Evaluation of thermodynamic functions relative to cavity formation in liquids: uses and misuses of Scaled Particle Theory

NICOLE MOREL-DESROSIERS AND JEAN-PIERRE MOREL[1]

Laboratoire d'Etude des Interactions Solutés–Solvants, Université de Clermont II, B.P. 45, 63170 Aubière, France

Received May 2, 1980

NICOLE MOREL-DESROSIERS and JEAN-PIERRE MOREL. Can. J. Chem. **59**, 1 (1981).

The Scaled Particle Theory (SPT) is probably the most powerful theory presently available, that enables the calculation of the thermodynamic functions relative to the formation of cavities in liquids. We give the general relationship between the enthalpy of vaporization and the enthalpy of formation of a molecular cavity in a pure normal liquid; the good agreement with the experimental data constitutes one of the strongest arguments justifying the application of SPT to real liquids. However, we show that SPT can lead to uncertain cavity terms if the molecular diameters of the studied liquids are not well-known. We compare, on the other hand, the cavity terms (G and H) calculated from Sinanoglu's theory, since this theory has been used to that end recently, with those obtained from SPT.

NICOLE MOREL-DESROSIERS et JEAN-PIERRE MOREL. Can. J. Chem. **59**, 1 (1981).

La "Scaled Particle Theory" (SPT) est sans doute la théorie la plus puissante disponible actuellement pour calculer les fonctions thermodynamiques relatives à la formation de cavités dans les liquides. Nous établissons la relation générale reliant l'enthalpie de vaporisation et l'enthalpie de création d'une cavité moléculaire pour un liquide normal; le bon accord avec l'expérience constitue un des meilleurs arguments justifiant l'application de la SPT aux liquides réels. Cependant, nous montrons que lorsque les diamètres moléculaires des liquides étudiés sont mal connus, la SPT peut conduire à des résultats incertains. Nous comparons d'autre part les termes de cavité (G et H) obtenus à l'aide de la théorie de Sinanoglu, théorie assez souvent utilisée à cette fin, avec ceux donnés par la SPT.

Introduction

Scaled Particle Theory (SPT) has often been applied, during the last years, to the investigation of solution properties. Recently, it has been used to predict Gibbs free energies, enthalpies, and entropies of transfer of large organic solutes from water to various solvents (1–3). The cavity terms calculated from SPT have also been compared (2, 3) to those obtained, unfortunately in an arguable way, from the macroscopic theory of Sinanoglu (4, 5) and the discrepancy between both sets of results has been used as the argument to question the validity of SPT.

After reading these controversial papers one feels it is necessary to recall some important points, unfortunately too often underestimated, relative to the application of SPT to real solutions and to clearly indicate some of its limitations. SPT is probably the most powerful theory available, at present, to calculate cavity terms corresponding to the introduction of a hard sphere at infinite dilution in a hard sphere fluid (6–8). We shall see that, without making use of any adjustable parameter, it leads, for a pure normal liquid, to an energy of cavity which is equal to the energy of vaporization of the liquid, this being a very important and severe criterion showing the validity of the theory. Of course, as soon as we leave the domain of simple molecules and try to apply SPT to sophisticated systems we cannot reasonably expect an accurate evaluation of the cavity terms. Consequently, we shall clearly indicate how dependent on the accuracy of the molecular parameters of the studied species the calculations are. We shall finally try to seriously compare the cavity terms calculated from SPT with those obtained from the theory of Sinanoglu, taking care to create in both cases cavities of comparable size.

Discussion

Theory

(a) Hard Spheres

The statistical mechanical theory of fluids employing distance scaling as a coupling procedure and hence called Scaled Particle Theory has been developed twenty years ago by Reiss *et al.* (6–8). The formalism of the theory has been extensively given in Reiss' comprehensive review (8). We shall only recall that SPT is concerned primarily with systems of particles having spherical symmetry and hard cores repelling one another with infinite force. It studies the probability that no molecule has its center within a spherical cell of radius r, this cavity being created, for instance, by insertion of a hard molecule of diameter σ_2 within the original fluid of molecules of diameter σ_1. The radius of the cavity is thus given by

$$[1] \qquad r = (\sigma_1 + \sigma_2)/2$$

This theory leads to an approximate expression for the reversible work expended in creating the

[1]To whom all correspondence should be addressed.

0008-4042/81/010001-07$01.00/0

©1981 National Research Council of Canada/Conseil national de recherches du Canada

Can. J. Chem. Downloaded from www.nrcresearchpress.com by 210.87.254.5 on 09/05/12
For personal use only.

Can. J. Chem. Downloaded from www.nrcresearchpress.com by 210.87.254.5 on 09/05/12
For personal use only.

cavity (the expression is exact for $r \leq \sigma_1/2$). It also leads to an analytical expression for the equation of state of a hard sphere fluid which is exact up to the third virial coefficient, which agrees over the entire range of fluid density with the equations of state obtained through the medium of machine computation and which is identical to the equation of state obtained from the exact solution of the Percus–Yevick equation (8).

(b) Real Liquids

The theory is extended to the study of real liquids through the introduction of the experimental density and the use of the model which considers the attractive part of the intermolecular potential of a real liquid as acting primarily to establish the density, i.e., the volume of a pseudo-container to which the molecules are confined (8). The real liquid in this pseudo-container may then be considered as a hard sphere fluid which is susceptible to treatment by SPT. However, although the theory gives the possibility to take implicitly into account the soft part (non-hard-core part) of the intermolecular potential of real solvents it requires that the solute molecule be like a hard billiard ball which interacts with solvent molecules only through their hard cores (8).

To check the validity of SPT when applied to real liquids, we shall now limit ourselves to the study of a pure liquid and derive the general relationship between the enthalpy of cavity and the enthalpy of vaporization.

We shall first consider the vaporization, under normal conditions (25°C, 1 atm), of a pure liquid to the ideal vapor. Assuming the internal degrees of freedom are the same in both phases, i.e. limiting our study to the particular case of a normal liquid, and using the results of statistical thermodynamics as expressed by Pierotti (9) for the decomposition of the chemical potentials, we can write

$$[2] \qquad \mu_g^0 = RT \ln q^{-1} + RT \ln \rho_g \Lambda^3$$

$$[3] \qquad \mu_l^0 = RT \ln q^{-1} + \mu_c^0 + \mu_i^0 + RT \ln \rho_l \Lambda^3$$

where $\rho_g = P^0/kT$ and $\rho_l = N/V^0$, P^0 being the pressure (1 atm), T the temperature, V^0 the molar volume of the liquid, k Boltzmann's constant, N Avogadro's number, and R the gas constant. Λ is the thermal de Broglie wavelength and q is the molecular partition function for the internal degrees of freedom. μ_c^0 is the chemical potential corresponding to the creation of a cavity at some fixed position in the fluid whereas μ_i^0 is the chemical potential corresponding to the interaction of one molecule, introduced into the cavity, with the neighbouring molecules. For the molar free energy of vaporization we thus have

$$[4] \qquad \Delta G_v^0 = \mu_g^0 - \mu_l^0 = RT \ln (P^0 V^0/RT) - \mu_c^0 - \mu_i^0$$

By simple derivation we get the standard molar enthalpy of vaporization

$$[5] \qquad \Delta H_v^0 = - H_c^0 - H_i^0 - \alpha RT^2 + RT$$

where H_c^0 and H_i^0 are the enthalpies of cavity and of interaction, respectively, and α is the coefficient of thermal expansion of the pure liquid.

We shall now look at the interaction term. It follows from statistical mechanics that the molar energy of vaporization of a normal liquid is approximately given by (10)

$$[6] \qquad \Delta E_v \simeq -\frac{N\rho}{2} \int u(r) g(r) 4\pi r^2 \, dr$$

where $u(r)$ is a pairwise additive intermolecular potential energy and $g(r)$ is the radial distribution function. On the other hand, the molar energy of interaction can be written as

$$[7] \qquad E_i = N\rho \int u(r) g(r) 4\pi r^2 \, dr$$

Hence, it follows that for such a liquid

$$[8] \qquad \Delta E_v = - E_i/2$$

as qualitatively described by Eyring (11) many years ago. By introducing into eq. [8] the relation $E = H - PV$ we simply get, under standard conditions (since the vapor is ideal and the PV terms for the liquid phase are negligible),

$$[9] \qquad H_i^0 = 2RT - 2\Delta H_v^0$$

Finally, by introducing eq. [9] into eq. [5] we get the following relation for the standard molar enthalpy of vaporization

$$[10] \qquad \Delta H_v^0 = H_c^0 + \alpha RT^2 + RT$$

This general equation should be satisfied by any theory leading to cavity terms.

Let us then check to which extent SPT can satisfy it, the enthalpy of cavity of the pure liquid being given, under standard conditions, by

$$[11] \qquad H_c^0 = \alpha RT^2 \left(\frac{y}{1-y}\right) \times \left\{\frac{6}{(1-y)} + \frac{9y}{(1-y)^2} + 1\right\}$$

where

$$[12] \qquad y = N\pi\sigma_1^3/6V^0$$

By introducing eq. [11] into eq. [10] we get

Can. J. Chem. Downloaded from www.nrcresearchpress.com by 210.87.254.5 on 09/05/12
For personal use only.

$$[13a] \quad \Delta H_v^0 = RT + \alpha RT^2 + \alpha RT^2\left(\frac{y}{1-y}\right) \times \left\{\frac{6}{(1-y)} + \frac{9y}{(1-y)^2} + 1\right\}$$

$$[13b] \quad = RT + \alpha RT^2\left\{\frac{(1+2y)^2}{(1-y)^3}\right\}$$

Reiss *et al.* (7) have arrived at eq. [13*b*] from a completely different starting-point. In fact, they studied the gas–liquid equilibrium at saturation pressure and differentiated along the line of coexistence between liquid and vapor phases to get the enthalpy of vaporization at this pressure. At the same temperature, their equation and ours give the same result since ΔH_v and α are almost pressure-independent. Wilhelm and Battino (12) have shown that the ΔH_v calculated from Reiss' equation for nonpolar, normal liquids are in good agreement (better than 10%) with the experimental enthalpies of vaporization. This constitutes a severe criterion showing the validity of SPT for the determination of the enthalpy of cavity of real simple systems. More recently, the study of the enthalpy, volume, and heat capacity of cavity of adamantane and of cyclohexane in cyclohexane, *n*-hexane, and carbon tetrachloride has also provided an interesting test of the validity of SPT for simple liquids (13).

Unfortunately, it is much less evident to check whether or not SPT gives satisfactory results when applied to the creation of a spherical cavity into liquids involving strong, directional, and nonadditive interactions. For such liquids, the enthalpy of vaporization method cannot serve as a test since eq. [8] is valid for "normal" liquids only. The enthalpy of vaporization test implies that the "solute" introduced into the cavity is simply one molecule of solvent (since we study pure liquids). Since SPT imperatively requires that the solute be as hard and spherical as possible, it obviously appears that this test cannot be used for liquids such as alcohols, water, dimethyl sulfoxide, etc.

With these solvents, one can look at binary solutions, provided the solute is almost hard sphere. The method devised by Pierotti (14) and using the solubility measurements of many simple gases in various solvents for the determination of the diameter of the solvent molecules constitutes an excellent test of the validity of SPT whatever the solvent. Pierotti has shown that the diameter of water determined in this manner (2.75 Å) is in excellent agreement with the value deduced from second virial coefficient (15). Wilhelm and Battino (16) and de Ligny and van der Veen (17, 18) have used this method to determine the diameter of many polar and nonpolar solvents. The results they have obtained, even for solvents involving strong interactions (e.g., methanol, ethanol, acetone, ...), are in very good agreement with the diameters deduced from various methods (19). Such an agreement for many polar substances cannot be fortuitous and, hence, seems to show that, provided the studied solute is as hard sphere as possible, SPT can also be used for the calculation of cavity terms in solvents involving nonadditive interactions.

We must note, however, that the gaseous solutes used in Pierotti's method are of rather small size. This is a fortunate situation since there seems to be, as we shall see, some restriction on the size of the hard sphere solute when we apply the original version of SPT to solvents involving strong interactions. This has been shown after Stillinger (20) has improved upon SPT original version in the particular case of pure water by explicitly incorporating surface tensions and radial distribution functions. Lucas and Bury (21) have compared the original SPT with Stillinger's modified version for the free energies, enthalpies, and entropies of transfer of hard sphere solutes of various sizes from gaseous state to water at infinite dilution, at 4°C. They have concluded that both versions lead to cavity terms which are pretty close (less than 10% difference) provided σ_2 is smaller than 4 Å. Unfortunately, such a comparison cannot be done, at present, for other liquids involving strong interactions since Stillinger's version requires the knowledge of the radial distribution function and its derivative with temperature.

Anyhow, it seems that SPT can give, provided the solutes are judiciously chosen, satisfactory cavity terms in all solvents. One must, however, be aware of the fact that the calculated cavity terms are extremely dependent on the uncertainty of the molecular diameters of the involved species. Desrosiers and Desnoyers (22) have shown the tremendous dependence of the volume and of the heat capacity of cavity on the diameter of the solvent molecules. Let us now examine the behaviour of the free energy and of the enthalpy.

Uncertainty of the Calculated Cavity Terms

According to SPT the free energy of cavity is given by

$$[14] \quad G_c = K_0 + K_1 r + K_2 r^2 + K_3 r^3$$

where

$$K_0 = RT\left\{-\ln(1-y) + \frac{9}{2}\left(\frac{y}{1-y}\right)^2\right\} - \frac{N\pi\sigma_1^3 P}{6}$$

$$K_1 = -\frac{RT}{\sigma_1}\left\{6\left(\frac{y}{1-y}\right) + 18\left(\frac{y}{1-y}\right)^2\right\} + N\pi\sigma_1^2 P \qquad [15]$$

$$K_2 = \frac{RT}{\sigma_1^2}\left\{12\left(\frac{y}{1-y}\right) + 18\left(\frac{y}{1-y}\right)^2\right\} - 2N\pi\sigma_1 P$$

$$K_3 = \frac{4}{3}N\pi P$$

r being calculated from eq. [1] and y from eq. [12].

The enthalpy of cavity is then

$$H_c = \alpha RT^2\left(\frac{y}{1-y}\right) \times \left\{\frac{6B}{(1-y)} + \frac{36yD}{(1-y)^2} + 1\right\} \qquad [16]$$

where

$$B = 2(r/\sigma_1)^2 - (r/\sigma_1)$$
$$D = (r/\sigma_1)^2 - (r/\sigma_1) + 1/4 \qquad [17]$$

The calculated cavity terms are extremely sensitive to the choice of the diameter of the studied solvent since σ_1 is raised to the sixth power in the calculations. To illustrate this phenomena we have calculated the free energies and the enthalpies of cavity corresponding to the introduction of an arbitrary solute of $\sigma_2 = 4$ Å into four rather different solvents (H_2O, CH_3OH, DMSO, c-C_6H_{12}). We have varied σ_1 by ± 0.1 Å around Wilhelm and Battino's values (16). These results are reported in Fig. 1 and the various parameters used for the calculations are given in Table 1. We see that for a $\delta\sigma_1$ as small as 0.1 Å G_c and H_c can vary by as much as 4 kJ mol^{-1}. This corresponds to a relative uncertainty of 10 to 20% for G_c and of 20 to 30% for H_c depending on the solvent. Furthermore, the uncertainty may be much larger for transfer functions.

On the other hand, it is easy to show from eqs. [14] and [16] that the cavity terms are much less sensitive to the choice of the diameter of the solute. For $\delta\sigma_2 = \pm 0.1$ Å (around $\sigma_2 = 4$ Å) G_c and H_c vary by about 0.5–1.0 kJ mol^{-1}, this corresponding to a relative uncertainty of 4% for each function. However, for a transfer process the uncertainty due to $\delta\sigma_2$ almost cancels.

Finally, we must add that since H_c is directly proportional to α it is necessary to know the thermal expansion coefficient of the pure solvent with good accuracy.

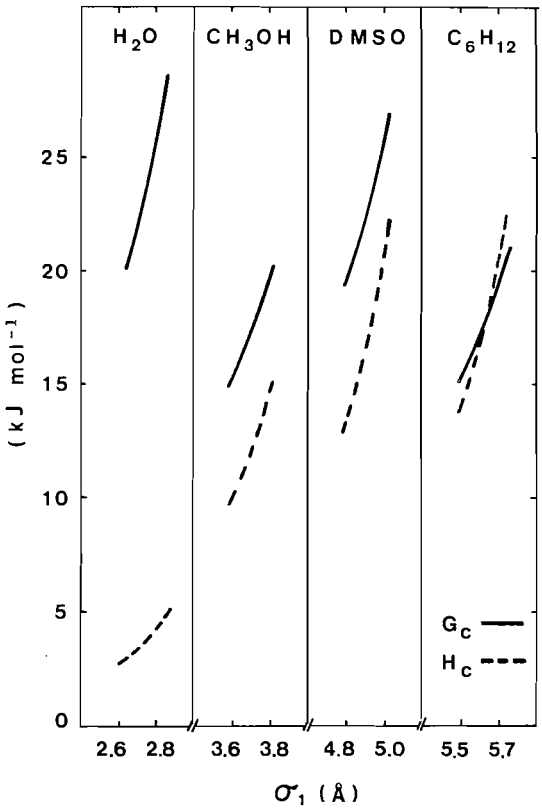

FIG. 1. Variation of the free energy and of the enthalpy of cavity with the diameter of the solvent σ_1, for a solute of $\sigma_2 = 4$ Å in water, methanol, dimethyl sulfoxide, and cyclohexane, at 25°C.

Since the uncertainty in the calculated terms can be very important, it is necessary to be extremely cautious when applying SPT to real systems especially if their molecular parameters are not very well-known. The interaction terms obtained by subtracting the cavity terms from the experimental thermodynamic functions (1, 2) may thus be very dubious and their interpretation hazardous.

Comparison of Cavity Terms Calculated from SPT and from Sinanoglu's Theory

The validity of SPT has been questioned recently (2, 3) on the sole basis of the discrepancy observed between two sets of cavity terms: those calculated from SPT and those obtained from the theory of Sinanoglu (4, 5). Unfortunately, this comparison was misleading since cavities of very different sizes were created in both cases (SPT calculations were done for a solute of $\sigma_2 = 8.4$ Å or $N\pi\sigma_2^3/6 = 187$ cm^3 mol^{-1} whereas Sinanoglu's theory was applied to a solute volume of 296 cm^3 mol^{-1}). Fur-

Can. J. Chem. Downloaded from www.nrcresearchpress.com by 210.87.254.5 on 09/05/12
For personal use only.

TABLE 1. Molecular parameters and physical properties of pure water, methanol, dimethyl sulfoxide, and cyclohexane, at 25°C. $K_1^e(1)$ and $K_1^s(1)$ are Sinanoglu's microscopic cavity factors

Liquid	σ_1 (Å)	V^0 (cm^3 mol^{-1})	$10^3\alpha$ (K^{-1})	γ^0 (dyn cm^{-1})	$\partial\gamma/\partial T^0$ (dyn cm^{-1} K^{-1})	$K_1^e(1)^g$	$K_1^s(1)^g$
H_2O	2.75[a]	18.0687[c]	0.257[c]	72.00	−0.157	1.277	1.235
CH_3OH	3.69[b]	40.73[b]	1.101[d]	22.20	−0.086	1.776	1.609
DMSO	4.91[b]	71.37[b]	0.88[e]				
c-C_6H_{12}	5.63[b]	108.75[b]	1.215[f]	24.38	−0.120	0.621	0.466

[a]From ref. 14.
[b]From ref. 16.
[c]Reference 27.
[d]Reference 28.
[e]Reference 29.
[f]Reference 30.
[g]From ref. 5.

thermore, one can wonder if it is realistic to expect the results obtained from a macroscopic theory (relating the bulk surface tension to the energy of formation of a molecular-sized cavity) to be as meaningful as or comparable to those obtained from a theory based on statistical mechanics and using molecular parameters. Anyhow, it can be interesting to calculate both sets of terms in a less questionable way.

The central idea of the development of Sinanoglu's theory is that the work W of expanding the spherical cavity radius from r to $r + \partial r$ can be written as a sum of a volume and a surface contribution. For sufficiently large r it follows that

$$[18] \quad W(r) \simeq \tfrac{4}{3}P\pi r^3 + 4\pi r^2\gamma$$

γ being a surface tension. For cavities of microscopic size a term accounting for the curvature dependence of the surface work must be added. It is important to note, at this point, that γ does not represent the interfacial tension between a liquid and its vapor since the cavity is not a bubble filled with vapor. In fact, the creation of a cavity in a liquid is equivalent to the introduction of a hard sphere and, hence, γ is the interfacial tension between the liquid and a rigid wall (8).

Starting on this basis and neglecting the volume work, Sinanoglu (4) gives for the free energy of cavity formation the following relation

$$[19] \quad G_c = K_1^e S\gamma(1 - X)$$

$$[20] \quad X = \left(1 - \frac{K_1^s}{K_1^e}\right)\left\{\frac{\partial \ln \gamma}{\partial \ln T} + \frac{2}{3}\alpha T\right\}$$

where S is the geometric surface area and α the coefficient of thermal expansion of the cavity. K_1^e and K_1^s are the constants adjusting the planar surface energy and entropy to highly curved microscopic dimensions. The following approximations are made: γ and α are assumed equal to the surface tension and to the coefficient of thermal expansion of the pure solvent. It is hard to estimate the importance of such approximations but we know that the uncertainty in γ will be of primary importance since G_c is directly proportional to the surface tension. With this theory the solvent is a continuum and, hence, the radius of the cavity is assumed equal to the radius of the solute ($r = \sigma_2/2$). Then,

$$[21] \quad S = 4\pi r^2 = 4.836 v_2^{2/3}$$

v_2 being the intrinsic volume of one molecule of solute. Hence, according to Sinanoglu, it follows that the molar free energy of cavity, expressed in J mol^{-1}, is given by

$$[22] \quad G_c(\text{J mol}^{-1}) = 6.023K_1^e 4.836 v_2^{2/3}\gamma_1 \times \left\{1 - \left(1 - \frac{K_1^s}{K_1^e}\right)\left(\frac{\partial \ln \gamma_1}{\partial \ln T} + \frac{2}{3}\alpha_1 T\right)\right\}$$

γ_1 being in dyn cm^{-1} and v_2 in Å^3. In ref. 4 it is indicated that if the solute is not a liquid v_2 is estimated from space-filling models or from X-ray structures whereas if it is a liquid v_2 is obtained from the experimental density d_2 of the liquid. The latter seems rather peculiar since it is straightforward, because of the compacity of the liquid, that

$$[23] \quad v_2 = \tfrac{4}{3}\pi r^3 \neq V_2^0/N = M_2/d_2 N$$

M_2 being the solute molecular weight. One should instead rely, for liquid solutes, on the molecular diameters determined from viscosity data, second virial coefficients, or deduced from various theories of statistical mechanics (19). By no way should v_2 be confused with the experimental molar volume V_2^0 and, *a fortiori*, with a partial molar volume. Abraham and Nasehzadeh (2) have used the partial molar volume of Ph_4As^+ in water (Millero's value (23): 295.6 cm^3 mol^{-1}) instead of the intrinsic volume ($N\pi\sigma_2^3/6 = 187$ cm^3 mol^{-1} (1)) to calculate, using Sinanoglu's theory, the cavity terms of Ph_4As^+ in various solvents. Accordingly their calculated results cannot represent cavity

Can. J. Chem. Downloaded from www.nrcresearchpress.com by 210.87.254.5 on 09/05/12
For personal use only.

terms and, hence, cannot be compared to SPT results.

The main problem with Sinanoglu's theory is the determination of the constants K_1^e and K_1^s. These functions are approximately given, for nonpolar solvents, by the following relation empirically deduced from the solubility and mixing data of asymmetric systems (5) (K_1 corresponding either to K_1^e or K_1^s)

$$[24] \quad K_1 = 1 + \left(\frac{v_1}{v_2}\right)^{2/3} [K_1(1) - 1]$$

where v_1 and v_2 are the molecular volumes of the solvent and solute, respectively, and $K_1^e(1)$, $K_1^s(1)$ are the adjustable microscopic cavity factors for the pure solvent. The way $K_1^e(1)$ and $K_1^s(1)$ are evaluated is not clearly indicated in Sinanoglu's papers but some of these factors are tabulated, for many common solvents, in ref. 5. Sinanoglu (24) stipulates that these can be used wherever v_1 and v_2 are roughly comparable. To use these factors with very small σ_2 can lead, for many solvents, to negative K_1^e and K_1^s values (which can even be pretty large) and, consequently, to negative free energies and energies of cavity. Furthermore, it is impossible (whereas it is easy to do it with SPT) to estimate the free energy of cavity for a point solute ($\sigma_2 = 0$).

Finally, Sinanoglu uses eq. [24] for polar solvents as well without indicating, however, the uncertainty in K_1^e (directly reflected on G_c) resulting from such an approximation.

The molar energy of cavity is given (4) by the following relation

$$[25] \quad E_c(\text{J mol}^{-1}) = 6.023 K_1^e 4.836 v_2^{2/3} \gamma_1 \times \left\{1 - \frac{\partial \ln \gamma_1}{\partial \ln T} - \frac{2}{3}\alpha_1 T\right\}$$

Using eqs. [22] to [25] (assuming $H_c \simeq E_c$) we have thus calculated the free energy and the enthalpy corresponding to the creation of cavities of diameter increasing from 1 to 10 Å (being aware, for the reasons mentioned in the preceding paragraph, that the results for very small σ_2 may not be meaningful) in two very different solvents: water and cyclohexane. To perform these calculations we have used Sinanoglu's microscopic cavity factors and the physical properties of pure solvents given in Table 1. The molecular volume v_2 is obtained from $\pi\sigma_2^3/6$ whereas the molecular volume of the solvent v_1 is calculated (*a*) from the diameter σ_1 given in Table 1 and, for comparison, (*b*) from (as does Sinanoglu) the molar volume of the pure solvent V_1^0. We have reported all the calculated results

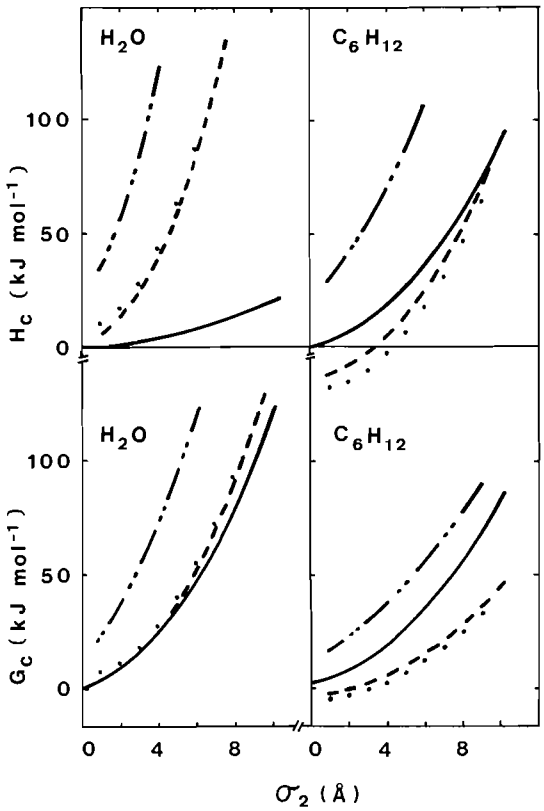

FIG. 2. Comparison of free energies and enthalpies of cavity calculated from SPT (—) and from Sinanoglu's theory (with $r = \sigma_2/2$ and the molecular diameter of the solvent (---); with $r = \sigma_2/2$ and the molar volume of the solvent (· · ·); with $r = (\sigma_1 + \sigma_2)/2$ (----)).

on Fig. 2 along with, for comparison, the corresponding STP cavity terms. We see that the two ways of evaluating v_1 (which appears only in eq. [24]) lead to not very different cavity terms. It is difficult to give the definition of the surface area of a cavity of microscopic dimensions (25). This is why we have also tried to perform the calculations by using eq. [1] to evaluate the cavity radius. The results of Fig. 2 show that G_c and H_c values increase very much by going from $r = \sigma_2/2$ to $r = (\sigma_1 + \sigma_2)/2$.

If we consider the particular process corresponding to the introduction of a molecule of cyclohexane ($\sigma_2 = 5.63$ Å) into pure cyclohexane, we see that H_c calculated from Sinanoglu's theory does not satisfy very well the general equation (eq. [10]) relating the enthalpy of vaporization and the enthalpy of cavity of pure normal liquids whereas the SPT term does ($\Delta H_v(\text{calcd})/\Delta H_v(\text{exp}) = 0.74$ with Sinanoglu's theory and 1.06 with SPT). SPT terms are probably the best cavity terms we can

Can. J. Chem. Downloaded from www.nrcresearchpress.com by 210.87.254.5 on 09/05/12
For personal use only.

get, at present, and as mentioned previously it may not be realistic to compare them with the cavity terms calculated from the macroscopic theory of Sinanoglu. Hence, we shall not analyse the results of Fig. 2 any more but only mention that the agreement between Sinanoglu (with $r = \sigma_2/2$) and SPT terms is, surprisingly, not so bad (except for H_c in water).

Sinanoglu's theory can thus be used to get gross approximations of the cavity terms but should never be preferred to SPT when the parameters necessary to apply the latter are known or can be evaluated (2, 3, 26).

Conclusion

The application of SPT, because of the bases of the theory, is restricted to the following species: (*a*) the solute must be as hard and spherical as possible and must not, of course, have strong and directional interactions with the solvent molecules. When such interactions are involved, the additivity of the cavity and interaction terms is itself arguable. (*b*) the solvent may be any real liquid. We have underlined, however, the tremendous importance of knowing the diameter of the solvent molecules with good accuracy. Since the various methods allowing the determination of the diameter lead to slightly different results, it is a coherent choice to determine it by applying SPT to gas solubility data (Pierotti's method).

Provided these conditions are respected and one is aware of the possible uncertainty in the results, SPT is the most powerful theory available, at present, to evaluate the thermodynamic data relative to the formation of spherical cavities in real liquids.

1. C. TREINER. Can. J. Chem. **55**, 682 (1977).
2. M. H. ABRAHAM and A. NASEHZADEH. Can. J. Chem. **57**, 71 (1979).
3. M. H. ABRAHAM and A. NASEHZADEH. Can. J. Chem. **57**, 2004 (1979).
4. O. SINANOGLU. Molecular associations in biology. Academic Press, NY. 1968. p. 427.
5. T. HALICIOGLU and O. SINANOGLU. Ann. New York Acad. Sci. **158**, 308 (1969).
6. H. REISS, H. L. FRISCH, and J. L. LEBOWITZ. J. Chem. Phys. **31**, 369 (1959).
7. H. REISS, H. L. FRISCH, E. HELFAND, and J. L. LEBOWITZ. J. Chem. Phys. **32**, 119 (1960).
8. H. REISS. Adv. Chem. Phys. **9**, 1 (1965); *In* Statistical mechanics and statistical methods in theory and application. *Edited by* U. Landman. Plenum Press. 1977. p. 99.
9. R. A. PIEROTTI. J. Phys. Chem. **67**, 1840 (1963).
10. J. H. HILDEBRAND and R. L. SCOTT. The solubility of nonelectrolytes. Dover, NY. 1964. p. 72.
11. H. EYRING. J. Chem. Phys. **4**, 283 (1936).
12. E. WILHELM and R. BATTINO. J. Chem. Phys. **58**, 3561 (1973).
13. N. MOREL-DESROSIERS and J. P. MOREL. J. Solution Chem. **8**, 579 (1979).
14. R. A. PIEROTTI. J. Phys. Chem. **69**, 281 (1965).
15. J. S. ROWLINSON. Trans. Faraday Soc. **47**, 120 (1951).
16. E. WILHELM and R. BATTINO. J. Chem. Phys. **55**, 4012 (1971).
17. C. L. DE LIGNY and N. G. VAN DER VEEN. Recl. Trav. Chim. **90**, 984 (1971).
18. C. L. DE LIGNY and N. G. VAN DER VEEN. Chem. Eng. Sci. **27**, 391 (1972).
19. J. O. HIRSCHFELDER, C. F. CURTISS, and R. B. BIRD. Molecular theory of gases and liquids. Wiley, NY. 1965.
20. F. H. STILLINGER. J. Solution Chem. **2**, 141 (1973).
21. M. LUCAS and R. BURY. J. Phys. Chem. **80**, 999 (1976).
22. N. DESROSIERS and J. E. DESNOYERS. Can. J. Chem. **54**, 3800 (1976).
23. F. J. MILLERO. Chem. Rev. **71**, 147 (1971).
24. O. SINANOGLU. Theor. Chim. Acta, **33**, 279 (1974).
25. A. BEN-NAIM. Hydrophobic interactions. Plenum Press, NY. 1980. p. 40.
26. J. J. MOURA RAMOS, M. LEMMERS, R. OTTINGER, M. L. STIEN, and J. REISSE. J. Chem. Res. (M), 0658 (1977).
27. G. S. KELL. J. Chem. Eng. Data, **12**, 66 (1967).
28. LANDOLT-BORNSTEIN. Zahlenwerte und funktionen aus physik, chemie, astronomie, geophysik, technik. Springer-Verlag. 1961. II band. 1 teil. p. 665.
29. J. N. BUTLER. J. Electroanal. Chem. **14**, 89 (1967).
30. M. B. EWING, K. N. MARSH, and R. H. STOKES. J. Chem. Thermodyn. **4**, 637 (1972).

Can. J. Chem. Downloaded from www.nrcresearchpress.com by 210.87.254.5 on 09/05/12
For personal use only.

Rate processes and nuclear magnetic resonance spectra of amine·SO_2 complexes + H_2O in liquid SO_2

KONRAD T. WU[1] AND ANDREW J. YENCHA[2]

Department of Chemistry, State University of New York at Albany, Albany, NY 12222, U.S.A.

Received March 10, 1980

KONRAD T. WU and ANDREW J. YENCHA. Can. J. Chem. **59**, 8 (1981).

A ^1H dnmr study has been performed on a series of addition compounds formed from the gaseous reactions of di- and trimethyl amine and triethyl amine with sulfur dioxide in the presence of a small amount of water in a liquid sulfur dioxide solvent. The dynamic system involves an equilibrium of the general form: amine·H^+ ⇄ amine·SO_2. The activation parameters for the exchange process were calculated. Large positive entropies of activation were found in the present systems that strongly suggest the formation of an ion pair in the transition state in which the activation process is controlled largely by solvation effects.

KONRAD T. WU et ANDREW J. YENCHA. Can. J. Chem. **59**, 8 (1981).

Faisant appel à la rmn dynamique du ^1H, on a étudié une série de composés d'addition formée au cours de réactions en phase gazeuse entre les di- et tri-méthylamines et triéthylamine et le bioxyde de soufre en présence d'une faible quantité d'eau dans du bioxyde de soufre liquide comme solvant. Le système dynamique implique un équilibre général de la forme: amine H^+ ⇄ amine·SO_2. On a calculé les paramètres d'activation de la réaction d'échange. Dans ces systèmes, on a trouvé que les entropies d'activation sont fortement positives; ceci suggère qu'il y a formation d'une paire d'ions dans l'état de transition dans lequel le processus d'activation est principalement contrôlé par des effets de solvatation.

[Traduit par le journal]

Introduction

It is well known that the protonation of an amine in aqueous solution is a diffusion controlled process (1). Steric hindrance arising from solvation and from formation of the transition-state complex has a noticeable effect on the rate of protonation (2), since the proton-transfer step is so fast that other steps become rate-determining. This steric effect has recently been shown to be responsible for the dramatic reduction in rate (3, 4) and for the large increase in entropy of activation (4) in various cases of protonation of nucleophilic addition reaction of amines. We wish to report an example of a similar type of reaction, i.e. protonation of a charge-transfer complex (amine·SO_2). We have examined this interesting effect employing dynamic nuclear magnetic resonance (dnmr) spectroscopy, which affords additional thermodynamic data and structural information on the protonation processes.

The dnmr method (5) has been used widely for the studies of intra- and intermolecular equilibrium processes of chemical systems involving the transfer of components of ions and molecules among different chemical environments in the solution phase. All of these studies deal with structural rearrangement of chemical exchange processes, either with or without changes in chemical bonding. The dnmr studies of the chemical system of amine·SO_2 + H_2O reported here involve more than one kind of exchange process taking place on the same temperature scale. From the observed dnmr spectra, some properties of these exchange processes can also be understood.

Experimental

The reactions between amines and sulfur dioxide to give molecular complex formation have been studied for many decades (6). Based on careful considerations on the active chemical nature of the species involved in this study and on the solubility of the substances under investigation, liquid sulfur dioxide was chosen as the solvent for this study. Liquid sulfur dioxide has been known as an excellent solvent for many years. A recent detailed discussion of its solvent properties has been given by Burow (7). An extremely successful use of liquid SO_2 as a solvent in nmr studies was demonstrated in the analyses of geometrical configurations of the cyclobutane protons in the study of the photodimers of coumarin and *N*-methylcarbostyril (8). The high solubility of the amine·SO_2 complexes in liquid SO_2 makes it appropriate as a solvent in the present study.

The reactions between the various amines and sulfur dioxide were carried out in a flask on a vacuum system. The mixing of the two reagents resulted in the rapid formation of particles in the gas phase with the evolution of considerable heat. The similar reaction of ammonia with sulfur dioxide has been shown to produce a heat of reaction of −125.5 kJ/mol (9). The reaction products were collected in an nmr tube mounted directly below the reaction vessel. The reaction system was then evacuated and the nmr tube containing the sample cooled to −78°C. Gaseous SO_2 was then slowly bled into the system where it was liquified in the sample tube. A small amount of liquid water (~2% by volume) was added through a septum in the reaction flask using a syringe and needle. The nmr tube was then sealed off and allowed to warm to room temperature.

Elemental analyses of the reaction products between di- and trimethyl amine (DMA and TMA) with SO_2 indicated the formation of a 1:1 adduct. Pure $(CH_3)_2NH·SO_2$ was a yellowish oily

[1]Present address: Department of Chemistry, State University of New York, College at Old Westbury, Old Westbury, NY 11568, U.S.A.

[2]To whom all correspondence should be addressed.

0008-4042/81/010008-06$01.00/0

©1981 National Research Council of Canada/Conseil national de recherches du Canada

Can. J. Chem. Downloaded from www.nrcresearchpress.com by 210.87.254.40 on 09/05/12
For personal use only.

Can. J. Chem. Downloaded from www.nrcresearchpress.com by 210.87.254.40 on 09/05/12
For personal use only.

liquid with the following elemental makeup (*Anal.* calcd.: C 22.01, H 6.46, N 12.83, S 29.38, O 29.32; found: C 21.55, H 6.61, N 12.47, S 29.85, O 27.81). The product $(CH_3)_3N{\cdot}SO_2$ was a white crystalline material whose elemental analysis yielded the following results (*Anal.* calcd.: C 29.25, H 7.37, N 11.37, S 26.03, O 25.98; found: C 29.56, H 7.54, N 11.55, S 26.20, O 25.82). Analysis of the reaction product between triethyl amine (TEA) and SO_2 was not performed. The white solid product obtained from the reaction of monomethyl amine (MMA) and SO_2 was found not to dissolve in liquid SO_2, which might indicate the formation of a polymeric compound.[3]

^1H nmr spectra were recorded using a 60-MHz Varian A-60A spectrometer in conjunction with a Varian V-4340 variable temperature probe. Temperature calibration was determined in the usual manner with methanol. A quadratic equation was used to fit the results (12). The readings were accurate to ±2–3°C.

Computed dnmr spectra of the di- and trimethyl amine systems were obtained through the use of the classical two-site line shape equations, modified by generating the coalescing multiplets for the corresponding components (5*f*). The signal strength was plotted against the frequency after proper normalization. Simulation spectra were obtained by adjusting the rate constant parameter for the exchange process until a good fit was achieved between the computed and experimental spectra. Linear relationships were assumed for both the population of the species (namely the equilibrium constant dependence) and the linewidth with temperature (13). The equilibrium concentration ratios, amine·H^+/amine·SO_2, at low temperatures were estimated by measuring the peak area of each species. Linear extrapolation ($\log k$ vs. $1/T$) was then made to obtain the population ratios at higher temperatures. The chemical shift difference ($\Delta\nu$) was also assumed to depend linearly upon temperature. Those values at fast exchange rates were thus similarly obtained by extrapolation. Ten experimental points were used in each case for such extrapolation measurements.

The gaseous reactant materials mono-, di-, and trimethyl amine and sulfur dioxide were obtained from Matheson Gas Products. Triethyl amine was obtained from the Eastman Kodak Co. All were of high purity, and no purification was performed.

Results and Discussion

The ^1H dnmr spectra of the TMA and DMA compounds at various temperatures together with the matching calculated spectra for the corresponding exchange rates are shown in Figs. 1 and 2, respectively. The identity of the ionic and complex amine compounds at low temperatures were established by obtaining the spectra in the presence of large amounts of water and in the absence of any water. In the former case, only alkylammonium ion exists. For the latter, the amine·SO_2 charge-transfer complex was the only product species found. The multiplets for the methyl groups attached to nitrogen in the ionic forms were further checked using a 100-MHz spectrometer to confirm that the splittings were caused by the indirect coupling of the N–H protons. At low temperature these components are separated by 5.6 Hz for the dimethylammonium ion and 5.1 Hz for the trimethylammonium ion, which are almost identical to those in aqueous solution (14). The rate of proton exchange increases with increasing temperature resulting in the coalescence of the multiplet components. At the same time, it is observed that the alkylammonium ion and complex compound sig-

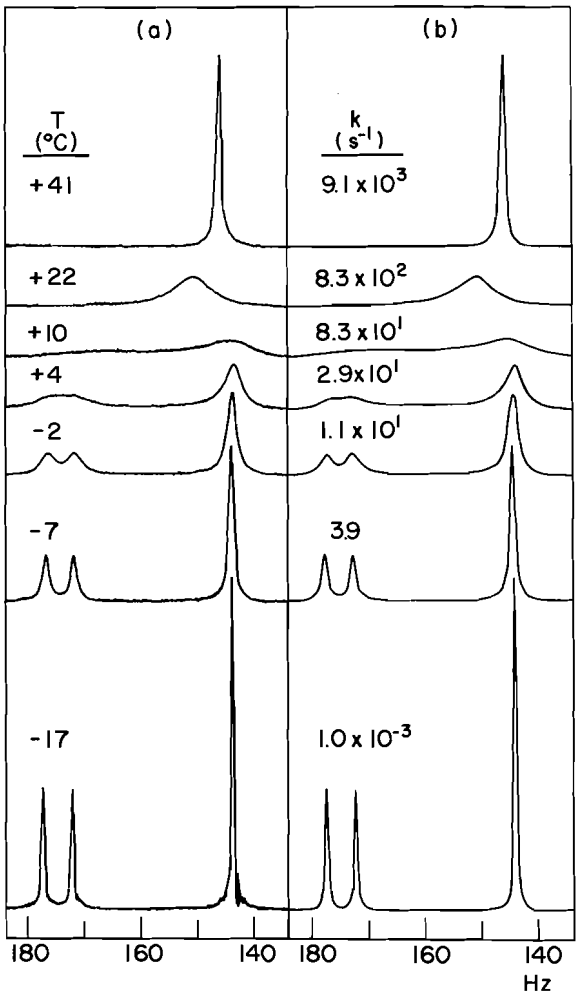

FIG. 1. Experimental 60-MHz ^1H dnmr spectra (*a*) of trimethyl amine·SO_2 + H_2O in liquid SO_2 at various temperatures and the corresponding simulated line-shape spectra, (*b*) with the rate constants for ion–complex exchange.

[3]Kinumaki and Hata (10) have proposed that the reaction of MMA and SO_2 proceeds as follows:

[*i*] $3CH_3NH_2 + 3SO_2 \rightarrow (CH_3NH_3)_2S_2O_5 + CH_3NSO$

where the pyrosulfite product, $(CH_3NH_3)_2S_2O_5$, is a solid and the product CH_3NSO, methylthionylamine, is a gas at room temperature. Since a pyrosulfite is expected to dissolve in liquid SO_2 that contains a small amount of water by virtue of the formation of a sulfite ion according to the equilibrium (11)

[*ii*] $S_2O_5^{2-} + H_2O \rightleftarrows 2HSO_3^-$

it does not appear that the solid product is a pyrosulfite.

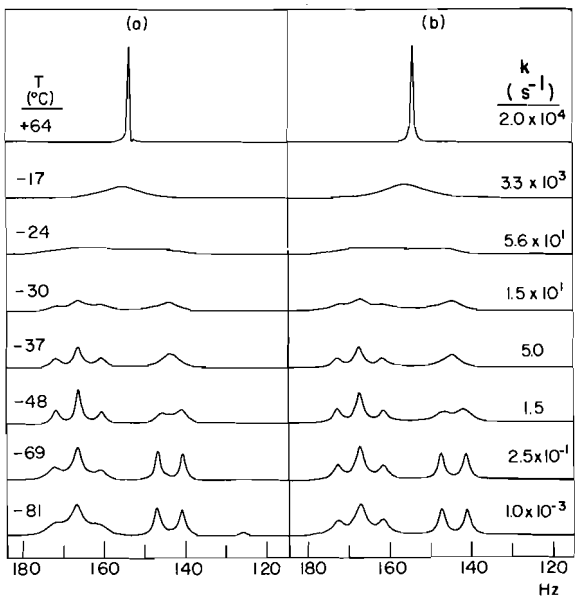

FIG. 2. Experimental 60-MHz ^1H dnmr spectra (*a*) of dimethyl amine·SO_2 + H_2O in liquid SO_2 at various temperatures and the corresponding simulated line-shape spectra, (*b*) with the rate constants for ion–complex exchange.

nals also collapse. This is obviously caused by the exchange of nuclei between different molecules. The broadening of the methyl signals at these intermediate exchange rates is due to the competition between hydrogen bonding to nitrogen and N—S charge-transfer bonding. Beyond these coalescing points, the signal shifts gradually towards higher fields, which results from increased dissociation of the complex compound. All observed exchange processes are reversible in the temperature range of interest.

The N—H proton absorptions of the ionic compounds (not shown in Figs. 1 and 2) were extensively broadened due to quadrupole effects. Integration of their signal strengths, however, confirmed their identity. The broadening of both the N—H proton absorption and the methyl signals of these ionic compounds give some definite indication about the exchange process between the ionic and non-ionic species. The small amount of water present in these systems may play some part in this process. The absence of an acidic proton signal in the spectra may be due to broadening resulting from a rapid equilibrium process. A similar feature has been observed previously in the literature (15). The N—H proton absorption signal of the $(CH_3)_2NH{\cdot}SO_2$ complex (not shown in Fig. 2) was broad in the absence of exchange, undetectable in the transition region, and a sharp line at fast exchange rates. No clear spectral pattern was observed for these N—H proton absorptions, thus a quantitative evaluation of the exchange broadening of these lines was judged to be impracticable.

The spin coupling of the methyl groups with the N—H proton of the DMA·SO_2 complex was also observed at low temperature (see Fig. 2). This coupling constant was measured to be 6.0 Hz. It has been observed that the small peak at 125.6 Hz emerges from beneath the charge-transfer complex peak as the temperature is lowered. Since this peak is quite different from the charge-transfer peak in both amplitude and shape (singlet vs. doublet) at low temperatures, the observed spectral pattern is thus not likely a result of a conformational effect due to a rotational process. The relative shift of these two bands was found to be concentration-dependent. Therefore, this small peak may arise from a polymeric aggregate. Because this peak appears at a much higher field than the doublet of $(CH_3)_2NH{\cdot}SO_2$, the structure of $[(CH_3)_2NH]_n{\cdot}SO_2$ is preferred rather than $[(CH_3)_2NH{\cdot}SO_2]_n$. A similar complex has been found (16) to be formed in the reaction of ammonia with SO_2 in the presence of H_2O. It seems to support our interpretation.

In Fig. 3 are shown the nmr spectra of the TMA compound dissolved in liquid SO_2 with D_2O added (upper trace) and H_2O added (lower trace) at −17°C. From this comparison it is clear that the low-field doublet in the H_2O added system is due to spin–spin splitting of the methyl protons of the ionic compound by an attached proton on the nitrogen atom. The two small peaks indicated by arrows in the D_2O added case are due to a small amount of H_2O impurity in the starting reactant materials. The line-widths of the deuterium compound system are expectedly broader than those of the hydrogen ones.

The dnmr spectra of the TEA system are shown in Fig. 4. As in the cases of the DMA and TMA systems, proton absorptions are detected for the species $(CH_3CH_2)_3NH^+$ and $(CH_3CH_2)_3N{\cdot}SO_2$. In both cases the three ethyl groups are equivalent. At the highest temperature measured, two well-defined groupings appear. At high-field (about 125 Hz), a triplet is observed that is due to methyl protons, while at low-field (about 280 Hz) a quartet is shown that is due to methylene protons. Both of these absorptions represent averaged signals due to rapid exchange between the ionic and complex species. As the temperature is lowered, individual absorptions are observed for the different compounds. As was the case for the DMA and TMA systems, the ionic form is located at a lower field compared to the complex. This is clearly discernible in the methylene proton absorptions. The ex-

Can. J. Chem. Downloaded from www.nrcresearchpress.com by 210.87.254.40 on 09/05/12
For personal use only.

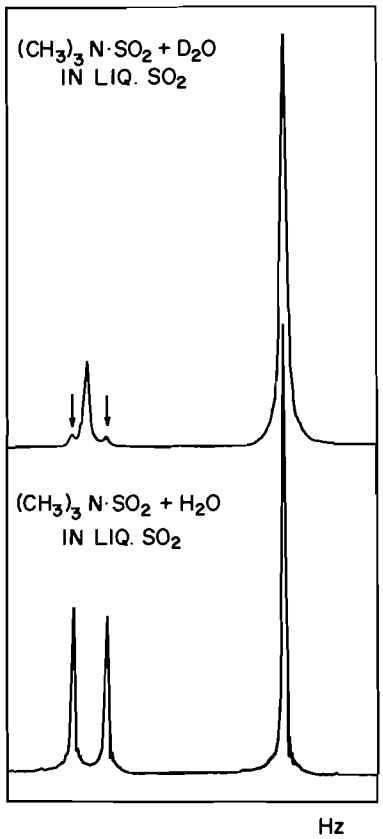

FIG. 3. Comparison of the 60-MHz ^1H nmr spectra at −17°C of $(CH_3)_3N{\cdot}SO_2$ dissolved in liquid SO_2 with D_2O added (upper trace) and H_2O added (lower trace). The two small peaks indicated by arrows in the D_2O added case are due to a small amount of H_2O impurity.

pected two triplet signals due to the methyl protons are not totally resolved in this figure but appear as an unsymmetrical quintet. For simplicity, the rate constant, as well as the free energy of activation at the coalescence temperature of this ion–complex exchange process, were estimated by the coalescing lineshape spectra of a two-site exchange system with unequal populations (5*f*).

In Table 1 are listed the free energies, enthalpies, and entropies of activation along with the Arrhenius activation energies for the ion–complex exchange process for various amine compounds. The $\Delta G_c^{\ddagger}$ values were calculated using the approximated rate constants at the coalescence temperature as given in Figs. 1, 2, and 4. The Arrhenius activation energy E_a for the ion to complex transformation processes for the DMA and TMA systems was determined from plots of log k versus reciprocal absolute temperature from the data given in Figs. 1 and 2. The $\Delta H_c^{\ddagger}$ and $\Delta S_c^{\ddagger}$ values given in Table 1 were calculated from the corresponding $\Delta G_c^{\ddagger}$ and E_a values in the standard way. Errors in the activation parameters were calculated (5*g*) from contributions of errors in rate constants, temperatures, and extrapolation.

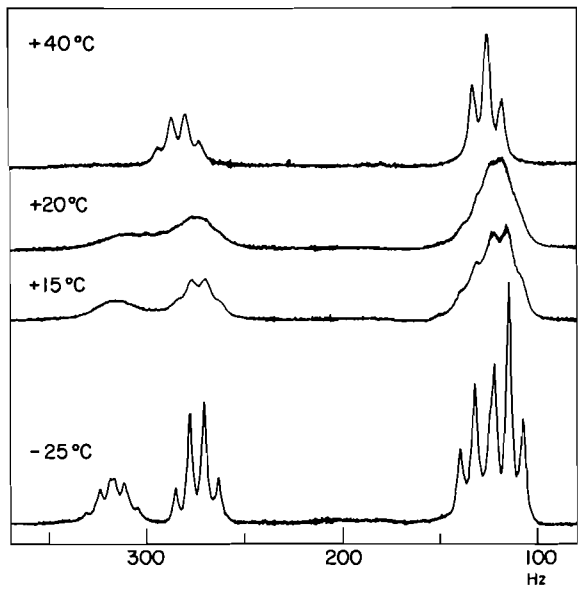

FIG. 4. Experimental 100-MHz ^1H dnmr spectra of triethyl amine·SO_2 + H_2O in liquid SO_2 at various temperatures.

Of considerable note in these data is both the sign and magnitude of the entropies of activation for the cases of DMA and TMA (213.4 ± 23.4 J/K mol and 187.9 ± 49.0 J/K mol, respectively). A positive entropy of activation means that the entropy of the activated complex is greater than the entropy of the reactants. To explain these rather unusual results, it is necessary to realize that we are dealing here with an ionic species that is being transformed into a neutral complex molecule. Solvation effects then are expected to play a major role in the entropy of activation. It is well known that electrostatic interactions in solution reactions have a profound effect on experimentally determined rate parameters (17). This is due to the fact that charged species are more strongly solvated than are neutral species. Thus, if one considers the entropy of activation of a charged reactant going to a less charged or neutral activated complex, a relative increase in entropy would be expected, hence, a positive entropy of activation. The magnitude of the entropy of activation tells us something about the type of electrostatic interaction that is operative in the formation of the activated complex, e.g. ion–dipole versus ion–ion interactions. It is predicted that reactions between oppositely charged ions will have a greater positive entropy of activation due to desolvation in the transition state (17).

Can. J. Chem. Downloaded from www.nrcresearchpress.com by 210.87.254.40 on 09/05/12
For personal use only.

TABLE 1. Free energies, enthalpies, and entropies of activation and Arrhenius activation energies for ion–complex exchange for various amine compounds*

Compound	T_c (K)	$\Delta G_c^{\ddagger}$ (kJ/mol)	$\Delta H_c^{\ddagger}$ (kJ/mol)	$\Delta S_c^{\ddagger}$ (J/deg mol)	E_a (kJ/mol)
DMA	249 ± 4	52.3 ± 1.7	105.4 ± 5.9	+213.4 ± 23.4	107.5 ± 5.9
TMA	283 ± 4	59.0 ± 1.7	112.1 ± 13.8	+187.9 ± 49.0	114.6 ± 13.8
TEA	293 ± 5	59.8 ± 2.5	nd	nd	nd

*nd = not determined.

A good example of this effect can be found in the reaction of 2,4,6-trimethyl pyridine (TMP) with iodine in nitrobenzene solvent to give the products $(TMP)_2I^+$ and I^- (18). The entropy of activation for this reaction was determined to be -211.7 ± 54.8 J/K mol. In many ways, the reverse of this reaction, namely iodine ion transfer, is quite analogous to the proton transfer reaction described here. Both the positive sign and magnitude of the entropy of activation of the reverse reaction agree with the results reported here.

By way of a contrast, consider the acid dissociation reaction of trimethylammonium ion in aqueous solution as follows:

[1] $(CH_3)_3NH^+ + H_2O \rightarrow (CH_3)_3N + H_3O^+$

In this case, Grunwald (19) found the entropy of activation to be +74.9 J/K mol compared to the +187.9 J/K mol found here for the acid dissociation for the same trimethylammonium ion but in liquid SO_2 solvent. This profound solvation effect has also been noted by Lichtin (20) in the entropy of activation for the dissociation of KBr in liquid SO_2. He reported a $\Delta S^{\ddagger}$ value of −154.0 J/K mol for this process.

Based on these considerations, we conclude that the formation of the activated complex in the ion → complex transformation involves, as the first step, a bimolecular reaction between a positively charged alkylammonium ion species and a negatively charged species produced from the dissociation of water in liquid SO_2 solvent.[4] The magnitude of the activation energies, as given in Table 1, seems to confirm the notion of electrostatic interaction contributions, for these experimentally determined values are some 25 to 30 kJ/mol higher than "normal" solution reactions and in general agreement with other known activation energies for oppositely charged ion–ion reaction systems (17).

The free energies of activation for the DMA, TMA, and TEA systems, as given in Table 1, suggest that steric factors may play a role in this exchange process. This steric effect may simply arise from different degrees of interference with the solvation of the protonated bases (2). Thus, it would not be unreasonable to rationalize that the formation of the transition state complex resulting from two differently charged species is the rate determining step in the conversion of the molecular ion into the molecular complex, during which solvation plays an important role.

[4]It is well known that H_2O and SO_2 react to produce a strong acid. However, the discussion of its chemical structure is ambiguous. Since the actual identity of the negative ion involved in the mechanism discussed here is not critical, it is thus not given specifically to avoid confusion.

1. (*a*) M. EIGEN. Angew. Chem. Int. Ed. **3**, 1 (1964); (*b*) E. GRUNWALD. J. Phys. Chem. **71**, 1846 (1967); (*c*) E. K. RALPH III and E. GRUNWALD. J. Am. Chem. Soc. **89**, 2963 (1967); (*d*) E. GRUNWALD and E. K. RALPH III. J. Am. Chem. Soc. **89**, 4405 (1967); (*e*) M. COCIVERA. J. Phys. Chem. **72**, 2520 (1968).
2. C. F. BERNASCONI and D. J. CARRÉ. J. Am. Chem. Soc. **101**, 2707 (1979) and references therein.
3. C. F. BERNASCONI and D. J. CARRÉ. J. Am. Chem. Soc. **101**, 2698 (1979).
4. (*a*) E. F. CALDIN and K. TORTSCHANOFF. J. Chem. Soc. Faraday Trans. I, **74**, 1804 (1978); (*b*) B. SCHREIBER, H. MARTINEK, P. WOLSCHANN, and P. SCHUSTER. J. Am. Chem. Soc. **101**, 4708 (1979); (*c*) E. L. SIMMONS. Prog. Reaction Kinet. **8**, 161 (1977).
5. (*a*) L. W. REEVES. Adv. Phys. Org. Chem. **3**, 187 (1965); (*b*) C. S. JOHNSON. Adv. Magn. Reson. **1**, 33 (1965); (*c*) J. E. ANDERSON. Q. Rev. **19**, 426 (1965); (*d*) G. BINSCH. Top. Stereochem. **3**, 97 (1968); (*e*) H. KESSLER. Angew. Chem. Int. Ed. **9**, 219 (1970); (*f*) I. O. SUTHERLAND. Ann. Rep. NMR Spectrosc. **4**, 71 (1971); (*g*) L. M. JACKMAN and F. A. COTTON. Dynamic nuclear magnetic resonance spectroscopy. Academic Press, New York. 1975; (*h*) S. F. LINCOLN. Prog. Reaction Kinet. **9**, 1 (1977); (*i*) S. SZYMANSKI, M. WITANOWSKI, and A. GRYFF-KELLER. Ann. Rep. NMR Spectrosc. **8**, 227 (1978).
6. (*a*) A. B. BURG. J. Am. Chem. Soc. **65**, 1629 (1943); (*b*) W. E. BYRD. Inorg. Chem. **1**, 762 (1962); (*c*) S. D. CHRISTIAN and J. GRUNDNES. Nature, **214**, 1111 (1967); (*d*) J. GRUNDNES and S. D. CHRISTIAN. J. Am. Chem. Soc. **90**, 2239 (1968); (*e*) J. GRUNDNES and S. D. CHRISTIAN. Acta Chem. Scand. **23**, 3583 (1969); (*f*) D. V. D. HELM, J. D. CHILDS, and S. D. CHRISTIAN. Chem. Commun. 887 (1969); (*g*) J. GRUNDNES, S. D. CHRISTIAN, V. CHEAM, and S. B. FARNHAM. J. Am. Chem. Soc. **93**, 20 (1971); (*h*) R. R. LUCCHESE, K. HABER, and H. F. SCHAEFER III. J. Am. Chem. Soc. **98**, 7617 (1976); (*i*) J. E. DOUGLAS and P. A. KOLLMAN. J. Am. Chem. Soc. **100**, 5226 (1978).
7. D. F. BUROW. The chemistry of nonaqueous solvents. Vol. III. *Edited by* J. J. Lagowski. Academic Press, New York. 1970.
8. L. PAOLILLO, H. ZIFFER, and O. BUCHARDT. J. Org. Chem. **35**, 38 (1970).

Can. J. Chem. Downloaded from www.nrcresearchpress.com by 210.87.254.40 on 09/05/12
For personal use only.

9. E. McLAREN, A. J. YENCHA, J. KUSHNIR, and V. MOHNEN. Tellus, **26**, 291 (1974).
10. (*a*) T. HATA and S. KINUMAKI. Nature, **203**, 1378 (1964); (*b*) S. KINUMAKI and T. HATA. Ann. Genie. Chim. **3**, 135 (1967).
11. (*a*) D. LYONS and G. NICKLESS. Inorganic sulfur chemistry. *Edited by* G. Nickless. Elsevier, Amsterdam. 1968. Chapt. 14; (*b*) F. A. COTTON and G. WILKINSON. Advanced inorganic chemistry. 3rd ed. Interscience, New York. 1972. p. 448.
12. A. L. VAN GEET. Anal. Chem. **42**, 679 (1970).
13. (*a*) A. JAESCHKE, H. MUENSCH, H. G. SCHMID, H. FRIEBOLIN, and A. MANNSCHRECK. J. Mol. Spectrosc. **31**, 14 (1969); (*b*) G. BINSCH and J. D. ROBERTS. J. Am. Chem. Soc. **87**, 5158 (1965).
14. A. LOEWENSTEIN and S. MEIBOOM. J. Chem. Phys. **27**, 1067 (1957).
15. N. MULLER and W. J. WALLACE. J. Org. Chem. **24**, 1151 (1959).
16. E. M. HARTLEY, JR. and M. J. MATTESON. Ind. Eng. Chem. Fundam. **14**, 67 (1975).
17. I. AMDUR and G. G. HAMMES. Chemical kinetics: principles and selected topics. McGraw-Hill, New York. 1966. pp. 115–119.
18. D. W. LARSEN and A. L. ALLRED. J. Am. Chem. Soc. **87**, 1219 (1965).
19. E. GRUNWALD. J. Phys. Chem. **67**, 2208 (1963).
20. N. N. LICHTIN. Progress in physical organic chemistry. Vol. 1. *Edited by* S. G. Cohen, A. Streitwieser, Jr., and R. W. Taft. Interscience, New York. 1963. p. 75.

Can. J. Chem. Downloaded from www.nrcresearchpress.com by 210.87.254.40 on 09/05/12
For personal use only.

Photo-oxidation of formic, acetic, and propionic acids with aqueous hydrogen peroxide[1]

YOSHIRO OGATA,[2] KOHTARO TOMIZAWA, AND KAORU TAKAGI

Department of Applied Chemistry, Faculty of Engineering, Nagoya University, Chikusa-ku, Nagoya, Japan

Received March 10, 1980

YOSHIRO OGATA, KOHTARO TOMIZAWA, and KAORU TAKAGI. Can. J. Chem. **59**, 14 (1981).

Photolytic oxidation of aliphatic acids with aqueous H_2O_2 has been studied. Formic acid gives CO_2 and H_2O. Acetic acid gives products containing CO_2, methane, formic, glycolic, and tartaric acids. Propionic acid gives CO_2, methane, ethane, acetic, formic, lactic, β-hydroxypropionic, malonic, and glycolic acids. A mechanism involving an initial H-atom abstraction by HO· formed via photo-dissociation of H_2O_2 is postulated and discussed.

YOSHIRO OGATA, KOHTARO TOMIZAWA et KAORU TAKAGI. Can. J. Chem. **59**, 14 (1981).

On a étudié l'oxydation photolytique des acides aliphatiques par du H_2O_2 aqueux. L'acide formique se décompose en CO_2 et H_2O. L'acide acétique donne un mélange de CO_2, de méthane et d'acides formique, glycolique et tartrique. L'acide propionique fournit du CO_2, du méthane, de l'éthane ainsi que les acides acétique, formique, lactique, β-hydroxypropionique, malonique et glycolique. On propose un mécanisme faisant intervenir au départ l'enlèvement d'un atome d'hydrogène par un HO· qui provient de la photodissociation de H_2O_2.

[Traduit par le journal]

Introduction

Recently, the removal of pollutants from waste water has become one of the biggest social problems. In this connection, the authors have reported previously on the photolysis of polyethylene glycol derivatives (1) and benzoic acid (2, 3) in the presence of H_2O_2. In general, lower aliphatic acids are resistant to ordinary chemical oxidation. The present paper deals with the photolysis of formic, acetic, and propionic acids with aqueous H_2O_2.

As to the photolysis of lower fatty acids with uv light (190–245 nm), formic acid gives hydrogen, carbon dioxide, and oxalic acid; acetic acid gives methane and carbon dioxide (4). No information is available on their oxidative photolysis, and we wish to report in the present paper the products and intermediates in the photolytic oxidation of these aliphatic acids with H_2O_2. The probable mechanism will be discussed on the basis of the observed products.

Results and Discussion

Acetic Acid (1)

In order to find the optimum conditions for the oxidation of acetic acid (**1**), the effect of the initial molar concentration ratio, $[H_2O_2]_0/[1]_0$, was examined under irradiation with 254 nm light (a Halos 60 W low-pressure Hg lamp). The estimation of H_2O_2 concentration was done iodometrically and that of **1** was performed with nmr and glc.

In the absence of H_2O_2, decomposition of **1** in aqueous solution did not occur after 15 h irradiation; hence, H_2O_2 was necessary for the decomposition of **1**; peracetic acid (CH_3CO_3H), which is expected from the acid-catalyzed reaction of **1** with H_2O_2, was not detected iodometrically after 15 h. Thus peracetic acid does not participate in this photolysis.

As shown in Table 1, the decomposition of **1** was almost complete with $[H_2O_2]_0/[1]_0 = 4.2$ after 15 h, but the efficiency of H_2O_2 for the decomposition of **1** was 0.23. This efficiency (0.23) is lower than the efficiency at the lower ratios, e.g., 0.47 at the ratio of 1.05, 0.31 at the ratio of 2.1, and 0.27 at the ratio of 3.15. This suggests that H_2O_2(or HO·) is consumed at higher concentration of H_2O_2 during later stages of the oxidation of **1** and/or by the self-decomposition to give O_2 and H_2O.

On the basis of the above results, the product analysis was carried out at the ratio of 4.21. The detected products were glycolic (**2**), tartaric (**3**), and formic acids (**4**), and methane and CO_2. The amounts of photolysis products (except for CO_2) from **1** varied with irradiation time and were so

TABLE 1. Effect of ratio of $[H_2O_2]_0/$[acetic acid (**1**)]$_0$ on the decomposition of **1** at 20°C[a]

$[H_2O_2]_0/[1]_0$	Irradiation time (h)	Dec. $[H_2O_2]$ (%)	Dec. [**1**] (%)
1.05	8	98.0	48.4
2.10	10	93.2	60.1
3.15	12	87.1	77.5
4.21	15	94.0	96.3

[a] Initial concentration of **1** is 0.251–0.304 *M* in aqueous solution under irradiation of 254 nm light.

[1] Contribution number 265.

[2] To whom all correspondence should be addressed.

[3] Glyoxylic acid (**5**) was obtained as the hydrated form: $OHC-CO_2H + H_2O \rightleftharpoons (HO)_2CHCO_2H$.

0008-4042/81/010014-05$01.00/0

©1981 National Research Council of Canada/Conseil national de recherches du Canada

Can. J. Chem. Downloaded from www.nrcresearchpress.com by 210.87.254.42 on 09/05/12
For personal use only.

TABLE 2. Comparison of photolysis of aqueous acetic (1), glycolic (2), and formic acids (4) at 20°C

	CH_3CO_2H (1)	$HOCH_2CO_2H$ (2)	HCO_2H (4)
$[Substrate]_0$ (*M*)	0.304	0.318	0.326
$[H_2O_2]_0$ (*M*)	1.34	0.798	0.372
$[H_2O_2]_0/[substrate]_0$	4.21	2.51	1.14
Irradiation time (h)	15	10	10
Dec. [substrate] (%)	96.3	98.2	100
Dec. $[H_2O_2]$ (%)	94.0	95.4	98.2
Yield of CO_2 (%)	103.8	122.8	86.3
Yield of O_2 (%)[a]	6.5	3.9	4.4

[a] The yield of O_2 is calculated by assuming evolution of 1 mol O_2 from 1 mol H_2O_2.

small that the estimation of their yields was difficult.

As shown in Table 2, glycolic (2) and formic acids (4) are more easily oxidized than acetic acid (1) at lower H_2O_2 concentration; further photo-oxidation of 2 with H_2O_2 gives 4, tartaric acid (3, trace), and glyoxylic acid (5, trace).[3] 5 (as hydrate) reacts with H_2O_2 in the dark to give formic acid (4) and CO_2. Photolysis of 4 in the presence of H_2O_2 gave CO_2 and H_2O. Therefore acetic acid (1) is more stable than the initial products (2 and 4) under these conditions (5, 6), so that only a trace amount of them remained in the products from 1.

Mechanism

The extinction coefficient of H_2O_2 ($\varepsilon_{254\ nm} = 20$) is much higher than that of acetic acid (1, $\varepsilon_{254\ nm} \simeq 0$), and the concentration of H_2O_2 is higher than that of 1, so that it is probable that H_2O_2 is photolyzed at first, forming radical HO·, followed by further reaction such as formation of HOO· etc. (7–10).

[1] $H_2O_2 \xrightarrow{h\nu} 2HO\cdot$

[2] $HO\cdot + H_2O_2 \longrightarrow HOO\cdot + H_2O$

[3] $HOO\cdot + H_2O_2 \longrightarrow HO\cdot + H_2O + O_2$

[4] $2HOO\cdot \longrightarrow H_2O_2 + O_2$

The radicals HO· and HOO· (reactions [1]–[4]) abstract a H-atom from the substrate, initiating the decomposition. The substrate radical thus formed couples with HO· and HOO·, affording more stable observed products as follows.

[5a] CH_3CO_2H (1) $\xrightarrow{HO\cdot} \cdot CH_2CO_2H$ (6) $+ H_2O$

[5b] CH_3CO_2H (1) $\xrightarrow{HO\cdot} CH_3CO_2\cdot$ (or $CH_3\cdot + CO_2$) $+ H_2O$

[5c] CH_3CO_2H (1) $\xrightarrow{h\nu} CH_4 + CO_2$ (trace)

[6a] $\cdot CH_2CO_2H$ (6) $\xrightarrow{HO\cdot} HOCH_2CO_2H$ (2)

[6b] $\cdot CH_2CO_2H$ (6) $\xrightarrow{HOO\cdot} HOOCH_2CO_2H$ (7)

[7] $HOCH_2CO_2H$ (2) $\xrightarrow{HO\cdot} HO\dot{C}HCO_2H$ (8) $+ H_2O$

[8] $HOOCH_2CO_2H$ (7) $\xrightarrow{h\nu} HO\cdot + \cdot OCH_2CO_2H$ (9)

[9a] $HO\dot{C}HCO_2H$ (8) $\xrightarrow{HO\cdot} (HO)_2CHCO_2H$ (10)

[9b] $HO\dot{C}HCO_2H$ (8) $\xrightarrow{\text{coupling}} HO_2CCH(OH)CH(OH)CO_2H$ (3)

Can. J. Chem. Downloaded from www.nrcresearchpress.com by 210.87.254.42 on 09/05/12
For personal use only.

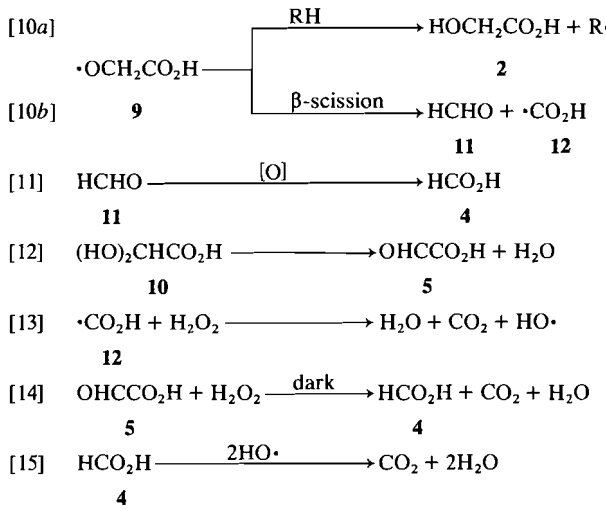

The decomposition of acetic acid (**1**) is expected to be initiated both by H-atom abstraction with HO· (reactions [5*a*] and [5*b*]) and by direct photolysis (reaction [5*c*]) (11). In this case, the main path of the decomposition of **1** should be [5*a*] because only a trace amount of methane was observed (reactions [5*b*] and [5*c*]). Substrate radical (·CH_2CO_2H, **6**) formed by reaction [5*a*] undergoes further reactions to give the observed products. α-Hydroperoxyacetic acid ($HOOCH_2CO_2H$, **7**) formed by reaction of radical **6** with HOO· decomposes to afford alkoxy radical **9** (reactions [6*b*] and [8]), which gives formaldehyde (**11**) by β-fission (reaction [10*b*]). Oxidation of the latter yields formic acid (**4**) (reaction [11]). The reaction of radical **12** with H_2O_2 gives CO_2 (reaction [13]) (8). Tartaric acid (**3**) is formed by dimerization of radicals, $HO\dot{C}HCO_2H$ (**8**) (reaction [9*b*]). As stated above, products **2**, **3**, **4**, methane, and CO_2 were detected in this photolysis.

Propionic Acid (13)

The photo-oxidation of propionic acid (**13**, 0.4–0.5 *M* initial concentration) was similarly carried out at various molar ratios of $[H_2O_2]_0/[\mathbf{13}]_0$. When H_2O_2 was completely decomposed, the decomposition of substrate **13** was 57% with equimolar H_2O_2, 75% with twice molar H_2O_2, and 100% with over triplicate molar H_2O_2. Thus, the time/conversion data were measured with 3.1-fold molar H_2O_2 as shown in Table 3.

An aqueous solution of 0.404 *M* **13** and 1.27 *M* H_2O_2 ($[H_2O_2]_0/[\mathbf{13}]_0 = 3.14$) was irradiated with 254 nm light. The products identified by nmr and glc were: CO_2, CH_3CO_2H (**1**), $HOCH_2CO_2H$ (**2**), HCO_2H (**4**), $CH_3CH(OH)CO_2H$ (**14**), $HOCH_2$-CH_2CO_2H (**15**), $HO_2CCH_2CO_2H$ (**16**), and CH_4 (trace). The yields of products dissolved in solution are plotted against the decomposition percentage of propionic acid (**13**) (Fig. 1).

The figure shows that yields of **1**, **2**, **4**, and **16** increase with the progress of the decomposition, while the yields of α- (**14**) and β-hydroxypropionic acids (**15**) decrease gradually after 50% decomposition of **13**. Hence, hydroxypropionic acids may be intermediates in the oxidation of **13** giving **1**, **4**, and others.

As to the evolution of CO_2, 1.15×10^{-2} mol of CO_2 was evolved on irradiation of a mixture of **13** (1.21×10^{-2} mol, 0.404 *M*) and H_2O_2 (3.81×10^{-2} mol, 1.27 *M*) after the consumption of 97.4% of **13**. Hence, CO_2 is evolved simultaneously with the oxidative degradation to lower molecular weight products, which are eventually oxidized to CO_2.

For the examination of the oxidative degradation of the intermediates, the following photo-oxidation of hydroxypropionic acids was carried out under the same conditions.

α-Hydroxypropionic acid (**14**, 0.374 *M*) in H_2O was photolyzed with H_2O_2 (1.24 *M*). The products in the 95% conversion of **14** were: **1** (58%), CO_2, traces of **2** and **4**, and pyruvic acid (**17**). Pyruvic acid is oxidized rapidly with H_2O_2 in the dark to give **1** and CO_2 (12, 13).

β-Hydroxypropionic acid (**15**, 0.374 *M*) in H_2O was photolyzed with H_2O_2 (1.24 *M*). The products in the 98% conversion of **15** were: **1** (10%), **2** (7%), **4** (52%), malonic acid (**16**, 18%), and CO_2.

Comparison of the evolution efficiency of CO_2 from a given amount of the decomposed H_2O_2 im-

TABLE 3. Conversion of propionic acid (**13**) and H_2O_2 by 254 nm irradiation in aqueous solution at 20°C

Irradiation time (h)	$[H_2O_2]$ (*M*)	Dec. $[H_2O_2]$ (%)	[**13**] (*M*)	Dec. [**13**] (%)
0	1.27	0	0.404	0
2	1.07	15.7	0.327	19.1
5	0.887	30.2	0.214	47.0
8	0.507	60.1	0.123	69.6
12	0.217	82.9	0.049	87.9
15	0.019	98.5	0.011	97.3

Can. J. Chem. Downloaded from www.nrcresearchpress.com by 210.87.254.42 on 09/05/12
For personal use only.

Can. J. Chem. Downloaded from www.nrcresearchpress.com by 210.87.254.42 on 09/05/12
For personal use only.

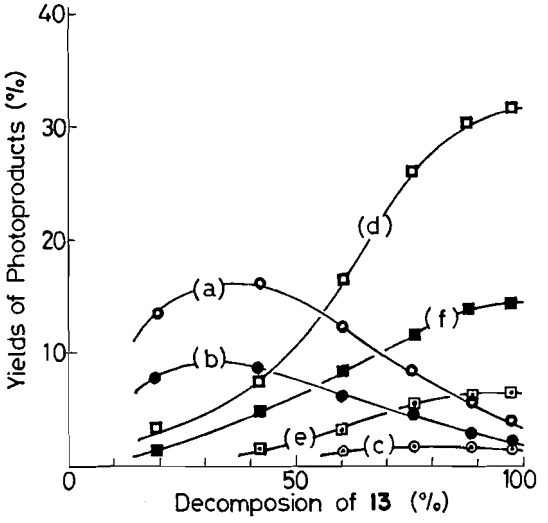

FIG. 1. Yields of products dissolved in solution against the photodecomposition percentage of propionic acid (**13**) with aqueous H_2O_2 at 20°C. Line (*a*), $CH_3CH(OH)CO_2H$ (**14**); (*b*), $HOCH_2CH_2CO_2H$ (**15**); (*c*), $HO_2CCH_2CO_2H$ (**16**); (*d*), CH_3CO_2H (**1**); (*e*), $HOCH_2CO_2H$ (**2**); (*f*), HCO_2H (**4**).

plies that the oxidation efficiency of the α-isomer (**14**) is 1.4 times higher than that of the β-isomer (**15**).

Mechanism

The above results suggest a mechanism which is analogous to that of acetic acid (**1**) and is initiated by the H-atom abstraction with the oxidative species HO· and HOO·. The primary reaction for propionic acid (**13**) degradation may be α- and β-hydrogen atom abstraction with HO·, since HO· is the strongest H-atom abstractor among the radical species in the system.

The radical species thus formed couples with HO· to give α- (**14**) and β-hydroxypropionic acid (**15**), and with HOO· to give the α- (**18**) and β-hydroperoxides (**19**), respectively, in a similar manner as above. Radical **20** ($CH_3\dot{C}(OH)CO_2H$) formed by α-H abstraction from **14** is converted mainly to pyruvic acid (**17**) which reacts easily with H_2O_2 in the dark to give **1** (reactions [16], [17]) (12, 13).

[16] $CH_3CH(OH)CO_2H \xrightarrow[-H_2O]{HO\cdot}$ (**14**)

$CH_3\dot{C}(OH)CO_2H \xrightarrow[-H_2O]{HO\cdot} CH_3COCO_2H$ (**20**, **17**)

[17] $CH_3COCO_2H + H_2O_2 \xrightarrow{dark} CH_3CO_2H + CO_2 + H_2O$ (**17**, **1**)

Diol **21** ($HOCH_2CH(OH)CO_2H$) formed by β-hydrogen abstraction from **14** followed by coupling with HO· leads to glycolic acid (**2**) via **23** similarly to pyruvic acid (**17**) (reactions [18], [19]), and peroxide **24** ($HOOCH_2CH(OH)CO_2H$) from **14** leads to radical **8** and formaldehyde (**11**) by photolytic O–O cleavage followed by β-scission of alkoxy radical (**25**) (reaction [20]) (14, 15).

[18] $HOCH_2CH(OH)CO_2H \xrightarrow[-H_2O]{HO\cdot}$ (**21**)

$HOCH_2\dot{C}(OH)CO_2H \xrightarrow[-H_2O]{HO\cdot} HOCH_2COCO_2H$ (**22**, **23**)

[19] $HOCH_2COCO_2H + H_2O_2 \xrightarrow{dark}$ (**23**)

$HOCH_2CO_2H + CO_2 + H_2O$ (**2**)

[20] $HOOCH_2CH(OH)CO_2H \xrightarrow[-HO\cdot]{h\nu}$ (**24**)

$\cdot OCH_2CH(OH)CO_2H \xrightarrow{\beta\text{-scission}} HCHO + HO\dot{C}HCO_2H$ (**25**, **11**, **8**)

β-Hydroxypropionic acid (**15**) also leads to glycolic acid (**2**) either via $HOCH_2COCO_2H$ (**23**) similar to reaction [16] or via hydroperoxide **26** ($HOCH_2CH(OOH)CO_2H$) (reaction [21]). Radical **28** ($HO\dot{C}HCH_2CO_2H$) formed from **15** gives malonic acid (**16**) via **29** (reaction [22]), which is directly decarboxylated to **1** or reacts with HO· to give **6** (11). β-Hydroperoxide ($HOOCH_2CH_2CO_2H$, **19**) leads to glycolic acid (**2**) and formic acid (**4**) analogously to peroxide **24**. Methane and ethane may be formed by photolysis of **1** (reaction [5*c*]) and **13**, respectively, and/or by H-abstraction from the carboxyl group by HO· followed by decarboxylation (11). In this photolysis of **13**, CO_2, **1**, **2**, **4**, **14**, **15**, and **16** should be formed, which were identified as products.

[21] $HOCH_2CH(OOH)CO_2H \xrightarrow[-HO\cdot]{h\nu}$ (**26**)

$HOCH_2\underset{O\cdot}{\overset{|}{C}}HCO_2H \xrightarrow[-H_2O]{HO\cdot} HOCH_2COCO_2H$ (**27**, **23**)

[22] $HO\dot{C}HCH_2CO_2H \xrightarrow{HO\cdot}$ (**28**)

$(HO)_2CHCH_2CO_2H \xrightarrow[-H_2O]{[O]} HO_2CCH_2CO_2H$ (**29**, **16**)

In conclusion, an aqueous solution of **1**, **4**, or **13** in the presence of excess H_2O_2 was decomposed almost completely with 254 nm light. A mechanism is postulated which involves the generation of HO· or HOO· from H_2O_2 followed by their abstraction of a H-atom from acids and/or their addition to substrate radicals.

Experimental

Materials

Formic acid, bp 100.0–101.0°C, acetic acid, bp 116.5–117.5°C, and propionic acid, bp 141.0–142.0°C were purified by fractionation. Hydrogen peroxide (90% guaranteed grade) was purchased from Mitsubishi Gas Chem. Co. Other reagents were of guaranteed reagent grade.

Photolysis

The substrate was mixed with aqueous H_2O_2, the solution was introduced into a quartz cell equipped with a gas buret (300 mL) connected with a capillary tube to the photolysis system, and irradiated with a Halos 60 W low-pressure Hg lamp at 20°C.

The concentration of H_2O_2 was measured by iodometry. The liquid products from the photolysis were identified and estimated *in situ* by nmr (a Hitachi R-24B spectrometer), and/or by glc (a Yanagimoto G 180 gas chromatograph with FID) and gc–ms (a Shimadzu GCMS-7000 mass spectrometer) with a column (2.5 mm × 2 m) packed with PEG 20M and Porapak QS after decomposition of remaining peroxides with $Na_2S_2O_3$, concentration of the solution, and then esterification by diazomethane. The gaseous products were analyzed by glc with FID and TCD using a 2.5 mm × 2 m column packed with Porapak QS and Molecular Sieve 5A with helium as a carrier gas. The evolved CO_2 was estimated by absorbing it in saturated aqueous $Ba(OH)_2$ followed by acidimetry with aqueous HCl. The evolved O_2 was absorbed in alkaline aqueous pyrogallol, and the volume of absorbed O_2 was estimated with a gas buret.

1. Y. Ogata, K. Tomizawa, and K. Fujii. Bull. Chem. Soc. Jpn. **51**, 2628 (1978).
2. Y. Ogata, K. Takagi, and S. Yamada. Bull. Chem. Soc. Jpn. **50**, 1629 (1977).
3. Y. Ogata, K. Tomizawa, and Y. Yamashita. J. Chem. Soc. Perkin Trans. II, 616 (1980).
4. K. Pfordte and G. Leuschner. Justus Liebigs Ann. Chem. **622**, 1 (1959).
5. C. Walling, G. M. El-Taliawi, and R. A. Johnson. J. Am. Chem. Soc. **96**, 133 (1974).
6. M. Anbar, D. Meyerstein, and P. Neta. J. Chem. Soc. B, 742 (1966).
7. J. Weiss. Discuss. Faraday Soc. 161 (1952).
8. G. V. Buxton and W. K. Wilmarth. J. Phys. Chem. **67**, 2835 (1963).
9. K. Omura and T. Matsuura. Tetrahedron, **24**, 3475 (1968).
10. T. Foster and P. R. West. Can. J. Chem. **52**, 3589 (1974).
11. W. T. Dixon, R. O. C. Norman, and A. L. Buley. J. Chem. Soc. 3625 (1964).
12. H. V. Euler and H. Hasselquist. Z. Naturforsch. **116**, 176 (1956); Chem. Abstr. **51**, 1339e (1957).
13. A. I. Brodskii, M. M. Aleksankin, and I. P. Gragerov. Zh. Obshch. Khim. **32**, 829 (1962); Chem. Abstr. **58**, 3287e (1963).
14. R. Ford, H-P. Schuchmann, and C. von Sonntag. J. Chem. Soc. Perkin Trans. II, 1338 (1975).
15. Y. Sawaki and Y. Ogata. J. Am. Chem. Soc. **98**, 7324 (1976).

Can. J. Chem. Downloaded from www.nrcresearchpress.com by 210.87.254.42 on 09/05/12
For personal use only.

Etude de l'adsorption de surfactants ioniques et non ioniques sur de la matière végétale carbonisée

FRANCIS PERINEAU ET ANTOINE GASET

Laboratoire de Chimie Organique et d'Agrochimie, Ecole Nationale Supérieure de Chimie, Institut National Polytechnique, 118 route de Narbonne, 31077 Toulouse Cedex, France

Reçu le 21 février 1980[1]

FRANCIS PERINEAU et ANTOINE GASET. Can. J. Chem. **59**, 19 (1981).

En vue de la valorisation des déchets ligneux dans le domaine de l'épuration d'effluents, nous avons étudié l'adsorption des trois principaux types de surfactant sur de la matière végétale ayant subi l'opération de carbonisage. Nous avons ainsi déterminé les conditions optimales de pH et de température. L'étude de l'influence de la variation de ces paramètres a en outre permis de mettre en évidence l'intervention de liaisons ioniques et hydrophobes, et d'identifier les groupements responsables de la fixation ionique. Puis l'analyse des courbes traduisant la fixation dans le temps en mileux eau pure et alcoolique nous a amené à proposer un mode d'adsorption. En outre nous avons tenté de caractériser le mode de diffusion des surfactants par le tracé des courbes de fixation en fonction de la racine du temps. Enfin la comparaison de l'adsorption de trois alkylsulfates de longueur de chaîne variable a confirmé la très grande importance des interactions hydrophobes et a permis de la relier à la valeur des cmc tensio-actives.

FRANCIS PERINEAU and ANTOINE GASET. Can. J. Chem. **59**, 19 (1981).

The aim of this investigation was to assess the possible use of sulfuric lignins for the purification of industrial liquid wastes. The adsorption of anionic (SDS), cationic (CPC), and non-ionic (NPPO) surfactants on charred plant material was carried out under various pH and temperature conditions. Ionic and hydrophobic interactions are involved in the adsorption process. The analysis of the adsorption kinetics in aqueous and alcoholic media allowed the mode of adsorption to be characterized. The plot of the surfactant uptake against the square root of time led to the determination of the mode of diffusion. The effect of the chain length of alkylsulfates on their adsorption corroborated the involvement of hydrophobic interactions and could be correlated with the values of their cmc.

Introduction

Dans le cadre de la valorisation du déchet issu de l'opération de carbonisage de la laine dans le domaine de l'épuration d'effluents riches en détergents (1), nous avons étudié l'adsorption de surfactants ioniques et non ioniques sur les lignines sulfuriques composant ce déchet. Le carbonisage a pour but d'éliminer la matière végétale profondément incrustée dans la laine. Cette opération a lieu par actions conjuguées de l'acide sulfurique et de la chaleur (2). Elle donne lieu à un déchet constitué de fibres modifiées et de matière végétale carbonisée et broyée composant en général plus de 50% de ce sous-produit. Celui-ci représente 5% du tonnage des laines carbonisées, soit 0,75% du tonnage des laines commercialisées. Aucune utilisation de ce déchet n'ayant été proposée, et en raison de ses caractéristiques ioniques et apolaires, nos travaux ont pour but de proposer sa valorisation dans le cadre de l'épuration des eaux polluées. Avant d'étudier l'adsorption des tensio-actifs sur le déchet global, nous avons étudié cette fixation sur chacun de ses composants: les fibres kératiniques modifiées et la matière végétale carbonisée. Ceci dans le but de mieux connaître les processus d'adsorption et d'utiliser ce sous-produit de façon optimale. En ce qui concerne plus particulièrement la partie végétale du déchet, le fait qu'elle se rencontre également à l'issue de divers tratitements de déchets d'origine végétale (rafle de maïs) constitue une motivation supplémentaire à cette étude.

Dans de telles conditions (H_2SO_4 29 *N*, 120°C) la matière végétale est hydrolysée. La cellulose et les hémicelluloses libèrent des sucres en C6 et C5. Seul le squelette ligneux est maintenu. Il subit en outre des réactions de sulfatation, ainsi que de façon plus secondaire de sulfonation. La température et le pH acide favorisent ces réactions au niveau de différents groupements fonctionnels (3–6), notamment des groupements alcooliques, des carbones éthyléniques et des noyaux phénoliques.

Parmi les travaux que l'on peut relever dans la littérature concernant l'adsorption de solutés sur les lignines sulfuriques on trouve essentiellement des résultats se rapportant à l'adsorption de phénols. L'analyse des isothermes tracées à différentes températures montre une adsorption physique pour ce produit (9, 10). L'adsorption de phénols a également été envisagée sur la lignine (11) mais il ne s'agit plus dans ce cas d'une simple adsorption puisqu'elle conduit à une condensation (12–14). Par ailleurs la fixation d'un colorant basique sur des fibres lignocellulosiques a été étudiée. Il a été montré que les fibres brutes ont un pouvoir adsorbant deux fois supérieur à celui de la cellulose pure en raison du caractère nucléophile des groupements carboxyliques et phénoliques

[1]Revision reçu le 2 juillet 1980.

0008-4042/81/010019-08$01.00/0

©1981 National Research Council of Canada/Conseil national de recherches du Canada

Can. J. Chem. Downloaded from www.nrcresearchpress.com by 210.87.254.40 on 09/05/12
For personal use only.

Can. J. Chem. Downloaded from www.nrcresearchpress.com by 210.87.254.40 on 09/05/12
For personal use only.

ionisés de la lignine (15). Par contre la capacité de fixation des lignines sulfonatées s'est avérée voisine de celle de la cellulose (16). En ce qui concerne l'adsorption de surfactants sur des matières végétales, son étude ne semble avoir été envisagée que sur de la cellulose sulfurique. La fixation de composés cationiques met principalement en oeuvre des liaisons ioniques. L'adsorption faible et réversible des tensio-actifs anioniques et non ioniques a lieu par liaisons hydrogènes (17).

Dans ces conditions il nous a paru intéressant d'étudier l'adsorption de ces trois types de composés tensio-actifs sur des lignines sulfuriques. Nous avons, dans un premier temps, déterminé les conditions optimales de pH et de température. Nous nous sommes ensuite attachés à faire ressortir les principaux types de liaisons mises en jeu, et à caractériser le mode de diffusion.

Partie expérimentale

1. Matériaux

1.1. Le déchet de carbonisage nous a été fourni par l'I.T.F.[2] Suld-Lecarim. La séparation de ses deux composants a lieu par tamisage. La granulométrie de la fraction végétale (lignines sulfuriques acides) recueillie est variable mais faible dans tous les cas. Le matériau est quasi pulvérulent. Il est ensuite lavé en colonne, de manière à éliminer l'acide sulfurique d'absorption avec de l'eau déminéralisée, jusqu'à ce que la valeur du pH d'équilibre soit de 4,2 (photo 1).

Les particules végétales issues du déchet de carbonisage ont été photographiées au microscope électronique. La photographie 1 met en évidence la présence de deux types de particules. Chacun d'eux a ensuite été photographié à un grossissement plus élevé (photos 2 et 3).

1.2. Les surfactants ioniques utilisés sont des produits Merck: dodécylsulfate de sodium (SDS) (réf. 2969); tétradécylsulfate de sodium (STS) (réf. 12 272); *n*-hexadécylsulfate de sodium (SHS) (réf. 12 184); chlorure de *N*-cétylpyridinium (CPC) (réf. 2340).

Le surfactant non ionique utilisé est un nonylphénoxypolyéthylèneoxyéthanol (NPPO) avec une longueur de chaîne correspondant à 9 mol d'oxyde d'éthylène (masse moléculaire 604). Ce produit nous a été fourni par la Société Montanoir.

2. Traitements

Le substrat (2 g) et la solution tensio-active (0,1 dm^3) de concentration 2 g/dm^3 sont mis en agitation mécanique pendant 20 min. Ceci fait exception lors de l'étude de la fixation d'alkylsulfates en fonction de la longueur de la chaîne. En effet, en raison de la mauvaise solubilité des STS et SHS, il n'est pas possible d'utiliser de fortes concentrations. Le substrat (2 g) est dans ce cas mis en agitation pendant 30 min avec 1,5 dm^3 de solution concentrée à 100 mg/dm^3. L'acidification a lieu par addition de H_2SO_4 36 *N* (le carbonisage se déroulant en présence de cet acide), tandis que les valeurs basiques du pH sont obtenues par emploi de NaOH 2 *N*. L'agitateur est placé dans une cuve thermostatée. Lignines sulfuriques et solution ne sont mises en contact que lorsque l'équilibre thermique est atteint. Les solutions alcooliques tensio-actives sont obtenues en dissolvant le surfactant dans un mélange isovolumétrique eau – éthanol.

[2]I.T.F.: Institut Textile de France.

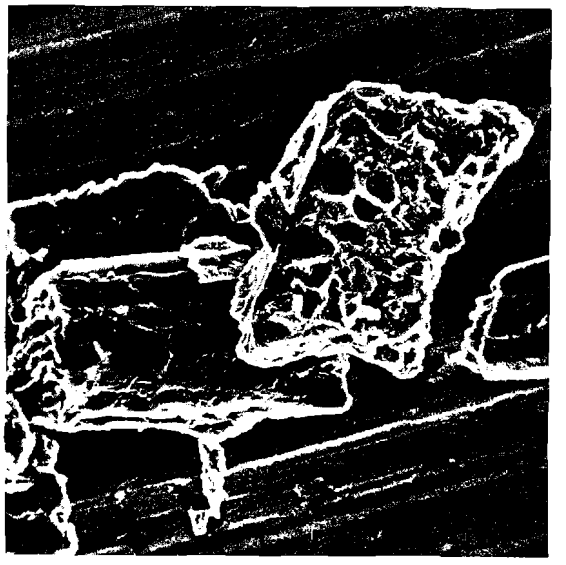

PHOTO 1. Particules végétales issues du déchet de carbonisage (grossies 350 fois).

PHOTO 2. Particule végétale de type tubulaire (grossie 1100 fois).

3. Techniques analytiques

La quantité de surfactant adsorbé (*X*) est calculée en déterminant la concentration résiduelle. Celle-ci est obtenue pour les tensio-actifs ioniques par la méthode de Longwell et Maniece (18). Les résultats ainsi acquis ont été confirmés par la méthode analytique consistant à former avec l'orthophénanthroline cuivrique un complexe extractible dans la méthylisobutylcétone et à le doser par spectrophotométrie d'absorption atomique (19). La concentration résiduelle en surfactant non ionique est déterminée par spectrophotométrie ultra-violette après complexation par le cobaltothyocyanate d'ammonium et extraction dans le benzène (20).

Can. J. Chem. Downloaded from www.nrcresearchpress.com by 210.87.254.40 on 09/05/12
For personal use only.

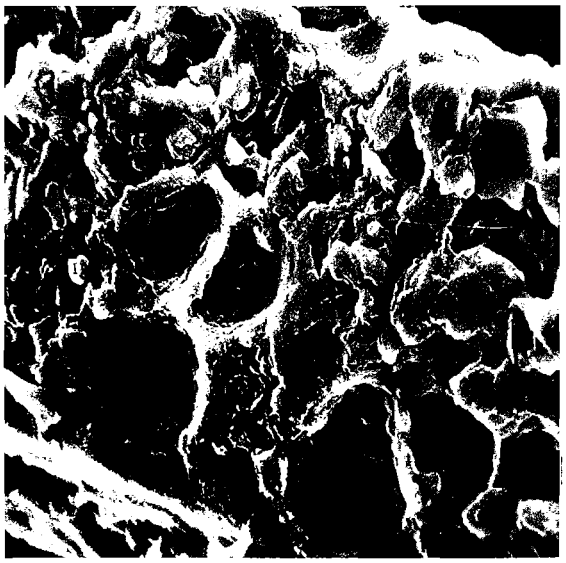

PHOTO 3. Particule végétale du type lamellaire (grossie 1100 fois).

Résultats et discussion

1. Influence du pH sur l'adsorption

1.1. D'un surfactant anionique: le dodécylsulfate de sodium (SDS)

On constate sur la fig. 1 que l'adsorption diminue lorsque le pH croît jusqu'à ce qu'il atteigne une valeur voisine de 9,5. Son importance est divisée par 6,7 entre les pH 0,5 et 9,5. Au-delà de cette valeur du pH, la quantité fixée augmente.

Cette chute de l'adsorption jusqu'à une valeur de pH de 9,5 peut être expliquée par l'intervention de liaisons ioniques. En effet la lignine peut réagir avec les amines pour former des ammoniums quaternaires (21). Ce greffage est favorisé en présence d'acide sulfurique et par action de la chaleur (22), c'est-à-dire par les conditions du carbonisage. De même les groupes méthoxys de la lignine peuvent donner lieu à des ions thiouroniums en présence de thiols aminés (15). Les analyses élémentaires des lignines sulfuriques composant le déchet de carbonisage font apparaître un taux d'azote de 5,1%. La lignine étant exempte de cet élément, on peut raisonnablement attribuer sa présence au greffage d'acides aminés kératiniques lors du carbonisage, dont certains portent une fonction thiol (cystéine provenant de l'hydrolyse de la cystine).

Nous retiendrons donc pour la fixation ionique du SDS à pH acide l'intervention des sites cationiques du type:

$$-CH=\overset{+}{N}-\underset{H}{} \quad \text{et} \quad -CH-S-C=\overset{+}{N}H_2 \qquad NH_2$$

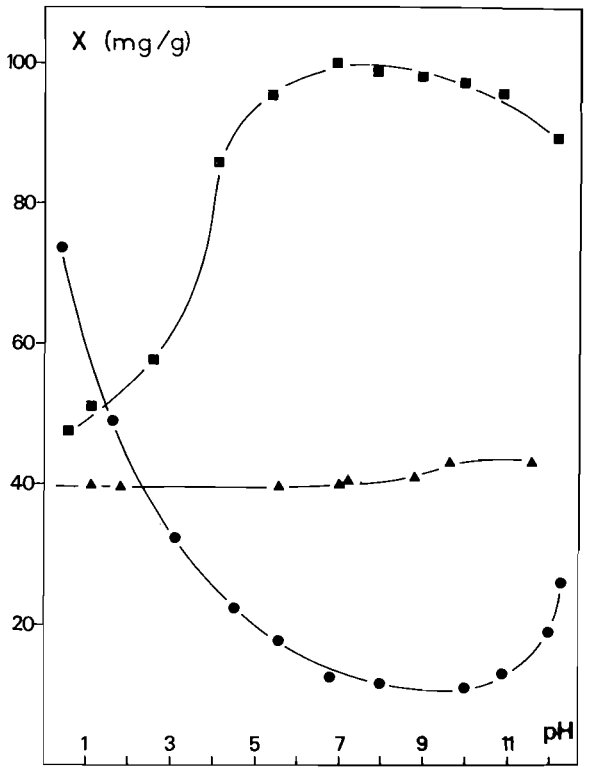

FIG. 1. Effet du pH sur l'adsorption (Co = 2 g/L, t = 20 min, θ = 22°C); ● SDS, ■ CPC, ▲ NPPO.

Au fur et à mesure que la valeur du pH croît, la proportion des sites cationiques mentionnés ci-dessus diminue, de même que l'adsorption du SDS. Son adsorption n'est cependant pas nulle. Ceci sous-entend l'intervention d'un autre type de liaisons telles que les interactions hydrophobes. Il est par contre étonnant de remarquer une augmentation de la fixation en milieu fortement basique. Ce phénomène est certainement lié à l'hydrolyse alcaline connue de la lignine (23, 24) et des lignosulfonates (25–28) que nous avons d'ailleurs observée sous forme d'une solubilisation partielle des particules végétales. Elle se traduit principalement par une dépolymérisation de la macromolécule (23–25). Au niveau des lignines sulfuriques, ce processus s'accompagne aussi d'une désulfonation (25–28). Ceci a pour conséquence de réduire le potentiel électronégatif du substrat et donc la répulsion vis-à-vis des anions. On peut également interpréter cette augmentation de la fixation pour des pH supérieurs à 9,5 par une ouverture de la structure macromoléculaire permettant des interactions hydrophobes substrat – SDS plus nombreuses et mettant en jeu une plus importante surface d'adsorption.

Nous avons pu vérifier que les phénomènes d'ad-

Can. J. Chem. Downloaded from www.nrcresearchpress.com by 210.87.254.40 on 09/05/12
For personal use only.

TABLEAU 1. Tensions superficielles de solutions de SDS, CPC et NPPO à 22°C en fonction du pH

	Tension superficielle (dyn/cm)		
pH	SDS (0,2 m*M*/L)	CPC (0,2 m*M*/L)	NPPO (0,156 m*M*/L)
2	58	40	31,5
6,3	64	45	31
11	65	40	31,5

sorption observés en fonction du pH ne sont pas dus à la dégradation de la molécule tensio-active. En effet la valeur de la tension superficielle des trois solutions tensio-actives reste stable sur la gamme de pH considérée (tableau 1). En outre nous avons vérifié que l'amélioration du pouvoir adsorbant liée à l'hydrolyse alcaline est définitive. Ainsi après avoir maintenu le substrat durant 20 min à pH 12,1, ce dernier a ensuite été ramené à 8,6. Le taux de fixation déterminé dans ces conditions est comparable à celui obtenu à pH 12.

1.2. D'un surfactant cationique: le chlorure de N-*cétylpyridinium (CPC)*

Inversement l'adsorption du CPC croît avec le pH. Elle est multipliée par le coefficient 2,1 entre les pH 0,5 et 7 (fig. 1). Ceci est en grande partie attribué à la dissociation des groupements sulfates ainsi qu'à celles des groupements sulfonates et phénoliques de façon secondaire. Notons que des analyses élémentaires du matériau ont fait apparaître une teneur en soufre de 2,6%. Or la lignine est en principe dépourvue de cet élément. Cela confirme donc sa sulfatation lors du carbonisage. Elle représenterait 0,21 mol équivalent pour 100 g de substrat et permettraient dans des conditions d'équilibre et de saturation une fixation de CPC égale à 640 mg/g.

L'adsorption du CPC en milieu acide peut être attribuée à des interactions hydrophobes, à l'intervention des doublets libres des hétéroatomes ainsi qu'à des liaisons ioniques. En effet les sulfates acides et les acides sulfoniques sont forts et certains restent sous forme dissociée à des pH très acides. Un autre argument expliquant cette adsorption en milieu acide met en jeu l'intervention de complexes entre les électrons π des noyaux aromatiques de la lignine et la partie cationique du surfactant (29). Quant à la diminution de la fixation à pH supérieur à 8, elle peut s'expliquer par la désulfonation partielle (25–28) mentionnée auparavant.

1.3. D'un surfactant non-ionique: le nonylphénoxypolyéthylèneoxyéthanol (NPPO)

Un tel soluté non ionique n'est en principe pas concerné par les liaisons ioniques. Son adsorption ne devrait pas être influencée par les variations du pH. Cependant les atomes d'oxygène des liaisons éthers des surfactants non ioniques à chaîne polyoxyéthylène peuvent être protonés à bas pH (29). Il est donc possible que le NPPO se fixe par liaisons ioniques sur les lignines sulfuriques du fait de la force des sulfates acides et des acides sulfoniques. Néanmoins les liaisons hydrogènes et les interactions hydrophobes contribuent certainement de façon plus importante à l'adsorption de ce type de soluté.

D'autre part il peut paraître surprenant d'observer une légère amélioration du taux de fixation (7,5%) à pH supérieur à 7,5 (fig. 1). Ce phénomène peut aussi être expliqué par l'hydrolyse du matériau qui aurait les mêmes conséquences que celles mentionnées pour le SDS. D'ailleurs, comme pour le SDS, nous avons constaté que cette amélioration du taux de fixation se maintient après avoir soumis le substrat à un pH de 11,6. Son pouvoir adsorbant vis-à-vis du NPPO à une valeur du pH ramenée à 1,8 est égale à celui obtenu à pH 11,6. Ceci semble donc confirmer l'hypothèse selon laquelle la plus grande adsorption du NPPO en milieu basique est due à l'hydrolyse du matériau et non pas à la dégradation de la molécule de NPPO dont la stabilité au pH est rapportée dans le tableau 1.

2. Influence de la température sur l'adsorption

Il ressort des résultats portés sur la fig. 2 que l'adsorption des trois surfactants choisis est fortement favorisée par l'élévation de la température. Ceci est particulièrement vrai pour les tensio-actifs ioniques. Les taux de fixation du SDS, CPC et NPPO sont respectivement multipliés entre 20°C et 55°C par 1,7, 1,27 et 1,3, et entre 20°C et 75°C par 1,8, 1,75 et 1,4. Ces résultats peuvent trouver leurs principales justifications au niveau: du substrat (modification de sa structure); du surfactant (modification de sa diffusion); de l'interaction substrat–surfactant.

Il est connu que la macromolécule de lignine gonfle lorsque la température du milieu s'élève, ce qui implique la dilatation des pores (30, 31), d'autant plus que la sulfonation de la lignine induit une destruction des liaisons transversales et donc une ouverture préalable des pores (3–8). Dans de telles conditions le soluté diffuse plus facilement, et la surface d'adsorption augmente. De ce fait le nombre de sites d'adsorption croît. Par ailleurs la concentration micellaire critique (cmc) des surfactant augmente avec la température, de telle sorte que le nombre de molécules tensio-actives indépendantes croît. Leur diffusion à l'intérieur des pores est par conséquent facilitée. Ainsi pour le

Can. J. Chem. Downloaded from www.nrcresearchpress.com by 210.87.254.40 on 09/05/12
For personal use only.

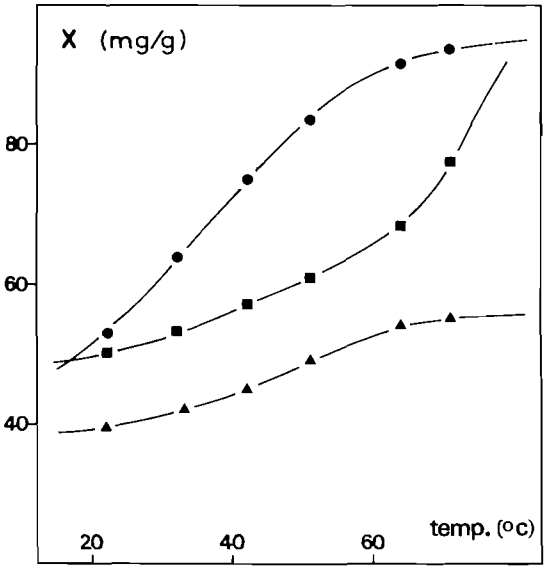

FIG. 2. Effet de la température sur l'adsorption (Co = 2 g/L, t = 20 min, pH = 1,8); ● SDS, ■ CPC, ▲ NPPO.

SDS la cmc passe entre 20°C et 70°C de 8,25 mM/L à 11,4 mM/L. Pour le CPC elle augmente de 0,9 mM/L à 2,36 mM/L entre 25°C et 80°C. Par contre celle du NPPO croît très faiblement de $6{,}23 \times 10^{-2}$ mM/L à $6{,}54 \times 10^{-2}$ mM/L entre 25°C et 75°C (32). Ceci pourrait expliquer l'effet décroissant de la température sur les adsorptions du SDS, CPC et NPPO, d'autant plus que la cmc traduit la possibilité qu'ont les surfactants à réduire leur surface.

Cette amélioration de la fixation liée à l'élévation de la température peut surtout s'expliquer par l'intervention de liaisons endothermiques telles que les interactions hydrophobes. La structure de la lignine est maintenue par des liaisons hydrogènes et des interactions hydrophobes (31). Lorsque la lignine est gonflée par un solvant polaire comme l'eau, les chaînes prennent une conformation telle qu'elle permet la formation d'interactions hydrophobes entre les chaînes apolaires de la lignine (30, 31). On conçoit que ces interactions puissent également s'établir entre les chaînes apolaires des surfactants et de la lignine. Outre celles du type lignine–surfactant, ces interactions hydrophobes peuvent être du type surfactant–surfactant. En effet il est généralement admis que l'adsorption des tensioactifs sur une surface polaire est tout d'abord ionique (29). Les résidus hydrophobes de ces premières molécules adsorbées sont donc orientés vers le solvant. Ils peuvent alors fixer de nouvelles molécules tensio-actives par interactions hydrophobes, selon le processus d'hémicellisation (29). L'adsorption ionique préalable du SDS et du CPC favorise ce phénomène et peut donc également expliquer l'effet plus important de la température sur leur fixation que sur celle du NPPO. Par ailleurs les liaisons hydrogènes entre les groupes acides carboxyliques et phénoliques dissociés et non dissociés de la lignine (31) peuvent être rompues lors de la diffusion des surfactants induisant ainsi une ouverture de la structure de la macromolécule, et par conséquent une accessibilité plus grande de ses sites hydrophobes aux molécules tensio-actives.

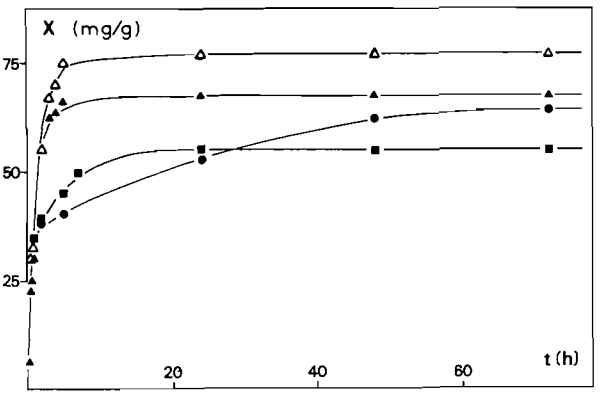

FIG. 3. Influence du temps de réaction sur l'adsorption (Co = 2 g/L, pH = 1,8); ● SDS 22°C, ■ CPC 22°C, ▲ NPPO 22°C, △ NPPO 56°C.

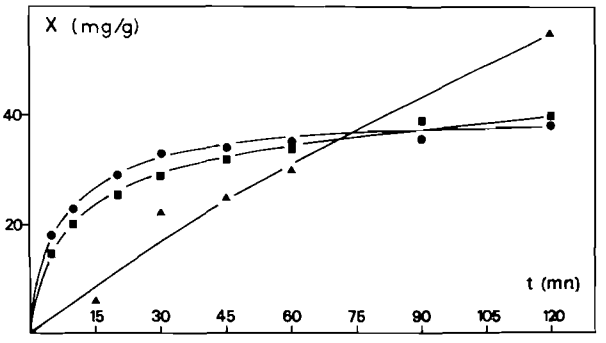

FIG. 4. Influence du temps de réaction sur l'adsorption (Co = 2 g/L, pH = 1,8, θ = 22°C); ● SDS, ■ CPC, ▲ NPPO.

3. Analyse des modes d'adsorption et de diffusion

3.1. D'un surfactant anionique: le SDS

Dans les conditions opératoires choisies, la fixation est très rapide lors des deux premières heures, puis une adsorption lente s'établit jusqu'à l'équilibre atteint en 72 h (fig. 3). L'agrandissement de la première partie de la courbe (fig. 4) fait ressortir deux étapes: une phase rapide lors des 30 premières minutes qui peut être attribuée à l'établissement de liaisons ioniques, comme nous le verrons lors de l'étude de l'adsorption en milieu alcoolique; suivie d'une phase lente qui correspond à l'adsorption hydrophobe. Si on se réfère à la fig. 3,

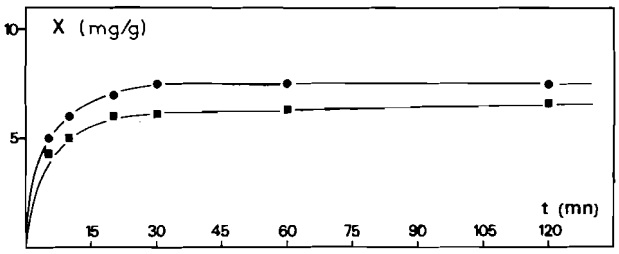

FIG. 5. Adsorption en milieu éthanolique (Co = 2 g/L, pH = 1,8, θ = 22°C); ● SDS, ■ CPC.

on peut remarquer que ces interactions s'établissent rapidement puis lentement après environ 2 h. Les premières semblent donc correspondre à des interactions hydrophobes lignine–SDS, rapides à s'établir en raison de la très grande hydrophobie de certains sites. Les deuxièmes correspondent alors à des interactions hydrophobes de seconde couche soit SDS–SDS à partir des molécules tensio-actives fixées ioniquement, soit lignine–SDS en raison de l'augmentation de l'hydrophobie de certains sites du fait de l'adsorption hydrophobe préalable.

En milieu alcoolique les interactions hydrophobes sont inhibées et la stabilité de la structure de la lignine est assurée par les groupements polaires (30, 31). Dans ces conditions seule l'adsorption ionique peut s'exprimer. On constate que dans un tel milieu la fixation est achevée en 30 min (fig. 5). Ceci semble donc correspondre à la cinétique rapide des liaisons ioniques, et corrobore l'interprétation proposée précédemment en ce qui concerne la succession des modes d'adsorption. Notons que nous avons étudié l'influence de la température sur l'adsorption du SDS en milieu éthanolique et que, conformément à ce qui était attendu, aucune variation de fixation n'a été observée. L'adsorption est dans ces conditions de 7,5 mg/g soit de $2{,}84 \times 10^{-2}$ mM/g. Elle représente seulement 12% de la quantité fixée à l'équilibre et 23% en 30 min en milieu eau pure. Il ne semble donc pas que l'adsorption lors de la première heure soit purement ionique. Ceci permet de penser qu'elle s'accompagne soit d'une adsorption hydrophobe lignine–SDS, soit qu'il s'agit d'une adsorption ionique de micelles, chaque micelle comportant en moyenne 4,25 molécules de SDS.

Par analogie aux études de diffusion de solutés dans la laine (33–35) nous avons tracé les courbes d'adsorption en fonction de la racine du temps ($\sqrt{t}$). Elles donnent lieu pour le SDS à la succession de deux droites avant le palier d'équilibre (fig. 6). Le fait de ne pas obtenir une seule droite peut être interprété en ceci que toutes les particules végétales ne sont pas identiquement accessibles.

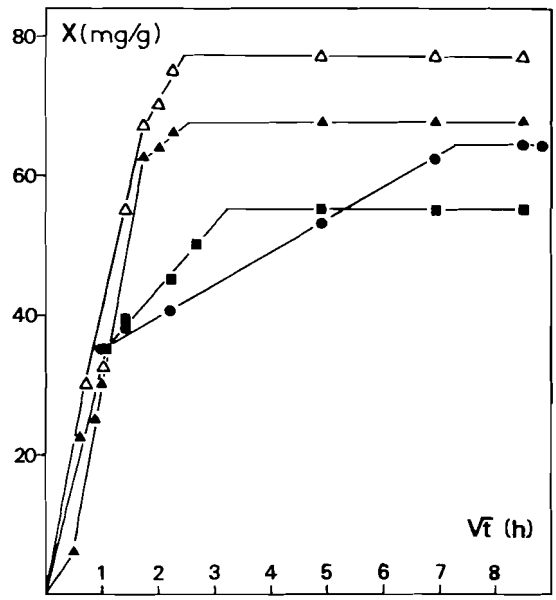

FIG. 6. Influence du temps de réaction sur l'adsorption (Co = 2 g/L, pH = 1,8); ● SDS 22°C, ■ CPC 22°C, ▲ NPPO 22°C, △ NPPO 56°C.

En effet leur granulométrie est suffisamment différente pour que le temps nécessaire à la diffusion dans les particules soit variable. Il est en outre apparu à travers les photos 1 à 3 que les particules végétales comportent des porosités de types différents. Ceci peut aussi être la cause de vitesses de diffusion différentes. Par ailleurs on constate l'absence d'une phase lente d'initiation. On peut pour cette raison préconiser la formation très rapide d'une couche à la surface des particules du fait de liaisons ioniques puis une diffusion par échanges ioniques et ouverture des liens hydrophobes dans toute la masse de la lignine.

3.2. D'un surfactant cationique: le CPC

En se référant aux figs 3 et 4, on retrouve les mêmes étapes d'adsorption pour le CPC que celles observées pour le SDS. La fixation du CPC en milieu alcoolique (fig. 5) s'élève à 6 mg/g en 30 min et à 6,5 mg/g en 120 min. Ceci confirme l'intervention de liaisons ioniques entre le CPC et les lignines sulfuriques à pH très acide. L'absence d'équilibre rapide peut s'expliquer par la mise en jeu d'interactions entre les groupements ammoniums du CPC et les doublets des hétéroatomes du substrat. Les taux de fixation du CPC en milieu alcoolique par rapport aux taux obtenus en milieu eau pure en 30 min et à l'équilibre sont respectivement de 11% et 20,7%. Comme pour le SDS il semble donc que l'adsorption lors de la première demi-heure ne soit pas strictement ionique, mais qu'elle s'accom-

Can. J. Chem. Downloaded from www.nrcresearchpress.com by 210.87.254.40 on 09/05/12
For personal use only.

Can. J. Chem. Downloaded from www.nrcresearchpress.com by 210.87.254.40 on 09/05/12
For personal use only.

pagne d'une adsorption hydrophobe. L'hypothèse d'une adsorption ionique de micelles n'est toutefois pas à exclure. Dans ce cas les micelles comporteraient en moyenne 4,85 molécules tensio-actives, c'est-à-dire un peu plus que les micelles de SDS. Cette plus grande taille des agrégats cationiques est en accord avec les pouvoirs de micellisation de ces surfactants traduits par les valeurs de leur cmc.

En se référant à la fig. 6 on observe une courbe analogue à celle du SDS, témoignant donc de l'hétérogénéité des particules végétales et d'un même mode de diffusion.

3.3. D'un surfactant non ionique: le NPPO

Il est normal de constater une adsorption nulle du NPPO en milieu alcoolique. Par ailleurs, si on considère la fixation en début de réaction (fig. 4), on remarque que la variation de la pente de la tangente en chaque point de la courbe du NPPO est négligeable par rapport à celles du SDS et du CPC. Cette observation semble confirmer le rôle prépondérant des liaisons ioniques en début de réaction pour les surfactants ioniques. D'autre part si on se réfère à la fig. 6 on note que son allure est la même que celle des courbes du SDS et du CPC. Son interprétation est donc analogue. Remarquons néanmoins qu'une phase d'initiation apparait en début de réaction (figs 4, 6). Sa cinétique est moins rapide que celle de la phase suivante de diffusion. On peut expliquer cette phase d'initiation non observée pour les surfactants ioniques par l'absence de la formation très rapide d'une couche de molécules tensio-actives à la surface des particules par liaisons ioniques.

A 56°C l'adsorption du NPPO est plus rapide du fait de l'absence de la phase lente d'initiation, et plus importante (figs 3, 6). Ces deux observations peuvent être interprétées d'une part par la dilatation des pores permettant une diffusion rapide dès le début de la réaction et induisant un accroissement de la surface d'adsorption, d'autre part par le caractère endothermique des interactions hydrophobes. De plus l'augmentation de la cmc a pour conséquence une diffusion plus rapide et une possibilité plus grande pour la molécule tensio-active de réduire sa surface.

Remarque: influence de la longueur de la chaîne tensio-active sur l'adsorption

Il apparaît dans le tableau 2 que l'adsorption des alkylsulfates de sodium croît avec la longueur de la chaîne tensio-active. Des résultats analogues ont été obtenus avec d'autres substrats (29). Par contre la cmc est inversement proportionnelle à la longueur de la chaîne (32). Celle des alkylsulfates est divisée par quatre lorsque la chaîne hydrophobe augmente de deux atomes de carbone (tableau 2).

TABLEAU 2. Comparaison de l'adsorption d'alkylsulfates de sodium de différentes longueurs de chaîne

Alkylsulfates	SDS	STS	SHS
cmc à 40°C (mM/L) (36)	8,60	2,21	0,54
x/m (μM/g)	124,8	142,2	187,2

Cela correspond à une diminution de la solubilité des surfactants dans l'eau et à un accroissement de leur pouvoir tensio-actif qui conduisent tout naturellement les molécules tensio-actives à s'adsorber sur les surfaces des matériaux en présence desquelles elles sont. Par ailleurs l'énergie libre du surfactant décroît d'où une augmentation de l'adsorption du fait de l'augmentation du nombre de forces dispersées mises en jeu (29). D'autre part la surface de la molécule tensio-active augmentant, l'établissement de liaisons de Van der Waals entre chaînes hydrophobes augmente. Ainsi l'augmentation de la longueur de la chaîne tensio-active se traduit par une accroissement des interactions hydrophobes tant lignine–surfactant que surfactant–surfactant conduisant à une adsorption pseudo-micellaire, c'est-à-dire à une adsorption par micellisation hydrophobe du surfactant sur les chaînes hydrophobes tensio-actives préalablement fixées.

Conclusion

L'influence importante du pH sur l'adsorption du SDS a mis en évidence l'intervention de liaisons ioniques, ce qui permet de proposer la formation d'ammoniums quaternaires et d'ions thiouroniums sur la lignine lors du carbonisage par réaction avec les acides aminés kératiniques. L'effet de ce paramètre sur la fixation du CPC a fait ressortir le rôle d'une très importante sulfatation de la lignine lors du carbonisage. Par ailleurs une légère amélioration du taux de fixation du NPPO à pH basique indique une hydrolyse alcaline du substrat également observée lors de l'adsorption du SDS se traduisant par un accroissement de sa fixation, et lors de l'adsorption du CPC se traduisant par une diminution de sa fixation.

L'étude de l'influence de la température sur l'adsorption des trois surfactants a montré l'intervention d'interactions hydrophobes, également mise en évidence lorsqu'on a fait varier la longueur de la chaîne tensio-active. Cette adsorption hydrophobe en relation inversement proportionnelle avec la cmc des surfactants s'avère plus importante pour le NPPO que pour les tensio-actifs ioniques, ce qui ressort de l'étude de la fixation dans le temps.

Le mode d'adsorption des surfactants ioniques est successivement ionique et hydrophobe. Enfin l'étude de la diffusion du SDS, CPC et NPPO

réalisée à partir des courbes d'adsorption tracées en fonction de $\sqrt{t}$ a mis en évidence l'hétérogénéité de la granulométrie et de la porosité des particules végétales. Elle a également fait apparaître l'absence de phase d'initiation en ce qui concerne le SDS et le CPC en raison de l'intervention rapide de liaisons ioniques. Quant à la phase d'initiation observée à 22°C pour le NPPO, elle disparaît à 56°C du fait de l'ouverture des pores du substrat, et du plus grand nombre d'interactions hydrophobes.

Remerciements

Ce travail a été réalisé grâce à l'aide financière du Ministère de l'Environnement et du Cadre de Vie. Nous remercions également l'ITF Sud Lecarim à travers la personne de Monsieur Sergent.

1. F. PERINEAU, J. MOLINIER et A. GASET. Proc. 1st Mediterranean Cong. Chem. Eng., Barcelone, **2**, 1050 (1978).
2. B. K. PATEL et T. N. RAMAMURTHY. Wool Woolens India, **13**, 49 (1976).
3. N. MIGITA, R. MITSUKAWA, J. NAKANO et M. ICHINO. J. Jpn. Tappi, **8**, 2 (1954).
4. L. IVNAS et B. LINDBERG. Acad. Chem. Scand. **15**, 1081 (1961).
5. B. D. BOGOMOLOV, O. F. GORDBUNOVA et S. V. PALMOVA. Tr. Arkhang. Lesotekh. Inst. **32**, 47 (1972).
6. V. F. FELICETTA, D. W. GLENNIE et J. L. MCCARTHY. Tappi, **50**, 170 (1967).
7. H. ERDTMAN. Research (London), **3**, 63 (1950).
8. A. BJORKMÄN et B. PEARSON. Sven. Papperstidn. **60**, 285 (1957).
9. G. P. GRIGOREV, T. M. VASILEVA, K. I. VLASOVA, V. P. KAPRANOVA et N. V. GAIVORONSKAYA. Tr. Leningrad Tekhnol. Inst. Tsellyul., Bumazh. Prom. **27**, 216 (1970).
10. G. P. GRIGOREV, T. M. VASILEVA, K. I. VLASOVA, L. N. SMIRNOVA et V. P. KAPRANOVA. Tr. Leningrad Tekhnol. Inst. Tsellyul., Burn. Prom. Sti. **13**, 30 (1973).
11. R. R. SHARIFOV, E. V. SHULLTS et N. A. ABBASOVA. Tr. Bakin Fil. Vses. Nauch., Issled. Inst. Vodosnabzh. Kanaliz, Gidrotekh. Sooruzh. Inzh. Gidrogeol. **6**, 230 (1971).
12. R. KITAMURA et S. SUZUKI. J. Pharm. Soc. Jpn. **57**, 659 (1937).
13. A. WACEK. Intern. Holzmarkt. **20**, 50 (1949).
14. L. P. GOLMAN, L. G. MATUSEVICH et V. M. REZNIKOV. Khim. Drev. **9**, 93 (1971).
15. G. G. ALLAN, P. MAURANEN, M. D. DESERT et W. M. REIF. Pap. Puu, **50**, 539 (1968).
16. K. V. SARKANEN et C. SCHUERCH. Anal. Chem. **27**, 1245 (1955).
17. G. K. MALINOVSKAYA, N. P. SHPENZER et S. L. TALMUD. Zh. Prikl. Khim. **51**, 2043 (1978).
18. J. LONGWELL et D. MANIECE. Analyst, **80**, 167 (1955).
19. M. MAUZAC, S. GUERARD, J. MATHIEU et J. LAROCHE. Analusis, **4**, 236 (1976).
20. R. A. GREFF, E. A. SETZKORN et W. D. LESLIE. J. Am. Oil Chem. Soc. **42**, 180 (1965).
21. T. HARADA et Z. NIKUNI. J. Agric. Chem. Soc. Jpn. **23**, 415 (1950).
22. L. N. MOZHEIKO, V. N. SERGEEVA, V. R. YAUNZEMS et D. Y. BALTSERE. Inst. Khimili Drev., A.N. Latv. SSR, 1971.
23. G. V. CHUIKO, E. I. CHUPKA, A. V. OBOLENSKAYA et V. M. NIKITIN. Khim. Drev. **10**, 133 (1971).
24. M. WAYMAN et T. I. OBIAGA. Can. Wood Chem. Symp. **4**, 19 (1973).
25. G. H. TOMLINSON et H. HIBBERT. J. Am. Chem. Soc. **58**, 345 (1936).
26. E. ADLER et L. ELLMER. Acta Chem. Scand. **2**, 839 (1948).
27. E. ADLER et S. HÄGGROTH. Acta Chem. Scand. **3**, 86 (1949).
28. K. KRATZL et J. SPONA. Halzforschung, **20**, 27 (1966).
29. J. M. ROSEN. J. Am. Oil Chem. Soc. **52**, 431 (1975).
30. I. A. PEARL. Chem. Eng. News, **42**, 80 (1964).
31. I. A. PEARL. Annal Review of Lignin Chemistry, Appleton, Wisconsin, The Institute of Paper Chemistry. 1973.
32. P. MUKERJEE et K. J. MYSSELS. Natl. Bur. Stand. **36**, 1 (1971).
33. J. B. SPEAKMAN et G. S. SMITH. J. Soc. Dyers Colour. **52**, 121 (1936).
34. J. H. SHINKLE. Text. Res. J. **25**, 861 (1955).
35. J. H. BRADBURY. Text. Res. J. **30**, 128 (1960).

Can. J. Chem. Downloaded from www.nrcresearchpress.com by 210.87.254.40 on 09/05/12
For personal use only.

Synthesis of tris(aminomethyl)phosphine oxide and its carbon dioxide adduct from tetrakis(hydroxymethyl)phosphonium salts via their methyl carbamate derivatives[1]

ARLEN W. FRANK

Southern Regional Research Center[2], New Orleans, LA 70179, U.S.A.

Received March 3, 1980

ARLEN W. FRANK. Can. J. Chem. **59**, 27 (1981).

Tris(aminomethyl)phosphine oxide (**6**) can be synthesized from octakis(hydroxymethyl)diphosphonium sulfate (**1*b***) in an overall yield of 54.6% via the methyl carbamate derivatives **2*b***, **3**, and **4**. On a preparative scale, the last step is complicated by the formation of a cyclic by-product **8** in amounts up to 20% of the total. The triamine **6** forms a 1:1 adduct (**11**) with carbon dioxide, whose structure, established by ^{1}H and ^{13}C nmr, consists of equimolar amounts of carbamate **A** and dicarbamate **BC**. The components **A**, **B**, and **C** can be separated by ion exchange. Thermolysis of **11** regenerates **6** smoothly, providing a convenient method for purifying the triamine.

ARLEN W. FRANK. Can. J. Chem. **59**, 27 (1981).

On peut synthétiser l'oxyde de tris(aminoéthyl)phosphine (**6**) avec un rendement global de 54,6% à partir du sulfate d'octakis-(hydroxyméthyl)diphosphonium (**1*b***) par l'intermédiaire des dérivés **2*b***, **3** et **4** du carbamate de méthyle. A l'échelle préparative, la formation du produit cyclique secondaire **8** dans une proportion de 20% complique la dernière étape. La triamine **6** forme avec le bioxyde de carbone un adduit 1:1 (**11**) dont on a établi la structure par la rmn du ^{1}H et du ^{13}C. Cet adduit consiste en des quantités équimoléculaires de carbamate **A** et de dicarbamate **BC**. On peut séparer les composants **A**, **B** et **C** des résidus par échangeurs d'ions. La thermolyse du composé **11** regénère le composé **6** de façon douce, fournissant ainsi une méthode de purification de la triamine.

[Traduit par le journal]

Introduction

As part of a program on the synthesis of new flame retardants for cotton, a supply of tris-(aminomethyl)phosphine oxide (**6**) was needed in quantities suitable for fabric testing. Until recently, **6** was accessible only from tetrakis(hydroxymethyl)phosphonium chloride (THPC, **1*a***)[3] by a five-step synthesis via tris(chloromethyl)phosphine oxide in a overall yield of 28.8% (1–5). The last step of this synthesis, a Gabriel reaction (5), was ill suited for scale-up. Recently, we described an alternate synthesis of **6** from **1*a*** via the four-step carbamate route outlined in Scheme 1. The overall yield of **6**, isolated as the crystalline trihydrobromide **7*b***, was 44.5% (6, 7).

In this paper, I describe some improvements in the carbamate method, changes that make it useful for synthesizing **6** in the laboratory on a preparative scale. The most significant changes are (*i*) substitution of THPS (**1*b***) for **1*a*** as the starting material, (*ii*) oxidation of the tertiary phosphine **3** with aqueous hydrogen peroxide *in situ*, and (*iii*) hydrolysis of the tertiary phosphine oxide **4** under alkaline rather than acid conditions. Finally, I describe a novel method of purifying **6** through its 1:1 adduct with carbon dioxide, a method that is potentially useful for the purification of other water-soluble, non-volatile primary or secondary amines.

Results and Discussion

The original starting material, THPC (**1*a***), is no longer manufactured in the United States because it is a potential source of formaldehyde and hydrogen chloride, precursors of the carcinogen bis-(chloromethyl) ether (8). In its place, other tetrakis-(hydroxymethyl)phosphonium salts are available commercially: the sulfate (**1*b***) THPS (Hooker Chemicals and Plastics Corp., Niagara Falls, NY) or TKO, the oxalate TKS, and the mixed phosphate/acetate TKP (Pyroset Series, American Cyanamid Co., Bound Brook, NJ). THPC is still available from foreign sources (Tetrakis-80, Aceto Chemical Co., Inc., Flushing, NY).

Reaction of methyl carbamate with **1*b*** under the conditions employed with **1*a*** (6) gave a quantitative yield of the diphosphonium sulfate **2*b***. This product, unlike the phosphonium chloride **2*a***, could not be induced to crystallize. It was characterized by ir and nmr spectroscopy and by conversion to **2*a*** with barium chloride.

Hydrolysis of **2*b*** with ammonium hydroxide under the conditions employed with **2*a*** (6) gave a quantitative yield of the tertiary phosphine **3**, mp 110–115°C, identical (ir, nmr) to the product obtained from **2*a***.

Oxidation of the tertiary phosphine **3** with hy-

[1]Dedicated to Dr. Léo Marion, with whom the author served as NRCC Postdoctorate Fellow, 1954–1955.

[2]One of the facilities of the Southern Region, Science and Education Administration, U.S. Department of Agriculture.

[3]Names of companies or commercial products are given solely for the purpose of providing specific information; their mention does not imply recommendation or endorsement by the U.S. Department of Agriculture over others not mentioned.

0008-4042/81/010027-07$01.00/0

©1981 National Research Council of Canada/Conseil national de recherches du Canada

Can. J. Chem. Downloaded from www.nrcresearchpress.com by 210.87.254.105 on 09/05/12
For personal use only.

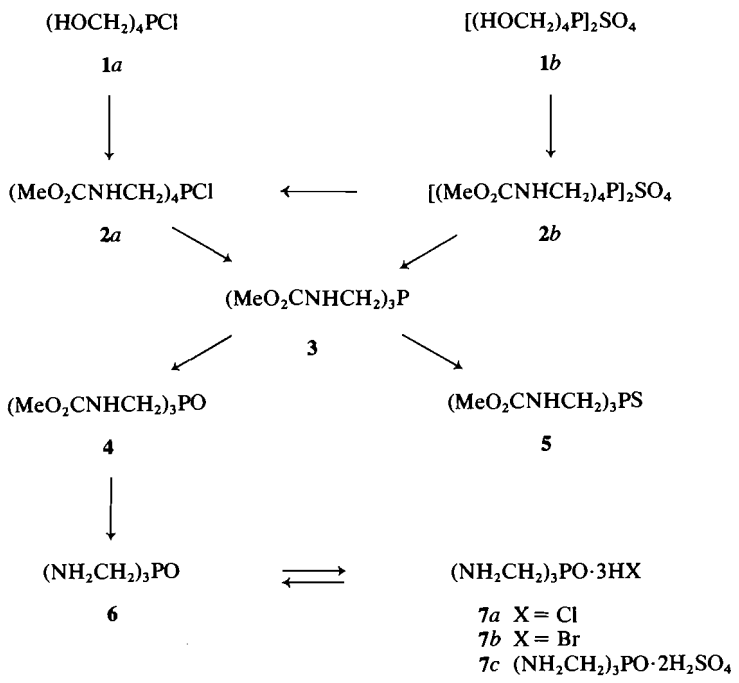

SCHEME 1. Synthesis of **6** from **1***a* or **1***b* via the carbamate route.

drogen peroxide in acetone, as described previously (6), gives the tertiary phosphine oxide **4** in yields of 69% to 84%. Although I have carried out this oxidation on numerous occasions without incident, the use of acetone poses a hazard because mixtures of acetone and hydrogen peroxide are potentially explosive (9). Water is just as effective as a solvent, and the hydrolysis by-products need not be removed before oxidation. Hydrolysis of **2***b* with ammonium hydroxide, followed by oxidation *in situ* with hydrogen peroxide, gave **4** in 88% yield, compared to 89% when the excess ammonium hydroxide and by-products were removed before oxidation. The phosphonium salts **2***a* and **2***b* are stable to hydrogen peroxide in the absence of base. The preferred procedure, described in the Experimental, gave a 70.6% yield of recrystallized **4**, based on **1***b*, without pausing to isolate either of the intermediates **2***b* or **3**.

The tertiary phosphine sulfide **5**, previously prepared in 73.4% yield by the reaction of **3** with sulfur in benzene (6), was prepared from **1***b* in 48.9% overall yield by condensation with methyl carbamate, hydrolysis with ammonium hydroxide, and sulfurization *in situ* with ammonium polysulfide.

Hydrolytic cleavage of carbamates to primary amines under alkaline conditions is practiced much less frequently than cleavage under acid conditions (10, 11). Hydrolysis of the tertiary phosphine oxide **4** with sodium hydroxide for 5 h at 100°C produced no visible change, but extensive gassing occurred when the solution was acidified. The product, identified by ir and nmr, was the triamine trihydrochloride **7***a*. The product was difficult to separate from the sodium chloride because of their similar solubility characteristics; the mixture was therefore neutralized with sodium hydroxide, giving the triamine **6** in 81.7% yield.

This difficulty was avoided by hydrolyzing **4** with barium hydroxide instead of sodium hydroxide. Barium carbonate separated during the reaction, enabling the progress of the reaction to be observed (eq. [1]). The excess base was destroyed by carbonation with Dry Ice while the reaction mixture was still hot. No gassing occurred when the filtrate was acidified, and the triamine trihydrochloride **7***a* was obtained in 93.2% yield. Neutralization of **7***a* with sodium hydroxide gave pure **6** in quantitative yield.

$$[1]\quad \underset{\mathbf{4}}{(MeO_2CNHCH_2)_3PO} + 3Ba(OH)_2 \rightarrow \underset{\mathbf{6}}{(NH_2CH_2)_3PO} + 3BaCO_3 + 3MeOH$$

If the filtrate was acidified with sulfuric acid instead of hydrochloric acid, the triamine was isolated as the crystalline bis(dihydrogen sulfate) **7***c* in 90.3% yield. Neutralization with barium hydroxide, followed by carbonation with Dry Ice at 100°C to destroy the excess base, gave pure **6** in quantitative yield.

If the filtrate was not acidified, the triamine **6** could be isolated directly. The crude product was

Can. J. Chem. Downloaded from www.nrcresearchpress.com by 210.87.254.105 on 09/05/12
For personal use only.

Can. J. Chem. Downloaded from www.nrcresearchpress.com by 210.87.254.105 on 09/05/12
For personal use only.

almost pure **6**, together with a by-product from which it was easily separated. The by-product was 5-aminomethyl-1,3-diaza-5-phosphorinan-2,5-dione (**8**).[4]

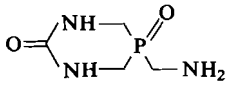

8

This by-product is a white, crystalline solid, mp 204–206°C, that forms crystalline 1:1 salts (**9***a*,*b*) with hydrochloric acid and sulfuric acid. The formation of **8**, a cyclic monomeric urea derivative, was surprising in view of a study of the condensation of urea with **1***a*. In that study (12), the products and their derivatives were invariably polymeric. Because the starting material **4** contained no **8** (by nmr), the by-product must have been formed during the hydrolysis, probably by degradation of a carbomethoxylamino group to an isocyanate group, followed by ring closure with an adjacent amino group. The yield of the by-product was highest (15–20%) in the preparative scale reactions. Attempts to hydrolyze **8** to **6** or to synthesize **8** from **6** and urea (13) were unsuccessful.

For large-scale preparations, it was more convenient to use calcium hydroxide as the base. The yield of **6**, isolated as the hydrate, was 74.8% based on **4**, or 54.6% overall based on **1***b*.

Reaction of 6 with Carbon Dioxide

Pure **6** did not absorb carbon dioxide in the absence of a solvent, but when a stream of carbon dioxide was passed into a solution of **6** in methanol or ethanol, a white solid separated immediately. The product was a fluffy solid (**10**), mp 57°C, that changed into a compact solid (**11**), mp 138°C dec., on exposure to the air. The final product (**11**) was a 1:1 adduct of **6** and carbon dioxide. Its elemental composition, molecular weight, and ir and ^{1}H nmr spectra are consistent with structure **A**, an intramolecular carbamate salt.

The ^{1}H nmr spectrum of **11** in D_2O showed a pair of doublets for the three methylene groups in a ratio of 4:2. The stronger doublet, δ 3.38 (J = 6.0 Hz), appearing slightly downfield of the doublet in **6**, represents the two aminomethylene groups, averaged by proton exchange between the nitrogens. The weaker doublet, δ 3.77 (J = 7.5 Hz), appearing further downfield. represents the carboxylaminomethylene group. These assignments were verified by subsequent experiments.

The ^{13}C nmr spectrum of **11** in D_2O (Table 1) exhibited separate signals for the three methylene groups, each split into a doublet of triplets because of coupling with phosphorus (1:1) and hydrogen (1:2:1). A small unsplit signal for the carboxyl carbon *d* appeared far downfield at δ 164.3. The weak doublet at δ 38.0 was assigned to the carboxylaminomethylene carbon *c*. The intensities of the signals were consistent with the assignments, but the nonequivalence of the aminomethylene carbons *b* was incompatible with structure **A**.

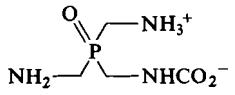

A

Addition of NaOD to a solution of **11** in D_2O altered its ^{1}H nmr spectrum, shifting the weak doublet to δ 3.66 (J = 5.5 Hz) and splitting the strong doublet into a pair of equal overlapping doublets, δ 3.15 (J = 5.5 Hz) and 3.17 (J = 6.0 Hz). The doublet at δ 3.17 coincided with **6**. No barium carbonate separated when barium chloride was added. The spectrum remained unchanged as the temperature was raised from 30°C to 60°C, but at 70°C it changed irreversibly, the doublet at δ 3.17 increasing in intensity at the expense of the other doublets. Similar behavior was produced by other strong bases such as ammonia or trimethylamine, but not by weak bases such as pyridine. Bases have a stabilizing influence on carbamates (14).

These experiments ruled out nonequivalence of the methylene hydrogens caused by restricted rotation or internal asymmetry (15). The displacement of **6** from **11** without hydrolysis suggested the alternate structure **BC**, an intermolecular dicarbamate salt.

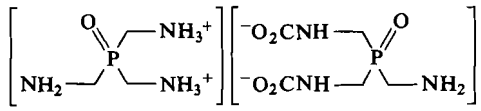

B **C**

This structure is compatible with the elemental composition, molecular weight, and ir and nmr spectra of **11**, but not with the molar ratios observed after treatment with base. The spectra can, however, be reconciled if **11** is comprised of structures **A** and **BC** in a 1:1 molar ratio. At this ratio, there are three *a* groups in structure **B**, and three *b*, *c*, and *d* groups apiece distributed between structures **A** and **C**. Separate signals are observed for the four groups in the ^{13}C nmr spectrum. The signals for *a* and *b* coincide in the ^{1}H nmr spectrum, but separate when base is added, liberating **B** as the free amine **6**.

It occurred to me that Kunin's method for

[4]Models of this compound have a rigid ring structure with no boat or chair forms. The P oxygen, however, may be axial or equatorial.

TABLE 1. ^{13}C nmr data for **6** and its derivatives

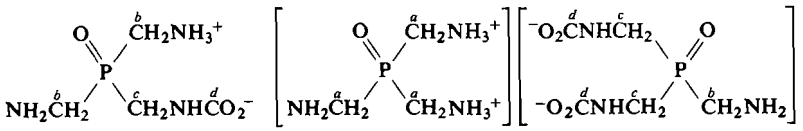

A **B** **C**

Compound	Formula	Intensity (%)	Assignment	δ_C (ppm)	J_{PC} (Hz)	J_{HC} (Hz)
6	$(NH_2\overset{a}{C}H_2)_3PO$	100	*a*	35.7	66.9	137.0
7a	$(NH_3^+\overset{a}{C}H_2)_3PO\ 3Cl^-$	100	*a*	36.8	71.4	144.8
11	**A** + **BC**	100	*a* (or *b*)	35.8	65.4	140.9
		85	*b* (or *a*)	36.0	72.3	139.3
		60	*c*	38.0	72.9	139.2
		17	*d*	164.3	0	0

separating the amino acids into acid, neutral, and basic classes by ion exchange (16, 17) might be useful for separating **11** into its components **A**, **B**, and **C**. Cation exchange resins and acidic reagents were avoided because of the sensitivity of carbamates to acids. Rexyn 203, a weak base anion exchange resin, did not adsorb any of the components, but Rexyn 201, a strong base anion exchange resin, adsorbed the acid component **C**, allowing the neutral component **A** and the basic component **B** (displaced as **6**) to pass through. The dicarbamate **C** could be displaced from the resin by sodium hydroxide but not by ammonium hydroxide; barium hydroxide gave an insoluble precipitate. Two-thirds (67%) of the carbon dioxide in **11** was present as the dicarbamate, confirming a 1:1 stoichiometry for **A**:**BC**.

Analogous structures have been invoked for the 1:1 adducts of carbon dioxide with ethylenediamine (18, 19) and other diamines (18, 20) to explain their behavior toward reagents such as phosgene and diazomethane. Estimates of the percentage of carbon dioxide present as the dicarbamate ranged from 20% (19) to 50% (18), falling to 0% after aging (20).

The initial fluffy product (**10**) of the reaction of **6** and carbon dioxide could be isolated by vacuum drying, preferably after rinsing with carbon tetrachloride. It seemed to be stable indefinitely if not exposed to the air; the original sample was unchanged after storage for a year. The composition, ^1H nmr spectrum, and behavior of **10** toward barium chloride, NaOD, and ammonia were identical to those of **11**, but the ir spectra differed in the 800–900 cm^{-1} region.

The transformation of **10** to **11** upon exposure to air (moisture) is seen to be a hydrogen bond breaking process that allows the product to rearrange to a more compact crystalline form. The transformation can be accelerated by adding a little water to the solution of **6** in ethanol before passing in the carbon dioxide.

Treatment of **6** with carbon dioxide in an aqueous solution at room temperature yielded no solids, but after stripping the product was a 3:1 mixture of **6** and **11**. No carbamate formed in boiling water, methanol, or ethanol. A slurry of **11** in ethanol decomposed to **6** and carbon dioxide when heated to reflux. If the carbon dioxide was swept out with argon, nothing separated on cooling, but if the reaction was carried out in a carbon dioxide atmosphere, the carbamate **10** separated on cooling.

In a paper ionophoresis study of the reaction of mono-, di-, and polyamines with carbon dioxide, Frahn and Mills (21) reported that polyamines form mixtures of mono-, di-, and polycarbamates. The upper limit for each was equal to the number of amino groups the polyamine contained. To see if **6** was capable of forming a tricarbamate, the monocarbamate **11** was dissolved in D_2O and saturated with carbon dioxide; the ratio of the doublets in the ^1H nmr spectrum changed from 2:1 to 1:1. If every free amino group in **A** and **BC** acquired either a carboxyl anion or a proton, the product would be a sesquicarbamate (3:2 adduct of CO_2 and **6**) whose *a*,*b*:*c* ratio is 1:1. No further reaction is possible.

When a solution of **11** in D_2O was treated with ammonia before saturation with carbon dioxide, however, the *a*,*b* doublet was almost completely suppressed in favor of a strong *c* doublet at δ 3.64 (J = 4.5 Hz). The product, which was not isolated, was presumably the ammonium salt $[NH_4^+]_3[P(O)(CH_2NHCO_2^-)_3]$ (**12**). Similar spectra, though not as sharply defined, were produced by solutions

Can. J. Chem. Downloaded from www.nrcresearchpress.com by 210.87.254.105 on 09/05/12
For personal use only.

Can. J. Chem. Downloaded from www.nrcresearchpress.com by 210.87.254.105 on 09/05/12
For personal use only.

of **11** in D_2O containing ammonium carbonate, or sodium carbonate after saturation with carbon dioxide.

Thermolysis of 11

The carbamate **11** decomposed cleanly when heated gently over a gas flame, leaving pure **6** as a colorless, anhydrous oil. This way to purify **6** is more convenient than the other methods available, provided that care is taken to prevent the reabsorption of carbon dioxide on cooling. Thermolysis proceeded smoothly when the solid was heated in an oil bath under vacuum, or in a drying pistol with a high boiling solvent such as xylene.

Pure **6** is a colorless hygroscopic oil, n_D^{20} 1.5682. On exposure to air, it rapidly forms a hydrate, n_D^{20} 1.5628. Neither substance has the properties ascribed to **6** in the literature (5). The hydrate, the product isolated when aqueous reagents are employed, can be dehydrated by drying under vacuum at 100°C or by azeotropic distillation with benzene. The carbamates **10** and **11** yield the anhydrous product directly.

A 20% solution of **6** in water is almost neutral (pH 7.80). The ^{13}C nmr spectrum, which has not been reported previously, exhibits only one signal for the three methylene carbons, split into a doublet of triplets because of coupling with phosphorus (1:1) and hydrogen (1:2:1). The spectrum of the trihydrochloride **7***a* exhibits a similar pattern, slightly expanded and slightly downfield (Table 1). Other properties of **6** and its salts are reported elsewhere (7).

Hydrolysis of Other Compounds

Hydrolysis of **2***a*, **2***b*, or **3** with barium hydroxide under the conditions employed with **4** gave the tertiary phosphine oxide **6**, isolated as the trihydrochloride **7***a*, in 75% to 78% yield, even though air was excluded and the excess base was destroyed with carbon dioxide from a cylinder instead of Dry Ice. There was no evidence of alkyl-nitrogen fission. Hydrolysis of the tertiary phosphine sulfide **5** with barium hydroxide was complete in 2 h, but the product was a mixture of unidentified amine salts.

Urea derivatives of **1***a* and **1***b* were difficult to hydrolyze and gave even poorer results. Hydrolysis of the urea derivative **13***a* (22) with barium hydroxide was 55% complete after 4 h refluxing and 84% complete after 10 h (eq. [2]). The yield of **14***a*, isolated as the trihydrochloride **7***a*, was 52%. Hydrolysis of the 1,3-dimethylurea derivative **13***b* (22) with barium hydroxide was 58% complete after 16 h refluxing. The products, separated into neutral and amine salt fractions by ion exchange chromatography (6), were complex mixtures whose high CH_3/CH_2 ratios, coupled with the identification of 1,1,3-trimethylurea as one of the products, provided evidence of C—P bond cleavage. The use of 75% ethylene glycol to raise the bp to 120°C increased the extent of hydrolysis to 87% after 30 h refluxing, but the product (**14***b*) was destroyed. The results were no better when the urea derivatives were hydrolyzed with sodium hydroxide or hydrobromic acid.

[2] $$\underset{\mathbf{13}}{[RNHCON(R)CH_2]_3PO} + 3Ba(OH)_2 \rightarrow \underset{\mathbf{14}}{(RNHCH_2)_3PO} + 3BaCO_3 + 3RNH_2$$

a R = H
b R = CH_3

Experimental

Melting points were corrected. Elemental analyses were performed by Galbraith Laboratories, Inc., Knoxville, TN. The ir spectra were taken on a Perkin-Elmer 137B (w weak, m medium, s strong, vs very strong); ^1H nmr spectra were taken on a Varian EM-360L with DSS as an internal lock, ^{13}C nmr spectra on a Varian CFT-20 with dioxane as an internal reference, and ^{31}P nmr spectra on a JEOL C60-HL at 24.3 MHz with 85% H_3PO_4 as an external reference (s singlet, d doublet, t triplet, m multiplet). All reagents were used as obtained.

Octakis(N-carbomethoxylaminomethyl)diphosphonium Sulfate (2b)

A mixture of 75% aqueous **1***b* (270.8 g, 0.5 mol) and methyl carbamate (300.2 g, 4 mol) was heated to reflux with constant stirring, held at 100–108°C for 2 h, allowed to cool, and stripped of water under reduced pressure, giving 443.8 g (102.9%) of **2***b* as an almost colorless tacky glass. Infrared (KBr): 1010 (m), 1110 (s), 1250 (vs), 1515 (s) (NH, amide II), 1720 (vs) (C=O, amide I), and 3300 m (NH) cm^{-1}; ^1H nmr (D_2O) δ: 3.74 (br s, 24H, CH_3) and 4.41 (br s, 16H, CH_2) ppm; ^{31}P nmr (H_2O) δ: 28.8 ppm.

On a fivefold scale it is advisable to add the methyl carbamate in 3 to 4 portions to the **1***b* at 70°C and heat to reflux between additions.

Tetrakis(N-carbomethoxylaminomethyl)phosphonium Chloride (2a)

A solution of **2***b* (8.88 g, 0.01 mol) in water (25 mL) was mixed with a solution of barium chloride (2.08 g, 0.01 mol) in water (25 mL), resulting in an immediate separation of solids. The mixture was heated to boiling to coagulate the solids, allowed to cool, and filtered, giving 2.31 g (99.0%) of barium sulfate. The filtrate, stripped under vacuum, left a crystalline residue that was rinsed with ethanol and dried, giving 5.62 g (67.1%) of **2***a*, mp 187.5–188°C dec., identical (ir, ^1H nmr) to the product prepared from **1***a* (6).

Tris(N-carbomethoxylaminomethyl)phosphine (3)

A solution of **2***b* (400.0 g, 0.464 mol) in water (500 mL) was purged with argon and treated with concentrated ammonium hydroxide (200 mL) over 15 min at 21–26°C. Solids started to separate after a few min, and after 2 h another 200 mL of water was added to facilitate stirring. After 4 h the solids were collected on a filter, rinsed with water, and dried, giving 280.0 g

Can. J. Chem. Downloaded from www.nrcresearchpress.com by 210.87.254.105 on 09/05/12
For personal use only.

(102.2%) of crystalline **3**, mp 110–115°C, identical (ir, ^{1}H nmr) to the product prepared from **2***a* (6).

*Tris(*N*-carbomethoxylaminomethyl)phosphine Oxide (4)*

A. From 3

Hydrogen peroxide (30%) was added dropwise to a well-stirred slurry of **3** (1476.2 g, 5 mol) in water (2000 mL) under an argon atmosphere, with ice-bath cooling applied as needed to keep the reaction temperature between 20 and 30°C. The addition was stopped after 3.5 h, when 550.6 g (4.85 mol) of hydrogen peroxide had been added; an iodine test for unreacted **3** was negative, and the product, which had separated during the reaction, abruptly foamed to the surface. The solids were collected on a filter, rinsed with water, and air-dried, giving 826.6 g (53.1%) of crystalline **4**, mp 179–180°C; ^{1}H nmr (Me_2SO-d_6) δ: 3.60 (s, 9H, CH_3), 3.55 (t, 6H, CH_2, J = 5.0 Hz), and 7.34 (m, 3H, NH) ppm, identical to the product prepared with acetone as the solvent (6).[5]

*B. From 2*b

A solution of **2**b (1078.4 g, 1.25 mol) in water (1600 mL) was purged with argon, stirred, and treated with concentrated ammonium hydroxide (500 mL) over 5 min at room temperature. In a few min, solids started to separate and the mixture warmed to the touch. After 2 h, the mixture, still containing the excess ammonia and by-products, was treated dropwise with 30% hydrogen peroxide (283.4 g, 2.5 mol) over a 2 h period, with ice-bath cooling applied as needed to keep the temperature below 30°C. The next day, the solids were collected on a filter, rinsed with ethanol, and air-dried, giving 435.9 g (56.0%) of crystalline **4**, mp 176–178°C dec. Work-up of the filtrate gave another 131.8 g (16.9%) of **4**, for a total yield of 73.0%. The products were combined and recrystallized from water (550 mL), giving 549.1 g (70.6%) of **4**, mp 180–181°C, identical (ir, ^{1}H nmr) to the product prepared from **3**.

*Tris(*N*-carbomethoxylaminomethyl)phosphine Sulfide (5)*

Concentrated ammonium hydroxide (500 mL) was added to a solution of **2***b* (1078.4 g, 1.25 mol) in water (1500 mL) in an apparatus previously purged with argon. Solids started to separate within min. After 2 h, the mixture, still containing the excess ammonia and by-products, was treated dropwise with 20% ammonium polysulfide (977 g, 2.87 mol) over 2 h at 25–30°C. The next day, the solids were collected on a filter, rinsed thoroughly with water, and air-dried, giving 521.4 g of crude **5**, mp 120–125°C. One recrystallization from ethanol gave 398.3 g (48.9%) of **5**, mp 132–135°C, identical (ir, ^{1}H nmr) to the product prepared from **3** (6).

Tris(aminomethyl)phosphine Oxide (6)

A. From 4

A slurry of **4** (311.2 g, 1 mol), calcium hydroxide (237.1 g, 3.2 mol), and water (2500 mL) was heated to reflux in an apparatus fitted with a mechanical stirrer and a K-head reflux condenser. Some of the methanol-containing distillate was drawn off from time to time and replaced by sufficient water to maintain the original volume. After 5 h at 98°C, the mixture was carbonated with Dry Ice until neutral through a tube extending through the reflux condenser and under the surface. The mixture was then purged with argon[6] and allowed to cool. The next day, the mixture was filtered to remove the calcium carbonate (323.5 g, 101.0%) and stripped under reduced pressure. After drying, the residue was shaken with ethanol, filtered to remove the by-product **8** (see below), and stripped again, giving 116.0 g (74.8%) of **6** hydrate as a colorless oil, n_D^{20} 1.5655, identical (ir, ^{1}H nmr) to the product prepared from **7***a* (7).

A portion of the product was dried by azeotropic distillation with benzene, with an efficient stirrer, an oil bath, and a Dean-Stark trap to collect the water. The refractive index (n_D^{20}) of the dried product was 1.5682. Another portion of the product was recovered unchanged after 5 h refluxing with calcium hydroxide.

*B. From 7*c

A hot solution of barium hydroxide octahydrate (31.55 g, 0.1 mol) in water (250 mL) was added to a hot solution of **7***c* (13.33 g, 0.04 mol) in water (250 mL). Solids separated at once. After 1 h at 65°C, the excess base was destroyed by passing a stream of carbon dioxide from a Dry Ice generator under the surface of the mixture until the contents were neutral. The mixture was heated to boiling, filtered through Celite filter aid, and stripped under vacuum, giving 6.20 g (100.0%) of **6** hydrate as a colorless oil, n_D^{20} 1.5538, identical (ir, ^{1}H nmr) to the product prepared from **7***a* (7). A portion of the product, dried in a drying pistol at 100°C, had a refractive index (n_D^{20}) of 1.5684.

C. From 11 (or 10)

Two 1-g samples of **11** were weighed in small vials and heated in a drying pistol by xylene (bp 139°C) at 0.7 Torr until the effervescence ceased. Weight loss, calcd.: 24.30%; found: 25.05, 24.88%. The product was a colorless oil, n_D^{20} 1.5681, identified as **6** by ir and ^{1}H nmr. Under the same conditions, **10** lost 30.00% of its weight, giving **6** as a colorless oil, n_D^{20} 1.5687, identical (ir, ^{1}H nmr) to the product obtained from **11**.

5-Aminomethyl-1,3-diaza-5-phosphorinan-2,5-dione (8)

The ethanol-insoluble by-product of the hydrolysis of **4** with calcium hydroxide (see **6**, method A, above) was a white, crystalline solid, 23.9 g (14.6%), mp 198–200°C. A portion of the substance was recrystallized from ethanol–water for analysis, mp 204–206°C; ir (KBr): 760–780 (s), 927 (m), 1155 (vs) (P=O), 1235 (s), 1290 (m), 1410 (m), 1520 (s) (NH, amide II), 1640 (m), 1670 (vs) (C=O, amide I), 2900 (m), 3100 (s), and 3270 (vs) (NH) cm^{-1}; ^{1}H nmr (D_2O) δ: 3.37 (d, 2H, chain CH_2, J = 5.5 Hz), 3.62 (t, 2H, J = 1.5 Hz), and 3.82 (s, 2H) ppm.

Anal. calcd. for $C_4H_{10}N_3O_2P$: C 29.45, H 6.18, N 25.77, P 18.99; *Mol. Wt.* 163.12; found: C 29.13, H 6.30, N 25.99, P 18.98; *Mol. Wt.* (osmometric in H_2O) 162.

The product (**8**) is soluble in water and insoluble in organic solvents. After 5 h refluxing with calcium hydroxide in water, most of it (86.9%) was recovered unchanged; the remainder contained no **6**.

Salts of 8

A solution of **8** (4.89 g, 0.03 mol) in water (15 mL) was treated with concentrated hydrochloric acid (25 mL), stripped under vacuum, shaken with ethanol, and filtered, giving 5.39 g (90.0%) of the HCl salt **9***a* as a white, crystalline solid, dec. 244°C. Infrared (Nujol): 746 (m), 834 (m), 935 (m), 1075 (m), 1115 (m), 1175 (vs) (P=O), 1240 (s), 1510 (vs) (NH, amide II), 1600 (s), 1650 (vs) (C=O, amide I), and 3130 (vs) (NH) cm^{-1}; ^{1}H nmr (D_2O) δ: 3.85 (d, 2H, chain CH_2, J = 7.5 Hz) and 3.92 (d, 4H, ring CH_2, J = 12.0 Hz) ppm.

Anal. calcd. for $C_4H_{11}ClN_3O_2P$: C 24.07, H 5.56, Cl 17.77, N 21.06, P 15.52; found: C 24.04, H 5.66, Cl 17.95, N 20.83, P 15.56.

The H_2SO_4 salt **9***b*, a white, crystalline solid, dec. 237°C, was similarly prepared from **8** and concentrated sulfuric acid in 98.8% yield. Infrared (Nujol): 862 (m), 1040 (s), 1170 (s) (P=O),

[5]The ^{1}H nmr spectrum of **4** was erroneously reported to show a signal for the CH_2 hydrogens at δ 3.47 (t, 6H, CH_2, J = 9.0 Hz) ppm (6). The corrected values for the original spectrum are identical to those of the present paper.

[6]Purging with an inert gas was necessary to prevent the carbon dioxide from reacting with the product after the mixture was cooled.

Can. J. Chem. Downloaded from www.nrcresearchpress.com by 210.87.254.105 on 09/05/12
For personal use only.

1240 (m), 1495 (s) (NH, amide II), 1650 (s) (C=O, amide I), and 3200 (s) (NH) cm^{-1}; ^1H nmr (D_2O) δ: 3.85 (d, 2H, chain CH_2, $J = 7.5$ Hz) and 3.92 (d, 4H, ring CH_2, $J = 12.0$ Hz) ppm.

The salts **9***a* and **9***b* are soluble in water and insoluble in organic solvents. Unlike **7***a* and **7***c*, they are also soluble in concentrated HCl and H_2SO_4, respectively. Neutralization with a base such as sodium hydroxide or calcium hydroxide regenerates the amine (**8**) quantitatively.

(Bis(aminomethyl)phosphinyl)methylcarbamic Acid (11)

A stream of carbon dioxide from a Dry Ice generator was passed into a solution of **6** (13.71 g, 0.1 mol) in ethanol (300 mL) over 1 h with constant stirring. Solids started to separate at once. The solids were collected on a filter, rinsed thoroughly with ethanol, sucked dry, and set aside for 24 h in an uncovered dish. On standing, the product changed from a light, fluffy solid to a compact solid covered with a layer of ethanol. The solids were once again collected on a filter, rinsed with ethanol, and dried under vacuum, giving 15.97 g (88.2%) of **11** as a white, crystalline solid, mp 138°C dec. Infrared (KBr): 840 (m), 880 (s), 1115 (s), 1140 (vs) (P=O), 1330 (vs), 1375 (w), 1470 (s), 1570 (vs) (C=O), 2950 (m), and 3300 (s) (NH) cm^{-1}; ^1H nmr (D_2O) δ: 3.38 (d, 4H, $C_{a,b}H_2$, $J = 6.0$ Hz) and 3.77 (d, 2H, C_cH_2, $J = 4.5$ Hz) ppm; see Table 1 for ^{13}C nmr data and identification of carbon atoms *a–c*.

Anal. calcd. for $C_4H_{12}N_3O_3P$: C 26.52, H 6.68, N 23.20, P 17.10; *Mol. Wt.* 181.14; found: C 26.64, H 6.61, N 23.24, P 17.10; *Mot. Wt.* (osmometric in H_2O) 190.

The carbamate **11** is soluble in water and insoluble in organic solvents. Its aqueous solution is neutral. Acids such as acetic acid produce gassing, but bases such as sodium hydroxide or barium hydroxide give stable solutions. Efforts to recrystallize the carbamate were unsuccessful. The product oils out from ethanol–water but solidifies on standing and can be recovered unchanged.

Separation of 11 into its Components

A solution of **11** (3.26 g, 18 mmol) in water (5 mL) was transferred to a 50-mL buret containing a 17-cm column of Rexyn 201 (OH form) ion exchange resin and eluted at a flow rate of 1 mL/min. The effluent (250 mL) was stripped to low volume under vacuum, treated cautiously (gassing) with concentrated HCl (50 mL), diluted with ethanol (50 mL), and filtered, giving 2.97 g (12.05 mmol, 100.4%) of **7***a*. The resin was then eluted with 4% NaOH. The effluent (200 mL) was treated with barium chloride (5.00 g, 24 mmol), boiled for 1 h, cooled, and filtered, giving 2.32 g (11.76 mmol, 98.0%) of barium carbonate.

Acknowledgements

I thank Gordon J. Boudreaux for taking the ^{31}P and ^{13}C nmr spectra, and Donald J. Daigle for helpful discussions and experimental verification of the synthetic scheme.

1. A. Hoffman. J. Am. Chem. Soc. **52**, 2995 (1930).
2. E. I. Grinshtein, A. B. Bruker, and L. Z. Soborovskii. Dokl. Akad. Nauk SSSR, **139**, 1359 (1961).
3. D. M. Jones and T. M. Noone. J. Appl. Chem. London, **12**, 397 (1962).
4. M. Grayson. J. Am. Chem. Soc. **85**, 79 (1963).
5. E. B. Trostyanskaya, E. S. Venkova, and Yu. A. Mikhailin. Zh. Obshch. Khim. **37**, 1655 (1967).
6. A. W. Frank and G. L. Drake, Jr. J. Org. Chem. **42**, 4040 (1977).
7. A. W. Frank and D. J. Daigle. J. Org. Chem. In press.
8. B. L. van Duuren, A. Sivak, B. M. Goldschmidt, C. Katz, and S. Melchionne. J. Natl. Cancer Inst. **43**, 481 (1969).
9. Kirk–Othmer. Encyclopedia of Chemical Technology. Vol. 11. 2nd ed. Wiley–Interscience, New York. 1966. pp. 407–408.
10. P. A. Adams and F. A. Baron. Chem. Rev. **65**, 567 (1965).
11. F. Möller. Methoden Org. Chem. (Houben-Weyl). 4th Ed., **11/1**, 948-952 (1957).
12. A. W. Frank. Paper presented at the 30th Southeastern Regional Meeting, American Chemical Society, Savannah, GA. November 8, 1978.
13. C. E. Schweitzer. J. Org. Chem. **15**, 471 (1950).
14. F. Christensson, H. C. S. Koefoed, A. C. Petersen, and K. Rasmussen. Acta Chem. Scand. Ser. A, **32**, 15 (1978).
15. D. W. Mathieson. Nuclear magnetic resonance for organic chemists. Academic Press, London. 1967. pp. 39–41.
16. R. Kunin. Ion exchange resins. 2nd ed. John Wiley and Sons, Inc., New York. 1958. p. 289.
17. J. C. Winters and R. Kunin. Ind. Eng. Chem. **41**, 460 (1949).
18. E. Katchalski, C. Berliner-Klibanski, and A. Berger. J. Am. Chem. Soc. **73**, 1829 (1951).
19. A. Jensen and R. Christensen. Acta Chem. Scand. **9**, 486 (1955).
20. W. Siefken. Justus Liebigs Ann. Chem. **562**, 75 (1949).
21. J. L. Frahn and J. A. Mills. Aust. J. Chem. **17**, 256 (1964).
22. A. W. Frank. Phosphorus Sulfur, **5**, 19 (1978).

The alkaloids of *Podopetalum ormondii*

STEWART MCLEAN, RENUKA MISRA, AND VIJAYA KUMAR
Department of Chemistry, University of Toronto, Toronto, Ont., Canada M5S 1A1
AND
JOHN A. LAMBERTON
Division of Applied Chemistry, Commonwealth Scientific and Industrial Research Organization, P.O. Box 4331, Melbourne, VIC. 3001, Australia

Received June 27, 1980

STEWART MCLEAN, RENUKA MISRA, VIJAYA KUMAR, and JOHN A. LAMBERTON. Can. J. Chem. **59**, 34 (1981).

The major alkaloids of *Podopetalum ormondii* have been shown to be (−)-podopetaline, (−)-ormosanine, and 6-epipodopetaline. A constant-melting substance, mp 160–161°C, isolated from the extract proved to be a quasiracemate of (−)-podopetaline and (−)-ormosanine; the absolute configuration of (−)-ormosanine consequently followed from the established absolute configuration of (−)-podopetaline. Both (−)-6-epipodopetaline, mp 118–119°C, and its racemic form, mp 174–175°C, were isolated from the extract. A constant-melting ternary mixture, mp 178–179°C, of the three major alkaloids has also been isolated.

STEWART MCLEAN, RENUKA MISRA, VIJAYA KUMAR et JOHN A. LAMBERTON. Can. J. Chem. **59**, 34 (1981).

On a montré que les alcaloides principaux de la *Podopétalum ormondii* sont la (−)podopétaline, la (−)ormosanine et l'épi-6 podopétaline. Des extraits bruts, on a isolé une substance qui a été recristallisé jusqu'à un point de fusion constant de 160–161°C et qui semble être le quasi racémate de la (−)podopétaline et de la (−)ormosanine. On en a donc déduit la configuration absolue de la (−)ormosanine, basée sur la configuration connue de la (−)podopétaline. Des extraits bruts, on a isolé la (−) épi-6 podopétaline de pf 118–119°C et son racémique de pf 174–175°C. On a également isolé un mélange ternaire à point de fusion constant pf 178–179°C comprenant les trois alcaloides principaux.

[Traduit par le journal]

The Ormosia alkaloids (1) are a group of bases structurally related to the pentacyclic $C_{20}H_{35}N_3$ alkaloid ormosanine (I); they were originally isolated from *Ormosia* species, but have subsequently been found in a number of related leguminous plants. Structural variations have not been common in this group of alkaloids and most of the complexity has arisen from stereochemical features. Ormosanine is a member of a set of diastereoisomers containing sixteen pairs of enantiomers, of which four other members have been identified as natural products and most of the rest have been obtained synthetically or semisynthetically. Since these compounds are saturated and contain three basic nitrogens, the shortage of suitable functional groups has made investigation by chemical methods extremely challenging and the common spectroscopic techniques provide little useful information. X-ray analysis has consequently been of paramount importance in structural studies, the first of these analyses (2) being of (±)-jamine (II), the so-called homo derivative of ormosanine, formed by condensation with formaldehyde. With the skeletal features of this key alkaloid established, much subsequent work was carried out using both chemical methods and X-ray analysis to determine the stereochemistry of other members of the diastereoisomeric set. It became apparent during this study that some alkaloids occur as racemic modifications in some plants and as single enantiomers in others.

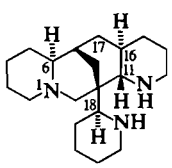

I [ormosanine]

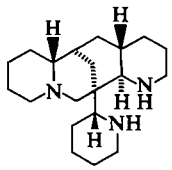

I′ [(−)-ormosanine]

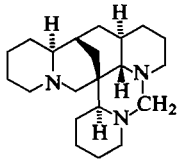

II [jamine]

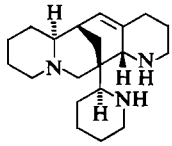

III[(−)-podopetaline]

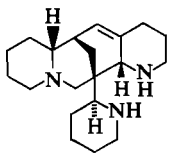

IV [6-epipodopetaline]

Note. Where the absolute configuration of an alkaloid has been established, the sign of rotation is indicated and the proper absolute configuration is depicted; otherwise, only the relative configuration is implied.

One of the few structural variants found in the

0008-4042/81/010034-04$01.00/0
©1981 National Research Council of Canada/Conseil national de recherches du Canada

Can. J. Chem. Downloaded from www.nrcresearchpress.com by 210.87.254.40 on 09/05/12
For personal use only.

Can. J. Chem. Downloaded from www.nrcresearchpress.com by 210.87.254.40 on 09/05/12
For personal use only.

Ormosia alkaloids is the presence of an ethylenic double bond between carbon atoms 16 and 17. These $C_{20}H_{33}N_3$ alkaloids belong to a second set of diastereoisomers containing eight pairs of enantiomers, each formally related to a pair of C-16 epimers of the ormosanine set.

In an earlier investigation of the alkaloids of *Podopetalum ormondii* (3), podopetaline (III), a $C_{20}H_{33}N_3$ base, was isolated and shown to be identical with one of the alkaloids of *O. semicastrata* (4). The structure and absolute configuration of (−)-podopetaline from *P. ormondii* was established by X-ray analysis of its hydrobromide (3). We now report on our further studies of the *P. ormondii* alkaloids.

A gc–ms examination of the total basic extract revealed that the strongest gc peak had the same retention time as podopetaline and showed ms peaks corresponding only to material of formula $C_{20}H_{33}N_3$ (M^+ 315). There were two other prominent gc peaks: the first was resolved from the podopetaline peak only under optimal conditions and corresponded to $C_{20}H_{35}N_3$ (M^+ 317) material; the second corresponded to $C_{20}H_{33}N_3$ material. A number of much smaller gc peaks indicated the presence of other alkaloids of this group, but it appeared unlikely that isolation of these alkaloids would be feasible. We have used a variety of techniques for separating the alkaloids of the total extract and we have identified three chemically distinct alkaloids, each corresponding to one of the major gc peaks; it is almost certain, therefore, that these peaks correspond to chemically homogeneous substances. The major alkaloid is clearly podopetaline (III), the $C_{20}H_{35}N_3$ alkaloid is ormosanine (I), and the second $C_{20}H_{33}N_3$ alkaloid is 6-epipodopetaline (IV). However, during the investigation other crystalline substances were isolated that initially suggested that the extract contained other isolable alkaloids. Our present results show that this is not the case, but the nature of these crystalline substances is intrinsically interesting and provides information of particular significance to the study of Ormosia alkaloids.

The major alkaloid, (−)-podopetaline (III) was readily isolated by any of the techniques we used. We isolated (−)-6-epipodopetaline (IV), mp 118–119°C, by first partitioning the total extract between an alkaline buffer and ether, and then fractionally crystallizing the material obtained from the organic phase. The structure and relative configuration of this alkaloid were determined by X-ray crystal structure analysis using the direct method (5). This analysis did not provide the absolute configuration of the molecule but it is clear that the crystal examined was configurationally homogeneous. The melting point of the sample remained constant after repeated recrystallizations, and despite the low value of its optical rotation, $[\alpha]_D$ −3.2° (MeOH), this material appears to consist of a single enantiomer. In another separation which employed chromatography and fractional crystallizations of the original alkaloidal extract, a small amount of a crystalline fraction, mp 174–175°C, $[\alpha]_D$ 0°, was isolated. This material proved to have the same spectroscopic and chromatographic properties as (−)-6-epipodopetaline, and is consequently identified as (±)-6-epipodopetaline. It follows that the 6-epipodopetaline of *P. ormondii* is partially racemic with a large excess of the levorotatory enantiomer.

Another fraction, obtained from the ether phase after the total extract had been partitioned between an alkaline buffer and ether, was obtained crystalline, mp 160–161°C, and this melting point was constant after repeated recrystallizations. However, it was clear from gc–ms analysis that this was not a homogeneous compound but a mixture of a $C_{20}H_{33}N_3$ component with the same retention time as podopetaline and a $C_{20}H_{35}N_3$ component with the same retention time as ormosanine. These components were conveniently separated by first converting them to their "homo" derivatives (see II) by condensation with formaldehyde. By this means it was established that the two components are (−)-podopetaline and ormosanine. The co-crystal was of considerable crystallographic interest since it was made up of a monoclinic component sandwiched between triclinic components. This provided a challenging problem for X-ray crystal analysis that was solved by Nyburg and his colleagues (6). The analysis confirmed the structural assignments made above, but went further by showing that the components form a quasiracemate of podopetaline and ormosanine of opposite absolute configurations. The co-crystal is levorotatory in methanol, $[\alpha]_D$ −33.9°; the podopetaline component has been shown to be (−)-podopetaline, $[\alpha]_D$ −48°, by its conversion to (−)-homopodopetaline; the ormosanine component has not been isolated directly, but was converted to (−)-homoormosanine (i.e. (−)-jamine). It follows from these figures that the ormosanine component is also levorotatory. Since the absolute configuration of (−)-podopetaline (shown in III) has been established previously (3), the absolute configuration of (−)-ormosanine follows from the X-ray crystal analysis, and is shown here as I′. This assignment

Can. J. Chem. Downloaded from www.nrcresearchpress.com by 210.87.254.40 on 09/05/12
For personal use only.

corroborates that made by Cannon *et al.* (7), who interrelated (−)-ormosanine and (−)-templetine. (−)-Ormosanine, $[\alpha]_D$ −19°, has been obtained by chemical reduction of (−)-panamine (8), and we have previously isolated ormosanine with $[\alpha]_D$ −9° from *O. semicastrata*; (−)-jamine has been obtained from *O. costulata* (9).

The separation procedure that provided the binary mixture also afforded a small amount of a crystalline fraction, mp 178–179°C, which also proved to be a constant-melting mixture, this time apparently of three components. The gc–ms analysis of this material indicates that it is composed of the three major alkaloids in the extract, podopetaline, 6-epipodopetaline, and ormosanine, but no further work has been carried out on this material.

It is clear from the results reported here that the Ormosia alkaloids have a strong tendency to co-crystallize. Furthermore, as has been noted previously, there are difficulties in using the spectroscopic techniques to provide criteria of purity and identity. It is probable that other investigations have been made more difficult because of these features, and this may have led to some of the confusion in the literature in this field. The existence of alkaloids in either an optically active or a racemic form, the melting points of which may be quite different, is a further possible source of confusion. Our present results take this point a step further by demonstrating that an alkaloid may be found in a partially racemic form. Whether or not the racemic form and the enantiomer present in excess can be separated by fractional crystallization depends on their crystal properties. The observation of optical activity does not, therefore, provide evidence that a single enantiomer has been isolated, and the differences in rotations reported for some alkaloids may arise in this way.

The biogenesis of these alkaloids has been a matter for conjecture only (10, 11), but in a reasonable hypothesis it has been proposed that there is a route to a symmetrical intermediate that incorporates all of the skeletal atoms of the Ormosia alkaloids, and subsequent ring-closure steps determine the chirality at each centre in the alkaloid and its absolute configuration. It appears improbable that separate enzyme-mediated routes exist that lead in one case to a racemic alkaloid and in another to a single enantiomer. Podopetaline and ormosanine are obviously structurally closely related, but the present study shows that they occur together with opposite absolute configurations. It seems even more improbable that two enzymatic systems of opposite chirality coexist to form these two alkaloids. The original hypothesis (10) can therefore be extended by the postulate that the common biosynthetic route leads all the way to racemic alkaloids, and it is in the subsequent metabolism of these alkaloids that chiral selection occurs. Thus (±)-ormosanine could be formed first and then (+)-ormosanine could be oxidized selectively to (−)-podopetaline. Conversely, if (±)-podopetaline were formed first, the next step would require a stereospecific reduction of one enantiomer. Now that we have demonstrated the presence in *P. ormondii* of partially racemic 6-epipodopetaline, with a large excess of the levorotatory isomer, the postulate that the dextrorotatory isomer has been stereospecifically but incompletely metabolized is attractive.

This type of phenomenon may be common in some other alkaloidal families, but it may have gone unrecognized because of the absence of reliable information concerning the absolute configuration of the alkaloids. Examples of partially racemic alkaloids are known, and the case of (±)-kreysigine and (−)-floramultine, two homoaporphines of *Kreysigia multiflora*, may be cited (12) as an example of the co-occurrence in a single plant of an optically active alkaloid and a closely related but racemic congener. It is recognized, however, that in those cases where there is a common precursor that can racemize by equilibration of one chiral centre (or possibly a limited number of such centres), different reaction channels may lead from the common precursor to either racemic or optically active products. It may be difficult to find other examples corresponding to the case of the Ormosia alkaloids where such racemization can be ruled out and the co-occurrence of optically active and racemic alkaloids requires effectively the resolution of a complex racemic precursor possessing a number of chiral centres by selective metabolism of one enantiomer to produce the optically active alkaloid.

Experimental

Melting points were determined on a Thomas-Kofler micro hot stage. A CEC 21-490 mass spectrometer was used for routine spectra and an AEI MS902 spectrometer was used for mass measurements. For gc–ms measurements a 2 m × 2 mm-id glass column containing 3% OV-17 on GCQ was used with linear temperature programming (200–250°C at 12°C/min) and coupled to the 21-490 spectrometer.

Isolation Procedures

The total bases of the bark of *P. ormondii* were extracted by standard procedures and obtained as a brownish syrup.

(The Toronto and Melbourne laboratories used different isolation procedures. In each laboratory attention was focussed on selected fractions; subsequently it has become apparent that fractions that were initially set aside can provide substances that were isolated more conveniently by a different procedure. This

Can. J. Chem. Downloaded from www.nrcresearchpress.com by 210.87.254.40 on 09/05/12
For personal use only.

report confines itself to a description of the procedures used to isolate materials discussed in this paper.)

(a) Chromatography

A solution of the crude basic extract in benzene was chromatographed on alumina (Woelm activity 1, pretreated with 1% of water). Elution with benzene and then 9:1 benzene–ether provided fractions from which crystalline podopetaline (3), mp 77.5–79°C, $[\alpha]_D$ −48° (*c* 0.95, methanol) was isolated (7.5%). Elution with chloroform provided fractions which contained the binary mixture of podopetaline and ormosanine. Elution with 9:1 chloroform–methanol provided fractions from which a crystalline material (~0.25%) was obtained; repeated recrystallization from acetone of this material gave (±)-6-epipodopetaline, mp 174–175°C; $[\alpha]_D$ 0° (*c* 0.29, methanol); M^+ at *m/e* 315. *Anal.* calcd. for $C_{20}H_{33}N_3$: C 76.1, H 10.5, N 13.3; found: C 76.3, H 10.6, N 12.8.

(b) Liquid–Liquid Extraction

The crude basic extract was dissolved in a minimum of dilute hydrochloric acid, and the solution was brought to pH 8.4 by the addition of a glycine – sodium hydroxide buffer. This solution was continuously extracted with ether; the ether was periodically removed, the aqueous solution was treated with sodium hydroxide to raise the pH by about 0.2 units, and this solution was extracted with fresh ether. Evaporation of the ether extracts afforded a series of alkaloidal fractions. Fractional crystallization of the first fraction (~10% of total crude) gave a small amount (~0.25%) of a crystalline substance, mp 178–179°C; gc–ms analysis showed that this was a mixture of three components in about equal amounts and with characteristics corresponding to podopetaline, 6-epipodopetaline, and ormosanine. This fractional crystallization also afforded a material (~1%) which was recrystallized from acetone to give (−)-6-epipodopetaline, mp 118–110°C; $[\alpha]_D$ −3.2° (methanol); M^+ at *m/e* 315 (315.2674). *Anal.* calcd. for $C_{20}H_{33}N_3$: C 76.14, H 10.54, N 13.32; found: C 75.95, H 10.38, N 13.60. This material showed the same ir, uv, nmr, and tlc characteristics as the racemic material, mp 174–175°C, described in (*a*) above.

The second fraction from the continuous extraction provided a material (~60% of total crude) which appeared on gc–ms examination to consist of two main components (*m/e* 317 and 315). Repeated recrystallization of this material from acetone provided a substance, mp 160–161°C; this melting point remained constant after further recrystallizations. This material $[\alpha]_D$ −33.9° (methanol), consisted of (−)-podopetaline and (−)-ormosanine in approximately equal amounts. (A sample was submitted for X-ray crystal structure analysis (6).)

Separation of Podopetaline/Ormosanine as "Homo" Derivatives

A solution of the above mixture of podopetaline and ormosanine (125 mg) in 5 mL of 88% formic acid and 3 mL of 37% formaldehyde was refluxed for 2.5 h; additional formic acid (2.5 mL) and formaldehyde (1.5 mL) were added and reflux was continued for a further 18 h. The solution was cooled and diluted with 75 mL of water, extracted with ether, made basic with ammonia, and thoroughly extracted with ether. The latter ether extract afforded a solid residue (127 mg) which was separated by preparative layer chromatography on silica gel with elution by diethylamine–hexane (1:18, then 1:9). The homopodopetaline fraction was obtained, after recrystallization from acetone, as plates (64 mg), mp 117–118.5°C; $[\alpha]_D$ −147.7° (*c* 0.2, methanol); ms *m/e*: 327 (100), 326 (28), 312 (11), 284 (15), 270 (8), 244 (31), 233 (29), 230 (19), 229 (51), 98 (75), and 84 (28). *Anal.* calcd. for $C_{21}H_{33}N_3$: C 77.01, H 10.16, N 12.83; found: C 76.82, H 10.06, N 12.64. This material was identical in every respect with a sample prepared in the same way from authentic (−)-podopetaline.

The ormosanine derivative, jamine (II), was recrystallized from acetone and obtained as needles (29 mg), mp 125–126.5°C; $[\alpha]_D$ −81° (*c* 0.3, methanol). This material was identical with a sample of (−)-jamine (9) obtained through the courtesy of Dr. K. L. Rinehart, Jr.

Acknowledgements

The work in Toronto was supported by the National Research Council of Canada. Part of this work was carried out by one of us (V.K.) while on leave from the University of Sri Lanka and supported as an International Development Research Centre Research Associate. We gratefully acknowledge the support we have received.

1. Z. VALENTA and H.-J. LIU. *In* International review of science. Organic Chem. Series 2. Vol. 9. *Edited* by K. Wiesner. Butterworths, London. 1976. Chapt. 1.
2. I. L. KARLE and J. KARLE. Acta Crystallogr. **17**, 1356 (1964).
3. N. K. HART, S. R. JOHNS, J. A. LAMBERTON, M. F. MACKAY, A. McL. MATHIESON, and L. SATZKE. Tetrahedron Lett. 5333 (1972); M. F. MACKAY, L. SATZKE, and A. McL. MATHIESON. Tetrahedron, **31**, 1295 (1975).
4. S. McLEAN, M. L. ROY, H. -J. LIU, and D. T. CHU. Can. J. Chem. **50**, 1639 (1972); S. McLEAN and R. MISRA. Can. J. Chem. **52**, 1907 (1974).
5. P.-T. CHENG, S. McLEAN, R. MISRA, and S. C. NYBURG. Tetrahedron Lett. 4245 (1976).
6. R. MISRA, W. WONG-NG, P.-T. CHENG, S. McLEAN, and S. C. NYBURG. J. Chem. Soc. Chem. Commun. 659 (1980).
7. J. R. CANNON, J. R. WILLIAMS, J. F. BLOUNT, and A. BROSSI. Tetrahedron Lett. 1683 (1974).
8. P. NAEGELI, W. C. WILDMAN, and H. A. LLOYD. Tetrahedron Lett. 2069 (1963).
9. J. K. FRANK, E. N. DUESLER, N. N. THAYER, R. HECKENDORN, K. L. RINEHART, I. C. PAUL, and R. MISRA. Acta Crystallogr. Sect. B, **34**, 2316 (1978).
10. P. DESLONGCHAMPS, Z. VALENTA, and J. S. WILSON. Can. J. Chem. **44**, 2539 (1966).
11. E. M. WILSON. Tetrahedron, **21**, 2561 (1965).
12. A. F. BEECHAM, N. K. HART, S. R. JOHNS, and J. A. LAMBERTON. Aust. J. Chem. **21**, 2829 (1968).

Solid state properties of poly-β-hydroxybutyrate and of its oligomers[1]

R. H. MARCHESSAULT,[2] SUZANNE COULOMBE, HIROMICHI MORIKAWA, KEIZO OKAMURA, AND J. F. REVOL

Department of Chemistry, Université de Montréal, C.P. 6210, Succ. A, Montréal (Qué.), Canada H3C 3V1

Received November 29, 1979[3]

R. H. MARCHESSAULT, SUZANNE COULOMBE, HIROMICHI MORIKAWA, KEIZO OKAMURA, and J. F. REVOL. Can. J. Chem. **59**, 38 (1981).

The solid state properties of poly-β-hydroxybutyrate (PHB) were investigated for samples with degrees of polymerization ($\overline{DP_n}$) from 4 to 994. The observed melting points ranged from 47°C to 180°C. Electron diffractograms on carefully prepared single crystals of a high molecular weight sample provided data which confirmed the reported *a* and *b* parameters from X-ray fiber diffraction and provided clear justification for the $P2_12_12_1$ space group. The observed intensities in the electron diffractogram, corresponding to (*hk*0) reflections, were compared with the predicted intensities for two proposed structures in the literature. The observed and calculated structure factors for both structures were in good agreement. Small angle X-ray diffraction of the meridional maximum for annealed "cold drawn" and "hot drawn" fibers showed a distinctly different dependence on temperature than the maximum for stacks of lamellar single crystals. For oligomers a long spacing was observed which was about twice the length of the sample $\overline{DP_n}$ multiplied by the crystalline advance per monomer.

R. H. MARCHESSAULT, SUZANNE COULOMBE, HIROMICHI MORIKAWA, KEIZO OKAMURA et J. F. REVOL. Can. J. Chem. **59**, 38 (1981).

Les propriétés de cristaux du poly-β-hydroxybutyrate (PHB) d'un degré de polymérisation ($\overline{DP_n}$) allant de 4 à 994 sont rapportées. Les points de fusion vont de 47°C à 180°C. Les absences systématiques observées en diffraction éléctronique sur monocristaux de forte masse confirment le groupe spatiale $P2_12_12_1$ proposé à partir du diagramme à fibre (rayons-X). Les intensités observées des réflections (*hk*0) du cliché de diffraction électronique sont en accord avec celles prédites à partir de deux structures crystallines proposées dans la literature et basées sur les données du diagramme à fibre. La diffusion méridionale des rayons-X aux petits angles pour des fibres étirées "à froid" et "à chaud" a été enrégistrée et la variation des maxima de diffusion, en fonction de la température, diffère sensiblement de ce qui est observé pour la variation de l'épaisseur de lamelles monocristallines. Pour des oligomères cristallins l'observation d'une tache de diffraction dont l'espacement est deux fois la longueur de la chaine dans sa conformation crystalline mène à proposer une maille avec deux chaines bout à bout selon l'axe *c*.

Introduction

Poly-β-hydroxybutyrate (PHB), discovered by Lemoigne (1) in 1927, is an important storage material in a wide variety of bacteria. It has been shown (2–5) that PHB is a linear head-to-tail polyester based on D(−)β-hydroxybutyric acid with the following formula:

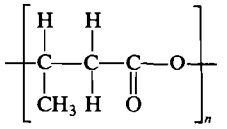

This optically active polymer occurs in bacteria in a native form which is described as crystalline hydrophobic granules (6). The size, shape, and internal morphology of these granules have been discussed in a paper which proposed a spherulite model for the granules with tangentially oriented and fibrillar organized chains (7). It was proposed that during biosynthesis simultaneous polymerization and crystallization limited chain-folding in the crystalline native granules (7). From X-ray diffraction studies, it was found that, in the crystalline state, PHB adopts a regular helical conformation with space group $P2_12_12_1$ which implies antiparallel chains for this polar macromolecule. The orthorhombic unit cell with dimensions $a = 5.76$ Å, $b = 13.20$ Å, and c(fiber axis) = 5.96 Å contains two antiparallel chains (8–10). The crystalline structure of PHB was refined by energy minimization methods (9, 10).

As reported in the present paper, the solid state properties of PHB and of its oligomers were investigated by differential scanning calorimetry, small and wide angle X-ray diffraction, and electron microscopy and diffraction. From these studies basic information on the crystallizing behaviour of this uniquely stereoregular and chiral polymer is sought in order to better understand the native morphology and its process of morphogenesis.

Experimental

Samples

The physical characteristics of PHB samples used in this study are referred to in Table 1. A to H samples (isolated from different bacterial cultures using different extraction recipes) and I to M samples (prepared by fractionating a low molecular

[1]This study is derived in part from the M.Sc. thesis of S.C. submitted to the Université de Montréal (1977) and the Ph.D. thesis of K.O. submitted to the College of Forestry, Syracuse, NY (1967).

[2]To whom correspondence should be addressed.

[3]Revision received September 3, 1980.

0008-4042/81/010038-07$01.00/0

©1981 National Research Council of Canada/Conseil national de recherches du Canada

Can. J. Chem. Downloaded from www.nrcresearchpress.com by 210.87.254.42 on 09/05/12
For personal use only.

Can. J. Chem. Downloaded from www.nrcresearchpress.com by 210.87.254.42 on 09/05/12
For personal use only.

weight sample ($\overline{M}_n$ = 694) on a Sephadex LH-20 column) are polydisperse and their number average molecular weight were measured with a Mechrolab High Speed Membrane Osmometer Model 501 and a Mechrolab Vapor Pressure Osmometer. N to R samples are monodisperse samples of PHB oligomers from octamer to tetramer. These monodisperse oligomer samples, isolated and purified by thin-layer chromatography (11), were provided by M. Bernard Hauttecoeur, Institut Pasteur, Paris.

Annealing

The single crystal powder was placed in a glass capillary and annealed in an oven whose temperature could be controlled to ±1°C. A system of purified, dry nitrogen was circulated at all times after initial evacuation-flushing. A thermometer near the sample registered the temperature. A typical heating schedule required about 30 min to reach the annealing temperature which was then maintained for 2 h. The samples were then gradually cooled to room temperature over a period of about 1 h by turning off the heating elements.

Melting Point and Differential Scanning Calorimetry

The melting point of the polymer samples was determined with a Mel-Temp melting point apparatus of which the heating rate was adjusted to 2°C/min.

The melting point and heat of fusion were also measured with a Perkin-Elmer differential scanning calorimeter model 1B. Indium was used as a melting point (156.4°C) and heat of fusion (12.43 cal/g) standard. A peak area of fusion which is proportional to heat of fusion was measured with Keuffel and Esser Compensating Polar Planimeters. The scanning speed of 10°C/min was used both for the standard (indium) and samples.

Wide Angle X-ray Diffraction

Crystalline oligomers (N to R samples) were submitted to wide angle X-ray diffraction. Powder diagrams were recorded on a cylindrical Debye-Scherrer camera which had a radius of 57.3 mm. A Philips X-ray unit operated at 40 kV and 20 mA was used with a Cu-tube as a radiation source. The Cu-K_α radiation (λ = 1.541 Å) was monochromatized by means of a Ni-filter. All samples were exposed to the X-ray beam for 7 h.

TABLE 1. Melting point and molecular weight of PHB samples used

Sample	$\overline{M}_n$	$\overline{DP}_n$	T_m (°C) Optical	T_m (°C) DSC[a]	Δh_f*(cal/g)
A	85 500	994	180	180	35.7
B	52 400	609	180	180	28.4
C	42 000	488	174	172	32.9
D	31 360	365	171	170	32.4
E	20 400	237	170	173	29.2
F	15 100	176	165	168	37.1
G	4 970	58	146	147	32.4
H	1 870	22	114	116	35.4
I	1 027	12			
J	569	6.4			
K	458	5.1			
L	395	4.4			
M	382	4.2			
N	688	8	101		
O	602	7	89		
P	516	6	81		
Q	430	5	65		
R	344	4	47		

[a]Differential scanning calorimetry.

Single Crystal Growth

The preparation of PHB single crystals has been previously reported (6, 10). In order to obtain monolamellar single crystals, the growth conditions were optimized in the following way. One milligram of PHB was dissolved in 4 mL of a mixture of ethanol and chloroform (2:1, v/v) in a sealed tube at a temperature of 73°C. The solution was then cooled to 60°C and kept at this temperature for 24 h. In order to selfseed the solution, the precipitate formed was dissolved again at 73°C. Immediately after the disappearance of the precipitate, the solution was again cooled to 60°C and kept at this temperature for 24 h.

Small Angle X-ray Diffraction

A to M samples were studied by small angle X-ray diffraction in order to determine the thickness of polymer single crystal lamellae. For each sample from A to M, a single crystal suspension was made and sedimented to form a mat under suction. Small angle X-ray diffraction from these mats with the X-ray beam parallel to the mat plane gave a very sharp small angle maximum from which "*d*" spacing, the lamella thickness, was deduced.

A Warhus camera with double pinhole collimation and adjustable specimen to film distance (17–29 cm) was used. A Norelco X-ray unit operated at 35 kV and 20 mA was used with a fine focus Cu-tube as a radiation source. The Cu-K_α line (1.542 Å) was monochromatized by means of a Ni-filter. The exposure time ranged from 8 to 48 h depending upon the specimen size, the film to specimen distance, and the diameter of collimator.

Electron Microscopy and Diffraction

Samples C, M, and N were studied by electron microscopy and electron diffraction. Drops of the crystal suspension were deposited on carbon-coated grids and the solvent was allowed to evaporate. Observations were made with a Philips EM 300 electron microscope operating at 80 kV for images and at 100 kV for diffraction. The crystals were observed either unshadowed or after shadowing with tungsten. Gold was evaporated on the crystal preparations for diffraction calibration. The intensities of the observed reflections were measured by integration with a Joyce-Loebl recording microdensitometer.

Results and Discussion

Electron Diffraction Studies of the Crystalline Structure of PHB and of its Oligomers

The electron micrograph and diffractogram of sample C illustrated in Fig. 1 is characteristic of PHB single crystals. The crystal thickness was estimated to be 50 Å from the shadow length. A total of 28 reflections were observed in a quadrant of the diffractogram. From this diffraction pattern, the unit cell base plane parameters *a* and *b* were respectively 5.76 Å and 13.20 Å which agrees with those reported by previous authors (8–10) based on the analysis of the PHB X-ray fiber diagram. Consequently the electron diffractogram is an (*hk*0) section of the PHB reciprocal lattice and indicates (6, 8) that in the crystal and molecular chains are perpendicular to the lamella surface. The diffractogram also confirmed the *pgg* base plane symmetry since only even reflections are observed along (*h*00) and (0*k*0) directions. This confirms the

Can. J. Chem. Downloaded from www.nrcresearchpress.com by 210.87.254.42 on 09/05/12
For personal use only.

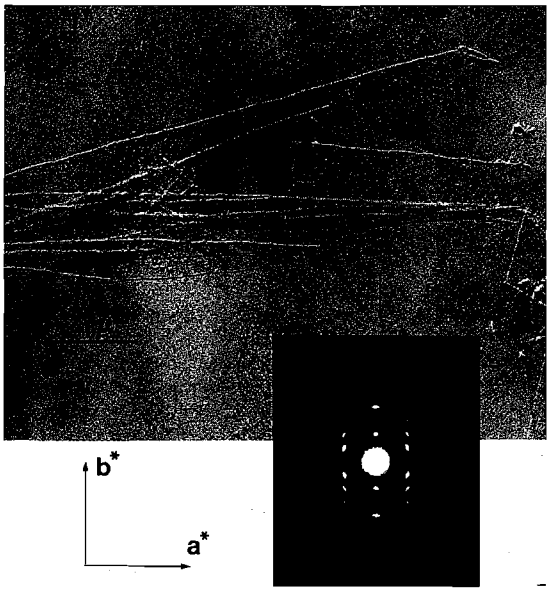

FIG. 1. Electron micrograph and diffractogram of sample C ($\bar{M}_n$ = 42 000 g/mol) where the PHB single crystals were shadowed with tungsten. The arrow in the micrograph points from the crystal region where the diffractogram was recorded with the orientation shown.

proposed orthorhombic $P2_12_12_1$ space group (8–10).

Cornibert and Marchessault (9) and Yokouchi *et al.* (10) independently proposed crystalline structure models of PHB based on X-ray diffraction and conformational analysis. Between these models the atomic coordinates of the C and O atoms in the asymmetric unit are in good agreement: the largest observed difference in the coordinates of the atoms was less than 0.18 Å. We next attempted a refinement of the models against the electron diffraction data using a least-squares refinement procedure with a scale factor K and an overall isotropic temperature factor B. Minimization of the quantity $\Sigma(F_o - F_c)^2$ was examined where F_o and F_c are the observed and calculated structure factors, respectively. F_o was derived from the observed intensity I_o by assuming $F_o = (I_o)^{1/2}$ (12). The electron scattering factors for C, O, and H atoms were taken from International tables for X-ray crystallography, vol. IV (13).

The lowest value of the discrepancy factor, defined by $R = \Sigma|F_o - F_c|/\Sigma F_o$ was 0.33 ± 0.01 with $K = 6.0 \pm 1.0$ and $B = 9.0 \pm 3.0$ Å^2 for the model of Yokouchi *et al.* (10). The same result was obtained with the Cornibert and Marchessault model (9) in which the scattering factor of oxygen was used for the methyl group since the exact coordinates of the hydrogen atoms of the group are not described. The F_o and F_c values are listed in Table 2. The assigned temperature factor of 9.0 ± 3.0 Å^2 is reasonable (10, 14) and the discrepancy factor R of 0.33 is acceptable in view of the fact that no effort was made to refine the structure, e.g., a small rotational movement of the chains about their axes has an important effect on ($hk0$) intensities.

Much lower values of the R factor have been reported by refinement of the models against X-ray diffraction data (9, 10). Cornibert and Marchessault (9) have reported that the R_I factor, defined $R_I = \Sigma|I_o - I_c|/\Sigma I_o$ where I_o and I_c are the observed and calculated intensities, respectively, is 0.24 by using all reflections in the diffractogram and an overall temperature factor for all atoms. Yokouchi *et al.* (10) have reported that the R factor is reduced to 0.135 by refinement of the atomic coordinates and temperature factors by the diagonal least-squares method.

It is noteworthy that the (120) reflection which

TABLE 2. Comparison of observed (F_o) and calculated (F_c) structure factors for reflections obtained by electron diffraction

h	k	l	F_o	F_c^a	F_c^b
0	2	0	100.0	80.0	82.1
0	4	0	64.0	78.7	79.7
0	6	0	14.0	2.2	2.3
0	8	0	14.0	11.0	4.4
1	1	0	100.0	95.1	81.4
1	2	0	40.0	28.1	49.1
1	3	0	26.5	13.8	26.1
1	4	0	22.4	9.5	21.7
1	5	0	17.3	4.7	10.9
1	6	0	10.0	7.8	5.9
1	7	0	10.0	3.2	0.1
1	8	0	14.1	15.3	17.7
2	0	0	17.3	6.5	2.9
2	1	0	14.1	1.0	1.9
2	2	0	14.1	4.3	5.3
2	3	0	10.0	2.6	2.4
2	4	0	22.4	25.7	23.4
2	5	0	(7.1)[c]	0.2	1.4
2	6	0	20.0	17.4	17.4
2	7	0	(7.1)[c]	1.4	1.1
2	8	0	14.1	2.1	4.5
3	1	0	17.3	17.7	18.7
3	2	0	(7.1)[c]	8.5	7.2
3	3	0	14.1	10.2	4.1
3	4	0	14.1	9.7	7.6
3	5	0	10.0	5.9	2.4
3	6	0	10.0	10.6	10.3
3	7	0	17.3	16.9	14.4
3	8	0	10.0	5.5	2.9
3	9	0	10.0	3.8	6.5
3	10	0	10.0	5.2	3.5

[a]Calculated by using the atomic coordinates proposed by Cornibert and Marchessault (9).
[b]Calculated by using the atomic coordinates proposed by Yokouchi *et al.* (10).
[c]For unobserved reflections, intensities were assumed to be half of the weakest observed intensity.

Can. J. Chem. Downloaded from www.nrcresearchpress.com by 210.87.254.42 on 09/05/12
For personal use only.

was very weak or unobservable in the X-ray diffraction pattern (9, 10), was clearly present in the electron diffractogram (see Table 2). The observed difference in the "sensitivity" of this reflection with respect to X-rays vs. electrons is explainable in terms of the structure factors based on the polymer crystal structure (9, 10). Whatever the reason for the intensity weakness of this observed X-ray reflection, the normalized calculated structure factor of the (120) reflection for X-rays is 20.1 (10). Furthermore the normalized structure factor for electrons is 60.3 (derived from data in column 4 of Table 2), where the structure factor for the (110) reflection is taken as 100. The better agreement between calculated and observed intensities of the (120) reflection is an example of how electron diffraction on polymer single crystals can add to one's confidence in polymer crystal structure determination.

Finally, a packing analysis to optimize molecular position in the unit cell in accordance with the method described by Williams (15) and modified by Sarko and Zugenmaier (16) was undertaken. The atomic coordinates of Yokouchi *et al.* (10) were used for the trial packing molecular model which aimed at minimization of the interchain interaction energy by changing rotational and translational positioning of the chains. In order to avoid local minima, different starting positions of the chains were examined. The degree of interaction between atoms of adjacent chains is measured by the packing index: $R_p = \Sigma w(d_0 - d_{ij})^2$ where d_0 is an empirical cut-off distance, d_{ij} is the distance between atoms i and j for the current trial model, and w is a weighting factor. The values of d_0 and w used here were those of Sarko and Zugenmaier (16). The minimum value of the index R_p obtained was 7.68 kcal mol^{-1}, which was very close to the value of 9.10 kcal mol^{-1} obtained with the model proposed by Yokouchi *et al.* (10). This result clearly indicates that in the model the chains are packed in close vicinity of the position of minimum packing energy.

In conclusion, all of these results indicate that the two independent structure determinations for PHB (9, 10) are in good agreement and account satisfactorily for the observed electron diffraction data. Furthermore, the electron diffraction approach, here outlined, with the single crystals is recommended as a valuable complement to X-ray diffraction analysis of polymer fibers.

The PHB octamer (sample N) electron diffraction pattern reveals that the plane *ab* of the octamer unit cell is a rectangular one. From this electron diffraction pattern, octamer unit cell dimensions in plane *ab* have been calculated: $a = 5.67$ Å and $b = 13.19$ Å. If we compare these results with those obtained for PHB polymer (orthorhombic unit cell with $a = 5.76$ Å and $b = 13.20$ Å), we can state that the octamer unit cell is similar to that of the polymer in the plane *ab*.

The sample M ($\overline{DP}_n = 4.2$) electron diffraction data are exactly the same as those of the polymer single crystal with systematic absences in the two dimensional reciprocal net up to the tenth order along the *b* axis. This confirms that the oligomers have the same crystal structure as the polymer at least as regards helical conformation and packing in the *ab* plane.

Lamella Thickness and Annealing of Single Crystals

The measured heats of fusion listed as Δh_f^* in Table 1 reflect differences in degree of crystallinity. This is an extensive quantity and could be used to evaluate the crystalline fraction if Δh_f (heat of fusion of the perfect crystal) were known.

Lamella thickness (long period) of single crystals prepared from samples A to M were determined from small angle X-ray diffraction patterns obtained with the X-ray beam parallel to the plane of the mat. These lamella thickness data are plotted against the number average molecular weight in Fig. 2. The molecular length calculated for each oligomer from $\overline{DP}_n$ and the repeat distance of 2.98 Å found from PHB polymer X-ray data for the structural unit is also shown in Fig 2 where it can be seen that the lamella thickness at first increases with increasing molecular weight and then becomes constant. For PHB molecules greater than $\overline{DP}_n = 12$ ($\overline{M}_n = 1000$), we observe that the length of the molecule is longer than the lamella thickness in keeping with the chainfolding hypothesis. Interestingly, the lamella thickness or the long period of oligomers from dimer to hexamer is approximately twice as much as their molecular length. This suggests, as illustrated in Fig. 3, that with these oligomers the lamella involves two molecules with the polar groups oriented toward each other. When these oligomers were annealed at a temperature 10°C below their melting point in a nitrogen atmosphere no increase of long period was observed which indicates that the molecules are extended in the crystal. Finally for oligomers from heptamer to undecamer, we can assume that the oligomer behaves in the lamella in a way intermediate between the two cases mentioned above.

It is well known that the long period, and thus the thickness of polyethylene lamellae, is dependent on the temperature of crystallization. The closer the

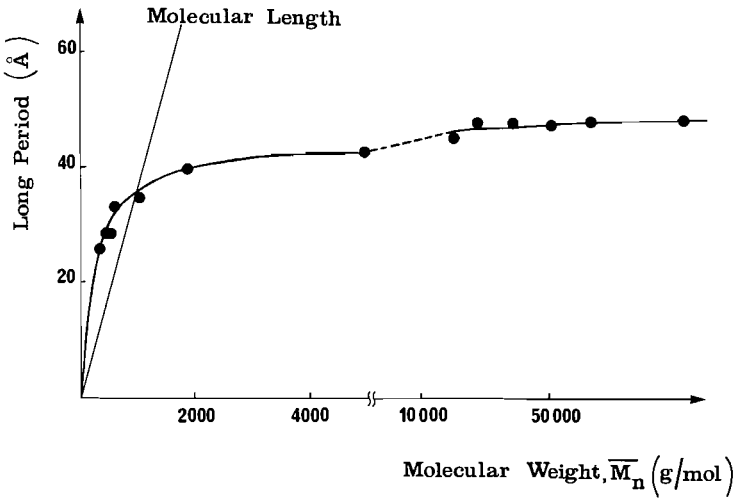

FIG. 2. Observed long period (lamella thickness) for single crystals of PHB as a function of number average molecular weight. For reference, the straight line corresponding to the calculated molecular length of the crystalline state is shown.

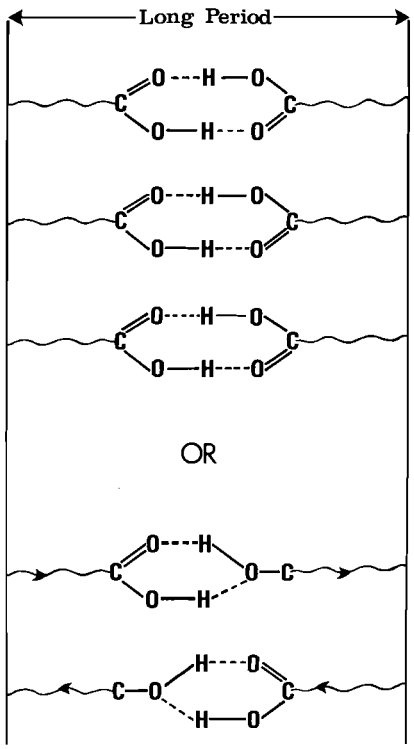

FIG. 3. Schematic representation of molecular arrangement in single crystals of extended chain PHB oligomers. Two possible arrangements are shown with either "head-to-tail" or "head-to-head" packing.

latter to the true melting point, the greater is the lamella thickness (17). Evidence has been presented that the long period of polyethylene single crystal lamellae can be increased by annealing at a temperature below the melting point (18).

Annealing studies were conducted on sample D single crystals ($\overline{M}_n$ = 31 360 g/mol). The X-ray results showed a nearly twofold increase in lamellar thickness over the temperature range studied. Theory predicts (19) development of infinitely long folds, i.e. completely extended chains, as the annealing temperature approaches more and more closely to the true melting point. The crystallization temperature, T_x, can be expressed by the following equation

$$T_x = T_m^0\left(1 - \frac{2\sigma_e}{\Delta h_f L^*}\right)$$

where T_m^0 = the melting point of a crystal of infinite fold period (K), σ_e = end surface free energy (erg/cm^2), Δh_f = the heat of fusion (erg/cm^3), L^* = the equilibrium fold length (cm). Figure 4 is a plot of the crystallization temperature against the reciprocal value of the observed fold length for PHB single crystals. The intercept leads to a predicted value of T_m^0 close to 200°C. For comparison, the same plot for oriented fibers is included which leads to the same predicted value for T_m^0 but the slope is considerably greater. Since the latter is the ratio $\sigma_e/\Delta h_f$ it must be concluded that the "end surface free energy" is much greater for the fiber orientation (melt crystallized) than for the single crystals (solution crystallized). This observation is in keeping with recent concepts concerning chainfold organization in these two systems (20, 21).

X-ray Diffraction Studies of PHB Oligomers

Crystalline Structure

Powder diagrams of all monodisperse samples of oligomers (from tetramer to octamer) were re-

Can. J. Chem. Downloaded from www.nrcresearchpress.com by 210.87.254.42 on 09/05/12
For personal use only.

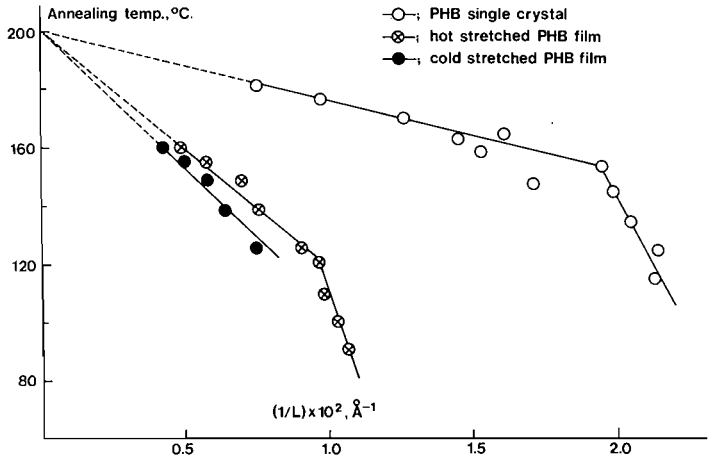

FIG. 4. Dependence of the long period for PHB on the annealing temperature for single crystals (lamellar thickness) and "drawn" film strips.

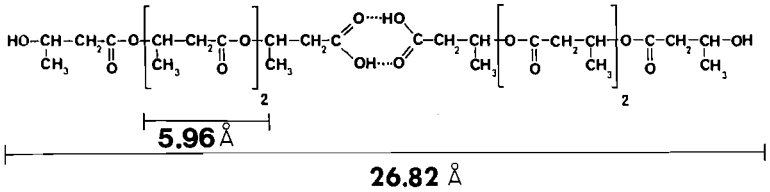

FIG. 5. Representation of the two tetramers contained along the *c* axis of the unit cell and bound together by a hydrogen bond.

corded. From the studies of these powder diagrams combined with the electron diffraction results it is assumed that oligomers crystallize as the polymer, i.e. in an orthorhombic unit cell with parameters $a = 5.76$ Å and $b = 13.20$ Å and with space group $P2_12_12_1$ and that only unit cell dimension c changes from one oligomer to the other. Starting with the tetramer powder diagram and considering the systematic extinctions of the space group $P2_12_12_1$ and the value of unit cell dimensions a and b, we assign the first line of the powder diagram as (002) so that the unit cell dimension c is found to be 26.6 Å.

These tetramer unit cell parameters were refined by minimizing the sum of the squares of the differences between the d-spacings (n of them) derived from the location of the diffraction spots and those calculated from the unit cell. An R-factor, which must be as small as possible for a good refinement, is defined by the following equation:

$$R = \frac{\sum|\sin^2 \theta_{obs} - \sin^2 \theta_{cal}|^{1/2}}{n - 3}$$

The refinement of the tetramer unit cell parameters leading to an R-factor of 1.7% yields the following results: $a = 5.76$ Å, $b = 13.14$ Å, $c = 26.82$ Å.

The c axis parameter of 26.82 Å thus obtained corresponds approximately to the length of eight (two tetramers) repeating units of the polymer (2.98 Å × 8) plus the length of one hydrogen bond (ca. 2.9 Å). In the light of this result and considering the small angle X-ray diffraction data, which suggest that two tetramers make up one lamella, it is reasonable to assume that the unit cell contains two tetramer molecules bound together by a hydrogen-bond along the c axis (Fig. 5). In this model the length of the terminal structural units (i.e. the hydroxyl and carboxylic acid end) should be different from that of the internal structural unit which corresponds to the repeat distance of the polymer. Accordingly the two end structural units of one tetramer taken together must equal a length of 7.45 Å.

We next attempted a calculation of the c parameters for the other oligomers (pentamer to octamer) by using the same refinement method as described for the tetramer. In the calculation two extreme cases were examined: the unit cell contains along the c axis either two oligomers bound together by a hydrogen bond or just one oligomer. For each of these two cases, the starting c parameter for each oligomer was derived by using the same values of the lengths of internal and terminal structural units as assumed for the tetramer model

Can. J. Chem. Downloaded from www.nrcresearchpress.com by 210.87.254.42 on 09/05/12
For personal use only.

TABLE 3. Unit cell parameters and R-factor for PHB oligomers

	If unit cell contains just one oligomer along c axis				If unit cell contains along c axis two oligomers bound together by a H bond			
Polymer	a	b	c	R	a	b	c	R
Tetramer[a]	3.21	7.43	8.00	11.4	5.76	13.14	26.82	1.7
Pentamer	5.81	13.4	16.42	2.9	5.75	13.19	32.3	1.8
Hexamer	5.73	13.19	19.64	2.1	5.79	13.24	38.67	2.1
Heptamer	5.67	13.18	22.39	1.7	5.69	13.18	44.74	2.0
Octamer	5.77	13.19	25.23	1.6	5.84	13.40	49.62	4

[a]Since electron diffraction data (8) clearly showed that $a = 5.76$ and $b = 13.2$, the very high value of R and the unacceptable refined values of a and b indicate either an error in measurement of certain reflections in the powder pattern or the total unacceptability of the "one chain" unit cell for the tetramer.

in Fig. 5. The same values of the a and b parameters as those for the polymer unit cell were again assumed for these oligomers. The refined unit cell parameters and R-factors for the oligomers are summarized in Table 3.

The data in Table 3 for the tetramer and pentamer case support the model where along the c axis two oligomers are bound together by a hydrogen bond. For the octamer, the model in which the unit cell contains just one oligomer along the c axis is preferred. For hexamer and heptamer, it is impossible with the results shown in Table 3 to find which form is preferred because the R-factor is the same in the two cases. Clearly one is seeing the results of a delicate energetic balance between "packing" energy and "surface" free energy for a polymer with a chain "sense". Once a minimum molecular weight is reached, chain folding is the dominant mechanism for achieving a packing with alternating chain "sense" as required by the space group.

Acknowledgements

The authors are pleased to acknowledge helpful discussions with Professor F. Brisse of this department and Dr. B. Hauttecoeur of the Institut Pasteur in Paris. The continued financial support of the National Research Council of Canada and the Ministère de l'Education du Québec made this study possible.

1. M. LEMOIGNE. Ann. Inst. Pasteur, **41**, 148 (1927).
2. M. LEMOIGNE. Bull. Soc. Chim. Biol. **8**, 770 (1926).
3. M. LEMOIGNE. Ann. Inst. Pasteur, **39**, 144 (1925).
4. I. OLSON, J. M. MERRICK, and I. J. GOLDSTEIN. Biochemistry, **4**, 453 (1965).
5. R. H. MARCHESSAULT, K. OKAMURA, and C. J. SU. Macromolecules, **3**, 735 (1970).
6. R. ALPER, D. G. LUNDGREN, R. H. MARCHESSAULT, and W. A. CÔTÉ. Biopolymers, **1**, 545 (1963).
7. D. ELLAR, D. G. LUNDGREN, K. OKAMURA, and R. H. MARCHESSAULT. J. Mol. Biol. **35**, 489 (1968).
8. K. OKAMURA. Ph.D. Thesis, Sunny College of Forestry, Syracuse, NY. 1967.
9. J. CORNIBERT and R. H. MARCHESSAULT. J. Mol. Biol. **71**, 735 (1972).
10. M. YOKOUCHI, Y. CHATANI, H. TADOKORO, K. TERANISHI, and H. TANI. Polymer, **14**, 267 (1973).
11. B. HAUTTECOEUR, M. JOLIVET, and R. GAVARD. C. R. Acad. Sci. Paris, **280**, 2801 (1975).
12. D. L. DORSET. Acta Crystallogr. A**32**, 207 (1976).
13. International tables for X-ray crystallography. Vol. IV. Kynoch Press, Birmingham. 1974.
14. B. K. VAINSHTEIN. Structure analysis by electron diffraction. MacMillan Company, New York. 1964. p. 143.
15. D. E. WILLIAMS. Acta Crystallogr. A**25**, 464 (1969).
16. P. ZUGENMAIER and A. SARKO. Acta Crystallogr. B**28**, 3158 (1972).
17. D. C. BASSETT and A. KELLER. Philos. Mag. **7**, 1553 (1962).
18. A. KELLER and A. O'CONNOR. Discuss. Faraday Soc. **25**, 114 (1958).
19. J. D. HOFFMAN and J. J. WEEKS. J. Res. Natl. Bur. Stand. **66A**, 13 (1962).
20. P. J. FLORY and D. Y. YOON. Nature, **272**, 226 (1978).
21. D. M. SADLER and A. KELLER. Science, 263 (1979).

Can. J. Chem. Downloaded from www.nrcresearchpress.com by 210.87.254.42 on 09/05/12
For personal use only.

The retroaldol reaction of 3-penten-2-one: equilibrium constant for hydration and rate constants for the hydration and retroaldol reactions in base

J. PETER GUTHRIE[1]

Department of Chemistry, University of Western Ontario, London, Ont., Canada N6A 5B7

Received April 24, 1980

J. PETER GUTHRIE. Can. J. Chem. **59**, 45 (1981).

In aqueous sodium hydroxide solutions at 25°C, 3-penten-2-one undergoes retroaldol cleavage to acetone and acetaldehyde. The kinetics can be followed spectrophotometrically, and show two exponential phases with rather different rate constants. By a new analysis of the mathematical solution to this system we have been able to derive an improved method for calculating the microscopic rate constants. These rate constants are $k_{hyd} = 2.89 \times 10^{-3}\ M^{-1}\ s^{-1}$, $k_{dehyd} = 4.04 \times 10^{-4}\ M^{-1}\ s^{-1}$, and $k_{retro} = 3.36 \times 10^{-4}\ M^{-1}\ s^{-1}$. The equilibrium constant for hydration of 3-penten-2-one (standard state for water is the pure liquid) is 7.13.

J. PETER GUTHRIE. Can. J. Chem. **59**, 45 (1981).

Dans des solutions aqueuses d'hydroxyde de sodium à 25°C, la pentèn-3 one-2 subit une rupture rétroaldolique et conduit à l'acétone et à l'acétaldéhyde. Les données cinétiques obtenues par spectrophotométrie montrent deux phases exponentielles avec des vitesses différentes. A l'aide d'une nouvelle analyse de la solution mathématique de ce système, nous avons pu mettre au point une meilleure méthode de calcul des constantes de vitesse microscopique. Ces constantes sont: $K_{hyd} = 2{,}89 \times 10^{-3}\ M^{-1}\ s^{-1}$, $K_{déhyd} = 4{,}04 \times 10^{-4}\ M^{-1}\ s^{-1}$ et $K_{rétro} = 3{,}36 \times 10^{-4}\ M^{-1}\ s^{-1}$. La constante d'équilibre d'hydratation de la pentèn-3 one-2 (l'état normal pour l'eau est le liquide à l'état pur) est de 7,13.

[Traduit par le journal]

Introduction

We recently published the results of an indirect evaluation of the equilibrium constants for aldol condensation reactions of simple compounds (1). In order to investigate the possibility of finding useful rate–equilibrium correlations we plan to study the rates of the aldol or retroaldol reactions of as many as possible of the systems for which equilibrium constants are now available. As part of this program, we have examined the behavior of 3-penten-2-one, for which some studies have been reported (2, 3), although in the published work the retroaldol reaction was not of primary interest. To our surprise, our results are not in satisfactory agreement with the literature values. Accordingly it seemed important to publish the results of the present investigation without delay. In analysing our kinetic data we have devised a better algebraic approach to extracting the microscopic rate constants from the experimental parameters than that which we reported previously (4).

Results and Discussion

The kinetics showed biphasic behavior as shown in Fig. 1. The experimental points were fitted to eq. [1] by the method of least squares (4–7). For the

$$[1] \quad OD = OD_\infty + \alpha \exp(-\lambda_2 t) + \beta \exp(-\lambda_3 t)$$

mechanism shown in Scheme 1, we can derive integrated rate equations for the concentrations of the three species (4), following the method of Frost and Pearson (8); this gives eqs. [2]–[4]. Then it is possible to derive an expression, eq. [6], for the optical density (OD) as a function of time:

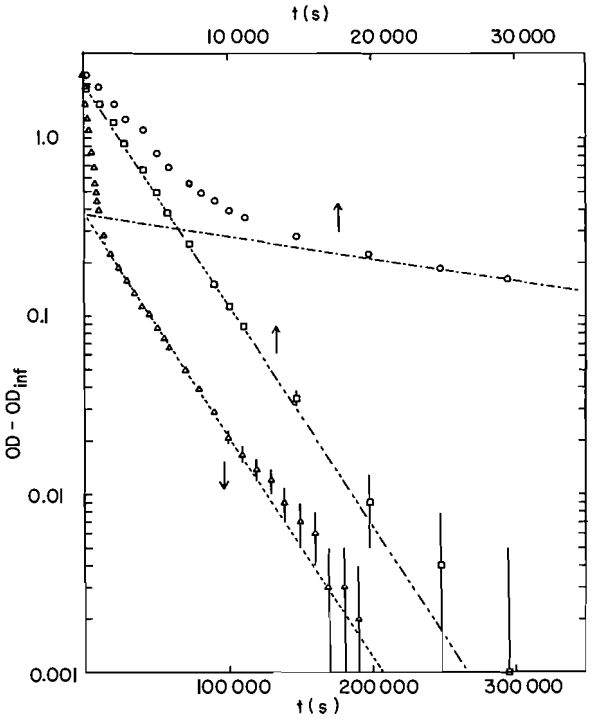

FIG. 1. First order plots, showing the two phase nature of the kinetics. (---) Lower abscissa, $OD - OD_{inf}$; (— · —) upper abscissa, $OD - OD_{inf}$; (— · · —) upper abscissa ($OD - OD_{inf}$) observed – extrapolated. 3-Penten-2-one in 0.1 *M* NaOH at ionic strength 1.0 *M*.

[1]Alfred P. Sloan Fellow, 1975–1979.

0008-4042/81/010045-05$01.00/0

©1981 National Research Council of Canada/Conseil national de recherches du Canada

Can. J. Chem. Downloaded from www.nrcresearchpress.com by 210.87.254.6 on 09/05/12
For personal use only.

Can. J. Chem. Downloaded from www.nrcresearchpress.com by 210.87.254.6 on 09/05/12
For personal use only.

$$[2]\quad [A_1] = [A_1]^0\left\{\frac{k_{12}(\lambda_2 - k_{23})}{\lambda_2(\lambda_2 - \lambda_3)}\exp(-\lambda_2 t) + \frac{k_{12}(k_{23} - \lambda_3)}{\lambda_3(\lambda_2 - \lambda_3)}\exp(-\lambda_3 t)\right\}$$

$$[3]\quad [A_1] = [A_1]^0\left\{-\frac{k_{12}}{\lambda_2 - \lambda_3}\exp(-\lambda_2 t) + \frac{k_{12}}{\lambda_2 - \lambda_3}\exp(-\lambda_3 t)\right\}$$

$$[4]\quad [A_3] = [A_1]^0\left\{\frac{k_{12}k_{23}}{\lambda_2\lambda_3} + \frac{k_{12}k_{23}}{\lambda_2(\lambda_2 - \lambda_3)} \times \exp(-\lambda_2 t) - \frac{k_{12}k_{23}}{\lambda_3(\lambda_2 - \lambda_3)}\exp(-\lambda_3 t)\right\}$$

$$[5]\quad OD = \varepsilon_1[A_1] + \varepsilon_2[A_2] + \varepsilon_3[A_3]$$

$$[6]\quad OD = [A_1]^0\varepsilon_3 + \alpha\exp(-\lambda_2 t) + \beta\exp(-\lambda_3 t)$$

where

$$[7]\quad \alpha = \frac{[A_1]^0 k_{12}(\lambda_2 - k_{23})\varepsilon_1}{\lambda_2(\lambda_2 - \lambda_3)} \times \left\{1 - \frac{\varepsilon_2}{\varepsilon_1}\frac{\lambda_2}{\lambda_2 - k_{23}} + \frac{\varepsilon_3}{\varepsilon_1}\frac{k_{23}}{\lambda_2 - k_{23}}\right\}$$

$$[8]\quad \beta = \frac{[A_1]^0 k_{12}(k_{23} - \lambda_3)\varepsilon_1}{\lambda_2(\lambda_2 - \lambda_3)} \times \left\{1 - \frac{\varepsilon_2}{\varepsilon_1}\frac{\lambda_3}{k_{23} - \lambda_3} - \frac{\varepsilon_3}{\varepsilon_1}\frac{k_{23}}{k_{23} - \lambda_3}\right\}$$

$$[9]\quad \lambda_{2,3} = (p \pm q)/2$$

$$[10]\quad p = k_{12} + k_{21} + k_{23}$$

$$[11]\quad q = (p^2 - 4k_{12}k_{23})^{1/2}$$

Thus far the derivation is rigorously correct for Scheme 1. Equations [7] and [8] are too complicated for convenient manipulation; fortunately it is possible in the present case to simplify these equations without serious error.

Since the extinction coefficient for 4-hydroxy-2-pentanone, ε_2, will be approximately equal to that

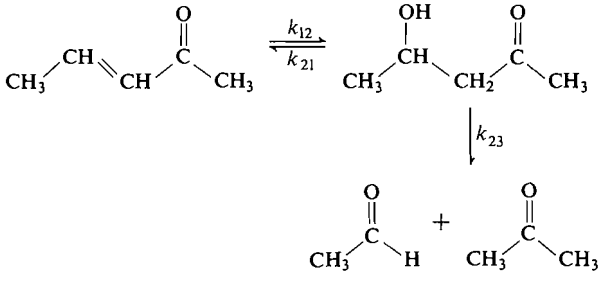

SCHEME 1

for acetone, and ε_3,' the sum of the apparent extinction coefficients for acetone and acetaldehyde, will be similar to that for acetone because much of the acetaldehyde will be present as the hydrate or hydrate anion (4, 9, 10) we make the simplifying approximation that $\varepsilon_2 = \varepsilon_3$. In any case these extinction coefficients are small at 225 nm.[2] Then we may write:

$$[12]\quad \alpha = \frac{[A_1]^0 k_{12}(\lambda_2 - k_{23})\varepsilon_1}{\lambda_2(\lambda_2 - \lambda_3)}\left\{1 - \frac{\varepsilon_3}{\varepsilon_1}\right\}$$

$$[13]\quad \beta = \frac{[A_1]^0 k_{12}(k_{23} - \lambda_3)\varepsilon_1}{\lambda_3(\lambda_2 - \lambda_3)}\left\{1 - \frac{\varepsilon_3}{\varepsilon_1}\right\}$$

Substitution of the values of the rate constants, derived by making the assumption that $\varepsilon_3 = \varepsilon_2$, into eqs. [7] and [8] shows that the error introduced by the approximation is, for any reasonable ε values, quite negligible, being less than 1%.

One can now derive a solution based upon eqs. [9], [12], and [13]. First we note that:

$$[14]\quad \lambda_2 + \lambda_3 = k_{12} + k_{21} + k_{23}$$

$$[15]\quad \lambda_2\lambda_3 = k_{12}k_{23}$$

$$[16]\quad \frac{\alpha}{\beta} = \frac{\lambda_3(\lambda_2 - k_{23})}{\lambda_2(k_{23} - \lambda_3)}$$

These three equations can now be solved for the three unknowns:

$$[17]\quad k_{23} = \left\{\lambda_2 + \lambda_3\left(\frac{\alpha\lambda_2}{\beta\lambda_3}\right)\right\} \Big/ \left\{1 + \left(\frac{\alpha\lambda_2}{\beta\lambda_3}\right)\right\}$$

$$[18]\quad k_{12} = \lambda_2\lambda_3/k_{23}$$

$$[19]\quad k_{21} = \lambda_2 + \lambda_3 - k_{12} - k_{23}$$

In order to assess the precision of these pseudo first order rate constants, we carried out a full error analysis (5) using the covariance matrix generated by the least squares program (6–8).

The kinetics results are found in Table 1; the derived rate constants are found in Table 2. Figure 2 shows that the microscopic rate constants are first order in hydroxide, as expected. The figure shows that there is some scatter in the values of the rate constants from run to run, particularly in the case of k_{23}. However, all values which deviated from the line had markedly larger estimated standard deviations from the least squares procedure. Clearly the calculations do not adequately determine the uncertainties in k_{23} etc., because the error bars do not reach the best fit line. On the other hand the relative

[2]The spectrum for 2-butanone in water, which should be a good model, shows an extinction coefficient of about 1 at 225 nm (11).

Can. J. Chem. Downloaded from www.nrcresearchpress.com by 210.87.254.6 on 09/05/12
For personal use only.

TABLE 1. Kinetic parameters for the hydration and retro-aldol reactions of 3-penten-2-one in aqueous NaOH[a]

[NaOH]	A_1	A_2	$10^3 \times A_3$[b]	A_4	$10^3 \times A_5$[b]
(*a*) Ionic strength 1.10[c]					
0.03	0.173(0.001)	0.548(0.002)	6.50(0.03)	0.100(0.002)	0.597(0.017)
0.03	0.228(0.002)	1.444(0.009)	6.22(0.05)	0.346(0.009)	1.03 (0.03)
0.05	0.273(0.005)	1.489(0.013)	10.9 (0.1)	0.368(0.012)	1.27 (0.08)
0.05	0.159(0.001)	0.548(0.002)	10.9 (0.1)	0.095(0.002)	0.834(0.030)
0.07	0.319(0.002)	1.521(0.005)	14.8 (0.1)	0.243(0.004)	1.16 (0.04)
0.10	0.156(0.001)	0.542(0.001)	23.1 (0.1)	0.140(0.001)	1.86 (0.03)
0.10	0.260(0.0002)	0.519(0.002)	20.5 (0.1)	0.111(0.001)	2.27 (0.04)
0.10	0.313(0.0002)	1.886(0.005)	18.3 (0.1)	0.324(0.002)	1.69 (0.01)
0.10	0.261(0.0002)	1.024(0.002)	19.4 (0.1)	0.183(0.001)	1.75 (0.01)
(*b*) Ionic strength 1.00[c]					
0.10	0.312(0.004)	1.502(0.014)	19.3 (0.4)	0.340(0.013)	2.19 (0.17)
0.10	0.335(0.0003)	2.100(0.010)	17.0 (0.1)	0.377(0.002)	1.71 (0.01)
0.10	0.233(0.0002)	1.371(0.003)	18.4 (0.04)	0.216(0.001)	1.52 (0.01)
0.10	0.173(0.0002)	0.516(0.002)	19.4 (0.1)	0.074(0.001)	2.32 (0.05)
0.30	0.432(0.002)	1.493(0.004)	49.9 (0.2)	0.233(0.004)	4.80 (0.21)
0.70	0.589(0.001)	1.393(0.004)	148 (1.0)	0.237(0.003)	10.7 (0.3)
1.00	0.640(0.001)	1.449(0.005)	227 (1.0)	0.235(0.003)	17.2 (0.4)

[a]All in aqueous solution at 25°C. Absorbance–time data were fitted to eq. [6] by least squares, leading to the parameters shown. Values in parentheses are the uncertainties estimated by the least-squares procedure, based on scatter of the experimental points about the calculated line.
[b]In min^{-1}.
[c]Ionic strength was maintained using KCl.

TABLE 2. Rate and equilibrium constants for individual steps[a]

[NaOH]	$10^4 \times k_{23}$	$10^3 \times k_{12}$	$10^4 \times k_{21}$	K[b]
(*a*) Pseudo first order rate constants at 0.1 *M* ionic strength				
0.03	0.116(0.003)	0.0931(0.0003)	0.136(0.002)	6.85
0.03	0.204(0.008)	0.0869(0.0004)	0.134(0.003)	6.48
0.05	0.256(0.016)	0.150 (0.001)	0.273(0.010)	5.49
0.05	0.161(0.006)	0.157 (0.001)	0.227(0.004)	6.92
0.07	0.221(0.008)	0.216 (0.001)	0.285(0.006)	7.58
0.1	0.383(0.008)	0.312 (0.001)	0.651(0.009)	4.79
0.1	0.448(0.008)	0.289 (0.002)	0.466(0.006)	6.20
0.1	0.324(0.002)	0.264 (0.001)	0.363(0.003)	7.27
0.1	0.337(0.002)	0.278 (0.001)	0.399(0.002)	6.97
(*b*) Second order rate constants at 0.1 *M* ionic strength[c]				
	3.37 (0.014)	2.90 (0.003)	4.06 (0.015)	7.13
(*c*) Pseudo first order rate constants at 1.0 *M* ionic strength				
0.1	0.437(0.036)	0.269 (0.002)	0.455(0.018)	5.91
0.1	0.331(0.003)	0.246 (0.001)	0.345(0.003)	7.13
0.1	0.289(0.001)	0.268 (0.001)	0.346(0.001)	7.75
0.1	0.434(0.010)	0.288 (0.001)	0.308(0.004)	9.35
0.3	0.91 (0.04)	0.730 (0.002)	0.902(0.014)	8.00
0.7	2.06 (0.06)	2.13 (0.01)	3.05 (0.04)	6.98
1.0	3.28 (0.08)	3.30 (0.02)	4.46 (0.06)	7.40
(*d*) Second order rate constants at 1.0 *M* ionic strength[c]				
	3.00 (0.013)	2.67 (0.004)	3.47 (0.10)	7.60
(*e*) Literature values of second order rate constants at 0.1 *M* ionic strength[d]				
	1.4	2.1	5	4.6

[a]All in aqueous solution at 25°C. Dimensions are s^{-1} for pseudo first order rate constants and $M^{-1}\,s^{-1}$ for second order rate constants.
[b]$K = k_{12}/k_{21} = [CH_3CH(OH)CH_2COCH_3]/[CH_3CH{=}CH{-}CO{-}CH_3]$.
[c]Calculated by least squares fit of the pseudo first order rate constants to the equation $y = ax$; the rate constants are defined as $k_{hyd} = k_{12}/[OH^-]$; $k_{dehyd} = k_{21}/[OH^-]$; and $k_{retro} = k_{23}/[HO^-]$.
[d]Calculated by J. L. Jensen from data in refs. 2 and 3 (personal communication).

Can. J. Chem. Downloaded from www.nrcresearchpress.com by 210.87.254.6 on 09/05/12
For personal use only.

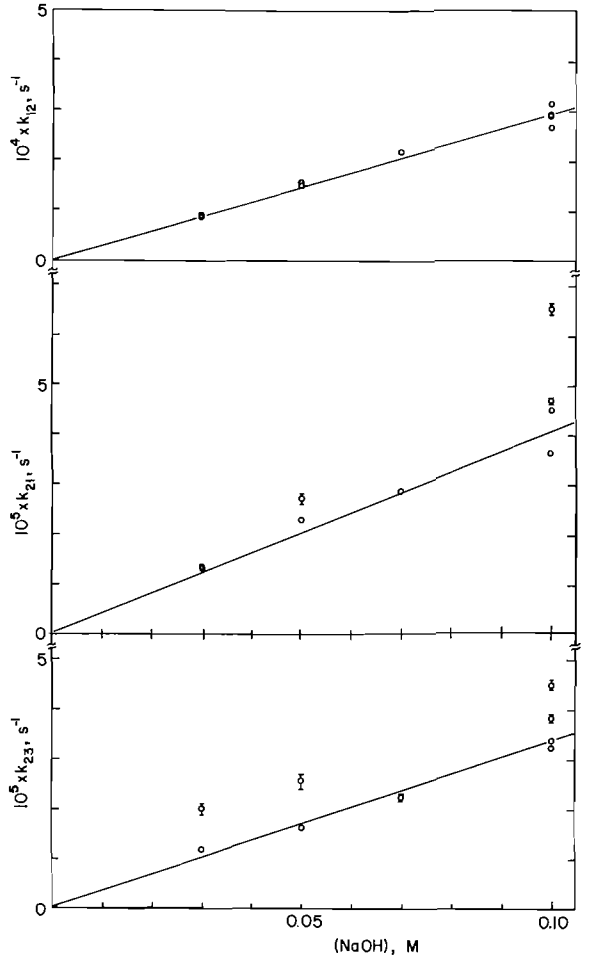

FIG. 2. Observed pseudo first order rate constants as a function of hydroxide concentration for ionic strength 0.1 *M*. Error bars are drawn using the standard deviations from Table 2.

reliability of different k values seems to be correct. There was no obvious reason to discard the runs given rise to these aberrant points. However weighted least squares fitting gave rise to the lines shown in Fig. 2, and the less reliable points have had little effect. (Weights were based on the least squares standard deviations in Table 2.)

The second phase of the reaction, for which the apparent rate constant is λ_3, is slow at 25°C, and the optical density change is small. This presumably makes the results sensitive to artefacts and leads to the observed scatter. The derived values of k_{21} and k_{23} are dependent upon the value of λ_3, whereas k_{12} is much less sensitive to it, being largely determined by λ_2.

The corresponding second order rate constants are found in Table 2; these values were calculated by least squares. Experiments were carried out at ionic strengths of 0.1 and 1.0 (maintained by KCl); the effect of ionic strength is seen to be small, but cannot be neglected. Table 2 also gives the equilibrium constant for hydration. The rate constant (3) and equilibrium constant (2) for hydration which have been reported by other workers are given in Table 2. The agreement is reasonable for k_{hyd}, not bad for K and k_{21} (considering the extrapolations involved) but is poor for k_{23}. Our work was carried out over a period of time, using several batches of pentenone independently purified by preparative gas chromatography. The pentenone used for kinetics showed clean nmr spectra totally consistent with the structure. Accordingly we feel that our numbers are correct, although we do not know the reason for the discrepancy.

Experimental

3-Penten-2-one (tech) from Aldrich could not be purified by distillation (a second component which we believe to be mesityl oxide was not separable), but could be obtained pure by preparative gas chromatography (SE30 column at 100°C). The pure material had a suitable nmr spectrum ($CDCl_3$) δ 1.9, doublet (each peak broadened) J = 7 Hz, 3H; δ 2.2, singlet, 3H; 6.0 doublet (each peak broadened) half of an AB quartet, J = 16 Hz; 6.8 doublet of quartets, other half of the AB quartet, J_{AB} = 16 Hz, J_{BX} = 7 Hz.

Stock solutions of the enone were prepared in tetrahydrofuran which had been freshly purified by passage through Grade I neutral alumina (Fisher). NaOH solutions were prepared from Fisher concentrates to give 0.1 or 1.0 *N* solutions. Other concentrations were prepared by dilution with the appropriate KCl solution. Samples of NaOH (3.0 mL) in quartz cuvettes with Teflon stoppers (1 cm path length) were thermostatted in the cell compartment of a Gilford Model 240 spectrophotometer equipped with an automatic sample changer. Reactions were initiated by addition of a suitable volume of the enone solution (Hamilton syringe). The reactions were followed at 225 nm and either recorded on a Heath Model SR205 recorder or else punched on paper tape using a Digitizer built in this department for use with the Gilford. Calculations were carried out on a Xitan microcomputer using programs written in BASIC or FORTRAN.

Acknowledgments

I wish to thank the Natural Sciences and Engineering Research Council of Canada, the Academic Development Fund of the University of Western Ontario, and the Alfred P. Sloan Foundation for financial support of this work. Technical assistance by Susan F. Vice and some preliminary experiments carried out in the course of a fourth year thesis project by Kevin J. Cooper are gratefully acknowledged.

1. J. P. GUTHRIE. Can. J. Chem. **56**, 962 (1978).
2. J. L. JENSEN and D. J. CARRE. J. Org. Chem. **39**, 2103 (1974).
3. J. L. JENSEN and H. HASHTROUDI. J. Org. Chem. **41**, 3299 (1976).
4. J. P. GUTHRIE. Can. J. Chem. **52**, 2037 (1974).
5. P. R. BEVINGTON. Data reduction and error analysis for the physical sciences. McGraw-Hill, New York. 1969.
6. W. E. DEMING. Statistical adjustment of data. Dover Publications, New York. 1964.
7. W. E. WENTWORTH. J. Chem. Educ. **42**, 96 (1965); **42**, 162 (1965).
8. A. A. FROST and R. G. PEARSON. Kinetics and mechanism. Wiley, New York. 1961. pp 173–177.
9. J. L. KURZ. J. Am. Chem. Soc. **89**, 3524 (1967).
10. R. P. BELL and D. P. ONWOOD. Trans. Faraday Soc. **58**, 1557 (1962).
11. U.V. atlas of organic compounds. Vol. 1. Butterworths, London. 1966. Spectrum B1/6.

Can. J. Chem. Downloaded from www.nrcresearchpress.com by 210.87.254.6 on 09/05/12
For personal use only.

Erratum: On the chemistry and high field nuclear magnetic resonance spectroscopy of rapamycin

JOHN A. FINDLAY
Chemistry Department, University of New Brunswick, Fredericton, N.B., Canada E3B 5A3
AND
LAJOS RADICS
NMR Laboratory, Central Research Institute for Chemistry, P.O. Box 17, H-1525 Budapest, Hungary

Ref.: Can. J. Chem. **58**, 579 (1980).
Received October 9, 1980

The configuration at C-28 of rapamycin is opposite to that depicted in structure **1** (*S* and not *R*). Reference 2 should read D. C. N. Swindells, P. S. White, and J. A. Findlay. Can. J. Chem. **56**, 2491 (1978).

A ^{31}P nmr spectroscopic study of complexation of tin(II) and lead(II) by some phosphines, phosphine oxides, and related ligands, with the ^{31}P nuclear magnetic resonance spectra of two tetratertiary phosphine tetraoxides and the analogous tetra-sulfides and -selenides[1,2,3]

PHILIP A. W. DEAN,[4] DONALD D. PHILLIPS, AND LIJANA POLENSEK

Department of Chemistry, University of Western Ontario, London, Ont., Canada N6A 5B7

Received May 14, 1980

PHILIP A. W. DEAN, DONALD D. PHILLIPS, and LIJANA POLENSEK. Can. J. Chem. **59**, 50 (1981).

^{31}P nmr has been used to show that, in $MeNO_2$, $M(SbF_6)_2$ (M = Sn or Pb) forms 1:1 complexes with $Ph_2P(CH_2)_2PPh_2$, $PhP[(CH_2)_2PPh_2]_2$, $MeC(CH_2PPh_2)_3$, $[Ph_2P(CH_2)_2]_2P(CH_2)_2\overset{+}{P}HPh_2$, $Ph_2P[(CH_2)_2PPh]_2(CH_2)_2\overset{+}{P}HPh_2$, $P[(CH_2)_2PPh_2]_3$, and $Ph_2P[(CH_2)_2PPh]_2(CH_2)_2PPh_2$. The phosphonium ligands are formed *in situ*. Spectra characteristics of slow inter- and intramolecular exchange were obtained in all cases except, perhaps, those involving the last two ligands, which may be involved in rapid intramolecular exchange. For the first five ligands, the maximum denticity is achieved and unambiguous one-bond M(II)—^{31}P (M = $^{117/119}Sn$ or ^{207}Pb) coupling constants are reported and discussed. In the presence of $M(SbF_6)_2$ (M = Sn or Pb), PPh_3 is protonated in $MeNO_2$, while in acetone $Sn(SbF_6)_2$ forms a 1:1 complex with PPh_3 which appears to be solvent-inserted, $[Sn—O—CMe_2PPh_3]^{2+}$.

Reduced temperature ^{31}P nmr spectroscopy has allowed the detection of 1:2 and 1:3 (M:L) complexes of $OPPh_3$, and 1:1 complexes of $Ph_2P(O)(CH_2)_2P(O)Ph_2$, $PhP(O)[(CH_2)_2P(O)Ph_2]_2$, and $(O)P[(CH_2)_2P(O)Ph_2]_3$, with both tin(II) and lead(II). The 1:1 complexes with polydentate ligands are isolable; nmr shows that the maximum denticity occurs except with the last ligand which behaves in a tridentate manner. Several two-bond M—O—P coupling constants have been obtained. Also, the changes which complexation produces in the P—P couplings are compared with changes produced in the analogous phosphine complexes.

The synthesis and characterization of $Ph_2P(E)[(CH_2)_2P(E)Ph]_2(CH_2)_2P(E)Ph_2$ (E = S or Se) and $(Se)P[(CH_2)_2P(Se)Ph_2]_3$ are reported. The ^{31}P nmr spectra of these compounds are compared with those of the parent tetraphosphines and other members of the corresponding tetraoxide–tetrachalcogenide series.

PHILIP A. W. DEAN, DONALD D. PHILLIPS et LIJANA POLENSEK. Can. J. Chem. **59**, 50 (1981).

On a utilisé la rmn du ^{31}P pour montrer que dans le $MeNO_2$, le $M(SbF_6)_2$ (M = Sn ou Pb) forme des complexes 1:1 avec les composés suivants: $Ph_2P(CH_2)_2PPh_2$, $PhP[(CH_2)_2PPh_2]_2$, $MeC(CH_2PPh_2)_3$, $[Ph_2P(CH_2)_2]_2P(CH_2)_2\overset{+}{P}HPh_2$, $Ph_2P[(CH_2)_2PPh]_2(CH_2)_2\overset{+}{P}HPh_2$, $P[(CH_2)_2PPh_2]_3$ et $Ph_2P[(CH_2)_2PPh]_2(CH_2)_2PPh_2$. Les ligands phosphonium sont formés *in situ*. Dans tous les cas, excepté peut être dans les cas des deux derniers ligands qui peuvent subir un échange intermoléculaire rapide, on a observé des spectres caractéristiques d'échanges inter- et intramoléculaire lents. Dans les cas des 5 premiers ligands tous les points d'attaches sont utilisés; on a aussi observé d'une façon non ambigue des constantes de couplage pour une liaison simple M(II)—^{31}P (M = $^{117/119}Sn$ ou ^{207}Pb que l'on discute. En présence du $M(SbF_6)_2$ (M = Sn ou Pb), PPh_3 est protoné dans le $MeNO_2$ alors que dans l'acétone le composé $Sn(SbF_6)_2$ forme un complexe 1:1 avec le PPh_3 qui semble être inséré dans le solvant, $[Sn—O—CMe_2PPh_3]^{2+}$.

A basse température, la spectroscopie de rmn du ^{31}P permet de déceler les complexes 1:2 et 1:3 (M:L) du $OPPh_3$ et les complexes 1:1 des composés $Ph_2P(O)(CH_2)_2P(O)Ph_2$, $PhP(O)[(CH_2)_2P(O)Ph_2]_2$ et $(O)P(CH_2)_2P(O)Ph_2]_3$ avec l'étain(II) ainsi que le plomb(II). On peut isoler les complexes 1:1 impliquant des ligands polydentates; la rmn montre que tous les sites des ligands sont liés à l'exception du dernier ligand qui se comporte de manière tridentate. On a obtenu plusieurs constantes de couplage MOP à travers deux liaisons. On a également comparé les changements produits par la complexation sur les constantes de couplage P—P avec les changements produits dans les complexes analogues de phosphines.

On rapporte la synthèse et la caractérisation du $Ph_2P(E)[(CH_2)_2P(E)Ph]_2(CH_2)_2P(E)Ph_2$ (E = S ou Se) et $(Se)P[(CH_2)_2P(Se)Ph_2]_3$. On a comparé les spectres de rmn du ^{31}P de ces composés à ceux des tétraphosphines apparentées et à ceux d'autres membres des séries correspondantes de tétraoxyde–tétrachalcogénures.

[Traduit par le journal]

Introduction

We report here an nmr spectroscopic investigation, involving primarily ^{31}P nmr, of the complexation of tin(II) and lead(II) by a variety of phosphorus donor ligands, most notably chelating tertiary phosphines. The primary object of this work, successfully achieved, was to establish the hitherto unknown (1–3) MP_n kernels for the two divalent Group IVA elements. During this study, we have been able to measure several one-bond tin(II)– and lead(II)–phosphorus coupling constants. (^{119}Sn, ^{117}Sn, and ^{207}Pb, all have spin $I = 1/2$, and natural abundances of 8.68, 7.67, and 21.11%, respectively.) These appear to be the first unambiguous examples of such couplings; the couplings involving tin(II) can usefully be compared with Sn–P coupling in tin(IV)–phosphine complexes (4, 5). In addition, the ^{31}P nmr spectra of complexes with

[1]Presented, in part, at the 2nd Joint CIC/ACS Conference, Montreal, P.Q., Canada, June, 1977.

[2]Abstracted, in part, from the M.Sc. thesis of D.D.P., University of Western Ontario, 1978.

[3]No reprints available.

[4]To whom all correspondence should be addressed.

0008-4042/81/010050-12$01.00/0

©1981 National Research Council of Canada/Conseil national de recherches du Canada

Can. J. Chem. Downloaded from www.nrcresearchpress.com by 210.87.254.42 on 09/05/12
For personal use only.

Can. J. Chem. Downloaded from www.nrcresearchpress.com by 210.87.254.42 on 09/05/12
For personal use only.

some of the polydentate phosphines yield P–P coupling constants which can be correlated with those found in complexes of other elements (e.g. refs. 6–9).

In the present study, strong acid salts of tin(II) and lead(II) have been used to minimize ligand–counterion competition at the coordination sites. Similarly, solvents of low Donor Number (10) were chosen, to reduce ligand–solvent competition. Nitromethane proved useful in many instances. It was thought that some oxidation of the ligands might occur in this medium, however, so as a precaution the ^{31}P nmr spectra of the related phosphine oxide complexes have been obtained; they are given here also. We could find no earlier report of the ^{31}P nmr spectra of two of the polydentate phosphine oxides used, $(O)P[(CH_2)_2P(O)Ph_2]_3$ and $Ph_2P(O)[(CH_2)_2P(O)Ph]_2(CH_2)_2P(O)Ph_2$; the spectra are given here together with those of the corresponding tetra-sulfides and -selenides (three of which seem to be new compounds) for comparison.

To our knowledge the only lead(II)–phosphine complexes which have been reported previously are $PbBr_2(dppe)$ and $[Pb(dppe)_2](ClO_4)_2$ (11)[5]; no nmr data are available for these compounds. At the outset of our study, tin(II)–phosphine complexes, in contrast to their tin(IV) analogs, had been little studied (1, 2). More recently, the only tin(II)–phosphine complexes which have been well-characterized are a limited number of 1:1 complexes of monodentate phosphines with stannous halides (12–14). In solution, even the complexes with such strongly basic phosphines as Bu^t_3P and $(Me_2N)_3P$ are labile on the nmr timescale (12, 13) and are partly solvolyzed by THF (12). However, when $SnCl_2(PBu^t_3)$ is coordinated to $W(CO)_5$ through tin, exchange of the phosphine is slow and no solvolysis by THF occurs (15). These last observations suggest that stable non-labile tin(II)–phosphine complexes should be preparable when the Lewis acidity of the tin centre is high. Our results demonstrate that this is so for tin and that analogous lead complexes can be prepared under similar conditions.

[5]Abbreviations used in this paper: $P(OMe)_3$ = tmp; $OP(OMe)_3$ = tmpO; $OPMe(OMe)_2$ = dmmp; $Ph_2P(CH_2)_2PPh_2$ = dppe; $Ph_2P(O)(CH_2)_2P(O)Ph_2$ = $dppeO_2$; $(Ph_2PCH_2)_3CMe$ = tripod; $[Ph_2P(CH_2)_2]_2PPh$ = etp; $[Ph_2P(CH_2)_2]_3P$ = PP_3; $[Ph_2P(O)(CH_2)_2]_3PO$ = PP_3O_4; $[Ph_2P(CH_2)_2]_2PPh(CH_2)_2\overset{+}{P}HPh_2]$ = $PP_2(PH)^+$; $[Ph_2P(CH_2)_2PPhCH_2]_2$ = P_2P_2; $Ph_2P(CH_2)_2PPh(CH_2)_2PPh(CH_2)_2\overset{+}{P}HPh_2$ = $PPP(PH)^+$; $[Ph_2P(O)(CH_2)_2P(O)PhCH_2]_2$ = $P_2P_2O_4$.

Experimental

Materials

The purity of all ligands was checked by ^{31}P and/or ^1H nmr. All liquids (except SbF_5) were stored over 3A Molecular Sieves.

Triphenylphosphine (Eastmen Kodak Co.) and tris(4-fluorophenyl)phosphine (Maybridge Chemical Co.) were recrystallized from ethanol. Dimethyl methylphosphonate (dmmp) and trimethyl phosphate (tmpO), both from Aldrich Chemical Co. Inc., were purified by distillation under dry N_2 at 1 atm. Trimethyl phosphite (tmp) (Strem Chemicals, Inc.) showed no significant impurity after reduced pressure distillation under dry N_2. Phosphorus-31 nmr showed the absence of appreciable impurities in 1,1,1-tris(diphenylphosphinomethyl)-ethane (tripod) and bis(2-diphenylphosphinoethyl)phenyl-phosphine (etp), both from Strem Chemicals, Inc., as well as tris(2-diphenylphosphinoethyl)phosphine, "Tetraphos II" (PP_3) and 1,1,4,7,10,10-hexaphenyl-1,4-7,10-tetraphosphadecane, "Tetraphos I" (P_2P_2),[6] both from Pressure Chemical Co.; these were pumped *in vacuo*, but otherwise were used as received.

1,2-Bis(diphenylphosphino)ethane was prepared by the standard method (17). Several of the phosphine oxides were prepared as part of an earlier study (18). PP_3O_4 (19) was prepared using I_2/OH^-, as previously. $P_2P_2O_4$ was prepared by the literature method (20). For comparison with the ^{31}P nmr spectra[7] of PP_3O_4 and $P_2P_2O_4$ (Table 1), the analogous tetrachalcogenides have been prepared. PP_3S_4 is a known compound (19). $P_2P_2S_4$ was obtained from a mixture of P_2P_2 and a slight deficiency of sulfur under reflux in benzene; the product was recrystallized from CH_2Cl_2–Bu^nOH.M.Pt (uncorr) 285–288°C. $P_2P_2Se_4$ was prepared by refluxing P_2P_2 with excess Se shot in benzene. After removal of solvent, the crude product was triturated with boiling Bu^nOH.M.Pt. (uncorr) 256–258°C. PP_3Se_4 was prepared similarly and recrystallized from Bu^nOH.M.Pt (uncorr) 203–204°C. The ^{31}P nmr spectra given in Table 1 characterize the new ligands.

Nitro-benzene and -methane were purified by distillation. Acetone-d_6 and nitromethane-d_3 (both MSD) and methylene chloride (Fisher "Spectranalyzed") were dried at least 12 h over 3A Molecular Sieves before use. Sulfur dioxide (Matheson Anhydrous Grade) was dried by standing in the gas phase over 3A Molecular Sieves for at least 12 h.

Antimony pentafluoride (PCR) was distilled twice under dry N_2, while arsenic pentafluoride (Ozark-Mahoning Co.), pure by tensimetry, was used as bought.

SnF_2 and PbF_2, both "Ultrapure" grade, were from Alfa-Ventron. $Sn(SbF_6)_2$ was synthesized by the literature method (23).

Manipulations

All glassware was baked out at 140°C for 12–24 h before use. Liquid SbF_5 was dispensed in a dry-N_2 filled glove box using an all glass syringe. Solids for the preparation of nmr samples were weighed out in the glove box. Solvents (except SO_2) and liquid ligands were added by standard N_2-vacuum techniques or in a dry-N_2 filled glovebag. SO_2 was condensed into samples and preparative mixtures from a glass–Teflon vacuum line.

Preparation of Lead Salts

Lead(II) hexafluoroantimonate, $Pb(SbF_6)_2$, was synthesized in a manner exactly analogous to that used for $Sn(SbF_6)_2$ (23); it

[6]This is thought to be the *meso*-form (16); our nmr data are consistent with the presence of a single isomer.

[7]These were not reported previously due to poor solubility in the solvents used (19).

Can. J. Chem. Downloaded from www.nrcresearchpress.com by 210.87.254.42 on 09/05/12
For personal use only.

TABLE 1. ^{31}P-{^1H} nuclear magnetic resonance spectra of $[Ph_2P(CH_2)_2PCH_2]_2$ (= P_2P_2) and $[Ph_2P(CH_2)_2]_3PPh$ (= PP_3) and their tetra-oxides, -sulfides, and -selenides[a,b]

Compound	δ_P(ppm)[c] P_A[d]	P_B[d]	$\lvert^3J(P_A—P_B)\rvert$[e] (Hz)	$\lvert^3J(P_B—P_{B'})\rvert$[e] (Hz)	$\lvert^1J(P—^{77}Se)\rvert$[f,g] (Hz)
P_2P_2	−14.6	−18.1	28.6±0.2	23.3±0.2	
$P_2P_2O_4$[h]	36.8	46.2	55.8±0.4	54.6±0.3	
$P_2P_2S_4$	39.1	45.8	58.5±0.2	60.6±0.2	
$P_2P_2Se_4$	31.0	37.3	62.8±0.3	60.4±0.4	$J(P_A—Se)$ = 737.7±0.6 $J(P_B—Se)$ = 738±1
PP_3	−14.5	−18.8	25.9±0.2		
PP_3O_4	26.1	43.6	46.1±0.3		
PP_3S_4[i]	39.3	49.9	55.4±0.3		
PP_3Se_4	31.8	38.1	56.2±0.4		$J(P_A—Se)$ = 739±3 $J(P_B—Se)$ = 740.0±0.1

[a]At 308 K in CH_2Cl_2 unless otherwise noted.
[b]P_2P_2, $P_2P_2O_4$, and ^{77}Se-free $P_2P_2Se_4$ give rise to AA'BB' spectra, PP_3, PP_3O_4, PP_3S_4, and ^{77}Se-free PP_3Se_4 to A_3B spectra; the ^{77}Se satellites of $P_2P_2Se_4$ constitute two superimposed AA'BB'X spectra, those of PP_3Se_4 superimposed AA'$_2$BX and A_3BX spectra.
[c]Relative to external 2% $OP(OMe)_3$ in $(CD_3)_2CO$ ($\delta_{OP(OMe)_3} = \delta_{H_3PO_4} - 1.72$ ppm); all errors in δ are < 0.1 ppm.
[d]P_A = —PPh_2 or —$P(E)Ph_2$; P_B = >PPh, >P(E)Ph, >P—, or >P(E)—; assignments for P_2P_2 and $P_2P_2E_4$ (E = O, S, or Se) are made by comparison with the spectra of etp and $etpE_3$, respectively (19, 21).
[e]$^6J(P—P)$ = 0 (21).
[f]$^1J(P—Se)$ is known to be negative (22).
[g]The various $^4J(P—^{77}Se)$ could not be determined with confidence due to signal overlap; they are probably small (21).
[h]In liquid SO_2; the compound is poorly soluble in CH_2Cl_2.
[i]A partial ^{31}P nmr spectrum of this compound has been reported previously (19).

is insoluble in SO_2. *Anal.* calcd. for $F_{12}PbSb_2$: Pb 30.49; found (by AA): Pb 30.3 ± 0.2.

The very SO_2-soluble $Pb(AsF_6)_2 \cdot xSO_2$ was prepared similarly, from PbF_2 and an excess of AsF_5 in SO_2. On removal of volatiles *in vacuo*, the product was of variable composition, the strongly held SO_2 of solvation being difficult to remove. Because of this variability, the AsF_6^- salt was not used further in the present work. A typical sample showed Pb (by AA): AsF_6^- (by precipitation as the Ph_4As^+ salt (24)): SO_2 (by difference) = 1:2.04:0.95. The presence of SO_2 in the solid was confirmed by the occurrence of a strong band at 1164 ± 2 cm^{-1} in the infrared spectrum.

Isolation of Tin(II) and Lead(II) Complexes with Polydentate Phosphine Oxides

Partial dissolution of insoluble $Sn(SbF_6)_2$ on $Pb(SbF_6)_2$ occurs on adding an SO_2 solution of a slightly less than equimolar amount of the appropriate ligand to a slurry of the metal salt in SO_2 in an H-shaped filter apparatus of a type described earlier (23). After stirring the mixture for ca. 5 min, filtration and removal of solvent from the filtrate yields the product. This method was used to prepare $Sn(SbF_6)_2(dppeO_2)$ (*Anal.* calcd. for $C_{26}H_{24}F_{12}O_2P_2Sb_2Sn$: C 30.60, H 2.37; found: C 30.30, H 2.27), $Pb(SbF_6)_2(dppeO_2)$ (*Anal.* calcd. for $C_{26}H_{24}F_{12}O_2P_2PbSb_2$: C 28.16, H 2.18, Pb 18.68; found: C 27.96, H 2.31, Pb 19.0), and $Pb(SbF_6)_2(PP_3O_4)$ (*Anal.* calcd. for $C_{42}H_{42}F_{12}O_4P_4PbSb_2$: C 35.67, H 2.99; found: C 36.15, H 3.10). Similarly, 1:1 complexes are formed between $Sn(SbF_6)_2$ and $etpO_3$ or PP_3O_4, and $Pb(SbF_6)_2$ and $etpO_3$; these appear to be solvated. (Elemental analyses (C and H) correspond to $Sn(SbF_6)_2 \cdot etpO_3 \cdot 2SO_2$, $Sn(SbF_6)_2 \cdot PP_3O_4 \cdot 3.5SO_2$, and $Pb(SbF_6)_2 \cdot etpO_3 \cdot SO_2$.)

Preparation of Nuclear Magnetic Resonance Samples

Proton nmr samples were made up in standard 5 mm od nmr tubes using CH_2Cl_2 as internal reference ($\delta_{CH_2Cl_2}(int) = \delta_{TMS}(int) - 4.72$ ppm (25)), and ^{13}C nmr samples similarly. For the latter, the residual solvent ($(CD_3)_2CO$) signal was used as internal reference ($\delta_{((CD_3)_2CO)}(int) = \delta_{TMS}(int) - 29.8$ ppm). Fluorine-19 nmr samples were prepared in medium-walled 5 mm od nmr tubes attached to 9 mm od special walled tubing to facilitate filling and heat sealing (see following); C_6F_6 was added from a vacuum line as internal reference ($\delta_{C_6F_6}(int) = \delta_{CFCl_3}(int) + 164.9$ ppm). Phosphorus-31 nmr samples of ligands alone were prepared in tubes handmade from 10 mm od Pyrex tubing. Ligand–metal salt mixtures were usually made up in similar tubes to which was attached a length of 9 mm od special wall tubing to facilitate sealing under vacuum as described earlier (21); however, samples containing insoluble excess metal salt in SO_2 were prepared in a filter apparatus of a previously described (26) type.

Nuclear Magnetic Resonance Spectra

Ambient probe temperature CW ^1H nmr spectra were measured using either a Varian T-60, or a Varian EM-360 or a Varian XL-100-12 Spectrometer System. The XL-100-12 Spectrometer System was used for all CW ^{19}F and FT ^{31}P spectra. An XL-100-15A Spectrometer System was used to provide ^{13}C-{^1H} spectra.

For spectral analysis of P_2P_2, $P_2P_2O_4$, $P_2P_2S_4$, $P_2P_2Se_4$, PP_3S_4, and PP_3Se_4, the program LOACN3 (27) was used; most probable errors are quoted.

Infrared Spectra

A Perkin-Elmer 621 Infrared Spectrophotometer was used to obtain infrared spectra. Samples were prepared as (dry) Nujol mulls between AgCl plates.

Elemental Analysis

Lead analyses were performed using a Varian Techtron Model 1200 AA Spectrometer. Carbon and hydrogen microanalyses were carried out by either the Analytische Laboratorien, Elbach, W. Germany or Schwarzkopf Microanalytical Laboratory, N.Y.C.

Results and Discussion

Complexes with Polydentate Phosphines

Both $Sn(SbF_6)_2$ and $Pb(SbF_6)_2$ are soluble exothermically in nitromethane. Dppe, etp, tripod, PP_3, and P_2P_2 have moderate to poor solubility in this solvent, but in the presence of an equimolar or

TABLE 2. ^{31}P-{^{1}H} nuclear magnetic resonance spectra of some complexes of tin(II) and lead(II) with chelating phosphines[a]

Complex[b]	δ_P(ppm)[c] and ($\Delta\delta_P$(ppm))[d]		$\lvert^1J(M—P)\rvert$ (Hz)[f]		$\lvert^3J(P_A—P_B)\rvert$[g] (Hz)
	P_A[e]	P_B[e]	P_A[e]	P_B[e]	
$Sn(dppe)^{2+}$	33.1(47.4)		1665		
$Pb(dppe)^{2+}$	102.6(116.9)		1714		
$Sn(etp)^{2+}$	24.9(39.5)	47.7(65.8)	1587	1369[h]	10[i]
$Pb(etp)^{2+}$	66.0(80.6)	90.2(108.3)	1836	1863	6[i,j]
$Sn(tripod)^{2+}$	−11.3(16.0)		1279		
$Pb(tripod)^{2+}$	13.8(41.1)		1786		
$Sn(PP_3)^{2+}$[k]	2.5(17.1)	36.8(55.7)	705	1482	40[l]
$Pb(PP_3)^{2+}$[k]	27.5(42.1)	80.1(99.0)	476[h]	2136	44[l]
$Sn(PP_2(PH))^{3+}$[k]	22.9(37.5)[m]	47.3(66.2)[m]	1574	~1400[o]	$J(P_A—P_B)$ = 11
	7.3(21.9)[m,n]		—		$J(P_{A'}—P_B)$ = 49
$Pb(PP_2(PH))^{3+}$[k]	65.6(80.2)[m]	86.8(105.7)[m]	1841	1772	$J(P_A—P_B)$ = 7
	7.7(22.3)[m,p]				$J(P_{A'}—P_B)$ = 43
$Sn(P_2P_2)^{2+}$[k,q]	0.9(15.5)[r]	27.2(45.3)[r]	[s]	~1380	40[t]
$Pb(P_2P_2)^{2+}$[k,q]	21.4(36.0)[r]	69.6(87.7)[r]	790[h]	1820[h]	37[t]
$Sn(PPP(PH))^{3+}$[k,q]	24.2(38.8)[u]	46.0(64.1)[u]	~1490[o,v]	~1480[o,v]	$J(P_A—P_B)$ = 13
	8.2(22.8)[u,w]	19.5(37.6)[u,x]	—	~1460[o,v]	$J(P_{A'}—P_{B'})$ = 32
					$J(P_B—P_{B'})$ = 17
					$J(P_A—P_{B'})$ = ~30
$Pb(PPP(PH))^{3+}$[k,q]	66.3(80.9)[u]	91.6(109.7)[u]	1717	~2020	$J(P_A—P_B)$ not obsd
	9.0(23.6)[u,w]	52.1(70.2)[u,x]	—	~1380	$J(P_{A'}—P_{B'})$ = 27
					$J(P_B—P_{B'})$ not obsd
					$J(P_A—P_{B'})$ = 38

[a]At 308 K in $MeNO_2$ unless otherwise noted.
[b]For abbreviations used, see footnote 5.
[c]In ppm relative to external 2% $OP(OMe)_3$ in $(CD_3)_2CO$ ($\delta_{OP(OMe)_3} = \delta_{H_3PO_4} - 1.72$ ppm).
[d]In ppm; $\Delta\delta_P = \delta_P$(complex in $MeNO_2$) − δ_P(free ligand in CH_2Cl_2).
[e]P_A = —PPh_2, P_B = >PPh or >P—, unless noted otherwise.
[f]For tin complexes, M = ^{119}Sn, for lead complexes, M = ^{207}Pb, and estimated error = ±2 Hz, except where noted.
[g]Estimated error ±1 Hz.
[h]Estimated error ±5 Hz.
[i]$|^3J(P—P)| = 29 \pm 1$ Hz in free etp.
[j]At 260 K; poorer resolution was obtained at 308 K.
[k]For discussion of these complexes, see text.
[l]$|^3J(P—P)| = 25.9 \pm 0.2$ Hz in free PP_3 (Table 1).
[m]Assignments are those shown in structure **1**.
[n]$P_{A'}$; $|^1J(^{31}P—^1H)| \approx 500$ Hz.
[o]$|^1J(^{117/119}Sn—^{31}P)_{ave}|$.
[p]$P_{A'}$; $|^1J(^{31}P—^1H)| \approx 530$ Hz.
[q]At 260 K; irreversible decomposition occurs on standing at 308 K.
[r]These assignments might be reversed.
[s]Could not be observed with certainty.
[t]Probably $|^3J(P_A—P_B) + {}^6J(P_A—P_{B'})|/2$ (see text).
[u]Assignments are those shown in structure **2**.
[v]The satellites were overlapping complex multiplets.
[w]$P_{A'}$.
[x]$P_{B'}$.

greater than equimolar amount of either metal salt, significant enhancement of solubility occurs.[5] The Sn(or Pb)$(SbF_6)_2$ – polydentate phosphine solutions in $MeNO_2$ are stable indefinitely at or below about 273 K. At 308 K all the solutions except those containing P_2P_2 show little decomposition during the time (a few hours at most) required to collect nmr data, but they gel on standing for longer periods. The spectra of the P_2P_2 solutions indicate extensive decomposition at room temperature.

The ^{31}P nmr spectra of freshly-made solutions containing L/M ≤ 1 (L = dppe, etp, or tripod; M = Sn or Pb) provided unambiguous evidence for the formation of 1:1 complexes; these undergo rapid intermolecular ligand exchange with the soluble part of any excess ligand when L/M > 1. A typical spectrum, that of $Pb(etp)^{2+}$, is shown in Fig. 1(*a*). Details of the ^{31}P nmr spectra of the various complexes are given in Table 2. From the data in this table, the qualitative similarity of the spectral patterns for analogous tin and lead complexes can be seen. Oxidation of Pb(II) to Pb(IV) in the medium used is very unlikely, and thus we surmise that all the complexes contain the central element in the divalent oxidation state. (We note that, in the same medium, or in liquid SO_2, no oxidation of the divalent metals occurs using phosphine oxides as ligands (see below)). The magnitude of the ^{119}Sn–^{31}P and ^{207}Pb–^{31}P coupling constants (1279–1665 Hz and 1714–1863 Hz for the ^{119}Sn and ^{207}Pb satellite splittings, respectively) confirms that direct metal–phosphorus bond formation occurs. For

Can. J. Chem. Downloaded from www.nrcresearchpress.com by 210.87.254.42 on 09/05/12
For personal use only.

Can. J. Chem. Downloaded from www.nrcresearchpress.com by 210.87.254.42 on 09/05/12
For personal use only.

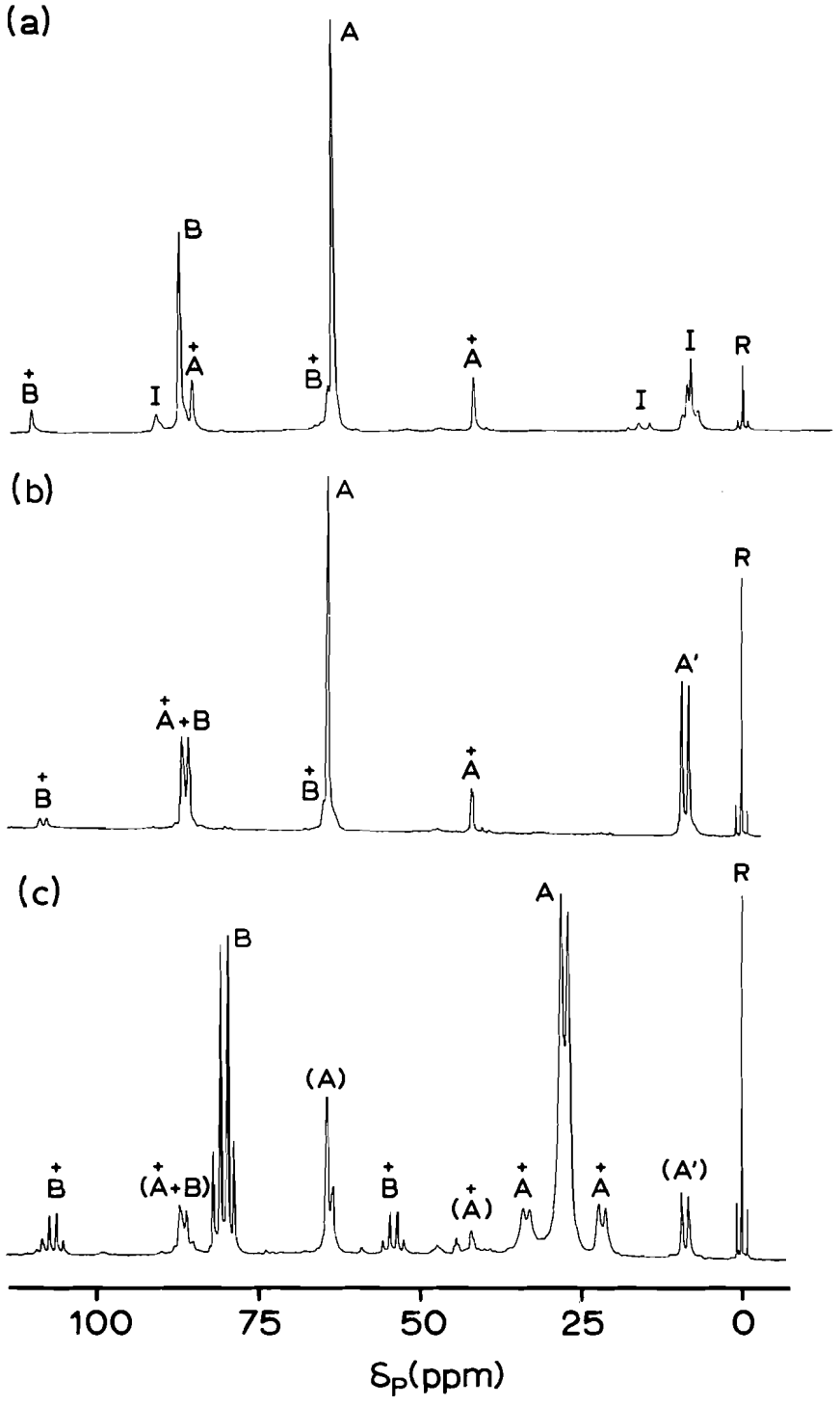

FIG. 1. The 308 K 40.54 MHz $^{31}P-\{^1H\}$ nmr spectrum of an $MeNO_2$ solution containing (*a*) etp/$Pb(SbF_6)_2 \approx 0.78$, showing the spectrum of $Pb(etp)^{2+}$; (*b*) $PP_3/Pb(SbF_6)_2 \approx 0.45$, showing the spectrum of $Pb(PP_2(PH))^{3+}$; (*c*) $PP_3/Pb(SbF_6)_2 \approx 0.75$, showing, the spectrum of $Pb(PP_3)^{2+}$ and superimposed (parenthesized assignments) $Pb(PP_2(PH))^{3+}$. R = reference signal; I = spectrum(a) of unidentified minor product(s); + = ^{207}Pb satellites; assignments are those used in the text.

Can. J. Chem. Downloaded from www.nrcresearchpress.com by 210.87.254.42 on 09/05/12
For personal use only.

comparison, $|^1J(^{119}Sn—^{31}P)|$ is 2280, 2383, and 2256 Hz when R_3 is Bu^n_3, Et_3, and Et_2Ph, respectively, in *trans*-$SnCl_4(PR_3)_2$ (4, 5, 28), and 1560 Hz in $(OC)_5WSnCl_2(PBu^t_3)$ (which could be regarded as a tin(II) complex) (15), while two-bond $^{117/119}Sn—^{31}P$ and $^{207}Pb—^{31}P$ couplings are an order of magnitude smaller than observed in the phosphine complexes, as discussed below. The comparatively small ranges observed for the metal–phosphorous couplings are evidence that dppe, etp, and tripod each achieve their maximum denticities in the 1:1 complexes, probably in complexes of similar stereochemistry. The coordination geometry cannot be deduced from our results, but in the etp and tripod complexes, at least, is most probably pseudotetrahedral with a pyramidal MP_3 kernel and a stereochemically-active lone pair of electrons. In the dppe complexes, a coordination number exceeding two may be achieved by solvent/counterion coordination.

The order of complexation shifts, i.e., Pb > Sn, is consistent with that observed for monophosphine complexes of tin(II) and germanium(II) halides (12, 13), i.e., Sn > Ge. For a constant metal ion, the complexation shifts of phosphorus atoms involved in five-membered chelate rings (in the dppe and etp complexes) are significantly larger than the shift found for the phosphorus atoms of $M(tripod)^{2+}$, which are involved in six-membered chelate ring formation. The unusually large (and cumulative) ^{31}P nmr deshielding associated with five-membered chelate ring formation has been extensively documented, for example, in refs. 29 and 30.

Two different complexes involving PP_3 were identified for both tin and lead. For both elements, the ^{31}P nmr spectrum found when $PP_3/M \lesssim 0.5$ had three regions of resonance, as exemplified by the spectrum of the lead complex given in Fig. 1(*b*). As can be seen by a comparison of Fig. 1 (*a*) and (*b*), the most deshielded resonance, a doublet of triplets, intensity 1, had both chemical shift and metal satellite splitting very close to those of P_B of the corresponding etp complex. Similarly, a doublet, intensity 2, had chemical shift and satellite splitting resembling those of P_A of the etp analogue. The third, most shielded, resonance, intensity 1, was satellite-free; in the $^{31}P-\{^1H\}$ nmr spectrum it was a doublet from three-bond P—P coupling, but showed an additional doublet splitting of ca. 500 Hz in the coupled spectrum. This large coupling is good proof of the occurrence of a protonated phosphine (31). We interpret this spectrum in terms of the formation, in the metal-rich mixtures, of the complex $M(PP_2(PH))^{3+}$, with the ligand bound as shown schematically in **1** (in which a pyramidal $M(P_A)_2P_B$ kernel is likely (see above)).

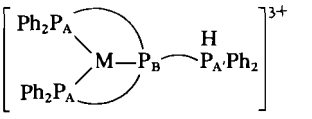

1

Details of the spectra of the $M(PP_2(PH))^{3+}$ complexes are given in Table 2.

To our surprise, the solvent $MeNO_2$ is not the source of the proton used in formation of $M(PP_2(PH))^{3+}$: the proton-coupled ^{31}P nmr spectra are unchanged on switching from CH_3NO_2 to CD_3NO_2 as solvent.[8] We were unable to identify the active protonic acid unambiguously, though it clearly involves the metal salts. However, reproducible results for $M(PP_2(PH))^{3+}$ and other protonated species (see below) were obtained using various batches of metal salts, ligands, and solvent.[8]

In the range $1 \gtrsim PP_3/M > 0.5$, tin and lead both form a second, 1:1, complex, which, at L/M > 1, exchanges with excess ligand. In each case this second complex gives a ^{31}P nmr spectrum consisting of a doublet, intensity 3, coupled to a quartet, intensity 1, both resonances having metal satellites. The spectrum of the lead complex is given in Fig. 1(*c*), and the spectral parameters of the two $M(PP_3)^{2+}$ complexes are included in Table 2. The most obvious interpretation of the doublet–quartet spectrum is in terms of a complex having the MP_4 kernel, with the ligand behaving in a tetradentate manner. The one-bond $M–P_A$ coupling appears anomalously small compared with the one-bond couplings found in the analogous dppe, etp, tripod, and $PP_2(PH)^+$ complexes, but the effect of an increase in coordination number is difficult to assess. A second possible interpretation is in terms of a complex in which PP_3 is tridentate and intramolecular P_A(bound)–P_A(free) exchange occurs rapidly:

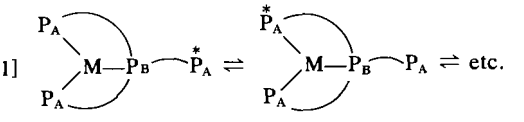

[8]We thank a referee for suggesting the experiments with CD_3NO_2 as solvent. The acidic proton cannot come from coordinated $CD_xH_{3-x}NO_2$, resulting from proton exchange between CD_3NO_2 and adventitious trace amounts of water: even after several days at RT no proton exchange is evident by ^1H nmr in $M(SbF_6)_2/CD_3NO_2/H_2O$ ($\approx$2/23/1) solutions. Also, no water could be detected by ^1H nmr in the dry CD_3NO_2 itself; the amount present is certainly less than required for the protonation observed. However, the coordinated water in the $M(SbF_6)_2/CD_3NO_2/H_2O$ solutions *is* clearly acidic: addition of the salt causes proton deshielding by ~6.4 and ~3.7 ppm for the tin- and lead-containing samples respectively.

Can. J. Chem. Downloaded from www.nrcresearchpress.com by 210.87.254.42 on 09/05/12
For personal use only.

(It should be noted that the "normal" chemical shift of P_B and value of $|^1J(M—^{31}P_B)|$ suggest that P_B is always bound.) In $Pb(PP_3)^{2+}$, at least, the broadness of the signal from P_A, compared with that for P_B (ca. 20 Hz vs. $\leq$5 Hz) (see Fig. 1(*c*)) suggests the presence of an exchange process, but the limited liquid range of $MeNO_2$ precluded further study.

Our spectra of $M(PP_2(PH))^{3+}$ and $M(etp)^{2+}$ (Table 2 and Fig. 1 (*a*) and (*b*)) show that the chemical shifts and satellite splittings of the bound phosphorus atoms are quite insensitive to the substituent on P_B (and vice versa), and Meek and co-workers, in very recent work on tridentate PP_3 and etp (*inter alia*) complexes of rhodium(I), have demonstrated similar insensitivities in that case also (9). Therefore the averaging process shown in ref. 2 should give parameters for P_B very similar to those in $M(etp)^{2+}$, while δ_{P_A} and $|^1J(M—^{31}P_A)|$ should be given by $((2/3)\delta_{P_A(M(etp))^{2+}} + (1/3)\delta_{P_A(PP_3(free))})$ (i.e. 11.7 ppm for Sn, 39.2 ppm for Pb), and $(2/3)|^1J(M—P_{A(M(etp))^{2+}}|$ (i.e. 853 Hz for Sn, 1191 Hz for Pb). In addition, $|^3J(P_A—P_B)|$ in $M(PP_3)$ should be given by $((2/3)|^3J(P_A—P_B)|_{M(etp)^{2+}} + (1/3) \times |^3J(P_A—P_B)|_{PP_3})$ (i.e. $\gtrsim$ 15 Hz for Sn, $\gtrsim$ 13 Hz for Pb). The correlation between calculated and found values is sufficiently poor as to disfavour a complex involving tridentate PP_3, in favour of one having the ligand tetradentate. However, it is possible that in solution there exists more than one species involved in rapid intramolecular exchange. Much more work will be necessary to resolve the structural ambiguity presented by $M(PP_3)^{2+}$.

The behaviour of the systems P_2P_2–$M(SbF_6)_2$–$MeNO_2$ (M = Sn or Pb) resembles that of the PP_3-containing systems in that, depending on the L/M ratio, one or the other or both of two complexes can be formed for each metal. In general, the P_2P_2 systems were more difficult to study because formation of side products is more extensive than in the PP_3-containing systems. When $P_2P_2/M \lesssim 0.5$, the major species formed for each element shows in the $^{31}P-\{^1H\}$ nmr spectrum four regions of resonance, all equally intense. The three less shielded resonances exhibit metal satellites, while the fourth signal is in the same region as $P_{A'}$ of **1**. Thus by comparison with the data for $M(etp)^{2+}$ and $M(PP_2(PH))^{3+}$, the species formed in these metal-rich mixtures is readily identified from its spectrum as $M(PPP(PH))^{3+}$, with the ligand bound as shown schematically in **2** which contains a tri-coordinate, probably pseudotetrahedrally coordinated ion. The spectral parameters for the two $M(PPP(PH))^{3+}$ complexes are listed in Table 2. Particularly noteworthy in both cases is the comparatively large

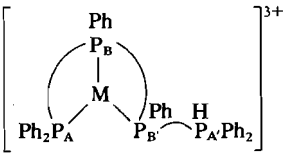

2

coupling between P_A and $P_{B'}$, which are separated by six bonds on the ligand backbone: this coupling must be transmitted largely via the metal. The difference in the chemical shifts of P_B and $P_{B'}$ in the spectra of the $M(PPP(PH))^{3+}$ complexes is a manifestation of the cumulative nature of the ^{31}P nmr five-membered chelate effect mentioned above: P_B, with the larger complexation shift, is involved in two chelate rings, while $P_{B'}$, with the smaller, is involved in only one.

In the region $0.5 < L/M \lesssim 1$, a second major species occurs, which, when $L/M > 1$, exchanges with excess ligand. The second species is evidently of 1:1 stoichiometry: for both tin and lead it is characterized in the ^{31}P nmr spectrum by two equally intense resonances, both "triplets". ^{207}Pb satellites are evident about both resonances in the spectrum of the lead complex but the $^{117/119}Sn$ satellites of P_A in the tin complex were obscured by the spectra of various side products. The 1:1 complex appears to be $M(P_2P_2)^{2+}$ in which the ligand has C_2 symmetry at least on a time average: the triplets then constitute a deceptively simple AA'XX' spectrum. Ambiguities arise about the structure of $M(P_2P_2)^{2+}$, as they did for $M(PP_3)^{2+}$. Compared with the data for metal-bound phosphorus in the analogous dppe, etp, $PP_2(PH)^+$, and $PPP(PH)^+$ complexes, $|^1J(M—P_B)|$ and $\delta_{P_B}(\Delta\delta_{P_B})$ fall in the "normal" range for both tin and lead. However, in $Pb(P_2P_2)^{2+}$, $|^1J(^{207}Pb—^{31}P_A)|$ appears anomalously small, and $\delta_{P_A}(\Delta\delta_{P_A})$ are subnormal for both the tin and the lead complex.

As in the case of $M(PP_3)^{2+}$ (see above), basically two interpretations of the spectra of $M(P_2P_2)^{2+}$ are possible: either the ligand could be behaving in a tetradentate manner or rapid free-bound intramolecular exchange could be occurring in a complex involving tridentate P_2P_2, as in [2]:

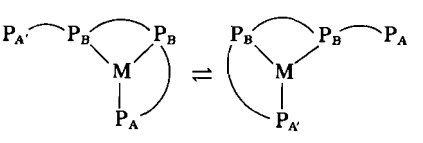

3a ***3b***

By comparison with the data for $M(PPP(PH))^{3+}$, and using our previous logic, the exchange process [2] should give rise to $\delta_{P_B} = (\delta_{P_B(M(PPP(PH))^{3+})} + \delta_{P_{B'}(M(PPP)PH))^{3+}})/2$ (i.e. 27.3 ppm for Sn, 71.9 ppm

Can. J. Chem. Downloaded from www.nrcresearchpress.com by 210.87.254.42 on 09/05/12
For personal use only.

for Pb), $|^1J(M—P_B)| = |^1J(M—P_B)_{(M(PPP(PH))^{3+})} + {}^1J(M—P_{B'})_{(M(PPP)PH))^{3+}}|/2$ (i.e. ~ 1470 Hz for Sn, ~ 1700 Hz for Pb), $\delta_{P_A} = (\delta_{P_A(M(PPP(PH))^{3+})} + \delta_{P_A(P_2P_2)})/2$ (i.e. 4.8 ppm for Sn, 25.9 ppm for Pb), and $^1J(M—P_A) = (^1J(M—P_A)_{(M(PPP(PH))^{3+})}/2$ (i.e. ~ 750 Hz for Sn, ~ 860 Hz for Pb). The expected results of averaging the chemical shifts and one-bond M–P coupling constants via [3] are in semi-quantitative agreement with those observed, and for that reason we hold a slight preference for structure **3** for the complexes $M(P_2P_2)^{2+}$. However, the values of the apparent P–P coupling are larger than can reasonably be explained, even though estimation is difficult because of a lack of information on the signs of the various couplings, and it must be emphasized that we have not ruled out with any certainty the occurrence of an MP_4 kernel.

Attempts to Prepare Complexes with Monodentate Phosphorus-donor Ligands

We were unable to obtain unambiguous evidence for the formation of a direct tin(or lead)–phosphorus bond with any monodentate phosphorus-donor ligand studied.

In acetone, $MeNO_2$, or $PhNO_2$ solutions of tmp–$M(SbF_6)_2$ at ambient probe temperature, a rearrangement of the tmp to dmmp occurs;[9] this is an example of the well-known Arbusov rearrangement which requires a cationic catalyst (32). In $MeNO_2$ solutions of $M(SbF_6)_2$ with PPh_3, the major product species was $HPPh_3^+$, identified by comparison of its ^1H-coupled and -decoupled ^{31}P nmr spectra with those reported in the literature (31).

In an attempt to reduce protonation arising in $MeNO_2$ as solvent (see above), PPh_3–$M(SbF_6)_2$ mixtures were investigated further using acetone as a solvent.[10] No evidence for any coordination of PPh_3 was found in acetone solutions containing $Pb(SbF_6)_2$. However, ^{31}P and ^{13}C nmr showed that in acetone $Sn(SbF_6)_2$ forms a 1:1 complex with PPh_3, which, at ca. 233 K or below, does not exchange with excess ligand.[11] In the ^{31}P nmr spectrum, δ_P and $\Delta\delta_P$ are 26.1 and 32.3 ppm, respectively, while in the ^{13}C spectrum the chemical shifts of the 1-, 2-, 3-, and 4-aryl carbons are 117.5, 135.2, 130.6, 135.4 ppm, respectively, the corresponding complexation shifts, $\Delta\delta_C(=\delta_{C,bound} - \delta_{C,free})$, being −19.5, 1.4, 1.5, and 6.0 ppm. In addition, the ^{13}C spectrum shows that changes in the various ^{31}P—^{13}C couplings are associated with complexation: $^1J(P—C)$, $^2J(P—C)$, $^3J(P—C)$, and $^4J(P—C)$ are 11, 19, 7, and ~0 Hz in the free ligand, but 78, ~9, 12, and ~0 Hz in the complexed ligand. Qualitatively, the changes in the ^{31}P and ^{13}C spectra of PPh_3 are those expected for coordination via the phosphorus atom, but no $^{117/119}Sn$ satellites were observed in the slow-exchange ^{31}P nmr spectrum, whereas $^1J(^{117/119}Sn—^{31}P)$ should be ca. 1500 Hz (see Table 2) for formation of a direct Sn—P bond. For this reason we suggest that the 1:1 complex is not $[Sn—PPh_3]^{2+}$, but is the solvent-inserted species

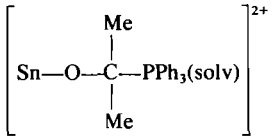

The ^{31}P and ^{13}C nmr parameters of the coordinated PPh_3 are close to those of, for instance, $MePPh_3^+$ (33),[12] and nucleophilic attack of phosphorus donors at carbonyl carbons is a well-established reaction (e.g. refs. 35–37).[13] We are presently extending our studies of acetone-inserted metal phosphine complexes.

Complexes of Phosphine Oxides

Both nitromethane and SO_2 were investigated as solvents for the tin(II) and lead(II) complexes of the phosphine oxides $OPPh_3$, $dppeO_2$, $etpO_3$, PP_3O_4, and $P_2P_2O_4$. $Sn(SbF_6)_2$ and $Pb(SbF_6)_2$ are soluble in nitromethane as noted earlier, but are insoluble in SO_2. However, the addition of an appropriate amount (see below) of phosphine oxide causes dissolution in SO_2, and over their common temperature range essentially identical nmr spectra are obtained using either solvent. As the phosphine oxide complexes are more labile than the analogous phosphine complexes (see above), SO_2, with its lower freezing point, was the better solvent for our study. Earlier, SO_2 has been used as a solvent for complexes of Cd(II) and Hg(II) with several polyphosphine oxides (18).

Addition of ca. 1.5 mol of $OPPh_3$ per mol of metal salt causes the complete dissolution of $Sn(SbF_6)_2$ or

[9]Separate experiments confirmed that the final metal-containing product is $M(dmmp)_3^{2+}$, and that no tmpO is formed. Detailed study of the tin(II) systems showed that δ_P and $\Delta\delta_P$ are 38.0 and 6.5, and −5.4 and −5.7 ppm, for $Sn(dmmp)_3^{2+}$ and $Sn(tmpO)_3^{2+}$, respectively, in $PhNO_2$ at 308 K.

[10]In acetone at 233 K, dppe forms at 1:1 complex with Sn^{2+} having δ_P and $\Delta\delta_P$ = 28.0 and 41.5 ppm respectively, and $|^1J(^{119}Sn—^{31}P)| = 1810$ Hz.

[11]^{19}F nmr of $Sn(SbF_6)_2$—$P(p\text{-}C_6H_4F)_3$ in acetone produces similar results. At 253 K, the *p*-fluorine of the complex is shielded by 10.4 ppm, from a shift of −113.9 (from $CFCl_3$) for the free ligand, and concurrently $^5J(^{31}P—^{19}F)$ is reduced in magnitude, from 4.5 Hz in the free ligand to $\lesssim 1$ Hz in the complex.

[12]Note, however, that direct coordination to some metals produces similar results; see, e.g., ref. 34.

[13]Other σ-donors attack coordinated carbonyl groups also. See, e.g., refs. 38 and 39.

Can. J. Chem. Downloaded from www.nrcresearchpress.com by 210.87.254.42 on 09/05/12
For personal use only.

TABLE 3. ^{31}P-{^{1}H} nuclear magnetic resonance spectra of complexes of tin(II) and lead(II) with triphenyl phosphine and some polyphosphine oxides[a]

Complex[b]	δ_P(ppm)[c] and ($\Delta\delta_P$(ppm))[d]		$\lvert^2J$(M—O—P)$\rvert$[f]		
	P_A[e]	P_B[e]	P_A[e]	P_B[e]	$\lvert^3J$(P—P)$\rvert$[g]
$Sn(OPPh_3)_2^{2+}$	44.8(12.3)		229[g,h]		
$Sn(OPPh_3)_3^{2+}$	44.1(11.6)		201[g,h]		
$Pb(OPPh_3)_2^{2+}$(?)	42.4(9.9)		[i]		
$Pb(OPPh_3)_3^{2+}$	41.5(9.0)		45[g]		
$Sn(dppeO_2)^{2+}$	52.1(15.2)		158		
$Pb(dppeO_2)^{2+}$	50.1(13.2)		[i]		
$Sn(etpO_3)^{2+}$	50.7(13.5)	61.8(15.4)	152	91	3[j]
$Pb(etpO_3)^{2+}$	49.4[k](12.2)	58.5[k](12.1)	[i]	[i]	20[j,l]
$Sn(PP_3O_4)^{2+}$[m]	50.5[n](14.2)	71.0(16.1)	144[n]	85	60[o,p], 2[p,q]
	58.5[r](22.2)				
$Pb(PP_3O_4^{2+})$	44.6(8.3)	63.0(8.1)	[i]	[i]	30[p]

[a]At 209 K in SO_2.
[b]For abbreviations used, see footnote 5.
[c]In ppm for external 2% $OP(OMe)_3$ in $(CD_3)_2CO$; $\delta_{OP(OMe)_3} = \delta_{H_3PO_4} - 1.72$ ppm.
[d]$\Delta\delta_P = \delta_P$(complex) $- \delta_P$(free ligand).
[e]P_A = —P(O)Ph_2; P_B = >P(O)Ph or >P(O)—.
[f]M = $^{117/119}$Sn(ave) for tin complexes, ^{207}Pb for lead complexes, except where noted; estimated error ± 2 Hz except where noted.
[g]Estimated error ± 1 Hz.
[h]$\lvert^2J(^{119}Sn—O—P)\rvert$.
[i]Not observed.
[j]$\lvert^3J$(P—P)$\rvert$ = 54 Hz for free ligand in SO_2 at 209 K.
[k]Broad signal.
[l]At 308 K; estimated from exchange averaged signal of a solution with excess ligand; probably of opposite sign to free ligand.
[m]See text for discussion of this species; assignments are those of structure 4.
[n]P_A of structure 4.
[o]$\lvert^3J(P_B—P_{A'})\rvert$; assignments are given in structure 4.
[p]^3J(P—P) = 54 Hz for free ligand in SO_2 at 209 K.
[q]$\lvert^3J(P_B—P_A)\rvert$; assignments are given in structure 4.
[r]$P_{A'}$ of structure 4.

$Pb(SbF_6)_2$ in SO_2. In the reduced temperature ^{31}P nmr spectra, evidence was found for the 1:3 and 1:2 complexes, $M(OPPh_3)_3^{2+}$ and $M(OPPh_3)_2^{2+}$, as the major species when L/M = 3 and 2, respectively. The ^{31}P nmr spectral parameters of these complexes are given in Table 3. When $2 < L/M < 3$, the 1:3 and 1:2 complexes coexist, while the 1:2 species persists as the major species when $1.5 \lesssim L/M < 2$. We were unable to identify the other species formed in the salt-rich solutions. ^{19}F nmr provided evidence for 1:3 and 1:2 complexes in the system $Sn(SbF_6)_2$–$OP(p\text{-}C_6H_4F)_3$–SO_2 also. At 233 K, the ^{19}F chemical shifts of the 1:3 and 1:2 complexes are −100.6 and −101.3 ppm, respectively (from $CFCl_3$), deshielded by 4.5 and 3.8 ppm, respectively, from the free ligand resonance. $^5J(^{31}P—^{19}F)$ is not affected significantly by the complexation.

In both $OPPh_3$–Sn(II) and $OP(p\text{-}C_6H_4F)_3$–Sn(II) mixtures, exchange is rapid at ambient probe temperature for all L/M ratios, and at reduced temperatures for L/M > 3. In the latter instance, the spectrum obtained is a weighted average of the free ligand and SnL_3^{2+} spectra. Three is clearly the highest number of the monodentate phosphine oxides which can be stably bound in these systems, and the rapid intermolecular exchange which occurs only in the presence of excess ligand shows that the 1:3 complexes undergo ligand exchange by an associative process, which seems reasonable as coordination numbers above the very common three are well-established for tin(II) (2, 3, 40).

The ^{207}Pb satellites of $Pb(OPPh_3)_3^{2+}$ are observed only when $OPPh_3$/Pb is very close to 3, and we were unable to observe the ^{207}Pb satellites of $Pb(OPPh_3)_2^{2+}$ in any solution studied. When $OPPh_3$/Pb > 3, $Pb(OPPh_3)_3^{2+}$ exchanges slowly: no ^{207}Pb satellites are observed, but the chemical shift is unchanged. The species with which this exchange occurs is not simply excess $OPPh_3$: the position of the second line observed moves towards that of free $OPPh_3$ as $OPPh_3$/Pb is increased. Apparently higher than 3 coordination of lead(II) by $OPPh_3$ is possible, but we were unable to identify the complex(es) involved.

The chelating polyphosphine oxides $dppeO_2$, $etpO_3$, and PP_3O_4 all cause dissolution of $Sn(SbF_6)_2$ or $Pb(SbF_6)_2$ in SO_2 when present in equimolar amounts or greater. The 1:1 complexes can be isolated from the supernatant liquor of mixtures where L/M < 1 (see Experimental Section). The 1:1 complexes of tin(II) are further characterized by slow-exchange ^{13}P nmr spectra which are obtained at reduced temperature. Details of the spectra of $Sn(dppeO_2)^{2+}$, $Sn(etpO_3)^{2+}$, and $Sn(PP_3O_4)^{2+}$ are

Can. J. Chem. Downloaded from www.nrcresearchpress.com by 210.87.254.42 on 09/05/12
For personal use only.

given in Table 3. The observation of $^{117/119}$Sn satellites at the bound phosphoryl groups is good evidence that intermolecular exchange is slow at 209 K. On warming these solutions from 209 K, gradual collapse of the satellites occurs until at ca. 273 K an exchange-averaged spectrum is observed. Also, exchange-averaged spectra are observed at all temperatures when L/Sn > 1.

The spectrum of $Sn(PP_3O_4)^{2+}$ deserves further comment. At 209 K it consists of three regions of resonance with $\delta_{OP(OMe)_3}$ = 50.5, 58.5, and 71.0 ppm, and relative intensities 2, 1, and 1. The upper and lower resonances have complexation shifts close to those of $Sn(etpO_3)^{2+}$ (see Table 3) and only these two resonances have $^{117/119}$Sn satellites and thus have their origin in bound phosphoryl groups. The three-bond P–P coupling between the bound phosphoryl groups is small, as it is in $Sn(etpO_3)^{2+}$, but the unbound P=O group shows a large coupling to the least shielded resonance. The spectrum of $Sn(PP_3O_4)^{2+}$ is in accord with the ligand being bound as shown schematically in **4**, in which the potentially tetradentate PP_3O_4 behaves in a tridentate manner, though the sizeable downfield "coordination" shift of the free phosphoryl phosphorus, $P_{A'}$, seems odd. The SnO_3 kernel in **4** is probably pyramidal (see below). Consis-

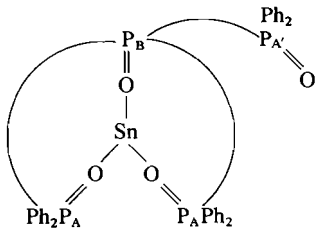

4

tent with intermolecular exchange (or a combination of inter- and intra-molecular exchange) involving **4**, two lines from the least shielded, broad "doublet" resonance of P_B (the small $^3J(P_A—P_B)$ is not resolved for either P_A or P_B at 209 K) remain sharp as the temperature is raised, while the two more shielded resonances, from P_A and $P_{A'}$, collapse together. From the two sharp lines of the P_B resonance the magnitude of $^3J(P_A—P_B)$ and relative signs of $^3J(P_A—P_B)$ and $^3J(P_{A'}—P_B)$ can be established.

The tridenticity of PP_3O_4 in $Sn(PP_3O_4)^{2+}$ again suggests that a maximum of three phosphoryl groups can be accommodated about tin under the conditions used in our experiments. Our results provide no evidence for the coordination geometry around the tin, but, as suggested for the chelating phosphines (see earlier), a pseudotetrahedral stereochemistry seems probable.

The 1:1 complexes of lead(II) with $dppeO_2$, $etpO_3$, and PP_3O_4 apparently are more labile than either their tin(II) analogues or $Pb(OPPh_3)_3^{2+}$: in their ^{31}P nmr spectra no ^{207}Pb satellites were observed even at reduced temperature in the absence of excess ligand. Though $|^2J(^{207}Pb—^{31}P)| < |^2J(^{117/119}Sn—^{31}P)|$ in $M(OPPh_3)_3^{2+}$ (see Table 3), it seems unlikely that the ^{207}Pb satellite splitting is too small to observe in all three polyphosphine oxide complexes of lead; thus we conclude that intermolecular exchange of ligand between lead centres is rapid. The complexation shifts of the lead complexes are similar to, though a little smaller than, those of their tin analogues with which they are probably isostructural.

$Sn(SbF_6)_2$ and $Pb(SbF_6)_2$ are soluble in SO_2 solutions containing $P_2P_2O_4$, when $P_2P_2O_4/M \gtrsim 0.33$, and it seems likely therefore that $P_2P_2O_4$ behaves as a bridging ligand, at least in metal-rich mixtures. At low temperatures the ^{31}P nmr spectra of the system $Pb(SbF_6)_2$–$P_2P_2O_4$ generally gave broad lines, while the system $Sn(SbF_6)_2$–$P_2P_2O_4$ either gave similar results, or gave complicated spectra which we were unable to analyze. As a result of these problems, no structural information is available on the $P_2P_2O_4$ complexes. However, from the sharp, exchange-averaged spectra observed at 308 K, it is evident that complexation is associated with a large decrease in $|^1J(P_A—P_B) + {}^3J(P_A—P_{B'})|$, from 56 Hz in free $P_2P_2O_4$ (Table 1) to ~6 Hz in the Sn(II) system and ~9 Hz in the Pb(II) system at L/M = 1.

Phosphorus–Phosphorus Coupling in Complexes of Polydentate Phosphines and Phosphine Oxides

There is ample evidence to show that coupling between adjacent phosphorus atoms changes in magnitude on formation of a chelate ring about a transition element, e.g. refs. 6–9, and a change of sign may occur also (6, 7). For the formation of a five-membered chelate ring with a hydrocarbon backbone, a reduction in magnitude is found (e.g. refs. 6, 8, 9) and a change in sign is thought to occur (6). Grim and co-workers (6, 7) have suggested that the through-ligand contribution to J(P—P) is unchanged on coordination (implying minimal conformation dependence (6)), but that chelate ring formation introduces a new coupling mechanism, through the metal, which is of opposite sign to the coupling through the ligand backbone. Our results for Sn(II) and Pb(II) complexes of etp, $PP_2(PH)^+$, and $PPP(PH)^+$ (see Table 2) show that "$^3J(P_A—P_B)$" (and, for the $PPP(PH)^+$ complexes,

Can. J. Chem. Downloaded from www.nrcresearchpress.com by 210.87.254.42 on 09/05/12
For personal use only.

"$^3J(P_B—P_{B'})$") is greatly reduced in magnitude on coordination, suggesting that the trends outlined hold for these two Main Group elements also. Further, as described above, our analysis of the spectra of the two M(PPP(PH))$^{3+}$ complexes shows the existence of a sizeable through-metal coupling from P_A to $P_{B'}$, in concert with the suggestion of Grim *et al.* (6, 7). It is disconcerting, therefore, to find that the coupling between adjacent phosphorus atoms of polyphosphine oxides is reduced markedly on chelate ring formation also (Table 3 and ref. 18). These results suggest either that the four-bond P—O—M—O—P coupling is significant, which would be surprising, or that there is a conformation dependence for the through-ligand coupling in chelate rings formed by polyphosphine oxides, when none exists, apparently, for rings formed by the corresponding polyphosphines. Both these possibilities are currently under investigation.

One-bond Metal–Phosphine Coupling Constants in Tin(II)), Tin(IV), and Lead(II) Phosphine Complexes

$|^1J(^{119}Sn—^{31}P)|$ in the tin(II) phosphine complexes ranges in magnitude from 705–1665 Hz (Table 2), outside the observed range (2256–2383 Hz) of $|^1J(^{119}Sn—^{31}P)|$ in the relatively few tin(IV) phosphine complexes which have been studied by ^{31}P nmr to date (4, 5). This difference may be of some diagnostic value. For example the combined data suggest that $(OC)_5WSnCl_2(PBu^t_3)$, for which $|^1J(^{119}Sn—^{31}P)|$ is 1560 Hz (15), is best regarded as a tin(II) complex. It should be noted though, that values of $|^1J(^{119}Sn—^{31}P)| \gtrsim 50$ Hz are known;[14] in all cases where the sign has been determined $^1J(^{119}Sn—^{31}P)$ is absolutely positive (42). It has been suggested (28) that the Sn(IV)—P bond in *trans*-$SnCl_4(PR_3)_2$ contains extensive tin 5*s* character. If this is true for the Sn(II)—P bond also, then the smaller magnitude of $|^1J(^{119}Sn—^{31}P)|$ in the tin(II) complexes may reflect mainly the expected reduction in $\Psi_{5s}^2(O)$ on changing from Sn(IV) to Sn(II).

The close similarity between the variation in $|^1J(^{119}Sn—^{31}P)|$ and $|^1J(^{207}Pb—^{31}P)|$ over a range of analogous complexes has been mentioned above. The magnetogyric ratios of ^{207}Pb and $^{117/119}Sn$ are of opposite sign, so it appears that $^1J(^{207}Pb—^{31}P)$ and $^1J(^{117/119}Sn—^{31}P)$ must be also. (The reduced coupling constants, $K_{M—P}$, will be of the same sign.) In general, the one-bond M—P couplings are larger in magnitude for ^{207}Pb than for ^{119}Sn, e.g. for the first three lead(II) complexes in Table 2, $|^1J(^{207}Pb—^{31}P)|_{ave} = 1800$ Hz, while for the tin(II) analogues $|^1J(^{119}Sn—^{31}P)|_{ave} = 1475$ Hz. Using these average values, $(K_{Pb—P}/K_{Sn—P})^{1/2} = 1.78$, reasonably close to Z_{Pb}/Z_{Sn} (= 1.64). Thus, using the arguments of Reeves and Wells (43), it appears that differences in $\Psi_{nx}^2(O)$ between tin(II) and lead(II) in the basically isostructural complexes are responsible for the different values of $K_{M—P}$.

[14]Reference 41 gives an up-to-date tabulation.

Acknowledgements

We wish to thank Kim Cornell, who examined tin(II) complexes of tmp, dmmp, and tmpO as part of her Honours research project, and the Natural Sciences and Engineering Research Council of Canada who provided financial support.

1. W. Levason and C. A. McAuliffe. Coord. Chem. Rev. **19**, 180 (1976).
2. P. G. Harrison. Coord. Chem. Rev. **20**, 1 (1976).
3. J. A. Zubieta and J. J. Zuckerman. Prog. Inorg. Chem. **24**, 251 (1978).
4. J. F. Malone and B. E. Mann. Inorg. Nucl. Chem. Lett. **8**, 819 (1972).
5. A. Yamasaki and E. Fluck. Z. Anorg. Allg. Chem. **396**, 297 (1973).
6. S. O. Grim, R. Barth, J. Mitchell, and J. DelGaudio. Inorg. Chem. **16**, 1776 (1977).
7. S. O. Grim, W. Briggs, R. Barth, C. A. Tolman, and J. P. Jesson. Inorg. Chem. **13**, 1095 (1974).
8. K. D. Tau, R. Uriarte, T. J. Mazanec, and D. W. Meek. J. Am. Chem. Soc. **101**, 6614 (1979).
9. T. J. Mazanec, K. D. Tau, and D. W. Meek. Inorg. Chem. **19**, 85 (1980).
10. V. Gutmann and E. Wychera. Inorg. Nucl. Chem. Lett. **2**, 257 (1966); V. Gutmann. Coordination chemistry in non-aqueous solvents. Springer Verlag, Vienna. 1968. Chapt. 2.
11. C. E. Wymore and J. C. Bailar. J. Inorg. Nucl. Chem. **14**, 42 (1960).
12. W-W. duMont, B. Neudert, G. Rudolph, and H. Schumann. Angew. Chem. Int. Edn. Engl. **15**, 308 (1976).
13. W-W. duMont and B. Neudert. Z. Anorg. Allg. Chem. **441**, 86 (1978).
14. B. L. Papke and J. T. Yoke. J. Inorg. Nucl. Chem. **41**, 461 (1979).
15. W-W. duMont. J. Organomet. Chem. **153**, C11 (1978).
16. I. S. Butler and N. J. Coville. J. Organomet. Chem. **66**, 111 (1974).
17. W. Hewertson and H. R. Watson. J. Chem. Soc. 1490 (1962).
18. P. A. W. Dean and M. K. Hughes. Can. J. Chem. **58**, 180 (1980).
19. R. B. King and P. R. Heckley. Phosphorus, **3**, 209 (1974).
20. K. Moedritzer. Thermochim. Acta, **16**, 173 (1976).
21. P. A. W. Dean. Can. J. Chem. **57**, 754 (1979).
22. W. McFarlane and D. S. Rycroft. J. Chem. Soc. Dalton, 2162 (1973).
23. T. Birchall, P. A. W. Dean, and R. J. Gillespie. J. Chem. Soc. A, 1777 (1971).
24. H. M. Dess, R. W. Parry, and G. L. Vidale. J. Am. Chem. Soc. **78**, 5734 (1956).
25. G. P. Nilles and R. D. Schuetz. J. Chem. Educ. **50**, 267 (1973).
26. P. A. W. Dean. Can. J. Chem. **51**, 4024 (1973).

27. A. A. BOTHNER-BY and S. M. CASTELLANO. LAOCN3. The Mellon Institute, Pittsburg.
28. G. G. MATHER, G. M. MCLAUGHLIN, and A. PIDCOCK. J. Chem. Soc. Dalton, 1823 (1973).
29. P. E. GARROU. Inorg. Chem. **14**, 1435 (1975).
30. R. MASON and D. W. MEEK. Angew. Chem. Int. Ed. Engl. **17**, 183 (1978).
31. S. O. GRIM and A. W. YANKOWSKY. J. Org. Chem. **42**, 1236 (1977) and references therein.
32. R. F. HUDSON. Structure and mechanism in organophosphorus chemistry. Academic Press, London. 1965. Chapt. 5.
33. T. A. ALBRIGHT, W. J. FREEMAN, and E. E. SCHWEIZER. J. Am. Chem. Soc. **97**, 2942 (1975).
34. P. A. W. DEAN and D. G. IBBOTT. Can. J. Chem. **54**, 177 (1976).
35. V. MARK. J. Am. Chem. Soc. **85**, 1884 (1963).
36. G. B. BOROWITZ, D. SCHNESSLER, W. MCCOMASS, L. I. BLAINE, K. B. FIELD, P. WARD, P. RAHN, B. V. RAHN, W. GLOVER, F. RAMAN, and I. J. BOROWITZ. Phosphorus, **2**, 91 (1972).
37. L. V. NESKROV, N. E. KREPYSHEVA, R. A. SABIROVA, and G. N. LIPKINA. J. Gen. Chem. USSR, **48**, 722 (1978).
38. A. R. BOATE and D. R. EATON. Can. J. Chem. **55**, 2432 (1977).
39. M. L. MANION-SCHILLING, H. D. ROTH, and W. C. HERNDON. J. Am. Chem. Soc. **102**, 4271 (1980).
40. J. D. DONALDSON. Prog. Inorg. Chem. **8**, 287 (1967).
41. P. S. PREGOSIN and R. W. KUNZ. ^{31}P and ^{13}C nmr of transition metal phosphine complexes. Springer-Verlag, Berlin. 1979. Table 11. p. 103.
42. W. MCFARLANE and D. S. RYCROFT. J. Chem. Soc. Dalton, 1977 (1974).
43. L. W. REEVES and E. J. WELLS. Can. J. Chem. **41**, 2698 (1963).

Can. J. Chem. Downloaded from www.nrcresearchpress.com by 210.87.254.42 on 09/05/12
For personal use only.

The fortuitous direct electrochemical synthesis of some copper(I) complexes

FAROUQ F. SAID AND DENNIS G. TUCK
Department of Chemistry, University of Windsor, Windsor, Ont., Canada N9B 3P4

Received June 9, 1980

FAROUQ F. SAID and DENNIS G. TUCK. Can. J. Chem. **59**, 62 (1981).

The electrochemical oxidation of copper in the presence of RX (R = CH_3, C_6H_5, $C_6H_5CH_2$; X = Cl, Br, I, not all combinations) and either 2,2′-bipyridine or $(C_2H_5)_4NX$ gives rise to neutral or anionic copper(I) halide complexes. The current efficiency shows that CuX is produced at the anode; the subsequent solution chemistry influences the complex formation processes.

FAROUQ F. SAID et DENNIS G. TUCK. Can. J. Chem. **59**, 62 (1981).

L'oxydation électrochimique du cuivre en présence de RX (R = CH_3, C_6H_5, $C_6H_5CH_2$; X = Cl, Br, I, pas toutes les combinaisons) et de bipyridine-2,2′ ou du $(C_2H_5)_4NX$ conduit à la formation de complexes halogénés du cuivre(I) sous la forme neutre ou sous la forme anionique. L'efficacité du courant montre qu'il se forme du CuX à l'anode; la solution chimique résultante influence le mode de formation du complexe.

[Traduit par le journal]

Introduction

In previous papers from this laboratory on the direct electrochemical synthesis of organometallic compounds, we have described the use of cells of the type $Pt_{(-)}$/RX + organic solvent/$M_{(+)}$ to prepare a variety of organometallic halides of main group metals (1–5). Less attention has been given to parallel studies of transition metals, although RMX (M = Ni, Pd) (6) and R_2MX_2 (M = Ti, Zr, Hf) (7) derivatives have been obtained by these methods. We have recently turned our attention to the electrochemical oxidation of the coinage metals, in the hope of once again synthesizing organohalides of these elements.

The present paper shows that in the case of copper expectation outran performance, in that although oxidation occurred the products were generally anionic or neutral inorganic complexes of copper(I). In one system (RX = C_6H_5Br) both copper(I) and copper(II) derivatives were isolated.

Experimental

General

Copper metal was in the form of turnings, approximately 1 cm^2 area, 1 g mass. The purification of solvents, etc., and the spectroscopic investigation of product materials, were carried out as described in earlier papers (1–7). All experiments were carried out under dry nitrogen.

Copper analysis was by atomic absorption spectrophotometry, and halide analysis by Volhard titration. Microanalysis was carried out by Guelph Chemical Laboratories Ltd. The presence of the tetraethylammonium cation, or of 2,2′-bipyridine (bipy), in the appropriate products was confirmed by conventional infrared spectroscopy.

Electrochemical Synthesis

A piece of copper, suspended on a platinum wire, formed the anode of a cell of the general type

$$Pt_{(-)}/CH_3CN + RX + bipy/Cu_{(+)}$$

or

$$Pt_{(-)}/CH_3CN + RX + (C_2H_5)_4NX/Cu_{(+)}$$

The actual solution compositions used are shown in Table 1, together with the initial applied voltage and current, and the weight of copper dissolved. The isolation of the anionic complexes followed conventional routes, as dictated by the solubilities involved. Reduction of the volume of the electrolyte phase by approximately 50% resulted in the precipitation of a solid, which was washed and/or recrystallized and dried *in vacuo*. The yields were of the order of 80%, based on the quantity of copper consumed.

$Cu/CH_4CN + C_6H_5Br$ + 2,2′-Bipyridine

This system merits special description in view of the findings. Early studies using an undivided cell yielded products which could not be characterized, and later experiments were therefore performed in a two-arm cell, with the electrode compartments joined via a narrow arm (2 mm id) lightly plugged with glass wool. For the experimental conditions listed in line 6 of Table 1, we observed the formation of a brown solution phase, together with a green solid which deposited in the anode compartment. The brown solution, on treatment with diethyl ether, yielded solid CuBr·bipy. The green solid is not apparently a single compound; microanalysis showed C, H, and N in the ratios required for 2,2′-bipyridine, but neither the absolute values for these elements, nor those for Cu and Br, lead to any obvious stoichiometry. In one experiment, however, a green single crystal grew on the copper anode, and X-ray studies (8) identified this as $[Cu(bipy)_2Br]Br$. We therefore conclude that the non-stoichiometric green solids referred to above are probably mixtures of this copper(II) salt with CuBr·bipy; for example, one product had C 43.3, H 3.5, N 10.5, and a mixture of 40% CuBr·bipy and 60% $CuBr_2$·2bipy requires C 43.5, H 2.9, N 10.2.

Results and Discussion

The organometallic chemistry of copper is apparently restricted to those compounds in which the element is the +I oxidation state (9), and it is therefore not surprising that the electrochemical oxidation did not give rise to the RCuX species which might have been expected by analogy with other previous experiments. The two main discus-

0008-4042/81/010062-03$01.00/0
©1981 National Research Council of Canada/Conseil national de recherches du Canada

Can. J. Chem. Downloaded from www.nrcresearchpress.com by 210.87.254.105 on 09/05/12
For personal use only.

TABLE 1. Reaction conditions for the electrochemical synthesis of copper(I) halide complexes

System	Solution composition RX (cm^3)	CH_3CN (cm^3)	bipy (g)	$(C_2H_5)_4NX$ (g)	Initial Voltage (V)	Initial Current (mA)	Time of electrolysis (h)	Cu dissolved (mg)
1	C_6H_5Cl 15	45	0	1.0	5	20	3.2	190
2	$C_6H_5CH_2Cl$ 15	40	0	1.0	5	20	5	290
3	C_6H_5Br 15	25	0	1.0	5	20	6	110
4	CH_3I 10	50	0	1.0	3.5	20	3	82
5	C_6H_5I 10	40	0	1.0	5	30	3	210
6	C_6H_5Br 20	10	0.5	0.015	50	Small	24	31
7	CH_3I 10	40	1.0	0.030	20	20	7	[a]

[a]Not recorded, since the cathode disintegrated during the electrolysis.

TABLE 2. Analytical results for copper(I) complexes

System	Product	Colour	Found (%) Cu	Found (%) Halogen	Calculated (%) Cu	Calculated (%) Halogen
1	$[(C_2H_5)_4N]_3[Cu_2Cl_5]$	Yellow	25.3	18.3	25.5	18.3[a]
2	$[(C_2H_5)_4N]\,[Cu_2Cl_3]$	Yellow	30.1	35.0	29.3	34.9[b]
3	$[(C_2H_5)_4N]_2[CuBr_3]$	Brown	42.6	11.6	42.6	11.3
4	$[(C_2H_5)_4N]_3[CuI_4]$	Pale yellow	52.9	6.5	52.8	6.6
5	$[(C_2H_5)_4N]\,[CuI_2]$	Pale brown	55.1	14.0	56.8	14.2
6	CuBr·bipy	Brown	20.9	26.7	21.2	26.7[c]
7	CuI·bipy	Brown	—	36.8	—	36.6

[a]Found C 39.8, H 8.8, N 5.5; calcd. C 41.4, H 8.7, N 6.0.
[b]Found C 24.9, H 5.6, N 3.2; calcd. C 26.4, H 5.5, N 3.8.
[c]Found C 39.0, H 2.8, N 9.1; calcd. C 40.1, H 2.7, N 9.3.

sion points to be addressed are the reaction pathway, and the structure of the products obtained.

The anionic copper(I) complexes listed in Table 2 are generally of known stoichiometries (cf. ref. 11), although few, if any, have been stabilized with bulky organic cations in previous studies. The structures of the various anionic copper(I) complexes are based on linked tetrahedra (10); the anion CuI_4^{3-}, which apparently has not been reported previously, may be a rare example of an isolated mononuclear anionic copper(I) tetrahedral species. No doubt salts with cations other than $(C_2H_5)_4N^+$ could be prepared by the electrochemical method, although the uncertainties about the solution chemistry involved (see below) require clarification before any claim can be made about predicting the identity of any products.

As in our previous work, we have measured the current efficiency, here expressed as moles of copper dissolved per Faraday of charge, for two typical systems, namely

$$Pt_{(-)}/CH_3CN + C_6H_5Cl + (C_2H_5)_4NCl/Cu_{(+)}$$
$$Pt_{(-)}/CH_3CN + C_6H_5Br + (C_2H_5)_4NBr/Cu_{(+)}$$

for which $E_F = 1.06$ and 1.10 mol F^{-1} respectively. These values correspond to the anode reaction

[1] $X^- + Cu \rightarrow CuX + e$

and in those systems where $(C_2H_5)_4NX$ is present in some quantity, the anion is clearly derived from this salt. In other cases, the reduction $RX + e \rightarrow R' + X^-$ is a source of halide ion (1, 11); there is a resultant significant difference in the operating voltage depending upon the presence or absence of $(C_2H_5)_4NX$ (see Table 1).

The disproportionation of copper(I) species formed by the anode reaction (1) will not occur in acetonitrile solution (12), and complex formation can then occur by reaction with excess halide ion, or with 2,2′-bipyridine. The absence of stable organo-copper(II) compounds eliminates reactions such as $CuX + RX \rightarrow RCuX + X$, but the presence of the organic halide is apparently crucial in the formation of the copper(I) complexes isolated, since cells which contain R_4NX but no RX give rise to a different group of copper compounds (yet to be characterized (13)) which precipitate immediately, in contrast to the present systems in which precipitation only occurs during the work-up following electrolysis. It is worth noting in this context that the exchange reaction between aryl halide and copper(I) halide has been discussed in terms of possible solvated four-centre ArXCuY intermediate species (14), so that the stabilization and solvation of similar complexes, or of analogues

Can. J. Chem. Downloaded from www.nrcresearchpress.com by 210.87.254.105 on 09/05/12
For personal use only.

involving CuX_2^-, etc. may well play an important role in the present syntheses. In general, this point apart, it seems that the production of CuX, and the subsequent complex formation, are in keeping with the known chemistry of the element.

The formation of copper(II) species was only observed in the presence of 2,2′-bipyridine, and we therefore tentatively conclude that complexing by this ligand allows the reaction

[2] $2CuX{\cdot}bipy \rightarrow Cu(bipy)_2X_2 + Cu$

to proceed significantly, even in acetonitrile. The insolubility of $Cu(bipy)_2X_2$ in acetonitrile may be important in this respect.

Acknowledgement

This work was supported in part by Operating Grants from the Natural Sciences and Engineering Research Council of Canada.

1. J. J. Habeeb and D. G. Tuck. J. Organomet. Chem. **134**, 363 (1977).
2. J. J. Habeeb and D. G. Tuck. J. Organomet. Chem. **146**, 213 (1978).
3. A. Osman and D. G. Tuck. J. Organomet. Chem. **169**, 255 (1979).
4. J. J. Habeeb, A. Osman, and D. G. Tuck. J. Organomet. Chem. **185**, 117 (1980).
5. J. J. Habeeb, F. F. Said, and D. G. Tuck. J. Organomet. Chem. **190**, 325 (1980).
6. J. J. Habeeb and D. G. Tuck. J. Organomet. Chem. **139**, C17 (1977).
7. F. F. Said and D. G. Tuck. Can. J. Chem. **58**, 1673 (1980).
8. M. Khan and D. G. Tuck. Unpublished results.
9. A. G. Massey. *In* Comprehensive inorganic chemistry. Vol. 3. *Edited by* A. F. Trotman-Dickenson. Pergamon Press. 1973. p. 1.
10. F. H. Jardine. Adv. Inorg. Radiochem. **17**, 115 (1975).
11. D. G. Tuck. Pure Appl. Chem. **51**, 2005 (1979).
12. I. M. Kolthoff and J. F. Coetzee. J. Am. Chem. Soc. **79**, 1852 (1957).
13. C. Oldham, F. F. Said, and D. G. Tuck. Unpublished results.
14. R. G. R. Bacon and H. A. O. Hill. J. Chem. Soc. 1097 (1964); Q. Rev. **19**, 95 (1965).

Can. J. Chem. Downloaded from www.nrcresearchpress.com by 210.87.254.105 on 09/05/12
For personal use only.

Nitrogen- and sulfur-containing models for metallo-enzymes. Part I. Synthesis and physical studies of 2(2-pyridyl)-1,3-dithioalkyl-2-propanols, 2(2-pyridyl)- and 2(2-imidazolyl)-1,3-dimercapto-2-propanols

N. J. CURTIS AND R. S. BROWN

Department of Chemistry, University of Alberta, Edmonton, Alta., Canada T6G 2G2

Received May 28, 1980

Can. J. Chem. Downloaded from www.nrcresearchpress.com by 210.87.254.105 on 09/05/12
For personal use only.

N. J. CURTIS and R. S. BROWN. Can. J. Chem. **59**, 65 (1981).

Several compounds of the title class have been synthesized as small-molecule analogues for the metal-binding sites in such biochemical systems as ADH. The ligands containing pyridine and two thioethers do not bind divalent metals (Co^{2+}, Zn^{2+}, Cu^{2+}, Ni^{2+}), strongly suggesting that thioethers are poorly chelated. However, the analogues containing free SH groups bind divalent metals very strongly, producing complexes with limited solubility at pH values in excess of 6. Titration of the latter ligands in the presence of 1 equiv. Zn^{2+} indicates the consumption of 3 equiv. OH^- by pH 6, one for the $\overset{+}{N}$—H → N: ionization, and one for each S—H bound to Zn^{2+}. On the basis of these data the resulting complexes are considered to neutral bis-thiolates. The relationship of these data to the state of ionization of the Zn^{2+}-cysteine SH's in ADH is discussed.

N. J. CURTIS et R. S. BROWN. Can. J. Chem. **59**, 65 (1981).

On a synthétisé plusieurs composés de la classe de ceux mentionnés dans le titre en tant qu'analogue des petites molécules des sites de liaison métallique de certains systèmes tel le ADH. Les ligands contenant la pyridine et deux thioéthers ne se lient pas au métaux bivalents (Co^{2+}, Zn^{2+}, Cu^{2+}, Ni^{2+}) suggérant ainsi fortement que les thioéthers sont chélatés faiblement. Cependant les analogues contenant des groupes SH libres se lient fortement aux métaux bivalents, produisant des complexes à solubilité limitée à un pH supérieur à 6. Le titrage des derniers ligands en présence de 1 éq. de Zn^{2+} démontrent qu'à un pH de 6, trois éq. de OH^- sont utilisés; un éq. pour l'ionisation de $\overset{+}{N}$—H→N: et un pour chacun des groupes S—H lié au Zn^{2+}. En se basant sur ces données, on en a déduit que les complexes résultant sont des bis-thiolates neutres. On discute de la relation entre ces données et l'état d'ionisation de la Zn^{2+}–cystéine SH dans l'ADH.

[Traduit par le journal]

Introduction

Many biological systems contain metal-binding sites containing (along with other residues) cysteine sulfhydryl and/or methionine thiomethyl groups (1, 2). Among these are the Zn-containing enzymes aspartate transcarbamylase (1*a*), superoxide dismutase (1*b*), metallothioneine (1*c*), porphobilinogen synthase (1*d*), and the alcohol dehydrogenases (1*e*–*h*). The structure of an inhibited ternary complex of horse liver alcohol dehydrogenase (HLADH), reduced nicotinamide adenine dinucleotide (NADH), and dimethyl sulfoxide shows that the catalytic Zn^{2+} ion is bound by cys 46, his 67, and cys 174. The fourth ligand site is occupied by the non-reducible DMSO oxygen as shown in Fig. 1 (1*g*) and the reducing agent (NADH) is positioned close to the Zn^{2+}-bound sulfoxide.

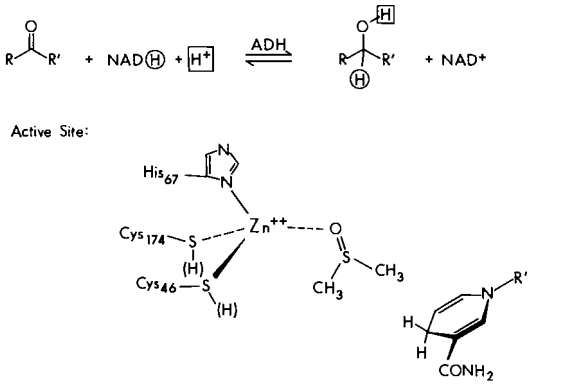

FIG. 1. The active site structure of a DMSO inhibited ternary complex of horse liver alcohol dehydrogenase depicting the Zn^{2+} binding site (1*g*).

The unusual "type 1" copper–blue proteins such as plastocyanin, stellacyanin, and azurin (2) contain a Cu^{2+} ion bound by cys, his, and/or met groups. The recently determined crystal structure of plastocyanin (2*a*) indicates that the Cu^{2+} ion is bound in a distorted tetrahedral geometry by two histidine imidazoles, a methionine SCH_3, and a cysteine SH. Stellacyanin (2*d*, *c*) contains no methionine so its copper binding site must differ from that of plastocyanin by at least one residue, but as yet no X-ray structure for the former is available. Several sulfur- and nitrogen-containing small molecules have been investigated as models for these proteins (3).

On the other hand, for the small molecules which have been investigated as models for NADH dependent oxido-reductases (4), no attempt has been made to approximate the known catalytic sites in the enzyme. It seemed to us that since the ADH's

0008-4042/81/010065-11$01.00/0

©1981 National Research Council of Canada/Conseil national de recherches du Canada

Can. J. Chem. Downloaded from www.nrcresearchpress.com by 210.87.254.105 on 09/05/12
For personal use only.

isolated from mammalian, yeast, or bacterial sources, while differing in their tertiary structures, have very similar catalytic sites (1*e*), that any model system for ADH should at least incorporate two thiols and an imidazole or pyridine nitrogen as a Zn^{2+} binding site. For this reason we have synthesized and studied a new class of S-, N-containing ligands of general structure **1** and **2**. Inspection of

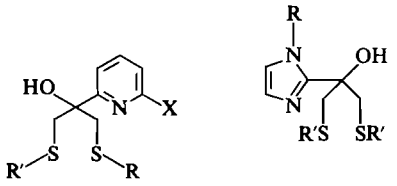

1 **2**

molecular models indicates that the unique connectivity of **1** and **2** orients the metal-binding groups (S and N) to form a tridentate chelate which might be a reasonable model for the active site depicted in Fig. 1. In the cases where X is a carbonyl-containing moiety as in **3**, one might observe reduction of the (possibly) coordinated C=O by 1,4-dihydropyridines to form an alcohol(ate) (**4**) as in reaction [1].

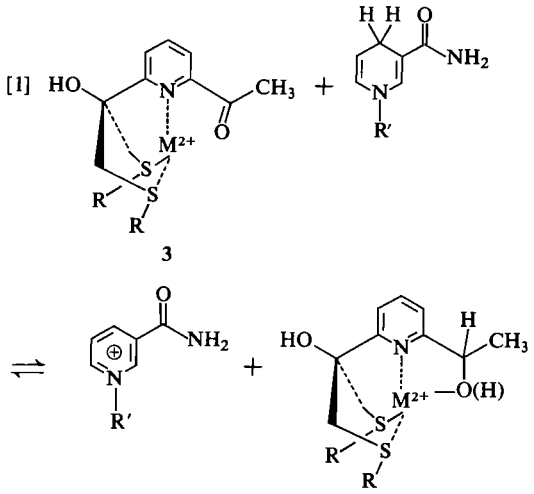

3

4

In this report we present the synthesis of the type **1** and **2** ligands, studies of their metal binding abilities, and some titration data of their 1:1 Zn^{2+} complexes. Subsequent publications will consider the kinetic and mechanistic aspects of the redox process.

Results

(A) Syntheses

The basic approach to these unknown ligands involves the nucleophilic addition of the appropriate 2-pyridyl (5) or 2-imidazolyl anions to the bis-1,3-dithioethers of acetone (**5**) as in reaction [2].

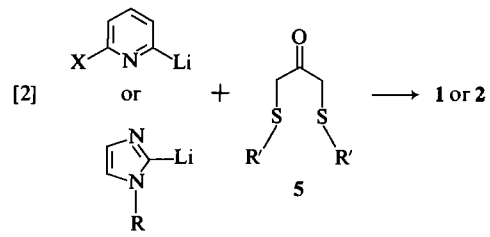

While 1 equiv. of 2-pyridyl lithium adds to acetone to provide reasonable yields of **16** (*vide infra*) at least 2 equiv. of this anion must be used per equiv. of **5** to obtain product, and even with 3 equiv. of anion the yields are not high (≤42%). On the other hand, methyl magnesium chloride gave satisfactory yields (~50%) of the corresponding addition product with **5** at a 1:1 ratio. The dithio ketones themselves (**5***a*–*h*) can be made in 30 to 90% yields by the bis displacement on 1,3-dichloroacetone by the appropriate thiolate anion (6). In order to obtain the free thiols of **1** and **2** (R = R′ = H) two routes were considered which utilize a suitably protected derivative of **5**. The first of these utilizing ketone **5***i* (7) (produced by the route outlined in reaction [3]) was deemed inappropriate since the oxidation of alcohol **7** proceeded in low and variable yield.

An alternative ketone (**5***j*) can be prepared in 80% yield by the double displacement of the bis-lithio anion of "1,3-dimercapto acetone"[1] (8) on chloromethylethyl ether. Deprotection of the hemithioacetal group (9) was accomplished by stirring **1** or **2** (R = R′ = $CH_2OCH_2CH_3$) in a 4:1 mixture of CH_3CN:H_2O with $HgCl_2$ to give a thick precipitate (presumably **8**) from which the free thiol could be liberated by H_2S treatment as in reaction [4]. We believe **8** is deprotonated as shown since the reaction mixture becomes very acidic as soon as $HgCl_2$ is added to the mixture.

In order to produce the 2,6-disubstituted pyridines (**1** X = $\overset{O}{\overset{\|}{C}}CH_3$; X = $CHOHCH_3$ (**14** and **15**,

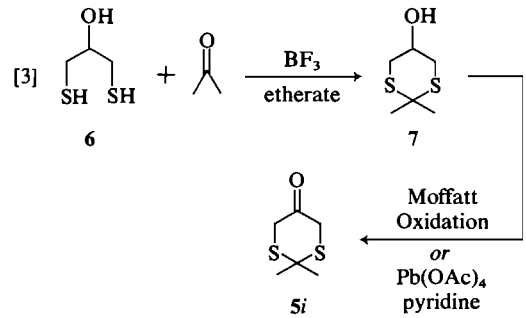

6 **7** **5***i*

[1] Schotte has proposed that this material exists as a dimer (8), a fact which is verified by mass spectral and infrared measurements.

Can. J. Chem. Downloaded from www.nrcresearchpress.com by 210.87.254.105 on 09/05/12
For personal use only.

[4]

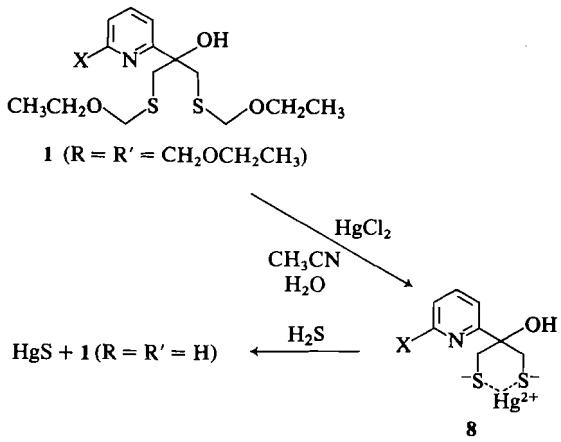

respectively)), the pathway shown in Scheme 1 was adopted. When the reaction mixture containing the fully protected material **9** was washed with 0.1 *N* HCl, debrominated residual unreacted starting pyridine was removed; further extraction of the reaction mixture with 3 *N* HCl gave **9** which on standing for 24 h in 3 *N* HCl at room temperature afforded the partially deblocked **1** (X = $COCH_3$, R = R′ = $CH_2OCH_2CH_3$). Deblocking of the thiol was accomplished as in reaction [4].

Finally compound **17** (*vide infra*) was produced by the route outlined in reaction [5].

[5]

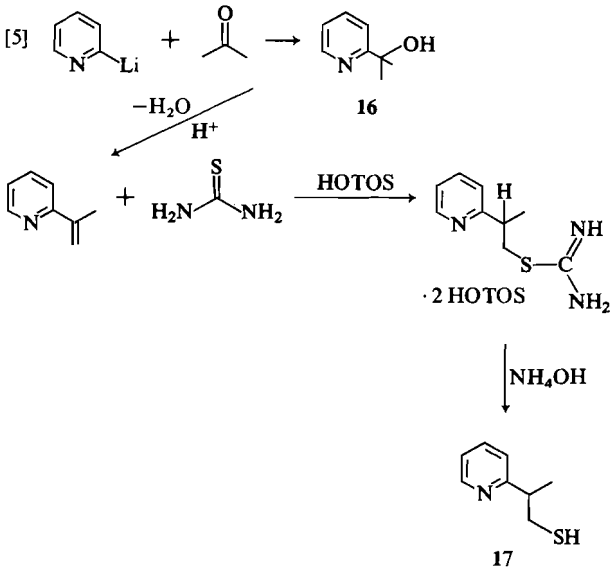

2(2-Pyridyl)propene (ref. 10*a*, prepared by acid-catalysed dehydration of **16**) when treated with 2.1 equiv. of *p*-toluenesulfonic acid (HOTOS) and 1 equiv. of thiourea (10*b*) gives the corresponding thiouronium salt which analysed as the ditosylate. Deprotection of this material in 4:1 NH_4OH:H_2O for 1 h gave **17**.

Table 1 lists the yields and physical data for ketones **5***a*–*j*, and in Table 2 are listed the physical data for thioethers **1***a*–*i* (X = H). Table 3 lists the data for thiols **10**–**17**.

(B) Titration and Metal Stability Constants

(*i*) pK_a measurements (11) were performed on thioethers **1***a*–*i* and thiols **10**–**13**, **16**, and **17** at concentrations of 4×10^{-3} *M* in 50% (v/v) aqueous dioxane at 25°C and constant ionic strength of I = 0.3 *M* $NaNO_3$. The data were analysed by a modified computer version of Simms' method (12, 13) and are given in Table 4. A general trend emerges when one compares the pK_a's of the substituted aryl thioethers **1***d*–*h*; electron withdrawing groups on the phenyl ring reduce the pK_a's in this medium substantially. Since the sulfur atoms are each four atoms removed from the site of protonation, the pK_a change of 0.56 units in passing from the *p*-OCH_3 to *m*-CF_3 derivatives seems appropriate for a simple through bond inductive effect or field effect. It is shown in Table 4 that each of the pyridine-sulfur containing species is a weaker base than is **16**; **17** might be considered an exception, but the latter contains no electron withdrawing α-OH group so its basicity is higher.

(*ii*) *Metal stability constants*, $pK_{M^{2+}}$ values for weak binding ligands **1***a*–*i* and **16** were determined by potentiometric titration methods (14*a*) on roughly 5×10^{-3} *M* solutions of ligand containing a 20-fold excess of metal (I = 0.3 *M*, T = 25°C) and the results are compiled in Table 5. For the Cu^{2+} complexes where the $pK_{M^{2+}}$ values are larger, titration methods outlined in ref. 13 were used successfully.

On the basis of the data given in Table 5 one can see that ligands **1***a*–*i* bind the divalent ions weaker than does **16**. Thus it appears that the thioether functionality does not contribute constructively to the complex formation, an observation noted by earlier workers (14*b*). Comparison of the data for **16** with those for pyridine (15) and α-picoline (16) (Table 5) shows that the former binds the divalent ion more tightly, probably by involvement of the α-OH group as in **18**. Since in general the thioethers bind more poorly than **16** but better than α-picoline; we cannot tell unambiguously whether their chelates resemble **18** or **19**, although one notes that the electron-withdrawing groups on the aryl ring decrease the binding ability as they do the pK_a's in Table 4. Thus probably a similar inductive mechanism is operative in both H^+ and M^{2+} binding.

The determination of the stability constants for the thiol containing ligands **10**–**15** and **17** is not as simple a task as for the thioethers since precipitation invariably accompanies the titration. Relatively few $pK_{M^{2+}}$ values for thiols have been re-

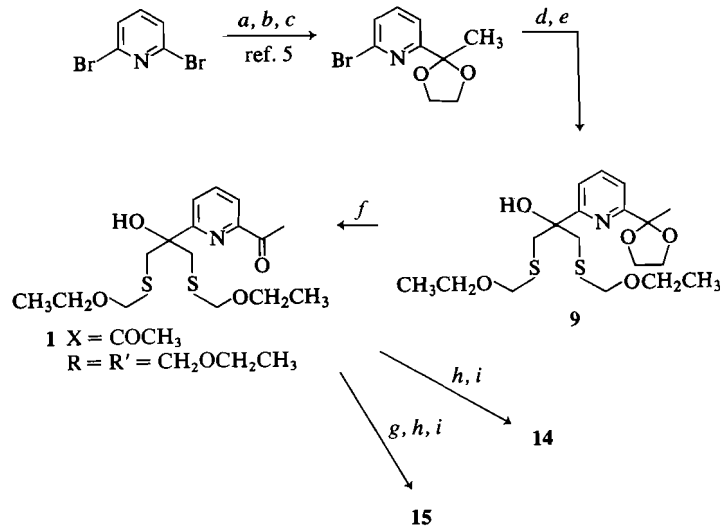

SCHEME 1. *a*, *n*BuLi, ether; *b*, dimethylacetamide; *c*, HOTOS, 2,2-dimethoxypropane, ethylene glycol; *d*, *n*BuLi, ether; *e*, **5***j*; *f*, HCl/H_2O; *g*, $NaBH_4$, ethanol; *h*, $HgCl_2$, CH_3CN/H_2O; *i*, H_2S.

ported (17). However, the reported values are large for 1,2-dithioethane (ref. 17*a*, $pK_{Ni^{2+}} = 20.7$) and 2,3-dimercapto-1-propanol (ref. 17*b*, $pK_{Zn^{2+}} = 13.5$). Utilizing the titration methods in ref. 12 one finds that the monothiol pyridine **13** also binds

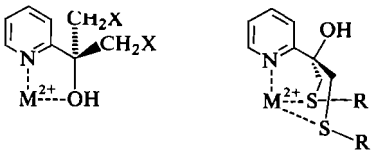

18, X = H **19**

Zn^{2+}, Co^{2+}, and Ni^{2+} very strongly, the respective $pK_{M^{2+}}$ values being 10.8, 10.9, and 10.8. It is therefore expected that the remaining thiols will be strong chelators as well, and although we do not have reliable $pK_{M^{2+}}$ values we believe that they are bound strongly through sulfur.

(iii) Titration of ligands **1**a, *11, 12, and 17 in the presence and absence of* Zn^{2+}. Thiols undoubtedly bind metals strongly as deprotonated thiolate complexes (17, 18), which is supported by the observation that when the neutral thiols and metals are mixed, H^+ ion is released. Since most of the mechanisms postulated for the action of ADH (*vide infra*) require a strongly electrophilic metal (i.e., as a Lewis acid for polarizing the presumably coordinated carbonyl), we were concerned about the state of ionization of the thiols at various pH values in the presence of Zn^{2+}. As a control experiment, weakly binding thioether **1***a* was titrated in 50% aq. dioxane ($I = 0.3$ *M*, $T = 25$°C) both in the absence, and presence of 1 equiv. of Zn^{2+}. Figure 2 shows the titration curves and it is seen that the pyridine–H^+ ionization is perturbed only slightly when Zn^{2+} is added. It is important to note that for the latter titration only 1 equiv. of OH^- is consumed up to a pH ~ 6; further addition of OH^- resulted in precipitation of $Zn(OH)_2$.

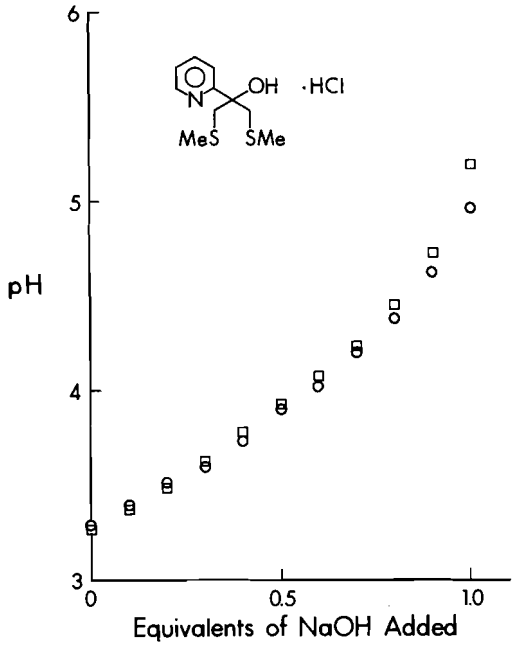

FIG. 2. A plot of the titration curve for **1***a* (pH vs. equivalents of NaOH added) in the absence (□) and presence (○) of 1 equiv. of Zn^{2+} in 50% aq. dioxane, $I = 0.3$, $T = 25$°C.

On the other hand, similar titration experiments performed on pyridine mono thiol **17** (Fig. 3) showed (in the absence of metal) a pK_a of 4.21 corresponding to the pyridinium → pyridine titra-

Can. J. Chem. Downloaded from www.nrcresearchpress.com by 210.87.254.105 on 09/05/12
For personal use only.

TABLE 1. Physical data for dithio ketones **5***a–k*[a]

Compound R = R′		Method	Yield (%)	Mp:Bp (°C/Torr)	Ir (cm^{-1})	Nmr (**8**, $CDCl_3$)
CH_3	(**5***a*)	A	87	53/0.55[b]	1706	2.11 (s, 6H); 3.42 (s, 4H)
CH_3CH_2	(**5***b*)	A	73	58/0.14[c]	1704	1.24 (t, 6H); 2.55 (q, 4H); 3.45 (s, 4H)
p-$(CH_3)_2\ddot{N}$–C$_6$H$_4$–	(**5***c*)[a]	B	43	61–62	1700	2.92 (s, 12H); 3.64 (s, 4H); 6.5–7.4 (m, 8H)
p-CH_3O–C$_6$H$_4$–	(**5***d*)[a]	B	31	38	1706	3.70, 3.78 (s, s, 10H); 6.7–7.5 (m, 8H)
p-CH_3–C$_6$H$_4$–	(**5***e*)	B	68	65–66[d]	1705	2.26 (s, 6H); 3.73 (s, 4H); 6.9–7.3 (m, 8H)
H–C$_6$H$_5$	(**5***f*)	B	58	36–37[e]	1705	3.82 (s, 4H); 7.3 (m, 10H)
p-Cl–C$_6$H$_4$–	(**5***g*)	B	67	78–79[f]	1705	3.80 (s, 4H); 7.2 (m, 8H)
m-CF_3–C$_6$H$_4$–[g]	(**5***h*)[a]	B	59	50–51	1725	3.90 (s, 4H); 7.4–7.7 (m, 8H)
CH_3 CH_3	(**5***i*)	Exptl.	—	51/0.2[i]	—	1.78 (s, 6H); 3.46 (s, 4H)
$CH_3CH_2OCH_2$—	(**5***j*)[a]	Exptl.	80	115/0.1	1708	1.18 (t, 6H); 3.55, 3.56 (s, q, 8H); 4.65 (s, 4H)
CH_3=R $CH_3CH_2OCH_2$=R′	(**5***k*)[h]	Exptl.	24	75/0.05	1704	1.19 (t, 3H); 2.08 (s, 3H); 3.35, 3.37, 3.56 (s, s, q, 6H)

[a]New compounds were identified by spectral methods and combustion analysis (±0.3%, C, H, N, S). Methods A or B refer to those given in Experimental.
[b]Lit. 107–109°C/9 Torr, ref. 8*b*.
[c]Lit. 123–124°C/11 Torr, ref. 8*b*.
[d]Lit. 66–67°C, ref. 32.
[e]Lit. 62°C, ref. 6.
[f]Lit. 89–91°C (from benzene), ref. 33.
[g]C, H analysis.
[h]Did not analyse correctly.
[i]Lit. 57.5–59°C/0.5 Torr, ref. 34.

TABLE 2. Physical data for thioethers **1***a–i* (X = H)[a,b]

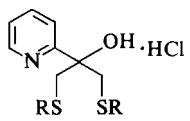

R[a]		Yield (%)	Mp (°C)	Purification	Nmr (δ, $CDCl_3$)[b]
CH_3	(**1***a*)	41	170–172	$CHCl_3/CH_3OH$	2.02 (s, 6H); 3.19 (ABq, 4H); 4.7 (s, 1H); 7.1–7.8 (m, 3H); 8.6 (m, 1H)
C_2H_5	(**1***b*)	42	152–154	$CHCl_3$	1.14 (t, 6H); 2.36 (q, 4H); 3.15 (ABq, 4H); 4.6 (s, 1H); 7.1–7.8 (m, 3H); 8.6 (m, 1H)
p-CH_3OPh	(**1***d*)	34	184–186	$CHCl_3/CH_3OH$	3.46 (ABq, 4H); 3.72 (s, 6H); 4.8 (s, 1H); 6.6–7.6 (m, 1H); 8.4 (m, 1H)
p-CH_3Ph	(**1***e*)	30	165–167	Acetone/C_2H_5OH	2.22 (s, 6H); 3.51 (ABq, 4H); 4.8 (s, 1H); 6.9–7.6 (m, 11H); 8.4 (m, 1H)
Ph	(**1***f*)	18	120–122	$CHCl_3$/benzene	3.59 (ABq, 4H); 4.9 (s, 1H); 6.9–7.6 (m, 11H); 8.4 (m, 1H)
P-ClPh	(**1***g*)	20	175–178	$CHCl_3/CH_3OH$	3.51 (ABq, 4H); 4.9 (s, 1H); 6.9–7.6 (m, 11H); 8.4 (m, 1H)
m-CF_3Ph	(**1***h*)	14	139–140	$CHCl_3$/ether	3.57 (ABq, 4H); 5.0 (s, 1H); 6.9–7.6 (m, 11H), 8.4 (m, 1H)
CH_3 CH_3	(**1***i*)[c]	23	46–47	Silica gel	1.64 (s, 3H), 1.93 (s, 3H); 2.50 (d, 2H, J = 14 Hz); 3.86 (d, 2H, J = 14 Hz); 4.5 (s, 1H); 7.1–7.9 (m, 3H); 8.5 (m, 1H)

[a]Compounds isolated as white or off-white HCl salt and were identified by spectral measurements, and combustion analysis (C, H, N ±0.3%).
[b]Nmr spectra of neutral compound.
[c]Not the HCl salt.

Can. J. Chem. Downloaded from www.nrcresearchpress.com by 210.87.254.105 on 09/05/12
For personal use only.

Can. J. Chem. Downloaded from www.nrcresearchpress.com by 210.87.254.105 on 09/05/12
For personal use only.

TABLE 3. Physical data for thiol-containing ligands

Compound[a]		Mp (°C)	Overall yield (%)	Nmr (δ)
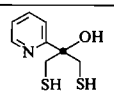	**(10)**[b]	158–160	25	3.29 (s, 4H); 8.0–8.2 (m, 2H); 8.6–8.9 (m, 2H)[c]
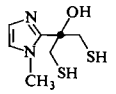	**(11)**	119–121	17	1.6 (dd, 2H); 2.8–3.5 (m, 4H); 3.87 (s, 3H); 4.9 (s, 1H); 6.8 (m, 2H)[d,e]
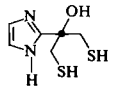	**(12)**	106–107	20	3.02 (s, 4H); 6.96 (s, 2H)[f]
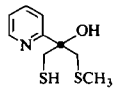	**(13)**[b]	162–164	21	2.35 (s, 3H); 3.58, 3.61 (s, s, 4H); 8.3–8.6 (m, 2H); 8.8–9.2 (m, 2H)[c]
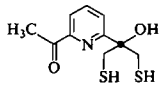	**(14)**	Gel	11	1.36 (t, 2H); 2.70 (s, 3H); 2.9–3.3 (m, 4H); 4.4 (s, 1H); 7.7–8.1 (m, 3H)[e]
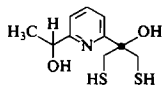	**(15)**	140–142	9	1.85 (d, 3H); 3.46 (s, 4H); 5.60 (q, 1H); 8.1–8.3 (m, 2H); 8.7–9.0 (m, 1H)[c]

[a]New compounds were identified by spectral properties and combustion analysis (C, H, N ±0.3%). Compound **12** has C, S analysis ±0.4%. Overall yield refers to the steps outlined in both reactions [1] and [4].
[b]HCl salt.
[c]D_2O solution.
[d]−50°C.
[e]$CDCl_3$.
[f]CD_3OD.

TABLE 4. pK_a's for thioethers **1***a–i* and thiols **10–13, 16, 17**[a,b]

Compound	pK_1[c]	Compound	pK_1[c]	pK_2[d]
1*a*	3.60	**10**	3.55	10.00
1*b*	3.61	**11**	5.38	9.61
1*d*	3.54	**12**	5.45	9.37
1*e*	3.47	**13**	3.66	10.71
1*f*	3.37	**16**	4.18	—
1*g*	3.16	**17**	4.21	≃10
1*h*	2.98			
1*i*	3.22			

[a]Obtained by potentiometric titration of 4–5 × 10^{-3} *M* solutions of compound in 50% (v/v) aqueous dioxane at 25°C and I = 0.3 ($NaNO_3$).
[b]Precision ±0.01 unit. Reported values are the averages of 3 determinations.
[c]pK_1 refers to $HL^+ \rightleftarrows H^+ + L$.
[d]pK_2 refers to the thiol proton L—SH $\rightleftarrows LS^- + H^+$.

TABLE 5. Metal stability constants for ligands **1***a–i*, **16**[a]

	$pK_{M^{2+}}$[b,c]			
Ligand	Co^{2+}[d]	Ni^{2+}[e]	Cu^{2+}[f]	Zn^{2+}[g]
1*a*	1.21	1.82	3.08	1.23
1*b*	1.17	1.60	3.13	1.20
1*d*	0.84	1.22	—	1.05
1*e*	0.86	1.18	2.92	0.86
1*f*	0.81	1.11	3.01	0.88[h]
1*g*	0.66	0.80	2.84	0.83[h]
1*h*	0.45	0.50	2.87	0.68
1*i*	1.16	1.71[i]	2.70	1.21[j]
16	1.99	2.56	3.53	1.88
[j]	—	1.85	2.54	1.07
[k]	—	≤1	1.3	≤1

[a]T = 25°C, I = 0.3, [ligand] = 4–5 × 10^{-3} *M*, 50% aq. dioxane.
[b]K_M is defined for $LM^{2+} \rightleftarrows L + M^{2+}$.
[c]Each value is the average of three determinations and has a precision of ±0.06 units or better.
[d]0.0904 *M*.
[e]0.0812 *M*.
[f]Determined as in ref. 12.
[g]0.0854 *M*.
[h]0.0867 *M*.
[i]0.0406 *M*.
[j]Reference 14.
[k]Reference 15.

tion, and a thiol → thiolate ionization at pH ≈ 10. In the presence of Zn^{2+}, however, the titration curve is markedly displaced with 2 equiv. of OH^- being consumed by pH < 6. At pH's in excess of 6.5 visible precipitation occurred which was tied to the consumption of additional OH^-. For best comparison of the data, it is clearly desirable to perform the analogous titrations on pyridine dithiol **10**, but its metal complex precipitated even at low pH. How-

Can. J. Chem. Downloaded from www.nrcresearchpress.com by 210.87.254.105 on 09/05/12
For personal use only.

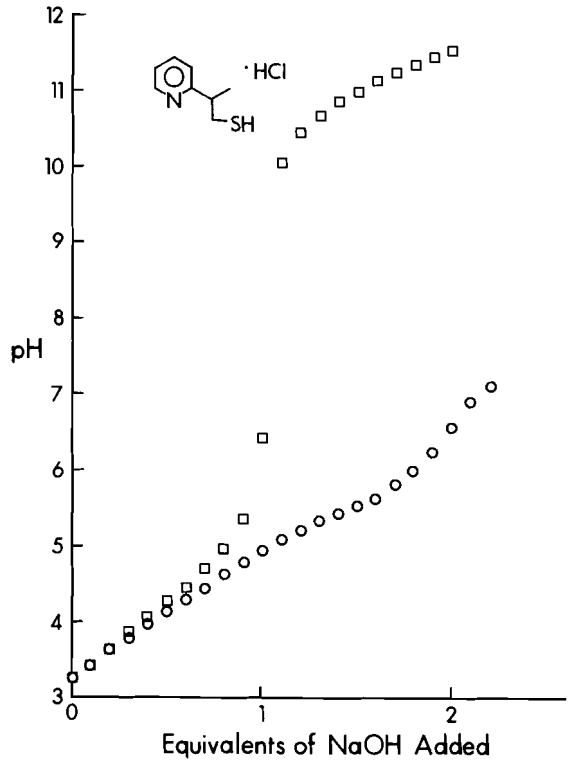

FIG. 3. A plot of the titration curve for **17** (pH vs. equivalents of NaOH added) in the absence (□) and presence of 1 equiv. of Zn^{2+} in 50% aq. dioxane, $I = 0.3$, $T = 25°C$. The deviation in the latter plot at pH > 6.5 is tied to visible precipitation of some species.

ever, the analogous imidazoles **11** and **12** proved more soluble, and their titration curves are shown in Fig. 4. For both species in the absence of metal one sees the imidazolium → imidazole pK_a of ~5.4, and a further titration of thiol at ~pH 9.4 (Table 4). In the presence of Zn^{2+}, however, the situation is very different, and in both cases one sees the consumption of 3 equiv. of OH^- at pH values less than 6. While no visible precipitation occurs up to pH 6, at higher values the complexes precipitated.

On the basis of the above, the additional consumption of 2 equiv. of OH^- can be most adequately explained as having arisen from the formation of stable thiolate complexes such as **20** which may neutralize the metal's charge sufficiently to render the complex insoluble.

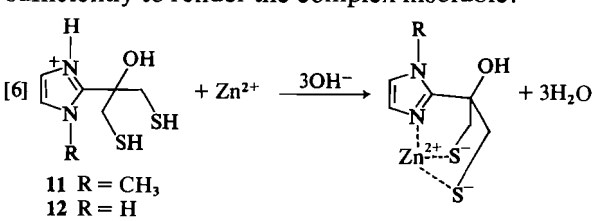

11 R = CH_3
12 R = H

Discussion

Mechanisms for the reduction of carbonyls by ADH involve the active site Zn^{2+} acting as a Lewis acid catalyst to activate the carbonyl for the reduction by NADH by inner sphere coordination of the carbonyl oxygen (1*e*, *g*, 19). Spectroscopic measurements on a chromophoric aldehyde support direct coordination of the aldehyde carbonyl (19*b*, *c*), and electronic substituent effects on the ADH catalysed reduction of substituted benzaldehydes have been used to support the Lewis acid mechanism (19*e*). Variations of this general mechanism which involve concerted H^- delivery from the NADH to the Zn^{2+} coordinated carbonyl and syncronous (20*a*) or stepwise (20*b*) delivery of H^+ from an additional Zn^{2+} coordinated H_2O. (For a recent review of other evidence for involvement of substrate and Zn^{2+} in the active site see ref. 21.)

An alternative role for the Zn^{2+} ion was proposed (22) based on nmr studies of the Co^{2+} substituted enzyme and involves a Zn^{2+} bound water molecule which functions as a protonic acid base catalyst in the facilitation of hydride transfer from the NADH to the C=O.

Additional mechansims involving electron transfer followed by H· transfer from the NADH to the metal-coordinated carbonyl have been proposed (23, 24). Recent work of van Eikeren *et al.* (25) has demonstrated the viability of the electron transfer mechanism in reductions of pyridyl ketones with *N*-propyl-1,4-dihydronicotinamides and supports this previously suggested mechanism. It is not clear, however, whether the metal-ion catalysed reductions proceed by a stepwise electron, H· transfer. Recent work by Ohno *et al.* (26) on the Mg^{2+} catalysed reduction of thiopivalophenone and methyl benzoyl formate by 1-benzyl-1,4-dihydronicotinamide (BNAH) leads these authors to propose that in some cases, a metal ion can lower the transition state for electron transfer from the dihydronicotinamide to the coordinated carbonyl; in other cases, the metal stabilizes the overall transition state for reduction. Additional workers (27) have reported on the basis of the discrepancy between kinetic isotope effects and product isotope yields, the existence of at least one intermediate in the reduction of α,α,α-trifluoroacetophenone (27) and 1,10-phenanthroline-2-carboxaldehyde (4*b*) by BNAH or its analogs.

It would appear that regardless of the exact mechanism which is adopted by the enzyme during reduction, the *positive* character of the metal must be involved either as a Lewis acid for C=O polarization, ketyl radical anion stabilization, or to re-

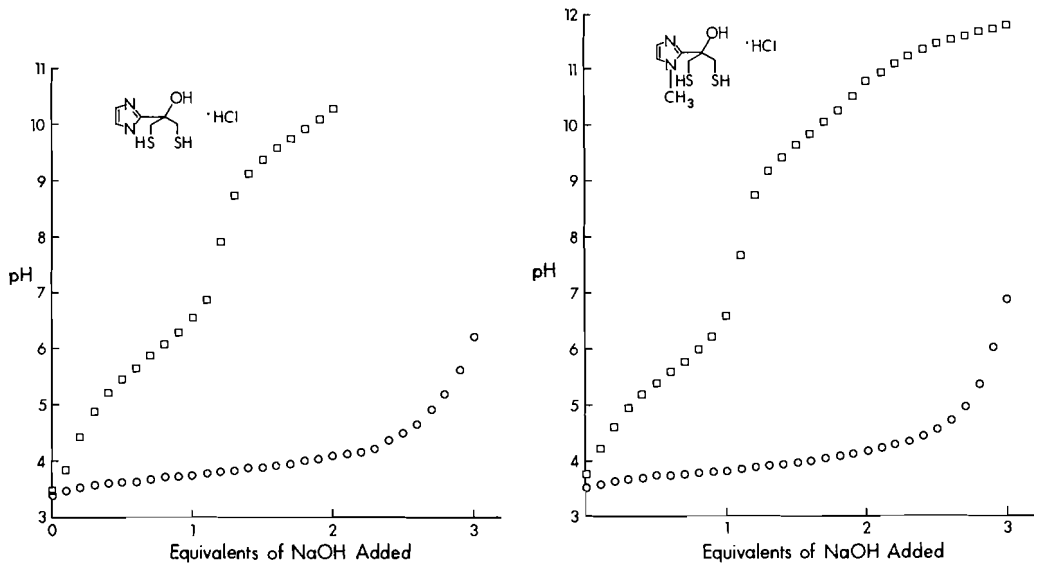

FIG. 4. A plot of the titration curves for imidazoles **11** and **12** (pH vs. equivalents of NaOH added) in the absence (□) and presence (○) of 1 equiv. of Zn^{2+} in 50% aq. dioxane, $I = 0.3$, $T = 25°C$. The similarity of both curves in the presence of Zn^{2+} indicates that the titration of an imidazole (N—H) proton is not occurring.

duce the pK_a of a Zn^{2+} bound H_2O enough to facilitate proton transfer reactions which accompany the reduction. It is expected then that inside the active site of the enzyme the net (+) charge of the metal at the time of C=O reduction should be an important factor. The titration data on the metal complexes of ligands **11** and **12**, however, indicate that at pH values in excess of 6 (where the enzyme operates), both thiols are completely deprotonated and therefore the Zn^{2+} charge is effectively neutralized. A hydrophobic environment in the active site would only serve to favor this charge neutralization.

In a preliminary form we have looked at the reduction of ligand **14** which contains an acetyl group at the 6-position of the pyridine. For reasons of solubility of the Zn^{2+} complex, the solvent system required to dissolve 3×10^{-3} *M* in each of **14**, $ZnCl_2$, and *N*-propyl-1,4-dihydronicotinamide (PNAH) was 90% (v/v) HMPA/H_2O. With 2 equiv. of added HCl (to make an acidic environment), a rapid loss of PNAH was observed by monitoring the absorbance at 350 nm. This was clearly tied to the acid catalysed hydration of PNAH (25, 28) as was evidenced by a characteristic isosbestic point at 310–315 nm. For **14**, PNAH, and $ZnCl_2$ in the same solvent system but with 1 equiv. of added NaOH, we observed a slow loss of PNAH (14% over 21 h) which again was tied to the formation of the hydrated product. Apparently in this medium we have no evidence to support a Zn^{2+} promoted reduction of **14** by PNAH. This seems disturbing in light of the considerable number of examples of 2-pyridyl aldehyde and ketone reduction by PNAH or BNAH which are catalysed by Zn^{2+} or Mg^{2+} (4, 26, 29). However, none of the latter examples utilizes a metal-binding site which contains an anionic ligand and therefore the electrophilicity of the metal in these cases was considerable. Metal coordinated acetyl acetonates also do not reduce under conditions where α-pyridyl ketones or α-keto esters do, presumably because the negatively charged acetylacetonate deadens the M^{2+} charge (26*b*). Although we do not know the detailed reasons for the lack of reducibility of Zn^{2+} bound **14**, we believe it is due to the fact that the deprotonated thiols reduce the electrophilicity of the metal sufficiently so that it either does not bind the pyridyl ketone, or does not interact sufficiently with the C=O group to promote reduction. While on the basis of the above one can only speculate about the analogous catalytic process in the enzyme, one might wonder about the Zn^{2+} electrophilicity if both the cysteine thiolates are coordinated to the metal during the reduction step. Similarly one might wonder about mechanisms which involve a $Zn^{2+}—OH_2 \rightleftarrows Zn^{2+}—OH$ ionization which facilitates proton transfers during the reduction (2) if Zn^{2+} already has two anionic groups attached to it. More work will be required to assess the importance of the state of ionization of the Zn^{2+}-bound sulfhydryl groups in the redox process, and further work is in progress in these laboratories to this end.

Can. J. Chem. Downloaded from www.nrcresearchpress.com by 210.87.254.105 on 09/05/12
For personal use only.

Can. J. Chem. Downloaded from www.nrcresearchpress.com by 210.87.254.105 on 09/05/12
For personal use only.

Experimental

Melting and boiling points are uncorrected. Routine ir and nmr spectra were respectively obtained using a Nicolet FTIR Spectrophotometer ($CHCl_3$ cast film) and either a Varian A-60 or Varian HA-100-15 (Fourier transform modifications provided by a Digilab FTS NMR-3 System). Titration data were obtained using equipment and methods outlined in ref. 12.

Ketones (5)

Syntheses of the thio ether containing ketones were accomplished by one of two methods outlined below for the preparation of bis-1,3-dithiomethyl acetone (**5***a*, method A) and bis-1,3-di(*p*-tolylthio)acetone (**5***e*, method B).

Method A

To a solution of 8.0 g (0.2 mol) NaOH in 100 mL of 95% ethanol held at −20°C was added 9.2 g (0.2 *m*) of CH_3SH which had previously been condensed in a cold trap. After warming to room temperature, this solution was added over 30 min to a stirred solution of 12.7 g (0.1 mol) of 1,3-dichloroacetone[2] in 100 mL of 95% ethanol. After stirring for 12 h, the resultant mixture was poured onto 100 g of ice and left for 30 min. After extraction of this mixture with CH_2Cl_2 (3 × 100 mL), the combined extracts were dried (Na_2SO_4), and stripped of solvent to yield an oil which was distilled to give 13.0 g (87%) of **5***a* (bp 53°C/0.55 Torr, lit. 106–109°C/9 Torr (Table 1)).

Method B

A solution of 8.0 g (0.2 mol) NaOH in 150 mL 98% EtOH was added over a 30 min period at room temperature to a stirred solution of 24.8 g (0.2 mol) *p*-methylthiophenol and 12.7 g (0.1 mol) 1,3-dichloroacetone.[2] After stirring for 12 h the mixture was poured onto 100 g ice, and the mixture left for 30 min. The resulting solid was filtered and recrystallized from methanol to give 20.6 g (68%) of **5***e* (mp 65–66°C; lit. 66–67°C, Table 1).

*Ketone 5*i

(3,5-Dithia-4,4-dimethylcyclohexanone (**5***i*)) was prepared from 3,5-dithia-4,4-dimethylcyclohexanol (**7**) as below.

To a solution of 24.8 g (0.2 mol) 1,3-dimercapto-2-propanol (**6**) and 11.8 g (0.2 mol) dry acetone in 200 mL $CHCl_3$ cooled to 0°C was cautiously added 10 mL BF_3:etherate. After 18 h at 5°C, the opaque mixture was washed with 100 mL aq. Na_2CO_3, water, and dried over Na_2SO_4. Following solvent removal, the residue was fractionally distilled to give 19.5 g (59%) of the alcohol (**7**) as a colorless oil (bp 58°C/0.08 Torr). Considerable decomposition of the material accompanies distillation but nmr analysis of the crude product indicates >90% yield. Nmr ($CDCl_3$) δ: 1.62 (s, 3H); 1.74 (s, 3H); 2.6–3.3 (m, 4H); 3.6 (d, 1H); 3.9 (m, 1H). *Anal.* calcd. for $C_6H_{12}S_2O$: C 43.87, H 7.36, S 39.03; found: C 43.61, H 7.38, S 38.86.

The ketone (**5***i*) (Table 1) was prepared from **7** in low and erratic yields by either pyridine/$Pb(OAc)_4$ oxidation (30*a*) or Moffatt oxidation (30*b*).

*Ketone 5*j

1,3-Dimercapto acetone[1] (12.2 g, 0.1 mol) in 300 mL dry THF was cooled to −5°C and 0.2 mol of *n*BuLi were added such that the temperature did not exceed 0°C. After stirring an additional 1 h, the cream-colored suspension was cooled to −65°C and 20.8 g (0.22 mol) of $ClCH_2OCH_2CH_3$ in 50 mL dry THF was added over 30 min. The mixture was left to warm up and stir overnight and then 200 mL H_2O were added, the THF layer separated, and the aqueous layer extracted with 2 × 100 mL ether. The combined organic extracts were dried and the solvent removed *in vacuo*. Distillation of the residue from a preheated oil bath (130°C) yielded 18.8 g (80%) of **5***j* as a pale yellow liquid; bp 115°C/0.1 Torr, nmr (Table 1). *Anal.* calcd. for $C_9H_{18}O_2S_2$: C 45.35, H 7.61, S 26.90; found: C 45.36, H 7.67, S 26.88.

*Ketone 5*k

This was prepared in a similar fashion to **5***j* by the sequential addition of 1 equiv. *n*BuLi (−50°C) 1 equiv. $ClCH_2OCH_2CH_3$ (−65°C), 1 equiv. *n*BuLi (−65°C) and 1.2 equiv. CH_3I to a stirred solution of 1,3-dimercaptoacetone in THF. After warming to room temperature overnight, 100 mL H_2O was added, and the mixture worked up as for **5***j*. Yield (after 3 fractional distillations) 4.7 g (24%) as a pale yellow liquid, bp 75°C/0.05 Torr. Satisfactory analyses could not be obtained for **5***j* so it was subjected to the pyridyl formation in an impure state (*vide infra*).

The alcohols in Table 2 were prepared by the general method outlined below.

*2-Lithiopyridine (5*a)

A solution of 14.2 g (0.09 mol) of 2-bromopyridine in 150 mL dry THF or ether was cooled to −65°C under N_2. Then 0.09 *m* of *n*BuLi (~2 *M* in hexane) was added via syringe at such a rate that the temperature did not rise above −55°C. After 15 min stirring at −50°C (not above −50°C to avoid decomposition) the red-brown solution was cooled to −65°C for subsequent use.

*Preparation of Alcohol 1*a

A solution of 4.50 g (0.03 mol) of ketone **5***a* in 50 mL of dry THF was added dropwise to 0.09 mol of 2-lithio pyridine (prepared as above) at −65 to −60°C. After stirring for 2 h at −65°C and having warmed to −40°C, the mixture was quenched by the addition of 50 mL water, and then brought to room temperature. Then 50 mL more H_2O were added, and the THF layer separated. The remaining aqueous layer was extracted with 2 × 100 mL ether, and the combined organic layers dried (Na_2SO_4), stripped, and the residue put on a vacuum line to remove pyridine. This residue was taken up in 200 mL ether, and dry HCl gas passed into the solution until no more precipitate appeared. The oily precipitate was triturated with acetone and recrystallized twice from $CHCl_3/CH_3OH$ to give 3.24 g (42%) of **1***a* as its HCl salt; mp 170–172°C. *Anal.* calcd. for $C_{10}H_{10}NOS_2Cl$: C 45.11, H 6.02, N 5.26; found: C 45.08, H 6.12, N 5.35. Spectral data are given in Table 2.

The alcohols which contain the free thiol functionality (Table 3) were prepared as follows.

Preparation of Alcohol 10

A solution of 0.09 mol of 2-pyridyl lithium was prepared as above (150 mL ether) and kept at −65°C. Ketone **5***j* (7.14 g, 0.03 mol) in 50 mL of ether was added over 30 min and the mixture stirred at −65°C. It was then warmed to −40°C and 50 mL saturated NH_4Cl added. After the solution had been brought to >0°C, 200 mL H_2O was added, the ether layer was separated, and the aqueous layer extracted with ether (2 × 100 mL). The combined ether extracts were dried (Na_2SO_4) and the volatiles removed *in vacuo*. The residue was then dissolved in ether (200 mL) and extracted with 6 × 50 mL of 3 *M* aq. HCl. Neutralization of the acid extracts with solid K_2CO_3 followed by $CHCl_3$ extraction (4 × 100 mL), drying and evaporation gave the addition product in reasonably pure form; nmr ($CDCl_3$) δ: 1.2 (t); 3.3 (ABq); 3.5 (q); 4.6 (s); 5.0 (s, Br); 7.0–7.7 (m); 8.4–8.6 (m).

This residue was then dissolved in 20 mL of 4:1 (v/v) CH_3CN/H_2O, and a solution of 16.3 g (0.06 mol) $HgCl_2$ in 130 mL of 20% aq. CH_3CN added which caused the rapid formation of a precipitate accompanied by H^+ release (solution became acidic). After 4 h stirring, the mixture was filtered and the precipitate washed with 200 mL H_2O. The solid was then slurried with 200 mL H_2O with rapid stirring and H_2S passed

[2]1,3-Dichloroacetone is a powerful lachrymator and vesicant and should be handled with due caution.

Can. J. Chem. Downloaded from www.nrcresearchpress.com by 210.87.254.105 on 09/05/12
For personal use only.

through for 6 h after which the resultant black mixture was treated with solid K_2CO_3 to raise the pH to 8, and then continuously extracted with ether under a nitrogen atmosphere. The ether extract was dried, filtered, and dry HCl passed through. The resultant oil crystallized on standing, and the solid material vacuum dried to give 1.75 g (25%) of **10** as pale yellow crystals: mp 158–160°C. *Anal.* calcd. for $C_8H_{12}NOS_2Cl$: C 40.41, H 5.09, N 5.89, Cl 14.91; found: C 40.54, H 5.14, N 6.07, Cl 14.87.

Alcohol 13 was obtained similarly but using ketone **5***k* as a starting material; mp 162–164°C (HCl) (Table 3). *Anal.* calcd. for $C_9H_{14}NOS_2Cl$: C 42.93, H 5.60, N 5.60, S 25.47; found: C 42.96, H 5.64, N 5.51, S 25.34.

Alcohol 11

This was obtained by the addition of 2-lithio-*N*-methylimidazole (prepared analogously to 2-lithio pyridine but by H^+ abstraction from *N*-methylimidazole) to ketone **5***j*. Workup as for alcohol **10** with the exception of the final HCl salt formation with dry HCl gave **11**, mp 119–121°C. *Anal.* calcd. for $C_7H_{12}N_2OS_2$: C 41.15, H 5.92, N 13.71, S 31.39; found: C 41.28, H 5.90, N 13.70, S 31.55.

Alcohol 12

This was prepared by the addition of 2-lithio-1-(bisethoxy methyl)imidazole (31) to ketone **5***j*. Deprotection of the imidazole nitrogen was followed by a similar extraction and isolation procedure as for **11**, mp 106–107°C (Table 3). *Anal.* calcd. for $C_6H_{10}N_2S_2O$: C 37.87, H 5.30, N 14.72, O 8.41, S 33.70; found: C 38.21, H 5.24, N 14.51, O 8.64, S 34.03.

Alcohol 14

This was prepared by the addition of the ethylene ketal of 6-acetyl-2-lithiopyridine to ketone **5***j* analogously to the procedure for **10**. The reaction mixture after the addition of saturated aq. NH_4Cl was washed with 3 × 150 mL of 0.1 *M* HCl followed by 4 × 100 mL of 3 *M* HCl; the latter extracts contained the addition product. After standing for 24 h (to hydrolyse the ethylene ketal) the latter acid extract was neutralized with solid K_2CO_3 and extracted with $CHCl_3$ (3 × 100 mL). The cleavage of the ethoxymethylthio groups was effected as before, and the product was obtained as a colorless gel after column chromatography over SiO_2 ($CHCl_3$) of the material isolated from the continuous ether extract; mp (Table 3). *Anal.* calcd. for $C_{10}H_{13}NO_2S_2$: C 49.36, H 5.38, N 5.76, O 13.15; found: C 49.65, H 5.28, N 5.99, O 13.02.

Alcohol 15

This was prepared following the route described for **14** except that the 6-acetyl group on the pyridine (ethoxymethylthio) compound was reduced with 200 mol% $NaBH_4$ in absolute ethanol at room temperature. TLC analysis showed the reaction to be completed in less than 1 h. The product was prepared analogously to **14** except that it was isolated as its HCl salt without chromatography (Table 3). *Anal.* calcd. for $C_{10}H_{15}NO_2S_2 \cdot HCl$: C 42.62, H 5.72, N 4.97, O 11.35, S 22.75; found: C 42.65, H 5.60, N 4.78, O 11.63, S 22.70.

Acknowledgements

The authors gratefully acknowledge the support of the University of Alberta and the Natural Sciences and Engineering Research Council of Canada.

1. (*a*) J. P. Rosenbusch and K. Weber. Proc. Natl. Acad. Sci. U.S.A. **68**, 1019 (1971); (*b*) G. Rotilio, L. Calabrese, F. Bossa, D. Barra, A. F. Agro, and B. Mondovi. Biochemistry, **11**, 2182 (1972); (*c*) J. H. R. Kägi and B. L. Vallee. J. Biol. Chem. **236**, 2435 (1961); (*d*) D. R. Bevin, P. Bodlaender, and D. Shemin. J. Biol. Chem. **255**, 2030 (1980); (*e*) C. I. Brändén, H. Jörnvall, H. Eklund, and B. Furugren. *In* The enzymes. Vol. 11. *Edited by* P. D. Boyer. 1975. p. 103; (*f*) C. I. Brändén *et al.* Proc. Natl. Acad. Sci. U.S.A. **70**, 2439 (1973); (*g*) H. Eklund and C. I. Brändén. J. Biol. Chem. **254**, 3458 (1979); (*h*) J. B. Jones and J. F. Beck. *In* Application of biochemical systems in organic chemistry. Vol. 1. J. Wiley and Sons, New York, NY. 1976. p. 107.
2. (*a*) P. M. Colman, H. C. Freeman, J. M. Guss, M. Murata, V. A. Norris, J. A. M. Ramshaw, and M. P. Venkatappa. Nature, **272**, 319 (1978), and references therein; (*b*) A. J. Fee. Struct. Bonding, Berlin, **23**, 1 (1975); (*c*) B. Reinhammer. *In* Advances in inorganic biochemistry. Vol. 1. *Edited by* G. L. Eichhorn and L. G. Marzilli. Elsevier, New York. 1979. pp. 91–118; (*d*) C. Bergman, E. K. Gandvik, P. O. Nyman, and L. Strid. Biochem. Biophys. Res. Commun. **77**, 1052 (1977); (*e*) J. Peisach, W. G. Levine, and W. E. Blumberg. J. Biol. Chem. **242**, 2847 (1967).
3. (*a*) R. D. Bereman, M. R. Churchill, and G. Shields. Inorg. Chem. **18**, 3117 (1979) and references therein; (*b*) J. V. Dagdigian and C. A. Reed. Inorg. Chem. **18**, 2623 (1979) and references therein; (*c*) T. E. Jones, D. B. Rorabacher, and L. A. Ochrymowicz. J. Am. Chem. Soc. **97**, 7485 (1975); (*d*) V. Srinivasan, E. I. Stiefel, A. Elsberry, and R. A. Walton. J. Am. Chem. Soc. **101**, 2611 (1979) and references therein; (*e*) V. M. Miskowski, J. A. Thich, R. Solomon, and H. J. Schugar. J. Am. Chem. Soc. **98**, 8344 (1976); (*f*) J. S. Thompson, T. J. Marks, and J. A. Ibers. J. Am. Chem. Soc. **101**, 4180 (1979) and references therein.
4. (*a*) D. J. Creighton and D. S. Sigman. J. Am. Chem. Soc. **93**, 6314 (1971); (*b*) D. J. Creighton, J. Hajdu, and D. S. Sigman. J. Am. Chem. Soc. **98**, 4619 (1976); (*c*) S. Shinkai and T. C. Bruice. Biochemistry, **12**, 1750 (1973); (*d*) S. Shinkai and T. C. Bruice. J. Am. Chem. Soc. **94**, 8258 (1972); (*e*) S. Trivić and V. Leskovac. J. Mol. Catal. **2**, 129 (1977); (*f*) A. Ohno, T. Kimura, S. G. Kim, H. Yamamoto, S. Oka, and Y. Ohnishi. Bioorg. Chem. **6**, 21 (1977); (*g*) Y. Ohnishi, M. Kagami, and A. Ohno. J. Am. Chem. Soc. **97**, 4766 (1975); (*h*) L. E. Overman. J. Org. Chem. **37**, 4214 (1972); (*i*) R. A. Gase and U. K. Pandit. J. Am. Chem. Soc. **101**, 7059 (1979).
5. (*a*) J. E. Parks, B. E. Wagner, and R. H. Holm. J. Organomet. Chem. **56**, 53 (1973); (*b*) J. E. Parks, B. E. Wagner, and R. H. Holm. Inorg. Chem. **10**, 2472 (1971).
6. H. Stetter, K. Dieminger, and E. Rauscher. Ber. **92**, 2057 (1959).
7. E. Howard and R. V. Lindsey. J. Am. Chem. Soc. **82**, 152 (1960).
8. (*a*) L. Schotte. Acta Chem. Scand. **4**, 1364 (1950); (*b*) Ark. Kemi, **5**, 533 (1953).
9. E. J. Corey and M. G. Bock. Tetrahedron Lett. 3269 (1975).
10. (*a*) B. Emmert and E. Asendorf. Chem. Ber. **72**, 1188 (1939); (*b*) L. Bauer and L. A. Gardella. J. Org. Chem. **26**, 82 (1961).
11. A. Albert and E. P. Serjeant. Ionization constants of acids and bases. J. Wiley and Sons, New York, NY. 1962.
12. H. S. Simms. J. Am. Chem. Soc. **48**, 1239 (1920).
13. R. S. Brown and J. Huguet. Can. J. Chem. **58**, 889 (1980).
14. (*a*) K. Kahmann, H. Sigel, and H. Erlenmeyer. Helv. Chim. Acta, **47**, 1754 (1964); (*b*) E. Gonick, W. C. Fernelius, and B. E. Douglas. J. Am. Chem. Soc. **76**, 4671 (1954).
15. (*a*) J. Bjerrum. Chem. Rev. **46**, 381 (1950); (*b*) R. J. Bruehlmann and F. H. Verhoek. J. Am. Chem. Soc. **70**,

1401 (1948); (*c*) A. GERO and J. J. MARKHAM. J. Org. Chem. **16**, 1835 (1951).
16. (*a*) H. C. BROWN and X. R. MIHM. J. Am. Chem. Soc. **77**, 1723 (1955); (*b*) C. GOLUMBIC and M. ORCHIN. J. Am. Chem. Soc. **72**, 4145 (1950).
17. (*a*) E. E. MARTELL and R. M. SMITH. Critical stability constants. Vol. 3. Plenum Press, New York. 1977; (*b*) D. L. LEVSSING and T. N. TISCHER. J. Am. Chem. Soc. **83**, 65 (1961).
18. D. L. LEVSSING and G. S. ALBERTS. J. Am. Chem. Soc. **82**, 4458 (1970).
19. (*a*) R. H. ABELES, R. F. HUTTON, and F. WESTHEIMER. J. Am. Chem. Soc. **79**, 712 (1957); (*b*) M. F. DUNN and J. S. HUTCHINSON. Biochemistry, **12**, 4882 (1973); (*c*) M. F. DUNN, J.-F. BIELLMANN, and G. BRANLANT. Biochemistry, **14**, 3176 (1975); (*d*) H. R. MAHLER and J. DOUGLAS. J. Am. Chem. Soc. **79**, 1159 (1957); (*e*) J. W. JACOBS *et al.* Biochemistry, **13**, 60 (1974).
20. (*a*) R. T. DWORSCHACK and B. V. PLAPP. Biochemistry, **16**, 2716 (1977); (*b*) J. SCHMIDT, J. CHEN, M. DETRAGLIA, D. MINKEL, and J. T. MCFARLAND. J. Am. Chem. Soc. **101**, 3634 (1974).
21. M. HUGHES and R. H. PRINCE. Bioorg. Chem. **6**, 137 (1977).
22. D. SLOAN, M. YOUNG, and A. S. MILDVAN. Biochemistry, **14**, 1988 (1975).
23. E. M. KOSOWER. *In* Flavins and flavoproteins. *Edited by* E. Slater. Elsevier, Amsterdam. 1966. p. 1.
24. (*a*) T. C. BRUICE. *In* Progress in bioorganic chemistry. Vol. 4. *Edited by* E. T. Kaiser and F. J. Kezdy. Wiley-Interscience. 1976. p. 1; (*b*) M. F. DUNN. Struct. Bonding, **23**, 61 (1975).
25. P. VAN EIKEREN, D. L. GRIER, and J. ELIASON. J. Am. Chem. Soc. **101**, 7406 (1979) and references therein.
26. (*a*) A. OHNO, S. YASUI, H. YAMAMOTO, S. OKA, and Y. OHNISHI. Bull. Chem. Soc. Jpn. **51**, 294 (1978); (*b*) A. OHNO. Private communication; (*c*) A. OHNO, S. YASUI, and S. OKA. Bull. Chem. Soc. Jpn. In press.
27. J. J. STEFFENS and D. M. CHIPMAN. J. Am. Chem. Soc. **93**, 6694 (1971).
28. C. C. JOHNSTON, J. L. GARDNER, C. SUELTER, and D. E. METZLER. Biochemistry, **2**, 689 (1963).
29. (*a*) A. OHNO, S. YASUI, R. A. GASE, S. OKA, and U. K. PANDIT. Bioorg. Chem. **9**, 199 (1980); (*b*) A. OHNO, S. YASUI, and S. OKA. Bull. Chem. Soc. Jpn. To be published.
30. (*a*) R. E. PARTCH. J. Org. Chem. **30**, 2498 (1968); (*b*) J. G. MOFFATT. Org. Synth. Coll. Vol. V, 242 (1973).
31. N. J. CURTIS and R. S. BROWN. J. Org. Chem. **45**, 4038 (1980).
32. J. HILL. J. Chem. Soc. C, 463 (1970).
33. C. PIANTADOSI, I. H. HALL, S. D. WYNCK, and K. S. ISHAQ. J. Med. Chem. **19**, 222 (1976).
34. E. G. HOWARD and R. V. LINDEY. J. Am. Chem. Soc. **82**, 158 (1960).

Can. J. Chem. Downloaded from www.nrcresearchpress.com by 210.87.254.105 on 09/05/12
For personal use only.

Photolysis of heptamethylbenzenonium cation in aqueous acids. Preparation of pentamethylcyclopentadiene

RONALD F. CHILDS, MAUNG ZEYA, AND ROBERT P. DAIN
Department of Chemistry, McMaster University, Hamilton, Ont., Canada L8S 4M1

Received July 9, 1980

RONALD F. CHILDS, MAUNG ZEYA, and ROBERT P. DAIN. Can. J. Chem. **59**, 76 (1981).

Irradiation of heptamethylbenzenium ion in a variety of aqueous acids using light of wavelength greater than 350 nm leads to the formation of pentamethylcyclopentadiene and acetone. In 50% HBF_4 and 70% $HClO_4$ this photolysis is very clean and can be used as a convenient preparation of pentamethylcyclopentadiene. A mechanism is proposed for the reaction.

RONALD F. CHILDS, MAUNG ZEYA et ROBERT P. DAIN. Can. J. Chem. **59**, 76 (1981).

En irradiant l'ion heptaméthylbenzénium dans différentes solutions aqueuses d'acide, par une lumière dont la longueur d'onde est supérieure à 350 nm, on obtient le pentaméthylcyclopentadiène et l'acétone. Dans le HBF_4 à 50% et dans le $HClO_4$ à 70%, cette photolyse se fait proprement et peut être utilisée comme méthode convenable de préparation du pentaméthylcyclopentadiène. On propose un mécanisme pour cette réaction.

[Traduit par le journal]

Benzenonium ions undergo an efficient and very clean photoisomerization to give bicyclo[3.1.0]-hexenyl cations (1–3). This seemingly very general photoisomerization could be a synthetically useful route to derivatives of bicyclo[3.1.0]hexene. However, the usefulness of this reaction is curtailed by two factors. The first of these is the facile thermal valence isomerization of the bicyclohexenyl cations to the starting benzenonium ions which necessitates the use of low temperatures for the photoreaction. Secondly, the recovery of the photoproducts from large volumes of such strong acids as FSO_3H and H_2SO_4 which are generally used for these reactions becomes problematical as the reactions are scaled up.

In an attempt to overcome these difficulties we have examined the photoreactions (1, 2) of heptamethylbenzenonium ion, **1** (4, 5), in a variety of weaker acids. The intent of this study was to try and find an acid medium in which **1** was stable but its photoproduct **2** would react with a nucleophile

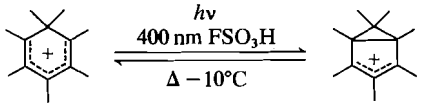

1 **2**

to give a kinetically stable material. This could allow the photoreaction to be carried out at room temperature and, if a weaker acid were used, facilitate product isolation Precedent for this type of approach comes from the early work of van Tamelen and co-workers on the tropylium, trityl, and cyclopropenium cations (6).

Results and Discussion

Cation **1** was obtained by protonation of **3** (4, 5). The triene **3** is a sufficiently basic hydrocarbon ($pK_a = 1.38$ (7)) to allow preparation of solutions of **1** in a variety of acids. Those used in this study included 96%, 24%, and 13% H_2SO_4, 5 *M* HCl, 70% $HClO_3$, 50% HBF_4, and CF_3COOH. ^1H nuclear magnetic resonance spectra of solutions of **3** in

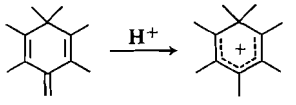

3 **1**

these acids indicated complete protonation and the presence of **1**. Over the time span of the photochemical reactions these solutions of **1** were stable at room temperature. When left for extended periods of time, particularly with aqueous HCl, **1** slowly degraded to hexamethylbenzene (4).

Irradiations of **1** were carried out using light of wavelength greater than 350 nm to ensure that the cation was the only absorbing species. A series of qualitative irradiations were carried out in nmr tubes using the acids listed above. The extent of reaction was monitored by ^1H nmr spectroscopy. With the exception of 96% H_2SO_4, a photoreaction was observed in all the acid solutions as shown by the loss of the resonances attributable to **1**. In the case of 96% H_2SO_4 no reaction could be detected when the solution was irradiated for 20 times the length of time required for complete reaction in the other acids.

With 24 and 13% H_2SO_4 and 5 *M* HCl as solvents a precipitate was formed during the course of the

0008-4042/81/010076-04$01.00/0
©1981 National Research Council of Canada/Conseil national de recherches du Canada

Can. J. Chem. Downloaded from www.nrcresearchpress.com by 210.87.254.6 on 09/05/12
For personal use only.

TABLE 1. Summary of photoreactions[a]

Solvent	Observation	^{1}H nmr spectrum of acid solution		Products after neutralization			
					Composition[d]		
		Acetone/H^{+b}	4/5	Recovery	4	HMB[e]	Involatile
96% H_2SO_4	No reaction						
24% H_2SO_4	Precipitate	2.20	B[c]	92%	84%	—	16%
13% H_2SO_4	Precipitate	2.20	B[c]	—			
5% H_2SO_4	Precipitate	2.20	B[c]	—			
5 *M* HCl	Precipitate	2.20	B[c]	99	8	—	92
CF_3COOH	Homogeneous	2.20	5[f]	81	64		36
70% $HClO_4$	Homogeneous	2.67	5[f]	88	97		—
50% HBF_4	Oily layer	2.17	B[c]	90	88	7	—

[a]All reactions at 25°C using light of wavelength greater than 350 nm.
[b]^{1}H nmr chemical shift of singlet associated with acetone.
[c]B, broad signal centered at δ 1.4.
[d]By glpc analysis.
[e]Hexamethylbenzene.
[f]Signals at δ 3.43, 3.08, 2.80, 2.13, 1.42, and 1.34.

irradiation. The ^{1}H nmr spectrum of the solution obtained after all **1** had been photoreacted showed a sharp singlet at δ 2.2 and a broad signal at δ 1.4. Neutralization of the acid led to a high recovery of organic material (>90%) containing varying quantities of a volatile compound and an intractable "polymer". The volatile component was identified as pentamethylcyclopentadiene, **4**, by comparison

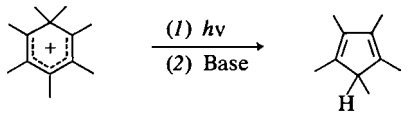

1 **4**

5 *M* HCl, 24 and 13% H_2SO_4

of its properties with an authentic sample (8). The yield of **4** was much higher in the H_2SO_4 solutions (78% in 24% H_2SO_4) than with the HCl solutions, Table 1.

When $HClO_4$ and CF_3COOH were used as solvents no precipitate was formed on irradiation of **1**. Instead the ^{1}H nmr spectrum indicated the presence of the *cis* and *trans* isomers of protonated pentamethylcyclopentadiene, **5** (9), together with a sharp singlet whose position varied according to the acid used (δ 2.67, $HClO_4$; δ 2.20, CF_3COOH). Addition of a small amount of acetone to each of these solutions caused these signals to be enhanced in intensity and it would appear that the other photoproduct of these reactions is acetone. The

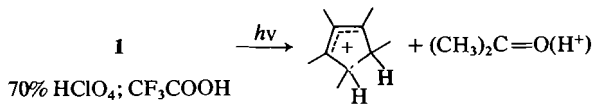

5

cis/*trans* isomers

position of the signals due to the methyl-group resonances of acetone is very dependent on the acid medium used, reflecting different degrees of its protonation (10). Neutralization of these acid solutions led to the recovery of **4** in high yield.

Mechanistic Considerations

A likely sequence of events linking **1** with **4** and acetone is shown in Scheme 1. The photochemically induced isomerization of **1** to **3** is well established to occur in FSO_3H at low temperatures. The reverse thermal isomerization of **2** to **1** is symmetry forbidden and in practice involves a substantial activation energy, $\Delta G^{\ddagger} = 83$ kJ/mol in FSO_3H (1). Provided **2** remains ionic, this barrier appears to be essentially independent of medium and counter-ion changes. In the more nucleophilic, weak acids used in this study, **2** would be expected to either lose a proton or react with a nucleophile to form **6** (11), **7**, **8**, or **9** (12). Ring protonation of **9** would lead to **10** which could fragment to give **4** and protonated acetone. Comparable cleavage reactions have been reported on protonation of 5-acylpentamethylcyclopentadiene and other cyclopentenone derivatives (13).

Support for this scheme comes from the treatment of **8**, prepared by reaction of CH_3Li with 1,3,4,5,6,6 - hexamethylbicyclo[3.1.0]hex - 3 - en - 2-one (5), with 24% H_2SO_4. The ^{1}H nmr spectrum of the solution so obtained was the same as that produced photochemically from **1** in the same medium and neutralization of the acid led to the recovery of **4**.

Synthetic Considerations

Pentamethylcyclopentadiene has been widely used as a ligand in organometallic chemistry. There

Can. J. Chem. Downloaded from www.nrcresearchpress.com by 210.87.254.6 on 09/05/12
For personal use only.

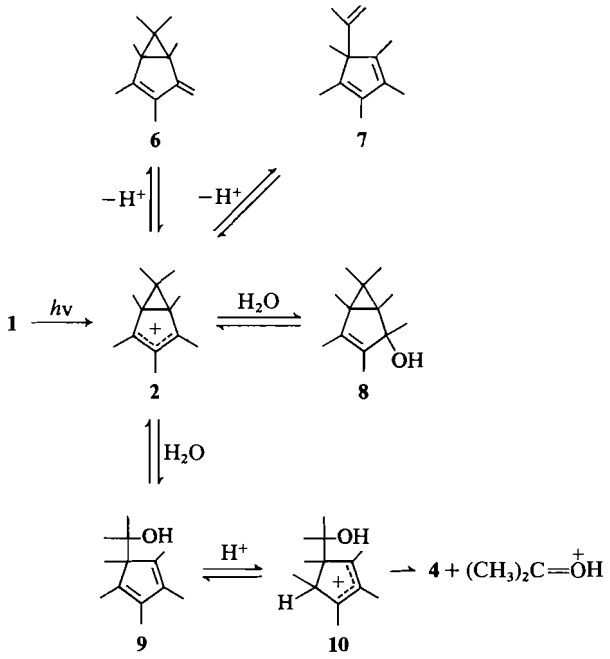

SCHEME 1

are several syntheses reported for this compound. These seem to fall into two main groups, those based on an elaboration of the five-membered ring from acyclic precursors and others based on hexamethyldewarbenzene (8, 14). The results described above suggested an alternative route starting from hexamethylbenzene.

Using a Friedel–Crafts reaction of hexamethylbenzene with $AlCl_3$ and methyl chloride it is possible to obtain the tetrachloroaluminate salt of **1** or the triene **3** in very high yields (4). Irradiation of a solution of **1** (1.5 g) in aqueous HBF_4 using a medium pressure mercury lamp and Pyrex filter led to the production of pentamethylcyclopentadiene in an 80% isolated yield. There seems to be no reason why the reaction could not be scaled up beyond this level and this two-step reaction sequence represents one of the easiest routes to **4**.

Experimental

The nmr spectra were recorded using a Varian EM-390 spectrometer. The chemical shifts of the samples in the aqueous acids were referenced to internal tetramethylammonium tetrafluoroborate taken as δ 3.10. Gas chromatographic analyses were performed using a Varian 3700 gas chromatograph coupled with a Varian CDS 111 integrator, and using a 5 ft × 1/8 in. column packed with 15% Carbowax on Chromasorb W.

Preparation of Acid Solutions of 1

The triene **3** (0.5 g) was dissolved in the appropriate acid by stirring at 0°C. With the aqueous H_2SO_4 solutions it was found to be more convenient to use a smaller amount of a stronger acid in the dissolution step and then add water to the resulting solution to give the appropriate concentration.

Photolyses were carried out using a Phillips SP 500 W super pressure mercury arc lamp. The light beam was arranged to pass through a water filter to remove infrared light and then through a Corning filter No. 3060 with a cutoff at 350 nm. Samples to be irradiated were placed in 10 mm Pyrex tubes and the reactions monitored by ^1H nmr to see when all **1** had been consumed. A typical reaction on the scale indicated above took some 3 h. Results obtained in a variety of acids are summarized in Table 1.

Recovery of photoproducts from the acid solutions was achieved by the slow addition of the acid to a stirred slurry of Na_2CO_3 (10 g) in ether (25 mL) at −78°C. The mixture was allowed to warm to room temperature and the ether layer separated, washed with water (1 × 20 mL), and dried. Removal of the ether *in vacuo* gave an oily residue which was weighed, vacuum transferred (160°C/15 Torr) nm, and analysed by glpc. Results are summarized in Table 1.

Preparative Scale Photolysis

The triene **3** (1.48 g) was added in small quantities to fluoroboric acid (120 mL, 50%) kept at 0°C. The resulting red solution was irradiated with a 125 W Hanovia medium pressure mercury lamp for 24 h at room temperature. (The photoreaction was monitored by ^1H nmr.) An oily liquid separated during the photolysis and this was subsequently extracted with ether (3 × 50 mL). The ether was washed with aqueous $NaHCO_3$ until neutral, with water (1 × 50 mL), and dried over $MgSO_4$. Removal of the ether *in vacuo* gave an oil (1.03 g) which consisted of **4** (90%), hexamethylbenzene (7%), and some minor unidentified components.

3-Methylene1,2,4,5,6,6-hexamethylcyclohex-1,4-diene 3 (4, 5)

Hexamethylbenzene (1.62 g) and $AlCl_3$ (2.0 g) were mixed and placed in a Parr pressure reactor. The reactor was cooled and CH_3Cl (25 g) was added and the mixture allowed to stand at room temperature for 16 h. The excess CH_3Cl was vented off, the remaining solid added to ice/water (80 mL)/ether (20 mL) mixture and the solution basified with NaOH. The ether layer was separated, the aqueous phase reextracted with ether (1 × 20 mL), and the combined ether extracts dried ($MgSO_4$). Removal of the ether *in vacuo* gave **3** (1.70 g, 96.5% yield) contaminated with less than 0.5% hexamethylbenzene.

1,2,3,4,5,6,6-Heptamethylbicyclo[3.1.0]hex-3-en-2-ol, 8

1,3,4,5,6,6-Hexamethylbicyclo[3.1.0]hex-3-en-2-one (0.77 g) in anhydrous ether (20 mL) was treated with methyllithium (6.7×10^{-3} mol in ether) at 25°C for 6 h. Saturated ammonium chloride solution (25 mL) was added and the ether layer separated, washed with water, and dried ($MgSO_4$). Removal of the ether gave **8** as an oil (0.81 g), bp 150°C at 0.5 Torr; ir (film): 3460, 2940, 2880, 1645 cm^{-1}; ^1H nmr δ: 1.85 (s, 1H), 1.55 (s, 6H), 1.20, 1.12, 1.05, and 1.02 (all s, 3H). *Anal.* calcd. for $C_{13}H_{22}O$: C 80.34, H 11.42; found: C 80.50, H 11.22%.

Rearrangement of 8 in 24% H_2SO_4

The alcohol **8** (1 g) was dissolved in 48% H_2SO_4 (20 mL) by stirring at 0°C. Water (20 mL) was added slowly with cooling and the resulting solution allowed to warm to room temperature for 0.5 h. The solution was cooled to 0°C and neutralized by the addition of Na_2CO_3. The organic material was extracted into ether (2 × 20 mL), the ether extract dried ($MgSO_4$), and the ether removed to give an oil (0.69 g). The oil was distilled at 160°C/15 Torr to give 0.65 g of a material which by its ^1H nmr spectrum consisted mainly of **4**. The glpc analysis showed 4 (91%) and hexamethylbenzene (9%) to be the only volatile constituents.

Acknowledgement

This work was supported by the Natural Sciences and Engineering Research Council of Canada.

Can. J. Chem. Downloaded from www.nrcresearchpress.com by 210.87.254.6 on 09/05/12
For personal use only.

1. R. F. CHILDS and S. WINSTEIN. J. Am. Chem. Soc. **96**, 6409 (1974).
2. I. S. ISAEV, V. I. MAMATYUK, L. I. KUZUBOVA, T. A. GORDYMOVA, and V. A. KOPTYUG. Zh. Org. Khim. **6**, 2482 (1970); V. A. KOPTYUG, L. I. KUZUBOVA, I. S. ISAEV, and V. I. MAMATYUK. Zh. Org. Khim. **6**, 2258 (1970); G. A. OLAH, G. LIANG, and S. P. JINDAL. J. Org. Chem. **40**, 3259 (1975).
3. B. D. PARRINGTON and R. F. CHILDS. Chem. Commun. 1581 (1970); R. F. CHILDS, M. SAKAI, B. D. PARRINGTON, and S. WINSTEIN. J. Am. Chem. Soc. **96**, 6403 (1974); J. W. PAVLIK and R. J. PASTERIS. J. Am. Chem. Soc. **96**, 6107 (1974); N. FILIPESCU and J. W. PAVLIK. J. Am. Chem. Soc. **92**, 6062 (1970); R. F. CHILDS, B. D. PARRINGTON, and M. ZEYA. J. Org. Chem. **44**, 4912 (1979).
4. W. VON E. DOERING, M. SAUNDERS, H. G. BOYTON, H. W. EARHART, E. F. WADLEY, and W. R. EDWARDS. Tetrahedron, **4**,178 (1958).
5. H. HART, P. M. COLLINS, and A. J. WARING. J. Am. Chem. Soc. **88**,1005 (1966).
6. E. E. VAN TAMELEN and T. M. COLE. J. Am. Chem. Soc. **93**, 6158 (1971); E. E. VAN TAMELEN, R. H. GREELEY, and H. SCHUMACHER. J. Am. Chem. Soc. **93**, 6151 (1971).
7. H. KUURA and U. HALDNA. Reakts. Sposobn. Org. Soedin. **3**,162 (1966); Chem. Abstr. **66**, 119381c (1967).
8. L. DE VRIES. J. Org. Chem. **25**, 1838 (1960).
9. T. S. SORENSEN, I. J. MILLER, and C. M. URNESS. Can. J. Chem. **48**, 3374 (1970); D. M. BROUWER and J. A. VAN DOORN. Recl. Trav. Chim. Pays-Bas, **89**, 333 (1970).
10. M. BROOKHART, G. C. LEVY, and S. WINSTEIN. J. Am. Chem. Soc. **89**, 1735 (1967); D. M. BROUWER. Recl. Trav. Chim. Pays-Bas, **86**, 879 (1967).
11. H. HART, J. D. DE VRIEZE, R. M. LANGE, and A. SHELLER. Chem. Commun. 1650 (1968).
12. R. CRIEGEE, H. GRUNER, D. SCHONLEBER, and R. HUBER. Chem. Ber. **103**, 3696 (1970).
13. R. F. CHILDS and M. ZEYA. Can. J. Chem. **53**, 3425 (1975); H. HART, I. HUANG, and P. LAVRICK. J. Org. Chem. **39**, 999 (1974).
14. U. BURGER, A. DELAY, and F. MAZENOID. Helv. Chim. Acta, **94**, 3773 (1972); D. FEITLER and G. M. WHITESIDES. Inorg. Chem. **15**, 466 (1976).

Can. J. Chem. Downloaded from www.nrcresearchpress.com by 210.87.254.6 on 09/05/12
For personal use only.

Towards a general scheme for estimating the heats of formation of organic ions in the gas phase. Part I. Odd-electron cations[1]

JOHN L. HOLMES[2] AND MERVIN FINGAS
Department of Chemistry, University of Ottawa, Ottawa, Ont., Canada K1N 9B4
AND
F. P. LOSSING
Division of Chemistry, National Research Council of Canada, Ottawa, Ont., Canada K1A 0R6
Received July 30, 1980

JOHN L. HOLMES, MERVIN FINGAS, and F. P. LOSSING. Can. J. Chem. **59**, 80 (1981).

It is shown that gas-phase heats of formation of homologous odd-electron organic cations can be well represented by an equation of the form $\Delta H_f[\text{ion}]^{+\cdot} = A - Bn + C/n$, where A, B, and C are constants and n is the total number of atoms in the molecule. Values for A, B, and C have been determined for the linear homologous series: alkanes, olefins, alkynes, alkanols, aliphatic ethers, aliphatic aldehydes, aliphatic ketones, alkanoic acids, alkyl chlorides, bromides, and iodides. For each of these series, correction terms for chain branching, double-bond position, and asymmetry effects are also given. These equations can be applied to molecules containing 40 or more atoms. The data base for this work is also presented.

JOHN L. HOLMES, MERVIN FINGAS et F. P. LOSSING. Can. J. Chem. **59**, 80 (1981).

On montre que les chaleurs de formation en phase gazeuse des électrons célibataires des cations organiques homologues, peuvent être représentées par une équation de la forme $\Delta H_f[\text{ion}]^{+\cdot} = A - Bn + C/n$ où A, B et C sont des constantes et n est le nombre total d'atomes de la molécule. On a déterminé les valeurs de A, B et C pour les séries homologues suivantes: alcanes, oléfines, alcynes, alcanols, éthers aliphatiques, aldéhydes aliphatiques, cétones aliphatiques, acides alcanoiques, chlorures, bromures et iodures d'alkyle. Pour chacune de ces séries, on rapporte les termes de correction pour les chaînes latérales, la position de doubles liaisons et les effets d'asymétrie. Ces équations peuvent être appliquées aux molécules contenant 40 atomes ou plus. On présente également les données de base de ce travail.

[Traduit par le journal]

Introduction

Sufficient data for the heats of formation of neutral organic molecules have been accumulated to make possible the development of a general additivity scheme for calculating ΔH_f^{298} for a very wide range of simple organic compounds (1).

For ionised organic molecules no such scheme has so far been established even though there are now probably more accurate data for molecular ionisation energies than for heats of combustion. The latest collection of data for organic cations (2) contains some 1500 values but the literature covered extends only to the end of 1971. The compilation includes many observations of ionization energies (IE) and appearance energies (AE) from which no heat of formation was derived owing to the possible unreliability of the observations. For example, IE and AE values obtained by electron impact using a conventional mass spectrometer are generally unreliable; ambiguities can also arise in AE measurements where the structure of the neutral product of the fragmentation is uncertain. Such matters are discussed by Rosenstock in the introduction to the aforementioned data collection (2).

We have accumulated some 8000 IE and AE values from the post-1971 literature and from our own laboratories. These data have sufficed for the construction of the general correlation scheme described in this paper. The present equations have been determined empirically but their form corresponds to the fact that ΔH_f(molecular ion) = ΔH_f(neutral) + IE (i.e., the equations contain terms relating to these two components). In this paper we present results only for odd-electron (molecular) ions. Even-electron ions will be dealt with in a subsequent publication.

Equations such as those described here are not only useful for predicting new ΔH_f^{298} values but also for revealing misfits which could indicate incorrect values for ΔH_f(neutral) or IE, or, more interestingly, an ion structure having special stabilizing or destabilizing properties.

Method

Of several possible approaches we elected to devise relationships which would permit direct calculation of ionic heats of formation rather than ionisation energies. For homologous series of ions, the data clearly show that, unlike their neutral counterparts (1, 3), ionic heats of formation cannot be reproduced satisfactorily by any additivity sys-

[1]NRCC No. 18717.
[2]To whom all correspondence should be addressed.

0008-4042/81/010080-14$01.00/0
©1981 National Research Council of Canada/Conseil national de recherches du Canada

Can. J. Chem. Downloaded from www.nrcresearchpress.com by 210.87.254.42 on 09/05/12
For personal use only.

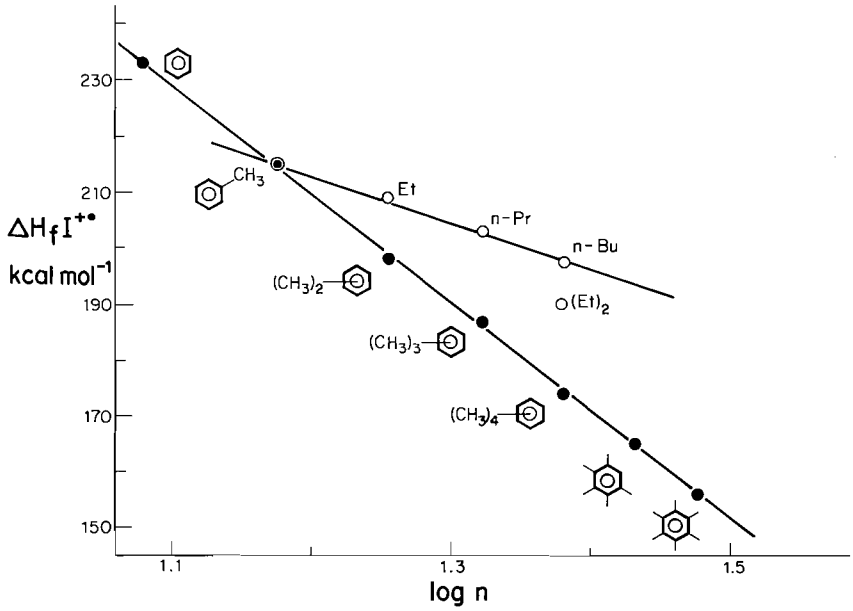

FIG. 1. Differentiation between a true homologous series and multiple substitution effects as discussed in the text. Data from refs. 2, 4, 5, and 6.

tem using constant atom and/or group equivalents. The reason for this is that whereas ΔH_f(neutral) for neighbouring homologues differ by a constant increment (1), the IE values decrease approximately exponentially with increasing homologue size. Thus ΔH_f(molecular ion) = ΔH_f(neutral) + IE cannot be incremental.

We will show here that ΔH_f for homologous series of odd electron organic cations can be calculated using as a basis empirical equations of the form $\Delta H_f[M]^{+\cdot} = A - Bn + C/n$ where A, B, and C are constants and n is the total number of atoms in the molecule. Such an equation, derived for a series of *unbranched homologous molecular ions*, will be referred to hereafter as the *generic* equation for that series. Once the generic equation for an homologous series had been derived, structural parameters for isomeric members of the series were established, for example, positional effects of chain branching, substituent size effects, double bond position, etc. The correction terms were found to be additive and characteristic of the particular homologous series but different from corresponding terms for their neutral counterparts.

These equations are valid up to ca. twenty C atoms and reproduce very satisfactorily the available experimental values to within 2 kcal mol^{-1}. Heats of formation of homologous series for which insufficient data are available to permit useful evaluation of A, B, and C, can be represented by a simple linear equation of the form $\Delta H_f[M]^{+\cdot} = \alpha - \beta \log n$, where α and β are constants and n again is the total number of atoms in the molecule; such equations hold only up to 8 to 10 carbon atoms. Indeed all series investigated can be fitted by the simpler equation over the above range but extension above ca. C_8 requires the three-term generic equation. As will be shown below, the simpler equation permits useful graphical representation of the data.

It is essential to note that for all homologous series with π-bonds, the smallest molecule to which the generic equation may be applied is not the member with *smallest n* but the first member containing a *methyl group* (e.g., $CH_3CH{=}CH_2$ not $CH_2{=}CH_2$). This characteristic of an homologous series is illustrated in Fig. 1, in which ΔH_f data for two series of aromatic ions are presented in simple graphical form as a function of log n. Both series fit simple linear equations $\Delta H_f[M]^+ = \alpha - \beta \log n$. The alkyl benzenes constitute a *true* homologous series, starting at toluene, whereas the series of multi-methyl substituted benzenes having benzene as its first member, illustrates the cumulative effect of multiple substitution by a functional group (in this case $CH_3^{\bullet}$) at a single atom or group of atoms. Note that this series is represented in the graph by the most stable positional isomers. The experimental value of ΔH_f for [diethylbenzene]$^{+\cdot}$ is also shown in Fig. 1; this point is co-linear with [benzene]$^{+\cdot}$ and [ethylbenzene]$^{+\cdot}$.

Our methods are readily applicable to other such

Can. J. Chem. Downloaded from www.nrcresearchpress.com by 210.87.254.42 on 09/05/12
For personal use only.

TABLE 1. Generic equations $\Delta H_f = A - Bn + C/n$ (kcal mol^{-1}) and correction terms

Series	A	B	C	Correction terms: Description	Correction terms: Magnitude
Alkanes	224	2.2	298	For each branch	−3
1-Olefins	231.6	1.61	110	For branch on carbon-2	−13
				For each remote branch	−2.5
x-Olefins (*trans*)	219.6 − x	1.61	110	(For $x \geq 2$)	
				For each branch on doubly-bonded carbon	−13
				For each branch elsewhere	−2.5
				cis corrections (same as for neutral compounds (1)):	
				For one *cis* correction	+1
				For two *cis* corrections around one double bond	+3
				When one group is *t*-butyl	+4
				When both groups are *t*-butyl	∼+10
1-Alkynes	278	1.57	110	For each branch (provisional)	−4
2-Alkynes	260	1.57	110	For each branch (provisional)	−4
3-Alkynes	257	1.57	110	For each branch (provisional)	−4
4-Alkynes	257	1.57	110	For each branch (provisional)	−4
5-Alkynes	256	1.57	110	For each branch (provisional)	−4
Alkanols	175	1.59	216	For each branch adjacent to —OH	−6
				For each branch elsewhere	−2
Aliphatic ethers	157	1.41	368	For each branch adjacent to —O—	−4.5
				For each branch elsewhere	−3
				Asymmetry correction, per carbon[a]	+1
Aliphatic aldehydes	188	1.65	135	For each branch adjacent to C=O	−5
				For each branch elsewhere	−3
Aliphatic ketones	166	1.78	252	For each branch adjacent to C=O	−3.5
				For each branch elsewhere	−1.5
				Asymmetry correction, per carbon[a]	+1.5
Alkanoic acids	142	1.90	112	For each branch adjacent to C=O	−3.5
				For each branch elsewhere	−1.5
Chloroalkanes	236	1.98	57	For each branch adjacent to halogen	−5
Bromoalkanes	219	1.40	115		
Iodoalkanes	222	1.69	44	For each branch elsewhere	−3

[a] The asymmetry correction, applicable to ethers and ketones having different numbers of C-atoms on either side of the functional group, refers to the smallest number of C-atoms which must be transferred to give the most symmetrical species, e.g. for methyl pentyl ketone the asymmetry correction is +3 kcal mol^{-1}.

substitutional series; these effects will be described in a forthcoming publication.

The Generic Equations

The function of the generic equations is to achieve a correct balance between the heats of formation of the neutral homologues, which become incrementally more negative with increasing molecular size, and the ionization energy, which falls approximately linearly with $1/n$. The three constants A, B, and C for a number of unbranched homologous series of odd-electron ions are given in Table 1. These have been fitted to the corresponding experimental ΔH_f(ion) values given in Tables 2 to 10, which we have selected as the most reliable and self-consistent. For many homologues, experimental heats of formation of the neutral species are not available; a few show irregular incremental changes along the series. Where such is the case, we have used heats of formation calculated by additivity. We have used spectroscopic or photon impact experimental values for the adiabatic ionization energies where these are available, supplemented where necessary by measurements made in this laboratory using mono-energetic electrons.

Structural Parameter Correction Terms

Having established the generic equation for an

Can. J. Chem. Downloaded from www.nrcresearchpress.com by 210.87.254.42 on 09/05/12
For personal use only.

TABLE 2. Alkanes

Formula	Structure	ΔH_f(neutral)[a] (kcal mol^{-1})	Ionization energy[c] (eV)	Reference	ΔH_f(ion) (kcal mol^{-1}) Expl.	Calcd.
CH_4	—	−17.9	≤12.615 (B)	2	273	273
C_2H_6	—	−20.2	11.52 (A)	2	245	244
C_3H_8	—	−24.8	10.95 (B)	2	228	227
C_4H_{10}		−30.4	10.55 (B)	2	213	214
		−32.4	10.57 (B)	2	211	211
C_5H_{12}		−35.1	10.35 (B)	2	204	204
		−36.9	10.20 (A)	7	198	201
		−40.3	10.21 (A)	8	195	198
C_6H_{14}	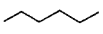	−39.9	10.18 (B)	2	195	195
		−41.8	10.12 (B)	2	192	192
		−41.1	10.08 (B)	2	191	192
		−44.9	10.06 (B)	2	187	189
		−42.6	10.02 (B)	2	188	189
C_7H_{16}		−44.9	9.99av. (B)	2	186	186
C_8H_{18}		−56.8[b]	9.86 (B)	2	171	169

[a]Reference 9.
[b]Calculated by additivity (1).
[c]Method: A refers to photoelectron spectroscopy, B to photoionization.

unbranched series of homologues, it is then necessary to apply correction terms for structural effects. These are described below.

(*1*) Chain branching on or adjacent to a functional group generally has a larger stabilizing effect than a remote branch.

(*2*) For olefins, the effect of substitution (branching) on a doubly bonded C-atom has a much larger stabilizing influence and this special type of branching on a functional group can be treated by a constant correction term. For these homologues adjacent and remote branching have equal effects.

(*3*) For non-terminal olefins the equations are for the *trans*-isomers. The corrections for *cis*-isomers given in Table 1 are the same as those for the neutral molecules (1).

(*4*) For alkynes, generic equations are given for different triple bond positions; branching effects appear to be non-specific.

(*5*) In addition to the branching coefficients, asymmetry corrections are required for ethers and ketones; these are described in Table 1.

(*6*) Ring strain effects are discussed in detail below but it is important to note that the magnitude of such effects in ions appears to be closely similar to that for the neutral species.

Calculations

Calculation of an ionic heat of formation involves the following steps, using the data in Table 1:

(*1*) the appropriate *generic equation* is solved, using the total number of atoms n.

(*2*) the structural parameter corrections applicable to the ion are then added to or subtracted from the number derived in (*1*).

Ionic heats of formation calculated by our method are presented in Tables 2–10, together with the data base for this work. The agreement between the experimental and calculated ΔH_f(ion) values is excellent, generally within 2 kcal mol^{-1}.

It must be emphasized that the values of the coefficients in the generic equations are those which yield results closest to presently available experimental values of acceptable accuracy. When

Can. J. Chem. Downloaded from www.nrcresearchpress.com by 210.87.254.42 on 09/05/12
For personal use only.

Can. J. Chem. Downloaded from www.nrcresearchpress.com by 210.87.254.42 on 09/05/12
For personal use only.

TABLE 3. Olefins

Formula	Structure	ΔH_f(neutral) (kcal mol^{-1})	Ionization energy[c] (eV)	Reference	ΔH_f(ion) (kcal mol^{-1}) Expl.	Calcd.
	Linear 1-olefins					
C_3H_6		4.88[a]	9.73 (B)	2	229	229
C_4H_8		−0.20[a]	9.625 (A)	10	222	221
C_5H_{10}		−5.33[a]	9.524 (A)	10	214	215
C_6H_{12}		−9.95[a]	9.478 (A)	10	209	209
C_7H_{14}		−14.8[a]	9.442 (A)	10	203	203
C_8H_{16}		−19.4[a]	9.43 (B)	2	198	198
C_9H_{18}		−24.7[b]	—	—	—	192
$C_{10}H_{20}$		−29.7[b]	9.48 (C)	This work	189	187
$C_{11}H_{22}$		−34.6[b]	—	—	—	182
$C_{12}H_{24}$		−39.5[b]	—	—	—	177
$C_{13}H_{26}$		−44.5[b]	9.38 (C)	This work	172	172
$C_{14}H_{28}$		−49.4[b]	—	—	—	167
	Linear 2-olefins					
C_4H_8	*cis*	−1.86[a]	9.124 (A)	10	209	208
	trans	−2.99[a]	9.122 (A)	10	207	207
C_5H_{10}	*cis*	−7.00[a]	9.036 (A)	10	201	202
	trans	−7.93[a]	9.036 (A)	10	200	201
C_6H_{12}	*cis*	−11.7[b]	8.969 (A)	10	195	196
	trans	−12.7[b]	8.966 (A)	10	194	195
C_7H_{14}	*cis-trans*	−16.6[b]	8.84 (A)	11	187	189
	Linear 3-olefins					
C_6H_{12}	*cis*	−11.5[b]	8.954 (A)	10	195	195
	trans	−12.5[b]	8.965 (A)	10	194	194
C_7H_{14}	*cis-trans*	−16.5[b]	8.77 (A)	11	186	—
	trans	−17.5[b]	8.92 (C)	This work	188	188
C_8H_{16}	*cis*	−21.4[b]	8.849 (A)	10	183	184
	Linear 4-olefins					
C_8H_{16}	*cis*	−21.4[b]	8.841 (A)	10	182	183
	trans	−22.4[b]	8.830 (A)	10	181	182
	Linear 5-olefins					
$C_{10}H_{20}$	*cis*	−31.3[b]	8.766 (A)	10	171	171
	trans	−32.3[b]	8.760 (A)	10	170	170
	Branched 1-olefins					
C_4H_8		−4.26[a]	9.239 (A)	10	209	208
C_5H_{10}		−8.55[a]	9.148 (A)	10	202	202
		−6.61[a]	9.533 (A)	10	213	212
C_6H_{12}		−13.3[b]	9.076 (A)	10	196	196
		−11.7[b]	9.44 (C)	12	206	206
		−12.0[b]	9.452 (A)	10	206	206
		−14.7[b]	9.072 (A)	10	194	193
		−13.7[b]	9.450 (A)	10	204	204
		−13.1[b]	9.061 (A)	10	196	196
C_7H_{14}		−18.2[b]	9.039 (A)	10	190	190
		−20.3[b]	9.025 (A)	10	188	188
		−20.9[b]	9.016 (A)	10	187	185

TABLE 3 (*Continued*)

Formula	Structure	ΔH_f(neutral) (kcal mol^{-1})	Ionization energy[c] (eV)	Reference	ΔH_f(ion) (kcal mol^{-1}) Expl.	Calcd.
C_8H_{16}		−26.5[b]	8.909 (A)	10	179	180
$C_{10}H_{20}$		−38.5[b]	8.795 (A)	10	164	164
	Branched 2-olefins					
C_5H_{10}		−10.3[b]	8.682 (A)	10	190	189
C_6H_{12}		−15.1[b]	8.58 (C)	12	183	183
		−15.1[b]	8.58 (C)	12	183	183
		−13.5[b]	8.976 (A)	10	193	193
		−14.5[b]	8.972 (A)	10	192	192
		−16.6[b]	8.271 (A)	10	174	172
C_7H_{14}	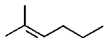	−20.0[b]	8.62 (C)	This work	179	177
		−18.7[b]	8.917 (A)	10	187	188
		−19.5[b]	8.912 (A)	10	186	187
		−19.7[b]	8.919 (A)	10	186	187
		−21.4[b]	8.213 (A)	10	168	166
		−17.5[b]	8.922 (A)	10	188	188
		−21.5[b]	8.908 (A)	10	184	184
C_8H_{16}	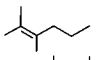	−26.4[b]	8.186 (A)	10	162	161
		−28.2[b]	8.165 (A)	10	160	158
	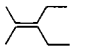	−26.2[b]	8.170 (A)	10	162	161
C_9H_{18}	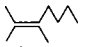	−31.3[b]	8.145 (A)	10	157	155
$C_{10}H_{20}$	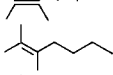	−36.3[b]	8.132 (A)	10	151	150
	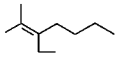	−36.1[b]	8.101 (A)	10	151	150
	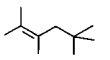	−41.1[b]	8.097 (A)	10	146	145
	Branched 3-olefins					
C_8H_{16}	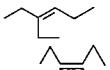	−24.6[b]	8.480 (A)	10	171	171
		−26.2[b]	8.172 (A)	10	162	160
	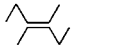	−26.2[b]	8.156 (A)	10	162	160
	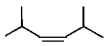	−25.1[b]	8.846 (A)	10	179	179
	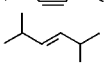	−26.1[b]	8.838 (A)	10	178	178
C_9H_{18}	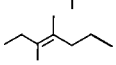	−31.1[b]	8.077 (A)	10	155	154

Can. J. Chem. Downloaded from www.nrcresearchpress.com by 210.87.254.42 on 09/05/12
For personal use only.

TABLE 3 (*Concluded*)

Formula	Structure	ΔH_f(neutral) (kcal mol^{-1})	Ionization energy[c] (eV)	Reference	ΔH_f(ion) (kcal mol^{-1}) Expl.	Calcd.
$C_{11}H_{22}$	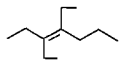	−40.6[b]	8.041 (A)	10	145	144
$C_{12}H_{24}$	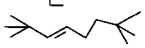	−50.4[b]	8.346 (A)	10	142	143
$C_{13}H_{26}$		−55.8[b]	8.307 (A)	10	136	135
$C_{14}H_{28}$		−56.8[b]	8.169 (A)	10	132	134

[a]Reference 9.
[b]Calculated by additivity (1).
[c]Method: A, photoelectron spectroscopy; B, photoionization; C, electron monochromator.

TABLE 4. Alkynes

Formula	Structure	ΔH_f(neutral)[b] (kcal mol^{-1})	Ionization energy[c] (eV)	Reference	ΔH_f(ion) (kcal mol^{-1}) Expl.	Calcd.
	1-Alkynes					
C_3H_4		+44.4[a]	10.36 (B, C)	2	283	283
C_4H_6		+39.5[a]	10.18 (B, C)	2	274	273
C_5H_8	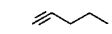	+34.7	10.05 (C) (10.10) (A)	This work[d]	266	266
		+32.6	9.97 (C) (10.05) (A)	This work[d]	263	262
C_6H_{10}		+29.8	9.95 (C) (10.07) (A)	13[d]	259	260
	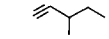	+27.7	9.79 (C) (9.98) (A)	13[d]	253	255
	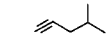	+27.7	9.83 (C) (10.05) (A)	13[d]	254	255
	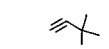	+25.7	9.80 (C) (9.92) (A)	13[d]	252	251
C_7H_{12}	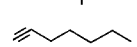	+24.9	(10.04) (A)	[d]	(256)	254
C_8H_{14}	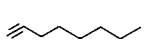	+19.9	9.95 (A)	14	249	248
C_9H_{16}	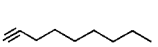	+14.9	9.93 (A)	14	244	243
$C_{10}H_{18}$	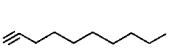	+10.0	9.91 (A)	14	239	238
$C_{11}H_{20}$	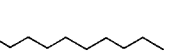	+5.0	9.90 (A)	14	233	233
$C_{12}H_{22}$	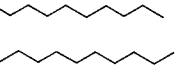	+0.1	9.90 (A)	14	228	228
$C_{13}H_{24}$	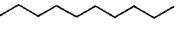	−4.9	9.90 (A)	14	223	223
$C_{14}H_{26}$	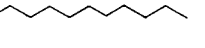	−9.8	9.89 (A)	14	218	218
	2-Alkynes					
C_4H_6	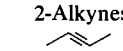	+34.7[a]	9.56 (C)	2	255	255

Can. J. Chem. Downloaded from www.nrcresearchpress.com by 210.87.254.42 on 09/05/12
For personal use only.

TABLE 4 (*Concluded*)

Formula	Structure	ΔH_f(neutral)[b] (kcal mol^{-1})	Ionization energy[c] (eV)	Reference	ΔH_f(ion) (kcal mol^{-1}) Expl.	Calcd.
C_5H_8		+30.2	9.45 (C) 9.439 (A)	2 d	248	248
C_6H_{10}	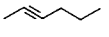	+25.3	9.37 (C) 9.366 (A)	13 d	241	242
		+23.1	9.31 (C) 9.346 (A)	13 d	238	238
	Unbranched					
C_7H_{12}		+20.4	9.326 (A)	d	235	236
C_8H_{14}		+15.4	9.31 (A) 9.302 (A)	14 d	230	230
C_9H_{16}		+10.4	9.32 (A) 9.289 (A)	14 d	225	225
$C_{10}H_{18}$		+5.5	9.30 (A)	14	220	220
$C_{11}H_{20}$		+0.5	9.28 (A)	14	215	215
$C_{12}H_{22}$		−4.4	9.29 (A)	14	210	210
$C_{13}H_{24}$		−9.4	9.28 (A)	14	205	205
$C_{14}H_{26}$		−14.3	9.26 (A)	14	199	200
	3-Alkynes unbranched					
C_6H_{10}		+25.5	9.34 (C) 9.323 (A)	13 d	240	239
C_7H_{12}		+20.6	9.260 (A)	d	234	233
C_8H_{14}		+15.6	9.22 (A) 9.222 (A)	14 d	228	227
C_9H_{16}		+10.7	9.20 (A) 9.202 (A)	14 d	223	222
$C_{10}H_{18}$		+5.8	9.19 (A) 9.19 (A)	14 d	218	217
$C_{11}H_{20}$		+0.8	9.17 (A)	14	212	212
$C_{12}H_{22}$		−4.1	9.17 (A)	14	207	207
$C_{13}H_{24}$		−9.1	9.14 (A)	14	202	202
$C_{14}H_{26}$		−14.0	9.17 (A)	14	197	197
	4-Alkynes unbranched					
C_8H_{14}		+15.7	9.20 (A) 9.196 (A)	14 d	228	227
C_9H_{16}		+10.7	9.17 (A)	14	222	222
$C_{10}H_{18}$		+5.8	9.17 (A)	14	217	217
$C_{11}H_{20}$		+0.8	9.13 (A)	14	211	212
$C_{12}H_{22}$		−4.1	9.14 (A)	14	207	207
$C_{13}H_{24}$		−9.1	9.07 (A)	14	200	202
$C_{14}H_{26}$		−14.0	9.11 (A)	14	196	197
	5-Alkynes unbranched					
$C_{10}H_{18}$		+5.8	9.14 (A) 9.125 (A)	14 d	216	216
$C_{11}H_{20}$		+0.8	9.11 (A)	14	211	211
$C_{12}H_{22}$		−4.1	9.09 (A)	14	206	206
$C_{13}H_{24}$		−9.1	9.09 (A)	14	201	201
$C_{14}H_{26}$		−14.0	9.10 (A)	14	196	196

[a]Reference 9.
[b]Calculated by additivity (1).
[c]Method: A, photoelectron spectroscopy; B, photoionization; C, electron monochromator.
[d]The IE values in parentheses in the earlier part of this table are from the work of Carlier et al. (32). Note that these ions are "hot" with respect to their fragmentation to yield the very abundant m/z 67, $[C_5H_7]^+$ ion and the given IE values correspond closely to those observed by ourselves (13) for the AE of m/z 67 in these compounds. The photoelectron values (d) did not include mass analysis and so could be subject to error. For this reason we have selected the results for ref. 13 for these ΔH_f values.

Can. J. Chem. Downloaded from www.nrcresearchpress.com by 210.87.254.42 on 09/05/12
For personal use only.

Can. J. Chem. Downloaded from www.nrcresearchpress.com by 210.87.254.42 on 09/05/12
For personal use only.

TABLE 5. Alkanols

Formula	Structure	ΔH_f(neutral) (kcal mol^{-1})	Ionization energy[c] (eV)	Reference	ΔH_f(ion) (kcal mol^{-1}) Expl.	Calcd.
	Primary					
CH_3OH		−48.1[a]	10.84 (A, B)	2	202	202
C_2H_5OH		−56.2[a]	10.47 (A, B)	2	185	185
C_3H_7OH		−61.2[a]	10.22 (A, B)	2	174	174
C_4H_9OH		−65.8[a]	10.07 (A, B)	2	166	166
$C_5H_{11}OH$		−71.3[b]	10.00 (A)	11	159	158
$C_6H_{13}OH$		−76.3[b]	9.89 (A)	11	152	152
$C_7H_{15}OH$		−81.2[b]	9.84 (A)	11	146	146
	Other					
C_3H_7OH		−65.1[a]	10.15 (A, B)	2	169	168
C_4H_9OH		−70.0[a]	9.88 (C)	This work	158	160
		−67.8[a]	10.09 (A) 10.12 (C)	2 This work	165	164
		−74.7[a]	9.97 (A)	2	155	154
$C_5H_{11}OH$	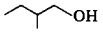	−72.2[a]	9.86 (C)	This work	155	156
		−75.2[a]	9.78 (C)	This work	150	152

[a]Reference 9.
[b]Calculated by additivity (1).
[c]Method: A, photoelectron spectroscopy; B, photoionization; C, electron monochromator.

TABLE 6. Aliphatic ethers

Formula	Structure	ΔH_f(neutral) (kcal mol^{-1})	Ionization energy[c] (eV)	Reference	ΔH_f(ion) (kcal mol^{-1}) Expl.	Calcd.
C_2H_6O		−43.2[a]	9.95 (S, A)	2	186	185
C_3H_8O		−51.7[a]	9.72 (C)	This work	172	171
$C_4H_{10}O$		−60.2[a]	9.52 (A, B)	2	159	160
		−60.2[a]	9.42 (C)	This work	157	156
$C_5H_{12}O$	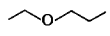	−65.2[b]	9.45 (D)	15	153	152
	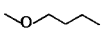	−61.7[b]	9.54 (C)	This work	158	153
$C_6H_{14}O$	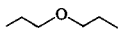	−69.9[a]	9.30 (A, B)	2	144	145
		−76.2[a]	9.20 (B)	2	136	136
	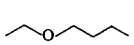	−70.2[b]	9.36 (C)	[c]	146	146
		−74.5[b]	9.32 (C)	This work	140	140
$C_7H_{16}O$	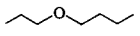	−75.0[b]	—	—	—	138
$C_8H_{18}O$	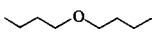	−79.8[a]	—	—	—	133
	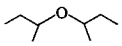	−86.3[a]	9.11 (C)	This work	124	124
		−87.1[a]	8.81 (A)	16	116	115

[a]Reference 9.
[b]Calculated by additivity (1). Note that the group equivalent for O—$(C)_2$ required to reproduce the data in Table IX (ref. 1, Chem. Rev. p. 288) is −23.1 kcal mol^{-1} and not −23.7 as given in Table XXXIV.
[c]Method: S, spectroscopy; A, photoelectron spectroscopy; B, photoionisation; C, electron monochromator; D, field ionisation.

TABLE 7. Aliphatic aldehydes

Formula	Structure	ΔH_f(neutral) (kcal mol^{-1})	Ionization energy[c] (eV)	Reference	ΔH_f(ion) (kcal mol^{-1}) Expl.	Calcd.
C_2H_4O		−39.7[a]	10.23 (S)	2	196	196
C_3H_6O		−45.5[a]	9.95 (A)	17, 18	184	185
C_4H_8O		−48.9[a]	9.83 (A)	18, 19	178	177
		−52.3[a]	9.70 (A)	18	171	172
$C_5H_{10}O$	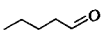	−54.6[b]	9.74 (A) 9.72 (C)	18 This work	170	170
		−56.5[b]	9.59 (A)	18	165	165
		−56.7[b]	9.69 (A) 9.72 (C)	18 This work	167	167
		−58.3[b]	9.50 (A)	18	161	160
$C_6H_{12}O$	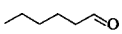	−59.5[b]	9.72 (A) 9.62 (A)	18 11	163	164
	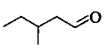	−61.6[b]	9.68 (C)	This work	162	161
		−61.5[b]	9.54 (C)	This work	159	159
		−64.3[b]	9.61 (A)	18	157	158
$C_7H_{14}O$		−64.5[b]	9.65 (A)	11	158	158
		−68.5[b]	9.44 (C)	This work	149	150

[a]Reference 9.
[b]Calculated by additivity (1).
[c]Method: S, spectroscopy; A, photoelectron spectroscopy; B, photoionization; C, electron monochromator.

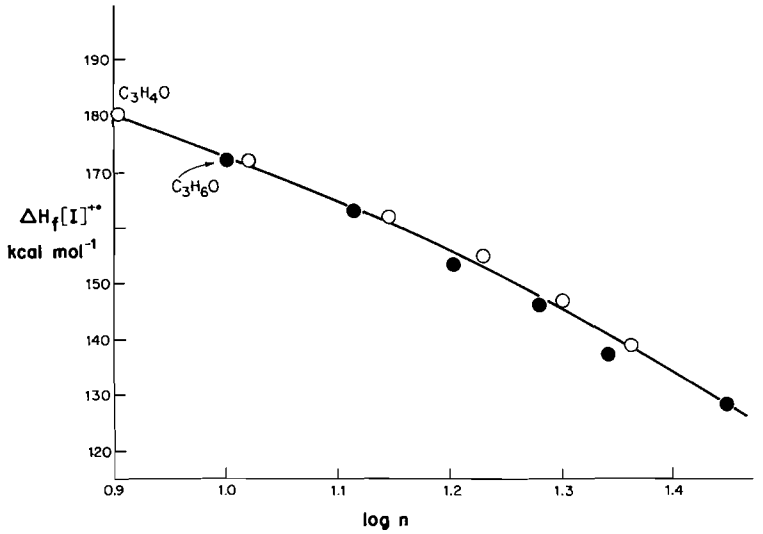

FIG. 2. Heats of formation of ketones plotted against log n. Closed circles are experimental values from Table 8 for di-n-alkyl ketones. Open circles are apparent ΔH_f values for cyclic ketones obtained by combining experimental IE with ΔH_f(neutral) values calculated by additivity (1) *but using no ring strain correction term* (references for cyclic ketone IE: 2, 28–30).

Can. J. Chem. Downloaded from www.nrcresearchpress.com by 210.87.254.42 on 09/05/12
For personal use only.

Can. J. Chem. Downloaded from www.nrcresearchpress.com by 210.87.254.42 on 09/05/12
For personal use only.

TABLE 8. Ketones

Formula	Structure	ΔH_f(neutral) (kcal mol^{-1})	Ionization energy[c] (eV)	Reference	ΔH_f(ion) (kcal mol^{-1}) Expl.	Calcd.
C_3H_6O		−51.9[a]	9.705 (S)	20	172	173
C_4H_8O		−57.0[a]	9.52 (A)	18	163	162
$C_5H_{10}O$		−61.7[a]	9.30 (A, C)	18, this work	153	153
		−61.7[b]	9.38 (A)	18	155	155
		−62.8[a]	9.29 (A)	18	151	151
$C_6H_{12}O$	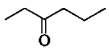	−66.6[b]	9.12 (A) 9.30 (C)	11 This work	146	145
		−66.9[a]	9.33 (A) 9.24 (A)	18 11	147	147
		−68.4[a]	9.09 (A)	18	141	142
		−68.6[b]	9.29 (A)	18	146	146
		−68.5[b]	9.20 (A) 9.22 (C)	18 This work	144	143
		−69.3[a]	9.11 (A)	18	141	140
$C_7H_{14}O$	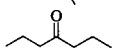	−71.6[b]	9.10 (A) 9.02 (A)	18 11	137	138
	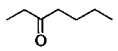	−71.6[b]	9.04 (A) 9.26 (C)	18 This work	139	139
	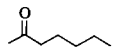	−71.5[b]	9.29 (A) 9.18 (A)	18 11	142	141
	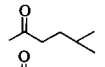	−73.6[b]	9.28 (A)	18	140	140
		−73.5[b]	9.22 (C)	This work	139	138
		−76.3[b]	9.22 (A)	18	136	138
		−75.2[b]	9.01 (A)	18	133	134
		−74.4[a]	8.96 (A) 8.94 (A)	2 18	132	131
$C_8H_{16}O$		−82.1[b]	8.79 (A)	18	121	121
$C_9H_{18}O$	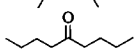	−82.4[a]	9.07 (C)	This work	127	125
	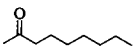	−81.4[b]	9.16 (C)	This work	130	130
		−85.6[b]	8.98 (A)	18	121	122
		−88.9[b]	8.67 (A)	18	111	111

[a]Reference 9.
[b]Calculated by additivity (1)
[c]Method: S, spectroscopy; A, photoelectron spectroscopy; B, photoionization; C, electron monochromator.

TABLE 9. Alkanoic acids

Formula	Structure	ΔH_f(neutral) (kcal mol^{-1})	Ionization energy[c] (eV)	Reference	ΔH_f(ion) (kcal mol^{-1}) Expl.	Calcd.
$C_2H_4O_2$		−103.3[a]	10.70 (A) 10.63 (A) 10.66 (C)	21 22 This work	143	141
$C_3H_6O_2$		−108.4[a]	10.51 (A) 10.24 (B) 10.41 (C)	22 2 This work	131	131
$C_4H_8O_2$	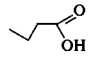	−112.8[b]	10.16 (B) 10.24 (C)	2 This work	122	123
$C_5H_{10}O_2$	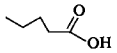	−117.7[b]	—	—	—	116
		−119.8[b]	—	—	—	115
		−119.6[b]	—	—	—	113
		−122.4[b]	10.08 (C)	This work	110	109
$C_6H_{12}O_2$	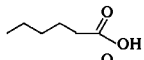	−122.7[a]	≤10.12 (C)	This work	≤111	110
	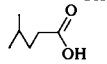	−124.5[b]	—	—	—	108
		−127.4[b]	—	—	—	103
		−126.6[b]	—	—	—	105
	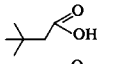	−122.4[b]	—	—	—	107
	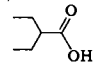	−124.5[b]	—	—	—	106

[a]Reference 9.
[b]Calculated by additivity (1, 27).
[c]Method: A, photoelectron spectroscopy; B, photoionization; C, electron monochromator.

TABLE 10. Haloalkanes

Formula	Structure	ΔH_f(neutral) (kcal mol^{-1})	Ionization energy[c] (eV)	Reference	ΔH_f(ion) (kcal mol^{-1}) Expl.	Calcd.
	Chlorides					
CH_3Cl		−20.6[a]	11.22 (S)	2	238	238
C_2H_5Cl		−26.1[a]	10.97 (A, B)	2, 23	227	227
C_3H_7Cl		−31.0[a]	10.82 (B) 10.88 (A)	2 24	219	219
		−33.6[a]	10.78 (B)	2	215	214
C_4H_9Cl		−35.1[a]	10.67 (B)	2	211	212
		−38.1[a]	10.66 (B)	2	208	209
		−38.6[a]	10.65 (B)	2	207	206

Can. J. Chem. Downloaded from www.nrcresearchpress.com by 210.87.254.42 on 09/05/12
For personal use only.

TABLE 10. (*Concluded*)

Formula	Structure	ΔH_f(neutral) (kcal mol^{-1})	Ionization energy[c] (eV)	Reference	ΔH_f(ion) (kcal mol^{-1}) Expl.	Calcd.
		−43.7[a]	10.61 (B)	2	201	201
	Bromides					
CH_3Br		−9.1[a]	10.54 (S) 10.53 (B, C)	2 2, this work	234	235
C_2H_5Br		−15.2[a]	10.29 (S, A, B)	2	222	222
C_3H_7Br		−20.5[a]	10.13 (A, B) 10.18 (A)	2 24	214	214
		−23.5[a]	10.08 (B) 10.12 (A)	2 2	209	209
C_4H_9Br		−25.6[a]	10.18 (A, B)	2	209	208
		−27.5[b]	10.09 (A, B)	2	205	206
		−28.9[a]	9.98 (B)	2	201	204
		−30.6[b]	9.89 (B) 9.95 (A)	2 2	198	199
$C_5H_{11}Br$		−30.3[b]	10.10 (B)	2	203	202
		−35.1[b]	10.04 (A)	2	196	196
	Iodides					
CH_3I		+3.4[a]	9.53 (A)	2	223	222
C_2H_5I		−2.0[a]	9.35 (S, A, B)	2, 26	214	214
C_3H_7I		−7.1[a]	9.26 (A, B)	2	206	207
		−9.8[a]	9.18 (A, B)	2	202	202
C_4H_9I		−12.1[b]	9.22 (A, B)	2	201	201
		−14.0[b]	9.18 (A, B)	2	198	198
		−14.4[b]	9.09 (B)	2	195	196
		−17.2[b]	9.02 (A, B)	2	191	191
$C_5H_{11}I$		−17.1[b]	9.18 (A, B)	2	195	196
		−19.1[b]	9.17 (A)	2	192	192
		−22.2[b]	8.93 (A)	2	184	185
$C_6H_{13}I$		−22.0[b]	9.17 (A)	26	189	190

[a]Reference 9.
[b]Calculated by additivity (1).
[c]Method: S, spectroscopy; A, photoelectron spectroscopy; B, photoionization; C, electron monochromator.

more precise observations are made small corrections to the coefficients will undoubtedly be necessary. Nevertheless the general applicability of the method will be unaffected.

Ring Strain Effects

Figure 2 shows the simple (logarithmic) plot for the unbranched dialkyl ketones. Data points are also shown for cyclic ketones obtained from the

Can. J. Chem. Downloaded from www.nrcresearchpress.com by 210.87.254.42 on 09/05/12
For personal use only.

Can. J. Chem. Downloaded from www.nrcresearchpress.com by 210.87.254.42 on 09/05/12
For personal use only.

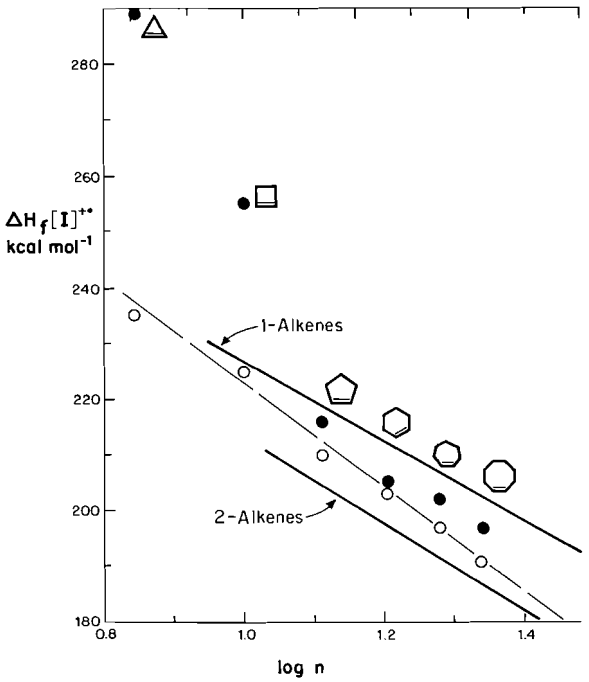

FIG. 3. Heats of formation of alkenes plotted against log n. Closed circles are experimental values for cyclo-alkenes (2), the designated lines for 1-alkenes and 2-alkenes are from data in Table 2. Open circles are the apparent ΔH_f values for the cyclic compounds obtained by subtraction from the closed circle values of the ring strain energy (1) for the neutral species.

experimental ionisation energy plus ΔH_f(neutral) calculated by additivity (1) but *omitting* the ring strain energy correction. All the points lie close to a common line. Thus for these ions, in which the ionised group is not within the ring, size (n) can be regarded as the major criterion affecting their heats of formation and that the ring strain energy in the cyclic ions is similar to that for the neutral cyclic compounds.

Figure 3 shows similar plots for cyclic olefins. Here the ionised π-system is within the ring and the ΔH_f values, again obtained from an experimental IE and omitting the neutral ring strain energy correction, lie between those for the 1-alkenes and 2-alkenes. Again it may be concluded that the ring strain energy in the ions is also similar to that obtained in the neutral cycloalkenes.

Acknowledgements

J.L.H. thanks the Natural Sciences and Engineering Research Council of Canada for continuing support of this work. The authors wish to thank Ms. K. Margittai and Ms. L. Hutchings for invaluable experimental assistance.

1. S. W. BENSON, F. R. CRUICKSHANK, D. M. GOLDEN, G. R. HAUGEN, H. E. O'NEAL, A. S. RODGERS, R. SHAW, and R. WALSH. Chem. Rev. **69**, 279 (1969); S. W. BENSON. Thermochemical kinetics. 2nd ed. John Wiley and Sons, New York. 1976.
2. H. M. ROSENSTOCK, K. DRAXL, B. W. STEINER, and J. T. HERRON. J. Phys. Chem. Ref. Data Suppl. 1, **6** (1977).
3. J. L. FRANKLIN. Ind. Eng. Chem. **41**, 1070 (1949); J. Chem. Phys. **21**, 2029 (1953).
4. R. G. MCLOUGHLIN, J. D. MORRISON, and J. C. TRAEGER. Org. Mass Spectrom. **14**, 104 (1979).
5. J. P. MAIER and D. W. TURNER. J. Chem. Soc. Faraday Trans. II, **69**, 196 (1973).
6. S. G. LIAS and P. AUSLOOS. J. Am. Chem. Soc. **100**, 6027 (1978).
7. G. BIERI, F. BURGER, E. HEILBRONNER, and J. P. MAIER. Helv. Chim. Acta, **60**, 2213 (1977).
8. A. E. JONES, G. K. SCHWEITZER, F. A. GRIMM, and T. A. CARLSON. J. Electron Spectrosc. Relat. Phenom. **1**, 29 (1972).
9. J. D. COX and G. PILCHER. Thermochemistry of organic and organometallic compounds. Academic Press. 1970.
10. P. MASCLET, D. GROSJEAN, G. MOUVIER, and J. DUBOIS. J. Electron Spectrosc. Relat. Phenom. **2**, 225 (1973).
11. F. S. ASHMORE and A. R. BURGESS. J. Chem. Soc. Faraday Trans. II, **74**, 734 (1978).
12. F. P. LOSSING and J. C. TRAEGER. Int. J. Mass Spectrom. Ion Phys. **19**, 9 (1976).
13. P. WOLKOFF, J. L. HOLMES, and F. P. LOSSING. Can. J. Chem. **58**, 251 (1980).
14. S. RANG and E. MARTENSON. Izv. Akad. Nauk Est. SSR, **27**, 44 (1978).
15. I. V. GOLDENFELD, I. Z. KOROSTYCHEVSKY, and B. G. MISCHANCHUK. Int. J. Mass Spectrom. Ion Phys. **13**, 297 (1974).
16. R. S. BROWN. Can. J. Chem. **53**, 3439 (1975).
17. R. H. STALEY, R. W. WIETING, and J. L. BEAUCHAMP. J. Am. Chem. Soc. **99**, 5964 (1977).
18. R. HERNANDEZ, P. MASCLET, and G. MOUVIER. J. Electron Spectrosc. Relat. Phenom. **10**, 333 (1977).
19. K. KIMURA, S. KATSUMATA, T. YAMAZAKI, and H. WAKABAYASHI. J. Electron Spectrosc. Relat. Phenom. **6**, 41 (1975).
20. R. H. HUEBNER, R. J. CELOTTA, S. R. MIELCZAREK, and C. E. KUYATT. J. Chem. Phys. **59**, 5434 (1973).
21. D. A. SWEIGERT and D. W. TURNER. J. Am. Chem. Soc. **94**, 5592 (1972).
22. F. M. BENOIT and A. G. HARRISON. J. Am. Chem. Soc. **99**, 3980 (1977).
23. B. P. TSAI, A. S. WERNER, and T. BAER. J. Chem. Phys. **63**, 4384 (1975).
24. K. KIMURA, S. KATSUMATA, Y. ACHIBA, H. MATSUMOTO, and S. NAGAKURA. Bull. Chem. Soc. Jpn. **46**, 373 (1973).
25. B. P. TSAI, T. BAER, A. S. WERNER, and S. F. LIN. J. Phys. Chem. **79**, 570 (1975).
26. R. A. BOSCHI and D. R. SALAHUB. Mol. Phys. **24**, 289 (1972).
27. J. L. HOLMES and F. P. LOSSING. J. Am. Chem. Soc. **102**, 1591 (1980).
28. P. C. MARTINO, P. B. SHEVLIN, and S. D. WORLEY. J. Am. Chem. Soc. **99**, 8003 (1977).
29. W. R. HARSHBARGER, M. A. KUEBLER, and M. B. ROBIN. J. Chem. Phys. **60**, 345 (1974).
30. G. HENTRICH, E. GUNKEL, and M. KLESSINGER. J. Mol. Struct. **21**, 231 (1974).
31. C. BATICH, P. BISCHOF, and E. HEILBRONNER. J. Electron Spectrosc. Relat. Phenom. **1**, 333 (1972).
32. P. CARLIER, J. E. DUBOIS, P. MASCLET, and G. MOUVIER. J. Electron Spectrosc. Relat. Phenom. **7**, 55 (1975).

Synthesis and structure of *N,N'*-ethylenebis(salicylideneiminato)chlorogallium(III) and its methyl analog

KENNETH S. CHONG, STEVEN J. RETTIG, ALAN STORR, AND JAMES TROTTER

Department of Chemistry, University of British Columbia, Vancouver, B.C., Canada V6T 1Y6

Received June 20, 1980

KENNETH S. CHONG, STEVEN J. RETTIG, ALAN STORR, and JAMES TROTTER. Can. J. Chem. **59**, 94 (1981).

The synthesis and physical properties of *N,N'*-ethylenebis(salicylideneiminato)chlorogallium(III) and *N,N'*-ethylenebis-(salicylideneiminato)methylgallium(III) are described. Crystals of *N,N'*-ethylenebis(salicylideneiminato)chlorogallium(III) dichloromethane are monoclinic, $a = 13.049(1)$, $b = 9.525(1)$, $c = 15.459(2)$ Å, $\beta = 92.452(5)°$, $Z = 4$, space group $P2_1/a$. The structure was solved by Patterson and Fourier syntheses and was refined by full-matrix least-squares procedures to $R = 0.042$ and $R_w = 0.051$ for 1815 reflections with $I \geq 3\sigma(I)$. The gallium atom is bonded to one chlorine atom and to the tetradentate *N,N'*-ethylenebis(salicylideneiminato) ligand to give a coordination geometry which is intermediate between square pyramidal and trigonal bipyramidal. Important bond lengths (corrected for libration) are: Ga—Cl, 2.228(2), Ga—O, 1.868(4) and 1.883(4), Ga—N, 2.019(6) and 2.035(5) Å. The crystal structure consists of discrete $(C_{16}H_{14}N_2O_2)GaCl$ and CH_2Cl_2 molecules linked by a C—H···O hydrogen bond (O···H = 2.31, O···C = 3.295(9) Å, C—H—O = 176°) to form complex-solvate units.

KENNETH S. CHONG, STEVEN J. RETTIG, ALAN STORR et JAMES TROTTER. Can. J. Chem. **59**, 94 (1981).

On décrit la synthèse et les propriétés physiques du *N,N'*-éthylène bis(salicylidèneiminato)chlorogallium(III) et du *N,N'*-éthylène bis(salicylidèneiminato)méthylgallium(III). Les cristaux de *N,N'*-éthylène bis(salicylidèneiminato)chlorogallium(III) dichlorométhane sont monocliniques et appartiennent au groupe d'espace $P2_1/a$ avec $a = 13,049(1)$, $b = 9,525(1)$, $c = 15,459(2)$ Å, $\beta = 92,452(5)°$, $Z = 4$. On a résolu la structure par les synthèses de Fourier et de Patterson et on l'a affinée par la méthode des moindres carrés (matrice entière) jusqu'à une valeur de R de 0,042 et de R_w de 0,051 pour 1815 réflexions avec $I > 3\sigma(I)$. L'atome de gallium est lié à un atome de chlore et au ligand tétradentate *N,N'*-éthylène bis(salicylidèneiminato) pour donner une géométrie de coordination qui est intermédiaire entre la pyramide carrée et la bipyramide trigonale. Les longueurs de liaisons importantes (corrigées pour la libration) sont: Ga—Cl, 2,228(2), Ga—O, 1,868(4) et 1,883(4), Ga—N, 2,019(6) et 2,035(5) Å. La structure du cristal consite en des molécules individuelles de $(C_{16}H_{14}N_2O_2)$ GaCl et de CH_2Cl_2 liées par une liaison hydrogène C—H···O (O···H = 2,31, O···C = 3,295(9) Å, C—H—O = 176°) conduisant à la formation d'unités de complexes solvatés.

[Traduit par le journal]

Introduction

In a previous paper (1) we described the reaction of trimethyl gallium with *N,N'*-ethylenebis-(salicylideneimine) in which either one dimethyl gallium moiety was bound to the ligand system in a postulated six-coordinate gallium complex, or two dimethyl gallium moieties were incorporated in the product if an excess of the gallium alkyl starting material was employed. The present study was undertaken to determine if five-coordinate gallium complexes could be produced using this type of ligand system and thereby extend our previous investigations in this area (2–6) to include square-pyramidal gallium complexes. Two complexes, **1**, have been characterized and the crystal structure of the compound **1***a* has been determined.

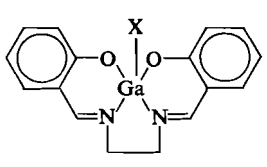

1
a X = Cl
b X = Me

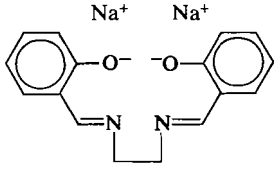

2

Experimental

Starting Materials

All solvents were dried and distilled before use and reactions were carried out in a glove box filled with dry nitrogen or in a nitrogen-blanketed apparatus. Methyl gallium dichloride was prepared by a standard procedure (7) from gallium trichloride (8) and tetramethylsilane. *N,N'*-Ethylenebis(salicylideneimine), prepared from ethylenediamine and salicylaldehyde by standard methods, was converted to its disodium salt, **2**, by reaction with sodium hydride in THF solvent. The disodium salt was isolated as a white solid.

N,N'-*Ethylenebis(salicylideneiminato)chlorogallium(III), 1*a

This compound was prepared by reacting the disodium salt, **2**, (2.713 g, 8.69 mmol) with gallium trichloride (1.530 g, 8.69 mmol) in THF at room temperature. The reaction mixture was stirred for several days to ensure complete reaction. It was then filtered and the crude product, obtained from the filtrate after removal of solvent under vacuum, was recrystallized from benzene (Soxhlet extraction) to give pale yellow crystals in ~ 50% yield. *Anal.* calcd. for **1***a*: C 51.6, H 3.8, N 7.5; found: C 51.1, H 3.9, N 7.7. The mass spectrum of **1***a* (recorded on a Varian MAT CH4B mass spectrometer at 70 eV with an ion source temerature of approximately 70°C) was dominated by two very strong signals due to the parent ion and to the parent ion minus the Cl group. ^1H nmr (d^6-acetone solution): $\tau_{-CH_2-CH_2-} = 6.10$ ppm singlet, $\tau_{HC=N} = 1.49$ ppm singlet, $\tau_{d^6\text{-acetone}} = 8.17$ ppm.

N,N'-*Ethylenebis(salicylideneiminato)methylgallium(III), 1*b

The methyl gallium derivative was prepared in a similar manner to that described above for the chloro compound. The di-

0008-4042/81/010094-06$01.00/0

©1981 National Research Council of Canada/Conseil national de recherches du Canada

Can. J. Chem. Downloaded from www.nrcresearchpress.com by 210.87.254.105 on 09/05/12
For personal use only.

Can. J. Chem. Downloaded from www.nrcresearchpress.com by 210.87.254.105 on 09/05/12
For personal use only.

sodium salt, **2**, (1.110 g, 3.55 mmol) was reacted with methyl gallium dichloride (0.550 g, 3.55 mmol) in THF at room temperature for 12 h. The sodium chloride precipitated was then filtered off and the crude product isolated from the filtrate by removal of solvent under vacuum. This crude product was recrystallized from benzene/THF to yield a pale yellow solid in ~ 80% yield. *Anal.* calcd. for **1***b*: C 58.2, H 4.9, N 8.0; found: C 58.6, H 5.7, N 7.9. The mass spectrum of compound **1***b* shows a very weak parent ion signal and was dominated by the very strong signal due to the parent ion minus the Me group. In addition a weak signal due to the doubly charged parent minus Me group ion was also evident in this spectrum. ^{1}H nmr (d^6-acetone solution): τ_{GaMe} = 10.73 ppm singlet, $\tau_{\text{"}CH_2\text{—}CH_2\text{"}}$ = 6.25 ppm complex multiplet, $\tau_{HC=N}$ = 1.69 ppm singlet, $\tau_{d^6\text{-acetone}}$ = 8.17 ppm.

X-ray Crystallographic Analysis of N,N'-*Ethylenebis(salicylideneiminato)chlorogallium(III) Dichloromethane*

Crystals suitable for X-ray analysis were obtained by recrystallization from benzene/dichloromethane. The crystal chosen was mounted in a general orientation and had dimensions of ca. 0.50 × 0.42 × 0.10 mm. Unit-cell parameters were refined by least-squares on 2 sin θ/λ values for 25 reflections measured on a diffractometer with Mo K_α radiation (λ = 0.71073 Å). Crystal data (at 22°C) are:

$C_{17}H_{16}Cl_3GaN_2O_2$ fw = 456.1

Monoclinic, a = 13.049(1), b = 9.525(1), c = 15.459(2) Å, β = 92.452(5)°, V = 1919.6(4) Å^3, Z = 4, ρ_c = 1.285 g cm^{-3}, $F(000)$ = 920, μ(Mo K_α) = 19.38 cm^{-1}. Absent reflections: $h0l$, $h \neq 2n$ and $0k0$, $k \neq 2n$ define uniquely the space group $P2_1/a$ (non-standard setting of $P2_1/c$, C_{2h}^5, No. 14).

Intensities were measured with graphite monochromatized Mo K_α radiation on an Enraf-Nonius CAD4-F diffractometer. An ω–2θ scan at 1.18–10.06° min^{-1} over a range of (0.75 + 0.35 tan θ) degrees in ω (extended by 25% on both sides for background measurement) was employed. Data were measured to 2θ = 50°. The intensities of 3 check reflections, measured every 3600 s throughout the data collection, remained constant to within ±4%. After data reduction, an absorption correction was applied using the Gaussian integration method (9, 10). Transmission factors ranged from 0.439 to 0.836 for 208 sampling points. Of the 3379 independent reflections measured, 1815 (54%) had intensities greater than 3σ(I) above background where $\sigma^2(I) = S + 2B + (0.04(S - B))^2$ with S = scan count and B = background count.

The positions of the gallium and the chlorine bonded to it were determined from the Patterson function and those of the remaining non-hydrogen atoms from a subsequent Fourier synthesis. After full-matrix least-squares refinement of the non-hydrogen atoms with anisotropic thermal parameters to R = 0.053, a difference map gave positions for all hydrogen atoms except those associated with the solvate. The solvent hydrogen atom positions were calculated and kept fixed during subsequent cycles of refinement while the remaining hydrogen atoms were refined with isotropic thermal parameters. The scattering factors of ref. 11 were used for non-hydrogen atoms and those of ref. 12 for hydrogen atoms. Anomalous scattering factors from ref. 13 were used for the Ga and Cl atoms. The weighting scheme, $w = 1/\sigma^2(F)$ where $\sigma^2(F)$ is derived from the previously defined $\sigma^2(I)$ gave uniform average values of $w(|F_o| - |F_c|)^2$ over ranges of $|F_o|$ and was employed in the final stages of refinement. Convergence was reached at R = 0.042 and R_w = 0.051 for 1815 reflections with $I \geq 3\sigma(I)$. For all 3379 reflections R = 0.107 and R_w = 0.057. The function minimized was $\Sigma w(|F_o| - |F_c|)^2$, $R = \Sigma||F_o| - |F_c||/\Sigma|F_o|$ and $R_w = (\Sigma w(|F_o| - |F_c|)^2/\Sigma w|F_o|^2)^{1/2}$.

On the final cycle of refinement the mean and maximum parameter shifts corresponded to 0.02 and 0.21σ respectively. The mean error in an observation of unit weight was 1.634. A final difference map showed maximum fluctuations of ±0.75 e Å^{-3} near the Ga and Cl atoms and ±0.20 e Å^{-3} elsewhere. The final positional and thermal parameters appear in Tables 1 and 2[1] respectively. Measured and calculated structure factors have been placed in the Depository of Unpublished Data.[1]

The ellipsoids of thermal motion for the non-hydrogen atoms are shown in Fig. 1. The thermal motion has been analysed in terms of the rigid-body modes of translation, libration, and screw motion (14) using the computer program MGTLS. The

TABLE 1. Final positional parameters (fractional × 10^4, Ga and Cl(1) × 10^5, H × 10^3) with estimated standard deviations in parentheses. Equivalent positions: ±(x, y, z; 1/2 + x, 1/2 − y, z)

Atom	x	y	z
Ga	27355(4)	38261(8)	31464(4)
Cl(1)	18010(10)	40856(18)	43051(10)
Cl(2)	3705(3)	6864(4)	415(3)
Cl(3)	1974(3)	8170(5)	1045(2)
O(1)	1821(3)	4353(5)	2232(2)
O(2)	3462(3)	5464(5)	2929(3)
N(1)	2537(4)	1792(6)	2827(3)
N(2)	3989(3)	2976(6)	3769(3)
C(1)	1041(4)	3612(9)	1899(4)
C(2)	953(5)	2155 (9)	1979(4)
C(3)	97(6)	1456(12)	1609(5)
C(4)	−653(7)	2199(17)	1165(6)
C(5)	−563(6)	3617(16)	1057(5)
C(6)	257(5)	4336(11)	1427(4)
C(7)	1744(5)	1323(9)	2395(4)
C(8)	3329(5)	827(9)	3188(5)
C(9)	4367(4)	5889(8)	3253(4)
C(10)	5029(4)	5057(8)	3780(3)
C(11)	5971(5)	5631(11)	4075(4)
C(12)	6277(5)	6913(11)	3851(5)
C(13)	5650(6)	7737(10)	3321(5)
C(14)	4704(6)	7215(10)	3029(5)
C(15)	4810(4)	3648(9)	3996(4)
C(16)	3828(5)	1517(9)	3981(5)
C(17)	2716(7)	6687(12)	1010(6)
H(3)	7(5)	48(7)	168(5)
H(4)	−112(6)	177(9)	100(5)
H(5)	−114(7)	420(10)	84(7)
H(6)	38(4)	526(6)	132(4)
H(7)	172(4)	36(5)	238(3)
H(8a)	387(5)	71(7)	272(4)
H(8b)	310(4)	−7(5)	331(3)
H(11)	631(5)	501(7)	442(4)
H(12)	687(5)	736(7)	406(4)
H(13)	583(5)	867(7)	316(4)
H(14)	431(4)	770(6)	269(4)
H(15)	522(5)	315(7)	432(4)
H(16a)	347(5)	143(7)	444(4)
H(16b)	440(5)	103(6)	426(4)
H(17a)	228	588	77
H(17b)	294	637	160

[1]The structure factor table and Table 2 (thermal parameters) are available, at a nominal charge, from the Depository of Unpublished Data, CISTI, National Research Council of Canada, Ottawa, Ont., Canada K1A 0S2.

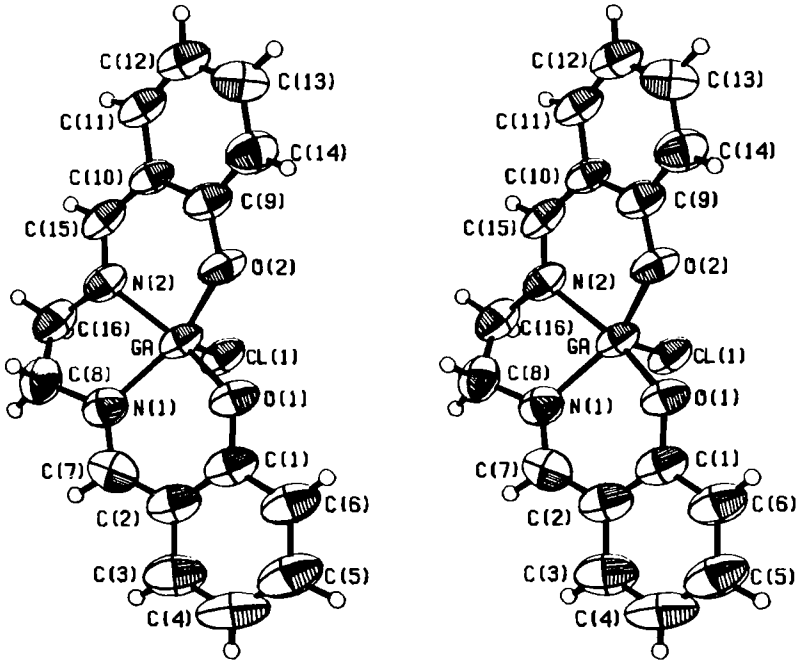

FIG. 1. Stereo view of the *N,N'*-ethylenebis(salicylideneiminato)chlorogallium(III) molecule, 50% thermal ellipsoids are shown for the non-hydrogen atoms.

rms standard error in the temperature factors σU_{ij} (derived from the least-squares analysis) is 0.0046 Å^2. Analysis of all non-hydrogen atoms except those of the solvent of crystallization gave rms $\Delta U_{ij} = 0.0070$ Å^2 and physically reasonable results. The appropriate bond distances have been corrected for libration (15), using shape parameters q^2 of 0.08 for all atoms involved. Corrected bond lengths are given along with the uncorrected values in Table 3 and the corrected bond angles do not differ from the uncorrected values listed in Table 4 by more than one standard deviation. Intra-annular torsion angles defining the conformations of the chelate rings are given in Table 5.

Results and Discussion

The two complexes reported here extend the series of five-coordinate gallium complexes structurally characterized to include an example of a severely distorted square-pyramidal geometry about the gallium atom. Thus the structure of the present chloro gallium complex, **1***a*, discussed below displays the gallium atom in a setting intermediate between square-pyramidal and trigonal bipyramidal in the mononuclear complex. Other five-coordinate gallium species which have been structurally characterized are better described as containing the gallium atom in a distorted trigonal bipyramidal environment and these compounds include a chain-like polymer (6), four binuclear gallium species (2, 3, 5), a cage structure involving eight gallium atoms two of which are five-coordinate (4), and a mononuclear species (16, 17).

The compounds **1***a* and **1***b* were easily prepared in good yield by reacting gallium trichloride or methyl gallium dichloride with a stoichiometric amount of the disodium salt of *N,N'*-ethylenebis-(salicylideneimine) in THF solvent. The compound **1***a* was obtained as an air-stable crystalline material suitable for X-ray investigations but numerous attempts to prepare similar quality crystals of the gallium methyl compound **1***b* were not successful. Interestingly the ^{1}H nmr in d^6-acetone solution of the chloro gallium compound, **1***a*, shows a singlet for the "CH_2—CH_2" protons whereas the compound **1***b* in d^6-acetone shows a very complex multiplet in the "CH_2—CH_2" region of the ^{1}H nmr spectrum. A rapidly fluxional process must occur for compound **1***a* in solution at room temperature since it is evident from the solid state structure that the four "CH_2—CH_2" protons are inequivalent. The compound **1***b*, on the other hand, must possess a more rigid structure in solution or undergo some interaction with the solvent which allows complex coupling to occur among the four "CH_2—CH_2" protons. Another notable difference between the two compounds **1***a* and **1***b* became evident from their mass spectra. The compound **1***a* displayed very strong signals for *both* the parent ion and the parent ion minus the Cl group. On the other hand the compound **1***b* displayed only a very weak signal due to the parent ion and its mass spectrum was dominated by the signal due to the parent ion minus

Can. J. Chem. Downloaded from www.nrcresearchpress.com by 210.87.254.105 on 09/05/12
For personal use only.

Can. J. Chem. Downloaded from www.nrcresearchpress.com by 210.87.254.105 on 09/05/12
For personal use only.

TABLE 3. Bond lengths (Å) with estimated standard deviations in parentheses

(*a*) Non-hydrogen atoms

Bond	Length		Bond	Length	
	Uncorr.	Corr.		Uncorr.	Corr.
Ga —Cl(1)	2.223(2)	2.228	C(2) —C(7)	1.432(9)	1.435
Ga —O(1)	1.879(4)	1.883	C(3) —C(4)	1.369(14)	1.372
Ga —O(2)	1.863(4)	1.868	C(4) —C(5)	1.366(13)	1.370
Ga —N(1)	2.014(6)	2.019	C(5) —C(6)	1.374(11)	1.376
Ga —N(2)	2.030(5)	2.035	C(8) —C(16)	1.513(11)	1.515
O(1)—C(1)	1.324(7)	1.326	C(9) —C(10)	1.407(8)	1.410
O(2)—C(9)	1.326(6)	1.328	C(9) —C(14)	1.387(9)	1.389
N(1)—C(7)	1.287(8)	1.288	C(10)—C(11)	1.403(8)	1.403
N(1)—C(8)	1.475(9)	1.477	C(10)—C(15)	1.415(9)	1.418
N(2)—C(15)	1.285(7)	1.286	C(11)—C(12)	1.335(10)	1.338
N(2)—C(16)	1.445(9)	1.447	C(12)—C(13)	1.379(11)	1.381
C(1)—C(2)	1.389(9)	1.402	C(13)—C(14)	1.388(9)	1.389
C(1)—C(6)	1.410(10)	1.414	C(17)—Cl(2)	1.625(10)	
C(2)—C(3)	1.402(9)	1.403	C(17)—Cl(3)	1.715(11)	

(*b*) Bonds involving hydrogen atoms

Bond	Length	Mean
C(sp^2)—H	0.77–0.98(5–9)	0.90(6)
C(sp^3)—H	0.87–1.03(5–7)	0.95(7)

TABLE 4. Bond angles (deg) with estimated standard deviations in parentheses, non-hydrogen atoms

Bonds	Angle (deg)	Bonds	Angle (deg)
Cl(1)—Ga —O(1)	102.9(1)	C(1) —C(2) —C(7)	121.9(6)
Cl(1)—Ga —O(2)	110.7(1)	C(3) —C(2) —C(7)	117.9(8)
Cl(1)—Ga —N(1)	103.6(1)	C(2) —C(3) —C(4)	120.0(10)
Cl(1)—Ga —N(2)	97.0(1)	C(3) —C(4) —C(5)	120.6(9)
O(1) —Ga —O(2)	87.3(2)	C(4) —C(5) —C(6)	120.7(10)
O(1) —Ga —N(1)	90.1(2)	C(1) —C(6) —C(5)	120.4(10)
O(1) —Ga —N(2)	159.4(2)	N(1) —C(7) —C(2)	126.1(7)
O(2) —Ga —N(1)	145.3(2)	N(1) —C(8) —C(16)	107.9(6)
O(2) —Ga —N(2)	90.8(2)	O(2) —C(9) —C(10)	124.2(6)
N(1) —Ga —N(2)	79.9(2)	O(2) —C(9) —C(14)	118.0(6)
Ga —O(1)—C(1)	127.1(4)	C(10)—C(9) —C(14)	117.7(6)
Ga —O(2)—C(9)	129.7(4)	C(9) —C(10)—C(11)	118.5(7)
Ga —N(1)—C(7)	123.6(6)	C(9) —C(10)—C(15)	123.0(6)
Ga —N(1)—C(8)	115.2(5)	C(11)—C(10)—C(15)	118.4(6)
C(7) —N(1)—C(8)	121.0(7)	C(10)—C(11)—C(12)	122.7(8)
Ga —N(2)—C(15)	125.2(5)	C(11)—C(12)—C(13)	119.8(7)
Ga —N(2)—C(16)	111.7(4)	C(12)—C(13)—C(14)	119.2(8)
C(15)—N(2)—C(16)	123.0(6)	C(9) —C(14)—C(13)	122.1(8)
O(1) —C(1)—C(2)	124.0(6)	N(2) —C(15)—C(10)	125.7(7)
O(1) —C(1)—C(6)	117.9(8)	N(2) —C(16)—C(8)	107.2(7)
C(2) —C(1)—C(6)	118.0(7)	Cl(2)—C(17)—Cl(3)	113.3(6)
C(1) —C(2)—C(3)	120.2(8)		

the Me group. These observations suggest a much stronger Ga—Cl link as compared with the Ga—Me link, as expected.

Attempts to replace the Cl group with other groups by treating the chlorogallium compound **1***a* with Na^+X^- salts (where X^- = Br^-, I^-, OEt^-, *n*-Bu^-, pyrazolide, or 3,5-dimethylpyrazolide) were unsuccessful, again indicating the presence of a relatively strong and highly covalent Ga—Cl link in compound **1***a*.

X-ray Crystallographic Analysis of ($C_{16}H_{14}N_2O_2$)-*GaCl*·CH_2Cl_2

The crystal structure of *N*,*N*′-ethylenebis-

TABLE 5. Intra-annular torsion angles (deg) chelate rings

Bond	Angle (deg)	Bond	Angle (deg)
Ga —O(1)	29.0(4)	Ga —O(2)	−12.0(4)
O(1) —C(1)	−21.3(6)	O(2) —C(9)	7.7(6)
C(1) —C(2)	−3.6(8)	C(9) —C(10)	2.2(7)
C(2) —C(7)	9.2(8)	C(10)—C(15)	−2.1(7)
C(7) —N(1)	8.7(7)	C(15)—N(2)	−6.7(7)
N(1) —Ga	−22.6(4)	N(2) —Ga	11.4(4)
Ga —N(1)	0.6(4)		
N(1) —C(8)	22.9(6)		
C(8) —C(16)	−42.6(6)		
C(16)—N(2)	44.8(5)		
N(2) —Ga	−25.9(4)		

(salicylideneiminato)chlorogallium(III) dichloromethane consists of discrete $(C_{16}H_{14}N_2O_2)GaCl$ and CH_2Cl_2 molecules linked by a C—H···O hydrogen bond (O(2)···H(17b) = 2.31, O(2)···C(17) = 3.295(9) Å, C—H—O = 176°) to form complex-solvate units. All other intermolecular distances correspond to normal van der Waals contacts.

The gallium atom is coordinated to a chlorine and to the two nitrogen and two oxygen atoms of the tetradentate *N,N'*-ethylenebis(salicylideneiminato) ligand resulting in a coordination geometry which closely resembles the C_s "twisted wedge" described by King (18). This geometry is intermediate between square pyramidal in which the chlorine is apical and trigonal bipyramidal with N(2) and O(1) occupying the axial coordination sites (see Fig. 1). Neither the large differences between axial and equatorial bond lengths expected for trigonal bipyramidal coordination nor the equality of basal bond lengths expected for idealized square pyramidal geometry are observed. The Ga—O and Ga—N bond lengths are, however, consistent with the observed intermediate geometry. The "axial" distances are longer than their counterparts by 0.015 Å (2.7σ) for Ga—O and by 0.016 Å (2.1σ) for Ga—N.

The Ga—Cl(1) distance of 2.228(2) Å is slightly, but significantly, longer than the equatorial Ga—Cl distance (2.190(2) and 2.195(5) Å for two independent structure determinations) in the trigonal bipyramidal complex chlorobis(8-hydroxy-2-methylquinolinato)gallium(III) (16, 17). The mean[2] Ga—O and Ga—N bond lengths of 1.876(8) and 2.027(8) Å are similar to the corresponding values of 1.885(1) and 2.038(5) Å observed for the tetrahedrally coordinated gallium atoms in *N,N'*-ethylenebis(salicylideneiminato)bis(dimethylgallium) (1) and lie within the ranges observed for equatorially coordinated O and N in trigonal bipyramidal gallium complexes (1.845–1.967 and 1.949–2.035 Å respectively for Ga—O and Ga—N) (2–6, 16, 17).

The $(C_{16}H_{14}N_2O_2)GaCl$ molecule contains a system of five fused rings. Both of the terminal aromatic rings are slightly distorted from planarity (χ^2 = 9.0 and 8.9 respectively for the rings containing C(1) and C(9)), the maximum deviation of any atom from the mean planes being 0.017(8) Å. The intra-annular torsion angles for the chelate rings (Table 5) show that the two six-membered chelate rings are conformationally non-equivalent, that containing O(1) being significantly less planar than the other. The central five-membered chelate ring has an envelope conformation with C(16) displaced from the plane defined by the four other atoms. The internal geometry of the organic ligand is as expected (see Tables 3 and 4).

The overall geometry of the $(C_{16}H_{14}N_2O_2)GaCl$ molecule is very similar to that of the analogous Fe(III) complex $(C_{16}H_{14}N_2O_2)FeCl$ (19). The coordination about the metal atoms is nearly identical, corresponding valence angles being in excellent agreement. The M—Cl and M—O distances are equal within experimental error while the M—N distances are somewhat longer in the Fe complex (mean Fe—N = 2.082, mean Ga—N = 2.027 Å).

[2]Here and elsewhere in this report mean values refer to weighted means with rms deviations from the mean in parentheses.

Acknowledgments

We thank the Natural Sciences and Engineering Research Council of Canada for financial support and the University of British Columbia Computing Centre for assistance. We are grateful to Mr. P. Borda for C, H, N analyses and to Dr. S. Chan for ^1H nmr spectra.

1. K. S. CHONG, S. J. RETTIG, A. STORR, and J. TROTTER. Can. J. Chem. **55**, 2540 (1977).
2. S. J. RETTIG, A. STORR, and J. TROTTER. Can. J. Chem. **52**, 2206 (1974).
3. S. J. RETTIG, A. STORR, and J. TROTTER. Can. J. Chem. **53**, 58 (1975).
4. S. J. RETTIG, A. STORR, and J. TROTTER. Can. J. Chem. **53**, 753 (1975).
5. S. J. RETTIG, A. STORR, and J. TROTTER. Can. J. Chem. **54**, 1278 (1976).
6. K. R. BREAKELL, S. J. RETTIG, A. STORR, and J. TROTTER. Can. J. Chem. **55**, 4174 (1977).
7. H. SCHMIDBAUER and W. FINDEISS. Angew. Chem. Int. Ed. **3**, 696 (1964).
8. N. N. GREENWOOD and K. WADE. J. Chem. Soc. 1527 (1956).

Can. J. Chem. Downloaded from www.nrcresearchpress.com by 210.87.254.105 on 09/05/12
For personal use only.

9. P. COPPENS, L. LEISEROWITZ, and D. RABINOVICH. Acta Crystallogr. **18**, 1035 (1965).
10. W. R. BUSING and H. A. LEVY. Acta Crystallogr. **22**, 457 (1967).
11. D. T. CROMER and J. B. MANN. Acta Crystallogr. Sect. A, **24**, 321 (1968).
12. R. F. STEWART, E. R. DAVIDSON, and W. T. SIMPSON. J. Chem. Phys. **42**, 3175 (1965).
13. D. T. CROMER and D. LIBERMAN. J. Chem. Phys. **53**, 1891 (1970).
14. V. SCHOMAKER and K. N. TRUEBLOOD. Acta Crystallogr. Sect. B, **24**, 63 (1969).
15. D. W. J. CRUICKSHANK. Acta Crystallogr. **9**, 747 (1956); **9**, 754 (1956); **14**, 896 (1961).
16. M. SHIRO and Q. FERNANDO. Anal. Chem. **43**, 1222 (1971).
17. K. DYMOCK and G. J. PALENIK. J. Chem. Soc. Chem. Commun. 884 (1973).
18. R. B. KING. J. Am. Chem. Soc. **91**, 7211 (1969).
19. M. GERLOCH and F. E. MABBS. J. Chem. Soc. A, 1598 (1967).

Can. J. Chem. Downloaded from www.nrcresearchpress.com by 210.87.254.105 on 09/05/12
For personal use only.

Thermolysis of 5,5-dimethyl-4-aryl-Δ^1-1,2,4-triazolin-3-ones in solution. Products, kinetics, substituent effects, and solvent effects

LUBOMIRA M. CABELKOVA-TAGUCHI AND JOHN WARKENTIN
Department of Chemistry, McMaster University, Hamilton, Ont., Canada L8S 4M1

Received June 23, 1980

LUBOMIRA M. CABELKOVA-TAGUCHI AND JOHN WARKENTIN. Can. J. Chem. **59**, 100 (1981).

A series of 5,5-dimethyl-4-aryl-Δ^1-1,2,4-triazolin-3-ones (Ar = C_6H_5, *p*-$C_6H_4CH_3$, *p*-$C_6H_4OCH_3$, *p*-C_6H_4Cl, and *p*-C_6H_4Br) were prepared from the corresponding 4-arylsemicarbazones of acetone by oxidative cyclization on alumina. The triazolinones decompose in solution to N_2, CO, and isopropylidene aryl amine, with first order kinetics, in the temperature range 148–200°C. Average activation parameters are $\Delta H^{\ddagger} = 35$ kcal mol^{-1} and $\Delta S^{\ddagger} = 8$ cal K^{-1} mol^{-1}. Substituent effects are correlated through σ-constants but the thermolyses are relatively insensitive to substituents, with $\rho = -0.17$ at 172.5°C. Solvent effects indicate a transition state that is less polar than the ground state.

It is tentatively concluded that the triazolinone fragmentation, like the analogous thermolysis of a Δ^3-1,3,4-oxadiazolin-2-one, may be a fully-concerted but nonsynchronous process with a transition state involving little, if any, charge separation. Other mechanisms, except for those involving highly polar (e.g. zwitterionic) transition states, have not been ruled out.

LUBOMIRA M. CABELKOVA-TAGUCHI et JOHN WARKENTIN. Can. J. Chem. **59**, 100 (1981).

On a préparé une série de diméthyl-5,5 aryl-4 Δ^1-triazoline-1,2,4 ones-3 (Ar = C_6H_5, *p*-$C_6H_4CH_3$, *p*-$C_6H_4OCH_3$, *p*-C_6H_4Cl et *p*-C_6H_4Br) par une cyclisation oxydante sur l'alumine des aryl-4 semicarbazones de l'acétone appropriée. Dans l'intervalle de température de 148 à 200°C les triazolinones en solution se décomposent en N_2, CO et isopropylidène d'arylamine selon une cinétique d'un premier ordre. Les paramètres moyens d'activation sont: $\Delta H^{\ddagger} = 35$ kcal mol^{-1} et $\Delta S^{\ddagger} = 8$ cal K^{-1} mol^{-1}. On établi une corrélation entre les effets se substituants et les constantes σ, les substituants n'ont toutefois que peu d'effet sur les thermolyses puisque $\rho = 0{,}17$ à 172,5°C. Les effets de solvants indiquent un état de transition moins polaire que l'état fondamental.

On conclut d'une façon préliminaire que la fragmentation de la triazolinone, comme la thermolyse analogue de la Δ^3-oxadiazoline-1,3,4 one-2, peut être un processus pleinement concerté mais non synchrone avec un état de transition impliquant peu de séparation de charges. On n'a pas éliminé d'autres mécanismes, à l'exception de ceux mettant en jeu des états de transition fortement polaires (i.e. zwittérions).

[Traduit par le journal]

Introduction

The thermolysis chemistry of Δ^3-1,3,4-oxadiazoline systems (**1**) shows the interesting dichotomy represented by eq. [1]. Thus, compounds

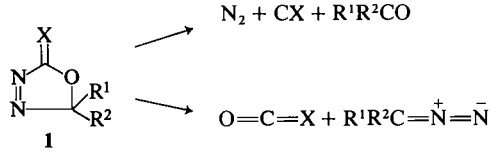

[1]

1

a $R^1 = R^2 =$ Ar; X = NAr
b $R^1 = R^2 =$ alkyl; X = NAr
c $R^1 = R^2 =$ alkyl; X = O
d $R^1 =$ alkyl, $R^2 =$ aryl; X = O
e $R^1 = R^2 =$ aryl; X = O
f $R^1 = R^2 =$ alkyl; X = N—N=$C(Ar)_2$
g $R^1 = R^2 =$ alkyl; X = N—N=CHAr

1*a* decompose to form aryl isocyanide and diaryl ketone as well as aryl isocyanate and diaryl diazomethane (1). Analogous fragmentations occur on thermolysis of **1***b* (2),[1] **1***c* (2–4), **1***d* (4), and **1***e* (3). The partitioning between the two thermolysis pathways is sensitive to the solvent polarity (3, 4), the substituents at C5 (1–4), and the exocyclic substituent (X) at C2 (2). In systems **1***f* and **1***g* the two piece fragmentation pathway can account for all of the observations and there may be little competition from the three-piece pathway (5).

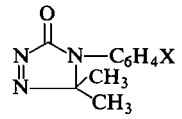

2

a X = H
b X = *p*-CH_3
c X = *p*-OCH_3
d X = *p*-Cl
e X = *p*-Br

We have been interested also in the role that the ring oxygen plays in determining the fragmentation pathway of choice and we report here the thermolysis chemistry of 5,5-dimethyl-4-aryl-Δ^1-1,2,4-triazolin-3-ones, **2**, in solution.

Experimental

Syntheses

Triazolinones **2** were prepared by the method of Landquist (6) who cyclized 4-arylthiosemicarbazones and 4-arylsemicarbazones of ketones (**3**) on basic alumina, eq. [2]. Acetone-4-arylsemicarbazones, **3**, were prepared from acetone semicarbazone by transamidation with the appropriate *p*-substituted aniline, following the method of Borsche (7). In a typical preparation,

[1]Studies of **1***b* include unpublished work of A. M. Cameron and J. B. Fulton.

0008-4042/81/010100-06$01.00/0
©1981 National Research Council of Canada/Conseil national de recherches du Canada

Can. J. Chem. Downloaded from www.nrcresearchpress.com by 210.87.254.105 on 09/05/12
For personal use only.

Can. J. Chem. Downloaded from www.nrcresearchpress.com by 210.87.254.105 on 09/05/12
For personal use only.

TABLE 1. 4-Arylsemicarbazones of acetone, $(CH_3)_2C{=}NNHCONHAr$[a] (3)

Ar	Melting point (°C)	Melting point (°C) (lit.)	^{1}Hmr (δ, $CDCl_3$)[b]
C_6H_5	154–155	155–156(7)	1.97 (s, 3H); 2.05 (s, 3H); 7.3–7.6 (m, br, 5H)
p-$C_6H_4CH_3$	173–174	174–175(7)	1.95 (s, 3H); 2.00 (s, 3H); 2.25 (s, 3H); 6.95–7.40 (m, 4H); 8.10 (s, br, 1H); 8.31 (s, br, 1H)
p-$C_6H_4OCH_3$	169–170	167–169[c]	1.90 (s, 3H); 2.00 (s, 3H); 3.65 (s, 3H); 6.8–7.4 (m, br, 4H)
p-C_6H_4Cl	170	169–170[c]	1.95 (s, 3H); 2.05 (s, 3H); 7.2–7.6 (m, br, 4H); 8.45 (s, br, 1H); 9.21 (s, br, 1H)
p-C_6H_4Br	172–173	174(8)	1.95 (s, 3H); 2.05 (s, 3H); 7.4–7.8 (m, br, 4H); 8.50 (s, br, 1H); 9.25 (s, br, 1H)

[a]All compounds in the table absorb between 1680 and 1690 cm^{-1} in the infrared.
[b]Abbreviations: s= singlet, m = multiplet, br = broad.
[c]Satisfactory analyses were obtained for the new semicarbazones. Unpublished work of A. M. Cameron.

[2] $(CH_3)_2C{=}NNHCONHAr \xrightarrow[CHCl_3]{Al_2O_3}$ 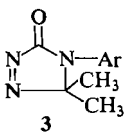

2 3

acetone semicarbazone (58 g, 0.5 mol) was heated at 145–165°C with aniline or p-substituted aniline (1.0 mol) in bis(2-methoxyethyl)ether (200 mL) to afford crude acetone-4-arylsemicarbazone in 25–35% yield. Purification by recrystallization (7) gave materials with the properties and spectral characteristics given in Table 1. A 5,5-dimethyl-4-aryl-Δ^1-1,2,4-triazolin-3-one, **2**, was prepared from the appropriate semicarbazone (**3**, ca.2 g) by stirring it at room temperature for 7 days with a slurry of alumina (Fisher Certified Reagent, Activity 1, 20–200 mesh, ca. 50 g) and dry chloroform (100 mL). Filtration, evaporation of the chloroform, and recrystallization of the crude solid residue from 95% ethanol yielded the triazolinone in 25–80% yield. Table 2 lists data for compounds **2**.

Solvents

Because of the high reactivities of isopropylidenearyl amines and of aryl isocyanates (the other potential products of thermolysis of **2**) carefully purified, dry solvents were used throughout.

Benzene and toluene (Mallinckrodt Analytical Reagent grade) were warmed with concentrated H_2SO_4. The hydrocarbon layers were separated, washed thoroughly with water, and dried over $CaCl_2$. The decanted liquids were then refluxed for 2 h in the presence of sodium wire before they were distilled. Fractions boiling at 80–81°C (benzene) and 110–111°C (toluene) were collected and stored over molecular sieves (5Å).

Chlorobenzene (Fisher Certified Reagent) was shaken repeatedly with portions of H_2SO_4 until the acid layer remained colourless. The chlorobenzene layer was washed with water and with potassium bicarbonate solution before it was dried over $CaCl_2$ and distilled. The fraction boiling at 130–131°C was redried over P_2O_5 and redistilled. Nitrobenzene (BDH, Analytical Reagent) was dried over P_2O_5 and distilled. It was stored over molecular sieves in a brown bottle.

Products of Thermolysis of 2a

A solution of **2*a*** (0.075 g, 4.0 × 10^{-4} mol) in 3 mL of dry benzene (see above) was degassed, sealed under vacuum, and heated at 175°C for 5 h. Quantitative analysis of the ^{1}H nmr spectrum (Varian HA-100 instrument) using a peak height calibration chart showed the presence of 0.052 g (98% yield) of acetone anil (isopropylidenephenyl amine). The ir spectrum contained a strong band at 1660 cm^{-1} ($\nu_{C=N}$) but none at 2270 cm^{-1} (ν_{ArNCO}). Gas chromatographic analysis (5 ft × $\frac{1}{4}$ in., 15% SE30 on 60–80 mesh Chromosorb P column) showed the presence of acetone, aniline, and acetone anil. Injection of freshly prepared acetone anil also led to acetone and aniline signals. These were therefore attributed to hydrolysis of the anil during handling or in the column.

The other triazolinones, **2*b*–*e***, gave analogous products as judged from the ^{1}H nmr and ir spectra of spent solutions. In no case were isocyanate bands near 2270 cm^{-1} evident in the ir spectra.

Kinetics

A stock solution of a triazolinone and internal standard toluene was loaded, in 0.3 mL portions, into Pyrex tubes which were sealed after at least three freeze–pump–thaw degassing cycles. Such tubes were mounted in a controlled temperature oil bath. Tubes withdrawn from time to time were cooled rapidly and stored cold. They were then warmed and opened, and the contents were transferred to an nmr tube for analysis. At least five scans of the reference signal and of the C-5 methyl signals from starting material were recorded. The average normalized peak height for starting material was converted to a concentration using a calibration chart and such concentrations were fitted to the first order rate law using a standard linear least-squares computer program. The program also gave the activation energies. Tables 3, 4, and 5 summarize the data for one of the compounds, **2*a***, while Table 6 summarizes the substituent effects. A typical Eyring plot is shown as Fig. 1 and the Hammett correlation is shown as Fig. 2.

Results and Discussion

Like oxadiazolinones (**1**) compounds **2** decompose in solution with first-order kinetics (Table 3). However, compounds **2** show no evidence for thermolysis by both of the competing pathways

Can. J. Chem. Downloaded from www.nrcresearchpress.com by 210.87.254.105 on 09/05/12
For personal use only.

TABLE 2. 5,5-Dimethyl-4-aryl-Δ^1-1,2,4-triazolin-3-ones[a] (2)

X	Melting point (°C)	Ultraviolet (95% EtOH) λ_{max} (log E)	^{1}H nmr (δ, $CDCl_3$)	Analysis (%)[b] C	H	N	X
H	142–143[c]	275(3.35) 375(2.63)	1.58 (s, 6H) 7.0–7.6 (m, 5H)				
p-CH_3	109–110	280(3.45) 385(2.69)	1.60 (s, 6H) 2.40 (s, 3H) 7.0–7.6 (m, 4H)	64.72 65.02	6.34 6.40	20.73 20.69	
p-OCH_3	230	285(3.41) 390(2.87)	1.55 (s, 6H) 3.70 (s, 3H) 6.7–7.6 (m, 4H)	60.31 60.27	6.09 5.94	19.03 19.18	
p-Cl	107	281(3.47) 378(2.64)	1.60 (s, 6H) 7.0–8.2 (m, 4H)	53.82 53.69	4.50 4.47	18.88 18.79	16.05 15.92
p-Br	126–127	282(3.67) 378(3.02)	1.58 (s, 6H) 7.0–8.2 (m, 4H)	44.88 44.77	3.96 3.73	15.55 15.67	29.68 29.85

[a]Carbonyl stretching frequency in the ir between 1750 cm^{-1} and 1755 (CCl_4).
[b]Lower numbers in each set are the calculated values.
[c]Literature (6), mp 143–144°C.

TABLE 3. Concentration dependence of k_{obsd} for thermolysis of 2*a* at 152.5°C

Solvent	[2*a*] (initial) *M*[a]	$k \times 10^4$ s^{-1}
Benzene	0.0142	4.56
	0.0284	4.58
	0.0568	4.57
	0.1136	4.52
Nitrobenzene	0.0113	2.81
	0.0226	2.77
	0.0452	2.79
	0.0904	2.77

[a]Single determination at each concentration.

TABLE 4. Kinetics of thermolysis of 2*a*

Temperature (°C)	$k \times 10^4$ (s^{-1})[a] C_6H_6	C_6H_5Cl	$C_6H_5NO_2$
148.0	2.55 ± 0.01	1.92 ± 0.01	1.12 ± 0.01
152.5	4.54 ± 0.02	3.54 ± 0.01	2.79 ± 0.01
157.1	7.57 ± 0.03	5.20 ± 0.02	4.64 ± 0.04
161.8	9.82 ± 0.05	7.65 ± 0.03	5.99 ± 0.05
166.6	16.4 ± 0.1	12.8 ± 0.1	7.74 ± 0.07
172.5	31.1 ± 0.2	21.2 ± 0.1	12.2 ± 0.1

[a]Estimated errors are standard deviations for average values of several runs.

TABLE 5. Activation parameters for 2*a*[a]

Solvent	$\Delta H^{\ddagger}$ (kcal mol^{-1})	$\Delta S^{\ddagger}$ (cal K^{-1} mol^{-1})
C_6H_6	35.7 ± 1.2	9.2 ± 2.6
C_6H_5Cl	34.9 ± 0.5	6.8 ± 1.1
$C_6H_5NO_2$	36.1 ± 0.3	8.5 ± 1.5

[a]Errors are those returned by least-squares analysis. Actual errors are probably larger: ca. ± 1 kcal mol^{-1} for $\Delta H^{\ddagger}$ and ± 3 cal K^{-1} mol^{-1} for $\Delta S^{\ddagger}$.

TABLE 6. Substituent effects on thermolysis of 2 in $C_6H_5NO_2$ at 172.5°C

p-Substituent	σ	$k \times 10^4$ (s^{-1})
H	0.0	12.2 ± 0.1
CH_3	−0.170	13.0 ± 0.1
OCH_3	−0.268	13.4 ± 0.1
Cl	0.227	11.1 ± 0.1
Br	0.227	11.1 ± 0.1

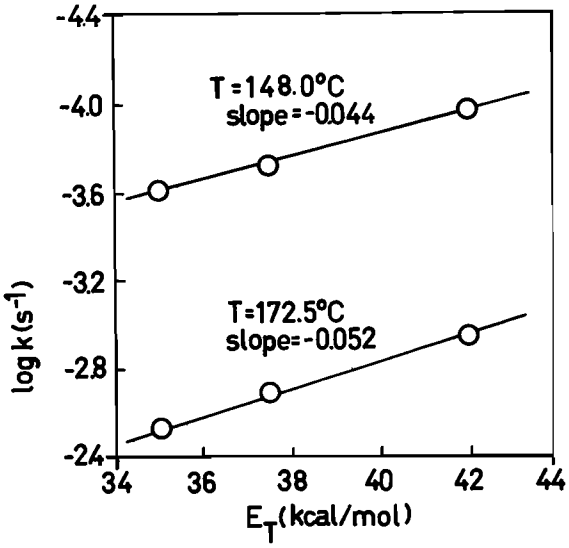

FIG. 1. Eyring plot for thermolysis of 2*a* in chlorobenzene.

characteristic of 1 (1–4). Only the three-piece fragmentation occurs, eq. [3]. The evidence against two-piece fragmentation rests on the absence of detectable concentrations of either aryl isocyanates or diazoalkanes from thermolysis of 2 in pure, dry solvents which do not react with either under the

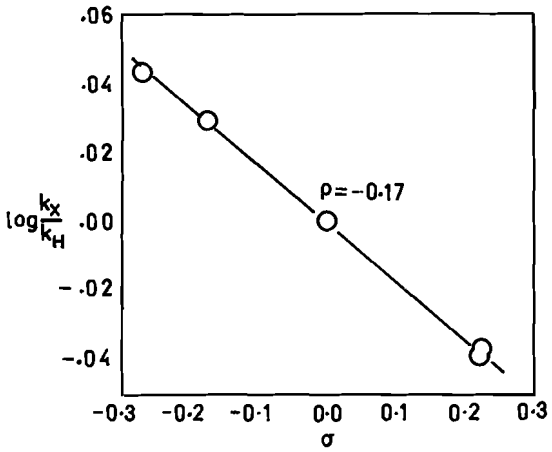

FIG. 2. Hammett correlation for thermolysis of **2** in nitrobenzene at 172.5°C.

reaction conditions (Experimental). Moreover, neither acetone azine, the product of self destruction of 2-diazopropane (9), nor the known products[2] of reaction between arylisocyanates and 2-diazopropane were detected. It follows that the isopropylidene aryl amine, obtained in high yield, came from a unidirectional fragmentation. Specifically ruled out is a dual fragmentation pathway (eq. [3]) in which the two-piece component is reversible.

[3] 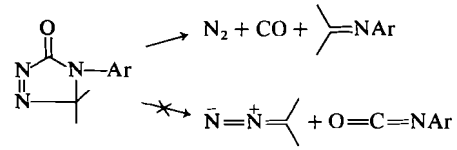

The preference for three-piece fragmentation shown by **2** is not the consequence of a lowered free energy of activation, relative to that for three-piece fragmentation of **1***c*. For example, **1***c* ($R^1 = R^2 = CH_3$) fragments to N_2, CO, and acetone with $\Delta H^{\neq} = 30.3 \pm 0.3$ kcal mol^{-1} and $\Delta S^{\neq} = 7.4 \pm 0.9$ cal K^{-1} mol^{-1}, in toluene (4). Thus **2**, with $\Delta H^{\neq} \simeq 35$ kcal mol^{-1} and $\Delta S^{\neq} \simeq 8$ cal K^{-1} mol^{-1} (Tables 5, 6) are more stable, kinetically, and they are particularly stabilized against decomposition to aryl isocyanate and diazoalkane. Their isomers **1***b*, in sharp contrast, decompose by the dual pathways of eq. [1].[3] Such dependence of fragmentation modes on structure is not predictable on the basis of casual inspection. A rationale, based on the thermodynamics of the processes, will be offered in a forthcoming paper.

Many mechanisms need to be considered for a process involving the breaking of three bonds (4). For example, there are six ways of reaching the products by breaking the three bonds, one at a time, in successive, homolytic steps, and many more if heterolytic pathways, as well as combinations of homolytic and heterolytic steps, are considered. To these must be added a large number of two-bond and three-bond, concerted mechanisms with nonpolar or dipolar transition states.

Stepwise processes involving breaking of either bond to sp^2 carbon (C3), out of concert with another bond breaking process, seem unlikely because those bonds are expected to be shorter,[4] and stronger, than the bonds from sp^3 carbon to ring nitrogens. A consequence of this line of reasoning is that N1—C5 bond breaking should be part (or all) of what happens in the slow step, since N4—C5 bond breaking is ruled out on the basis of product identity. If the above postulate is accepted, only transition states with the gross features of **4**, **5**, and **6** need to be considered. Fine features include the

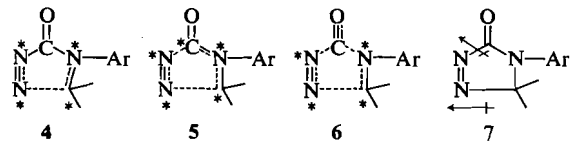

homolytic or heterolytic character of the bond ruptures and, for the latter character, the sense and the magnitude of the charge separation.[5] In the following paragraphs we examine the evidence in terms of those transition states. That evidence includes the solvent effects, the substituent effects, and the activation parameters.

The solvent effects on rate constants (Fig. 3) indicate that the transition state is less polar than the ground state as is the case for analogous fragmentation of **1***c* (4). An inverse relationship between rate and solvent polarity is a well-known feature of the thermolysis chemistry of *cis* azo compounds (11) and has been explained in terms of a large dipole moment for compounds having the *cis* azo function. We are therefore not restricted by the observed solvent effects to consideration of non-polar transition states. In fact, all types of

[2]Oxindoles, hydantoins, and oxazolidones. These compounds were prepared and studied concurrently in this laboratory by J. B. Fulton and their spectra and physical properties were known to us; J. B. Fulton and J. Warkentin, manuscript in preparation.

[3]Unpublished work of A. M. Cameron.

[4]An X-ray crystal structure (10) of **1***b* (Ar = *p*-C_6H_4Br) indicated that the oxadiazoline ring bonds to sp^2 carbon are shorter (N—C(sp^2) = 1.444 Å; O—C(sp^2) = 1.349 Å), than the ring bonds to sp^3 carbon (N—C(sp^3) = 1.472 Å; O—C(sp^3) = 1.458 Å).

[5]The sites at which radical or ionic character might develop are marked with an asterisk in **4**, **5**, and **6**.

Can. J. Chem. Downloaded from www.nrcresearchpress.com by 210.87.254.105 on 09/05/12
For personal use only.

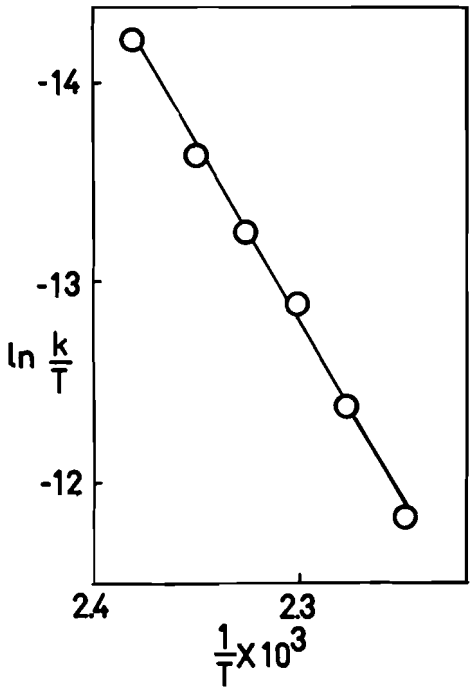

FIG. 3. Solvent effects on rate constants for thermolysis of **2***a*. The three solvents are, from left to right: benzene, chlorobenzene, and nitrobenzene and the average slope, including the other temperatures from Table 4, is -0.038 ± 0.012.

transition states (**4**, **5**, **6**) could be polar, but less polar than the ground state, because one or both of the major ground state dipole vectors (**7**) are partly lost. Thus, the solvent effect criterion is useful only for narrowing the choice of transition states, to exclude any with substantial charge separation, such as zwitterionic structures.

A Hammett rho (ρ) value of -0.17 at 172.5°C suggests that there is a small increase in electron demand at N4 in the transition state of the rate-determining step. This result was not expected, for N4 should already be depleted of electron density in the ground state by virtue of its attachment to the electron-withdrawing azocarbonyl group. Transition state **4** might accommodate both the small value and the solvent effects if it were essentially diradical-like with very limited charge separation, in the sense of **8**.

Transition state **5**, involving concerted breaking of two bonds, can not be excluded on the basis of the substituent and solvent effects. It could have some of the characteristics of a 1,3-dipole (**9**)[6] in which there is a formal positive charge on nitrogen. Thus, a negative ρ value of small magnitude could

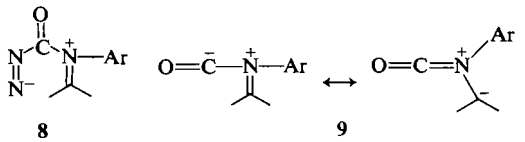

8 **9**

be accommodated without requiring that transition state **5** should be more polar than the *cis* azo compound **2**. However, the absence of $M - 28$ peaks or M to $M - 28$ metastable peaks in the mass spectra of **2** suggests that **9** is not an intermediate in the mass spectral fragmentation of **2**. In view of that, **9** can be regarded as an unlikely intermediate from thermolysis of **2** in solvents of low polarity and the suitability of **5** to describe the transition state is put in doubt.

A fully concerted mechanism (transition state **6**) accommodates the solvent and substituent effects readily. In reaching transition state **6** the system has partly lost both of the major vectors (see **7**) contributing to the polarity of the ground state. If the fragmentation were nonsynchronous, with N1—C5 bond breaking running ahead of N2—C3 and N4—C3 bond-breaking motions,[7] then a small increase in electron demand at N4 would be expected. Insofar as N4 is concerned, the nonsynchronous but fully concerted fragmentation has the characteristics of **4**, which, it was pointed out earlier, also fits the polarity factors.

Interpretation of activation entropies requires caution and, preferably, support from other criteria of mechanism. The observed values of $\Delta S^{\ddagger}$ for **2** (8 cal K^{-1} mol^{-1}, Table 5) are compatible with either of the concerted processes, transition states **5** or **6**. Dissociative, concerted reactions do not show the large, positive values of $\Delta S^{\ddagger}$ that are expected on the basis of $\Delta S^{0}_{(reaction)}$. The reason for this is that the reaction fragments are still restricted at the transition state, with loosening of interfragment interactions partly compensated for by greater intrafragment rigidity as π-bonding in the fragments develops. For example the thermolyses of *cis*-3,5-diphenyl-1-pyrazoline (12) and those of *cis*- and *trans*-3,5-divinyl-1-pyrazoline (13) have $\Delta S^{\ddagger}$ values near zero.[8] Without conjugating substituents like phenyl or vinyl, whose rotations "freeze out" at the transition state, pyrazolines fragment with higher activation entropies. Nine methyl-substituted or unsubstituted pyrazolines (14) fragment with $\Delta S^{\ddagger}$ values between 2.9 and 11.2; the average being 8.7 cal K^{-1} mol^{-1} (14).[8] The

[6]The resonance depicted in **9** clearly requires a geometry that **5** can only approach if the transition state comes very late on the reaction coordinate.

[7]Nonsynchroneity, in the proposed sense, is in keeping with the qualitative order of bond strengths inferred from bond lengths of a model compound; footnote 4.

[8]For evidence that these are concerted reactions, see the appropriate references.

Can. J. Chem. Downloaded from www.nrcresearchpress.com by 210.87.254.105 on 09/05/12
For personal use only.

latter are fair models for **2** and two-bond, concerted fragmentation of **2**, via transition state **5**, would fit well with the observed $\Delta S^{\neq}$. However, the thermolysis of **1***c* to ketone, nitrogen, and carbon monoxide is probably a three-bond, concerted fragmentation (4). The value of $\Delta S^{\neq}$ (**1***c*, R = CH_3, 5.9 cal K^{-1} mol^{-1}, average for three solvents) is not significantly different from that observed for **2** and thus the $\Delta S^{\neq}$ criterion is also inconclusive.

Since a more exhaustive set of mechanistic criteria suggested that the three-piece fragmentation of compounds **1***c* involves concerted scission of three bonds (4), the weight of analogy is on the side of **6** as the most likely transition state for thermolysis of **2**.

Although concerted thermolyses of **1***c* and **2** into three products are thermally allowed, $\sigma 2s + \sigma 2s + \sigma 2s$, chelotropic processes, there is a subtle difference between the two systems. For the oxadiazolinone system, the geometric change required, other than bond breaking motions, is flattening at C5 (eq. [4]). The triazolinone system, however, can

[4] 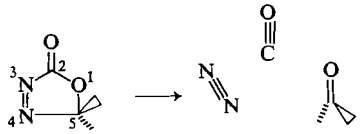

not reach the geometries of the products as economically. As eq. [5] shows, concerted fragmentation of **2** involving only flattening at C5 produces imine product with a 90° twist. The extra motion required to get to ground state product geometry in the latter case may be responsible, in part, for the higher activation enthalpy.

[5] 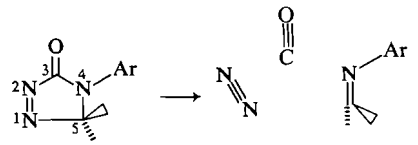

Acknowledgements

We are indebted to Dr. A. J. Paine for helpful discussions and to the Natural Sciences and Engineering Research Council of Canada for financial support.

1. P. R. West and J. Warkentin. J. Org. Chem. **33**, 2089 (1968).
2. G. A. MacAlpine and J. Warkentin. Can. J. Chem. **56**, 308 (1978).
3. S. L. Lee, A. M. Cameron, and J. Warkentin. Can. J. Chem. **50**, 2326 (1972).
4. A. J. Paine and J. Warkentin. Can. J. Chem. **57**, 2681 (1979).
5. P. C. Ip, K. Ramakrishnan, and J. Warkentin. Can. J. Chem. **52**, 3671 (1974).
6. J. K. Landquist. J. Chem. Soc. C, 63 (1970).
7. W. Borsche. Chem. Ber. **38**, 831 (1905).
8. A. S. Wheeler. J. Am. Chem. Soc. **2**, 167 (1934).
9. M. T. H. Liu and K. Ramakrishnan. Tetrahedron Lett. 3139 (1977).
10. A. Prakash, C. Calvo, J. Warkentin, and A. M. Cameron. J. Cryst. Mol. Struct. **3**, 71 (1973).
11. A. Schulz and C. Rüchardt. Tetrahedron Lett. 3893 (1976).
12. M. Schneider and H. Strohäcker. Tetrahedron, **32**, 619 (1976).
13. R. J. Crawford and M. Ohno. Can. J. Chem. **52**, 3134 (1974).
14. R. J. Crawford and A. Mishra. J. Am. Chem. Soc. **88**, 3963 (1966).

Can. J. Chem. Downloaded from www.nrcresearchpress.com by 210.87.254.105 on 09/05/12
For personal use only.

Biosynthesis of the quinolizidine alkaloids.[1] Incorporation of Δ^1-piperideine into matrine

FINIAN J. LEEPER,[2] GUNNAR GRUE-SØRENSEN, AND IAN D. SPENSER
Department of Chemistry, McMaster University, Hamilton, Ont., Canada L8S 4M1

Received July 3, 1980

FINIAN J. LEEPER, GUNNAR GRUE-SØRENSEN, and IAN D. SPENSER. Can. J. Chem. **59**, 106 (1981).

Label from [6-^{14}C]-Δ^1-piperideine is incorporated nonrandomly into the carbon skeleton of the quinolizidine alkaloid, matrine, in *Sophora tetraptera* and *S. microphylla*. The distribution of radioactivity was determined by a new chemical degradation sequence. On the basis of the results, one of two previously postulated biogenetic schemes must be discarded. A modified biogenetic scheme is presented which is consistent with the present results and also leads to the correct stereochemistry of matrine.

FINIAN J. LEEPER, GUNNAR GRUE-SØRENSEN et IAN D. SPENSER. Can. J. Chem. **59**, 106 (1981).

Dans la *Sophora tétraptera* et dans la *S. microphylla*, le ^{14}C en position 6 de la Δ^1-pipéridéine n'est pas incorporé au hasard dans le squelette carboné de la matrine, un alcaloïde du type quinolizidine. On a déterminé la distribution de la radioactivité à l'aide d'une nouvelle séquence pour la dégradation chimique. En se basant sur les résultats obtenus, on doit mettre de côté l'un des deux schémas biogénétiques proposé antérieurement. On présente un schéma biogénétique modifié qui est en accord avec nos résultats et qui conduit également à la stéréochimie appropriée de la matrine.

[Traduit par le journal]

Introduction

Matrine (**3**) is the major alkaloid of the genus *Sophora*. Its C_{15} skeleton, like that of its isomer, the lupine alkaloid lupanine (**4**)[3], is generated from three C_5 units which are derived from lysine (**1**) via cadaverine (**2**), a symmetrical (C_{2v}) molecule (Scheme 1). Thus, label from [2-^{14}C]lysine (2,3) and from [1-^{14}C]cadaverine (2–4) enters six carbon atoms of matrine, C-2, -6, -10, -11, -15, and -17. The evidence that activity is located at these six carbon atoms is conclusive for C-15 (2–4), adequate for C-2, C-10, (2, 3), and C-11 (2), circumstantial for C-17 (3), and inferred for C-6. It is assumed, but not rigorously demonstrated, that each of the labelled carbon atoms carries one sixth of the activity of intact matrine.

Δ^1-Piperideine (**5**) which has been shown to lie on the route from lysine and cadaverine into several lysine-derived alkaloids (anabasine (5), decodine (6), lycopodine (7), lupanine (1)) serves as a precursor of matrine (2). Label from [6-^{14}C]-Δ^1-piperideine was incorporated into C-15, and into C-2 and/or C-10. Significantly, the incorporation of label into C-15 (10% of the recovered specific activity) was much lower than the mean incorporation of label into C-2 and C-10 (45% of the recovered specific activity) (2). The reaction employed to gain access to C-2 and C-10 yielded degradation products which did not permit discrimination between these two carbon atoms. It is therefore unknown whether C-2 and C-10 were equally labelled (45% of recovered specific activity at each site) or not (e.g.

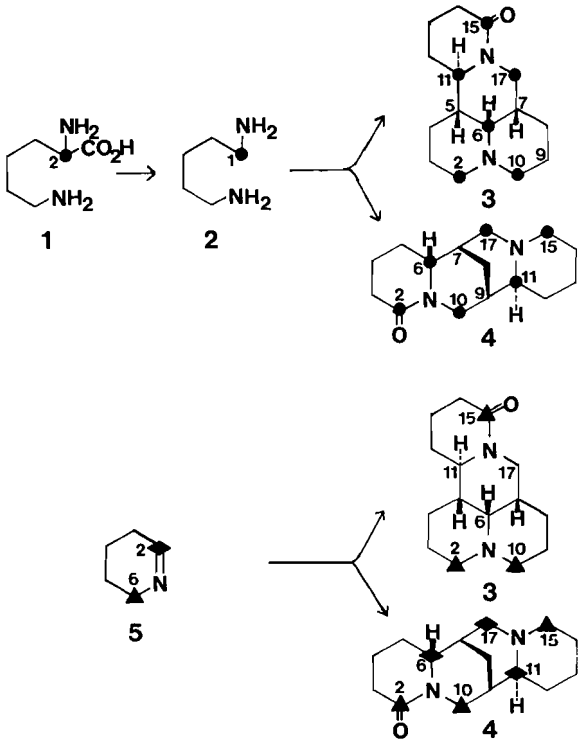

SCHEME 1. Incorporation of labelled precursors into matrine (**3**) and lupanine (**4**).

[1]This paper is dedicated to the memory of Léo Marion, on the anniversary of his death at the age of 80, on July 15th, 1979. It was in Léo Marion's laboratory, at the National Research Council of Canada Laboratories, Sussex Drive, Ottawa, that the very first tracer experiments, designed to test biogenetic hypotheses of the origin of natural products, were conducted during the period 1951–1954. One of us was privileged to participate in the design and execution of some of these pioneering studies.

[2]Present address: Department of Chemistry, University of Cambridge, Cambridge, England.

0008-4042/81/010106-10$01.00/0
©1981 National Research Council of Canada/Conseil national de recherches du Canada

Can. J. Chem. Downloaded from www.nrcresearchpress.com by 210.87.254.6 on 09/05/12
For personal use only.

Can. J. Chem. Downloaded from www.nrcresearchpress.com by 210.87.254.6 on 09/05/12
For personal use only.

10% and 80% of recovered specific activity at one and at the other carbon atom, respectively, assuming equal yields of degradation product from each of the two sites).

We recently suggested that matrine should be regarded as a modified trimer of Δ^1-piperideine and advanced one of several possible biogenetic schemes based on this notion (1). As will be shown in the discussion that follows, and contrary to published statements (cf ref. 8), this idea is not inconsistent with the observed unequal incorporation of label from [6-^{14}C]-Δ^1-piperideine into different sites of matrine (2).

We have reinvestigated the incorporation of [6-^{14}C]-Δ^1-piperideine into matrine, in *Sophora tetraptera* and *S. microphylla*. Our results, based on a new degradation sequence which permits individual assay of the activity at each of the three crucial sites, C-2, -10, and -15, lead to a new biogenetic model of the origin of matrine, which is consistent with all experimental results and accounts for the stereochemistry of the alkaloid.

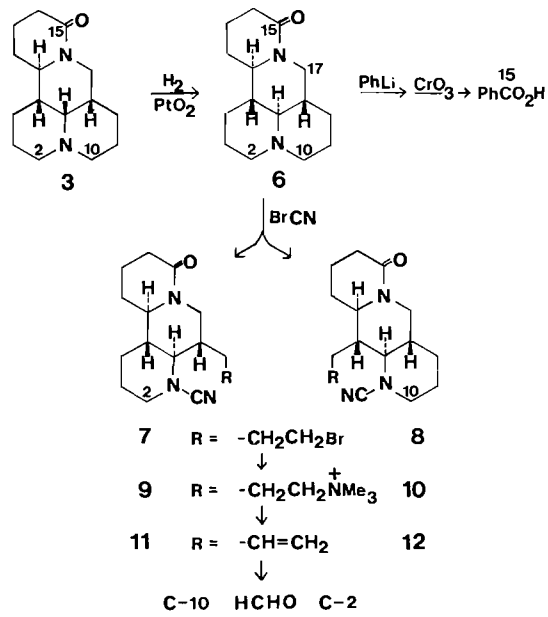

SCHEME 2. Degradation of matrine.

Methods and Results

[6-^{14}C]-Δ^1-Piperideine, prepared from [6-^{14}C]-lysine by oxidation with *N*-bromosuccinimide (7), was administered by the wick method, in separate experiments, to intact stocks of *Sophora tetraptera* (Experiment 1) and *S. microphylla* (Experiment 2). After three days in contact with the tracer, the plants were harvested and extracted. The alkaloid fraction of the extract yielded radioactive matrine (**3**). The matrine was diluted with inactive carrier and converted into allomatrine (**6**) (9) by heating with platinum oxide in an atmosphere of hydrogen. This isomerization under reducing conditions removed traces of a radioactive impurity, which was not removed by persistent chromatography and by repeated recrystallization of matrine. This impurity was probably a trimer of Δ^1-piperideine, e.g., α-tripiperideine, whose R_f value corresponds to that of matrine in a number of solvent systems, including those used in the purification of matrine. Hydrogenation of α-tripiperideine (10), under conditions used in the isomerization of matrine into allomatrine, yields piperidine which is volatile and would evaporate with solvent during work-up.

The three carbon atoms of matrine (**3**) (C-2, -10, -15) predicted to be the sites of label derived from [6-^{14}C]-Δ^1-piperideine, were obtained individually by degradation of allomatrine. The degradation sequence is shown in Scheme 2.

The carbonyl carbon (C-15) was extruded as benzoic acid, by reaction of allomatrine with phenyl lithium, followed by oxidation of the basic products of this reaction with Jones' reagent. A small amount of benzophenone, resulting from addition of two moles of phenyl lithium, was also isolated.

Carbon-2 and carbon-10 of matrine were obtained individually as formaldehyde (isolated as the dimedone derivative), as follows. Von Braun reaction of allomatrine (**6**) with cyanogen bromide (cf. ref. 11) yields two bromocyanamides, A (**7**) and B (**8**), which were separated and converted into the corresponding trimethylammonium salts (**9** and **10**) and then, by Hofmann elimination, into the alkenes (**11** and **12**). Oxidative cleavage with sodium metaperiodate in the presence of catalytic amounts of osmium tetroxide then yielded formaldehyde. The overall yield of formaldehyde dimethone was 58% and 43%, from bromocyanamide A and B, respectively.

The results of the degradation of the samples of matrine from the two experiments are shown in Table 1. In each case, the carbonyl carbon atom (C-15, benzoic acid) accounted for approximately one sixth of the total activity of matrine, whereas C-2 (formaldehyde dimethone) and C-10 (formaldehyde dimethone) each account for one quarter of the activity of the intact matrine. The three sites account for only two-thirds of the total activity of matrine.

TABLE 1. Incorporation of [6-^{14}C]-Δ^1-piperideine into matrine

Product	C-atoms of matrine	Experiment 1 *Sophora tetraptera* SA[a]	Experiment 1 *Sophora tetraptera* RSA[b]	Experiment 2 *Sophora microphylla* SA[a]	Experiment 2 *Sophora microphylla* RSA[b]
Allomatrine (**6**)	All	1.25±0.01	100±1	1.56±0.01	100±1
Benzoic acid	C-15	0.20±0.01	16±0.4	0.27±0.01	17±0.4
Bromocyanamide A (**7**)	All	1.25±0.01	100±1	1.58±0.02	101±1
Formaldehyde dimethone from bromocyanamide A	C-10	0.32±0.01	25±0.5	0.39±0.01	25±0.5
Bromocyanamide B (**8**)	All	1.26±0.01	101±1	1.60±0.02	102±1
Formaldehyde dimethone from bromocyanamide B	C-2	0.33±0.02[c]	26±2	0.39±0.01	25±0.5

[a]SA = Specific activity (dpm per mmol) × 10^{-4}.
[b]RSA = Relative specific activity (per cent) (allomatrine = 100).
[c]*This formaldehyde dimethone was obtained from a sample of bromocyanamide B which had been prepared from the original* bromocyanamide B, specific activity 1.26 (±0.01) × 10^4 dpm per mmol, by 2.64-fold dilution with inactive carrier. The result shown (0.33 (±0.02) × 10^4 dpm per mmol) is the corrected value.

Discussion

The Biosynthesis of Matrine

Radioactivity from [2-^{14}C]lysine (2, 3) and from [1-^{14}C]cadaverine (2–4) is incorporated nonrandomly into matrine (Scheme 1). Partial degradation of the radioactive matrine showed that in each case approximately one sixth of the radioactivity of the intact molecule was present at the carbonyl carbon (C-15) (2–4). Other degradation results were interpreted to indicate that each of five other carbon atoms, C-2, C-6, C-10, C-11, and C-17, also carried one sixth of the label. It was inferred that the carbon skeleton of matrine originates from three C_5 fragments which are derived from lysine via its decarboxylation product, cadaverine, and are incorporated in symmetrical fashion and with equal efficiency into each of the three C_5-segments of the alkaloid.

A number of biogenetic hypotheses have been advanced to rationalize this derivation of matrine. Each of these models finds a parallel in the schemes which have been proposed for the origin of lupanine from the same precursors.[3] The distribution of label from [^{14}C]lysine or [^{14}C]cadaverine, while serving to provide a general framework for the biogenetic models, has not yet provided a basis for discrimination between them.

The distribution of radioactivity from [2-^{14}C]- and [6-^{14}C]-Δ^1-piperideine within lupanine (**4**) is quite different from that of label from [2-^{14}C]- and [6-^{14}C]lysine, in that the individuality of C-2 and C-6 of Δ^1-piperideine is maintained on the route into the alkaloid and only three sites become labelled (1). Similarly, label from [6-^{14}C]-Δ^1-piperideine enters three sites of matrine (2). Thus, as in the case of the Lycopodium (7) and the Decodon (6) alkaloids, randomization of C-2 and C-6 of lysine occurs at some stage of the biosynthetic route between lysine (**1**) and Δ^1-piperideine (**5**), presumably during conversion of the decarboxylation product of lysine, i.e. cadaverine (**2**), into Δ^1-piperideine. Once the latter has been formed, equilibration of these carbon atoms does not occur. A study of the distribution of label within matrine derived from [6-^{14}C]-Δ^1-piperideine might serve to distinguish among the biogenetic models that have been proposed, particularly since activity from this source is not equally distributed among the three carbons of matrine which become labelled (2).

The biogenetic models that have been advanced to account for the origin of matrine differ from one another in the sequence in which the three C_5 units are assembled and in the intermediates that are invoked. In principle, each model envisages the formation of a C_{10} intermediate which, in a subsequent step, is converted into the C_{15} skeleton of the alkaloid by reaction with the third C_5 unit. Since label from [6-^{14}C]-Δ^1-piperideine enters one site only within each of the three C_5 units, C_5 compounds with C_{2v} symmetry (e.g., glutardialdehyde) cannot be relays between Δ^1-piperideine and the alkaloid. Several postulated biogenetic models (e.g. ref. 12) are thereby eliminated.

The C_{10} compounds ($C_{10}N$ or $C_{10}N_2$) that have been postulated as intermediates in the remaining models (1–3, 12–14) are derivable from tetrahydroanabasine (**13**), a dimer of Δ^1-piperideine. In aqueous solution at pH 6–8, Δ^1-piperideine dimerizes readily and within a few hours 80–90% of the compound has been converted into dimer (13). The labelling pattern of tetrahydroanabasine, derived from [6-^{14}C]-Δ^1-piperideine, is shown in Scheme 3. It is a necessary consequence of the dimerization process that the two labelled centres

[3]For a summary of the relevant literature see ref. 1.

Can. J. Chem. Downloaded from www.nrcresearchpress.com by 210.87.254.6 on 09/05/12
For personal use only.

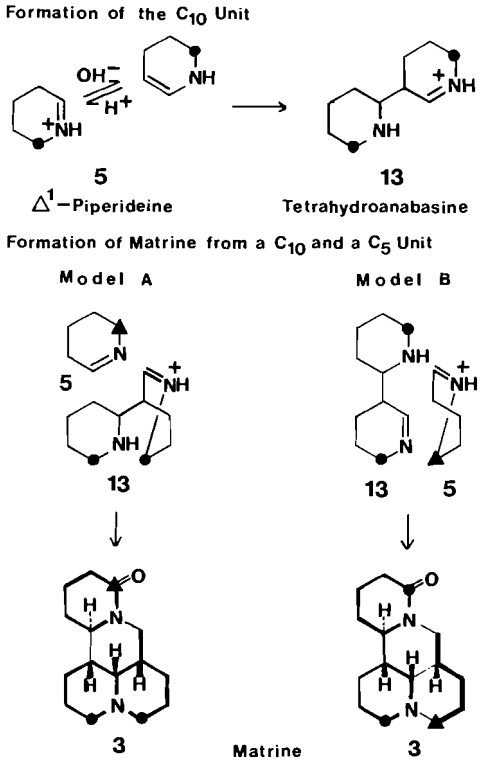

SCHEME 3. Two models for the derivation of matrine from tetrahydroanabasine (C_{10}) (**13**) and Δ^1-piperideine (C_5) (**5**).

of the dimer have the same molar specific activity, i.e. each of the labelled carbon atoms contains 50% of the activity of the intact molecule.

When [6-^{14}C]-Δ^1-piperideine is synthesized by oxidation of [6-^{14}C]lysine, the solution contains not only monomer, but also dimer. Entry of the mixture of labelled monomer and dimer into the plant will be followed by mixing of each component with the corresponding inactive material, if the latter is a normal component of the plant. Since it is unlikely that the two components will be diluted to the same extent, or that, after dilution, they will fully equilibrate with one another in the plant within the experimental period, it can be expected that the specific activity of the monomer unit present within the cell at any one time will not be the same as that of the two equally labelled centres of the dimer unit. As a consequence, the monomer-derived C_5-fragment of matrine will show a specific activity different (either higher or lower) from that of the two equally labelled centres within the dimer-derived C_{10} unit.[4]

[4]It is, of course, possible but not very likely that conditions may prevail which lead, quite fortuitously, to equal specific activity at the three labelled centres.

The variants of matrine biogenesis that have been proposed can all be accommodated by one or the other of two models (Scheme 3) which differ from one another in that different segments of matrine are derived from the C_{10} unit. An experiment with [6-^{14}C]-Δ^1-piperideine can serve as a critical test to distinguish between the two models, provided a degradation is available which permits individual assay of radioactivity at each of the three labelled carbon atoms, C-2, C-10, and C-15 of matrine. In such an experiment, the two labelled carbon atoms of matrine (**3**) supplied by the C_{10}-unit (●) must have the same specific activity. The labelled centre of matrine (▲) whose specific activity is different from that of the other two must be supplied by the C_5 unit.

Labelled matrine had been obtained from an experiment with [6-^{14}C]-Δ^1-piperideine in *Sophora flavescens* (2). Degradation showed that 10% of the recovered activity was located at the carbonyl carbon (C-15). The rest of the recovered activity was distributed over C-2 and C-10. Since the degradation that was employed did not permit individual assay of radioactivity at these two centres, the result that was obtained (2) cannot distinguish between the two models of Scheme 3 (Model A demands: C-2 of matrine, 45%; C-10, 45%; average 45%; model B demands: C-2 of matrine, 10%; C-10, 80%, average 45%; observed: average of C-2 and C-10, 45% (2)). By a new degradation sequence which was designed to recover C-2 and C-10 of matrine individually (see below), it is now shown (Table 1) that, in labelled matrine obtained from [6-^{14}C]-Δ^1-piperideine in each of two Sophora species, *S. tetraptera* (Experiment 1) and *S. microphylla* (Experiment 2), C-2 and C-10 show the same molar specific activity and are therefore supplied by the C_{10}-unit, whereas C-15 shows a different, lower, molar specific activity, and is therefore supplied by the C_5 unit. These results conclusively disprove all variants of model B, including the aldotripiperideine route of matrine biogenesis (1). The data are consistent with model A (Scheme 3).

It will be noted that in each case the three labelled centres that were recovered account for only two thirds of the activity of intact matrine (Table 1). A similar incomplete recovery of label within C-2, -10, and -15 of matrine derived from [6-^{14}C]-Δ^1-piperideine may have been encountered by Shibata and Sankawa (2). The remaining activity is presumably distributed over C-6, C-11, and C-17 of matrine, carbon atoms which would become labelled if [6-^{14}C]lysine or [1-^{14}C]cadaverine were available to the plant. Since [6-^{14}C]-Δ^1-piperideine was

Can. J. Chem. Downloaded from www.nrcresearchpress.com by 210.87.254.6 on 09/05/12
For personal use only.

Can. J. Chem. Downloaded from www.nrcresearchpress.com by 210.87.254.6 on 09/05/12
For personal use only.

prepared by oxidation of [6-^{14}C]lysine, it is possible that traces of [6-^{14}C]lysine were present in the solution of Δ^1-piperideine that was fed to the plant. It has been reported that incorporation of lysine into matrine is more efficient than incorporation of Δ^1-piperideine (2). Residual [6-^{14}C]lysine in the feeding solution might then make a disproportionate contribution to the labelling of the product.

Another, more likely, explanation why the label is partially randomized may be that the conversion of cadaverine into Δ^1-piperideine in Sophora is reversible. It has recently been reported that the generation of lupine alkaloids from cadaverine in *Lupinus polyphyllus* is catalyzed by a cadaverine–pyruvate transaminase system, referred to as 17-oxosparteine synthase (15). Enzyme-bound 5-aminopentanal, i.e. Δ^1-piperideine, is postulated as the first intermediate. Transaminase-catalyzed reactions are, in general, readily reversible. The presence of an analogous enzyme system in Sophora would allow the partial reconversion of Δ^1-piperideine into cadaverine, and would thus account for the partial conversion of [6-^{14}C]- into [2-^{14}C]-Δ^1-piperideine, and the partial scrambling of label in matrine.

Many variations are possible for a route leading to matrine from a C_{10} unit, tetrahydroanabasine (**13**), and a C_5 unit, Δ^1-piperideine (**5**), which are consistent with model A (Scheme 3). Three of these variations are outlined in Scheme 4. They lead to the stereochemistry of matrine and relate its origin to that of the C_{15} lupine alkaloids. The starting point of two of these routes is the all-*trans* isomer of isotripiperideine (**14**), one of the trimers of Δ^1-piperideine. The same trimer was invoked also as the starting point for lupanine biogenesis (1). The scheme also includes another compound (**17**) which lies on the postulated route to lupanine.

Matrine (**3**) is generated in a series of unexceptional oxidation–reduction and cyclization steps. The stereochemistry of the four chiral centres of matrine is created in the course of bond-formation between C-5 and C-11,[5] and in the reduction at C-6. If ring-closure proceeds through a chair-like transition state (e.g. **18**, **20**) the hydrogen atoms at C-5 and C-11 of the newly formed ring in **19** and in **23**

[5]The numbering system for matrine which is adopted in this paper was introduced by Schütte *et al.* (3). It corresponds to the customary numbering system of the ring system of the $C_{15}N_2$ lupine alkaloids, and shows the biogenetic correspondence of the carbon atoms of the matrine and of the lupine skeleton. The difference between this numbering system and that used by Chemical Abstracts is minor but significant. Several other numbering systems for matrine have also been used.

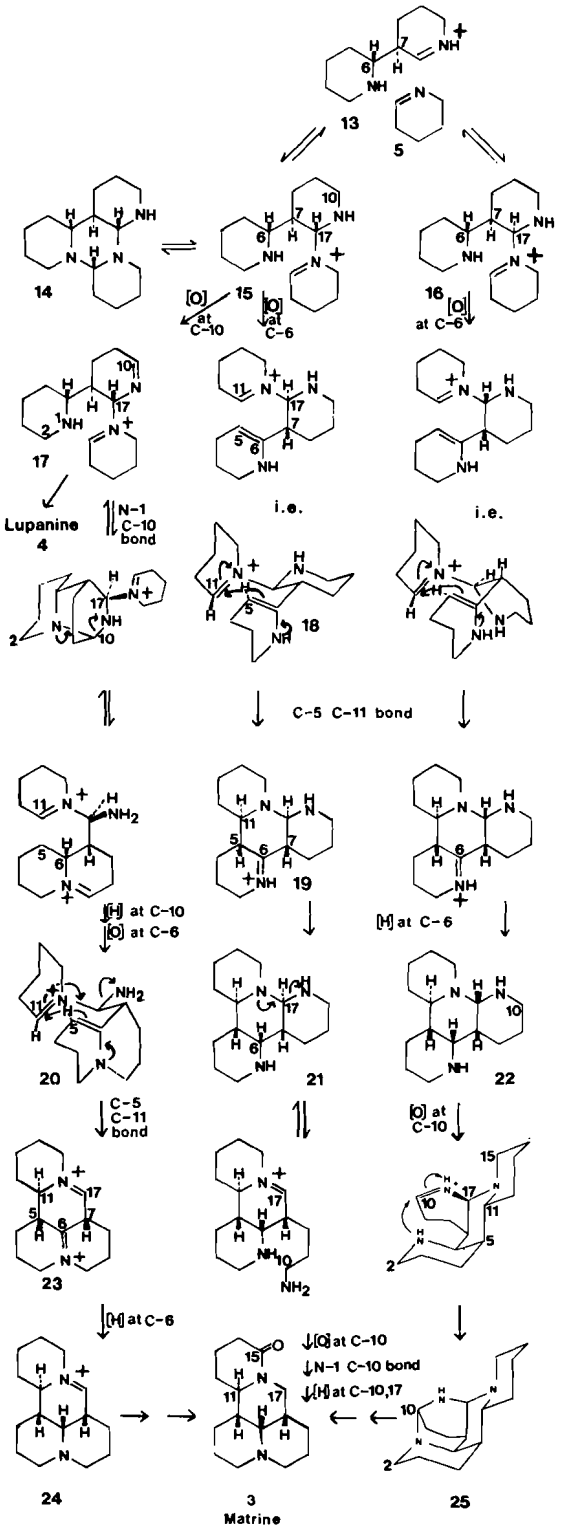

SCHEME 4. Biogenesis of matrine.

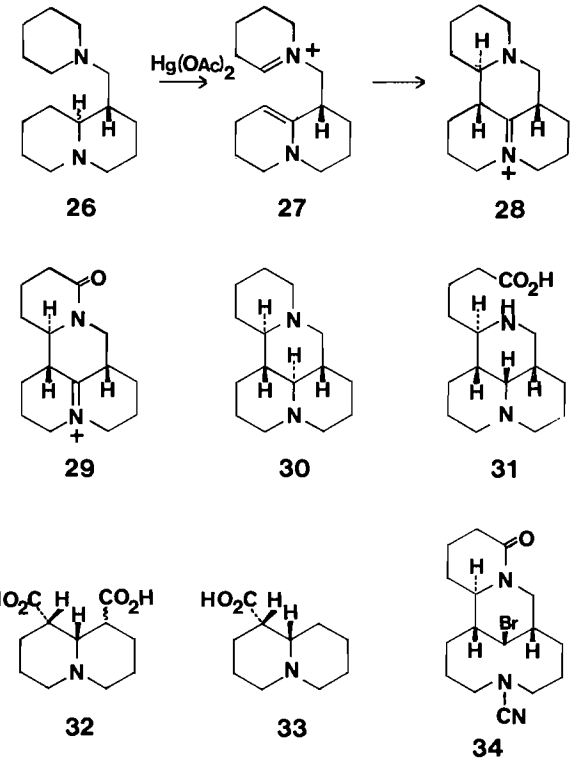

will be *cis* and *trans*, respectively, to the hydrogen at C-7. There is chemical analogy for this postulate. Mercuric acetate oxidation (16) of **26** is reported to give, among other products, dehydromatridine (**28**), formed by spontaneous cyclization of **27**.

If in the reduction of the iminium salts **19** and **23**, generated in the above cyclization, the hydride approaches C-6 *trans* to the hydrogen atoms at C-5 and -7, the resulting product would have the favoured all-*trans* allomatridine (**30**) configuration. Inspection of a model shows, however, that the iminium salts are not planar, and that the less hindered approach to C-6 is *cis* to the adjacent hydrogen atoms. Thus, it is not the thermodynamically favoured allomatridine (**30**) configuration but the matridine configuration (**24**) which is likely to be kinetically favoured in this reduction. Indeed, chemical reduction of dehydromatrine (**29**) yields matrine (**3**) and not allomatrine (**6**) (17).

The 5*R*,6*S*,7*S*,11*R* stereochemistry of matrine (**3**) is not the only one found in the Sophora alkaloids. Other naturally occurring stereoisomers are accessible through the proposed biogenetic model. Thus, allomatrine (**6**) (5*R*,6*R*,7*S*,11*R*) could be generated in the reduction step at C-6. Epimers at C-7 (e.g. sophoridine, 5*R*,6*S*,7*R*,11*R*) and C-5 can result from equilibration of the appropriate iminium ion (e.g. **19** or **23**) with the corresponding enamine.

Our earlier scheme for the biogenesis of matrine (1) had invoked intermediacy of a "prematrine trimer" (**25**), generated in two steps from one of the stereoisomers (**22**) of aldotripiperideine, which was, in turn, derived as a variant of Model B (Scheme 3) in a single step from tetrahydroanabasine (**13**) and Δ^1-piperideine (**5**). The results now presented show that aldotripiperideine generated in this manner cannot serve as a precursor of matrine. Nevertheless, the notion that aldotripiperideine is implicated in matrine biogenesis remains attractive. Aldotripiperideine (of unknown stereochemistry) is converted into allomatridine (**30**) by treatment with Raney Nickel (18), conditions similar to those that convert matridine into allomatridine (19) and matrine into allomatrine (9). Furthermore, an aldotripiperideine of unknown stereochemistry occurs naturally (20). The aldotripiperideine (**22**) which yields the "prematrine trimer" by intramolecular cyclization is accessible from tetrahydroanabasine and Δ^1-piperideine not only by the route which is forbidden since it is a variant of Model B (1), but also by another route which is allowed since it is a variant of Model A. The first intermediate of this route is **16**, the C-17 epimer of **15**. The desired aldotripiperideine **22** is obtained from **16** by steps which parallel the route from **15** to the C-17 epimeric aldotripiperideine **21** (Scheme 4).

The Chemical Degradation of Matrine

For a complete investigation of the mode of incorporation into matrine of label from [2-^{14}C]- and [6-^{14}C]lysine and from [1-^{14}C]cadaverine, six carbon atoms, C-2, -6, -10, -11, -15, and -17 must be extruded for individual assay of radioactivity. Three of these, C-2, -10, and -15, must be obtained individually for an interpretation of the mode of incorporation of label from [6-^{14}C]-Δ^1-piperideine. Only one of these carbons, C-15, has been obtained directly, in the form of benzoic acid, by treatment of matrine with phenylmagnesium bromide (2) or phenyl lithium (3, 4), followed by chromic acid (2) or permanganate (3, 4) oxidation of the phenyldihydro derivative. Estimation of label at other centres was indirect, depending on the assay of products which were obtained by oxidative fragmentation of matrine and either contained more than one of the crucial carbon atoms or arose from two or more sites within the molecule.

These products were glutaric acid (2), succinic acid (2, 3), γ-aminobutyric acid (2, 3), β-alanine (2, 3), glycine (3), quinolizidine-5,7-dicarboxylic acid

Can. J. Chem. Downloaded from www.nrcresearchpress.com by 210.87.254.6 on 09/05/12
For personal use only.

Can. J. Chem. Downloaded from www.nrcresearchpress.com by 210.87.254.6 on 09/05/12
For personal use only.

(**32**) (3), and quinolizidine-5-carboxylic acid (**33**) (3). Glutaric acid, generated from the C_5 chain, C-11 to C-15, contains C-11 and -15, which cannot be differentiated from one another. Succinic acid can originate from four different C_4 units within the molecule. These are nonequivalent and would yield the compound at unequal rates.[6] These C_4 units contain C-2, -10, -11, and -15. Each of these carbon atoms would yield one of the carboxyl groups of succinic acid and cannot thus be assayed individually.[7] γ-Aminobutyric acid and β-alanine are each generated from two nonequivalent sites, encompassing C-2 and C-10, respectively, whose individual activity cannot therefore be determined. Similarly, glycine may be generated from three nonequivalent sites, embracing C-2, C-10, and C-17.

As far as the quinolizidine carboxylic acids **32** and **33** are concerned, we were unable to duplicate the oxidation of matrine which is reported (3, 22) to yield these products.[8] Under the conditions described in ref. 3 the sole reaction that occurs is hydrolysis, yielding matrinic acid (**31**) together with unreacted matrine. When more vigorous conditions were employed (22) γ-aminobutyric acid, β-alanine, and glycine were also obtained, in poor yield (5–15%).

Thus, reactions previously employed in the degradation of labelled matrine were unsuitable for gaining individual access to C-2 and C-10. A new degradation was developed for this purpose (Scheme 2).

The key to this degradation was the von Braun reaction with cyanogen bromide. Matrine does not undergo this reaction, but its conformationally stable all-*trans* stereoisomer, allomatrine (**6**), does (24), and isomerization of matrine into allomatrine proceeds in high yield (9). Reaction with cyanogen bromide converts allomatrine into two bromocyanamides, mp 126°C (24) and 166°C (24), 167–168°C (11), of which only the latter had been characterized (11). These two compounds were obtained in high yield and their separation proved possible. The ^{1}H nmr analysis of the neutral fraction from the reaction of allomatrine with cyanogen bromide revealed the presence of two compounds, in the ratio 3:2. The starting material, allomatrine (**6**), shows a double doublet δ 4.6 (J = 13 and 4 Hz), well separated from the rest of the spectrum, due to the equatorial 17-hydrogen atom which is coplanar with the carbonyl group and therefore significantly deshielded. The ^{1}H nmr spectrum of matrine shows a similar signal. The spectrum of the mixture of neutral reaction products showed two sets of double doublets, centered at δ 5.0 (major product A) and δ 4.7 (minor product B), respectively.

The two products resisted chromatographic separation (silica gel or reversed phase), but were eventually separated by repeated fractional crystallization from ethyl acetate/petroleum ether, by employing the double doublets at δ 5.0 and δ 4.7, respectively, as diagnostic indicators for the purity of the two products, mp 134–135°C, the major product (A), and mp 168–169°C, rising to 174–176°C after repeated recrystallization, the minor product (B). The structure of bromocyanamide B was determined by single crystal X-ray diffraction (25). It was shown to have structure **8**.

The two bromocyanamides, A and B, were each taken through a sequence of conventional steps which eventually led to the recovery of C-10 and C-2, respectively, as formaldehyde. Treatment with trimethylamine gave the quaternary ammonium salts, **9** and **10**, respectively. Hofmann elimination using potassium *tert*-butoxide yielded the alkenes, **11** and **12**. Their ^{1}H nmr spectra showed the pattern of signals characteristic for the protons of a terminal double bond, thus providing

---

[6]It had previously been assumed (3) that the sole source of succinic acid in the oxidation of matrine is the C_4 chain C-12, -13, -14, -15. That this assumption is in error is indicated by the report (21) that succinic acid is obtained in the oxidation of sophocarpine (i.e. 13,14-dehydromatrine).

[7]The uncertainty of the degradation is illustrated by the following. It is reported (3) that matrine, specific activity 13.7×10^4 cpm per mmol, gave succinic acid, specific activity 2.26×10^4 cpm per mmol, which was diluted with inactive carrier, to give a sample, specific activity 7.32×10^3 cpm per mmol. Whatever the source of this succinate from within the skeleton of matrine, only one of its carboxyl groups can be labelled. Yet, when this succinic acid was further degraded by a Schmidt reaction to yield inactive ethylene diamine and labelled carbon dioxide, the specific activity of the latter was 6.90×10^3 cpm per mmol, i.e. essentially identical with that of the succinic acid from which it was derived. This is clearly impossible, unless the degradation reaction is accompanied by a large reverse isotope effect.

[8]It is reported (22) that the quinolizidine mono- and dicarboxylic acids obtained by oxidation of matrine were optically active. This is surprising; the dicarboxylic acid thus apparently did not retain the stereochemistry of matrine. Furthermore, the physical constants reported for the monocarboxylic acid (referred to as *d*-lupininic acid) (mp 255°C; hydrochloride mp 275°C (dec.), $[\alpha]_D$ +37.78° (CH_3OH) (22)) correspond to those reported (23) for (+)epilupininic acid ((1*S*-*cis*)-2*H*-octahydroquinolizine-1-carboxylic acid) (mp 255°C, $[\alpha]_D^{15}$ +25.2° (*c* 1.6, H_2O); hydrochloride, mp 273°C, $[\alpha]_D^{15}$ +36.2° (*c* 1.9, H_2O)) rather than to those predicted for (+)lupininic acid (**33**) (reported (23) for (−)lupininic acid ((1*R*-*trans*)-2*H*-octahydroquinolizine-1-carboxylic acid), mp 172°C, $[\alpha]_D^{20}$ −7.2° (*c* 2.2, H_2O); hydrochloride, mp 258–259°C, $[\alpha]_D^{15}$ −9.5° (*c* 2.9, H_2O)).

Can. J. Chem. Downloaded from www.nrcresearchpress.com by 210.87.254.6 on 09/05/12
For personal use only.

early evidence that the two bromocyanamides were **7** and **8**, and that the third possible bromocyanamide (**34**) of allomatrine had not been produced. The alkene derived from bromocyanamide B was contaminated by the corresponding *tert*-butyl ether (ca. 20%). Formaldehyde, isolated as the dimethone, was obtained by oxidative cleavage of each alkene. Since the structures **7** and **8** are assigned to the bromocyanamides, A and B, respectively, the sample of formaldehyde from bromocyanamide B is derived from C-2, and that from bromocyanamide A from C-10 of matrine. It is of interest, however, that the interpretation of the tracer results did not depend on these assignments and was possible without them.

No more than 200 mg matrine was required to complete the degradation leading to assay of activity of C-15 (benzoic acid) and of each of C-2 and C-10 (formaldehyde dimethone). The sequence includes three compounds which retain all carbon atoms of matrine (allomatrine, bromocyanamides A and B) and must therefore show identical molar specific activity, serving as independent check of radiochemical purity.

Experimental

Administration of [6-^{14}C]-Δ^1-Piperideine to Sophora Spp.

Stocks of *Sophora microphylla* and *S. tetraptera* were obtained from Hillier Nurseries, Winchester, England. The stocks were planted in the greenhouse in April 1978, broke dormancy within two weeks and were allowed to grow normally for three months. The tracer experiments were conducted in July 1978.

The tracer, [6-^{14}C]-Δ^1-piperideine, was prepared (7) from a sample of DL-[6-^{14}C]lysine monohydrochloride (nominal specific activity 48 mCi per mmol, nominal total activity 0.3 mCi, Commissariat a l'Energie Atomique, France) to which had been added nonradioactive DL-lysine monohydrochloride (42 mg). The oxidation was carried out using *N*-bromosuccinimide (90 mg), yielding [6-^{14}C]-Δ^1-piperideine (nominal specific activity 1.3 mCi per mmol). A radioscan of a thin layer chromatogram of the product (silica gel; 1-butanol/acetic acid/water 2:1:1) showed the presence of a small amount of a second radioactive component, R_f 0.06, probably [2,10-^{14}C$_2$]tetrahydroanabasine, in addition to [6-^{14}C]-Δ^1-piperideine, R_f 0.28. Only traces of [6-^{14}C]lysine, R_f 0.09, could have been present. In each of two experiments, a solution of the radioactive product (0.07 mCi) was administered to 3 stocks of *S. tetraptera* (Experiment 1) and *S. microphylla* (Experiment 2) by infusion into the stems through cotton wicks. The plants were allowed to grow in contact with tracer for three days and were then harvested. The material, roots, stems, and leaves, was dried at 60°C.

Extraction of Matrine from Sophora microphylla

The dried plant material (34 g) was ground in a blender and extracted 10 h in a Soxhlet apparatus with acetic acid in ethanol (2% v/v, 250 mL). The extract was concentrated *in vacuo* to 50 mL, aqueous hydrochloric acid (2% v/v, 100 mL) was added, and concentration continued until all ethanol was removed. The mixture was then cooled in ice and filtered through Celite. The filtrate was extracted with chloroform (3 × 10 mL), neutralized with sodium carbonate, and made strongly alkaline with sodium hydroxide. The alkaline solution was extracted with chloroform (4 × 10 mL) and the extracts dried over sodium sulfate, filtered, and evaporated to dryness *in vacuo*. The residue was dissolved in chloroform and applied to a column of silica gel (Baker, 60–200 mesh, 15 × 1.5 cm) and eluted with $CHCl_3$/MeOH/0.880 NH_3 (97:3:0.3). The fractions containing matrine were identified by tlc (see below), concentrated, and then applied to a column of silica gel (Merck prepacked, size A) and eluted with $CHCl_3$/MeOH (97:3). The uv absorbance of the eluate was continuously monitored at 254 nm. The crude matrine (11 mg) which emerged (65–115 mL) was diluted with nonradioactive matrine (177 mg) and the carrier-diluted mixture was converted to allomatrine without further purification.

Extraction of Matrine from S. tetraptera

Labelled matrine (5 mg) was obtained from *S. tetraptera* (40 g dry weight) by essentially the same procedure. The crude product was diluted with nonradioactive matrine (270 mg) and converted into allomatrine.

The experimental details that follow are those used in the degradation of matrine from Experiment 2. The procedure followed in Experiment 1 differed only in minor details.

Conversion of Matrine (3) into Allomatrine (6)

Matrine (188 mg) was dissolved in acetic acid (8 mL), platinum dioxide (70 mg) was added, and the mixture was heated 15 h (bath temperature 105°C) with continuous stirring under an atmosphere of hydrogen. The composition of the mixture was monitored by tlc (silica gel; $CHCl_3$/MeOH/0.880 NH_3; 90:10:0.5) and the alkaloids visualized by spraying with Dragendorff's reagent (26) (matrine R_f 0.62, allomatrine R_f 0.50; R_f values are lower, 0.5 and 0.4 respectively, if the compounds are applied directly in acetic acid solution). If the conversion was not complete, the hydrogenation was continued after addition of fresh catalyst (70 mg, twice a day) until tlc showed that no matrine remained. When the reaction was complete, the catalyst was filtered off and washed with water and the filtrate was evaporated to dryness *in vacuo*. The residue was dissolved in 0.25 *M* sulfuric acid (10 mL) and the solution extracted with chloroform (2 × 3 mL). The acidic solution was neutralized with sodium carbonate and made strongly basic with sodium hydroxide. This alkaline solution was extracted with chloroform (5 × 3 mL) and the extract was dried over sodium sulfate, filtered, and evaporated to dryness *in vacuo*. The residue was dissolved in light petroleum (bp 30–60°C) and filtered through Celite, and the filtrate was concentrated. Upon cooling crystals appeared which were filtered off and recrystallized from light petroleum, yield 112 mg. Evaporation of the mother liquor yielded a residue from which further product was obtained by chromatography on a Merck prepacked silica gel column (size A) with $CHCl_3$/MeOH (96:4) as eluant. The total yield was 166 mg (88%).

This material was diluted with inactive allomatrine (85 mg) and recrystallized three times to constant radioactivity (mp 105–105.5°C; lit. (9) mp 103–105°C).

Degradation of Allomatrine

Carbon-15 as Benzoic Acid

Allomatrine (45.5 mg, 0.18 mmol) was dissolved in dry ether (2 mL) under an atmosphere of nitrogen. Phenyl lithium (2.7 *M*, in benzene/ether, 0.25 mL, 0.7 mmol) was injected and the solution stirred for 19 h. The solution was then cooled in an acetone/Dry Ice bath, methanol (0.5 mL) was injected, and the mixture was allowed to warm to room temperature. Sulfuric acid (0.25 *M*, 10 mL) was added and the mixture extracted with

Can. J. Chem. Downloaded from www.nrcresearchpress.com by 210.87.254.6 on 09/05/12
For personal use only.

chloroform (3 × 4 mL). The aqueous layer was neutralized with sodium carbonate and made strongly alkaline with sodium hydroxide. This alkaline solution was extracted with chloroform (4 × 4 mL) and the extract dried over sodium sulfate, filtered, and evaporated to dryness *in vacuo*. The residue was dissolved in ethanol (2 mL), concentrated hydrochloric acid (3 drops) was added, and the solution evaporated to dryness *in vacuo*. The residue was dissolved in sulfuric acid (2 *M*, 1.5 mL) and 2.7 *M* chromium trioxide in 4 *M* sulfuric acid (0.5 mL) was added. This mixture was heated 1 h at reflux in a bath at 125°C with stirring. The mixture was cooled, water (8 mL) was added, and the solution extracted with chloroform (4 × 4 mL). The chloroform extract was extracted with aqueous sodium bicarbonate (5% w/v, 2 × 5 mL) and the aqueous extract was acidified with concentrated hydrochloric acid and extracted with chloroform (4 × 3 mL). This chloroform extract was dried over sodium sulfate, filtered, and evaporated to dryness *in vacuo* to yield benzoic acid (15 mg, 67%) which was recrystallized twice from water, mp 121–122°C.

Carbon-2 and Carbon-10 as Formaldehyde

Bromocyanamides A and B (7 and 8). Allomatrine (166 mg, 0.67 mmol) was dissolved in a solution of cyanogen bromide in dry benzene (0.25 *M*, 5 mL, 1.25 mmol) which had been stored over anhydrous potassium carbonate. The solution was heated 1.5 h at reflux with stirring and was then evaporated to dryness *in vacuo*. Sulfuric acid (0.25 *M*, 10 mL) was added to the residue and the mixture extracted with chloroform (4 × 4 mL). The extract was dried over sodium sulfate, filtered, and evaporated to dryness. The product was a mixture of two isomeric bromocyanamides (A(**7**) and B(**8**)) in the ratio 3:2, as determined from the ^{1}H nmr spectrum. Each of these compounds shows a distinct double doublet (J = 13 and 4 Hz), centered at δ 5.00 and 4.73 ppm, respectively. The isomers were separated by fractional crystallization from ethyl acetate/light petroleum (bp 30–60°C). The ratio of products in each batch of crystals was determined by ^{1}H nmr. When seed crystals were available, the following procedure was employed. The mixture of products was dissolved in ethyl acetate (2 mL) at room temperature. Light petroleum was added until the solution turned cloudy. Seed crystals of bromocyanamide B were added and the mixture kept 1 h at 5°C. The crystals that appeared were pure or nearly pure bromocyanamide B (**8**). The mother liquor was evaporated to dryness *in vacuo* and the recrystallization procedure was repeated except that seed crystals of bromocyanamide A (**7**) were added. Pure or nearly pure bromocyanamide A was then obtained. The mother liquor of this second recrystallization yielded a further crop of bromocyanamide B. If impure crystals were obtained, a further recrystallization yielded pure product (^{1}H nmr). Each bromocyanamide was recrystallized from ethyl acetate/light petroleum.

Products: Bromocyanamide A (**7**): 90 mg (38%), mp 134–135°C (lit. (24) mp 126°C); $[\alpha]_D^{20}$ +153° (*c* 2.1, C_2H_5OH); ir ($CHCl_3$) ν: no *trans*-quinolizidine bands, 2210 (C≡N), 1660 (C=O) cm^{-1}; ^{1}H nmr ($CDCl_3$) δ: 5.00 (dd, J = 4 and 13 Hz, 1H), 3.45 (t, J = 5 Hz, 2H), 3.6–0.9 (m, 21H) ppm; ^{13}C nmr ($CDCl_3$) δ: 169.0, 115.5, 66.1, 59.2, 51.6, 45.1, 44.7, 37.7, 33.6, 32.7, 29.7, 28.2, 26.5, (2C), 23.9, 18.9 ppm; ms *m/e*: 355, 353(M^+), 274, 248, 247, (100%). *Anal.* calcd. for $C_{16}H_{24}N_3OBr$: C 54.24, H 6.83, N 11.86, Br 22.56; found: C 54.42, H 6.92, N 11.74, Br 22.40.

Bromocyanamide B (**8**): 78 mg (33%), mp 174–176°C (lit. (11) mp 167–168°C); $[\alpha]_D^{20}$ +32° (*c* 2.0, C_2H_5OH); ir ($CHCl_3$) ν: no *trans*-quinolizidine bands, 2210 (C≡N), 1660 (C=O) cm^{-1}; ^{1}H nmr ($CDCl_3$) δ: 4.73 (dd, J = 4 and 13 Hz, 1H), 3.45 (t, J = 5 Hz, 2H), 3.6–0.9 (m, 21H) ppm; ^{13}C nmr ($CDCl_3$) δ: 169.3, 115.5, 65.2, 59.0, 52.3, 45.8, 43.9, 38.0, 33.7, 32.6, 28.6, 27.8, 27.2, 25.9, 23.7, 18.9 ppm; ms *m/e*: 355, 353(M^+), 274, 248, 247 (100%). *Anal.* calcd. for $C_{16}H_{24}N_3OBr$: C 54.24, H 6.83, N 11.86; found: C 54.38, H 6.94, N 11.76.

Formaldehyde Dimethone. The bromocyanamide (A or B) (60 mg, 0.17 mmol) was dissolved in methanol (1 mL) and a solution of trimethylamine in methanol (25% w/w, 0.5 mL) was added. The solution was allowed to stand 3 days in a stoppered flask and was then evaporated to dryness and the residue dried *in vacuo*. Potassium metal (34 mg) was added to dry *tert*-butyl alcohol (2 mL) and, when it had all dissolved, a portion (1 mL, 0.43 mmol) of the solution was added to the above residue. The mixture was heated 3 h at reflux and then cooled. Water (10 mL) and sodium hydroxide (10% w/v, 2 mL) were added and the mixture extracted with chloroform (4 × 4 mL). The extract was dried over sodium sulfate, filtered, and evaporated to dryness *in vacuo*. The ^{1}H nmr of the residue indicated an almost quantitative yield of alkene from bromocyanamide A but only about 80% from B. Sodium metaperiodate (70 mg, 0.33 mmol for A; 58 mg, 0.27 mmol for B), water (1 mL), and a solution of osmium tetroxide in ethyl acetate (5 mg/mL, 0.5 mL, 0.01 mmol), was added to the residue. The mixture was vigorously stirred at room temperature for 2.5 h. Water (2 mL) was added and the mixture was extracted with chloroform (3 × 1 mL) to remove organic material other than formaldehyde. The chloroform extract was back-extracted with water (1 × 1 mL) and the combined aqueous extracts were then reextracted with light petroleum (bp 30–60°C) (1 × 2 mL) to remove traces of chloroform. Nitrogen was bubbled through the aqueous solution for a few minutes to remove the last traces of organic solvent and a solution of dimedone (48 mg, 0.34 mmol, for A; 39 mg, 0.27 mmol, for B) in 95% ethanol (0.5 mL) was then added. Formaldehyde dimethone started to precipitate almost immediately. After 1 h it was filtered off, washed with water, and dried *in vacuo*. Yield of formaldehyde dimethone: 29 mg (58%) from bromocyanamide A (**7**), (C-10); 21.5 mg (43%) from bromocyanamide B (**8**), (C-2). The product was recrystallized twice from ethanol/water, mp 190–191°C (lit. (ref. 26, p. 79) mp 189°C).

Determination of Radioactivity

Radioactivity was assayed by liquid scintillation counting (Mark 1 liquid scintillation computer, Model 6860, Nuclear Chicago). Samples were dissolved in toluene (4 drops) and the solution dispersed in A.C.S. (Amersham). Triplicate samples of each compound were counted under comparable conditions of quenching. Confidence limits shown in Table 1 are standard deviations from the mean.

Acknowledgments

This investigation was supported by a grant from the Natural Sciences and Engineering Research Council of Canada.

We are grateful to Professor Ushio Sankawa, Faculty of Pharmaceutical Sciences, University of Tokyo, for a generous gift of matrine *N*-oxide. We thank Professor R. C. Cambie, University of Auckland, New Zealand, for a sample of matrine from the collection of the late Professor L. H. Briggs, University of Auckland, and to Professor Ernest Wenkert, Rice University, Houston, TX for his services as a go-between.

1. W. M. Golebiewski and I. D. Spenser. J. Am. Chem. Soc. **98**, 6726 (1976).
2. S. Shibata and U. Sankawa. Chem. Ind. 1161 (1963).

3. H. R. SCHÜTTE, J. LEHFELDT, and H. HINDORF. Justus Liebigs Ann. Chem. **685**, 194 (1965).
4. H. R. SCHÜTTE, H. ASLANOW, and C. SCHÄFER. Arch. Pharm. Weinheim, **295**, 34 (1962).
5. E. LEETE. J. Am. Chem. Soc. **91**, 1697 (1969).
6. R. N. GUPTA, P. HORSEWOOD, S. H. KOO, and I. D. SPENSER. Can. J. Chem. **57**, 1606 (1979).
7. M. CASTILLO, R. N. GUPTA, Y. K. HO, D. B. MACLEAN, and I. D. SPENSER. Can. J. Chem. **48**, 2911 (1970).
8. R. B. HERBERT. *In* The alkaloids. Vol. 8. Specialist periodical reports. *Edited by* M. F. Grundon. The Chemical Society, London. 1978. p. 1.
9. E. OCHIAI, S. OKUDA, and H. MINATO. Yakugaku Zasshi, **72**, 781 (1952); Chem. Abstr. **48**, 2724i (1954).
10. C. SCHÖPF, A. KOMZAK, F. BRAUN, E. JACOBI, M.-L. BORMUTH, M. BULLNHEIMER, and I. HAGEL. Justus Liebigs Ann. Chem. **559**, 1 (1948).
11. K. TSUDA and H. MISHIMA. J. Org. Chem. **23**, 1179 (1958).
12. C. SCHÖPF, H. ARM, G. BENZ, and H. KRIMM. Naturwissenschaften, **38**, 186 (1951).
13. C. SCHÖPF, F. BRAUN, and A. KOMZAK. Chem. Ber. **89**, 1821 (1956).
14. E. K. NOWACKI and G. R. WALLER. Rev. Latinoam. Quim. **8**, 49 (1977).
15. M. WINK and T. HARTMANN. FEBS Lett. **101**, 343 (1979); M. WINK, T. HARTMANN, and H.-M. SCHIEBEL. Z. Naturforsch. **34c**, 704 (1979).
16. F. BOHLMANN, E. WINTERFELDT, and U. FRIESE. Chem. Ber. **96**, 2251 (1963).
17. F. BOHLMANN, W. WEISE, D. RAHTZ, and C. ARNDT. Chem. Ber. **91**, 2176 (1958).
18. C. SCHÖPF and W. SCHWETER. Naturwissenschaften, **40**, 165 (1953).
19. K. A. ASLANOV, A. S. SADYKOV, V. B. LEONT'EV, and A. I. BEGISHEVA. Khim. Prir. Soedin. 93 (1969); Chem. Abstr. **71**, 61616t (1969).
20. K.-H. MICHEL, F. SANDBERG, F. HAGLID, and T. NORIN. Acta Pharm. Suec. **4**, 97 (1967).
21. B. A. ABDUSALAMOV, K. A. ASLANOV, and A. S. SADYKOV. Khim. Prir. Soedin. 549 (1977); Chem. Abstr. **87**, 164322d (1977).
22. A. S. SADYKOV and Y. I. PAKANAEV. Dokl. Akad. Nauk SSSR, **129**, 588 (1959); Dokl. Chem. Engl. **129**, 1037 (1959).
23. R. LUCKENBACH (*Editor*). Beilsteins Handbuch der Organischen Chemie. 4th ed. Vol. 22. 3rd and 4th Supplement. Part 1. Springer Verlag, Berlin. 1979. p. 213.
24. K. TSUDA and H. MISHIMA. Chem. Pharm. Bull. Jpn. **5**, 285 (1957).
25. R. FAGGIANI and C. J. L. LOCK. To be published.
26. R. M. C. DAWSON, D. C. ELLIOTT, W. H. ELLIOTT, and K. M. JONES (*Editors*). Data for biochemical research. 2nd ed. Oxford University Press, Oxford. 1969. p. 519.

Can. J. Chem. Downloaded from www.nrcresearchpress.com by 210.87.254.6 on 09/05/12
For personal use only.

An electron spin resonance and CIDEP study of the primary processes in the photoreductions of furaldehyde, furyl methyl ketone, and acetylthiophene by phenols

KUANG S. CHEN AND JEFFREY K. S. WAN

Department of Chemistry, Queen's University, Kingston, Ont., Canada K7L 3N6

Received July 28, 1980

KUANG S. CHEN and JEFFREY K. S. WAN. Can. J. Chem. **59**, 116 (1981).

The primary processes in the photoreduction of 2-furaldehyde, 2-furyl methyl ketone, and 2-acetylthiophene by phenol, 2,6-di-*tert*-butylphenol, and pentachlorophenol, respectively, were studied by esr and time-resolved CIDEP techniques. These furan derivatives, in their excited triplet states, can abstract a hydrogen atom from phenol via either the carbonyl group or the carbon–carbon double bond. The present results suggest that they all behave in the primary processes predominantly as carbonyl compounds. The spin–lattice relaxation times of all transient and polarized radicals observed in these photochemical systems were estimated by the CIDEP technique. The photoreductions of furaldehyde and furyl methyl ketone were also examined by high-field CIDNP. The nuclear polarization is mainly due to the cage products and the results are consistent with triplet carbonyl abstraction mechanism. Secondary radical addition to the carbon–carbon double bond of the furan ring was also observed in the furaldehyde–phenol system.

KUANG S. CHEN et JEFFREY K. S. WAN. Can. J. Chem. **59**, 116 (1981).

On a étudié par la rpe et par les techniques de PEDIC à temps résolu le processus primaire de la photoréduction du furaldéhyde-2, de la furyl-2 méthylcétone et de l'acétyl-2 thiophène par le phénol, le di-*tert*-butyl-2,6 phénol et le pentachlorophénol respectivement. Ces dérivés furanniques, dans leurs états triplets excités, peuvent enlever un atome d'hydrogène du phénol par l'intermédiaire du carbonyle ou de la double liaison carbone–carbone. Les résultats obtenus suggèrent que dans le processus primaires ils se comportent tous principalement comme des composés carbonylés. Grâce à la technique PEDIC, on a évalué les temps de relaxation spin–réseau de tous les radicaux intermédiaires et polarisés observés dans ces systèmes photochimiques. On a également étudié les photoréductions du furaldéhyde et de la furylméthylcétone grâce à la PNDIC à haut champ. La polarisation nucléaire est due principalement aux produits encagés et les résultats sont en accord avec le mécanisme d'élimination par le triplet du carbonyle. On a également observé l'addition secondaire d'un radical sur la double liaison carbone–carbone du cycle furane dans le système furaldéhyde/phénol.

[Traduit par le journal]

Introduction

The photoreductions of quinones by phenols have been used extensively in this laboratory as model systems for chemically induced magnetic polarization studies (1). While quinones contain both carbonyl groups and conjugated olefinic bonds, they behave essentially as carbonyl compounds in the photoreduction by phenols. Similarly, uranyl ions and organometals such as organotin and organomercury quench the excited triplet quinones mainly via the carbonyl moiety (2–4). Recently we began a systematic examination of the photoreductions of other diketones which contain also a reactive carbon–carbon double bond. Thus, the photoexcited "polarized" triplet malelic anhydride undergoes a primary hydrogen atom abstraction from the solvent molecule via its carbonyl oxygen. This is followed by a rapid rearrangement of the primary ketyl radical with the transfer of the hydroxylic proton to the neighboring C=C double bond (5). In general, it is much less obvious in the photoreactions of malelic anhydrides and maleimides (6) whether the triplet reacts exclusively via the carbonyl group or via the olefinic bond. In this report we examine another interesting class of compounds, the furan derivatives which contain a carbonyl group and adjacent olefinic bonds enclosed separately in a furan ring. Earlier we have developed the furilphenol system as a model to examine the detailed theory involved in low-field CIDNP studies (7–9). The esr and CIDEP results (10) show that two furil derived radicals were observed in the photoreduction: one is the "polarized" semidione radical and the other is an allyl radical formed by secondary radical addition to the furan ring. With 2-furaldehyde and 2-furyl methyl ketone, the present study shows that their excited triplet states behave mainly as a carbonyl compound in the primary processes of the photoreduction by phenol. To probe the effect of the heteroatom of the furan ring on the primary photochemical processes, the photoreduction of 2-acetylthiophene was examined and compared to that of 2-furyl methyl ketone.

Experimental

The chemicals were purchased from: MCB (2-furaldehyde and 2-furyl methyl ketone), Aldrich (2-acetylthiophene, phenol, 2,6-di-*tert*-butylphenol, and pentachlorophenol), and Canlab (2-propanol, toluene). The phenols and the furan derivatives were vacuum sublimed or distilled before use.

0008-4042/81/010116-07$01.00/0

©1981 National Research Council of Canada/Conseil national de recherches du Canada

Can. J. Chem. Downloaded from www.nrcresearchpress.com by 210.87.254.42 on 09/05/12
For personal use only.

Can. J. Chem. Downloaded from www.nrcresearchpress.com by 210.87.254.42 on 09/05/12
For personal use only.

Sample solutions contained in suprasil tubings were degassed and the tubings were sealed off under vacuum. The concentrations of the reactants were adjusted to give the optimum CIDEP effect. Cw esr spectra were recorded while the samples were directly photolyzed (200 W super pressure Hg lamp) within the cavity of an X-band Varian E-3 spectrometer employing 100 kHz field modulation. The temperature of the sample in the cavity was controlled by flowing thermostatted nitrogen gas by the sample cell and the temperature was continuously monitored by a copper–constant thermocouple. For g-factor measurements, the magnetic field was measured by a Bruker nmr oscillator and the klystron frequency was determined with a Hewlett-Packard 5342 frequency counter.

CIDEP experiments were carried out using a Molectron UV24 pulsed N_2 megawatt laser and a time-resolved dc detection system described previously (11). The spin–lattice relaxation times of the "polarized" transient radicals were estimated by the time-resolved CIDEP technique (11), and the data were applied to determine the lower limits of the rate of the secondary radical addition reactions.

Results and Discussion

Photoreduction of 2-Furaldehyde by Phenols

Photolyses of 10% 2-propanol/90% toluene solutions of 2-furaldehyde (FHCO) and various phenols led to the observation of the primary "polarized" phenoxy radical (PhO*) and a furaldehye derived radical which was not polarized. Since phenols are much more efficient than 2-propanol in the quenching of the carbonyl triplets (10), the primary photochemical process which readily accounts for the initial polarization of the phenoxy radical, is the following:

$$[1]\quad \text{FHCO} + h\nu \xrightarrow{\text{ISC}} {}^3[\text{FHCO}]^* \xrightarrow[-80^\circ\text{C}]{\text{PhOH}} \text{PhO}^* + \text{FHCOH}^*$$

Despite the low temperature and the high sensitivity of CIDEP measurements, the primary radical FHCOH escaped experimental observation. Instead, the observed transient radical derived from furaldehyde was assigned to the adduct of a phenoxyl radical to ground state furaldehyde:

$$[2]\quad \text{PhO} + \text{FHCO} \xrightarrow[-56^\circ\text{C}]{k_a} \text{(I)}$$

(I)

At very low temperatures only the phenoxy radical was observed. As the temperature was gradually increased, the ratio of the signal intensity of the furan derived radical to that of the phenoxy radical also increased. When pentachlorophenol was used, the observed esr spectrum was simplified and all the hyperfine lines due to the protons in the radical adduct **I** could be resolved. These hyperfine coupling constants and their experimental assignments are: $a_1^H = 14.3$ G; $a_2^H = 8.2$ G; $a_3^H = 1.3$ G; and $a_4^H = 6.6$ G; $g = 2.0030 \pm 0.0001$. These assignments are consistent with a similar OH radical adduct to furaldehyde reported by Shiga and Isomoto (12). The magnitude of the coupling constants for protons 2 and 3 is characteristic of the allylic protons.

None of the hyperfine structure observed in the furan derived radical showed any temperature dependence. Along with the fact that this radical intensity increases relative to phenoxy radical at higher temperatures, we conclude that the esr spectrum observed cannot be due to the primary ketyl radical and therefore the assignment of the secondary radical adduct **I** is most reasonable. Since the primary phenoxy radical exhibited strong initial polarization, the fact that the adduct formed in reaction [2] did not retain any polarization can be used to estimate the *upper limit* of the rates of the secondary reactions, provided the spin–lattice relaxation times T_1s of the phenoxy radicals are known. Figure 1*a* shows a typical transient response of the unsubstituted phenoxy radical at a constant field with Fig. 1*b* showing the corresponding transient response of the 2,6-di-*tert*-butylphenoxy radical (DTB—PhO*) in the same furaldehyde photoreduction system, at −56°C. The estimated values of T_1 are 3.9 μs for the unsubstituted phenoxy radical and 6.5 μs for DTB—PhO, respectively. With these data and the knowledge of the approximate concentration of the furaldehyde in the sample concentration of the furaldehyde in the sample solutions, the upper limits of the rates of the secondary reactions at −56°C are found to be:

$$[2a]\quad \text{PhO}^* + \text{FHCO} \xrightarrow{k_a < 2.6 \times 10^5\ M^{-1}\ s^{-1}} \text{I}$$

$$[2b]\quad \text{DTB—PhO}^* + \text{FHCO} \xrightarrow{k_a < 1.5 \times 10^5\ M^{-1}\ s^{-1}} \text{I}$$

It is apparent that although DTB—PhO has a longer T_1 than PhO, its addition to furaldehyde would still be slower due to steric hindrance caused by the two bulky *t*-butyl groups. The results also suggest that the phenoxy radicals generally add slower to the olefinic bonds in furaldehyde than the corresponding additions to quinones and malelic anhydrides.

The failure of observing the primary furaldehyde radical cannot be used to argue that furaldehyde behaves as a carbonyl compound. Rather, it remains equally possible that the primary abstraction from the phenol is via the carbon–carbon double bond. In this regard we examined the high-field CIDNP effect in the photoreduction of furaldehyde

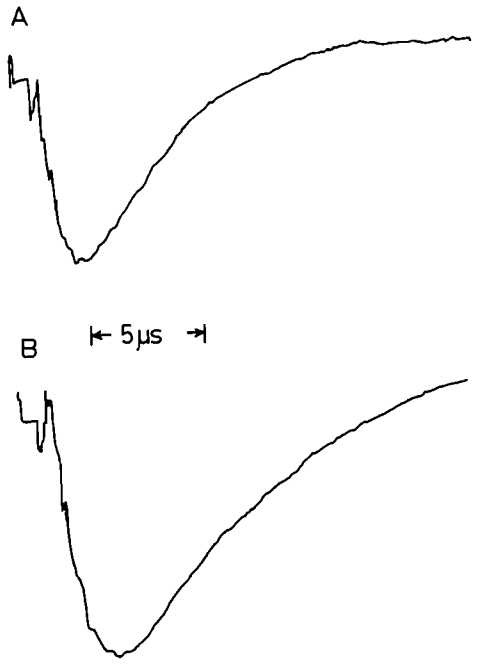

FIG. 1. The transient responses of (*a*) phenoxy radical and (*b*) 2,6-di-*tert*-butylphenoxy radical at −56°C observed in the laser flash photolysis of 2-furaldehyde in 10% 2-propanol/90% toluene containing the corresponding phenol. B_1 is 40 mG. The curve represents the difference between the on-resonance and off-resonance responses.

by pentachlorophenol in $CDCl_3$. The experiments were performed in a Bruker 60 MHz FT nmr spectrometer with a light pulsing device described by deBoer and Wan (13). Sample solutions containing furaldehyde and pentachlorophenol in $CDCl_3$ were vacuum degassed and sealed. The *net* CIDNP spectrum, i.e. the difference between dark and light observations, is presented in Fig. 2. At 14 kG (the spectrometer field), the net effect is predominant, although appreciable multiplet effects are shown by the furan proton H_3 which is adjacent to the carbonyl group.

The strong enhanced absorption of the aldehydic proton at δ 9.7 can be readily explained by the Kapteins's rules at high field (14) according to the following reaction scheme:

[1] $FHCO + h\nu \xrightarrow{ISC} {}^3[FHCO]$

[3] $^3[FHCO] + C_6Cl_5OH \rightleftharpoons$ T

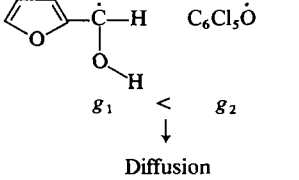

In addition to the cage recombination process, an alternate mechanism involving the exchange reaction between the primary radical and the diamagnetic parent molecule could lead to the aldehydic proton polarization as well:

[3*a*]

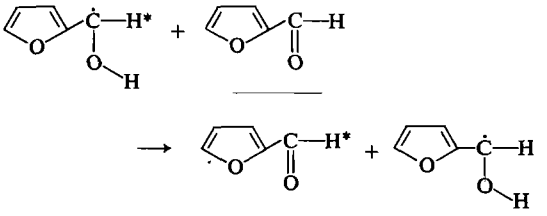

Previous CIDNP studies (15, 16) have proposed such an exchange mechanism in the photoreduction of other aldehydes. These reactions can be very efficient in transferring nuclear spin polarization from the primary radicals to diamagnetic products. However, we have pointed out earlier (17) that if these exchange reactions are reversible, they can also convert an already polarized product to a radical with subsequent destruction of the polarization by relaxation.

By analogy of the furil and pentachlorophenol system (10), g_2 is expected to be larger than g_1 in the primary radical pair and the hyperfine coupling constant of the aldehydic proton would be negative. With these assumptions and the triplet furaldehyde as the precursor, the cage product would exhibit CIDNP with the aldehydic proton strongly enhanced absorptive. With the same transient furaldehyde "ketyl" radical, the furan proton H_3 adjacent to the carbon radical centre is expected to have the largest hyperfine coupling constant and thus showing appreciable multiplet effect. On the other hand, if the primary photochemical process involves the triplet FHCO abstracting a hydrogen atom via the carbon–carbon double bond giving an allylic type of radical similar to that of **I**, the esr parameters would change to a positive hyperfine coupling constant for the aldehydic proton with the proton H_1 having the largest hyperfine coupling constant. This reaction mechanism will lead to a cage product of the furaldehyde with the aldehydic proton in the emissive mode and with a lesser multiplet effect for the proton H_3.

The conclusion that the primary photochemical abstraction process of the triplet furaldehyde involves the carbonyl group is consistent with the CIDNP results. This is more than just a mere coincidence as the CIDNP results for the furyl methyl ketone described in the next section are consistently correlated with the same conclusion.

Can. J. Chem. Downloaded from www.nrcresearchpress.com by 210.87.254.42 on 09/05/12
For personal use only.

Can. J. Chem. Downloaded from www.nrcresearchpress.com by 210.87.254.42 on 09/05/12
For personal use only.

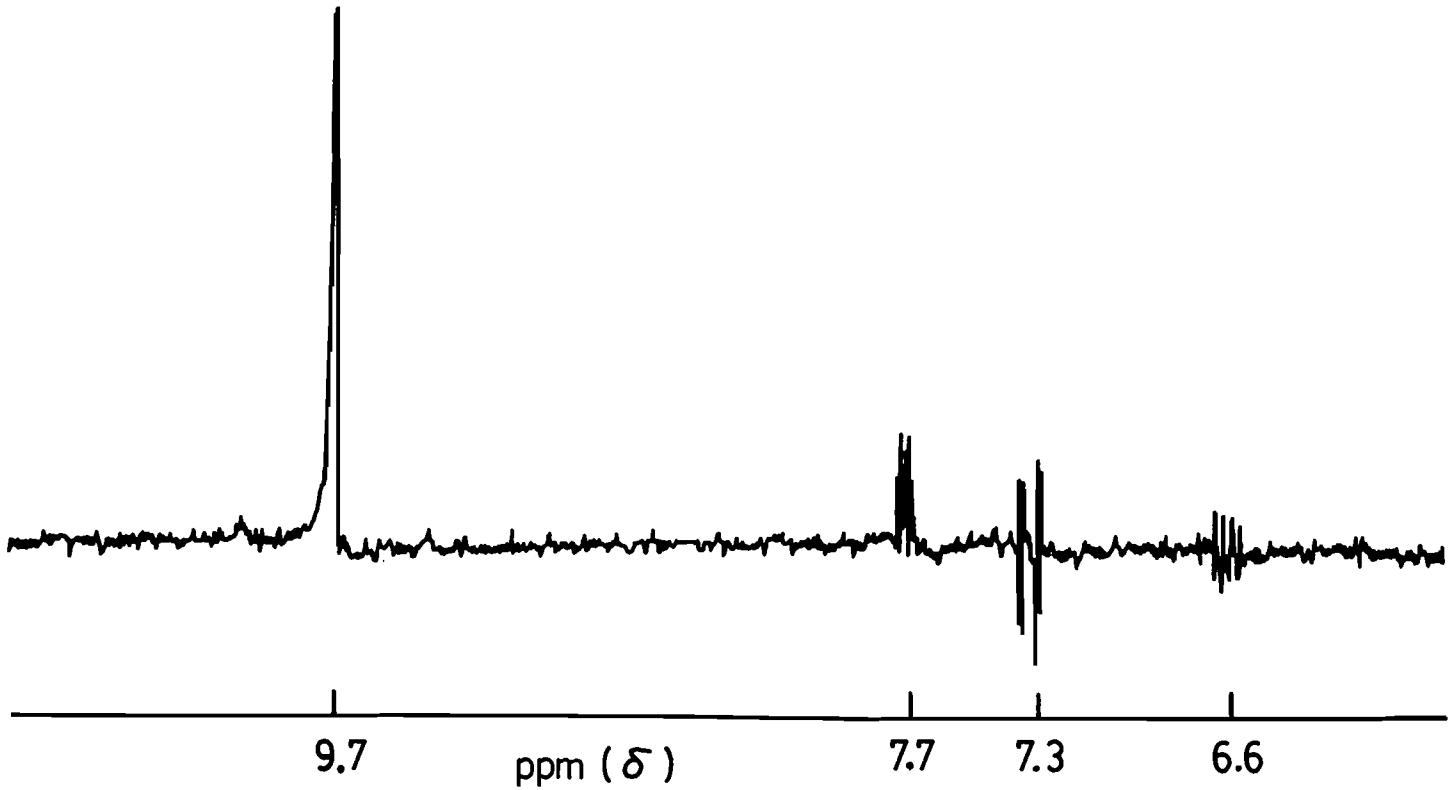

FIG. 2. The *net* proton-FT CIDNP spectrum of 2-furaldehyde obtained in the photoreduction of furaldehyde by pentachlorophenol in $CDCl_3$.

Can. J. Chem. Downloaded from www.nrcresearchpress.com by 210.87.254.42 on 09/05/12
For personal use only.

Photoreduction of 2-Furyl Methyl Ketone by Phenols

Two radicals were observed by esr when 2-furyl methyl ketone (FCOMe) was photoreduced by phenol at −60°C in a 10% 2-propanol/90% toluene solution. One of the radicals is the primary phenoxy radical and its esr spectrum changes to correspond to the particular substituted phenol used. CIDEP experiments show that both radicals exhibit initial polarization and that they have different values of T_1. In the 2,6-di-*tert*-butylphenol/ FCOMe system at −60°C, the values of T_1 are 6 μs for 2,6-di-*tert*-butylphenoxy radical and 4.3 μs for the other counter radical. Unlike the FHCO system, no new radicals were observed when the temperature was raised.

The results from both the esr and CIDEP observations support the following primary photochemical processes:

[4] FCOMe + $h\nu \xrightarrow{\text{ISC}}$ ^{3}[FCOMe]*

$$\xrightarrow[-80°C]{PhOH} \left[\text{2-furyl-C(OH)(}\dot{}\text{)-CH}_3\right]^* + \text{PhO}\dot{}\text{*}$$

II

The hyperfine coupling constants and their assignments to the ketyl radical II are: $a_1^H = 5.5$ G; $a_2^H = 1.3$ G; $a_3^H = 8.4$ G; $a_{CH_3}^H = 14.5$ G; and $a_{OH}^H = 1.29$ G (at −80°C). The last coupling constant is temperature dependent. These assignments are consistent with other ketyl radicals such as the furil ketyl radical (10) and the acetophenone ketyl radical (18). A *g*-factor of 2.0031 was measured for the ketyl radical II.

It is interesting to note that the addition of the primary phenoxy radical to the ground state FCOMe does not seem to be at all efficient. No esr spectrum could be observed for the adduct. On the other hand, it is not too surprising that the primary ketyl radical II is more stable (and thus observable) than the corresponding primary furaldehyde "ketyl" radical.

The mechanism of the primary photochemical reaction of FCOMe in reaction [4] was further supported by CIDNP results. Sample solutions containing FCOMe and pentachlorophenol in $CDCl_3$ exhibited a *net* CIDNP high field spectrum as shown in Fig. 3. Again the predominant polarization is underlined by the net effect and the strong emission of the methyl protons of the caged product FCOMe at δ 2.5 corresponds to a positive hyperfine coupling constant for the methyl protons which is expected in the ketyl radical II.

Thus, we conclude that both furaldehyde and furyl methyl ketone undergo primary photochemical abstraction reactions via their carbonyl group.

Photoreduction of 2-Acetylthiophene by Phenols

To study the effect of the heteroatom of the furan ring on the primary photochemical processes of furyl methyl ketone, we have carried out the photoreduction of 2-acetylthiophene by various phenols in 2-propanol and in 10% 2-propanol/90% toluene solvents. At −80°C, two radicals were observed; one was the phenoxy radical and the other counter radical was derived from the acetylthiophene. CIDEP experiments show that the phenoxy radical was polarized but the initial polarization magnitude was much weaker relative to that observed in the furyl methyl ketone/phenol system under identical conditions. Furthermore, repeated efforts failed to show positively the polarization from the acetylthiophene derived radical. These results can be discussed in terms of the following mechanism:

[5] $$\text{thienyl-C(=O)-CH}_3 + h\nu \xrightarrow{\text{ISC}} {}^3[\text{thienyl-C(=O)-CH}_3]^*$$

[6] $$^3[\text{thienyl-C(=O)-CH}_3]^* + \text{PhOH} \longrightarrow \text{PhO}\dot{}\text{*} + \text{thienyl-C(OH)(}\dot{}\text{)-CH}_3\text{*}$$

[7] $$\text{thienyl-C(OH)(}\dot{}\text{)-CH}_3 \longrightarrow \text{1,2,3-thienyl-C(O}^-\text{)(}\dot{}\text{)-CH}_3 + \text{H}^+$$

(III)

The totally emissive polarization observed in the phenoxy radical indicates the operation of the phototriplet CIDEP mechanism (19). However, the relatively much smaller magnitude of the initial polarization can be attributed to three different reasons. Firstly, the initial electron polarization of the acetylthiophene triplet in reaction [5] which arises from the unequal intersystem crossing rates to the three triplet sublevels may not be as large as that in the triplet furyl methyl ketone. The presence of the S atom may have influenced substantially the intersystem crossing processes and the characteristics of the triplet sublevels. Secondly, the initial polarization transferred to the phenoxy radical in reaction [6] depends heavily upon the rate of that chemical reaction, which must compete effectively with the spin depolarization rate of the polarized

Can. J. Chem. Downloaded from www.nrcresearchpress.com by 210.87.254.42 on 09/05/12
For personal use only.

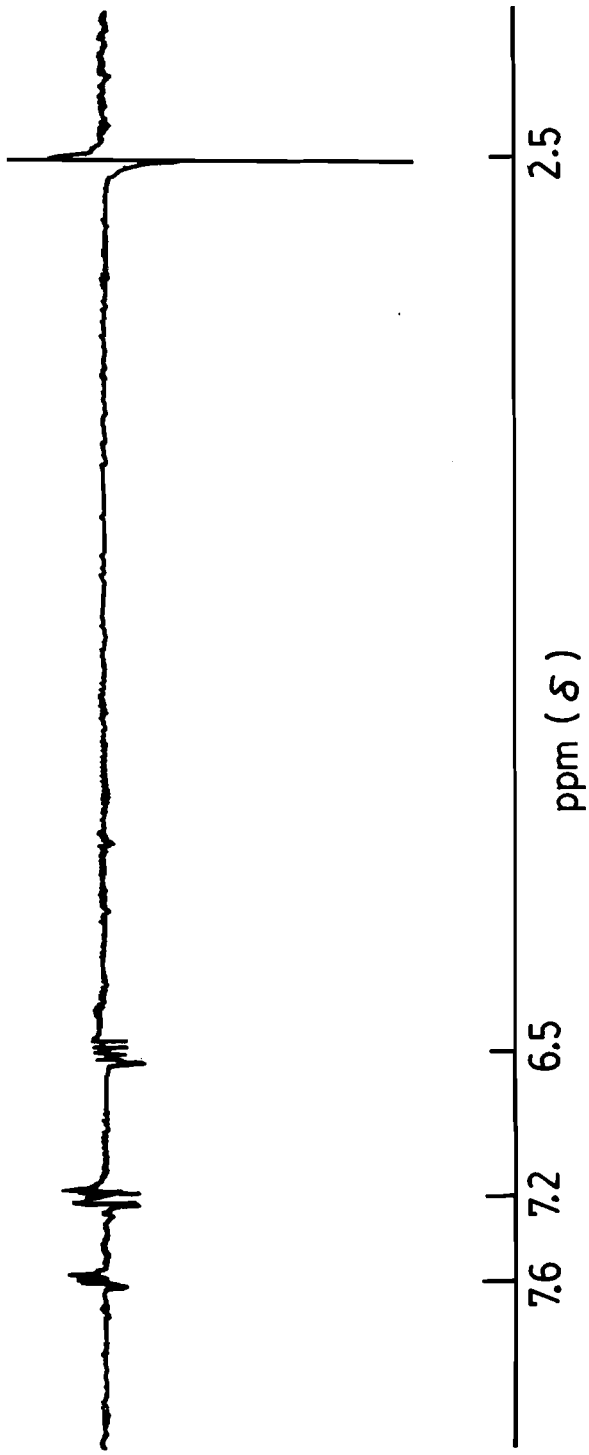

FIG. 3. The *net* proton-FT CIDNP spectrum of 2-furyl methyl ketone obtained in the photoreduction of the parent ketone by pentachlorophenol in $CDCl_3$.

triplet. In this regard, we have compared the cw signal intensity of the phenoxy radicals generated in both the acetylthiophene and the furyl methyl ketone systems under almost identical experimental conditions. The comparable intensity suggests that reaction [6] does not seem to be appreciably slower than reaction [4]. A third possible reason is that the spin–lattice relaxation rate of the polarized triplet acetylthiophene is faster than that of furyl methyl ketone, as the S atom has a larger spin–orbit coupling than the O atom. Indeed, the failure of observing polarization from the counter acetylthiophene derived radical can be partly attributed to the short T_1 of such radical.

The esr observation of the acetylthiophene radical during the photolysis is assigned to its radical anion **III**. The hyperfine coupling constants and their assignments are: $a_1^H = 7.40$ G; $a_2^H = 1.9$ G; $a_3^H = 7.6$ G; and $a_{CH_3}^H = 12.1$ G. These assignments are in good agreement with those observed by Hudson and Lewis (20) who generated the radical anions by the photolysis of acetylthiophene in methanol in the presence of sodium methoxide. In their systems they were able to observe the two conformers of the radical anion at equilibrium:

[8] 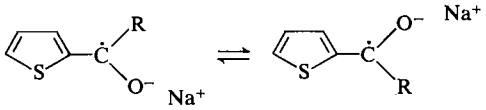

In our photochemical system, the reduction proceeds via the triplet abstraction mechanism, reaction [6], and the radical anion **III** is subsequently formed by the ionization of the "ketyl" radical. The ionization is more favored in 2-propanol solution than in a 10% 2-propanol/90% toluene solution. It is interesting to note that no radical anion was observed when we photolysed a methanol solution of furyl methyl ketone in the presence of sodium methoxide, although with acetylthiophene we obtained essentially the same results as reported by Hudson and Lewis (20). This suggests that acetylthiophene is a much better electron acceptor than furyl methyl ketone and it accounts for the rapid ionization process in reaction [7] but not for the analogous ketyl radical of furyl methyl ketone.

Acknowledgment

This research is supported by the Natural Sciences and Engineering Research Council of Canada.

1. J. K. S. WAN. Adv. Photochem. **12**, 283 (1980).
2. J. W. M. DEBOER, K. S. CHEN, Y. C. CHAN CHUNG, and J. K. S. WAN. J. Am. Chem. Soc. **101**, 5425 (1979).
3. K. S. CHEN, R. SMITH, and J. K. S. WAN. Can. J. Chem. **56**, 2503 (1978).
4. J. K. KOCHI, K. S. CHEN, and J. K. S. WAN. Chem. Phys. Lett. **73**, 557 (1980).
5. K. S. CHEN, T. FOSTER, and J. K. S. WAN. J. Phys. Chem. In press.
6. P. B. AYSCOUGH, T. H. ENGLISH, G. LAMBERT, and A. J. ELLIOT. J. Chem. Soc. Faraday I, **73**, 1302 (1977).
7. H. M. VYAS and J. K. S. WAN. Mol. Phys. **34**, 887 (1977).
8. J. W. M. DEBOER, D. A. HUTCHINSON, and J. K. S. WAN. Chem. Phys. Lett. **62**, 300 (1979).
9. J. W. M. DEBOER, D. A. HUTCHINSON, R. HAWLEY, and J. K. S. WAN. Chem. Phys. **43**, 81 (1979).
10. A. J. ELLIOT and J. K. S. WAN. Can. J. Chem. **56**, 2499 (1978).
11. J. W. M. DEBOER, Y. C. CHAN CHUNG, and J. K. S. WAN. Can. J. Chem. **57**, 2971 (1979).
12. T. SHIGA and A. ISOMOTO. J. Phys. Chem. **73**, 1139 (1969).
13. J. W. M. DEBOER and J. K. S. WAN. Mol. Photochem. **9**, 303 (1979).
14. R. KAPTEIN. J. Am. Chem. Soc. **94**, 6251 (1972).
15. G. CLOSS and D. PAULSON. J. Am. Chem. Soc. **92**, 7229 (1970).
16. H. CHEN, M. COCIVERA, and S. VAISH. Can. J. Chem. **53**, 2548 (1975).
17. F. J. ADRIAN, H. M. VYAS, and J. K. S. WAN. J. Chem. Phys. **65**, 1454 (1976).
18. R. WILSON. J. Chem. Soc. B, 1581 (1968).
19. J. K. S. WAN and A. J. ELLIOT. Acc. Chem. Res. **10**, 161 (1977).
20. A. HUDSON and J. W. E. LEWIS. Tetrahedron, **26**, 4413 (1970).

Can. J. Chem. Downloaded from www.nrcresearchpress.com by 210.87.254.42 on 09/05/12
For personal use only.

Osmotic and activity coefficients of sodium sulphate in water from 50 to 150°C

OM. N. BHATNAGAR AND ALAN N. CAMPBELL
University of Manitoba, Department of Chemistry, Winnipeg, Man., Canada R3T 2N2

Received June 26, 1980

OM. N. BHATNAGAR and ALAN N. CAMPBELL. Can. J. Chem. **59**, 123 (1981).

The vapour pressure lowering, ΔP, of sodium sulphate solutions in water was measured in the concentration range 0.4 to 1.8 *m* and the temperature range 50 to 150°C by the use of a differential manometer. ΔP values were used to calculate the osmotic coefficient of sodium sulphate solutions. Pitzer's equation for osmotic coefficients was used to evaluate $\beta_{MX}^{(0)}$, $\beta_{MX}^{(1)}$, and C_{MX}^{ϕ} at each temperature. An attempt has been made to explain the changes in these constants in terms of the ion–ion and ion–solvent interactions. Using these constants, the mean activity coefficients, $\gamma_{\pm}$, of sodium sulphate were calculated at different temperatures and concentrations using Pitzer's equation.

OM. N. BHATNAGAR et ALAN N. CAMPBELL. Can. J. Chem. **59**, 123 (1981).

Faisant appel à un manomètre différentiel et opérant à des températures allant de 50 à 150°C, on a mesuré l'abaissement de la vapeur, ΔP, de solutions de sulfate de sodium dans l'eau à des concentrations allant de 0,4 à 1,8 *m*. On a utilisé les valeurs de ΔP pour calculer le coefficient osmotique des solutions de sulfate de sodium. On a utilisé l'équation de Pitzer relative aux coefficients osmotiques pour évaluer $\beta_{MX}^{(0)}$, $\beta_{MX}^{(1)}$ et C_{MX}^{ϕ} à chaque température. On a tenté d'expliquer les variations de ces constantes en fonction d'interactions ion–ion et ion–solvant. En utilisant ces constantes et l'équation de Pitzer, on a calculé les coefficients d'activité moyens, $\gamma_{\pm}$, du sulfate de sodium à différentes températures et à différentes concentrations.

[Traduit par le journal]

Introduction

Fundamental studies of electrolyte solutions at high temperatures have lagged behind those on pure gases and solids because experiments are difficult and their interpretation requires much sophistication. Until recently, the data available at high temperature lacked precision but recently some excellent work on thermodynamic properties of electrolyte solutions in water has been reported (1–7). In a previous paper (8) the authors reported the osmotic and activity coefficients of lithium chloride derived from measurements of the lowering of vapour pressure in the temperature range 50 to 150°C. In this paper the authors report the osmotic and activity coefficients of sodium sulphate in the concentration range 0.4 to 1.8 *m* and the temperature range 50 to 150°C.

Experimental

Analytical grade sodium sulphate was used without further purification. The concentrations of solution were determined after each experiment by gravimetric analysis of the solution as barium sulphate (9*a*). The experimental procedure was essentially the same as before (8). The only changes were that silicone oil was used in the bath, since it does not deteriorate at high temperatures. Also, four multijunction thermocouples were used to monitor the bath temperature constantly. These thermocouples were strategically located in the oil bath around the vapour pressure cell. The vapour pressure lowering was measured with a differential manometer as before (8).

Results and Discussion

The observed lowering of vapour pressure, ΔP, in Torr, was corrected to the density of mercury at 0°C. The size of the bulbs in the vapour pressure cell was reduced to minimize the vapour space and hence it was not necessary to make any temperature corrections to concentrations due to evaporation.

The possibility of HSO_4^- ion formation according to the reaction

$$SO_4^{2-} + H_2O \rightleftharpoons HSO_4^- + OH^-$$

was looked into. The second dissociation constant of sulphuric acid has been reported at high temperature by Marshall and Jones (9*b*). This was used to calculate the HSO_4^- ion concentration in the temperature and concentration range of present work. The HSO_4^- ion concentration was of the order of 10^{-5} *m* and was considered insignificant.

The osmotic coefficients were calculated from the following equation:

$$[1] \quad \phi = \frac{1000}{\nu m M_1 RT}\left[RT \ln (P^0/P) - \int_P^{P^0} \xi \mathrm{d}p - \overline{V}_1^{\,0}(\mathrm{l})\Delta P\right]$$

where ϕ is the osmotic coefficient, T the absolute temperature, R the gas constant, M_1 the molecular weight of water, m the molality, v the number of ions resulting from complete ionization of one molecule, P^0 and P are the vapour pressure of pure water and solution respectively, assuming the solute to be non-volatile.

The first term in the bracket gives the osmotic coefficient at low vapour pressures, the second term gives the corrections for the deviations of the vapour from the perfect gas law, and the third term is an

0008-4042/81/010123-04$01.00/0
©1981 National Research Council of Canada/Conseil national de recherches du Canada

Can. J. Chem. Downloaded from www.nrcresearchpress.com by 210.87.254.6 on 09/05/12
For personal use only.

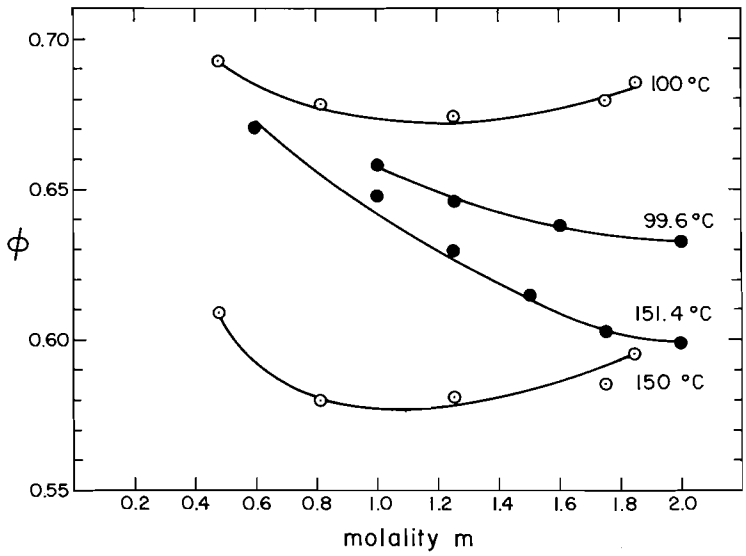

FIG. 1. Osmotic coefficient vs. molality m of sodium sulphate in water. ○ Data from present work, ● data from refs. 15 and 16.

adequate approximation for the isothermal compression of the solution from its own vapour pressure to that of pure water. The integrand ξ was calculated using the equation given by Smith, Keyes, and Gerry (10). $V^0(l)$ the molar volume of pure water and P^0 were calculated from the equations given in ref. 10. $\bar{V}_1{}^0(l)$ is used instead of $\bar{V}_1(l)$, the partial molar volume of water, because under these conditions the difference is negligibly small. Recently Pitzer (11) has developed a set of equations for thermodynamic properties of electrolyte solutions which are very general and can be applied to any valency type compounds. These equations are semi-empirical in nature but are quite successful in predicting the thermodynamic properties of electrolyte solutions up to 6 M (12–14). The relevant equations for osmotic and activity coefficients for a pure electrolyte are given as follows.

$$[2]\quad \phi - 1 = -|Z_M Z_X| A\phi \frac{I^{1/2}}{1 + bI^{1/2}} + \frac{m2\nu_M\nu_X}{\nu}[\beta_{MX}{}^{(0)} + \beta_{MX}{}^{(1)} \exp(-\alpha I^{1/2})] + \frac{m^2 2(\nu_M\nu_X)^{3/2} C_{MX}{}^{\phi}}{\nu}$$

$$[3]\quad \ln \gamma_{\pm} = -|Z_M Z_X| A\phi \left[\frac{I^{1/2}}{1 + bI^{1/2}} + \frac{2}{b}\ln(1 + bI^{1/2})\right] + \frac{m2\nu_M\nu_X}{\nu}\left\{2\beta_{MX}{}^{(0)} + \frac{2\beta_{MX}{}^{(1)}}{\alpha^2 I}\left[1 - \left(1 + \alpha I^{1/2} - \frac{\alpha^2 I}{2}\right)\exp(-\alpha I^{1/2})\right]\right\} + \frac{3m^2 2(\nu_M\nu_X)^{3/2} C_{MX}{}^{\phi}}{2\nu}$$

where Z_M and Z_X are the positive and negative ionic charges in electronic units. Likewise ν_M and ν_X are the number of ions of each type in the formulae and $\nu = \nu_M + \nu_X$. I is the ionic strength and $A\phi$ is the Debye–Hückel coefficient for the osmotic functions given by:

$$[4]\quad A\phi = 1/3\left(\frac{2\pi N_0 \rho\omega}{1000}\right)^{1/2}\left(\frac{e^2}{DkT}\right)^{3/2}$$

where all terms have the usual meaning and are explained elsewhere (14). The values of $A\phi$ in water at various temperatures for the present calculations were taken from ref. 14. The coefficients $\beta_{MX}{}^{(0)}$ and $\beta_{MX}{}^{(1)}$ account for the various short range interactions between M and X and for cosphere overlap effects, while $C_{MX}{}^{\phi}$ accounts for triple ion interaction and is important at high concentrations. The parameters α and b were given a value of 2 and 1.2 respectively for the present calculations, and were treated as independent of temperature. Pitzer and Mayorga (12) have used the same values of α and b for all different types of electrolytes and found them satisfactory. The experimental values of ϕ and m were used to evaluate the best values of $\beta_{MX}{}^{(0)}$, $\beta_{MX}{}^{(1)}$, and $C_{MX}{}^{\phi}$ which were in turn used to calculate the mean activity coefficient, $\gamma_{\pm}$, by eq. [3]. These activity coefficients were compared with those obtained by eq. [5] using graphical integration.

$$[5]\quad \ln \gamma_{\pm} = -(1 - \phi) - 2\int_0^{m^{1/2}} \frac{1 - \phi}{m^{1/2}}\, dm^{1/2}$$

Can. J. Chem. Downloaded from www.nrcresearchpress.com by 210.87.254.6 on 09/05/12
For personal use only.

Can. J. Chem. Downloaded from www.nrcresearchpress.com by 210.87.254.6 on 09/05/12
For personal use only.

The osmotic coefficients of sodium sulphate at various temperatures and concentrations are given in Table 1. For comparison the results have been plotted in Fig. 1 at 100 and 150°C and those reported by Soldano and co-workers (15, 16) at 99.6 and 151.4°C using the isopiestic method. There is a great difference in the two sets of data. Similar differences were observed for the LiCl data (8). Recently, Holmes, Baes, and Mesmer (7) determined the osmotic coefficients of KCl, $CaCl_2$, and $MgCl_2$ by the isopiestic method, and compared them with the earlier isopiestic results of Soldano and co-workers (16); they found the agreement to be fair to poor above 100°C.

Equation [2] uses experimental osmotic coefficients and concentrations to determine $\beta_{MX}^{(0)}$, $\beta_{MX}^{(1)}$, and C_{MX}^{ϕ}. Table 2 gives the values of $\beta_{MX}^{(0)}$, $\beta_{MX}^{(1)}$, and C_{MX}^{ϕ} at each temperature from 50 to 150°C. The second virial coefficient in Pitzer's equation (11) is a complicated function of many interactions and its physical interpretation in terms of molecular quantities is not simple. As has been discussed by Pitzer (11) the principal contributions to $\beta_{MX}^{(1)}$ will come from short range interactions of unlike charged ions while the interactions of like and unlike charged ions will both contribute to $\beta_{MX}^{(0)}$. Since the second virial coefficient is a weighted mean of the interactions of pairs of ions with signs $++$, $+-$, and $--$, it was shown by Pitzer and Mayorga (12) that the relative weighting of $+-$ interactions is greatest at low ionic strength and $++$ and $--$ terms become more important at higher ionic strength, but never equal to the weight of $+-$ interactions. The $\beta_{MX}^{(0)}$ in Table 2 increases with increasing temperature, reaches a maximum at around 125°C, and then decreases. Similar behaviour was observed for $\beta_{MX}^{(0)}$ values for NaCl (14). The $\beta_{MX}^{(1)}$ steadily decreases with increasing temperature, but this is not the case for NaCl (14). This would indicate that with increase in temperature the short range interactions between like and unlike charged ions, $+-$ type, become greater and the repulsive forces of the type $++$ and $--$ decrease with increase in temperature. The change of $\beta_{MX}^{(0)}$ and $\beta_{MX}^{(1)}$ for Na_2SO_4 with temperature is similar to that found for KCl and NaCl in water–methanol mixture (17). By addition of methanol to water the dielectric constant of the solvent mixture decreases and in the present work the same effect results by raising the temperature. However, it is interesting that $\beta_{MX}^{(1)}$ for NaCl (14) in water increases with increasing temperature while $\beta_{MX}^{(1)}$ for NaCl in methanol–water mixture (17) decreases with higher methanol content. In water sodium and sulphate ions are hydrated to a certain extent, and due to the difference in the ionic sizes and surface charge density

TABLE 1. Osmotic coefficient of sodium sulphate in water*

	50°C			75°C			100°C			125°C			150°C		
m	ΔP (Torr)	ϕ_{exp}	ϕ_{fit}	ΔP (Torr)	ϕ_{exp}	ϕ_{fit}	ΔP (Torr)	ϕ_{exp}	ϕ_{fit}	ΔP (Torr)	ϕ_{exp}	ϕ_{fit}	ΔP (Torr)	ϕ_{exp}	ϕ_{fit}
0.4745	1.67	0.708	0.709	5.21	0.703	0.704	13.60	0.693	0.693	30.30	0.665	0.667	57.94	0.609	0.608
0.8112	2.71	0.676	0.675	8.60	0.683	0.681	22.64	0.679	0.677	50.97	0.659	0.655	93.70	0.580	0.583
1.2507	4.03	0.657	0.656	12.91	0.670	0.671	34.40	0.674	0.675	77.56	0.655	0.658	143.90	0.581	0.578
1.7471	5.55	0.653	0.657	17.94	0.673	0.675	47.97	0.680	0.682	109.59	0.670	0.671	203.52	0.585	0.590
1.8535	5.95	0.662	0.659	19.16	0.679	0.677	51.20	0.685	0.683	116.99	0.675	0.674	216.30	0.596	0.593

*ϕ_{exp} are the calculated values of osmotic coefficient using eq. [1]; ϕ_{fit} are the values obtained by fitting the ϕ_{exp} and m values to a least-squares programme using eq. [2].

TABLE 2. Parameter for thermodynamic functions for Na_2SO_4

T (°C)	$\beta_{MX}^{(0)}$	$\beta_{MX}^{(1)}$	C_{MX}^{ϕ}
50	0.0477	1.37	0.00237
75	0.0894	1.29	−0.00613
100	0.1230	1.25	−0.01250
125	0.1390	1.17	−0.01400
150	0.1040	1.10	−0.00551

TABLE 3. Mean activity coefficients of sodium sulphate*

	50°C		75°C		100°C		125°C		150°C	
m	$\gamma_{\pm}'$	$\gamma_{\pm}''$	$\gamma_{\pm}'$	$\gamma_{\pm}''$	$\gamma_{\pm}'$	$\gamma_{\pm}''$	$\gamma_{\pm}'$	$\gamma_{\pm}''$	$\gamma_{\pm}'$	$\gamma_{\pm}''$
0.4745	0.281	0.279	0.265	0.265	0.245	0.243	0.217	0.215	0.178	0.176
0.8112	0.229	0.228	0.220	0.218	0.204	0.202	0.178	0.178	0.140	0.137
1.2507	0.192	0.190	0.189	0.187	0.177	0.175	0.154	0.154	0.116	0.114
1.7471	0.168	0.167	0.170	0.168	0.160	0.158	0.139	0.139	0.102	0.101
1.8535	0.164	0.161	0.167	0.166	0.157	0.156	0.137	0.136	0.099	0.098

*$\gamma_{\pm}'$ = activity coefficients calculated from Pitzer's eq. [3]; $\gamma_{\pm}''$ = activity coefficients calculated from eq. [5].

their hydrated sizes will be different. If the hydrated size of the ion decreases with increasing temperature, it will result in decrease of $\beta_{MX}^{(1)}$ and increase in $\beta_{MX}^{(0)}$ values. The mean activity coefficient, $\gamma_{\pm}$, calculated from Pitzer's eq. [3] and by eq. [5], are in good agreement if the inevitable errors of graphical integration are considered (Table 3). The activity coefficients show little change with temperature up to 100°C. Above this temperature the change is considerable. It is also interesting to note that the $\gamma_{\pm}$ values of Na_2SO_4 are much smaller as compared to NaCl at comparable concentrations and temperatures. Further measurements at higher concentrations and temperature are being carried out with greatly modified equipment in order to understand better the behaviour of Na_2SO_4 and other electrolytes in aqueous solutions.

Acknowledgments

We want to thank Atomic Energy of Canada Ltd. for their financial support and for the use of their computer and programming services.

1. E. R. GARDNER, P. J. JONES, and H. J. DE NORDWALL. Trans. Faraday Soc. **59**, 1994 (1963).
2. W. L. GARDNER, R. E. MITCHELL, and J. W. COBBLE. J. Phys. Chem. **73**, 2025 (1964).
3. C. M. CRISS and J. W. COBBLE. J. Am. Chem. Soc. **86**, 5385 (1964).
4. E. R. GARDNER. Trans. Faraday Soc. **65**, 91 (1969).
5. C. LIU and W. T. LINDSAY, JR. J. Phys. Chem. **74**, 341 (1970).
6. C. LIU and W. T. LINDSAY, JR. J. Solution Chem. **1**, 45 (1972).
7. H. F. HOLMES, C. F. BAES, JR., and R. E. MESMER. J. Chem. Thermodyn. **10**, 983 (1978).
8. A. N. CAMPBELL and OM. N. BHATNAGAR. Can. J. Chem. **57**, 2542 (1979).
9. (*a*) I. M. KOLTHOFF, E. B. SANDELL, E. J. MEEHAN, and S. BRUCKENSTEIN. Qualitative chemical analysis. IVth ed. The MacMillan Company, New York, NY; (*b*) W. L. MARSHALL and E. V. JONES. J. Phys. Chem. **70**, 4028 (1966).
10. L. B. SMITH, F. G. KEYES, and H. T. GERRY. Proc. Am. Acad. Arts Sci. **69**, 137 (1934).
11. K. S. PITZER. J. Phys. Chem. **77**, 268 (1973).
12. K. S. PITZER and G. MAYORGA. J. Phys. Chem. **77**, 2300 (1973).
13. K. S. PITZER and G. MAYORGA. J. Solution Chem. **3**, 539 (1974).
14. L. F. SILVESTER and K. S. PITZER. J. Phys. Chem. **81**, 1822 (1977).
15. C. S. PATTERSON, L. O. GILPATRICK, and B. A. SOLDANO. J. Chem. Soc. 2730 (1960).
16. B. A. SOLDANO and P. B. BIEN. J. Chem. Soc. A, 1825 (1966).
17. A. R. GUPTA. J. Phys. Chem. **83**, 2986 (1979).

Can. J. Chem. Downloaded from www.nrcresearchpress.com by 210.87.254.6 on 09/05/12
For personal use only.

Activity coefficients, densities, dipole moments, and surface tensions of the system triethylamine–methylethylketone–water

ALAN N. CAMPBELL

Department of Chemistry, University of Manitoba, Winnipeg, Man., Canada R3T 2N2

Received May 5, 1980

ALAN N. CAMPBELL. Can. J. Chem. **59**, 127 (1981).

The properties named in the title have been determined by standard methods. Viscosity, molar volume, and orientation polarisation all indicate abnormalities of the nature of association between the components.

The most interesting result is that of surface tension which indicates that, in the case of the binary system triethylamine–water, a surface layer of constant composition is formed over a wide range of total composition. When, by a rise in temperature of two or three degrees, this layer becomes unstable, it splits into two phases of different composition. The surface layer may then be instantaneously reformed and so on. A mechanism for the generation of a two-phase system is thus established. The data for the three-phase, isothermal, system are not so convincing, for reasons that are suggested.

ALAN N. CAMPBELL. Can. J. Chem. **59**, 127 (1981).

On a déterminé les propriétés mentionnées dans le titre en utilisant des méthodes normales. La viscosité, le volume molaire et l'orientation de la polarisation révèlent tous des anomalies dans la nature de l'association entre les composants.

Le résultat le plus intéressant est celui de la tension superficielle; il révèle que dans le cas du système binaire triéthylamine–eau, il se forme une couche de surface dont la composition est constante pour des compositions totales très variables. Quand cette surface devient instable, par suite d'une augmentation de la température de 2 à 3°C, elle se sépare en deux phases de compositions différentes. La couche de surface peut se reformer instantanément et ainsi de suite. On a donc établi un mécanisme de formation d'un système à deux phases. Pour les raisons invoquées les données relatives à un système isotherme à trois phases ne sont pas convaincantes.

[Traduit par le journal]

Introduction

A recent paper by the author (1) has defined the compositions of equilibrium liquid layers of the system triethylamine – methylethyl ketone – water, at constant temperatures lying between 0 and 160°C. The problem of why some liquid pairs (or triplets) separate into two layers, while others do not, has been approached via the different theories of solution. As an attempt to have a better description of the problem, the properties mentioned in the title have been studied. Some interesting results as to the mechanism of separation result from a study of surface tension.

Since the mere existence of two layers implies a large degree of non-ideality, it is to be expected that the activity coefficients in at least one layer should deviate widely from unity, and this was found to be so.

It seems obvious that there must be some connection between dielectric constant and partial miscibility though what that connection is, is not obvious. Nevertheless, the dielectric constants and refractive indices were determined, and the derived quantities, distortion polarisation, and orientation polarisation calculated.

The determination of surface tension at 16°C for the system triethylamine–water, at which temperature all mixtures are homogeneous and at 25°C for the ternary system triethylamine–methylethylketone–water was carried out as a matter of routine but the results were found to be very instructive.

Perhaps the best method, at least the one most free from approximations and assumptions, of obtaining activities and activity coefficients, is that of vapour pressure determination. Provided the pressures are low (not greater than 100 Torr) the vapours may be assumed to obey the ideal gas laws, and the simple relationship

$$[1] \quad a_1 = p_1/p_1^0$$

applies, where p_1 is the partial pressure of component 1, and p_1^0 the vapour pressure in the pure state. If the vapour pressures are higher, as in the determination of activity coefficients at higher temperatures (above 100°C) (2), the assumption of ideality can no longer be justified and a more complicated equation of state must be used. This usually requires the use of a computer programme. Worse still, no equation of state, except perhaps the virial equation with a sufficient number of terms, is entirely satisfactory. At room temperature, however, say 25°C, the simple relationship of eq. [1] is entirely satisfactory.

Since the compositions of congruent layers at 25°C (and other temperatures) have already been determined (1), it remained only to find the total vapour pressure (same for both layers) and the composition of the vapour from one or both layers.

0008-4042/81/010127-05$01.00/00

©1981 National Research Council of Canada/Conseil national de recherches du Canada

Can. J. Chem. Downloaded from www.nrcresearchpress.com by 210.87.254.40 on 09/05/12
For personal use only.

Can. J. Chem. Downloaded from www.nrcresearchpress.com by 210.87.254.40 on 09/05/12
For personal use only.

Applications of Dalton's law then gives the partial pressures. Activity coefficients result from eq. [2]

[2] $a_1 = \gamma_1 N_1$

where N_1 is the mole fraction of component 1 in the liquid state. Since N_1 is very different in the two congruent layers, the activity coefficients of the same component are very different.

Experimental

For the investigation of equilibrium layers, a mixture of composition such as would give roughly equal volumes of each layer was stirred for 24 h at 25°C; samples of each (homogeneous) layer were then removed by suction.

Total vapour pressure was determined with a closed manometer and vapour composition by the air saturation method (error ±0.1 Torr). The latter method is not good for the determination of total vapour pressure because of the difficulty of ensuring complete saturation of the air and of knowing the exact volume of air (or nitrogen) passed through. The method, however, is very good for the determination of vapour composition, where it is not necessary to know the volume of gas passed through. The method has been frequently described by the author and by others (3). In this investigation, a presaturator at 30°C preceded the saturator at 25°C. The vapour was condensed in absorption tubes immersed in liquid nitrogen and analysed for triethylamine by conductimetric titration with standard hydrochloric acid. This figure, together with a determination of density, gave the total composition. The error in this analysis is ±1% of total content.

Densities were determined with large (50 cm^3) pyknometers and dielectric constants with a Sargent oscillometer. The error in density is not more than ±0.001 and in dielectric constant 0.1 unit.

Surface tension was determined at 16°C, a temperature at which all compositions of the triethylamine–water system are homogeneous. As the temperature of tap-water in Winnipeg in the winter is never above 10°C, it was easy to maintain a thermostat at 16°C by using a mercury–toluene regulator connected to a pumping system, so that the pump was activated whenever the temperature rose above 16°C. The capillary rise method, in the form of the two capillary method of Sugden (4), was used. The radii of cross-section of the capillaries were 9.800×10^{-3} cm and 2.260×10^{-2} cm respectively. With such fine capillaries, the capillary rise for water was 8.34 cm. Error of measurement equals ±0.01 cm.

Results

Vapour pressures, partial pressures, activities, and activity coefficients of TriE, MEK, H_2O are given in Table 1. Table 2 lists the dielectric constants, densities, refractive indices, distortion and orientation polarisations for the triethylamine–water system at 16°C. These results are shown graphically in Figs. 1 and 2.

The results of Campbell and Lam (5) show a pronounced viscosity maximum over the miscibility gap.

The surface tension of the triethylamine–water mixtures at 16°C is shown in Table 3.

In a recent investigation (1), the author studied

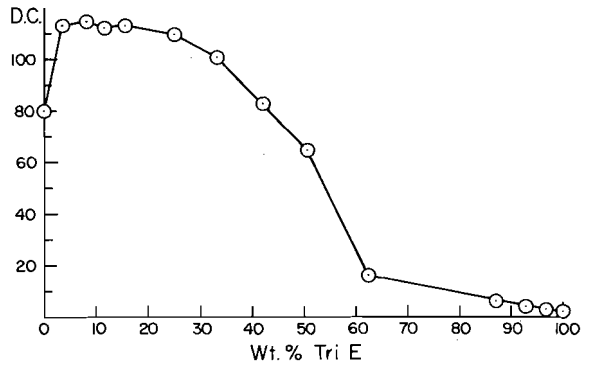

FIG. 1. Dielectric constant vs. wt.% triethylamine.

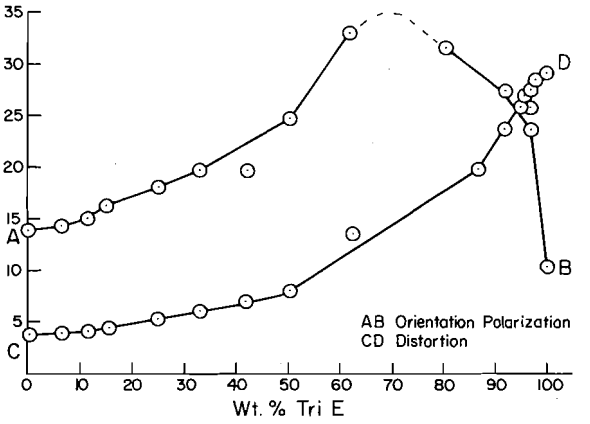

FIG. 2. Distortion and orientation polarisation vs. wt.% triethylamine.

the equilibrium conditions in the system triethylamine–methylethylketone–water and showed that at 25°C, there are two areas of heterogeneity: one, the larger, based on two layers containing water and triethylamine only. With addition of methylethylketone the area shrinks, giving rise to an isothermal critical composition (plait point). By analogy with the work just described on the triethylamine–water system it would seem that a series of compositions, tangential to the three-component system, should also show constant surface tension and constant composition of surface layer. Accordingly, eight mixtures were made up, lying on a straight line (in the triangular diagram) running from 12 wt.% methylethylketone – 88% water, to the point 37% triethylamine – 63% methylethylketone. The densities and surface tensions are given in Table 4.

Discussion

The densities, though crude, are sufficient to allow the showing of the trend in molar volume as shown in Fig. 3. In the system triethylamine–wa-

Can. J. Chem. Downloaded from www.nrcresearchpress.com by 210.87.254.40 on 09/05/12
For personal use only.

TABLE 1

(*A*) Vapour pressures

Compound	Vapour pressure (Torr)
Triethylamine	72.5
Methylethylketone	89.30
Water	23.76

(*B*) Partial pressures, activities, and activity coefficients

(*a*) Results of expt. 1, total vapour pressure = 94.75 Torr

Parameter	Value		
	TriE	MEK	H_2O
Composition in wt.%			
Lower layer	4.025	25.7	70.28
Vapour from lower layer	12.6	77.57	9.83
Upper layer	11.90	68.1	20.0
Vapour from upper layer	9.243	82.76	8.0
Mean vapour composition	10.92	80.17	8.90
Partial pressure (Torr)	5.69	61.45	27.34
Activities	0.082	0.6853	1.190
Activity coefficient			
Lower layer	8.864	1.113	1.311
Upper layer	1.515	8.269	1.311

(*b*) Results of expt. 2, total vapour pressure = 92.4 Torr

Parameter	Value		
	TriE	MEK	H_2O
Composition in wt.%			
Lower layer	8.948	14.6	77.05
Upper layer	30.60	28.4	41.0
Vapour	45.64	39.36	15.0
Partial pressure	22.77	27.55	42.07
Activities	0.3141	0.3085	1.771
Activity coefficients			
Lower layer	16.20	7.254	1.888
Upper layer	3.088	2.330	2.312

(*c*) Results of expt. 3, total vapour pressure = 84.3 Torr

Parameter	Vapour		
	TriE	MEK	H_2O
Composition in wt.%			
Lower layer	7.436	—	92.564
Upper layer	51.04	10.00	38.96
Vapour	57.70	36.8	5.5
Partial pressure	34.68	30.84	18.59
Activities	0.4897	0.3696	0.8013
Activity coefficient			
Lower layer	29.20	—	0.2237
Upper layer	2.296	7.455	0.2861

TABLE 1 (*Concluded*)

(*d*) Summary of activity coefficients

Expt.	Lower layer			Upper layer		
	TriE	MEK	H_2O	TriE	MEK	H_2O
1	8.864	1.113	1.311	1.515	1.577	2.328
2	16.20	7.254	1.888	3.088	2.330	2.312
3	29.20	—	0.2237	2.296	7.455	0.2861

(*e*) Ratio of activity coefficients in equilibrium layers: lower layer/upper layer

Expt.	Ratio		
	TriE	MEK	H_2O
1	5.851	0.7058	0.5631
2	5.246	3.113	0.8167
3	12.72	—	0.7819

ter, the molar volume increases slowly and uniformly up to 60 wt.% triethylamine, but after this concentration, it increases much more rapidly to the value for pure triethylamine. This indicates that in solutions containing less than 60 wt.% (0.21 mole fraction triethylamine), the triethylamine is bound in some way to the water: further increases in triethylamine content leave the triethylamine more or less free to exhibit its own large molar volume. The viscosity results can be explained in the same way.

That the activity coefficients of triethylamine and of methylethylketone should be greater than unity is not surprising. That they should be so much greater than unity is not unknown. The activity coefficients of water are much smaller. The ratio of the activity coefficients of the same substance in the two layers is not constant, nor is there any reason why it should be. The deduction from the above that all the components of the homogeneous phases, when two liquid layers are found, are markedly non-ideal is to be expected.

In the binary system triethylamine–water, when dielectric constant is plotted against triethylamine content, it appears that the dielectric constant rises slowly up to 5% triethylamine, though there may be some doubt as to this because of the not inappreciable electric conductance of these weak solutions. After this apparent maximum, however, the dielectric constant falls rapidly up to 60 wt.% triethylamine (the same concentration as for molar volume) after which it decreases slowly and regularly to that of pure triethylamine. Much the same behaviour is shown by the distortion polarisation (obtained from the refractive index) and the orien-

Can. J. Chem. Downloaded from www.nrcresearchpress.com by 210.87.254.40 on 09/05/12
For personal use only.

TABLE 2. Dielectric constants, densities, refractive indices, distortion and orientation polarisations for the triethylamine–water system at 16°C

Composition								
In wt.%		In mole fraction						
TriE	H_2O	TriE	H_2O	Density	Refractive index	Dielectric constant	Distortion polarisation	Orientation polarisation
100	—	1.00	—	0.7255	1.4020	2.42	33.98	10.84
—	100	—	1.00	0.9982	1.3330	80.37	3.712	14.12
3.767	96.26	0.007257	0.9928	0.9894	1.3367	113.5*	3.910	14.42
7.956	92.04	0.01516	0.9848	0.9847	1.3442	115*	4.150	14.93
11.75	88.25	0.0293	0.9707	0.9820	1.3486	113*	4.201	15.39
15.71	84.29	0.03489	0.9654	0.9701	1.3522	113*	4.664	16.33
25.01	74.99	0.05606	0.9440	0.9488	1.3550	110.5*	5.228	18.12
32.94	67.06	0.0804	0.9196	0.9314	1.3700	101*	5.996	19.74
42.08	57.92	0.1144	0.8855	0.9120	1.3856	83	7.081	19.57
50.32	49.68	0.1527	0.8473	0.8874	1.3856	65	8.120	24.93
62.74	37.26	0.2305	0.7695	0.8245	1.4035	16	13.66	32.94
86.97	13.03	0.5430	0.4573	0.7805	1.4048	6.2	19.83	31.50
92.63	7.393	0.6903	0.3097	0.7652	1.4048	4.3	24.15	27.48
95.88	4.116	0.8058	0.1944	0.7511	1.4040	3.7	27.68	25.94
97.01	2.994	0.8522	0.1478	0.7450	1.4028	3.4	29.10	23.92
98.34	1.659	0.9134	0.08913	0.7410	1.4020	3.24	30.91	23.34

*It may be that the apparent high dielectric constant is due to conductance but the work of Campbell and Lam (5) indicates a specific conductance for this solution of about 1.144×10^{-3} mhos cm^{-1} with $\alpha = 2.8\%$.

TABLE 3. Surface tension of triethylamine–water mixtures at 16°C

Wt.% TriE	Surface tension (dyn/cm)
100.00	28.05
8.864	26.74
16.62	21.00
25.05	21.27
33.55	20.63
43.48	21.17
52.69	22.70
66.25	21.02
74.40	21.88
84.14	21.24
92.93	20.77
00.00	73.49 (lit.)

TABLE 4. Density and surface tension of the MEK–H_2O–TriE system

Composition in wt.%				
MEK	H_2O	TriE	Density	Surface tension (dyn/cm)
100	—	—	0.8096	24.49
12.48	87.52	—	0.9860	37.52
21.90	69.97	8.115	0.9569	29.63
16.90	78.80	4.30	0.9730	28.52
29.39	57.65	12.96	0.9310	26.07
37.51	44.60	17.89	0.9024	24.68
44.22	33.35	22.43	0.8774	25.47
50.14	22.36	27.5	0.8495	24.59
61.00	6.327	32.67	0.8049	23.79
68.42	—	31.58	0.7826	22.75

tation polarisation (from the dielectric constant and the distortion polarisation) (Fig. 2). Up to 50 wt.% triethylamine, both distortion and orientation polarisation increase slowly and regularly, but after this concentration, the rate of increase is much greater, leading, for the orientation polarisation, to a maximum at 70 wt.%.

If the (unlikely) assumption is made that water is acting merely as a diluent, and preserves its molar polarisation of 14.12, it is possible to calculate the molar polarisation of the triethylamine in solution. For example, a solution containing 74.14 wt.% triethylamine (mole fraction = 0.3378) has an experimental molar polarisation of 32.94.

$$32.94 = 0.3378x + (0.6625)(14.12)$$

$$x = 69.70$$

When this is done, however, and the results plotted, they appear very irregular: no obvious meaning can be attached to the curve.

When the surface tension results for the binary system are plotted (Fig. 4), it appears that the surface tension drops rapidly from that of water to a value of 21.30, which is below that of pure triethylamine, constant within the limits of experimental error. This value is reached with an addition of 16 wt.% triethylamine and continues constant up to 93% triethylamine: these are roughly the limits of the miscibility gap. In terms of the Gibbs adsorption theorem, this means that a surface layer of constant composition is formed by all mixtures lying within the gap. Since a rise in temperature of

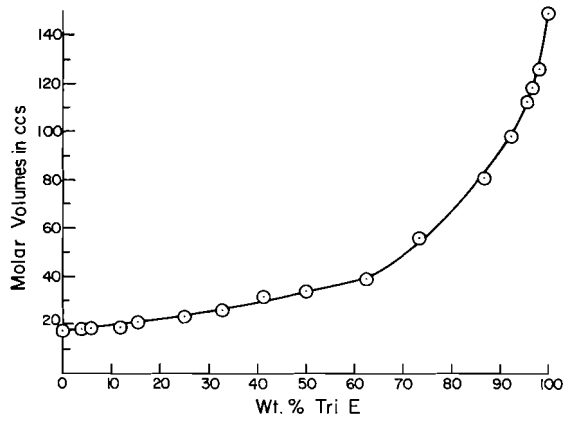

FIG. 3. Molar volume vs. wt.% triethylamine.

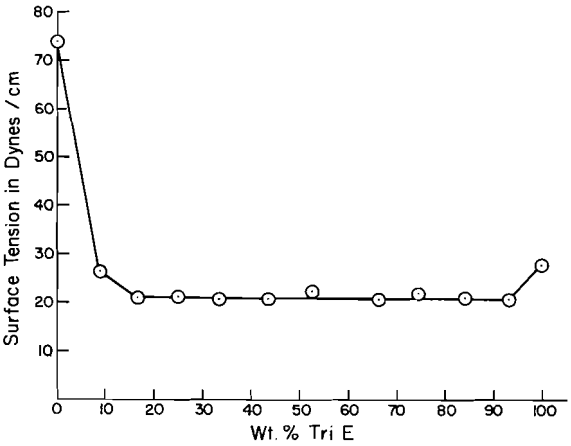

FIG. 4. Surface tension vs. wt.% triethylamine.

two or three degrees causes the mixtures to separate into two layers, it would seem that the surface layer becomes unstable and separates into two phases, only to be immediately reformed from the body of the liquid. The constancy of composition of the surface layer could easily be proved experimentally by means of a surface balance, but this seems unnecessary in view of the validity of the Gibbs theorem.

For the surface tension experiments on the three-component system, it is apparent that constancy cannot be claimed and indeed it should not be expected. The minimum on the temperature composition curve for the two-component system is very flat so that the tangential line is never very far from the heterogeneous region. The corresponding curve for the three-component system, however, shows high curvature, so that some compositions on the tangential line are far removed from heterogeneity. If the surface tension figures are plotted against triethylamine content, it appears that the surface tension drops from 36.52 dyn/cm at 12.48 wt.% MEK, 87.52% H_2O, to 27.07 dyn/cm at 20.39% MEK and 12.96% TriE, from which point the surface tension varies between 26 and 22 dyn/cm up to the binary system MEK–TriE. Probably if the mixtures had been chosen not on a straight line but so as to run parallel to the boundary of heterogeneity, a closer approach to constancy would have been found.

1. A. N. CAMPBELL. Can. J. Chem. **58**, 846 (1980).
2. A. N. CAMPBELL and O. N. BHATNAGAR. Can. J. Chem. **57**, 2542 (1979).
3. A. N. CAMPBELL, E. M. KARTZMARK, and S. C. ANAND. Can. J. Chem. **49**, 2184 (1971); F. R. V. BICHOWSKY and H. V. STORCH. J. Am. Chem. Soc. **37**, 2696 (1915).
4. S. SUGDEN. J. Chem. Soc. **119**, 1483 (1921).
5. A. N. CAMPBELL and S.-Y. LAM. Can. J. Chem. **51**, 551 (1973).
6. A. N. CAMPBELL and S.-Y. LAM. Can. J. Chem. **51**, 4005 (1973).

Can. J. Chem. Downloaded from www.nrcresearchpress.com by 210.87.254.40 on 09/05/12
For personal use only.

The outer-sphere oxidation of ascorbic acid by the thioureapentacyanoferrate(III) ion

DONAL H. MACARTNEY AND ALEXANDER MCAULEY[1]

The Department of Chemistry, University of Victoria, Victoria, B.C., Canada V8W 2Y2

Received July 25, 1980

DONAL H. MACARTNEY and ALEXANDER MCAULEY. Can. J. Chem. **59**, 132 (1981).

The oxidation of ascorbic acid by thioureapentacyanoferrate(III) has been investigated over the pH range 0.8–7.2 at an ionic strength of 1.0 *M* ($NaClO_4$). The variations in the rates of oxidation with hydrogen ion concentration are consistent with a reaction scheme involving three pH-related species; ascorbic acid (H_2A) ($k_1 = 0.111\ M^{-1}\ s^{-1}$, $\Delta H_1^{\ddagger} = 5.1$ kcal mol^{-1}, $\Delta S^{\ddagger} = -46$ cal deg^{-1} mol^{-1}), the ascorbic anion, (HA^-) ($k_2 = 66\ M^{-1}\ s^{-1}$, $\Delta H_2^{\ddagger} = 5.4$ kcal mol^{-1}, $\Delta S_2^{\ddagger} = -32$ cal deg^{-1} mol^{-1}) and the ascorbic dianion, (A^{2-}) ($k_3 = 8.78 \times 10^7\ M^{-1}\ s^{-1}$, $\Delta H_3^{\ddagger} = 3.1$ kcal mol^{-1}, $\Delta S_3^{\ddagger} = -12$ cal deg^{-1} mol^{-1}). The low reduction potential of $Fe(CN)_5TU^{2-}$ ($E^0 = 0.35$ V) permits the measurement of the rate of oxidation of the ascorbate dianion, not previously investigated with metal complexes. The second acid dissociation constant of ascorbic acid ($HA^- \rightleftharpoons A^{2-} + H^+$) has been measured in 1.0 *M* $NaClO_4$ over the temperature range studied. A relationship between the rate of oxidation and the reduction potentials of the ascorbic acid species is shown.

DONAL H. MACARTNEY et ALEXANDER MCAULEY. Can. J. Chem. **59**, 132 (1981).

On a étudié l'oxydation de l'acide ascorbique par le thiouréepentacyanoferrate(III) dans un intervalle de pH allant de 0,8 à 7,2 et à une force ionique de 1,0 *M* ($NaClO_4$). Les variations des vitesses d'oxydation avec la concentration en ions hydrogène sont en accord avec un processus réactionnel impliquant 3 espèces reliées au pH; l'acide ascorbique (AH_2) ($k_1 = 0{,}111\ M^{-1}\ s^{-1}$, $\Delta H_1^{\ddagger} = 5{,}1$ kcal mol^{-1}, $\Delta S^{\ddagger} = -46$ cal deg^{-1} mol^{-1}), l'anion ascorbate (AH^-) ($k_2 = 66\ M^{-1}\ s^{-1}$, $\Delta H_2^{\ddagger} = 5{,}4$ kcal mol^{-1}, $\Delta S_2^{\ddagger} = -32$ cal deg^{-1} mol^{-1}) et le dianion ascorbate (A^{2-}) ($k_3 = 8{,}78 \times 10^7\ M^{-1}\ s^{-1}$, $\Delta H_3^{\ddagger} = 3{,}1$ kcal mol^{-1}, $\Delta S_3^{\ddagger} = -12$ cal deg^{-1} mol^{-1}). Le faible potentiel de réduction du $Fe(CN)_5TU^{2-}$ ($E^0 = 0{,}35$ V) permet de mesurer la vitesse d'oxydation du dianion ascorbate dont l'oxydation par des complexes métalliques n'a pas été étudiée antérieurement. On a mesuré la deuxième constante de dissociation de l'acide ascorbique ($HA^- \rightleftharpoons A^{2-} + H^+$) dans une solution de $NaClO_4$ 1,0 *M* dans l'intervalle de température utilisée. On met en évidence une relation entre la vitesse d'oxydation et les potentiels de réduction de l'acide ascorbique et de ses deux anions.

[Traduit par le journal]

Introduction

The oxidation of ascorbic acid to dehydroascorbic acid has been investigated using a number of metal complexes as oxidizing agents (1–7). Among the various metal ions, complexes of iron(III) have frequently been used. The reactions of ascorbic acid with tris(1,10-phenanthroline)-iron(III) and its derivatives have been studied (2) with the differences in oxidation rates discussed in terms of free energy changes as related by the Marcus theory (8) to outer-sphere electron-transfer reactions.

These previous studies have involved primarily metal complexes with reduction potentials in the range 0.80–1.25 V. As a result, the rate constants for the acid-dependent pathway involving the ascorbate anion often approach the diffusion-controlled limit (3). In order to obtain the specific rates of oxidation of ascorbic acid (H_2A) and the ascorbate anion (HA^-) such kinetic studies were performed in solutions which were 0.01–1.0 *M* in acid. With thioureapentacyanoferrate(III) as the oxidizing agent the lower reduction potential (0.35 V) allows the measurement of rate constants in solutions up to pH 7. Under the latter conditions, a third species, the ascorbate dianion (A^{2-}), is involved in the reduction process. In this paper we present rate data on the various reactions, and using reduction potentials, correlate the rates of oxidation to the E^0 values for the ascorbic acid species.

Experimental Section

Reagents

Thioureapentacyanoferrate(III) solutions were prepared by adding a ten-fold excess of recrystallized thiourea (Fisher) to freshly prepared solutions of aquopentacyanoferrate(III) (1×10^{-4} *M*). Sodium pentacyanoammineferrate(II) was prepared by a standard procedure (ref. 9, p. 1511) from sodium nitroprusside, and recrystallized several times from concentrated ammonia. The pentacyanoammineferrate(III) may be formed by oxidation of the iron(II) complex with sodium nitrite (ref. 9, p. 1512). The corresponding aquo species was produced in solution by addition of NaOH (~pH 11) followed 15 min later by $HClO_4$ to ~pH 4. The concentration of $Fe(CN)_5OH_2^{2-}$ solutions was determined from absorbances in the visible spectrum (11) (λ340 nm; ε = 748 M^{-1} cm^{-1}, λ394 nm; ε = 743 M^{-1} cm^{-1}). The thiourea was then added, prior to the possible onset of any dimerization of the iron(III) species (11). Ascorbic acid (Sigma) solutions ($0.2–8.0 \times 10^{-2}$ *M*) were prepared in degassed buffered solutions just prior to their use.

Kinetic Measurements

The kinetic experiments were carried out using a stopped-flow apparatus described previously (12). Reactions were studied at temperatures between 10.4 and 32.5°C with thermostatting to ±0.05°C. The reduction of $Fe(CN)_5TU^{2-}$ was followed at 600 nm, its λ_{max} in the visible region. Perchloric acid was used to control the acidity of solutions in the 0.8–2.2 pH range, while phthalate, phosphate, or borate buffers were used

[1]To whom all correspondence should be addressed.

0008-4042/81/010132-06$01.00/0

©1981 National Research Council of Canada/Conseil national de recherches du Canada

Can. J. Chem. Downloaded from www.nrcresearchpress.com by 210.87.254.105 on 09/05/12
For personal use only.

Can. J. Chem. Downloaded from www.nrcresearchpress.com by 210.87.254.105 on 09/05/12
For personal use only.

at higher pH levels. The ionic strength was maintained at 1.0 *M* in all cases using $NaClO_4$.

All kinetic measurements were made under pseudo-first-order conditions with ascorbate acid in at least a ten-fold excess. Data obtained from oscilloscope traces of photomultiplier output were collected by a PCM-12 minicomputer. Plots of $\ln (A_t - A_\infty)$ were linear for at least 3 half-lives.

Dissociation Constants

The second acid dissociation constant of ascorbic acid was measured at four temperatures between 10 and 34°C at 1.0 *M* ($NaClO_4$) ionic strength. A Radiometer 26 instrument with a GK2311C combination electrode, calibrated (13) at several pH values, was used. The ascorbic acid solutions were prepared in degassed distilled water and nitrogen was bubbled into the thermostatted (±0.1°C) cell throughout the titrations.

Spectra

A Varion Techtron 635 spectrophotometer was employed in the measurement of the visible spectra and in the determination of the stoichiometry of the redox reaction.

Cyclic Voltammetry

The reduction potential of $Fe(CN)_5TU^{2-/3-}$ was determined by cyclic voltammetry using a Princeton Applied Research Model 173 instrument with a PAR Model 175 Universal Programmer. Platinum wire working and counter electrodes and a saturated (NaCl) calomel reference electrode were employed.

Results[2] and Discussion

The complex $Fe(CN)_5TU^{2-}$ (TU = thiourea) is formed in the substitution reaction of aquopentacyanoferrate(III) with thiourea. This species is blue in aqueous solution with a maximum absorbance in the visible region at 600 nm ($\varepsilon = 2300\ M^{-1}\ cm^{-1}$). Reduction of the iron(III) complex by ascorbic acid yields a pale yellow–green solution with a visible maximum at 406 nm ($\varepsilon = 325\ M^{-1}\ cm^{-1}$). This peak is identical to that found for $Fe(CN)_5TU^{3-}$, formed in the reaction of aquopentacyanoiron(II) with thiourea (14). The visible spectra of the thioureapentacyanoferrate(II)/(III) species are shown in Fig. 1.

The stoichiometry of the reaction was determined by spectrophotometric (600 nm) titrations of a fixed concentration of $Fe(CN)_5TU^{2-}$ with varying amounts of ascorbic acid. The oxidant:reductant ratio was found to be 2.01 ± 0.05:1. The overall reaction may be written as

$$[1] \quad 2Fe(CN)_5TU^{2-} + H_2A \rightarrow 2Fe(CN)_5TU^{3-} + A + 2H^+$$

The first acid dissociation constant, K_1, for ascorbic acid ($H_2A \rightleftharpoons HA^- + H^+$) has been measured under various conditions of ionic strength and temperature (1–4, 15–17). The values used in this work

[2]Complete set of detailed rate data is available, at a nominal charge, from the Depository of Unpublished Data, CISTI, National Research Council of Canada, Ottawa, Ont., Canada K1A 0S2.

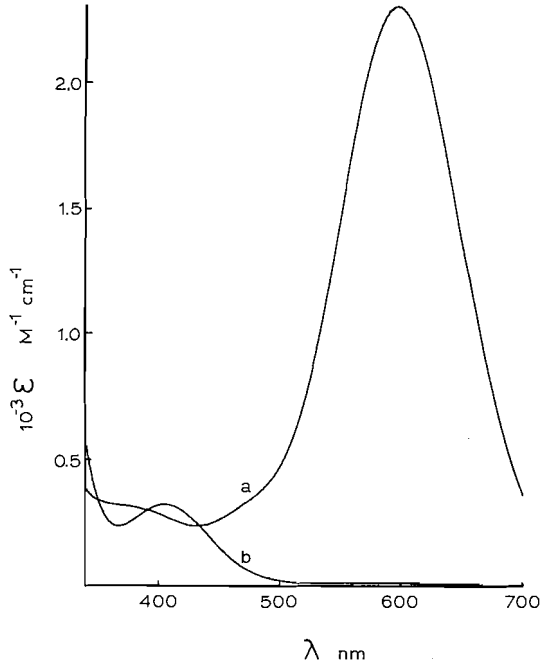

FIG. 1. Visible spectra of thioureapentacyano iron(III) and iron(II): (*a*) $Fe^{III}(CN)_5TU^{2-}$, (*b*) $Fe^{II}(CN)_5TU^{3-}$ formed upon addition of ascorbic acid.

(Table 2) are from interpolations of these literature values. The value of the second dissociation constants, K_2 ($HA^- \rightleftharpoons A^{2-} + H^+$), is less accurately known (4, 15, 16) for the temperature range and ionic strength used in this study and was therefore determined under the present conditions. At an ionic strength of 1.0 *M* ($NaClO_4$) the following values were found: at 10.0°C; $3.47 \pm 0.20 \times 10^{-12}\ M$, 16.2°C; $4.17 \pm 0.20 \times 10^{-12}\ M$, 25.4°C; $5.89 \pm 0.20 \times 10^{-12}\ M$, 34.0°C; $8.32 \pm 0.20 \times 10^{-12}\ M$.

Kinetics and Mechanism

The reaction between ascorbic acid and $Fe(CN)_5TU^{2-}$ was carried out under pseudo-first-order conditions with the reductant in excess. Plots of $\ln (A_t - A_\infty)$ against time were linear for at least three half-lives. The reaction is also first-order in ascorbic acid as shown in Fig. 2 where the rates have been measured at several acidities. The rate law may be expressed as

$$[2] \quad -d[Fe(CN)_5TU^{2-}]/dt = 2k_0[Fe(CN)_5TU^{2-}][H_2A]$$

Oxidations of ascorbic acid have been generally considered to take place in two one-electron steps with the formation of an ascorbate radical intermediate which is further oxidized to dehydroascorbic acid (A) (1–7). Previous studies (1–7) have

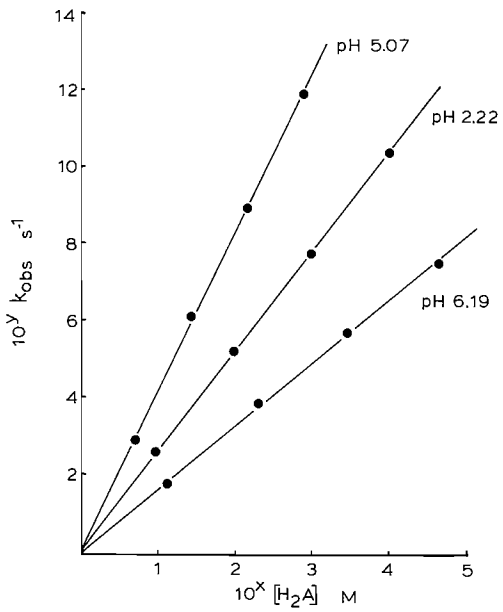

FIG. 2. Plots of k_{obs} against ascorbic acid concentration: pH 2.22; $x = 2, y = 2$, pH 5.07; $x = 3, y = 1$, pH 6.19; $x = 4, y = 1$.

demonstrated the dependence of the rate on the hydrogen ion concentration in the range $[H^+] = 0.01–1.0\ M$. This is attributed to two reacting forms of the reductant, the undissociated ascorbic acid (H_2A), and the ascorbate anion (HA^-). In the reduction of $Fe(CN)_5TU^{2-}$, where in the range pH 2–7.5 there is no change in the spectrum of the oxidant, the acid dependence continues as the acidity is decreased above pH 5. This can be attributed to a third reducing agent, the ascorbate dianion (A^{2-}).

The following reaction scheme is consistent with the data at pH 0.8–2.2:

$$[3] \quad H_2A \overset{K_1}{\rightleftharpoons} HA^- + H^+$$

$$[4] \quad HA^- \overset{K_2}{\rightleftharpoons} A^{2-} + H^+$$

$$[5] \quad Fe(CN)_5TU^{2-} + H_2A \xrightarrow{k_1} Fe(CN)_5TU^{3-} + HA^{\cdot} + H^+$$

$$[6] \quad Fe(CN)_5TU^{2-} + HA^- \xrightarrow{k_2} Fe(CN)_5TU^{3-} + A^{-\cdot} + H^+$$

$$[7] \quad HA^{\cdot} \overset{K_r}{\rightleftharpoons} A^{-\cdot} + H^+$$

Under the conditions used in this study the ascorbate intermediate is a radical anion. Only at high acid concentrations is the first pK_a of the $A^{-\cdot}$ species approached (18) ($pK_r = -0.45$).

At higher pH's (2.2–7.0) the additional reaction pathway is observed.

$$[8] \quad Fe(CN)_5TU^{2-} + A^{2-} \xrightarrow{k_3} Fe(CN)_5TU^{3-} + A^{-\cdot}$$

$$[9] \quad Fe(CN)_5TU^{2-} + A^{-\cdot} \xrightarrow{\text{fast}} Fe(CN)_5TU^{3-} + A$$

The reaction rates at various acidities at $T = 25°C$ are presented in Table 1. The observed second-order rate constant, k_0, may be expressed as:

$$[10] \quad k_0 = \frac{k_1[H^+]^2 + k_2K_1[H^+] + k_3K_1K_2}{[H^+]^2 + K_1[H^+] + K_1K_2}$$

It is of interest that over the pH range studied, k_0 increases by a factor of $> 3 \times 10^4$.

(i) $[H^+] > 0.01$ M

In this acidity range where there is no contribution from k_3 (eq. [8]), eq. [10] may be reduced to

$$[11] \quad k_0 = k_1 + k_2K_1/[H^+]$$

Treatment of the data from pH 0.8–2.2 according to eq. [11] is shown in Fig. 3 where the slope and intercept are equal to k_2K_1 and k_1 respectively. The values of k_1 and k_2 for the four temperatures studied are found in Table 2.

(ii) pH 4.8–7.2

Under these conditions the reaction pathway involving the undissociated ascorbic acid (eq. [5]) may be neglected, with the reduction of eq. [10] to the form

$$[12] \quad k_0 = k_2 + k_3K_2/[H^+]$$

Treatment of the data with eq. [12] is shown in Fig. 4, from which values of k_2 and k_3 are determined. Values of k_3 for the four temperatures are presented in Table 2. Values of k_2 determined from slopes using eq. [11] were used in calculating activation parameters. A much greater degree of uncertainty is associated with the values from the

TABLE 1. Variation of the second-order rate constant, k_0, with pH at 25.0°C, $I = 1.0\ M$ ($NaClO_4$)

pH	k_0 (M^{-1} s^{-1})	pH	k_0 (M^{-1} s^{-1})
0.82	0.172	4.14	67.5
1.27	0.238	4.74	131
1.55	0.375	4.80	136
1.84	0.570	4.88	153
1.90	0.715	4.95	194
2.10	0.990	5.37	254
2.18	1.22	5.93	574
2.22	1.30	6.12	816
3.23	12.9	6.34	1196
3.31	15.0	6.73	2930
3.44	19.8	6.90	4113
3.65	28.6	7.03	5686

Can. J. Chem. Downloaded from www.nrcresearchpress.com by 210.87.254.105 on 09/05/12
For personal use only.

Can. J. Chem. Downloaded from www.nrcresearchpress.com by 210.87.254.105 on 09/05/12
For personal use only.

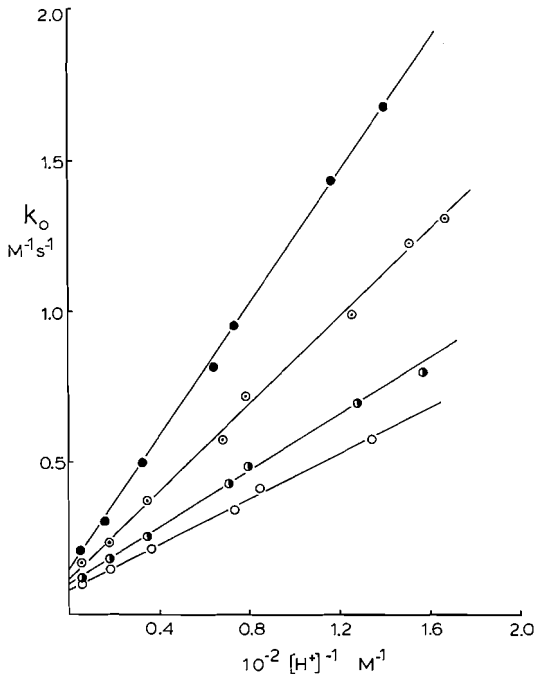

FIG. 3. Plots of second-order rate constants, k_0, against $[H^+]^{-1}$ using values from pH 0.8–2.2 according to eq. [11]. T = 10.4°C ○, 18.5°C ◑, 25.0°C ⊙, and 32.5°C ●.

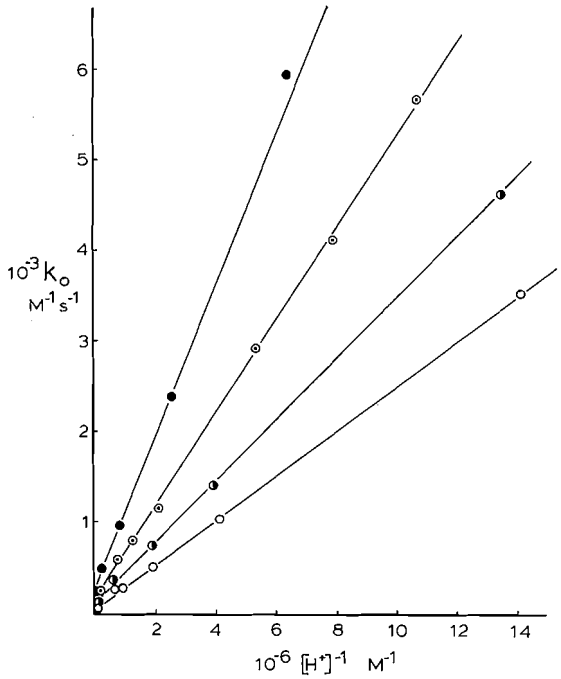

FIG. 4. Plots of second-order rate constants, k_0, against $[H^+]^{-1}$ using values from pH 4.8–7.2 according to eq. [12]. T = 10.4°C ○, 18.5°C ◑, 25.0°C ⊙, and 32.5°C ●.

TABLE 2. Specific rate and dissociation constants and activation parameters for the reduction of $Fe(CN)_5TU^{2-}$ by ascorbic acid

T (°C)	10^2k_1 (M^{-1} s^{-1})	10^5K_1 (M)	k_2 (M^{-1} s^{-1})	$10^{12}K_2$ (M)	$10^{-7}k_3$ (M^{-1} s^{-1})
10.4	7.44	8.81	39.9	3.63	6.46
18.5	9.16	9.91	47.7	4.47	7.72
25.0	11.1	10.9	66.0	5.75	8.78
32.5	13.1	12.2	84.4	7.94	10.3

$\Delta H_1^*(H_2A) = 5.1 \pm 1.0$ kcal mol^{-1}
$\Delta S_1^*(H_2A) = -46 \pm 5$ cal deg^{-1} mol^{-1}
$\Delta H_2^*(HA^-) = 5.4 \pm 0.5$ kcal mol^{-1}
$\Delta S_2^*(HA^-) = -32 \pm 2$ cal deg^{-1} mol^{-1}
$\Delta H_3^*(A^{2-}) = 3.1 \pm 0.5$ kcal mol^{-1}
$\Delta S_3^*(A^{2-}) = -12 \pm 2$ cal deg^{-1} mol^{-1}

intercepts in Fig. 4. Agreement between the two sets of data was, however, considered reasonable. For example, a slope of 66 ± 8 M^{-1} s^{-1} (Fig. 3) may be compared with the intercept 105 ± 25 M^{-1} s^{-1} (Fig. 4), T = 25°C.

From a knowledge of the specific rate constants and acid dissociation data, a pH profile may be constructed using eq. [10]. The calculated profile together with the experimental points at 25.0°C are shown in Fig. 5. Very good agreement was obtained for all four temperatures over the pH range 0.8–7.2.

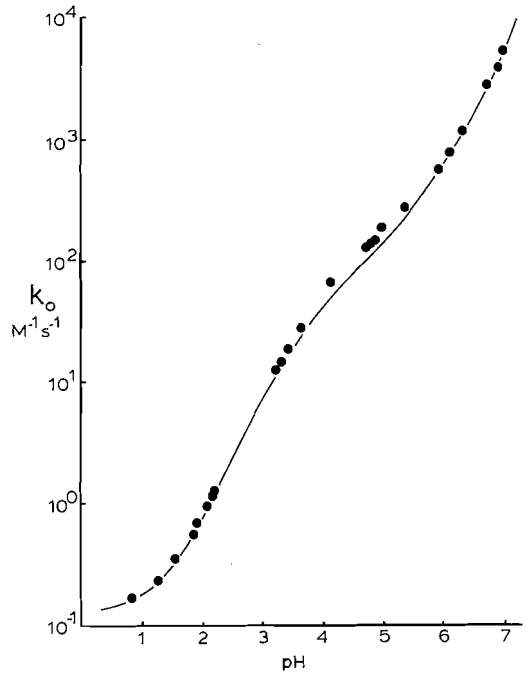

FIG. 5. pH profile of rates of oxidation of ascorbic acid by $Fe(CN)_5TU^{2-}$ at 25.0°C. The solid line is derived from eq. [10] using the values found in Table 2.

Can. J. Chem. Downloaded from www.nrcresearchpress.com by 210.87.254.105 on 09/05/12
For personal use only.

The activation parameters corresponding to the specific rate constants of the three reaction pathways are shown in Table 2. In each case $\Delta H^{\ddagger}$ has a small positive value with $\Delta S^{\ddagger}$ being large and negative. The values of $\Delta H_1^{\ddagger}$ and $\Delta S_1^{\ddagger}$ are similar to those parameters ($\Delta H^{\ddagger} = 0$–5 kcal mol^{-1} and $\Delta S^{\ddagger} = -30$ to -40 cal deg^{-1} mol^{-1}) found for other metal complexes reacting with the undissociated ascorbic acid (1–3). Similarly $\Delta H_2^{\ddagger}$ and $\Delta S_2^{\ddagger}$ fall in the range ($\Delta H^{\ddagger} = 0$–5 kcal mol^{-1} and $\Delta S^{\ddagger} = -12$ to -32 cal deg^{-1} mol^{-1}) associated with the oxidation of the ascorbate anion (1–3). The values of $\Delta H_3^{\ddagger}$ and $\Delta S_3^{\ddagger}$ are consistent with trend to a smaller $\Delta H^{\ddagger}$ and less negative $\Delta S^{\ddagger}$ on going from H_2A to HA^- to A^{2-}. The trend in $\Delta G^{\ddagger}$ values; $\Delta G_1^{\ddagger}$ (18.8 kcal mol^{-1}) > $\Delta G_2^{\ddagger}$ (14.9 kcal mol^{-1}) > $\Delta G_3^{\ddagger}$ (6.6 kcal mol^{-1}), reflects the reactivity of the three species; $k_1 < k_2 < k_3$. The ratio $k_2{:}k_1$ ($T = 25$°C) for this system is about 6×10^2, fairly close to the value of 1.25×10^3 for the hexacyanoferrate(III) system (5).

For outer-sphere electron transfer reactions a relationship between the free energy of activation, ΔG_{12}^*, and the free energy of reaction ΔG_{12}^0, has been derived by Marcus (8). This correlation may be written in the form

$$[13] \quad \Delta G_{12}^* = W_{12} + \lambda(1 + G_{12}^0/\lambda)^2/4$$

where $\lambda = 2(\Delta G_{11}^* + \Delta G_{22}^*)$ with ΔG_{11}^* and ΔG_{22}^* referring to the self-exchange reactions of the reductant and oxidant. At the ionic strength used in this study the work term, W_{12}, is small, reducing eq. [13] to the form

$$[14] \quad \Delta G_{12}^* = 0.50\Delta G_{12}^0 + \text{constant}$$

This equation is equivalent to the linear correlation of the rate of electron transfer ($\log k_0$) with the standard reduction potentials of the ascorbate species if the reactions occur via an outer-sphere mechanism. Wong and Kochi (19) have presented this relationship in the equivalent form:

$$[15] \quad \log k_0 = 8.5E^0 + \text{constant}$$

Several estimates of the reduction potentials of the ascorbic acid/ascorbate radical and ascorbic anion/ascorbate radical have been reported. The estimated potentials vary depending on the extent of protonation postulated for the radical intermediate. If it is assumed that electron transfer occurs without simultaneous proton loss then the redox couples are $H_2A^{+\cdot}/H_2A$; $E^0 \simeq 1.35$ V (1, 3) and $HA^{\cdot}/HA^-$; $E^0 \simeq 0.93$ V (2). It can also be postulated that with the large acid dissociation constants of the ascorbate radical (18), pK_{r_2} ($H_2A^{+\cdot} \rightleftharpoons HA^{\cdot} + H^+$) $\ll -2$ and pK_{r_1} ($HA^{\cdot} \rightleftharpoons A^{-\cdot} + H^+$) = -0.45, proton loss occurs simultaneously with the electron transfer yielding a common intermediate, $A^{-\cdot}$ ($HA^{\cdot}$ at very high (> 1 M) acid concentrations). On this basis, the potential $E^0(pH_i)$ (at any pH value i) can be calculated using the expression (20)

$$[16] \quad E^0(pH_i) = E^0(pH_0) + 0.059 \log \frac{K_1K_2 + K_1[H^+] + [H^+]^2}{K_r + [H^+]}$$

where $E^0(pH_0)$ has been extrapolated from data at pH's 11 and 13.5 to be 0.99 V (21). This value is lower than that derived from kinetic data at $[H^+] = 1.0$ M. Using $E^0(pH_0) = 1.33$ V (3), however, yields a value for $E^0(A^{-\cdot}/HA^-)$ of 0.87 V, closely similar to that of 0.93 V derived earlier by Pelizzetti *et al.* (2). Using eq. [16] with this higher $E^0(pH_0)$ value we have calculated the potentials for the various species over the pH range studied.

Figure 6 shows a plot of $\log k_0$ against reduction potentials derived in this manner. The correlation is linear between pH 1 and pH 6 with a slope of 8.5 ± 0.1, in agreement with the form of the Marcus relationship in eq. [15]. This indicates that the three

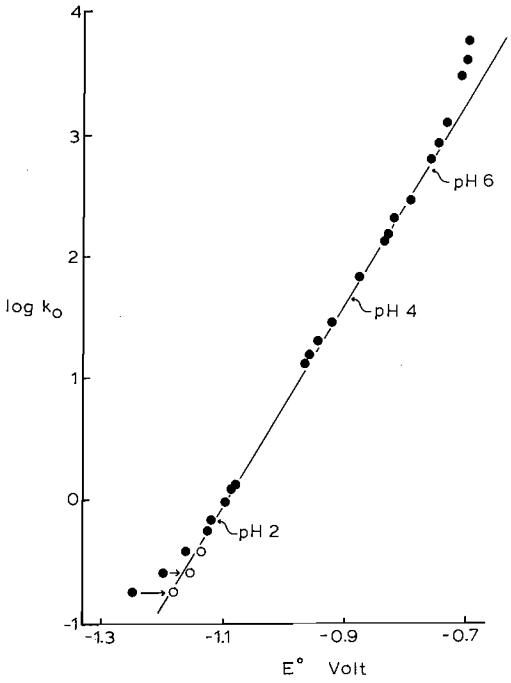

FIG. 6. Plot of $\log k_0$ against E^0, the reduction potential for the ascorbic acid/ascorbate radical couple. E^0 values are derived from eq. [16]. The unfilled circles show the corrections made for the protonation of $Fe(CN)_5TU^{2-}$ as discussed in the text.

ascorbate species, all contributing to the reaction rates in this pH range, react with thioureapentacyanoferrate(III) in an outer-sphere mechanism.

Using $E^0(pH_0) = 0.99$ V causes a shift of ~350 mV in the abscissa but produces no change in the slope of the line. There is some deviation in the fit (Fig. 6) below pH 2 and above pH 6. The derivation assumes a constant reduction potential of the Fe^{III}/Fe^{II} couple over the pH range studied. At low pH, however, there is likely to be some protonation of the iron(III) species, resulting in an increase in the potential. The following E^0 values at various acidities were measured by cyclic voltammetry: pH = 0.94, $E^0 = 0.41$ V; pH = 1.32, $E^0 = 0.39$ V; pH = 1.84, $E^0 = 0.37$ V; and pH = 5.80, $E^0 = 0.35$ V.

These potential changes suggest an estimated pK_a for $Fe(CN)_5TU^{2-}$ of ~1.8. Similar changes in E^0 with pH have been observed (22) in other $Fe(CN)_5L$ couples where L = H_2O, substituted thioureas and thioisonicotinamide. Insertion of the corrected E^0 values in Fig. 6 moves the experimental points (unfilled circles) closer to the observed line. At the higher pH's deviations may be due to the nature and concentration of added electrolytes (10) or possibly due to the uncertainty in the values chosen for $E^0(pH_0)$. Further studies in progress may help to clarify this situation.

Acknowledgements

One of us (D.H.M.) wishes to thank the University of Victoria for a Graduate Fellowship. Assistance from the Natural Sciences and Engineering Research Council of Canada is also acknowledged.

1. Z. AMJAD, J. C. BRODOVITCH, and A. McAULEY. Can. J. Chem. **55**, 3581 (1977).
2. E. PELIZZETTI, E. MENTASTI, and E. PRAMAURO. Inorg. Chem. **15**, 2898 (1976).
3. E. PELIZZETTI, E. MENTASTI, and E. PRAMAURO. Inorg. Chem. **17**, 1181 (1978).
4. M. M. TAQUI-KHAN and A. E. MARTELL. J. Am. Chem. Soc. **90**, 3386 (1968).
5. U. S. MEHROTRA, M. C. AGRAWAL, and S. P. MUSHRAW. J. Phys. Chem. **73**, 1996 (1969).
6. R. A. RICHMAN, R. L. SORENSON, K. O. WATKINS, and G. DAVIES. Inorg. Chem. **16**, 1570 (1977).
7. E. PELIZZETTI, E. MENTASTI, and E. PRAMAURO. J. Chem. Soc. Dalton Trans. 61 (1978).
8. R. A. MARCUS. J. Phys. Chem. **72**, 891 (1968).
9. G. BRAUER. Handbook of preparative inorganic chemistry. 2nd ed. Academic Press, New York. 1965.
10. A. D. PETHYBRIDGE and J. E. PRUE. Prog. Inorg. Chem. **17**, 327 (1972).
11. J. H. ESPENSON and S. G. WOLENUK. Inorg. Chem. **11**, 2034 (1972).
12. K. J. ELLIS and A. McAULEY. J. Chem. Soc. Dalton Trans. 1533 (1973).
13. A. I. VOGEL. Quantitative inorganic analysis. 3rd ed. Longmans, London. 1961. p. 1160.
14. D. H. MACARTNEY and A. McAULEY. Inorg. Chem. **18**, 2891 (1979).
15. A. E. MARTELL and R. M. SMITH. Critical stability constants. Vol. 3. Plenum Press, New York. 1977. p. 264.
16. O. WAHLBERG and P. ULMGREN. Acta Chem. Scand. **21**, 2759 (1967).
17. M. M. TAQUI-KHAN and A. E. MARTELL. J. Am. Chem. Soc. **91**, 4668 (1969).
18. G. P. LAROFF, R. W. FESSENDEN, and F. H. SCHULER. J. Am. Chem. Soc. **94**, 9062 (1972).
19. C. L. WONG and J. K. KOCHI. J. Am. Chem. Soc. **101**, 5593 (1979).
20. Y. L. ILAN, G. CZAPSKI, and D. MEISEL. Biochim. Biophys. Acta, **430**, 209 (1976).
21. E. PELIZZETTI, D. MEISEL, W. A. MULAC, and P. NETA. J. Am. Chem. Soc. **101**, 6954 (1979).
22. D. H. MACARTNEY and A. McAULEY. To be published.

Can. J. Chem. Downloaded from www.nrcresearchpress.com by 210.87.254.105 on 09/05/12
For personal use only.

Five-coordinated halogenomercurate(II) complexes: crystal structures of bis(L-tryptophanium) trichloromercurate(II) and bis(D,L-homocysteine thiolactonium) tetrabromomercurate(II)

LANGFORD BOOK, ARTHUR J. CARTY, AND CHUNG CHIEH

Guelph–Waterloo Centre for Graduate Work in Chemistry, University of Waterloo, Waterloo, Ont., Canada N2L 3G1

Received June 5, 1980

Can. J. Chem. Downloaded from www.nrcresearchpress.com by 210.87.254.40 on 09/05/12
For personal use only.

LANGFORD BOOK, ARTHUR J. CARTY, and CHUNG CHIEH. Can. J. Chem. **59**, 138 (1981).

Reactions of L-tryptophan and D,L-homocysteine with mercury(II) halides in acidic ethanol/water solutions result in the formation of bis(L-tryptophanium) trichloromercurate(II) (TPTC) and bis(D,L-homocysteine thiolactonium) tetrabromomercurate(II) (HTTB) respectively. Their crystal structures consist of halide-bridged polymeric chains of quasi HgX_3^- units. The coordination geometry around Hg(II) in both anions is distorted trigonal bipyramidal. There are no chemical bonds between the amino acid cations and the mercury(II) ions. TPTC is monoclinic, space group $P2_1$ with a = 16.688(5), b = 5.626(1), c = 14.022(5) Å, β = 108.17(3)°. The structure was solved and refined from 2433 independent counter measured reflections to an R factor of 0.062. The two independent tryptophan molecules per asymmetric unit form a single cation via a strong hydrogen bond between the carboxylate groups. Thus the compound can be represented by $MHgCl_3$ where M is the cation. One of the three Cl^- ions is strongly bonded to one Hg(II) ion and weakly bonded to two other Hg(II) ions. In addition to the three short Hg—Cl distances of 2.403(3), 2.376(4), and 2.614(4) Å, there are two long Hg—Cl bonds of 2.833(4) and 2.888(4) Å to each Hg(II), from the weakly bridged chloride ions. HTTB is orthorhombic, space group *Pnma* with a = 8.068(3), b = 24.985(7), and c = 8.828(3) Å. The structure was refined to an R value of 0.066 for 819 observed reflections ($I \geq 3\sigma(I)$), however, inclusion of unobserved reflections did not change the parameters. The homocysteine free base used in the reaction was lactonised under the experimental conditions to a thiolactonium ion. There are three relatively short Hg—Br interactions (2.566(3) twice, 2.662(4) Å) within the distorted trigonal bipyramidal stereochemistry of each mercury atom and two longer Hg—Br bonds (2.917(6) and 3.087(5) Å). The polymeric, anion chains arrange in layers on the mirror planes ($y = \pm 1/4$) with these layers sandwiched by two layers of cations.

LANGFORD BOOK, ARTHUR J. CARTY et CHUNG CHIEH. Can. J. Chem. **59**, 138 (1981).

Les réactions du L-tryptophane et de la (D,L)-homocystéine avec les halogénures de mercure(II) dans des solutions acides d'éthanol/eau conduisent respectivement à la formation du trichloromercurate(II) de bis(L-tryptophanium) (TCTP) et de tétrabromomercurate(II) de bis(D,L-homocystéine thiolactonium) (TBHT). La structure de ces cristaux consiste en des chaînes polymérisées de quasi-unités HgX_3^- avec des halogènes en position de pont. La géométrie de coordination autour du Hg(II) dans les deux anions est déformée de façon trigonale bipyramidale. Il n'y a pas de liaisons chimiques entre les cations d'acides aminés et les ions mercure(II). Le TCTP est monoclinique avec a = 16,688(5), b = 5,626(1), c = 14,022(5) Å, β = 108,17(3)° groupe d'espace $P2_1$. On a résolu la structure à partir de mesures relatives à 2433 réflexions indépendantes et on l'a affinée jusqu'à une valeur conventionnelle R de 0,062. Les deux molécules indépendantes de triptophane par unité asymétrique forment un cation simple par l'intermédiaire de fortes liaisons hydrogènes entre les groupements carboxylates. Dans ce cas, le composé peut être représenté par la formule $MHgCl_3$ où M est le cation. L'un des trois ions chlorures est fortement lié à un ion Hg(II) et faiblement lié aux deux autres ions Hg(II). De plus, aux trois courtes liaisons HgCl de 2,403(3), 2,376(4) et 2,614(4) Å s'ajoutent deux longues liaisons de 2,833(4) et 2,088(4) Å dues aux ions halogénures liés faiblement aux ions Hg(II). Le THBT est orthorombique avec a = 8,068(3), b = 24,985(7) et c = 8,828(3) Å groupe d'espace *Pnma*. On a résolu la structure et on l'a affinée jusqu'à une valeur de R de 0,066 pour 819 réflexions observées ($I > 3\sigma(I)$). Cependant l'inclusion de réflexions non observées n'affecte nullement les paramètres. Dans les conditions expérimentales utilisées, l'homocystéine sous forme de base libre se transforme en ion thiolactum. Il y a trois interactions relativement courtes Hg—Br (deux mesurant 2,566(3) et une 2,662(4) Å) à l'intérieur de la stéréochimie déformée de façon trigonale bipyramidale de chaque atome de mercure et deux longues liaisons Hg—Br de (2,917(6) et 3,087(5) Å). La chaîne polymère d'anions s'arrange en couches dans les plans d'un miroir ($y = \pm\frac{1}{4}$). Ces couches sont comprimés entre deux couches de cations.

[Traduit par le journal]

Introduction

Mercury(II) ions interact with many biological sites through coordination with deprotonated thiol, imidazole, disulfide, thioether, amino, or carboxylate groups (1). A great deal of effort has been devoted to the characterisation and quantitation of these interactions in both model systems (1) and proteins (2). For obvious reasons much less attention has been focused on another important group of ligands, the halide ions. At physiological pH halide ion does not compete favourably with thiols or imidazole for primary coordination sites on Hg^{2+}, thus mercury–halide interactions are generally of secondary importance (3) unless there is an excess of Hg^{2+} over strong binding sites available. Nevertheless, there is a great deal of evidence pointing to the significance of mercury–halide complexation in biological systems. Thus, the reactivity of calf rennin towards mercurials is strongly modified in 2 *M* NaCl (2) and the uptake of methylmercury into the bloodstream via the stomach wall is influenced by the low pH and high

0008-4042/81/010138-06$01.00/0

©1981 National Research Council of Canada/Conseil national de recherches du Canada

Can. J. Chem. Downloaded from www.nrcresearchpress.com by 210.87.254.40 on 09/05/12
For personal use only.

Cl^- concentration in this organ (4). Both neutral mercuric halides and halogeno anions have been extensively used as probes of biological activity in proteins; although displacement of halide ion or pseudohalide from the halogenomercurates(II) or pseudo-halomercurates(II) by anionic cysteine can occur as in lamprey haemoglobin (2, 5), numerous examples are known in which intact anionic mercurates interact electrostatically with the protein in a specific site. A notable illustration of the latter is the binding of HgI_3^- in myoglobin (6). The potential significance of Hg^{2+}/Cl^- binding in biological systems when covalent $HgCl_2$ is used as a reagent under acidic conditions is shown by the relatively strong Hg---Cl interactions in the model compounds $HgCl_2[SCH_2CH(NH_3)COOH]$ (3) and $Hg_2Cl_4[SCMe_2CH(NH_3)COOH]\cdot 2H_2O$ (7). For non-sulfhydryl containing proteins, there are frequently positively charged groups such as the guanidinium group of arginine and the terminal amino group of lysine. These groups are capable of interacting with mercurate anions via tight ion pair formation. While histidine imidazole will interact with mercurials via halide displacement at physiological pH, protonation at lower pH may effect a change to ionic binding between the positively charged histidine and an available anion.

As part of a more general program designed to prove certain aspects of mercury–halide binding in competition with other ligands under various conditions of salinity and pH we have investigated the reactions of two amino acids, one an important sulfhydryl containing amino acid homocysteine and the other a non-sulfhydryl molecule tryptophan with Hg^{2+}. In acidic solution protonation of the amino acids would be expected and we describe herein the synthesis and X-ray structures of two ionic complexes bis(D,L-homocysteine thiolactonium) tetrabromomercurate(II) and bis(L-tryptophanium) trichloromercurate(II) containing unusual mercury(II) anions formed under these conditions.

Experimental

Preparation of Compounds

Bis(L-tryptophanium) trichloromercurate(II) (TPTC) was prepared by mixing equal volumes of an aqueous solution of L-tryptophan (Sigma Chemical Co., St. Louis, MO) and an ethanol solution of mercury(II) chloride (BDH Chemicals, Toronto). Many attempts were made to crystallise products from solutions containing approximately 5 mmol of mercury chloride and 2.5 to 10 mmol of tryptophan. In all of the attempts, the small amounts of precipitate initially formed were removed by filtration and slow evaporation of the clear filtrates at 298 K gave bundles of very light brown but transparent crystals which were washed with a small amount of ethanol. The surface color of the dried crystals eventually turned brown on standing. *Anal.* calcd. for $C_{22}H_{25}Cl_3HgN_4O_4$: C 36.88, H 3.52, N 7.82, Cl 14.85; found: C 36.90, H 3.64, N 7.75, Cl 15.76.

Bis(D,L-homocysteine thiolactonium) tetrabromomercurate(II) (HTTB) was prepared by mixing an aqueous solution containing 4 mmol of D,L-homocysteine free base (Sigma) with an alcoholic solution containing 2 mmol of $HgBr_2$ (BDH). A large amount of white precipitate formed initially was redissolved by adding concentrated HBr thus changing the pH from ~4 to ~1. On evaporation rectangular colorless crystals were obtained. *Anal.* calcd. for $C_8H_{16}Br_4HgN_2O_2S_2$: C 12.70, H 2.13, N 3.70, Br 42.25; found: C 12.87, H 2.17, N 3.65, Br 40.82.

Elemental analyses were carried out by Galbraith Laboratories, Knoxville, TN.

X-ray Studies

Preliminary rotation, Weissenberg, and precession photographs were taken for space group determination and unit cell constant estimates. Suitable crystals were then selected for intensity measurements. The crystal sizes for TPTC and HTTB were 0.13 × 0.23 × 0.20 mm and 0.07 × 0.06 × 0.07 mm respectively, along the three crystallographic axes. These crystals were mounted on a Syntex $P2_1$ diffractomer. Unit cell parameters and orientation matrices were determined by least-squares fits of 15 low angle (10–25°) reflections for each compound. The crystal data are:

Bis(L-tryptophanium) Trichloromercurate(II)

$C_{22}H_{25}Cl_3HgN_4O_4$ fw = 716.20

Monoclinic, space group $P2_1(C_2^2$, No. 4, from systematic absences and structural analysis), $a = 16.688(5)$, $b = 5.626(1)$, $c = 14.022(5)$ Å, $\beta = 108.17(3)°$, $V = 1249.0(7)$ Å^3, $\rho_m = 1.90$ (by flotation in CCl_4/*s*-$C_2H_2Br_4$ mixtures), $Z = 2$, $\rho_c = 1.822$ (298 K; MoKα, $\lambda = 0.71069$ Å), μ(MoKα) = 66.4 cm^{-1}, $\mu R = 0.76$.

Bis(D,L-homocysteine Thiolactonium) Tetrabromomercurate(II)

$C_8H_{16}Br_4HgN_2O_2S_2$ fw = 756.58

Orthorhombic, space group *Pnma* (D_{2h}^{16}, No. 62, from systematic absences and structural analysis), $a = 8.068(3)$, $b = 24.985(7)$, $c = 8.828(3)$ Å, $V = 1780(1)$ Å^3, $\rho_m = 2.76$ (by flotation in CCl_4/*s*-$C_2H_2Br_4$ mixtures), $Z = 4$, $\rho_c = 2.822$ (298 K; MoKα, $\lambda = 0.71069$ Å), μ(MoKα) = 182.6 cm^{-1}, $\mu R = 0.64$.

All independent reflections with $2\theta \leq 50°$ were measured using the θ–2θ scan method with graphite monochromated MoKα radiation. The scan ranges were 0.8° below 2θ of MoKα_1 and above that of MoKα_2 and variable scan speeds in the range of 2–30° min^{-1} were used, to minimize counting errors for weak reflections. Background counts for half of the time used in the scan were measured at both extremes of the scan range.

Two strong reflections were repeatedly measured after every 50 reflections for monitoring purposes. No significant change in intensity with time was noted. The standard deviations, $\sigma(I)$, of intensities were calculated from counting statistics. Among 2433 reflections measured for TPTC, 2173 (89%) had $I > \sigma(I)$ and were considered observed. For HTTB, among 1614 reflections measured, 819 with $I > 3\sigma(I)$ and were considered as observed. The majority of unobserved reflections were in the reciprocal space with $2\theta > 40°$. Intensities were measured with a scintillation counter equipped with a pulse height analyzer. Lorentz-polarization corrections were applied in the derivation of structure amplitudes.

The coordinates of the mercury atoms were determined from three-dimensional Patterson maps. For TPTC, the indeterminable *y* coordinate was arbitrarily assigned a value of 1/4 and for

Can. J. Chem. Downloaded from www.nrcresearchpress.com by 210.87.254.40 on 09/05/12
For personal use only.

HTTB, the mercury atom was situated on a mirror plane. Thus for TPTC Fourier maps based on the phase calculated from the mercury atom alone contained false mirror images and care was exercised in choosing peaks for other non-hydrogen atoms corresponding to the correct configuration of the amino acids. Atomic scattering factors from the International tables for X-ray crystallography (8) with anomalous dispersion corrected for Hg and Br atoms were used. When only observed reflections were included with isotropic temperature factors for all non-hydrogen atoms, the R $(=\Sigma||F_o| - |F_c||/\Sigma|F_o|)$ factors were 0.11 and 0.15 respectively for TPTC and HTTB, from full-matrix least-squares refinements. For TPTC, further refinement with unobserved reflections included and using anisotropic temperature parameters with a weighting scheme of $w = (30 - |F_o| + 0.013 \times F_o^2)^{-1}$ gave R and R_w $(= \{\Sigma w|F_o| - |F_c|)^2/\Sigma w|F_o|^2\}^{1/2}$ of 0.062 and 0.064 respectively. This scheme gave uniform values of $(\Sigma\omega|\Delta F|)/(n - p)$ for various ranges of F_o except the unobserved reflections. When unobserved reflections were excluded, R was 0.058. The shifts of parameters were less than 0.2σ in the last cycle of refinement and the final difference Fourier map showed only ripples (1.5 e/Å^3) around the mercury atom. The atomic coordinates are given in Table 1.[1]

For HTTB, the weighting function used was $w = (80 - |F_o| + 0.0063F_o^2)^{-1}$. The final R and R_w values were both 0.14 when all reflections were included. A final difference Fourier calculated using all measured reflections showed ripples (2.4 e/Å^3) around the Hg and Br atoms. The exclusion of unobserved reflections, however, gave much more satisfactory R and R_w values of 0.066 and 0.087 respectively. The shifts of parameters in the final cycle of refinement were less than 0.2σ. Atomic parameters obtained in refinements with or without weak reflections were not significantly different. Atomic coordinates are given in Table 2.[1] Computer programs used in the reduction, solution, and refinement of X-ray data have been described elsewhere (9).

Results and Discussion

Reaction of L-tryptophan with mercuric chloride in acidic aqueous alcohol solutions gives preferentially the ionic compound bis(L-tryptophanium) trichloromercurate(II) (TPTC) even when an excess amount of mercuric chloride was used. In contrast, bis(D,L-homocysteine thiolactonium) tetrabromomercurate(II) (HTTB) was obtained only when 2 mol of amino acid per mole of mercuric salt were used. Amorphous intractable solids were obtained for 1:1 molar ratios of reactants.

Both structures contain protonated amino acid cations and polymeric chains of halogenomercurates(II); the simple, monomeric ions HgX_3^- and HgX_4^{2-} found in other systems (10) are not present in TPTC and HTTB. However, in TPTC a cation consisting of two amino acid residues linked by a strong hydrogen bond (*vide infra*) is present whereas in HTTB the charge on the tetrabromomercurate(II) is balanced by two homocysteine thiolactone cations. Thus the formation of HTTB involves the lactonisation of homocysteine free base in acid solution.

In neither complex is there any evidence for close contact between ligating atoms on the amino acids and the metal ions. The immediate stereochemistry of the mercury atoms in both TPTC and HTTB is distorted trigonal bipyramidal, with two terminal and three triply bridging chloride

TABLE 1. Atomic coordinates for TPTC

Atom	x	y	z
Hg	0.08343(4)	0.25000	0.09060(5)
Cl(1)	0.0421(2)	0.262(3)	0.2401(2)
Cl(2)	0.2084(2)	0.241(2)	0.0435(3)
Cl(3)	−0.0546(2)	0.255(2)	−0.0626(3)
O(1)	0.1202(9)	0.351(2)	0.782(1)
O(2)	0.1770(8)	0.485(3)	0.6696(8)
O(3)	0.0455(8)	0.125(3)	0.493(1)
O(4)	0.1753(9)	0.090(3)	0.602(1)
N(1)	0.4107(7)	0.293(4)	0.922(1)
N(2)	0.1562(8)	0.733(6)	0.897(1)
N(3)	0.2853(9)	0.431(4)	0.287(1)
N(4)	0.0571(7)	0.768(5)	0.3855(9)
C(1)	0.357(1)	0.418(4)	0.843(1)
C(2)	0.330(1)	0.614(3)	0.885(1)
C(3)	0.3689(8)	0.604(3)	0.989(1)
C(4)	0.3661(9)	0.741(7)	1.072(1)
C(5)	0.413(1)	0.684(3)	1.169(1)
C(6)	0.458(1)	0.468(4)	1.188(1)
C(7)	0.464(1)	0.325(3)	1.109(1)
C(8)	0.4183(8)	0.394(3)	1.011(1)
C(9)	0.2728(9)	0.806(3)	0.825(1)
C(10)	0.1773(9)	0.741(7)	0.800(1)
C(11)	0.156(1)	0.512(4)	0.750(1)
C(12)	0.233(1)	0.632(4)	0.288(1)
C(13)	0.245(1)	0.696(3)	0.383(1)
C(14)	0.3081(9)	0.532(3)	0.448(1)
C(15)	0.346(1)	0.520(4)	0.551(1)
C(16)	0.408(1)	0.341(4)	0.587(2)
C(17)	0.432(1)	0.188(4)	0.523(2)
C(18)	0.392(1)	0.196(4)	0.416(2)
C(19)	0.331(1)	0.370(3)	0.383(1)
C(20)	0.2049(9)	0.899(3)	0.422(1)
C(21)	0.1361(9)	0.826(3)	0.467(1)
C(22)	0.116(1)	0.036(3)	0.524(1)

TABLE 2. Atomic coordinates for HTTB

Atom	x	y	z
Hg	0.2437(3)	0.2500	−0.0542(2)
Br(1)	0.2899(4)	0.1504(1)	0.0028(3)
Br(2)	0.1037(5)	0.2500	−0.3273(4)
Br(3)	−0.0192(7)	0.2500	0.1726(7)
S	0.233(1)	0.0162(3)	0.533(1)
O	0.095(4)	0.0608(8)	0.298(2)
N	0.197(3)	0.1620(8)	0.376(2)
C(1)	0.189(3)	0.065(1)	0.400(3)
C(2)	0.286(4)	0.115(1)	0.438(4)
C(3)	0.322(5)	0.120(1)	0.603(3)
C(4)	0.379(4)	0.061(1)	0.647(5)

[1]Tables of observed and calculated structure factor amplitudes, of temperature factors, and of bond lengths and angles in TPTC and that of the homocysteine thiolactone molecule within HTTB are available, at a nominal charge, from the Depository of Unpublished Data, CISTI, National Research Council of Canada, Ottawa, Ont., Canada K1A 0S2.

Can. J. Chem. Downloaded from www.nrcresearchpress.com by 210.87.254.40 on 09/05/12
For personal use only.

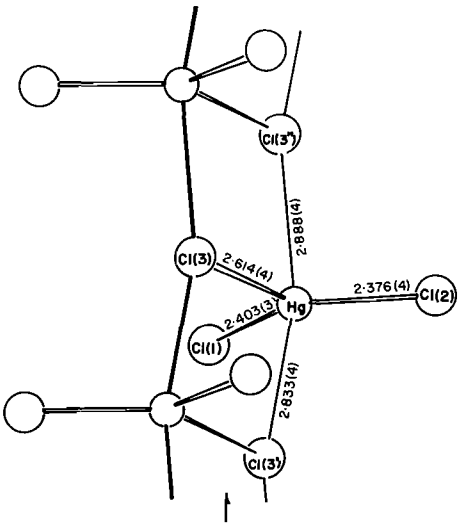

FIG. 1. Double chain of quasi $HgCl_3^-$ ions linked by bridging Cl^- ions.

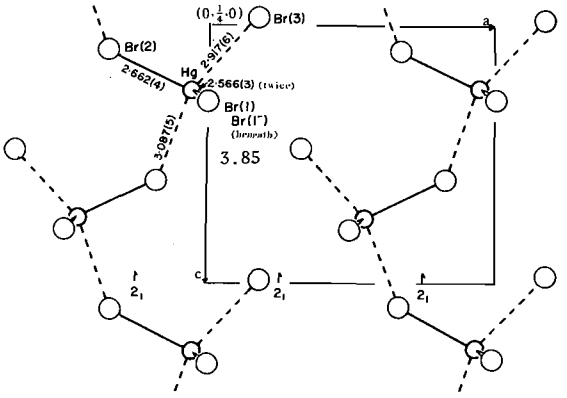

FIG. 2. The mirror plane with $y = 1/4$ containing a layer of $[HgBr_3—Br]_n$ chains.

ions in the former and three terminal and two doubly bridging bromide ions in the latter (Figs. 1 and 2).

The five Hg—Cl bonds in TPTC, all of which are at distances less than the sum of the van der Waals radii (3.3 Å), can be divided into two groups. Amongst a group of three short Hg—Cl bonds defining an approximately trigonal $HgCl_3^-$ unit are two metal interactions with terminal halide ions and a third bond to a triply bridging chloride ion (Fig. 1). Two other halide ions Cl(3″) and Cl(3′) from neighbouring units at longer distances from Hg lie above and below this trigonal plane, thus defining the vertices of an approximate trigonal bipyramid. The angle Cl(3′)—Hg—Cl(3″) is 159.1(2)° and the angles between axial and equatorial bonds are in the range 79.1–96.1° (Table 3). The triply bridging chloride ion Cl(3) links the $HgCl_3^-$ units into a

TABLE 3. Comparison of bond angles (deg) around the mercury(II) ion in TPTC and HTTB

(*i*) In TPTC[a]

Among equatorial bonds		Others	
Bonds	Angle	Bonds	Angle
Cl(1)HgCl(2)	139.3(2)	Cl(3′)HgCl(1)	93.8(2)
Cl(2)HgCl(3)	113.4(2)	Cl(3′)HgCl(2)	93.8(2)
Cl(3)HgCl(1)	107.3(2)	Cl(3′)HgCl(3)	80.1(2)
Σ	360.0	Cl(3″)HgCl(1)	90.6(2)
		Cl(3″)HgCl(2)	96.1(2)
		Cl(3″)HgCl(3)	79.1(2)
		Cl(3″)HgCl(3′)	159.2(2)

[a]Equivalent positions: prime denotes $\bar{x}$, $-0.5 + y$, $\bar{z}$; double prime denotes $\bar{x}$, $0.5 + y$, $\bar{z}$.

(*ii*) In HTTB[a]

Among equatorial bonds		Others	
Bonds	Angle	Bonds	Angle
Br(1)HgBr(1)	151.8(1)	Br(1)HgBr(2*)	86.0(1)
Br(1)HgBr(2)	103.8(1)	Br(1⁻)HgBr(2*)	86.0(1)
Br(1⁻)HgBr(2)	103.8(1)	Br(2)HgBr(2*)	95.3(1)
Σ	359.4	Br(1)HgBr(3)	88.3(1)
		Br(1⁻)HgBr(3)	88.3(1)
		Br(2)HgBr(3)	108.2(1)
		Br(2*)HgBr(3)	156.5(1)

[a]Equivalent positions; super minus denotes x, $0.5 - y$, z; asterisk denotes $0.5 + x$, $0.5 - y$, $-0.5 + z$.

double chain extending along the 2_1 screw axis as shown in Fig. 3. The average Hg—Cl bond length within the quasi $HgCl_3^-$ unit (2.464 Å) compares favourably with the average equatorial distance of 2.415 Å in $(S_4N_3)HgCl_3$ (11) which consists of a structurally similar double chain of $HgCl_3^-$ units.

The atoms Hg, Br(2), and Br(3) in HTTB lie on the mirror plane at $y = 1/4$, but Br(1) occupies a general position. As in the case of TPTC the five Hg—X distances shown in Fig. 2 can be divided into two groups, with three short and two long bonds. It is interesting that while the stoichiometry is indicative of an $HgBr_4^{2-}$ ion, polymerisation via single Br^- bridges produces a structure containing quasi $HgBr_3^-$ units linked into elongated trigonal bipyramids via long axial Hg—Br interactions. As can be seen from a comparison of angles in Tables 3 for TPTC and HTTB, the polyhedron defined by the five bromide ions coordinated to Hg in the latter is considerably more distorted than in the chloride complex. As is the case for TPTC, the symmetry responsible for generating the polymeric linkage in HTTB is a 2_1 screw axis.

Although there are two amino acid residues in TPTC only a monovalent cation is required to balance the charge on the counterion. The X-ray data did not allow the location of hydrogen atoms on the amino acids but an analysis of intermolecular dis-

tances strongly suggested that the two tryptophan moieties were linked by a strong, possibly symmetrical hydrogen bond between carboxylate entities. Thus the O(2)---O(4) distance between the two independent tryptophan molecules is only 2.41(2) Å. This value lies at the lower end of the normal range of 2.40–2.45 Å for symmetrical O---H---O hydrogen bonds (12, 13) and compares for example with the value of 2.44(2) Å for the O---O distance in $Hg(SCH_2CH(NH_3)COO)(SCH_2CH(NH_3)COOH)Cl\cdot 0.5H_2O$ (3). We suggest therefore that the cation in TPTC is as shown below:

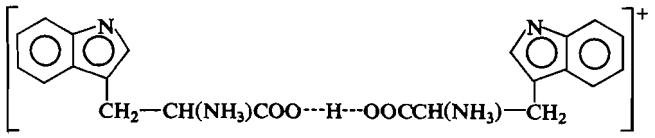

The remaining bond lengths and angles for the amino acid residues appear normal and have been deposited as supplementary data.[1] A packing diagram for TPTC is shown in Fig. 3. Tryptophan molecules can be divided into two parts: the hydrophobic ring and the hydrophilic amino-carboxylate tail. The tails arrange themselves around the double chain possibly due to N—H---Cl hydrogen bonding whereas the rings are packed back to back in the unit cell. Some of the shortest distances between the nitrogen atom of the amino group and Cl^- are: N(2)---Cl(1) (at $-x, 0.5+y, 1-z$), 3.27(1) Å; N(2)---Cl(3) (at $-x, 0.5+y, 1-z$), 3.28(1) Å; N(2)---Cl(2) (at $x, y, 1+z$), 3.39(2) Å; N(4)---Cl(1) (at $x, 1+y, z$), 3.41(2) Å. The shortest non-bonding distance between Cl^- and any oxygen atom is 3.50(2) Å.

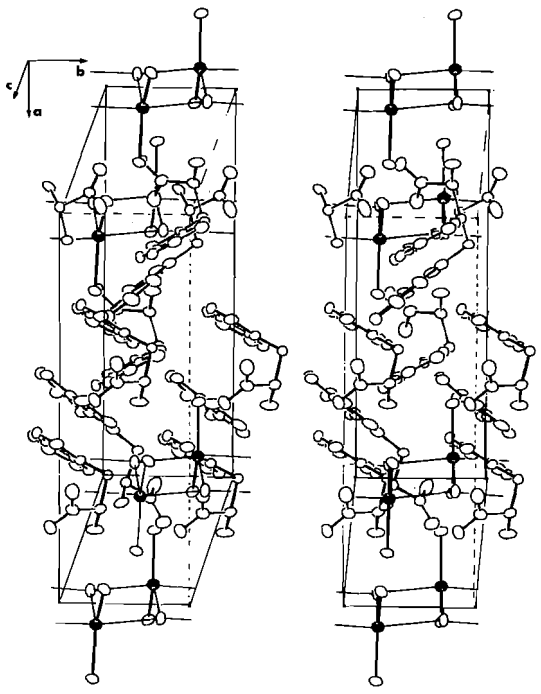

FIG. 3. Packing diagram of TPTC.

The puckered five-member ring of the thiolactonium ion in HTTB has the normal envelope conformation and the C(=O)—S bond length of 1.73(3) Å is shorter than the $C(H_2)$—S of 1.91(3) Å. The bond lengths and angles are normal[1] when compared to those in homocysteine thiolactone hydrochloride (14). The packing diagram (Fig. 4) illustrates $[Hg(Br_3)—Br]_n$ chains packed in layers on mirror planes with $y = \pm 1/4$. These layers are sandwiched between two layers, one as the mirror image of the other, of thiolactonium cations with the amino groups extended towards the bromide ions lying on the mirror planes. As a result, each nitrogen atom has five neighbouring Br^- ions within a range of 3.50 Å: N...Br(1), 3.39(2); N...Br(1) (at $0.5+x, y, 0.5+z$), 3.47(2); N...Br(2) (at $x, y, 1+z$), 3.50(2); N...Br(3), 3.33(2); N...Br(3) (at $0.5+x, 0.5-y, 0.5-z$), 3.20(2) Å. Some of these are probably due to the formation of N—H---Br hydrogen bonds. These three-layer sandwiches are stacked on top of each other alternating their orientations so that there are centers of symmetry between them.

In the two structures reported here, both Hg(II) ions have an effective coordination number of 5 with distorted trigonal bipyramidal stereochemistry. This coordination geometry is not particularly common for halogenomercurates(II), the only other examples of which we are aware being $[Me_3S][HgCl_3]$ (14), $[S_4N_3][HgCl_3]$ (11), $[Me_4N][HgBr_3]$ (15), $[Hg_3I_6(en)_2]$ (16), and $[Cr(NH_3)_6][HgCl_5]$ (17). It is interesting that the first four of these structures contain polymeric anions with axially elongated trigonal bipyramidal stereochemistry at mercury somewhat related to that in TPTC whereas $[Cr(NH_3)_6][HgCl_5]$ (17) has a more regular trigonal bipyramidal arrangement of halide ions around the metal with Hg—Cl(equatorial) of 2.640 Å and Hg—Cl(axial) of 2.518 Å. For halogenomercurates(II) of the HgX_3^- type, other com-

Can. J. Chem. Downloaded from www.nrcresearchpress.com by 210.87.254.40 on 09/05/12
For personal use only.

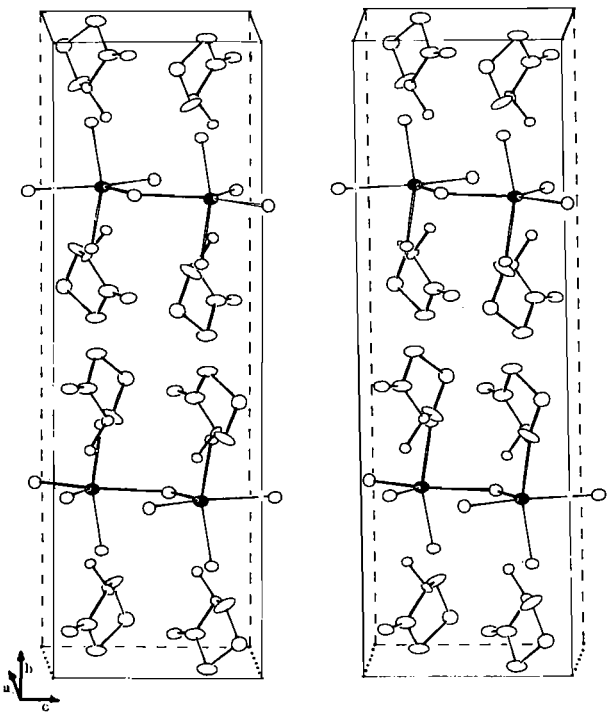

FIG. 4. Packing diagram of HTTB.

mon structures are the distorted octahedron with two long and four short bonds (18), the simple, unassociated three coordinate structure (19), and the distorted tetrahedron (20). By far the most frequently encountered structural unit in HgX_4^{2-} species is the tetrahedron (21). Clearly the structure of the ion is not necessarily indicated by the stoichiometry. In a biological sense the occurrence of structures containing polymeric $HgCl_3^-$ and $HgBr_4^{2-}$ ions, each having quasi HgX_3^- units present as structural units in conjunction with large organic cations may be significant since it suggests the possible appearance of such units in protein structures. The corresponding trigonal ion HgI_3^- has already been identified in myoglobin (6).

Acknowledgement

We are grateful to the Natural Sciences and Engineering Research Council for support of this work.

1. A. J. CARTY and S. F. MALONE. *In* the biogeochemistry of mercury in the environment. *Edited by* J. O. Nriagu. Elsevier/North Holland Biomedical Press, Amsterdam. 1979. p. 433.
2. T. L. BLUNDELL and J. A. JENKINS. Chem. Soc. Rev. 139 (1977).
3. N. J. TAYLOR and A. J. CARTY. J. Am. Chem. Soc. **99**, 6143 (1977).
4. D. L. RABENSTEIN and C. A. EVANS. Bioinorg. Chem. **8**, 115 (1978).
5. W. E. LOVE. Private communication.
6. R. H. KRETSINGER, H. C. WATSON, and J. C. KENDREW. J. Mol. Biol. **31**, 305 (1968).
7. A. J. CARTY and N. J. TAYLOR. J. Chem. Soc. Chem. Commun. 214 (1976).
8. International tables for X-ray crystallography. Vol. III. Kynock Press, Birmingham. 1968.
9. L. BOOK and C. CHIEH. Acta Crystallogr. B**36**, 300 (1980).
10. D. GRDENIC. Q. Rev. **19**, 303 (1965).
11. K. WEIDENHAMMER and M. L. ZIEGLER. Z. Anorg. Allg. Chem. **434**, 152 (1977).
12. W. H. HAMILTON and J. A. IBERS. Hydrogen bonding in solids. W. A. Benjamin, New York, NY. 1968.
13. S. N. VINOGRADOV and R. H. LINNELL. Hydrogen bonding. Van Nostrand Reinhold, New York, NY. 1971.
14. S. T. FREER and J. KRAUT. Acta Crystallogr. **19**, 992 (1965).
15. J. G. WHITE. Acta Crystallogr. **16**, 397 (1963).
16. D. GRDENIC, M. SIKIRICA, and I. VICKOVIC. Acta Crystallogr. B**33**, 1630 (1977).
17. W. CLEGG, D. A. GREENHALGH, and B. P. STRAUGHAN. J. Chem. Soc. Dalton Trans. 2591 (1975).
18. K. SAGISAWA, K. KITAHAMA, H. KIRIYAMA, and R. KIRIYAMA. Acta Crystallogr. B**30**, 1603 (1974).
19. R. H. FENN. Acta Crystallogr. **20**, 20 (1966).
20. R. MASON, G. B. ROBERTSON, and G. A. RUSHOLME. Acta Crystallogr. B**30**, 894 (1973).
21. B. KAMENAR and A. NAGL. Acta Crystallogr. B**32**, 1414 (1976).

Can. J. Chem. Downloaded from www.nrcresearchpress.com by 210.87.254.40 on 09/05/12
For personal use only.

N,O- and S,O-bonded Hg(II) complexes with S-substituted amino acids: synthesis and crystal structures of bis(*S*-methyl-L-cysteinato)mercury(II) and bis(D,L-ethioninato)-mercury(II) diperchlorate

LANGFORD BOOK, ARTHUR J. CARTY, AND CHUNG CHIEH

Guelph–Waterloo Centre for Graduate Work in Chemistry, University of Waterloo, Waterloo, Ont., Canada N2L 3G1

Received July 17, 1980

Can. J. Chem. Downloaded from www.nrcresearchpress.com by 210.87.254.5 on 09/05/12
For personal use only.

LANGFORD BOOK, ARTHUR J. CARTY, and CHUNG CHIEH. Can. J. Chem. **59**, 144 (1981).

Complexes $Hg[CH_3SCH_2CH(NH_2)COO]_2$ and $Hg[CH_3CH_2SCH_2CH_2CH(NH_3)COO]_2(ClO_4)_2$ obtained from reactions of yellow HgO with *S*-methyl-L-cysteine and ethionine respectively have been characterized by X-ray diffraction methods. The former is monoclinic, space group $P2_1$ with $a = 13.790(4)$, $b = 4.994(1)$, $c = 9.898(2)$ Å, and $\beta = 106.20(2)°$. The R and R_w factors were 0.063 and 0.075 respectively for 980 independent reflections. The *S*-methyl-L-cysteine complex is N,O bonded with two Hg—N bond lengths of 2.16(3) and 2.13(3) Å and ∠N—Hg—N=172(2)°. There are eight Hg···O distances within the range of 2.54–3.75 Å. The three shortest of these are distributed in an equatorial plane with respect to the N—Hg—N moiety. The Hg—O bond length of 2.54(2) Å is associated with the chelate ligand.

The ethionine complex is triclinic, space group $P\bar{1}$ with $a = 11.376(7)$, $b = 12.009(8)$, $c = 9.495(6)$ Å, $\alpha = 94.74(6)$, $\beta = 108.01(5)$, and $\gamma = 71.78(5)°$. The R and R_w values for all 3526 reflections were 0.083 and 0.10 respectively but R became 0.058 for only observed reflections ($I > 3\sigma(I)$). The Hg^{2+} is bonded to two sulfur, Hg—S = 2.436(5) and 2.537(4) Å, and two oxygen, Hg—O = 2.28(1) and 2.259(9) Å, atoms in a distorted tetrahedron. The Hg^{2+}–carboxylate interactions are stronger in the S-bonded than the N-bonded complex probably indicating a preference for Hg–amine coordination. At low pH when the amino group is protonated, Hg–thioether coordination becomes important for S-substituted amino acids.

LANGFORD BOOK, ARTHUR J. CARTY et CHUNG CHIEH. Can. J. Chem. **59**, 144 (1981).

On a caractérisé, par les méthodes de diffraction de rayons-X, les complexes $Hg[CH_3SCH_2CH(NH_2)COO]_2$ et $Hg[CH_3CH_2SCH_2CH_2CH(NH_3)COO]_2(ClO_4)_2$ obtenus respectivement par réaction du HgO jaune avec les *S*-méthyle L-cystéine et éthionine. Le premier est monoclinique et appartient au groupe d'espace $P2_1$ avec $a = 13,790(4)$, $b = 4,994(1)$, $c = 9,898(2)$ Å, et $\beta = 106,20(2)°$. Les facteurs R et R_w sont respectivement de 0,063 et 0,075 pour 980 réflexions indépendantes. Le complexe de *S*-méthyle L-cystéine est lié par N,O et comporte deux liaisons Hg—N de 2,16(3) et 2,13 Å et un angle ∠N—Hg—N de 172(2)°. Il y a huit distances Hg···O de l'ordre de 2,54 à 3,75 Å. Les trois distances les plus courtes sont distribuées dans un plan équatorial par rapport au fragment N—Hg—N. On attribue au ligand chélaté la liaison Hg—O de 2,54(2) Å.

Le complexe de l'éthionine est triclinique et appartient au groupe d'espace $P\bar{1}$ avec $a = 11,376(7)$, $b = 12,009(8)$, $c = 9,495(6)$ Å, $\alpha = 94,74(6)$, $\beta = 108,01(5)$, et $\gamma = 71,78(5)°$. Les valeurs de R et de R_w sont respectivement de 0,083 et 0,10 pour l'ensemble des 3526 réflexions mais la valeur de R devient égale à 0,058 pour les réflexions observées avec ($I > 3\sigma(I)$). L'ion Hg^{2+} est lié à deux atomes de soufre, Hg—S = 2,436(5) et 2,537(4) Å, et à deux atomes d'oxygène, Hg—O = 2,28(1) et 2,259(9) Å, selon un tétraèdre déformé. Les interactions Hg^{2+}–carboxylate sont plus fortes dans les complexes liés par le soufre que dans ceux liés par l'azote indiquant ainsi une préférence pour une coordination Hg–amine. Si le pH est faible, le groupe amine est protoné et la coordination Hg–thioéther devient importante pour les acides aminés ayant un substituant sur les soufre.

[Traduit par le journal]

Introduction

S-substituted amino acids have three possible binding sites towards metal ions, namely, the thioether, amino, and carboxylate groups. Towards mercuric ion (Hg^{2+}) the binding mode is pH dependent. Although early potentiometric work (1) suggested little or no involvement of thioether coordination to Hg^{2+} for methionine, ethionine, or *S*-methylcysteine, it later became apparent from ^1H (2–5) and ^{13}C nmr (4–6) studies of Hg^{2+}/methionine, ethionine, or *S*-methyl-L-cysteine solutions that under acidic conditions ($pD \leq 2$) Hg^{2+} was bound exclusively to the thioether sulfur atom.

This result thus parallels the behaviour of methionine towards CH_3Hg^+ (7). However, on raising the pH to 7.0 or above a reversal of binding site occurs; for methionine, Natusch and Porter (2) predicted N,O chelation at alkaline pH whereas in contrast the shorter alkyl chain of *S*-methyl-L-cysteine allowed S,N chelation under similar conditions (2). For isolated solids the paucity of sound structural information for methionine, ethionine, and *S*-methylcysteine complexes of Hg^{2+} gave rise to considerable speculation as to solid state structures. Livingston and Nolan (8) synthesised an ethionine complex $Hg(ethH)_2(ClO_4)_2$ from acidic solution and on the basis of ir measurements proposed a linear configuration at mercury with bonding localised at the amino group. On the other hand, the methionine derivative $Hg[CH_3SCH_2CH_2CH(NH_2)COO]_2$ prepared initially by McAuliffe *et al.* (9) and later by Birgersson, Drakenberg, and Neville (5) was formulated as an

0008-4042/81/010144-07$01.00/0

©1981 National Research Council of Canada/Conseil national de recherches du Canada

Can. J. Chem. Downloaded from www.nrcresearchpress.com by 210.87.254.5 on 09/05/12
For personal use only.

N,O chelate in the solid state by the former workers (9) and as an amine-bonded species with weaker carboxylate bonding by Sze, Davis, and Neville (10). Thus despite abundant nmr evidence for thioether bonding in acid solution, none of the available spectroscopic data for solids pointed to sulfur bonding in isolated complexes. This apparent anomaly was recently resolved by an X-ray analysis of $Hg(CH_3SCH_2CH_2CH(NH_3)COO)_2(ClO_4)_2 \cdot 2H_2O$, isolated from acid solution, which demonstrated not only strong Hg^{2+}–thioether bonding but also additional important *intermolecular* interactions to carboxylate units of neighbouring molecules (11). This result and the remaining anomalies apparent in the literature concerning the solution and solid state structures of ethionine and *S*-methylcysteine complexes of Hg^{2+} prompted us to synthesise the ethionine complex $Hg(ethH)_2(ClO_4)_2$ by the method reported by Livingstone and Nolan (8) and a halide-free *S*-methylcysteine compound $Hg(S\text{-}Me\text{-}cyst)_2$ for X-ray analysis. We report the preparation and full structural characterisation of these species in this paper.

Experimental

Preparation of Compounds

$Hg(S\text{-}Me\text{-}cyst)_2$

Yellow mercuric oxide (5 mmol) was stirred in 200 mL water and a solution of *S*-methyl-L-cysteine (10 mmol in 50 mL water) was gradually added. The yellow HgO dissolved completely within 5 min of the addition of the *S*-methyl-L-cysteine solution. The resultant colourless solution had a pH of ~6. After stirring for 10 min, a white precipitate formed. Recrystallisation from hot aqueous solution by slow cooling and evaporation gave large thin triangular or rhomboidal crystals. The crystals were fragile and generally fragmented when attempts were made to cleave them. Considerable care was exercised in choosing an unflawed crystal for X-ray analysis. The data crystal produced good quality unstreaked Weissenberg photographs. *Anal.* calcd. for $C_8H_{16}HgN_2O_4S_2$: C 20.49, H 3.44, N 5.97; found: C 20.52, H 3.48, N 5.98.

$Hg(ethH)_2(ClO_4)_2$

Yellow mercuric oxide (5 mmol) was dissolved in a solution of D,L-ethionine (10 mmol in 50 mL water) with stirring. Concentrated perchloric acid (1 mL) was added to acidify the resultant solution to a pH of 1.0. The solution was then allowed to evaporate slowly at room temperature and flattened ellipsoidal crystals were isolated. *Anal.* calcd. for $C_{12}H_{26}Cl_2HgN_2O_{12}S_2$: C 19.85, H 3.61, N 3.86; found: C 19.61, H 3.62, N 3.86.

X-ray Structural Analysis

Weissenberg and precession photographs were taken for space group and cell constant determinations. The latter were refined by least-squares methods from the angles of 15 reflections for each crystal measured on a Syntex $P2_1$ diffractometer. Crystal data and information pertaining to structural analysis are listed in Table 1.

Intensities were collected at 298 ± 1 K using graphite monochromated MoKα radiation on a Syntex $P2_1$ diffractometer employing a θ–2θ scan mode. Two standard reflections were repeatedly measured at intervals of 25 reflections to monitor the stability during data collection. Their intensities decreased by 14% at the end of data collection owing to slow decomposition of the $Hg(S\text{-}Me\text{-}cyst)_2$ crystal in the X-ray beam. This decrease was used as a base for scaling the intensities of reflections collected after the standard reflections. For $Hg(ethH)_2(ClO_4)_2$ the intensities of standard reflections fluctuated within 4% during the course of data collection. Backgrounds were measured at both extremes of the scan. Lorentz and polarization corrections were applied to the derivation of structure amplitudes.

Both structures were solved by the heavy atom method. For $Hg(S\text{-}Me\text{-}cyst)_2$, the indeterminable *y* coordinate was arbitrarily assigned a value of 1/4. There were pseudo mirror planes at $y = \pm 1/4$ on the Fourier map based on the phase of the Hg atom alone. This pseudo symmetry was removed gradually by including initially one of the S atoms, then both S atoms in the phasing process for a Fourier synthesis. The L-configuration was chosen to agree with the amino acid used. Non-hydrogen atoms were located in successive Fourier or difference Fourier maps.

Least-squares refinements were carried out when all atoms were located and anisotropic temperature parameters were introduced at appropriate stages. Atomic scattering factors with anomalous dispersion coefficients were taken from ref. 12. Computer programs utilized in the solution and refinement of X-ray data have been described elsewhere (13).

Just before the conclusion of refinement, difference Fourier maps were synthesised; these indicated that the methyl groups in both structures were disordered. Two sites were given for the carbon atom of one of the methyl groups bonded to S in $Hg(S\text{-}Me\text{-}cyst)_2$ as C(24A) and C(24B). Similarly, C(12A) and C(12B) were due to the disorder of the terminal —CH_3 in one of the ethyl groups attached to the S atom in $Hg(ethH)_2(ClO_4)_2$. The ratios of occupancy factors were 3:1 and 2:1 respectively for the cysteine and ethionine compounds. Including these atoms in the refinement gave the *R* and R_w factors in Table 1. There were no significant peaks other than those in the vicinity of the Hg atom in the final difference Fourier maps. The refinement stopped when the shifts of parameters were less than 0.25 and the final difference Fourier maps showed only ripples (max. 1.0 e $Å^{-3}$) around the Hg atoms. Atomic parameters for the two crystal structures are given in Tables 2 and 3.[1]

Results and Discussion

In $Hg(S\text{-}Me\text{-}cyst)_2$ the Hg^{2+} ion is bonded to two amino groups with Hg—N bond lengths of 2.16(3) and 2.13(3) Å at an angle of 172(1)°. Short Hg—N bonds of this length are usually associated with two-coordinate, linear mercury complexes as in $(CH_3Hg)_2$(D,L-penicillamine)$\cdot 2H_2O$ (2.13 Å) (14), CH_3Hg(L-methionine) (2.06 Å) (15), CH_3Hg(L-tyrosine)$\cdot H_2O$ (2.17 Å) (16), $(PhHg)_2$(H-creatinine)(NO_3) (2.00 and 2.06 Å) (17), $(CH_3Hg)_2$(9-Me-adenine)(ClO_4) (2.08 and 2.09 Å) (18), $(CH_3Hg)_2$(adenine)$(NO_3)\cdot 2H_2O$ (2.08 and

[1]Tables of observed and calculated structure factor amplitudes and anisotropic temperature factors are available, at a nominal charge, from the Depository of Unpublished Data, CISTI, National Research Council of Canada, Ottawa, Ont., Canada K1A 0S2.

Can. J. Chem. Downloaded from www.nrcresearchpress.com by 210.87.254.5 on 09/05/12
For personal use only.

TABLE 1. Crystal data

Compound	$Hg(S\text{-}Me\text{-}cyst)_2$	$Hg(ethH)_2(ClO_4)_2$
Formula	$C_8H_{16}HgN_2O_4S_2$	$C_{12}H_{26}Cl_2HgN_2O_{12}S_2$
fw	469.6	725.9
System	Monoclinic	Triclinic
a	13.790(4)	11.376(7)
b	4.994(1)	12.009(8)
c	9.898(2)	9.495(6)
α		94.74(6)
β	106.20(2)	108.01(5)
γ		71.78(5)
Space group	$P2_1$	$P\bar{1}$
V (Å^3)	654.6(3)	1172(1)
ρ_o (g cm^{-3})	2.378	2.02
ρ_c (g cm^{-3})	2.379	2.057
Z	2	2
μ (MoKα, cm^{-1})	121.6	70.8
μR	1.7	0.78
2θ range (deg)	≤ 45	≤ 45
Scan range		
Below MoKα_1 (deg)	0.9	1.0
Above MoKα_2 (deg)	1.3	1.0
Standard reflections	2 1 1	$\bar{1}$ $\bar{1}$ 2
	1 1 3	0 1 1
Change in I	Drop by 14%	$\pm 4\%$
Size of crystal (mm)	$0.09 \times 0.28 \times 0.17$	$0.08 \times 0.10 \times 0.22$
Number of reflections	980	3526
No. unobserved	85	1036
R (all reflections)	0.067	0.083
(observed only)	0.063	0.058
R_w (all reflections)	0.079	0.10
w^{-1}	$(150 - \lvert F_o \rvert + 0.015F_o^2)$	$(35 - \lvert F_o \rvert + 0.017F_o^2)$

TABLE 2. Fractional coordinates of non-hydrogen atoms in $Hg(S\text{-}Me\text{-}cyst)_2$

Atom	x	y	z
Hg	0.01050(8)	0.25000	0.2538(1)
S(1)	−0.3562(8)	0.026(3)	0.183(1)
S(2)	0.3597(9)	0.439(6)	0.321(2)
O(11)	−0.059(2)	0.24(1)	0.571(2)
O(12)	−0.159(2)	0.599(9)	0.535(4)
O(21)	0.063(2)	−0.007(6)	0.064(2)
O(22)	0.132(2)	0.127(6)	−0.107(2)
N(1)	−0.117(2)	0.064(7)	0.302(3)
N(2)	0.124(2)	0.481(9)	0.201(3)
C(11)	−0.126(3)	0.37(1)	0.496(4)
C(12)	−0.180(2)	0.24(2)	0.345(3)
C(13)	−0.282(3)	0.15(1)	0.358(4)
C(14)	−0.381(6)	0.33(1)	0.084(8)
C(21)	0.120(3)	0.140(9)	0.013(4)
C(22)	0.180(3)	0.350(9)	0.114(3)
C(23)	0.271(3)	0.22(2)	0.206(4)
C(24A)	0.442(6)	0.27(3)	0.428(8)
C(24B)	0.427(8)	0.50(2)	0.222(9)

2.09 Å) (18), and $Hg(1\text{-methylthymine})_2$ (2.04 Å) (19). Bonds of similar length are also found in mercuric chloride complexes of biologically important nitrogen bases such as $[HgCl_2(1\text{-Me-cytosine})]_2$ (2.17 Å) (20) and $[HgCl_2(guanosine)]$ (2.16 Å) (21) where the N—Hg—N bond system approaches linearity and other metal ligand interactions are weak. In addition to these strong Hg—N bonds, there are eight carboxylate oxygen atoms situated at distances less than 3.75 Å from the mercury atom, Table 4. Among these, three short Hg—O bonds (Hg—O(21) = 2.54(2) Å, Hg—O(12^{I}) = 2.60(4) Å, and Hg—O(22^{II}) = 2.82(3) Å) define an equatorial, trigonal plane with respect to the almost linear N—Hg—N moiety. Thus, N(1), N(2), O(21), O(12^{I}), and O(22^{II}) lie at the apices of a distorted trigonal bipyramid as shown in Fig. 1. A least-squares plane containing Hg and these three equatorial oxygen atoms has the equation $0.727X + 0.676Y - 0.121Z = 0.366$ referring to orthogonal axes X, Y, and Z. The displacements of the atoms Hg, O(21), O(12^{I}), O(22^{II}), N(1), and N(2) from this plane are −0.220, 0.040, 0.092, 0.088, −2.28, and 1.89 Å respectively. The shortest Hg—O bond length (Hg—O(21) of 2.54(2) Å) is from the same amino acid which is N-bonded to Hg^{2+}. Thus this amino acid is quite strongly N,O-chelated to the mercury atom. One of the carboxylate oxygen atoms of the other amino acid in the molecule is not coordinated since the Hg—O(11) distance (3.53(2) Å) is well outside the sum of Van der Waals radii for mercury and oxygen (~3.0 Å). Thus not only are

Can. J. Chem. Downloaded from www.nrcresearchpress.com by 210.87.254.5 on 09/05/12
For personal use only.

TABLE 3. Fractional coordinates of non-hydrogen atoms in $Hg(ethH)_2(ClO_4)_2$

Atom	x	y	z
Hg	0.02400(6)	0.30452(5)	0.18300(7)
Cl(1)	0.6687(5)	0.1193(5)	0.4514(6)
Cl(2)	0.3641(5)	0.2541(4)	−0.0579(6)
S(1)	−0.1789(4)	0.2995(4)	0.0003(5)
S(2)	−0.1188(4)	0.4721(3)	0.2001(5)
O(1)	−0.208(1)	−0.152(1)	−0.203(1)
O(2)	−0.096(1)	−0.104(1)	0.016(1)
O(3)	−0.043(1)	0.695(1)	0.573(1)
O(4)	0.017(1)	0.855(1)	0.617(1)
O(11)	0.570(2)	0.096(2)	0.489(2)
O(12)	0.783(2)	0.083(3)	0.557(3)
O(13)	0.643(4)	0.241(2)	0.449(5)
O(14)	0.686(2)	0.063(2)	0.320(2)
O(21)	0.240(2)	0.317(2)	−0.048(2)
O(22)	0.390(3)	0.142(2)	−0.061(6)
O(23)	0.449(3)	0.287(4)	0.049(4)
O(24)	0.381(4)	0.276(4)	−0.185(4)
N(1)	−0.427(2)	0.004(2)	−0.219(2)
N(2)	−0.050(1)	0.908(1)	−0.328(1)
C(1)	−0.195(1)	−0.086(1)	−0.094(2)
C(2)	−0.311(2)	0.017(2)	−0.096(2)
C(3)	−0.289(2)	0.133(2)	−0.108(2)
C(4)	−0.194(2)	0.160(2)	0.033(2)
C(5)	−0.308(2)	0.406(2)	0.049(3)
C(6)	−0.298(3)	0.407(2)	0.214(3)
C(7)	−0.022(1)	0.784(1)	0.536(2)
C(8)	−0.051(2)	0.793(1)	0.368(2)
C(9)	0.046(1)	0.696(1)	0.309(2)
C(10)	0.028(2)	0.575(1)	0.312(2)
C(11)	0.282(2)	0.411(3)	0.331(6)
C(12A)	0.367(6)	0.476(4)	0.377(8)
C(12B)	0.307(7)	0.377(7)	0.464(6)

TABLE 4. Interatomic distances (Å) and angles (deg) for $Hg(S\text{-Me-cyst})_2$*

Atom pairs	Distance (Å)	Bonds	Angle (deg)
(A) Around Hg^{2+}			
Hg—N(1)	2.16(3)	N(1)—Hg—N(2)	172(1)
Hg—N(2)	2.13(3)	N(1)—Hg—O(12^{I})	102(1)
Hg—O(12^{I})	2.60(4)	N(1)—Hg—O(21)	111(1)
Hg—O(21)	2.54(2)	N(1)—Hg···O(22^{II})	84.7(9)
Hg···O(22^{II})	2.82(3)	N(2)—Hg—O(12^{I})	84(1)
Hg···O(11^{III})	2.92(4)	N(2)—Hg—O(21)	73(1)
Hg···O(11^{I})	3.09(4)	N(2)—Hg···O(22^{II})	88(1)
Hg···O(21^{II})	3.26(2)	O(12^{I})—Hg—O(21)	97(1)
Hg···O(11)	3.53(2)	O(12^{I})—Hg···O(22^{II})	152.9(9)
Hg···O(22^{IV})	3.75(3)	O(21)—Hg···O(22^{II})	105.0(7)
(B) Ligands			
S(1)—C(14)	1.79(6)	C(14)—S(1)—C(13)	102(3)
S(1)—C(13)	1.86(4)	S(1)—C(13)—C(12)	108(2)
C(13)—C(12)	1.52(6)	C(13)—C(12)—C(11)	104(2)
C(12)—C(11)	1.61(6)	C(13)—C(12)—N(1)	121(2)
C(12)—N(1)	1.38(7)	C(11)—C(12)—N(1)	112(2)
C(11)—O(11)	1.23(6)	C(12)—C(11)—O(11)	114(3)
C(11)—O(12)	1.33(6)	C(12)—C(11)—O(12)	121(3)
S(2)—C(24A)	1.6(1)	O(11)—C(11)—O(12)	125(2)
S(2)—C(24B)	1.6(1)	C(11^{I})—O(12^{I})—Hg	103(2)
S(2)—C(23)	1.79(7)	C(24A)—S(2)—C(23)	110(5)
C(23)—C(22)	1.49(7)	C(24B)—S(2)—C(23)	98(4)
C(22)—C(21)	1.54(6)	S(2)—C(23)—C(22)	115(2)
C(22)—N(2)	1.44(5)	C(23)—C(22)—C(21)	107(3)
C(21)—O(21)	1.28(5)	C(23)—C(22)—N(2)	110(3)
C(21)—O(22)	1.25(4)	C(21)—C(22)—N(2)	114(2)
		C(22)—C(21)—O(21)	115(2)
		C(22)—C(21)—O(22)	118(2)
		O(21)—C(21)—O(22)	127(2)
		C(21)—O(21)—Hg	110(2)

*Equivalent positions: I = $-x, -1/2 + y, 1 - z$; II = $-x, 1/2 + y, -z$; III = $-x, 1/2 + y, 1 - z$; IV = $-x, -1/2 + y, -z$.

the two amino acids coordinated differently to mercury, but the presence of several additional marginal intermolecular carboxylate interactions gives rise to a rather complex coordination environment at the metal atom. Molecules of $Hg(S\text{-Me-cyst})_2$ are linked together by these intermolecular Hg^{2+}–carboxylate interactions forming polymeric chains along the 2_1 axes. Interactions between these chains are via Van der Waals forces. A packing diagram is shown in Fig. 2. It is interesting that Natusch and Porter (2) predicted an S,N bonding mode for the 1:2 Hg^{2+}/*S*-methyl-L-cysteine complex in basic solution, a result in obvious conflict with the present structural work unless there is a dramatic change in amino acid coordination to mercury on dissolution of $Hg(S\text{-Me-cyst})_2$. Although no X-ray data are yet available for the bis(methionine) complex $Hg[CH_3SCH_2CH_2CH(NH_2)COO]_2$ it is worth noting that the structural assignment for this molecule based on vibrational data (10), namely strong Hg^{2+}–amine and weaker Hg^{2+}–carboxylate bonding, compares reasonably with the structure of $Hg(S\text{-Me-cyst})_2$ prepared in the present work. From nmr measurements (2) it had been predicted that these two amino acids would bond differently to Hg^{2+} in neutral or basic solution due to the superior S,N chelating ability of *S*-methyl-L-cysteine.

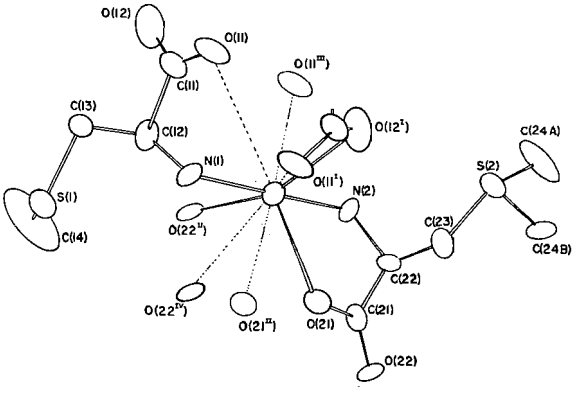

FIG. 1. Crystal structure of $Hg(S\text{-Me-cyst})_2$.

Can. J. Chem. Downloaded from www.nrcresearchpress.com by 210.87.254.5 on 09/05/12
For personal use only.

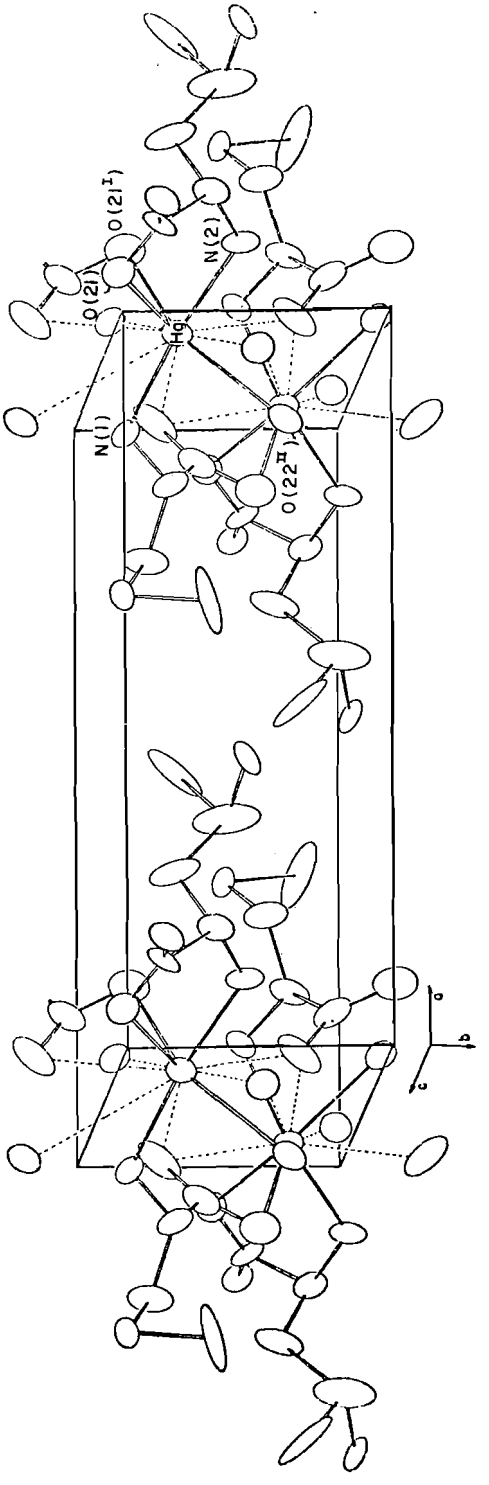

FIG. 2. Packing diagram for Hg(S-Me-cyst)$_2$.

In $Hg(ethH)_2(ClO_4)_2$ (Fig. 3) the Hg^{2+} ion is tetrahedrally bonded to two thioether sulfur and two carboxylate oxygen atoms as in the corresponding methionine complex (11). Previous conclusions regarding the aminoacid bonding in this complex (8) are thus erroneous. The principal structural features of the ethionine complex are the relatively strong Hg—S bonds of 2.436(5) and 2.537(4) Å, which are accompanied by two strong and two weak intermolecular Hg—O bonds. The two strong Hg—O bonds in $Hg(ethH)_2(ClO_4)_2$, 2.28(1) and 2.259(9) Å (and those for $Hg(methH)_2(ClO_4)_2 \cdot 2H_2O$: 2.27(1) and 2.32(1) Å (11)) are much stronger than the equatorial Hg—O bonds in Hg(S-Me-cyst)$_2$. Together with the other, weaker Hg—O interactions (3.00(1) and 3.03(1) Å) the coordination can be described as (4 + 2) to differentiate the primary coordination shell and the additional long range contacts (22). It is noteworthy that the Hg—S bond lengths in $Hg(ethH)_2(ClO_4)_2$ (ave. 2.487 Å) are significantly longer than those in the bis(cysteinato)mercury complex $Hg[SCH_2CH(NH_3)COO][SCH_2CH(NH_3)COOH]Cl \cdot 0.5H_2O$ (ave. 2.341 Å (23)) where coordination is to anionic sulfur.

Recognising that the shortest primary Hg—O contacts in Hg(S-Me-cyst)$_2$ (Hg—O(21) of 2.54(2) Å and Hg—O(12^{I}) of 2.60(4) Å) are considerably longer than the distances Hg—O(1^{I}) (2.28(1) Å) and Hg—O(3^{II}) (2.259(9) Å) in $Hg(ethH)_2(ClO_4)_2$ (Table 5) and also that the N—Hg—N angle (172(1)°) in the former is much closer to the ideal angle for digonal coordination than S(1)—Hg—S(2) of 123.2(1)° in the latter, it is tempting to suggest that amine coordination in Hg(S-Me-cyst)$_2$ is stronger than thioether bonding in $Hg(ethH)_2(ClO_4)_2$ or in $Hg(methH)_2(ClO_4)_2 \cdot 2H_2O$ (11). Greater *residual* Lewis acidity for mercury coordinated to two thioethers then promotes stronger carboxylate interactions.

Bonding sites of Hg^{2+} on S-substituted amino acids such as *S*-methylcysteine and ethionine are

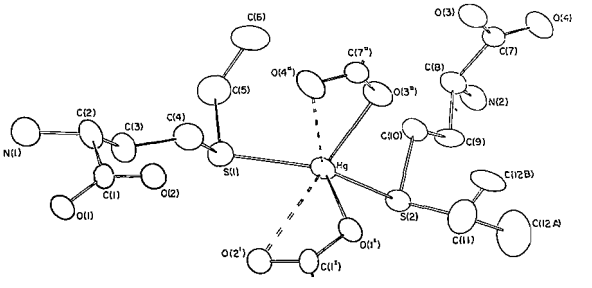

FIG. 3. Crystal structure of $Hg(ethH)_2(ClO_4)_2$.

TABLE 5. Interatomic distances (Å) and angles (deg) for $Hg(ethH)_2(ClO_4)_2$*

Atom pairs	Distance (Å)	Bonds	Angle (deg)	Bonds	Angle (deg)
(A) Around Hg^{2+}					
Hg—S(1)	2.436(5)	S(1)—Hg—S(2)	123.2(1)	S(2)—Hg···O(4^{II})	139.9(2)
Hg—S(2)	2.537(4)	S(1)—Hg—O(1^{I})	120.0(2)	O(1^{I})—Hg···O(2^{I})	47.2(3)
Hg—O(1^{I})	2.28(1)	S(1)—Hg···O(2^{I})	74.2(2)	O(1^{I})—Hg···O(3^{II})	94.5(3)
Hg···O(2^{I})	3.00(1)	S(1)—Hg—O(3^{II})	119.9(3)	O(1^{I})—Hg···O(4^{II})	81.5(3)
Hg—O(3^{II})	2.259(9)	S(1)—Hg···O(4^{II})	89.0(2)	O(2^{I})—Hg—O(3^{II})	130.2(3)
Hg···O(4^{II})	3.03(1)	S(2)—Hg—O(1^{I})	98.7(2)	O(2^{I})···Hg···O(4^{II})	91.1(2)
		S(2)—Hg···O(2^{I})	118.5(2)	O(3^{II})—Hg···O(4^{II})	46.3(3)
		S(2)—Hg—O(3^{II})	94.1(2)		
(B) Ligands					
S(1)—C(5)	1.78(2)	Hg—S(1)—C(5)	108.1(8)	C(9)—C(8)—C(7)	112.5(8)
S(1)—C(4)	1.80(2)	Hg—S(1)—C(4)	104.0(7)	C(9)—C(8)—N(2)	109.5(8)
C(5)—C(6)	1.53(4)	S(1)—C(5)—C(6)	105(1)	N(2)—C(8)—C(7)	109.8(6)
C(4)—C(3)	1.52(3)	S(1)—C(4)—C(3)	106.0(8)	C(8)—C(7)—O(3)	111.9(8)
C(3)—C(2)	1.51(3)	C(4)—C(3)—C(2)	112(1)	C(8)—C(7)—O(4)	121.3(8)
C(2)—C(1)	1.50(3)	C(3)—C(2)—C(1)	113(1)	O(3)—C(7)—O(4)	126.9(7)
C(1)—O(1)	1.25(2)	C(3)—C(2)—N(1)	111(1)	Hg—O(1^{I})—C(1^{I})	111.5(6)
C(1)—O(2)	1.25(2)	N(1)—C(2)—C(1)	110(1)	Hg···O(2^{I})—C(1^{I})	76.7(6)
C(2)—N(1)	1.51(3)	C(2)—C(1)—O(1)	115.8(9)	Hg—O(3^{II})—C(7^{II})	111.3(6)
S(2)—C(11)	1.84(4)	C(2)—C(1)—O(2)	119.6(9)	Hg···O(4^{II})—C(7^{II})	75.1(6)
S(2)—C(10)	1.84(2)	O(1)—C(1)—O(2)	124.6(7)		
C(11)—C(12A)	1.37(7)	C(4)—S(1)—C(5)	105(1)		
C(11)—C(12B)	1.28(8)	Hg—S(2)—C(11)	102(1)		
C(10)—C(9)	1.53(2)	Hg—S(2)—C(10)	100.1(5)		
C(9)—C(8)	1.54(2)	S(2)—C(11)—C(12A)	121(3)		
C(8)—C(7)	1.53(3)	S(2)—C(11)—C(12B)	126(3)		
C(7)—O(3)	1.26(2)	S(2)—C(10)—C(9)	109.9(7)		
C(7)—O(4)	1.20(2)	C(10)—S(2)—C(11)	104(1)		
C(8)—N(2)	1.47(2)	C(10)—C(9)—C(8)	112.8(9)		
(C) Perchlorate Groups					
Cl(1)—O(11)	1.39(3)	O(11)—Cl(1)—O(12)	112(2)	O(21)—Cl(2)—O(24)	112(2)
Cl(1)—O(12)	1.34(3)	O(11)—Cl(1)—O(13)	108(2)	O(22)—Cl(2)—O(23)	112(3)
Cl(1)—O(13)	1.40(2)	O(11)—Cl(1)—O(14)	112(1)	O(22)—Cl(2)—O(24)	101(3)
Cl(1)—O(14)	1.47(2)	O(12)—Cl(1)—O(13)	103(2)	O(23)—Cl(2)—O(24)	107(3)
Cl(2)—O(21)	1.41(2)	O(12)—Cl(1)—O(14)	107(2)		
Cl(2)—O(22)	1.28(2)	O(13)—Cl(1)—O(14)	115(2)		
Cl(2)—O(23)	1.30(4)	O(21)—Cl(2)—O(22)	116(2)		
Cl(2)—O(24)	1.34(4)	O(21)—Cl(2)—O(23)	108(2)		
(D) Possible Hydrogen Bonding					
O(2^{IV})···N(2)	2.84(1)	O(12^{V})···N(2)	2.93(3)	O(14^{VI})···N(2)	2.99(3)
O(11^{I})···N(1)	2.97(3)	O(14^{I})···N(1)	3.14(3)	O(22^{III})···N(1)	2.95(5)

*Equivalent positions: I = $-x, -y, -z$; II = $-x, 1-y, 1-z$; III = $-1+x, y, z$; IV = $x, 1+y, z$; V = $1-x, 1-y, 1-z$; VI = $-1+x, 1+y, z$.

pH dependent. In acid solutions, protonation of amino groups prevents their coordination to Hg^{2+} and S-coordination becomes important (2–6). Otherwise, amino-coordination is favourable and this is partly supported by the fact that the Hg—O(carboxylate) bonds are shorter in the S-bonded complex than in the N-bonded one. The strong Hg^{2+}–carboxylate interactions seen in these structures may extend beyond the solid state domain and play important roles in solution chemistry.

Finally we note that the use of HgO in reactions with amino acids has obvious significance for the synthesis of halide free mercury complexes.

Acknowledgement

This work was supported by grants from the Natural Sciences and Engineering Research Council of Canada.

1. G. R. LENZ and A. E. MARTELL. Biochemistry, **3**, 745 (1964).
2. D. F. S. NATUSCH and L. J. PORTER. J. Chem. Soc. A, 2527 (1971).
3. B. JEZOWSKA-TRZEBIATOWSKA, T. KOWALIK, and M. KOZLOWSKI. Bull. Acad. Polon. Sci. **25**, 57 (1977).

Can. J. Chem. Downloaded from www.nrcresearchpress.com by 210.87.254.5 on 09/05/12
For personal use only.

4. G. A. NEVILLE and T. DRAKENBERG. Can. J. Chem. **52**, 616 (1974).
5. B. BIRGERSSON, T. DRAKENBERG, and G. A. NEVILLE. Acta Chem. Scand. **27**, 3953 (1973).
6. R. G. KHALIFAH. Inorg. Chim. Acta, **32**, L53 (1979).
7. M. T. FAIRHURST and D. L. RABENSTEIN. Inorg. Chem. **14**, 1413 (1975).
8. S. E. LIVINGSTON and J. D. NOLAN. Inorg. Chem. **7**, 1447 (1968).
9. C. A. MCAULIFFE, J. V. QUAGLIANO, and L. M. VALLARINO. Inorg. Chem. **5**, 1996 (1966).
10. Y. K. SZE, A. R. DAVIS, and G. A. NEVILLE. Inorg. Chem. **14**, 1969 (1975).
11. A. J. CARTY and N. J. TAYLOR. J. Chem. Soc. Chem. Commun. 214 (1976).
12. International tables for X-ray crystallography. Vol. III. Kynoch Press, Birmingham. 1968. p. 202.
13. L. BOOK and C. CHIEH. Acta Crystallogr. B**36**, 300 (1980).
14. Y. S. WONG, A. J. CARTY, and C. CHIEH. J. Chem. Soc. Dalton Trans. 1801 (1977).
15. Y. S. WONG, A. J. CARTY, and C. CHIEH. J. Chem. Soc. Dalton Trans. 1157 (1977).
16. N. W. ALCOCK, P. A. LAMPE, and P. MOORE. J. Chem. Soc. Dalton Trans. 1324 (1978).
17. A. J. CANTY, M. FYFE, and B. M. GATEHOUSE. Inorg. Chem. **17**, 1467 (1978).
18. L. PRIZANT, M. J. OLIVIER, R. RIVEST, and A. L. BEAUCHAMP. J. Am. Chem. Soc. **101**, 2765 (1979).
19. L. D. KOSTURKO, C. FOLZER, and R. F. STEWART. Biochemistry, **13**, 3949 (1974).
20. M. AUTHIER-MARTIN and A. L. BEAUCHAMP. Can. J. Chem. **55**, 1213 (1977).
21. M. AUTHIER-MARTIN, J. HUBERT, R. RIVEST, and A. L. BEAUCHAMP. Acta Crystallogr. B**34**, 273 (1978).
22. D. GRDENIC. Q. Rev. **19**, 303 (1965).
23. A. J. CARTY and N. J. TAYLOR. J. Am. Chem. Soc. **99**, 6143 (1977).

Can. J. Chem. Downloaded from www.nrcresearchpress.com by 210.87.254.5 on 09/05/12
For personal use only.

Hydrogen bonding solvent effect on the basicity of primary amines CH_3NH_2, $C_2H_5NH_2$, and $CF_3CH_2NH_2$

YAN K. LAU AND P. KEBARLE

Chemistry Department, University of Alberta, Edmonton, Alta., Canada T6G 2G2

Received July 9, 1980

YAN K. LAU and P. KEBARLE. Can. J. Chem. **59**, 151 (1981).

The equilibria $RNH_3^+(H_2O)_{n-1} + H_2O = RNH_3^+(H_2O)_n$ were measured for R = CH_3, C_2H_5, and CF_3CH_2 from $n = 1$ to $n = 3$ with a pulsed electron beam high ion source pressure mass spectrometer. The proton and hydrate transfer equilibria $CH_3NH_3^+(H_2O)_n + C_2H_5NH_2 = CH_3NH_2 + C_2H_5NH_3^+(H_2O)_n$ were measured for $n = 0$ to $n = 3$. These data allow the evaluation of ΔH^0 and ΔG^0 for the reactions: $R_0NH_3^+(H_2O)_n + RNH_3^+ = R_0NH_3^+ + RNH_3^+(H_2O)_n$. $\Delta H^0 = \delta\Delta H^0_{0,n}(RNH_3^+)$, $\Delta G = \delta\Delta G^0_{0,n}(RNH_3^+)$. These data are compared with $\delta\Delta E_{0,3}$ (STO-3G) evaluated by Hehre and Taft. In general good agreement is observed at $n = 3$. The $\delta\Delta H^0_{0,3}(RNH_3^+) \approx \delta\Delta E_{0,3}(RNH_3^+)$ are also found close to the ion hydration free energy difference in aqueous solutions.

YAN K. LAU et P. KEBARLE. Can. J. Chem. **59**, 151 (1981).

Utilisant un spectromètre de masse ayant comme source d'ions à haute pression un faisceau pulsé d'électron, on a mesuré l'équilibre $RNH_3^+(H_2O)_{n-1} + H_2O = RNH_3^+(H_2O)$ où R = CH_3, C_2H_5 et CF_3CH_2 et n varie de 1 à 3. On a mesuré l'équilibre de transfert du proton et de l'hydrate: $CH_3NH_3^+(H_2O)_n + C_2H_5NH_2 = CH_3NH_2 + C_2H_5NH_3^+(H_2O)_n$ pour des valeurs de n allant de 0 à 3. Ces données permettent d'évaluer le ΔH^0 et le ΔG^0 des réactions: $R_0NH_3^+(H_2O)_n + RNH_3^+ = R_0NH_3^+ + RNH_3^+(H_2O)_n$. $\Delta H^0 = \delta\Delta H^0_{0,n}(RNH_3^+)$, $\Delta G = \delta\Delta G^0_{0,n}(RNH_3^+)$. On a comparé ces données avec la valeur de $\delta\Delta E_{0,3}$ (STO-3G) évaluée par Hehre et Taft. En général, on observe une bonne corrélation lorsque $n = 3$. On a également trouvé que les valeurs $\delta\Delta H^0_{0,3}(RNH_3^+) \approx \delta\Delta E_{0,3}(RNH_3^+)$ sont voisines de la différence d'énergie libre de l'hydratation de l'ion en solutions aqueuses.

[Traduit par le journal]

Introduction

"Understanding solvent effects" to the practicing non-specialist chemist really means having a qualitative description of the role of the solvent in terms of some easily recognizable properties of the ion and the solvent or solvent molecules. Early work on solvent effects was often based on the Born equation. The focus of such predictions was on the radius of the ion and the dielectric constant of the solvent. However, the models used were often over-simplified and at times amounted to using two variable parameters, the dielectric constant, variable because of the unknown extent of dielectric saturation, and the radius of the ion variable for reasons which become obvious when one considers the problem of describing an organic ion with charged functional group and some charge delocalization.

A continuing effort from this laboratory (1, 2) has been to try to show that some of the major features of ionic solvation in condensed media can be explained on basis of the interactions of the ion with a small number of solvent molecules. The pertinent experimental data are obtained from measurement of gas phase ion, $Ion^{\pm}$, solvent molecules, Sl, equilibria $(n - 1, n)$, as in reaction [1].

[1] $\quad Ion^{\pm}(Sl)_{n-1} + Sl = Ion^{\pm}(Sl)_n$

These provide $\Delta G^0_{n-1,n}$ and $\Delta H^0_{n-1,n}$. The key demonstration of the pertinence of the approach is given by plots of $\delta\Delta G^0_{0,n}$ (or $\delta\Delta H^0_{0,n}$) versus n, where $\Delta G^0_{0,n} = \Delta G^0_{0,1} + \Delta G^0_{1,2} + \cdots + \Delta G^0_{n-1,n}$. Consider two ions like B_0H^+ and BH^+, $\delta\Delta G^0_{0,n}$ is then given by $\delta\Delta G^0_{0,n} = \Delta G^0_{0,n}(BH^+) - \Delta G^0_{0,n}(B_0H^+)$. Plots of $\delta\Delta G^0_{0,n}$ versus n have shown, for a number of systems, that the $\delta\Delta G_{0,n}$ approaches the difference of the solvation energies of the ions in the liquid solvent already for some small n like $n =$ 5 or 6 or 7. (For examples of such plots see ref. 2 and Fig. 3 of this paper.) The success of this approach has a great attraction for the chemist since the formidable appearing problem of liquid solvent interactions is reduced to the familiar chemistry of ion–molecule, i.e. molecule–molecule interactions. An additional very important advantage is that the energetics, geometries, and even the thermodynamics (ΔH, ΔG, and ΔS) of an ion surrounded by a small number of molecules are amenable to theoretical calculations. The energetics and structures of small ion-molecule clusters — by quantum mechanical calculations (3), the energetics of large clusters — by pair potential calculations (4) and the thermodynamics with Monte Carlo calculations (4, 5). While such calculations can be executed with great computational input (large basis sets, large number of solvent molecules, periodic boundary conditions etc.) and the results can be of great significance, the effort may not be justified for a large number of different systems. Furthermore important qualitative insights may often be lost. It

0008-4042/81/010151-05$01.00/0

©1981 National Research Council of Canada/Conseil national de recherches du Canada

Can. J. Chem. Downloaded from www.nrcresearchpress.com by 210.87.254.40 on 09/05/12
For personal use only.

Can. J. Chem. Downloaded from www.nrcresearchpress.com by 210.87.254.40 on 09/05/12
For personal use only.

is therefore desirable to have also more limited but skillfully applied calculations which provide qualitative insights. One such recent approach by Taagepera, DeFrees, Hehre, and Taft (6) is based on reactions [2]–[4].

[2] $R_0NH_3^+{}_{(g)} + RNH_{2(g)} = R_0NH_{2(g)} + RNH_3^+{}_{(g)}$

[3] $R_0NH_3^+{}_{(aq)} + RNH_{2(aq)} = R_0NH_3^+{}_{(aq)} + RNH_{2(aq)}$

[4] $R_0NH_3^+(H_2O)_3 + RNH_2(H_2O)_k = R_0NH_2(H_2O)_k + RNH_3^+(H_2O)_3$

Hehre and Taft (6) represent the aqueous medium effect $\delta\Delta G^0{}_{am}(exp)$ on the proton transfer between two primary amines as the difference between the energy for the proton transfer in the gas phase, reaction [2], and proton transfer in aqueous solution, reaction [3]. The medium effect is then given by eq. [5].

[5] $\delta\Delta G^0{}_{am}(exp) = \Delta G^0{}_2 - \Delta G^0{}_3$

Aqueous proton transfer [3] is then modelled by the process [4]. The aqueous ammonium ions are represented by the trihydrates involving the three strong primary hydrogen bonds, while the aqueous bases are variously modelled as containing zero, one, or three water molecules. One obtains a theoretical aqueous medium effect $\delta\Delta E_{am}$(STO-3G) by calculating the electronic energies of the

[6] $\delta\Delta E_{am}(STO\text{-}3G) = \Delta E_2 - \Delta E_4$

molecules entering reactions [2] and [4] with the minimal basis set STO-3G method. The authors (6) were able to show for several systems that $\delta\Delta E_{am}$ is very close to $\delta\Delta G^0{}_{am}$. For example, for $R_0 = C_2H_5$ and $R = CF_3CH_2$, $\delta\Delta G^0{}_{am}(exp) = -7.7$ kcal/mol, while $\delta\Delta E_{am}(STO\text{-}3G) = -7.3$ kcal/mol (for $k = 0$). Changes of $k = 0$ to $k = 1$ (one water molecule as proton donor to the nitrogen of the free base) and to $k = 3$ (additional two molecules as proton acceptors from the NH_2 group of the free base) did not improve the agreement with $\delta\Delta G_{am}(exp)$ significantly.

Since the accuracy of the STO-3G method can be questioned even when applied to an isodesmic process like [4], we were encouraged by Professor Taft to check the data by means of ion–molecule equilibria measurements. The outcome of these measurements is described in the following sections.

Experimental

The measurements were made with one of our pulsed electron beam high ion source pressure mass spectrometers using a quadrupole mass analyzer (7).

The clustering equilibria $(n - 1, n)$ (see reaction [7] and section on Results and Discussion) were measured in the presence of very small pressures of RNH_2 in order to avoid the formation of the protonated dimers $(RNH_2)_2H^+$. Typical gas mixtures were 0.1 mTorr RNH_2, 0.02–2 Torr H_2O, third gas CH_4 at ~4 Torr. Changes of water pressures by a factor of ~5 left the equilibrium constants $K_{n-1,n}$ invariant. The reaction sequence in the above mixture is: CH_5^+, $C_2H_5^+$ from CH_4 react very rapidly with H_2O leading to $H^+(H_2O)_n$. The proton hydrates react with RNH_2 forming $RNH_3(H_2O)_n^+$. The proton hydrates disappear completely as the $n - 1, n$ equilibria of the ammonium ions become established.

The proton and hydrate transfer equilibria (see reaction [8] and section on Results and Discussion) were measured with known mixtures of the two amines CH_3NH_2 and $C_2H_5NH_2$. The ratio methyl to ethyl amine was large in order to keep the methyl and ethylammonium intensities of similar magnitude. The constancy of the equilibrium constants was checked by varying the water pressure and the neutral amine concentration ratio.

Results and Discussion

As mentioned in the Experimental part, two types of equilibria measurements were made. The first kind were clustering equilibria $(n - 1, n)$ shown in reaction [7] for $R = CH_3$, C_2H_5, and CF_3CH_2 and $n = 1, 2, 3$.

[7] $RNH_3^+(H_2O)_{n-1} + H_2O = RNH_3^+(H_2O)_n$

The van't Hoff plots for these measurements are shown in Fig. 1. The thermochemical data resulting from the plots, $\Delta H^0{}_{n-1,n}$, $\Delta G^0{}_{n-1,n}$, and $\Delta S^0{}_{n-1,n}$ are shown in Table 1. A second set of experiments involved the measurement of equilibria [8] which involve proton and hydrate transfer.

[8] $R_0NH_3^+(H_2O)_n + RNH_2 = R_0NH_2 + RNH_3^+(H_2O)_n$

The van't Hoff plots for the equilibrium constants of reaction [8] for $R_0 = CH_3$ and $R = C_2H_5$ and $n = 0$ to 3 are shown in Fig. 2. The corresponding ΔG^0, ΔH^0, and ΔS^0 values are given in Table 1. Unfortunately equilibria [8] for $R_0 = C_2H_5$ and $R = CF_3CH_2$ could not be measured directly because of the large difference between the proton affinities of ethyl and trifluoroethyl amine.

The van't Hoff plots for reaction [8], Fig. 2, illustrate in a very graphic manner the attenuating effect of the aqueous medium on the proton transfer between methyl and ethyl amine. As n is increased from 0 to 3 there is a progressive decrease of slope, i.e. decrease of the exothermicity for the enthalpy change and a progressive lowering of the respective van't Hoff lines which signals a decrease of the exothermicity for the free energy change, with water addition. The corresponding numerical changes of ΔH^0 and ΔG^0 with n, in Table 1, permit a direct comparison with the $\Delta H^0{}_{(aq)}$ and $\Delta G^0{}_{(aq)}$ for proton transfer in the liquid aqueous medium (8) also given in Table 1. Increase of n leads to a progressive approach of the gas phase results to the aqueous values. At $n = 3$ the two sets of values come to within less than 1 kcal/mol.

The Taft–Hehre (6) measure of the aqueous medium effect: $\delta\Delta E_{am}$(STO-3G) (eq. [6]) corres-

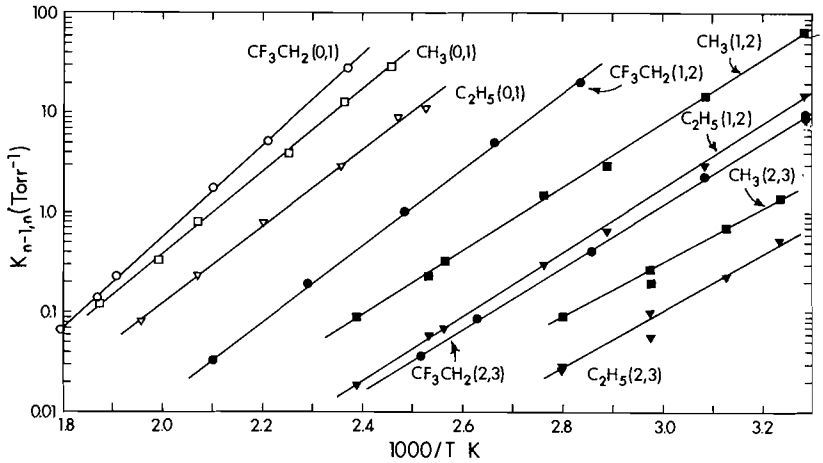

FIG. 1. van't Hoff plots of equilibrium constants $K_{n-1,n}$ for reactions $RNH_3^+(H_2O)_{n-1} + H_2O = RNH_3^+(H_2O)_n$. Numbers beside plots give value for $n-1,n$. The formulas give identity of R.

TABLE 1. Summary of thermodynamic data[a]

Hydration reactions	$n-1, n$	$-\Delta H^0$ (kcal/mol)	$-\Delta S^0$ (cal/K mol)	$-\Delta G^0_{298}$ (kcal/mol)
[1] $CF_3CH_2NH_3^+(H_2O)_{n-1} + H_2O = CF_3CH_2NH_3^+(H_2O)_n$	0,1	21.1 ± 0.2	30.0 ± 0.3	12.1 ± 0.2
	1,2	17.3 ± 0.2	29.9 ± 0.4	8.4 ± 0.2
	2,3	14.2 ± 0.1	29.2 ± 0.4	5.5 ± 0.2
[2] $CH_3NH_3^+(H_2O)_{n-1} + H_2O = CH_3NH_3^+(H_2O)_n$	0,1	18.8 ± 0.3	26.3 ± 0.7	11.0 ± 0.4
	1,2	14.6 ± 0.3	26.7 ± 0.7	6.7 ± 0.3
	2,3	12.4 ± 0.8	26.4 ± 2.3	4.5 ± 1.0
[3] $CH_3CH_2NH_3^+(H_2O)_{n-1} + H_2O = CH_3CH_2NH_3^+(H_2O)_n$	0,1	17.5 ± 0.4	25.9 ± 0.9	9.8 ± 0.5
	1,2	14.7 ± 0.2	29.7 ± 0.7	5.8 ± 0.3
	2,3	13.2 ± 1.2	30.8 ± 3.6	4.0 ± 1.6
Proton and hydrate transfer reactions	n	$-\Delta H^0$	$-\Delta S^0$	$-\Delta G^0_{298}$
$CH_3NH_3^+(H_2O)_n + C_2H_5NH_2 = CH_3NH_2 + C_2H_5NH_3^+(H_2O)_n$	0	3.4 ± 0.3	0.7 ± 0.6	3.2 ± 0.3
	0	2.9[c]		2.9[c]
	1	2.8 ± 0.3	2.3 ± 0.6	2.1 ± 0.3
	2	1.5 ± 0.7	0.1 ± 2.2	1.5 ± 1.0
	3	1.0 ± 0.4	1.0 ± 1.1	0.7 ± 0.5
$CH_3NH_3^+(aq) + C_2H_5NH_2(aq) = CH_3NH_2(aq) + C_2H_5NH_2^+(aq)$	(aq)	0.5[b]	−1.7[b]	0.02[b]
$CF_3CH_2NH_3^+ + C_2H_5NH_2 = CF_3CH_2NH_2 + C_2H_5NH_3^+$	0	15.5[d]		15.5[d]
		14.6[c]		14.6[c]
$CF_3CH_2NH_3^+(aq) + C_2H_4NH_2(aq) = CF_3CH_2NH_2(aq) + C_2H_5NH_3^+(aq)$	(aq)	5.4[b]	5.0[b]	6.9[b]

[a] Error limits given with data correspond to standard deviation of van't Hoff plot. Actual absolute error unknown but believed to be ~2 kcal/mol for $\Delta H_{n-1,n}$, ~1 kcal for $\Delta G^0_{n-1,n}$, 4 cal/deg for $\Delta S^0_{n-1,n}$, and half of the above values for the proton and hydrate transfer equilibria.
[b] From ref. 8.
[c] From ref. 6.
[d] From proton transfer equilibria ladder (Lau and Kebarle, unpublished results).

ponds actually to the difference of the hydrogen bonding energies for the formation of the ionic trihydrates, eq. [9], when $k = 0$, i.e. when the neutral bases are not hydrated.

$$R_0NH_3^+(H_2O)_3 + RNH_3^+ = R_0NH_3^+ + RNH_3^+(H_2O)_3$$

$$[9] \quad -\delta\Delta E_{am}(\text{STO-3G}) = \Delta E_{0,3}(RNH_3^+) - \Delta E_{0,3}(R_0NH_3^+) \quad (k = 0)$$

The clustering $(n-1, n)$ equilibria data reaction [7] can be used to obtain a corresponding expression with variable n which is shown in eq. [10].

$$[10] \quad -\delta\Delta H^0_{am}(\text{clust}) = \Delta H^0_{0,n}(RNH_3^+) - \Delta H^0_{1,n}(R_0NH_3^+) = \delta\Delta H^0_{0,n}(RNH_3^+)$$

(identical equations also for ΔG^0). Data from Table

Can. J. Chem. Downloaded from www.nrcresearchpress.com by 210.87.254.40 on 09/05/12
For personal use only.

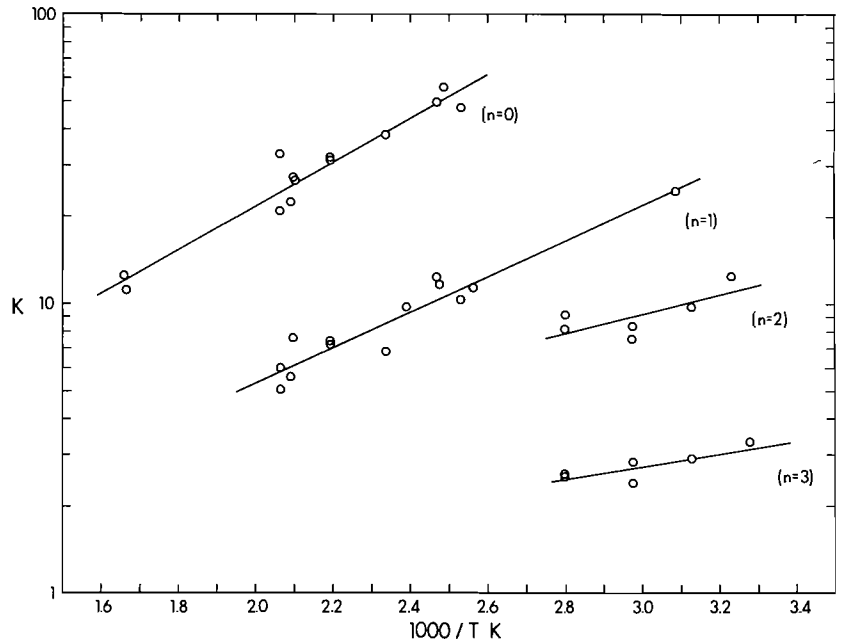

FIG. 2. van't Hoff plots of proton and hydrate transfer equilibria: $CH_3NH_3^+(H_2O)_n + C_2H_5NH_2 = CH_3NH_2 + C_2H_5NH_3^+(H_2O)_n$.

1 provide numerical values for eq. [10] with $n = 1$ to $n = 3$ for two base pairs: $R_0 = CH_3$, $R = C_2H_5$ and $R_0 = C_2H_5$, $R = CF_3CH_2$ dealt with by Hehre and Taft. For the pair CH_3, C_2H_5 a second set of $\delta\Delta H^0_{am}$(clust), and corresponding $\delta\Delta G^0$ can be obtained from the proton and hydrate transfer equilibra [8] by means of eq. [11], i.e. by subtracting the energy change for proton transfer in the absence of water

$$[11] \quad -\delta\Delta H^0_{0,n}(RNH_3^+) = \Delta H_8(n = n) - \Delta H_8(n = 0)$$

A summary of the data and a comparison with the STO-3G results is given in Fig. 3 which shows plots of $\delta\Delta H^0_{0,n}(RNH_3^+)$ and $\delta\Delta G^0_{0,n}(RNH_3^+)$ versus n. For the pair C_2H_5, CF_3CH_2 one finds very good agreement between the $\delta\Delta H^0_{0,3}$ and $\delta\Delta E_{0,3}$ results. The very close agreement is certainly fortuitous. Since the $\Delta H^0_{n-1,n}$ data have an error of some ± 1 kcal/mol, the cumulative error in the $\Delta H_{0,3}$ and $\delta\Delta H^0_{0,3}$ could easily be of the order of 2–3 kcal/mol.

Hehre and Taft (6) compared the $\delta\Delta E_{am}$(STO-3G) with the *free energy* $\delta\Delta G^0_{am}$(exp), see eq. [5]. The free energy rather than the enthalpy was chosen for the following reason. The $\delta\Delta E_{am}$ models only the hydrogen bonding solvent effect. In aqueous solution there are additional effects due to cavity formation CAV, structure making hydrophobic effects STR, van der Waals effects VDW, etc. (8). A partial cancellation of the $\delta\Delta H$ and $\delta(-T\Delta S)$ of the CAV, STR, VDW effects occurs so that the hydrgen bonding effect in the aqueous medium is quite well represented by the free energy difference $\delta\Delta G^0_{am}$(exp). Examination of Fig. 3 shows that for C_2H_5, CF_3CH_2 the gas phase hydrogen bonding data at $n = 3$ are in agreement with the corresponding $\delta\Delta G^0_{am}$, as was pointed out by Hehre and Taft (6) on the basis of $\delta\Delta E$(STO-3G).

As mentioned before, two sets of gas phase equilibria results are available for the pair $R_0 = CH_3$, $R = C_2H_5$, the data derived from the $(n-1, n)$ equilibria and the data from the proton and hydrate transfers, reaction [8]. For $\delta\Delta G^0_{0,n}(C_2H_5NH_3^+)$ the results from the two equilibrium determinations are in very good agreement. The $\delta\Delta G^0_{0,3}$ results are seen to be close to the $\delta\Delta G^0_{am}$(exp) and $\delta\Delta G^0_{aq}(C_2H_5NH_3^+)$ and the $\delta\Delta E_{am}$(STO-3G). Unfortunately the values obtained for $\delta\Delta H^0_{0,n}(C_2H_5NH_3^+)$ by the two different equilibrium measurements are not in good agreement. The largest differences ($\sim$2 kcal/mol) occurs for $n = 3$. The 0,3 value obtained from the $n-1, n$ equilibria (slopes of six van't Hoff plots) probably contains a larger accumulated error. Therefore these results are more suspect. If they are discounted, then one finds the $\delta\Delta E_{0,3}$(STO-3G) results of Hehre and Taft within less than 1 kcal/mol of the $\delta\Delta H_{0,3}$ results (equilibria [8]).

The present results fit into a more general trend, which is, that substituent effects on basicity and acidity are attenutaed in water due to hydrogen bonding to the ions, and particularly due to the

Can. J. Chem. Downloaded from www.nrcresearchpress.com by 210.87.254.40 on 09/05/12
For personal use only.

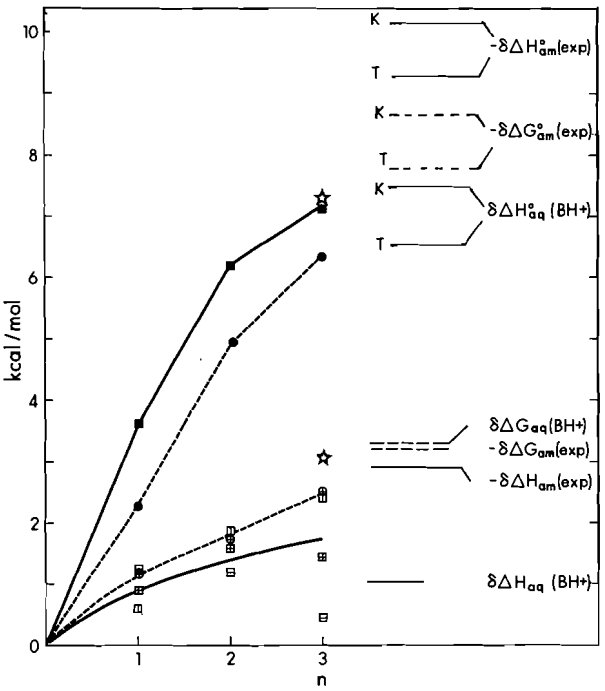

FIG. 3. Energy changes for hydrate transfer reactions:
[*a*] $C_2H_5NH_3(H_2O)_n^+ + CF_3CH_2NH_3^+ = C_2H_5NH_3^+ + CF_3CH_2NH_3(H_2O)_n^+$
■ $\Delta H^0 = \delta\Delta H^0_{0,n}(CF_3CH_2NH_3^+)$; ● $\Delta G = \delta\Delta G^0(CF_3CH_2NH_3^+)$; *$\Delta E$(STO-3G) Hehre and Taft (6). These data should be compared with $\delta\Delta H^0_{aq}(BH^+) = \Delta H^0_{aq}(CF_3CH_2NH_3^+) - \Delta H^0_{aq}(C_2H_5NH_3^+)$. Related quantities are also the aqueous medium effect: $\delta\Delta G^0_{am}$ and $\delta\Delta H^0_{am}$. Two sets of values: *K* and *T*, are shown for these data. This arises from differences in proton transfer in gas phase determinations (see footnotes *c* and *d* in Table 1). Read ordinate negative for reaction [*a*].
[*b*] $CH_3NH_3^+(H_2O)_n + C_2H_5NH_3^+ = CH_3NH_3^+ + C_2H_5NH_3^+(H_2O)_n$
$\Delta H^0 = \delta\Delta H^0_{0,n}(C_2H_5NH_3^+)$, ⊟ from $n-1,n$ equilibria Fig. 1, ◫ from equilibria [8] Fig. 2, ⊞ average of above, ⊕ $\Delta G^0 = \delta\Delta G^0_{0,n}(C_2H_5NH_3^+)$ average from $(n-1,n)$ equilibria and equilibria [8], results from the two types of equilibria are very close therefore only average is given in Table 1 and present figure. Read ordinate positive for reaction [*b*].

initial strong hydrogen bonds. Thus substituents that decrease the gas phase basicity of say RNH_2 increase the hydrogen bonding hydration of RNH_3^+. This automatic attenuation effect is simply expressed by the observation (9, 10) that hydrogen bonds in onium ions $BH^+...(OH_2)_n$ increase in strength as the acidity of BH^+ is increased, i.e., as the basicity of B is decreased. The operation of this rule is quite general and its important consequence on gas phase and aqueous substituent effects and the success of Hammet type plots based on aqueous acidities of benzoic acids has been discussed elsewhere (10). It may be pointed out that the van't Hoff plots in Fig. 1 provide one more illustration of the rule. The gas phase acidities of the onium ions RNH_3^+ increase in the order R = CF_3CH_2, CH_3, and C_2H_5. The van't Hoff lines for the (0, 1) interaction with water change slope and decrease in position in the same order. The interactions at higher $(n-1, n)$ follow the same trends, but the decreases of slope (ΔH) are somewhat less distinct than the decreases in height (ΔG).

Acknowledgements

A discussion with Professor R. W. Taft is gratefully acknowledged. The present work was supported by the Natural Science and Engineering Research Council of Canada.

1. I. DZIDIC and P. KEBARLE. J. Phys. Chem. **74**, 1466 (1970); P. KEBARLE. *In* Ions and ion pairs in organic reactions. *Edited by* M. Szwarc. Wiley Interscience. 1972; P. KEBARLE. *In* Modern aspects of electrochemistry. Vol. 9. *Edited by* B. E. Conway and J. O'M. Bockris. Plenum Press. 1974; P. KEBARLE. Ann. Rev. Phys. Chem. **28**, 445 (1977).
2. P. KEBARLE, W. R. DAVIDSON, M. FRENCH, J. B. CUMMING, and T. B. MCMAHON. Faraday Discuss. Chem. Soc. **64**, 220 (1977).
3. G. H. F. DIERCKSEN and W. P. DRAEMER. Theor. Chim. Acta, Berlin, **23**, 387 (1972); **23**, 393 (1972); P. A. COLLMAN and L. C. ALLEN. J. Am. Chem. Soc. **92**, 6101 (1970); A. PULLMAN and A. M. ARMBUSTER. Chem. Phys. Lett. **36**, 558 (1975); H. KISTENMACHER, H. POPKIE, and E. CLEMENTI. J. Chem. Phys. **61**, 699 (1974).
4. E. CLEMENTI. *In* Lecture notes in chemistry. Vol. 2. Springer Verlag. 1976.
5. F. F. ABRAHAM and M. R. MRUZIK. Faraday Discuss. Chem. Soc. **61**, 34 (1976).
6. M. TAAGEPERA, D. D. DEFREES, W. J. HEHRE, and R. W. TAFT. J. Am. Chem. Soc. **102**, 424 (1980).
7. A. J. CUNNINGHAM, J. D. PAYZANT, and P. KEBARLE. J. Am. Chem. Soc. **94**, 7627 (1972).
8. R. W. TAFT, J. L. WOLF, J. L. BEAUCHAMP, G. SCORRANO, and E. M. ARNETT. J. Am. Chem. Soc. **100**, 1240 (1978).
9. W. R. DAVIDSON, J. SUNNER, and P. KEBARLE. J. Am. Chem. Soc. **93**, 7139 (1971).
10. T. B. MCMAHON and P. KEBARLE. J. Am. Chem. Soc. **99**, 2222 (1977).

Can. J. Chem. Downloaded from www.nrcresearchpress.com by 210.87.254.40 on 09/05/12
For personal use only.

Nitroxide derivatives of acetylacetone as spin-labelled ligands

D. PLANCHEREL[1] AND D. R. EATON

Department of Chemistry, McMaster University, Hamilton, Ont., Canada L8S 4M1

Received July 7, 1980

D. PLANCHEREL and D. R. EATON. Can. J. Chem. **59**, 156 (1981).

Electron spin resonance spectra are reported from a number of radicals derived from 2,4-pentadione substituted at the 3 position with nitroxide-containing groups. If the substituent is *t*-butyl nitroxide no metal complexes are formed. This is attributed to steric factors which prevent the formation of the enol form of the β-diketone. If the substituent is trifluoromethyl nitroxide two types of metal complex have been observed. The esr spectra of the first type are very similar to that of the uncomplexed radical. Such complexes are formed with Co(III) and Al(III). The esr spectra of the second type show considerably increased ^{14}N and ^{19}F hyperfine coupling constants and in some cases large couplings to the metal nucleus. Complexes for the second type have been observed with Pd(II), Pt(II), and Rh(III). The possible structures of these radicals are discussed.

D. PLANCHEREL et D. R. EATON. Can. J. Chem. **59**, 156 (1981).

On rapporte les spectres de rpe d'un certain nombre de radicaux provenant de la pentadione-2,4 portant en position 3 un substituant contenant le groupe nitroxyde. Il ne se forme pas de complexes métalliques si le substituant est le *tert*-butylnitroxyde. On attribue ce fait à des facteurs stériques qui empêchent la formation de l'énol de la β-dicétone. Si le substituant est le trifluorométhylnitroxyde, on observe deux types de complexes métalliques. Le spectre de rpe du premier type est très semblable à celui du radical non complexé. De tels complexes se forment avec le Co(III) et le Al(III). Dans les spectres rpe du deuxième type, on note une augmentation considérable des constantes de couplage hyperfin du ^{14}N et du ^{19}F et dans certains cas de grands couplages avec le métal. On a observé des complexes du deuxième type avec le Pd(II), le Pt(II) et le Rh(III). On discute des structures possibles de ces radicaux.

[Traduit par le journal]

Introduction

Nitroxide radicals have been extensively used in chemistry and biochemistry as spin labels (1–3). The synthesis of a variety of compounds suitable for this purpose has been reported (4). Some years ago (5) we discussed the use of 4-pyridyl-*t*-butyl nitroxide as a spin-labelled ligand. The use of pyridine as the ligand moiety has some disadvantages. The complexes tend to be relatively labile, the esr spectra are fairly complex, and the nitroxide spin label is too far removed from the metal atom to make the observation of metal hyperfine coupling probable.

The intent of the present research was to investigate nitroxide substituted β-diketones as possible spin-labelled ligands. Specifically the potentialities of the anion radicals

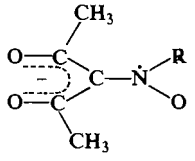

R = *t*-butyl, CF_3

to serve as spin-labelled ligands have been explored. β-Diketone anions form very stable complexes with a wide variety of metal ions. The above radicals should give rather simple esr spectra — the *t*-butyl group does not give resolvable hyperfine splitting and at worst a small splitting can be anticipated from the methyl groups. At the same time, earlier nmr studies (6) have shown that relatively small modifications in metal–ligand bonding can give rise to large substituent effects at the γ position of β-diketone complexes.

Results

We report two sets of experiments, the first directed towards the synthesis of *t*-butyl nitroxide labelled metal complexes and the second towards the synthesis of trifluoromethyl nitroxide labelled complexes. The first set was unsuccessful as regards the primary objective. The results are nevertheless reported since they provide some interesting information on the stereochemistry of this class of radical. In the second set of experiments radicals containing metal ions are clearly formed but the chemistry is complex. Two different types of metal-containing radicals are involved, one with no hyperfine coupling to the metal and the other with large metal hyperfine coupling constants.

t-*Butyl Nitroxide Radicals*

The radicals are formed (7) by the reactions of *t*-butyl magnesium chloride with appropriate nitro compounds. There are two approaches to the formation of the spin-labelled acetylacetonate

[1]Present address: Institut de Chimie inorganique et analytique de l'Université Perolles, CH-1700 Fribourg, Switzerland.

0008-4042/81/010156-08$01.00/00

©1981 National Research Council of Canada/Conseil national de recherches du Canada

Can. J. Chem. Downloaded from www.nrcresearchpress.com by 210.87.254.6 on 09/05/12
For personal use only.

Can. J. Chem. Downloaded from www.nrcresearchpress.com by 210.87.254.6 on 09/05/12
For personal use only.

complexes — synthesis of the radical ligand followed by metal complex formation or nitration of acetylacetonate complexes followed by reaction with the Grignard reagent. Both approaches have been tried.

3-Nitro-2,4-pentanedione was prepared by literature methods (8, 9, 22) and reacted with *t*-butyl magnesium chloride in ether. The product could be extracted with other solvents. An esr spectrum in carbon tetrachloride is shown in Fig. 1(*a*) and the coupling constants are given in Table 1. The spectrum is entirely consistent with the radical **1***a*.

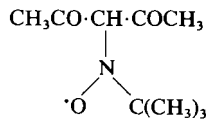

(**1***a*)

The coupling constants are within the range shown by similar nitroxides (10). 3-Nitro-2,4-pentanedione was deuterated by reaction with D_2O and after drying was reacted with *t*-butyl magnesium chloride. The esr spectrum shown in Fig. 1(*b*) results. Clearly the doublet splitting arises from the hydrogen at the 3 position. Treatment of the solution giving rise to spectrum 1*b* with water leads to no proton exchange. In another experiment an excess of base (cyclohexylamine) was added to a solution of the radical **1**, and again produced no change. It appears that this radical cannot exist in the enol form **1***b*.

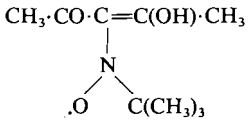

(**1***b*)

Treatment of solutions of **1***a* with a variety of metal salts and complexes in several solvents leads to no new esr spectra.

Complexes of Co(III) 3-nitroactylacetone were prepared by the method of Collman *et al.* (8, 11) and separated by chromatography. No radicals were obtained by reaction with *t*-butyl magnesium chloride. Analogous Al(III) complexes are too labile to separate by chromatography. Reaction of a mixture of nitration products with *t*-butyl magnesium chloride leads to the formation of radical **1***a* and a second short-lived radical. The quality of the esr spectra of the latter species were inadequate for analysis. The nitration of Zn(II) acetylacetonate was unsuccessful, only Zn(II) acetate being isolated. We note that Statsko and co-workers (12) have reported the production of an anion radical of acetylacetone by the reaction of Grignard reagents with metal acetylacetonates. This radical was not observed in the present work.

All of the above results indicate that radical **I** can exist only in its keto form. It is difficult to rationalise this conclusion on the basis of electronic effects. The nitro compound is predominantly in the enol form (22) and there seems no good electronic reason why the nitroxide should be vastly different. A more likely explanation lies in steric effects. Molecular models indicate that the enolate is only possible if the π system of the acetylacetonate ring is perpendicular to the π N—O bond — the bulky *t*-butyl group prevents coplanarity. The keto isomer on the other hand is relatively sterically unhindered. The keto isomer though is only capable of forming weak complexes with metal ions (13). It appears that a less sterically hindered nitroxide is necessary to produce a good spin-labelled ligand (18).

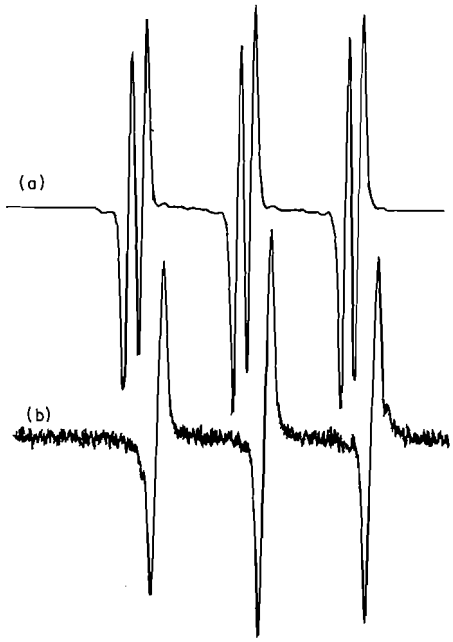

FIG. 1. (*a*) Electron spin resonance spectrum of 3 *t*-butyl nitroxide 2,4-pentanedione, in CCl_4; (*b*) esr spectum of this radical deuterated at the 3 positions in ether.

TABLE 1. Electron spin resonance data of *t*-butyl nitroxides

Molecule	a_N (G)	a_H (G)	ΔH (G)	g	Solvent
I	14.0_9	1.75	0.93	2.0066	CCl_4
	13.96	1.81		2.0064	Benzene
	13.88	1.72		2.0064	Et_2O
3-*d* **I**	13.88		1.04	2.0064	Et_2O

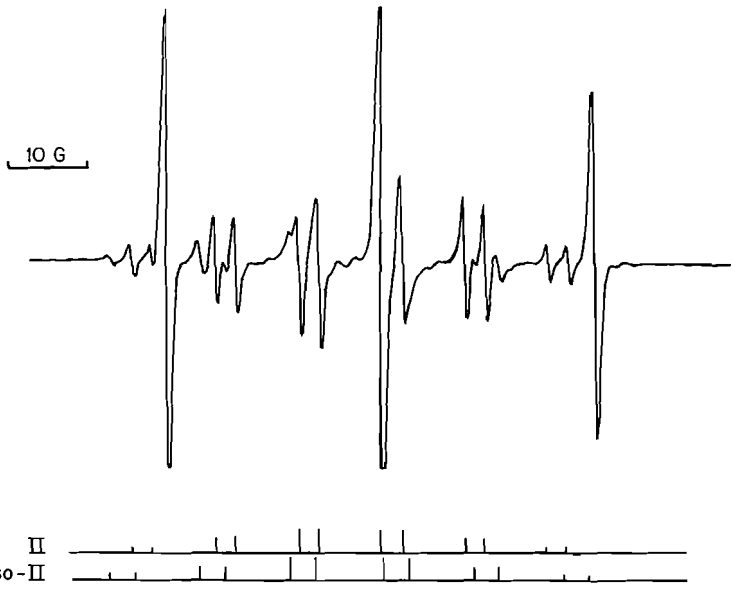

FIG. 2. Electron spin resonance spectrum from the reaction of equimolar acetylacetone and trifluoronitrosomethane, in CCl_4. The three intense lines are assigned to the iminoxy radical (**IV**) and the less intense lines arise from the diketo radicals (**II**) and (iso-**II**). The keto enol (**III**) is not visible in this spectrum.

Trifluoromethyl Nitroxide Radicals

Booth *et al.* (14) have studied the reaction between trifluoronitrosomethane and acetylacetone and have reported the radical products **II** to **V**.

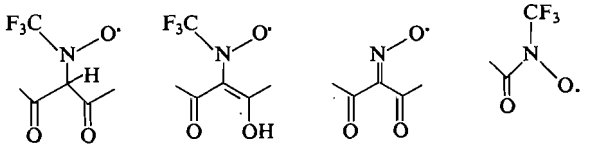

II **III** **IV** **V**

The occurrence of the enol radical **III** suggests that replacement of the *t*-butyl group by the trifluoromethyl group could circumvent the steric problems encountered above. We have therefore examined the reaction of trifluoronitrosomethane with both acetylacetone and with a variety of metal acetylacetonates.

Reaction of Trifluoronitrosomethane and Acetylacetone

The esr spectra obtained by this reaction are broadly in agreement with those reported by Booth *et al.* (14). A typical spectrum is shown in Fig. 2. The three most intense lines are assigned to the iminoxy radical **IV**. This radical decays relatively rapidly and after 30 min the main radical species present is the diketo radical **II** with smaller concentrations of the enol radical **III** and an unidentified species labelled iso-**II** in the figure. From the similarity of the coupling constants, we suspect that iso-**II** may be a geometric isomer of **II** possibly with the two keto group *trans*. We did not observe the radical **V**. Coupling constants are given in Table 2.

Reaction of Trifluoronitrosomethane with Aluminum Acetylacetonate

A spectrum obtained from this reaction is shown in Fig. 3. This spectrum represents the situation $2\frac{1}{2}$ h after the reaction was started. At earlier times radicals **II** and **IV** are present but appear to be less stable than in the case of the reaction with acetylacetone. The spectrum of Fig. 3 gives coupling constants and a *g* value similar to those reported for **III**. The differences, although small, are significant (see Table 2). The simplicity of the spectrum arises from the accidental equivalence of the ^{19}F and ^{14}N coupling constants. This radical is much more stable than those described above and can be easily detected 24 h after mixing the reactants. On the basis of the hyperfine coupling constants and the stability we assign it to the Al(III) complex of the anion of radical **III**. Note that no ^{27}Al hyperfine coupling can be detected.

Reaction of Trifluoronitrosomethane with Cobalt(III) Acetylacetonate

This reaction appears to be very similar to that with the aluminum complex. Again radicals **II** and **IV** appear in a transitory manner but the most stable species (remaining for more than 24 h) gives a spectrum very similar to the keto enol radical **III**. In this case (Table 2) the esr parameters are not significantly different. No ^{59}Co coupling is ob-

Can. J. Chem. Downloaded from www.nrcresearchpress.com by 210.87.254.6 on 09/05/12
For personal use only.

TABLE 2. Electron spin resonance data of trifluoromethyl nitroxides

CF_3NO +	a_N	a_F	$\bar{a}_{N,F}$	a_{other}	g
acacH	9.82	8.88			2.00668
	9.75 ± 0.07	8.87 ± 0.07	9.22		2.0067
$Al(acac)_3$			9.57 ± 0.17		2.0073
$Co(acac)_3$	9.84 ± 0.15	9.05 ± 0.18			2.0073
$Rh(acac)_3$	14.7 ± 0.3	12.5 ± 0.3		a^{Rh}: 4.3 ± 0.3	2.0060
$Pd(acac)_2$	α13.87 ± 0.15	12.68 ± 0.18		a^H: 2.52 ± 0.2	2.015
	β13.92 ± 0.16	11.95 ± 0.19			2.013
$Pt(acac)_2$	13.80 ± 0.38	11.40 ± 0.34		a^{Pt}: 63.6 ± 0.4	2.0134
Diketo **II**	10.5	10.7	10.6	a^H: 2.56	2.0063
iso **II**			11.7	a^H: 2.48	2.0063
Iminoxy **IV**	27.5				2.004

served. On the basis of the greatly enhanced stability (note that with acetylacetone we never observe the enol as more than a relatively minor component of the mixture) and by analogy with the Al(III) results we attribute the long-lived esr spectrum to a Co(III) complex of the anion of **III**.

Reaction of Trifluoronitrosomethane with Palladium(II) Acetylacetonate

This reaction gives quite different results to those described above. Initially radicals **II** and **IV** are observed with rather low intensities but these disappear completely after 12 h. There is also some indication of iso-**II**. After an induction period of 1 to 2 days two new radical species, labelled α and β in Fig. 4 appear. These spectra persist for 5 to 7 days with β being the longer-lived and predominating towards the end of this period. Both species can be analysed in terms of coupling to a ^{14}N atom and a CF_3 group, but both of these coupling constants are very much larger (12–14 G as opposed to 8–9 G) than those encountered previously. In addition the α radical has a further small coupling (2.5 G) with an $I = 1/2$ nucleus, presumably H. A typical spectrum, together with a computer simulation, is shown in Fig. 4. The agreement between the observed and simulated spectrum is sufficiently close to give confidence in the analysis. No ^{105}Pd coupling is observed but since the lines from the splitting due to this $I = 5/2$ nucleus would have only 3.5% of the main line intensities, this is not surprising. From the large changes in hyperfine coupling and the greatly enhanced stability it seems certain that the species responsible for these spectra contain

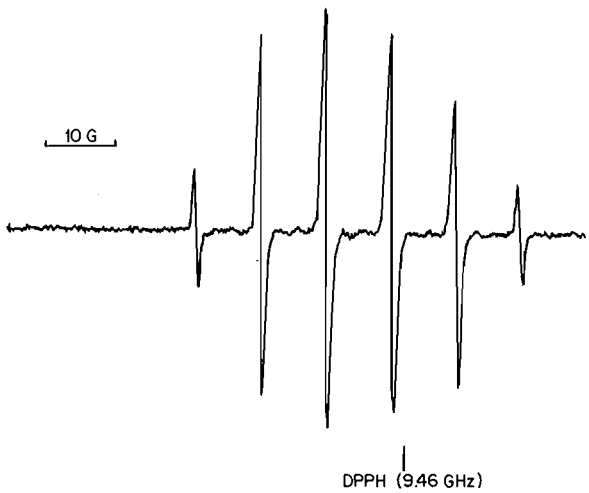

FIG. 3. Electron spin resonance spectrum from the reaction of $Al(acac)_3$ with trifluoronitrosomethane (1:3 mole ratio) in CCl_4. The only radical species present is the Al(III) complex of radical **III**.

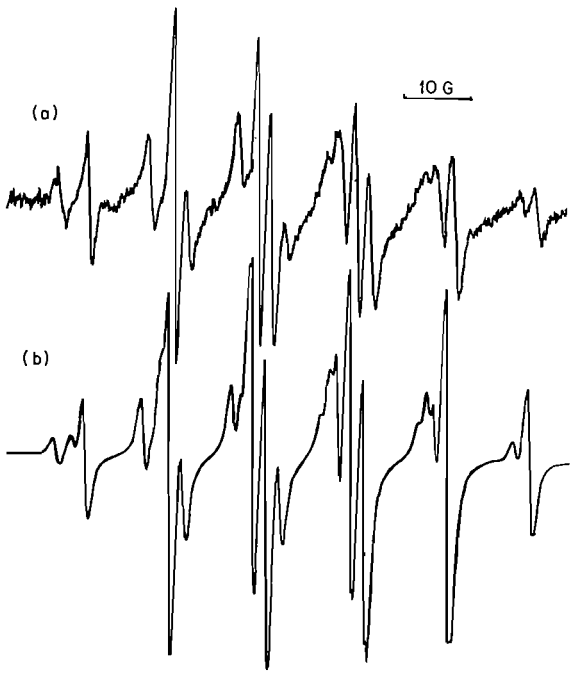

FIG. 4. (*a*) Electron spin resonance spectrum of the product from the reaction of $Pd(acac)_2$ with trifluoronitrosomethane (1:2 mole ratio) in CCl_4 after 6 days; (*b*) simulated spectrum using the parameters for the αPd and βPd radicals given in Table 2 and a Lorentzian line width of 1.0 G. The assumed concentration ratio of the αPd radical to the βPd radical is 0.3:1.0.

Can. J. Chem. Downloaded from www.nrcresearchpress.com by 210.87.254.6 on 09/05/12
For personal use only.

Can. J. Chem. Downloaded from www.nrcresearchpress.com by 210.87.254.6 on 09/05/12
For personal use only.

the metal ion. Electron spin resonance parameters are given in Table 2. Possible structures will be discussed below.

Reaction of Trifluoronitrosomethane with Platinum(II) Acetylacetonate

This reaction proceeds in a similar manner to that with the palladium analogue. There is only a single final product with ^{14}N and ^{19}F coupling constants quite similar to those of the β-palladium compound. In this case though there is an additional large coupling (63.2 G) ascribed to the 33.8% of ^{195}Pt with $I = 1/2$. A typical spectrum together with the computer simulation is shown in Fig. 5 and the measured parameters are given in Table 2. The final radical is stable for 8 to 12 days. In the early stages of the reaction there is some evidence for an additional "precursor" radical but the intensity was insufficient to allow analysis of the esr spectrum of this radical.

Reaction of Trifluoronitrosomethane with Rhodium(III) Acetylacetonate

This reaction shows some of the features of both the cobalt acetylacetonate and the palladium/platinum acetylacetonate reactions. Initially **II** and **IV** plus apparently some uncomplexed **III** are observed. After a few hours a new spectrum with large ^{14}N and ^{19}F couplings grows in intensity. This spectrum shows a ^{103}Rh coupling of 4.3 G (data in Table 2). However, this radical is much less stable than the Pd and Pt analogues and disappears after 5 or 6 h. Finally a weak spectrum (Fig. 6) remains. We do not believe that this represents a metal-containing species.

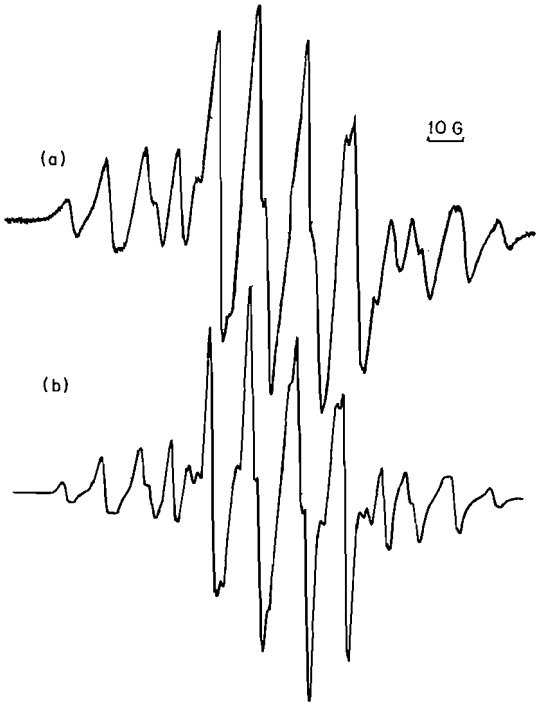

FIG. 5. (*a*) Electron spin resonance spectrum of the product from the reaction of $Pt(acac)_2$ with trifluoronitrosomethane (1:3 mole ratio) in CCl_4 after 1 day; (*b*) simulated spectrum using the parameters of Table 2 and a Lorentzian line width of 2.35 G.

Reaction of Trifluoronitrosomethane with Iridium(III) Acetylacetonate

We have been unable to positively identify any metal-containing radical species in this reaction. Early in the reaction **II**, **IV**, and iso-**II** are all present as is the keto enol **III**. This latter radical shows very similar coupling constants to the version obtained from free acetylacetone and the stability is not significantly enhanced. There is therefore no real evidence for complex formation. After standing for several days the weak spectrum of Fig. 6 remains.

Discussion

The failure of the radical **I** to form metal complexes is almost certainly steric in origin. In its enol form the central carbon of the acetylacetone must be planar and this leads to steric hindrance between the methyl groups of the acetylacetone and the *t*-butyl substituent on the nitroxide. In the keto form the central carbon is tetrahedral and the steric hindrance is less. It has been reported elsewhere (15) that sterically hindered β-diketones exist exclusively in the keto form.

From the results of the reactions with aluminium (III) acetylacetonate and cobalt(III) acetylacetonate it seems very probable that the radical **III** does form metal complexes but that the effects of the metal are minimal. This is not therefore a satisfactory spin-labelled ligand. It is well established (5) that spin density from the nitroxide groups can be delocalized to neighbouring π systems when the stereochemistry is favourable. We must assume in this case that the π system of the nitroxide and that of the β diketone are fixed in mutually perpendicular planes to minimize steric interactions. We note that the ^{14}N and ^{19}F hyperfine coupling constants for radical **III** are not substantially different from those reported for the trifluoromethyl phenyl nitroxide (2).

The most interesting radicals are those formed in the reactions with Pd, Pt, and Rh acetylacetonates. Nitroxide radicals can be regarded as resonance hybrids of the two structures

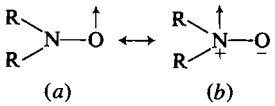

(*a*) (*b*)

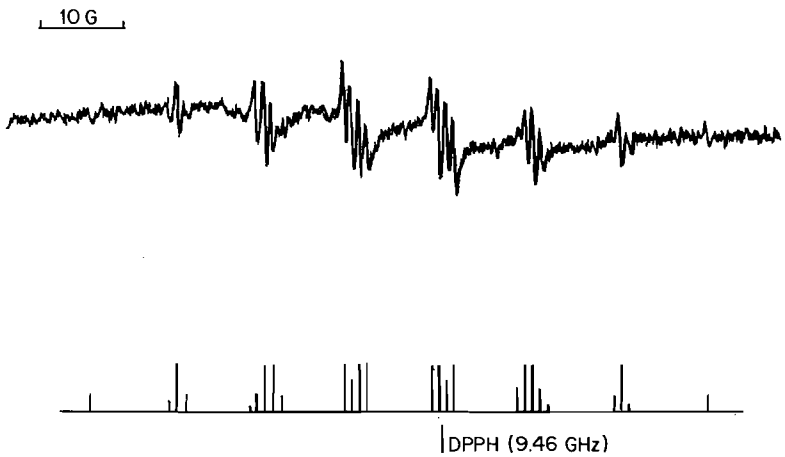

FIG. 6. Electron spin resonance spectrum of the final radical species from the reaction of $Rh(acac)_3$ or $Ir(acac)_3$ with trifluoronitrosomethane. Solvent CCl_4; 5 days reaction time. The analysis shown is for $H{\cdot}NO{\cdot}CF_3$ assuming the parameters given in the text.

The greater the contribution of structure *b* the larger will be the ^{14}N hyperfine coupling since it is this structure which places the unpaired electron on the nitrogen. The large increase in ^{14}N hyperfine coupling for the Pd, Pt, and Rh radicals indicates that structure *b* is favoured. The observation of metal hyperfine coupling demands a radical which places the metal close to the nitroxide group. It may be noted that the numerical value of the ^{103}Rh coupling constant is much smaller than that of the ^{195}Pt coupling. Part of this difference arises from the smaller magnetic moment of ^{103}Rh.

We have considered three possible types of structure for these radicals.

(*i*) One of the features of the chemistry of the β-diketonate complexes of the heavy transition metals in the formation of C bonded complexes in addition to O bonded complexes (16, 17).

Thus structures of the type

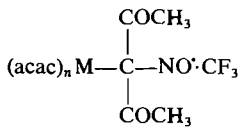

are possible.

(*ii*) The direct addition of nitroxide radicals to metal complexes with a vacant coordination site has been reported (1); i.e. structures of the type

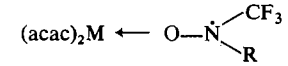

where R could be any of the groups corresponding to radicals **II**, **III**, or **V** or even a completely different group.

(*iii*) Formation of a metal nitroxide bond could be combined with bonding to the β-diketonate function. There are two modifications of this possibility. The ligand could remain bidentate in which case an NO bond replaces a CO bond, i.e.

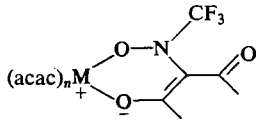

Alternatively the ligand could become tridentate, i.e.

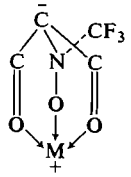

In this case the central carbon has become tetrahedral, with the resultant loss of aromaticity in the β-diketonate moiety, but with the added stability associated with a tridentate ligand. In either case there is the possibility of protonating the central carbon. A model indicates that the tridentate structure has very little strain.

The large ^{14}N coupling constant argues against alternative (*i*). It has been shown (19) that for phenyl nitroxide radicals electron withdrawing substituents favour resonance form (*a*) and decrease the ^{14}N coupling. Coordination of the carbon to a positive metal centre would be expected to have a similar effect. Neither does this structure provide a ready explanation of the additional ^{1}H coupling in the Pd α radical. Coordination of the nitroxide oxygen on the other hand would favour resonance structure (*b*) and increase the ^{14}N coupling. Alternative (*ii*) is satisfactory in this respect but cannot account for the additional ^{1}H coupling. Alternative (*iii*) is satisfactory in both respects. We favour the tridentate ligand since this will also ac-

Can. J. Chem. Downloaded from www.nrcresearchpress.com by 210.87.254.6 on 09/05/12
For personal use only.

count for the slow rate of formation of the radical (considerable molecular reorganization is necessary) and the high stability of the final product. It also provides a ready explanation of the greater stability of the Pd and Pt compounds compared with the Rh compound since in the former cases an additional coordination site is already available whereas in the latter case an acetylacetonate must be displaced. However, this assignment must remain tentative.

Booth *et al.* (14) have discussed possible mechanisms for the reaction of trifluoronitrosomethane with β-diketones and have rationalized the production of the various radicals observed. Their mechanisms are equally applicable to complexed β-diketones and we can add little to this discussion.

Finally we comment on the radical giving rise to the spectrum of Fig. 6. The esr spectrum can be fitted to that expected for the radical

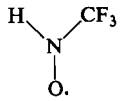

with $a_F = 11.1 \pm 0.1$ G, $a_N = 12.0 \pm 0.1$ G, $a_H = 21.2 \pm 0.1$ G, and $g = 2.0069$. We have no ready explanation for the formation of this radical and the assignment must remain tentative. The radical anion CF_3NO^- has been reported (20) but the analysis of the spectrum is unclear.

Experimental

The majority of spectra were obtained using a JEOLCO-JES-3BS-X spectrometer operating at 9400 MHz. A few spectra were obtained with a Varian E-line spectrometer (University of Guelph) which has a higher sensitivity. Metal acetylacetonates were purchased from Research Organic/Inorganic Chemical Co.

Cobalt(III) [Bis(acetylacetonate)(3-nitroacetylacetonate)]

This complex was synthesized by analogy with the cobalt(III) [bis(3-nitroacetylacetonate)] (8) and the mixed ligand chromium(III) complexes (11). Finely ground $Cu(NO_3)_2 \cdot 3H_2O$ (1.6 g, 6.5 mmol) was dissolved in 100 mL acetic anhydride and stirred 30 min at 0°C. Cobalt(III) trisacetylacetonate (4.2 g, 1.8 mmol) was then added in 2–3 min. The mixture was stirred 3 h at 0°C and 1 h at room temperature, then poured into 1 L water/ice (1:1) and 11 g sodium acetate; this was again stirred 1 to 2 h. This solution (or suspension if any precipitate was present) was extracted three times with 300 mL chloroform. The chloroform solution was washed four times with 125 mL aqueous sodium acetate (5%) and twice with 200 mL water. The solution was dried over Na_2SO_4. The chloroform was then distilled off under vacuum and the dry residue was chromatographed on silica gel (60–120 mesh) with ethylacetate/benzene (1 to 2:100) as eluent. The column was approximately 30 cm long and 5 cm in diameter.

The products come in the order tri-, di-, mono-nitro derivatives; the separation of the di- and mono-nitro derivatives is reasonable and becomes excellent when a fractionator is used.

The purity was checked by thin layer chromatography and nmr (21). The complexes were recrystallized in chloroform/methanol. Yield: mono-nitro, 1.65 g (35%); di-nitro, 0.32 g (6%); unseparated ~ 1 g.

Copper(II) [Bis(3-nitroacetylacetonate)]

This was synthesized by the procedure of Collman and coworkers (8). It is interesting to note that the addition of copper nitrate must be carried out very slowly and carefully. There is an induction period of a few minutes before the very exothermic reaction starts.

3-Nitroacetylacetone

The procedure described by Yoshida *et al.* (22) was followed but 15 g of EDTA disodium salt were used instead of 150 g (probably a mistake) of EDTA diammonium salt.

3-d 3-Nitroacetylacetone

3-Nitroacetylacetone (0.1 mL) was dissolved in 5 mL $CDCl_3$ and shaken twice with 0.2 mL D_2O. The $CDCl_3$ solution was dried over Na_2SO_4 and then the $CDCl_3$ was removed under vacuum. The complete replacement of the methine and enol protons was checked by ^{1}H-nmr. The 3-*d* 3-nitroacetylacetone was used without further purification.

t-*Butylnitroxides*

General procedure: An approximately 0.2 *M* ethereal solution of *t*-butyl magnesium chloride was used in all cases.

Typically a 0.5 *M* to 3 *M* ethereal solution of the nitro derivative was slowly mixed with a stoichiometric excess of *t*-butyl magnesium chloride, and stirred 30 min at 0°C. After neutralization with ammonium chloride the mixture was extracted with ether and dried over sodium sulphate. If necessary, the ethereal solution was concentrated under vacuum.

3-(t-Butylnitroxyl)acetylacetone

The above general procedure was carried out with 0.65 g of 3-nitroacetylacetone (4.4 mmol) in 5 mL of dry ether. After neutralization and extraction, the ether was distilled off under vacuum, and the yellow product was chromatographed on a small column (Pasteur pipette; silica gel 60–200 mesh) with benzene as eluant. It was not possible to determine the purity of the obtained product but it was assumed to be between 50% and 80% as pure nitroxide.

3-d 3-(t-Butylnitroxyl)acetylacetone

The general procedure was used, starting with 3-*d* 3-nitroacetylacetone and using pure D_2O (without NH_4Cl) for the neutralization. The ethereal extract was concentrated or evaporated to dryness but not further purified. Experiments with this radical were mainly qualitative.

Some water (H_2O) was added to an ethereal solution of the deuterated nitroxide and no proton exchange was observed in the esr spectrum.

Trifluoronitrosomethane (CF_3NO) (14, 23, 24)

Silver trifluoroacetate was synthesized by reaction of trifluoroacetic acid with silver oxide (23). Then the procedure described by Taylor, Brice, and Wear (25) was followed. The obtained yield (23%) is lower than the value given in the literature (56%). The CF_3NO was distilled twice.

It is a blue compound as vapour (room temperature), liquid, or solid (77 K).

Trifluoronitroxyl Radicals (14)

Carbon tetrachloride was dried over molecular sieves (type 4A) and deoxygenated by bubbling dry nitrogen through it. Due to the different solubilities the solutions had the following concentration ranges: 0.05 *M* to 0.1 *M*: acacH; Co(III) and Al(III) acetylacetonates 0.01 *M* to 0.03 *M*: Rh(III), Ir(III), Pd(II), and Pt(II) acetylacetonates. The standard procedure was to make up a solution of the above mentioned concentration in carbon tet-

Can. J. Chem. Downloaded from www.nrcresearchpress.com by 210.87.254.6 on 09/05/12
For personal use only.

rachloride. Dry nitrogen was bubbled a few minutes through this solution. Then 0.5 mL to 1 mL was transferred into an nmr tube and was degased using standard vacuum techniques. The required amount of trifluoronitrosomethane was then distilled into this tube from a vacuum system, before the tube was sealed under vacuum. The ratio of trifluoronitrosomethane and acetylacetone (free or complexed) was between 0.3:1 and 2:1. This means, e.g., a ratio $Co(acac)_3$:CF_3NO between 1:1 and 1:6 respectively.

The sealed tube was then warmed up from 77 K to room temperature in less than 2 min, and the esr spectra recorded.

With all metal complexes a precipitate was slowly formed. This was negligible in the case of $Al(acac)_3$ but was important with the other complexes, making any nmr measurement inaccurate (if the precipitate was suspended) or unreal (if it was centrifugated to the upper end of the tube, outside the measured solution). This precipitate was white (Al(III)) or brown to dark brown (Co, Rh, Ir, Pd, Pt).

Acknowledgements

We are indebted to the Natural Sciences and Engineering Research Council for financial support, to the Swiss National Science Foundation for scholarship support (D.P.), and to Dr. E. G. Janzen of the University of Guelph for use of esr facilities.

1. S. S. Eaton and G. R. Eaton. Coord. Chem. Rev. **26**, 207 (1978).
2. E. G. Janzen. Top. Stereochem. **6**, 177 (1971).
3. J. F. W. Keana. Chem. Rev. **78**, 37 (1978).
4. E. G. Rozantsev and V. D. Sholle. Synthesis, 190 (1971); 401 (1971).
5. C. T. Cazianis and D. R. Eaton. Can. J. Chem. **52**, 2454 (1974); **52**, 2463 (1974).
6. D. R. Eaton and K. L. Chua. Can. J. Chem. **49**, 56 (1971); **51**, 2260 (1973).
7. H. Lemaire, Y. Marechal, R. Ramasseul, and A. Rassat. Bull. Soc. Chim. 372 (1965).
8. J. P. Collman, R. L. Marshall, W. L. Young, and S. D. Goldby. Inorg. Chem. **1**, 704 (1962).
9. P. R. Singh and R. Sahai. Aust. J. Chem. **20**, 649 (1967).
10. A. Rockenbauer, S. A. Abdel-Monem, G. Moger, and L. Sumegi. J. Mol. Struct. **46**, 169 (1978).
11. J. P. Collman and M. Yamada. J. Org. Chem. **28**, 3017 (1963).
12. A. Stasko, A. Tkac, V. Laurinc, and L. Malik. Org. Magn. Reson. **8**, 237 (1976).
13. P. W. N. M. Van Leeuwen and A. P. Praat. Inorg. Chim. Acta, **4**, 101 (1970).
14. B. L. Booth, D. J. Edge, R. N. Haszeldine, and R. G. G. Holmes. J. Chem. Soc. Perkin II, 7 (1977).
15. N. N. Shapet'ko. J. Org. Chem. USSR, **8**, 2275 (1972).
16. D. Gibson. Coord. Chem. Rev. **4**, 225 (1969).
17. J. P. Fackler, Jr. Prog. Inorg. Chem. **7**, 361 (1966).
18. A. Rassat, R. Briere, and P. Rey. J. Am. Chem. Soc. **100**, 343 (1978).
19. E. G. Janzen. Acc. Chem. Res. **2**, 279 (1969).
20. V. A. Ginsburg, A. N. Medvedev, L. L. Martynova, P. O. Gitel', and G. E. Nikolaenko. J. Org. Chem. USSR, **8**, 491 (1972).
21. A. J. Brown, O. W. Howarth, and P. Moore. J. Am. Chem. Soc. **100**, 713 (1978).
22. Z. Yoshida, H. Ogoshi, and T. Tokumitsu. Tetrahedron, **26**, 5691 (1970).
23. R. N. Haszeldine. J. Chem. Soc. 584 (1951).
24. W. D. Blackley and R. R. Reinhard. J. Am. Chem. Soc. **87**, 802 (1965).
25. C. W. Taylor, T. J. Brice, and R. L. Wear. J. Org. Chem. **27**, 1064 (1962).

Can. J. Chem. Downloaded from www.nrcresearchpress.com by 210.87.254.6 on 09/05/12
For personal use only.

Ouverture de dichlorocyclopropanes en présence d'un nucléophile interne. Absence de participation intramoléculaire. Réarrangement concerté en chlorures allyliques

LAURENT CHICHE, HENRI CHRISTOL, JACQUES COSTE, FRANCINE PIETRASANTA ET FRANÇOISE PLÉNAT
ERA No 610, Laboratoire de Chimie Organique, E.N.S. Chimie, 8, rue de l'Ecole Normale, 34075 Montpellier, France
Reçu le 25 avril 1980

LAURENT CHICHE, HENRI CHRISTOL, JACQUES COSTE, FRANCINE PIETRASANTA et FRANÇOISE PLÉNAT. Can. J. Chem. **59**, 164 (1981).

On montre qu'un nucléophile interne convenablement placé (groupement carboxylate), n'intervient pas au cours du réarrangement d'un dichlorocyclopropane en chlorures allyliques. Ce résultat paraît en faveur d'un mécanisme concerté, de type $\sigma_s^2 + \sigma_a^2$, pour ce réarrangement. Dans les composés obtenus, le chlore allylique peut ensuite être déplacé soit par le solvant (H_2O) pour conduire à des alcools, soit par le groupement carboxylique interne pour conduire à une lactone.[1]

LAURENT CHICHE, HENRI CHRISTOL, JACQUES COSTE, FRANCINE PIETRASANTA, and FRANÇOISE PLÉNAT. Can. J. Chem. **59**, 164 (1981).

It is shown that a conveniently placed internal nucleophile (carboxyl group) is not involved with the rearrangement of a dichlorocyclopropane into an allylic chloride. This result appears to support a concerted mechanism of a $\sigma_s^2 + \sigma_a^2$ type for this rearrangement. In the products obtained, the allylic chloride may undergo displacement either by solvent (H_2O), leading to alcohols, or by the internal carboxyl group, leading to a lactone.

[Journal translation]

On sait que les halocyclopropanes conduisent par thermolyse à des halogénures d'allyle. L'ouverture du microcycle est presque toujours considérée comme concertée avec le départ de l'halogène et se conforme aux règles de Woodward–Hoffmann (schéma 1, étape a) (2). La paire d'ions intermédiaire **1** est suffisamment intime pour que le retour de l'halogène en position allylique se montre stéréospécifique (étape b) (2, 3). Jefford a proposé un autre mécanisme possible rendant bien compte de la stéréospécificité globale observée (2); il s'agirait d'une transposition 1,3 sigmatropique selon un processus $\sigma_s^2 + \sigma_a^2$, processus totalement concerté (étape c).

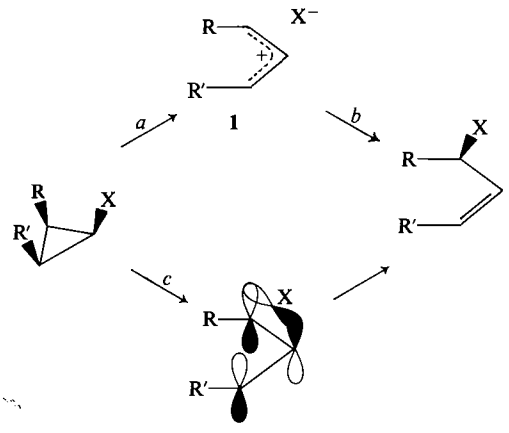

2

SCHÉMA 1

La distinction entre ces deux mécanismes s'est révélée délicate (3, 4). Toutefois, dans la première hypothèse, le développement d'une charge positive sur les carbones 2 et 3 devrait permettre à un nucléophile interne, convenablement placé et suffisamment puissant, d'intervenir pour conduire à des produits de cyclisation intramoléculaire. La participation d'un hydroxyle interne a ainsi déjà été suggérée (5); mais il n'a pas été démontré que l'éther cyclique obtenu dans ce cas ne résulte pas de la cyclisation, dans le milieu basique utilisé, de composés à chlore allylique qui auraient été primitivement formés par réarrangement thermique. De façon contradictoire, une absence de participation a été constatée pour le réarrangement des composés tricycliques **3** et **4** qui conduisent exclusivement aux esters à chlore allylique (4, 6):

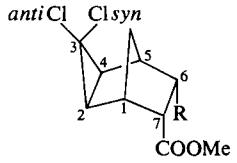

3 R = H
4 R = COOMe

FIG. 1

Ce résultat pouvait être utilisé comme un argument en faveur d'un mécanisme totalement concerté. Cependant d'autres interprétations sont possibles; dans le cas d'un mécanisme ionique (schéma 1, étapes a et b), la participation d'un nucléophile interne peut entrer en jeu pendant ou après la formation de la paire d'ions **1**. Si elle est concomitante,

[1]Une partie de ce travail a fait l'objet d'une communication préliminaire (1).

0008-4042/81/010164-11$01.00/0
©1981 National Research Council of Canada/Conseil national de recherches du Canada

Can. J. Chem. Downloaded from www.nrcresearchpress.com by 210.87.254.5 on 09/05/12
For personal use only.

Can. J. Chem. Downloaded from www.nrcresearchpress.com by 210.87.254.5 on 09/05/12
For personal use only.

l'attaque du nucléophile interne est attendue avec inversion de configuration, comme l'était celle d'un nucléophile externe (3), ce qui n'est pas possible pour les composés **3** et **4**. D'un autre côté, une fois la paire d'ions **1** formée, cette contrainte stéréoélectronique n'existe plus, mais il y a alors possibilité de compétition entre le retour de l'halogène et l'attaque du nucléophile interne, et on peut craindre qu'à ce titre une fonction ester méthylique ne soit pas assez puissante.

Nous avons choisi pour notre part comme substrats les composés **5** qui présentent les avantages suivants. D'une part la souplesse relative de la molécule doit laisser au nucléophile interne la possibilité d'attaquer avec la stéréochimie requise, comme le suggèrent les résultats obtenus par Marshall et Ellison (7) dans la solvolyse de cyclopropyls–carbinols de même squelette. D'autre part, la tension de cycle, suffisamment faible pour que les composés dichlorocyclopropaniques puissent être isolés, demeure cependant assez forte pour que l'extension de cycle reste facile. Il sera dès lors possible de modifier le nucléophile interne (acide carboxylique ou carboxylate) et de faire varier les conditions de l'ouverture du noyau cyclopropanique, ce qui n'était pas le cas pour les composés **3** et **4**, ceux-ci se réarrangeant dans les conditions même de leur synthèse.

L'ouverture des composés **5** conduit, dans des proportions variables suivant les essais (Tableau 1), à la formation de la lactone **6**, des produits de réarrangement **7**, **9**, **11** et **13**, et de trois alcools **8**, **10** et **12**.

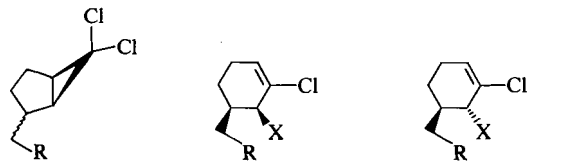

5a R = COOMe **7** X = Cl; **8** X = OH **9** X = Cl; **10** X = OH
b R = COOH
c R = COONa

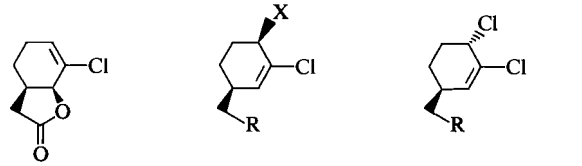

6 **11** X = Cl; **12** X = OH **13**

SCHÉMA 2

Synthèses et structures

Composés bicycliques 5a *et* 5b

Les composés **5***a* ont été préparés par action du trichloracétate de méthyle, en présence de méthylate de sodium, sur le (cyclopenténYl-3)acétate de méthyle. Le spectre de rmn du produit d'addition, en présence d'$Eu(DPM)_3$, indique l'obtention des deux isomères *cis* et *trans* dans les proportions 25:75. L'hydrolyse basique de ce mélange conduit aux acides **5***b* dont l'isomère majoritaire a été isolé par l'intermédiaire du sel de dicyclohexylamine correspondant. Après régénération de l'acide, l'isomère **5***b* majoritaire est estérifié (CH_2N_2); l'identification a été faite à ce niveau et repose sur des corrélations chimiques (schéma 3): par réduction (Na/NH_3), puis régression de la chaîne latérale, on obtient le composé **15**-*trans*. L'isomère **15**-*cis* a été préparé par ailleurs (8) à partir du composé **16**-*cis* connu (9).

On démontre ainsi la stéréochimie *trans* de l'isomère **5** majoritaire. Par ailleurs, la réduction du mélange des isomères **5***a* (*cis*/*trans* = 25:75) conduit au mélange des isomères **14**-*cis* et *trans* connu (8), ce qui confirme la nature *cis* de l'isomère **5** minoritaire.

Composés d'extension de cycle

Les principales preuves chimiques utilisées dans les attributions de structure sont exposées sur le schéma **4**.

Le caractère γ-lactonique du composé **6** apparaît en ir ($\nu_{C=O}$ = 1780 cm^{-1}). Le spectre de rmn correspond bien à la structure proposée; la faible valeur de la constante de couplage entre H-2 et H-1 (J = 5,5 Hz) indique une jonction de cycle *cis* (10); en effet, les lactones de ce type à jonction de cycle *trans* présentent des constantes de couplage nettement supérieures ($J \geq$ 10 Hz (11)). La structure de ce composé a été confirmée par voie chimique par corrélation avec la lactone saturée **17** connue (fig. 2). La réduction en présence de palladium a été conduite sur le sel de sodium correspondant à la lactone **6**, en milieu basique fort, afin d'éviter l'hydrogénolyse de la liaison alkyle–oxygène (11*c*, 12).

L'hydrolyse basique de la lactone **6** conduit à l'hydroxyacide **8***b* qui est donc de stéréochimie *cis*; en effet, en présence d'une base suffisamment concentrée, l'hydrolyse des esters se fait uniquement par rupture de la liaison acyle–oxygène (13), donc ici avec rétention de configuration du carbone C-2. Pour confirmation, on constate que l'hydroxyacide **8***b* redonne la lactone **6** par cyclisation spontanée. En outre, l'hydroxy-ester **8***a* conduit, par réduction, à l'ester **18** qui, par cyclisation, donne la lactone saturée *cis* **17** connue. Les structures de la lactone **6** et des composés **8***b* et **8***a* (obtenu par estérification de l'acide **8***b*) sont ainsi établies sans ambiguité.

Can. J. Chem. Downloaded from www.nrcresearchpress.com by 210.87.254.5 on 09/05/12
For personal use only.

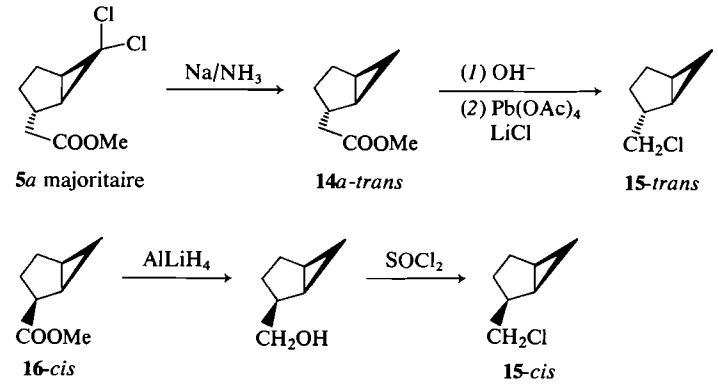

5*a* majoritaire 14*a*-*trans* 15-*trans*

16-*cis* 15-*cis*

SCHÉMA 3

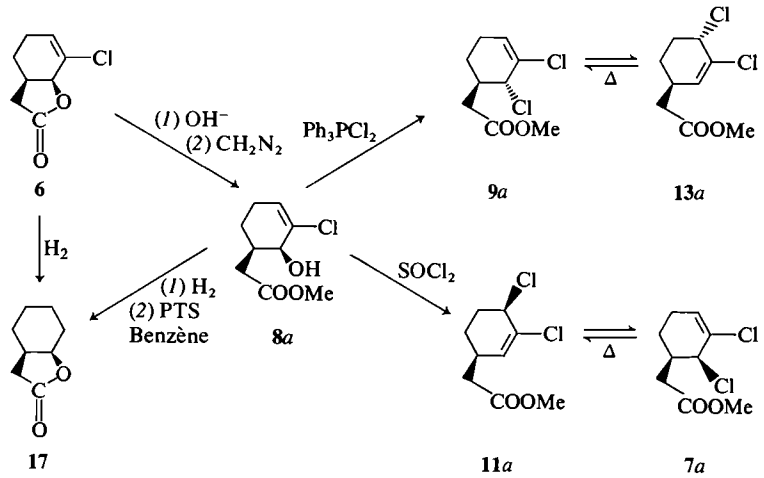

6 9*a* 13*a*

8*a*

17 11*a* 7*a*

SCHÉMA 4

Les alcools **10***b* et **12***b* conduisent, par catalyse acide (benzène, acide *p*-toluènesulfonique) à la lactone **6**; cela indique un même squelette de base pour ces trois composés (et pour les esters dérivés **10***a* et **12***a*). Le composé **10***a* dont le spectre de rmn est voisin de celui du composé **8***a* (en particulier le proton éthylénique résonne sous la forme d'un triplet) est donc l'isomère *trans* indiqué. La structure de l'alcool **12***a*, en accord avec ses propriétés spectrographiques (en particulier le proton éthylénique résonne en rmn sous la forme d'un doublet), a été établie par réduction puis hydrolyse en hydroxy-acide **19**, connu (14).

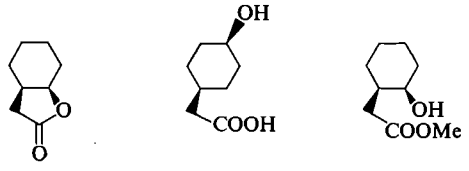

17 19 18

FIG. 2

Les quatre isomères dichlorés **7**, **9**, **11** et **13**, obtenus en mélange par chauffage des composés **5**, n'ont pu être séparés directement, ni en tant qu'esters, ni en tant qu'acides. Cependant, par hydrolyse basique douce du mélange d'esters, les deux isomères **9***a* et **11***a* se cyclisent en lactone **6**, ce qui a permis d'isoler le mélange de **7***b* + **13***b*, dont la chromatographie sur colonne, permet d'isoler de très faibles quantités de chacun des deux isomères purs.

Les composés **9***a* et **11***a* ont du être préparés par d'autres voies, puis identifiés comme composants du mélange **7***a* + **9***a* + **11***a* + **13***a* par rmn. Le composé **9***a* a été obtenu à partir de l'alcool **8***a* par action du dichlorure de triphénylphosphine. Etant donné l'inversion de configuration généralement induite par l'utilisation de ce réactif (15, 3*b*), nous avons attribué la stéréochimie *trans* au composé **9***a*; le composé **7***a*, voisin de **9***a* en rmn, doit donc être l'isomère *cis*. Par isomérisation thermique, le composé **9***a* conduit, de façon majoritaire au composé **13***a*; étant donné que de tels réarrangements

TABLEAU 1. Ouverture des composés **5** et réactivité du composé **7***c*; produit réactionnel en % relatifs

Conditions	Essai No	Produit de départ	Avancement	Produit réactionnel 6	7	9	11	13
Chauffage des produits purs en tubes scellés à 130°C	1	**5***a*[a]	33	5	3	37	4	51
			72	9	7	35	9	39
			95	17	21	18	28	16
	2	**5***a*[b]	50	Trace	21	25	20	34
			93	5	17	24	13	41
			97	7	16	23	13	41
	3	**5***b*[b]	62	31	19	9	11	30
	4	**5***b*[a]	58	44	Trace	17	Trace	39
Chauffage 165 h à 40°C dans H_2O/acétone 70:30	5	**5***a*[b]	16	5	25	20	23	27
	6	**5***b*[b]	17	47	26	0	4	23
						8	**10**	**12**
	7	**5***c*[b]	88[c]	80	5	0	3,5	11,5
	8	**5***c*[a]	80	91,5	0	0	3,5	5
	9	**7***c*	43	15	57	0	5	23

[a] Isomère *trans* pur.
[b] Mélange d'isomères *cis*/*trans* dans le rapport 25:75.
[c] Le rapport *cis*/*trans* des composés **5***a* qui n'ont pas réagi est de 7:93.

de chlore allylique se font rapidement de façon synfaciale par un mécanisme de type S_Ni' (2, 13*b*), nous avons attribué la stéréochimie *trans* au composé **13***a*.

Le composé **11***a* n'a pu être obtenu pur, mais seulement comme composante majoritaire d'un mélange contenant les quatre isomères **7***a*, **9***a*, **11***a* et **13***a*, par action du chlorure de thionyle sur l'alcool **8***a*. La stéréochimie du composé **11***a* ainsi obtenu, qui doit être *cis* en accord avec le mécanisme S_Ni' souvent invoqué pour l'action du chlorure de thionyle (3*b*, 13*a*, 13*b*), a été confirmée de la même façon que ci-dessus par réarrangement allylique du composé **7***a*; ce dernier conduit en effet, par chauffage, à un mélange dans lequel le composé **11***a* est majoritaire.

La connaissance des signaux fournis en rmn par les composés **7**, **9**, **11** et **13**, a permis par la suite d'analyser qualitativement et quantitativement les mélanges de ces composés par rmn à 100 MHz.

Résultats et discussion

Le composé **5***a*-*trans* conduit, par chauffage, aux quatre composés à chlore allylique **7***a*, **9***a*, **11***a* et **13***a*, accompagnés de faibles quantités de la lactone **6** (cf. tableau 1, essai 1). Cependant, l'extrapolation, pour un avancement très faible de la réaction, des proportions relatives des isomères **7***a* et **11***a* et de la lactone **6** est proche de zéro, alors que les composés **9***a* et **13***a* sont présents en quantité importante. Il est donc très vraisemblable que les trois composés **7***a*, **11***a* et **6** ont été formés par réarrangement thermique de **9***a* et **13***a*. Dans les mêmes conditions, le mélange des isomères **5***a* conduit à une proportion notable des isomères *cis* **7***a* et **11***a*, et cela même pour un avancement réduit de la transposition (essai 2). Le réarrangement cyclopropyle–allyle observé est donc stéréospécifique: l'isomère **5***a*-*trans* conduit aux composés *trans* **9***a* et **13***a* avec une stéréospécificité proche de 100%, et l'isomère *cis* conduit aux composés *cis* **7***a* et **11***a* avec, toutefois, un degré de stéréospécificité qu'il ne nous a pas été possible de mesurer. La règle de Woodward–Hoffmann–De Puy implique que c'est le chlore disposé en *syn* qui quitte la molécule (2, 16): par conséquent la stéréospécificité observée montre que l'atome de chlore revient sur la molécule du côté où il est parti, conformément aux observations précédentes reportées en série tricyclique et bicyclique (2, 3).

En ce qui concerne la participation du groupement méthoxycarbonyle, on constate que le pourcentage de la lactone **6** est relativement faible, et que, par extrapolation pour un avancement très faible de la réaction il tend vers zéro (essais 1 et 2). Ce résultat traduit clairement l'absence de participation à l'ouverture du noyau cyclopropanique, le peu de lactone **6** observé provenant d'une cyclisation des composés d'extension de cycle initialement formés **7***a*, **9***a*, **11***a* et **13***a*. Dans les composés **5***a*, le groupement méthoxycarbonyle est en mesure d'attaquer le noyau cyclopropanique avec inversion de configuration (cf. plus haut); l'absence

Can. J. Chem. Downloaded from www.nrcresearchpress.com by 210.87.254.5 on 09/05/12
For personal use only.

Can. J. Chem. Downloaded from www.nrcresearchpress.com by 210.87.254.5 on 09/05/12
For personal use only.

de participation n'est donc pas due à des contraintes stéréoélectroniques: elle pourrait, par contre provenir d'une nucléophilie insuffisante de l'ester carboxylique.

L'ouverture des acides carboxyliques **5***b*, dans lesquels le nucléophile interne est plus puissant que précédemment (17), conduit en effet à un pourcentage supérieur de la lactone **6** (essais 3 et 4). Mais les résultats obtenus dans ce cas peuvent être interprétés de deux façons. *Voie 1*. Il y aurait réarrangement thermique préalable en composés à chlore allylique, puis cyclisation d'une partie du mélange obtenu en lactone **6**. *Voie 2*. Il y aurait formation initiale de la lactone **6** par participation de l'acide carboxylique interne; la lactonisation entraînant la présence d'HCl dans le milieu réactionnel, cet acide pourrait alors ouvrir la lactone **6** pour conduire aux composés à chlore allylique **7***b*, **9***b*, **11***b* et **13***b*.

Il est donc très difficile de déterminer, dans ce cas, l'origine exacte des produits formés. Tout au plus, la comparaison des résultats fournis par le mélange des isomères **5***b* (*cis*/*trans* = 25:75; essai 3) et par l'isomère **5***b*-*trans* seul, essai 4, montre que dans le cas du mélange, une partie au moins des composés dichlorés ne provient pas de la lactone **6**; en effet, les composés **7***b* et **11***b*, présents dans le premier cas, sont absents dans le second et proviennent donc directement de l'isomère **5***b*-*cis*. En conséquence, la participation directe de l'acide carboxylique (voie 2 du schéma 5), si elle existe, n'entre pas seule en jeu. Afin de mieux appréhender le mécanisme qui intervient, nous avons réalisé l'ouverture des composés **5** dans des conditions différentes; en effet, l'utilisation de températures plus basses pouvait modifier les rapports de vitesse entre ouverture puis lactonisation (voie 1), ou lactonisation par participation et ouverture de la lactone (voie 2), et ainsi permettre d'opter pour l'un ou l'autre mécanisme. L'ouverture ne pouvait alors être atteinte en des temps raisonnables qu'en présence d'un solvant de grande constante diélectrique dont la fonction est d'accélérer le processus (18).

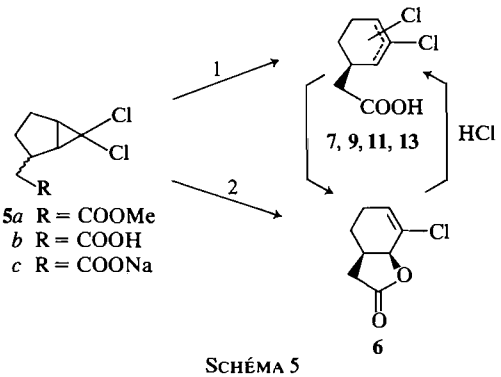

SCHÉMA 5

Nous avons choisi un solvant aqueux. Il fallait alors vérifier que l'emploi d'un tel solvant ne modifiait pas de façon notable le mécanisme, contrairement à ce qui est parfois proposé dans la littérature. En effet, l'ouverture dans de telles conditions des esters **5***a* (essai 5) conduit aux quatre composés à chlore allylique et à de faibles quantités de lactone **6**, comme c'était le cas lors de la thermolyse (essai 2); le caractère ionisant et dissociant du solvant utilisé n'implique donc pas, comme on pouvait le craindre, l'obtention directe d'un cation allylique dissocié, c'est à dire non impliqué dans une paire d'ions de type **1**, car celui-ci aurait conduit à des alcools par attaque du solvant (19*a*, *b*), et éventuellement à la lactone **6** par cyclisation intramoléculaire. Ce résultat mérite d'être souligné car l'obtention directe de cations allyliques à été invoquée (19), et récemment encore (20), lors d'ouverture d'halocyclopropanes en solution dans l'eau ou l'acide acétique. Après cette vérification, il était possible de poursuivre l'étude de l'ouverture des acides **5***b* en effectuant la réaction en présence de solvant polaire (essai 6); on obtient ici 47% de lactone **6** (dont nous avons vérifié la stabilité dans le milieu réactionnel) et 53% des composés à chlore allylique **7**, **11** et **13**; par conséquent, on met, ici en évidence que trois des composés à chlore allylique proviennent directement d'un réarrangement préalable en composés à chlore allylique (voie 1 du schéma 5). Les pourcentages relatifs observés pour ces composés sont alors très bien interprétés en fonction de leurs vitesses de lactonisation respectives, déterminées dans des conditions voisines, qui suivent l'ordre **9** > **11** ≫ **13** ≫ **7** (1); on comprend en effet aisément les taux très faible et nul des composés **11** et **9**, ceux-ci conduisant rapidement à la lactone **6**. Nous concluons donc, dans ce cas encore, à l'absence de participation du nucléophile interne à l'ouverture du noyau dichlorocyclopropanique; ce résultat paraît nettement en faveur d'un transfert de l'atome de chlore en position allylique totalement concerté (état de transition de type **2**), qui interdit la participation de tout nucléophile.

Nous avons enfin étudié le comportement des sels de sodium **5***c* dans lesquels le nucléophile interne est encore plus puissant. Ceux-ci conduisent (essais 7 et 8) à de fortes proportions de la lactone **6**, ce qui pouvait *a priori* faire penser à l'entrée en jeu d'une participation nucléophile interne. Mais nous savons que, dans des conditions semblables, les composés **9***c*, **11***c* et **13***c*, se lactonisent rapidement en composé **6** (1); nous avons

TABLEAU 2. Réactivité des composés **5***a*, **7***b* et **13***b* en milieu basique; produit réactionnel en % relatifs

Conditions[a]	Produit de départ	Avancement	Produit réactionnel[b]			
			5*b*	**8***b*	**10***b*	**12***b*
MeOH–H_2O (80:20)	**5***a*[c]	97	100	—	—	—
H_2O	**5***a*[c]	95	58[d]	27	2,5	12,5
	7*b*	100	—	25	4	71
	13*b*	100	—	82	2	16

[a]Les réactions sont menées en présence de 5 équivalents de soude.
[b]L'analyse a été réalisée dans tous les cas après estérification par le diazométhane.
[c]Mélange d'isomères *cis*/*trans* dans le rapport 25:75.
[d]Mélange d'isomères *cis*/*trans* dans le rapport 19:81.

également constaté que le composé **7***c*, pourtant le plus stable, évolue dans les conditions de l'ouverture (tableau 1, essai 9). On peut donc envisager, ici aussi, un réarrangement préalable en composés à chlore allylique, suivi d'une lactonisation rapide de trois d'entre eux (voie 1 du schéma 5). La présence du composé **7***c* en est révélatrice et cela d'autant plus que le pourcentage observé pour ce composé est inférieur au pourcentage réellement obtenu (le produit à réagi en partie) et que d'autre part ce pourcentage doit être rapporté à la proportion du composé **5***c*-*cis* dans le mélange d'isomères utilisé. On note également, lors de l'ouverture des composés **5***c*, la présence des alcools **10***c* et **12***c*; or leur formation directe par attaque des ions hydroxyles du solvant (rendu légèrement basique par la présence de sels de sodium d'acides carboxyliques) sur les composés **5***c* est improbable (3). Ces alcools peuvent donc résulter d'une attaque des ions hydroxyles, soit sur les composés **7***c*, **9***c*, **11***c* et **13***c* intermédiaires, soit sur la lactone **6**.[2] En milieu basique fort, on a vu que la lactone **6** conduit exclusivement à l'alcool **8**. Pourtant, dans ces conditions, l'ouverture des composés **5***c* donne également naissance aux alcools **10** et **12** (tableau 2, hydrolyse basique de **5***a*); par conséquent dans ce dernier cas au moins, et probablement dans le cas précédent, on peut conclure que les alcools observés résultent de l'hydrolyse des composés à chlore allylique et sont donc révélateurs de la formation intermédiaire de ces derniers (nous avons vérifié, cf. Tableau 2, que les composés **7***c* et **13***c*, issus des acides **7***b* et **13***b*, conduisent effectivement aux alcools **10***c* et **12***c* dans de telles conditions).

[2]On sait qu'en milieu faiblement basique, voire "neutre", l'hydrolyse d'esters peut se faire par rupture de la liaison alkyle–oxygène, ce qui permet, si le reste alkyle est un groupement allyle, l'entrée en jeu de réarrangements allyliques (21); la lactone **6** est donc théoriquement susceptible de conduire aux alcools **10** et **12**.

Conclusion

Malgré la présence d'un nucléophile interne puissant (groupement carboxylate), les composés **5***c* s'ouvrent donc eux aussi, comme les esters **5***a* et les acides **5***b*, en composés à chlore allylique selon la voie 1 du schéma 5. Ce résultat suggère, pour le réarrangement, un mécanisme concerté plutôt que par paire d'ions (schéma 1); en effet, nous avons montré par ailleurs (1) que pour les composés **9***c* et **11***c*, le groupement carboxylate interne déplace le chlore allylique très rapidement par participation intramoléculaire selon des processus S_N et S_N'; cette participation devrait donc se faire *à fortiori* sur une éventuelle paire d'ions intermédiaire de type **1** et conduire exclusivement à la lactone **6**.

Il faut donc remarquer que les résultats obtenus ici sont en désaccord avec ceux de Remy *et al.* qui concluent à l'existence de phénomènes de participation dans l'ouverture thermique d'halocyclopropanes (22).

Partie expérimentale

Indications générales

Les points de fusion, non corrigés, ont été déterminés en capillaire à l'aide de l'appareil du Dr. Tottoli. Les chromatographies en phase vapeur (cpv) ont été réalisées dans l'une des conditions suivantes précisée pour chaque cas; condition A: appareil Carlo Erba Fractovap GT série 200 à ionisation de flamme équipé d'une colonne de 2 m × 2 mm de remplissage 5% SE 30 sur CGLA 80/100 mesh; condition B: appareil Intersmat IGC 120 DFL à ionisation de flamme équipé d'une colonne de 1,5 m × 1/8 in. de remplissage 10% SE 30 sur PAW 80/100 mesh; on indiquera le temps de rétention (t_r), la température de colonne (T_c) et la pression de gaz vecteur (P). Les spectres ir ont été enregistrés sur spectrophotomètre Perkin Elmer 221 ou 377 en solution 0,2 *M* sauf indication contraire. Les spectres de rmn ont été enregistrés à 60 MHz et température ambiante sur appareil Varian modèle EM-360 ou A-60; pour les spectres enregistrés à 90 et 100 MHz (précisé dans chaque cas) nous avons utilisé les modèles EM-390 et HA-100; les déplacements chimiques sont donnés en ppm (référence interne TMS); les lettres s, d, t, q et m signifient respectivement singulet, doublet, triplet, quadruplet et multiplet. Les analyses centésimales ont été effectuées au laboratoire de Microanalyse du C.N.R.S. à l'E.N.S.C. de Montpellier.

Can. J. Chem. Downloaded from www.nrcresearchpress.com by 210.87.254.5 on 09/05/12
For personal use only.

Can. J. Chem. Downloaded from www.nrcresearchpress.com by 210.87.254.5 on 09/05/12
For personal use only.

(Dichloro-6,6 bicyclo[3.1.0]hexyl-2) acétates de méthyle cis *et* trans, *5*a

La cyclopropanation du (cyclopenténYl-3)acétate de méthyle est réalisée selon réf. 23, sous atmosphère d'azote sec. Pour 14 g d'oléfine, on utilise 18,5 g de MeONa et 59 g de CCl_3—COOMe. On obtient par distillation 2,7 g d'un mélange d'oléfine de départ et de composés d'addition **5***a*, puis 18,5 g (83%) de ces derniers: $Eb_{0,5}$ 100°C; cpv (conditions A) t_r 10 min 40 s, T_c 130 à 180°C (4°C/min), P 1,55 à 1,75 bar; ir ($CHCl_3$): 1735 (C=O) cm^{-1}; rmn ($CDCl_3$) δ: 3,71 (s, 3H, COOMe), 1,2 à 3,0 (m, 9H); rmn ($CDCl_3$ avec 0,1 mol d'Eu(DPM)$_3$ par mol de substrat) principaux signaux à δ: 4,26 (s, 0,75H, COOMe de **5***a-cis*), 4,05 (s, 2,25H, COOMe de **5***a-trans*).

Acides (dichloro-6,6 bicyclo[3.1.0]hexyl-2) acétiques cis *et* trans, *5*b

On agite 1 h à 20°C, 25 g des esters **5***a* dans 200 cm^3 de MeOH–H_2O (80:20) contenant 22,5 g de NaOH. On élimine le méthanol sous pression réduite sans chauffer. Les eaux sont lavées à l'éther et acidifiées à froid (HCl 50%). On extrait à l'éther; les éthers sont lavés (H_2O), séchés (Na_2SO_4), puis concentrés, ce qui laisse 22,8 g (97%) des acides **5***b* homogènes en ccm. Un échantillon très pur du mélange a été obtenu par filtration sur colonne de silice avec éther–éther de pétrole – acide formique (29,5:69,5:1); ir ($CHCl_3$): 1710 (C=O) cm^{-1}; rmn ($CDCl_3$) δ: 11,3 (s, large, 1H, COOH), 1,25 à 3,0 (9H). *Anal.* calc. pour $C_8H_{10}Cl_2O_2$: C 45,93, H 4,78, Cl 33,97; trouvée: C 46,1, H 5,0, Cl 34,2%.

Séparation de l'isomère 5b-trans

Selon la technique de Fouquey *et al.* (24), on ajoute à froid 21,8 g de dicyclohexylamine à 25 g d'acides **5***b*. Le sel formé cristallise rapidement en présence de quelques gouttes d'acétate d'éthyle; F 126–127°C (AcOEt). Celui-ci est dissous dans 50 cm^3 d'eau et 200 cm^3 de méthanol. On ajoute à froid une solution aqueuse de soude 0,5 *N* jusqu'à pH ≃ 10. Le méthanol est éliminé sous pression réduite à 20°C. Les eaux sont lavées (Et_2O), acidifiées (HCl 50%) et extraites à l'éther. Les éthers sont lavés (H_2O), séchés (Na_2SO_4) et concentrés. On recueille ainsi 5,2 g (20,8%) d'acide **5***b-trans* dont 2,0 g sont estérifiés par un excès de diazométhane en solution éthérée conduisant à 2,0 g (94%) d'ester **5***a-trans*: ir (film): 3030 C—H cyclopropyliques), 1740 C=O) cm^{-1}; rmn ($CDCl_3$) δ: 3,71 (s, 3H, COOMe), 1,2 à 3,00 (m, 9H); rmn ($CDCl_3$ avec 0,13 mol d'Eu(DPM)$_3$ par mol de substrat) principaux signaux à δ: 4,4 (s, 0,09H, COOMe de **5***a-cis*), 4,15 (s, 2,91H, COOMe de **5***a-trans*). *Anal.* calc. pour $C_9H_{12}Cl_2O_2$: C 48,43, H 5,38; trouvée: C 49,0, H 5,6%.

(Bicyclo[3.1.0]hexyl-2) acétate de méthyle-trans, ***14***a

On opère selon réf. 25; dans un ballon de 250 cm^3 balayé par de l'azote sec et muni d'une ampoule à égalisation de pression, on piège, en refroidissant à −70°C, 75 cm^3 d'ammoniac. On y additionne 1,8 g de sodium, puis goutte à goutte, 7 g d'ester **5***a-trans* en solution dans 35 cm^3 d'éther anhydre. Après 1/2 h d'agitation, on ajoute 4,2 g de chlorure d'ammonium, laisse évaporer l'excès d'ammoniac, ajoute un peu d'eau, puis extrait à l'éther. Les éthers sont séchés (Na_2SO_4) puis concentrés. Par chromatographie sur colonne de silice avec éther – éther de pétrole (10:90), on isole 1,24 g (18%) d'ester **5***a-trans* (ccm, rmn), et 1,65 g (34%) de composé **14***a-trans*. Infrarouge (CCl_4): 3070 et 3030 (C—H cyclopropylique), 1750 (C=O) cm^{-1}; rmn (CCl_4) δ: 3,60 (s, 3H, COOMe), 0,6 à 0,26 (m, 9H), 0,0 à 0,6 (m, 2H). Par addition d'Eu(DPM)$_3$ le singulet correspondant à COOMe se dédouble, laissant apparaître moins de 3% de **14***a-cis*.

Acide (bicyclo[3.1.0]hexyl-2)acétique trans, ***14***b

On agite 1,54 g d'ester **14***a* dans 25 cm^3 de MeOH–H_2O (80:20) contenant 2 g de soude pendant 2 h à 20°C. On élimine le méthanol sous pression réduite sans chauffer, puis lave à l'éther. On acidifie à froid (HCl 50%) et extrait à l'éther. Les éthers sont lavés (H_2O), séchés (Na_2SO_4) et concentrés sous pression réduite, ce qui laisse 1,25 g (89% d'acide **14***b-trans* homogène en ccm; ir (CCl_4): 1710 (C=O) cm^{-1}; rmn (CCl_4) δ: 11,5 (s large 1H, COOH), 2,1 à 2,7 (m, 3H), 1,0 à 2,1 (m, 6H) 0,0 à 0,6 (m, 2H). *Anal.* calc. pour $C_8H_{12}O_2$: C 68,57, H 8,57; trouvée: C 68,2, H 8,6%.

Chlorométhyl-2 bicyclo[3.1.0]hexane-trans, ***15***

On traite 1,12 g d'acide **14***b* selon la méthode de Kochi (26). On obtient ainsi 470 mg (45%) du composé **15***-trans* homogène en ccm; ir (film): 3070 et 3040 (C—H cyclopropylique) cm^{-1}; rmn (CCl_4, 100 MHz) δ: 3,35 et 3,26 (parties A et B de ABX, J_{AB} = 10,4 Hz, J_{AX} = 7,1 Hz, J_{BX} = 7,6 Hz, CH_2Cl), 2,28 (quatre raies, partie X de ABX dédoublée avec $J \simeq 7$, *CH*—CH_2Cl), 0,7 à 1,8 (m, 8H).

Chlorométhyl-2 bicyclo[3.1.0]hexane-cis, ***15***

A une suspension agitée de 1,52 g d'$AlLiH_4$ dans 30 cm^3 d'éther, on ajoute lentement 7 g d'ester **16***-cis* obtenu selon (9). On observe un reflux puis agite encore à température ambiante pendant 3 h. Après hydrolyse par le sel de Seignette, on décante la phase organique puis distille. On recueille 3,9 g (62%) d'hydroxyméthyl-2 bicyclo[3.1.0]hexane-*cis*; Eb = 87°C; ir (CCl_4): 3630 et 3100 à 3600 (O—H) cm^{-1}; rmn (CCl_4) δ: 4,12, (s, 1H, se déplace par dilution, O*H*), 3,50 (d, 2H, J = 7 Hz, CH_2OH), 2,0 à 2,7 (m, 1H, *CH*—CH_2OH), 0,5 à 2,0 (6H), 0,0 à 0,5 (m, 2H). *Anal.* calc. pour $C_7H_{12}O$: C 75,00, H 10,71; trouvée: C 75,0, H 10,5%.

Dans un ballon à deux tubulures équipé d'un réfrigérant avec garde à H_2SO_4 et ampoule à brome, on place 3,7 g de l'alcool précédent et 2,6 g de pyridine dans 40 cm^3 d'éther anhydre. On ajoute lentement à 0°C 4,28 g de $SOCl_2$; le chlorhydrate de pyridinium précipite immédiatement. Lorsque l'addition est terminée, on porte au reflux 2 h, filtre, concentre sous pression réduite et distille. On isole 1,5 g (35%) du composé **15** *cis* homogène en ccm; ir (film): 3072 et 3040 (C—H cyclopropyliques) cm^{-1}; rmn (CCl_4, 100 MHz) δ: 3,46 et 3,37 (parties A et B de ABX, J_{AB} = 10,5 Hz, J_{AX} = 7,4 Hz, J_{BX} = 6,9 Hz, 2H, CH_2Cl), 2,30 à 2,70 (m, 1H, *CH*—CH_2Cl), 0,5 à 2,0 (6H), 0,0 à 0,5 (m, 2H). *Anal.* calc. pour $C_7H_{11}Cl$: C 64,36, H 8,43; trouvée: C 64,5, H 8,4%.

Mélange des isomères cis *et* trans *du (bicyclo[3.1.0]hexyl-2)-acétate de méthyle,* ***14***a

La méthode utilisée ci-dessus pour l'obtention du composé **14***a-trans*, a été appliquée à 2,2 g de mélange des isomères **5***a* (*cis*/*trans* = 25:75). Après traitement identique, on obtient 0,33 g (15%) de mélange d'isomères **5***a* (ccm, rmn) et 0,48 g (32%) de mélange d'isomères **14***a*; ir (CCl_4): 3070 et 3030 (C—H cyclopropyliques), 1750 (C=O) cm^{-1}; rmn (CCl_4) δ: 3,60 (s, 3H, COO*M*e), 0,6 à 0,26 (m, 9H), 0,0 à 0,6 (m, 2H). Par addition d'Eu(DPM)$_3$ le singulet correspondant à COOMe se dédouble, indiquant la présence des isomères *cis* et *trans* dans les proportions respectives de 25:75.

(Dichloro-2,3 cyclohexényl-6)acétate de méthyle-cis, ***11***a

A 10 g d'alcool **8***a*, on additionne lentement à froid sous azote 11,9 g de chlorure de thionyle fraîchement distillé, puis agite 2 h à température ambiante (l'avancement est suivi par ccm). On étend à l'éther, basifie à froid (Na_2CO_3 10%) et décante la phase organique; celle-ci est lavée (H_2O/NaCl), séchée (Na_2SO_4) et concentrée. On recueille 9,3 g de mélange des produits **6** (60%) et **7***a*, **9***a*, **11***a* et **13***a* (40%) d'après la ccm et la rmn. Par chromatographie sur colonne de silice avec éther – éther de pétrole (20:80) de 5 g de mélange, on isole 132 mg (2,25%) de mélange possédant la composition suivante: **7***a* (3%), **9***a* (26%), **11***a* (61%), **13***a* (10%) et 2,03 g (33,4%) de mélange des mêmes produits dans les proportions respectives de 11%, 34%, 45% et

Can. J. Chem. Downloaded from www.nrcresearchpress.com by 210.87.254.5 on 09/05/12
For personal use only.

10%. La rmn du mélange contenant le composé **11***a* à 61% permet d'attribuer à ce dernier les signaux suivants ($CDCl_3$, 90 MHz) δ: 5,88 (dd, 1H, J = 2,3 et 0,9 Hz, H éthylénique), 4,48 (m, 1H, $W_{\frac{1}{2}}$ = 7,5 Hz, CHCl), 3,70 (s, 3H, COOMe).

(Dichloro-2,3 cyclohexényl-4)acétate de méthyle-trans-*9*a

Ce composé a été préparé à partir de 3,3 g de Ph_3P et 1,0 g d'alcool **8***a* selon la technique décrite par Fleming et Thomas (3). On récupère 3,8 g de produit brut contenant la lactone **6** et un mélange des composés dichlorés dans les proportions 30:70 (ccm, rmn). Par chromatographie sur colonne de silice avec éther – éther de pétrole (30:70), on isole les composés dichlorés: 649 mg (60%) de **9***a* (souillé toutefois par 15% de son isomère **11***a*); ir (CCl_4): 1742 (C=O), 1647 (C=C) cm^{-1}; rmn ($CDCl_3$, 100 MHz) δ: 6,04 (t, 1H, J = 3,9 Hz, H éthylénique), 4,3 (m à allure de d, $J \simeq 3,5$ Hz, CHCl), 3,69 (s, 3H, COOMe), 1,4 à 2,8 (m, 7H). *Anal.* calc. pour $C_9H_{12}Cl_2O_2$: C 48,43, H 5,38, Cl 31,83; trouvée: C 48,2, H 5,3, Cl 30,8%.

Acides (dichloro-2,3 cyclohexényl-4) et (dichloro-2,3 cyclohexényl-6)acétiques 7b *et* 13b. *Esters méthyliques correspondants* 7a *et* 13a

On prépare 9,3 g de mélange des isomères **7***a*, **9***a*, **11***a* et **13***a* et de la lactone **6** par action du chlorure de thionyle sur l'alcool **8***a* (cf. ci-dessus). Le mélange est enrichi en composés recherchés **7***a* et **13***a* par chauffage 5 h à 160°C (équilibrage thermodynamique), puis hydrolysé par agitation 1 h à 20°C avec une solution de 4 g de NaOH dans 80 cm^3 de méthanol et 20 cm^3 d'eau. On étend à l'eau, acidifie à froid (HCl 50%) et extrait par une quantité importante d'acétate d'éthyle. La phase organique est lavée (H_2O), séchée (Na_2SO_4) et concentrée, ce qui laisse 9 g de produit brut contenant les composés **7***b*, **13***b* et **6** (ccm, rmn). Par chromatographie sur colonne de silice avec éther – éther de pétrole – acide formique (29,5:69,5:1), on parvient à isoler avec difficulté 400 mg (3,9%) d'acide **7***b* et 300 mg (2,9%) d'acide **13***b*; 140 mg du premier et 125 mg du second ont été estérifiés par action d'un excès de diazométhane en solution éthérée pour conduire respectivement à 140 mg (94%) d'ester **7***a* et 126 mg (94%) d'ester **13***a*.

Acide **7***b*: F 156–158°C (éther – éther de pétrole); ir (KBr): 1700 (C=O) cm^{-1}; rmn ($CDCl_3$) δ: 9,44 (s, 1H, COOH), 6,05 (t élargi, 1H, J = 4 Hz, H éthylénique), 4,69 (s, 1H, $W_{\frac{1}{2}}$ = 4,6 Hz, CHCl), 1,5 à 2,9 (7H). *Anal.* calc. pour $C_8H_{10}Cl_2O_2$: C 45,93, H 4,78, Cl 33,97; trouvée C 46,2, H 4,8, Cl 33,8%.

Ester **7***a*: rmn ($CDCl_3$) δ: 5,97 (t, 1H, J = 3,8 Hz, H éthylénique), 4,61 (s, 1H, $W_{\frac{1}{2}}$ = 5 Hz, CHCl), 3,69 (s, 3H, COOMe), 2,1 à 2,9 (5H), 1,2 à 1,9 (2H).

Acide **13***b*: rmn (acétone-d_6) δ: 6,1 (d, 1H, J = 4,5 Hz, H éthylénique), 4,63 (t mal résolu, 1H, J = 4,2 Hz, CHCl), 1,0 à 3,0 (m, 7H).

Ester **13***a*: rmn ($CDCl_3$) δ: 5,97 (d, 1H, J = 4,5 Hz, H éthylénique), 4,47 (t, 1H, J = 3,5 Hz, CHCl), 3,70 (s, 3H, COOMe), 1,2 à 3,1 (7H).

Traitement basique des composés 5a, 7b *et* 13b: *obtention de la lactone* 6 *et des alcools* 10 *et* 12

(*a*) On agite 20 h à 20°C, 10 g de **5***a* (*cis*/*trans* = 25:75) dans 105 cm^3 d'une solution de soude à 8%. On lave à l'éther, acidifie à froid (HCl 50%) et extrait à AcOEt. La phase organique est lavée (H_2O/NaCl), séchée (Na_2SO_4), concentrée puis estérifiée immédiatement par action d'un excès de diazométhane en solution éthérée. On recueille un mélange composé des produits **5***a*, **8***a*, **10***a* et **12***a* (ccm, rmn); 4,3 g de ce mélange sont chromatographiés sur colonne de silice avec éther – éther de pétrole (25:75). L'alcool **8***a* se cyclise en lactone **6** sur la colonne et on recueille 100 mg d'alcool **10***a* souillé de lactone **6**, 360 mg d'alcool **12***a* souillé de lactone **6** et 780 mg (23,5%) de cette lactone. Deux nouvelles chromatographies permettent d'isoler 78 mg (1,8%) d'alcool **10***a* et 306 mg (7,9%) d'alcool **12***a*. L'analyse quantitative du produit de la réaction est indiquée ci-dessous en (*c*).

γ-*Lactone de l'acide (chloro-2 hydroxy-3 cyclohexényl-4)-acétique*-cis, *6*: F 76–77°C (ether–acétone); cpv (conditions B) t_r 15 min 50 s, T_c 130 à 170°C (4°C/min), P 1,2 à 1,3 bar; ir ($CHCl_3$): 1780 avec inflexion à 1755 (C=O), 1650 (C=C) cm^{-1}; rmn ($CDCl_3$, 100 MHz) δ: 6,21 (t, 1H, J = 4,2 Hz, H éthylénique), 4,76 (d, 1H, J = 5,5 Hz, CH—O—CO), 1,2 à 3,0 (m, 7H). *Anal.* calc. pour $C_8H_9ClO_2$: C 55,65, H 5,22, Cl 20,58; trouvée: C 55,5, H 5,2, Cl 20,5%.

(Chloro-2 hydroxy-3 cyclohexényl-4) acétate de méthyle-trans *10*a: F 48–53°C; ir ($CHCl_3$): 3596 et 3450 large (O—H), 1730 (C=O), 1650 (C=C) cm^{-1}; rmn ($CDCl_3$) δ: 5,97 (t, 1H, J = 3,8 Hz, H éthylénique), 3,97 (d, 1H, J = 5,5 Hz, CH—OH), 3,71 (s, 3H, COOMe), 3,60 (s, 1H, se déplace par dilution, H hydroxylique), 1,2 à 1,3 (m, 7H). *Anal.* calc. pour $C_9H_{13}ClO_3$: C 52,94, H 6,37, Cl 17,15; trouvée: C 53,4, H 6,4, Cl 16,4%.

(Chloro-2 hydroxy-3 cyclohexényl-6) acétate de méthyle-cis, *12*a: rmn ($CDCl_3$) δ: 5,84 (d, 1H, J = 2,5 Hz, éthylénique), 4,17 (t mal résolu, 1H, $J \simeq 5$ Hz, H carbinolique), 3,70 (s, 3H, COOMe), 3,45 (s large, se déplace par dilution, H hydroxylique), 1,2 à 2,8 (7H).

(*b*) *Obtention des acides* 10b *et* 12b

On agite 1 h, à 20°C, 440 mg de **10***a* dans 5 cm^3 de H_2O–MeOH (20:80) contenant 440 mg de NaOH; on étend à l'eau, lave à l'éther, acidifie à froid (HCl 50%) et extrait à l'éther. Les éthers, lavés (H_2O), séchés (Na_2SO_4) et concentrés conduisent à 350 mg (87%) d'acide **10***b* homogène en ccm: F 107–109°C; rmn (acétone-d_6) δ: 6,5 à 7,5 (m, 2H, —COOH et —OH), 5,93 (t, 1H, J = 4,0 Hz, H éthylénique), 3,93 (d, 1H, J = 6,0 Hz, H carbinolique), 1,2 à 3,0 (m, 7H). De la même façon, à partir de 592 mg de **12***a* on recueille 500 mg (90%) d'acide **12***b*: rmn ($CDCl_3$) δ: 7,51 (s large, 2H, COOH et OH), 5,92 (d, 1H, J = 2,0 Hz, H éthylénique), 4,18 (s, 1H, $W_{\frac{1}{2}}$ = 7,0 Hz, H carbinolique), 2,2 à 2,9 (m, 3H), 1,5 à 3,2 (m, 4H).

(*c*) La détermination des pourcentages des composants avant séparation a été réalisée en partie par rmn à 100 MHz; nous avons ensuite acétylé le produit brut précédent. Si les principaux signaux fournis en rmn par les composés **8***a* et **10***a* sont superposés, il n'en est pas de même au niveau des acétates correspondants. (La synthèse de ces derniers est indiquée ci-dessous en (*d*).) L'acétylation est menée sur 1 g de produit brut par 1,4 cm^3 d'anhydride acétique dans 14 cm^3 de pyridine; après 15 h d'abandon à 20°C, on ajoute de la glace et extrait à l'acétate d'éthyle. La pyridine est éliminée par lavage avec une solution saturée de $CuSO_4$ jusqu'à absence de changement de couleur. On lave à l'eau, au carbonate de sodium 10% et enfin avec une solution saturée de NaCl. On sèche (Na_2SO_4), concentre et chromatographie sur colonne de silice avec éther – éther de pétrole (10:90 varie graduellement jusqu'à 40:60) ce qui conduit à 410 mg (41%) de **5***a* (*cis*/*trans* = 19:81) et 525 mg de mélange des acétates correspondants à **8***a*, **10***a* et **12***a* (47,5%).

(*d*) Cent milligrammes de l'alcool **10***a* et 288 mg de l'alcool **12***a* sont acétylés séparément par la technique utilisée plus haut. On isole, par chromatographie sur colonne de silice avec éther – éther de pétrole (30:70), 37 mg (31%) d'acétate correspondant à **10***a*; rmn ($CDCl_3$) δ: 6,10 (t, 1H, J = 4,07 Hz, H éthylénique), 5,30 (signal large, 1H, $W_{\frac{1}{2}}$ = 8,3 Hz, CHOAc), 3,70 (s, 3H, COOMe), 1,3 à 2,7 (10H avec s à 2,11, $OCOCH_3$). On obtient par ailleurs 237 mg (68%) d'acétate correspondant à **12***a*; ir ($CHCl_3$): 1735 (C=O), 1650 (C=C) cm^{-1}; rmn ($CDCl_3$) δ: 6,05 (d, 1H, J = 2,2 Hz, H éthylénique), 5,36 (signal large, 1H, $W_{\frac{1}{2}}$ = 8 Hz, CHOAc), 3,70 (s, 3H, COOMe), 1,0 à 3,0 (m, 10H). *Anal.* calc. pour $C_{11}H_{15}ClO_4$: C 53,55, H 6,09; trouvée: C 53,8, H 6,3%.

(*e*) *Réactivité des composés* 7b *et* 13b

On place séparément 135 mg des composés **7***b* et **13***b* dans les conditions de l'hydrolyse des composés **5***a* (cf. plus haut en (*a*))

Can. J. Chem. Downloaded from www.nrcresearchpress.com by 210.87.254.5 on 09/05/12
For personal use only.

puis traite de façon identique. La composition des mélanges obtenus est déterminée comme paragraphe (*c*), mais l'absence de composés de type **5** a rendu inutile la chromatographie du mélange obtenu par acétylation. Les valeurs obtenues sont portées dans le tableau 2.

(Chloro-2 hydroxy-3 cyclohexényl-4)acétate de méthyle-cis, *8*a

On agite 20 h, à 20°C, 5 g de lactone **6** et 5,8 g de NaOH dans 67 cm³ d'eau. Puis on lave à l'éther, acidifie (HCl 50%) et extrait à l'acétate d'éthyle. La phase organique est lavée à l'eau, séchée (Na_2SO_4), concentrée sous pression réduite et immédiatement estérifiée par action d'un excès de diazométhane en solution éthérée. Après traitement on recueille 5,7 g (96%) de **8***a* contenant une trace de lactone **6** (ccm, rmn). Le composé a été purifié par filtration sur colonne de silice avec éther – éther de pétrole (70:30). Dans ces conditions le produit se cyclise intensivement en lactone **6**, mais on parvient à isoler 400 mg d'alcool **8***a* pur; ir ($CHCl_3$): 1729 (C=O), 1652 (C=C) cm^{-1}; rmn ($CDCl_3$) δ: 5,94 (t, 1H, J = 4,0 Hz, H éthylénique), 4,10 (dd, 1H, J = 5,5 et 3,5 Hz, H carbinolique), 3,65 (s, 3H, COOMe), 3,02 (d, 1H, J = 5,5 Hz, OH), 1,9 à 2,8 (m, 5H), 1,3 à 1,7 (m, 2H); par addition de CF_3COOH, le produit se lactonise rapidement en lactone **6**; on note auparavant les transformations suivantes: 4,1 (d, J = 3,5 Hz, H carbinolique), disparition du signal à 3,02. *Anal.* calc. pour $C_9H_{13}ClO_3$: C 52,94, H 6,37, Cl 17,15; trouvée: C 52,9, H 6,4, Cl 17,0%.

Ce composé a été acétylé selon la technique habituelle pour obtenir un composé présentant le spectre de rmn suivant, δ: 6,10 (t, 1H, J = 4,0 Hz, H éthylénique), 5,5 (signal large, 1H, $W_{\frac{1}{2}}$ = 6,0 Hz, CHOAc), 3,67 (s, 3H, COOMe), 0.7 à 2,8 (10H avec s à 2,1; O—$COCH_3$).

Réduction de la lactone 6; lactone de l'acide (hydroxy-2 cyclohexyl)acétique cis, *17*

Selon réf. 27, on agite 1 h, à 20°C, 400 mg de lactone **6** dans une solution THF–H_2O (30:70) 0,3 *M* en NaOH, puis hydrogène 2 h 30 min à 20°C, sous pression atmosphérique, en présence de 200 mg de Pd/C 10%. On filtre, acidifie à froid (HCl 50%) et extrait à l'acétate d'éthyle. La phase organique est lavée (H_2O), séchée (Na_2SO_4) et concentrée, puis chauffée 1/2 heure en présence de benzène et d'acide *p*-toluène sulfonique dans un ballon équipé d'un décanteur à eau. On étend à l'éther, lave rapidement ($NaHCO_3$ dilué), séche (Na_2SO_4) et concentre. Par chromatographie sur colonne de silice avec éther – éther de pétrole (20:80) on isole 80 mg (48%) de lactone **17** identique à un échantillon authentique (8).

*Réduction de l'alcool 8*a: *(hydroxy-2 cyclohexyl)acétate de méthyle* cis, *18*

On hydrogène 18 h à 20°C et sous pression atmosphèrique 1 g d'alcool **8***a* en présence de 430 mg de Pd/C 10% dans 50 cm³ de méthanol et 1 cm³ de pyridine. On étend à l'éther, filtre, extrait à AcOEt. La phase organique est lavée à l'eau, puis avec une solution saturée de sulfate de cuivre (jusqu'a absence de changement de coloration), enfin à l'eau, séchée (Na_2SO_4) et concentrée. Par chromatographie sur colonne de silice avec éther – éther de pétrole (30:70), on obtient 406 mg (48%) d'alcool **18** homogène en ccm; ir ($CHCl_3$): 3610 et 3460 large (O—H), 1729 (C=O) cm^{-1}; rmn ($CDCl_3$) δ: 3,9 (signal large, 1H, H carbinolique), 3,68 (s, 3H, COOMe), 1,1 à 2,7 (m, 12H avec pic à 2,53 qui se déplace par dilution, OH). *Anal.* calc. pour $C_9H_{16}O_3$: C 62,79, H 9,30; trouvée: C 63,3, H 9,2%.

Cyclisation de l'alcool 18: lactone 17

On agite 1 h 45 min, à 20°C, 400 mg de **18** dans 100 cm³ de MeOH–H_2O (80:20) contenant 0,48 g de soude. On étend à l'eau, élimine le méthanol sous pression réduite, lave à l'éther, acidifie à froid (HCl 50%) et extrait à l'acétate d'éthyle. La phase organique est lavée à l'eau, séchée (Na_2SO_4) et concentrée. Le produit brut est chauffé 1 h 15 min au reflux du benzène en présence d'acide *p*-toluène sulfonique dans un ballon muni d'un décanteur à eau. Puis on lave à l'eau, sèche (Na_2SO_4) et concentre. Par chromatographie sur colonne de silice avec éther – éther de pétrole (20:80), on recueille 229 mg (70%) de lactone **17** (ccm, rmn, ir).

*Réduction de l'alcool 12*a: *hydroxy acide 19*

Quatre cent dix milligrammes d'alcool **12***a* sont réduits comme ci-dessus (réduction de **8***a*). On isole 159 mg (50%) de (hydroxy-4 cyclohexyl)acétate de méthyle *cis*; ir (CCl_4): 3645 et 3480 large (O—H), 1750 (C=O) cm^{-1}; rmn ($CDCl_3$) δ: 3,96 (signal large, 1H, H carbinolique), 3,69 (s, 3H, COOMe), 3,3 (signal large, 1H, O—H), 2,1 à 2,4 (2H), 0.8 à 2,0 (9H). *Anal.* calc. pour $C_9H_{16}O_3$: C 62,79, H 9,30; trouvée: C 63,2, H 9,5%.

Cent trente-cinq milligrammes de cet ester sont agités 48 h à 20°C dans 3,7 cm³ de soude à 8% dans MeOH–H_2O (80:20). On étend à l'eau, élimine le méthanol sous pression réduite, lave (Et_2O), acidifie à froid (HCl 20%) et extrait AcOEt. La phase organique est séchée (Na_2SO_4), concentrée et chromatographiée sur colonne de silice avec éther – éther de pétrole – acide formique (69,5: 29,5:1). On récupère ainsi 27 mg du composé **19** identique à l'échantillon authentique préparé ci-dessous (F, ccm, ir).

Préparation de l'hydroxy-acide 19

On oxyde selon réf. 7 1,7 g de bicyclo [2.2.2] octanone-2 (14) par 3,1 g d'acide *m*-chloroperbenzoïque et 1,15 g de $NaHCO_3$ dans 100 cm³ de CH_2Cl_2. On lave par NaOH 5%, puis à l'eau saturée de NaCl, sèche (Na_2SO_4) et concentre sous pression réduite. Par chromatographie sur colonne de silice avec éther – éther de pétrole (60:40), on isole (*a*) 235 mg d'un composé de F 170°C; rmn ($CDCl_3$) δ: 4,30 (d, 2H, J = 3,6 Hz), 1,4 à 3,0 (10 H); (*b*) 1,1 g (57%) de lactone de l'acide (hydroxy-4 cyclohexyl)-acétique: F 146°C (litt. (14) F 145–148°C); rmn ($CDCl_3$) δ: 4,52 (signal large, 1H, $W_{\frac{1}{2}}$ = 4 Hz, CHOCO), 2,86 (d, 2H, J = 3,5 Hz, CH_2COO), 1,5 à 2,4 (9H).

On agite 2 h, à 20°C, 500 mg de la lactone de F 146°C obtenue ci-dessus dans 30 cm³ de soude aqueuse à 5%. On acidifie à froid (HCl 50%), puis extrait à l'acétate d'éthyle. La phase organique est séchée (Na_2SO_4) et concentrée. Après recristallisation on isole 385 mg (68%) d'acide **19**; F 139–140°C (AcOEt) (litt. (14) F 139–140°C); ir (KBr): 2400 à 3400 et 3440 (O—H), 1711 (C=O) cm^{-1}.

*Equilibrage thermique des composés 7*a, *9*a *et 11*a

Chacun des produits est chauffé, sous pression atmosphérique, à 160 ± 1°C. L'avancement est suivi par rmn à 60 MHz. Lorsque les pourcentages relatifs des quatre isomères ne varient plus que lentement, on enregistre le spectre de rmn à 100 MHz qui permet l'analyse du mélange obtenu (pour le réarrangement du composé **9***a*, la composition du produit obtenu a été évaluée à partir du spectre de rmn à 60 MHz). On obtient les résultats suivants:

		Produit de réarrangement en % relatifs				
Produit de départ	t_h	**6**	**7***a*	**9***a*	**11***a*	**13***a*
7*a* (140 mg)	2,5	9	28	14	38	11
9*a* (571 mg)	6	9	6	31	9	45
11*a* (126 mg)	5	17	12	18	19	34

Can. J. Chem. Downloaded from www.nrcresearchpress.com by 210.87.254.5 on 09/05/12
For personal use only.

Lactonisation des composés 8b, *10*b *et 12*b

Dans un ballon de 250 cm³ équipé d'un décanteur à eau, on place 527 mg formés de 74% de **8***b*, 8% de **10***b* et 18% de **12***b*, 70 cm³ de benzène anhydre et 350 mg d'acide *p*-toluènesulfonique. On porte au reflux du benzène et suit l'avancement en ccm; après 2 h 30 min, on étend à l'éther, lave au carbonate de sodium 2% puis à l'eau. La phase organique, séchée (Na_2SO_4) puis concentrée, laisse 740 mg (98%) de lactone **6**. La phase aqueuse basique est acidifiée à froid (HCl 50%) puis extraite à l'acétate d'éthyle; après séchage (Na_2SO_4) et concentration, on obtient 70 mg de résidu contenant seulement des traces de lactone **6**.

Ouverture thermique des composés 5

Les produits sont placés en ampoules scellées (300 mg par ampoule) dans un bain d'huile à 130 ± 1°C. Les ampoules, prélevées une à une, sont refroidies par un bain de glace. L'avancement est déterminé, en rmn (60 MHz) par intégration des protons vinyliques apparus. La composition des mélanges réactionnels est déterminée par analyse du spectre de rmn à 100 MHz (après estérification par le diazométhane dans le cas des acides **5***b*, sauf pour l'acide **5***b-trans* pour lequel la composition est évaluée d'après le spectre de rmn à 60 MHz du mélange d'acides obtenu). Les résultats sont consignés dans le tableau 1.

Ouverture en solution des acides 5a *et* 5b

On agite 165 h, à 40°C, 2 g de mélange d'esters **5***a* (*cis*/*trans* = 25:75) dans 210 cm³ d'acétone et 91 cm³ d'eau. On prélève 75 cm³ que l'on étend à l'eau; l'acétone est éliminée sous pression réduite à 20°C puis on extrait à l'éther. Les éthers, lavés (H_2O/NaCl), séchés (Na_2SO_4) puis concentrés, laissent 498 mg de produit brut dont la composition est déterminée par analyse du spectre de rmn à 100 MHz. L'avancement de l'ouverture est mesuré, comme dans le cas de l'ouverture thermique, par l'intégration, en rmn, des signaux dus aux protons vinyliques des produits formés. On traite de la même façon 1,1 g de mélange d'acides **5***b* (*cis*/*trans* = 25:75). Ce produit brut est cependant estérifié par un excès de diazométhane en solution éthérée pour l'analyse par rmn à 100 MHz. La stabilité, dans ces conditions, de la lactone **6** a été établie ainsi: on agite 165 h, à 40°C, 330 mg de la lactone **6** dans 144 cm³ d'eau et 234 cm³ d'acétone contenant 2 mmol d'HCl (on travaille en présence d'HCl car la lactonisation des composés dichlorés **5***b* ou **7***b*, **9***b*, **11***b* et **13***b* libère une quantité stoechiométrique de cet acide). On élimine l'acétone sous pression réduite à 20°C puis extrait à l'éther; les éthers, séchés (Na_2SO_4) et concentrés mènent à 317 mg (96%) de lactone **6** inchangée.

Ouverture en solution des composés 5c *et réactivité du composé* 7c

A. A 4 g de **5***b* (*cis*/*trans* = 25:75) dissous dans 186 cm³ d'eau et 427 cm³ d'acétone, on ajoute 0,68 g de soude puis agite 165 h à 40°C. On élimine l'acétone sous pression réduite à 20°C. Par extraction à l'éther on isole 2,0 g de lactone **6** (rmn). La phase aqueuse est acidifiée par HCl 50% puis extraite à l'éther. Les éthers sont lavés (H_2O), séchés (Na_2SO_4), concentrés et immédiatement estérifiés par action d'un excès de diazométhane en solution éthérée. Après traitement on obtient un mélange présentant six taches en ccm. Par chromatographie sur colonne de silice avec éther – éther de pétrole (20:80, varie graduellement jusqu'à 50:50) on isole: (*1*) 631 mg d'esters **5***a* contenant d'après le spectre de rmn 28% du composé **7***a*. En présence d'Eu(DPM)$_3$ il est possible d'observer trois signaux dus aux COOMe des composés **5***a-cis*, **5***a-trans* et **7***a*. Les deux premiers ont pu être reconnus par ajout d'un mélange connu de **5***a cis* et *trans*; leur rapport d'intégration indique la proportion *cis*/*trans* de 7:93 pour **5***a*; (*2*) 108 mg (3,1%) d'alcool **10***a* (rmn); (*3*) 351 mg (10,1%) d'alcool **12***a* (rmn); (*4*) 60 mg de lactone **6** (rmn), ce qui, compte-tenu des 2 g isolés par extraction directe, conduit à un rendement de 70,4%.

B. Un gramme d'acide **5***b-trans*, soumis aux mêmes conditions, conduit à: (*1*) 590 mg (72%) de la lactone **6** (rmn) par extraction directe; (*2*) un produit brut présentant, après estérification, quatre taches en ccm et dont la composition précise a été déterminée par la méthode déjà utilisée pour l'analyse du produit de l'hydrolyse basique des composés **5***a*. Les résultats sont portés dans le tableau 1.

C. Réactivité du composé **7***c*: on place 140 mg d'acide **7***b* dans les conditions des réactions précédentes. On élimine ensuite l'acétone sous pression réduite à 20°C, puis acidifie à froid (HCl 20%) et extrait à l'éther. Les éthers sont lavés (H_2O), séchés (Na_2SO_4), concentrés et immédiatement soumis à l'action d'un excès de diazométhane en solution éthérée. Après traitement on récupère 150 mg d'un produit brut dont l'analyse est réalisée par rmn à 100 MHz, et rmn à 60 MHz du produit obtenu par acétylation. Le composé **7***a* est facilement mis en évidence et dosé en rmn à 100 MHz (signal à 4,61 Hz). Les résultats obtenus sont portés dans le tableau 1.

1. L. CHICHE, H. CHRISTOL, J. COSTE et F. PLÉNAT. Tetrahedron Lett. 3251 (1978).
2. C. W. JEFFORD. Chimia, **24**, 357 (1970).
3. (*a*) I. FLEMING et E. J. THOMAS. Tetrahedron Lett. 2485 (1971); (*b*) Tetrahedron, **28**, 4989 (1972).
4. C. W. JEFFORD, D. T. HILL, J. GORÉ et B. WAEGELL. Helv. Chim. Acta, **55**, 790 (1972).
5. (*a*) T. SASAKI, S. EGUCHI et T. KIRIYAMA. J. Org. Chem. **38**, 2230 (1973); (*b*) B. CAPON et S. MCMANUS. Neighbouring group participation. Vol. 1. Plenum Press, New York. 1976. p. 181.
6. L. GHOSEZ et P. LAROCHE. Proc. Chem. Soc. 90 (1963).
7. J. A. MARSHALL et R. H. ELLISON. J. Org. Chem. **40**, 2070 (1975).
8. L. CHICHE. Thèse d'Etat, Montpellier, 1978.
9. P. K. FREEMAN, F. A. RAYMOND, J. C. SUTTON et W. R. KINDLEY. J. Org. Chem. **33**, 1448 (1968).
10. Y. ASAKAWA, J. C. MULLER, G. OURISSON, J. FOUSSEREAU et G. DUCOMBS. Bull. Soc. Chim. Fr. 1465 (1976).
11. (*a*) S. DANISHEFSKY, M. Y. TSAI et T. KITAHARA. J. Org. Chem. **42**, 394 (1977); (*b*) M. BERTRAND, J. P. DULCERE, G. GIL, J. GRIMALDI et P. SYLVESTRE-PANTHET. Tetrahedron Lett. 3305 (1976); (*c*) P. CRABBÉ et A. GUZMAN. Tetrahedron Lett. 2293 (1976).
12. A. E. GREEN, J. C. MULLET et G. OURISSON. J. Org. Chem. **39**, 186 (1974).
13. (*a*) E. S. GOULD. Mechanism and structure in organic chemistry. Holt–Dryden, New York. 1959. p. 342; (*b*) P. D. DELAMARE. Molecular rearrangements. Vol. 1. *Edité par* P. de Mayo. Interscience, New York. 1963. p. 69.
14. J. MEINWALD et E. FRAUENGLASS. J. Am. Chem. Soc. **82**, 5235 (1960).
15. (*a*) G. A. WILEY, R. L. HERSHKOWITZ, B. M. REIN et B. C. CHUNG. J. Am. Chem. Soc. **86**, 964 (1964); (*b*) Tetrahedron Lett. 2509 (1964); (*c*) S. J. CRISTOL, R. M. STROM et D. P. STULL. J. Org. Chem. **43**, 1150 (1978).
16. L. GHOSEZ, G. SLINCKX, M. GLINEUR, P. HOET et P. LAROCHE. Tetrahedron Lett. 2773 (1967).
17. B. GIESE. Chem. Ber. **108**, 2998 (1975).
18. R. D. DE SELMS et C. M. COMBS. J. Org. Chem. **28**, 2206 (1963).

19. (*a*) P. v. R. SCHLEYER, W. F. SLIWINSKI, G. W. VAN DINE, U. SCHOLLKOPF, J. PAUST et K. FELLENBERGER. J. Am. Chem. Soc. **94**, 125 (1972); (*b*) W. F. SLIWINSKI, T. M. SU et P. v. R. SCHLEYER. J. Am. Chem. Soc. **94**, 133 (1972); (*c*) J. H. ONG et R. E. ROBERTSON. Can. J. Chem. **52**, 2660 (1974).
20. (*a*) H. P. M. THIELLER, G. J. KOOMEN et U. K. PANDIT. Tetrahedron, **33**, 2603 (1977); (*b*) Y. BESSIÈRE, D. N. H. SAVARY et M. SCHLOSSER. Helv. Chim. Acta, **60**, 1739 (1977).
21. G. MEYER, P. VIOUT et P. RUMPF. Bull. Soc. Chim. Fr. 4436 (1968).
22. D. C. REMY, P. S. ANDERSON, M. E. CHRISTY et B. E. EVANS. J. Org. Chem. **43**, 4311 (1978).
23. D. JOULAIN et F. ROUESSAC. Bull. Soc. Chim. Fr. 1428 (1973).
24. C. FOUQUEY, L. LACOMBE, J. JACQUES et G. AZADIAN-BOULANGER. Bull. Soc. Chim. Fr. 469 (1976).
25. O. M. NEFEDOV, N. N. NOVITSKAYA et A. D. PETROV. Proc. Acad. Sci. USSR, **152**, 752 (1963).
26. J. K. KOCHI. J. Org. Chem. **30**, 3265 (1965).
27. R. T. LALONDE, J. DING et M. A. TOBIAS. J. Am. Chem. Soc. **89**, 6651 (1967).

Can. J. Chem. Downloaded from www.nrcresearchpress.com by 210.87.254.5 on 09/05/12
For personal use only.

Action de l'hydroxyurée sur les esters α-acétyléniques

CHRISTIANE LASSALVY, CLÉMENT PETRUS[1] ET FRANÇOISE PETRUS

Laboratoire de Synthèse et d'Etudes Physicochimiques d'Hétérocycles Azotés, Université des Sciences et Techniques du Languedoc, Place E. Bataillon, 34060 Montpellier, France

Reçu le 2 avril 1980

CHRISTIANE LASSALVY, CLÉMENT PETRUS et FRANÇOISE PETRUS. Can. J. Chem. **59**, 175 (1981).

L'addition-1,4 de l'hydroxyurée sur les esters α-acétyléniques par l'oxanion $H_2N—CO—NHO^-$ conduit aux β-uréidoxy esters éthyléniques *E* et *Z*. Avec le tétrolate et le phényl propiolate d'éthyle, l'isomère *E* est isolé et identifié. L'isomère *Z* se cyclise *in situ* pour conduire, à partir du tétrolate, à la carboxamido-2 méthyl-5 isoxazolone-3. A partir du phényl propiolate, l'hydroxy-3 phényl-5 isoxazole est directement obtenu, le dérivé *N*-carboxamido intermédiaire n'étant pas isolé. Avec le propiolate d'éthyle, la cyclisation *in situ* de l'isomère *Z* conduit aussi à l'hydroxy-3 isoxazole. Le β-uréidoxy acrylate *E* n'est pas isolé; il réagit avec le solvant, dans une addition de Michaël, puis se cyclise en *N*-carboxamido-2 éthoxy-5 isoxazolidinone-3.

CHRISTIANE LASSALVY, CLÉMENT PETRUS, and FRANÇOISE PETRUS. Can. J. Chem. **59**, 175 (1981).

Hydroxyurea, in its oxanion form $NH_2—CO—NHO^-$, reacts in basic medium by a 1,4-addition to α-acetylenic esters leading to the *E* and *Z* ethylenic β-ureidoxy ester isomers. The *E* isomer can be isolated and identified from reaction with ethyl tetrolate and ethyl propiolate. The *Z* isomer undergoes cyclisation *in situ* to give the 2-carboxamido-5-methyl-3-isoxazolone. With phenyl propiolate, the 3-hydroxy-5-phenyl isoxazole is directly obtained without isolation of the intermediate *N*-carboxamido derivative. In the case of ethyl propiolate two cyclic compounds are obtained: 3-hydroxyisoxazole and 2-*N*-carboxamido-5-ethoxy-3-isoxazolidinone. The formation of the former is due to the *in situ* cyclisation of the *Z* isomer. The isolation of the latter compound can be explained by solvent addition to the *E* β-ureidoxyacrylate intermediate in a Michaël addition followed by cyclisation.

Introduction

L'hydroxyurée s'étant révélée une hydroxylamine *N*-protégée, ne réagissant que par son oxanion $NH_2—CO—NHO^-$, dans différentes réactions de substitutions nucléophiles (1) et additions de Michaël sur des dérivés éthyléniques (2), il nous a paru intéressant d'étudier le comportement de ce réactif avec les esters α-acétyléniques. Rappelons que Iwai et Nakamura (3) montrent que l'action de l'hydroxylamine sur les esters α-acétyléniques implique uniquement l'attaque par le doublet de l'azote qui peut conduire, suivant les conditions expérimentales, à une addition-1,4 pour donner des β-hydroxyaminoesters qui se cyclisent en isoxazolones-5, ou par action sur la fonction ester à des acides hydroxamiques qui se cyclisent en isoxazolones-3. D'où l'intérêt d'étudier l'action d'une hydroxylamine *N*-protégée, telle que l'hydroxyurée, sur les esters α-acétyléniques.

Nous avons donc réalisé cette étude en prenant comme esters de départ les propiolate, phényl propiolate et tétrolate d'éthyle en vue de comparer les effets de substituants.

Si dans tous les cas une addition-1,4 de l'hydroxyurée impliquant l'oxygène du réactif est observée, l'évolution des intermédiaires dans le milieu réactionnel est différente et nous expliciterons successivement les résultats obtenus à partir du tétrolate, phényl propiolate et propiolate d'éthyle.

[1]Auteur à qui toute correspondance sera adressée.

Résultats et discussion

Action de l'hydroxyurée sur le tétrolate d'éthyle

En milieu éthylate de sodium, on obtient un mélange de β-uréidoxy crotonate d'éthyle **1***a* et de carboxamido-2 méthyl-5 isoxazolone-3 **1***b*. Dans une première étape, l'addition-1,4 de l'hydroxyurée conduit aux deux β-uréidoxy crotonates d'éthyle *E* et *Z*, puis hétérocyclisation *in situ* de l'isomère *Z* par l'azote en α de l'oxygène (5-*exo*-trig), favorisée d'après les règles de Baldwin (4), pour donner le composé **1***b*. Le β-uréidoxy crotonate d'éthyle **1***a* obtenu, remis en présence d'éthylate de sodium, ne s'est pas cyclisé, la configuration *E* de ce composé ne permettant pas la cyclisation (schéma 1).

Action de l'hydroxyurée sur le phényl propiolate d'éthyle

Les résultats obtenus à partir de cet ester sont comparables à ceux observés précédemment. L'hydroxyurée réagit dans une addition-1,4 sur la triple liaison conjuguée au groupement ester, pour donner les β-uréidoxy cinnamates d'éthyle *E* et *Z*. Nous isolons l'isomère *E* non cyclisable **2***a* et l'hydroxy-3 phényl-5 isoxazole **2***c* à côté d'une petite quantité d'ester de départ non réagi. La formation du composé **2***c* est expliquée par le processus suivant: cyclisation 5-*exo*-trig de l'isomère *Z* par l'atome d'azote en α de l'oxygène conduisant à la carboxamido-2 phényl-5 isoxazolone-3 non isolée, qui évolue en hydroxy-3 phényl-5 isoxazole **2***c* (schéma 1).

0008-4042/81/010175-05$01.00/0

©1981 National Research Council of Canada/Conseil national de recherches du Canada

Can. J. Chem. Downloaded from www.nrcresearchpress.com by 210.87.254.40 on 09/05/12
For personal use only.

Can. J. Chem. Downloaded from www.nrcresearchpress.com by 210.87.254.40 on 09/05/12
For personal use only.

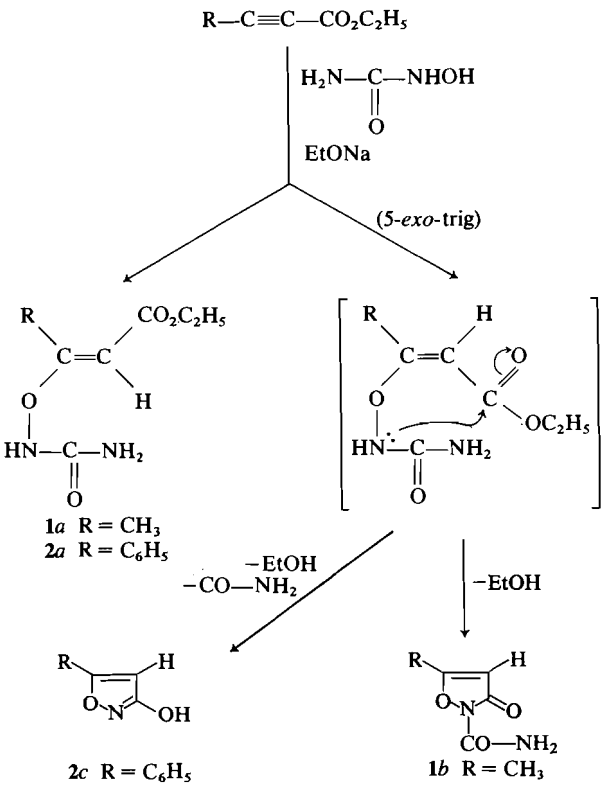

SCHÉMA 1

Action de l'hydroxyurée sur le propiolate d'éthyle

Nous isolons l'hydroxy-3 isoxazole **3***c* et la carboxamido-2 éthoxy-5 isoxazolidinone-3 **3***d*. La formation de composés d'addition du solvant, β-éthoxy acrylate et β-diéthoxy propionate d'éthyle, abaisse le rendement de la réaction en produits cycliques.

Le processus de formation de **3***c* est comparable à celui donné plus haut pour le composé **2***c*: cyclisation 5-*exo*-trig du β-uréidoxy acrylate d'éthyle *Z*, formation de la carboxamido-2 isoxazolone-3 **3***b*, perte du groupement carboxamido pour donner l'hydroxy-3 isoxazole **3***c*.

Nous discutons maintenant la formation de **3***d* qui admet comme intermédiaire le β-uréidoxy acrylate d'éthyle *E* non isolé. En effet, en faisant réagir le propiolate d'éthyle avec un excès d'hydroxyurée (1 mol d'ester pour 2,5 mol de réactif) en présence d'éthylate de sodium, le diuréidoxy-3,3 propanoate d'éthyle **3***f* est obtenu à côté de l'hydroxy-3 isoxazole **3***c*. Il y a donc addition-1,4 de l'hydroxyurée sur la double liaison du β-uréidoxy acrylate d'éthyle *E*.

Sans excès d'hydroxyurée, l'éthylate s'additionne pour donner le β-uréidoxy β-éthoxy propionate dont l'hétérocyclisation 5-*exo*-trig conduit à l'isoxazolidinone **3***d*.

En l'absence d'hydroxyurée, nous observons l'addition de l'éthylate sur le propiolate conduisant à l'acide β-diéthoxy propionique.

Il apparaît ainsi que la cyclisation du β-uréidoxy acrylate d'éthyle *Z* est favorisée par rapport à l'addition de Michaël. D'autre part, nous notons une exaltation de la réactivité de la double liaison du β-uréidoxy acrylate *E* par rapport aux autres β-uréidoxy esters insaturés qui ne donnent pas d'addition de Michaël dans les mêmes conditions (schéma 2).

Identification des composés

Les uréidoxyesters sont identifiés par des méthodes spectrales ir et rmn (tableaux 1 et 2). Leurs spectres ir présentent les bandes d'un groupement carboxamide $H_2N—\underset{\underset{O}{\|}}{C}—NH$: $\nu_{C=O}$ à 1690–1700 cm^{-1}, ν_{NH_2} vers 3350–3500 cm^{-1}, δ_{NH_2} à 1600 cm^{-1} et en outre la bande ν_{CO} ester vers 1730–1750 cm^{-1} et la bande $\nu_{C=C}$ à 1640 cm^{-1} pour les esters éthyléniques. Ces données sont comparables à celles des spectres ir des uréidoxy esters (1*e*) et uréidoxy cétones cités dans la littérature (2*c*). Les spectres rmn corroborent les structures proposées.

Parmi les produits cycliques, l'hydroxy-3 isoxazole **3***c* et l'hydroxy-3 phényl-5 isoxazole **2***c* sont identifiés aisément par leur spectre rmn par comparaison avec les données de la littérature (3). Pour la carboxamido-2 méthyl-5 isoxazolone-3 **1***b*, nous notons les bandes à 1600 cm^{-1} dues à δ_{NH_2} et 3 bandes à 1630 cm^{-1}, 1690 cm^{-1} et 1750 cm^{-1}. Par comparaison avec les isoxazolones-3 *N*-substituées (5), les bandes à 1630 et 1690 cm^{-1} sont attribuées à $\nu_{C=C}$ et ν_{CO} cyclique; celle à 1750 cm^{-1} correspond à $\nu_{CO—NH_2}$, en accord avec Olive *et al.* (2*b*) qui notent la présence de $\nu_{N—CO—N}$ à 1735–1740 cm^{-1} pour des carboxamido-2 isoxazolidinones-3. Nous avons confirmé la structure de ce composé en synthétisant l'autre isomère, la carboxamido-2 méthyl-3 isoxazolone-5 par action du cyanate de potassium sur la méthyl-3 isoxazolone-5.

Son spectre présente les bandes à 1590 cm^{-1}, 1630 cm^{-1}, attribuées à δ_{NH_2} et $\nu_{C=C}$. La bande ν_{CO} à 1730 cm^{-1} est caractéristique des isoxazolones-5 *N*-substituées (6); celle à 1760 cm^{-1} correspond bien à $\nu_{CO—NH_2}$ confirmant les attributions précédentes.

Les spectres rmn confirment la structure isoxazolone-3 du composé (5*b*). Le spectre rmn de ce dernier est tout à fait comparable à celui de l'acétyl-2 méthyl-5 isoxazolone-3 donné dans la littérature (7) (tableau 3).

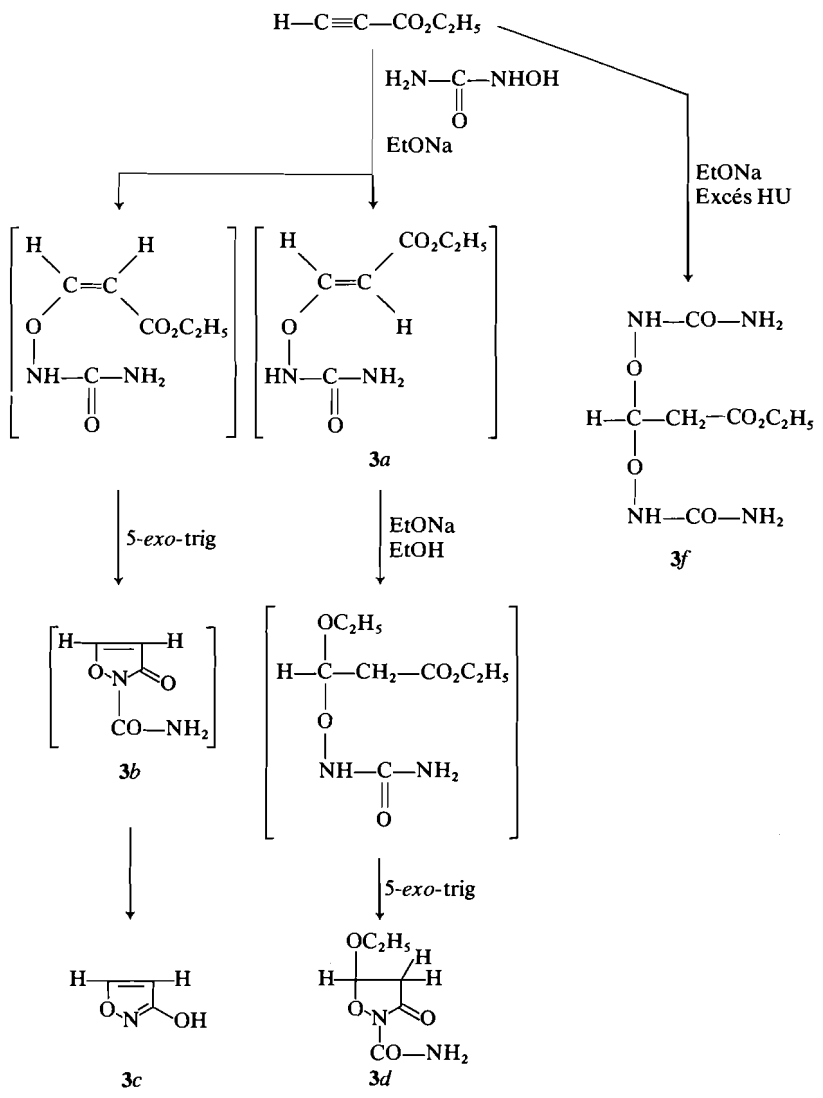

SCHÉMA 2

Le spectre ir de la carboxamido-2 éthoxy-5 isoxazolidinone-3 **3***d* présente les bandes du groupement carboxamido: δ_{NH_2} à 1600 cm^{-1}, ν_{CO-NH_2} à 1760 cm^{-1} et ν_{NH_2} à 3390 cm^{-1}. La bande à 1730 cm^{-1} correspondrait au CO du cycle.

Le spectre rmn dans le DMS-d_6 présente un système ABX dégénéré correspondant aux protons en 4 et 5 que nous avons résolu par double résonance, à côté des signaux du C_2H_5 et de NH_2; δ_{HA} = 2,6 ppm; δ_{HB} = 3,4 ppm; δ_{HX} = 5,63 ppm; J_{AB} = 17,4 Hz; J_{AX} = 0; J_{BX} = 5,6 Hz; δ_{CH_3} = 1,17 ppm; δ_{OCH_2} = 6 ppm; δ_{NH_2} = 7,25 ppm.

Conclusion

Nous avons montré que l'hydroxyurée réagissait sur les esters α-acétyléniques dans une addition-1,4 impliquant l'oxygène du réactif pour conduire à des β-uréidoxyesters éthyléniques *E* et *Z*. L'hétérocyclisation régiospécifique 5-*exo*-trig par l'azote en α de l'oxygène est une nouvelle voie de synthèse des isoxazolones-3.

Partie expérimentale

Mode opératoire général

A une solution de 0,1 mol de méthylate de sodium dans le méthanol (ou d'éthylate de sodium dans l'éthanol), on ajoute à température ambiante 0,1 mol d'hydroxyurée sous agitation; après dissolution de l'hydroxyurée, 0,1 mol d'ester acétylénique sont additionnés goutte à goutte à ce mélange.

L'agitation est maintenue suivant les cas durant une période de 24 à 48 h. Après évaporation du solvant à pression normale, le résidu réactionnel est repris par l'eau et extrait à l'éther.

La phase aqueuse est acidifiée par une solution d'acide chlorhydrique à 40% jusqu'à pH 3–4, constant.

(a) A partir du tétrolate d'éthyle

Le tétrolate d'éthyle est préparé suivant la méthode de

Can. J. Chem. Downloaded from www.nrcresearchpress.com by 210.87.254.40 on 09/05/12
For personal use only.

Can. J. Chem. Downloaded from www.nrcresearchpress.com by 210.87.254.40 on 09/05/12
For personal use only.

TABLEAU 1. Spectres infrarouges (DMS-d_6)

No.	$\nu_{C=O}$ ester	$\nu_{-C(=O)-NH_2}$	δ_{NH_2}	ν_{NH_2}	$\nu_{C=C}$
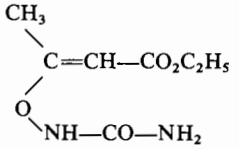 **1a**	1750	1690	1600	3360	1630
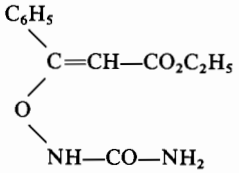 **2a**	1730	1690	1600	3400	1640
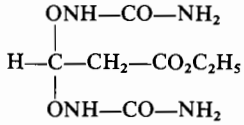 **3f**	1760	1690	1600	3400	—

TABLEAU 2. Spectres rmn ^{1}H (DMS-d_6)

No.		H_α[a]	NH_2	NH	OCH_2		CH_3
1a	CH_3 2,27[b]	5,57[b]	6,57	9,60	4,03(q)	$J = 7$ Hz	1,13(t)
2a	C_6H_5 7,50	5,83	6,56	9,77	3,96(q)	$J = 7$ Hz	1,10(t)
3f	H 5,13	2,93 $J_{H_\alpha H} = 6$ Hz	6,60	9,00	4,17(q)	$J = 7$ Hz	1,20(t)

[a]H_α désigne le ou les protons en α du groupement ester.
[b]Pic élargi.

TABLEAU 3. Spectres rmn ^{1}H

	Solvant	H	CH_3	NH_2	CO—CH_3
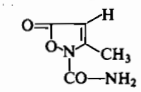	DMS-d_6	5,5	2,57	7,73	—
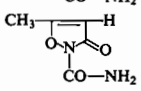	DMS-d_6	5,83	2,27	7,57	—
	$CDCl_3$	5,63	2,40	7,43	—
1b 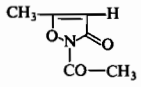	$CDCl_3$	5,55 $J = 0,9$ Hz	2,32	—	2,56
Litt.(7)					

Can. J. Chem. Downloaded from www.nrcresearchpress.com by 210.87.254.40 on 09/05/12
For personal use only.

Nazarov *et al.* (8); Eb 60°C/25 Torr (litt. (9) Eb 163°C/752 Torr). Temps de réaction 4 jours.

A partir du résidu de la phase éthérée, le β-uréidoxy crotonate d'éthyle **1***a* est séparé par filtration, et purifié par recristallisation. La phase aqueuse est ensuite traitée comme précédemment; le solide est purifié par recristallisation dans l'éthanol. On obtient la carboxamido-2 méthyl-5 isoxazolone-3 **1***b*.

β-Uréidoxy crotonate d'éthyle **1***a*: F (éthanol) 138°C; Rdt 20%. *Anal.* calc. pour $C_7H_{12}N_2O_4$: C 44,68, H 6,43; trouvée: C 44,51, H, 6,25%.

Carboxamido-2 méthyl-5 isoxazolone-3 **1***b*: F (éthanol) 141°C; Rdt 50%. *Anal.* calc. pour $C_5H_6N_2O_3$: C 42,25, H 4,26; trouvée: C 42,17, H 4,28%.

(b) A partir du phényl propiolate d'éthyle

Temps de réaction 48 h. A partir du résidu de la phase éthérée, on sépare par filtration le β-uréidoxy cinnamate d'éthyle **2***a* et l'ester de départ non réagi (10%). Le précipité de la phase aqueuse est filtré. On isole ainsi l'hydroxy-3 phényl-5 isoxazole **2***c* qui est recristallisé dans l'éthanol.

β-Uréidoxy cinnamate d'éthyle **2***a*: F 130°C; Rdt 20%. *Anal.* calc. pour $C_{12}H_{14}N_2O_4$: C 57,59, H 5,64; trouvée: C 57,50, H 5,59%.

Hydroxy-3 phényl-5 isoxazole **2***c*: F 163–165°C (litt. (3) F 163–165°C); Rdt 50%; rmn (**5***b*) (DMS-d_6 à 60 MHz): 6,48 (s, H-4), 7,5 (m, C_6H_5), 11,4 (s, OH) ppm. *Anal.* calc. pour $C_9H_7NO_2$: C 67,07, H 4,38; trouvée: C 67,09, H 4,51%.

(c) A partir du propiolate d'éthyle

Temps de réaction 36 h. Le résidu de la phase éthérée est distillé; on obtient un mélange (50:50) de β-éthoxy acrylate d'éthyle et de β-diéthoxy propionate d'éthyle caractérisé par rmn avec un rendement global de 50%.

β-Éthoxy acrylate d'éthyle; rmn ($CDCl_3$ à 60 MHz): 7,56 (d, H_β), 5,13 (d, H_α, J = 12 Hz), 3,56 (m, O—CH_2), 4,13 (q,), 1,23 (m, CH_3) ppm.

β-Diéthoxy propionate d'éthyle; rmn: 4,87 (t, H), 2,63 (d, CH_2, J = 6 Hz), 3,56 (m, O—CH_2), 4,13 (q, 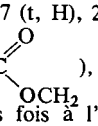), 1,23 (m, CH_3) ppm.

La phase aqueuse est extraite plusieurs fois à l'acétate d'éthyle. Les extraits combinés sont séchés sur sulfate de sodium; l'acétate d'éthyle est évaporé sous pression réduite. Le solide récupéré est chromatographié sur colonne de silice (éluant: éther). On obtient l'hydroxy-3 isoxazole **3***c* et le carboxamido-2 éthoxy-5 isoxazolidinone-3 **3***d*.

Hydroxy-3 isoxazole **3***c*: F (hexane) 98–99°C (litt. (3) F 98–99°C); Rdt 25%; rmn (DMS-d_6 à 60 MHz): 6,13 (d, H-4), 8,57 (d, H-5, $J_{4,5}$ = 2 Hz), 11,1 (s large, OH) ppm. *Anal.* calc. pour $C_3H_3NO_2$: C 42,36, H 3,56; trouvée: C 42,57, H 3,56%.

Carboxamido-2 éthoxy-5 isoxazolidinone-3 **3***d*: F (éthanol) 126°C; Rdt 15%. *Anal.* calc. pour $C_6H_{10}N_2O_4$: C 41,38, H 5,79; trouvée: C 41,36, H 5,81%.

Cas particuliers

Action de l'hydroxyurée en excès

A une solution de 0,05 mol d'éthylate de sodium dans l'éthanol, on ajoute à température ambiante 0,125 mol d'hydroxyurée sous agitation et 0,05 mol de propiolate d'éthyle. L'agitation est maintenue pendant trois jours. Après évaporation du solvant, le résidu est repris par de l'eau; une petite quantité de diuréidoxy-3,3 propanoate d'éthyle précipite et est séparée par filtration. On acidifie jusqu'à pH ≃ 3–4. On extrait à l'acétate d'éthyle, on sèche sur sulfate de sodium. Cette phase est concentrée et le dérivé diuréidoxy qui précipite est séparé par filtration. En évaporant à sec le filtrat, on récupère l'hydroxy-3 isoxazole caractérisé par comparaison avec un échantillon authentique (3).

Diuréidoxy-3,3 propanoate d'éthyle: F (éthanol): 156–157°C. *Anal.* calc. pour $C_7H_{14}N_4O_6$: C 33,60, H 5,64, N 22,39; trouvée: C 33,60, H 5,76, N 22,30%.

En l'absence d'hydroxyurée

Le mode opératoire général est repris sans hydroxyurée. Temps de réaction 48 h. La phase aqueuse acidifiée est extraite à l'éther. La phase éthérée, séchée sur sulfate de sodium, est concentrée sous vide. On obtient l'acide β-diéthoxy propionique caractérisé par rmn et spectre de masse; rmn ($CDCl_3$ à 60 MHz): 2,66 (d, H), 4,90 (t, CH_2, J = 6 Hz), 7,00 (OH), 3,61 (m, OCH_2), 1,20 (t, CH_3, J = 6 Hz) ppm. Spectre de masse: pic moléculaire à *m/e* 162 (faible intensité); *m/e* 161, 117, 103 (forte intensité) caractéristiques d'un acétal (10).

Techniques utilisées

Les points de fusion non corrigés ont été mesurés en tube capillaire (appareil Büchi).

Les analyses ont été déterminées par le laboratoire Central de Microanalyse du CNRS.

Les spectres rmn ^1H ont été réalisés soit au moyen d'un appareil Varian modèle T60 ou Brucker WP 80. Les déplacements chimiques sont exprimés en ppm par rapport au TMS pris comme référence interne. Les spectres ir ont été enregistrés sur un appareil Perkin Elmer 297.

1. (*a*) O. Exner. Collect. Czech. Chem. Commun. **23**, 272 (1958); **26**, 701 (1961); (*b*) W. Klotzer, H. Bretschneider, E. Fitz, R. Reiner et G. Bader. Monatsh. Chem. **101**, 1109 (1970); H. Bretschneider, E. Fitz et W. Klotzer. U.S. No du brevet 3242189 (1966); (*c*) O. Fuchs, T. Lang et A. Nemes. Hung. Peljes, 8443 (1974); Chem. Abstr. **82**, 43392g (1974); (*d*) U. Krueger et G. Zinner. Arch. Pharm. **311**, 579 (1978); (*e*) C. Bennouna, F. Petrus et J. Verducci. J. Heterocycl. Chem. **16**, 161 (1979); (*f*) H. El Meslouhi. Thèse 3ème Cycle, Montpellier, 1979.
2. (*a*) J. Olive, C. Petrus et F. Petrus. Bull. Soc. Chim. Fr. 1144 (1973); (*b*) J. Olive, C. Petrus et F. Petrus. Bull. Soc. Chim. Fr. 1589 (1976); (*c*) R. Jacquier, J. Olive, C. Petrus et F. Petrus. Tetrahedron Lett. 2337 (1975); (*d*) R. Jacquier, J. Olive, C. Petrus et F. Petrus. Tetrahedron Lett. 2979 (1975).
3. I. Iwai et N. Nakamura. Chem. Pharm. Bull. **14**, 1277 (1966).
4. J. Baldwin. J. Chem. Soc. Chem. Commun. 734 (1976).
5. (*a*) A. Boulton, A. Katritzky, A. Majid et S. ØKsne. Tetrahedron, **20**, 2835 (1964); (*b*) R. Jacquier, C. Petrus, F. Petrus et J. Verducci. Bull. Soc. Chim. Fr. 1978 (1970).
6. (*a*) A. Boulton et A. Katritzky. Tetrahedron, **12**, 41 (1961); (*b*) A. Katritzky, S. ØKsne et A. Boulton. Tetrahedron, **18**, 777, (1962); (*c*) R. Jacquier, C. Petrus, F. Petrus et J. Verducci. Bull. Soc. Chim. Fr. 2690 (1970).
7. H. Goth, A. Gagneux, C. Eugster et H. Schmid. Helv. Chim. Acta, **50**, 137 (1967).
8. I. Nazarov, S. Ananchenko et I. Torgov. Chem. Abstr. **53**, 16085e (1959).
9. F. Stolz. Beilstein's Handbuch der Organishen Chemie. Band II. 480 (1943).
10. R. Friedel et A. Sharkey. Anal. Chem. **28**, 940 (1956).

The interaction of a soil fulvic acid with precipitating hydrous ferric oxide at pH = 6[1]

COOPER H. LANGFORD,[2] SHUI MUI WONG, AND ALAN W. UNDERDOWN
Metal Ions Group, Department of Chemistry, Carleton University, Ottawa, Ont., Canada K1S 5B6

Received August 4, 1980

COOPER H. LANGFORD, SHUI MUI WONG, and ALAN W. UNDERDOWN. Can. J. Chem. **59**, 181 (1981).

A kinetic method of analysis which distinguishes Fe(II) from Fe(III) and Fe(III) forms of various labilities from each other is based on spectrophotometric monitoring of the reaction of Fe(II) with ferrozine. Reduction of Fe(III) with hydroxylamine hydrochloride allows the single colourimetric reagent to detect all forms of Fe. The method is applied to study of the effects of a well characterized soluble soil organic acid sample, a fulvic acid, on the speciation of Fe(III) under conditions (pH = 6) where Fe(III) forms a colloidal hydrous oxide in the absence of fulvic acid, The effect of fulvic acid is to greatly increase the lability of Fe(III) compared to that in a hydrous oxide colloid. However, ultrafiltration and light scattering experiments indicate that the Fe(III) – fulvic acid species is larger than the hydrous ferric oxide colloid particles. Kinetic studies in the absence of hydroxylamine hydrochloride show that fulvic acid can act as a reducing agent for iron in the presence of an Fe(II) complexing agent like ferrozine but neither kinetic studies with an Fe(III) reagent nor Mössbauer spectra suggest significant initial presence of Fe(II) in the aged Fe(III) – fulvic acid samples.

COOPER H. LANGFORD, SHUI MUI WONG et ALAN W. UNDERDOWN. Can. J. Chem. **59**, 181 (1981).

Faisant appel à la détection spectrophotométrique de la réaction du Fe(II) avec la ferrozine, on a développé une méthode cinétique d'analyse qui permet de distinguer le Fe(II) du Fe(III) et des formes de Fe(III) de labilité variable. La réduction du Fe(III) par le chlorhydrate d'hydroxylamine permet de détecter toutes les formes de Fe à l'aide d'un seul réactif colorimétrique. On a appliqué cette méthode à l'étude des effets d'un échantillons d'un acide organique de sol soluble bien caractérisé, l'acide fulvique, sur la différenciation de Fe(III) dans des conditions (pH 6) où le Fe(III) forme un oxyde hydraté colloidal en l'absence d'acide fulvique. L'acide fulvique a comme effet d'augmenter fortement la labilité du Fe(III) par rappport à celle de l'oxyde hydraté colloidal. Cependant l'ultrafiltration et les expériences de diffraction lumineuse indiquent que l'entité Fe(III) – acide fulvique est plus volumineuse que les particules colloidals d'oxyde ferrique hydraté. Les études cinétiques, en l'absence du chlorhydrate d'hydroxylamine, montrent que l'acide fulvique peut agir comme agent réducteur du fer en présence d'un agent complexant du Fe(II) tel la ferrozine; toutefois ni les études cinétiques impliquant un réactif de Fe(III) ni le spectres Mossbauer ne suggèrent une présence initiale significative de Fe(II) dans les vieux échantillons de Fe(III) – acide fulvique.

[Traduit par le journal]

Introduction

Using sulfosalicylic acid (SSA) as a spectrophotometric reagent for kinetic analysis, we have studied complexation of Fe(III) by the well characterized soil fulvic acid sample which was derived from a Prince Edward Island Podzol Bh horizon by the Agriculture Canada group (1). In acid solution, a "1:1 complex" was found with conditional stability constant showing complex pH dependence (2). In solution at pH = 4, evidence was obtained for "dissolution" of colloidal hydrous ferric oxide by fulvic acid and some reduction of Fe(III) by fulvic acid was observed (3). Unfortunately, the spectrophotometric sensitivity of SSA is not adequate for analysis of true natural water models. The low solubility of Fe(III) at intermediate pH values (pH = 6–8) recommends study of quite dilute samples.

In this report a new kinetic reagent system which has good sensitivity for iron is described. It uses the sensitive Fe(II) spectrophotometric reagent ferrozine (the disodium salt of 3-(2-pyridyl)-5,6-bis(4-phenyl-sulfonic acid)-1,2,4-triazine) introduced by Stookey in 1970 (4). Determination of Fe(III) is accomplished by including the reducing agent hydroxylamine hydrochloride in the reagent solution. The new kinetic reagent is applied (as SSA was) to distinguishing species of different lability under pseudo first order kinetic conditions. Information about lability of iron species at pH = 6 is complimented with structural studies using light scattering, ultrafiltration, and Mössbauer spectroscopy.

The kinetic method of analysis depends upon the formation of a *common product* from one or more initial species present in the sample. Under first order or pseudo first order conditions, the kinetics of formation of the common product may be written:

$$[1] \quad P = A_0[1 - \exp(-k_A t)] + B_0[1 - \exp(-k_B t)] + \ldots + X$$

where P represents a concentration proportional parameter of the product, A_0 the concentration of species A initially present in the sample (expressed

[1]Supported by grants from the Natural Sciences and Engineering Research Council of Canada.

[2]To whom all correspondence should be addressed at Department of Chemistry, Concordia University, Montreal, P.Q., Canada H3G 1M8.

0008-4042/81/020181-06$01.00/0

©1981 National Research Council of Canada/Conseil national de recherches du Canada

Can. J. Chem. Downloaded from www.nrcresearchpress.com by 210.87.254.40 on 09/06/12
For personal use only.

Can. J. Chem. Downloaded from www.nrcresearchpress.com by 210.87.254.40 on 09/06/12
For personal use only.

in the same units as P), B_0 the initial concentration of species B, X a time-independent term including any concentrations of fast reacting species plus blank, and k_A, k_B the corresponding rate constants. In a sample containing two species with rate constants appropriate to the time scale of the experiment, the problem is to fit four parameters; A_0, B_0, k_A, and k_B. A_0 and B_0 are the "quantitative" parameters. k_A and k_B are the "qualitative" parameters which allow recognition of distinct species. In this work, the four parameters are obtained by a non-linear least-squares fitting procedure based on a library program using the Marquardt algorithm which has been extensively tested elsewhere (5). Tests in ref. 5 suggest that successful resolution of up to three components which differ in rate constant by a factor of three or more is achievable.

Experimental

Materials

Ferrozine was a generous gift of Diagnostic Chemicals, Ltd., Charlottetown, P.E.I. Fe(III) stock solutions were prepared by dissolution of A.R. grade iron wire in concentrated A.R. grade HNO_3. Fe(II) stocks were prepared from A.R. grade ferrous ammonium sulfate (used as a weighing form). Other reagent grade materials used as received were sulfosalicyclic acid, a TRIS buffer (2-amino-2-(hydroxymethyl)-1,3 propanediol), and trisodium phosphate. The sample of fulvic acid was prepared from a sample of the Armadale Bh horizon podzol described in ref. 1 according to the method cited there. Acidimetric titration curves agree with those for the sample described in ref. 1. Water for solutions was "tap" distilled water redistilled from permanganate in an all glass apparatus.

Solution Preparation

The kinetic reagent solution employed in most experiments was composed of 3.00×10^{-3} M ferrozine, 6.00×10^{-3} M $NH_2OH \cdot HCl$, and 1.0×10^{-2} M $HClO_4$. This solution determines final values of both the pH and ionic strength of all mixtures prepared from mixing equal quantities of it with the various sample solutions of this study. Consequently, rate constants are evaluated for constant solution conditions. Runs are also always pseudo first order in ferrozine and $NH_2OH \cdot HCl$. Iron-containing samples were prepared by diluting stock solutions, adjusting pH (as measured with an Orion 701A digital pH/mV meter) slowly by titration with TRIS, and finally aging for 27 h to provide for preliminary pseudo equilibration. That is, the solutions are equilibrated with respect to faster homogeneous processes, but probably not with respect to all heterogeneous processes. As before (3), 27 h was chosen as a common point for comparisons.

Kinetic Studies

Two types of experiments were conducted. For slower reactions equal volumes of reagent and sample were mixed and thermostated at 25.0°C. Aliquots were pipetted into 1 cm quartz cells in a Coleman 124 Spectrophotometer. The monitoring wavelength was 562 nm. The extinction coefficient of ferrozine at pH = 2.00 is $1.27 \pm 0.01 \times 10^4$ M^{-1} cm^{-1}. For faster reactions, kinetic data were collected using a Durrum–Gibson stopped flow spectrophotometer thermostated at 25.0°C.

Filtration, Light Scattering, and Mössbauer

The fraction of "larger" particles in each of solutions of Fe(III) equilibrated at pH = 6 and solutions of Fe(III) plus FA so equilibrated was estimated by filtration through 0.45 or 0.4 μm pore filters. Since such filters can have ion exchange properties, three types were compared (suppliers in parentheses); 0.45 μm cellulose acetate (Gelman), 0.45 μm cellulose acetate (Millipore), and 0.4 μm polycarbonate (Bio-Rad Laboratories). Two types of filter supports were used; glass and polycarbonate.

Light scattering studies were carried out using a Phoenix light scattering apparatus modified to accept the beam of a 5 mW He–Ne laser. Absorption corrections are based on data from the "straight through" orientation of the detector. Such experiments are more fully described elsewhere (6).

Mössbauer measurements were made using an instrument assembled in the laboratories of D. R. Wiles and described fully elsewhere (7). Briefly, it is a constant acceleration design operating in transmission geometry with a 0.2 mCu ^{57}Co(Pd) source. A 1024 channel multichannel analyzer collects count rates with a velocity increment of 0.03 mm s^{-1} per channel. Data analysis used a non-linear least-squares regression program (7).

Results

Fe(III) Hydrous Oxide Colloids

Solutions of initial Fe(III) concentrations of 5.00×10^{-5} M were adjusted to pH = 6.0 and aged. On mixing with the ferrozine/$NH_2OH \cdot HCl/HClO_4$ reagent the largest part of the Fe(III) reacted with a pseudo first order rate constant of $4.9 \pm 0.3 \times 10^{-3}$ s^{-1}. The concentration of this species yielded by the fitting routine was $4.8 \pm 0.1 \times 10^{-5}$ M. Mass balance considerations suggest the presence of a small quantity of a faster reacting component. This was detected on a sample subjected to filtration through a 0.45 μm filter and then run on the Durrum–Gibson stopped flow. The stopped flow data could be fitted kinetically as two components with pseudo first order rate constants of 1.5×10^{-1} s^{-1} and $4.8 \pm 0.2 \times 10^{-3}$ s^{-1} respectively. A large part of the total iron was removed by the filtration step. We conclude that about 4.8×10^{-5} M Fe(III) is present as a hydrous oxide colloid and about 2×10^{-6} M Fe(III) is present as small "dissolved" species.

Mixtures of Fe(II)/Fe(III)

The capacity of the system to discriminate Fe originally present in the 2+ oxidation state was tested on samples prepared by combining Fe(II) and Fe(III) stocks to give 2.5×10^{-5} M concentrations in each. The solution was titrated to pH = 6 with TRIS and aged for 27 h. A distinction between the initial Fe(II) and Fe(III) was clearly achieved. A quite rapid component appeared in the kinetics which is attributed to Fe(II). A slower component was fitted to a pseudo first order rate constant of 4.3 $\pm 0.5 \times 10^{-3}$ s^{-1}. The rate constant for this component is in satisfactory agreement with the value above. However, the concentrations of the fast (Fe(II)) component and the slower one do not add up to the original 5.0×10^{-5} M Fe concentration. In three runs, the concentrations found were: (*1*)

Can. J. Chem. Downloaded from www.nrcresearchpress.com by 210.87.254.40 on 09/06/12
For personal use only.

Fe(III), 2.4×10^{-5} *M*, Fe(II), 1.8×10^{-5} *M*, Fe(total), 4.2×10^{-5} *M*; (*2*) Fe(III), 2.6×10^{-5} *M*, Fe(II) 1.7×10^{-5} *M*, Fe(total), 4.3×10^{-5} *M*; (*3*) Fe(III), 2.6×10^{-5} *M*, Fe(II), 1.8×10^{-5} *M*, Fe(total), 4.4×10^{-5} *M*. Some ~13% of the total iron is not recovered. The loss was reproducible over 10 runs. The fate of this iron was traced by employing an ASTM Standard Method (8). Allowing a reaction time of over a month, 100 ± 5% of the total iron was recovered. Interestingly, it appears that Fe(II) (in solution *not* O_2-free) catalyzes formation of *insoluble* iron oxide precipitates. This phenomenon is reminiscent of the role of Cr^{2+} in dissolution of anhydrous $CrCl_3$.

Kinetics in Solutions of Fe(III) with Fulvic Acid

The fulvic acid sample used has the following functionality: 3.3 mequiv. g^{-1} phenolic-OH near carboxylates; 7.71 mequiv. g^{-1} of carboxylate; and 3.6 mequiv. g^{-1} of alcoholic-OH (1). It is assumed on the basis of "blocking experiments" (9) that all of the phenolic-OH is placed so that it can participate in salicylate like chelation and a "1:1 ratio with Fe(III)" is taken to be one phenolate group on FA to one Fe(III). The molecular weight was reported to be 951 (1). On this basis solutions were prepared to contain 1.50 mg mL^{-1} of FA. These are intended to be approximately 1.67×10^{-5} *M* and to provide an approximate 1:1 ratio of binding sites to the 5.00×10^{-5} *M* Fe(III) concentration prepared from Fe(III) stocks. Such 1:1 solutions were adjusted to pH = 6 with TRIS and aged for 27 h.

Kinetics on these samples were carried out with three reagent solutions. The first was the same as that used in the previous experiments, the second was the same except that the reducing agent $HONH_2 \cdot HCl$, was omitted, and the third was the less sensitive but direct Fe(III) reagent solution, based on sulfosalicyclic acid (SSA), which was described at length in ref. 3. Absorbance–time curves for a typical run in each of these cases are given in Fig. 1.

Non-linear regression yielded two components in the first case, a major one with a rate constant of 1.49 ± 0.03 s^{-1} and a minor one with a rate constant fast compared to the time scale of manual kinetics. The parameters are collected in Table 1. The first noteworthy observation is that both components found react faster than any component in the absence of FA. Clearly, FA affects all the Fe(III) hydrous oxide colloids. The second point is that one or both components *may* be an Fe(II) species prior to the addition of ferrozine reagent. This requires testing.

It is because of the second observation that kinetics were run with omission of $HONH_2 \cdot HCl$ and

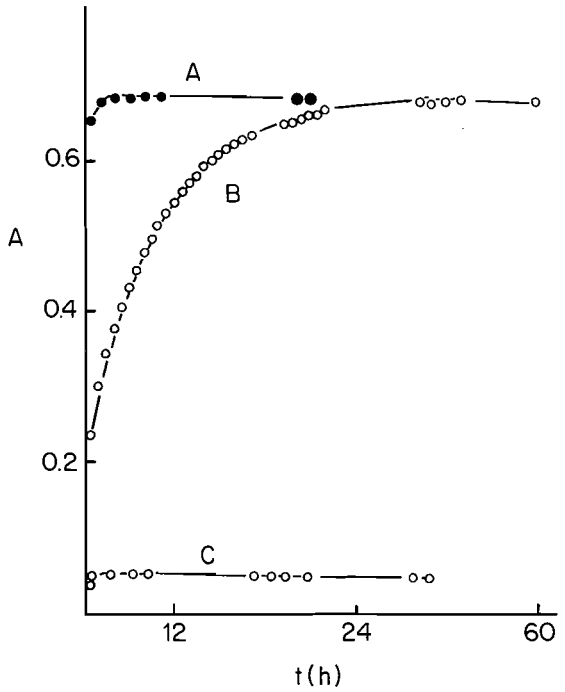

FIG. 1. Absorbance–time curves for reactions of samples containing fulvic acid. *A*, reagent contains ferrozine plus $NH_2OH \cdot HCl$; *B*, reagent contains ferrozine without an added reducing agent; *C*, reagent is SSA in acid, an Fe(III) reagent.

with the SSA reagent solution. The fifth and sixth entries in Table 1 show the results of using the Fe(III) reagent, SSA. SSA does not allow the low detection limit associated with ferrozine. Thus, results at total Fe equal to 5.00×10^{-5} are of low precision. However, there appears to be a single component. The SSA runs were repeated with total Fe raised to 1.00×10^{-4} *M*. In this case, the precision of the rate constant for three trials was quite good, supporting a single kinetic component. This component accounts for 100 ± 5% of the Fe at both concentration levels. The simplest interpretation is that all of the Fe is present in Fe(III) species.

However, the third and fourth entries in Table 1 show that 100% of the Fe can be delivered to the Fe(II) reagent, ferrozine in the absence of a reducing agent in the *reagent* solution. That is, FA can act as a reducing agent. Reduction by fulvic acid has *two* kinetic components as suggested by the apparent deviation of curve *B* of Fig. 1 from a single exponential; the figure does not clearly resolve the faster component (present in smaller quantity). The order of magnitude of the rate constant given in Table 1 for the fast component was adequately confirmed by five stopped-flow runs which yielded a rate constant from *initial rate* measurements of $1.13 \pm 0.13 \times 10^{-1}$ s^{-1}. (This value is not corrected for small contributions of the slower component.)

TABLE 1. Concentrations and rate constants for kinetically identified components present in samples prepared from Fe(III) and FA (all rate constants are averages of two or more runs; uncertainties are standard deviations from mean)

Sample	Reagent	Component	Rate constant (s^{-1})	Concentration (M)
Fe(III):FA	Fz:$NH_2OH \cdot HCl$[a]	Slow	1.49 ± 0.3	$4.27 \pm 0.08 \times 10^{-5}$
		Fast	—	$0.48 \pm 0.06 \times 10^{-5}$
	Fz[b]	Slow	$8.55 \pm 0.35 \times 10^{-3}$	3.50×10^{-5}
		Fast	$1.5 \pm 0.1 \times 10^{-1}$	$1.6 \pm 0.1 \times 10^{-5}$
	SSA[c]	Single	$3.2 \pm 0.8 \times 10^{-1}$	$4.9 \pm 0.1 \times 10^{-5}$
Fe(III):FA×2[d]	SSA	Single	$3.12 \pm 0.08 \times 10^{-1}$	$1.05 \pm 0.05 \times 10^{-4}$
Fe(III):FA:PO_4	Fz	Slow	$7.2 \pm 0.2 \times 10^{-3}$	$4.13 \pm 0.03 \times 10^{-5}$
		Fast	$1.2 \pm 0.1 \times 10^{-1}$	$0.91 \pm 0.01 \times 10^{-5}$

[a]This designates the reagent ferrozine plus $NH_2OH \cdot HCl$.
[b]This reagent omits $NH_2OH \cdot HCl$.
[c]This is the SSA reagent of ref. 3.
[d]"×2" indicates doubling of Fe(III) concentration.

TABLE 2. Filtration of samples through 0.45 μm cellulose acetate and 0.4 μm polycarbonate filters

	Cellulose acetate (Gelman)		Cellulose acetate (Millipore)		Polycarbonate (Bio-Rad Labs)	
Sample[a]	A[b]	B	A	B	A	B
Fe(III)	48.0%	—	0	0	58.5%	63.0%
Fe(III):FA	21.0%	—	25.0%	21.0%	22.3%	16.3%

[a]Samples are: Fe(III) = 5.00×10^{5} M Fe(III) stock adjusted to pH = 6; Fe(III): FA = 5.0×10^{-5} M from F(III) stock + 1.67×10^{-5} M from FA stock adjusted to pH = 6.
[b]A = glass filter support disc; B = polycarbonate filter support disc.

The observation that FA reduces Fe with at least two components in the kinetics confirms a preliminary observation reported in ref. 3 where phenanthroline was used as an Fe(II) reagent. There appear to be at least two distinguishable reducing sites on FA that must be used in the complete reduction of Fe(III) to Fe(II) by "one equivalent of FA chelate complexing sites". This illustrates once more the polydisperse mixture character (1) of even carefully purified FA.

Mössbauer Experiments

In order to provide support for the suggestion above that Fe in the presence of FA remains in the Fe(III) form until an Fe(II) reagent induces reduction, solid samples from the 27 h aged Fe:FA samples were obtained by freeze drying and Mössbauer spectra were recorded. A symmetric doublet was observed with an isomer shift of 0.440 mm/s and a quadrupole splitting of 0.770 mm/s. Half widths and areas of the two components of the doublet are very close. This is consistent with Fe(III). No Fe(II) signal was observable.

Filtration Studies

Since Fe(III) bound to FA is considerably more labile than Fe(III) in the hydrous oxide colloids at the same pH after the same period of aging, it is tempting to think of FA as a simple solubilizing complexing agent. But this may be a considerable oversimplification. Solutions of 5.00×10^{-5} M Fe(III) with and without "one equivalent" of FA, exactly, parallel to those used in kinetic experiments, were prepared and aged for 24 h. Aliquots were analyzed by atomic absorption to confirm 100% recovery of Fe then the samples were filtered through 0.45 μm cellulose acetate and 0.4 μm polycarbonate filters and Fe content of the *filtrate* was determined. Percentage Fe recovery in the filtrate is shown in Table 2. Making allowance for the known ion exchange properties of cellulose acetate, it seems clear that the Fe(III):FA sample has a *larger* fraction of particles of size greater than 0.4 μm than the Fe(III) hydrous oxide colloid. Fe(III) FA complexes would appear to be *aggregated despite* their *kinetic lability*.

Light Scattering

To confirm the aggregation effects in Fe(III):FA complexes from the opposite point of view. The Rayleigh scattering ratio at 90° (R_{90}) is shown in Fig. 2 as a function of added Fe(III) to a solution of 0.100 mg/mL of FA. Light scattering begins to increase rapidly above 1 mmol of Fe per mmol of FA. Under the above assumption this corresponds to

Can. J. Chem. Downloaded from www.nrcresearchpress.com by 210.87.254.40 on 09/06/12
For personal use only.

Can. J. Chem. Downloaded from www.nrcresearchpress.com by 210.87.254.40 on 09/06/12
For personal use only.

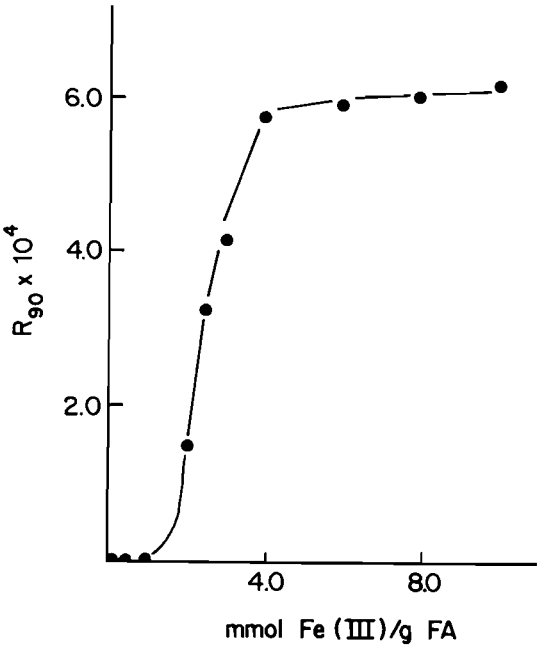

FIG. 2. Light scattering at 90° (R_{90}) as a function of added Fe(III) concentration for a solution of fulvic acid. It should be noted that the intercept at zero Fe(III) is *not* zero. The instrument has another order of magnitude of resolution.

one Fe to 3 mequiv. of fulvic acid. A limit is approached near 4 mequiv. of Fe to 3 mequiv. of FA. The figure suggests aggregation is extensive under the conditions of the kinetic studies.

Phosphate Effects

Another constituent of natural systems that interacts with iron is phosphate. Consequently, kinetic experiments on the Fe(III):FA system were repeated with the addition of 5.0×10^{-5} *M* Na_3PO_4. Solutions were still adjusted to pH = 6 and the ratio is 1:1:1 Fe(III):FA:PO_4. Again samples were aged 27 h. Phosphate effects are not large. The fact that phosphate has an effect is most clearly seen in the induced reduction of Fe(III) by FA. A typical pair of runs is illustrated in Fig. 3. Rate constants and concentrations are shown in the last two lines of Table 1. Phosphate retards the FA reduction reactions slightly. This probably implies the existence of a ternary complex.

Discussion

The concentration of FA used in these experiments corresponds to less than 10 mg per litre of "dissolved organic carbon". This is a value which realistically models natural waters. Moreover, titrations of lake water organic matter (10) and fractionated organic matter from a stream (11) suggest that our soil FA is a good model of a leading (often

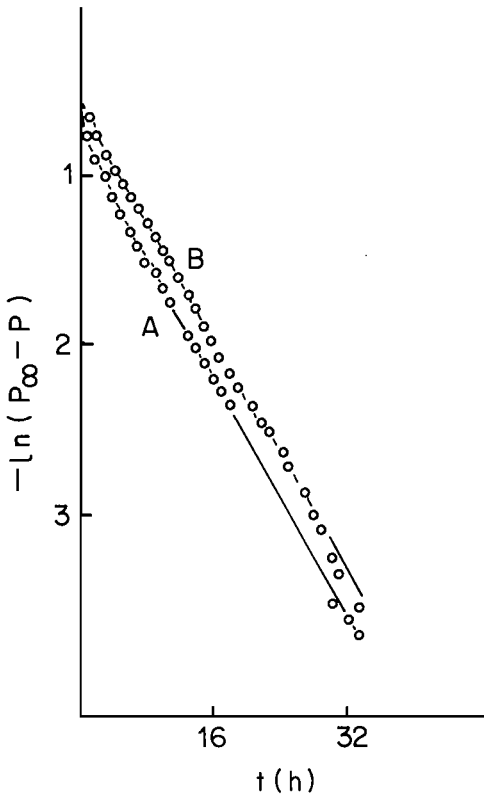

FIG. 3. The effect of added Na_3PO_4 on the kinetics of reduction of Fe(III) by fulvic acid. *A*, no phosphate; *B*, 1 equiv. of phosphate added (5×10^{-5} *M*).

dominant) component of natural water organic matter.

Recently, metal ion titrimetric studies (12) and light scattering as a function of pH (6) studies have confirmed the Schnitzer–Gamble (1) model of FA as a *polydisperse* mixture of predominantly phenol-polycarboxylate units with a limited degree of polymerization via covalent linkages but with extensive aggregation via hydrogen bonding and other labile interactions. This picture of FA can be used to construct a consistent interpretation of the *mechanism* by which FA "dissolves" hydrous ferric oxide colloids. Individual Fe ions or small fragments of hydroxo iron polymer are coordinated at FA sites analogous to the salicylic acid functionality. (A small fraction may be reduced to Fe(II) and, indeed, transient reduction *may* play a catalytic part in the "dissolution" mechanism as it does in a number of slow dissolutions known to inorganic chemistry.) The Fe ions coordinated to one fulvic acid unit bridge to other fulvic acid units to give the aggregates that are often of larger particle size than the hydrous oxide colloids. These aggregated complexes, however, remain comparatively labile.

The rate constant for reaction with SSA in a pH = 2 reagent solution is similar to that reported earlier for decomposition of a monomeric Fe(III)–FA complex that forms in strong acid media.

A recent field study of the organic ligands in the Indian River, Almonte, Ontario (13) emphasized a role for the reducing power of aquatic humic substances as well as their complexing power in metal ion mobilization. (Mobilization by dissolved organic acids appears to follow the order Fe > Mn > Ni ~ Cu.) The evidence of ease of ferrozine *induced* Fe reduction by fulvic acid suggests reductive steps in dissolution of metals from hydrous oxide sediments as a mechanism for the effect observed in the field.

The results on mixtures of Fe(II) and Fe(III) do illustrate the role of electron transfer steps in hydrolytic precipitate growth. Microscopic reversibility implies a role for electron transfer in the reverse process.

Acknowledgements

We thank Mr. Claude Bordeleau and Dr. D. R. Wiles for the Mössbauer spectra. Dr. J. R. Duffy suggested ferrozine and some of its homologs for our evaluation.

1. D. S. GAMBLE and M. SCHNITZER. *In* Trace metals and metal–organic interactions in natural waters. *Edited by* P. C. Singer. Ann Arbor Science, Ann Arbor. 1973.
2. C. H. LANGFORD and T. R. KHAN. Can. J. Chem. **53**, 2979 (1975).
3. C. H. LANGFORD, R. KAY, G. W. QUANCE, and T. R. KHAN. Anal. Lett. **10**, 1247 (1977).
4. L. L. STOOKEY. Anal. Chem. **42**, 779 (1970).
5. M. K. S. MAK. Ph.D. Thesis, Carleton University. 1980.
6. A. W. UNDERDOWN, C. H. LANGFORD, and D. S. GAMBLE. J. Am. Chem. Soc. To be published.
7. C. BORDELEAU. Ph.D. Thesis, Carleton University. 1980.
8. 1974 Annual Book of ASTM Standards, American Society for Testing and Materials, Philadelphia, 1974. Part 31, p. 332.
9. M. SCHNITZER and J. R. M. SKINNER. Soil Sci. **99**, 278 (1965).
10. J. BUFFLE, F. GRETER, and W. HAERDI. Anal. Chem. **49**, 216 (1977).
11. C. H. LANGFORD and T. R. KHAN. Inorg. Nucl. Chem. Lett. **15**, 291 (1979).
12. D. S. GAMBLE, A. W. UNDERDOWN, and C. H. LANGFORD. Anal. Chem. In press.
13. T. R. KHAN. Ph.D. Thesis, Carleton University. 1979.

Can. J. Chem. Downloaded from www.nrcresearchpress.com by 210.87.254.40 on 09/06/12
For personal use only.

The redetermination of the crystal structure of trisulphur dinitrogen dioxide

GREG MACLEAN, JACK PASSMORE, AND PETER S. WHITE

Department of Chemistry, University of New Brunswick, Fredericton, N.B., Canada E3B 5A3

AND

ARTHUR BANISTER AND JAMES A. DURRANT

Department of Chemistry, University of Durham, Science Laboratories, South Road, Durham, England DH1 3LE

Received July 28, 1980

GREG MACLEAN, JACK PASSMORE, PETER S. WHITE, ARTHUR BANISTER, and JAMES A. DURRANT. Can. J. Chem. **59**, 187 (1981).

The crystal structure of $S_3N_2O_2$ has been redetermined and the structure refined to a final R of 0.057 and R_w of 0.076 for 550 reflections with $I \geq 2\sigma(I)$. $S_3N_2O_2$ is planar and of C_{2v} symmetry, as previously found by Weiss. The central S—N distances and angle are 1.647(3) Å, NŜN 97.3(2)°, with adjacent N—S distances and angles of 1.535(3) Å, SN̂S 124.3(2)°, and terminal S—O distances and angles of 1.446(4) Å, NŜO 118.0(2)°. The infrared and Raman spectra are reported and some assignments are made.

GREG MACLEAN, JACK PASSMORE, PETER S. WHITE, ARTHUR BANISTER et JAMES A. DURRANT. Can. J. Chem. **59**, 187 (1981).

On a déterminé de nouveau la structure cristalline du $S_3N_2O_2$ et on l'a affinée jusqu'à une valeur finale de $R = 0{,}057$ et $R_w = 0{,}076$ pour 550 réflexions avec $I \geq 2\sigma(I)$. Tel que Weiss l'avait établi antérieurement, la molécule de $S_3N_2O_2$ est planaire et possède une symétrie C_{2v}. Pour les S—N du centre, les distances et les angles sont respectivement de 1,647(3) Å et NŜN 97,3(2)°; pour les N—S adjacents les distances et les angles sont respectivement de 1,535(3) Å et SN̂S 124,3(2)° alors que les distances des S—O terminaux sont de 1,446(4) Å avec un NŜO de 118,0(2)°. On rapporte les spectres infrarouges et Raman; on a aussi procédé à quelques attributions de bandes.

[Traduit par le journal]

Introduction

In a recent survey (1) of structural data for inorganic and organic compounds containing two coordinate nitrogens attached to sulphur, it was shown that for unstrained S—N—S^{IV} compounds there is an inverse relationship between the nitrogen bond angle and the mean N—S distance, as given by eq. [1][1]

[1] $d_{NS} = 179.99 - 0.1599\hat{N}$

where $\hat{N}$ is the SNS bond angle in degrees, d_{NS} is the arithmetic mean (in pm) of the two adjacent NS distances. All available structural data were accommodated by eq. [1], except those for $S_3N_2O_2$ (3) and $N(SCl)_2^+$ in $N(SCl)_2BCl_4$ (4) (and recently $N(SCl)_2AlCl_4$ (5)). The published structure of $S_3N_2O_2$ (3) included a very short S^{IV}—O bond length of 1.37 Å, however standard deviations were not given. In the course of our work single crystals of $S_3N_2O_2$ were obtained and in view of the above, the crystal structure was redetermined.

Experimental

Preparation of $S_3N_2O_2$

Unless otherwise specified, the apparatus and techniques employed were the same as those described in refs. 6 and 7.

In a typical reaction SO_2 (3.69 g, 57.6 mmol) was condensed onto a mixture of $NS_2Br_2AsF_6$ (0.494 g, 1.56 mmol) (8) and CsF (0.421 g, 2.77 mmol) in one bulb of a two-bulb vessel incorporating a sintered glass frit. The mixture was stirred for 2 days at room temperature, the insoluble and soluble products were separated and the volatiles (SO_2, Br_2, and OSF_2) were slowly removed by evacuation. The insoluble portion (0.496 g) contained $CsAsF_6$ and a small amount of an unidentified species.

The orange soluble product (0.327 g) was held at 45°C for 30 min under a dynamic vacuum and a small quantity (ca. 0.1 g) of yellow plate-like crystals were formed above the heated zone. The crystals were identified as $S_3N_2O_2$.

The infrared spectrum of a Nujol mull using KBr plates was similar to that of an infrared spectrum of $S_3N_2O_2$ obtained by Chivers (9) and Durrant (10). Peaks were observed at 1185 vs, 1150 sh, 1086 mw, 1036 s, 1015 sh, 993 mw, 722 m (Nujol?), 684 ms, 656 w, 555 m, 503 m, 372 ms cm^{-1}. The Raman spectra of a sample of crystals in a melting point tube was obtained using a Ramalab Spex Spectrometer, with a slit width of 2 cm^{-1} and approximately 200 mW of power of the 5145 Å emitting laser line. Peaks were recorded at 1199 mw, 1165 vvw, 1039 vs, 1025 sh, 996 vvw, 806 vvw, 718 vvw, 687 mw, 656 vvw, 555 vvw, 515 mw, 385 vvw, 354 vvw, 236 mw, 166 vvw, 125 vvw, 108 w, 91 w, 59 m cm^{-1}.

Structure Determination

A crystal of dimensions 0.50 × 0.35 × 0.25 mm was mounted under nitrogen in a dried glass capillary as described previously (11) with the modification that crystals were examined and manipulated with the help of a Wild M3 microscope of long focal length mounted outside the dry box.

Preliminary precession photographs showed the space group to be $C2/c$ or Cc and cell parameters to be similar to those of Weiss (3). Accurate cell dimensions were obtained from a least-squares fit to the centered positions of 21 Friedel pairs of reflections on a Picker FACS-I diffractometer ($31° < 2\theta < 42°$). Graphite monochromated Mo $K_{\bar{\alpha}}$ radiation was used throughout

[1]Data giving rise to eqs. [1]–[4] have also been treated by a more sophisticated statistical model to give slightly different equations (2), but these changes do not affect the conclusions drawn here using eqs. [1]–[4] (which are based on a least-squares treatment).

0008-4042/81/020187-04$01.00/0

©1981 National Research Council of Canada/Conseil national de recherches du Canada

Can. J. Chem. Downloaded from www.nrcresearchpress.com by 210.87.254.42 on 09/05/12
For personal use only.

Can. J. Chem. Downloaded from www.nrcresearchpress.com by 210.87.254.42 on 09/05/12
For personal use only.

the investigation. Relevant crystallographic data are:

$S_3N_2O_2$ f.w. = 156.20
Monoclinic, $C2/c$, $a = 16.389(3)$ Å, $b = 4.5719(6)$ Å, $c = 6.790(1)$ Å, $\beta = 96.64(2)°$, $V = 505.3$ Å^3, $Z = 4$, $\rho_c = 2.053$ Mg m^{-3}, $F(000) = 312$, μ(Mo $K_{\bar{\alpha}}$) = 1.27 mm^{-1}, $\lambda = 0.71069$ Å.

Intensity data were collected using an ω–2θ scan of 2 deg, corrected for dispersion of the K_α doublet. Backgrounds were estimated from standing counts at both ends of the scan and an analysis of the profile of the peak. Standards monitored throughout the data collection showed no significant deviation from their mean value. Data were collected for $2\theta \leq 60°$ which resulted in 741 unique reflections of which 550 were considered observed ($I \geq 2\sigma(I)$) and included in the subsequent refinement. After data reduction, the structure was refined by least squares using the positions of Weiss (3) as a starting point. The function minimized by the procedure was $\sum w(|F_o| - |F_c|)^2$ with $w = 1/(\sigma(F) + 0.005|F|^2)^2$, $\sigma(F)$ being derived from counter statistics and the factor 0.005 from an analysis of the statistics of the standards. Atomic scattering factors were those given in the International tables (12) and were corrected for anomalous dispersion. The final reliability indices were $R = 0.057$, $R_w = 0.076$ (0.077 and 0.081 respectively including unobserved reflections) and all shifts were zero in the final cycle of least squares. An attempt to refine the structure in the acentric space group Cc did not result in a significant improvement in the reliability factor indicating that $C2/c$ is the correct choice. Final positional parameters are given in Table 1.[2]

TABLE 1. Final positional parameters for $S_3N_2O_2$ with estimated standard deviations in parentheses

Atom	x	y	z
S(1)	0.5000(0)	0.1280(3)	0.2500(0)
S(2)	0.34669(5)	0.2826(3)	0.3676(2)
N(1)	0.4306(2)	0.3660(7)	0.3047(5)
O(1)	0.1728(2)	0.4752(9)	0.1194(6)

Results and Discussion

The reaction leading to $S_3N_2O_2$ and other products, described in the Experimental section, is complex and presumably involves participation of the solvent SO_2. The compound $S_3N_2O_2$ can be prepared more easily and in good yield by a variety of reported methods (13–15).

The packing of $S_3N_2O_2$ in the unit cell is shown in Fig. 1, and the structure of $S_3N_2O_2$ is depicted in Fig. 2, with bond distances and angles given in Table 2. The units of $S_3N_2O_2$ are planar with a perpendicular distance of 2.335 Å between the adjacent planes[2] (see Fig. 1).

The overall geometry of $S_3N_2O_2$ is the same as that reported by Weiss (3). The NSO groups are *cis* with respect to the central sulphur atom. Similar *cis* configurations, and bond distances and angles within the NSO groups have been found in *cis*-HNSO (16), ClNSO (17), $PhSO_2NSO$ (18), and PhNHNSO (19). The S—O distance (1.446(4) Å) in $S_3N_2O_2$ is also similar to that found in these related molecules.

The overall bonding in $S_3N_2O_2$ may, to a first order of approximation, be depicted by valence bond structures **1**, **2**, and **3**.

The central S—N bond distance 1.647(3) Å is somewhat less than that of other formally single S—N bonds (20) (cf. S_7NH, 1.73 Å (21) or H_3NSO_3, 1.775 Å (22)) and suggests that there is some delocalisation of the π system across the central suphur atom, thus, accounting for the planarity of the molecule. Using Pauling's (23) approach, the central SN, NS, and SO bonds have bond orders 1.37, 1.88, and 1.93 respectively. Similar SN bond orders are derived by Nyburg's relationship between bond order and bond distance for SN species (24). Planarity and a *cis–cis* configuration may also in part result as a consequence of weak bonding or electrostatic attraction between the central sulphur atom and terminal oxygen atoms. A related geometry has been found for the

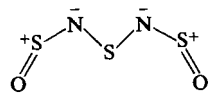

1

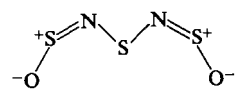

2

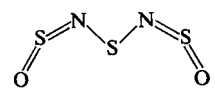

3

NS_4^- (25, 26) and it has been suggested from calculations that the *cis* configuration arises from electrostatic attraction between a partially positively charged sulphur atom and negatively charged terminal sulphur.

Observed sulphur nitrogen bond distances and bond angles have been shown (1, 27) to be related by eqs. [1] and [2],

$$[2] \quad d_{SN} = 211.37 - 0.4661\hat{S}$$

where in eq. [2], d_{SN} is the average sulphur–nitrogen bond distance (in pm) adjacent to the $\hat{NSN}$ angle (in deg) (27). Table 3 shows that the new data are consistent with those obtained for other related unstrained sulphur nitrogen species.

The vibrational spectrum of $S_3N_2O_2$ is complex, however it seems reasonable to assign the 1185 (vs) cm^{-1} peak in the ir as the ν_{asym}(NSO) stretch, and the 1039 (vs) cm^{-1} peak in the Raman as the ν_{sym}(NSO) stretch. The relationship between these two stretching frequencies fits that found for other

[2]Tables of the structure factors, thermal parameters, and atomic deviations from the least-squares plane of $S_3N_2O_2$ may be obtained, at a nominal charge, from the Depository of Unpublished Data, CISTI, National Research Council of Canada, Ottawa, Ont., Canada K1A 0S2.

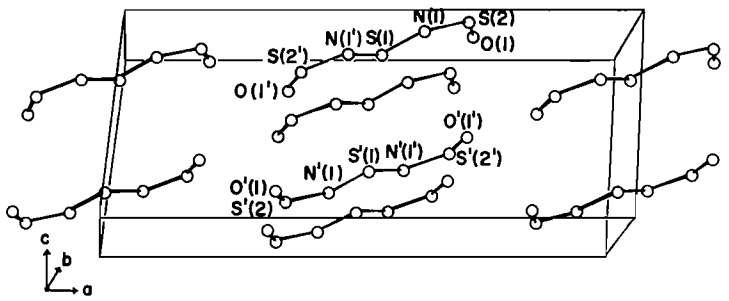

FIG. 1. The crystal packing in $S_3N_2O_2$.

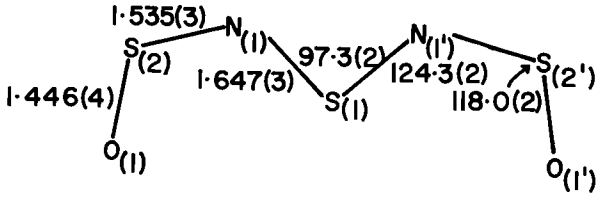

FIG. 2. Configuration of $S_3N_2O_2$, with distances in Å and angles in degrees.

TABLE 2. Bond distances (Å) and angles (deg) in $S_3N_2O_2$ with estimated standard deviations in parentheses that are not given in Fig. 2

Intramolecular contacts		Intermolecular contacts*	
Bond	Distance or angle	Bond	Distance
S(1)—S(2)	2.8132(9)	S(1)—S'(1)	3.5908(8)
S(1)—O(1)	3.142(4)	S(2)—O'(1')	3.185(4)
N(1)—S(1)—S(2)	26.8(1)		
N(1)—S(1)—O(1)	54.2(1)		
S(2')—S(1)—O(1)	178.28(9)		

*Includes all S—S distances ≤3.81 Å, and all S—O distances ≤3.24 Å.

NSO compounds (20, 28). It has been shown (28) that ν_{sym}(NSO) is largely associated with ν(NS) and ν_{asym}(NSO) with ν(SO). Therefore the 1185 cm^{-1} peak can also be assigned as ν_{SO}, and the 1039 cm^{-1} as ν_{SN}. The emprical relationship

[3] $\lambda_{SO}(\mu) = 0.251 d_{SO} - 27.809$

has been derived (10) relating λ_{SO} stretching wavelength with d_{SO} in pm. A d_{SO} value of 144.6 pm in eq. [3] gives a ν_{SO} of 1178 cm^{-1} which supports the assignment of the 1185 cm^{-1} peak in the ir as ν(SO). Similarly (10) eq. [4] has been found to relate $S^{(IV)}$—N distances to wavelengths.

[4] $d_{SN} = 4.672\lambda_{SN} + 110.12$

Consequently for d_{SN} = 153.5 pm, a ν(SN) of 1077 cm^{-1} is derived from eq. [4], again supporting the assignment of the very strong 1039 cm^{-1} peak in the Raman as ν(SN).

TABLE 3. Observed vs. calculated average SN bond length estimated by eqs. [1] and [2]

	Observed data		
Atom	Bond angle (deg)	Average d_{SN} (Å)	Calculated d_{SN} (Å)
N(1)	124.3(2)	1.591(7)	1.60 (eq. [1])
S(1)	97.3(2)	1.647(7)	1.66 (eq. [2])

Although one expects a strongly delocalised and vibrationally coupled system in $S_3N_2O_2$, the distance/wavelength correlations fit remarkably well; however, the assignments must be regarded as tentative.

NOTE ADDED IN PROOF:

An excellent paper reporting the X-ray structure of $S_3N_2O_2$ at −105°C, and an assignment of vibrational spectrum has now appeared, and is in essential agreement with our results (29).

Acknowledgements

We thank the Natural Sciences and Engineering Research Council of Canada for financial support, N.A.T.O. for a travel grant no. 1459 (J.P. and A.J.B.), and T. Chivers for helpful discussions.

1. A. J. BANISTER and J. A. DURRANT. J. Chem. Res. (S), 150 (1978).
2. A. J. BANISTER and R. S. ROBERTS. To be published.
3. J. WEISS. Z. Naturforsch. **16B**, 477 (1961).
4. O. GLEMSER, B. KREBS, J. WEGENER, and E. KINDLEN. Angew. Chem. Int. Ed. **8**, 598 (1969).
5. O. GLEMSER, E. KINDLEN, B. KREBS, R. MEWS, F. M. SCHNEPEL, and J. WEGENER. Z. Naturforsch, **35B**, 657 (1980).
6. J. PASSMORE and P. TAYLOR. J. Chem. Soc. Dalton, 804 (1976).
7. J. PASSMORE, E. K. RICHARDSON, and P. TAYLOR. Inorg. Chem. **17**, 1681 (1978).
8. G. MACLEAN and J. PASSMORE. Unpublished results.
9. T. CHIVERS. Private communication.
10. J. A. DURRANT. Ph.D. Thesis, University of Durham, Durham, England. 1977.
11. R. F. DUNPHY, C. LAU, H. LYNTON, and J. PASSMORE. J. Chem. Soc. Dalton, 2533 (1973).

Can. J. Chem. Downloaded from www.nrcresearchpress.com by 210.87.254.42 on 09/05/12
For personal use only.

12. C. H. DAUBEN and D. H. TEMPLETON. International tables for X-ray crystallography. Vol. III. Kynoch Press, Birmingham. 1962. p. 213, Table 3.3.2A.
13. W. L. JOLLY and M. BECKE-GOEHRING. Inorg. Chem. **1**, 76 (1962).
14. D. A. ARMITAGE and A. W. SINDEN. Inorg. Chem. **11**, 1151 (1972).
15. D. A. ARMITAGE and A. W. SINDEN. J. Inorg. Nucl. Chem. **36**, 993 (1974).
16. W. H. KIRCHHOFF. J. Am. Chem. Soc. **91**, 2437 (1969).
17. H. OBERHAMMER. Z. Naturforsch. **25A**, 1497 (1970).
18. G. DÉLÉRIS, C. COURSEILLE, J. KOWALSKI, and J. DUNOGUÈS. J. Chem. Res. (S), 122 (1979).
19. A. GIEREN and B. DEDERER. Angew. Chem. Int. Ed. **16**, 179 (1977).
20. A. J. BANISTER, L. F. MOORE, and J. S. PADLEY. Spectrochim. Acta, **23A**, 2705 (1967).
21. J. WEISS and H. S. NEUBERT. Acta Crystallogr. **18**, 815 (1965).
22. J. W. BATS, P. COPPENS, and T. F. KOETZLE. Acta Crystallogr. **33B**, 37 (1977).
23. L. PAULING. The nature of the chemical bond. 3rd ed. Cornell University Press, Ithaca, NY. 1960.
24. S. C. NYBURG. J. Crystallogr. Mol. Struct. **3**, 331 (1973).
25. T. CHIVERS and R. T. OAKLEY. J. Chem. Soc. Chem. Commun. 752 (1979).
26. T. CHIVERS, W. G. LAIDLAW, R. T. OAKLEY, and M. TRSIC. J. Am. Chem. Soc. **102**, 5773 (1980).
27. A. J. BANISTER and J. A. DURRANT. J. Chem. Res. (S), 152 (1978).
28. H. H. EYSEL. J. Mol. Struct. **5**, 275 (1970).
29. R. STEUDEL, J. STEIDEL, and N. RAUTENBERG. Z. Naturforsch. **35B**, 792 (1980).

Can. J. Chem. Downloaded from www.nrcresearchpress.com by 210.87.254.42 on 09/05/12
For personal use only.

Solvent effects on the visible absorption spectrum of crystal violet[1]

J. KORPPI-TOMMOLA[2] AND R. W. YIP
Division of Chemistry, National Research Council of Canada, Ottawa, Ont., Canada K1A 0R6

Received July 28, 1980

J. KORPPI-TOMMOLA and R. W. YIP. Can. J. Chem. **59**, 191 (1981).

Addition of polar solvents to non-polar solutions of crystal violet results in dramatic changes in the visible absorption spectra. The observed changes are explained in terms of crystal violet existing as an ion-pair in non-polar solutions and as a solvated ion in polar solutions.

The spectrum of crystal violet in toluene and in acetone solution remains virtually unchanged over a wide temperature range. However in methanol, as was reported for ethanol (1), the short wavelength component of the absorption in the visible region disappears as the temperature is lowered. The spectral behaviour in alcoholic solutions suggests a decreasing solvent–solute interaction around the dye cation due to increased self-association of the solvent molecules as the temperature is decreased. Our observations have a direct application in interpreting some of the results of the photodynamics of crystal violet in solution.

J. KORPPI-TOMMOLA et R. W. YIP. Can. J. Chem. **59**, 191 (1981).

L'addition de solvants polaires aux solutions non polaires du cristal violet provoque des changements majeurs dans le spectre d'absorption visible. On explique les changements observés en fonction du fait que le cristal violet existe sous forme d'une paire d'ions dans les solutions non polaires et sous forme d'ion solvaté dans les solutions polaires.

Dans le toluène et dans une solution d'acétone, le spectre du cristal violet reste inchangé sur une large échelle de température. Cependant, dans le méthanol et tel que rapporté pour l'éthanol (1), la composante de courte longueur d'onde de l'absorption dans la région du visible, disparait lorsqu'on abaisse la température. Le comportement spectral dans les solutions alcooliques suggère une diminution de l'interaction solvant–soluté autour du cation colorant, provenant de l'augmentation de l'auto-association des molécules du solvant lorsque la température diminue. Nos observations trouvent une application directe dans l'interprétation de quelques résultats de la photodynamique du cristal violet en solution.

[Traduit par le journal]

Introduction

The phenyl rings of the dye cation crystal violet (CV) (tri-*p*-dimethylamino phenylcarbonium ion), like other triphenylmethane dyes, are forced out of the molecular plane by rotation about the central bonds because of steric hindrance between the rings (1). If all of the rings are rotated in the same sense over the same angle, then the cation resembles a propeller with D_3 symmetry. Within the Hückel approximation, this symmetry gives rise to a doubly degenerate lowest excited state (x, y polarized in the molecular plane) (2).

In dilute solution, crystal violet shows two overlapping absorption bands in the 550–600 nm region. These bands are not due to aggregation which has been observed in more concentrated solution (3). The presence of the two overlapping absorption bands can be due to a single species with a symmetry less than D_3 (giving rise to two non-degenerate states) or due to two species.

Early on, Lewis and co-workers (1) suggested that the bands are due to two rotamers; a symmetrical D_3 propeller-like species, and an unsymmetrical species with one of the phenyl rings rotated in the opposite sense with respect to the other two rings. This suggestion was based on the important observation that as the temperature is lowered, one of the bands (the one at short wavelength) tends to disappear while the other band increases in absorption. The observation clearly rules out the interpretation that the band structure represents a partially resolved vibrational structure of a single electronic state. Recent experiments on the picosecond recovery times of the two absorption bands on excitation with a single 530 nm picosecond pulse suggests the presence of two species in solution at room temperature (4). The recovery time proved to be dependent on the monitoring wavelength. A recent resonance Raman study suggests that CV exists as a single D_3 species in solution (5). Magnetic circular dichroism studies are also consistent with a single propeller-like species (either with symmetrical or unsymmetrical angles of twist of the phenyl group) with splitting of the degenerate E states (6).

The fluorescent properties of CV do not rule out the presence of two ground state species which can be rapidly transformed in the excited state. Independent of the exciting wavelength, CV shows only a single fluorescent band which mirrors the long wavelength absorption band (1, 2). The fluorescence polarized excitation spectrum shows a different polarization ratio for the two absorption

[1]NRCC No. 18756.
[2]NRCC Research Associate.

0008-4042/81/020191-04$01.00/0
©1981 National Research Council of Canada/Conseil national de recherches du Canada

Can. J. Chem. Downloaded from www.nrcresearchpress.com by 210.87.254.5 on 09/05/12
For personal use only.

Can. J. Chem. Downloaded from www.nrcresearchpress.com by 210.87.254.5 on 09/05/12
For personal use only.

bands (2), indicating the presence of two electronic transitions.

To resolve the apparently conflicting results on CV, we have carried out a visible absorption study of CV in different solvents and solvent mixtures and a study of CV absorption at different temperatures. The results enable us to formulate a consistent picture of CV in solution which satisfactorily explains the visible absorption, fluorescence, and time-dependent recovery properties of CV in solution.

Results and Discussion

The visible absorption band of CV acetate in solution is a well resolved doublet in non-polar solvents but is a heavily overlapped doublet in polar solvents. The separation of the band maxima in non-polar solvents is about 65 nm while that in polar solvents is about 30 nm (Tables 1 and 2). The absorption spectrum of CV perchlorate in toluene (maxima at 535, 605 nm) is, within experimental error, identical with the spectrum of the acetate salt. To further investigate the two different band shapes, toluene solutions of CV were titrated with several polar and non-polar solvents. Results from the titrations are given in Fig. 1. The curves shown were obtained by measuring the peak height at 600 nm. Parallel behaviour is obtained for the short wavelength component in all titrations.

Adding benzene in toluene solution of the dye (2×10^{-5} *M*) left the molar absorption coefficient (ε) almost unchanged. Addition of acetonitrile and chloroform first decreases ε slightly and then increases it until the bulk is reached. Alcohol titrations result in most dramatic changes in the spectra (Fig. 1). Adding small amounts of alcohol reduces to less than one half of its initial value. Further addition of alcohol increases ε from its minimum value towards a final bulk ε in alcoholic solutions, the relative increase being over 400%. Saturation is reached by a mole fraction of 0.3. In *t*-butyl alcohol mixtures, ε remains low throughout the concentration region. Acetone titration shows an intermediate behaviour, which could be understood in terms of a keto–enol equilibrium in acidic acetone solutions. Beside changes in ε, addition of a polar solvent in toluene solutions of CV non-linearly shifts the wavelengths of the two absorption components. The short wavelength component (at 540 nm in toluene shifting to 560 nm in polar solvents) seems to be more sensitive to the addition of titrant than is the long wavelength component (Fig. 2). The wavelength shifts occur in the same concentration region as that observed for the sharp increase in ε (Fig. 1). Addition of non-polar solvent leaves the wavelengths of both absorption components unchanged.

TABLE 1. Absorption wavelengths of crystal violet in non-polar solvents

Solvent	λ_1 (nm)	λ_2 (nm)	$\Delta\lambda$ (nm)
CS_2	609	542	67
Cyclohexane	595	531	64
Decalin	602	532	70
Benzene	605	538	67
Toluene	603	537	66
Mesitylene	605	539	66
Hexafluorobenzene	593	529	64

TABLE 2. Absorption wavelengths of crystal violet in polar solvents

Solvent	λ_1 (nm)	λ_2 (nm)	$\Delta\lambda$ (nm)
Water	590	552	38
Methanol	586	553	33
Ethanol	589	560	29
t-Butyl alcohol	588	558	30
Glycerol	595	560	35
Chloroform	587	560	27
Acetonitrile	587	558	29
Acetone	588	558	30
Fluorobenzene	593	560	33
Chlorobenzene	593	562	31
Benzonitrile	593	565	28

The results from our temperature measurements are shown in Fig. 3. Decreasing temperature decreases the intensity of the short wavelength component in the methanol spectra (Fig. 3*C*). The observation is similar to that reported by Lewis and co-workers (1) for ethanol solution. However in toluene solution (Fig. 3*A*), where the two components are well resolved, no significant relative intensity changes are observed over the temperature range from +50°C to −50°C. In acetone solutions, we observed some changes in the band shape as the sample was cooled, but disappearance of the short wavelength components does not occur as in methanol solutions (Fig. 3*B*). Overall increase in all spectra studied is partly due to narrower line widths and partly to solvent contraction at lower temperature.

To explain the doublet structure of the CV absorption band in the different solvents, we suggest that the "free" cation degeneracy (*E* state) is perturbed differently depending on the environment of the dye. In a non-polar solvent such as toluene, CV salt likely exists as ion pairs in solutions (1, 2), whereas in a polar solution such as methanol, all of the ions are solvated. The degenerate *E* state of the

Can. J. Chem. Downloaded from www.nrcresearchpress.com by 210.87.254.5 on 09/05/12
For personal use only.

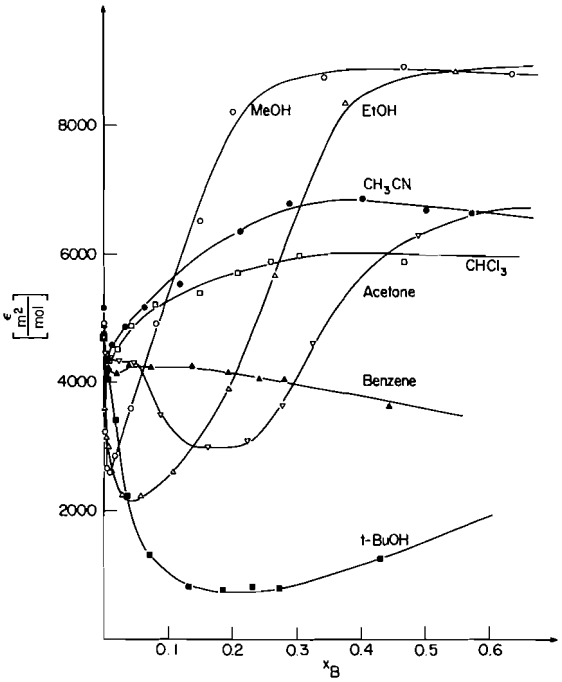

FIG. 1. Molar absorption coefficient ($\varepsilon_{600\,nm}$) as a function of molar fraction of titrant in toluene solutions of crystal violet acetate: ○ = methanol, △ = ethanol, ● = CH_3CN, □ = $CHCl_3$, ▲ = benzene, ▽ = acetone, and ■ = *t*-butyl alcohol.

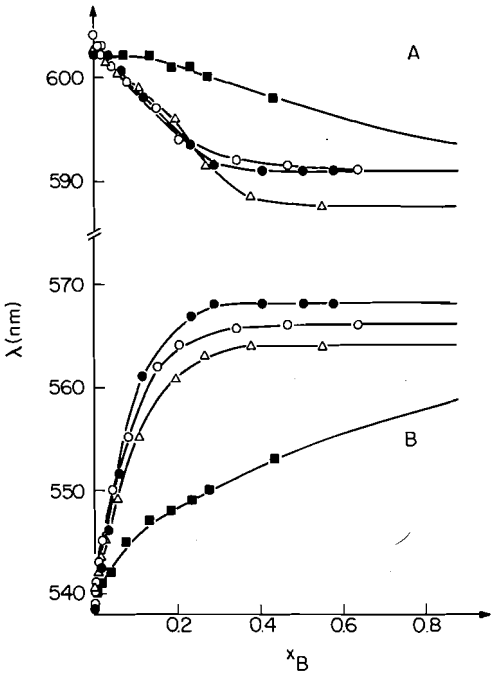

FIG. 2. Wavelengths of the two absorption components of crystal violet in toluene as a function of molar fraction of titrant: ○ = methanol, △ = ethanol, ● = chloroform, and ■ = *t*-butyl alcohol.

"free" cation will then be perturbed by dye cation–solvent interactions in polar solution and by the tightly bound counter anion in non-polar solution; the perturbation being larger in the latter case. The doublet structure does not appear to critically depend on the nature of the counter ion. The absorption spectrum of the perchlorate salt (more symmetric counter anion) was identical with that of the acetate salt in toluene. The sharp decrease in ε after adding small amounts of polar solvent in toluene solution of CV indicates one of the species in solution is disappearing, while the increase in ε with the further addition of titrant implies a new species is being formed. The initial decrease in ε could be explained by the disappearance of tight ion pairs in solution due to solvation of the counter ions. If the spectrum of CV in polar solvents is due to completely solvated dye cation, then further addition of polar solvent should increase the ε of the solution. Since solvated CV is assumed to have a more strongly overlapping band than does CV in an ion-pair, the further addition of polar solvent increases the overlap of the two absorbing components (Fig. 2) and increases the ε of the solution (Fig. 1). In acetonitrile and in chloroform titrations, the rising part of titration curve follows closely the above picture. In alcoholic titrations, the basic scheme is the same but the changes in ε are much more dramatic. Direct hydrogen bonding of alcohol monomers to the nitrogen atoms of the dye cation may be involved. Other phenomena such as self-association of the solvent and, in the case of *t*-butyl alcohol, steric hindrance may contribute to the overall behaviour of the titration curves.

The temperature dependence of the visible absorption spectrum of CV in alcoholic solutions (Fig. 3*C*) can be understood in terms of solvation changes with temperature. In addition to being a polar solvent, alcohols tend to self-associate. In dilute alcohol solution, dimer aggregates can be identified while in neat liquid only a few of the molecules remain in monomeric form (7). Reducing the temperature decreases the number of monomeric species in alcohols. Assuming that solvation is mainly due to the interaction of alcohol monomers and the dye cation, reducing the temperature decreases the number of solvent molecules capable of solvating the dye and finally trapping an almost "free" dye cation in a polymer matrix. Accordingly the degeneracy of the first excited state is returned and we see only one absorbing component in the spectra (Fig. 3*C*, ref. 1). It may be mentioned that in concentrated alcoholic dye solutions ($C > 5 \times 10^{-4}\,M$), the temperature behaviour is reversed to what we observed in dilute dye solutions, indicat-

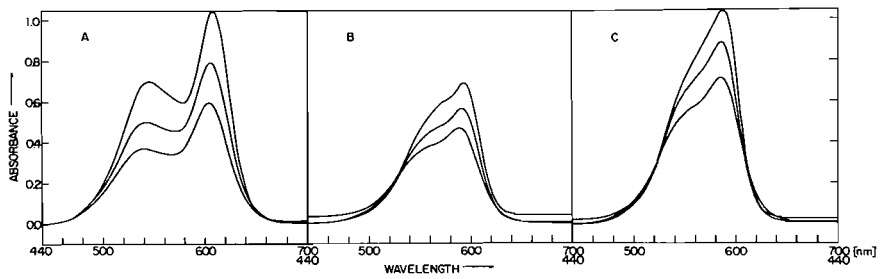

FIG. 3. Temperature dependence of crystal violet spectrum: (*A*) in toluene, temperatures from top to bottom $T = -50°C$, $+5°C$, and $+46°C$; (*B*) in acetone, $T = -87°C$, $-39°C$, and $+23°C$; (*C*) in methanol, $T = -70°C$, $-29°C$, and $+50°C$.

ing clustering of the dye molecules in the more concentrated solution (3).

The temperature dependence of the absorption spectrum of CV in ethanol was previously interpreted by Lewis and co-workers (1) in terms of an equilibrium between two rotamers (one absorbing at 500 nm and the other absorbing at 600 nm). Our results for the temperature studies of the absorption changes of CV in toluene suggests that this interpretation is incorrect and that the temperature behaviour of dilute CV in solution is best understood in terms of solvation changes. If there were two rotamers of the dye in alcohol solution, there is no reason why these should not be present in a solvent like toluene and give rise to a temperature dependence. Within experimental error, toluene spectra show no temperature dependence (Fig. 3*A*).

Our suggestion that the solvated and "free" CV in alcohol solution have different absorption spectra has a very important implication on the understanding of the excited state and recovery properties of triphenylmethane dyes in solution. If we assume that desolvation occurs in the excited state, the species which is undergoing non-radiative deactivation and fluorescence is the unsolvated dye cation having a single absorption band at 600 nm. This assumption is consistent with the observation of a single fluorescence band which mirrors the 600 nm absorption band (1, 2).

To explain our recovery kinetics (4), we propose a two-step mechanism, that is the decay of the unsolvated excited molecules is followed by resolvation of the ground state. If the first step is fast compared to the second solvation step, the first recovery monitored at 600 nm measures the decay of the unsolvated excited molecules. The slower recovery time observed at 550 nm would then be due to resolvation of the ground state. The exact kinetic picture depends on the relative magnitudes of the two rate constants and the kinetics has to be treated in terms of a two series first order reaction scheme. Our model implies a non-exponential recovery kinetics of CV in solution. Indeed, a poor single exponential fit particularly at 550 nm, was observed for the recovery of CV in glycerol (4). The important implication of the above model is that viscosity dependent radiationless decay rates cannot be obtained from recovery kinetics without considering solvation processes. Experiments on the photodynamics of CV in solution to test the above mechanism are in progress.

Experimental

Crystal violet carbinol was prepared by shaking methanol solution of the chloride (Baker Chemical) with excess of 1 *M* NaOH. The carbinol was then extracted from and recrystallized in hexane. Crystal violet acetate solutions (2×10^{-5} *M*) were made by dissolving the carbinol in the solvent and by adding acetic acid (0.05 *M*). Further addition of the acid did not increase the absorption of the solution. Crystal violet perchlorate was prepared from the carbinol and perchloric acid.

The spectra were recorded on a Cary 118 double beam spectrometer using 1 cm pathlength cells. Low temperatures were produced by boiling off liquid nitrogen through a cell holder. The temperature was measured right beside the sample cell using a copper–constantan thermocouple.

Acknowledgement

We would like to thank Dr. Roland Bonneau (Université de Bordeaux I) for stimulating discussion of the problem.

1. G. N. LEWIS, T. T. MAGEL, and D. LIPKIN. J. Am. Chem. Soc. **64**, 1774 (1942).
2. F. C. ADAM and W. T. SIMPSON. J. Mol. Spectrosc. **3**, 363 (1959).
3. L. V. LEVSHIN and V. K. GORSHKOV. Opt. Spectrosc. **10**, 401 (1961).
4. J. M. GRZYBOWSKI, S. E. SUGAMORI, D. F. WILLIAMS, and R. W. YIP. Chem. Phys. Lett. **65**, 456 (1979).
5. L. ANGELONI, G. SMULEVICH, and M. P. MARZOCCHI. J. Raman Spectrosc. **8**, 305 (1979).
6. H. P. J. M. DEKKERS and E. C. M. KIELMAN-VAN LUYT. Mol. Phys. **31**, 1001 (1976).
7. J. KORPPI-TOMMOLA. J. Mol. Struct. **40**, 13 (1977).

Can. J. Chem. Downloaded from www.nrcresearchpress.com by 210.87.254.5 on 09/05/12
For personal use only.

Synthesis of *cis*- and *trans*-platinum compounds with pyrimidine and crystal structures of *trans*-[Pt(pyrimidine)$_2$X$_2$] where X = Cl and Br

F. D. ROCHON, P. C. KONG, AND R. MELANSON

Département de chimie, Université du Québec à Montréal, C.P. 8888, Montréal (Qué.), Canada H3C 3P8

Received June 6, 1980

F. D. ROCHON, P. C. KONG, and R. MELANSON. Can. J. Chem. **59**, 195 (1981).

cis- and *trans*-[Pt(pm)$_2$X$_2$] where pm = pyrimidine and X = Cl, Br, have been synthesized. The *cis*-compounds were isolated from the reaction of K_2PtCl_4 and pm in water, while the *trans*-isomers were obtained by isomerization of *cis*-[Pt(pm$_2$X$_2$] in DMF in the presence of pm.

The crystal structures of the two compounds *trans*-[Pt(pm)$_2$X$_2$] have been determined by X-ray diffraction. The two compounds (X = Br and Cl) are isostructural. The crystals belong to the monoclinic $P2_1/c$ space group. The cell parameters are $a = 4.787(3)$, $b = 14.257(7)$, $c = 8.503(3)$ Å and $\beta = 99.33(4)°$ when X = Cl and $a = 4.826(3)$, $b = 14.822(5)$, $c = 8.516(5)$ Å and $\beta = 101.26(4)°$ when X = Br. The platinum atom is located on a centre of symmetry at the origin and $Z = 2$. The residual factors are $R = 0.029$ and $R_w = 0.036$ (X = Cl) and $R = 0.036$ and $R_w = 0.035$ (X = Br).

F. D. ROCHON, P. C. KONG et R. MELANSON. Can. J. Chem. **59**, 195 (1981).

Les complexes *cis* et *trans*-[Pt(pm)$_2$X$_2$] où pm = pyrimidine et X = Cl et Br ont été synthétisés. Les composés *cis* ont été isolés de la réaction de K_2PtCl_4 et pm dans l'eau, tandis que les isomères *trans* ont été obtenus par l'isomérisation de *cis*-[Pt(pm)$_2$X$_2$] dans le DMF en présence de pm.

La structure cristalline des deux composés *trans*-[Pt(pm)$_2$X$_2$] a été déterminée par diffraction des rayons X. Les deux composés (X = Cl et Br) sont isostructuraux. Les cristaux appartiennent au groupe spatial monoclinique $P2_1/c$. Les paramètres de maille sont $a = 4,787(3)$, $b = 14,257(7)$, $c = 8,503(3)$ Å et $\beta = 99,33(4)°$ pour X = Cl et $a = 4,826(3)$, $b = 14,822(5)$, $c = 8,516(5)$ Å et $\beta = 101,26(4)°$ pour X = Br. L'atome de platine se trouve sur un centre de symétrie à l'origine et $Z = 2$. Les facteurs résiduels sont $R = 0,029$ et $R_w = 0,036$ (X = Cl) et $R = 0,036$ et $R_w = 0,035$ (X = Br).

Introduction

Since the discovery of the antitumour properties of *cis*-[Pt(NH$_3$)$_2$Cl$_2$], a large research effort was made to synthesize complexes of the type *cis*-[Pt(L)$_2$Cl$_2$] (L = amine derivative) in order to extend the screening range of platinum complexes. In recent years, we have been involved in a program of synthesizing new platinum complexes and of studying their reactions and structures in solution and in the solid state. We have been studying the interaction between platinum compounds and amine ligands, since the antitumour properties of the platinum complexes were related to an interaction with the bases of cellular DNA. Since *trans*-[Pt(L)$_2$Cl$_2$] has no antitumour activity, and the *cis*-isomers may isomerize to the *trans*-isomers under certain conditions, the study of these isomerization reactions is important.

Platinum compounds of pyridine (py) and pyrimidine (pm) show some similar reactivity in non-aqueous solvents. For example, *cis*-[Pt(L)$_2$Cl$_2$] (L = py and pm) isomerise to the *trans*-isomers in dimethylsulphoxide (DMSO) or in dimethylformamide (DMF) in the presence of free L (1). In aqueous solution, the reactivities are different. In this paper, the chemical reactions of these compounds in aqueous solution are compared.

We have isolated *cis*- and *trans*-[Pt(pm)$_2$X$_2$] where pm = pyrimidine and X = Cl and Br. They were identified by infrared spectroscopy. The far infrared region was very similar to the spectra of *cis*- and *trans*-[Pt(pm)$_2$X$_2$] (where pm = 2-aminopyrimidine, 4-phenylpyrimidine, and 4-methylpyrimidine) reported earlier (1). In order to confirm the *cis* and *trans* configurations of the complexes, we decided to determine the crystal structures of the isomers. Unfortunately, only the *trans* isomers gave suitable crystals for X-ray diffraction. The crystal structures of both compounds *trans*-[Pt(pm)$_2$X$_2$] where X = Cl and Br are therefore reported below.

Experimental

cis-*[Pt(pm)$_2$Cl$_2$]*

Pyrimidine (0.2 g) is added to 0.415 g of K_2PtCl_4 dissolved in 10 mL of water. A yellow precipitate appears immediately. Two hours later, the precipitate is filtered off, washed with water, and dried under vacuum in the presence of P_2O_5 at room temperature. Yield: 85%. *Anal.* calcd.: C 22.54, H 1.88, Cl 16.67; found: C 22.22, H 1.91, Cl 17.06.

trans-*[Pt(pm)$_2$Cl$_2$]*

cis-[Pt(pm)$_2$Cl$_2$] (0.426 g) and 5 drops of pyrimidine are added to 5 mL of DMF. The mixture is left standing at room temperature for two weeks and yellow crystals appear slowly. The crystals are then collected by filtration and washed with a small amount of DMF and then with ether. Yield: 40%. The filtrate is diluted with ether and a precipitate appears immediately. Infrared spectroscopy has shown that the precipitate is the same as the crystals collected previously. Total yield: 75%. *Anal.* calcd.: C 22.54, H 1.88, N 13.15, Cl 16.67; found: C 22.59, H 1.85, N 12.83, Cl 16.89.

0008-4042/81/020195-04$01.00/0

©1981 National Research Council of Canada/Conseil national de recherches du Canada

Can. J. Chem. Downloaded from www.nrcresearchpress.com by 210.87.254.6 on 09/05/12
For personal use only.

TABLE 1. Final positional structure parameters, estimated standard deviations ($\times 10^4$), and temperature factors (U_{eq} Å^2)*

trans-[Pt(pyrimidine)$_2$Cl$_2$]					*trans*-[Pt(pyrimidine)$_2$Br$_2$]				
Atom	x	y	z	U_{eq}	Atom	x	y	z	U_{eq}
Pt	0	0	0	280.8	Pt	0	0	0	295.3
Cl	231.9(4)	−179.5(1)	2701.6(3)	456.9	Br	323.5(2)	−153.7(1)	2867.4(1)	523.4
N(1)	1691(11)	1287(4)	343(8)	338	N(1)	1568(13)	1261(5)	306(8)	315
N(3)	5329(13)	2266(5)	1666(10)	510	N(3)	5166(14)	2238(6)	1600(9)	504
C(2)	4111(14)	1448(5)	1363(10)	388	C(2)	4016(19)	1459(7)	1297(12)	433
C(4)	4024(17)	3002(6)	915(13)	591	C(4)	3777(21)	2922(7)	829(13)	592
C(5)	1538(17)	2933(5)	−153(11)	484	C(5)	1294(22)	2812(7)	−204(13)	635
C(6)	438(13)	2031(5)	−432(10)	383	C(6)	224(18)	1968(7)	−463(11)	433

*$U_{eq} = \frac{1}{3}(U_{11} + U_{22} + U_{33} + 2U_{13}\cos\beta)$.

cis-[Pt(pm)$_2$Br$_2$] and trans-*[Pt(pm)$_2$Br$_2$]*

The same methods as the ones used for the chloro analogues were used. The solution of K_2PtBr_4 was prepared according to ref. 1.

The crystals *trans*-[Pt(pm)$_2$X$_2$] where X = Cl and Br used for X-ray diffraction were obtained as thin plates directly from the isomerization reaction of *cis*-[Pt(pm)$_2$X$_2$] and pm in DMF. After two weeks of standing in a stoppered flask, crystals started to appear.

A set of precession photographs for both crystals showed that the $h0l$, $l = 2n + 1$ and $0k0$, $k = 2n + 1$ reflections were systematic absences indicating the monoclinic space group $P2_1/c$. The cell parameters were obtained by least-squares refinement from the setting angles of 15 automatically centred reflections on a Syntex P$\bar{1}$ diffractometer using graphite-monochromatized MoKα radiation.

Crystal Data

$C_8H_8Cl_2N_4Pt$ $M_r = 426.17$

Monoclinic, $P2_1/c$, $a = 4.787(3)$, $b = 14.257(7)$, $c = 8.503(3)$ Å, $\beta = 99.33(4)°$, $V = 572.7(5)$ Å^3, $Z = 2$, $D_x = 2.471$, $D_m = 2.46(2)$ Mg m^{-3}, λ(MoKα) = 0.71069 Å, μ(MoKα) = 13.32 mm^{-1}, and T = 295 K.

$C_8H_8Br_2N_4Pt$ $M_r = 515.09$

Monoclinic $P2_1/c$, $a = 4.826(3)$, $b = 14.822(5)$, $c = 8.516(5)$ Å, $\beta = 101.26(4)°$, $V = 597.5(5)$ Å^3, $Z = 2$, $D_x = 2.863$, $D_m = 2.86(2)$ Mg m^{-3}, λ(MoKα) = 0.71069 Å, μ(MoKα) = 19.40 mm^{-1}, and T = 295 K.

Collection and Reduction of Intensity Data

The intensity data were collected from a crystal of *trans*-[Pt(pyrimidine)$_2$Cl$_2$] measuring 0.34 × 0.34 × 0.06 mm, the short dimension parallel to the a axis. The *trans*-[Pt(pyrimidine)$_2$Br$_2$] crystal measured 0.32 × 0.262 × 0.076 mm. A total of 1681 independent reflections (1747 for the bromo analogue) were measured in the region of $2\theta < 60°$ by the $2\theta/\theta$ scan technique using Mo Kα radiation. During the data collection three standard reflections were measured after every 47 reflections as a test of crystal and instrument stability. Their variations were less than 3% from their respective means. The 1108 reflections (1209 for the bromo analogue) for which the intensities were greater than $2.5\sigma(I)$ were considered observed. The standard deviation $\sigma(I)$ was calculated as already described (2). An absorption correction based on the equations of the crystal faces was applied to all the reflections of both crystals. The transmission factors varied from 0.061 to 0.452 for the chloro compound and from 0.018 to 0.224 for the bromo analogue. The data were corrected for the Lorentz and polarization effects. The scattering factors of Cromer and Waber (3) were used for platinum, bromine, chlorine, nitrogen, and carbon, those of Stewart, Davidson, and Simpson (4) were used for hydrogen. The anomalous dispersion terms (5) of platinum, bromine, and chlorine were included in the calculations.

Structure Determination

The position of the platinum atom in each structure determination was easily located on a centre of symmetry at the origin, from the three-dimensional Patterson map. The positions of all the other atoms, except the hydrogen atoms, were obtained by structure factor and Fourier map calculations. The refinement of the parameters was carried out by full-matrix least-squares methods. In the early stages of refinement, unit weight was assigned to all observed reflections. Later individual weights $w = 1/\sigma^2(F)$ (6) were applied. The hydrogen atoms on the pyrimidine ring were fixed at their calculated position and assigned isotropic thermal parameters of 6.0 Å^2. The refinement of the scale factor, the coordinates, and anisotropic temperature factors of all the non-hydrogen atoms converged to $R = \Sigma||F_o| - |F_c||/\Sigma|F_o| = 0.029$ (0.036 for the bromine compound) and $R_w = [\Sigma w(|F_o| - |F_c|)^2/\Sigma w|F_o|^2]^{1/2} = 0.036$ (0.035 for the bromine compound). The final difference Fourier map did not show peaks higher than ±0.8 e Å^{-3}.

The calculations were carried out with a Cyber 73 computer and the programs used have already been described (2). A table of observed and calculated structure factors is available from the Depository of Unpublished Data.[1]

Results and Discussion

The two analyzed compounds [Pt(pyrimidine)$_2$X$_2$] (X = Cl and Br) are isostructural. The refined atomic parameters for the two crystals are listed in Table 1. A list of the anisotropic temperature factors is available.[1] A labelled diagram of the two analyzed compounds is shown in Fig. 1. The bond lengths and the bond angles are shown in Table 2.

The platinum atom in the crystal lies on a centre of symmetry at the origin. The compounds have therefore the *trans* configuration as shown by infrared spectroscopy. The coordination around the platinum atom is square planar. The angles around platinum are close to the expected 90°. The Pt—Cl (2.296 Å) and the Pt—Br (2.427 Å) bonds

[1]Lists of structure factors and anisotropic thermal parameters are available, at a nominal charge, from the Depository of Unpublished Data, CISTI, National Research Council of Canada, Ottawa, Ont., Canada K1A 0S2.

Can. J. Chem. Downloaded from www.nrcresearchpress.com by 210.87.254.6 on 09/05/12
For personal use only.

Can. J. Chem. Downloaded from www.nrcresearchpress.com by 210.87.254.6 on 09/05/12
For personal use only.

TABLE 2. Bond distances (Å) and bond angles (deg) in *trans*-[Pt(pyrimidine)$_2$X$_2$]

Bond	Distance X = Cl	Distance X = Br
Pt—X	2.296(2)	2.427(1)
Pt—N(1)	2.008(5)	2.014(7)
N(1)—C(2)	1.350(10)	1.343(11)
N(1)—C(6)	1.338(9)	1.335(12)
N(3)—C(2)	1.311(10)	1.285(14)
N(3)—C(4)	1.329(11)	1.317(14)
C(4)—C(5)	1.378(13)	1.351(15)
C(5)—C(6)	1.395(10)	1.355(14)

Bonds	Angle X = Cl	Angle X = Br
X—Pt—N(1)	90.2(2)	90.5(2)
Pt—N(1)—C(2)	122.2(5)	123.1(6)
Pt—N(1)—C(6)	121.0(5)	122.0(6)
C(2)—N(1)—C(6)	116.8(6)	114.9(7)
C(2)—N(3)—C(4)	116.6(7)	115.7(9)
N(1)—C(2)—N(3)	125.9(7)	127.9(9)
N(1)—C(6)—C(5)	121.3(7)	120.8(9)
N(3)—C(4)—C(5)	123.3(8)	122.15(10)
C(4)—C(5)—C(6)	116.1(8)	118.6(10)

are normal and agree well with published values (2, 7–12).

The Pt—N distances (2.008 Å and 2.014 Å) are normal for bonds in position *trans* to nitrogen ligands which have a relatively low *trans* influence. The values agree well with the values found in other platinum–nitrogen base crystals (11, 13, 14).

The pyrimidine ring is planar in both compounds. The dihedral angles between the platinum coordination planes and the pyrimidine planes are 52.5° (chlorine compound) and 54.3° (bromine compound). The N—C bonds (1.29–1.35 Å are slightly shorter than the C—C bonds (1.35–1.40 Å). The values agree well with the values published for pyrimidine (15) and for pyrimidin-2-one (16). The pyrimidine ring angles vary from 116 to 126° for the chlorine compound and from 115 to 128° for the bromine compound. As Singh (17) has pointed out, the internal ring angle at a N atom is smaller if the N atom is not covalently bound to an extra-annular H atom. Here the internal angles at the N atoms are 117 and 115° at N(1) and 117 and 116° at N(3) for the chloro and the bromo analogues respectively. The binding of N(1) to the platinum atom does not change the internal angle at the nitrogen atom as it does in the hydrochlorides of pyrimidine and pyrimidin-2-one. The protonation at N(1) in both these compounds increases the ring angle at the nitrogen atom by about 6° (18). This effect shown by Singh (17) is not observed when platinum is the

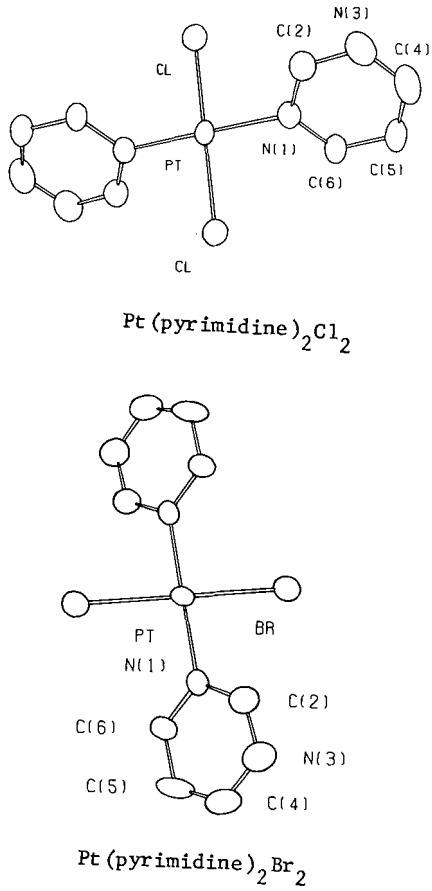

FIG. 1. Labelled diagrams of *trans*-[Pt(pyrimidine)$_2$Cl$_2$] and *trans*-[Pt(pyrimidine)$_2$Br$_2$].

exocyclic bonded group. Similar results have been observed in other platinum compounds (11, 19, 20). Therefore, coordination to the platinum atom does not affect the structure of the pyrimidine ligand.

Packing diagrams of the two crystals are shown on Fig. 2. The platinum coordination planes are almost parallel to the *bc* plane. All the pyrimidine rings are stacked in one direction parallel to the *c* axis and they are located approximately at $x = 0$ and at $x = \frac{1}{2}$. The packing therefore consists of alternate layers of pyrimidine rings and $PtCl_2$ moieties parallel to the *ac* plane. Since all the hydrogen atoms are located on carbon atoms, no strong hydrogen bonding was expected.

cis-[Pt(pm)X$_2$] were isolated from the reaction of K_2PtCl_4 and pm in water. The *trans*-isomers were prepared from the isomerization of the *cis*-isomers in DMF in the presence of pm. The reactivities of both isomers were compared to the reactivities of the pyridine analogues which we have studied in aqueous and non-aqueous solvents (1). Both *cis* and *trans*-[Pt(pm)$_2$Cl$_2$] are slowly soluble in 4 *M*

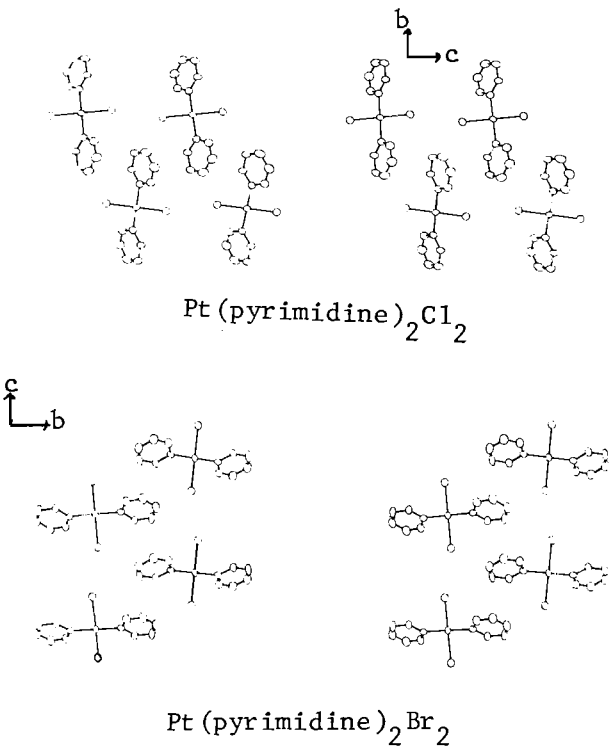

FIG. 2. Stereoscopic diagrams of the packing in the two crystals *trans*-[Pt(pyrimidine)$_2$Cl$_2$] and *trans*-[Pt(pyrimidine)$_2$Br$_2$].

HCl solution at 80–100°C. After filtrating, the yellow solution can be cooled to room temperature without the appearance of any precipitate. The reaction is the following:

$$[Pt(pm)_2Cl_2] \xrightarrow{HCl} (pmH)^+[Pt(pm)Cl_3]^-$$

The solution can be evaporated to dryness and redissolved in water a few times. Then, the product is not soluble in water any more. It is also not soluble immediately in 4 *M* HCl solution at room temperature. Infrared spectroscopy has shown that the product is *cis*-[Pt(pm)$_2$Cl$_2$]. The same product was obtained no matter which isomer was used in the above reaction. The scheme in acid medium is therefore as follows:

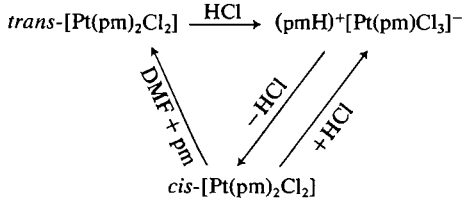

In contrast, pyridine compounds, *trans*-[Pt(py)$_2$Cl$_2$], can be isolated from concentrated HCl solution on a steam bath (21). *trans*-[Pt(py)$_2$Cl$_2$] cannot be converted to the *cis*-isomer as the pyrimidine compound. The pyrimidine compounds dissolve easily in acid medium probably because the proton H^+ can easily approach the uncoordinated nitrogen atom of the pyrimidine ring, causing the coordinate bond to weaken and pyrimidine to dissociate from platinum.

Acknowledgments

Grateful acknowledgments are made to the Natural Sciences and Engineering Research Council of Canada, to the Ministère de l'Education (FCAC) for financial support, and to Johnson Matthey Inc. for the loan of potassium tetrachloroplatinite.

1. P. C. KONG and F. D. ROCHON. Can. J. Chem. **57**, 526 (1979).
2. R. MELANSON, J. HUBERT, and F. D. ROCHON. Can. J. Chem. **53**, 1139 (1975).
3. D. T. CROMER and J. T. WABER. Acta Crystallogr. **18**, 104 (1965).
4. R. F. STEWART, E. R. DAVIDSON, and W. T. SIMPSON. J. Chem. Phys. **42**, 3175 (1965).
5. D. T. CROMER and D. LIBERMAN. J. Chem. Phys. **53**, 1891 (1970).
6. G. H. STOUT and L. H. JENSEN. X-ray structure determination. Macmillan Co., New York. 1968. p. 454.
7. G. ZANOTTI, A. DEL PRA, G. BOMBIERI, and A. M. TAMBURRO. Acta Crystallogr. B**34**, 2138 (1978).
8. F. D. ROCHON, P. C. KONG, and R. MELANSON. Can. J. Chem. **58**, 97 (1980).
9. J. BRITTEN and C. J. L. LOCK. Acta Crystallogr. B**35**, 3065 (1979).
10. R. MELANSON and F. D. ROCHON. Acta Crystallogr. B**33**, 3571 (1977); B**34**, 941 (1978); B**34**, 1125 (1978).
11. R. FAGGIANI, B. LIPPERT, and J. C. L. LOCK. Inorg. Chem. **19**, 295 (1980).
12. R. MELANSON, F. D. ROCHON, and J. HUBERT. Acta Crystallogr. B**35**, 736 (1979).
13. F. D. ROCHON and R. MELANSON. Acta Crystallogr. B**35**, 2313 (1979).
14. R. MELANSON and F. D. ROCHON. Acta Crystallogr. B**34**, 3594 (1978); Can. J. Chem. **57**, 57 (1979).
15. P. J. WHEATLEY. Acta Crystallogr. **13**, 80 (1960).
16. S. FURBERG and J. SOLBAKK. Acta Chem. Scand. **24**, 3230 (1970).
17. C. SINGH. Acta Crystallogr. **19**, 861 (1965).
18. S. FURBERG and J. B. AAS. Acta Chem. Scand. A**29**, 713 (1975).
19. C. J. L. LOCK, R. A. SPERANZINI, and J. POWELL. Can. J. Chem. **54**, 53 (1976).
20. R. MELANSON and F. D. ROCHON. Inorg. Chem. **17**, 679 (1978).
21. G. B. KAUFFMAN. Inorg. Synth. **1**, 249 (1963).

Can. J. Chem. Downloaded from www.nrcresearchpress.com by 210.87.254.6 on 09/05/12
For personal use only.

Conformational analysis and photochemical behavior of sulfoxides in the naphtho[1,2-*b*]thiopyran and naphtho[2,1-*b*]thiopyran series

IAN W. J. STILL,[1] PARKASH C. ARORA, S. KHAQAN HASAN, GERALD W. KUTNEY, LAWRENCE Y. T. LO,[2] AND KENNETH TURNBULL

Erindale College, University of Toronto, Mississauga, Ont., Canada L5L 1C6

Received February 11, 1980[3]

IAN W. J. STILL, PARKASH C. ARORA, S. KHAQAN HASAN, GERALD W. KUTNEY, LAWRENCE Y. T. LO, and KENNETH TURNBULL. Can. J. Chem. **59**, 199 (1981).

The sulfoxides derived from 2,3-dihydro-4*H*-naphtho[1,2-*b*]thiopyran and its 4-phenyl and 4-oxo derivatives, as well as the analogous sulfoxides in the 2,3-dihydro-1*H*-naphtho[2,1-*b*]thiopyran series, have been synthesized and their structures established by spectroscopic methods, especially ^1H and ^{13}C nmr. On photolysis these sulfoxides have been found to react by a rather inefficient photochemical deoxygenation pathway.

IAN W. J. STILL, PARKASH C. ARORA, S. KHAQAN HASAN, GERALD W. KUTNEY, LAWRENCE Y. T. LO et KENNETH TURNBULL. Can. J. Chem. **59**, 199 (1981).

On a synthétisé les sulfoxydes provenant du dihydro-2,3 4*H*-naphto[1,2-*b*] thiopyranne et ses dérivés phényl-4 et oxo-4 ainsi que les sulfoxydes analogues des séries dihydro-2,3 1*H*-naphto[2,1-*b*] thiopyranne et on a établi leurs structures en utilisant des méthodes spectroscopiques, plus particulièrement la rmn du ^1H et du ^{13}C. On a trouvé que la photolyse de ces sulfoxydes se produit par un processus de déoxygénation photochimique qui est relativement inefficace.

[Traduit par le journal]

Introduction

As an extension of our earlier photochemical studies of sulfoxides in the 4-thiochromanone series (1), we have undertaken the synthesis and examined the photochemistry of the analogous naphtho-fused 4-thiopyranone 1-oxides. Since we were interested in discovering whether the photochemical behavior of these sulfoxides was dependent on the location of the S=O group at the α- or β-positions in the naphthalene nucleus, we have prepared the two possible isomeric 4-oxo sulfoxides. We have also synthesized the analogous sulfoxides with the C=O group in the above sulfoxides replaced by a methylene unit, because we suspected that the carbonyl group may play a fundamental role in modifying the photochemical behavior of these sulfoxides. Finally, we have synthesized the sulfoxides in the above series where the carbonyl group is replaced by a $-CHC_6H_5-$ unit. Interest in this type of system arose from the report several years ago by Schultz and Schlessinger (2) of the photochemical dehydration of a naphtho-fused thiopyran oxide bearing the sulfinyl functionality at the 2-position in the naphthalene unit, and with phenyl substituents located both α- and γ- to the S=O group, in the hetero-ring. For comparative purposes, we have synthesized the *cis*- and *trans*-isomers, in both the 1-sulfinyl and the 2-sulfinyl naphthalene series.

The syntheses, the structural assignments for the various sulfoxides, and the photochemical results will be discussed in turn.

Results and Discussion

The syntheses of 2,3-dihydro-4*H*-naphtho[1,2-*b*]thiopyran **5** and its sulfoxide **6** and the analogous ketosulfide **7** and ketosulfoxide **8**, from 1-naphthalenethiol, via 3-(1-naphthylthio)propanoic acid **1**, were carried out essentially by literature procedures, as shown in Scheme 1. Neither of the sulfoxides had been reported previously. The syntheses of the phenyl-substituted sulfide **9** and its epimeric sulfoxides **10***a*,*b*, again starting from 1-naphthalenethiol, by way of the ketone **3** and the corresponding alcohol **4**, were also relatively straightforward, as outlined in Scheme 2. The total yield of the isomeric sulfoxides obtained by oxidation was 79%, the *trans*-isomer predominating, as expected from similar oxidations (3), in the ratio of almost 5:1. Evidence for the assignments of the *cis*- and *trans*-structures will be discussed in the next section. It is worth noting that, as an alternative route to **5**, an analogous attempt to cyclize the known alcohol 3-(1-naphthylthio)-1-propanol **2** by the stannic chloride procedure (Scheme 2) was unsuccessful, indicating that this reaction does not work for primary alcohols, at least in this series.

Starting from 2-naphthalenethiol, essentially similar synthetic routes led to the analogous sulfide **11** and ketosulfide **13** and their sulfoxides **12** and **14**, respectively. As observed in the 1-naphthyl series above, cyclization of the primary alcohol 3-(2-

[1]Author to whom correspondence should be addressed.
[2]Undergraduate research participant.
[3]Revision received September 26, 1980.

0008-4042/81/020199-11$01.00/0
©1981 National Research Council of Canada/Conseil national de recherches du Canada

Can. J. Chem. Downloaded from www.nrcresearchpress.com by 210.87.254.5 on 09/05/12
For personal use only.

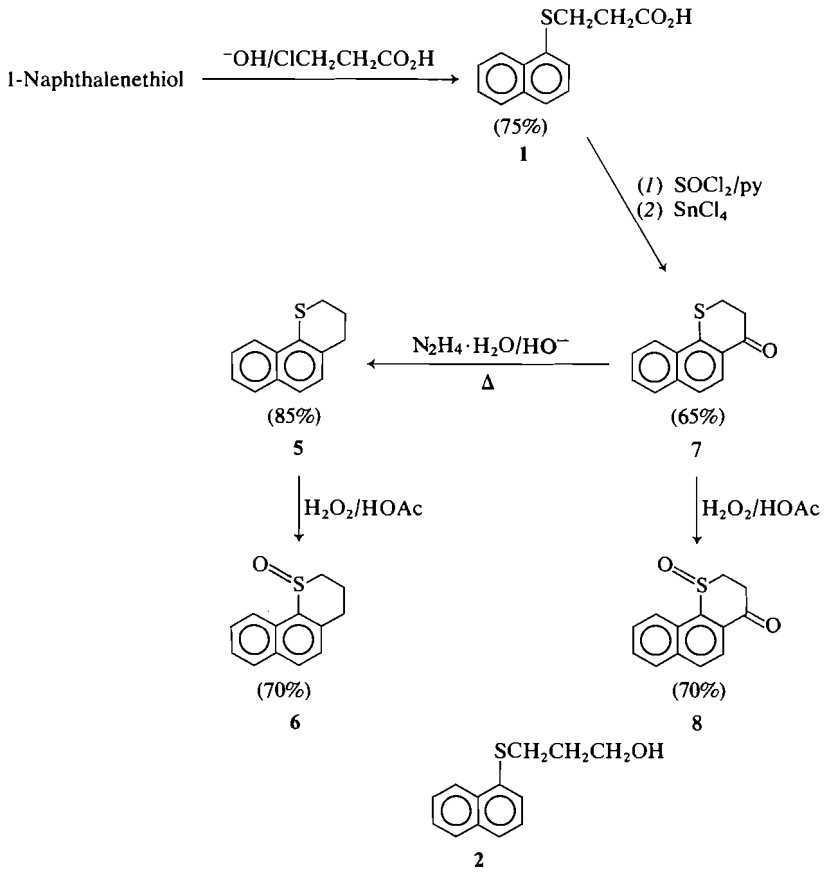

SCHEME 1

naphthylthio)-1-propanol, in an attempt to produce **11**, was unsuccessful. Oxidation of the phenyl derivative **15** produced a mixture of *cis*- and *trans*-sulfoxides **16***a*,*b* in 69% yield, the *trans*:*cis* ratio being slightly greater than 4:1.

Before proceeding to a discussion of the photochemical behavior of these sulfoxides we felt that it would be appropriate to examine their ^1H and ^{13}C nmr spectra, with the aim of assigning configurations to the *cis*- and *trans*-phenyl-substituted pairs of sulfoxides **10***a*,*b* and **16***a*,*b*, as it was felt initially that the photochemical behavior of these sulfoxides might show a stereochemical dependence. The 60 MHz ^1H nmr spectra for these compounds (see Experimental) look very complex and were rather uninformative. Somewhat better results, especially for compound **10***b*, were obtained with the 220 MHz spectra, the data from which are reported for the phenyl-substituted sulfoxides, as well as the parent-sulfoxides **6** and **12**, in Tables 1 and 2. Partial assignments could be made by analyzing those coupling constants which were obtained, by analogy with simple model systems, such as thiane 1-oxide (4), and also by running comparison spectra in C_6D_6, which had some effect in simplifying the spectra for first order analysis because of the greater spread of chemical shift values compared with those in $CDCl_3$. One interesting feature of the aromatic region in these spectra, allowing an immediate distinction to be made between the 1- and the 2-sulfinylnaphthalene series, is the fact that only in those sulfoxides where the sulfoxide group is at the 1-position (see numbering system in Tables) is a one-proton signal observed well downfield, at $\delta \approx 8.6$–8.8 (H-10). For the 4-sulfoxides (Table 2) with an adjacent *peri* aromatic proton at C-5, on the other hand, no aromatic proton downfield of $\delta \approx 8$ ppm is observed. (This is in accord with the fact that in the simple 4-thiochromanone 1-oxide system (1) only *one* aromatic proton is shifted well downfield, the one *peri* to the carbonyl group.) Even larger downfield shifts of the H-10 proton (to $\delta \approx 9.1$ ppm) were observed for the ketosulfide and ketosulfoxide **13** and **14**, due to analogous effects of the C-1 carbonyl group.

In terms of the immediate problem of assigning the *cis*- and *trans*-configurations to the sulfoxide mixtures **10** and **16**, however, the results in Tables 1

Can. J. Chem. Downloaded from www.nrcresearchpress.com by 210.87.254.5 on 09/05/12
For personal use only.

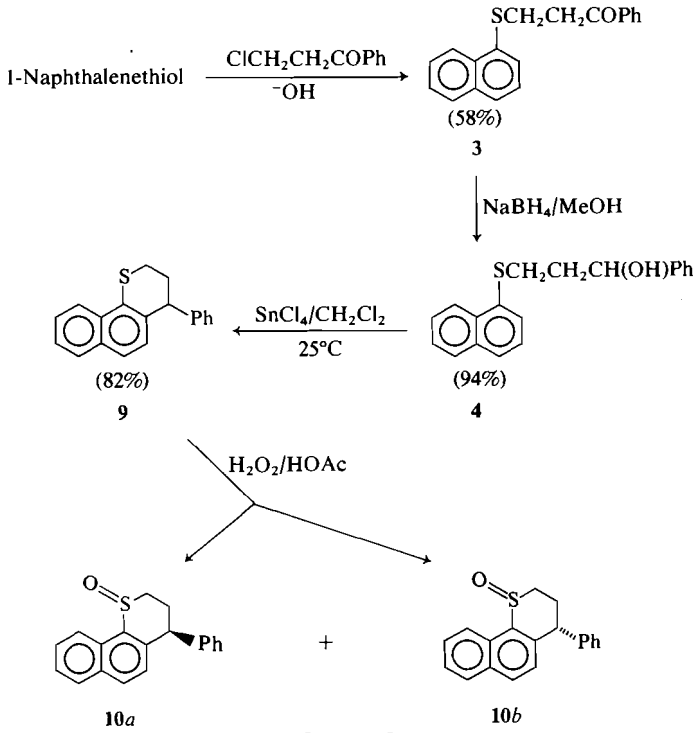

SCHEME 2

and 2 were not very helpful. Inspection of Dreiding models of both the 4-phenyl-2,3-dihydro-4*H*-naphtho[1,2-*b*]thiopyran 1-oxide **10** and 1-phenyl-2,3-dihydro-1*H*-naphtho[2,1-*b*]thiopyran 4-oxide **16** structures revealed an interesting clue in the latter case. (It has been shown (5) that benzo-fused thiopyrans prefer the "sofa" type conformation, but even if the "pseudo-chair" form is preferred here it does not invalidate the following discussion.) If the phenyl group is placed in an equatorial position in **16**, it is found that severe steric interaction with the H-10 proton would render free rotation of the phenyl ring virtually impossible. Since no evidence has been found in any of the nmr spectra (^1H or ^{13}C) for nonequivalent *ortho*- and *meta*-positions in the phenyl ring, we assume that in both **16***a* and **16***b* the phenyl substituent must be *axial* (strictly, pseudo-axial). Given the normal preference for the axial orientation in thiane oxides (4) and the preference for *trans*-sulfoxide formation in the oxidation of substituted cyclic sulfides (3) we can, with some confidence, assign the major isomer **16***b* the *trans*-diaxial conformation *B* and the minor *cis*-isomer **16***a* must therefore be assigned conformation *A*.

Attempts to substantiate this conclusion by carrying out a series of lanthanide-induced shift (LIS) studies, using gradually increasing amounts of the shift reagent ($Eu(fod)_3$) (6), were inconclusive, mainly because of the complexity of the ^1H nmr spectra already referred to. Qualitatively, however, one could observe that, as expected from coordination of the reagent with the sulfoxide oxygen atom, the H-1 proton was shifted by the smallest amount while, of the four remaining hetero-ring protons, two were clearly shifted by larger amounts.

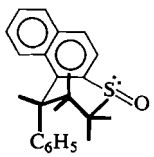

A **16***a*

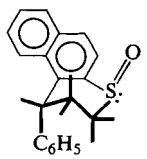

B **16***b*

If our proposal that the configurational isomerism in **16** can be ascribed to a change in the S=O bond orientation (axial vs. equatorial) is correct, then evidence in support of this should be available from the ^{13}C chemical shift of the β-carbon (C-2) in the two isomers. This can be seen readily from Table 4 where the much more upfield position ($\delta = 22.6$) observed for C-2 in **16***b* is consistent with the *gauche* relationship between the C-2/C-3 bond and the axial S=O bond. In contrast, the δ value for C-2 in the *cis*-isomer ($\delta = 27.1$) is much closer to the value observed ($\delta = 30.2$) in the analogous sulfide **15**. The $\Delta\delta$ of -7.6 ppm for C-2 between **16***b* and **15** in fact is in very good agree-

Can. J. Chem. Downloaded from www.nrcresearchpress.com by 210.87.254.5 on 09/05/12
For personal use only.

Can. J. Chem. Downloaded from www.nrcresearchpress.com by 210.87.254.5 on 09/05/12
For personal use only.

TABLE 1. ^{1}H nmr data (in $CDCl_3$) for naphtho[1,2-*b*]thiopyran sulfoxides, at 220 MHz[a]

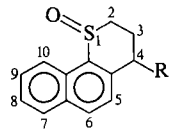

R	δ[b]						
	H_{2e}	H_{2a}	H_{3e}	H_{3a}	H_{4e}	H_{4a}	H_{arom}
H **6**	3.01[c]	3.39[c]	2.06[c]	2.69[c]	2.69[c]	3.01[c]	7.16, d (J = 8.7), H5 7.52–7.76 (4H), H6, H7, H8, and H9 8.61, br d ($J \approx 9$), H10
(*cis*) C_6H_5 **10***a*	3.48[c]	2.37[c]		3.00[c] (2H)	—	4.28 ($w_{1/2} \approx 18$ Hz)	7.10, d (J = 8.5), H5 7.31 (5H), C_6H_5 7.59–7.81 (4H), H6, H7, H8, and H9 8.81, dd (J = 8.2, 0.5), H10
(*trans*) C_6H_5 **10***b*	3.20 ddd (J = 14.5, 4.8, 2.2)	2.98 ddd (J = 14.5, 14.0, 2.2)	2.20 dddd (J = 13.5, 4.8, 2.5, 2.2)	3.30 dddd (J = 14.0, 13.5, 5.0, 2.2)	4.65 dd (J = 5.0, 2.5)	—	6.96 (2H), *ortho*-C_6H_5 protons 7.19–7.90 (5H) 7.30 (3H), remaining C_6H_5 protons 8.82, br d ($J \approx 9$), H10

[a]Assignments were made from a study of the coupling constants (^2J and ^3J) and, in some cases, by using spin decoupling.
[b]Signals indicated appeared as multiplets, unless otherwise specified.
[c]Individual assignments for these protons must be regarded as tentative since, due to the complexity of the first-order spectra even at 220 MHz, individual coupling constants could not always be extracted.

TABLE 2. ^{1}H nmr data (in $CDCl_3$) for naphtho[2,1-*b*]thiopyran sulfoxides, at 220 MHz[a]

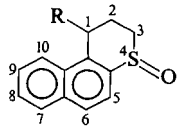

R	δ[b] H_{1e}	H_{1a}	H_{2e}	H_{2a}	H_{3e}	H_{3a}	H_{arom}
H **12**	3.15[c] (3H)		2.27[c]	2.72[c]	3.50[c] dt (J = 18.5, 5.5)	3.15[c] (3H)	7.68 (5H), H6, H7, H8, H9, H10 8.03, d (J = 9.5), H5
(*cis*)C_6H_5 **16***a*	4.97 t (J = 4.5)	—	2.57[c] (2H)		3.25[c] (2H)		7.23–7.92 (11H), all aromatic protons
(*trans*)C_6H_5 **16***b*	5.02 dt (J = 4.5, 3.5)	—	2.31[c]	3.12[c] (3H)	3.12[c] (3H)		6.91 (2H), *ortho*-C_6H_5 protons 7.25 (3H), remaining C_6H_5 protons 7.40–7.88 (6H), H5, H6, H7, H8, H9, and H10

[a]Assignments were made from a study of the coupling constants (^2J and ^3J) and, in some cases, by using spin decoupling.
[b]Signals indicated appeared as multiplets, unless otherwise specified.
[c]Individual assignments for these protons must be regarded as tentative since, due to the complexity of the first-order spectra even at 220 MHz, individual coupling constants could not always be extracted.

ment with the Δδ of −9.5 ppm for C-2 between the parent sulfide and sulfoxides **11** and **12** and indicates that in **12** the S=O bond also adopts the axial arrangement. The Δδ values found for the same (β) carbon atom in thiane compared to thiane 1-oxide are −12.7 (S=O axial) and −4.9 (S=O equatorial) ppm (7).

Turning to the isomeric sulfoxides **10***a*,*b*, inspection of Dreiding models this time revealed no clear-cut preference for the orientation of the phenyl substituent. However, reference to the ^{13}C nmr data in Table 3, and analogy with the arguments used above for the other isomeric pair of sulfoxides, show again a (β)Δδ, this time for C-3, between **9** and **10***a* and **10***b* of −8.7 and −9.7 ppm, respectively. Between **5** and **6** the comparable Δδ value is −10.6 ppm, indicating that *all* of the sulfoxides in this series adopt the S=O axial orientation. Thus, in contrast to the *cis*/*trans* isomerism in the case of **16** where the phenyl substituent adopts an axial orientation in both isomers, in the case of the *cis*/*trans* isomers of **10**, the S=O bond adopts an axial orientation in both isomers, with the phenyl substituent also being axial in the predominant *trans*-isomer **10***b*, but equatorial in the minor *cis*-isomer **10***a* (in the 2,3-dihydro-4*H*-naphtho[1,2-*b*]thiopyran series an equatorial phenyl group is quite free to rotate). These assignments are in accord with the ^{1}H nmr data for **10***a*,*b* reported in Table 1. If our structural deductions from the ^{13}C nmr data, as well as the related evidence provided by Dreiding models and the oxidation results are correct, the only one of the two pairs of epimeric

TABLE 3. ^{13}C nmr chemical shifts[a,b] for hetero-ring carbons in 2,3-dihydro-4*H*-naphtho[1,2-*b*]thiopyran derivatives

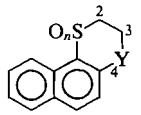

	Y	*n*	C-2	C-3	C-4
5	CH_2	0	21.5	22.9	30.3
9	CHC_6H_5	0	22.9	30.6	44.7
6	CH_2	1	45.0	12.3	29.9
10*a*	CHC_6H_5(*cis*-)[c]	1	44.2	21.9	46.8
10*b*	CHC_6H_5(*trans*-)[c]	1	40.4	20.9	43.9

[a]Chemical shifts in ppm downfield from TMS, in $CDCl_3$.
[b]Reference was made to the known pattern of chemical shifts in thiane and its oxide (axial and equatorial conformers) (7), as well as the peak multiplicities in arriving at these assignments.
[c]For a detailed discussion of the stereochemical assignment of these isomers, see text.

sulfoxides **10** and **16** which should possess an *axial* methine proton is the minor *cis*-isomer **10***a*, which might therefore be expected to reveal this distinction in its ^{1}H nmr spectrum. Indeed, this expectation is fulfilled, as reference to Table 1 shows δ = 4.28 ppm for the (H-4) methine signal, a value well upfield from those recorded for the methine protons (δ = 4.65–5.02 ppm) in the other three phenyl-substituted sulfoxides. Furthermore, although the methine signal at 4.28 ppm in **10***a* was not clearly resolved even in the 220 MHz spectrum, the line width ($W_{\frac{1}{2}} \approx$ 18 Hz) is clearly very much in accord with an axial conformation for this proton. This result provides valuable corroboration for the correctness of our stereochemical assignments.

Can. J. Chem. Downloaded from www.nrcresearchpress.com by 210.87.254.5 on 09/05/12
For personal use only.

TABLE 4. ^{13}C nmr chemical shifts[a,b] for hetero-ring carbons in 2,3-dihydro-1*H*-naphtho[2,1-*b*]thiopyran derivatives

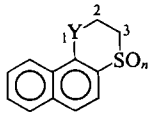

	Y	*n*	C-1	C-2	C-3
11	CH_2	0	27.1	23.3	24.9
15	CHC_6H_5	0	39.2	30.2	21.8
12	CH_2	1	25.3	13.8	45.5
16*a*	CHC_6H_5	1 (*cis*-)[c]	41.3	27.1	42.3
16*b*	CHC_6H_5	1 (*trans*-)[c]	40.2	22.6	41.4

[a]Chemical shifts in ppm downfield from TMS, in $CDCl_3$.
[b]Reference was made to the known pattern of chemical shifts in thiane and its oxide (axial and equatorial conformers) (7), as well as the peak multiplicities, in arriving at these assignments.
[c]For a detailed discussion of the stereochemical assignment of these isomers, see text.

As in the case of the isomeric sulfoxides **16***a*,*b* an attempted LIS effect-analysis on **10***a*,*b* proved disappointing, although again it was clear that two of the C-2/C-3 protons, presumably those on the same side of the hetero-ring as the axial S=O bond, were being preferentially shifted.

The remaining effects observable from the ^{13}C nmr data in Tables 3 and 4 were reasonably in accordance with expectation. For example, the (α)-downfield shifts produced by converting the sulfide sulfur to sulfoxide lie in the range +17.5 → 21.3 ppm, compared with the average value of +19.7 ppm for thiane systems quoted by Lambert *et al.* (7). The β-effects have already been discussed and the γ-effects of converting sulfide into sulfoxide are very small (±2 ppm), as expected (7). The effects of introducing the phenyl substituent are in the range +12.1 → 16.9 ppm, for the α-effects and +6.9 → 9.6 ppm, for the β-effects (with one exception), well within the ranges expected (8). It is significant that the one exception is an apparent β(C_6H_5) effect of +13.3 ppm for the *cis*-sulfoxide, **16***a*. However, it will be noted that, according to our earlier arguments, **16***a* is the only one of the two isomeric pairs of sulfoxides with an S=O equatorial bond and it is thus much more likely that this is the correct explanation for the apparent anomaly, rather than an unusual β-effect of the phenyl substituent.

Rather surprisingly, given the variety of photochemical pathways observed in the 4-thiochromanone 1-oxide series (1), the sole photochemical reaction observed for the present sulfoxides in all experiments but one (see below), is a rather inefficient photochemical deoxygenation reaction to afford the corresponding sulfides. The

TABLE 5. Results of irradiation of sulfoxides[a,b]

Compound	Recovery of starting material (%)	Sulfide (%)[c]
6	57	Trace
12	84	8
8	—	57
14	27	28
10*a*,*b*	30[d]	38[d]
16*a*,*b*	25[d]	27[d]

[a]Irradiations were carried out for 24 h, in degassed benzene, unless otherwise stated (see Experimental).
[b]For relevant uv data, see Table 6 (Experimental).
[c]Corrected for recovered starting material.
[d]Irradiation for 5.5 h.

results of these irradiations,[4] carried out in benzene, are summarized in Table 5. Photochemical deoxygenation has been observed before (1, 9) but we have earlier characterized it as a reaction which normally occurs only when other photochemical processes (such as rearrangements via ring expansion to cyclic sulfenates, or reactions involving β- or γ-hydrogen abstraction processes) are disfavored (1). The deoxygenations observed here proceed more readily when the irradiation source is a medium-pressure mercury arc (115 or 400 W), emitting radiation mainly at 313 and 366 nm, essentially no reaction being observed when a low-pressure mercury source (4 W) was used, with the exception of the case discussed in detail below. Surprisingly, as is evident from Table 5, the keto-sulfoxides show little difference in behavior from the simpler sulfoxides, whereas they might have been expected to form products similar to those obtained in the thiochromanone series (1). However, the yields of sulfide obtained were somewhat better and relatively little starting material was recovered from the irradiation of compounds **8** and **14**. No major difference could be detected in the photochemical behavior of compounds **10** and **16**, whether single pure isomers were used or the *cis*/*trans* mixtures. In the latter case, however, significant changes in composition of the mixtures from *trans*:*cis* ratio's of ~4:1 to ~1:1 were observed, indicating that photo-epimerization of the sulfoxides was occurring to a significant extent.

The exceptional case referred to above was encountered when the mixture of *cis*- and *trans*-sulfoxides **16***a*,*b* was irradiated in benzene for a prolonged period (70 h) with the 4 W light source. In addition to recovered starting material (76%) and a small amount (12%) of the sulfide, a third product (4%) was obtained, in a very small quantity. The presence of a characteristic ^1H nmr signal at δ 9.75,

[4]Relevant uv spectral data are collected in the Experimental (Table 6).

Can. J. Chem. Downloaded from www.nrcresearchpress.com by 210.87.254.5 on 09/05/12
For personal use only.

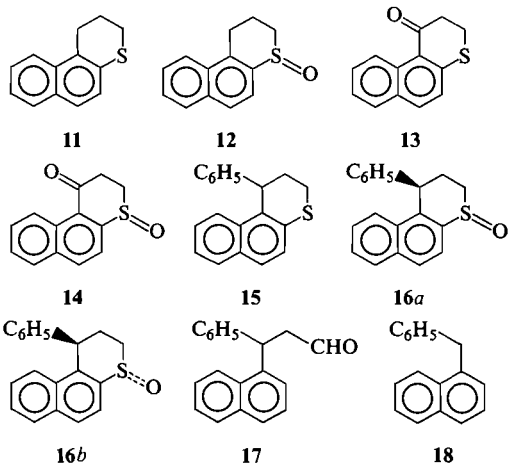

as well as infrared bands at ν 2840, 2740 cm^{-1}, indicated that this product is an aldehyde. The apparent molecular ion at $m/e = 260$ and analogy with similar photochemical transformations already observed in the 4-thiochromanone 1-oxide series (1) lead us to propose structure **17** for this minor photoproduct. The structure of this photoproduct[5] was confirmed by a straightforward synthesis of **17** by the addition of bromoacetaldehyde diethyl acetal to 1-benzylnaphthalene **18**, in the presence of sodium amide, followed by acid hydrolysis. The photochemical rearrangement of **16***a*,*b* to **17** may be regarded as another example of the process which we have previously categorized (1) as a type B (sulfoxide) photoreaction. Thus, initial rearrangement of **16***a*,*b* to the corresponding seven-membered cyclic sulfenate, followed by S—O bond homolysis, loss of a sulfur atom, and (intramolecular) hydrogen atom transfer would lead to the observed aldehyde. The much lower yield encountered in the present case may be due to further photochemical degradation of the aldehyde, which is of a simple aliphatic type, unlike the β-ketoaldehydes produced from the thiochromanone sulfoxides (1).

The nature of the photochemical deoxygenation of sulfoxides is itself an interesting mechanistic question, touched upon by Gurria and Posner (9). Although we feel that this question is deserving of further study, the present sulfoxide systems are structurally not well suited for this purpose. We can, however, definitely rule out the possibility that the sulfoxides examined in this study (photochemically) disproportionate to equimolar amounts of sulfide and sulfone, since no traces of sulfone were ever found and since independent irradiation of the sulfone analogue of **8** (which gave the highest yield of sulfide in Table 5) under identical reaction conditions led to no change. We have also conducted an experiment involving the irradiation of **8** in the presence of cyclohexene in an attempt to trap any singlet oxygen, which may arise during the deoxygenation reaction, in the manner described by Gurria and Posner (9). No peroxide could be detected by spot tests, indicating that $^1O_2$ is not being formed and that the oxygen lost from the S=O group must be accounted for in some as yet unexplained fashion.

[5]The ^1H nmr spectrum of the authentic material (see Experimental) is much better resolved than that of the photoproduct, since the larger amount of material available allowed a greater degree of purification.

Experimental

The ir spectra were recorded on a Perkin-Elmer 257 grating spectrophotometer, uv spectra on a Unicam SP-8000 instrument, and ^1H nmr spectra on a Varian EM-360 spectrometer, with additional 220 MHz spectra being recorded for some of the sulfoxides studied. Natural abundance, proton decoupled ^{13}C nmr spectra were obtained on a Varian XL-100-15 spectrometer at 25.16 MHz, in the pulsed Fourier transform mode. The temperature of the probe was 32 ± 3°C. Spectral widths of 6000 Hz were routinely used, with acquisition times of 0.666 s and pulse widths of 12 μs. Mass spectra were routinely recorded with a Bell and Howell 21-490 instrument.

Elemental analyses were performed by the Scandinavian Micro-analytical Laboratory, Box 25 DK 2730, Herlev, Denmark. All melting points are uncorrected.

1-Naphthalenesulfonyl Chloride[6]

1-Naphthalenesulfonic acid (10.0 g, 0.040 mol) was dissolved in distilled water (75 mL). Sodium hydrogen carbonate (3.36 g, 0.040 mol) was slowly added to neutralize the solution. The solution was then brought to boiling and sodium chloride (7 g) added with stirring. Upon cooling, white crystals formed, which were collected and redissolved in a boiling solution of sodium chloride (10 g) in water (100 mL). Again, cooling and subsequent filtration gave sodium 1-naphthalenesulfonate as fine white crystals (5.8 g, 62%), after drying at 110°C.

Sodium 1-naphthalenesulfonate (9.00 g, 0.039 mol) was mixed with phosphorus pentachloride (8.13 g, 0.039 mol), and the mixture was heated at 170–180°C for 3 h (under anhydrous conditions), with intermittent shaking. Ice-cold water (~80 mL) was carefully poured onto the cooled solid mass with shaking and the aqueous phase was extracted with carbon tetrachloride (2 × 50 mL). The organic extracts were washed (H_2O, dried $MgSO_4$) and evaporated *in vacuo* to yield a brown oil, which crystallized on cooling. Recrystallization from hexane afforded pale tan needles of the title compound (6.0 g, 68%); mp 60–62°C (lit. (12) mp 67.5°C).

1-Naphthalenethiol[6]

1-Naphthalenesulfonyl chloride (5.48 g, 0.024 mol) was slowly added at −5°C to a mixture of crushed ice (60 g) and 98% sulfuric acid (11 mL) in a 250-mL 3-necked flask. Zinc dust (10.0 g), purified by stirring 3 min in 10% hydrochloric acid,

[6]An essentially identical procedure was used to make the analogous 2-naphthalene derivatives.

Can. J. Chem. Downloaded from www.nrcresearchpress.com by 210.87.254.5 on 09/05/12
For personal use only.

TABLE 6. Ultraviolet absorption data

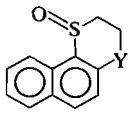
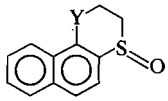

Y	λ_{max} nm (log ε)	Y	λ_{max} nm (log ε)
>CH_2 **6**	227 (4.29) 288 (3.52)	>CH_2 **12**	233 (4.25) 280 (3.25) 292[a](3.12)
>C=O **8**	249[a](4.59) 255 (4.66) 299 (3.85) 345 (3.32)	>C=O **14**	252 (4.56) 335 (3.88)
>CHPh (*cis*-) **10***a*	224 (4.60) 237 (4.42) 289[b](3.70)	>CHPh (*cis*- + *trans*-) **16***a* + **16***b*	234 (4.77) 283 (3.80) 293[a](3.61)
1-$C_{10}H_7$S(=O)CH_3[c]	225 (4.81) 280[a](3.90) 288 (3.95)	2-$C_{10}H_7$S(=O)CH_3[c]	227 (4.69) 277 (3.78) 288 (3.62)
1-$C_{10}H_7$C(=O)CH_3[d]	240 (4.36) 293 (3.77) 320[a](3.55)	2-$C_{10}H_7$C(=O)CH_3[d]	246 (4.71) 282 (4.04) 366[b](3.25)

[a]Inflexion.
[b]Plateau.
[c]Reference 10.
[d]Reference 11.

filtering, washing with H_2O/acetone, and then drying, was then added with vigorous stirring. After 1.5 h the mixture was brought to room temperature and then refluxed (90–100°C) for 5 h. On cooling, water (80 mL) was added and the mixture extracted with ether (2 × 100 mL). The organic layers were combined, dried ($MgSO_4$), and evaporated *in vacuo* to yield a pale yellow oil (3.3 g, 85%) of adequate purity, as indicated by tlc. Spectral properties of the oil were identical with those of an authentic sample.

3-(1-Naphthylthio)propanoic Acid, 1

1-Naphthalenethiol (1.74 g, 0.011 mol) was added to an aqueous solution of 1% sodium hydroxide (88 mL), followed by 3-chloropropanoic acid (1.18 g, 0.011 mol) in methanol (22 mL), with stirring. After refluxing for 4 h and subsequent cooling, 4 *M* hydrochloric acid was added until the solution reached pH 3. Extraction with dichloromethane (2 × 100 mL), combination and drying ($MgSO_4$) of the extracts, followed by evaporation *in vacuo* afforded a colorless solid which was digested with hexane and filtered. Recrystallization from benzene/hexane gave the title compound (2.0 g, 82%); mp 84–86°C (lit. (13) mp 89–90°C).

3-(2-Naphthylthio)propanoic Acid

This compound was prepared in 86% yield by essentially the same procedure, mp 101–102°C (lit. (13) mp 104–105°C).

*2,3-Dihydro-4*H*-naphtho[1,2-*b*]thiopyran-4-one, 7*

A mixture of 3-(1-naphthylthio)propanoic acid (0.5 g, 2.15 mmol), dry pyridine (0.015 mL), dry ether (5 mL), and thionyl chloride (0.54 g, 4.5 mmol), added in the above order, was refluxed for 45 min (14). The excess thionyl chloride was removed *in vacuo*, benzene (2 mL) was added, and again the solvent was removed *in vacuo*. The residual oil was dissolved in dry benzene (5 mL) and cooled to 2°C. Two precooled (2°C) solutions of stannic chloride (0.40 g) in dry benzene (0.5 mL) were added, separated by an interval of 20 min, and the mixture was left overnight under anhydrous conditions. The product was isolated by pouring the reaction mixture on to ice-water (80 mL) containing 11 *M* hydrochloric acid (10 mL), and extracting with dichloromethane (2 × 60 mL). The organic extracts were washed (10% $NaHCO_3$, H_2O), dried ($MgSO_4$), and evaporated to yield a pale yellow solid (0.4 g, 85%); mp (EtOH) 107–108°C (lit. (13) mp 107°C); ir ($CHCl_3$) ν: 1670 (CO) cm^{-1}; ^1H nmr ($CDCl_3$) δ: 3.15–3.80 (4H, A_2B_2 system), 7.5–8.7 (6H, m).

*2,3-Dihydro-1*H*-naphtho[2,1-*b*]thiopyran-1-one, 13*

This compound was prepared by an essentially identical method, adapted from that of Young and Ohnmacht (15), in 81% yield; mp (EtOH) 64–66°C (lit. (13) mp 68–69°C); ir ($CHCl_3$) ν: 1667 (CO) cm^{-1}; ^1H nmr ($CDCl_3$) δ: 3.2 (4H, A_2B_2 system), 7.1–7.8 (5H, m), 9.1 (1H, dd, J = 8.0, 2.0 Hz).

*2,3-Dihydro-4*H*-naphtho[1,2-*b*]thiopyran-4-one 1-Oxide, 8*

A solution of ketosulfide 7 (0.53 g, 2.5 mmol) in glacial acetic acid (5 mL) was cooled to a slush; 30% hydrogen peroxide (0.28 g, 2.5 mmol) was then added slowly with stirring. After 17 h at 25°C, the mixture was diluted with water (100 mL), neutralized with solid sodium hydrogen carbonate, extracted with dichloromethane (2 × 100 mL), dried ($MgSO_4$), and evaporated to yield an off-white solid (400 mg, 70%), recrystallized from hexane; mp 184–186°C; ir ($CHCl_3$) ν: 1675 (CO), 1025 (SO) cm^{-1}; ^1H nmr ($CDCl_3$) δ: 2.7–4.0 (4H, m), 7.4–8.2 (5H, m), 8.45–8.90 (1H, m); ms *m/e*: 230 (21), 212 (91), 186 (100), 158 (49),

Can. J. Chem. Downloaded from www.nrcresearchpress.com by 210.87.254.5 on 09/05/12
For personal use only.

Can. J. Chem. Downloaded from www.nrcresearchpress.com by 210.87.254.5 on 09/05/12
For personal use only.

126 (22). *Anal.* calcd. for $C_{13}H_{10}O_2S$: C 67.82, H 4.38, S 13.90; found: C 67.44, H 4.35, S 13.91.

*2,3-Dihydro-1*H*-naphtho[2,1-*b*]thiopyran-1-one 4-Oxide, **14***

This compound was prepared by essentially the procedure described above for the isomeric sulfoxide and isolated in 45% yield; recrystallized from benzene–hexane; mp 109–110°C; ir ($CHCl_3$) ν: 1675 (CO), 1050 (SO) cm^{-1}; ^1H nmr ($CDCl_3$) δ: 2.5–3.7 (4H, m), 7.4–8.3 (5H, m), 9.05 (1H, dd, J = 8.0, 3.0 Hz); ms *m/e*: 230 (20), 214 (12), 212 (11), 202 (100), 186 (28), 158 (18), 146 (37), 126 (18). *Anal.* calcd. for $C_{13}H_{10}O_2S$: C 67.82, H 4.38, S 13.90; found: C 67.82, H 4.43, S 13.89.

*2,3-Dihydro-1*H*-naphtho[2,1-*b*]thiopyran, **11***

This compound was readily obtained, although in a lower yield (37%) than previously reported in the literature (16), by the Wolff–Kishner reduction of the corresponding cyclic keto-sulfide; mp (*n*-hexane) 86–88°C (lit. (16) mp 91–92°C); ^1H nmr ($CDCl_3$) δ: 2.0–2.5 (2H, m), 2.9–3.2 (4H, m), 7.0–8.0 (6H, m); ms *m/e*: 200 (100). *Anal.* calcd. for $C_{13}H_{12}S$: C 77.98, H 6.04, S 15.98; found: C 78.09, H 6.07, S 15.84.

*2,3-Dihydro-4*H*-naphtho[1,2-*b*]thiopyran, 5*

As for the isomeric sulfide above, this compound was obtained in 74% yield (lit. (17) 82%) as a pale yellow oil; ^1H nmr ($CDCl_3$) δ: 1.9–3.2 (6H, m), 6.9–8.2 (6H, m); ms *m/e*: 200 (100).

*2,3-Dihydro-1*H*-naphtho[2,1-*b*]thiopyran 4-Oxide, **12***

A solution of the sulfide **11** (0.03 g, 1.5 mmol) in glacial acetic acid (4 mL) was cooled to a slush; hydrogen peroxide (30%) (0.17 g, 1.52 mmol) was added slowly with stirring. After 5 h at 25°C the mixture was diluted with water (100 mL), neutralized with solid $NaHCO_3$, and extracted with dichloromethane (2 × 100 mL). The organic extract was washed with water (1 × 100 mL), brine (1 × 100 mL), and dried ($MgSO_4$). Evaporation *in vacuo* afforded a pink solid (0.25 g, 77%); mp 125–127°C; ^1H nmr ($CDCl_3$) δ: 1.9–3.7 (6H, m), 7.3–8.7 (6H, m); ms *m/e*: 216 (32), 200 (35), 199 (100), 166 (54), 165 (29), 115 (22). *Anal.* calcd. for $C_{13}H_{12}OS$: C 72.21, H 5.59, S 14.81; found: C 72.05, H 5.61, S 14.53.

*2,3-Dihydro-4*H*-naphtho[1,2-*b*]thiopyran 1-Oxide, 6*

Essentially the same procedure was used as for the isomeric sulfoxide described above. Evaporation of the CH_2Cl_2 extracts *in vacuo* gave pale yellow needles (from dichloromethane–hexane) (0.62 g, 60%); mp 139–142°C; ^1H nmr ($CDCl_3$) δ: 1.9–3.9 (6H, m), 6.9–8.2 (5H, m), 8.7 (1H, dd, J = 8.5, 2.0 Hz). *Anal.* calcd. for $C_{13}H_{12}OS$: C 72.21, H 5.59, S 14.81; found: C 72.24, H 5.66, S 14.81.

3-(2-Naphthylthio)-1-phenyl-1-propanone

2-Naphthalenethiol (6.4 g, 0.04 mol) was added to a 1% aqueous sodium hydroxide solution (160 mL), followed by 3-chloro-1-phenyl-1-propanone (6.8 g, 0.04 mol) in methanol (80 mL), with stirring. After refluxing (4 h), the starting cloudy mixture had changed to two well-defined layers. After cooling, the crude product was extracted with methylene chloride. Washing the combined methylene chloride extracts (aqueous 10% NaOH, H_2O), drying ($MgSO_4$), and evaporation gave the crude product. This crude product was then recrystallized from 95% ethanol to give 3-(2-naphthylthio)-1-phenyl-1-propanone as a white solid (9.7 g, 83%), mp 70–72°C (dichloromethane – *n*-hexane) (lit. (18) mp 92°C); ir ($CHCl_3$) ν: 1690 (C=O) cm^{-1}; ^1H nmr ($CDCl_3$) δ: 3.48 (4H, s), 7.3–8.15 (12H, m); ms *m/e*: 292 (16), 160 (100), 132 (29), 128 (21), 115 (32), 105 (76), 77 (46). *Anal.* calcd. for $C_{19}H_{16}OS$: C 78.06, H 5.52, S 10.95; found: C 77.81, H 5.55, S 11.14.

3-(2-Naphthylthio)-1-phenyl-1-propanol

3-(2-Naphthylthio)-1-phenyl-1-propanone (5.8 g, 0.02 mol) was dissolved in methanol (150 mL). Sodium borohydride (0.20 g, 0.0053 mol) was then added to the solution, and the mixture was stirred at 25°C for 3.5 h. Additional sodium borohydride (0.06 g) was then added and the mixture stirred for a further 1.5 h. The solution was poured into 2 *N* hydrochloric acid solution (180 mL) and the product extracted with dichloromethane. Washing (H_2O, 10% NaOH, H_2O), drying ($MgSO_4$), and evaporation of the solvent yielded 3-(2-naphthylthio)-1-phenyl-1-propanol (5.6 g, 96%) as a white solid; mp 64–66°C (dichloromethane – *n*-hexane); ^1H nmr ($CDCl_3$) δ: 1.97 (2H, q, J = 6.0 Hz), 2.21 (1H, s, exchanges with D_2O), 2.98 (2H, t, J = 7.0 Hz), 4.73 (1H, t, J = 6.0 Hz), 7.2–7.8 (12H, m); ms *m/e*: 294 (2), 276 (93), 247 (35), 199 (12), 117 (100), 105 (26), 91 (13). *Anal.* calcd. for $C_{19}H_{18}OS$: S 10.89; found: S 10.68.

*1-Phenyl-2,3-dihydro-1*H*-naphtho[2,1-*b*]thiopyran, 15*

3-(2-Naphthylthio)-1-phenyl-1-propanol (5.2 g, 0.018 mol) was dissolved in dichloromethane (180 mL). Stannic chloride (2.5 mL, 0.021 mol) was added dropwise during 10 min to the stirred solution. The color of the solution changed from colorless to yellow after the addition of stannic chloride. After stirring 2 h at 25°C, 2 *N* hydrochloric acid (180 mL) was added to the solution with disappearance of the yellow color. The organic layer separated, and the mixture was thoroughly extracted with dichloromethane. Washing the combined organic extracts (H_2O, 10% $NaHCO_3$), drying ($MgSO_4$), and evaporation gave 1-phenyl-2,3-dihydro-1*H*-naphtho[2,1-*b*]thiopyran as a pale grey solid (4.3 g, 88%); mp 131–133°C, on recrystallization from dichloromethane – *n*-hexane: ^1H nmr ($CDCl_3$) δ: 2.1–3.1 (4H, m), 4.87 (1H, t, J = 3.5 Hz), 7.0–7.8 (11H, m); ms *m/e*: 276 (100), 247 (38), 215 (11), 199 (13), 166 (9), 165 (8). *Anal.* calcd. for $C_{19}H_{16}S$: C 82.56, H 5.83, S 11.60; found: C 82.67, H 5.84, S 11.59.

cis- *and* trans-*1-Phenyl-2,3-dihydro-1*H*-naphtho[2,1-*b*]thiopyran 4-Oxide, **16a** and **16b***

1-Phenyl-2,3-dihydro-1*H*-naphtho[2,1-*b*]thiopyran (3.6 g, 0.013 mol) was dissolved in warm acetic acid (150 mL). After cooling to 10°C, 30% hydrogen peroxide (2.0 mL, 0.017 mol) was added dropwise to the cold solution during 10 min. The mixture was continuously stirred for 6 h at 25°C. The solution was then diluted with water (150 mL), and saturated with sodium acetate before extracting with dichloromethane. Washing the combined extracts (saturated NaCl, 10% $NaHCO_3$, saturated NaCl), drying ($MgSO_4$), and evaporation gave a milky white oil (3.6 g). After purification by chromatography on silica gel and elution with dichloromethane–acetone mixture (10:1), a mixture of *cis*- and *trans*-sulfoxides was obtained as a white solid (2.74 g, 69%); mp 155–160°C; ^1H nmr ($CDCl_3$) δ: 2.2–2.6 (2H, m), 2.8–3.3 (2H, m), 5.0 (1H, t), 6.8–7.9 (11H, m).

Separation of the *cis*- and *trans*-mixture (380 mg) by chromatography on silica gel (CH_2Cl_2:CH_3COCH_3 = 7:1) gave pure *cis*-isomer (65 mg); mp 207–209°C (dichloromethane – *n*-hexane) and pure *trans*-isomer (283 mg), mp 157–159°C (same solvent); ^1H nmr (*cis*) ($CDCl_3$) δ: 2.3–2.7 (2H, m), 3.0–3.3 (2H, m), 4.85 (1H, t), 6.8–7.9 (11H, m); ms *m/e*: 292 (18), 275 (100), 247 (19), 242 (30), 215 (20), 165 (12), 115 (14), 91 (88). *Anal.* calcd. for $C_{19}H_{16}OS$: C 78.06, H 5.52, S 10.95; found: C 77.80, H 5.53, S 10.90. ^1H nuclear magnetic resonance (*trans*) ($CDCl_3$) δ: 2.1–2.6 (2H, m), 2.75–3.15 (2H, m), 5.0 (1H, t), 6.8–8.0 (11H, m); ms *m/e*: 292 (6), 276 (100), 275 (36), 247 (37), 215 (15), 199 (13), 166 (10), 115 (12), 91 (44). *Anal.* calcd. for $C_{19}H_{16}OS$: C 78.06, H 5.52, S 10.95; found: C 77.64, H 5.56, S 10.79.

*4-Phenyl-2,3-dihydro-4*H*-naphtho[1,2-*b*]thiopyran, 9*

This compound was prepared by an analogous procedure to that described above for the isomeric naphtho[2,1-*b*] thiopyran derivative, starting from 1-naphthalenethiol, a comparable yield

Can. J. Chem. Downloaded from www.nrcresearchpress.com by 210.87.254.5 on 09/05/12
For personal use only.

(82%) being obtained in the cyclization step. The pale yellow oil had ^{1}H nmr ($CDCl_3$) δ: 1.9–3.2 (4H, m), 4.4 (1H, m), 6.9–8.1 (11H, m); ms *m/e*: 276 (100). *Anal.* calcd. for $C_{19}H_{16}S$: C 82.56, H 5.83, S 11.60; found: C 82.69, H 5.92, S 11.30.

cis- *and* trans-*4-Phenyl-2,3-dihydro-4*H-*naphtho[1,2-*b*]thiopyran 1-Oxide, 10*a *and 10*b

The thiopyran (3.1 g, 11.2 mmol) was dissolved in a mixture of glacial acetic acid (130 mL) and acetone (40 mL). At 25°C, 30% hydrogen peroxide (1.34 g, 11.76 mmol) was added dropwise, and after 4 h the solution was diluted with water (150 mL) and saturated with sodium acetate. It was then extracted with dichloromethane (2 × 100 mL), washed with NaOH solution (10%, 100 mL), water (2 × 100 mL), and dried ($MgSO_4$). Evaporation afforded a yellow oil (2.6 g, 79%), shown to be a mixture of isomers (approx. 5:1) by tlc. The mixture could not be separated by column chromatography since the isomers were so close in R_f value, but preparative tlc (run in dichloromethane–ethylacetate 3:1) afforded partial purification and a white solid (mixture); mp 186–192°C.

Further chromatographic separation of this mixture gave the two pure isomeric sulfoxides: *trans*-sulfoxide; mp 182–184°C, from dichloromethane–hexane; ^{1}H nmr ($CDCl_3$) δ: 1.9–3.5 (4H, m), 4.55 (1H, m), 6.7–8.0 (10H, m), 8.75 (1H, dd, J = 8.0, 2.0 Hz). *Anal.* calcd. for $C_{19}H_{16}OS \cdot \frac{1}{2}H_2O$: C 75.75, H 5.65, S 10.63; found: C 75.68, H 5.45, S 10.81; *cis*-sulfoxide; mp 201–202°C, from dichloromethane–hexane; ^{1}H nmr ($CDCl_3$) δ: 2.0–3.5 (4H, m), 3.9–4.3 (1H, m), 6.8–7.95 (10H, m), 8.75 (1H, dd, J= 8.0, 2.0 Hz). *Anal.* calcd. for $C_{19}H_{16}OS$: C 78.06, H 5.52, S 10.95; found: C 77.91, H 5.53, S 10.91.

3-(1-Naphthylthio)-1-propanol, 2

This alcohol was prepared in 68% yield as a pale yellow oil by the procedure of Cagniant and Cagniant (14) and showed the expected spectral characteristics. Attempted cyclization to **5** by the already described procedure using $SnCl_4$ was unsuccessful.

3-(2-Naphthylthio)-1-propanol

This alcohol was also prepared, in 90% yield, by the above procedure; mp 59–61°C (lit. (14) mp 63°C); ^{1}H nmr ($CDCl_3$) δ: 1.98 (2H, quintet, J = 7 Hz), 3.20 (2H, t, J = 7 Hz), 3.85 (2H, t, J = 7 Hz), 7.25–8.05 (8H, m, arom. and O*H*).

1-Methylsulfinylnaphthalene (Methyl 1-Naphthyl Sulfoxide)

To a solution of 1-methylthionaphthalene (19) (0.91 g, 5.23 mmol) in glacial acetic acid (15 mL) at 10–15°C, 30% hydrogen peroxide (0.593 g, 5.23 mmol) was added dropwise and the mixture stirred for 5 h. Work-up consisted of dilution with water (20 mL), extraction with dichloromethane (2 × 20 mL), washing (5% $NaHCO_3$ (4 × 20 mL), water (20 mL)), drying ($MgSO_4$), and evaporation to give a pale yellow solid (0.75 g, 75%); mp 64–66°C (lit. (10) mp 66–67°C); ir ($CHCl_3$) ν: 1065 cm^{-1}.

2-Methylsulfinylnaphthalene (Methyl 2-Naphthyl Sulfoxide)

Oxidation of 2-methylthionaphthalene (20) was carried out as for the 1-isomer above to give the sulfoxide in 70% yield; mp 104–106°C (lit. (21) mp 104–105°C); ir ($CHCl_3$) ν: 1060 cm^{-1}.

Irradiation of Sulfoxides

The irradiations were routinely conducted under nitrogen in degassed benzene as solvent, at concentrations around 0.2–0.5%, for varying periods of time. The ultraviolet source used was either a low-pressure (4 W) mercury arc, emitting mainly at 254 nm, or a medium-pressure arc (115 W or 400 W), emitting mainly at 313 and 366 nm. A typical example appears below.

*Irradiation of 1-Phenyl-2,3-dihydro-1*H-*naphtho[2,1-*b*]thiopyran 4-Oxide, 16*a,b

The *trans*/*cis* sulfoxide mixture (>4:1) (0.5 g) was irradiated in dry benzene in a quartz vessel for 70 h, using the low-pressure source. Evaporation of the solvent and chromatographic separation on silica gel gave three pure compounds: (*a*) a white solid (380 mg), shown to be a mixture of the starting sulfoxides. Further chromatography led to the isolation of almost equal amounts of the pure *cis*- (115 mg) and *trans*- (131 mg) isomers of the starting sulfoxide; (*b*) a solid of mp 122–125°C, shown to be identical with 1-phenyl-2,3-dihydro-1*H*-naphtho[2,1-*b*]thiopyran by mp, mmp, and spectral comparisons was obtained (14 mg, 12% based on starting material consumed); and (*c*) the final product (4 mg, 4%) was a pale yellow liquid (**17**); ir ($CHCl_3$) ν: 2840, 2740 (C*H*O), 1730 (CO) cm^{-1}; ^{1}H nmr ($CDCl_3$) δ: 3.2 (2H, br d), 5.3 (1H, m), 6.8–8.2 (12H, m), 9.75 (1H, br s); ms *m/e*: 260 (53), 242 (16), 217 (100), 202 (47), 165 (11), 155 (84), 128 (21), 127 (63), 105 (42), 77 (58).

3-(1-Naphthyl)-3-phenylpropanal, 17

Following the general procedure of Kuznetsov and Libman (22), 1-benzylnaphthalene (23) **18** (2.31 g, 10.60 mmol) in dry ether (10 mL) was slowly dropped into a mixture of sodium amide (prepared from sodium) in liquid ammonia (0.45 g, 19.57 mmol and 20 mL liquid ammonia) cooled in a methanol – Dry Ice bath at −35°C.

After stirring for 1 h at −35°C, bromoacetaldehyde diethyl acetal (2.30 g, 11.68 mmol) was added over a period of 15 min. Ammonium chloride was added and the ammonia was allowed to evaporate. Water was added and the mixture was extracted with diethyl ether.

The ether layer was evaporated and the resulting oil was refluxed for 1 h in acetic acid (10 mL), water (5 mL), and hydrochloric acid (0.5 mL). Extraction with diethyl ether, washing with sodium carbonate solution, drying (Na_2SO_4), and evaporation of the ether gave an oil. Column chromatography (SiO_2, CH_2Cl_2) yielded 3-(1-naphthyl)-3-phenylpropanal, **17** (1.06 g, 25%). The infrared and mass spectral characteristics of this material were identical with those of the product of irradiation of **16***a,b*. The authentic material, however, after careful purification, afforded white crystals, mp 101–102°C (hexanes); ^{1}H nmr ($CDCl_3$) δ: 3.25 (2H, dd, J = 7 Hz, 2 Hz), 5.4 (1H, t, J = 7 Hz), 7.0–8.2 (12H, m), 9.75 (1H, t, J = 2 Hz).

Singlet Oxygen Trapping Experiment (9)

2,3-Dihydro-4*H*-naphtho[1,2-*b*]thiopyran-4-one 1-oxide **8** (0.14 g, 0.61 mmol) in degassed cyclohexene (10 mL) and glacial acetic acid (5 mL) was irradiated (medium-pressure arc, 400 W) for 22 h. Placing a drop of the solution on potassium iodide – starch paper did not leave a brown stain nor did a blue spot appear when a drop of water was added, indicating the absence of peroxide (24). A more sensitive spot test (from $FeSO_4 \cdot 7H_2O$ (0.90 g), 5 *M* hydrochloric acid (5 mL), zinc, and sodium thiocyanate (1.70 g)) also proved negative.

Acknowledgements

Financial support of this study by the National Research Council of Canada and by the University of Toronto is gratefully acknowledged. It is a pleasure to acknowledge the contribution of undergraduate research participants S. Persad, M. Wagner, and R. A. Wong in performing some of the preliminary synthetic experiments and to acknowledge the very generous assistance of Dr. A. A. Grey

of the University of Toronto in obtaining and assigning the 220 MHz ^{1}H nmr spectra. One of us (IWJS) also acknowledges the generous hospitality provided by Professor B. Zwanenburg during a sabbatical leave spent early in 1980 at the Laboratorium voor Organische Chemie, Katholieke Universiteit, Nijmegen, The Netherlands.

1. I. W. J. STILL, P. C. ARORA, M. S. CHAUHAN, M.-H. KWAN, and M. T. THOMAS. Can. J. Chem. **54**, 455 (1976).
2. A. G. SCHULTZ and R. H. SCHLESSINGER. Tetrahedron Lett. 4787 (1973).
3. C. R. JOHNSON and D. MCCANTS. J. Am. Chem. Soc. **87**, 1109 (1965).
4. J. B. LAMBERT and S. I. FEATHERMAN. Chem. Rev. **75**, 611 (1975).
5. W. D. COTTERILL, C. J. FRANCE, R. LIVINGSTONE, J. R. ATKINSON, and J. COTTAM. J. Chem. Soc. Perkin Trans. I, 787 (1972).
6. K. A. KIME and R. E. SIEVERS. Aldrichimica Acta, **10**, 54 (1977), and references therein.
7. J. B. LAMBERT, D. A. NETZEL, H. SUN, and K. K. LILIANSTROM. J. Am. Chem. Soc. **98**, 3778 (1976).
8. J. B. STOTHERS. Carbon-13 nmr spectroscopy. Academic Press, New York, NY. 1972. p. 67.
9. G. M. GURRIA and G. H. POSNER. J. Org. Chem. **38**, 2419 (1973).
10. A. MANGINI, M. PALLOTTI, M. TIECCO, A. DONDONI, and P. VIVARELLI. Int. J. Sulfur Chem. Part A, **2**, 69 (1972).
11. L. SKULSKI. Bull. Acad. Pol. Sci. **17**, 253 (1969).
12. Chem. Zentralbl. (II), 929 (1927).
13. F. KROLLPFEIFFER and H. SCHULTZE. Chem. Ber. **56**, 1819 (1923).
14. P. CAGNIANT and D. CAGNIANT. Bull. Soc. Chim. Fr. 2037 (1966).
15. T. E. YOUNG and C. J. OHNMACHT. J. Org. Chem. **32**, 444 (1967).
16. W. E. TRUCE and G. A. TOREN. J. Am. Chem. Soc. **76**, 695 (1954).
17. E. CAMPAIGNE and B. G. HEATON. J. Org. Chem. **29**, 2372 (1964).
18. B. D. TILAK and G. T. PANSE. Indian J. Chem. **7**, 191 (1969).
19. F. TABOURY. Bull. Soc. Chim. Fr. **31**, 1183 (1904).
20. H. STAUDINGER, H. GOLDSTEIN, and E. SCHLENKER. Helv. Chim. Acta, **4**, 342 (1921).
21. F. KROLLPFEIFFER and W. HAHN. Chem. Ber. **86**, 1049 (1953).
22. S. G. KUZNETSOV and N. M. LIBMAN. J. Org. Chem. USSR, **1**, 1418 (1965).
23. K. DZIEWONSKI and S. DZIECIELEWSKI. Bull. Acad. Pol. Sci. 273 (1927); Chem. Abstr. **22**, 2164a (1928).
24. F. FEIGL. Spot tests in organic analysis. 6th ed. Elsevier, Amsterdam. 1960. pp. 534, 535.

Can. J. Chem. Downloaded from www.nrcresearchpress.com by 210.87.254.5 on 09/05/12
For personal use only.

Selective transformations of secologanin: dihydroxylation

JOHN RICHARD PURDY, RAYMOND G. HAMILTON, LALARUKH AKHTER, AND STEWART MCLEAN
Department of Chemistry, University of Toronto, Toronto, Ont., Canada M5S 1A1

Received August 5, 1980

JOHN RICHARD PURDY, RAYMOND G. HAMILTON, LALARUKH AKHTER, and STEWART MCLEAN. Can. J. Chem. **59**, 210 (1981).

Sweroside tetraacetate (**2***b*) has been converted in high yield by osmylation to the epimeric glycols **3** and **4** (R = H) which have been separated. This reaction proceeds with high chemoselectivity for reaction at the vinyl side chain but with low stereoselectivity, leading to a small excess of the 3-*R* isomer. Secologanin derivatives appear to show a much lower chemoselectivity in this reaction, but the stereoselectivity is considerably higher, and opposite to that in the sweroside example. Conditions have been found for oxidizing the dimethylacetal **5***b* of secologanin tetraacetate in useful yields to the epimeric glycols **6** and **7** (R = H); in this reaction a large excess of the 3-*S* isomer is formed. The reasons for these differences in selectivity appear to be related to differences between the two series in conformational preference.

JOHN RICHARD PURDY, RAYMOND G. HAMILTON, LALARUKH AKHTER et STEWART MCLEAN. Can. J. Chem. **59**, 210 (1981).

La réaction du tétraacétate de sweroside avec le tétroxyde d'osmium conduit avec d'excellents rendements aux glycols épimères **3** et **4** (R = H) qu'on a pu séparer. Cette réaction se produit avec une haute régiosélectivité du côté de la chaîne latérale vinylique, mais avec une faible stéréosélectivité; elle conduit à un léger excès de l'isomère 3-*R*. Les dérivés de la sécologanine semblent exhiber une plus faible régiosélectivité au cours de cette réaction mais la stéréosélectivité est considérablement plus élevée et est à l'opposé de celle observée avec la sweroside. On a mis au point des conditions permettant d'oxyder du diméthylacétal (**5***b*) du tétraacétate de sécologanine en glycols épimères **6** et **7** (R = H) avec des rendements convenables; dans cette réaction, l'isomère 3-*S* est produit en grand excès. Les causes de ces différences de sélectivité semblent être reliées aux différences de préférence conformationnelle entre les deux séries.

[Traduit par le journal]

Secologanin (**1***a*) is an iridoid glycoside of considerable biosynthetic significance, particularly in the field of indole alkaloids (1), where it represents the common last nonnitrogenous precursor to a vast and diverse array of alkaloids. It appears to be established that it is after secologanin has been linked to a tryptophan-derived component that diversification takes place by further chemical modifications of the intermediate. Secologanin is of chemical interest itself as a molecule that incorporates a dense aggregation of sensitive functional groups and chiral centres. A study of the selective chemical transformations of secologanin could consequently afford results of synthetic and biosynthetic importance. We report here our studies of the dihydroxylation of the olefinic side chain.

Secologanin and its closely related congener sweroside (**2***a*) are readily available constituents of various *Lonicera* species. The osmium tetroxide oxidation of sweroside tetraacetate (**2***b*) has been described by Bock *et al.* (2) who isolated a modest yield of the diols resulting from a chemoselective oxidation of the vinyl side chain. Stereoselectivity was low, and they obtained an inseparable mixture of epimeric glycols. The acetylated glycols **3** and **4** (R = Ac) were, however, separated, and their configurations were assigned by correlation with secogalioside, the configuration of which was established by the nuclear Overhauser enhancement technique.

This reaction appeared to serve as an excellent model for our purpose, and in our hands optimization of the osmylation reaction, using the catalytic system with *N*-methylmorpholine *N*-oxide (3), has led to the conversion of sweroside tetraacetate to the epimeric mixture of glycols in over 80% yield. Furthermore, separation of the glycols themselves has been accomplished by chromatography, and each epimer has been isolated in a crystalline form; the ratio of **3** to **4** (R = H) produced in the reaction is 2:3. Each epimer has been acetylated to form the derivatives **3** and **4** (R = Ac) reported previously (2).

Despite the close similarity between secologanin and sweroside, the selective dihydroxylation of secologanin tetraacetate (**1***b*) proved to be a much more difficult task, even when the free aldehyde was protected as its dimethyl acetal (**5***b*). It appears probable that the cause of this difficulty is that the endocyclic double bond is more susceptible to oxidation in this series than in the sweroside series, and this oxidation leads to uncharacterizable products. It appears that the vinyl side chain is osmylated with some selectivity in the early stages of the reaction, but attempts to carry the reaction to completion inevitably lead to over-oxidation and diminished yields of the desired product. The best conversion of **5***b* to the glycols **6** and **7** (R = H) was achieved by carrying out the osmylation under carefully controlled conditions and stopping the reaction when somewhat less than half of the start-

0008-4042/81/020210-05$01.00/0
©1981 National Research Council of Canada/Conseil national de recherches du Canada

Can. J. Chem. Downloaded from www.nrcresearchpress.com by 210.87.254.6 on 09/05/12
For personal use only.

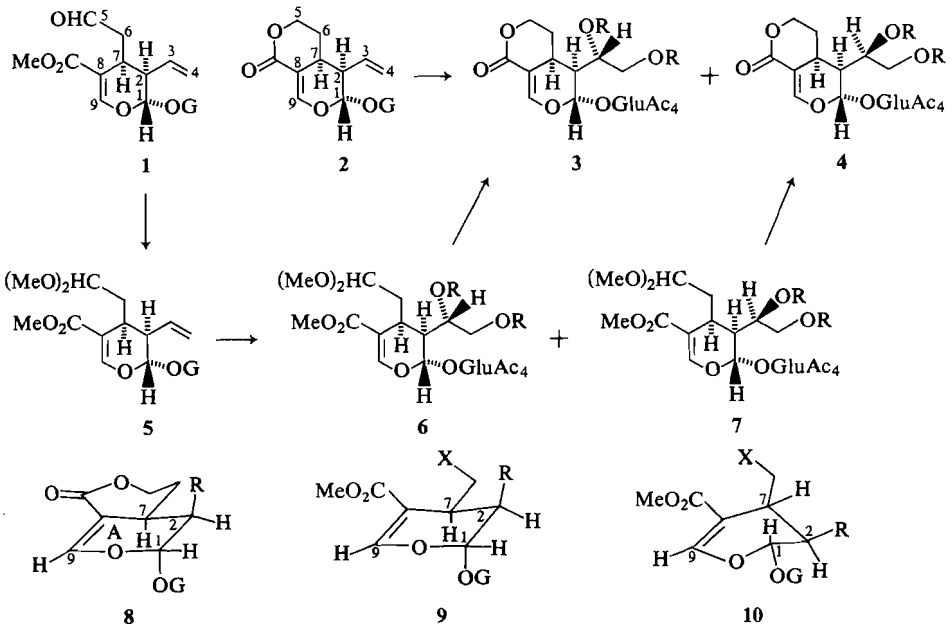

(*a*) G = β-D-glucopyranosyl
(*b*) G = tetraacetyl-β-D-glucopyranosyl

ing material had reacted; after work-up, unchanged **5***b* could be conveniently recovered and the mixture of glycols could be isolated in yields of 40–45% based on unrecovered **5***b*. The nmr spectrum of the product shows that it contains the two epimeric glycols in a 10:1 ratio. The major epimer was isolated as a gum by chromatography, and samples enriched in the minor epimer were obtained, but these always contained some of the major epimer.

The configurations of the glycols were determined by converting the acetylated derivatives **6** and **7** (R = Ac) obtained from the glycol mixture to the corresponding derivatives **3** and **4** (R = Ac) in the sweroside series. The dimethyl acetal function was first hydrolyzed and the resulting aldehyde was reduced to the alcohol in high yield (86%) by sodium cyanoborohydride; acidic conditions caused the hydroxy esters to cyclize to the lactones **3** and **4** (R = Ac). Chromatography afforded the major epimer in crystalline form, isolated in 60% yield, and this was shown to be identical in every respect with **3** (R = Ac), the minor epimer obtained from sweroside. The minor epimer **4** (R = Ac) from secologanin was identical in chromatographic and spectroscopic characteristics with the major epimer from sweroside. Since the configurations of the glycols in the sweroside series appear secure (2), it follows that the glycols **6** and **7** (R = H) were obtained in the ratio of 10:1 in the secologanin series, and that the osmylation of **5***b* had taken place with a high degree of stereoselectivity to form the 3-*S* derivative.

The high stereoselectivity but low chemoselectivity in the secologanin series contrasts strikingly with the high chemoselectivity but low stereoselectivity in the sweroside series; furthermore, it is the 3-*R* isomer that is produced in small excess in the latter case. Another difference between the two series is in the conformational preferences of the molecules as revealed in their nmr spectra, and it seems probable that selectivity and conformational factors are interrelated. The conformation of the dihydropyran, ring A, that is common to all of these compounds could be judged from the coupling constant ($J_{1,2}$) between the configurationally *trans* protons at C-1 and C-2; other data, especially the magnitude of the allylic coupling between the protons at C-7 and C-9, were also of value. (Table 1 lists the key data).

In the sweroside series the conformational situation is uncomplicated. All of the derivatives examined show $J_{1,2}$ values characteristic of vicinal diequatorial protons, and relatively large values for allylic coupling with $J_{7,9}$ values in the range 2–2.5 Hz; values reported by others (4) for compounds in this series are in the same ranges. It follows that ring A retains the conformation depicted in **8** when the C-2 substituent is vinyl or a

Can. J. Chem. Downloaded from www.nrcresearchpress.com by 210.87.254.6 on 09/05/12
For personal use only.

TABLE 1. Selected nmr data for derivatives of sweroside and secologanin[a]

Compound	Chemical shift C-1—H(τ)	$J_{1,2}$ (Hz)	Chemical shift C-9—H(τ)	$J_{7,9}$ (Hz)	Comments
Sweroside derivatives:					
Sweroside (*2a*)	4.43	1.5	2.39	2.0	In D_2O, see ref. 4
Tetraacetate *2b*	4.65	~1	2.46	2.0	See also ref. 4
3,4-Dihydro-*2b*	4.55	1.5	2.48	2.0	See ref. 4
Glycol **3** (R = H)	4.50	1.5	2.50	2.5	
Derivative **3** (R = Ac)	4.44	1.5	2.46	2.5	See also ref. 2
Glycol **4** (R = H)	4.18	1.5	2.40	2.0	
Derivative **4** (R = Ac)	4.35	1.5	2.46	2.5	See also ref. 2
Secologanin derivatives:					
Secologanin (*1a*)	5.20	7.0	2.42	1.0	In D_2O, see also ref. 5
Tetraacetate *1b*	4.73	3.0	2.60	1.5	
Dimethyl acetal *5b*	4.79	2.5	2.76	~1	In CCl_4
Glycol **6** (R = H)	4.61	10.0	2.67	~0	
Derivative **6** (R = Ac)	4.50	9.0	2.51	~0	
Glycol **7** (R = H)	4.43	10.0	(2.67)	~0	Mixture with **6** (R = H); C-9 signals probably coincide

[a]Spectra obtained with $CDCl_3$ solutions, unless otherwise indicated.

more heavily substituted derivative and the C-1 substituent is a glucose residue or its tetraacetate, and the conformation is the same in aqueous or organic solvents. The presence of the fused lactone and the anomeric effect of the C-1 glycoside together appear sufficient to maintain ring A in the conformation **8** having an axial C-2 substituent in all of these compounds.

In the secologanin series, however, the conformational preference varies. Secologanin itself (*1a*) has been observed in aqueous (D_2O) solution (where the aldehyde exists largely in the hydrated form) and, in agreement with others (5), we have found $J_{1,2}$ = 7.0 Hz and $J_{7,9}$ = 1.0 Hz. In $CDCl_3$ solution, however, its tetraacetate *1b* exhibits $J_{1,2}$ = 3.0 Hz and $J_{7,9}$ = 1.5 Hz; the corresponding assignments of 2.5 and ~1 Hz for a carbon tetrachloride solution of its dimethyl acetal *5b* are made with less confidence because of interference from other signals. These results indicate that the equilibrium between the two conformations of ring A, **9** (corresponding to the sweroside conformation) and **10**, is more finely balanced; the effect of an aqueous medium leads to a preference for **10**, while in a nonaqueous solvent, **9** is preferred, and it is probable that the minor conformation is a significant component of the dynamic equilibrium in both media since the coupling constants do not correspond to the extreme values associated with either pure conformation. In the major glycol **6** (R = H) derived from *5b*, the values $J_{1,2}$ = 9.5 and $J_{7,9}$ ~ 0 Hz were observed, and the values for the minor glycol **7** (R = H) present in the reaction mixture were very similar. It seems clear that conformation **10** becomes strongly dominant when the bulk of the substituent R at C-2 increases and the preference of this group for an equatorial environment outweighs the combined effect of an axial C-7 substituent and an equatorial substituent at the anomeric centre C-1. The nmr spectra of intermediates in the conversion of **6** and **7** to **3** and **4** showed $J_{1,2}$ and $J_{7,9}$ values corresponding to conformation **10** until the lactone ring was closed.

These differences in conformational preference in the two series provide an explanation for the differences in the selectivity of the osmylation reaction. In the sweroside series the vinyl side chain is clearly axial and there is little difference in steric hindrance to approach by the reagent to either face. The C-2 substituent remains axial in the product glycol, as does the C-1 glycoside moiety; under these circumstances the internal 8,9 double bond appears to resist attack by osmium tetroxide. In the more conformationally mobile secologanin derivative, on the other hand, the osmylation shows a high degree of stereoselectivity for reaction at the vinyl side chain, and the C-2 substituent in the product glycol is equatorial. It is reasonable to propose that the steric environment of the vinyl side chain differs from that in the sweroside series during the osmylation process, and that reaction through conformation **10** is preferred as the bulky osmate develops (6), adopting an equatorial orientation in which there is more steric difference between the two faces of the side chain. The low chemoselectivity for reaction at the vinyl side chain may be attributed to the increased reactivity of the endocyclic double bond when the substituents at

Can. J. Chem. Downloaded from www.nrcresearchpress.com by 210.87.254.6 on 09/05/12
For personal use only.

Can. J. Chem. Downloaded from www.nrcresearchpress.com by 210.87.254.6 on 09/05/12
For personal use only.

C-1 and C-2 are both equatorial. This is the presumed conformation in the osmylated intermediate and the evidence presented above does indicate that over-oxidation increases as the concentration of osmylated material builds up. The possibility that some of the starting material **5***b* undergoes oxidation at the endocyclic double bond through the small amount of the reactive conformation present in the equilibrium can not be ruled out since no characterizable products of oxidation at this site in starting material or products have been isolated. The weight of the evidence indicates that osmylation in the secologanin series shows some chemoselectivity for the vinyl side chain and the reaction is stereoselective, but the product formed is susceptible to further oxidation at the endocyclic double bond. In any event, these studies have provided a useful route to secologanin derivatives carrying an oxidized C-2 side chain of established chirality; these are valuable synthetic intermediates.

Experimental

Melting points were determined on a calibrated Thomas-Kofler micro hot stage. Infrared spectra were measured on a Perkin-Elmer 337 spectrometer; the wavelengths (μ) of selected absorptions of solutions in chloroform are reported. Ultraviolet spectra were measured on a Unicam SP 1800 spectrometer; the λ_{max} values (nm) followed by the log ε values in parentheses for solutions in methanol are reported. Proton nmr data reported were measured at 220 MHz at the Canadian 220 MHz NMR Centre; unless otherwise indicated, solutions in $CDCl_3$ were used, and chemical shifts are reported on the τ scale followed by an indication of the multiplicity (initial letter) of the signal, the coupling constants (in Hz) when available, and the number of protons associated with the signal. (More detailed analyses than those reported are available in a number of cases.) A Waters Associates Prep LC/system 500 with PrepPak-500 cartridge (30 × 5.7 cm) was used for hplc separations.

Secologanin and sweroside were isolated from local *Lonicera* species (mainly *L. tatarica*).

Dihydroxylation of Sweroside Tetraacetate

Sweroside tetraacetate (13.05 g; 23.4 mmol), prepared by treatment of sweroside (**2***a*) with acetic anhydride in pyridine, was dissolved in a mixture of 80 mL of tetrahydrofuran and 50 mL of water containing *N*-methylmorpholine *N*-oxide dihydrate (5.36 g; 34.5 mmol) under argon, and a solution of osmium tetroxide (213 mg; 0.84 mmol) in 8 mL of *tert*-butyl alcohol was carefully added to the stirred reaction mixture (3). Stirring was continued at room temperature for 23 h, a slurry of 12 g of Florisil, 1 g of sodium hydrogen sulfite, and 80 mL of water was added, and the mixture was filtered. The filtrate was reduced in volume on a rotary evaporator until an aqueous slurry remained, and this was extracted with methylene chloride. The extract was thoroughly washed with 5% hydrochloric acid followed by 5% aqueous sodium bicarbonate and then brine, dried, and evaporated to dryness. A solid residue (10.89 g; 19.4 mmol) was obtained; its nmr spectrum showed that it was a 2:3 mixture of diols **3** and **4** (R = H). The diol mixture was separated by hplc on silica gel with elution by 1:9 methanol–ether. Isomer **3** (R = H) was isolated, after recrystallization from ether–methanol, as white crystals (2.5 g), mp 112–114°C; ir: 2.70, 2.77, 5.68, 5.84, 6.15; uv: 242 (3.68); nmr: 2.50 (d, J = 2.5; 1), 4.50 (d, J = 1.5; 1), 4.7–5.2 (complex; 4), 5.4–5.9 (complex; 4), 6.2–6.4 (complex; 4), 7.00 (m, 1), 7.45 (d, J = 4; 1; removed by D_2O), 7.76 (complex; 2; 1 after D_2O wash), 7.8–8.0 (complex; 2), 7.86 (s, 3), 7.91 (s, 3), 7.95 (s, 3), 8.02 (s, 3). *Anal.* calcd. for $C_{24}H_{32}O_{15}$: C 51.43, H 5.75; found: C 51.25, H 5.80. On acetylation this formed **3** (R = Ac), mp 172–173°C (lit. (2) mp 171–172°C), with spectroscopic characteristics corresponding to published values (2). Isomer **4** (R = H) was obtained in the same way as white crystals (4.1 g), mp 92–93°C; ir: 2.70, 2.77, 5.68, 5.84, 6.15; uv: 243 (3.79); nmr: 2.40 (d, J = 2; 1), 4.18 (d, J = 1.5; 1), 4.7–5.2 (complex; 4), 6.2–6.6 (complex; 4), 6.90 (m, 1), 6.94 (d, J = 4; 1; removed by D_2O), 7.32 (m, 1; removed by D_2O), 7.81 (m, 1), 7.82 (s, 3), 7.98 (s, 3), 8.00 (s, 3), 8.05 (s, 3), 8.15–8.3 (complex; 2). *Anal.* calcd. for $C_{24}H_{32}O_{15}$: C 51.43, H 5.75; found: C 51.31, H 5.81. On acetylation this formed **4** (R = Ac) with spectroscopic characteristics corresponding to published values but a somewhat higher mp, 150–151°C (lit. (2) mp 133.5–134.5°C).

*Dimethylacetal of Secologanin Tetraacetate (***5***b)*

A solution of secologanin (1.0 g) in 10 mL of methanol was stirred with Amberlite IR 120(H) ion-exchange resin (1.0 g) for one day. After filtration and evaporation of the solvent, the acetal **5***a* was isolated in essentially quantitative yield as a white amorphous solid; ir: 2.98 (broad), 5.90, 6.18; nmr complex, included: 2.58 (br. s, 1), 6.28 (s, 3), 6.68 (s, 6). *Anal.* calcd. for $C_{19}H_{30}O_{11}$: C 52.53, H 6.96; found: C 52.67, H 6.92. This was converted by treatment with acetic anhydride in pyridine to the tetraacetate **5***b*, an amorphous white solid; ir: 5.70, 5.87, 6.14; uv: 233 (3.97), 305 (shoulder); nmr (CCl_4): 2.76 (br. s, 1), 4.42 (ddd, J values 18, 10, 4; 1), 4.70 (dd, J values 18,2; 1), 4.74 (dd, J values 10,2; 1), 4.79 (d, J = 2.5; 1), 4.9–6.3 (complex; 8), 6.34 (s, 3), 6.75 (s, 3), 6.78 (s, 3), 7.31 (complex; 2), 7.8–8.2 (complex; 2), 7.94 (s, 3), 8.02 (s, 3), 8.04 (s, 3), 8.14 (s, 3).

Alternatively, the sequence could be reversed, producing first secologanin tetraacetate (**1***b*) and then **5***b*.

Dihydroxylation of the Secologanin Derivative **5**b

A solution of **5***b* (e.g. 2 g) and about a molar equivalent of osmium tetroxide in redistilled pyridine (e.g. 10 mL) was stirred at room temperature for 4 h. The black solution was stirred with aqueous sodium hydrogen sulfite (e.g. 3 g/150 mL) until its color had been discharged, and then it was thoroughly extracted with chloroform. The extract was washed with 5% aqueous sodium hydrogen carbonate and then brine, dried, and evaporated to dryness. A colorless residue was obtained, which was chromatographed on a silica gel column pretreated with water (3%); 3:7 hexane – ethyl acetate followed by 1:9 methanol – ethyl acetate were used for elution. (Solvents were pretreated with potassium carbonate.) Starting material (50–60%) was obtained from early fractions and the mixture of glycols **6** and **7** (R = H) was isolated from later fractions in yields corresponding to 40–45% of unrecovered **5***b*. The nmr spectrum showed the mixture to contain **6** and **7** in a 10:1 ratio. Repeated chromatography on the same system led to the isolation of the major epimer **6** (R = H) as a colorless oil; ir: 2.85 (broad), 5.75, 5.85; uv: 234 (3.94); nmr: 2.67 (s, 1), 4.61 (d, J = 10.0; 1), 4.7–6.3 (complex; 11), 6.35 (s, 3), 6.58 (s, 3), 6.72 (s, 3), 6.97 (m, 1), 7.80 (m, 1), 7.83 (s, 3), 7.89 (s, 6), 7.92 (s, 3), 8.01 (m, 1), 8.70 (m, 1). A homogeneous sample of the minor epimer was not isolated, but fractions enriched in this isomer were obtained and the signals characteristic of **7** (R = H) could be deduced from the nmr spectrum of the enriched mixture. *Anal.* calcd. for $C_{27}H_{40}O_{17}$: C 50.94, H 6.33; found: C 50.94, H 6.08.

The acetylated derivatives **6** and **7** (R = Ac) could be prepared from the glycols by standard procedures. They could be obtained more conveniently by treatment of the mixture obtained

from the osmylation reaction with acetic anhydride in pyridine for 12 h at room temperature. Chromatography of the product on silica gel with ether elution afforded unchanged **5***b* in the early fractions and the acetates **6** and **7** (R = Ac) in later fractions.

Conversion to the Sweroside Series

A solution of the mixture of **6** and **7** (R = Ac) (150 mg; 0.24 mmol) described above in a mixture of 3 mL of tetrahydrofuran and 5 mL of 0.1 *N* hydrochloric acid was stirred at room temperature for about 4 h to hydrolyze the dimethyl acetal function (monitored by tlc); sodium cyanoborohydride (15 mg; 0.24 mmol) was added and stirring was continued for about 10 min to reduce the aldehyde function (monitored by tlc). The solution was concentrated by evaporation under reduced pressure and then extracted with methylene chloride. The extract afforded the alcohol (120 mg; 0.20 mmol) which was dissolved in 10 mL of tetrahydrofuran containing 60 mg of concentrated hydrochloric acid. The solution was stirred at room temperature for about 7 h (monitored by tlc) and then worked up; tlc analysis of the residue (133 mg) showed two components with the same retention times as the sweroside derivatives **3** and **4** (R = Ac). The major component of the mixture was isolated after repeated preparative tlc as white crystals, mp 172–173°C, identical with the sample of **3** (R = Ac) obtained from sweroside (see above).

Acknowledgement

The financial support of the Natural Sciences and Engineering Research Council of Canada is gratefully acknowledged.

1. A. I. SCOTT. MTP International Review of Science. Organic Chemistry, Series One, Vol. 9. *Edited by* K. F. Wiesner. Butterworths, London. 1973. p. 105.
2. K. BOCK, S. R. JENSEN, and B. J. NIELSEN. Acta Chem. Scand. Ser. B, **30**, 743 (1976).
3. V. VAN RHEENEN, R. C. KELLY, and D. Y. CHA. Tetrahedron Lett. 1973 (1976).
4. H. INOUYE, S. UEDA, and Y. NAKAMUSA. Tetrahedron Lett. 5229 (1966); Chem. Pharm. Bull. **18**, 1856 (1970); H. INOUYE, T. YOSHIDA, Y. NAKAMURA, and S. TOBITA. Chem. Pharm. Bull. **18**, 1889 (1970).
5. A. R. BATTERSBY, A. R. BURNETT, and P. G. PARSONS. J. Chem. Soc. C, 1187 (1969).
6. S. G. HENTGES and K. B. SHARPLESS. J. Am. Chem. Soc. **102**, 4263 (1980).

Can. J. Chem. Downloaded from www.nrcresearchpress.com by 210.87.254.6 on 09/05/12
For personal use only.

The conversion of sweroside to secologanin

RAYMOND G. HAMILTON AND STEWART MCLEAN
Department of Chemistry, University of Toronto, Toronto, Ont., Canada M5S 1A1

Received August 5, 1980

RAYMOND G. HAMILTON and STEWART MCLEAN. Can. J. Chem. **59**, 215 (1981).

A chemical route from sweroside (**2***a*) to secologanin (**1***a*) has been established. The lactone ring of sweroside tetraacetate (**2***b*) was opened by trimethylsilyl iodide. The unstable iodo carboxylic acid **3** (R = H; X = I) was then formed and immediately converted to its methyl ester. The iodo function was displaced by formate, and the formate was selectively methanolized under neutral conditions. The resulting alcohol **3** (R = Me; X = OH) was oxidized by pyridinium chlorochromate to the aldehyde, secologanin tetraacetate (**1***b*). With care, the conversion from the sweroside series to the secologanin series can be carried out in excellent yield. Secologanin can readily be recovered from its tetraacetate.

RAYMOND G. HAMILTON et STEWART MCLEAN. Can. J. Chem. **59**, 215 (1981).

On a établi une voie d'accès à la sécolaganine (**1***a*) à partir de la sweroside (**2***a*). On a ouvert le cycle lactonique du tétraacétate de sweroside (**2***b*) en utilisant l'iodure de triméthylsilyle. Il se forme alors l'acide iodocarboxylique **3** (R = H; X = I) qui est instable et qui se transforme immédiatement en son ester méthylique. L'iode est ensuite déplacé par un formate que l'on méthanolyse dans des conditions neutres. L'oxydation de l'alcool **3** (R = Me; X = OH) qui en résulte par le chlorochromate de pyridinium conduit à l'aldéhyde (**1***b*) le tétraacétate de sécologanine. En prenant des précautions, on peut, avec d'excellents rendements transformer des composés de la sweroside en composés de la série sécologanine. On peut récupérer facilement la sécologanine à partir de son tétraacétate.

[Traduit par le journal]

Secologanin (**1***a*), an iridoid of biosynthetic importance, is readily available as a constituent of various *Lonicera* species, where it occurs along with the related iridoid, sweroside (**2***a*). The chemical conversion of **1***a* to **2***a* can readily be carried out, and was used in the elucidation of the structure of secologanin (1). As part of one of our investigations we wished to demonstrate that the reverse process, the oxidative conversion of **2***a* to **1***a* could also be carried out chemically.

Sweroside tetraacetate (**2***b*) reacted rapidly with trimethylsilyl iodide (2) in chloroform at room temperature, and aqueous work-up produced a good yield of the unstable iodo carboxylic acid **3** (R = H; X = I), which was extremely prone to reclose to **2***b*. Immediate treatment of the intermediate acid with diazomethane converted it to its ester **3** (R = Me; X = I), which was obtained crystalline. Many attempts to replace the iodo function under oxidative or hydrolytic conditions failed, often because the intermediate recyclized. Conversion to the formate **3** (R = Me; X = OCHO) was successful when the iodide was treated with sodium formate in hexamethylphosphoric triamide, and selective methanolysis of the formate group was accomplished by prolonged treatment of **3** (R = Me; X = OCHO) with neutral methanol in refluxing tetrahydrofuran. The product alcohol **3** (R = Me; X = OH), which is also susceptible to lactonization, was successfully oxidized by pyridinium chlorochromate (3) to the aldehyde **1***b*, identical in every respect with a sample prepared by the acetylation of

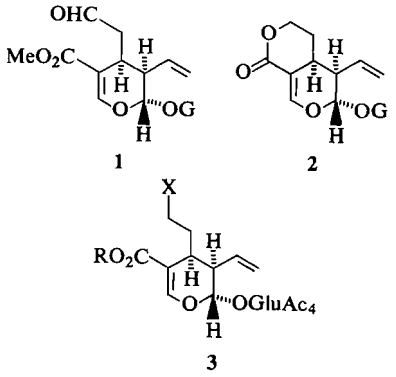

(*a*) G = β-D-glucopyranosyl
(*b*) G = tetraacetyl-β-D-glucopyranosyl

secologanin. With care, all of these transformations can be carried out in very high yields. Problems arise principally from the ease with which intermediates relactonize to the sweroside derivatives. In the oxidation step our yield was only 80%, but the amount of sweroside tetraacetate recovered from the reaction corresponded to the undesired lactonization of 13% of the precursor **3** (R = Me; X = OH). With allowance made for recovered **2***b*, the series of reactions was carried out with 88% conversion of **2***b* to **1***b*. Secologanin (**1***a*) can readily be liberated from its tetraacetate by brief treatment with methanol containing a catalytic amount of potassium carbonate; it is preferable to protect the aldehyde group as its dimethyl acetal during this operation.

0008-4042/81/020215-02$01.00/0
©1981 National Research Council of Canada/Conseil national de recherches du Canada

Can. J. Chem. Downloaded from www.nrcresearchpress.com by 210.87.254.42 on 09/05/12
For personal use only.

Can. J. Chem. Downloaded from www.nrcresearchpress.com by 210.87.254.42 on 09/05/12
For personal use only.

Experimental

Melting points were determined on a calibrated Thomas–Kofler micro hot stage. Infrared spectra were measured on a Unicam SP3-200 spectrometer; the wavelengths (μ) of selected absorptions of solutions in chloroform are reported. Ultraviolet spectra were measured on a Unicam SP800A spectrometer; the λ_{max} values (nm) followed by the log ε values in parentheses for solutions in methanol are reported. Proton nmr spectra were recorded on a Varian T-60 spectrometer or at the Canadian 220 MHz NMR Centre; the chemical shifts for solutions in $CDCl_3$ are reported on the τ scale followed in parentheses by an indication of the multiplicity (initial letter) of the signal, the coupling constants (in Hz) when available, and the number of protons associated with the signal.

Secologanin and sweroside were isolated from local *Lonicera* species (mainly *L. tatarica*).

Iodo Ester 3(R = Me; X = I)

Crystalline sweroside tetraacetate, **2***b*, (2.0 g; 3.8 mmol) was dissolved in 11 mL of freshly-distilled chloroform under argon and treated with trimethylsilyl iodide (0.9 g; 4.5 mmol). The solution was stirred for 1 h, further trimethylsilyl iodide (0.2 g) was added, and stirring was continued for 10 min. The solution was shaken with 50 mL of water, and the aqueous phase was thoroughly reextracted with chloroform. The combined organic solutions were concentrated under reduced pressure to a volume of about 25 mL, and treated with excess ethereal diazomethane. After the reaction was complete, acetic acid was added to remove the excess diazomethane, and the solution was evaporated under reduced pressure. The gummy residue was dissolved in methylene chloride, washed with 5% aqueous sodium thiosulfate and then brine, dried, and evaporated to dryness. The residue (2.4 g; 3.6 mmol) was substantially pure **3** (R = Me; X = I) which, on recrystallization from ether, formed needles, mp 156–159°C; ir: 5.70, 5.85, 6.13; uv: 230 (3.65); nmr (220 MHz): 2.65 (d, J = 1.5; 1), 4.38 (m, 1), 4.6–5.2 (complex; 7), 5.65–5.9 (complex; 2), 6.23 (m, 1), 6.27 (s, 3), 6.75–6.95 (complex; 2), 7.2–7.3 (complex; 2), 7.50 (m, 1), 7.89 (s, 3), 7.96 (s, 3), 7.99 (s, 3), 8.06 (s, 3), 8.17 (m, 1). *Anal.* calcd. for $C_{25}H_{33}O_{13}I$: C 44.93, H 4.97, I 18.98; found: C 44.81, H 4.86, I 19.29.

Formate 3(R = Me; X = OCHO)

The above iodo ester (102 mg; 0.15 mmol) and sodium formate (25 mg; 0.37 mmol) were dissolved together in 3 mL of hexamethylphosphoric triamide and stirred in a stoppered vessel at room temperature for 22 h. The solution was diluted with 60 mL of water and extracted with ether. The extract was washed with brine, dried, and evaporated to dryness. The residue, after recrystallization from ether, yielded **3** (R = Me; X = OCHO) (90 mg; 0.15 mmol) as needles, mp 152–154°C; ir: 5.70, 5.81, 6.13; uv: 230 (3.72); nmr (60 MHz): 2.09 (br.s, 1), 2.75 (br.s, 1), 4.4–5.25 (complex; 8), 5.6–6.3 (complex; 5), 6.33 (s, 3), 7.2–7.5 (complex; 2), 7.93 (s, 3), 8.00 (s, 3), 8.03 (s, 3), 8.10 (s, 3), 8.0–8.2 (complex; 2). *Anal.* calcd. for $C_{26}H_{34}O_{15}$: C 53.24, H 5.84; found: C 53.15, H 5.85.

Alcohol 3(R = Me; X = OH)

A solution of the above formate (45 mg; 0.075 mmol) in 3 mL of 1:1 methanol–tetrahydrofuran was refluxed for 1 week. Extraction with chloroform with standard work-up provided the alcohol **3** (R = Me; X = OH) as a residue (39 mg; 0.07 mmol) which after recrystallization from ether formed needles, mp 120–121°C; ir: 2.87 (broad), 5.70, 5.88, 6.13; uv: 233 (3.99); nmr (60 MHz): 2.70 (br.s, 1); 4.4–5.2 (complex; 8), 5.65–5.75 (complex; 2), 6.28 (s, 3), 6.3–6.6 (complex; 3), 7.1–7.7 (complex; 3), 7.97 (s, 3), 8.00 (s, 3), 8.02 (s, 3), 8.04 (s, 3), 8.1–8.4 (complex; 2). *Anal.* calcd. for $C_{25}H_{34}O_{14}$: C 53.76, H 6.14; found: C 53.77, H 6.16.

*Secologanin Tetraacetate 1*b

A solution of the above alcohol (125 mg; 0.224 mmol) in 11 mL of freshly distilled methylene chloride was transferred into a septum-capped flask that contained pyridinium chlorochromate (193 mg; 0.895 mmol), sodium acetate (15 mg; 0.179 mmol), and 1.1 g of Celite under argon (4). The reaction mixture was stirred at room temperature for 1 h, the solvent was pumped off, and the powder that remained was loaded onto a column of silica gel (15 g) and eluted with ether. Early fractions provided **1***b* (99 mg; 0.178 mmol) identical in the behavior, and ir, uv, and nmr spectroscopic characteristics with a sample prepared by acetylation of secologanin. Later fractions afforded sweroside tetraacetate (15 mg; 0.029 mmol).

*Secologanin 1*a

A solution of tetraacetate **1***b* (31 mg) in 5 mL of methanol was stirred with 240 mg of Amberlite 1R 120(H) ion exchange resin for 14 h at room temperature. The mixture was filtered, and the filtrate was stirred with 9 mg of potassium carbonate for 0.5 h at room temperature. The mixture was filtered, the filtrate was evaporated to dryness under reduced pressure, and the residue remaining was dissolved in a mixture of 1 mL of water and 4 mL of tetrahydrofuran to which 45 mg of concentrated hydrochloric acid was added. After 2 h, solid sodium hydrogen carbonate was added to neutralize the acid, and the mixture was stirred and then filtered. Removal of the solvent left secologanin as a residue; the conversion was essentially quantitative.

Acknowledgement

The financial support of the Natural Sciences and Engineering Research Council of Canada is gratefully acknowledged.

1. I. Souzu and H. Mitsuhashi. Tetrahedron Lett. 191 (1970).
2. M. E. Jung and M. A. Lyster. J. Am. Chem. Soc. **99**, 968 (1977).
3. E. J. Corey and J. W. Suggs. Tetrahedron Lett. 2647 (1975).
4. P. A. Grieco, E. Williams, and T. Sugahara. J. Org. Chem. **44**, 2194 (1979).

Stability of the 1,4-bis(2′-haloethyl)-1,4-diazabicyclo[2.2.1]heptane dication[1]

GEORGE R. PETTIT,[2] DONALD P. GIESCHEN, WILLIAM E. PETTIT, AND THOMAS E. RAWSON
Cancer Research Institute and Department of Chemistry, Arizona State University, Tempe, AZ 85281, U.S.A.

Received May 21, 1980

GEORGE R. PETTIT, DONALD P. GIESCHEN, WILLIAM E. PETTIT, and THOMAS E. RAWSON. Can. J. Chem. **59**, 217 (1981).

Certain derivatives of the 1,4-bis(2′-haloethyl)-1,4-diazabicyclo[2.2.1]heptane dication system ranging from dibromide **2***b* to ethanesulfonate **2***g* were found to be quite stable under essentially neutral conditions. A very convenient synthesis of 1,4-bis(2′-chloroethyl)-1,4-diazabicyclo [2.2.1]heptane dichloride (**2***d*) was developed in order to compare the relative stability of this system with that of dibromide **2***b*. While dichloride **2***d* was found to be less stable than dibromide **2***b*, it did prove very useful for rapid preparation of other anion derivatives such as dinitrate **2***e*, dihydrogen dimaleate **2***h*, diperiodate **2***i*, tetrachloroplatinate **2***j*, and tetrachloroaurate **2***k*. *At temperatures near 150°C, or upon ignition (in the open) or gentle shock, diperiodate* **2***i detonated violently*. The ethanesulfonate **2***g* was obtained from diperchlorate **2***a* employing an ion-exchange procedure. Stabilization of dication **2** provides an unusual heterocyclic system with exceptional anticancer properties.

GEORGE R. PETTIT, DONALD P. GIESCHEN, WILLIAM E. PETTIT et THOMAS E. RAWSON. Can. J. Chem. **59**, 217 (1981).

On a trouvé que certains dérivés du système dication bis(halo-2′ éthyl)-1,4 diaza-1,4 bicyclo[2.2.1] heptane allant du dibromure **2***b* à l'éthane sulfonate **2***g* sont tout à fait stables dans des conditions essentiellement neutres. On a mis au point une synthèse très pratique du dichlorure du bis(chloro-2′ éthyl)-1,4 diaza-1,4 bicyclo[2.2.1]heptane (**2***d*) dans le but de comparer la stabilité relative de ce système à celle du dibromure **2***b*. Bien que le dichlorure **2***d* soit moins stable que le dibromure **2***b*, il s'est révélé très utile pour une préparation rapide d'autres anions tels le dinitrate **2***e*, le dimaléate **2***h*, le diperiodate **2***i*, le tétrachloroplatinate **2***j* et le tétrachloroaurate **2***k*. *A des températures voisines de 150°C ou par allumage (à l'air libre) ou par un léger choc, le diperiodate* **2***i détonne violemment*. On a obtenu l'éthanesulfonate, **2***g*, à partir du diperchlorate, **2***a*, en utilisant un procédé d'échange d'ions. La stabilisation du dication **2** fournit un système hétérocyclique inhabituel qui a des propriétés anticancérigènes exceptionnelles.
[Traduit par le journal]

The unusual 1,4-diazabicyclo[2.2.1]heptane dication represents a chemically and theoretically interesting heterocyclic system. The methylene bridge carbon forms a relatively strained (96.8°) N—C—N bond and is derived from formaldehyde. Due to just these properties a substantial degree of reactivity can be anticipated. In 1964 we summarized discovery and preliminary antineoplastic activity of the 1,4-bis(2′-haloethyl)-1,4-diazabicyclo[2.2.1] heptane dication (2). Subsequently, detailed chemical (3*a*–*c*), structural (3*a*, 4), and biological (3*d*) studies of this novel ring system were described. The crystal structure of diperchlorate **2***a* was unequivocally confirmed by X-ray crystallographic analysis (4). Because of the broad spectrum anticancer properties displayed by 1,4-bis(2′-chloroethyl)-1,4-diazabicyclo[2.2.1]heptane diperchlorate (**1***a* → **2***a*) an evaluation of some selected anion derivatives was undertaken (3*d*). Since the methylene bridge carbon–nitrogen bond was found very susceptible to nucleophilic attack, preparation of salts derived from anions such as acetate was precluded. In contrast to the reaction of *N*,*N*-bis(2-chloroethyl)amine with formalin where the product required isolation as the diperchlorate derivative (**2***a*), the analogous diaminomethane formation and intramolecular cyclization (5) (**1***b* → **2***b*) with *N*,*N*-bis(2-bromoethyl)amine caused rapid separation of dibromide **2***b* from the reaction mixture and greatly simplified isolation. Interest in both the stability of dibromide **2***b* and in the preparation of other halide salts for biological evaluation led us to reexamine the structure and

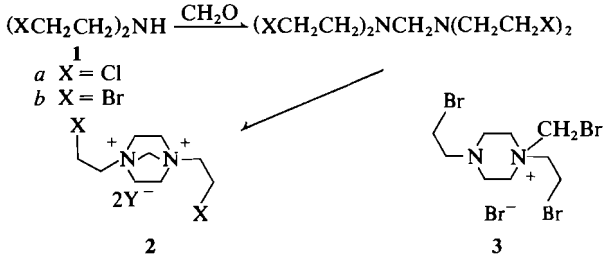

a X = Cl, Y = ClO_4^-
b X = Br, Y = Br^-
c X = Br, Y = ClO_4^-
d X = Cl, Y = Cl^-
e X = Cl, Y = NO_3^-
f X = Cl, Y = F^-
g X = Cl, Y = $CH_3CH_2SO_3^-$
h X = Cl, Y = CO_2^-, CO_2H
i X = Cl, Y = IO_4^-
j X = Cl, Y = $PtCl_4^{-2}/2$
k X = Cl, Y = $AuCl_4^-$

[1]Antineoplastic Agents 66. For previous contribution see ref. 1.

[2]Author to whom correspondence should be addressed.

0008-4042/81/020217-05$01.00/0
©1981 National Research Council of Canada/Conseil national de recherches du Canada

Can. J. Chem. Downloaded from www.nrcresearchpress.com by 210.87.254.5 on 09/05/12
For personal use only.

Can. J. Chem. Downloaded from www.nrcresearchpress.com by 210.87.254.5 on 09/05/12
For personal use only.

stability of this substance, particularly in respect to intramolecular attack by bromide ion yielding an isomer such as **3**.

A specimen of dibromide **2***b* prepared in our laboratories approximately 16 years ago and stored at ambient temperatures was compared with a freshly prepared sample by potentiometric titration for bromide content and spectral techniques. The potentiometric titration established the presence of two bromide ions in each set of samples and the infrared spectra were identical. The ^{1}H and ^{13}C nmr spectra showed the expected methylene bridge protons and carbon at 5.64 and 82.8 δ respectively. Any remaining uncertainty about structure **2***b* was removed by observing the single natural abundance (6) ^{15}N nmr signal exhibited by both old and new specimens at −294 ppm. The preceding experiments established the reasonable stability of dibromide **2***b* under essentially neutral conditions and treatment with perchloric acid readily gave another useful derivative, diperchlorate **2***c*.

Establishment of the structure and stability behavior of dibromide **2***b* encouraged further efforts on the isolation of dichloride **2***d*. The amine **1***a* → **2***d* transformation was reexamined and eventually it was found that dichloride **2***d* could be selectively precipitated from the ethanol–water reaction mixture by employing 1,2-dimethoxyethane. By this means 54% yields of dichloride **2***d* were realized.[3] But interestingly, this halide derivative proved to be less stable than dibromide **2***b*. Dichloride **2***d* proved fairly unstable thermally and began to decompose (turn a straw color to brown) at temperatures above 60°C, while dibromide **2***b* appeared stable to ca. 160°C. Also, heating the dichloride (**2***d*) in refluxing ethanol for 6 h resulted in extensive degradation to *N*,*N*′-bis(2′-chloroethyl)piperazine hydrochloride. After similar treatment the corresponding diperchlorate (**2***a*) was recovered virtually unchanged.

Fortunately dichloride **2***d* did seem stable enough to serve as a very convenient intermediate for preparation of more useful derivatives. Our previous study (**3***d*) indicated that stabilization of dication **2** requires an anion of limited nucleophilicity. An anion corresponding to an acid with pK_a 2 or less seemed most desirable. Further evidence for this observation and its limitation with certain halide acids was provided by the following experiments. Reactions of silver nitrate or silver fluoride with a solution of dichloride **2***d* easily provided dinitrate **2***e* or difluoride **2***f*. Interestingly difluoride **2***f* proved to be very unstable, resisted purification and suggested a very real decrease in stability for the series bromide > chloride > fluoride. Therefore the sterically much larger iodide as anion should be superior to bromide ion and this possibility will be explored in the future. When the present evaluation of dication **2** stability was in progress a number of other possible anion derivatives seemed more attractive and the useful results uncovered will now be reviewed.

Dinitrate **2***e*, as predicted, proved to be quite stable and was routinely prepared as just described or by ion-exchange methods (3*d*) using diperchlorate **2***a*. With acids yielding silver salts of very limited solubility such as ethanesulfonic acid the latter ion-exchange procedure was best and the stable diethanesulfonate **2***g* was obtained in high yield. Except for eliminating trace amounts of silver from the product the reaction of dichloride **2***d* with a soluble silver salt was most simply performed. By this means reaction of dichloride **2***d* with silver hydrogen maleate provided an alternative (3*d*) synthesis of dihydrogen dimaleate **2***h*.

As soon as dichloride **2***d* became readily available many other potentially convenient and simple reactions leading to stabilization of dication **2** became practical. Illustrative was the facile preparation of diperiodate **2***i* and tetrachloroplatinate **2***j* using aqueous solutions of the dichloride (**2***d*) with sodium *meta*-periodate and chloroplatinic acid. The low thermal and shock stability of diperiodate **2***i* was surprising. *At temperatures approaching 150°C the diperiodate (***2***i) violently detonates*. The same result was obtained by gentle striking on a metal surface. Diperiodate **2***i* appears to be a potentially useful explosive and/or propellant.

The property of certain platinum–nitrogen bonded square planar complexes to inhibit tumor growth is well known (7).[4] Presumably the antineoplastic activity of such substances is due to DNA–platinum coordination. Since even gold chloride ($HAuCl_4$) forms a DNA complex (8) a selection of gold compounds should be evaluated (see also ref. 9). Here, for a beginning, tetrachloroaurate **2***k* was prepared from chloroauric acid trihydrate and dichloride **2***d* in hydrochloric acid.

Both dibromide **2***b* (102% life extension at 100 mg/kg) and tetrachloroplatinate **2***j* (87% life

[3]Dichloride **2***d* (melting at 174°C) was originally prepared in 4% yield by treating *N*,*N*,*N*′,*N*-tetrakis(2-chloroethyl)diaminomethane with diethyl ether (3*c*).

[4]The tetrachloroplatinate (**2***j*) was of special interest as a potentially useful cancer chemotherapeutic drug. Rationale was based on the observation that *cis*-platinum II diamine dichloride (the well-known platinum square planar coordination compound earlier found to have antibiotic effects) is now finding application in human cancer treatment, especially for testicular carcinoma.

Can. J. Chem. Downloaded from www.nrcresearchpress.com by 210.87.254.5 on 09/05/12
For personal use only.

extension at 50 mg/kg) were found to markedly inhibit growth of the National Cancer Institute's murine P388 lymphocytic leukemia (3*d*). The other derivatives of dication **2** reported herein are presently being evaluated.

Experimental

All solvents including water were redistilled (through glass). Melting points (capillary tube, oil bath) are uncorrected. Solvent extracts of aqueous solutions were dried over anhydrous magnesium sulfate. The infrared spectra were observed (Perkin-Elmer 299 Spectrophotometer) in potassium bromide and reported as ν_{max} in cm^{-1}. Nuclear magnetic resonance spectra were determined as follows: ^1H nmr (in ppm, δ) with respect to internal tetramethylsilane or sodium 2,2-dimethyl-2-silapentane-5-sulfonate using a Varian Associates T-60A or XL-100; ^{13}C nmr (at 22.6 MHz using a Bruker WH-90 nmr spectrometer) in ppm downfield from internal tetramethylsilane or, if observed in deuterium oxide solution, *p*-dioxane (67.4 ppm) was used as internal reference and chemical shifts were recalculated with respect to tetramethylsilane; and ^{15}N nmr in water with a 1 *M* solution of sodium nitrate (nitrogen-15) in deuterium oxide as external reference employing the same Bruker instrument. Unless otherwise noted the nmr spectra were determined in deuterium oxide solution. The potentiometric titrations were conducted using a digital millivoltmeter and Hewlett-Packard plotter to record volume vs. emf data. Element composition analyses were determined in the Spang Microanalytical Laboratory, Eagle Harbor, MI or the Mikroanalytisches Laboratorium, Fritz-Pregl-Strasse 14–16, West Germany.

1,4-Bis(2'-bromoethyl)-1,4-diazabicyclo[2.2.1]heptane Dibromide (2b)

Procedure A

The method we previously described (3*b* and *d*) was further developed (cf. **2***a*) and applied to the preparation of dibromide **2***b*. Immediately upon removal (rotary evaporation ice-bath) of solvent from the colorless oily *N,N*-bis(2-bromoethyl)amine (10, 11) (*caution, unstable and can vigorously decompose*) it was dissolved in absolute ethanol–formalin (37%).

Procedure B

To a solution of *N*-bis(2-bromoethyl)amine hydrochloride (**1***b*, ref. 10) (50.0 g) in 95% ethanol (300 mL) was added a solution prepared from water (45 mL), potassium hydroxide (10.7 g), and 95% ethanol (150 mL). The precipitate of potassium chloride was collected and 37% formalin (50 mL) was added to the filtrate. After remaining at room temperature overnight dibromide **2***b* (18.3 g) was collected. Addition of 70% perchloric acid (27 mL) to the reaction mixture filtrate and removal of the crystalline product 2 h later afforded 11.6 g of diperchlorate **2***c* (see below). By this means conversion of starting amine **1***b* to dibromide **2***b* and diperchlorate **2***c* amounted to 66% overall. Recrystallization from water–ethanol gave colorless plates of the monohydrate decomposing at 178.5–179.5°C as previously noted (3*b*); ir: 3600–3400, 3080–2980, 1460, 1370, 1120, 890, 660 (C—Br); ^1H nmr: 5.64 (s, 2H), 4.44 (s, 8H), 4.5–4.3 (t, 4H), 4.0–3.8 (t, 4H); ^{13}C nmr: 82.8, 60.0, 59.6, 59.4, 37.6, 22.8; and ^{15}N nmr δ: −294.6.[5] A specimen of dibromide **2***b* prepared 16 years earlier again showed only a single signal at −294.7 in the nitrogen-15 nmr spectrum.

A freshly prepared specimen of dibromide **2***b* and another sample prepared approximately 16 years earlier were found identical by spectral (ir and nmr) comparisons and by results of potentiometric titration experiments assessing bromide ion content. A 0.106 *M* solution of silver nitrate was employed to titrate, a 0.3531 g sample of the 1962 preparation of dibromide **2***b* and a 0.4370 g sample of the freshly prepared counterpart. The former specimen required 14.7 mL (14.8 calcd.) of silver nitrate solution and the latter required 17.8 mL (18.3 calcd.). Each set of titration curves (electrode/potential vs. calomel electrode) confirmed the presence of 2 bromide ions in each sample.

Three recrystallizations from 0.5% aqueous perchloric acid (recrystallization from water appeared to cause partial hydrolysis of the side chain carbon–bromine bond) afforded a pure specimen of *1,4-bis(2-bromoethyl)-1,4-diazabicyclo[2.2.1]-heptane diperchlorate* (**2***c*) as colorless prisms decomposing at 175–176°C; ir: 3080–2980, 1460, 1370, 1220–950 (ClO_4^-), 660 (C—Br); ^1H nmr: 5.65 (s, 2H), 4.5 (s, 8H), 4.5–4.3 (t, 4H), 4.1–3.9 (t, 4H); ^{13}C nmr (acetonitrile): 82.6, 60.0, 59.7, 59.2, 37.8, 22.7.[5] *Anal.* calcd. for $C_9H_{18}Br_2Cl_2N_2O_8$: C 21.07, H 3.54, Br 31.16, Cl 13.83, N 5.46; found: C 20.91, H 3.85, Br 31.12, Cl 13.75, N 5.39.

1,4-Bis(2'-chloroethyl)-1,4-diazabicyclo[2.2.1]heptane Dichloride (2d)

In a typical experiment 300 mL of 1,2-dimethoxyethane (glyme) was added to the reaction mixture resulting from condensation of *N*-bis(2-chloroethyl)amine (from 7.14 g of the hydrochloride) and 37% formalin (75 mL) in ethanol (125 mL) at room temperature for 24 h. Application of diglyme for this purpose also proved very useful. Upon cooling 32.0 g (54%) of dichloride **2***d* was collected and recrystallized from 10:3 ethanol–methanol to afford 18.6 g decomposing at 169–171°C; ir: 3060–2880, 1472, 1448–1436, 1118, 882, 670–668; ^1H nmr: 4.16–4.41 (m, 8H), 4.46 (s, 8H), 5.68 (s, 2H); ^{13}C nmr: 37.56 (—CH_2CH_2Cl), 59.63 (ring —CH_2CH_2—), 59.96 (—CH_2-CH_2Cl), 83.10 (ring —CH_2—).

After prolonged drying periods dichloride **2***d* was still found to retain some water. The following calculated elemental compositions were based on the results of careful Karl Fischer water determinations. *Anal.* calcd. for $C_9H_{18}Cl_4N_2 \cdot 0.31\ H_2O$: C 35.75, H 6.23, Cl 46.90; found: C 35.74, H 6.03, Cl 46.85, H_2O 2.09 (analytical specimen dried for 4 h at room temperature and at 0.1 Torr).

Anal. calcd. for $C_9H_{18}Cl_4N_2 \cdot 0.21\ H_2O$: C 36.05, H 6.19, Cl 47.29; found: C 36.10, H 6.03, Cl 47.05, H_2O 1.27 (analytical sample dried to constant weight at room temperature and at 0.1 Torr).

Substitution of tetrahydrofuran for glyme in this experiment caused separation of dichloride **2***d* as an oil that required separate crystallization from ethanol.

Stability of the 1,4-Bis(2'-chloroethyl)-1,4-diazabicyclo-[2.2.1] heptane Cation in Refluxing Ethanol–Water

Procedure A (With Dichloride 2d)

A solution of dichloride **2***d* (1.0 g) in 99% ethanol–water (25 mL) was heated at reflux for 6 h. Upon cooling 0.7 g of colorless crystalline material separated from the reaction mixture and was identified as *N,N'*-bis(2'-chloroethyl)piperazine hydrochloride by spectral comparison (ir and ^1H nmr) with an authentic sample

Procedure B (With Diperchlorate 2a)

A solution of diperchlorate **2***a* (1.0 g) in 83% ethanol–water (31 mL) was heated at reflux for 5.5 h. Upon cooling, 0.4 g of crystalline diperchlorate **2***a* separated from the reaction mixture. The filtrate was concentrated *in vacuo* and the residue was found to be mostly unchanged perchlorate **2***a*.

1,4-Bis(2-Chloroethyl)-1,4-diazabicyclo[2.2.1]heptane Dinitrate (2e)

Procedure A

Dichloride **2***d* (3.1 g) was dissolved in water (20 mL) and 10 mL (21 mmol) of 2.1 *M* aqueous silver nitrate was added. The

Can. J. Chem. Downloaded from www.nrcresearchpress.com by 210.87.254.5 on 09/05/12
For personal use only.

mixture was diluted to 150 mL with water and the solution was filtered through sintered glass and lyophilized to yield 3.3 g of colorless solid dinitrate **2***e*. Due to traces of silver impurities the product rapidly (ca. 1 h) darkened. Four recrystallizations from absolute methanol (sintered glass filtration) afforded colorless needles decomposing at 149–150°C (rapid heating).

Procedure B

Amberlite IRA-400 (170 mL, chloride form, ca. 2-fold excess) was placed in a chromatography column and converted to the resin hydroxide by washing with 8 L of 1 *N* sodium hydroxide. Excess sodium hydroxide was removed by elution with water and the resin was converted to the IRA-400 nitrate by elution with 400 mL of 1 *N* nitric acid. Excess nitric acid was removed with water until the eluate was neutral to Hydrion pH paper. A 1 L water solution of 1,4-bis(2′-chloroethyl)-1,4-diazabicyclo-[2.2.1]heptane diperchlorate (**2***a*, 21.2 g, 50 mmol) was passed slowly over the resin. Lyophilization of the resulting eluate afforded 16.2 g (93%) of dinitrate **2***e*. Three recrystallizations from methanol provided an analytical specimen decomposing at 149–150°C (rapid heating); ir: 3020 (H_2O), 2990, 1475, 1445, 1385, 1125, 895 (NO_3^-); ^1H nmr: 4.27–4.38 (m, 8H), 4.52 (s, 8H), 5.70 (s, 2H). *Anal.* calcd. for $C_9H_{18}N_4Cl_2O_6$: C 30.96, H 5.20, N 16.05, Cl 20.31, O 27.49; found: C 31.06, H 5.19, N 16.12, Cl 20.26, O 27.37.

Upon ignition (Bunsen burner flame) dinitrate **2***e* burned rapidly but not violently.

Decomposition of the 1,4-Bis(2′-chloroethyl)-1,4-diazabicyclo-[2.2.1]heptane Cation by Fluoride Ion

The hydroxide form of Amberlite IRA-400 (170 mL) was prepared as described above (Procedure B). The resin was converted to the fluoride form by transferring from the chromatography column to a plastic beaker and treating (twice) with 1 *N* hydrofluoric acid (250 mL). The resin fluoride was washed three times with water (250 mL), returned to the chromatography column, and washed with additional water (1 L). The column eluate at this stage was still acidic (ca. pH 3 using Hydrion pH paper). A solution of diperchlorate **2***a* (21.2 g, 0.05 mol) in 1 L of water was passed through the resin column. The resin was washed with additional water (200 mL) and both eluates were combined and lyophilized. The difluoride (**2***f*) remained colorless until lyophilization was nearly complete whereupon it darkened to an orange-brown tar-like mixture.

1,4-Bis(2′-chloroethyl)-1,4-diazabicyclo[2.2.1]heptane Diethanesulfonate (2g)

After conversion of Amberlite IRA-400 (170 mL chloride form) to the hydroxide form (cf. procedure B above) the resin was further converted to the ethanesulfonate form by elution with 1 *N* ethane sulfonic acid (300 mL). The resin was washed with water (400 mL) until a neutral (Hydrion pH paper) eluate was obtained. A solution of the diperchlorate **2***a* (10.6 g) in water (500 mL) was passed over the resin followed by 100 mL of water. The combined eluates were collected and lyophilized to yield colorless crystals. After dissolution in hot ethanol (15 mL) and reprecipitation by adding acetone 9.4 g (85%) of diethanesulfonate **2***g* were obtained as colorless crystalline plates. Recrystallization from isopropanol afforded a pure specimen: mp 195°C (dec.); ^1H nmr (XL-100) δ: 1.26 (triplet, 6H), 2.90 (quadruplet, 4H), 4.12–4.40 (complex, 8H), 4.46 (singlet, 8H), 5.67 (singlet, 2H). *Anal.* calcd. for $C_{13}H_{28}Cl_2N_2O_6S_2$: C 35.21, H 6.36, Cl 15.99, N 6.32, O 21.65, S 14.46; found: C 35.11, H 6.22, Cl 16.04, N 6.33, O 22.04, S 14.26.

1,4-Bis(2′-chloroethyl)-1,4-diazabicyclo[2.2.1]heptane Dihydrogen Dimaleate (2h)

To a solution of maleic acid (2.32 g, 0.02 mol) in water (10 mL) was added 6.21 mL (0.02 mol) of 3.22 *M* ammonium hydroxide followed by 10.0 mL of 2.10 *M* silver nitrate solution. The colorless silver salt, which precipitated immediately, was collected, washed (twice with cold water and once with acetone), and dried in a vacuum desiccator; yield, 2.85 g. The silver salt was dissolved in 500 mL of hot water and 1.95 g of dichloride **2***d* in water (10 mL) was added. After removal of precipitated silver chloride by filtering the solution through sintered glass, the filtrate was lyophilized to afford 2.68 g (46.0%) of a pinkish-gray solid. By comparison of infrared and proton magnetic resonance spectra the product was found identical with an authentic sample (3*d*).

1,4-Bis(2′-chloroethyl)-1,4-diazabicyclo[2.2.1]heptane Diperiodate (2i)

A solution of dichloride **2***d* (0.49 g), sodium metaperiodate (0.711 g, 0.0033 mol), and 4 mL of water was prepared by warming (steam bath). Upon cooling (ice bath) colorless needles of diperiodate **2***i* formed; yield, 0.56 g (55%). After recrystallization from water, the *diperiodate displayed an explosive decomposition temperature of 150°C and moderate shock sensitivity*; ir: 3040, 3020, 2985, 2970, 1468, 1438, 1360, 1110, 900, 835, and 667; ^1H nmr: 4.25 (4H), 4.33 (4H), 4.47 (8H), and 5.67 (2H). *Anal.* calcd. for $C_9H_{18}Cl_2I_2N_2O_8$: C 17.81, H 2.99, Cl 11.68, I 41.82, N 4.62; found: C 17.86, H 3.16, Cl 11.70, I 41.85, N 4.60.

When a few milligrams of diperiodate **2***i* were placed on an anvil and tapped with a hammer it consistently detonated with a loud report. Also, *when heated and/or ignited (in the open air) the diperiodate detonated with a vigorous report*. Great caution must be exercised when preparing and handling this substance.

1,4-Bis(2′-chloroethyl)-1,4-diazabicyclo[2.2.1]heptane Tetrachloroplatinate (2j)

A 0.7 g calculated amount (0.0017 mol) of potassium tetrachloroplatinate was prepared (12) (alternatively 0.7 g of commercial K_2PtCl_4 in 100 mL of 0.5 *N* hydrochloric acid may be used) by heating 0.82 g (0.0017 mol) of potassium hexachloroplatinate and 0.089 g (0.00085 mol) of hydrazine dihydrochloride in 20 mL of water at 55°C for 2.5 h. The resulting dark red solution was filtered and diluted to 90 mL with 0.5 *N* hydrochloric acid. At this point 0.5 g (0.0017 mol) of dichloride **2***d* was added and the mixture was heated at reflux to afford a light orange solution. Upon filtration (hot) and cooling, light orange needles of the tetrachloroplatinate (**2***j*) separated to yield 0.67 g (71%). Following recrystallization from 0.5 *N* hydrochloric acid the platinate decomposed at 235–243°C (without melting); ir: 3010, 1460, 1420, 1120, 910, and 655; ^1H nmr (dimethylsulfoxide-d_6): 4.27 (2H) and 4.30 (overlapping peaks 16H), and 5.71 (2H). *Anal.* calcd. for $C_9H_{18}Cl_6N_2Pt$: C 19.23, H 3.23, Cl 37.85, Pt 34.71; found: C 19.23, H 3.26, Cl 37.87, Pt 34.65.

1,4-Bis(2′-chloroethyl)-1,4-diazabicyclo[2.2.1]heptane Ditetrachloroaurate (2k)

To a solution of chloroauric acid trihydrate (0.97 g, 2.47 mmol) in 6 *N* hydrochloric acid was added dichloride **2***d* (0.37 g, 1.24 mmol) dissolved in 6 *N* hydrochloric acid. An immediate bright orange precipitate separated. The mixture was heated at reflux until the solid dissolved. The reaction mixture was cooled to room temperature and the orange crystalline product (plates and needles) collected. Yield, 0.58 g (52%); mp 185°C. An analytical specimen was obtained by three recrystallizations from 3 *N* hydrochloric acid; orange needles (mp 177°C (dec.)) and plates (mp 185°C (dec.)): ir: 3140, 2990, 1470, 1448, 1108, 1104, 892, 878, 696, 672; ^1H nmr δ: 4.22 (singlet, 16H) and 5.43 (singlet, 2H). *Anal.* calcd. for $C_9H_{18}Au_2Cl_{10}N_2$: C 11.97, H 2.01, Au 43.64, Cl 39.27, N 3.10; found: C 11.89, H 1.85, Au 43.58, Cl 39.50, N 3.22.

Acknowledgements

This investigation was supported by Grant No. CA-16049-02-06 awarded by the National Cancer Institute, The Department of Health, Education, and Welfare, Mrs. Mary Dell Pritzlaff, the Fannie E. Rippel Foundation, the Olin (Spencer T. and Ann W.) Foundation, Mr. Robert B. Dalton, Mr. Jack Whiteman, the Phoenix Coca Cola Bottling Co., and the Achievement Rewards for College Scientists Foundation, Phoenix Chapter. We gratefully acknowledge this necessary assistance. We wish to thank Drs. D. Gust and J. Witschel, Jr. for providing the nmr spectra.

1. J. POLONSKY, Z. VARON, C. MORETTI, G. R. PETTIT, C. L. HERALD, J. A. RIDEOUT, S. B. SAHA, and H. N. KHASTGIR. J. Nat. Prod. **43**, 503 (1980).
2. G. R. PETTIT and J. A. SETTEPANI. Chem. Ind. London, 1805 (1964).
3. (*a*) G. R. PETTIT, D. C. FESSLER, and J. A. SETTEPANI. J. Org. Chem. **34**, 2978 (1969); (*b*) D. C. FESSLER, G. R. PETTIT, and J. A. SETTEPANI. J. Med. Chem. **12**, 542 (1969); (*c*) H. BÖHME and H. ORTH. Arch. Pharm. **300**, 148 (1967); (*d*) G. R. PETTIT, D. P. GIESCHEN, and W. E. PETTIT. J. Pharm. Sci. **68**, 1539 (1979).
4. D. J. ABRAHAM, R. D. ROSENSTEIN, and G. R. PETTIT. J. Med. Chem. **14**, 1141 (1971).
5. W. SCHULZE. Pharmazie, **30**, 265 (1975).
6. K. L. WILLIAMSON, L. G. PEASE, and J. D. ROBERTS. J. Am. Chem. Soc. **101**, 714 (1979); S. N. Y. FANSO-FREE, G. T. FURST, P. R. SRINIVASAN, R. L. LICHTER, R. B. NELSON, J. A. PANETTA, and G. W. GRIBBLE. J. Am. Chem. Soc. **101**, 1549 (1979); D. H. LIVE, H. R. WYSSBROD, A. J. FISCHMAN, W. C. AGOSTA, C. H. BRADLEY, and D. COWBURN. J. Am. Chem. Soc. **101**, 474 (1979); I. I. SCHUSTER, S. H. DOSS, and J. D. ROBERTS. J. Org. Chem. **43**, 4693 (1978).
7. S. K. CARTER and M. SLAVIK. Cancer Treat. Rev. **3**, 451 (1976); S. K. CARTER. Cancer Chemother. Pharmacol. **1**, 15 (1978); C. T. BAHNER, T. C. PATTERSON, L. M. RIVES, and H. D. HARMON. J. Med. Chem. **22**, 575 (1979); Proceedings of the National Cancer Institute Conference on *cis*-Platinum and Testicular Cancer. Cancer Treat. Rep. **63**, No. 9–10 (1979).
8. V. G. ALBANO, P. L. BELLON, M. MANASSERO, and M. SANSONI. J. Chem. Soc. Chem. Commun. 1210 (1970).
9. R. J. PUDDEPHATT. The chemistry of gold. Monograph 16. Elsevier Scientific Publishing Co., Amsterdam, The Netherlands. 1978. p. 252.
10. G. R. PETTIT, M. R. CHAMBERLAND, D. S. BLONDA, and M. A. VICKERS. Can. J. Chem. **42**, 1699 (1964).
11. G. R. PETTIT, J. A. SETTEPANI, and R. A. HILL. Can. J. Chem. **43**, 1792 (1965).
12. G. B. KAUFFMAN and D. O. COWAN. Inorg. Synth. **7**, 239 (1973).

Can. J. Chem. Downloaded from www.nrcresearchpress.com by 210.87.254.5 on 09/05/12
For personal use only.

Adsorption of *N*-methylacetamide and L-arginine onto apatitic phosphates

J. V. GARCIA-RAMOS AND P. CARMONA
Instituto de Optica, C.S.I.C. Serrano, 121. Madrid-6. Spain
Received May 20, 1980

J. V. GARCIA-RAMOS and P. CARMONA. Can. J. Chem. **59**, 222 (1981).

The adsorption of *N*-methylacetamide and of L-arginine on apatitic phosphates has been studied by infrared spectroscopy. During the initial adsorption, the bands of adsorbed *N*-methylacetamide indicate the presence of the *trans* form attached to surface cations via the carbonyl group. The position of the amide I band is found to give a linear correlation with q/r for apatitic cations (where q is the charge and r the radius of a cation). At higher amounts of adsorbed amide, hydrogen bonding arises either from the self-association of amide molecules or from the binding of these to the surface phosphate anions. L-Arginine can be adsorbed through the groups containing NH bonds or through the carboxyl group. Infrared spectra of calcinated samples as well as the Ca/P ratio determinations point out that a substitution of L-arginine positive ions for surface cations takes place upon adsorption of this amino acid on apatitic calcium phosphate.

J. V. GARCIA-RAMOS et P. CARMONA. Can. J. Chem. **59**, 222 (1981).

On a étudié par la spectroscopie infrarouge l'adsorption de la *N*-méthylacétamide et de la L-arginine sur les phosphates apatitiques. Pendant l'adsorption initiale, les bandes de la *N*-méthylacétamide adsorbée indiquent la présence de la forme *trans* attachée à la surface des cations par l'intermédiaire du groupe carbonyle. On a trouvé que la position de la bande I de l'amide donne une corrélation linéaire avec le rapport q/r des cations apatitiques (où q est la charge et r le rayon du cation). Pour de plus grandes quantités d'amide, il se forme des liaisons hydrogènes soit à partir de l'auto-association des molécules d'amide soit à partir de leur point d'attache à la surface des anions phosphate. La L-arginine peut être adsorbée soit par le biais des groupes contenant les liaisons NH soit au moyen du groupe carboxylique. Les spectres infrarouges d'échantillons calcinés ainsi que les déterminations du rapport Ca/P révèlent qu'il se produit une substitution des ions positifs de la L-arginine à la surface du cation au lieu de l'adsorption de cet acide aminé sur le phosphate de calcium apatitique.

[Traduit par le journal]

Can. J. Chem. Downloaded from www.nrcresearchpress.com by 210.87.254.6 on 09/05/12
For personal use only.

Introduction

Any investigation of conditions governing the formation and prevention of growth of hydroxyapatite is helpful for the treatment of urolithiasis (1). Apatitic calcium phosphate is a constituent of urinary calculi and frequently forms the nuclei of renal stones (2).

It has long been known that the addition of certain compounds to a crystallising medium can influence the growth rate of the crystals. Because renal stones consist predominantly of crystalline materials, prevention and retardation of their formation may be accomplished by the addition of compounds which are adsorbed onto certain crystal faces of some crystalline constituent. Elucidation of the adsorption mechanism of natural macromolecules onto apatitic calcium phosphate is hindered by the complexity of these molecules. In order to gain an insight into the prevention of stone formation, it is necessary to define the conditions that modify the crystal growth of the individual crystalline components. The effort in this work was to develop a model system in which each factor (individually and in combination) can be assessed. This model system overcomes the complexities encountered when a biological system is used as adsorbate where it is difficult to determine or isolate the factors or agents which promote or inhibit the growth of renal stone crystals. Therefore, it seems more convenient to use, as an initial step, smaller molecules with a low number of functional groups (e.g. *N*-methylacetamide, which contains the peptide group, L-arginine which bears a positively charged guanidinium group) as adsorbates.

Although the binding sites of amides for ions have been determined in solution (3) the present paper emphasizes spectroscopic aspects obtained from the adsorption of *N*-methylacetamide and of L-arginine onto apatitic calcium phosphate, with special reference to the form of the adsorbed species and the nature of its bonding to the surface.

Experimental

N-Methylacetamide (NMA) was prepared by Hofmann's procedure (4) and subjected to vacuum distillation (mp 28°C) several times. Its purity was checked by referring to its infrared spectrum. The deuteration of NMA was carried out by isotopic exchange in heavy water. The sample was dried over P_2O_5. This operation was repeated three times in a glovebox until it was concluded by infrared spectroscopy that deuteration was complete. The sample of L-arginine was purchased from Sigma Chemical Co. and was used as such.

The procedures for the preparation of apatitic calcium phosphate (ACP) and the determination of its specific surface have been described in a previous paper (5). Deuterated calcium, strontium, and barium apatite samples were obtained in the same way by using Na_2DPO_4 and $Ca(NO_3)_2$, $Sr(NO_3)_2$, and $Ba(NO_3)_2$ in heavy water solutions (pD = 10).

The adsorption of NMA was done in a glovebox. Finely

0008-4042/81/020222-05$01.00/0
©1981 National Research Council of Canada/Conseil national de recherches du Canada

Can. J. Chem. Downloaded from www.nrcresearchpress.com by 210.87.254.6 on 09/05/12
For personal use only.

ground deuterated ACP on an agate mortar (30 mg) were placed in 0.5 mL of deuterium oxide. A few drops of this suspension were placed on a CaF_2 infrared window which was then dried in a vacuum desiccator over P_2O_5. This CaF_2 crystal containing the dried polycrystalline film of ACP was used as a window of the closed adsorption cell shown in Fig. 1, so that the ACP film was exposed to the vapor of the liquid NMA placed in the bottom of the cell (Fig. 1). The adsorption experiments were carried out this way at 35–37°C, and the infrared spectra were recorded every hour by using another cell containing liquid NMA and the adsorption cell pathlength to compensate for the NMA vapor not adsorbed onto the ACP polycrystalline film.

The procedure to determine the adsorption isotherm of L-arginine was as follows: aqueous solutions of 0.15, 1.50, 3.00, 4.50, and 7.50 m*M* L-arginine at pH 8 were prepared. Each solution (2 mL) was then added to 200 mg of apatitic calcium phosphate in test tubes. These were then placed in a water bath at 37°C for an hour and shaken every 10 min. The tubes were then centrifuged at 5000 g for 10 min and aliquots of supernatant were taken for chemical analysis according to the procedures of Moore and Stein (6) and Spies (7). The amounts adsorbed were obtained as differences between the initial and final amino acid concentrations. The amounts adsorbed per gram of calcium apatite (Q) versus equilibrium concentrations (C) constitute the adsorption isotherms for the amino acid considered.

Infrared spectra of the solid samples were studied using two Perkin-Elmer infrared spectrophotometers, models 457 and 225. Infrared spectra of aqueous solutions and films were recorded on the same instruments using CaF_2 cells with 0.1 mm pathlength.

About 2 g of calcium apatite containing adsorbed L-arginine, and the same weight of pure calcium apatite were heated at 800°C for 2 h. Infrared spectra of the calcinated products, in KBr, were then recorded.

The quantitative determinations of calcium were carried out by means of a double-beam Perkin-Elmer 305B atomic absorption spectrophotometer. Phosphorus was determined by the use of the conventional colorimetric procedures (8).

Results and Discussion

Vibrational spectroscopy has enabled us to identify the specific interactions between the peptide group and ACP by using hydrogen bond methods. According to literature (9), the *N*-methylacetamide molecule is stabilized by the resonance between the two structures

$$CH_3C{=}ONHCH_3 \leftrightarrow CH_3O^-C{=}N^+HCH_3$$

This resonance is affected by the formation of hydrogen bonds and by adsorption of the apatitic surface. We have compared the infrared spectra of this adsorbed substance with those of the liquid amide and in CCl_4 solution, in order to estimate the strength of the bonding between this amide group and apatitic phosphates (Table 1).

The infrared spectrum of a *N*-deuterated NMA liquid sample shows adsorption bands at 2480, 1635, and 1480 cm^{-1} which are observed at 2578, 1688, and 1406 cm^{-1}, respectively, in diluted CCl_4 solution (Table 1). These bands have been assigned to ν(N—D), amide I and amide II modes, respectively.

All these shifts in the frequencies can be explained by the nature of the vibrations as follows: the amide I band mainly arises from the ν(C=O) vibration and the amide II band from the δ(N—D) and ν(C—N) modes (10). Therefore, the frequency decrease of the amide I band indicates the decrease of the double bond character of the C=O bond, and the frequency increase of the amide II band may be explained considering that the N—D bond is fixed through the deuterium atom. In addition, part of the amide II band potential energy comes from the ν(C—N) vibration (10). Therefore, the frequency increase of the amide II band can also arise from the increase of the double bond character of the C—N group. In the same directions relative to this case, band shifts from the NMA spectrum in CCl_4 solution occur when NMA is adsorbed on the apatitic surface, as described below.

Figures 2 and 3 show the infrared spectra from adsorbed *N*-deuterated *N*-methylacetamide on ACP. Figures 2*a* and 3*a* are two background spectra from a dried polycrystalline film of ACP. During adsorption on this phosphate, the first detectable infrared bands (Figs. 2*b* and 3*b*) arise at 2569, 1563, and 1425 cm^{-1} (Table 1). The former can be assigned to the ν(N—D) vibration and its frequency is slightly lower than the one which corresponds to the same mode for this amide in diluted CCl_4 solution, 2578 cm^{-1} (Table 1). The band at 1563 cm^{-1} arises from carbonyl groups attached to the surface, and the 1425 cm^{-1} band can be assigned to the amide II mode, the frequency of which

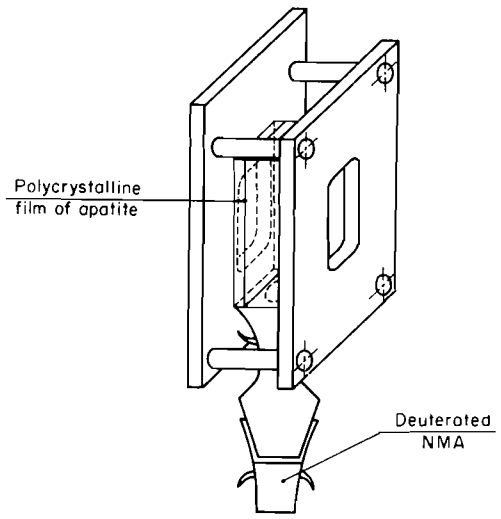

FIG. 1. Adsorption infrared cell.

TABLE 1. Positions of infrared bands of deuterated NMA in CCl_4 solution, in the liquid state and adsorbed on apatitic phosphates

NMA in CCl_4 solution (1.5%)	Liquid NMA	NMA adsorbed on apatitic surfaces*			Assignment
		ACP	ASP	ABP	
2578	2480	2569	2570	2571	ν(N—D)
1688	1635	1563	1568	1571	Amide I
1406	1480	1425	1424	1422	Amide II

*ACP: apatitic calcium phosphate, ASP apatitic strontium phosphate, and ABP apatitic barium phosphate.

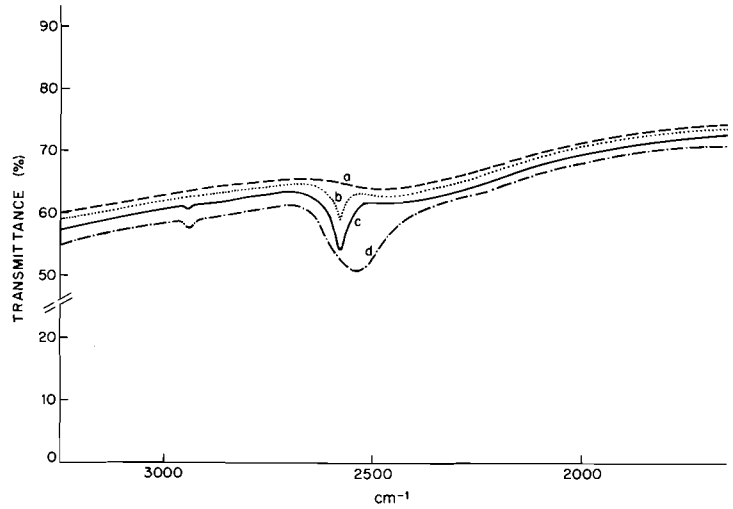

FIG. 2. Infrared spectra (3000–2000 cm^{-1}) of adsorbed *N*-deuterated NMA on ACP. (*a*) ACP; (*b*) after 2 h of adsorption; (*c*) after 5 h of adsorption; (*d*) after 24 h of adsorption.

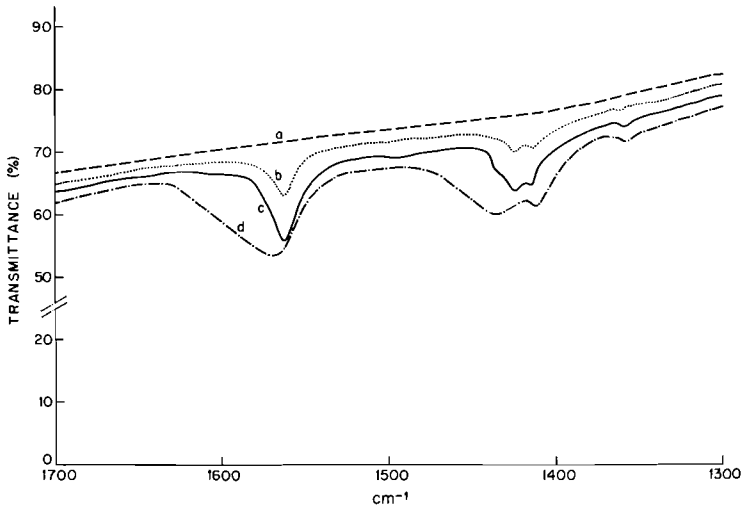

FIG. 3. Infrared spectra (1700–1300 cm^{-1}) of adsorbed *N*-deuterated NMA on ACP. (*a*) ACP; (*b*) after 2 h of adsorption; (*c*) after 5 h of adsorption; (*d*) after 24 h of adsorption.

Can. J. Chem. Downloaded from www.nrcresearchpress.com by 210.87.254.6 on 09/05/12
For personal use only.

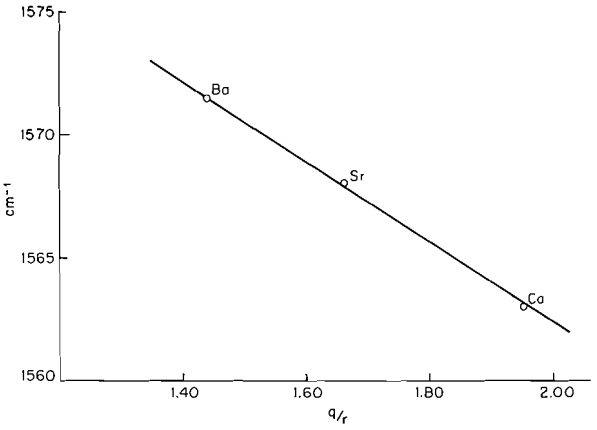

FIG. 4. The position of the amide I band of *N*-deuterated NMA adsorbed on different apatite phosphates as a function of q/r (eau $Å^{-1}$).

being higher than the one which arises from the same mode of *N*-deuterated NMA in the gaseous state (1385 cm^{-1}) (11) and from its isotopic species in CCl_4 solution (1406 cm^{-1}). As described above for liquid NMA, one could think that these band shifts from the NMA spectrum in CCl_4 solution are characteristic of adsorbed molecules being able to find phosphate anions (HPO_4^{2-}) to form hydrogen bonds (e.g. C=O...HPO_4^{2-}). However, the position of the amide I band is found to give a linear correlation with q/r for the apatitic cations (Fig. 4) where q is the cation charge and r its radius as taken from ref. 12, strongly suggesting that the main initial adsorption is at cation sites. In addition, the values for the amide I frequencies indicate that during the initial adsorption, the amide–apatite interactions can be described in terms of strongish ion–dipole binding between the carbonyl group and apatitic cations.

On the other hand, during the first stages of adsorption (Fig. 2*a*, 2*b*) the N—D groups are expected to be free of hydrogen-bonding. In fact, the ν(N—D) band is sharp and appears at a frequency near the corresponding value for the free NMA *trans* form in CCl_4 solution, 2578 cm^{-1} (9) (Table 1). The fact that the ν(N—D) frequency is slightly lower in the first case can be explained by considering that cation binding to the C=O group can increase the acidity of the N—D group (3). These results suggest that the adsorbed molecules probably take the *trans* form. Moreover, the wavenumber of the ν(N—D) vibration of the free *cis* form, 2540 cm^{-1} (9), would not be expected to move toward higher frequencies (2569 cm^{-1}) if adsorption of the NMA molecules had taken place keeping the *cis* conformation on the apatitic surface.

In the 1500–1400 cm^{-1} region, the strongest bands correspond to the amide II and $\delta_s N$ modes (10, 11) and therefore, only these bands are visible around 1420 and 1400 cm^{-1} during the initial adsorption (Fig. 3*b*). When the amount of adsorbate increases (Fig. 3*c*), C—H deformation modes appear at 1455 cm^{-1} these being posteriorly masked by the amide II band (Fig. 3*b*). This figure shows that the amide I and amide II bands become broader, increase in intensity, and shift to higher frequencies, 1610 and 1450 cm^{-1}, respectively. The same can be said for the ν(N—D) vibration, but this one varies in opposite direction, that is, toward lower values (about 2500 cm^{-1}). These changes arise from hydrogen bonding originated either in the self-association of NMA molecules or in the binding of these to the surface phosphate anions. This type of situation may be expected at high coverage due to the reduced availability of sites for cation binding to the carbonyl groups.

Infrared bands of L-arginine were assigned in a previous paper (13). Figure 5 includes the infrared spectrum of this substance adsorbed onto ACP showing a band at 1620 cm^{-1}, due to the ν_{as}(OCO)

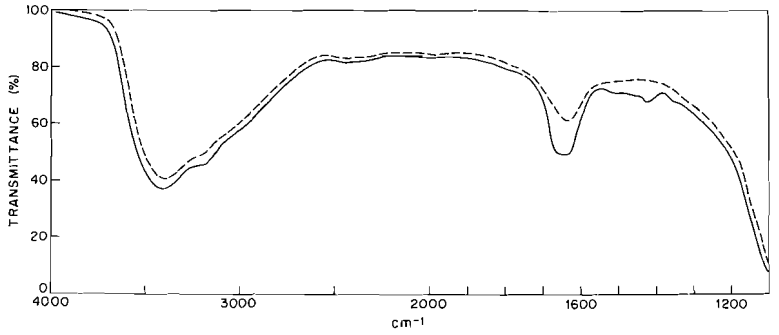

FIG. 5. Infrared spectra of ACP (dashed line) and of adsorbed L-arginine on ACP (full line), in KBr.

Can. J. Chem. Downloaded from www.nrcresearchpress.com by 210.87.254.6 on 09/05/12
For personal use only.

TABLE 2. Adsorption isotherm of L-arginine on ACP

$C_0 \times 10^6$ (mol/mL)	$C \times 10^6$ (mol/mL)	$Q \times 10^6$ (mol/g)	C/Q (g/mL)
1.00	0.74	2.56	0.29
1.50	1.02	4.80	0.21
2.00	1.59	4.10	0.39
2.50	1.93	5.75	0.34
3.00	2.21	7.93	0.28
4.00	2.87	11.13	0.26

vibration, superimposed on the apatitic water deformation band at 1635 cm^{-1}. In addition, the ν(N—H) and δ(N—H) bands appear at 3185 and 1515 cm^{-1}, respectively. The vibrations involving the NH groups in this substance appear at frequencies very near to those of the same modes for this amino acid in the solid state (13), which suggests that L-arginine is hydrogen bonded, via the guanidinium or amino groups, to surface anions on ACP. On the other hand, adsorption of L-arginine resulted in an upward shift of the ν_s(OCO) band (1420 cm^{-1}) with respect to the frequency of the same mode for L-arginine in aqueous solution (1395 cm^{-1}) (13). This occurs upon formation of calcium salts of carboxylic acids (14) where calcium ions are bound to carboxyl groups, and suggests that L-arginine can also bind to surface cations through the carboxyl group.

Table 2 gives the analytical figures used to obtain the adsorption isotherm. A Langmuir-type adsorption model did not fit the experimental results probably due to the fact that L-arginine can bind to ACP surface through several functional groups, as described above. Finally, calcium pyrophosphate is formed on calcination of ACP (15). Since the infrared spectra of calcinated samples show that the amount of pyrophosphate decreases when the adsorbate/adsorbent ratio increases, a substitution of L-arginine positive ions for surface cations will be expected. This is in agreement with the Ca/P ratio determinations showing that this ratio varies in the opposite direction to that of the adsorbate/adsorbent.

1. D. J. SUTOR. Br. J. Urol. **41**, 179 (1969).
2. W. H. BOYCE. Am. J. Med. **45**, 673 (1968).
3. C. DE LOZE, M. H. BARON, and F. FILLAUX. J. Chim. Phys. **75**, 631 (1978).
4. W. H. HOFMANN. W. Ber. W. Dent. W. Chem. Ges. **14**, 2730 (1881).
5. P. CARMONA, J. V. GARCIA-RAMOS, P. F. GONZALES-DIAZ, L. CIFUENTES-DELATTE, and A. HIDALGO. Pathogenese und Klinik der Harnsteine VI. *Edited by* W. Vahlensieck and G. Gasser. Dr. Dietrich Steinkopff Verlag. Darmstadt. 1978. p. 77.
6. S. MOORE and W. H. STEIN. J. Biol. Chem. **176**, 367 (1948).
7. J. R. SPIES. Methods in enzymology. Vol. III. *Edited by* S. Colowich and N. Kaplan. Academic Press, New York and London. 1951.
8. C. K. FISKE and J. SUBBAROW. J. Biol. Chem. **66**, 375 (1925).
9. J. SMOLIKOVA, A. VITEK, and K. BLAHA. Collect. Czech. Chem. Commun. **38**, 548 (1973).
10. M. REY-LAFONT, M. T. FOKEL, and C. GARRIGOU-LAGRANGE. Spectrochim. Acta, **29A**, 471 (1973).
11. T. MIYAZAWA, T. SHIMANOUCHI, and S. MIZUSHIMA. J. Chem. Phys. **24**, 408 (1956).
12. Handbook of chemistry and physics. 49th ed. C.R.C. Press, Cleveland, OH. 1968–1969.
13. J. V. GARCIA-RAMOS and P. CARMONA. Opt. Pur. Appl. **13**, 35 (1980).
14. R. A. PECKAUSKAS, J. D. TERMINE, and I. PULLMAN. Biopolymers, **15**, 569 (1976).
15. P. F. GONZALEZ-DIAZ, J. V. GARCIA-RAMOS, and M. SANTOS. Calcif. Tissue Int. **28**, 215 (1979).

Can. J. Chem. Downloaded from www.nrcresearchpress.com by 210.87.254.6 on 09/05/12
For personal use only.

The addition of simple aromatic hydrocarbons to condensed aromatic thiophenes promoted by aluminum chloride. Part I. Naphtho[2,1-*b*]thiophene

PETER DAVID CLARK AND DAVID M. MCKINNON

Department of Chemistry, The University of Manitoba, Winnipeg, Man., Canada R3T 2N2

Received August 5, 1980

PETER DAVID CLARK and DAVID M. MCKINNON. Can. J. Chem. **59**, 227 (1981).

Naphtho[2,1-*b*]thiophene undergoes addition of aromatic hydrocarbons across the 1,2-bond in the presence of aluminum chloride. At 20°C 1-aryl-1,2-dihydronaphtho[2,1-*b*]thiophenes are the major products and at higher temperatures 2-arylnaphtho[2,1-*b*]thiophenes result. 1-Arylnaphtho[2,1-*b*]thiophenes may be prepared by treatment of the dihydro-addition products with 2,3-dichloro-5,6-dicyano-1,4-benzoquinone thus giving a new synthesis of 1- and 2-arylnaphtho[2,1-*b*]thiophenes from the parent heterocycle.

PETER DAVID CLARK et DAVID M. MCKINNON. Can. J. Chem. **59**, 227 (1981).

En présence de chlorure d'aluminium, les hydrocarbures aromatiques s'additionnent au naphto[2,1-*b*]thiopène à travers la double liaison en 1,2. A 20°C, les aryl-1 dihydro-1,2 naphto[2,1-*b*]thiones sont les produits principaux et, à des températures plus élevées, il se forme des aryl-2 naphto[2,1-*b*]thiophènes. Les aryl-1 naphto[2,1-*b*]thiopènes peuvent être préparés par une réaction entre les produits d'addition dihydro et la dichloro-2,3 dicyano-5,6 benzoquinone-1,4; on a ainsi développé une nouvelle synthèse des aryl-1 et aryl-2 naphto[2,1-*b*]thiopènes à partir de l'hétérocycle apparenté.

[Traduit par le journal]

Can. J. Chem. Downloaded from www.nrcresearchpress.com by 210.87.254.5 on 09/05/12
For personal use only.

Introduction

To date, only one synthesis of 1- and 2-arylnaphtho[2,1-*b*]thiophenes (**2***a*, *b*) has been described (1). This method involves the cyclodehydration of suitable (arylnaphthylthio)acetones (**1**) and, while satisfactory, it necessitates the individual preparation of these compounds. Also their cyclodehydration may give unwanted side products (2, 3). In recent work (4) it was shown that simple aromatic hydrocarbons add to the 2- or 3-positions of benzo[*b*]-thiophene (**3***a*) under very mild conditions. Either 2-arylbenzo[*b*]thiophenes (**3***b*) or 3-aryl-2,3-dihydrobenzo[*b*]thiophenes (**4***a*) were obtained by varying the reaction conditions. The dihydro products **4***a* readily dehydrogenated to 3-arylbenzo[*b*]thiophenes (**3***c*) thus giving a synthesis of either 2- or 3-arylbenzo[*b*]thiophenes from the parent heterocycle. In this paper we have investigated the reaction of naphtho[2,1-*b*]thiophene (**2***c*) with some aromatic hydrocarbons in the presence of aluminum chloride with a view to developing a general synthesis of 1- and 2-arylnaphtho[2,1-*b*]thiophenes (**2***a*, *b*).

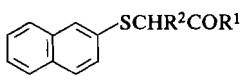

1

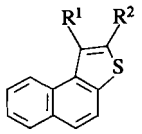

2

a R^1 = Ar, R^2 = H
b R^1 = H, R^2 = Ar
c R^1 = H, R^2 = H
d R^1 = C_6H_5, R^2 = H
e R^1 = H, R^2 = C_6H_5
f R^1 = C_6H_4-4′-Me, R^2 = H
g R^1 = H, R^2 = C_6H_4-4′-Me
h R^1 = C_6H_4-4′-Et, R^2 = H
i R^1 = H, R^2 = C_6H_4-4′-Et
j R^1 = H, R^2 = C_6H_3-3′,4′-$(Me)_2$
k R^1 = C_6H_5CHMe, R^2 = H
l R^1 = H, R^2 = C_6H_5CHMe

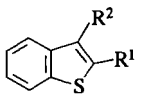

3

a R^1 = R^2 = H
b R^1 = Ar, R^2 = H
c R^1 = H, R^2 = Ar

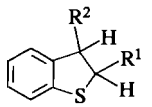

4

a R^1 = H, R^2 = Ar
b R^1 = Ar, R^2 = H

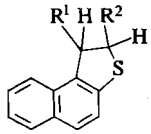

5

a R^1 = R^2 = H
b R^1 = Ar, R^2 = H
c R^1 = H, R^2 = Ar
d R^1 = C_6H_5, R^2 = H
e R^1 = C_6H_4-4′-Me, R^2 = H
f R^1 = C_6H_4-4′-Et, R^2 = H
g R^1 = H, R^2 = C_6H_3-3′,4′-$(Me)_2$
h R^1 = H, R^2 = C_6H_3-2′,5′-$(Me)_2$

Results and Discussion

In a typical experiment naphtho[2,1-*b*]thiophene (**2***c*) was dissolved in excess of an aromatic hydrocarbon, two mol equivalents of aluminum chloride[1] were added, and the reaction mixtures were stirred either at 20°C or heated under reflux. An intense deep red color which always developed on addition of the aluminum chloride dissipated on addition of

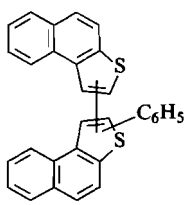

6

[1]The reactions proceed more slowly with one mol equivalent of aluminum chloride.

0008-4042/81/020227-05$01.00/0

©1981 National Research Council of Canada/Conseil national de recherches du Canada

TABLE 1. The reactions of naphtho[2,1-*b*]thiophene with aromatic hydrocarbons and aluminum chloride

Aromatic hydrocarbon	Temp. (°C)	Time (h)	Dihydronaphtho[2,1-*b*] derivatives (**5**) (%) 1-Ar	Dihydronaphtho[2,1-*b*] derivatives (**5**) (%) 2-Ar	Aromatic derivatives (**2**) (%) 2-Ar
Benzene	20	24	88		
	80	24			71
Toluene	20	3	80		
	110	5			48
Ethylbenzene	20	1	76		
	136	3			[a]
1,2-Dimethylbenzene	20	2		35	38
	142	2			41
1,4-Dimethylbenzene	20	7		45	
Anisole	20	4	[b]		
N-Methylaniline	20	24	[c]		

[a]1,2-Dihydronaphtho[2,1-*b*]thiophene (**5***a*) was isolated.
[b]Phenol and polymeric material were isolated.
[c]Naphtho[2,1-*b*]thiophene was recovered.

dilute acid during the isolation of the products. The results of these reactions are summarized in Table 1.

A comparison of the results given in Table 1 with those obtained with benzo[*b*]thiophene (**3***a*) (4) reveals that, in general, the two systems react in a similar fashion. For example, treatment of a solution of naphtho[2,1-*b*]thiophene (**2***c*) in an aromatic hydrocarbon with aluminum chloride at 20°C results in good yields of 1-aryl-1,2-dihydronaphtho[2,1-*b*]-thiophenes (**5***b*). The isolation of these products was relatively simple and their further treatment with 2,3-dichloro-5,6-dicyano-1,4-benzoquinone gave 1-arylnaphtho[2,1-*b*]thiophenes (**2***a*) in excellent yields (Table 4). Nevertheless, not all reactions at 20°C followed the results obtained with benzo[*b*]thiophene (**3***a*). For example, while the reaction of naphtho-[2,1-*b*]thiophene (**2***c*) with benzene gave 1-phenyl-1,2-dihydronaphtho[2,1-*b*]thiophene (**5***d*), under identical conditions benzo[*b*]thiophene (**3***a*) failed to react with benzene and self-addition occurred, resulting in a mixture of 2- and 3-(2′- and 3′-benzo[*b*]thienyl)-2,3-dihydrobenzo[*b*]thiophenes (4). It is significant that the reaction of naphtho[2,1-*b*]thiophene with benzene is very slow compared to other reactions (see Table 1). With benzo[*b*]thiophene the alternative pathway of self-addition is possible, but with naphtho[2,1-*b*]thiophene self-addition does not occur, possibly due to steric factors, and a slow reaction with benzene takes place. An attempt was made to force naphtho[2,1-*b*]thiophene to undergo self-addition by treatment of the solution in dichloromethane with aluminum chloride. Although the reaction mixture turned the usual deep red color no other reaction was apparent on work-up after 12 h. On prolonged reaction all naphtho[2,1-*b*]thiophene was consumed, but only polymeric products were obtained. Nevertheless, a mixture of products as a result of self-addition was isolated from the reaction of naphtho-[2,1-*b*]thiophene with benzene and aluminum chloride at 78°C. Although attempts to elucidate the precise structure of this mixture by hydrodesulfurization were unsuccessful, it is probable that it was a mixture of the compounds **6** (tlc, nmr, and mass spectra).

While the reaction mechanisms suggested (4) for benzo[*b*]thiophene almost certainly apply to naphtho[2,1-*b*]thiophene, Scheme 1 gives a brief outline of these. As was the case for benzo[*b*]thiophene (**3***a*), the formation of the aryl-1,2-dihydronaphtho-[2,1-*b*]thiophenes (**5***b*, *c*) was reversible (Scheme 1) since, when 1,2-dihydro-1-(4′-methylphenyl)naphtho-[2,1-*b*]thiophene (**5***e*) was treated with aluminum chloride in benzene solution at 20°C over 24 h, 1,2-dihydro-1-phenylnaphtho[2,1-*b*]thiophene (**5***d*) was isolated. Interestingly, the reactions of naphtho-[2,1-*b*]thiophene with 1,2- and 1,4-dimethylbenzene at 20°C resulted in reaction at C-2 rather than the usual reaction at C-1. This may be rationalized in terms of steric interference between the methyl groups of the hydrocarbons and the C—H bond at C-9 of the carbonium ion **8** so that products derived from carbonium ion **7** are observed.

Generally, when a mixture of naphtho[2,1-*b*]-thiophene and aluminum chloride in an aromatic hydrocarbon was heated, 2-arylnaphtho[2,1-*b*]thiophenes (**2***b*) were obtained (Table 1). This parallels the results with benzo[*b*]thiophene (4). 1,2-Dihydronaphtho[2,1-*b*]thiophene (**5***a*) was also obtained from the reaction in boiling ethylbenzene and probably results from hydride abstraction from ethylbenzene

Can. J. Chem. Downloaded from www.nrcresearchpress.com by 210.87.254.5 on 09/05/12
For personal use only.

TABLE 2. ^{1}H nuclear magnetic resonance data for aryl-1,2-dihydronaphtho[2,1-*b*]thiophenes (**5**) and their *S*,*S*-dioxide derivatives (**9**)

Ar	Compound	H_A[a]	H_B	H_X (δ ppm)[b]	J_{AB} (Hz)[c]
1-C_6H_5	**5***d*	4.00	3.22	5.12	−11.6
1-C_6H_5	**9***a*	4.10	3.55	5.33	−13.6
1-(C_6H_4-4′-Me)	**5***e*	4.00	3.32	5.16	−11.0
1-(C_6H_4-4′-Me)	**9***b*	4.07	3.60	5.15	−13.5
1-(C_6H_4-4′-Et)	**5***f*	4.02	3.30	5.16	−11.5
1-(C_6H_4-4′-Et)	**9***c*	4.05	3.58	5.14	−13.8
2-(C_6H_3-3′,4′-$(Me)_2$)	**5***g*	4.05	3.60	5.16	−16.0
2-(C_6H_3-3′,4′-$(Me)_2$)	**9***d*	4.10	3.55	4.70	−16.2
2-(C_6H_3-2′,5′-$(Me)_2$)	**5***h*	4.05	3.60	5.40	−16.5
2-(C_6H_3-2′,5′-$(Me)_2$)	**9***e*	4.10	3.70	5.20	−16.3

[a]H_X refers to the proton on the aryl-substituted carbon atom.
[b]All values are ±0.02 ppm.
[c]All values are ±0.2 Hz.

by the carbonium ions, **7** and **8**. Hydride abstractions from 1,2- and 1,4-dimethylbenzene have been observed previously (4, 5).

To summarize, it has been shown that it is possible to prepare either 1- or 2-arylnaphtho[2,1-*b*]thiophenes (**2***a*, *b*) as a result of the addition of aromatic compounds to the parent heterocycle **2***c*. This has given a more versatile synthesis of these compounds, and since naphtho[2,1-*b*]thiophene (**2***c*) shows little tendency for self-addition, it should be possible to extend the method to less reactive benzene derivatives. The method is limited to those benzene derivatives which do not coordinate strongly with aluminum chloride, as reactions with anisole and *N*-methylaniline failed to give addition products.

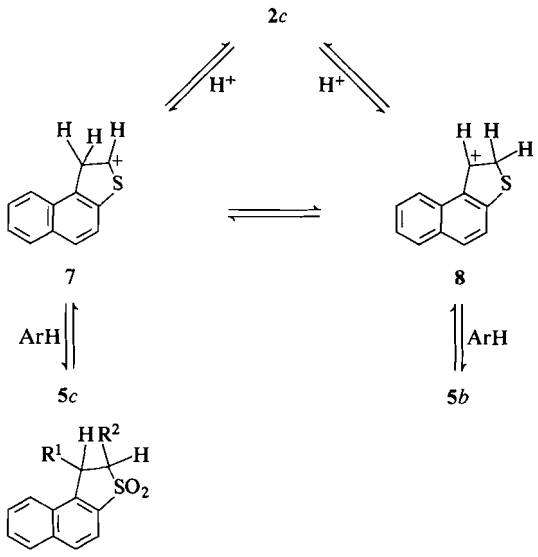

a $R^1 = C_6H_5$, $R^2 = H$
b $R^1 = C_6H_4$-4′-Me, $R^2 = H$
c $R^1 = C_6H_4$-4′-Et, $R^2 = H$
d $R^1 = H$, $R^2 = C_6H_3$-3′,4′-$(Me)_2$
e $R^1 = H$, $R^2 = C_6H_3$-2′,5′-$(Me)_2$

SCHEME 1. Mechanisms for the addition of aromatic compounds to naphtho[2,1-*b*]thiophene.

Product Analysis

Differentiation between 1- and 2-aryl-1,2-dihydronaphtho[2,1-*b*]thiophenes (**5***b*, *c*) was difficult, but could be accomplished by a combination of analysis of ^{1}H nmr signals of the dihydro protons and by desulfurization with Raney nickel. Similar difficulties were experienced during work with 2- and 3-aryl-2,3-dihydrobenzo[*b*]thiophenes (**4***a*, *b*) (4). There it was found that the geminal coupling J_{AB} in **4***b* (−15 Hz) is considerably larger than that in **4***a* (−11 Hz). Also oxidation of **4***b* to its *S*,*S*-dioxide leaves the value of J_{AB} relatively unchanged, while oxidation of **4***a* produces a much bigger change (−2.6 Hz) in J_{AB}. It seemed likely that the values of J_{AB} for the aryldihydronaphtho[2,1-*b*]thiophenes (**5***b*, *c*) should be similar to those for the benzo[*b*]thiophenes and so provide structural information. To test this, several hydrodesulfurizations were carried out (see Experimental) and in each case the spectral assignments were confirmed.[2] The ^{1}H nmr data for the aryldihydronaphtho[2,1-*b*]thiophenes (**5***b*, *c*) and their oxidized derivatives **9** are given in Table 2.

Experimental

The ^{1}H nmr spectra were obtained in deuteriochloroform solution, unless stated otherwise, on a Varian model EM360 spectrometer using tetramethylsilane as an internal standard. Melting points are uncorrected.

*Naphtho[2,1-*b*]thiophene (**2c**)*

This was prepared by the method of Tilak (6) and had mp 114–115°C (lit. (6) mp 114–115°C).

[2]Full characterization of products from Raney nickel hydrodesulfurizations was not carried out since analyses of the ^{1}H nmr spectra gave the necessary structural information.

Can. J. Chem. Downloaded from www.nrcresearchpress.com by 210.87.254.5 on 09/05/12
For personal use only.

Can. J. Chem. Downloaded from www.nrcresearchpress.com by 210.87.254.5 on 09/05/12
For personal use only.

Addition Reactions of Naphtho[2,1-b]thiophene at 20°C to Form 1- and 2-Aryl-1,2-dihydronaphtho[2,1-b]thiophenes (5)

(a) General Procedure

Aluminum chloride (Fisher, technical grade) (2.88 g, 0.020 mol) was added to a solution of naphtho[2,1-*b*]thiophene (2.0 g, 0.010 mol) in the appropriate aromatic hydrocarbon (100 mL). The organic material was isolated by extraction with ethyl acetate. Evaporation of the washed (H_2O) and dried ($MgSO_4$) organic extracts gave the products as oils which either yielded crystalline material from hexane solution or were purified further by chromatography on alumina and elution with hexane – ethyl acetate (20:1).

(b) With Benzene

The oily residue was dissolved in hexane (50 mL) and on keeping this solution at −5°C for 24 h 1,2-dihydro-1-phenylnaphtho[2,1-*b*]thiophene (**5***d*) was deposited as colorless needles (2.52 g, 88%), mp 129–130°C. The nmr spectrum δ: 6.9–7.9 (m, the aromatic protons).[3] The mass spectrum: M^+ 262; calcd.: 262. *Anal.* calcd. for $C_{18}H_{14}S$: C 82.45, H 5.35, S 12.20; found: C 82.05, H 5.30, S 12.15%.

(c) With Toluene

1,2-Dihydro-1-(4′-methylphenyl)naphtho[2,1-*b*]thiophene (**5***e*) was obtained as colorless prisms (2.2 g, 80%), mp 102–103°C from hexane solution. The nmr spectrum δ: 2.23 (s, Me) and 6.9–7.8 (m, the aromatic protons). The mass spectrum: M^+ 276; calcd.: 276. *Anal.* calcd. for $C_{19}H_{16}S$: C 82.60, H 5.80, S 11.60; found: C 82.50, H 5.75, S 11.55%.

The structure of this product was confirmed by hydrodesulfurization with Raney nickel. A mixture of the compound (0.5 g) and Raney nickel (1 g) in 95% aqueous ethanol was heated under reflux for 8 h. The reaction mixture was filtered and the filtrate was evaporated leaving an oily residue. Short path distillation (130°C at 0.2 Torr) of this oil gave 1-(4-methylphenyl)-1-(1′-naphthyl)ethane (92%) as a clear oil (8).[2] The nmr spectrum δ: 1.69 (d, CH—Me), 2.2 (s, Me), 4.88 (q, CH—Me), and 6.95–8.15 (m, the aromatic protons). The mass spectrum: M^+ 246; $C_{19}H_{18}$ requires M 246.

(d) With Ethylbenzene

1,2-Dihydro-1-(4′-ethylphenyl)naphtho[2,1-*b*]thiophene (**5***f*) was obtained as colorless needles (2.4 g, 76%), mp 94–95°C from hexane solution. The nmr spectrum δ: 1.15 (t, Me), 2.65 (q, CH_2), and 6.9–7.9 (m, the aromatic protons). The mass spectrum: M^+ 290; calcd.: 290. *Anal.* calcd. for $C_{20}H_{18}S$: C 82.75, H 6.20, S 11.05; found: C 82.50, H 6.30, S 11.25%.

(e) With 1,2-Dimethylbenzene

The semi-solid product was dissolved in hexane at 20°C and slowly 2-(3′,4′-dimethylphenyl)naphtho[2,1-*b*]thiophene (**2***j*) crystallized out as pale yellow needles (1.2 g, 38%), mp 229–230°C. The nmr spectrum δ: 2.0 (s, 2 Me) and 6.9–8.2 (m, the aromatic protons). The mass spectrum: M^+ 288; calcd.: 288. *Anal.* calcd. for $C_{20}H_{16}S$: C 83.35, H 5.55, S 11.10; found: C 83.50, H 5.45, S 11.25%.

Concentration of the mother liquors and cooling to −5°C gave 1,2-dihydro-2-(3′,4′-dimethylphenyl)naphtho[2,1-*b*]thiophene (**5***g*) (1.1 g, 35%), mp 62–64°C as colorless microcrystals. The nmr spectrum δ: 2.2 (s, 2 Me) and 7.0–8.2 (m, the aromatic protons). The mass spectrum: M^+ 290; calcd.: 290. *Anal.* calcd. for $C_{20}H_{18}S$: C 82.75, H 6.20, S 11.05; found: C 83.0, H 6.20, S 10.95%.

Raney nickel hydrodesulfurization of either of the foregoing products in hot ethanolic solution gave 1-(3′,4′-dimethylphenyl)-2-(1′-naphthyl)ethane as a colorless viscous oil.[2] The nmr spectrum δ: 2.25 (s, 2 Me), 2.7–3.4 (m, CH_2—CH_2), and 7.0–8.3 (m, the aromatic protons). The mass spectrum: M^+ 260; calcd. for $C_{20}H_{20}$: M 260.

(f) With 1,4-Dimethylbenzene

Chromatography of the crude product gave 1,2-dihydro-2-(2′,5′-dimethylphenyl)naphthol[2,1-*b*]thiophene (**5***h*) as a pale yellow oil (1.42 g, 45%).[4] The nmr spectrum δ: 2.28 (s, Me), 2.40 (s, Me), and 7.0–8.1 (m, the aromatic protons). The mass spectrum: M^+ 290; calcd. for $C_{20}H_{18}S$: M 290.

Aryl-1,2-dihydronaphtho[2,1-b]thiophene-S,S-dioxides (9)

The aryl-1,2-dihydronaphtho[2,1-*b*]thiophenes described were characterized as their *S,S*-dioxides (**9**) as an aid to structural elucidation (see Discussion). The relevant ^1H nmr data for these compounds are given in Table 2. They were prepared by oxidation with hydrogen peroxide in glacial acetic acid (see ref. 7) and crystallized from ethanol. Their properties are summarized in Table 3.

Addition Reaction of Naphtho[2,1-b]thiophene Above 20°C to Form 2-Arylnaphtho[2,1-b]thiophenes

(a) General Procedure

These reactions were carried out as described for the reactions at 20°C except that each experiment was carried out at the boiling point of the aromatic hydrocarbon.

(b) With Benzene

Chromatography of the dark residue gave a white solid which afforded colorless microcrystals of 2-phenylnaphtho[2,1-*b*]thiophene (**2***e*) (2.0 g, 71%), mp 107–108°C, lit. (1) mp 106–108°C. The nmr spectrum δ: 7.1–8.5 (m, the aromatic protons). The mass spectrum: M^+ 260; calcd.: 260. *Anal.* calcd. for $C_{18}H_{12}S$: C 83.10, H 4.60, S 12.30; found: C 82.80, H 4.50, S 12.20%.

Further elution of the column with hexane – ethyl acetate (1:1) gave a pale yellow solid (assigned as structure **6**) (0.25 g, 17%), mp 225–250°C. The nmr spectrum (DMSO-d_6) δ: 7.0–8.5 (m, the aromatic protons). The mass spectrum: M^+ 442.

Discussion of this product was given earlier.

(c) With Toluene

Chromatography of the crude product gave a pale yellow oil. This oil was dissolved in hexane and on cooling to −5°C, pale yellow microcrystals of 2-(4′-methylphenyl)naphtho[2,1-*b*]thiophene (**2***g*) (1.44 g, 48%), mp 110–112°C, were deposited. The nmr spectrum δ: 2.35 (s, Me), 7.0–8.5 (m, the aromatic protons). The mass spectrum: M^+ 274; calcd.: 274. *Anal.* calcd. for $C_{19}H_{14}S$: C 83.20, H 5.10, S 11.70; found: C 83.50, H 5.25, S 11.55%.

Hydrodesulfurization of this product with Raney nickel using the method described earlier gave 1-(4′-methylphenyl)-2-(1′-naphthyl)ethane (bp 150°C at 0.2 Torr) as a pale yellow oil (8).[2] The nmr spectrum δ: 2.35 (s, Me), 2.7–3.5 (m, CH_2—CH_2), and 7.0–8.5 (m, the aromatic protons). The mass spectrum: M^+ 246; $C_{19}H_{18}$ requires M 246.

(d) With 1,2-Dimethylbenzene

Chromatography of the crude product and crystallization of the resulting solid from hexane gave 2-(3′,4′-dimethylphenylnaphtho[2,1-*b*]thiophene (**2***j*) as pale yellow needles (1.28 g, 41%), mp 229–230°C. This product was identical (spectral properties, mixture melting point) to that obtained from the experiment with 1,2-dimethylbenzene at 20°C.

(e) With Ethylbenzene

Chromatography of the crude product gave a pale yellow oil. This was redissolved in hexane and on keeping this solution at

[3]Analysis of the dihydro signals for all aryl-1,2-dihydronaphtho[2,1-*b*]thiophenes is presented in Table 2.

[4]Complete purification of **5***h* was not possible, but this compound was characterized fully as its *S,S*-dioxide, **9***e*.

TABLE 3. Aryl-1,2-dihydronaphtho[2,1-*b*]thiophene-*S*,*S*-dioxides (**9**)

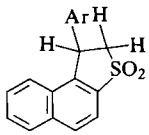

9*a–c*

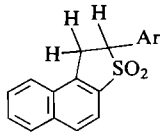

9*d*,*e*

Aryl group	Compound	Melting point (°C)	Yield (%)	Analysis (%) Calculated C	H	S	Found C	H	S
1-(C_6H_5)	**9***a*	185–185.5	89	73.45	4.75	10.90	73.20	4.75	10.75
1-(C_6H_4-4′-Me)	**9***b*	206–207	100	74.00	5.20	10.40	74.10	5.05	10.35
1-(C_6H_4-4′-Et)	**9***c*	198–200	86	74.55	5.60	9.95	74.45	5.55	9.80
2-(C_6H_3-3′,4′-$(Me)_2$)	**9***d*	139–140	76	74.55	5.60	9.95	74.65	5.65	9.79
2-(C_6H_3-2′,5′-$(Me)_2$)	**9***e*	210–212	100	74.55	5.60	9.95	74.30	5.70	9.85

TABLE 4. 1-Arylnaphtho[2,1-*b*]thiophenes (**2**)

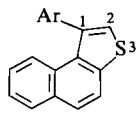

Compound	Melting point (°C)	Yield (%)	Analysis (%) Calculated C	H	S	Found C	H	S
2*d*	83–84 (lit. (1) mp 84–86)	86	83.10	4.60	12.30	82.90	4.50	12.15
2*f*	95–96	70	83.20	5.10	11.70	83.10	5.20	11.55
2*h*	[a]	76	83.35	5.55	11.10	83.30	5.45	10.95
2*j*	229–230	82	83.35	5.55	11.10	83.50	5.45	11.25

[a]Obtained as an oil.

−10°C for 24 h, pale yellow microcrystals of 1,2-dihydronaphtho[2,1-*b*]thiophene (**5***a*) (0.70 g, 35%), mp 78–79°C were formed. The nmr spectrum δ: 3.5 (s, CH_2—CH_2) and 7.0–8.0 (m, the aromatic protons). The mass spectrum: M^+ 186, calcd. 186. *Anal.* calcd. for $C_{12}H_{10}S$: C 77.40, H 5.40, S 17.20; found: C 77.45, H 5.40, S 17.35%.

Evaporation of the mother liquors gave a pale yellow oil (1.6 g). Analysis of the mass and ^1H nmr spectra indicated compounds **2***h* or *i* and **2***k* or *l* were present, but resolution of the mixture could not be achieved. The nmr spectrum δ: 1.16 (t) and 2.60 (q) due to —CH_2CH_3 of **2***h* or *i*, 1.60 (d) and 4.14 (q) due to $CHCH_3$ of **2***k* or *l*, and 6.9–8.1 (m, the aromatic protons). The mass spectrum: M^+ 288.

*The Preparation of 1-Arylnaphtho[2,1-*b*]thiophenes*

General Procedure

A mixture of a 1-aryl-1,2-dihydronaphtho[2,1-*b*]thiophene (1 g) and 2,3-dichloro-5,6-dicyano-1,4-benzoquinone (1.25 mol equiv.) in benzene (50 mL) was heated under reflux for 2 h. The reaction mixture was cooled and then was filtered through a short (ca. 5 cm) alumina (tlc grade) column. The colorless filtrate was evaporated to dryness and the residue was crystallized from hexane at −5°C. The results are summarized in Table 4.

Acknowledgments

We wish to thank the Natural Sciences and Engineering Research Council of Canada for financial support of this work, and Mr. W. Buchannon for the preparation of mass spectra.

1. O. DANN and M. KOKORUDZ. Chem. Ber. **91**, 172 (1958).
2. D. S. RAO and B. D. TILAK. J. Sci. Ind. Res. India, Sect. B, **18**, 77 (1958).
3. B. D. TILAK, L. J. PANDYA, T. S. MURTHY, and V. S. PALKAR. 4th Ann. Rept. Res., Petroleum Research Fund, American Chemical Society. 1960. p. 19.
4. P. D. CLARK, K. CLARKE, D. F. EWING, and R. M. SCROWSTON. J. Chem. Soc. Perkin Trans. I, 677 (1980).
5. B. S. FRIEDMAN, F. L. MORRITZ, C. J. MORRISEY, and R. KONCOS. J. Am. Chem. Soc. **80**, 5867 (1958).
6. B. D. TILAK. Proc. Indian Chem. Soc. Sect. A, **33**, 71 (1951).
7. B. IDDON and R. M. SCROWSTON. Adv. Heterocycl. Chem. **11**, 177 (1970).
8. N. D. KUSHCH, G. V. TKACHENKO, N. K. MOSCHINSKAYA, and P. I. BURYAK. Izv. Vyssh. Uchebn. Zaved. Khim. Khim. Teknol. **20**, 1559 (1977).

Can. J. Chem. Downloaded from www.nrcresearchpress.com by 210.87.254.5 on 09/05/12
For personal use only.

Dielectric absorption of a few aromatic amines in a polystyrene matrix

S. P. TAY[1] AND S. WALKER

Department of Chemistry, Lakehead University, Thunder Bay, Ont., Canada P7B 5E1

Received April 10, 1980

S. P. TAY and S. WALKER. Can. J. Chem. **59**, 232 (1981).

Dielectric absorption studies in the ranges 77–373 K and 10^2–10^7 Hz have been made on aniline, poly(4-aminostyrene), *p*-toluidine, 4-chloroaniline, 1-aminopyrene, and 4-aminobiphenyl in a polystyrene matrix. An intramolecular process has been observed in poly(4-aminostyrene) and 1-aminopyrene with enthalpies of activation of 25 and 26 kJ mol^{-1} respectively. The enthalpy of activation of the intramolecular process is of the same order as that found for the torsional barrier in aniline and 4-fluoroaniline. The most likely candidate for the intramolecular process appears to be rotation of the amino group about the carbon–nitrogen bond.

S. P. TAY et S. WALKER. Can. J. Chem. **59**, 232 (1981).

On a étudié, dans les intervalles de 77 à 373 K et de 10^2 à 10^7 Hz, l'absorption diélectrique des composés suivants sur un support de polystyrène: aniline, poly(amino-4 styrène), *p*-toluidine, chloro-4 aniline, amino-1 pyrène et amino-4 biphényle. Dans les cas du poly(amino-4 styrène) et de l'amino-1 pyrène, on a observé une réaction intramoléculaire avec des enthalpies d'activation respectives de 25 et 26 kJ mol^{-1}. L'enthalpie d'activation des processus intramoléculaires est du même ordre de grandeur que celle qu'on a observé pour la barrière de torsion de l'aniline et de la fluoro-4 aniline. La rotation du groupe amino autour de la liaison carbon–azote semble être le phénomène le plus couramment observé lors des réactions intramoléculaires.

[Traduit par le journal]

Introduction

Numerous dielectric studies have been made in the microwave region on the intramolecular motion associated with aromatic amines in the pure liquid and solution (1–5). Internal rotation about the C—N bond of the non planar $C_{aromatic}$—NH_2 grouping or nitrogen inversion or both may be considered as the possible relaxation process(es) giving rise to dielectric absorption at higher frequencies in addition to the lower-frequency one for molecular rotation (6). Nevertheless, the dielectric data have not been sufficiently conclusive in the high frequency range to justify a clear-cut assignment of the intramolecular relaxation time, τ_2, which is, for example, 2.1×10^{-12} s for aniline in cyclohexane at 298 K (4). In addition, our previous work (7) has shown that little reliance can be placed on the τ_2 value from a Budó analysis (8) when the weight factor C_1 for the molecular relaxation time τ_1 is much larger than the weight factor C_2 for the intramolecular relaxation time τ_2, and also when $C_1 \simeq C_2$ for τ_2 values smaller than 4.3×10^{-12} s which seems to be the case in aniline. The angle (θ) of inclination of the dipole moment (μ) towards the principal axis of rotation in aniline is estimated from group moment calculations to be 48°. The perpendicular component (μ_2) and the parallel component (μ_1) of the dipole moment are $\mu \sin\theta$ and $\mu \cos\theta$. The relationship of $C_1/C_2 = \mu_1^2/\mu_2^2$ follows the Budó theory. By taking the dipole moments of aniline, chlorobenzene, and toluene as 1.51, 1.58, and 0.37 D respectively (9), we note that $C_1 = 1 - C_2 = 0.44$ in the case of aniline whereas in 4-chloroaniline $C_1 = 0.84$. In *p*-toluidine $C_1 = 0.25$ which is a condition for a good Budó analysis for τ_2. In the present work it has been anticipated that the rate of molecular relaxation would be more retarded in the medium of a polystyrene matrix than the intramolecular relaxation processes which could well be detected separately from the molecular one, and consequently accurate barriers could possibly be determined (10, 11).

Experimental and Results

Dielectric measurements on solutes dispersed in a polystyrene matrix and the evaluation of the results have been described previously (10–25). The polystyrene matrix was prepared in the way described by Davies and Swain (10). We have also adopted their experimental and analytical procedures for obtaining relaxation times and distribution parameters by means of the Fuoss–Kirkwood equation and the enthalpy of activation from the Eyring equation. All the solutes were purified before use. The polystyrene used here had a weight average molecular weight, $\bar{M}_W$, of 230 000. The dielectric data ε_m'', ν_m, β, and ε_∞ have been placed in the Depository of Unpublished Data and the results of Eyring equation analyses of these data are given in Table 1.[2]

Standard statistical techniques were employed to fit the function of temperature data to the Eyring equation. The 95% confidence intervals on ΔH_E were typically ±10% of the nominal values or ±3 kJ mol^{-1}, whichever is the greater, and in agreement with the work of Davies and Swain (10). For the ΔS_E term, these confidence intervals were of the order of ±50% of

[1]Present address: Bell Northern Research, Department 5R13, P.O. Box 3511, Station C, Ottawa, Ont., Canada K1Y 4H7.

[2]Complete set of data may be obtained, at a nominal charge, from the Depository of Unpublished Data, CISTI, National Research Council of Canada, Ottawa, Ont., Canada K1A 0S2.

0008-4042/81/020232-06$01.00/0

©1981 National Research Council of Canada/Conseil national de recherches du Canada

Can. J. Chem. Downloaded from www.nrcresearchpress.com by 210.87.254.42 on 09/05/12
For personal use only.

Can. J. Chem. Downloaded from www.nrcresearchpress.com by 210.87.254.42 on 09/05/12
For personal use only.

the nominal values in some cases, since this term is often a small part of the intercept, $\{\ln (h/k_B) - \Delta S_E/R\}$, of the ln $(T\tau)$ versus $(1/T)$ plot (Figs. 1 and 2).

Discussion

Numerous dielectric absorption studies have now been made of solutes at low concentration in a polystyrene matrix (10–25). It should be noted that:

(*1*) For a single dielectric process the absorption curves are very broad and symmetrical and fit the Fuoss–Kirkwood curve well within the limits of experimental error (10, 11, 15). When asymmetrical absorption curves are obtained, this may suggest overlap of absorption (11, 22).

(*2*) From around room temperature to 95°C (the glass transition temperature of polystyrene), there is the possibility of observing a co-operative process involving both the polystyrene and the solute molecule since the latter lowers the glass transition temperature. Such a process is characterized by large ΔH_E (>100 kJ mol^{-1}) and ΔS_E values and is unlikely to be confused with an intramolecular process which has much smaller ΔH_E and ΔS_E values (26).

(*3*) The loss of the polystyrene itself is very small in the given frequency and the temperature region, and this is subtracted from the measured loss of the disk containing the solute (10, 11, 14). When the concentration of the solute in the polystyrene matrix is low (<5 to 7 mol%), the ΔH_E value for the molecular process is independent of concentration (27). For intramolecular processes this is also the case (15). As is apparent in the studies of Davies and Swain, the energy barrier for an intramolecular process is independent within experimental error of the polystyrene matrix (10). For example, an intramolecular process studied by the nmr technique in dilute liquid solution yields the same barrier as the dielectric study carried out in the polystyrene matrix (10). The latter work was extended by a most detailed study by Tay, Walker, and Wyn-Jones (11) where ΔH_E values obtained from the dielectric, ultrasonic and nmr techniques for a variety of intramolecular processes were compared. All three methods employed different solvent media but yielded intramolecular energy values in agreement well within experimental error. Furthermore, the results are readily repeatable. Numerous examples are now available where the polystyrene matrix approach enables the complete separation of group and molecular rotation and where the energy barrier for group rotation is similar in value to that obtained by other methods (10, 11, 15, 17, 19, 20).

(*4*) Electric dipole moment values deduced from the dispersion data agree only with literature values when the absorption occurs around room temperature (10, 23). At lower temperatures the moments

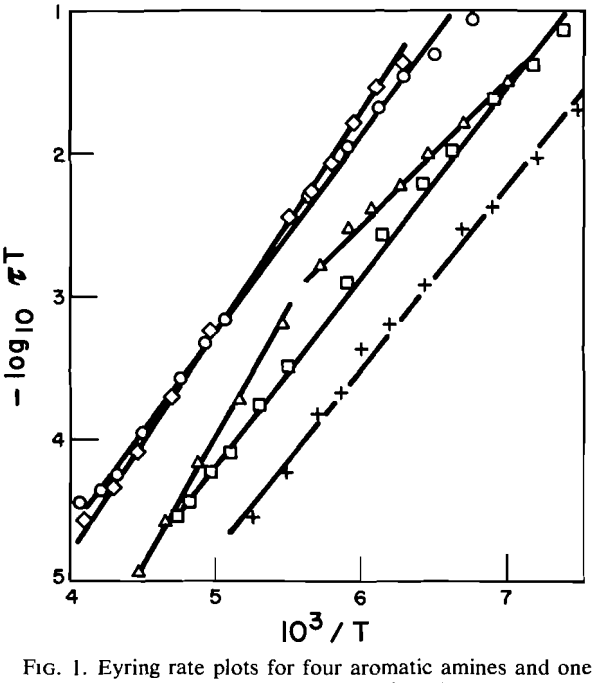

FIG. 1. Eyring rate plots for four aromatic amines and one rigid molecule: +, poly(4-aminostyrene) in polystyrene; △, *p*-toluidine in polystyrene; ◇, 4-chlorotoluene in polystyrene; □, 4-chloroaniline in polystyrene; ○, 1-aminopyrene in polystyrene.

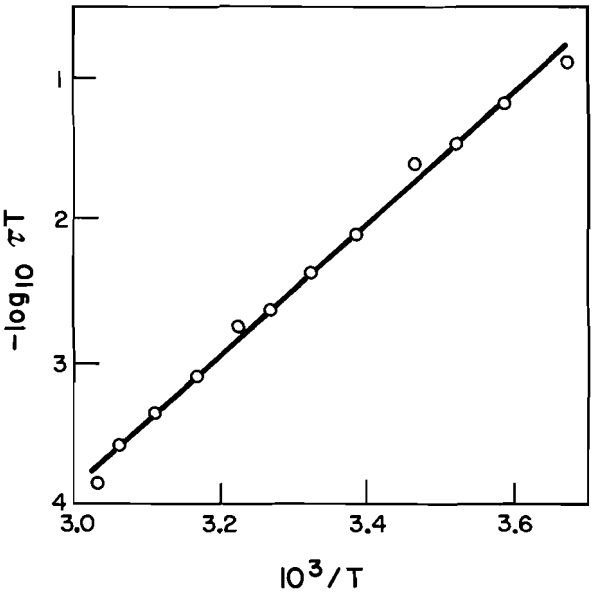

FIG. 2. Eyring rate plot for 4-aminobiphenyl in polystyrene.

TABLE 1. Relaxation and activation energy parameters for some aromatic amines in polystyrene matrices

Compound (mol L^{-1})	Temperature range (K)	$\log_{10}\nu$ (Hz)	Relaxation times τ (s) 150 K	200 K	300 K	ΔG_E (kJ mol^{-1}) 150 K	200 K	300 K	ΔH_E (kJ mol^{-1})	ΔS_E (J K^{-1} mol^{-1})
Aniline (1.147)	89–131	2.7–6.1	2×10^{-8}			14			17 ± 1*	26 ± 10
Chlorobenzene‡ (0.881)	81–111	2.5–4.5	2×10^{-7}			17			11 ± 1	−40 ± 8
Poly(4-aminostyrene) (0.701)	125–198	2.3–6.3	1×10^{-5}			22			25 ± 1	18 ± 5
p-Toluidine	144–175	2.9–4.3	1×10^{-4}			25			20 ± 1	−32 ± 8
(0.849)	174–223	4.3–6.5		5×10^{-7}			24		32 ± 2	41 ± 8
4-Chlorotoluene† (0.380)	160–244	2.8–6.2	1×10^{-3}	3×10^{-6}		28	27		29 ± 1	10 ± 3
4-Chloroaniline (0.532)	136–222	2.5–6.4	8×10^{-5}	3×10^{-7}		24	23		26 ± 1	12 ± 4
1-Aminopyrene (0.770)	149–265	2.4–6.6	5×10^{-4}	6×10^{-6}		27	27		26 ± 1	−5 ± 4
4-Aminobiphenyl (0.544)	272–330	2.6–5.6			2×10^{-5}			46	86 ± 5	135 ± 16
4-Chlorobiphenyl§ (0.576)	283–313	2.8–4.4			3×10^{-5}			48	85 ± 10	123 ± 34

*The ΔH_E errors quoted are for 95% confidence limits.
†Reference 39.
‡Reference 40.
§Reference 31.

evaluated may be substantially smaller than the true value (10).

(5) The enthalpy of activation for the molecular relaxation of a solute in polystyrene is highly dependent on size for a particular type of solute molecule (14). Thus, for the series chlorobenzene, 4-chlorotoluene, and 4-chlorobiphenyl (see Table 1), the ΔH_E values are 11, 29, and 85 kJ mol^{-1} respectively. Hence, in the study of group relaxation the molecular and group processes may be sorted out by varying the size of the molecule to which the flexible group is attached.

We shall now discuss each of the solute molecules in turn and the first one to be considered is poly(4-aminostyrene) which from the dielectric point of view is the simplest since any absorption in our frequency and temperature ranges could not be attributable to relaxation of single molecules.

Poly(4-aminostyrene)

Previous work has indicated that it is feasible to study an intramolecular process by attachment of the molecular unit to the backbone of a polymer. For example, Heijboer (28) has shown that inversion of the cyclohexane ring can be readily detected in a dielectric study of poly(4-chlorocyclohexyl methacrylate). The activation enthalpy of 48 kJ mol^{-1} agrees within experimental error with that of 43 kJ mol^{-1} for ring inversion in cyclohexyl chloride from an nmr study (29), and with a value of 42.2 kJ mol^{-1} for the same process in cyclohexyl chloride in a polystyrene matrix determined by Davies and Swain (10) using a dielectric technique similar to that we currently employ. This work has also been repeated in this laboratory, and a value of 43 kJ mol^{-1} was obtained. Fielding-Russell and Wetton (30) studied the dielectric absorption of poly(4-ethoxystyrene) and observed a γ-relaxation in a temperature range of 93–163 K over a frequency range of 10^2–10^7 Hz in addition to the α- and β-relaxations which occurred above room temperature in the same frequency range. These authors suggest two motional possibilities to account for the γ-relaxation: (*a*) onset of rotation of the CH_2—CH_3 bond about the preceding O—CH_2 bond as axis; and (*b*) some form of large angle libration of the ethoxy group. They estimated an Arrhenius activation enthalpy of 21 kJ mol^{-1} for the γ-relaxation process. The clear separation of the γ-relaxation from the β-relaxation in poly(4-ethoxystyrene) suggests the possibility of an uncomplicated study of intramolecular motions of the amino group in poly(4-aminostyrene). The $\ln \tau T$ versus $1/T$ plot for poly(4-aminostyrene) in polystyrene is given in Fig. 1, and well within the limits of experimental error the data fit a straight line. The absorption occurs in the 125–198 K range and cannot be ascribed to α- and β-relaxation processes

Can. J. Chem. Downloaded from www.nrcresearchpress.com by 210.87.254.42 on 09/05/12
For personal use only.

Can. J. Chem. Downloaded from www.nrcresearchpress.com by 210.87.254.42 on 09/05/12
For personal use only.

which would occur at higher temperatures in the 10^2–10^6 Hz frequency range. It would seem that the relatively low ΔH_E value for poly(4-aminostyrene) in Table 1 can be attributed to an intramolecular process with an activation enthalpy of 25 kJ mol^{-1}.

Aniline, 4-Chloroaniline, and p-*Toluidine*

We have noted earlier that the Budó weight factors for molecular (C_1) and intramolecular (C_2) relaxations are approximately the same in the case of aniline. In *p*-toluidine the latter is larger whereas in 4-chloroaniline the reverse is true. Thus, it is expected that the intramolecular relaxation process would contribute more to the dielectric absorption in *p*-toluidine than the molecular one. On the contrary, dielectric loss arising from the molecular relaxation process would dominate the dielectric absorption in 4-chloroaniline. This is indeed observed in the present work. The ΔH_E value of 26 kJ mol^{-1} for 4-chloroaniline is very similar to that of 29 kJ mol^{-1} for the rigid molecule 4-chlorotoluene. Both molecules are of a similar size and shape with the latter molecule being just slightly larger which fits in with their relative ΔH_E values and also their ΔG_E values. Thus, as judged by the activation parameters for 4-chloroaniline, there is no indication of a contribution to the dielectric absorption from group rotation. This may be accounted for by the fact that $C_1 \gg C_2$.

The Eyring rate plot for *p*-toluidine in Fig. 1 indicates two limiting slopes from the low and high temperature data. The low frequency data yield ΔH_E and ΔS_E of 20 ± 1 kJ mol^{-1} and -32 ± 8 J K^{-1} mol^{-1} respectively, while the high frequency data yield the corresponding parameters of 32 ± 2 kJ mol^{-1} and 41 ± 8 J K^{-1} mol^{-1}, respectively. This is to be contrasted with the previously observed result that an Eyring rate plot for a single relaxation process is linear over the frequency range of 10^2–10^7 Hz regardless of the nature of the relaxation process. Some examples are 1-iodonaphthalene in polystyrene (14), 1,4-dinitrobenzene in polystyrene (16), furan-2-carbaldehyde in polystyrene (11), 1-fluoro-1,1,2,2-tetrachloroethane in polystyrene (11), and certainly, 4-chloroaniline in polystyrene in the present study (Fig. 1). The higher energy barrier of 32 kJ mol^{-1} for *p*-toluidine agrees better with the one of 29 kJ mol^{-1} for molecular relaxation in 4-chlorotoluene. Certainly, the lower barrier of 20 kJ mol^{-1} is much too low to be ascribed to the molecular relaxation of *p*-toluidine. When it is borne in mind that a value of 25 kJ mol^{-1} has been determined for the intramolecular process in poly(4-aminostyrene) and that in each case the absolute accuracy in ΔH_E is not better than ± 3 kJ mol^{-1}, then the lower barrier in *p*-toluidine would be in harmony with this. Certainly, it may be concluded that the dielectric absorption of *p*-toluidine indicates the presence of more than one relaxation process and most likely it is the overlap of the molecular and an intramolecular process.

Broad dielectric absorption is observed for aniline in polystyrene in the temperature range of 89.0–130.8 K which is about 40° lower than that for poly(4-aminostyrene). The loss curves (Fig. 3) are slightly asymmetrical, being somewhat steeper on the low frequency side. This is to be contrasted with the symmetrical curves observed for various rigid molecules where there is just one process (14). A reasonably linear Eyring plot yields ΔH_E and ΔS_E of 17 kJ mol^{-1} and 26 J K^{-1} mol^{-1} respectively which are to be compared with the corresponding values of 11 kJ mol^{-1} and -40 J K^{-1} mol^{-1} for chlorobenzene in polystyrene. In view of the asymmetry of the curves and the fact that the ΔH_E value does not match that for the molecular process, it would seem that overlap of intramolecular and molecular processes most likely occurs and that the Eyring parameters are not meaningful.

1-Aminopyrene and 4-Aminobiphenyl

The dielectric absorption in 1-aminopyrene is noteworthy. Such a large molecule with four fused rings would be expected to encounter a high energy barrier to molecular rotation, a lower limit of this being the 60 kJ mol^{-1} for 4-fluorobiphenyl in polystyrene (31). The barrier of 26 kJ mol^{-1} could not possibly be attributed to molecular relaxation and is best ascribed to an intramolecular process. This value agrees well with that for the intramolecular process in poly(4-aminostyrene). In

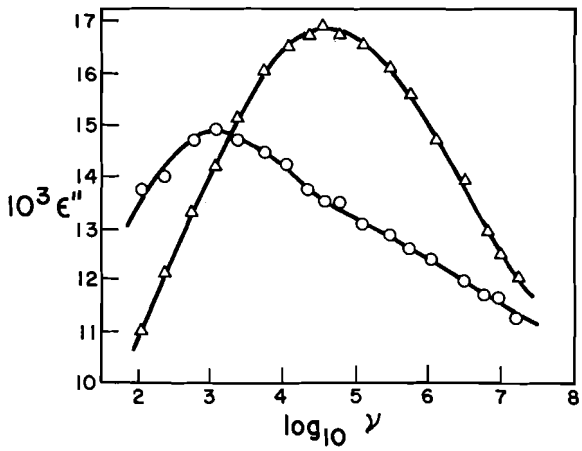

FIG. 3. Dielectric loss curves for aniline in polystyrene: ○, 94 K; △, 110.6 K.

Can. J. Chem. Downloaded from www.nrcresearchpress.com by 210.87.254.42 on 09/05/12
For personal use only.

contrast to 1-aminopyrene, 4-aminobiphenyl exhibits a broad dielectric absorption near room temperature, that is at about 120° higher than that for 1-aminopyrene. The ΔH_E value which emerges from the Eyring rate plot (Fig. 2) is 86 kJ mol^{-1}. By comparison with the ΔH_E value of 85 kJ mol^{-1} for 4-chlorobiphenyl (31) which is a rigid molecule of similar size and shape the relaxation process observed in 4-aminobiphenyl may be readily characterized as a molecular one. The presence of the molecular process in one case and its absence in the other could be accounted for by the molecular process of the much larger molecule, 1-aminopyrene, being at lower frequencies than we had available which would correspond with a higher free energy of activation than was the case for 4-aminobiphenyl. In fact, the temperature (330 K) used in the study of 4-aminobiphenyl is within about 20° of our upper limit. Thus, the absence of the molecular process for 1-aminopyrene may be accounted for.

Conclusions

Examination of poly(4-aminostyrene) and 1-aminopyrene in a polystyrene matrix has enabled a complete separation of an intramolecular process from that of a molecular one. Previous dielectric absorption studies of aniline (3), *m*-toluidine (4), and *p*-toluidine (4), in inert solvents in the microwave region revealed very little variation of the intramolecular relaxation time with temperatures over a 40, 25, and 35° range respectively and, consequently, a negligible enthalpy of activation. The present studies indicate a value of ~25 kJ mol^{-1} for an intramolecular process in 1-aminopyrene, and poly(4-aminostyrene). There are also signs of a similar process in *p*-toluidine. The two most likely candidates for the intramolecular process are nitrogen inversion or internal rotation of the amine group.

Relative intensity measurement of rotational transitions in the 0^+ and 0^- inversion states by the microwave spectroscopic technique has indicated that the inversion frequency for aniline itself is close to 46 cm^{-1} (32). An inversion barrier of 6.7 kJ mol^{-1} has been found for aniline from a vibrational analysis of the 294 nm band of its vapour (33). Semi-empirical calculations have yielded values between 2.9 and 14 kJ mol^{-1} for the barrier to pyramidal inversion in aniline (34). Recently, a far infrared investigation of aniline, aniline-ND_2, aniline-NHD, monohalosubstituted anilines, 2-aminopyrimidine, and 3-aminopyridine in the vapour phase has been reported (35–38), and an inversion barrier of 6.3 kJ mol^{-1} for aniline has been determined (35, 36). Inversion barriers for the nine *ortho*-, *meta*-, and *para*-substituted fluoro-, chloro-, and bromoanilines range between 4.6 and 7.2 kJ mol^{-1} for the extreme cases of *o*-bromoaniline and *p*-fluoroaniline respectively (37). For 3-aminopyridine the inversion barrier is 6.0 kJ mol^{-1}, whereas it is only 0.75 kJ mol^{-1} for 2-aminopyrimidine (38).

Thus, from the available physical evidence we note there is a small inversion barrier. Further it is improbable that the inversion will appreciably disturb the surrounding medium. Hence, it is unlikely that this inversion frequency would be shifted from the far infrared region to the radiofrequency range in our experiments by lowering the temperature or by changing to a more viscous medium. Thus, it would seem unlikely that nitrogen inversion is the candidate for the intramolecular process which we have observed. Far infrared studies of aniline and 4-fluoroaniline have resulted in rotational energy barriers of 24 and 18.8 kJ mol^{-1} (35). The value for aniline is almost coincident with that which we have found for the intramolecular process in poly(4-aminostyrene) and 1-aminopyrene. In the case of poly(4-aminostyrene), the ΔH_E value obtained is for an intramolecular process while in the case of 1-aminopyrene the value is much too small to be attributed to a molecular process. Altogether, it would seem that the most likely candidate for the intramolecular process observed for both these molecules is rotation of the amino group about the C—N bond.

1. E. L. Grubb and C. P. Smyth. J. Am. Chem. Soc. **83**, 4879 (1961).
2. E. N. DiCarlo and C. P. Smyth. J. Am. Chem. Soc. **84**, 3638 (1962).
3. S. K. Garg and C. P. Smyth. J. Chem. Phys. **46**, 373 (1967).
4. S. W. Tucker and S. Walker. Can. J. Chem. **47**, 681 (1969).
5. S. W. Tucker and S. Walker. J. Chem. Phys. **52**, 2545 (1970).
6. C. P. Smyth. *In* Internal rotation in molecules. *Edited by* W. J. Orville-Thomas. Wiley. 1974. p. 48.
7. J. Crossley, S. P. Tay, and S. Walker. Adv. Mol. Relax. Processes, **6**, 79 (1974).
8. A. Budó. Z. Phys. **39**, 706 (1938).
9. A. L. McClellan. Tables of experimental dipole moments. W. H. Freeman and Co., San Francisco and London. 1963; Vol. 2. Rahara Enterprises, CA. 1974.
10. M. Davies and J. W. Swain. Trans. Faraday Soc. **67**, 1637 (1971).
11. S. P. Tay, S. Walker, and E. Wyn-Jones. Adv. Mol. Relax. Interact. Processes, **13**, 47 (1978).
12. M. Davies and A. Edwards. Trans. Faraday Soc. **63**, 2163 (1967).
13. M. Davies and J. W. Swain. Chem. Phys. Lett. **2**, 42 (1968).
14. S. P. Tay and S. Walker. J. Chem. Phys. **63**, 1634 (1975).

15. C. K. McLellan and S. Walker. Can. J. Chem. **55**, 583 (1977).
16. J. Kraft, S. P. Tay, and S. Walker. J. Phys. Chem. **80**, 303 (1976).
17. A. Lakshmi, S. Walker, N. A. Weir, and J. H. Calderwood. J. Phys. Chem. **82**, 1091 (1978).
18. A. Lakshmi, S. Walker, N. A. Weir, and J. H. Calderwood. J. Chem. Phys. **68**, 4662 (1978).
19. A. Lakshmi, S. Walker, N. A. Weir, and J. H. Calderwood. J. Chem. Soc. Trans. Faraday II, **74**, 727 (1978).
20. M. A. Mazid, J. P. Shukla, and S. Walker. Can. J. Chem. **56**, 1800 (1978).
21. A. Lakshmi, S. Walker, N. A. Weir, and J. H. Calderwood. Adv. Mol. Relax. Interact. Processes, **13**, 287 (1978).
22. J. Crossley, M. A. Mazid, C. K. McLellan, P. F. Mountain, and S. Walker. Adv. Mol. Relax. Interact. Processes, **12**, 239 (1978).
23. J. Crossley, M. A. Mazid, C. K. McLellan, P. F. Mountain, and S. Walker. Can. J. Chem. **56**, 567 (1978).
24. J. P. Shukla, S. Walker, and S. Warren. J. Chem. Soc. Trans. Faraday II, **74**, 2045 (1978).
25. J. Crossley, J. P. Shukla, S. P. Tay, M. S. Walker, and S. Walker. Can. J. Chem. **57**, 2843 (1979).
26. J. Chao. Private communication.
27. T. I. Borisova and V. N. Chirkov. Russ. J. Phys. Chem. **47**, 949 (1973).
28. J. Heijboer. Koll. Z. **171**, 7 (1960).
29. E. Eliel. Angew. Chem. **4**, 761 (1968).
30. G. S. Fielding-Russell and R. E. Wetton. Chem. Soc. Spec. Publ. No. 20, 95 (1966).
31. A. Khwaja. Private communication.
32. D. G. Lister, J. M. MacDonald, and N. L. Owen. Internal rotation and inversion. Academic Press. 1978. p. 192.
33. J. C. D. Brand, D. R. Williams, and T. J. Cook. J. Mol. Spectrosc. **20**, 359 (1966).
34. A. Rauk, J. D. Andose, W. G. Frick, R. Tang, and K. Mislow. J. Am. Chem. Soc. **93**, 6507 (1971).
35. N. W. Larsen, E. L. Hansen, and F. W. Nicolaisen. Chem. Phys. Lett. **43**, 584 (1976).
36. R. A. Kydd and P. J. Krueger. Chem. Phys. Lett. **49**, 539 (1977).
37. R. A. Kydd and P. J. Krueger. J. Chem. Phys. **60**, 827 (1978).
38. R. A. Kydd. Abstract of Papers, 62nd Canadian Chemical Conference, CIC, Vancouver, June 1979. p. 148.
39. S. P. Tay. Unpublished results.
40. M. Mazid. Private communication.

Can. J. Chem. Downloaded from www.nrcresearchpress.com by 210.87.254.42 on 09/05/12
For personal use only.

Crystal structures and conformations of 1-α-D-xylofuranosylcytosine and its protonated form (HCl salt)[1]

MICHAEL L. POST,[2] CAROL P. HUBER, AND GEORGE I. BIRNBAUM
Division of Biological Sciences, National Research Council of Canada, Ottawa, Ont., Canada K1A 0R6
AND
DAVID SHUGAR
Institute of Biochemistry and Biophysics, Academy of Sciences, 02-532 Warsaw, Poland
Received July 24, 1980
This paper is dedicated to Prof. Raymond U. Lemieux on the occasion of his 60th birthday

MICHAEL L. POST, CAROL P. HUBER, GEORGE I. BIRNBAUM, and DAVID SHUGAR. Can. J. Chem. **59**, 238 (1981).

The structures of 1-α-D-xylofuranosylcytosine, $C_9H_{13}N_3O_5$ (**1**), and its hydrochloride salt, $C_9H_{13}N_3O_5$·HCl (**1**·HCl), have been determined by X-ray diffraction from diffractometer data, using direct method techniques. Both compounds crystallize in the orthorhombic system with $Z = 4$. Space group and cell parameters are, for **1**: $P2_12_12$, $a = 18.706$, $b = 8.127$, $c = 7.007$ Å; and for **1**·HCl: $P2_12_12_1$, $a = 16.800$, $b = 8.045$, $c = 8.897$ Å. Refinement by block-diagonal least-squares calculations gave a final R of 0.033 on 873 reflections and 0.034 on 914 reflections for **1** and **1**·HCl, respectively. The glycosyl torsion angles are in the *anti* domain, $\chi_{CN} = -25.1°$ (**1**) and $-28.6°$ (**1**·HCl), and the sugar puckers are nearly pure ${}_2^3T$ (**1**) and ${}^3E$ (**1**·HCl) forms. The C(4′)—C(5′) rotamer is *trans–gauche* in both cases. No intramolecular hydrogen bonding occurs in the xylofuranosyl rings. Lattice packing in the crystal structures occurs via intermolecular hydrogen bonding, with base stacking in pairs about one of the 2-fold axes for the neutral form, and with no base-stacking interactions for the protonated form. The biological implications of the structure and conformation of α-nucleosides are examined.

MICHAEL L. POST, CAROL P. HUBER, GEORGE I. BIRNBAUM et DAVID SHUGAR. Can. J. Chem. **59**, 238 (1981).

On a déterminé les structures de la 1-α-D-xylofurannosylcytosine $C_9H_{13}N_3O_5$ (**1**) et de son chlorhydrate par diffraction de rayons-X, en se basant sur des données obtenues par des méthodes directes. Les deux composés cristallisent dans le système orthorhombique avec $Z = 4$. Le groupe spatial et les dimensions de la maille sont pour le composé **1**: $P2_12_12$, $a = 18{,}706$, $b = 8{,}127$, $c = 7{,}007$ Å; et pour son chlorhydrate $P2_12_12_1$, $a = 16{,}800$, $b = 8{,}045$, $c = 8{,}897$ Å. On a affiné les structures par la méthode des moindres carrés (bloque diagonal) jusqu'à une valeur de $R = 0{,}033$ pour 873 réflexions et de 0,034 pour 914 réflexions respectivement pour le composé **1** et son chlorhydrate. Les angles de torsion glycosidiques sont dans le domaine *anti* $\chi_{CN} = -25{,}1°$ (**1**) et $-28{,}6°$ (**1**·HCl), et le plissement des cycles furannoses conduit à des formes presque parfaites ${}_2^3T$ (**1**) et ${}^3E$ (**1**·HCl). Dans les deux cas le rotamère C(4′)—C(5′) est *trans–gauche*. Il n'y a pas de liaison hydrogène intramoléculaire dans les cycles xylofurannosyles. L'organisation des molécules dans le cristal se fait par l'intermédiaire de liaisons hydrogène intermoléculaires; les bases s'entassent par paires le long de l'un des axes binaires de symétrie dans le cas de la forme neutre et sans interactions d'entassement des bases pour la forme protonée. On a examiné les implications biologiques de la structure et de la conformation des α-nucléosides.
[Traduit par le journal]

Introduction

Nucleotide residues hitherto found in natural nucleic acids occur exclusively in the β-anomeric configuration. There are, however, a number of examples of α-nucleosides and nucleotides, in the free state or as constituents of more complex molecules, such as the vitamin B_{12} group, in living cells (ref. 1, and references cited therein). Some α-nucleoside 5′-phosphates are substrates of 5′-nucleotidase (2, 3); α-5-formyluridine is sufficiently effective as a non-competitive inhibitor of *Escherichia coli* DNA-dependent RNA polymerase to permit the affinity labelling of the latter (4). Other α-nucleosides have also been found to be substrates for, and inhibitors of, a variety of enzymes (5, 6).

Increasingly widespread interest in the biological and physico-chemical properties of α-anomeric nucleosides and nucleotides derives largely from the unexpected findings that some are potent antimetabolites with antitumour and antiviral activities (7–11) which, in several instances, are comparable to, or even in excess of, those of the corresponding β-anomers (6, 10, 11). Undoubtedly the most striking illustration is α-2′-deoxy-6-thioguanosine, which is presently undergoing clinical trials (12). It is readily phosphorylated by kinase(s) in some tumour cells (13) and is incorporated into the terminal position of small oligodeoxynucleotides (14, 15), thus acting as a chain terminator. The foregoing has raised some questions as to the presumed gross structural dissimilarity between α- and β-anomeric nucleoside pairs, and led to the chemical synthesis of the two anomers of 3′-(hydroxymethyl)-branched 2′-deoxynucleosides of 6-thioguanine. *Both* of these, in agreement with expecta-

[1]NRCC No. 18677.
[2]Present address: Division of Chemistry, National Research Council of Canada, Ottawa, Ont., Canada K1A 0R9.

0008-4042/81/020238-08$01.00/0
©1981 National Research Council of Canada/Conseil national de recherches du Canada

Can. J. Chem. Downloaded from www.nrcresearchpress.com by 210.87.254.40 on 09/05/12
For personal use only.

Can. J. Chem. Downloaded from www.nrcresearchpress.com by 210.87.254.40 on 09/05/12
For personal use only.

tions, were found to be not only *equally* effective as inhibitors of the growth of WI-L2 human lymphoblastoid cells, but to be even more effective in this regard than the parent α-2′-deoxy-6-thioguanosine (6).

It has also been found that the α-anomers of at least two arabinosyl nucleosides exhibit antiviral activities comparable to those of the corresponding β-anomers (10). Since substrate and/or inhibitor properties of a given class of compounds are dependent, amongst other factors, on conformational parameters, it is of obvious interest to compare the conformations of the two anomeric forms of nucleosides. However, only very limited structural and conformational solid state data are at present available for α-nucleosides (see ref. 1 and references cited therein). The utility of such solid state data in the interpretation of solution conformations obtained by nmr spectroscopy has already been admirably illustrated in the case of ribo- and deoxyribonucleosides (16, 17). We report here on the solid state structure and conformation of α-xylofuranosylcytosine (**1**) and of its hydrochloride salt

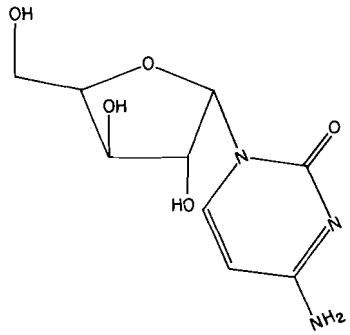

1

(**1**·HCl). The antimetabolic properties of some β-D-xylofuranosyl nucleosides have been well documented (18–21). It has been shown that 9-β-D-xylofuranosyladenine interferes with methylation of nuclear RNA (21) via inhibition of the synthesis of *S*-adenosyl-L-methionine (22). Insofar as we are aware, no attempts have yet been made to examine the possible antimetabolic properties of α-xylofuranosyl nucleosides, but their properties in some enzyme systems have received some attention as discussed below.

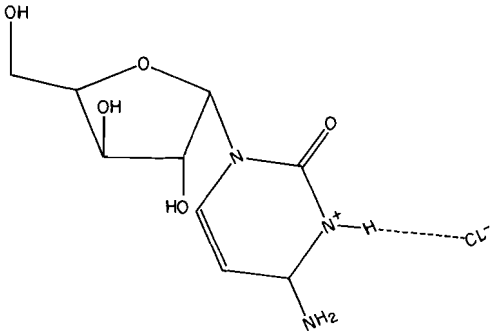

1·HCl

Experimental

Preparation of 1-α-D-Xylofuranosylcystosine (1) and 1·HCl

O^2,2′-anhydro-1-α-D-xylofuranosyluracil, obtained by the method of Holy (2), was heated under reflux with aqueous triethylamine (10% v/v) to produce 1-α-D-xylofuranosyluracil. The latter was then acetylated and treated with P_2S_5 in dioxane to give the 4-thio derivative (3) which, when aminated with methanolic ammonia in a sealed tube at 105°C, yielded **1**. Passage through a Dowex-50W (H^+) column followed by crystallization from anhydrous ethanol yielded pure **1**, mp 263–264°C (decomp.). The mother liquors from the crystallization were treated with excess HCl (2 *N*) and brought to dryness, to give the hydrochloride salt (**1**·HCl), which was then recrystallized several times from anhydrous ethanol to yield the pure product, mp 190–191°C (uncorr.).

X-ray Analysis of 1 and 1·HCl

Crystals of **1** and **1**·HCl were grown from anhydrous ethanol. Weissenberg and precession photographs were used to determine the space groups and preliminary cell constants. Accurate lattice parameters were obtained by least-squares treatment of the 2θ values of 19 and 14 (**1** and **1**·HCl, respectively) reflections centered on a diffractometer. Intensity data for both compounds were collected with Ni-filtered CuKα radiation (λ = 1.54178 Å) on a Picker diffractometer equipped with a scintillation detector and pulse height discriminator; θ–2θ scans were employed and background counts of 20 s were taken at each end of the scan range. Threshold levels for "unobserved" data were experimentally determined as the larger of 0.1 × total background *or* 50 counts (for **1**) and 48 counts (for **1**·HCl), and reflections with intensities lower than these values were excluded during structure refinement. Lorentz, polarization, and scaling factors (calculated with regard to frequently monitored check reflections) were applied to the raw data, but no corrections were made for absorption or secondary extinction. Crystal data and other pertinent details are as follows:

$C_9H_{13}N_3O_5$ (**1**) fw = 243.22
Orthorhombic, a = 18.706(4), b = 8.127(2), c = 7.007(1) Å, V = 1065.2 Å^3, Z = 4, ρ_{calcd} = 1.516, ρ_{meas} = 1.52 g cm^{-3} (20°C, CuKα Ni-filtered), μ = 10.8 cm^{-1}, crystal size 0.24 × 0.08 × 0.05 mm, $2\theta_{max}$ = 120°, scan speed 1° min^{-1} in 2θ, scan widths 1.7° for 2θ ≤ 90°; 2.0° for 90° < 2θ ≤ 120°, reflections observed/accessible = 873/947 (92%). Absences $h00$, $h = 2n + 1$; $0k0$, $k = 2n + 1$, space group $P2_12_12$.

$C_9H_{13}N_3O_5$·HCl (**1**·HCl) fw = 279.70
Orthorhombic, a = 16.800(3), b = 8.045(1), c = 8.897(1) Å, V = 1202.6 Å^3, Z = 4, ρ_{calcd} = 1.544, ρ_{meas} = 1.54 g cm^{-3} (20°C, CuKα Ni-filtered), μ = 30.4 cm^{-1}, crystal size 0.21 × 0.09 × 0.04 mm, $2\theta_{max}$ = 130°, scan speed 2° min^{-1} in 2θ, scan widths 1.4° for 2θ ≤ 80°, 1.6° for 80 < 2θ ≤ 105°, 1.8° for 105 < 2θ ≤ 130°, reflections observed/accessible = 914/1209 (76%). Absences $h00$, $h = 2n + 1$; $0k0$, $k = 2n + 1$; $00l$, $l = 2n + 1$, space group $P2_12_12_1$.

The structures were solved by direct methods using the symbolic addition procedure with tangent refinement and a multisolution approach. In each case, all nonhydrogen atoms were located in *E*-maps calculated with 119 and 144 phased *E*'s ≥ 1.45

Can. J. Chem. Downloaded from www.nrcresearchpress.com by 210.87.254.40 on 09/05/12
For personal use only.

TABLE 1. Final atomic positional coordinates ($\times 10^4$) for the non-H atoms, estimated standard deviations are in parentheses

	1			**1**·HCl		
Atom	*x/a*	*y/b*	*z/c*	*x/a*	*y/b*	*z/c*
N(1)	4746(1)	7156(3)	9701(3)	6655(2)	3420(4)	2654(3)
C(2)	5333(1)	8097(4)	9148(4)	6682(2)	3318(6)	4206(4)
O(2)	5440(1)	8352(3)	7425(3)	6146(2)	3827(5)	4992(3)
N(3)	5772(1)	8727(3)	10514(3)	7352(2)	2580(5)	4777(3)
C(4)	5639(1)	8417(4)	12357(4)	7948(2)	1918(5)	3950(4)
N(4)	6080(1)	9001(3)	13692(4)	8535(2)	1170(5)	4653(4)
C(5)	5034(2)	7461(4)	12938(4)	7895(2)	2056(5)	2379(4)
C(6)	4602(2)	6862(4)	11570(4)	7248(2)	2792(5)	1782(3)
C(1′)	4269(1)	6543(4)	8187(4)	5912(2)	4086(5)	2009(4)
O(1′)	3898(1)	5153(3)	8893(3)	6060(2)	4709(3)	561(3)
C(2′)	3693(1)	7784(4)	7560(4)	5275(2)	2714(5)	1855(4)
O(2′)	3426(1)	8708(3)	9123(3)	5622(1)	1127(3)	1692(3)
C(3′)	3105(2)	6616(4)	6885(4)	4867(2)	3181(4)	379(4)
O(3′)	3270(1)	5989(3)	5044(3)	4290(1)	4449(3)	605(3)
C(4′)	3153(2)	5240(4)	8348(4)	5561(2)	3852(5)	−539(4)
C(5′)	2945(1)	3525(4)	7682(4)	5364(2)	5112(5)	−1738(4)
O(5′)	2181(1)	3423(3)	7450(3)	4954(2)	4345(4)	−2946(3)
Cl^-	—	—	—	7842(1)	2242(2)	8097(1)

TABLE 2. Final hydrogen atom positional coordinates ($\times 10^3$) and isotropic thermal parameters ($Å^2 \times 10^2$), estimated standard deviations are in parentheses

	1				**1**·HCl			
Atom	*x/a*	*y/b*	*z/c*	U_{iso}	*x/a*	*y/b*	*z/c*	U_{iso}
H(1)	598(2)	894(4)	1497(5)	65(10)	901(3)	74(6)	416(6)	81(16)
H(2)	645(2)	966(5)	1337(6)	62(11)	852(3)	104(7)	560(6)	79(16)
H(3)	—	—	—	—	736(4)	235(7)	574(7)	108(22)
H(5)	499(2)	707(4)	1430(4)	46(8)	833(2)	151(6)	183(5)	54(13)
H(6)	417(2)	616(6)	1181(6)	76(13)	712(2)	296(5)	77(4)	44(11)
H(1′)	459(1)	621(4)	700(4)	37(9)	575(2)	499(4)	265(4)	23(9)
H(2′)	387(1)	859(4)	656(4)	36(8)	490(2)	272(5)	281(4)	44(11)
H(O2′)	374(2)	962(6)	946(6)	92(15)	572(2)	75(5)	261(5)	60(13)
H(3′)	265(1)	713(4)	693(4)	26(8)	461(2)	222(5)	−2(4)	26(9)
H(O3′)	309(2)	684(7)	409(7)	118(18)	398(3)	393(6)	94(6)	77(16)
H(4′)	286(1)	552(4)	956(4)	31(8)	582(2)	285(5)	−93(5)	47(11)
H(5′1)	316(2)	338(5)	639(6)	70(12)	502(2)	587(5)	−128(4)	32(9)
H(5′2)	309(1)	269(3)	882(4)	25(7)	583(2)	583(5)	−207(5)	51(12)
H(O5′)	199(2)	351(6)	839(7)	96(15)	527(3)	402(8)	−356(6)	86(17)

and ≥ 1.50 for **1** and **1**·HCl, respectively. Refinement was carried out using block-diagonal least squares with the non-H atoms initially having isotropic, and then anisotropic, thermal motion. Hydrogen atoms were located in difference Fourier syntheses and their contribution was included in the refinement with isotropic thermal parameters. The function minimized throughout was $\Sigma w(|F_o| - |F_c|)^2$ with weights, w, in the form $\sqrt{w} = |F_o|/M$ for $|F_o| \leq M$; $\sqrt{w} = M/|F_o|$ for $|F_o| > M$ with $M = 12.4$ and 10.4 for **1** and **1**·HCl. These weighting schemes made the average values of $w(\Delta F^2)$ independent of $|F_o|$ and $\sin^2\theta$. Convergence was attained at an R of 0.033 and 0.034 for the observed data (0.043 and 0.061 for all data)[3] and an R_w of 0.034 and 0.040,[4] the figures for **1** being given first. Scattering factors were taken from ref. 23 and ref. 24 (for H) and those for O and Cl^- were corrected for the real and imaginary components of anomalous dispersion (23). The absolute configuration was chosen with respect to the known D-xylofuranosyl moiety in each structure. Programs used were from the NRC crystallographic set (25) and most figures are based on ORTEP II (26) plots. The final atomic parameters are given in Tables 1 and 2.

[3]Tables of observed and calculated structure factors, anisotropic thermal parameters, least-squares planes, and bond angles involving hydrogen atoms are available, at a nominal charge, from the Depository for Unpublished Data, CISTI, National Research Council of Canada, Ottawa, Ont., Canada K1A 0S2.

[4]$R_w = \Sigma\sqrt{w}(|F_o| - |F_c|)/\Sigma\sqrt{w}|F_o|$.

Results and Discussion

Views of the two molecules, together with the atom numbering scheme, are exhibited in Fig. 2. Bond lengths and bond angles for each structure are listed in Table 3, and conformational parameters, together with those for the related ribofuranoside, α-cytidine (data from ref. 1), are summarized in Table 4.

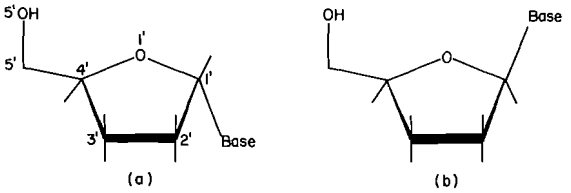

FIG. 1. The α (*a*) and β (*b*) anomeric configurations for a nucleoside.

Each structure exhibits the α-anomeric glycosyl linkage at C(1′) (see Fig. 1) with torsion angles, χ_{CN} (Table 5), of −25.1° and −28.6° for **1** and **1**·HCl, respectively, hence both in the *anti* domain. The glycosidic torsion angles are close to those reported for α-cytidine (1) and α-5-formyluridine (4), −28° and −22°, respectively, so that a χ_{CN} in this range appears reasonably typical for α-nucleosides with a 2′-hydroxyl *cis* to the aglycone.

Sugar Moieties

The pucker of the sugar rings is similar in the two structures: C(2′)*exo*—C(3′)*endo* in **1** and C(3′)*endo* in **1**·HCl. The former conformation is that observed in α-cytidine (1), and the latter in α-5-formyluridine (4), as well as in the α-nucleotide moiety of vitamin B_{12} (27). Furthermore, in the two crystallographically independent molecules of 9-α-D-arabinofuranosyladenine, the sugar moiety of one is C(2′)*exo*—C(3′)*endo*, and that of the other C(3′)*endo* (28). While it may be tempting to consider this narrow range of sugar conformations as preferred for nucleosides with the 2′-OH and the aglycone *cis* oriented, it should nonetheless be noted that a much broader range has been observed in the case of β-arabinofuranosyl nucleosides (29), as well as in other α-nucleosides (30).

This *cis* orientation of the 2′-OH and the aglycone results in a close approach between O(2′) and the ring N(1), which may be alleviated by various distortions. In **1** the $^{3}_{2}T$ pucker leads to the O(2′)—C(2′) and C(1′)—N(1) bonds being more staggered than in **1**·HCl, the difference in the torsion angle about C(1′)—C(2′) being 10° (Table 5). Furthermore, the N(1)—C(1′)—C(2′) bond angle is about 3° larger in **1** than in **1**·HCl. Consequently the N(1)···O(2′) contact in **1** is increased to 2.802 Å. On the other hand, the entire pyrimidine ring in **1**·HCl is displaced away from O(2′), as is clear from the large displacement (0.129 Å) of C(1′) from the ring plane. A similar, even larger, displacement (0.145 Å) was found in α-5-formyluridine (4). However, such distortion is not as effective in relieving the O(2)···N(1) interaction, this distance in **1**·HCl being a relatively short 2.674 Å. It follows that, in nucleosides in which the aglycone is *cis* to the O(2′), the sugar ring is unlikely to have ^{4}E or $_{4}E$ puckers, with the N(1)—C(1′)—C(2′)—O(2′) torsion angle approaching 0°, unless such a pucker is imposed by some structural features as, e.g. in the case of the cyclic O^{2},2′-anhydro-1-α-D-xylofuranosyluracil (31).

In both **1** and **1**·HCl, the conformation about the C(4′)—C(5′) bond is *trans–gauche*. In the case of ribonucleosides, the most commonly encountered conformation of the exocyclic 5′-CH_2OH is *gauche–gauche*. It is consequently of interest that

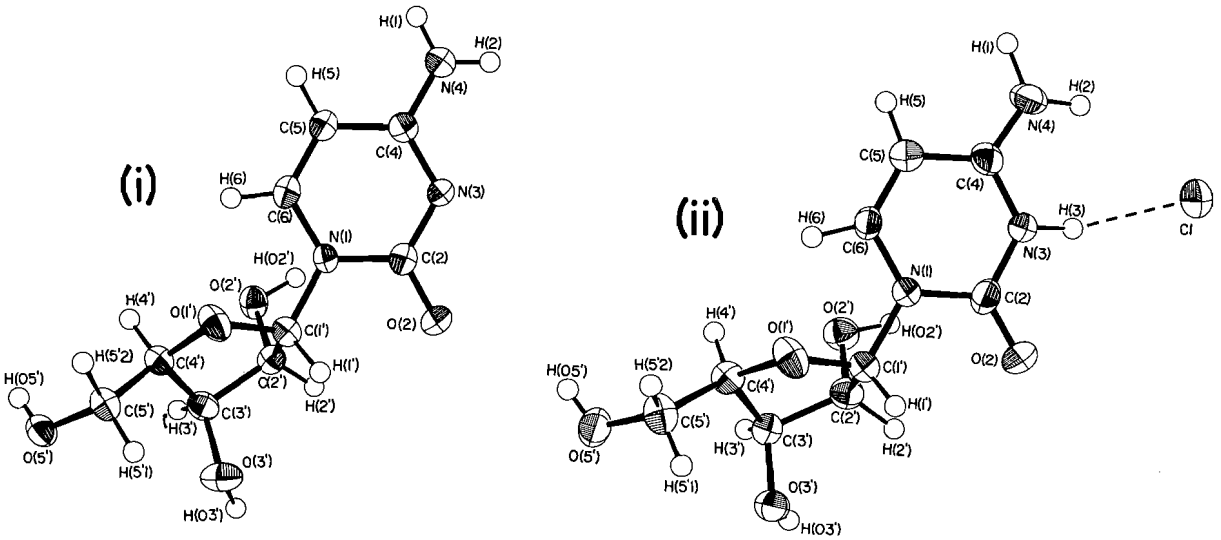

FIG. 2. Perspective views of (*i*) α-D-xylofuranosylcytosine (**1**), and (*ii*) α-D-xylofuranosylcytosine hydrochloride (**1**·HCl). Non-H atoms are represented by 50% probability thermal ellipsoids and H atoms by spheres of arbitrary radius.

Can. J. Chem. Downloaded from www.nrcresearchpress.com by 210.87.254.40 on 09/05/12
For personal use only.

Can. J. Chem. Downloaded from www.nrcresearchpress.com by 210.87.254.40 on 09/05/12
For personal use only.

TABLE 3. Bond lengths (Å) and angles (deg), with estimated standard deviations in parentheses

	Length			Length	
Bond	1	1·HCl	Bond	1	1·HCl
N(1)—C(2)	1.393(4)	1.385(5)	C(4′)—C(5′)	1.520(4)	1.509(5)
C(2)—O(2)	1.241(3)	1.211(5)	C(5′)—O(5′)	1.441(3)	1.418(5)
C(2)—N(3)	1.361(4)	1.370(5)	N(4)—H(1)	0.92(4)	0.97(5)
N(3)—C(4)	1.339(4)	1.352(5)	N(4)—H(2)	0.90(4)	0.85(5)
C(4)—N(5)	1.334(4)	1.314(5)	N(3)—H(3)	—	0.88(6)
C(4)—C(5)	1.432(4)	1.405(5)	C(5)—H(5)	1.01(4)	0.98(4)
C(5)—C(6)	1.345(4)	1.347(5)	C(6)—H(6)	1.00(4)	0.93(4)
C(6)—N(1)	1.358(4)	1.360(4)	C(1′)—H(1′)	1.05(3)	0.97(3)
N(1)—C(1′)	1.473(4)	1.475(5)	C(2′)—H(2′)	1.02(3)	1.06(4)
C(1′)—C(2′)	1.540(4)	1.544(5)	O(2′)—H(O2′)	0.97(4)	0.88(5)
C(2′)—O(2′)	1.418(4)	1.411(5)	C(3′)—H(3′)	0.95(3)	0.96(4)
C(2′)—C(3′)	1.528(4)	1.528(5)	O(3′)—H(O3′)	1.02(4)	0.73(5)
C(3′)—O(3′)	1.421(4)	1.421(4)	C(4′)—H(4′)	1.03(3)	0.98(4)
C(3′)—C(4′)	1.520(4)	1.523(5)	C(5′)—H(5′1)	1.00(4)	0.94(4)
C(4′)—O(1′)	1.446(3)	1.460(5)	C(5′)—H(5′2)	1.08(3)	1.02(4)
O(1′)—C(1′)	1.416(4)	1.404(4)	O(5′)—H(O5′)	0.75(5)	0.81(5)

	Angle			Angle	
Bonds	1	1·HCl	Bonds	1	1·HCl
C(2)—N(1)—C(6)	121.4(2)	121.6(3)	N(1)—C(1′)—C(2′)	114.1(2)	111.2(3)
C(2)—N(1)—C(1′)	117.6(2)	115.9(3)	O(1′)—C(1′)—C(2′)	106.2(2)	107.3(3)
C(6)—N(1)—C(1′)	121.0(2)	122.2(3)	C(1′)—C(2′)—C(3′)	100.7(2)	102.2(3)
N(1)—C(2)—N(3)	119.1(2)	114.9(3)	C(1′)—C(2′)—O(2′)	111.9(2)	111.7(3)
N(1)—C(2)—O(2)	119.3(2)	122.2(3)	O(2′)—C(2′)—C(3′)	108.3(2)	108.6(3)
O(2)—C(2)—N(3)	121.6(3)	122.9(3)	C(2′)—C(3′)—C(4′)	101.9(2)	101.8(3)
C(2)—N(3)—C(4)	119.7(2)	125.3(3)	C(2′)—C(3′)—O(3′)	110.4(2)	111.1(3)
N(3)—C(4)—C(5)	121.5(3)	117.6(3)	O(3′)—C(3′)—C(4′)	109.6(2)	110.1(3)
N(3)—C(4)—N(4)	119.7(3)	118.5(3)	C(3′)—C(4′)—O(1′)	105.7(2)	104.3(3)
N(4)—C(4)—C(5)	118.9(3)	123.8(4)	C(4′)—O(1′)—C(1′)	110.0(2)	110.2(3)
C(4)—C(5)—C(6)	118.0(3)	118.5(4)	C(3′)—C(4′)—C(5′)	116.9(2)	116.7(3)
C(5)—C(6)—N(1)	120.3(3)	122.0(3)	O(1′)—C(4′)—C(5′)	106.4(2)	106.4(3)
N(1)—C(1′)—O(1′)	108.4(2)	109.7(3)	C(4′)—C(5′)—O(5′)	110.0(2)	110.5(3)

TABLE 4. Conformational features for 1, 1·HCl, and α-cytidine (α-C)[a]

	Value		
Parameter	1	1·HCl	α-C[b]
Glycosyl torsion angle, χ_{CN}	−25.1	−28.6	−28.4
Pseudorotation angle, P	−1.9	18.1	−3.0
Sugar pucker	${}_2^3T$	${}^3E$	${}_2^3T$
Maximum angle of pucker, τ_m	38.4	37.1	39.0
ϕ_{OO}	169.3	173.5	−57.8
ϕ_{OC}	−72.9 } *tg*	−70.6 } *tg*	59.4 } *gg*

[a]All values expressed in deg.
[b]Data from ref. 1.

solution studies on a series of analogues of 9-β-D-xylofuranosyladenine demonstrated a relatively low (< 30%) population of the *gauche–gauche* form (32). Furthermore, in the solid state structure of 1-β-D-lyxofuranosyluracil in which both the 2′-OH and 3′-OH are "up", i.e. *cis* to the 5′-CH_2OH, the conformation of the latter is *gauche–trans*, while in solution the *gauche–gauche* populations for the neutral form and for the neutral and protonated forms of 1-β-D-lyxofuranosylcytosine are exceptionally low, from 10% to 20% (33). Similarly low *gauche–gauche* populations of the exocyclic 5′-CH_2OH have been reported for the solution conformations of the α- and β-xylofuranosides of oxidized and reduced nicotinamides (34). This effect has been ascribed to steric and electrostatic effects of the "up" 3′-OH, which is *cis*, and adjacent, to the 5′-CH_2OH group (33).

Can. J. Chem. Downloaded from www.nrcresearchpress.com by 210.87.254.40 on 09/05/12
For personal use only.

TABLE 5. Some torsional angles

Bonds	Torsional angle (deg) 1	1·HCl
C(6)—N(1)—C(1′)—O(1′):χ_{CN}	−25.1	−28.6
O(1′)—C(4′)—C(5′)—O(5′):ϕ_{OO}	169.3	173.5
C(3′)—C(4′)—C(5′)—O(5′):ϕ_{OC}	−72.9	−70.6
O(1′)—C(1′)—C(2′)—C(3′)	−32.8	−22.9
C(1′)—C(2′)—C(3′)—C(4′)	38.4	35.3
C(2′)—C(3′)—C(4′)—O(1′)	−31.8	−36.0
C(3′)—C(4′)—O(1′)—C(1′)	11.5	22.7
C(4′)—O(1′)—C(1′)—C(2′)	13.8	0.3
N(1)—C(1′)—C(2′)—O(2′)	−37.4	−26.9

Effects of Base Protonation

In the case of **1**·HCl, protonation occurs at the ring N(3), as might have been anticipated from previous X-ray studies (35), as well as from nmr solution data (36). Values of bond lengths in this portion of the cytosine ring are closely similar to those found in other protonated 1-substituted cytosines (35, 37–40). Thus, relative to the parent **1**, bonds C(2)—O(2) and C(4)—N(4) are shorter, and C(2)—N(3) and N(3)—C(4) slightly longer. This is accompanied by a decrease in bond angle at N(3)—C(4)—C(5) and N(1)—C(2)—N(3) of about 4°, with a similar increase at C(2)—N(3)—C(4). All of these changes are compatible with delocalization of the positive charge between the ring N(3) and the exocyclic N(4) (38, 39), as also observed in solution by ^{15}N nmr spectroscopy (36). In the neutral form, **1**, the heterocyclic ring atoms are planar within the limits of error, whereas in **1**·HCl N(3) is significantly displaced (0.012 Å) towards the chloride ion to which it is hydrogen bonded. The deviations of most of the hydrogen bond donor/acceptor atoms in the cytosine ring are in a direction such that a closer approach between H-bonded atom pairs occurs.

Hydrogen Bonding

All the hydrogen bonding in both structures is intermolecular (Table 6). In contrast to O^2,2′-1-α-D-xylofuranosyluracil, where *intra*molecular hydrogen bonding is observed between O(3′) and O(5′), viz. O(3′)—H···O(5′), in the solid state (31), no such intramolecular bonds are present in either **1** or **1**·HCl, where both the *trans–gauche* orientation at C(4′)—C(5′) and the C(3′)*endo* sugar pucker preclude its formation on purely geometrical grounds. Furthermore, for 9-β-D-xylofuranosyladenine in solution, where side chain and sugar ring conformations are not subject to crystal packing forces, no such hydrogen bonding occurs to any appreciable extent, if at all, for the neutral and protonated forms, or even in strongly alkaline medium where the sugar hydroxyl(s) ionize (32).

Crystal Packing

The modes of lattice packing are illustrated in Fig. 3, in which the hydrogen bonding interactions are also indicated. For the protonated form there is no overlap of bases in the solid state, the translational symmetry elements (see Fig. 3) ensuring, in this instance, the absence of close approaches of base atoms to symmetry-related molecules.

The situation is quite different for the neutral form, with mean base plane separations of 3.37 and 3.36 Å, these distances being between planes symmetrically related by the two unique 2-fold axes at $(\frac{1}{2}, 1)$ and $(\frac{1}{2}, \frac{1}{2})$, respectively, in the *ab* plane. The result is a base-stacking type of interaction (41) which is appreciable and occurs through the crystal lattice along a direction parallel to the *b*-axis. This is similar to the stacking pattern referred to as type III by Motherwell *et al.* (42), a pattern which is not the energetically preferred one and which is observed only infrequently. The perpendicularly projected overlap of bases amounts to approximately 30% in the case of the bases related by the $(\frac{1}{2}, 1)$ 2-fold axes, and approximately 0% for the $(\frac{1}{2}, \frac{1}{2})$ related bases. Consequently, extended base stacking is not predominant in the solid state. The

TABLE 6. Hydrogen bond distances (in Å) and angles (in deg)

Compound	*D*	*A*	*A* at	Distance H···*A*	Distance *D*···*A*	Angle *D*—H···*A*
1	O(2′)—H···N(3)		$1-x, 2-y, z$	1.79	2.747	169
	O(5′)—H···O(2)		$\frac{1}{2}-x, -\frac{1}{2}+y, 2-z$	1.92	2.667	177
	O(3′)—H···O(5′)		$\frac{1}{2}-x, \frac{1}{2}+y, 1-z$	1.75	2.771	176
	N(4)—H(1)···O(2)		$x, y, 1+z$	2.06	2.925	158
	N(4)—H(2)···O(5′)		$\frac{1}{2}+x, 1\frac{1}{2}-y, 2-z$	2.15	3.043	169
1·HCl	N(3)—H···Cl⁻		x, y, z	2.25	3.079	158
	O(3′)—H···Cl⁻		$-\frac{1}{2}+x, \frac{1}{2}-y, 1-z$	2.30	3.018	169
	O(2′)—H···O(3′)		$1-x, -\frac{1}{2}+y, \frac{1}{2}-z$	1.90	2.761	163
	O(5′)—H···O(2)		$x, y, -1+z$	1.96	2.748	165
	N(4)—H(1)···O(5′)		$\frac{1}{2}+x, \frac{1}{2}-y, \bar{z}$	1.93	2.856	160
	N(4)—H(2)···O(2′)		$1\frac{1}{2}-x, \bar{y}, \frac{1}{2}+z$	2.46	2.952	118

Can. J. Chem. Downloaded from www.nrcresearchpress.com by 210.87.254.40 on 09/05/12
For personal use only.

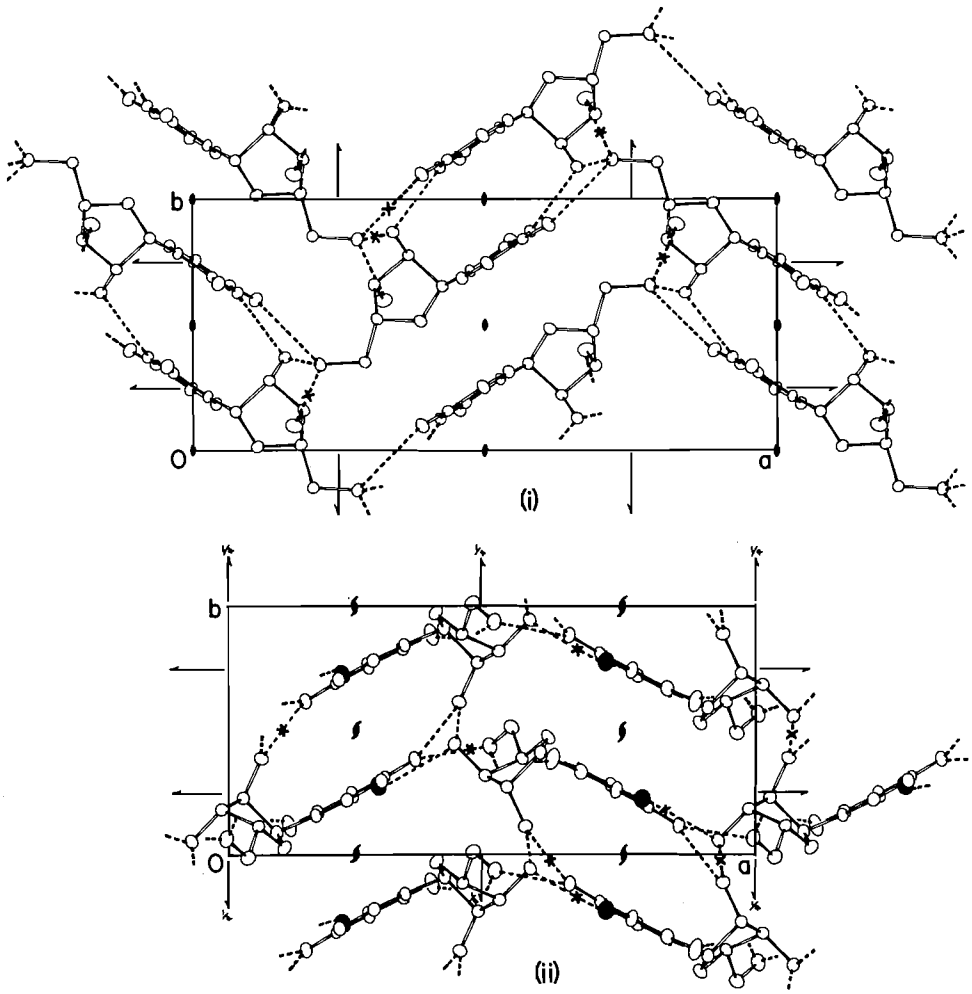

FIG. 3. Packing diagrams for (*i*) α-D-xylofuranosylcytosine (**1**) and (*ii*) α-D-xylofuranosylcytosine hydrochloride (**1**·HCl). In each case the view direction is parallel to the *c*-axis. Broken lines represent H-bond interactions with a cross to indicate that one of the molecules involved is related to that shown by a cell translation along *c*. In (*ii*), the chloride ion is shaded.

position of N(3), which is close to the centre of its "paired" base, when viewed in projection, is closely similar to the arrangement in the solid state structure of α-cytidine (1). Since protonation of N(3) usually precludes base stacking (38), this position may possibly be preferred for certain stacking modes (41), and is one which cannot be maintained on protonation, owing to the proximity of positive charges. It should, nonetheless, be noted that base stacking has been observed in the solid state structures of cytosine hydrochloride (38) and 1-methyl-N^4- hydroxycytosine hydrochloride (43).

Furthermore, in a study on the structure of the (1-methylcytosine)–(1-methylcytosine·H^+) complex, the two molecules were found to form asymmetrically hydrogen-bonded dimers, which were stacked in such a manner that molecular overlap was between charged and neutral bases (40). The mean stacking distance was 3.22 Å. The resulting base stacking mode, which is of obvious significance in relation to the solution conformation of protonated poly(rC), was considered to be favoured by overlapping of protonated with neutral species. It is, consequently, of interest to note that in the crystal structure of 1-methyl-N^4-hydroxycytosine·HCl, base overlapping is at least as extensive as in the foregoing complex, with an interplanar distance of about 3.25 Å (43); furthermore, the protonated N(3) atoms of the stacked molecules are even closer to each other in the latter structure than the protonated and non-protonated N(3) atoms in the (1-methylcytosine)–(1-methylcytosine·H^+) structure.

Biological Aspects

In the absence of data regarding antimetabolic

Can. J. Chem. Downloaded from www.nrcresearchpress.com by 210.87.254.40 on 09/05/12
For personal use only.

activities of α-xylofuranosyl nucleosides, it is perhaps premature to discuss the conformational features of the present structures which may be of significance in various enzymatic systems. Model building studies do not reveal structural analogies between the α- and β-anomers of xylofuranosylcytosine as in the case of the anomers of 2′- deoxy-6-thioguanosine (6). However, some data of Bennett and Hill (44) are relevant to the foregoing. These authors examined the substrate properties towards adenosine kinase of a variety of anomeric nucleosides of adenine and 8-azaadenine in which the sugar moieties included arabinofuranose, xylofuranose, and lyxofuranose. Amongst these 9-β-D-xylofuranosyl-8-azaadenine and 9-α-L-lyxofuranosyladenine were good substrates. In general, it appeared that substrate activity required the presence of a 2′-hydroxyl *trans* to the aglycone, and a considerable degree of freedom about the glycosidic bond; with these conditions, it was irrelevant whether the 3′-hydroxyl or the exocyclic carbinol group are *cis* or *trans* relative to the aglycone. From these criteria it is obvious that the α-anomer of xylofuranosyladenine should not be a substrate, but this analogue was apparently not available. In view of the known importance of intracellular conversion of nucleoside analogues to their 5′-phosphates, which are the active analogues, it will obviously be of interest to examine the substrate properties towards pyrimidine nucleoside kinase(s) of the title compound of this study, the more so in that the α-anomers of a number of ribo-, deoxyribo-, and arabino-furanosyl nucleosides have been established as potent antimetabolites.

Acknowledgments

We are indebted to Dr. J. Giziewicz for synthesis of the title compounds. One of us (M.L.P.) is grateful to the National Research Council of Canada for the award of a Research Associateship (1975–1978) during the course of this investigation. The support of the Polish National Cancer Research Program (PR-6/1701, to D.S.) is also acknowledged.

1. M. L. Post, G. I. Birnbaum, C. P. Huber, and D. Shugar. Biochim. Biophys. Acta, **479**, 133 (1977).
2. A. Holy. Coll. Czech. Chem. Commun. **38**, 100 (1973).
3. T. Kulikowski and D. Shugar. J. Med. Chem. **17**, 269 (1974).
4. V. W. Armstrong, H. Sternbach, and F. Eckstein. Biochemistry, **15**, 2086 (1976).
5. A. J. Grant and L. M. Lerner. J. Med. Chem. **22**, 1016 (1979).
6. E. M. Acton, R. N. Goerner, H. S. Uh, K. J. Ryan, D. W. Henry, C. E. Cass, and G. A. LePage. J. Med. Chem. **22**, 518 (1979).
7. C. W. Smith, R. W. Sidwell, R. K. Robins, and R. L. Tolman. J. Med. Chem. **15**, 883 (1972).
8. D. Shugar. FEBS Lett. **40** (Suppl.), S48 (1974).
9. L. L. Bennett, W. M. Shannon, P. W. Allan, and G. Arnett. Ann. N.Y. Acad. Sci. **255**, 342 (1975).
10. L. L. Bennett, J. A. Montgomery, R. W. Brockman, and Y. F. Shealy. Adv. Enz. Regul. **16**, 255 (1978).
11. P. B. Sehgal and I. Tamm. Biochem. Pharmacol. **27**, 2475 (1978).
12. DCT Bulletin, Cancer Therapy Evaluation Program, N.C.I., No. 3 (1979).
13. A. Peery and G. A. LePage. Cancer Res. **29**, 617 (1969).
14. Y. Nakai and G. A. LePage. Cancer Res. **32**, 2445 (1972).
15. T. Tamaoki and G. A. LePage. Cancer Res. **35**, 1015 (1975).
16. M. Sundaralingam. Ann. N.Y. Acad. Sci. **255**, 3 (1975).
17. C. Altona and M. Sundaralingam. J. Am. Chem. Soc. **95**, 2333 (1973).
18. P. Roy-Burman. Recent Results Cancer Res. **25**, 1 (1970).
19. J. F. Henderson, C. M. Smith, F. F. Snyder, and G. Zombor. Ann. N.Y. Acad. Sci. **255**, 489 (1975).
20. G. A. LePage and S. Naik. Ann. N.Y. Acad. Sci. **255**, 481 (1975).
21. R. I. Glazer and A. L. Peale. Biochem. Biophys. Res. Commun. **81**, 521 (1978).
22. R. I. Glazer and A. L. Peale. Cancer Lett. **6**, 193 (1979).
23. J. A. Ibers and W. C. Hamilton (*Editors*). International tables for X-ray crystallography. Vol. IV. Kynoch Press, Birmingham. 1974.
24. R. F. Stewart, E. R. Davidson, and W. T. Simpson. J. Chem. Phys. **42**, 3175 (1965).
25. F. R. Ahmed, S. R. Hall, M. E. Pippy, and C. P. Huber. J. Appl. Crystallogr. **6**, 309 (1973).
26. C. K. Johnson. ORTEP Report ORNL-3794. 2nd revision. Oak Ridge, TN. 1970.
27. P. G. Lenhert. Proc. R. Soc. Ser. A, **303**, 45 (1968).
28. S. J. Cline and D. J. Hodgson. Biochim. Biophys. Acta, **563**, 540 (1979).
29. G. I. Birnbaum, E. Darzynkiewicz, and D. Shugar. J. Am. Chem. Soc. **97**, 5904 (1975).
30. M. Sundaralingam. J. Am. Chem. Soc. **93**, 6644 (1971).
31. G. I. Birnbaum, J. Giziewicz, C. P. Huber, and D. Shugar. J. Am. Chem. Soc. **98**, 4640 (1976).
32. I. Ekiel, E. Darzynkiewicz, L. Dudycz, and D. Shugar. Biochemistry, **17**, 1530 (1978).
33. I. Ekiel, E. Darzynkiewicz, G. I. Birnbaum, and D. Shugar. J. Am. Chem. Soc. **101**, 4724 (1979).
34. N. J. Oppenheimer. J. Carbohydr. Nucleosides Nucleotides, **5**, 251 (1978).
35. J. J. Guy, L. R. Nassimbeni, G. M. Sheldrick, and R. Taylor. Acta Crystallogr. Sect. B, **32**, 2909 (1976).
36. V. Markowski, G. R. Sullivan, and J. D. Roberts. J. Am. Chem. Soc. **99**, 714 (1977).
37. J. S. Sherfinski and R. E. Marsh. Acta Crystallogr. Sect. B, **29**, 192 (1973).
38. N. S. Mandel. Acta Crystallogr. Sect. B, **33**, 1079 (1977).
39. M. A. Viswamitra, B. S. Reddy, G. H.-Y. Lin, and M. Sundaralingam. J. Am. Chem. Soc. **93**, 4565 (1971).
40. T. J. Kistenmacher, M. Rossi, and L. Marzilli. Biopolymers, **17**, 2581 (1978).
41. C. E. Bugg, J. M. Thomas, M. Sundaralingam, and S. T. Rao. Biopolymers, **10**, 175 (1971).
42. W. D. S. Motherwell, L. Riva di Sanseverino, and O. Kennard. J. Mol. Biol. **80**, 405 (1973).
43. G. I. Birnbaum, T. Kulikowski, and D. Shugar. Can. J. Biochem. **57**, 308 (1979).
44. L. L. Bennett and D. L. Hill. Mol. Pharmacol. **11**, 803 (1975).

Thione photochemistry. Dual pathways in aralkyl thione cyclizations[1]

S. Basu, Axel Couture, Kam W. Ho, Mikio Hoshino, Paul de Mayo, and R. Suau
Photochemistry Unit, Department of Chemistry, University of Western Ontario, London, Ont., Canada N6A 5B7

Received June 12, 1980

This paper is dedicated to Prof. Raymond U. Lemieux on the occasion of his 60th birthday

S. Basu, Axel Couture, Kam W. Ho, Mikio Hoshino, Paul de Mayo, and R. Suau. Can. J. Chem. **59**, 246 (1981).

It is shown that aralkyl thiones, which possess an oxygen atom at the δ position in the side chain, can therefore not undergo the preferred δ insertion, and insert at the γ and ε positions. Although ε insertion occurs only from the $^1(\pi,\pi^*)$ state, γ abstraction (followed by cyclization or cleavage) occurs from both $^1(\pi,\pi^*)$ and $^3(n,\pi^*)$ states. The quantum yields of photocyclization of **2***c*, **2***d*, and **2***g* change little with solvent polarity, which suggests that a thione–ether charge transfer interaction contributes little to the cyclization. Fluorescence and product quenching studies are reported which support this.

S. Basu, Axel Couture, Kam W. Ho, Mikio Hoshino, Paul de Mayo et R. Suau. Can. J. Chem. **59**, 246 (1981).

On montre que les aralkylthiones qui, dans la chaîne latérale, possèdent un atome d'oxygène en position δ ne peuvent pas subir une insertion privilégiée en position δ mais seulement en positions γ et ε. Quoique l'insertion ε se produise seulement à partir de l'état $^1(\pi,\pi^*)$, l'élimination en position γ (suivie d'une cyclisation ou d'une rupture) a lieu à partir des deux états $^1(\pi,\pi^*)$ et $^3(n,\pi^*)$. Les rendements quantiques de la photocyclisation de **2***c*, **2***d* et **2***g* qui changent à peine avec la polarité du solvant suggèrent que l'interaction de transfert de charge éther–thione contribuent faiblement à la cyclisation. On rapporte les études de fluorescence et de rupture des produits qui appuient cette suggestion.

[Traduit par le journal]

Can. J. Chem. Downloaded from www.nrcresearchpress.com by 210.87.254.42 on 09/05/12
For personal use only.

Introduction

In the previous papers of this series (1) we have shown that aralkyl thiones containing a hydrocarbon side chain, upon irradiation into the π,π^* band, cyclize to yield cyclopentane thiols. No such reaction was observed following excitation into the n,π^* state. In fact, the quantum yield of disappearance of such a thioketone is $\sim 10^{-2}$ upon π,π^* excitation and $\leq 10^{-5}$ upon n,π^* excitation.

Typically, in the thione **2***d*, ~40% of the thione molecules in the π,π^* state underwent δ-H abstraction, the remainder decaying radiationlessly. The hydrogen abstraction (Scheme 1) gave a 1,5-biradical whose lifetime was $< 10^{-8}$ s, and only one-tenth of these biradicals cyclized to product **3**, the remainder disproportionating to regenerate the thione.

No γ- or ε-cyclizations were observed in those thiones containing only hydrocarbon side chains, even when there were more ε-hydrogen atoms than δ-hydrogen atoms, as in 1-phenyl-2,2,5,5-tetramethylthiohexanone **6** and 1-phenyl-2-2-5-trimethylthiopentanone **7**.

We report here[2] that in those cases such as **2***g*, where the δ-carbon is replaced by an oxygen atom, S_2 excitation leads to the formation of both four-membered **4** and six-membered ring thiols **5**

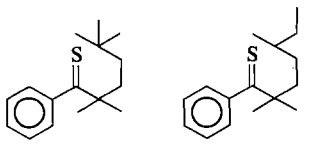

6 **7**

(Scheme 2). Furthermore, Type II reaction products, i.e. ethyl vinyl ether and cyclobutanethiol, **4**, are now isolated upon n,π^* excitation and lead us to conclude that there are two routes to the Type II products.

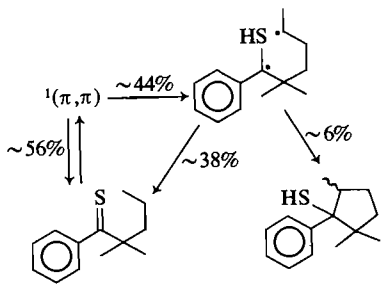

2*d* **3**

Scheme 1

Results

Preparative

The thiones **2**, *a–f*, have already been described (1*b*). Of the remainder, **2***i* will be described elsewhere, **2***g* and **2***j* were prepared from the corre-

[1]Photochemical Synthesis 79. Part No. 246 from the Photochemistry Unit, University of Western Ontario.

[2]Part of the material reported has been described in preliminary form (1*a*).

0008-4042/81/020246-09$01.00/0

©1981 National Research Council of Canada/Conseil national de recherches du Canada

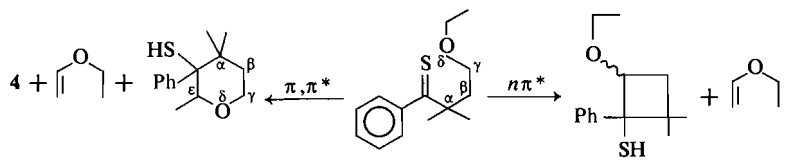

5 2g 4

SCHEME 2

sponding ketones **1***g* and **1***j* which were, in turn, prepared by condensing the enolate anion of isobutyrophenone with the appropriate bromide. The ketone **1***h* was obtained by condensing the anion of isobutyrophenone with allyl bromide, followed by hydroxylation of the olefin with potassium permanganate to give the vicinal diol which was then methylated with methyl iodide. All thiones had closely similar absorption spectra, and this, together with the constant reduction potential (Table 2), suggested that there was insignificant interaction between the ground state thiocarbonyl function and any side chain, even when the latter was oxygenated.

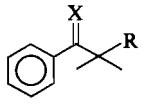

1 X=O
2 X=S

a R = CH_2CH_3
b R = $CH_2CH_2CH_3$
c R = $CH_2CH(CH_3)_2$
d R = $CH_2CH_2CH_2CH_3$
e R = CH_3
f R = $CH_2CH_2CH(CH_3)_2$
g R = $CH_2CH_2OCH_2CH_3$
h R = $CH_2CH(OCH_3)(CH_2OCH_3)$
i R = CH_2OCH_3
j R = $CH_2CH_2CH_2OCH_3$

Preparative irradiations were conducted with benzene as solvent through Pyrex (excitation of S_1, S_2) and through a Corning filter 3-72 (S_1 only).

Irradiation of **2***g* through Pyrex gave **4** (45%), ethyl vinyl ether (5%), together with **5** (40%) (Scheme 2). Excitation of **2***g*, at $\lambda > 445$ nm slowly gave a complex mixture from which **4** (45%) and ethyl vinyl ether (10%) were isolated; no **5** could be detected. Irradiation of **2***h* gave **10** (32%) as a mixture of isomers and **11** (36%); at >450 nm **2***h* gave a mixture from which **10** and **11** were both absent. Both β-methoxy **2***i* and δ-methoxy **2***j* thiones underwent δ-cyclization in high yields to give thiols **12** (85%) and **13** (100%), respectively, when irradiated through Pyrex, but irradiation at $\lambda > 445$ nm did not lead to appreciable reaction; there was no change in the nmr spectrum after 2 weeks of using two 450 W lamps.

All the thiols were identified by the absorption at $\sim 2580\,cm^{-1}$ and the presence of an exchangeable (D_2O) uncoupled proton ~δ 2.0 in the ^1H nmr spectra. All five aromatic protons remained. No molecular ion peak was observed in the mass spectra, but M − H_2S and M − (H_2S + CH_3) were evident. Also, the thiols **10**, **11**, and **12**, were converted into olefins **14**, **15**, and **16**, respectively, in high yields, by the action of mercuric acetate.

Mechanistic Studies

The quantum yields of disappearance of **2***j* and formation of **13** were measured in benzene and acetic acid, both stereoisomers of **13** being estimated separately (Table 1). The ratios of the quantum yield of product formation and of disappearance in both solvents were ~0.85, consistent with the isolated yield of product. The drop in quantum yield from benzene to acetic acid is not attributed to solvent–thione interaction since there is no appreciable change in the π,π* band (297 nm); there is a blue shift (565 → 550 nm) in the *n*,π* absorption. The quantum yields of disappearance (2) of **2***j* and **2***i* were 2.7×10^{-2} and 4.9×10^{-2} at short wavelength (313 ± 5 nm), but at long wavelength were $\leq 10^{-4}$. The quenching of formation of **4** and **5** from **2***g* by biacetyl was possible at 313 nm with correction for quencher absorption; the plots of reciprocal quantum yield against biacetyl concentration are given in Fig. 1. The quantum yield of **5** ($7.4 \pm 0.5 \times 10^{-3}$) was unchanged in the presence of 1.7 *M* piperylene ($7.4 \pm 0.5 \times 10^{-3}$). Attempted

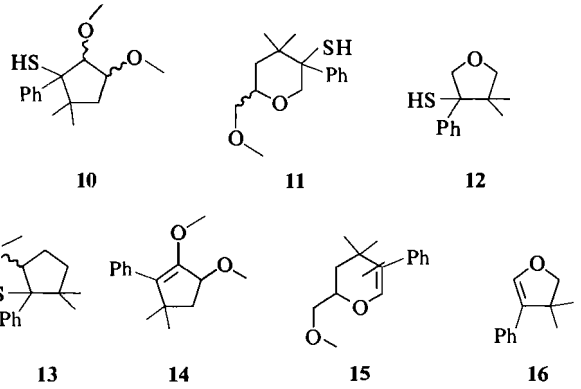

10 **11** **12**

13 **14** **15** **16**

Can. J. Chem. Downloaded from www.nrcresearchpress.com by 210.87.254.42 on 09/05/12
For personal use only.

TABLE 1. Quantum yields of photocyclization of thioketone **2***j* at room temperature

	Concentration (M)	$\Phi_R{}^{1\,a}$	$\Phi_R{}^{2\,a}$	$\Phi_{dis}{}^{b}$	Conversion (%)
Benzene	7.2×10^{-3}	2.1×10^{-2}	2.1×10^{-2}	0.048	4.4
	9.7×10^{-3}	2.0×10^{-2}	2.1×10^{-2}	0.056	3.7
	1.7×10^{-2}	2.0×10^{-2}	2.1×10^{-2}		
Acetic acid	1.9×10^{-2}	1.0×10^{-2}	1.3×10^{-2}	0.028	1.6
	1.1×10^{-2}	1.1×10^{-2}	1.5×10^{-2}	0.026	2.8

[a]The quantum yields of formation of the cyclopentane thiols. The superscripts 1 and 2 indicate the different thiols in order of elution from the vpc column.
[b]The quantum yield of disappearance of the thioketone.

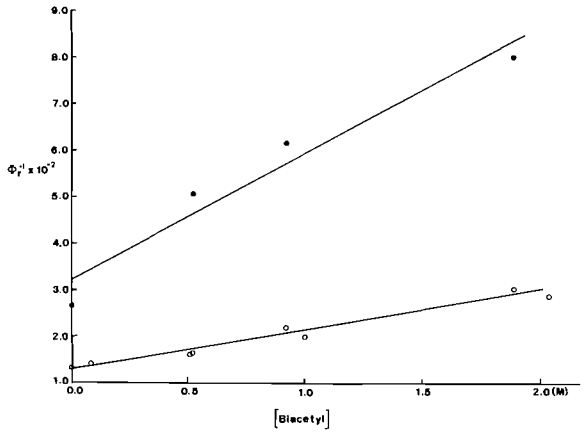

FIG. 1. The quantum yields of formation at **4** (●) and **5** (○) from the π,π^* excited thione **2***g* in the presence of biacetyl in benzene. The slope of **4** is $2.7 \times 10^{-2}\,M^{-1}$, intercept 320; the slope of **5** is $89\,M^{-1}$, intercept 125.

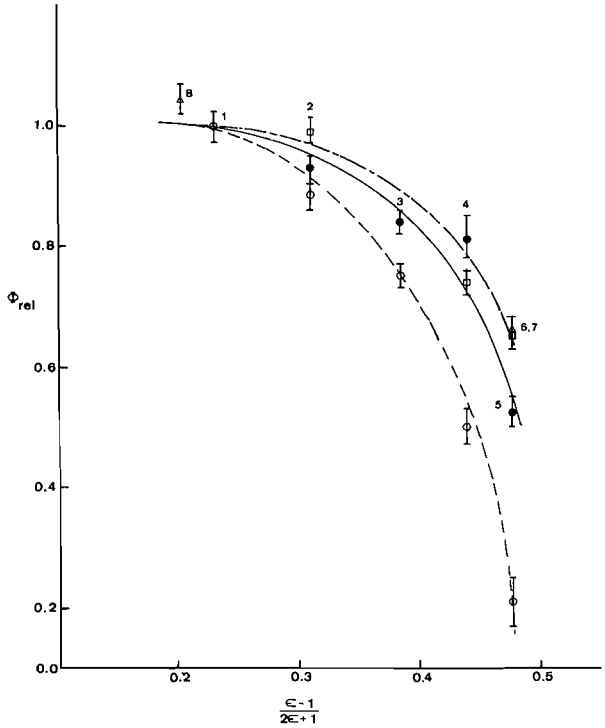

FIG. 2. Solvent effect on the quantum yield of photocyclization of π,π^* excited thiones at room temperature. The quantum yields (Φ_{rel}) are expressed relative to that in benzene. Solvents: 1, benzene; 2, 1,2-dimethoxyethane; 3, ethyl acetate; 4, *tert*-butyl alcohol; 5, ethanol; 6, acetic acid; 7, acetonitrile; 8, cyclohexane. Reactions studied are **2***g* → **4** (○), **2***g* → **5** (●), photocyclization of **2***c* (△) and **2***d* (□).

sensitization of the reaction with benzophenone, 2-acetonaphthone, and chrysene (E_T 69, 59.4, and 56.6 kcal/mol) was unsuccessful.

The photocyclization of **2***d* and **2***g* was studied at short wavelength in solvents of different polarities. The results, together with those observed previously for **2***c*, are given relative to that in benzene, and are plotted against the solvent polarity function $\{2(\varepsilon - 1)/2\varepsilon + 1\}$ (3) (Fig. 2). All efficiencies decrease with increasing polarity, **4** being most sensitive.

Charge Transfer Studies

The fluorescence of **2***a* was quenched by a variety of molecules whose excited states were higher than the π,π^* state of the thione. Using hexane and acetonitrile as solvents, the logarithms of the quenching rate constants were plotted against the ionization potential of the quenchers (Figs. 3 and 4). Two values for **2***b* (triethylamine and ethyl vinyl ether) are included in Fig. 3. The excited thiones appear to act as electron acceptors with regard to all species except acrylonitrile and fumaronitrile, towards which they act as donors. The photocyclization itself is also quenched by electron donors; the quenching of **2***c* and **2***d* by triethylamine has already been reported (1*c*); the quenching of the cyclization of **2***c* by di-*n*-butyl sulfide is shown in Fig. 5.

Reduction Potentials of Thiones

In Table 2 are presented the polarographic half-wave potentials of aromatic thioketones in dry acetonitrile containing 0.1 M tetraethylammonium perchlorate at 20°C. The potentials were measured against a silver – silver chloride electrode (aqueous) after removal of oxygen by purging with nitro-

Can. J. Chem. Downloaded from www.nrcresearchpress.com by 210.87.254.42 on 09/05/12
For personal use only.

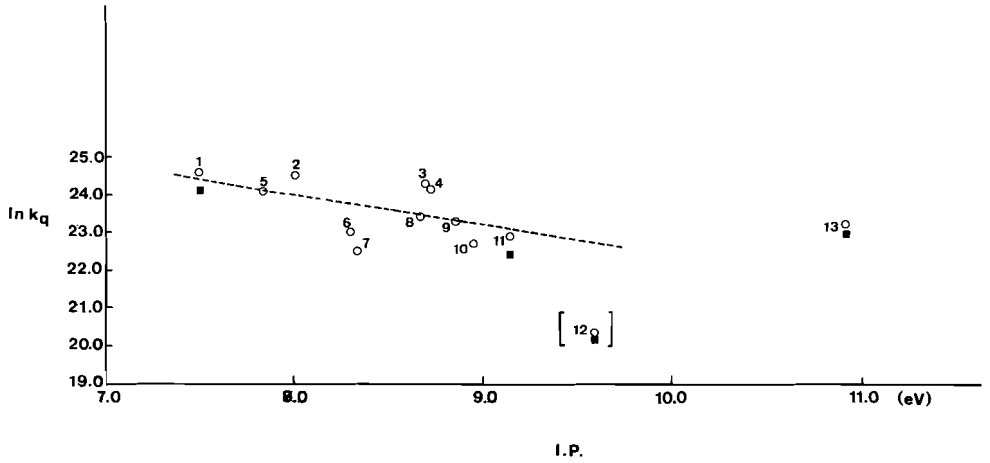

FIG. 3. Plot of the logarithm of fluorescence quenching rate constant against the ionization potential of quencher in hexane at 20°C. Thiones studied are **2***a* (○) and **2***b* (■). Quenchers: 1, triethylamine; 2, diethylamine; 3, 2-butylamine; 4, 2-propylamine; 5, 2,5-dimethyl-2,4-hexadiene; 6, di-*n*-butylsulfide; 7, 2,3-dihydropyran; 8, 2-methyl-2-butene; 9, isoprene; 10, cyclohexene; 11, ethyl vinyl ether; 12, diethyl ether (at the limit of detection; value may not be real); 13, acrylonitrile. The slope obtained by least-squares fitting method was $-0.86\,eV^{-1}$ (diethyl ether and acrylonitrile were excluded).

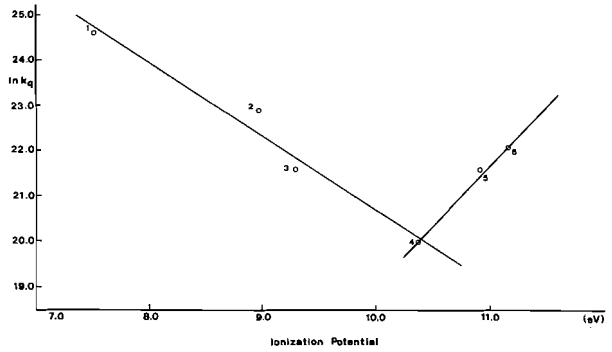

FIG. 4. Plot of logarithm of the fluorescence quenching rate constant against the ionization potential of quencher for thione **2***a* in acetonitrile at 20°C. Quenchers: 1, triethylamine; 2, cyclohexene; 3, pyridine; 4, acetic acid; 5, acrylonitrile; 6, fumaronitrile. The slopes of both lines obtained by least-squares fitting method were $-1.63\,eV^{-1}$ for donors and $2.7\,eV^{-1}$ for acceptors.

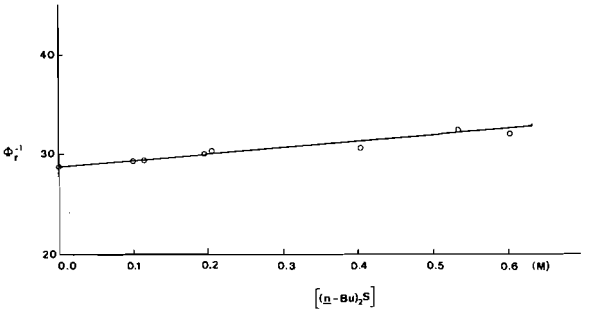

FIG. 5. Plot of the reciprocal of quantum yield of photocyclization of **2***c* against the concentration of di-*n*-butylsulfide in benzene. Slope and intercept obtained by least-squares fitting method were $6.1\,M^{-1}$ and 28.7.

gen. The polarographic current–voltage curves were obtained using a PAR model 170 system.

The reduction potentials of the thiones can also be estimated by the two following equations.

(*a*) Elofson's equation (4) (eq. [1]):

$$[1]\quad \text{Absorption maximum of the } {}^1n,\pi^* \text{ band (eV)} = (-0.59 \pm 0.04)E_{\frac{1}{2}}^{Red} + (1.46 \pm 0.11)$$

The $E_{\frac{1}{2}}^{Red}$ is the half-wave potential of the reduction of thioketone measured against the SCE. The energy of the maximum of the ${}^1n,\pi^*$ band of aralkyl thioketone is 2.14 eV. Therefore, the estimated reduction potential of aralkyl thioketone, against the SCE, is −1.17 V. Similarly, the reduction potential of thiobenzophenone is estimated to be −0.91 V.

(*b*) Loutfy's equation (5) (eq. [2]):

$$[2]\quad E_{\frac{1}{2}}^{Red}(C{=}S) = 1.06\,E_{\frac{1}{2}}^{Red}(C{=}O) - 0.79$$

vs. $(Ag/AgCl_s)$ electrode in acetonitrile.

Taking the reduction potential of acetophenone (−1.99 V in DMF) against the SCE (6) the thiones may be estimated as −1.32 V against $Ag/AgCl_s$ in acetonitrile (solvent correction −0.4 V (7)); correction for $Ag/AgCl_s$ in water against SCE at 20°C is

TABLE 2. Reduction potentials of aromatic thioketones in acetonitrile at 20°C

Thione	Concentration ($M \times 10^{-3}$)	$E_{\frac{1}{2}}^{red}$(V)
Thiobenzophenone	4.28	−1.03
2*e*	3.06	−1.35
2*f*	2.19	−1.30
2*g*	2.19	−1.35

Can. J. Chem. Downloaded from www.nrcresearchpress.com by 210.87.254.42 on 09/05/12
For personal use only.

Can. J. Chem. Downloaded from www.nrcresearchpress.com by 210.87.254.42 on 09/05/12
For personal use only.

−0.04 V (7). The assumption is made that alkyl sidechains have no effect. The estimated potential of thiobenzophenone (−1.17 V vs. SCE in MeCN) is −1.13 V vs. $Ag/AgCl_s$.

Discussion

From the results reported a number of conclusions can be drawn: (*a*) in the absence of ethereal oxygen abstraction occurs only at the δ position; (*b*) with an ethereal oxygen at the δ position, and if no other δ hydrogen is available, abstraction occurs at ε and γ positions (the latter being accompanied by Type II cleavage); (*c*) when activated ε (primary) and δ (secondary) hydrogen is available (as in **2***h*) roughly equal amounts of δ and ε cyclization products are obtained. As might have been expected, the position of attack is the result of balanced stereochemical and energetic factors and the former is not, as was originally thought in the absence of results from the ethers, overwhelming.

Although the Type II process is observed in **2***g* (Scheme 2), following excitation into both upper and lower excited states, they follow essentially separate paths; that is, the product derived from excitation into the S_2 state is *not* in large measure obtained by preliminary internal conversion to the lower excited state. This follows because the quantum yield of formation of one of the stereoisomers of the cyclobutane thiols **4** was 3.5×10^{-3} from S_2 as against $< 10^{-4}$ upon excitation into the S_1 state. Further, this Type II reaction could not be sensitized with the higher efficiency with sensitizers of energy from 55–69 kcal/mol, nor could it, when initiated from S_2, be quenched with piperylene. There are, therefore, two distinct pathways for the Type II cleavage and closure, whereas the accompanying product from S_2 excitation, **5** ($\phi = 7 \times 10^{-3}$), is not formed on S_1 excitation and is derived by a single pathway.

In the short wavelength excitation of **2***g* both **4** and **5** formation should, then, derive from a single intermediate. Both processes are quenched by biacetyl, and the Stern–Volmer plots (Fig. 1) indicate, within experimental error, the same lifetime for the common responsible excited state (170 and 140 ps respectively). The rates of formation of **4** and **5** are $2.1 \times 10^7\ s^{-1}$ and $5.2 \times 10^7\ s^{-1}$ respectively. The entropy required to freeze an internal C—C rotation in achieving the transition state is 4–5 gibbs (8) yet, despite the fact that two more rotations have to be frozen in its formation, **5** is generated faster than **4**. We attribute this to the difficulty the γ-hydrogen has in attaining the reactive volume of space (π) above and below the plane of the thione group (9).

In view of the efficient intersystem crossing in thiones the Type II products derived from S_1 excitation probably derive from the triplet (10). The difference in quantum yield obtained by this pathway to these products and that obtained from S_2 has at least three sources.

Firstly, the abstractions themselves differ in efficiency for energetic reasons. Good values are not available for the thiocarbonyl group, but a crude approximation using Benson's data (11) suggests that from the triplet (E_T = 46 kcal/mol) biradical formation might be close to thermoneutral, depending upon the value chosen for the conjugated thione and the weakening of S—H bond by an adjacent carbon-centered radical. Similarly, one may assume that the π bond energy of the C=S linkage is roughly equal to that of the triplet,[3] when the overall reaction involves the additional C—H cleavage and SH formation. Biradical formation, on the other hand, from the S_2 state is very exothermic (1*c*). Secondly, the geometry of the abstractions, as discussed elsewhere (9), is different. Since n,π^* and π,π^* abstractions occur in orthogonal planes, the conformational requirements in the transition state differ, γ abstraction from S_2 appearing markedly more difficult. Thirdly, the n,π^* pathway leads first to a triplet biradical. In its longer lifetime conformational change may occur to favour one or other of the chemical processes (elimination closure and disproportionation) open to it after spin relaxation to the singlet. The S_2 pathway presumably leads directly to the singlet.

It is interesting that the biradical **17***b* derived from **17***a* gives cyclobutanol and methyl vinyl ether in a ratio of 1:2.5 (13) whereas the biradical **18** derived from β-phenylethylthiobenzoate (14) gives only the elimination product. From **2***g* (Scheme 2) the ratio of cyclobutanethiol **4** to ethyl vinyl ether (n,π^*) was found to be 4:1. The lack of elimination from the biradical may be attributed to the presence of the two α-methyl substituents which in the transoid conformation for elimination are eclipsed with the thiol and phenyl groups **19**. This effect may also be observed in the ratio of cyclization and elimination of biradicals derived from thiobenzoate abstraction. As the β-substituent becomes larger the cyclization becomes more important, and becomes the major process when a *tert*-butyl group is present, as in **20**.

[3]This appears to be approximately true for carbonyl compounds. It is in approximate agreement with Benson's estimate of 55 kcal/mol for the π strength of thioformaldehyde (11). The energy of the $^3n,\pi^*$ state of thioformaldehyde was calculated to be 36–44 kcal/mol (12).

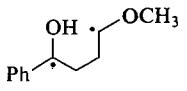

17*b*

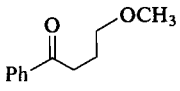

17*a*

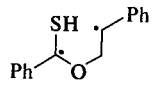

18

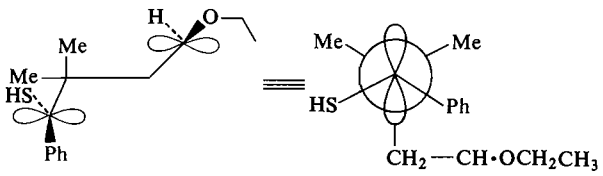

19

We have considered the possibility that intramolecular charge transfer occurs from the oxygen to the excited thione, followed by proton transfer. We believe this to be excluded both because of the poor quenching of the $^1\pi,\pi^*$ thione by ether and because of the decrease in the quantum yields of **4**, **5**, and other cyclopentane thiols with increasing solvent polarity (Fig. 2). The invariance of the π,π^* absorption band of **2***d* and **2***j* with solvent is also indicative of a lack of interaction. The small decrease in quantum yield observed may be because of different conformation populations in the various solvents, given that the conformers have different dipole moments.[4] Further, in protic solvents hydrogen bonding to the ethereal oxygen may also cause conformer population changes.

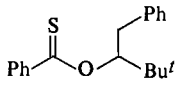

20

Charge Transfer in the $^1\pi,\pi^*$ Excited Thiones

The interactions of the π,π^* excited thioketone and some electron-donating and electron-accepting quenchers were studied in two ways: the change of the fluorescence quantum yield and the change of the quantum yield of photocyclization in the presence of charge transfer quenchers.

The free energy change for the formation of a charge transfer complex, ΔG_{CT}, in the excited state is given by eq. [3] (17).

$$[3] \quad \Delta G_{CT} = E(D/D^+) = E(A^-/A) = \Delta E_{o,o} + \Delta$$

where $E(D/D^+)$ is the oxidation potential of the donor, $E(A^-/A)$ is the reduction potential of the acceptor, $\Delta E_{o,o}$ is the excitation energy of the thioketone, Δ is the interaction term including the Coulombic term and entropy of interaction. Since the ionization potential, IP, and electron affinity, EA, of a molecule are linearly related to its oxidation potential and reduction potential, respectively, the above equation can be written as in eq. [4] (18).

$$[4] \quad \Delta G_{CT} \approx IP - EA - \Delta E_{o,o} + C$$

For the same chromophore, with a system of donors, ΔG_{CT} and the logarithm of the rate constant of fluorescence quenching, k_q, are linearly proportional to the ionization potential of the quencher (18). The relation for **2***a* and **2***b* is shown in hexane in Fig. 3 and for **2***a* in acetonitrile in Fig. 4. With the exception of acrylonitrile and fumaronitrile an approximately linear relationship is obtained. These substances have high ionization potentials and we conclude that here the excited thione is acting as a donor.

The slopes of these plots are for **2***a* and **2***b* $-0.86\,eV^{-1}$ (hexane) and for **2***a* $-1.63\,eV^{-1}$ and $2.7\,eV^{-1}$ for donors and acceptors respectively in acetonitrile. These values are far less than the value, $17.06\,eV^{-1}$ (18, 19), predicted for systems in which quenching of fluorescence occurs via complete electron transfer. A 3% charge transfer contribution in the exciplexes of aromatic thiones and olefins has been claimed by Turro and Ramamurthy (20).

This small charge-transfer interaction in the encounter complex was also observed in the variation of the quantum yield of photocyclization of **2***c* with the concentration of amine and sulfide: di-*n*-butyl sulfide, having a higher ionization potential, quenches the cyclization at a lower rate constant (Fig. 5, $k_q = 9 \times 10^8\,M^{-1}\,s^{-1}$) than triethylamine (1*c*). Although only these two quenchers were studied, their ionization potentials and quenching rate constants suggest also a small charge-transfer interaction between the excited thione and donor.

The processes of formation of **5** and the photocyclization of **2***c* and **2***d* appear very similar in solvents of various polarities, as shown in Fig. 2. Since there cannot be any intramolecular charge transfer in **2***c* and **2***d*, this parallel behaviour suggests that the formation of **5** should also involve only a neutral biradical intermediate with no charged species preceding it. This is consistent with the observed very small (if real) charge transfer interaction between the π,π^* thione and ether. The intramolecular charge transfer mechanism leading to **5** is thus excluded. Obviously, the formation of **4** cannot involve charged species either, for similar reasons. Such sensitivity to solvent as is shown in the formation of **4** may be attributed to solvent dependent conformational changes.

[4]See, for instance, ref. 15. The thiocarbonyl group has a similar dipole moment to that of the carbonyl group (16).

Can. J. Chem. Downloaded from www.nrcresearchpress.com by 210.87.254.42 on 09/05/12
For personal use only.

Can. J. Chem. Downloaded from www.nrcresearchpress.com by 210.87.254.42 on 09/05/12
For personal use only.

Experimental

General Procedures

The ^{1}H nmr spectra were obtained in carbon tetrachloride solution unless otherwise stated and are given in parts per million from internal Me_4Si. Mass spectra were obtained on an M-66 at 70 eV, relative intensities being given parenthetically. Melting points and boiling points are uncorrected; temperatures recorded for bulb-to-bulb distillation are external; petroleum ether (PE) refers to the fraction of boiling range 60–80°C. For vapor-phase chromatography (vpc) the following columns were used: (A) 15% FFAP on Chromosorb W, 80/100 (HP), $\frac{1}{4}$ in. × 6 ft; (B) 10% SE 30 on Chromosorb W, 80/100 (acid washed), $\frac{1}{4}$ in. × 6 ft.

Purifications of Solvents and Reagents

Commercial spectrograde benzene and cyclohexane were used without further treatment, while commercial spectrograde hexane was passed through a column of dry alumina; acetic acid was first distilled over chromium trioxide, and then fractionally distilled, after stirring with molecular sieve (4A) at 116°C, *tert*-butyl alcohol was fractionated twice over sodium after refluxing overnight; dimethoxyethane was obtained by distilling commercial product over calcium hydride (CaH_2). Acetonitrile was refluxed over CaH_2 for 12 h and fractionally distilled; cyclohexene was distilled over P_2O_5 at 83°C under nitrogen; isopropanol and ethyl benzene were fractionally distilled over sodium; 2,5-dimethyl-2,4-hexadiene was first distilled and then purified by vpc (5% DCC30). Acrylonitrile and ethyl vinyl ether were freshly distilled under nitrogen before use; commercial anhydrous analytical grade diethyl ether was distilled over molecular sieve (5A) before use; triethylamine, isopropyl amine, *sec*-butyl amine, diethyl amine, and pyridine were freshly distilled over sodium hydroxide pellets under nitrogen. Biacetyl was distilled under nitrogen and kept under reduced pressure; isoprene was distilled over lithium aluminium hydride; 2,3-dihydropyran was refluxed over CaH_2 and freshly distilled; diethyl maleate was fractionated through a spinning band column; fumaronitrile was sublimed. All thioketones were purified by vpc (Column B at 120°C); piperylene was freshly distilled.

Preparative Photochemistry

The reactions were carried out near room temperature using a 450-W Hanovia medium-pressure lamp.

Ketone Preparations

The ketones were prepared as described previously by condensing the enolate anion of isobutyrophenone and the appropriate bromide in boiling toluene or benzene.

1-Phenyl-3-methoxy-2,2-dimethylpropanone (1i)

This was prepared from isobutyrophenone (7.4 g, 0.05 mol), sodium amide (2 g), and chloromethyl methyl ether (8 g, 0.1 mol) in refluxing toluene (150 mL). The yield was 85% (8.3 g): bp 56°C (0.5 Torr); ^{1}H nmr δ: 7.35 (m, 5, arom), 3.39 (s, 2), 3.2 (s, 3), 1.2 (s, 6, CMe_2); mass spectrum *m/e*: 176 (M^+, 0.3), 148 (7), 105 (100), and 77 (54).

1-Phenyl-5-methoxy-2,2-dimethylpentanone (1j)

3-Methoxy propanol was prepared by the method of Smith and Sprung (21) in 71% yield. Phosphorus tribromide (6 g) was added to the alcohol (18 g, 0.2 mol) slowly with stirring at −15°C. The mixture was distilled after being stirred for 2 h at room temperature. The fraction boiling below 135°C was collected, washed with water, dried with $CaCl_2$, and redistilled to give 1-bromo-3-methoxypropane (6.1 g, 40%) bp 130–133°C (lit. (22) bp 132–133°C). Condensation of isobutyrophenone enolate anion (from 5.7 g of ketone and 1.8 g of sodium amide in 80 mL of toluene) with this bromide (6.1 g, 0.04 mol) gave the ketone **1o** in 59% yield (4.6 g): bp 105–106°C (0.25 Torr); ^{1}H nmr δ: 7.5–7.26 (m, 5, arom), 3.13 (m, 5), 1.7 (m, 4), 1.26 (s, 6, CMe_2); mass spectrum *m/e*: 220 (M^+, 2), 188 (8), 148 (3), 115 (38), 105 (100), and 77 (32). *Mol Wt.* calcd. for $C_{14}H_{20}O_2$: 220.1462; found (ms): 220.1468.

1-Phenyl-4-ethoxy-2,2-dimethylbutanone (1g)

This was prepared from 1-bromo-2-ethoxyethane and isobutyrophenone in 39% yield: bp 94–95°C (0.2 Torr); ^{1}H nmr δ: 7.13 (m, 5, arom), 3.34 (t, 2, J = 7 Hz), 3.26 (q, 2, J = 6.5 Hz), 2.0 (t, 2, J = 7.0 Hz), 1.26 (s, 6, CMe_2), 1.00 (t, 3, J = 6.5 Hz); mass spectrum *m/e*: 220 (M^+, 3) 148 (90), 105 (100). *Mol. Wt.* calcd. for $C_{14}H_{20}O_2$: 220.1462; found (ms): 220.1469.

1-Phenyl-2,2-dimethyl-pent-4-enone

This was prepared by condensing isobutyrophenone enolate anion (from 40 g of ketone and 10.7 g of sodium amide in 700 mL of toluene) with allyl bromide (36 g, 0.3 mol) in 87% yield (44 g): bp 68–72°C (0.1 Torr); ^{1}H nmr δ: 7.4 (m, 5, arom), 4.36–6.0 (m, 3), 2.46 (d, 2, J = 7 Hz), 1.26 (s, 6, CMe_2); mass spectrum *m/e*: 188 (M^+, 5), 105 (95), and 77 (100). *Mol. Wt.* calcd. for $C_{13}H_{16}O$: 188.1200; found (ms): 188.1201.

1-Phenyl-4,5-dimethoxy-2,2-dimethylpentanone (1h)

To a cooled solution (−10°C) of the ethylene ketal of the previous ketone (18.8 g, from the ketone ethylene glycol in benzene containing *p*-toluenesulfonic acid) in *tert*-butyl alcohol (800 mL) and ice-water (560 mL), $KMnO_4$ (19 g) and NaOH (4 g) in water (640 mL) at 0°C were added with vigorous stirring. After 5 min the mixture was bubbled with SO_2 until the manganese dioxide was dissolved. After isolation ($CHCl_3$) the diol was obtained as white crystals (21 g). The crude diol (mp 77–79°C) was then methylated with methyl iodide (18 mL) in 1,2-dimethoxyethane (125 mL, distilled from LAH) and sodium hydride (3 g) slowly added below 50°C. After 4 h the mixture was poured into water and the crude ketal isolated ($CHCl_3$). This was added to methanol–water (4:1, 300 mL) containing HCl (3 mL) and stirred at 60°C (12 h). After neutralization, isolation and distillation gave **1h** in 77% yield (15.5 g): bp 90–92°C (0.05 Torr); ^{1}H nmr δ: 7.3 and 7.6 (m, 5, arom), 3.36 (m, 3), 3.26 (s, 3), 3.16 (s, 3) 1.60–2.40 (m, 2), 1.23 (s, 6, CMe_2); mass spectrum *m/e*: 205 (100), 148 (9), 105 (85), and 89 (76). *Anal.* calcd. for $C_{15}H_{22}O_3$: C 71.97, H 8.86; found: C 72.04, H 8.91.

Thioketone Preparations

The thioketones were prepared from the corresponding ketones using previously reported methods (23).

1-Phenyl-3-methoxy-2,2-dimethylthiopropanone (2i)

The thione was prepared from **1i** and P_2S_5 in refluxing pyridine in 61% yield: λ_{max} (C_6H_{12}): 558, 296, and 226 nm (ε 110, 4980, and 13 600); ^{1}H nmr δ: 7.2 (m, 5, arom), 3.5 (s, 2), 3.28 (s, 3), 1.35 (s, 6, CMe_2); mass spectrum *m/e*: 208 (M^+, 15), 176 (25), 143 (34), 121 (55), 77 (30), and 45 (100). *Mol. Wt.* calcd. for $C_{12}H_{16}OS$: 208.0921; found (ms): 208.0914.

1-Phenyl-5-methoxy-2,2-dimethylthiopentanone (2j)

This compound was prepared from ketone **1j** with H_2S and HCl in absolute ethanol at −78°C in 45% yield, bulb-to-bulb distillation 82–90°C (0.2 Torr); λ_{max}(C_6H_{12}): 567, 297, and 229 (ε 105, 3850, and 9480; ^{1}H nmr δ: 7.13 (m, 5, arom), 3.18 (s, 3), 3.20 (m, 2), 1.70 (m, 4), 1.34 (s, 6, CMe_2); mass spectrum *m/e*: 236 (M^+, 37), 204 (12), 165 (52), 122 (100), 121 (58), and 113 (28). *Mol. Wt.* calcd. for $C_{14}H_{20}OS$: 236.1234; found (ms): 236.1215.

1-Phenyl-4-ethoxy-2,3-dimethylthiobutanone (2g)

The reaction of ketone **1g** and H_2S, HCl in absolute ethanol at −78°C gave thione **2g** in 55% yield, bulb-to-bulb distillation at 65–70°C (0.08 Torr); λ_{max}(C_6H_{12}): 566, 297, and 228 nm (ε 110,

Can. J. Chem. Downloaded from www.nrcresearchpress.com by 210.87.254.42 on 09/05/12
For personal use only.

3830, and 8960); ^{1}H nmr δ: 7.13 (bs, 5, arom), 3.45 (t, 2, J = 7.0 Hz), 3.42 (q, 2, J = 6.5 Hz), 2.10 (t, 2, J = 7.0 Hz), 1.40 (s, 6, CMe_2), 1.09 (t, 3, J = 6.5 Hz); mass spectrum *m/e*: 236 (M^+, 2) 164 (100), 121 (92). *Mol. Wt.* calcd. for $C_{14}H_{20}OS$: 236.1234; found (ms): 236.1217.

*1-Phenyl-4,5-dimethoxy-2,2-dimethylthiopentanone (2*h)

This compound was prepared from the corresponding ketone with H_2S and HCl in absolute ethanol at −78°C in 45% yield, bulb-to-bulb distillation at 82–90°C (0.2 Torr); $\lambda_{max}(C_6H_{12})$: 558, 295, and 228 nm (ε 111, 3730, and 8570); ^{1}H nmr (CCl_4 + pyridine) δ: 3.30 (m, 3), 3.23 (s, 3), 3.15 (s, 3), 2.65 (m, 2), 1.42 (s, 3), 1.33 (s, 3); mass spectrum *m/e*: 234 (5), 221 (10), 164 (100), and 121 (50). *Anal.* calcd. for $C_{15}H_{22}O_2S$: C 67.64, H 8.33, S 12.01; found: C 68.39, H 8.32, S 11.68.

*Irradiation of 2*i

(a) Above 445 nm

The thione (156 mg) in benzene (150 mL) was irradiated through Corning filter 3-72 for 5 days. The ^{1}H nmr spectrum showed no change.

(b) Above 290 nm

The thione (210 mg) in benzene (200 mL) was irradiated through Pyrex to complete conversion (12 h). The solvent was evaporated *in vacuo*. The residue was dissolved in chloroform (3 mL) and glacial acetic acid (7 mL), and mercury acetate (400 mg) was added with stirring. After 2 h, the mixture was diluted with chloroform and filtered through Celite. The filtrate was washed with dilute sodium bicarbonate and dried over $MgSO_4$. Thin-layer chromatography gave 1,2-dihydrofuran **16** (148 mg, 85%) mp 32°C; ^{1}H nmr δ: 7.18 (m, 5, arom), 6.41 (s, 1), 4.05 (s, 2), 1.32 (s, 6, CMe_2); mass spectrum *m/e*: 174 (M^+, 55) 159 (73), 121 (30), 117 (100), and 47 (44). *Mol. Wt.* calcd. for $C_{12}H_{14}O$: 174.1044; found (ms): 174.1038.

*Irradiation of 2*j

The thione (153 mg) in bezene (10 mL) was irradiated (Pyrex) to complete conversion (8 h) to give **13** in virtually quantitative yield; bp 78–85°C (0.4 Torr). The ^{1}H nmr data indicated a 50:50 mixture of isomers, most clearly in the duplication of the methoxy peaks (3.33, 3.26), SH (2.31, 1.78), and geminal methyl groups (1.24, 1.17 (*trans* to phenyl); 0.82, 0.55 (*cis* to phenyl)); mass spectrum *m/e*: 202 (27), 187 (100), 129 (10), and 91 (9). *Anal.* calcd. for $C_{14}H_{20}OS$: C 71.16, H 8.53, S 13.54; found: C 71.24, H 8.70, S 13.52.

*Irradiation of 2*g

(a) Through Pyrex

A solution of thione (600 mg) in benzene (30 mL) was irradiated (Pyrex) for 40 h (>90% conversion). Preparative tlc (pet. ether/CH_2Cl_2, 5:2) afforded a partial separation into one stereoisomer, **4***a*, (112 mg, 19%, faster band) and a mixture of another isomer of **4***b* and **5** (396 mg, 60%). The thiol **4***a* (distilled 50–52°C/0.05 Torr); ^{1}H nmr δ: 7.96 and 7.32 (m, 5, arom), 4.41 (t, 1, X part of ABX, $J_{AX} = J_{BX}$ = 8 Hz), 3.62 (q, 2, J = 6.6 Hz), 2.2–1.85 (m, 2, AB part of ABX, J_{AB} = 11 Hz), 1.95 (s, 1, SH), 1.31, 0.67 (s, 3H each, CMe_2), 1.16 (t, 3, J = 6.6 Hz); mass spectrum *m/e*: 202 (100) and 187 (55). *Anal.* calcd. for $C_{14}H_{20}OS$: C 71.16, H 8.53, S 13.54; found: C 71.09, H 8.42, S 13.45.

The separation of **4***b* and **5** was achieved by vpc (column B, 165°C). The thiol **4***b* was eluted first (49 min, 29%), followed by **5** (70 min, 40%). The former (distilled 50–55°C/0.08 Torr) had ^{1}H nmr δ: 7.95 and 7.32 (m, 5, arom), 4.40 (t, X part of ABX, $J_{AX} = J_{BX}$ = 8 Hz), 3.55 (q, 2, J = 7 Hz), 2.12–1.79 (m, 2, AB part of ABX, J_{AB} = 11 Hz), 1.99 (s, 1, SH), 1.35 and 0.8 (s, 3H each, CMe_2), 1.23 (t, 3, J = 7 Hz); mass spectrum *m/e*: 236 (M^+, 2), 202 (100), and 187 (22). *Mol. Wt.* calcd. for $C_{14}H_{20}OS$: 236.1234; found (ms): 236.1218. The tetrahydropyran **5** was purified by tlc, distilled (61–65°C/0.04 Torr); ^{1}H nmr δ: 7.16 (m, 5, arom), 4.14 (q, 1, J = 6.5 Hz), 3.87 (m, 2), 1.70–2.24 (m, 2) (AA′BB′, J_{AB} = 14 Hz, $J_{AA'} = J_{AB'}$ = 2, $J_{BA'}$ = 10, $J_{BB'}$ = 7 Hz), 1.2 (s, 1, D_2O exchangeable), 1.38 (d, 3, J = 6.5 Hz), 1.12 and 0.67 (s, 3H each, CMe_2); mass spectrum *m/e*: 236 (M^+, 30), 202 (51), and 187 (100). *Mol. Wt.* calcd. for $C_{14}H_{20}OS$: 236.1234; found (ms): 236.1222.

Reaction of **5** (40 mg) with mercuric acetate in acetic acid gave the corresponding dihydropyran (27 mg, 77%) distilled at 50–53°C/0.05 Torr; $\lambda_{max}(C_6H_{12})$: 246 nm (ε 4500); ^{1}H nmr δ: 7.13 (m, 5, arom), 3.98 (m, 2), and 1.73 (m, 2) (AA′BB′: J_{AB} = 5, $J_{AB'}$ = 5.4, $J_{AB'} = J_{BA'}$ = 1.4, $J_{AA'} = J_{BB'}$ = 4 Hz), 1.38 (s, 3, vinyl methyl), 0.97 (s, 6, CMe_2); mass spectrum *m/e*: 202 (M^+, 25) and 187 (100). *Mol. Wt.* calcd. for $C_{14}H_{18}O$: 202.1357; found (ms): 202.1363.

(b) Above 445 nm

The thione (23 mg) in benzene (5 mL) was irradiated (two 450-W lamps, Corning filter 3-72, 6 days, 60% conversion); vpc analysis (Column A, 170°C) showed the presence of three major peaks: (20 min, 20%; 26 min, 25%), the two isomers of **4**, and (36 min) the thione. The thiols were collected and identified by ir spectra. The tetrahydropyran **5** was absent.

Identification of Ethyl Vinyl Ether

A solution of thione **2***g* (209 mg) in benzene (10 mL) was irradiated (Pyrex, 90% conversion, 24 h) and the product examined by vpc (Column B, 40°C).[5] A peak corresponding to ethyl vinyl ether (~5%) was observed, and the substance identified by collection and comparison of ir spectra. By irradiation at λ > 445 nm the yield of ether was ca. 10%.

*Irradiation of 2*h

The thione (500 mg) in benzene (45 mL) was irradiated to complete conversion (Pyrex, 24 h). Preparative tlc (pet. ether/ethyl acetate, 21:4) gave two major fractions A (slow) and B. Fraction A, after rechromatography, was recrystallized from ethanol to give **11** (180 mg, 36%); mp 60–61°C; ^{1}H nmr (C_6D_6) δ: 3.97, 4.22 (AB quartet, 2, J = 12 Hz), 3.85 (m, 1), 3.25 (m, 3), 3.14 (s, 3, OCH_3), 1.8 (dd, 1, J_1 = 10, J_2 = 14 Hz), 1.16 (s, 1, SH), 1.09, 0.84 (s, 3H each, CMe_2), 0.96 (dd, 1, J_1 = 2.5, J_2 = 14 Hz); (CCl_4): 4.05, 4.11 (AB quartet, 2H, J = 12 Hz), 3.9 (m, 1), 0.89 (s, 3); mass spectrum *m/e*: 232 (80), 217 (37), and 121 (100).

The thiol was dethiolated (200 mg) with mercuric acetate, purified by preparative tlc (CH_2Cl_2) to give **15** (111 mg, 70%), distilled at 76–80°C/0.08 Torr; $\lambda_{max}(C_6H_{12})$: 246 (ε 4600); ^{1}H nmr δ: 7.13 (s, 5, arom), 6.10 (s, 1, vinyl hydrogen), 4.05 (m, 1), 3.32 (s, 3, OCH_3), 2.88 (m, 2, AB part of ABX, J_{AB} = 10, $J_{AX} = J_{BX}$ = 5 Hz), 1.65 (m, 2, AB part of ABX, J_{AB} = 13.5, J_{AX} = 5, J_{BX} = 7 Hz), 1.20, 0.92 (s, 3H each, CMe_2); mass spectrum *m/e*: 232 (M^+, 100) and 217 (37). *Mol. Wt.* calcd. for $C_{15}H_{20}O$: 232.1462; found (ms): 232.1463.

Fraction B (200 mg) was rechromatographed using multi-development (pet. ether/ethyl acetate, 20:1, five developments) to give fractions C (80 mg) and D (110 mg). Fraction C, distilled 75–80°C (0.08 Torr), was **10**; ^{1}H nmr δ: 4.49 (d, 1H, J = 6 Hz), 3.9 (m, 1), 3.00, 2.78 (s, 3H each, OMe), 2.44 (s, 1, SH), 1.70–1.47 (m, 2, AB part of ABX, J_{AB} = 14, J_{AX} = 2.5, J_{BX} = 5 Hz), 1.13, 0.68 (s, 3H each, CMe_2); mass spectrum *m/e*: 232 (49) and 217 (100). This thiol was converted with mercuric acetate into the dimethoxy-dihydrofuran **14** (70 mg, 80%) described below.

The fraction D was treated with mercuric acetate and the olefin **14** (69 mg, 71%) was isolated by preparative tlc (pet. ether/ethyl acetate, 75:6), distilled (56–60°C/0.05 Torr); $\lambda_{max}(C_6H_{12})$: 254 (ε 4400); ^{1}H nmr δ: 7.34 (s, 5, arom), 4.22 (dd, 1,

[5]Care was taken to ensure the absence of the corresponding ketone. No isobutyrophenone was detected in the product.

$J_1 = 3.5$ Hz, $J_2 = 7$ Hz), 3.42, 3.36 (s, 3H each, OCH_3), 1.94 (dd, 1, $J_1 = 13.5$, $J_2 = 7$ Hz), 1.71 (dd, 1, $J_1 = 13.5$, $J_2 = 3.5$ Hz), 1.12, 0.98 (s, 3H each, CMe_2); mass spectrum *m/e*: 232 (M^+, 31) and 217 (100). *Mol. Wt.* calcd. for $C_{15}H_{20}O_2$: 232.1462; found (ms): 232.1460.

Irradiation of 2h *Above 445 nm*

A solution of **2***h* (190 mg) in benzene (40 mL) was irradiated to complete conversion (30 days). Vapor phase chromatographic analysis of the product (10% Carbowax 20M on Chromosorb P, 80/100, acid washed, ¼in. × 6 ft, 170°C) showed the presence of four main components (retention time 51, 54, 68, 77 minutes) but the above thiols (retention time **11**, 62, **10**, 64, and 70.5 min) were absent; column B at 175°C showed the absence of the tetrahydropyran.

Kinetic Studies

The samples were excited either with an Osram HBO 200 W high pressure mercury arc using an interference filter Schott #6672-02 (313 ± 5 nm) with ferrioxalate actinometry, or with an Ushio UXL-2003D Xenon ZKW discharge lamp in a calibrated Jasco Spectroirradiator at the appropriate wavelengths. Thiols were analyzed by vpc on a 6 ft glass column, using a flame detector (Aerograph 2400). Various conditions were used for different thiols.

Thiol	Calibration compound	Column temperature (°C)
13	*p*-Bromobiphenyl	140
4, 5	β-Acetonaphthalene	150

Fluorescence measurements were carried out on a Perkin Elmer MPF-4 spectrophotometer. The optical density of the samples was less than 0.1. The disappearance of thioketone was followed by the change of the optical density at the maximum of the n,π^* band.

Reduction Potentials

The half-wave potentials of the thioketones were measured in acetonitrile solution in a nitrogen atmosphere at room temperature with a PAR model 170 electroanalytical system. The potentials were measured with a dropping mercury electrode against the silver – silver chloride electrode. Each solution contained 0.1 *M* tetraethylammonium perchlorate and 10^{-3} *M* thioketone.

1. (*a*) P. DE MAYO and R. SUAU. J. Am. Chem. Soc. **96**, 6807 (1974); (*b*) A. COUTURE, K. HO, M. HOSHINO, P. DE MAYO, R. SUAU, and W. R. WARE. J. Am. Chem. Soc. **98**, 6218 (1976); (*c*) K. W. HO and P. DE MAYO. J. Am. Chem. Soc. **100**, 5725 (1979).
2. S. KATO, S. MINAGAWA, and M. KOIZUMI. Bull. Chem. Soc. Jpn. **34**, 1026 (1961).
3. L. ONSAGER. J. Am. Chem. Soc. **58**, 1486 (1936); F. C. FRANK. Trans. Faraday Soc. **42A**, 19 (1946); J. G. KIRKWOOD. Trans. Faraday Soc. **42A**, 7 (1946).
4. R. M. ELOFSON, F. F. GADALLAH, and L. A. GADALLAH. Can. J. Chem. **47**, 3979 (1969).
5. R. O. LOUTFY and R. O. LOUTFY . J. Phys. Chem. **76**, 1640 (1972).
6. M. PEOVER. Electroanalytical chemistry. Vol. 2. *Edited by* A. J. Bard. Dekker, New York, NY. 1966. p. 298.
7. H. SIEGERMAN. Technique in electroorganic synthesis. Part II. *Edited by* N. L. Weinberg. John Wiley & Sons, Inc., New York. 1975. p. 667.
8. H. E. O'NEAL and S. W. BENSON. J. Phys. Chem. **71**, 2903 (1967).
9. D. S. L. BLACKWELL, K. H. LEE, P. DE MAYO, G. L. R. PETRASIUNAS, and G. REVERDY. Nouv. J. Chim. **3**, 123 (1979).
10. J. R. HUBER and M. MAHANEY. Chem. Phys. Lett. **30**, 410 (1975); O. SERAFIMOV, H. J. HAINK, and J. R. HUBER. Ber. Bunsenges. Phys. Chem. **80**, 536 (1976).
11. S. W. BENSON. Chem. Rev. **78**, 23 (1978).
12. J. FABIAN and A. MELHORN. Z. Chem. **9**, 271 (1969); N. C. BAIRD and J. R. SWENSON. J. Phys. Chem. **77**, 277 (1973).
13. P. J. WAGNER and A. E. KEMMPAINEN. J. Am. Chem. Soc. **94**, 7495 (1972).
14. S. ACHMATOWICZ, D. H. R. BARTON, P. D. MAGNUS, G. A. POULTON, and P. J. WEST. J. Chem. Soc. Perkin Trans. I, 1567 (1973), and subsequent papers in this series; Y. OGATA, K. TAGAI, and S. IHDA. J. Chem. Soc. Perkin Trans. I, 1725 (1975); J. WIRZ. J. Chem. Soc. Perkin Trans. II, 1307 (1973).
15. J. LOOYENGA. Mol. Phys. **9**, 501 (1964).
16. O. H. LEBLANC, JR., V. W. LAURIE, and W. D. GWINN. J. Chem. Phys. **33**, 598 (1960); L. C. KRISHNER and E. B. WILSON, JR. J. Chem. Phys. **31**, 882 (1959); J. C. SWALEN and C. C. COSTAIN. J. Chem. Phys. **31**, 1562 (1959); K. C. LAL. J. Sci. Ind. Res. India Sect. B, **20**, 181 (1961).
17. H. KNIBBE, D. REHM, and A. WELLER. Ber. Bunsenges. Phys. Chem. **73**, 839 (1969).
18. J. B. GUTTENPLAN and S. G. COHEN. J. Am. Chem. Soc. **94**, 4040 (1972).
19. D. REHM and A. WELLER. Ber. Bunsenges. Phys. Chem. **73**, 834 (1969).
20. N. J. TURRO and V. RAMAMURTHY. Tetrahedron Lett. 2423 (1976).
21. L. I. SMITH and J. SPRUNG. J. Am. Chem. Soc. **65**, 1276 (1943).
22. R. PAUL. Ann. Chim. **18**, 303 (1932).
23. J. W. SCHREEREN, P. H. J. OOMS, and R. J. F. NIVARD. Synthesis, 149 (1973).

Can. J. Chem. Downloaded from www.nrcresearchpress.com by 210.87.254.42 on 09/05/12
For personal use only.

One-stage glycosylation using protected glycose: the synthesis of *O*-β-D-glucopyranosyl-(1→3)-*O*-[β-D-glucopyranosyl-(1→6)]-D-glucopyranose

SHINKITI KOTO,[1,2] SHIGERU INADA, TOYOSAKU YOSHIDA, MIYAKO TOYAMA, AND SHONOSUKE ZEN

School of Pharmaceutical Sciences, Kitasato University, Shirokane, Minato-ku, Tokyo, Japan 108

Received June 25, 1980

This paper is dedicated to Prof. Raymond U. Lemieux on the occasion of his 60th birthday

SHINKITI KOTO, SHIGERU INADA, TOYOSAKU YOSHIDA, MIYAKO TOYAMA, and SHONOSUKE ZEN. Can. J. Chem. **59**, 255 (1981).

The one-stage β-glucosylation of benzyl 3-*O*-acetyl-2,4-di-*O*-benzyl-α-D-glucopyranoside (**1**) with 2,3,4,6-tetra-*O*-benzyl-α-D-glucopyranose (**2**) using a mixture of *p*-nitrobenzenesulfonyl chloride, silver trifluoromethanesulfonate, and triethylamine, followed by deacetylation, gave benzyl *O*-(2,3,4,6-tetra-*O*-benzyl-β-D-glucopyranosyl)-(1→6)-2,4-di-*O*-benzyl-α-D-glucopyranoside (**3**). The disaccharide derivative **3** was then subjected to the β-glucosylation, followed by catalytic hydrogenation, to afford *O*-β-D-glucopyranosyl-(1→3)-*O*-[β-D-glucopyranosyl-(1→6)]-D-glucopyranose (**4**). The key intermediate **1** was prepared from D-glucose by way of a Fischer reaction, triphenylmethylation, a controlled benzylation, and detriphenylmethylation.

SHINKITI KOTO, SHIGERU INADA, TOYOSAKU YOSHIDA, MIYAKO TOYAMA et SHONOSUKE ZEN. Can. J. Chem. **59**, 255 (1981).

Un mélange de chlorure de *p*-nitrobenzènesulfonyle, de trifluorométhane sulfonate d'argent et de triéthylamine, provoque la β-glucosylation en une étape du *O*-acétyl-3 di-*O*-benzyl-2,4 α-D-glucopyrannoside de benzyle (**1**) par le tétra-*O*-benzyl-2,3,4,6 α-D-glucopyrannose (**2**) qui, suivie d'une déacétylation, donne le *O*-(tétra-*O*-benzyl-2,3,4,6 β-D-glucopyrannosyl)-(1→6)di-*O*-benzyl-2,4 α-D-glucopyrannoside de benzyle (**3**). La β-glucosylation du disaccharide **3**, suivie d'une hydrogénation catalytique, conduit au dérivé *O*-β-D-glucopyrannosyl-(1→3) *O*-[β-D-glucopyrannosyl-(1→6)]-D-glucopyrannose (**4**). On a préparé l'intermédiaire principal **1** à partir du D-glucose en le soumettant successivement à une réaction de Fischer, à une triphénylméthylation, à une benzylation contrôlée et finalement à une élimination du groupe triphénylméthyle.

[Traduit par le journal]

Introduction

In the past decade, various approaches to systematic synthesis of oligosaccharides have been reported (1). We ourselves have also presented a scheme for oligosaccharide synthesis systematically using a set of protecting groups (2). In all the approaches reported so far, however, building units have been coupled by modified Koenigs–Knorr reactions which always require the preparation of reactive intermediates such as glycosyl halides. Recently, we have found that an equimolar mixture of *p*-nitrobenzenesulfonyl chloride, silver trifluoromethanesulfonate, and triethylamine (3) is of use for activation of the hemiacetal hydroxyl groups of a stable intermediate, 2,3,4,6-tetra-*O*-benzyl-α-D-glucopyranose (**2**), even in the presence of alcohol (4). This enabled us to develop a one-stage β-glucosylation with **2** (5). In order to show the utility of our novel method, we attempted to synthesize *O*-β-D-glucopyranosyl-(1→3)-*O*-[β-D-glucopyranosyl-(1→6)]-D-glucopyranose (**4**), a branched-chain trisaccharide which builds the polyglucan, sclerotan, of the sclerotia of *Sclerotinia libertiana* (6) as well as the anti-tumor polyglucans, lentinan (7*a*) and schizophyllan (7*b*). This trisaccharide has been synthesized as a by-product of the condensation of 2,3,4,6-tetra-*O*-acetyl-α-D-glucopyranosyl bromide and benzyl 4,6-*O*-benzylidene-β-D-glucopyranoside (8).

Results and Discussion

Prior to preparing the key intermediate, benzyl 3-*O*-acetyl-2,4-di-*O*-benzyl-α-D-glucopyranoside (**1**), we investigated the controlled benzylation (9) of methyl 6-*O*-triphenylmethyl-α-D-glucopyranoside (**5**) (10). The benzylation of **5** by short heating in benzyl chloride containing a limited amount of potassium hydroxide gave the di-*O*-benzyl derivative **6** in a 62% yield. The structure of this compound was determined by measuring ^{1}H nmr of the acetate **7**; the spin system of H-1, H-2, and H-3 was analyzed by double resonance technique. The observed chemical shift value of H-3 shows that the acetyl group is at the C-3 position. The structure of **6** was alternatively confirmed as follows: **6** was detriphenylmethylated, methylated, and hydrogenated to give methyl 3,6-di-*O*-methyl-α-D-glucopyranoside (**9**) (11*a*) which was not oxidized by sodium periodate. The triphenylmethyl group of **7** was removed by mild acid hydrolysis to give the partially protected methyl glucoside **10** which has two kinds of protecting groups, benzyl (persistent) and acetyl (temporary) groups.

The preparation of **1** was then carried out. Benzyl α-D-glucopyranoside, conveniently prepared

[1]Post-doctoral fellow, University of Alberta, 1972–1974.

[2]Author to whom all correspondence should be addressed.

0008-4042/81/020255-05$01.00/0

©1981 National Research Council of Canada/Conseil national de recherches du Canada

Can. J. Chem. Downloaded from www.nrcresearchpress.com by 210.87.254.40 on 09/05/12
For personal use only.

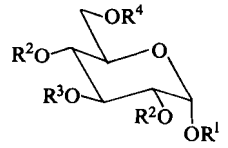

	R^1	R^2	R^3	R^4
1	Bn	Bn	Ac	H
2	H	Bn	Bn	Bn
5	Me	H	H	Tr
6	Me	Bn	H	Tr
7	Me	Bn	Ac	Tr
8	Me	Bn	H	H
9	Me	H	Me	Me
10	Me	Bn	Ac	H
11	Bn	H	H	Tr
12	Bn	Bn	H	Tr
13	Bn	Bn	Ac	Tr
14	Bn	Bn	H	αG
15	Bn	Bn	βG	βG
16	Bn	Bn	αG	βG

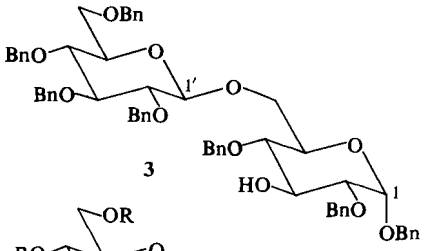

3

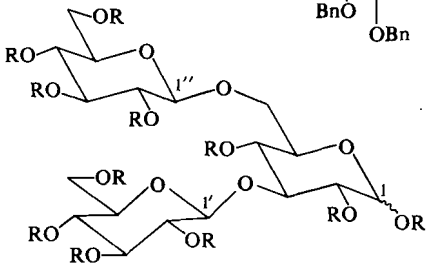

4 R = H
17 R = Ac

Ac = Acetyl
Bn = Benzyl
αG = 2,3,4,6-Tetra-*O*-benzyl-α-D-glucopyranosyl
βG = 2,3,4,6-Tetra-*O*-benzyl-β-D-glucopyranosyl
Me = Methyl
Tr = Triphenylmethyl

by a Fischer reaction of D-glucose with benzyl alcohol in the presence of *p*-toluenesulfonic acid, was converted into the 6-*O*-triphenylmethyl derivative **11**. The controlled benzylation of **11** afforded the partially benzylated monosaccharide **12** in a 35% yield. The selectivity of the reaction became less prominent than in the case of **6** mentioned above. The structure of **12** was determined by ^{1}H nmr of the acetate **13**; again, the spin system of H-1, H-2, and H-3 was unequivocally assigned. The location of the signal of H-3 shows that the acetyl group is at the C-3 position. Mild hydrolysis of **13** removed the triphenylmethyl groups to furnish the desired intermediate **1**.

Compound **1** thus prepared was then glucosylated with **2** using our one-stage β-glucosylation. Treatment of an equimolar mixture of **1** and **2** in dichloromethane with the reagent mixture of *p*-nitrobenzenesulfonyl chloride, silver trifluoromethanesulfonate, and triethylamine (5), followed by deacetylation and subsequent chromatography, gave the partially protected benzyl α-gentiobioside **3** in a 69% yield; the isomaltose derivative **14** was also obtained in a 21% yield. Compound **3** was again glucosylated with **2** using the same reagent mixture to give the fully benzylated branched-chain trisaccharide **15** in a 29% yield; the α(1→3), β(1→6) trisaccharide derivative **16** (19%) was separated by chromatography. ^{13}C nuclear magnetic resonance of **15** in $CDCl_3$ shows that the compound has the β,β-configuration.

Catalytic hydrogenation of **15** over palladium black in moist acetic acid afforded the trisaccharide **4**; ^{13}C nmr of **4** in D_2O shows that the trisaccharide is an equilibrium mixture of the anomeric forms. A pair of the anomeric carbons (C-1) of the pyranose appears at δ 93.2 and 96.9. A pair of the signals of the C-3 are at δ 83.3 and 85.7, resembling the case of anomeric laminaribiose (12). The latter value is almost equal to that of the C-3 of laminaran (δ 85.5) and lentinan (δ 85.3) (13). The C-6 resonates at δ 69.9, agreeing with the case of anomeric gentiobiose (δ 70.2) (12) and the β(1→6) glucan (δ 70.0) (13). Acetylation of **4** with acetic anhydride and sodium acetate afforded the totally acetylated trisaccharide **17**.

It is noted that **1** with a primary hydroxyl group gives β-glucoside more selectively than does **3** with a secondary group. We interpreted this as follows. Compound **1** effectively consumes the glucosyl sulfonate immediately after its generation from **2** so that the ratio of alcohol to the sulfonate is kept high; this favors β-glucoside formation (14).

In conclusion, we have shown that our one-stage β-glucosylation with **2** using the reagent mixture is of use for oligosaccharide synthesis, employing benzyl (persistent) and acetyl (temporary) groups.

NOTE ADDED IN PROOF: one of the referees has

Can. J. Chem. Downloaded from www.nrcresearchpress.com by 210.87.254.40 on 09/05/12
For personal use only.

Can. J. Chem. Downloaded from www.nrcresearchpress.com by 210.87.254.40 on 09/05/12
For personal use only.

suggested that the glycosylation reaction could proceed via the protected glycosyl chloride.

Experimental

Melting points were determined by an MP-1 melting point apparatus (Yanagimoto); uncorrected values are given. Specific rotations were measured in a jacketed 1-dm cell by a DIP-180 automatic polarimeter (Japan Spectroscopic) at 20°C. Infrared spectra were measured with a JASCO IRA-1 grating infrared spectrophotometer. The ^{1}H nmr values were determined with a JEOL-PS-100 spectrometer; ^{13}C nmr values were observed with a JEOL-PS-100 spectrometer equipped with a JEOL-EC-100 computer. Column chromatography was done on silica gel (Kanto Kagaku); each fraction was examined by tlc on silica gel (Merck, No. 7731). Evaporation was done under reduced pressure using a rotary evaporator (Tokyo Rika-kikai) equipped with a WP-33 aspirator (Yamato) at 35–40°C, unless otherwise stated.

*Methyl 2,4-Di-*O*-benzyl-6-*O*-triphenylmethyl-α-*D*-glucopyranoside (6)*

A mixture of the triphenylmethyl derivative **5** (10) (1.0 g, 2.3 mmol), benzyl chloride (Tokyo Kasei, 15 mL, 130 mmol), and crushed potassium hydroxide (1.0 g, 18 mmol) was stirred at 95°C for 2 h. The cooled mixture was diluted with benzene, filtered, and evaporated *in vacuo* on a boiling water bath. The residue was chromatographed on a silica gel column with benzene–butanone (100:1→5:1, gradient) as solvent. This gave pure **6** (0.88 g, 62%), mp 63–66°C; $[\alpha]_D$ +49° (*c* 0.6, chloroform). *Anal.* calcd. for $C_{40}H_{40}O_6$: C 77.89, H 6.54; found: C 77.90, H 6.51.

*Methyl 3-*O*-Acetyl-2,4-di-*O*-benzyl-6-*O*-triphenylmethyl-α-*D*-glucopyranoside (7)*

The partially benzylated compound **6** (703 mg, 1.14 mmol) was treated with acetic anhydride (7 mL) in pyridine (7 mL) for 90 min. The mixture was diluted with cold methanol (70 mL), evaporated *in vacuo* at 60°C, and then purified on a silica gel column with benzene–butanone (30:1) as solvent. This afforded a pure sirup of **7** (750 mg, 100%); $[\alpha]_D$ +37° (*c* 0.8, chloroform); ^{1}H nmr ($CDCl_3$, TMS) δ: 1.94 (s, 3H, CH_3CO), 3.18 (dd, $J_{5,6}$ = 4.8 Hz, $J_{6,6'}$ = 10 Hz, 1H, H-6), 3.44 (s, 3H, CH_3O), 3.57 (dd, $J_{1,2}$ = 3.8 Hz, $J_{2,3}$ = 9.0 Hz, 1H, H-2), 3.64 (t, $J_{3,4}$ = $J_{4,5}$ = 9.0 Hz, 1H, H-4), 3.88 (m, $J_{4,5}$ = 9.0 Hz, $J_{5,6}$ = 4.8 Hz, $J_{5,6'}$ = 2.0 Hz, 1H, H-5), 4.25 and 4.35 (AB system, J_{AB} = 11 Hz, 2H, CH_2Ph-4), 4.66 (s, 2H, CH_2Ph-2), 4.84 (d, $J_{1,2}$ = 3.8 Hz, 1H, H-1), 5.54 (t, $J_{2,3}$ = $J_{3,4}$ = 9.0 Hz, 1H, H-3). *Anal.* calcd. for $C_{42}H_{42}O_7$: C 76.57, H 6.43; found: C 77.09, H 6.47.

*Methyl 3-*O*-Acetyl-2,4-di-*O*-benzyl-α-*D*-glucopyranoside (10)*

The acetate **7** (791 mg, 1.2 mmol) was dissolved in *p*-dioxane (8 mL) containing dilute sulfuric acid (3 *M*, 1.2 mL). The solution was heated at 82–92°C for 60 min. The cooled solution was neutralized carefully with powdered sodium hydrogen carbonate under stirring, evaporated, and chromatographed on a silica gel column with benzene–butanone (100:1→3:1, gradient). This afforded pure **10** (332 mg, 66%), mp 61–62°C; $[\alpha]_D$ +67° (*c* 1.0, chloroform); ir(film): 1750 (CH_3COO) cm^{-1}; ^{1}H nmr($CDCl_3$, TMS) δ: 1.87 (s, 1H, OH), 1.95 (s, 3H, CH_3CO), 3.35 (s, 3H, CH_3O), 4.60 (s, 4H, CH_2Ph-2 and -4), 4.65 (d, $J_{1,2}$ = 3.8 Hz, 1H, H-1), 5.55 (t, $J_{2,3}$ = $J_{3,4}$ = 9.5 Hz, 1H, H-3). *Anal.* calcd. for $C_{23}H_{28}O_7$: C 66.65, H 6.78; found: C 66.30, H 6.86.

*Methyl 2,4-Di-*O*-benzyl-α-*D*-glucopyranoside (8) and the Structural Proof*

A mixture of **6** (150 mg, 0.24 mmol), *p*-dioxane (1.5 mL), and dilute sulfuric acid (3 *M*, 0.23 mL) was heated at 85°C for 1 h. The mixture was diluted with benzene, extracted with aqueous sodium hydrogen carbonate (5%) and water, evaporated, and purified on a silica gel column with benzene–butanone (5:1) as solvent. This afforded pure **8** (75 mg, 83%), mp 74–75°C; $[\alpha]_D$ +88° (*c* 0.6, chloroform) (lit. (11*b*) mp 75°C; $[\alpha]_D^{23}$ +87°(*c* 1.18, chloroform)). *Anal.* calcd. for $C_{21}H_{26}O_6$: C 67.36, H 7.00; found: C 67.10, H 6.90.

Compound **8** (50 mg, 0.13 mmol) was reacted with methyl iodide (Tokyo Kasei, 0.3 mL) and powdered barium oxide (0.37 g) in *N*,*N*-dimethylformamide (1 mL) at 82°C for 3 h under vigorous stirring. The mixture was diluted with benzene, filtered, and evaporated *in vacuo* at 80°C. The residue was purified on a silica gel column with benzene–butanone (100:1→20:1, gradient) to give a homogeneous sirup of the dimethyl compound (52 mg, 97%); ^{1}H nmr ($CDCl_3$, TMS) spectrum contains three singlets of methoxyl group at δ 3.33, 3.36, and 3.69. This compound (49 mg, 0.12 mmol) was hydrogenated twice over palladium black (14 mg) in a mixture of methanol (3 mL), water (0.5 mL), and acetic acid (0.3 mL) at 340 kPa using a Paar hydrogenation apparatus to give methyl 3,6-di-*O*-methyl-α-D-glucopyranoside (**9**) (27 mg, 100%); $[\alpha]_D$ +145° (*c* 0.7 ethanol) (lit. (11) $[\alpha]_D$ +141.6° (*c* 1.22, ethanol)). *Anal.* calcd. for $C_9H_{18}O_6$: C 48.64, H 8.16; found: C 48.80, H 8.13. The ^{1}H nmr (D_2O, ext. TMS) spectrum has three singlets of methoxyl group at δ 3.84, 3.87, and 4.14. Monitoring tlc showed that compound **9** (2.2 mg, 0.01 mmol) did not react with sodium periodate (2.2 mg) in water (0.10 mL) at room temperature overnight, whereas methyl 4,6-di-*O*-methyl-α-D-glucopyranoside (15) was completely exhausted during the same reaction.

*Benzyl 6-*O*-Triphenylmethyl-α-*D*-glucopyranoside (11)*

Anhydrous D-glucose (Wako, 10 g, 55 mmol), benzyl alcohol (Wako, 10 mL), and *p*-toluenesulfonic acid monohydrate (Tokyo Kasei, 3 g, 16 mmol) were placed in a round-bottomed flask and the reaction was stirred well at 60–70°C for 4 h. Thin-layer chromatography of the reaction mixture showed that the main product was benzyl α-D-glucopyranoside (16); the β-anomer (17) was also detected. The mixture was diluted with chloroform (100 mL) containing triethylamine (Wako, 4.4 mL) and filtered. The filtrate was evaporated *in vacuo* on a boiling water bath and chromatographed on a silica gel column with chloroform–methanol (100:1→3:1, gradient) as solvent. This gave a sirup (5.7 g, 36%) of benzyl α-D-glucopyranoside; ^{13}C nmr (D_2O, ext. TMS) δ: 61.6 (C-6), 70.8 (C-4), 70.9 (CH_2Ph), 72.5 (C-2), 73.1 (C-5), 74.3 (C-3), 98.9 (C-1), 129.6, 129.9, 138.2 (phenyl). The slower-moving product was the β-anomer (0.6 g, 4%); ^{13}C nmr (D_2O, ext. TMS) δ: 62.0 (C-6), 70.8 (C-4), 72.6 (CH_2Ph), 74.3 (C-2), 77.0 (C-5), 77.1 (C-3), 102.4 (C-1), 129.6, 129.8, 137.1 (phenyl).

The α-glucoside (8.9 g, 31.5 mmol) was reacted with triphenylmethyl chloride (Tokyo Kasei, 9.2 g, 33 mmol) in pyridine (35 mL) at 60°C for 3 h. The mixture was diluted with chloroform and extracted with aqueous sodium hydrogen sulfate (5%) and water. After evaporation the residue was chromatographed on a silica gel column with benzene–butanone (10:1→1:1, gradient). This gave a pure solid of **11** (6.2 g, 36%), mp 75–77°C; $[\alpha]_D$ +25° (*c* 0.4, chloroform). *Anal.* calcd. for $C_{32}H_{32}O_6$: C 74.98, H 6.29; found: C 74.27, H 6.65.

*Benzyl 2,4-Di-*O*-benzyl-6-*O*-triphenylmethyl-α-*D*-glucopyranoside (12)*

A mixture of the triphenylmethyl compound **11** (6.1 g, 12 mmol), benzyl chloride (82 mL), and crushed potassium hydroxide (6.1 g) was stirred at 98°C for 2.5 h. The cooled mixture was processed as described for **6** and chromatographed on a

Can. J. Chem. Downloaded from www.nrcresearchpress.com by 210.87.254.40 on 09/05/12
For personal use only.

column of silica gel. Gradient elution with benzene–butanone (100:1→10:1) gave pure **12** (2.9 g, 35%); $[\alpha]_D$ +72° (*c* 1.0, chloroform). *Anal.* calcd. for $C_{46}H_{44}O_6$: C 79.74, H 6.40; found: C 79.56, H 6.47.

Benzyl 3-O-Acetyl-2,4-di-O-benzyl-6-O-triphenylmethyl-α-D-glucopyranoside (13)

The partially benzylated product **12** (2.2 g, 32 mmol) was reacted with acetic anhydride (13 mL) and pyridine (6.5 mL) overnight. The cooled mixture was diluted with cold methanol (100 mL), evaporated *in vacuo* at 70°C, and purified on a silica gel column with benzene–butanone (100:1→20:1, gradient) as solvent. This gave pure **13** (2.4 g, 97%), mp 147–148°C; $[\alpha]_D$ +65°(*c* 1.0, chloroform); ^{1}H nmr ($CDCl_3$, TMS) δ: 1.95 (s, 3H, CH_3CO), 3.12 (dd, $J_{5,6}$ = 4.0 Hz, $J_{6,6'}$ = 10.0 Hz, 1H, H-6), 3.45 (dd, $J_{5,6'}$ = 2.0 Hz, $J_{6,6'}$ = 10.0 Hz, 1H, H-6'), 3.56 (dd, $J_{1,2}$ = 3.8 Hz, $J_{2,3}$ = 9.5 Hz, 1H, H-2), 3.65 (t, $J_{3,4} = J_{4,5}$ = 9.5 Hz, 1H, H-4), 3.91 (m, $J_{4,5}$ = 9.5 Hz, $J_{5,6}$ = 4.0 Hz, $J_{5,6'}$ = 2.0 Hz, 1H, H-5), 4.21 and 4.33 (AB system, J_{AB} = 10.0 Hz, 2H, CH_2Ph-4), 4.53 (s, 2H, CH_2Ph-2), 4.59 and 4.75 (AB system, J_{AB} = 12.0 Hz, 2H, CH_2Ph-1), 4.98 (d, $J_{1,2}$ = 3.8 Hz, 1H, H-1), 5.55 (t, $J_{2,3} = J_{3,4}$ = 9.5 Hz, 1H, H-3). *Anal.* calcd. for $C_{48}H_{46}O_7$: C 78.45, H 6.31; found: C 78.86, H 6.23.

Benzyl 3-O-Acetyl-2,4-di-O-benzyl-α-D-glucopyranoside (1)

The acetate **13** (625 mg, 0.85 mmol) was dissolved in *p*-dioxane (6 mL) containing dilute sulfuric acid (3 *M*, 0.4 mL). The reaction was stirred at 80°C for 60 min. The cooled mixture was diluted with benzene, then extracted with dilute sodium hydrogen carbonate (5%) and water. The solvent was evaporated and the residue was purified on a silica gel column with benzene–butanone (100:1→10:1, gradient) as solvent. This gave pure **1** as long needles (330 mg, 76%), mp 128–129°C; $[\alpha]_D$ +100°(*c* 0.3, chloroform); ir(KBr): 1740 (CH_3COO) cm^{-1}. *Anal.* calcd. for $C_{29}H_{32}O_7 \cdot H_2O$: C 68.22, H 6.71; found: C 68.03, H 6.22. Heating this at 105°C *in vacuo* gave the anhydrous form, mp 129–130°C. *Anal.* calcd. for $C_{29}H_{32}O_7$: C 70.71, H 6.55; found: C 70.96, H 6.62.

Benzyl O-(2,3,4,6-Tetra-O-benzyl-β-D-glucopyranosyl)-(1→6)-2,4-di-O-benzyl-α-D-glucopyranoside (3) and the α(1→6) Isomer (14)

Triethylamine (140 μL, 1.0 mmol) was added to a stirred mixture of **1** (492 mg, 1.0 mmol), **2** (18) (540 mg, 1.0 mmol), *p*-nitrobenzenesulfonyl chloride (222 mg, 1.0 mmol), and silver trifluoromethanesulfonate (257 mg, 1.0 mmol) in dichloromethane (5 mL) at −40°C. The bath temperature was allowed to rise to 0°C, at which temperature the reaction was agitated overnight. The reaction mixture showing a single main spot was diluted with benzene, filtered, and chromatographed on a silica gel column with benzene–butanone (100:1→5:1, gradient). This afforded a solid mixture (966 mg) of products giving the main spot. The solid was then dissolved in a mixture of methanol (10 mL), *p*-dioxane (2 mL), and acetone (6 mL). Dilute sodium methoxide (0.2 *M*, 5 mL) was added to the solution. After standing overnight, the solution showing two spots (R_f 0.38 and 0.31, benzene–butanone (10:1)) was neutralized with acetic acid, evaporated, and chromatographed on a silica gel column with benzene–butanone (100:1→10:1, gradient) as solvent. The faster-moving product was **14** (212 mg, 21%), mp 72–74°C; $[\alpha]_D$ +96°(*c* 1.0, chloroform); ^{13}C nmr ($CDCl_3$, TMS) showed two kinds of anomeric carbons at δ 94.4 (C-1) and 97.1 (C-1'). *Anal.* calcd. for $C_{61}H_{64}O_{11} \cdot H_2O$: C 73.92, H 6.71; found: C 73.66, H 6.62. Drying this at 105°C *in vacuo* gave anhydrous sirup. *Anal.* calcd. for $C_{61}H_{64}O_{11}$: C 75.29, H 6.63; found: C 74.97, H 6.58. The slower-moving product was **3** (683 mg, 69%), mp 88–91°C; $[\alpha]_D$ +82°(*c* 0.5, chloroform); ^{13}C nmr ($CDCl_3$, TMS) showed the presence of two anomeric carbons at δ 94.8 (C-1) and 103.8 (C-1'). *Anal.* calcd. for $C_{61}H_{64}O_{11} \cdot 0.5H_2O$: C 74.59, H 6.47; found: C 74.24, H 6.56. Dehydration of this at 105°C *in vacuo* gave an anhydrous sirup. *Anal.* calcd. for $C_{61}H_{64}O_{11}$: C 75.29, H 6.63; found: C 75.10, H 6.63.

Benzyl O-(2,3,4,6-Tetra-O-benzyl-β-D-glucopyranosyl)-(1→3)-O-[2,3,4,6-tetra-O-benzyl-β-D-glucopyranosyl-(1→6)]-2,4-di-O-benzyl α-D-glucopyranoside (15) and the α(1→3), β(1→6) Isomer (16)

To a stirred mixture of **2** (18) (147 mg, 0.27 mmol), **3** (251 mg, 0.26 mmol), *p*-nitrobenzenesulfonyl chloride (60 mg, 0.27 mmol), and silver trifluoromethanesulfonate (70 mg, 0.27 mmol) in dichloromethane (1.5 mL), triethylamine (38 μL, 0.27 mmol) was added at −40°C and the reaction was conducted as described above. The processed reaction mixture was chromatographed on a column of silica gel with benzene–butanone (100:1→10:1, gradient). This gave three fractions: fraction A (**15**, **16**, and octa-*O*-benzyl α,β-trehalose (19), 275.9 mg), fraction B (the self-condensation product and **3**, 96 mg), and fraction C (**2**, 20 mg). Rechromatography of fraction A gave fraction D (**15** and **16**, 133.2 mg) and then fraction E (**16** and the trehalose derivative, 122.3 mg). Fraction D was again chromatographed to give pure **15** (112.8 mg, 29%); $[\alpha]_D$ +38°(*c* 0.6, chloroform); ^{13}C nmr ($CDCl_3$, TMS) showed the presence of three anomeric carbons at δ 94.3 (C-1), 102.6 (C-1'), and 103.8 (C-1''). *Anal.* calcd. for $C_{95}H_{98}O_{16}$: C 76.28, H 6.60; found: C 76.15, H 6.54. Chromatography of fraction E gave pure **16** (73.7 mg, 19%); $[\alpha]_D$ +59°(*c* 1.4, chloroform); ^{13}C nmr ($CDCl_3$, TMS) showed the presence of three anomeric carbons at δ 94.6 (C-1), 97.3 (C-1'), and 103.6 (C-1''). *Anal.* calcd. for $C_{95}H_{98}O_{16}$: C 76.28, H 6.60; found: C 76.01, H 6.98.

O-β-D-Glucopyranosyl-(1→3)-O-[β-D-glucopyranosyl-(1→6)]-D-glucopyranose (4)

The fully benzylated trisaccharide **15** (100 mg, 0.067 mmol) was hydrogenated over palladium black (100 mg) in acetic acid (5 mL) containing water (0.05 mL) at 410 kPa overnight. The mixture was filtered, concentrated, and hydrogenated again over the catalyst (100 mg) in acetic acid (5 mL) containing water (3 mL). After repetition of a similar hydrogenation, the residual glass obtained was crystallized with ethanol to give **4** (30 mg, 89%), mp 183–188°C; $[\alpha]_D$ −1.1° (*c* 1.5, water) (lit. (8) mp 197–199°C; $[\alpha]_D$ −0.6° (*c* 1.15, water)); ^{13}C nmr (D_2O, ext. TMS) δ: 61.9 (73, C-6' and C-6), 69.2 (14, C-4), 69.9 (11, C-6), 70.8 (97, C-4' and C-4), 72.1 (29, C-2α and C-5α), 73.9 (23, C-2β), 74.3 (45, C-2), 74.6 (54, C-2'), 75.7 (11, C-5β), 76.8 (100, C-5' and C-5), 77.0 (66, C-3), 77.1 (65, C-3'), 83.3 (11, C-3α), 85.7 (10, C-3β), 93.2 (14, C-1α), 96.9 (15, C-1β), 104.0 (50, C-1), 104.3 (28, C-1'). *Anal.* calcd. for $C_{18}H_{32}O_{16}$: C 42.86, H 6.39; found: C 42.82, H 6.77.

O-(2,3,4,6-Tetra-O-acetyl-β-D-glucopyranosyl)-(1→3)-O-[2,3,4,6-tetra-O-acetyl-β-D-glucopyranosyl-(1→6)]-1,2,4-tri-O-acetyl-D-glucopyranose (17)

The trisaccharide **4** (20 mg, 0.04 mmol) was reacted with acetic anhydride (1 mL) and sodium acetate (100 mg) under stirring at 100°C for 6 h. After dilution with chloroform, filtration, and evaporation at 80°C *in vacuo*, the residue obtained was purified on a silica gel column with benzene–butanone (2:1) as solvent. This gave a pure glass of **17** (35 mg, 91%); ^{13}C nmr ($CDCl_3$, TMS) showed that the glass was an anomeric mixture (δ 88.9 (C-1α) and 91.6 (C-1β) (20)). The glass was crystallized with ethanol, mp 233–235°C; $[\alpha]_D$ −2.1° (*c* 0.7, chloroform) (lit. (6) mp 226–227°C; lit. (8) mp 237°C; $[\alpha]_D^{20}$ −2.56° (*c* 1.33, chloroform)). *Anal.* calcd. for $C_{40}H_{54}O_{27}$: C 49.69, H 5.63; found: C 49.81, H 6.05.

1. (*a*) J. M. Fréchet and C. Schuerch. J. Am. Chem. Soc. **93**, 492 (1971); (*b*) R. D. Guthrie, A. D. Jenkins, and J. Stehlicek. J. Chem. Soc. C, 2690 (1971); (*c*) K. Takiura,

S. HONDA, T. ENDO, and K. KAKEHI. Chem. Pharm. Bull. **20**, 438 (1972); (*d*) P. J. PFÄFFLI, S. H. HIXON, and L. ANDERSON. Carbohydr. Res. **23**, 195 (1972); (*e*) N. BELORIZKY, G. EXOFFIER, D. GAGNAIRE, J.-P. UTILLE, M. VIGNON, and P. VOTTERO. Bull. Soc. Chim. Fr. 4749 (1972); (*f*) U. ZEHAVI and A. PATCHORNIK. J. Am. Chem. Soc. **95**, 5673 (1973); (*g*) V. ESCHENFELDER, R. BROSSMER, and H. WACHTER. Angew. Chem. Int. Ed. Engl. **14**, 715 (1975).

2. S. KOTO, T. UCHIDA, and S. ZEN. Bull. Chem. Soc. Jpn. **46**, 2520 (1973).
3. S. KOTO, Y. HAMADA, and S. ZEN. Chem. Lett. 587 (1975).
4. S. KOTO, N. MORISHIMA, T. SATO, and S. ZEN. 26th Intern. Congr. Pure Appl. Chem., Tokyo. 1977. 8B407.
5. S. KOTO, T. SATO, N. MORISHIMA, and S. ZEN. Bull. Chem. Soc. Jpn. **53**, 1761 (1980).
6. H. KITAHARA and Y. TAKEUCHI. J. Agric. Chem. Soc. Jpn. **35**, 468 (1961).
7. (*a*) G. CHIHARA, Y. MAEDA, J. HAMURO, T. SASAKI, and F. FUKUOKA. Nature, **222**, 687 (1969); (*b*) N. KOMATSU, S. KUBO, S. KIKUMOTO, K. KIMURA, G. SAITO, and S. SAKAI. Gann, **60**, 137 (1969).
8. A. KLEMER and K. HOMBERG. Chem. Ber. **93**, 1643 (1960); Chem. Ber. **94**, 2727 (1961), cf. K. TAKEO. Carbohydr. Res. **77**, 131 (1977).
9. S. KOTO, Y. TAKEBE, and S. ZEN. Bull. Chem. Soc. Jpn. **45**, 291 (1972).
10. B. HELFERICH and J. BECKER. Justus Liebigs Ann. Chem. **440**, 1 (1924).
11. (*a*) H. OKABE, N. KOSHITO, K. TANAKA, and T. KAWASAKI. Chem. Pharm. Bull. **19**, 2394 (1971); (*b*) J. M. KUESTER and I. DYONG. Justus Liebigs Ann. Chem. 2179 (1975).
12. T. USUI, N. YAMAOKA, K. MATSUDA, K. TSUZIMURA, H. SUGIYAMA, and S. SETO. J. Chem. Soc. Perkin Trans. I, 2425 (1973).
13. H. SAITO, T. OHKI, N. TAKASAKA, and T. SASAKI. Carbohydr. Res. **58**, 293 (1977).
14. F. J. KRONZER and C. SCHUERCH. Carbohydr. Res. **27**, 379 (1973).
15. D. J. BELL and J. LORBER. J. Chem. Soc. 453 (1940).
16. E. V. PIEL and C. B. PURVES. J. Am. Chem. Soc. **61**, 2978 (1939).
17. K. H. SLOTTA and H. HELLER. Chem. Ber. **63**, 1024 (1930).
18. S. KOTO, N. MORISHIMA, Y. MIYATA, and S. ZEN. Bull. Chem. Soc. Jpn. **49**, 2639 (1976).
19. S. KOTO, N. MORISHIMA, and S. ZEN. Bull. Chem. Soc. Jpn. **52**, 784 (1979).
20. M. R. VIGNON and P. J. A. VOTTERO. Carbohydr. Res. **53**, 197 (1977).

Can. J. Chem. Downloaded from www.nrcresearchpress.com by 210.87.254.40 on 09/05/12
For personal use only.

Approaches to some carbohydrate-derived sultones

BERT FRASER-REID,[1] KING MO SUN, AND RAYMOND Y-K. TSANG

Guelph–Waterloo Centre for Graduate Work in Chemistry, University of Waterloo, Waterloo, Ont., Canada N2L 3G1

AND

PIERRE SINAŸ AND MARCK PIETRASZKIEWICZ

Laboratoire de Biochemie Structurale, E.R.A., 739 U.E.R. de Sciences Fondementales et Appliquées, 45046 Orleans, France

Received June 9, 1980

This paper is dedicated to Prof. Raymond U. Lemieux on the occasion of his 60th birthday

BERT FRASER-REID, KING MO SUN, RAYMOND Y-K. TSANG, PIERRE SINAŸ, and MARCK PIETRASZKIEWICZ. Can. J. Chem. **59**, 260 (1981).

Under some conditions deprotonation of various mixed disulfonate ester derivatives of carbohydrates leads to intramolecular displacement yielding a product in which a sultone is fused to the sugar ring. The procedure seems to work best when a mesylate and a benzenesulfonate are involved. Examples with both pyranose and furanose sugars are described.

BERT FRASER-REID, KING MO SUN, RAYMOND Y-K. TSANG, PIERRE SINAŸ et MARCK PIETRASZKIEWICZ. Can. J. Chem. **59**, 260 (1981).

Dans certaines conditions, la déprotonation de divers esters disulfoniques mixtes de carbohydrates donne lieu à un déplacement intramoléculaire conduisant à un produit dans lequel une sultone est fusionnée au cycle du sucre. La méthode semble mieux fonctionner quand on utilise un mésylate ou un benzènesulfonate. On décrit des exemples avec les sucres des types pyrannose et furannose.

[Traduit par le journal]

In a previous publication by one of us (1) it was shown that the reaction of methanesulfonyl chloride with a sugar α-keto-alcohol in the presence of sodium hydride caused efficient formation of a bicyclic system in which a sultone was fused to a pyranoside ring.[2] Bicyclic sultones are of interest in view of their potential for biological activity (3). In this communication we describe other routes from readily available sugars, which make these interesting, novel binuclear heterocyclic systems available for further use.

The present series of investigations began with the observation that a number of mixed disulfonates, upon treatment with organometal reagents, gave sultones in high yields. Thus the mesylate-tosylate **2** reacted with lithium acetylide – ethylenediamine complex to give the seven-membered sultone **3** in 98% yield as a crystalline substance. The structure of **3** follows from the elemental analysis, the nmr data indicating the retention of the isopropylidine group, and the ir data for the sulfonate (1170, 1345 cm^{-1}). A homologue was also prepared from the mesylate-tosylate **5** which gave the six-membered sultone **6** in 90% yield.

Analogous reactions in the pyranose series also occur. Thus the mesylate-tosylate **7***c* reacted with the dianion of ethyl acetoacetate, **8**, (4) to give **9** as a noncrystalline substance in 74% yield which was then hydrogenated over palladium to the saturated analogue **10**, as a crystalline substance.

A number of experiments were carried out to determine some of the requirements for the formation of sultones in these systems. The results in eqs. (a), (b), and (c), Scheme 1, indicate that in all cases the tosylate (or benzenesulfonate) was displaced, implying that the mesylate had been deprotonated and thereby producing a nucleophile. The pK_a data indicate that a mesylate group is eight times more acidic than a tosylate (5), hence under the reaction conditions the latter is the preferred leaving group.

With regard to compound **7***d*, even if one of the tosyl groups should be deprotonated, the planar aromatic ring would prevent the resulting anion from achieving an acceptable geometry to effect the displacement of the other tosyl group. It is therefore not surprising that when **7***d* was treated with the dianion **8**, the material was recovered unchanged. The same geometric constraints do not apply to the dimesylate **7***e*, which could conceivably give the analogues **9** and/or **11**. However, this substrate was also recovered unchanged after treatment with dianion **8**, even though a generous excess of base had been used.

Comparison of the results with **7***c* and **7***e* suggests that it is advantageous to have sulfonates of

[1]Author to whom correspondence may be addressed at the Chemistry Department, University of Maryland, College Park, MD 20742, U.S.A.

[2]This result is reminiscent of the work of Durst and Tin (2) who showed that the mesylate of the *trans*-bromohydrin of cyclohexene gave a cyclic sultone upon treatment with *n*-butyl lithium.

0008-4042/81/020260-04$01.00/0

©1981 National Research Council of Canada/Conseil national de recherches du Canada

Can. J. Chem. Downloaded from www.nrcresearchpress.com by 210.87.254.6 on 09/05/12
For personal use only.

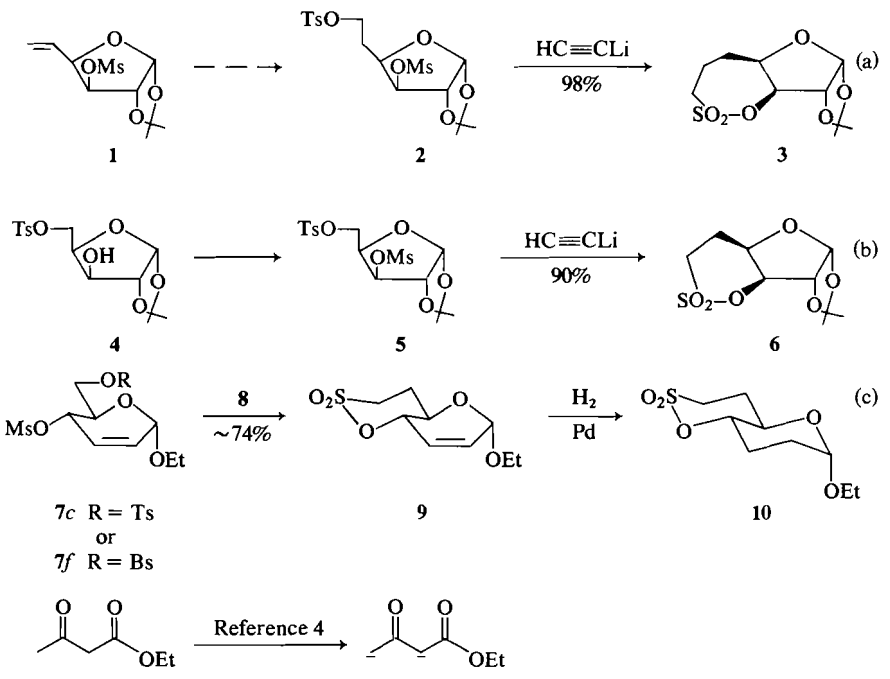

SCHEME 1

different reactivities so that one can be deprotonated preferentially while the other would be the favoured leaving group. These conditions are met with the mesylate-benzenesulfonate **7***f*. Although LDA in THF/HMPA did cause initial formation of **9** as detected by tlc, gross decomposition set in rapidly. However, some success was obtained with sodium hydride, and **9** was obtained in ~60% yield although an appreciable amount of starting material **7***f* was also recovered.

The properties and synthetic utility of these interesting sultones are being investigated in our laboratories and will be described in future publications.

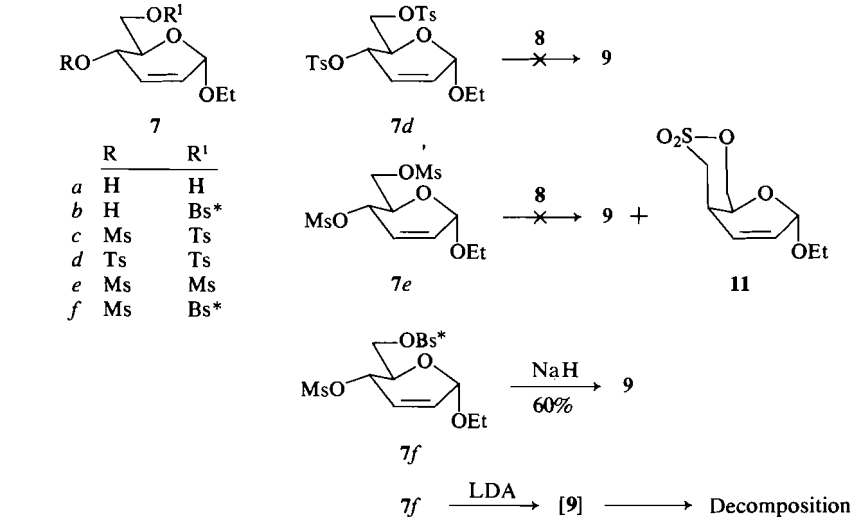

	R	R¹
a	H	H
b	H	Bs*
c	Ms	Ts
d	Ts	Ts
e	Ms	Ms
f	Ms	Bs*

*Bs = benzenesulfonate

SCHEME 2

Can. J. Chem. Downloaded from www.nrcresearchpress.com by 210.87.254.6 on 09/05/12
For personal use only.

Can. J. Chem. Downloaded from www.nrcresearchpress.com by 210.87.254.6 on 09/05/12
For personal use only.

Experimental

General

Melting points were determined on a Fisher-Johns heating stage or a Büchi apparatus, and are uncorrected. The nmr spectra were determined, unless otherwise stated, in deuteriochloroform containing 1% tetramethylsilane as internal standard with a Varian HR 220, Varian HA 100, Varian T-60, or a Perkin-Elmer R-32 (90 MHz) spectrometer. Coupling constants were obtained by measuring spacings of spectra judged to be first order.

Thin-layer chromatography (tlc) was performed on precoated 0.2 mm silica gel sheets (E. Merck, F-254) and developed with the solvent indicated. The chromatograms were first viewed under ultraviolet light, then sprayed with concentrated sulfuric acid and heated in an oven for complete visualization.

For column chromatography, E. Merck silica gel (0.05–0.20 mm, 70–325 mesh A.S.T.M.) was used.

Elemental analyses were carried out by Service Central d'Analyse, 69390 Vernaison, France, or Guelph Chemical Laboratories Ltd., Guelph, Ontario.

*5-Deoxy-1,2-*O*-isopropylidene-3-*O*-mesyl-6-*O*-tosyl-α-*D*-glucofuranose (2)*

A 1 *M* solution of diborane in tetrahydrofuran (1 mL) was added to a solution of the mesylate **1** (264 mg) (6) in tetrahydrofuran (5 mL). The mixture was stirred for 2 h at room temperature, then water (1 mL) was added, followed by a 30% hydrogen peroxide solution (0.7 mL) and a 30% sodium hydroxide solution (0.6 mL). The reaction was stirred for 1.5 h, evaporated, and the residue extracted with chloroform. The chloroform layer was evaporated and the residue was treated directly with tosyl chloride (280 mg) in dry pyridine (2 mL). After 12 h at room temperature, work-up gave a residue which was chromatographed on silica gel (5 g); elution with benzene – ethyl acetate (10:9) gave pure fractions of compound **2** (158 mg, 36%), mp 78–80°C; $[\alpha]_D^{20}$ −11° (*c* 0.86, $CHCl_3$); nmr data (acetone-d_6) δ: 1.30 and 1.43 (6H, 2s, Me), 1.90–2.20 (2H, m, CH_2), 2.45 (3H, s, Ts), 3.10 (3H, s, Ms), 3.90–4.40 (3H, m, CH_2 and H-4), 4.70–4.85 (2H, 2d, H-2 and H-3), 5.85 (2H, d, 4 Hz, H-1). *Anal.* calcd. for $C_{17}H_{24}O_9S_2$: C 46.78, H 5.54, S 14.69; found: C 46.83, H 5.52, S 14.74.

*5,6,7-Trideoxy-1,2,*O*-isopropylidene-α-*D*-xylo-heptofuranose-3,7-sultone (3)*

A solution of 5-deoxy-1,2-*O*-isopropylidene-3-*O*-mesyl-6-*O*-tosyl-α-D-glucofuranose (**2**, 87.2 mg) and lithium acetylide – ethylenediamine complex (46 mg) in dry dimethylsulfoxide (1 mL) was stirred for 20 min at room temperature. After addition of water (5 mL), the reaction mixture was extracted with ether (10 mL). The ether layer was distilled off and the residue was chromatographed on silica gel (3 g) to give the sultone **3** (57.1 mg, 98%), mp 148°C (chloroform–hexane); nmr data δ: 1.33 and 1.50 (6H, 2s, Me), 1.70–2.50 (4H, m, —CH_2—), 3.30–3.55 (2H, m, —CH_2SO_2—), 4.45–4.70 (1H, m, H-4), 4.80 (1H, d, 4 Hz, H-2), 5.07 (1H, d, 3 Hz, H-3), 6.00 (1H, d, H-1). *Anal.* calcd. for $C_{10}H_{16}O_6S$: C 45.45, H 6.10, S 12.11; found: C 45.20, H 5.74, S 11.94.

*1,2-*O*-Isopropylidene-3-*O*-mesyl-5-*O*-tosyl-α-*D*-xylofuranose (5)*

1,2-*O*-Isopropylidene-5-*O*-tosyl-α-D-xylofuranose (**4**, 6.88 g) was treated with mesyl chloride (1.7 mL) in pyridine (20 mL) during 12 h at 0°C. After work-up, compound **5** was obtained (7.88 g, 97%) mp 104–105°C (from ethyl acetate – hexane, 1:4); $[\alpha]_D^{20}$ −36° (*c* 0.43, $CHCl_3$); nmr data (acetone-d_6) δ: 1.30 and 1.40 (6H, 2s, Me), 2.45 (3H, s, Ts), 3.20 (3H, s, Ms), 4.15–4.60 (3H, m, H-4, H-5, H-5'), 4.85 (3H, d, 4 Hz, H-2), 5.07 (3H, d, 3 Hz, H-3 .), 6.00 (3H, d, H-1). *Anal.* calcd. for $C_{16}H_{22}O_9S_2$: C 45.49, H 5.25, S 15.18; found: C 45.63, H 5.22, S 14.91.

*5,6-Dideoxy-1,2-*O*-isopropylidene-α-*D*-xylo-hexofuranose-3,6-sultone (6)*

A solution of 1,2-*O*-isopropylidene-3-*O*-mesyl-5-*O*-tosyl-α-D-glucofuranose (**5**, 406 mg) and lithium acetylide – ethylenediamine complex (243 mg) in dry dimethylsulfoxide (7 mL) was stirred for 1 h at room temperature. After addition of water (20 mL), the reaction mixture was extracted with chloroform (3 × 20 mL). The chloroform layer was washed with water and run through a layer of silica gel. The solvent was distilled off and the residue dissolved in benzene (50 mL), washed with water (60 mL), and evaporated to give a white solid **6** (216 mg, 90%), only slightly soluble in many organic solvents at room temperature, mp 190–200°C (dec); nmr data ($CDCl_3$) δ: 1.32 and 1.50 (6H, 2s, Me), 2.50–2.70 (2H, m, CH_2), 3.05–3.25 (2H, m, CH_2SO_2), 4.25–4.40 (1H, m, H-4), 4.65 (1H, d, 4 Hz, H-2), 4.97 (1H, d, 1.5 Hz, H-3), 6.00 (1H, d, H-1). *Anal.* calcd. for $C_9H_{14}O_6S$: C 43.20, H 5.64, S 12.79; found: C 43.21, H 5.77, S 12.77.

*Ethyl 2,3-Dideoxy-4-*O*-mesyl-6-*O*-benzenesulfonyl-α-*D*-erythro-hex-2-enopyranoside (7*d*)*

A solution of ethyl 2,3-dideoxy-α-D-*erythro*-hex-2-enopyranoside (*7a*, 2.5 g) (7) in dry pyridine (100 mL) and methylene chloride (100 mL) was cooled to −40°C, and benzenesulfonyl chloride (2.5 g) dissolved in methylene chloride (20 mL) was added in small portions over 2 h. The reaction mixture was kept at −10°C for 3 days, and the residue after work-up was separated on a silica gel column. The monobenzenesulfonate *7b* (2.7 g; 60%) was then treated with mesyl chloride (2.0 mL) in pyridine (100 mL) at room temperature for 12 h giving *7d* (2.92 g; 87%). For *7d*, $[\alpha]_D^{20}$ +51.6° (*c* 5.44, $CHCl_3$); nmr data ($CDCl_3$) δ: 1.19 (3H, t, CH_3—CH_2O), 3.20 (3H, s, CH_3SO_3), 3.33–3.90 (2H, m, CH_3—CH_2—O), 4.00 (1H, m, H-5), 4.22 (2H, m, 2H-6), 4.96 (1H, bs, H-1), 5.01 (1H, bd, H-4), 5.62–6.12 (2H, q, H-2, H-3), 7.53–8.00 (5H, m, $PhSO_3$); ms *m/e* 347 (M^+ − OEt).

*Ethyl 2,3,6,7-Tetradeoxy-α-*D*-erythro-hept-2-enopyranosid-4,-7-sultone (9)*

(a) The dianion **8** was generated in the standard manner (4). Ethyl acetoacetate (5 g) was added dropwise to a suspension of 50% sodium hydride (1.5 g; 31 mmol) in ice-cold tetrahydrofuran. The solution became clear and after 10 min *n*-butyllithium (15 mL of 2.4 *M*; 36 mmol) was added dropwise whereupon the colour became orange-yellow. Hexamethylphosphoramide (20 mL) was then added and after stirring for another 20 min, the sugar *7c* (3) (1.0 g, 2.5 mmol) in tetrahydrofuran (5 mL) was added. Thin-layer chromatography in ethyl acetate – petroleum ether (1:4) showed the reaction to be complete after 15 min and water was added. After the extraction and washing with solutions of ammonium chloride and sodium bicarbonate, the material was chromatographed to give **9** (0.43 g, 74%) as a syrupy substance.

(b) In a similar experiment to the foregoing, the mesylate-benzenesulfonate, *7f*, (1.0 g, 2.6 mmol) (8) afforded compound **9** (0.43 g) also in 74% yield.

(c) Sodium hydride (50 mg of 50%; 1.04 mmol) was suspended in dry tetrahydrofuran (5 mL) and compound *7f* (0.1 g, 0.26 mmol), dissolved in 5 mL of the same solvent and 5 mL of hexamethylphosphoramide, was added. After stirring at room temperature for 18 h, tlc in ethyl acetate – petroleum ether (1:4) still showed the presence of starting material. Work-up and separation by preparative layer chromatography afforded some starting material, *7f* (15 mg), and the title compound **9** (31 mg) in 60% yield based on unrecovered starting material. For **9**, $[\alpha]_D^{20}$ 3.4 (*c* 5.62, $CHCl_3$); nmr data ($CDCl_3$) δ: 1.10 (3H, t, CH_3—

CH_2O—), 2.00–2.20 (2H, m, CH_2—CH_2SO_2—), 3.12–3.46 (2H, m, CH_3—CH_2—O—), 3.50 (1H, m, H-5), 4.35 (1H, d, H-4), 4.46 (1H, s, H-1), 5.16–5.34 (2H, q, H-2, H-3); ms *m/e* 234 (M^+).

*Ethyl 2,3,6,7-Tetradeoxy-α-D-*erythro*-heptopyranosid-4,7-sultone (**10**)*

The sultone **9** (200 mg) was hydrogenated over 5% palladium on carbon in ethanol. Preparative layer chromatography using methanol – methylene chloride (1:24) afforded 150 mg (75%) of **10**, mp 119–120°C; $[\alpha]_D^{20}$ 57.2°(*c* 1.02, $CHCl_3$); nmr data ($CDCl_3$) δ: 1.20 (3H, t, CH_3—CH_2O—), 1.78–2.40 (6H, m, 2H-2, 2H-3, 2H-6), 3.10–3.41 (2H, m, CH_2—SO_3—), 3.78 (1H, m, H-5), 4.22 (1H, q, H-4), 4.70 (1H, t, H-1). *Anal.* calcd. for $C_9H_{16}O_5S$: C 45.75, H 6.83, S 13.57; found: C 45.75, H 6.98, S 13.46.

Acknowledgements

We are grateful to the Natural Sciences and Engineering Research Council of Canada, the Centre National de la Recherche Scientifique, and Boehringer of France for support for this work.

1. M. B. YUNKER and B. FRASER-REID. J. Chem. Soc. Chem. Commun. 325 (1978).
2. T. DURST and K.-C. TIN. Can. J. Chem. **48**, 845 (1970).
3. J. F. PILICHOWSKI and J. LHOMME. Tetrahedron, **33**, 1113 (1977).
4. S. N. HUCKIN and L. WEILER. J. Am. Chem. Soc. **96**, 1082 (1974).
5. C. L. BUMGARDNER, J. R. LEVER, and S. T. PURRINGTON. J. Org. Chem. **45**, 748 (1980).
6. J. K. N. JONES and J. L. THOMPSON. Can. J. Chem. **35**, 955 (1957), and references cited.
7. R. J. FERRIER and N. PRASAD. J. Chem. Soc. C, 570 (1969).
8. M. B. YUNKER. Ph.D. Thesis, University of Waterloo, Waterloo, Ont., Canada. 1975.

Can. J. Chem. Downloaded from www.nrcresearchpress.com by 210.87.254.6 on 09/05/12
For personal use only.

The formation of azoxyalkanes in reactions of some organometallic reagents with *N*-nitroso-*O*,*N*-dialkylhydroxylamines: the nonphotochemical synthesis of an acyclic (*E*)-azoxyalkane

A. C. M. MEESTERS, H. RÜEGER, K. RAJESWARI, AND M. H. BENN[1]

Chemistry Department, The University, Calgary, Alta., Canada T2N 1N4

Received July 10, 1980

This paper is dedicated to Prof. Raymond U. Lemieux on the occasion of his 60th birthday

A. C. M. MEESTERS, H. RÜEGER, K. RAJESWARI, and M. H. BENN. Can. J. Chem. **59**, 264 (1981).

Azoxyalkanes were found to be regiospecifically formed in the reactions of some alkyllithium and Grignard reagents with *N*-nitroso-*O*,*N*-dialkylhydroxylamines. Remarkably, although (*Z*)-stereomers were usually produced, in one case the (*E*)-isomer was predominant.

A. C. M. MEESTERS, H. RÜEGER, K. RAJESWARI et M. H. BENN. Can. J. Chem. **59**, 264 (1981).

On a trouvé que les azoxyalcanes se forment de façon régiospécifique dans les réactions des alkyllithium et des réactifs de Grignard avec les *N*-nitroso *O*,*N*-dialkylhydroxylamines. On a notamment trouvé un cas où l'isomère (*E*) est le produit principal en dépit du fait qu'il y a généralement formation des stéréoisomères (*Z*).

[Traduit par le journal]

Introduction

Faced with a need for some unsymmetrical azoxyalkanes (**1**, $R^1 \neq R^2$), it occurred to us that as an alternative to the existing methods (1), they might be prepared by the reaction of *N*-nitroso-*O*,*N*-dialkylhydroxylamines (**2**) with organometallic reagents (**3**), a process schematically portrayed by eq. [1], and apparently not previously investigated.

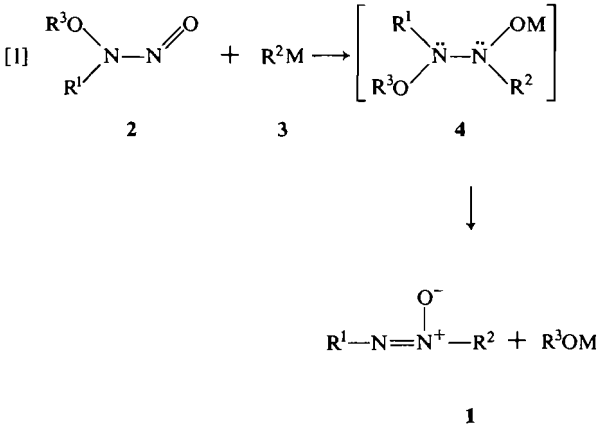

[1]

2 **3** **4**

1

We were encouraged to investigate this possibility by the report that alkyllithium reagents added to the nitroso function of *N*-nitrosoamines (2), and the observation that the *N*-alkoxy-*N'*-hydroxy intermediates **5***a* and *b*, closely related to **4**, regiospecifically eliminated methanol to afford the azoxyalkanes **6***a* and **6***b* (1*b*), eq. [2].

However, we anticipated problems arising as a result of such competing processes as α-metallation of the nitrosohydroxylamine, eq. [3], and further, "over-reaction" of the azoxyalkane products with the organometallic reagents, cf. eqs. [4] and [5] (3).

Results and Discussion

In fact, exploratory experiments in which methyllithium was allowed to react with *N*-nitroso-*O*,*N*-dimethylhydroxylamine, in ether, at ca. −65°C, gave (*Z*)-azoxymethane in 10–20% yield. Accordingly we decided to probe further.

Our experiences, summarized by the examples given in Table 1, and further illustrated in the Experimental (3), suggest that the reaction of *N*-nitroso-*O*,*N*-dialkylhydroxylamines with some organometallic reagents *can* result in the regiospecific formation of azoxyalkanes. Unfortunately, the synthesis is at present effectively restricted to primary alkyllithium reagents, and is of dubious preparative value on account of the low yields, the major products indeed being those corresponding to "over-reactions". However, during this work we made the following striking discovery.

The reaction of methyllithium with *N*-nitroso-*O*-methyl-*N*-*n*-butylhydroxylamine gave two isomeric ($C_5H_{12}N_2O$) products (*A* and *B*), both of which were obtained as liquids, homogeneous by glc analysis. Some spectroscopic properties of these two compounds are listed in Table 2.

The less polar, minor isomer *A* was thus identified as the expected (*Z*)-azoxyalkane (**7**). When *B* was heated (in boiling toluene solution) it was cleanly but slowly converted into *A* (the pro-

[1]Author to whom correspondence may be addressed.

0008-4042/81/020264-05$01.00/0

©1981 National Research Council of Canada/Conseil national de recherches du Canada

Can. J. Chem. Downloaded from www.nrcresearchpress.com by 210.87.254.105 on 09/05/12
For personal use only.

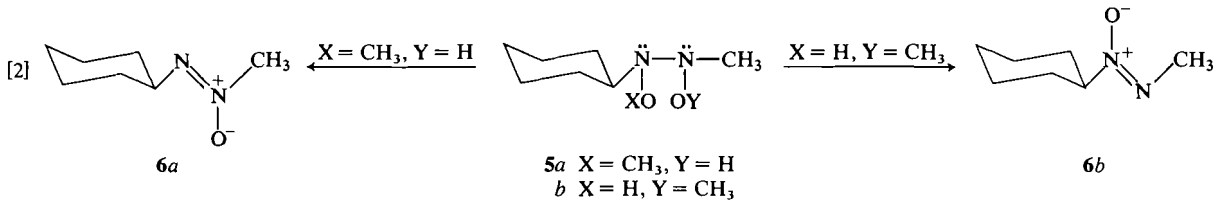

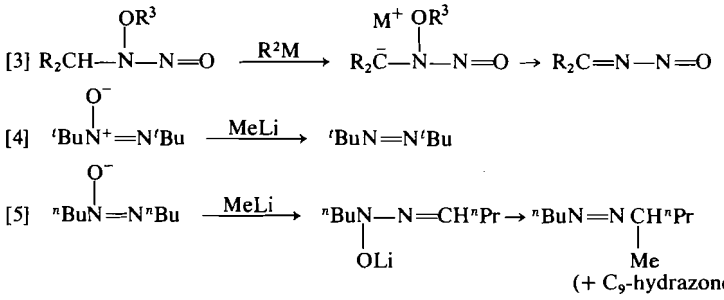

cess was almost complete after 24 h). The ir and uv spectra of *B* are inconsistent (4, 5) with it being the oxadiazirine (**8**), but are in accord (4, 5) with the (*E*)-azoxyalkane structure (**9**); as are the nmr data (which also exclude the regioisomeric (*E*)- and (*Z*)-(**10**)).

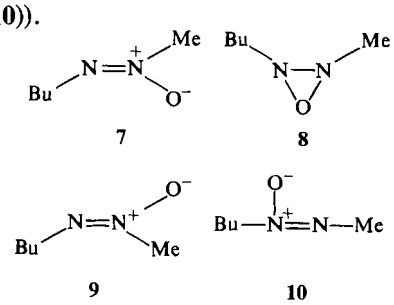

This finding surprised us, for in all the other cases the azoxyalkanes were isolated as (*Z*)-stereomers. To account for the formation of **9** we offer the following rationalization. The *N*-nitroso compound exists predominantly in the (*Z*)-conformation (as shown in **2**, Scheme 1) (6). Addition of methyllithium reagent then yields an intermediate (**4***a*) in which the barrier to inversion at nitrogen is sufficiently high that elimination of methoxide is faster, with the consequence that **9** is kinetically favoured over **7**.

If this were the case, why are (*E*)-azoxyalkanes not the usual isomers isolated? We suggest that as the steric bulk of either, or both, of the two alkyl substituents is increased, thermal isomerization to the more stable (*Z*)-stereomer becomes easy; and/or that in cases where there are more hydrogens attached to the distal (to oxidized nitrogen) α-carbon atom than on the proximal, isomerization via a distal anionic species becomes a facile process,[2] i.e. under our reaction conditions the process *E*-**1** ⇄ *E*-**11** ⇄ *Z*-**11** ⇄ *Z*-**1** may permit thermodynamic (equilibrium) control of azoxyalkane product-formation, with the consequence that *Z*-**1** is isolated (Scheme 2).

Of all the examples which we studied, only the reaction of methyllithium with *N*-nitroso-*N*-*n*-butyl-*O*-methylhydroxylamine would be expected

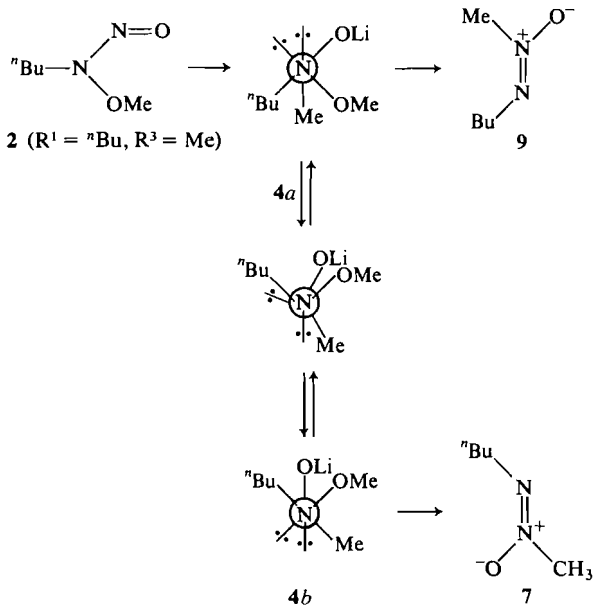

SCHEME 1. A suggestion for the reaction of methyllithium with *N*-nitroso-*N*-*n*-butyl-*O*-methylhydroxylamine.

[2]Assuming the kinetic acidity is as for *Z*-azoxymethane, cf. ref. 7.

Can. J. Chem. Downloaded from www.nrcresearchpress.com by 210.87.254.105 on 09/05/12
For personal use only.

Can. J. Chem. Downloaded from www.nrcresearchpress.com by 210.87.254.105 on 09/05/12
For personal use only.

TABLE 1. A synopsis of the formation of azoxyalkanes by the reactions[a] of some organometallic reagents with *N*-nitroso-*O*,*N*-dialkylhydroxylamines

2		3		1[b]		
R^1	R^3	R^2	M	R^1	R^2	Yield[c] (%)
Me	Me	Me	Li	Me	Me	10–20
Me	Me	^{n}Bu	Li	Me	^{n}Bu	7
Me	Me	^{n}Bu	MgBr	Me	^{n}Bu	4
Me	Me	^{n}Bu$_2$	CuLi	Me	^{n}Bu	5
^{n}Bu	Me	Me	Li	^{n}Bu	Me	29–50[d]
^{n}Bu	Me	^{n}Bu	Li	^{n}Bu	^{n}Bu	30
^{i}Pr	Me	Me	Li	^{i}Pr	Me	19
^{i}Pr	Me	^{n}Bu	Li	^{i}Pr	Bu	12
^{i}Pr	Me	Ph	MgBr	^{i}Pr	Ph	6
^{t}Bu	Me	Me	Li	^{t}Bu	Me	Trace
^{t}Bu	^{t}Bu	Me	Li	^{t}Bu	Me	0
Et	Et	^{n}BuC≡C	Li	Et	^{n}BuC≡C	0

[a]See Experimental for typical conditions.
[b](*Z*)-Isomers, except where noted.
[c]Isolated products, >95% pure by glc analysis. The major products were usually azoalkanes, hydrazones, and hydrazines (cf. Experimental).
[d](*E*)-Isomer also (see text, Experimental).

TABLE 2. Spectroscopic properties of the isomers *A* and *B*

Property	Isomer *A*	Isomer *B*
ν_{max} (film)	1510, 1420, 1328, and 1108 cm^{-1}	1510, 1416, 1315, and 1105 cm^{-1}
^{1}H nmr δ($CDCl_3$, TMS = 0)	0.95 (3H, J = 7 H), 1.1–2.0 (4H, m), 3.40 (2H, t, J = 7 Hz), 4.05 (3H, s)	0.95 (3H, t, J = 7 Hz), 1.2–2.0 (4H, m), 3.50 (2H, t, J = 7 Hz), 3.98 (3H, s)
^{13}C nmr δ($CDCl_3$, TMS = 0)	13.8(q), 20.9(t), 29.2(t), 52.1(q), and 56.7(t)	13.7(q), 20.5(t), 30.5(t), 52.7(q), and 55.0(t)
Mass spectrum (ions > 15%)	99(26) (M − 17), 74(27), 73(21), 57(38), 45(33), 43(100), and 41(47) amu	99(23) (M − 17), 74(23), 73(10), 57(32), 45(19), 43(100), and 41(35) amu
λ_{max} (EtOH) (log ε)	219 nm (3.51)	233 nm (3.84)

to yield an azoxyalkane which was relatively sterically unhindered, and possessed more proximal α-hydrogen atoms than distal, i.e. where the preferred anion would be the proximal one, with less of a tendency to undergo $E \rightarrow Z$ isomerization than the distal anion.

We also suspect that formation of the proximal carbanion may protect an azoxyalkane from "over-reactions" (i.e. prevent reactions such as that of eq. [6]), and so be responsible for the relatively good yields of **9** obtained under our reaction conditions.

We hoped that we might be able to supress reactions such as [6] by selecting an organometallic reagent which retained high nucleophilicity, but was less basic than an alkyllithium. However, the

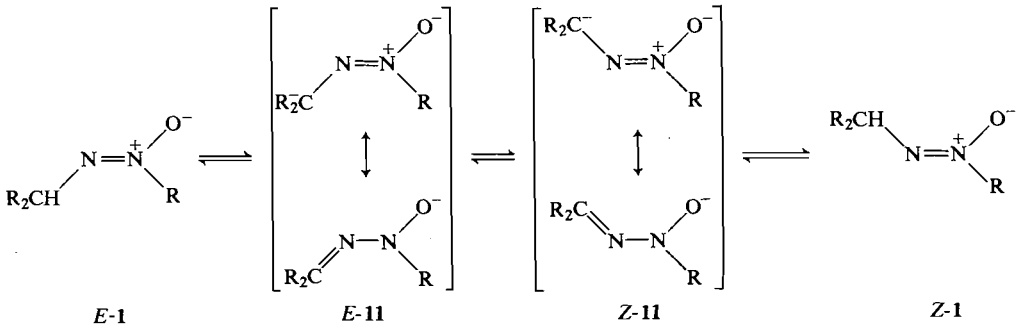

E-1 *E*-11 *Z*-11 *Z*-1

SCHEME 2. The isomerism of (*E*)- and (*Z*)-azoxyalkanes via an anionic intermediate.

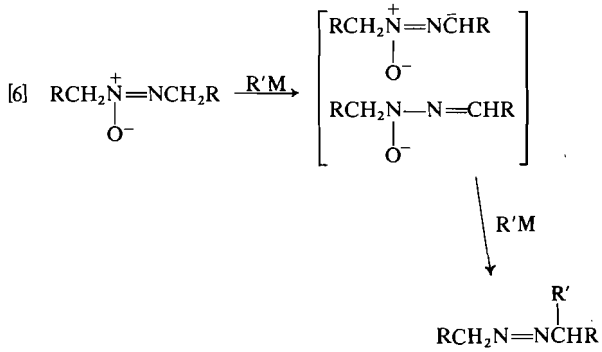

use of Grignard or cuprate reagents gave even lower yields of isolated azoxyalkanes (cf. Table 1), with concomitant increased production of reduction products.

As matters thus rest, the reaction of *N*-nitroso-*O*,*N*-dialkylhydroxylamines with organometallic reagents is seen to be a tantalizingly restricted route to azoxyalkanes.

Experimental

Physical Measurements

Boiling points are uncorrected.

Elemental analyses were performed by the Schwartzkopf Microanalytical Laboratory, Woodside, NY. The ^{1}H nmr spectra were measured on Hitachi Perkin-Elmer R24B, and Bruker WH-90 FT spectrometers, and ^{13}C nmr on the latter instrument. All samples were dissolved in $CDCl_3$, and shift values are quoted on the δ scale in ppm from a tetramethylsilane internal standard. Infrared spectra (ir) were recorded on Perkin-Elmer 337 or 467 grating spectrometers, liquids being examined as thin films. Mass spectra (ms) were measured on a Varian Associates MAT CH-5 spectrometer, while analyses involving ms of gas chromatographically separated samples (gc–ms) were made with a Hewlett-Packard 5992A system equipped with glass columns (17.0 cm × 0.75 (id) cm) packed with OV-101 or OV-17 (3%) on Chromosorb WHP 80/100.

Analytical gas chromatography (glc) was performed using a Bendix 2500 instrument, also using glass columns, packed with OV-1 or OV-17 liquid phases (3%). Preparative glc (pglc) was carried out with an Aerograph 90P unit, fitted with a 2 m × 3 mm column packed with SE-30 (10%) on Chromosorb W 60/80. Ultraviolet spectra (uv) were measured on a Cary 15 spectrophotometer, using 1 cm quartz cells.

Materials

Methyl- and *n*-butyllithium reagents were commercially available (Aldrich Chemical Co.) as solutions in diethyl ether and hexane respectively, and were used as received.

The *N*-nitroso-*O*,*N*-dialkylhydroxylamines were prepared by nitrosation (8) of the corresponding hydroxylamines, characterized spectroscopically, and used directly. (CAUTION! *N*-nitroso-*O*,*N*-diethylhydroxylamine is known (9) to cause cancer in rats, so it, and its homologues, should be handled with great care.) Of the hydroxylamines, *O*,*N*-dimethylhydroxylamine hydrochloride was obtained as a commercial product (Aldrich Chemical Co.), the others were synthesized by a standard procedure (10) or the sodium cyanoborohydride reduction (11) of the *O*-alkyl oximes (themselves obtained by condensing the appropriate *O*-alkylhydroxylamines and aldehydes). Exceptional was *O*,*N*-di-*tert*-butylhydroxylamine, for which we had to devise a special synthesis (12).

The Reaction of Organometallic Reagents with N-*Nitroso*-O,N-*dialkylhydroxylamines*

Typically, one or two equivalents of the organometallic reagent were added to one of the nitroso compounds dissolved in anhydrous diethyl ether, at ca. −75°C, under an atmosphere of dry argon. When optimizing conditions, aliquots of the reaction mixture were withdrawn periodically (with a syringe, via a serum-capped sampling port), quenched in aqueous ammonium chloride, and the solution analysed by glc. When the nitroso reactant was seen to have been consumed, the reaction mixture was stopped. Product isolation involved extracting the azoxyalkanes from the acidified reaction mixture, a procedure which facilitated their separation from basic, "over-reaction" products. However, it should be noted that (*E*)-azoxyalkanes are more polar than their (*Z*)-stereomers, and correspondingly more soluble in water, so continuous extraction may be required. Column chromatography (Merck Silica Gel 60 70/230 mesh), or pglc was also required. The examples given below provide details of these methods.

The Reaction of n-*Butyllithium with* N-*Nitroso*-O,N-*dimethylhydroxylamine: The Preparation of* (Z)-*1*-n-*Butyl-2-methyldiazene-1-oxide* (Z)-*1* (R^1 = *Me*, R^2 = ^{n}*Bu*)

A hexane solution of *n*-butyllithium (1.6 *M*, 35 mL, 56 mmol) was added dropwise over 30 min to a stirred solution of *N*-nitroso-*O*,*N*-dimethylhydroxylamine (3.6 g, 40 mmol) in diethyl ether (50 mL) maintained at −78°C, under an argon atmosphere. The light yellow suspension which formed was stirred for a further hour at −78°C, and then quenched at −60°C by the addition of saturated aqueous ammonium chloride solution (20 mL). When this mixture had warmed to 0°C, the yellow ether phase was separated from the colourless aqueous phase, washed with hydrochloric acid (3 *M*, 3 × 10 mL) and brine (1 × 10 mL), then dried ($MgSO_4$), and evaporated to yield a yellow oil (X-1) (1.5 g).

The aqueous phase from the quenched reaction was combined with the various aqueous washes, basified with aqueous ammonia,[3] and extracted with diethyl ether (3 × 100 mL). The combined ether extracts were then dried ($MgSO_4$) and evaporated to yield a second yellow oil (X-2) (1.6 g).

A gc–ms analysis of X-1 revealed three major products: X-1-*1* (ca. 20%, P^+ 99 amu); X-1-*2* (ca. 8%, P^+ 142 amu), and X-1-*3* (ca. 72%, P^+ 156 amu). Of these, X-1-*1* and X-1-*3* were isolated by pglc, and purified by bulb-to-bulb distillation (18 Torr pressure, bath ca. 80°C). X-1-*2* was recognized as identical with X-2-*1* (identical gc–ms data) and identified as described below.

As thus obtained X-1-*1* was a near colourless liquid; λ_{max} (EtOH) (log ε): 218 (ca. 3.7); ir ν_{max}: 1515, 1385, and 1328 cm^{-1}; ^{1}H nmr δ: 0.95 (3H, t, *J* = 7 Hz), 1.1–1.6 (2H, m), 1.97 (2H, p, *J* = 7 Hz), 3.20 (3H, s), and 4.20 (2H, t, *J* = 7 Hz); ^{13}C nmr δ: 13.5 (q), 19.7 (t), 29.8 (t), 39.4 (q), and 69.4 (t); ms: 99 (100) (*M* − 17), 61 (32), 60 (25), 57 (68), 43 (98), and 41 (98) amu, all consistent with this product being (*Z*)-1-*n*-butyl-2-methyldiazene-1-oxide ((*Z*)-**1**, R^1 = Me, R^2 = *n*-Bu). *Anal.* calcd. for $C_5H_{12}N_2O$: C 51.70, H 10.42, N 24.12%; found: C 52.10, H 10.35, N 24.23%.

Similarly X-1-*3* was obtained as a nearly colourless oil; ir ν_{max}: 2950, 2870, 1470, 1438, and 1382 cm^{-1}; ^{1}H nmr δ: 0.85 (3H, t, *J* = 7 Hz), 0.90 (3H, t, *J* = 7 Hz), 1.2–2.2 (10H, m), 3.80 (4H, t, *J* = 7 Hz); ^{13}C nmr δ: 14.0 (two coincident signals, q), 20.6 (t), 22.5

[3]If the acidic solution was extracted continuously with dichloromethane for 24 h and the dried ($MgSO_4$) extracts were evaporated, only a trace of yellow oil was obtained.

Can. J. Chem. Downloaded from www.nrcresearchpress.com by 210.87.254.105 on 09/05/12
For personal use only.

Can. J. Chem. Downloaded from www.nrcresearchpress.com by 210.87.254.105 on 09/05/12
For personal use only.

(t), 27.4 (t), 29.6 (t), 29.8 (t), 68.9 (t), and 69.2 (t); ms: 156 (14), 56 (62), 43 (100), and 41 (62) amu, all consistent with this being *N*-*n*-butyl-*N'*-*n*-pentyldiazene. *Anal.* calcd. for $C_9H_{20}N_2$: C 69.18, H 12.81%; found: C 69.00, H 13.05%.

Analysis of X-2 by gc–ms revealed the presence of two major products X-2-*1* (ca. 40%, P^+ 142 amu) and X-2-*2* (ca. 60%, P^+ 156 amu). These were isolated by pglc, and purified by bulb-to-bulb distillation as before.

As thus obtained, X-2-*1* was a colourless oil; ^{1}H nmr δ: 0.91 (3H, t, J = 7 Hz), 1.2–2.1 (4H, m), and 3.75 (2H, t, J = 7 Hz); ^{13}C nmr δ: 13.9 (q), 20.5 (t), 29.8 (t), and 69.0 (t); ms: 142 (15), 57 (95), and 41 (100) amu, all consistent with this being *N*,*N'*-di-*n*-butyldiazene. *Anal.* calcd. for $C_8H_{18}N_2$: C 67.49, H 12.74, N 19.76%; found: C 67.38, H 12.55, N 19.83%.

Similarly X-2-*2* was obtained as a near colourless oil; ^{1}H nmr δ: 0.92 (3H, t, J = 7 Hz), 0.94 (3H, t, J = 7 Hz), 1.2–1.6 (6H, m), 2.35 (2H, q, J = 7.5 Hz), 2.65 (3H, s), 3.07 (2H, t, J = 6.8 Hz), and 6.63 (1H, t, J = 5.5 Hz); ^{13}C nmr δ: 13.7 (q), 14.0 (q), 20.3 (t), 21.2 (t), 29.0 (t), 35.2 (t), 38.3 (q), 58.3 (t), and 138.2 (d); ms: 156 (16), 113 (100), and 44 (28) amu, all consistent with this being butanal *N*-*n*-butyl-*N*-methylhydrazone, and presumably the (*E*)-stereomer. *Anal.* calcd. for $C_9H_{20}N_2$: N 18.00%; found: N 17.43%.

The Preparation of (E)-, *and* (Z)-*1-Methyl-1-*n*-butyldiazene-1-oxides* (*(E)-9, and (Z)-9*)

A solution of methyllithium (1.9 *M* in diethyl ether, 12.9 mL, 21.6 mmol) was added, over the course of 10 min, to a stirred solution of *N*-nitroso-*N*-*n*-butyl-*O*-methylhydroxylamine (1.43 g, 10.8 mmol) in diethyl ether (60 mL), maintained at ca. −60°C, under an atmosphere of argon. After about 0.5 equiv. of the methyllithium had been added a yellow precipitate began to separate. After addition was complete, the reaction mixture was stirred at ca. −60°C for 30 min. A sample (0.5 mL) was then withdrawn, quenched in a saturated aqueous solution of ammonium chloride (1 mL), the ether phase separated, dried ($MgSO_4$), and analysed by glc. Little nitrosohydroxylamine remained, so the main bulk of the reaction mixture was allowed to warm up. At about 0°C the precipitate was almost completely dissolved, and the solution was orange coloured. The mixture was then shaken with saturated aqueous ammonium chloride solution (10 mL). The ether phase was separated, washed with dilute hydrochloric acid (3 *M*, 3 × 10 mL), and again with saturated aqueous ammonium chloride solution (1 × 10 mL), before being dried ($MgSO_4$) and concentrated (at atmospheric pressure) to a yellow oil (fraction X-1, 0.85 g), which still contained some ether.

The aqueous phase from the quenching of the reaction mixture was combined with the other aqueous washings and the whole (ca. 60 mL, pH ca. 1) was extracted continuously with dichloromethane, for 8 h. The organic extract was then dried ($MgSO_4$) and evaporated at atmospheric pressure to yield another yellow oil (X-2, 2.07 g).

The aqueous phase was brought to pH ca. 4 (indicator paper) with aqueous ammonia, and extracted continuously with dichloromethane for a further 24 h. Processing of the organic extract as before yielded a little more yellow oil (X-3, 0.19 g).

A glc analysis of X-1 (on 10% SE-30 at 80°C) revealed the presence of one major component. This was isolated after column chromatography (monitored by glc) as a nearly colourless oil (eluted with CH_2Cl_2), >98% pure by glc analysis (60 mg). This material, isomer *A*, was purified for analysis by bulb-to-bulb distillation under reduced pressure (80°C bath, at 20 Torr). *Anal.* calcd. for $C_5H_{12}N_2O$: C 51.70, H 10.42, N 24.12%; found: C 51.48, H 10.50, N 24.15%. The spectroscopic data collected from isomer *A* ((*Z*)-**9**) are presented in Table 2 (see text), and revealed this to be the (*Z*)-azoxyalkane (**7**).

The glc analyses of X-2 and X-3 revealed them to be very similar (containing small amounts of isomer *A*, and many other minor products, together with major amounts of a new component). Accordingly, these fractions were combined and subjected to column chromatography (as before, monitoring the separation by glc). Small amounts of isomer *A* (ca. 20 mg) were isolated from the initial (CH_2Cl_2) eluates, while a major component appeared in the later (CH_2Cl_2–Et_2O 1:1 (v/v)) fractions. Removal of the solvent afforded this second substance as a pale yellow oil (295 mg), >98% pure by glc. This material, isomer *B*, was also purified for analysis by bulb-to-bulb distillation. Found: C 51.76, H 10.41, N 23.90% cf. isomer *A*. The spectroscopic data collected for isomer *B* ((*E*)-**9**) are also presented in Table 2, and showed it to be the (*E*)-azoxyalkane (**9**).

Thermal Isomerization of B

A solution of *B* (30 mg) in toluene (5 mL) was boiled under reflux and the reaction mixture monitored by glc. After 24 h, *B* appeared to have been destroyed. After removal of toluene, under reduced pressure (ca. 20 Torr) at room temperature, an ^{1}H nmr spectrum of the residue (20 mg) revealed it to be the isomer *A* (**7**); together with traces of residual *B* and toluene.

Acknowledgements

We thank the Natural Sciences and Engineering Research Council of Canada for a grant-in-aid (A4547 to M.H.B.) which supported this research. Thanks are also due to Dr. R. Yamdagni, who carried out the mass spectroscopic analyses.

1. (*a*) V. Nelson, A. Serianz, and P. Kovacic. J. Org. Chem. **41**, 1751 (1976); (*b*) K. G. Taylor, S. R. Isaac, and M. S. Clark, Jr. J. Org. Chem. **41**, 1135 (1976); (*c*) R. A. Moss and G. M. Love. J. Am. Chem. Soc. **95**, 3070 (1973), and references cited in these papers.
2. D. Seebach and D. Enders. Angew. Chem. Int. Ed. Engl. **11**, 301 (1972).
3. A. C. M. Meesters. Ph.D. Thesis, University of Calgary, 1978.
4. F. D. Greene and S. S. Hecht. J. Org. Chem. **35**, 2482 (1970).
5. K. G. Taylor, S. R. Isaac, and J. L. Swigert. J. Org. Chem. **41**, 1146 (1976); K. G. Taylor and T. Riehl. J. Am. Chem. Soc. **94**, 250 (1972).
6. T. Axenrod, M. J. Wieder, and G. W. A. Milne. Tetrahedron Lett. 401 (1969); A. H. Lamberton and H. M. Yusuf. J. Chem. Soc. Chem. Commun. 397 (1969).
7. M. H. Benn and P. Kazmaier. J. Chem. Soc. Chem. Commun. 886 (1972).
8. A. B. Boese, Jr., L. W. Jones, and R. T. Major. J. Am. Chem. Soc. **53**, 3530 (1931).
9. M. Wiessler and D. Schmael. Z. Krebsforsch. Klin. Onkol. **83**, 205 (1975); Chem. Abstr. **83**, 109573 (1975).
10. N. Kreutzkamp and P. Messinger. Chem. Ber. **100**, 3463 (1967).
11. R. F. Borch, M. D. Bernstein, and H. D. Durst. J. Am. Chem. Soc. **93**, 2897 (1971).
12. A. C. M. Meesters and M. H. Benn. Synthesis, 679 (1978).

A total synthesis of the enantiomer of anhydromyriocin (anhydrothermozymocidin)[1]

DANIEL R. PAYETTE[2] AND GEORGE JUST

Department of Chemistry, McGill University, Montreal, P.Q., Canada H3A 2K6

Received July 2, 1980

This paper is dedicated to Prof. Raymond U. Lemieux on the occasion of his 60th birthday

DANIEL R. PAYETTE and GEORGE JUST. Can. J. Chem. **59**, 269 (1981).

The optical antipode of anhydromyriocin, the γ-lactone derived from the antibiotic myriocin (thermozymocidin), was synthesized from L-arabinose, establishing the absolute configuration of myriocin as **47**. In contrast to its natural enantiomer, it showed but little antifungal activity.

DANIEL R. PAYETTE et GEORGE JUST. Can. J. Chem. **59**, 269 (1981).

L'antipode optique de l'anhydromyriocine, la γ-lactone obtenue à partir de l'antibiotique myriocine (thermozymocidine) a été synthétisé à partir du L-arabinose, établissant ainsi **47** comme étant la configuration absolue de la myriocine. Contrairement à son énantiomère naturel, ce produit ne montra que peu d'activité fungicide.

Can. J. Chem. Downloaded from www.nrcresearchpress.com by 210.87.254.42 on 09/05/12
For personal use only.

In 1972, two antifungal agents, myriocin and thermozymocidin, were isolated from *Myriococcum albomyces NRRL 3858* (1) and *Albomyces 20,349* (2) respectively. They were both identified as 2-amino-2-hydroxymethyl-3,4-dihydroxy-14-oxo-eicos-6-enoic acid (3, 4). Some ambiguity remained concerning their identity and relative stereochemistries. Their absolute configuration was not reported. Bagli *et al.* (3) suggested the stereochemistry **1** for anhydromyriocin, whereas Kuo and Wendler (5) assigned the configuration **2**, based on spectral comparison of various synthetic racemic isomers of the lactonic ester **3** with Bagli's products. This was in accord with the relative stereochemistry obtained by X-ray diffraction for thermozymocidin.[3]

We decided to synthesize anhydrothermozymocidin from chiral precursors, and compare it to the γ-lactone derived from natural myriocin, thus (*a*) confirming the identity or nonidentity of the two compounds and (*b*) proving their absolute and relative configuration.

Synthetic Approach

The best candidate for a precursor seemed to be arabinose which already contains the desired *vic*-diol in a *threo* configuration and of which both D and L isomers are available. In the approach described, the two main problems were (*a*) elongation of the pentose at C-1 by at least one carbon atom permitting the introduction of a *trans* double bond and the hydrocarbon chain, and (*b*) selective protection of the 4-hydroxy function, allowing its conversion at a later stage to a ketone and hence to a cyanoamine and amino acid.

We first studied the use of phosphorus ylids on partially protected pentofuranoses, hoping to effect simultaneous homologation at C-1 and opening of the sugar, thus allowing subsequent protection of the free hydroxyl group. The use of stabilized ylids is limited by the ease with which the products cyclize via a Michael-type addition (6), restricting the choice of hydroxyl protecting groups. It was our experience that although nonstabilized ylids react sluggishly with closed sugars, others, of intermediate reactivity, such as thiomethylmethylenetriphenylphosphorane, did give the desired intermediate. However, we also found that hydrolysis of the resulting terminal vinyl sulfides to the free aldehydes presented major difficulties.

We then decided to use the sugar in the open form and concentrate on the homologation itself. We describe several approaches involving (*a*) attempted displacement of mesylate or iodide functions with an acetylenic anion (**6** → **7** → **8** → **9** →); (*b*) a two-carbon elongation via a stabilized ylid leading to a carboxylic acid, followed by oxidative decarboxylation and ultimately the formation of a terminal phosphonium salt (**6** → **11** → **12** → **13** → **19** →); (*c*) formation, via a Wittig reaction, of a model α,β-unsaturated ketone followed by reduction, with a borane reagent, of the corresponding tosylhydrazone accompanied by migration of the double bond (**6** → **14** → **15** → **16**); and finally, (*d*) the method which proved to be the most practical: a one carbon elongation using nitromethane addition with eventual transformation to a terminal bromide or an aldehyde, permitting the formation of the double bond by a Wittig reaction (**6** → **17** → **18** → **19** or **18** → **20** → **21**).

Results and Discussion[4]

2,3,5-Tri-*O*-benzyl-D-arabinose diethyl dithio-

[1]Abstracted from the Ph.D. thesis of D.R.P., McGill University, 1980.

[2] Holder of an N.S.E.R.C. scholarship, 1974–1976.

[3]C. Scolastico, as quoted in ref. 5.

[4]For a preliminary communication of this work see ref. 7.

0008-4042/81/020269-14$01.00/0

©1981 National Research Council of Canada/Conseil national de recherches du Canada

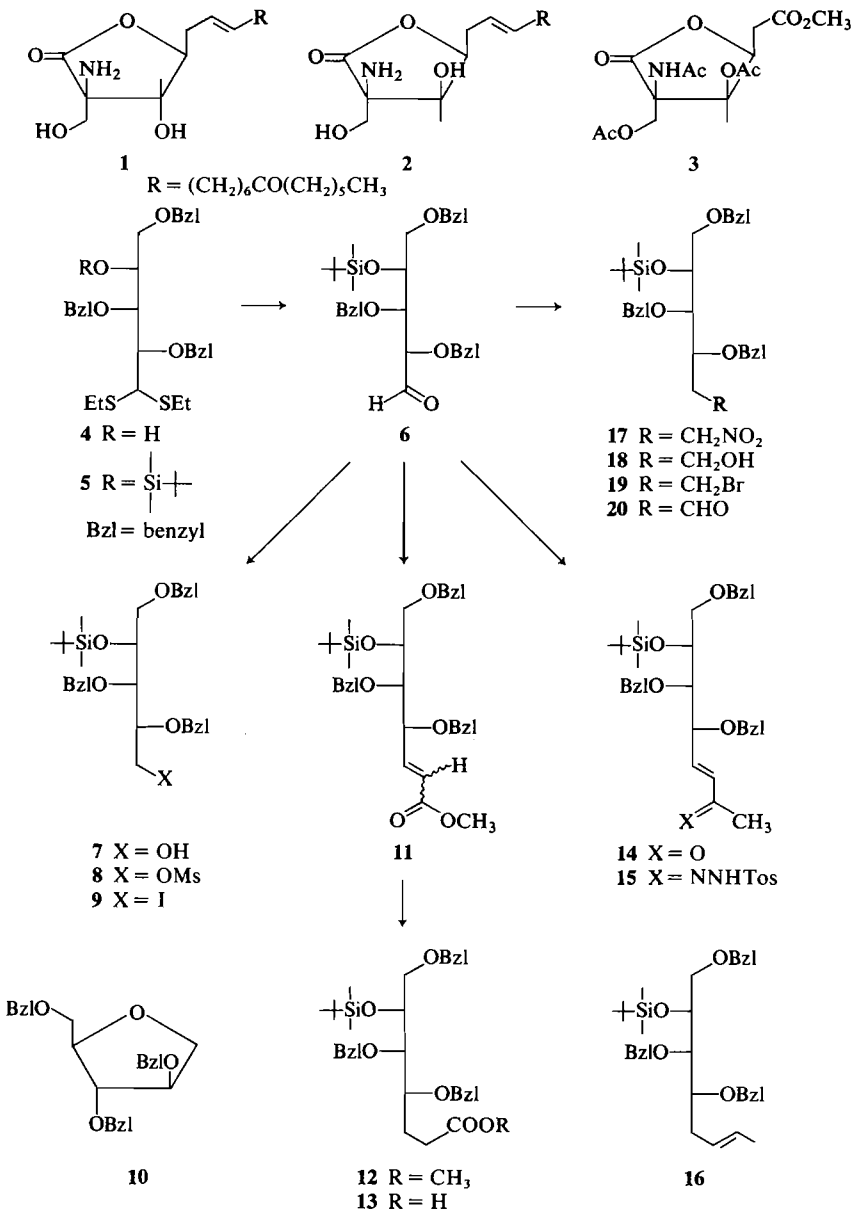

acetal **4** (8) was protected as its *tert*-butyldimethylsilyl ether **5** (9) and converted to the free aldehyde **6** (10). Reduction with sodium borohydride gave alcohol **7** which was transformed to the mesylate **8** (11) and then to the iodide **9** by refluxing **8** in 2-butanone with excess sodium iodide (12). Reaction of **8** or **9** with the lithium salt of a model acetylene (1-octyne) in 10% HMPT/THF gave exclusively, and regardless of temperature, elimination products. Furthermore, formation of iodide **9** from mesylate **8** was complicated by the competing formation of tetrahydrofuran derivative **10**, so that no more than 40% **9** could be isolated.

Next, aldehyde **6** was treated with carbomethoxymethylenetriphenylphosphorane in methanol to give a mixture of *E* and *Z* olefins **11**, which was reduced to the saturated methyl ester with sodium borohydride in the presence of nickelous chloride (13). Treatment with lithium *n*-propylmercaptide in HMPT (14) gave the free acid **13**, but all attempts to convert **13** through Hunsdiecker-type (15) reactions to bromide **19**

Can. J. Chem. Downloaded from www.nrcresearchpress.com by 210.87.254.42 on 09/05/12
For personal use only.

Can. J. Chem. Downloaded from www.nrcresearchpress.com by 210.87.254.42 on 09/05/12
For personal use only.

failed. However, this terminal bromide **19**, which we hoped to convert to the corresponding phosphonium salt, was produced by a different route as will be discussed later in the text.

The first successful formation of a *trans* double bond at the appropriate position (**16**) was accomplished by the catecholborane reduction (16) of tosylhydrazone **15**, obtained by reaction of aldehyde **6** with 1-triphenylphosphoranylidene-2-propanone in DMF, followed by reaction of the resulting *trans* α,β-unsaturated ketone **14** with tosylhydrazine (17) in ethanol at 20°C. However, the low yields, the relative instability of **15**, and the difficulties in obtaining it in a pure state prompted us to look for a more practical approach.

Wollenberg and Miller (18) reported a very efficient method of converting aldehydes into saturated nitro compounds having one more carbon atom by the addition of nitromethane, using fluoride ions as base, followed by acetylation and reduction with sodium borohydride. We found that, although this method failed on closed sugars, it could be applied successfully on aldehydo sugars such as **6**, giving the nitro compound **17** in 76% overall yield. Ozonolysis of the sodium nitronate salt (19) of **17** in ethanol, followed by reductive work-up with sodium borohydride, gave alcohol **18**, which could then be converted to bromide **19** by Hanessian's method (20). Attempts were made to form the corresponding phosphonium bromide by reaction with triphenylphosphine in various refluxing solvents such as toluene, ethanol, or dimethylformamide (21), but they resulted in either recovery of the starting material or its complete destruction.

Oxidation of **18** with pyridinium chlorochromate (22) gave the base sensitive aldehyde **20** which could, in principle, be submitted to the action of an appropriate Wittig reagent.

Wittig reactions involving nonstabilized ylids generally produce, in the absence of soluble lithium salts, predominately *cis* olefins (23). Schlosser and Christmann (24) reported recently a modification of this reaction, whereby the intermediate betaine is isomerized to its more stable *threo* form by adding a second equivalent of base. Conflicting reports have appeared concerning the generality of this procedure (25). When we treated aldehyde **6** with the ylid generated from a model *n*-alkyltriphenylphosphonium iodide, following exactly Schlosser's procedure using freshly prepared phenyl lithium as base and a 1:1 mixture of THF/diethyl ether as solvent, we obtained at best a nonseparable 1:1 mixture of *cis* and *trans* olefins as determined by ^{13}C nmr. We then decided to prepare the *cis*-olefin using the standard Wittig reaction conditions and isomerize it chemically to its *trans* isomer. For this, we needed the phosphonium bromide salt **31** which was prepared as follows.

Reaction of cyclooctanone with *n*-hexylmagnesium bromide in refluxing ether and dehydration of the resulting tertiary alcohol **26** with iodine in refluxing xylene (26) gave 1-hexylcyclooctene. Ozonolysis in ethanol at −70°C, followed by reductive work-up with sodium borohydride, gave the conveniently crystalline diol **27**. Selective oxidation of the secondary alcohol function with bromine–HMPT (27) afforded 1-hydroxy-8-tetradecanone **28** which was ketalized with either ethylene glycol or 2,2-dimethyl-1,3-propanediol in refluxing benzene with *p*-toluenesulfonic acid as catalyst to afford **29***a* or **29***b*. Alcohols **29** were then converted to the corresponding bromides **30** with *N*-bromosuccinimide and triphenylphosphine in DMF (20). Treatment of **30***a* with triphenylphosphine under argon at 140°C for 5.5 h gave **31***a* as a glassy material, which had to be purified by fractional precipitation. However, the infrared and nmr spectra of **31***a* showed partial hydrolysis of the ketal function (10 to 30%). This problem was later solved by using the less acid sensitive ketal **30***b* instead of **30***a*, and carrying out the reaction in acetonitrile in the presence of trimethyl orthoformate. The phosphonium salt **31***b* thus obtained was also purified by repeated precipitation.

Aldehyde **20** was submitted to the action of the ylid generated from **31***a* in THF at −70°C. *Cis*-olefin **21**, contaminated with less than 5% of its *trans* isomer, was obtained in 67% yield. The conditions of this reaction proved to be critical. Too rapid an addition of aldehyde to the cold ylid solution or higher reaction temperature resulted in the formation of elimination products. The isomerization of the *cis* to the *trans*-olefin **22** was carried out according to the method of Vedejs and Fuchs (28) which involves epoxidation, followed by reaction with lithium diphenylphosphide, quaternization with methyl iodide, and decomposition of the intermediate betaine. Desilylation of **22** with tetra-*n*-butylammonium fluoride in THF (9) and oxidation with dimethyl sulfoxide – acetic anhydride (29) gave ketone **24**. Treatment with sodium cyanide and ammonium chloride in methanolic ammonia for 4 days at 20–25°C produced the two isomeric cyanoamines **25** which were separated by high pressure liquid chromatography but could not be assigned definite structures. Debenzylation using published procedures (30) was unfortunately not

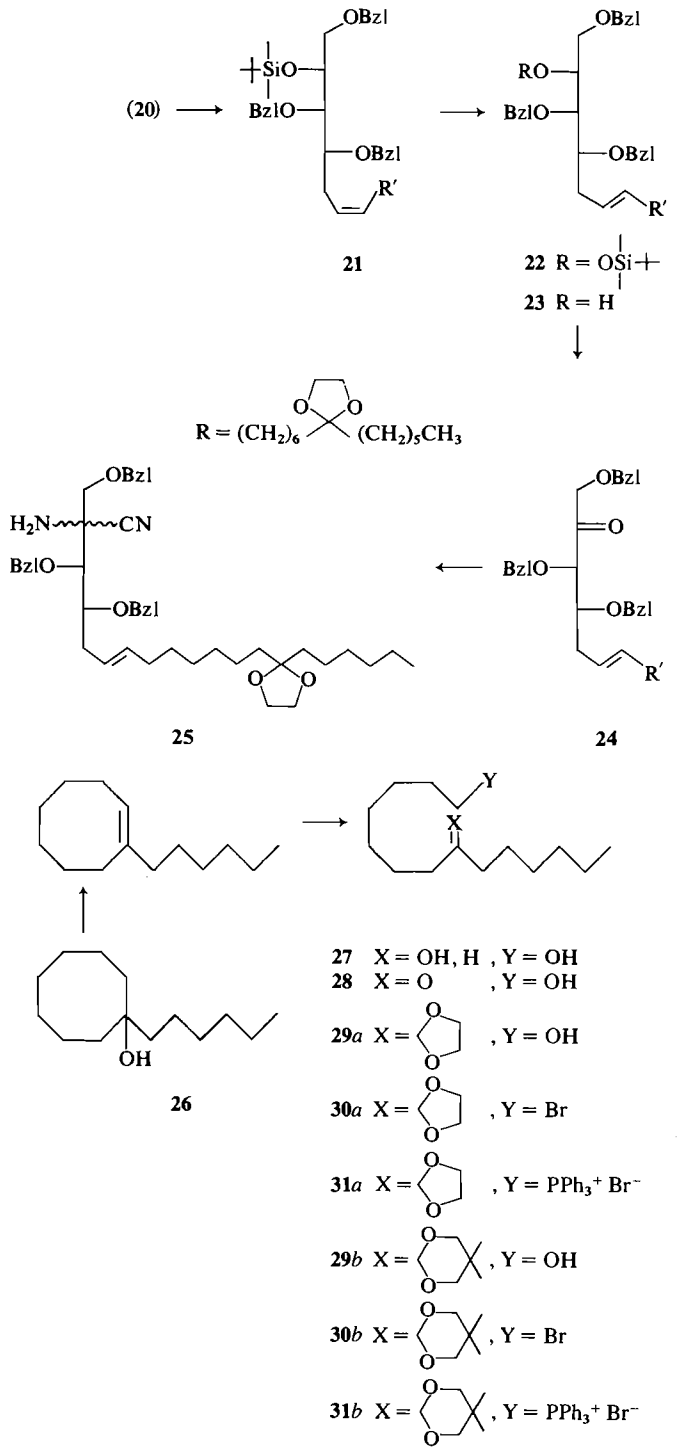

successful. Even hydrogenolysis over palladium on charcoal in ethanol – acetic acid, which, we hoped, would have given the saturated debenzylated product, failed, **25** acting, as could be demonstrated, as a very effective catalyst poison. The complete sequence was therefore repeated using acid labile protecting groups.

The L-arabinose derivative **32** (31) was tritylated and, without purification, silylated (9) to give the fully protected dithioacetal **33**, which was trans-

Can. J. Chem. Downloaded from www.nrcresearchpress.com by 210.87.254.42 on 09/05/12
For personal use only.

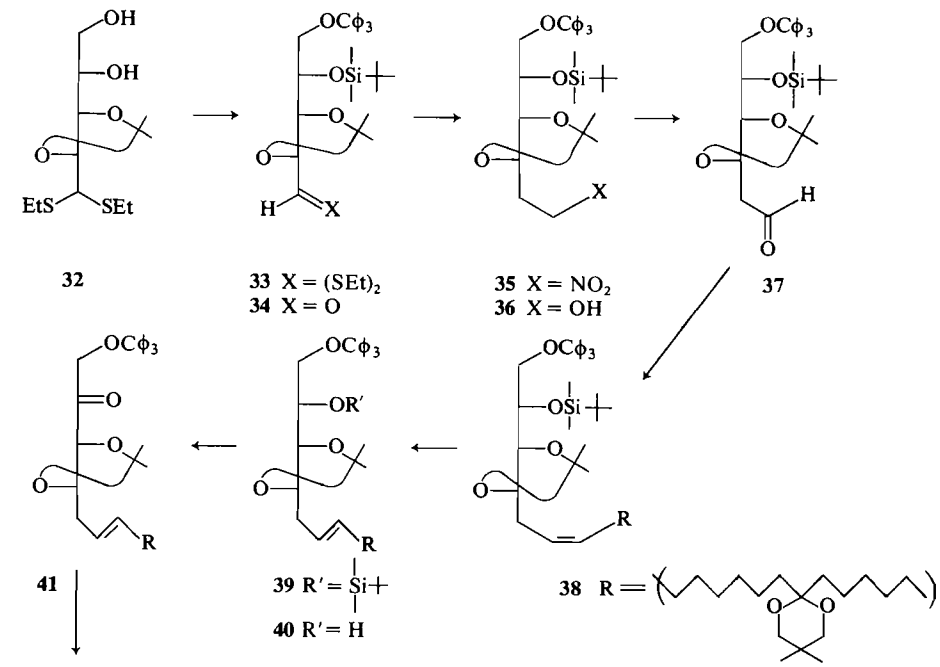

32 33 X = $(SEt)_2$ 34 X = O 35 X = NO_2 36 X = OH 37 38 R = 39 R′ = Si+ 40 R′ = H 41

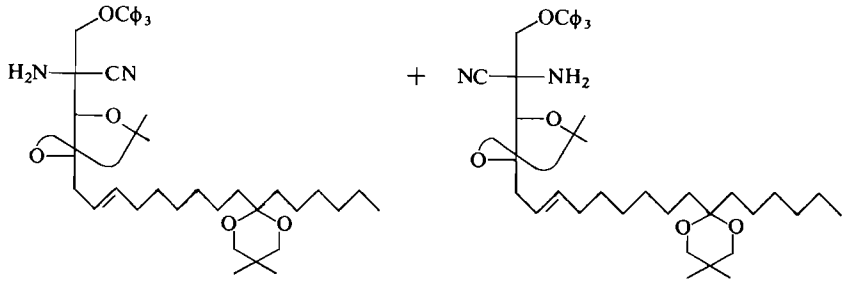

42 43

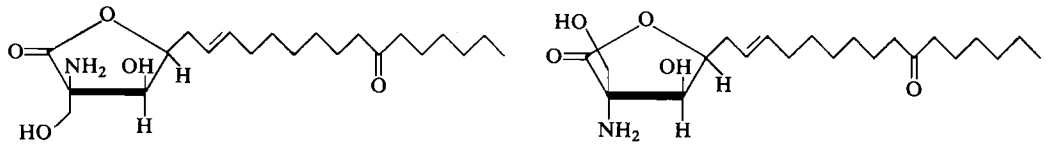

44 45

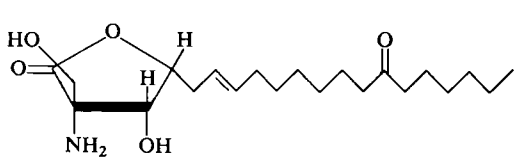

46 Anhydromyriocin

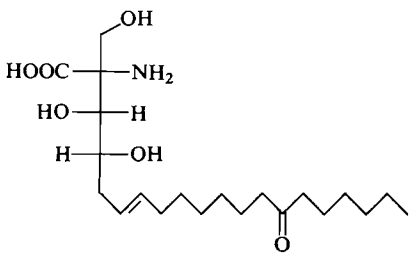

47 Myriocin

Can. J. Chem. Downloaded from www.nrcresearchpress.com by 210.87.254.42 on 09/05/12
For personal use only.

Can. J. Chem. Downloaded from www.nrcresearchpress.com by 210.87.254.42 on 09/05/12
For personal use only.

formed into the 2-deoxy aldehyde **37** (**33** → **34** → **35** → **36** → **37**) as described in the benzylated series (**5** to **20**). The Wittig reaction was performed with the phosphonium salt **31***b* rather than **31***a* giving a much improved yield of *Z*-olefin **38**. Epoxidation of **38** was best carried out in cyclohexane and gave a mixture of products, the two major components of which were assumed to be the two *erythro* epoxides and were therefore not separated. The use of more polar solvents, such as CH_2Cl_2 and dichloroethylene, or the addition of a buffer solution (32) resulted in more complex reaction mixtures.

Successive treatment of the epoxides with lithium diphenylphosphide and methyl iodide produced the *E*-olefin **39**[5] in 81% yield from **38**. Desilylation and oxidation as from **22** to **24** gave ketone **41** which, upon treatment with sodium cyanide and ammonium chloride for 8 days, gave cyanoamines **42** and **43** in a 4:5 ratio and 71% total yield. The reaction could easily be monitored by tlc which indicated, more clearly than with **25**, the rapid formation of the corresponding cyanohydrins, followed by their slow conversion to the more polar cyanoamines. Heating only resulted in a very modest increase in reaction rate and the formation of more impurities. Separation of the cyanoamines could this time be achieved by "flash" column chromatography (33).

The final step, consisting of the simultaneous acid hydrolysis of all protecting groups and acid catalyzed lactonization, was first attempted by treating **42** with 90% aqueous trifluoroacetic acid at 25°C for 10 min. Deprotection of the different functionalities seemed complete from the presence of ketone (1710 cm^{-1}) and hydroxyl (3200–3600 cm^{-1}) absorptions in the infrared spectrum of the major product, and also from its polarity on tlc, as compared with "natural" anhydromyriocin; but no lactone or carboxylic acid absorption could be detected. However, treatment of **42** with wet methanolic HCl for 3 h at 45°C, gave lactone **44**, in 56% yield, the ir, 200 MHz ^{1}Hmr, and ms spectra of which were superimposable with that of the γ-lactone derived from natural myriocin (3). This, and comparison of the optical rotation of **44** in methanol and methanolic HCl, with that reported for anhydromyriocin $[\alpha]_D^{24}$ + 33.4° (*c* 0.718, MeOH) (3) and for anhydrothermozymocidin hydrochloride $[\alpha]_D^{25}$ + 33° (*c* 1.0, MeOH) (4*b*), clearly demonstrated (*a*) the identity of myriocin and thermozymocidin, and (*b*) that **44** is the optical antipode of their γ-lactone, proving **46** to be their absolute configuration.

The other cyanoamine **43** was similarly transformed into lactone **45**, the different spectra of which, while confirming the structure, showed significant differences to that of **44**.

Biological Activity

Lactones **44** and **45** did not show any significant in vitro antimicrobial activity against Candida, Dermatophytes, and Trichomonads.

Experimental

General

Mass spectra (ms) were obtained on a HP 5984 or LKB-9000 mass spectrometer. Infrared (ir) spectra were obtained on a Perkin Elmer 297 spectrophotometer. Proton and carbon-13 magnetic resonance spectra were recorded on Varian T-60, T-60A, XL-200, and on Brucker FT 90 spectrometers. High pressure liquid chromatography separations were performed on an Altex 300 instrument, using "Spherisorb S10W" silica gel (Technical Marketing Associates). Chemical shifts were measured using tetramethylsilane as internal standard. Thin-layer chromatography was carried out using precoated Kieselgel 60 F_{254} silica gel plates. All column chromatography was performed using the "flash chromatography" technique described by Still *et al.* (33) and using 32–63 μ (400–230 mesh) silica gel (ICN).[6] Microanalyses were carried out by Mid-West Microlab Ltd., Indianapolis, IN. Melting points were determined on a Gallenkamp block and are uncorrected unless otherwise mentioned. The following abbreviations were used: rt (room temperature), tlc (thin layer chromatography), s (singlet), d (doublet), m (multiplet), etc., b (broad or badly defined), pe (petroleum ether 30–60°C), HMPT (hexamethylphosphoric triamide), EI (electron impact), and CI-IB (chemical ionization/isobutane).

*2,3,5-Tri-*O*-benzyl-4-*O*-*tert*-butyldimethylsilyl-*D*-arabinose Diethyl Dithioacetal (5)*

A solution of alcohol **4** (8) (9.4 g, 18 mmol) in dry DMF (100 mL) was treated with *tert*-butyldimethylsilyl chloride (3.5 g, 23 mmol) and imidazole (3.5 g, 51 mmol) under argon, for 3 days at ambient temperature. Water (200 mL) was added and the product was extracted with pe (6 × 100 mL). The combined extracts were washed with water (3 × 100 mL), dried ($MgSO_4$), and concentrated *in vacuo* to a colorless oil. Chromatography (by successive elution of a 55 mm column with 400 mL pe and 1000 mL 8% EtOAc/pe) gave 11.1 g of pure **5** (95%): $[\alpha]_D^{22}$ −13.0° (*c* 13.3, $CHCl_3$); ir (film) ν_{max}: 1250 and 830 (Si—C) cm^{-1}; ^{1}Hmr ($CDCl_3$) δ: 0.09, 0.13 (2s, 6H, $Si(CH_3)_2$), 0.90 (s, 9H, $SiBu^t$), 1.11, 1.19 (2t, 6H, J = 7.5 Hz, SCH_2CH_3), 2.51, 2.75 (2q, 4H, J = 7.5 Hz, SCH_2CH_3), 3.3–5.0 (m's, 12H) and 7.23 (s, 15H, phenyls) ppm; ms (EI, 15 eV, 60°C) *m/e*: 640 (0.2, M^+), 583 (9), 579 (2), 505 (9), 267 (71), and 91 (100); *Anal.* calcd. for $C_{36}H_{52}O_4S_2Si$: C 67.45, H 8.18, S 10.00; found: C 67.26, H 8.07, S 9.89.

*2,3,5-Tri-*O*-benzyl-4-*O*-*tert*-butyldimethylsilyl-*aldehydo-*D*-arabinose (6)*

A solution of **5** (1.05 g, 1.64 mmol), $HgCl_2$ (0.90 g, 3.3 mmol), and HgO (0.90 g, 4.1 mmol) in 20 mL of 90% aqueous acetone

[5]The isomeric purity of the olefin was established by ^{13}C nmr of the final product **44**, which showed no detectable amount of *cis*-olefin carbons.

[6]I.C.N. Nutritional Biochemicals, 26201 Miles Road, Cleveland, OH.

Can. J. Chem. Downloaded from www.nrcresearchpress.com by 210.87.254.42 on 09/05/12
For personal use only.

was stirred at rt for one hour. Hexane (50 mL) was added and the mixture was filtered through Celite. The filtrate was concentrated *in vacuo* to about 20 mL causing the precipitation of more mercuric salts which were filtered off. This filtrate, diluted with 30 mL hexane, was washed with 5% KI (2 × 60 mL) and water. Drying ($MgSO_4$) and evaporation of the solvent left 0.87 g (99%) of colorless aldehyde **6** which, as shown by tlc and ir spectroscopy, needed neither purification nor dehydration. An analytical sample was obtained by chromatography (8% EtOAc/hexane); $[\alpha]_D^{22}$ −12° (*c* 10.2, $CHCl_3$); ir (film)ν_{max}: 2895 and 1736 (aldehyde) cm^{-1}; ^{1}Hmr ($CDCl_3$) δ: 0.07 (s, 6H, $Si(CH_3)_2$), 0.90 (s, 9H, $SiBu^t$), 3.40–4.32 (m's, 5H), 4.45 (s, 2H, CH_2Ph), 4.56 (s, 2H, CH_2Ph), 4.40, 4.60, 4.67, 4.87 (ABq, 2H, *J* = 11 Hz, CH_2Ph), 7.23, 7.26 (2s, 15H), and 9.8 (apparent s, 1H, CHO) ppm.

Alcohol 7

Aldehyde **6** (1.27 g, 2.38 mmol) was reduced by treatment with sodium borohydride (90 mg, 2.37 mmol) in 15 mL methanol for 30 min. The solvent was evaporated and replaced by hexane (50 mL), and the mixture was acidified with 10% aqueous acetic acid. The aqueous phase was extracted with hexane and the combined extracts were washed with saturated $NaHCO_3$ and water. Drying ($MgSO_4$) and evaporation of the solvent left 1.15 g (91%) of pure **7**; $[\alpha]_D^{22}$ −8° (*c* 17, $CHCl_3$); ir (film) ν_{max}: 3200–3600 (hydroxyl) cm^{-1}; ^{1}Hmr ($CDCl_3$) δ: 0.08 (s, 6H, $Si(CH_3)_2$), 0.90 (s, 9H, $SiBu^t$), 2.68 (bs, 1H, OH), 3.40–3.95 (m's, 6H), 4.00–4.32 (m, 1H), 4.43, 4.59, 4.68 (3s, 2H each, CH_2Ph), and 7.23 (s, 15H) ppm; ms (EI, 15 eV, 20°C) *m/e*: 481 (0.4), 446 (2), 340 (24), and 181 (100); *Anal.* calcd. for $C_{32}H_{44}O_5Si$: C 71.60, H 8.26; found: C 71.44, H 8.49.

Mesylate 8 (ref. 11)

Methanesulfonyl chloride (0.41 mL, 5.26 mmol) was added dropwise to a cold solution (ice–salt bath) of alcohol **7** (1.99 g, 3.71 mmol) and triethylamine (1.04 mL, 7.43 mmol) in dry pentane. After 5 min, hexane (70 mL) was added and the mixture was washed successively with 1 *N* HCl (2 × 50 mL), water (50 mL), and saturated $NaHCO_3$. Drying ($MgSO_4$) and evaporation of the solvent left a colorless oil which was chromatographed (18% EtOAc/hexane) to give 2.04 g (89%) of mesylate **8**; $[\alpha]_D^{22}$ −5.5° (*c* 6.5, CCl_4); ir (film)ν_{max}: 1182 (—SO_2—O—)cm^{-1}; ^{1}Hmr ($CDCl_3$) δ: 0.06 (s, 6H, $Si(CH_3)_2$), 0.89 (s, 9H, $SiBu^t$), 2.78 (s, 3H, OSO_2CH_3), 3.36–4.16 (m's, 7H), 4.26–4.84 (m's, 6H, 3× CH_2Ph), and 7.25 (s, 15H) ppm; ms (CI-IB, 25–130°C) *m/e*: 615 (0.6, $M^+ + 1$), 211 (100).

Iodide 9 and Tetrahydrofuran 10 (ref. 12)

A solution of mesylate **8** (494 mg, 0.81 mmol) and anhydrous sodium iodide (1.2 g, 8.0 mmol) in 15 mL freshly distilled 2-butanone was refluxed for 80 min, at which time production of the desired iodide **9** had stopped as indicated by tlc (15% EtOAc/hexane). Hexane and water (20 mL each) were added. The aqueous phase was extracted with hexane (3 × 10 mL) and the combined extracts were washed successively with aqueous sodium thiosulfate, saturated $NaHCO_3$, and water. After drying ($MgSO_4$) and concentration *in vacuo*, chromatography (4%, EtOAc/hexane) afforded 188 mg (36%) of iodide **9**. When the reaction was allowed to continue, iodide **9** was all converted to a by-product, identified as **10**, after the same work-up as above and chromatography (14% EtOAc/hexane); iodide **9**: $[\alpha]_D^{22}$ −4.3° (*c* 9.0, CCl_4); ^{1}Hmr (CCl_4) δ: 0.09 (s, 6H, $Si(CH_3)_2$), 0.91 (s, 9H, $SiBu^t$), 3.26–4.16 (m's, 7H), 4,42, 4.61, 4.70 (3s, 2H each, CH_2Ph), and 7.24 (s, 15H) ppm; ms (CI-IB, 23–125°C) *m/e*: 647 (45, $M^+ + 1$), 181 (100); tetrahydrofuran **10**: $[\alpha]_D^{22}$ −10° (*c* 1.2, CCl_4); ^{1}Hmr (CCl_4) δ: 3.38–3.60 (m, 2H), 3.77–4.05 (m, 5H), 4.39 (s, 2H, CH_2Ph), 4.51 (s, 4H, CH_2Ph), and 7.23 (s, 15H) ppm; ms (CI-IB, 24–120°C) *m/e*: 405 (43, $M^+ + 1$), 181 (100).

Unsaturated Ester 11

A solution of aldehyde **6** (1.88 g, 3.52 mmol) and carbomethoxymethylenetriphenylphosphorane (1.41 g, 4.23 mmol) in 20 mL methanol was kept at rt for 18 h. The solvent was evaporated and replaced by 100 mL hexane. The precipitate was filtered off and washed with hexane. The filtrate was concentrated *in vacuo* to leave a colorless oil which appeared on tlc as a clean pair of spots, in a 3 to 2 ratio, the major component being the less polar one. It was possible, by flash chromatography (7% EtOAc/hexane), to obtain a small amount of the two components in sufficient purity to identify them as the *cis* (major) and *trans* (minor) isomers of **11**. The total yield of the purified mixture of isomers was 2.00 g (96%); *cis* isomer: ir (film) ν_{max}: 1738 (α,β-unsaturated ester) and 1652 (C=C) cm^{-1}; ^{1}Hmr ($CDCl_3$) δ: 0.05 (s, 6H, $Si(CH_3)_2$), 0.91 (s, 9H, $SiBu^t$), 3.49–4.26 (m's, 7H, $COOCH_3$ singlet at 3.62), 4.48 (s, 4H, CH_2Ph), 4.67 (s, 2H, CH_2Ph), 5.29 (d of d, M part of an ABMX pattern, 1H, $J_{3,4}$ = 8.5 Hz, $J_{2,4}$ < 1 Hz, $J_{4,5}$ = 4 Hz, C-4), 5.73, 5.92, 6.10, 6.23, 6.28, 6.41 (AB part of the ABMX, 2H, $J_{2,3}$ = 11 Hz, C-2,3), and 7.24 (s, 15H) ppm; ms (EI, 70 eV, 105°C) *m/e*: 577 (0.1), 533 (0.3), 482 (0.1), 425 (1), 181 (12), and 91 (100); *trans* isomer: ir (film) ν_{max}: 1742 (α,β-unsaturated ester), 1655 (C=C) cm^{-1}; ^{1}Hmr ($CDCl_3$) δ: 0.05 (s, 6H, $Si(CH_3)_2$), 0.95 (s, 9H, $SiBu^t$), 3.43–3.89 (m's, 6H, $COOCH_3$ singlet at 3.70), 3.97–4.76 (m's, 8H), 5.90, 6.16 (B part of an apparent ABX pattern, 1H, $J_{2,3}$ = 17 Hz, $J_{3,4}$ = 6 Hz, $J_{2,4}$ < 1Hz, C-2), 6.79, 6.89, 7.06, 7.16 (A part of the ABX, 1H, C-3), and 7.24 (s, 15H) ppm; ms (EI, 70 eV, 85°C) *m/e*: 533 (0.1), 482 (0.2), 425 (0.3), 181 (15), and 91 (100).

Methyl Ester 12 (ref. 13)

To a solution of unsaturated esters **11** (2.00 g, 3.39 mmol) in 25 mL methanol cooled in an ice bath, nickelous chloride hexahydrate (0.081 g, 0.34 mmol) was added and the mixture was stirred until dissolution was complete. Then, sodium borohydride (0.259 g, 6.79 mmol) was added slowly, followed, after five minutes, by 5 mL water. Most of the methanol was evaporated off and replaced by hexane (50 mL), and the mixture was acidified with 10% aqueous acetic acid. The aqueous phase was separated and extracted with hexane (3 × 50 mL). The combined organic phases were washed with saturated $NaHCO_3$ and water, dried over $MgSO_4$, and concentrated *in vacuo* to give, after chromatography (10% EtOAc/hexane), 1.80 g (90%) of **12**; $[\alpha]_D^{22}$ +2.5° (*c* 9.1, $CHCl_3$); ir (film) ν_{max}: 1735 (ester) cm^{-1}; ^{1}Hmr ($CDCl_3$) δ: 0.07 (s, 6H, $Si(CH_3)_2$), 0.89 (s, 9H, $SiBu^t$), 1.72–2.51 (m's, 4H, CH_2CH_2COOR), 3.53–4.25 (m's, 8H, $COOCH_3$ singlet at 3.57), 4.49 (s, 2H, CH_2Ph), 4.35, 4.55, 4.61, 4.81 and 4.52, 4.71, 4.76, 4.95 (2 ABq, 2H each, *J* = 11 Hz, CH_2Ph), and 7.25 (s, 15H) ppm; ms (EI, 15 eV, 22°C) *m/e*: 536 (0.3), 502 (0.3), 337 (11), 245 (25), and 181 (100); *Anal.* calcd. for $C_{35}H_{48}O_6Si$: C 70.91, H 8.16; found: C 70.76, H 8.34.

Carboxylic Acid 13 (ref. 14)

A solution of 1-propanethiol (1.26 mL, 14 mmol) in 10 mL dry THF, was treated under argon with *n*-butyl lithium (6.9 mL, 1.6 *M* solution in hexane, 11 mmol) for 5 min at room temperature. Then, 10 mL HMPT was added, followed after 5 min by a solution of methyl ester **12** (1.65 g, 2.79 mmol) in 25 mL HMPT. After 2.5 h, the mixture was poured in 200 mL 5% aqueous acetic acid and several extractions with diethyl ether (4 × 60 mL) were performed. The combined ether extracts were shaken with 100 mL 10% aqueous silver nitrate and the solids were filtered off before the organic phase could be separated. Drying ($MgSO_4$) and evaporation of the solvent gave an oil still containing some HMPT and acetic acid. This oil was then taken up in hexane (100 mL), washed with water (5 × 50 mL), dried, and concentrated again. Chromatography of the residue (a 55 mm column was eluted with successive 500 mL portions of 20%, 50%

Can. J. Chem. Downloaded from www.nrcresearchpress.com by 210.87.254.42 on 09/05/12
For personal use only.

EtOAc in hexane, and pure EtOAc) gave 1.40 g of pure **13** (88%); $[\alpha]_D^{22}$ +1.2° (*c* 6.9, $CHCl_3$); ir (film) ν_{max}: 3400–2500 and 1710 (carboxylic acid) cm^{-1}; ^{1}Hmr ($CDCl_3$) δ: 0.08 (s, 6H, $Si(CH_3)_2$), 0.90 (s, 9H, $SiBu^t$), 1.96 (m, 2H, C-3), 2.30 (m, 2H, C-2), 3.40–4.22 (m's, 5H), 4.47 (s, 2H, CH_2Ph), 4.34, 4.53, 4.62, 4.80 and 4.51, 4.69, 4.75, 4.93 (2 ABq, 2H each, J = 11 Hz, CH_2Ph), 7.24 (s, 15H), and 11.15 (bs, 1H, COOH) ppm; ms (EI, 15 eV, 20–100°C) *m/e*: 523 (0.2), 521 (0.6), 489 (1.2), 381 (3), and 91 (100); *Anal.* calcd. for $C_{34}H_{46}O_6Si$: C 70.54, H 8.01; found: C 70.71, H 8.25.

Unsaturated Ketone 14

Aldehyde **6** (1.26 g, 2.36 mmol), in 15 mL dry DMF, was treated with 1-triphenylphosphoranylidene-2-propanone (900 mg, 2.83 mmol) in the presence of benzoic acid (14 mg, 0.11 mmol) for 16 h at rt and 2.5 h at 80°C. Water (100 mL) was added and the mixture was extracted with hexane (6 × 50 mL). The combined extracts were washed with saturated $NaHCO_3$ and water (3 × 50 mL), dried over $MgSO_4$, and concentrated *in vacuo*. Chromatography (7% EtOAc/hexane) afforded 0.95 g (70%) of ketone **14**; $[\alpha]_D^{22}$ −13° (*c* 6.5, $CHCl_3$); ir (film) ν_{max}: 1691 (α,β-unsaturated ketone) and 1630 (C=C) cm^{-1}; ^{1}Hmr ($CDCl_3$) δ: 0.06 (s, 6H, $Si(CH_3)_2$), 0.89 (s, 9H, $SiBu^t$), 2.11 (s, 3H, $COCH_3$), 3.41–3.86 (m's, 3H), 3.96–4.46 (m's, 2H), 4.49, 4.70 (2s, 4H and 2H, CH_2Ph), 6.08, 6.35, 6.59, 6.69, 6.86, 6.96 (AB part of an apparent ABX pattern, 2H, J_{AB} = 17 Hz, J_{AX} = 6 Hz, J_{BX} < 1 Hz, CH=CH), and 7.26 (s, 15H) ppm; ms (CI-IB, 27–130°C) *m/e*: 575 (2.4, M^+ +1), 107 (100); *Anal.* calcd. for $C_{35}H_{46}O_5Si$: C 73.13, H 8.07; found: C 73.25, H 8.29.

Tosylhydrazone 15 (ref. 17)

A solution of ketone **14** (574 mg, 1.65 mmol) and *p*-toluenesulfonylhydrazine (338 mg, 1.82 mmol) in 15 mL absolute ethanol was stirred at rt for 3 h. The solvent was evaporated off at rt and the residue chromatographed (22% EtOAc/hexane) to yield 0.51 g (42%) of unstable hydrazone **15** as a yellow oil; $[\alpha]_D^{22}$ +3° (*c* 13, $CHCl_3$); ir (film) ν_{max}: 3220 (N—H), 1603 (olefin), and 1172 (SO_2—N) cm^{-1}; ^{1}Hmr ($CDCl_3$) δ: 0.02, 0.04 (2s, 6H, $Si(CH_3)_2$), 0.87 (s, 9H, $SiBu^t$), 1.77 (s, 3H, C-1), 2.40 (s, 3H, $PhCH_3$), 3.33–4.72 (m's, 11H), 5.73, 5.83, 6.00, 6.10, 6.23, 6.50 (AB part of an ABX, 2H, J_{AB} = 16 Hz, J_{AX} < 1 Hz, J_{BX} = 6 Hz, CH=CH), 7.17–7.38, 7.76–7.99 (m's, 19H), and 8.24 (bs, 1H, NH) ppm.

Olefin 16 (ref. 16)

Catecholborane (0.1 mL, 0.9 mmol) was added to a solution of tosylhydrazone **15** (500 mg, 0.67 mmol) in chloroform (5 mL) under argon. After one hour at 0°C and one more hour at rt, sodium acetate trihydrate (300 mg, 2.2 mmol) was added and the mixture was refluxed for 3 h. Most of the chloroform was evaporated and replaced by 50 mL hexane. This solution was washed twice with water and the aqueous phases were extracted with hexane (30 mL). The combined organic phases were dried ($MgSO_4$) and concentrated to give a yellow oil which was chromatographed (4% EtOAc/hexane) yielding 220 mg (58%) of olefin **16**; $[\alpha]_D^{22}$ −11° (*c* 2.6, CCl_4); ir (film) ν_{max}: 970 (*trans* olefin) cm^{-1}; ^{1}Hmr ($CDCl_3$) δ: 0.06 (s, 6H, $Si(CH_3)_2$), 0.89 (s, 9H, $SiBu^t$), 1.63 (d, 3H, J = 4 Hz, allylic CH_3), 2.32 (m, 2H, allylic CH_2), 3.40–4.26 (m's, 5H), 4.47, 4.57 (2s, 2H each, CH_2Ph), 4.52, 4.70, 4.75, 4.93 (ABq, 2H, J = 11 Hz, CH_2Ph), 5.42 (m, 2H, CH=CH), and 7.26 (s, 15H) ppm; *Anal.* calcd. for $C_{35}H_{48}O_4Si$: C 74.95, H 8.63; found: C 75.15, H 8.80.

Nitrosugar 17 → Cyanoamine 25

Most compounds in the **17** to **25** series were prepared using similar or identical procedures and work-up as compounds **35** to **43**. For additional details, the reader is referred to the procedures of the latter series.

3,4,6-Tri-O-benzyl-5-O-tert-butyldimethylsilyl-1,2-dideoxy-1-nitro-D-arabino-hexitol (17)

Similarly to the preparation of **35**, aldehyde **6** (500 mg, 0.90 mmol) was treated successively with (*a*) nitromethane (0.14 mL, 2.6 mmol), anhydrous KF (3 mg, 0.05 mmol), and 18-crown-6 (12 mg, 0.05 mmol) in isopropanol for 3 h at rt; (*b*) acetic anhydride (0.12 mL, 1.3 mmol) and 4-dimethylaminopyridine (10 mg, 0.09 mmol) in anhydrous Et_2O for 18 h; and (*c*) $NaBH_4$ (100 mg, 2.8 mmol) in absolute EtOH (5 mL) in an ice bath. The same tlc solvent (9% EtOAc/pe) was used for each step. After work-up and chromatography (7% EtOAc/pe), 411 mg of nitro compound **17** (76%) was obtained; $[\alpha]_D^{22}$ +2.0° (*c* 13.5, $CHCl_3$); ir (film) ν_{max}: 1548 (RNO_2) cm^{-1}; ^{1}Hmr ($CDCl_3$) δ: 0.08 (s, 6H, $Si(CH_3)_2$), 0.90 (s, 9H, $SiBu^t$), 1.85–2.45 (m, 2H, $CH_2CH_2NO_2$), 3.39–3.9 (m's, 4H), 3.9–4.45 (m's, 3H, including a triplet at 4.28 for CH_2NO_2, J = 7 Hz), 4.47–4.92 (m's, 6H, CH_2Ph), 7.23 and 7.27 (2s, 15H) ppm; ms (CI-IB, 135°C) *m/e*: 580 (2.5, M^+ +1), 181 (100); *Anal.* calcd. for $C_{33}H_{45}NO_6Si$: C 68.36, H 7.82, N 2.41; found: C 68.21, H 7.75, N 2.46.

3,4,6-Tri-O-benzyl-5-O-tert-butyldimethylsilyl-2-deoxy-D-arabino-hexitol (18)

As for **36**, alcohol **18** was prepared by ozonolysis of the sodium nitronate salt of **17** in EtOH followed by reductive work-up with $NaBH_4$. The yield after chromatography (25% EtOAc/pe) amounted to 83%; $[\alpha]_D^{22}$ +3.4° (*c* 17.6, $CHCl_3$); ir (film) ν_{max}: 3450 (hydroxyl) cm^{-1}; ^{1}Hmr ($CDCl_3$) δ: 0.08 (s, 6H, $Si(CH_3)_2$), 0.90 (s, 9H, $SiBu^t$), 1.83 (t, 2H, J = 6 Hz, CH_2CH_2OH), 2.28 (s, 1H, OH), 3.40–4.28 (m's, 7H), 4.48 (s, 2H, CH_2Ph), 4.38, 4.57, 4.64, 4.83 (ABq, 2H, J = 11 Hz, CH_2Ph), 4.52, 4.71, 4.78, 4.96 (ABq, 2H, J = 11 Hz, CH_2Ph), 7.23 and 7.27 (2s, 15H) ppm; ms (CI-IB, 55°C) *m/e*: 551 (17, M^+ +1), 181 (100); *Anal.* calcd. for $C_{33}H_{46}O_5Si$: C 71.96, H 8.42; found: C 71.78, H 8.51.

3,4,6-Tri-O-benzyl-1-bromo-5-O-tert-butyldimethylsilyl-1,2-dideoxy-D-arabino-hexitol (19) (ref. 20)

To a solution of alcohol **18** (272 mg, 0.49 mmol) and triphenylphosphine (142 mg, 0.54 mmol) in dry DMF (1.0 mL), was slowly added *N*-bromosuccinimide (97 mg, 0.54 mmol). After 15 min, methanol (0.2 mL) was added followed after 5 min by water (5 mL). This mixture was extracted with hexane (4 × 10 mL) and the combined extracts washed with water (3 × 20 mL). Drying ($MgSO_4$) and evaporation of the solvent left a semi-crystalline residue containing some triphenylphosphine oxide. Chromatography (9% EtOAc/pe) afforded 211 mg (70%) of bromide **19** as a colorless oil; $[\alpha]_D^{22}$ +16° (*c* 2.65, $CHCl_3$); ^{1}Hmr ($CDCl_3$) δ: 0.05 (s, 6H, $Si(CH_3)_2$), 0.90 (s, 9H, $SiBu^t$), 2.04 (q, 2H, J = 7 Hz, C-2), 3.36 (t, 2H, J = 7 Hz, CH_2Br), 3.50–4.18 (m's, 5H), 4.47 (s, 2H, CH_2Ph), 4.37, 4.56, 4.63, 4.82 (ABq, 2H, J = 11 Hz, CH_2Ph), 4.48, 4.67, 4.72, 4.90 (ABq, 2H, J = 11 Hz, CH_2Ph), and 7.26 (s, 15H) ppm; ms (CI-IB, 10–100°C) *m/e*: 615, 613 (4.9, 4.5, M^+ +1), 181 (100); *Anal.* calcd. for $C_{33}H_{45}BrO_4Si$: C 64.58, H 7.39, Br 13.02; found: C 64.43, H 7.39, Br 13.31.

3,4,6-Tri-O-benzyl-5-O-tert-butyldimethylsilyl-2-deoxy-aldehydo-D-glucose (20)

A solution of alcohol **18** (618 mg, 1.12 mmol) in 5 mL dry CH_2Cl_2 was treated at rt with pyridinium chlorochromate (22) (360 mg, 1.67 mmol) in the presence of Celite (360 mg) and anhydrous sodium acetate (45 mg, 0.55 mmol). The reaction was in general complete in less than two hours. Hexane (15 mL) was added and the mixture was stirred for another 15 min, until the precipitate took a granular aspect. The mixture was filtered through Celite and the solids washed with several portions of hexane. The combined filtrates were concentrated *in vacuo* at rt to a colorless oil which was chromatographed (17% EtOAc/hexane) giving 474 mg (77%) of pure aldehyde **20**. This

Can. J. Chem. Downloaded from www.nrcresearchpress.com by 210.87.254.42 on 09/05/12
For personal use only.

product was always used immediately because of its relative instability; $[\alpha]_D^{22}$ −6.4° (*c* 7.85, $CHCl_3$); ir (film) ν_{max}: 1722, 2720 (aldehyde) cm^{-1}; ^{1}Hmr($CDCl_3$) δ: 0.07 (s, 6H, $Si(CH_3)_2$), 0.89 (s, 9H, SiBu^t), 2.67 (d of d, 2H, *J* = 2, 6 Hz, CH_2CHO), 3.40–4.33 (m's, 5H), 4.47 (s, 2H, CH_2Ph), 4.59 (s, 2H, CH_2Ph), 4.45, 4.64, 4.70, 4.89 (ABq, 2H, *J* = 11 Hz, CH_2Ph), 7.24, 7.28 (2s, 15H), and 9.64 (t, 1H, *J* = 2 Hz, CHO) ppm.

Z-Olefin 21

In a procedure similar to the preparation of **38**, the freshly prepared aldehyde **20** (490 mg, 0.89 mmol) was added to a solution at −70°C of the ylid previously prepared by the action of *n*-butyl lithium (0.60 mL, 1.6 *M* in hexane, 0.95 mmol) on phosphonium salt **30***a* (660 mg, 1.1 mmol). The same work-up and purification by chromatography (7% EtOAc/hexane) yielded 472 mg (67%) of olefin **21**, the isomeric purity of which, as determined by ^{13}C nmr, was approximately 95% (*cis*); $[\alpha]_D^{22}$ −4.4° (*c* 10, $CHCl_3$); ir (film): no detectable absorption at 973 cm^{-1} (*trans* olefin); ^{1}Hmr ($CDCl_3$) δ: 0.08 (s, 6H, $Si(CH_3)_2$), 0.91 (apparent s, 12H, SiBu^t and CH_2CH_3), 1.10–1.80 (m's, 20H), 1.80–2.22 (m, 2H, C-8), 2.39 (m, 2H, C-5), 3.41–3.78 (m, 4H), 3.86 (s, 4H, dioxolane CH_2's), 3.93–4.27 (m, 1H), 4.48, 4.57 (2s, 2H each, CH_2Ph), 4.50, 4.69, 4.74, 4.93 (ABq, 2H, *J* = 11 Hz, CH_2Ph), 5.42 (m, 2H, CH=CH), and 7.24 (s, 15H); ^{13}C nmr ($CDCl_3$) δ: 132.03, 125.39 (C-7, C-6), 29.58, and 27.53 (C-5,8) ppm; the corresponding carbons of the *trans* isomer at 133.21, 125.93, 34.44, and 32.66 ppm were barely detectable (approximately 5%); ms (EI, 15 eV, 86°C) *m/e*: 786 (1.4, M^+), 731 (2), 701 (16), and 157 (100); *Anal.* calcd. for $C_{50}H_{76}O_6Si$: C 74.86, H 9.36; found: C 75.12, H 9.44.

E-*Olefin 22*

The *Z*-olefin **21** (957 mg, 1.22 mmol) in CH_2Cl_2 (20 mL) was treated at rt with *m*-chloroperbenzoic acid (283 mg, approximately 85% peroxyacid, 1.40 ± 0.07 mmol) for 3 h. More peroxyacid (25 mg, 0.12 mmol) was then added and the stirring continued for 1.5 h. Hexane (30 mL) was added and this mixture was washed successively with 5% aqueous Na_2SO_3 (50 mL), saturated $NaHCO_3$, and water. Drying ($MgSO_4$), concentration *in vacuo*, and chromatography (11% EtOAc/hexane) gave 884 mg (90%) of epoxide, presumably a mixture of *erythro* isomers not separated on tlc; ^{1}Hmr ($CDCl_3$) δ: 0.08 (s, 6H, $Si(CH_3)_2$), 0.91 (apparent s, 12H, SiBu^t and C-20), 1.10–2.01 (m's, 24H), 2.91 (m, 2H, C-6,7), 3.30–3.82 (m's, 3H), 3.82–4.24 (m's, 6H), 4.39–4.90 (m's, 6H, CH_2Ph), and 7.24 (s, 15H) ppm; ms (EI, 70eV, 93°C) *m/e*: 746 (0.2), 745 (0.3), 717 (1.3), 91 (100).

As in the preparation of **39**, the epoxides derived from **21** (884 mg, 1.10 mmol) were treated, in dry THF and under argon, with lithium diphenylphosphide (28) (2.3 mL of a 0.50 *M* solution in THF, 1.15 mmol) for 30 min followed by methyl iodide (0.1 mL, 1.6 mmol) for another 30 min. Chromatography (7% EtOAc/hexane) afforded 708 mg (74% from **21**) of *E*-olefin **22**. The ^{13}C nmr spectrum showed this olefin to be at least 95% *trans*; $[\alpha]_D^{22}$ −4.4° (*c* 10.6, $CHCl_3$); ir (film) ν_{max}: 973 (*trans* olefin) cm^{-1}; ^{1}Hmr ($CDCl_3$) δ: essentially identical to that of **21**; ^{13}C nmr ($CDCl_3$) δ: 133.21, 125.93 (C-7, C-6), 34.44, and 32.66 (C-5,8) ppm, all four carbons showing the characteristic downfield shift (34) from the *cis* isomer; *Anal.* calcd. for $C_{50}H_{76}O_6Si$: C 74.86, H 9.36; found: C 75.01, H 9.64.

Alcohol 23

To a solution of silyl ether **22** (818 mg, 1.04 mmol) in dry THF (7 mL) under argon, was added 1.75 mL of 0.65 *N* tetra-*n*-butylammonium fluoride (9) (1.13 mmol) in THF. After 7 h at rt, hexane (30 mL) was added, the solution was washed with water (2 × 50 mL), dried ($MgSO_4$), and concentrated *in vacuo*. The residue was chromatographed (28% EtOAc/hexane) to give 590 mg (84%) of pure **23**; $[\alpha]_D^{22}$ −1° (*c* 7.4, $CHCl_3$); ir (film) ν_{max}: 3300–3600 (hydroxyl) cm^{-1}; ^{1}Hmr ($CDCl_3$) δ: 0.90 (bt, 3H, *J* = 6 Hz, C-20), 1.10–1.75 (m's, 20H), 1.93 (m, 2H, C-8), 2.41 (bt, 2H, *J* = 6 Hz, C-5), 3.09 (bs, 1H, OH), 3.32–3.75 (m, 4H), 3.86 (s, 4H, dioxolane CH_2's), 3.88–4.25 (m, 1H), 4.50 (s, 2H, CH_2Ph), 4.57 (s, 4H, CH_2Ph), 5.39 (m, 2H, CH=CH), 7.23 and 7.25 (2s, 15H, phenyls) ppm; *Anal.* calcd. for $C_{43}H_{60}O_6$: C 76.75, H 8.99; found: C 76.52, H 9.11.

Ketone 24

Alcohol **23** was oxidized with a 3:2 mixture of dimethylsulfoxide and acetic anhydride, exactly as described in the preparation of **41**, to give a 74% yield of ketone **24** after chromatography (20% EtOAc/hexane); $[\alpha]_D^{22}$ −26° (*c* 9.4, $CHCl_3$); ir (film) ν_{max}: 1732 (ketone) cm^{-1}; ^{1}Hmr ($CDCl_3$) δ: 0.90 (bt, 3H, *J* = 6 Hz, C-20), 1.08–1.73 (m's, 20H), 1.87 (m, 2H, C-8), 2.35 (bt, 2H, *J* = 6 Hz, C-5), 3.64–4.07 (m's, 6H, dioxolane CH_2's singlet at 3.86), 4.27–4.71 (m's, 8H), 5.27 (m, 2H, CH=CH), and 7.25 (s, 15H) ppm.

Cyanoamines 25

Ketone **24** (411 mg, 0.61 mmol) was dissolved in 12 mL methanol previously saturated with ammonia. Sodium cyanide (60 mg, 1.2 mmol) and ammonium chloride (60 mg, 1.1 mmol) were added and the mixture was stirred at rt for 4 days. Ammonia gas was occasionally bubbled in to insure saturation. The reaction was monitored by tlc (25% EtOAc/hexane). The solvent was evaporated off and the residue was taken up in Et_2O (30 mL) and water (30 mL). The separated aqueous phase was extracted with ether (10 mL) and the combined organic phases were washed with saturated $NaHCO_3$ and water. Drying ($MgSO_4$) and evaporation of the solvent left a yellow oil which was filtered on a short silica gel column (10 g, eluted with 30% EtOAc/hexane) to remove polar impurities. The two cyanoamines, separated by high pressure liquid chromatography (230 psi, 20% EtOAc and 0.1% MeOH in hexanes), amounted to 155 mg (37%) of the less polar isomer and 137 mg (32%) of the more polar one; *less polar isomer*: $[\alpha]_D^{22}$ +2° (*c* 5.4, $CHCl_3$); ir (film) ν_{max}: 3390, 3320 (R—NH_2), 2220 (nitrile), and 972 (*trans* olefin) cm^{-1}; ^{1}Hmr ($CDCl_3$) δ: 0.90 (bt, 3H, *J* = 6 Hz, C-20), 1.04–2.22 (m's, 24H), 2.51 (bt, 2H, *J* = 6 Hz, C-5), 3.29–3.79 (m's, 4H), 3.86 (s, 4H, dioxolane CH_2's), 4.31, 4.49, 4.56, 4.74 (ABq, 2H, *J* = 11 Hz, CH_2Ph), 4.49, 4.69 (2s, 2H each, CH_2Ph), 5.39 (m, 2H, CH=CH), and 7.24 (s, 15H, phenyls) ppm; ms (EI, 70 eV, 89°C) *m/e*: 641 (0.3), 584 (5), 476 (5), 240 (30), 157 (49), and 91 (100); *Anal.* calcd. for $C_{44}H_{60}N_2O_5$: C 75.83, H 8.68, N 4.02; found: C 75.55, H 8.69, N 4.07; *more polar isomer*: $[\alpha]_D^{22}$ +5° (*c* 5.4, $CHCl_3$); ir (film): identical to that of the other isomer; ^{1}Hmr ($CDCl_3$) δ: differs from the spectrum of the other isomer only in the 3.3–4.7 ppm region: 3.33–3.96 (m's, 8H, dioxolane CH_2's singlet at 3.86), 4.41, 4.61, 4.68, 4.87 (ABq, 2H, *J* = 11 Hz, CH_2Ph), 4.51, and 4.56 (2s, 2H each, CH_2Ph) ppm; ms (EI, 70 eV, 73°C) *m/e*; 669 (0.2), 584 (2), 476 (11), 240 (10), 157 (52), and 91 (100); *Anal.* calcd. for $C_{44}H_{60}N_2O_5$: C 75.83, H 8.68, N 4.02; found: C 75.54, H 8.61, N 4.25.

1-n-Hexylcyclooctanol (26)

A solution of 1-bromohexane (42 mL, 0.3 mol, in 50 mL dry Et_2O) was added to a stirred suspension of 14 g magnesium turnings (0.6 mol) in 400 mL dry Et_2O (under an argon atmosphere) at a rate which maintained a gentle reflux. After the addition was complete, the reflux was continued for 30 min. Then, a solution of cyclooctanone (40 g, 0.32 mol) in 50 mL Et_2O was added dropwise, again at a rate sufficient to maintain reflux which was continued for 30 min after the addition.

The cooled mixture was poured into 800 mL ice-water containing 80 mL concentrated H_2SO_4. After separation, the aqueous phase was extracted twice with ether and the combined organic phases were washed twice with water. Neutralization

Can. J. Chem. Downloaded from www.nrcresearchpress.com by 210.87.254.42 on 09/05/12
For personal use only.

(saturated $NaHCO_3$), drying ($MgSO_4$), and evaporation of the solvent left a yellow liquid. Distillation gave 24.9 g of product, bp 100–115°C/0.03 Torr, which still contained about 23% unreacted cyclooctanone as determined by glc (3 ft column, 3% OV-101, 250°C). Further purification was found unnecessary before the following reaction. Nevertheless, a small sample was later redistilled and a fraction collected at 104°C/0.005 Torr (found to be 96% pure by gc) was used for characterization; ir (film) ν_{max}: 3200–3600 (hydroxyl) cm^{-1}; ms (EI, 70 eV, 25°C) *m/e*: 194 (0.6, $M^+ - 18$), 183 (0.4), 169 (1.2), 155 (5.3), 141 (16), and 127 (100, $M^+ - 85$).

1,8-Tetradecanediol (27)

The mixture obtained previously (containing about 77% of alcohol **26** (90 mmol) and 23% cyclooctanone) was refluxed in 250 mL xylene in the presence of 150 mg iodine (0.6 mmol) (26) using a Dean-Stark trap, and the progress of the reaction was followed by glc (3% OV-101, 230°C). After 30 min, the solvent was distilled off and the residue taken up in 100 mL hexane. This solution was washed with 1.5% $Na_2S_2O_3$ (5 × 50 mL) and once with water. Drying ($MgSO_4$) and evaporation of the solvent gave a yellow liquid which was dissolved in absolute ethanol and treated with excess ozone at −70°C. After purging with a stream of nitrogen, $NaBH_4$ (10 g, 263 mmol) was added and the stirred solution allowed to warm up to rt (2 h). Most of the solvent was evaporated off and replaced by $CHCl_3$ (100 mL). The mixture was acidified with 10% aqueous AcOH and the aqueous phase extracted with $CHCl_3$. The $CHCl_3$ extracts were washed twice with water and neutralized with saturated $NaHCO_3$. Drying ($MgSO_4$) and evaporation to dryness gave a colorless oil which was crystallized from cold hexane (−50°C). After recrystallization, a 17.1 g yield (25% from bromohexane) of diol **27** was obtained; mp: 47.5–48.5°C; ir ($CHCl_3$) ν_{max}: 3300–3550 and 3610 (hydroxyls) cm^{-1}; ^{1}Hmr ($CDCl_3$) δ: 0.7–2.0 (m, 25H), 2.44 (s, 2H, OH), and 3.45–3.70 (m, 3H, CH_xOH) ppm; ms (EI, 70 eV, 21°C) *m/e*: 213 (0.2), 211 (0.2), 194 (0.4), 166 (0.5), 145 (19), 127 (19), 109 (90), and 55 (100); *Anal.* calcd. for $C_{14}H_{30}O_2$: C 72.98, H 13.13; found: C 73.12, H 13.17.

1-Hydroxy-8-tetradecanone 28 (ref. 27)

To a mixture of diol **27** (9.9 g, 43 mmol) and hexamethyl phosphoric triamide (1.62 g, 9.1 mmol), in 350 mL CH_2Cl_2 and 250 mL of 8% $NaHCO_3$ at 5°C, was added dropwise a solution of Br_2 (7.9 g, 49 mmol) in 90 mL CH_2Cl_2 with vigorous stirring. The reaction, monitored by tlc (Et_2O) during and after the addition, was not allowed to go to completion since significant amounts of impurities, that proved difficult to remove, started to appear towards the end. The reaction was stopped by adding "reagent" hexane, which contains small amounts of olefins, until the orange color disappeared. The CH_2Cl_2 phase was separated and concentrated *in vacuo*, and replaced by hexane/Et_2O (1:1, 200 mL). After washing this solution several times with water to remove the HMPT, drying ($MgSO_4$) and evaporation of the solvent afforded a white crystalline mass, which could not be purified by crystallization. Chromatography (45% EtOAc/hexane) gave 7.1 g (72%) of colorless crystals. A sample recrystallized from cold hexane was used for characterization; mp 52.0–53.0°C; ir ($CHCl_3$) ν_{max}: 1710 (ketone), 3300–3550 and 3620 (hydroxyl) cm^{-1}; ^{1}Hmr ($CDCl_3$) δ: 0.65–1.8 (m, 21H), 2.36 (t, 4H, J = 6.5 Hz, —CH_2CO—), 2.73 (s, 1H, OH), and 3.54 (t, 2H, J = 6 Hz, —CH_2OH) ppm; ms (EI, 70 eV, 35°C) *m/e*: 228 (0.5, M^+), 227 (0.3), 211 (0.6), 210 (0.4), 158 (6.7), 143 (7.6), 128 (27), 113 (40), and 43 (100); *Anal.* calcd. for $C_{14}H_{28}O_2$: C 73.63, H 12.36; found: C 73.27, H 12.68.

2-(7-Hydroxy-n-heptyl)-2-n-hexyl-1-3-dioxolane (29a)

A solution of ketone **28** (6.6 g, 29 mmol) in 1800 mL benzene was refluxed in the presence of $TsOH \cdot H_2O$ (900 mg, 5 mmol) and ethylene glycol (50 mL) using a Dean-Stark trap. The reaction was monitored by glc (OV-101, 200–280°C), product and starting material having the same R_f on tlc. After 4.5 h the mixture was concentrated *in vacuo* to about half its volume. The benzene phase was separated, washed with saturated $NaHCO_3$ (2 × 100 mL), and dried over $MgSO_4$. Evaporation of the solvent left a yellow liquid which was treated with $NaBH_4$ (0.4 g, 11 mmol) in 70 mL EtOH for 0.5 h to reduce any residual ketone to the more polar diol **27**. The solvent was evaporated *in vacuo*, replaced by hexanes (200 mL), and the mixture was acidified with 10% aqueous AcOH. Neutralization (saturated $NaHCO_3$), drying ($MgSO_4$), evaporation of the solvent, and purification by chromatography (45% EtOAc/hexane) gave 6.75 g pure **29*a*** (86%); ir (film) ν_{max}: 3200–3600 (hydroxyl) cm^{-1}; ^{1}Hmr ($CDCl_3$) δ: 0.7–2.0 (m, 25H), 2.90 (s, 1H, OH), 3.50 (t, 2H, J = 6.5 Hz, CH_2OH), and 3.85 (s, 4H,dioxolane CH_2's) ppm; ms (CI-IB, 34°C) *m/e*: 273 (100, $M^+ + 1$); *Anal.* calcd. for $C_{16}H_{32}O_3$: C 70.54, H 11.84; found: C 70.30, H 11.93.

5,5-Dimethyl-2-(7-hydroxy-n-heptyl)-2-n-hexyl-1,3-dioxane (29b)

A solution of the hydroxyketone **28** (7.6 g, 31 mmol), 2,2-dimethyl-1,3-propanediol (13 g, 125 mmol), and $TsOH \cdot H_2O$ (150 mg, 0.8 mmol) in one liter of benzene was refluxed overnight using a Dean-Stark trap. The solvent was evaporated off *in vacuo* and the residue was treated with $NaBH_4$ (150 mg, 3.9 mmol) in 50 mL EtOH for 0.5 h to reduce any residual ketone to the more polar diol **27**. The ethanol was evaporated off, replaced with 100 mL hexanes, and the mixture was acidified with 10% aqueous AcOH. After neutralization with saturated $NaHCO_3$ and drying ($MgSO_4$), the solvent was removed *in vacuo* to give a yellowish liquid which was chromatographed (35% EtOAc/hexane) to give 9.5 g of pure ketal **29*b*** (97%); ir (film) ν_{max}: 3100–3600 (hydroxyl) cm^{-1}; ^{1}Hmr ($CDCl_3$) δ: 0.7–2.0 (m, 31H, including a singlet at 0.90 for $C(CH_3)_2$), 2.8 (bs, 1H, OH), and 3.25–3.70 (m, 6H, dioxane ring CH_2's and CH_2OH) ppm; ms (EI, 15 eV, 80°C) *m/e*: 231 (1.3), 230 (13), 229 (100), and 199 (91).

2-(7-Bromo-n-heptyl)-2-n-hexyl-1,3-dioxolane (30a)

This material was prepared in 86% yield from alcohol **29*a*** by the same procedure used for **30*b***, and was purified by flash chromatography using 5% EtOAc/hexane as eluent; ^{1}Hmr ($CDCl_3$) δ: 0.7–2.1 (m, 25H), 3.38 (t, 2H, J = 6.5 Hz, CH_2Br), and 3.87 (s, 4H, dioxolane CH_2's) ppm; ms (CI-IB, 30°C) *m/e*: 337 (100, $M^+ + 1$) and 335 (95, $M^+ + 1$); *Anal.* calcd. for $C_{16}H_{31}BrO_2$: C 57.31, H 9.32, Br 23.83; found: C 57.22, H 9.33, Br 24.00.

2-(7-Bromo-n-heptyl)-5,5-dimethyl-2-n-hexyl-1,3-dioxane (30b) (ref. 20)

To a solution of alcohol **29*b*** (9.5 g, 30 mmol) and triphenylphosphine (9.50 g, 36.3 mmol) in 50 mL dry DMF was added slowly *N*-bromosuccinimide (6.50 g, 36.5 mmol) at 10°C. The reaction followed by tlc (20% EtOAc/hexane), was generally complete in less than 30 min. This mixture was then extracted with hexanes (80 mL). Water was added to the DMF phase until triphenylphosphine oxide started precipitating out and 6 more hexane extractions (80 mL) were performed. The combined hexane phases were washed twice with water, dried ($MgSO_4$), and evaporated to dryness. The residue was purified by flash chromatography (2% EtOAc/hexane) affording 9.92 g pure **30*b*** (87%) as a colorless liquid; ^{1}Hmr ($CDCl_3$) δ: 0.6–2.2 (m, 31H, including a singlet at 0.90 for $C(CH_3)_2$), 3.30 and 3.32 ((t, J = 6.3 Hz, CH_2Br) and (s, dioxane ring CH_2's), total integration 6H) ppm; ms (EI, 15 eV, 85°C) *m/e*: 294 (5), 293 (44), 292 (6), 291

Can. J. Chem. Downloaded from www.nrcresearchpress.com by 210.87.254.42 on 09/05/12
For personal use only.

(42), 200 (13), and 199 (100); *Anal.* calcd. for $C_{19}H_{37}BrO_2$: C 60.47, H 9.88, Br 21.17; found: C 60.49, H 10.17, Br 21.21.

*7-(2-*n*-Hexyl-1,3-dioxolan-2-yl)-*n*-heptyl-triphenylphosphonium Bromide (31a)*

A mixture of bromide **30***a* (4.25 g, 12.7 mmol) and triphenylphosphine (3.80 g, 14.5 mmol) was heated at 140°C under argon for 5.5 h. The glassy material obtained was dissolved in a minimum of acetone and the phosphonium salt was precipitated by adding (slowly at first) anhydrous Et_2O (400 mL). The precipitate was allowed to settle overnight and the clear solution decanted. The residue was pumped dry (2 h) leaving 5.3 g (70%) of phosphonium salt **31***a* as a thick foam. This method of preparation of phosphonium salts containing a ketal function proved unreliable since a variable amount (10–30%) of ketone, resulting from partial hydrolysis of the ketal function, could be detected in the ir spectrum: ir (film) ν_{max}: 1590 (C=C) and 1710 (variable intensity) (ketone) cm^{-1}; ^{1}Hmr ($CDCl_3$) δ: 0.7–2.0 (m, 25H), 3.5–3.85 (bs, 2H, CH_2—P^+), 3.87 (s, 4H, dioxolane CH_2's), and 7.2–8.0 (m, 15H, phenyls) ppm.

*7-(5,5-Dimethyl-2-*n*-hexyl-1-3-dioxan-2-yl)-*n*-heptyl-triphenylphosphonium Bromide (31b)*

In a flask stoppered with a septum, a mixture of bromide **30***b* (3.06 g, 8.12 mmol), triphenylphosphine (3.22 g, 12.3 mmol), and trimethyl orthoformate (1.8 mL) in dry acetonitrile (7.0 mL) was heated under argon, in an oil bath kept at 90°C, for 14 h. The solvents were evaporated *in vacuo* and the residue was dissolved in a minimum of dry tetrahydrofuran. The phosphonium salt was precipitated out by adding (slowly at first) anhydrous Et_2O (250 mL). The precipitate was allowed to settle overnight (under an argon atmosphere) and the ether solution decanted. Another precipitation from THF with Et_2O was performed and the residue was dried on a pump for 2 h to yield 4.4 g (85%) of a very thick foam.

When the precipitate was kept under an ether layer and under a dry atmosphere (argon) for a few days, partial crystallization occurred, but collection and storage of the crystals was complicated by their highly hygroscopic nature which caused them to turn back into an oil; ir (film) ν_{max}: 1590 (C=C) cm^{-1}, no trace of carbonyl absorption; ^{1}Hmr (CCl_4) δ: 0.6–2.0 (m, 31H), 3.35 (s, 4H, dioxane ring CH_2's), 3.9–4.5 (bs, 2H, CH_2—P^+), and 7.1–8.3 (m, 15H, phenyls) ppm.

*4-*O*-tert-Butyldimethylsilyl-2,3-*O*-isopropylidene-5-*O*-triphenylmethyl-*L*-arabinose Diethyl Dithioacetal (33)*

A solution of 2,3-*O*-isopropylidene-L-arabinose diethyl dithioacetal **32** (31) (14.3 g, 48.3 mmol), triphenylmethyl chloride (16.2 g, 58.2 mmol), and 4-dimethylaminopyridine (0.3 g, 2.45 mmol) in 25 mL dry pyridine was stirred at room temperature for two days. Then 50 mL dry DMF was added, followed by *tert*-butyldimethylsilyl chloride (11.0 g, 73.1 mmol) and imidazole (11.0 g, 162 mmol). After stirring at rt for 24 h, water (100 mL) was added and the mixture was extracted with hexanes (6 × 100 mL). The combined hexane phases were washed successively with 1*N* HCl, saturated $NaHCO_3$, and water. Drying over $MgSO_4$ and evaporation of the solvent afforded a colorless oil which partially crystallized. Recrystallization from absolute ethanol and purification of the residue by chromatography (2% EtOAc/petroleum ether) gave a total yield of 27.0 g (86% from **33**); mp 92–93°C; $[\alpha]_D^{22}$ −33° (*c* 12, $CHCl_3$); ir (film) ν_{max}: 1590 (aromatic) cm^{-1}; ^{1}Hmr ($CDCl_3$) δ: −0.09, 0.07 (2s, 6H, $Si(CH_3)_2$), 0.83 (s, 9H, SiBu^t), 1.27, 1.29 (2t, 6H, J = 7.5 Hz, CH_3CH_2S—), 1.33, 1.47 (2s, 6H, $C(CH_3)_2$), 2.67 (q, 4H, J = 7.5 Hz, CH_3CH_2S—), 3.05–3.4 (m, 2H), 3.8–4.6 (m, 4H), and 7.05–7.55 (m, 15H, trityl) ppm; *Anal.* calcd. for $C_{37}H_{52}O_4S_2Si$: C 68.05, H 8.02, S 9.82; found: C 68.29, H 7.88, S 10.10.

*4-*O*-tert-Butyldimethylsilyl-2,3-*O*-isopropylidene-5-*O*-triphenylmethyl-aldehydo-*L*-arabinose (34)*

The dithioacetal **33** (5.0 g, 7.7 mmol) was dissolved in 90 mL acetone, and 5 mL water was added followed by HgO (3.7 g, 17 mmol) and $HgCl_2$ (4.6 g, 17 mmol). The mixture was refluxed until no starting material could be detected by tlc (15% EtOAc/hexanes, 1.5 h). Hexane (200 mL) was added to the cooled suspension and a vigorous stirring maintained for 10 min. After filtration through Celite, the solids were washed with several portions of hexane and the combined filtrates concentrated *in vacuo* to about half their volume. The solution was decanted from the precipitated mercuric salts, washed with 5% aqueous KI (5 × 100 mL), and washed once with water. Drying over $MgSO_4$ and evaporation of the solvent left a colorless oil which was purified by flash chromatography (12% EtOAc/hexanes). The ^{1}Hmr and ir spectra showed that the aldehyde group was at least 50% hydrated. Therefore, the product was refluxed for 30 min, in 100 mL benzene using a Dean-Stark trap. Evaporation of the solvent left 4.6 g of a viscous oil which still contained some mercuric salts (as demonstrated by the immediate appearance of elemental mercury when a small amount of this aldehyde was treated with $NaBH_4$ in methanol). In general, no further purification was performed and this material was used directly in the following step.

In a subsequent run, an analytical sample was obtained by repeating the same sequence (treatment with KI and chromatography) until no mercuric salts could be detected. After dehydration in refluxing benzene, the following data could be obtained: $[\alpha]_D^{22}$ +3° (*c* 8, $CHCl_3$); ir (film) ν_{max}: 2800, 2710, 1735 (aldehyde) cm^{-1}; ^{1}Hmr (CCl_4) δ: −0.12, 0.02 (2s, 6H, $Si(CH_3)_2$), 0.83 (s, 9H, SiBu^t), 1.30, 1.40 (2s, 6H, $C(CH_3)_2$), 3.1 (apparent d, 2H), 3.7–4.0 (m, 1H), 4.25 (bs, 2H), 7.03–7.45 (m, 15H, trityl), and 9.55 (bs, 1H, CHO) ppm.

*5-*O*-tert-Butyldimethylsilyl-1,2-dideoxy-3,4-*O*-isopropylidene-1-nitro-6-*O*-triphenylmethyl-*L*-arabino-hexitol (35) (ref. 18)*

The aldehyde **34**, freshly prepared from 5.0 g of the dithioacetal **33** (7.7 mmol), was dissolved in 25 mL dry isopropanol. Nitromethane (2.0 mL, 37 mmol), anhydrous KF (50 mg, 0.86 mmol), and 18-crown-6 (120 mg, 0.45 mmol) were added and the mixture was stirred at room temperature for 3 h. The course of the reaction was followed by tlc (10% Et_2O/benzene).

The isopropanol was removed *in vacuo* at rt. The foamy material obtained was dissolved in 30 mL dry Et_2O and treated with acetic anhydride (2.0 mL, 21 mmol) and 4-dimethyl-aminopyridine (60 mg, 0.50 mmol). Thin-layer chromatography (2.5% Et_2O/benzene) indicated that after 50 min, all the β-hydroxynitro compound had been replaced by two less polar spots. The ether was evaporated off and replaced by 100 mL absolute EtOH. This solution was cooled in an ice bath and $NaBH_4$ (2.2 g, 58 mmol) was added very slowly. After one hour, a new spot on tlc (benzene), which had gradually appeared between the two original ones, had completely replaced them. The solvent was evaporated *in vacuo*, hexanes (100 mL) and water (50 mL) were added to the residue, and this mixture, in an ice bath, was slowly acidified with 10% aqueous AcOH. The aqueous phase was separated and washed twice with hexanes (100 mL). The combined organic phases were washed with water (3 × 100 mL), neutralized with saturated $NaHCO_3$, washed with water again, dried over $MgSO_4$, and concentrated *in vacuo* to a very thick syrup. Chromatography (8% EtOAc/hexanes) yielded 3.8 g of pure **35** (83% from **33**); $[\alpha)_D^{22}$ −1.1° (*c* 10,

Can. J. Chem. Downloaded from www.nrcresearchpress.com by 210.87.254.42 on 09/05/12
For personal use only.

$CHCl_3$); ir (film) ν_{max}: 1553 (NO_2) cm^{-1}; ^{1}Hmr (CCl_4) δ: −0.08, 0.03 (2s, 6H, $Si(CH_3)_2$), 0.83 (s, 9H, $SiBu^t$), 1.29, 1.35 (2s, 6H, $C(CH_3)_2$), 2.05 (bt, 2H, J = 7.5 Hz, $—CH_2CH_2NO_2$), 2.75–3.4 (m, 2H), 3.75–4.05 (m, 3H), 4.28 (t, 2H, J = 7.5 Hz, $—CH_2NO_2$), and 7.03–7.42 (m, 15H, trityl) ppm; *Anal.* calcd. for $C_{34}H_{45}NO_6Si$: C 69.00, H 7.66, N 2.36; found: C 69.21, H 7.93, N 2.55.

*5-O-tert-Butyldimethylsilyl-2-deoxy-3,4-O-isopropylidene-6-O-triphenylmethyl-*L*-arabino-hexitol (36) (ref. 19)*

A solution of nitro compound **35** (3.8 g, 6.4 mmol) in absolute EtOH was treated with 13 mL of freshly prepared 0.59*N* EtONa/EtOH and the solution was kept stirring under nitrogen for 15 min. O_3 (36 mmol/h) was bubbled through the solution at −70°C for 17 mins (10 mmol). After purging the excess ozone with a stream of nitrogen, $NaBH_4$ (500 mg) was added, and the stirred solution was allowed to warm up to room temperature (2 h). Most of the solvent was evaporated off and replaced with hexanes (50 mL) and water (20 mL). The mixture was acidified with 10% aqueous AcOH and the separated aqueous phase washed with hexanes (2 × 50 mL). The combined organic phases were washed twice with water, neutralized with saturated $NaHCO_3$, and washed again with water. Drying ($MgSO_4$) and evaporation of the solvent gave a colorless oil which was chromatographed (27% EtOAc/hexanes) giving 3.3 g of pure **36** (92%); $[\alpha]_D^{22}$ +1.4° (*c* 11, $CHCl_3$); ir (film) ν_{max}: 3200–3600 (alcohol hydrogen bonding) cm^{-1}; ^{1}Hmr (CCl_4) δ: −0.10, 0.02 (2s, 6H, $Si(CH_3)_2$), 0.83 (s, 9H, $SiBu^t$), 1.30, 1.37 (2s, 6H, $C(CH_3)_2$), 1.68 (bt, 2H, J = 5.5 Hz, $—CH_2CH_2OH$), 2.0 (bs, 1H, OH), 2.9–3.3 (m, 2H), 3.56 (t, 2H, J = 5.5 Hz, $—CH_2OH$), 4.9 (bs, 3H), and 7.05–7.45 (m, 15H, trityl) ppm; *Anal.* calcd. for $C_{34}H_{46}O_5Si$: C 72.56, H 8.24; found: C 72.30, H 8.04.

*5-O-tert-Butyldimethylsilyl-2-deoxy-3,4-O-isopropylidene-6-O-triphenylmethyl-*aldehydo-L-*glucose (37)*

A solution of **36** (3.3 g, 5.9 mmol) in 180 mL dry methylene chloride was treated with pyridinium chlorochromate (2.5 g, 11.6 mmol) (22) in the presence of Celite (2.5 g) and anhydrous NaOAc (500 mg, 6.1 mmol) for 4 h, at ambient temperature, with vigorous stirring. Hexane (300 mL) was added and stirring was continued for a few minutes, until the precipitate had taken a granular aspect. The suspension was then filtered through Celite and the solids washed several times with hexane. The combined filtrates were concentrated *in vacuo* (water bath at 25°C) to about 100 mL and filtered again through Celite. The solvent was evaporated and the residue chromatographed (flash, 13% EtOAc/hexane) to yield 2.8 g (85%) of pure aldehyde. This product was always prepared just prior to use; $[\alpha]_D^{22}$ −1.1° (*c* 8.6, $CHCl_3$); ir (film) ν_{max}: 2820, 2720, and 1728 (aldehyde) cm^{-1}; ^{1}Hmr (CCl_4) δ: −0.10, 0.01 (2s, 6H, $Si(CH_3)_2$), 0.83 (s, 9H, $SiBu^t$), 1.33 (bs, 6H, $C(CH_3)_2$), 2.42 (d of d, 2H, J = 2, 5.5 Hz, CH_2CHO), 2.8–3.4 (m, 2H), 3.8–4.6 (m, 3H), 7.1–7.5 (m, 15H, trityl), and 9.65 (t, 1H, J = 2 Hz, CHO) ppm.

Z-Olefin 38

A solution of the phosphonium salt **31***b* (4.4 g, 6.9 mmol) in dry THF (30 mL) under argon was treated with 1.6*N* *n*-BuLi in hexane (3.5 mL, 5.6 mmol) at 25°C for 10 min, then cooled to −70°C. A solution of the freshly prepared aldehyde **37** (2.8 g, 5.0 mmol) in 20 mL dry THF was added dropwise (one drop per second). After stirring at −70°C for 5 min, 1 mL *t*-BuOH in 5 mL THF was added, the mixture was warmed up to 20°C, and stirred for 20 min. Et_2O (50 mL) was added and the mixture was washed with water (4 × 50 mL), dried ($MgSO_4$), and concentrated *in vacuo* to a volume of about 10 mL. Hexane (100 mL) was added, causing precipitation of Ph_3PO which was filtered off. The filtrate was concentrated again *in vacuo* to half its volume, cooled in an ice bath, and Ph_3PO filtered again. Evaporation of the solvent to dryness left a yellow oil which was purified by flash chromatography as follows. Half of the crude material was applied on a 55 mm id column as a 30% (approx.) solution in 2% EtOAc/hexane and the column was eluted successively with 2% and 3% EtOAc/hexane (1000 mL each); 50 mL fractions were collected. Fractions 16–34 contained pure olefin **38**; total yield: 3.6 g (86%); $[\alpha]_D^{22}$ −4° (*c* 10, $CHCl_3$); ir (film) ν_{max}: 3000–3100 (aromatic C—H), 2800–3000 (aliphatic C—H, large), 1601 (C=C), and no detectable absorption at 971 cm^{-1} (*trans* olefin) which was present in the spectrum of the *trans* isomer **38**; ^{1}Hmr (CCl_4) δ: −0.11, 0.02 (2s, 6H, $Si(CH_3)_2$), 0.6–2.5 (m's, 48H), 3.0–3.25 (m, 2H), 3.33 (s, 4H, dioxane ring CH_2's), 3.86 (m, 3H), 5.2–5.8 (m, 2H, CH=CH), and 7.05–7.55 (m, 15H, trityl) ppm; *Anal.* calcd. for $C_{53}H_{80}O_6Si$: C 75.67, H 9.59; found: C 75.60, H 9.85.

E-Olefin 39

A solution of *Z*-olefin **38** (3.1 g, 3.7 mmol) in 80 mL cyclohexane was treated with *m*-chloroperbenzoic acid (0.95 g, approximately 85% peroxyacid, 4.7 ± 0.3 mmol) for 30 min at 5°C and 90 min at ambient temperature. More peroxyacid (0.30 g, 1.4 ± 0.1 mmol) was added. After one hour, hexane (70 mL) was added and the solution was washed successively with 5% aqueous Na_2SO_3 (2 × 50 mL), saturated $NaHCO_3$, and water. Drying ($MgSO_4$) and evaporation of the solvent *in vacuo* left a crude material which appeared on tlc (15% EtOAc/hexane) as three very close spots. The two major components presumed to be the two possible *erythro* epoxides were separated from the minor (least polar) one by repeated flash chromatography, each time using successively 5 and 10% EtOAc/hexane. A total yield of 3.0 g (95%) of *erythro* epoxides was obtained; ^{1}Hmr (CCl_4) δ: −0.07 and 0.02, −0.05 and 0.02 (two pairs of s, 6H, $Si(CH_3)_2$), 0.6–2.3 (m's, 48H), 2.5–3.5 (m's, 8H, with a singlet at 3.33 for dioxane CH_2's), 3.7–4.2 (m, 3H), and 7.02–7.55 (m, 15H, trityl) ppm.

A 0.45*M* solution of lithium diphenylphosphide (28) was prepared by treating chlorodiphenylphosphine (0.18 mL, 1.0 mmol) in 20 mL dry tetrahydrofuran with excess lithium (28 mg) for 3 h at room temperature, under an argon atmosphere; 8.3 mL of this solution (3.7 mmol) was added with a syringe to a solution of the epoxides (3.0 g, 3.5 mmol) in 20 mL dry THF under argon. After 25 min at 20°C, methyl iodide (0.5 mL, 8.1 mmol) was added and stirring was continued for 90 min. The mixture was then poured in 100 mL saturated $NaHCO_3$ and the separated aqueous phase was extracted with hexane (4 × 50 mL). The combined organic phases were washed with water (3 × 50 mL), dried over $MgSO_4$, and concentrated *in vacuo*. Purification by chromatography (4% EtOAc/hexane) afforded 2.5 g (85%) of pure olefin **39** (81% from **38**); $[\alpha]_D^{22}$ −6.7° (*c* 5.5, $CHCl_3$); ir (film) ν_{max}: identical with that of *Z*-olefin **37** plus a 970 cm^{-1} absorption for *trans* olefin; ^{1}Hmr (CCl_4) δ: −0.11, 0.01 (2s, 6H, $Si(CH_3)_2$), 0.6–2.3 (m's, 48H), 3.0–3.25 (m, 2H), 3.33 (s, 4H, dioxane ring CH_2's), 3.83 (m, 3H), 5.25–5.50 (m, 2H, —CH=CH—), and 7.05–7.55 (m, 15H, trityl) ppm.

Alcohol 40

Tetra-*n*-butylammonium fluoride trihydrate (1.8 g, 5.7 mmol) was azeotroped with benzene, the benzene evaporated, and dry THF (40 mL) was added. A solution of the silyl ether **39** (2.5 g, 3.0 mmol) in dry THF (20 mL) was then introduced and the mixture was refluxed until the reaction appeared complete on tlc (14% EtOAc/hexane, 2 to 3 h), the reaction being carried out under argon. Hexane (50 mL) was added, the solution was washed with water (2 × 50 mL), dried ($MgSO_4$), and concentrated *in vacuo*. Chromatography of the residue (14% EtOAc/hexane) gave 1.9 g of alcohol **40** (88%); $[\alpha]_D^{22}$ −6° (*c* 13, CCl_4); ir (film) ν_{max}: 3300–3600 (hydroxyl) cm^{-1}; ^{1}Hmr (CCl_4) δ: 0.90 (apparent s, 9H, dioxane $C(CH_3)_2$ and CH_2CH_3), 1.05–2.40

Can. J. Chem. Downloaded from www.nrcresearchpress.com by 210.87.254.42 on 09/05/12
For personal use only.

(m, 30H), 2.4–2.7 (bs, 1H, OH), 3.1–4.1 (m's, 9H, dioxane CH_2's singlet at 3.33), 5.30–5.55 (m, 2H, CH=CH), and 7.1–7.55 (m, 15H, trityl) ppm.

Ketone 41

Alcohol **40** (1.9 g, 2.6 mmol) was dissolved in 10 mL of a 3:2 mixture of dry dimethyl sulfoxide and acetic anhydride. The solution was stirred at room temperature under argon for 18 h. Water (50 mL) was added and the mixture was extracted with hexane (6 × 50 mL). The combined hexane solutions were washed with water (2 × 50 mL), dried over $MgSO_4$, and stripped of solvent *in vacuo* at rt. The residue was chromatographed by the successive elution of a 55 mm column with 5% and 10% EtOAc/hexane (1000 mL each) which yielded 1.65 g of pure ketone **41** (87%); $[\alpha]_D^{22}$ +8° (*c* 9.5, CCl_4); ir (film) ν_{max}: 1737 (ketone) cm^{-1}; ^{1}Hmr (CCl_4) δ: 0.7–2.4 (m's, 39H), 3.33 (s, 4H, dioxane CH_2's), 3.70–3.90 (m, 2H), 4.00 (m, 2H), 5.25–5.50 (m, 2H, CH=CH), and 7.0–7.55 (m, 15H, trityl) ppm.

Cyanoamines 42 and 43

Ketone **41** (1.60 g, 2.21 mmol) was dissolved in 80 mL methanol previously saturated with ammonia. Sodium cyanide (350 mg, 7.1 mmol) and ammonium chloride (350 mg, 6.5 mmol) were added and the mixture was stirred at 20–25°C for 8 days with daily bubbling in of ammonia to ensure saturation. As shown by tlc (20% EtOAc/hexane), the ketone was rapidly converted into two more polar compounds, identical in R_f's with the products obtained by treating **41** with sodium cyanide and sodium bisulfite in methanol, and therefore probably the cyanohydrins. In the following days, the cyanohydrins were slowly replaced by the even more polar cyanoamines. The solvent was removed *in vacuo* and replaced with hexane (100 mL). This solution was washed with water, dried ($MgSO_4$), and concentrated to a yellow oil. Repeated flash chromatography on a 55 mm column (15% EtOAc/hexane) allowed the isolation of cyanoamines **42** (more polar) and **43** (less polar) in respective yields of 0.51 g (31%) and 0.66 g (40%); cyanoamine **42**: $[\alpha]_D^{22}$ −4° (*c* 6, $CHCl_3$); ir (film) ν_{max}: 3320 and 3390 (R—NH_2), 973 (*trans* olefin) cm^{-1}, nitrile absorption too small to be observed; ^{1}Hmr (CCl_4) δ: 0.7–2.4 (m's, 41H), 3.07 (bs, 2H), 3.20–3.75 (m, 6H, dioxane CH_2's singlet at 3.33), 3.80–4.25 (m, 2H), 5.10–5.40 (m, 2H, CH=CH), and 7.05–7.55 (m, 15H, trityl) ppm; *Anal.* calcd. for $C_{48}H_{66}N_2O_5$: C 76.76, H 8.86, N 3.73; found: C 76.61, H 9.04, N 3.58; cyanoamine **43**: $[\alpha]_D^{22}$ −26° (*c* 8.0, $CHCl_3$); ir (film) ν_{max}: 3330 and 3400 (R—NH_2), 975 (*trans* olefin) cm^{-1}, nitrile absorption too small to be observed; ^{1}Hmr (CCl_4) δ: essentially identical to that of **41**, apparent broad singlet at 3.07 ppm replaced by a multiplet: 2.85–3.20 (2H) ppm; *Anal.* calcd. for $C_{48}H_{66}N_2O_5$: C 76.76, H 8.86, N 3.73; found: C 76.90, H 8.97, N 3.55.

Lactone 44

To a solution of cyanoamine **42** (430 mg, 0.57 mmol) in 2.0 mL methanol was added 8.0 mL of 3% water in methanol previously saturated with HCl gas. The mixture was kept in a water bath at 45°C for 3 h. The solvent was then removed *in vacuo* and replaced by 30 mL chloroform. This solution was washed several times with saturated K_2CO_3, then with water (until neutrality), dried over $MgSO_4$, and concentrated *in vacuo*. Chromatography (flash, on a 10 mm column, 11% methanol in chloroform) followed by recrystallization from diethyl ether/hexane gave 125 mg (56%) of crystalline **44**. An analytical sample was obtained by further recrystallization from the same solvents until a constant melting point of 79.5–80.0°C (corrected) was recorded; $[\alpha]_D^{22}$ −24° (*c* 3.0, methanol) and −38° (*c* 0.55, 0.037 *N* HCl in methanol); ir (CH_2Cl_2) ν_{max}: 3100–3650 with maxima at 3310, 3390, and 3605 (R—NH_2 and R—OH), 1774 (γ-lactone), 1709 (ketone) and 970 (*trans* olefin) cm^{-1}; ^{1}Hmr, 200 MHz, ($CDCl_3$) δ: 0.86 (t, 3H, J = 7 Hz, C-20), 1.00–1.42 (m's, 12H), 1.54 (p, 4H, J = 7 Hz, C-12,16), 2.00 (q, 2H, J = 6.5 Hz, C-8), 2.38 (t, 4H, J = 7 Hz, C-13,15), 2.56 (t, 2H, J = 6.5 Hz, C-5), 3.62, 3.67, 3.74, 3.79 (ABq, 2H, J = 11 Hz, CH_2OH), 4.11 (d, 1H, J = 3.5 Hz, C-3), 4.46 (t of d, 1H, J = 3.5, 6.5 Hz, C-4), and 5.52 (m, 2H, $J_{6,7}$ = 16 Hz, $J_{5,6}$ = $J_{7,8}$ = 6.5 Hz, δ_6 = 5.43, δ_7 = 5.61) ppm, exchangeable protons not included; ^{13}C nmr ($CDCl_3$): the olefinic carbons C-6 and C-7 appear at 123.72 and 134.78 ppm respectively, with no detectable amount of the carbons from the corresponding *cis*-olefin which would normally appear at slightly higher field (34); ms (EI, 70 eV, 22–130°C) *m/e*: 383 (M^+, 0.5), 256 (60), 200 (12), 113 (17), 104 (35), and 102 (100); all spectra were superimposable with that of anhydromyriocin, prepared as described by Bagli *et al.* (3) from natural myriocin.

Lactone 45

Cyanoamine **43** (450 mg, 0.60 mmol) was treated as described above with wet methanolic HCl for 3 h at 45°C. After work-up, the crude product was purified by chromatography (10 mm column, 5% MeOH/$CHCl_3$) and recrystallized from Et_2O/hexane to give 140 mg (60%) of pure **45**, melting at 76.0–76.5°C (corrected); $[\alpha]_D^{22}$ −54° (*c* 2.7, methanol); ir (CH_2Cl_2) ν_{max}: 3200–3650 with maxima at 3310, 3380, and 3590 (R—NH_2 and R—OH), 1772 (γ-lactone), 1709 (ketone) and 970 (*trans* olefin) cm^{-1}; ^{1}Hmr, 200 MHz, ($CDCl_3$) δ: 0.86 (t, 3H, J = 7 Hz, C-20), 1.00–1.44 (m's, 12H), 1.54 (p, 4H, J = 7 Hz, C-12, 16), 2.00 (q, 2H, J = 6.5 Hz, C-8), 2.38 (t, 4H, J = 7 Hz, C-13,15), 2.54 (m, 2H, C-5), 3.78, 3.83, 3.94, 3.99 (ABq, 2H, J = 11 Hz, CH_2OH), 4.11 (d, 1H, J = 3.5 Hz, C-3), 4.70 (t of d, 1H, J = 3.5, 6.5 Hz, C-4), and 5.52 (m, 2H, $J_{6,7}$ = 16 Hz, $J_{5,6}$ = $J_{7,8}$ = 6.5 Hz, δ_6 = 5.41, δ_7 = 5.62 ppm) ppm, exchangeable protons not included; ms (EI, 70 eV, 23–135°C) *m/e*: 383 (M^+, 0.2), 256 (13), 200 (2), 113 (17), 104 (48), and 102 (100).

Acknowledgements

We are grateful to the Natural Sciences and Engineering Research Council of Canada for financial support. We also thank Mr. A. Ugolini, Dr. W. Dawson, Dr. J. Everett, and Ms. L. Ayotte for ^{13}C and 200 MHz ^{1}Hmr spectra; Dr. O. A. Mamer, Dr. V. Taguchi, and Ms. J. Montgomery for the mass spectra; and Dr. N. Elmore, Imperial Chemical Industries, Macclesfield, for making available the biological testing results. The gift of an authentic sample of myriocin from Dr. J. Bagli, Ayerst Laboratories, Montreal, Canada, is gratefully acknowledged.

1. D. Kluepfel, J. F. Bagli, H. Baker, M.-P. Charest, A. Kudelski, S. N. Sehgal, and C. Vézina. J. Antibiot. **25**, 109 (1972).
2. (*a*) R. Craveri, P. L. Manachini, and F. Aragazzini. Experientia, **28**, 867 (1972); (*b*) R. Craveri, P. L. Manachini, and F. Aragazzini. U.S. Patent No. 3,758,529 (1973).
3. J. F. Bagli, D. Kluepfel, and M. St-Jacques. J. Org. Chem. **38**, 1253 (1973).
4. (*a*) F. Aragazzini, P. L. Manachini, R. Craveri, B. Rindone, and C. Scolastico. Experientia, **28**, 881 (1972); (*b*) Tetrahedron, **28**, 5493 (1972).
5. C. H. Kuo and N. L. Wendler. Tetrahedron Lett. 211 (1978), and references therein.
6. J. G. Buchanan, A. R. Edger, M. J. Power, and P. D. Theaker. Carbohydr. Res. **38**, C22 (1974).

7. G. JUST and D. R. PAYETTE. Tetrahedron Lett. 3219 (1980).
8. H. G. FLETCHER, JR. and H. W. DIEHL. J. Org. Chem. **30**, 2321 (1965).
9. E. J. COREY and A. VENKATESWARLU. J. Am. Chem. Soc. **94**, 6190 (1972).
10. J. F. W. MCOMIE. Protective groups in organic chemistry. Plenum Press, New York. 1973. p. 334.
11. R. K. CROSSLAND and K. L. SERVIS. J. Org. Chem. **35**, 3195 (1970).
12. M. B. GRAVESTOCK, W. S. JOHNSON, B. E. MCCARRY, R. J. PARRY, and B. E. RATCLIFFE. J. Am. Chem. Soc. **100**, 4274 (1978).
13. T. SATCH, K. NANBA, and S. SUZUKI. Chem. Pharm. Bull. **19**, 817 (1971).
14. P. A. BARTLETT and W. S. JOHNSON. Tetrahedron Lett. 4459 (1970).
15. (*a*) J. CASON and D. M. WALBA. J. Org. Chem. **37**, 669 (1972); (*b*) E. C. TAYLOR, Y. MAKI, and A. MCKILLOP. J. Org. Chem. **34**, 1172 (1969).
16. G. W. KABALKA, D. T. C. YANG, and J. D. BAKER, JR. J. Org. Chem. **41**, 574 (1976).
17. R. O. HUTCHINS, M. KACHER, and L. RUA. J. Org. Chem. **40**, 923 (1975).
18. R. H. WOLLENBERG and S. J. MILLER. Tetrahedron Lett. 3219 (1978).
19. J. E. MCMURRY, J. MELTON, and H. PADGETT. J. Org. Chem. **39**, 259 (1974).
20. S. HANESSIAN, M. M. PONPIPOM, and B. LAVALLÉE. Carbohydr. Res. **24**, 45 (1978).
21. P. BECK. Organic phosphorus compounds. Vol. 2. Wiley-Interscience, New York. 1972. p. 191.
22. E. J. COREY and J. W. SUGGS. Tetrahedron Lett. 2647 (1975).
23. H. O. HOUSE. Modern synthetic reactions. W. A. Benjamin Inc., Don Mills, Ont. 1972.
24. M. SCHLOSSER and K. F. CHRISTMANN. Angew. Chem. Int. Ed. Engl. **5**, 126 (1966).
25. W. S. JOHNSON and G. E. DUBOIS. J. Am. Chem. Soc. **98**, 1038 (1976); A. CORVERS, J. H. VAN MIL, M. M. E. SAP, and H. M. BUCK. Recl. Trav. Chim. Pays-Bas, **96**, 18 (1977); A. CORVERS, P. C. H. SCHEERS, J. W. DE HAANN, and H. M. BUCK. Recl. Trav. Chim. Pays-Bas, **96**, 279 (1977); R. J. ANDERSON and C. A. HENRICK. J. Am. Chem. Soc. **97**, 4327 (1975).
26. R. RIEMSCHNEIDER and G.-A. HOYER. Monatsh. Chem. **99**, 642 (1968).
27. M. AL NEIRABEYEH, J.-C. ZIEGLER, B. GROSS, and P. CAUBÈRE. Synthesis, 811 (1976).
28. E. VEDEJS and P. L. FUCHS. J. Am. Chem. Soc. **95**, 822 (1973).
29. W. W. EPSTEIN and F. W. SWEAT. Chem. Rev. **67**, 247 (1967).
30. (*a*) T. MORITA, Y. OKAMOTO, and H. SAKURAI. Chem. Commun. 874 (1978); G. A. OLAH, S. C. NARANG, B. C. BALARAM GUPTA, and R. MALHOTRA. J. Org. Chem. **44**, 1246 (1979); (*b*) J. N. BEMILLER, R. E. WING, and C. Y. MEYERS. J. Org. Chem. **33**, 4292 (1968).
31. M. ZINNER, G. REMBARZ, and H.-P. KLÖCHING. Ber. **90**, 2688 (1957).
32. W. K. ANDERSON and T. VEYSOGLU. J. Org. Chem. **38**, 2267 (1973).
33. W. CLARK STILL, M. KAHN, and A. MITRA. J. Org. Chem. **43**, 2923 (1978).
34. D. E. DORMAN, M. JAUTELAT, and J. D. ROBERTS. J. Org. Chem. **36**, 2757 (1971).

Can. J. Chem. Downloaded from www.nrcresearchpress.com by 210.87.254.42 on 09/05/12
For personal use only.

Synthesis of colchifoline from deacetylcolchiceine

MARIA A. IORIO AND MARISA MOLINARI

Laboratory of Pharmaceutical Chemistry, Istituto Superiore di Sanità, 00161 Rome Italy

AND

ARNOLD BROSSI

Medicinal Chemistry Section, Laboratory of Chemistry, NIAMDD, National Institutes of Health, Bethesda, MD 20205, U.S.A.

Received June 23, 1980

This paper is dedicated to Prof. Raymond U. Lemieux on the occasion of his 60th birthday

MARIA A. IORIO, MARISA MOLINARI, and ARNOLD BROSSI. Can. J. Chem. **59**, 283 (1981).

Treatment of a mixture of deacetylcolchicine and deacetylisocolchicine, obtained by diazomethane methylation of deacetylcolchiceine, with trifluoroacetylglycolyl chloride in pyridine, afforded directly colchifoline and isocolchifoline. The two ether isomers could be separated by chromatography and the material eluted first proved to be identical with colchifoline isolated from commercial samples of colchicine.

MARIA A. IORIO, MARISA MOLINARI et ARNOLD BROSSI. Can. J. Chem. **59**, 283 (1981).

Un mélange de déacétylcolchicine et de déacétylisocolchicine, obtenu par la méthylation de la déacétylcolchicéine par le diazométhane, réagit avec le chlorure de trifluoroacétylglycolyle dans la pyridine et conduit directement à la colchifoline et à l'isocolchifoline. On peut séparer les deux éthers isomères par chromatographie. Le premier produit élué est identique à la colchifoline que l'on a isolé à partir d'un échantillon commercial de colchicine.

[Traduit par le journal]

Colchifoline (**5**) is a novel congener of colchicine (**3**), recently detected and isolated from commercial samples of colchicine (1). It is chemically the *O*-methyl ether of 2-demethylcolchifoline (**7**), an alkaloid isolated by Šantavý and co-workers (2) from the leaves of *Colchicum autumnale L.* The finding of hydroxyacetylated alkaloids besides colchicine and *N*-formyl congeners is interesting, and suggests that these alkaloids are possibly related to each other through a biooxidative degradation of the *N*-acetyl group of colchicine.

We now would like to report a synthesis of colchifoline (**5**) from deacetylcolchiceine (**8**), readily available from colchicine (**3**) (3).

A mixture of **1** and **2** was obtained from deacetylcolchiceine (**8**) by the procedure of Raffauf *et al.* (4). This mixture, when treated with trifluoroacetylglycolyl chloride in pyridine, afforded, judged by tlc, a mixture of the two hydroxyacetylated derivatives **5** and **6**. Trifluoroacetylglycolyl chloride, a novel hydroxyacetylating agent, was prepared from glycolic acid by treatment with trifluoroacetic anhydride and treatment of the acid with refluxing thionyl chloride in the form of a colorless liquid (see Experimental). The reaction mixture obtained after usual work-up was separated by chromatography over silica gel. The first eluted material was identical with colchifoline (**5**), a minor contaminant of commercial colchicine (1). The second compound, obtained in at least equal amounts, was assigned the structure of isocolchifoline (**6**). The two ethers **5** and **6** are converted by refluxing 0.1 *N* HCl into colchifoleine (**9**), illustrated with the same arrangements of the oxygen functionalities in ring C as in colchiceine (**10**) (5).

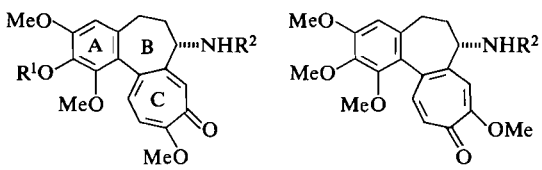

1 R^1 = Me, R^2 = H **2**
3 R^1 = Me, R^2 = COMe **4**
5 R^1 = Me, R^2 = $COCH_2OH$ **6**
7 R^1 = H, R^2 = $COCH_2OH$

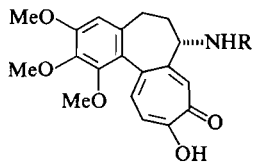

8 R = H
9 R = $COCH_2OH$
10 R = COMe

Structure Assignments

The colchicine-like nature of ring C in colchifoline (**5**) and the *iso* structure of isocolchifoline (**6**) were evident from a comparison of their ^1H nmr spectra (aromatic protons) with those of reference substances (**3**, **4**) reported recently (6–8). Mass spectra of colchifoline (**5**) and isocolchifoline (**6**) showed the same fragmentation pattern with the

0008-4042/81/020283-02$01.00/0

©1981 National Research Council of Canada/Conseil national de recherches du Canada

Can. J. Chem. Downloaded from www.nrcresearchpress.com by 210.87.254.5 on 09/05/12
For personal use only.

TABLE 1. ^{1}H nuclear magnetic resonance spectral data[a]

Compound	H—C-4	H—C-8	H—C-11	H—C-12
Colchifoline (**5**)	6.56 s	7.78 s	6.95 d (*J* 11)	7.44 d (*J* 11)
Colchicine (**3**)[b]	6.57 s	7.67 s	6.93 d (*J* 11)	7.40 d (*J* 11)
Isocolchifoline (**6**)	6.62 s	7.22 s	7.23 d (*J* 13)	7.57 d (*J* 13)
Isocolchicine (**4**)[b]	6.60 s	7.22 s	7.13 d (*J* 13)	7.47 d (*J* 13)
Colchifoleine (**9**)	6.60 s	7.60 s	7.35 d (*J* 12)	7.65 d (*J* 12)
Colchiceine (**10**)[b]	6.60 s	7.66 s	7.39 d (*J* 12)	7.65 d (*J* 12)

[a]Chemical shifts (δ) in $CDCl_3$ (TMS internal standard) at 100 MHz.
[b]References 6 and 7.

same base peak, *m/z* 312, but varied somewhat in peak intensity. In the mass spectrum of **6** the fragment ions corresponding to $(M - COCH_2OH)^+$, *m/z* 356 (13%); $(M - NH_2COCH_2OH)^{+\cdot}$, *m/z* 340 (35%); and $(M - (CO + COCH_2OH))^+$, *m/z* 328 (18%), are of much higher intensity than the same fragments in colchifoline (**5**) (1).

Experimental

Melting points (uncorrected) were determined in open glass capillaries on a Büchi-Tottoli apparatus. Microanalyses were performed by the Microanalytical Section (ISS) under the direction of Dr. A. Mazzeo-Farina. Optical rotations were measured with a Perkin-Elmer model 141. Fourier transform ^{1}H nmr spectra were recorded at 100 MHz with a Varian XL 100 spectrometer at 29°C and mass spectra with a LKB 2091 spectrometer (70 eV) equipped with a Digital PDP 11 data processing system, samples applied by direct inlet, and probe usually heated from 25 to 200°C. Thin-layer chromatography utilized silica gel plates (Stratocrom SI F254, C. Erba).

Trifluoroacetylglycolic Acid

To a stirred and ice-cooled suspension of glycolic acid (5 g, 66 mmol) in 100 mL dichloromethane a solution of trifluoroacetic anhydride (12 mL, 86 mmol) in 50 mL dichloromethane was added dropwise during 2 h. The homogeneous solution was then stirred at room temperature for two days, evaporated under vacuum, and distilled at 95–98°C (10 Torr) to afford 9.3 g (82%) of the title compound in the form of a colorless liquid: $n_D^{24} = 1.3690$; nmr ($CDCl_3$) δ: 4.93 (s, 2H, CH_2), 10.3 (s, 1H, OH). *Anal.* calcd. for $C_4H_3F_3O_4$ (172.07): C 27.92, H 1.76; found: C 27.68, H 1.99.

Trifluoroacetylglycolyl Chloride

Trifluoroacetylglycolic acid (9 g, 52 mmol) was refluxed for 6 h in 10 mL of thionyl chloride. After this period excess thionyl chloride was removed under vacuum at room temperature and the residue distilled to afford 7.8 g (78%) of the acid chloride: bp 30–32°C (10 Torr); $d^{18} = 1.505$; nmr ($CDCl_3$) δ: 5.18 (s, CH_2). *Anal.* calcd. for $C_4H_2ClF_3O_3$ (190.51): C 25.22, H 1.06; found: C 24.94, H 1.14.

Colchifoline (5) and Isocolchifoline (6) from a Mixture of 1 and 2

To a crude mixture of **1** and **2**, prepared from 2 g of **8**, dissolved in 30 mL dichloromethane and 1.50 mL of pyridine, and cooled in an ice-bath, was carefully added dropwise, under stirring and under anhydrous conditions, 1.2 mL (9.5 mmol) of trifluoroacetylglycolyl chloride. After each drop a red color developed but disappeared quickly on stirring. After standing overnight the solution contained two new major products by tlc (SiO_2 F254, $CHCl_3$–MeOH–NH_4OH 90:9:1) with R_f 0.49 and 0.31 and identical with the isolated products **5** and **6**. The solution was washed twice with water (2 × 3 mL) before drying (Na_2SO_4). The reaction products obtained after evaporation were dissolved in chloroform and chromatographed on a column (2.5 × 80 cm) of silica gel-60 (0.04–0.06 mm) packed in $CHCl_3$, and eluted with $CHCl_3$ containing 5% MeOH and 0.5% NH_4OH. The first compound isolated was colchifoline **5** (500 mg), which crystallized from ethyl acetate. This compound retains solvent firmly and loses it after prolonged heating at 100°C (0.5 Torr). The melting point rises to 151–152°C; $[\alpha]_D^{22}$ −149° (*c* 0.94, $CHCl_3$). *Anal.* calcd. for $C_{22}H_{25}NO_7$ (415.44): C 63.60, H 6.07, N 3.37; found: C 63.47, H 5.91, N 3.17.

This compound was identical with a sample isolated from commercial colchicine (1) by tlc, mixture mp, and spectral data. The second component (660 mg) was isocolchifoline (**6**) which was crystallized from ethyl acetate – dichloromethane: mp 220–221°C; $[\alpha]_D^{22}$ −297° (*c* 1, $CHCl_3$). *Anal.* calcd. for $C_{22}H_{25}NO_7$ (415.44): C 63.60, H 6.07, N 3.37; found: C 63.40, H 6.12, N 3.33.

Colchifoleine (9)

This enol was obtained by refluxing **5** or **6** during 1 h (100 mg) in 0.1 *N* HCl (6 mL). The crystalline precipitate was filtered, washed with cold water, and crystallized from H_2O–MeOH: mp 227–228°C, $[\alpha]_D^{22}$ −254° (*c* 0.65, $CHCl_3$). *Anal.* calcd. for $C_{21}H_{23}NO_7$ (401.41): C 62.83, H 5.78, N 3.49; found: C 62.52, H 5.86, N 3.60.

1. M. A. IORIO, A. MAZZEO-FARINA, G. CAVINA, L. BONIFORTI, and A. BROSSI. Heterocycles, **14**, 625 (1980).
2. P. SEDMERA, H. POTESILOVÁ, V. MALICHOVÁ, V. PREININGER, and F. ŠANTAVÝ. Heterocycles, **12**, 337 (1979).
3. H. FERNHOLZ. Angew. Chem. **65**, 319 (1953).
4. R. F. RAFFAUF, A. L. FARREN, and G. E. ULLYOT. J. Am. Chem. Soc. **75**, 5292 (1953).
5. J. V. SILVERTON. Acta Crystallogr. Sect. B, **35**, 2800 (1979).
6. M. A. IORIO, A. BROSSI, and J. V. SILVERTON. Helv. Chim. Acta, **61**, 1213 (1978).
7. H. G. CAPRARO and A. BROSSI. Helv. Chim. Acta, **62**, 965 (1979).
8. C. D. HUFFORD, H. G. CAPRARO, and A. BROSSI. Helv. Chim. Acta, **63**, 50 (1980).

Can. J. Chem. Downloaded from www.nrcresearchpress.com by 210.87.254.5 on 09/05/12
For personal use only.

The leaf oil terpene composition of incense cedar and coast redwood[1,2]

E. VON RUDLOFF

Prairie Regional Laboratory, National Research Council of Canada, Saskatoon, Sask., Canada S7N 0W9

Received June 17, 1980

This paper is dedicated to Prof. Raymond U. Lemieux on the occasion of his 60th birthday

E. VON RUDLOFF. Can. J. Chem. **59**, 285 (1981).

Analysis by an on-line computerized gas chromatographic – mass spectral method of the volatile leaf oils of the North American incense cedar and coast redwood revealed unusual percentage compositions of the major terpenes and presence of unique minor components. The chemosystematic implications are discussed briefly.

E. VON RUDLOFF. Can. J. Chem. **59**, 285 (1981).

L'analyse, par chromatographie en phase gazeuse couplée à une spectromètre de masse relié à un ordinateur, des huiles volatiles des feuilles du cèdre aromatique nord américain et du séquoia de mer révèle la présence de pourcentages inhabituels des principaux terpènes ainsi que la présence de constituants secondaires uniques. On discute brièvement des implications chimiosystématiques.
[Traduit par le journal]

Introduction

Recently, we reported on a gas chromatographic (gc) – mass spectrographic method for the identification of known terpenes in complex essential oils, such as the volatile conifer leaf oils (1). On-line computerized comparisons of mass spectra (ms) and relative retention times (rrt) facilitate quick and reliable assignment of peak identities even with the many terpenes that have similar ms. Of course the problem with unknown components, for which no reference spectra are available, remains. However, this is not a major drawback in chemosystematic studies because similarity or dissimilarity of unknowns with the same rrt in different or related species, varieties, hybrids, etc. can be established quite readily. We have improved this method by use of high efficiency glass capillary columns and although not all separation problems were solved, most components of several complex juniper leaf oils could be identified (2–4). The present communication deals with a similar analysis of the volatile leaf oils of incense cedar, *Calocedrus decurrens* (Torr.) Florin (syn. *Libocedrus decurrens* Torr.; fam. *Cupressaceae*) and for comparison also coast redwood, *Sequoia sempervirens* (D. Don) Endl. (fam. *Taxodiaceae*). Both sets of leaf samples were collected in the dormant season in northern California. The oil of incense cedar does not appear to have been analyzed by modern methods, whereas that of coast redwood was analyzed by gc and infrared (ir) spectroscopy by Levinson and co-workers in 1968 (5). Hilal *et al.* (6) reported on some bactericidal properties of redwood leaf oil components and the terpenoids of the pocket resin were investigated by Anderson and co-workers (7).

Results and Discussion

The mean relative percentage composition from 5 trees each of incense cedar and coast redwood is shown in Table 1. The terpene pattern of incense cedar is unusual among North American conifers, having relatively large amounts of limonene, car-3-ene, α-pinene, myrcene, and α-terpinyl acetate and low amounts of β-pinene, β-phellandrene, and the camphene group of terpenes (8). The presence of small amounts of 3-methylenebicyclo[3.2.1.]oct-2-ene, two possible isomers (rrt 0.252 and 0.394), and at least some of the 11 unknown minor components in the oxygenated monoterpene range is unique. The paucity of sesquiterpenes (no sesquiterpene hydrocarbon that may be correlated with Schorger's "libocedrene" (9) was found), but the presence of cedrol, as well as the absence of allyl phenyl ethers are also noteworthy. Trace components that could be identified were: tetrahydrofuran, oct-1-en-3-ol, *cis*- and *trans*-sabinene hydrate, borneol, *trans*-carveol, and methyl thymol. The quantitative variation from one tree to another was relatively small (8), although car-3-ene varied from 10 to 30%.

The major components of the leaf oil of coast redwood from northern California (α-pinene, limonene, β-phellandrene, γ-terpinene, myrcene, terpinolene, terpinen-4-ol, and eudesmol isomers) are the same as those reported by Levinson and co-workers (5). However, we found more sabinene than β-pinene, less α-terpineol and its acetate, and only traces of citronellol and geraniol. These dif-

[1]Gas–liquid chromatography of terpenes. Part XXI. For part XX, see ref. 17.

[2]NRCC No. 18647.

0008-4042/81/020285-03$01.00/0

©1981 National Research Council of Canada/Conseil national de recherches du Canada

Can. J. Chem. Downloaded from www.nrcresearchpress.com by 210.87.254.42 on 09/05/12
For personal use only.

TABLE 1. The major (2% and more) and minor (0.2–2%) components of the volatile leaf oils of incense cedar (IC) and coast redwood (CR) from northern California

Compound	Relative retention time[a]	IC %[b]	CR %[b]	Compound	Relative retention time[a]	IC %[b]	CR %[b]
Hex-2-en-1-al	0.186	1.5	0.1	Unknown (MW150)	0.870	0.7	—
3-Methylene-bicyclo-[3.2.1]oct-2-ene	0.240	0.5	—	Piperitol	0.872	—	0.2
Unknown (MW120)	0.252	1.1	—	Unknown (MW152)	0.876	0.4	—
Tricyclene	0.316	0.2	0.1	Unknown (MW180)	0.886	0.8	—
α-Thujene	0.327	0.2	0.6	(Carvone)	0.906	0.7[c]	—
α-Pinene	0.338	9.2	24.9	Unknown (MW152)	0.912	0.3[c]	—
α-Fenchene	0.358	0.6	—	Unknown (MW182)	0.916	0.4[c]	—
Camphene	0.360	0.2	0.2	Piperitone	0.922	0.3	0.2
Unknown (MW120)	0.394	0.2	—	Unknown (MW182)	0.970	0.3	—
Sabinene	0.406	0.4	6.0	Bornyl acetate	1.000	0.5	0.4
β-Pinene	0.411	0.5	1.8	Unknown	1.012	0.9	—
Myrcene	0.446	8.0	4.7	(Verbenone)	1.027	0.9[c]	—
α-Phellandrene	0.465	Trace	0.4	Piperityl acetate	1.080	1.0	—
Car-3-ene	0.483	21.0	0.3	α-Terpinyl acetate	1.117	5.7	0.8
α-Terpenene	0.493	0.3	1.4	α-Copaene	1.182	—	0.5
p-Cymene	0.502	0.2	1.2	β-Elemene	1.202	0.2	0.3
β-Phellandrene	0.512	0.3	9.9	β-Caryophyllene	1.248	—	1.2
Limonene	0.159	31.3	8.6	Humulene	1.304	—	0.3
trans-Ocimene	0.561	Trace	0.3	Germacrene-D	1.347	0.2	5.5
γ-Terpinene	0.578	0.8	6.2	α-Muurolene	1.378	—	0.3
Fenchone	0.609	0.5	—	α-Cadinene + γ-Muurolene	1.413	—	1.6
Unknown	0.632	0.3[c]	—	Elemol	1.455	Trace	1.1
Terpinolene	0.634	3.9	2.6	Elemol isomer	1.455	0.2	6.3
Unknown (MW150)	0.642	0.3	—	C_{15} alcohol (MW222)	1.494	0.2	—
Linalool	0.667	0.3	0.1	Cedrol	1.530	0.8	0.1
Unknown (MW152)	0.709	0.3	—	γ-Eudesmol	1.582	0.1	1.8
Unknown (MW152)	0.713	0.2[c]	—	β-Eudesmol	1.602	Trace	0.9
Unknown (MW152)	0.716	0.4[c]	—	α-Eudesmol + Cadinol isomer	1.612	Trace	2.5
Terpinen-4-ol	0.801	1.4	5.6				
α-Terpineol	0.832	0.7	0.8				
p-Cymenol	0.839	0.4	0.1				

[a]Relative retention time for bornyl acetate = 1.000.
[b]Relative percentages as obtained by integration and summation of peak areas.
[c]Impure.

ferences may be the result of variation from one population to another. In addition to the compounds listed in the table, we also identified trace amounts of isopentenyl isovalerate (an unusual hemiterpenoid ester found in yellow cedar, *Chamaecyparis nootkatensis* (D. Don) Spach (10) and Sitka Spruce, *Picea sitchensis* (Bong.) Carr. (11) leaf oils), hex-3-en-1-ol, tetrahydrofuran, oct-1-en-3-ol, 2-nonanone, 2-undecanone, *cis*-ocimene, *cis*- and *trans*-sabinene hydrate, camphene hydrate, borneol, neryl and geranyl acetate (but no citronellyl acetate), α-cubebene, β-bourbonene (like some of the cadinene–muurolene isomers a possible rearrangement product of germacrene-D (12)), thujopsene, β-selinene, β-cubebene, as well as several elemene, germacrene, cadinene and muurolene isomers, calamenene, 4:10-dimethyl-7-isopropylbicyclo[4.4.0]deca-1:4-diene (13), three cadinol isomers, torreyol, and possibly bisabolol. The elemol isomer with rrt 1.466 is not hedycaryol, the potential precursor of elemol and eudesmol isomers (14, 15), nor did its ms correspond to that of δ-elemol. At least 8 trace components in the monoterpene range and 15 in the sesquiterpene range remain to be identified. The great diversity of sesquiterpenes contrasts strongly with their paucity in incense cedar leaf oil and is, together with the relatively large amounts of the terpinene isomers, terpinen-4-ol, germacrene-D, and the elemol and eudesmol isomers, of chemosystematic value (8). Also, it is unusual in conifer leaf oils to find α-pinene as the main component, the only other North American species with this trait being the common juniper, *Juniperus communis* L. and yellow cedar (some trees only) (8).

Although not all of the leaf oil components of incense cedar and coast redwood could be identified, much data that are of chemosystematic value were readily obtained by the improved gc–ms

Can. J. Chem. Downloaded from www.nrcresearchpress.com by 210.87.254.42 on 09/05/12
For personal use only.

Can. J. Chem. Downloaded from www.nrcresearchpress.com by 210.87.254.42 on 09/05/12
For personal use only.

method. Presence or absence of compounds of interest (even those with unknown ms) can be established without having to resort to more time-consuming separation techniques that require larger amounts of oil. By using the total ion count for each gc peak, relative percentages can be obtained simultaneously. These percentages correspond fairly well with those obtained with a thermal conductivity detector.

Incense cedar and coast redwood are monotypic species of the order *Cupressales* and their leaf oil patterns reflect their separate taxonomic classification. Whereas there is some similarity of the monoterpene hydrocarbon patterns with that of yellow cedar, the oxygenated monoterpenes and sesquiterpenes differ greatly (8, 10). Gough and Mills (16) have found unusual diterpenes in the wood of incense cedar.

Experimental

The leaves and twigs from 5 trees each of incense cedar near Gasquet and coast redwood east of Crescent City, northern California, were collected in the fall of 1977. These were transported and stored in the cold and dark. The leaves were separated from the twigs and steam-distilled for 6 h (4, 8, 17, 18). Whereas the recovery of volatile oil from coast redwood leaves was complete (0.4–0.7%, based on fresh weight), that of the incense cedar was incomplete and distillation was continued for a further 18 h (yield 0.6–0.9%). The relative percentages of the individual components were determined by analysis on four different packed gc columns (Apiezon-L, PEG 20M-OV 17, PEG 20M-QFI, and EGPN (17, 18); helium as carrier gas, TCD) (17–19). Aliquots (1 μL) of the leaf oils in ether (1:20 v/v) were analyzed by gc–ms on a deactivated 30 m SP 2100 glass capillary column (J + W Scientific) (1:30 split ratio, helium as carrier gas) on a Finnigan model 4000 quadropole gc – mass spectrometer (2), temperature-programming from 55°C (held for 6 min after injection) to 220°C (held for 15 min) at 3°/min. Mass spectral scans were taken every second. The recorded ms were compared by the computerized method (1) with those in our own file as well as the Finnigan Library of the National Bureau of Standards. Spectra of unknown compounds were also compared with those in the literature (e.g. ref. 13). The ms of peak 2 of incense cedar showed a "purity" of 900 (max. 1000) for 3-methylenebicyclo[3.2.1]oct-2-ene in the Finnigan NBS library, which represents a high degree of similarity. Mass spectrum of the elemol isomer: 121(100), 93(78), 41(71), 105(64), 67(61), 107(56), 91(52), 81(49), 79(44), 119(42) (just as with elemol, the parent ion peak mass 220 was not recorded); ms of sesquiterpene alcohol, rrt 1.530, *m/e*: 222(2), 95(100), 150(72), 43(63), 151(58), 41(51), 81(40), 93(35), 69(35), 107(33), 55(28). The ir and ^{1}Hmr spectra of the main components of incense cedar leaf oil were recorded for the fractions isolated in preparative gc (17–19).

Acknowledgements

The guidance during the early part of my career and continued inspiration and encouragement by Prof. R. U. Lemieux, as well as technical assistance by L. R. Hogge and M. Granat are gratefully acknowledged.

1. R. P. Adams, M. Granat, L. R. Hogge, and E. von Rudloff. J. Chromatogr. Sci. **17**, 75 (1979).
2. R. P. Adams, E. von Rudloff, and T. A. Zanoni. Biochem. Syst. Ecol. **8**, 35 (1980).
3. R. P. Adams, E. von Rudloff, T. A. Zanoni, and L. R. Hogge. J. Nat. Prod. (Lloydia), **42**, 417 (1980).
4. E. von Rudloff, L. Hogge, and M. Granat. Phytochemistry, **19**, 1701 (1980).
5. D. E. Gregonis, R. D. Portwood, W. H. Davidson, D. A. Durfee, and A. S. Levinson. Phytochemistry, **7**, 975 (1968).
6. S. M. Hilal, H. H. Zedan, M. Y. Haggag, and F. M. Soliman. Egypt. J. Pharm. Sci. **18**, 85 (1979).
7. R. Riffer, A. B. Anderson, and A. Wong. Phytochemistry, **8**, 923 (1969).
8. E. von Rudloff. Biochem. Syst. Ecol. **2**, 131 (1975).
9. A. W. Schorger. J. Ind. Eng. Chem. **8**, 22 (1916).
10. Y. S. Cheng and E. von Rudloff. Phytochemistry, **9**, 2517 (1970).
11. E. von Rudloff. Phytochemistry, **17**, 127 (1977).
12. K. Yoshihara, Y. Ohta, T. Sakai, and Y. Hirose. Tetrahedron Lett. 2263 (1969).
13. E. von Sydow, K. Anjou, and G. Karlsson. Arch. Mass Spectral Data, Vol. 1. SIK Rapport No. 279. Goteborg, Sweden. 1970.
14. R. V. H. Jones and M. D. Sutherland. Chem. Commun. 1229 (1968).
15. M. Kodama, Y. Matsuki, and S. Ito. Tetrahedron Lett. 1121 (1976).
16. L. J. Gough and J. S. Mills. Phytochemistry, **13**, 1612 (1974).
17. E. von Rudloff. Gas–liquid chromatography of terpenes. *In* Recent advances in chromatography. Vol. 10. *Edited by* J. C. Giddings and R. A. Keller. M. Dekker, Inc., New York. 1974. p. 173.
18. E. von Rudloff. Scope and limitations of gas–liquid chromatography of terpenes in chemosystematic studies. *In* Recent advances in phytochemistry. Vol. 2. *Edited by* M. K. Seikel and V. C. Runeckles. Appleton-Century-Crofts, New York. 1969. p. 128.
19. R. S. Hunt and E. Von Rudloff. Can. J. Bot. **52**, 477 (1974).

Applications of the ene reaction. Synthesis and properties of substituted α-methylene-γ-lactones[1,2]

ALFRED W. HANSON, ARCHIBALD W. MCCULLOCH, AND A. GAVIN MCINNES

Atlantic Research Laboratory, National Research Council of Canada, 1411 Oxford Street, Halifax, N.S., Canada B3H 3Z1

Received July 7, 1980

This paper is dedicated to Prof. Raymond U. Lemieux on the occasion of his 60th birthday

ALFRED W. HANSON, ARCHIBALD W. MCCULLOCH, and A. GAVIN MCINNES. Can. J. Chem. **59**, 288 (1981).

Substituted dimethyl 1,4-pentadiene-1,2-dicarboxylates (**1** or **3**) may be prepared by $AlCl_3$-promoted or thermal ene reaction of olefins with dimethyl acetylenedicarboxylate. Lactonization of these adducts is catalyzed by acid. In the presence of 80% H_2SO_4 the predominant product (ca. 80%) is a (*Z*)-dihydro-3-carbomethoxymethylene-2(3*H*)-furanone (**2** or **4**). Cyclization with anhydrous HCl affords a mixture of products, the composition of which depends on the starting material; major products include the corresponding (*E*)- and δ-lactone isomers (**6** and **7**). Detailed ^1H and ^{13}C nmr data are reported for all compounds. The structures of the (*E*)-4,5,5-trimethyl-, (*Z*)-4,5,5-trimethyl-, and (*Z*)-4,4,5,5-tetramethyl furanone derivatives (**6***a*, **2***a*, and **2***b*) have been established by X-ray crystallography. The properties of some of these lactones are discussed, as are possible methods of removal of the carbomethoxyl from **2**.

ALFRED W. HANSON, ARCHIBALD W. MCCULLOCH et A. GAVIN MCINNES. Can. J. Chem. **59**, 288 (1981).

Les pentadiène-1,4 dicarboxylates-1,2 de diméthyle substitués (**1** ou **3**) peuvent être préparés par une réaction ène favorisée par $AlCl_3$ ou par une réaction thermique des oléfines avec l'acétylènedicarboxylate de diméthyle. L'acide catalyse la lactonisation de ces adduits. En présence de H_2SO_4 à 80%, les produits majoritaires (ca. 80%) sont les (*Z*) dihydrocarbométhoxyméthylène-3 (3*H*)-furannones-2 (**2** ou **4**). La cyclisation par du HCl anhydre conduit à un mélange de produits dont la composition dépend du produit de départ; les produits principaux comprennent les isomères (*E*) et les δ-lactones correspondants (**6** et **7**). On rapporte les données détaillées de la rmn du ^1H et du ^{13}C de tous les composés. Utilisant la diffraction des rayons-X, on a déterminé les structures des dérivés des (*E*)-triméthyl-4,5,5, (*Z*)-triméthyl-4,5,5 et (*Z*)-tétraméthyl-4,4,5,5 furannones (**6***a*, **2***a* et **2***b*). On discute des propriétés de quelques-unes de ces lactones ainsi que des méthodes possibles d'élimination du groupe carbométhoxyle du composé **2**.

[Traduit par le journal]

Introduction

As an extension of our studies on the effect of Lewis acids on Diels–Alder additions of dimethyl acetylenedicarboxylate (DMAD) (2), we have investigated the effect of $AlCl_3$ on ene reactions involving this compound. As anticipated, the Lewis acid causes dramatic acceleration of the reactions of DMAD with various olefins, and is particularly useful in the case of volatile olefins (see below). The adducts **1** are structurally suited as intermediates for the synthesis of substituted α-methylene-γ-lactones, which are potential antitumor agents (refs. 3, 4, and references therein) and in which there has thus been considerable recent synthetic interest (5, 6). Our observation of such compounds as by-products of certain $AlCl_3$-promoted reactions encouraged us to undertake a detailed study of the effect of acids on adducts **1**.

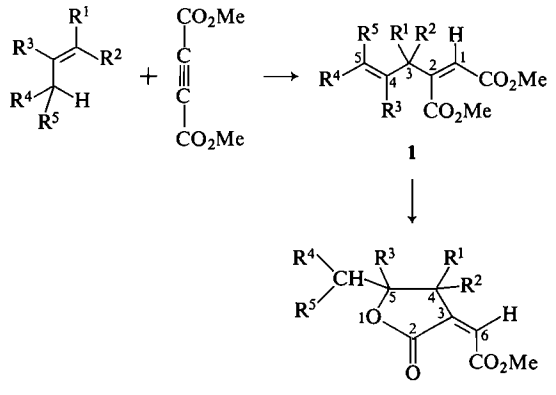

a $R^1 = R^3 = CH_3$; $R^2 = R^4 = R^5 = H$
b $R^1 = R^2 = R^3 = CH_3$; $R^4 = R^5 = H$
c $R^1 = R^2 = R^5 = H$; $R^3 + R^4 = (CH_2)_4$
d $R^1 = CH_3$; $R^2 = R^5 = H$; $R^3 + R^4 = (CH_2)_4$
e $R^1 = R^2 = R^5 = H$; $R^3 + R^4 = CH{\cdot}CH_2{\cdot}CH{\cdot}CH_2$, $C(CH_3)_2$

Results and Discussion

Ene Reactions

Adducts **1***a*, *b*, and **3** were prepared by $AlCl_3$-promoted reactions of 2-methyl-2-butene, 2,3-dimethyl-2-butene, and 1-methylcyclohexene with DMAD. No reaction occurred in the absence of the Lewis acid, even on extended reflux. The $AlCl_3$-promoted ene reaction with DMAD appears to be limited to 1,1-di-, tri-, and tetrasubstituted olefins, since similar reactions involving mono- or 1,2-disubstituted olefins afford chiefly cyclobu-

[1]Issued as NRCC No. 18660.

[2]For a preliminary account of some of this work see ref. 1.

0008-4042/81/020288-14$01.00/0

©1981 National Research Council of Canada/Conseil national de recherches du Canada

Can. J. Chem. Downloaded from www.nrcresearchpress.com by 210.87.254.105 on 09/05/12
For personal use only.

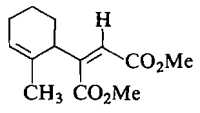

3

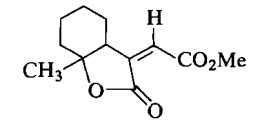

4

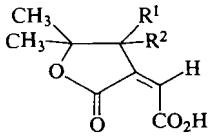

5

a $R^1 = CH_3$; $R^2 = H$
b $R^1 = R^2 = CH_3$

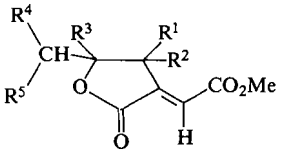

6

a $R^1 = R^3 = CH_3$; $R^2 = R^4 = R^5 = H$
b $R^1 = R^2 = R^3 = CH_3$; $R^4 = R^5 = H$
c $R^1 + R^3 = (CH_2)_4$; $R^2 = R^4 = R^5 = H$

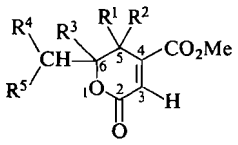

7

a $R^1 = R^3 = CH_3$; $R^2 = R^4 = R^5 = H$
b $R^1 + R^3 = (CH_2)_4$; $R^2 = R^4 = R^5 = H$

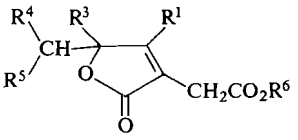

8

a $R^1 = R^3 = R^6 = CH_3$; $R^4 = R^5 = H$
b $R^1 + R^3 = (CH_2)_4$; $R^4 = R^5 = H$; $R^6 = CH_3$
c $R^1 = R^3 = CH_3$; $R^4 = R^5 = R^6 = H$

tenes (1).[3] Similar results have been reported by Snider *et al.* using propiolate esters as enophiles (7); since our submission of this manuscript they have also published an account of related work using DMAD (8). Although we obtained **1***a* and **3** in 55–60% yield our isolated yield of pure **1***b* was low (28%) and by-products included **2***b* (17%) and **6***b* (8%).

Adducts **1***c–e* were most conveniently prepared by thermal reaction of methylenecyclohexane, ethylidenecyclohexane, and β-pinene with DMAD.

Lactonization

Cyclization of **1** was catalyzed by acid, the product composition being dependent upon the type of acid used. The reagent of choice for the conversion of **1***a–d* to **2***a–d* (or of **3** to **4**) was 80% sulfuric acid. The products were obtained in 80–85% yield after only a few minutes at room temperature. Similar conditions have been reported for cyclization of *cis* 2,5-dienoic acids and esters to δ-lactones (9). As expected, strongly acidic conditions caused rearrangement of the α-pinene derivative **1***e*.

In contrast to the behavior with H_2SO_4, treatment of **1***a* with anhydrous HCl over a period of 5 days led to a mixture of products, the chief of which was **6***a* (37%). The isomers **7***a* (3%) and **8***a* (6%) were also obtained, as were the chlorinated derivatives **9***a* (5%) and **9***b* (6%). Compound **2***a* was shown to isomerize readily to **8***a* under the same conditions. Similar reaction of **1***b* with anhydrous HCl afforded a 3:1 mixture of **6***b* and **2***b*. In contrast, although **6***c* was formed in the HCl-catalyzed reaction of **3** it was obtained only as a minor product (3%), as was **8***b* (6%) resulting from isomerization of **4**. The predominant product in this case was **7***b* (35%).

Properties

Although reaction of **2***a* with anhydrous HCl rapidly afforded **8***a* (together with a small amount of **9***a*), **6***a* was unaffected under similar conditions. Overnight treatment of either **2***a* or **6***a* with refluxing triethylamine, however, caused conversion to **8***a*.

With refluxing 50% H_2SO_4 the hydrolysis product from **2***a* was **8***c*. Hydrolysis without migration of the double bond, to give **5***a*, was achieved using 65% H_2SO_4 at 25°C (slow) or refluxing 10% NaOH.

Catalytic reduction of either **2***b* or **6***b* over 5% Pd/C proceeded smoothly to give **10***c*. Reduction of **6***a* gave **10***a* as the only product. Hydrogenation of **2***a* under identical conditions yielded **10***a* (15%) and **10***b* (22%), as well as the unexpected **8***a* (54%).[4]

[3]This work will be detailed elsewhere.

[4]Although not separated and characterized, a similar mixture of products was obtained on catalytic reduction of **2***d*; in contrast, no olefinic material was detected in the product of hydrogenation of **2***c*.

Can. J. Chem. Downloaded from www.nrcresearchpress.com by 210.87.254.105 on 09/05/12
For personal use only.

Can. J. Chem. Downloaded from www.nrcresearchpress.com by 210.87.254.105 on 09/05/12
For personal use only.

We have investigated removal of the carbomethoxyl group to give the parent α-methylene lactones. Our first attempts utilized the reported oxidative decarboxylation of lactone acetic acids (10, 11). Thus, **10***d*, obtained by saponification of **10***c*, afforded **11** in 15% yield. Significantly improved product quality and yield (79%) resulted when direct copper/quinoline decarboxylation of **5***b* was employed. Our preliminary evidence suggests that the direct decarboxylation is limited to lactone acids of type **5** in which C-4 is fully substituted.

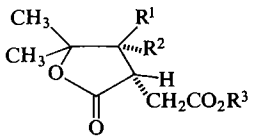

10

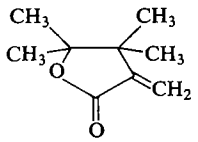

11

a $R^1 = R^3 = CH_3$; $R^2 = H$
b $R^1 = H$; $R^2 = R^3 = CH_3$
c $R^1 = R^2 = R^3 = CH_3$
d $R^1 = R^2 = CH_3$; $R^3 = H$

Antitumor screening of **2***a*, **2***b*, **4**, **6***a*, and **11** has revealed no activity against P388 lymphocytic leukemia.

Structures

The structures of all new compounds were established largely from spectral considerations. Mass spectra (including accurate mass determinations) and infrared absorptions are given in the experimental section. Full ^1H nmr data are presented in Tables 1 (adducts) and 2 (lactones). Detailed high-resolution ^{13}C nmr data are given in Tables 3 (adducts), 4, and 5 (lactones).

Adducts

The ^1H and ^{13}C nmr spectra of **1***a–e* are entirely consistent with the structure and stereochemistry anticipated from consideration of the ene reaction mechanism (12). The *cis* relationship of the two ester groups is established both from the high-field chemical shift (ca. δ 5.8) of H-1, and the characteristic *trans* coupling ($^3J_{CH} \sim$ 12 Hz) between the ester carbonyl carbon (at C-2) and H-1 (13). The endocyclic double bond of **3** results from isomerization of the initially formed adduct. Analogous adducts with propiolate esters have been reported by Snider *et al.* (7).

Lactones 2a, 2b, *and* 6a

The structures of these three compounds were determined from their spectral properties (see below). X-ray crystal structure analyses, which were performed to obtain conformations in the solid state, served also to confirm these structures. Comparable views of the molecules are given in Fig. 1. Some torsion angles and, for the lactone rings, the equivalent conformation parameters (14) are given in Table 8; these data, together with the final atomic positions (Table 6) have been placed in the Depository of Unpublished Data.[5] The ring conformations are intermediate between the extremes of envelope and "half-chair". The methyl substituents at C-4 are unequivocally "equatorial" or "axial". In **2***b* (with two substituents at C-4) the axial bond is significantly longer than the equatorial (1.560 (3)Å, compared to 1.510 (3)Å). In **2***a* the lone substituent at C-4 is in the equatorial position. The molecule is otherwise similar to **2***b* except that the carbomethoxyl group is (perhaps because of packing forces) rotated by about 180°. In **6***a* the carbomethoxyl group is *trans* to the ring carbonyl, and this configuration brings O-7′ quite close to the position which would be occupied by an equatorial substituent (H-4 is 2.67Å from O-7′; other things being equal, the corresponding methyl substituent would be even closer). It is presumably for this reason that the substituent at C-4 is found in the axial position.

Other Lactones

The combined nmr evidence limited the structural possibilities for the three isomers **2***a*, **6***a*, and **7***a*. The latter, not identified by X-ray analysis, shows characteristic ir absorption centered at 1718 cm^{-1}, in contrast to the γ-lactones which show carbonyl absorptions near 1760 cm^{-1}.

Couplings ($^3J_{CH}$) involving α,β-unsaturated carbonyl systems depend on the double bond stereochemistry, being significantly larger when the coupled hydrogen is *trans* to the carbonyl carbon (13). In the case of **2***a* and **6***a* the *trans*- and *cis*-orientations of the lactone carbonyl carbon and the olefinic hydrogen are reflected by $^3J_{CH}$ values of 12.5 and 6.4 Hz respectively. In **7***a* the lactone carbonyl carbon is coupled only to the geminal olefinic hydrogen (^2J = 3.7 Hz), while the ester carbonyl carbon shows a characteristic *cis* $^3J_{CH}$ of 6.0 Hz with this hydrogen.

The nmr spectra of **4**, **6***c*, and **7***b* are very similar to those of the analogues **2***a*, **6***a*, and **7***a*, with the obvious exceptions due to replacement of two methyl groups by a cyclohexane ring. Similarly, the spectra of **2***b* and **6***b* are closely comparable to those of **2***a* and **6***a*. The structures of the spirocyclic derivatives **2***c* and **2***d* also followed from their obvious spectral similarities to **2***a*.

That **8***a* and **8***b* were isomeric with **2***a* and **2***b* respectively was established by accurate mass

[5]These tables are available, at a nominal charge, from the Depository of Unpublished Data, CISTI, National Research Council of Canada, Ottawa, Ont., Canada K1A 0S2.

Can. J. Chem. Downloaded from www.nrcresearchpress.com by 210.87.254.105 on 09/05/12
For personal use only.

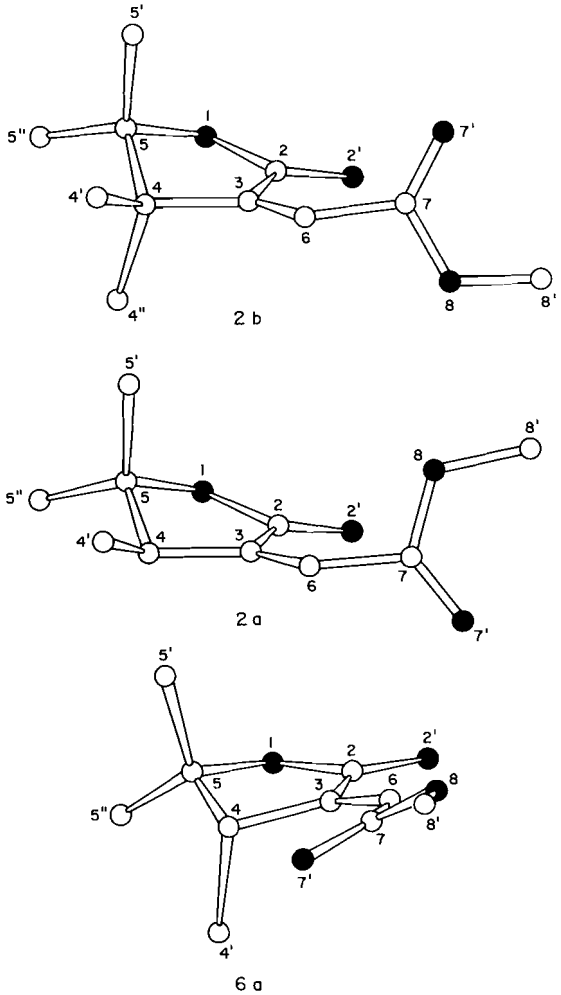

FIG. 1. Equivalent views of the three molecules studied by X-ray crystallography. Solid circles O, open circles C.

measurements. The presence of the endocyclic double bond in these compounds was shown by the appearance of nmr signals for allylic methyl (**8***a*; δ_H 2.00; δ_C 11.33 ppm) and methylene (**8***a* and **8***b*; $\delta_H \sim$ 3.3; $\delta_C \sim$ 28 ppm) groupings and for two quaternary olefinic carbons (116–120 and 167–170 ppm).

The mass spectra of the reduction products **10***a–c* showed that these compounds were derived by addition of one mole of hydrogen to the appropriate lactones (see above). This was confirmed by their nmr spectra which showed that the products possessed saturated rings carrying a $-CH_2CO_2CH_3$ grouping. Differentiation of isomers **10***a* and **10***b* was based on the observed vicinal couplings of 10.9 and 7.8 Hz between the two ring hydrogens, indicative of *trans* and *cis* relationships respectively (15).

The structures of the four acids **5***a*, **5***b*, **8***c*, and **10***d* followed from their characteristic ir and ^{1}H nmr

TABLE 1. ^{1}H nuclear magnetic resonance of adducts **1** and **3**

Compound	Chemical shift δ_H (ppm) (multiplicity, J_{HH} (Hz))				
	H-1	H-3	H-5	OCH_3(s)	CH_3 and ring H
1*a*	5.81 (d, $J_{1,3}$ 1.5)	3.20 (qm, $J_{1,3}$ 1.5, J_{3,CH_3} 7.0)	4.85 (m, $J_{5a,5b}$ 1.5, $J_{5a,3}$ 0.8, J_{5a,CH_3} 0.9) 4.89 (qu, $J_{5a,5b}$ 1.5, J_{5b,CH_3} 1.5)	3.70 3.76	1.25 (d, J_{3,CH_3} 7.0, CH_3 at C-3) 1.70 (m, $J_{CH_3,5a}$ 0.9, $J_{CH_3,5b}$ 1.5, CH_3 at C-4)
1*b*	5.83 (s)		4.93 (bs)	3.80	1.29 (s, CH_3 at C-3); 1.73 (bs, CH_3 at C-4)
1*c*	5.80 (t, $J_{1,3}$ 1.5)	2.95 (bs)	5.53 (bm)	3.70, 3.78	1.40–1.75 (m, 4H); 1.80–2.15 (m, 4H)
1*d*	5.78 (d, $J_{1,3}$ 1.5)	3.09 (bq, J_{3,CH_3} 7.0)	5.55 (bm)	3.70, 3.77	1.21 (d, J_{3,CH_3} 7.0, CH_3 at C-3); 1.40–1.70 (m, 4H); 1.75–2.15 (m, 4H)
1*e*	5.80 (t, $J_{1,3}$ 1.5)	3.00 (m, $J_{3a,3b}$ 16.0)	5.38 (bm)	3.70, 3.78	0.81 (s, CH_3); 1.27 (s, CH_3); 1.16 (d, 8.4, 1H); 1.90–2.55 (m, 5H)
3	5.75 (d, $J_{1,3}$ 1.1)	2.98 (bm)	5.69 (bm)	3.71, 3.82	1.64 (m, J_{3,CH_3} 0.6, J_{5,CH_3} 1.5, CH_3 at C-4); 1.25–2.15 (m, 6H)

Can. J. Chem. Downloaded from www.nrcresearchpress.com by 210.87.254.105 on 09/05/12
For personal use only.

TABLE 2. ^{1}H nuclear magnetic resonance of lactones

Compound	Chemical shift δ_H (ppm) (multiplicity, J_{HH} (Hz))					
	CH_3 at C-4[a]	CH_3 at C-5[a](s)	H-4[a]	H-6	OCH_3(s)	Other H
2*a*	1.18 (d, J_{4,CH_3} 6.9)	1.23, 1.49	2.88 (dq, $J_{4,6}$ 3.1, J_{4,CH_3} 6.9)	6.13 (d, $J_{4,6}$ 3.1)[b]	3.82	
2*b*	1.16 (s)	1.31		6.08 (s)[c]	3.81	
2*c*			2.77 (d, $J_{4,6}$ 2.5)	6.32 (t, $J_{4,6}$ 2.5)	3.79	1.25–1.95 (m, 10H, ring CH_2)
2*d*	1.16 (d, J_{4,CH_3} 6.9)		2.77 (dq, $J_{4,6}$ 3.0, J_{4,CH_3} 6.9)	6.11 (d, $J_{4,6}$ 3.0)	3.81	1.30–1.90 (m, 10H, ring CH_2)
4		1.49	2.83 (bdt, $J_{4,6}$ 2.9, J_{4,CH_2} 5.0)	6.16 (d, $J_{4,6}$ 2.9)	3.81	1.10–2.00 (m, 8H, ring CH_2)
5*a*	1.27 (d, J_{4,CH_3} 6.9)	1.37, 1.60	3.10 (dq, $J_{4,6}$ 3.1, J_{4,CH_3} 6.9)	6.33 (d, $J_{4,6}$ 3.1)		11.00 (bs, OH)
5*b*[d]	1.25 (s)	1.40		6.34 (s)		8.90 (bs, OH)
6*a*	1.20 (d, J_{4,CH_3} 7.2)	1.37, 1.45	3.55 (dq, $J_{4,6}$ 1.8, J_{4,CH_3} 7.2)	6.73 (d, $J_{4,6}$ 1.8)	3.82	
6*b*	1.30 (s)	1.32		6.79 (s)	3.80	
6*c*		1.28	3.48 (m)	6.65 (d, $J_{4,6}$ 1.5)	3.80	1.00–2.40 (m, 8H, ring CH_2)
7*a*	1.17 (d, J_{5,CH_3} 7.0)	1.44, 1.48	2.78 (q, J_{5,CH_3} 7.0)	6.72 (s)	3.89	
7*b*		1.35	2.62 (dd, $J_{5,7t}$ 11.8, $J_{5,7e}$ 4.8)	6.73 (s)	3.87	0.90–2.25 (m, 8H, ring CH_2)
8*a*	2.00 (t, J_{6,CH_3} 0.6)	1.46		3.29 (bs)	3.71	
8*b*		1.48		3.30 (bs)	3.70	2.76 (m, 1H), 1.20–2.40 (m, 7H)
8*c*	2.01 (t, $J_{CH_3,6}$ 0.5)	1.48		3.34 (d, J_{6,CH_3} 0.5)		6.94 (bs, OH)
9*a*	1.15 (d, J_{4,CH_3} 6.8)	1.28, 1.47	2.56 (dq, $J_{3,4}$ 12.1, J_{4,CH_3} 6.8)	4.66 (d, $J_{3,6}$ 3.2)	3.85	3.23 (dd, $J_{3,4}$ 12.1, $J_{3,6}$ 3.2, H-3)
9*b*	1.05 (d, J_{4,CH_3} 6.8)	1.28, 1.47	2.60 (dq, $J_{3,4}$ 11.7, J_{4,CH_3} 6.8)	4.97 (d, $J_{3,6}$ 3.6)	3.83	3.20 (dd, $J_{3,4}$ 11.7, $J_{3,6}$ 3.6, H-3)
10*a*	1.07 (d, J_{4,CH_3} 6.8)	1.27, 1.44	2.15 (bdq, $J_{3,4}$ 10.9, J_{4,CH_3} 6.8)	2.35–3.00 (m)	3.70	2.35–3.00 (m, H-3)
10*b*	0.90 (d, J_{4,CH_3} 7.3)	1.36, 1.46	2.47 (dq, $J_{3,4}$ 7.8, J_{4,CH_3} 7.3)	2.45 (dd, $J_{6a,6b}$ 17.0, $J_{3,6a}$ 10.0) 2.82 (dd, $J_{6a,6b}$ 17.0, $J_{3,6b}$ 5.0)	3.72	3.47 (ddd, $J_{3,6a}$ 10.0, $J_{3,6b}$ 5.0, $J_{3,4}$ 7.8, H-3)
10*c*	0.93 (s), 1.05 (s)	1.33, 1.39		AB part of ABX, 2.50, $\Delta\nu_{AB}$ 33.0, J_{AB} 16.2, J_{AX} = J_{BX} = 7.0	3.73	X part of ABX 3.22
10*d*	0.93 (s), 1.07 (s)	1.33, 1.38		AB part of ABX, 2.55, $\Delta\nu_{AB}$ 33.8, J_{AB} 16.5, J_{AX} 7.1, J_{BX} 6.8		X part of ABX, 3.20 8.90 (bs, OH)
11	1.13 (s)	1.30		5.43 (s), 6.13 (s)		

[a]In the case of **7***a* the shifts listed are for CH_3 groups at C-5 and C-6, and for H-5.
[b]In DMSO-d_6, irradiation of the methyl at δ 1.10 caused a 21% nOe of the signal for H-6 at δ 6.52.
[c]In DMSO-d_6, irradiation of the methyl at δ 1.10 caused a 35–40% nOe of the signal for H-6 at δ 6.53.
[d]In acetone-d_6.

Can. J. Chem. Downloaded from www.nrcresearchpress.com by 210.87.254.105 on 09/05/12
For personal use only.

TABLE 3. ^{13}C nuclear magnetic resonance of adducts **1** and **3**

Compound	Chemical shift δ_C (ppm) (multiplicity, $^nJ_{CH}$ (Hz)[a])						
	C-1	C-2	C-3	C-4	C-5	C=O	Other C
1*a*	118.94 dd ^1J 164.8, ^3J 5.3	153.76 m	45.23 dm $^1J \sim 128$	144.82 m	113.07 tqu ^1J 155.9, ^3J 5.3	165.45 dq ^2J 1.9, ^3J 3.8 168.80 dqu ^3J 12.3, ^3J 4.0	17.09 qd, ^1J 128.1, ^2J 4.9 (CH_3 at C-3), 20.11 qddd, ^1J 126.2, ^3J 10.6, ^3J 6.6, ^3J 3.8 (CH_3 at C-4)
1*b*	117.85 d ^1J 164.9	158.68 m	44.41 m	148.55 m	111.93 tq ^1J 155.8, ^3J 5.8	165.44 dq ^2J 1.6, ^3J 3.8 168.37 dq ^3J 12.1, ^3J 4.0	19.91 qdd, ^1J 126.4, ^3J 11.3, ^3J 6.4 (CH_3 at C-4), 26.22 qq, ^1J 128.1, ^3J 4.8 (CH_3 at C-3)
1*c*	120.17 dt ^1J 165.3, ^3J 5.9	149.44 m	43.02 tm $^1J \sim 129.5$	132.59 bm	126.29 dbm*	165.28 dq ^2J 1.9, ^3J 3.9 168.88 dq ^3J 12.1, ^3J 4.0	22.30, 23.00, 25.53, 27.92 (all tm)[b]
1*d*	118.14 dd ^1J 165.0, ^3J 5.2	155.00 bm	45.57 dm $^1J \sim 130$	136.98 bm	124.31 dbm*	165.49 dq ^2J 1.9, ^3J 3.8 169.07 dq ^3J 12.1, ^3J 3.9	16.59 qd, ^1J 127.8, ^2J 4.8 (CH_3 at C-3), 22.46, 22.96, 25.45, 25.99 (all tm)[b]
1*e*	121.04 dt ^1J 165.0, ^3J 6.0	147.87 t ^2J 7.3	41.85 tm $^1J \sim 129$	142.71 m	121.14 dm*	165.17 dq ^2J 2.3, ^3J 3.9 168.66 dq ^3J 12.1, ^3J 4.0	20.97 qm, ^1J 124.0 (CH_3), 26.25 qm, ^1J 124.7 (CH_3), 31.51 (tm), 31.91 (tm), 38.07 (m), 40.59 (dm), 45.49 (dm)*
3	120.87 dd ^1J 165.4, ^3J 5.9	152.38 bm	43.57 dm $^1J \sim 130$	131.36 bm	126.59 dm*	165.59 dq, ^2J 2.3, ^3J 4.0 169.46 dq ^3J 12.0, ^3J 4.0	22.31 qm* (CH_3), 17.10, 25.08, 26.73 (all tm)[b]

[a]Values of $^nJ_{CH}$ were obtained from first order spectral analysis. Coupling constants of resonances marked * could not be determined due to signal overlap. Each compound showed two methoxyl resonances in the range 51.59–52.26 (^1J = 147.0–147.4 Hz).
[b]Cyclohexyl methylene carbons were observed as tm, with ^1J = 128–130 Hz.

Can. J. Chem. Downloaded from www.nrcresearchpress.com by 210.87.254.105 on 09/05/12
For personal use only.

TABLE 4. ^{13}C nuclear magnetic resonance of lactones: chemical shift data

	Chemical shift δ_C (ppm)									
Compound	CH_3 at C-4	CH_3 at C-5	C-2	C-3	C-4	C-5	C-6	OCH_3	C=O	Ring CH_2
2*a*	12.18	22.91, 26.84	166.44	140.56	45.42	85.41	125.56	52.17	165.75	
2*b*	22.70	23.49	166.51	145.87	46.06	87.12	124.40	52.11	165.73	
2*c*			166.58	134.44	40.05	83.95	127.18	52.30	165.69	22.45, 24.68, 37.41
2*d*	12.62		166.57	140.83	45.55	86.57	125.44	52.30	165.83	21.41, 22.30, 24.99, 31.79, 36.12
4		25.16	166.94	139.37	46.42	83.66	124.90	52.19	165.70	20.33, 21.87, 24.64, 36.03
5*b*[a]	22.91	23.51	170.55	147.73	47.45	90.73	128.56		164.85	
6*a*	15.11	22.46, 29.91	169.08	150.05	43.55	85.48	123.81	51.99	165.31	
6*b*	21.36	23.55	169.37	149.30	46.50	87.63	124.56	51.96	165.05	
6*c*		29.75	169.86	150.48	45.04	83.65	122.56	51.99	165.68	20.57, 22.69, 29.61, 33.63
7*a*[b]	15.11	25.43, 26.97	163.34	124.35	149.62	37.16	82.81	52.81	165.12	
7*b*[b]		26.44	164.00	124.81	149.05	39.90	81.18	52.76	165.04	21.17, 24.29, 30.10, 37.40
8*a*	11.33	24.55	172.08	119.67	167.73	86.19	28.76	52.06	169.80	
8*b*		22.11	172.39	116.45	(170.01)	85.27	28.37	52.07	(170.36)	22.80, 25.74, 27.23, 40.15
9*a*	12.87	22.15, 27.03	172.44	51.33	42.43	85.55	55.04	53.46	167.88	
9*b*	13.12	22.31, 26.78	173.28	50.64	40.93	85.80	56.04	53.41	168.37	
10*a*	12.73	21.52, 26.98	176.28	(43.17)	(45.46)	85.21	32.83	51.77	171.65	
10*b*	11.18	23.79, 27.41	176.72	(40.85)	(41.24)	85.10	30.55	52.01	172.10	
10*c*	19.40, 21.22	22.10, 23.63	176.06	46.54	43.66	87.19	29.84	51.86	172.04	
10*d*[a]	19.60, 21.37	22.33, 23.82	176.67	47.04	44.21	87.59	30.14		173.38	
11	23.27	23.47	169.88	147.07	45.18	87.00	118.71			

[a]In acetone-d_6.
[b]In **7***a* and **7***b* the methyl groups are located at C-5 and C-6.

Can. J. Chem. Downloaded from www.nrcresearchpress.com by 210.87.254.105 on 09/05/12
For personal use only.

TABLE 5. ^{13}C nuclear magnetic resonance of lactones: ^{13}C—^{1}H coupling constants[a,b]

Compound	Multiplicity $^{n}J_{CH}$ (Hz)				
	C-2	C-3	C-4	C-6	C=O
2*a*	dd, ^{3}J 12.5, ^{3}J 1.7	m	dm, ^{1}J 130.1	dd, ^{1}J 164.2, ^{3}J 5.0	dq, ^{2}J 1.9, ^{3}J 3.9
2*b*	d, ^{3}J 12.5	m	m	d, ^{1}J 163.6	dq, ^{2}J 1.7, ^{3}J 3.9
2*c*	dt, ^{3}J 12.4, ^{3}J 3.8	dt, ^{2}J 2.5, ^{2}J 6.9	btm, $^{1}J \sim 135$	dt, ^{1}J 164.5, ^{3}J 4.8	dq, ^{2}J 1.9, ^{3}J 3.9
2*d*	dd, ^{3}J 12.4, ^{3}J 2.2	m	dm, $^{1}J \sim 130$	dd, ^{1}J 163.7, ^{3}J 5.0	dq, ^{2}J 2.0, ^{3}J 4.0
4	dd, ^{3}J 12.9, ^{3}J 2.4	m	bdm, $^{1}J \sim 133$	dd, ^{1}J 163.8, ^{3}J 5.0	ddq, ^{4}J 1.9, ^{2}J 1.9, ^{3}J 3.8
5*b*	d, ^{3}J 13.0	m	m	d, ^{1}J 163.3	s
6*a*	t, ^{3}J 6.4, 6.4	m	dm, ^{1}J 140.0	dd, ^{1}J 167.5, ^{3}J 2.5	m
6*b*	d, ^{3}J 7.6	m	m	d, ^{1}J 165.0	dq, ^{2}J 1.3, ^{3}J 3.9
6*c*	t, ^{3}J 6.7, 6.7	m	bdm, $^{1}J \sim 140$	dd, ^{1}J 167.4, ^{3}J 1.9	dq, ^{2}J 1.6, ^{3}J 3.7
7*a*	d, ^{2}J 3.7	dd, ^{1}J 174.6, ^{3}J 4.5	m	m	dqu, ^{3}J 6.0, ^{3}J 3.8
7*b*	d, ^{2}J 3.8	dd, ^{1}J 174.6, ^{3}J 4.3	bd, ^{2}J 8.0	bm	dqu, ^{3}J 5.9, ^{3}J 3.8
8*a*	t, ^{3}J 4.7	tq, $^{2}J = {}^{3}J = 5.6$	m	t, ^{1}J 130.1	tq, ^{2}J 7.6, ^{3}J 3.8
8*b*	t, ^{3}J 4.6	m	m	t, ^{1}J 130.1	m
9*a*	t, $^{2}J = {}^{3}J = 7.2$	dm, $^{1}J \sim 127$	bdm, $^{1}J \sim 127.5$	ddd, ^{1}J 150.7, ^{2}J 4.6, ^{3}J 3.4	dqu, ^{2}J 6.2, ^{3}J 3.7
9*b*	dd, ^{2}J 7.1, ^{3}J 3.1	dm, $^{1}J \sim 127$	bdm, $^{1}J \sim 128$	ddd, ^{1}J 154.3, ^{2}J 5.1, ^{3}J 2.1	m
10*a*	m	(dm, $^{1}J \sim 130$)	(bdm, ^{1}J 128.7)	tt, ^{1}J 130.2, $^{2}J = {}^{3}J = 4.9$	m
10*b*	m	(dm, $^{1}J \sim 135$)	(dm, ^{1}J 129.5)	td, ^{1}J 129.8, ^{2}J 5.1	m
10*c*	ddd, ^{2}J 7.5, ^{3}J 4.1, 5.4	dm, ^{1}J 128.1	bm	bt, ^{1}J 127.3	tqu, ^{2}J 7.6, ^{3}J 3.8
10*d*	ddd, ^{2}J 7.6, ^{3}J 4.5, 5.4	dm, $^{1}J \sim 127$	m	td, ^{1}J 130.3, ^{2}J 7.9	dt, ^{3}J 4.1, ^{2}J 7.3
11	dd, ^{3}J 13.7, ^{3}J 7.0	m	bm	dd, ^{1}J 159.5, ^{1}J 163.2	

[a]Values of $^{n}J_{CH}$ were obtained from first-order spectral analysis.

[b](*i*) All C-methyl resonances were q (^{1}J 126.3–129.4) and in addition were coupled to geminal and vicinal hydrogens; (*ii*) C-5 was a m (showing geminal and vicinal couplings), except in **7***a* and **7***b* where it was a dm (^{1}J 130–133); (*iii*) each OCH_3 carbon was a q (^{1}J 147.0–148.3); (*iv*) all cyclohexane methylenes were btm (^{1}J 128–130).

Can. J. Chem. Downloaded from www.nrcresearchpress.com by 210.87.254.105 on 09/05/12
For personal use only.

signals for carboxyl groups and from the very close similarity of their remaining spectral properties to those of the corresponding esters **2***a*, **2***b*, **8***a*, and **10***c*.

In the case of the chloro compounds **9***a* and **9***b* the structure followed from their mass spectra, which indicated a molecular formula $C_{10}H_{15}O_4Cl$ and a close structural resemblance to **10***a* and **10***b*, and from their combined ^1H and ^{13}C nmr spectra. The ^1H nmr spectrum of each compound was characterized by *trans* couplings (J = 11.7 and 12.1 Hz respectively) between the two ring hydrogens (15). Finally, stereospecific dehydrochlorination of **9***a* to **2***a* and of **9***b* to **6***a* on silica gel (see Experimental) can only be explained on the basis of **9***a* and **9***b* being diastereoisomers, epimeric at the chloro-substituted carbon C-6 (Scheme 1).

The presence of the unsubstituted *exo* methylene group in **11** was established by ^1H nmr (single proton resonances at 5.43 and 6.13 ppm, with characteristically small geminal coupling (16)) and ^{13}C nmr (in which C-6 appeared as the X part of an ABX, with outer spacing = $J_{AX} + J_{BX}$ = 322.7 Hz). As expected, the carbonyl carbon showed both *cis* (^3J = 7.0 Hz) and *trans* (^3J = 13.7 Hz) couplings to the olefinic hydrogens (13).

Mechanisms

The mechanistic alternatives for the $AlCl_3$-promoted ene reaction have been reviewed by Snider *et al.* (7, 8).

Protonation of **1** and subsequent cyclization and hydrolysis (Scheme 2) gives **2** (or **4**), the original stereochemistry of the ester-substituted double bond being retained. Pathways explaining the formation of all major products isolated from the HCl-catalyzed reaction of **1***a* are illustrated in Scheme 3. Protonation of the double bond and cyclization can occur as above (a); the product in this case is the (*Z*)-isomer **2***a*, which immediately isomerizes to **8***a*. Isolation of the (*E*)-lactone **6***a* and δ-lactone **7***a* suggests that there is appreciable

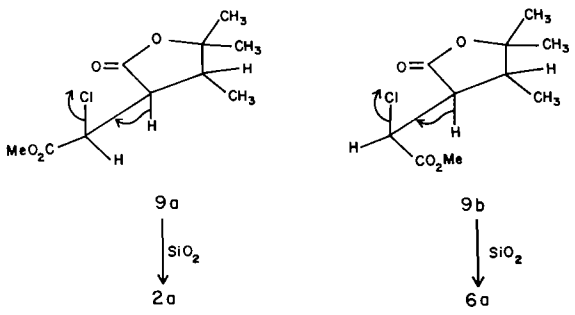

SCHEME 1

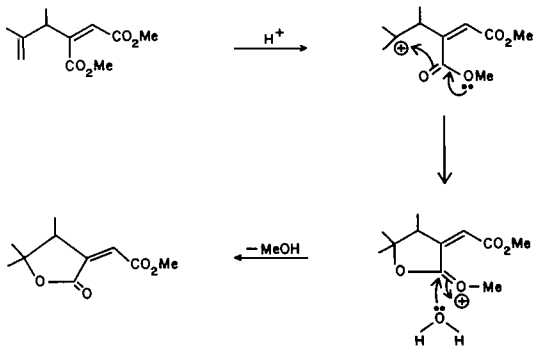

SCHEME 2

isomerization of the ester-substituted double bond of **1***a*, possibly through an HCl addition/elimination pathway. Cyclization can then proceed in either conformer as shown (b or c). Finally, addition of HCl to the ester-bearing double bond of **1***a* could also result in a chlorine-containing intermediate which could cyclize in such a way (d) as to produce the two chloro-lactones **9***a* and **9***b*, both having the more favorable *trans* orientation of the bulky side-chain at C-3 and the methyl substituent at C-4. Similar mechanisms must operate in the HCl-promoted cyclizations of **1***b* to **2***b* and **6***b*, and of **3** to **4** (which isomerizes to **8***b*), **6***c*, and **7***b*.

The properties of the lactones are for the most part unexceptional. The behavior of **2***a* and **6***a* during catalytic reduction is of interest. The product of reduction of **6***a* does not correspond to that predicted from classical theory, but can be explained on the basis of steric interaction in the diadsorbed substrate (17). Thus, although classical theory would predict approach of the catalyst on the less sterically hindered side of the molecule (opposite to the methyl at C-4), such attachment would introduce severe steric interaction between the methyl at C-4 and the carbomethoxyl group. Thus, the net result is preferred approach on the same side as the methyl at C-4 and consequently hydrogenation to give **10***a*. In the case of **2***a* much less steric strain is introduced by adsorption on the side opposite the methyl group. Such "classical" approach leads to **10***b*. Sterically favored catalyst abstraction of H-4 in the diadsorbed intermediate, followed by desorption, affords the dominant product **8***a*. The isolation of small amounts of **10***a* from the reduction of **2***a* indicates that the catalyst may also approach from the same side as the C-4 methyl.

Although the cyclization of substituted 1,4-pentadiene-1,2-dicarboxylates offers a useful synthetic route to γ-lactones of type **2**, it is limited at present to adducts **1** in which R^3 is an alkyl group.

Can. J. Chem. Downloaded from www.nrcresearchpress.com by 210.87.254.105 on 09/05/12
For personal use only.

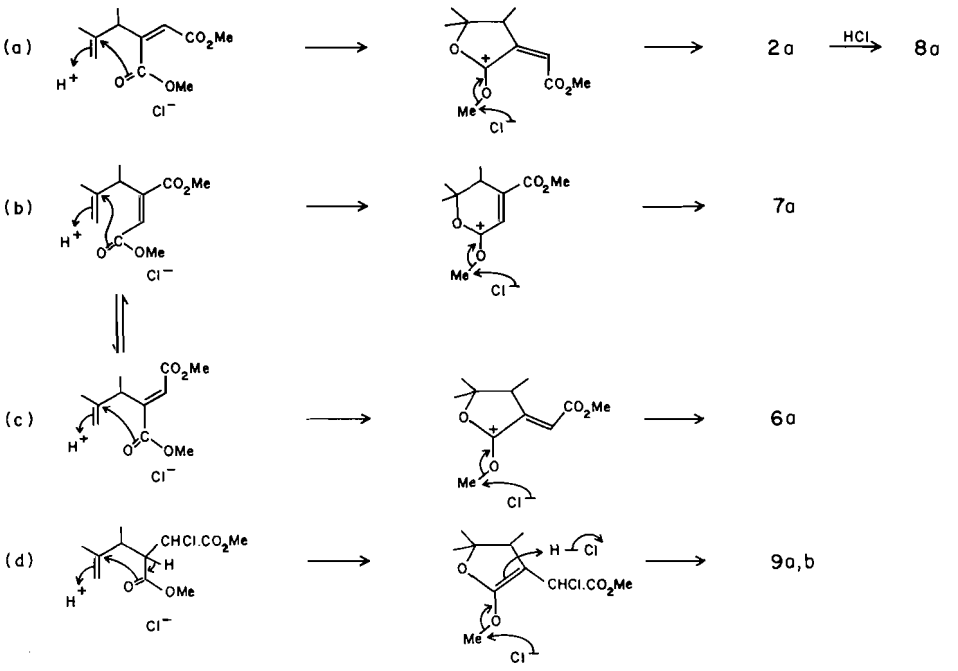

SCHEME 3

Procedures for lactonization of **1** (R^3 = H) are currently being explored, as are alternative methods of removing the ester group from **2**. Since it has been suggested that antitumor activity may require not only an α-methylene-γ-lactone moiety, but also a second α,β-unsaturated carbonyl system elsewhere in the molecule (4), work is in progress to extend our approach to more complex compounds.

Experimental

All nmr spectra were measured in $CDCl_3$ unless stated otherwise. Standard abbreviations used in the tabulated data are as follows: b broad, s singlet, d doublet, t triplet, q quartet, qu quintet, m multiplet. All ^1H nmr spectra were recorded on a Varian HA-100D spectrometer. The ^{13}C nmr spectra were recorded on a Varian XL-100-15 spectrometer under the following conditions; frequency 25.16 MHz; acquisition time 0.8 or 1.6 s (data accuracy ±0.6 or ±0.3 Hz); spectral width 5120 Hz; flip angle 30°; internal ^2H lock to solvent; temperature about 30°C. ^1H irradiation at 100 MHz: (*a*) $\gamma H_2/2\pi$ ca. 3800 Hz, broadband irradiation by 0–180° phase modulation at 150 Hz; (*b*) as for (*a*), but irradiation only applied for 1.6 s between data acquisition periods (high-resolution spectrum with retained nOe).

High-resolution mass spectral measurements were made with a Dupont-CEC 21-110B double-focussing mass spectrometer, using electrical detection for mass measurements. Infrared absorptions were measured on Perkin-Elmer 521 or 180 spectrometers. Column chromatographic separations were carried out on Mallinckrodt silicic acid (100 mesh) and preparative thin-layer chromatography (plc) on 2.0 mm Merck silica gel F-254 precoated plates.

$AlCl_3$-promoted Ene Reactions

*Preparation of 1*a

A solution of DMAD (14.2 g, 0.1 mol) in CH_2Cl_2 (150 mL) was added to an ice-cooled, vigorously stirred suspension of $AlCl_3$ (13.3 g, 0.1 mol) in CH_2Cl_2 (250 mL). To this was then added 2-methyl-2-butene (14.0 g, 0.2 mol). There was a vigorous exothermic reaction. After 1 h at room temperature the reaction mixture was poured into ice-water/CH_2Cl_2. The organic phase and CH_2Cl_2 extracts of the aqueous phase were combined, dried, and evaporated. Column chromatography (50% benzene/chloroform) of the orange oily residue afforded pure *(Z)-dimethyl-3,4-dimethyl-1,4-pentadiene-1,2-dicarboxylate* **1***a* as a straw-colored oil (12.74 g, 60%) n_D^{22} = 1.4669; ν_{max} (liq. film) 1729, 1641 cm^{-1}. Molecular ion (2%) at *m/e* 212.1049 ($C_{11}H_{16}O_4$ requires 212.10486); base peak at *m/e* 152.0834 ($C_9H_{12}O_2$ requires 152.08373); ions at *m/e* 197.0819 (8%) ($C_{10}H_{13}O_4$ requires 197.08139) and *m/e* 93.0703 (74%) (C_7H_9 requires 93.07043).

Other column fractions contained **1***a* with unreacted DMAD as a contaminant.

*Preparation of 1*b

A reaction employing $AlCl_3$ (15.96 g, 0.12 mol), DMAD (17.04 g, 0.12 mol), and 2,3-dimethyl-2-butene (20.16 g, 0.24 mol) in CH_2Cl_2 (480 mL), for 90 min at room temperature, was worked up as before to give a reddish oil. Chromatography (50% benzene/$CHCl_3$) gave (*i*) unreacted DMAD (2.902 g); (*ii*) a yellow oil (0.597 g), composed of **1***b* (see below) heavily contaminated by dimethyl chloromaleate (δ_H 6.33) and dimethyl chlorofumarate (δ_H 7.17); (*iii*) a yellow oil (2.745 g), composed of **1***b* slightly contaminated by the two chloro olefins; (*iv*) *dimethyl 3,3,4-trimethyl-1,4-pentadiene-1,2-dicarboxylate* **1***b* which was obtained as a pale yellow oil (7.59 g, 28%) n_D^{25} = 1.4552; ν_{max} (liq. film) 1731, 1637 cm^{-1}. Molecular ion (6%) at *m/e* 226.1211 ($C_{12}H_{18}O_4$ requires 226.12051); base peak at *m/e* 170; (*v*) **6***b* (1.92 g, 8%) (see below); (*vi*) dimethyl ethoxymaleate (contaminant from DMAD?), which was obtained as a pale yellow oil (0.442 g); ν_{max} (liq. film) 1749, 1715, 1621 cm^{-1}. Molecular ion (66%) at *m/e* 188.0675 ($C_8H_{12}O_5$ requires 188.06848); base peak at *m/e* 101; ions at *m/e* 173.0454 (73%) ($C_7H_9O_5$ requires 173.04500) and *m/e* 157.0500 (87%) ($C_7H_9O_4$

Can. J. Chem. Downloaded from www.nrcresearchpress.com by 210.87.254.105 on 09/05/12
For personal use only.

requires 157.05009); (*vii*) pure **2***b*, obtained as a colorless solid (4.418 g, 17%) (see below).

Preparation of **3**

A solution of DMAD (14.20 g, 0.1 mol) in CH_2Cl_2 (100 mL) was added to a stirred suspension of $AlCl_3$ (13.3 g, 0.1 mol) in CH_2Cl_2 (150 mL). To this was added 1-methylcyclohexene (10.56 g, 0.11 mol) at a rate such that the temperature did not rise above 30°C. After 1 h at room temperature, work-up as above followed by column chromatography (50% benzene/chloroform) gave **3** as a pale yellow oil (13.33 g, 56%) n_D^{25} = 1.4940; ν_{max} (liq. film) 1735 (sh), 1726, 1642 cm^{-1}. Molecular ion (7%) at *m/e* 238.1213 ($C_{13}H_{18}O_4$ requires 238.12051); base peak at *m/e* 206.0941 ($C_{12}H_{14}O_3$ requires 206.09430); ion at *m/e* 178.0995 (93%) ($C_{11}H_{14}O_2$ requires 178.09938).

Thermal Ene Reactions

Preparation of **1**c

A mixture of methylenecyclohexane (5.00 g, 0.052 mol) and DMAD (6.66 g, 0.047 mol) was heated at 110°C for 6 days; ^1H nmr analysis indicated 70% conversion to **1***c*. Repeated column chromatography ($CHCl_3$) and plc (10% acetone/petroleum ether) afforded **1***c* as an almost colorless oil, n_D^{21} = 1.4873; ν_{max} (liq. film) 1725 cm^{-1}. Molecular ion (7%) at *m/e* 238.1196 ($C_{13}H_{18}O_4$ requires 238.12051); base peak at *m/e* 119.

Preparation of **1**d

A mixture of ethylidenecyclohexane (12.12 g, 0.110 mol) and DMAD (14.21 g, 0.100 mol) was heated at 120°C for 72 h. Chromatography ($CHCl_3$) of the crude product afforded (*a*) unreacted ethylidenecyclohexane (0.812 g); (*b*) a mixture (3:2) of DMAD and **1***d* (1.890 g); (*c*) pure **1***d* as an almost colorless oil (12.47 g, 50%), n_D^{25} = 1.4898; ν_{max} (liq. film) 1737 cm^{-1}. Molecular ion (6%) at *m/e* 252.1350 ($C_{14}H_{20}O_4$ requires 252.13616); base peak at *m/e* 133.1020 ($C_{10}H_{13}$ requires 133.10173).

Preparation of **1**e

A mixture of β-pinene (5.44 g, 0.04 mol) and DMAD (6.24 g, 0.044 mol) was heated at 130°C for 5 h. Chromatography (50% benzene/$CHCl_3$) of the yellow oil obtained gave (*a*) colorless oil (3.693 g), consisting of **1***e* and about 10% DMAD, and (*b*) pure **1***e* as a colorless oil (5.033 g, 45%), n_D^{21} = 1.4952; ν_{max} (liq. film) 1736 cm^{-1}. Molecular ion (34%) at *m/e* 278.1517 ($C_{16}H_{22}O_4$ requires 278.15181); base peak at *m/e* 203.0710 ($C_{12}H_{11}O_3$ requires 203.07082).

Cyclizations Catalyzed by 80% Sulfuric Acid

Conversion of **1**a *to* **2**a

Diene **1***a* (212 mg) was dissolved in 80% sulfuric acid (1 mL). After 2 min the mixture was poured into ice-water/CH_2Cl_2. The organic phase and CH_2Cl_2 extracts of the aqueous phase were combined, dried, and evaporated to give a pale yellow oil (188 mg), plc (25% acetone/petroleum ether) of which afforded pure (Z)-*dihydro-3-carbomethoxymethylene-4,5,5-trimethyl-2(3H)-furanone* **2***a* (167 mg, 84%). Recrystallization from petroleum ether gave colorless prisms, mp 51–51.5°C; ν_{max} (KBr) 1762, 1737, 1677 cm^{-1}. Molecular ion (2%) at *m/e* 198.0893 ($C_{10}H_{14}O_4$ requires 198.08921); base peak at *m/e* 140.0471 ($C_7H_8O_3$ requires 140.04735).

Cyclization of **1***a* to **2***a* did not occur using 50% H_2SO_4; with 65% H_2SO_4 reaction occurred slowly, but gave mainly the hydrolyzed product **5***a*.

Conversion of **1**b *to* **2**b

Diene **1***b* (1.00 g) was dissolved in 80% H_2SO_4 (5 mL). After 20 min at room temperature the mixture was worked up as above. The residue on plc ($CHCl_3$) gave (Z)-*dihydro-3-carbomethoxymethylene-4,4,5,5-tetramethyl-2(3H)-furanone* **2***b* (746 mg, 80%). Recrystallization from petroleum ether/ethyl acetate gave colorless prisms, mp 73.5–74.5°C; ν_{max} (KBr) 1760, 1733 cm^{-1}. Molecular ion not observed ($C_{11}H_{16}O_4$ requires 212); base peak at *m/e* 154.0630 ($C_8H_{10}O_3$ requires 154.06300); ions at *m/e* 197.0806 (2%) ($C_{10}H_{13}O_4$ requires 197.08139), 181.0865 (8%) ($C_{10}H_{13}O_3$ requires 181.08647), and 126.0687 (76%) ($C_7H_{10}O_2$ requires 126.06801).

Conversion of **1**c *to* **2**c

Treatment of **1***c* (750 mg) with 80% H_2SO_4 (3 mL) for 10 min at room temperature gave an orange oil. Chromatography (50% benzene/$CHCl_3$) afforded **2***c* as an almost colorless oil (586 mg, 83%), n_D^{22} = 1.5014; ν_{max} (liq. film) 1766, 1742, 1680 cm^{-1}. Molecular ion (18%) at *m/e* 224.1051 ($C_{12}H_{16}O_4$ requires 224.10486); base peak at *m/e* 126.0318 ($C_6H_6O_3$ requires 126.03170).

Conversion of **1**d *to* **2**d

Reaction of **1***d* (2.00 g) with 80% H_2SO_4 (6 mL) for 10 min at room temperature afforded a yellow oil which crystallized. Recrystallization from petroleum ether gave **2***d* as cream-colored prisms (1.47 g, 78%), mp 81–82.5°C; ν_{max} (liq. film) 1758, 1738 cm^{-1}. Molecular ion (5%) at *m/e* 238.1203 ($C_{13}H_{18}O_4$ requires 238.12051); base peak at *m/e* 140.0472 ($C_7H_8O_3$ requires 140.04735).

Conversion of **3** *to* **4**

Reaction of **3** (714 mg) with 80% H_2SO_4 (3 mL) for 10 min at room temperature followed by plc (25% acetone/petroleum ether) gave **4** as a colorless crystalline solid (535 mg, 79%), mp 60–61°C; ν_{max} (KBr) 1760, 1742, 1675 cm^{-1}. Molecular ion (65%) at *m/e* 224.1051 ($C_{12}H_{16}O_4$ requires 224.10486); base peak at *m/e* 93.0703 (C_7H_9 requires 93.07043).

Cyclizations Catalyzed by HCl

Conversion of **1**a *to* **6**a, **7**a, **8**a, **9**a, *and* **9**b

A solution of **1***a* (7.20 g) in CH_2Cl_2 (175 mL) was saturated with HCl(gaseous). The solution was allowed to stand at room temperature, with periodic addition of HCl(gaseous) for 5 days. The residue obtained on evaporation was chromatographed (2% acetone/petroleum ether) to give a solid (2.78 g), crystallization of which from petroleum ether gave (E)-*dihydro-3-carbomethoxymethylene-4,5,5-trimethyl-2(3H)-furanone* **6***a* as colorless prisms (2.49 g, 37%), mp 54–55°C; ν_{max} (KBr) 1759, 1726 cm^{-1}. Molecular ion (< 1%) at *m/e* 198.0895 ($C_{10}H_{14}O_4$ requires 198.08921); base peak at *m/e* 112; ion (82%) at *m/e* 140.0470 ($C_7H_8O_3$ requires 140.04735). Continued elution with 5% acetone/petroleum ether gave (*a*) a solid, crystallization of which from petroleum ether gave the pyranone **7***a* as colorless prisms (223 mg, 3.3%), mp 54–55.5°C; ν_{max} (KBr) 1718 (br) cm^{-1}. Molecular ion (1%) at *m/e* 198.0895 ($C_{10}H_{14}O_4$ requires 198.08921); base peak at *m/e* 140.0467 ($C_7H_8O_3$ requires 140.04735); (*b*) a solid (628 mg); crystallization from petroleum ether gave **9***b* as colorless prisms (472 mg, 5.9%), mp 70–71°C; ν_{max} (CCl_4) 1772, 1740 (sh) cm^{-1}. Very weak (< 1%) molecular ions at *m/e* 236 and 234 ($C_{10}H_{15}O_4$ ^{37}Cl and $C_{10}H_{15}O_4$ ^{35}Cl require 236 and 234); base peak at *m/e* 113.0606 ($C_6H_9O_2$ requires 113.06026); ions at *m/e* 221.0401 (4%) ($C_9H_{12}O_4$ ^{37}Cl requires 221.03946) and *m/e* 219.0430 (13%) ($C_9H_{12}O_4$ ^{35}Cl requires 219.04236); (*c*) a solid (500 mg); crystallization from petroleum ether/ethyl acetate gave **9***a* as colorless prisms (403 mg, 5.1%), mp 67–68°C: ν_{max} (CCl_4) 1775, 1745 (sh) cm^{-1}. Very weak (< 1%) molecular ions at *m/e* 236 and 234 ($C_{10}H_{15}O_4$ ^{37}Cl and $C_{10}H_{15}O_4$ ^{35}Cl require 236 and 234); base peak at *m/e* 113.0605 ($C_6H_9O_2$ requires 113.06026); ions at *m/e* 221.0401 (4%) ($C_9H_{12}O_4$ ^{37}Cl requires 221.03946) and *m/e* 219.0425 (10%) ($C_9H_{12}O_4$ ^{35}Cl requires 219.04236).

The column was now eluted with 50% acetone/petroleum ether. This gave **8***a* as an almost colorless oil (399 mg, 5.9%), n_D^{24} = 1.4689. On standing at 0°C this solidified, mp 36–38°C; ν_{max} (liq. film) 1760 (sh), 1741, 1685 cm^{-1}. Molecular ion (73%) at

Can. J. Chem. Downloaded from www.nrcresearchpress.com by 210.87.254.105 on 09/05/12
For personal use only.

m/e 198.0899 ($C_{10}H_{14}O_4$ requires 198.08921); base peak at *m/e* 155.0711 ($C_8H_{11}O_3$ requires 155.07082).

NOTE: On prolonged (>72 h) exposure to silica gel, either on stirring in $CHCl_3$ or adsorbed to plc plates, **9***a* was quantitatively converted to **2***a*, while **9***b* was quantitatively converted to **6***a*.

Conversion of **1**b *to* **2**b *and* **6**b

A solution of **1***b* (0.450 g) in CH_2Cl_2 (15 mL) was saturated with HCl(gas) and allowed to stand at room temperature for 24 h. The product was shown by ^1H nmr to be a 3:1 mixture of **6***b* and **2***b*. These isomers were readily separated by plc ($CHCl_3$). *(E)-Dihydro-3-carbomethoxymethylene-4,4,5,5-tetramethyl-2(3H)-furanone* **6***b* was obtained as a pale yellow oil, n_D^{25} = 1.4760, which could not be induced to crystallize; ν_{max} (liq. film) 1762, 1728 cm^{-1}. Molecular ion not observed ($C_{11}H_{16}O_4$ requires 212); base peak at *m/e* 126.0685 ($C_7H_{10}O_2$ requires 126.06801); ion at *m/e* 154.0632 (67%) ($C_8H_{10}O_3$ requires 154.06300).

Conversion of **3** *to* **6**c, **7**b, *and* **8**b

Crude **3** derived from reaction of 1-methylcyclohexene (3.664 g, 0.038 mol) with dimethyl acetylenedicarboxylate (4.927 g, 0.035 mol) and $AlCl_3$ (4.614 g, 0.035 mol) was dissolved in CH_2Cl_2 (200 mL) and the solution saturated with HCl(gas). The mixture was allowed to stand at room temperature, with periodic addition of HCl(gas), for 11 days. The residue obtained on evaporation was chromatographed ($CHCl_3$) to give (*a*) an initial fraction (599 mg), containing some unreacted acetylenic ester; (*b*) a yellow oil (2.8 g). Column chromatography (10% acetone/petroleum ether) of this gave (*i*) an oil (718 mg), repeated plc (75% benzene/$CHCl_3$) of which afforded pure **6***c* as a pale yellow oil (225 mg, 3%), which crystallized, mp 27–30°C; ν_{max} (liq. film) 1761, 1723 cm^{-1}. Molecular ion (7%) at *m/e* 224.1048 ($C_{12}H_{16}O_4$ requires 224.10486); base peak at *m/e* 177.0545 ($C_{10}H_9O_3$ requires 177.05517); and (*ii*) compound **7***b* (773 mg) (see below); (*c*) pure **7***b* as a colorless solid (2.003 g, total yield 35%), mp 81–82°C; ν_{max} (KBr) 1715 (br) cm^{-1}. Molecular ion (100%) at *m/e* 224.1048 ($C_{12}H_{16}O_4$ requires 224.10486); (*d*) a yellow oil (950 mg), half of which (estimated yield 5–6%) was **8***b*. Pure **8***b* was obtained from this fraction only after repeated plc ($CHCl_3$) as a colorless crystalline solid, mp 80.5–82°C; ν_{max} (KBr) 1731, 1675 cm^{-1}. Molecular ion (19%) at *m/e* 224.1040 ($C_{12}H_{16}O_4$ requires 224.10486); base peak at *m/e* 181.0862 ($C_{10}H_{13}O_3$ requires 181.08647).

Reactions of Lactones

Conversion of **2**a *to* **8**a

A solution of **2***a* (260 mg) in CH_2Cl_2 (25 mL) was saturated with HCl(gas) and the mixture stirred at room temperature for 24 h. The residue obtained on evaporation was subjected to plc ($CHCl_3$; 10% acetone/petroleum ether), which gave **8***a* as an almost colorless oil (156 mg, 60%) (see above). Signals for **9***a* were present in the ^1H nmr spectrum of the crude product, but this compound did not survive plc. A quantitative yield of **8***a* was also obtained when a solution of **2***a* (100 mg) in triethylamine (15 mL) was refluxed for 17 h.

Conversion of **6**a *to* **8**a

A solution of **6***a* (133 mg) in CH_2Cl_2 (20 mL) was saturated with HCl(gas) and the mixture stirred at room temperature for 42 h. Evaporation gave an oil (135 mg), ^1H nmr of which indicated unchanged **6***a*. However, an almost quantitative conversion of **6***a* to **8***a* was observed when the former (100 mg) was refluxed in triethylamine (15 mL) for 20 h.

Conversion of **4** *to* **8**b

A solution of **4** (240 mg) in CH_2Cl_2 (15 mL) was saturated with HCl(gas) and stirred at room temperature for 24 h. Evaporation gave an oily residue, plc ($CHCl_3$) of which afforded **8***b* as a colorless crystalline solid (197 mg, 82%).

Conversion of **2**a *to* **8**c

Lactone **2***a* (200 mg) was refluxed in 50% H_2SO_4 (10 mL) for 1 h, and the cooled solution then extracted with ether. Drying and evaporation gave the acid **8***c* as cream-colored rosettes (164 mg, 88%), mp 113–115°C; ν_{max} (KBr) 3700–2400 (br. env., with maxima at 3530 and 3410), 1726, 1712, 1685 cm^{-1}. Molecular ion (15%) at *m/e* 184.0740 ($C_9H_{12}O_4$ requires 184.07356); base peak at *m/e* 141.0549 ($C_7H_9O_3$ requires 141.05517); ion at *m/e* 169.0502 (45%) ($C_8H_9O_4$ requires 169.05009).

Conversion of **2**a *to* **5**a

Lactone **2***a* (200 mg) was refluxed for 1 h in 10% NaOH (10 mL). After cooling the solution was extracted with ether, then acidified. Ether extraction of the acid solution afforded acid **5***a* as a pale yellow oil (153 mg, 82%), n_D^{25} = 1.4920; ν_{max} (liq. film) 3700–2400 (br. env. with maxima at 2760 and 2660 cm^{-1}), 1759 (sh), 1730 (br.) cm^{-1}. Molecular ion (22%) at *m/e* 184.0740 ($C_9H_{12}O_4$ requires 184.07356); base peak at *m/e* 141; ion at *m/e* 169.0495 (48%) ($C_8H_9O_4$ requires 169.05009).

Conversion of **2**b *to* **5**b

A solution of **2***b* (1.00 g) in 10% NaOH (30 mL) was heated at 100°C for 3 h. Similar work-up to that used for **5***a* above gave a virtually quantitative yield of **5***b*. The latter crystallized from petroleum ether/ethyl acetate as colorless needles, mp 75.5–77°C; ν_{max} (KBr) 3500–2500 (br. env.), 1730 (br), 1640 (br) cm^{-1}. Molecular ion not observed ($C_{11}H_{16}O_4$ requires 212); base peak at *m/e* 140.0468 ($C_7H_8O_3$ requires 140.04735).

Catalytic Reduction of **6**a

The unsaturated lactone **6***a* (212 mg) in methanol (20 mL) was hydrogenated over 5% Pd/C (70 mg). After uptake of H_2 had ceased (30 min) the normal work-up gave **10***a* as a colorless oil (205 mg, 96%) n_D^{24} = 1.4529; ν_{max} (liq. film) 1764, 1737 cm^{-1}. Molecular ion not detected ($C_{10}H_{16}O_4$ requires 200); base peak at *m/e* 114.0685 ($C_6H_{10}O_2$ requires 114.06808); ion at *m/e* 185.0808 (24%) ($C_9H_{13}O_4$ requires 185.08139).

Catalytic Reduction of **2**a

A solution of **2***a* (756 mg) in methanol (40 mL) was hydrogenated over 5% Pd/C (230 mg). When uptake of H_2 abruptly ceased (10 min) the solution was filtered and evaporated to give a pale yellow oil (750 mg), plc ($CHCl_3$) of which afforded (*a*) a pale yellow oil (283 mg), ^1H nmr of which showed a mixture of **10***a* and **10***b* in an approximate ratio of 2:3. Repeated plc (25% acetone/petroleum ether; $CHCl_3$) gave **10***b* as a pale yellow oil (90 mg), n_D^{24} = 1.4546; ν_{max} (liq. film) 1762, 1736 cm^{-1}. Molecular ion (< 1%) at *m/e* 200.1047 ($C_{10}H_{16}O_4$ requires 200.10486); base peak at *m/e* 114; ion at *m/e* 185.0811 (46%) ($C_9H_{13}O_4$ requires 185.08139); (*b*) a pale orange oil, further plc ($CHCl_3$) of which gave **8***a* (408 mg, 54%).

Similar results were obtained using Adams' catalyst in place of 5% Pd/C, or EtOAc as solvent.

No conversion of **2***a* to **8***a* was observed on treatment with methanol and 5% Pd/C. No **8***a* was formed upon "hydrogenation" of a mixture of **10***a* and **10***b* for 3 h over 5% Pd/C. In addition **8***a* could not be reduced under these conditions.

When the reduction of **2***a* was carried out with deuterium the **8***a* isolated was shown by ^1H nmr to have a single deuterium located at C-6.

Conversion of **2**b *(or* **6**b*) to* **10**d

(*a*) The unsaturated lactone **2***b* or **6***b* (400 mg) in methanol (35 mL) was hydrogenated over 5% Pd/C (60 mg). When uptake of H_2 ceased (2–4 h) the usual work-up gave **10***c* in almost quantitative yield as a colorless oil.

(*b*) The saturated lactone **10***c* (3.10 g) obtained as in (*a*) was dissolved in 10% NaOH (50 mL) and refluxed for 1 h. The cooled solution was extracted with ether, then acidified. Ether extraction of the acid solution gave **10***d* as a colorless solid (2.638 g, 91%). Recrystallization from petroleum ether/ethyl acetate af-

Can. J. Chem. Downloaded from www.nrcresearchpress.com by 210.87.254.105 on 09/05/12
For personal use only.

forded prisms, mp 137–139°C; ν_{max} (KBr) 3650–2500 (br. env. with max. at 3450), 1749, 1700 cm^{-1}. Molecular ion (< 1%) at *m/e* 200.1049 ($C_{10}H_{16}O_4$ requires 200.10486); base peak at *m/e* 114.0685 ($C_6H_{10}O_2$ requires 114.06808); ion at *m/e* 185.0812 (30%) ($C_9H_{13}O_4$ requires 185.08139).

Preparation of **11**

(a) Oxidative Decarboxylation of **10***d* (cf. ref. 18)

A mixture of **10***d* (400 mg), $Cu(OAc)_2 \cdot H_2O$ (87 mg), and pyridine (53 mg) in benzene (20 mL) was stirred at room temperature for 45 min. Lead tetraacetate (2.96 g) in benzene (30 mL) was then added. The resulting mixture was stirred in the dark for 2 h and was then refluxed under N_2 for 19 h. The green solution was washed twice with water, dried, and evaporated. The residue (192 mg) was shown by ^1H nmr to be a mixture of **10***d* and **11** (see below) in a molar ratio of 2.4:1 (estimated conversion to **11**, 15%).

(b) Decarboxylation of **5***b*

A stirred mixture of **5***b* (5.40 g), copper powder (530 mg) and quinoline (120 mL) was heated at 200°C for 6 h. The mixture was cooled, washed with 2 *N* HCl, filtered, and extracted with ether. Evaporation of solvent from the dried extract yielded a yellow oil. Column chromatography afforded **11** (3.309 g, 79%) as an apparently volatile colorless oil which crystallized at low temperature, with mp 14–17°C; ν_{max} ($CHCl_3$) 1753 cm^{-1}. Molecular ion (< 1%) at *m/e* 154.0995 ($C_9H_{14}O_2$ requires 154.09938); base peak at *m/e* 96.0580 (C_6H_8O requires 96.05752).

The above decarboxylation can also be achieved using Cu powder and pyridine. However, the reaction is slower and the quality of the product inferior to that obtained using quinoline.

Crystallography

The several space groups were determined from single-crystal photographs. The unit cell constants were derived from least-squares analyses of the settings of a Picker four-circle diffractometer for twelve or more reflections in the range $98 < 2\theta < 130°$. The intensities of all independent reflections with $2\theta < 130°$ were measured with θ–2θ scans, using Ni-filtered CuKα radiation ($\lambda\alpha_1$ = 1.5405 Å). Individual reflection profiles were analysed as described by Grant and Gabe (19). The standard deviations of the measured intensities were evaluated from counting statistics, and reflections for which $I(\text{net}) < 2\sigma(I(\text{net}))$ were treated as unobserved.

All structures were solved uneventfully with the aid of MULTAN (20). Refinement was by block-diagonal least squares, minimizing $\Sigma w\Delta F^2$, where $1/w = \sigma^2(F_o) + kwF_o^2$. Hydrogen atoms were included in the refinement, with initial positions reasonably assumed, or inferred from difference-Fourier syntheses. The parameters refined were atomic coordinates, temperature factors (anisotropic for C and O), scale factor, and secondary extinction coefficient *g* (21). The computer programs used are identified in ref. 22. The atomic scattering factors were taken from ref. 23. The final atomic coordinates are given in Table 6. (Tables of final atomic positions, bond lengths, torsion angles, thermal parameters, and F_o and F_c have been placed in the Depository of Unpublished Data.[5])

Crystal Data and Refinement Details

Compound **2**b

Monoclinic, $P2_1/a$, (systematic absences: $0k0$ for k odd; $h0l$ for h odd) a = 11.585 (1), b = 15.884 (1), c = 6.7238 (5) Å, β = 111.61 (3)°, V = 1150.3 Å^3, ρc = 1.225, Z = 4, specimen dimensions 0.2 × 0.3 × 0.6 mm, no absorption corrections (μ = 0.78 mm^{-1}), g for secondary extinction 4.36 × 10^4 Å, kw in weighting scheme, 0.0002. 1955 reflections were scanned, and of these 1658 were observed. For the latter only, the final R index was 0.049 (Rw = 0.074). The esd's of bond lengths and angles (C and O only) are 0.002 to 0.003 Å and 0.1 to 0.2°.

Compound **2**a

(Because of severe decomposition problems, the specimen was maintained at −150°C with the use of a modified Syntex cryostat.) Triclinic, $P\bar{1}$, a = 8.518 (1), b = 9.554 (1), c = 6.723 (1)Å, α = 101.34 (1), β = 88.20 (1), γ = 109.29 (1)°, V = 506.0 Å^3, ρc = 1.301 g cm^{-3}, Z = 2, specimen dimensions 0.05 × 0.3 × 0.3 mm, no absorption corrections (μ = 0.83 mm^{-1}), g for secondary extinction 2.6 × 10^4Å, kw in weighting scheme, 0.0004. 1714 reflections were scanned, and of these 1506 were observed. For the latter only, the final R index was 0.037 (Rw = 0.052). The esd's of bond lengths and angles are 0.002 Å and 0.1°.

Compound **6**a

(To prevent rapid decomposition in air, the specimen was sealed in a thin-walled glass tube). Monoclinic, $P2_1/n$, (systematic absences: $0k0$ for k odd; $h0l$ for $h + l$ odd), a = 9.061 (1), b = 18.630 (2), c = 6.292 (1)Å, β = 96.77 (1)°, V = 1054.7 Å^3, ρc = 1.248 g cm^{-3}, Z = 4, specimen dimensions 0.3 × 0.5 × 0.7 mm, no absorption corrections (μ = 0.79 mm^{-1}), g for secondary extinction, 6.5 × 10^3Å, kw in weighting scheme, 0.0005. 1801 reflections were scanned, and of these 1398 were observed. For the latter only, the final R index was 0.041 (Rw = 0.066). The esd's of bond lengths and angles are 0.002 to 0.003 Å, and 0.1 to 0.2°.

Acknowledgments

We wish to thank Mrs. M. G. Flack for her excellent technical assistance and J. Hiltz (NRCC summer student, 1976) for his contribution to this work. Our thanks go also to J. Van Ingen for ^1H nmr data, P. F. Seto for ir data, and D. J. Embree for accurate mass determinations. We thank the Drug Evaluation Branch, National Cancer Institute, Bethesda, MD for conducting antitumor screening.

1. A. W. McCulloch and A. G. McInnes. Tetrahedron Lett. 1963 (1979).
2. A. W. McCulloch, B. Stanovnik, D. G. Smith, and A. G. McInnes. Can. J. Chem. **47**, 4319 (1969).
3. J. M. Cassady, S. R. Byrn, I. K. Stamos, S. M. Evans, and A. McKenzie. J. Med. Chem. **21**, 815 (1978).
4. I. H. Hall, K.-H. Lee, C. O. Starnes, S. A. Eigebaly, T. Ibuka, Y-S. Wu, T. Kimura, and M. Haruna. J. Pharm. Sci. **67**, 1235 (1978).
5. P. A. Grieco. Synthesis, 67 (1975).
6. R. B. Gammill, C. A. Wilson, and T. A. Bryson. Synth. Commun. **5**, 245 (1975).
7. B. B. Snider, D. J. Rodini, R. S. E. Conn, and S. Sealfon. J. Am. Chem. Soc. **101**, 5283 (1979).
8. B. B. Snider, D. M. Roush, D. J. Rodini, D. Gonzalez, and D. Spindell. J. Org. Chem. **45**, 2773 (1980).
9. G. Agnes and G. P. Chiusoli. Chim. Ind. Milan, **50**, 194 (1968); Chem. Abstr. **69**, 35352t (1968).
10. T-L. Ho and C. M. Wong. Synth. Commun. **4**, 133 (1974).
11. K. J. Divakar, P. P. Sane, and A. S. Rao. Tetrahedron Lett. 399 (1974).
12. H. M. R. Hoffmann. Angew. Chem. Int. Ed. Engl. **8**, 556 (1969).
13. U. Vogeli and W. Von Philipsborn. Org. Magn. Reson. **7**, 617 (1975).
14. C. Altona, H. J. Geise, and C. Romers. Tetrahedron, **24**, 13 (1968).

15. D. SAVOSTIANOFF and M. PFAU. Bull. Soc. Chim. Fr. 4162 (1967).
16. Z. SAMEK. Collect. Czech. Chem. Commun. **43**, 3210 (1978).
17. S. SIEGEL and J. R. COZORT. J. Org. Chem. **40**, 3594 (1975).
18. J. D. BACHA and J. K. KOCHI. Tetrahedron, 2225 (1968).
19. D. F. GRANT and E. J. GABE. J. Appl. Crystallogr. **11**, 114 (1978).
20. G. GERMAIN, P. MAIN, and M. M. WOOLFSON. Acta Crystallogr. Sect. A, **27**, 368 (1971).
21. A. C. LARSON. Crystallographic computing. Munksgaard, Copenhagen, Denmark. 1970. p. 291.
22. A. C. LARSON and E. J. GABE. Computing in crystallography. Delft University Press, Delft, Holland. 1978. p. 81.
23. International tables for X-ray crystallography. Vol. IV. Kynoch Press, Birmingham, England. 1974. Table 2.2B ('SDS' for H, 'RHF' for C and O).

Can. J. Chem. Downloaded from www.nrcresearchpress.com by 210.87.254.105 on 09/05/12
For personal use only.

The brex-5-yl system. A uniquely structured norbornyl homolog

ALEX NICKON, RAYMOND C. WEGLEIN, AND C. THOMAS MATHEW
Department of Chemistry, The Johns Hopkins University, Baltimore, MD 21218, U.S.A.

Received July 21, 1980

This paper is dedicated to Prof. Raymond U. Lemieux on the occasion of his 60th birthday

ALEX NICKON, RAYMOND C. WEGLEIN, and C. THOMAS MATHEW. Can. J. Chem. **59**, 302 (1981).

The brexane skeleton functionalized at C-5 is perceived as potentially useful for various mechanistic studies. Our present objective was to prepare and characterize brex-5-yl derivatives and to seek spectroscopic evidence for geometric distortion in the skeleton. The structures synthesized include brex-4-ene, brexan-5-one, both of the epimeric brexan-5-ols, and various derivatives of these compounds. Spectroscopic data (ir, ^{1}H nmr, and uv) are compared with those from relevant model compounds and are most simply interpreted on the basis of a twist in the brexyl skeleton. This distortion imparts more *exo* character to the C—H bonds at C-4 and more *endo* character to the C—H bonds at C-5. As an extension of the useful terms geminal and vicinal, we propose the word *hominal* to represent a 1,3-relationship between two groups.

ALEX NICKON, RAYMOND C. WEGLEIN et C. THOMAS MATHEW. Can. J. Chem. **59**, 302 (1981).

On croit que le squelette brexane ayant une fonction en C-5 pourrait s'avérer utile pour diverses études de mécanisme. Notre objectif est de préparer et de caractériser des brexanes substitués en position 5 et de chercher les preuves spectroscopiques de la déformation géométrique du squelette. Parmi les composés synthétisés on note le brexène-4, la brexanone-5, les deux brexanols-5 épimères et plusieurs dérivés de ces composés. On a comparé les données spectroscopiques ir, rmn du ^{1}H et uv de ces composés avec celles de composés modèles appropriés et on les a interprété uniquement en fonction d'une torsion du squelette brexyle. Cette déformation donne aux liaisons C—H en position 4 un caractère fortement *exo* et à celles en C-5 un caractère fortement *endo*. Comme extension des termes géminal et vicinal très utilisés nous proposons le mot *hominal* pour représenter la relation 1,3 entre deux groupes.

[Traduit par le journal]

Tricyclo[4.3.0.0^{3,7}]nonane (**1**), trivially named brexane, is an intriguing homolog of bicyclo-[2.2.1]heptane because it is comprised of two partially superposed norbornyl units with one cyclopentyl ring in common. The norbornyl moieties are revealed in **1***a* and **1***b* by bold lines, and the common ring is numbered **1**, **2**, **3**, **7**, and **6**. Previ-

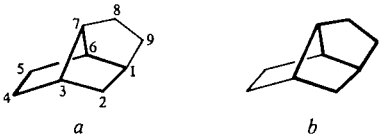

a *b*

1

ously, we prepared and characterized this tricyclic hydrocarbon and its C-2 and C-4 monofunctional derivatives (1). In this paper we draw attention to some potentially useful aspects of C-5 functionalized brexanes and describe their syntheses, characterization, and some transformations. As illustrated in the *exo* derivative **2** (shown in two perspectives, **2***a* and **2***b*, and also in a mirror image perspective, **2***c*), a departing group Z at C-5 apparently has "norbornyl-like" surroundings. However, the remote two-carbon bridge (C-8, C-9) restricts the skeletal changes that might accompany (or follow) ionization of Z. To illustrate, let us consider the three general types of rearrangements observed in norbornyl cations. With conventional norbornyl numbering, these rearrangements are termed 3,2-hydrogen shifts, 6,2-hydrogen shifts, and Wagner–Meerwein ring-bond shift (2). Of these processes the 3,2-H shift (i.e. the *vicinal* H shift) is by far the slowest (2*d*). It is barely detectable in acetolysis of *exo*-norbornyl brosylate (3, 4) but was observed in formolysis (3) and in a low temperature ^{1}H nmr study of the norbornyl cation in $SbF_5/SO_2/SO_2F_2$ (5). For the vicinal shift in substituted norbornyl cations, an *exo*-H rearranges much faster than does an *endo*-H, and some researchers relate this stereochemical preference to structural peculiarities of norbornyl cations (6). By analogy a vicinal H shift in the brex-5-yl cation to

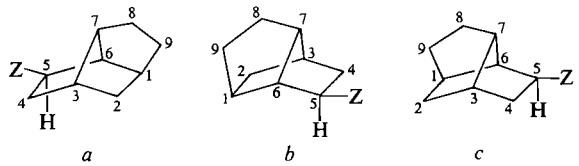

a *b* *c*

2

produce **4** appears possible and would be easily detected from a product study.[1] In contrast, cation **3** should resist the other two types of "norbornyl"

[1]The rearranged cation **4** has been generated other ways in HOAc, and its fate is known (refs. 1, 7, 8). For example, prior to capture, much of it undergoes Wagner–Meerwein shift to the brendyl cation **6**.

0008-4042/81/020302-12$01.00/0
©1981 National Research Council of Canada/Conseil national de recherches du Canada

Can. J. Chem. Downloaded from www.nrcresearchpress.com by 210.87.254.5 on 09/05/12
For personal use only.

Can. J. Chem. Downloaded from www.nrcresearchpress.com by 210.87.254.5 on 09/05/12
For personal use only.

rearrangements. Thus, hydride transfer from C-1 to C-5 (analogous to the norbornyl 6,2-H shift and which we term a *hominal*[2] shift) is unlikely because it produces the bridgehead cation **5**, whose instability should parallel that of the bridgehead 1-norbornyl cation (9). A conventional Wagner–Meerwein shift (**3** → **7**) is also unfavourable, because it would produce the twist-brendyl skeleton **7**, which is considerably more strained than the initial skeleton (10).[3] Clearly, if the brex-5-yl system is denied this Wagner–Meerwein shift capability, then a complete mechanistic study of its ionization behavior becomes important because the "nonclassical" ion interpretation of norbornyl chemistry requires onset of such a shift during ionization of *exo*-derivatives (2), whereas other interpretations do not (11). Other workers have independently recognized the potential value of constrained skeletons for mechanistic study and have prepared tricyclic and pentacyclic structures like **8***a* (12*a*) and **8***b* (12*b*, *c*). Although **8***b* contains a brexyl unit within its skeleton (see heavy lines), this pentacycle has extra nonbonded interactions and other complicating features that would preclude direct comparison with the norbornyl system.

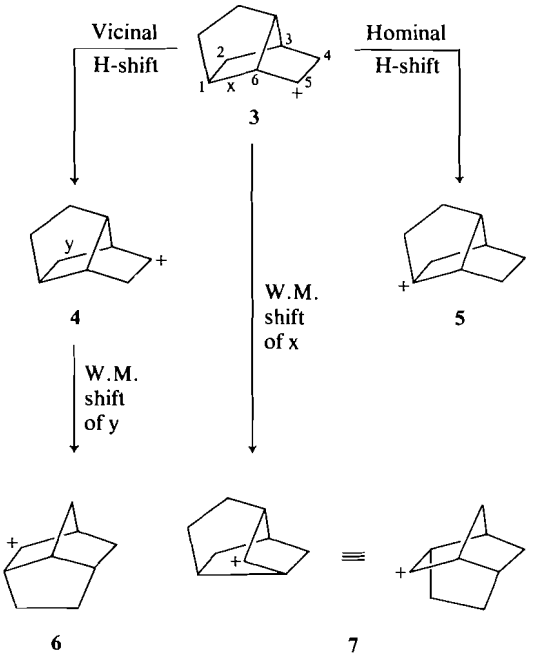

3 4 5 6 7

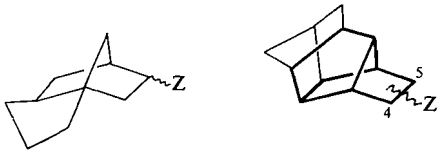

8*a* 8*b*

Another worthwhile mechanistic study would compare brex-5-yl (**3**) and brex-4-yl (**4**) behavior, because the latter cation generated solvolytically does rearrange via Wagner–Meerwein shift to the brend-2-yl system **6** (7, 8). Such comparison is especially meaningful if the surroundings of a substituent at C-5 and C-4 are similar enough so that differences in kinetic behavior could not be attributed to differences in nonbonded interactions. Because molecular models of brexane suggest that the ethano bridge twists[4] the "norbornyl" portion somewhat, it becomes essential to learn experimentally how this twist affects the local environ-

[2]Chemists use *geminal* and *vicinal* to designate, respectively, attachment to the same atom (i) and to adjacent atoms (ii). However, no convenient word serves for iii, the next stage in

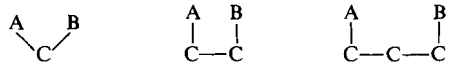

i ii iii

geminal *vicinal* *hominal*

this progression; and clarity sometimes suffers. For example, a 1,5-H shift in the brexyl cation **3** corresponds structurally to a 6,2-H shift in the norbornyl cation; and both represent 1,3-H shifts in the generalized sense. To avoid possible misinterpretation of the numerals, chemists frequently resort to awkward terms such as "6,2-norbornyl type" or "1,3-type" to describe this general class of H-shift. Since "homo" is widely used to denote a homologous counterpart (cf. homoenolate ion, homoconjugation, homoaromaticity, etc.), we propose "hominal" to signify a 1,3-relationship between two groups. (The ending *inal* rather than *onal* keeps its spelling and pronunciation as in gem*inal* and vic*inal*.) Thus, a hominal elimination is a 1,3- or γ-elimination. And, we may speak of hominal proton coupling in nmr (J_{hom}), of hominal orbital overlap, of hominal insertions by carbenes, of *hom*-dihalides, of hominal H-loss from a cation, of hominal axial interactions in a cyclohexane chair, etc.

[3]The strain in twist-brendane has been estimated (ref. 10*b*) to exceed that in brexane by 5.2–8.7 kcal/mol (21.8–36.4 kJ/mol).

[4]Altona and Sundaralingham (13) would describe this distortion as a *synchro*-twist. Thus, if perspective **2***b* of brexane is viewed along the C-6 · · · C-3 vector, the *rear* atoms (C-2 and C-4) of the *norbornyl unit* are both displaced in the *same twist sense* (i.e. both counterclockwise or both clockwise) relative to the front atoms (C-1 and C-5). For the enantiomer depicted in **2***b*, the *synchro* twist is counterclockwise (as shown in i), whereas

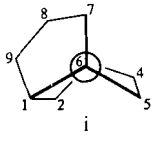

i

for the mirror image **2***c* the *synchro* twist is clockwise. When the rear atoms of a substituted norbornyl unit are displaced in opposite twist senses (i.e. one clockwise and one counterclockwise), the twist is termed *contra*.

Can. J. Chem. Downloaded from www.nrcresearchpress.com by 210.87.254.5 on 09/05/12
For personal use only.

ments at C-4 and C-5 relative to each other and relative to their norbornyl counterparts. We shall first outline our syntheses and characterization of brexanes functionalized at C-5. Then we shall describe relevant spectral features of the C-5 and C-4 derivatives as probes for geometric distortion in the brexyl skeleton. These studies provide a necessary foundation for later interpretation of kinetic behavior.

Our starting point was deltacyclane (**10**) (1), obtained by Wolff–Kishner reduction of deltacyclan-8-one (**9**) (1, 14) and also by hydrogenation of deltacyclene (15). In this work we improved considerably the reported (14) two-step synthesis of ketone **9** from norbornadiene and α-chloroacrylonitrile. Then, by a known three-step sequence, we converted hydrocarbon **10** to a mixture of brexan-4-one (**11**) and brendan-2-one (**12**), readily separated by gas chromatography (1). We tried, unsuccessfully, to convert **11** to brex-4-ene (14) by the Shapiro–Heath (16) modification of the Bamford–Stevens reaction, but we satisfactorily accomplished this change by bromination, reduction with $NaBH_4$, and reductive elimination of the bromohydrins with zinc. This sequence was carried through without characterization of intermediates and has the added advantage that it can be applied to a mixture of **11** and **12**. The latter ketone, being nonenolizable, is not brominated and ends up as alcohols, from which we separated liquid olefin **14** by column chromatography. A different route to brex-4-ene is now available through discovery by Brieger and Anderson (17) that 1-(3′-butenyl)-1,3-cyclopentadiene (**13**) at 180°C undergoes diene isomerization followed by intramolecular Diels–Alder addition to give an olefin identical with our brex-4-ene.[5]

Osmium tetroxide converted olefin **14** to the *exo*–*cis*-diol **15**, for ir and ^1H nmr studies. Although we have no rigorous proof, the *exo* stereochemistry for **15** is indicated by the lack of nmr coupling between each of the carbinyl protons at C-4 and C-5 and its adjacent bridgehead proton. Furthermore, as will soon become evident, *exo* attack is highly favored in other additions to brex-4-ene.

Hydroboration of olefin **14** produced virtually only two alcohols, in ca. 72:28 ratio. The minor component corresponded to the known *exo*-brexan-4-ol (**16**) (1). Acetylation of the mixture and separation by preparative gas chromatography afforded the known *exo*-brexan-4-ol acetate (**17**) (1) and the major product, *exo*-brexan-5-ol acetate (**19**). This new, liquid acetate was fully characterized and was reduced with $LiAlH_4$ to crystalline *exo*-brexan-5-ol (**18**), which gave a solid brosylate **20** by treatment with brosyl chloride in pyridine. The *exo* stereochemistry in compounds **18**–**20** follows from several spectral correlations to be discussed later.

In contrast to hydroboration, which gave *exo* products almost exclusively, oxymercuration of brex-4-ene (**14**) followed by acetylation produced ca. 35 rel.% of *endo*-brexan-5-ol acetate (**22**) together with *exo*-4-OAc **17** (54%) and *exo*-5-OAc **19** (11%). The pure, liquid *endo*-5-OAc **22** was separated by gas chromatography and was reduced with $LiAlH_4$ to solid *endo*-brexan-5-ol (**21**). This alcohol gave a crystalline brosylate (**23**) by action of methyl lithium and brosyl chloride. Each of the epimeric alcohols **18** and **21** was oxidized to brexan-5-one (**24**), but we used the (more plentiful) *exo*-alcohol to get this liquid ketone in quantity. We reconverted brexan-5-one to brex-4-ene (**14**) by a Bamford–Stevens sequence (18) and so proved that the brexane skeleton remains intact in ketone **24**. Let us now compare spectral properties of our tricyclic molecules with their norbornyl counterparts to probe for distortions in the brexane skeleton (19).[6]

Spectral Characteristics

Infrared carbonyl stretching frequencies in cyclic ketones have been used to estimate C—CO—C bond angles (20) and to assess strain in secondary, cycloalkyl cations (21). In carbon tetrachloride the ketone bands (cm^{-1}) in brexan-5-one (1749), brexan-4-one (1751) (7), and brexan-2-one (1751) (7) are very close to that in norbornan-2-one (1751) (7, 20*b*, *d*). In this respect, therefore, the brexyl skeleton is clearly "norbornyl-like."[7]

From studies of the near infrared spectral region, Gassman and Hooker (23) found that norbornenes show an overtone of the olefinic C—H stretch between 6083–5977 cm^{-1}. The band position depends on skeletal structure, and on the number of substituents and their electronic and stereochemical nature. Norbornene itself absorbs at 6013 cm^{-1}, and we find that brex-4-ene is very similar, with absorption at 6010 cm^{-1}.

Another infrared spectral comparison involves

[5]We thank Dr. G. Brieger for helpful exchange of information.

[6]For extensive tables that also include other polycyclic systems in these comparisons, see ref. 19.

[7]In contrast, the pentacyclic ketones related to **8***b* represent distorted norbornyl homologs because the 4-one absorbs at 1746 and the 5-one at 1744 (22). For a stretching frequency of 1751 the C—CO—C angle is estimated at 101.5° (20*d*); and 1744 corresponds to 104.8°. Note, however, that similarity to norbornan-2-one, and not absolute value, is the relevant aspect. The tricyclic ketone related to **8***a* has a "norbornyl-type" carbonyl at 1749 (12*a*).

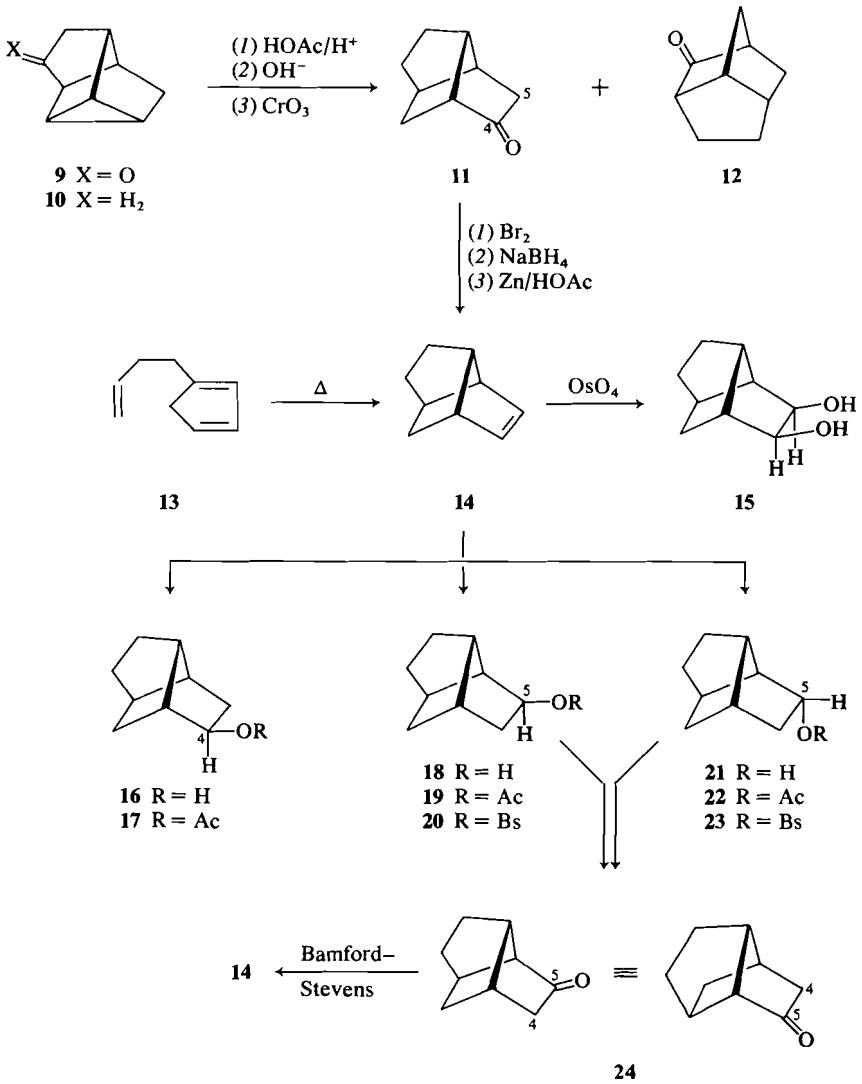

intramolecular H-bonding in vicinal diols recorded at high dilution. An important factor determining the difference (Δν) in O—H stretching frequency between the "bonded" and "nonbonded" OH bands is the dihedral angle between the adjacent oxygens; the larger the dihedral angle the smaller the Δν (24).

Our *exo–cis*-brexane-4,5-diol (**15**) in carbon tetrachloride has Δν 92.4 cm^{-1} (Table 1, Entry 1), which is somewhat less than the values (Δν 103 and 102) for *cis*-norbornanediols (Entry 2). In this respect, therefore, the brexanediol differs from its norbornyl counterparts. Viewed most simply this smaller Δν indicates a skeletal twist, which increases the dihedral angle between the two C—O bonds relative to that in norbornanediol.

However, several selected known *cis* diols shown in Table 1 reveal that factors other than dihedral angle can influence Δν. For example, although the vicinal C—O bonds in camphane (Entry 3) seem as rigidly eclipsed as those in norbornane, the Δν's for the camphanediols (90–96 cm^{-1}) are lower and more like that in brexanediol. Also, the homoadamantanediol (Entry 4) exhibits a still smaller Δν (89 cm^{-1}), and yet molecular mechanics calculations for the parent hydrocarbon favour C_{2v} symmetry, i.e. a nontwisted ethano bridge, with a near 0° dihedral angle for vicinal bonds (25). Finally, noradamantane-3,7-diol (Entry 5) has a surprisingly low Δν (37 cm^{-1}) despite its locked framework, and a dihedral angle of 0° imposed by symmetry (26). Evidently, other factors (such as H—O—C and C—C—O angles) also influence Δν, and these factors might also help explain why Δν for

Can. J. Chem. Downloaded from www.nrcresearchpress.com by 210.87.254.5 on 09/05/12
For personal use only.

TABLE 1. Δν (O—H) for *cis*-diols in bridged polycyclics

Entry	Diol	Δν (cm^{-1})	Reference
1	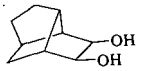	92.4 (*exo–cis*)	This work
2	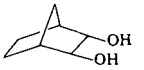	103 (*exo–cis*) 102 (*endo–cis*)	24
3	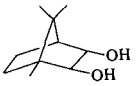	90, 91, 96 (*exo–cis*) 95 (*endo–cis*)	24
4	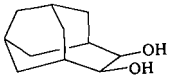	89	25
5	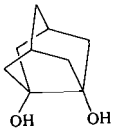	37	26

brexan-4,5-diol (Entry 1) is lower (by ca. 10 cm^{-1}) than that for the norbornanediols. However, because molecular models clearly suggest a synchro twist (13) in the norbornyl units of brexane, and because this tricyclic skeleton has no steric interactions that might impose unusual H—O—C or C—C—O angles, we are inclined to accept a noneclipsed arrangement (i.e. dihedral angle > 0°) for the vicinal bonds in brexanediol.

Proton nmr also provides clues about distortions in brexyl derivatives. We shall first examine olefinic analogs and then derivatives containing only sp^3 carbons. Table 2 summarizes chemical shifts and coupling constants for the olefinic hydrogens in norbornene, brex-4-ene, and pertinent model compounds. In norbornene (Entry 1), our reference model (27, 28), the olefinic hydrogens are equivalent (δ 5.94), but their mutual coupling (J = 5.8 Hz) has been determined indirectly from ^{13}C nmr (28*c*). This equivalence is lost and the skeleton is distorted when a *trans*-fused, five-membered ring is attached as shown in Entry 2 (29). In this tricycle the vinyl hydrogens H-2 and H-3 differ appreciably in location (Δδ = 0.75), and each hydrogen couples differently (ΔJ = 0.50) with its vicinal bridgehead proton. These differences may arise in part from changes in ring angles at each trigonal carbon (i.e. rehybridization) (29) and in part from skeletal twisting. A synchro twist induced by the remote *trans*-fused ring swings H-2 slightly downward (*endo* direction) and H-3 slightly upward (*exo* direction). The dihedral angles change such that the coupling constant $J_{3,4}$ should be greater than $J_{1,2}$ as was observed. Also, relative to norbornene, the chemical shifts for H-2 and H-3 are displaced in opposite directions, and this feature is expected based on published ^1H nmr studies of saturated and unsaturated norbornyl compounds (30). Those studies showed that *exo* hydrogens appear generally at lower field (larger δ) than do *endo* hydrogens. Whatever the theoretical basis for these *exo–endo* differences,[8] olefinic H's that acquire *endo* or *exo* character due to ring-twist might be expected to change their chemical shifts correspondingly. Interestingly, the vinyl–vinyl coupling constant $J_{2,3}$ in this distorted molecule (Entry 2) and in norbornene are virtually the same. Probably this coupling is simply not sensitive enough to reveal a skeletal twist. Alternatively, a compensating effect on $J_{2,3}$ might be produced by changes in olefin-carbon hybridization, because the magnitude of vinyl–vinyl coupling is known to depend on the H—C=C angles (31).

In the pentacyclic brexyl homolog, Entry 3, the olefinic H's were not dissimilar enough[9] to show distinct signals with discernible couplings (22, 32). Therefore, unlike the case in Entry 2, ^1H nmr gives no information about distortion in the pentacyclic olefin.

Brex-4-ene (Entry 4) represents a situation between those of Entries 2 and 3. Thus, the vinyl H's have distinctly different chemical shifts and these accord with a synchro twist that increases the *exo* character of H-4 (larger δ) and increases the *endo* character of H-5 (smaller δ). But, the difference (Δδ = 0.24) is less than that in Entry 2 (Δδ = 0.75), and this smaller change might reflect a smaller distortion. The coupling constants, $J_{3,4}$ and $J_{5,6}$, in Entry 4 give no structural clues, because they are equal to each other and comparable to the corresponding couplings in norbornene (Entry 1).

In 9-oxo-brex-4-ene (Entry 5), the remote polar carbonyl group slightly perturbs the olefinic chemical shifts. But, relative to norbornene, the Δδ's and ΔJ's follow the same trends as in brex-4-ene (19).[6] In summary, the chemical shift differences for the olefinic hydrogens in brex-4-ene support a synchro twist in which H-4 becomes more *exo*-like and H-5 becomes more *endo*-like, with the practical consequence that *exo* approach by reagents should be easier at C-5 than at C-4. *Endo*-approach might also be partly influenced by this twist, but could be

[8]Musher (ref. 30*a*) suggested that the bicyclo[2.2.1]heptane ring skeleton has an inherent magnetic anisotropy that deshields *exo* hydrogens relative to *endo* hydrogens.

[9]Private communication from R. K. Howe (ref. 22) to R.C.W.

Can. J. Chem. Downloaded from www.nrcresearchpress.com by 210.87.254.5 on 09/05/12
For personal use only.

TABLE 2. ^{1}H nuclear magnetic resonance of olefinic hydrogens in brex-4-ene and related polycycles

Entry		δ (H site)	*J* (Hz) Vinyl–vinyl	*J* (Hz) Vinyl–bridgehead	Reference
1[a]	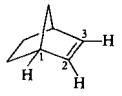	5.94	5.8±0.1[b]	2.95±0.10	27, 28
2[c]	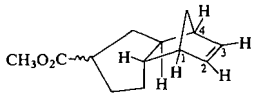	5.82 (C-2) 6.57 (C-3)	5.75	2.85 ($J_{1,2}$) 3.35 ($J_{3,4}$)	29
3	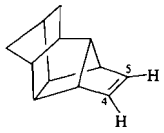	5.82 (C-4,C-5)[d]	—[e]	—[e]	22,32
4[a]	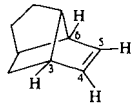	5.77 (C-5) 6.01 (C-4)	5.7	3.0 (C-5,C-6) 3.0 (C-3,C-4)	This work
5[f]	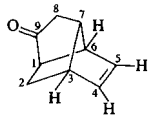	5.88 (C-5) 6.35 (C-4)	5.5	3.2 (C-5,C-6) 3.2 (C-3,C-4)	33[g]

[a]CCl_4 solution.
[b]Obtained from ^{13}C nmr (28c).
[c]$CDCl_3$ solution.
[d]Center of unresolved multiplet ($W_{1/2}$ 8Hz) from H's at C-4 and C-5; solvent unspecified.[9]
[e]Not discernible from the unresolved multiplet.[9]
[f]Solvent not specified.
[g]We are grateful to Adams and Trecker (ref. 33) for privately informing us of their synthesis of 9-oxo-brex-4-ene (Table 2, Entry 5) and for providing a sample. We confirmed their proposed structure by catalytic hydrogenation of the double bond to give authentic brexan-4-one, and not (as reported in ref. 33) by Wolff–Kishner reduction to give brex-4-ene.

dominated by interactions with the transannular *endo* hydrogens at C-1 and C-2.

We now turn to our saturated brexyl systems to seek evidence for skeletal twist relative to their norbornyl counterparts (34). Electron diffraction studies (35) on norbornane reveal a skeleton with C_{2v} symmetry and, therefore, virtually eclipsed vicinal hydrogens at the sides of the boat-shaped ring, i.e. C—H dihedral angles of 0° and 120°. X-ray studies on a small number of norbornanes show that substitution can distort the ring slightly in a *synchro* or *contra* manner to change these dihedral angles (13).[10] Therefore the reported ranges for ^{1}H nmr shifts and for coupling constants (derived from a large number of substituted norbornanes) already embrace molecules slightly distorted from true C_{2v} symmetry and from the corresponding true dihedral angles. Marchand *et al.* (36) have pointed out that even for norbornane itself and for its non-distorted analogs, *exo–exo* vicinal coupling exceeds *endo–endo* coupling, and they proposed a theoretical interpretation involving transannular interactions of the C-2 and C-3 bonds with the C-7 methylene bridge (37). Therefore, an in-depth understanding of couplings in our brexanes relative to those in norbornanes should take into account these hominal interactions as well as vicinal ones. Qualitatively, however, we might probe for distortion in the brexyl skeleton through the Karplus relationship between vicinal dihedral angle and J_{HH} (38). Although the literature is replete with accurate *J*'s for unsaturated norbornyl derivatives (34, 36, 37), the data for saturated norbornanes are meagre. Table 3 lists the available information (Entries 1 and 2) and also summarizes the chemical shifts and coupling constants for our monofunctional brexanes (Entries 3 through 7). Although the norbornyl analogs are of little help, we can infer a twist in the saturated brexyl skeleton from the following

[10]Although calculations suggest that *synchro* twist should prevail when substituents are at C-2 and/or C-3, one example of *contra* twist has been observed, namely, in *exo*-norbornan-2-ol tosylate, where the O—S bond and the aryl ring may exert their own special influence (ref. 13).

Can. J. Chem. Downloaded from www.nrcresearchpress.com by 210.87.254.5 on 09/05/12
For personal use only.

TABLE 3. Nuclear magnetic resonance of carbinyl protons in brexyl and norbornyl derivatives

Entry	Compound	Chemical shifts (δ) and coupling constants (J)[a] Z = OH	Z = OAc	Z = OBs	Reference
1	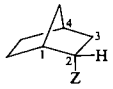	4.18[b] $W_{1/2} = 20$[d]	4.86[c] $W_{1/2} = 20$[d]	4.82[b] $W_{1/2} = 20$[d]	1
2	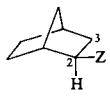	3.71[b] $J_{2n,3n} = 6$	4.52[c] $J_{2n,3n} = 6$	4.49[b] $J_{2n,3n} = 4.5$	1
3	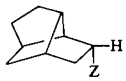	4.20[b] $W_{1/2} = 20$	4.90[b] $W_{1/2} = 22$	4.74[c] $W_{1/2} = 20$	1
4	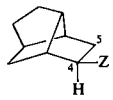	3.71[b] 3.58[c] $J_{4n,5n} = 6$	4.59[b] 4.46[c] $J_{4n,5n} = 6.2$[e] $J_{4n,5x} = 1.5$	4.36[c] $J_{4n,5n} = 5$	1, This work
5	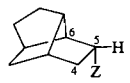	4.30[c,f]	5.05[c] $J_{5x,4x} = 8.5$ $J_{5x,4n} = 1.5$ $J_{5x,6} = 5.0$	4.96[c] $J_{5x,4x} = 9.0$ $J_{5x,4x} = 1.5$ $J_{5x,6} = 5.0$	This work
6	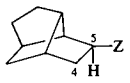	3.95[c] $J_{5n,4n} = 7.0$ $J_{5n,4x} = 4.0$	4.79[c] $J_{5n,4n} = 7.2$[e] $J_{5n,4x} = 4.0$[e]	4.67[c,f]	This work
7	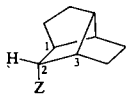	3.71[c] $J_{2,3} = 6$[g]	4.47[b] $J_{2,3} = 5.5$[g]	4.38[b] $J_{2,3} = 5.5$[g]	1

[a]When J's are not extractable from multiplets owing to poor resolution, we report $W_{1/2}$, i.e. the width (Hz) of the multiplet at half-height. Subscripts x = *exo*, n = *endo*.
[b]Recorded in $CDCl_3$.
[c]Recorded in CCl_4.
[d]Couplings in these specific compounds do not appear to be reported. However, for various bicyclo[2.2.1]heptane derivatives (saturated and unsaturated), typical J ranges are as follows: $J_{x,x} = 7.4–11.6$; $J_{x,n} = 2.1–4.6$; $J_{1,2x} = 2.9–4.3$; $J_{1,2n} = 0$; $J_{2x,6x} = 1.0–1.8$; $J_{2n,7anti} = 2–4$. See refs. 19 and 34.
[e]This value (±0.5 Hz) was confirmed by stereospecific preparation of monodeuterated analogs (ref. 18).
[f]Coupling constants not recorded.
[g]Note in the formula as written and numbered in entry 7, if the H and Z at C-2 were interchanged, then this coupling would be $J_{1,2}$.

line of reasoning. For the eclipsed, i.e. norbornyl-type, geometry (see **25**), the vicinal couplings, $J_{2x,3n}$ and $J_{3x,2n}$, both correspond to a dihedral angle of ca. 120° because of symmetry; and, therefore, whether an *exo* substituent (for example) is at C-2 or C-3 makes no difference in the *exo–endo* coupling of the remaining hydrogens. In contrast, for a brexane that is synchro-twisted by θ° (see **26**), an *exo* substituent at C-4 should leave the $J_{4n,5x}$ with a decreased coupling (i.e. dihedral angle 120 − θ°), whereas an *exo* substituent at C-5 should leave $J_{5n,4x}$ with an increased coupling (i.e. dihedral angle ca. 120 ± θ°).

The $J_{n,x}$ couplings in three brexyl compounds in Table 3 were identifiable, and those in Entries 4 and 6 constitute a relevant pair for comparison. The 1.5 Hz for $J_{4n,5x}$ in Entry 4 (Z = OAc) is appreciably smaller than the 4.0 Hz for $J_{5n,4x}$ in Entry 6, in accord with a synchro twist.

As a final nmr indication of geometric distortion, we note that the observed couplings ($J \sim 5–6$ Hz) involving an *exo*-H and a vicinal bridgehead hydrogen in two brexyl derivatives (viz. $J_{5x,6}$ in Entry

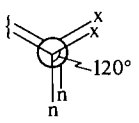

25

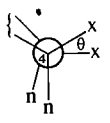

26

Can. J. Chem. Downloaded from www.nrcresearchpress.com by 210.87.254.5 on 09/05/12
For personal use only.

Can. J. Chem. Downloaded from www.nrcresearchpress.com by 210.87.254.5 on 09/05/12
For personal use only.

5, and $J_{2,3}$ in Entry 7) are markedly higher than those in saturated norbornanes (ca. 3.5 Hz, ref. 39).

In ultraviolet excitation of alkenes, a rotation around the double bond increases the wave length of absorption, and Coulson and Stewart have shown theoretically for ethylene how the angle of twist alters the ground state and excited states (40). Our gas phase ultraviolet measurements gave λ_{max} 200 nm for brex-4-ene and λ_{max} 195 nm for norbornene. This difference is consistent with a twist in the tricyclic olefin although by itself is not persuasive, because factors other than olefinic twist could also affect the absorption. Interestingly, 9-oxo-brex-4-ene (Table 2, Entry 5) gave λ_{max} 195 nm. The carbonyl group should widen the ring angle at C-9 and thus lessen the twist. This expectation agrees with the shorter wave length absorbed by the keto-olefin relative to that in brex-4-ene. Thus, the combined evidence from ir, ^{1}H nmr and uv qualitatively supports a synchro twist in the brexyl skeleton, although it cannot define the atomic positions quantitatively. We have previously used computer calculations to estimate dihedral angles in other bridged molecules (10). Now applied to brexane, these calculations lead to a twist of 12.1° for the *exo* bonds and 13.1° for the *endo* bonds, away from the eclipsed array (see **26**). We emphasize, however, that these estimates pertain to the saturated hydrocarbon, and not necessarily to substituted or unsaturated derivatives (41).

Experimental

General

Unless stated otherwise, the following applies. Melting points were determined in sealed Pyrex capillaries, are corrected, and are rounded to the nearer half degree. For distillations we used a 20–30 cm Vigreux column equipped with a cold-finger condenser and a fraction cutter. Reduced pressures refer to millimeters of Hg (Torr). Elemental analyses were by M—H—W Laboratories, Garden City, MI. Routine infrared spectra were run on a Perkin-Elmer Model 337 grating instrument; special spectra (e.g. for H-bonding) were obtained with Perkin-Elmer Model 521 (grating), and near-infrared were recorded with Cary Model 14 spectrometers. Band positions refer to cm^{-1} and the letters sh, w, m, s, and br refer to shoulder, weak, medium, strong, and broad. Ultraviolet spectra refer to the gas phase and were recorded at atmospheric pressure in 1 cm quartz cells on Cary Model 14 and Model 15 spectrometers equipped with a nitrogen flush.

^{1}H nuclear magnetic resonance spectra were run on Varian Associates, Inc., A-60 and HA-100 instruments. The 100 MHz instruments were used in most cases where J values were measured and were operated by Mr. William Ellis, by Dr. James Alderfer (Johns Hopkins School of Hygiene and Public Health, courtesy of Professor Paul O. P. Ts'o), by Dr. Haruhiko Yagi (National Institutes of Health, courtesy of Dr. B. Witkop), and by Mr. Robert Confer (Pennsylvania State University, courtesy of Professor L. M. Jackman), whom we thank.

Analytical gas chromatography (glc) was conducted on a Perkin-Elmer Model 900 analytical instrument equipped with a hydrogen flame ionization detector linked to a Model 16 Honeywell recorder and disc integrator. Preparative glc was done with a Wilkins Aerograph "Autoprep" Model A-700 fitted with a thermal conductivity detector and Honeywell recorder. Temperatures were routinely 180 ± 10°C for the injector and 230 ± 10°C for the detector. The carrier gas was always helium. Retention times (t_R) are in minutes, and relative percentages were determined from disc integration data and represent the average of at least two determinations. Column designation, column temperature, and column inlet pressure are included for each case.

Analytical Columns

A-1: Golay R 300 ft (0.01 in. id) with polypropylene glycol liquid phase (UCON-oil LB-550-X). A-2: Golay FFAP, 100 ft (0.02 in. id) with Varian's Free Fatty Acid Phase. A-3: 9 ft (1/8 in. od) 15% Carbowax 20M on 80/100 Chromosorb W. A-4: 9 ft (1/8 in. od) 20% Reoplex 400 on 80/100 Chromosorb W. A-5: 9 ft (1/8 in. od) 10% Carbowax 20M on 80/100 Chromosorb W. A-6: 9 ft (1/8 in. od) 20% MBMA (*m*-bis-(*m*-phenoxy)benzene + Apiezon L Grease) on Chromosorb W 80/100. A-7: Golay Reoplex 400, 300 ft (0.01 in. id).

Preparative Columns

P-1: 50 ft (1/4 in. od) 20% Reoplex 400 on 80/100 Chromosorb W. P-2: 20 ft (3/8 in. od) 30% Carbowax 20M on 40/60 Chromosorb W. P-3: 18 ft (3/8 in od) 27% diethylene glycol succinate (DEGS) on 80/100 Chromosorb W.

Solvents and Reagents

Brown's oxidation reagent containing two oxygen milliequivalents per milliliter consisted of a solution of sodium dichromate (50 g, 0.168 mol) in 96% sulfuric acid (37.5 mL) and distilled water (150 mL), made up to a final volume of 253 mL with more distilled water (42). *Preoxidized ether*: twice the volume of diethyl ether necessary for an oxidation was stirred with one-tenth of its volume of Brown's reagent for 1 h. The ether layer was washed successively with 1/10 volume proportions of water, saturated sodium bicarbonate, and brine. The ether was dried over $MgSO_4$. *Dry ether* was obtained by distillation from lithium aluminum hydride. To purify n-*pentane* we stirred commercial pentane for 24 h with 1/4 its volume of a 1:1 solution of concentrated and fuming sulfuric acids. The pentane layer was washed repeatedly with water and saturated sodium bicarbonate. It was dried over $MgSO_4$ and finally was distilled (bp 35–36°C) from sodium wire. *Methylene chloride* was stirred (24 h) with concentrated sulfuric acid, was washed repeatedly with water, then with saturated sodium carbonate. It was dried over calcium chloride and finally distilled (bp 39–40°C) from phosphorous pentoxide. *Chromium trioxide – pyridine complex* was obtained by addition of CrO_3 (6 molar equivalent, vacuum dried before use) to a magnetically stirred solution of pyridine (12 molar equivalent) in purified methylene chloride (ca. 15 mL per 1.0 mmol of alcohol to be oxidized) protected with a calcium chloride drying tube. After 1–2 h stirring at room temperature, we added the alcohol to be oxidized.

Deltacyclan-8-one (9)

(a) Diels–Alder Reaction

A degassed mixture of freshly distilled norbornadiene (44.0 g, 0.48 mol), freshly distilled α-chloroacrylonitrile (40.3 g, 0.46 mol, Marbon Chemical Division of Borg-Warner), and hydroquinone (0.3 g) was heated 14 h at 200°C in a thick, vacuum-sealed Pyrex tube. The cooled mixture was poured into pentane (1 L), was filtered to remove polymer, and was concentrated on a rotary evaporator. Distillation of the residue gave 56.3 g (68%) of *8-cyano-8-chlorodeltacyclane*; bp 73–75°C at 1 Torr (lit. (14) bp 89–94°C at 0.1 Torr). The characteristic ir (neat) and ^{1}H nmr bands agreed with those reported (14).

Can. J. Chem. Downloaded from www.nrcresearchpress.com by 210.87.254.5 on 09/05/12
For personal use only.

(b) Hydrolysis

The adduct (43 g) was hydrolyzed in dimethyl sulfoxide – aqueous KOH essentially as reported (14). The residue from work-up gave 18.7 g (58%) of deltacyclan-8-one (bp 104°C, 21 Torr), whose ir, ^{1}H nmr, and glc were identical to those of an authentic sample (1).

Deltacyclane (10)

Wolff–Kishner reduction of ketone **9** as reported gave this hydrocarbon, whose ir and glc (A-6, 100°C, 40 psi) were identical to those of an authentic sample (1). We also obtained deltacyclane by hydrogenation (10 h at 50 psi) of deltacyclene (15) (33.4 g) in pentane (80 mL) over prereduced PtO_2 (0.06 g in 20 mL pentane). Filtration and evaporation left 33.5 g of pure deltacyclane. Near ir (not previously reported in ref. 1) (CCl_4): 5992 cm^{-1}, ε 0.960.

Brexan-4-one (11) and Brendan-2-one (12)

The cyclopropyl ring in deltacyclane was opened with $HOAc/H_2SO_4$, and the derived mixture of *exo*-4-brexyl and *exo*-2-brendyl acetates was saponified to an alcohol mixture, which was directly oxidized to a mixture of ketones **11** and **12** (ratio typically ~ 1:1.2) as described (1*b*). Preparative glc (P-2, 185°C, 60 psi) of 200 μL batches of neat, liquid mixture separated the ketones with collection efficiency of 65% and a purity for each of > 99% (A-3, 170°C, 40 psi). However, for routine preparation of brex-4-ene, we were able to use the ketone mixture rather than pure brexan-4-one because brendan-2-one has no readily enolizable hydrogens.

Brex-4-ene (14)

(a) Halohydrin Route

A mixture (typically 1:1.2) of ketones **11** and **12** (4.63 g, 34 mmol) was treated with pyridinium hydrobromide perbromide (43*a*) (5.43 g, 17 mmol) in glacial acetic acid (35 mL) for 40 min at 55°C. The solution was added to water (450 mL) and extracted with methylene chloride (3 × 30 mL), which was then washed successively with 0.1 *N* sodium thiosulfate (50 mL) and saturated sodium bicarbonate (100 mL). The organic layer was dried over $MgSO_4$ and evaporated to leave 5-bromobrexan-4-one and brendan-2-one as a mixture (5.5 g), which was reduced directly with $NaBH_4$ (0.322 g, 8.5 mmol) in ethanol (15 mL). After 1 h at room temperature the reaction mixture was added to water (350 mL) and extracted with ether (5 × 20 mL), which was then washed with brine (50 mL), dried over $MgSO_4$, and evaporated to leave a mixture (5.45 g) of bromohydrins and brendan-2-ol.[11] This mixture in glacial acetic acid (10 mL) containing water (1 mL) was stirred 30 min at room temperature with zinc (2.2 g). After addition of water (200 mL) and extraction with pentane (3 × 20 mL) the extract was washed with saturated sodium bicarbonate and dried over anhydrous sodium carbonate. The residue (3.06 g) from evaporation was chromatographed on Alcoa F-20 alumina (100 g). Elution with pentane (100 mL) gave liquid brex-4-ene (0.71 g, 36% based on ketone **11**), which was > 98% pure by glc (A-6, 100°C, 40 psi). Ultraviolet λ_{max}: 200 ± 0.2 nm (gas phase, atmospheric pressure). Under the same conditions norbornene had λ_{max} 195 nm. Infrared ν (CCl_4): 6010 cm^{-1}, ε 0.724; ν (CS_2): 3050 (m), 1340 (m), 702 (s, *cis* olefin CH) cm^{-1}; ν (neat): 1615 cm^{-1}; ^{1}H nmr (CCl_4) δ: 6.01 and 5.77 (olefinic hydrogens at C-4 and C-5, respectively, each signal is a double doublet, $J_{4,5}$ = 5.7 Hz, $J_{3,4}$ = $J_{5,6}$ = 3.0 Hz), 2.53 (broad s, 1), 2.38 (broad s, 1), 2.10 (broad s, 1), 1.83–1.49 (m, 3), 1.49–1.03 (m, 3), 0.86 (m, 1).[12]

Anal. calcd. for C_9H_{12}: C 89.94, H 10.06; found: C 89.72, H. 10.18.

(b) Intramolecular Diels–Alder Route

Sodium (4.82 g, 0.21 mol) was finely dispersed in boiling xylene. The bulk of the xylene was decanted from the cooled mixture, and dry tetrahydrofuran (50 mL) was added, then decanted. Addition and decantation of tetrahydrofuran was repeated three times to remove xylene, which is difficult to separate from brex-4-ene. Finally, dry tetrahydrofuran (100 mL) was added, and the ice-cooled mixture was stirred in a nitrogen atmosphere as cyclopentadiene (20 mL) from pyrolysis of dicyclopentadiene (43*b*) was added over 30 min. After an additional 45 min, 4-bromobutene (27 g, 0.2 mol, Columbia Organic Chemicals Co.) was added over 45 min, and the mixture was stirred an additional 2.5 h. Work-up as described by Brieger and Anderson (17) gave crude 1-(3′-butenyl)-1,3-cyclopentadiene (**13**, 20.2 g, 84%), with ir and ^{1}H nmr absorption as reported (17). The crude triene was immediately dissolved in benzene (50 mL) and heated in a sealed tube for 4 h at 180°C. Removal of the benzene on a rotary evaporator and vacuum distillation of the residue gave 17.3 g (72%) of brex-4-ene; bp 84–86°C (100 Torr), > 99% pure by glc (A-6, 100°C, 40 psi), and identical in all respects to olefin from the bromohydrin route.

exo–cis-*Brexane-4,5-diol (15)*

Osmium tetroxide (0.5 g, 1.97 mmol) in ether (6 mL) was added at once to a stirred, carbon tetrachloride (3 mL) solution of brex-4-ene (0.25 g, 2.08 mmol), which was freshly purified by preparative glc (P-2, 100°C, 18 psi). Though exothermic, the reaction did not require cooling. After 84 h pyridine (10 mL), water (10 mL), and sodium bisulfite (0.5 g, 4.8 mmol) were added and stirring was continued 1 h to reduce the osmate ester. Water (25 mL) was added, the mixture was extracted with methylene chloride (5 × 20 mL), which was then washed with 5% hydrochloric acid (10 mL) and with saturated sodium bicarbonate (10 mL), and dried ($MgSO_4$). Evaporation left 0.072 g (24%) of diol, which was recrystallized twice from hexane, mp 98–99°C (0.049 g). Infrared ν (CCl_4): 3620 (m), 3550–3340 (m), 1080 (m), 1060 (s). At high dilution (5 × 10^{-3} *M* in CCl_4), a spectrum recorded with scale expansion on a Perkin-Elmer Model 521 showed a sharp "free" OH at 3631.0 and a broader "bonded" OH at 3538.6 (Δν 92.4 cm^{-1}). ^{1}H nuclear magnetic resonance (CCl_4) δ: 3.95 (d, 1, C-5 H, $J_{4,5}$ = 6.0 Hz), 3.66 (d, 1, C-4 H, $J_{4,5}$ = 6.0 Hz), 2.99 (broad s, 2, OH), 2.46 (broad s, 1), 2.08–1.78 (m, 3), 1.77–1.05 (m, 4), 1.01–0.78 (m, 2). *Anal.* calcd. for $C_9H_{14}O_2$: C 70.10, H 9.15; found: C 70.04, H 9.02.

exo-*Brexan-5-ol Acetate (19)*

Dropwise (75 min) addition of a solution of sodium borohydride (0.34 g, 8.98 mmol) in dry diglyme (9 mL) to freshly distilled boron trifluoride etherate (2.3 mL, 16.2 mmol) in dry diglyme (2 mL) generated diborane, which was continuously passed into a stirred solution of brex-4-ene (3.61 g, 30 mmol) by a stream of nitrogen. The reaction flask was vented to a scrubber containing acetone. The diborane generator was heated 3 h with an air gun and then was recharged with the same amounts of reactants, and the whole cycle was repeated. After the diborane generator was finally heated for an extra 3 h, water (2 mL) was slowly added to the stirred reaction flask to decompose the excess of diborane. After 15 min sodium hydroxide solution (3.2 mL, 3 *N*) was added, followed by hydrogen peroxide (3.2 mL, 30%). The mixture was warmed to 50°C, held there for 1 h, and then poured into a solution of saturated sodium chloride (20 mL) that contained an excess of solid sodium chloride to ensure saturation. The tetrahydrofuran layer was separated, and the aqueous layer was extracted with ether (3 × 15 mL). The combined organic extracts were dried (Na_2SO_4) and evaporated under vacuum. The solid (2.95 g) was almost entirely a mixture of *exo*-brexan-5-ol (18) and *exo*-brexan-4-ol (16) whose approximate ratio (ca.

[11]The brendan-2-ol is largely *endo*. Compare $LiAlH_4$ reduction of brendan-2-one (ref. 1*b*).

[12]Proton assignments at C-4 and C-5 are unambiguous, because we also had 4-deuteriobrex-4-ene from another project (ref. 18).

Can. J. Chem. Downloaded from www.nrcresearchpress.com by 210.87.254.5 on 09/05/12
For personal use only.

3:1) was estimated from their C*H*—O nmr signals in CCl_4 at δ 3.95 and 3.58,[13] respectively. More accurate analysis (glc, A-1, 110°C, 50 psi) revealed a ratio of 72:28 (t_R 110.0 and 112.4 min, respectively). The latter retention time was identical to that of an authentic sample of *exo*-brexan-4-ol (1).

The alcohol mixture (2.45 g) was acetylated with acetic anhydride (5.2 g) in pyridine (10 mL) for 6 h at 25°C and then 10 min on the steam bath. Ether (125 mL) was added and the solution was washed successively with 5% hydrochloric acid (2 × 100 mL), saturated sodium bicarbonate (2 × 50 mL), and saturated sodium chloride (50 mL), and was dried ($MgSO_4$). Evaporation left the acetates as a 72:28 mixture with t_R 30 and 32 min, respectively, (A-4, 125°C, 50 psi). These acetates were separated by preparative glc (P-2, 180°C, 30 psi, t_R 77 min and 90 min). The liquid *exo*-brexan-5-ol acetate (**19**) was rechromatographed on a Reoplex column (P-1, 155°C, 30 psi) and was 99.9% pure. Infrared ν (CCl_4): 1740 (s), 1250 (vs), 1230 (m), 1062 (m), 1045 (w), 1025 (m) cm^{-1}; ^1H nmr (CCl_4) δ: 4.79 (doublet of doublets, 1, CH—O, $J_{4x,5n}$ = 4 Hz, $J_{4n,5n}$ = 7.2 Hz), 2.12 (broad s, 1), 2.07–1.15 (m, 12), 1.01 (broad s, 2). A $OCOCH_3$ singlet at 1.92 protrudes sharply from its surrounding multiplets.[14] *Anal.* calcd. for $C_{11}H_{16}O_2$: C 73.30, H 8.94; found: C 73.23, H 8.96.

exo-*Brexan-5-ol (18)*

exo-Brexan-5-ol acetate (0.36 g) was reduced with lithium aluminum hydride (0.15 g) in ether (50 mL) for 12 h at room temperature and 30 min at reflux. After cautious addition of a little saturated ammonium chloride, the ether was decanted and the residual salts were washed with ether. After being dried ($MgSO_4$) and evaporated, the ether left 0.25 g (90%) of liquid *exo*-brexan-5-ol, which gave the analytical sample (0.21 g) after one bulb-to-bulb distillation at 0.9 Torr at a bath temperature of 90–110°C. Infrared ν (CCl_4): 3605 (m), 1068 (m), 1012 (m) cm^{-1}; ^1H nmr (CCl_4) δ: 3.95 (double doublet, 1, CH—O, $J_{4x,5n}$ = 4.0 Hz, $J_{4n,5n}$ = 7.0 Hz), 2.60 (s, 1), 2.19 (broad s, 1), 2.0–1.05 (m, 9), 0.95 (broad s, 2). *Anal.* calcd. for $C_9H_{14}O_2$: C 78.21, H 10.21; found: C 78.37, H 10.39.

exo-*Brexan-5-ol* p-*Bromobenzenesulfonate (20)*

Brosyl chloride (0.50 g) and *exo*-brexan-5-ol (0.13 g) in benzene (1 mL) and dry pyridine (2 mL) stood three days in the freezer. The precipitated pyridine hydrochloride was removed and washed with ether. The combined ether–benzene solution was washed with cold 5% hydrochloric acid (3 × 10 mL), with saturated sodium bicarbonate (2 × 10 mL), and with 10 mL of saturated sodium chloride, and was dried over $MgSO_4$. Evaporation left 0.35 g of oil, which was taken up in pentane and treated for 30 min with Norite. Filtration through Celite followed by concentration and cooling to −78°C gave a solid, which was collected and recrystallized twice from ether–pentane; 0.13 g, mp 72–73.5°C (remelts at 71–73°C); ir ν (CCl_4): 1190 (s), 1180 (m), 1100 (m), 1075 (m), 1015 (m), 970 (m), 948 (m), 932 (m), 895 (m), 882 (m), 606 (m), 550 (m) cm^{-1}; ^1H nmr (CCl_4) δ: 7.83 (s, 4), 4.67 (double doublet, 1, C*H*—O), 2.3–0.8 (m, 12). *Anal.* calcd. for $C_{15}H_{17}BrO_3S$: C 50.42, H 4.76; found: C 50.15, H 4.82.

endo-*Brexan-5-ol Acetate (22)*

Brex-4-ene (**14**, 12.01 g, 0.1 mol) in tetrahydrofuran (5 mL) was oxymercurated–demercurated with mercuric acetate (35.05 g, 0.11 mol) in water (100 mL) – tetrahydrofuran (100 mL) by a reported general procedure (44). Work-up left an oil (12.3 g, 89%) that contained the following mixture of brexyl alcohols and acetates as revealed by glc (A-1, 110°C, 50 psi): *endo*-5-ol (33%), *exo*-5-ol (10%), *exo*-4-ol (48%), *endo*-5-OAc (2.8%), *exo*-5-OAc (1.3%), *exo*-4-OAc (5.3%). This mixture was combined with acetic anhydride (65 mL) and pyridine (10 mL) and, after 8 h at room temperature, ice was added, the mixture was stirred 30 min, and then combined with water (500 mL) and ether (100 mL). Work-up as described earlier for acetylation left 12.5 g (78.5%) of oil, shown by glc (A-1, 110°C, 50 psi) to consist of: *endo*-5-OAc (35%), *exo*-5-OAc (11%), and *exo*-4-OAc (54%) in that order of elution. Separation by preparative glc (P-1, 158°C, 30 psi) gave pure, liquid *endo*-brexan-5-ol acetate; ir ν (CCl_4): 1740 (s), 1375 (m), 1365 (m), 1248 (s), 1148 (m), 1132 (m), 1036 (m) cm^{-1}; ^1H nmr (CCl_4) δ: 5.05 (double doublet and fine structure, 1, J = 8.5, 5.0, 1.5 Hz, CH—O), 2.3–0.95 (m, 15). *Anal.* calcd. for $C_{11}H_{16}O_2$: C 73.20, H 8.94; found: C 73.36, H 9.06.

endo-*Brexan-5-ol (21)*

Reduction of *endo*-brexan-5-ol acetate (0.133 g) in ether (20 mL) with lithium aluminum hydride (0.056 g) for 13 h at room temperature left 0.106 g of solid on normal work-up; mp 65–66°C. Recrystallization from pentane gave the analytical sample (0.092 g, 90%), mp 68–69.5°C; ir ν (CCl_4): 3601 (m), 1148 (w), 1128 (w), 1078 (m), 1040 (m,), 992 (m); ^1H nmr (CCl_4) δ: 4.30 (m, 1, CH—O), 2.23 (broad d, 1), 2.08–1.75 (m, 4), 1.62–1.18 (m, 6), 1.18–0.92 (m, 2). *Anal.* calcd. for $C_9H_{14}O$: C 78.21, H 10.21; found: C 78.09, H 10.03.

endo-*Brexan-5-ol* p-*Bromobenzenesulfonate (23)*

Methyl lithium (100 μL, 1.8 *M*, Alpha Inorganics, Inc.) was added by syringe to a stirred solution of *endo*-brexan-5-ol (0.023 g, 0.168 mmol, mp 65–66.5°C) in dry ether (1 mL). After 10 min, brosyl chloride (0.045 g, 0.174 mmol) in ether (2 mL) was added by syringe. After 1 h the mixture was diluted with ether and was washed successively with water (20 mL), saturated sodium bicarbonate (20 mL), and saturated sodium chloride (20 mL), and was dried over sodium sulfate and potassium carbonate. Evaporation left 0.060 g (99%) of oil, which was crystallized from pentane at −78°C; 0.012 g, mp 71.5–72.5°C (remelts at 71–71.5°C); ir ν (CCl_4): 1401 (m), 1385 (m), 1190 (s), 1100 (w), 1070 (m), 950 (w), 880 (m) cm^{-1}; ^1H nmr (CCl_4) δ: 7.65 (m, 4, aromatic), 4.96 (double doublet with extra splitting, 1, J = 5.0, 9.0, 1.5 Hz, CH—O), 2.20 (m, 2), 2.0–1.0 (m, 10). *Anal.* calcd. for $C_{15}H_{17}BrO_3S$: C 50.42, H 4.76; found: C 50.42, H 5.00.

Brexan-5-one (24)

exo-Brexan-5-ol (0.54 g, 0.39 mmol) was treated with chromium trioxide – pyridine complex (5.98 mmol) in methylene chloride (45). After 45 min the reaction mixture was taken up in ether (100 mL) and washed with 5% hydrochloric acid (2 × 50 mL), saturated sodium bicarbonate solution (2 × 50 mL), and with saturated sodium chloride. The dried ($MgSO_4$) ether gave 0.049 g (93%) of liquid ketone, which was distilled bulb-to-bulb (90–100°C at 0.9 Torr) to give the analytical sample. Infrared ν (CCl_4): 1749 (s), 1460 (w), 1415 (m), 1320 (m), 1275 (m), 1160 (m), 1145 (m), 1060 (m) cm^{-1}; ^1H nmr (CCl_4) δ: 2.5–2.1 (m, 3), 1.98 (broad s, 1), 1.85 (s, 1), 1.80–1.35 (m, 5), 1.26 (broad s, 2). *Anal.* calcd. for $C_9H_{12}O$: C 79.37, H 8.88; found: C 79.21, H 9.01.

We have reconverted brexan-5-one to brex-4-ene by a Bamford–Stevens sequence (18) as extra proof of skeletal integrity.

9-Oxo-brex-4-ene (Table 2, Entry 5)

Adams and Trecker isolated this compound in low yield from dye-sensitized photooxygenation of 2-ethylidenebicyclo-[2.2.1]hept-4-ene (33). The enone is liquid but gives a crystalline 2,4-dinitrophenylhydrazone (mp 165–166°C), and also a pyrrolidine iminium perchlorate (mp 164–165°C), from which the pure enone is regenerated by alkaline hydrolysis. Dr. Adams kindly provided a sample of his enone, the following infrared and ^1H nmr data, and experimental details. Infrared ν: 3051 (w, olefin CH), 1748 (s, C=O), 1570 (w, C=C), 1404 (m, CH_2CO),

[13]In $CDCl_3$, the CH—O doublet in *exo*-brexan- 4-ol is at δ 3.71 (ref. 1*b*).

[14]Assignment of coupling constants was straightforward, because we had on hand 4-*exo*-deuterio-*exo*-brexan-5-ol acetate and 4-*endo*-deuterio-*exo*-brexan-5-ol acetate (ref. 18).

703, 722 (s, *cis* olefin CH) cm^{-1}; ^1H nmr δ: 1.25 (m, 1, 2-*endo*), 1.65 (m, 1, 2-*exo*), 2.05 (m, 2, C-8 CH_2), 2.35 (m, 1, C-7 H), 2.67 (m, 1, C-3 H), 2.93 (m, 1, C-6 H), 5.88 (m, 1, C-5 H), 6.37 (m, 1, C-4 H). Adams and Trecker derived these nmr assignments and the following coupling constants by appropriate double irradiation techniques: $J_{2n,2x} = 12.9, J_{1,2n} = 6.2, J_{4,5} = 5.5, J_{2x,3} = 5.0, J_{3,4} \sim J_{5,6} = 3.2, J_{1,2x} \sim J_{2n,3} = 0$ Hz. We duplicated their synthesis and also confirmed the structure of the enone by catalytically hydrogenating the double bond to give brexan-4-one, identical in all respects with an authentic sample (1). We measured the near-infrared spectrum of 9-oxo-brex-4-ene in CCl_4: λ: 6031 cm^{-1} (ε 1.044). The gas-phase uv had λ_{max} 195 nm.

Acknowledgements

The research was supported by grants from the National Science Foundation and the National Institutes of Health. We thank Drs. Fu-chih Huang, Donald M. Sainsbury, and Gopalkrishna D. Pandit for experimental help. We thank Professor T. J. Kistenmacher for assistance in computer calculations, and Professor P. von R. Schleyer and D. Khoury for information about their molecular mechanics computer programs.

1. (*a*) A. Nickon, H. Kwasnik, T. Swartz, R. O. Williams, and J. B. DiGiorgio. J. Am. Chem. Soc. **87**, 1613 (1965); **87**, 1615 (1965); (*b*) A. Nickon, H. R. Kwasnik, C. T. Mathew, T. D. Swartz, R. O. Williams, and J. B. DiGiorgio. J. Org. Chem. **43**, 3904 (1978).
2. (*a*) H. C. Brown. The nonclassical ion problem. Plenum Press, New York, NY. 1977; (*b*) G. D. Sargent. Q. Rev. Chem. Soc. **20**, 301 (1966); (*c*) G. E. Greame. Rev. Pure Appl. Chem. **16**, 25 (1966); (*d*) J. A. Berson. Molecular rearrangements. *Edited by* P. de Mayo. Interscience, New York, NY. 1963. Chapt. 3; (*e*) B. Capon, M. J. Perkins, and C. W. Rees. Organic reaction mechanism-1965. Interscience, New York, NY. 1966. Chapt. 1.
3. J. D. Roberts, C. C. Lee, and W. H. Saunders, Jr. J. Am. Chem. Soc. **76**, 4501 (1954); J. D. Roberts and C. C. Lee. J. Am. Chem. Soc. **73**, 5009 (1951).
4. (*a*) C. C. Lee and L. K. M. Lam. J. Am. Chem. Soc. **88**, 2831 (1966); (*b*) J. B. Stothers, C. T. Tan, A. Nickon, F. Huang, R. Sridhar, and R. Weglein. J. Am. Chem. Soc. **94**, 8581 (1972).
5. M. Saunders, P. von R. Schleyer, and G. Olah. J. Am. Chem. Soc. **86**, 5680 (1964).
6. (*a*) J. A. Berson, J. H. Hammons, A. W. McRowe, R. G. Bergman, A. Remanick, and D. Houston. J. Am. Chem. Soc. **89**, 2590 (1967); (*b*) C. J. Collins and B. M. Benjamin. J. Am. Chem. Soc. **89**, 1652 (1967); (*c*) P. von R. Schleyer. J. Am. Chem. Soc. **89**, 699 (1967); (*d*) A. J. Jones, E. Huang, R. Haseltine, and T. S. Sorensen. J. Am. Chem. Soc. **97**, 1133 (1975), and references cited there.
7. T. D. Swartz. Ph.D. Dissertation, The Johns Hopkins University, Baltimore, MD. 1966.
8. R. S. Bly, R. K. Bly, A. O. Redenbaugh, and O. R. Vail. J. Am. Chem. Soc. **89**, 880 (1967).
9. G. J. Gleicher and P. von R. Schleyer. J. Am. Chem. Soc. **89**, 582 (1967).
10. (*a*) A. Nickon and R. C. Weglein. J. Am. Chem. Soc. **97**, 1271 (1975); (*b*) E. M. Engler, J. D. Andose, and P. von R. Schleyer. J. Am. Chem. Soc. **95**, 8005 (1973).
11. (*a*) F. R. Jensen and B. E. Smart. J. Am. Chem. Soc. **91**, 5688 (1969); (*b*) G. A. Olah, J. R. DeMember, C. Y. Lui, and R. D. Porter. J. Am. Chem. Soc. **93**, 1442 (1971); (*c*) T. G. Traylor, W. Hanstein, H. J. Berwin, N. A. Clinton, and R. S. Brown. J. Am. Chem. Soc. **93**, 5715 (1971).
12. (*a*) E. J. Corey and R. S. Glass. J. Am. Chem. Soc. **89**, 2600 (1967); (*b*) R. K. Howe, P. Carter, and S. Winstein. J. Org. Chem. **37**, 1473 (1972); (*c*) R. K. Howe and S. Winstein. J. Org. Chem. **38**, 2797 (1973).
13. C. Altona and M. Sundaralingham. J. Am. Chem. Soc. **92**, 1995 (1970).
14. P. K. Freeman, D. M. Balls, and D. J. Brown. J. Org. Chem. **33**, 2211 (1968).
15. (*a*) L. G. Cannell. Tetrahedron Lett. 5967 (1966); (*b*) T. J. Katz, J. C. Carnahan, Jr., and R. Boecke. J. Org. Chem. **32**, 1301 (1967).
16. R. H. Shapiro and M. J. Heath. J. Am. Chem. Soc. **89**, 5734 (1967).
17. G. Brieger and D. R. Anderson. J. Org. Chem. **36**, 243 (1971).
18. A. Nickon, F. Huang, R. Weglein, K. Matsuo, and H. Yagi. J. Am. Chem. Soc. **96**, 5264 (1974).
19. R. W. Weglein. Ph.D. Dissertation, The Johns Hopkins University, Baltimore, MD. 1973.
20. (*a*) J. O. Halford. J. Chem. Phys. **24**, 830 (1956); (*b*) R. Zbinden and H. K. Hall, Jr. J. Am. Chem. Soc. **82**, 1215 (1960); (*c*) R. C. Lord and R. W. Walker. J. Am. Chem. Soc. **76**, 2518 (1954); (*d*) P. von R. Schleyer and R. D. Nicholas. J. Am. Chem. Soc. **83**, 182 (1961); (*e*) S. Bank, W. D. Closson, and L. T. Hodgins. Tetrahedron, **24**, 381 (1968).
21. (*a*) C. S. Foote. J. Am. Chem. Soc. **86**, 1853 (1964); (*b*) P. von R. Schleyer. J. Am. Chem. Soc. **86**, 1854 (1964); **86**, 1856 (1964).
22. R. K. Howe. Ph.D. Dissertation, University of California, Los Angeles, CA. 1965.
23. P. G. Gassman and W. M. Hooker. J. Am. Chem. Soc. **87**, 1079 (1965).
24. M. Tichy. *In* Advances in organic chemistry: methods and results. Vol. 5. *Edited by* R. A. Raphael, E. C. Taylor, and H. Wynberg. John Wiley and Sons, Inc., New York, NY. 1965. p. 115.
25. P. von R. Schleyer, E. Funke, and S. H. Liggero. J. Am. Chem. Soc. **91**, 3965 (1969).
26. T. M. Gorrie. Ph.D. Dissertation, Princeton University, Princeton, NJ. 1972.
27. K. B. Wiberg and B. J. Nist. J. Am. Chem. Soc. **83**, 1226 (1961).
28. (*a*) O. L. Chapman. J. Am. Chem. Soc. **85**, 2014 (1963); (*b*) G. V. Smith and H. Kriloff. J. Am. Chem. Soc. **85**, 2016 (1963); (*c*) P. Laszlo and P. von R. Schleyer. J. Am. Chem. Soc. **85**, 2018 (1963).
29. G. B. Clemans, M. N. Essiet, and R. L. Tyson. J. Org. Chem. **37**, 2312 (1972).
30. (*a*) J. I. Musher. Mol. Phys. **6**, 93 (1963); (*b*) A. P. Marchand and N. W. Marchand. Tetrahedron Lett. 1365 (1971).
31. M. A. Cooper and S. L. Manatt. Org. Magn. Reson. **2**, 511 (1970).
32. L. de Vries and S. Winstein. J. Am. Chem. Soc. **82**, 5363 (1960).
33. W. R. Adams and D. J. Trecker. Tetrahedron, **28**, 2361 (1972).
34. (*a*) M. Barfield and B. Chakrabarti. Chem. Rev. **69**, 757 (1969); (*b*) T. J. Flautt and W. F. Erman. J. Am. Chem. Soc. **85**, 3212 (1963); (*c*) P. Laszlo and P. von R. Schleyer. J. Am. Chem. Soc. **86**, 1171 (1964); (*d*) A. P. Marchand and J. E. Rose. J. Am. Chem. Soc. **90**, 3724 (1968).

Can. J. Chem. Downloaded from www.nrcresearchpress.com by 210.87.254.5 on 09/05/12
For personal use only.

35. A. YOKOZEKI and K. KUCHITSU. Bull. Chem. Soc. Jpn. **44**, 2356 (1971), and references cited there.
36. A. P. MARCHAND, N. W. MARCHAND, and A. L. SEGRE. Tetrahedron Lett. 5207 (1969).
37. J. L. MARSHALL, S. R. WALTER, M. BARFIELD, A. P. MARCHAND, N. W. MARCHAND, and A. L. SEGRE. Tetrahedron, **32**, 537 (1976).
38. (*a*) M. KARPLUS. J. Chem. Phys. **30**, 11 (1959); (*b*) J. Am. Chem. Soc. **85**, 2870 (1963).
39. P. M. SUBRAMANIAN, M. T. EMERSON, and N. A. LEBEL. J. Org. Chem. **30**, 2624 (1965), and ref. 34*b–d*.
40. C. A. COULSON and E. T. STEWART. *In* The chemistry of alkenes. Vol. 1. *Edited by* S. Patai. John Wiley and Sons, New York, NY. 1964. Chapt. 1.
41. M. R. SMITH and J. M. HARRIS. J. Org. Chem. **43**, 3588 (1978).
42. H. C. BROWN and C. P. CARG. J. Am. Chem. Soc. **83**, 2952 (1961).
43. L. F. FIESER. Organic experiments. 1st ed. D. C. Heath and Co., Boston, MA. 1964. (*a*) p. 68; (*b*) p. 84.
44. H. C. BROWN and P. J. GEOGHEGAN, JR. J. Org. Chem. **35**, 1844 (1970).
45. R. RATCLIFFE and R. RODEHORST. J. Org. Chem. **35**, 4000 (1970).

Can. J. Chem. Downloaded from www.nrcresearchpress.com by 210.87.254.5 on 09/05/12
For personal use only.

Stereoselective syntheses of *O*- and *S*-nitrophenyl glycosides. Part III.[1] Syntheses in the α-D-galactopyranose and α-maltose series

MARCEL APPARU,[2] MICHÈLE BLANC-MUESSER, JACQUES DEFAYE, AND HUGUES DRIGUEZ

Centre de Recherches sur les Macromolécules Végétales, Centre National de la Recherche Scientifique,[3] 53 X, 38041 Grenoble, France

Received June 19, 1980

This paper is dedicated to Prof. Raymond U. Lemieux on the occasion of his 60th birthday

MARCEL APPARU, MICHÈLE BLANC-MUESSER, JACQUES DEFAYE, and HUGUES DRIGUEZ. Can. J. Chem. **59**, 314 (1981).

The action of *p*-nitrophenol on penta-*O*-acetyl-β-D-galactopyranose in dichloromethane, in the presence of stannic tetrachloride, gave *p*-nitrophenyl α-D-galactoside in fair yield. This technique failed when *o*-nitrophenol was used. Tetra-*O*-acetyl-β-D-galactopyranosyl and hepta-*O*-acetyl-β-maltosyl chlorides were converted to *p*- or *o*-nitrophenyl α-D-glycosides and *p*-nitrophenyl α-D-1-thioglycosides in good yield using hexamethylphosphoramide as a solvent and the sodium salt of the phenols as nucleophiles. The galactosides have been functionalized for further condensation at the C-4 position by selective benzoylation.

MARCEL APPARU, MICHÈLE BLANC-MUESSER, JACQUES DEFAYE et HUGUES DRIGUEZ. Can. J. Chem. **59**, 314 (1981).

L'action du *p*-nitrophénol en présence de chlorure stannique sur le penta-*O*-acetyl-β-D-galactopyranose dissous dans du dichlorométhane conduit au *p*-nitrophényl-α-D-galactoside. Cette technique n'aboutit pas à la formation de galactoside lorsque l'*o*-nitrophénol est utilisé. Les chlorures de tétra-*O*-acétyl-β-D-galactopyranosyle et d'hepta-*O*-acétyl-β-maltosyle dissous dans l'hexaméthylphosphoramide et traités par le sel de sodium des *p*- ou *o*-nitrophénol ou du *p*-nitrothiophénol, conduisent avec de bons rendements aux glycosides correspondants. Les galactosides ont été fonctionnalisés par benzoylation sélective pour des condensations ultérieures impliquant la position C-4.

Introduction

Within the framework of a program on the mechanism of action of α-amylase using the substrate analogs approach we have undertaken the synthesis of some derivatives of nitrophenyl maltosides and maltotriosides in which the oxygen atoms at C-1, C′-1 and/or C″-1 might be replaced by a sulfur atom.

In former articles in this series (1) the steric control in 1-thioglycosylation was achieved by a S_N2 type of reaction involving the action of a thiolate anion on glycosyl halides. The reverse displacement of a leaving group by a 1-thioglycose is an alternative approach (2), Scheme 1. The present paper deals with the application of this method to derivatives of D-galactose and maltose suitable for the above purpose.

Results and Discussion

Nitrophenyl α-D-galactopyranosides and α-maltosides are well known and even commercially available. However, their preparation has been found cumbersome by us, as well as by others (3, 4), leading to much poorer yields than those reported (5, 6).

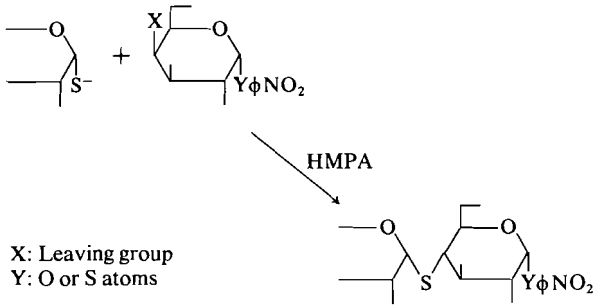

SCHEME 1

In 1953 Lemieux and Shyluk (7) pointed out that the reaction between phenol and penta-*O*-acetyl-β-D-glucopyranose in benzene solution for short periods at reflux temperature, in the presence of anhydrous stannic chloride as a catalyst, gave phenyl β-D-glucopyranoside. This work was reinvestigated ten years ago by Ingle and Bose (8) and more recently this method was used for the synthesis of alkyl β-D-glycosides (9) and their α-anomers through *in situ* anomerization of the former compounds.

Since 1,2-*cis* aryl glycosides with electron withdrawing groups on the aglycon have not yet been prepared extensively by the application of the above method, we have investigated the possible synthesis of *p*- and *o*-nitrophenyl α-D-galactopyranosides and maltosides, starting from their corresponding β-acetates and using stannic chloride as a catalyst.

[1]For part I and part II, see refs. 1*a* and *b*.

[2]Post-doctoral fellow 1977; present address: Université Scientifique et Médicale, Département de chimie organique, 53 X, 38041 Grenoble, France.

[3]Laboratoire propre du C.N.R.S., associé à l'Université Scientifique et Médicale de Grenoble.

0008-4042/81/020314-07$01.00/0

©1981 National Research Council of Canada/Conseil national de recherches du Canada

Can. J. Chem. Downloaded from www.nrcresearchpress.com by 210.87.254.6 on 09/05/12
For personal use only.

TABLE 1. Proton nuclear magnetic resonance data for the *O*-acylated galactosides **2–4, 12, 20–26**[a]

Compound	Solvent	H-1 $J_{1,2}$	H-2 $J_{2,3}$	H-3 $J_{3,4}$	H-4 $J_{4,5}$	H-5 $J_{5,6a}$ $J_{5,6b}$	H-6a $J_{6a,6b}$	H-6b	OH $J_{4,OH}$
2	Chloroform-*d*	5.92 d (4)	5.35 dd (10)	5.58 m (3)	5.56 sl	4.29 tl (6)	4.12 m		
3	Chloroform-*d*	5.15 d (8)	5.49 dd (10)	5.11 dd (4)	5.45 dl		4.12 m		
4	Chloroform-*d*	5.91 d (4)	5.27 dd (11)	5.53 dd (3)	5.61 dl	4.45 tl (7)	4.13 m		
12	Chloroform-*d*	6.22 d (5.5)	5.41 dd (11)	5.29 dd (3.5)	5.52 dl (1.5)	4.62 tl (6)	4.09 m		
20	Acetone-*d*	6.61 d (5.5)	6.12 dd (11)	5.72 dd (3)	4.66 ddl	4.90 ddl (3) (8)	4.71 dd (12)	4.58 dd	5.30 d (5)
21	Acetone-*d*	6.44 d (6)	4.96 ql (10)	5.62 dd (3)	6.03 dl	5.10 m (8) (4)	4.56 dd (12)	4.45 dd	5.40 d (4)
22	Acetone-*d*	6.63 d (6)	5.81 dd (11)	4.64 m (3)	5.98 dl	5.05 tl (6.5)	4.49 m		5.24 d (6)
23	Acetone-*d*	6.77 d (5.5)	6.15 dd (10.5)	6.04 dd (3)	6.22 dl	5.28 ddl (8) (4)	4.64 dd (12)	4.55 dd	
24	Dimethyl-sulfoxide-*d*	6.30 d (6)	4.60 dd (11)	5.14 ddl (3)	4.24 sl		4.44 m		
25	Benzene-*d*	5.90 d (4)	6.13 dd (10.5)	6.04 dd (3)	4.00 m	3.93 ddl (3.5) (8.5)	4.62 dd (12)	4.29 dd	2.38 d (4.5)
26	Benzene-*d*	5.88 d (3.5)	6.23 dd (10.5)	6.08 dd (3)	4.27 m	4.11 ddl (3.5) (8.5)	4.69 dd (12)	4.29 dd	3.18 d (5)

[a]Abbreviations: d doublet, dd doublet of doublets, t triplet, m multiplet, l large (splitting < 1.5 Hz).

The reaction of 1,2-*trans* per-*O*-acetylated sugars in dichloromethane was monitored by tlc and the crude product, after work-up, was examined by ^{13}C nmr. Several experimental conditions (temperature, variable ratio of stannic chloride – sugar, delayed addition of the phenol) were tried. Glycoside formation was invariably complete within 6 h at 60°C when 2 mol/equiv. of stannic tetrachloride were added to a dichloromethane solution of 1,2,3,4,6-penta-*O*-acetyl-β-D-galactopyranose (**1**) containing 1.5 mol/equiv. of *p*-nitrophenol.

A substantial part (30–40%) of the more abundant α-anomer **2** was easily isolated by crystallization and the two anomeric acetylated glycosides remaining in the mother liquor were separated by column chromatography.

In contrast with the results obtained in the synthesis of alkyl α-D-glycosides (9), it appears that the *p*-nitrophenyl α-D-galactoside **2** formed did not result from anomerization. Indeed, when pure β-anomer **3** was treated with stannic chloride under dichloromethane in the above conditions, tlc or ^{13}C nmr spectroscopy showed no α-galactoside formation, in good agreement with the known fact that phenyl β-D-glycosides are not easily subject to anomerization (3, 10). This would suggest that pathways alternative to those proposed by Banoub and Bundle (9) are possible.

From the preceding result, it could be expected that *o*-nitrophenyl α-D-galactoside **4** would be formed from the condensation of penta-*O*-acetyl-β-D-galactopyranose **1** with *o*-nitrophenol using the

Can. J. Chem. Downloaded from www.nrcresearchpress.com by 210.87.254.6 on 09/05/12
For personal use only.

Can. J. Chem. Downloaded from www.nrcresearchpress.com by 210.87.254.6 on 09/05/12
For personal use only.

TABLE 2. Proton nuclear magnetic resonance data for the *O*-acetylated maltosides **7**, **8**, and **13** in chloroform-*d*[a,b]

	H-1	H-2	H-3	H-4	H-5	H-6a	H-6b	H′-1	H′-2	H′-3	H′-4	H′-5	H′-6a	H′-6b
7	5.76	4.97	5.74		4.08	4.43	4.21	5.46	4.88	5.37	5.08	3.95	4.26	4.06
	d	dd	m		m	dd	dd	d	dd	tl	t	m	dd	dd
	(3.5)	(10)				(2) (12.5)	(4.5)	(4)	(11)	(10)	(10)		(4) (12)	(2)
8	5.73	4.92	5.73	4.08	4.28	4.08 or 4.28		5.46	4.88	5.37	5.07	3.97	4.08 or 4.49	
	d	dd	dd	m	m	m		d	dd	t	t	m	m	
	(3.5)	(10)	(9)					(4)	(10)	(10)	(10)			
13	6.01	5.10	5.42	3.97		4.00–4.44		5.42	4.91	5.39	5.08		4.00–4.44	
	d	dd	t	dd		m		d	dd	t	t		m	
	(6)	(9)	(9)	(10)				(4)	(10)	(10)	(10)			

[a]The primed numbers refer to the protons of the non reducing unit.
[b]Abbreviations: d doublet, dd doublet of doublets, m multiplet.

same technique. Unexpectedly, under similar conditions no glycoside formation was detected and the major product isolated from the reaction was penta-*O*-acetyl-α-D-galactopyranose **5**. Lemieux and Brice (11) have shown that the treatment of **1** with stannic chloride in chloroform led to its α-anomer **5** in the absence of an alcohol. Thus, under the conditions used, one can postulate that an interaction occurred between stannic chloride and the vicinal nitro and hydroxyl groups on the benzene ring which hindered the ability of the hydroxyl function to participate in the formation of a glycosidic linkage.

This above disappointing experiment led us to investigate, for these syntheses, the application of a method earlier developed in the *manno* and *gluco* series (1*a*, *b*). The technique involves a strong dipolar aprotic solvent, hexamethylphosphoramide (HMPA) and the *in situ* activation of the nucleophile as its sodium salt. An inversion occurs at C-1 of the per-*O*-acetyl halides notwithstanding the presence of vicinal *O*-acyl participating groups.

Addition of tetra-*O*-acetyl-β-D-galactopyranosyl chloride (12) **6** to a solution of the sodium salt of *p*- or *o*-nitrophenol in HMPA gave, by direct crystallization after work-up, the expected products in 40 and 51% yield respectively. The advantage of this method was further demonstrated by the specific

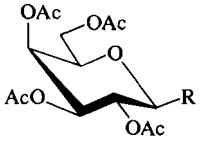

1 R = OAc
3 R = $OC_6H_4NO_2p$
6 R = Cl

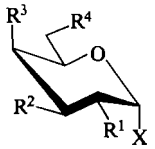

2 $R^1 = R^2 = R^3 = R^4 = OAc$; $X = OC_6H_4NO_2p$
4 $R^1 = R^2 = R^3 = R^4 = OAc$; $X = OC_6H_4NO_2o$
5 $R^1 = R^2 = R^3 = R^4 = X = OAc$
12 $R^1 = R^2 = R^3 = R^4 = OAc$; $X = SC_6H_4NO_2p$
14 $R^1 = R^2 = R^3 = R^4 = OH$; $X = OC_6H_4NO_2p$
15 $R^1 = R^2 = R^3 = R^4 = OH$; $X = OC_6H_4NO_2o$
16 $R^1 = R^2 = R^3 = R^4 = OH$; $X = SC_6H_4NO_2p$
20 $R^1 = R^2 = R^4 = OBz$; $R^3 = OH$; $X = SC_6H_4NO_2p$
21 $R^1 = OH$; $R^2 = R^3 = R^4 = OBz$; $X = SC_6H_4NO_2p$
22 $R^2 = OH$; $R^1 = R^3 = R^4 = OBz$; $X = SC_6H_4NO_2p$
23 $R^1 = R^2 = R^3 = R^4 = OBz$; $X = SC_6H_4NO_2p$
24 $R^1 = R^3 = OH$; $R^2 = R^4 = OBz$; $X = SC_6H_4NO_2p$
25 $R^1 = R^2 = R^4 = OBz$; $R^3 = OH$; $X = OC_6H_4NO_2p$
26 $R^1 = R^2 = R^4 = OBz$; $R^3 = OH$; $X = OC_6H_4NO_2o$
27 $R^1 = R^2 = R^3 = R^4 = OBz$; $X = OC_6H_4NO_2p$
28 $R^1 = R^2 = R^3 = R^4 = OBz$; $X = OC_6H_4NO_2o$

TABLE 3. Carbon-13 nuclear magnetic resonance shifts for the anomeric carbons in chloroform-*d* for glycosides **2–4, 7, 8, 12, 13** and in methanol-*d* for glycosides **14–19**

	2	3	4	7	8	12	13	14	15	16	17	18	19
C-1	95.0	98.6	96.5	94.3	95.6	84.0	83.2	99.5	99.7	89.5	98.9	99.3	88.8
C'-1				96.0	96.0		96.1				102.8	102.7	102.9

syntheses of *p*- and *o*-nitrophenyl maltoside derivatives **7** and **8**; these two compounds were obtained with 45 and 37% yield respectively from **9** by direct crystallization via the hepta-*O*-acetyl-β-maltosyl chloride **10**. It is worthwhile to note that, in our hands, application of the stannic chloride procedure did not give pure **7** without chromatographic purification, the β-anomer **11** being always present as a side product.

In the same way, addition of glycosyl halides **6** or **10** to a solution of the sodium salt of *p*-nitrothiophenol gave after chromatography the 1,2-*cis*-thioglycosides **12** and **13** in 73 and 60% yields respectively. These compounds, potential inhibitors of glycosidases, are usually obtained in low yield together with their 1,2-*trans* anomers by reaction of an aldose with a thiol under strongly acidic conditions, or by fusion of a fully acetylated sugar with thiols in the presence of a Lewis acid.[4]

The de-*O*-acetylated compounds **14–19** were obtained by careful addition of sodium methoxide. In the presence of an excess of this reagent a mixture of *O*-phenyl isomers was obtained which probably arose from migration of the *O*-phenyl group from the anomeric to the C-2 or C-3 position as demonstrated by Horton and Luetzow (14) using aqueous alkali.

The hydroxyl free *galacto* compounds **14–16** were converted to suitable derivatives for further condensation (see Scheme 1) by selective benzoylation with benzoyl chloride in pyridine at −20°C. A difference in selectivity was observed between the *O*- and *S*-compounds. Partial benzoylation of *p*-nitrophenyl 1-thio-α-D-galactoside **16** with 3.3 mol/equiv. of the acylating reagent afforded mainly the 2,3,6-tri-*O*-benzoyl derivative **20** (57% yield) together with several minor compounds such as the 3,4,6- and 2,4,6-tribenzoates **21** and **22** (3 and 2% yield respectively), the tetrabenzoate **23**, and the 3,6-di-*O*-benzoyl derivative **24** (15 and 2% yield respectively). However, with the *p*- and *o*-nitrophenyl compounds **14** and **15**, the 2,3,6-tri-*O*-benzoates **25** and **26** were the only partially substituted products isolated (70 and 79% yield respectively), together with about 5–10% yield of the perbenzoylated products **27** and **28**.

[4]For a review see refs. 1 and 13.

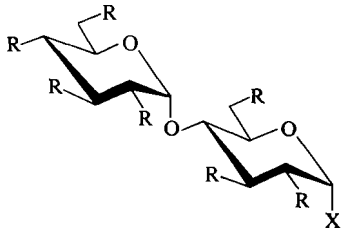

7 R = OAc; X = $OC_6H_4NO_2p$
8 R = OAc; X = $OC_6H_4NO_2o$
13 R = OAc; X = $SC_6H_4NO_2p$
17 R = OH; X = $OC_6H_4NO_2p$
18 R = OH; X = $OC_6H_4NO_2o$
19 R = OH; X = $SC_6H_4NO_2p$

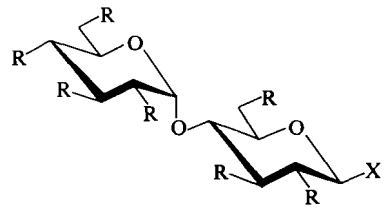

9 R = X = OAc
10 R = OAc; X = Cl
11 R = OAc; X = $OC_6H_4NO_2p$

This decreasing of the selectivity from the *O*-glycosyl to *S*-glycosyl series may be due either to a lack of hydrogen bonding between acyl pyridinium ions and the aglycon (15) or to a steric hindrance of the bulky sulfur atom which may lead to a distorted chair conformation. In this last eventuality, it is well known that a preferential acylation may be related to the orientation of vicinal groups, since high yields of substitution at the equatorial hydroxyl vicinal to the axial hydroxyl are usually obtained (16, 17).

All the compounds showed the expected proton magnetic resonance spectra (Tables 1 and 2), but for the aryl 1-thio-α-D-glycosides the anomeric coupling constants had a value of 5.5–6 Hz versus 4 Hz found for their *O*-analogs, and H-1 was deshielded by about 0.3 ppm. The ^{13}C nmr parameters are recorded in Table 3.

Conclusion

The results presented in this paper show that *p*-nitrophenyl α-D-galactopyranosides and maltosides can be obtained by both stannic chloride or HMPA methods. However, stannic chloride can-

Can. J. Chem. Downloaded from www.nrcresearchpress.com by 210.87.254.6 on 09/05/12
For personal use only.

Can. J. Chem. Downloaded from www.nrcresearchpress.com by 210.87.254.6 on 09/05/12
For personal use only.

TABLE 4. Chromatographic solvents, melting point, optical rotation, and analytical data for compounds **2**, **4**, **7**, **8**, **12**–**26**

Compound (yield)	Chromatographic solvent	Melting point (°C) (cryst. solvent)	Specific rotation $[\alpha]_D^{RT}$ (*c*) solvent	Analytical data									
				Calculated:				Found:				Lit. mp °C	Lit. $[\alpha]_D$ (ref.)
				C	H	N	S	C	H	N	S		
2 (40%)[a]	Ether–hexane 2:1	132–133 (Ethanol)	+204° (0.68) Chloroform	$C_{20}H_{23}NO_{12}$ 51.17	4.94	2.98		51.44	5.00	2.97		129–130,	+275° (20)
4 (51%)[a]	Dichloromethane–ether–hexane 40:4:8	168–169 (Ethanol)	+199° (0.56) Chloroform	$C_{20}H_{23}NO_{12}$ 51.17	4.94	2.98		51.06	4.78	2.91		169–170,	+187.9° (20)
7 (45%)[a]	Ethyl acetate – hexane 2:1	163–165 (Methanol)	+184° (0.44) Chloroform	$C_{32}H_{39}NO_{20}$ 50.74	5.19	1.85		50.86	5.15	1.80		138–139, 176–178,	+103° (3) +223° (5)
8 (37%)[a]	Ethyl acetate – hexane 2:1	234–236 (Methanol)	+226° (0.28) Chloroform	$C_{32}H_{39}NO_{20}$ 50.74	5.19	1.85		50.58	5.16	1.83		185–187,	+222° (5)
12 (66%)[a]	Dichloromethane–ether 20:1	168–169 (Ethanol)	+332° (0.53) Chloroform	$C_{20}H_{23}NSO_{11}$ 49.48	4.77	2.80	6.60	49.33	4.68	2.82	6.6		
13 (60%)[a]	Dichloromethane–ether 8:1	Foam	+247° (0.35) Chloroform	$C_{32}H_{39}NSO_{19}$ 49.67	5.08	1.81	4.14	49.91	5.12	1.82	4.38		
14 (100%)[b]	Chloroform–methanol–water 65:25:4	170–171 (Ethanol) 165–167 (Freeze dry)	+220° (0.4) Water	$C_{12}H_{15}NO_8$ 47.84	5.02	4.65		47.86	5.22	4.70		169, 82–84,	+225° (6) +305° (20)
15 (100%)[b]	Chloroform–methanol–water 65:25:4	145–147 (Ethanol)	+198° (0.6) Water	$C_{12}H_{15}NO_8$ 47.84	5.02	4.65		47.66	5.08	4.50		145–147,	+224° (21)
16 (100%)[b]	Chloroform–methanol–water 65:25:4	188–189 (Freeze dry)	+328° (0.5) Water	$C_{12}H_{15}NSO_7 \cdot 0.5\,H_2O$ 44.17	4.94	4.29	9.82	43.87	4.68	4.33	10.0		
17 (100%)[b]	Chloroform–methanol–water 65:25:4	132–133 (Freeze dry)	+186° (0.27) Water	$C_{18}H_{25}NO_{13} \cdot 0.5\,H_2O$ 45.76	5.55	2.96		45.70	5.55	2.95		145–146, 140 105,	+265° (5) (4) +134.7° (3)
18 (100%)[b]	Chloroform–methanol–water 65:25:4	110–112 (Freeze dry)	+174° (0.7) Water	$C_{18}H_{25}NO_{13} \cdot H_2O$ 44.90	5.65	2.91		44.92	5.70	2.87		153–155, 101	+245° (5) (4)

Can. J. Chem. Downloaded from www.nrcresearchpress.com by 210.87.254.6 on 09/05/12
For personal use only.

TABLE 4 (*Concluded*)

Compound (yield)	Chromatographic solvent	Melting point (°C) (cryst. solvent)	Specific rotation $[\alpha]_D^{RT}$ (*c*) solvent	Analytical data									
				Calculated:				Found:				mp °C	Lit. $[\alpha]_D$ (ref.)
				C	H	N	S	C	H	N	S		
19 (100%)[b]	Chloroform–methanol–water 65:25:4	121–123 (Freeze dry)	+345° (0.35) Water	$C_{18}H_{25}NSO_{12}\cdot 0.5\ H_2O$ 44.26	5.37	2.87	6.56	44.41	5.49	2.80	6.79		
20 (57%)[c]	Dichloromethane–acetone 32:1	193 (Methanol–chloroform)	+260° (0.56) Acetone	$C_{33}H_{27}NSO_{10}$ 62.95	4.32	2.22	5.09	62.88	4.56	1.96	5.14		
21 (3%)[c]	Dichloromethane–acetone 32:1	190–191 (Dichloromethane–methanol)	+323° (0.51) Acetone	$C_{33}H_{27}NSO_{10}$ 62.95	4.32	2.22	5.09	62.80	4.44	2.38	5.30		
22 (1.5%)[c]	Dichloromethane–acetone 32:1	80–85 Foam	+199° (0.29) Acetone	$C_{33}H_{27}NSO_{10}$ 62.95	4.32	2.22	5.09	62.87	4.55	2.27	5.14		
23 (15%)[c]	Dichloromethane–acetone 32:1	179–180 (Dichloromethane–methanol)	+186° (0.58) Chloroform	$C_{40}H_{31}NSO_{11}$ 65.47	4.26	1.91	4.37	65.51	4.35	1.84	4.44		
24 (2%)[c]	Dichloromethane–acetone 32:1	211–213 (Acetone–methanol)	+433° (0.49) Acetone	$C_{26}H_{23}NSO_9$ 59.42	4.41	2.66	6.10	59.45	4.57	2.81	6.09		
25 (70%)[c]	Dichloromethane–ether 15:1	168–171 (Ethanol)	+177° (0.47) Chloroform	$C_{33}H_{27}NO_{11}$ 64.60	4.44	2.28		64.67	4.44	2.52			
26 (79%)[c]	Dichloromethane–ether 15:1	158–159 (Ethanol)	+178° (0.4) Chloroform	$C_{33}H_{27}NO_{11}$ 64.60	4.44	2.28		64.59	4.56	2.10			

[a]From the per-*O*-acetylated derivative.
[b]From the corresponding acetylated glycoside.
[c]From the hydroxyl free glycoside.

not be applied for the syntheses of *o*-nitrophenyl derivatives nor 1-thio-α-D-glycosides. The simplicity of the HMPA procedure, together with its versatility, suggest that this method may have considerable potential for this type of synthesis, and constitutes a useful alternative to other methods.

Experimental

Solutions were dried (sodium sulfate) and evaporated *in vacuo* at temperatures below 45°C. Thin layer chromatography (tlc) was performed on silica gel (Merck F 254, Merck, Darmstadt, Germany). Preparative chromatography used silica gel (Merck 60, 70–230 mesh). Optical rotations were determined with a Quick polarimeter (Roussel et Jouan) at room temperature. The ^{1}H nmr spectra were recorded at 250 MHz with a Cameca spectrometer. Assignments were confirmed by double irradiation or the INDOR technique. The ^{13}C nmr spectra at 25.18 MHz were recorded with a Bruker WP 100 instrument. The chemical shifts are reported in δ (ppm) relative to internal TMS and the coupling constants (in brackets) in Hz.

General Procedure for the Preparation of Nitrophenyl Glycosides 2, 4, 7, 8, 12, and 13 in HMPA

Chlorides **6** or **10** prepared from their per-*O*-acetylated precursors (10 g) by using dichloromethyl methyl ether and boron trifluoride as described (12), were added to a solution of HMPA (40 mL for **6** or 25 mL for **10**) containing the sodium salt of nitrophenol (1.6 mol/equiv.) or nitrothiophenol (2.0 mol/equiv.) prepared from the phenol or thiophenol and sodium hydride (1*b*). The mixture was stirred at 40°C for 6 h, then overnight at room temperature. An ice-water mixture (150 mL) was added and the precipitate filtered on a Celite bed, washed with water, then dissolved in dichloromethane (150 mL). The organic layer was poured into water (100 mL), which was then extracted with dichloromethane (2 × 150 mL), and each portion washed with water (2 × 100 mL). After solvent removal, crystallization from ethanol or purification by column chromatography for the thioderivatives **12** and **13**, yielded the pure glycosides **2**, **4**, **7**, **8**, **12**, and **13**. The yields, physical constants, and migration solvents for these compounds are reported in Table 4.

p-*Nitrophenyl 2,3,4,6-Tetra-*O*-acetyl-α-D-galactopyranoside (2) (by the Stannic Chloride Method)*

Stannic tetrachloride (6 mL, 55 mmol) was added to a solution of penta-*O*-acetyl-β-D-galactose **1** (10 g, 25 mmol) and *p*-nitrophenol (5.2 g, 37 mmol) in dichloromethane (50 mL). After 5 h at 60°C, dichloromethane (50 mL) was added and the reaction mixture was poured into an ice-cold saturated bicarbonate solution, then neutralized with solid sodium bicarbonate, filtered on Celite bed, and extracted with chloroform (2 × 100 mL). The organic phase was washed again with ice-cold saturated bicarbonate solution and water (100 mL). Crystallization of the crude product afforded pure **2** (3.9 g, 33%, Table 4). Column chromatography of the mother liquor provided an additional 1.2 g of **2** and its β-anomer **3** (0.35 g, 3%), identical with an authentic sample (18) by ^{1}H and ^{13}C nmr spectra and its melting point 141–143°C, lit. (18) mp 145–146°C.

*De-*O*-acetylation of Nitrophenyl Glycosides 2, 4, 7, 8, 12, and 13*

In a typical experiment the acetylated glycoside (**8**, 1 mmol) was suspended in methanol (150 mL), 0.4 mL of 1 *M* sodium methoxide was added, and the reaction mixture stirred overnight. The clear solution was neutralized with Amberlite IR 120 (H^+), filtered, concentrated to dryness, and freeze-dried. The solid foam obtained in quantitative yield can be recrystallized from ethanol or used without crystallization. Confirmation of the expected structure was obtained by ^{13}C nmr spectroscopy (Table 3). Physical constants and analytical data are recorded in Table 4.

Selective O*-Benzoylation of Glycosides 14–16*

Compounds **14**, **15**, or **16** (9 mmol) were dissolved in anhydrous pyridine (45 mL), cooled to −20°C, and then benzoyl chloride (3.78 mL, 30.4 mmol) in pyridine (4 mL) was added slowly. After 18 h, methanol (20 mL) was poured into the flask and the solution was evaporated to dryness. The reaction mixture of compounds **14** or **15** was dissolved in dichloromethane (100 mL) and washed with water (2 × 100 mL). The aqueous layer was back-extracted with dichloromethane (2 × 100 mL). The crude product showed only two spots on tlc corresponding to perbenzoylated glycosides and the expected compounds **25** and **26**, which were obtained pure after chromatography (Table 4). The solid obtained from **16**, insoluble in dichloromethane, was dissolved in methanol (100 mL); silica gel (10 g) was added and the suspension evaporated to dryness, the powder was applied to the top of a wet chromatography column (100 g), and eluted. The first fraction was characterized as *p*-nitrophenyl 2,3,4,6-tetra-*O*-benzoyl-1-thio-α-D-galactopyranoside (**23**), then the 3,4,6-tri-*O*-benzoyl derivative **21**, followed by its 2,4,6-tri-*O*-benzoyl isomer **22**, appeared. The main fraction to be eluted from the column was pure *p*-nitrophenyl 2,3,6-tri-*O*-benzoyl-1-thio-α-D-galactopyranoside (**20**).

Acknowledgments

We wish to thank Mrs. F. Bouhet for her technical assistance. Nuclear magnetic resonance spectra were carried out by Miss M.-L. Dheu and Mr. H. Reutenauer.

1. (*a*) M. Blanc-Muesser, J. Defaye, and H. Driguez. Tetrahedron Lett. 4307 (1976); (*b*) M. Blanc-Muesser, J. Defaye, and H. Driguez. Carbohydr. Res. **67**, 305 (1978).
2. M. Blanc-Muesser. Doctorat d'Etat Thesis, University of Grenoble, Grenoble, France. 1980.
3. P. M. Barna. Aust. J. Chem. **24**, 673 (1971).
4. K. Wallenfels, P. Földi, H. Niermann, H. Bender, and D. Linder. Carbohydr. Res. **61**, 359 (1978).
5. S. Matsubara. Bull. Chem. Soc. Jpn. **34**, 718 (1961).
6. G. Siewert and O. Westphal. Justus Liebigs Ann. Chem. **720**, 188 (1968).
7. R. U. Lemieux and W. P. Shyluk. Can. J. Chem. **31**, 528 (1953).
8. T. R. Ingle and J. L. Bose. Carbohydr. Res. **12**, 459 (1970).
9. J. Banoub and D. Bundle. Can. J. Chem. **57**, 2085 (1979).
10. E. M. Montgomery, N. K. Richtmyer, and C. S. Hudson. J. Am. Chem. Soc. **64**, 690 (1942).
11. R. U. Lemieux and C. Brice. Can. J. Chem. **30**, 295 (1952).
12. I. Farkas, I. F. Szabó, and R. Bognár. Carbohydr. Res. **48**, 136 (1976).
13. J. Schneider, H. H. Liu, and Y. C. Lee. Carbohydr. Res. **39**, 156 (1975).
14. D. Horton and A. E. Luetzow. J. Chem. Soc. Chem. Commun. 79 (1971).
15. J. M. Knoblich, J. M. Sugihara, and T. Yamazaki. J. Org. Chem. **36**, 3407 (1971).
16. G. J. F. Chittenden and J. G. Buchanan. Carbohydr. Res. **11**, 379 (1969).
17. R. W. Jeanloz and D. A. Jeanloz. J. Am. Chem. Soc. **79**, 2579 (1957).
18. T. Iversen and R. Johansson. Synthesis, 823 (1979).
19. B. Helferich and K. H. Jung. Justus Liebigs Ann. Chem. **589**, 77 (1954).
20. C. J. Porter, R. Holmes, and B. F. Crocker. J. Gen. Physiol. **37**, 271 (1953).

Can. J. Chem. Downloaded from www.nrcresearchpress.com by 210.87.254.6 on 09/05/12
For personal use only.

9-Oxobenzomorphans. IV. 9-Oxo-5-[3″-(1″-hydroxypropyl)]- and 9-oxo-5-[3″-(1″-sulfidrylpropyl)]-6,7-benzomorphans as cyclic hemiketals and hemithioketals

GERRY KAVADIAS[1] AND STEPHAN VELKOF

Bristol Laboratories of Canada, 100 Industrial Boulevard, Candiac, P.Q., Canada J5R 1J1

Received July 2, 1980

This paper is dedicated to Prof. Raymond U. Lémieux on the occasion of his 60th birthday

GERRY KAVADIAS and STEPHAN VELKOF. Can. J. Chem. **59**, 321 (1981).

The syntheses of 9-oxobenzomorphans **10** and **12** are described. Both products exist in the cyclic forms **11** and **13** respectively. Hydrobromide and oxalate salts of the 9-oxobenzomorphan **1** when crystallized from methanol form stable methylhemiketals **4** and **5**. Bromination of **5** yielded benzomorphan **8** which on treatment with sodium hydroxide produced, via **10**, the cyclic hemiketal **11**. Reaction of **8** with sodium hydrogen sulfide afforded, via **12**, the cyclic hemithioketals **13**.

GERRY KAVADIAS et STEPHAN VELKOF. Can. J. Chem. **59**, 321 (1981).

On décrit les synthèses des oxo-9 benzomorphanes **10** et **12**. Les deux produits existent respectivement sous les formes cycliques **11** et **13**. Si l'on recristallise le bromhydrate et l'oxalate de l'oxo-9 benzomorphane **1** dans le méthanol, il y a formation des méthylhémicétals stables **4** et **5**. La bromation de **5** donne le benzomorphane **8** qui réagit avec l'hydroxyde de sodium pour conduire à l'hémicétal cyclique **11** par l'intermédiaire du composé **10**. Le composé **8** réagit avec le sulfure acide de sodium et conduit, par l'intermédiaire du dérivé **12**, aux hémithioacétals cycliques **13**.

[Traduit par le journal]

In our search for new structures as medicinally useful analgesics, the benzomorphans of the general structure I (Fig. 1, X = O, S) appeared as promising candidates. Interest in these classes of compounds has been generated from the anticipation that these products would exist predominantly or entirely in the cyclic hemiketalic form II, thus resembling known structures which have important analgesic activity. It was recently reported that several 14-hydroxymorphinans (III) (1) and 8-oxomorphinans (IV) (2) possess valuable pharmacological activities as analgesics and narcotic antagonists. Compounds of formula II combine in a single structure both the structural elements which appear to be associated with the biological properties of III and IV, i.e. the hydroxy group and the heteroatom at the 14- and 8-positions, respectively.

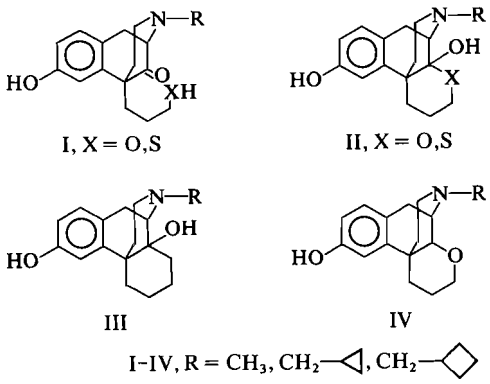

FIG. 1.

The present paper describes the preparation of the cyclic hemiketal **11** and the cyclic hemithioketals **13***a* and **13***c* (Scheme 3). We have previously presented the syntheses of 9-oxobenzomorphans **1***a*, *b* (3–5) and these compounds served as starting materials in the present syntheses.

The first goal was to prepare the bromides **8***a–c*, the key intermediates of our synthetic scheme. Initially, an attempt was made to synthesize **8***a*,*b* by bromination of 5-allyl-9-oxobenzomorphans **1***a*,*b* but this approach was unsuccessful. Thus, reaction of **1***a* with bromine in methanol solution and in the presence of silver acetate (6) failed to produce the desired **8***a* but instead yielded a product mixture (4 components) from which the tetrahydrofurano compound **3** was isolated (Scheme 1).

The preparation of **8***a*,*b* was accomplished by bromination of **5***a*,*b* (Scheme 2) as will be discussed later. It is appropriate at this point to describe briefly the syntheses and properties of the methyl hemiketals **4***a*,*b* and **5***a*,*b*. When the oxalate or hydrobromide salts of **1***a*,*b* were dissolved in methanol and the solution permitted to stand for sufficient time (6–10 h) before crystallization was induced, the respective hemiketals **4***a*,*b* and **5***a*,*b* were formed in good yields. Two isomers were predicted for each individual hemiketal salt and apparently both were formed. Separation of the isomers was readily accomplished by fractional crystallization. Interestingly, the hemiketal salts **4***a*

[1]Author to whom correspondence may be addressed.

0008-4042/81/020321-05$01.00/0

©1981 National Research Council of Canada/Conseil national de recherches du Canada

Can. J. Chem. Downloaded from www.nrcresearchpress.com by 210.87.254.5 on 09/05/12
For personal use only.

Can. J. Chem. Downloaded from www.nrcresearchpress.com by 210.87.254.5 on 09/05/12
For personal use only.

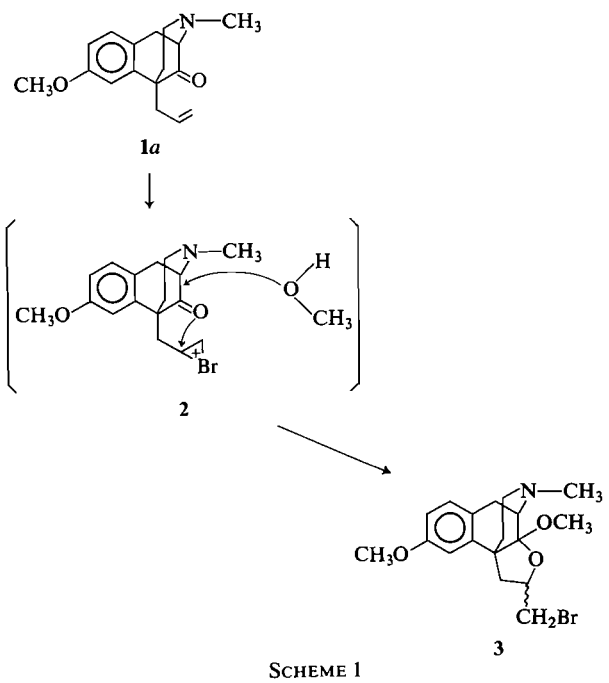

SCHEME 1

and **5***a* when treated with base did not generate the precursor ketone **1***a* as might have been expected but instead provided the methyl hemiketal free base **6** as a stable crystalline product (mp 107–111°C). Compound **6** was stable both in the crystalline form and in solution and could be recrystallized from ethanol without appreciable decomposition. Regeneration of the precursor ketone **1***a* could be effected by treatment of **6** with aluminum oxide or by refluxing of **6** in methanol solution. Structural assignment to **6** as the methyl hemiketal was based on elemental analysis, ir and ^{1}Hmr spectroscopy, and by the fact that it could be converted to **1***a* as mentioned above. The ir spectrum of **6** showed strong absorption at 3380 cm^{-1} (OH) and lacked the carbonyl absorption band (~1700 cm^{-1}) and the ^{1}Hmr spectrum was in accord with the proposed structure (see Experimental). Base treatment of the methyl hemiketal hydrobromide **5***b* generated the ketone **1***b*, not the hemiketal free base as might have been anticipated from the above discussion.

Bromination of the methyl hemiketal **6** or its hydrobromide salt **5***a* in chloroform at 0°C produced in quantitative yield **8***a* hydrobromide as a mixture of two stereoisomers. One isomer was predominant in the mixture and was isolated in 70% yield by crystallization. The structure of **8***a* was established by analytical and spectroscopic data (see Experimental) and further confirmed by chemical transformation to the ketone **9**. Treatment of **8***a* with sodium hydride in DMF followed by acid hydrolysis yielded the ketone **9**, thus establishing the relative positions of bromine and methoxy group on the side chain of the molecule.

Bromination of the hemiketal hydrobromide **5***b* in chloroform yielded **8***b* hydrobromide (100%) as a mixture of two stereoisomers (isomerism at C—OCH_3) in a ratio of approximately 1:1, separated by fractional crystallization. The configuration of the carbon attached to the methoxy group in **8***b* was not

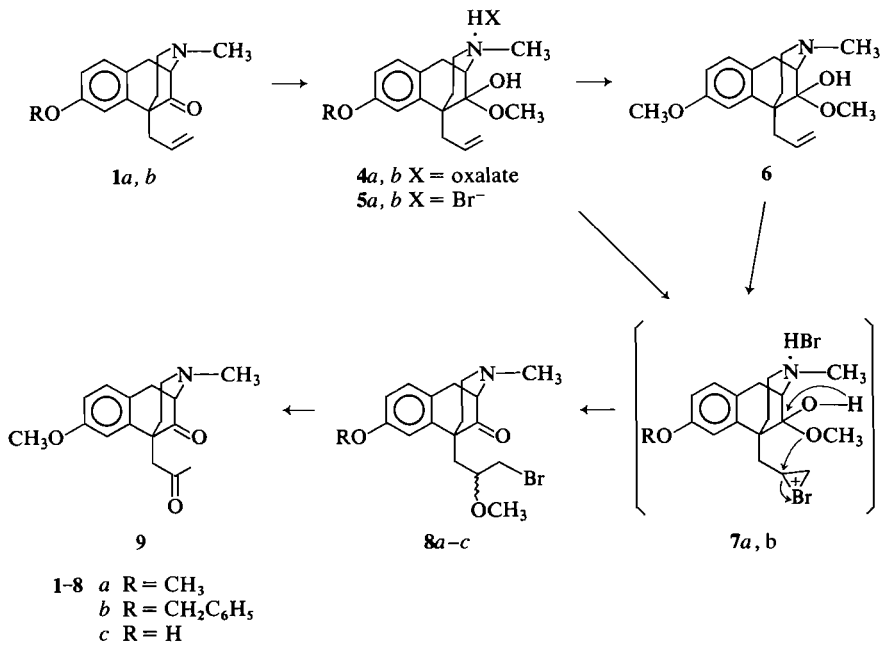

SCHEME 2

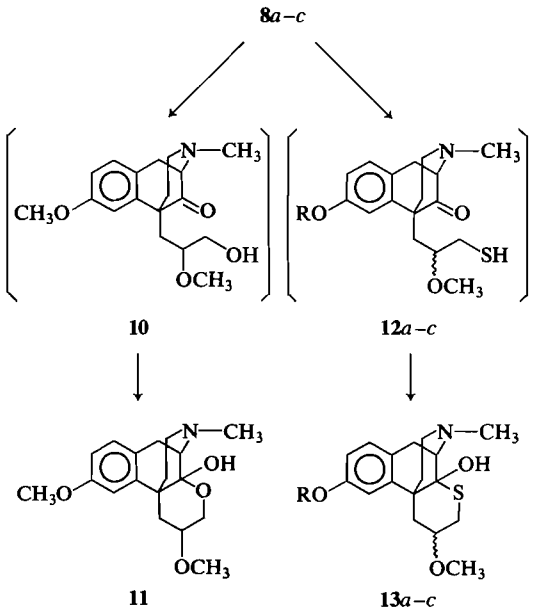

12,13 *a* R = CH_3
b R = $CH_2C_6H_5$
c R = H

SCHEME 3

established and for classification purposes the two isomers were designated as A- and B-isomers.

The mechanism of the reaction of the methyl-hemiketals **5***a,b* and **6** with bromine can be envisioned as occurring with initial formation of the bromonium ion **7***a,b* followed by migration of the methoxy group to form **8***a–c*.

Treatment of each isomer of **8***b* with trifluoroacetic acid (7) removed the benzyl group and afforded the respective isomers of **8***c*.

Treatment of **8***a* with sodium hydroxide in aqueous ethanol at room temperature produced, via **10**, the cyclic hemiketal **11** in 53% yield (Scheme 3). The ir spectrum of **11** lacked carbonyl absorption in the area of 1700 cm^{-1} thus indicating that the compound existed entirely in the cyclic form.

Reaction of **8***a* with sodium hydrogen sulfide in aqueous ethanol at reflux temperature gave, via **12***a*, the cyclic product **13***a* in 75% yield. In a similar manner, each isomer of **8***c* upon treatment with sodium hydrogen sulfide produced respective isomers of **13***c* in 75–80% yield. Lack of carbonyl absorption on the ir spectra of **13***a,c* was taken as evidence for the cyclic nature of these products.

Compound **11** did not exhibit significant analgesic activity whereas compounds **13***a,c* were moderately active (see Table 1).

Experimental

The melting points were determined on a Mel-Temp melting point apparatus and are not corrected. The ir spectra were recorded on a Unicam SP-200G grating ir spectrometer. The

TABLE 1. Analgesic activities of **13***a–c*

Compound	ED_{50}, mg/Kg[a] Analgesic act (mouse writhing)
13*a*	4.3
13*c* (A-isomer)	4.5
13*c* (B-isomer)	0.15
Morphine·H_2SO_4	0.56

[a]Subcutaneous administration.

^{1}Hmr spectra were taken with a Varian A-60A spectrometer. Tetramethylsilane (for solutions other than deuterium oxide) and sodium 4,4-dimethyl-4-silapentane-1-sulfonate (for solutions of deuterium oxide) were used as internal standards. Thin-layer chromatography (tlc) was carried out on microscope slides coated with silica gel G (E. Merck, A. G., Darmstadt) and the spots were visualized with sulfuric acid. The analysis were performed by Micro-Tech Laboratories, Skokie, IL.

*Tetrahydrofuranobenzomorphan 3. Bromination of 5-Allyl-9-oxo-6,7-benzomorphan 1*a

A solution of bromine (4.9 g, 30.5 mmol) in methylene chloride (10 mL) was added dropwise during 15 min to a stirred mixture of **1***a* (3–5) (7.32 g, 27 mmol) and silver acetate (5.09 g, 30.5 mmol) in methanol (100 mL) at 0°C. After stirring for 1 h at 0°C, the reaction mixture was filtered. The filtrate was evaporated and the residue was partitioned between a saturated solution of sodium bicarbonate (100 mL) and ether (100 mL). The ether solution, after drying, was evaporated to give 8.0 g of a syrup which on tlc (silica, 5% ethanol in ether) showed four spots. This product was dissolved in ethanol (20 mL), treated with a hot solution of picric acid (7.2 g) in ethanol (120 mL), and the precipitate was collected to give 5.0 g of the picrate salt of **3**, mp 170–179°C. The mp of this salt was unchanged after two more recrystallizations from ethanol. Treatment of the picrate salt of **3** with sodium bicarbonate and extraction with ether afforded the free base (**3**) as a syrup; ir ($CHCl_3$): 1610, 1505 cm^{-1}; ^{1}Hmr ($CDCl_3$) δ: 2.41 (s, 3H, NCH_3), 3.20 (s, 3H, OCH_3), 3.73 (s, 3H, Ar—OCH_3), 3.66–3.86 (m, 2H, CH_2Br), 4.20–4.80 (m, 1H, O—C—H), 6.5–7.0 (m, 3H, ArH).

The oxalate salt of **3** had mp 164–169°C (ethanol–ether, 1:1). *Anal.* calcd. for $C_{18}H_{24}BrNO_3 \cdot C_2H_2O_4$: C 50.85, H 5.54, Br 16.91; found: C 50.48, H 5.51, Br 17.21.

5-Allyl-2′,9-dimethoxy-9-hydroxy-2-methyl-6,7-benzomorphan Oxalate (4a)

A mixture of 19.8 g of 5-allyl-2′-methoxy-2-methyl-9-oxo-6,7-benzomorphan (**1***a*) oxalate (anhydrous salt) and 250 mL of dry methanol was heated under reflux until all the solids had dissolved and then the solution was allowed to cool gradually to room temperature. Crystallization usually commenced after 4–5 h; if solids were formed prior to this time, they were redissolved by heating the mixture. After standing at room temperature for 18 h, the crystalline precipitate was collected by filtration to give 11.0 g of methyl hemiketal oxalate **4***a*, mp 158–160°C. Concentration of the filtrate under reduced pressure and trituration of the residue with methanol (50 mL) afforded another 1.6 g of **4***a*, mp 156–160°C. The two crops were combined to a total of 12.6 g (59%). *Anal.* calcd. for $C_{20}H_{27}NO_7$: C 61.06, H 6.91, N 3.55; found: C 60.95, H 6.90, N 3.52.

*5-Allyl-2′,9-dimethoxy-9-hydroxy-2-methyl-6,7-benzomorphan Hydrobromide (5*a)

A solution of 10.5 g of 5-allyl-2′-methoxy-2-methyl-9-oxo-6,7-benzomorphan (**1***a*) in dry ether (50 mL) was mixed with a solution of hydrogen bromide in ether and the precipitated **1***a* hydrobromide collected by filtration. A mixture of this salt and

Can. J. Chem. Downloaded from www.nrcresearchpress.com by 210.87.254.5 on 09/05/12
For personal use only.

Can. J. Chem. Downloaded from www.nrcresearchpress.com by 210.87.254.5 on 09/05/12
For personal use only.

dry methanol (50 mL) was heated under reflux until all the solids had dissolved and then the solution was left to stand at room temperature. Samples of the reaction mixture were taken at intervals, diluted with chloroform, and examined by ir; the carbonyl band of **1***a* hydrobromide slowly decreased and completely disappeared after 6 h indicating that the formation of **5***a* was completed. At this point, the solution was diluted with anhydrous ether (50 mL) and the resulting solution was allowed to slowly crystallize at room temperature overnight. The crystalline precipitate was collected by filtration to provide 10.7 g (72%) of methyl hemiketal hydrobromide **5***a*, mp 165–167°C, resolidified and melted at 195–200°C (dec.); ir (Nujol): 3300, 2600, 1605, 1505 cm^{-1}. *Anal.* calcd. for $C_{18}H_{25}NO_3 \cdot HBr$: C 56.26, H 6.81, N 3.64; found: C 56.20, H 6.79, N 3.62.

When a solution of **1***a* hydrobromide in methanol, soon after it was prepared, was induced to crystallize by the addition of ether, unchanged starting material was recovered.

A solution of **1***a* hydrobromide in methanol allowed to stay at room temperature for 1 h and then evaporated gave a mixture of starting material and **5***a* (OH and CO bands on ir).

5-Allyl-2',9-dimethoxy-9-hydroxy-2-methyl-6,7-benzomorphan (6)

Into a separatory funnel were added 100 mL of water, 7 mL of concentrated ammonium hydroxide, 12.65 g of methyl hemiketal oxalate **4***a*, and 50 mL of methylene chloride and the mixture was shaken until the solids had dissolved. The organic layer was separated and the aqueous phase extracted with methylene chloride (50 mL). Evaporation of the combined extracts at 30°C and crystallization of the residue from ether (25 mL) gave 7.1 g of **6**, mp 107–111°C. Another 0.5 g of **6** was obtained by evaporation of the mother liquor and crystallization of the residue from ether (10 mL). The two crops were combined to give a total yield of 7.6 g (77.5%) of **6**; ir ($CHCl_3$): 3380, 1610, 1505 cm^{-1}; ^{1}Hmr ($CDCl_3$) δ: 2.35 (s, 3H, NCH_3), 3.25 (s, 3H, OCH_3), 3.68 (s, 3H, Ar—OCH_3), 4.23 (s, 1H, OH), 4.83–5.25 (m, 2H, C=CH_2), 5.8–6.43 (m, 1H, CH=C), 6.5–7.0 (m, 3H, ArH). *Anal.* calcd. for $C_{18}H_{25}NO_3$: C 71.25, H 8.30, N 4.61; found: C 71.45, H 8.42, N 4.58.

A sample of **6** was dissolved in boiling ethanol and the solution allowed to crystallize. The crystalline product, mp 105–110°C was identical in all respects (ir, ^{1}Hmr) with **6**, thus indicating the stability of the compound in this solvent.

Compound **6** when dissolved in boiling methanol and the solution evaporated was converted quantitatively to the ketone **1***a*.

Treatment of a solution of **6** in chloroform with aluminum oxide gave the ketone **1***a* (100%).

5-Allyl-2'-benzyloxy-9-hydroxy-9-methoxy-2-methyl-6,7-benzomorphan Hydrobromide (5b)

To a solution of 6.0 g of 5-allyl-2'-benzyloxy-2-methyl-9-oxo-6,7-benzomorphan (**1***b*) (3–5) in dry ether was added an ethereal solution of hydrogen bromide and the precipitated **1***b* hydrobromide collected by filtration (7.4 g). A mixture of this salt and 40 mL of dry methanol was heated under reflux and, after the solids had dissolved, the solution was allowed to stay at room temperature. Crystallization usually commenced after 6–7 h; when solids were formed before this period of time, they were redissolved by heating the mixture. After standing at room temperature for 24 h, the crystalline precipitate that was formed was collected by filtration to give 4.4 g (55%) of methyl hemiketal hydrobromide **5***b*, mp 115–120°C; ir (Nujol): 3300, 2650, 1605, 1505 cm^{-1}. *Anal.* calcd. for $C_{24}H_{29}NO_3HBr$: C 62.64, H 6.56; found: C 62.45, H 6.53.

The mother liquor was evaporated and the residue was crystallized from methanol (5 mL) to give 2.6 g (32%) of the other isomer of **5***b*, mp 150–160°C; ir (Nujol): 3300, 2650, 1605, 1505 cm^{-1}. *Anal.* found: C 62.55, H 6.55.

Treatment of **5***b* (either isomer) with a base and extraction with ether produced the ketone **1***b*.

In another experiment, 6.0 g of **1***b* hydrobromide was dissolved with an excess of methanol (150 mL) and the solution was let stand 48 h at room temperature. Removal of the solvent under reduced pressure and trituration of the residue with ether gave 6.45 g (100%) of crystalline **5***b*, as a mixture of two isomers. This material was used in the bromination reaction.

2'-Methoxy-2-methyl-9-oxo-5-[3"-(1"-bromo-2"-methoxypropyl)]6,7-benzomorphan (8a)

A. Bromination of the Methyl Hemiketal 6

To a stirred solution of 2.24 g (14 mmol) of bromine in 150 mL chloroform at 0°C was quickly added a solution of 4.23 g (14 mmol) of **6** in 70 mL chloroform and the reaction mixture stirred at 0°C for 15 min. Removal of the solvent *in vacuo* gave 6.5 g (100%) of **8***a* hydrobromide as a mixture of two isomers. A sample of this salt was converted to the free base and examined by tlc on alumina plates using 1% methanol in chloroform as eluent; it showed two spots of R_f 0.28 (major) and 0.49 (minor) for the two isomers of **8***a*. Recrystallization of the crude salt from dry acetone afforded 4.5 g (70%) of **8***a* hydrobromide as a single isomer, mp 132–134°C; ir (Nujol): 2500, 1740, 1610, 1505 cm^{-1}. *Anal.* calcd. for $C_{18}H_{24}BrNO_3 \cdot HBr$: C 46.67, H 5.44, Br 34.50; found: C 46.40, H 5.36, Br 34.32.

The free base **8***a* was regenerated from its hydrobromide salt by treatment with ammonium hydroxide followed by extraction with chloroform. Compound **8***a* thus obtained showed a single spot on tlc of R_f 0.28; ir ($CHCl_3$): 1725, 1610, 1505 cm^{-1}; ^{1}Hmr ($CDCl_3$) δ: 2.43 (s, 3H, CH_3), 3.25 (s, 3H, OCH_3), 3.76 (s, 3H, Ar—OCH_3), 6.6–7.1 (m, 3H, ArH).

B. Bromination of Methyl Hemiketal Hydrobromide 5a

To a stirred solution of bromine (3.87 g, 24.2 mmol) in chloroform (240 mL) at 0°C was quickly added a solution of **5***a* (9.3 g, 24.2 mmol) in methanol–chloroform mixture (60 mL, 1:3) and the reaction mixture stirred at 0°C for 15 min. Removal of the solvent by evaporation left a residue which was basified with 1 *N* sodium hydroxide and extracted with ether. The ether extract, after drying ($MgSO_4$), was treated with a solution of hydrogen bromide in dry ether and the mixture evaporated to dryness. The residual oil crystallized from acetone to give 7.3 g (65%) of **8***a* hydrobromide, mp 132–134°C, identical in all respects (mixture mp, ir, ^{1}Hmr) with that from the previous preparation.

2'-Benzyloxy-2-methyl-9-oxo-5-[3"-(1"-bromo-2"-methoxypropyl)]-6,7-benzomorphan (8b) (A- and B-Isomers)

A solution of the hemiketal hydrobromide **5***b* (5.08 g, 11 mmol) in chloroform (120 mL) was added in one lot to a stirred solution of bromine (1.76 g, 11 mmol) in chloroform (140 mL) at 0°C. After stirring for 15 min, the reaction mixture was evaporated under reduced pressure to give 5.9 g (100%) of **8***b* hydrobromide (mixture of two isomers) as a syrup. The syrupy product was dissolved in dry acetone (20 mL), the solution diluted with dry ether (10 mL), and the resulting solution allowed to crystallize at room temperature. The crystalline precipitate was collected by filtration to give 2.7 g, mp 100–110°C. This product was suspended in dry acetone (20 mL), the mixture was heated under reflux with stirring, and then cooled to room temperature. The solids were collected by filtration to give 1.8 g of one isomer of **8***b* hydrobromide (A-isomer), mp 132–135°C. *Anal.* calcd. for $C_{24}H_{28}BrNO_3 \cdot HBr$: C 53.45, H 5.42, Br 29.63; found: C 52.98, H 5.28, Br 30.12.

The free base **8***b* (A-isomer) was quantitatively regenerated from the above salt by treatment with sodium bicarbonate and extraction with chloroform. Thin-layer chromatography (Al_2O_3, 1% MeOH–$CHCl_3$) showed one major spot of R_f 0.40 and a trace of a spot of R_f 0.61 (the other isomer); ir (neat): 1725, 1605,

Can. J. Chem. Downloaded from www.nrcresearchpress.com by 210.87.254.5 on 09/05/12
For personal use only.

1500 cm^{-1}; ^{1}Hmr ($CDCl_3$) δ: 2.33 (s, 3H, NCH_3), 3.13 (s, 3H, OCH_3), 3.55 (m, 2H, CH_2Br), 5.0 (s, 2H, CH_2Ar), 6.7–7.4 (m, 8H, ArH).

The mother liquor and the acetone extract were combined and evaporated. The residue crystallized from an acetone–ether mixture (40 mL, 1:1) to give 1.9 g, mp 148–158°C. This product contained mainly (~85%) the hydrobromide salt of the other isomer **8***b* (B-isomer). *Anal.* calcd. for $C_{24}H_{28}BrNO_3 \cdot HBr$: C 53.45, H 5.42, Br 29.63; found: C 52.81, H 5.42, Br 30.08.

The above salt was converted to the free base **8***b* (B-isomer) by treatment with sodium bicarbonate and extraction with chloroform. The free base **8***b* thus obtained showed on tlc (Al_2O_3, 1% MeOH–$CHCl_3$) one major spot of R_f 0.61 (B-isomer) and a minor of R_f 0.40 (A-isomer); ir (neat): 1725, 1605, 1500 cm^{-1}, ^{1}Hmr ($CDCl_3$) δ: 2.43 (s, 3H, NCH_3), 3.03 (s, 3H, OCH_3), 3.81 (m, 2H, CH_2Br), 5.0 (s, 2H, CH_2Ar), 6.7–7.4 (m, 8H, ArH).

*2'-Hydroxy-2-methyl-9-oxo-5-[3"-(1"-bromo-2"-methoxypropyl)]-6,7-benzomorphan (**8***c*) *(A- and B-Isomers)*

A-Isomer

To 1.2 g (2.6 mmol) of compound **8***b* (A-isomer) was added 19 mL of trifluoroacetic acid (7) at 25°C. The solution was let stand at 25°C for 72 h and then evaporated. The residue was chromatographed on alumina (130 g, Activity II) with 2% methanol in methylene chloride as eluent to yield 0.7 g (72.5%) of **8***c* (A-isomer), mp 166–168°C (dec.); ir ($CHCl_3$): 3300, 1730, 1605, 1505 cm^{-1}; ^{1}Hmr ($CDCl_3$) δ: 2.38 (s, 3H, NCH_3), 3.21 (s, 3H, OCH_3), 6.6–7.2 (m, 3H, ArH). *Anal.* calcd. for $C_{17}H_{22}NBrO_3$: C 55.44, H 6.02, Br 21.69; found: C 55.38, H 6.05, Br 21.62.

B-Isomer

In a manner analogous to that given above for the preparation of the A-isomer, 1.06 g of **8***b* (B-isomer) was treated with trifluoroacetic acid (7) and the product purified by chromatography on alumina to give 0.72 g (85%) of the B-isomer of **8***c*; ir ($CHCl_3$): 3300, 1730, 1605, 1505 cm^{-1}; ^{1}Hmr ($CDCl_3$) δ: 2.44 (s, 3H, NCH_3), 3.05 (s, 3H, OCH_3), 6.6–7.2 (m, 3H, ArH). *Anal.* found: C 55.28, H 5.98, Br 21.65.

*2'-Methoxy-2-methyl-9-oxo-5-[3"-(2"-oxopropyl)]-6,7-benzomorphan (**9**)*

To a suspension of 0.85 g of sodium hydride (from a 55% mineral oil dispersion washed three times with benzene) in 20 mL of dry DMF was added a solution of 10.2 g (26.4 mmol) of **8***a* in 15 mL of DMF and the mixture was stirred at 70°C for 6 h and at room temperature for 18 h. The reaction mixture was diluted with water (100 mL) and extracted with ether (3 × 100 mL). The combined extracts, after being washed with water and dried, were evaporated to dryness. The residue (5.8 g) was dissolved in 1 *N* aqueous hydrochloric acid (40 mL) and the solution was allowed to stand at room temperature for 1 h. The reaction mixture was then neutralized with 10% sodium bicarbonate solution and extracted with ether. The ether extract, after drying, was evaporated and the residue chromatographed on silica with 3% methanol in chloroform as eluent, to give 3.0 g (40%) of **9**; ir ($CHCl_3$): 1730, 1610, 1510 cm^{-1}; ^{1}Hmr ($CDCl_3$) δ: 2.18 (s, 3H, C(=O)—CH_3), 2.45 (s, 3H, NCH_3), 3.05 (s, 2H, CH_2CO), 3.73 (s, 3H, OCH_3), 6.5–7.2 (m, 3H, ArH). *Anal.* calcd. for $C_{17}H_{21}NO_3$: C 71.05, H 7.36, N 4.87; found: C 70.82, H 7.48, N 4.81.

*3,6-Dimethoxy-14-hydroxy-17-methyl-8-oxomorphinan (**11**)*

A solution of **8***a* (3.0 g, 6.5 mmol) and sodium hydroxide (0.64 g, 16 mmol) in 65% ethanol–water mixture (12 mL) was stirred at room temperature for 48 h. The reaction mixture was concentrated under reduced pressure and the residue partitioned between water and chloroform. The chloroform and the organic extracts were combined, dried, and evaporated. The residue was chromatographed on 80 g of alumina (activity II) with 2% methanol in methylene chloride to give 1.1 g (53%) of **11**, mp 141–142°C; ir ($CHCl_3$): 3300, 1610, 1505 cm^{-1}; ^{1}Hmr ($CDCl_3$) δ: 2.38 (s, 3H, NCH_3), 3.43 (s, 3H, OCH_3), 3.78 (s, 3H, $ArOCH_3$), 6.6–7.2 (m, 3H, ArH). *Anal.* calcd. for $C_{18}H_{25}NO_4$: C 67.68, H 7.88, N 4.38; found: C 67.58, H 7.92, N 4.35.

*3,6-Dimethoxy-14-hydroxy-17-methyl-8-thiomorphinan (**13**a)*

Hydrogen sulfide was bubbled for 15 min into a solution of potassium hydroxide (0.7 g, 12.5 milliequiv.) in 90% ethanol (15 mL). To the resulting solution of potassium hydrosulfide was added a solution of **8***a* (1.15 g, 3 mmol) in 90% ethanol (5 mL) and the reaction mixture was heated under reflux for 1.5 h while hydrogen sulfide was bubbled into the solution. The reaction mixture, after cooling to room temperature, was diluted with water (50 mL) and extracted twice with 50 mL portions of chloroform. The combined chloroform extracts were washed with water (60 mL), dried over sodium sulfate, and filtered. Evaporation of the filtrate gave 1.0 g of crystalline product which showed on tlc (alumina, 2% MeOH–CH_2Cl_2) a single spot of R_f 0.59. Recrystallization from ethanol afforded 0.75 g (75%) of **13***a*, mp 176–177°C; ir ($CHCl_3$): 3600, 3400, 1610, 1505 cm^{-1}; ^{1}Hmr ($CDCl_3$) δ: 2.32 (s, 3H, NCH_3), 3.40 (s, 3H, OCH_3), 3.70 (s, 3H, $ArOCH_3$), 4.90 (s, 1H, OH), 6.4–7.0 (m, 3H, ArH). *Anal.* calcd. for $C_{18}H_{25}NO_3S$: C 64.44, H 7.51, S 9.56; found: C 64.54, H 7.58, S 9.39.

*3,14-Dihydroxy-6-methoxy-17-methyl-8-thiomorphinal (**13**c)*

A-Isomer

A mixture of 0.5 g (1.35 mmol) of **8***c* (A-isomer) and 0.47 g (6.5 mmol) of potassium hydrosulfide in 14 mL of 90% ethanol was heated under reflux for 3 h while hydrogen sulfide was bubbled into the solution. The reaction mixture was evaporated to dryness and the residue partitioned between chloroform (80 mL) and water (10 mL). The organic phase was separated and the aqueous phase extracted with chloroform (2 × 15 mL). The combined chloroform extracts, after drying, were evaporated and the residue was chromatographed over silica gel (50 g) with 3% methanol in chloroform as eluting solvent to give 0.35 g (80%) of **13***c* (A-isomer), mp 227–229°C. Thin layer chromatography (silica, 5% MeOH–ether) showed a single spot of R_f 0.38; ir (Nujol): 3300, 1605, 1505 cm^{-1}. *Anal.* calcd. for $C_{17}H_{23}NO_3S$: C 63.52, H 7.21, S 9.97; found: C 63.48, H 7.09, S 9.88.

B-Isomer

Using the procedure described above for the preparation of the A-isomer, 0.7 g (1.9 mmol) of **8***c* (B-isomer) were reacted with potassium hydrosulfide (9 mmol) in 90% ethanol (20 mL) to provide 0.48 g (78%) of the B-isomer of **13***c*, mp 245–246°C (ethanol); ir (Nujol): 3300, 1605, 1505 cm^{-1}. *Anal.* calcd. for $C_{17}H_{23}NO_3S$: C 63.52, H 7.21, N 4.35, S 9.97; found: C 63.29, H 7.73, N 4.40, S 7.92.

1. I. Monković, H. Wong, A. W. Pircio, Y. G. Perron, I. J. Pachter, and B. Belleau. Can. J. Chem. **53**, 3094 (1975).
2. Y. Lambert, J. P. Daris, and I. Monković. Can. J. Chem. **55**, 2523 (1977).
3. G. Kavadias, S. Velkof, and B. Belleau. Can. J. Chem. **57**, 1852 (1979).
4. G. Kavadias, S. Velkof, and B. Belleau. Can. J. Chem. **57**, 1861 (1979).
5. G. Kavadias, S. Velkof, and B. Belleau. Can. J. Chem. **57**, 1866 (1979).
6. R. U. Lemieux and B. Fraser-Reid. Can. J. Chem. **42**, 532 (1964).
7. J. P. Marsh, Jr. and L. Goodman. J. Org. Chem. **30**, 2491 (1965).

A novel synthesis of 2,4,6-trithiaheptane and its conversion into 2,6-bis(methylthio)thiane. Spectral properties of some thiaalkanes

J. STUART GROSSERT,[1] DONALD L. HOOPER, AND WILLIAM M. NEAVES

Chemistry Department, Dalhousie University, Halifax, N.S., Canada B3H 4J3

Received June 9, 1980

This paper is dedicated to Prof. Raymond U. Lemieux on the occasion of his 60th birthday

J. STUART GROSSERT, DONALD L. HOOPER, and WILLIAM M. NEAVES. Can. J. Chem. **59**, 326 (1981).

2,4,6-Trithiaheptane (**1***a*) has been prepared by lithium tetrahydridoaluminate reduction of the methiodide of 1,3,5-trithiane (**2**). Treatment of **1***a* with strong bases permitted formation of 3-alkylated derivatives (**3**) which could in turn be converted into diastereomeric mixtures of 3,5-dialkyl derivatives (**4**). A two-step alkylation of **1***a* with 1-bromo-3-chloropropane led to the formation of 2,6-bis(methylthio)thiane (**5**). Proton and ^{13}C nmr spectral studies on these compounds, including the measurement of long-range carbon–proton coupling constants, are described; their mass spectra showed elimination of methanethiol as a characteristic major fragmentation pathway.

J. STUART GROSSERT, DONALD L. HOOPER et WILLIAM M. NEAVES. Can. J. Chem. **59**, 326 (1981).

On a préparé le trithia-2,4,6 heptane (**1***a*) en réduisant le méthyliodure du trithianne-1,3,5 (**2**) par le tétrahydroaluminate de lithium. La réaction du composé **1***a* avec des bases fortes conduit à la formation de dérivés alkylés (**3**) qui peuvent être ensuite transformés en des mélanges diastéréoisomères de dérivés (**4**) dialkylés en 3 et 5. Une alkylation en deux étapes de **1***a* par le bromo-1 chloro-3 propane conduit à la formation du bis(méthylthio)-2,6 thianne (**5**). On décrit les études spectrales de ces composés en rmn du ^1H et du ^{13}C, y compris les mesures des constantes de couplage à longue distance carbon–proton; leurs spectres de masse indiquent que l'élimination de méthanethiol est une caractéristique du processus principal de fragmentation.

[Traduit par le journal]

Introduction

As part of a continuing interest in the preparation and properties of sulfur-containing organic molecules (1), we wished to explore the preparation and spectral properties of compounds derived from 2,4,6-trithiaheptane, **1***a* (2). In particular, we were interested in examining whether **1***a* would form a sulfur-stabilized carbanion which could be usefully alkylated, especially since it was known that alkylation of simple, acyclic mercaptals is not generally a synthetically useful reaction (3).

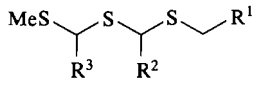

1*a* $R^1 = R^2 = R^3 = H$
b $R^1 = I; R^2 = R^3 = H$
c $R^1 = R^3 = H; R^2 = Li$
d $R^1 = H; R^2 = R^3 = Li$
e $R^1 = H; R^2 = Li; R^3 =$ alkyl

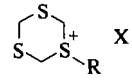

2*a* R = Me; X = I
b R = Me; X = $OCOCF_3$

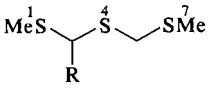

3*a* R = Me
b R = *n*Bu
c R = D
d R = $CH_2CH_2CH_2Cl$

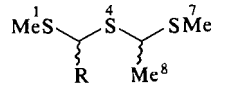

4*a* R = Me[9]
b R = $\overset{9}{C}H_2CH_2CH_2\overset{12}{C}H_3$

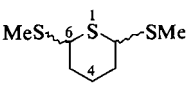

5

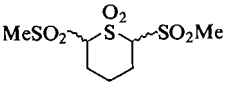

6

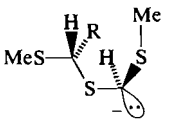

7

Preparative Results

Fehér and Vogelbruch first prepared 2,4,6-trithiaheptane, **1***a*, using a classical condensation of chloromethyl methyl sulfide with sodium sulfide (2). It seemed possible that **1***a* could be derived also by hydride reduction of an *S*-methyl sulfonium salt of *s*-trithiane, e.g. **2***a*. Such a reduction is precedented, although it does not appear to have been used widely (4). The preparation of **2***a* has been reported (5). We found it to be rather unstable both in solution and in the crystalline state, especially if it had not been carefully recrystallized; however, the pure solid was adequately stable if stored in a freezer. Attempts to record an ^1H nmr spectrum of **2***a* were frustrated by its insolubility in solvents such as chloroform and by its rapid decomposition in solvents such as DMSO-d_6. Spectra obtained showed peaks that could be attributed to **1***b*, **2***a*, *s*-trithiane, and iodomethane. However, **2***a* dissolved in trifluoroacetic acid and when treated with an equimolar amount of silver trifluoroacetate gave a

[1]Author to whom correspondence may be addressed.

0008-4042/81/020326-07$01.00/0

©1981 National Research Council of Canada/Conseil national de recherches du Canada

Can. J. Chem. Downloaded from www.nrcresearchpress.com by 210.87.254.105 on 09/05/12
For personal use only.

Can. J. Chem. Downloaded from www.nrcresearchpress.com by 210.87.254.105 on 09/05/12
For personal use only.

solution which had the expected ^{1}H nmr spectrum of **2***b*. As might be expected **2***a* decomposed over a wide temperature range when heated. Obviously, a less nucleophilic counterion than iodide was required if **2***a* was to be studied further. Nevertheless, reduction of **2***a* was successfully achieved in reasonable yield with lithium tetrahydridoaluminate in THF, to give **1***a* identical by glc, tlc, spectra, and odor with the material prepared by Fehér and Vogelbruch's method.

As a bis-thioacetal, **1***a* could be expected to form a monolithio derivative, **1***c*, (3) or perhaps even a dilithio derivative (**1***d*); this latter might have been susceptible to oxidation (6) or to dialkylation with ring formation (7), as below:

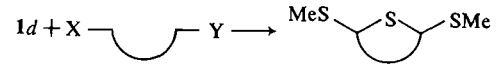

We have found that **1***c* could be generated readily under standard conditions (3) and that it reacted efficiently with standard electrophiles, such as iodomethane to give 3-methyl-2,4,6-trithiaheptane, **3***a*, or with 1-bromobutane to yield the *n*-butyl derivative, **3***b*. Quenching **1***c* with deuteroacetic acid gave **3***c*, but of more interest was the reaction of **1***c* with 1-bromo-3-chloropropane which gave **3***d*, a compound that had potential for ring closure by a two-step reaction. Possibility of direct ring formation via an ambident electrophile and **1***d* as outlined above was ruled out when we found that several reactions of **1***a* with two equivalents of *n*-butyllithium followed by quenching with different proton donors failed to regenerate **1***a*. It appears therefore that **1***d* is quite unstable.

Compounds **3***a–c* were foul-smelling oils which could be distilled and were subjected to spectral studies that are detailed presently. As might be expected, **3***d* was less stable and decomposed on standing or on attempted distillation.

Before attempting ring closure of **3***d*, we explored further alkylation of **3***a* and **3***b* by metallation with lithium diisopropylamide (LDA) and alkylation with iodomethane, which resulted in the rapid formation of 3,5-dialkylated 2,4,6-trithiaheptanes, **4***a* and **4***b*, as mixtures of two diastereomers. It is not apparent from the data we have obtained which is the predominant diastereomer although it can be argued[2] that the *erythro* diastereomer should be formed more readily than the *threo* (*dl* pair) isomer. We are investigating this point further. The nmr spectra and glc analyses showed no significant amounts of 3,3-dialkylation products.

Overnight reaction of **3***d* with LDA gave **5** as a thick foul-smelling oil, that was a ca. 5:1 diastereomeric mixture. Formation of this bis-substituted thiane was confirmed when it was oxidized by H_2O_2–HOAc to a tris-sulfone, **6**, that had a correct combustion analysis for $C_7H_{14}O_6S_2$ and an ir spectrum which indicated sulfone groups. The ^{1}H and ^{13}C nmr spectra of **6** were consistent with its structure and with it being a mixture of two components. The mass spectrum showed a molecular ion corresponding to the molecular weight of **6**, as well as peaks at $M^+ \cdot - 79$ and *m/z* 79, indicative of an $MeSO_2$— group.

Mass Spectra

The mass spectra of the trithiaheptanes (**1***a*, **3***a–d*, **4***a*, *b*) all showed loss of MeSH as a major initial fragmentation (cf. Table 1[3] and Scheme 1, **A** → **D**). This fragmentation was supported in all cases by a metastable ion and it has been observed previously in bis(alkylthio) alkanes (10, 11).[4] Ions **B** and **C** can be formed by standard fragmentations of thioethers (10); **G** and **H** are readily explicable as arising from **D** although it is conceivable that they could derive from **C** or **B** respectively. Thiane **5** also showed loss of CH_3SH as the initial fragmentation process (for spectrum, see Experimental), although in this case subsequent fragmentation appeared to occur chiefly by loss of MeS· since *m/z* 99 is the base peak of the spectrum. Presumably the ion at *m/z* 97 is the thiacyclohexatriene cation derived from *m/z* 99. There is some precedent for this type of fragmentation pattern from the mass spectra of methylthianes (10, 12).

Nuclear Magnetic Resonance Spectra

The nmr spectra of the trithiaheptanes (Tables 2–4) showed a number of interesting features. The "gated" ^{13}C nmr spectra of **1***a* and **3***a* were especially informative due to very clearly defined three-bond ^{13}C—^{1}H couplings across sulfenyl sulfur which permitted unambiguous assignment of all the resonances in the spectrum of **3***a*. In fact, the particular structures of **1***a* and **3***a* make them ideal

[2]This argument derives from the assumption (8, 9) that the most stable configuration and conformation of the carbanions derived from **3***a*, *b*, or *d* would have the anion orbital *trans*, antiparallel to both adjacent C—S bonds, cf. **7**.

[3]Table 1 is available, at a nominal charge, from the Depository of Unpublished Data, CISTI, National Research Council of Canada, Ottawa, Ont., Canada K1A 0S2.

[4]This type of fragmentation has subsequently proved valuable in structure determination of substituted 2,4,6-trithiaheptanes, J. S. Grossert and M. Langman, to be published.

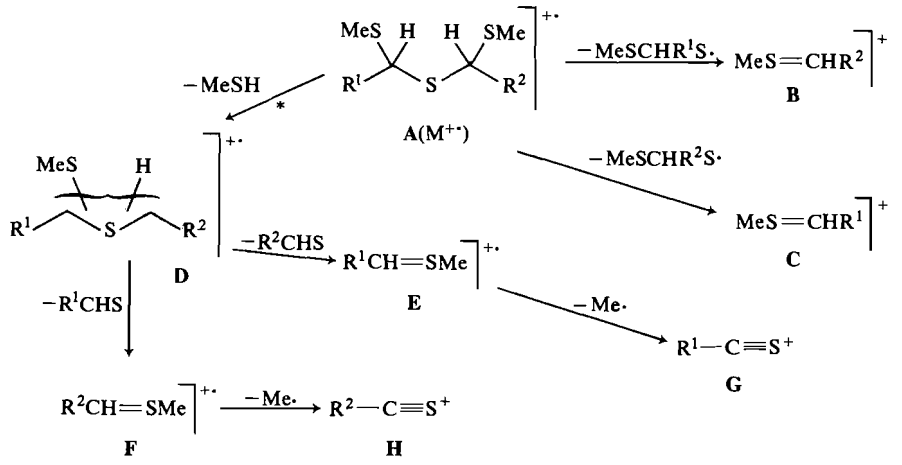

SCHEME I

molecules for observing high-resolution ^{13}C nmr spectra without wide-band ^{1}H decoupling (13).

The assignment of the ^{1}H nmr spectra (Table 2) is straightforward, save for the assignment of the SMe groups. This was carried out by a combination of heteronuclear decoupling methods and is reported elsewhere[5] as an example of a general method of assigning XCH_3 signals. The transmission of chirality effects through sulfenyl sulfur as evidenced by the appearance of methylene AB quartets in **3** is noteworthy. This type of observation is precedented, albeit uncommonly (14).

The ^{13}C nmr assignments (Table 3) are the result of spectra measured under conditions of full ^{1}H decoupling, single-frequency off-resonance decoupling (SFORD) (15) and "gated" ^{1}H decoupling (16). The SFORD spectra were used to distinguish methyl, methylene, and methine carbon signals and to assign the signals of the *n*-butyl carbons of **3***b* and **4***b*. In these SFORD spectra each methylene resonance for a carbon of the *n*-butyl chain showed second-order lines between the components of the first-order triplet, as expected (17) for the SFORD signals of carbons coupled to a tightly-coupled proton spin system. For each of **3***a* and **3***b* the C(1) and C(7) SMe signals were distinguished by the distinctive patterns observed in gated decoupling experiments. In each case, C(1) was a quartet of doublets and C(7) was a quartet of triplets, with the fine doublet or triplet splitting arising from three-bond coupling through sulfenyl sulfur to the methine proton at C(3) or to the methylene protons at C(5). Similarly, in **4***a* and **4***b* the CMe and SMe signals were distinguished by the splitting patterns observed under gated decoupling conditions. The two SMe signals of an individual diastereomer could not be differentiated in this way and the assignments of C(1) and C(7) for **4***a* and **4***b* in Table 3 may have to be reversed. The signals of the two diastereomers could, of course, be distinguished by their different integrals in the fully decoupled spectrum of a mixture.

The coupling across sulfenyl sulfur atoms, which we have exploited in making some of the above assignments, proved to be a considerable complication in extracting values of $^{2}J_{CH}$ and $^{3}J_{CH}$ for C(3) and C(5). The coupling constants reported in Table 4 were extracted from the gated decoupling spectra by first-order analysis. Cases for which $^{3}J_{CH}$ values are not reported in Table 4 were those in which C(3) and C(5) are subject to so many 2- and 3-bond couplings with protons that the first-order patterns could not be distinguished within the resolution of the experiment.

The parameters reported in Tables 3 and 4 usefully supplement data available (18–23) for open-chain organosulfur compounds. For example, it is known (18) that the α, β, γ, and δ substituent effects of a sulfenyl sulfur atom in simple sulfides are little different from those of a carbon atom. The ^{13}C chemical shifts of the trithiaheptanes reported in Table 3 confirm this. For C(1), the terminal methyl group of heptane, δ (^{13}C) = 13.9 which changes to δ 13.7 for the corresponding carbon of di-*n*-propyl sulfide (18) and to δ 14.2 in **1***a*, where heptane carbons C(2), C(4), and C(6) are all replaced by sulfur atoms. The change in chemical shift for C(3) in the same series is from δ 32.4 to δ 34.6 to δ 35.8. The greatest experimental chemical shift changes for the trithiaheptanes are the result of 3- and/or 5-alkyl substitution. These chemical shift changes,

[5]D. L. Hooper, J. S. Grossert, and W. M. Neaves, to be published.

Can. J. Chem. Downloaded from www.nrcresearchpress.com by 210.87.254.105 on 09/05/12
For personal use only.

TABLE 2. The ^{1}H nmr spectral parameters of substituted 2,4,6-trithiaheptanes

Compound	*C*-Methyl resonance	*S*-Methyl resonances	Methylene resonances	Methine resonances	Other resonances
1*a*	—	δ 2.15(s)*	δ 3.75(s)	—	—
3*a*	1.59(d, J = 6.9†)	2.10, s, C(7) 2.16, s, C(1)	3.72(J_{AB} 13.6)	4.08(q, J = 6.9)	—
3*b*	0.90(dist. t)	2.05, s, C(7) 2.15, s, C(1)	3.73(J_{AB} 13.7)	3.93(t, J = 6.8)	1.05–2.00(6H, b, m)
3*c*	—	2.15(s)	3.77(s)	3.77(s)	—
3*d*	—	2.03, s, C(7) 2.13, s, C(1)	3.73(J_{AB} 13.5)	3.95(t, $J \sim 6$)	1.88–2.14(m, 4H) 3.40–3.73(m, 2H)
4*a* Major	1.61(d, J = 6.8)	2.16(s)	—	3.96(q, J = 6.8)	—
Minor	1.58(d, J = 7.1)	2.10(s)	—	4.11(q, J = 7.1)	—
4*b* Major	1.59(d, J = 6.6)	2.11, 2.15(s, s)	—	3.80(t, J = 6.6)H(3) 3.98(q, J = 6.6)H(5)	0.91(dist. t) (butyl methyl)
Minor	1.58(d, J = 7.0)	2.06, 2.08(s, s)	—	3.87(t, J = 6.5)H(3) 4.17(q, J = 7.0)H(5)	1.05–2.00 (6H, b, m)

*Abbreviations: s = singlet, d = doublet, t = triplet, q = quartet, dist. = distorted, m = multiplet, b = broad.
†All coupling constants (J) were measured directly from the spectra and are reported in Hz.

referred to trithiaheptane **1***a* as a base, are listed as Δ^{exp} in Table 3. The values Δ^{calc} in this table are the calculated substituent effects for the corresponding carbons of heptane, using the substituent parameters of Lindeman and Adams (ref. 24; see also ref. 25). The agreement between Δ^{exp} and Δ^{calc} is such that it appears quite acceptable to use the hydrocarbon substituent parameters to predict chemical shifts in acyclic compounds containing sulfenyl sulfur, once again emphasizing the similarity of carbon and sulfur for this particular aspect of ^{13}C spectroscopy.

The directly bonded carbon—proton coupling constants (Table 4) were almost invariant for a particular carbon throughout the series **1***a*–**4***b*. This is the expected result, as the dominant factor for $^1J_{CH}$ is known (26) to be the electronegativity of the atoms bonded to the carbon of the ^{13}C—H fragment. A calculation using Malinowski's ζ values (27) gave $^1J_{CH}$ = 138.0 Hz for C(1) and C(7), $^1J_{CH}$ = 150.9 for a C(3) or C(5) methylene group, and $^1J_{CH}$ = 151.8 for a C(3) or C(5) methine group.

In discussing the experimental $^3J_{CH}$ values for the series, reference must be made to the work of Dorman, Bauer, and Roberts (28) on "long-range" carbon—proton coupling in methyl ethers. They observed a strong decrease in the coupling $^3J_{CH}$ of the methoxyl carbon to the α-proton(s) with increasing bulk of the α-substituents, and a less striking decrease in the three-bond coupling of the methoxyl protons to the α-carbon. The $^3J_{CH}$ values in Table 4 are in general agreement with these trends and with similar values reported by Dauphin and Cuer (23). In **1***a*, **3***a*, and **3***b* the splitting patterns of C(3) and C(5) showed $^3J_{C(3),H(5)}$ and $^3J_{C(5),H(3)}$ to be somewhat smaller than $^3J_{C(3),H(1)}$ and $^3J_{C(5),H(7)}$ which indicates the effect of sulfenyl sulfur as a substituent to the coupling fragment C—S—C—H. We are not aware of any published data on the effect of sulfenyl sulfur as a substituent on the corresponding fragment C—C—C—H, but a similar effect would be predicted.

The smaller values 3.5 Hz and 3.8 Hz for $^3J_{C(1),H(5)}$ in the spectra of the major diastereomers of **4***a* and **4***b* indicated a larger contribution of *gauche* $^3J_{CH}$ values in comparison with the contribution to $^3J_{CH}$ in the minor diastereomer, and hence a greater population of conformers with either the —CHRS— chain or an alkyl group *anti* to the terminal S-methyl group.

The ^{13}C nmr spectrum of **5** showed 4 lines, with appropriate chemical shifts and off-resonance multiplicities, for the major diastereomer. This was presumed to have a *cis* configuration, support for which came from the ^{1}H nmr spectrum which showed a single intense S-methyl peak. The minor component (ca. 15%) showed two methylene, one methine, and two S-methyl ^{13}C resonances, as would be expected from the *trans* compound. The two methyl peaks were not sufficiently intense to enable both to be seen clearly in either the off-resonance ^{13}C spectrum or in the ^{1}H spectrum, in this latter case, due to overlapping methylene resonances.

Conclusions

The alkylation reactions discussed in this paper represent a further development in methods for the

Can. J. Chem. Downloaded from www.nrcresearchpress.com by 210.87.254.105 on 09/05/12
For personal use only.

Can. J. Chem. Downloaded from www.nrcresearchpress.com by 210.87.254.105 on 09/05/12
For personal use only.

TABLE 3. ^{13}C chemical shifts in some 2,4,6-trithiaheptanes

Compound	C(1)			C(3)			C(5)			C(7)			*C*-Methyl resonances	Other resonances
	δ	Δ^{exp}	Δ^{calc}	δ	Δ^{exp}	Δ^{calc}	δ	Δ^{exp}	Δ^{calc}	δ	Δ^{exp}	Δ^{calc}		
1*a*	14.2	—	—	35.8	—	—	35.8	—	—	14.2	—	—	—	—
3*a*	11.3	−2.9	−3.0	45.4	9.6	14.6	36.4	0.6	−2.7	14.2	0.0	0.0	21.9	—
3*b*	12.1	−2.1	−2.5	52.2	16.4	16.1	37.0	1.2	−1.7	15.0	0.8	0.0	13.9	22.3, 29.9, 34.8
4*a* Major diastereomer	12.8	−1.4	−3.0	46.3	10.5	9.5	46.3	10.5	9.5	12.8	−1.4	−3.0	22.3	—
4*a* Minor diastereomer	11.4	−2.8	−3.0	46.9	11.1	9.5	46.9	11.1	9.5	11.4	−2.8	−3.0	21.6	—
4*b* Major diastereomer	12.8	−1.4	−3.0	46.0	10.2	9.5	52.0	16.2	14.0	12.4	−1.8	−2.5	13.6(C(12)) 22.3(C(8))	22.0(C(11)), 29.1(C(10)) 34.9(C(9))
4*b* Minor diastereomer	11.0	−3.2	−3.0	46.4	10.6	9.5	52.6	16.8	14.0	11.2	−3.0	−2.5	13.6(C(12)) 21.4(C(8))	21.9(C(11)), 29.3(C(10)) 34.2(C(9))

TABLE 4. ^{13}CH coupling constants in some 2,4,6-trithiaheptanes

Compound	$^1J_{CH}$ (Hz)					$^3J_{CH}$ (Hz)				$^2J_{CH}$ (Hz)
	C(1)	C(3)	C(5)	C(7)	Others	C(1)	C(3)	C(5)	C(7)	C—CH_3
1*a*	139.0	150.7	150.7	139.0	—	4.7	5.0(C(3), H(1)) 4.3(C(3), H(5))	5.0(C(5), H(7)) 4.3(C(5), H(3))	4.7	—
3*a*	138.9	151.6	150.7	138.8	129.2(C(8))	4.0	4.7(C(3), H(1)) *	4.8(C(5), H(7)) 3.9(C(5), H(3))	4.5	3.5
3*b*	138.7	150.6	149.8	138.8	125.1(C(11))	4.2	4.1(C(3), H(1)) *	4.9(C(5), H(7)) 3.9(C(5), H(3))	4.5	3.5
4*a* Major diastereomer	138.8	151.3	151.3	138.8	129.1(C(8,9))	3.5	*	*	3.5	3.5
4*a* Minor diastereomer	138.9	151.1	151.1	138.9	129.0(C(8,9))	4.2	*	*	4.2	3.7
4*b* Major diastereomer	138.8	*	*	139.0	129.0(C(8)) 124.8(C(12))	3.8	*	*	3.7	3.3
4*b* Minor diastereomer	138.7	*	*	138.8	129.1(C(8)) 124.8(C(12))	4.0	*	*	4.2	3.9

*Not observed, or strongly distorted splitting pattern.

Can. J. Chem. Downloaded from www.nrcresearchpress.com by 210.87.254.105 on 09/05/12
For personal use only.

umpolung of carbonyl reactivity (3, 29). Of particular interest in this case is the availability of a second acidic proton for cyclization reactions to produce compounds such as **5**, a masked glutaraldehyde. We are actively exploring ways to extend the synthetic versatility of these reactions and to explore stereochemical consequences that arise from the particular geometry that molecules such as **1***e* adopt in the formation of **4** and **5**.

Experimental

General

Proton nmr spectra were measured on either a T-60 or a CFT-20 spectrometer and the chemical shifts are reported with respect to internal TMS. Carbon nmr spectra were recorded (CFT-20) in $CDCl_3$ which served as solvent, lock signal, and internal reference. The ^{13}C chemical shifts are reported with respect to TMS, δ ($^{13}CDCl_3$) = 76.90 (30). All gated decoupling experiments used the maximal acquisition time allowed for the minimum spectral width which could avoid "foldover" of spectral lines. These experiments used 90° pulses with 2–5 s delay between pulses. Typically, 20 000 pulses were required for the 50–75% solutions of trithiaheptanes in $CDCl_3$. The carbon—proton coupling constants reported were extracted from the experimental splitting of resonance signals in the gated decoupling experiments. Cases showing obvious second-order characteristics are not reported here.

Mass spectra were obtained from a DuPont-CEC 21-104 spectrometer with a glass probe inserted directly into the source, which operated at 70 eV and ca. 150°C. Gas–liquid chromatographic analyses were run on an H-P 5750 f.i.d. instrument using an SE30 column (5% on Chromosorb W) at 140–160°C, with N_2 carrier gas. Thin-layer chromatographic analyses were on Merck HF-254 silica gel, developed with 1.5–3.0% EtOAc in isooctane and visualized by uv light or by cerate spray (31). Tetrahydrofuran (THF) was distilled first from P_2O_5 and then, immediately before use, from $NaAlH_4$ under dry N_2. Diisopropylamine (iPr$_2$NH), hexamethylphosphoric-triamide (HMPTA), and *N,N,N,N*-tetramethylethylenediamine (TMEDA) were distilled at the appropriate pressure from CaH_2. *n*-Butyllithium (*n*BuLi) was 2.4 *M* in hexane (Alfa Inorganics) and its molarity was checked by the method of Watson and Eastham (32). Other chemicals were obtained from Fisher Scientific, Eastman Organic, or Aldrich and were purified only if necessary. Bulb-to-bulb distillations were carried out using a set of bulbs which rotated on a Chemquip rotary evaporator and which were heated by an oven fashioned from a pair of concentric glass tubes, Nichrome heating wire, and Transite ends. Combustion analyses were by Dr. F. Pascher, Bonn, West Germany.

*Preparation of Methylthionia-3,5-dithiacyclohexane Iodide, 2*a

s-Trithiane was treated with $(MeO)_2SO_2$, followed by KI, according to the method of Lee and Dougherty (5) to give the sulfonium iodide **2***a*, which was thrice rapidly recrystallized from DMSO–CH_2Cl_2. The colorless crystals of **2***a* were washed with cold CH_2Cl_2, dried *in vacuo* and stored at −15°C.

Reduction of **2**a *to 2,4,6-Trithiaheptane, 1*a

A stirred suspension of **2***a* (3.62 g, 12.9 mmol) in dry THF (150 mL) was cooled (ice bath) and treated cautiously with $LiAlH_4$ (0.5 g). The reaction was stirred overnight at room temperature, the excess hydride was destroyed with acetone, and the slurry filtered through Celite, which was Soxhlet extracted with CH_2Cl_2. The filtrate and CH_2Cl_2 extracts gave on evaporation a yellow oil which was chromatographed (CH_2Cl_2, silica gel) to give **1***a* as a pale yellow oil (1.26 g, 63%) that on distillation gave **1***a* as a colorless oil, identical in all respects to material prepared by Fehér and Vogelbruch's method (2), bp 52–54°C, 0.05 Torr; for ms see Table 1; for nmr see Tables 2–4.

Preparation of 3-Substituted 2,4,6-Trithiaheptanes, 3

(a) General Procedure and Preparation of **3**a

A solution of 2,4,6-trithiaheptane (**1***a*, 2.46 mL, 19.0 mmol) in THF (25 mL) was cooled by a ca −80°C bath (liquid N_2 – acetone slush) in an N_2 atmosphere with magnetic stirring. *n*-Butyllithium (7.9 mL, 19.0 mmol) was added by syringe, followed after 30 min by iodomethane (1.5 mL, 24.1 mmol). After 15–30 min a precipitate was observed, and the reaction was allowed to warm to room temperature (ca. 60 min), after which it was poured into an aqueous buffer solution (10% NH_4Cl, 10% NaOAc, 100 mL). This was extracted with CH_2Cl_2 (1 × 25, 3 × 15 mL) which was washed with water, dried ($MgSO_4$), and rotary evaporated to a pale yellow oil which was distilled to give 3-methyl-2,4,6-trithiaheptane, **3***a*, as a colorless oil (2.7 g, 85%), bp 54–56°C/0.05 Torr.

(b) Preparation of Butyl Derivative, **3**b

Compound **1***a* (3.11 mL, 23.8 mmol) was reacted as in (*a*) with *n*BuLi (9.9 mL, 23.8 mmol) and 1-bromobutane (2.8 mL, 26.2 mmol). The reaction warmed slowly and was stirred overnight at room temperature. It gave **3***b* as a colorless oil (4.37 g, 87%), bp 75°C/0.08 Torr.

(c) Preparation of Deuterioderivative, **3**c

The reaction as under (*a*) was quenched with DOAc to give **3***c* as a colorless oil. Compounds **3***a–c* were homogeneous by tlc and glc.

(d) Preparation of γ-Chloropropyl Derivative, **3**d

Compound **1***a* (5.1 mL, 39 mmol) was reacted as in (*b*) with *n*BuLi (17.0 mL, 40 mmol) and 1-bromo-3-chloropropane (8.0 mL, 75 mmol) to give **3***d* which was not distilled since it was essentially clean (^1H nmr), yield 8.18 g (91%), ms: 232, 230 (0.3, 0.8, $M^{+\cdot}$), 184 (0.6), 182 (1.4), 171 (0.3), 169 (0.8), 153 (25), 105 (29), 87 (24), 61 (100), 45 (89); nmr see Table 2.

Preparation of 3,5-Disubstituted 2,4,6-Trithiaheptanes, 4

(a) Preparation of Dimethyl Compound, **4**a

Lithium diisopropylamide (LDA) was prepared at ca. −80°C in THF from iPr$_2$NH (0.43 mL, 3.1 mmol) and *n*BuLi (1.3 mL, 3.1 mmol) and to this was added a solution of **3***a* (521 mg, 3.1 mmol) in THF (20 mL). Procedures as for **3***a* gave **4***a* as a yellow oil (427 mg, 76%) which was distilled (0.01 Torr, bulb-to-bulb) to give a colorless oil (250 mg), ratio of two components (glc) 2.38:1. A repeat experiment on **3***a* (644 mg, 3.8 mmol) with only *n*BuLi (not LDA) as base gave **4***a* (580 mg, 83%) which was distilled to give a colorless oil (446 mg), ratio of components 2.35:1.

(b) Preparation of n*-Butylmethyl Compound,* **4**b

Compound **3***b* (1.00 g, 4.76 mmol) was treated with LDA as for the preparation of **4***a*, to give a pale yellow oil, **4***b* (729 mg, 74%), which was distilled (0.01 Torr, bulb-to-bulb) to give a colorless semisolid oil, diastereomer ratio (glc) 3.6:1.

Preparation of 2,6-Bis(methylthio)thiane, 5

LDA was prepared from iPr$_2$NH (5.4 mL, 38.4 mmol) and *n*BuLi (16.0 mL, 3.84 mmol) in THF (50 mL). To this was added HMPTA (3.8 mL) and **3***d* (8.81 g, 35.6 mmol). The mixture was allowed to warm to room temperature at which it was stirred for 20 h. After work-up, the crude product was chromatographed on silica gel, with toluene–isooctane (2:3, 500 mL) as eluant, which gave **5** as a pale yellow oil (3.29 g, 48%) that appeared to be clean by nmr and mass spectrometry, but which decomposed on attempted distillation; ^1H nmr ($CDCl_3$) δ: 4.05 (m, major, CH), 3.80 (m, minor, CH), 2.5–1.8 (m, CH_2 envelope), 2.20 (s, minor, SMe), 2.18 (s, major, SMe); ^{13}C

nmr, major δ: 47.19 C(2, 6), 32.66 C(3, 5), 21.89 C(4), 14.09 (SMe); minor δ: 47.91 C(2, 6), 32.87 C(3, 5), 26.73 C(4), 14.60, 12.82 (SMe); ms: 194 (9, $M^{+\cdot}$), 147 (11), 146 (43), 99 (100), 98 (26), 97 (42), 87 (40), 76 (61), 65 (18), 47 (54), 45 (82).

*Preparation of 2,6-Bis(methanesulfonyl)thiane-*S,S*-dioxide, 6*

A stirred, cooled solution of **5** (490 mg, 2.5 mmol) in glacial acetic acid (10 mL) was treated with 50% H_2O_2 (3 mL). After 10 min, the ice bath was removed and the reaction was stirred at room temperature for 65 h. The mixture was poured into 10% $NaHSO_3$ solution (100 mL) which was extracted with ethyl acetate (3 × 50 mL), from which **6** (300 mg, 41%) was obtained as a pale yellow solid. Two recrystallizations from acetone and a sublimation (130°C, 0.3 Torr) gave pure **6**, mp 253–254°C; ir: 1340, 1325, 1168, 1158, 790 cm^{-1}; ^1H nmr (DMSO-d_6) δ: 1.4–2.7 (m, CH_2 + DMSO), 3.30, 3.33 (2 × s, $MeSO_2$—), 4.9–5.4 (m, CH); ^{13}C nmr (DMSO-d_6), major component δ: 19.50 C(4), 24.79 C(3, 5), 42.78 (SO_2Me), 76.97 C(2, 6); minor component: δ: 21.93, 25.09, 43.02, 78.39; *Anal.* calcd. for $C_7H_{14}O_6S_3$: C 28.95, H 4.86, S 33.13%; found: C 29.00, H 4.90, S 32.86%.

Acknowledgments

We thank the National Research Council of Canada and Dalhousie University for financial support and Dr. J-H. Kim for recording the mass spectra.

1. J. S. Grossert, M. M. Bharadwaj, R. F. Langler, T. S. Cameron, and R. E. Cordes. Can. J. Chem. **56**, 1183 (1978); J. S. Grossert, M. M. Bharadwaj, J. B. Faught, and A. Terzis. Can. J. Chem. **58**, 1106 (1980).
2. F. Fehér and K. Vogelbruch. Chem. Ber. **91**, 996 (1958).
3. D. Seebach and E. J. Corey. J. Org. Chem. **40**, 231 (1975), and references therein.
4. S. Ašperger, D. Stefanović, D. Hegedić, D. Pavlović, and L. Klasinc. J. Org. Chem. **33**, 2526 (1968); P. Wilder, Jr., L. A. Feliu-Otero, and G. A. Diegnan. J. Org. Chem. **39**, 2153 (1974); V. Ceré, A. Guenzi, S. Pollicino, E. Sandri, and A. Fava. J. Org. Chem. **45**, 261 (1980).
5. S. W. Lee and G. Dougherty. J. Org. Chem. **4**, 48 (1939).
6. J. S. Grossert, J. Buter, E. W. H. Asveld, and R. M. Kellogg. Tetrahedron Lett. 2805 (1974).
7. M. P. Cooke, Jr. and R. Goswami, J. Am. Chem. Soc. **95**, 7891 (1973).
8. N. D. Epiotis, W. R. Cherry, S. Shaik, R. Yates, and F. Bernardi. Top. Curr. Chem. **70**, 185 (1977).
9. A. G. Abatjoglou, E. L. Eliel, and L. F. Kuyper. J. Am. Chem. Soc. **99**, 8262 (1977).
10. J. H. Beynon, R. A. Saunders, and A. E. Williams. The mass spectra of organic molecules. Elsevier, Amsterdam. 1968. pp. 360–365.
11. T. H. Shuttleworth. Appl. Spectrosc. **18**, 78 (1964); D. G. I. Kingston, B. W. Hobrock, M. M. Bursey, and J. T. Bursey. Chem. Rev. **75**, 693 (1975).
12. Q. N. Porter and J. Baldas. Mass spectrometry of heterocyclic compounds. Wiley-Interscience, New York. 1971. pp. 236–241.
13. G. C. Levy and D. C. Dittmer. Org. Magn. Reson. **4**, 107 (1972).
14. W. B. Jennings. Chem. Rev. **75**, 307 (1975); M. Brink and E. Larsson. Tetrahedron, **27**, 3875 (1971).
15. R. R. Ernst. J. Chem. Phys. **45**, 3845 (1966).
16. J. Feeney, D. Shaw, and P. J. S. Pauwels. J. Chem. Soc. Chem. Commun. 554 (1970).
17. E. W. Hagaman. Org. Magn. Reson. **8**, 389 (1976).
18. G. Barbarella, P. Dembech, A. Garbesi, and A. Fava. Org. Magn. Reson. **8**, 108 (1976).
19. A. Hoppmann, P. Weyerstahl, and W. Zummack. Justus Liebigs Ann. Chem. 1547 (1977).
20. C. M. Hall and J. Wemple. J. Org. Chem. **42**, 2118 (1977).
21. J. V. Paukstelis, E. F. Byrne, T. P. O'Connor, and T. E. Roche. J. Org. Chem. **42**, 3941 (1977).
22. R. G. Petrova, I. I. Kandror, V. I. Dostovalova, T. D. Churkina, and R. Kh. Freidlina. Org. Magn. Reson. **11**, 406 (1978).
23. G. Dauphin and A. Cuer. Org. Magn. Reson. **12**, 557 (1979).
24. L. P. Lindeman and J. Q. Adams. Anal. Chem. **43**, 1245 (1971).
25. F. W. Wehrli and T. Wirthlin. Interpretation of carbon-13 nmr spectra. Heyden and Son, London. 1976.
26. N. Muller and D. E. Pritchard. J. Chem. Phys. **31**, 1471 (1959).
27. E. R. Malinowski. J. Am. Chem. Soc. **83**, 4479 (1961).
28. D. E. Dorman, D. Bauer, and J. D. Roberts. J. Org. Chem. **40**, 3729 (1975).
29. D. Seebach, N. R. Jones, and E. J. Corey. J. Org. Chem. **33**, 300 (1968); R. D. Balanson, V. M. Kobal, and R. R. Schumaker. J. Org. Chem. **42**, 393 (1977).
30. J. B. Stothers. Carbon-13 nmr spectroscopy. Academic Press, New York. 1972.
31. J. S. Grossert and R. F. Langler. J. Chromatogr. **97**, 83 (1974).
32. S. C. Watson and J. F. Eastham. J. Organomet. Chem. **9**, 165 (1967).

Can. J. Chem. Downloaded from www.nrcresearchpress.com by 210.87.254.105 on 09/05/12
For personal use only.

Regioselective eliminations in reactions of carbohydrate derivatives with superoxide, or with borohydride in 2-propanol

VANGA S. RAO AND ARTHUR S. PERLIN

Department of Chemistry, McGill University, Montreal, P.Q., Canada H3C 3G1

Received July 9, 1980

This paper is dedicated to Prof. Raymond U. Lemieux on the occasion of his 60th birthday

VANGA S. RAO and ARTHUR S. PERLIN. Can. J. Chem. **59**, 333 (1981).

The reaction between 2,3,4,6-tetra-*O*-benzyl-1,5-di-*O*-mesyl-D-glucitol (**2**) and potassium superoxide resulted in the loss of H-4 and the 5-mesyloxy (as well as 1-mesyloxy) substituent, and an almost quantitative conversion into enol ether **4**, i.e., 1,3,4,5-tetra-*O*-benzyl-3-dehydro-2-deoxy-L-*threo*-hex-2-enitol. When the reaction was performed with **8**, in which the 1-*O*-mesyl group (of **2**) is replaced by *O*-(methoxy)trityl, the outcome was wholly different: an olefin was formed through the removal of a primary (H-6) rather than a secondary (H-4) proton, and nucleophilic displacement also took place. Results similar to those for **8** were obtained with the 2-epimer of **2**, i.e., 2,3,4,6-tetra-*O*-benzyl-1,5-di-*O*-mesyl-D-mannitol (**12**). It is suggested that selective displacement of the 1-*O*-mesyl group of **2** by superoxide generates a 1-peroxy anion (**6**) that abstracts H-4 intramolecularly, promoting concomitant loss of the 5-mesyloxy group. The transition state for proton abstraction within anion **6** appears to be more stable than that of the corresponding anion in the *manno* series, accounting for the different reaction routes for **2** and **12**. Elimination occurred also in the reduction of 2,3,4,6-tetra-*O*-benzyl-D-glucopyranose with sodium borohydride in 2-propanol, en route to **2**, affording 2,4,6-tri-*O*-benzyl-2-dehydro-3-deoxy-D-*threo*-hex-2-enitol (**21**). The ^{1}H nmr spectra of alditol derivatives **2**, **8**, and **12** show that these molecules depart substantially from extended zigzag conformations, in contrast to configurationally related peracetylated acyclic derivatives.

VANGA S. RAO et ARTHUR S. PERLIN. Can. J. Chem. **59**, 333 (1981).

Par réaction avec le superoxyde de potassium le tétra-*O*-benzyl-2,3,4,6 di-*O*-mésyl-1,5 D-glucitol (**2**) perd le proton en H-4 et le groupe mésyloxy-5 (ainsi que le mésyloxy-1) et se transforme presque quantitativement en éther énolique **4** soit le tétra-*O*-benzyl-1,3,4,5 déhydro-3 déoxy-2 L-*thréo*-hexène-2 itol. Si l'on effectue la même réaction sur le composé **8** qui correspond au remplacement du groupe *O*-mésyl-1 (de **2**) par un groupe *O*-(méthoxy)trityl, la réaction est très différente. Il se forme une oléfine par l'intermédiaire d'une élimination de l'hydrogène primaire (H-6) plutôt que par celle du proton (H-4) et il se produit ainsi un déplacement nucléophile. Avec l'épimère du composé **2**, soit le tétra-*O*-benzyl-2,3,4,6 di-*O*-mésyl-1,5 D-mannitol (**12**), on obtient des résultats semblables à ceux que donne le composé **8**. On suggère que le déplacement sélectif du groupe *O*-mésyl-1 du composé **2** par le superoxyde, engendre un anion péroxy (**6**) qui enlève intramoléculairement H-4 en favorisant la perte concomitante du groupe mésyloxy en position 5. L'état de transition lors de l'élimination du proton dans l'anion (**6**) semble être plus stable que celui dérivant de l'anion correspondant des séries *manno*; ceci explique les réactions différentes de **2** et **12**. Lors de la réduction du tétra-*O*-benzyl-2,3,4,6 D-glucopyranose par le borohydrure de sodium dans le propanol-2, il se produit également une élimination qui conduit au tri-*O*-benzyl-2,4,6 déhydro-2 déoxy-3 D-*thréo*-hexène-2 itol (**21**) plutôt qu'au composé **2** attendu. Les spectres rmn du ^{1}H des dérivés alditol **2**, **8**, et **12** indiquent que ces molécules s'éloignent de façon marquées des conformations en zig zag en contradiction avec les configurations des dérivés acycliques peracétylés apparentés.

[Traduit par le journal]

Introduction

In examining possibilities for a novel synthesis of L-idose, 2,3,4,6-tetra-*O*-benzyl-1,5-di-*O*-mesyl-D-glucitol (**2**) was prepared[1] by hydride reduction of 2,3,4,6-tetra-*O*-benzyl-D-glucopyranose (**1**), followed by mesylation. It was anticipated that the use of potassium superoxide (KO_2) to displace the mesyloxy substituents of **2**, by analogy with corresponding S_N2 reactions in the acyclic and alicyclic series (1, 2) would yield 1,3,4,5-tetra-*O*-benzyl-L-iditol (**3**), potentially a suitable precursor to L-idose. Instead, an uncommon type of elimination process ensued. Another unexpected elimination reaction was encountered during the reduction of **1** with sodium borohydride in 2-propanol. These, and related, observations form the subject of the present article.

Results and Discussion

Reaction between 2,3,4,6-Tetra-O-benzyl-1,5-di-O-mesyl-D-glucitol and Potassium Superoxide

When alditol **2** was subjected to reaction with KO_2, in 1:1 methyl sulfoxide – dimethylformamide containing 18-crown-6 (1, 2) an almost quantitative yield was obtained of an unstable monohydroxy compound, characterized as **4**. That is, the ^{1}H nmr spectrum of **4** contained an appropriate downfield triplet (δ 5.20) attributable to H-2, as well as an OH-6 doublet of doublets (δ 2.77, eliminated by deuterium exchange). Moreover the acetylation of **4** with acetic anhydride – pyridine produced a syrupy monoacetate (**5**), characterized by ^{13}C resonance signals attributable to the enol ether moiety

[1]V. S. Rao and A. S. Perlin, unpublished results.

0008-4042/81/020333-06$01.00/0

©1981 National Research Council of Canada/Conseil national de recherches du Canada

Can. J. Chem. Downloaded from www.nrcresearchpress.com by 210.87.254.105 on 09/05/12
For personal use only.

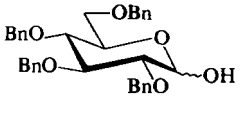

1

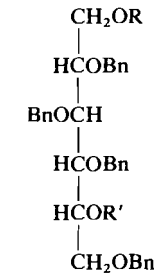

2 R = R′ = Ms
6 R = O⁻; R′ = Ms
8 R = MeOTr; R′ = Ms
18 R = R′ = H
19 R = R′ = Ac

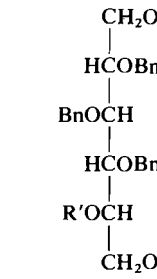

3 R = R′ = H
9 R = MeOTr; R′ = H
10 R = R′ = Ac

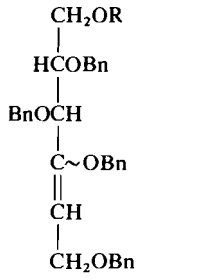

4 R = H
5 R = Ac
14 R = Ac (D-*erythro*)

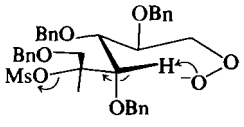

7

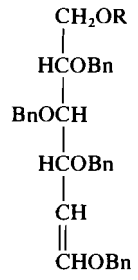

11 R = MeOTr
13 R = Ac (D-*arabino*)

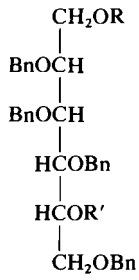

12 R = R′ = Ms
15 R = O⁻; R′ = Ms
24 R = R′ = Ac

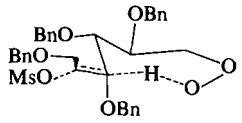

16

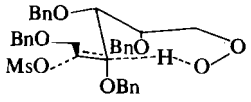

17

(C-3 at δ 154.2 and C-2 at δ 101.3), as well as by a simple A_2X spin system anticipated for H-1,1′ (δ 4.17) and olefinic H-2 (δ 5.18).[2]

To account for the high degree of regioselectivity observed in this reaction[3] it is suggested that, initially, only the 1-*O*-mesyl group of **2** is displaced by O_2^-, and subsequent electron transfer (2) generates an intermediate peroxy monomesylate (**6**). A large difference in reactivity of this magnitude between the 1-*O*-mesyl substituent and that at position 5 is to be expected, in the light of comparative rates of displacement of primary vs. secondary sulfonyloxy groups in alditol derivatives (3–5). Intramolecular abstraction[4] of H-4 by the anion and extrusion of the sulfonyloxy group at C-5 then follow, as in **7**, giving rise to the enol ether (**4**). The stereochemistry of the elimination process is not known, however, as the configuration of the enol moiety in **4** has yet to be determined.

Support for the requirement of such an intermediate as **6** is furnished by the fact that the reaction characteristics of **8**, the 1-*O*-(methoxy)trityl analog of **2**, are markedly different. That is, although several products were formed in the reaction of **8** with superoxide under the same conditions, an olefin corresponding to **4** was not among those detected. According to the ^{1}H nmr spectrum of the peracetylated reaction mixture, the main products (about 40% each) were an L-iditol derivative (**9**; based on close similarities to the spectrum of 1,5-di-*O*-acetyl-2,3,4,6-tetra-*O*-benzyl-L-iditol

[2]Catalytic de-*O*-benzylation of **5** gave a mixture of products that was not separated. However, a major signal in the ^{1}H nmr spectrum of the mixture was a triplet at δ 2.99 (J = 6.0 Hz), attributable to the 2-methylene group of a 2-deoxy-3-keto structure (—CO—CH_2—CH_2OH) expected when the enolic ether substituent of **5** is removed.

[3]The isolation of a single product precludes the possibility that a 1-enolate was formed originally, and then isomerized to **4**, as a mixture of *cis* and *trans* isomers of **4** should have been encountered (6).

[4]An intramolecular elimination process involving superoxide has been cited (7), although details are as yet unavailable.

Can. J. Chem. Downloaded from www.nrcresearchpress.com by 210.87.254.105 on 09/05/12
For personal use only.

Can. J. Chem. Downloaded from www.nrcresearchpress.com by 210.87.254.105 on 09/05/12
For personal use only.

(**10**)), and a 1-hexenitol (**11**) (δ 6.42 (1 H, d, H-1); $J_{1,2}$ = 13.0 Hz).[5] The latter olefin, in fact, should be one product ordinarily formed in an E_2 process (8), as its formation is initiated by the abstraction of a primary proton. For the same reason, a product analogous to **11** is to be expected in an elimination reaction of **2** whereas, by contrast, the formation of **4** requires the exclusive removal of a secondary proton (H-4).

The proton–proton coupling constants (Table 1), obtained from 200 MHz spectra of **2** and **8**, show that these two alditols are closely similar in conformation. Furthermore, it is evident from the discussion to be presented later that the molecules are not primarily in an extended zigzag conformation. As **8** cannot give rise to an anionic intermediate analogous to **6**, its reaction with superoxide is unexceptional. For alditol **2**, however, molecular models suggest that in rotamers commensurate with the coupling constants of protons 2–5, the introduction of a peroxy anion moiety at C-1 could allow for a facile intramolecular attack by this anion on H-4, and lead to the formation of the regioselective elimination product (**4**). Moreover, the transition state envisaged for this route appears to be favorable, especially when the result obtained from **2** is compared with that from its *manno* epimer.

That is, in the reaction of 2,3,4,6-tetra-*O*-benzyl-1,5-di-*O*-mesyl-D-mannitol (**12**) with potassium superoxide, a mixture of displacement and elimination products was formed comparable to that described for the *O*-mesyl-*O*-(methoxy)trityl derivative (**8**), and there was no indication whatever that an enol ether corresponding to **4** had been produced. Hence, the ^{1}H nmr spectrum of the peracetylated reaction mixture, which showed that the *O*-mesyl substituents had been completely removed, contained a prominent doublet (δ 6.42, $J_{1,2}$ = 13.0 Hz) commensurate with a 1-hexenitol structure (**13**) analogous to **11**. By contrast, there was no signal in the vicinity of δ 5.2, as would be expected for **14**, an enol ether analogous to **5**. Therefore, the elimination product from **12** is the normal one, due to abstraction of a primary proton (H-6 or H-6′).

Although the extended zigzag conformation should be more readily favored (9) by **12** than by **2**, because in this conformation the substituents on C-2 to -5 are staggered, coupling data (Table 1) show that there must be a substantial population of other rotameric states, as discussed below. However, as $J_{2,3}$ could not be determined, it is unclear if the anionic function of the 1-peroxy intermediate (**15**) expected from **12** would be in close proximity to H-4, as already proposed for **6**. Nevertheless, intramolecular proton abstraction within **15** should involve a less favorable transition state than one for **6**. That is, in comparing transition states **16** and **17**, corresponding to **6** and **15**, respectively, it is found that the 2- and 4-benzyloxy substituents of **17** are eclipsed, whereas there are no comparable destabilizing interactions in **16**. Differences such as these help to account for the fact that the *manno* isomer (**12**) follows a conventional reaction course with superoxide, whereas the *gluco* isomer (**2**) undergoes the highly regioselective, unusual, elimination reaction described.

*Elimination Accompanying the Reduction of 2,3,4,5-Tetra-*O*-benzyl-*D*-glucopyranose (1) with Borohydride in 2-Propanol*

For the preparation of **2**, described at the outset, 2,3,4,6-tetra-*O*-benzyl-D-glucopyranose (**1**) was reduced to the corresponding D-glucitol derivative (**18**) with sodium borohydride in 7:3 tetrahydrofuran–water. In a separate attempt to prepare **18**, employing 2-propanol under reflux as the solvent, a mixture of two products was formed. The mixture was acetylated and separated by column chromatography on silica gel. About half of the material consisted of the diacetate of the reduction product anticipated, i.e., 1,5-di-*O*-acetyl-2,3,4,6-tetra-*O*-benzyl-D-glucitol (**19**), prepared also by acetylation of **18**. The second component was shown by ^{1}H nmr spectroscopy to be a 2-enitol (**20**); it contains two *O*-acetyl groups, three *O*-benzyl substituents, and an olefinic proton on C-3 (δ 4.97, d, $J_{3,4}$ = 9.2 Hz). H-1 and -1′ of **20** give rise to an AB pair of signals (J = 12.0 Hz), and these two signals were replaced by two broad singlets when sodium borodeuteride was used in the reduction. These data received support from the ^{13}C spectrum, which exhibited signals at δ 153.2 (C-2) and 111.4 (C-3) commensurate with the enol ether structure proposed for **20**. Consequently, the formation of diol **21** (from which **20** was derived by acetylation) involved not only the reduction of the hemiacetal moiety of **1**, but also the elimination of H-2 and the 3-benzyloxy substituent.

Although 2-propanol is widely employed (10) as a solvent for reductions with sodium borohydride, it leads (11) to formation of the corresponding tetraboronate ion and, on dissociation of the latter, of a strong base:

$$B(OiPr)_4^- \rightleftharpoons B(OiPr)_3 + OiPr^-$$

[5] A minor product was the corresponding D-glucitol derivative. The latter could have arisen through hydrolysis, due to a trace of moisture present, or possibly also due to limited attack of O_2^- on sulfur.

Can. J. Chem. Downloaded from www.nrcresearchpress.com by 210.87.254.105 on 09/05/12
For personal use only.

Accordingly, is has been reported (12) that some carbonyl reductions in 2-propanol are accompanied by extensive enolization, leading to epimeric or racemic products. The formation of **21** also may be accounted for by an initial enolization (**22**), which then is followed by migration of the double bond and concomitant elimination of the benzyloxy group on C-3 (**23**),[6] and hydride reduction. However, as there was no trace of the D-mannitol derivative (**24**) that would be obtained through prior epimerization of **1**, the rate of the migration–elimination step (**23**) likely exceeds that of enolization (**22**). It is worth noting that the C-2 epimer of **1**, namely 2,3,4,6-tetra-*O*-benzyl-D-mannose was largely reduced to the corresponding alditol under the same reaction conditions. That is, ^{1}H nmr analysis of the product, after acetylation, indicated that a 9:1 mixture of alditol **24** and olefin **20** was obtained (the *gluco* isomer **19** was not detected). However, the mannose derivative may well be expected to undergo elimination less extensively than **1**, because the rate of base-catalysed enolization is more rapid in the *gluco* than in the *manno* series (13), whereas the relative rates of reduction with diborane are reversed (14).

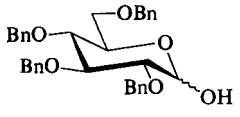

1

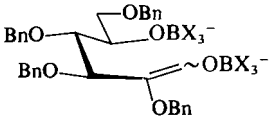

22

(X = H or/and O*i*Pr)

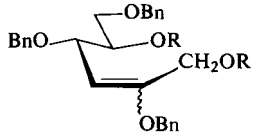

20 R = Ac
21 R = H

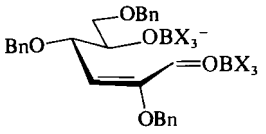

23

Conformations of Alditol Derivatives

Reference has been made above to proton–proton couplings (Table 1) obtained at 200 MHz for the alditol derivatives. As coupling data are available from a number of studies (9) dealing with the conformations of acyclic carbohydrate derivatives, it was of interest to compare the present results with those obtained with configurationally-related compounds. For this purpose, coupling parameters (15) for the hexaacetates of D-glucitol (**25**) and D-mannitol (**26**) are included in Table 1.

There are some substantial differences between our results and those for the hexaacetates. Particularly noteworthy are the much larger values of $J_{4,5}$ exhibited by the latter compounds, which are characterized (9) by conformations in which protons -4 and -5 are mainly *trans*. Other acyclic derivatives in the *gluco* and *manno* series show analogous properties; e.g. a recent study (16) on hexononitrile pentaacetates reports $J_{4,5}$ values of 8.4 Hz (*gluco*) and 9.2 Hz (*manno*). Consequently, the alditols described here are unusual in being represented prominently by arrangements of chain carbon atoms in which H-4 and H-5 are *gauche*, and thus depart from extended zigzag conformations. As $J_{3,4}$, $J_{4,5}$, and $J_{5,6}$ are essentially constant ($J_{5,6'}$ is altered noticeably) for alditols **2**, **8**, and **19**, as well as **12** and **24**, a change in the C-5 substituent from *O*-acetyl to *O*-mesyl has only a minor influence on conformation. Hence differences observed with respect to the peracetylated alditols may be attributed to the *O*-benzyl substituents, although molecular models have provided little insight as to possible steric causes for these changes.

Experimental

General Methods

Solutions were usually evaporated below 40°C under diminished pressure. Solvents were dried by conventional procedures, distilled, and stored over molecular sieves (Type 4A). Potassium superoxide was obtained from Ventron Corp., 18-crown-6 from Aldrich Chemicals, and 2,3,4,6-tetra-*O*-benzyl-D-glucose from Pfanstiehl Laboratories (Waukegan, IL). Silica gel for column chromatography was obtained from Macherey Nagel and Co. (Germany). Microanalyses were performed by Guelph Chemical Laboratories, Ltd. (Guelph, Ont.). Proton magnetic resonances were recorded with a Varian T-60, HA-100, or XL-200 spectrometer, using $CDCl_3$ as the solvent. Chemical shifts (δ) are reported with reference to tetramethylsilane and, together with the coupling constants given, were obtained by first-order analysis of 200 MHz spectra with the aid of homonuclear decoupling experiments. Carbon-13 nmr spectra were recorded with a Bruker WH-90 spectrometer. Mass spectra were obtained with an LKB 9000 spectrometer at an ion source of 70 eV.[7]

*1,3,4,5-Tetra-*O*-benzyl-L-gulitol (18)*

Sodium borohydride (5 g) was added to a stirred solution of 2,3,4,6-tetra-*O*-benzyl-D-glucopyranose (**1**) (5.0 g) in 7:3 tetrahydrofuran–water (70 mL), the solution was heated under reflux for 18 h, and then evaporated. Water was introduced, followed by chloroform, and the chloroform layer was washed successively with 5% hydrochloric acid, saturated sodium hydrogen carbonate, and water, dried (anhydrous sodium sulfate), and evaporated, to give a colorless, viscous syrup (5.12 g); $[\alpha]_D$ +8.2 (*c* 5.1, $CHCl_3$); ^{1}H nmr data for **18**: δ: 2.15 (1H, t, OH-6, J = 6.0), 2.85 (1H, d, OH-2, J = 6.0), 3.3–4.0 (8H, overlapped m, H-1 to -6′), 4.20, 4.30, 4.36, 4.40 (8H, s, OCH_2), 6.8–6.9 (20H, overlapped m, C_6H_5).

[6]As kindly pointed out by a referee, an *intramolecular* elimination of the 3-benzyloxy group of **22** is a plausible alternative.

[7]Chemical ionization (isobutane; HP 5980 A spectrometer) was also used for most of the compounds described. In general, with both electron impact and chemical ionization, parent ions were not detected and only fragments of relatively low molecular weight were observed.

Can. J. Chem. Downloaded from www.nrcresearchpress.com by 210.87.254.105 on 09/05/12
For personal use only.

TABLE 1. Proton–proton coupling constants (Hz) for alditol derivatives[a]

	D-*gluco*				D-*manno*		
J	**2**	**8**	**19**	**[25][b]**	**12**	**24**	**[26][b]**
1,1′	−11.1	−10.8	−12.0	−12.0	−11.4	−12.0	−12.3
1,2	2.7	2.8	4.0	4.0	1.8	3.5	2.6
1′,2	7.2	5.1	6.4	6.1	4.8	—	5.3
2,3	5.1	5.2	5.2	6.4	—	—	9.0
3,4	5.1	5.2	5.2	4.3	3.9	4.0	2.2
4,5	3.0	2.4	4.0	6.8	3.0	4.0	9.0
5,6	3.0	2.4	4.0	3.6	3.0	4.5	2.6
5,6′	7.2	7.6	5.6	5.6	7.2	4.0	5.3
6,6′	−11.1	—	−10.8	−12.6	−11.4	−11.0	−12.3

[a]Data acquired at 200 MHz; solvent, $CDCl_3$.
[b]Data from ref. 15; solvent, $CDCl_3$.

*2,3,4,6-Tetra-*O*-benzyl-1,5-di-*O*-mesyl-*D*-glucitol (2)*

A solution of methanesulfonyl chloride (1.4 g) in pyridine (10 mL) was added through a septum to a solution of **18** (2.7 g) in pyridine (20 mL) cooled in an ice-bath. After 48 h in the cold, the reaction mixture was poured into ice-water, and a thick syrupy deposit that formed was extracted with chloroform. The extract was washed successively with 5% hydrochloric acid, saturated sodium hydrogen carbonate, and water, dried (anhydrous sodium sulfate), and evaporated, affording a colorless, viscous syrup (3.0 g); $[\alpha]_D$ +7.6 (*c* 9.1, $CHCl_3$); ^1H nmr data for **2**: δ: 2.96 and 3.08 (2 × 3H, s, CH_3), 3.84 (1H, t, H-3), 3.9 (1H, dd, H-6′), 4.0 (1H, dd, H-6), 4.04 (1H, m, H-2), 4.18 (1H, dd, H-4), 4.39 (1H, dd, H-1′), 4.61 (1H, dd, H-1), 5.17 (1H, dt, H-5), 4.60 (2H, s, OCH_2), 4.69 (2H, s, OCH_2), 4.70 and 4.81 (2H, AB, *J* = 11.4, OCH_2), 4.76 and 4.89 (2H, AB, *J* = 11.4, OCH_2), 7.36–7.64 (20H, m, C_6H_5). Other coupling data are given in Table 1. *Anal.* calcd. for $C_{36}H_{42}O_{10}S_2$: S 9.18; found: S 8.74.

*1,3,4,5-Tetra-*O*-benzyl-3-dehydro-2-deoxy-*L*-threo-hex-2-enitol (4)*

To a vigorously stirred solution of potassium superoxide (0.51 g, 7.15 mmol; finely ground and weighed under dry nitrogen) and 18-crown-6 (0.95 g, 3.57 mmol) in 1:1 methylsulfoxide–dimethylformamide (5 mL), cooled in an ice-bath and under dry nitrogen, was added a solution of **2** (0.5 g, 0.71 mM) in the same solvent mixture (5 mL). An orange-yellow color developed briefly, and then the original yellow color returned, the coolant was removed, and 24 h later additional 18-crown-6 (0.95 g in 4 mL of the solvent mixture) was introduced. Following a further period of 3 h, the reaction mixture was poured into ice-water saturated with sodium chloride, extracted with chloroform, and the extract was washed successively with cold 10% hydrochloric acid, sodium hydrogen carbonate, and water, dried (anhydrous sodium sulfate), and evaporated. The syrupy residue was freed from 18-crown-6 by passage through a column of silica gel using 1:1 chloroform – ethyl acetate as eluant, and recovered by evaporation; yield, 0.23 g. ^1H nuclear magnetic resonance data for **4**: δ: 2.77 (1H, dd, OH-6, $J_{OH\text{-}6,H\text{-}6}$ = 7.8, $J_{OH\text{-}6,H\text{-}6'}$ = 4.2), 3.64 (1H, m, H-6′, $J_{5,6'}$ = 4.5, $J_{6,6'}$ = 12.5), 3.80 (1H, m, H-6, $J_{5,6}$ = 3.5, $J_{6,6'}$ = 12.5), 4.0 (1H, m, H-5, $J_{4,5}$ = 7.8, $J_{5,6} \simeq J_{5,6'} \simeq 4$), 4.09 (2H, d, H-1, 1′, $J_{1,2}$ = 7.8), 4.51 and 4.59 (2H, AB, OCH_2, *J* = 11.4), 4.58 and 4.78 (2H, AB, OCH_2, *J* = 11.4), 4.61 (1H, d, H-4, $J_{4,5}$ = 7.8), 4.81 and 5.01 (2H, AB, OCH_2, *J* = 11.4), 4.93 (2H, s, OCH_2), 5.20 (1H, t, H-2, $J_{1,2}$ = $J_{1',2}$ = 7.8), 7.35–7.65 (20H, m, C_6H_5).

*6-O-Acetyl-1,3,4,5-tetra-*O*-benzyl-3-dehydro-3-deoxy-*L*-threo-hex-2-enitol (5)*

The title compound was prepared in quantitative yield by acetylation of **4** with 1:2 acetic anhydride – pyridine. The ^1H nmr data for **5** were δ: 2.04 (3H, s, CH_3), 4.09–4.19 (3H, overlapping m, H-5, 6,6′), 4.17 (2H, d, H-1, 1′, $J_{1,2}$ = 7.25), 4.49 (1H, d, H-4, $J_{4,5}$ = 7.0), 4.53 (2H, s, OCH_2), 4.56 and 4.78 (2H, AB, OCH_2, *J* = 11.8), 4.78 and 4.89 (2H, AB, OCH_2, *J* = 11.8), 4.90 (2H, s, OCH_2), 5.18 (1H, t, H-2, $J_{1,2}$ = $J_{1',2}$ = 7.25), 7.35–7.61 (20H, m, C_6H_5); ^{13}C nmr data: δ: 20.8 (CH_3), 64.1, 65.1 (2×), 69.6, 70.9, 72.4, 74.1 (2×) (4 CH_2, C-1, -4, -5, -6), 101.3 (C-2), 128.5–127.7 (C-2′ to C-6′ of C_6H_5), 138.2, 138.8 (3×) (C-1′ of C_6H_5), 154.2 (C-3), 170.8 (C=O). *Mol. wt.* calcd. for $C_{36}H_{38}O_6$: 566.7; found: M^+ 566.

*5-O-Mesyl-1-O-(methoxy)trityl-2,3,4,6-tetra-O-benzyl-*D*-glucitol (8)*

A solution of **18** (7.8 g) and (methoxy)trityl chloride (5.0 g) in dry pyridine (50 mL) was stirred for 48 h at 5°C, ice-water was introduced, the mixture was extracted with chloroform, and the extract was washed successively with 5% hydrochloric acid, sodium hydrogen carbonate, and water, dried (anhydrous sodium sulfate), and evaporated. The syrupy residue (12.1 g) was treated with methanesulfonyl chloride as described above under **2**, affording **8** as a hygroscopic foam; $[\alpha]_D$ +12.6 (*c* 5.0, $CHCl_3$); ^1H nmr data for **8**: δ: 2.95 (3H, s, CH_3SO_2), 3.29 (1H, dd, H-1′), 3.85 (3H, s, OCH_3), 3.59 (1H, dd, H-1), 3.81 (1H, dd, H-6′), 3.93–4.02 (3H, overlapping m, H-2, 4, 6), 4.06 (1H, t, H-3), 4.22 and 4.65 (2H, AB, OCH_2, *J* = 11.2), 4.51 and 4.53 (2H, AB, OCH_2, *J* = 11.2), 4.71 and 4.80 (2H, AB, OCH_2, *J* = 11.2), 4.72 and 4.83 (2H, AB, OCH_2, *J* = 11.2), 5.01 (1H, m, H-5), 7.11–7.71 (20H, m, C_6H_5). Other coupling data are given in Table 1. *Anal.* calcd. for $C_{55}H_{56}O_9S$: C 73.97, H 6.32; found: C 73.88, H 6.41.

*2,3,4,6-Tetra-*O*-benzyl-1,5-di-*O*-mesyl-*D*-mannitol (12)*

2,3,4,6-Tetra-*O*-benzyl-D-mannopyranose[8] was reduced with sodium borohydride in aqueous tetrahydrofuran, as described above under **18**, and then methanesulfonated, as described under **2**. The product was a viscous syrup; $[\alpha]_D$ +12.1 (*c* 3.0, $CHCl_3$); ^1H nmr data for **12**: δ: 2.89, 2.94 (2 × 3H, s, CH_3), 3.77–3.86 (2H, overlapping m, H-2, 3), 3.78 (1H, dd, H-6′), 3.89 (1H, dd, H-6), 4.04 (1H, dd, H-4), 4.39 (1H, dd, H-1′), 4.41 and 4.64 (2H, AB, OCH_2, *J* = 11.4), 4.46 (2H, s, OCH_2), 4.55 and 4.75 (2H, AB, OCH_2, *J* = 11.4), 4.71 (2H, s, OCH_2), 4.69 (1H, dd, H-1), 4.99 (1H, m, H-5). Other coupling data are presented in Table 1. The mass spectrum was closely similar to that of **2**.

1,5-di-O-Acetyl-2,4,6-tri-O-benzyl-2-dehydro-3-deoxy-D-threo-hex-2-enitol (20) and 1,5-Di-O-acetyl-2,3,4,6-tetra-O-benzyl-D-glucitol (19)

2,3,4,6-Tetra-*O*-benzyl-D-glucopyranose (5.0 g) was dis-

[8]Kindly furnished by R. G. S. Ritchie.

solved in boiling 2-propanol, sodium borohydride (5.0 g) was introduced, refluxing was continued for 24 h, and the solution was evaporated. Water was added to the residue, followed by chloroform, and the chloroform layer was washed successively with 1% hydrochloric acid, sodium hydrogen carbonate, and water, dried (anhydrous sodium sulfate), and evaporated (yield, 4.9 g). The syrupy residue was acetylated with 1:2 acetic anhydride – pyridine (yield, 5.4 g), and the acetylation product (1.0 g) was chromatographed on a column of silica gel packed in petroleum ether, using gradient elution with mixtures of petroleum ether – chloroform. Compound **19** emerged first (yield, 0.4 g); $[\alpha]_D$ +6.6 (*c* 3.9, $CHCl_3$); its ^1H nmr spectrum was indistinguishable from the diacetate prepared from **18**. The ^1H nmr data for **19** were δ: 1.96 and 2.01 (2 × 3H, s, CH_3), 3.72 (1H, dd, H-3), 3.74 (1H, dd, H-6′), 3.81–3.91 (1H, m, H-2), 3.86 (1H, dd, H-6), 3.97 (1H, dd, H-4), 4.17 (1H, dd, H-1′), 4.29 (1H, dd, H-1), 4.15 and 4.51 (2H, AB, OCH_2, J = 12), 4.62 and 4.65 (2H, AB, OCH_2, J = 12), 4.63 (2H, s, OCH_2), 4.68 (2H, s, OCH_2), 5.3 (1H, m, H-5), 7.27–7.41 (20H, m, C_6H_5); other coupling data are given in Table 1. Continued elution of the column afforded **20** (yield, 0.35 g); $[\alpha]_D$ +15.6 (*c* 2.8, $CHCl_3$); ^1H nmr data for **20**: δ: 2.08 and 2.11 (2 × 3H, s, CH_3), 3.68 (2H, d, H-6,6′, $J_{5,6}$ = 5.2), 4.34 and 4.50 (2H, AB, OCH_2, J = 12), 4.48 and 4.58 (2H, AB, OCH_2, J = 12), 4.87 (2H, s, OCH_2), 4.65 and 4.72 (2H, AB, H-1,1′, J = 13.6), 4.69 (1H, dd, H-4, $J_{3,4}$ = 9.2, $J_{4,5}$ = 5.6), 4.97 (1H, d, H-3, $J_{3,4}$ = 9.2), 5.26 (1H, dd, H-5, $J_{4,5}$ = $J_{5,6}$ = 5.2), 7.27–7.43 (15H, m, C_6H_5). The ^{13}C nmr data were δ: 20.9, 21.1 (2 CH_3), 62.3, 68.7, 70.5, 71.3, 71.6, 73.0, 73.3 (3 CH_2, C-1, -4, -5, -6), 111.4 (C-3), 127.7–128.3 (C-2′ to C-6′ of C_6H_5), 137.0, 138.2, 138.5 (C-1′ of C_6H_5), 153.2 (C-2), 170.3 (C=O).

Acknowledgements

The authors express their gratitude to the Natural Sciences and Engineering Research Council of Canada for generous support. The 200 MHz ^1H nmr spectra were kindly recorded by W. Dawson, L. Ayotte, and J. Everett, and mass spectra by O. A. Mamer. 2,3,4,6-Tetra-*O*-benzyl-D-mannose was furnished by R. G. S. Ritchie.

1. (*a*) J. San Filippo, Jr., C.-J. Chern, and J. S. Valentine. J. Org. Chem. **40**, 1678 (1975); (*b*) E. J. Corey, K. C. Nicolaou, M. Shibasaki, Y. Machida, and C. S. Shiner. Tetrahedron Lett. 3183 (1975).
2. (*a*) E. Lee-Ruff. Chem. Soc. Rev. **6**, 195 (1977); (*b*) D. T. Sawyer and M. J. Gibian. Tetrahedron, **35**, 1471 (1979).
3. R. S. Tipson. Adv. Carbohydr. Chem. **8**, 107 (1953).
4. M. A. Bukhari, A. B. Foster, J. M. Webber, and J. Lehmann. Carbohydr. Res. **1**, 485 (1966).
5. D. H. Ball and F. W. Parrish. Adv. Carbohydr. Chem. Biochem. **24**, 139 (1969).
6. D. J. Cram and R. T. Uyeda. J. Am. Chem. Soc. **86**, 5466 (1964).
7. R. A. Johnson, E. A. Nidy, L. Baczynskyj, and R. R. Gorman. J. Am. Chem. Soc. **99**, 7738 (1977).
8. W. B. Chiao and W. H. Saunders, Jr. J. Org. Chem. **45**, 1319 (1980).
9. P. L. Durette and D. Horton. Adv. Carbohydr. Chem. Biochem. **26**, 49 (1971).
10. H. O. House. Modern synthetic reactions. 2nd ed. Benjamin, New York. 1972. p. 55.
11. M. R. Johnson and B. Rickborn. J. Org. Chem. **35**, 1041 (1970).
12. V. Hach, E. C. Fryberg, and E. McDonald. Tetrahedron Lett. 2629 (1971).
13. M. L. Wolfrom and W. L. Lewis. J. Am. Chem. Soc. **50**, 837 (1928).
14. S. S. Bhattacharjee, J. A. Schwarcz, and A. S. Perlin. Carbohydr. Res. **42**, 259 (1975).
15. S. J. Angyal, R. Le Fur, and D. Gagnaire. Carbohydr. Res. **23**, 121 (1972).
16. L. M. Sweeting, B. Coxon, and R. Varma. Carbohydr. Res. **72**, 43 (1979).

Can. J. Chem. Downloaded from www.nrcresearchpress.com by 210.87.254.105 on 09/05/12
For personal use only.

Conversion of hydroxyl groups into bromo groups in carbohydrates with inversion of configuration

BJÖRN CLASSON, PER J. GAREGG, AND BERTIL SAMUELSSON

Department of Organic Chemistry, Arrhenius Laboratory, University of Stockholm, S-106 91 Stockholm, Sweden

Received August 6, 1980

This paper is dedicated to Prof. Raymond U. Lemieux on the occasion of his 60th birthday

BJÖRN CLASSON, PER J. GAREGG, and BERTIL SAMUELSSON. Can. J. Chem. **59**, 339 (1981).

A novel reagent system is described for the efficient, one-step transformation of hydroxyl groups in carbohydrates to bromodeoxy groups. The reaction proceeds with inversion of configuration. The reagent system consists of triphenylphosphine, tribromoimidazole, and imidazole in toluene at elevated temperature. The carbohydrate need not be soluble in toluene. The examples given include substitution of isolated primary and secondary hydroxyl groups in otherwise protected carbohydrates as well as disubstitution involving one primary and one secondary position in hexopyranosides. High yields are obtained in the replacement of hydroxyl by bromine in the 2-position of 3,4,6-protected methyl α-D-gluco- and -mannopyranosides.

BJÖRN CLASSON, PER J. GAREGG et BERTIL SAMUELSSON. Can. J. Chem. **59**, 339 (1981).

On décrit un nouveau système de réactif qui permet de transformer efficacement une seule étape les groupes hydroxyles des carbohydrates en groupes bromodéoxy. La réaction se fait avec inversion de configuration. Le système de réactif est constitué de triphénylphosphine, de tribromoimidazole et de l'imidazole dans le toluène à haute température. Il n'est pas nécessaire que le carbohydrate soit soluble dans le toluène. Les exemples donnés comprennent la substitution de groupe hydroxyle primaire et secondaire de carbohydrates par ailleurs protégés ainsi que la disubstitution impliquant une position primaire et une position secondaire des hexopyrannosides. On a obtenu des rendements élevés en remplaçant l'hydroxyle par le brome en position 2 des α-D-gluco- et mannopyrannosides de méthyle protégés en positions 3,4,6.

[Traduit par le journal]

Introduction

Replacements of hydroxyl groups in carbohydrates by halogen, giving rise to halogeno sugars, represent important synthetic transformations. Halogeno sugars are useful intermediates for obtaining *inter alia* amino sugars and deoxy sugars.

We have previously reported transformations using novel reaction systems consisting of triphenylphosphine together with either iodine and imidazole or triiodoimidazole **1** and imidazole in toluene at elevated temperature (1–4). These reagent systems convert vicinal hydroxyl groups in hexopyranosides into the corresponding dideoxyhexenopyranosides (1, 2). Single hydroxyl groups are converted, with inversion of configuration, into the corresponding deoxyiodo compounds including the 2-position in hexopyranosides. Partial iodinations, at primary positions in unprotected hexopyranosides, are possible in good yields (3, 4). An obvious extension of this work is the use of this type of reaction for obtaining bromodeoxy sugars. Some of our work in this area is the subject of this paper. The examples include the disubstitutions of methyl hexopyranosides and a facile synthesis of methyl 3,6-dideoxy-α-D-*ribo*-hexopyranoside ("methyl α-paratoside") from methyl α-D-glucopyranoside. Previous work on the synthesis of bromodeoxy sugars has been reviewed (5).

Results and Discussion

The reagent system used consists of triphenylphosphine, tribromoimidazole, and (usually) imidazole in toluene at elevated temperature. In the various brominations described below, we found that the addition of a few equivalents of imidazole sometimes resulted in improved yields and cleaner reactions. The reason for this is not obvious, although we have noted that whenever a hard precipitate is formed in the reaction mixture no further reaction takes place. The addition of imidazole, however, dissolves this complex and the reaction then proceeds. Yields of products thus obtained are given in brackets in Scheme 1, which shows the various compounds obtained in the present work.

Reactions at Single Hydroxylated Positions

The examples include the methyl 3,4,6-tri-*O*-benzyl-D-hexopyranosides with the α-D-*manno*- (**3**), α-D-*gluco*- (**5**), and β-D-*gluco*- (**7**) configurations as well as methyl 2,3-*O*-isopropylidene-β-D-ribofuranoside (**9**) and 1,2:3,4-di-*O*-isopropylidene-α-D-galactopyranose (**11**). Of the various substrates examined in the present reaction system, serious difficulty was encountered with 1,2:5,6-di-*O*-isopropylidene-α-D-glucofuranose only. In the corresponding iodination (3, 4) 3-deoxy-3-iodo-1,2:5,6-di-*O*-isopropylidene-α-D-allofuranose was

0008-4042/81/020339-05$01.00/0

©1981 National Research Council of Canada/Conseil national de recherches du Canada

Can. J. Chem. Downloaded from www.nrcresearchpress.com by 210.87.254.42 on 09/05/12
For personal use only.

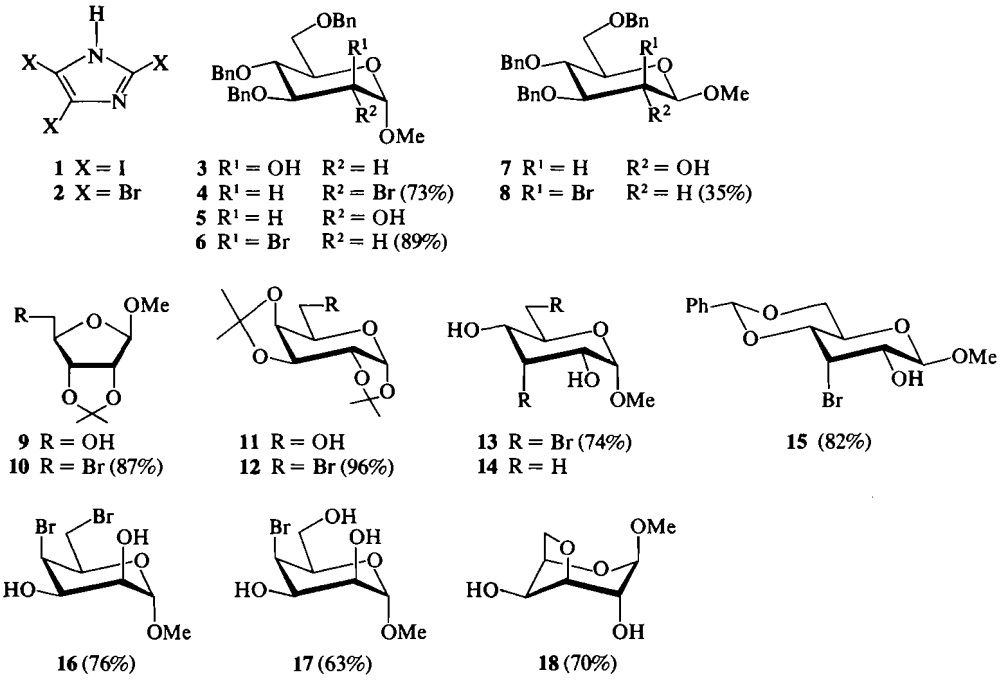

SCHEME 1

obtained in a 78% yield. The bromination, however, yielded mainly olefin and only about 30% of 3-bromo-3-deoxy-1,2:5,6-di-*O*-isopropylidene-α-D-allofuranose. Nuclear magnetic resonance data were obtained showing the corresponding characteristic H-2 triplet previously observed for the corresponding iodide (6, 7), ^{1}H nmr (100 MHz, $CDCl_3$) δ: 4.70 (t, $J_{1,2} \sim J_{2,3} \sim 3.7$ Hz, H-2). We find the ease by which bromination in the 2-position occurs particularly significant. A plausible mechanism for the product-forming reaction in these substitutions could be of a "push–pull" type:

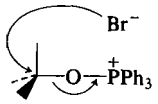

Reactions of Methyl Hexopyranosides

Dibromination of methyl α-D-glucopyranoside produced the dibromide **13**. The *allo* configuration was established by ^{1}H nmr spin decoupling experiments. Catalytic hydrogenation yielded methyl α-paratoside **14** (8). This constitutes an excellent route to **14** from methyl α-D-glucopyranoside.

The factors determining the substitution pattern in **13** are not obvious. Jennings and Jones (9) have shown that methyl α-D-glucopyranoside reacts with sulfuryl chloride in pyridine–chloroform to give methyl 4,6-dichloro-4,6-dideoxy-α-D-galactopyranoside 2,3-di(chlorosulfate) in 84% yield. The corresponding β-anomer, however, gave the 3,6-dichloro-3,6-dideoxy as well as the 4,6-dichloro-4,6-dideoxy compound. Similar substitution patterns were observed with the methanesulfonyl chloride – dimethyl formamide reagent (10). The lack of reactivity at C-3 in methyl α-D-glucopyranoside in these chlorination reactions was ascribed to steric interference by a 1,3-diaxial interaction between the α-methoxyl group in the $^4C_1$ conformation and the incoming nucleophile. In the present bromination reactions this might be overcome by conformational inversion at the elevated temperatures through cyclic phosphonium diester formation bridging *O*-2 and *O*-4 in the $^1C_4$ conformation in the reaction intermediates. No such intermediates have, however, been isolated and this explanation is therefore highly tentative. In the product obtained (**13**) the *cis*-relationship between OH-2, Br-3, and OH-4 makes epoxide formation from **13** impossible, contributing to the high yield obtained.

Monobromination of methyl 4,6-*O*-benzylidene-α-D-glucopyranoside gave a mixture of products in low yields in agreement with the above considerations. The corresponding β-anomer, however, for which no 1,3-diaxial hindrance to 3-substitution in the $^4C_1$ conformation exists, yielded the bromodeoxy glycoside **15** in 82% yield. Bundle (11) chlorosulfated the same starting material to obtain crystalline methyl 4,6-*O*-benzylidene-β-D-glucopy-

Can. J. Chem. Downloaded from www.nrcresearchpress.com by 210.87.254.42 on 09/05/12
For personal use only.

Can. J. Chem. Downloaded from www.nrcresearchpress.com by 210.87.254.42 on 09/05/12
For personal use only.

ranoside 2,3-bis(chlorosulfate) in 77% yield. This, upon reaction with tetraethylammonium bromide in chloroform, gave **15** as the 2-(chlorosulfate) in 84% yield (11).

Dibromination of methyl α-D-mannopyranoside gave **16** in 76% yield. The structure of **16** was ascertained by ^{1}H nmr spin decoupling experiments performed with the derived 2,3-acetate of **16**. Monobromination of methyl 6-*O*-(triphenylmethyl)-α-D-mannopyranoside followed by detritylation similarly gave **17**. Jennings and Jones obtained only methyl 6-chloro-6-deoxy-α-D-mannopyranoside 2,3,4-tri(chlorosulfate) from the reaction of methyl α-D-mannopyranoside with sulfuryl chloride (9). This was attributed to a 1,3-diaxial interaction between OH-2 and incoming nucleophile approaching the 4-position (12) in the $^4C_1$ conformation rendering 4-substitution unlikely, similarly nucleophilic substitution at C-3 would be hindered by axial OCH_3. Forced reaction conditions towards nucleophilic displacement at C-4 have resulted in ring contraction and substitution at C-5, presumably via *O*-5 participation. Thus, methyl 6-deoxy-2,3-*O*-isopropylidene-α-D- and α-L-mannopyranoside carrying a sulfonyloxy substituent at C-4 upon treatment with azide anion gave methyl 5-azido-5,6-dideoxy-2,3-*O*-isopropylidene-α-D- and α-L-talofuranosides together with smaller amounts of the corresponding allofuranosides (13, 14). The reactivity at C-4 in the present brominations therefore seems surprising. A tentative explanation, analogous to the one given above for the results obtained with methyl α-D-glucopyranoside might be that methyl α-D-mannopyranoside forms a cyclic phosphonium diester across *O*-2 and *O*-3.

In contrast to the results described above, attempted dibrominations of methyl α-D- and β-D-galactopyranosides gave low yields of reaction products and no dibromodideoxy compounds. Attempted monobromination of methyl β-D-galactopyranoside gave a 70% yield of the 3,6-anhydrosugar **18** and this is a convenient route to **18**.

Experimental

General Methods

Melting points are corrected. Concentrations were performed at reduced pressure and a bath temperature below 40°C. Optical rotations were obtained using a Perkin-Elmer 241 polarimeter. The nmr spectra were recorded using a Jeol JNM FX 100 instrument. Chemical shifts are given in ppm downfield from tetramethylsilane. The nmr spectra which were recorded for all new compounds were invariably in agreement with the postulated structures. Only selected nmr data are given below. Thin layer chromatography was carried out using precoated silica gel plates (F_{250} Merck) and the spots were detected by charring with 8% aqueous sulfuric acid. All reactions were monitored by tlc. The yields given below are for purified products. Column chromatography was performed using silica gel 60 (0.040–0.063 mm, Merck).

Tribromoimidazole 2 (15)

Compound **2** was prepared by adding bromine (3 equivalents) to imidazole (4 equivalents) in water, filtering off the product, and recrystallizing from ethanol–water.

Work-up Procedure A (for water-insoluble products)

After cooling to room temperature the product was stirred for 5 min with an equal volume of saturated aqueous sodium hydrogen carbonate. Iodine was added portion-wise. When the organic phase remained iodine-coloured it was stirred for another 10 min. Aqueous sodium thiosulfate was added to remove the excess iodine. The mixture was then transferred to a separating funnel. Any material remaining in the reaction vessel was dissolved in the minimum amount of acetone and added to the main bulk of material. After diluting with toluene, the organic phase was extracted with water, dried ($MgSO_4$), filtered, and concentrated. In small-scale preparations the residue was subjected to column chromatography directly; in larger-scale preparations it was found to be advantageous to precipitate triphenylphosphine oxide with diethyl ether, filtering and concentrating before proceeding to purification by means of column chromatography (toluene – ethyl acetate 4:1).

Work-up Procedure B (for products soluble in both water and organic solvents)

The procedure was the same as that described above until after the transfer of the product to a separating funnel. The organic phase was then separated and the aqueous phase was extracted four times with dichloromethane. The combined organic phases were dried ($MgSO_4$), concentrated, and then subjected to column chromatography (toluene – ethyl acetate 1:1).

Reaction Conditions

The conditions used in individual preparations are described below. The reaction is normally completed in a few hours at elevated temperatures and results in a high-density *liquid phase* immiscible with toluene. If a hard precipitate is formed, a few molar equivalents of imidazole should be added to the reaction mixture.

Methyl 3,4,6-Tri-O-benzyl-2-bromo-2-deoxy-α-D-glucopyranoside (4)

A mixture of **3** (16) (0.30 g, 0.64 mmol), triphenylphosphine (0.93 g, 3.54 mmol), tribromoimidazole (0.54 g, 1.77 mmol), and imidazole (0.12 g, 1.77 mmol) in toluene (50 mL) was stirred for 1 h at 80°C and then under reflux at a bath temperature of 120°C overnight. Work-up (procedure A) yielded **4** (0.25 g, 73%), $[\alpha]_D^{22}$ +85° (*c* 1.0, $CHCl_3$); ^{13}C nmr (25 MHz, $CDCl_3$) δ: 51.16 (C-2), 55.74 (OCH_3), 68.38 (C-6), 99.77 (C-1). *Anal.* calcd. for $C_{28}H_{31}O_5Br$: C 63.8, H 5.92, Br 15.2; found: C 63.9, H 5.99, Br 15.3.

Methyl 3,4,6-Tri-O-benzyl-2-bromo-2-deoxy-α-D-mannopyranoside (6)

A mixture of **5** (17) (0.37 g, 0.80 mmol), triphenylphosphine (0.92 g, 3.51 mmol), **2** (0.54 g, 1.77 mmol), and imidazole (0.12 g, 1.76 mmol) in toluene (35 mL) was stirred under reflux at a bath temperature of 120°C for 6 h. Work-up (procedure A) yielded **6** (0.39 g, 89%), $[\alpha]_D^{22}$ +21° (*c* 1.0, $CHCl_3$); ^{13}C nmr (25 MHz, $CDCl_3$) δ: 51.38 (C-2), 55.26 (OCH_3), 69.02 (C-6), 101.16 (C-1). *Anal.* calcd. for $C_{28}H_{31}O_5Br$: C 63.8, H 5.92, Br 15.2; found: C 63.7, H 5.84, Br 15.2.

Methyl 3,4,6-Tri-O-benzyl-2-bromo-2-deoxy-β-D-mannopyranoside (8)

A mixture of **7** (17) (0.25 g, 0.54 mmol), triphenylphosphine

Can. J. Chem. Downloaded from www.nrcresearchpress.com by 210.87.254.42 on 09/05/12
For personal use only.

(0.565 g, 2.15 mmol), **2** (0.328 g, 1.08 mmol), and imidazole (0.148 g, 2.15 mmol) in toluene (25 mL) was stirred under reflux at a bath temperature of 120°C for 5 h. Work-up (procedure A) yielded **8** (0.10 g, 35%), $[\alpha]_D^{22}$ −43° (*c* 1.25, $CHCl_3$); ^{13}C nmr (25 MHz, $CDCl_3$) δ: 53.6 (C-2), 57.0 (OCH_3), 99.2 (C-1). Due to instability a satisfactory analysis could not be obtained for this compound.

*Methyl 5-Bromo-5-deoxy-2,3-*O*-isopropylidene-β-*D*-ribofuranoside (10)*

A mixture of **9** (18) (0.50 g, 2.45 mmol), triphenylphosphine (1.28 g, 4.88 mmol), **2** (0.91 g, 2.98 mmol), and imidazole (0.20 g, 2.98 mmol) in toluene (50 mL) was stirred for 1 h at 70°C and then for 2 h at 90°C. Work-up (procedure A) yielded **10** (0.57 g, 87%), $[\alpha]_D^{22}$ −79° (*c* 1.0, $CHCl_3$) (lit. (19) $[\alpha]_D^{25}$ −80° (*c* 2.61, $CHCl_3$)). The ^1H nmr shifts and coupling constants were in agreement with those published (19).

*6-Bromo-6-deoxy-1,2:3,4-di-*O*-isopropylidene-α-*D*-galactopyranose (12)*

A mixture of **11** (20) (1.00 g, 3.84 mmol), triphenylphosphine (2.02 g, 7.70 mmol), **2** (1.17 g, 3.84 mmol), and imidazole (0.26 g, 3.82 mmol) in toluene (50 mL) was stirred for 1 h at 70°C and then for 2 h at 95°C. Additional tribromoimidazole (0.58 g, 1.90 mmol) was added and the mixture was stirred for 2 h at 95°C. Work-up (procedure A) yielded **12** (1.19 g, 96%), $[\alpha]_D^{22}$ −47° (*c* 1.0, $CHCl_3$) (lit. (11) $[\alpha]_D$ −58.9° (*c* 1.15, $CHCl_3$)); ^1H nmr (100 MHz, $CDCl_3$) δ: 1.35 (2 × s, 6H), 1.44 (s, 3H), 1.54 (s, 3H, isopropylidene H), 3.46 (dd, 2H, H-6, H-6′), 4.10 (dt, H-5), 4.28–4.42 (m, H-2, H-4), 4.64 (dd, 1H, H-3), 5.54 (d, 1H, H-1), $J_{1,2}$ = 5.2 Hz, $J_{2,3}$ = 7.8 Hz, $J_{3,4}$ = 2.4 Hz, $J_{4,5}$ = 2.0 Hz, $J_{5,6}$ = 3.7 Hz, $J_{5,6}$ = 4.1 Hz.

*Methyl 3,6-Dibromo-3,6-dideoxy-α-*D*-allopyranoside (13)*

A mixture of methyl α-D-glucopyranoside (0.50 g, 2.57 mmol, finely ground), **2** (1.57 g, 5.15 mmol), and triphenylphosphine (2.70 g, 10.3 mmol) in toluene (50 mL) was stirred for 1 h at 75°C and then at a bath temperature of 110°C for 4 h. Work-up (procedure B) yielded **13** (0.613 g, 74%), $[\alpha]_D^{22}$ +86° (*c* 1.0, $CHCl_3$). Material crystallized from ethanol decomposed at 150°C; ^{13}C nmr (25 MHz, $CDCl_3$) δ: 32.8 (C-6), 56.0 (OCH_3), 62.6 (C-3), 98.8 (C-1). *Anal.* calcd. for $C_7H_{12}O_4Br_2$: C 26.3, H 3.78, Br 50.0; found: C 26.3, H 3.64, Br 50.0. For the 2,4-di-*O*-acetyl derivative of **13**, ^1H nmr (100 MHz, $CDCl_3$) δ: 4.73 (dd, 1H, H-4), $J_{3,4}$ = 3.7 Hz, $J_{4,5}$ = 9.5 Hz.

*Methyl 3,6-Dideoxy-α-*D*-ribo-hexopyranoside (14)*

Catalytic hydrogenation of **13** (0.10 g, 0.31 mmol) in ethanol (10 mL) containing triethylamine (1 mL) was hydrogenated over 10% palladium on carbon at atmospheric pressure for 24 h. The mixture was filtered (Celite), concentrated, diluted with water, passed through an anion exchanger, and concentrated to yield **14** (0.043 g, 85%), $[\alpha]_D^{22}$ +169° (*c* 1.0, $CHCl_3$) (lit. (8) $[\alpha]_{578}^{33}$ +170° ($CHCl_3$)). A ^{13}C nmr spectrum of **14** was superimposable on that given by an authentic sample (8).

*Methyl 4,6-*O*-Benzylidene-3-bromo-3-deoxy-β-*D*-allopyranoside (15)*

A mixture of methyl 4,6-*O*-benzylidene-β-D-glucopyranoside (0.25 g, 0.886 mmol), **2** (0.81, 2.66 mmol), triphenylphosphine (1.39 g, 5.32 mmol), and imidazole (0.181 g, 2.66 mmol) in toluene (25 mL) was stirred for 4 h at 75°C. Work-up (procedure B, but using isooctane – ethyl acetate 1:2 for column chromatography instead of toluene – ethyl acetate) yielded **15** (0.25 g, 82%), which crystallized from ethyl acetate – light petroleum, mp 118–120°C; $[\alpha]_D^{22}$ −9° (*c* 1.5, $CHCL_3$) (lit. (11) mp 97–99°C, $[\alpha]_D^{22}$ −23° ($CHCl_3$)). The ^1H nmr data corresponded to those published (11).

*Methyl 4,6-Dibromo-4,6-dideoxy-α-*D*-talopyranoside (16)*

A mixture of methyl α-D-mannopyranoside (0.50 g, 2.57 mmol, finely ground), **2** (1.57 g, 5.15 mmol), and triphenylphosphine (2.70 g, 10.3 mmol) in toluene (50 mL) was reacted and worked up as described for **13**, to yield **16** (0.624 g, 76%) which crystallized from toluene, mp 106–110°C; $[\alpha]_D^{22}$ +77° (*c* 1.0, $CHCl_3$); ^{13}C nmr (25 MHz, $CDCl_3$) δ: 32.4 (C-6), 55.6 (OCH_3), 57.6 (C-4), 65.1, 68.8, and 70.5 (C-2, C-3, and C-5), 102.0 (C-1). *Anal.* calcd. for $C_7H_{12}O_4Br_2$: C 26.3, H 3.78, Br 50.0; found: C 26.2, H 3.63, Br 50.1. Compound **16** was acetylated to give methyl 2,6-di-*O*-acetyl-4,6-dibromo-4,6-dideoxy-α-D-talopyranoside which had ^1H nmr (100 MHz, $CDCl_3$) δ: 2.10 (s, 3H, CH_3CO), 2.15 (s, 3H, CH_3CO), 3.46 (s, 3H, OCH_3), 3.58 (dd, 2H, H-6, H-6′), 4.13 (dt, 1H, H-5), 4.53 (dd, 1H, H-4), 4.77 (d, 1H, H-1), 5.10 (m, 1H, H-2), 5.26 (dd, 1H, H-3), $J_{1,2}$ = 1.3 Hz, $J_{2,3}$ = 4.1 Hz, $J_{3,4}$ = 4.2 Hz, $J_{4,5}$ = 2.0 Hz.

*Methyl 4-Bromo-4-deoxy-α-*D*-talopyranoside (17)*

A mixture of methyl 6-*O*-(triphenylmethyl)-α-D-mannopyranoside (0.40 g, 0.92 mmol), **2** (0.59 g, 1.83 mmol), triphenylphosphine (0.48 g, 1.83 mmol), and imidazole (0.124 g, 1.82 mmol) in toluene (40 mL) was stirred for 1 h at 80°C and then for 4 h at 100°C. Work-up (procedure B) excluding column chromatography yielded presumed methyl 4-bromo-4-deoxy-6-*O*-(triphenylmethyl)-α-D-talopyranoside which was detritylated by treatment with 80% aqueous acetic acid for 4 h at 65°C. The reaction mixture was concentrated and partitioned between water and dichloromethane. The aqueous phase was concentrated and the product purified by column chromatography (water-saturated ethyl acetate) to yield **17** (0.15 g, 63%) which crystallized from ethyl acetate – light petroleum, mp 105°C; $[\alpha]_D^{22}$ +102° (*c* 1.0, H_2O). *Anal.* calcd. for $C_7H_{13}O_5Br$: C 32.7, H 5.10, Br 31.1; found: C 32.7, H 4.99, Br 31.0. Compound **17** was acetylated to give methyl 2,3,6-tri-*O*-acetyl-4-bromo-4-deoxy-α-D-talopyranoside; ^1H nmr (100 MHz, $CDCl_3$) δ: 2.06 (s, 3H, CH_3CO), 2.08 (s, 3H, CH_3CO), 2.12 (s, CH_3CO), 3.38 (s, OCH_3), 4.08–4.32 (m, 3H, H-5, H-6, H-6′), 4.40 (d, 1H, H-4), 4.75 (s, 1H, H-1), 5.12 (dd, 1H, H-2), 5.23 (t, 1H, H-3), $J_{1,2}$ = 0.2 Hz, $J_{2,3}$ = 4 Hz, $J_{3,4}$ = 4 Hz, $J_{4,5} \sim 0$ Hz; ^{13}C nmr (25 MHz, $CDCl_3$) δ: 20.8 (CH_3CO), 47.3 (C-4), 55.2 (OCH_3), 65.4, 66.0, 66.5, 67.1 (C-2, C-3, C-5, C-6), 99.4 (C-1), 169.9 (CH_3CO).

*Methyl 3,6-Anhydro-β-*D*-galactopyranoside (18)*

A mixture of methyl β-D-galactopyranoside (0.50 g, 2.57 mmol, finely ground), **2** (1.15 g, 3.79 mmol), triphenylphosphine (1.99 g, 7.57 mmol), and imidazole (0.860 g, 12.6 mmol) in toluene (50 mL) was stirred at 100°C for 2.5 h. The reaction mixture was extracted with water. The combined aqueous extracts were concentrated and the residue acetylated. The product was purified by column chromatography (toluene – ethyl acetate 2:1) to yield **18** as the diacetate (0.438 g, 70%). Deacetylation and crystallization from ethyl acetate yielded **18**, mp 117°C; $[\alpha]_D^{22}$ −112° (*c* 1.0, H_2O) (lit. (21) mp 119°C, $[\alpha]_D^{18}$ −115° (H_2O)).

Acknowledgements

We are indebted to Professor Bengt Lindberg for his interest, to the Swedish Natural Science Research Council for financial support, and to Smitts Fond and Stipendium Berzelianum (The Royal Swedish Academy of Sciences) for maintenance grants (to B.S.).

1. P. J. GAREGG and B. SAMUELSSON. Synthesis, 469 (1979).
2. P. J. GAREGG and B. SAMUELSSON. Synthesis, 813 (1979).
3. P. J. GAREGG and B. SAMUELSSON. J. Chem. Soc. Chem. Commun. 978 (1979).

4. P. J. GAREGG and B. SAMUELSSON. J. Chem. Soc. Perkin Trans. I. In press.
5. S. HANESSIAN. Methods Carbohydr. Chem. **VI**, 183 (1972); A. H. HAINES. Adv. Carbohydr. Chem. Biochem. **33**, 72 (1976).
6. H. KUNZ and P. SCHMIDT. Tetrahedron Lett. 2123 (1979).
7. R. W. BINKLEY and D. G. HEHEMANN. J. Org. Chem. **43**, 3244 (1978).
8. G. EKBORG and S. SVENSSON. Acta Chem. Scand. **27**, 1437 (1973).
9. H. J. JENNINGS and J. K. N. JONES. Can. J. Chem. **43**, 2372 (1965).
10. R. G. EDWARDS, L. HOUGH, A. C. RICHARDSON, and E. TARELLI. Carbohydr. Res. **35**, 111 (1974).
11. D. BUNDLE. J. Chem. Soc. Perkin Trans. I, 2751 (1979).
12. A. C. RICHARDSON. Carbohydr. Res. **10**, 395 (1969).
13. S. HANESSIAN. J. Chem. Soc. Chem. Commun. 796 (1966).
14. J. JARY, P. NOVAK, and Z. SAMEK. Justus Liebiegs Ann. Chem. **40**, 98 (1970).
15. G. WYSS. Ber. **10**, 1370 (1877).
16. N. E. FRANKS and R. MONTGOMERY. Carbohydr. Res. **6**, 286 (1968).
17. G. EKBORG, B. LINDBERG, and J. LÖNNGREN. Acta Chem. Scand. **26**, 3287 (1972).
18. N. J. LEONARD and K. L. CARRAWAY. J. Heterocycl. Chem. **3**, 485 (1966); P. A. LEVENE and E. T. STILLER. J. Biol. Chem. **104**, 299 (1934).
19. S. HANESSIAN, M. M. PONPIPOM, and P. LAVALLEE. Carbohydr. Res. **24**, 45 (1972).
20. A. L. RAYMOND and E. F. SCHROEDER. J. Am. Chem. Soc. **70**, 2785 (1948).
21. B. A. LEWIS, F. SMITH, and A. M. STEPHEN. Methods Carbohydr. Chem. **II**, 172 (1963).

Can. J. Chem. Downloaded from www.nrcresearchpress.com by 210.87.254.42 on 09/05/12
For personal use only.

Synthesis of some bicyclo[2.2.2]oct-5-en-2-ones and bicyclo[2.2.2]octan-2-ones. Rearrangements accompanying oxidative decarboxylation with lead tetraacetate

PETER YATES AND GORDON E. LANGFORD[1]

Lash Miller Chemical Laboratories, University of Toronto, Toronto, Ont., Canada M5S 1A1

Received June 25, 1980

This paper is dedicated to Prof. Raymond U. Lemieux on the occasion of his 60th birthday

PETER YATES and GORDON E. LANGFORD. Can. J. Chem. **59**, 344 (1981).

1-Methoxy-2-methyl-1,4-cyclohexadiene (**3**), 2-methoxy-1-methyl-1,3-cyclohexadiene (**2**), and 2-methoxy-1,5,5-trimethyl-1,3-cyclohexadiene (**14**) on heating with maleic anhydride give 1-methoxy-*endo*-7-methylbicyclo[2.2.2]oct-5-ene-*syn*-2,3-dicarboxylic acid anhydride (**7**) and its 6-methoxy-1-methyl (**16***a*) and 6-methoxy-1,8,8-trimethyl (**16***b*) analogues, respectively. On hydrolysis **16***a* and **16***b* give the corresponding keto dicarboxylic acids, **18***a* and **18***b*, via keto anhydrides **17***a* and **17***b*. Treatment of **18***b* with lead tetraacetate gives 1,8,8-trimethylbicyclo[2.2.2]oct-5-en-2-one (**19**) together with products in which rearrangement to a bicyclo[3.2.1]octane system has occurred. Treatment of **17***b* with bis(triphenylphosphino)nickel dicarbonyl gives only **19**; similar treatment of **17***a* gives 1-methylbicyclo[2.2.2]oct-5-en-2-one (**1**). Reaction of bicyclo[2.2.2]octane-2,3-dione (**27**) with methyllithium gives 3-hydroxy-3-methylbicyclo[2.2.2]octan-2-one (**28**), its dimer **31**, and a diol **30**. Treatment of 5-*exo*-acetoxy-1, 5-*endo*-dimethyl-6-oxobicyclo[2.2.2]octane-*anti*-2,3-dicarboxylic acid (**37**) with lead tetraacetate gives 3-*endo*-acetoxy-1,3-*exo*-dimethylbicyclo[2.2.2]oct-5-en-2-one (**33**) as a minor product; the major product is derived by rearrangement to a bicyclo[3.2.1]octane system. It is proposed that this rearrangement, like that of **18***b*, involves oxidative decarboxylation of a single carboxylic acid group to give a carbonium ion that undergoes rearrangement via a 1,2-acyl migration.

PETER YATES et GORDON E. LANGFORD. Can. J. Chem. **59**, 344 (1981).

Par chauffage avec l'anhydride maléique, le méthoxy-1 méthyl-2 cyclohexadiène-1,4 (**3**), le méthoxy-2 méthyl-1 cyclohexadiène-1,3 (**2**) et le méthoxy-2 triméthyl-1,5,5 cyclohexadiène-1,3 (**14**) donnent respectivement l'anhydride de l'acide méthoxy-1 méthyl-7-*endo* bicyclo[2.2.2] octène-5 dicarboxylique-2,3-*syn* (**7**) et ses analogues méthoxy-6 méthyl-1 (**16***a*) et méthoxy-6 triméthyl-1,8,8 (**16***b*). Par hydrolyse, les composés **16***a* et **16***b* donnent les acides céto dicarboxyliques **18***a* et **18***b* correspondants par l'intermédiaire des anhydrides cétoniques **17***a* et **17***b*. Le composé **18***b* réagit avec le tétraacétate de plomb et donne la triméthyl-1,8,8 bicyclo[2.2.2] octène-5 one-2 (**19**) aux côtés de produits qui se sont transposés en des dérivés du bicyclo[3.2.1]octane. La réaction du composé **17***b* avec le bis(triphénylphosphino) nickel dicarbonyle donne seulement le dérivé **19**; par une réaction analogue, **17***a* fournit le méthyl-1 bicyclo[2.2.2] octène-5 one-2 (**1**). La réaction de la bicyclo[2.2.2] octadione-2,3 (**27**) avec le méthylithium fournit l'hydroxy-3 méthyl-3 bicyclo[2.2.2] octanone-2 (**28**), son dimère **31** et un diol **30**. L'acide acétoxy-5-*exo* diméthyl-1,5-*endo* oxo-6 bicyclo[2.2.2] octanedicarboxylique-2,3-*anti* (**37**) réagit avec le tétraacétate de plomb pour fournir l'acétoxy-3-*endo* diméthyl-1,3-*exo* bicyclo[2.2.2] octène-5 one-2 (**33**) comme produit secondaire; le produit principal provient d'une transposition en un système bicyclo[3.2.1]octane. On suggère que cette transposition, comme celle du composé **18***b*, implique une décarboxylation oxydante d'un seul groupement carboxyle conduisant à un carbocation qui subit une transposition par l'intermédiaire d'une migration acyle-1,2.

[Traduit par le journal]

During the course of ^{13}C nmr spectroscopic studies (1) and other work (2, 3) on bicyclo[2.2.2]oct-5-en-2-ones and bicyclo[2.2.2]octan-2-ones we had occasion to synthesize several members of these series. We report this work here because we consider that it includes several features of intrinsic interest.

1-Methylbicyclo[2.2.2]oct-5-en-2-one and Related Compounds

1-Methylbicyclo[2.2.2]oct-5-en-2-one (**1**) was first obtained by routes *A* and *B* in Scheme 1 (4). In each case **1** was formed as a component of a complex mixture of products and it was isolated by preparative gas–liquid chromatography. Subsequently **1** was prepared in good yield by route *C* in Scheme 1 (5). Although the "ortho effect" greatly favours the desired regiochemistry of the Diels–Alder reaction in route *C*, alkyl substitution is rarely found to lead to regiospecific addition (6), and indeed it was observed (4) that the product mixture from route *A* contained a small amount of 4-methylbicyclo[2.2.2]oct-5-en-2-one, the regioisomer of **1**. We therefore thought it worthwhile to investigate an alternative route for the preparation of the latter, and chose 1-methyl-2-methoxy-1,3-hexadiene (**2**) as the diene component of a Diels–Alder reaction pathway to the desired product.

It has been reported (7) that Birch reduction of *o*-methylanisole gives a mixture of the 1,4-dienes **3** and **4**, which is converted on treatment with potassium amide in liquid ammonia to a mixture of the 1,3-dienes **2** and **5**, in which the former is the major component; the structures of the conjugated dienes were inferred from the Diels–Alder adducts that they formed. However, although the Birch reduc-

[1]Present address: Raylo Chemicals, Ltd., 8045 Argyll Road, Edmonton, Alta., Canada T6C 4A9.

0008-4042/81/020344-12$01.00/0

©1981 National Research Council of Canada/Conseil national de recherches du Canada

Can. J. Chem. Downloaded from www.nrcresearchpress.com by 210.87.254.6 on 09/05/12
For personal use only.

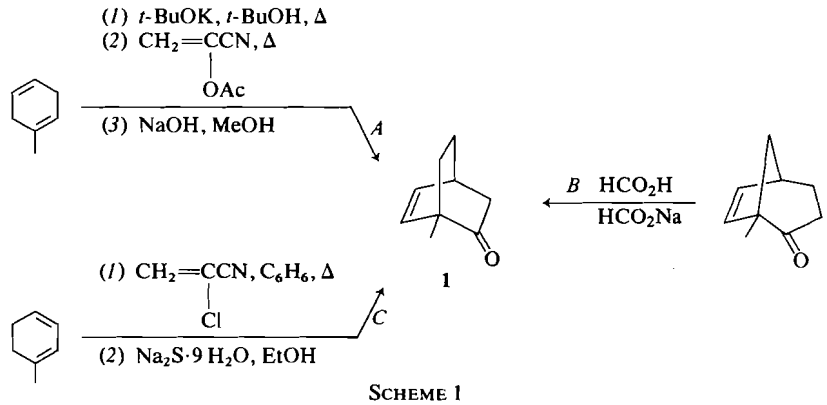

SCHEME 1

tion gave the expected unconjugated diene **3**, identified by ^1H and ^{13}C nmr spectroscopy, treatment of this with potassium amide in liquid ammonia gave in our hands a conjugated diene as the major product together with a substantial amount of the rearomatization product, *o*-methylanisole

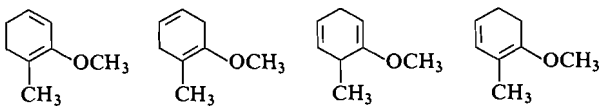

2 **3** **4** **5**

(Scheme 2). The ^1H nmr spectrum of the crude reaction product (signals at δ 1.03 (d, $J = 7$ Hz, 3H), 3.57 (s, 3H), 4.88 (d, $J = 6$ Hz, 1H), 5.2–5.5 (m, 1H), 5.7–6.0 (m, 1H)) clearly established that the conjugated diene has structure **6** and showed, furthermore, none of the signals observed for an authentic sample of **2** (*vide infra*). The preferential formation of **6** from **3** can be interpreted in terms of thermodynamic control of the reaction, in which catalytic quantities of base are used. Of the conjugated dienes that can be formed **6** is expected to be the most stable because an oxygen lone pair of electrons is in linear, rather than cross, conjugation with the conjugated diene system, and steric interaction between the methoxyl and methyl groups is minimized.

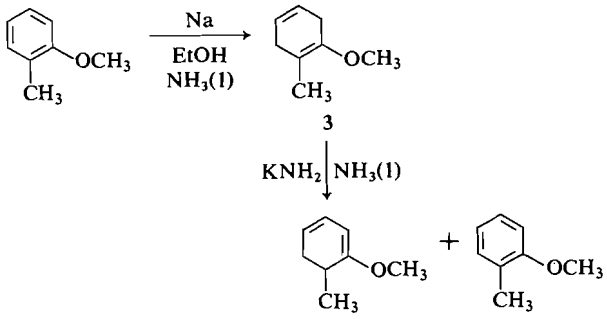

SCHEME 2

The product of the Birch reduction was further characterized by the preparation of Diels–Alder adducts of its conjugated isomer. Because of the instability of the conjugated diene and the difficulty of preparing it free from *o*-methylanisole, the isomerization and addition were performed simply by heating **3** in the presence of the dienophile (8).

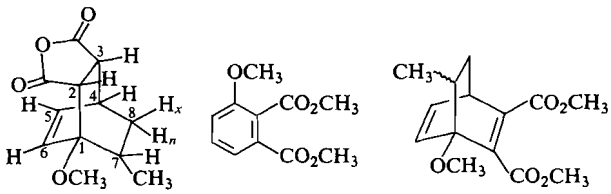

7 **8** **9**

Reaction with maleic anhydride at 140°C gave the adduct **7**,[2] whose gross structure is assigned on the basis of its ir and ^1H and ^{13}C nmr spectra (Table 1). Although no first order analysis of the coupling constants was possible in the ^1H nmr spectrum in deuteriochloroform, several coupling constants could be derived from the spectrum in hexadeuterioacetone. In particular H(3) is observed to be vicinally coupled to H(2) ($J = 9$ Hz) and H(4) ($J = 3$ Hz) but has no long-range coupling. This leads to the assignment of the endo stereochemistry of the anhydride ring with respect to the double bond as in **7**, since if the anhydride ring were exo a longe-range "W" coupling of ~2 Hz would be expected between H(3) and *endo*-H(8) (9). The methyl group is assigned the endo configuration as in **7** because it and one of the methylene protons (*endo*-H(8)) are strongly shielded (10); the exo protons at C(7) and C(8) are both ~1 ppm less shielded than *endo*-H(8).

[2]All chiral compounds were obtained as racemates and their structural representations do not imply absolute configurations.

Can. J. Chem. Downloaded from www.nrcresearchpress.com by 210.87.254.6 on 09/05/12
For personal use only.

TABLE 1. ^1H and ^{13}C nuclear magnetic resonance spectra of compound **7**[a,b]

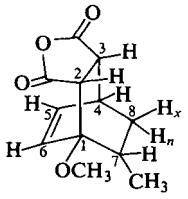

7

	$^H\delta(CDCl_3)$	$^H\delta(CD_3COCD_3)$		$^C\delta(CDCl_3)$
H(2)	2.9–3.6 (m)	3.75 (d, 9 Hz)	C(1)	80.3
H(3)		3.48 (dd, 9, 3 Hz)	C(2)	46.3
H(4)		2.8–3.15 (m)	C(3)	44.2
H(5)	5.9–6.4 (m)	6.25 (dd, 9, 6 Hz)	C(4)	31.2*
H(6)		6.00 (br d, 9, ~2 Hz)	C(5)	130.3
H(7)	1.8–2.4 (m)	1.9–2.2 (m)	C(6)	134.5
H(8x)		2.2–2.5 (m)	C(7)	31.8*
H(8n)	0.8–1.3 (m)	0.8–1.2 (m)	C(8)	33.9
$CH_3(7)$	0.83 (d, 7 Hz)	0.77 (d, 7 Hz)	$CH_3(7)$	17.4
CH_3O	3.48 (s)	3.47 (s)	CH_3O	49.8
			CO	169.0, 172.3

[a] The intensities of the proton signals are in accord with the assignments; signal multiplicities and coupling constants are given in parentheses.
[b] The multiplicities of the ^{13}C signals in the single frequency off-resonance decoupled spectrum are in accord with assignments; the individual assignments of ^{13}C signals marked with asterisks are uncertain.

This assignment is in accord with the similarity of the chemical shifts of H(2) and H(3); if the methyl group had the exo configuration, it would be anticipated that it would exert a deshielding steric repulsion effect on H(2) (11).

Reaction of **3** with dimethyl acetylenedicarboxylate at 180–195°C gave dimethyl 3-methoxyphthalate (**8**), which must be formed by loss of propene from the adduct **9** (Alder–Rickert reaction (12)). Thus in the case of the thermal as in the base-catalyzed isomerization of **3** the conjugated diene formed is **6** not **2**.

The alternative route to **2** from 3-methyl-2-cyclohexenone (**10**) shown in Scheme 3 was therefore adopted. This is based on the synthesis of the closely related diene **14** from isophorone (**10***b*) (13). The latter synthesis was first repeated to determine optimum conditions for each step and to obtain **14** as a precursor to the corresponding bicyclo[2.2.2]octenone. It was found that the compounds in the monomethyl series are much more reactive than their trimethyl analogues and that reaction conditions had to be controlled carefully. Whereas **10***b* is epoxidized smoothly at 15–20°C and is unreactive at lower temperatures, the yield of epoxide **11***a* from **10***a* increased from 35 to 92% when the reaction temperature was lowered to 0–5°C; this is considered to be due to hydrolytic

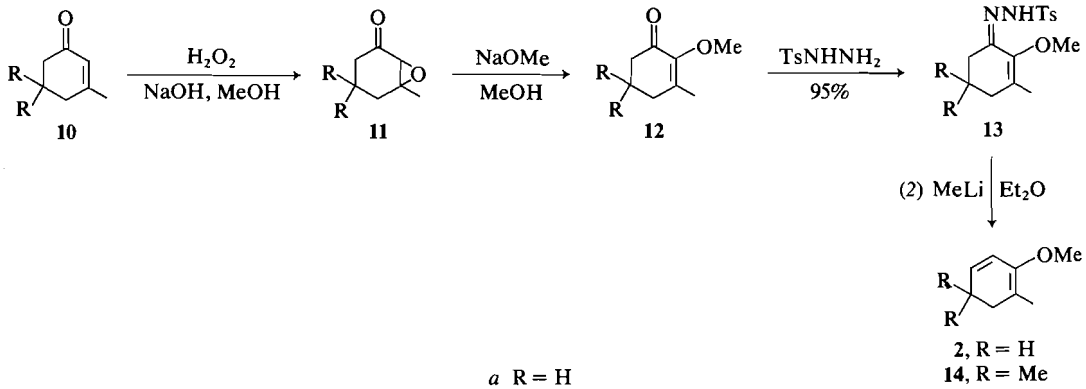

a R = H
b R = Me

SCHEME 3

Can. J. Chem. Downloaded from www.nrcresearchpress.com by 210.87.254.6 on 09/05/12
For personal use only.

Can. J. Chem. Downloaded from www.nrcresearchpress.com by 210.87.254.6 on 09/05/12
For personal use only.

opening of the epoxide ring of **11***a* at the higher temperature. The reaction temperature is also critical for the conversion of **11***a* to **12***a*. Curiously, although **11***a* reacts rapidly with methanolic sodium methoxide at 0–5°C, the best yields of **12***a* were obtained when the epoxide was added dropwise to boiling methanolic sodium methoxide; competing reactions leading to polymer formation appear to predominate at low temperatures. The corresponding reaction occurs much more slowly in the case of **11***b*, analysis of whose ^{1}H nmr spectrum shows it to have the conformation **15** in which the axial methyl group at C(5) hinders rearside attack by methoxide on the epoxide at C(2). In both series formation of the tosylhydrazones **13***a* and **13***b* and conversion of these to the dienes **2** and **14** could be effected in high yield under appropriate conditions (see Experimental) and the overall yields of the dienes from **10***a* and **10***b*, respectively, were ~50 and 63%.

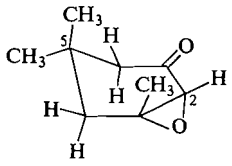

15

Diene **2** was identified by its ^{1}H nmr spectrum and the relationship of this spectrum to that of **14** (Table 2). Both dienes decomposed on standing and it was found to be best to convert them immediately to their adducts with maleic anhydride. Gross structures corresponding to **16***a* and **16***b* are assigned to these adducts based on their ir, ^{1}H nmr (Table 3), and ^{13}C nmr (1) spectra. Acid-catalyzed hydrolysis of **16***a* and **16***b* with one equivalent of water gave the keto anhydrides **17***a* and **17***b*, respectively; in the presence of excess water the keto dicarboxylic acids **18***a* and **18***b*, respectively, were formed. The stereochemistry of **17***b*, and thus of **16***b* and **18***b*, is assigned on the basis of an analysis of its

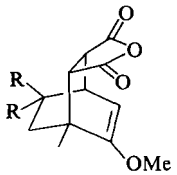

16*a* R = H
16*b* R = Me

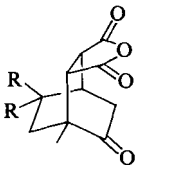

17*a* R = H
17*b* R = Me

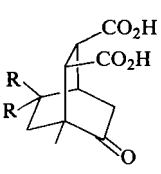

18*a* R = H
18*b* R = Me

^{1}H nmr spectrum (Table 3). The long-range "W" coupling of ~2 Hz observed between H(3) and H(5n) is only possible with the stereochemistry shown (9), demonstrating that maleic anhydride added in the normal endo fashion. Corroboration for this stereochemical assignment derives from the large downfield shifts of H(3) and H(5n) relative to H(2) and H(5x), respectively, which can be attributed to the deshielding steric compression effects of the *gem*-dimethyl groups (11). Independent evidence for the stereochemistry of **16***b* is provided by the absence of long-range coupling between H(2) and H(7n), since in the exo stereoisomer the corresponding protons would have a "W" relationship. Although the spectrum of the keto anhydride **17***a* could not be analyzed in detail, the absence of long-range coupling in the spectrum of **16***a* between H(2) and H(7n) and between H(3) and H(8n) demonstrates that this, and thus **17***a* and **18***a*, have the endo stereochemistry shown.

The keto acid **18***b* has been prepared previously by hydrolysis of the Diels–Alder adduct of the enol acetate of **10***b* and maleic anhydride and converted to 1,8,8-trimethylbicyclo[2.2.2]oct-5-en-2-one (**19**) in undisclosed yield by oxidative bisdecarboxylation with lead tetraacetate in pyridine (14). In our hands such treatment of **18***b* gave a mixture containing **19** (30–40%) and three other compounds that are considered to be the rearrangement products **20–22** (Scheme 4). Compound **19** was identified by its ir, ^{1}H nmr (Table 4), and ^{13}C nmr (1) spectra. Compound **20** was obtained as a crystalline solid, but **21** and **22** were not separated from each other. The structures **20–22** are assigned on the basis of spectroscopic (see Experimental) and mechanistic considerations (Scheme 5), and although they have not been established rigorously they gain authentication from their relationship to the structure of the rearrangement product formed in a related reaction (*vide infra*).

Because of these complications associated with the preparation of **19** by reaction of **18***b* with lead

TABLE 2. ^{1}H nuclear magnetic resonance spectra of compounds **2** and **14**[a]

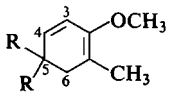

$^H\delta(CDCl_3)$

	2 (R = H)	**14** (R = CH_3)
H(3)	5.6–6.1 (m)	5.46 (d, 10 Hz)
H(4)		5.80 (d, 10 Hz)
H(5)	1.8–2.4 (m)	—
H(6)		2.0–2.1 (m)
CH_3(1)	1.72 (s)	1.68 (br s)
CH_3(5)	—	1.00 (s)
CH_3O	3.54 (s)	3.54 (s)

[a]See footnote *a* in Table 1.

TABLE 3. ^{1}H nuclear magnetic resonance spectra of compounds **16***a*, **16***b*, **17***a*, and **17***b*[a]

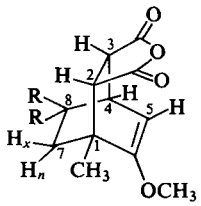

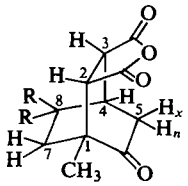

	$^H\delta(CDCl_3)$			$^H\delta(CDCl_3)$	$^H\delta^b$
	16*b* (R = Me)	**16***a* (R = H)		**17***b* (R = Me)	**17***a* (R = H)
H(2)	2.76 (d, 9 Hz)	2.82 (d, 9.5 Hz)	H(2)	3.15 (d, 10.5 Hz)	3.3–3.7 (m)
H(3)	3.50 (dd, 9, 3.5 Hz)	3.14 (dd, 9.5, 3 Hz)	H(3)	3.74 (ddd, 10.5, 3.2, 2.1 Hz)	
H(4)	2.71 (dd, 7, 3.5 Hz)	3.24 (m)	H(4)	2.34 (ddd, 3.2, 3.1, 2.2 Hz)	2.6–2.9 (m)
H(5)	4.88 (d, 7 Hz)	4.87 (d, 7 Hz)	H(5x)	2.02 (dd, 19.5, 2.2 Hz)	2.2–2.4 (m)
H(7)	1.23 (s)	1.47 (br s)	H(5n)	2.72 (ddd, 19.5, 3.1, 2.1 Hz)	
H(8)	—		H(7)	1.58 (s)	1.6–2.0 (m)
CH_3(1)	1.38 (s)		H(8)	—	
CH_3(8)	0.95 (s), 1.10 (s)	—	CH_3(1)	1.28 (s)	1.28 (s)
CH_3O	3.50 (s)	3.47 (s)	CH_3(8)	1.13 (s), 1.22 (s)	—

[a]See footnote *a* in Table 1.
[b]In $CDCl_3$–CD_3COCD_3(3:2).

tetraacetate, its preparation by treatment of the keto anhydride **17***b* with bis(triphenylphosphino)nickel dicarbonyl[3] was investigated (15). This procedure gave **19** in essentially quantitative yield and the formation of rearrangement products was not observed. It is of interest that application of the procedure to the enol ether **16***b* gave only *o*-methylanisole in addition to recovered **16***b*. The preparation of the original target molecule, 1-methylbicyclo[2.2.2]oct-5-en-2-one (**1**) from the keto anhydride **17***a* was also accomplished by this method (Scheme 6). The weight and ^{1}H nmr spectra of the crude product indicated that again the bicyclo[2.2.2]octenone was formed in essentially quantitative yield; however, losses during chromatography attributable to its very high volatility reduced the yield of isolated product to 52%. Its

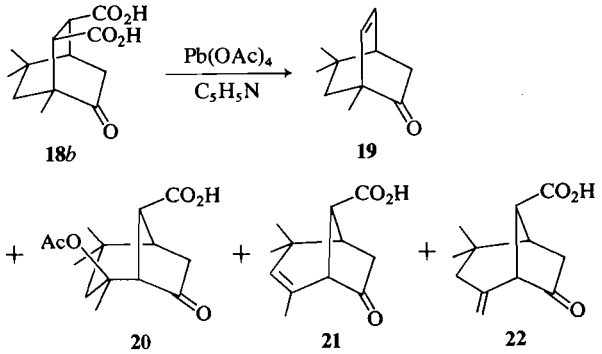

SCHEME 4

[3]We thank Professor D. N. Butler, York University, for a generous supply of this compound.

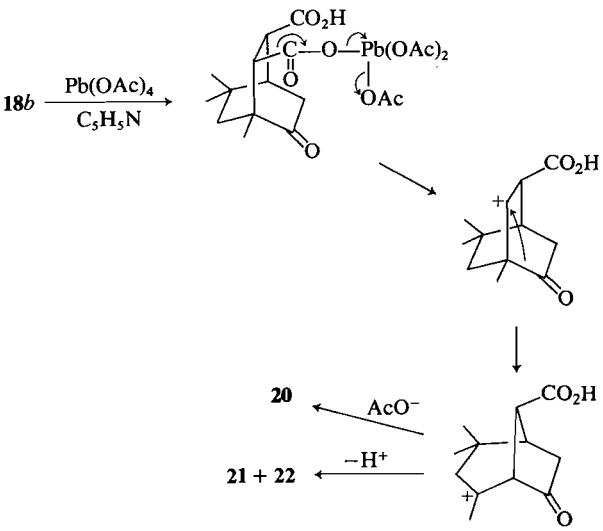

SCHEME 5

structure was established by its ir, ^{1}H nmr (Table 4), and ^{13}C nmr (1) spectra.

Catalytic hydrogenation of **1** and **19** gave the corresponding bicyclo[2.2.2]octanones **23** and **24**, respectively (Scheme 6). The former has been obtained previously by other routes (16, 17). Their ir, ^{1}H nmr (Table 4), and ^{13}C nmr (1) spectra are in accord with expectation.

Compounds Related to 3-Hydroxybicyclo[2.2.2]-octan-2-one

3-Hydroxybicyclo[2.2.2]octan-2-one (**25**) (18) and its *O*-acetyl derivative (**26**) (19) have been prepared previously from bicyclo[2.2.2]octane-2,3-dione

Can. J. Chem. Downloaded from www.nrcresearchpress.com by 210.87.254.6 on 09/05/12
For personal use only.

Can. J. Chem. Downloaded from www.nrcresearchpress.com by 210.87.254.6 on 09/05/12
For personal use only.

TABLE 4. ^{1}H nuclear magnetic resonance spectra of compounds **1**, **19**, **23**, and **24**[a]

	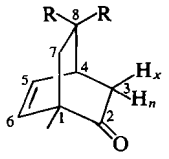 $^H\delta(CDCl_3)$		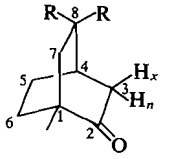 $^H\delta(CDCl_3)$	
	1 (R = H)	**19** (R = Me)	**23** (R = H)	**24** (R = Me)
H(3n)	1.9–2.3 (m)	1.90 (dd, 19, 3.5 Hz)	2.0–2.3 (m)	1.95 (dd, 19, 2.5 Hz)
H(3x)		2.43 (dd, 19, 2.5 Hz)		2.53 (ddd, 19, 3, 3 Hz)
H(4)	2.8–3.1 (m)	2.2–2.5 (m)		1.8–2.2 (m)
H(5)	6.45 (dd, 8, 6.5 Hz)	6.55 (dd, 8, 6.5 Hz)	1.4–1.9 (m)	1.4–1.8 (m)
H(6)	5.83 (dd, 8, 1.6 Hz)	5.78 (dd, 8, 1.5 Hz)		
H(7)	1.4–1.9 (m)	1.38 (AB,[b] 13.5 Hz)		1.33 (br s)
H(8)		—		—
CH_3(1)	1.22 (s)	1.15 (s)	0.93 (s)	0.83 (s)
CH_3(8)	—	1.02 (s), 1.10 (s)	—	0.91 (s), 1.07 (s)

[a]See footnote *a* in Table 1.
[b]$\Delta\nu \approx 6$ Hz.

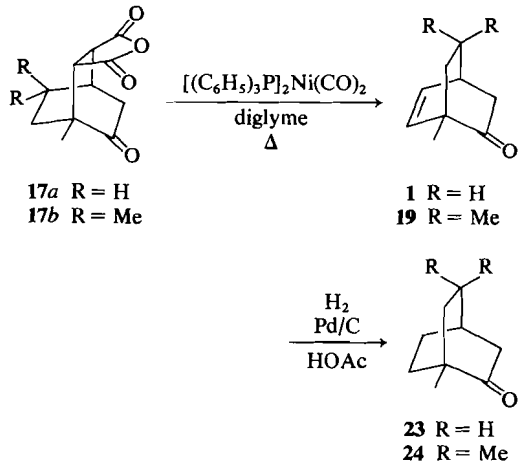

17*a* R = H
17*b* R = Me

1 R = H
19 R = Me

23 R = H
24 R = Me

SCHEME 6

(**27**) and bicyclo[2.2.2]octanone by the routes shown in Scheme 7. We wished to prepare the corresponding 3-methyl compound, 3-hydroxy-3-methylbicyclo[2.2.2]octan-2-one (**28**). Preparation of **28** was approached by reaction of methyllithium with dione **27**. Slow dropwise addition of methyllithium to **27** in ether led to decolorization after the addition of 0.5 equivalent. Work-up of the reaction mixture at this stage gave a product $C_{17}H_{24}O_4$, whose spectra showed it to be one of the stereoisomers **29**, derived by reaction of **28** with unconsumed **27** (Scheme 8).[4] When a slight excess (~1.1 equiv.) of methyllithium was added to **27** a complex product mixture was obtained from which three major components were isolated by chromatography. These were identified spectroscopically as the desired ketol **28**, a diol of type **30**,[5] and a dimer **31** of **28**. The facile formation of dimers from α-ketols is well known (20); in the present case the dimer may have a structure of type **31***a* or **31***b*. It seems likely that dimers of the latter type will have, as a result of equilibration, *cis* fusions of the dioxane ring with the bicyclo[2.2.2]octane rings. In this event they will have a symmetry element absent in dimers of type **31***a*. Since the ^{13}C nmr spectrum of the dimer showed sixteen discrete signals

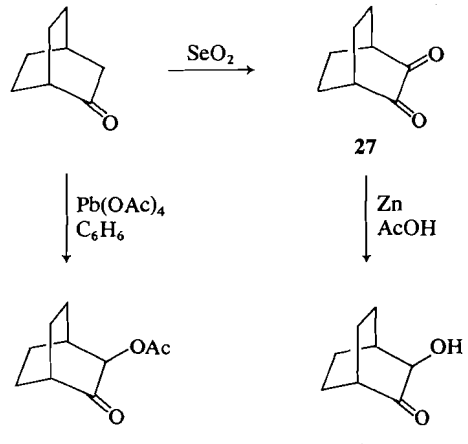

27

26

25

SCHEME 7

[4]It is probable that both stereoisomers were formed, but only one was isolated on crystallization of the crude reaction product.

[5]In an earlier investigation,[6] two such diols were isolated; the diol isolated in the present work corresponds to the major product isolated previously, which was tentatively assigned structure **30** on the basis of ir spectroscopic comparison.

[6]P. Yates and K. E. Stevens, unpublished results.

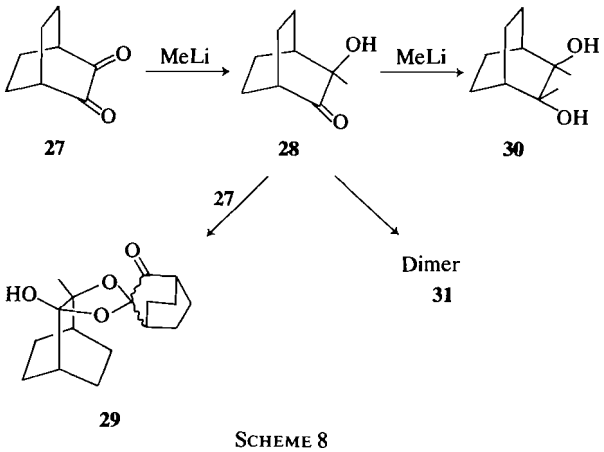

SCHEME 8

(including two methyl signals), it is concluded that the structure of the dimer isolated is of type **31***a*.

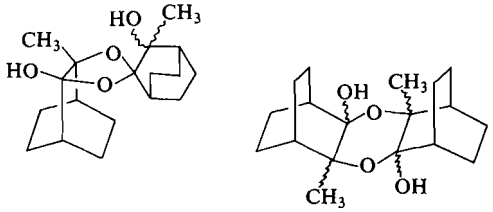

31*a* **31***b*

The final synthetic objectives in this work were the compounds **32–34**. These could be obtained from the known compounds **35** and **36** (19) by the routes shown in Scheme 9. However, in contrast to the cases of compounds **17***a* and **17***b*, the yields in the reactions of **35** and **36** with bis(triphenylphosphino)nickel dicarbonyl were abysmal (5–10%) and insufficient **32** and **33** could be isolated from these routes for full characterization. Interestingly, **32** was accompanied by 2,6-dimethylphenol, a plausible route for whose formation is shown in Scheme 10. Oxidative bisdecarboxylation with lead tetraacetate and pyridine of **37**, the dicarboxylic acid derived from mild hydrolysis of **36** also gave **33** in very low yield, but sufficient material was obtained for characterization of this and its hydrogenation product **34** (Table 5).

TABLE 5. ^{1}H nuclear magnetic resonance spectra of compounds **33** and **34**[a]

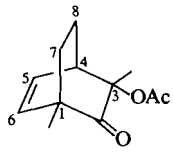

33

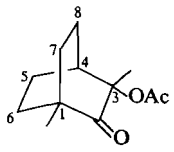

34

	$^H\delta(CDCl_3)$		$^H\delta(CDCl_3)$
H(4)	3.6–3.9 (m)	H(4)	2.7–2.9 (m)
H(5)	6.37 (dd, 8, 6 Hz)	H(5)	1.5–1.9 (m)
H(6)	5.88 (dd, 8, 2 Hz)	H(6)	
H(7)	1.3–1.9 (m)	H(7)	
H(8)		H(8)	
CH_3(1)	1.27 (s)	CH_3(1)	0.99 (s)
CH_3(3)	1.60 (s)	CH_3(3)	1.59 (s)
CH_3CO	1.95 (s)	CH_3CO	2.03 (s)

[a]See footnote *a* in Table 1.

The major product from the reaction of **37** with lead tetraacetate and pyridine was a compound $C_{13}H_{16}O_5$ that is assigned structure **38**; this undergoes ready hydrolysis of the acetate group to give **39**. These structural assignments are based on spectroscopic data (see Experimental). Compound **38** is thought to be formed as in Scheme 11. The rearrangement of the bicyclo[2.2.2]octane to a bicyclo[3.2.1]octane system in the course of this

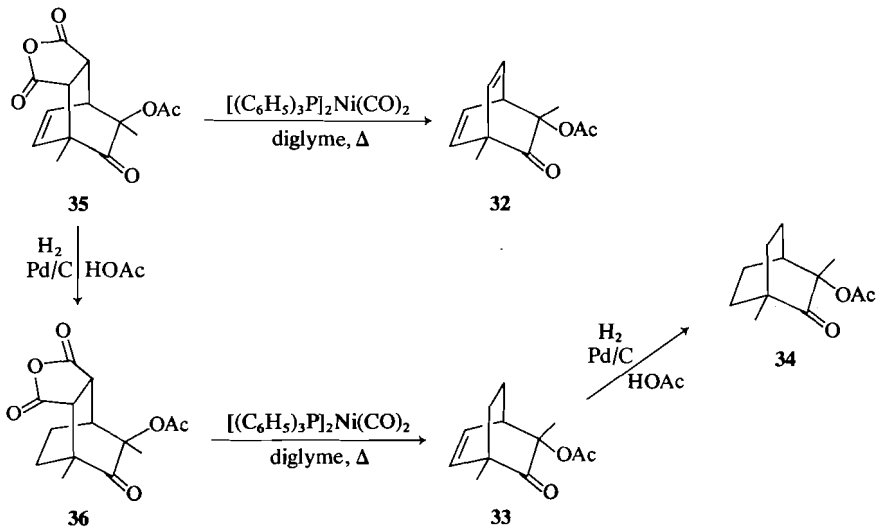

SCHEME 9

Can. J. Chem. Downloaded from www.nrcresearchpress.com by 210.87.254.6 on 09/05/12
For personal use only.

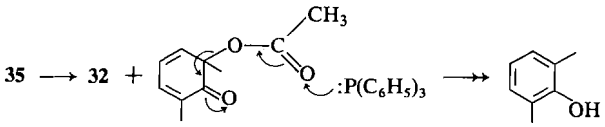

SCHEME 10

reaction and the analogous rearrangement when **18*b*** is treated with lead tetraacetate and pyridine (*vide supra*) is of considerable interest. Carbonium ions of type **40** have been previously implicated as intermediates in the oxidative bisdecarboxylation reaction (21), and the unusual competition between rearrangement and decarboxylation of such intermediates in the present cases is attributable to the high migratory aptitude of the acyl group and the formation of a tertiary carbonium ion. The final formation of a lactone from this ion in the case of **37**, but of products derived by deprotonation and attack of acetate ion in the case of **18*b***, reflects the difference in the stereochemical relationship between the carboxylic acid groups and the ketone group in the two series.

Experimental

Unless otherwise specified, melting points are uncorrected, ir spectra were recorded for $CHCl_3$ solutions, ^1H and ^{13}C nmr spectra were recorded for $CDCl_3$ solutions, and solutions in organic solvents were dried over anhydrous $MgSO_4$.

Birch Reduction of 2-Methylanisole. Formation of 1-Methoxy-2-methyl-1,4-cyclohexadiene (3)

2-Methylanisole was prepared by methylation of *o*-cresol with dimethyl sulfate (22). It was reduced by the method of Birch (7, 23) to the 1,4-diene **3**; ^1H nmr δ: 1.65 (br s, 3H), 2.6–2.9 (m, 4H), 3.54 (s, 3H), 5.6–5.8 (m, 2H); ^{13}C nmr δ: 145.6 (s), 124.6 (d), 123.7 (d), 111.4 (s), 55.9 (q), 33.0 (t), 26.2 (t), 14.9 (q).

Treatment of 3 with Potassium Amide. Formation of 1-Methoxy-6-methyl-1,3-cyclohexadiene (6) and o-Methylanisole

Liquid ammonia (~50 mL) was distilled into a 100-mL three-necked flask containing a polyethylene-covered magnetic stirring bar and fitted with a dry-ice condenser with a soda-lime guard tube. Potassium (0.17 g, 4.4 mg-atom) was added with stirring, forming a dark blue solution. After a few minutes, ferric nitrate nonahydrate (42 mg) was added and 10 min later more potassium (0.09 g, 2.3 mg-atom) was added. The solution was stirred for 40 min and then the 1,4-diene **3** (1.28 g, 10.3 mmol) was added dropwise. The mixture was stirred for a further 30 min and water (20 mL) was carefully added dropwise. The condenser was removed and stirring was continued for 2.5 h. The residue was extracted with dichloromethane (3 × 50 mL). The extracts were dried (K_2CO_3) and evaporated to give an oil whose ^1H nmr spectrum showed two major components, *o*-methylanisole (~30%) and **6** (~60%); ^1H nmr δ: 1.03 (d, J = 7 Hz, 3H), 3.57 (s, 3H), 4.88 (d, J = 6 Hz, 1H), 5.2–5.5 (m, 1H), 5.7–6.0 (m, 1H), a broad, unresolved absorption at δ 1.5–3.0 includes the signals of the other three aliphatic protons. Increased proportions of *o*-methylanisole were isolated with longer reaction times.

*Reaction of 3 with Maleic Anhydride. Formation of 1-Methoxy-7-*endo*-methylbicyclo[2.2.2]oct-5-ene-*syn*-2,3-dicarboxylic Acid Anhydride (7)*

A sample of crude diene **3** (1.71 g, ~75% pure), obtained as above, and maleic anhydride (1.9 g) were stirred together. In a few minutes the mixture became warm and the anhydride dissolved, forming a clear red solution. The solution was heated under nitrogen in an oil bath at 140°C overnight and then volatile material was removed on a vacuum line starting at 20°C (10 Torr) and going to 65°C (0.05 Torr). The residue was a dark brown viscous oil (2.39 g). It was chromatographed on silica gel (60 g) with 2:1 hexanes – ethyl acetate and the major fraction (R_f 0.26) was recrystallized from chloroform–hexanes to give white crystalline **7**, mp 136–138°C; ir λ_{max}: 5.40 (w), 5.67 μm; ^1H and ^{13}C nmr: see Table 1; *m/e*: 180.0422 ((M − C_3H_6)$^+$ 180.0422). *Anal.* calcd. for $C_{12}H_{14}O_4$: C 64.85, H 6.35; found: C 64.55, H 6.43.

Reaction of 3 with Dimethyl Acetylenedicarboxylate. Formation of Dimethyl 3-Methoxyphthalate (8)

A sample of crude diene **3** (2.08 g, ~75% pure) obtained as above was heated with dimethyl acetylenedicarboxylate (2.38 g, ~33% excess) in an oil bath with stirring under reflux. The bath temperature was raised to 180°C over 30 min and then maintained at 180–195°C for 90 min. Distillation of the residue yielded crude **8** (1.86, ~66%), bp 135–142°C (0.9 Torr). A portion of the distillate was chromatographed on silica gel with 3:1 hexanes – ethyl acetate, and the material thus obtained was recrystallized from 95% ethanol to give pure, crystalline **8**, mp 75–76°C (lit. (24) mp 72–72.5°C, (7) mp 77–77.5°C); ir λ_{max}: 5.82 (br), 6.32 (m) μm; ^1H nmr δ: 3.85 (s, 3H), 3.88 (s, 3H), 3.95 (s, 3H), 7.0–7.7 (m, 3H); *m/e*: 224.0685 (M$^+$ 224.0685).

2-Methoxy-1,5,5-trimethyl-1,3-cyclohexadiene (14) (13)

Isophorone oxide (**11*b***) was prepared by treatment of isophorone with alkaline hydrogen peroxide in methanol (25).

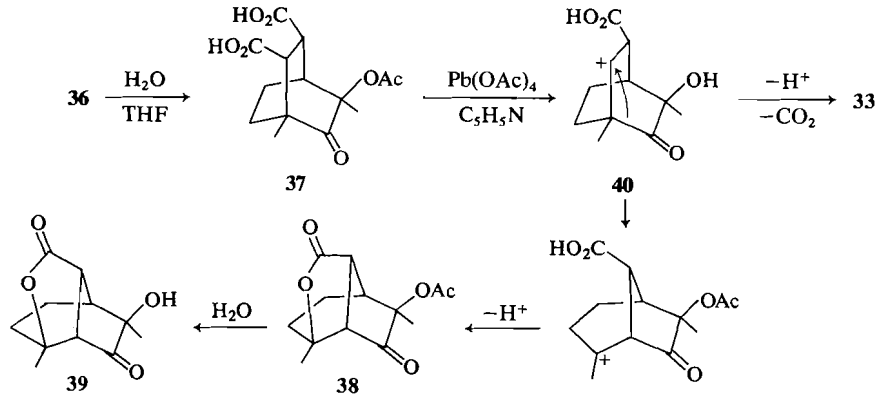

SCHEME 11

Can. J. Chem. Downloaded from www.nrcresearchpress.com by 210.87.254.6 on 09/05/12
For personal use only.

Can. J. Chem. Downloaded from www.nrcresearchpress.com by 210.87.254.6 on 09/05/12
For personal use only.

A solution of **11***b* (36.0 g, 0.214 mol) in methanol (25 mL) was added dropwise with stirring to a solution of sodium (9.0 g, 0.39 g-atom) in methanol (175 mL) at room temperature under nitrogen. The mixture was boiled under reflux for 2 h, cooled, and poured into ice water (500 mL). After extraction with dichloromethane (4 × 150 mL) the organic phase was washed with saturated brine, dried, and evaporated to give a brown liquid. Distillation of the crude product yielded **12***b* (35.3 g, 90%) as a colorless liquid, bp 78–80°C (2.8 Torr); ^{1}H nmr δ: 1.06 (s, 6H), 1.90 (s, 3H), 2.2–2.4 (m, 4H), 3.65 (s, 3H).

Ketone **12***b* (2.84 g, 16.9 mmol) was heated with *p*-toluenesulfonylhydrazine (3.15 g, 16.9 mmol) in 60% aqueous methanol at ~65°C for 2 h. The hot solution separated into two phases, and on cooling the lower phase solidified. The solid was filtered and recrystallized from 95% ethanol to give crystalline tosylhydrazone **13***b* (5.02 g, 88%), mp 123–124.5°C; ^{1}H nmr δ: 0.96 (s, 6H), 1.76 (s, 3H), 2.04 (s, 2H), 2.15 (s, 2H), 2.41 (s, 3H), 3.53 (s, 3H), 7.2–7.5 (m, 2H), 7.8–8.1 (m, 2H) ppm. *Anal.* calcd. for $C_{17}H_{24}N_2O_3S$: C 60.69, H 7.19, N 8.33; found: C 60.41, H 7.09, N 8.29.

Tosylhydrazone **13***b* (10.27 g, 30.6 mmol) in dry ether (100 mL) was stirred under nitrogen in a three-necked flask fitted with a reflux condenser and dropping funnel. A solution of methyllithium in ether (1.23 *M*; 53 mL, 65 mmol) was added dropwise at room temperature over 1 h. The mixture was boiled under reflux for 1 h and cooled in an ice bath, and water (50 mL) was added dropwise. The aqueous phase was washed twice with ether (400 mL total), and the combined ether extracts were washed with saturated brine, dried, and evaporated to give **14** as an oil; ^{1}H nmr δ: 1.00 (s, 6H), 1.68 (br s, 3H), 2.0–2.1 (m, 2H), 3.54 (s, 3H), 5.46 (d, J = 10 Hz, 1H), 5.80 (d, J = 10 Hz, 1H). This was treated immediately with maleic anhydride to give **16***b* (*vide infra*).

2-Methoxy-1-methyl-1,3-cyclohexadiene (2)

A solution of 30% hydrogen peroxide (11.8 *M* by iodometric titration; 20 mL, 0.33 mol) in methanol (100 mL) was stirred in an ice bath and 3-methyl-2-cyclohexen-1-one (11.0 g, 0.100 mol) was added. A solution of 6 *N* aqueous sodium hydroxide (8.4 mL, 0.05 mol) was placed in a dropping funnel. When the solution in the flask had cooled to 0°C, a few drops of aqueous sodium hydroxide were added cautiously with monitoring of the temperature. The temperature rose slowly to 5°C and remained there for about 15 min. When the temperature fell to 3.5°C, a few more drops of aqueous sodium hydroxide were added, and the temperature again rose to 5°C. After 15 min the temperature had fallen below 2°C, and the remainder of the aqueous sodium hydroxide was added more rapidly over about 10 min while keeping the temperature below 5°C. The mixture was stirred for a further 45 min in the ice bath, and then poured onto ice (100 g) and extracted quickly with dichloromethane (4 × 60 mL). The extracts were dried and evaporated, and the residue was distilled to give the epoxide **11***a* (11.60 g, 92%), bp 66–68°C (5.5 Torr); ^{1}H nmr δ: 1.45 (s, 3H), 1.4–2.7 (m, 6H), 3.08 (s, 1H); *m/e*: 126.0681 (M^+ 126.0680). *Anal.* calcd. for $C_7H_{10}O_2$: C 66.65, H 7.99; found: C 66.17, H 8.04.

A solution of epoxide **11***a* (12.8 g, 0.101 mol) in methanol (10 mL) was added dropwise over 10 min with stirring under reflux to a boiling solution obtained by reaction of sodium (3.4 g, 0.15 g-atom) with methanol (65 mL). After 5 min the mixture was cooled in an ice bath and poured onto crushed ice (100 g), and the mixture was extracted with dichloromethane (4 × 50 mL). The combined extracts were washed with saturated brine, dried, and evaporated to give enol ether **12***a* (12.9 g, 91%) as a brown oil, which was used for conversion to the tosylhydrazone **13***a*. Pure **12**a was obtained by distillation; bp 73–75°C (3.0 Torr); ^{1}H nmr δ: 1.8–2.2 (m, 2H), 1.93 (br s, 3H), 2.3–2.6 (m, 4H), 3.65 (s, 3H); *m/e*: 140.0836 (M^+ 140.0836). *Anal.* calcd. for $C_8H_{12}O_2$: C 68.55, H 8.63; found: C 68.14, H 8.58.

Compound **12***a* (7.90 g, 56 mmol) and *p*-toluenesulfonylhydrazine (10.60 g, 57 mmol) were warmed gently together in 95% ethanol (25 mL) until they dissolved, and the solution was allowed to cool slowly to room temperature and stand overnight. Yellow crystals of tosylhydrazone **13***a* separated and the mother liquor assumed a dark red-brown color. The yellow product was filtered, washed with ethanol, and recrystallized from 95% ethanol to give **13***a* (15.65 g, 90%), as pale yellow needles, mp 160–162°C; ^{1}H nmr δ: 1.5–2.5 (m, ~6H), 1.81 (s, 3H), 2.41 (s, 3H), 3.60 (s, 3H), 7.30 (m, 2H), 7.90 (m, 2H); *m/e*: 308.1203 (M^+ 308.1188). *Anal.* calcd. for $C_{15}H_{20}N_2O_3S$: C 58.42, H 6.54, N 9.08; found: C 58.32, H 6.55, N 8.91.

Tosylhydrazone **13***a* (0.346 g, 1.12 mmol) was stirred in dry ether (10 mL) and a solution of methyllithium in ether (1.2 *M*; 2.7 mL, 3.2 mmol) was added dropwise under nitrogen. The mixture was boiled under reflux for 15 min, allowed to stand for 45 min, and then cooled in an ice bath. Aqueous 5% sodium carbonate (10 mL) was added dropwise and the mixture was extracted with dichloromethane (4 × 20 mL). The combined extracts were dried and evaporated to give **2** (0.117 g, 84%) as an oil; ^{1}H nmr δ: 1.72 (s, 3H), 1.8–2.4 (m, 4H), 3.54 (s, 3H), 5.6–6.1 (m, 2H). This was treated immediately with maleic anhydride to give **16***a* (*vide infra*).

*Reaction of 2 with Maleic Anhydride. Formation of 6-Methoxy-1-methylbicyclo[2.2.2]oct-5-ene-*syn*-2,3-dicarboxylic Acid Anhydride (16a)*

Crude diene **2** freshly prepared from tosylhydrazone **13***a* (5.09 g, 16.5 mmol) was dissolved in dry benzene (20 mL) under nitrogen, and the solution was cooled in an ice bath. A solution of maleic anhydride (1.6 g, 16.3 mmol) in dry benzene (20 mL) was added slowly with stirring. The solution was stored overnight at 8°C. The solvent was evaporated and the solid residue (3.23 g) was sublimed at 0.005 Torr (at this pressure, excess maleic anhydride does not condense on the cold finger, but sublimes into the liquid nitrogen trap). A viscous oil condensed on the cold finger and then crystallized to a pale yellow solid (2.56 g). Recrystallization of the sublimate from chloroform–hexanes gave the Diels–Alder adduct **16***a* (2.37 g, 65%), as white crystals, mp 103–106°C. An analytical sample was obtained by a second recrystallization, mp 105–107°C; ir λ_{max}: 5.42 (w), 5.50 (w), 5.68, 6.17 (m) μm; ^{1}H nmr: see Table 3: ^{13}C nmr δ: 173.1 (s), 172.2 (s), 160.6 (s), 93.0 (d), 55.0 (q), 50.1 (d), 46.4 (d), 39.3 (s), 32.9 (t), 32.5 (d), 25.8 (t), 17.8 (q). *Anal.* calcd. for $C_{12}H_{14}O_4$: C 64.85, H 6.35; found: C 64.48, H 6.39.

*Reaction of 14 with Maleic Anhydride. Formation of 6-Methoxy-1,8,8-trimethylbicyclo[2.2.2]oct-5-ene-*syn*-2,3-dicarboxylic Acid Anhydride (16b)*

Crude diene **14**, freshly prepared from tosylhydrazone **13***b* (10.27 g, 30.6 mmol), was dissolved in benzene (10 mL) and maleic anhydride (50 g, 51 mmol) was added. The solution was stirred at room temperature overnight. The solvent was evaporated, and the residue was heated on a vacuum line at 50–65°C for 1 h. Recrystallization of the brown residue from dichloromethane–hexanes yielded needles of adduct **16***b*. A further small crop was obtained by recrystallization from ether of the residue obtained by concentration of the mother liquors. The yield of **16***b* was 5.83 g, (76% based on tosylhydrazone **13***b*). An analytical sample was prepared by recrystallization from ether; mp 138–139°C; ir λ_{max}: 5.40 (w), 5.66, 6.15 (m) μm; ^{1}H nmr: see Table 3; ^{13}C nmr δ: 173.8 (s), 171.1 (s), 159.2 (s), 93.7 (d), 55.2 (q), 49.5 (t), 48.8 (d), 43.9 (d), 43.7 (d), 41.3 (s), 34.6 (s), 30.5 (q), 29.3 (q), 17.8 (q); *m/e*: 250.1202 (M^+ 250.1205). *Anal.* calcd. for $C_{14}H_{18}O_4$: C 67.18, H 7.25; found: C 67.11, H 7.19.

Can. J. Chem. Downloaded from www.nrcresearchpress.com by 210.87.254.6 on 09/05/12
For personal use only.

Hydrolysis of **16**a. *Formation of 1-Methyl-6-oxobicyclo[2.2.2]octane*-syn-*2,3-dicarboxylic Acid Anhydride (***17***a) and Acid (***18***a)*

Enol ether **16***a* (2.00 g, 9.0 mmol) was dissolved in warm tetrahydrofuran (10 mL). Concentrated hydrochloric acid (0.15 mL) was added dropwise with stirring. Crystals began to separate immediately. After standing for 30 min at room temperature the mixture was evaporated to dryness, and the white crystalline residue was washed with dry ether. The crystals, which were insoluble in ether, were pure keto anhydride **17***a* (1.76 g, 94%). By concentration of the ether washings a further crop of **17***a* was obtained, 0.059 g (3%). An analytical sample was prepared by recrystallization from chloroform; mp 216–215°C; ir λ_{max}: 5.32 (w), 5.62, 5.76 μm; ^{1}H nmr: see Table 3. *Anal.* calcd. for $C_{11}H_{12}O_4$: C 63.45, H 5.81; found: C 63.37, H 5.85.

If, after a few minutes, water was added to the reaction mixture, and the mixture was boiled under reflux for 1 h, a mixture of **17***a* and the corresponding dicarboxylic acid **18***a* was formed; ir λ_{max}: 2.9–4.2, 5.2 (w), 5.80 (br) μm. The latter was not obtained in pure form.

Hydrolysis of **16**b. *Formation of 1,8,8-Trimethyl-6-oxobicyclo[2.2.2]octane*-syn-*2,3-dicarboxylic Acid Anhydride (***17***b) and Acid (***18***b)*

Enol ether **16***b* (2.2 g, 8.8 mmol) was stirred in tetrahydrofuran (20 mL) with 3 *N* hydrochloric acid (2 mL) for 1 h. Evaporation gave an oil, shown by ^{1}H nmr spectroscopy to be a mixture of **16***b* (30%) and **17***b* (70%). The mixture was redissolved in tetrahydrofuran (20 mL), stirred with 6 *N* hydrochloric acid (2.0 mL) for 2 h, and evaporated to give an oil. Dichloromethane was added and the white precipitate of **18***b* was filtered. The filtrate was evaporated to give a solid, which was washed with ether, leaving **17***b* as an amorphous white solid (1.82 g, 87%), mp 133.5–134°C; ir λ_{max}: 5.36 (w), 5.62, 5.78 μm; ^{1}H nmr: see Table 3; *m/e*: 236.1050 (M^+ 236.1048). *Anal.* calcd. for $C_{13}H_{16}O_4$: C 66.09, H 6.83; found: C 65.93, H 6.89.

The fraction from the hydrolysis of **16***b* that was insoluble in dichloromethane was crystallized from aqueous acetone to give diacid **18***b* (0.123 g, 5.5%) as white needles, mp 199–201°C; ir λ_{max} (KBr): 3.0–4.0, 5.80, 5.87 μm; ^{1}H nmr δ (acetone-d_6 + D_2O): 0.94 (s, 3H), 0.97 (s, 3H), 1.15 (s, 3H), 1.32 (d, J = 14 Hz, 1H), 1.63 (d, J = 14 Hz, 1H), ~2.15 (m, under acetone-d_5 signal, 1H) 2.41 (ddd, J = 19, 3.5, 2 Hz, 1H), 2.94 (dd, J = 19, 2.2 Hz, 1H), 3.15 (d, J = 12 Hz, 1H), 3.58 (ddd, J = 12, 2, 2 Hz, 1H). *Anal.* calcd. for $C_{13}H_{18}O_5$: C 61.41, H 7.14; found: C 61.31, H 7.10.

Lead Tetraacetate Oxidation of **18**b. *Formation of 1,8,8-Trimethylbicyclo[2.2.2]oct-5-en-2-one (***19***) and Compounds 20–22*

Diacid **18***b* (427 mg, 1.68 mmol) and dry lead tetraacetate (930 mg, 2.15 mmol) were combined in a small flask and then dried on a vacuum line (0.005 Torr) for 2 h at room temperature. Pyridine (dried by distillation from calcium hydride onto freshly activated molecular sieves; 5 mL) was syringed into the flask under nitrogen and the mixture was heated with stirring for 5 min in an oil bath at 60–64°C. Gas was evolved and the mixture darkened. The mixture was then cooled in an ice bath and slowly added to ice-cold 2 *N* nitric acid (40 mL). The solution was extracted with dichloromethane (5 × 12 mL) and the combined extracts were washed with 2 *N* nitric acid (5 mL) and saturated brine (5 mL), dried, and evaporated to give an orange oil (300 mg).

The oil was chromatographed on silica gel with 10:1 hexanes – ethyl acetate to give enone **19** (92 mg, 33%), which had a distinctive, camphor-like odor; sublimation gave colorless crystals, mp 42–44°C; ir λ_{max} 5.85 μm; ^{1}H nmr: see Table 4; *m/e*: 164.1180 (M^+ 164.1201).

On further elution of the silica gel column with 2:1 hexanes – ethyl acetate two further fractions were isolated. The first (79 mg) was an oil, considered to be a mixture of **21** and **22**; ^{1}H nmr: signals (~1:1:2) at δ 4.75 (br s), 4.85 (br s), and 5.2 (br s); ^{13}C nmr: two strong signals at 133.2 (d) and 129.3 (s), and two weaker signals at 142.0 (s) and 111.9 (t) and signals at δ 208.3 (s) and 179.5 (s). The second (35 mg) was a crystalline solid, mp 170–172°C, considered to be **20**; ir λ_{max}: 3.0–3.7, 5.70 (br) μm; ^{1}H nmr: δ 2.00 (s), no vinyl proton signals; *m/e*: 268.1359 (M^+ 268.1311).

Treatment of **17**b *with bis(Triphenylphosphino)nickel Dicarbonyl. Formation of 1,8,8-Trimethylbicyclo[2.2.2]oct-5-en-2-one (***19***)*

Anhydride **17***b* (0.123 g, 0.52 mmol), bis(triphenylphosphino)nickel dicarbonyl (0.327 g, 0.51 mmol), and a small magnetic stirring bar were placed in a small two-necked flask fitted with a rubber septum and dried on a vacuum line with gentle warming from a heat gun. Diglyme (dried by distillation from sodium and stored over molecular sieves under nitrogen; 2.0 mL) was syringed into the flask under nitrogen. The mixture was boiled under reflux under nitrogen for 3 h with stirring. The diglyme was distilled from the mixture under high vacuum into a liquid nitrogen trap; additional diglyme (~3 mL) was added to the residue, and the distillation was repeated. The distillates were combined and added to water (100 mL), and the mixture was extracted with pentane (4 × 50 mL). The pentane extracts were washed repeatedly with water (5 × 100 mL) with very vigorous shaking to remove diglyme and with saturated brine (50 mL) and dried. The pentane was carefully distilled at 0.5–1.0 atm to give **19** in essentially quantitative yield. Chromatography on silica gel with 10:1 pentane – ethyl acetate yielded pure **19**, identical in spectroscopic properties with the sample prepared by lead tetraacetate oxidation of **18***b* (*vide supra*).

Treatment of **16**b *with bis(Triphenylphosphino)nickel Dicarbonyl. Formation of* o-*Methylanisole*

Treatment of anhydride **16***b* with bis(triphenylphosphino)-nickel dicarbonyl following the procedure described above for the preparation of **19** gave a crude product that was shown by ^{1}H nmr spectroscopy to contain *o*-methylanisole together with unconsumed **16***b*.

*1-Methylbicyclo[2.2.2]oct-5-ene-2-one (***1***)*

Enone **1** was prepared by treatment of anhydride **17***a* with bis(triphenylphosphino)nickel dicarbonyl, following the procedure described above for the preparation of **19**. The conversion appeared to be quantitative by ^{1}H nmr spectroscopy but, due to the volatility of **1**, the isolated yield was only 52% after chromatography; **1** was obtained as a colorless oil; ir λ_{max}: 5.86 μm; ^{1}H nmr: see Table 4; *m/e*: 136.0892 (M^+ 136.0888).

*1-Methylbicyclo[2.2.2]octan-2-one (***23***)*

Enone **1** (87 mg, 0.64 mmol) was dissolved in glacial acetic acid (5 mL) and the solution was stirred with 5% palladium on carbon (50 mg) under hydrogen (1 atm) for 3 h. The catalyst was filtered and washed with dichloromethane, and the filtrate and washings were basified by addition to a cold solution of potassium hydroxide (10 g) in water (50 mL). The mixture was extracted with dichloromethane (4 × 15 mL), and the organic phase was dried and evaporated to yield **23** (64 mg, 73%) as a colorless oil (lit. (16) mp 36–37°C, (17) 30–31°C); ir λ_{max}: 5.83 μm; ^{1}H nmr: see Table 4; *m/e*: 138.1043 (M^+ 138.1044).

*1,5,5-Trimethylbicyclo[2.2.2]octan-2-one (***24***)*

Enone **19** (100 mg, 0.61 mmol) was dissolved in glacial acetic acid (2.0 mL) and 5% palladium on carbon catalyst (50 mg) was added. The mixture was stirred overnight under hydrogen

Can. J. Chem. Downloaded from www.nrcresearchpress.com by 210.87.254.6 on 09/05/12
For personal use only.

(1 atm), although gas uptake appeared to be complete within 10 min. The catalyst was removed by filtration through Celite and washed with dichloromethane. The combined filtrate and washings were added to aqueous 5% sodium carbonate (50 mL), and the mixture was extracted with dichloromethane (4 × 12 mL). The extracts were washed with aqueous sodium carbonate (5 mL), dried, and evaporated to give **24** (90 mg, 89%) as a colorless oil with a camphor-like odour. Chromatography on silica gel with 15:1 hexanes – ethyl acetate yielded pure **24**; ir λ_{max}: 5.80 μm; ^{1}H nmr: see Table 4; *m/e*: 166.1357 (M^+ 166.1357).

Reaction of Bicyclo[2.2.2]octane-2,3-dione (27) with 0.5 Equivalent of Methyllithium. Formation of Compound 29

Bicyclo[2.2.2]octane-2,3-dione (**27**; 0.46 g, 3.3 mmol) was stirred in dry ether (40 mL) under nitrogen; the yellow crystals did not dissolve completely. A solution of methyllithium in ether (1.67 *M*) was slowly added by syringe. The yellow solution abruptly turned white when 1.0 mL (1.67 mmol) of methyllithium had been added. After standing overnight the reaction mixture was treated with a little isopropyl alcohol and then water. The aqueous phase was saturated with sodium chloride, separated, and washed with chloroform (4 × 40 mL). The combined organic solution and extracts were dried and evaporated to give oily pale yellow needles. After one recrystallization from hexanes and two from diethyl ether, **29** (0.10 g) was obtained as white needle-shaped crystals, mp 161.5–162°C (corr); ir λ_{max}: 2.96 (w), 5.78 μm; ^{1}H nmr δ 1.0–2.6 (m, ~20H), 1.33 (s, 3H), 5.30 (s, 1H); ^{13}C nmr δ: 218.8, 106.6, 104.0, 87.1, 42.9, 38.5, 36.8, 35.5, 24.5, 22.1, 22.0, 21.1, 21.0, 20.9, 20.5, 20.4, 20.2 (17 lines); *m/e*: 264.1729 ($M - CO)^+$ 264.1725). *Anal.* calcd. for $C_{17}H_{24}O_4$: C 69.84, H 8.27; found: C 69.63, H 8.28.

Reaction of Bicyclo[2.2.2]octane-2,3-dione (27) with 1.1 Equivalents of Methyllithium. Formation of 3-Hydroxy-3-methylbicyclo[2.2.2]octan-2-one (28) and Compounds 30 and 31

Dione **27** (0.559, 4.0 mmol) was treated in dry ether (50 mL) with methyllithium (4.4 mmol) and the reaction mixture was worked up as above. Three major components were identified in the crude product mixture by tlc (silica gel, 4:1 hexanes – ethyl acetate) and isolated by column chromatography: **31** (R_f 0.33; 0.11 g, 18%), **28** (R_f 0.25; 0.20 g, 32%) and **30** (R_f 0.17; 0.19 g, 28%). The relative yields of the products were found to vary.

Compound **31** was a white powder sparingly soluble in hexane. It was purified by washing with hexanes; mp 195–197°C (corr, sealed cap); ir λ_{max}: 2.85–2.95 μm; ^{1}H nmr δ: 1.2–2.0 (m, ~20H), 1.4 (s, 6H); ^{13}C nmr δ: 111.4 (s), 104.8 (s), 86.2 (s), 76.4 (s), 40.1 (d), 37.9 (d), 37.3 (d), 36.3 (d) 25.3 (q), 23.0 (t), 22.5 (t), 21.6, 21.1, 21.0, 20.8, 20.3;[7] *m/e*: 308.1992 (M^+ 308.1988). *Anal.* calcd. for $C_{18}H_{28}O_4$: C 70.10, H 9.15; found: C 70.11, H 9.08.

Compound **28** was recrystallized from hexanes; mp 116–121°C; ir λ_{max}: 2.84 (w), 5.78 μm; ^{1}H nmr δ: 1.2–2.1 (m, 9H), 1.33 (s, 3H), 2.2–2.4 (m, 1H), 2.7 (br s, 1H, exchanges with D_2O); ^{13}C nmr δ: 220.7 (s), 75.6 (s), 41.8 (d), 38.2 (d), 25.4 (t), 23.3 (q), 22.1 (t), 21.9 (t), 20.6 (t); *m/e*: 154.1033 (M^+ 154.0993). *Anal.* calcd. for $C_9H_{14}O_2$: C 70.10, H 9.15; found: C 69.98, H 9.13.

Compound **30** was recrystallized from hexanes; mp 190–192°C; ir λ_{max}: 2.88, 2.95 μm; ^{1}H nmr δ: 1.27 (s, 6H), 1.3–1.8 (m, 8H), 1.8–2.1 (m, 2H), 2.8 (br s, 2H, exchanges with D_2O); ^{13}C nmr δ: 73.4 (s), 38.8 (d), 24.7 (q), 22.8 (t), 20.7 (t); *m/e*: 170.1313 (M^+ 170.1307). *Anal.* calcd. for $C_{10}H_{18}O_2$: C 70.55, H 10.66; found: C 70.49, H 10.63.

Treatment of 35 and 36 with bis(Triphenylphosphino)nickel Dicarbonyl. Formation of Compounds 32 and 33

Treatment of the anhydrides **35** and **36** (19) with bis(triphenylphosphino)nickel dicarbonyl following the procedure described above for the preparation of **19** gave mixtures whose ^{1}H nmr spectra indicated the presence of **32** and **33**, respectively. However, the very low yields (5–10%) of these products and difficulties in their purification precluded their full characterization. The formation of **33** was established by comparison of the ^{1}H nmr spectrum of the crude product with that of **33** obtained by treatment of **37** with lead tetraacetate (*vide infra*). Compound **32** was isolated by preparative tlc (silica, dichloromethane) as an amorphous solid (R_f 0.2–0.4); ^{1}H nmr δ: 1.58 (s, 6H), 1.96 (s, 3H), 4.7 (m, 1H), 6.08 (dd, J = 6.5, 2 Hz, 2H), 6.35 (t, J = 6.5 Hz, 1H), 6.42 (t, J = 6.5 Hz, 1H). A second product isolated from the chromatogram (R_f 0.5–0.7) was shown to be 2,6-dimethylphenol by ^{1}H and ^{13}C nmr spectroscopic comparison with an authentic sample.

Lead Tetraacetate Oxidation of 37. Formation of 3-endo-Acetoxy-1,3-exo-dimethylbicyclo[2.2.2]oct-5-en-2-one (33) and Compounds 38 and 39

Anhydride **36** (1.20 g) was dissolved in tetrahydrofuran (20 mL), water (20 mL) was added, and the mixture was stirred overnight. Evaporation of the clear solution yielded crude **37** as a white solid; ir λ_{max}: 2.9–4.2, 5.76 (br) μm; ^{1}H nmr δ: 1.13 (s, 3H), 1.65 (s, 3H), 2.10 (s, 3H).

Crude diacid **37** (1.09 g, 3.7 mmol) was dried in vacuum and dissolved under nitrogen in pyridine that had been dried by distillation from barium oxide and saturated with oxygen. Lead tetraacetate (recrystallized from glacial acetic acid and dried in vacuum; 2.42 g, 5.5 mmol) was added to the solution, which became warm. When the nitrogen stream from the reaction flask was bubbled through fresh limewater, the latter rapidly turned milky. The reaction mixture was heated for 8 min in an oil bath at 67 ± 2°C, cooled, and slowly added dropwise with stirring to dilute nitric acid at 6–7°C (ice bath). The clear yellow solution was extracted with ether and the organic phase was washed with aqueous sodium bicarbonate followed by saturated brine, and dried. Evaporation yielded an oil from which compounds **33** and **38** were isolated by column chromatography with 4:1 hexanes – ethyl acetate on silica gel (50 g).

The first compound eluted (R_f 0.45) was **33** (42 mg, 5.5%), which was obtained as needles; ^{1}H nmr: see Table 5; *m/e*: 166.0997 ($(M - C_2H_2O)^+$ 166.0994).

The major fraction (R_f 0.18) from the chromatogram was compound **38**, which was obtained as an oil that could not be crystallized; ir λ_{max}: 5.62–5.78 μm; ^{1}H nmr δ: 1.1–2.1 (m, 4H), 1.53 (s, 6H), 2.04 (s, 3H), 3.1–3.4 (m, 3H) (in C_6D_6 the 6H singlet at δ 1.53 was resolved into two 3H singlets); ^{13}C nmr (C_6D_6) δ: 206.3 (s), 174.3 (s), 169.3 (s), 86.7 (s), 86.0 (s), 60.2 (d), 47.9 (d), 43.2 (d), 30.8 (t), 24.0 (q), 22.2 (t), 20.8 (q), 16.2 (q); *m/e*: 252 (M^+ 252).

After storage for 6 months at room temperature, the oil **38** had changed into a new, solid product. Recrystallization of this solid from dichloromethane yielded a crystalline compound **39**. The same substance had been isolated as a minor product (R_f 0.09) in the chromatographic separation of the original crude product from the lead tetraacetate reaction. Compound **39** had mp 167–168°C; ir λ_{max}: 2.87 (w), 5.62, 5.73 μm; ^{1}H nmr δ: 1.2–2.1 (m, 4H), 1.38 (s, 3H), 1.52 (s, 3H), 2.08 (s, 1H, absent after D_2O treatment), 2.5–2.8 (m, 1H), 3.17 (dt, J = 5.5, 1.8 Hz, 1H), 3.58 (t, J = 5.5 Hz, 1H); ^{13}C nmr δ: 210.9, 175.8 (or 176.8),[8] 86.5,

[7]The sample was not sufficiently soluble in $CDCl_3$ to determine the multiplicities of the signals in the δ 21.6–20.3 range; in $CDCl_3$ – pyridine-d_5 one of these signals is a quartet (δ 21.0) and the others are triplets. Two of the signals in the δ 20–23 range must each correspond to two different carbon atoms, since only 16 signals were observed.

[8]Owing to the low solubility of **39**, this signal could not be identified unambiguously.

78.9, 59.8, 47.6, 44.3, 30.8, 24.3, 21.9, 18.2; *m/e*: 210.0884 (M^+ 210.0892). *Anal.* calcd. for $C_{11}H_{14}O_4$: C 62.85, H 6.71; found: C 62.74, H 6.60.

3-Acetoxy-1,3-dimethylbicyclo[2.2.2]oct-2-anone (34)

Enone **33** was hydrogenated in glacial acetic acid over 5% Pd/C at 1 atm and 20°C for 43 h. The catalyst was filtered. The filtrate was evaporated, and the residue was dissolved in dichloromethane, washed with aqueous sodium bicarbonate, and dried. Evaporation yielded an oil whose ^1H nmr spectrum showed no vinyl proton signals. The crude product was chromatographed on silica gel with 5:1 hexanes–ethyl acetate to give **34** as an oil; ^1H nmr: see Table 5; *m/e*: 168.1142 ($(M - C_2H_2O)^+$ 168.1150).

Acknowledgement

We thank the Natural Sciences and Engineering Research Council of Canada for support of this work.

1. P. YATES, H. AUKSI, J. A. GOSBEE, G. E. LANGFORD, and F. N. MACLACHLAN. Org. Magn. Reson. **14**, 153 (1980); G. E. LANGFORD, H. AUKSI, J. A. GOSBEE, F. N. MACLACHLAN, and P. YATES. Tetrahedron. In press.
2. P. YATES and H. AUKSI. Can. J. Chem. **57**, 2853 (1979).
3. P. YATES. J. Photochem. **5**, 91 (1976).
4. I. ALFARO, W. ASHTON, K. L. RABONE, and N. A. J. ROGERS. Tetrahedron, **30**, 559 (1974); K. L. RABONE and N. A. J. ROGERS. Chem. Ind. London, 1838 (1965).
5. R. P. GREGSON and R. N. MIRRINGTON. Aust. J. Chem. **29**, 2037 (1976); J. Chem. Soc. Chem. Commun. 598 (1973).
6. H. WOLLWEBER. Diels–Alder reaktion. Georg Thieme Verlag, Stuttgart. 1972. p. 33.
7. A. J. BIRCH and P. HEXTALL. Aust. J. Chem. **8**, 96 (1955).
8. I. ALFARO, W. ASHTON, L. D. MCMANUS, R. C. NEWSTEAD, K. L. RABONE, N. A. J. ROGERS, and W. KERNICK. Tetrahedron, **26**, 201 (1970); A. J. BIRCH and K. P. DASTAR. J. Chem. Soc. Perkin Trans. I, 1650 (1973).
9. M. BARFIELD and B. CHAKRABARTI. Chem. Rev. **69**, 757 (1969).
10. S. GERIBALDI, G. TORRI, and M. AZZARO. Bull. Soc. Chim. Fr. 2521 (1973).
11. L. A. PAQUETTE, G. KLEIN, and C. W. DOECKE. J. Am. Chem. Soc. **100**, 1595 (1978).
12. K. ALDER and H. F. RICKERT. Justus Liebigs Chem. Ann. **524**, 180 (1936); Chem. Ber. **70**, 1354 (1937).
13. K. M. PATEL and W. REUSCH. Synth. Commun. **5**, 27 (1975).
14. S. GERIBALDI, G. TORRI, and M. AZZARO. Bull. Soc. Chim. Fr. 2836 (1973).
15. B. M. TROST and F. CHEN. Tetrahedron Lett. 2603 (1971).
16. W. KRAUS, C. CHASSIN, and R. CHASSIN. Tetrahedron, **25**, 3681 (1969).
17. H. FELKIN and C. LION. Tetrahedron, **27**, 1375 (1971).
18. R. J. CRAWFORD. Ph.D. Thesis, University of Toronto, Toronto, Ont. 1965.
19. H. AUKSI. Ph.D. Thesis, University of Toronto, Toronto, Ont. 1978.
20. J. C. SHEEHAN, R. C. O'NEILL, and M. A. WHITE. J. Am. Chem. Soc. **72**, 3376 (1950); W. H. URRY, D. J. TRECKER, and D. A. WINEY. Tetrahedron Lett. 609 (1962).
21. R. A. SHELDON and J. K. KOCHI. Org. React. **19**, 279 (1972).
22. H. H. HODGSON and J. NIXON. J. Chem. Soc. 2166 (1930).
23. A. J. BIRCH. J. Chem. Soc. 1551 (1950).
24. D. G. DAVIES and P. HODGE. J. Chem. Soc. C, 3158 (1971).
25. R. L. WASSON and H. O. HOUSE. Org. Syn. Coll. Vol. 4, 552 (1963).

Can. J. Chem. Downloaded from www.nrcresearchpress.com by 210.87.254.6 on 09/05/12
For personal use only.

Betylates. 1. Synthesis and reactions of an isolable [0]betylate, *N,N*-dimethyl-*N*-(phenoxysulfonyl)methanaminium fluorosulfate[1]

JAMES FREDERICK KING AND TERESA MEE-LING LEE

Department of Chemistry, University of Western Ontario, London, Ont., Canada N6A 5B7

Received July 21, 1980

This paper is dedicated to Prof. Raymond U. Lemieux on the occasion of his 60th birthday

JAMES FREDERICK KING and TERESA MEE-LING LEE. Can. J. Chem. **59**, 356 (1981).

Phenyl [0]betylate fluorosulfate (**2**), the first example of a "[0]betylate" (trialkylammoniosulfate ester), has been prepared by methylation of phenyl *N,N*-dimethylsulfamate with methyl fluorosulfate. Nucleophiles react with **2** either by attack on the sulfur or methyl carbon atoms, but with no sign of any products derived from benzyne or the phenyl cation. A synthesis of enol *N,N*-dimethylsulfamates has been devised using a reagent, $Me_2NSO_2\overset{+}{N}Me_3\ FSO_3^-$, prepared from tetramethylsulfamide and methyl fluorosulfate, but no satisfactory method was found for converting the sulfamic ester to the [0]betylate. Evidence is presented that phenyl chlorosulfate reacts with trimethylamine to give the phenyl [0]betylate which then undergoes further reaction.

JAMES FREDERICK KING et TERESA MEE-LING LEE. Can. J. Chem. **59**, 356 (1981).

On a préparé le fluorosulfate de [0]bétylate de phényle (**2**) le premier exemple d'un "[0]bétylate" (ester de trialkylammoniosulfate) par la méthylation du *N,N*-diméthylsulfamate de phényle à l'aide du fluorosulfate de méthyle. Les nucléophiles réagissent avec le composé **2** par attaque sur les atomes de soufre ou de carbone du méthyle; on n'a toutefois isolé aucun composé pouvant provenir du benzyne ou du cation phényle. On a mis au point une synthèse de *N,N*-diméthylsulfamates d'énol en utilisant le réactif $Me_2NSO_2\overset{+}{N}Me_3\ FSO_3^-$, préparé à partir de la tétraméthylsulfamide et du fluorosulfate de méthyle; on n'a toutefois pas trouvé de méthode satisfaisante permettant de transformer l'ester sulfamique en [0]bétylate. On rapporte des données indiquant que le chlorosulfate de phényle réagit avec la triéthylamine pour conduire au [0]bétylate de phényle qui subit alors d'autres réactions.

[Traduit par le journal]

Introduction

We have recently pointed to the synthetic utility of "betylates", i.e. esters of the general formula $R_3\overset{+}{N}(CH_2)_nSO_2OR'X^-$, especially those in which $n = 2$ or 3, which we refer to as [2]- or [3]betylates (1–3).[2] As an extension of this work it was natural to consider the properties to be expected in the lowest member of this series, the [0]betylates or trialkylammoniosulfates, $R_3\overset{+}{N}SO_2OR'X^-$. The direct attachment to the sulfonyl group of a function as electron withdrawing as a trialkylammonio group would be expected to lead to a total grouping $R_3\overset{+}{N}SO_2O$ with very high nucleofugality[3] indeed. One difficulty with the synthesis of a highly reactive functional group is that many species containing the grouping may be too short-lived for isolation and characterization. Because phenyl derivatives are commonly the most readily obtained of the isolable compounds containing a powerfully nucleofugal group, we chose to explore first the preparation of a phenyl [0]betylate salt.

Accordingly this paper describes the preparation, characterization, and some reactions of the first [0]betylate or ammoniosulfate ester, *N,N,*-dimethyl-*N*-(phenoxysulfonyl)methanaminium fluorosulfate (**2**). The accompanying paper reports analogous experiments aimed at providing *alkyl* [0]betylates; as is described there, these reactions gave substitution, elimination, or rearrangement products derived in all likelihood from highly reactive alkyl [0]betylate intermediates.[4]

Results and Discussion

A Stable [0]Betylate, N,N-*Dimethyl*-N-*(phenoxysulfonyl)methanaminium Fluorosulfate*

The synthesis of the first isolated and characterized [0]betylate was achieved very simply. Recalling that sulfonamides react with powerful alkylating reagents to form sulfonylammonium salts (6–8), we treated phenyl *N,N*-dimethylsulfamate (**1**) with an excess of neat methyl fluorosulfate.

[1]Part 22 in the series Organic Sulfur Mechanisms. Part 21: Can. J. Chem. **57**, 3278 (1979).

[2]We have proposed the trivial name "betylates" (which originates from their formation of betaines by simple nucleophilic substitution) to encompass those compounds which in current Chemical Abstracts usage might be called ω-alkoxysulfonyl-*N,N,N*-trialkyl-1-alkanaminium (or ω-aryloxysulfonyl-*N,N,N*-trialkyl-1-alkanaminium) salts and *N*-alkoxysulfonyl-*N,N*-dimethylmethanaminium (or *N*-aryloxysulfonyl-*N,N*-dimethylmethanaminium) salts. The name betylate, with or without a numerical descriptor, has the advantage of very simply denoting a class of structurally similar species in a manner easily conveyed in both spoken and written form. It is neither suited to be nor intended as a formal substitute for official nomenclature in naming individual chemical species.

[3]In this and the following paper we use "nucleofuge" as a synonym for the more familiar "leaving group", along with "nucleofugal" and "nucleofugality" as the most felicitous derived forms (4).

[4]A preliminary account of both aspects of this work has appeared elsewhere (5).

0008-4042/81/020356-06$01.00/0

©1981 National Research Council of Canada/Conseil national de recherches du Canada

Can. J. Chem. Downloaded from www.nrcresearchpress.com by 210.87.254.42 on 09/05/12
For personal use only.

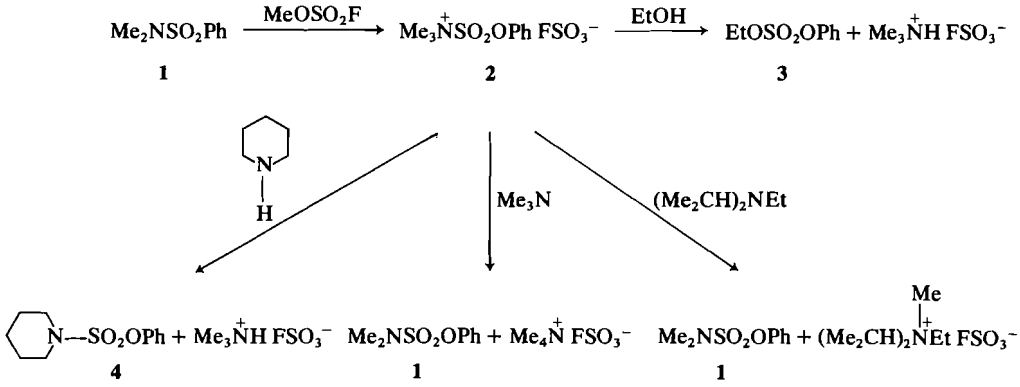

SCHEME 1

Reaction for 18 h at 50°C gave an 88% yield of the [0]betylate (**2**) as a white crystalline solid which gave correct element analyses. The proton nmr spectrum showed only a methyl singlet at 3.70 (9H) and the aromatic protons at 7.56 ppm (5H). Strong bands at 1445 and 1210 cm^{-1} were found in the infrared spectrum, as expected for a sulfonyl group flanked by strongly electron withdrawing groups (9).

The further reactions in Scheme 1 serve both to confirm the assigned structure and to illustrate some of the reactions of the new functional group. Displacement at sulfur occurs very readily at room temperature with either alcohol or piperidine, forming trimethylammonium ion and, respectively, ethyl phenyl sulfate (**3**) and the sulfamic ester **4**.

Simple displacement at sulfur of trimethylamine by trimethylamine must of course simply give back **2**, and so reaction with this amine was tried with the possibility in mind that we might see a different, and more interesting, reaction course such as cleavage of the Ph—O bond, possibly with formation of benzyne. What we observed, however, was a rapid, slightly exothermic methyl transfer giving **1** and tetramethylammonium fluorosulfate. Use of hindered amines did not help. Diisopropylethylamine reacted more slowly than trimethylamine, but by essentially the same route, to give **1** and the quaternary ammonium salt. 2,6-Di-*tert*-butylpyridine probably did not react directly with **2** at all; the reaction mixture after one week at 60°C appeared to consist, in addition to unreacted **2**, of **1** and the tetramethylammonium cation, suggesting that the products were formed via slow hydrolysis followed by reaction of the trimethylamine as above. Other workers have encountered a similar failure to detect either phenyl cations or benzyne with so-called "super sulfonate" esters (10).

Preparation of Enol N,N-*Dimethylsulfamates and Attempted Formation of the Corresponding [0]Betylates*

Enol trifluoromethanesulfonates (triflates) are well known as useful precursors of vinyl cations (11), although ionization even of such a strongly nucleofugal group as triflate can be slow. It therefore seemed worthwhile to determine if [0]betylates could be used to form vinyl cations, especially those not readily obtained in other ways. Difficulties, unfortunately, arose.

The first problem appeared in the preparation of enol *N,N*-dimethylsulfamate esters. Whereas the procedure of Binkley and Degering (12), involving reaction of a sodium alkoxide or aryloxide with *N,N*-dimethylsulfamoyl chloride, had worked well for aryl and alkyl *N,N*-dimethylsulfamates (see Table 1 and the accompanying paper), the corresponding reaction of sodium or lithium cyclohexenoxide, for example, gave no sign of the sulfamate ester. The only identified product from this reaction was tetramethylsulfamide (**5**). Since sulfamoyl chlorides appear to show the usual tendency for the chlorosulfonyl group to undergo reduction (13), and since enolates react with arenesulfonyl chlorides to give the α-chlorinated carbonyl compound and the arenesulfinate anion (14), it seems likely that alkali cyclohexenoxides attacked the chlorine rather than the sulfur atom of the sulfamoyl chloride to form 2-chlorocyclohexanone and the sulfinimidate anion, $Me_2NSO_2^-$, which then reacted with more sulfamoyl chloride to give tetramethylsulfamide (**5**) and sulfur dioxide.

The behaviour of the chlorosulfonyl group is readily systematized in hard–soft acid–base terms (15), i.e. "hard" nucleophiles attack preferentially at the sulfonyl sulfur, the "hard" electrophile, whereas "soft" nucleophiles attack at chlorine, the

Can. J. Chem. Downloaded from www.nrcresearchpress.com by 210.87.254.42 on 09/05/12
For personal use only.

Can. J. Chem. Downloaded from www.nrcresearchpress.com by 210.87.254.42 on 09/05/12
For personal use only.

TABLE 1. *N,N*-Dimethylsulfamic esters and amides of general structure Me_2NSO_2Z

	Z	Boiling and/or melting point (°C); yield	Spectra		
			^{1}H nmr (in ppm from Me_4Si)	^{13}C nmr (in ppm from Me_4Si)	Infrared (in cm^{-1}, major peaks only)[a]
Esters	OC_6H_5 (1)	bp 78–79/0.4 Torr; 93%	2.91(s, 6H), 7.2–7.4(m, 5H)	38.7(CH_3), 121.8(CH), 126.8(CH), 129.8(CH), 150.3(C)	1490, 1375, 1200, 1170, 1150, 975, 860, 785, 750, 690
	OC_6H_4-*p*-NO_2	mp 124–127; 78%	3.02(s, 6H), 7.42(d, 2H, J = 9 Hz), 8.25(d, 2H)	38.8(CH_3), 122.1(CH), 125.6(CH), 145.8(C), 155.0(C)	1525, 1485, 1380, 1350, 1180, 1150, 975, 865, 840 ($CHCl_3$)
	(8)	bp 80–83/0.6 Torr; 75%	0.9–1.8(m, 4H), 2.0–2.8(m, 4H), 2.93(s, 6H), 5.65(m, 1H)	[b]	1360, 1170, 1085, 960, 860, 800, 750
	OCH=C(CH_3)$_2$ (7)	bp 72–74/2 Torr; 59%	1.65(d, 3H, J = 2 Hz), 1.73(d, 3H, J = 2 Hz) 2.92(s, 6H), 6.26(septet, 1H)	15.4(CH_3), 19.3(CH_3), 38.6(CH_3), 122.7(C), 130.5(CH)	1375, 1180, 1095, 970, 800
Amides	NMe_2	mp 73; 73%	2.82(s)[c]	[b]	1330, 1150, 955, ($CHCl_3$)
		bp 83–87/0.6 Torr; mp 45–48; 63%	2.84(s, 6H), 7.08(br s, 1H) 7.21(br s, 1H), 7.81(br s, 1H)	[b]	1460, 1385, 1175, 1145, 1050, 960, 720

[a]Determined using neat liquid except where the solvent is indicated.
[b]^{13}C spectrum not determined.
[c]Determined on the Varian T-60 instrument.

"soft" electrophile. What is therefore required in the present instance is a reagent Me_2NSO_2Z in which Z is a good nucleofuge but a poor electrophile (especially not "soft"), so that the preferred reaction would then be simply the reaction of the "hard" oxygen atom of the enolate with the "hard" sulfur atom. Such a reagent was found in *N,N*-dimethyl-*N*-dimethylsulfamoylmethanaminium fluorosulfate (**6**), which was readily prepared by reaction of tetramethylsulfamide (**5**) with methyl fluorosulfate. Reaction of **6** with the appropriate lithium enolates gave the enol sulfamic esters **7** and **8** (see Table 1). We have not explored the generality of the reaction nor made any serious attempt to optimize yields, but the procedure appears to provide a serviceable route to enol (and presumably other) dialkylsulfamate esters. The method provides an illustration of the usefulness of the strongly nucleofugal properties of a trialkylammonio group when attached to sulfonyl sulfur, already encountered above in the reactions of **2** (see Scheme 1).

We did not, however, succeed in making the [0]betylates from the enol sulfamates. The products from reaction with methyl fluorosulfate were typically dark purple-brown mixtures from which we isolate nothing except (from **7**) a small amount of the betaine, $Me_3\overset{+}{N}SO_3^-$; suggesting formation of perhaps a small amount of the [0]betylate; further work is clearly in order.

Before we had found the method for making enol sulfamates via **6**, we examined other possible candidates for the reagent Me_2NSO_2Z specified above. We readily obtained compounds in which Z was *p*-nitrophenyl and 1-imidazolyl, respectively, but both proved unreactive to lithium cyclohexenoxide. An attempt at making 2,4-dinitrophenyl *N,N*-dimethylsulfamate by reaction of sodium 2,4-dinitrophenoxide with *N,N*-dimethylsulfamoyl chloride gave no sign of the desired ester.

Other Possible Routes to [0]Betylates

If we examine the general structural formula of the [0]betylate cation below, we can readily see five potential routes to its synthesis, labelled (a) to (e), according to which bond is formed in the final step.

Can. J. Chem. Downloaded from www.nrcresearchpress.com by 210.87.254.42 on 09/05/12
For personal use only.

Route (a), i.e. final formation of the bond labelled (a), is of course the method used in this study. Alkylation with reagents other than methyl fluorosulfate is an obvious variation. Methyl triflate was tried and found to give exactly analogous results with phenyl *N*,*N*-dimethylsulfamate; an nmr experiment showed the peaks expected of the triflate salt of **2**.

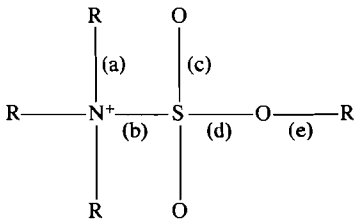

Route (b) is embodied in a suggestion by Charalambous *et al.* (16) to account for formation of alkyl chlorides on treatment of alkyl chlorosulfates with pyridine or triethylamine.

$$ROSO_2Cl + C_5H_5N \rightarrow [ROSO_2\overset{+}{N}C_5H_5] + Cl^- \rightarrow RCl + C_5H_5\overset{+}{N}SO_3^-$$

To test this idea and explore the synthetic value of this route, we treated phenyl chlorosulfate with excess trimethylamine and obtained phenyl *N*,*N*-dimethylsulfamate (**1**) and tetramethylammonium chloride, precisely what would be expected from initial formation of the [0]betylate (**2**) followed by its rapid reaction with trimethylamine as shown in Scheme 1. Use of a limited amount of the amine gave the same products plus unreacted starting material, with no sign of the intermediate (**2**) visible in the nmr spectrum. We had already observed that **2** on reaction with tetraethylammonium chloride for 1 min at room temperature gave a roughly 2:1 mixture of phenyl chlorosulfate and phenyl *N*,*N*-dimethylsulfamate (**1**), the latter, as before, being derived from reaction of **2** with trimethylamine, the coproduct of the initial reaction. It is evident that both displacement of chloride ion from phenyl chlorosulfate by trimethylamine to form **2**, and the reverse process, are rapid reactions. In the hope of obtaining direct spectroscopic evidence for formation of **2**, we treated phenyl chlorosulfate with a mixture of trimethylamine and silver hexafluoroantimonate. A limited amount of the amine gave a product showing mostly unreacted phenyl chlorosulfate in the nmr spectrum, but characteristic signals due to **2** at 3.70 and 7.56 ppm (in roughly 10% yield) were clearly in evidence. In another experiment with more trimethylamine the proportion of **2** did not appear to increase but rather the starting material diminished and peaks showing the presence of **1** and tetramethylammonium cation appeared. Route (b) is probably of limited use as a procedure for isolating [0]betylates, but these experiments serve to confirm the original suggestion of Charalambous *et al.* (16) that reaction of chlorosulfate esters with tertiary amines proceeds by way of a transitory [0]betylate. The reaction may well prove of value as an easy method of making a highly reactive, short-lived [0]betylate in the presence of chloride ion (or, with the use of silver salts, in the presence of any of a considerable choice of other ions as well).

Charalambous *et al.* (16) used pyridine for most of these experiments and it might be momentarily surprising to note that we saw little or no reaction in an nmr experiment with phenyl chlorosulfate and pyridine in carbon tetrachloride. This observation does not preclude reaction of pyridine with phenyl chlorosulfate, but does require that if such reaction occurs, the equilibrium constant must strongly favour the starting materials. The speed of the reaction of phenyl [0]betylates (e.g. **2**) with chloride ion, as discussed above, is entirely consistent with this conclusion.

The other routes indicated in the above structure need only brief comment. Route (c) we have not tried at all; possible precursors such as the sulfinic analogue of a [0]betylate do not appear to be readily available. Route (d) might be practicable if one could obtain a compound of the type $R_3\overset{+}{N}SO_2\overset{+}{N}R_3$, but in our preparation of the monocation **6** we saw no sign of further alkylation to the dication. One version of route (e) would be alkylation of the betaine $Me_3\overset{+}{N}SO_3^-$, but it is evident that a much less nucleophilic anion than fluorosulfate or triflate is required as the counterion of the potential [0]-betylate, since the experiments in the accompanying paper clearly show that with these anions the equilibrium lies far on the side of betaine and ester rather than that of the betylate. Whether or not such reagents as trimethyloxonium fluoroborate or methyl fluoride–antimony pentafluoride would alkylate the betaine remains to be demonstrated.

It is evident that much more work is required to find all of the possible pathways to [0]betylates and to assess their merits. The present paper describes only the beginning: we have found a preparative route leading to this class of compounds and thereby demonstrated its existence by actual isolation and characterization. The accompanying paper explores the application of this route to alkyl derivatives, in which the exclusive, and very rapid, mode of reaction is C—O cleavage with formation of the betaine $Me_3\overset{+}{N}SO_3^-$, a reaction which displays the extraordinary leaving-group ability of the [0]betylate grouping.

Can. J. Chem. Downloaded from www.nrcresearchpress.com by 210.87.254.42 on 09/05/12
For personal use only.

Experimental

Infrared spectra were determined using a Beckman IR-20A instrument and NaCl cells. Routine ^{1}Hmr spectra were obtained with a Varian T-60 instrument unless otherwise indicated; ^{1}Hmr spectra of pure compounds (except where otherwise specified) and ^{13}Cmr spectra were determined using Varian XL-100 spectrometers. Mass spectra were run on a Varian MAT-311A instrument. Normal reaction work-up procedure included drying with anhydrous sodium sulfate and evaporation of the solvent under reduced pressure using a rotary evaporator. Methyl fluorosulfate, as supplied (labelled "Magic Methyl") by Aldrich Chemical Co., Milwaukee, WI, U.S.A., was distilled before use.

Phenyl N,N-*Dimethylsulfamate (1)*

Phenol (4.7 g, 50 mmol) was added to a suspension of sodium hydride (1.2 g, 50 mmol, oil-free, obtained by washing 2.4 g of the 50% suspension with hexanes) in 1,2-dimethoxyethane (50 mL). After hydrogen evolution had slowed, *N,N*-dimethylsulfamoyl chloride (12) (7.9 g, 55 mmol) was added; the temperature of the reaction mixture rose to 40–50°C. The mixture was stirred without heating overnight, and most of the solvent then removed on the rotary evaporator. The residue was worked up by extraction with a mixture of chloroform and water. The organic layer was dried and evaporated. Distillation of the crude product gave **1** (9.39, 93%); ms: M^+ calcd. 201.0459; found 201.0456; other properties are given in Table 1.

N,N-*Dimethyl*-N-*phenoxysulfonylmethanaminium Fluorosulfate (Phenyl[0]Betylate Fluorosulfate, 2)*

A solution of phenyl *N,N*-dimethylsulfamate (**1**) (2 g, 10 mmol) in methyl fluorosulfate (3 mL) was heated at 50°C for 18 h, after which time the mixture had solidified. Dry CH_2Cl_2 (20 mL) was added, the solid mass broken up, and the supernatant liquid decanted; three further washes with CH_2Cl_2 gave a white solid (2.76 g, 88%) which was dried under vacuum; mp 122–125°C; ir ν_{max} (Nujol): 1575 (m), 1445 (vs), 1280 (vs), 1210 (s), 1115 (s), 1070 (s), 910 (s), 770 (s), 705 (s), 650 (s) cm^{-1}; ^{1}Hmr δ: 7.56 (5H, broad s), 3.70 (9H, s) ppm. *Anal.* calcd. for $C_9H_{14}NO_6S_2F$: C 34.29, H 4.44, N 4.44, S 20.32; found: C 34.37, H 4.49, N 4.36, S 20.21.

Reactions of Phenyl [0]Betylate Fluorosulfate (2) with Nucleophiles

(a) Ethanol

Just enough ethanol was added to **2** (254 mg, 0.81 mmol) to give a solution, which was allowed to stand for 1 h. It was then taken up in water and extracted twice with $CHCl_3$. The organic layer was dried and the solvent evaporated. The residue after distillation (0.6 Torr, bath 110°C) gave **3** as a colorless oil (100 mg, 61%); ir ν_{max}: 1595 (m), 1400 (vs), 1210 (vs), 1000 (s) cm^{-1}; ^{1}Hmr δ: 7.16 (5H, m) 4.38 (2H, q, J = 7 Hz), 1.40 (3H, t) ppm; ms *m/e*: calcd. M^+ 202.0300; found 202.0297.

(b) Piperidine

Piperidine (85 mg, 1 mmol) was added to a solution of **2** (315 mg, 1 mmol) in acetonitrile (4 mL). A mildly exothermic reaction ensued and the mixture turned yellow-green; after ½ h the mixture was diluted with $CHCl_3$ and the solution extracted six times with water. The $CHCl_3$ layer was dried and the solvent removed; the residue (209 mg) was distilled (0.6 Torr, bath 125°C) to give **4** as a colorless oil which subsequently solidified, mp 57–59°C; ir ν_{max}: 1585 (m), 1380 (vs), 1190 (vs), 950 (s) cm^{-1}; ^{1}Hmr δ: 7.2 (5H, m), 3.2–3.4 (4H, br t), 1.5–1.7 (6H br s) ppm; ms *m/e*: calcd. M^+ 241.0772; found 241.0772.

The combined aqueous layers were made strongly basic with NaOH and nitrogen passed over the solution and into a solution of picric acid in absolute ethanol. The yellow precipitate was collected and washed with ether; yield 109 mg (38%) melting at 212–216°C; reported mp for trimethylammonium picrate 216°C (17).

(c) Trimethylamine

Excess gaseous trimethylamine was added (from a syringe) to **2** (88 mg, 28 mmol) dissolved in acetonitrile-d_3 (0.5 mL); mild evolution of heat and formation of a precipitate were observed as the amine was added. The liquid phase was decanted, diluted with water, and extracted twice with $CHCl_3$. The organic layer was dried and concentrated by evaporation; dry ether was added and the ethereal solution decanted from insoluble material and evaporated. The nmr and ir spectra of the residue (39 mg) were identical to those of an authentic sample of phenyl *N,N*-dimethylsulfamate; yield 70%.

The precipitate formed in the reaction was washed with dry ether and dried; the nmr spectrum (D_2O) was identical to that of an authentic specimen (mp > 360°C) of tetramethylammonium fluorosulfate prepared by reaction of trimethylamine with methylfluorosulfate.

(d) N,N-*Diisopropyl*-N-*ethylamine*

N,N-Diisopropyl-*N*-ethylamine (193 mg, 1.5 mmol) and **2** (472 mg, 1.5 mmol) were dissolved in dry acetonitrile (2 mL); the mixture gradually turned brown. After one day at room temperature the mixture was diluted with water and extracted twice with $CHCl_3$. Evaporation of the solvent gave an oil (245 mg, 81%) which was distilled (139 mg, 46%) and which showed nmr and ir spectra identical to those of authentic phenyl *N,N*-dimethylsulfamate (**1**).

The aqueous layer was evaporated to dryness and the residue taken up in isopropyl alcohol and the solution filtered. Evaporation of the filtrate gave a white solid (163 mg, 45%), mp 289–292°C (dec.); the nmr spectrum was identical with that of an authentic specimen of *N,N*-diisopropyl-*N*-ethyl-*N*-methylammonium fluorosulfate (mp 292°C with decomposition) prepared by reaction of the amine with methyl fluorosulfate.

(e) 2,6-Di-tert-*butylpyridine*

The amine (290 mg, 1.5 mmol) and **2** (478 mg, 1.5 mmol) in CD_3CN (1.5 mL) appeared from nmr spectra to react only very slowly. After one week about 55% of the initial amount of **2** was consumed. Peaks at 7.2 and 2.9 ppm in the nmr were assigned to phenyl *N,N*-dimethylsulfamate (**1**) (and confirmed by addition of authentic **1**), and a peak at 3.1 ppm to tetramethylammonium fluorosulfate; a strong peak at 1.5 ppm, presumably due to either di-*tert*-butyl pyridinium or di-*tert*-butyl-*N*-methylpyridinium cation, was also present.

(f) Tetraethylammonium Chloride

To a solution of **2** (139 mg, 0.44 mmol) in dry acetonitrile (1 mL), carefully dried tetraethylammonium chloride (241 mg, 1.45 mmol) also in dry acetonitrile (0.5 mL) was added. After 1 min the mixture was diluted with water and the solution extracted twice with $CHCl_3$. The solvent was evaporated to yield a clear liquid (64 mg), shown by peaks at 7.3, 7.2, and 3.9 ppm to consist almost entirely of a roughly 2:1 mixture of phenyl chlorosulfate and phenyl *N,N*-dimethylsulfamate.

N,N-*Dimethyl*-N-*Dimethylsulfamoylmethanaminium Fluorosulfate (6)*

Tetramethylsulfamide (**5**) (0.4 g, 2.6 mmol), prepared from dimethylamine and *N,N*-dimethylsulfamoyl chloride as described by Behrend (18), was dissolved in dry CH_2Cl_2 and allowed to react with methyl fluorosulfate (0.5 mL, 6.2 mmol) for 1 day, whereupon dry CH_2Cl_2 (20 mL) was added and the crystalline product collected by filtration, washed twice with CH_2Cl_2, and dried under reduced pressure. The product (5.2 g, 74%) was a white solid, mp 163–164°C; ^{1}Hmr δ: 3.26 (6H, s), 3.30 (9H, s). *Anal.* calcd. for $C_5H_{15}FN_2O_5S_2$: C 22.55, H 5.63, N 10.52, S 24.06; found: C 22.68, H 5.67, N 10.39, S 23.98.

2-Methylpropenyl N,N-*Dimethylsulfamate (7)*

Lithium 2-methylpropenoxide was generated in DME from methyllithium (15 mmol) and trimethylsilyl 2-methylpropenyl

Can. J. Chem. Downloaded from www.nrcresearchpress.com by 210.87.254.42 on 09/05/12
For personal use only.

ether (2.16 g, 15 mmol) as described by Stang *et al.* (19). To the solution of the enolate at −70°C, **6** (1.33 g, 5 mmol) was added in portions. The mixture was then allowed to warm to room temperature and stirred overnight. The volatile components were removed on the rotary evaporator, water was added to the residue, and the mixture extracted twice with $CHCl_3$. The organic extract was dried and the solvent evaporated and the residue distilled to give a colourless liquid (0.53 g, 59%) which solidified to needles on cooling; ms: M^+ calcd. 179.0616; found 179.0615; other properties are listed in Table 1.

1-Cyclohexenyl N,N-*Dimethylsulfamate (8)*

Redistilled cyclohexanone (1.67 g, 17 mmol) and oil-free sodium hydride (20 mmol, from the 50% suspension in mineral oil, 1 g) in dry 1,2-dimethoxyethane (DME) (30 mL) were heated under N_2 at 70°C for 3 h. The reaction mixture was cooled in ice and **6** (4.79 g, 18 mmol) added in portions via a solid-addition tube. After 1 h at room temperature water was added and the mixture extracted with three portions of $CHCl_3$. The combined $CHCl_3$ extracts were dried and the solvent evaporated to give an orange oil which was distilled to give **8** as a colourless liquid (2.63 g, 75%) with the properties summarized in Table 1.

p-*Nitrophenyl* N,N-*Dimethylsulfamate*

p-Nitrophenol (7.0 g, 50 mmol) was added in portions to a suspension of oil-free sodium hydride (50 mmol, from 2.4 g of 50% suspension in mineral oil) in DME. After hydrogen evolution had slowed, *N,N*-dimethylsulfamoyl chloride (6.46 g, 45 mmol) was added to the bright orange suspension. The mixture was heated at 70°C overnight and then cooled and worked up by distribution in water–benzene. The benzene layer was washed with dilute NaOH and water and dried, and the solvent evaporated to give a light-yellow solid. On recrystallization from benzene–hexanes this yielded a very pale yellow solid (8.6 g, 78% yield), mp 124–127°C; ms: M^+ calcd. 246.0310; found 246.0313; other properties are recorded in Table 1.

Dimethylsulfamoyl-1-imidazole

N,N-Dimethylsulfamoyl chloride (4.3 g, 30 mmol) and imidazole (4.1 g, 60 mmol) in $CHCl_3$ (50 mL) were allowed to react at 25°C for 30 min. The mixture was then taken up in water and extracted with benzene. The organic layer was washed with water, dried, and the solvent evaporated leaving a colourless liquid, which on distillation gave a solid (mp 45–48°C, 3.3 g, 63%); ms: M^+ calcd. 175.0415; found 175.0415; other properties are listed in Table 1.

Reaction of Phenyl Chlorosulfate with Trimethylamine

To a solution of phenyl chlorosulfate (216 mg, 1.1 mmol) (20) in $CDCl_3$ (0.5 mL) excess trimethylamine (80 to 90 mL vapour) was added from a syringe. After 15 min the mixture was partitioned between CCl_4 and water. The CCl_4 layer was dried and the solvent evaporated leaving a pale yellow oil (170 mg, 75%), the nmr and ir spectra of which were identical to those of authentic phenyl *N,N*-dimethylsulfamate (**1**). In a separate experiment the solid precipitate was shown to be tetramethylammonium chloride; addition of authentic tetramethylammonium fluorosulfate enhanced the nmr signal (in D_2O solution).

In another experiment silver hexafluoroantimonate (276 mg of the complex with two benzene molecules, 0.55 mmol) was dissolved in dry acetonitrile (0.3 mL) and dry trimethylamine gas (4 mL) added. Another flask containing phenyl chlorosulfate (109 mg, 0.57 mmol) in dry acetonitrile (0.2 mL) was cooled to −40°C and kept cold while the Me_3N–$AgSbF_6$ solution was added dropwise. The nmr spectrum of the solution (after it had come to room temperature) showed a singlet at 3.7 ppm characteristic of the $Me_3\overset{+}{N}SO_2OPh$ cation; addition of authentic **2** enhanced the signal. Other signals in the same spectrum corresponded to unreacted phenyl chlorosulfate, benzene, acetonitrile, and perhaps a small amount of trimethylammonium ion. In another experiment using different quantities, phenyl chlorosulfate (41 mg, 0.21 mmol), silver hexafluoroantimonate – benzene complex (119 mg, 0.24 mmol), and trimethylamine (5 mL of gas) in CH_3CN, the size of the peak at 3.7 ppm ascribed to the $Me_3\overset{+}{N}SO_2OPh$ cation was about the same but additional peaks at 3.1 and 2.9 ppm, probably due to Me_4N^+ cation and **1**, respectively, were observed; the peak at 7.5 ppm due to phenyl chlorosulfate was diminished relative to the peak at 7.35 ppm due to benzene.

Reaction of Phenyl N,N-*Dimethylsulfamate (1) with Methyl Trifluoromethanesulfonate*

The nmr spectrum of a solution of **1** in excess methyl trifluoromethanesulfonate (triflate) kept at room temperature, was observed at intervals. The reaction was characterized by replacement of the signals at 2.9 and 7.3 ppm due to **1** by peaks at 3.7 and 7.5 ascribed to phenyl [0]betylate triflate, and was about half complete in 6 h and about 95% complete after 24 h. Only trace amounts of materials other than starting materials and the [0]betylate product were visible in the nmr spectrum.

Acknowledgements

We thank Professor J. B. Stothers for the ^{13}C nmr spectra, Mrs. Heather Schroeder for the 100 MHz ^1H spectra, and Mr. Doug Hairsine for the mass spectra. This work was supported by the National Research Council of Canada.

1. J. F. KING, S. M. LOOSMORE, J. D. LOCK, and M. ASLAM. J. Am. Chem. Soc. **100**, 1637 (1978).
2. J. F. KING, M. ASLAM, and J. D. LOCK. Tetrahedron Lett. 3615 (1979).
3. J. F. KING and M. ASLAM. Synthesis, 285 (1980).
4. C. J. M. STIRLING. Acc. Chem. Res. **12**, 198 (1979).
5. J. F. KING and T. M. LEE. J. Chem. Soc. Chem. Commun. 48 (1978).
6. R. W. ALDER. Chem. Ind. London, 983 (1973).
7. T. OISHI, K. KAMATA, S. KOSUDA, and Y. BAN. J. Chem. Soc. Chem. Commun. 1148 (1972).
8. J. F. KING and J. R. DU MANOIR. J. Am. Chem. Soc. **97**, 2566 (1975).
9. F. K. BUTCHER, J. CHARALAMBOUS, M. J. FRAZER, and W. GERRARD. Spectrochim. Acta, Part A, **23**, 2399 (1967).
10. L. R. SUBRAMANIAN, M. HANACK, L. W. K. CHANG, M. A. IMHOFF, P. v. R. SCHLEYER, F. EFFENBERGER, W. KURTZ, P. J. STANG, and T. E. DUEBER. J. Org. Chem. **41**, 4099 (1976).
11. P. J. STANG. Prog. Phys. Org. Chem. **10**, 276 (1973).
12. W. W. BINKLEY and E. F. DEGERING. J. Am. Chem. Soc. **61**, 3250 (1939).
13. T. DURST and M. J. O'SULLIVAN. J. Org. Chem. **35**, 2043 (1970).
14. F. MUTH. *In* Methoden der organischen Chemie (Houben-Weyl). Vol. 9. 4th ed. Georg Thieme Verlag, Stuttgart. 1955. p. 310.
15. R. G. PEARSON. Hard and soft acids and bases. Dowden, Hutchinson, and Ross, Inc., Stroudsburg, PA. 1973.
16. J. CHARALAMBOUS, M. J. FRAZER, and W. GERRARD. J. Chem. Soc. 5480 (1964).
17. M. DELEPINE. C. R. Acad. Sci. **122**, 1272 (1896).
18. R. BEHREND. Justus Liebigs Ann. Chem. **222**, 116 (1884).
19. P. J. STANG, M. G. MANGUM, D. P. FOX, and P. HAAK. J. Am. Chem. Soc. **96**, 4562 (1974).
20. F. SINN and K. SCHIMMELSCHMIDT. *In* Methoden der organischen Chemie (Houben-Weyl). Vol 6/2. 4th ed. Georg Thieme Verlag, Stuttgart. 1963. p. 469.

Betylates. 2. The formation and high reactivity of alkyl [0]betylates[1]

JAMES FREDERICK KING AND TERESA MEE-LING LEE

Department of Chemistry, University of Western Ontario, London, Ont., Canada N6A 5B7

Received July 21, 1980

This paper is dedicated to Prof. Raymond U. Lemieux on the occasion of his 60th birthday

JAMES FREDERICK KING and TERESA MEE-LING LEE. Can. J. Chem. **59**, 362 (1981).

Unhindered primary alkyl *N*,*N*-dimethylsulfamates (**1**) react with methyl fluorosulfate to give the corresponding alkyl fluorosulfates (**3**) and the betaine, $Me_3\overset{+}{N}SO_3^-$ (**4**), evidently by way of the intermediate alkyl [0]betylate fluorosulfate (**2**); with certain other alkyl esters (**1**) products of substitution, elimination, and rearrangement are formed. The reaction not only provides a potentially useful route to simple alkyl fluorosulfates, but serves to demonstrate the powerful nucleofugality of the [0]betylate group. To obtain a method for predicting the reactivity of [0]betylates, we have compared substituent parameters with rate constants in four series of nucleophilic displacements involving esters of the general structure $ROSO_2Z$; correlation (of log *k*) with σ^* is mediocre but a new parameter, σ^*_{15} with a "15% resonance" contribution as defined by Swain and Lupton, gives good to excellent agreement in the four reaction series. Evidence is presented for formation of the 7-norbornyl cation via the [0]betylate from 7-norbornyl *N*,*N*-dimethylsulfamate and methyl fluorosulfate. Comparison with what is known of the reactivities of 7-norbornyl *p*-toluenesulfonate and trifluoromethanesulfonate esters serves to confirm that [0]betylates are among the most nucleofugal functions of which a derivative has been fully characterized.

JAMES FREDERICK KING et TERESA MEE-LING LEE. Can. J. Chem. **59**, 362 (1981).

Les *N*,*N*-diméthylsulfamates d'alkyles (**1**) primaires non encombrées réagissent avec le fluorosulfate de méthyle pour donner les fluorosulfates d'alkyles correspondants (**3**) et la bétaine $Me_3\overset{+}{N}SO_3^-$ (**4**), manifestement par l'intermédiaire du fluorosulfate de [0]bétylate d'alkyle (**2**). Il se forme des produits de substitutions, d'élimination et de transposition avec d'autres esters d'alkyles (**1**). La réaction ne fournit pas seulement une voie d'accès très pratique aux fluorosulfates d'alkyle, mais sert également à démontrer le puissant caractère nucléofuge du groupe [0]bétylate. Dans le but d'obtenir une méthode permettant de prédire la réactivité des [0]bétylate nous avons comparé les paramètres des substituants avec les constantes de vitesse de quatre séries de déplacements nucléophiles impliquant des esters de structure générale $ROSO_2Z$. La corrélation entre le log de *k* et σ^* est médiocre, mais un nouveau paramètre, σ^*_{15} comprenant une contribution de "résonance de 15%" telle que définie par Swain et Lupton, fournit une bonne corrélation avec les 4 séries de réactions. On prouve la formation du cation norbornyle-7 par l'intermédiaire du [0]bétylate à partir du *N*,*N*-diméthylsulfamate de norbornyle-7 et du fluorosulfate de méthyle. En se basant sur les données connues au sujet des réactivités des *p*-toluènesulfonates et trifluorométhanesulfonate de norbornyle-7, on a pu confirmer le fait que les [0]bétylates font partie des fonctions les plus nucléofuges dont on a pu caractériser complètement un dérivé.

[Traduit par le journal]

Introduction

In the accompanying paper (1) we have reported that phenyl *N*,*N*-dimethylsulfamate reacts with methyl fluorosulfate to yield the first example of an isolable "[0]betylate" (i.e. trialkylammoniosulfate) ester.[2]

$$Me_2NSO_2OPh + MeOSO_2F \rightarrow Me_3\overset{+}{N}SO_2OPh\ FSO_3^-$$

The [0]betylate group, $R_3\overset{+}{N}SO_2O$, would be predicted to be highly nucleofugal, i.e. to be a powerful leaving group, since the attachment of such strongly electron-withdrawing functions as the fluoro or trifluoromethyl groups directly to the sulfonyl sulfur has led to sulfonic esters of high reactivity, the so-called "super sulfonates". In fact, by a quantitative method of assessment described in detail later in this paper, we estimate that [0]betylates should be a number of orders of magnitude more reactive than even the "super sulfonates". Accordingly when we had determined that an aryl [0]betylate could be prepared from an aryl *N*,*N*-dimethylsulfamate, we quickly turned our attention to the corresponding reaction of *alkyl N*,*N*-dimethylsulfamates. This paper describes our study of this reaction and our observation of the remarkable nucleofugality (leaving group activity) of the [0]betylate function.[3] In addition, as is described in the final part of this paper, the latter point has led to the development of a simple linear free energy relationship based on the Swain–Lupton treatment of electronic effects of substituents (3), which enables prediction of the variation in reactivity of compounds of the type $ROSO_2Z$ with change in Z.

Results and Discussion

Alkyl [0]Betylates, Their Formation and Potent Alkylating Properties

Reaction of alkyl *N*,*N*-dimethylsulfamates (**1**)

[1]Part 23 in the series Organic Sulfur Mechanisms. Part 22: preceding paper.

[2]For the definition of the trivial name "betylate" see footnote 2 of the accompanying paper (1).

[3]A preliminary account of this work has appeared (2).

0008-4042/81/020362-11$01.00/0

©1981 National Research Council of Canada/Conseil national de recherches du Canada

Can. J. Chem. Downloaded from www.nrcresearchpress.com by 210.87.254.6 on 09/05/12
For personal use only.

Can. J. Chem. Downloaded from www.nrcresearchpress.com by 210.87.254.6 on 09/05/12
For personal use only.

with methyl fluorosulfate has not in our hands led to the isolation of an alkyl [0]betylate (**2**), though from the results given in this section it will become evident that this is indeed the usual first step and that the [0]betylate simply undergoes further reaction. With simple primary alkyl *N*,*N*-dimethylsulfamates the isolated products are the alkyl fluorosulfate (**3**) and the betaine (**4**). The yields and spectroscopic properties of a number of alkyl fluorosulfates produced in this manner are given in Table 1. No attempt has been made to optimize these yields but it would appear that this is a serviceable general procedure for converting unhindered primary alcohols into their fluorosulfate esters.[4] Some of the limitations of this route are displayed by the reactions of isobutyl and neopentyl *N*,*N*-dimethylsulfamates, which gave respectively isobutene and *tert*-butyl fluoride, and 2-methyl-2-butene. Reaction of isopropyl *N*,*N*-dimethylsulfamate appeared to give the fluorosulfate ester which was evidently unstable under the reaction conditions. Because the procedure of Ahmed *et al.* (4) for specifically making ethyl fluorosulfate is easier we did not try to make it by our route on a preparative scale, but an nmr experiment showed that the reaction in fact gives ethyl fluorosulfate and the betaine efficiently. Similarly the reaction of methyl *N*,*N*-dimethylsulfamate with methyl fluorosulfate appears, at least in part, to give **4** plus another molecule of methyl fluorosulfate; a fuller discussion of this reaction is given later in this section.

The available evidence is nicely consistent with the route shown in Scheme 1, i.e. initial formation of the [0]betylate, a process which is exactly parallel to the formation of the phenyl derivative (**1**), and then, as the second step, conversion of the ion-pair (**2**) into the alkyl fluorosulfate (**3**) and the betaine (**4**). The latter conversion may be regarded as a "substrate–reagent ion-pair" (SRIP) reaction (6), a process we have found in the reactions of [2]- and [3]betylates to be a surprisingly facile process, even for anions of very low nucleophilicity. The perchlorate or trifluoromethanesulfonate (triflate) salts of 1-hexadecyl [2]betylate, for example, are converted almost quantitatively into 1-hexadecyl perchlorate or 1-hexadecyl triflate, respectively, by refluxing in toluene for one hour (6). In this context rapid formation of the primary alkyl fluorosulfates (**3**) from the ion-pair (**2**) is entirely expected in view of the high nucleofugality predicted for the

$$\underset{\mathbf{1}}{Me_2NSO_2OR} + MeOSO_2F \longrightarrow \underset{\mathbf{2}}{[Me_3\overset{+}{N}SO_2OR\ FSO_3^-]}$$

$$\downarrow$$

$$\underset{\mathbf{3}}{ROSO_2F} + \underset{\mathbf{4}}{Me_3\overset{+}{N}SO_3^-}$$

SCHEME 1

[0]betylate grouping. It should perhaps be pointed out, however, that the fluorosulfate salts of 1-alkyl [2]betylates have not, in our hands, given 1-alkyl fluorosulfates, but rather the di-1-alkyl sulfates (6). These are believed to arise via the comparatively rapid hydrolysis of the fluorosulfate anion by adventitious moisture, followed by SRIP reactions with the bisulfate and alkylsulfate betylate ion-pairs. With the present scheme, however, this complication does not arise, perhaps because the nucleofugality of the [0]betylate group is such that displacement is readily effected at temperatures at which fluorosulfate is stable, or possibly simply because any water entering the system is rapidly scavenged by reaction with methyl fluorosulfate. It may be noted here that use of methyl trifluoromethanesulfonate (triflate) instead of the fluorosulfate gave the analogous result; the nmr spectrum of a mixture of excess methyl triflate with 3-phenyl-1-propyl *N*,*N*-dimethylsulfamate (**1**, R = $PhCH_2CH_2CH_2$) showed, after an interval, peaks identical to those of an authentic specimen of 3-phenyl-1-propyl triflate.

In the hope of finding at least an occasional isolable alkyl [0]betylate, we gave especial attention to those alkyl groups which are particularly reluctant to undergo nucleophilic substitution (or elimination) reactions. Recalling the low reactivity of 2,2,2-trifluoroethyl sulfonic esters (7), we synthesized 2,2,2-trifluoroethyl *N*,*N*-dimethylsulfamate (**1**, R = CF_3CH_2). Its reaction with methyl fluorosulfate was very slow, presumably because of the effect of the strongly electron-withdrawing trifluoromethyl group on the reactivity of the free electron pair of the nitrogen atom. The course of the reaction, however, was the same as that found with other alkyl groups, giving the fluorosulfate ester (**3**) in moderate yield. Extending the substitution by a trifluoromethyl group one step further led to complete deactivation of the nitrogen atom; 1,1,1,3,3,3-hexafluoro-2-propyl *N*,*N*-dimethylsulfamate (**1**, R = $(CF_3)_2CH$) showed little or no reaction with neat methyl fluorosulfate even after five weeks at 50°C.

It would appear that the inhibition of [0]betylate

[4]Previous methods have been conveniently summarized by Olah *et al.* (5).

Can. J. Chem. Downloaded from www.nrcresearchpress.com by 210.87.254.6 on 09/05/12
For personal use only.

TABLE 1. Alkyl fluorosulfates: yield from the alkyl *N,N*-dimethylsulfamate and spectroscopic properties

Alkyl group	Percentage yield[a]	Nuclear magnetic resonance absorption			Major peaks in the infrared spectrum (in cm^{-1})
		^{19}F in ppm from $CFCl_3$	^{1}H in ppm from Me_4Si	^{13}C in ppm from Me_4Si[b]	
Methyl[c]	—	−31.4	4.20	62.5(CH_3)	1455, 1430, 1230, 1000, 840, 745
Ethyl[c]	—	−35.2 (J_{HF}0.9)	1.52(3H, t of d), 4.62(2H, q, J = 3.5)	14.5(CH_3), 74.8(CH_2)	1435, 1230, 990, 955, 825
1-Propyl	45	−34.6	1.04(3H, t, J = 7, 1.89(2H, sextet), 4.44(2H, t)	9.7(CH_3), 22.4(CH_2), 79.8(CH_2)	1440, 1230, 970
1-Butyl	68	−34.6	0.97(3H, t), 1.46(2H, sextet), 1.82(2H, quintet), 4.53(2H, t, J = 7)	13.3(CH_3), 18.5(CH_2) 30.7(CH_2), 77.9(CH_2)	1440, 1230, 965
2,2,2-Trifluoroethyl	36	−38.3(q, J_{FF}2.6) 74.6(t of d, J_{HF}7.4)	4.74(quartet)	69.5(CH_2, q, J_{CF} = 39.8)[d]	1460, 1446(sh), 1293, 1231, 1184, 1042, 962, 855, 810
3-Phenyl-1-propyl	52(86)	−34.7	1.95–2.30(2H, quintet), 2.76(2H, t) 4.49(2H, t, J = 7), 7.18(5H, d)	30.1(CH_2), 31.1(CH_2), 76.8(CH_2) 126.6(CH), 128.5(CH), 128.8(CH), 139.6(C)	1438, 1226, 963
7-Norbornyl	32(60)	−36.9	1.2–2.0(8H, m), 2.41(2H, s), 4.88(1H, s)	25.5(CH_2), 26.5(CH_2), 39.0(CH) 95.1(CH)	1440, 1230, 975 934, 792

[a]Yields with parentheses refer to crude products, those without to distilled products.
[b]^{13}C chemical shifts were obtained from ^{1}H noise-decoupled spectra. The number of hydrogens on each carbon was deduced from off-resonance spectra.
[c]The spectrum of methyl fluorosulfate was obtained from a redistilled sample of the commercial material, that of ethyl fluorosulfate from a sample prepared by the method of Ahmed *et al.* (4).
[d]No signal was observed for the CF_3 carbon.

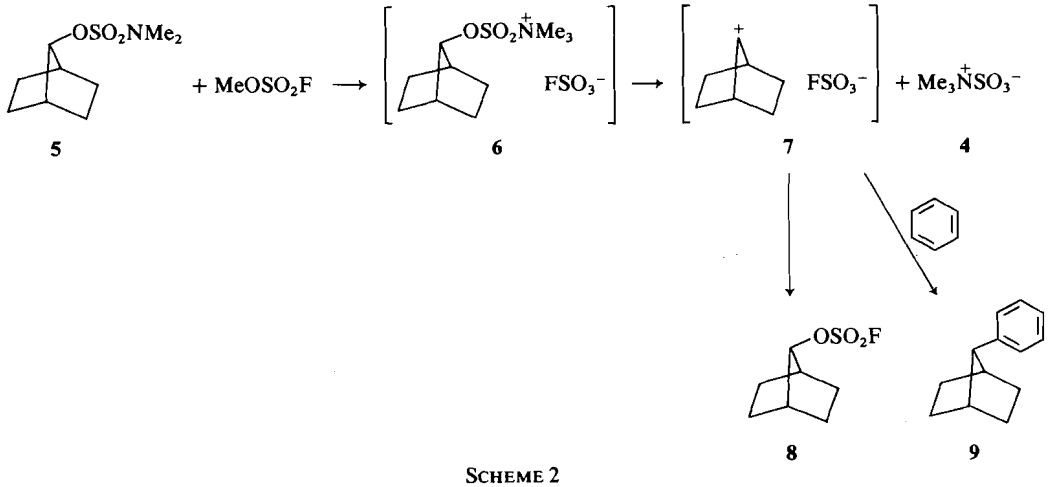

5 6 7 4 8 9

SCHEME 2

formation outweighs the possible benefits of having trifluoromethyl groups present, and we turned to another quarter in our attempts to find an isolable alkyl[0]betylate. 7-Norbornyl derivatives are known to be very slow to solvolyze (8). This has been ascribed by Schleyer and Nicholas (9) principally to the added angle strain required by carbonium ion formation. Bimolecular displacement in this system would be expected to show the same increase in angle strain, and, in addition, to have nonbonding repulsions of nucleophile and nucleofuge with the *exo*-hydrogens,[5] in the fashion suggested by Schleyer and co-workers (10) as one of the factors contributing to "limiting" (S_N1) character in the solvolysis of 2-adamantyl derivatives. We found that 7-norbornyl *N*,*N*-dimethylsulfamate (**5**) with methyl fluorosulfate formed the betaine (**4**) and 7-norbornyl fluorosulfate (**8**) in about 60% yield. Clearly the [0]betylate (**6**) had again been formed and had reacted further. Further insight was provided by reaction in the presence of benzene (three equivalents with respect to **5**), which gave 7-phenylnorbornane (**9**) as the major product (58% yield) in addition to a 17% yield of the fluorosulfate ester (**8**). The structure of **9** followed readily from elemental analysis and spectra, especially the ^{13}Cmr spectrum which showed in the saturated carbon region only the characteristic four signal pattern appropriate to the symmetrical 7-norbornyl skeleton. The formation of **9** is simply explained as a Friedel–Crafts reaction involving the norbornyl cation (**7**) as in Scheme 2. Since 7-norbornyl fluorosulfate gave no reaction with benzene under these conditions, the [0]betylate (**6**) is presumably the immediate precursor of the cation (**7**). The formation of the Friedel–Crafts product from the 7-norbornyl *N*,*N*-dimethylsulfamate (**5**), is to be contrasted with the reactions of the ethyl and 2,2,2-trifluoroethyl esters (**1**), which, as expected for a simple concerted (S_N2) displacement, gave no sign of the alkylbenzene when benzene was included in the reaction mixture. An even clearer indication of the same point is the reaction of 3-phenyl-1-propyl *N*,*N*-dimethylsulfamate; there was no sign in the nmr spectrum of the crude product of any indane, the intramolecular Friedel–Crafts product.

Reaction of isopropyl *N*,*N*-dimethylsulfamate (**1**, R = Me_2CH), on the other hand, gave some cumene, pointing to the presence of isopropyl cation in the reaction mixture. The known ability of isopropyl fluorosulfate to form cumene with benzene (5), taken with the presence in the nmr spectrum as the reaction proceeds of peaks ascribable to isopropyl fluorosulfate, points to the following sequence.

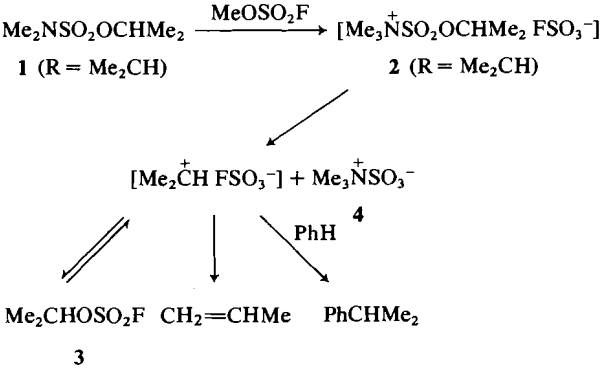

Still pursuing the goal of isolating an alkyl [0]betylate we attempted to prepare 1-apocamphyl

[5]Gassman *et al.* (11) report that sodium methoxide in methanol reacts with 7-norbornyl tosylate by way of S—O cleavage to form 7-norbornanol with no trace of the products of S_N2 attack on C-7 with C—O cleavage.

Can. J. Chem. Downloaded from www.nrcresearchpress.com by 210.87.254.6 on 09/05/12
For personal use only.

Can. J. Chem. Downloaded from www.nrcresearchpress.com by 210.87.254.6 on 09/05/12
For personal use only.

and 1-norbornyl[6] [0]betylates, but were thwarted by difficulties in obtaining the *N*,*N*-dimethylsulfamate ester from the alcohol.

As was mentioned, the reaction of methyl *N*,*N*-dimethylsulfamate (**1**, R = Me) is different in one important respect from that of all of the other *N*,*N*-dimethylsulfamate esters: methyl fluorosulfate is a product of the reaction as well as a reagent. The picture is further complicated by the fact that the methyl ester (**1**, R = Me) rearranges to the betaine (**4**) merely on standing at room temperature for an extended period (12, 13), and the question then arises, does the betaine (**4**) which is produced when the methyl ester (**1**, R = Me) is mixed with methyl fluorosulfate come from the previously known uncatalyzed rearrangement, or is it formed as in Scheme 1? Our limited observations indicate that the latter route accounts for at least part of the product. Whereas "a period of several weeks" is reported (14) as the time required for complete rearrangement of neat methyl *N*,*N*-dimethylsulfamate (**1**, R = Me) at room temperature, we found that in the presence of methyl fluorosulfate (about 30 mol%) the ester (**1**, R = Me) was converted to **4** in seven days. The roughly first order disappearance of **1** (R = Me) as followed by nmr spectra gave $k \approx 6 \times 10^{-5}\ s^{-1}$, or $t_{1/2} = 21$ h; the amount of methyl fluorosulfate remained constant. In another nmr experiment using methyl-d_3 fluorosulfate, a peak at 4.20 ppm characteristic of methyl fluorosulfate (and which was initially absent) gradually developed; this is precisely what would be expected from the Scheme 1 route, but not from a reaction in which methyl fluorosulfate is merely a spectator. The rate of the rather slow reaction of a solution (1.8 *M*) of **1** (R = Me) in chloroform-*d* containing methyl fluorosulfate (0.8 *M*) was also followed by nmr. The amount of methyl fluorosulfate remained constant while that of **1** (R = Me) decreased steadily. The reaction was more than 90% complete after six weeks at 40°C, but neither first nor second order plots showed acceptable linearity. The data suggested rather a mixed order reaction such as might arise if the reaction were proceeding in part as in Scheme 1 and in part by a second order process. The nature of the latter is uncertain but it could be alkylation of the ester (**1**) by the intermediate ion pair (**2** FSO_3^-) to form the betaine (**4**) plus another ion pair (**2** FSO_3^-). With the aid of the steady state assumption (which is justified by the absence of any peaks ascribable to **2** in the nmr spectra), one may readily show that such a chain propagation step, **2** $FSO_3^- + \mathbf{1} \rightarrow \mathbf{4} + \mathbf{2}\ FSO_3^-$, would lead to a second order dependence on the ester (**1**, R = Me).

Another possibility is that the putative second order reaction is simply the uncatalyzed rearrangement that occurs in the absence of methyl fluorosulfate. The mechanism of this reaction has in fact been studied by Ziegler and Orchin (13) who report a first order rate constant for the rearrangement in 1,2,4-trichlorobenzene at 130–132°C. They also observed, however, the formation of crossed products from reaction of a mixture of two sulfamic esters and concluded that their "experiments suggest that the rearrangement proceeds through some type of ion pair", which they represent as a methyl cation – *N*,*N*-dimethylsulfamate ion pair. This route, however, appears highly improbable in the light of recent information on the difficulty of intramolecular transfer of a methyl group between nucleophilic centres (15, 16). It is evident on examination of a fuller description of this work (14) that the experimental difficulties were such that a reaction order of greater than unity for the rearrangement of **1** (R = Me) is not precluded.[7] In the context of the present paper it is tempting to suggest that the first step of the reaction is a bimolecular methyl transfer to form the [0]betylate sulfamate ion pair, $Me_3\overset{+}{N}SO_2OMe\ Me_2NSO_3^-$, and that this may then either collapse to form two molecules of the betaine (**4**), or else undergo methyl transfer chain propagation steps with unreacted ester (**1**, R = Me); such a scheme would lead to second or higher order dependence on the ester (**1**, R = Me).[8] If the first step in the uncatalyzed rearrangement is indeed methylation of the ester (**1**, R = Me) by another molecule of the same ester, it is highly unlikely that such a process would compete with methylation by methyl fluorosulfate, a far more powerful methylating agent.[9] This would suggest that the uncatalyzed rearrangement is not the second (or higher) order process which appears to be present in the reaction of the ester (**1**, R = Me) with methyl fluorosulfate, but it is evident that further work is required to make any definite pronounce-

[6]We are grateful to Dr. D. F. Tavares (University of Calgary) for his patient efforts in this frustrating endeavour.

[7]NOTE ADDED IN PROOF: Recent crossing experiments with a mixture of deuterium-labelled and unlabelled **1** (R = Me) show the rearrangement to **4** to be entirely *intermolecular* in acetonitrile solution starting with total concentrations of either 0.08 *M* or 2.0 *M* (see ref. 34).

[8]Kinetic analysis of an exactly analogous scheme is given in a discussion of the closely related intramolecular rearrangement of $Me_2N(CH_2)_4SO_2OMe$ to the corresponding betaine (16).

[9]The quantitative relationships developed in the next section predict that methyl fluorosulfate methylates water and triethylamine respectively 10^5 and 10^8 times faster than does methyl *N*,*N*-dimethylsulfamate (**1**, R = Me).

TABLE 2. Rate constants for nucleophilic substitution reactions of ZSO_2OR

	R = Methyl		R = Ethyl	
Z	H_2O[a] (s^{-1})	Sodium *p*-nitrophenoxide[b] ($M^{-1}s^{-1}$)	Triethylamine[c] ($M^{-1}s^{-1}$)	Sodium ethyl acetoacetate[d] ($M^{-1}s^{-1}$)
Methyl	1.66×10^{-7}	—	3.6×10^{-7}	—
Phenyl	3.78×10^{-7}	—	—	—
p-Tolyl	—	0.0196	1.2×10^{-6}	1.3×10^{-5}
Methoxyl[e]	2.79×10^{-6}	0.43	—	—
Ethoxyl[e]	—	—	1.5×10^{-5}	4.0×10^{-4}
Fluoro	1.45×10^{-3}	—	0.17	6.1
Trifluoromethyl	4.38×10^{-3}	1300	—	17.8

[a]Hydrolysis at 0.3°C; values for Z = F and CF_3 are from Kevill and Lin (17), the others are calculated from the data of Robertson (18).
[b]Reaction of sodium *p*-nitrophenoxide in sulfolane at 42°C (19).
[c]Reaction with triethylamine in acetonitrile at 0°C (4).
[d]Reaction with the sodium enolate of ethyl acetoacetate in dimethoxyethane at 0°C (both C- and O-alkylation) (20).
[e]Statistically corrected (i.e. *k*/2).

ment on the formation of the betaine (**4**) from the ester (**1**, R = Me) other than that Scheme 1 is followed for at least part of the reaction in the presence of methyl fluorosulfate.

Prediction of the Rates of Reaction of [0]Betylates and Other Alkyl Esters of General Formula $ROSO_2Z$

It is evident from both this and earlier work that change of Z in compounds of the general formula $ROSO_2Z$ can have a very large effect on the ease of nucleophilic displacement of the R group. In this section we examine previously reported data with an eye to finding a useful predictive relationship, and then check to see if this and our admittedly limited information on [0]betylate reactivity are consistent.

Previous rate data on compounds of the general formula $ROSO_2Z$ having quite different substituent groups, Z, are summarized in Table 2. One may see immediately that electron-withdrawing substituents accelerate these reactions, but closer inspection shows that this is not a direct function of a simple inductive (or field) effect. Log *k* values for these reactions correlate only indifferently with the Taft σ^* values, for example, with correlation coefficients (*r*) ranging from 0.88 to 0.94. Note particularly the two series having both Z = CF_3 and F; in both cases the triflate reacts faster than the fluorosulfate even though σ^* (or σ_I) is greater for a fluoro than a trifluoromethyl substituent. The data are not without pattern, however; a least-squares linear regression analysis of each of the three other reactions with respect to the hydrolysis at 0.3°C yields correlation coefficients that are all greater than 0.997.

Perhaps the simplest solution to the problem is to postulate resonance:

$$ROSO_2\text{—}\ddot{Z} \leftrightarrow RO\bar{S}O_2{=}Z^+$$

This hypothesis is, of course, not new, an excellent case for electron donation into the sulfonyl group having been made some time ago by Bordwell *et al.* (21). Such electron delocalization would be expected to be important in stabilizing the ground state (as shown) and also in inhibiting the development of a partial negative charge on the dicoordinated oxygen atom in the transition state. We find, in fact, that the use of a modified σ^* parameter which specifically includes a resonance component gives quantitative support for this idea. The new parameter, which we call σ_x^*, is derived directly from the field and resonance parameters of Swain and Lupton (3) with scaling to facilitate comparison with conventional σ^* and ρ^* values.[10] In particular, σ_{15}^* and σ_{20}^* values, i.e. σ^* values with respectively "15% resonance" and "20% resonance" components (3), yield quite acceptable correlations having *r* values ranging from 0.969 to 1.000. Tables 3 and 4 list the results obtained on the basis of "15% resonance"; correlations with σ_{20}^* values are not very different, being slightly better with the hydrolysis and triethylamine reactions and rather poorer with the *p*-nitrophenoxide and enolate displacements. Table 4 also reports, in parentheses,

[10]We define σ_x^* from the Swain-Lupton relation $\sigma = f\mathcal{F} + r\mathcal{R}$, as follows:

(*i*) $(\sigma_x^*)_z = 2.60\,[\mathcal{F}_z + 1.6\mathcal{R}_z x/(100 - x)] + 0.49$

where $x = \%\mathcal{R}$ the "percent resonance" or "sensitivity to resonance effects", and $\mathcal{F}_z$ and $\mathcal{R}_z$ are the field and resonance parameters for substituent Z, all as defined by Swain and Lupton (3). The constants 2.60 and 0.49 (which were obtained from $\sigma_H^* = 0.49$ and $\sigma^*_{Me_3N^+} = 4.29$[11]) give σ_x^* values such that in the absence of resonance effects (i.e. either $x = 0$ for a reaction or $\mathcal{R} = 0$ for a substituent) then $(\sigma_x^*)_z \equiv \sigma_z^*$ (if calculated from $\mathcal{F}$ and $\mathcal{R}$).

[11]The value $\sigma^*_{Me_3N^+} = 4.29$ was obtained from the expression $pK_a = 4.81 - 0.69\sigma^*$ relating pK_a values of acids of the type ZCH_2COOH to the calculated σ^* values of Takahashi *et al.* (22) (J. P. Guthrie, private communication).

Can. J. Chem. Downloaded from www.nrcresearchpress.com by 210.87.254.6 on 09/05/12
For personal use only.

TABLE 3. σ^*_{15} values[a]

Z	$\mathscr{F}$	$\mathscr{R}$	σ^*_{15}
CH_3	−0.052	−0.141	0.25
C_6H_5[b]	0.139	−0.088	0.79
C_2H_5O	0.363	−0.444	1.11
CH_3O	0.413	−0.500	1.20
F	0.708	−0.336	2.08
CF_3	0.631	0.181	2.26

[a]$\mathscr{F}$ and $\mathscr{R}$ values are from Swain and Lupton (3), the σ^*_{15} values are calculated from $\sigma^*_{15} = 2.60\,(\mathscr{F} + 0.282\,\mathscr{R}) + 0.49$.
[b]The same values were assigned to *p*-tolyl.

results obtained assuming $\sigma^*_{15} = \sigma^*_0 = 2.13$ for the CF_3 group, i.e. that there is no resonance contribution with this substituent. The proposed resonance involves electron donation from the Z group, whereas the positive value of the $\mathscr{R}$ parameter of the CF_3 group signifies electron withdrawal. It is at least arguable that no such electron withdrawal will occur between sulfonyl and trifluoromethyl groups and hence that a different substituent parameter is appropriate. It is evident, however, from Table 4 that the results are much the same with or without a trifluoromethyl resonance component.

The addition of an adjustable parameter can be expected, of course, to improve any correlation, but it should be specifically noted in the present discussion that the *same* value, i.e. "15% resonance", gives a good fit for *four* separate reaction series. When this is taken with the considerable body of other evidence supporting electron donation into a sulfonyl group (21), the present treatment is in our view eminently sensible; it is clearly capable of direct application not only to reactions of other sulfonyl compounds but, in principle, also to reactions of any system in which resonance occurs between the substituent and the reacting centre.

From the final column in Table 4 we note that the rate constants predicted for the corresponding reactions of [0]betylate are indeed high, and that our failure to isolate or even in most instances to see any direct sign of an alkyl [0]betylate is therefore not surprising.

The one reaction which may have given such a sign was that of 7-norbornyl *N,N*-dimethylsulfamate (**5**), which showed a small peak at 3.75 ppm as the reaction proceeded. The position of this signal was close to that for the methyl group in phenyl [0]betylate fluorosulfate, i.e. 3.70 ppm (**1**); if it was indeed due to **6** then the size of the peak would indicate a maximum of about 10% of **6** during the reaction. From this value plus a rough estimate of the rate constant of about $6 \times 10^{-5}\,s^{-1}$ for disappearance of **5**, we may arrive at a first order rate constant of about $4 \times 10^{-4}\,s^{-1}$ for the reaction **6** → **7** in methyl fluorosulfate; this number is a minimum value since if the peak in question is not due to **6**, then in the absence of any larger appropriate peaks to assign to **6**, we must assume that **6** reacts even more quickly.

For comparison, the reported rate constants for the acetolyses of 7-norbornyl *p*-tosylate and triflate at 25°C are respectively $6.36 \times 10^{-15}\,s^{-1}$ (8) and $1.37 \times 10^{-9}\,s^{-1}$ (23). We have no direct information on the relative ease of ionization reactions in methyl fluorosulfate vs. acetic acid, but we may hazard a guess via the Hildebrand solubility parameter δ, which has been correlated by Herbrandson and Neufeld (24) with the Winstein–Grunwald solvent parameter **Y**. The relation $\mathbf{Y} = 0.524\,\delta_{25} - 8.25$ and $\delta_{25} = 9.9$ gives a **Y** value of −3.6 for methyl fluorosulfate.[12] For acetic acid **Y** = −1.639 (27), and hence the rate of ionization of *tert*-butyl chloride is estimated to be about 100 times faster in acetic acid than in methyl fluorosulfate. If we may apply the same factor to the ionization of **6** then we obtain $4 \times 10^{-2}\,s^{-1}$ for acetolysis of **6** at 25°C. This estimate, though very rough, is remarkably close to the rate constant, $3 \times 10^{-2}\,s^{-1}$, that we may calculate from the acetolysis rates of the tosylate and triflate taken with σ^*_{15} values given in Table 3; using $\sigma^*_{15} = 2.13$ for trifluoromethyl (as discussed) gives $5 \times 10^{-1}\,s^{-1}$ for the acetolysis of the [0]betylate (**6**). Though the approximations made in this analysis are both many and crude, the results are in full agreement with the mechanism in Scheme 2.

It should perhaps be explicitly noted that although the modified Taft equation gives us a quantitative picture of the reactivity of [0]betylates, the simple qualitative conclusion that [0]betylates are highly nucleofugal is quite independent of any such treatment. Whereas the rate constant for acetolysis of 7-norbornyl triflate at room temperature is about $10^{-9}\,s^{-1}$, the lower limit for the specific rate of the reaction **6** → **7** in methyl fluorosulfate, which is in all likelihood a less polar medium, is about $10^{-4}\,s^{-1}$. A [0]betylate is therefore more nucleofugal than a triflate, itself a "super sulfonate", by at least five orders of magnitude, and must be one of the most powerful nucleofuges for which a derivative has been isolated and characterized. This conclusion invites comparison of [0]betylates with diazonium ions, the simple alkyl derivatives of which are highly reactive transient species whereas aryl and certain specially constructed alkyl derivatives

[12]The value of δ_{25} was calculated from $d = 1.424$ and bp 92°C (25) as described by Hildebrand and Scott (26).

Can. J. Chem. Downloaded from www.nrcresearchpress.com by 210.87.254.6 on 09/05/12
For personal use only.

TABLE 4. Correlation of the reactions of ZSO_2OR with σ_{15}^*

Reagent[a]	ρ_{15}^{*}[b]	log k_0[b]	r[b]	Estimated[c] $k_{Me_3N}^{+}$
Water (R = Me)	2.36 (2.45)[d]	−7.90 (−7.95)	0.978 (0.973)	$2 \times 10^2\ s^{-1}$ $(4 \times 10^2\ s^{-1})$
Sodium nitrophenoxide (R = Me)	3.28 (3.62)[d]	−4.30 (−4.63)	1.000 (1.000)	$6 \times 10^9\ M^{-1}\ s^{-1}$ $(8 \times 10^{10}\ M^{-1}\ s^{-1})$
Triethylamine (R = Et)	3.25	−7.93	0.969	$1 \times 10^6\ M^{-1}\ s^{-1}$
Sodium ethylacetoacetate (R = Et)	4.23 (4.48)[d]	−9.93 (−10.18)	0.999 (0.999)	$2 \times 10^8\ M^{-1}\ s^{-1}$ $(1 \times 10^9\ M^{-1}\ s^{-1})$

[a]In the reactions described in Table 2.
[b]Slope (ρ_{15}^{*}), intercept (log k_0), and correlation coefficient (r) obtained by least-squares linear regression.
[c]Rate constant estimated for $Me_3\overset{+}{N}SO_2OR$ using $\sigma_{15}^{*} = \sigma^{*} = 4.29$[10] and the linear regression parameters.
[d]Values in parentheses are calculated using $\sigma_{15}^{*} = \sigma_0^{*} = 2.13$ for CF_3, i.e. assuming no electron-withdrawing resonance (see text).

are isolable. The evidence for formation of phenyl cations from aryldiazonium salts (28), taken with our failure to observe any analogous reactions from phenyl [0]betylate (1), would suggest that, in this particular system, at least, the diazonium ion is probably the more nucleofugal group.

It seems likely that the high reactivity of the [0]betylate function and its ease of formation from a hydroxylic precursor will combine to make it a synthetically useful as well as mechanistically interesting group. The present papers, however, constitute only the initial survey of the chemistry of [0]betylates and the numerous unanswered questions raised here, and many others as well, must await further experimentation.

Experimental

Spectrometers and general procedures are the same as those given in the accompanying paper (1). The ^{19}Fmr spectra were also determined on a Varian XL-100 instrument. Vapour phase chromatography was carried out with a F + M 700 Chromatograph using 6 ft × 1/4 in. columns containing silicone rubber SE 30 on Chromosorb W. The alcohols used in the preparation of **1** were commercial materials except for 7-norbornanol which was made from norbornene by a known route (29).

Preparation of Alkyl N,N-*Dimethylsulfamates (1)*

A suspension in 1,2-dimethoxyethane of the sodium alkoxide, generated by reaction of the alcohol with oil-free sodium hydride, was treated with *N,N*-dimethylsulfamoyl chloride (30). The scale of the preparations varied from 1 to 50 mmol; the limiting reagent with low boiling alcohols was the sulfamoyl chloride but with the others was the hydroxylic starting material. The properties and yields are summarized in Table 5. The methyl ester (**1**, R = Me) was used in further experiments without any attempt at purification by distillation; this ester rearranges readily to **4** on heating and is reported to be undistillable (12).

Reaction of Methyl Fluorosulfate with Alkyl N,N-*Dimethylsulfamate Esters (1)*

A preliminary examination of each reaction was carried out by observing the proton nmr spectrum (T-60) after standing for intervals (with or without heating) of a solution of the sulfamic ester (**1**) (about 0.3 mmol) in methyl fluorosulfate (0.3 mL) in a sealed nmr tube. Yields and spectra of products from preparative runs are given in Table 1.

(a) Ethyl N,N-*Dimethylsulfamate (1, R = Et)*

After one day at room temperature the proton nmr spectrum (XL-100) of a mixture of ethyl *N,N*-dimethylsulfamate (53 mmol) and benzene (80 mmol) in excess methyl fluorosulfate showed peaks at 1.55 (t), 4.61 (q), and 7.43 (s) (all relative to the singlet at 4.20 ppm due to $MeOSO_2F$); no sign of any signals appropriate to the ethyl group of ethyl benzene was observed; the ^{19}F spectrum showed a peak at −35.0 relative to the peak due to methyl fluorosulfate at −31.42 ppm.

(b) 1-Butyl N,N-*Dimethylsulfamate (1, R = $CH_3CH_2CH_2CH_2$)*

The nmr tube experiment indicated the reaction to be about half complete after 6 h, and complete after 5 days at room temperature.

The butyl ester (**1**, R = $CH_3CH_2CH_2CH_2$) (6.2 g, 34 mmol) and methyl fluorosulfate (3.1 g, 27 mmol) were allowed to stand at room temperature in a sealed ampoule for 6 days, whereupon the brown supernatant liquid was decanted from the white deposit of the betaine (**4**). The solid was washed with dry CH_2Cl_2 and the combined liquid phases distilled. The initial distillate at atmospheric pressure was mostly CH_2Cl_2 and was discarded. Distillation under reduced pressure (about 25 Torr) gave 1-butyl fluorosulfate (bp 57°C, 2.9 g, 68%).

(c) Propyl N,N-*Dimethylsulfamate (1, R = $CH_3CH_2CH_2$)*

The nmr experiment showed roughly 80% reaction after 24 h at room temperature. In the preparative experiment a mixture of methyl fluorosulfate (3.3 g, 29 mmol) and the propyl ester (6 g, 36 mmol) were allowed to stand at room temperature and then worked up in the same way as the product from the 1-butyl ester, to give propyl fluorosulfate (1.85 g, 45%).

(d) 2,2,2-Trifluoroethyl N,N-*Dimethylsulfamate (1, R = CF_3CH_2)*

The nmr experiment (with added benzene) after 3 days at 60°C showed about 80% conversion to 2,2,2-trifluoroethyl fluorosulfate, which gave a quartet at 4.8 ppm (i.e. 0.6 ppm downfield from the singlet of methyl fluorosulfate); there was no sign of any product derived from alkylation of the benzene. The white precipitate showed a peak at 3.1 ppm (CD_3CN) appropriate to the betaine (**4**).

A mixture of the sulfamic ester (**1**, R = CF_3CH_2) (5.8 g, 28 mmol) and methyl fluorosulfate (2.51 g, 22 mmol) was heated in a sealed ampoule at 70°C for 12 days. Work-up and distillation (at atmospheric pressure) as with the butyl ester gave a sample

Can. J. Chem. Downloaded from www.nrcresearchpress.com by 210.87.254.6 on 09/05/12
For personal use only.

Can. J. Chem. Downloaded from www.nrcresearchpress.com by 210.87.254.6 on 09/05/12
For personal use only.

TABLE 5. Alkyl *N,N*-dimethylsulfamate esters, Me_2NSO_2OR

R	Boiling point (°C); yield	Spectra		
		^{1}Hmr (in ppm from Me_4Si)	^{13}Cmr (in ppm from Me_4Si)	Infrared (in cm^{-1}, neat sample, major peaks only)
Methyl	—	2.86(s, 6H), 3.80(3H)[a]	[b]	1355, 1165, 995, 965, 770
Ethyl	63–64/3.4 Torr; 83%	1.34(t, 3H, J = 7 Hz), 2.83(s, 6H) 4.17(q, 2H)	14.8(CH_3), 38.4(CH_3), 66.9(CH_2)	1350, 1160, 1000, 955, 900, 760
Propyl[c]	79/2.6 Torr; 81%	1.00(t, 3H, J = 7 Hz), 1.76(sextet, 2H), 2.86(s, 6H), 4.12(t, 2H)	10.1(CH_3), 22.6(CH_2), 38.4(CH_3), 72.2(CH_2)	1360, 1170, 950, 745
Isopropyl	90/5 Torr; 87%	1.39(d, 6H, J = 7 Hz), 2.84(s, 6H), 4.79(septet, 1H)	[b]	1355, 1170, 915, 870
Butyl	72.4/1.7 Torr; 71%	0.90(t, 3H, J = 7 Hz), 1.25–1.9(m, 8H), 2.89(s, 6H), 4.18(t, 2H, J = 6 Hz)	13.5(CH_3), 18.8(CH_2), 31.1(CH_2), 38.5(CH_3), 70.5(CH_2)	1355, 1170, 940
Isobutyl	68–72/2 Torr; 97%	0.99(d, 6H, J = 7 Hz), 2.04(m, 1H), 2.89(s, 6H), 3.93(d, 2H, J = 7 Hz)	[b]	1345, 1155, two unresolved peaks at 970 and 935, 800
Neopentyl[d]	90/5 Torr; 87%	0.99(s, 9H), 2.90(s, 6H), 3.81(s, 2H)	26.1(CH_3), 31.9(C), 38.5(CH_3), 79.3(CH_2)	1360, 1170, three unresolved peaks at 985, 955, and 935, 825
3-Phenyl-1-propyl	132–134/1 Torr; 10%[e]	1.9–2.2(m, 2H), 2.5–2.9(?)(2H, m), 2.82(s, 6H), 4.08(t, 2H, J = 6 Hz)[a]	[b]	1360, 1170, 965, 935, 745, 700
2,2,2-Trifluoroethyl	68–71/10 Torr; 71%	2.93(s, 6H), 4.45(q, 2H, J_{HF} = 8 Hz)	38.5(CH_3), 65.3(CH_2, J_{CF} = 38 Hz)[f]	1380, 1290, 1180, 1050, 970, 790
1,1,1,3,3,3-Hexafluoro-2-propyl	65–67/8 Torr; 83%	2.93(s, 6H), 5.05(septet, 1H, J_{HF} = 6 Hz)	[b]	1390, 1365(8h), 1290, four unresolved peaks at 1250, 1240, 1205, and 1185, 1110, 1085, 980, 880, 795
7-Norbornyl	75–79/0.6 Torr;[g] 78%	1.1–1.9(m, 8H), 2.31(br s, 2H), 2.84(s, 6H), 4.56(br s, 1H)	25.9(CH_2), 26.8(CH_2), 38.5(CH_3) 39.0(CH), 87.4(CH)	1350, 1165, 995, 960, 850

[a]Determined on the Varian T-60 instrument.
[b]^{13}C spectrum not determined.
[c]Mass spectrum: M^+ calcd. 167.0616; found 167.0612.
[d]Mass spectrum: M^+ calcd. 195.0929; found 195.0925.
[e]Compound extensively decomposed on distillation (crude product satisfactory for most purposes).
[f]^{19}F nmr: δ_{CFCl_3} 78.4(t, J_{HF} = 8 Hz); the CF_3 carbon was not observed in the ^{13}C spectrum; ms: M^+ calcd. 275.0051; found 275.0048.
[g]Melting point 39–42°C.

Can. J. Chem. Downloaded from www.nrcresearchpress.com by 210.87.254.6 on 09/05/12
For personal use only.

of 2,2,2-trifluoroethyl fluorosulfate (1.46 g, 36%) which appeared to contain a minor amount of impurity; the purest fraction boiled at 82–83°C. *Anal.* calcd. for $C_2H_2F_4O_3S$: C 13.19, H 1.10; found: C 12.94, H 1.23.

(e) 3-Phenyl-1-propyl N,N-*Dimethylsulfamate (1, R = $PhCH_2CH_2CH_2$)*

The nmr experiment indicated that reaction was complete in 2 h at 60°C. Reaction of the ester (**1**, R = $PhCH_2CH_2CH_2$) (3 g, 12 mmol) and methyl fluorosulfate (4 mL, 50 mmol) at 60°C for 5 h, followed by work-up as above, gave a brown liquid (2.3 g, 86% crude yield) the nmr spectrum of which indicated the product to be >90% 3-phenyl-1-propyl fluorosulfate with no sign of any peaks ascribable to indane. Distillation gave a colorless oil (1.4 g, 52%) boiling at 75–77°C/0.8 Torr. Mass spectrum: M^+ calcd. 218.0409; found 218.0413.

(f) 7-Norbornyl N,N-*Dimethylsulfamate (5)*

The nmr experiment (with added benzene) showed 30% reaction (as measured by the shrinkage of the signal at 2.9 ppm) after 75 min and 50% reaction after 210 min corresponding to a rate constant for disappearance of **5** of about 6×10^{-5} s^{-1}. An extra signal about 0.1 ppm upfield from that of benzene pointed to formation of an aromatic product, and a small peak at 3.75 ppm consistent with the intermediacy of **6** (~10%) was present in the spectra observed after 75 and 210 min of reaction.

In a preparative run the ester (**5**, 0.6 g, 2.7 mmol) and methyl fluorosulfate (1.5 mL, 18.5 mmol) were allowed to react for 60 h at room temperature. Carbon tetrachloride was added to the reaction mixture and the liquid phase separated from the solid; the latter was washed twice with more CCl_4 and the CCl_4 solutions combined and the solvent evaporated leaving a crude product (0.32 g, 60%) which appeared from its nmr spectrum to consist of the fluorosulfate ester (**8**) containing a small amount (<10%) of starting sulfamate (**5**). Two distillations under reduced pressure (20 Torr, bath 115°C) gave the pure product (0.17 g, 32%). *Anal.* calcd. for $C_7H_{11}FO_3S$: C 43.30, H 5.67, S 16.50; found: C 43.22, H 5.82, S 16.32.

In another reaction a mixture of **5** (0.28 g, 1.3 mmol) and methyl fluorosulfate (0.3 mL, 3.7 mmol) with benzene (0.3 g, 3.9 mmol) was allowed to stand at room temperature for 20 h, after which time the mixture consisted of a dark purple liquid and a white solid. The volatile constituents were evaporated and the residue mixed with ether; the ether solution was separated from the solid (**4**), and the solvent evaporated. The residue was then mixed with hexanes, the solution separated from the small amount of coloured oil, and the solvent evaporated. The crude product (0.17 g) appeared from its nmr spectrum to consist almost entirely of 7-phenylnorbornane (**9**) and 7-norbornyl fluorosulfate (**8**); the relative areas of the peaks at 2.9 and 4.9 ppm indicated a 3:1 ratio of **9** to **8**, or yields of about 58% and 17%, respectively. The product from five similar small scale runs was chromatographed on a column of silica gel. 7-Phenylnorbornane (**9**) was eluted with hexanes and distilled (bath 105°C/6 Torr). Infrared ν_{max}: 2955 (vs), 1600 (m), 1495 (s), 1450 (s), 720 (s), 695 (s) cm^{-1}; ^{1}Hmr δ: 7.18 (5H, m), 2.86 (1H, br s), 2.53 (2H, br s), 1.0–1.8 (8H, m) ppm; ^{13}Cmr δ: 23.9 (CH_2), 26.8 (CH_2), 35.9 (CH), 50.0 (CH), 122.0 (CH), 124.3 (CH), 124.6 (CH), 138.2 (C) ppm. *Anal.* calcd. for $C_{13}H_{16}$: C 90.70, H 9.31; found: C 90.47, H 9.51.

When a small sample of the crude reaction product (i.e. before any work-up), derived from reaction of **5** with methyl fluorosulfate without benzene, was treated with excess benzene and allowed to stand for 19 h at room temperature, the nmr spectrum showed no sign of any 7-phenylnorbornane (**9**).

(g) Isobutyl N,N-*Dimethylsulfamate (1, R = Me_2CHCH_2)*

The nmr experiment showed the reaction to be complete after about 18 h at room temperature (as judged by the virtual disappearance of the original peak at 2.9 ppm); extensive signal broadening perhaps due to the presence of a solid phase (**4**) made interpretation difficult, but strong peaks at 0.9 to 1.1 and 1.2 to 1.3 ppm suggested dimeric and perhaps oligomeric products from isobutene.

In a preparative experiment nitrogen was passed over a mixture of isobutyl *N,N*-dimethylsulfamate (2 g, 11 mmol) and methyl fluorosulfate (4 mL, 49.5 mmol) and the gas stream passed through a trap cooled in a Dry Ice – acetone bath. After 4 h a visible condensate had collected in the trap. The nmr spectrum of this material ($CDCl_3$) showed broad "singlets" at 1.7 and 4.6 ppm identical with those of an authentic sample of isobutene, and, in addition two peaks of equal intensity ascribable to *tert*-butyl fluoride, δ 1.33 ppm, J_{HF} = 20.4 Hz; reported: 1.30 ppm, J_{HF} = 20 Hz (neat) (31) and 1.33 ppm, J_{HF} = 20.5 Hz (CCl_4) (32). The infrared spectrum (gas phase) showed peaks at 2970, 1770, 1655, 1455, and 890 cm^{-1} as shown by authentic isobutene, plus additional strong peaks at 1380, 1260, and 1200 cm^{-1}; the gas phase ir spectrum of *tert*-butyl fluoride is reported to show strong bands at 1380, 1260, 1205, and 890 cm^{-1} (33).

In another experiment nitrogen was passed over a mixture of the sulfamic ester (1 g, 5.5 mmol), methyl fluorosulfate (1.5 mL, 18.6 mmol), and calcium carbonate (1 g) at room temperature for 2.5 h while the gas stream passed through a trap cooled in a Dry Ice – isopropyl alcohol mixture. Pentane (0.34 g) was added to the trap and the solution analyzed by vpc; the quantity of isobutene in the trap was thereby estimated to be about 50 mg (16% yield).

(h) Neopentyl N,N-*Dimethylsulfamate (1, R = Me_3CCH_2)*

A mixture of the sulfamate ester (**1**, R = Me_3CCH_2) (1.8 g, 9.2 mmol) and methyl fluorosulfate (3 mL, 37 mmol) was allowed to stand at room temperature for 1.5 h. Nitrogen was passed through the mixture of liquid and solid (**4**) and then through a trap cooled in Dry Ice. The nmr spectrum of the product was found by comparison with authentic spectra to correspond to a 2:1 mixture of methyl fluorosulfate and 2-methyl-2-butene. In another experiment the volatile products were analyzed by vpc; addition of an authentic specimen of 2-methyl-2-butene enhanced the signal of the major volatile product.

(i) Isopropyl N,N-*Dimethylsulfamate (1, R = Me_2CH)*

The nmr experiment showed new peaks at 1.6 (d) and 5.2 (m) ppm strongly suggestive of isopropyl fluorosulfate. These peaks reached maximum intensity around 2 to 3 h after start of the reaction and then gradually disappeared. A mixture of the sulfamate ester (43 mg, 0.3 mmol), methyl fluorosulfate (0.2 mL, 2.5 mmol), and benzene (182 mg, 2.3 mmol) was observed by nmr; the starting material had virtually disappeared after 7 h at room temperature. Signals in both the nmr spectrum and vpc assigned to cumene were enhanced on addition of authentic cumene.

(j) Methyl N,N-*Dimethylsulfamate (1, R = Me)*

A mixture of the methyl ester (**1**, R = Me), methyl fluorosulfate, and benzene (added as the nmr integration standard) in a molar ratio of 8:3:1 a sealed nmr tube was allowed to stand at room temperature. After an initial drop (in the first 3 h) perhaps due to adventitious hydrolysis, the methyl fluorosulfate signal stayed constant while the disappearance of the methoxy methyl signal (at 3.8 ppm) followed a first order rate law to >90% reaction, $k = 9.6 \times 10^{-6}$ s^{-1} ($r = 0.995$).

In another experiment a solution of the ester (**1**, R = Me) (94 mg, 0.68 mmol, 1.8 *M*), methyl fluorosulfate (34 mg, 0.3 mmol, 0.8 *M*), and benzene (24 mg, 0.3 mmol, 0.8 *M*) in $CDCl_3$ (364 g, 243 μL) in a sealed nmr tube was heated in an oil bath at 40.2°C. The nmr spectrum was determined at intervals over a period of about 6 weeks at the end of which time the concentration of the ester was <30% of the initial concentration; the methyl fluorosulfate concentration was unaltered. The ester was half consumed after about 240 h. A plot of ln[ester] vs. time was distinctly curved, the slope diminishing at longer times;

plots of 1/[ester] and 1/[ester]$^{1/2}$ vs. time were also curved with the slopes increasing at longer times.

Reaction of 3-Phenyl-1-propyl N,N-*Dimethylsulfamate (1, R = $PhCH_2CH_2CH_2$) with Methyl Trifluoromethanesulfonate*

The nmr spectrum of a mixture of the sulfamic ester and excess methyl triflate held at room temperature was observed at intervals. The triplet at 4.1 ppm due to the sulfamic ester (and which was partly obscured by the singlet at 4.1 of the methyl triflate) gradually disappeared while a new triplet appeared at 4.5 ppm. Other peaks were observed at 7.1 (s), 2.6–3.0 (m), and 1.9–2.4 (m). The reaction appeared complete after about 24 h; the product consisted of a white solid (presumed to be **4**) and a light brown liquid. Addition of a sample of 3-phenyl-1-propyl triflate prepared by reaction of sodium 3-phenyl-1-propoxide with triflic anhydride enhanced the above signals.

Acknowledgements

We thank Professor J. B. Stothers for the ^{13}Cmr spectra, Mrs. Heather Schroeder for the ^{19}F and the XL-100 ^{1}Hmr spectra, and Mr. Doug Hairsine for the mass spectra. This work was supported by a grant from the National Research Council of Canada.

1. J. F. King and T. M. Lee. Can. J. Chem. **59**, 356 (1981).
2. J. F. King and T. M. Lee. J. Chem. Soc. Chem. Commun. 48 (1978).
3. C. G. Swain and E. C. Lupton, Jr. J. Am. Chem. Soc. **90**, 4328 (1968).
4. M. G. Ahmed, R. W. Alder, G. H. James, M. L. Sinnott, and M. C. Whiting. Chem. Commun. 1533 (1968).
5. G. A. Olah, J. Nishimura, and Y. K. Mo. Synthesis, 661 (1973).
6. J. F. King, S. M. Loosmore, J. D. Lock, and M. Aslam. J. Am. Chem. Soc. **100**, 1637 (1978).
7. R. L. Hansen. J. Org. Chem. **30**, 4322 (1965), and references cited.
8. S. Winstein, M. Shatavsky, C. Norton, and R. B. Woodward. J. Am. Chem. Soc. **77**, 4183 (1955).
9. P. v. R. Schleyer and R. D. Nicholas. J. Am. Chem. Soc. **83**, 182 (1961).
10. J. L. Fry, C. J. Lancelot, L. K. M. Lam, J. M. Harris, R. C. Bingham, D. J. Raber, R. E. Hall, and P. v. R. Schleyer. J. Am. Chem. Soc. **92**, 2538 (1970).
11. P. G. Gassman, J. M. Hornback, and J. M. Pascone. Tetrahedron Lett. 1425 (1971).
12. W. Traube, H. Zander, and H. Gaffron. Ber. **57**, 1045 (1924).
13. P. F. Ziegler and M. Orchin. J. Org. Chem. **33**, 443 (1968).
14. P. F. Ziegler. Ph.D. Thesis, University of Cincinnati, Cincinnati, OH. 1963.
15. L. Tenud, S. Farooq, J. Seibl, and A. Eschenmoser. Helv. Chim. Acta, **53**, 2059 (1970).
16. J. F. King and M. J. McGarrity. J. Chem. Soc. Chem. Commun. 1140 (1979).
17. D. N. Kevill and G. M. L. Lin. Tetrahedron Lett. 949 (1978).
18. R. E. Robertson. Prog. Phys. Org. Chem. **4**, 213 (1967).
19. E. S. Lewis and S. Vanderpool. J. Am. Chem. Soc. **99**, 1946 (1977).
20. P. Sarthou, F. Guibé, and G. Bram. J. Chem. Soc. Chem. Commun. 377 (1974).
21. F. G. Bordwell, N. R. Vanier, W. S. Matthews, J. B. Hendrickson, and P. L. Skipper. J. Am. Chem. Soc. **97**, 7160 (1975), and references cited.
22. S. Takahashi, L. A. Cohen, H. K. Miller, and E. G. Peake. J. Org. Chem. **36**, 1205 (1971).
23. T. M. Su, W. F. Sliwinski, and P. v. R. Schleyer. J. Am. Chem. Soc. **91**, 5386 (1969).
24. H. F. Herbrandson and F. R. Neufeld. J. Org. Chem. **31**, 1140 (1966).
25. G. A. Sokol'skii. J. Gen. Chem. **36**, 817 (1966); J. Meyer and G. Schramm. Z. Anorg. Allge. Chem. **206**, 24 (1932).
26. J. H. Hildebrand and R. L. Scott. Regular solutions. Prentice-Hall, Englewood Cliffs, NJ. 1962. pp. 166*ff*.
27. A. H. Fainberg and S. Winstein. J. Am. Chem. Soc. **78**, 2770 (1956).
28. H. Zollinger. Angew. Chem. Int. Ed. Engl. **17**, 141 (1978).
29. H. M. Walborsky and D. F. Loncrini. J. Org. Chem. **22**, 1117 (1957).
30. W. W. Binkley and E. F. Degering. J. Am. Chem. Soc. **61**, 3250 (1939).
31. G. A. Olah, W. S. Tolgyesi, S. J. Kuhn, M. E. Moffatt, I. J. Bastien, and E. B. Baker. J. Am. Chem. Soc. **85**, 1328 (1963).
32. H. Vahrenkamp and H. Nöth. J. Organomet. Chem. **12**, 281 (1968).
33. D. E. Mann, N. Acquista, and D. R. Lide, Jr. J. Mol. Spectrosc. **2**, 575 (1958).
34. D. Marquarding, A. Schutz, and I. Ugi. Chem. Ber. **110**, 2656 (1977).

Can. J. Chem. Downloaded from www.nrcresearchpress.com by 210.87.254.6 on 09/05/12
For personal use only.

Reaction des glycosyl isonitriles avec les amines et les alcools

DANIELLE MARMET, PAUL BOULLANGER ET GÉRARD DESCOTES

Université Claude Bernard Lyon I, Ecole Supérieure de Chimie Industrielle de Lyon, ERA 689 du C.N.R.S., 69622 Villeurbanne, France

Reçu le 28 mai 1980

Ce papier est dédié au Prof. Raymond U. Lemieux pour son 60ème anniversaire

DANIELLE MARMET, PAUL BOULLANGER et GÉRARD DESCOTES. Can. J. Chem. **59**, 373 (1981).

Après complexation par les métaux, les glycosylisonitriles **1** peuvent réagir avec les alcools pour conduire principalement à des orthoesters si le carbone C-2 porte un groupe participant et (ou) à des alkyl glycosides sans stéréosélectivité particulière. Avec les amines, l'α-addition sur **1** conduit à des formamidines avec de bons rendements. La synthèse stéréospécifique d'une glucosyl quinazolinone **15** est décrite par hétérocyclisation ultérieure de la formamidine obtenue avec l'anthranilate de méthyle.

DANIELLE MARMET, PAUL BOULLANGER, and GÉRARD DESCOTES. Can. J. Chem. **59**, 373 (1981).

After complexation with metals, glycosylisonitriles **1** react with alcohols to give mainly orthoesters, if C-2 bears a participating group, and/or alkyl glycosides without particular stereoselectivity. In the case of amines, formamidines are obtained by α-addition to **1** in good yields. An example of further heterocyclisation is given with the stereospecific synthesis of the glucosyl-quinazolinone **15**.

Can. J. Chem. Downloaded from www.nrcresearchpress.com by 210.87.254.40 on 09/05/12
For personal use only.

Introduction

Notre récente synthèse de glycosylisonitriles (1) nous a permis d'étudier leur réactivité comme synthons et de la comparer avec celle d'isonitriles non glucidiques.

De nombreuses données de la littérature en série aliphatique permettaient d'envisager des réactions d'α-métallation à l'aide de bases fortes (2) ou d'α-additions de composés à hydrogène mobile par complexation avec divers métaux ou sels métalliques (3) (Schéma 1).

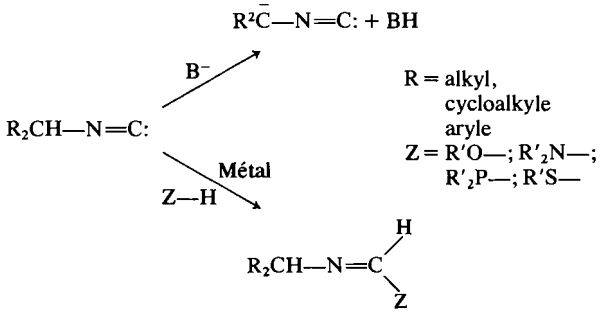

SCHÉMA 1

Nos essais d'arrachement du proton anomère par métallation se sont révélés négatifs quels que soient la base ou le glycosylisonitrile utilisés. Ce manque de réactivité, qui peut être raisonnablement attribué à l'effet mésomère donneur défavorable de l'oxygène du cycle, peut être rapproché des récents échecs de Nolte *et al.* (4) au cours d'essais d'anomérisation par diverses bases fortes d'un glucosylisonitrile de configuration β.

Par contre, l'étude de la réactivité, vis-à-vis de composés à hydrogène mobile, des glucosylisonitriles complexés par des sels métalliques a permis de mettre en évidence une différence importante entre les amines qui donnent une réaction d'α-addition (5) et les alcools qui ne donnent lieu qu'à une réaction de substitution non observée en série aliphatique.

La complexation des glucosylisonitriles avec des métaux et sels métalliques et la réactivité des complexes ainsi obtenus avec quelques alcools et amines font l'objet de cette publication.

Résultats et discussion

Complexation de glucosylisonitriles avec divers métaux et sels métalliques

Comme l'ont montré Saegusa *et al.* les α-additions d'alcools (6) et d'amines (5) sur les isonitriles ne peuvent être réalisées que par la formation de complexes intermédiaires σ entre les isonitriles et des sels métalliques ou métaux des groupes IB (Cu, Ag, Au) ou IIB (Zn, Cd, Hg) (Schéma 2). Les métaux et leurs chlorures peuvent catalyser l'addition des amines aliphatiques à température ambiante (6); les métaux et leurs oxydes celle des alcools à 120°C (6).

La formation de ces complexes peut être mise en évidence en spectroscopie infrarouge par l'observation d'un déplacement vers les courtes longueurs d'onde de la bande isonitrile après complexation (7). La valeur absolue du déplacement ν N=C :) complexé − ν (N=C :) libre donne une

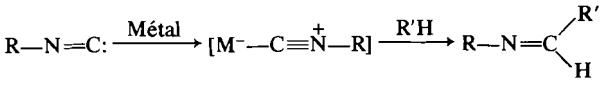

SCHÉMA 2

0008-4042/81/020373-06$01.00/0

©1981 National Research Council of Canada/Conseil national de recherches du Canada

Can. J. Chem. Downloaded from www.nrcresearchpress.com by 210.87.254.40 on 09/05/12
For personal use only.

indication sur la stabilité du complexe formé puisqu'un grand déplacement de bande indique un complexe stable et peu réactif et un déplacement faible, un complexe moins stable et plus réactif (3).

La complexation du tétra-*O*-acétyl-2,3,4,6-β-D-glucopyranosylisonitrile **1** avec divers métaux et sels métalliques, étudiée dans divers solvants a montré que la valeur ν (N≡C :) complexé − ν (N≡C:) libre était indépendante du solvant (éther, dichlorométhane, acétonitrile) excepté dans le cas du chlorure d'argent. En spectroscopie infrarouge on observe à côté de la bande isonitrile libre à 2145 cm^{-1} une faible bande due à l'isonitrile complexé et correspondant à un déplacement moyen de 40 à 50 cm^{-1} en accord avec ceux précédemment décrits par Saegusa et Ito (3).

Les résultats de ces complexations sont résumés dans le Tableau 1.

Les résultats du Tableau 1 montrent que deux systèmes catalytiques provoquent la formation de complexes de plus faible stabilité dont la stoechiométrie n'a pas été étudiée: le chlorure d'argent dans l'acétonitrile et le chlorure mercurique dans le dichlorométhane ou l'acétonitrile (δ:ν (N≡C:) = 39 cm^{-1} et 33 cm^{-1} respectivement). Leur utilisation ultérieure a confirmé leur meilleure réactivité dans la réaction avec les alcools pour le chlorure d'argent et dans l'α-addition des amines aromatiques pour le chlorure mercurique.

Réactivité des alcools avec les glucosylisonitriles complexés

Le manque de réactivité des alcools sur les glucosylisonitriles libres, indépendemment de la température, ou complexés à température ambiante, quels que soient le sel métallique ou l'alcool saturé utilisés est en accord avec les résultats obtenus en série aliphatique par Saegusa *et al.* (5).

A température plus élevée cependant (≥ 70°C), deux types de réactions sont observés en fonction de l'agent complexant utilisé. Les complexes formés avec les oxydes cuivreux ou cuivriques (meilleurs catalyseurs d'α-addition d'alcools selon Saegusa (6)) subissent une décomposition, suivie en spectroscopie infrarouge, pour régénérer l'isonitrile libre initial.

Avec le cuivre, le chlorure cuivreux et principalement avec le chlorure d'argent dans l'acétonitrile (complexe le moins stable d'après l'étude infrarouge), l'alcool réagit sur le glycosylisonitrile pour conduire à un mélange d'orthoesters *endo* et *exo* (**3***a*, **4***a*, **5***a*, **6***a*) majoritaires et de glucosides (**3***b*, **4***b*, **5***b*, **6***b*). Dans chaque cas, l'isomère *exo* de **3***a* à **6***a* est formé très majoritairement (≥ 90%) par rapport à l'isomère *endo* comme le montrent les paramètres rmn ^1H (en particulier le déplacement chimique du groupement méthyle *endo* de l'orthoester) par référence aux résultats de la littérature (8, 9). En l'absence de groupe participant en position C-2 (cas du tétra-*O*-méthyl-2,3,4,6-β-D-glucopyranosyl isonitrile **2**) (1), seuls les glycosides **7** de configuration α (57%) et β (35%) sont formés dans cette réaction. Le formimidate attendu **8** n'est jamais observé dans les produits de réaction (Schéma 3).

Le complexe isonitrile – chlorure d'argent peu stable dans l'acétonitrile (Tableau 1) semble réagir comme groupe partant en présence d'alcool à haute température; la formation d'un ion oxocarbenium suggérée par la participation de l'acétate en C-2 dans le cas de **1** et par le manque de stéréospécificité de la réaction dans le cas de **2** pourrait expliquer la formation des produits observés (**4** à **7**) par un mécanisme inverse de celui avancé pour la formation des glycosylisonitriles par substitution nucléophile (1) (Schéma 3).

La fragilité de la liaison C—N anomère dans les glycosylisonitriles due à la facilité de formation d'un ion oxocarbénium assistée par la participation de l'oxygène du cycle pyrannique peut donc expliquer la différence de réactivité de ceux-ci vis-à-vis des alcools par rapport à leurs homologues aliphatiques.

Réactivité des amines sur les glucosylisonitriles complexés

Comme précédemment observé en série aliphatique (5), les amines aliphatiques réagissent

TABLEAU 1. Complexation du glucosylisonitrile **1** avec quelques sels métalliques

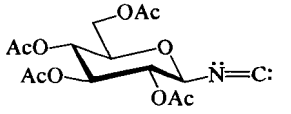

1

Métal ou sel métallique[a]	ν (N≡C) complexé cm^{-1}[b]
Cu	2192
CuO	2191
Cu_2O	2192
CuCl	2192
$HgCl_2$	2178
Ag_2O	2195
AgCl[c]	2194

[a]Isonitrile (40 μmol); solvant (acétonitrile ou dichlorométhane) (1,5 mL); sel métallique (4 μmol); température ambiante; 24 h de complexation.
[b]Mesures infrarouge réalisées avec un appareil Perkin–Elmer 225.
[c]Valeur obtenue dans le dichlorométhane; dans ce cas seulement, une différence importante est observée dans l'acétonitrile (ν (N≡C): 2184).

Can. J. Chem. Downloaded from www.nrcresearchpress.com by 210.87.254.40 on 09/05/12
For personal use only.

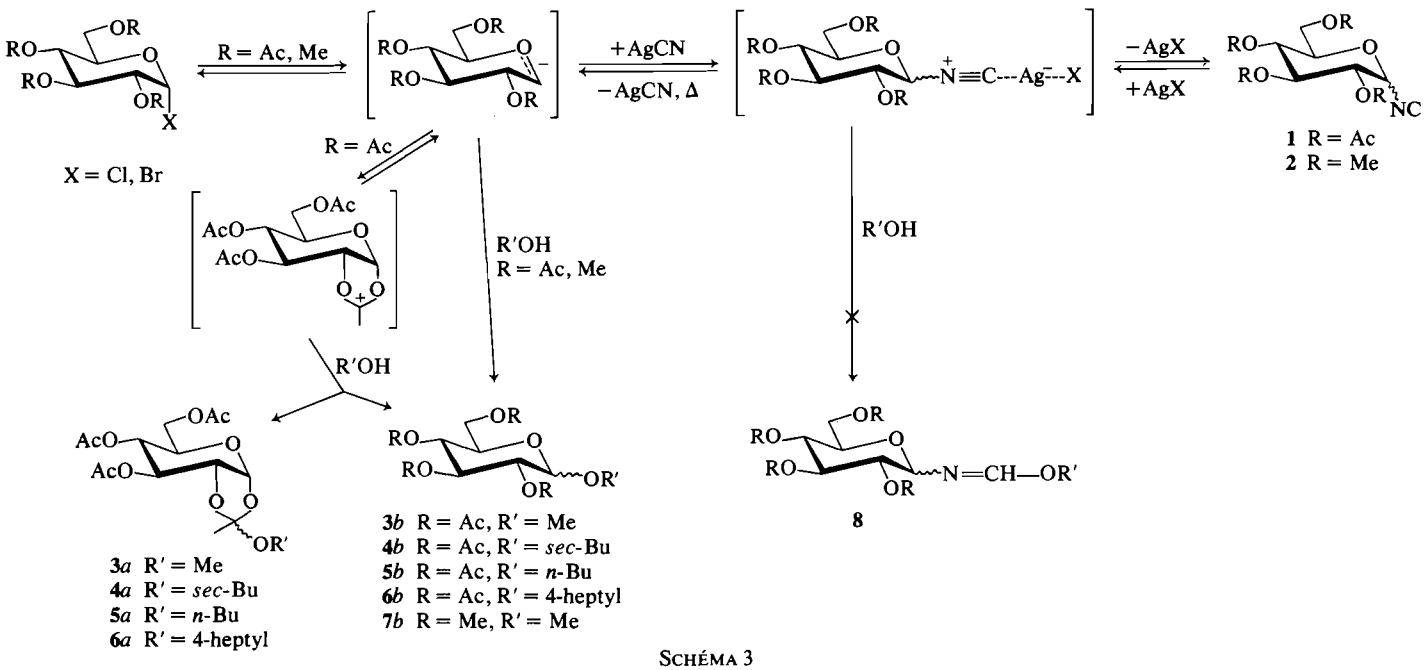

SCHÉMA 3

TABLEAU 2. Synthèse de glucosylformamidines[a] obtenues à partir du tétra-*O*-acétyl-2,3,4,6-β-D-glucopyranosylisonitrile **1**

Amine	Temps de réaction (min)	Rendement (%)	Produit obtenu	
Pipéridine	15	90	RR′ = —$CH_2(CH_2)_3CH_2$—	**9**
Diéthylamine	20	92	R = R′ = Et	**10**
Dibutylamine	20	93	R = R′ = *n*-Bu	**11**
Isobutylamine	30	98	R = *iso*-Bu; R′ = H	**12**
Aniline	20[b]	99	R = Ph; R′ = H	**13**

[a]Formamidines obtenues par réaction d'une amine (3,3 mmol) sur l'isonitrile 1 (1 mmol) en présence de chlorure d'argent (0,07 mmol) dans le dichlorométhane (0,8 mL) à 0°C.
[b]Catalyseur utilisé: chlorure mercurique.

sur les glucosylisonitriles complexés par les chlorures métalliques, à température ambiante, pour conduire par α-addition à des formamidines (**9** à **13**) (Tableau 2) (10). Cette addition semble être stéréospécifique, excepté dans le cas de **13**, puisqu'un seul des isomères *Z* ou *E* de **9** à **12** est isolé comme le montrent les spectres de résonance magnétique nucléaire ^1H et ^{13}C. Les conditions opératoires utilisées, la stabilité des formamidines obtenues au cours de chauffage à des températures voisines de 50°C et la facilité de cyclisation de la formamidine **14** en quinazolinone **15** semblent indiquer que seul l'isomère thermodynamique de configuration *E* est isolé au cours de cette addition. Ces résultats sont en accord avec les récents travaux de Hegarty et Chandler (11, 12) qui indiquent que le produit cinétique *Z* d'addition d'une amine secondaire sur un isonitrile s'isomérise à température ambiante en produit thermodynamique de configuration *E*.

Les meilleurs rendements sont obtenus par complexation avec le chlorure d'argent dans le dichlorométhane ou l'acétonitrile. Dans le cas des amines aromatiques (aniline ou anthranilate de méthyle) de bons résultats ont été obtenus en utilisant comme agent complexant le chlorure mercurique à température ambiante. Ces données sont en accord avec la stabilité présumée des complexes étudiés en spectroscopie infrarouge (Tableau 1).

Utilisés à température ambiante ou à 0°C, les glucosylisonitriles complexés sont donc susceptibles de conduire à des réactions d'α-addition comme leurs homologues aliphatiques; ce n'est qu'à température plus élevée que le groupement isonitrile complexé peut se comporter comme groupe partant et conduire à une substitution nucléophile en position anomère avec les alcools; cette dualité de réactivité n'a pas, à notre connaissance, été signalée en série aliphatique.

Les résultats satisfaisants obtenus dans la synthèse des formamidines ont permis d'envisager une application de cette α-addition à la préparation de nucléosides de configuration définie. Dans ce but, l'anthranilate de méthyle a été condensé sur le glucosylisonitrile **1** complexé par le chlorure d'argent ou le chlorure mercurique.

Dans le premier cas, la formamidine **14** obtenue reste complexée au chlorure d'argent même après un chauffage prolongé. La catalyse par le chlorure mercurique, complexant plus faible (Tableau 1), permet de réaliser une hétérocyclisation directe en quinazolinone **15** précédemment préparée par une autre voie (13), par simple reflux dans le dichloroéthane (Schéma 4). Une telle hétérocyclisation directe a déjà été mentionnée dans la synthèse des 1 *N*-(ribofuranosyl) adénines par Imbach et coll. (14).

Cet exemple de synthèse stéréospécifique de la quinazolinone **15** permet d'éviter la non régio- et stéréosélectivité observées lors de la substitution d'halogénures de glycosyles par l'hydroxy-4 quinazoline (formation de dérivés d'O- et C-substitution (13) et des anomères α et β (15)). Les glycosylisonitriles acétylés représentent donc de nouveaux synthons osidiques (16) à configuration anomérique définie utilisables en synthèse

Partie expérimentale

Les points de fusion sont déterminés en tube capillaire sur un appareil Buchi et ne sont pas corrigés. Les pouvoirs rotatoires sont mesurés sur un polarimètre Perkin Elmer 141 dans des cellules de 1 dm. Les spectres infrarouge sont enregistrés sur spectromètres Perkin Elmer 225 et 237. Les spectres de rmn ^1H sont enregistrés sur appareil Varian A 60 et Varian HA 100 (référence: Me_4Si interne); les spectres de rmn ^{13}C sur appareil Varian XL 100 opérant à 25.2 MHz (référence Me_4Si interne). Les chromatographies sont réalisées sur gel de silice Merck (230–400 mesh).

Tétra-O-acétyl-2,3,4,6-β-D-glucopyranosylisonitrile 1

Préparé selon le mode opératoire de Nolte *et al* (4) à partir du bromure de tétra-*O*-acétyl-2,3,4,6-α-D-glucopyranosyle (17), les

Can. J. Chem. Downloaded from www.nrcresearchpress.com by 210.87.254.40 on 09/05/12
For personal use only.

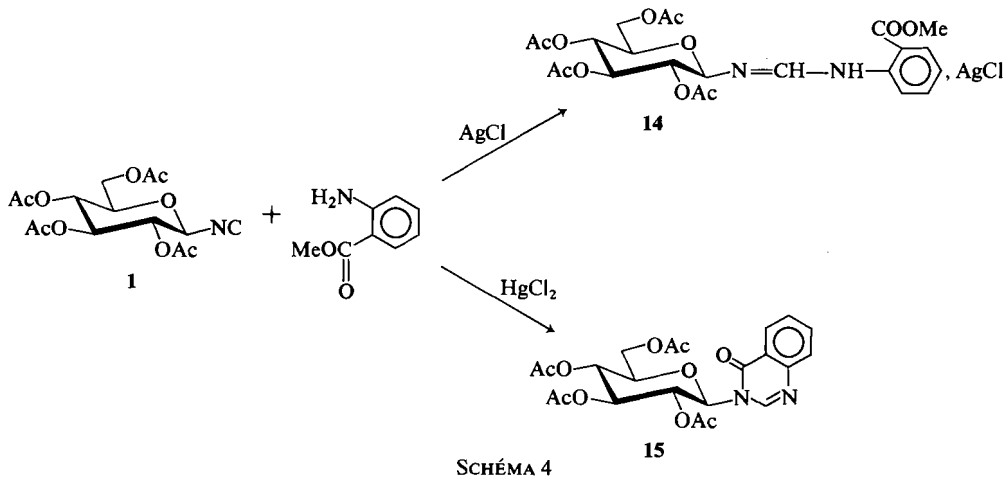

SCHÉMA 4

propriétés physiques et spectrales de **1** sont en accord avec celles décrites par Martin-Lomas et Chacon-Fuertes (18).

Tétra-O-méthyl-2,3,4,6-β-D-glucopyranosylisonitrile 2
Préparé selon le mode opératoire précédemment publié (1).

Réaction du glucopyranosylisonitrile complexé 1 avec les alcools

A l'isonitrile **1** (357 mg, 1 mmol) en solution dans l'acétonitrile (1 mL) est ajouté du chlorure d'argent anhydre (10 mg, 7×10^{-2} mmol). Après solubilisation, l'alcool (2 mmol) est ajouté à la solution qui est portée à reflux jusqu'à disparition complète de la bande infrarouge ν (N=C:) du groupement isonitrile.

Après précipitation du chlorure d'argent par dilution dans le solvant réactionnel et évaporation du solvant, les mélanges obtenus sont chromatographiés sur gel de silice (éluant acétate d'éthyle – hexane 1:1). Les produits principaux ainsi récupérés sont les orthoesters *exo* **3***a* à **6***a*, identifiés par référence aux produits décrits dans la littérature et par les spectres rmn ^1H caractéristiques de ces composés (8, 9).

*Tri-O-acétyl-3,4,6-(1-méthoxyéthylidène)-1,2-O-α-D-glucopyranose 3*a
Obtenu après 3 h de reflux avec un rendement de 84%. Huile incolore, $[\alpha]_D^{20}$ +50,6° (*c*, 1,6, $CHCl_3$) (litt. (19) $[\alpha]_D$ +48,3° ($CHCl_3$)). Spectre rmn ^1H en accord avec celui décrit dans la littérature (8).

*Tri-O-acétyl-3,4,6-[1-(méthyl-1-propyloxyéthylidène)]-1,2-O-α-D-glucopyranose 4*a
Obtenu après 3 h de reflux avec un rendement de 52%. Solide blanc, F = 67°C (alcool 95°C); $[\alpha]_D^{20}$ +39° (*c* 2,4, $CHCl_3$); rmn ^1H (CD_3CN) δ ppm: 5,60 (d, 1H, H-1, $J_{1,2}$ = 5,2 Hz); 5,03 (t, 1H, H-3, $J_{2,3}$ = 2,7 Hz, $J_{3,4}$ = 2,7 Hz); 4,90–4,65 (m, 1H, H-4, $J_{4,5}$ = 8,8 Hz); 4,40–4,0 (m, 3H, H-2, H-6, H-6′); 3,90–3,50 (m, 1H, H-5); 1,67 (s, 3H, CH_3 orthoester): 1,50–0,80 (m, 9H, *n*-butyl). *Anal.* calc. pour $C_{18}H_{28}O_{10}$: C 53,46, H 6,98, O 39,56; trouvé: C 53,33, H 6,76, O 39,73.

*Tri-O-acétyl-3,4,6-(1-n-butoxyéthylidène)-1,2-O-α-D-glucopyranose 5*a
Préparé dans le butanol comme solvant et avec le cuivre métallique comme catalyseur le produit est obtenu après 10 h de reflux avec un rendement de 35%. Les constantes physiques de **5***a* sont en accord avec celles décrites dans la littérature (20). Huile incolore, $[\alpha]_D^{20}$ +41° (*c* 1,5, $CHCl_3$) (litt. (20) $[\alpha]_D$ +33,8° ($CHCl_3$)).

*Tri-O-acétyl-3,4,6-[1-(propyl-1-butyloxyéthylidène)]-1,2-O-α-D-glucopyranose 6*a
Obtenu après 6 h de reflux avec une rendement de 47%. Huile incolore, $[\alpha]_D^{20}$ +22° (*c* 4,4, $CHCl_3$); rmn ^1H (CD_3CN) δ ppm: 5,70 (d, 1H, H-1, $J_{1,2}$ = 5,0 Hz); 5,15–4,65 (m, 2H, H-3, H-4); 4,43–4,23 (m, 1H, H-2); 4,20–3,50 (m, 3H, H-6, H-6′, H-5); 1,63 (s, 3H, CH_3 orthoester); 1,50–0,60 (m, 15H, heptyl). *Anal.* calc. pour $C_{21}H_{34}O_{10}$: C 56,49, H 7,68; trouvé: C 56,35, H 7,62.

Réaction du glucopyranosylisonitrile 1 complexé avec les amines

A l'isonitrile **1** (357 mg, 1 mmol) dans le dichlorométhane (0,8 mL) à 0°C est ajouté le chlorure d'argent (10 mg, 7×10^{-2} mmol) pour les amines aliphatiques ou le chlorure mercurique (19 mg, 7×10^{-2} mmol) pour les amines aromatiques. Après solubilisation, l'amine (3,3 mmol, Tableau 2) est ajoutée à la solution et l'agitation poursuivie pendant 30 min jusqu'à disparition de la bande infrarouge du groupement isonitrile ν(N=C:). Après concentration et filtration, de l'hexane (2 × 2 mL) est ajouté à la solution pour précipiter le sel métallique; le filtrat est alors concentré et repris avec un mélange éther – éther de pétrole (45–60°C) pour cristallisation éventuelle du produit d'α-addition. Les formamidines de configuration probable *E*, excepté dans le cas de **13** (*Z* + *E*) sont caractérisées par rmn ^1H (proton —N=C*H*—N< très déblindé 7,3–7,5 ppm) et infrarouge (ν(—N=C<) 1630 cm^{-1}).

N-*(Tétra-O-acétyl-2,3,4,6-β-D-glucopyranosyl)-N′,N′-pentaméthylène formamidine 9*
Obtenue avec un rendement de 90%. Solide blanc, pf 107–108°C (éther); $[\alpha]_D^{20}$ = +2,3° (*c* 2,4, $CHCl_3$); ir (KBr) ν_{max}: 1620 cm^{-1} (>C=N—); rmn ^1H (CD_3COCD_3) δ ppm: 7,48 (s, 1H, —N=C*H*—N<); 5,30–4,70 (m, 3H, H-2, H-3, H-4); 4,50 (d, 1H, H-1, $J_{1,2}$ = 8,2 Hz); 4,25–3,90 (m, 3H, H-5, H-6, H-6′); 3,50–3,20 (m, 4H, H αα′pipéridine); 1,75–1,40 (m, 6H, Hββ′γ pipéridine); rmn ^{13}C (CD_3COCD_3) δ ppm: 156,2 (>*C*=N); 94,4 (C-1); 74,2–74,0–73,7 (C-2, C-3, C-5); 69,8 (C-4); 63,2 (C-6). *Anal.* calc. pour $C_{20}H_{30}O_9N_2$: C 54,29, H 6,83, N 6,33; trouvé: C 54,28, H 6,86, N 6,28.

N-*(Tétra-O-acétyl-2,3,4,6-β-D-glucopyranosyl)-N′,N′-éthyl formamidine 10*
Obtenue avec un rendement de 92%. Solide blanc, pf 83–85°C (éther – éther de pétrole); $[\alpha]_D^{20}$ = +1,6° (*c* 3,1, $CHCl_3$); ir (KBr) ν_{max}: 1620 cm^{-1} (>C=N—); rmn ^1H (CD_3COCD_3) δ

Can. J. Chem. Downloaded from www.nrcresearchpress.com by 210.87.254.40 on 09/05/12
For personal use only.

ppm: 7,50 (s, 1H, —N=C*H*—N<); 5,25–4,70 (m, 3H, H-2, H-3, H-4); 4,45 (d, 1H, H-1, $J_{1,2}$ = 7,8 Hz); 4,20–3,07 (m, 3H, H-5, H-6, H-6′); 3,27 (q, 4H, CH_2); 1,05 (t, 6H, CH_3); rmn ^{13}C (CD_3COCD_3) δ ppm: 156,1 (>*C*=N—); 94,7 (C-1); 74,1–73,9–73,7 (C-2, C-3, C-5); 69,8 (C-4); 63,2 (C-6). *Anal.* calc. pour $C_{19}H_{30}O_9N_2$: C 53,01, H 7,03, N 6,51; trouvé: C 53,07, H 6,90, N 6,54.

N-(*Tétra*-O-*acétyl-2,3,4,6*-β-D-*glucopyranosyl*)-N′,N′-*butylformamidine 11*

Obtenue avec un rendement de 93%, sa purification impossible par chromatographie sur colonne (décomp.) est rendue difficile car le composé n'est pas cristallin. Huile claire; $[\alpha]_D^{20}$ −6,3° (*c* 2,5, $CHCl_3$); ir (film) ν_{max}: 1620 cm^{-1} (>C=N—); rmn ^1H (CD_3COCD_3) δ ppm: 7,50 (s, 1H, —N=C*H*—N<); 5,30–4,65 (m, 3H, H-2, H-3, H-4); 4,50 (d, 1H, H-1, $J_{1,2}$ = 7,5 Hz); 4,25–3,70 (m, 3H, H-5, H-6, H-6′); 3,30–3,0 (m, 4H, CH_2 butylamine); 1,70–0,70 (m, 14H, CH_2 et CH_3 butylamine). *Anal.* calc. pour $C_{23}H_{38}O_9N_2$: C 56,76, H 7,87, N 5,76; trouvé: C 55,75, H 7,63, N 5,17.

N-(*Tétra*-O-*acétyl-2,3,4,6*-β-D-*glucopyranosyl*)-N′-*isobutylformamidine 12*

Obtenue avec un rendement de 98%. Solide blanc, pf 97–99°C (éther); $[\alpha]_D^{20}$ −16,3° (*c* 2,1, $CHCl_3$); ir (KBr) ν_{max}: 1630 cm^{-1} (—N=C<); rmn ^1H (CD_3COCD_3) δ ppm: 7,60 (s, 1H, —N=C*H*—N<); 6,0–5,5 (m, 1H, >N*H*); 5,30–4,70 (m, 3H, H-2, H-3, H-4); 4,50 (d, 1H, H-1, $J_{1,2}$ = 7,8 Hz); 4,20–3,70 (m, 3H, H-5, H-6, H-6′); 3,0 (m, 2H, —CH_2—); 1,1–0,75 (m, 7H, —$CH(CH_3)_2$); rmn ^{13}C (CD_3COCD_3) δ ppm: 155,1 (—N=*C*<); 85,8 (C-1); 74,5 (C-5); 73,4 (C-3); 72,0 (C-2); 68,7 (C-4); 62,5 (C-6). *Anal.* calc. pour $C_{19}H_{30}O_9N_2$: C 53,01, H 7,03, N 6,51; trouvé: C 53,11, H 7,08, N 6,79.

N-(*Tétra*-O-*acétyl-2,3,4,6*-β-D-*glucopyranosyl*)-N′-*phénylformamidine 11*

Obtenue avec un rendement de 99%. Huile incolore; $[\alpha]_D^{20}$ +38° (*c* 2,9, $CHCl_3$); ir (film) ν_{max}: 1650 cm^{-1} (—N=C<); rmn ^1H (CD_3COCD_3) δ ppm: 8,30 et 8,0 (2s, 1H, —N=C*H*—N< *Z* et *E* obtenus en pourcentages voisins); 7,50–7,0 (m, 5H, aromatiques); 6,30–5,60 (m, 1H, >NH); 5,40–4,70 (m, 4H, H-1, H-2, H-3, H-4); 4,40–3,70 (m, 3H, H-5, H-6, H-6′). *Anal.* calc. pour $C_{21}H_{26}O_9N_2$: C 55,99, H 5,82, N 6,22; trouvé: C 55,87, H 5,93, N 6,71.

*3*N-(*Tétra*-O-*acétyl-2′,3′,4′,6′*-β-D-*glucopyranosyl*)-*quinazolinone-4 15*

La réaction réalisée selon le mode opératoire usuel dans le dichloroéthane à reflux pendant 3 h conduit directement au produit d'hétérocylisation **15** qui cristallise dans l'éther (rendement 72%). Solide blanc, pf 180–182°C (éther) (litt. (13) pF 190°C); $[\alpha]_D^{20}$ +12° (*c* 1,5, $CHCl_3$) (litt. (13) $[\alpha]_D$ 0° ($CHCl_3$); ir (KBr) ν_{max}: 1730 cm^{-1} (C=O quinazolinone); 1680 cm^{-1} (—N=C<); rmn ^1H (CD_3COCD_3) δ ppm: 8,47 (s, 1H, H-2); 8,15 (d, 1H, H-5, $J_{5,6}$ = 7,8 Hz); 7,90–7,35 (m, 3H, H-6, H-7, H-8); 6,35 (d, 1H, H-1′, $J_{1',2'}$ = 7,8 Hz); 5,62–5,15 (m, 3H, H-2′, H-3′, H-4′); 4,42–4,15 (m, 3H, H-5′, H-6′, H-6″). *Anal.* calc. pour $C_{22}H_{24}O_{10}N_2$: C 55,46, H 5,08, N 5,88; trouvé: C 55,51, H 4,87, N 6,06.

Remerciements

Nous remercions le Professeur A. F. Hegarty, University College Dublin, pour ses intéressantes suggestions concernant les configurations des glycosylformamidines.

1. P. Boullanger, D. Marmet et G. Descotes. Tetrahedron, **35**, 163 (1979).
2. U. Schöllkopf. Angew. Chem. Int. Ed. Engl. **16**, 339 (1977).
3. T. Saegusa et Y. Ito. Isonitrile chemistry. *Edité par* I. Ugi. Academic Press, New York, London. 1971. p. 65.
4. R. J. M. Nolte, J. A. J. Van Zomeren et J. W. Zwikker. J. Org. Chem. **43**, 1972 (1978).
5. T. Saegusa, Y. Ito, S. Kobayashi, K. Hirota et H. Yoshioka. Bull. Chem. Soc. Jpn. **42**, 3310 (1969).
6. T. Saegusa, Y. Ito, S. Kobayashi, K. Hirota et N. Takeda. Can. J. Chem. **47**, 1217 (1969).
7. F. A. Cotton et F. Zingales. J. Am. Chem. Soc. **83**, 351 (1961).
8. R. U. Lemieux et A. R. Morgan. Can. J. Chem. **43**, 2199 (1965).
9. A. S. Perlin. Can. J. Chem. **41**, 399 (1963).
10. D. Marmet, P. Boullanger et G. Descotes. Tetrahedron Lett. 1459 (1980).
11. A. F. Hegarty et A. Chandler. Tetrahedron Lett. 885 (1980).
12. A. F. Hegarty et A. Chandler. J. Chem. Soc. Chem. Commun. 130 (1980).
13. G. Wagner et F. Suess. Pharmazie, **24**, 35 (1969).
14. B. Rayner, C. Tapiero et J. L. Imbach. Carbohydr. Res. **59**, 111 (1977).
15. M. G. Start et R. K. Robins. J. Heterocycl. Chem. **6**, 89 (1969).
16. G. Gosselin, J. L. Barascut et J. L. Imbach. Actual. Chim. **3**, 7 (1969); **4**, 13 (1969).
17. R. U. Lemieux. Methods Carbohydr. Chem. **2**, 221 (1963).
18. M. Martin-Lomas et M. E. Chacon-Fuertes. Carbohydr. Res. **59**, 604 (1977).
19. T. Ogawa et M. Matsui. Carbohydr. Res. **51**, C 13 (1976).
20. S. Hanessian et J. Banoub. Carbohydr. Res. **44**, C 14 (1975).

Can. J. Chem. Downloaded from www.nrcresearchpress.com by 210.87.254.40 on 09/05/12
For personal use only.

Conformational analysis in carbohydrate chemistry. V.[1] Formation of glycosidic anhydrides from heptoses

STEPHEN JOHN ANGYAL AND TRUNG QUANG TRAN

School of Chemistry, University of New South Wales, Kensington, N.S.W. 2033, Australia

Received July 11, 1980

This paper is dedicated to Prof. Raymond U. Lemieux on the occasion of his 60th birthday

STEPHEN JOHN ANGYAL and TRUNG QUANG TRAN. Can. J. Chem. **59**, 379 (1981).

The position of the equilibrium between aldoheptoses and their glycosidic anhydrides depends crucially on the configuration of the heptose. Depending on that configuration, the 1,6-anhydropyranose, the 1,7-anhydropyranose, or the 1,6-anhydrofuranose is the major product, its proportion varying from 99% to less than 1%. The position of the equilibrium is predictable from conformational considerations. 1,7-Anhydrofuranoses have not been encountered. The 1,3-dioxane ring of the 1,7-anhydropyranoses was found to assume a skew form.

STEPHEN JOHN ANGYAL et TRUNG QUANG TRAN. Can. J. Chem. **59**, 379 (1981).

La position de l'équilibre entre les aldoheptoses et leurs anhydrides glycosidiques dépend fondamentalement de la configuration de l'heptose. Dépendant de la configuration, le produit majoritaire est soit l'anhydro-1,6 pyrannose, soit l'anhydro-1,7 pyrannose ou soit l'anhydro-1,6 furannose et ses proportions varient de 99% à moins de 1%. On peut prédire la position de l'équilibre à partir des considérations conformationnelles. On n'a pas mis en évidence la présence de l'anhydro-1,7 furannose. On a trouvé que le cycle dioxanne des anhydro-1,7 pyrannoses présente une forme décalée.

[Traduit par le journal]

Introduction

Although the 1,6-anhydrides of the aldohexoses have been extensively studied and widely used as synthetic intermediates (2), very little was known until recently about the glycosidic anhydrides of the aldoheptoses. These anhydrides are formed from, and are in equilibrium with, the parent aldoses in boiling aqueous solutions containing a strong acid. In this way, Richtmyer and his coworkers obtained the 1,6-anhydropyranose (3) from D-*glycero*-D-*ido*-heptose, and the 1,6- and 1,7-anhydropyranoses (4) from D-*glycero*-D-*gulo*-heptose. Recently, Angyal and Beveridge (1) prepared the 1,6-anhydropyranoses of D-*glycero*-L-*manno*-, D-*glycero*-L-*allo*-, and D-*glycero*-L-*altro*-heptoses. These anhydrides were found to be present in the equilibrium mixtures in much higher proportion than were the 1,6-anhydrides in the equilibria with the respective aldohexoses. The higher stability of the heptose anhydrides, compared with the hexose anhydrides, was attributed (1) to the ring closure occurring through a secondary, rather than through a primary, hydroxyl group.

The proportion of 1,6-anhydropyranose in equilibrium with an aldohexose ranges from 0.2% for glucose to 76% for idose (5). These proportions have been explained in terms of nonbonded interactions (5). With the recognition that the tendency for ring formation through primary hydroxyl groups is different from that through secondary hydroxyl groups, it is possible now to discuss the conformational analysis of anhydroheptoses by analogy to that of the anhydrohexoses, and to make predictions about the proportion of the anhydroheptoses at equilibrium. Some of these predictions have now been tested.

For the aldoheptoses, three different types of glycosidic anhydrides are significant: the 1,6- and 1,7-anhydro-pyranoses and the 1,6-anhydrofuranoses. The 1,7-anhydrofuranoses, which contain fused five- and seven-membered rings, would have low stability and have, in fact, not been encountered in our work. Other types of anhydrides, such as the 1,4-anhydropyranoses (6), would occur in very small amounts only.

There are sixteen possible diastereomeric aldoheptoses (counting each pair of enantiomers only once); we have not investigated all of them. The synthesis of some of the aldoheptoses is quite cumbersome and it was felt that not all of them would yield worthwhile information. Thus, the discussion which follows will allow us to predict with confidence, even though we were not able to test our prediction, that D-*glycero*-L-*ido*-heptose would be converted to an extent of over 99% into the 1,6-anhydropyranose, and that D-*glycero*-D-*gluco*-heptose would yield no anhydride in a proportion over 0.1%.

Results and Discussion

1,6-Anhydropyranoses

The proportions of 1,6-anhydropyranose in equilibrium with each aldohexose are (5): glucose,

[1]For part IV, see ref. 1.

0008-4042/81/020379-05$01.00/0

©1981 National Research Council of Canada/Conseil national de recherches du Canada

Can. J. Chem. Downloaded from www.nrcresearchpress.com by 210.87.254.42 on 09/05/12
For personal use only.

Can. J. Chem. Downloaded from www.nrcresearchpress.com by 210.87.254.42 on 09/05/12
For personal use only.

0.2; mannose, 0.8; galactose, 0.8; talose, ≧2.8; allose, ≧14; altrose, 65; gulose, 65; and idose, 76%. When the additional hydroxymethyl group in the 1,6-anhydroheptoses is *exo*, the proportion of the anhydride in equilibrium was found to be considerably higher (1), namely, 15% for D-*glycero*-L-*manno*-heptose, 54% for D-*glycero*-L-*allo*-heptose, and 98% for D-*glycero*-L-*altro*-heptose. It is reasonable to assume that similar increases would occur in going from the other hexoses to the homomorphous D-*glycero*-L-heptoses (and their L-*glycero*-D-heptose enantiomers), the anhydrides of which all have *exo* hydroxymethyl groups. In fact, we found that on equilibration D-*glycero*-L-*gluco*-heptose gave 7.5%, D-*glycero*-L-*galacto*-heptose 18%, and D-*glycero*-L-*talo*-heptose 31% of the 1,6-anhydropyranose. The structures of these anhydrides were not proven because we had insufficient material for their isolation but, by analogy with the other heptoses, it is very likely that they are 1,6-anhydropyranoses. The other anhydrides of these heptoses would have very unfavourable interactions. The remaining heptoses of this group, D-*glycero*-L-*gulo*- and D-*glycero*-L-*ido*-heptose, were not available but, by analogy with D-*glycero*-L-*altro*-heptose, one can confidently predict that they would be converted into the 1,6-anhydropyranoses to the extent of at least 98%.

The 1,6-anhydropyranoses of the D-*glycero*-D-heptoses (and their L-*glycero*-L-heptose enantiomers) have the hydroxymethyl group in the *endo* configuration (**1**) and are therefore less stable than the homomorphous hexose derivatives. Thus we found that D-*glycero*-D-*gulo*-heptose yields only 11%, and D-*glycero*-D-*ido*-heptose 35%, of the 1,6-anhydropyranose (compared with 65 and 76% for the hexoses). One would then predict that D-*glycero*-D-*altro*-heptose would give the 1,6-anhydride in a proportion similar to that of the *gulo* compound, and that D-*glycero*-D-*gluco*-, -D-*manno*-, -D-*galacto*-, and -D-*talo*-heptose would yield only traces of the anhydride. In fact, on equilibration of the *galacto* and *talo* isomers we found (by glc) only very small amounts (<0.5%) of compounds which could be the 1,6-anhydropyranoses. D-*glycero*-D-*allo*-Heptose yielded approximately 3% of the 1,6-anhydride; this is about the proportion one would have predicted by comparison with allose (14%).

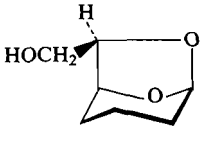

1

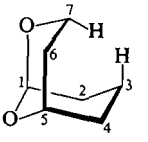

2

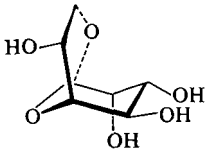

3

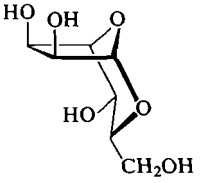

4

1,7-Anhydropyranoses

Only one anhydride of this type has been described, 1,7-anhydro-D-*glycero*-β-D-*gulo*-heptopyranose, obtained in about 10% yield[2] from the heptose on equilibration (4). We found that D-*glycero*-D-*ido*-heptose gave 40% of the 1,7-anhydride. The ring system contained in these anhydrides (analogous to the bicyclo[3,3,1]nonane system) is inherently unstable owing to the interaction, in the twin-chair form (**2**), between the *endo* hydrogen atoms on C-3 and C-7. The strain in bicyclo[3,3,1]nonane has been estimated (7) to be ~42 kJ mol^{-1}. The 1,7-anhydrides appear to be about equal in stability to the 1,6-anhydrides with an *endo* hydroxymethyl group; judging by models, the configuration of C-6 does not appear to affect the stability to any significant extent, except in those cases when O-4 is equatorial: the 1,7-anhydride of a D-*glycero*-L-heptose would then have a parallel 1,3-interaction between O-4 and O-6.

These considerations indicate that D-*glycero*-D-*altro*-heptose (which we did not have) would give about 10% of the 1,7-anhydride, and D-*glycero*-D-*allo*-heptose, about 4%. In fact, equilibration of the latter compound produced an anhydride in 4.3% yield; this we believe to be the 1,7-anhydride. The 1,7-anhydride of D-*glycero*-L-*altro*-heptose would have a stability similar to that of the D-*glycero*-D-*altro* compound but would hardly be detectable in the presence of the overwhelming proportion (98%) of the 1,6-anhydride. None of the other heptoses would yield a substantial proportion of the 1,7-anhydropyranose.

In fact, the other heptoses we investigated did not yield any compound that we could recognize as the 1,7-anhydropyranose. D-*glycero*-L-*allo*-Heptose gave two minor components (beside the 1,6-anhydropyranose); one of these is probably the 1,7-anhydropyranose.

In order to identify the anhydride obtained from D-*glycero*-D-*ido*-heptose as the 1,7-anhydride, we studied its nmr spectrum and, for comparison, also

[2]Angyal and Dawes (5) reported a much higher conversion (66%) but we were unable to repeat their results. Even after 72 h boiling with 5% sulfuric acid, only 11.4% of the 1,7-anhydride was found to be present, and the amount no longer increased with time.

Can. J. Chem. Downloaded from www.nrcresearchpress.com by 210.87.254.42 on 09/05/12
For personal use only.

those of 1,7-anhydro-D-*glycero*-D-*gulo*-heptopyranose and of the 1,6-anhydrides of these two heptoses. In all of these spectra, only the signal of H-1 could be distinguished, the other signals overlapping extensively. However, when these compounds were acetylated, the signals of H-2, H-3, H-4, and either H-6 or H-7 and H-7′ shifted downfield, and all the spectra could be fully analysed. In the spectra of the acetylated 1,6-anhydrides, the signals of H-5 and H-6 were at highest field, showing thereby that C-5 and C-6 do not carry acetoxy groups. On the other hand, in the spectra of the acetylated 1,7-anhydrides, the signals of H-5, H-7, and H-7′ were at highest field.

The conformations of these 1,7-anhydrides are of interest. Bicyclo[3,3,1]nonane, in the absence of *endo* substituents which would cause steric interaction, is predominantly in the twin-chair form, with the chairs somewhat flattened (8). It has been suggested, however, that in the 1,7-anhydropyranoses the interaction between H-3 and H-7 may be sufficiently large to encourage the 1,3-dioxan ring to exist, at least partially, in a boat conformation (9). In fact, the nmr spectra of the acetates clearly show that the anhydride ring is not in the chair form (**2**): in that form, $J_{5,6}$, $J_{6,7}$, and $J_{6,7'}$ would all have values of ~3.5 Hz. In the spectrum of tetraacetyl-1,7-anhydro-D-*glycero*-β-D-*gulo*-heptose these values are 1.2, 7.1, and 9.0 Hz, respectively, which seems to indicate that the 1,3-dioxan ring is in the $^{a6}S_{a2}$ skew form (**3**). The *ido* anhydride has somewhat smaller coupling constants (1.0, 5.3, 5.1 Hz); there seems to be more of the twin-chair form in equilibrium with the skew form. Accordingly, the pyranose ring is somewhat flattened ($J_{2,3}$ and $J_{3,4}$ are less than 10 Hz).

1,6-Anhydrofuranoses

No anhydrofuranose derivative of an aldoheptose has so far been reported. From the aldohexoses, small amounts (0.04–2.5%) of the 1,6-anhydrofuranoses are produced on equilibration in acid solution (5, 6, 10), in addition to the predominant 1,6-anhydropyranoses. The anhydrofuranoses of talose and altrose occur in the highest proportion (2.5 and 1.6%), followed by those of allose (1.0%) and galactose (0.95%). Since the formation of the 1,6-anhydrofuranose from an aldoheptose would involve ring formation through a secondary hydroxyl group, it is predictable that the anhydride will be formed in a considerably higher proportion than it is from the homologous hexose, provided that the additional hydroxymethyl group is *exo* and therefore its presence does not introduce an unfavourable steric interaction.

Of all the diastereomers, the 1,6-anhydrofuranose of D-*glycero*-D-*talo*-heptose would be the energetically most favourable one: O-2, O-3, and C-7 are *exo* and O-5 is equatorial. It was found that this heptose gave one anhydride in 11.2% yield. The nmr spectrum of its acetate proved that this is, indeed, the anhydrofuranose (**4**): $J_{1,2}$ and $J_{3,4}$ are smaller than 0.5 Hz and $J_{2,3}$ is 6.7 Hz. The spectrum is similar to that of the acetate of 1,6-anhydro-α-D-talofuranose (5). The six-membered anhydro-ring is in the chair form ($J_{5,6}$ is 10.0 Hz).

The 1,6-anhydrofuranoses of D-*glycero*-D-*galacto*- and D-*ido*-heptose would differ from the preceding anhydride only in having an *endo* hydroxyl group on C-2 and C-3, respectively, and would therefore also be energetically favourable. D-*glycero*-D-*galacto*-Heptose produced, on equilibration, 7.5% of an anhydride, which was shown to be the 1,6-anhydrofuranose by the nmr spectrum of its acetate; this is closely similar to the spectrum of the acetate of 1,6-anhydro-α-D-*galacto*-furanose (11). Although D-*glycero*-D-*ido*-heptose is converted into the two anhydropyranoses in a yield of nearly 75%, glc shows the presence of another anhydride (1.3%) which presumably is the anhydrofuranose.

In the D-*glycero*-L-heptose series, the 1,6-anhydrofuranoses of the *gluco*, *allo*, and *altro* configuration have the most favourable structures (C-7 *exo* and no, or only one, *endo* hydroxyl group). In the equilibrium mixtures formed from the *gluco* and *allo* isomers, glc shows the presence of an anhydride in a proportion higher than that of the anhydrofuranose of glucose and allose, respectively; these we presume to be the 1,6-anhydrofuranoses though we have not isolated them. Since D-*glycero*-L-*altro*-heptose is converted to the 1,6-anhydropyranose to the extent of 98%, the anhydrofuranose was not detected. Additional small peaks are also seen in the glc curves of the equilibrium mixtures from D-*glycero*-L-*galacto*- and D-*glycero*-L-*talo*-heptoses. These are also believed to represent anhydrofuranoses; although they would have *endo* hydroxymethyl groups, ring closure through a secondary hydroxyl group would compensate for this steric effect; the proportion of 1,6-anhydrofuranose is about the same as that formed from the homologous hexoses. From D-*glycero*-L-*talo*-heptose, yet another anhydride appears to be produced; since the 1,7-anhydropyranose would be energetically unfavourable, we cannot guess its structure.

Chaby and Szabó (12) distinguished the 1,6- and 1,7-anhydroheptopyranoses from each other by the mass spectra of their acetates. The spectra show the same peaks but in different proportions. We recorded the mass spectra of the acetates of the two

TABLE 1. Anhydrides (%) formed by acid-catalysed equilibration of aldohexoses in aqueous solution

D-*glycero*-	1,6-Pyr	1,6-Pyr	1,6-Fur	D-*glycero*-	1,6-Pyr	1,7-Pyr	1,6-Fur
D-*gluco*-	(<0.1)*	(—)	(—)	L-*gluco*-	8.5†	—	0.7†
D-*manno*-	(<0.2)	(—)	(—)	L-*manno*-	15‡	—	—
D-*galacto*-	Trace	Trace	8.5	L-*galacto*-	18†	—	0.6†
D-*talo*-	Trace	—	12.2	L-*talo*-	31†	—	2.8†
D-*allo*-	2.9†	4.3†	—	L-*allo*-	54‡	1†	2†
D-*altro*-	(10)	(10)	(—)	L-*altro*-	98‡	—	—
D-*gulo*-	10.8	11.4	—	L-*gulo*-	(98)	(—)	(—)
D-*ido*-	33.5	39	1.3†	L-*ido*-	(99)	(—)	(—)

*NOTE: figures in parentheses are estimates based on analogy.
†The structure of this compound has not been unequivocally determined.
‡Reference 1.

1,6-anhydrofuranoses and again found the same peaks in proportions somewhat similar to those in the spectra of the 1,7-anhydrides. The proportions were not the same in the spectra of the *galacto* and the *talo* isomer. In view of these results we are disinclined to rely on mass spectra for the determination of the structures of the anhydroheptoses.

The results obtained are summarized in Table 1. For those heptoses which we did not investigate, we estimated the proportion of the anhydrides in equilibrium by analogy with the homologous hexoses and the other heptoses; these estimates are shown in parentheses. Those components whose structures we have not determined are also indicated.

Experimental

General

Solvents were evaporated under diminished pressure in rotary evaporators. All solvents used for chromatography were distilled. "Light petroleum" refers to the fraction boiling between 60 and 80°C; "ethanol" refers to 95% ethanol; mixed solvents were prepared on a v/v basis.

Column chromatography was performed on Merck Silica Gel H (Type 60). Gas–liquid chromatography (glc) was carried out with a custom-built instrument, using nitrogen as carrier gas with a flow-rate of 60–80 mL per min, and a hydrogen flame-ionization detector. The 1.5 m coiled glass column was filled with 3% SP-2401 on Chromosorb W (AW-DMCS) and was kept at 210 or 215°C. Peaks were cut out and weighed; it was assumed that all compounds gave equal detector responses. The compounds were analysed by glc as their acetates. Most reaction mixtures showed small amounts of very volatile compounds (R_t < 1 min) which could be dianhydrides or decomposition products. The pure heptoses gave up to four peaks after acetylation: those of the two pyranoses and of the two furanoses.

Thin-layer chromatograms (tlc) were run on Merck Silica Gel G (Type 60), supported on microscope slides, without activation. The compounds were detected by spraying with 20% sulfuric acid in ethanol and then heating on a hot-plate.

Proton magnetic resonance spectra were recorded with JEOL JNM-4H-100 and JNM-FX-100 spectrometers. The spectra described here were run in deuteriated benzene, using Me_4Si as internal standard; most of the spectra were also run in deuteriochloroform but those spectra could not be fully analysed. Mass spectra were recorded with an AEI MS-12 spectrometer by electron impact at 70 eV from a direct insertion probe at 25°C and a source temperature of 230°C. Optical rotations were determined with a Bendix NPL Automatic Polarimeter 143C, equipped with a JANUS digital readout, in a 2 cm cell. Microanalyses were carried out by Mr. J. Sussman in the School's microanalytical laboratory.

Establishment of Equilibria

A solution containing the heptose in 5% aqueous sulfuric acid (20 parts) was heated on a steam-bath for 48 h. Samples removed from time to time, and analysed by glc after acetylation, showed that in every case equilibrium had been reached by that time. The acid was removed by stirring with Amberlite IRA 400 resin in the hydrogen carbonate form until the solution was neutral. Evaporation gave a syrup. In those cases where a large proportion of the heptose remained unchanged, some of it was recovered by crystallization at this stage. The mixture was then treated with acetic anhydride–pyridine (1:1) on a steam-bath for 2 h, evaporated, the residue dissolved in chloroform, and washed first with *M* sulfuric acid, then with saturated sodium hydrogencarbonate solution. After evaporation, the residue was chromatographed on a column of silica gel; the acetates of the anhydrides emerged before those of the heptoses. Some of the acetates crystallized; those that did not, were distilled at a pressure of 0.2–0.3 Torr.

Equilibration of D-glycero-L-gluco-*Heptose (13)*

The glc peaks (215°C): 0.7% (R_t 2.1 min), 8.5% 1,6-anhydropyranose (2.7 min), 51% β-pyranose (6.0 min), and 40% α-pyranose (7.2 min).

Equilibration of D-glycero-L-galacto-*Heptose (14)*

The glc peaks (215°C): 0.6% (2.2 min), 18% 1,6-anhydropyranose (3.2 min), 40% β-pyranose (6.7 min), 13.6% furanose (?) (7.5 min), and 29% α-pyranose (8.3 min).

Equilibration of D-glycero-L-talo-*Heptose (14)*

The glc peaks (210°C): 2.8% (3.5 min), 2.5% (4.2 min), 31% 1,6-anhydropyranose (5.1 min), 37% heptose (15.0 min), and 26% heptose (17.8 min). The substance appearing at 4.2 min is formed more slowly than the other products; after 24 h it amounts to only 1.4%.

Equilibration of D-glycero-D-gulo-*Heptose (15)*

The glc peaks (210°C): 11.4% 1,7-anhydropyranose (4.8 min), 10.8% 1,6-anhydropyranose (6.2 min), and four heptose peaks: 68.5% (12.6 min), 2.5% (17 min), 3.6% (19.5 min), 3.2% (22.5 min). The 1,7-anhydride is formed at a slower rate than the 1,6-anhydride; after 24 h the composition was 5.0, 9.0, 73.9, 2.1, 4.6, and 5.4%, respectively.

Column chromatography with ether – petroleum ether (1:3) as eluant gave, in fractions 7–12, 2,3,4,6-tetra-*O*-acetyl-1,7-anhydro-D-*glycero*-β-D-*gulo*-heptopyranose, $[\alpha]_D^{22}$ +48.9° (*c* 1.43, $CHCl_3$); nmr δ: 1.44, 1.62, 1.71, 1.91 (Ac), 3.59 (dd, H-7′, $J_{6,7'}$ = 9.0, $J_{7,7'}$ = −10.8), 3.71 (H-7, $J_{6,7}$ = 7.1), 4.59 (dd, H-5, $J_{4,5}$ = 6.3, $J_{5,6}$ = 1.2), 5.06 (d, H-1, $J_{1,2}$ = 1.8), 5.14 (ddd, H-6),

Can. J. Chem. Downloaded from www.nrcresearchpress.com by 210.87.254.42 on 09/05/12
For personal use only.

Can. J. Chem. Downloaded from www.nrcresearchpress.com by 210.87.254.42 on 09/05/12
For personal use only.

5.57 (dd, H-2, $J_{2,3}$ = 3.8), 5.59 (dd, H-4, $J_{3,4}$ = 10.3), 5.85 (dd, H-3). *Anal.* calcd. for $C_{15}H_{20}O_{10}$: C 50.00, H 5.59; found: C 50.23, H 5.56.

Fractions 21–39 gave 2,3,4,7-tetra-*O*-acetyl-1,6-anhydro-D-*glycero*-β-D-*gulo*-heptopyranose, $[\alpha]_D^{22}$ +20.1° (*c* 1.61, $CHCl_3$); nmr δ: 1.59 (Ac), 1.64 (Ac), 1.68 (2Ac), 3.99 (quin, H-6), 4.27 (t, H-5, $J_{4,5} = J_{5,6}$ = 4.1), 4.35 (dd, H-7′, $J_{6,7'}$ = 4.2, $J_{7,7'}$ = −12), 4.49 (dd, H-7, $J_{6,7}$ = 7.5), 5.30 (d, H-1, $J_{1,2}$ = 2.3), 5.44 (dd, H-2, $J_{2,3}$ = 5.0), 5.52 (dd, H-4, $J_{3,4}$ = 9.6), 5.84 (dd, H-3). *Anal.* calcd. for $C_{15}H_{20}O_{10}$: C 50.00, H 5.59; found: C 49.90, H 5.37.

Equilibration of D-glycero-D-ido-*Heptose (15)*

The glc peaks (210°C): 39% 1,7-anhydropyranose (2.5 min), 33.5% 1,6-anhydropyranose (2.8 min), 1.3% anhydrofuranose (?) (4.4 min), and four peaks of the heptose: 3.2% (7.7 min), 4.2% (10.6 min), 15.4 (11.8 min), 3.4% (14.5 min).

Column chromatography with ethyl acetate – light petroleum (1:4) as eluant gave, in fractions 28–40, 2,3,4,6-tetra-*O*-acetyl-1,7-anhydro-D-*glycero*-β-D-*ido*-heptopyranose which crystallized from benzene – light petroleum as needles, mp 74–76°C; $[\alpha]_D^{26}$ −34.5° (*c* 1.48, $CHCl_3$); nmr δ: 1.51, 1.66, 1.73, 1.85 (Ac), 3.60 (dd, H-7′, $J_{6,7'}$ = 5.1, $J_{7,7'}$ = −12.7), 3.80 (dd, H-7, $J_{6,7}$ = 5.3), 4.36 (broad d, H-5), 4.93 (dt, H-6, $J_{5,6}$ = 1.0), 5.11 (dd, H-2, $J_{1,2}$ = 3.7, $J_{2,3}$ = 9.0), 5.28 (broad d, H-1), 5.32 (dd, H-4, $J_{3,4}$ = 9.5, $J_{4,5}$ = 6.6), 5.99 (t, H-3). There appears to be long-range coupling between H-1 and H-5. *Anal.* calcd. for $C_{15}H_{20}O_{10}$: C 50.00, H 5.59; found: C 50.92, H 5.80.

Fractions 46–56 gave 2,3,4,7-tetra-*O*-acetyl-1,6-anhydro-D-*glycero*-β-D-*ido*-heptopyranose, $[\alpha]_D^{23}$ −53° (*c* 1.15, $CHCl_3$); nmr δ: 1.59, 1.60, 1.65, 1.70 (Ac), 4.03 (quin, H-6), 4.14 (t, H-5, $J_{5,6}$ = 4.2), 4.34 (dd, H-7′, $J_{6,7'}$ = 6.2, $J_{7,7'}$ = −12.1), 4.50 (dd, H-7, $J_{6,7}$ = 7.6), 5.05 (d, H-2, $J_{1,2}$ = 1.7, $J_{2,3}$ = 8.0), 5.28 (ddd, H-4, $J_{3,4}$ = 9.0, $J_{4,5}$ = 4.5, $J_{4,6}$ = 1.1), 5.43 (d, H-1), 5.87 (dd, H-3). *Anal.* calcd. for $C_{15}H_{20}O_{10}$: C 50.00, H 5.59; found: C 50.79, H 5.84.

Equilibration of D-glycero-D-allo-*Heptose (16)*

The glc peaks (215°C): 4.3% 1,7-anhydropyranose (?) (3.0 min), 2.9% 1,6-anhydropyranose (?) (3.8 min), 71.6% β-pyranose (8.3 min), and three other forms of the heptose: 10.8% (10.5 min), 4.2% (11.6 min), 6.1% (13.5 min).

Equilibration of D-glycero-D-galacto-*Heptose (17)*

The glc peaks (210°C): 8.5% 1,6-anhydrofuranose (6.8 min), 0.5% (9.3 min), 0.5% (10.1 min), 47.5% heptose (16.5 min) and 43.5% (23.3 min). Column chromatography over silica gel (10 parts) with ether – petroleum ether (1:2) (10 mL fractions) gave, in fractions 14–21, 2,3,5,7-tetra-*O*-acetyl-1,6-anhydro-D-*glycero*-β-D-*galacto*-heptofuranose, $[\alpha]_D^{22}$ +151.3° (*c* 1.25, $CHCl_3$); nmr δ: 1.51 (Ac), 1.62 (Ac), 1.82 (2Ac), 4.0–4.35 (m, 3H, H-6, 7, 7′), 4.67 (d, H-4, $J_{4,5}$ = 4.6), 5.09 (dd, H-5, $J_{5,6}$ = 9.1), 5.18 (ddd, H-2, $J_{1,2}$ = 4.8, $J_{2,3}$ = 2.5, $J_{2,5}$ = 0.6), 5.40 (d, H-3, $J_{3,4}$ = 0), 5.63 (d, H-1). Mass spectrum *m/e* (relative abundance): 43 (100), 81 (8), 82(8), 110 (10), 111 (11), 115 (15), 153 (8), 157 (11). *Anal.* calcd. for $C_{15}H_{20}O_{10}$: C 50.00, H 5.59; found: C 50.47, H 5.64.

Equilibration of D-glycero-D-talo-*Heptose (17)*

The glc peaks (210°C): 12.2% 1,6-anhydrofuranose (5.7 min), trace (7.8 min), and three peaks of the heptose: 22.5% (11.6 min), 58% (15.5 min), 7.5% (17.7 min). Column chromatography, as above, gave in fractions 11–18, 2,3,5,7-tetra-*O*-acetyl-D-*glycero*-α-D-*talo*-heptofuranose, $[\alpha]_D^{23}$ +106.5° (*c* 1.3, $CHCl_3$); nmr δ: 1.60, 1.64, 1.71, 1.81 (Ac), 3.29 (dt, H-6, $J_{5,6}$ = 10.0, $J_{6,7} + J_{6,7'}$ = 7.0), 4.10 (dd, H-7′, $J_{7,7'}$ = −12.1), 4.11 (dd, H-7), 4.76 (d, H-4, $J_{4,5}$ = 4.6), 5.04 (dd, H-5), 5.33 (d, H-3, $J_{2,3}$ = 6.7, $J_{3,4}$ = < 0.5), 5.39 (s, H-1, $J_{1,2}$ = 0), 5.43 (d, H-2). Mass spectrum *m/e* (relative abundance): 43 (100), 63 (6), 81 (8), 82 (7), 97 (6), 110 (15), 111 (12), 115 (20), 153 (8), 157 (11). *Anal.* calcd. for $C_{15}H_{20}O_{10}$: C 50.00, H 5.59; found: C 51.38, H 5.70.

Acknowledgments

This work was supported by a grant from the Australian Research Grants Committee. The authors are grateful to Mrs. Donna Range for carrying out some of the preliminary experiments and to Dr. V. Bílik (Bratislava) for a gift of samples of D-*glycero*-L-*galacto*- and D-*glycero*-L-*talo*-heptoses.

1. S. J. ANGYAL and R. J. BEVERIDGE. Carbohydr. Res. **65**, 229 (1978).
2. M. ČZERNÝ and J. STANĚK. Adv. Carbohydr. Chem. Biochem. **34**, 23 (1977).
3. J. W. PRATT, N. K. RICHTMYER, and C. S. HUDSON. J. Am. Chem. Soc. **75**, 4503 (1953).
4. L. C. STEWART and N. K. RICHTMYER. J. Am. Chem. Soc. **77**, 424 (1955).
5. S. J. ANGYAL and K. DAWES. Aust. J. Chem. **21**, 2747 (1968).
6. P. KÖLL. Chem. Ber. **106**, 3559 (1973).
7. W. PARKER, W. V. STEELE, and I. WATT. J. Chem. Thermodyn. **9**, 307 (1977).
8. W. A. C. BROWN, J. MARTIN, and G. A. SIM. J. Chem. Soc. 1844 (1965); M. DOBLER and J. D. DUNITZ. Helv. Chim. Acta, **47**, 695 (1964); N. C. WEBB and M. R. BECKER. J. Chem. Soc. B, 1317 (1967); E. L. OSINA, V. L. MASTRYUKOV, L. V. VILKOV, and N. A. BELIKOVA. J. Chem. Soc. Chem. Commun. 12 (1976); M. R. VEGAR and R. J. WELLS. Tetrahedron Lett. 2847 (1971).
9. J. F. STODDART. Stereochemistry of carbohydrates. Wiley-Interscience, New York. 1971. p. 227.
10. K. HEYNS and P. KÖLL. Chem. Ber. **105**, 2228 (1972).
11. R. U. LEMIEUX and R. NAGARAJAN. Can. J. Chem. **42**, 1270 (1964).
12. R. CHABY and P. SZABÓ. Carbohydr. Res. **49**, 489 (1976).
13. J. C. SOWDEN and D. R. STROBACH. J. Am. Chem. Soc. **82**, 954 (1960).
14. H. S. ISBELL. J. Res. Natl. Bur. Stand. **19**, 639 (1937).
15. N. K. RICHTMYER. Methods Carbohydr. Chem. **1**, 160 (1962).
16. J. W. PRATT and N. K. RICHTMYER. J. Am. Chem. Soc. **77**, 6326 (1955).
17. J. C. SOWDEN and R. SCHAFFER. J. Am. Chem. Soc. **73**, 4662 (1951).

2-Alkoxy-5(4*H*)-oxazolones from *N*-alkoxycarbonylamino acids and their implication in carbodiimide-mediated reactions in peptide synthesis

N. Leo Benoiton and Francis M. F. Chen

Department of Biochemistry, University of Ottawa, Ottawa, Ont., Canada K1N 9A9

Received June 27, 1980

This paper is dedicated to Prof. Raymond U. Lemieux on the occasion of his 60th birthday

N. Leo Benoiton and Francis M. F. Chen. Can. J. Chem. **59**, 384 (1981).

Reaction of N-ethyl,N′-(γ-dimethylaminopropyl)-carbodiimide·HCl with one equiv. of *N*-*tert*-butoxycarbonyl-L-valine (**3***a*) in dichloromethane at 23°C gives, besides the symmetrical anhydride (**5***a*), the optically pure 2-*tert*-butoxy-4-isopropyl-5(4*H*)-oxazolone (**4***a*) which can be obtained in 50% yield under selected conditions. The 2-benzyloxycarbonyl-4-isopropyl-5(4*H*)-oxazolone (**4***b*) is similarly obtainable from *N*-benzyloxycarbonyl-L-valine (**3***b*). Anhydrous acid converts **4***a* to the oxazolidinedione. Simple preparations of the *N*-carboxyanhydrides of valine and isoleucine have been devised from these reactions. Compound **4** reacts with **3** to give **5**. Compound **4** reacts with an amino acid ester to give the optically pure peptide even in the presence of salts, but partial racemization occurs for reactions in the presence of a tertiary amine. Evidence for the implication of 2-alkoxy-5(4*H*)-oxazolones in the couplings of *N*-alkoxycarbonylamino acids is presented. Compound **4***a* has been isolated in 6–11% yield from carbodiimide-mediated reactions of **3***a* with itself or amino acid methyl esters which have been terminated before completion.

N. Leo Benoiton et Francis M. F. Chen. Can. J. Chem. **59**, 384 (1981).

La réaction du chlorohydrate de *N*-éthyl,*N*′(γ-diméthylaminopropyl)carbodiimide avec un équivalent de *N*-*tert*-butoxycarbonyl-L-valine (**3***a*) dans le dichlorométhane à 23°C donne en plus de l'anhydride symétrique (**5***a*), le composé *tert*-butoxy-2 isopropyl-4 (4*H*)oxazolone-5 (**4***a*) que l'on peut obtenir dans des conditions choisies avec un rendement de 50%. D'une façon analogue, on obtient le benzyloxycarbonyl-2 isopropyl-4 (4*H*)oxazolone-5 (**4***b*) à partir de la *N*-benzyloxycarbonyl-L-valine (**3***b*). L'acide anhydre transforme le composé **4***a* en oxazolidinedione. A partir de ces réactions, on a mis au point des préparations simples de *N*-carboxyanhydrides de la valine et de l'isoleucine. Le composé **4** réagit avec **3** et donne le composé **5**. Le produit **4** réagit avec un ester d'acide aminé pour conduire au peptide optimiquement pur même en présence de sels, mais il se produit une racémisation partielle au cours des réactions conduites en présence d'une amine tertiaire. On présente la preuve de l'implication des alkoxy-2 (4*H*)oxazolones-5 dans les couplages des acides aminés *N*-alkoxycarbonylés. On a isolé le composé **4***a* à partir des réactions d'autocondensation du composé **3***a* ou de sa condentation sur les esters méthyliques d'acides aminés en présence de carbodiimide qui s'arrêtent avant d'avoir totalement réagi.

[Traduit par le journal]

When an acylamino acid or a protected peptide (**1**) is coupled with a nucleophile (amine or phenol), racemization frequently occurs. The change in stereochemistry is the result of the formation of the 2-alkyl-5(4*H*)-oxazolone (**2**) by cyclization of the activated *N*-substituted amino acid moiety. Compound **2** racemizes faster than it couples with the nucleophile. However, no racemization occurs when an *N*-alkoxycarbonylamino acid (**3**) is coupled, as is done successively during the build-up of a peptide chain starting from the *C*-terminus. The reason accepted to explain the preservation of stereochemistry has been that the corresponding 2-alkoxy-5(4*H*)oxazolones (**4**) are not formed because of the unique nature of the urethane carbonyl group (1). We describe here results which are incompatible with this basic tenet of peptide chemistry. As a follow-up on our work on the synthesis of symmetrical anhydrides (**5**) of *N*-alkoxycarbonylamino acids (2), we describe the preparation and characterization of the 2-alkoxy-5(4*H*)-oxazolones **4***a* and **4***b* derived from Boc-Val (**3***a*) and Z-Val (**3***b*) respectively,[1] as well as their isolation from reaction mixtures similar to those used in peptide synthesis.[2]

Reaction of the soluble carbodiimide EDC (**6**) with two equiv. of **3** in dichloromethane followed by washing with aqueous citric acid and sodium hydrogen carbonate gave 70–80% yields of symmetrical anhydride (**5**) for several Boc- and Z-amino acids but lower yields for Boc-Val and Boc-Ile (2). Attempts to increase the yield of **5** by using more EDC (1 equiv.) produced a second stable neutral product which could be obtained pure (yield, 20% by weight) after removal of solvent by precipitating out the anhydride with light petro-

[1]Abbreviations: Boc, *tert*-butoxycarbonyl; Bzl, benzyl; Z, benzyloxycarbonyl; DCC, *N*,*N*′-dicyclohexylcarbodiimide; EDC, *N*-ethyl,*N*′-(γ-dimethylaminopropyl)-carbodiimide·HCl; EDU, *N*-ethyl,*N*′-(γ-dimethylaminopropyl)-urea; NMM, *N*-methylmorpholine; Val, valine. Amino acid symbols represent the L-isomer.

[2]Part of this work was presented at the Sixth American Peptide Symposium, Washington, DC, June 1979 (3).

0008-4042/81/020384-06$01.00/0

©1981 National Research Council of Canada/Conseil national de recherches du Canada

Can. J. Chem. Downloaded from www.nrcresearchpress.com by 210.87.254.40 on 09/05/12
For personal use only.

Can. J. Chem. Downloaded from www.nrcresearchpress.com by 210.87.254.40 on 09/05/12
For personal use only.

leum. ^{1}H nuclear magnetic resonance spectroscopy indicated it to be a derivative of valine with a *tert*-butyl group displaced 0.13 ppm downfield from that of a Boc or *tert*-butyl ester group, and which had lost its —N—H proton, as evidenced by the sharp α-proton doublet (4.13 ppm). Reaction with anhydrous methylamine gave a quantitative yield of Boc-Val-$NHCH_3$ thus establishing it to be an activated form of Boc-Val. Elemental analysis corresponded with Boc-Val which had lost one mole of water. Infrared absorption at 1845 and 1700 cm^{-1} combined with the absence of absorption at 3400 (—N—H) and 1770 (urethane carbonyl) cm^{-1} indicated the 5(4*H*)-oxazolone structure (4, 5). The compound is therefore 2-*tert*-butoxy-4-isopropyl-5(4*H*)-oxazolone (**4***a*). The aziridinone structure is excluded on the basis of the mass spectrum and the absence of absorption for a urethane carbonyl group (4) in the ir spectrum. The high specific rotation (−49.6° in $CHCl_3$) indicated that the compound was not appreciably racemized. A test for optical purity (see below) established it to be optically pure (<0.1% D-isomer).

Compound **4***a* could be detected and quantitated in the presence of other derivatives of Boc-Val by integration of the *tert*-butyl peaks of nmr spectra. No **4***a* could be detected after reaction of EDC with two equiv. of Boc-Val, or after a reaction carried out in dimethylformamide. More **4***a* was formed at 23°C (35%) than at 0°C (30%); the yield of **5***a* was greater at 0°C (55%) than 23°C (40%). Other factors increased the yield of **4***a*. Maximum yield (55%; isolated) was achieved by adding the Boc-Val dropwise to a dilute solution containing excess EDC and some triethylamine·HCl. Compound **4***a* was stable in deuterochloroform at −5°C for 5 days, in dimethylformamide at 23°C for 2 h, and in dichloromethane–ethanol (20:1) at 23°C for 20 h. It slowly decomposes in solutions containing water giving rise to *tert*-butanol, and is converted to valine *N*-carboxyanhydride (**7***a*) on standing in *tert*-butanol, anhydrous acid, or *in vacuo*. Since **5***a* is also converted to **7***a* by dry HCl, the mixture of **4***a* and **5***a* obtained from the reaction of Boc-Val and EDC serves as a convenient source for the preparation of **7***a*.[3] The valine hydrochloride liberated from **5***a* can be eliminated by simple filtration of the solution of **7***a* in dichloromethane.

Evidence for the formation of the 2-*tert*-butoxy-5(4*H*)-oxazolones (**4**) from the following Boc-amino acids, using one equiv. of EDC, was also obtained (% yield): alanine, 15; leucine, 5; isoleucine, 45; phenylalanine, 15. But in no case could the product be isolated pure because the symmetrical anhydride could not be precipitated out completely. The best product from Boc-Ile contained 5% of anhydride. The mixture of **4***c* and **5***c* obtained from Boc-Ile and EDC could be used to prepare **7***c* in good yield.[3]

When EDC was reacted with Z-Val (**3***b*) as described for reactions with Boc-Val, the analogous 2-benzyloxy-5(4*H*)-oxazolone (**4***b*), $[\alpha]_D$ −55.8° ($CHCl_3$), was obtained in 20% yield using one equiv. of EDC, and in 55% yield using the conditions giving maximum yield. Elemental analysis, nmr, ir, and mass spectra were in accord with this structure. The compound is readily detected and quantitated in a mixture on the basis of the methyleneoxy protons of the nmr spectrum which are 0.20 ppm downfield from those of a Z-group. Compound **4***b* is more stable than **4***a*, not decomposing *in vacuo*, or on standing in *tert*-butanol or wet dichloromethane for 24 h. After 36 h in ethanol, it had been completely converted to the ethyl ester. It reacted with *p*-nitrophenol to give the ester, and with Z-Val to give the symmetrical anhydride (**5***b*), but did not react with *p*-nitroaniline. Catalytic hydrogenation of **4***b* gave **7***a*.

Compound **4***a* reacted with an equiv. of Z-Val and **4***b* with an equiv. of Boc-Val to give quantitative yields of identical products whose nmr and ir curves were consistent with the anhydride structure BocNH—$((CH_3)_2CH)$CH—CO—O—CO—$CH(CH(CH_3)_2)$—NHZ.[4] Unequivocal proof of the absence of the anhydrides **5***a* or **5***b* in the product cannot be provided.

Other 2-benzyloxy-5(4*H*)-oxazolones isolated from reactions using conditions giving maximum yields were those from Z-Phe (**4***d*; 25%), Z-Gly (5%), and Z-Cys(Bzl) (3%). All were pure as evidenced by nmr spectroscopy, but only **4***d* was completely characterized.

When EDC was reacted with two equiv. of **3***a* for 30 min as for the preparation of **5***a*, after work-up the sole product was **5***a*. However, when such a synthesis was terminated at 3 min by the addition of aqueous sodium bicarbonate, and the products were examined after removal of the water-soluble side-products, a 37% yield of an equimolar mixture of **4***a* and **5***a* was found. This corresponds to a 12% yield of **4***a*. An additional experiment established that **4***a* is present in the reaction mixture before

[3]The generality of this approach for the preparation of *N*-carboxyanhydrides is under investigation.

[4]The mp previously reported for this compound which is an oil is an error (3).

Can. J. Chem. Downloaded from www.nrcresearchpress.com by 210.87.254.40 on 09/05/12
For personal use only.

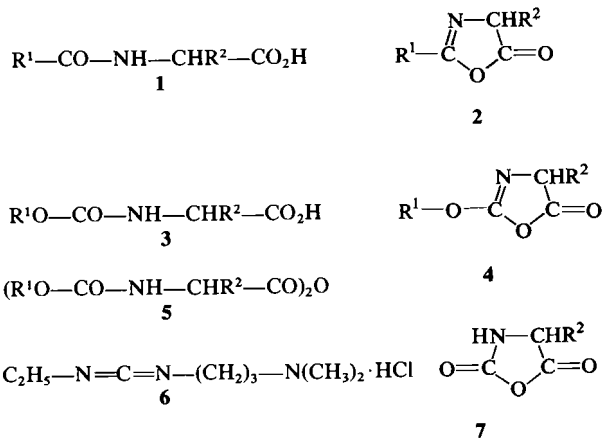

1 **2** **3** **4** **5** **6** **7**

	R^1	R^2
a	$(CH_3)_3C$—	$(CH_3)_2CH$—
b	$C_6H_5CH_2$—	$(CH_3)_2CH$—
c	$(CH_3)_3C$—	$C_2H_5(CH_3)CH$—
d	$C_6H_5CH_2$—	$C_6H_5CH_2$—

contact with water. Compound **4***a* does not decompose upon standing in dichloromethane at 23°C, and reacts within minutes with **3***a* to give **5***a*. Compound **5***a* did not give rise to any **4***a* when it was left several hours in dichloromethane, even in the presence of triethylamine·HCl. We therefore conclude that **4***a* is an intermediate in the reaction of EDC with **3***a* to give **5***a*. When **3***a* is not present in amount sufficient to react with all of the activated **3***a*, **4***a* accumulates, to the extent of >25%. The initial product of the reaction of EDC with **3***a* is the *O*-acylisourea (**8**);[5] **8** then reacts with **3***a* to give **5***a*. But some of **8** must cyclize to form **4***a* which then reacts with **3***a* to give **5***a* (Scheme 1).

Having succeeded in isolating **4***a* from a reaction mixture containing an oxygen nucleophile, an attempt was made to isolate it from a mixture containing a nitrogen nucleophile. A normal coupling of Boc-Val with Val-OMe·HCl (NMM) mediated by EDC (3 mmol of each) was terminated after 3 min by the addition of aqueous citric acid. Work-up as usual followed by precipitation of the protected dipeptide with light petroleum and removal of solvent by evaporation gave 45 mg (7.5% yield) of pure **4***a*. A similar experiment using DCC gave essentially the same results except that the product was contaminated with an equal amount of non-peptide Boc-derivative (*N*-acylurea). Since **4***a* is known to react with amines to give amides, and since there is no **4***a* in the above reaction mixtures if they are left for 30 min, we conclude that **4***a* is an intermediate in the carbodiimide-mediated coupling of Boc-Val with Val-OMe. As in the previous case, some *O*-acylisourea must cyclize to form **4***a* which then reacts with Val-OMe to give the protected peptide **9** (Scheme 1). An additional possibility is that some of the **4***a* reacts with **3***a* to form **5***a* which then reacts with Val-OMe to give the peptide. Evidence pointing to this comes from the following competitive experiment. When **4***a* was added to a mixture of Z-Val and Val-OMe (1 equiv. of each), the product consisted of Z-Val-Val-OMe (15%) in addition to Boc-Val-Val-OMe. Formation of the anhydride (or **4***b*) must be invoked to account for the appearance of Z-Val-Val-OMe. Implication of the anhydride in these couplings, however, would run contrary to the contention that the *O*-acylisourea and not the symmetrical anhydride is the activated intermediate for synthesis in solution (6). Other competitive experiments were carried out, but these could not be rationalized because of the complexity of the system examined.

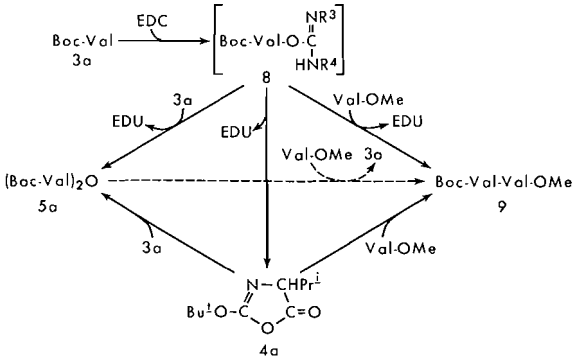

SCHEME 1

The question which immediately arises with respect to the implication of 2-alkoxy-5(4*H*)-oxazolones in couplings is whether it is a phenomenon general to carbodiimide-mediated couplings. The results of an attempt to answer this question are given in Table 1. The 2-alkoxy-5(4*H*)-oxazolone was detectable in most of the reaction mixtures examined, the amount being independent of the nature of the carbodiimide or the side-chain of the amino acid ester nucleophile involved. Three factors had an important bearing on the amounts isolated: temperature, *N*-protecting group, and residue activated. The amount was 6–11% for Boc-Val and Boc-Ile at 23°C. It dropped to 0.3–1% at 0°C, or for Boc-Leu and Z-Val at 23°C; No 5(4*H*)-oxazolone was detectable for Z-Val or Boc-Leu at 0°C. The amount detected represents the balance between the rate of formation of the 5(4*H*)-oxazolone and its rate of reaction with the ester. Failure to detect the 5(4*H*)-oxazolone in the latter cases can-

[5]See ref. 1, p. 115.

Can. J. Chem. Downloaded from www.nrcresearchpress.com by 210.87.254.40 on 09/05/12
For personal use only.

TABLE 1. 2-Alkoxy-5(4*H*)-oxazolones isolated from coupling mixtures[a]

3	Ester[b]	Reagent	Temperature °C	4 % yield
Boc-Val	Val-OMe	EDC	23	7.5[c]
Boc-Val	Ala-OMe	EDC	23	6.4[c]
Boc-Val	Val-OMe	DCC	23	6[d]
Boc-Ile	Ala-OMe	EDC	23	8[e]
Boc-Ile	Val-OMe	DCC	23	11[d]
Boc-Leu	Leu-OMe	EDC	23	0.3[f]
Boc-Ile	Ala-OMe	EDC	0	0.9[f]
Boc-Ile	Ala-OMe	DCC	0	>1[f]
Z-Val	Val-OMe	EDC	23	0.8[f]
Z-Val	Leu-OMe	EDC	23	0.3[f]
Z-Val	Ala-OMe	EDC	0	0
Boc-Leu	Ala-OMe	EDC	0	trace[f]

[a]Couplings (3 mmol) in dichloromethane were terminated after 3 min. Yields represent neutral product remaining in mother liquor after normal work-up followed by precipitation of peptide and *N*-acylurea with light petroleum.
[b]Used as hydrochloride, neutralized with *N*-methylmorpholine.
[c]Isolated pure (40–45 mg).
[d]Mixed with an equal amount of inert unesterified Boc-derivative (*N*-acylurea).
[e]Mixed with 1/5 of its weight of peptide.
[f]Not pure. Addition of methylamine eliminated the α-hydrogen doublet in the nmr spectrum producing the CH_3NH doublet of the methylamide.

not be taken as proof that it was not formed. Kinetic data are required before the results can be completely rationalized. We nevertheless conclude that the data in Table 1 provide compelling evidence in favor of the tenet that the 2-alkoxy-5(4*H*)-oxazolone is implicated generally in the carbodiimide-mediated couplings of **3**.

Both **4***a* and **4***b* were shown to be optically pure when assessed by a procedure used routinely in our laboratory. The method consists in coupling the Boc-amino acid, in this case the 5(4*H*)-oxazolone, with L-Lys(Z)-OBzl followed by deprotection and analysis for the diastereomeric peptides with an amino acid analyzer (7). The ester is used as the hydrochloride salt, which is neutralized by adding NMM. Besides demonstrating the optical integrity of the 2-alkoxy-5(4*H*)-oxazolones, the test also demonstrated that they couple without racemization, even in the presence of salt. These results were mandatory if the 2-alkoxy-5(4*H*)-oxazolones are to be implicated in coupling reactions which are known to proceed without racemization. So there is no inconsistency between the results and the proposals. The chiral stability of the 2-alkoxy-5(4*H*)-oxazolones (**4**) contrasts with that of the 2-alkyl-5(4*H*)-oxazolones (**2**) which cannot be coupled without extensive racemization (1, 8). When **4***a* and **4***b* were coupled in the presence of a tertiary amine base, however, some racemization did occur, 6 and 15%, respectively, in the presence of 0.2 equiv. of triethylamine. As much as 50% of **4***b* was racemized when it was coupled in the presence of 1.0 equiv. of triethylamine. The difference in the chiral stabilities of the two types of 5(4*H*)-oxazolones is therefore one of degree.

In view of the above, we submit that the tenet that **3** does not racemize when it is coupled because it does not form the 5(4*H*)-oxazolone must now be rejected. The 5(4*H*)-oxazolone can and does form in some cases. The reason no racemization obtains is that even if the 2-alkoxy-5(4*H*)-oxazolone does form, it is chirally stable under normal conditions of coupling. Caution with technique should be exercised, however, because **4** can racemize in the presence of excess base.

When **4***a* was first encountered by us, the only reference in the literature to the existence of a 2-alkoxy-5(4*H*)-oxazolone was a communication by Jones and Witty (9). They reported that the cyclic compound derived from Z-Phe and phosgene or thionyl chloride followed by triethylamine, which had been described as the *N*-benzyloxycarbonyl-3-benzylaziridin-2-one (10), was in fact the 2-benzyloxy-5(4*H*)-oxazolone **4***d*. The so-called *N*-acylaziridinones had been suggested for use in peptide synthesis since they reacted with amino acid esters to give unracemized products (10). The full paper by Jones and Witty (11) became available to us shortly after our presentation at the Washington Symposium. They have shown with kinetic data that **4***d* reacts with amine nucleophiles (anilines) more quickly, and racemizes in the presence of a tertiary amine base more slowly, than the corresponding 2-phenyl-5(4*H*)-oxazolone. Our results are in complete harmony with those of Jones and Witty as well as with the observations of Miyoshi (10).

Our conclusion on the chiral stability of 2-alkoxy-5(4*H*)-oxazolones is the same as that of Jones and Witty (11). As pointed out by them, it has already been clearly demonstrated that the 4-proton in the analogous 2-alkoxy- 5(4*H*)-thiazolone is much less acidic than that in the corresponding 2-alkyl-5(4*H*)-thiazolone (12), so the observations are as expected.

Explanations invoked to account for the apparent reluctance of **3** to form **4** have been the lower acidity of the —N—H (11, 13) and the lower nucleophilicity of the carbonyl (14) of the urethane group. Cyclization of **3** is considered to require an exceptionally good leaving group such as chloride at the carboxyl group (1, 11) and, until the report of Jones and Witty, was considered to be accompanied by expulsion of the alkyl group giving rise to the *N*-carboxyanhydride **7** (1). Cyclization without loss of the alkyl group obviously does occur, and it occurs under conditions less forcing than previously thought. In fact, the conditions used to make

Can. J. Chem. Downloaded from www.nrcresearchpress.com by 210.87.254.40 on 09/05/12
For personal use only.

2-alkyl-5(4*H*)-oxazolones (**2**) using EDC (15) are identical with those used here to make the 2-alkoxy-5(4*H*)-oxazolones (**4**) except that 0°C is used in the former case, to avoid racemization. The differences in nature between the amide and urethane groups of the two substrates are therefore of little consequence in the cyclization. A more important difference resides in the fate of the products once formed. Compound **2** undergoes no apparent reaction with the substrate, while **4** reacts to form **5**. This can account in part for the much higher yields of **2** than **4** from the reactions.

Our results on the racemization attending couplings of **4** in the presence of base indicate that the 2-*tert*-butoxy group allowed less racemization than the 2-benzyloxy group. This is consistent with the report that the racemizing tendency of the *tert*-butoxycarbonyl group is four times lower than that of the benzyloxycarbonyl group (16). It suggests also that the lability of the 4-proton in **4** is affected by the electron donating property of the 2-alkoxy substituent. Inspection of molecular models indicates that steric effects cannot be invoked to explain the different ionizing tendencies of the 4-proton in 5(4*H*)-oxazolones. The electronic effects of the 2-alkoxy substituent must also be responsible for the unusually low acidity of the 4-proton in **4** relative to that in **2**.

Experimental

General

EDC (17) was purchased from Sigma Chemical Co., St. Louis. Light petroleum refers to the 30–60°C fraction, from Baker (Canlab). Magnesium sulfate was used as drying agent. Solvents were removed at room temperature using a rotary evaporator. Melting points were taken by the capillary method and are uncorrected. Optical rotations were measured with a Perkin-Elmer model 141 polarimeter using a 1-dm tube. The ir spectra were taken on a Unicam SP1100 spectrometer. Proton and carbon-13 nmr spectra were taken on Varian T60 and FT80 instruments, respectively. Chemical shifts are given in ppm relative to tetramethylsilane as internal standard for solutions in deuterochloroform. Elemental analyses were done by Mr. H. Seguin, National Research Council, Ottawa. The stereochemical purities of **4** and **7** were established by adding the products (0.5 mmol) to a solution of L-Lys(Z)-OBzl·HCl (NMM) in dichloromethane. Peptide products were isolated, deprotected, and analyzed for the diastereomers as previously described (7). For assessing the racemization of **4***a* and **4***b* during couplings in the presence of base, the base was added to the solution of the ester.

2-tert-*Butoxy-4-isopropyl-L-5(4*H*)-oxazolone* (**4***a*)

(i) Using Reactants in Equimolar Amounts

A solution of Boc-Val (434 mg; 2 mmol) and EDC (384 mg; 2 mmol) in 20 mL of CH_2Cl_2 was stirred at 0°C for 30 min. The solution was washed with cold 10% aqueous citric acid (20 mL), saturated aqueous $NaHCO_3$ (20 mL), and water (20 mL) and dried. The solvent was removed and light petroleum was added to the residue. After 18 h at −5°C, the crystalline symmetrical anhydride (**5***a*) (207 mg; 50%) mp 84–85°C was filtered off and the solvent was removed to leave a clear oil (80 mg; 20%); $[\alpha]_D^{23}$ −49.6° (*c* 2.0, $CHCl_3$); ir (liquid film): 1845, 1700 cm^{-1}; ^1H nmr δ: 0.94 (d, 3, *J* = 7 Hz), 1.06 (d, 3, *J* = 7 Hz), 1.60 (s, 9), 2.18 (m, 1), 4.13 (d, 1, *J* = 4 Hz); ^{13}C nmr δ: 175.7 (s, C=O), 155.9 (s, C=N), 85.4 (s, $C(CH_3)_3$), 71.0 (d, C—N), 31.1 (d, $C(CH_3)_2$), 27.5 (q, $C(CH_3)_3$), 18.8 and 17.3 (q, $C(CH_3)_2$); ms *m/e*: 199 (M^+ absent), 184 (2, $M^+ - CH_3$), 144 (2, **7***a*H^+), 116 (5, **7***a*H^+ − CO), 101 (20, $(CH_3)_3COCO^+$), 57 (100, $(CH_3)_3C^+$), 41 (90, $C_3H_5^+$). *Anal.* calcd. for $C_{10}H_{17}NO_3$ (Boc-Val − H_2O): C 60.28, H 8.60, N 7.03; found: C 60.04, H 8.47, N 7.02; optical purity >99.8%.

(ii) Conditions Giving Maximum Yield

Boc-Val (2 mmol) in 20 mL of CH_2Cl_2 was added dropwise over 20 min to a stirred solution of EDC (3 mmol) and $Et_3N \cdot HCl$ (3 mmol) in 100 mL of CH_2Cl_2. Work-up as in (*i*) gave a 20% yield of **5***a* and a 50% yield (200 mg) of **4***a*.

(iii) From a Prematurely Terminated Synthesis of **5**a

A solution of Boc-Val (2 mmol) and EDC (1 mmol) in 20 mL of CH_2Cl_2 was stirred at 23°C for 3 min. The mixture was washed with acid and aqueous bicarbonate as in (*i*), and the solvent was removed. Analysis showed the residue (160 mg; ≈37%) was an equimolar mixture of **4***a* and **5***a*. Removal of **5***a* by precipitation (−5°C) with light petroleum and elimination of solvent gave pure **4***a* (40 mg, 10%). When the reactants were stirred for 20 min before work-up, no **4***a* could be detected in the product.

(iv) From a Prematurely Terminated Coupling

To a stirred solution of Boc-Val, Val-OMe·HCl, and NMM (3 mmol of each) in 60 mL of CH_2Cl_2 at 23°C was added EDC (3 mmol). After 3 min the solution was washed and dried as in (*i*), the solvent was removed, and light petroleum was added. After 15 h at −5°C, the Boc-Val-Val-OMe and any **5***a* were filtered off. Elimination of the solvent gave **4***a* (45 mg; 7.5%).

Similar work-up after 3 min of a coupling mixture containing DCC instead of EDC gave a 6% yield of **4***a* mixed with an equiv. of inert Boc-derivative (see Table 1). The presence of **5***a* in the mixture is excluded on the basis of reaction of the mixture with CH_3NH_2 in ether. Extraction of the solution with *N* hydrochloric acid, and analysis of the aqueous extract (nmr) showed the presence of Val-$NHCH_3$ but no valine.

*2-Benzyloxy-4-isopropyl-L-5(4*H*)-oxazolone* (**4***b*)

A synthesis starting with Z-Val (2 mol) and EDC (2 mmol) carried out as described in (*i*) for the preparation of **4***a* gave crystalline **5***b* (243 mg; 50%) mp 99–101°C, followed by **4***b* as an oil (93 mg; 20%); $[\alpha]_D^{23}$ −55.8° (*c* 1.0, $CHCl_3$); ir (liquid film): 1845, 1700 cm^{-1}; ^1H nmr δ: 0.93 (d, 3, *J* = 8 Hz), 1.07 (d, 3, *J* = 8 Hz), 4.20 (d, 1, *J* = 4 Hz), 5.40 (s, 2), 7.48 (s, 5); ^{13}C nmr δ: 175.3 (s, C=O), 158.3 (s, C=N), 134.4–128.6 (aryl carbons), 71.6 (t, Ph*C*), 71.0 (d, C—N), 31.0 (d, $C(CH_3)_2$), 18.6 and 17.2 (q, $C(CH_3)_2$); ms *m/e*: 233 (3, M^+), 205 (8, M^+ − CO), 152 (17, $PhCH_2OCONH_3^+$), 107 (20, $PhCH_2O^+$), 91 (100, $PhCH_2^+$). *Anal.* calcd. for $C_{13}H_{15}NO_3$: C 66.93, H 6.48, N 6.01; found: C 67.10, H 6.65, N 6.15; optical purity >99.8%.

Under conditions giving maximum yield as in (*ii*) Z-Val (2 mmol) gave 160 mg of **5***b*, followed by 253 mg (54%) of **4***b*.

*2-Benzyloxy-4-benzyl-L-5(4*H*)-oxazolone* (**4***d*)

Using the conditions giving maximum yield as in (*ii*) Z-Phe (2 mmol) gave 140 mg (25%) of **4***d* which could be crystallized from ether – light petroleum. Melting point 65–66°C; $[\alpha]_D^{23}$ −36.5° (*c*, 1.5, tetrahydrofuran) (lit. (11) mp 73–73.5°C; $[\alpha]_D$ −36.0°); ^1H nmr δ: 3.14 (d, 1, *J* = 6 Hz), 3.16 (d, 1, *J* = 5 Hz), 4.60 (2d, 1, *J* = 5 and 6 Hz), 5.33 (s, 2), 7.22 (s, 5), 7.40 (s, 5). *Anal.* calcd. for $C_{17}H_{15}NO_3$: C 72.58, H 5.36, N 4.98; found: C 72.32, H 5.52, N 4.89.

Can. J. Chem. Downloaded from www.nrcresearchpress.com by 210.87.254.40 on 09/05/12
For personal use only.

Reaction of **4a** *with Methylamine*

To **4***a* (153 mg) was added excess CH_3NH_2 in anhydrous ether, obtained by extraction from an aqueous solution saturated with NaCl, and the solvent was removed after 10 min. The residue was dissolved in ether, and the solution was washed with 5% aqueous citric acid and aqueous $NaHCO_3$, dried, and the solvent was removed. The residue (mp 98–102°C) was recrystallized from CH_2Cl_2 – petroleum ether to give 165 mg (94%) of Boc-Val-$NHCH_3$, mp 113–114°C; ^{1}H nmr δ: 0.95 (d, 6), 1.42 (s, 9), 2.10 (m, 1), 2.82 (d, 3, J = 5 Hz), 3.90 (dd, 1, J = 9 and 5 Hz), 5.10 (br, 1), 6.1 (br, 1). *Anal.* calcd. for $C_{11}H_{22}N_2O_3$: C 57.4, H 9.6, N 12.2; found: C 57.2, H 9.5, N 12.1.

Reactions of **4** *with* **3** *to give* **5**

To **4***a* in CH_2Cl_2 was added an equiv. of **3***a*. After 15 min, the solution was washed with aqueous $NaHCO_3$, dried, and the solvent was removed. Addition of light petroleum gave **5***a* (>90% yield). Compound **5***b* was obtained similarly from **4***b* and **3***b*. Reaction of **4***a* with **3***b*, or **4***b* with **3***a*, gave the same product (oil) whose nmr spectrum indicated one Boc-group and one Z-group per two isopropyl side-chain groups of valine.[4]

*L-Valine-N-carboxyanhydride (***7a***)*

(i) Synthesis from Boc-Val

A solution of Boc-Val (2 mmol) was treated with EDC under conditions giving a maximum yield of **4***a*. After work-up and removal of solvent, the residue (0.36 g) containing **5***a* (34%) and **4***a* (50%) was left in 20 mL of CH_2Cl_2 saturated with dry HCl at 0°C for 2 h. The solvent was removed by evaporation, more was added, and evaporation was repeated. CH_2Cl_2 was added and the mixture was filtered. The solvent was removed, and the residue was recrystallized from $CHCl_3$ – light petroleum to give 185 mg (65%) of *N*-carboxyanhydride **7***a*, mp 57–58°C; $[\alpha]_D^{24}$ −45.0° (*c* 1.0, acetone) (lit. (18) mp 71°C; $[\alpha]_D$ −43°; lit. (19) mp 67–69°C, $[\alpha]_D$ −44.4°); ir ($CHCl_3$): 3345, 1860, and 1795 cm^{-1}; ^{1}H nmr δ: 1.06 (d, 3, J = 6 Hz), 1.10 (d, 3, J = 6 Hz), 2.30 (m, 1), 4.28 (d, 1, J = 4 Hz), and 7.15 (br, 1). *Anal.* calcd. for $C_6H_9NO_3$: C 50.34, H 6.34, N 9.79; found: C 50.36, H 6.49, N 9.77; optical purity >99.8%. The product is completely soluble in $CHCl_3$ indicating the absence of polymer.[6]

(ii) Reaction of **4a** *with Hydrogen Chloride*

When **4***a* was left in CH_2Cl_2 containing dry HCl at 0°C, a 90% yield of **7***a* was obtained.

(iii) Catalytic Hydrogenation of **4b**

When **4***b* was hydrogenated in *tert*-butanol in the presence of 5% palladium-on-charcoal catalyst, a quantitative yield of **7***a* was obtained.

*L-Isoleucine-N-carboxyanhydride (***7c***)*

This compound was obtained from Boc-Ile as described for the preparation of **7***a*. Yield: 65%; mp 65–66°C;[6] $[\alpha]_D^{24}$ −27.0° (*c* 2.0, acetone) (no data reported (19, 20)); ir ($CHCl_3$): 3360, 1860, and 1795 cm^{-1}; ^{1}H nmr δ: 1.05 (m, 6), 1.45 (m, 2), 2.00 (br, 1), 4.25 (d, 1, J = 4 Hz), and 7.10 (br, 1). *Anal.* calcd. for $C_7H_{11}NO_3$: C 53.49, H 7.06, N 9.91; found: C 53.66, H 7.18, N 8.89; optical purity >99.8%.

Isolation of **4** *from Prematurely Terminated Couplings (Table 1)*

Reactions and work-up were as described for the isolation of **4***a* according to (*iv*). The identity of the products was confirmed by adding anhydrous methylamine and noting the change in the nmr spectrum.

[6]The mp gradually increases after storage of the *N*-carboxyanhydride at −5°C (4° in four days). Removal of polymerized material by taking up the mixture in chloroform and filtering, gives product (80% recovery) with the original mp.

Acknowledgements

We thank the Medical Research Council of Canada for financial support, Mr. H. Seguin for the elemental analyses, and Dr. J. H. Jones for the free exchange of information subsequent to our initial presentation.[2] N.L.B. is Career Investigator of the M.R.C.C.

1. M. Bodanszky, Y. S. Klausner, and M. A. Ondetti. Peptide synthesis. 2nd ed. Wiley-Interscience, New York, NY. 1976. p. 137.
2. F. M. F. Chen, K. Kuroda, and N. L. Benoiton. Synthesis, 928 (1978).
3. N. L. Benoiton and F. M. F. Chen. *In* Peptides: structure and biological function. *Edited by* E. Gross and J. Meienhofer. Pierce Chemical Co., Rockford, IL. 1979. p. 261.
4. M. W. Williams and G. T. Young. J. Chem. Soc. 3701 (1964).
5. M. Goodman and W. J. McGahren. J. Am. Chem. Soc. **87**, 3028 (1965).
6. J. Rebek and D. Feitler. J. Am. Chem. Soc. **96**, 1606 (1974).
7. N. L. Benoiton, K. Kuroda, S. T. Cheung, and F. M. F. Chen. Can. J. Biochem. **57**, 776 (1979).
8. D. S. Kemp. *In* The peptides. Analysis, synthesis, biology. Vol. 1. Major methods of peptide bond formation. *Edited by* E. Gross and J. Meienhofer. Academic Press, New York, NY. 1979. p. 317.
9. J. H. Jones and M. J. Witty. J. Chem. Soc. Chem. Commun. 281 (1977).
10. M. Miyoshi. Bull. Chem. Soc. Jpn. **43**, 3221 (1970); **46**, 212 (1973); **46**, 1489 (1973).
11. J. H. Jones and M. J. Witty. J. Chem. Soc. Perkin Trans. I, 3203 (1979).
12. J. H. Davies, R. H. Davis, and R. A. G. Carrington. J. Chem. Soc. Perkin Trans. I, 1983 (1972).
13. I. Antanovics, A. L. Heard, J. Hugo, M. W. Williams, and G. T. Young. *In* Peptides. Proc. Sixth European Peptide Symposium, Athens, 1963. *Edited by* L. Zervas. Pergamon Press, Oxford. 1966. p. 139; G. T. Young. *In* Peptides. Proc. Eighth European Peptide Symposium, Noordwijk, 1966. *Edited by* H. C. Beyerman, A. Van de Linde, and W. Massen Van den Brink. North-Holland, Amsterdam. 1967. p. 55.
14. H. Determann, J. Heuer, P. Pfaender, and M. L. Reinartz. Ann. Chem. **694**, 190 (1966).
15. F. M. F. Chen, K. Kuroda, and N. L. Benoiton. Synthesis, 230 (1979).
16. J. Kovacs, R. Cover, G. Jham, Y. Hsieh, and T. Kalas. *In* Peptides: chemistry, structure and biology. *Edited by* R. Walter and J. Meienhofer. Ann. Arbor Science Publishers, Ann Arbor, MI. 1975. p. 317.
17. J. C. Sheehan, P. A. Cruickshank, and G. L. Boshart. J. Org. Chem. **26**, 2525 (1961).
18. M. Oya, R. Katakai, H. Naki, and Y. Iwakura. Chem. Lett. 1143 (1973).
19. R. Hirschmann, H. Schwam, R. G. Strachan, E. F. Schoenewaldt, H. Barkemeyer, S. M. Miller, J. B. Conn, V. Garsky, D. V. Veber, and R. G. Denkewalter. J. Am. Chem. Soc. **93**, 2746 (1971).
20. P. Pfaender, E. Kuhnle, B. Krahl, A. Backmansson, G. Gnauck, and H. Blecher. Hoppe-Seyler's Z. Physiol. Chem. **354**, 267 (1973).

Evidence for the generation of free hydroxyl radicals from certain quinone antitumor antibiotics upon reductive activation in solution[1]

J. WILLIAM LOWN AND HSIAO-HSIUNG CHEN

Department of Chemistry, University of Alberta, Edmonton, Alta., Canada T6G 2G2

Received June 4, 1980

This paper is dedicated to Prof. Raymond U. Lemieux on the occasion of his 60th birthday

J. WILLIAM LOWN and HSIAO-HSIUNG CHEN. Can. J. Chem. **59**, 390 (1981).

The nature of the reactive oxygen species generated from certain quinone antitumor antibiotics upon reductive activation in aqueous solution was investigated. A kinetic criterion was employed involving the relative rate of trapping of hydroxyl and formate radicals by the spin-trap 5,5-dimethyl-1-pyrroline-*N*-oxide (DMPO) in conjunction with epr spectroscopy. By comparison with a system involving the photolysis of hydrogen peroxide as a standard free hydroxyl system it was concluded that at pH 7 and at 37°C reductive activation of adriamycin, daunorubicin, mitomycin B, mitomycin C, and streptonigrin gives rise to free hydroxyl radicals in direct contrast with, for example, the photolysis of quinones in solution.

J. WILLIAM LOWN et HSIAO-HSIUNG CHEN. Can. J. Chem. **59**, 390 (1981).

On a étudié la nature des espèces réactives d'oxygène produites à partir de certaines quinones antibiotiques antitumescentes par une activation réductrice en solution aqueuse. On a utilisé un critère cinétique faisant intervenir la vitesse de piégeage des radicaux hydroxyle et formate par le capteur de spin, *N*-oxyde de diméthyl-5,5 pyrroline-1 (ODMP), conjointement avec la spectroscopie de rpe. Par comparaison avec un système impliquant la photolyse du peroxyde d'hydrogène en tant que système de référence pour le groupe hydroxyle libre, on a conclu qu'à un pH de 7 à 37°C l'activation réductrice de l'adriamycine, de la daunorubicine, de la mitomycine B, de la mitomycine C et de la streptonigrine produit des radicaux hydroxyles libres contrairement à ce qui se produit lors de la photolyse des quinones en solution.

[Traduit par le journal]

Introduction

There is accumulating evidence that reactive oxygen species, including the superoxide anion radical, hydrogen peroxide, and the hydroxyl radical are generated in vivo during the metabolism and/or molecular mechanism of cytotoxic action of certain antitumor antibiotics, especially those containing quinone moieties (see Fig. 1) (1–9). Oxidizing agents have many deleterious effects on cells including lipid peroxidation, macromolecule depolymerization, and membrane damage (2, 10–12). Many of these effects have been directly attributed to the hydroxyl radical owing to its high reactivity (13–17). Thus it became important from the viewpoint of elucidating the mechanism of action of antibiotics to determine the exact nature of the oxygen species produced. In a previous paper we reported the detection of superoxide and hydrogen peroxide formed in solution from a group of reductively activated quinone antibiotics (7). The formation of hydroxyl radicals was strongly implicated but not unambiguously proven. In the present work we provide evidence using kinetic criteria in conjunction with epr spectroscopy for the generation of hydroxyl radicals from certain quinone antibiotics, some of which are of clinical use in the treatment of cancer.

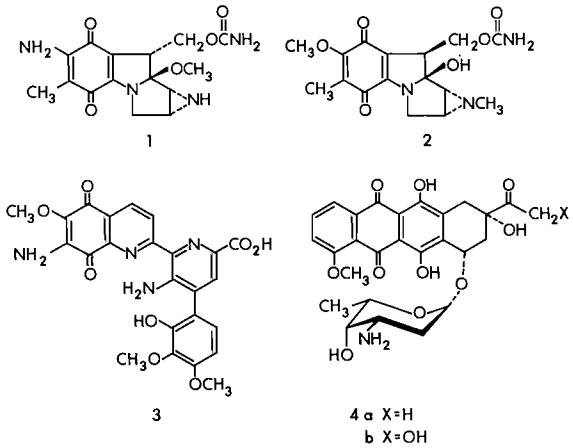

FIG. 1. Structures of quinone antitumor antibiotics. 1, Mitomycin C; 2, mitomycin B; 3, streptonigrin; 4a, daunorubicin; and 4b, adriamycin.

Results

Ultraviolet photolysis of dilute hydrogen peroxide solutions is known to generate OH· radicals (18). Whereas the OH radical itself is too short lived to permit a steady state epr signal, added DMPO (19), however, produces a steady state DMPO·OH spin-adduct spectrum (Fig. 2A) with its characteristic four-line pattern (19, 20). Addition of sodium formate also introduced the typical six-line epr spectrum of the DMPO·formyl spin-adduct (21,

[1]Studies related to antitumor antibiotics. Part XXII.

0008-4042/81/020390-06$01.00/0

©1981 National Research Council of Canada/Conseil national de recherches du Canada

Can. J. Chem. Downloaded from www.nrcresearchpress.com by 210.87.254.42 on 09/05/12
For personal use only.

Can. J. Chem. Downloaded from www.nrcresearchpress.com by 210.87.254.42 on 09/05/12
For personal use only.

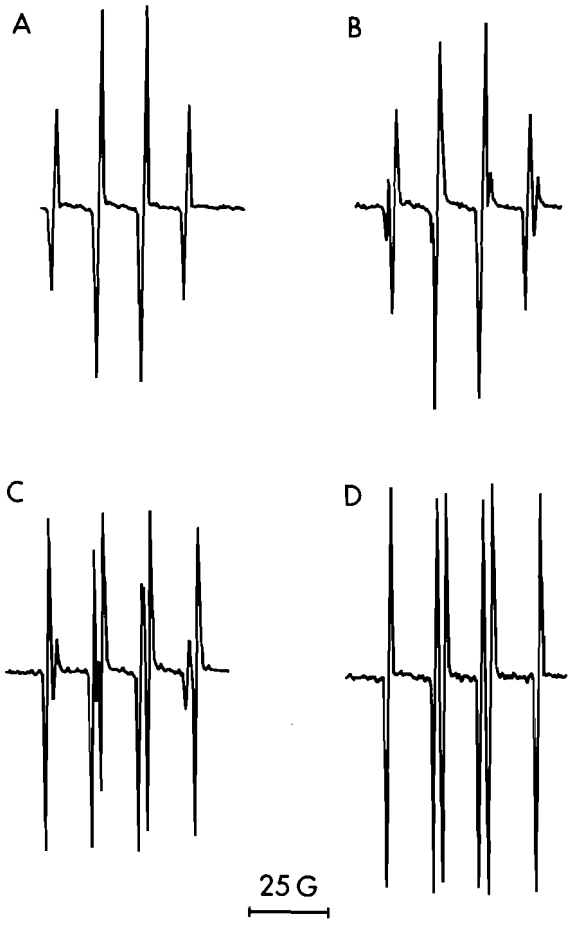

FIG. 2. Electron paramagnetic resonance spectra (microwave power 4 mW, modulation amplitude 0.05 G, scan time 1000 s) of DMPO spin-trapped radicals obtained by incubating 1×10^{-2} *M* mitomycin C reduced with 3×10^{-2} *M* sodium borohydride in the presence of different concentrations of sodium formate at pH 7.0. A(none); B, 7.5 m*M*; C, 62.5 m*M*; D, 100 m*M*. Spectrum A shows only the DMPO·OH spin adduct, hfs $a^N = 15.0$ G, $a^H = 15.0$ G. Spectrum D shows only the formyl DMPO spin adducts, hfs $a^N = 15.6$ G, $a^H = 18.8$ G. Spectra C and B show a superimposition of the spectra of the two spin adducts.

22) (Fig. 2D). As the concentration of the sodium formate increased, the signal strength of the DMPO·formyl species increased at the expense of the DMPO·OH adduct (e.g. Figs. 2B, C). The peroxide solution under uv photolysis was used as the free OH radical system (18) against which the antibiotics systems were compared.

Mitomycin C, when reduced with slightly in excess of one equivalent of sodium borohydride in aqueous solution and exposed to oxidation by air, gives rise to a semiquinone species which was identified by its epr hyperfine spectrum which in turn had been subject to computer simulation analysis (7). Care was taken to ensure that the excess of the sodium borohydride was removed before addition of the DMPO to prevent its reduction (*vide infra*). Addition of DMPO and incubation at pH 7 in phosphate buffer and at 37°C gave rise to the superimposition of the epr signals due to the semiquinone together with the characteristic 1:2:2:1 DMPO·OH pattern.

It was established in control experiments that the spin-trapping agent DMPO in the pH 7.0 buffer solution did not give rise to radical species in the absence of the antibiotics. The reason why it was essential to remove excess of the reducing agent sodium borohydride before addition of the DMPO is that we had observed that phenyl *N-tert*-butylnitrone (PBN) in the presence of sodium borohydride is reduced to benzyl *tert*-butyl hydroxylamine, subsequent air oxidation of which gives rise to the benzyl *tert*-butyl nitroxide which affords a 9-line epr spectrum with hyperfine couplings $a^N = 16.2$ G, $a^H = 10.5$ G (7). Therefore DMPO was reduced with sodium borohydride in solution and the product exposed to air oxidation in order that the corresponding radical species produced from DMPO could be recognized if it was formed. Electron paramagnetic resonance examination shows a well-resolved 9-line spectrum with $a^N = 16.0$ G, $a^H_{CH_2} = 21.5$ G (Fig. 3).

As the concentration of the added sodium formate increased, the epr signal strength of the DMPO·formyl species increased at the expense of the DMPO·OH adduct. The ratio of the DMPO·OH peak height to the sum of the OH and formyl adduct

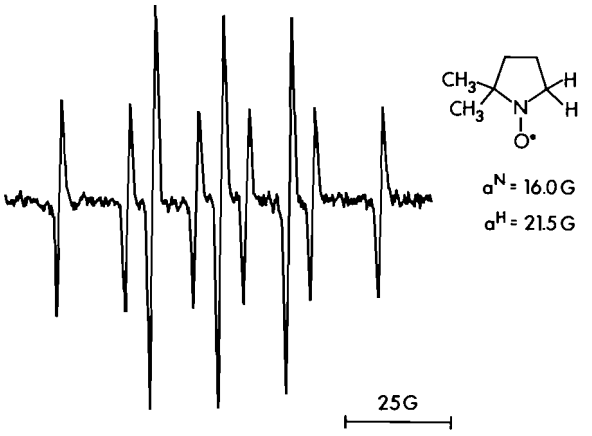

FIG. 3. Electron paramagnetic resonance spectrum (microwave power 8 mW, modulation amplitude 0.1 G, scan time 1000 s) of 2,2-dimethyltetrahydropyrrole *N*-oxide radical obtained from the reduction of DMPO with sodium borohydride followed by air oxidation; hfs $a^N = 16.0$ G, $a^H_{CH_2} = 21.5$ G.

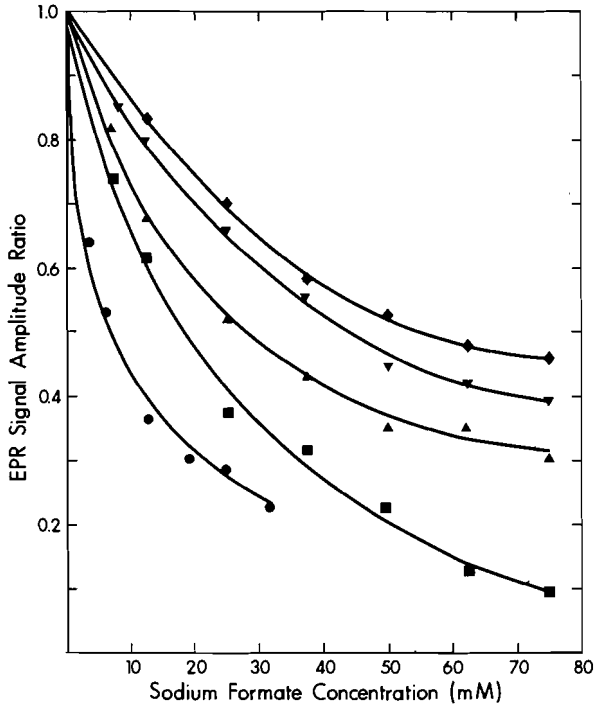

FIG. 4. Plot of the ratio (amplitude DMPO·OH adduct epr signal):(amplitude DMPO·formyl adduct + amplitude DMPO·OH adduct epr signals) versus concentration of added sodium formate for different antibiotics: ◆ mitomycin B; ▼ adriamycin; ▲ daunorubicin; ■ mitomycin C; ● streptonigrin.

peak heights was determined and plotted against formate concentration. The sodium formate concentration at which the DMPO·OH and DMPO·CO_2^- spin-adduct concentrations are equal was thus determined (Fig. 4).

Similar procedures were adopted to investigate the behavior of mitomycin B, daunorubicin, adriamycin, and streptonigrin. In the case of daunorubicin the radical generation, spin-trapping, and the epr analysis were performed at the three buffered pH's of 6, 7, and 8. The results of the determinations in each case of the formate concentration at which the DMPO·OH and DMPO·CO_2 spin adduct concentrations are equal are summarized in Table 1.

TABLE 1. Ratios of rate constants for reaction of hydroxyl species with formate anion and DMPO for quinone antibiotics at pH 7

Antibiotic	(k_9/k_{10})†	
Adriamycin	0.28 ± 0.15	
Daunorubicin*	0.18 ± 0.09	
Mitomycin B	0.37 ± 0.19	
Mitomycin C	0.11 ± 0.06	
Streptonigrin	0.05 ± 0.03	
H_2O_2 system	0.23 ± 0.12	
Benzoquinone	4.8 ± 0.4	(ref. 42)

*Value of (k_9/k_{10}) at pH $6.0 = 0.18 \pm 0.09$, and at pH $8.0 = 0.15 \pm 0.08$.
†Values of (k_9/k_{10}) were calculated for the antibiotics when the concentrations of the DMPO·OH and DMPO·formyl radicals were equal (see text).

Discussion

There is growing evidence that the generation of reactive oxygen species is intimately associated with the primary cytotoxic and, in some cases, secondary toxic effects of certain antitumor antibiotics. For example it has been shown that the glycopeptide antitumor antibiotics bleomycin and tallysomycin bind to DNA and through the intermediacy of an iron complex undergo redox cycling in vivo to generate reactive oxygen species (most probably O_2^- and OH·) which cleave DNA (23–26). Since these antibiotics bind at particular sequences in the genome they have been characterized as site-specific radical generators (3). Also, the anthracyclines daunorubicin and adriamycin exhibit many effects in vivo including interference with cell respiration and lipid peroxidation especially in heart tissue (27). There is evidence that these effects are associated with the generation of reactive oxygen radicals and may be causally related to the severe dose-related cardiotoxicity (1–3, 28–32). The surveillance system that ordinarily protects the cell against damage by oxygen species consists of superoxide dismutase which removes O_2^- and functions in tandem with the enzymes glutathione peroxidase and catalase (which remove H_2O_2) (33). Part of the selectivity expressed by antitumor agents such as bleomycin and mitomycin C which generate reactive oxygen species may therefore be attributed to the suppressed levels of superoxide dismutase and of catalase in neoplastic tissue (34). Because of the existence of these enzymes the intermediacy of superoxide and hydrogen peroxide in the action of quinone antitumor antibiotics is unambiguously established by their selective enzymatic removal (with consequent protection of macromolecules against damage), by superoxide dismutase and by catalase, respectively (4, 7, 25, 26).

By contrast, there appears to be no specific cell surveillance enzyme to remove OH·. The cell seems to rely on the removal of the precursor components O_2^- and H_2O_2 (from which OH· may arise) to prevent formation of hydroxyl radicals. The intermediacy of OH· and its role in antibiotic action has had to be inferred by indirect means, e.g. suppression of DNA scission by free radical scavengers like mannitol or sodium benzoate (7). In view of the high reactivity of OH· (which is arguably the most powerful oxidant encountered in biological

Can. J. Chem. Downloaded from www.nrcresearchpress.com by 210.87.254.42 on 09/05/12
For personal use only.

Can. J. Chem. Downloaded from www.nrcresearchpress.com by 210.87.254.42 on 09/05/12
For personal use only.

systems) it becomes essential to establish whether or not free OH· radicals are generated.

Alternative mechanisms may be envisaged for the formation of the hydroxyl radical from quinone antibiotics.

[1] $AB + [2H] \rightarrow ABH_2$

[2] $ABH_2 + O_2 \rightarrow ABH^{\cdot} + HO_2^{\cdot}$

[3] $HO_2^{\cdot} \rightarrow H^+ + O_2^{-}$

[4] $2O^{-} + 2H^+ \xrightarrow{SOD} H_2O_2 + O_2$

[5] $2H_2O_2 \xrightarrow{catalase} 2H_2O + O_2$

[6] $CMX{\cdot}Fe^{3+} + O_2^{-} \rightarrow CMXFe^{2+} + O_2$

[7] $CMX{\cdot}Fe^{2+} + H_2O_2 \rightarrow CMXFe^{3+} + OH^{\cdot} + OH^{-}$

In the above scheme AB represents a reducible antibiotic. SOD represents superoxide dismutase. *CMX*· Fe signifies iron complexed in vivo to either protein or ATP, or in the case of the glycopeptide antibiotics bleomycin and tallysomycin to the antibiotics themselves. This scheme gains support from (*a*) electrochemical measurements that show the redox potentials of the antibiotics to be compatible with reductants available in vivo (35, 36), (*b*) from the unambiguous identification of the semiquinone species ABH· by epr (7) and of O_2^{-} and H_2O_2 by employing SOD and catalase, respectively (4, 7, 25, 26).

Although hitherto the generation of OH· species in vivo had been attributed to the Haber–Weiss reaction [8] this is improbable since it has recently

[8] $H_2O_2 + O_2^{-} \rightarrow OH^{\cdot} + OH^{-} + O_2$

been shown to be quite slow ($k < 0.3\ M^{-1}\ s^{-1}$) (37–39) and therefore is unlikely to represent the source of OH· species. Instead it has been suggested that the OH· radical is produced by reaction of O_2^{-} with Fe(III) complexed with protein or ATP since traces of iron are present in most biological systems (40). The release of free radicals in close proximity to DNA in the case of "site-specific free radical generators" e.g. bleomycin, adriamycin, daunorubicin, is necessary because of the high reactivity of OH·. Its rate constants are so large for most compounds that it will react with the first molecule it encounters. Thus, in order to damage DNA, OH must be released close to it.

A number of alternative mechanisms may be envisaged for the formation of "bound" hydroxyl radicals, i.e., via a species which is capable of donating a hydroxyl group to the spin-trap. In the case of quinone-containing antibiotics these could include for example a hydration pathway e.g.

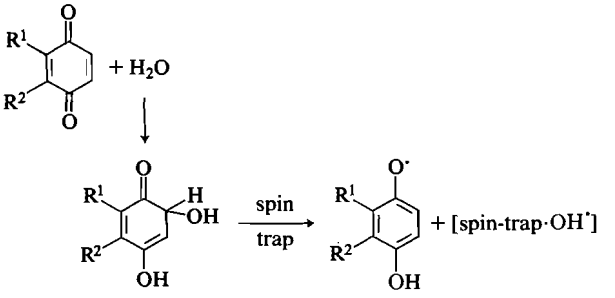

The intermediate hydrated form of the activated antibiotic could serve, in effect, as an hydroxyl radical donor or a "bound hydroxyl radical". A mechanism such as this has precedence in the known photoinduced hydration of *p*-benzoquinone which is able to transfer a hydroxyl group to a spin-trap such as DMPO (41, 42). Another related reaction is the observed hydration of certain spin-traps in solution to give a hydroxylamine which is readily oxidizable to a stable nitroxide giving rise to a "false spin adduct", as observed by Janzen *et al.* in the case of the α-4-pyridyl-1-oxide *N-tert*-butyl nitrone (43).

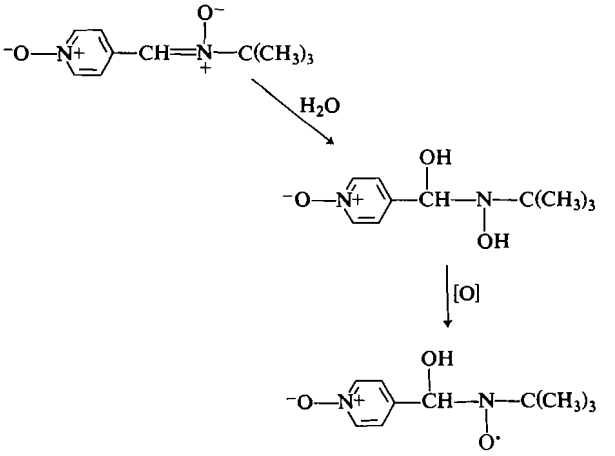

In view of these mechanistic alternatives the kinetic criteria implicit in the formate procedure of Harbour and co-workers (21, 22) were applied to discriminate between a true free hydroxyl species and a "bound" hydroxyl species (hereafter referred to as X) generated from these antibiotics.[2] The basis of the method is as follows. Formate ion reacts rapidly with OH radicals to generate the formyl radical (44) with a rate constant of $2.7 \times 10^9\ M^{-1}\ s^{-1}$ at pH 7.0 (45).

$$HCOO^{-} + OH^{\cdot} \rightarrow CO_2^{-} + H_2O$$

The formyl radical thus produced can react with the

[2]The authors are indebted to Dr. J. R. Bolton for suggesting the application of their procedure to the present problem.

Can. J. Chem. Downloaded from www.nrcresearchpress.com by 210.87.254.42 on 09/05/12
For personal use only.

spin-trap to produce a superposition of the OH and formyl radical spin-adduct spectra. At low formate concentrations most of the X will react directly with DMPO. At higher concentrations of formate, however, X will react to generate more of the formyl radical with a resultant increase in formyl adduct spectrum intensity. If X represents the free OH radical, the benzoquinone system should react identically with a system known to involve free OH, e.g. the kinetics of the two systems should be identical. If X is an intermediate other than OH, the systems are expected to behave differently.

Czapski and Bielski have established that uv photolysis of dilute hydrogen peroxide solutions produces free OH radicals (18) and for this reason it was chosen as the free OH radical system against which the antibiotic systems were compared. The relative concentrations of the OH and formyl spin-adducts were determined as a function of formate concentration for each system. This was done by measuring the amplitude of the low field peak of each spin-adduct signal. A correction for linewidth was made where necessary

$$I \propto \gamma'_{max}(\Delta H_{pp})^2$$

where I = approximate relative intensity, $2\gamma'$ = peak to peak amplitude, and ΔH_{pp} = peak to peak linewidth. Thus, corrected peak amplitude is proportional to peak area and radical concentration.

The competing reactions may be represented as follows

[9] $X + DMPO \xrightarrow{k_9}$ 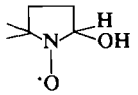

[10] $X + HCOO^- \xrightarrow{k_{10}} CO_2^{\cdot-} + H_2O$

[11] $CO_2^{\cdot-} + DMPO \xrightarrow{k_{11}}$ 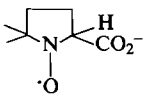

Reaction [11] is common for the antibiotics and hydrogen peroxide systems regardless of the nature of X. The two competing reactions are [9] and [10]

$$\text{Rate [9]} = k_9[X][DMPO]$$

$$\text{Rate [10]} = k_{10}[X][HCOO^-]$$

When the concentrations of OH and formyl spin-adducts are equal, then Rate [9] = Rate [10]. Then, assuming that reaction [11] goes to completion:

$$k_9[X][DMPO] = k_{10}[X][HCOO^-]$$

$$[HCOO^-]/[DMPO] = k_9/k_{10}$$

The concentrations of formate and DMPO under these conditions are known. If a particular antibiotic system involves a free OH radical, the ratio of the rate constants must be similar to that for the hydrogen peroxide system. It may be seen from the table that the ratios of (k_9/k_{10}) at pH 7 for adriamycin, daunorubicin, mitomycin B, mitomycin C, and streptonigrin are quite similar to that recorded for the hydrogen peroxide systems. In the example of daunorubicin (k_9/k_{10}) does not vary significantly over the pH range 6.0 to 8.0. By contrast the system involving the photolysis of *p*-benzoquinone, from which the stable products are hydroquinone and 2-hydroxy-1,4-benzoquinone, gives a very different value for (k_9/k_{10}) of 4.8 indicative of the intermediacy of a "bound" hydroxyl radical donor (42).

It has been suggested by a referee that owing to the high reactivity of the OH· radical some attack of this species on susceptible groups in the antibiotics (e.g. CH_3O, $\diagdown CH—OH$, $\diagdown CH—OR$) may be anticipated to compete with trapping of the OH· by formate anion. The radicals produced from such reactions should also be trapped by DMPO but since there was no evidence of addition epr signals in addition to the primary spin-adducts one may conclude such processes do not occur to a detectable extent.

The results demonstrate that these antibiotics are giving rise to the hydroxy radical by a mechanism similar to that given in reactions [1] to [7] and that it is free in solution. The results should assist in the understanding of the molecular mechanism of anticancer action and of the cytotoxicity of these antibiotics.

Experimental

Materials

Mitomycin C was purchased from Calbiochem. Mitomycin B was a gift from Dr. K. Shirahata, Kyoway Hakko Kogyo Co. Ltd., Tokyo, Japan. Streptonigrin was supplied by Dr. H. R. Wood, Jr., National Cancer Institute, Washington, DC. Daunorubicin and adriamycin were generous gifts from Dr. F. Arcamone, Farmitalia, Milan.

5,5-Dimethyl-1-pyrroline-*N*-oxide (DMPO) was purchased from Aldrich Chemical Co. and was purified by charcoal decolorization just before use. A standard solution of DMPO, 0.64 *M* was prepared in 0.1 *M* phosphate buffer, pH = 7.0.

Electron Paramagnetic Resonance Spectroscopy

The epr spectra were obtained on a Bruker ER-400 EPR spectrometer fitted with a Varian V3601 12-inch magnet with VFR Hall effect controller. Hyperfine couplings were obtained by comparison with peroxylamine disulfonate (triplet, spacing 13.0 G) and *g* values were obtained by direct Fieldial measurements.

Spin Trapping and EPR Detection of Radical Species from Reduced Quinone Antibiotics

A standard reaction solution was prepared for each run on a 400 μL scale with deionized water containing 5 mmol of EDTA, 25 mmol phosphate buffer pH 7.0, 0.16 mol DMPO, and either 0, 7.5 m*M*, 12.5 m*M*, 25 m*M*, 37.5 m*M*, 50 m*M*, 62.5 m*M*, or 75 m*M* sodium formate.

Separately, the semiquinone of each antibiotic was prepared

Can. J. Chem. Downloaded from www.nrcresearchpress.com by 210.87.254.42 on 09/05/12
For personal use only.

by treating 1000 μL of a 1×10^{-2} *M* solution of the antibiotic with 300 μL of 3×10^{-2} *M* sodium borohydride, incubated at room temperature and protected from the light in the presence of atmospheric oxygen for different periods of time depending on the redox potential of the antibiotics; ca. 3 min for mitomycin B, 6 min for streptonigrin, 10 min for daunorubicin, 15 min for mitomycin C, and 25 min for adriamycin. Care was taken to ensure that the excess of sodium borohydride was discharged before addition of the spin-trap to avoid the reduction of DMPO and its reoxidation to form the nitroxide which would have given rise to the 9-line epr spectrum shown in Fig. 3. After the room temperature incubation, 200 μL of the semiquinone solution was added into the prepared DMPO – sodium formate solution and incubated at 37°C for 2.5 h before the epr study.

The addition of sodium formate permits the detection of the hydroxyl radical which thereby gives rise to the formyl spin-trapped nitroxide according to the method of Harbour and Bolton (22). In the present study, however, the formate concentration was systematically varied. A plot of the relative peak heights of spin-adduct spectra versus formate concentration was made for each antibiotic. The relative concentrations of the OH and formyl spin adducts were determined by measuring the amplitude of the low field peak of each spin-adduct signal. Some decay of the signals occurred during the 1000 s scan time. Therefore, the spectrometer scans from low to high field, using the low field peaks, to minimize any error introduced by signal decay.

In control experiments it was established that in the presence of sodium formate and buffer the spin-trapping agent DMPO did not give rise to radicals in the absence of sodium borohydride treated antibiotics.

Acknowledgements

This research was supported by grants to J.W.L. from the National Cancer Institute of Canada, the Natural Sciences and Engineering Research Council of Canada, and the University of Alberta. We are indebted to Professor J. R. Bolton and Mr. J. Hern of the University of Western Ontario for giving us the details of their formate spin-trapping procedure.

1. W. S. Thayer. Chem.-Biol. Interactions, **19**, 265 (1977).
2. J. Goodman and P. Hochstein. Biochem. Biophys. Res. Commun. **77**, 797 (1977).
3. N. R. Bachur, S. L. Gordon, and M. V. Gee. Mol. Pharmacol. **13**, 901 (1977).
4. R. Cone, S. K. Hasan, J. W. Lown, and A. R. Morgan. Can. J. Biochem. **54**, 219 (1976).
5. H. L. White and J. R. White. Mol. Pharmacol. **4**, 549 (1968).
6. H. L. White and J. R. White. Biochim. Biophys. Acta, **123**, 648 (1966).
7. J. W. Lown, S. K. Sim, and H. H. Chen. Can. J. Biochem. **56**, 1042 (1978).
8. L. W. Oberley and G. R. Buettner. FEBS Lett. **97**, 47 (1979).
9. M. Tomasz. Chem.-Biol. Interactions, **13**, 89 (1976).
10. I. Fridovich. Adv. Enzymol. **41**, 35 (1974).
11. W. Bors, M. Saran, E. Lengfelder, R. Spöttl, and C. Michel. Curr. Top. Radiat. Res. Q. **9**, 247 (1974).
12. B. Halliwell. New Phytol. **73**, 1075 (1974).
13. S. J. Weiss, G. W. King, and A. F. Lobuglio. J. Clin. Invest. **60**, 370 (1977).
14. A. I. Tauber and B. M. Babior. J. Clin. Invest. **60**, 374 (1977).
15. B. Halliwell and S. Ahluwalia. Biochem. J. **153**, 513 (1976).
16. K. L. Fong, P. B. McCay, J. L. Poyer, B. B. Keele, and H. Misra. J. Biol. Chem. **248**, 7792 (1973).
17. C. Beauchamp and I. Fridovich. J. Biol. Chem. **245**, 4641 (1970).
18. G. Czapski and H. J. Bielski. J. Phys. Chem. **67**, 2180 (1963).
19. E. G. Janzen and J. I.-P. Liu. J. Magn. Reson. **9**, 510 (1973).
20. E. G. Janzen, D. E. Nutter, E. R. Davis, B. J. Blackburn, J. L. Poyer, and P. B. McCay. Can. J. Chem. **56**, 2237 (1978).
21. J. F. Harbour, V. Chow, and J. R. Bolton. Can. J. Chem. **52**, 3549 (1974); J. R. Harbour and M. L. Hair. Can. J. Chem. **57**, 1150 (1979).
22. J. R. Harbour and J. R. Bolton. Photochem. Photobiol. **28**, 231 (1978).
23. E. A. Sausville, J. Peisach, and S. B. Horwitz. Biochemistry, **17**, 2740 (1978).
24. R. M. Burger, J. Peisach, W. E. Blumberg, and S. B. Horwitz. J. Biol. Chem. **254**, 10906 (1979).
25. J. W. Lown and S. K. Sim. Biochem. Biophys. Res. Commun. **77**, 1150 (1977).
26. J. W. Lown and A. V. Joshua. Biochem. Pharmacol. **29**, 521 (1980).
27. A. Di Marco, F. Arcamone, and F. Zunino. *In* Antibiotics III. Mechanism and action of antimicrobial and antitumor agents. *Edited by* J. W. Corcoran and F. E. Hahn. Springer Verlag, New York. 1975. p. 104.
28. J. W. Lown, H. H. Chen, J. A. Plambeck, and E. M. Acton. Biochem. Pharmacol. **28**, 2563 (1979).
29. T. Kishi, T. Watanabe, and K. Folkers. Proc. Natl. Acad. Sci. U.S.A. **73**, 4653 (1976).
30. Y. Iwamoto, I. L. Hansen, T. H. Porter, and K. Folkers. Biochem. Biophys. Res. Commun. **58**, 633 (1974).
31. E. Bachmann, E. Weber, and G. Zbinden. Agents Actions, **515**, 383 (1975).
32. G. Zbinden, E. Bachmann, and C. Holdnegger. Antibiot. Chemother. **23**, 255 (1978).
33. I. Fridovich. *In* Biochemical and medical aspects of active oxygen. *Edited by* O. Hayaishi and K. Asada. University Park Press, Baltimore. 1977. p. 171.
34. A. V. Peskin, Ya. M. Koen, I. B. Zbarsky, and A. A. Konstantinov. FEBS Lett. **78**, 41 (1977).
35. J. C. Dabrowiak and F. S. Santillo. J. Electrochem. Soc. **126**, 2091 (1979).
36. G. M. Rao, A. Begleiter, J. W. Lown, and J. A. Plambeck. J. Electrochem. Soc. **124**, 199 (1977).
37. J. J. Van Hemmen and W. J. A. Meuling. Arch. Biochem. Biophys. **182**, 743 (1977).
38. G. J. McClune and J. A. Fee. FEBS Lett. **67**, 294 (1976).
39. B. Halliwell. FEBS Lett. **72**, 8 (1976).
40. G. Czapski and Y. A. Ilan. Abstract C-11. International conference on singlet oxygen and related species in chemistry and biology. Pinawa, Manitoba. August 21–26, 1977.
41. M. Shirai, T. Awatsuji, and M. Tanaka. Bull. Chem. Soc. Jpn. **48**, 1329 (1975).
42. J. Hern. B.Sc. Fourth year research thesis, University of Western Ontario, London, Ont. 1979.
43. E. J. Janzen, Y. Y. Wang, and R. V. Shetty. J. Am. Chem. Soc. **100**, 2923 (1978).
44. O. P. Chawla and R. W. Fessenden. J. Phys. Chem. **79**, 2693 (1975).
45. L. S. Myers, J. F. Ward, W. T. Tsukamoto, D. E. Holmes, and J. P. Julia. Science, **148**, 1234 (1965).

Synthesis of fluoro derivatives of 2-amino-2-deoxy-D-galactose and -D-glucose

LESLIE HOUGH, ANNA A. E. PENGLIS, AND ANTHONY C. RICHARDSON
Department of Chemistry, Queen Elizabeth College, London W8 7AH, Great Britain

Received July 2, 1980

This paper is dedicated to Prof. Raymond U. Lemieux on the occasion of his 60th birthday

LESLIE HOUGH, ANNA A. E. PENGLIS, and ANTHONY C. RICHARDSON. Can. J. Chem. **59**, 396 (1981).

Selective fluoride displacement of the 6-mesyloxy group of methyl 2-benzamido-3-*O*-benzyl-2-deoxy-4,6-di-*O*-mesyl-α-D-glucopyranoside **4** gave the 6-fluoride **5**. Subsequent removal of the blocking substituents afforded 2-amino-2,6-dideoxy-6-fluoro-D-glucose, isolated as its hydrochloride **11** and its *N*-acetyl derivative **12**. Nucleophilic displacement of the remaining 4-mesyloxy group of the intermediary 6-fluoro-4-mesylate **5**, by benzoate anion afforded derivatives of 2-amino-2,6-deoxy-6-fluoro-D-galactose (**18**). An interplay of similar substitutions on **4** gave, after deprotection, methyl 2-acetamido-4,6-difluoro-2,4,6-trideoxy-α-D-galactopyranoside (**22**), methyl 2-acetamido-3-*O*-acetyl-4,6-difluoro-2,4,6-trideoxy-α-D-glucopyranoside (**27**), and methyl 2-benzamido-3-*O*-benzyl-6-fluoro-2,4,6-trideoxy-β-L-*threo*-hex-4-enopyranoside (**28**).

Methyl 2-acetamido-2,4-dideoxy-4-fluoro-α-D-glucopyranoside diacetate (**31**) was synthesized from the 4-*O*-mesyl-6-*O*-trityl-galactopyranoside **29**.

LESLIE HOUGH, ANNA A. E. PENGLIS et ANTHONY C. RICHARDSON. Can. J. Chem. **59**, 396 (1981).

Le déplacement sélectif du groupe mésyloxy-6 du benzamido-2 *O*-benzyl-3 déoxy-2 di-*O*-mésyl-4,6 α-D-glucopyrannoside de méthyle (**4**) par un fluorure donne le dérivé fluoré en 6 (**5**). L'élimination subséquente des substituants protecteurs conduit à l'amino-2 didéoxy-2,6 fluoro-6 D-glucose que l'on a isolé sous forme de chlorhydrate (**11**) et de dérivé *N*-acétylé (**12**). Le déplacement nucléophile du groupe mésyloxy-4 du fluoro-6 mésylate-4 intermédiaire (**5**) par l'anion benzoate conduit aux dérivés de l'amino-2 déoxy-2,6 fluoro-6 D-galactose (**18**). Une séquence analogue de substitutions sur le composé **4** conduit, après déprotection, à l'acétamido-2 difluoro-4,6 tridéoxy-2,4,6 α-D-galactopyrannoside de méthyle (**22**), à l'acétamido-2 *O*-acétyl-3 difluoro-4,6 tridéoxy-2,4,6 α-D-glucopyrannoside de méthyle (**27**) et au benzamido-2 *O*-benzyl-3 fluoro-6 tridéoxy-2,4,6 β-L-*thréo*-hexéno-4 pyrannoside de méthyle (**28**).

On a synthétisé le diacétate de l'acétamido-2 didéoxy-2,4 fluoro-4 α-D-glucopyrannoside de méthyle (**31**) à partir du *O*-mésyl-4 *O*-trityl-6 galactopyrannoside (**29**).

[Traduit par le journal]

Substitution of fluorine into certain natural products, notably steroids, has sometimes markedly enhanced their biological activities. These effects have been explained in terms of the greater electronegativity of fluorine, which affects the acidity of neighbouring protons, coupled with the ability of fluorine to accept a hydrogen bond in the same way as oxygen. The latter property has motivated a considerable effort into the synthesis of carbohydrate derivatives in which one or more hydroxyl groups have been replaced by fluorine. For example, fluorinated analogues of D-glucose and D-galactose have been synthesized (1–3) for biochemical studies and the probing of molecular conformation by the use of ^{19}F nmr spectroscopy has added a new dimension to structural studies of carbohydrates in solution (3, 4). However, the anticipation that such fluorinated sugars would function as highly effective inhibitors of various enzymes (cf. fluorocitric acid (5) formed from fluoroacetic acid in vivo) has not been realized, although some do act as weak reversible inhibitors. For example, we have shown that 6-deoxy-6-fluorotrehalose is a good reversible inhibitor of insect trehalase (6).

In view of the wide distribution of D-glucosamine and D-galactosamine in the animal kingdom, the synthesis of specifically fluorinated analogues was investigated. Meanwhile the syntheses of derivatives of 2-amino-2,6-dideoxy-6-fluoro-D-glucose (**11**) and -D-galactose and 2-amino-2,4-dideoxy-4-fluoro-D-glucose have been reported (7–9), but by different and less convenient routes than those described herein, although the method described by Sharma and Korytnyk (8), in which primary hydroxyl groups could be displaced directly with fluorine by treatment with diethylaminosulphur trifluoride, was particularly convenient for the preparation of 6-deoxy-6-fluorohexosamine derivatives.

The most rational approach for the introduction of fluorine into 2-amino-2-deoxy-D-glucose and -D-galactose is by nucleophilic fluoride displacement of a sulphonyloxy group in a suitably blocked but readily available *gluco*-analogue. Thus, for the synthesis of the 6-fluorides, methyl 2-benzamido-3-*O*-benzyl-2-deoxy-4,6-di-*O*-mesyl-α-D-glucopyranoside (**4**) was considered appropriate. It was prepared from methyl 2-benzamido-4,6-*O*-benzylidene-2-deoxy-α-D-glucopyranoside (10) by sequential benzylation, mild acid hydrolysis, and mesylation in an overall yield of 55%. Selective

0008-4042/81/020396-10$01.00/0
©1981 National Research Council of Canada/Conseil national de recherches du Canada

Can. J. Chem. Downloaded from www.nrcresearchpress.com by 210.87.254.6 on 09/05/12
For personal use only.

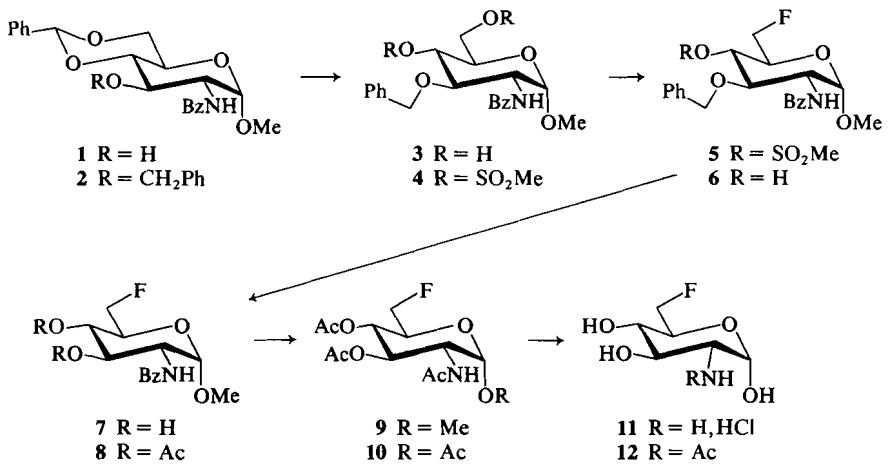

nucleophilic displacement of the primary ester of the 4,6-dimesylate **4** was readily achieved by reaction with tetrabutylammonium fluoride in acetonitrile (2, 3) for 1 h at reflux. The 6-fluoride **5** was isolated in 87% yield, and its structure confirmed by the ^{19}F nmr spectrum (Table 2) which displayed a triplet of doublets ($J_{H\text{-}6a,6\text{-}F} = J_{H\text{-}6b,6\text{-}F} = 47.5$, $J_{H\text{-}5,6F} = 22.5$ Hz) typical of a 6-deoxy-6-fluoroglucopyranoside (3, 11). Removal of the remaining mesyl group was accomplished by boiling methanolic sodium hydroxide, which gave methyl 2-benzamido-3-*O*-benzyl-2,6-dideoxy-6-fluoro-α-D-glucopyranoside (**6**), crystalline in 93% yield. Hydrogenolysis of the 3-*O*-benzyl-6-fluoride **6** in the presence of acid then gave crystalline methyl 2-benzamido-2,6-dideoxy-6-fluoro-α-D-glucopyranoside (**7**), which was also characterized as its diacetate **8**, the ^1H and ^{19}F nmr parameters of which were in complete accord with the structure (Tables 1 and 2). Hydrolysis of the diacetate **8** with hydrochloric acid afforded crystalline 2-amino-2,6-dideoxy-6-fluoro-α-D-glucose hydrochloride (**11**) in 90% yield. *N*-Acetylation of the amine salt **11** was accomplished by deionization of a solution of **11** followed by treatment with acetic anhydride (12) to give crystalline 2-acetamido-2,6-dideoxy-6-fluoro-α-D-glucose (**12**).

An alternative route to the *N*-acetyl derivative (**12**) involved treatment of methyl 3,4-di-*O*-acetyl-2-benzamido-2,6-dideoxy-6-fluoro-α-D-glucopyranoside (**8**) with a boiling mixture of acetic acid and acetic anhydride (13), thereby replacing the *N*-benzoyl substituent with *N*-acetyl. The reaction mixture was either processed directly to give methyl 2-acetamido-3,4-di-*O*-acetyl-2,6-dideoxy-6-fluoro-α-D-glucopyranoside (**9**) in 65% yield, or cooled and treated with a little sulphuric acid in order to acetolyze the glycosidic group. This latter treatment afforded a crystalline mixture of triacetates of 2-acetamido-2,6-dideoxy-6-fluoro-D-glucose which was mainly the α-pyranose, but which could not be resolved into a pure anomer by recrystallization. The pure α-pyranose tri-*O*-acetate (**10**) was, however, obtained from the 2-acetamido sugar (**12**) by acetylation with acetic anhydride in pyridine.

For the synthesis of the *galacto* isomer (**18**), the 6-fluoro-4-mesylate (**5**) was readily available. Nucleophilic displacement of the sulphonyloxy group by benzoate anion in hexamethylphosphoric triamide afforded the 4-*O*-benzoyl-galactoside (**13**) crystalline in 80% yield. Its ^1H nmr spectrum was indicative of the *galacto* configuration showing the H-3 and H-4 resonances as double doublets ($J_{2,3}$ 10.5 Hz, $J_{3,4}$ 3.2 Hz, $J_{4,5}$ 1.3 Hz) (14). On the other hand, the ^{19}F nmr spectrum was highly second order, as found with other 6-deoxy-6-fluorogalactopyranosides (6, 15).

The 4-*O*-benzoyl group was removed from the 6-fluoride (**13**) by transesterification with methanolic sodium methoxide, giving methyl 2-benzamido-3-*O*-benzyl-2,6-dideoxy-6-fluoro-α-D-galactopyranoside (**14**) in 80% yield. The ^{19}F nmr spectrum of **14** (Table 2), was first order and showed $J_{6F,5H} = 14.6$ Hz which was within the expected range for a galactoside (3, 11). Hydrogenolysis of the benzyl group of **14** in the usual manner yielded methyl 2-benzamido-2,6-dideoxy-6-fluoro-α-D-galactopyranoside (**15**), which was isolated as its crystalline diacetate (**16**). Acetolysis of the *N*-benzoyl group in **16** with a boiling mixture of acetic anhydride and acetic acid afforded methyl 2-acetamido-3,4-di-*O*-acetyl-2,6-dideoxy-6-fluoro-α-D-galactopyranoside (**17**) in 74% yield, de-*O*-acetylation of

Can. J. Chem. Downloaded from www.nrcresearchpress.com by 210.87.254.6 on 09/05/12
For personal use only.

Can. J. Chem. Downloaded from www.nrcresearchpress.com by 210.87.254.6 on 09/05/12
For personal use only.

TABLE 1. First-order ^{1}H nmr parameters (τ and Hz)

	4[a,c]	**8**[b,d]	**9**[a,d]	**10**[b,d]	**13**[b,d]	**16**[b,c]	**17**[b,d]	**24**[a,c]	**26**[b,d]	**27**[b,d]	**30**[a,d]	**31**[b,d]
H-1	5.11 d	5.13 d	5.26 d	3.83 d	4.97 d	5.02 d	5.22 d	5.61 d	—	—	5.17 t	5.33 t
H-2	—	5.49 m	5.68 td	5.56 cm				5.29 cm	—	—	5.58 cm	—
H-3	—	4.60 t	4.94 t		6.20 dd	4.71 dd	4.84 dd	5.79 dd	4.51 ddd	6.67 td	4.52 ddd	4.70 ddd
H-4	4.92 t	4.88 t	4.84 t		4.16 dd	4.50 dd	4.62 dd	4.63 dd	—	—	5.41 dt	5.30 dt
H-5		6.02 cm	6.36 ddt	6.03 cm				5.61 cm	—	—	5.58 d	—
H-6, 6′		5.54 cm	5.54 cm	5.58 cm			5.60 cm	5.61 cm	—	—	5.56 cm	—
N*H*	2.34 d	3.64 d	4.29 d	4.35 d	4.04 s		4.36 d	—	3.57 d	4.20 d	3.58 d	4.27 d
$J_{1,2}$	4.0	3.5	3.5	3.5	3.3	3.5	3.5	3.7	—	—	3.31	—
$J_{2,3}$		10	10		10.5	10	11	11.4	10.6	11.0	11.31	
$J_{3,4}$	9.7	10	10		3.2	3.5	3.2	2.7	8.7	8.7	9.7	
$J_{4,5}$	9.7	10	10.5		1.3	1	1	0.5			9.7	
$J_{5,6}$	—	—	—	—	—	—	—	—	—	—	1.8	—
$J_{5,6'}$	—	—	—	—	—	—	—	—	—	—	11.3	—
$J_{2,NH}$	9	9.5	9.5	8.0	8.5		10	9.0	9.0	9.0	9.0	9.0
$J_{F\text{-}4,H\text{-}1}$	—	—	—	—	—	—	—	—	—	—	3.3	—
$J_{F\text{-}4,H\text{-}3}$	—	—	—	—	—	—	—	—	14.0	14.0	13.0	14.0
$J_{F\text{-}4,H\text{-}5}$	—	—	—	—	—	—	—	—	—	—	4.4	—
$J_{F\text{-}6,H\text{-}6}$	—	—	—	—	—	—	46.0	—	—	—	—	—

[a]At 220 MHz.
[b]At 100 MHz.
[c]In $(CD_3)_2CO$.
[d]In $CDCl_3$.

TABLE 2. ^{19}F nmr parameters at 56.46 MHz in δ (ppm relative to external C_6F_6) and Hz

	5[a]	**6**[a]	**7**[b]	**8**[b]	**9**[d]	**10**[a]	**11**[c]	**12**[d]	**13**[d]	**14**[a]	**15**[d]	**16**[a]	**17**[a]	**18**[d]	**19**[a]	**20**[a]	**21**[a]	**22**[d]	**25**[d]	**26**[d]	**26**[b]	**27**[d]	**27**[b]	**28**[a]	**30**[a]	**30**[d]	**31**[a]
F-4															61.05	60.50	60.00	62.10	35.15	37.40	39.60	37.50	39.30	—	34.00	36.85	35.40
F-6	74.9	76.8	76.1	74.4	73.8	75.1	77.0	75.8	73.3[e]	72.3	72.0	73.3[e]	75.1[e]	72.1	73.55	74.85	64.80	73.80	77.20	77.95	80.50	77.85	79.97	61.15	—	—	—
$J_{F\text{-}4,H\text{-}3}$	—	—	—	—	—	—	—	—	—	—	—	—	—	—	26.4	25.9	28.1	33.8	—	15.8	14.6	13.5	13.5	—	12.4	16.4	14.7
$J_{F\text{-}4,H\text{-}4}$	—*	—	—	—	—	—	—	—	—	—	—	—	—	—	55.1	54.0	54.0	63.0	—	48.4	54.0	48.4	52.9	—	49.7	50.8	49.7
$J_{F\text{-}4,H\text{-}5}$	—	—	—	—	—	—	—	—	—	—	—	—	—	—	26.4	25.9	28.1	33.8	—	1.1	—	2.8	2.8	—	—	—	—
$J_{F\text{-}6,H\text{-}5}$	22.5	28.0	26.0	23.5	23.5	25	30.5	29.3	—	14.5	14.5	—	—	15.8	16.9	12.4	13.5	13.5	—	25.9	27.0	24.8	27.0	—	—	—	—
$J_{F\text{-}6,H\text{-}6a}$	47.5	49.5	49.5	48.5	48.5	48.5	49.5	48.5	—	48.5	46.0	—	—	47.5	48.9	47.3	45.0	47.3	—	47.3	50.6	47.3	48.4	48.1	—	—	—
$J_{F\text{-}6,H\text{-}6b}$	47.5	49.5	49.5	48.5	48.5	48.5	49.5	48.5	—	48.5	46.0	—	—	47.5	48.9	47.3	45.0	47.3	—	47.3	50.6	47.3	48.4	48.1	—	—	—

[a]In $CDCl_3$.
[b]In $(CD_3)_2CO$.
[c]In D_2O.
[d]In C_5D_5N.
[e]Second-order multiplet.

Can. J. Chem. Downloaded from www.nrcresearchpress.com by 210.87.254.6 on 09/05/12
For personal use only.

which gave the crystalline methyl 2-acetamido-2,6-dideoxy-α-D-galactopyranoside (**18**).

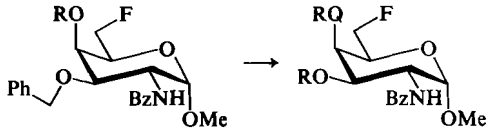

13 R = COPh
14 R = H

15 R = H
16 R = Ac

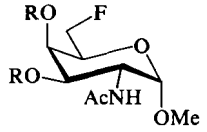

17 R = Ac
18 R = H

The 4,6-di-*O*-mesylglucopyranoside (**4**) was a suitable precursor of 2-amino-4,6-difluoro-2,4,6-trideoxy-α-D-galactopyranoside derivatives by prolonged treatment with tetrabutylammonium fluoride in acetonitrile for several days. The ^{19}F nmr spectrum of the crude concentrated reaction mixture showed the expected triplet of doublets due to F-6 at 73.3 ppm and a doublet of triplets due to F-4 at 61.7 ppm above external C_6F_6. The observed coupling constants of the F-6 signal were: $J_{H\text{-}6a,6F} = J_{H\text{-}6b,6F} = 45$ Hz, $J_{F,5H}$ 15.8 Hz. The corresponding parameters of the F-4 signal were $J_{F,4H}$ 53.5 Hz, $J_{F,3H} = J_{F,5H} = 31.5$ Hz. These were in complete accord with those expected for **19** with a primary fluorine substituent at C-6 and an axial secondary fluorine substituent at C-4 of a galactopyranoside (3, 4); the product **19** was subsequently isolated in 77% yield. However, the 4,6-difluoride **19** could be conveniently prepared in 62% yield by refluxing a solution of the 4,6-dimesylate (**4**) and anhydrous potassium fluoride in dry ethane-1,2-diol for 15–20 min. In general, the displacement of secondary esters on pyranosides by potassium fluoride has not been successful (3). There was no reason to suspect extensive introduction of the —OCH_2CH_2OH group in the molecule as previously reported (*4a*, 16) or any interference by the benzyloxy group at C-3 (17), although some nonspecific decomposition was observed.

The 4,6-difluorogalactoside (**19**) was hydrogenolyzed to give methyl 2-benzamido-4,6-difluoro-2,4,6-trideoxy-α-D-galactopyranoside which was acetylated immediately after work-up, to give the acetate (**20**). The ^1H nmr spectrum was complex due to extensive ^{19}F–^1H coupling; however, the ^{19}F nmr spectrum showed clearly the two expected resonances and both were first-order. The coupling constants (Table 1) were consistent with the *galacto* configuration.

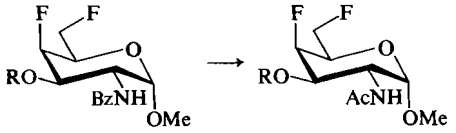

19 R = CH_2Ph
20 R = Ac

21 R = Ac
22 R = H

Treatment of the *N*-benzoate **20** with acetic anhydride – acetic acid gave methyl 2-acetamido-3-*O*-acetyl-4,6-difluoro-2,4,6-trideoxy-α-D-galactopyranoside (**21**). The ^1H nmr spectrum of the *N*-acetate (**21**) was not amenable to first-order analysis, but the ^{19}F nmr spectrum (Table 2) was readily interpreted. A triplet of doublets was observed for F-6 at 74.80 ppm, $J_{F,6H} = J_{F,6'H} = 45.0$ Hz, $J_{F,5H}$ 13.5 Hz, and a triplet of doublets (with the two middle lines coalescing) corresponding to the F-4 signal, at 60.0 ppm above external C_6F_6; $J_{F,5H}$ 28.1 Hz, $J_{F,4H}$ 54.0 Hz, $J_{F,3H}$ 28.1 Hz. De-*O*-acetylation of **21** with sodium methoxide in methanol gave methyl 2-acetamido-4,6-difluoro-2,4,6-trideoxy-α-D-galactopyranoside (**22**).

The synthesis of fluorinated analogues of 2-amino-2-deoxy-D-glucose from **4** was then investigated by nucleophilic displacements involving double inversion at C-4, as employed in the synthesis of 4-deoxy-4-fluoro-D-glucose (18), 4,4′-dideoxy-4,4′-difluoro-α,α-trehalose and 4,6,4′,6′-tetrafluoro-α,α-trehalose (19) from suitable *gluco*-derivatives. Thus the dimesylate **4** was treated with lithium benzoate in hexamethylphosphoric triamide to give the syrupy 4,6-di-*O*-benzoylgalactopyranoside which, after de-*O*-acylation followed by mesylation, afforded crystalline methyl 2-benzamido-3-*O*-benzyl-2-deoxy-4,6-di-*O*-mesyl-α-D-galactopyranoside (**24**). The ^1H nmr spectrum confirmed the assigned structure (Table 1). The dimesylate existed in the $^4C_1$ conformation with the lowest field ring proton signal (H-4) at τ 4.63; $J_{1,2}$ 3.7 Hz, $J_{2,3}$ 11.4 Hz, $J_{3,4}$ 2.7 Hz, $J_{4,5}$ 0.5 Hz, (Table 1) were indicative of the *galacto* configuration.

Reaction of the 4,6-di-*O*-mesylgalactopyranoside (**24**) with potassium fluoride in boiling ethane-1,2-diol gave a mixture of the 4,6-difluoride (**25**) and the unsaturated 6-fluoride (**28**), separated by silica gel column chromatography in the ratio of 3:2 and in 65% overall yield. The ^{19}F nmr spectrum of **28** showed the expected triplet at 61.15 ppm (above external C_6F_6), $J_{F,6H} = J_{F,6'H} = 48.1$ Hz (Table 2). The 4,6-difluoride (**25**) was obtained in 39% yield, which was de-*O*-benzylated and then

Can. J. Chem. Downloaded from www.nrcresearchpress.com by 210.87.254.6 on 09/05/12
For personal use only.

acetylated to give methyl 3-*O*-acetyl-2-benzamido-4,6-difluoro-2,4,6-trideoxy-α-D-glucopyranoside (**26**). The *N*-benzoate **26** was then converted to the *N*-acetate **27**. The ^{19}F nmr spectra of **26** and **27** were first-order (Table 1), the coupling constants being indicative of the glucopyranoside in the $^4C_1$ conformation.

In an attempt to improve the proportion of substitution product, attempts were made to fluorinate the 4,6-di-*O*-mesylgalactopyranoside (**24**) with potassium fluoride in ethane-1,2-diol at lower temperatures (100°C) but the reaction failed to proceed. Elimination reactions usually accompany substitution at C-4 of galactopyranosides because of the favourable *trans*–diaxial relationship between the substituent at C-4 and H-3 and H-5, enhanced in this case by the high basicity of the fluoride anion.

Treatment of **24** with tetrabutylammonium fluoride in boiling acetonitrile for 24 h gave three products; ^{19}F nmr spectroscopic examination of the reaction mixture indicated the presence of the unsaturated 6-fluoride (**28**) (F-6, 60.60 ppm, above external C_6F_6), and the 4,6-difluoride **25**, (F-6, 77.70 ppm); the yields of the latter were variable (0–40%). The third product (5%) was separated by column chromatography but it gave no ^{19}F nmr signal.

The synthesis of methyl 2-acetamido-3,6-di-*O*-acetyl-2,4-dideoxy-4-fluoro-α-D-glucopyranoside (**31**) utilized a similar sequence involving double inversion at C-4. Thus, the 4,6-*galacto*-diol (**23**) was selectively and sequentially tritylated and mesylated to give methyl 2-benzamido-3-*O*-benzyl-2-deoxy-4-*O*-mesyl-6-*O*-trityl-α-D-galactopyranoside (**29**). The 4-mesylate **29** was fluorinated using tetrabutylammonium fluoride in acetonitrile for 24 h when tlc examination indicated the presence of one major compound. ^{19}F nuclear magnetic resonance spectroscopy confirmed that inversion of configuration had taken place at C-4 since the signal obtained was that expected for equatorial fluorine (3, 11), namely a double doublet at 34.0 ppm (above external C_6F_6), $J_{F,4}$ 50.8 Hz, $J_{F,3}$ 15.8 Hz, $J_{F,5}$ 2.5 Hz. No fluorination was observed on treatment of **29** with potassium fluoride in boiling ethane-1,2-diol, as evidenced by ^{19}F nmr spectroscopic examination. This result is not surprising, in view of the fact that in a parallel synthesis of 4-deoxy-4-fluoro-D-glucose (18), methyl 4-*O*-mesyl-2,3-di-*O*-methyl-6-*O*-trityl-α-D-galactopyranoside failed to react with caesium fluoride in ethane-1,2-diol, whereas the 4-*O*-mesyl group was displaced in the absence of the trityl ether group. Likewise, removal of the trityl group from **29** gave the 4-mesylate which reacted with potassium fluoride in ethane-1,2-diol to give methyl 2-benzamido-3-*O*-benzyl-2,4-dideoxy-4-fluoro-α-D-glucopyranoside in 25–40% yield.

After removal of the trityl group from the 4-fluoride by methanolysis, followed by hydrogenolysis of the 3-*O*-benzyl group, the resultant 3,6-diol was acetylated to give the crystalline methyl 2-benzamido-3,6-di-*O*-acetyl-2,4-dideoxy-4-fluoro-α-D-glucopyranoside (**30**).

The ^1H nmr spectrum of the 3,6-diacetate **30** (Table 1) was characteristic of a glucopyranoside structure in the $^4C_1$ conformation, with a typical long range coupling (3, 11) between H-1e and F-4e, as observed, for example, in the spectra of 4-deoxy-4-fluoro-D-glucopyranose (18). Methyl 2-acetamido-3,6-di-*O*-acetyl-2,4-dideoxy-4-fluoro-α-D-glucopyranoside (**31**) was then prepared from the *N*-benzoate **30** by treatment with acetic anhydride and acetic acid.

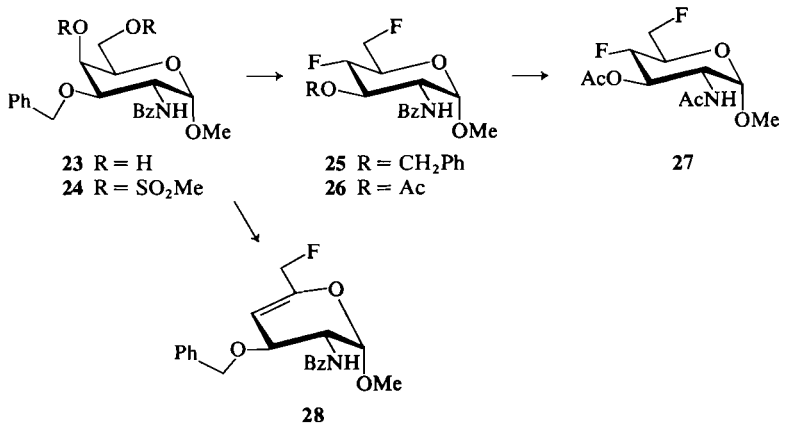

23 R = H
24 R = SO_2Me

25 R = CH_2Ph
26 R = Ac

27

28

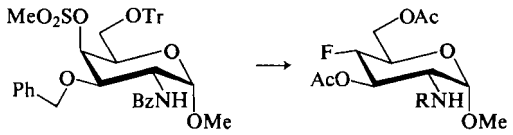

29 30 R = COPh 31 R = Ac

Experimental

Optical rotations are quoted for chloroform solutions at 20°C unless otherwise stated. Light petroleum refers to the fraction boiling at 60–80°C. For general experimental procedures see ref. 6.

Anhydrous Tetrabutylammonium Fluoride (TBAF) (20)

To a stirred solution of hydrogen fluoride (5.8 g) in water (60 mL) was slowly added 40% aqueous tetrabutylammonium hydroxide. The pH of the mixture was then adjusted to approximate neutrality by the addition of either further acid or base and the solution then diluted to ca. 800 mL. Upon storage at 0–5°C the clatherate $(4Bu_4NF \cdot H_2O)_8$ crystallized and was filtered off and washed with ice-cold water. It was then dried *in vacuo* over phosphorus pentoxide over the course of about two weeks with regular changes of desiccant. Yield 53 g (80%).

Methyl 2-Benzamido-3-O-benzyl-4,6-O-benzylidene-2-deoxy-α-D-glucopyranoside (2)

To a vigorously stirred solution of the 4,6-*O*-benzylidene acetal (**1**, 10) (19.3 g, 50 mmol) in dry *N*,*N*-dimethylformamide (100 mL) was added benzyl chloride (55 mL) followed by sodium hydride (2.4 g of 50% oil dispersion, 50 mmol). Further small quantities of sodium hydride (5 × 0.24 g) were added over a period of 2–3 h. Benzylation appeared to be rapid (tlc) and some of the product crystallized out of the reaction mixture. The reaction mixture was stirred overnight at room temperature and decomposed by the addition of ethanol (20 mL) and the resulting solid product filtered off. A further crop of product was obtained by concentration of the filtrate to smaller bulk. The combined crops were extracted with dichloromethane, and inorganic matter removed by filtration (Hyflo Supercel). Addition of diethyl ether to the extract yielded the crude benzyl ether (19.5 g, 82%). Recrystallization from dichloromethane–ethanol gave the 3-*O*-benzyl ether **2**, mp 254–255°C, $[\alpha]_D$ +143.5° (*c* 0.4). *Anal.* calcd. for $C_{28}H_{29}NO_6$ (475): C 70.7, H 6.15, N 2.95; found: C 70.8, H 6.0, N 2.9.

Methyl 2-Benzamido-3-O-benzyl-2-deoxy-α-D-glucopyranoside (3)

A suspension of the 3-*O*-benzyl ether (**2**) (20 g, 421 mmol) in glacial acetic acid – water (400 mL, 3:1 v/v) was heated under reflux for 20–30 min and the resulting clear solution evaporated to dryness. The residue was codistilled with water and toluene at 40–50°C to remove the last traces of acetic acid and dried *in vacuo* over P_2O_5 and sodium hydroxide pellets at 40–50°C. The crude solid so obtained (13 g, 79%) was sufficiently pure for the following stages, but an analytical sample was obtained by recrystallization from methanol – diethyl ether, mp 202.5–204°C, $[\alpha]_D$ +145° (*c* 0.5, methanol). *Anal.* calcd. for $C_{21}H_{25}NO_6$ (387): C 65.1, H 6.5, N 3.6; found: C 64.9, H 6.5, N 3.6.

Methyl 2-Benzamido-3-O-benzyl-2-deoxy-4,6-di-O-mesyl-α-D-glucopyranoside (4)

To an ice-cold solution of the 4,6-diol (**3**) (8 g, 20.7 mmol) in dry pyridine (50 mL) was added dropwise mesyl chloride (2 mL, 25 mmol). The reaction mixture was kept at ca. 5°C overnight and then poured slowly into vigorously stirred ice-water. The resulting solid was filtered off and extracted with dichloromethane. The extract was dried ($MgSO_4$), decolourized (charcoal), filtered (Hyflo Supercel), and evaporated to a small volume. Addition of ether gave the crystalline *dimesylate* (9.5 g, 85%), mp 196–197°C, $[\alpha]_D$ +115.5° (*c* 0.65). *Anal.* calcd. for $C_{23}H_{29}NO_{10}S_2$ (543): C 50.8, H 5.4, N 2.6; found: C 51.1, H 5.6, N 2.9.

Methyl 2-Benzamido-3-O-benzyl-2,6-dideoxy-6-fluoro-4-O-mesyl-α-D-glucopyranoside (5)

To a solution of the dry 4,6-dimesylate (**4**) (6 g, 11 mmol) in dry acetonitrile (30 mL) was added dry tetrabutylammonium fluoride (26 g, 100 mmol) and the mixture heated under reflux for 1 h. Thin-layer chromatography indicated complete conversion of the starting material to a single product. The reaction mixture was then cooled and slowly poured into ice-water. The solid, which separated, was filtered off and extracted with dichloromethane. The extract was washed with water, dried ($MgSO_4$), and evaporated to dryness to give the crude crystalline 6-fluoride (5.2 g, 87%) which was suitable for subsequent reactions. An analytically pure sample of the *6-fluoride* (**5**) was obtained from dichloromethane–ethanol, mp 187.5–189.5°C, $[\alpha]_D$ +136.5° (*c* 0.72). *Anal.* calcd. for $C_{22}H_{26}FNO_7S$ (467): C 56.5, H 5.6, N 3.0; found: C 56.7, H 5.5, N 2.95.

Methyl 2-Benzamido-3-O-benzyl-2,6-dideoxy-6-fluoro-α-D-glucopyranoside (6)

To a solution of the 4-mesylate (**5**) (4.8 g, 10.3 mmol) in dry methanol (50 mL) was added sodium hydroxide (4.4 g) and the mixture heated under reflux for 1 h. After cooling and dilution with water, the mixture was extracted three times with chloroform and the combined extracts then washed with water, dried ($MgSO_4$), and evaporated to dryness. Recrystallization of the solid residue from chloroform – diethyl ether gave the 6-fluoride (3.7 g, 93%), mp 162.5–165°C, $[\alpha]_D$ +105° (*c*, 1). *Anal.* calcd. for $C_{21}H_{24}FNO_5$ (389): C 64.8, H 6.2, N 3.6; found: C 64.5, H 6.15, N 3.5.

Methyl 2-Benzamido-2,6-dideoxy-6-fluoro-α-D-glucopyranoside (7)

A solution of the 3-*O*-benzyl ether (**6**) (0.5 g, 1.29 mmol) in methanol (50 mL) was hydrogenated at room temperature at 50 psi over 5% palladium-on-charcoal (0.1 g) in the presence of concentrated hydrochloric acid (2 mL). The reaction time varied from 1.5–18 h, depending on the particular batch of catalyst used. On completion of the reaction, the mixture was neutralized ($BaCO_3$) and, after removal of most of the inorganic salts, the filtrate was evaporated to dryness with a little silica gel (0.20 g) which was then applied to the top of a short column of silica gel (15 g). Elution with acetone gave the required 3,4-diol, free of inorganic material. Recrystallization from methanol gave **7** (0.3 g, 78%), mp 178.5–180°C, $[\alpha]_D$ +127° (*c* 0.44, methanol). *Anal.* calcd. for $C_{14}H_{18}FNO_5$ (299): C 56.2, H 6.05, N 4.7, F 6.35; found: C 56.1, H 6.0, N 4.6, F 6.6.

Methyl 3,4-Di-O-acetyl-2-benzamido-2,6-dideoxy-6-fluoro-α-D-glucopyranoside (8)

To a solution of **7** (0.25 g, 0.836 mmol) in pyridine (30 mL) was added acetic anhydride (5 mL) and the reaction mixture was allowed to stand at room temperature overnight. The mixture was evaporated to dryness and the residue was dissolved in dichloromethane and washed with saturated sodium bicarbonate, dried ($MgSO_4$), and then evaporated to dryness. The resulting crystalline diacetate (0.3 g, 91%) was sufficiently pure for subsequent reactions, but an analytical sample from ethyl acetate – cyclohexane had mp 120–122.5°C, $[\alpha]_D$ +139.5° (*c* 1.13).

Can. J. Chem. Downloaded from www.nrcresearchpress.com by 210.87.254.6 on 09/05/12
For personal use only.

Can. J. Chem. Downloaded from www.nrcresearchpress.com by 210.87.254.6 on 09/05/12
For personal use only.

Anal. calcd. for $C_{18}H_{22}FNO_7$ (383): C 56.4, H 5.8, N 3.7; found: C 56.4, H 5.9, N 3.8.

*Methyl 2-Acetamido-3,4-di-*O*-acetyl-2,6-dideoxy-6-fluoro-α-*D*-glucopyranoside (9)*

A solution of the *N*-benzoate (**8**) (1 g, 2.6 mmol) in acetic anhydride – acetic acid (250 mL, 4:1 v/v) was heated under reflux for 24 h. The reaction mixture was then cooled and slowly poured into an ice-cold mixture of dichloromethane and saturated aqueous sodium hydrogen carbonate mixture with vigorous stirring. The dichloromethane layer was separated, washed with water, dried ($MgSO_4$), evaporated to dryness, and the product recrystallized from acetone – light petroleum to give the *N*-*acetate* (0.55 g, 65%), mp 143.5–145.5°C, $[\alpha]_D$ +110° (*c* 1.05). *Anal.* calcd. for $C_{13}H_{20}FNO_7$ (321): C 48.6, H 6.2, N 4.35; found: C 48.8, H 6.2, N 4.3.

*2-Acetamido-1,3,4-tri-*O*-acetyl-2,6-dideoxy-6-fluoro-α,β-*D*-glucopyranose*

The above reaction was repeated but after the reflux the reaction mixture was cooled (5°C), concentrated sulphuric acid (3 mL) was added dropwise, and the mixture stored at room temperature for 24 h. It was then processed as above to give a crystalline mixture of anomeric 1,3,4-triacetates (0.3 g, 33%) which was mainly the α-anomer (nmr), mp 163.5–169.5°C (dichloromethane – diethyl ether – light petroleum); mixture mp with the pure α-anomer (**10**), 156–157°C, $[\alpha]_D$ +118.5° (*c* 0.6).

*2-Acetamido-2,6-dideoxy-6-fluoro-α-*D*-glucopyranose (12)*

A solution of either methyl 2-benzamido-2,6-dideoxy-6-fluoro-α-D-glucopyranoside (**7**) (0.5 g, 1.67 mmol) or its 3,4-diacetate (**8**) (0.64 g, 1.67 mmol) in 2 *M* hydrochloric acid (50 mL) and tetrahydrofuran (5 mL) was heated under reflux for 2.5 h when tlc (8:2 ether–methanol and 5:1:3:1 2-propanol – ethyl acetate – water – concentrated ammonia) showed the presence of one spot which gave a positive reaction with the ninhydrin and *p*-anisidine phthalate spray. The reaction mixture was evaporated to dryness and the residue codistilled twice with absolute ethanol to give the crude crystalline hydrochloride (**11**) (0.29 g, 90%). A solution of the hydrochloride in water–methanol (22 mL, 10:1) was added to Dowex-1(CO_3^{2-}) ion exchange resin (24 mL) and acetic anhydride (0.5 mL). The mixture was then stirred vigorously at 0–5°C for 90 min and filtered. The filtrate and washings were then passed through a column of Amberlite IR-120(H^+) (5 mL) and the eluate evaporated to dryness. Recrystallization from methanol gave the acetamide (0.3 g, 79%), mp 188–190°C (dec.), $[\alpha]_D$ +62.5° (5 min) → +33.2° (18 h) (*c* 0.28, water) (lit. (7) mp 209–210°C (dec.), $[\alpha]_D$ +64° → +33°). *Anal.* calcd. for $C_8H_{14}FNO_5$ (223): C 43.05, H 6.3, N 6.3; found: C 43.25, H 6.7, N 5.9.

*2-Acetamido-1,3,4-tri-*O*-acetyl-2,6-dideoxy-6-fluoro-α-*D*-glucopyranose (10)*

Acetylation in the usual way with acetic anhydride (3 mL) and pyridine (12 mL) of the *N*-acetate (**12**), (0.2 g, 0.9 mmol) gave **10** (0.2 g, 90%), mp 171–173°C after crystallisation from dichloromethane–ether – light petroleum, $[\alpha]_D$ +106.5° (*c* 0.61). *Anal.* calcd. for $C_{14}H_{20}FNO_8$ (349): C 48.1, H 5.7, N 4.0; found: C 48.1, H 5.8, N 4.15.

*Methyl 2-Acetamido-2,6-dideoxy-6-fluoro-α-*D*-glucopyranoside*

A solution of the 3,4-diacetate (**9**) (0.2 g, 0.62 mmol) in dry methanol (25 mL) which contained a catalytic amount of sodium methoxide was stored at room temperature overnight. Neutralization with Amberlite IR-120 (H^+) and evaporation to dryness gave the crystalline 3,4-diol (0.1 g, 67%) which was recrystallized from methanol–ether–cyclohexane, mp 163–165°C, $[\alpha]_D$ +120° (*c* 0.14, methanol). *Anal.* calcd. for $C_9H_{16}FNO_5$ (237): C 45.55, H 6.8, N 5.9; found: C 45.7, H 6.75, N 6.05.

*Methyl 2-Benzamido-4-*O*-benzoyl-3-*O*-benzyl-2,6-dideoxy-6-fluoro-α-*D*-galactopyranoside (13)*

To a suspension of the 4-mesylate (**5**) (4.6 g, 9.85 mmol) in hexamethylphosphoric triamide (10 mL) was added lithium benzoate (8 g) and the reaction mixture was stirred at 140°C for 24 h. After completion of the reaction, the mixture was cooled and slowly poured into vigorously stirred ice-water, and the resulting solid was filtered off. A solution of the solid in dichloromethane was washed once with water, dried ($MgSO_4$), and evaporated to give the 4-benzoate (3.9 g, 80%), mp 128–130°C when crystallized from dichloromethane – light petroleum, $[\alpha]_D$ +202° (*c* 0.68). *Anal.* calcd. for $C_{28}H_{28}FNO_6$ (493): C 68.15, H 5.7, N 2.85; found: C 67.9, H 5.65, N 2.9.

*Methyl 2-Benzamido-3-*O*-benzyl-2,6-dideoxy-6-fluoro-α-*D*-galactopyranoside (14)*

To a solution of the 4-benzoate (**13**) (3.5 g, 7.1 mmol) in anhydrous methanol (60 mL) was added *M* sodium methoxide (50 mL) and the mixture kept at room temperature overnight. The solution was then neutralized (Amberlite IR-120(H^+) resin) and evaporated to give a crystalline residue. The product **14** so obtained (2.5 g, 90%) was sufficiently pure for the next stage, but a small portion was recrystallized from chloroform–ether – light petroleum to give **14** mp 165–169.5°C, $[\alpha]_D$ +122.5° (*c* 0.67). *Anal.* calcd. for $C_{21}H_{24}FNO_5$ (389): C 64.8, H 6.2, N 3.6; found: C 64.9, H 6.2, N 3.5.

*Methyl 3,4-Di-*O*-acetyl-2-benzamido-2,6-dideoxy-6-fluoro-α-*D*-galactopyranoside (16)*

A solution of the 3-*O*-benzyl ether **14** (1.5 g, 3.85 mmol) in methanol (120 mL) was hydrogenated at room temperature at 50 psi over 5% palladium-on-charcoal (0.3 g) in the presence of concentrated hydrochloric acid (2 mL) as before. After completion (tlc) the reaction mixture was neutralized ($PbCO_3$) and evaporated to dryness, to give syrupy methyl 2-benzamido-2,6-dideoxy-6-fluoro-α-D-galactopyranoside (**15**). The diol (**15**) was acetylated immediately with acetic anhydride (5 mL) in pyridine (40 mL) at room temperature in the usual way. After 12 h the reaction mixture was evaporated to dryness and the residue dissolved in dichloromethane and washed successively with dilute hydrochloric acid, water, saturated sodium hydrogen carbonate, and water. The organic layer was dried ($MgSO_4$) and evaporated to dryness. The crystalline 3,4-diacetate (1.2 g, 80%) was sufficiently pure for the next stage, but recrystallization from chloroform–ether – light petroleum gave **16**, mp 141–143°C, $[\alpha]_D$ +111.5° (*c* 0.77). *Anal.* calcd. for $C_{18}H_{22}FNO_7$ (383): C 56.4, H 5.75, N 3.65, F 4.95; found: C 56.1, H 5.75, N 3.7, F 4.7.

*Methyl 2-Acetamido-3,4-di-*O*-acetyl-2,6-dideoxy-6-fluoro-α-*D*-galactopyranoside (17)*

A solution of the *N*-benzoate (**16**) (0.5 g, 1.3 mmol) in acetic anhydride – acetic acid (25 mL, 4:1 v/v) was heated under reflux for 24 h when tlc indicated the presence of one product. The reaction mixture was poured slowly into an ice-cold mixture of dichloromethane and aqueous sodium hydrogen carbonate with vigorous stirring. The organic layer was separated, washed with water, dried ($MgSO_4$), and evaporated to dryness, to give the syrupy *N*-acetate (0.31 g, 74%) which was recrystallized from dichloromethane–ether–cyclohexane, mp 122–126°C (sublim. and dec. from 115°C), $[\alpha]_D$ +105° (*c* 0.73). *Anal.* calcd. for $C_{13}H_{20}FNO_7$ (321): C 48.75, H 6.00, N 4.35; found: C 48.5, H 6.3, N 4.1.

Methyl 2-Acetamido-2,6-dideoxy-6-fluoro-α-D-galactopyranoside (18)

A solution of the diacetate **17** (0.2 g, 0.62 mmol) in dry methanol (25 mL), containing a catalytic amount of sodium

Can. J. Chem. Downloaded from www.nrcresearchpress.com by 210.87.254.6 on 09/05/12
For personal use only.

methoxide was kept at room temperature overnight, neutralized (Amberlite resin IR-120 (H^+)), and evaporated to dryness to give a crystalline residue. Recrystallization from ethanol–ether gave needles (0.11 g, 73%), mp 201–206°C (sublim. and dec.) with change in crystalline form at ca. 140°C, $[\alpha]_D$ +200° (*c* 0.53). *Anal.* calcd. for $C_9H_{16}FNO_5$ (237): C 45.6, H 6.75, N 5.9; found: C 45.2, H 6.65, N 5.7.

Methyl 2-Benzamido-3-O-benzyl-4,6-difluoro-2,4,6-trideoxy-α-D-galactopyranoside (19)

(*a*) A solution of the 4,6-dimesylate (**4**) (2 g, 3.68 mmol) and tetrabutylammonium fluoride (10 g) in dry acetonitrile (5 mL) was heated under reflux for 4–5 days. The reaction mixture was cooled, poured into ice-water, and the resultant solid filtered off. The solid was extracted with dichloromethane and the organic extract washed with water, dried (sodium sulphate), and decolourized (charcoal). Evaporation of the filtrate gave a semi-solid residue which was recrystallized from chloroform – diethyl ether – light petroleum to give the 4,6-difluoride **19** (1.1 g, 77%), mp 199–201°C, $[\alpha]_D$ +131.5° (*c* 0.40). *Anal.* calcd. for $C_{21}H_{23}F_2NO_4$ (391): C 64.45, H 5.9, N 3.6; found: C 64.15, H 5.85, N 3.7.

(*b*) A solution of the dimesylate **4** (4 g, 7.37 mmol) and dry potassium fluoride (4 g) in dry ethane-1,2-diol (4 mL) was heated under reflux for 25–30 min. The reaction mixture was cooled, poured into water, and the solid material filtered off. A solution of the solid in dichloromethane was washed with water, dried (magnesium sulphate), then decolourized (charcoal), and evaporated to dryness to give a solid (1.8 g, 62%) with identical ^1H nmr and ^{19}F nmr to that obtained above.

Methyl 3-O-Acetyl-2-benzamido-4,6-difluoro-2,4,6-trideoxy-α-D-galactopyranoside (20)

De-*O*-benzylation of the crude 4,6-difluoro-3-*O*-benzyl ether **19** (1.8 g, 4.6 mmol) was carried out in the presence of 5% palladium-on-charcoal in methanol and hydrochloric acid (2 mL) to give methyl 2-benzamido-4,6-difluoro-2,4,6-trideoxy-α-D-galactopyranoside which, without further purification, was acetylated in the usual way (acetic anhydride – pyridine) to give the 3-acetate **20** (1.1 g, 70%), mp 124.5–129°C from chloroform – diethyl ether – light petroleum, $[\alpha]_D$ +120° (*c* 0.62). *Anal.* calcd. for $C_{16}H_{19}F_2NO_5$ (343): C 56.0, H 5.55, N 4.1; found: C 56.05, H 5.8, N 4.2.

Methyl 2-Acetamido-3-O-acetyl-4,6-difluoro-2,4,6-trideoxy-α-D-galactopyranoside (21)

A solution of the *N*-benzoate **20** (0.8 g, 2.33 mmol) in acetic anhydride – acetic acid (200 mL, 4:1 v/v) was heated under reflux for 24 h. The reaction mixture was then cooled and slowly poured with vigorous stirring into an ice-cold mixture of dichloromethane and saturated sodium hydrogen carbonate. The dichloromethane layer was washed with water, dried (magnesium sulphate), and then evaporated to give a crystalline compound. Recrystallization from acetone–dichloromethane – light petroleum gave the *N*-acetate **21** (0.42 g, 64%), mp 203–205.5°C (sublimation and pre-softening at 198°C), $[\alpha]_D$ +142° (*c* 0.5). *Anal.* calcd. for $C_{11}H_{17}F_2NO_5$ (281): C 47.0, H 6.05, N 5.0; found: C 47.15, H 6.1, N 5.05.

Methyl 2-Acetamido-4,6-difluoro-2,4,6-trideoxy-α-D-galactopyranoside (22)

A solution of the 3-acetate **21** (0.3 g, 1.07 mmol) in methanol (30 mL) was treated as previously described with a catalytic amount of sodium methoxide in methanol to give, after neutralization, the title compound **22** (0.27 g, 87%) which was recrystallized from methanol, mp 211–214°C, crystalline change from dense plates to fine needles, 172–185°C, $[\alpha]_D$ +196° (*c* 0.71, methanol). *Anal.* calcd. for $C_9H_{15}F_2NO_4$ (239): C 45.2, H 6.25, N 5.9; found: C 45.05, H 6.3, N 6.0.

Methyl 2-Benzamido-3-O-benzyl-2-deoxy-α-D-galactopyranoside (23)

To a suspension of methyl 2-benzamido-3-*O*-benzyl-2-deoxy-4,6-di-*O*-mesyl-α-D-glucopyranoside **4** (15 g, 27.6 mmol) in hexamethylphosphoric triamide (60 mL) was added lithium benzoate (10 g) and the reaction mixture stirred at 140°C for 24–36 h. After completion of the reaction, the mixture was cooled and slowly poured into vigorously stirred ice-water. The solid so obtained was filtered off, dissolved in dichloromethane and washed with water, dried (magnesium sulphate), and evaporated to dryness to give the syrupy 4,6-dibenzoate (13.5 g, 70%). A solution of the syrup in methanol (150 mL) containing a catalytic amount of sodium methoxide was heated under reflux for 15 min. After cooling the mixture was neutralized with Amberlite IR-120 (H^+), the resin was filtered off and the filtrate was evaporated to dryness and recrystallized from dichloromethane–ethanol to give the 4,6-*galacto*-diol **23** (5.5 g, 52%), mp 167–168.5°C, $[\alpha]_D$ +141° (*c* 1.29, methanol). *Anal.* calcd. for $C_{21}H_{25}NO_6$ (387): C 65.1, H 6.5, N 3.6; found: C 65.2, H 6.55, N 3.8.

Methyl 2-Benzamido-3-O-benzyl-2-deoxy-4,6-di-O-mesyl-α-D-galactopyranoside (24)

The 4,6-dimesylate **24** was prepared as above from the diol **23** (4.7 g) in 90% yield. Recrystallization from dichloromethane–ethanol gave **24**, mp 213–215°C, $[\alpha]_D$ +118° (*c* 0.64). *Anal.* calcd. for $C_{23}H_{29}NO_{10}S_2$ (543): C 50.8, H 5.4, N 2.6, S 11.8; found: C 50.7, H 5.65, N 2.75, S 11.8.

Methyl 2-Benzamido-3-O-benzyl-4,6-difluoro-2,4,6-trideoxy-α-D-glucopyranoside (25) and Methyl 2-Benzamido-3-O-benzyl-6-fluoro-2,4,6-trideoxy-β-L-threo-hex-4-enopyranoside (28)

(*a*) A solution of the 4,6-dimesylate **24** (5 g, 9.2 mmol) and dry potassium fluoride (5 g) in dry ethanediol (4 mL) was heated under reflux for 20–30 min. Thin-layer chromatography (ethyl acetate – cyclohexane, 3:7) indicated two products in the ratio 2:3. The reaction mixture was poured into water; the solid material so obtained was filtered and extracted into dichloromethane. After washing once with water, drying (magnesium sulphate), and decolourizing (charcoal), the organic layer was evaporated to dryness. Silica gel chromatography (ethyl acetate – cyclohexane 1:4) effected separation of the two compounds. The unsaturated 6-fluoride (**28**) was eluted first and was recrystallized from dichloromethane – diethyl ether – light petroleum (0.87 g, 25%), mp 108.5–113.5°C (repeated crystallizations resulted in a wider melting range), $[\alpha]_D$ +154° (*c* 0.53). *Anal.* calcd. for $C_{21}H_{22}FNO_4$ (371): C 67.9, H 5.9, N 3.8; found: C 68.0, H 5.8, N 3.6. The second fraction contained the crystalline 4,6-difluoride (**25**), (1.4 g, 39%), mp 208.5–209.5 (from methanol), $[\alpha]_D$ +122.5° (*c* 0.5). *Anal.* calcd. for $C_{21}H_{23}F_2NO_4$ (391): C 64.4, H 5.9, N 3.6; found: C 64.0, H 5.8, N 3.6.

(*b*) To a solution of the 4,6-dimesylate (**24**) (0.5 g, 0.92 mmol) in dry acetonitrile (5 mL) was added tetrabutylammonium fluoride (2.5 g) and the mixture was heated under reflux. Thin-layer chromatography showed that after 2 h no starting material remained, with the formation of two faster moving compounds. Silica column chromatography (ethyl acetate – cyclohexane, 1:4) gave a fastest moving compound (0.08 g), which contained no fluorine as indicated by ^{19}F nmr ($CDCl_3$) spectroscopy, and a slower moving compound which corresponded to the unsaturated 6-fluoride **28** (0.3 g), which gave a triplet at 60 ppm upfield from external C_6F_6, with $J_{F,6}$ 48 Hz.

Methyl 3-O-Acetyl-2-benzamido-4,6-difluoro-2,4,6-trideoxy-α-D-glucopyranoside (26)

Hydrogenolysis of the 4,6-difluoride **25** (1.2 g, 3.07 mmol) was carried out as described previously to give methyl 2-

Can. J. Chem. Downloaded from www.nrcresearchpress.com by 210.87.254.6 on 09/05/12
For personal use only.

benzamido-4,6-difluoro-2,4,6-trideoxy-α-D-glucopyranoside (0.77 g, 83%) which, without further purification, was treated with acetic anhydride (3 mL) in pyridine (12 mL) to give the crystalline 3-acetate **26** (0.72 g, 83%), mp 159–160.5°C (dichloromethane–ethanol), $[\alpha]_D$ +73.5° (*c* 0.95). *Anal.* calcd. for $C_{16}H_{19}F_2NO_5$ (343): C 56.0, H 5.55, N 4.1; found: C 56.2, H 5.5, N 4.2.

Methyl 2-Acetamido-3-O-acetyl-4,6-difluoro-2,4,6-trideoxy-α-D-glucopyranoside (27)

The *N*-benzoate (**26**) (0.6 g, 1.75 mmol) was treated as previously described for **20** and the resultant *N*-acetate **27** (0.4 g, 83%) recrystallized from dichloromethane – light petroleum, mp 179–180°C (plates → needles at 142–152°C), $[\alpha]_D$ +50° (*c* 0.35). *Anal.* calcd. for $C_{11}H_{17}F_2NO_5$ (281): C 47.0, H 6.05, N 5.0; found: C 47.2, H 6.05, N 5.1.

Methyl 2-Benzamido-3-O-benzyl-2-deoxy-4-O-mesyl-6-O-trityl-α-D-galactopyranoside (29)

To a stirred solution of methyl 2-benzamido-3-*O*-benzyl-2-deoxy-α-D-galactopyranoside (**23**) (5.5 g, 14.2 mmol) in pyridine (50 mL) was added trityl chloride (6 g, 19.75 mmol). The reaction mixture was left at room temperature for 2–3 days, when tlc showed complete reaction. It was then cooled to 0°C and mesyl chloride (3 mL) was added dropwise. The reaction mixture was then kept at 0–5°C overnight, then slowly poured into water, and after standing for 1 h the resulting solid was filtered off and dissolved in dichloromethane. The solution was then decolourized by filtration through a Hyflo Supercel charcoal pad. The filtrate was concentrated to dryness and the residue was codistilled with small quantities of toluene, followed by carbon tetrachloride to remove the last traces of pyridine. On evaporation to dryness it gave a solid residue. The material was dissolved in dichloromethane and addition of ethanol effected crystallization (6 g, 60%). The material so obtained was sufficiently pure for subsequent reaction. The crystalline, analytically pure, 4-mesylate **29** was obtained after several recrystallizations from dichloromethane–ethanol, mp 193–196.5°C, $[\alpha]_D$ +72° (*c* 0.045). *Anal.* calcd. for $C_{41}H_{41}NO_8S$ (707): C 69.55, H 5.8, N 2.0; found: C 69.15, H 5.75, N 1.9.

Methyl 3,6-Di-O-acetyl-2-benzamido-2,4-dideoxy-4-fluoro-α-D-glucopyranoside (30)

To a solution of the 4-mesylate **29** (0.5 g, 0.71 mmol) in dry acetonitrile (10 mL) was added tetrabutylammonium fluoride (2.5 g) and the reaction mixture refluxed for 18 h when tlc indicated the formation of one major product. The reaction mixture was cooled and poured into ice-water and the solid so obtained was filtered and dissolved in dichloromethane. The solution was washed once with water, dried (sodium sulphate), and evaporated to dryness to give the 4-fluoride (0.3 g, 67%). The ^{19}F nmr spectrum (CD_3COCD_3/CH_2Cl_2) gave the characteristic low field quartet at 37 ppm above external C_6F_6; $J_{F,4}$ 50.8 Hz, $J_{F,3}$ 15.8 Hz, $J_{F,5}$ 2.5 Hz. The 4-fluoride (0.2 g) was then dissolved in methanol–chloroform (30 mL, 1:1 v/v), concentrated hydrochloric acid (0.2 mL) was added, and the solution stirred at room temperature for 3 h. Thin-layer chromatography indicated complete cleavage of the trityl group. The mixture was neutralized (lead carbonate), filtered, and the filtrate and washings (together with silica gel (0.5 g)) were evaporated to dryness. This material was loaded on a silica gel column (25 g). Elution with toluene removed the triphenylmethanol completely, and elution with toluene–acetone (1:4) gave methyl 2-benzamido-3-*O*-benzyl-2,4-dideoxy-4-fluoro-α-D-glucopyranoside (0.17 g, 94%). The material so obtained was suspended in methanol (50 mL) containing 5% Pd/C and concentrated hydrochloric acid (2 mL). The suspension was hydrogenated at room temperature at 50 psi. The mixture was neutralized (lead carbonate) and the catalyst and inorganic salts were filtered off. The filtrate and washings were evaporated to dryness and the solid so obtained, methyl 2-benzamido-2,4-dideoxy-4-fluoro-α-D-glucopyranoside (0.11 g, 85%), was dissolved in pyridine (30 mL). Acetic anhydride (8 mL) was added and the reaction mixture kept at room temperature overnight. Evaporation of the reagent and solvent was followed by dissolution of the residue in dichloromethane. The dichloromethane layer was washed with dilute hydrochloric acid, water, saturated sodium hydrogen carbonate, and water. It was then dried (magnesium sulphate), filtered (Hyflo Supercel), and concentrated to dryness. The crystalline 3,6-diacetate (**30**) (0.12 g, 85%) was obtained from dichloromethane – diethyl ether – light petroleum, mp 148.5–150.5°C, $[\alpha]_D$ +88 ± 10° (*c* 0.01). Mass spectrum *m/e*: 383 (M^+); 340 ($M^+ - CH_3CO$); 323 ($M^+ - HOAc$); 310 ($M^+ - OCH_3 - CH_2CO$). *Anal.* calcd. for $C_{18}H_{22}FNO_7$ (383): C 56.4, H 5.75, N 3.65; found: C 57.3, H 6.25, N 3.7.

Methyl 2-Acetamido-3,6-di-O-acetyl-2,4-dideoxy-4-fluoro-α-D-glucopyranoside (31)

The *N*-benzoate **30** (0.09 g, 0.24 mmol) was treated with a boiling mixture of acetic anhydride – acetic acid, as previously described, to give the *N*-acetate **31** (0.05 g, 69%), which was recrystallized from chloroform – light petroleum, mp 116–118°C, $[\alpha]_D$ +57.2 ± 10° (*c* 0.028). Mass spectrum *m/e*: 321 (M^+), 290 ($M^+ - OCH_3$), 278 ($M^+ - HOAc$), 261 ($M^+ - OCH_3 - CH_2CO$). *Anal.* calcd. for $C_{13}H_{20}FNO_7$ (321): C 48.60, H 6.25, N 4.35; found: C 49.7, H 6.4, N 4.5.

Acknowledgments

One of us (A.A.E.P.) thanks the University of London for a scholarship. We are indebted to the Physical Chemical Measurements Unit (Harwell) for 100 and 220 MHz ^1H nmr spectra.

1. P. W. KENT. Chem. Ind. 1129 (1969); *In* Carbon–fluorine compounds. C.I.B.A. Foundation Symposium. Elsevier. 1972. p. 169.
2. A. B. FOSTER and J. H. WESTWOOD. Pure Appl. Chem. **35**, 147 (1973).
3. A. A. E. PENGLIS. Adv. Carbohydr. Chem. Biochem. In press.
4. L. EVELYN and L. D. HALL. Carbohydr. Res. **47**, 285 (1976), and references therein.
5. (*a*) R. A. PETERS. Proc. R. Soc. London, Ser. B, **139**, 145 (1952); (*b*) R. A. PETERS, R. W. WAKELIN, P. BUFFA, and L. C. THOMAS. Proc. R. Soc. London, Ser. B, **140**, 497 (1953).
6. A. F. HADFIELD, L. HOUGH, and A. C. RICHARDSON. Carbohydr. Res. **63**, 51 (1978).
7. M. L. SHULMAN and A. YA KHORLIN. Carbohydr. Res. **27**, 141 (1973).
8. M. SHARMA and W. KORYTNYK. Tetrahedron Lett. 573 (1977).
9. J. PACAK, P. DRASAR, D. STROPOVA, M. CERNY, and M. BUDENSINSKY. Collect. Czech. Chem. Commun. **38**, 3936 (1973).
10. C. F. GIBBS, L. HOUGH, and A. C. RICHARDSON. Carbohydr. Res. **1**, 290 (1965).
11. L. PHILLIPS and V. WRAY. J. Chem. Soc. B, 1618 (1971).
12. S. ROSEMAN and J. LUDOWIEG. J. Am. Chem. Soc. **76**, 301 (1954).
13. P. A. GENT and R. GIGG. J. Chem. Soc. Perkin Trans. I, 1858 (1973).
14. (*a*) G. BIRCH and A. C. RICHARDSON. J. Chem. Soc. C, 749 (1970); (*b*) P. L. DURETTE and D. HORTON. Org. Magn. Reson. **3**, 417 (1971).

15. L. HOUGH, A. K. PALMER, and A. C. RICHARDSON. J. Chem. Soc. Perkin Trans. I, 2513 (1972).
16. (*a*) J. E. G. BARNETT. Adv. Carbohydr. Chem. **22**, 177 (1967); (*b*) A. B. FOSTER and R. HEMS. Carbohydr. Res. **10**, 168 (1969); (*c*) I. D. BLACKBURNE, P. M. FREDERICKS, and R. D. GUTHRIE. Aust. J. Chem. **29**, 381 (1976); (*d*) H. S. SRIVASTAVA and V. K. SRIVASTAVA. Carbohydr. Res. **60**, 210 (1978).
17. L. D. HALL and P. R. STEINER. Can. J. Chem. **48**, 451 (1970).
18. A. B. FOSTER, R. HEMS, and J. H. WESTWOOD. Carbohydr. Res. **15**, 41 (1970).
19. L. HOUGH, A. K. PALMER, and A. C. RICHARDSON. J. Chem. Soc. Perkin Trans. I, 784 (1973).
20. P. W. KENT and R. C. YOUNG. Tetrahedron, **27**, 4057 (1971).

Can. J. Chem. Downloaded from www.nrcresearchpress.com by 210.87.254.6 on 09/05/12
For personal use only.

Synthesis and conformations of α-aminoadipyl- and glycyl-α-aminoadipylthiazepine sulfoxides

SAUL WOLFE, RAYMOND JOHN BOWERS, SYED KHAQAN HASAN, AND PETER MICHAEL KAZMAIER

Department of Chemistry, Queen's University, Kingston, Ont., Canada K7L 3N6

Received July 4, 1980

This paper is dedicated to Prof. Raymond U. Lemieux, on the occasion of his 60th birthday

SAUL WOLFE, RAYMOND JOHN BOWERS, SYED KHAQAN HASAN, and PETER MICHAEL KAZMAIER. Can. J. Chem. **59**, 406 (1981).

The title compounds, having the *R*-absolute configurations at sulfur, and labelled with ^{14}C at carbons 5, 6, and 7 of the seven-membered ring, have been synthesized by condensation of isotopically labelled 3D-benzhydryloxycarbonyl-6L-amino-2,2-dimethyl-5-oxoperhydro-1,4-thiazepine with *N*-Boc- and α-benzhydryl-protected L-α-aminoadipic acid and glycyl-L-α-aminoadipic acid, followed by oxidation with *m*-chloroperoxybenzoic acid and complete deprotection with formic acid. The conformations of the sulfoxides, and related thiazepines and thiazepine sulfoxides, have been examined by ^{1}Hmr spectroscopy. All thiazepines, and the two title sulfoxides, appear to exist in a twist boat conformation. Most other sulfoxides exist in a chair conformation, which is stabilized by an internal hydrogen bond between the sulfinyl oxygen and the amide proton at C6; when this hydrogen bond is not present, both chair and twist boat conformations may be observable. The title compounds are of interest as possible intermediates in penicillin biosynthesis from glycyl-δ-(L-α-aminoadipyl)-L-cysteinyl-D-valine (GACV) or ACV, according to a new theory, which deals, in particular, with the stereochemical course of the biosynthesis at the beta (β) carbon atom of valine.

SAUL WOLFE, RAYMOND JOHN BOWERS, SYED KHAQAN HASAN et PETER MICHAEL KAZMAIER. Can. J. Chem. **59**, 406 (1981).

On a synthétisé les composés mentionné dans le titre, ayant des configurations absolues *R* au niveau du soufre et marqués au carbone-14 en positions 5, 6 et 7 du cycle à 7, en condensant le produit marqué benzhydryloxycarbonyl-3D amino-6L diméthyl-2,2 oxo-5 perhydrothiazépine-1,4 sur les acides L-α-aminoadipique et glycyl-L-α-aminoadipique portant des groupes protecteurs *N*-Boc et α-benzhydryle. Cette étape est suivie d'une oxydation par l'acide *m*-chloroperoxybenzoique puis d'une déprotection complète par l'acide formique. On a étudié, par la spectroscopie de rmn du ^{1}H les conformations des sulfoxydes, des thiazépines apparentées et des sulfoxydes de diazépines. Toutes les thiazépines et les deux sulfoxydes mentionnés dans le titre semblent exister selon une conformation bateau-croisé. La plupart des autres sulfoxydes ont une conformation chaise qui est stabilisée par une liaison hydrogène intramoléculaire entre l'oxygène du sulfinyle et le proton de l'amide en position C-6. En l'absence de cette liaison hydrogène, on peut observer les deux conformations chaise et bateau-croisé. Les composés mentionnés dans le titre sont intéressants en tant qu'intermédiaires éventuels dans la biosynthèse de la pénicilline à partir de la glycyl-δ-(L-α-aminoadipyl)-L-cystéinyl)-D-valine (GACV) ou ACV selon une nouvelle théorie, qui traite, en particulier de l'aspect stéréochimique de la biosynthèse au niveau du carbone beta (β) de la valine.

[Traduit par le journal]

Introduction

The biosynthesis of Isopenicillin N (**1**) proceeds via the tripeptide δ-(L-α-aminoadipyl)-L-cysteinyl-D-valine (**2**) (ACV). This conversion has been established using cell-free extracts of the eukaryotic organisms *Penicillium chrysogenum* and *Cephalosporium acremonium* (1, 2), and also the prokaryotic organism *Streptomyces clavuligerus*.[1] A tetrapeptide containing glycine in addition to the elements of ACV has been isolated from the mycelium of *C. acremonium* (3) and also from *Paecilomyces persicinus P-10* (4) and found, in the latter case, to have the constitution Gly-Aad-Cys-Val (**3**) (GACV). The role of this tetrapeptide is not known.

The oxidative cyclization of **2** to **1** occurs with loss of only two carbon-bound hydrogens, viz., the β hydrogen of the valinyl moiety (5),[2] and the pro-*S* hydrogen of the cysteinyl moiety (6). Loss of these hydrogens accompanies the formation of the C2—S and C5—N bonds of the penicillin nucleus, and both of these bonds are formed with retention of configuration at carbon (7).

Although little is known concerning the nature of the species which lie between ACV (or GACV) and penicillin (2, 8), thiazepines have often been considered as possible penicillin precursors (9). The early work of Arnstein and Crawhall (*9a*), which established that L-valine is incorporated into penicillin with loss of the α hydrogen, led to the proposal that a cysteinyl-α,β-dehydrovalinyl peptide **4** is cyclized, initially to the 3D,6L-thiazepine **5**, and then to penicillin. This pathway was tested some years ago (*9b,c*), with negative results.

It was recognized only later that examination of the post-peptide stages of penicillin biosynthesis requires a cell-free system, and that the presence of an L-α-aminoadipyl side chain may be essential. It has also become clear that a thiazepine intermediate cannot arise via a dehydropeptide precursor, since the L- to D-isomerization of valine occurs

[1] S. E. Jensen, D. W. S. Westlake, R. J. Bowers, H. Auksi, and S. Wolfe. Unpublished results.

[2] Also R. J. Bowers, D. A. Lowe, R. B. Morin, and S. Wolfe. Unpublished results.

0008-4042/81/020406-16$01.00/0

©1981 National Research Council of Canada/Conseil national de recherches du Canada

Can. J. Chem. Downloaded from www.nrcresearchpress.com by 210.87.254.42 on 09/05/12
For personal use only.

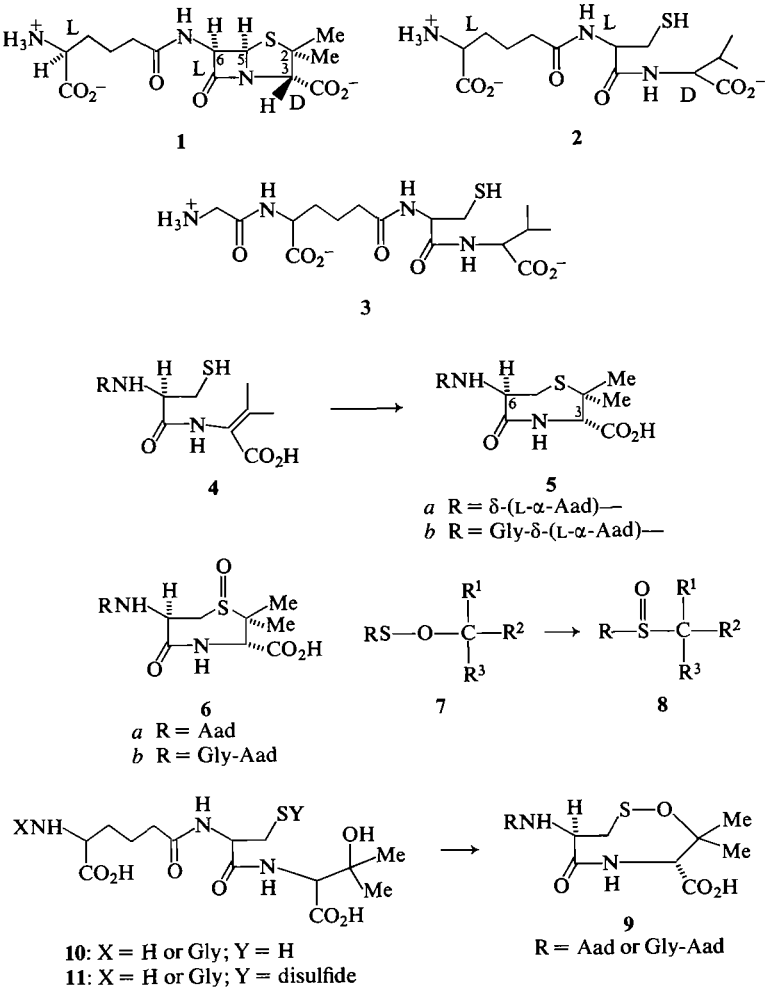

during the incorporation of this amino acid into ACV, and the α hydrogen of this amino acid is then retained during the late stages of the biosynthesis (2, 10).

The present work was founded on the following considerations. First, syntheses of the thiazepines **5***a* and **5***b* have not yet appeared in the literature. Secondly, oxidative cyclization of **5** to penicillin can be envisaged to occur via an intramolecular Pummerer reaction (11) of the derived sulfoxides **6**. As discussed elsewhere (12), such a process can account for the stereochemical course of penicillin biosynthesis at the β carbon of the cysteinyl moiety. Thirdly, a pathway to sulfoxides **6** exists that does not involve oxidation of a thiazepine precursor or loss of the α hydrogen of the valinyl moiety. This is the rearrangement of a sulfenate to a sulfoxide (**7** → **8**), which takes place with retention of configuration at carbon (13, 14). The required sulfenate in the present case is **9**, which could arise from the known β-hydroxyvaline-containing peptides **10** (3, 4) or their derived disulfides **11** (15). Since oxygenation at the β carbon of the valinyl moiety is expected to proceed with retention of configuration (16), a sequence **10** → **11** → **9** → **6** can account for the stereochemical course of penicillin biosynthesis at the β carbon of the valinyl moiety, and for the retention of the α hydrogen of this amino acid. It should be noted that the thermal sulfenate → sulfoxide rearrangement is slow in nonpolar media, although there is some evidence (13) of rate enhancement in polar solvents; the reaction is not known to occur in aqueous solution.

On the basis of these considerations, we have become interested in the syntheses of the thiazepines **5***a* and **5***b*, and the thiazepine sulfoxides **6***a* and **6***b*. These syntheses form part of a more general interest in the substrate specificities

Can. J. Chem. Downloaded from www.nrcresearchpress.com by 210.87.254.42 on 09/05/12
For personal use only.

Can. J. Chem. Downloaded from www.nrcresearchpress.com by 210.87.254.42 on 09/05/12
For personal use only.

of cell-free systems derived from both eukaryotic and prokaryotic organisms. A synthesis of ACV, necessary for a demonstration of the efficacy of the systems to be employed, has already been published (17). The synthesis of GACV has also been achieved, and will be reported separately.[3]

Synthetic Studies

The syntheses were based on the successful strategy devised for ACV (17), which employed benzhydryl ester protection for carboxyl groups and *tert*-butoxycarbonyl (Boc) protection for amino groups. The syntheses of **5***a* and **6***a* therefore required the aminoadipic acid derivative **12**, already described (17). The syntheses of **5***b* and **6***b* required the glycylaminoadipic acid derivative **13**, which was prepared without difficulty from the α-benzhydryl ester **14** (17), by coupling with the *N*-hydroxysuccinimide ester of Boc-glycine (**15**). An alternative route to **5***b* was also worked out, as described below.

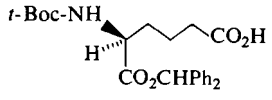

12

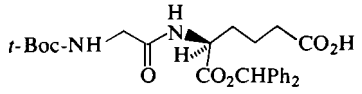

13

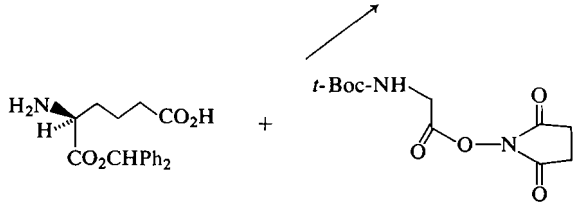

14 **15**

The syntheses also required the carboxyl-protected thiazepine **16**. Several routes to this compound were examined. Initially, it was considered that a stereospecific route might be feasible, by aminophosphine-promoted extrusion of a sulfur atom from the cyclic disulfide **17** (18). As summarized in Scheme 1, carbobenzoxy-*S*-trityl-L-cysteine (**18**) was condensed with the methyl ester of D-penicillamine, using *N*-ethoxycarbonyl-2-ethoxy-1,2-dihydroquinoline (EEDQ) (21). The resulting peptide (**19**), obtained in quantitative yield, was converted to the crystalline disulfide **17** in 65–70% yield upon exposure to a solution of iodine

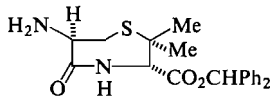

16

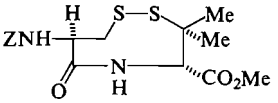

17 Z = $PhCH_2OCO$—

in methanol at low temperature. Treatment of the disulfide with aminophosphines did not afford the desired thiazepine **20** under a variety of reaction conditions.[4]

Eventually it was found that **20** was formed in approximately 10% yield upon reaction of **17** with sodium cyanide in dimethylformamide (22), but the compound could not be isolated in pure form. This route was, therefore, abandoned.

The nonstereospecific synthesis of Leonard and Ning (23) was examined next. As shown in Scheme 2, methyl carbobenzoxyaminoacrylate (**21**) was allowed to react under a hydrogen atmosphere for six days with D-penicillamine in absolute methanol containing triethylamine. Trituration of the crude product with chloroform gave the crystalline 3D,-6L-thiazepine **22** in 18–22% yield. The 3D,6D-epimer of this compound could be crystallized from the chloroform filtrates in ca. 15% yield.

The dehydroalanine derivative **21** was prepared in two ways. The more efficient procedure, which was employed for the synthesis of unlabelled thiazepines, involved treatment of the methyl ester of carbobenzoxycysteine (**23**) with silver carbonate (24) or with Fetizon's reagent (25). This sequence afforded **21** in 77% overall yield from L-cystine. Alternatively, alanine was converted to the carbobenzoxy methyl ester **24**; successive treatment with freshly prepared *tert*-butyl hypochlorite and 1,5-diazabicyclo[5.4.0]undec-5-ene (DBU) produced a 1:1 mixture of **21** and **24** (26). The recovery of **24** from this two-step procedure is unexplained, since it could be demonstrated that the *N*-chloro compound **25** is formed in the first step in quantitative yield. The 1:1 mixture of **21** and **24** did not require purification. Reaction with D-penicillamine, as described above, led to crystalline thiazepine **22** and recovered crystalline **24**, which could be recycled. This latter sequence, beginning with L-[^{14}C(U)]-alanine, was used to prepare **22**, ^{14}C-labelled at C5, C6, and C7.

The conversion of **22** to the benzhydryl ester salt **26** is summarized in Scheme 3. Treatment with a solution of hydrogen bromide in glacial acetic acid gave the salt **27** in 91% yield (23), which could be neutralized with pyridine (23) to the amino acid **28** and then converted to **26** as a foam, following successive reactions with *p*-toluenesulfonic acid (*p*-

[3]S. Wolfe, H. Auksi, and R. J. Bowers. Unpublished results.

[4]R. J. Bowers and S. Wolfe. Unpublished results.

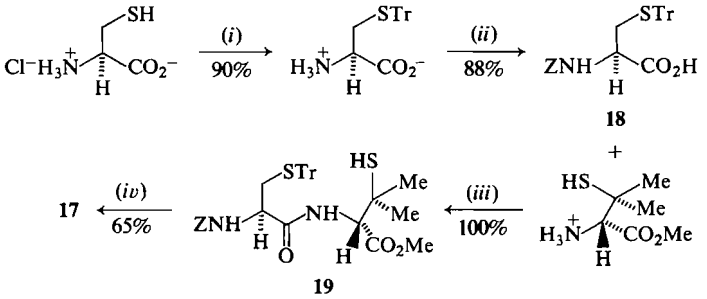

SCHEME 1. Reagents: (*i*) TrOH, AcOH, $BF_3 \cdot Et_2O$ (19); (*ii*) $PhCH_2OCOCl$, NaOH, dioxane (20); (*iii*) EEDQ, Et_3N, CH_2Cl_2; (*iv*) I_2, CH_3OH, 0–10°C.

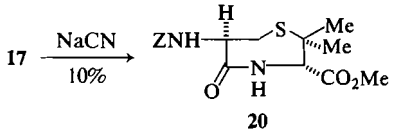

TsOH) and diphenyldiazomethane (DDM) (26). The overall yield of **26** from **27** in this manner was 53%. Alternatively, **27** was converted to the ammonium salt **29**, by successive treatment with Amberlite 120/H^+ and *N* ammonium hydroxide. Successive treatment with DDM, *followed* by *p*-TsOH, afforded *crystalline* **26**, in 74% overall yield from **27**.

Neutralization of **26**, and coupling with **12** and **13** using EEDQ, led to crystalline **30** (84%) and to **31** (78%) as a foam, respectively. The Boc-protected aminoadipylthiazepine **30** could also be converted to **31**, in an overall 50% yield, by selective removal of Boc (*p*-TsOH, Et_2O, CH_2Cl_2, reflux, 12 h (27)), followed by neutralization and condensation with **15**. Complete deprotection of **30** and **31** was achieved initially using a mixture of trifluoroacetic acid and anisole, as described previously (17). Subsequently, overnight treatment with formic acid was found to be equally effective.[5]

The oxidation of the thiazepines was examined at several stages in the sequence, and using a variety of reagents. These studies indicated that the introduction of the sulfoxide moiety was best accomplished following protection of the amino and

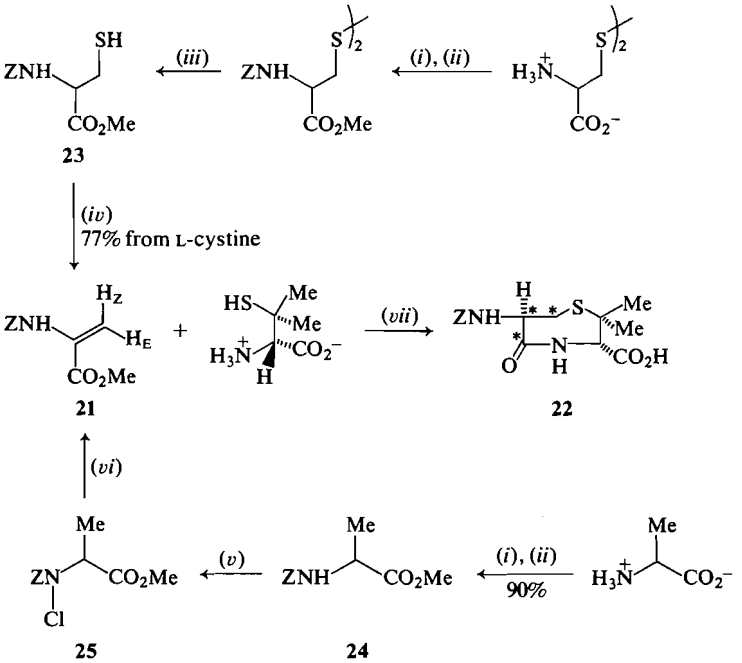

SCHEME 2. Reagents: (*i*) $PhCH_2OCOCl$, NaOH; (*ii*) CH_2N_2; (*iii*) Zn, HCl/MeOH, 0°C; (*iv*) Ag_2CO_3; (*v*) *t*-BuOCl, NaOMe; (*vi*) DBU, CH_2Cl_2; (*vii*) Et_3N, MeOH, H_2.

[5]C. C. Shaw. Personal communication.

Can. J. Chem. Downloaded from www.nrcresearchpress.com by 210.87.254.42 on 09/05/12
For personal use only.

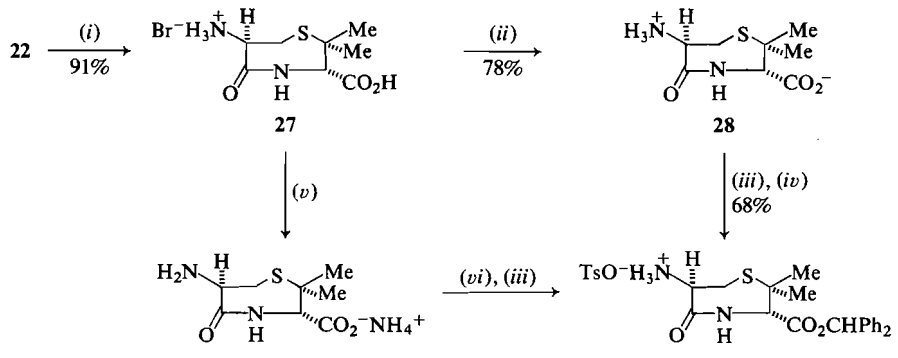

SCHEME 3. Reagents: (*i*) HBr, HOAc; (*ii*) pyridine, $CHCl_3$, EtOH; (*iii*) *p*-TsOH; (*iv*) DDM, DMF, 50°C; (*v*) Amberlite 120/H^+, NH_4OH; (*vi*) DDM, CH_2Cl_2, MeOH.

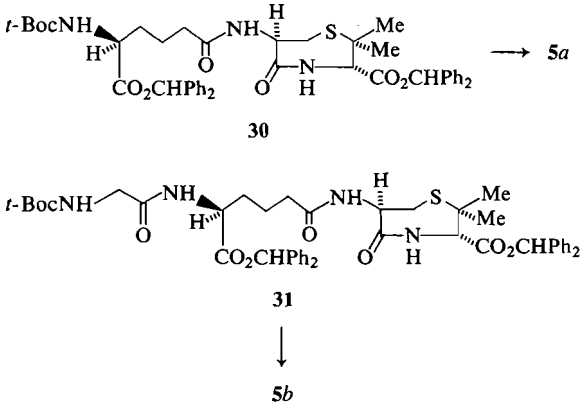

carboxyl groups, and that *m*-chloroperbenzoic acid (MCPBA) was the most effective oxidizing agent. In each case, a single sulfoxide (**32***a*–*e*) resulted, in near quantitative yield.

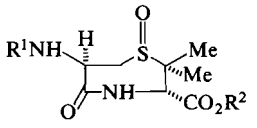

32

a R^1 = Z; R^2 = $CHPh_2$
b R^1 = Z; R^2 = C_6H_4-*p*-NO_2
c R^1 = *epi*-Z; R^2 = $CHPh_2$
d R^1 = protected Aad; R^2 = $CHPh_2$
e R^1 = protected Gly-Aad; R^2 = $CHPh_2$
f R^1 = Aad; R^2 = H
g R^1 = Gly-Aad; R^2 = H

As a preliminary to the deprotection of the sulfoxides, optically active benzyl methyl sulfoxide and benzyl *o*-carboxyphenyl sulfoxide were exposed to a mixture of trifluoroacetic acid and anisole. This treatment led to rapid racemization at sulfur (28). Use of these conditions for the removal of Boc and benzhydryl protecting groups from the sulfoxides **32***d* and **32***e* was, therefore, considered to be inappropriate. A single experiment with **32***a* confirmed this conclusion; at −20°C the sulfoxide was converted to a complex mixture within 5 min. Deprotection via overnight treatment with 98–100% formic acid[5] was then found to be completely satisfactory and application of these conditions to **32***d* and **32***e* led to the fully deprotected thiazepine sulfoxides **32***f* (≡ **6***a*) and **32***g* (≡ **6***b*), respectively.

^{1}H Nuclear Magnetic Resonance Data and Conformational Analysis of the Thiazepines and Thiazepine Sulfoxides

Table 1 summarizes salient features of the ^{1}Hmr spectra of thirteen 3D,6L-thiazepines **33***a*–*m* and four 3D,6D-thiazepines **33***n*–*q* prepared during the present work. The following points can be made: (*i*) the vicinal H3–C3–N4–H4 coupling constants are in the range 7–8 Hz, suggesting that H3 and H4 have dihedral angles in the range 0–20° (*syn*) or 130–150° (*anti*) (29). In each case the seven-membered ring may adopt a chair or a twist-boat conformation (30), so that four conformations may, in principle, be considered, viz., the *syn*-chair (**A**), the *syn*-boat (**B**), the *anti*-chair (**C**) and the *anti*-boat (**D**); (*ii*) the chemical shift of H6 does not change significantly in the 3D,6L-isomers upon the introduction of benzhydryl or *p*-nitrobenzyl ester substituents on the C3-carboxyl group. This suggests that H6 does not lie in the shielding region of the carboxyl group, and that conformations **C** and/or **D** are preferred; (*iii*) in the 3D,6L-epimers, the two H6–H7 coupling constants range from 2.5–6.2 and 8.0–11.5 Hz; in the 3D,6D-epimers, these coupling constants are nearly equal, ca. 6 Hz. The vicinal coupling constants of the 3D,6L-epimers are close to the values expected (29) for 60° and 180° dihedral angles. In the cyclic disulfide L-cysteinyl-L-cysteine (**34**), whose crystal struc-

Can. J. Chem. Downloaded from www.nrcresearchpress.com by 210.87.254.42 on 09/05/12
For personal use only.

Can. J. Chem. Downloaded from www.nrcresearchpress.com by 210.87.254.42 on 09/05/12
For personal use only.

TABLE 1. Proton magnetic resonance data for various thiazepines **33**

Compound	R^1	R^2	Configuration at C6	Solvent	Chemical shift (ppm) H3	H6	H7*R*	H7*S*	Coupling constant (Hz) H6–H7*R*	H6–H7*S*	H3–N4*H*
a	H·HBr	H	L	A[a]	4.27	5.02	3.29	2.82	11.5	2.5	—
b	H·TsOH	H	L	A	4.14	4.85	3.20	2.70	11.5	2.8	—
c	H	H	L	B[b]	3.89	5.09	3.24	2.80	11.5	2.9	—
d	Z[c]	H	L	B	4.33	4.87	2.88		—	—	—
e	Aad	H	L	A	4.30	4.77	2.94	2.78	9.0	6.1	—
f	Gly-Aad	H	L	A	4.32	4.77	3.00	2.86	—	—	—
g	Z	Me	L	C[d]	4.22	4.73	2.87		—	—	7.5
h	Z	Bzhl[e]	L	C	4.35	4.72	2.85	2.92	9.0	5.0	8.0
i	Z	*p*-NB[f]	L	C	4.27	4.77	2.90		—	—	8.0
j	H·TsOH	Bzhl	L	C	4.07	4.69	3.07		—	—	7.0
k	H	Bzhl	L	C	4.63	3.95	2.62	2.92	8.0	4.0	7.5
l	Protected Aad[g]	Bzhl	L	C	4.25	4.78	2.77	2.84	10.2	2.8	8.0
m	Protected Gly-Aad[g]	Bzhl	L	C	4.32	4.83	2.81	2.78	8.5	6.2	6.0
n	H	H	D	B	4.18	4.35	2.81	3.09	5.6	7.8	—
o	H·HCl	H	D	A	4.47	4.80	3.28, 3.70		6.0	6.0	—
p	Z	Me	D	C	4.58	4.70	2.85, 2.95		6.0	6.0	7.0
q	Z	Bzhl	D	C	4.72	4.73	2.89		—	—	7.5

[a] D_2O.
[b] D_2O/K_2CO_3.
[c] Carbobenzoxyamino.
[d] $CDCl_3$.
[e] Benzhydryl.
[f] *p*-Nitrobenzyl.
[g] Spectrum recorded at 360 MHz.

ture (**35**) is known (31), the dihedral angles with H6 are 71° and 196°, respectively, for the pro-*S* and pro-*R* hydrogens of the *N*-terminus, and the observed coupling constants are 3.5 and 12.1 Hz, respectively (32).

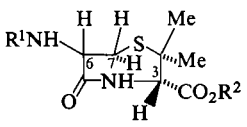

33

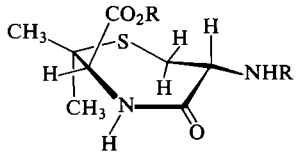

Chair **A**

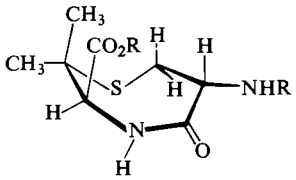

Boat **B**

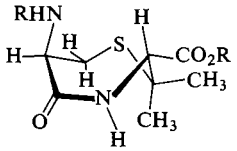

Chair C

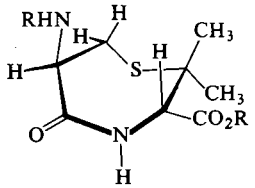

Boat **D**

In the chair conformation **C**, the estimated dihedral angles with H6 are ca. 20° (for the pro-*R* hydrogen) and ca. 100° (for the pro-*S* hydrogen). On the other hand, dihedral angles of ca. 60° and 180°

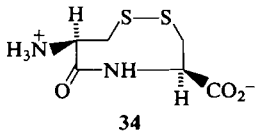

34

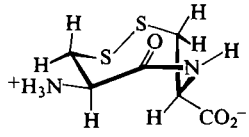

35

can be achieved in the flexible boat conformation **D**. It can be concluded, tentatively, that the 3D,6L-thiazepines exist in conformation **D**. As will be seen, most of the 1*R*,3D,6L-thiazepine sulfoxides adopt conformation **C**. An analogous conformational change has been observed during the transformation of penicillins to penicillin-*S*-sulfoxides (33). It must also be pointed out that **C** and **D** were earlier considered by Leonard and Wilson (9) (see also ref. 30) to be the most probable conformations of the 3D,6D-thiazepine **33** having $R^1 = PhCH_2CO$ and $R^2 = CH_3$.

Table 2 summarizes a variety of data concerning the seven thiazepine sulfoxides **32***a–g*. A first point of interest is the dextrorotatory change in $[\alpha]_D$ (+25 to +30°) following oxidation of the thiazepines. Since penicillin esters exhibit a dextrorotatory change in $[\alpha]_D$ of ca. +50 to +60° upon conversion to β-sulfoxides **36**, and a levorotatory change of ca. −150° upon conversion to α-sulfoxides **37** (34), this is a first indication that all sulfoxides prepared in this work have the *R*-configuration at sulfur. It is especially noteworthy that the 6D-isomer **32***d* also has the *R*-configuration at sulfur since, by analogy

TABLE 2. $\Delta[\alpha]_D$[a] and $\Delta\nu$[b] data and coupling constants associated with the thiazepine sulfoxides **32**

Compound	R^1	R^2	Solvent	$\Delta[\alpha]_D$ (°)	Δν (ppm) H3	Δν (ppm) H6	Δν (ppm) NH6	Coupling constant (Hz) H6–H7*R*	Coupling constant (Hz) H6–H7*S*	Coupling constant (Hz) H3–N4*H*
a	Z[c]	Bzhl[d]	$CDCl_3$	+24	−0.87	−0.05	−1.07	7.2	1.6	8.0
b	Z	*p*-NB[e]	$CDCl_3$	+3.4	−0.95	−0.02	−1.40	5.9	2.2	8.0
c	*epi-Z*	Bzhl	$CDCl_3$	+32.5	−0.43	−0.64	+0.15	—	—	7.0
d	Protected Aad	Bzhl	$CDCl_3$	+29	−0.93	−0.05	−1.55	7.0	2.8	8.0
e	Protected Gly-Aad[f]	Bzhl	$CDCl_3$	+17	−1.03	−0.04	−1.27	8.7	<1.0	7.5
f	Aad[f]	H	D_2O	+41	−0.10	−0.28	—	10.2	2.4	—
g	Gly-Aad[f]	H	D_2O		−0.08	−0.25	—	10.3	2.6	—

[a] $[\alpha]_D$**32** − $[\alpha]_D$**33**.
[b] **v33** − **v32**.
[c] Carbobenzoxyamino.
[d] Benzhydryl.
[e] *p*-Nitrobenzyl.
[f] 360 MHz spectrum.

with penicillin chemistry (34), the *S*-configuration might have been expected in this case.

The ^{1}Hmr data confirm these configurational assignments, and indicate that conformation **C** (see **38**) is adopted by sulfoxides **32***a*,*b*,*d*, and *e*. Thus, in these compounds, oxidation results in a large (1.0–1.7 ppm) shift to lower field of the N—H6 proton, indicative of hydrogen bonding of this proton to the sulfoxide oxygen, a ca. 0.9 ppm shift to lower field of H3, indicative of a *syn*-axial effect (35), and only a small downfield shift of H6. In addition, the H6–H7 coupling constants, ca. 7–8 Hz for H6–H7*R* and ca. 1–3 Hz for H6–H7*S*, are consistent with the ca. 20° and 100° dihedral angles estimated earlier for conformation **C**. These various observations are those expected for **38**, in which H3, the β-substituent at C6, and the S—O bond all point in the same direction.

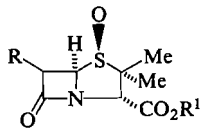

36

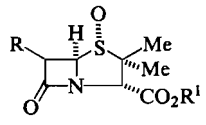

37

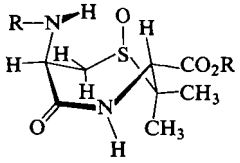

38

In the 6D-isomer **32***c*, both H3 and H6 exhibit shifts to lower field, and the N—H6 proton shows a small *upfield* shift, indicating absence of the internal hydrogen bond. The small downfield shifts of H3 and H6 in this compound, compared to those observed for H3 in **32***a*,*b*,*d*, and *e*, suggest that when this hydrogen bond is not present both conformations **C** and **D** may be significantly populated.

The data for the Aad- and Gly-Aad-sulfoxides indicate that these compounds exist mainly in conformation **D** in aqueous solution. Thus both H3 and H6 show small downfield shifts, consistent with an electrostatic (but not *syn*-axial) effect of the sulfoxide moiety (35), and the H6–H7 coupling constants have values close to those found in the thiazepines.[6]

The chemical properties of the thiazepine sulfoxides provide further support for the configurational assignments. Oxidation of **33***k* afforded a product whose ^{1}Hmr spectrum revealed the presence of a dehydrovaline moiety. Oxidation of **33***j*

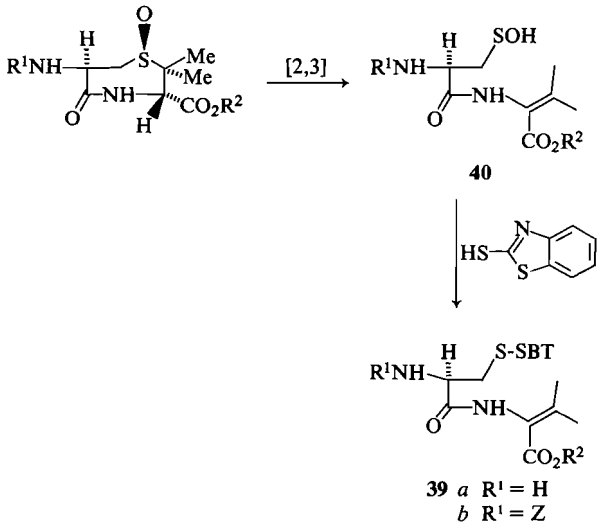

39 *a* R^1 = H
b R^1 = Z

[6] An alternative interpretation of these latter observations is that *R*- to *S*-epimerization of the sulfoxides occurs under the formic acid deprotection conditions. However, this could be ruled out on the basis of the optical activity data for the protected and deprotected α-aminoadiphylthiazepine sulfoxides, together with the finding that optically active benzyl 2-carboxyphenyl sulfoxide is configurationally stable in formic acid solvent.

Can. J. Chem. Downloaded from www.nrcresearchpress.com by 210.87.254.42 on 09/05/12
For personal use only.

Can. J. Chem. Downloaded from www.nrcresearchpress.com by 210.87.254.42 on 09/05/12
For personal use only.

gave a product which appeared to be sulfoxide; however, neutralization again led to decomposition, with appearance of a dehydrovaline moiety in the ^{1}Hmr spectrum. Addition of mercaptobenzothiazole yielded the disulfide **39***a* (15*c*,*d*), characterized further as its carbobenzoxy derivative **39***b*. These observations are consistent with the occurrence of a [2,3] sigmatropic rearrangement of an *R*-sulfoxide to the sulfenic acid **40**. Such a reaction necessarily requires a *syn*-diaxial relationship between H3 and the sulfoxide oxygen, the rearrangement being facilitated by the *syn*-amino group at C6.

Experimental

General

Melting points were determined on a Mel-Temp apparatus, and are uncorrected. Optical rotations were obtained on a Perkin Elmer 141 polarimeter. Infrared spectra were recorded on either Perkin Elmer 180 or Acculab 6 instruments. Proton nmr spectra were recorded on Varian EM360, Bruker HX60, or Nicolet NT-360 spectrometers. Chemical shifts are reported in δ values relative to tetramethylsilane, acetone (δ 2.225 ppm), or 2,2-dimethyl-2-sila-pentane-5-sulfonate as internal standards. Mass spectra were obtained on a Jeol JMS-OISC instrument under electron impact conditions at 76 eV. Chemical ionization mass spectra were obtained on a Dupont 21-491B mass spectrometer by Mr. P. R. Gordon, whom we thank. Radioactive samples were counted in a toluene–cellosolve (2:1) scintillation solution on a Searle Delta 300 Model 6891 liquid scintillation counter. Analytical thin-layer chromatography (tlc) was performed on precoated Merck silica gel 60 F-254 plates, with aluminium or glass backing. Spots were observed under short wave ultraviolet light, or were visualized with iodine vapour, ninhydrin (Boc-derivatives were detected by spraying initially with 3:1 formic acid – concentrated hydrochloric acid, followed by ninhydrin), or with palladium chloride (for sulfur containing compounds). Preparative thin-layer chromatography (plc) was performed on Merck silica gel 60 F-254 precoated 20 × 20 cm plates (layer thickness 2 mm) or, alternatively, glass plates were coated with a slurry of Macherey Nagel silica gel G-HR and calcium sulfate. Lumilux green ZS was used as a fluorescent indicator. Merck 60 mesh silica gel was used for column chromatography. High performance liquid chromatography (hplc) utilized Merck prepacked Lobar columns, a Fluid Metering Inc. model RP-SY pump, and model PD-60-LF pulse dampener. Solvents were distilled before use and were dried, as necessary, by literature procedures. Unless stated, magnesium sulfate was used routinely as a drying agent. Microanalyses were carried out by Galbraith Laboratories, Knoxville, TN.

S-*Trityl-L-cysteine (19)*

L-Cysteine hydrochloride monohydrate (7.0 g, 40 mmol) was dissolved in a mixture of absolute methanol (15 mL) and chloroform (10 mL) and the solution was evaporated to dryness. This process was repeated twice and the resultant amorphous solid was finally treated with chloroform (15 mL) and again evaporated to dryness. The solid was dried overnight under high vacuum. To the anhydrous L-cysteine hydrochloride were added successively trityl alcohol (10.4 g, 40 mmol), freshly distilled acetic acid (40 mL), and boron trifluoride etherate (5.6 mL). The orange mixture was then placed in a preheated oil bath (40°C) and heated with stirring to 100°C over a period of 25 min. During this time most of the trityl alcohol dissolved and, after a further 15 min at 100°C, a clear amber-coloured solution resulted. Heating was discontinued and the solution was allowed to cool to room temperature (45 min), during which time a white precipitate formed. The reaction was quenched by addition of ethanol (60 mL), which discharged the amber colour, and the solid dissolved. Water (40 mL) was added, followed by anhydrous sodium acetate (12 g). The mixture was stirred until all of the solid had dissolved and was then diluted with water (140 mL). The product precipitated as a colourless oil, which rapidly crystallized as a fluffy white solid. This was collected the next day, washed well with water and acetone, and dried, finally under high vacuum to give a white amorphous solid, 13.06 g (90%) mp 150–155°C (lit. (19) mp 181–182°C), which was used without purification for the next step.

N-*Benzyloxycarbonyl*-S-*trityl-L-cysteine (18)*

A vigorously stirred solution of *S*-trityl-L-cysteine (7.2 g, 20 mmol), in 1 *N* sodium hydroxide (20 mL) and freshly distilled dioxane (20 mL), was cooled to 0°C in an ice-salt bath, and two drops of phenolphthalein indicator were added. Benzyl chloroformate (4.0 mL, 4.8 g, 28 mmol) and 1 *N* sodium hydroxide (30 mL) were then added dropwise from separate syringes, at such a rate that the solution remained slightly alkaline. Towards the end of the addition a white solid precipitated which masked the colour of the indicator, but the addition of the reagents was maintained at approximately the same rate. The addition was complete within 10 min and, after stirring for an additional 15 min at room temperature, the mixture was diluted with water (50 mL). The solid did not dissolve, and dioxane (10 mL) was added. To the resulting solution (pH 7.5) was added 2 *N* hydrochloric acid (10 mL), whereupon the product precipitated as a finely divided oil. The dioxane was evaporated rapidly under reduced pressure, and the residual white gum was extracted into ethyl acetate (4 × 50 mL). The organic extract was washed with dilute brine (2 × 50 mL), followed by saturated brine (30 mL), and was then dried and evaporated to leave a light, golden syrup. This was dissolved in methylene chloride (50 mL) and the solvent was reevaporated. Upon removal of the last traces of solvent, under high vacuum, the product became a white foam (10.57 g). The crude product was dissolved in ether (70 mL) and treated with dicyclohexylamine (4.0 mL, 20 mmol). A gelatinous precipitate formed rapidly, and the mixture soon became solid. Additional ether (50 mL) was added, and the mixture was left for 3 h at 5°C with occasional scratching. The crystals were collected, washed with cold ether, and dried under vacuum to give a white, microcrystalline solid, 11.90 g (88%). A portion of this solid was recrystallized twice from ethanol to give fine colourless needles mp 189–190°C (lit. (36*b*) mp 140–142°C); $[\alpha]_D^{24}$ +18.65 (*c* 2.0, CH_3OH) (lit. (36*b*) $[\alpha]_D^{20}$ +1.0 (*c* 2.0, CH_3OH)); ir (Nujol): 3430 (s, NH), 3062 (s, ArH), 2370 (br, m, NH_2^+), 1725 (s, urethane C=O), 1621 (s, CO_2^-), 1566 (s, amide II) cm^{-1}; ^{1}Hmr ($CDCl_3$) δ: 0.66–2.16 (20H, m, cyclohexyl methylene protons), 2.66 (2H, m, C3 methylene protons), overlapping with 2.88 (2H, m, cyclohexyl methine protons), 4.15 (1H, m, C2 methine), 5.05 (2H, s, $PhCH_2$), 5.72 (1H, d, $J = 7$ Hz, slow exchange with D_2O, urethane N*H*), 6.75–7.8 (20H, m, Ar*H*), overlapping with 7.8–9.0 (2H, br, exchange with D_2O, NH_2^+). *Anal.* calcd. for $C_{42}H_{50}N_2O_4S$: C 74.30, H 7.42, N 4.12, S 4.72; found: C 74.00, H 7.27, N 4.37, S 5.15.

A suspension of the dicyclohexylammonium salt (3.0 g) in ether (75 mL) was shaken with 20% aqueous citric acid (40 mL) until all of the solid had dissolved. The ether layer was then washed with water (4 × 50 mL), followed by saturated brine (25 mL), dried, and evaporated to leave a white foam, 2.22 g (100%) mp 56–65°C (lit. (36*a*) mp 114–115°C); $[\alpha]_D^{24}$ +7.1° (*c* 0.45, CH_3OH) (lit. (36*a*) $[\alpha]_D^{25}$ +17° (*c* 1.41, CH_3OH)); ir ($CHCl_3$): 3700–2300 (br), 2630 (br, CO_2H), 1715 (s, urethane and carboxylic acid (C=O), 1495 (s, amide II) cm^{-1}; ^{1}Hmr ($CDCl_3$) δ:

Can. J. Chem. Downloaded from www.nrcresearchpress.com by 210.87.254.42 on 09/05/12
For personal use only.

2.67 (2H, br d, C3 methylene), 4.23 (1H, m, C2 methine), 5.05 (2H, s, PhCH_2), 5.22 (1H, br d, J = 8 Hz, NH), 7.05–7.50 (20H, m, ArH), 8.42 (1H, s, CO_2H).

In view of the large difference between the melting point and rotation of the dicyclohexylamine salt observed in the present work and those of ref. 36*b*, the diethylamine salt was also prepared; mp (ethanol) 166–170°C (lit. (36*a*) 169°C); $[\alpha]_D^{26}$ +21.1 (*c* 2.15, CH_3OH) (lit. (36*a*) $[\alpha]_D$ +21.4 (*c* 5, CH_3OH)). It appears that the literature data for the dicyclohexylamine salt are in error.

D-Penicillamine Methyl Ester Hydrochloride

A solution of D-4-carboxy-2,2,5,5-tetramethylthiazolidine hydrochloride (4.45 g, 20 mmol) in water (100 mL) was treated with concentrated hydrochloric acid (1.0 mL) and refluxed for 9 min. The solution was cooled and evaporated to dryness. The crystalline residue was dissolved in methanol (30 mL) and benzene (10 mL), and the solvent was evaporated. This process was repeated once more, the product was suspended in benzene (30 mL), and the solvent was again evaporated to leave white platelets. The resultant anhydrous D-penicillamine hydrochloride was dissolved in anhydrous methanol (70 mL) and the solution was cooled to 0°C in a ice-salt bath, saturated with hydrogen chloride, warmed to room temperature (10 h), and then again recooled to 0°C and resaturated with hydrogen chloride. The mixture was again warmed slowly to room temperature (6 h) and then refluxed for 2.5 h, cooled, and evaporated to dryness. The crystalline residue was dissolved in methanol (40 mL) and the solvent was evaporated. This process was repeated, first with methanol (40 mL), and then with benzene (2 × 40 mL). The residual solid was dried under high vacuum for 1 h and then crystallized from dry *tert*-butanol (100 mL) to give fine, colourless needles, 2.42 g, (60%) mp 188–189.5°C (lit. (37) mp 180–182°C; lit (38) mp 186–188°C); $[\alpha]_D^{23.4}$ −10.82° (*c* 10, H_2O) (lit. (38) $[\alpha]_D$ −7.4° (H_2O)); ir (KBr): 3260–2520 (br, s, NH_3^+), 2480 (m, NH_3^+), 1744, 1734 (s, C=O), 1520, 1500 (s, NH_3^+) cm^{-1}; ^{1}Hmr ($CDCl_3$, trace CF_3CO_2H) δ: 1.50 (3H, s, CH_3), 1.67 (3H, s, CH_3), 2.18 (1H, s, exchange with D_2O, —SH), 3.90 (3H, s, CO_2CH_3), 4.17 (1H, m, collapses to singlet with D_2O exchange, CH), 7.65 (3H, br, exchange with D_2O, NH_3^+).

N-*Benzyloxycarbonyl*-S-*trityl*-L-*cysteinyl*-D-*penicillamine Methyl Ester* (*19*)

A solution of *N*-benzyloxycarbonyl-*S*-trityl-L-cysteine (497 mg, 1.0 mmol), in chloroform (6.0 mL), was stirred at room temperature and treated with EEDQ (247.3 mg, 1.0 mmol). After 5 min, D-penicillamine methyl ester hydrochloride (200 mg, 1.0 mmol) was added in one portion, followed by triethylamine (0.15 mL, 1.1 mmol). The resulting solution was stirred at room temperature for 24 h, and then diluted with chloroform (15 mL) and washed successively with 20% aqueous citric acid (3 × 10 mL), saturated sodium bicarbonate (2 × 10 mL), and saturated brine (10 mL). The organic layer was dried and evaporated to give a pale golden syrup, which, upon removal of the last traces of solvent under high vacuum, gave a white foam, 611.9 mg (100% yield); $[\alpha]_D^{25.6}$ +9.38° (*c* 4.0, CH_3OH); ir ($CDCl_3$): 3415 (m, NH), 3090, 3065 (w, ArH), 1736, 1718, 1686 (s, ester, urethane, amide C=O), 1595 (w, C=C), 1495 (s, amide II) cm^{-1}; ^{1}Hmr ($CDCl_3$) δ: 1.29 (3H, s, CH_3), 1.45 (3H, s, CH_3), 1.95 (1H, s, exchange with D_2O, SH), 2.70 (2H, d, J = 7.5 Hz, cysteinyl CH_2—), 3.68 (3H, s, —CO_2CH_3), 3.99 (1H, m, cysteinyl —CH—), 4.60 (1H, d, J = 10 Hz, collapses to a singlet on exchange with D_2O/CF_3CO_2H, penicillamine CH—), 5.10 (2H, s, PhCH_2—), 5.28 (1H, d, J = 7.5 Hz, exchange with D_2O/CF_3CO_2H, urethane NH—), 6.90 (1H, d, J = 10 Hz, slow exchange with D_2O/CF_3CO_2H, amide NH), 7.09–7.66 (20H, m, ArH).

L-*Carbobenzoxyamino*-4D-*carbomethoxy*-3,3-*dimethyl*-6-*oxoperhydro*-1,2,5-*dithiazocine* (*17*) (*39*)

A solution of iodine (317 mg, 1.25 mmol) in methanol (14 mL) was stirred at room temperature and a solution of the dipeptide **19** (306 mg, 0.5 mmol) in methanol (8.0 mL) was added dropwise during 1 h. The reaction mixture was stirred for an additional 15 min, and the solution was then cooled to 0°C and the excess iodine destroyed by addition of 5% sodium thiosulfate solution (5.2 mL). The mixture was neutralized with saturated sodium bicarbonate (1.3 mL) and then evaporated to dryness. The residual solid was partitioned between ethyl acetate (25 mL) and water (25 mL). The organic layer was washed with brine (15 mL), dried, and evaporated to leave an amber gum. Trituration with hexane (2 × 10 mL) afforded a creamy white solid, which was collected by filtration and dried under high vacuum. The crude product (170 mg) was purified by plc on two plates (methylene chloride – ethyl acetate, 5:1). One major band (R_f 0.57–0.80) was isolated as a white foam, 113 mg (58% yield). Recrystallization from acetone–hexane gave colourless prisms, mp 123–124.5°C; $[\alpha]_D$ +284° (*c* 1.77, $CHCl_3$); ir (KBr): 3330, 3280 (s, NH), 1738, 1710, 1664 (s, ester, urethane, amide C=O), 1515 (s, amide II) cm^{-1}; ^{1}Hmr ($CDCl_3$) δ: 1.48 (6H, s, CH_3), 2.80–3.60 (2H, A and B of ABX, J_{AB} = 14 Hz, J_{AX} = 10.5 Hz, J_{BX} = 5.0 Hz, C8 methylene), 3.75 (3H, s, CO_2CH_3), 4.28–4.83 (1H, m, C7 methine), 4.98 (1H, d, J = 11 Hz, C4 methine), 5.17 (2H, s, PhCH_2), 5.90 (1H, d, J = 8 Hz, urethane NH), 7.38 (1H, br d, J = 11 Hz, ring NH) overlapping with 7.42 (5H, s, Ph); ms (350°C, 76 eV) *m/e* (relative intensity > 20%): 399 (*M* + 1, 100), 334 (32), 91 (50); CIMS (isobutane): 457 (*M* + 57). *Anal.* calcd. for $C_{17}H_{22}N_2O_5S_2$: C 51.24, H 5.57, N 7.03, S 16.09; found: C 51.53, H 5.82, N 7.24, S 16.01.

Higher yields (65–70%) of **17** were obtained by addition of the peptide **19** to the iodine solution at 0°C. After the addition was complete the reaction mixture was warmed to 10°C over 20 min and then recooled, quenched with 5% sodium thiosulfate solution, and worked up as described above. A similar reaction involving addition of the dipeptide to the iodine solution at 10°C gave a 58% yield of **17**. A further reaction, maintained at 0°C throughout, failed to cleave the *S*-trityl group.

Reaction of 17 with Sodium Cyanide (*22*)

A solution of **17** (117 mg, 0.295 mmol) in freshly distilled dimethylformamide (5.0 mL) was stirred at room temperature under dry nitrogen and sodium cyanide (14.7 mg, 0.30 mmol) was added. The solid dissolved slowly to form a yellow solution. After 16 h, the reaction mixture was poured into water (40 mL), and the resultant fine white precipitate was extracted into ethyl acetate (2 × 40 mL). Saturated brine was added during the extraction to minimize emulsion formation. The combined extracts were washed with dilute brine (3 × 50 mL), saturated brine (15 mL), dried, and evaporated to leave a pale yellow solid (90 mg). Purification by plc (methylene chloride – ethyl acetate, 2:1) afforded two major bands, at R_f 0.68 (22.4 mg) and R_f 0.48 (24.4 mg). Analysis of the less polar band by ^{1}Hmr revealed it to be a 1:3 mixture of the cyclic disulfide **17** and the 3D,6D-thiazepine **33***p*. The more polar band contained an approximately 1:1 mixture of a dehydrovalinyl dipeptide and the 3D, 6L-thiazepine **33***g*.

N,N′-*Dibenzyloxycarbonyl*-L-*cystine*

A solution of L-cystine (9.6 g, 40 mmol) in 1 *N* sodium hydroxide (80 mL) was cooled below 5°C, and benzyl chloroformate (20.4 g, 120 mmol) and 1 *N* sodium hydroxide (160 mL) were added separately in portions, with vigorous stirring, at such a rate that the pH remained between 10 and 12. Addition of the reagents required 2 h, and a white precipitate formed as the reaction progressed. The cooling bath was then removed and the mixture was allowed to warm to room temperature, with con-

Can. J. Chem. Downloaded from www.nrcresearchpress.com by 210.87.254.42 on 09/05/12
For personal use only.

tinued stirring. Most of the solid dissolved to give a slightly cloudy solution (pH 9.2), which was transferred to a separatory funnel and washed with ether (2 × 50 mL). The aqueous layer was then quickly added to 4 *N* hydrochloric acid (40 mL) and the resultant gummy precipitate extracted into ethyl acetate (3 × 100 mL). The combined extracts were dried and evaporated to leave a pale amber syrup, which became a white foam (22.65 g) upon removal of the last traces of solvent under high vacuum. The product was dried *in vacuo* for 8 h and then triturated with chloroform (100 mL). The foam dissolved initially, and the product rapidly crystallized out. The mixture was cooled at 5°C overnight and the crystals were then collected. The product was washed well with cold chloroform and dried (21.86 g, mp 102–117°C). A portion was recrystallized from chloroform containing a small amount of ethanol to give microneedles, mp 118–122°C (lit. (40) mp 113–114°C; lit. (41) mp 123°C); ir (Nujol): 3335 (s, NH), 3500–2200 (br, CO_2H), 1715 (s, urethane C=O), 1680 (s, CO_2H), 1530 (s, amide II).

N,N′-*Dibenzyloxycarbonyl-L-cystine Dimethyl Ester*

A solution of *N,N′*-dibenzyloxycarbonyl-L-cystine (508 mg, 1.0 mmol), in ethyl acetate (25 mL), was stirred at 0°C and treated with a slight excess of ethereal diazomethane. After 15 min, the excess diazomethane was destroyed by addition of a few drops of glacial acetic acid, and the mixture was evaporated to dryness. The syrupy residue was dissolved in methylene chloride (25 mL) and washed with saturated sodium bicarbonate (10 mL). The organic layer was dried and evaporated to leave a colourless syrup (531 mg, 99%). The product solidified, on standing, to a white solid, mp 67–72°C (lit. (36*a*) mp 73–75°C); ir (neat): 3330 (s, NH), 1720 (s, br, C=O), 1510 (s, amide II); ^{1}Hmr ($CDCl_3$) δ: 3.14 (4H, d, J = 5 Hz, —S—CH_2—), 3.71 (6H, s, CO_2CH_3), 4.38–4.78 (2H, m, —C*H*—), 5.08 (4H, s, Ph—CH_2—), 5.67 (2H, br d, J = 8 Hz, N*H*), 7.30 (10H, s, Ph).

N-Benzyloxycarbonyl-L-cysteine Methyl Ester (23)

A solution of *N,N′*-dibenzyloxycarbonyl-L-cystine dimethyl ester (10.78 g, 20.1 mmol) was stirred in methanol (150 mL) at 0°C. Ice-cold concentrated hydrochloric acid (13.0 mL) was then added dropwise at such a rate that the temperature remained below 5°C. The solution was then cooled to 0°C and zinc dust (6.0 g) was added in small portions over a 15 min period. When the addition was complete the mixture was stirred for a further 15 min at 0°C and then filtered into ice-cold saturated sodium bicarbonate (100 mL). The resultant mixture was concentrated under reduced pressure at 30°C until all of the methanol had been removed, and the residual slush was partitioned between ethyl acetate (150 mL) and water (200 mL). The aqueous layer was further extracted with ethyl acetate (2 × 100 mL) and the combined organic layers were washed successively with 2.5 *N* hydrochloric acid (2 × 30 mL), water (50 mL), saturated bicarbonate (30 mL), water (30 mL), and saturated brine (30 mL), and evaporated to a colourless syrup (10.53 g, 97%), which solidified on freezing. Infrared (film): 3350 (m, br, NH), 2578 (w, SH), 1735, 1718 (s, C=O), 1516 (s, amide II), 1211 (s, C—O) cm^{-1}; ^{1}Hmr ($CDCl_3$) δ: 1.42 (1H, t, J = 9 Hz, S*H*, exchange with D_2O), 3.01 (2H, q, J = 9 Hz, 5 Hz, S—CH_2, collapses to doublet J = 5 Hz on shaking with D_2O), 3.79 (3H, s, CO_2CH_3), 4.62 (1H, quintet, J = 5 Hz, 10 Hz, C*H*, collapses to triplet, J = 5 Hz on shaking with CF_3CO_2D/D_2O), 5.13 (2H, s, PhCH_2—), 5.77 (1H, br d, J = 10 Hz, N*H* exchange with CF_3CO_2D/D_2O), 7.38 (5H, s, *Ph*).

N-*Benzyloxycarbonyl Dehydroalanine Methyl Ester (21)*

Using Silver Carbonate (24)

N-Benzyloxycarbonyl-L-cysteine methyl ester (360 mg, 1.34 mmol) was treated with silver carbonate (555 mg, 1.5 equiv.). After a few min the mixture became hot and began to effervesce. The vigorous reaction was quenched by the addition of methanol (25 mL), and the resulting mixture was refluxed, with stirring, for 9 h. During this time the green suspension of silver carbonate became brown and then black. The mixture was cooled, filtered, the black filter cake washed well with ethyl acetate, and the combined filtrates were evaporated to dryness. The residue, which contained a trace of black solid, was dissolved in methylene chloride (20 mL) and filtered. A few crystals of hydroquinone were added to the filtrate and the solvent was then removed *in vacuo*. The unstable product was dried briefly under high vacuum to give a colourless syrup, 299 mg (95% crude yield) which was stored at −15°C (lit. (9*b*) mp 34–35°C); ir (film): 3420, 3360 (m, NH), 1740, 1720 (s, C=O), 1640 (m, C=C), 1525 (s, amide II) cm^{-1}; ^{1}Hmr ($CDCl_3$) δ: 3.77 (3H, s, CO_2CH_3), 5.10 (2H, s, PhCH_2), 5.72 (1H, d, J = 1 Hz, H_E), 6.19 (1H, d, J = 1 Hz), 7.30 (6H, s, overlapping *Ph*CH$_2$ and N*H*). In a later experiment, which employed absolute methanol as the solvent, the reaction was incomplete after 9 h and, on washing the black filter cake with ethyl acetate, the washings became rich brown in colour. After evaporation of the solvent, the brown residue was extracted with warm hexane. Evaporation of these extracts afforded the dehydroalanine derivative in 68% yield.

Using Fetizon's Reagent (25)

A solution of *N*-carbobenzoxy-L-cysteine methyl ester (10.53 g, 39 mmol) in dry methanol (160 mL) was treated with water (1.0 mL), followed by Fetizon's reagent (23.4 g). The resulting mixture was stirred and heated to reflux at 75–80°C for 8.5 h. After this time, the colour of the reagent had changed from green to black, and an aliquot of the reaction mixture, swirled with ethyl acetate, did not impart any colour to the solvent. The black suspension was filtered and the solids washed with methanol. The combined filtrates were evaporated to leave an amber syrup containing some fine black particles, which were removed by dissolution of the product in methylene chloride (100 mL) and passage of this solution through two short columns (1 in. × 1 in.) of Celite with the aid of additional methylene chloride. A trace of hydroquinone was added to the filtered solution and the solvent was evaporated to leave an amber syrup that was dried briefly under high vacuum (8.50 g, 92%). The ir and nmr spectra of this syrup were identical to those of the material described above.

6L-Carbobenzyloxyamino-3D-carboxy-2,2-dimethyl-5-oxoperhydro-1,4-thiazepine (22) (23)

A solution of *N*-carbobenzoxydehydroalanine methyl ester (7.0 g, 30 mmol) in dry methanol (150 mL) was stirred under hydrogen at room temperature. D-Penicillamine (4.46 g, 30 mmol) was then added, followed by triethylamine (5.0 mL, 3.64 g, 36 mmol). Most of the solid dissolved to give a slightly cloudy solution, which cleared within 1 h. After eight days, the resultant amber solution was evaporated to dryness to leave a light golden foam. The product was dissolved in water (60 mL), layered with ethyl acetate (75 mL), and acidified to pH 2 with 2.5 *N* hydrochloric acid (13 mL). The layers were separated and the aqueous layer was extracted with ethyl acetate (2 × 50 mL). The combined organic layers were washed with saturated brine (25 mL) and dried. Evaporation of the solvent gave an off-white solid, which was triturated with chloroform (50 mL) and allowed to stand at room temperature for 24 h. The 3D,6L-thiazepine **22** was collected by filtration, washed with chloroform, and dried under high vacuum to give a white solid 2.28 g (22%) mp 203–206°C. Recrystallization from *n*-butanol (20 mL) gave a white, microcrystalline solid (1.62 g) mp 211–213°C (lit. (23) mp 222–222.5°C); $[\alpha]_D$ −12.6° (*c* 1.0, 7% $NaHCO_3$) (lit. (23) $[\alpha]_D$ −16° (*c* 1.0, 5% $NaHCO_3$)); ir (KBr): 3410 (m) and 3280 (m) (NH), 3600–2200 (br, OH), 1700 (sh) and 1693 (s) (CO_2H and

Can. J. Chem. Downloaded from www.nrcresearchpress.com by 210.87.254.42 on 09/05/12
For personal use only.

urethane C=O), 1615 (s, amide C=O); ^{1}Hmr (D_2O/K_2CO_3) δ: 1.30 (3H, s, CH_3), 1.57 (3H, s, CH_3), 2.88 (2H, br m, C7 methylene protons), 4.33 (1H, s, C3 methine), overlapping with 4.87 (1H, m, C6 methine), 5.16 (2H, s, PhCH_2), 7.44 (5H, s, Ar). Evaporation of the chloroform filtrate gave a pale golden foam (6.51 g) which was dissolved in ethyl acetate (75 mL) and extracted with saturated bicarbonate (3 × 30 mL). The combined aqueous extracts were washed with ethyl acetate (15 mL), layered with ethyl acetate (50 mL), and acidified to pH 2.4 with 2.5 *N* hydrochloric acid. The layers were separated and the aqueous layer was extracted with ethyl acetate (20 mL). The combined organic layers were washed with saturated brine (2 × 10 mL) and dried. Evaporation of the solvent gave a gummy foam which was dissolved in methylene chloride (40 mL) and again evaporated to dryness and dried under high vacuum to leave a pinkish yellow foam (5.21 g). When this was dissolved in benzene (25 mL) and the solution seeded with **22**, a second crop of material (1.0 g) mp 175–195°C (sealed tube) was obtained. The benzene mother liquor was evaporated to dryness and dissolved in ethanol (10 mL). Water was added to this solution until it became cloudy, and the 3D,6D-isomer crystallized slowly as an off-white solid (2.0 g). Recrystallization from *n*-butanol gave a white microcrystalline solid (1.4 g) mp 130–150°C (lit. (23) mp 125–150°C; $[\alpha]_D^{25}$ −10, $[\alpha]_{365}^{25}$ −34.5 (*c* 1.0, saturated $NaHCO_3$) (lit. (23) $[\alpha]_D$ −11° (*c* 1.0, 5% $NaHCO_3$)); ir (Nujol): 3400, 3300 (m, NH), 1725, 1698, 1615 (s, urethane, carboxyl, amide C=O); ^{1}Hmr (D_2O/K_2CO_3) δ: 1.21 (3H, s, CH_3), 1.44 (3H, s, CH_3), 2.71 (2H, br m, C7 methylene protons), 4.13 (1H, s, C3 methine proton), 4.64 (1H, m, C6 methine proton), 4.99 (2H, s, PhCH_2), 7.23 (5H, s, Ar).

6L-Carbobenzoxyamino-3D-carboxy-2,2-dimethyl-5-oxoperhydro-1,4-thiazepine Benzhydryl Ester (33h)

A suspension of **22** (176 mg, 0.5 mmol), in methylene chloride (3.0 mL), was treated during 5 min with a solution of diphenyldiazomethane (97 mg, 0.5 mmol) in methylene chloride (3.0 mL). The resulting pink solution was treated with formic acid (1 drop), the solvent was then evaporated, and the residue was dried under high vacuum, to leave a light yellow foam (269.5 mg). This crystallized upon addition of ether to give 199 mg, (79%) mp 162–163°C, $[\alpha]_D$ −24°, $[\alpha]_{365}$ −115°(*c* 1.0, CH_3OH); ir ($CHCl_3$): 3400 (m, NH), 1714, 1660 (s, amide, ester, urethane C=O), 1488, 1450 (s, amide II) cm^{-1}; ^{1}Hmr ($CDCl_3$) δ: 1.38 (6H, s, CH_3), 2.83 (2H, m, C7 methylene protons), 4.27 (1H, d, J = 8 Hz, C3 methine), 4.68 (1H, m, C6 methine), 5.03 (2H, s, PhCH_2), 6.23 (1H, d, J = 5 Hz, urethane NH), 6.78 (1H, d, J = 8 Hz, amide NH), 6.97 (1H, s, benzhydryl methine), 7.33 (5H, s, Ar). *Anal.* calcd. for $C_{29}H_{30}N_2O_5S$: C 67.16, H 5.83, N 5.40; found: C 66.95, 67.20, H 6.00, 5.87, N 5.34, 5.34.

6L-Amino-3D-benzhydryloxycarbonyl-2,2-dimethyl-5-oxoperoxoperhydro-1,4-thiazepine p-*Nitrobenzyl Ester (33i)*

A solution of **22** (176 mg, 0.5 mmol) and *p*-nitrobenzyl bromide (119 mg, 0.55 mmol), in DMF (6.0 mL), was treated with anhydrous potassium carbonate (42 mg, 0.3 mmol) and stirred at room temperature for 21 h. During this period the crystalline potassium carbonate dissolved and was replaced by a fine white precipitate. The reaction mixture was poured into water (50 mL) and the product was extracted with ethyl acetate (2 × 20 mL). The combined organic layers were washed sequentially with water (4 × 25 mL), saturated sodium bicarbonate (20 mL), again with water (25 mL), and then dried. Evaporation of the solvent gave a white solid (249 mg), which was crystallized from acetone as white microneedles (188 mg, 77% yield), mp 191–192°C; $[\alpha]_D$ −26.4°, $[\alpha]_{436}$ −69.0° (*c* 2.0, CH_2Cl_2); ir (KBr): 3300, 3270 (m, NH), 1735, 1710, 1660 (s, ester, urethane, amide C=O), 1514 (s, $ArNO_2$), 1335 (s, $ArNO_2$) cm^{-1}; ^{1}Hmr ($CDCl_3$) δ: 1.47 (6H, s, CH_3), 2.90 (2H, m, C7 methylene), 4.27 (1H, d, J = 8 Hz, C3 methine), 4.77 (1H, m, C6 methine), 5.10 (2H, s, ArCH_2), 5.30 (2H, s, ArCH_2), 6.17 (1H, br s, urethane NH), 6.63 (1H, d, J = 8 Hz, amide NH), 7.35 (5H, s, Ph), 7.57 (2H, d, J = 8 Hz, *p*-nitrobenzyl *H2* and *H6*, 8.25 (2H, d, J = 8 Hz, *p*-nitrobenzyl *H3* and *H5*). *Anal.* calcd. for $C_{23}H_{25}N_3O_7S$: C 56.66, H 5.17, N 8.62; found: C 56.54, 56.76, H 5.36, 5.25, N 8.57, 8.52.

6L-Amino-3D-carboxy-2,2-dimethyl-5-oxoperhydro-1,4-thiazepine Hydrobromide Salt (27) (23)

To a solution of 1 *M* hydrogen bromide in anhydrous acetic acid (10 mL) was added **22** (704 mg, 2.0 mmol). After 30 min stirring, most of the solid had dissolved and the mixture was allowed to stand while the product crystallized from solution. After a total of 4 h at room temperature, the product was collected by filtration, washed well with ether, and dried under high vacuum overnight to yield a white microcrystalline solid, 484 mg (81%), mp 229–232°C (dec.) sealed tube (lit. (23) mp 241–243°C (dec.)); $[\alpha]_D$ −65.0°, $[\alpha]_{365}$ −245° (*c* 2.0, CH_3OH); ir (KBr): 3700–2400 (s, br, CO_2H), 3582 (m), 3515 (m, NH_3^+), 1718 (s, CO_2H), 1650 (s, amide I) cm^{-1}; ^{1}Hmr (D_2O) δ: 1.62 (3H, s, CH_3), 1.67 (3H, s, CH_3), 2.82 (1H, q, J_{AB} = 14.9, J_{AX} = 2.5 Hz), 3.29 (1H, q, J_{AB} = 14.9, J_{BX} = 11.5 Hz) (A and B quartets for C7 geminal protons), 4.27 (1H, s, C3 methine), 5.02 (1H, q, J_{AX} = 2.5, J_{BX} = 11.5 Hz, X-quartet for C6 methine).

6L-Amino-3D-benzhydryloxycarbonyl-2,2-dimethyl-5-oxoperhydro-1,4-thiazepine p-*Toluenesulfonic Acid Salt (26)*

A slurry of Amberlite 1R 120 (H) (6 g) in water was added to a small glass column and the resin was washed with 2.5 *N* hydrochloric acid (30 mL) followed by deionized water (2 × 30 mL) until the column was neutral. A solution of **27** (273 mg, 0.91 mmol), in water (3.0 mL), was added to the column. The column was washed with deionized water (60 mL) until the washings were neutral and the thiazepine was then eluted with 1 *N* ammonium hydroxide (200 mL). Evaporation of the eluate gave a white solid, which was dissolved in water (20 mL) and reevaporated. Drying under high vacuum gave a mixture of the free thiazepine and its ammonium salt (194.3 mg) mp > 260°C; ir (KBr): 3320, 3100, 2600 (br, NH_3^+), 3230 (s, br, NH_4^+), 1652 (s, amide I), 1550 (s, br, CO_2^-), 1390 (s, NH_4^+ and CO_2^-); analytical tlc (Silica Gel): R_f 0.43 (2-butanone – acetic acid – water 4:1:1), ninhydrin yellow. The crude thiazepine (194 mg) was stirred for 18 h at 24°C with methylene chloride (3.6 mL), methanol (4.8 mL), and diphenyldiazomethane (345 mg, 1.8 mmol). The resulting red solution was filtered to remove a trace of suspended solid and evaporated to dryness. The residue was treated with acetone (2.5 mL), followed by anhydrous *p*-toluenesulfonic acid (155 mg, 0.9 mmol), to give a clear red solution. Dilution with dry ether (40 mL) precipitated the product as a white solid, which was collected after cooling overnight at 4°C. The product was washed with ether and air dried to give 374 mg (74% from the hydrobromide), mp 172–177°C (sealed tube). Recrystallization from boiling acetonitrile (4.5 mL) gave white microneedles (278 mg), mp 181–183°C (sealed tube) (an analytical sample had mp 187–189°C (sealed tube)); $[\alpha]_D^{24}$ −24.7°, $[\alpha]_{365}^{24}$ −117.3° (*c* 1.5, CH_3OH); ir (KBr): 3670–2400 (br, NH_3^+), 1735 (s, ester C=O), 1667 (s, amide I), 1160 (s, br, SO_3^-) cm^{-1}; ^{1}Hmr ($CDCl_3$) δ: 1.26 (6H, s, CH_3), 2.34 (3H, s, ArCH_3), 2.5–3.47 (2H, m, C7 methylene), 3.98 (1H, d, J = 7 Hz, collapses to singlet with D_2O exchange, C3 methine), 4.69 (1H, m, C6 methine), 6.87 (1H, s, ester methine), 6.95 (2H, d, J = 8 Hz, tosyl *H3* and *H5*), 7.20 (5H, s, Ph) overlapping with 7.26 (5H, s, Ph), overlapping with 7.62 (2H, d, J = 8 Hz, tosyl *H2* and *H6*, overlapping with 7.5–8.37 (4H, br s, exchange with D_2O, NH_3^+ and amide NH). *Anal.* calcd. for $C_{28}H_{32}N_2O_6S_2$: C 60.41, H 5.79, N 5.03; found: C 60.19, H 5.98, N 4.92.

Can. J. Chem. Downloaded from www.nrcresearchpress.com by 210.87.254.42 on 09/05/12
For personal use only.

3D-Carboxy-6L-carbobenzoxyamino-2,2-dimethyl-5-oxoperhydro-1,4-thiazepine Methyl Ester (33g)

A suspension of **22** (102.4 mg) in ethyl acetate (10 mL) was stirred, cooled to 0°C, and a slight excess of ethereal diazomethane (8 mL) was added in portions. The solid dissolved to form a clear yellow solution, which was allowed to warm to room temperature during 1 h. The excess diazomethane was destroyed by the dropwise addition of acetic acid and the solvent was evaporated to give colourless microneedles, which were dried under high vacuum, mp 142–143.5°C. Recrystallization from chloroform–hexane gave colourless microprisms, mp 144–145°C; ir ($CHCl_3$): 3400 (m, NH) 1725, 1710, 1655 (s, urethane, ester, amide C=O) cm^{-1}; ^{1}Hmr ($CDCl_3$) δ: 1.42 (6H, s, CH_3), 2.87 (2H, br d, C7 methylene), 3.75 (3H, s, CO_2CH_3), 4.22 (1H, d, J = 7.5 Hz, C3 methine), 4.73 (1H, m, C6 methine), 5.03 (2H, s, PhCH_2), 6.28 (1H, d, J = 5 Hz, urethane NH), 6.93 (1H, d, J = 7.5 Hz, amide NH), 7.27 (5H, s, Ph).

The 6D-epimer **33***p* was prepared analogously to give colourless microprisms from chloroform–hexane, mp 142.5–143°C; ir ($CHCl_3$); 3390, 3370 (m, NH), 1730, 1710, 1670 (s, urethane, ester, amide C=O) cm^{-1}; ^{1}Hmr ($CDCl_3$) δ: 1.32 (6H, s, CH_3), 2.90 (2H, m, C7 methylene), 3.77 (3H, s, CO_2CH_3), 4.58 (1H, d, J = 7 Hz, C3 methine), overlapping with 4.70 (1H, m, C6 methine), 5.05 (2H, s, PhCH_2), 6.28 (2H, m, overlapping urethane and amide NH), 7.32 (5H, s, Ph).

3D-Benzhydryloxycarbonyl-6L-carbobenzoxyamino-2,2-dimethyl-5-oxoperhydro-1,4-thiazepine-1-oxide (32a)

A solution of **33***h* (259.0 mg, 0.5 mmol) in methylene chloride (10 mL) was stirred at 4°C and an ice-cold solution of 85% *m*-chloroperoxybenzoic acid (102.0 mg, 0.5 mmol), in methylene chloride (10 mL), was added dropwise during 25 min. The resultant solution was stirred at 4°C for an additional 2.5 h and then washed sequentially with 3.5% sodium bicarbonate (10 mL), 2% sodium thiosulfate (10 mL), 3.5% sodium bicarbonate (10 mL), and saturated brine (10 mL). The organic layer was then dried and evaporated to leave a white foam (262 mg, 98%), $[\alpha]_D$ 0.0°, $[\alpha]_{365}$ 0.0° (*c* 1.0, CH_2Cl_2); ir ($CHCl_3$): 3350 (m, NH), 1715, 1670 (s, urethane, ester, amide C=O), 1042 (s, sulfoxide) cm^{-1}; ^{1}Hmr ($CDCl_3$) δ: 1.17 (3H, s, CH_3), 1.25 (3H, s, CH_3), 2.93 (1H, q, J = 1.6, 15.1 Hz, *H7S*), 3.18 (1H, q, J = 7.2, 15.1 Hz, *H7R*), 4.67 (1H, m, C6 methine), 5.09 (2H, s, CH_2), 5.22 (1H, d, J = 8 Hz, C3 methine), 6.66 (1H, d, J = 8 Hz, NH), 7.32 (6H, Ar and urethane NH). *Anal.* calcd. for $C_{29}H_{30}N_2O_6S$: C 65.15, H 5.66, N 5.24; found: C 65.29, H 6.01, N 5.12.

Sulfoxide **32***c*: white foam, $[\alpha]_D$ +18°, $[\alpha]_{365}$ +73° (*c* 2.02, CH_2Cl_2); ir ($CHCl_3$): 3400, 3375 (m, NH), 1725, 1670 (s, ester, urethane, amide C=O), 1045 (s, sulfoxide) cm^{-1}; ^{1}Hmr ($CDCl_3$) δ: 1.12 (6H, s, CH_3), 2.6–3.5 (2H, m, C7 methylene), 5.02 (2H, s, PhCH_2), overlapping with 5.15 (1H, d, J = 7 Hz, C3 methine) and 5.37 (1H, m, C6 methine), 6.20 (1H, d, J = 8 Hz, urethane NH), 6.57 (1H, d, J = 7 Hz, amide NH), 6.92 (1H, s, benzhydryl methine), 7.27 (15H, s, Ph).

Sulfoxide **32***b*: pale yellow foam, $[\alpha]_D$ −23.0°, $[\alpha]_{436}$ −51° (*c* 2.2, methylene chloride); ir ($CHCl_3$): 3390, 3350 (m, NH), 1725, 1715, 1673 (s, ester, urethane, amide C=O), 1343 (s, $ArNO_2$), 1040 (m, sulfoxide) cm^{-1}; ^{1}Hmr ($CDCl_3$) δ: 1.32 (6H, s, CH_3), 2.98 (1H, q, J = 2.2, 15.0 Hz, *H7S*), 3.33 (1H, q, J = 5.9, 15.0 Hz, *H7R*), 4.75 (1H, m, C6 methine), 5.05 (2H, s, ArCH_2), 5.25 (2H, s, ArCH_2), overlapping with 5.22 (1H, d, C3 methine), 6.55 (1H, d, J = 8 Hz, NH), 7.28 (5H, s, Ph), 7.52 (2H, m), overlapping with 7.57 (1H, br, NH), 8.22 (2H, m).

Preparation of N-tert-*Butoxycarbonylglycyl-L-α-aminoadipic Acid α-Benzhydryl Ester (13)*

A suspension of L-α-aminoadipic acid α-benzhydryl ester (596.6 mg, 1.82 mmol), in dry methanol (28 mL) and dimethoxyethane (8 mL), was treated with dicyclohexylamine (0.37 mL, 1.82 mmol) and the mixture was stirred for 5 min to give a slightly cloudy solution. Then the succinimidyl ester **15** (495.5 mg, 1.82 mmol) was added and stirring was continued for 30 min, at which time additional dicyclohexylamine (0.37 mL, 1.82 mmol) was added. The stirring was then continued for 24 h. Removal of the solvent gave a gummy yellow solid which was dissolved in methylene chloride (50 mL) and washed with 10% potassium bisulfate (3 × 25 mL) and saturated brine (25 mL) and dried over sodium sulfate. Evaporation of the solvent gave a sticky yellow foam (823 mg), which was purified on silica gel (50 g), (ethyl acetate – methanol, 10:1) to give a colourless foam (786.3 mg, 90%) $[\alpha]_D^{26}$ −20.8 (*c* 2.0, CH_3OH); ir ($CHCl_3$): 3580–2440 (br, CO_2H), 3410, 3360 (m, NH), 1710, 1680 (s, urethane, ester, carboxylic acid C=O) cm^{-1}; ^{1}Hmr ($CDCl_3$) δ: 1.40 (9H, s, *t*-Bu), overlapping with 1.17–2.50 (6H, m, α-aminoadipyl methylene), 3.80 (2H, d, J = 5.5 Hz, glycyl methylene), 4.70 (1H, m, α-aminoadipyl methine), 5.53 (1H, br, urethane NH), 6.90 (1H, s, benzhydryl methine), 7.13 (1H, d, J = 8 Hz, amide NH), overlapping with 7.32 (10H, s, Ph), 8.30 (1H, br, CO_2H).

3D-Benzhydryloxycarbonyl-6L-amino-2,2-dimethyl-5-oxoperhydro-1,4-thiazepine (16 ≡ 33k)

A suspension of the thiazepine benzhydryl ester *p*-toluenesulfonic acid salt **26** (270 mg, 0.485 mmol) in ethyl acetate (10 mL) was stirred with saturated sodium bicarbonate (5 mL) until all of the solid had dissolved. The organic layer was washed with sodium bicarbonate (5 mL), dried, and evaporated to leave a colourless syrup. This was dissolved in methylene chloride (15 mL) and the solvent was evaporated to leave a colourless foam, which was dried under high vacuum (178.5 mg, 96%). The product crystallized as colourless needles by slow evaporation from chloroform; mp 137–138.5°C; ir ($CHCl_3$): 3400, 3380 (m, NH, NH_2), 1740 (s, ester C=O), 1665 (s, amide C=O) cm^{-1}; ^{1}Hmr ($CDCl_3$) δ: 1.27 (3H, s, CH_3), 1.35 (3H, s, CH_3), 1.90 (2H, s, NH_2), 2.62 (1H, q, J_{AB} = 15.5 Hz, J_{BX} = 8.0 Hz), 2.92 (1H, q, J_{AB} = 15.5 Hz, J_{AX} = 4.0 Hz, AB quartet of ABX for C7 methylene), 3.95 (1H, q, J_{AX} = 8.0, J_{BX} = 4.0 Hz, C6 methine), 4.63 (1H, d, J = 7.5 Hz, C3 methine), 6.60 (1H, d, J = 7.5 Hz, amide NH), 6.92 (1H, s, benzhydryl methine), 7.28 (10H, s, Ph).

Fully Protected α-Aminoadipylthiazepine (30)

A solution of **12** (195.7 mg, 0.458 mmol) and EEDQ (116.1 mg, 0.47 mmol) in ethyl acetate (8.0 mL) was stirred for 5 min. To this was added the benzhydryl ester **33***k* (176.0 mg, 0.458 mmol), and the resultant solution was stirred for 72 h. The reaction mixture was then diluted to 25 mL with ethyl acetate and washed with 10% potassium bisulfate (2 × 10 mL), saturated brine (10 mL), dried, and evaporated to leave a syrup, which was dissolved in methylene chloride (15 mL) and again evaporated. Repetition of this process with more methylene chloride (15 mL) afforded an off-white foam (335.8 mg). Purification of a portion (172 mg) by plc, 2 plates, (chloroform – ethyl acetate, 1:1) gave one major band, R_f 0.38–0.60, which yielded a white foam (94 mg). This crystallized upon slow evaporation from ethyl acetate to give white microneedles, mp 193–197°C; $[\alpha]_D$ −41.5°, $[\alpha]_{365}$ −159° (*c* 1.2, CH_3OH); $[\alpha]_D$ −30.0°, $[\alpha]_{365}$ −114° (*c* 1.18, CH_2Cl_2); ir (KBr): 3320 (m, br, NH), 1735, 1700, 1657 (s, ester, urethane, amide C=O) cm^{-1}; ^{1}Hmr ($CDCl_3$) δ: 1.39 (3H, s, CH_3), 1.43 (9H, s, Boc), 1.46 (3H, s, CH_3), 1.57–1.93 (4H, m, CH_2CH_2), 2.16 (2H, m, CH_2CO), 2.77 (1H, q, J_{BX} = 10.2, J_{AB} = 15.0, *H7R*), 2.84 (1H, q, J_{AX} = 2.8, J_{AB} = 15.0, *H7S*), 4.25 (1H, d, J = 8 Hz, C3 methine), 4.41 (1H, m, Aad methine), 4.78 (1H, m, C6 methine), 5.12 (1H, d, J = 9 Hz, urethane NH), 6.24 (1H, d, J = 8 Hz, N4H), 6.78 (1H, d, J = 5 Hz, NH at C6), 6.88 (1H, s, benzhydryl CH), 6.99 (1H, s, benzhydryl CH), 7.32 (20H, m, Ar). *Anal.* calcd. for $C_{45}H_{51}N_3O_8S$: C 68.07, H 6.48, N 5.29; found: C 68.26, H 6.64, N 5.29.

Can. J. Chem. Downloaded from www.nrcresearchpress.com by 210.87.254.42 on 09/05/12
For personal use only.

Fully Protected Glycyl α-Aminoadipylthiazepine (31)

*A. From the Thiazepine 33*k

A solution of **13** (28.5 mg, 0.0588 mmol), in methylene chloride (0.3 mL), was stirred at room temperature with EEDQ (16.8 mg, 0.068 mmol). After 5 min the thiazepine **33***k* (22.6 mg, 0.0588 mmol), in methylene chloride (1 mL), was added. The volume was reduced by passing a stream of dry nitrogen over the surface of the solution, and was then adjusted to 0.5 mL. After 48 h the solvent was evaporated and the residual syrup was dissolved in ethyl acetate (2 mL) and washed with 10% potassium bisulfate (2 × 1 mL), saturated brine (1 mL), and dried over sodium sulfate. Evaporation gave a syrup, which was dissolved in methylene chloride (4 mL) and evaporated. Repetition of this process with more methylene chloride (4 mL) gave a creamy white foam, 47.6 mg. Purification by plc (methylene chloride – methanol, 9:1) gave one major band, R_f 0.48–0.65, as a white foam 39.2 mg (78% yield); $[\alpha]_D$ −23.3°, $[\alpha]_{365}$ −82.7° (*c* 1.74, CH_2Cl_2); ir ($CHCl_3$): 3390 (m, NH), 1725, 1660 (s, urethane, amide, ester C=O) cm^{-1}; ^{1}Hmr ($CDCl_3$) δ: 1.34 (3H, s, C*H*$_3$), 1.42 (9H, s, Boc), 1.49 (3H, s, C*H*$_3$), 1.52–1.95 (4H, m, C*H*$_2$C*H*$_2$), 2.18 (2H, m, C*H*$_2$CO), 2.78 (1H, q, J_{BX} = 6.2, J_{AB} = 15 Hz, *H7S*), 2.81 (1H, q, J_{AX} = 8.5, J_{BX} = 15 Hz, *H7R*), 3.75 (1H, octet, J_{AB} = 16 Hz, J_{AX} = 5.5, 6.0 Hz, glycyl CH_2), 4.32 (1H, br s, C3 methine), 4.69 (1H, sextet, Aad methine), 4.83 (1H, br s, C6 methine), 5.30 (1H, br s, urethane N*H*), 6.54 (1H, br d, *J* ~ 6 Hz, N4*H*), 6.87 (1H, s, benzhydryl C*H*), 6.98 (1H, s, benzhydryl C*H*), overlapping with 7.01 (1H, br d, *J* ~ 7.5 Hz, N*H*), 7.14 (1H, br s, N*H*), 7.24–7.40 (20H, m, Ar). *Anal.* calcd. for $C_{47}H_{54}N_4O_9S$: C 66.33, H 6.40, N 6.58; found: C 65.88, H 6.42, N 6.44.

B. Via the Fully Protected α-Aminoadipylthiazepine 30

The fully protected thiazepine **30** (81.0 mg, 0.102 mmol) was dissolved in methylene chloride (2 mL), and the solution was evaporated to a golden oil, which dissolved readily in dry ether (6.0 mL). Anhydrous *p*-TsOH (17.6 mg, 0.102 mmol) was added, and the mixture was refluxed for 5 h. A gum precipitated during this time but tlc analysis (ethyl acetate) of the ether soluble material indicated that starting material was still present. Reflux was continued for an additional 5 h and the solvent was then evaporated to leave an amber, gummy solid, which was triturated with ether (5 mL) to give an off-white solid 81.1 mg. Analysis by tlc (ethyl acetate) showed the presence of one major ninhydrin-positive spot, R_f 0.8, a very minor ninhydrin-positive impurity at R_f 0.65, and a trace of starting material, R_f 0.95, which was ninhydrin-negative. The crude salt was dissolved in methylene chloride (2 mL) and stirred with saturated sodium bicarbonate (1 mL). The organic layer was removed and the aqueous layer was extracted with methylene chloride (1 mL). The combined organic layers were dried over sodium sulfate, filtered, and stirred for 20 h at room temperature with **15** (27.2 mg, 0.10 mmol). The reaction mixture was then washed with water (2 × 2 mL), saturated brine (1 mL), and dried over sodium sulfate. Evaporation of the solvent gave an amber syrup, which was partially purified by precipitation from ethyl acetate (0.5 mL) with hexane to give an oil (69.3 mg). Further purification by rapid chromatography on silica gel (5 g) (ethyl acetate – methylene chloride, 1:2 then 1:1) gave a white foam (43.3 mg, 50% from **30**) which was identical by tlc and ^{1}Hmr with the material prepared above.

*Oxidation of the Fully Protected α-Aminoadipylthiazepine 30 to the Sulfoxide 32*d

A solution of the fully protected α-aminoadipyl thiazepine **30** (28.1 mg, 0.0354 mmol), in methylene chloride (0.5 mL), was stirred at 2°C and an ice-cold solution of 85% *m*-chloroperoxybenzoic acid (0.071 *M*, 0.5 mL) was added during 2 h. After stirring an additional 0.5 h at 0°C, the solution was washed with saturated sodium bicarbonate (2 × 1 mL), saturated brine (1 mL), dried, and evaporated to leave a colourless foam (28.2 mg, 98%) $[\alpha]_D$ −12.9, $[\alpha]_{365}$ −48.8 (*c* 4.12, CH_2Cl_2); ir (KBr): 3300 (m, br, NH), 1735, 1700, 1685, 1660 (s, urethane, ester, amide C=O) cm^{-1}; ^{1}Hmr ($CDCl_3$) δ: 1.20 (3H, s, C*H*$_3$), 1.25 (3H, s, C*H*$_3$), 1.68 (4H, m, C*H*$_2$C*H*$_2$), 2.10 (2H, m, C*H*$_2$CO), 2.94 (1H, q, *J* = 2.8, 15 Hz, *H7S*), 3.38 (1H, q, *J* = 7.0, 15 Hz, *H7R*), 4.38 (1H, m, Aad methine), 4.83 (1H, m, C6 methine), 5.18 (1H, d, *J* = 8 Hz, C3 methine), 5.18 (1H, d, *J* = 10 Hz, urethane N*H*), 6.45 (1H, d, *J* = 8 Hz, ring N*H*), 6.87 (1H, s, benzhydryl methine), 6.98 (1H, s, benzhydryl methine), 7.28 (20H, s, Ar), 8.33 (1H, br d, amide N*H*).

*Oxidation of the Fully Protected Glycyl α-Aminoadipylthiazepine 31 to the Sulfoxide 32*e

A solution of the fully protected glycyl α-aminoadipylthiazepine (34.7 mg, 0.041 mmol), in methylene chloride (0.5 mL), was stirred at 2°C and an ice-cold solution of 85% *m*-chloroperoxybenzoic acid (0.082 *M*, 0.5 mL) was added over 20 min. The solution was stirred at 2°C for an additional 20 min and was then washed with sodium thiosulfate (1 mL), saturated sodium bicarbonate (2 × 1 mL), saturated brine (1 mL), and dried over sodium sulfate. Evaporation of the solvent gave a white foam 32.3 mg, 91% yield $[\alpha]_D$ −6.16, $[\alpha]_{365}$ −61.6 (*c* 3.6, CH_2Cl_2); ir ($CHCl_3$): 3390, 3330 (m, NH), 1730, 1680, 1675 (s, ester, urethane, amide C=O) cm^{-1}; ^{1}Hmr ($CDCl_3$) δ: 1.20 (3H, s, C*H*$_3$), 1.23 (3H, s, C*H*$_3$), 1.42 (9H, s, *t*-Bu), 1.45–1.96 (4H, m, C*H*$_2$C*H*$_2$), 2.25 (2H, m, C*H*$_2$CO), 2.91 (1H, d, *J* = 15 Hz, *H7S*), 3.30 (1H, q, *J* = 8.7, 15 Hz, *H7R*), 3.78 (2H, br octet, J_{AB} = 17.0, J_{AX} = J_{BX} = 5 Hz, glycyl C*H*$_2$), 4.66 (1H, m, Aad methine), 4.87 (1H, m, C6 methine), 5.35 (1H, br, C3 methine), 6.40 (1H, br, urethane N*H*), 6.84 (1H, d, *J* = 7.5 Hz, ring N*H*), 6.86 (1H, s, benzhydryl methine), 6.98 (1H, s, benzhydryl methine), 7.33 (20 H, m, Ar), 8.28 (1H, br, N*H*). *Anal.* calcd. for $C_{47}H_{54}N_4O_{10}S$: C 65.11, H 6.28, N 6.46; found: C 65.04, H 6.68, N 6.29.

*Deprotection of the Fully Protected α-Aminoadipylthiazepine 30. Preparation of 5*a

A solution of the fully protected α-aminoadipylthiazepine (38.1 mg, 0.048 mmol), in anhydrous formic acid (3.0 mL), was stirred at room temperature for 18 h, and then evaporated to dryness. The residue was partitioned between water (5 mL) and ether (5 mL). The ether layer was extracted with water and the combined aqueous layers were evaporated to leave a glass (20.4 mg). Analytical tlc (silica gel): R_f 0.26 (2-butanone – acetic acid – water, 4:1:1), visible as a salmon-pink spot with ninhydrin, or yellow spot with palladium chloride. Very minor ninhydrin positive impurities were detected at R_f 0.50 and 0.63; $[\alpha]_D^{25}$ −48.8, $[\alpha]_{365}^{25}$ −172.4 (*c* 1.7, H_2O); ^{1}Hmr (D_2O) δ: 1.32 (3H, s, C*H*$_3$), 1.47 (3H, s, C*H*$_3$), 1.80 (4H, br m, C*H*$_2$C*H*$_2$), 2.35 (2H, m, C*H*$_2$CO), 2.78 (1H, q, *J* = 6.1, 15 Hz, *H7S*), 2.94 (1H, q, *J* = 9.0, 15 Hz, *H7R*), 3.82 (1H, br q, Aad methine), 4.30 (1H, s, C3 methine), 4.77 (1H, q, *J* = 6.1, 9.0, C6 methine). *Anal.* calcd. for $C_{14}H_{23}N_3O_6S{\cdot}H_2O$: C 44.32, H 6.64, N 11.07; found: C 43.89, H 6.77, N 11.01.

*Deprotection of the Fully Protected Glycyl-α-aminoadipylthiazepine 31. Preparation of 5*b

A solution of the fully protected glycyl-α-aminoadipylthiazepine (41.4 mg, 0.0486 mmol) in 97% formic acid (4.0 mL) was stirred at room temperature for 14 h. The formic acid was then evaporated and the residual syrup dissolved in methylene chloride (5 mL) and again evaporated. This process was repeated with more methylene chloride (5 mL) to leave a solid residue, which was partitioned between water (5 mL) and ether (2 mL). The aqueous layer was washed with more ether (2 mL) and then evaporated to leave a whitish glass (21.0 mg). Analytical tlc (silica gel): R_f 0.26 (2-butanone – acetic acid – water,

Can. J. Chem. Downloaded from www.nrcresearchpress.com by 210.87.254.42 on 09/05/12
For personal use only.

4:1:1), visible as an orange-yellow spot with ninhydrin or yellow spot with palladium chloride; ^{1}Hmr (D_2O) δ: 1.30 (3H, s, CH_3), 1.54 (3H, s, CH_3), 1.76 (4H, br m, CH_2CH_2), 2.36 (2H, m, CH_2CO), 2.85 (1H, q, J = 15.3, 3.3 Hz, C7 proton), 2.96 (1H, q, J = 15.3, 10.4 Hz, C7 proton), 3.88 (2H, s, glycyl CH_2), 4.32 (1H, s, C3 methine), 4.63 (1H, m, Aad methine), 4.77 (1H, m, C6 methine).

Deprotection of the Fully Protected α-Aminoadipylthiazepine Sulfoxide **32**d. *Preparation of* **6**a

A solution of the fully protected α-aminoadipylthiazepine sulfoxide (3.9 mg, 0.0048 mmol) in anhydrous formic acid (0.30 mL) was stirred at room temperature for 19 h. The formic acid was then evaporated and the residual oil partitioned between water (2 mL) and ether (2 mL). The ether layer was extracted with water (2 × 2 mL) and the combined aqueous layers were evaporated to leave a colourless glass (0.8 mg). Analytical tlc (silica gel): R_f 0.12 (2-butanone – acetic acid – water, 4:1:1), visible as an orange spot with ninhydrin or as a grey spot with palladium chloride and heating. Very minor, ninhydrin-positive impurities were present at R_f 0.23 and 0.53; $[\alpha]_D^{27}$ −7.6, $[\alpha]_{365}^{27}$ −28.5 (*c* 1.65, H_2O); ^{1}Hmr (D_2O) δ: 1.32 (2H, m, CH_3), 1.53 (3H, s, CH_3), 1.83 (4H, m, CH_2CH_2), 2.41 (2H, m, $COCH_2$), 3.29 (1H, q, J = 2.4, 13.7 Hz, *H7S*), 3.36 (1H, q, J = 10.2, 13.7 Hz, *H7R*), 3.85 (1H, m, Aad methine), 4.38 (1H, s, *H3*), 5.05 (1H, q, J = 2.4, 10.2 Hz, *H6*).

Deprotection of the Fully Protected Glycyl α-Aminoadipylthiazepine Sulfoxide **32**e. *Preparation of* **6**b

A solution of the fully protected glycyl α-aminoadipylthiazepine sulfoxide (43.2 mg, 0.0498 mmol), in 97% formic acid (4.0 mL), was stirred at room temperature for 14 h. The formic acid was then evaporated and the residue was dissolved in methylene chloride (5 mL) and again evaporated. Repetition of this process with more methylene chloride (5 mL) gave a solid residue, which was partitioned between water (4 mL) and ether (2 mL). The aqueous phase was washed again with ether (2 mL) and evaporated to leave a white glass (20.3 mg, 85%). Analytical tlc (silica gel): R_f 0.13 (2-butanone – acetic acid – water, 4:1:1) visualized as a yellow spot with ninhydrin and brown spot with palladium chloride and heating. A minor, ninhydrin-negative, palladium chloride-positive impurity was detected at R_f 0.34; ^{1}Hmr (D_2O) δ: 1.36 (3H, s, CH_3), 1.56 (3H, s, CH_3), 1.64–1.94 (4H, m, CH_2CH_2), 2.38 (2H, m, CH_2CO), 3.26 (1H, q, J = 2.6, 13.8 Hz, *H7S*), 3.36 (1H, q, J = 10.3, 13.8 Hz, *H7R*), 3.89 (1H, s, glycyl CH_2), 4.40 (2H, m, Aad methine and C3 methine), 5.02 (1H, br d, C6 methine).

Synthesis of Isotopically Labelled Thiazepines

To DL-alanine (800.2 mg, 8.98 mmol) was added a 2% ethanolic solution of L-[U-^{14}C]alanine (500 μCi, 171 mCi/mmol) and the resulting solution was evaporated to dryness. The residue was dissolved in water (10 mL) containing sodium bicarbonate (1.9 g, 22.5 mmol), and benzyl chloroformate (1.6 mL, 2.01 g, 11.8 mmol) was added dropwise, with stirring at room temperature during 5 min. The mixture was stirred for an additional 2 h and was then extracted with ether (3 × 20 mL). The aqueous phase was acidified to pH 2, whereupon an oil precipitated, which crystallized rapidly on cooling to give labelled carbobenzoxyalanine (1.525 g, 76%), mp 104–106°C. This was treated at 0°C with excess ethereal diazomethane, and the mixture was allowed to stand overnight and then filtered and evaporated to dryness to give labelled **24** (1.53 g, 95%) as a colourless syrup, which crystallized on scratching, mp 38–40°C. To this material (1.33 g, 5.96 mmol), in anhydrous methanol at 0°C, were added freshly prepared *tert*-butyl hypochlorite (42) (1.1 mL, 1.0 g, 9.2 mmol) and 0.17 mL of a 1% solution of sodium methoxide in dry methanol. The mixture was stirred for 2.5 h at 0°C and then evaporated and the residue dissolved in methylene chloride (20 mL). This solution was washed with saturated brine (10 mL), dried and evaporated to give labelled **25** as a colourless syrup (1.39 g, 90%); ^{1}Hmr ($CDCl_3$) δ: 1.5 (3H, d, J = 7.0 Hz), 3.7 (3H, s), 5.0 (1H, q, J = 7.0 Hz), 5.2 (2H, s), 7.36 (5H, s). A solution of the labelled **25** in methylene chloride (10 mL) was placed in a 50 mL three-necked flask equipped with a magnetic stirrer and fitted with two serum caps and a condenser topped with a drying tube. The flask was placed in a water bath maintained at 45°C, and DBU (775 mg, 5.1 mmol) was added, followed by additional methylene chloride (5 mL). The mixture was refluxed for 20 min, cooled, and extracted successively with water (10 mL), 3 *N* hydrochloric acid (10 mL), saturated sodium bicarbonate (10 mL), and water (10 mL). To the dried solution was added one crystal of 2,6-di-*tert*-butyl-4-methylphenol, and the solvent was then removed to yield a light brown syrup (1.26 g). Although the ^{1}Hmr spectrum of this material indicated that it was a 1:1 mixture of **21** and **24**, it was used without purification in the next step, reaction with D-penicillamine (822 mg, 5.5 mmol) in dry methanol (15 mL) containing triethylamine (0.85 mL, 6.0 mmol), as described earlier for the preparation of unlabelled **22**. Work-up in the same manner afforded 135.6 mg of **22**, 610 mg of the 3D,6D-epimer and, from the ethyl acetate extracts, 524 mg of recovered **24**, specific activity 30 μCi/mmol.

The crude **22** was recrystallized from hot *n*-butanol (1.1 mL) to give 120.5 mg, mp 203.5–204°C (dec.) (sealed tube), $[\alpha]_D^{29}$ −13° (*c* 0.5, $NaHCO_3$), specific activity 30 μCi/mmol. This material, ^{14}C-labelled at C5, C6, and C7, was used to prepare radioactive samples of the four thiazepines **5***a*, **5***b*, **6***a*, and **6***b*.

Conversion of **33**j *to* **39**a *and* **39**b

A solution of **33***j* (157.0 mg, 0.3 mmol) in methylene chloride (10 mL) was stirred at 2°C. An ice-cold solution of 85% *m*-chloroperoxybenzoic acid (60.9 mg, 0.3 mmol) in methylene chloride (5 mL) was added in small portions during 25 min. Stirring was continued for a further 1 h at 2°C and, during this time, a white precipitate formed which was collected by filtration and dried under high vacuum to give 51.8 mg, mp 144–150°C. The filtrate was stirred with 5% sodium thiosulfate (5 mL) followed by water (5 mL). Solid 2-mercaptobenzothiazole (50.1 mg, 0.3 mmol) was next added and the mixture was stirred at room temperature until this solid had dissolved. Saturated aqueous sodium bicarbonate (5 mL) was then added and the mixture was stirred for 10 h. After this time a solution of saturated brine (5 mL) was added to facilitate separation of the organic layer, which was then washed with saturated brine (5 mL), dried over sodium sulfate, and evaporated to leave a cloudy gum. The product was redissolved in methylene chloride, filtered to remove a fine suspension, and reconcentrated to a white foam (98.2 mg). Analysis by tlc (methylene chloride – ethyl acetate, 4:1) indicated the presence of two major components, at R_f 0.76 (2-mercaptobenzothiazole) and R_f 0.15, ninhydrin:yellow, palladium chloride:orange. This latter component was unstable on silica gel.

The mixture was subjected to flash chromatography on silica gel H (2 g) using methylene chloride (80 mL) to elute the 2-mercaptobenzothiazole (31.5 mg), and ethyl acetate (120 mL) to elute the polar component. The ethyl acetate eluent was evaporated and the gummy product was dissolved in methylene chloride (5 mL), filtered, and concentrated to give **39***a* as a white foam (56.0 mg, 48.7%). Infrared (CCl_4): 3335 (br, m, amide NH and NH_2), 1716 (s, ester C=O), 1682 (s, amide C=O) cm^{-1}; ^{1}Hmr ($CDCl_3$) δ: 1.83 (3H, s, vinyl CH_3), overlapping with 1.95 (2H, s, rapid exchange with D_2O, NH_2), 2.15 (3H, s, vinyl CH_3), 2.68–3.95 (3H, m, cysteinyl methylene and methine protons), 6.82 (1H, s, benzhydryl methine), 7.02–7.95 (~14H, ArH), 8.72 (1H, br s, rapid exchange with D_2O, amide NH).

Can. J. Chem. Downloaded from www.nrcresearchpress.com by 210.87.254.42 on 09/05/12
For personal use only.

The amine **39***a* (44.0 mg, 0.08 mmol) was treated with a solution of 0.096 *M* dicyclohexylamine in methylene chloride (1.0 mL, 1.2 equiv.) and stirred at 0°C. To this solution was added, during 1 min, a solution of benzyl chloroformate (19 mg, 0.11 mmol) in methylene chloride (1 mL). The resulting solution was stirred for 3 h at 0°C, and the solvent was evaporated and the residue partitioned between ethyl acetate (10 mL) and saturated sodium bicarbonate (10 mL). The organic layer was washed successively with saturated bicarbonate (10 mL), 10% potassium bisulfate (2 × 10 mL), saturated brine (10 mL), dried over sodium sulfate, and evaporated to leave a gummy foam (53.1 mg). The product was purified by plc (methylene chloride – ethyl acetate, 9:1) and the band R_f 0.45–0.65 was isolated (36 mg). Crystallization from chloroform–hexane gave **39***b* as an off-white solid (16.6 mg, 30%) mp 124–127°C; ir (Nujol): 3290 (s, amide and urethane NH), 1722, 1696, 1655 (s, ester, urethane, amide C=O), 1527 (s, amide II) cm^{-1}; ^{1}Hmr ($CDCl_3$) δ: 1.87 (3H, s, vinyl CH_3), 2.18 (3H, s, vinyl CH_3), 3.04 (1H, q, J_{AX} = 7.3, J_{AB} = 14.6 Hz), 3.43 (1H, q, J_{BX} = 4.5, J_{AB} = 14.6 Hz, cysteinyl CH_2), 4.78 (1H, m, cysteinyl C*H*) overlapping with 5.08 (2H, s, PhCH_2O), 6.59 (1H, br d, J = 7 Hz, urethane N*H*), 6.92 (1H, s, benzhydryl methine), 7.02–8.00 (20H, m, ArH), 9.19 (1H, br s, amide NH).

Acknowledgements

This research was supported by grants from the Atkinson Charitable Foundation, Toronto, and the Natural Sciences and Engineering Research Council of Canada. The authors also thank Dr. Chia-Cheng Shaw for the suggestion that formic acid be used to remove Boc and benzhydryl protecting groups.

1. J. O'Sullivan, R. C. Bleaney, J. A. Huddleston, and E. P. Abraham. Biochem. J. **184**, 421 (1979); T. Konomi, S. Herchen, J. E. Baldwin, M. Yoshida, N. A. Hunt, and A. L. de Main. Biochem. J. **184**, 427 (1979).
2. B. Meesschaert, P. Adriaens, and H. Eyssen. J. Antibiot. **33**, 722 (1980).
3. P. B. Loder and E. P. Abraham. Biochem. J. **123**, 471 (1971); **123**, 477 (1971).
4. L. A. Eriquez and M. A. Pisano. Antimicrob. Agents Chemother. **16**, 392 (1979).
5. H. Kluender, F.-C. Huang, A. Fritzberg, H. Schnoes, C. J. Sih, P. Fawcett, and E. P. Abraham. J. Am. Chem. Soc. **96**, 4054 (1974); P. Adriaens, B. Meesschaert, H. Vanderhaeghe, and H. Eyssen. Arch. Int. Physiol. Biochim. **84**, 767 (1976).
6. D. W. Young, D. J. Morecombe, and P. K. Sen. Eur. J. Biochem. **75**, 133 (1977); P. Adriaens, H. Vanderhaeghe, B. Meesschaert, and H. Eyssen. Antimicrob. Agents Chemother. **8**, 15 (1975).
7. D. J. Aberhart. Tetrahedron, **33**, 1545 (1977); H. Kluender, C. H. Bradley, C. J. Sih, P. Fawcett, and E. P. Abraham. J. Am. Chem. Soc. **95**, 6149 (1973); N. Neuss, C. H. Nash, J. E. Baldwin, P. A. Lemke, and J. B. Grutzner. J. Am. Chem. Soc. **95**, 3797 (1973).
8. N. Neuss, R. D. Miller, C. A. Affolder, W. Nakatsukasa, J. Mabe, L. L. Huckstep, N. de la Higuera, A. H. Hunt, J. L. Occolowitz, and J. H. Gilliam. Helv. Chim. Acta, **63**, 1119 (1980).
9. (*a*) H. R. V. Arnstein and J. C. Crawhall. Biochem. J. **67**, 180 (1957); D. J. D. Hockenhull, K. Ramachandran, and T. K. Walker. Arch. Biochem. **23**, 160 (1949); (*b*) H. R. V. Arnstein and M. E. Clubb. Biochem. J. **68**, 528 (1958); (*c*) B. Sjöberg, H. Thelin, L. Nathorst-Westfelt, E. E. van Tamelen, and E. R. Wagner. Tetrahedron Lett. 281 (1965); (*d*) N. J. Leonard and G. E. Wilson, Jr. J. Am. Chem. Soc. **86**, 5307 (1964); (*e*) P. Blondeau, R. Gauthier, C. Berse, and D. Gravel. Can. J. Chem. **49**, 3866 (1971); M. H. Benn and R. E. Mitchell. Can. J. Chem. **50**, 2195 (1972).
10. P. A. Fawcett, J. J. Usher, J. A. Huddleston, R. C. Bleaney, J. J. Nisbet, and E. P. Abraham. Biochem. J. **157**, 651 (1976).
11. S. Oae and T. Numata. *In* Isotopes in organic chemistry. Vol. 5. *Edited by* E. Buncel and C. C. Lee. Elsevier, Amsterdam. 1980. In press; S. Wolfe and P. M. Kazmaier. Can. J. Chem. **57**, 2388 (1979); **57**, 2397 (1979); S. Wolfe, P. M. Kazmaier, and H. Auksi. Can. J. Chem. **57**, 2404 (1979); **57**, 2412 (1979).
12. P. M. Kazmaier. PhD Thesis. Queen's University, Kingston, Ont. 1978.
13. S. Braverman and B. Sredni. Tetrahedron, **30**, 2379 (1974).
14. E. G. Miller, D. R. Rayner, H. T. Thomas, and K. Mislow. J. Am. Chem. Soc. **90**, 4861 (1968).
15. (*a*) R. B. Morin, E. M. Gordon, and J. R. Lake. Tetrahedron Lett. 5213 (1973); (*b*) J. E. Baldwin, S. B. Haber, and J. Kitchin. J. Chem. Soc. Chem. Commun. 790 (1973); (*c*) D. H. R. Barton, P. G. Sammes, M. V. Taylor, C. M. Cooper, G. Hewitt, B. E. Looker, and W. G. E. Underwood. Chem. Commun. 1137 (1971); (*d*) T. Kamiya, T. Teraji, Y. Sato, M. Hashimoto, O. Nakaguchi, and T. Oku. Tetrahedron Lett. 3001 (1973).
16. K. R. Hanson and I. A. Rose. Acc. Chem. Res. **8**, 1 (1975).
17. S. Wolfe and M. G. Jokinen. Can. J. Chem. **57**, 1388 (1979).
18. D. N. Harpp, J. Adams, J. G. Gleason, D. Mullins, and K. Steliou. Tetrahedron Lett. 3989 (1978).
19. R. G. Hiskey and J. B. Adams, Jr. J. Org. Chem. **30**, 1340 (1965).
20. R. G. Hiskey and W. P. Tucker. J. Am. Chem. Soc. **84**, 4794 (1962).
21. B. Belleau and G. Malek. J. Am. Chem. Soc. **90**, 1651 (1968).
22. K. Tanaka, J. Hayami, and A. Kaji. Bull. Chem. Soc. Jpn. **45**, 536 (1972).
23. N. J. Leonard and R. Y. Ning. J. Org. Chem. **31**, 3928 (1966).
24. D. Gravel, R. Gauthier, and C. Berse. Chem. Commun. 1322 (1972).
25. V. Balogh, M. Fétizon, and M. Golfier. J. Org. Chem. **36**, 1339 (1971).
26. A. A. Aboderin, G. R. Delpierre, and J. S. Fruton. J. Am. Chem. Soc. **87**, 5469 (1965).
27. J. Goodacre, R. J. Ponsford, and I. Stirling. Tetrahedron Lett. 3609 (1975).
28. E. Jonsson. Acta Chem. Scand. **21**, 1277 (1967).
29. V. F. Bystrov. Prog. Nucl. Magn. Reson. Spectrosc. **10**, 41 (1976); K. D. Kopple, G. R. Wiley, and R. Tauke. Biopolymers, **12**, 627 (1973); J. Feeney. J. Magn. Reson. **21**, 473 (1976).
30. O. Ermer and S. Lifson. J. Am. Chem. Soc. **95**, 4121 (1973); E. A. Noe and J. D. Roberts. J. Am. Chem. Soc. **93**, 7261 (1971); G. Favini and A. Nava. Theor. Chim. Acta, **31**, 261 (1973); H. Ogura, H. Takayanagi, and K. Furuhata. J. Chem. Soc. Perkin Trans. I, 665 (1976); D. N. J. White and M. J. Bovill. J. Chem. Soc. Perkin Trans. II, 1610 (1977); N. L. Allinger and J. T. Sprague. J. Am. Chem. Soc. **94**, 5734 (1972).

31. S. CAPASSO, C. MATTIA, L. MAZZARELLA, and R. PULITI. Acta Crystallogr. Sect. B, **33**, 2080 (1977).
32. S. CAPASSO, L. MAZZARELLA, and T. TANCREDI. Biopolymers, **18**, 1555 (1979).
33. R. D. G. COOPER, P. V. DE MARCO, J. C. CHENG, and N. D. JONES. J. Am. Chem. Soc. **91**, 1408 (1969).
34. R. D. G. COOPER, P. V. DE MARCO, and D. O. SPRY. J. Am. Chem. Soc. **91**, 1528 (1969); D. H. R. BARTON, F. COMER, and P. G. SAMMES. J. Am. Chem. Soc. **91**, 1529 (1969).
35. R. LETT and A. MARQUET. Tetrahedron, **30**, 3379 (1974).
36. (*a*) L. ZERVAS and I. PHOTAKI. J. Am. Chem. Soc. **84**, 3887 (1962); (*b*) H. AROLD and M. HARTMANN. J. Prakt. Chem. **21**, 59 (1963).
37. H. M. CROOKS. *In* The chemistry of penicillin. *Edited by* H. T. Clarke, J. R. Johnson, and R. Robinson. Princeton University Press, Princeton, NJ. 1949. p. 471.
38. B. J. SWEETMAN, M. M. VESTLING, S. T. TICARIC, P. L. KELLY, L. FIELD, P. MERRYMAN, and I. A. JAFFE. J. Med. Chem. **14**, 868 (1971).
39. B. KAMBER. Helv. Chim. Acta, **54**, 927 (1971).
40. F. WEYGAND and R. GEIGER. Chem. Ber. **90**, 634 (1957).
41. M. BERGMAN and L. ZERVAS. Chem. Ber. **65**, 1192 (1932).
42. M. J. MINTZ and C. WALLING. Org. Synth. Coll. Vol. V, 184 (1973).

Can. J. Chem. Downloaded from www.nrcresearchpress.com by 210.87.254.42 on 09/05/12
For personal use only.

Biosynthesis of elsinochromes C and D. Pattern of acetate incorporation determined by ^{13}C and ^{2}H nmr[1]

ITSUO KUROBANE[2] AND LEO C. VINING
Biology Department, Dalhousie University, Halifax, N.S., Canada B3H 4J1
AND
A. GAVIN MCINNES, DONALD G. SMITH, AND JOHN A. WALTER
Atlantic Research Laboratory, National Research Council of Canada, 1411 Oxford St., Halifax, N.S., Canada B3H 3Z1
Received July 8, 1980
This paper is dedicated to Prof. Raymond U. Lemieux on the occasion of his 60th birthday

ITSUO KUROBANE, LEO C. VINING, A. GAVIN MCINNES, DONALD G. SMITH, and JOHN A. WALTER. Can. J. Chem. **59**, 422 (1981).

Elsinochromes C and D have been isotopically labelled by supplementing cultures of the producing fungus with sodium [1-^{13}C]-, [2-^{13}C]-, [1,2-^{13}C]-, or [2-^{13}C, 2-$^{2}H_3$]acetate and the distribution of isotope has been determined by ^{13}C and ^{2}H nuclear magnetic resonance spectroscopy. The pattern of ^{13}C labelling is consistent with assembly of the elsinochrome carbon skeleton from two heptaketide chains with loss of the terminal carboxyl groups, and dimerization to generate the 1,2-dihydrobenzo (*ghi*)-perylene ring system. Elsinochrome D was converted to the more soluble triacetate to examine the fate of ^{2}H presented to the culture as [2-^{13}C, 2-$^{2}H_3$]acetate. Deuterium labelling was restricted to the C-14 and C-16 methyl groups, a result consistent with these belonging to the "starter" C_2 units of polyketide intermediates. Carbon-13 enrichment data for elsinochromes labelled from [1,2-^{13}C]acetate indicated that the polyketide chains were formed from a highly enriched precursor pool with subsequent dilution accounting for a much lower average incorporation. Presence of spin–spin coupling between linked carbons derived from separate polyketide precursors implies that dilution occurs after the dimerization step. From the combined evidence a plausible pathway for elsinochrome biosynthesis is deduced.

ITSUO KUROBANE, LEO C. VINING, A. GAVIN MCINNES, DONALD G. SMITH et JOHN A. WALTER. Can. J. Chem. **59**, 422 (1981).

On a marqué isotopiquement les elsinochromes C et D en additionnant, aux milieux de cultures du champignon producteur, de l'acétate de sodium[^{13}C-1], [^{13}C-2], [^{13}C-1,2] ou [^{13}C-2, $^{2}H_3$-2]; on a déterminé la distribution des isotopes par la rmn du ^{13}C et du ^{2}H. Le modèle de marquage en ^{13}C est en accord avec l'élaboration du squelette carboné de l'elsinochrome à partir de deux chaînes d'heptacétide avec la perte des groupes carbonyles terminaux et une dimérisation qui produisent le système cyclique dihydro-1,2 benzo(*ghi*)-pérylène. On a transformé l'elsinochrome D en son triacétate plus soluble pour étudier le sort du ^{2}H introduit dans le milieu de la culture sous forme d'acétate [^{13}C-2, $^{2}H_3$-2]. Le marquage au deutérium est limité aux carbones C-14 et C-16 des groupes méthyles; ce résultat est en accord avec le fait que ces groupes appartiennent aux unités C_2 de départ des polycétides intermédiaires. Les données d'enrichissement au ^{13}C des elsinochromes marqués à partir de l'acétate [^{13}C-1,2] indiquent que les chaînes polycétides se forment à partir d'un ensemble de précurseurs fortement enrichis et dont la dilution subséquente est responsable du faible taux d'incorporation. La présence d'un couplage spin–spin entre les carbones liés provenant de précurseurs isolés de polycétide implique que la dilution se produit après l'étape de dimérisation. On a déduit, à partir de l'ensemble des données un cheminement possible pour la biosynthèse de l'elsinochrome.

[Traduit par le journal]

Introduction

Fungi of the phytopathogenic genus *Elsinoë* and its imperfect stage *Sphaceloma*, produce the bright-red photosensitizing elsinochromes A (**1**), B (**2**), C (**3**), and D (**4**). Their structures, except for the absolute configuration of the chiral centers which remains undetermined, were deduced from chemical spectroscopic evidence (1–6). These pigments have, so far, been described only from *Elsinoë* or *Sphaceloma* strains. An earlier report of their formation by *Phyllosticta caryae* was withdrawn when this organism proved to be a misidentified strain of *Elsinoë randii* (3). While working with strains of the onion pink-root-disease fungus, *Pyrenochaeta terrestris*, we observed that one culture was exceptional and produced a mixture of red pigments subsequently recognized as elsinochromes. The main components were identified as **3** and **4**. Although **4** has been reported as only a minor component of *Elsinoë* species, where either **1** or a mixture of **2** and **3** usually predominate, it is possible that our culture of *P. terrestris* represents another example of a misidentified species. Unfortunately, this fungus no longer produces sexual structures so its true identity cannot be established.

Biosynthetic enrichment of **1** with [^{14}C]formate has shown that the methoxyl groups originate from the one-carbon pool of *Elsinoë araliae* (7). Partial chemical degradation of material labelled with [1-^{14}C]acetate gave results which suggested (5, 7) that the remaining carbons were derived from acetate and which were consistent with the involvement of two polyketide chains as depicted in Fig. 1A. Similar

[1]Issued as NRCC No. 18735.
[2]Guest scientist at ARL 1975–1979.

0008-4042/81/020422-09$01.00/0
©1981 National Research Council of Canada/Conseil national de recherches du Canada

Can. J. Chem. Downloaded from www.nrcresearchpress.com by 210.87.254.42 on 09/05/12
For personal use only.

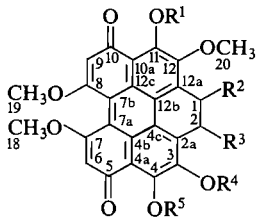

1 $R^1 = R^5 = H$, $R^2 = \underset{13}{COCH_3}$, $R^3 = \underset{15}{COCH_3}$, $R^4 = \underset{17}{CH_3}$

2 $R^1 = R^5 = H$, $R^2 = \underset{13}{COCH_3}$, $R^3 = \underset{15}{CH(OH)}\underset{16}{CH_3}$, $R^4 = \underset{17}{CH_3}$

3 $R^1 = R^5 = H$, $R^2 = \underset{13}{CH(OH)}\underset{14}{CH_3}$, $R^3 = \underset{15}{CH(OH)}\underset{16}{CH_3}$, $R^4 = \underset{17}{CH_3}$

4 $R^1 = H$, $R^2 = \underset{13}{CH(OH)}\underset{14}{CH_3}$, $R^3 = \underset{15}{CH(OH)}\underset{16}{CH_3}$, $R^4 + R^5 = \underset{17}{CH_2}$

6 $R^1 = COCH_3$, $R^2 = \underset{13}{CH(OCOCH_3)}\underset{14}{CH_3}$, $R^3 = \underset{15}{CH(OCOCH_3)}\underset{16}{CH_3}$, $R^4 + R^5 = \underset{17}{CH_2}$

conclusions (5, 7, 9) have been drawn from a ^{13}C nmr investigation of ^{13}C-enriched samples of cercosporin (**5**), a closely related perylenequinone produced by the fungus, *Cercospora kikuchii*, which causes purple-speck disease of soybeans (8). The aromatic and side-chain carbon atoms of cercosporin were alternately labelled by [1-^{13}C]- and [2-^{13}C]acetate while the methoxy and methylenedioxy carbon atoms were derived from [^{13}C]formate (9).

However, none of this evidence strictly excludes the possibility that **1** and **5** are constructed from a single polyketide chain. An intermediate of the kind shown in Fig. 1B, where n may be any number including zero, might be processed by excising $n + 1$ internal carbon atoms and the carboxyl terminal group to give a product with the same distribution of isotopically labelled acetate carbon atoms as would be obtained from two chains originating as in Fig. 1A. To distinguish between these two possibilities it is necessary to determine the arrangement of intact two-carbon units derived from[1-$^{13}C_{0;1;1}$, 2-$^{13}C_{1;0;1}$]acetate (abbreviated in this paper to [1,2-^{13}C]acetate). However, an initial single-chain polyketide intermediate processed as shown in Fig. 1C would, by appropriate fusion of the fragments, give a product indistinguishable in labelling pattern from that of Fig. 1A. Thus the number of *de novo* polyketide chains used in the construction of these molecules can be firmly established only by identifying the chain-initiating units. This is difficult for symmetrical molecules like **1** and **5** and was not attempted in the preceding investigations.

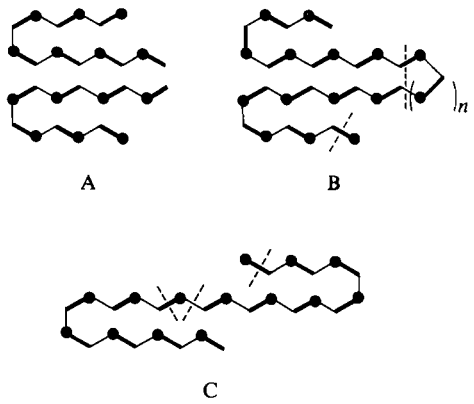

FIG. 1. Possible polyketide intermediates en route to elsinochromes and cercosporin.

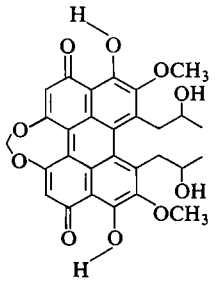

5

In this communication we provide the necessary evidence that the biosynthesis of elsinochromes involves two polyketide chains. Evidence of their polyketide origin was obtained by labelling **3** and the unsymmetrical **4** from [1-^{13}C]-, [2-^{13}C]-, and [1,2-^{13}C]acetate and determining the enrichment patterns by ^{13}C nmr spectrometry. The pressure of two chain-initiating units was established by enriching **4** with [2-$^{13}C_{0;1}$, 2-$^{2}H_{3;3}$]acetate (abbreviated to [2-^{13}C, 2-$^{2}H_3$]acetate throughout) and using ^{13}C and ^{2}H nmr to pinpoint the carbons bonded to ^{2}H in the metabolite.

Can. J. Chem. Downloaded from www.nrcresearchpress.com by 210.87.254.42 on 09/05/12
For personal use only.

Can. J. Chem. Downloaded from www.nrcresearchpress.com by 210.87.254.42 on 09/05/12
For personal use only.

Materials and Methods

Culture

Pyrenochaeta terrestris was obtained from the Centraalbureau voor Schimmelcultures, Baarn, where it is catalogued as CBS 322.62. It was maintained on Sabouraud-dextrose agar. Three substrains were isolated from the stock culture and CBS 322.62B, which produced the highest yields of elsinochromes C and D, was used in the study. To obtain a uniform vegetative inoculum, spores and mycelium from a slant were incubated for 4 days in a D-glucose (1%) – neopeptone (0.5%) – corn steep liquor (0.5%) medium. These and all subsequent liquid cultures were grown in 250 mL Erlenmeyer flasks containing 50 mL of medium and incubated at 25°C on a rotary shaker (220 rpm, 3.8 cm eccentricity). The vegetative inoculum was homogenized in a Waring blender and added in 2.5 mL portions to 50 mL of soluble starch (5%) – neopeptone (1%) production medium.

To establish the most efficient feeding regimen sterile solutions of [1-^{14}C]acetate (20 μCi/L) were added to cultures on the first, second, or third day of fermentation and incubation was continued until the tenth day before harvesting. The precursor concentration in the culture was 2 or 5 m*M*. Solutions of sodium [1-^{13}C]-, [2-^{13}C]-, [1,2-^{13}C]-, and [2-^{13}C, 2-^{2}H$_3$]-acetate were fed on the third day at final concentrations 5 m*M*. In all experiments the pigments were isolated on the tenth day from 1 L of culture broth.

Labelled Precursors

Sodium [1-^{14}C]acetate was obtained from New England Nuclear Corporation, Boston, MA. Sodium [1-^{13}C]-, [2-^{13}C]-, and [1,2-^{13}C]acetates (all 90% ^{13}C) were supplied by Merck, Sharp and Dohme Canada, Ltd., Pointe Claire, P.Q. Sodium [2-^{13}C, 2-^{2}H$_3$]acetate (90% ^{13}C; >95% ^{2}H) was prepared by dissolving sodium [2-^{13}C]acetate (90% ^{13}C; 37.1 mmol) in sodium deuteroxide solution (7.42 mmol sodium in 22.5 mL $^{2}H_2O$ (99.7% ^{2}H)) and heating in a sealed stainless steel tube for 20 h at 137°C to exchange protons for deuterons (10). This exchange process was repeated four times. After each treatment the solution was taken to dryness and the residue of partially deuterated sodium acetate was redissolved in a fresh aliquot of the sodium deuteroxide solution. The final sample of deuterated sodium acetate was dissolved in 10 mL $^{2}H_2O$ and acidified with H_2SO_4 to pH 2–3. This acidic solution was transferred to a microdistillation apparatus and the fraction distilling at 100°C was collected. A further 5 mL $^{2}H_2O$ was added to the remaining solution and the distillation repeated. Neutralization of the combined distillates with sodium hydroxide (pH 9.0–9.5) and removal of the solvent gave the required product in good yield (32.9 mmol) and with a high deuterium content (>95%) as determined by ^{1}H and ^{13}C nmr analyses.

Isotope Measurement

Radioactivity was determined with a Nuclear Chicago ISOCAP/300 liquid scintillation counter. Carbon-13 (25.16 MHz) and ^{2}H (15.36 MHz) spectra were obtained with a Varian XL-100/15 Fourier transform nmr spectrometer at 29°C, using 0.4 mL of solution in a 5 mm tube. Broadband (^{1}H)-decoupling at 100 MHz was achieved by phase modulation of the decoupling field ($\gamma H_2/2\pi$ ca. 3500 Hz) from 0 to 180° at 150 Hz; for ^{2}H-decoupling at 15.36 MHz, $\gamma H_2/2\pi$ was ca. 310 Hz, with phase modulation at 40 Hz.

Other experimental conditions for observing ^{13}C were as follows: (*a*) **3** at natural abundance (NA) or enriched with [1-^{13}C]- or [2-^{13}C]acetate: sweep width (SW) 5120 Hz, acquisition time (AT) 1.6 s (16384 data points), flip angle (FA) 30°, time constant (TC) for weighting free induction decay −0.4 s, sample concentration 130 mg/mL in C^2HCl_3, internal ^{2}H lock, {^{1}H} decoupled; high resolution (HR) spectrum of NA material, TC −0.8 s, decoupler off during AT, on for a pulse delay (PD) of 1.6 s; (*b*) **3** enriched with [1,2-^{13}C]acetate: conditions as for (*a*) but FA 55°, PD 1.6 s; (*c*) **4** at NA or from [1-^{13}C]- or [2-^{13}C]acetate: as for (*a*) but AT 0.8 s (8192 data points), TC −0.8 s, 142 mg/mL; (*d*) **4** from [1,2-^{13}C]acetate: as for (*a*) but FA 41°, TC −0.8 s, 140 mg/mL; (*e*) elsinochrome D triacetate (**6**) at NA: as for (*a*) but FA 54°, 226 mg/mL; (*f*) **6** from [2-^{13}C, 2-^{2}H$_3$]acetate: SW 5120 Hz, AT 3.2 s (32768 data points), FA 25°, TC −1.6 s, 141 mg/mL in C^1HCl_3/C_6F_6 (4:1), internal ^{19}F lock, {^{1}H} and {^{1}H, ^{2}H} decoupled.

Conditions for observing the ^{2}H spectrum of **6** biosynthesized from [2-^{13}C, 2-^{2}H$_3$]acetate (solution from (*f*) above) were: SW 500 Hz, AT 2.0 s (2000 data points), FA 90°, TC −0.8 s, internal ^{19}F lock, {^{1}H} decoupled.

Isolation of Elsinochromes

Mycelium, separated by vacuum filtration, was leached with acetone until the reddish-orange pigments were completely extracted. The aqueous concentrate from removing the acetone *in vacuo* was diluted with water and extracted several times with ethyl acetate. The solid residue left after removing the solvent *in vacuo* was redissolved in a small volume of ethyl acetate and chromatographed on a silicic acid column. Elution with a 3:1 ethyl acetate – acetone mixture gave **3**, whereas **4** was eluted by acetone–methanol (9:1). Both pigments crystallized from 2:1 chloroform–hexane. Their physical properties were identical to those reported previously (5, 6) and were confirmed by direct comparison with specimens kindly provided by Dr. R. J. J. Ch. Lousberg, Organisch Chemisch Laboratorium, Rijksuniversiteit te Utrecht.

Elsinochrome D (**4**) (0.093 mmol), dissolved in a mixture of pyridine (1.0 mL) and acetic anhydride (1.2 mL), was kept for 8 h at room temperature. The acetyl derivative (**6**) was isolated in the usual manner. It was purified by thin-layer chromatography (tlc) on silica gel 60 T-254 (E. Merck, Darmstadt). The chromatogram was developed three times with an 8:1:1 mixture of chloroform–benzene–methanol and the orange zone containing **6** was extracted with chloroform. The chloroform solution, washed with a 1 m*M* aqueous solution of ethylenediamine tetraacetic acid to remove paramagnetic impurities, was taken to dryness and the residue crystallized from 2:1 chloroform–hexane to give **6** (0.086 mmol) as orange needles, mp 114–115°C; $[\alpha]_D^{24}$ −733° (*c* 0.023, acetone); λ_{max} (log ε) (95% ethanol): 223 (4.63), 247 (4.43), 266 (4.34), 291 (shoulder) (4.07), 347 (broad) (3.96), 359 (3.97), 442 (4.29); ms *m/e*: 672 (M^+), 630 (*M* − 42).

Results

Production of Elsinochromes and Incorporation of [1-^{14}C]Acetate

Yields of **3** and **4** as a function of incubation time showed the most rapid accumulation to be in the interval from 3 to 8 days after inoculation. This information, combined with the measurement of radioactivity incorporated from [1-^{14}C]acetate given in Table 1, established that cultures should be supplemented on the third day with potential precursors at 5 m*M* concentration.

Incorporation of Sodium [1-^{13}C]-, [2-^{13}C], and [2-^{13}C, 2-^{2}H$_3$]Acetate

Procedures used to calculate ^{13}C-enrichment have been discussed in detail elsewhere (11). The distribu-

Can. J. Chem. Downloaded from www.nrcresearchpress.com by 210.87.254.42 on 09/05/12
For personal use only.

TABLE 1. Incorporation of radioactivity from sodium [1-^{14}C]-acetate into elsinochromes C (**3**) and D (**4**)

Sodium [1-^{14}C]acetate added[a]		Specific incorporation (%)[b]	
(day)	(m*M*)	**3**	**4**
1	5	8.5	8.6
2	5	10.7	10.4
3	5	16.5	24.9
	2	5.0	10.7

[a]Cultures (1 L) were supplemented at the time of inoculation with [1-^{14}C]acetate (20 μCi) plus unlabelled carrier to a final concentration of 2 or 5 m*M*.
[b]Specific incorporation estimated as 100 times specific activity of pigment divided by specific activity of precursor.

tion of isotopic label derived from [1-^{13}C]- and [2-^{13}C]acetates was determined by comparing ^{13}C nmr spectra of the enriched and natural abundance metabolites recorded under identical conditions.

Positions enriched by sodium [1-^{13}C]acetate were, in **3**: C-13, C-15, 0.6%; C-2a, C-12a, 0.5%; C-4b, C-12c, 0.6%; C-7, C-8, 0.4%; C-5, C-10, 0.3%; C-4, C-11, 0.3%; error ± 0.15%; in **4**: C-13, 2.5%; C-15, 2.3%; C-2a, 1.8%; C-12a, 1.8%; C-4b, 1.9%; C.12c, 2.2%; C-7, 1.5%; C-8, 1.8%; C-5, 1.6%; C-10, 1.7%; C-4, 2.2%; C-11, 1.8%; error ± 0.3%. Sites enriched by sodium [2-^{13}C]acetate were, in **3**: C-14, C-16, 1.1%; C-1, C-2, 1.0%; C-4c, C-12b, 1.2%; C-7a, C-7b, 1.7%; C-6, C-9, 0.9%; C-4a, C-10a, 1.5%, C-3, C-12, 1.3%; error ± 0.3%; in **4**: C-14, 4.7%; C-16, 4.7%; C-1, 4.3%; C-2, 4.3%; C-4c, 1.7%; C-12b, 2.2%; C-7a, 2.2%; C-7b, 2.4%; C-6, 4.9%; C-9, 4.3%; C-4a, 4.2%; C-10a, 3.4%; C-3, 3.2%; C-12, 3.0%; error ±1.1%.

The overall average enrichments at sites labelled by [1,2-^{13}C]acetate were determined by quantitative analysis of the multiplet patterns arising from ^{13}C—^{13}C spin–spin coupling in ^{13}C nmr spectra of the enriched metabolites. Sodium [1,2-^{13}C]acetate is nominally 90% ^{13}C-enriched and therefore contains the following mixture of isotopic species: $^{13}CH_3{}^{13}CO_2Na$, 81%; $^{13}CH_3{}^{12}CO_2Na$, 9%; $^{12}CH_3{}^{13}CO_2Na$, 9%; $^{12}CH_3{}^{12}CO_2Na$, 1%. Incorporation of this precursor into **3** and **4** was detected by one-bond ^{13}C—^{13}C spin–spin coupling which results in the presence of pairs of equally spaced doublet signals (total intensity I_d) as satellites of singlet resonances (intensity I_c) arising from isolated ^{13}C nuclei. Pairs of bonded carbons incorporated as ^{13}C—^{13}C were identified by matching coupling constants (Table 2). Both C-3 and C-12 were ^{13}C-enriched in **4** but neither was present as part of a ^{13}C—^{13}C unit.

Additional components of quartets (total intensity I_m), due to spin–spin coupling with two adjacent carbons, were observed about the resonances for C-1, C-2, C-4a, C-5, C-6, C-9, C-10, C-10a, C-11, and C-13 of **4**. Overlap of signals prevented quartets accompanying other carbon signals from being detected. The presence of the quartets demonstrated that a proportion of **4** had been biosynthesized from a precursor pool containing a high concentration of doubly labelled acetate. Thus $I_m/(I_m + I_d)$ for C_B of C_A—C_B—C_C gives the ^{13}C-probability at C_C (11) before the highly enriched **4** was diluted with natural abundance material, where C_A—C_B is an intact ^{13}C—^{13}C unit and C_B is any one of the carbons exhibiting quartet components. The main signal for C-3 was accompanied by low-intensity doublet ^{13}C—^{13}C satellites arising from approximately equal coupling to C-2a and C-4; similar satellites were symmetrically located about the signal for C-12 due to coupling with C-11 and C-12a. Probabilities of ^{13}C at carbons adjacent to C-3 and C-12 were determined from $I_d/2(I_c - I_{NA} + I_d)$ where I_{NA} is the ^{13}C natural abundance contribution to I_c, and the 2 in the denominator takes into account the superposition of satellites arising from equal coupling of C-3 and C-12 to adjacent carbons. Similar measurements on **3** enriched by doubly labelled acetate were not possible because the signal/noise ratio in the ^{13}C nmr spectrum was inadequate. The average enrichment at sites in ^{13}C-labelled **3** and **4** after in vivo dilution with natural abundance material may be calculated as reported previously (11) from $\%^{13}C = 1.11(I_d + I_m)/[I_c - f(I_d + I_m)]$, where $f = 1/9$. Enrichment data are reported in Table 2.

Incorporation of Sodium [2-^{13}C, 2-$^{2}H_3$]Acetate

The culture conditions used to obtain ^{13}C-enriched elsinochromes were also used to obtain **4** enriched with label from sodium [2-^{13}C, 2-$^{2}H_3$]acetate. At a ^{2}H content of 95% the methyl group of the precursor would possess the following mixture of isotopic species: $^{13}C^{2}H_3$, 77.16%; $^{13}C^{2}H_2H$, 12.18%; $^{13}C^{2}HH_2$, 0.64%; $^{12}C^{2}H_3$, 8.57%; $^{12}C^{2}H_2H$, 1.35%; $^{12}C^{2}HH_2$, 0.02%. As the enriched material contained carbons bonded to both hydrogen and deuterium, simultaneous ^{1}H- and ^{2}H-broadband decoupling was used to remove ^{13}C—^{1}H and ^{13}C—^{2}H spin–spin couplings and thus obtain singlet resonances in the ^{13}C nmr spectrum. The spectrometer was field-frequency locked to ^{19}F in hexafluorobenzene. Since the latter substance considerably reduces the solubility of **4** in chloroform, the more soluble triacetate derivative **6** was used. The ^{13}C chemical shifts for unlabelled **6** in chloroform were not significantly different from those obtained with 4:1 chloroform–hexafluorobenzene, the solvent mixture used for ^{13}C nmr spectral analysis of enriched **6**.

[2-^{13}C, 2-$^{2}H_3$]Acetate labelled the same sites in **6** as were previously found to be enriched in **4** by

TABLE 2. Average enrichments (% ^{13}C) after dilution with natural abundance material,[a] ^{13}C concentration in precursor at time of incorporation (in parentheses),[b] and $^{13}C—^{13}C$ spin–spin couplings ($^1J_{cc}$)[c] for **3** and **4** labelled from [1,2-^{13}C]acetate (90% ^{13}C)

	$^1J_{cc}$		% ^{13}C			$^1J_{cc}$		% ^{13}C	
Carbon pairs	**3**	**4**	**3**	**4**	Carbon pairs	**3**	**4**	**3**	**4**
C-13, C-14		39.3		2.7	C-7b, C-8		64.1		2.8
	38.8		1.1	(C-13, 44%)		66.4		0.6	(C-8, 33%)
C-15, C-16		39.4		2.7	C-7, C-7a		64.3		2.6
				(C-15, 44%)					(C-7, 40%)
C-1, C-12a		41.9		3.0	C-9, C-10		60.4		2.6
	41.2		0.8	(C-1, 46%)		64.1		0.9	
C-2, C-2a		40.7		2.9	C-5, C-6		60.0		2.6
				(C-2, 46%)					
C-12b, C-12c		61.9		2.2	C-10a, C-11		63.9		2.9
	61.7		0.6			61.8		0.8	(C-10a, 45%)
C-4c, C-4b		63.5		3.1	C-4, C-4a		74.0		2.8
									(C-4a, 42%)

[a]Average enrichments calculated from $1.11(I_d + I_m)/[I_c - f(I_d + I_m)]$ (see text). Average value ± standard deviation was 2.7 ± 0.2 for **4** and 0.80 ± 0.2 for **3**. In **4**, C-3 (2.3% ^{13}C) and C-12 (2.5% ^{13}C) were enriched but were not parts of $^{13}C—^{13}C$ units; labelling at the corresponding sites in **3** was not estimated because the signal/noise ratio in the ^{13}C spectrum was low.
[b]Values determined from $I_m/(I_d + I_m)$ (see text). Average value ± standard deviation for **4** was 42 ± 4% ^{13}C. Values were not determined for **3** because the signal/noise ratio in the ^{13}C spectrum was low.
[c]Data accuracy ± 0.3 Hz but error in $^1J_{cc}$ reduced by interpolation to peak centres between data points.

sodium [2-^{13}C]acetate. ^{13}C-enrichments were once again determined by comparing the ^{13}C nmr spectra of the enriched and natural abundance samples (11). Signal enhancements were observed for C-14 (3.0%), C-16 (3.0%), C-1 (2.0%), C-2 (2.0%), C-12b (1.9%), C-7b (2.0%), C-7a (2.0%), C-9 (1.9%), C-6 (1.8%), C-10a (1.8%), C-4a (2.0%), C-12 (2.1%), and C-3 (2.0%) (error ca. ±0.2%). Also, both side-chain methyl groups in **6** gave rise to a set of four singlet resonances (Fig. 1), one due to CH_3 and the others originating from methyl carbons bonded to deuterium and chemically shifted by an amount proportional to the number of deuteriums (12) (−0.27 ($^{13}C^2HH_2$), −0.52 ($^{13}C^2H_2H$), and −0.73 ppm ($^{13}C^2H_3$)). The latter resonances appear as a broad hump on the baseline of the ^{13}C nmr spectrum when the ^2H-decoupling field is removed because they are split into multiplets by $^{13}C—^2H$ spin–spin coupling. Intensity measurements on a spectrum in which nuclear Overhauser effects were suppressed with the relaxation reagent $Cr(acac)_3$ (13) and gated decoupling (14, 15) indicated that the methyl signals had the following fractional composition: $^{13}CH_3$, 0.33; $^{13}C^2HH_2$, 0.16; $^{13}C^2H_2H$, 0.21; $^{13}C^2H_3$, 0.31 (all ±0.02). Thus the methyl groups of **6** retained 53% [100 × (0.31 + 2/3 × 0.21 + 1/3 × 0.16) ÷ (0.86 + 2/3 × 0.14 + 1/3 × 0.01)] of the deuterium at C-2 of the precursor. Four-fifths of the intensity of the $^{13}CH_3$ signal has a natural abundance origin, enrichment accounting for the remainder. The C-1, C-2, C-6, and C-9 methine groups contained no deuterium although also derived from the methyl group of acetate.

The ^1H-broadband-decoupled ^2H nmr spectrum confirmed that only the methyl groups contained deuterium. Deuteriums bonded to ^{13}C appeared as a broad doublet ($^1J_{C^2H} \approx 20$ Hz) due to $^{13}C—^2H$ coupling whereas those bonded to ^{12}C gave a broad singlet. The line widths are determined mainly by the viscosity of $CHCl_3$ which influences the correlation times for molecular motion (16) although chemical shift nonequivalence of resonances due to the different isotopic species probably contributes.

Discussion

Assignment of Carbon Resonances

Resonances were identified from concordant evidence provided by chemical-shift trends, by characteristic multiplicities and $^{13}C—H$ spin–spin couplings in the high-resolution ^{13}C nmr spectrum and by $^{13}C—^{13}C$ spin–spin coupling introduced when **3** and **4** were labelled with [1,2-^{13}C]acetate.

For symmetry reasons each of the fifteen resonances observed for **3** arises from an equivalent pair of carbons. The assignment of signals due to carbons bearing hydrogen was straightforward as their nmr parameters (Tables 3 and 4) were different and distinctive. Four resonances at lowest field clearly originated from two equivalent pairs of carbons bearing oxygen. Geminal coupling of C-5 (C-10) to H-6 (H-9) distinguished these carbons from C-4, C-11 which give singlet resonances. Carbons bearing methoxyls were observed as multiplets due to three-bond coupling with the methoxy hydrogens and two-bond coupling to H-6, H-9 (C-7, C-8) or three-bond coupling to H-1, H-2 (C-12, C-3). Shielding by

Can. J. Chem. Downloaded from www.nrcresearchpress.com by 210.87.254.42 on 09/05/12
For personal use only.

TABLE 3. ^{13}C nuclear magnetic resonance chemical shift data (δ_c TMS) for elsinochrome C (**3**), D (**4**), and D-triacetate (**6**) in C^2HCl_3[a]

	δ_c											
Compound	C-1	C-2	C-2a	C-3	C-4	C-4a	C-4b	C-4c	C-5	C-6	C-7	C-7a
3	42.20	42.20	134.77	150.57	171.88	107.37	122.64	122.87	179.59	102.27	167.40	118.40
4	41.95	41.20	118.11	148.59	150.54	108.22	121.69	124.03	183.48	105.54	168.34	124.94
6	38.63	38.31	116.61	148.68	150.04	109.35	122.55	124.10	183.47	106.20	167.50	124.26

	δ_c											
Compound	C-7b	C-8	C-9	C-10	C-10a	C-11	C-12	C-12a	C-12b	C-12c	C-13	C-14
3	118.40	167.40	102.27	179.59	107.37	171.88	150.57	134.77	122.87	122.64	70.30	21.91
4	120.10	167.97	103.54	186.74	108.42	163.80	148.84	134.98	120.20	122.07	70.20	21.91
6	118.92	166.98	105.95	170.05	125.61	148.68	151.59	131.26	122.27	123.14	71.62	18.18

	δ_c									
Compound	C-15	C-16	C-17	C-18	C-19	C-20	11-O_2CCH_3	11-O_2CCH_3	13,15-O_2CCH_3	13,15-O_2CCH_3
3	70.30	21.91	61.16	56.42	56.42	61.16				
4	69.57	21.73	104.03	56.33	56.08	61.20				
6	71.62	18.01	103.99	56.29	56.17	61.63	168.84	21.39	170.02	20.94

[a]The assignments for C-13 and C-15 in **4**, and for the pairs C-14, C-16; C-18, C-19; and C-3, C-12 in **4** and **6**, may be interchanged.

adjacent hydroxyl groups (17) also distinguished the C-3, C-12 from the C-7, C-8 resonance. Furthermore, matching coupled carbons (Table 2) in the ^{13}C nmr spectrum of **3** enriched with [1,2-^{13}C]acetate identified the following pairs: C-13, C-14, (C-15, C-16); C-1, C-12a (C-2, C-2a); C-7b, C-8 (C-7a, C-7); C-9, C-10 (C-6, C-5); C-10a, C-11 (C-4a, C-4). The resonances for C-12b (C-4c) and C-12c (C-4b) which form a coupled AB system can be distinguished because C-12b (C-4c) is coupled to H-1 (H-2) whereas C-12c (C-4b) is not coupled and gives a singlet resonance. Methoxyl signals could be assigned by comparing the spectra of **3** and **4**.

Separate resonances are observed for thirty carbons in the unsymmetrical **4** (Table 3). In the spectrum of **6** three pairs of signals overlap; these arise from C-13 and C-15 and the methyl and carbonyl carbons of the acetate groups at C-13 and C-15. Coupled pairs of carbons in **4** enriched with [1,2-^{13}C]-acetate were matched in the same way as for **3**, but some assignments were ambiguous because chemical shifts and $^1J_{cc}$ values for similar carbons (e.g. C-7a, C-7b; C-7, C-8) were not significantly different. As expected, conversion of **4** to **6** influenced the chemical shifts of C-7b through C-12c more than those of other aromatic ring carbons (Table 3). This chemical shift correlation, combined with the ^{13}C—^{13}C spin–spin coupling information, provides reasonable grounds for our assignments. The methylenedioxy carbon gave a characteristic triplet resonance in the high resolution spectrum and the three-bond coupling of C-4 to the methylenedioxy hydrogens distinguished it from its counterpart C-11.

Assembly Pattern of Acetate in 3 and 4

Data for **4** enriched from [1,2-^{13}C]acetate indicate that the polyketide chains were formed from a precursor pool highly enriched (≈30%; Table 2) with doubly ^{13}C-labelled acetate, and that an additional ten-fold dilution with natural-abundance material occurred at a later stage in the biosynthetic pathway to give a final average enrichment of 2–3% at individual sites. As the same feeding conditions were used for all precursors, isotopic dilution must follow the same pattern with singly labelled precursors. If dilution occurred after **4** was formed, ^{13}C—^{13}C spin–spin coupling should be observed between the three pairs of directly bonded carbons (C-1, C-2; C-12b, C-4c; C-7b, C-7a) joining the two halves of the molecule. This coupling should be more easily detected with the sample enriched from [2-^{13}C]acetate because the ^{13}C nmr spectrum would not be complicated by one-bond spin–spin interactions between other pairs of carbons. Since, for these carbon pairs, chemical shift differences are comparable with $^1J_{cc}$ (Table 3), any ^{13}C—^{13}C coupled carbon resonances present would form an AB quartet. The expected average ratio I_s/I_c of intensity I_s of each half of the quartet to the corresponding central resonance intensity I_c (after subtraction of the component due to natural-abundance material) would be ca. 0.4 ($=0.3 \times 0.3 \div 0.3 \times 0.7$) under conditions identical to those used

Can. J. Chem. Downloaded from www.nrcresearchpress.com by 210.87.254.42 on 09/05/12
For personal use only.

Can. J. Chem. Downloaded from www.nrcresearchpress.com by 210.87.254.42 on 09/05/12
For personal use only.

TABLE 4. ^{13}C—H coupling constants ($^nJ_{CH}$) for elsinochrome C (**3**), D (**4**), and D-triacetate (**6**) in C^2HCl_3

	$^nJ_{CH}$ (Hz)											
Compound	C-1	C-2	C-2a	C-3	C-4	C-4a	C-4b	C-4c	C-5	C-6	C-7	C-7a
3	d;^1J 135.7	d;^1J 135.7	t;^3J 5.3	m	s	bs	s	d;^3J 4.4	d;^2J 2.5	d;^1J 162.5	dq;^2J, $^3J\sim3$	d;^3J 6.1
4	dm;$^1J\sim133$	dm;$^1J\sim133$	dd;$^3J\sim4.8$, 6.5	m	bs	d;$^3J\sim3$	s	d;^3J 4.5	s	d;^1J 163.1	dq;^2J 2.6 ^3J 3.7	d;^3J 6.3
6	dm;$^1J\sim134$	dm;^1J 134	m	m	s	d;^3J 3.8	s	d;^3J 4.5	d;^2J 2.0	d;^1J 163.0	dq;^2J 3.2 ^3J 4.2	d;^3J 4.3

	$^nJ_{CH}$ (Hz)											
Compound	C-7b	C-8	C-9	C-10	C-10a	C-11	C-12	C-12a	C-12b	C-12c	C-13	C-14
3	d;^3J 6.1	dq;^2J, $^3J\sim3$	d;^1J 162.5	d;^2J 2.5	bs	s	m	t;^3J 5.3	d;^3J 4.4	s	dm;$^1J\sim145$	q;^1J 125.6
4	d;^3J 5.5	dq;^2J 2.7 ^3J 4.3	d;^1J 163.8	s	d;$^3J\sim3$	d;^2J 2.6	m	dd;^3J 5.2, 6.3	d;^3J 5.5	s	dm;$^1J\sim142$	q;$^1J\sim125$
6	d;^3J 3.6	dq;^2J 3.2 ^3J 4.2	d;^1J 163.0	d;$^2J\sim3$	d;^3J 6.8	bs	dq;^3J 4.4	m	d;^3J 4.7	s	dm;$^1J\sim148$	q;^1J 128

	$^nJ_{CH}$ (Hz)									
Compound	C-15	C-16	C-17	C-18	C-19	C-20	11-O_2CCH_3	11-O_2CCH_3	13,15-O_2CCH_3	13,15-O_2CCH_3
3	dm;$^1J\sim145$	q;^1J 125.6	q;^1J 145.6	q;^1J 145.8	q;^1J 145.8	q;^1J 145.6				
4	dm;$^1J\sim142$	q;$^1J\sim125$	t;^1J 178.4	q;^1J 146.8	q;^1J 146.3	q;^1J 145.1				
6	dm;$^1J\sim148$	q;$^1J\sim128$	t;^1J 176.9	q;^1J 145.6	q;^1J 146.2	q;^1J 145.6	q;^2J 7.4	q;^1J 130.2	dq;^2J 6.5, ^3J 4.0	q;^1J 129.7

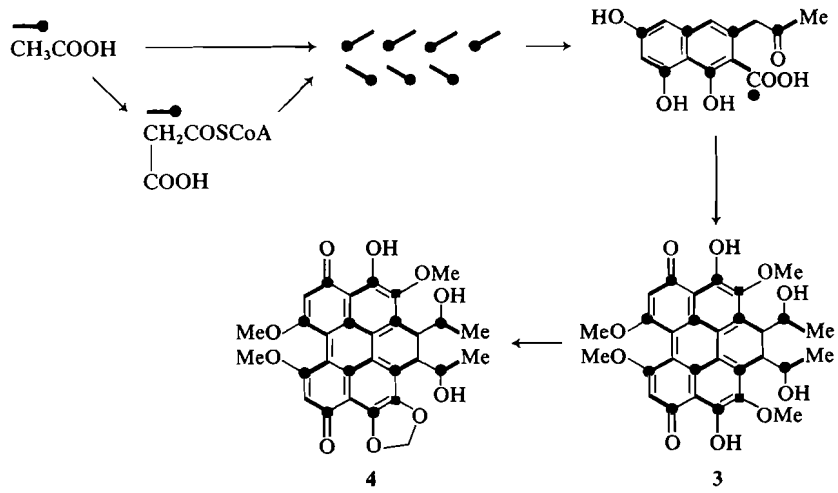

SCHEME 1. Plausible route for the biosynthesis of elsinochromes C and D.

for incorporation of the ^{13}C—^{13}C label. The inner components of such quartets are indeed visible for **4** labelled with [2-^{13}C]acetate, the outer components being masked by noise. Couplings of $^{1}J_{C\text{-}4c,C\text{-}12b} = 63 \pm 8$ Hz; $^{1}J_{C\text{-}7a,C\text{-}7b} = 61 \pm 9$ Hz were obtained from the spacings of the inner quartet components and $\Delta\nu$, but $^{1}J_{C\text{-}1,C\text{-}2}$ was not measurable. The average I_s/I_c was 0.6 ± 0.1, comparable with the expected value and confirming that no further dilution of label had occurred between the formation of the polyketide chains and the dimerization process. It is not possible to confirm this result for **3** labelled with [2-^{13}C]acetate since the pairs of nuclei which would be coupled are chemically equivalent.

Information on the fate of acetate hydrogens during elsinochrome biosynthesis was obtained from the ^{13}C and ^{2}H spectra of **6** enriched from [2-^{13}C, 2-$^{2}H_3$]acetate. Simultaneous ^{1}H- and ^{2}H-broadband decoupling ensured that carbons gave singlet resonances in the ^{13}C nmr spectrum. Carbons bearing deuterium were identified by the presence of one-bond deuterium isotope chemically-shifted ^{13}C signals which became multiplets if the ^{2}H-decoupling field was removed. Each methyl group of **6** gave a set of four signals arising from $^{13}CH_3$, $^{13}C^{2}HH_2$, $^{13}C^{2}H_2H$, and $^{13}C^{2}H_3$ and calculations show that approximately 47% of the original ^{2}H was exchanged for ^{1}H during biosynthesis. It is noteworthy that the C-1, C-2, C-6, and C-9 methine groups contained no deuterium although also derived from the methyl group of acetate. Acetyl coenzyme A – malonyl coenzyme A interconversion (23) can account for loss of deuterium at the acetyl groups but the complete removal of deuterium at other sites suggests facile exchange between the protons of water and the deuterium at activated methylene groups in malonyl coenzyme A (24, 25) or in the polyketide chain bound to the enzyme surface. The presence of deuterium at the methyl groups of **6** but not elsewhere was also confirmed by the ^{2}H spectrum, in which signals (intensity I_{13}) arising from deuteriums bonded to ^{13}C of the methyl groups were well separated by ^{13}C—^{2}H coupling from the corresponding signal (intensity I_{12}) of ^{2}H bonded to ^{12}C. The absence of additional signals clearly indicated that deuterium was not retained at other sites in the molecule. The ratio $I_{12}/(I_{12} + I_{13})$, determined from integrals and peak heights (with allowance for overlap of broadened peaks), is 0.19 + 0.01. Since the same ratio in the 90% ^{13}C-enriched precursor is 0.111, some of the ^{2}H lost from [^{13}C, ^{2}H] labelled acetate in forming malonate is not mixed with the medium but is sequestered by endogenous malonate to yield [^{12}C, ^{2}H] acetate. We observed similar behaviour in our study of fusarubin biosynthesis.[3]

Labelling patterns determined by ^{13}C nmr analysis of the metabolites following isotopic incorporation from [1,2-^{13}C]acetate suggest strongly that the carbocyclic rings and alkyl side chains were formed initially from 14 intact two-carbon units, two of which cleaved subsequently with the loss of a carbon to give C-3 and C-12. Singly enriched acetates labelled alternate carbons as expected (7) and showed that C-3 and C-12 originated from the methyl group of acetate. The distribution of two carbon units in **3** and **4** is incompatible with their biosynthesis via a single polyketide chain processed as in Fig. 1B and indicates that two chains, formed either *de novo* or by processing as in Fig. 1C, were involved. A decision between these alternatives can be based on the number of chain-initiating units detectable at C-13, C-14

[3]I. Kurobane, L. C. Vining, A. G. McInnes, and J. A. Walter. Unpublished results.

Can. J. Chem. Downloaded from www.nrcresearchpress.com by 210.87.254.42 on 09/05/12
For personal use only.

and C-15, C-16 in **4**. That these two-carbon groups represent two "starter" acetate units is established by the significant proportion of trideuteromethyl groups from [2-^{13}C, 2-$^{2}H_3$]acetate incorporated intact at C-14 and C-16. Thus the biosynthesis of **3** and **4** involves two heptaketide chains formed via the acetate–polymalonate pathway (18). A plausible pathway is suggested in Scheme 1. The chains first cyclize to a substituted naphthalene, two molecules of which oxidatively couple (19), before or after decarboxylation, to give **3**. A subsequent reaction between the C-3 methoxy and C-4 hydroxy groups (20, 21) would convert **3** to **4**. As noted earlier (5), apart from the dimerization process, the biosyntheses of elsinochromes and fusarubin,[3] or more correctly 4a,10a-dihydrofusarubin (22), appear to have many features in common.

Acknowledgements

We thank Dr. R. J. J. Ch. Lousberg of the University of Utrecht, and Dr. U. Weiss of the National Institute of Health, Bethesda, MD for specimens of elsinochromes. Mrs. S. Kurobane and C. Mofford provided valuable technical help. The work was supported by a research grant (to L.C.V.) from the National Research Council of Canada.

1. U. Weiss, H. Flon, and W. C. Burger. Arch. Biochem. Biophys. **69**, 311 (1957).
2. T. J. Batterham and U. Weiss. Proc. Chem. Soc. 89 (1963).
3. W. H. L. Hackeng, H. Copier, and C. A. Salemink. Recl. Trav. Chim. Pays-Bas, **82**, 322 (1963).
4. U. Weiss, H. Ziffer, T. J. Batterham, M. Bluner, W. H. L. Hackeng, H. Copier, and C. A. Salemink. Can. J. Microbiol. **11**, 57 (1965).
5. R. J. J. Ch. Lousberg, C. A. Salemink, U. Weiss, and T. J. Batterham. J. Chem. Soc. C, 1219 (1969).
6. R. J. J. Ch. Lousberg, C. A. Salemink, and U. Weiss. J. Chem. Soc. C, 2159 (1970).
7. C.-T. Chen, K. Nakanishi, and S. Natori. Chem. Pharm. Bull. Tokyo, **14**, 1434 (1966).
8. R. J. J. Ch. Lousberg, U. Weiss, C. A. Salemink, A. Armone, L. Metlini, and G. Masini. Chem. Commun. 1463 (1971); S. Yamazaki and T. Ogawa. Agric. Biol. Chem. **36**, 1707 (1972).
9. A. Okubo, S. Yamazaki, and K. Fuwa. Agric. Biol. Chem. **39**, 1173 (1975).
10. J. G. Atkinson, J. J. Csakvary, G. T. Herbert, and R. S. Stuart. J. Am. Chem. Soc. **90**, 498 (1968).
11. J. L. C. Wright, L. C. Vining, A. G. McInnes, D. G. Smith, and J. A. Walter. Can. J. Biochem. **55**, 678 (1967).
12. H. Batiz-Hernandez and R. A. Bernheim. Prog. Nucl. Magn. Reson. Spectrosc. **3**, 63 (1967).
13. R. Freeman, K. G. R. Pachler, and G. N. La Mar. J. Chem. Phys. **55**, 4586 (1971).
14. R. Freeman, H. D. W. Hill, and R. Kaptein. J. Magn. Reson. **7**, 327 (1972).
15. D. Shaw. Nuclear magnetic resonance specialist periodical reports. Vol. 2. Chemical Society, London. 1973. Chapt. 7. p. 269.
16. H. H. Mantsch, H. Saito, and I. C. P. Smith. Prog. Nucl. Magn. Reson. Spectrosc. **11**, 211 (1977).
17. J. B. Stothers. Carbon-13 nmr spectroscopy. Academic Press Inc., New York. 1972.
18. W. B. Turner. Fungal metabolites. Academic Press Inc., London. 1971. p. 74.
19. W. I. Taylor and A. R. Battersby (*Editors*). Oxidative coupling of phenols. Marcel Dekker Inc., New York. 1967.
20. D. H. R. Barton, G. W. Kirby, J. B. Taylor, and G. M. M. Thomas. J. Chem. Soc. 4545 (1963).
21. A. R. Battersby, R. Binks, S. W. Breuer, H. M. Fales, W. C. Wildman, and R. H. Highet. J. Chem. Soc. 1595 (1964).
22. I. Kurobane, L. C. Vining, A. G. McInnes, and D. G. Smith. Can. J. Chem. **56**, 1593 (1978).
23. C. Gregolin, E. Ryder, and M. D. Lane. J. Biol. Chem. **243**, 4227 (1968).
24. K. I. Arnstadt, G. Schindlbeck, and F. Lynen. Eur. J. Biochem. **55**, 561 (1975).
25. B. Sedgwick, J. W. Cornforth, S. J. French, R. T. Gray, E. Kelstrup, and P. Willadsen. Eur. J. Biochem. **75**, 481 (1977).

Can. J. Chem. Downloaded from www.nrcresearchpress.com by 210.87.254.42 on 09/05/12
For personal use only.

The photochemical addition of *N*-haloamides to olefins: the influence of various factors on the competition between 1,2-addition and hydrogen abstraction[1-3]

JEAN LESSARD, MARTINE MONDON (IN PART), AND DANIEL TOUCHARD[4]

Département de chimie, Université de Sherbrooke, Sherbrooke (Qué.), Canada J1K 2R1

Received May 22, 1980

This paper is dedicated to Prof. Raymond U. Lemieux on the occasion of his 60th birthday

JEAN LESSARD, MARTINE MONDON, and DANIEL TOUCHARD. Can. J. Chem. **59**, 431 (1981).

In the photodecomposition of *N*-haloamides (ZCONRX) in the presence of olefins, the 1,2-addition chain competes with the hydrogen abstraction chain(s) leading to the parent amide (the quantum yields for these processes are greater than unity). The following factors were shown to have an influence on this competition as measured by the yield of 1,2-addition and the yield of parent amide in methylene chloride solutions: (*i*) the *N*-halogen (higher yields of addition with X = Cl than with X = Br); (*ii*) the electronegativity of Z (increase of the yield of addition as the electronegativity of Z increases); (*iii*) the temperature (higher yields of addition at lower temperatures, and at −70°C, better yields of addition (>90%, R = H) for X = Br than for X = Cl); and (*iv*) the size of R (dramatic decrease of the yield of 1,2-addition in going from R = H to R = CH_3). Surprisingly, the presence of a scavenger for HX had no influence on the yield of 1,2-addition. Both the size and electronegativity of Z had an effect on the stereochemistry of 1,2-addition to cyclohexene. High yields of addition to a variety of olefins were obtained with *N*-chloroamides such as $ClCH_2CONHCl$, $C_2H_5OCONHCl$, $CF_3CONHCl$. Their addition to enol ethers at −70°C led to the synthesis of α-amido acetals or ketals (aldehydes or ketones) and to an α-amido glycoside in good yields.

JEAN LESSARD, MARTINE MONDON et DANIEL TOUCHARD. Can. J. Chem. **59**, 431 (1981).

Lors de la décomposition photochimique de *N*-haloamides (ZCONRX) en présence d'oléfines, l'addition-1,2 est en compétition avec l'abstraction d'hydrogène (ce sont des processus radicalaires en chaîne comme le montrent des rendements quantiques supérieurs à l'unité). On a démontré que les facteurs suivants exercent une influence sur cette compétiton en mesurant les rendements en addition-1,2 et en amide: (*i*) l'halogène X (rendements en addition plus élevés avec X = Cl qu'avec X = Br); (*ii*) l'électronégativité de Z (augmentation du rendement en addition avec l'électronégativité de Z); (*iii*) la température (rendements d'addition plus élevés à basse température et, à −70°C, les rendements en addition deviennent meilleurs (>90% pour R = H) avec les dérivés *N*-bromés qu'avec les dérivés *N*-chlorés); et (*iv*) la grosseur du substituant R (une diminution très marquée du rendement en addition en remplaçant l'hydrogène par un méthyle). Etonnamment, l'utilisation d'un capteur de HX n'a eu aucun effet sur le rendement en addition. La grosseur de même que l'électronégativité de Z influencent la stéréochimie de l'addition-1,2 au cyclohexène. On a obtenu d'excellents rendements d'addition à une grande variété d'oléfines avec les *N*-chloroamides suivants: $ClCH_2CONHCl$, $C_2H_5OCONHCl$, $CF_3CONHCl$. Leur addition aux ethers d'énol à −70°C à permis d'obtenir des α-amido acétals (aldéhydes ou cétones) et un α-amido glycoside en bons rendements.

Introduction

The photochemical decompositon of *N*-haloamides should lead to an amidyl radical and a halogen atom (reaction [1]).

[1] $ZCONR{-}X \xrightarrow{h\nu} ZCO\dot{N}R + X^{\cdot}$

In the presence of an olefin, three main radical chain processes can be operating and compete with each other: the 1,2-addition process and two halogenation processes. The 1,2-addition process should involve the nitrogen centered radical as the chain carrier (reactions [2] and [3]) and its addition

[2] $ZCO\dot{N}R + \rangle C{=}C\langle \rightarrow ZCONR{-}\overset{|}{C}{-}\overset{|}{C}{\cdot}$

[3] $ZCONR{-}\overset{|}{C}{-}\overset{|}{C}{\cdot} + ZCONR{-}X \rightarrow ZCONR{-}\overset{|}{C}{-}\overset{|}{C}{-}X + ZCO\dot{N}R$

to the carbon–carbon double bond (reaction [2]). The two halogenation processes should involve abstraction of hydrogen atoms (mainly allylic) from the olefin: (*i*) by the nitrogen centered radical (the Bloomfield (5) mechanism proposed for *N*-bromosuccinimide):

[4] $ZCO\dot{N}R + \rangle C{=}\overset{|}{C}{-}CH{-} \rightarrow \rangle C{=}\overset{|}{C}{-}\dot{C}\langle + ZCONHR$

[5] $\rangle C{=}\overset{|}{C}{-}\dot{C}\langle + ZCONR{-}X \rightarrow \rangle C{=}\overset{|}{C}{-}CX{-} + ZCO\dot{N}R$

and/or (*ii*) by the halogen atom (the Goldfinger (6) mechanism proposed for *N*-chloro and *N*-

[1]Part XI in the series "Radical reactions of *N*-haloamides with olefins". For parts X, IX, VIII, and VII, see refs. 1, 2*a* 2*b*, and 3.

[2]Part of the results were published in ref. 4 as communications.

[3]Abbreviated from the Ph.D. thesis of D. Touchard, Université de Sherbrooke, Sherbrooke (Qué.), 1974.

[4]France–Quebec Predoctorate Fellow, 1970–1972. Present address: Institut Universitaire de Technologie, Université de Nantes, 44606 Saint-Nazaire, France.

0008-4042/81/020431-20$01.00/0

©1981 National Research Council of Canada/Conseil national de recherches du Canada

Can. J. Chem. Downloaded from www.nrcresearchpress.com by 210.87.254.5 on 09/05/12
For personal use only.

bromosuccinimide):

[6] $X^{\cdot} + \rangle C{=}C{-}CH{-} \rightarrow \rangle C{=}C{-}\dot{C}\langle + HX$

[7] $ZCONRX + HX \rightarrow ZCONHR + X_2$

[8] $\rangle C{=}C{-}\dot{C}\langle + X_2 \rightarrow \rangle C{=}C{-}CX{-} + X^{\cdot}$

Both halogenation processes lead to the parent amide.

The purpose of our studies on the radical reactions of *N*-haloamides with olefins was to try to determine the relative importance of the above three radical chain processes and to determine the main factors which may affect the competition between them. This paper reports some of the results on the photochemical decomposition of ZCONRX (R = H: *N*-halo-*N*-hydroamides; R = alkyl: *N*-alkyl-*N*-haloamides) in the presence of olefins. We are going to examine the effect of X (X = Cl and Br), the influence of the electronegativity of Z, the effect of temperature, the effect of R (R = H and CH_3), and the effect of a scavenger for HX on the yield of 1,2-addition and the yield of the parent amide that is on the competition between the 1,2-addition process and the hydrogen abstraction processes (halogenation).[5] We will also try to evaluate the scope and limitations of the photochemical addition of *N*-haloamides to olefins for the synthesis of *N*-(2-haloalkyl)-amides (Scheme 1).

$$ZCONR{-}X + \rangle C{=}C\langle \xrightarrow{h\nu} ZCONR{-}C{-}C{-}X$$

SCHEME 1

Other methods of radical additon of *N*-haloamides to olefins (7, 8) are the thermal addition of *N*,*N*-dichlorourethane (9–11*a*, 11*c*), the photochemical addition of *N*-chlorourethane (11), and the chromous chloride promoted addition of *N*-halo-*N*-hydrocarboxamides and *N*-halo-*N*-hydrocarbamates (3, 12). Closely related are the photochemical addition to olefins of *N*-halo-succinimides (13, 14) and -glutarimides (13), of *N*,*N*-dichlorosulfonamides (15), of *N*-alkyl-*N*-chlorosulfonamides (16, 17), of *N*-chloro-*N*-methylcyanamide (17), and the spontaneous addition of *N*,*N*-dihalophosphoramides (18).

Results

Additions to Cyclohexene (Scheme 2)

To study the effect of various factors on the competition between the 1,2-addition process and

$$ZCONRX + \bigcirc \rightarrow \underset{X}{\overset{NRCOZ}{\bigcirc}} + ZCONHR$$

1 **2** *cis* **3** *trans*

SCHEME 2

the hydrogen abstraction processes, we have chosen cyclohexene as a representative olefin in order to give a fair chance to the hydrogen abstraction processes. Indeed, cyclohexene has allylic hydrogens which are quite reactive towards electrophilic radicals, more reactive per se than those of a terminal olefin (19, 20), and has an internal double bond which is normally less reactive than terminal ones in radical additions (20, 21). Furthermore, it was interesting to see if the various factors studied would have an effect on the stereochemistry of 1,2-addition.

The ultraviolet spectra of *N*-haloamides show a maximum in the 250–260 nm region with tailing up to about 260 nm (22). The photolyses were carried out in a Rayonnet reactor, under a nitrogen atmosphere, using Vycor glassware with the 254 nm lamps and Pyrex glassware with the 300 nm and 350 nm lamps. The results of Table 1 (entries 1 to 6) show that the more energetic the radiation, the shorter is the reaction time as expected. The wavelength has practically no effect on the relative yields of 1,2-adducts[6] and acetamide, and on the *cis*(**2**)/*trans*(**3**) ratio.

The photochemical addition of *N*-chloroacetamide (NCA, **1***b*) to cyclohexene was studied in three different solvents and in neat cyclohexene. In acetonitrile, the yield of 1,2-addition was comparable to that obtained in methylene chloride but the *cis*(**2***b*)/*trans*(**3***b*) ratio was much lower (compare entries 4 and 7 of Table 1). In methylene chloride, the *cis* isomer predominates (**2***b*/**3***b* = 2.7) whereas in acetonitrile, the *trans* isomer predominates (**2***b*/**3***b* = 0.65). This is due to the electrophilic chlorination of cyclohexene by the chlorine formed in the Goldfinger type hydrogen abstraction process (reaction [7]) and/or by NCA itself (Scheme 3); such ionic reactions should be favored in the more polar acetonitrile. Evidences for the occurrence of electrophilic chlorination in acetonitrile were provided (*i*) by the formation of the *trans* adduct **3***b* (Scheme 3, R^1 = H) in 18% and 19% yield respec-

[5]A detailed study of the influence of these factors on the halogenation products will be reported in a forthcoming paper.

[6]Many of the addition products to cyclohexene (12*a*) and to the other olefins (12, 23) have already been described. All new compounds had ir, ^{1}H nmr spectra, and elemental analysis, and/or a mass spectrum consistent with their structures. The ir and ^{1}H nmr spectra of the new adducts were similar to those of the known adducts (12, 23) except for the protons of R and Z.

Can. J. Chem. Downloaded from www.nrcresearchpress.com by 210.87.254.5 on 09/05/12
For personal use only.

TABLE 1. Addition of *N*-bromoacetamide (NBA, **1***a*) and *N*-chloroacetamide (NCA, **1***b*) to cyclohexene (Scheme 2)

Entry	*N*-Haloamide	Solvent[a] (mL)	>=</1 (mmol)	Lamps	Reaction time[b] (h)	Yield[c] of products: 2 + 3 (%)	(2/3)	Acetamide (%)
1	$CH_3CONHBr$ (**1***a*)	CH_2Cl_2 (10)	10/5	254 nm	0.5	25	(1.5)	67
2				300 nm	2	26	(1.4)	66
3				350 nm	5.5	29	(1.4)	62
4	$CH_3CONHCl$ (**1***b*)	CH_2Cl_2 (10)	10/5	254 nm	4.5	55	(2.7)	39
5				300 nm	12	57	(2.5)	38
6				350 nm	53	55	(2.4)	39
7		CH_3CN (10)	10/5	254 nm	4.5	53	(0.65)	41
8		C_6H_6 (40)	10/5	254 nm	10	42	(2.5)	49[d]
9		Cyclohexene (40)	395/5	254 nm	48	38	(2.2)	52

[a]Methylene chloride and acetonitrile were distilled over phosphorous pentoxide and benzene was distilled over sodium.
[b]The irradiations were carried out at 15–20°C and were stopped when the starch – iodide paper test was negative.
[c]The yields are based on the *N*-haloamide and represent yields of isolated pure products (preparative layer chromatography (plc)).
[d]Acetanilide was isolated in an 8% yield (material balance, 99%).

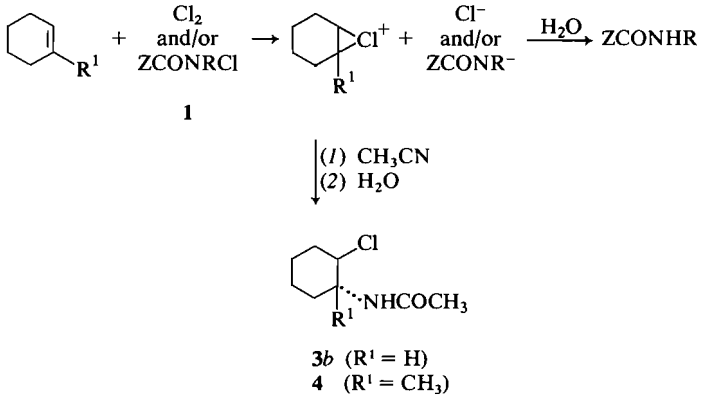

SCHEME 3

tively in the photolysis of *N*-chlorochloroacetamide (NCCA, **1***h*) and of *N*-chloro-*N*-methylacetamide (NCMA, **1***u*) in the presence of cyclohexene, and (*ii*) by the formation of the *trans* adduct **4** (Scheme 3, $R^1 = CH_3$) in 7 and 16% yield respectively in the photolysis of NCA and NCMA in the presence of 1-methylcyclohexene. In the ^1H nmr spectrum of **4**, the signal of the proton at δ 4.68 (dd, ΣJ = 14.5 Hz) was not altered by *N*-deuteriation. The NH signal at δ 5.85 is narrow (no vicinal proton) compared to the NH signal of adducts **11***b* and **12***b*[6] (see Table 8, entry 4 for their structures). The *trans* stereochemistry was assigned on the basis that, in the case of cyclohexene, *trans* **3***b* only was formed with NCMA (**1***u*) under the same reaction conditions (Scheme 3).

The photodecomposition of NCCA (**1***h*) in acetonitrile in the presence of cyclohexene gave, in addition to **3***b*, 72% of 1,2-adducts **2***h* and **3***h*[6] and 12% of chloroacetamide; NCMA (**1***u*) gave 68% of *N*-methylacetamide,[7] no 1,2-adduct being detected. With 1-methylcyclohexene, in addition to **4**, NCA (**1***b*) gave 54% of 1,2-adducts **18***b* and **19***b*[6] and 39% of acetamide; in the case of NCMA (**1***u*) no 1,2-adduct was formed and 76% of *N*-methylacetamide[7] was isolated. It is noteworthy that the *cis*/*trans* ratio is somewhat larger in acetonitrile (**2***h*/**3***h* = 5; **18***b*/**19***b* = 5) than in methylene chloride (**2***h*/**3***h* = 3.9, Table 2, entry 3; **18***b*/**19***b* = 4.8, Table 8, entry 4). In the dark, other conditions being the same as in Table 1, the reaction of NCA (**1***b*) with cyclohexene in acetonitrile took 35 days and gave about 14% of *trans* adduct **3***b*.

In benzene (Table 1, entry 8), the photochemical reaction of NCA with cyclohexene was slower and the yield of 1,2-addition lower than in methylene

[7]For the photolyses of NCMA (**1***u*) in acetonitrile, the 254 nm lamps were used. We found later (see Table 4) that, in methylene chloride, a better recovery of *N*-methylacetamide was obtained with the 300 nm lamps.

Can. J. Chem. Downloaded from www.nrcresearchpress.com by 210.87.254.5 on 09/05/12
For personal use only.

TABLE 2. Addition of *N*-halo-*N*-hydroamides (**1**, R = H) to cyclohexene (Scheme 2):[a] the influence of Z

Entry	*N*-Haloamide	Reaction time (h)	Yield[b] of products **2** + **3** (%)	(**2**/**3**)	Parent amide (%)
N-Chloro Derivatives					
1	$(CH_3)_3CCONHCl$ (**1***c*)	3	37	(11)	47
2	$CH_3CH_2CONHCl$ (**1***d*)	3	51	(2.4)	36
3	$CH_3CONHCl$ (**1***b*)[c,d]	4.5	55	(2.6)	39
4	$ClCH_2CH_2CONHCl$ (**1***e*)	3	66	(2.7)	28
5	$HCONHCl$ (**1***f*)	2.5	72	(2.6)	15
6	$BrCH_2CONHCl$ (**1***g*)	3.5	79	(3.1)	24
7	$ClCH_2CONHCl$ (**1***h*)	2.5	89	(3.9)	9
8	$FCH_2CONHCl$ (**1***i*)	2.5	91	(4.6)	7
9	$Cl_2CHCONHCl$ (**1***j*)	2.3	94	(5.2)	4
10	$CCl_3CONHCl$ (**1***k*)	2	99	(8.9)	0
11	$CF_3CONHCl$ (**1***l*)	1.5	97(100[e])	(7.3[e])	0
12	$C_2H_5OCONHCl$ (**1***m*)	1.5	84	(8.3)	15
N-Bromo Derivatives					
13	$CH_3CONHBr$ (**1***a*)[f]	2	26	(1.40)	66
14	$ClCH_2CONHBr$ (**1***n*)	1.5	61	(1.44)	37
15	$FCH_2CONHBr$ (**1***o*)	1.5	61	(1.54)	30
16	$Cl_2CHCONHBr$ (**1***p*)	1.5	71	(1.84)	26
17	$CCl_3CONHBr$ (**1***q*)[g]	1.5	84	(2.65)	14
18	$CF_3CONHBr$ (**1***r*)[h]	0.2	36	(0.70)	7

[a]Reaction conditions: 15–20°C, 254 nm lamps with ZCONHCl, 300 nm lamps with ZCONHBr, solutions 0.2 to 0.5 *M* in *N*-haloamide, 2 mol of olefin per mol of *N*-haloamide, CH_2Cl_2 as solvent.
[b]Yield of chromatographically (plc) pure products based on the *N*-haloamide.
[c]From Table 1, entry 4.
[d]The dark reaction took 45 days and no 1,2-adduct could be detected.
[e]By vapor phase chromatography (vpc). The two isomers were not separated by plc.
[f]From Table 1, entry 2.
[g]The dark reaction took 30 h and gave 30% of 1,2-adducts ($2q/3q = 0.5$).
[h]Only 70% of the material could be recovered from the silica gel plates. The fractions containing products other than **2***r*, **3***r*, and trifluoroacetamide were not investigated. The dark reaction took 2 days and led to 24% of *trans* adduct **3***r*. The *cis* adduct **2***r* could not be detected. Again the recovery of material from the plates was poor (65%) and the other products formed were not investigated.

chloride, the *cis*(**2***b*)/*trans*(**3***b*) ratio being about the same. The addition of NCA to benzene, leading to acetanilide (8%) after loss of hydrogen chloride, does compete with the addition to cyclohexene (42%). In neat cyclohexene, the reaction was still slower than in benzene, the yield of addition and the *cis*/*trans* ratio being practically the same (Table 1, entry 9).

From the results of Table 1, we selected methylene chloride as solvent to carry out the study of various factors on the competition between 1,2-addition and hydrogen abstraction. The reaction conditions are specified in footnote *a* of the various tables. The material balance (1,2-adduct(s) plus parent amide) was generally very high: 92–100%. The dark reactions either did not occur at all or occurred to a very small extent during the time required for the photochemical reaction to be completed. In a few cases, the dark reaction was allowed to go to completion and the results were quite different from those of the photochemical reaction (see Table 2, footnotes *d*, *g*, and *h*).

In the absence of an olefin, methylene chloride does react with the radicals formed in the photodecomposition of *N*-haloamides. Indeed, NCMA (**1***u*) led to the formation of substantial amounts of chloroform (>95%) and traces of 1,1,2,2-tetrachloroethane according to vpc analysis. The recovery of *N*-methylacetamide was low (about 8%) and some *N*-methyl-*N*,*N*′-methylenebisacetamide ($CH_3CON(CH_3)CH_2NHCOCH_3$), resulting probably from the addition of *N*-methylacetamide to $CH_3CON{=}CH_2$, was isolated in low yield (~6%). Other products were formed but were not investigated. The structure of the methylenebisacetamide was determined from its ir, ^1H nmr, and mass spectra (see Experimental section).

Effect of the Halogen (X)

The results of Table 1 and Table 2 show that the yields of 1,2-addition[6] are higher with *N*-chloro-*N*-hydro amides than with the corresponding *N*-bromo derivatives. Thus, the nature of X has an influence on the competition between 1,2-addition

Can. J. Chem. Downloaded from www.nrcresearchpress.com by 210.87.254.5 on 09/05/12
For personal use only.

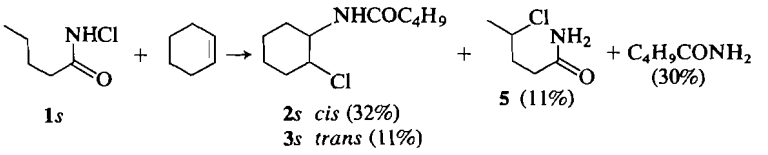

SCHEME 4

and hydrogen abstraction, the latter being less important when X = Cl than when X = Br. The *N*-halogen does have an influence also on the *cis*/*trans* ratio, the **2**/**3** ratio being larger for X = Cl than for X = Br as observed in the chromous chloride promoted addition of *N*-haloamides to cyclohexene (12*a*). Finally the reactions were faster in the case of the *N*-bromo derivatives.

Effect of Z

The results recorded in Table 2 show that, in the case of the *N*-chloro derivatives, the yield of 1,2-addition increases by changing Z in the order $(CH_3)_3C < CH_3CH_2 < CH_3 < ClCH_2CH_2 < H < BrCH_2 < ClCH_2 < FCH_2 < Cl_2CH < CCl_3 \sim CF_3$. A quantitative yield of addition was obtained for Z = CCl_3 and Z = CF_3 (entries 10 and 11). Steric effects are probably responsible for the lower yield of addition with Z = $(CH_3)_3C$ as compared to Z = CH_3CH_2 (entries 1 and 2). For the rest of the series, the increase of the yield of 1,2-addition parallels the acidity of the corresponding carboxylic acids (ZCOOH) (24) and the acidity of the *N*-chloro-*N*-hydro carboxamides themselves (25). Therefore, an increase of the electron-withdrawing power of the ZCO group favors 1,2-addition over hydrogen abstraction. *N*-Chlorourethane (NCU, **1***m*) (entry 2) led to a much better yield of addition than NCA (entry 3). Thus a carboalkoxy group appears to be more electron-attracting than an acetyl group, probably as a result of the inductive effect of the alkoxy group, although NCU is less acidic (pK_a = 8.02) than NCA (pK_a = 7.22) (25) due to the stabilization of the carboalkoxy group by resonance. Another interesting feature of Table 2 is the variation of the *cis*(**2**)/*trans*(**3**) ratio with Z. Both the size and electronegativity of Z appear to have an influence on this ratio. For instance it is much larger for Z = $(CH_3)_3C$ than for Z = CH_3CH_2 (entries 1 and 2): size effect. It increases in the order Z = $BrCH_2 < ClCH_2 < FCH_2$ (entries 6, 7, and 8) and it is larger for Z = C_2H_5O than for Z = CH_3CH_2 (entries 12 and 2): electronegativity effect. It is somewhat larger for Z = CCl_3 than for Z = CF_3, the size effect being probably more important than the electronegativity effect.

An interesting case is that of *N*-chloropentanamide (**1***s*) where the alkyl chain is long enough for intramolecular halogenation[8] to compete with the 1,2-addition process. These two processes involve the amidyl radical as the chain carrier and it is noteworthy that the intermolecular process is about 4 times faster than the intramolecular one as shown by the yields of 1,2-adducts **2***s* and **3***s* and of 4-chloropentanamide (**5**) (Scheme 4). The 4-chloro derivative **5** could not be separated from pentanamide by plc. Its yield was determined by microanalytical determination of chlorine. The mixture of **5** and pentanamide was treated with potassium tertiobutoxide in tertiobutanol at 80°C under nitrogen to afford pentanamide (22%) and 5-methyl-2-pyrrolidinone (**6**) (9%) (Scheme 5). Alkaline hydrolysis of a mixture of pentanamide and **5** obtained by photolysis of *N*-chloropentanamide (**1***s*) in the absence of olefin afforded pentanoic acid (15%) and γ-valerolactone (**8**) (59%) (Scheme 5).

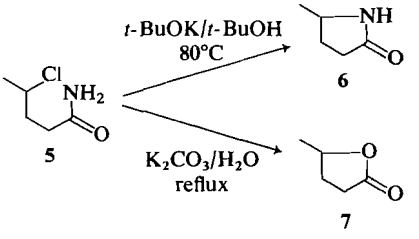

SCHEME 5

The yield of addition of the *N*-bromo-*N*-hydrocarboxamides to cyclohexene and the *cis*(**2**)/*trans*(**3**) ratio also increase with Z in the order: $CH_3 < ClCH_2 \simeq FCH_2 < Cl_2CH < CCl_3$ (Table 2, entries 13 to 17). However, the behavior of *N*-bromotrifluoroacetamide (**1***r*) was quite unexpected (entry 18). Not only the yield of 1,2-addition and the *cis*/*trans* ratio were much lower than in the case of *N*-bromotrichloroacetamide (**1***q*) (entry 17),[9] but the material balance was very poor in contrast

[8]The photolysis of *N*-chlorohexanamide in methylene chloride at ca. 20°C was reported to give, after alcaline hydrolysis of the crude product, 49% of γ-lactone arising from 4-chlorohexanamide (26).

[9]*N*-Bromotrichloroacetamide (**1***q*) and *N*-bromotrifluoroacetamide (**1***r*) were reported to undergo thermal addition (not in the dark) to neat cyclohexene (reaction exothermic enough to bring cyclohexene to a boil) (27). The yield of addition and the *cis*/*trans* ratio were also lower in the case of **1***r* (38%, **2***r*/**3***r* = 0) than in the case of **1***q* (60%, **2***q*/**3***q* = 2).

Can. J. Chem. Downloaded from www.nrcresearchpress.com by 210.87.254.5 on 09/05/12
For personal use only.

TABLE 3. The effect of temperature on the photochemical addition of *N*-halo-*N*-hydrocarboxamides (**1**, R = H) to cyclohexene (Scheme 2)[a]

Entry	*N*-Haloamide	Solvent % (v/v) CH_3OH in CH_2Cl_2	*T* (°C)	Reaction time (h)	Yield[b] of products: 2 + 3 (%)[c]	(2/3)	Parent amide (%)[c]	3-Halomethoxy-cyclohexane (%)[d]
1	$CH_3CONHBr$ (**1***a*)	0	15	2	25	(1.5)	68	0
2		0	−3	3.5	34	(1.4)	59	0
3		0.7	−24	5	52	(1.5)	46	1
4		1.3	−52	7.5	77	(1.5)	17	5
5		2.6	−70	11	91	(1.3)	5	4
6	$ClCH_2CONHBr$ (**1***n*)	0	20	2	61	(1.4)	36	0
7		3.8	−70	12	95	(1.1)	0	5
8		100	−70	17	64	(0.6)	31	27
9	$CH_3CONHCl$ (**1***b*)	0	15	4	54	(2.4)	41	0
10		2.4	−70	6	77	(1.7)	17	7

[a]Sclutions 0.06 *M* in *N*-halocarboxamide, 2 mol of olefin per mol of *N*-haloamide.
[b]Based on the *N*-haloamide.
[c]Of isolated products.
[d]By vpc.

to the addition of all the other *N*-haloamides of Table 2.[10] Processes other than 1,2-addition and halogenation must be involved but they were not investigated.

Finally, the rate of the photochemical decomposition of the *N*-halo-*N*-hydrocarboxamides in the presence of cyclohexene, as measured roughly by the reaction time, increases as the electronegativity of Z increases.

Effect of Temperature

As shown in Table 3, we have found that lowering the temperature favors the 1,2-addition of *N*-halo-*N*-hydrocarboxamides (**1**, R = H) over the hydrogen abstraction processes. The effect is less important in the case of NCA (**1***b*) (entries 9 and 10) than in the case of *N*-bromoacetamide (NBA, **1***a*) (entries 1 to 5) and *N*-bromochloroacetamide (**1***n*) (entries 6 and 7).[11] Thus very high yields of addition can be obtained with simple *N*-bromo-*N*-hydrocarboxamides. The 91% yield of addition with NBA is particularly worth noting since the photolysis in refluxing carbon tetrachloride was reported to give, as the primary product, *trans*-2-bromocyclohexyl-*N*-bromoacetamidate resulting from the ionic addition of *N*,*N*-dibromoacetamide and only 1% of *trans* 1,2-adduct **3***a* (28). The temperature has little influence on the *cis*(**2**)/*trans*(**3**) ratio. The smaller ratio observed at −70°C can probably be attributed to the presence of a significant amount of methanol (more than 2%) as in pure methanol, this ratio is much smaller (compare entries 7 and 8). All the irradiations of Table 3 were carried out with solutions 0.06 *M* in *N*-halocarboxamide which represents approximately a nine-fold dilution with respect to the conditions given in Table 2. Such a dilution had no effect on the relative importance of the competing radical chain processes: compare entries 1, 6, and 9 of Table 3 with entries 10, 11, and 1 respectively of Table 2. At low temperatures, methanol was added in order to ensure complete dissolution of the *N*-halocarboxamide. This led to the formation of *trans* 3-halomethoxycyclohexane through electrophilic halogenation of cyclohexene. In pure methanol as much as 27% of this product was formed (entry 8).

Effect of R

A comparison of the results of Table 4, entries 1 to 7, with those of Table 2, entries 13, 3, 7, and 11, shows that the replacement of the *N*-hydrogen by an *N*-methyl group has a drastic effect on the competition between 1,2-addition and hydrogen abstraction. The former is suppressed in the case of the *N*-methyl derivatives **1***t* and **1***u* even at −70°C (entries 1 to 5); it is suppressed also in the case of the *N*-methyl derivative **1***v* (entry 6). While the yield of addition of *N*-chlorotrifluoroacetamide (**1***l*) to cyclohexene was quantitative (Table 2, entry 11), the yield of addition of the corresponding *N*-methyl derivative **1***w* was 20% only (Table 4, entry 7). The fact that *N*-chloro-*N*-methyltrifluoroacetamide (**1***w*) does add to cyclohexene shows again that an electron attracting Z group favors

[10]The chromous chloride promoted addition of *N*-bromotrifluoroacetamide (**1***r*) to cyclohexene under the standard reaction conditions (12*a*) gave much better results than the photochemical reaction yielding 80% of 1,2-adduct **2***r* and **3***r* (**2***r*/**3***r* = 1.2) and 20% of trifluoroacetamide.

[11]A similar temperature effect has been reported recently for the photochemical reaction of *N*-bromosuccinimide with cyclohexene in acetonitrile and in the presence of ethylene oxide (14).

Can. J. Chem. Downloaded from www.nrcresearchpress.com by 210.87.254.5 on 09/05/12
For personal use only.

TABLE 4. The photochemical addition of *N*-halo-*N*-alkylcarboxamides (**1**, R = alkyl) to cyclohexene (Scheme 2)[a]

Entry	*N*-Haloamide	*T* (°C)	Lamps (nm)	Yield[b] of products: **2** + **3** (%)	Yield[b] of products: Parent amide (%)
1	CH_3CONBr (**1***t*)	15–20	300	0	93
2		−70	300	0	95
3	CH_3CONCl (**1***u*)	15–20	300	0	95–97
4		15–20	254	0	45[c]
5		−70	254	0	93
6	$ClCH_2CONCl$ (**1***v*)	15–20	300	0	90
7	CF_3CONCl (**1***w*)	15–20	254	20[d]	61

[a]Solutions 0.5 *M* (0.06 *M* at −70°C) in *N*-haloamide, 2 mol of olefin per mol of *N*-haloamide, CH_2Cl_2 as solvent.
[b]Yields of isolated products based on the *N*-haloamide.
[c]Besides the parent amide, $CH_3CON(CH_3)CH_2NHCOCH_3$ was isolated in 2% yield.
[d]Homogeneous by thin layer chromatography (tlc) but could be a mixture of *cis* (**2***w*) and *trans* (**3***w*) isomers.

the 1,2-addition process. The ^1H nmr spectrum of *N*-(2-chlorocyclohexyl)-*N*-methyltrifluoroacetamide (**2***w* and/or **3***w*) shows a complex absorption at δ 3.7–4.3 for protons H_1 and H_2 and two 1:3:3:1 quartets for the *N*-methyl group, one at δ 3.03 ($^5J_{H,F}$ = 1.5 Hz) and the other at δ 2.93 ($^5J_{H,F} < 1$ Hz, not completely resolved). These two quartets arise from two different orientations around the CO—N bond, the CH_3 and CF_3 being *syn* in one and *anti* in the other (29).

Effect of a Scavenger for HX

We have seen in the Introduction that one of the competing mechanisms in the photochemical decomposition of *N*-haloamides in the presence of olefins could be hydrogen abstraction via the halogen atom–HX–X_2 chain (the Goldfinger mechanism). The formation of substantial amounts of dichlorocyclohexane[5] in the photolysis of NCA (**1***b*) and of NCMA (**1***u*) in the presence of cyclohexene indicates that this mechanism is probably operating and also that the olefin acts as a scavenger for chlorine. With the aim of suppressing completely the chlorine atom–HCl–Cl_2 chain and hoping to increase the yield of 1,2-addition, we studied the effect of 2,4,6-trimethylpyridine (TMP) and cyclohexene oxide as HCl scavengers on the photodecomposition of NCA and NCMA in the presence of cyclohexene. TMP was used successfully by Johnson and Greene (22) to repress the chlorine atom–HCl–Cl_2 chain in the light-initiated chlorination of alcanes with *N*-chloroamides. Epoxides have been used to scavenge HBr in the bromination of ketones (30) and alkyl benzenes (31), and in the photochemical decomposition of *N*-bromosuccinimide in the presence of olefins (14). The results of Table 5 show that, contrary to our expectation, the presence of a scavenger for HCl did not favor the 1,2-addition process over hydrogen abstraction. No addition of NCMA was observed in the presence or in the absence of a scavenger (entries 4 to 7). The yields of 1,2-addition of NCA were even lower in the presence of a scavenger. NCA and NCMA as well as the 1,2-adducts **2***b* and **3***b*, dichlorocyclohexane, 3-chlorocyclohexene, and 4-chlorocyclohexene were stable toward TMP and cyclohexene oxide under the reaction conditions. The photodecomposition was slowed down by the addition of TMP and cyclohexene oxide. The most striking result of Table 5 is the large amount of HCl scavenged (see entries 5, 6, and 7). The yield of *trans* chlorocyclohexanol (entry 7) shows that cyclohexene oxide was effective in scavenging HCl.

Additions to 1-Dodecene

The reaction is depicted in Scheme 6. The structure of the 1,2-adducts **8** shows that the amido

Can. J. Chem. Downloaded from www.nrcresearchpress.com by 210.87.254.5 on 09/05/12
For personal use only.

TABLE 5. Effect of a scavenger for HCl on the photochemical addition of *N*-chlorocarboxamides (**1**, X = Cl) to cyclohexene (Scheme 2)[a]

Entry	*N*-Chloroamide	Scavenger	(Sc:NCl)[b]	Reaction time (h)	Scavenged HCl (%)	Yield[c] of products: 2 + 3 (%)	(2/3)	Parent amide (%)
1	$CH_3CONHCl$ (**1***b*)	None		4		51	(2.6)	40
2		TMP[d]	(1:1)	12	[e]	46	(2.1)	50
3		TMP[d]	(2:1)	26	[e]	44	(1.9)	51
4	$CH_3CONCl(CH_3)$ (**1***u*)	None[f]		3		0		45
5		TMP[d]	(1:1)	9	40[g]	0		82
6		TMP[d]	(2:1)	14	43[g]	0		74
7		Cyclohexeneoxide	(1.5:1)	6	55[h]	0		97[i]

[a]Solutions 0.2 *M* in *N*-haloamide; 15–20°C; 254 nm lamps; 2 mol of olefin per mol of *N*-haloamide; CH_2Cl_2 as solvent.
[b]Mole ratio of scavenger to *N*-chloroamide.
[c]Of isolated products unless stated otherwise.
[d]TMP = 2,4,6-trimethylpyridine.
[e]Not determined.
[f]Taken from Table 4, entry 4.
[g]The reaction mixture was treated with silver nitrate. The yield of silver chloride minus the yield of 3-chloro- and 4-chloro-cyclohexene determined by vpc represents the amount of TMP hydrochloride formed.
[h]Yield of *trans*-chlorocyclohexanol determined by vpc.
[i]By vpc.

$$ZCONRX + R^1CH_2CH=CH_2 \longrightarrow R^1CH_2\underset{X}{CH}-\underset{NRCOZ}{CH_2} + ZCONHR$$

1 **8**

SCHEME 6

$$CH_3(CH_2)_9\underset{Cl}{CH}-\underset{N(CH_3)COCF_3}{CH_2} \xrightarrow[CH_3OH/H_2O]{K_2CO_3} CH_3(CH_2)_9\underset{O}{CH}-\underset{N}{CH_2}$$

with the carbonyl group of **9** bonded to C and O, and CH_3 bonded to C.

8 **9**

SCHEME 7

group attached itself to the terminal carbon of the olefin. The spectral characteristics of adducts **8** where R = H are very similar to those of the 1,2-adducts to 1-octene (12*a*). Treatment of 1,2-adduct **8***w* by potassium carbonate in aqueous methanol gave the *N*-methyloxazolidone **9** (Scheme 7).

The results of Table 6 confirm the trends observed with cyclohexene: the yields of addition are higher with the *N*-chloroamides than with the corresponding *N*-bromo derivatives (compare entries 1 and 2 with entries 2 and 4); the 1,2-addition is favored by increasing the electron-attracting power of Z (entries 1 and 2, 3 and 4); lowering the temperature favors the 1,2-addition process (entries 6 and 7); the replacement of an *N*-hydrogen by an *N*-methyl group diminishes drastically the amount of 1,2-addition (entries 3 and 6); and, finally, the presence of a scavenger for HX (TMP) does not promote the 1,2-addition process (compare entries 8 and 9).

It is noteworthy that the yields of addition of *N*-chloro-*N*-methylchloroacetamide (**1***v*) and *N*-chloro-*N*-methyltrifluoroacetamide (**1***w*) to 1-dodecene (17 and 70% respectively, entries 6 and 10) are significantly higher than those obtained with cyclohexene (0 and 18% respectively, see entries 5 and 6 of Table 4). On the other hand, in the case of the *N*-halo-*N*-hydrocarboxamides, the yields of 1,2-addition are comparable with both olefins (e.g. compare entries 1 and 2 of Table 6 with entries 14 and 17 of Table 2).

Additions to Norbornene

Norbornene is an interesting olefin since it has a reactive double bond and no readily abstractable hydrogens. The reaction is depicted in Scheme 8

Can. J. Chem. Downloaded from www.nrcresearchpress.com by 210.87.254.5 on 09/05/12
For personal use only.

Can. J. Chem. Downloaded from www.nrcresearchpress.com by 210.87.254.5 on 09/05/12
For personal use only.

TABLE 6. Addition of ZCONRX (**1**) to 1-dodecene (Scheme 6)[a]

Entry	*N*-Haloamide	*T* (°C)	Yield[b] of products: **8** (%)	Parent amide (%)	CH_3 | ZCON—CH_2—NHCOZ (%)
1	$ClCH_2CONHBr$ (**1***n*)	15–20	62	30	
2	$CCl_3CONHBr$ (**1***q*)	15–20	82	13	
3	$ClCH_2CONHCl$ (**1***h*)	15–20	95	3	
4	$CCl_3CONHCl$ (**1***k*)	15–20	98	0	
5	CH_3CONCl (**1***u*)	15–20	0	74	~2
6	$ClCH_2CONCl$ (**1***v*)	15–20	17	77	[c]
7		−70[d]	24	69	[c]
8[e]	$C_2H_5OCONCl$ (**1***x*)	15–20	21	36[f]	35[f]
9[g]		15–20	23	50[h]	[i]
10	CF_3CONCl (**1***w*)	15–20	70(71[h])	26[h]	[c]

[a]Solutions 0.2 to 0.5 *M* in *N*-haloamide; 300 nm lamps with *N*-bromoamides and 254 nm lamps with *N*-chloro derivatives; 2 mol of olefin per mol of *N*-haloamide; CH_2Cl_2 as solvent.
[b]Yield of chromatographically pure products based on ZCONRX unless otherwise indicated.
[c]Not detected.
[d]Solution of 0.06 *M* in *N*-chloroamide.
[e]Addition to 1-octene.
[f]By ^1H nmr of a fraction consisting of a mixture of *N*-methylurethane and methylenebisurethane.
[g]Addition to 1-octene in the presence of 1 molar equivalent of 2,4,6-trimethylpyridine.
[h]By vpc.
[i]No attempt was made to isolate the product.

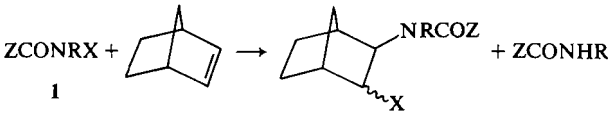

10 *cis*
11 *trans*

SCHEME 8

and the results are recorded in Table 7. The amido group in the 1,2-adducts **10** and **11** has the *exo* orientation. A number of features of Table 7 parallel those observed with cyclohexene: both the yield of 1,2-addition and the *cis*(**10**)/*trans*(**11**) ratio are higher when X = Cl than when X = Br (entries 1 and 3) and increase with the electronegativity and/or the size of Z (entries 2 to 4).[12] The 42% yield of addition of NCMA (**1***u*) (entry 5) is noteworthy since no addition was observed with cyclohexene (Table 4, entry 3) or 1-dodecene (Table 6, entry 5). For the *N*-halo-*N*-hydrocarboxamides (entries 1, 2, and 3), the yield of 1,2-addition is similar to that obtained with cyclohexene (Table 2) and 1-dodecene (Table 6). Entries 5 to 8 show that the size of the *N*-alkyl group has a marked effect on the

[12]A similar increase of the *cis*/*trans* ratio with Z was observed also in the chromous chloride promoted addition of *N*-halo-*N*-hydro amides to norbornene (12*a*).

TABLE 7. Addition of ZCONRX (**1**) to norbornene (Scheme 8)[a]

Entry	*N*-Haloamide	Yield[b] of products: **10** + **11** (%)	(**10**/**11**)	Parent amide (%)
1	$ClCH_2CONHBr$ (**1***n*)	77	(2.7)	30
2	$CH_3CONHCl$ (**1***b*)	56	(3.6)	40
3	$ClCH_2CONHCl$ (**1***h*)	88	(5.8)	10
4	$CCl_3CONHCl$ (**1***k*)	96	(5.8)	<2
5	$CH_3CON(CH_3)Cl$ (**1***u*)	42[c]		52
6	$CH_3CON(C_2H_5)Cl$ (**1***y*)	10[d]		87
7	$CH_3CON(i\text{-}C_3H_7)Cl$ (**1***z*)	0		89
8	$CH_3CON(t\text{-}C_4H_9)Cl$ (**1**α)	0		92

[a]Solutions 0.5 *M* in *N*-haloamide; 15–20°C; 2 mol of olefin per mol of *N*-haloamide; 300 nm lamps in entry 1 and 254 nm lamps in the others; CH_2Cl_2 as solvent.
[b]Yields of chromatographically pure products based on the *N*-haloamide.
[c]Homogeneous on tlc. The ^1H nmr spectrum shows two *N*-methyl groups.
[d]Homogeneous on tlc. The ^1H nmr spectrum shows two *N*-ethyl groups.

TABLE 8. Addition of ZCONHX (1, R = H) to various mono-olefins[a]

Entry	Olefin	*N*-Haloamide	Addition products: Structure		No.	Yield[b] (%)	Parent amide (%)
1	Styrene	$CH_3CONHCl$ (1*b*)	Inhibition of the photodecomposition[c]				
2	*cis*-3-Hexene	$CF_3CONHCl$ (1*l*)	$C_2H_5CH(Cl)-CH(NHCOCF_3)C_2H_5$	*threo*	**12***l*	64[d]	0
				erythro	**13***l*	27[d]	
3	*trans*-3-Hexene	$CF_3CONHCl$ (1*l*)	$C_2H_5CH(Cl)-CH(NHCOCF_3)C_2H_5$	*threo*	**12***l*	63[d]	0
				erythro	**12***l*	27[d]	
4	1-Methyl-cyclohexene	$CH_3CONHCl$ (1*b*)	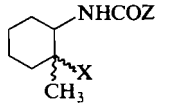	*cis*	**18***b* (Z = CH_3, X = Cl)	48	36
				trans	**19***b* (Z = CH_3, X = Cl)	10	
5		$ClCH_2CONHCl$ (1*h*)		*cis*	**18***h* (Z = CH_2Cl, X = Cl)	88	7
				trans	**19***h* (Z = CH_2Cl, X = Cl)	0	
6		$ClCH_2CONHBr$ (1*n*)		*cis*	**18***n* (Z = CH_2Cl, X = Br)	48	35
				trans	**19***n* (Z = CH_2Cl, X = Br)	14	
7	1,2-Dimethyl-cyclohexene	$ClCH_2CONHX$ (1*h*, X = Cl; 1*n*, X = Br)	No addition				91–92
8	Ethoxyethylene	$ClCH_2CONHCl$ (1*h*)[e]	$CH_2-CH(OC_2H_5)_2$ | NHCOZ		**23***h* (Z = CH_2Cl)	81	[f]
9		$CF_3CONHCl$ (1*l*)[e]			**23***l* (Z = CF_3)	92	[f]
10	1-Methoxy-cyclohexene	$ClCH_2CONHCl$ (1*h*)[g]	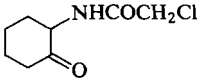		**24***h*	82	10[h]
11		$ClCH_2CONHBr$ (1*n*)[g]					
12	1-Chloro-cyclohexene	$ClCH_2CONHCl$ (1*h*)	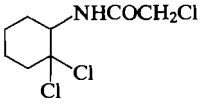		**24***h*	0	86[i]
					36*h*	35	59
13	1-Acetyl-cyclohexene[j]	$ClCH_2CONHCl$ (1*h*)	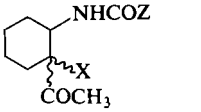	*cis*	**37***h* (Z = CH_2Cl, X = Cl)	16	30
				trans	**38***h* (Z = CH_2Cl, X = Cl)	54	
14		$C_2H_5OCONHCl$ (1*m*)		*cis*	**37***m* (Z = C_2H_5O, X = Cl)	11	32
				trans	**38***m* (Z = C_2H_5O, X = Cl)	24	
					39*m* (Z = C_2H_5O, X = H)	28	
15	1-Octyne	$ClCH_2CONHCl$ (1*h*)	No addition				93

[a]Unless stated otherwise, the reactions were carried out at 15–20°C in methylene chloride solutions 0.5 *M* in *N*-haloamide, with an excess of olefin (2 mo per mol of *N*-haloamide) using the 254 nm lamps with *N*-chloro derivatives and the 300 nm lamps with *N*-bromo derivatives. In the case of the enol ethers (entries 8 to 11) the reaction temperature was −70°C and the solutions were 0.06 *M* in *N*-haloamide.
[b]Yields of isolated (plc) products based on the *N*-haloamides unless otherwise indicated.
[c]After 80 h of irradiation, 95% of unreacted NCA (1*b*) was still present. Reduction of the reaction mixture by sodium bisulfite allowed the recovery of 96% of acetamide.
[d]By vpc.
[e]The photolysis was followed by the addition, at −70°C, of 1 equiv. of sodium ethoxide in dry ethanol.
[f]Not determined.
[g]Photolysis followed by the addition of water.
[h]α-Chlorocyclohexanone was formed in a 9% yield according to vpc analysis.
[i]Besides the parent amide, α-bromocyclohexanone was the sole product identified (57% by vpc).
[j]The 350 nm lamps were used.

1,2-addition process: 42% of addition for R = CH_3 compare to 10% for R = C_2H_5 then 0% for R = *i*-C_3H_7 and R = *t*-C_4H_9.

Additions to Various Mono-olefins

We chose mainly NCCA (1*h*), *N*-chlorotrifluoroacetamide (1*l*), and NCU (1*m*) to evaluate the scope and limitations of the method for the synthesis of *N*-(2-haloalkyl)amides since they gave a high yield of addition with the three olefins studied so far. The results are shown in Table 8. Styrene inhibited completely the photodecomposition of NCA (1*b*) (entry 1). The yield of addition of *N*-chlorotrifluoroacetamide (1*l*) to the isomeric 3-hexenes (entries 2 and 3) was somewhat lower than that obtained with cyclohexene (Table 2, entry 7). The

Can. J. Chem. Downloaded from www.nrcresearchpress.com by 210.87.254.5 on 09/05/12
For personal use only.

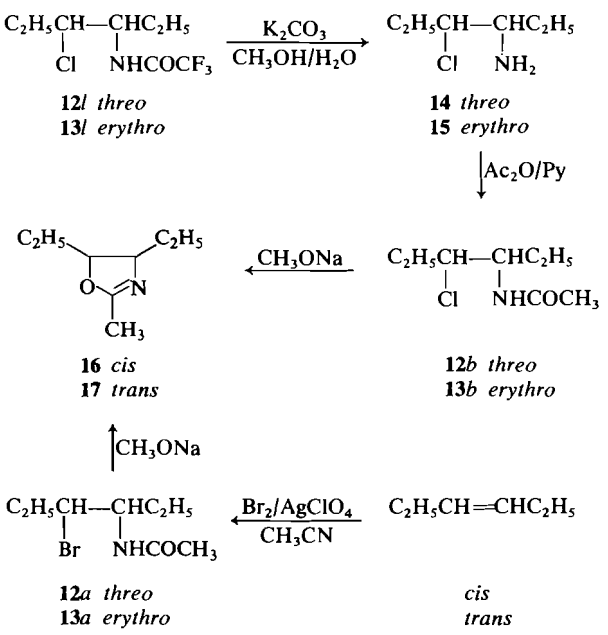

SCHEME 9

same *threo*(**12***l*)/*erythro*(**13***l*) ratio was obtained irrespective of the configuration of the olefin, thus showing that equilibration of the intermediate radical adduct, through inversion at the radical center and/or rotation around the central carbon–carbon bond, was much faster than its reaction with a molecule of *N*-chloroamide (chlorine-atom transfer, reaction [3]). The structure of **12***l* and **13***l* was proven by their conversion to the oxazolines **16** and **17** respectively as shown in Scheme 9. Authentic samples of **16** and **17** were obtained by the bromoacetamidation (32) of *cis*-3-hexene and *trans*-3-hexene respectively followed by treatment of the resulting β-bromoamide with sodium methoxide (Scheme 9).

For the additions to 1-methylcyclohexene (Table 8, entries 4 to 6), the yields were comparable to those obtained with cyclohexene but the *cis*(**18**)/*trans*(**19**) ratios were higher as observed in the chromous chloride promoted additions (12*a*). As with cyclohexene, both the yield of addition and the *cis*/*trans* ratio are higher for X = Cl than for X = Br and increase with the electronegativity of Z. No adduct could be detected with a tetrasubstituted olefin (entry 7) in contrast to the chromous chloride promoted additions (12*a*).

The addition of *N*-chlorotrifluoroacetamide (**1***l*) and NCU (**1***m*) to pregnenolone acetate (**20**) (equimolar quantities of *N*-chloroamide and olefin) is depicted in Scheme 10. The addition was regiospecific, the amido group being attached to the less substituted carbon atom (C-6) of the olefin. The transfer of chlorine onto the intermediate radical at C-5 was stereospecific giving the more stable *trans* A/B ring fusion. The predominant formation of the *trans* adduct with the amido group at C-6 β and axial shows the strong preference for the axial attack of the 5,6-double bond by an amidyl radical. The yields of addition were quite good (those between brackets take into account the recovery of pregnenolone acetate)[13] and the *cis*(**21**)/*trans*(**22**) ratio appears to vary with Z. The ^{1}H nmr spectra of **21***l* and **22***l* were similar to those of **21***m* and **22***m* whose structure has been unambiguously determined (12*a*). In particular, they show clearly that the proton at position 3 is axial in both isomers (*trans* A/B ring fusion) and that the proton at position 6 is axial in **21***l* and equatorial in **22***m* (see Experimental section).

The radical addition of *N*-haloamides to enol ethers followed by solvolysis of the intermediate α-haloether (1,2-adduct) should provide a way to synthesize α-amido acetals or ketals (aldehydes or ketones). *N*-Bromoamides cannot be used for that purpose since electrophilic bromination was much faster than light-initiated addition even at −70°C (Table 8, entry 11). With *N*-chloroamides however, electrophilic chlorination was usually negligible at −70°C and excellent yields of α-amido acetals **23** and α-amidocyclohexanone **24***h* were obtained from ethoxyethylene and 1-methoxycyclohexene respectively (Table 8, entries 8 to 10). When the photochemical addition of NCCA (**1***h*) to 1-methoxycyclohexene was followed by methanolysis of the intermediate α-chloroether, the α-amido ketal **25***h* was isolated in a 78% yield. Its hydrolysis to α-chloroacetamidocyclohexanone (**24***h*) was quantitative.

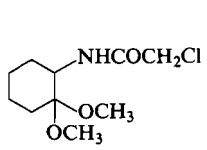

25*h*

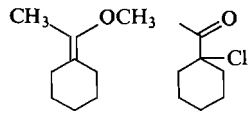

26 **27**

Neither NCCA (**1***h*) nor NCU (**1***m*) could be added to (1-methoxyethylidene)cyclohexane (**26**), a fully substituted enol ether, the parent amide being isolated in 95 and 93% yield respectively after treatment of the photolysate with water.[14] Beside

[13]The photochemical addition of NCU to cholesteryl acetate and to androst-5-en-3β-ol-17-one was reported to give only the corresponding *trans* 1,2-adduct in 34% and 9% yield respectively (33). The chromous chloride promoted addition of NCU in excess to pregnenolone acetate led to 21% of **21***m* and 79% of **22***m* (12*a*).

[14]In contrast, the chromous chloride promoted addition of NCU to **23** gave 62% of the expected α-amido ketone, 1-acetyl-1-ethoxycarbonylaminocyclohexane (23).

Can. J. Chem. Downloaded from www.nrcresearchpress.com by 210.87.254.5 on 09/05/12
For personal use only.

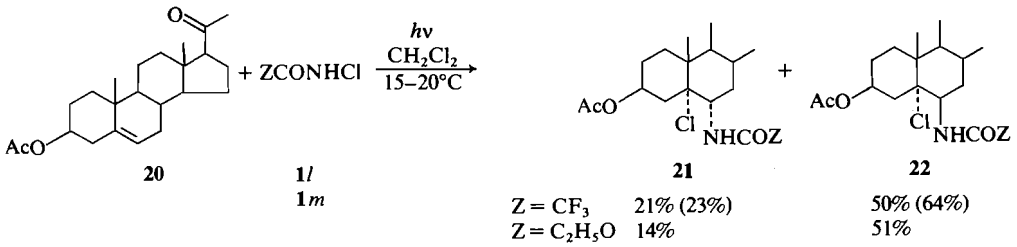

SCHEME 10

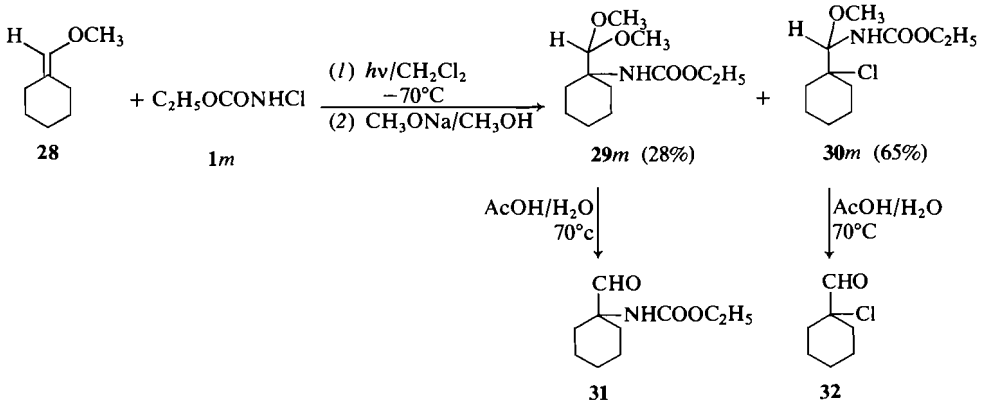

SCHEME 11

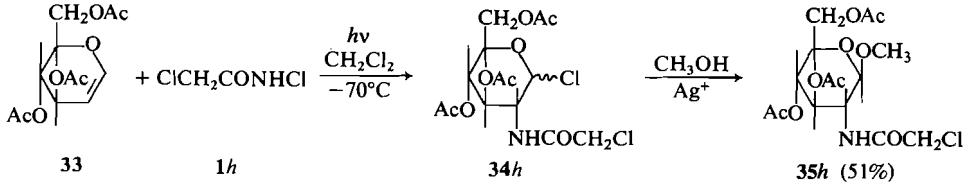

SCHEME 12

the parent amide some 1-acetyl-1-chlorocyclohexene (**27**), resulting from electrophilic chlorination of **26** was formed according to vpc analysis (~10–20%). The addition of NCU (**1***m*) to methoxymethylenecyclohexane (**28**) gave 28% only of α-amido acetal **29***m* but 65% of 1,2-adduct **30***m* resulting from the attack of the amidyl radical on the less substituted carbon atom of enol ether **29***m* (Scheme 11). The α-amido acetal **29***m* and the 1,2-adduct **30***m* were treated with 70% aqueous acetic acid at 70°C for 2 h to afford respectively the α-amido aldehyde **31** (88%, fully characterized as its 2,4-DNP derivative) and the known (34) α-chloro aldehyde **32** (70%) (Scheme 11).

We applied the reaction to triacetyl-D-glucal (**33**) and NCCA (**1***h*) using a slight excess of glucal (1.1 mol per mol of **1***h*). The reaction is described in Scheme 12. The 1,2-adduct **34***h* was not isolated. The crude product was treated with methanol under Koenigs–Knorr conditions to afford the α-amido β-D-glucoside **35***h* (23) in 51% yield (88% by taking into account the amount of unreacted **33** recovered). Thus the amidyl radical preferentially adds on the α face of triacetyl-D-glucal (**33**) as found in the chromous chloride promoted additions (23) and in contrast to the preferential addition of the thioacetyl radical on the β face (35).

The radical addition of *N*-chloroamides to ketene acetals should lead to α-amido esters (hence to α-amino acids) after hydrolysis of the 1,2-adducts. Unfortunately, with such electron-rich olefins (e.g. ketene diethyl acetal), electrophilic chlorination was very fast even at −70°C.

The addition of NCCA (**1***h*) to the electron-poor olefin 1-chlorocyclohexene (Table 8, entry 12) was less efficient than its addition to cyclohexene as

Can. J. Chem. Downloaded from www.nrcresearchpress.com by 210.87.254.5 on 09/05/12
For personal use only.

Can. J. Chem. Downloaded from www.nrcresearchpress.com by 210.87.254.5 on 09/05/12
For personal use only.

expected. However, the addition of NCCA and NCU (**1***m*) to 1-acetylcyclohexene, which is also an electron-poor but a conjugated olefin, was quite efficient (~70%; Table 8, entries 13 and 14). The *trans* adduct **38***m*, upon heating at 185°C under nitrogen, was converted to the oxazolidone **40**.

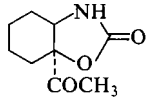

40

Under the same conditions, the *cis* isomer **37***m* was recovered unchanged. We have no satisfactory explanation for the fact that adduct **39***m* where X = H was the major product in the case of NCU whereas no such product was isolated in the case of NCCA. Finally, NCCA did not add to 1-octyne (Table 8, entry 15).

Additions to Dienes

The photodecomposition of NCCA (**1***h*) was inhibited by 1,3-cyclohexadiene. Indeed, after irradiating for 45 h, 94% of *N*-chloro derivative **1***h* was still present according to iodometric titration. Treatment with sodium bisulfite led to the recovery of 95% of chloroacetamide.

As depicted in Scheme 13, the addition of NCA (**1***b*) to norbornadiene led to a 66% yield of three isomeric 3,5-disubstituted nortricyclenes **42***b*, **43***b*, and **44***b* and to a small amount (7%) of 1,2-adduct **41***b*. The stereochemistry of the nortricyclene adducts has not been determined. They have already been described (12*b*). Hydrogenation of 1,2-adduct **41***b* over Adam's catalyst in ethyl acetate afforded the corresponding norbornane derivative **45***b* (Scheme 13) which was different from either of the 1,2-adducts **10***b* and **11***b* obtained from the photochemical addition of NCA (**1***b*) to norbornene (see Scheme 8). Therefore, the chloroacetamido group of **45***b* must be *endo*. The orientation of the chlorine substituent was not determined.

We have already reported that the photochemical addition of *N*-halo-*N*-hydro amides to 1,6-heptadiene gives rearranged 1,7-adducts as well as unrearranged 1,2-adducts (1). In contrast, the addition of NCCA (**1***h*) to 1,5-cyclooctadiene gave 50% of 1,2-adduct **46***h* and 44% of chloroacetamide (Scheme 14). No bicyclic compound resulting from transannular cyclization of the primary radical adduct was detected. Such bicyclic derivatives have been obtained in radical additions to 1,5-cyclooctadiene (36). The ^{1}H nmr spectrum of **46***h* shows a multiplet centered at δ 5.84 for the two olefinic protons and a complex absorption centered at δ 4.45 for the protons on the carbons bearing the substituents. The stereochemistry of adduct **46***h* was not determined.

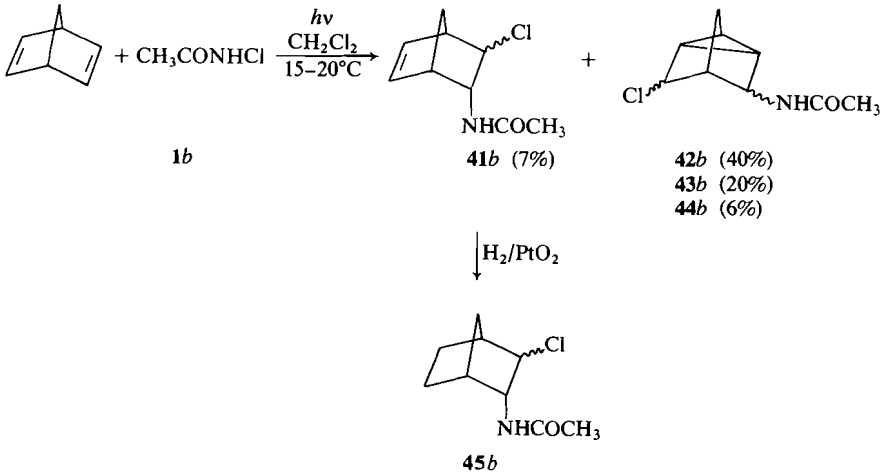

SCHEME 13

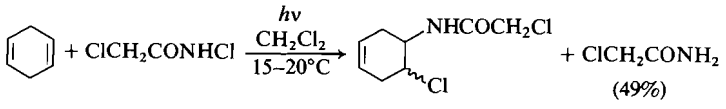

SCHEME 14

Can. J. Chem. Downloaded from www.nrcresearchpress.com by 210.87.254.5 on 09/05/12
For personal use only.

Discussion

The following observations indicate that the photochemical 1,2-addition of *N*-haloamides to olefins involves the attack of the π-bond by an amidyl radical (reaction [2]) followed by halogen-atom transfer onto the resulting adduct radical (reaction [3]): (*i*) the failure of the dark reactions; (*ii*) the orientation of the addition to unsymmetrical olefins (the amido group is attached to the less substituted carbon atom) and to norbornene (the amido group is *exo* (37)); (*iii*) the formation of rearranged adducts in the additions to norbornadiene and to 1,6-heptadiene (1); (*iv*) the inhibition of the 1,2-addition process by oxygen (see below); (*v*) quantum yields greater than unity for the formation of the addition products (see Table 9).

We have seen that, under a nitrogen atmosphere, the photoaddition of *N*-bromochloroacetamide (**1***n*) to cyclohexene in methanol – methylene chloride (1:25) at −70°C was complete after 12 h and gave 95% of 1,2-adducts **2***n* and **3***n* (**2***n*/**3***n* = 1.1) (Table 3, entry 7). Under the same conditions but bubbling oxygen instead of nitrogen through the solution, there was still 18% of unreacted *N*-bromoamide after 63 h and the yield of 1,2-addition was low (20%, **2***n*/**3***n* = 1.0). The main reaction products were 2-bromomethoxycyclohexane (48%) resulting from electrophilic bromination of cyclohexene and chloroacetamide (57%). Thus, the 1,2-addition process is inhibited by oxygen.

Quantum yields greater than unity are indicative of chain processes. From the values of the quantum yields for the formation of 1,2 adducts, Φ(addn), given in Table 9, entries 1 and 2, the 1,2-addition process involves a chain mechanism. The chain appears to be longer with a *N*-bromoamide than with its *N*-chloro analogue because bromine-atom transfers are faster than chlorine-atom transfers. We have indeed shown, using 1,6-heptadiene as the olefin, that the transfer step [3] of the 1,2-addition process is faster with an *N*-bromoamide than with its *N*-chloro analogue (1). The relatively low quantum yields could result from short chains[15] and/or from low efficiency of the primary processes.

TABLE 9. Quantum yields for the photolysis of *N*-haloamides in the presence of cyclohexene

Entry	*N*-Haloamide	Quantum yields[a] Φ(N—X)[b]	Φ(addn)[c]
1	$ClCH_2CONHCl$ (**1***h*)	2.4	2.4
2	$ClCH_2CONHBr$ (**1***n*)	16	10
3	$CH_3CON(CH_3)Cl$ (**1***u*)	6.2	[d]
4	$CH_3CON(CH_3)Br$ (**1***t*)	61	[d]

[a]Based on potassium ferioxalate actinometry, see ref. 38.
[b]Quantum yield for the disappearance of *N*-haloamide (iodometric titration).
[c]Quantum yield for the formation of 1,2-adducts 2 and 3 (isolated).
[d]No addition product was detected.

The quantum yields for the disappearance of *N*-haloamide, Φ(N—X), given in entries 3 and 4 (Table 9) where the addition process could not be detected, are larger than the Φ(addn) values of entries 1 and 2, thus showing that the hydrogen abstraction chain(s) is(are) longer than the 1,2-addition chain. This is shown also by the fact that in entry 3 where the yield of 1,2-addition was of the order of 60%, Φ(N—X) is larger than Φ(addn). In entry 1, the yield of 1,2-addition was greater than 90% and Φ(N—X) has the same value as Φ(addn).

Interestingly, while Φ(N—X) in entry 3 is about 2.6 times larger than Φ(addn) of entry 1 (*N*-chloro derivatives), Φ(N—X) in entry 4 is about 6 times larger than Φ(addn) in entry 2 (*N*-bromo derivatives). Therefore, in the case of *N*-bromoamides, hydrogen abstraction appears to compete more effectively with 1,2-addition than in the case of *N*-chloroamides. This would then explain why the yields of 1,2-addition of *N*-bromoamides are lower than those of the corresponding *N*-chloro derivatives (*Effect of X*). It also might indicate that the main hydrogen abstraction species is not the same whether the *N*-haloamide is an *N*-bromo or an *N*-chloro derivative as would be the case if hydrogen abstraction occurs mainly through the Goldfinger type mechanism (reactions [6] to [8]) when X = Br as well as when X = Cl.[16]

An increase of the electron-withdrawing power of the acyl group (ZCO) should increase the reactivity of the amidyl radical towards the π-bond of an olefin (reaction [2]) by rendering the radical more electrophilic.[17] Furthermore, we have shown that the reactivity of ZCONHX as an halogen-atom transfer agent towards a carbon radical (reaction [3]) increases with the electron-withdrawing power of ZCO (1). Therefore, both the rate of step [2] and that of step [3] of the 1,2-addition chain increase as the ZCO moiety becomes more electronegative and, then, the 1,2-addition process can compete more effectively with hydrogen abstraction. Ex-

[15]We did not isolate any product resulting from the coupling of two amidyls or the coupling of two intermediate adduct-radicals and other reactions are probably involved as chain-termination steps of the 1,2-addition chain.

[16]A more elaborate discussion on the nature of the hydrogen abstraction process(es) is outside the scope of this paper and will be given in a forthcoming paper.

[17]For an interpretation of the electrophilic character of radicals and of their reactivity towards alkenes in terms of frontier orbital interactions, see refs. 39 and 40. An application to the reactivity of alkoxy radicals towards olefins is given in ref. 41.

Can. J. Chem. Downloaded from www.nrcresearchpress.com by 210.87.254.5 on 09/05/12
For personal use only.

perimentally, this is translated into better yields of 1,2-addition (Tables 2 and 4) and shorter reaction times (Table 2). An alkanesulfonyl group should be more electron-withdrawing than an alkanoyl group and it is noteworthy that irradiation of *N*-chloro-*N*-methylethanesulfonamide in the presence of 1-hexene led to a 58% yield of addition (14) whereas NCMA (**1***u*) did not add to 1-dodecene (Table 4).

A conjugated olefin like styrene and conjugated dienes should be more reactive towards an electrophilic radical than an alkene.[17] Unfortunately, the photodecomposition of *N*-chloroamides at 254 nm were inhibited by styrene and 1,3-cyclohexadiene. This could be attributed to the fact that all the light was absorbed by the olefin which could not transfer its energy to the *N*-haloamide. We have not tried to use longer wavelengths. On the other hand, an electron-poor olefin like 1-acetylcyclohexene should be less reactive towards an electrophilic radical than a simple alkene.[17] However, the photochemical addition of NCCA (**1***h*) and NCU (**1***m*), using the 350 nm lamps, was quite efficient (~60%, Table 8). We do not know whether the photodecomposition occurs by direct excitation of the *N*-chloroamide or by indirect excitation, 1-acetylcyclohexene (present in excess) absorbing all the light ($n \rightarrow \pi^*$ excitation) and acting as a sensitizer. The lower yield of addition of NCCA (**1***h*) to 1-chlorocyclohexene (35%) as compared to cyclohexene (91%) is in agreement with the amidyl radical being electrophilic and 1-chlorocyclohexene being poorer in electrons than cyclohexene due to the inductive effect of chlorine.[17] The yields of addition to norbornene should be higher than those to cyclohexene and 1-dodecene since norbornene has a reactive double bond but no reactive allylic hydrogens (minimization of the hydrogen abstraction process(es)). In agreement with this, NCMA (**1***u*) did add to norbornene (42%) whereas it could not be added to cyclohexene or 1-dodecene and the addition of *N*-bromochloroacetamide (**1***n*) was somewhat more efficient with norbornene (77%) than with cyclohexene and 1-octene (62%). However, the yields of addition of NCA (**1***b*) to norbornene and to cyclohexene were exactly the same (50%).

The effect of temperature on the yield of 1,2-addition (Table 3) shows that the hydrogen abstraction process(es) is(are) retarded more than the 1,2-addition process as the temperature is lowered; and more so for an *N*-bromoamide than for its *N*-chloro analogue. This implies that the activation enthalpy of the hydrogen abstraction process(es) is higher than that of the 1,2-addition process. It also implies that the activation energy for hydrogen abstraction is higher with an *N*-bromoamide than with the corresponding *N*-chloro derivative, which could be readily explained: (*i*) if the main hydrogen abstractor is not the same whether X = Br or X = Cl (as suggested above from the Φ(N—X)/Φ(addn) ratio) and (*ii*) if the hydrogen abstractor is the halogen atom (Goldfinger mechanism, reactions [6] to [8]) since a bromine atom is less reactive than a chlorine atom (42).

The replacement of the *N*-hydrogen by an alkyl group (*Effect of R*) should decrease the reactivity of the amidyl radical towards the π-bond of an olefin (reaction [2]) mainly because an *N*-alkyl amidyl is bulkier than its *N*-hydro analogue at the reacting center. On the other hand, the effect of such a replacement on the halogen-atom transfer step [3] should be much smaller. In fact we do not know whether or not an *N*-halo-*N*-alkylamide is a better halogen atom donor than its *N*-hydro analogue. Therefore, the dramatic effect of an *N*-methyl group on the yield of 1,2-addition to cyclohexene ($CH_3CONHCl$, 55% and $CH_3CON(CH_3)Cl$, 0%; $CF_3CONHCl$, 97%, and $CF_3CON(CH_3)Cl$, 18%) and to 1-dodecene ($ClCH_2CONHCl$, 95%, and $ClCH_2CON(CH_3)Cl$, 17%) is most probably due to the retardation of the addition step [2]. The 1,2-addition chain would thus compete less effectively with the hydrogen abstraction chain(s) which should not be affected so much by the presence of an *N*-methyl substituent. Indeed, hydrogen abstraction by the amidyl radical (reaction [9], Bloomfield mechanism) should not be very sensitive to the steric bulk at the nitrogen and the Goldfinger chain (reactions [6] to [8]) should not be affected by the size of the nitrogen radical. The decrease of the yield of addition of $CH_3CONRCl$ to norbornene with R in the order $H > CH_3 > C_2H_5 > i\text{-}C_3H_7$ (Table 7) is in agreement with the addition step [2] being sensitive to the steric bulk of the nitrogen radical. However, contrary to our expectation, the decrease in yield was more pronounced in going from $R = CH_3$ (42%) to $R = C_2H_5$ (10%) than from R = H (56%) to $R = CH_3$ (42%).

We have seen that the yield of addition was lower for X = Br than for X = Cl, that the Φ(N—X)/Φ(addn) ratio was larger for X = Br than for X = Cl, and that the temperature had a more pronounced influence on the competition between 1,2-addition and hydrogen abstraction when X = Br than when X = Cl. These facts can be readily explained, as already pointed out, if hydrogen abstraction involves mainly the halogen atom (Goldfinger chain, reactions [6] to [8]) with both an *N*-bromo and an *N*-chloroamide. We would then expect that efficient scavenging of HX should at

Can. J. Chem. Downloaded from www.nrcresearchpress.com by 210.87.254.5 on 09/05/12
For personal use only.

least diminish the importance of the Goldfinger chain ($X^{\cdot}$–HX–X_2 chain) if it does not suppress it completely. As a result, the 1,2-addition chain (reactions [2] and [3]) should become more important or even take over and the yield of addition should increase. The scavenging of HCl by 2,4,6-trimethylpyridine and by cyclohexene oxide was quite efficient (40 to 55%) as we have seen. But, contrary to our expectation, it had no influence on the yield of 1,2-addition of *N*-chloroamides to cyclohexene (Table 5) or to 1-octene (Table 6, entries 8 and 9), although it did have an effect on the total amount and relative proportion of the halogenation products.[5] A similar observation has been recently reported concerning the effect of ethylene oxide as a scavenger for HBr in the photodecomposition of NBS in the presence of cyclohexene (14): the scavenger had practically no effect on the yield of addition but did affect the relative proportions of 3-bromocyclohexene and dibromocyclohexane.

Summary and Conclusions

The present work allowed us to show that the photochemical addition of *N*-haloamides (ZCONRX) to olefins is a radical chain process. An increase of the yield of addition was observed: (*i*) when replacing X = Br for X = Cl, (*ii*) when increasing the electron-withdrawing power of the ZCO moiety, and (*iii*) when lowering the temperature. Thus high yields of addition to a variety of olefins were obtained with *N*-chloro-*N*-hydroamides (R = H, X = Cl) such as $ClCH_2$-CONHCl (**1***h*), $CCl_3CONHCl$ (**1***k*), $CF_3CONHCl$ (**1***l*), and NCU (**1***m*) at 15–20°C. By carrying out the light-initiated reactions at ca. −70°C, it was possible to get excellent yields of addition with *N*-bromo-*N*-hydroamides (R = H, X = Br) even in the case of NBA (**1***a*). Therefore, the photochemical method can lead to almost quantitative yields of 1,2-addition of *N*-halo-*N*-hydroamides (ZCONHX) to olefins and can be useful to synthesize *N*-(2-haloalkyl)amides. From enol ethers and ZCONHCl, we have prepared α-amido acetals and ketals (aldehydes and ketones) and a 2-amido glycoside in good yields.

We have shown that replacing the *N*-hydrogen by an *N*-methyl group did cause a dramatic decrease in the yield of 1,2-addition which was attributed to a steric effect on the rate of addition of the amidyl radical to the double bond of the olefin (reaction [2]).

We have found that the *cis* isomer predominates over the *trans* isomer in the addition of ZCONHX to cyclohexene, 1-methylcyclohexene, and norbornene as in the chromous chloride promoted additions (12*a*), and furthermore that the *cis*/*trans* ratio varies with the electronegativity and the size of Z.[18]

Finally, although some of the facts (e.g. the variation of the Φ(N—X)/Φ(addn) ratio with X, the difference in the amplitude of the temperature effect with X) could be best explained by a competition between an addition chain involving the amidyl radical as the chain carrier and a halogen atom – HX – X_2 chain (Goldfinger mechanism) for hydrogen abstraction, the presence of an efficient HCl scavenger had practically no effect on the yield of 1,2-addition of *N*-chloroamides (it did have an effect, however, on the halogenation products).[5] Further work is necessary to clearly identify and recognize the pathways competing with the 1,2-addition process.

Experimental Section[19]

Most of the pertinent general information is the same as that given in ref. 12*a*. In addition to an OS-138 column, SE-30 (5% on dimethylsilylated Chromosorb W) and Carbowax 20 M (10% on dimethylsilylated Chromosorb W) columns were used for analytical and preparative vapor phase chromatography (vpc).

Olefins

They were obtained commercially except for 1-methoxycyclohexene which was prepared from cyclohexanone according to the method described by Schmidt and Grafin (44) in a 94% yield after distillation, bp 49°C/22 Torr (lit. (44) 36°C/12 Torr), and (1-methoxymethylene)cyclohexane (**26**) which was prepared from cyclohexanone by the method described by Wittig (45) in a 60% yield after distillation, bp 46–50°C/20–25 Torr (lit. (45) 74°C/48 Torr). The preparation of (1-methoxyethylidene)-cyclohexane (**26**) has been described (46).

Amides

With the exception of pentanamide, the amides were obtained commercially and were used without purification. Pentanamide was prepared from pentanoyl chloride and concentrated ammonium hydroxyde, and recrystallized from methylene chloride, mp 105–107°C (lit. (47) 106°C).

N-*Halo*-N-*hydroamides*

With the few exceptions given below, they were prepared by the sodium hypohalite method (48), their iodometric purity was greater than 94% except for *N*-chloroformamide (**1***f*) (86%), *N*-chloropentanamide (**1***s*) (83%), and *N*-bromo-2,2-dichloroacetamide (**1***p*) (83%). *N*-Chloro-2,2-dimethylpropionamide (**1***c*) was prepared from the parent amide and tertiobutylhypochlorite according to the method of Beckwith and Goodrich (26): yellow liquid, 98% iodometric purity, 65% yield. *N*-Bromo-2,2,2-

[18]The results of a study of the stereochemistry of the radical 1,2-addition of ZCONHX to a variety of acyclic and cyclic (conformationally rigid and flexible) olefins (43) will be reported later.

[19]For the new products not described in the Experimental section, the melting points together with the microanalytical and/or mass spectral data and the ir and ^1H nmr characteristic absorptions are available, at a nominal charge, from the Depository of Unpublished Data, CISTI, National Research Council of Canada, Ottawa, Ont., Canada K1A 0S2.

Can. J. Chem. Downloaded from www.nrcresearchpress.com by 210.87.254.5 on 09/05/12
For personal use only.

trichloroacetamide (**1***q*) was prepared from the parent amide and acetylhypobromite (49): mp 123–124°C (lit. (27) 125°C), 99% iodometric purity, 92% yield. The latter method was used also to prepare *N*-bromo-2,2,2-trifluoroacetamide (**1***r*) which was purified by sublimation: mp 61–62°C (lit. (27) 62°C), 100% iodometric purity, 82% yield.

N-*Halo*-N-*alkylamides*

Most of *N*-chloro-*N*-alkyl amides were prepared by treatment of a stirred solution (magnetic stirring) of the parent amide (0.02 mol) in water (25 mL) containing sodium bicarbonate (0.03 mol, not completely soluble) with chlorine at ca. 0°C (ice bath) until the solution was yellow. The *N*-chloroamide separated out as a deep yellow liquid. Methylene chloride was added. The two phases were separated and the organic phase washed once with water then dried. Evaporation under reduced pressure afforded the *N*-chloroamide as a colorless or slightly yellow liquid. *N*-Chloro-*N*-methylacetamide (**1***u*) was distilled under reduced pressure: bp 45–46°C/16 Torr (95% active chlorine, 73% yield). The other *N*-chloroamides were used without purification: *N*-chloro-*N*-ethylacetamide (**1***y*), 96% active chlorine, 75% yield; *N*-chloro-*N*-isopropylacetamide (**1***z*), 100% active chlorine, 70% yield; *N*-chloro-*N*-tertiobutylacetamide (**1**α), 95% active chlorine, 75% yield; *N*-chloro-*N*-methylchloroacetamide (**1***v*), 95% active chlorine, 60% yield.

N-Chloro-*N*-methylethylcarbamate (**1***x*) was prepared by treating the parent carbamate in methylene chloride with excess sodium hypochlorite (2*a*): 83% active chlorine (sample containing methylene chloride and unreacted parent amide according to the ^{1}H nmr spectrum), 80% yield. *N*-Chloro-*N*-methyltrifluoroacetamide (**1***w*) was obtained from the parent amide by the tertiobutylhypochlorite method (26) and purified by distillation: bp 65–70°C/170 Torr, 94% active chlorine, 60% yield.

N-Bromo-*N*-methylacetamide (**1***t*) was prepared directly in the photochemical cell from equimolar amounts of *N*-methylacetamide and tertiobutyl hypobromite according to the method described by Neale *et al.* (50) for the *N*-bromination of *N*-alkylcarboxamides except that methylene chloride was used as the solvent instead of carbon tetrachloride.

Photochemical Reactions

The uv irradiations were carried out in a Rayonnet RPR-100 reactor using Pyrex cells with the 300 and 350 nm lamps and Vycor cells with the 254 nm lamps. For the reactions at 15–20°C, the cells were cooled with tap water. For the reactions at lower temperatures, jacketed cells of the type described in ref. 1 were used. The reaction temperatures were measured with a copper–constantan thermocouple. The solvents used were dry: methylene chloride and acetonitrile freshly distilled from P_2O_5, absolute methanol. The *N*-haloamide (usually 5 mmol) and the solvent were placed in the cell and cooled to the desired temperature as nitrogen was passed through the solution (10 to 15 min). The olefin (usually 10 mmol), neat or dissolved in the solvent, was added slowly. The reaction mixture was degassed for a further 10 min before irradiating. The resulting solution was normally 0.2 to 0.5 *M* in *N*-haloamide for the reactions at 15–20°C and 0.06 *M* in *N*-haloamide for the reactions at low temperature. A slow stream of nitrogen was maintained throughout the irradiation which was stopped when no more *N*-haloamide was present (negative starch – iodide paper test). The reaction mixture was transferred into a volumetric flask. Aliquots were used for chromatographic separations, vpc, and other analyses.

(a) In the Presence of Cyclohexene

Aliquots were separated by preparative layer chromatography (plc) on silica gel to isolate the *cis* and *trans* adducts **2** and **3** and the parent amide (order of increasing polarity). The yields are recorded in Tables 1, 2, 3, and 4 and in Scheme 4.

An aliquot was treated with silver nitrate (10% ethanolic solution) in the dark at room temperature for 0.5 h. Under these conditions, 3-bromo- and 3-chlorocyclohexene as well as 4-chlorocyclohexene reacted completely to form AgX which was filtered, washed with water, and dried in an oven at 100°C to constant weight. Dichloro- and dibromocyclohexane, *trans* chloro- and bromomethoxycyclohexane, *trans*-chlorocyclohexanol, and the 1,2-adducts **2** and **3** did not react significantly with $AgNO_3$ under the same conditions. Thus the amount of AgX formed was related to the total yield of 3-halo- and 4-halocyclohexene. For the reactions carried out in the presence of 2,4,6-trimethylpyridine (TMP), the TMP hydrochloride formed also led to the formation of AgCl (Table 5).

Finally another aliquot was analysed by vpc for *trans*-chlorocyclohexanol (Carbowax 20 M) formed in the reactions carried out in the presence of cyclohexene oxide (Table 5), *trans*-chloro- and bromomethoxycyclohexane (OS-138) formed in the reactions carried out in the presence of methanol, 3-chloro- (SE-30 or Carbowax 20 M) or 3-bromocyclohexene (OS-138), 4-chlorocyclohexene (SE-30 or Carbowax 20 M), dichloro- or dibromocyclohexane (OS-138), and bicyclohexenyl (OS-138). Authentic samples either commercially available or readily prepared from well known methods were used as standards. The compounds were isolated by preparative vpc for full identification and spectral comparison with the authentic samples. The yields of 3-halocyclohexenes, 4-chlorocyclohexene, dihalocyclohexanes, and bicyclohexenyl will be reported and discussed in a forthcoming paper.

(b) In the Presence of cis *and* trans *3-Hexene*

The pure addition products were obtained by separation of aliquots by preparative vpc on OS-138. The yields were determined by analytical vpc on OS-138 using the pure products as standards (Table 8, entries 2 and 3).

(c) In the Presence of Enol Ethers

The reactions were carried out at −70°C. After the *N*-haloamide had reacted completely, 1 equiv. of sodium methoxide or ethoxide in methanol or ethanol (2 to 3% solution) was added and the reaction mixture was allowed to warm to room temperature. The solvent was removed and the crude product separated by plc on silica gel to isolate the adducts and the parent amide (see Table 8, entries 8 and 9, and Scheme 11). Alternatively, water was added to the reaction mixture which was then allowed to warm to room temperature. The solvent was evaporated and the crude product separated by plc on silica gel to yield the α-amido carbonyl derivative and the parent amide (see Table 8, entry 10). The α-haloketones resulting from electrophilic halogenation were separated by preparative vpc (OS-138) and compared with authentic samples. Their yield was determined by vpc using the pure samples as standards (see Table 8, entry 10, and 1-acetyl-1-chlorocyclohexane (**27**)).

(d) In the Presence of the Other Olefins

Aliquots were separated by plc or silica gel to isolate the addition product(s) and the parent amide. In the case of cyclic olefins (norbornene, 1-methylcyclohexene, pregnenolone acetate) the *cis* adduct was less polar than the *trans* isomer as in the case of cyclohexene. The yields are reported in Tables 6, 7, and 8 and in Schemes 10, 13, and 14.

Typical Procedures for the Photochemical Addition of N-*Haloamides to Olefins*

(a) Addition of N-*Chloropentanamide (1s) to Cyclohexene*

A solution of *N*-chloroamide **1***s* (732 mg, 83% active chlorine, 5 mmol) in CH_2Cl_2 (10 mL) was placed in a Vycor cell cooled with tap water. Nitrogen was bubbled through the solution for 10 min then cyclohexene (1 mL, ~10 mmol), freshly passed through alumina, was added. After degassing for a further

Can. J. Chem. Downloaded from www.nrcresearchpress.com by 210.87.254.5 on 09/05/12
For personal use only.

10 min, the solution was irradiated (254 nm lamps) until the starch–iodide paper test was negative (20 h) while maintaining a slow stream of nitrogen. The reaction mixture was transferred into a 25 mL volumetric flask with methylene chloride. The resulting solution was analyzed by vpc: dichlorocyclohexane, 22%; 3-chlorocyclohexene, 8%; 4-chlorocyclohexene, 3%; bicyclohexenyl, 9%. A 10 mL aliquot was treated with $AgNO_3$ (20 mL of a 10% alcoholic solution) for 30 min in the dark. The precipitate was filtered, washed with water, and dried: 38 mg of AgCl (13%). The remaining solution (15 mL) was evaporated *in vacuo*. The residue was separated by plc (ether–pentane 1:1) to give three main fractions. The less polar fraction consisted of cis N-*(2-chlorocyclohexyl)pentanamide* (**2***s*), mp 47–52°C (212 mg, 32%). Recrystallization from pentane afforded the analytical sample, mp 50–51°C; $\nu_{max}(CHCl_3)$ 3440 (NH), 1730 (C=O), 1520 cm^{-1} (NH); $\delta(CDCl_3)$, 0.91 (t, J = 6.5 Hz, 3H), 1.0–2.4 (6H), 4.10 (m, $\Delta\nu_{1/2}$ = 27 Hz, $\Delta\nu_{1/2}$ = 19 Hz after exchange with D_2O, H_1), 4.51 (q, $J \simeq$ 2.5 Hz, H_2), 6.33 ppm (br d, J = 8 Hz, NH); *m/e* 217, 219 (3:1, M^+). *Anal.* calcd. for $C_{11}H_{20}ClNO$: Cl 16.28; found: Cl 16.26.

The second fraction consisted of trans N-*(2-chlorocyclohexyl)pentanamide* (**3***s*), mp 83–86°C (70 mg, 11%). Recrystallization from pentane–ether afforded the analytical sample, mp 87°C; $\nu_{max}(CHCl_3)$ 3430 and 3320 (free and bonded NH), 1665 (C=O), 1520 cm^{-1} (NH); $\delta(CDCl_3)$, 0.90 (t, J = 6.5 Hz, 3H), 1.0–2.5 (6H), 3.84 (m, $\Delta\nu_{1/2} \sim$ 21 Hz, $H_1 + H_2$), 6.38 ppm (br, NH); *m/e* 217, 219 (3:1, M^+). *Anal.* calcd. for $C_{11}H_{20}ClNO$: Cl 16.28; found: Cl 16.06.

The third fraction (219 mg) consisted of a mixture of pentanamide and 4-chloropentanamide **5** which could not be separated. A microanalytical determination of chlorine gave 5.40% from which the relative proportion of pentanamide and **5** could be evaluated as 70:30 (30% yield of pentanamide, 11% yield of **5**). The ^1H nmr spectrum ($CDCl_3$) showed a doublet at 1.52 ppm (J = 6 Hz) for the methyl group of **5**. The mixture was dissolved in dry tertiobutanol (5 mL) then treated with *t*-BuOK (100 mg of K in 2.5 mL of *t*-BuOH) at 80°C for 12 h under a nitrogen atmosphere. Water was added and the mixture extracted with methylene chloride (2 × 25 mL). The organic phases were washed with water then dried. The solution was concentrated then analysed by vpc using pure samples as standards: pentanamide, 22%; 5-methyl-2-pyrrolidinone (**6**), 9%. The pure samples were obtained by preparative vpc and compared (ir and ^1H nmr) with authentic samples obtained commercially.

Alternatively, 5 mmol of *N*-chloropentanamide (**1***s*) was photolysed under the same conditions as above but in the absence of cyclohexene. The crude product was treated with base according to the procedure described by Beckwith and Goodrich (26) and the resulting mixture separated by plc (ether) to afford valeric acid (76 mg, 15%) and γ-valerolactone (295 mg, 59%). The lactone was purified by distillation and compared (ir and ^1H nmr) with an authentic sample.

(b) Addition of N-*Chloro-trifluoroacetamide (1l) to Pregnenolone Acetate (20)*

The reaction was carried out as in (*a*) with the following quantities: **1***l*, 263 mg, 100% active chlorine, 2 mmol in CH_2Cl_2 (5 mL); **20**, 717 mg, 2 mmol in CH_2Cl_2 (5 mL). The reaction took 1.75 h. The solvent was evaporated *in vacuo* and the crude product separated by plc (ether–pentane 1:1) to give three main fractions. The less polar fraction consisted of pregnenolone acetate, mp 147–150°C (137 mg, 19%), identical (ir, ^1H nmr) to that of an authentic sample.

The second fraction consisted of *3β-acetoxy-5α-chloro-6α-trifluoroacetylaminopregnan-20-one* (**21***l*), mp 183–185°C (201 mg, 21%). Recrystallization from ether afforded the analytical sample, mp 185–186°C; $\nu_{max}(CHCl_3)$ 3420 (NH), 1735 and 1710 (C=O of amide and acetate), 1250 and 1030 (acetate), 1170 cm^{-1} (CF_3); $\delta(CDCl_3)$ 0.63 (s, $18CH_3$), 1.19 (s, $19CH_3$), 2.02 (s, $COCH_3$), 2.11 (s, $OCOCH_3$), 4.36 (t, ΣJ = 20 Hz, H_6 axial; becomes a d, J = 9.5 Hz, upon irradiating the NH), 5.24 (m, $\Delta\nu_{1/2}$ = 33 Hz, H_3 axial), 6.41 ppm (br d, J = 9.5 Hz, NH). *Anal.* calcd. for $C_{25}H_{30}F_3ClNO_4$: C 59.34, H 6.97, N 2.76; found: C 59.12, H 7.14, N 2.63.

The third fraction consisted of *3β-acetoxy-5α-chloro-6β-trifluoroacetylaminopregnan-20-one* (**22***l*), mp 210–211°C (516 mg, 50%). Recrystallization from methylene chloride – methanol afforded the analytical sample, mp 205–206°C; $\nu_{max}(CHCl_3)$ 3460 (NH), 1740 and 1710 (C=O of amide and acetate), 1535 (NH), 1250 and 1035 (acetate), 1175 cm^{-1} (CF_3); $\delta(CDCl_3)$, 0.65 (s, $18CH_3$), 1.24 (s, $19CH_3$), 2.02 (s, $COCH_3$), 2.12 ($OCOCH_3$), 4.45 (dd, ΣJ = 14 Hz, H_6 equatorial; becomes a d, J = 3.8 Hz, upon irradiating the NH), 5.35 (m, $\Delta\nu_{1/2}$ = 32 Hz, H_3 axial), 6.52 ppm (br d, J = 9.5 Hz, NH). *Anal.* calcd. for $C_{25}H_{30}F_3ClNO_4$: C 59.34, H 6.97, N 2.76; found: C 59.28, H 6.81, N 2.80.

(c) Addition of N-*Chlorochloroacetamide (1h) to Triacetyl-*D-*glucal (33)*

A solution of *N*-chloroamide **1***h* (242 mg, 96% active chlorine, 2 mmol) in CH_2Cl_2 (80 mL) was placed in a Vycor jacketed cell (1) cooled with methanol saturated with dry ice. Nitrogen was bubbled through the solution for 10 min, then a solution of glycal **33** (599 mg, 2.2 mmol) in CH_2Cl_2 (20 mL) was added slowly. After degassing for a further 10 min, the reaction mixture was irradiated (254 nm lamps) for 3.25 h. The solvent was evaporated *in vacuo* at ca. 5–10°C. The residue was dissolved in absolute methanol (40 mL). Silver carbonate (3 g) and Drierite (3 g) were added and the mixture stirred for 12 h at room temperature. Filtration through celite, washing with methanol, and evaporation to dryness gave a crystalline residue (905 mg). Recrystallization from methylene chloride – ether afforded *methyl-2-deoxy-2-chloroacetylamino-3,4,6-tri-*O-*acetyl-β-*D-*glucopyranoside* (**35***h*), mp 148–152°C (351 mg, 44%). Further recrystallization gave a sample melting at 156–157°C; $[\alpha]_D^{25}$ −5° (*c* 1.0, $CHCl_3$) (lit. (51) mp 154–156°C; $[\alpha]_D^{0}$ −6.67 (*c* 0.75)); it proved identical (ir, ^1H nmr) to that of an authentic sample (23). Separation of the mother liquors by plc (ether) gave two fractions. The less polar fraction consisted of triacetyl-D-glucal (**33**), mp 43–48°C (251 mg, 42%) identified (ir, ^1H nmr) with an authentic sample. The second fraction consisted of β-glucopyranoside **35***h*, mp 150–156°C (97 mg, 12%; total yield: 56% (51% based on glucal **33**).

N-*Methyl Oxazolidone* **9**

N-(2-Chlorododecyl)-*N*-methyltrifluoroacetamide (**8***w*) (100 mg, 0.3 mmol) was treated with a 7% solution of potassium carbonate in methanol–water (5:2, 10 mL) at room temperature overnight. The reaction mixture was extracted with methylene chloride, the organic phases washed with water then dried. Removal of the solvent *in vacuo* afforded the N-*methyloxazolidone* **9**, mp 40–42°C (62 mg, 85%). Two recrystallizations from hexane afforded a sample melting at 44–44.5°C; $\nu_{max}(CHCl_3)$ 1760 cm^{-1} (C=O); $\delta(CDCl_3)$ 0.89 (m, terminal CH_3), 1.0–2.0 (18H), 2.88 (s, $\geq N—CH_3$), 3.01–3.74 (six lines, 2H), 4.44 ppm (m, $\Delta\nu_{1/2} \sim$ 30 Hz, 1H); *m/e* 241 (M^+).

cis-*Oxazoline* **16**

(a) From Bromoacetamidation of cis *3-Hexene*

A solution of bromine (3.2 g, 0.02 mol) and silver perchlorate (4.14 g, 0.02 mol) in acetonitrile (25 mL, distilled over P_2O_5) was cooled in an ice bath and *cis*-hexene (2.5 mL, ~0.02 mol) was added dropwise while stirring. The precipitation of silver bromide was immediate. After a few minutes, sodium hydroxide (10 mL of 0.01 *N* solution) was added. The mixture was extracted with methylene chloride and the organic phases washed

Can. J. Chem. Downloaded from www.nrcresearchpress.com by 210.87.254.5 on 09/05/12
For personal use only.

with water then dried. The solvent was removed *in vacuo* (2.30 g, 52%). Part of the residue (1.0 g) was dissolved in absolute methanol (25 mL). Sodium methoxide (0.105 g of sodium in 5 mL of methanol) was added and the mixture heated at 60°C for 12 h under nitrogen. Part of the methanol was evaporated *in vacuo* and the resulting solution treated with brine (10 mL) and then extracted with methylene chloride (3 × 25 mL). The combined organic phases were dried and the solvent evaporated to give cis-*4,5-diethyl-2-methyloxazoline* (**16**) (0.65 g, 94%) which was purified by microdistillation for analyis: $\nu_{max}(CHCl_3)$ 1665 (C=N), 1438 (C—N), 1268 cm^{-1} (C—O—C); $\delta(CDCl_3)$ 0.8–1.8 (10H); 1.93 (d, J = 1.5 Hz, N—CH_3), 3.85 (br sext, J = 7 and 9 Hz, H-4), 4.40 ppm (sext, J = 7 and 9 Hz, H-5). *Anal.* calcd. for $C_9H_{15}NO$: C 68.04, H 10.70, N 0.91; found: C 68.48, H 11.06, N 9.22.

(b) From threo N-*(4-Chloro-3-hexyl)trifluoroacetamide (12l)*

The *threo* 1,2-adduct **12***l* (462 mg, 2 mmol) was stirred with potassium carbonate (20 mL of a 7% solution in methanol–water 5:2) for 3 h at room temperature. The mixture was extracted with methylene chloride. The solvent was evaporated and the residue treated in acetic anhydride – pyridine at room temperature for 4 h. The solvent was removed *in vacuo* and the crude product treated with sodium methoxide (46 mg of sodium in 10 mL of methanol) at 65°C for 24 h. Work up as in (*a*) followed by microdistillation of the product gave the pure cis-*oxazoline* **16** (214 mg, 70%), identical (ir, ^1H nmr) to the sample obtained in (*a*).

trans-*Oxazoline* ***17***

(a) From Bromoacetamidation of trans *3-Hexene*

The procedure was exactly the same as that described in (*a*) above using the same quantities except that treatment with sodium methoxide was carried out on the whole crude β-bromoamide to give trans-*4,5-diethyl-2-methyloxazoline* (**17**) (2.97 g, 97%) which was purified by microdistillation: $\nu_{max}(CHCl_3)$, 1670 (C=N), 1440 (C—N), 1250 cm^{-1} (C—O—C); $\delta(CDCl_3)$, 0.95 (t, J = 7.5 Hz, 3H), 1.53 (m, 4H), 1.95 (d, J = 1.2 Hz, N—CH_3), 3.56 (br q, J = 6 Hz, H-4), 4.05 ppm (q, J = 6 Hz, H-5). *Anal.* calcd. for $C_9H_{15}NO$: C 68.04, H 10.70, N 9.91; found: C 68.07, H 10.92, N 9.40.

(b) From erythro N-*(4-Chloro-3-hexyl)trifluoroacetamide (13l)*

The procedure was exactly the same as that described in (*b*) above using the same quantities to give the *trans*-oxazoline **17** (236 mg, 77%), identical (ir, ^1H nmr) to the sample obtained in (*a*).

Hydrolysis of α-*Amido Acetal* ***29***m

The acetal **29***m* (95 mg, 0.39 mmol) was treated at 70°C with 70% aqueous acetic acid (5 mL) for 2 h. Evaporation to dryness in the presence of benzene gave an oil (70 mg, 88%); $\nu_{max}(CHCl_3)$ 3420 (NH), 2810 and 2710 (CH of aldehyde), 1730 (C=O of carbamate), 1710 (C=O of aldehyde), 1500 (NH), 1240 and 1100 cm^{-1} (C—O of carbamate); $\delta(CDCl_3)$ 1.24 (t, J = 7 Hz, OCH_2CH_3), 4.10 (q, J = 7 Hz, OCH_2CH_3), 5.24 (br, NH), 9.20 ppm (s, CHO); *m/e* 199 (M^+). The 2,4-DNP derivative (prepared in methanol) melted at 158–159°C.

Hydrolysis of ***30***m

The hydrolysis was carried out as above (95 mg of **30***m*, 0.4 mmol) except that the reaction was carried out in the presence of 2,4-dinitrophenylhydrazine (198 mg, 1 mmol) to give directly the 2,4-DNP derivative of α-chloro aldehyde **32** (104 mg, 80%), mp 214–215°C (lit. (34) mp 220–221°C).

Hydrogenation of ***41***b

Compound **41***b* (46 mg, 0.25 mmol) was hydrogenated over prehydrogenated platinum oxide (3 mg) in ethyl acetate (2 mL) over 1 h (3.6 mL of H_2 was absorbed). Filtration over celite and evaporation to dryness gave N-(endo-*3-chloro*-endo-*2-norbornyl)acetamide* (**45***b*), mp 127–128°C (40 mg, 100%). Recrystallization from ether – methylene chloride afforded the analytical sample, mp 129–130°C; $\nu_{max}(CHCl_3)$ 3430 (NH), 1670 (C=O), 1515 cm^{-1} (NH); $\delta(CDCl_3)$ 1.1–2.3 (6H), 1.98 (s, CH_3), 2.42 (m, $H_1 + H_4$), 2.42 (m, $H_2 + H_3$), 6.52 ppm (br, NH); *m/e* 187, 189 (3:1, M^+). *Anal.* calcd. for $C_9H_{14}ClNO$: C 57.60, H 7.57, N 7.46; found: C 57.45, H 7.70, N 7.65.

N-*Methyl*-N,N′-*methylenebisurethane* ($C_2H_5OCON(CH_3)CH_2COOC_2H_5$)

Urethane (7.12 g, 80 mmol), *N*-methylurethane (4.62 g, 40 mmol), formaldehyde (10 mL of a 37% solution, 123 mmol), and hydrochloric acid 0.1 *N* (120 mL) were stirred at room temperature for 4 days. The crude product obtained after methylene chloride extraction (3 × 150 mL) followed by the usual work up was distilled under reduced pressure. The fraction collected at 80–130°C (0.4 Torr) was redistilled to afford a fraction (1.4 g, 95–110°C/0.6 Torr) containing the desired product. An aliquot (0.350 g) was separated by plc on silica gel (hexane–ether 2:1) to give N-*methyl*-N,N′-*methylenebisurethane* (0.274 g, 16%) which was purified by microdistillation (90–100°C, 0.1 Torr) for analysis: $\nu_{max}(CHCl_3)$ 3460 (NH), 1730 and 1700 (C=O), 1505 (NH), 1235 and 1190 cm^{-1} (C—O—C); $\delta(CDCl_3)$ 1.24 (t, J = 7 Hz, 6H), 2.94 (s, $>$N—CH_3), 4.08 (q, J = 7 Hz, 4H), 4.59 (d, J = 7 Hz, $>$N—CH_2—NH—), 5.88 ppm (br, NH); *m/e* 204 (M^+). *Anal.* calcd. for $C_8H_{16}N_2O_4$: C 47.05, H 7.90, N 13.72; found: C 47.11, H 7.86, N 13.86.

The photochemical addition of *N*-chloro-*N*-methylethylcarbamate (0.83 g, 83% active chlorine, 5 mmol) to 1-octene (1.6 mL, 10 mmol) in CH_2Cl_2 (30 mL) was carried out in the usual way. Separation by plc on silica gel (ether–hexane 1:1) afforded two fractions. The less polar fraction consisted of the 1,2-adduct **8***x* (0.26 g, 21%) (see Tables 10, 11, and 12 for its characterization).[19] The other fraction (0.47 g) consisted of a mixture of *N*-methylethylcarbamate and *N*-methyl-*N*,*N*′-methylenebisurethane, the relative proportions of which were determined by ^1H nmr (see Table 6 for the yields). Further separation of the second fraction by plc allowed the isolation of a small amount of bisurethane identical (ir, ^1H nmr) to the authentic sample prepared above.

N-*Methyl*-N,N′-*methylenebisacetamide*

Attempts to prepare that compound from *N*-methylacetamide, acetamide, and formaldehyde in acidic medium as above were unsuccessful. *N*-Chloro-*N*-methylacetamide (**1***u*) was treated with triethylamine in the presence of *N*-methylacetamide in methylene chloride but no bisacetamide could be detected.

N-Chloro-*N*-methylacetamide (**1***u*) (565 mg, 95% active chlorine, 5 mmol) in CH_2Cl_2 (25 mL) was irradiated at 254 nm for 4 h. Vapor phase chromatography analysis showed the presence of a substantial amount of chloroform (>95%) and traces of 1,1,2,2-tetrachloroethane (SE-30 column, 35°C) and about 8% of *N*-methylacetamide (OS-138 column, 130°C). The solvent was evaporated and the residue separated by plc on silica gel (ether–hexane 4:1) to afford N-*methyl*-N,N′-*methylenebisacetamide* (21 mg, 6%) as an oil which was not purified further: $\nu_{max}(CHCl_3)$ 3430 and 3300 (free and bonded NH), 1672 and 1650 (C=O), 1510 cm^{-1} (NH); $\delta(CDCl_3)$ 1.98 (s, $COCH_3$), 2.06 (s, $COCH_3$), 3.14 (s, $>$N—CH_3), 4.71 (d, J = 7.5 Hz, $>$N—CH_2—NH), 6.67 ppm (br, NH); *m/e* 144.0903 (calcd. for $C_6H_{12}N_2O_2$, 144.0899).

A more polar fraction still contained some bisacetamide along with polymeric material according to the ^1H nmr spectrum and was not further investigated.

Acknowledgements

We are grateful to the Ministère de l'Education du Québec and the Natural Sciences and Engineering Research Council of Canada for their financial support. We acknowledge the helpful assistance of G. Caron, Y. Couture, D. Bérubé, and J. Y. Huot who carried out some of the reactions.

1. M. Mondon and J. Lessard. Can. J. Chem. **56**, 2590 (1978).
2. (*a*) J. Lessard, R. Cote, P. Mackiewicz, R. Furstoss, and B. Waegell. J. Org. Chem. **43**, 3750 (1978); (*b*) P. Mackiewicz, R. Furstoss, B. Waegell, R. Cote, and J. Lessard. J. Org. Chem. **43**, 3746 (1978).
3. H. Driguez, J. P. Vermes, and J. Lessard. Can. J. Chem. **56**, 119 (1978).
4. (*a*) D. Touchard and J. Lessard. Tetrahedron Lett. 4425 (1971); (*b*) D. Touchard and J. Lessard. Tetrahedron Lett. 3827 (1973).
5. G. F. Bloomfield. J. Chem. Soc. 114 (1944).
6. J. Adam, P. A. Gosselain, and P. Goldfinger. Nature, **171**, 704 (1953); P. A. Gosselain, J. Adam, and P. Goldfinger. Bull. Soc. Chim. Belg. **65**, 533 (1956).
7. R. S. Neale. Synthesis, 1 (1971).
8. P. Mackiewicz and R. Furstoss. Tetrahedron, **34**, 3241 (1978).
9. P. Chabrier. Ann. Chim. **17**, 353 (1942).
10. T. A. Foglia and D. Swern. J. Org. Chem. **31**, 3625 (1966).
11. (*a*) K. Schrage. Tetrahedron Lett. 5795 (1966); (*b*) Tetrahedron, **27**, 3033 (1967); (*c*) Tetrahedron, **27**, 3039 (1967).
12. (*a*) H. Driguez, J. M. Paton, and J. Lessard. Can. J. Chem. **55**, 700 (1977); (*b*) H. Driguez and J. Lessard. Can. J. Chem. **55**, 720 (1977).
13. J. C. Day, M. G. Katsaros, W. D. Kocher, A. E. Scott, and P. S. Skell. J. Am. Chem. Soc. **100**, 1950 (1978).
14. F. L. Lu, Y. M. A. Naguib, M. Kitadani, and Y. L. Chow. Can. J. Chem. **57**, 1967 (1979).
15. (*a*) F. A. Daniher and P. E. Butler. J. Org. Chem. **33**, 4336 (1968); (*b*) T. Ohashi, M. Sugie, M. Okahara, and S. Komori. Tetrahedron, **25**, 5349 (1969).
16. T. Ohashi, M. Sugie, M. Okahara, and S. Komori. Tetrahedron Lett. 4195 (1968).
17. R. S. Neale and N. L. Marcus. J. Org. Chem. **34**, 1808 (1969).
18. (*a*) A. Zwierzak and A. Koziara. Tetrahedron, **26**, 3527 (1970); (*b*) S. Zawadzki and A. Zwierzak. Tetrahedron, **29**, 315 (1973).
19. C. Walling, A. Rieger, and D. Tanner. J. Am. Chem. Soc. **85**, 3129 (1963).
20. M. L. Poutsma. J. Am. Chem. Soc. **87**, 2172 (1965).
21. (*a*) M. S. Kharasch and M. Sage. J. Org. Chem. **14**, 537 (1949); (*b*) R. P. Buckley and M. Szwarc. Proc. R. Soc. A, 396 (1957); (*c*) C. Walling and W. Helmreich. J. Am. Chem. Soc. **81**, 1144 (1959).
22. R. A. Johnson and F. D. Greene. J. Org. Chem. **40**, 2186 (1975).
23. H. Driguez, J. P. Vermez, and J. Lessard. Can. J. Chem. **56**, 119 (1978).
24. G. Kortüm, W. Vogel, and K. Andtrussow. Dissociation constants of organic acids in aqueous solution. Butterworth, London. 1961. pp. 294, 295.
25. H. Menard and J. Lessard. J. Chem. Eng. Data, **23**, 64 (1978).
26. A. L. J. Becwith and J. E. Goodrich. Aust. J. Chem. **18**, 747 (1965).
27. J. D. Park, H. J. Gerjovich, W. R. Lycan, and J. R. Lacher. J. Am. Chem. Soc. **74**, 2189 (1952).
28. S. Wolfe and D. V. C. Awang. Can. J. Chem. **49**, 1384 (1971).
29. M. T. Rogers and J. C. Woodrey. J. Phys. Chem. **66**, 540 (1962).
30. V. Calo, L. Lopez, and G. Pesce. J. Chem. Soc. Perkin Trans. 1, 501 (1977).
31. D. D. Tanner and N. Wada. J. Am. Chem. Soc. **97**, 2190 (1975).
32. A. Hassner, L. A. Levy, and R. Gault. Tetrahedron Lett. 3119 (1966).
33. Von K. Ponsold and W. Ihn. J. Prakt. Chem. **313**, 811 (1971).
34. G. Stork, W. S. Worrall, and J. J. Pappas. J. Am. Chem. Soc. **82**, 4315 (1960).
35. K. Igarashi and T. Honma. J. Org. Chem. **35**, 606 (1970).
36. R. P. A. Sneeden. Synthesis, 259 (1971).
37. N. A. Lebel. J. Am. Chem. Soc. **82**, 623 (1960); P. A. Bohm and P. I. Abell. Chem. Rev. **62**, 599 (1962); N. A. Lebel, P. D. Beirne, E. R. Karger, J. C. Powers, and P. Subramanian. J. Am. Chem. Soc. **85**, 3199 (1963); K. Kwart and J. L. Nyce. J. Am. Chem. Soc. **86**, 2601 (1964); C. L. Osborn, T. V. van Auken, and D. J. Trecker. J. Am. Chem. Soc. **86**, 201 (1964); D. I. Davies, L. T. Parfitt, C. K. Alden, and J. A. Claisse. J. Chem. Soc. C, 1585 (1969).
38. C. G. Hatchard and C. A. Parker. Proc. R. Soc. A**235**, 518 (1956).
39. J. Fossey. Thèse d'Etat, Université de Paris-Sud, 1974. pp. 69 *et seq*.
40. I. Fleming. Frontier orbitals and organic chemical reactions. John-Wiley and Sons, Ltd., New York, NY. 1976. pp. 182–188.
41. M. P. Bertrand and J. M. Surzur. Tetrahedron Lett. 3451 (1976).
42. W. A. Pryor. Free radicals. McGraw-Hill, Inc., New York, NY. 1966. pp. 154–156.
43. M. Mondon. Ph.D. Thesis, Université de Sherbrooke, Sherbrooke (Qué.). 1977.
44. V. Schmidt and P. S. Grafin. Ann. Chem. **656**, 100 (1962).
45. G. Wittig, W. Böll, and K. H. Kbück. Chem. Ber. **95**, 2514 (1962).
46. G. Caron and J. Lessard. Can. J. Chem. **51**, 981 (1973).
47. Handbook of chemistry and physics. CRC Press. 1972. p. C-411.
48. C. Bachand, H. Driguez, J. M. Paton, D. Touchard, and J. Lessard. J. Org. Chem. **39**, 3136 (1974).
49. T. R. Beebe and J. W. Wolfe. J. Org. Chem. **35**, 2056 (1976).
50. R. S. Neale, N. L. Marcus, and R. G. Schepers. J. Am. Chem. Soc. **88**, 3051 (1966).
51. T. Osawa. Chem. Pharm. Bull. Tokyo, **8**, 597 (1960).

Can. J. Chem. Downloaded from www.nrcresearchpress.com by 210.87.254.5 on 09/05/12
For personal use only.

Effects of protonation and hydrogen bonding on carbon-13 chemical shifts of compounds containing the >C=N̈— group[1,2]

MALWINA ALLEN[3] AND JOHN D. ROBERTS[4]

The Gates and Crellin Laboratories of Chemistry, California Institute of Technology, Pasadena, CA 91125, U.S.A.

Received March 4, 1980

This paper is dedicated to Prof. Raymond U. Lemieux on the occasion of his 60th birthday

MALWINA ALLEN and JOHN D. ROBERTS. Can. J. Chem. **59**, 451 (1981).

The effects of hydrogen bonding and protonation produced by changing solvent from chloroform to 2,2,2-trifluoroethanol to trifluoroacetic acid were determined for the ^{13}C chemical shifts of fourteen imines, four oximes, and two pyridines. Downfield shifts relative to chloroform were observed for the C=N carbon of the imines and oximes in both trifluoroethanol and trifluoroacetic acid, ranging from 1.5 to 27.5 ppm, which contrasts with upfield C_α shifts for the pyridines in trifluoroacetic acid. Substantial downfield and upfield shifts of from +10 to −15 ppm were found for the *para* and *ipso* carbons, respectively, of the aromatic rings attached to the C=N group in trifluoroacetic acid. Possible explanations of these shift changes are considered as well as their relation to the corresponding changes in ^{15}N shifts with the identical variations in solvent.

MALWINA ALLEN et JOHN D. ROBERTS. Can. J. Chem. **59**, 451 (1981).

Utilisant le chloroforme, la trifluoro-2,2,2 éthanol et l'acide trifluoroacétique comme solvants, on a déterminé les effets de la liaison hydrogène et de la protonation résultant du changement de solvant sur les déplacements chimiques du ^{13}C de 14 imines, de 4 oximes et de deux pyridines. On a observé des déplacements chimiques vers les champs faibles (allant de 1,5 à 27,5 ppm) du carbone C=N des imines et des oximes dans le trifluoroéthanol et dans l'acide trifluoroacétique; ces résultats contrastent avec les déplacements chimiques vers les champs forts observés pour les C_α des pyridines dans l'acide trifluoroacétique. Dans l'acide trifluoroacétique, on a observé des déplacements importants vers les champs faibles et vers les champs forts allant de +10 a −15 ppm pour les carbones respectivement en positions *para* et *ipso* des cycles aromatiques liés au groupe C=N.

On considère des explications probables de ces déplacements aussi bien que leur relation avec les changements correspondants dans les déplacements chimiques du ^{15}N avec des changements identiques de solvants.

[Traduit par le journal]

Introduction

In the preceding paper (1), we reported the changes in ^{15}N chemical shifts associated with the sequence of solvent changes, chloroform → 2,2,2-trifluoroethanol → trifluoroacetic acid for a number of imines, oximes, and pyridines. The corresponding changes in ^{13}C chemical shifts are discussed here.

Previous studies of the protonation of azaaromatics (2), amino acids (3), aliphatic amines (4), benzenamine (5), and nitriles (6) have demonstrated a general trend of upfield ^{13}C shifts, ranging from 1 to about 17 ppm, for the carbons directly attached to the nitrogens. Because imines, oximes, azaaromatics, and nitriles all have multiple bonds between nitrogen and carbon, and because the ^{15}N shifts of all of the substances move strongly *upfield* on protonation, it was of interest to determine whether the ^{13}C shifts of the carbons multiply bonded to the nitrogens change in a similarly uniform way.

Experimental Section

The compounds used were the same as in the earlier investigation (1). The ^{13}C spectra of 4 mol% solutions were taken with a Varian XL-100-15 spectrometer operating at 25.4 MHz in the Fourier-transform mode, with 12-mm od sample tubes, 20-μs pulses (45° flip angle), and 5-s repetition rates. Good signal-to-noise ratios could usually be obtained for all of the carbons with 200–300 scans. Tetramethylsilane (TMS) was used as internal reference, and a 5-mm coaxial tube containing deuterium oxide provided the external field frequency lock signal. The samples were at the ambient probe temperature, about 28°C. The data length was 8192 points for a spectral width of 5000 Hz. The reproducibility of the shifts was about ±0.05 ppm.

Results and Discussion

The ^{13}C chemical shifts of all of the compounds studied in this work in chloroform solution are summarized in Tables 1 to 4, wherein the compounds are grouped in accord with common structural features. Values for the shifts of some of these compounds have been reported previously (2, 7–9), but were redetermined to ensure constant experimental conditions. The assignments of resonances to particular carbons were generally

[1]Supported by the National Science Foundation, and by the Public Health Service, Research Grant No. GM-11072 from the Division of General Medical Sciences.

[2]Contribution No. 6180.

[3]On sabbatical leave from Framingham State College, Framingham, MA 01701, U.S.A.

[4]To whom all correspondence should be addressed.

0008-4042/81/020451-08$01.00/0

©1981 National Research Council of Canada/Conseil national de recherches du Canada

Can. J. Chem. Downloaded from www.nrcresearchpress.com by 210.87.254.42 on 09/05/12
For personal use only.

TABLE 1. ^{13}C chemical shifts of *N*-benzylideneanilines in chloroform

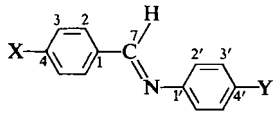

Compound	X	Y	δ, ppm from internal TMS									
			C7	C1	C2	C3	C4	C1′	C2′	C3′	C4′	C8[a]
1*a*	CH_3O	H	159.3	129.1	130.3	114.0	162.0	152.2	120.7	128.9	125.3	55.2
1*b*	CH_3	H	160.0	133.6	129.6	129.3	141.6	152.1	120.7	128.9	125.3	21.6
1*c*	H	H	160.1	136.0	128.5	128.5	131.1	151.8	120.6	129.0	125.7	
1*d*	O_2N	H	157.0	141.4	129.2	123.8	149.1	150.7	120.8	129.2	126.9	
1*e*	H	OCH_3	158.0	136.3	128.5	128.5	130.8	144.7	122.0	114.3	158.0	55.0
1*f*	H	NO_2	162.4	135.3	128.8	129.1	132.2	157.7	121.1	124.8	145.3	

[a]The substituent carbon.

TABLE 2. ^{13}C chemical shifts of *N*-benzylidenealkylamines in chloroform

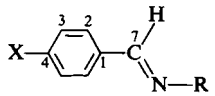

Compound	X	R	δ, ppm from internal TMS									
			C7	C1	C2	C3	C4	C1′	C2′	C3′	C4′	C8
2*a*	CH_3O		157.9	129.4	129.4	114.1	161.2	69.9	25.7	34.5	25.7	55.1
2*b*	O_2N		155.9	142.0	128.5	123.6	148.6	70.6	24.6	34.2	25.6	
2*c*	H	$CH(CH_3)_2$	158.0	136.4	127.9	128.3	130.2	61.7	24.2			
2*d*	H	$CH_2CH(CH_3)_2$	160.5	136.3	127.9	128.3	130.4	69.7	29.6	20.7		
2*e*	H	CH_2CH_3	160.2	136.2	127.8	128.4	130.3	55.8	16.3			

confirmed by single-frequency off-resonance decoupling, relative peak intensities, and comparisons with shift assignments already made for appropriately substituted benzene derivatives. For the imine, **3***a*, the phenyl rings attached to the C=N carbon are nonequivalent; the set of resonances similar to those of **3***b* was assigned to the *anti* phenyl carbons. This assumes the *anti* configuration of **3***b* suggested by Yoshida *et al.* (9) is correct. The resonances of **3***c* and **3***d* were made by analogy with those of the corresponding oximes (7).

The ^{13}C shifts of the imines of Table 1 and of the oximes of Table 4 have been discussed previously (7, 8). The C=N carbons of the imines in Table 2 are very similar to those of Table 1, and are rather insensitive to substituents, 4-nitro vs. 4-methoxy, in **2***a*–**2***b*, and to the various alkyl groups in **2***c*–**2***e*.[5]

The resonances of the C=N carbons of imines listed in Table 3 are farther downfield than those of Tables 1 and 2 (analogous to ketones vs. aldehydes) with deshielding increasing with the number of the aliphatic groups. Perhaps surprisingly, the change in ring size from six to five between **3***c* and **3***d* causes as large a shift change as going from **3***a* to **3***c*.

The *changes* in ^{13}C shifts (Δδ) which occur on changing the solvent from chloroform to trifluoroethanol and from chloroform to trifluoroacetic acid are listed in Tables 5 to 9.[6] The assignments of the resonances of the 2′ and 3′ carbons of **1***a*–**1***f* in trifluoroacetic acid and of the aliphatic carbons of **3***c*, **3***d*, and **4***b*, in trifluoroacetic acid are tentative, as therefore will be the Δδ values for these substances. Concentration effects on the ^{13}C resonances of representative compounds in the 2, 4, 8, and 10 mol% range were within 0.1 ppm (more

[5]The insensitivity of imines to substituents on adjacent rings is similar to that reported for acetophenones (10*a*), styrenes (10*b*), and chalconnes (10*c*).

[6]The reasons for choosing chloroform as the standard solvent were discussed earlier (1).

Can. J. Chem. Downloaded from www.nrcresearchpress.com by 210.87.254.42 on 09/05/12
For personal use only.

TABLE 3. ^{13}C chemical shifts of ketimines in chloroform

Compound	δ, ppm from internal TMS													
	C7	C1	C2	C3	C4	C5	C6	C1′	C2′	C3′	C4′	C1″	C4″	C8
3*a* 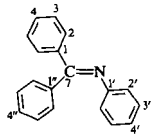	167.8	139.5	[a]	[a]	130.5			151.2	[a]	[a]	122.9	136.1	128.3	
3*b* 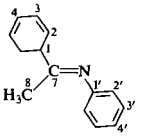	165.2	139.4	127.1	128.2	130.3			151.6	119.3	128.8	123.1			17.3
3*c* 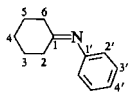		174.6	27.8	27.6	25.9	31.2	39.4	150.6	119.7	128.6	122.8			
3*d* 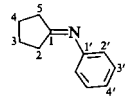		182.1	30.6	24.9	24.1	36.2		152.0	119.0	128.9	123.0			

[a]Resonance assignments for these atoms were not made.

TABLE 4. ^{13}C chemical shifts of oximes in chloroform

Compound	δ, ppm from internal TMS							
	C7	C1	C2	C3	C4	C5	C6	C8
4*a*[a] 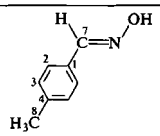	150.3	129.2	129.5	127.0	140.2			21.3
4*b* 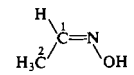		147.6	11.2					
4*c*[b] 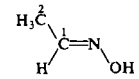		147.9	15.0					
4*d*[b] 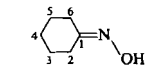		160.3	25.8	25.6	24.4	26.7	31.9	

[a]Configuration as given in ref. 8.
[b]A mixture of 4*b* and 4*c*, consisting mostly of one isomer, was used. The major signals were attributed to 4*b* on the basis of ref. 8.

substantial changes were noted at 20 mol%) and it appears that the shifts at infinite dilution are already well approximated by those at the 10 mol% level.

It will be seen from Tables 5 to 9 that changing from chloroform to either trifluoroethanol or trifluoroacetic acid produces substantial changes in many of the carbon chemical shifts of the compounds studied. Both upfield and downfield shift changes are observed, and it is especially interesting and significant that trifluoroethanol and trifluoroacetic acid may have effects which are not only different in magnitude but in sign as well. It is not wholly surprising that this be the case, because, as we have pointed out when discussing the ^{15}N shifts (1), trifluoroethanol is primarily a hydrogen-bonding solvent, while trifluoroacetic acid is a protonating solvent for imines. Protonation with trifluoroacetic acid is firmly established by observation of proton–^{15}N couplings with imines (1).

For the ^{15}N resonances of C=N nitrogens, both

Can. J. Chem. Downloaded from www.nrcresearchpress.com by 210.87.254.42 on 09/05/12
For personal use only.

TABLE 5. Effects of hydrogen bonding and protonation on ^{13}C chemical shifts of *N*-benzylideneanilines

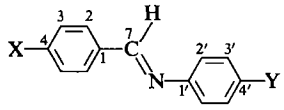

				$\Delta\delta^b = (\delta_{solvent} - \delta_{CHCl_3})$, ppm									
Compound	X	Y	Solvent[a]	C7	C1	C2	C3	C4	C1′	(C2′ C3′)[c]		C4′	C8[d]
1*a*	CH_3O	H	TFE	5.1	−0.2	2.3	1.7	2.7	0.1	1.5	1.8	2.5	0.9
			TFA	5.4	−8.6	7.3	4.1	9.7	−14.4	0.9	3.1	7.3	2.1
1*b*	CH_3	H	TFE	5.2	−0.1	1.6	1.6	3.2	0.0	1.3	1.7	2.2	0.0
			TFA	6.9	−8.4	5.3	4.3	14.4	−15.0	1.3	3.1	6.6	1.4
1*c*	H	H	TFE	5.3	0.2	1.6	1.6	2.4	0.2	1.6	1.5	2.3	
			TFA	7.7	−8.2	5.5	3.1	10.1	−14.5	1.4	3.6	7.9	
			HOAc	2.7	−2.8	1.1	0.9	4.4	[e]	1.2	0.9	1.5	
1*d*	O_2N	H	TFE	5.1	1.1	1.8	1.5	1.8	1.0	1.2	1.8	2.1	
			TFA	9.0	−8.1	6.1	3.0	5.5	−13.4	2.0	3.4	8.2	
1*e*	H	OCH	TFE	5.6	0.1	1.5	1.6	3.4	0.6	1.4	1.7	1.9	1.0
			TFA	7.1	−8.2	3.6	2.5	10.0	−13.7	1.9	3.3	6.0	1.7
1*f*	H	NO_2	TFE[f]	—	—	—	—	—	—	—	—	—	—
			TFA	9.2	−7.6	6.4	3.7	10.9	−15.1	3.0	2.9	5.2	

[a]TFE = CF_3CH_2OH, TFA = CF_3CO_2H, HOAc = CH_3CO_2H.
[b]Positive signs signify downfield shifts, negative signs upfield shifts.
[c]The ^{13}C assignments for these atoms are tentative, and perhaps larger solvent changes should be expected for C2′ than for C3′. However, other possible assignments gave Δδ's which were less consistent and, in fact, unreasonable in some instances.
[d]The substituent carbon.
[e]Signal not seen in the spectrum.
[f]Compound not sufficiently soluble to obtain a spectrum.

TABLE 6. Effects of hydrogen bonding and protonation on ^{13}C chemical shifts of *N*-benzylidenealkylamines

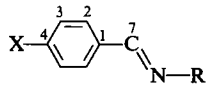

				$\Delta\delta^a = (\delta_{solvent} - \delta_{CHCl_3})$, ppm									
Compound	X—	—R	Solvent[a]	C7	C1	C2	C3	C4	C1′	C2′	C3′	C4′	C8
2*a*	CH_3O—		TFE	5.4	−0.1	2.1	1.3	2.5	1.4	0.5	0.7	0.5	0.9
			TFA	10.7	−9.1	7.1	3.7	9.6	−4.3	0.1	−0.8	0.1	2.0
2*b*	O_2N—		TFE	5.8	0.5	1.9	1.5	1.9	2.0	1.3	0.8	0.8	
			TFA	14.4	−9.1	6.1	6.0	5.7	−2.8	1.1	−1.0	0.1	
2*c*	H—	—$CH(CH_3)_2$	TFE	5.3	−0.2	2.0	1.9	2.4	1.3	−0.3			
			TFA	13.3	−9.8	5.3	3.6	10.5	−1.9	−2.3			
2*d*	H—	—$CH_2CH(CH_3)_2$	TFE	5.8	−0.2	1.6	1.7	2.5	0.3	0.8	0.0		
			TFA	13.5	−9.0	5.3	3.7	10.6	−7.3	0.8	−1.0		
			HOAc	12.1	−7.7	5.2	2.5	7.8	−7.9	−0.5	[b]		
2*e*	H—	—CH_2CH_3	TFA	13.1	−8.8	5.3	3.5	10.3	−5.0	−2.3			

[a]See Table 5.
[b]Overlapped by CH_3CO_2H resonance.

trifluoroacetic acid and trifluoroethanol uniformly cause *upfield* shifts, with the protonation shifts being several times the hydrogen-bonding shifts. These shift changes accord with the expected increases in the $n \rightarrow \pi^*$ transition energies, which are associated with very substantial second-order paramagnetic contributions to the chemical shifts of $>C{=}\ddot{N}-$ nitrogens. This does not mean to say that other effects on the ^{15}N chemical shifts are negligible, only that they appear to be largely

Can. J. Chem. Downloaded from www.nrcresearchpress.com by 210.87.254.42 on 09/05/12
For personal use only.

TABLE 7. Effects of hydrogen bonding and protonation on ^{13}C chemical shifts of ketimines

Compound	Solvent[a]	$\Delta\delta^a = \delta_{solvent} - \delta_{CHCl_3}$, ppm C7	C1	C2	C3	C4	C5	C6	C1′	C2′	C3′	C4′	C1″	C4″	C8
3*a*	TFE	6.8	1.5	[a]	[b]	1.8			−0.2	[b]	[b]	1.8	1.0	2.1	
	TFA	16.0	−5.3	[b]	[b]	8.9			−14.0	[b]	[b]	9.4	−5.5	8.8	
3*b*	TFE	7.8	1.7	1.3	1.8	2.1			−0.6	2.1	1.9	3.1			2.1
	TFA	23.5	−6.9	5.0	2.0	9.8			−15.5	6.6	3.1	10.1			3.4
3*c*	TFE		7.5	1.2	1.2	0.7	1.6	0.1	−0.9	2.2	1.9	3.0			
	TFA		27.5	(2.5	2.5	−0.5	2.5	−0.6)[c]	−15.9	5.6	5.6	10.0			
	HOAc		19.1	(0.1	0.0	−0.8	−3.3	2.7)[c]	−11.6	5.4	1.8	6.9			
3*d*	TFE		7.3	1.8	0.7	1.0	0.6		−1.1	2.0	1.5	3.0			
	TFA		26.7	(6.0	1.1	1.1	2.3)[c]		−15.4	4.6	3.9	8.8			

[a]See Table 5.
[b]Resonance assignments for these atoms were not made.
[c]These values based on tentative assignments.

TABLE 8. Effects of hydrogen bonding and protonation on ^{13}C chemical shifts of oximes

Compound	Solvent[a]	$\Delta\delta^a = \delta_{solvent} - \delta_{CHCl_3}$, ppm C7	C1	C2	C3	C4	C5	C6	C8
4*a*	TFE	3.5	0.7	1.5	1.4	2.8			0.2
	TFA	1.8	−5.9	7.0	5.2	11.5			1.2
4*b*[b]	TFE		4.0	0.2					
	TFA		11.0	1.9					
4*c*	TFE		4.5	0.2					
	TFA		11.3	−1.5					
4*d*	TFE		5.9	(1.0	1.0)[c]	1.5	1.2	0.9	
	TFA		20.3	(2.2	1.5	1.0	1.7	1.0)[c]	
	HOAc		1.2	(0.4	0.6)[c]	1.1	0.8	0.3	

[a]See Table 5.
[b]A mixture of 4*b* and 4*c*, consisting mostly of 4*b*, was used.
[c]Based on tentative assignments.

masked by the changes in second-order paramagnetic effects associated with partial or full bonding to the unshared electron pair on nitrogen. Because the carbons with which we are concerned have no unshared pairs, it is to be expected that different considerations are likely to apply in rationalizing the positions of their resonance signals.

In the following discussion, we will give special attention to the ^{13}C shift changes which are associated with hydrogen bonding and protonation of the carbons of the structural units, C—C=N—C of imines and pyridines, and C—C=N—OH of oximes. Perusal of Tables 5 to 9 shows that the aromatic carbon resonances, except for those of the *ipso* carbons, move downfield on both hy-

Can. J. Chem. Downloaded from www.nrcresearchpress.com by 210.87.254.42 on 09/05/12
For personal use only.

TABLE 9. Effects of hydrogen bonding and protonation on ^{13}C chemical shifts of pyridines

Compound	Solvent[a]	$\Delta\delta^b = \delta_{solvent} - \delta_{CHCl_3}$, ppm C2	C3	C4
5*a* Pyridine[c]	TFE	−0.5	2.3	3.4
	HOAc	−5.3	2.7	7.0
	TFA	−6.9	5.9	13.7
5*b* 2,6-Dimethylpyridine[d]	TFE	1.7	3.0	3.6
	TFA	−1.4	2.6	12.5

[a]See Table 5.
[b]12.5 mol% solutions.
[c]^{13}C shifts in $CHCl_3$ were: C2, 149.7; C3, 123.5; C4, 135.7, all in ppm.
[d]^{13}C shifts in $CHCl_3$ were: C2, 156.7; C3, 119.4; C4, 135.7.

drogen bonding and protonation, as befits conversion of the C=N groups into more electron-attracting groups. The changes in shift of these aromatic carbons are often large, especially on protonation, but there are no surprises in their general trends. The aliphatic carbon-shift changes outside of the structural units, C—C=N—C or C—C=N—OH, are generally small and somewhat erratic and will not be considered further.

One interesting aspect of the shift changes in Tables 5 to 9 is the fact that hydrogen bonding or protonation uniformly causes the resonances of C=N carbons in imines and oximes to move *downfield* while, in contrast, the resonances of C2,6 of pyridine move *upfield*. 2,6-Dimethylpyridine is different from pyridine in that its C2,6 resonances move downfield on hydrogen bonding and upfield on protonation. Also significant are the large and uniform *upfield* protonation shifts of aromatic *ipso* carbons which we shall henceforth designate as C1 and C1′ in the structural unit C^1—C=N—$C^{1'}$. When C1 is a saturated carbon, as in **3***b–d* and **4***b–d*, the corresponding protonation shifts (here, of the carbon actually labeled in the formulas variously as C8, C2,5, C2,6, or C2) are medium in size and *downfield*. However, as with **2***c–e*, when C1′ is aliphatic, the shift changes are medium and *upfield*.

The hydrogen-bonding shifts of the C1 and C1′ resonances are generally quite small compared to those of the C=N carbon resonances and may or may not have the same sign as the protonation shifts. To summarize (where C_{ar} = *ipso* aromatic ring carbon and C_{ali} = saturated carbon):

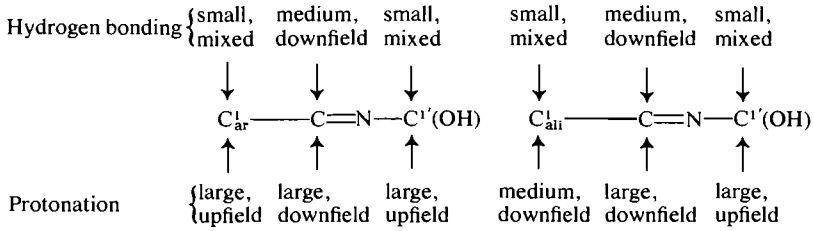

What sense can be made out of these patterns of shift changes? Let us consider the effects on the C=N carbon resonances first, remembering that the α-carbon resonances of pyridine go upfield on hydrogen bonding or protonation — opposite to the imine and oxime C=N resonances.

Partial or complete bonding to the lone pair of a C=N nitrogen by a proton donor is expected to raise the $n \rightarrow \pi^*$ transition energy and cause a very substantial upfield shift of the ^{15}N resonance. Such bonding will also be expected to change the character of the C=N bond, as can be rationalized by an increase in the contribution of resonance structures such as **6***b*. (The resonance structures, **6**, are written for convenience to correspond to full protonation, but the extension to a hydrogen-bonding situation should be obvious.)

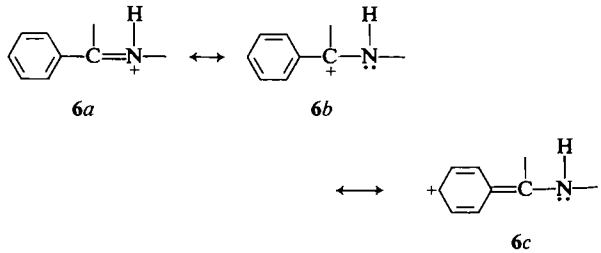

6*a* **6***b* **6***c*

Can. J. Chem. Downloaded from www.nrcresearchpress.com by 210.87.254.42 on 09/05/12
For personal use only.

Can. J. Chem. Downloaded from www.nrcresearchpress.com by 210.87.254.42 on 09/05/12
For personal use only.

If an aromatic ring is attached to the carbon of the C=N bond, then both hydrogen bonding and protonation could be expected to lead to electron delocalization from the ring, as symbolized by **6***c*, and this, of course, is expected to affect the shieldings of the ring carbons in a significant way in the *downfield* direction, as is observed. An important question is what part, if any, of the shift change at the C=N carbon could be a neighboring anisotropy effect arising from the decrease in the paramagnetic shielding of the nitrogen nucleus associated with hydrogen bonding or protonation. Such neighboring anisotropy effects have been used to account for the shielding of acetylenic and non-hydrogen bonded H—O, H—N, and H—F protons (11). Whether a change in the electron circulation around the nitrogen should be expected to shield or deshield a directly attached C=N carbon nucleus is not easy to predict with molecules as complex as the ones considered here. However, shielding at nitrogen and deshielding at carbon of C=N atoms as the result of changing the second-order paramagnetic contributions by hydrogen bonding to, or protonation of, the nitrogen is certainly not unreasonable.

Experimentally, for the compounds in Tables 5 to 8, the ratios of the changes produced by hydrogen bonding and protonation on the C=N carbon resonances are substantially smaller than are the ratios of the corresponding effects on the C4 resonances of the aromatic carbons. This fact, at least naively, seems to suggest a sizeable contribution to the downfield shift in the C=N shifts through the diamagnetic change in the nitrogen shielding as the result of hydrogen bonding. On full protonation, this contribution would be expected to be enhanced, but then might be masked by an opposing shift associated with drastic changes in the overall electron distribution ascribable to resonance structures **6***b* and **6***c*. These notions are in good agreement with the fact that the shifts of C1 and C1′ are only very slightly changed by hydrogen bonding but are greatly changed by protonation, as would be expected if there is not in fact much charge transfer on hydrogen bonding. Pyridine and 2,6-dimethylpyridine (Table 9), where the C=N atoms are part of aromatic rings, could well be different from imines and oximes because of different anisotropies of the second-order paramagnetic effect at their nitrogen atoms.

The results with compounds **1***a*–**1***d* indicate a qualitative relationship between shift changes on protonation and relative contributions of **6***b* and **6***c*. With **1***a* and **1***b*, which can enhance the contribution of **6***c*, the C4 shifts are larger and the C7 shifts smaller than for **1***d* with its 4-nitro group, which should favor **6***b* over **6***c*. That both the C7 and C4 shifts of **1***a* are smaller than **1***b* is expected because of electron delocalization from the methoxy group, **7**.

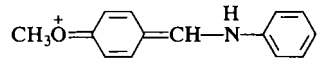

7

The large upfield shifts of the resonances of C1 and C1′ on protonation have several parallels in compounds where a positive center is generated adjacent to carbon. For example, formation of the conjugate acid of acetophenone with trifluoromethanesulfonic acid causes an upfield shift of the *ipso* carbon of 8 ppm (5), ionization of triphenylmethanol in sulfuric acid results in an upfield shift of 9.9 ppm for the *ipso* carbons (12), conversion of benzenamine to its salt with methanesulfonic acid gives an upfield C1 shift of 17.6 ppm (5). In all of these substances, as with the compounds studied here, the other ring-carbon resonances move downfield. The upfield shift changes produced by attachment of carbon to an atom undergoing a loss of electronic charge seems very likely to be largely an inductive effect. Clearly, conjugative unsaturation is not necessary, because conversion of a carboxylate salt to the acid results in an upfield shift of the carboxyl carbon (13) and the change of an aliphatic amine to the ammonium ion causes an upfield shift of the α carbon (4). The fact that protonation of imines is expected to call for an increase in conjugation involving C1 (**6***c*) and a decrease in conjugation involving C1′ (**8**) adds further weight to postulation of a nonconjugative origin to the resulting shift changes.

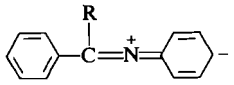

8

It has been pointed out to us by Reynolds that the π-inductive effect is likely to be especially important in these systems in determining the shifts of the *ipso* carbons and, furthermore, can help to account for the smaller shift changes of the *ortho* relative to the *para* carbons of the unsubstituted phenyl rings of **1***a*–**1***f*, **2***c*–**2***e*, and **3***b*–**3***d* on protonation (14, 15).

1. M. Allen and J. D. Roberts. To be published.
2. R. J. Pugmire and D. M. Grant. J. Am. Chem. Soc. **90**, 697 (1968).
3. A. R. Quirt, J. R. Lyerla, Jr., I. R. Pear, J. S. Cohen, W. F. Reynolds, and M. H. Freedman. J. Am. Chem. Soc. **96**, 570 (1974).
4. I. Morishima, K. Yoshikawa, K. Okada, T.

YONEZAWA, and K. GOTO. J. Am. Chem. Soc. **95**, 165 (1973).
5. G. L. NELSON, G. C. LEVY, and J. D. CARGIOLO. J. Am. Chem. Soc. **94**, 3089 (1972).
6. G. A. OLAH and T. E. KIOVSKY. J. Am. Chem. Soc. **90**, 4666 (1968).
7. G. E. HAWKES, K. HERWIG, and J. D. ROBERTS. J. Org. Chem. **39**, 1017 (1974).
8. N. INAMOTO, K. KUSHIDA, S. MASUDA, H. OHTA, S. SATOH, Y. TAMURA, K. TOKUMARU, K. TORI, and M. YOSHIDA. Tetrahedron Lett. **41**, 3617 (1974).
9. M. YOSHIDA, H. MINATO, and M. KOBAYASHI. Chem. Lett. 1097 (1976).
10. (*a*) K. S. DHAMI and J. B. STOTHERS. Can. J. Chem. **43**, 479 (1965); (*b*) K. S. DHAMI and J. B. STOTHERS. Can. J. Chem. **43**, 510 (1965); (*c*) E. SOL'ANIOVA, S. TOMA, and S. GRONOWITZ. Org. Magn. Reson. **8**, 439 (1976).
11. J. A. POPLE. Proc. R. Soc. London, A**239**, 550 (1957).
12. G. J. RAY, R. J. KURLAND, and A. K. COLTER. Tetrahedron, **27**, 735 (1971).
13. R. HAGEN and J. D. ROBERTS. J. Am. Chem. Soc. **91**, 4504 (1969).
14. W. F. REYNOLDS and G. K. HAMER. J. Am. Chem. Soc. **98**, 7296 (1976).
15. W. D. ADCOCK, B. D. GUPTA, and W. KITCHING. J. Org. Chem. **41**, 1498 (1976).

Can. J. Chem. Downloaded from www.nrcresearchpress.com by 210.87.254.42 on 09/05/12
For personal use only.

The twist angle approach to the stereoselectivity in reduction of ketones

MICHAEL R. GIDDINGS AND JOHN HUDEC

Department of Chemistry, The University, Southampton S09 5NH, Great Britain

Received July 3, 1980

This paper is dedicated to Prof. Raymond U. Lemieux on the occasion of his 60th birthday

MICHAEL R. GIDDINGS and JOHN HUDEC. Can. J. Chem. **59**, 459 (1981).

Semiempirical MO calculations show that the π^* orbital of the carbonyl carbon of asymmetric ketones deviates from orthogonality. These small deviations, measured by twist angles, are used to predict the configurations of the diastereoisomeric alcohols formed on reduction of the ketones with complex metal hydrides. The method is particularly suitable for predicting the changes in stereoselectivity when the carbonyl compound is substituted. This is illustrated by a number of examples of reduction of substituted rigid polycyclic ketones. It is proposed that a nucleophile approaches a carbonyl group preferentially from the side of obtuse angle with respect to the O—C bond. The twists incorporate the electronic nature of the substitent and help to understand the steric effect. The application of the twist angle approach to other reactions is briefly mentioned.

MICHAEL R. GIDDINGS et JOHN HUDEC. Can. J. Chem. **59**, 459 (1981).

Les calculs semi-empiriques de OM montrent que l'orbitale π^* du carbone du carbonyle des cétones asymétriques dévie de l'orthogonalité. On a utilisé ces petites déviations, mesurées par les angles de torsion, pour prédire les configurations des alcools diastéroisomères qui proviennent de la réduction des cétones par les hydrures métalliques complexes. Cette méthode convient particulièrement à la prédiction des changements de stéréosélectivité quand le composé carbonylé porte un substituant. Un grand nombre d'exemples de réductions des cétones polycycliques rigides substituées illustrent cette méthode. On propose qu'un nucléophile approche le groupe carbonyle préférentiellement du côté de l'angle obtus par rapport à la liaison O—C. Les torsions incorporent la nature électronique du substituant et aident à comprendre l'effet stérique. On mentionne brièvement l'application de l'angle de torsion d'approche à d'autres réactions.

[Traduit par le journal]

The search for a set of rules that would predict the stereoselectivity in the reduction of ketones by complex metal hydrides has been under continuous study since their introduction in the early 1950's. Virtually all the rationalisations, based on experimental data, incorporate some kind of steric effect. However, their predictive ability is very limited for the following reasons: (*i*) they are all based on the results obtained on substituted cyclohexanones (or acyclic ketones with assumed preferred conformations), (*ii*) the only substituent that is seriously considered is the methyl group, and (*iii*) the approach of the reagent nucleophile to the carbonyl group is assumed to be strictly perpendicular to the C—O bond from either side of the π/π^* MO's. For the sake of brevity, we do not discuss the merits and disadvantages of the various earlier proposals and refer the reader to a very recent review (1) in which the question of stereoselectivity is discussed and critically evaluated. We concentrate on the presentation of a different approach that incorporates some aspects of earlier proposals (2–4) and promises to be much more general.

We have shown recently (5) that the cd of the n→ π^* transition of a chiral carbonyl compound can be easily obtained by evaluating the twists of the n and π^* orbitals (HOMO and LUMO) localised on oxygen from an output of a simple program such as CNDO/2 (6). More importantly, these calculations predict quite accurately the *relative* changes in cd, both in sign and magnitude, when any one of the hydrogen atoms of the ketone is replaced by a substituent. Although our analysis showed that the π^* MO contributed very little to the overall rotary strength because it is mainly localised on the C=O group, it nevertheless interacts with the σ^* orbital of the substituent C—X bond. As the π^* orbital on the C atom of the carbonyl group is involved in the reactions with nucleophiles, we have re-examined it in order to see whether it undergoes any distortions (twists) on substitution. Such twists (Fig. 1), if present, should be a most useful guide for predicting the change in the ratio of diastereoisomeric alcohols on reduction of ketones, and more generally, in any reaction in which an electron deficient atom is present or produced that subsequently reacts with a nucleophile.

In principle, there can be two twists generated, one in the *xz* and one in the *xy* planes, either of which can be positive or negative.[1] Assuming that the nucleophile will react preferentially with the C=O group from the side of the "obtuse angle"

[1]The twist angles (all in minutes of a degree) are defined as

$$\text{tg}\,\theta_{(\pi^*xz)} = C(\pi^*z)/C(\pi^*x); \qquad \text{tg}\,\theta_{(\pi^*xy)} = C(\pi^*y)/C(\pi^*x)$$

where the coefficients C are the eigenvectors on the carbonyl carbon in the π^* (LUMO) molecular orbital. It should be noted that $\theta_{(\pi^*xz)}$ will have the same sign for any pair of antipodal ketones but $\theta_{(\pi^*xy)}$ will have opposite signs. Standard bond angles and bond lengths as well as idealised geometries were used in all calculations.

0008-4042/81/020459-09$01.00/0

©1981 National Research Council of Canada/Conseil national de recherches du Canada

Can. J. Chem. Downloaded from www.nrcresearchpress.com by 210.87.254.5 on 09/05/12
For personal use only.

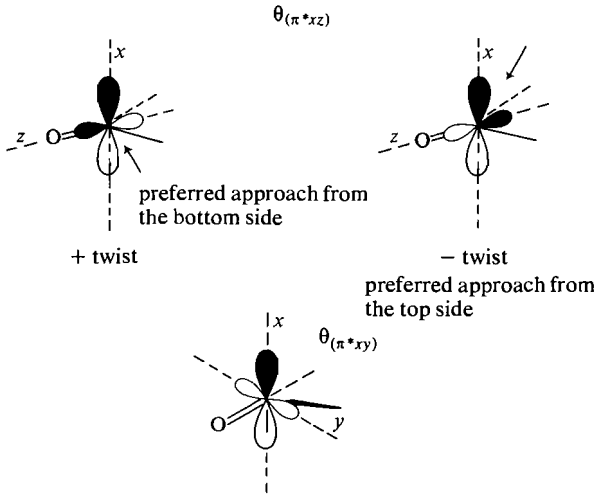

Positive twist attack from the front above or the back below
negative twist attack from the front below or the back above

FIG. 1. Distortions of π* orbitals on substitution.

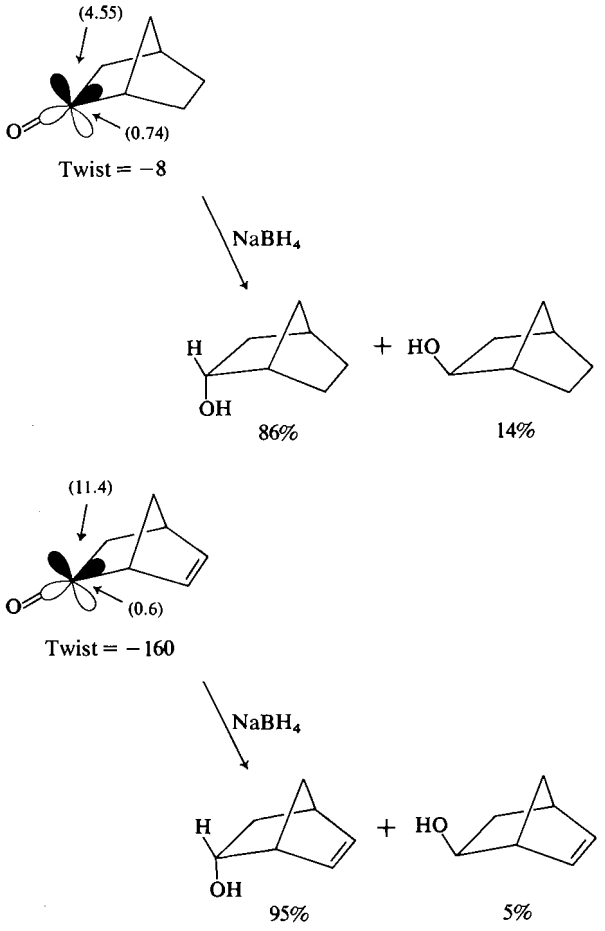

FIG. 2. Reduction of norbornene 2-ketones.

(2), it will come from the top preferentially if $\theta_{(\pi^*xz)}$ is negative and from the bottom if $\theta_{(\pi^*xz)}$ is positive. As there is still some doubt about the reduction of flexible cyclohexanones (1, 4), we have limited our analysis to rigid carbonyl systems.

The first systems we examined were norbornene 2- and 7-ketones and the corresponding saturated analogues (7) (Figs. 2 and 3). The increase in the *endo* alcohol of the 2-ketone was ascribed to the steric (and electrostatic) effect of the π electrons being larger than that of the ethano bridge. However, such a conclusion is immediately negated by the results of the 7-ketone. The change in the $\theta_{(\pi^*xz)}$ twist of the unsaturated ketones *relative* to the saturated ones reflect the change in the distribution of the alcohols: the positive twist in the 7-one series parallels preferential attack from the *syn* side, and the increased negative twist on going from saturated to the unsaturated compounds in the 2-one series parallels the increased attack from the *exo* side. Interestingly, in this case the change in twists reflects the change in the relative rates of reduction from the *exo* and *endo* sides — an increase in obtuse angle is proportional to the increase in relative rate. The dramatic decrease in the rate of addition from the *anti* side in the 7-one series is probably a reflection of the twist, the angle of attack becoming more acute. The decrease in rate from the *syn* side (instead of an increase) may be due to electrostatic and/or steric interaction between the π electrons of the double bond and the incoming nucleophile, BH_4^-. It thus appears that both the experiment and theory concur and indicate that a double bond as a substituent interacts with a carbonyl group in a variable way that is very strongly orientationally dependent (for another example, benzobicyclo-[2:2:2]octanone, see ref. 8).

We turned our attention next to 2-adamantanone system, which because of its symmetry (in the same way as 7-norbornanone), should show clearly the effect of substituents (F and Cl) at positions 4_{eq}- (9) and 5. The analysis of the $\theta_{(\pi^*xz)}$ twists provided an unexpected surprise as they predicted not only that fluorine and chlorine should give different isomers as the major products in both 4 and 5 substituted series but that the major fluoro alcohol in the 4-series will be *trans* with respect to the cyclohexane that carries both substituents and *cis* in the 5-series (vice versa for Cl). As no such results were available in the literature, we checked these predictions experimentally ourselves and found them to be in full agreement (Scheme 1).[2] The only surprising

[2]From general properties of halogens, Br and I are expected to follow progressively the enhanced trend of Cl. Unfortunately, our program is not parametrised for these elements.

Can. J. Chem. Downloaded from www.nrcresearchpress.com by 210.87.254.5 on 09/05/12
For personal use only.

Can. J. Chem. Downloaded from www.nrcresearchpress.com by 210.87.254.5 on 09/05/12
For personal use only.

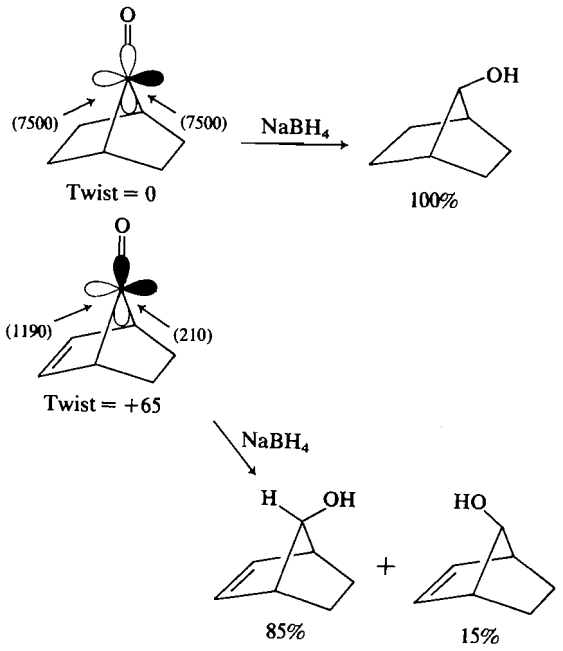

FIG. 3. Reduction of norbornene 7-ketones.

point about the experimental results is the larger inverse ratio of the fluoro isomers in the 5-series than in the 4-series. This is most likely due to differing steric requirements of the two reagents used; $LiAl(OBu^t)_3H$ was forced on us in the 4-series as

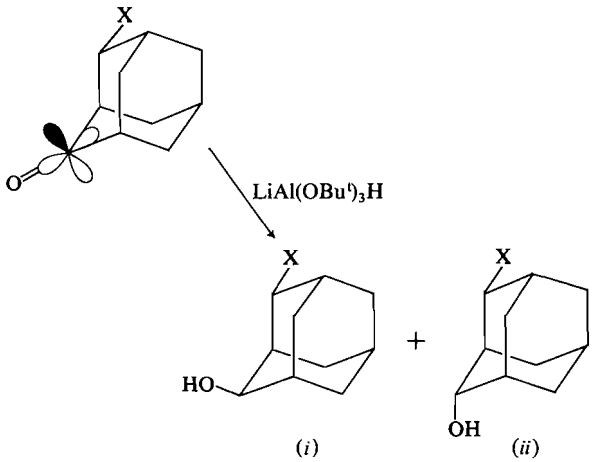

Substituent	Twist $\theta_{(\pi^*xz)}$	Twist $\theta_{(\pi^*xy)}$	Product (%) (*i*)	Product (%) (*ii*)
F	14	20	53	47
H	0	0	50	50
Cl	−46	−81	45	55
Br			43	57
I			34	66

SCHEME 1

$LiAlH_4$ or $NaBH_4$ gave in all cases (except X = H) the bicyclic unsaturated alcohol formed by Grob-type elimination.

In order to gain a better understanding of these results, we carried out the twist analysis on a γ-substituted pentanone that could serve as a model for *anti*-π-substituted camphors (10). Again, the $\theta_{(\pi^*xz)}$ twists predicted unexpected results that had to be checked experimentally. The $\theta_{(\pi^*xz)}$ twists showed the same trend as the 4-substituted adamantanone series and, gratifyingly, these predictions were borne out experimentally, despite the steric effect of the *syn*-7-methyl group. The apparent decrease in steric bulk of this methyl group on going from X = F to X = Cl can be explained by the utilisation of the twist in the *xy*-plane, $\theta_{(\pi^*xy)}$; its sign suggests that the nucleophile approaches the carbonyl carbon along a path between C-1 and C-7-*syn* methyl groups. An inspection of molecular models does agree that this direction of *exo* approach is less hindered than any other one (Scheme 3).

These results show that electronic substituent effects, transmitted through bonds, are responsible for the changes in the product ratios, as well as for the changes in the cd of the corresponding ketones; in fact, they parallel one another. For the same given orientation of a substituent X, as in 4-substituted adamantanones and in *anti*-π-substituted camphors, F has a dissignate contribution and Cl a consignate contribution to the cd of the parent unsubstituted ketone.

However, the behaviour of the $SnMe_3$ group, a strong σ-electron donor as observed in the cd of ketones (11), is at present difficult to rationalise, even though the result was predicted by the calculations. In this instance, $SnMe_3$ group acts in the same way as F, as a net electron acceptor, in contrast to Cl which is a net electron donor (12) (the balance between the σ-withdrawal and π-donation, both effects being conformationally dependent (5, 11)). In order to test this hypothesis, we calculated butanone and pentanone-2 with different electronegativities of the starred H atoms (Scheme 4).

The best way to assess the data in Scheme 4, so that they can be compared with the calculated data in Schemes 1 and 3, is to use twists relative to H of normal electronegativity, i.e. $\delta\theta = \theta^R_{(\pi^*)} - \theta^H_{(\pi^*)}$ where $\theta^R_{(\pi^*)}$ is H* with altered electronegativity. It then becomes immediately apparent that F in both series produces the twists of the same signs as the more electronegative H; Cl parallels the behaviour of the more electropositive H. As has been already mentioned, SiH_3 group (Scheme 3) behaves anomalously.

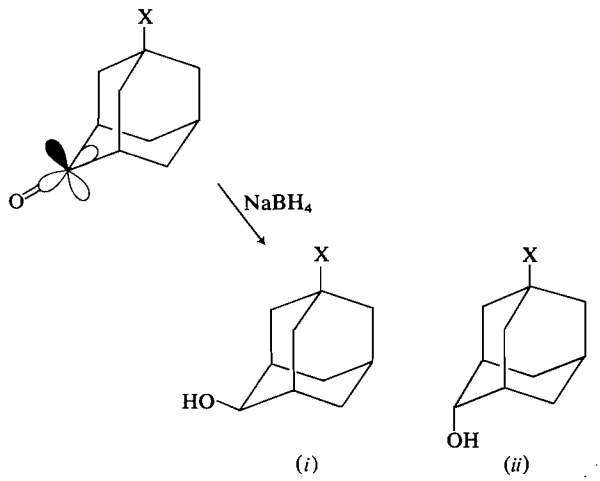

Substituent	Twist $\theta_{(\pi^*xz)}$	Twist $\theta_{(\pi^*xy)}$	Product (%) (i)	Product (%) (ii)
F	−4	0	38	62
H	0	0	50	50
Cl	+13	0	60/40	
Br			59/41	

SCHEME 2

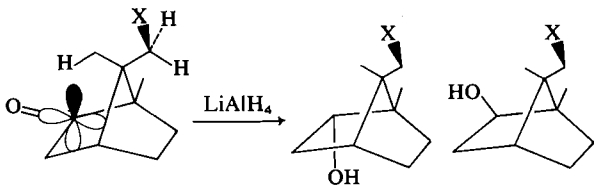

Substituent	Twist $\theta_{(\pi^*xz)}$	Twist $\theta_{(\pi^*xy)}$	Product (%) (i)	Product (%) (ii)
F	−4	−8	6	94
H	−11	−19	10	90
Cl	−23	−44	20	80
$SnMe_3$ (experiment)			4	96
SiH_3 (calculation)	14	−25		

SCHEME 3. Preferred conformation of the substituted *anti*-π-methyl group, as shown, is corroborated by X-rays on *anti*-π-trimethyltin camphor (unpublished work — we thank Dr. L. Alexander, Open University, for the information) and on substituted *anti*-π-camphor sulphonic acid derivatives (36).

The last system that we investigated computationally was the recently studied 3-substituted bicyclo[2:2:2]octanone-2 (13, 14). The results (Scheme 5) of reduction with $LiAlH_4$ (13) are startling — with R = H and Me, the ratio of *trans* to *cis* alcohols is 1, it increases on going from R = Et to Pr^i and then drops below 1 for R = Bu^t. This suggests that the steric bulk of Me is equal to H, Et and Pr^i get progressively smaller than Me, and only Bu^t is greater than H. The same trend is observed when the reduction is carried out with a much bulkier reagent, $LiAl(OBu^t)_3H$, when all *trans*/*cis* ratios are reduced by a nearly constant factor.

The calculations on a model molecule, R substituted acetone, in correct conformation help to understand the results. The twists, $\theta_{(\pi^*xz)}$, is negative (increasing from Me to Bu^t) for Me, Bu^t, and all conformations of Et and Pr^i, and thus we would expect the *trans* alcohol as the major product. However, the twist, $\theta_{(\pi^*xy)}$, is changing its sign on going from Me to Bu^t, leaning away from the substituent in the case of Me and towards it in the case of Bu^t. The results for the $LiAlH_4$ reduction can be explained on the following basis: the same *trans*/*cis* ratio of alcohols for the unsubstituted and the methyl ketone indicates that the steric interaction between the Me group and the incoming reagent is offset by the preferred lower energy approach from the side of the obtuse angle and away from the Me ($\theta_{(\pi^*xy)}$). The average of the $\theta_{(\pi^*xz)}$ increases for the two likely conformations of the Et group and hence an increase in the *trans* alcohol. There is a further increase in this angle for the single preferred conformation of the Pr^i group which should give considerably increased proportion of the *trans* alcohol. However, the change in sign of the $\theta_{(\pi^*xy)}$ twist now increases the steric interaction between the substituent and the incoming reagent and thus reduces the effect of the $\theta_{(\pi^*xz)}$ twist. The increase in the $\theta_{(\pi^*xz)}$ for Bu^t group is very small but the change in $\theta_{(\pi^*xy)}$ towards the substituent quite large, generating a big steric interaction with the approaching reagent; this leads to a dramatic decrease of the *trans* alcohol.

Perhaps the most revealing is the recent kinetic study of this system using the bulky $LiAl(OBu^t)_3H$ (14). It can be seen (Fig. 4) that the rate of reaction gradually decreases (relative to H when $\theta_{(\pi^*xz)} = 0$) for the *cis* alcohols, i.e. an approach from opposite side to the substituent. This must mean that the energy of the transition state increases as the angle of attack becomes more acute on going from R = H to Bu^t. The fact that the rates for the *syn* attack, leading to *trans* alcohols, for Me, Et, and Pr^i are all identical, means that there is a balancing effect between the increasing obtuse angle, which should lower the transition state energy (twist $\theta_{(\pi^*xz)}$), and the increasing steric interaction between the substituent and the incoming reagent (twist $\theta_{(\pi^*xy)}$), which should increase the energy. In these cases, they just balance. It is now possible to predict that the rate profile for the reduction of this system with $LiAlH_4$ should be virtually identical for the *anti* approach by the reagent. However, all the rates for

Can. J. Chem. Downloaded from www.nrcresearchpress.com by 210.87.254.5 on 09/05/12
For personal use only.

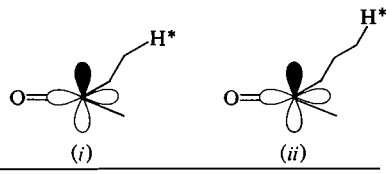

(*i*) (*ii*)

Electronegativity of H*	Twist (*i*)		Twist (*ii*)	
	$\theta_{(\pi^*xz)}$	$\theta_{(\pi^*xy)}$	$\theta_{(\pi^*xz)}$	$\theta_{(\pi^*xy)}$
3.15 (donor)	−15	−26	−16	−26
Normal	1	4	−11	−19
11.5 (acceptor)	24	33	−4	−6

SCHEME 4

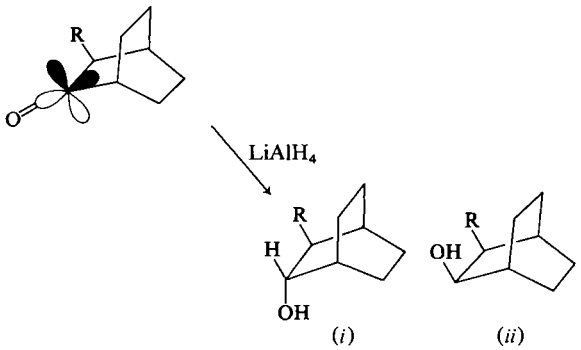

(*i*) (*ii*)

Substituent	Conformation of Me groups	Twist $\theta_{(\pi^*xz)}$	Twist $\theta_{(\pi^*xy)}$	Product (%) (*i*)	Product (%) (*ii*)
R					
Me		−8	+6	50	50
Et	a	−6	+9		
	b	−18	−7	68	32
	c	*−13*	*−3*		
Pr^i	a,b	−17	−6	72	28
	b,c	*−19*	*−11*		
	a,c	*−10*	*+1*		
Bu^t	a,b,c	−18	−11	15	85

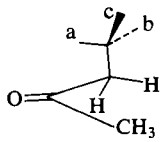

SCHEME 5. Conformation of Me groups in R = Et, Pr^i (and Bu^t) used in calculations. The conformations in italics above are unlikely to exist in the bicyclic ketone.

the *syn* approach would be faster, i.e. raised, so that the rates for the *syn* and *anti* approach for R = Me coincide.[3]

The steric effect of substituents is one of the basic concepts used by organic chemists in rationalising, and sometimes predicting, the outcome in reactions. Our calculations shed some light on its subtle changes which may arise as a consequence of a substitution in other parts of a molecule, e.g. in the *anti*-π-substituted camphors, which result in a change of the twist angles at the reaction centre. Similarly, we would like to suggest that the "buttressing effect" (7) which is responsible for a larger rate reduction of the attack from the *endo* side camphor relative to the norbornanone-2 is the consequence of the change in $\theta_{(\pi^*xz)}$. Our present work should also adequately account for the recently proposed anisotropic inductive effect (14) of alkyl groups.[4]

Another effect which is often invoked in reductions is electrostatic repulsion of the substituent (18) — our calculations have shown this to be unimportant in the substituted adamantanones. In fact, we predict that 3-chlorobicyclo[2:2:2]-

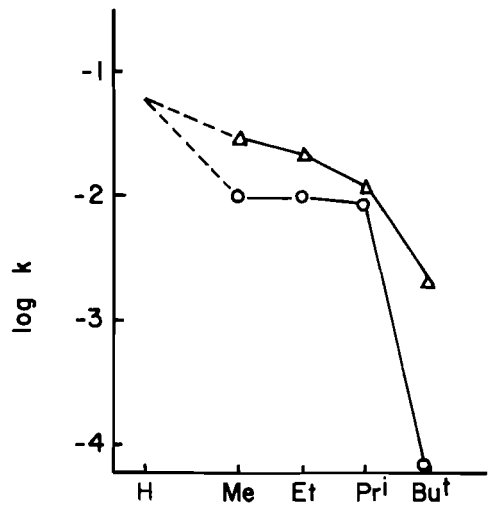

FIG. 4. log (rate) (○) for the formation of the *trans* alcohols and log (rate) (△) for the formation of the *cis* alcohols as a function of the substituent R in the reduction of 3-substituted bicyclo[2:2:2]octan-2-one with $LiAl(OBu^t)_3H$.

[3]Our calculations on the optical activity of the 3-alkylbicyclo[2:2:2]octan-2-ones indicate again a rough correspondence between the reduction and the magnitude of the Cotton effect — the Bu^t groups should behave anomalously in terms of the strict application of Octant Rule (15, 16).

[4]We have also carried out calculations on 4 ax-substituted adamantanones but the results did not warrant experimental product study unless detailed rate study was undertaken as well. The twists (reported as $\theta_{(\pi^*xz)}$, $\theta_{(\pi^*xy)}$) for F and Cl were 7; −11 and 10; −19 respectively, indicate a preference for the formation of the axial alcohol (with respect to the cyclohexane that carries the axial F and Cl). In terms of the rate studies, we would expect the rate of formation of the diaxial alcohol to be accelerated relative to half the rate of reduction of adamantanone, as would have been predicted on the basis of the inductive effect of an electron-withdrawing substituent (17). The twists of 4 ax-methyladamantanone were −3; 7 — these allow us to predict larger amounts of the diaxial alcohol at a retarded rate on the basis of the arguments already presented, again as might be predicted on the basis of an inductive effect of an electron donating substituent (17).

Can. J. Chem. Downloaded from www.nrcresearchpress.com by 210.87.254.5 on 09/05/12
For personal use only.

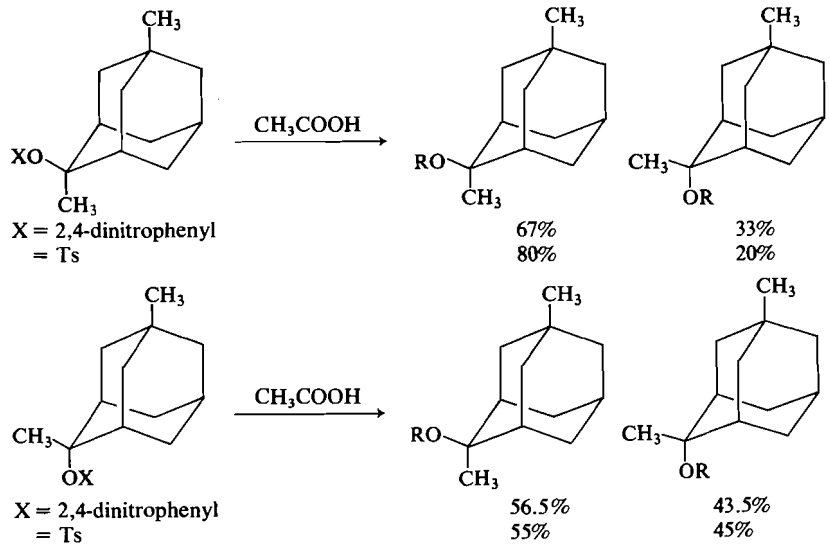

FIG. 5. Solvolysis of 2,5-dimethyladamantyl-2-(leaving group).

octanone-2 should give *trans* alcohol as the major product. On the other hand, the fact that the phenyl group leads to predominantly *cis* alcohol on reduction of 3-phenylbicyclo[2:2:2]octanone-2 (13) is mainly due to its restricted rotation — the balance between the favoured *syn* attack (negative $\theta_{(\pi^*xz)}$) is more than offset by the twist (negative $\theta_{(\pi^*xy)}$) that leads to steric hindrance to the approach. When such rotational restriction is removed, as in 2-phenylindanone-1 (13) or 1-phenylindanone-2 (13), the *trans* alcohol is the major isomer observed.[5]

Our preliminary investigations show that the application of the twist principle can be of help in other reactions, such as solvolysis. It was reported that both isomers of 2,5-dimethyladamantyl-2-(leaving group) (19) give more of the *cis* product on solvolysis (Fig. 5). This means that the compound with the *trans* leaving group solvolyses, under pseudo S_N1 conditions, with more inversion and the *cis* compound largely with retention of configuration. The same result is obtained in the methanolysis of the two epimeric 2-chloro-2-ethynyl-5-phenyladamantanes (20) — both give the same mixture of methoxy compounds (Fig. 6). The calculations on 5-methyl and 5-phenyl-2-adamantyl cation show a small $\theta_{(\pi^*xz)}$ twist towards the substituent (Me, − 1.5; Ph, − 3, which varies in magnitude but not in sign when the phenyl group is rotated). This result could be interpreted in terms of the involvement of solvent-separated ion-pairs which collapse into the product preferentially from the side of the obtuse angle, i.e. *cis* to the substituent.

Previous calculation on the reduction of ketones (2*b*) confirmed the experimentally derived conclusion (2*a*) that a nucleophile approaches the carbonyl group from the obtuse angle which varied from ca. 109° to 118° depending on the distance

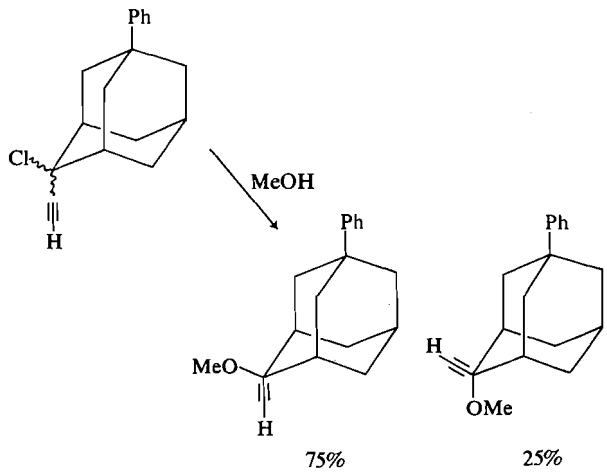

FIG. 6. Methanolysis of the two epimeric 2-chloro-2-ethynyl-5-phenyladamantanes.

[5]It should be pointed out that the twist angles vary not only when an asymmetric substituent X is rotated about the C—X bond but also with the rotation about O=C—C_α bond. Indeed, we find that $\theta_{(\pi^*xz)}$ changes its sign in the region of O=C—C—X dihedral angle of 80° to 100° for many substituents. Thus generalisations of preferred attack of a nucleophile on a carbonyl group in an acyclic system is difficult. The twist $\theta_{(\pi^*xy)}$ in a conformation of minimum energy may hinder the approach of the reagent from the obtuse angle side, thus raising the energy of the transition state to such an extent that a lower energy transition state may be obtained in a conformation of higher energy in which the twist $\theta_{(\pi^*xz)}$ has changed in sign.

Can. J. Chem. Downloaded from www.nrcresearchpress.com by 210.87.254.5 on 09/05/12
For personal use only.

Can. J. Chem. Downloaded from www.nrcresearchpress.com by 210.87.254.5 on 09/05/12
For personal use only.

between the nucleophile (H^-) and the carbonyl carbon (of formaldehyde). Thus the potential energy surface was evaluated. The stereochemistry of reduction was studied by considering the energy difference between two assumed and geometry unrelaxed reaction complexes some way along a reaction co-ordinate at an optimised angle of approach of 90° (4).

In contrast to these approaches, our calculations involve the evaluation of the twist angles (θ_{π^*}) of a ketone whose carbonyl group is perturbed asymmetrically by a substituent relative to the parent unsubstituted ketone or a suitably substituted analogue). Whilst it is relatively easy to appreciate the usefulness of calculations of the former approach vis-à-vis stereoselectivity and the mechanism of the reaction, it is, as yet, difficult to appreciate that an asymmetric ketone should have information built into its ground state as to how stereoselectively it will react with certain nucleophiles. Such an approach raises several questions that we will attempt to answer.

Perhaps the most important question is whether the twist approach has any physical significance and if so, how it governs the stereoselectivity. Extensive calculations on selected ketones have shown that the twist angles relate to the electron density distribution about an atom. The three dimensional shape of the electron density of the three 2*p* bonding electrons for the carbonyl carbon (2*s* electron has been omitted because of its spherical contribution) shows a flattening on the two diastereotopic sides which in turn have small indentations in them, representing a decrease in electron density — in effect small electron deficient wells. These indentations move relative to one another when the orientation (or position) of the substituent attached to the parent ketone is altered; the twist angles represent their relative positions with respect to the C—O bond.[6] Thus a nucleophile approaches the carbonyl carbon aiming for one of the electron deficient wells, preferably the one that is further away from the electron-rich oxygen in order to minimize the electrostatic repulsion.

The electron density distortion observed above is very similar to an early rationalisation for the reduction of cyclohexanones (3) based on orbital interactions. It was suggested that the π-electron density of the C=O bond is dissymmetrically distributed on the two faces because of the dissymmetric interaction with the α axial hydrogens on one side and the "axial" C_α—C_β bonds. This was later confirmed by more sophisticated calculations (21).

The next question that needs to be answered is the question of reaction rates. The calculations show quite clearly that net electron-withdrawing substituents (e.g. F) lower the energy of the LU molecular orbital of the C=O, resulting in an increased rate of reduction (17), whilst net electron-donating substituents (e.g. Me and other alkyl groups) hardly effect the LUMO energy or slightly raise it and hence decrease the rate of reaction (17) (the change is conformationally dependent). It is thus difficult at the moment to decide how much of the experimentally observed rate changes can be ascribed to the change in the LUMO energy (which should affect both diastereotopic sides of the carbonyl groups equally) and how much to the change in the twist angles. This aspect was investigated by another set of calculations on asymmetric ketones by bending the oxygen of the carbonyl group out of the plane. It was found that when the bending (up to 2° out of the plane) was in the direction that resulted in the decrease of the obtuse angle $\theta_{(\pi^*xz)}$, the ground state energy rose much more steeply than when the bending was in opposite direction (i.e. an increase in the obtuse angle). In some cases a small decrease in energy was observed which suggests that strongly perturbed carbonyl groups need not necessarily be strictly coplanar with the α-carbon atoms. Such experimental evidence is currently difficult to abstract from the X-ray crystallographic literature. Similar relaxations of molecular geometry were observed in carbonium ions (22). This would suggest that for any given partially bonding distance between the carbonyl carbon and the nucleophile, there will be more rehybridisation at lower energy cost when the nucleophile approaches from the obtuse angle side. Taken to limit, the transition state resulting from attack at an obtuse angle should be slightly more product-like irrespective of the final diastereoisomeric product distribution.

Another question of importance to organic chemists must be whether the twist angle approach is applicable not only to reductions with complex metal hydrides but also to other addition reactions to the carbonyl group. In order to classify the reagents, we have carried out calculations on protonated ketones and found that the twist angles of the protonated species are very different from those obtained on the corresponding ketones. Furthermore, the twist angles are different for ketones that do not contain a vertical plane of symmetry and that

[6]The same electron density distortion is observed on the oxygen of chiral ketones. This distortion, measured by $-(\theta_n - \theta_{\pi^*})$ is proportional to the rotatory strength of the $n \rightarrow \pi^*$ transition (5). Thus it must represent the direction as well as the relative magnitude of the electric transition moment.

Can. J. Chem. Downloaded from www.nrcresearchpress.com by 210.87.254.5 on 09/05/12
For personal use only.

are protonated from either side. We therefore conclude that any reactants, such as Grignard reagents, aluminium alkoxides, etc. that co-ordinate first to the carbonyl oxygen, will produce quite different stereoselectivity than those which add directly. Thus we do not distinguish between $NaBH_4$, $LiAlH_4$, modified complex hydrides, KCN (23), etc. Although the details of the mechanism of reduction of ketones with complex metal hydrides have yet to be fully established, it is beginning to be accepted that the transition state in sodium borohydride reductions has considerably more product developed character than the lithium aluminium hydride one (1). Our calculations do not tell us anything about it. The relative changes in the ratio of the products (with respect to H as a substituent) may arise partly to the changing steric requirements of the reagents and partly to their different degree of "hardness" (24), as has already been suggested (4).

Finally there is a question how the twist angles arise. This happens when *p* orbital on an atom mixes into itself a small amount of character from a second *p* orbital on the same atom, even though they are mutually orthogonal. Such mixing is possible when these two orthogonal orbitals can interact simultaneously with orbital on another atom; this phenomenon takes place extensively in aliphatic systems. Orbital mixing analyses have been performed on a number of systems in order to gain a better understanding of various chemical processes (25–27) and have been generalised in an Orbital Mixing Rule (27). The twist angles represent a simple way of evaluating the extent of orbital mixing both in magnitude and sign. We have attempted the orbital mixing analyses on our systems in order to derive some rules for predicting the twists; unfortunately, we have failed so far in this instance, even though we were quite successful in deriving rules for the prediction of the optical activity of chiral ketones (5) without recourse to the Octant Rule (15), which has sometimes failed to predict the correct absolute configuration (28). The same lack of predictability applies to the suggestion that the π electron density on the diastereotopic faces of a cyclohexanone is unequal (3) as has already been pointed out (29). We therefore hope that these simple semiempirical MO calculations will soon be utilised by practising organic chemists as they will not only help to rationalise many unexpected results,[7] but will also predict them.

Our work in this area strongly indicates that the twist approach can rationalise, and put on a semiquantitative basis, the recently proposed "Approach Vector Analysis" to stereoselectivity (31). It can also rationalise many other stereochemical outcomes of various reactions in which the effect of a differently oriented substituent has hitherto been explained in terms of opposing or reinforcing dipole–dipole and steric interactions (32). The twist angle approach will also be extremely useful in rationalising some aspects of chiral discrimination (33), in particular enantiomeric (34) and diastereomeric interactions — in the latter case, the application of the twist angle approach is obvious.

Experimental

General Procedure

The ketones (0.5 m*M*) were dissolved in a solvent (2 mL; Et_2O or MeOH), cooled to 0°C and the reducing agent (1 m*M* equiv.) added. The reactions were allowed to stand overnight at 0°C and worked up in the usual way (saturated aq. Na_2SO_4 for $LiAl(OBu^t)H$ and $LiAlH_4$ and aq. AcOH for $NaBH_4$). The worked up reaction solutions were then analysed by glc. The solvents were evaporated and changed to $CDCl_3$ for the nmr analyses. ^1H nmr spectra were run on Varian HA-100 or XL-100. The chemical shifts are quoted in ppm from TMS (internal); s = singlet, d = doublet, t = triplet, q = quartet, dt = double triplet, dq = double quartet. All J_{HF} coupling constants were confirmed by F decoupling.

trans-*4eq-X-adamantan-2-ols*

X = *F*: 4-H_{ax}, 4.99 t (J_{HF} = 50.3 Hz); 2-H, 4.08 br (J_{HF} ~ 3 Hz).
H = *Cl*: 4-H_{ax}, 4.74t; 2-H, 4.09t.
X = *Br* (35): 4-H_{ax}, 5.00t, 2-H, 4.04t.
X = *I*: 4-H_{ax}, 5.27t; 2-H, 4.02t.

cis-*4eq-X-adamantan-2-ols*

X = *F*: 4-H_{ax}, 4.60 (J_{HF} = 50.8 Hz); 2-H, 3.78 (J_{HF} ~ 0).

[7]For further example of an identical problem, see ref. 30*a*. Our understanding of our own CNDO/2 calculations on norbornene differs slightly from the interpretation of the explanation that is given in ref. 27 (ref. 3 of the above publication). The π electron density, which is equal on both *exo* and *endo* sides of the double bond, is concentrated into a smaller volume of space on the *exo* side. This can be seen from the θ_π twists (i.e. the $p\sigma$ components of the C_2—C_3 σ bond mix into the π system with such phasing as to create twists on C_2 and C_3 which tend to parallel C_1—C_7 and C_4—C_7 bonds respectively). We also observe from the twist angles, θ_π, that the *exo*-π electron density is tilted towards the C_7 bridge. The consequence of this latter tilt is that the energy minimizes when the hydrogens attached to the double bond are bent down (towards the ethano bridge — energy minimum at 3.9–4.0) and then rises again. The energy rises quite steeply on bending towards the C_7 bridge. The bending was carried out only in a plane perpendicular to the plane of the double bond — we have not examined the energy change when the hydrogens are at the same time pushed together. The less energy demanding rehybridisation in the *endo*-direction (for the C_2 and C_3 hydrogens), a consequence of orbital mixing, does account, in our opinion, not only for the preferential *exo*-addition of norbornene (also norbornyl cation) but also for the enhanced rates in cases when the reaction is controlled by HO(diene)/LU(norbornene) or LU(diene)/HO(norbornene) interactions. (θ_{π^*} is tilted away from the C_7 bridge, on the other side of the symmetry plane of the double bond with a very slightly more concentrated "electron hole" on the *exo*-side.) Bach *et al.* (30*b*) also reach the same conclusions in different systems.

Can. J. Chem. Downloaded from www.nrcresearchpress.com by 210.87.254.5 on 09/05/12
For personal use only.

X = *Cl*: 4-H_{ax}, 4.24t; 2-H, 3.85t.
X = *Br* (35): 4-H_{ax}, 4.45t; 2-H, 3.85t.
X = *I*: 4-H_{ax}, 4.72t; 2-H, 3.94t.

The *cis* alcohols (X = F to I) have shorter retention times than the *trans* alcohols on 10 ft PPGA 1/8 in. diameter columns: in contrast the *trans* alcohols (X = F to I) have higher R_F values on silica gel preparative plates than the *cis* alcohols when eluting with petroleum ether 40 – 60/ether mixtures.

5-X-adamantan-2-ols

X = *F*: *trans* isomer (major), 3.93t; *cis* isomer (minor), 3.75dt ($J_{HF} \sim 2$ Hz).
X = *Cl*: 3.77t (minor); 3.94t (major).
X = *Br*: 3.83t (minor); 3.97t (major).
The alcohols could not be separated by TLC.

anti-π-*Substituted Bornyl Alcohols*

(Only the mean chemical shift of the geminal protons of the substituted *anti*-π-methyl group is quoted.)

Isoborneols

X = *F*: 4.31dq (2H, $J_{AB} = -9.3$ Hz, $J_{HF} = 47.8$ Hz); 3.58dt (1H, *J*'s ca. 5.2 and 6.0 Hz, $J_{HF} = 2.5$ Hz); 1.18d (3H, $J_{HF} = 1.7$ Hz); 0.98s (3H).
X = *Cl*: 3.43q (2H, $J_{AB} = -10.9$ Hz, upfield H doublet is split into a quartet, $J = 1.0$ Hz); 3.65t (1H, *J*'s ca. 5.2 and 5.8 Hz); 1.21 (3H, $J = 1.0$ Hz); 0.95s (3H).
X = $SnMe_3$: 0.85q (2H, $J_{AB} = -12.7$ Hz, upfield H doublet is split into a quartet, $J = 1.4$); 3.64t (1H, *J*'s ca. 2 × 5.5 Hz); 1.07d (3H, $J = 1.4$); 0.91s (3H); 0.05s (9H, satellites with $J_{SnH} = 51.5$ and 49.0 Hz).

Borneols

X = *F*: 4.30dq (2H, $J_{AB} = -9.4$ Hz, $J_{HF} = 47.5$ Hz); 3.94dq (1H, *J*'s 9.8, 3.6, and 1.8 Hz); 0.965d (3H, J_{HF} ca. 1.5); 0.87s (3H).
X = *Cl*: 3.50q (2H, $J_{AB} = -11.0$, upfield H doublet is split into a quartet, $J = 0.9$ Hz); 4.04dq (1H, *J*'s, 9.7, 3.6, and 2.0 Hz); 1.03d (3H, $J = 0.9$ Hz); 0.89s (3H).
X = $SnMe_3$: ca. 0.93q (2H, $J_{AB} = -12.8$ Hz, upfield H doublet is split into a quartet, $J = 1.5$ Hz); 3.98dq (1H, *J*'s 10.1, 3.8, and 2.0 Hz); 0.895d (3H, $J = 1.5$ Hz); 0.88s (3H); 0.16s (9H, satellites with $J_{SnH} = 51.5$ and 49.5 Hz).

The reaction mixtures were analysed on a 10 ft 5% FFAP column and separated preparatively on silica gel plates eluting with petroleum ether 40 – 60/ether mixtures.

Acknowledgement

We would like to thank the Chemistry Department of the University of Alberta for their generosity in allowing us to use their facilities during our stay (J.H.: 1972–1974) when the major part of this work was carried out.

1. D. C. Wigfield. Report No. 61, Tetrahedron, **35**, 449 (1979).
2. (*a*) H. B. Bürgi, J. D. Dunitz, and E. Shefter. J. Am. Chem. Soc. **95**, 5065 (1973); (*b*) H. B. Bürgi, J. M. Lehn, and G. Wipff. J. Am. Chem. Soc. **96**, 1956 (1974).
3. J. Klein. Tetrahedron Lett. 4307 (1973).
4. N. T. Anh and O. Eisenstein. Tetrahedron Lett. 155 (1976); J. Huet, Y. Maroni-Barnaud, N. T. Anh, and J. Seyden-Penne. Tetrahedron Lett. 159 (1976).
5. E. Ernstbrunner, M. R. Giddings, and J. Hudec. Chem. Commun. 953 (1976); 954 (1976); 956 (1976).
6. J. A. Pople and A. Segal. J. Chem. Phys. **44**, 3289 (1966).
7. H. C. Brown and J. Muzzio. J. Am. Chem. Soc. **88**, 2811 (1966).
8. K. Tori, Y. Takano, and K. Kitahonoki. Chem. Ber. **97**, 2798 (1964).
9. G. Snatzke and G. Eckhardt. Tetrahedron, **24**, 4543 (1968).
10. M. T. Hughes and J. Hudec. Chem. Commun. 805 (1971).
11. J. Hudec. J. Chem. Soc. Perkin I, 1020 (1975).
12. K. B. Wiberg. J. Am. Chem. Soc. **102**, 1229 (1980); F. Bernardi, I. G. Csizmadia, and N. D. Epiotis. Tetrahedron, **31**, 3085 (1975).
13. D. Varech and J. Jacques. Tetrahedron Lett. 4443 (1973); M. J. Brienne, D. Varech, and J. Jacques. Tetrahedron Lett. 1233 (1974).
14. M. Cherest, H. Felkin, P. Tacheau, J. Jacques, and D. Varech. Chem. Commun. 372 (1977).
15. W. Moffitt, R. B. Woodward, A. Mozcowitz, W. Klyne, and C. Djerassi. J. Am. Chem. Soc. **83**, 4013 (1961).
16. T. D. Bouman and D. A. Lightner. J. Am. Chem. Soc. **98**, 3145 (1976).
17. H. C. Brown and K. Ichikawa. J. Am. Chem. Soc. **84**, 373 (1962).
18. M. G. Combe and H. B. Henbest. Tetrahedron Lett. 404 (1961); A. Calvert and J. Levisalles. Tetrahedron Lett. 2157 (1972).
19. J. A. Bone, J. R. Pitt, and M. C. Whiting. J. Chem. Soc. Perkin II, 1447 (1975).
20. J. W. le Noble, D.-M. Chiou, and Y. Okaya. Tetrahedron Lett. 1961 (1978).
21. N. T. Anh, O. Eisenstein, J-M. Lefour, and M-E. Tran Huu Dan. J. Am. Chem. Soc. **95**, 6146 (1973).
22. L. Radom, J. A. Pople, V. Buss, and P. Von R. Schleyer. J. Am. Chem. Soc. **94**, 311 (1972); Y Apeloig, P. von R. Schleyer, and J. A. Pople. J. Am. Chem. Soc. **99**, 5901 (1977).
23. P. G. Gassman and J. J. Talley. J. Am. Chem. Soc. **102**, 4138 (1980).
24. R. G. Pearson and J. Songstand. J. Am. Chem. Soc. **89**, 1827 (1967).
25. L. Libit and R. Hoffmann. J. Am. Chem. Soc. **96**, 1370 (1974).
26. A. Imamura and T. Hirano. J. Am. Chem. Soc. **97**, 4192 (1975).
27. S. Inagaki, H. Fujimoto, and K. Fukui. J. Am. Chem. Soc. **98**, 4054 (1976).
28. S. F. Mason, K. Schofield, and R. J. Wells. J. Chem. Soc. C, 626 (1967); S. Yamada and T. Kunieda. Chem. Pharm. Bull. Jpn. **15**, 490 (1967).
29. E. C. Ashby and J. R. Boone. J. Org. Chem. **41**, 2890 (1976).
30. (*a*) R. Huisgen, P. H. J. Ooms, M. Mingin, and N. L. Allinger. J. Am. Chem. Soc. **102**, 3951 (1980); (*b*) R. D. Bach and P. E. Blanchette. J. Am. Chem. Soc. **101**, 46 (1979).
31. J. E. Baldwin. Chem. Commun. 738 (1976).
32. H. B. Henbest. Proc. Chem. Soc. 159 (1963).
33. S. F. Mason. Ann. Reps. Chem. Soc. **73**, 53 (1976).
34. H. Wynberg and B. Feringa. Tetrahedron, **32**, 2831 (1976).
35. D. Farkasiu and P. von R. Schleyer. Tetrahedron Lett. 3835 (1973).
36. S. M. Johnson, I. C. Paul, K. L. Rinehart, and R. Srinivasan. J. Am. Chem. Soc. **90**, 136 (1968); W. H. Pirkle, R. L. Muntz, and I. C. Paul. J. Am. Chem. Soc. **93**, 2818 (1971).

Nucleosides. 118. Total syntheses of pentopyranine B and D. Cytosine nucleosides elaborated by *Streptomyces griseochromogenes*[1]

KYOICHI A. WATANABE AND AKIRA MATSUDA

Laboratory of Organic Chemistry, Sloan-Kettering Institute for Cancer Research, Sloan-Kettering Division of Graduate School of Medical Sciences, Cornell University, New York, NY 10021, U.S.A.

AND

TSUNEO ITOH

School of Pharmaceutical Sciences, Kitasato University, Shirokane, Minato-ku, Tokyo, 108, Japan

Received July 22, 1980

This paper is dedicated to Prof. Raymond U. Lemieux on the occasion of his 60th birthday

KYOICHI A. WATANABE, AKIRA MATSUDA, and TSUNEO ITOH. Can. J. Chem. **59**, 468 (1981).

Pentopyranine B and D, pentopyranosylcytosine nucleosides elaborated by *Streptomyces griseochromogenes*, have been synthesized from the common intermediate, methyl 4-*O*-benzoyl-3-deoxy-3-iodo- β-D-xylopyranoside (**1**). The synthetic products, 1-(2,3-dideoxy-β-D-*glycero*pentopyranosyl)cytosine (**18**) and 1-(3-deoxy-β-D-*erythro*pentopyranosyl)cytosine (**7**) were identical with the natural products, pentopyranine B and D, respectively.

KYOICHI A. WATANABE, AKIRA MATSUDA et TSUNEO ITOH. Can. J. Chem. **59**, 468 (1981).

Utilisant le *O*-benzyl-4 déoxy-3 iodo-3 β-D-xylopyrannoside de méthyle (**1**) comme intermédiaire commun, on a synthétisé les pentopyranines B et D, des nucléosides du type pentopyrannosylcytosine, élaborées par les *Strepstomyces griseochromogenes*. Les produits synthétiques (didéoxy-2,3 β-D-*glycéro*pentopyrannosyl)-1 cytosine (**18**) et (déoxy-3 β-D-*érythro*pentopyrannosyl)-1 cytosine (**7**) sont respectivement identiques aux produits naturels pentopyranine B et D.

[Traduit par le journal]

Nine nucleosides (Fig. 1) were isolated by Seto *et al.* (see ref. 1) from the culture filtrate of *Streptomyces griseochromogenes* during their studies on the biosynthesis of the important nucleoside antibiotic, blasticidin S, a potent antifungal agent against rice blast disease (2). The structures of pentopyranine A and C were proposed (3) as 1-(2,3-dideoxy-α-L-*glycero*pentopyranosyl)cytosine and 1-(3-deoxy-α-L-*threo*pentopyranosyl)-cytosine, respectively, and were confirmed by total syntheses (4, 5). Pentopyranine E, F, and G were identified by direct comparison with the known nucleosides, 1-(α-L-arabinopyranosyl)cytosine (6), 1-(β-D-xylopyranosyl)cytosine (6), and 1-(β-D-glucopyranosyl)cytosine (7), respectively. The total syntheses of pentopyranic acid (8) and pentopyranamine D (9), which is the nucleoside moiety of blasticidin H (10), have also been achieved. This report describes the total syntheses of the two remaining nucleosides, pentopyranine B and D (11).

The starting material for the syntheses of both pentopyranine B and D was methyl 4-*O*-benzoyl-3-deoxy-3-iodo-β-D-xylopyranoside (**1**) which was obtained in 7 steps from D-arabinose by the method

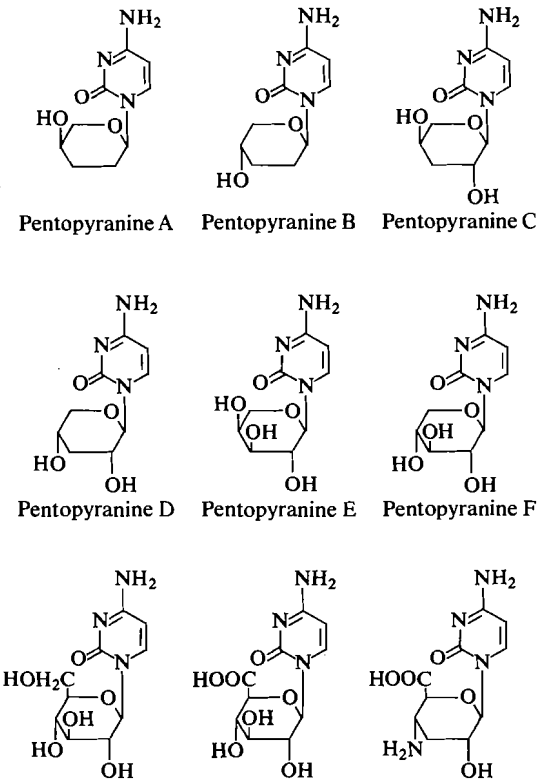

FIG. 1.

[1]This investigation was supported by funds from the National Cancer Institute, National Institutes of Health, U.S. Public Health Service Grant Nos. CA-08748 and CA-18601.

0008-4042/81/020468-05$01.00/0

©1981 National Research Council of Canada/Conseil national de recherches du Canada

Can. J. Chem. Downloaded from www.nrcresearchpress.com by 210.87.254.105 on 09/05/12
For personal use only.

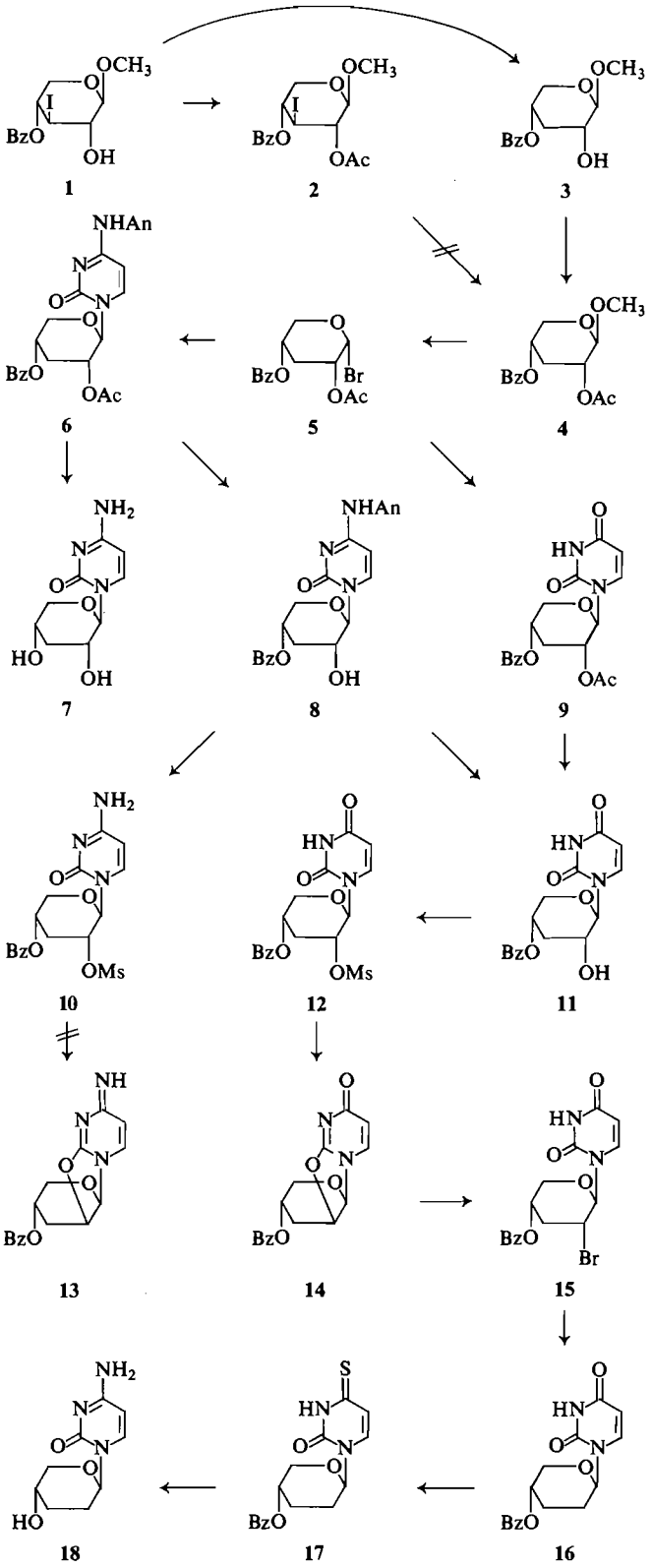

An = anisoyl

Can. J. Chem. Downloaded from www.nrcresearchpress.com by 210.87.254.105 on 09/05/12
For personal use only.

Can. J. Chem. Downloaded from www.nrcresearchpress.com by 210.87.254.105 on 09/05/12
For personal use only.

reported for the preparation of the β-L-counterpart by Lemieux *et al.* (12). Acetylation of the iodohydrin afforded the crystalline acetate **2**. Hydrogenation of **2** over Pd/C gave a product which was contaminated with considerable amounts of 2,3- and 3,4-dideoxysugars (13). However, reduction of **1** gave the corresponding 3-deoxysugar (**3**) which was acetylated to give the crystalline methyl 2-*O*-acetyl-4-*O*-benzoyl-3-deoxy-β-D-*erythro*pentopyranoside (**4**) in good yield. Compound **4** was treated with HBr/HOAc to give the corresponding glycosyl bromide (**5**) which was then condensed with trimethylsilylated N4-anisoylcytosine (5) to afford the crystalline protected nucleoside **6**. Deacylation of **6** with NaOMe/MeOH afforded the corresponding free nucleoside **7**, which was identical with the natural product, pentopyranine D.

The synthesis of pentopyranine B was achieved as follows: selective de-*O*-acetylation of **6** was achieved by treatment with HCl/MeOH, and the crystalline product **8** was mesylated to give the 2-*O*-mesylate **10**. Treatment of **10** with NaOMe under various conditions, however, did not afford the desired anhydronucleoside **13**, but always gave an intractable mixture. Compound **8** was, therefore, deaminated with aqueous HOAc to give the uracil nucleoside **11**. Compound **11** could also be prepared by condensation of the bromosugar **5** with trimethylsilylated uracil followed by de-*O*-acetylation of the protected nucleoside **9**. Mesylation of **11**, and subsequent base treatment of the mesylate **12**, afforded the desired 2,2′-anhydronucleoside **14** in good yield. Treatment of **14** with HBr–DMF complex in tetrahydrofuran gave the 2′-bromo-2′-deoxynucleoside **15**. Reductive debromination of **15** with *n*-Bu_3SnH (14) afforded the 2′,3′-dideoxy derivative **16**. Thiation of **16** with P_4S_{10} in dioxane and amination of the 4-thio nucleoside **17** with NH_3/MeOH gave the free cytosine nucleoside **18**, which exhibited identical uv, ir, and ^1H nmr spectral properties as those of the natural product, pentopyranine B.

Experimental

Microanalyses were performed by Galbraith Laboratories, Inc., Knoxville, TN, or by Spang Microanalytical Laboratory, Eagle Harbor, MI. Melting points were determined on a Thomas-Hoover capillary apparatus and are uncorrected. The ^1H nmr spectra were obtained on a Jeol PFT-100 spectrometer with Me_4Si as the internal standard for organic solvents and $Me_3Si(CH_2)_3SO_3Na$ for D_2O; chemical shifts are reported in parts per million (δ), and signals are quoted as s (singlet), d (doublet), t (triplet), q (quartet), or m (multiplet); *J* values are first order. Infrared spectra were recorded on a Perkin-Elmer Infracord using pressed KBr pellets.

Methyl 2-O-Acetyl-4-O-benzoyl-3-deoxy-3-iodo-β-D-xylopyranoside (2)

Compound **1** (21.3 g, 0.056 mol, prepared from D-arabinose according to Lemieux *et al.* (12)) was acetylated in pyridine (210 mL) with Ac_2O (15 mL). After 3 h the reaction mixture was diluted with CH_2Cl_2 (450 mL), MeOH (50 mL), and water (500 mL). The organic layer was washed with water (2 × 500 mL), dried (Na_2SO_4), and evaporated *in vacuo*. The residue was crystallized from EtOH to give 23 g (97%) of **2**, mp 105–106°C; ^1H nmr ($CDCl_3$) δ: 2.13 (3H, s, CH_3CO), 3.49 (3H, s, OCH_3), 3.44 (1H, q, H-5a, $J_{5a,5e}$ = 11.9, $J_{4,5a}$ = 8.3 Hz), 4.23 (1H, t, H-3, $J_{3,4} = J_{2,3}$ = 9.5 Hz), 4.36 (1H, q, H-5e, $J_{5a,5e}$ = 11.9, $J_{4,5e}$ = 3.9 Hz), 4.39 (1H, d, H-1, $J_{1,2}$ = 6.4 Hz), 5.20 (1H, t, H-2, $J_{1,2} = J_{2,3}$ = 6.4 Hz), 5.29 (1H, sextet, H-4, $J_{4,5a}$ = 8.3, $J_{3,4}$ = 8.5, $J_{4,5e}$ = 4.6 Hz), 7.2–8.2 (5H, m, aromatic). *Anal.* calcd. for $C_{15}H_{17}IO_6$: C 42.86, H 4.05, I 30.24; found: C 42.91, H 4.13, I 30.04.

*Methyl 4-O-Benzoyl-3-deoxy-β-D-*erythro*pentopyranoside (3)*

Compound **1** (20 g, 0.053 mol) was hydrogenated over 10% Pd/C (1 g) in EtOAc (250 mL) containing Et_3N (5.3 g). The catalyst was removed by filtration, and the filtrate was washed successively with water, 0.1 *M* $Na_2S_2O_3$, and water (250 mL each), dried (Na_2SO_4), and evaporated to dryness *in vacuo*. The colorless residue 11.8 g (89%) of **3** was sufficiently pure to be used in the next step; ^1H nmr ($CDCl_3$) ($^1C_4$ conformation) δ: 2.10 (1H, m, H-3e, $J_{3a,3e}$ = 14.7, $J_{2,3e} = J_{3e,4}$ = 4.5, $J_{1,3e} = J_{3e,5e}$ = 1.0 Hz), 2.30 (1H, dt, H-3a, $J_{3a,3e}$ = 14.7, $J_{2,3a} = J_{3a,4}$ = 4.00 Hz), 3.48 (3H, s, CH_3O), 3.68 (1.4H, m, H-2 and a part of H-5e), 3.81 (0.6H, q, part of H-5e, $J_{5a,5e}$ = 13.0, $J_{4,5e}$ = 3.4, $J_{3e,5e}$ = 1.8 Hz), 4.07 (1H, q, H-5a, $J_{5a,5e}$ = 13.0, $J_{4,5a}$ = 2.5 Hz), 4.57 (1H, d, H-1, $J_{1,2}$ = 2.7 Hz), 5.16 (1H, quintet, H-4, $J_{4,5a} = J_{4,5e} = J_{3a,4} = J_{3e,4}$ = 3.2 Hz), 7.3–8.2 (5H, m, aromatic).

An analytical sample (syrup) was purified by chromatography on a silica gel G60 column using C_6H_6–EtOAc (9:1) as the eluent. *Anal.* calcd. for $C_{13}H_{16}O_5$: C 61.90, H 6.35; found: C 61.69, H 6.53.

*Methyl 2-O-Acetyl-4-O-benzoyl-3-deoxy-β-D-*erythro*pentopyranoside (4)*

Acetylation of **3** (13 g, 0.052 mol) with Ac_2O (10 mL) in a mixture of CH_2Cl_2 (100 mL) and pyridine (30 mL) gave the acetate **4** which was crystallized from EtOH – *n*-heptane to afford 12.5 g (82%) of pure **4**, mp 66–67°C; ^1H nmr ($CDCl_3$) ($^1C_4$ conformation) δ: 2.01 (3H, s, CH_3CO), 2.27 (2H, m, H-3a,3e), 3.45 (3H, s, CH_3O), 3.73 (1H, dt, H-5e, $J_{5a,5e}$ = 12.8, $J_{4,5e} = J_{3,5e}$ = 2.0 Hz), 4.06 (1H, dd, H-5a, $J_{5a,5e}$ = 12.8, $J_{4,5a}$ = 2.1 Hz), 4.67 (1H, d, H-1, $J_{1,2}$ = 0.5 Hz), 4.80 (1H, quintet, H-4), 5.07 (1H, narrow m, H-2), 7.4–8.2 (5H, aromatic multiplet). *Anal.* calcd. for $C_{15}H_{18}O_6$: C 61.22, H 6.12; found: C 61.07, H 6.37.

*2-O-Acetyl-4-O-benzoyl-3-deoxy-D-*erythro*pentopyranosyl Bromide (5)*

Compound **4** (1.18 g, 4 mmol) was dissolved in 30% HBr/HOAc (10 mL); the mixture was stirred for 2 h at room temperature and partitioned between CH_2Cl_2 (100 mL) and water (50 mL). The organic layer was washed with water (2 × 50 mL), dried (Na_2SO_4), and concentrated to dryness *in vacuo*. Compound **5** was obtained in quantitative yield as a slightly yellow syrup which was not further purified but used directly in the next step.

*1-(2-O-Acetyl-4-O-benzoyl-3-deoxy-β-D-*erythro*pentopyranosyl)-N4-anisoylcytosine (6)*

$SnCl_4$ (0.7 mL, 6 mmol) was added to a mixture of the above bromo sugar **5** and crude N4,O2-bis(trimethylsilyl)-N4-anisoylcytosine (prepared from 1.47 g (6 mmol) of N4-anisoylcytosine (5)) in dry CH_2ClCH_2Cl (25 mL). The mixture was stirred at room temperature for 1 h, and then heated at 60°C for 20 min. The mixture was diluted with CH_2Cl_2 (25 mL) and poured into saturated $NaHCO_3$ (100 mL); the suspension was passed through a Celite pad. The filtrate was washed (water), dried (Na_2SO_4), and evaporated to dryness *in vacuo*. The residue was

Can. J. Chem. Downloaded from www.nrcresearchpress.com by 210.87.254.105 on 09/05/12
For personal use only.

crystallized from EtOH to give 879 mg (43.2%) of **6**, mp 240–242°C; ^{1}H nmr ($CDCl_3$) δ: 2.02 (3H, s, CH_3CO), 2.06 (1H, q, H-3′a, $J_{3'a,3'e} = J_{2',3'a} = J_{3'a,4'} = 11.6$ Hz), 2.75 (1H, m, H-3′e), 3.65 (1H, t, H-5′a, $J_{5'a,5'e} = J_{4',5'a} = 10.7$ Hz), 3.89 (3H, s, CH_3O), 4.37 (1H, dd, H-5′e, $J_{5'a,5'e} = 10.7$, $J_{5'e,4} = 5.2$ Hz), 5.36–4.69 (2H, m, 10 lines, H-2′,4′), 6.00 (1H, d, H-1′, $J_{1',2'} = 9.5$ Hz), 6.99 (1H, d, H-5, $J_{5,6} = 8.8$ Hz), 8.08–7.37 (6H, m, benzoyl and H-6), 8.58 (1H, broad s, NH). *Anal.* calcd. for $C_{26}H_{25}N_3O_8$: C 61.53, H 4.97, N 8.28; found: C 61.36, H 4.97, N 8.13.

*1-(3-Deoxy-β-D-*erythro*pentopyranosyl)cytosine (7)*

A suspension of **6** (177 mg, 0.35 mmol) in absolute MeOH (20 mL) was treated with 1 *N* NaOMe (1 mL). The reaction mixture was stirred overnight at room temperature and then neutralized with Amberlite IRC-50 (H^+). The resin was removed by filtration, and the filtrate was evaporated to dryness *in vacuo*. The residue was dissolved in water (20 mL) and extracted with $CHCl_3$ (2 × 20 mL). The aqueous phase was evaporated *in vacuo* to dryness. The residue was crystallized from MeOH–Et_2O to give 66.5 mg (84%) of **7**, mp 255–257°C (dec.) (lit. (11), mp 261°C (dec.)). A mixture mp with the natural sample was unchanged; ^{1}H nmr (DMSO-d_6) δ: 1.41 (1H, dd, H-3′a, $J_{2',3'a} = J_{3'a,3'e} = J_{3'a,4'} = 10.7$ Hz), 2.20 (1H, m, H-3′e), 3.06 (1H, t, H-5′a, $J_{5'a,5'e} = J_{4',5'a} = 9.0$ Hz), 3.70 (3H, m, H-2′, 4′, 5′e), 5.03 (2H, broad s, dissociable, 2′- and 4′-OH), 5.28 (1H, d, H-1′, $J_{1',2'} = 9.2$ Hz), 5.68 (1H, d, H-5, $J_{5,6} = 7.5$ Hz), 7.14 (2H, broad s, NH_2), 7.53 (1H, d, H-6, $J_{5,6} = 7.5$ Hz). The ^{1}H nmr spectrum taken in concentrated DCl was identical with that of the natural sample supplied by Dr. Seto.

*1-(4-O-Benzoyl-3-deoxy-β-D-*erythro*pentopyranosyl)-N4-anisoylcytosine (8)*

A solution of **6** (254 mg, 0.5 mmol) in 3% HCl/MeOH (50 mL) was stirred for 6 h at room temperature and then the mixture was stored at 4°C for 3 days. The solvent was removed *in vacuo* and the residue dried by several azeotropic distillations with EtOH. The residue was crystallized from EtOH to give 189 mg (81%) of **8**, mp 229–230°C; ^{1}H nmr (DMSO-d_6) δ: 1.85 (1H, q, H-3′a, $J_{2',3'a} = J_{3'a,3'e} = J_{3'a,4'} = 11.2$ Hz), 2.50 (1H, m, H-3′e), 3.56 (1H, t, H-5′a, $J_{4',5'a} = J_{5'a,5'e} = 10.4$ Hz) 3.84 (3H, s, CH_3O), 4.00 (1H, m, H-2′), 4.13 (1H, m, H-5′e), 5.21 (2H, m, H-4′ and 2′-OH), 5.58 (1H, d, H-1′, $J_{1',2'} = 9.2$ Hz), 7.05 (1H, d, H-5, $J_{5,6} = 8.9$ Hz), 7.31–8.26 (10H,m, aromatic and H-6). *Anal.* calcd. for $C_{24}H_{23}N_3O_7$: C 61.93, H 4.98, N 9.03; found: C 61.81, H 5.00, N 8.91.

*1-(4-O-Benzoyl-3-deoxy-2-O-mesyl-β-D-*erythro*pentopyranosyl)-N4-anisoylcytosine (10)*

A cold (0°C) solution of **8** (233 mg, 0.5 mmol) in dry pyridine (5 mL) was treated with MsCl (0.12 mL, 1.5 mmol). After 2 h, the mixture was poured into an ice–water mixture (100 mL). The precipitate was collected and washed with water and EtOH to give 261 mg (96%) of **10**, mp 155–157°C; ^{1}H nmr (DMSO-d_6) δ: 2.26 (1H, q, H-3′a, $J_{2',3'a} = J_{3'a,3'e} = J_{3'a,4'} = 11.9$ Hz), 2.81 (1H, m, H-3′e), 3.15 (3H, s, CH_3SO_2), 3.79 (1H, t, H-5′a, $J_{4',5'a} = J_{5'a,5'e} = 10.7$ Hz), 3.85 (1H, s, CH_3O), 4.22 (1H, dd, H-5′e, $J_{4,5e} = 4.8$, $J_{5'a,5'e} = 10.7$ Hz), 5.26 (2H, m, H-2′,4′), 5.99 (1H, d, H-1′, $J_{1',2'} = 8.9$ Hz), 7.05 (1H, d, H-5, $J_{5,6} = 8.9$ Hz), 8.32–7.36 (10H, m, aromatic and H-6), 11.18 (1H, broad s, NH). *Anal.* calcd. for $C_{25}H_{25}N_3O_9S$: C 55.24, H 4.64, N 7.73, S 5.90; found: C 55.03, H 4.53, N 7.68, S 6.04.

*1-(2-O-Acetyl-4-O-benzoyl-3-deoxy-β-D-*erythro*pentopyranosyl)uracil (9)*

A room temperature solution of **5** (prepared from 1.89 g, 6.43 mmol of **4**) and 2,4-bis(trimethylsilyloxy)pyrimidine (prepared from 1.08 g of uracil) in dry CH_2ClCH_2Cl (50 mL) was treated with $SnCl_4$ (0.53 mL, 4.5 mmol). After 3 h, saturated $NaHCO_3$ solution (100 mL) was added to the mixture, and the resulting suspension was filtered through a Celite pad. The filtrate was washed with water, dried (Na_2SO_4), and evaporated to dryness *in vacuo*. The residue was dissolved in $CHCl_3$ and placed on a column of silica gel G60 (4 × 31 cm), and the column was washed successively with $CHCl_3$ (500 mL), 0.5% EtOH in $CHCl_3$ (500 mL), and 1% EtOH in $CHCl_3$ (1000 mL). Compound **9** was obtained from the last fraction and was crystallized from EtOH to give 1.2 g (50%), mp 190–191°C; ^{1}H nmr ($CDCl_3$) δ: 2.04 (3H,s, CH_3CO), 2.07 (1H, q, H-3′a, $J_{2',3'a} = J_{3'a,3'e} = J_{3'a,4'} = 11.6$ Hz), 2.76 (1H, m, H-3′e), 3.63 (1H, t, H-5′a, $J_{4',5'a} = J_{5'a,5'e} = 10.7$ Hz), 4.33 (1H, ddd, $J_{5'a,5'e} = 10.7$, $J_{4',5'e} = 5.2$, $J_{3'e,5'e} = 2.0$ Hz), 5.08 (2H, m, H-2′, 4′), 5.73 (1H, d, H-1′, $J_{1',2'} = 9.2$ Hz), 5.81 (1H, dd, H-5, $J_{5,6} = 8.2$, $J_{5,NH} = 2.1$ Hz), 7.26–8.07 (6H, m, aromatic and H-6). *Anal.* calcd. for $C_{18}H_{18}N_2O_7$: C 57.75, H 4.85, N 7.48; found: C 57.52, H 4.95, N 7.35.

*1-(4-O-Benzoyl-3-deoxy-β-D-*erythro*pentopyranosyl)uracil (11)*

A mixture of **9** (450 mg, 1.2 mmol) in 3% HCl/MeOH (50 mL) was stirred at room temperature for 4.5 h and then evaporated to dryness *in vacuo*. The residue was coevaporated several times with EtOH until colorless crystals were obtained. The crystals were collected by suction filtration and washed with Et_2O to give 352 mg (88%) of **11**, mp 235–238°C; ^{1}H nmr ($CDCl_3$ – DMSO-d_6 4:1) δ: 1.86 (1H, q, H-3′a, $J_{2',3'a} = J_{3'a,3'e} = J_{3'a,4'} = 11.8$ Hz), 2.58 (1H, m, H-3′e) 3.53 (1H, t, H-5′a, $J_{4',5'a} = J_{5'a,5'e} = 10.4$ Hz), 3.81 (1H, m, H-2′), 4.23 (1H, m, H-5′e), 4.97 (1H, m, H-4′), 5.43 (1H, d, H-1′, $J_{1',2'} = 9.2$ Hz), 5.66 (1H, d, H-5, $J_{5,6} = 8.2$ Hz), 7.47–8.03 (6H, m, aromatic and H-6), 11.29 (1H, broad s, NH). *Anal.* calcd. for $C_{16}H_{16}N_2O_6$: C 57.83, H 4.85, N 8.43; found: C 57.81, H 4.85, N 8.38.

*1-(4-O-Benzoyl-3-deoxy-2-O-mesyl-β-D-*erythro*pentopyranosyl)uracil (12)*

A cold (0°C) solution of **11** (352 mg, 1.06 mmol) in dry pyridine (5 mL) was treated with MsCl (0.25 mL). After 3 h, the mixture was poured into an ice–water mixture, and the precipitate was collected and crystallized from EtOH to give **12** (391 mg, 90%), mp 158–159°C; ^{1}H nmr ($CDCl_3$) δ: 2.18 (1H, q, H-3′a, $J_{2',3'a} = J_{3'a,3'e} = J_{3'a,4'} = 11.0$ Hz), 2.90 (1H, m, H-3′e), 3.02 (3H, s, CH_3SO_2), 3.65 (1H, t, H-5′a, $J_{4',5'a} = J_{5'a,5'e} = 11.0$ Hz), 4.36 (1H, ddd, H-5′e, $J_{5'a,5'e} = 11.0$, $J_{4',5'e} = 5.3$, $J_{3'e,5'e} = 2.4$ Hz), 4.82 (1H, octet, H-2′, $J_{1',2'} = 8.9$, $J_{2',3'a} = 11.0$, $J_{2',3'e} = 5.2$ Hz), 5.23 (1H, 7 lines, H-4′, $J_{4',5'a} = 11.0$, $J_{4',5'e} = J_{3'e,4'} = 5.3$ Hz), 5.78 (1H, d, H-1′, $J_{1',2'} = 8.9$ Hz), 5.85 (1H, dd, H-5, $J_{5,6} = 8.4$, $J_{5,NH} = 2.1$ Hz), 7.27–8.07 (6H, m, H-6 and aromatic). *Anal.* calcd. for $C_{17}H_{18}N_2O_8S$: C 49.75, H 4.42, N 6.83, S 7.81; found: C 49.86, H 4.35, N 6.75, S 7.79.

*2,2′-Anhydro-1-(4-O-benzoyl-3-deoxy-β-D-*threo*pentopyranosyl)uracil (14)*

A suspension of **12** (511 mg, 1.25 mmol) in dry MeCN (100 mL) was treated with 1,8-diazabicyclo[5,4,0]undec-7-ene (0.25 mL, 1.6 mmol). The mixture was heated at reflux for 1 h and then cooled to room temperature. The solvent was removed *in vacuo*, and the residue was crystallized from EtOH to give 370 mg (94.4%) of **14**, mp 199–203°C; ^{1}H nmr ($CDCl_3$) δ: 2.23 (1H, octet, H-3′ down, $J_{3'down,\ 3'up} = 15.0$, $J_{2',3'down} = 7.9$, $J_{3'down,4'} = 3.7$ Hz), 2.99 (1H, octet, H-3′up, $J_{3'down,\ 3'up} = 15.0$, $J_{2',3'up} = 3.7$, $J_{3'up,4'} = 7.3$ Hz), 3.90 (2H, m, H-5′, 5″), 5.13–5.33 (2H, m, H-2′,4′), 5.89 (1H, d, H-1′, $J_{1',2'} = 6.1$ Hz), 6.11 (1H, d, H-5, $J_{5,6} = 7.6$ Hz), 7.26–8.09 (6H, m, H-6 and aromatic). *Anal.* calcd. for $C_{16}H_{14}N_2O_5$: C 61.15, H 4.49, N 8.91; found: C 61.23, H 4.40, N 8.84.

*1-(4-O-Benzoyl-2-bromo-2,3-dideoxy-β-D-*erythro*pentopyranosyl)uracil (15)*

A mixture of DMF–HBr complex (230 mg) and **14** (104 mg, 0.33 mmol) in dry THF (10 mL) was heated at reflux for 40 min. The solvent was removed *in vacuo*, and the residue was dissol-

Can. J. Chem. Downloaded from www.nrcresearchpress.com by 210.87.254.105 on 09/05/12
For personal use only.

ved in a small volume of THF and spotted on 2 sheets of glass plates (20 × 20 cm) coated with silica gel PF_{254} which were then developed in $CHCl_3$–EtOH (170:7). The major band was removed and extracted with EtOAc. After evaporation of the solvent, compound **15** (110 mg, 84%) was obtained as colorless crystals, mp 201–202°C; ^{1}H nmr ($CDCl_3$) δ: 2.34 (1H, q, H-3′a, $J_{2',3'a} = J_{3'a,3'e} = J_{3'a,4'} = 11.5$ Hz), 3.12 (1H, m, H-3′e), 3.73 (1H, t, H-5′a, $J_{4',5'a} = J_{5'a,5'e} = 11.5$ Hz), 4.08 (1H, octet, H-2′, $J_{1',2'} = 9.5$, $J_{2',3'a} = 11.5$, $J_{2',3'e} = 4.6$ Hz), 4.38 (1H, ddd, H-5′e, $J_{5'a,5'e} = 11.5$, $J_{4',5'e} = 5.2$, $J_{3'e,5'e} = 2.4$ Hz), 5.16 (1H, 7 lines, H-4′, $J_{3'e,4'} = J_{4',5'e} = 5.2$, $J_{3'a,4'} = J_{4',5'a} = 11.5$ Hz), 5.82 (2H, 2 doublets for H-1′ and H-5, $J_{1',2'} = 9.5$ Hz), 7.22–8.06 (6H, m, H-6 and aromatic). *Anal.* calcd. for $C_{16}H_{15}BrN_2O_5 \cdot 0.5H_2O$: C 47.54, H 3.98, Br 19.77, N 6.93; found: C 47.75, H 3.74, Br 19.75, N 6.85.

1-(4-O-Benzoyl-2,3-dideoxy-β-D-glycero-pentopyranosyl)uracil (16)

A mixture of **15** (271 mg, 0.69 mmol), *n*-Bu_3SnH (0.24 mL, 0.9 mmol), and 2,2′-azobis(2-methylpropionitrile) (~10 mg) in dry MeCN (40 mL) was heated under reflux for 5 h. The solvent was removed *in vacuo*, and the residue was crystallized from EtOH to give 191 mg of **16** (88%), mp 188–190°C; ^{1}H nmr ($CDCl_3$) δ: 1.79–2.20 (3H, m, H-2′a,2′e,3′a), 2.39 (1H, m, H-3′e), 3.63 (1H, t, H-5′a, $J_{4',5'a} = J_{5'a,5'e} = 10.7$ Hz), 4.31 (1H, ddd, H-5′e, $J_{5'a,5'e} = 10.7$, $J_{4',5'e} = 4.9$, $J_{3'e,5'e} = 2.1$ Hz), 5.09 (1H, m, H-4′), 5.72 (1H, q, H-1′, $J_{1',2'a} = 8.6$, $J_{1',2'e} = 2.0$ Hz), 5.80 (1H, q, H-5, $J_{5,6} = 8.2$, $J_{5,3NH} = 2.0$ Hz), 7.38–8.07 (6H, m, H-6 and benzoyl), 8.60 (1H, broad s, 3NH). *Anal.* calcd. for $C_{16}H_{16}N_2O_5$: C 60.75, H 5.10, N 8.85; found: C 60.66, H 5.18, N 8.76.

1-(4-O-Benzoyl-2,3-dideoxy-β-D-glycero-pentopyranosyl)-4-thiouracil (17)

To a stirred suspension of **16** (158 mg, 0.5 mmol) in dry dioxane (20 mL) was added P_4S_{10} (200 mg), and the mixture was heated under reflux for 45 min. A second charge of P_4S_{10} (100 mg) was added and the mixture refluxed for a further 45 min. The solvent was removed *in vacuo*, the residue extracted with $CHCl_3$ (10 mL), and the extract placed on a column of silica gel G60 (2.4 × 13 cm). The column was washed with $CHCl_3$, the uv absorbing fractions collected and evaporated, and the residual yellow powder purified by preparative tlc (20 × 20 cm glass plate coated with silica gel PF_{254}, C_6H_6–EtOAc 6:1 system) to give 58 mg of **17** which was sufficiently pure to be used directly in the next step.

1-(2,3-Dideoxy-β-D-glycero-pentopyranosyl)cytosine (18)

Compound **17** (58 mg, 0.17 mmol) was dissolved in saturated NH_3/MeOH (3 mL) in a test tube which was sealed and heated at 100°C for 36 h in a steel container. The yellow mixture was concentrated to dryness, the residue extracted with $CHCl_3$, and then crystallized from EtOH to afford 16 mg (43%) of **18**, mp 233–234°C (lit. (11) mp 241°C). When this compound was admixed with a sample of the natural product, no depression of melting point was observed; ^{1}H nmr (DMSO-d_6) δ: 1.49–1.78 (3H, m, H-2′a,2′e,3′a), 2.04 (1H, m, H-3′e), 3.16 (1H, t, H-5′a, $J_{4',5'a} = J_{5'a,5'e} = 9.9$ Hz), 3.54 (1H, m, H-4′), 3.87 (1H, m, H-5′e), 4.92 (1H, d, 4′OH), 5.48 (1H, m, H-1′), 5.69 (1H, d, H-5, $J_{5,6} = 7.5$ Hz), 7.14 (2H, broad s, NH_2), 7.57 (1H, d, H-6, $J_{5,6} = 7.5$ Hz). The ^{1}H nmr spectrum of this sample taken in concentrated DCl was identical with that of pentopyranine B supplied by Dr. Seto. The ir spectrum (KBr) of the synthetic compound **18** was not identical to that of the natural product. An approximately 10:1 mixture of the natural product and synthetic **18** gave an ir spectrum which was identical to that of the synthetic product. The reverse (an approximately 1:10 mixture of the natural product and synthetic **18**) did not alter the ir spectrum of the synthetic product.

Acknowledgements

The authors are indebted to Dr. Jack J. Fox for his warm and continued interest and encouragement. They also wish to thank Professor Haruo Seto of the Institute of Applied Microbiology, the University of Tokyo, for samples of pentopyranine B and D and the ir and ^{1}H nmr spectra of these natural products.

1. R. J. SUHADOLNIK. Nucleosides as biological probes. Wiley Interscience, New York. 1979. pp. 154–158.
2. K. FUKUNAGA. The rice blast disease. Proceedings of a Symposium at the International Rice Research Institute. The Johns Hopkins Press, Baltimore, MD. 1963. p. 406.
3. H. SETO, N. OTAKE, and H. YONEHARA. Tetrahedron Lett. 3991 (1972).
4. T. M. K. CHIU, H. OHRUI, K. A. WATANABE, and J. J. FOX. J. Org. Chem. **38**, 3622 (1973).
5. K. A. WATANABE, T. M. K. CHIU, D. H. HOLLENBERG, and J. J. FOX. J. Org. Chem. **39**, 2482 (1974).
6. J. J. FOX and I. GOODMAN. J. Am. Chem. Soc. **73**, 3256 (1951).
7. G. E. HILBERT and E. F. JANSEN. J. Am. Chem. Soc. **58**, 60 (1936).
8. K. A. WATANABE, D. H. HOLLENBERG, and J. J. FOX. J. Antibiot. Tokyo, **29**, 597 (1976).
9. K. A. WATANABE, T. M. K. CHIU, U. REICHMAN, C. K. CHU, and J. J. FOX. Tetrahedron, **32**, 1493 (1976).
10. H. SETO and H. YONEHARA. J. Antibiot. Tokyo, **30**, 1019 (1977).
11. H. SETO. Agric. Biol. Chem. **37**, 2415 (1973).
12. R. U. LEMIEUX, K. A. WATANABE, and A. A. PAVIA. Can. J. Chem. **47**, 4413 (1969).
13. A. F. RUSSELL, S. GREENBERG, and J. G. MOFFATT. J. Am. Chem. Soc. **95**, 4025 (1973).
14. G. L. GRADY and H. G. KUIVILLA. J. Org. Chem. **34**, 2014 (1969).

Un nouvel agent de glycosylation: l'anhydride trifluorométhanesulfonique. Synthèse des α et β *O*-glycosyl-L-sérine, -L-thréonine et -L-hydroxyproline

J. M. LACOMBE, A. A. PAVIA[1] ET J. M. ROCHEVILLE

Laboratoire de Chimie Bioorganique, Faculté des Sciences d'Avignon 33, rue Louis-Pasteur, 84000 Avignon, France

Reçu le 26 juin 1980

Ce papier et dédié au Prof. Raymond U. Lemieux à l'occasion de son 60ème anniversaire

J. M. LACOMBE, A. A. PAVIA et J. M. ROCHEVILLE. Can. J. Chem. **59**, 473 (1981).

La réaction à froid, dans le dichlorométhane ou l'acétonitrile, d'un dérivé benzylé d'un monosaccharide réducteur avec un hydroxyaminoacide convenablement protégé, en présence d'anhydride trifluorométhanesulfonique comme agent de condensation conduit avec un rendement variant entre 55 et 90% au mélange des *O*-glycosylaminoacides dans lequel les anomères α sont prépondérants. Les α et β *O*-D-galactosyl, D-glucosyl, D-xylosyl-et L-arabinosyl-L-sérine, -L-thréonine et -L-hydroxyproline ont été ainsi obtenus purs par cristallisation ou chromatographie sur colonne. Leur structure et leur stéréochimie s'appuient essentiellement sur la rmn du ^{13}C.

J. M. LACOMBE, A. A. PAVIA, and J. M. ROCHEVILLE. Can. J. Chem. **59**, 473 (1981).

When 2,3,4,6-tetra-*O*-benzyl-D-glucopyranose, -D-galactopyranose and 2,3,4-tri-*O*-benzyl-D-xylopyranose were allowed to react in the cold in dichloromethane or acetonitrile as solvent in the presence of trifluoromethanesulfonic (triflic) anhydride, with methyl or benzyl esters of the *N*-(benzyloxycarbonyl)-L-serine, -L-threonine, and -L-hydroxyproline, an anomeric mixture of the corresponding *O*-glycosylaminoacids was obtained (55 to 90% overall yield), with the α-anomer being predominant. The same experimental procedure was successfully applied to the condensation of the benzyl ester of the *N*-(benzyloxycarbonyl)-L-hydroxyproline with 2,3,4-tri-*O*-benzyl-L-arabinopyranose and 2,3,5-tri-*O*-benzyl-L-arabinofuranose affording the corresponding condensation products with similar yield. Pure α and β anomers were obtained after column chromatography or crystallization with 30 to 65% yield. Hydrogenolysis of benzyl derivatives afforded the unprotected compounds. Optical rotation, ^1H and ^{13}C nmr were the main methods used to assess structure and stereochemistry.

Introduction

La nature de la jonction entre la copule glucidique et le squelette peptidique constitue un des aspects essentiels de la chimie et de la biochimie des glycoprotéines et protéoglycanes. Les deux types de liaisons rencontrées diffèrent par leurs propriétés chimiques, leur stabilité vis-à-vis des bases en particulier (1). La liaison *N*-glycosidique entre le 2-acétamido-2-désoxy-β-D-glucopyranose et la L-asparagine, mise en évidence pour la première fois par Marshall et Neuberger au début des années 60 dans l'ovalbumine et fréquemment trouvée depuis dans un grand nombre de glycoprotéines, est stable en milieu basique. A l'exception de celles impliquant une liaison glycosidique avec l'hydroxylysine et l'hydroxyproline, les *O*-glycoprotéines sont fragiles en milieu basique. La liaison osidique entre le galactose et l'hydroxylysine est présente dans le collagène et les polymères apparentés (1); celle entre la sérine et/ou la thréonine et le 2-acétamido-2-désoxy-α-D-galactose prédomine dans de nombreuses mucoprotéines (1), les substances des groupes sanguins (1, 2), les immunoglobulines (1, 2), les glycoprotéines "antigel" (1, 3), et les glycoprotéines membranaires comme la glycophorine par exemple (1, 4).

Nous avons décrit récemment (5) la synthèse des 3-*O*-(2-acétamido-2-désoxy-α-D-galactopyranosyl)-L-sérine et L-thréonine qui constituent l'unité de base de ces macromolécules. De nombreux autres glycopeptides dans lesquels la sérine et la thréonine sont liés au D-glucose (6), L-fucose (7), D-galactose (8), D-mannose (6, 9, 10) et D-xylose (10) ont été décrits dans les toutes dernières années. Par ailleurs, le D-galactose (11, 12) et le L-arabinose (11, 13) sont présents dans la nature sous la forme de *O*-galactosyl et *O*-arabinosyl-L-hydroxyproline dans certaines glycoprotéines de la paroi des cellules végétales (11, 13).

Il apparait évident qu'une connaissance approfondie des propriétés physiques, chimiques et conformationnelles des glycoprotéines est nécessaire pour mieux apprécier les relations existant entre d'une part leur structure et d'autre part leur métabolisme, leur rôle biologique et leur pathologie (14, 15). Dans cette optique il nous a semblé important de développer une méthode permettant d'accéder à ces glycosylaminoacides et glycopeptides de base.

Résultats et discussion

Nous avons décrit récemment (16) la synthèse en une seule étape des dérivés benzylés du tréhalose et des analogues *galacto*, *manno*, *xylo*, *arabino*, *fructo* par autocondensation des monosaccharides

[1]Auteur à qui toute correspondance doit être adressée.

0008-4042/81/020473-09$01.00/0

©1981 National Research Council of Canada/Conseil national de recherches du Canada

Can. J. Chem. Downloaded from www.nrcresearchpress.com by 210.87.254.5 on 09/05/12
For personal use only.

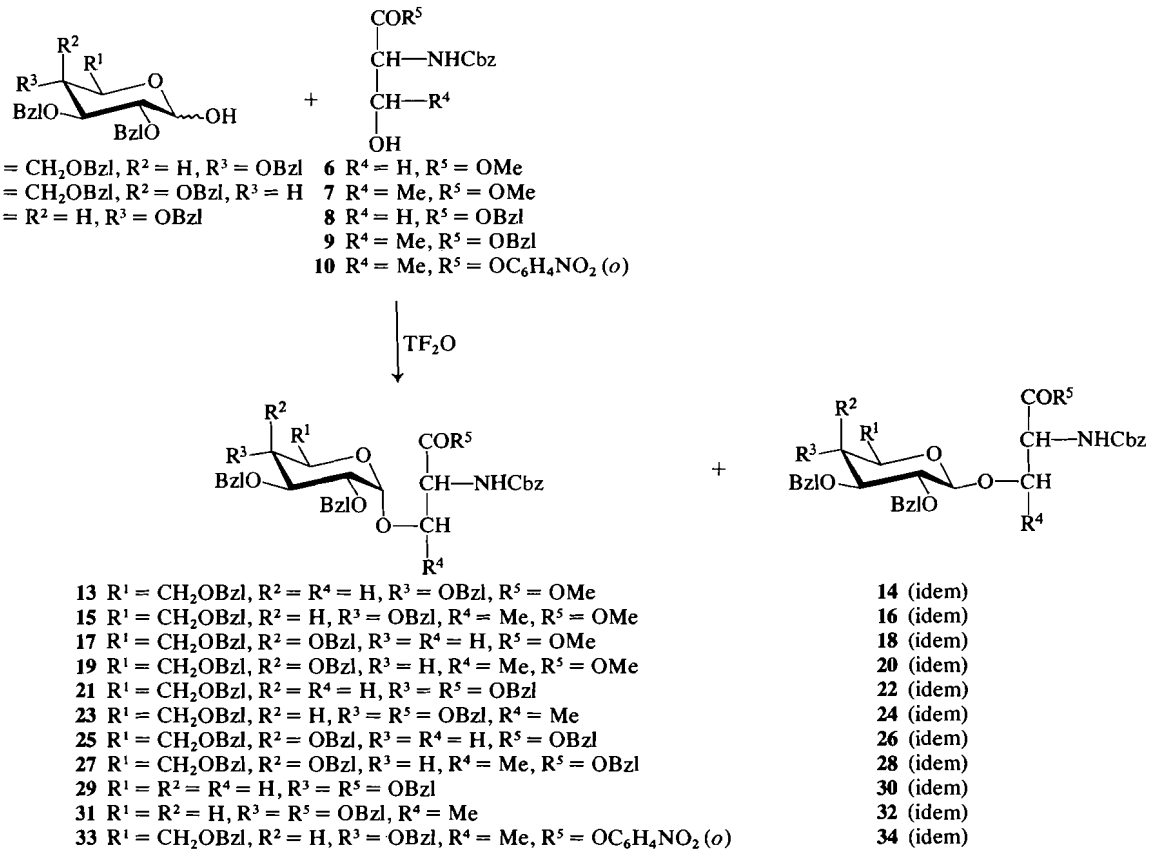

1 $R^1 = CH_2OBzl$, $R^2 = H$, $R^3 = OBzl$ **6** $R^4 = H$, $R^5 = OMe$
2 $R^1 = CH_2OBzl$, $R^2 = OBzl$, $R^3 = H$ **7** $R^4 = Me$, $R^5 = OMe$
3 $R^1 = R^2 = H$, $R^3 = OBzl$ **8** $R^4 = H$, $R^5 = OBzl$
9 $R^4 = Me$, $R^5 = OBzl$
10 $R^4 = Me$, $R^5 = OC_6H_4NO_2$ (*o*)

13 $R^1 = CH_2OBzl$, $R^2 = R^4 = H$, $R^3 = OBzl$, $R^5 = OMe$ **14** (idem)
15 $R^1 = CH_2OBzl$, $R^2 = H$, $R^3 = OBzl$, $R^4 = Me$, $R^5 = OMe$ **16** (idem)
17 $R^1 = CH_2OBzl$, $R^2 = OBzl$, $R^3 = R^4 = H$, $R^5 = OMe$ **18** (idem)
19 $R^1 = CH_2OBzl$, $R^2 = OBzl$, $R^3 = H$, $R^4 = Me$, $R^5 = OMe$ **20** (idem)
21 $R^1 = CH_2OBzl$, $R^2 = R^4 = H$, $R^3 = R^5 = OBzl$ **22** (idem)
23 $R^1 = CH_2OBzl$, $R^2 = H$, $R^3 = R^5 = OBzl$, $R^4 = Me$ **24** (idem)
25 $R^1 = CH_2OBzl$, $R^2 = OBzl$, $R^3 = R^4 = H$, $R^5 = OBzl$ **26** (idem)
27 $R^1 = CH_2OBzl$, $R^2 = OBzl$, $R^3 = H$, $R^4 = Me$, $R^5 = OBzl$ **28** (idem)
29 $R^1 = R^2 = R^4 = H$, $R^3 = R^5 = OBzl$ **30** (idem)
31 $R^1 = R^2 = H$, $R^3 = R^5 = OBzl$, $R^4 = Me$ **32** (idem)
33 $R^1 = CH_2OBzl$, $R^2 = H$, $R^3 = OBzl$, $R^4 = Me$, $R^5 = OC_6H_4NO_2$ (*o*) **34** (idem)

SCHÉMA 1

appropriés dans le dichlorométhane à froid en présence d'anhydride trifluorométhanesulfonique comme agent de condensation. Nous avons pu montrer que la réaction était du type acido-catalysé et que l'anhydride trifluorométhanesulfonique jouait le double rôle de "source de protons" et de "piège à eau".

Nous avons pu montrer également (16) que si la réaction était conduite en présence d'un excès (3 à 4 moles pour une) d'un hydroxyaminoacide, la réaction d'autocondensation était minimisée au profit de la formation des glycosylaminoacides. Le travail que nous rapportons ici représente la généralisation de l'observation précédente et l'extension de la méthode à la préparation des α et β-*O*-glycosylaminoacides naturels.

La réaction est effectuée dans le dichlorométhane ou dans un mélange dichlorométhane–acétonitrile, à froid, en présence d'anhydride trifluorométhanesulfonique (voir Partie expérimentale). Dans ces conditions, le dérivé benzylé du monosaccharide réducteur réagit en quelques minutes avec un excès de l'hydroxyaminoacide convenablement protégé pour donner avec un bon rendement (55 à 90%) le mélange des deux anomères du *O*-glycosylaminoacide correspondant. La chromatographie du mélange réactionnel sur gel de silice, permet d'une part de séparer les anomères α et β et d'autre part de récupérer la majeure partie de l'aminoacide qui n'a pas réagi.

La condensation des 2,3,4,6-tétra-*O*-benzyl-D-gluco (**1**) et galactopyranose (**2**) avec les esters méthyliques de la *N*-(benzyloxycarbonyl)-L-sérine (**6**), -L-thréonine (**7**) et -L-hydroxyproline (**11**) dans le dichlorométhane entre −70 et 0°C conduit au mélange des *O*-glycosylaminoacides correspondants, dans lequel l'anomère α est toujours prépondérant ou parfois même exclusif. La chromatographie sur colonne de gel de silice, des mélanges réactionnels permet d'isoler les anomères α (**13**, **15**, **17**, **19**, **35** et **37**) purs avec un rendement variant entre 32 et 65%.

En dehors de l'utilisation possible de ces composés comme preuve non ambiguë de structure, ou comme haptène, un des objectifs majeurs de notre travail est l'étude de leurs propriétés conformationnelles en solution aqueuse et à l'état solide.

Can. J. Chem. Downloaded from www.nrcresearchpress.com by 210.87.254.5 on 09/05/12
For personal use only.

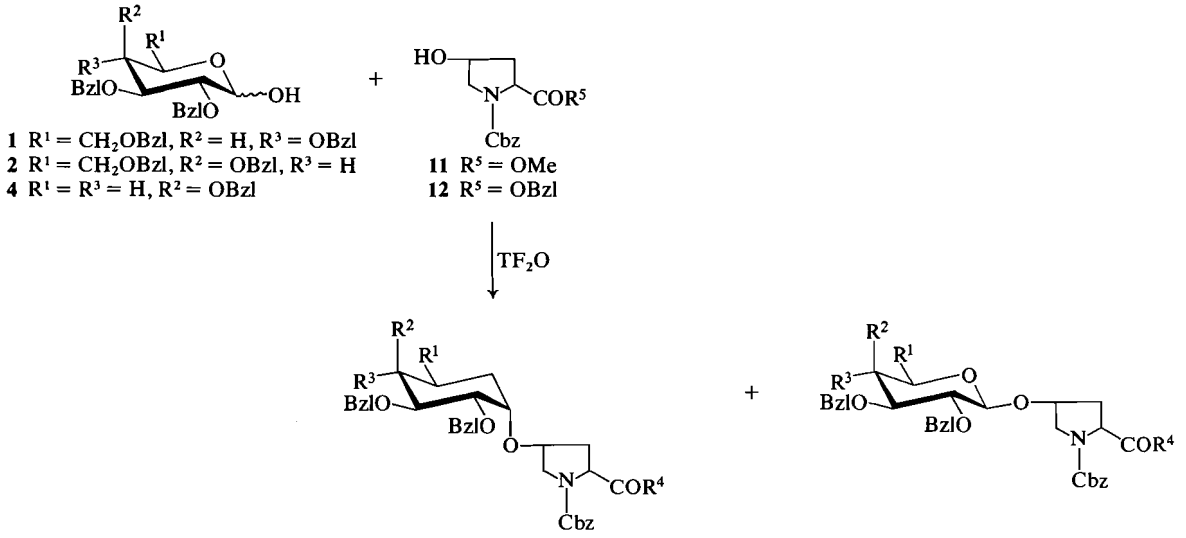

SCHÉMA 2

Il était donc nécessaire de prévoir des agents protecteurs qui puissent être éliminés facilement. C'est la raison pour laquelle nous avons choisi de protéger la fonction acide par l'ester benzylique. Dans une seconde série d'expériences la condensation a été réalisée entre −20° et +20°C dans un mélange dichlorométhane–acétonitrile. La réaction dure en moyenne 30 minutes et conduit avec un rendement compris entre 70 et 90% au mélange des deux anomères. C'est ainsi qu'ont été condensés les esters benzyliques des *N*-(benzyloxycarbonyl)-L-sérine (**8**) et -L-thréonine (**9**) avec les monosaccharides **1**, **2** et **3** pour conduire aux glycosylaminoacides correspondants de configuration α (**21**, **23**, **25**, **27**, **29** et **31**) et β (**22**, **24**, **26**, **28**, **30** et **32**) obtenus purs après chromatographie sur colonne avec des rendements variant entre 30 et 50% pour les anomères α, 30 et 40% pour les anomères β.

D'autre part, l'ester benzylique de la *N*-(benzyloxycarbonyl)-L-hydroxyproline (**12**) a été condensé selon le même protocole expérimental avec le 2,3,4,-tri-*O*-benzyl-L-arabinopyranose (**4**) pour donner les produits de condensation de configuration β-L- (**39**) et α-L- (**40**). Dans le cas du 2,3,5-tri-*O*-benzyl-L-arabinofuranose (**5**), seul l'anomère α-L- (**41**) a été isolé (rdt. 55%).[2]

[2]Le pouvoir rotatoire fortement négatif et la position du carbone anomère sont en faveur du composé de configuration α-L. Depuis l'envoi de ce manuscrit, nous avons pu synthétiser le β-L-arabinofuranosyl-L-hydroxyproline caractérisé en rmn du ^{13}C par δ(C-1) 100,90 ppm au lieu de 107,30 pour l'anomère α (voir Tableau 1).

Dans l'optique d'un allongement éventuel de la chaîne peptidique du côté C-terminal de l'aminoacide nous avons vérifié que la condensation pouvait être réalisée avec des aminoacides "activés" comme montré précédemment (18). Les esters *O*-nitrophénoliques de la *N*-(benzyloxycarbonyl)-3-*O*-(2,3,4,6-tétra-*O*-benzyl-D-glucopyranosyl)-L-thréonine α (**33**) et β (**34**) ont pu être obtenus de cette façon.

La déprotection est effectuée en une seule étape par hydrogénation du composé protégé en présence de palladium sur charbon dans le mélange éthanol–eau – acide acétique (17). Nous avons obtenu de façon quantitative les composés *O*-D-glucopyranosyl-L- thréonine α (**42**) et β (**43**), *O*-D-glucopyranosyl-L-sérine α (**46**) et β (**47**), *O*-D-galactopyranosyl-L-thréonine α (**44**) et β (**45**), *O*-D-galactopyranosyl-L-sérine α (**48**) et β (**49**), *O*-D-xylopyranosyl-L-thréonine α (**50**) et β (**51**), *O*-D-

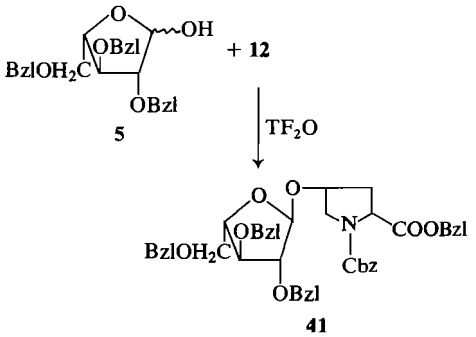

SCHÉMA 3

Can. J. Chem. Downloaded from www.nrcresearchpress.com by 210.87.254.5 on 09/05/12
For personal use only.

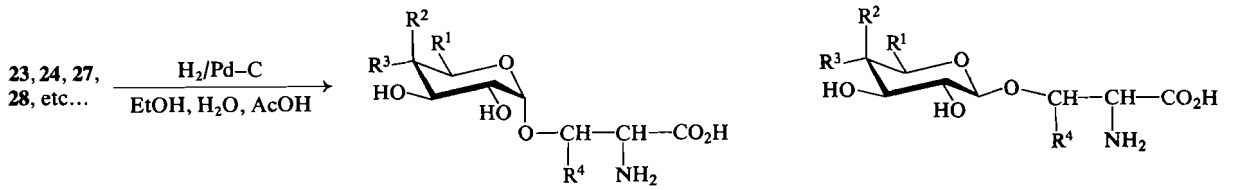

42 $R^1 = CH_2OH, R^2 = H, R^3 = OH, R^4 = CH_3$
44 $R^1 = CH_2OH, R^2 = OH, R^3 = H, R^4 = CH_3$
46 $R^1 = CH_2OH, R^2 = H, R^3 = OH, R^4 = H$
48 $R^1 = CH_2OH, R^2 = OH, R^3 = R^4 = H$
50 $R^1 = R^2 = H, R^3 = OH, R^4 = CH_3$
52 $R^1 = R^2 = R^4 = H, R^3 = OH$

43 $R^1 = CH_2OH, R^2 = H, R^3 = OH, R^4 = CH_3$
45 $R^1 = CH_2OH, R^2 = OH, R^3 = H, R^4 = CH_3$
47 $R^1 = CH_2OH, R^2 = H, R^3 = OH, R^4 = H$
49 $R^1 = CH_2OH, R^2 = OH, R^3 = R^4 = H$
51 $R^1 = R^2 = H, R^3 = OH, R^4 = CH_3$
53 $R^1 = R^2 = R^4 = H, R^3 = OH$

SCHÉMA 4

xylopyranosyl-L-sérine α (**52**) et β (**53**) et α-L-arabinofuranosyl-L-hydroxyproline (**54**) à partir des composés **21–32** et **41**.

La structure et la stéréochimie des composés décrits dans ce travail s'appuient fondamentalement sur les pouvoirs rotatoires, la rmn du proton et du ^{13}C. Le tableau 1 en résume les données essentielles.

L'examen des valeurs rapportées dans le tableau 1 appelle plusieurs commentaires.

(*1*). Pour les composés protégés (**13** à **41**), la stéréochimie de la liaison glycosidique est facilement déterminée à partir des déplacements chimiques des carbones anomères. Il faut noter néanmoins que la différence de déplacement chimique qui est en moyenne de 5 ppm pour les dérivés de la sérine ou de l'hydroxyproline n'est plus que de 3 ppm pour ceux de la thréonine. Dans ces derniers les C-1 dans la configuration β sont blindés d'environ 2,5 ppm par rapport à ceux de leurs homologues de la sérine ou de l'hydroxyproline.

(*2*). Parallèlement, le déplacement chimique du méthyl de la thréonine est très sensible à la stéréochimie de la liaison glycosidique et on observe une différence remarquablement constante de 1,5 ppm entre les deux valeurs. Le CH_3 des anomères β est blindé par rapport à ceux des anomères α, y compris dans les produits déprotégés **42–45** et **50–51**. Etant donné le petit nombre de groupements qui absorbent entre 10 et 20 ppm (voir le cas de la glucoamylase (6) par exemple), le méthyl de la thréonine pourrait servir de *sonde* et être d'une *aide considérable* dans l'étude des glycoprotéines pour (*i*) distinguer les résidus thréonine non glycosylés ($\delta CH_3 = 20,3$ ppm pour la thréonine) de ceux qui sont liés à des chaînes oligosaccharidiques ($\delta CH_3 < 19,3$ ppm); (*ii*) parmi ces derniers, identifier et doser ceux qui sont liés à la chaîne peptidique par des liaisons α ($\delta CH_3 \simeq 19,1$ ppm) et β ($\delta CH_3 \simeq 17,5$ ppm).

(*3*). La comparaison des valeurs relatives aux composés déprotégés semble montrer que (*i*) la position des carbones anomères de configuration β varie très peu après déprotection: 100,8 ppm pour **43** au lieu de 101,0, 101,5 et 101,3 dans **16**, **24** et **34**; 101,3 ppm pour **45** au lieu de 102,02 dans **20** et **28**; (*ii*) par contre, la déprotection s'accompagne d'un déblindage du carbone α d'environ 3 ppm. Il en résulte des déplacements chimiques extrêmement voisins entre les dérivés α (**42**, **44**, **50**) et les dérivés β (**43**, **45**, **51**); (*iii*) dans la mesure où cette observation peut être extrapolée aux spectres ^{13}C rmn de glycoprotéines natives, il apparait peu raisonnable d'utiliser les valeurs des déplacements chimiques des carbones anomères pour préciser la nature des monosaccharides liés à la protéine et la stéréochimie de la jonction entre la partie saccharidique et le squelette peptidique.

(*4*). Il faut enfin signaler que les dérivés de la L-hydroxyproline (**35–41**) présentent un dédoublement de certains signaux. Ce phénomène n'est pas le résultat d'une racémisation survenue lors de la condensation, puisque la *N*-(benzyloxycarbonyl)-L-hydroxyproline (**A**) possède un azote tertiaire qui interdit la formation de l'oxazolone intermédiaire. Par ailleurs, l'absence de racémisation est confirmée par le fait que (*i*) le dédoublement des signaux apparait déjà dans le composé **A** et s'accentue dans l'ester méthylique de la *N*-(benzyloxycarbonyl)-L-hydroxyproline (**B**); (*ii*) l'hydrogénolyse de **A** conduit à la L-hydroxyproline dont le spectre du ^{13}C rmn et le pouvoir rotatoire sont identiques à ceux du produit de départ; (*iii*) le pouvoir rotatoire $[\alpha]_D^{22} -71°$ et le point de fusion pf 106°C de **A** sont identiques à ceux rapportés dans la littérature (23). Ces valeurs sont fondamentalement différentes de celles données pour la D-allo ($[\alpha]_D^{22} +26,5°$) et L-allothréonine ($[\alpha]_D^{22} -23,7°$).

L'explication la plus plausible est celle d'un ralentissement de la vitesse d'inversion de l'atome d'azote intracyclique avec le remplacement de l'atome d'hydrogène. Le ralentissement a comme conséquence première une augmentation du temps

Can. J. Chem. Downloaded from www.nrcresearchpress.com by 210.87.254.5 on 09/05/12
For personal use only.

Can. J. Chem. Downloaded from www.nrcresearchpress.com by 210.87.254.5 on 09/05/12
For personal use only.

TABLEAU 1. Déplacements chimiques les plus caractéristiques en rmn du ^{13}C des *O*-glycosylaminoacides[a]

Composés		C-1		C-α			CH_3-thr	
		α	β	Ser	Thr	Hyp	α	β
Glc-Ser-OMe	**13**	98,67		54,70				
	14		103,85	54,62				
Glc-Thr-OMe	**15**	98,04			59,07		19,07	
	16		101,0		59,0			17,63
Gal-Ser-OMe	**17**	99,44		54,60				
	18		104,46	54,40				
Gal-Thr-OMe	**19**	98,27			58,60		19,07	
	20		102,27		58,90			17,89
Glc-Ser-OBzl	**21**	98,78		54,93				
	22		103,94	54,80				
Glc-Thr-OBzl	**23**	98,03			59,44		19,16	
	24		101,5		59,26			17,56
Gal-Ser-OBzl	**25**	99,65		55,07				
	26		104,35	54,84				
Gal-Thr-OBzl	**27**	98,55			59,36		19,11	
	28		102,02		59,22			17,52
Xyl-Ser-OBzl	**29**	98,32		54,86				
	30		104,48	54,75				
Xyl-Thr-OBzl	**31**	97,76			59,12		19,25	
	32		102,34		58,99			17,70
Glc-Thr-$OC_6H_4NO_2$	**33**	98,74			60,04		19,30	
	34		101,30		59,68			17,24
Glc-Hyp-OMe[b]	**35**	96,70 96,08				58,04 57,84		
	36		102,42 102,28			57,50 57,69		
Gal-Hyp-OMe[b]	**37**	97,76 97,04				58,03 58,20		
	38		103,30					
L-Ara-Hyp-OBzl[b]	**39**		97,6 97,42					
	40	102,48 Elargi				58,35 Elargi		
L-Ara-Hyp-OBzl[b]	**41**	105,35 Elargi				58,17 Elargi		
Glc-Thr	**42**	100,90 J(C-1-H_1) 169,8 Hz			58,50		19,10	
	43		100,80 J(C-1-H_1) 161,5 Hz		58,41			17,30
Gal-Thr	**44**	101,35			58,73		19,03	
	45		101,30		58,73			17,48
Glc-Ser	**46**	100,16		55, 44				
	47		102,92	55,5				
Gal-Ser	**48**	99,85		55,6				
	49		103,5	55,6				
Xyl-Thr	**50**	100,60			60,0		19,4	
	51		101,03		60,2			17,4
Xyl-Ser	**52**	99,92		54,1				
	53		103,6	55,4				
L-araf-Hyp	**54**	107,30				60,60		

[a]Tous les spectres des composés protégés **13** à **41** ont été enregistrés dans le chloroforme-*d*, avec le TMS comme référence interne; ceux des composés **42** à **47** dans l'oxyde de deutérium avec comme référence interne le dioxane dont la position par rapport au TMS a été prise égale à 67,4 ppm.
[b]Voir le texte pour l'origine du dédoublement des signaux dans les dérivés de la L-hydroxyproline.

de vie des deux conformères possibles qui deviennent observables par rmn.

Partie expérimentale

Méthodes générales

Le déroulement des réactions ainsi que l'homogénéité des composés décrits ont été contrôlés par chromatographie sur couche mince (ccm) de gel de silice (Merck F 254, Merck, Darmstadt, Allemagne), la révélation des plaques étant assurée par vaporisation d'une solution 10% d'acide sulfurique suivie du chauffage à 100°C. Les purifications ont été réalisées par chromatographie sur colonne de gel de silice (Merck 60). Les points de fusion ont été mesurés sur appareil Tottoli et sont rapportés non corrigés. Les pouvoirs rotatoires ont été mesurés sur un micro polarimètre Jobin-Yvon 11230. Les microanalyses ont été effectuées par le Service Central de Microanalyse du C.N.R.S., division de Montpellier. Les spectres de rmn ^1H ont été enregistrés à 80 MHz sur un appareil Bruker WP 80; sauf indications particulières ils ont été réalisés dans le chloroforme-*d* et les déplacements chimiques sont donnés en δ par rapport au tétraméthylsilane pris comme référence interne. Les spectres de rmn ^{13}C ont été enregistrés sur un appareil Bruker WP 80 à 20,115 MHz, les déplacements chimiques sont exprimés par rapport au tétraméthylsilane en référence interne. Dans le cas des solutions aqueuses, le déplacement chimique du dioxane utilisé comme référence est de 67,4 ppm.

Les 2,3,4,6-tétra-*O*-benzyl-D-glucopyranose (**1**), galactopyranose (**2**), 2,3,4-tri-*O*-benzyl-D-xylopyranose (**3**) et L-arabinopyranose (**4**) ont été préparés selon la technique de Koto *et al.* (19). Le 2,3,5-tri-*O*-benzyl-L-arabinofuranose (**5**) a été préparé selon le protocole expérimental décrit par Glaudemans et Fletcher (19). Les produits ont été purifiés par recristallisation ou chromatographie sur colonne de gel de silice et leurs caractéristiques physiques conformes à celles rapportées dans la littérature. Les dérivés méthylés **6**, **7**, **11** et benzylés **8**, **9**, **12**, des *N*-(benzyloxycarbonyl)-L-sérine, -L-thréonine et -L-hydroxyproline ont été préparés par les méthodes classiques (20–23) et leurs propriétés physiques conformes à celles rapportées (24–28). L'ester *O*-nitrophénylique de la *N*-(benzyloxycarbonyl)-L-thréonine (**10**) a été préparé selon la méthode de Bodansky *et al.* (29) et est conforme à celui décrit précédemment (18).

Conditions générales de glycosylation

Aucune condition particulière n'est à prendre concernant l'anhydricité des solvants et réactifs.

Première variante (utilisée pour la synthèse des composés **13–19**, **35–38**)

Le monosaccharide benzylé et l'aminoacide *N* et *C* protégé (2 à 3 mol par mol de monosaccharide) sont dissous dans le dichlorométhane (environ 15 mL pour 6 mmol de réactif) et la solution est refroidie à −70°C. A cette solution refroidie est ajouté l'anhydride trifluorométhanesulfonique en une seule fois de sorte que la proportion des réactifs dans le milieu réactionnel soit approximativement de 1,5 équivalents d'anhydride par mole de sucre. Le mélange ci-dessus est maintenu pendant cinq minutes à la température de −70°C puis le vase réactionnel est sorti du bain. On laisse la température revenir vers la température ambiante en suivant la disparition du monosaccharide benzylé en chromatographie couche mince. Lorsque la réaction est terminée (généralement de 10 à 25 min) le vase réactionnel est plongé dans le bain à −70°C et le mélange repris par l'eau puis extrait par du chloroforme, de l'éther ou du dichlorométhane. La phase organique est lavée par une solution d'hydrogénocarbonate de sodium, de l'eau jusqu'à neutralité, séchée sur sulfate de sodium et le solvant évaporé sous vide. Le produit brut est obtenu sous forme d'une huile que l'on purifie par chromatographie sur colonne de gel de silice (solvant B).

Seconde variante (utilisée pour la synthèse de tous les esters benzyliques)

L'aminoacide *N* et *C* protégé (4 mmol) est dissous dans l'acétonitrile (30 mL). A cette solution refroidie à −20°C est ajouté l'anhydride trifluorométhanesulfonique (1,5 mmol). Au mélange ci-dessus on additionne goutte à goutte la solution du monosaccharide benzylé (1 mmol) dans le dichlorométhane (10 mL) pendant environ 15 min, puis le vase réactionnel est sorti du bain froid et laissé réagir jusqu'à ce que le contrôle en ccm (solvant A) montre la disparition totale du monosaccharide (environ 30 min). Le mélange réactionnel est ensuite traité comme précédemment et le produit brut chromatographié (solvant B) ou recristallisé; le lavage de la colonne par du méthanol permet de récupérer 75 à 85% de l'aminoacide en excès.

Solvants utilisés pour la chromatographie; solvant A: chloroforme–éther, 90:10, v/v; solvant B: chloroforme–éther, 96:4, v/v.

Ester méthylique de la N-*(benzyloxycarbonyl)*-O-*(2,3,4,6-tétra*-O-*benzyl-D-glucopyranosyl)-L-sérine : α (13) et β (14)*

A une solution de Z-Ser-OMe (**6**) (1,020 g, 4 mmol) et de tétrabenzylglucose (**1**) (1,080 g, 2 mmol) dans le dichlorométhane (15 mL) refroidie à −70°C est ajouté l'anhydride trifluorométhanesulfonique (0,5 mL, 3 mmol). Après 15 min à température ambiante le mélange réactionnel est traité puis chromatographié sur gel de silice (250 g). L'élution par le solvant B donne une huile (0,87 g, 55%) qui est un mélange de deux anomères (2 spots en ccm, solvant A). Le composé **13** cristallise dans un mélange éther/éther de pétrole (0,500 g, 31,5%); pf 79–80°C; $[\alpha]_D^{22}$ +32 (*c* 1,7, $CHCl_3$); ^1H rmn: 4,72 (d, $J_{1,3}$ = 3,9 Hz, (H-1)), 3,51 (q, $J_{1,2}$ = 3,9 Hz, $J_{2,3}$ = 10 Hz, (H-2)), 5,97 (*J* = 9 Hz, (N—H)); ^{13}C rmn: 170,43 (CO ester), 156,11 (CO uréthane), 98,67 (C-1), 71,00 (C-5), 54,70 (C-α-Ser), 52,52 (CH_3 ester). *Anal.* calc. pour $C_{46}H_{49}N$: C 71,22, H 6,32, N 1,80; trouvée: C 70,90, H 6,34, N 1,85.

Les liqueurs mères de recristallisation contiennent un mélange de **13** et de son anomère β (**14**) dont le spectre ^{13}C est caractérisé par un signal à 103,85 (C-1) et 54,62 (C-α-Ser).

Ester méthylique de la N-*(benzyloxycarbonyl)*-O-*(2,3,4,6-tétra*-O-*benzyl-D-glucopyranosyl)-L-thréonine : α (15) et β (16)*

A une solution de Z-Thr-OMe (**7**) (1,068 g, 4 mmol) et de tétrabenzyl glucose (**1**) (1,080 g, 2 mmol) dans le dichlorométhane refroidie à −70°C est ajouté l'anhydride trifluorométhanesulfonique (0,5 mL, 3 mmol). Après 20 min à température ambiante le mélange réactionnel est traité puis chromatographié sur gel de silice (250 g) élué par le solvant B. Le composé **15** est obtenu pur (1,0 g, 64%) sous forme d'un solide blanc qui cristallise dans un mélange éther/éther de pétrole: pf 86–88°C; $[\alpha]_D^{22}$ +25,3 (*c* 1,8, $CHCl_3$); ^1H rmn: 4,85 (d, $J_{1,2}$ = 3,6 Hz, (H-1)), 3,43 (q, $J_{1,2}$ = 3,6 Hz, $J_{2,3}$ = 9 Hz, (H-2)), 4,36 (m, $J_{\alpha,\beta}$ = 7,2 Hz, (H-β-thr)), 4,32 (q, $J_{\alpha\text{-NH}}$ = 8,7 Hz, (H-α-thr)); ^{13}C rmn: 171,23 (CO ester), 156,84 (CO uréthane), 98,04 (C-1), 79,19 (C-β-thr), 71,13 (C-5), 68,54 (C-3), 67,13 (CH_2-benzyloxycarbonyl), 59,07 (C-α-thr), 52,38 (CH_3 ester), 19,07 (CH_3-thr).

Le spectre de rmn du produit contenu dans les liqueurs de recristallisation montre un signal à 101,0 (C-1), 59,0 (C-α-thr) et 17,63 (CH_3-thr).

Ester méthylique de la N-*(benzyloxycarbonyl)*-O*(2,3,4,6-tétra*-O-*benzyl-D-galactopyranosyl)-L-sérine: α (17) et β (18)*

A une solution de Z-Ser-OMe (**6**) (1,020 g, 4 mmol) et de tétrabenzyl galactose (**2**) (0,540 g, 1 mmol) dans le dichlorométhane (10 mL) refroidie à −70°C est ajouté l'anhydride trifluorométhanesulfonique (0,25 mL, 1,5 mmol). Après 5 minutes à −70°C le mélange réactionnel est sorti du bain et laissé

Can. J. Chem. Downloaded from www.nrcresearchpress.com by 210.87.254.5 on 09/05/12
For personal use only.

Can. J. Chem. Downloaded from www.nrcresearchpress.com by 210.87.254.5 on 09/05/12
For personal use only.

revenir à température ambiante (10 min). Le contrôle en chromatographie sur couche mince (solvant A) montre que le tétrabenzyl galactose a complètement réagi. Après traitement, l'huile obtenue (0,650 g, 80%)[3] est chromatographiée sur gel de silice (100 g), éluée par le solvant B. Deux fractions correspondant respectivement à l'anomère α (0,390 g, 45%) et au mélange d'anomères α et β (0,205 g, 30%) sont récupérées.

La première fraction cristallise dans un mélange éther/éther de pétrole pour donner **17**, pf 70–72°C; ^{13}C rmn: 170,50 (CO ester), 156,11 (CO uréthane), 99,44 (C-1), 54,6 (C-α-Ser), 52,38 (CH_3 ester).

Dans la deuxième fraction l'anomère β (**18**) est identifié par son spectre ^{13}C rmn: 170,89 (CO ester), 156,16 (CO uréthane), 104,46 (C-1), 54,4 (C-α-Ser), 52,43 (CH_3 ester).

Ester méthylique de la N-*(benzyloxycarbonyl)*-O-*(2,3,4,6-tétra*-O-*benzyl-*D*-galactopyranosyl)-*L*-thréonine: α (19) et* β *(20)*

A une solution de Z-Thr-OMe (**7**) (0,80 g, 3 mmol) et de tétrabenzyl galactose (**2**) (0,54 g, 1 mmol) dans le dichlorométhane (10 mL) refroidie à −70°C est ajouté l'anhydride trifluorométhanesulfonique (0,25 mL, 1,5 mmol). Après 5 minutes à −70°C et 20 min à température ambiante, le composé **2** a complètement disparu (ccm, solvant A). Le mélange réactionnel est traité et l'huile obtenue après évaporation (0,68 g, 90%) est chromatographiée sur gel de silice (150 g) éluée par le solvant B.

On obtient ainsi trois fractions correspondant respectivement à l'anomère α **19** (0,380 g, 49%), au mélange α et β (**19** et **20**) (0,121 g, 15%) et au composé β **20** (0,135 g, 17%). *Composé 19*: $[\alpha]_D^{22}$ +26,14 (*c* 1,075, $CHCl_3$); ^{13}C rmn: 171,17 (CO ester), 156,8 (CO uréthane), 98,27 (C-1), 58,60 (C-α-thr), 52,33 (CH_3 ester), 19,07 (CH_3-thr). *Anal.* calc. pour $C_{47}H_{51}N$: C 71,41, H 6,46; trouvée: C 70,64, H 6,35. *Composé 20*: $[\alpha]_D^{22}$ +0,257 (*c* 1,66, $CHCl_3$); ^{13}C rmn: 170,9 (CO ester), 156,7 (CO uréthane), 102,27 (C-1), 58,9 (C-α-thr), 52,33 (CH_3 ester), 17,90 (CH_3-thr).

Ester benzylique de la N-*(benzyloxycarbonyl)*-O-*(2,3,4,6-tétra*-O-*benzyl-*D*-glucopyranosyl)-*L*-sérine: α (21) et* β *(22)*

A une solution de Z-Ser-OBzl (**8**) (1,31 g, 4 mmol) dans l'acétonitrile (30 mL) refroidie à −20°C on ajoute 0,25 mL (1,5 mmol) d'anhydride trifluorométhanesulfonique. On additionne peu à peu (20 min) le tétrabenzyl glucose (**1**) (0,54 g, 1 mmol) en solution dans le dichlorométhane (10 mL) et le vase réactionnel est sorti du bain froid. Après 50 min **1** a disparu (ccm solvant A) et on traite le mélange réactionnel. L'huile obtenue est chromatographiée sur gel de silice (éluant B). On obtient trois fractions (rdt. global 0,75 g, 88%). La première fraction contient l'anomère α (**21**) (0,4 g, 48%) sous forme d'huile. La seconde fraction contient un mélange des anomères α et β (0,035 g, 4%). La troisième fraction contient l'anomère β (**22**) (0,31 g, 36%) qui cristallise. Le lavage de la colonne au méthanol permet de récupérer 80% (0,78 g) de l'excès d'aminoacide. *Composé* **21**: $[\alpha]_D^{22}$ +33 (*c* 1,1, $CHCl_3$); ^{1}H rmn: 6,05 (d, *J* = 8,5 Hz (NHCbz)); 7,25 (30H, C_6H_5); ^{13}C rmn: 170,1 (CO ester), 156,2 CO uréthane), 98,78 (C-1), 54,70 (C-α-Ser). *Anal.* calc. pour $C_{52}H_{53}O_{10}N$: C 73,32, H 6,22, N 1,64; trouvée: C 72,85, H 6,57, N 1,70. *Composé 22*: pf 80–81°C (éther – éther de pétrole); $[\alpha]_D^{22}$ +16,3 (*c* 0,55, $CHCl_3$); ^{1}H rmn: 7,25 (30H, C_6H_5), 5,75 (d, *J* = 6,3 Hz (NHCbz)); ^{13}C rmn: 170,0 (CO ester), 156,1 (CO uréthane), 103,9 (C-1), 69,7 (C-β-Ser), 68,8 (C-6), 54,62 (C-α-Ser).

Ester benzylique de la N-*(benzyloxycarbonyl)*-O-*(2,3,4,6-tétra*-O-*benzyl-*D*-glucopyranosyl)-*L*-thréonine: α (23) et* β *(24)*

A une solution de Z-Thr-OBzl (**9**) (1,38 g, 4 mmol) dans l'acétonitrile (30 mL) refroidie à −20°C, on ajoute 0,25 mL (1,5 mmol) d'anhydride trifluorométhanesulfonique. On additionne peu à peu (15 min) à la solution précédente le composé **1** (0,54 g, 1 mmol) dans le dichlorométhane (10 mL). Après la fin de l'addition on sort le vase réactionnel à température ambiante et on contrôle l'évolution par ccm (solvant A). Après traitement le mélange réactionnel est chromatographié sur gel de silice (solvant B). On obtient ainsi trois fractions: la première (0,380 g, 44%) sous forme d'huile correspond à l'anomère α (**23**), la deuxième (0,040 g, 5%) est un mélange des anomères α et β, la troisième (0,32 g, 37%) sous forme d'huile correspond à l'anomère β (**24**). *Composé 23*: $[\alpha]_D^{22}$ +40 (*c* 0,4, $CHCl_3$); ^{1}H rmn: 1,2 (d, *J* = 6 Hz (CH_3-thr)), 5,75 (d, *J* = 8,5 Hz (NH-Cbz)), 7,15 (30H, C_6H_5); ^{13}C rmn: 180,67 (CO ester), 155,4 (CO uréthane), 98,03 (C-1), 59,44 (C-α-thr), 19,16 (CH_3-thr). *Anal.* calc. pour $C_{53}H_{55}O_{10}N$: C 73,52, H 6,35, N 1,61; trouvée: C 73,35, H 6,55, N 1,44. *Composé 24*: $[\alpha]_D^{22}$ +14,5 (*c* 0,53, $CHCl_3$); ^{1}H rmn: 1,2 (d, *J* = 6 Hz (CH_3-thr)), 5,65 (d, *J* = 8,5 Hz (NH-Cbz)), 7,1 (30H, C_6H_5); ^{13}C rmn: 170,3 (CO ester), 155,6 (CO uréthane), 101,5 (C-1), 59,26 (C-α-thr), 17,6 (CH_3-thr).

Ester benzylique de la N-*(benzyloxycarbonyl)*-O-*(2,3,4,6-tétra*-O-*benzyl-*D*-galactopyranosyl-*L*-sérine: α (25) et* β *(26)*

A une solution de Z-Ser-OBzl (**6**) (1,31 g, 4 mmol) dans l'acétonitrile (30 mL) refroidie à −20°C sont ajoutés l'anhydride trifluorométhanesulfonique (0,25 mL, 1,5 mmol) puis lentement (15 min) le composé **2** (0,54 g, 1 mmol) en solution dans le dichlorométhane (10 mL). Trente minutes après avoir sorti le ballon du bain froid le composé **2** a disparu (ccm, éluant A). Après traitement habituel et chromatographie de l'huile résiduelle sur colonne (éluant B) on obtient trois fractions: l'anomère α **25** (0,34 g, 40%), un mélange des deux anomères α et β (0,13 g, 15%) et l'anomère β (**26**) (0,34 g, 40%). Le composé **6** est récupéré (0,8 g, 80%) par lavage de la colonne au méthanol. *Composé 25*: $[\alpha]_D^{22}$ +21 (*c* 1,1, $CHCl_3$); ^{1}H rmn: 6,15 (d, *J* = 8,5 Hz (NH-Cbz)), 7,25 (30H, C_6H_5); ^{13}C rmn: 170,19 (CO ester), 156,36 (CO uréthane), 99,65 (C-1), 69,03 (C-6), 55,07 (C-α-Ser). *Anal.* calc. pour $C_{52}H_{53}O_{10}N$: C 73,32, H 6,22, N 1,64; trouvée: C 73,68, H 6,26, N 1,48. *Composé 26*: $[\alpha]_D^{22}$ +5,2 (*c* 1,2, $CHCl_3$); ^{1}H rmn: 5,95 (d, *J* = 8,5 Hz (NH-Cbz)), 7,25 (30H, C_6H_5); ^{13}C rmn: 170,01 (CO ester), 156,32 (CO uréthane), 104,35 (C-1), 68,71 (C-6), 54,84 (C-α-Ser).

Ester benzylique de la N-*(benzyloxycarbonyl)*-O-*(2,3,4,6-tétra*-O-*benzyl-*D*-galactopyranosyl)-*L*-thréonine: α (27) et* β *(28)*

A une solution de Z-Thr-OBzl (**7**) (1,38 g, 4 mmol) dans l'acétonitrile (30 mL) refroidie à −20°C sont ajoutés 0,25 mL, 1,5 mmol d'anhydride trifluorométhanesulfonique et une solution de **2** (0,54 g, 1 mmol) dans le dichlorométhane (10 mL). Après 40 min traitement habituel et chromatographie, le composé **27** est obtenu sous forme d'huile (0,44 g, 50%) ainsi que le composé **28** (0,260 g, 30%). *Composé 27*: $[\alpha]_D^{22}$ +29 (*c* 2,8, $CHCl_3$); ^{1}H rmn: 1,3 (d, *J* = 6 Hz (CH_3-thr)), 6,0 (d, *J* = 8,5 Hz (NH-Cbz)), 7,3 (30H, C_6H_5); ^{13}C rmn: 170,78 (CO ester), 158,8 (CO uréthane), 98,55 (C-1), 59,36 (C-α-thr), 19,11 (CH_3-thr). *Anal.* calc. pour $C_{53}H_{55}O_{10}N$: C 73,52, H 6,35, N 1,61; trouvée: C 72,71, H 6,49, N 1,53. *Composé 28*: $[\alpha]_D^{22}$ −5,5 (*c* 1,8, $CHCl_3$); ^{1}H rmn: 1,25 (d, *J* = 6 Hz (CH_3-thr)), 5,85 (d, *J* = 8 Hz (NH-Cbz)), 7,3 (30H, C_6H_5); ^{13}C rmn: 170,42 (CO ester), 157,5 (CO uréthane), 102,02 (C-1), 59,22 (C-α-thr), 17,52 (CH_3-thr).

Ester benzylique de la N-*(benzyloxycarbonyl)*-O-*(2,3,4-tri*-O-*benzyl-*D*-xylopyranosyl)-*L*-sérine: α (29) et* β *(30)*

A une solution de Z-Ser-OBzl (**6**) (1,32 g, 4 mmol) dans l'acétonitrile (30 mL) refroidie à −20°C on ajoute 0,25 mL (1,5 mmol) d'anhydride trifluorométhanesulfonique, puis la solution de **3** (0,42 g, 1 mmol) dans le dichlorométhane (10 mL). Après disparition de **3** (20 min) traitement habituel et

[3]Dans tout ce qui suit le rendement global ainsi exprimé correspond en fait à celui obtenu après séparation de l'excès d'aminoacide, par chromatographie.

Can. J. Chem. Downloaded from www.nrcresearchpress.com by 210.87.254.5 on 09/05/12
For personal use only.

chromatographie on obtient les composés **29** (0,220 g, 30%) et **30** (0,220 g, 30%) sous forme de solides ainsi qu'un mélange de **29** et **30**. Après une nouvelle chromatographie des fractions en mélange la quantité totale de composés α est de (0,338 g, 45%) et β (0,27 g, 37%). *Composé 29*: pf 105–106°C ($CHCl_3$ – éther de pétrole); $[\alpha]_D^{22}$ +41 (*c* 1,4, $CHCl_3$); ^1H rmn: 5,8 (d, *J* = 8,5 Hz (NH-Cbz)), 7,3 (25H, C_6H_5); ^{13}C rmn: 170,14 (CO ester), 156,6 (CO uréthane), 98,32 (C-1), 54,86 (C-α-Ser). *Composé 30*: pf 76–78°C (éther-éther de pétrole); $[\alpha]_D^{22}$ +9 (*c* 1,1, $CHCl_3$); ^1H rmn: 5,62 (d, *J* = 8,2 Hz (NH-Cbz)), 7,3 (25H, C_6H_5); ^{13}C rmn: 170,01 (CO ester), 156,5 (CO uréthane), 104,48 (C-1), 54,75 (C-α-Ser). *Anal.* calc. pour $C_{44}H_{45}O_9N$: C 72,22, H 6,15, N 1,91; trouvée: C 72,08, H 6,30, N 1,80.

Ester benzylique de la N-*(benzyloxycarbonyl)*-O-*(2,3,4-tri*-O-*benzyl*-D-*xylopyranosyl)*-L-*thréonine: α (31) et β (32)*

La réaction de **7** (1,38 g, 4 mmol) dans l'acétronitrile (30 mL) à −20°C avec **3** (0,42 g, 1 mmol) en présence de l'anhydride trifluorométhanesulfonique (0,25 mL, 1,5 mmol), conduit après traitement habituel et chromatographie sur colonne de gel de silice (éluant B) à trois fractions dont une constituée d'un mélange d'anomères α **31** et β **32**. Après chromatographie de cette fraction on obtient **31** pur, sous forme d'huile avec un rendement de 50% et **32** cristallise avec un rendement de 34%. *Composé 31*: $[\alpha]_D^{22}$ +35 (*c* 3,2, $CHCl_3$); ^1H rmn: 1,3 (d, *J* = 6 Hz (CH_3-thr)), 5,95 (d, *J* = 8,2 Hz (NH-Cbz)), 7,3 (25H, C_6H_5); ^{13}C rmn: 170,72 (CO ester), 155,6 (CO uréthane), 97,76 (C-1), 59,12 (C-α-thr), 19,25 (CH_3-thr). *Anal.* calc. pour $C_{45}H_{47}O_9N$: C 72,48, H 6,30, N 1,87; trouvée: C 71,48, H 6,25, N 1,74. *Composé 32*: pf 71–72°C (éther – éther de pétrole); $[\alpha]_D^{22}$ −10 (*c* 0,8, $CHCl_3$); ^1H rmn: 1,25 (d, *J* = 6 Hz (CH_3-thr)), 5,55 (d, *J* = 8,5 Hz (NH-Cbz)), 7,3 (25H, C_6H_5); ^{13}C rmn: 170,42 (CO ester), 156,1 (CO uréthane), 102,34 (C-1), 58,99 (C-α-thr), 17,70 (CH_3-thr). *Anal.* calc. pour $C_{45}H_{47}O_9N$: C 72,48, H 6,30, N 1,87; trouvée: C 72,67, H 6,29, N 1,88.

Ester-O-*nitrophénolique de la* N-*(benzyloxycarbonyl)*-O-*(2,3,4,6-tétra*-O-*benzyl*-D-*glucopyranosyl)*-L-*thréonine: α (33) et β (34)*

A une solution de l'ester *O*-nitrophénolique de la *N*-(benzyloxycarbonyl)-L-thréonine (18) (0,75 g, 2 mmol) dans l'acétonitrile (15 mL) refroidie à −20°C sont ajoutés 0,125 mL (0,75 mmol) d'anhydride trifluorométhanesulfonique puis lentement la solution du composé **1** (0,270 g, 0,5 mmol) dans le dichlorométhane (5 mL). Après être sorti du bain froid la réaction est terminée au bout de 30 min (ccm, solvant. A, révélation par uv). Après traitement le résidu huileux, jaune est chromatographié sur colonne de gel de silice pour donner **33** (0,18 g, 40%) et **34** (0,14 g, 30%). *Composé 33*: $[\alpha]_D^{22}$ +17 (*c* 2,4, $CHCl_3$); ^{13}C rmn: 168,5 (CO ester), 155,3 (CO uréthane), 98,74 (C-1), 60,04 (C-α-thr), 19,3 (CH_3-thr). *Anal.* calc. pour $C_{52}H_{52}O_{12}N_2$: C 69,64, H 5,80, N 3,12; trouvée: C 69,52, H 5,92, N 2,92. *Composé 34*: $[\alpha]_D^{22}$ +12 (*c* 2,8, $CHCl_3$); ^{13}C rmn: 168,27 (CO ester), 155,36 (CO uréthane), 101,3 (C-1), 59,68 (C-α-thr), 17,24 (CH_3-thr). *Anal.* calc. pour $C_{52}H_{52}O_{12}N_2$: C 69,64, H 5,80, N 3,12; trouvée: C 69,22, H 5,83, N 3,02.

Ester méthylique de la N-*(benzyloxycarbonyl)*-O-*(2,3,4,6-tétra*-O-*benzyl*-D-*glucopyranosyl)*-L-*hydroxyproline: α (35) et β (36)*

A une solution de Z-Hyp-OMe (**8**) (1,116 g, 4 mmol) et de tétrabenzyl glucose (**1**) (1,080 g, 2 mmol) dans le dichlorométhane (15 mL) refroidie à −70°C est ajouté l'anhydride trifluorométhanesulfonique (0,5 mL, 3 mmol). Après 15 min à température ambiante le mélange réactionnel est traité et l'huile obtenue (1,95 g, 90%) purifiée par chromatographie sur colonne de gel de silice (250 g). L'élution par le solvant B permet de recueillir trois fractions. La première fraction (0,760 g, 47%) qui cristallise dans un mélange éther – éther de pétrole correspond à **35**: pf 59–62°C; ^{13}C rmn[4]: 172,98 (CO ester), 154,69 (CO uréthane), 96,1 et 96,70 (C-1), 57,84 et 58,08 (C-α-Hyp), 52,04 et 52,33 (CH_3 ester). *Anal.* calc. pour $C_{48}H_{51}O_{10}N$: C 71,91, H 6,36, N 1,74; trouvée: C 71,97, H 6,38, N 1,80. *Le composé 36*: pf 75–76°C (éther – éther de pétrole); ^{13}C rmn[4]: 172,78 (CO ester) 102,42 et 102,28 (C-1), 57,50 et 57,69 (C-α-Hyp), 52,04 et 52,33 (CH_3 ester). *Anal.* calc. pour $C_{48}H_{51}O_{10}N$: C 71,91, H 6,36, N 1,74; trouvée: C 71,85, H 6,36, N 1,82.

Ester méthylique de la N-*(benzyloxycarbonyl)*-O-*(2,3,4,6-tétra*-O-*benzyl*-D-*galactopyranosyl)*-L-*hydroxyproline: α (37) et β (38)*

A une solution de Z-Hyp-OMe (**8**) (0,84 g, 3 mmol) et de tétrabenzyl galactose (**2**) (0,54 g, 1 mmol) dans le dichlorométhane (7,5 mL) refroidie à −60°c est ajouté l'anhydride trifluorométhanesulfonique (0,25 mL, 1,5 mmol). Après 5 min à −60°C la réaction est laissée 20 min hors du bain froid. Le composé **2** ayant complètement disparu, le mélange réactionnel est alors traité comme précédemment. L'huile obtenue (0,570 g, 70%) est chromatographiée sur gel de silice (125 g) éluée par le solvant B. L'anomère α **37** (0,480 g, 60%) a été isolé pur; ^{13}C rmn[4]: 173,09 (CO ester), 97,76 et 97,04 (C-1), 58,03 et 58,26 (C-α-Hyp), 52,02 et 52,25 (CH_3 ester). *Anal.* calc. pour $C_{48}H_{51}O_{10}N$: C 71,91, H 6,36; trouvée: C 70,74, H 6,34. Le composé **38**, n'a pas été isolé pur. Le spectre ^{13}C du mélange montre un carbone anomère à 103,3 ppm.

Ester benzylique de la N-*(benzyloxycarbonyl)*-O-*(2,3,4-tri*-O-*benzyl*-L-*arabinopyranosyl)*-L-*hydroxyproline: β (39) et α (40)*

A une solution de Z-Hyp-OBzl (**12**) (1,42 g, 4 mmol) dans l'acétonitrile (30 mL) à −15°C sont ajoutés l'anhydride trifluorométhanesulfonique (0,25 mL, 1,5 mmol) et le composé **4** (0,42 g, 1 mmol) dissous dans le dichlorométhane (10 mL). Après 30 min à −15°C la réaction est terminée (ccm, solvant A). Après traitement habituel et chromatographie sur colonne de gel de silice, on obtient ainsi 0,65 g (rdt. 85%) du mélange des composés β **39** et α **40** qu'il ne nous a pas été possible de séparer. Les déplacements chimiques des carbones anomères mesurés sur le spectre du mélange sont rapportés dans le tableau 1.

Ester benzylique de la N-*(benzyloxycarbonyl)*-O-*(2,3,5-tri*-O-*benzyl*-α-L-*arabinofuranosyl)*-L-*hydroxyproline: (41)*

A une solution de **12** (1,42 g, 4 mmol) dans l'acétonitrile (30 mL) à −15°C est ajouté l'anhydride trifluorométhanesulfonique, (0,25 mL, 1,5 mmol) puis en 15 min le composé **5** (0,42 g, 1 mmol) en solution dans le dichlorométhane (10 mL). La réaction est terminée après 20 min à −15°C. Le contrôle de la réaction en ccm (solvant A) montre la présence de deux composés de R_f différents. Après traitement du milieu réactionnel et chromatographie, un seul des anomères subsiste isolé pur sous forme d'huile (0,38 g, 55%); $[\alpha]_D^{22}$ −62,4 (*c* 2,1, $CHCl_3$); ^{13}C rmn: 172,3 (CO ester), 155,1 (CO uréthane), 105,3 (C-1), 69,6 (C-5), 58,17 (C-α-Hyp).

Méthode générale de déprotection. Synthèse des composés 42–54

Le composé protégé (1 mmol) est dissous dans l'éthanol (40 mL), auquel est ajouté l'acide acétique (10 mL), l'eau (10 mL) et le Pd/C 10% (2,5 g). L'hydrogénation est réalisée à température ambiante sous une pression de 4 bars, pendant 24 h. Après filtration sur Célite et lavage du catalyseur avec de l'eau

[4]Voir texte pour l'origine du dédoublement des signaux des carbones de l'hydroxyproline.

Can. J. Chem. Downloaded from www.nrcresearchpress.com by 210.87.254.5 on 09/05/12
For personal use only.

bouillante (2 × 15 mL) le filtrat est concentré sous pression réduite en chauffant à 50°C. On reprend avec 10 mL d'eau, filtre et concentre à nouveau, puis on dissous à nouveau avec 10 mL d'eau et on désionise avec une résine acide faible Amberlite IRC 50. On concentre, on évapore sous pression réduite pour éliminer toutes traces d'acide acétique. Les composés ont été obtenus purs avec des rendements variant entre 85 et 95%.

O-D-glycopyranosyl-L-thréonine α (**42**) (rdt. 89%), pf. 220–230°C (dec.), $[\alpha]_D^{25}$ +39 (*c* 2,0, H_2O); β (**43**) (rdt 92%), hygroscopique, $[\alpha]_D^{25}$ −21 (*c* 1, H_2O).

O-D-galactopyranosyl-L-thréonine α (**44**) (rdt 97%), hygroscopique, $[\alpha]_D^{25}$ +36 (*c* 1,1, H_2O); β (**45**) (rdt 87%), hygroscopique, $[\alpha]_D^{25}$ −13 (*c* 1,2, H_2O).

O-D-glucopyranosyl-L-sérine α (**46**) (rdt 92%), hygroscopique, $[\alpha]_D^{25}$ +39 (*c* 1,2, H_2O); β (**47**) (rdt 94%), hygroscopique, $[\alpha]_D^{25}$ −14 (*c* 1,1, H_2O).

O-D-galactopyranosyl-L-sérine α (**48**) (rdt 91%), hygroscopique, $[\alpha]_D^{25}$ +79 (*c* 1,1, H_2O); β (**49**) (rdt 91%), pf. 235–240°C (dec.), $[\alpha]_D^{25}$ −7 (*c* 1,2, H_2O).

O-D-xylopyranosyl-L-thréonine α (**50**) (rdt 97%), hygroscopique. $[\alpha]_D^{25}$ +35 (*c* 1, H_2O); β (**51**) (rdt 90%), hygroscopique, $[\alpha]_D^{25}$ −24 (*c* 1,8, H_2O).

O-D-xylopyranosyl-L-sérine α (**52**) (rdt 91%), hygroscopique, $[\alpha]_D^{25}$ +34 (*c* 1,2, H_2O); β (**53**) (rdt. 98%), pf 230–235°C (dec.), $[\alpha]_D^{25}$ −12 (*c* 1, H_2O) (litt. (30) pf 230–240°C (dec.); $[\alpha]_{578}^{29}$ −65 (*c* 0,1, H_2O)).

O-α-L-arabinofuranosyl-L-hydroxyproline α (**54**) (rdt. 95%), pf 121–123°C, $[\alpha]_D^{25}$ −115 (*c* 1, H_2O).

Les valeurs les plus caractéristiques en ^{13}C rmn des composés ci-dessus sont rapportés dans le tableau 1.

Remerciements

Les auteurs remercient J. L. Durand, technicien 1 B, responsable du laboratoire de rmn pour sa collaboration technique.

1. R. G. SPIRO. Ann. Rev. Biochem. **39**, 599 (1970); R. D. MARSHALL et A. NEUBERGER. Adv. Carbohydr. Chem. Biochem. **25**, 407 (1970); N. SHARON. *Dans* Complex carbohydrates. *Edité par* N. Sharon. Addison-Wesley Publishing Company. 1975; M. I. Horowitz et W. Pigman (*Editeurs*). The glycoconjugates. Academic Press, New York. 1977; A. Gottschalk (*Editeur*). Glycoproteins. 2ième éd. Elsevier, New York. 1972.
2. E. A. KABAT (*Editeur*). *Dans* Structural concepts in immunology and immunotherapy. 2ième éd. Holt, Rinehart and Winston, New York. 1976.
3. W. N. GLÖCKNER, R. A. NEWMAN et G. UHLENBRUCK. Biochem. Biophys. Res. Commun. **66**, 701 (1975).
4. J. P. SEGREST, R. L. JACKSON et V. T. MARCHESI. Biochem. Biophys. Res. Commun. **13**, 964, (1973); J. P. SEGREST, I. KAHANE, R. L. JACKSON et V. T. MARCHESI. Arch. Biochem. Biophys. **155**, 165 (1973); H. FURTHMAY. Nature, **221**, 519 (1978).
5. B. FERRARI et A. A. PAVIA. Carbohydr. Res. **79**, C1 (1980).
6. K. DILL et A. ALLERHAND. J. Biol. Chem. **254**, 4524 (1979).
7. P. HALLGREN, A. LUNDBLAD et S. SVENSSON. J. Biol. Chem. **250**, 5312 (1975).
8. L. MUIR et Y. C. LEE. J. Biol. Chem. **245**, 502 (1970).
9. A. L. ROSENTHAL et J. H. NORDIN. J. Biol. Chem. **250**, 5295 (1975).
10. U. LINDAHL et L. RODEN. *Dans* Glycoproteins. *Édité par* A. Gottschalk. Elsevier, New York. 1972. pp. 491–517.
11. D. H. MILLER, D. T. A. LAMPORT et M. MILLER. Science, **176**, 918 (1972).
12. D. T. A. LAMPORT. *Dans* Biogenesis of plant cell wall polysaccharides. *Edité par* F. Loewus. Academic Press, New York. 1973. p. 149.
13. D. T. A. LAMPORT. Biochemistry, **8**, 1155 (1969).
14. R. C. HUGHES. Essays in Biochem. **11**, 1 (1975); E. KÖTTGEN, CH. BAUER, W. REUTTER et W. GEROCK. Klin. Wochenschr. **57**, 151 (1979); **57**, 199, (1979); R. MONTGOMERY. *Dans* The carbohydrates, chemistry and biochemistry. Vol. IIB. *Edité par* W. Pigman et D. Horton. Academic Press, New York. 1970. pp. 628–698; R. KORNFELD et S. KORNFELD. Ann. Rev. Biochem. **45**, 217 (1976); G. M. N. COOK et R. W. STODDART (*Editeurs*). *Dans* Surface carbohydrates of the eukariotic cell. Academic Press, London. 1973.
15. D. MAZAU et M. T. ESQUERRE. Plant Sci. Lett. **7**, 119 (1976); M. T. ESQUERRE, C. LAFITTE, D. MAZAU, A. TOPPAN et A. TOUZE. 5th International Symposium on Glycoconjugates, Kiel, Germany. Septembre 3–7, 1979. p. 699.
16. A. A. PAVIA, J. M. ROCHEVILLE et S. N. UNG. Carbohydr. Res. **79**, 79 (1980); S. N. UNG-CHHUN. Thèse de doctorat d'Etat, Faculté des Sciences d'Avignon, Université des Sciences et Techniques du Languedoc, 25 mars 1980; A. A. PAVIA et S. N. UNG-CHHUN. Can. J. Chem. **59**, 482 (1981); J. M. ROCHEVILLE. Thèse de doctorat de Spécialité, Faculté des Sciences d'Avignon, Université de Marseille III, 22 juin 1979.
17. P. J. GAREGG et T. NORBERG. Carbohydr. Res. **52**, 235 (1976).
18. J. MARTINEZ, A. A. PAVIA et F. WINTERNITZ. Carbohydr. Res. **50**, 15 (1976).
19. S. KOTO, N. MOROSHIMA, Y. MIYATA et S. ZEN. Bull Chem. Soc. Jpn. **49**, 2639 (1976); G. P. J. GLAUDEMANS et H. G. FLETCHER. J. Org. Chem. **28**, 3004 (1963).
20. M. BERGMANN et L. ZERVAS. Ber. **65**, 1192 (1932).
21. M. K. MILLER et H. WAELSH. J. Am. Chem. Soc. **82**, 1092 (1960).
22. M. A. TILAK. Tetrahedron, 6323 (1968).
23. J. P. GREENSTEIN et M. WINITZ. *Dans* Chemistry of the aminoacids. John Wiley and Sons, Inc., New York. 1961.
24. R. B. MERRIFIELD. J. Biol. Chem. **232**, 43 (1958).
25. J. K. N. JONES, J. P. MILLINGTON et M. B. PERRY. Can. J. Chem. **40**, 2229 (1962).
26. D. F. DE TAR, F. F. ROGERS et J. H. BACH. J. Am. Chem. Soc. **89**, 3039 (1967).
27. C. H. HASSALL et J. THOMAS. J. Chem. Soc. C, 1495 (1968).
28. A. A. PARCHETT et B. WITKOP. J. Am. Chem. Soc. **79**, 185 (1957).
29. M. BODANSKY, K. W. FUNK et M. L. FINK. J. Org. Chem. **38**, 3565 (1973); M. BODANSKY, M. KONDO, C. Y. LIN et G. F. SIGLER. J. Org. Chem. **39**, 444 (1974).
30. B. LINDBERG et B. G. SILVANDER. Acta Chem. Scand. **192**, 530 (1965).

Mécanisme de la réaction de glycosylation par réversion acide en présence d'anhydride trifluorométhane sulfonique comme agent de condensation

ANDRÉ A. PAVIA[1] ET SAK N. UNG-CHHUN

Laboratoire de Chimie Bioorganique, Faculté des Sciences, 33, rue Louis Pasteur, 84000 Avignon, France

Reçu le 26 juin 1980

Ce papier est dédié au Prof. Raymond U. Lemieux à l'occasion de son 60ème anniversaire

ANDRÉ A. PAVIA et SAK N. UNG-CHHUN. Can. J. Chem. **59**, 482 (1981).

Le caractère acido-catalysé de la réaction de synthèse des glycosylglycosides symétriques par autocondensation des dérivés benzylés des monosaccharides réducteurs en présence d'anhydride trifluorométhanesulfonique a été établi grâce à la rmn du fluor à basse température. L'efficacité de la méthode est justifiée par la propriété particulière de l'acide trifluorométhanesulfonique de former un sel d'hydroxonium $CF_3SO_3^- H_3O^+$ stable, insoluble dans le milieu réactionnel, permettant de déplacer l'équilibre vers la formation du glycoside. L'anhydride joue dans cette réaction le double rôle de source de protons et de piège à eau. Il est montré par ailleurs que le mécanisme le plus probable est celui passant par un intermédiaire oxonium cyclique et que l'α-stéréosélectivité résulte essentiellement de l'anomérisation *in situ* des composés β en composés α thermodynamiquement plus stables.

ANDRÉ A. PAVIA and SAK N. UNG-CHHUN. Can. J. Chem. **59**, 482 (1981).

The acid-catalysed mechanism of the reaction using trifluoromethanesulfonic anhydride to synthesize symmetrical 1,1′-glycosyl-glycosides such as trehalose and *galacto*, *manno*, *arabino*, *xylo* etc. analogues has been elucidated. The authors were able to prove by ^{19}F nmr study at low temperature that the efficiency of the system is due to the peculiar property of trifluoromethanesulfonic acid generated *in situ* to form a stable, insoluble hydroxonium trifluoromethanesulfonate $CF_3SO_3^- H_3O^+$. The procedure satisfies the two necessary conditions for a glycosylation reaction being workable: (*i*) the presence in catalytic amounts of free acid which is regenerated during the condensation step; (*ii*) a very efficient trapping of the water liberated during the protonation step which displaces the equilibrium towards the formation of the glycoside. The α-stereoselectivity of the reaction is discussed in terms of anomerisation of the β-anomers on to the thermodynamically more stable α ones, through a cyclic oxonium intermediate.

Introduction

Depuis les premiers travaux d'Haszeldine et coll. (1–3), l'acide trifluorométhanesulfonique et ses dérivés ont été de plus en plus utilisés en chimie organique (4, 5) et parmi eux les trifluorométhanesulfonates principalement comme agents d'alkylation. Ces dérivés sont connus pour être de très bons groupes partants et leur réactivité a été mise à profit dans des réactions de solvolyse impliquant des substrats réputés très peu ou pas réactifs. Ces esters constituent un moyen simple et efficace d'activer les groupements hydroxyles aussi leur utilisation dans la chimie des carbohydrates va en augmentant (6–14). Dans certains cas, l'anhydride trifluorométhanesulfonique a été utilisé pour promouvoir la formation *in situ* d'intermédiaires 1-*O*-trifluorométhanesulfonates comme dans le cas de la synthèse en une seule étape d'α-D-glucosides rapportée récemment (13, 14) par Leroux et Perlin.

Lorsque nous avons appliqué le protocole expérimental décrit par ces auteurs à la synthèse de *O*-glycosylaminoacides nous avons pu mettre en évidence dans le milieu réactionnel des quantités très faibles, mais décelables de 1,1′-glycosyl-glycosides. Cette observation nous a incité à reconsidérer le rôle de l'anhydride trifluorométhanesulfonique à la fois comme source de protons et comme agent de déshydratation, ces deux conditions étant nécessaires pour qu'une réaction de glycosylation acido-catalysée soit possible et efficace. C'est ainsi qu'ont pu être synthétisés par un processus simple, rapide et avec des rendements quasi-quantitatifs (≥95%) les mélanges d'α,α et α,β-tréhalose et ses analogues *galacto*, *manno*, à partir respectivement des dérivés benzylés du D-glucopyranose, D-galactopyranose, D-mannopyranose (15*a*). Dans chaque cas les anomères α,α sont obtenus de façon prépondérante.

De plus, quand la réaction est effectuée en présence d'un excès (deux à trois moles pour une) d'un second "alcool" (hydroxyaminoacide convenablement protégé ou monosaccharide non réducteur), le produit de condensation majoritaire est le *O*-glycosylaminoacide ou le disaccharide mixte (55 à 90%) (15*a*, *b*). Dans ce cas aussi l'anomère prépondérant et parfois même exclusif est l'anomère α. Nous sommes maintenant en mesure d'établir le mécanisme de la réaction.

Résultats et discussion

Les résultats décrits précédemment (15*a*) ont été confirmés par la synthèse des dérivés benzylés de l'α-D-xylopyranosyl-α-D-xylopyranoside (**1**), β-L-arabinopyranosyl-β-L-arabinopyranoside (**2**), β-L-

[1]Auteur a qui toute correspondance doit être adressée.

0008-4042/81/020482-08$01.00/0

©1981 National Research Council of Canada/Conseil national de recherches du Canada

Can. J. Chem. Downloaded from www.nrcresearchpress.com by 210.87.254.42 on 09/05/12
For personal use only.

Can. J. Chem. Downloaded from www.nrcresearchpress.com by 210.87.254.42 on 09/05/12
For personal use only.

arabinopyranosyl-α-L-arabinopyranoside (**3**), β-D-fructofuranosyl-β-D-fructofuranoside (**4**), α-D-fructofuranosyl-α-D-fructofuranoside (**5**). On peut à priori envisager deux modes de formation pour ces glycosides.

(*1*) Glycosylation directe par réaction entre une mole du monosaccharide réducteur et le dérivé 1-*O*-trifluorométhanesulfonate ou la paire d'ions correspondante, selon le schéma 1. Il est vraisemblable qu'en absence de base, la formation du triflate est très limitée. En fait un tel dérivé n'a jamais été décelé. Notons que dans cette hypothèse le milieu réactionnel doit s'enrichir en acide trifluorométhanesulfonique CF_3SO_3H.

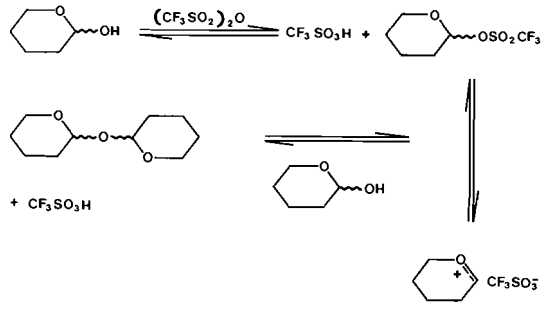

SCHÉMA 1

(*2*) Condensation par réversion acide. L'acide nécessaire pour catalyser la réaction peut être contenu à l'état d'impureté dans l'anhydride (cf. mode d'obtention (2)) soit provenir d'une hydrolyse partielle de l'anhydride par l'eau existant dans le solvant, soit encore d'une réaction d'estérification nécessairement limitée entre le sucre et l'anhydride (schéma 1). Cet acide est régénéré au cours de la réaction de condensation proprement dite. La différence essentielle avec le processus précédent réside dans la formation d'eau qui peut donner avec l'anhydride un sel d'hydroxonium (schéma 2).

La condensation dite par réversion acide ne représente qu'un cas particulier de la glycosylation acido-catalysée utilisée couramment pour la préparation des alkyl-glycosides simples. Dans ce cas l'alcool est utilisé en grand excès et l'équilibre est ainsi déplacé vers la formation du glycoside. Dans tous les autres cas où les réactifs sont en proportions voisines de la stoechiométrie, l'efficacité de la méthode dépend strictement de celle avec laquelle l'eau formée au cours de la réaction de condensation est éliminée du milieu réactionnel. Par l'étude en rmn du Fluor-19, nous apportons la preuve que l'efficacité de notre système est essentiellement due à la propriété particulière de l'acide trifluorométhanesulfonique libéré par hydrolyse de former avec l'eau un hydrate ou plus précisément un trifluorométhanesulfonate d'hydroxonium dont la formation résulte globalement de l'équation ci-dessus (schéma 2).

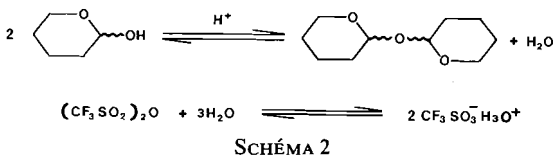

SCHÉMA 2

Vis-à-vis d'un acide aussi fort que l'acide trifluorométhanesulfonique, l'eau se comporte comme une base et sa "capture" est d'autant plus efficace que "l'hydrate" ainsi formé est insoluble dans le dichlorométhane, comme nous avons pu le montrer, à partir d'échantillons authentiques. Dans ces conditions, non seulement on minimise les dégradations que pourraient subir les sucres en présence d'un tel acide, mais on déplace l'équilibre de façon quasi-irréversible vers la formation du glycoside.

En dehors de ce sel d'hydroxynium stable, isolable (F 34°C) décrit dès les premiers travaux d'Haszeldine (1–3) sont également connus d'autres dérivés du même type. Les structures cristallines de $CF_3SO_3^-$ H_3O^+, $CF_3SO_3^-$ $H_5O_2^+$, $CF_3SO_3^-$ $H_3O^+ \cdot CF_3SO_3H$, que l'on peut assimiler sur le plan de la stoechiométrie à des monohydrate, dihydrate, hémihydrate, ont été déterminées par diffraction des rayons X (16). Les études cristallographiques montrent que dans $CF_3SO_3^-$ H_3O^+ et $CF_3SO_3^-$ H_3O^+, CF_3SO_3H, l'ion hydroxonium H_3O^+ est lié par liaison-hydrogène à 3 atomes d'oxygène appartenant à 3 ions trifluorométhanesulfonates selon un arrangement pyramidal. Dans l'hémihydrate il n'y a pas de liaison-hydrogène entre H_3O^+ et la seconde molécule d'acide qui est liée par son hydroxyle à l'un des trois ions $CF_3SO_3^-$ entourant H_3O^+. Il est probable qu'en solution aqueuse on peut envisager tout un éventail de combinaisons entre la molécule d'acide et les molécules d'eau.

L'hypothèse de la réversion acide est confirmée par les résultats suivants. Trois espèces fluorées sont susceptibles d'intervenir: l'anhydride $(CF_3SO_2)_2O$ (**A**), l'acide non dissocié CF_3SO_3H (**B**) et le sel d'hydroxonium $CF_3SO_3^-$ H_3O^+ (**C**). Les déplacements chimiques du groupement CF_3 dans **A**, **B** et **C**[2] en solution dans le dichlorométhane ont

[2]En fait **C** qui a été préparé comme indiqué (2) est à peu près insoluble dans le dichlorométhane. Le spectre de rmn a été réalisé sur une suspension obtenue par agitation de **C** avec le solvant. Malgré cette hétérogénéité la valeur du déplacement chimique est reproductible.

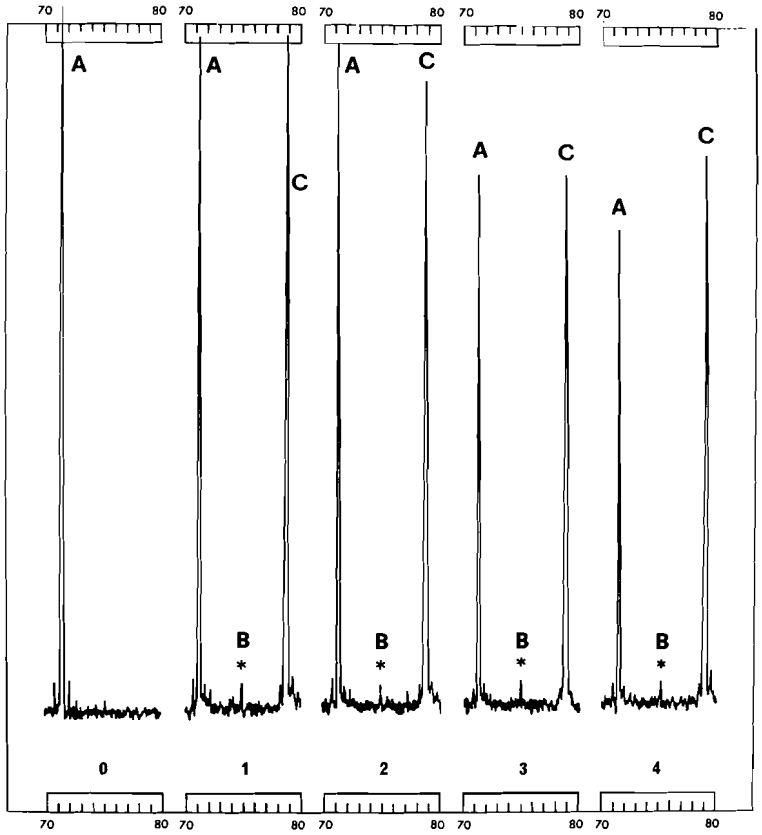

FIG. 1. Hydrolyse de l'anhydride trifluorométhanesulfonique contrôlé par les spectres de ^{19}F rmn (voir texte pour les explications).

été obtenus dans des conditions de concentration et de température (−40°C) identiques à celles utilisées pour le contrôle de la réaction proprement dite. Par rapport au trichlorofluorométhane utilisé en référence interne on note δ_A +71,5 ppm, δ_B +75,3 ppm, δ_C +78,8 ppm. Ces valeurs se retrouvent à ±0,4 ppm près dans le mélange **A** + **B** et dans le milieu réactionnel.

Lorsque les solutions de **A** et **B** dans le dichlorométhane sont agitées à température ambiante avec un égal volume d'eau, le contrôle en ^{19}F rmn montre que la phase organique ne contient plus ni **A** ni **B**. Par contre le spectre de la phase aqueuse montre dans les deux cas un signal CF_3 situé à +2,82 ppm par rapport à celui de l'acide trifluoroacétique pris comme référence interne. Dans les mêmes conditions, les spectres de **B**, **C** et du mélange des deux en solution aqueuse présentent le même signal CF_3 à +2,84 ppm.

Par ailleurs le spectre enregistré immédiatement après avoir agité à froid la solution **A** avec une goutte d'eau (la solution se trouble) fait apparaitre un changement significatif: l'intensité du signal CF_3-**A** a diminué tandis qu'apparait le signal **C** à 78,8 ppm. De plus, un troisième signal de faible intensité est présent à 75,3 ppm. A −40°C, dans les dix minutes qui suivent l'enregistrement du premier spectre, on note une diminution progressive du signal CF_3-**A** puis une stabilisation et une augmentation concomittante de CF_3-**C**, l'intensité de CF_3-**B** restant faible et apparemment constante (fig. 1).

Ces observations montrent que (*a*) l'acide trifluorométhanesulfonique est plus soluble dans l'eau que dans le dichlorométhane; (*b*) l'hydrolyse de l'anhydride est relativement rapide même à basse température; (*c*) le produit principal de l'hydrolyse est le sel d'hydroxonium; (*d*) le milieu ne contient que des quantités faibles (catalytiques) d'acide libre.

La réaction du tétrabenzylglucose avec l'anhydride triflique a été étudiée dans les conditions ci-après: on réalise le mélange comme décrit précédemment à −80°C, puis on laisse remonter la température en sortant le vase réactionnel hors du bain carboglace–acétone. L'évolution de la réaction est contrôlée de dix degrés en dix degrés, parallèlement par ccm et ^{19}F rmn. Les spectres sont

Can. J. Chem. Downloaded from www.nrcresearchpress.com by 210.87.254.42 on 09/05/12
For personal use only.

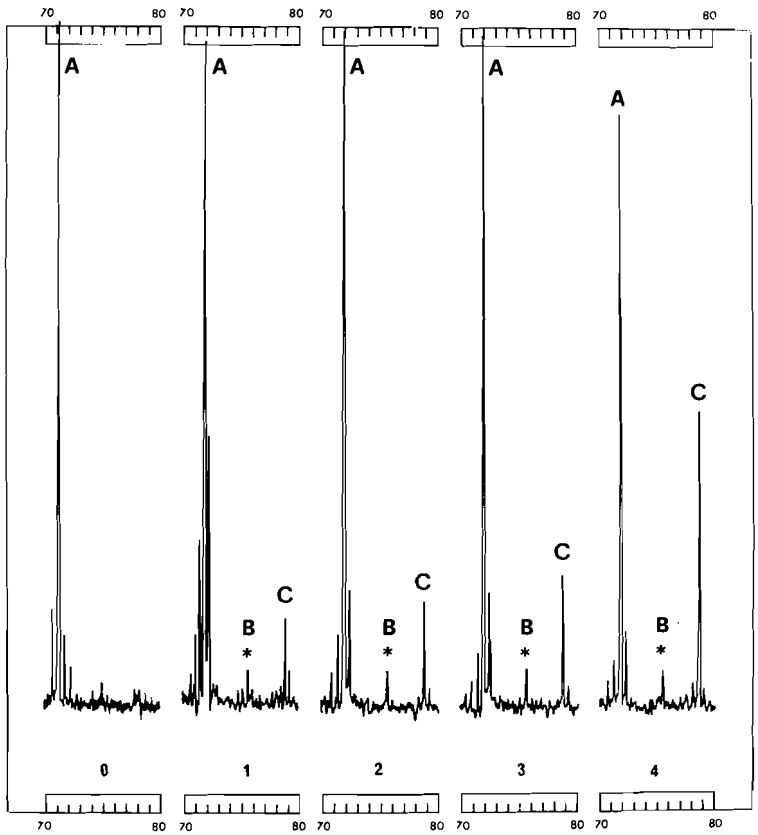

FIG. 2. Spectres de rmn du fluor de la réaction du 2,3,4,6-tétra-*O*-benzyl-D-glucopyranose en présence de $(CF_3SO_2)_2O$ au moment du mélange (0), en cours de réaction (1, 2, 3) et en fin de réaction (4).

réalisés à −46°C de façon à bloquer la réaction et minimiser les dégradations éventuelles pendant la durée de l'enregistrement. La figure 2 montre les modifications du spectre dans la région d'absorption des groupements CF_3. Elles sont analogues à celles observées dans l'expérience précédente.

La formation des disaccharides, confirmée par ccm s'accompagne de la diminution de la quantité d'anhydride au profit du sel d'hydroxonium. On note également l'apparition du signal à 75,3 ppm de faible intensité. La réaction est terminée lorsque la température du milieu réactionnel atteint ~+15°C et dure en moyenne 15 à 30 min selon le volume de la solution. La formation du sel d'hydroxonium implique nécessairement la libération d'eau et confirme la validité du mécanisme acido-catalysé.

Par ailleurs comme nous l'avions noté précédemment (15*a*) la réaction peut être réalisée en présence d'acide trifluorométhanesulfonique moyennant un contrôle strict des temps de réaction et des conditions de température, afin de minimiser les réactions de dégradation. L'examen de la réaction réalisé simultanément par ccm et ^{19}F rmn entre −80 et −40°C, montre que (*a*) à −60°C, 5 minutes seulement après que le mélange ait été sorti du bain froid, la moitié environ du D-glucose a été transformé en un mélange d'α,α et α,β-tréhalose, (*b*) à cette même température le milieu réactionnel ne contient déjà plus d'acide trifluorométhanesulfonique; le seul signal visible est celui situé à 78,8 ppm attribué à CF_3-**C**, d'intensité équivalente à celle du signal CF_3-**B** de la solution témoin, mesuré avant d'ajouter le tétrabenzylglucose. L'obtention de ce signal est une preuve supplémentaire de la libération d'eau en cours de réaction. Abstraction faite des traces d'eau susceptibles d'être contenues dans le solvant, la quantité d'acide est au moins égale à la quantité d'eau qui pourra être libérée par la réaction de condensation. Au moment du 1er contrôle il y a normalement un excès d'acide puisque la réaction n'a progressé que de moitié. Malgré celà, tout l'acide a disparu du milieu réactionnel. Il est probable que ce dernier s'est solubilisé dans la "phase aqueuse" correspondant à l'eau libérée au cours de la condensation.

Par ailleurs, si, en fin de réaction, on ajoute l'acide au milieu réactionnel, on ne voit apparaitre le signal à 75,6 ppm caractéristique de l'acide non

Can. J. Chem. Downloaded from www.nrcresearchpress.com by 210.87.254.42 on 09/05/12
For personal use only.

Can. J. Chem. Downloaded from www.nrcresearchpress.com by 210.87.254.42 on 09/05/12
For personal use only.

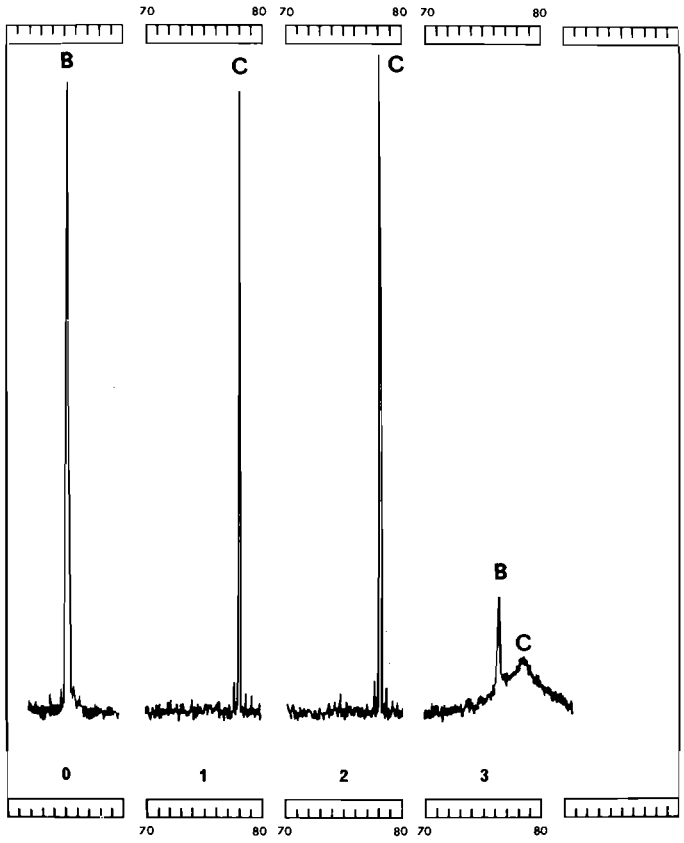

FIG. 3. Spectre de rmn du fluor de la réaction du 2,3,4,6-tétra-*O*-benzyl-D-glucopyranose en présence de CF_3SO_3H au moment du mélange (0), en cours de réaction (1, 2) et en fin de réaction (3).

dissocié, que lorsque ce dernier est ajouté en excès. Dans le même temps le signal à 78,8 ppm évolue sous forme d'un signal élargi.

Les résultats ci-dessus, s'ils confirment la validité d'un mécanisme acido-catalysé, ne nous permettent pas de trancher entre les deux voies possibles, celle passant par un oxonium acyclique (schéma 3A) et celle qui passe par un oxonium cyclique (schéma 3B).

Ces deux mécanismes ont été souvent discutés dans le cadre des réactions d'hydrolyse de glycosides simples (17, 18) bien qu'il soit difficile de les distinguer expérimentalement (19). Mora et Wood (20) s'appuient sur l'hypothèse 3A pour expliquer la polycondensation du glucose alors que Banks *et al.* (21) concluent en faveur du mécanisme 3B après étude de la méthanolyse des phénylglycopyranosides et des effets isotopiques mesurés lors de l'hydrolyse du méthyl-α-D-glucopyranoside. Cet ion oxonium cyclique n'est pas exclusivement capturé par l'eau puisque Overend *et al.* (22) notent la formation (5 à 10%) de disaccharides au cours de l'hydrolyse du méthyl α et β-D-glucopyranoside. Par ailleurs, l'addition de glucose au milieu réac-

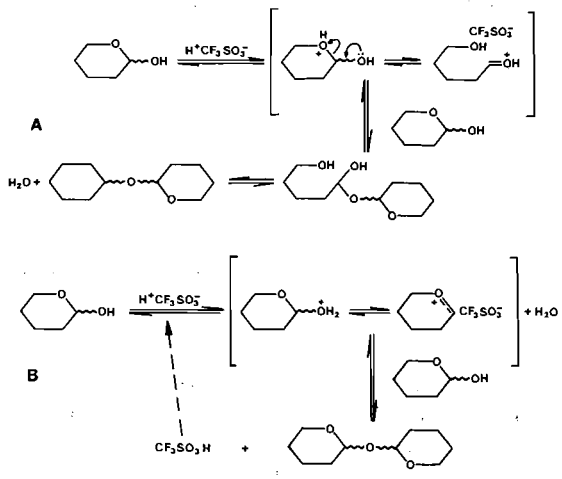

SCHÉMA 3

tionnel provoque une augmentation de la concentration en disaccharide sans que la vitesse d'hydrolyse soit modifiée. Cet intermédiaire est également impliqué dans les réactions d'alcoolyse d'halogénures de glycosyle (23).

Dans l'optique du choix entre les deux hypothè-

Can. J. Chem. Downloaded from www.nrcresearchpress.com by 210.87.254.42 on 09/05/12
For personal use only.

ses ci-dessus, nous avons réalisé l'autocondensation du 2,3,4,6-tétra-*O*-benzyl-5-thio-D-glucopyranose (**6**)[3] et du 2,3,6-tri-*O*-benzyl-D-glucopyranose. Dans le premier cas la réaction conduit au bout de 30 min au mélange des trois anomères de l'octa-*O*-benzyl-5,5′-dithiotréhalose (rdt. global 90%) d'où l'anomère α,α (**7**) a été isolé pur avec un rendement de 38% et caractérisé par les données de rmn[4] (H-1, 5,16 ppm, $J_{1,2}$ = 2,5 Hz). Dans l'hypothèse du schéma 3A, le remplacement d'un atome d'oxygène par un atome de soufre moins basique aurait dû se traduire par une diminution sensible de la vitesse de la réaction; en fait il n'en est rien.

De même, dans le cas du 2,3,6-tri-*O*-benzyl-D-glucopyranose il était possible d'envisager la formation de dérivés du type furanoside si la réaction obéissait au mécanisme du type 3A.

Pour tenir compte de la fragilité relative des formes furanoses, nous avons effectué des prélèvements en cours de réaction à des températures inférieures à 0°C, ces aliquots étant traités comme habituellement. En aucun cas nous n'avons pu mettre en évidence ni isoler des composés de condensation du type furanoside. Le mécanisme utilisant la voie passant par l'oxonium cyclique (schéma 3B) semble être le plus plausible et les résultats de l'anomérisation décrits ci-après plaident en sa faveur.

Tout au long de ce travail nous avons constaté (^{13}C rmn et ccm) que les anomères β(α,β et β,β) sont relativement abondants en début de réaction et que leur concentration diminue au fur et à mesure que la réaction progresse. Le processus d'anomérisation a été souvent mis en avant (18, 24, 25, 26) dans d'autres circonstances; il fait intervenir selon les auteurs un mécanisme du type 3A ou 3B. Si l'anomérisation des glycosides simples a donné lieu à de nombreux travaux, peu d'efforts ont été consacrés à celle de disaccharides et aucun à notre connaissance à celle des glycosyl-glycosides. Deux types d'expériences ont été réalisés: le premier en présence d'acide trifluorométhanesulfonique, le second, en reproduisant les conditions mêmes de la réaction de glycosylation en présence d'anhydride (15*a*). Les expériences ont été réalisées sur les substrats suivants: l'octa-*O*-benzyl-*galacto*-tréhalose α,α (**8**), α,β (**9**) et β,β (**10**), l'octa-*O*-benzyl-tréhalose α,β (**11**) et β,β (**12**), l'hexa-*O*-benzyl-L-*arabino*-tréhalose α,β (**3**) et l'octa-*O*-benzyl-1-thio-*galacto*-tréhalose β,β (**13**). En présence d'acide, on n'observe pas d'anomérisation proba-

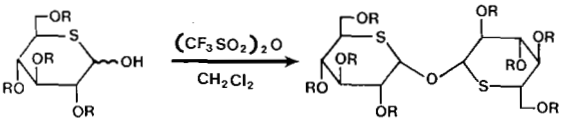

SCHÉMA 4

blement masquée par la réaction d'hydrolyse qui prédomine.

Les résultats obtenus en présence d'anhydride sont résumés dans le tableau 1 et appellent les commentaires suivants. (*a*) Comme on pouvait s'y attendre, le *galacto*-tréhalose α,α (**8**) reste inchangé, sans dégradation ni transformation. Par contre les anomères α,β et β,β sont convertis avec un bon rendement en anomère α,α, même en présence de quantités catalytiques d'anhydride (exp. 3). (*b*) l'α,β-L-*arabino*-tréhalose (**3**) est converti quantitativement en anomère β,β (**2**). (*c*) L'octa-benzyl-1-thio-D-*galacto*-tréhalose β,β (**13**) reste inchangé lorsqu'il est placé dans des conditions qui transforment son homologue **10** en son anomère α,α (**8**). Par ailleurs le contrôle de la réaction ne permet pas de mettre en évidence le produit d'hydrolyse. Cette expérience qui a été répétée plusieurs fois est particulièrement significative dans la mesure où elle indique clairement que l'étape déterminante dans le processus d'anomérisation comme dans celui de la glycosylation est bien la protonation de l'hétéroatome interglycosidique. Le remplacement de l'oxygène par un atome de soufre moins basique défavorise ce processus en diminuant considérablement la vitesse. L'ensemble des résultats discutés ci-dessus nous autorise à proposer le schéma réactionnel 5.

Les données rapportées dans ce travail sont toutes en faveur d'un mécanisme acido-catalysé.[5] L'efficacité de la méthode est expliquée par la "capture" de l'eau libérée au cours de la condensation sous la forme d'un sel d'hydroxonium, insoluble dans le dichlorométhane. Il a été montré également que l'α-stéréosélectivité est renforcée

[3]L'expérience a été réalisée pour le compte du laboratoire du Professeur Defaye de Grenoble et sur un échantillon de 2,3,4,6-tétra-*O*-benzyl-5-thio-D-glucopyranose fourni par ce laboratoire.

[4]J. Defaye, H. Driguez et B. Henrissat, résultats non publiés.

[5]On peut ajouter aux observations rapportées ci-dessus les précisions suivantes. (*a*) Si la réaction passait par un intermédiaire 1-*O*-triflate qui est extrêmement réactif il ne serait pas nécessaire de laisser la réaction évoluer jusqu'à température ambiante (~ +15°C) pour qu'elle soit complète, alors que toutes les réactions impliquant un tel intermédiaire sont faites à −78°C (8, 9, 10). (*b*) Seule l'hypothèse acido-catalysée permet d'expliquer (*1*) que la réaction ne se fasse pas (disaccharides à l'état de trace seulement, < 5%) lorsqu'elle est conduite en présence de pyridine ou collidine, alors que la formation du triflate devrait être favorisée dans de telles conditions; (*2*) que la réaction ait lieu et soit beaucoup plus rapide encore lorsque l'on remplace l'anhydride par l'acide; (*3*) que la réaction ait lieu lorsque l'on remplace l'anhydride triflique par l'anhydride phosphorique (résultats non encore publiés); (*4*) l'anomérisation des disaccharides-1,1,α,β et β,β en disaccharides α,α en présence d'anhydride trifluorométhanesulfonique.

Can. J. Chem. Downloaded from www.nrcresearchpress.com by 210.87.254.42 on 09/05/12
For personal use only.

TABLEAU 1. Anomérisation des glycosyl-glycosides en présence d'anhydride trifluorométhanesulfonique, dans les mêmes conditions que celles utilisées pour la synthèse

Expériences	Composés[a]	Conditions	Produits obtenus[b] α,α	β,β	Autres composés
1	*Galacto*-tréhalose α,α (**8**)	15 min, 0°C	**8** (97%)	—	Monomère (≃3%)
2	Mélange **8** (30%), **9** (58%), **10** (12%)	45 min, −10°C	**8** (75%)	—	Monomère + inconnu (25%)
3[c]	Mélange **9** (85%), **10** (15%)	15 h, 25°C	**8** (90%)	—	Monomère (≃10%)
4	*Arabino*-tréhalose α,β-L (**3**)	20 min, 0°C	—	**2** (100%) (β,β-L)	—
5	Tréhalose α,β (**11**)	20 min, −5°C	75%	—	Monomère
6	1-thio-*galacto*-tréhalose β,β (**13**)[e]	60 min, −10°C	—	**13** (100%)	—
7[d]	1-thio-*galacto*-tréhalose β,β (**13**)	14 h, 25°C	—	**13** (95%)	—

[a]Voir texte pour la nomenclature des produits.
[b]L'analyse du produit de la réaction est réalisée par ^{13}C rmn; les pourcentages sont mesurés à partir des intégrales des signaux des carbones anomères.
[c]Dans cette expérience, l'anhydride est utilisée en quantité catalytique (0,5%).
[d]Au bout de ce temps la solution a noirci.
[e]Produit Sigma no T 4012.

par l'anomérisation *in situ* des dérivés α,β et β,β en dérivés α,α.

Sur le plan du mécanisme proprement dit, le choix en faveur d'un processus réactionnel faisant intervenir un oxonium cyclique intermédiaire s'appuie sur différentes preuves chimiques dont (*a*) l'absence de dérivés furanosiques lorsque le substrat est un dérivé non protégé en position-4; (*b*) la non diminution de la réactivité et de la vitesse lorsque la réaction met en jeu un substrat du type 5-thio-glucose; (*c*) l'absence d'anomérisation du 1-thio-*galacto*-tréhalose β,β alors que l'α,β et le β,β-*galacto*-tréhalose sont, dans les mêmes conditions convertis en leur isomère α,α.

Partie expérimentale

Méthodes générales

Le déroulement des réactions ainsi que l'homogénéité des composés décrits ont été contrôlés par chromatographie sur couche mince (ccm), de gel de silice (Merck F 254, Merck, Darmstadt, Allemagne), la révélation des plaques étant assurée par vaporisation d'une solution 10% d'acide sulfurique suivie du chauffage à 100°C. Les purifications ont été réalisées par chromatographie sur colonne de gel de silice (Merck 60). Les points de fusion ont été mesurés sur appareil Tottoli et sont rapportés non corrigés. Les pouvoirs rotatoires ont été mesurés sur un polarimètre Jobin-Yvon, 11230. Les microanalyses ont été effectuées par le Service Central de Microanalyses du C.N.R.S., division de Montpellier. Les spectres de rmn du ^1H ont été enregistrés à 80 MHz sur un appareil Bruker WP 80; sauf indications particulières ils ont été réalisés dans le chloroforme-*d* et les déplacements chimiques sont donnés en δ par rapport au tétraméthylsilane pris comme référence interne. Les spectres de rmn du ^{13}C ont été enregistrés sur un appareil Bruker WP 80 à 20,115 MHz, les déplacements chimiques sont exprimés par rapport au tétraméthylsilane en référence interne. Dans le cas des solutions aqueuses, le déplacement chimique du dioxane utilisé comme référence interne est de 67,4 ppm.

Les monomères ont été obtenus selon les méthodes déjà décrites. Leurs caractéristiques physiques sont les suivantes.

2,3,4-Tri-*O*-benzyl-D-xylopyranose: F 129–130°C; $[\alpha]_D^{22}$ +18,5° (*c* 0,59, $CHCl_3$); ^{13}C rmn ($CDCl_3$): 92,65 ppm (C-1 anomère β), 91,44 ppm (C-1 anomère α).

2,3,4-Tri-*O*-benzyl-L-arabinopyranose: F 69–70°C; $[\alpha]_D^{22}$ +36,6° (*c* 1,83, $CHCl_3$); ^{13}C rmn ($CDCl_3$): 90,02 ppm (C-1 anomère α), pas de signal correspondant à l'anomère β.

Le 1,3,4,6-tétra-*O*-benzyl-D-fructofuranose a été obtenu par hydrolyse de l'octabenzyl saccharose en présence d'acide trifluorométhanesulfonique: $[\alpha]_D^{22}$ −12,5° (*c* 0,4 $CHCl_3$); ^{13}C rmn: 105,40 ppm (C-2 anomère β, 20%), 102,66 ppm (C-2 anomère α, 80%).

Les glycosyl-glycosides ont été préparés selon le protocole expérimental décrit précédemment (15*a*).

(2,3,4-Tri-*O*-benzyl-α-D-xylopyranosyl)-2,3,4-tri-*O*-benzyl-α-D-xylopyranoside (**1**): (rdt. 90%), $[\alpha]_D^{22}$ +96,10 (*c* 0,77, $CHCl_3$); ^{13}C rmn: 94,22 ppm (C-1). *Anal.* calc. pour $C_{52}H_{54}O_9$: C 75,91, H 6,56; trouvée: C 75,81, H 6,53.

(2,3,4-Tri-*O*-benzyl-β-L-arabinopyranosyl)-2,3,4-tri-*O*-benzyl-β-L-arabinopyranoside (**2**): (rdt. 97%): F 134–135°C; $[\alpha]_D^{22}$ +142° (*c* 1,15, $CHCl_3$); ^1H rmn: 5,75 (d, $J_{1,2}$ 3,5 Hz (2H, H-1), 4,08 (q, H-2) ppm; ^{13}C rmn: 94,66 ppm (C-1). *Anal.* calc. pour $C_{52}H_{54}O_9$: C 75,91, H 6,56; trouvée: C 75,69, H 6,55.

(2,3,4-Tri-*O*-benzyl-β-L-arabinopyranosyl)-2,3,4-tri-*O*-benzyl-α-L-arabinopyranoside (**3**). $[\alpha]_D^{22}$ +84,13 (*c* 0,72, $CHCl_3$); ^{13}C rmn: 102,91 ppm (C-1, α-L), 99,54 ppm (C-1 β-L). *Anal.* calc. pour $C_{52}H_{54}O_9$: C 75,91, H 6,56; trouvée: C 75,80, H 6,45.

1,2,4,6,1′,2′,4′,6′-Octa-*O*-benzyl-fructofuranosyl-fructofuranoside β,β (**4**) et α,α (**5**): le mélange réactionnel (rdt. global 53%) contient environ 85% du composé **4** et 15% de **5**. La chromatographie ne nous a pas permis de les séparer; ^{13}C rmn: 108,5 ppm (C-1 anomère β,β), 104,70 ppm (C-1 anomère α,α).

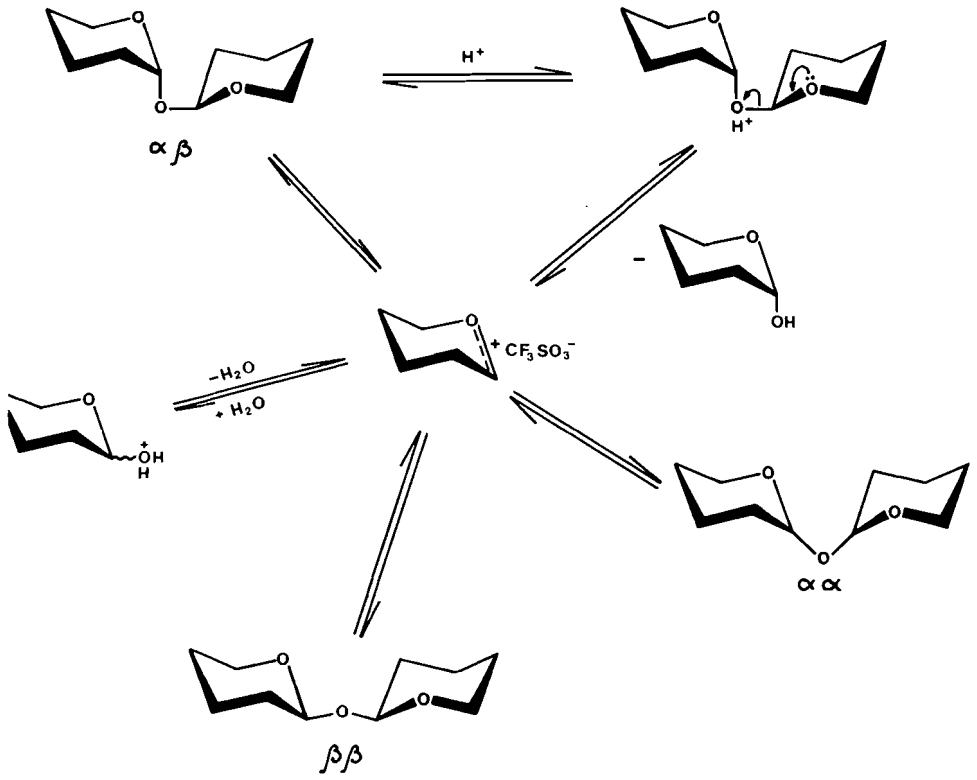

SCHÉMA 5

Réactions d'anomérisation

Les disaccharides α,α, α,β ou β,β octabenzylés (0,5 mmol) purs ou sous forme de mélange sont mis en réaction en présence de l'anhydride trifluorométhane sulfonique (1 à 1,5 mole par mole de sucre) dans le dichlorométhane (≈8 mL) de la même façon que pour les réactions de condensation des monosaccharides. La réaction est conduite, contrôlée et traitée comme précédemment (15*a*).

Remerciements

Les auteurs remercient la Mairie d'Avignon et le Conseil Général du Vaucluse pour l'aide matérielle qu'ils leur ont si généreusement accordée ainsi que Monsieur J. L. Durand, Technicien responsable du laboratoire de rmn pour sa collaboration technique.

1. R. N. HASZELDINE et J. M. KIDD. J. Chem. Soc. 4228 (1954).
2. T. GRAMSTADT et J. M. HASZELDINE. J. Chem. Soc. 173 (1956).
3. T. GRAMSTADT et J. M. HASZELDINE. J. Chem. Soc. 4069 (1957).
4. A. SENNING. Chem. Rev. **65**, 385 (1965).
5. R. D. HOWELLS et J. D. MCCOWN. Chem. Rev. **77**, 69 (1977).
6. R. U. LEMIEUX et K. KONDO. Carbohydr. Res. **35**, C4 (1974).
7. L. D. HALL et D. C. MILLER. Carbohydr. Res. **47**, 299 (1976); **40**, C1 (1975).
8. F. J. KRONZER et C. J. SCHUERCH. Carbohydr. Res. **27**, 379 (1973).
9. E. S. RACHAMAN, R. EBY et C. SCHUERCH. Carbohydr. Res. **67**, 147 (1978).
10. V. MAROUSECK, J. J. LUCAS, P. E. WHEAT et C. SCHUERCH. Carbohydr. Res. **60**, 85 (1978).
11. C. SCHUERCH. American Chemical Society Symposia, Série 87. 1973. p. 80.
12. R. L. SHONE. Tetrahedron Lett. **11**, 993 (1977).
13. J. LEROUX et A. S. PERLIN. Carbohydr. Res. **47**, C8 (1976).
14. J. LEROUX et A. S. PERLIN. Carbohydr. Res. **67**, 163 (1978).
15. (*a*) A. A. PAVIA, J. M. ROCHEVILLE et S. N. UNG. Carbohydr. Res. **79**, 79 (1980); (*b*) J. M. LACOMBE, A. A. PAVIA et J. M. ROCHEVILLE. Can. J. Chem. **59**, 473 (1981).
16. J. B. SPENEN et J. O. LUNDGREN. Acta Crystallogr. Sect. B, **29**, 1923 (1973); R. J. DELAPLANE, J. O. LUNDGREN et I. OLOVSON. Acta Crystallogr. Sect. B, **31**, 2202 (1975); R. J. DELAPLANE, J. O. LUNDGREN et I. OLOVSON. Acta Crystallogr. Sect. B, **31**, 2208 (1975).
17. J. N. BEMILLER. Adv. Carbohydr. Chem. **22**, 27 (1967).
18. B. CAPON. Chem. Rev. **69**, 415 (1969).
19. C. A. BUNTON, T. A. LEWIS, D. R. SEWELLYN et C. A. VERNON. J. Chem. Soc. 4419 (1955).
20. P. T. MORA et J. W. WOOD. J. Am. Chem. Soc. **80**, 685 (1958).
21. B. E. C. BANKS, Y. MEINWALD, A. J. RHIND-TUTT, I. SHEFT et C. A. VERNON. J. Chem. Soc. 3240 (1961).
22. W. G. OVEREND, C. W. REES et J. S. SEQUEIRA. J. Chem. Soc. 3429 (1962).
23. R. U. LEMIEUX, K. B. HENDRIKS, R. U. STICK et K. JAMES. J. Am. Chem. Soc. **97**, 4056 (1975).
24. R. U. LEMIEUX. Adv. Carbohydr. Chem. Biochem. **9**, 1 (1954); R. U. LEMIEUX et J. I. HAYAMI. Can. J. Chem. **43**, 2162 (1965).
25. B. CAPON et D. THACKER. J. Chem. Soc. B, 1010 (1967).
26. R. J. FERRIER, L. R. HATTON et W. G. OVEREND. Carbohydr. Res. **8**, 56 (1968).

Can. J. Chem. Downloaded from www.nrcresearchpress.com by 210.87.254.42 on 09/05/12
For personal use only.

A relative extrusibility scale and its application to the thermal fragmentation patterns of 5-membered ring diazenes[1]

ANTHONY JAMES PAINE[2]

Xerox Research Centre of Canada, 2480 Dunwin Drive, Mississauga, Ont., Canada L5L 1J9

AND

JOHN WARKENTIN

Department of Chemistry, McMaster University, Hamilton, Ont., Canada L8S 4M1

Received August 18, 1980

ANTHONY JAMES PAINE and JOHN WARKENTIN. Can. J. Chem. **59**, 491 (1981).

Extrusion of a stable molecular fragment (like N_2, CO_2, SO_2, CO, etc.) is a common chemical process. Using thermodynamic additivity concepts, group values, and heat of formation data, a Relative Extrusibility Scale (ΔH_{ex}^0) has been defined for these fragmentations:

$$\underset{\text{GMF}}{\text{R—X—R}} \rightarrow 2\text{R} + \text{X} \qquad \Delta H_{ex}^0(\text{X}) = \Delta H_f^0(\text{X}) - \Delta H_f^0(\text{GMF})$$

(GMF = generalized molecular fragment, can be cyclic or chain)

Twenty-four such extrusions spanning 150 kcal mol^{-1} have been compiled. Typical values include N_2 (−42.0), CO_2 (−2.6), HCN (13.8), CO (15.4), H_2CO (18.3), C_2H_4 (32.2), and $^1CH_2$ (109). Among other theoretical and mechanistic applications, this list should be useful when designing synthetic routes involving extrusion reactions.

In a particularly effective illustration of the usefulness of the scale, it rationalizes, for the first time, the variety of product types obtained from thermolyses of 14 different kinds of 5-membered ring diazenes. Heat of formation data on most of these compounds do not exist and they contain such sufficiently complicated functional group arrangements that most of the thermodynamic group equivalents are also unknown. This problem can be circumvented by thermodynamic cycles based on the Relative Extrusibility Scale, suitable models, and interfragment resonance corrections. Within an error framework of less than ± 5 kcal mol^{-1}, enthalpy estimates are sufficiently accurate to give heats of reaction capable of predicting which of the potential fragmentation routes actually occur. Formation of a 3-membered ring must be exothermic by at least 30 kcal mol^{-1} to contribute to the products, but 3-piece fragmentation and 1,3-dipolar cycloreversion will contribute to the observed products when the process is either thermoneutral or exothermic. The unimportance of entropy is also discussed.

ANTHONY JAMES PAINE et JOHN WARKENTIN. Can. J. Chem. **59**, 491 (1981).

L'expulsion d'un fragment moléculaire stable (comme N_2, CO_2, SO_2, CO, etc.) est un procédé chimique courant. Faisant appel à des concepts d'additivité thermodynamique, à des valeurs de groupe et à des données de chaleur de formation, on a défini une échelle relative d'expulsion (ΔH_{ex}^0) de ces fragments:

$$\underset{\text{FMG}}{\text{R—X—R}} \rightarrow 2\text{R} + \text{X} \qquad \Delta H_{ex}^0(\text{X}) = \Delta H_f^0(\text{X}) - \Delta H_f^0(\text{FMG})$$

(FMG = fragment moléculaire généralisé; peut être cyclique ou à chaîne ouverte)

On a compilé 24 exemples de telles expulsions couvrant une variation de 150 kcal mol^{-1}. Les valeurs typiques comprennent N_2 (−42,0), CO_2 (−2,6), HCN (13,8), CO (15,4), H_2CO (18,3), C_2H_4 (32,2) et $^1CH_2$ (109). Cette liste, parmi d'autres applications mécanistique et théorique, devrait être utile quand il s'agit de synthèse impliquant des réactions d'expulsion.

L'utilité de cette échelle est illustrée d'une façon particulièrement appropriée par le fait qu'elle rationalise pour la première fois la variété des produits obtenus au cours de la thermolyse de 14 sortes différentes de diazènes à cinq chaînons. Les données de chaleur de formation de la plupart de ces composés n'existent pas et ils contiennent tant d'arrangements de groupes fonctionnels compliqués que les équivalents de groupe thermodynamique sont également inconnus. Ce problème peut être évité en utilisant des cycles thermodynamiques basés sur l'échelle relative d'expulsion, sur des modèles appropriés et sur des corrections de résonance interfragment. Dans les limites d'erreur de ±5 kcal mol^{-1}, les évaluations d'enthalpie sont suffisamment précises pour donner les chaleurs de réaction susceptibles de prédire la voie de fragmentation qui serait potentiellement suivie. La formation d'un cycle à 3 chaînons doit être exothermique (au moins 30 kcal mol^{-1}) pour contribuer à la formation des produits; toutefois les fragmentations conduisant à des chaînons à 3 unités et la cycloinversion dipolaire-1,3 contribueront aux produits observés quand le processus est soit thermoneutre, soit exothermique. On discute également du fait que l'entropie n'est pas importante.

[Traduit par le journal]

Introduction

Thermodynamic considerations place a strong quantitative constraint on kinetics, but are often overlooked as criteria of chemical reactivity. Through the efforts of Benson *et al.* (1, 2) and others (3), additivity schemes have been developed which permit reasonably accurate estimation of thermodynamic parameters (ΔH_f^0, S^0, C_p^0) for many organic compounds. These estimates facilitate calculation of

[1]Presented in part at the 63rd Chemical Institute of Canada Conference in Ottawa, June 8–11, 1980.

[2]Author to whom correspondence may be addressed.

0008-4042/81/030491-15$01.00/0

©1981 National Research Council of Canada/Conseil national de recherches du Canada

Can. J. Chem. Downloaded from www.nrcresearchpress.com by 210.87.254.40 on 09/06/12
For personal use only.

Can. J. Chem. Downloaded from www.nrcresearchpress.com by 210.87.254.40 on 09/06/12
For personal use only.

thermodynamic state function changes associated with a very large number of reactions.

Nevertheless, there remain numerous reactions for which the heat of formation of a reactant or product is not only unmeasured, but the structure is also sufficiently complex that ΔH_f^0 cannot be estimated directly by summing group contributions. This paper demonstrates that some of these previously inestimable heats of formation can be crudely obtained from appropriate cycles based on a Relative Extrusibility Scale and Table of Interfragment Interactions developed herein. Although the method is more general, it is useful to develop the discussion in the context of rationalizing 5-membered ring diazene chemistry.

Extrusion Reactions

Extrusion of a stable molecular fragment like N_2, CO, CO_2, SO_2, etc., is a common chemical process. In the most general sense,[3] an extrusion reaction may be defined as a process whereby a molecule of some kind, either cyclic or acyclic, undergoes unimolecular thermal fragmentation to liberate a small molecule, X, together with some other stable molecular product(s) and/or short-lived intermediates, such as dipoles, diradicals, or biradicals, for example. Typical examples of extrusion reactions would be cycloreversions, diazene fragmentations, decarbonylations, and decarboxylations.

For a variety of reasons (synthetic, theoretical, mechanistic), it is desirable to know the relative ease of extrusion of various small molecules. For example, which of CO, SO_2, or SO is most easily extruded by the cheleotropic process in eq. [1]? Suppose a certain radical, R•, were a synthetic target. What fragments could be extruded together with R• to drive the synthesis?

[1] 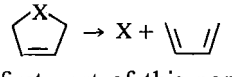 X = CO, SO, SO_2,...

The first part of this paper uses thermodynamics to derive a Relative Extrusibility Scale which addresses these kinds of questions. Such an approach ignores very important kinetic and mechanistic factors, but has several advantages. The thermodynamic scale is more generally applicable because the complicating variety of (often unknown) mechanistic types can be ignored. Furthermore, the relative thermodynamic scale may be anchored (made into an absolute scale) for a given reaction series using one known heat of reaction, thereby allowing computation of approximate values for other cases in the series. If such a calculation reveals that a specific extrusion is excessively endothermic, the relative scale will have predicted that the corresponding extrusion is kinetically inaccessible.

A Relative Extrusibility Scale from Group Values

Consider eq. [2] to describe a general extrusion reaction which releases a fragment X. The thermodynamic driving force for the extrusion is the free energy change, ΔG^0. If various X are to be compared for constant R and R′, however, entropy changes will be approximately independent of X, making differences between ΔG^0 and ΔH^0 very similar.

It is both convenient and instructive to arbitrarily define eq. [3] as the model process. Here, the end groups R and R′ of the more general eq. [2] have been set equal to carbon fragments whose group equivalents are readily available.[4] Structure **1** is obviously not a molecule in this formalism, but rather something we define as a generalized molecular fragment, whose heat of formation, ΔH_f^0 (GMF:X), can be calculated by summing the group equivalents for two [C—(X)(C)$(H)_2$] and one [X—$(C)_2$] (eq. [4], examples to come).

[2] R—X—R′ → R + X + R′

[3] C—CH_2—X—CH_2—C → 2″C—CH_2″ + X

GMF **1**

[4] ΔH_f^0(GMF:X) = [X—$(C)_2$] + 2[C—(X)(C)$(H)_2$]

[5] $\Delta H_{ex}^0(X) = \Delta H_f^0(X) - \Delta H_f^0$(GMF:X)

With eq. [3] as the model process, we arbitrarily define a *relative* scale of extrusibility, ΔH_{ex}^0 (X), as the difference between the heat of formation of X and the GMF containing X (eq. [5]). Such a definition intentionally ignores the constant contribution of the cofragments.

One advantage of this kind of relative enthalpy scale for a related set of reactions is that enthalpy contributions from ring strain, gauche interactions, solvent effects, or other factors are all approximately constant and cancel when two extrusions are compared.

Because additivity principles have been introduced in the thermodynamic calculation, the scale is really only defined for the gas phase. However, in most cases the results can be safely applied in solu-

[3]This definition differs from an earlier definition by Duke and Stark (4) by including acyclic cases.

[4]The thermodynamic additivity concepts of Benson and particularly the group values found in his 1976 text (2) together with heat of formation data in his 1969 review (1) and a text by Cox and Pilcher (3) have been used extensively throughout the present work. Whether directly measured, or reliably computed from group equivalents, all unreferenced heats of formation used in the following discussion are available from these sources. Space limitations prohibit including details of any straightforward computations. Units are universally assumed to be kcal mol^{-1} for *G* and *H* and cal mol^{-1} K^{-1} for *S*, and will not always be explicitly carried.

Can. J. Chem. Downloaded from www.nrcresearchpress.com by 210.87.254.40 on 09/06/12
For personal use only.

-X-	-N=N-	-CH=CH-
GMF:	C—CH_2—N=N—CH_2—C	C—CH_2—CH=CH—CH_2—C

Groups	ΔH_f^0	Groups	ΔH_f^0
2[N_A—(C)]	27.0 × 2	2[C—(C_D)(C)(H_2)]	−4.76 × 2
2[C—(N_A)(C)(H_2)]	−6.0 × 2	2[C_D—(C)(H)]	8.59 × 2
ΔH_f^0(GMF) = 42.0		ΔH_f^0(GMF) = 7.66	
$\Delta H_f^0(N_2)$ = 0.0		ΔH_f^0(CH≡CH) = 54.19	
		ΔH_{ex}^0(CH≡CH) = 46.53	

$$\Delta H_{ex}^0(N_2) = \Delta H_f^0(N_2) - \Delta H_f^0(\text{GMF}) = -42.0$$

SCHEME 1

tion if products and reactants are nonpolar. Whereas solvent can alter the kinetics quite considerably, particularly in the case of dipolar intermediates or dipolar transition states on a path to nonpolar products, it has a much less significant effect on the thermodynamics. If a solvent effect is severe, one can always calculate corrections for solvation differences between starting materials and products with greater ease than for transition states.

If similar extrusions occur by a concerted mechanism, then differences in ΔH_{ex}^0 may be used to predict or explain differences in $\Delta H_{obs}^{\ddagger}$, using the Hammond Postulate (5), thereby achieving a bridge between thermodynamics and kinetics. Even if the extrusion mechanisms are not concerted, or are not even the same, the Relative Extrusibility Scale may still be anchored to give approximate reaction enthalpies.

By way of example, consider the cases for extrusion of molecular nitrogen versus its carbon analogue, acetylene. For nitrogen, Scheme 1 shows the generalized azo compound, then sums the appropriate set of group equivalents to give ΔH_f^0 (GMF:N_2). Following eq. [5], the relative extrusibility of N_2, ΔH_{ex}^0 (N_2) is found to be −42.0 kcal mol^{-1}.

On the other side of Scheme 1, the generalized olefin is subjected to a similar calculation to yield the relative extrusibility of acetylene as 46.5 kcal. This little example shows that, all other factors being equal, the extrusion of molecular nitrogen (formation of an NN triple bond) from azo compounds is 88.5 kcal more exothermic than extrusion of acetylene (formation of a CC triple bond) from olefins.

Similar calculations may be performed for a number of different fragments (although not all the ones of interest, since key group equivalents are not available). Twenty-four such extrusions spanning 150 kcal have been compiled in Table 1. These ΔH_{ex}^0 do not correlate at all with the heat of formation of the extruded fragment; both ΔH_f^0 (GMF) and ΔH_f^0(X) are important. The last two columns of the table show the effect of methyl or phenyl substitution on ΔH_{ex}^0, in cases where enough group equivalents exist. Substitution typically lowers ΔH_{ex}^0 by conjugation with the newly-formed bond: a methyl group is worth 2 to 4 kcal; a phenyl typically 8–13. These corrections are reasonably significant, but are not available for key cases. In those instances, typical values for $\delta\Delta H$ may be used, but this will introduce additional error into the estimate of ΔH_{ex}^0.

In their 1967 book on extrusion reactions, Duke and Stark empirically ranked the ease of extrusion of inorganic molecules as $N_2 > CO_2 \gtrsim CO \gtrsim SO > SO_2 > O_2 \gtrsim S > O$, provided the mechanisms remain comparable (4). In reasonable agreement, Table 1 quantifies their qualitative observations.

Intergroup Interaction, ΔH_{int}^0 (Table 2)

Another important factor which must be considered when attempting thermodynamic estimates is the effect of intergroup interaction or resonance. This correction factor is employed when the extruded fragment is not bound to two CH_2 groups (as defined in the GMF), but rather is adjacent to another functional group. Intergroup interactions may either stabilize or destabilize a molecule, thereby affecting ΔH_{ex}^0. For example, if two adjacent functional groups X and Y are both -CH=CH-, then a resonance interaction will lower the energy of R—X—Y—R, increasing ΔH_{ex}^0(X) or ΔH_{ex}^0(Y). On the other hand, in peroxides (X = Y = O) and hydrazines (X = Y = NR) adjacency is destabilizing, and ΔH_{int}^0 is positive (Table 2).

Interfragment interaction corrections, ΔH_{int}^0, are defined here as the difference between heats of formation of a GMF containing the two functional groups in contact and one with an intervening 2-carbon bridge. For example, ΔH_{int}^0 (C=O/O) = ΔH_f^0 (**2**) − ΔH_f^0 (**3**) = −91.5 + 67.9 = −23.6 (eq. [6]; row 1, column 4 in Table 2).

[6]

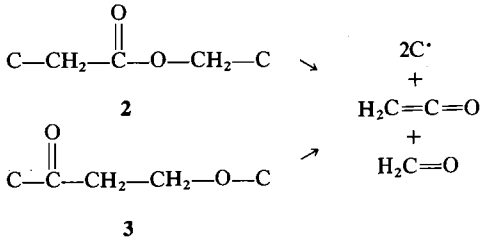

2 **3**

TABLE 1. Relative heats of extrusion (ΔH_{ex}^0) of various molecular fragments[a]

Case	-X- in GMF	ΔH_f^0(GMF)	X	$\Delta H_f^0(X)_{obs}$	ΔH_{ex}^0	$\delta\Delta H_{Me}$[b]	$\delta\Delta H_{Ph}$[c]
a	-N=N-	42.0	N_2	0	−42.0		
b	-C(=NH)-O-	−16.76	HNCO	−27.90[d]	−11.15		—
c	-C(=O)-O-	−91.5	CO_2	−94.05	−2.55		
d	-CH(OH)-O-	−90.43	HCOOH	−90.5	−0.1		—
e	-CH(OCH_3)-O-	−85.93	$HCOOCH_3$	−83.6	2.3	−2.4	—
f	-C(CH_3)(OAc)-O-	−145.33	$H_3CCOCCH_3$ (O O)	−137.9	7.4		
g	-C(CH_3)(CH_3)-O-	−63.23	$(CH_3)_2C{=}O$	−51.7	11.5		
h	-CH=N-	18.53	HCN	32.3	13.8	−4.6	−2.1
i	-S(=O)(=O)-	−85.1	SO_2	−70.9	14.2		
j	-C(=O)-	−41.8	CO	−26.4	15.4		
k	-C(CH_2)-O-	−26.97	$H_2C{=}C{=}O$	−11.4	15.6		—
l	-CH_2-O-	−44.33	$H_2C{=}O$	−26.0	18.3	−3.4	−12.7
m	-NH-C(=O)-	−49.0	HNCO	−27.90[d]	21.1		—

System **2** contains the same atoms as **3**, but is stabilized by 23.6 kcal by the interaction between carbonyl and oxygen groups. Both **2** and **3** may, in principle, decompose to the same products by eliminating one ketene plus one formaldehyde molecule in a multiextrusion reaction, but decomposition of **3** will be 23.6 kcal less endothermic (or more exothermic) than decomposition of **2**.

Significantly, ΔH_{int}^0 is only taken into consideration of ΔH_{ex}^0 when the bond between X and Y in R—X—Y—R is broken in the reaction. Again, not all the desirable numbers are available, and the estimation of missing values, even when facilitated by Table 2, can be somewhat crude.

Thermal Fragmentation Patterns of 5-Membered Ring Diazenes

In the second part of this paper, the concepts advanced in the previous section are developed to permit thermodynamic estimates which contribute to understanding the variety of product types arising from fragmentation of 5-membered ring diazenes. Among the product patterns observed in this series, three major fragmentation routes emerge: 3-membered ring formation, 1,3-dipolar cycloreversion, and 3-piece ($\sigma 2s + \sigma 2s + \sigma 2s$) fragmentation (Scheme 2).[5] In focussing on these three major routes, other

[5]It is possible that for certain cases, 3-piece fragmentation is not a distinct third option, but rather that the products result from further decomposition of a three-membered ring or diazo species formed in an earlier step. In none of the known cases of 3-piece fragmentations of these diazenes does the experimental evidence favour the intermediacy of a 3-membered ring. On the other hand, highly reactive diazo species like $A{=}\overset{+}{N}{=}\bar{N}$ could be short lived, high energy intermediates (e.g. $O{=}C{=}\overset{+}{N}{=}\bar{N}$) on the way to final products (e.g. CO + N_2). It is important to remember, however, that the present focus is on the insight *thermodynamics* offers, and therefore, the kinetic and mechanistic details of how the products are ultimately obtained are irrelevant to the present discussion.

Can. J. Chem. Downloaded from www.nrcresearchpress.com by 210.87.254.40 on 09/06/12
For personal use only.

TABLE 1 *(Concluded)*

Case	-X- in GMF	ΔH_f^0(GMF)	X	$\Delta H_f^0(X)_{obs}$	ΔH_{ex}^0	$\delta\Delta H_{Me}$[b]	$\delta\Delta H_{Ph}$[c]
n	$-\overset{\overset{NCH_3}{\|\|}}{C}-$	11.92	$H_3C\overset{+}{N}\equiv\bar{C}$	35.9	(24.0)[e]		—
o	-O—O-	−25.2	$^3O_2$	0	25.2[f]		
p	$-CH_2NH-$	−2.73	$H_2C{=}NH$	22.6[g]	25.3	N: −4.0 C: 0.9	−10.4 —
q	$-\overset{\overset{O}{\|\|}}{S}-$	−29.85	SO	1.5	31.4		
r	$-CH_2CH_2-$	−19.72	$H_2C{=}CH_2$	12.5	32.2	−1.1	−3.2
s	$-CH_2N{=}N-$	37.07	$H_2C{=}\overset{+}{N}{=}\bar{N}$	71	33.9		—
t	$-CH_2\overset{\overset{O}{\|\|}}{C}-$	−46.73	$H_2C{=}C{=}O$	−11.4	35.3		—
u	$-\overset{\overset{S}{\|\|}}{C}-$	17.6[h]	CS	55 ± 5	37.4		
v	$-CH_2—S-$	−5.1	$H_2C{=}S$	33.4[i]	38.5		—
w	$-CH{=}CH-$	7.66	$HC{\equiv}CH$	54.19	46.5	−2.2	+2.0
x	$-CH_2-$	−14.79	$^3CH_2$	86 ± 3	101[j]		−13.5

[a] See text for definitions and discussion. All units kcal mol^{-1}.
[b] The effect of methyl substitution on ΔH_{ex}^0.
[c] The effect of phenyl substitution on ΔH_{ex}^0. In cases where missing data prevent calculation, a dash is found.
[d] Reference 37.
[e] Due to the lack of available data for unsubstituted compounds, this X contains a methyl group.
[f] $\Delta H_{ex}^0(^1O_2) = \Delta H_{ex}^0(^3O_2) + 22$ kcal mol^{-1} (ref. 6).
[g] Calculated from group equivalents.
[h] Benson's compilation lists only one thiocarbonyl group equivalent, [CS—(N)$_2$] for thiourea, which is an assigned value (2). A crude estimate for the difference in ΔH_f^0 between a thiocarbonyl compound and the corresponding carbonyl compound may be obtained from the following (admittedly poor) models: $\Delta H_f^0(CS_2) - \Delta H_f^0(COS) = 61.9$; $\Delta H_f^0(COS) - \Delta H_f^0(CO_2) = 60.2$; $\Delta H_f^0(HNCS) - \Delta H_f^0(HNCO) = 57.9$; and $\Delta H_f^0(\text{thiourea})_s - \Delta H_f^0(\text{urea})_s = 57.6$. The average is 59.4 ± 2 kcal, giving [CS—(X)(Y)] ≡ [CO—(X)(Y)] + 59.4, assuming [X—(CS)( )...] = [X—(CO)( )...].
[i] Following footnote *h* above: $\Delta H_f^0(H_2CS) \simeq \Delta H_f^0(H_2CO) + 59.4 = -26.0 + 59.4 = 33.4$.
[j] $\Delta H_{ex}^0(^1CH_2) = \Delta H_{ex}^0(^3CH_2) + 8$ kcal mol^{-1} (ref. 7).

less frequent products (olefins from H or R migration in biradicals, bicyclic products, any products from bimolecular mechanisms, etc.) are ignored. The present discussion is meant to be quite general, and enthalpy estimates for specific alternative processes can usually be obtained in the conventional way.

Table 3 summarizes the various experimental observations on thermal fragmentation patterns of 14 types of 5-membered ring diazenes. Δ^1-Pyrazolines (**4**), Δ^3-1,3,4-oxadiazolines (**5**), and thiadiazolines (**6**) give 3-membered rings with stereochemistries consistent with the intervention of 1,3-biradicals. Although these rings are often synthesized by 1,3-dipolar cycloadditions, the synthesis is usually not reversible, except in very rare cases involving extremely large steric effects or very strongly-electron-withdrawing substituents. In contrast to these three systems, 3-*H* pyrazoles (**7**) are thermally stable. The less well-known series of carbonyl diazenes, **8** to **10**, is characterized by very facile 3-piece fragmentation, without the intervention of 3-membered rings. From pyrazoline **8**, the products are nitrogen, carbon monoxide, and olefin, in good yield at low temperature. The additional double bond in **9** lowers the yield of the thermal unimolecular process to form an alkyne, but the other two processes have been ruled out. In contrast to the case for structurally similar **9**, 3-piece fragmentation of **10** is a high yield process.

Warkentin and co-workers (26–34) have shown that a series of 3 triazolines (**12–14**) gives exclusive 3-piece fragmentation, whereas iminooxadiazoline **15**

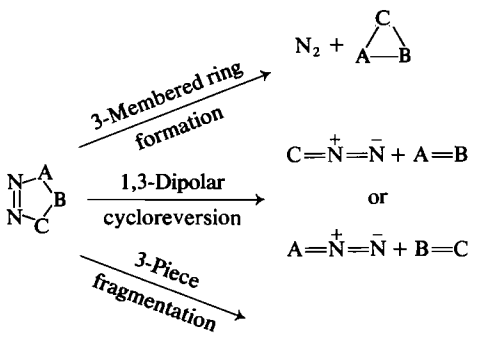

$C + A{=}B + N_2$ or $A + B{=}C + N_2$

A,B,C = CO, CR_2, O, S, CS, Se, NR, C=NR,...

SCHEME 2. Thermal fragmentation patterns of 5-membered ring diazenes

Can. J. Chem. Downloaded from www.nrcresearchpress.com by 210.87.254.40 on 09/06/12
For personal use only.

Can. J. Chem. Downloaded from www.nrcresearchpress.com by 210.87.254.40 on 09/06/12
For personal use only.

TABLE 2. Intergroup interactions (ΔH_{int}^0) in R—X—Y—R[a]

X	Y: O	NH	C=C			
O	37.4	—	−7.3	−23.6	−17.6	42.8
NH		11.0	—	−21.2[b]	—	—
C=C			−3.6	−8.8	−3.4	−2.1
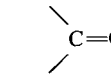				4.4	5.1	−7.1
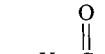					5.8	−1.1
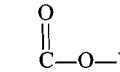						48.2

[a]See text for definitions and discussion. All values kcal mol^{-1}. Dashed lines indicate unavailable group values. Negative numbers are stabilizing interactions which raise ΔH_{ex}^0.
[b]ΔH_{int}^0(NPh/C=O) = −16.4.

and oxadiazolinone **16** demonstrate competing independent mechanisms for 1,3-dipolar cycloreversion and 3-piece fragmentation. In examining these systems over the past decade, it has been very unclear why such highly varied reactivity patterns have been observed. What gross molecular features influence the direction of fragmentation from case to case? Why do triazolines **12** to **14** not undergo 1,3-dipolar cycloreversion? Why do more highly-functionalized pyrazolines not form 3-membered rings? Why is there competition in some systems but not others?

Mechanistic work on **15** and **16** has determined how factors such as temperature, solvent, and substituent can affect the (kinetic) competition within a molecular type (30, 32–34), but it would be useful to develop generalizations capable of rationalizing all of the diverse chemistry in Table 3, and predicting product types for as-yet-unknown cases.

In this regard, it is extremely useful to examine the thermochemistry of the three major competitive fragmentation routes in these cyclic diazenes. To do this, however, is not simple; some potential 3-membered ring products are experimentally unknown, and only two relevant heats of formation have been reported: those of 3,3,5,5-tetramethylpyrazoline (**4***a*; ref. 35) and 5,5-dimethyloxadiazolinone (**16***a*; ref. 33). Many of the systems in Table 3 are too complex for normal additivity schemes to work; too many group equivalents are not available. Most of these problems can be overcome by applying the Relative Extrusibility Scale and the Table of Interfragment Interactions. These numbers can be manipulated with the scarce available data and with data for appropriate model compounds to estimate thermodynamic quantities of interest for these diazenes and their reactions. The reliability of the method will be established by a suitable test, estimating the heat of formation of **16***a*.

The Breakdown of Ordinary Additivity

Engel (35) measured the gas phase heat of formation of **4***a* as 9.4 kcal mol^{-1}, from which one may readily calculate, using ordinary additivity rules, the value for the unsubstituted pyrazoline (**4**) with eq. [7]. With this value, it is a routine matter to calculate the reaction enthalpies for the 5 different processes in Scheme 3.

[7] $\Delta H_f^0(\mathbf{4}) = \Delta H_f^0(\mathbf{4a}) - 4[\text{C—(C)(H)}_3] - 2[\text{C—(N}_A\text{)(C)}_3] + 2[\text{C—(N}_A\text{)(C)(H)}_2]$
$= 9.4 - 4(-10.20) - 2(-3.0) + 2(-6.0) = 44.2$ kcal

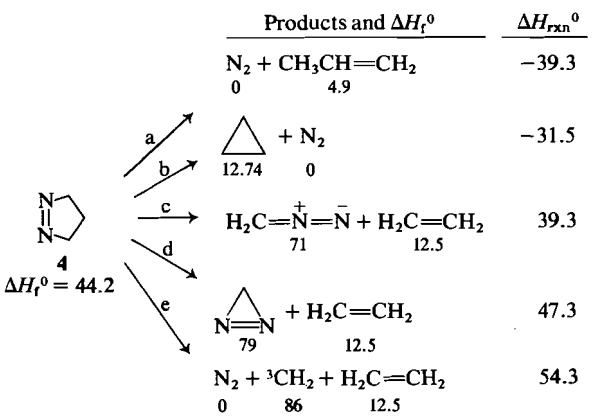

SCHEME 3. Thermochemistry of Δ^1-pyrazoline

TABLE 3. Classification of thermal fragmentation patterns of 5-membered ring diazenes

	Ring type[a]	3-Membered ring formation	1,3-Dipolar cycloreversion	3-Piece fragmentation	Temperature[b] comments, ref.
4		Dominant	—	—	200–250°C Some olefin (8–11)
5		Dominant	Only with CF_3 substituent (12)	—	30–120°C Other reactions (12–14)
6		Dominant	Only with extremely bulky substituent (15)	—	50–100°C (15, 16)
7		—	—	—	Thermally stable (17)
8		Ruled out	—	Almost quantitative N_2 + CO + olefin	−30°C Stereospecific (18–22)
9		Ruled out	—	1.3% N_2 + CO + alkyne	20°C Much dimeric and polymeric material (23)
10		—	—	95–99% N_2 + CO +nitrile	20°C (24)
11		—	Only observed product, trapped in unstated yield (25)	—	150°C (25)
12: Z = O **13**: Z = S **14**: Z = NPh		—	—	Quantitative :C=Z + N_2 +	100–200°C (26–28)
15		—	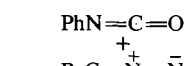	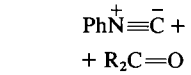	100°C Competition between independent mechanisms (29–31)
16		Ruled out	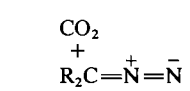	N_2 + CO + R_2C=O	85°C Competition between independent mechanisms (32–34)

[a]Specific substituents are not shown on these ring type structures unless only one compound was studied. In spite of these generalized structures, the parent (unsubstituted) compounds have seldom been isolated and studied. Alkyl or aryl substitution adjacent to the N=N is necessary to prevent tautomerization to cyclic hydrazone-like derivatives.
[b]In some cases, particularly for **8**, **9**, and **10**, the reaction temperature actually refers to the temperature at which the compound was formed *in situ* (usually by oxidation) and subsequently rapidly decomposed. As such then, these temperatures offer only a rough guide to relative reactivity.

Can. J. Chem. Downloaded from www.nrcresearchpress.com by 210.87.254.40 on 09/06/12
For personal use only.

Clearly, the thermodynamics are only favourable for olefin or 3-membered ring formation (paths a and b, respectively), which are exothermic by 30 to 40 kcal. Indeed, these are the only types of observed products in the vast majority of simple pyrazoline thermolyses. Other potential fragmentation routes, such as diazoalkane formation (path c), diazirine formation (path d), and 3-piece fragmentation (path e), are disfavoured by some 70–100 kcal, and are too endothermic to be feasible. The thermodynamics account for the chemistry. Such a successful result urges further application, for example, to oxadiazoline **5**, Table 3. Unfortunately, additivity eq. [8] cannot be solved because the group equivalent [C—(O) (N_A) $(H)_2$] is unknown. The situ-

[8] $\Delta H_f^0(\mathbf{5}) = \Delta H_f^0(\mathbf{4}) - 2[C—(N_A)(C)(H)_2] - [C—(C)_2(H)_2] + 2[C—(O)(N_A)(H)_2] + [O—(C)_2]$

ation worsens when one attempts to calculate the heat of formation of dimethyloxadiazolinone (**16***a*; Scheme 4). In this case, half of the required group equivalents are not known, and there is no way to estimate them. Group values are not intrinsic properties; Benson's scales are anchored by numerous assigned values, making it extremely hazardous to estimate values for missing groups because there are no patterns among the tabulated numbers. This is a major drawback of conventional application of Benson's additivity method. What can be done?

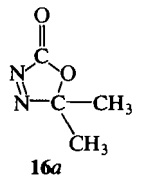

16*a*

$[O—(CO)(C)] = -43.1$
$[CO—(O)(N_A)] = ?$
$[N_A—(CO)] = ?$
$[N_A—(C)] = 27.0$
$[C—(O)(N_A)(C)_2] = ?$
$2[C—(C)(H)_3] = -10.2 \times 2$
Ring strain = ?
$\Delta H_f^0 = ???$

SCHEME 4. Heat of formation of dimethyloxadiazolinone

Thermodynamic Cycles Based on the Relative Extrusibility Scale

Equation [9] represents a thermodynamic cycle in which model pyrazoline **4***a*, whose heat of formation has been measured, extrudes isobutene, while the target molecule extrudes CO_2 in the other direction. Equations [10]–[12] summarize the algebra (recalling the definition in eq. [5] for the final step) to express the heat of formation of the target molecule in terms of GMF switches and an intergroup interaction term. Although Table 2 does not contain a value for ΔH_{int}^0 (N=N/CO_2), this method has the advantage that it is much easier to estimate this value by examining the other systems in Table 2 than it is to estimate 3 missing group equivalents in Scheme 4. At the present time, the approximation ΔH_{int}^0 (N=N/CO_2) ~ ΔH_{int}^0 (C=C/CO_2) = −3.4 kcal seems the most reasonable. This gives the numerical result at the end of eq. [12].

[9] 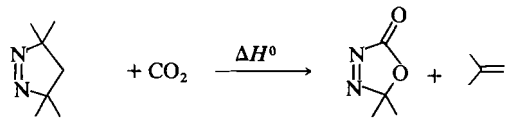

	Model (**4***a*)		Target (**16***a*)	
ΔH_f^0:	9.4	−94.05	?	−4.04

[10] $\Delta H^0 = \Delta H_f^0$ (target) + ΔH_f^0(>=) − ΔH_f^0 (CO_2) − ΔH_f^0 (model)

$= \Delta H_{ex}^0$(>=) − ΔH_{ex}^0(CO_2) + ΔH_{int}^0(N=N/CO_2)

so:

[11] ΔH_f^0 (target) = ΔH_{ex}^0(>=) − ΔH_{ex}^0(CO_2) + ΔH_{int}^0(N=N/CO_2) − ΔH_f^0(>=) + ΔH_f^0(CO_2) + ΔH_f^0 (model)

[12] ΔH_f^0 (target) = ΔH_f^0 (model) + ΔH_f^0 (GMF: new fragment) − ΔH_f^0 (GMF: old fragment) + ΔH_{int}^0

$= 9.4 + \Delta H_f^0$(C—CH_2—COO—CH_2—C) − ΔH_f^0(C—CH_2—C(Me)$_2$—CH_2—CH_2—C) + ΔH_{int}^0(N=N/CO_2)

$= 9.4 + (-91.5) - (-34.69) + (-3.4) = -50.8$

Can. J. Chem. Downloaded from www.nrcresearchpress.com by 210.87.254.40 on 09/06/12
For personal use only.

Can. J. Chem. Downloaded from www.nrcresearchpress.com by 210.87.254.40 on 09/06/12
For personal use only.

One is not restricted to any particular model, and Scheme 5 shows the results of similar calculations for 8 different models for oxadiazolinone, ranging from pyrazoline **4***a*, through various oxygenated rings, to cyclopentene and cyclopentane. Even the hydrocarbons (which require two fragment swaps) are reasonable models for **16***a*.

All eight models yield very similar estimates[6] for the heat of formation of the target molecule, the average being -50 ± 3 kcal, which is within experimental error of the measured value (33). The successful application of simple models, used with either one or two fragment switches, has severely challenged the GMF method, proving its utility in cases where errors of up to 5 kcal can be tolerated.

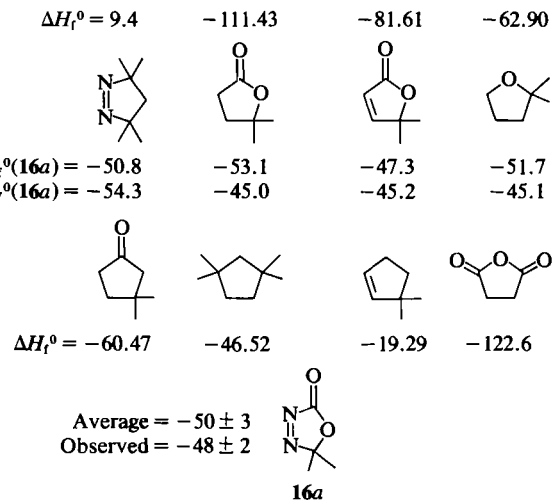

16*a*

SCHEME 5. Estimates for the heat of formation of dimethyloxadiazolinone from various models (34)

Reaction Enthalpies for 5-Membered Ring Diazenes

Similar calculations, summarized in the Appendix, have been performed for the other 5-membered ring diazenes in Table 3, permitting the first examination of some of their interesting thermochemistry. Table 4 contains the estimated reaction enthalpies for the three different processes for all 14 systems; circled values correspond to major observed routes.

As discussed earlier, pyrazoline (**4**) fragments to cyclopropane, releasing more than 30 kcal, while 1,3-dipolar cycloreversion and 3-piece fragmentation, at 39 and 54 kcal, are too endothermic to be feasible. Likewise, oxadiazoline (**5**) and thiadiazoline (**6**) form 3-membered rings by very exothermic processes, and the other alternatives are thermodynamically forbidden, at 25 to 60 kcal.

On the other hand, 3-*H* pyrazole (**7**) is much more stable because cyclopropene formation is thermoneutral, disfavoured by 30–40 kcal relative to analogous processes in systems **4**–**6**. Its alternatives are even worse.

Estimates for the three carbonyl diazenes **8**–**10** demonstrate that the observed 3-piece fragmentation is thermodynamically favoured. Thermal decomposition of pyrazolinone **8** to N_2 plus CO plus olefin is exothermic by 22 kcal. Although cyclopropanone formation is also slightly exothermic (by 10 kcal), it is still much less favourable than cyclopropane formation from pyrazoline, and would not be expected to compete with 3-piece fragmentation of **8** at the lower temperature.

The presence of the double bond in **9** shifts all values upwards from those for **8**, much the same as the result of switching to **7** from **4**. In this example, 3-piece fragmentation is roughly thermoneutral, but yield was only 1.3% (Table 3). Cyclopropenone is less accessible than cyclopropanone, and it is not possible to write a 1,3-dipolar cycloreversion without invoking an unlikely, high-energy N_2CO intermediate.

Nitrile formation by 3-piece fragmentation of **10** is also very exothermic, by 35 kcal. Table 1 shows that extrusion of HCN is one of the more favourable processes. The bracketed value of 14 kcal under 3-membered ring formation reflects the assumption that this value equals that for **9** (see Appendix).

Interestingly, phenyl substituted methylene oxadiazoline (**11**) undergoes thermoneutral 1,3-dipolar cycloreversion in preference to exothermic (by 14 kcal) 3-membered ring formation. However, the estimates predict that without C5 phenyl substitution, 1,3-dipolar cycloreversion and 3-piece fragmentation will be much more endothermic, perhaps inaccessible (footnote *c* in Table 4).

Now the discussion narrows to **12**–**16**, which spurred our initial interest. Like systems **8**–**10**, triazolines **12**–**14** have very exothermic 3-piece fragmentation routes. There are almost no data available for thiocarbonyl compounds, so that the error in the values for **13** is likely quite large, although it apparently fits the patterns. In this series, as in **8** and **11**, it seems that 3-membered ring formation is insufficiently exothermic to compete.

The last two systems in Table 4 show the interesting competition between independent mechanisms for 1,3-dipolar cycloreversion and 3-piece fragmentation. It is gratifying to see that amongst all the

[6]Some of these differences reflect differences in strain energy for the 9 systems in Scheme 5. This can be seen from the known ring strain contributions (1): THF (6.7), cyclopentanone (6.0), succinic anhydride (1.1). Subtraction of this factor would reduce the *scatter* in ΔH_f° (target), but it would give no greater *certainty* to that value because the ring strain contribution in **16***a* is unknown. Therefore, it is preferable to include this uncertainty in the apparent scatter in Scheme 5.

Can. J. Chem. Downloaded from www.nrcresearchpress.com by 210.87.254.40 on 09/06/12
For personal use only.

TABLE 4. Reaction enthalpy estimates for thermal fragmentation of 5-membered ring diazenes[a]

Compound		ΔH^0 (3-membered ring formation)	ΔH^0 (1,3-dipolar cycloreversion)	ΔH^0 (3-piece fragmentation)
4		(−31.5)	39	54
5		(−32)	25	40
6		(−39)	45	60
7		−1	58	73
8		−10	51	(−22)
9	R = Ph	14	Certainly ≫ 0	(2[b])
10		(14)	Certainly ≫ 0	(−35)
11	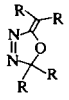 R = Ph[c]	−14	(0)	15[d]
12	Z = O	−3	12	(−31)
13	Z = S	(−3)	(12)	< (−8)
14	Z = NPh	(−3)	19	(−23)
15	*a* R = Me	(−14)	(−9)	(−21)
	b R = Ph	(−14)	(−26)	(−38)
16	*a* R = Me	2	(1)	(−30)
	b R = Ph	2	(−16)	(−47)

[a]Estimates refer to the gas phase (kcal mol^{-1}). Circled values correspond to observed products (Table 3). Values in parentheses are assumed the same as some other value in the table. See the Appendix for details.
[b]For R = H (**9***a*) this is −2 kcal.
[c]For R = H (**11***a*) these values are: −14, 24, and 39 kcal.
[d]This value, based on forming diphenylcarbene, assumes that the difference between 1,3-dipolar cycloreversion and 3-piece fragmentation in **11** is the same as in **4**, **5**, **6**, and **7**.

molecules in the table, only these two satisfy apparent thermodynamic criteria for both reactions; three-piece fragmentation is exothermic by the usual large amount and 1,3-dipolar cycloreversion is exothermic or thermoneutral. The unobserved 3-membered-ring-forming reactions, although slightly exothermic, are insufficiently so to compete with the other two processes.

As the details in the Appendix show, many of the heats of reaction appearing in Table 4 are crude and numerous approximations were necessary. Even though some of the final results may be in error by

Can. J. Chem. Downloaded from www.nrcresearchpress.com by 210.87.254.40 on 09/06/12
For personal use only.

more than ± 5 kcal, the differences among the numbers from system to system, and from reaction to reaction, are much greater, and the following gross trends are apparent: 3-membered ring formation must be exothermic by some 30 kcal or more in order for it to be important, but thermoneutral or exothermic 1,3-dipolar cycloreversion or 3-piece fragmentation can contribute to the observed products.

By identifying processes which are too endothermic to be reasonable, the reaction enthalpy estimates obtained from the Relative Extrusibility Scale are able to account for the gross features of the fragmentation patterns of 5-membered ring diazenes. *As thermochemical information, however, such data cannot explain why two processes, which differ in exothermicity by* 10–30 *kcal in systems* **15** *and* **16**, *have transition states of similar energy.* That is a kinetic problem which is no doubt related to the fact that the two processes have different mechanisms.

On Entropy and Temperature Dependence

As the introduction to the Relative Extrusibility Scale noted, entropy contributions cancel when comparing *similar* extrusions, for example, epoxide vs. cyclopropane formation, and differences in ΔH^0 parallel differences in ΔG^0. However, it may seem that comparing 2-piece to 3-piece fragmentations in Scheme 3 and Table 4 is rather akin to comparing apples to oranges. Typical values of the thermodynamic entropy change on forming two fragments from a 5-membered ring are about $+40$ eu. For 3-piece fragmentation this rises to about $+70$ eu. Should this difference be accounted for when estimating the thermodynamic driving force? Is it meaningful to compare ΔH^0 for 3-membered ring formation from pyrazolinone at -25°C to that for pyrazoline at 250°C?

In spite of large thermodynamic entropy changes associated with multipiece fragmentations, $\Delta S^{\neq}$ is usually quite small for these processes, on the order of 10 eu or less, and sometimes negative. This apparently reflects the fact that, regardless of the mechanism, the ring of atoms is largely unbroken at the transition state. Since it is the activation entropy which affects the competition between processes, and since these activation entropies are all similar, and smaller than the thermodynamic entropy changes, it is reasonable to view these irreversible fragmentation reactions as enthalpy driven. This differs from the situation in the reverse direction, where the driving force for cycloadditions is the free energy change. Because $\Delta S^{\neq}$ is large and negative, both enthalpy and entropy contribute to the barrier for cycloaddition.

Analogous arguments greatly reduce the effect of the heat capacity term to the subjective concept of "*driving force*", leaving ΔH^0, calculated at 25°C, as a reasonably valid index of thermodynamic influence over fairly wide temperature ranges, perhaps even the 300° span in Table 3. In most cases then, one does not have to be too concerned with entropy factors when comparing reactions carried out at different temperatures, or when comparing reactions which give different numbers of products.

Acknowledgements

The Natural Sciences and Engineering Research Council of Canada supported this work through an operating grant and through postgraduate scholarships to A.J.P.

1. S. W. Benson, F. R. Cruickshank, D. M. Golden, G. R. Haugen, H. E. O'Neal, A. S. Rodgers, R. Shaw, and R. Walsh. Chem. Rev. **69**, 279 (1969).
2. S. W. Benson. Thermochemical kinetics. Wiley–Interscience, New York, NY. 1976.
3. J. D. Cox and G. Pilcher. Thermochemistry of organic and organometallic compounds. Academic Press, New York, NY. 1970.
4. A. J. Duke and B. P. Stark. Extrusion reactions. Pergamon Press, Oxford, U.K. 1967.
5. G. S. Hammond. J. Am. Chem. Soc. **77**, 334 (1955).
6. F. A. Cotton and G. Wilkinson. Advanced inorganic chemistry. 3rd ed. Wiley–Interscience, New York, NY. 1972.
7. C. Wentrup. Tetrahedron, **30**, 1301 (1974).
8. R. J. Crawford and A. Mishra. J. Am. Chem. Soc. **88**, 3963 (1966).
9. R. J. Crawford and H. Tokunaga. Can. J. Chem. **52**, 4033 (1974).
10. O. P. Strausz, J. W. Lowa, and H. E. Gunning. *In* Comprehensive chemical kinetics. Vol. 5. *Edited by* C. H. Bamford and C. F. H. Tipper. Elsevier, Amsterdam. 1972. Chapt. 5. p. 566.
11. B. H. Al-Sader and R. J. Crawford. Can. J. Chem. **46**, 3301 (1968).
12. N. Shimizu and P. D. Bartlett. J. Am. Chem. Soc. **100**, 4260 (1978).
13. R. W. Hoffmann and H. J. Luthardt. Chem. Ber. **101**, 3861 (1968).
14. D. W. K. Yeung, G. A. MacAlpine, and J. Warkentin. J. Am. Chem. Soc. **100**, 1962 (1978).
15. F. Cordt, R. M. Frank, and D. Lenoir. Tetrahedron Lett. 505 (1979).
16. J. Buter, S. Wassenaar, and R. M. Kellog. J. Org. Chem. **37**, 4045 (1972).
17. G. L. Closs and W. A. Boll. J. Am. Chem. Soc. **85**, 3904 (1963).
18. W. Nagata and S. Kamata. J. Chem. Soc. C, 540 (7970).
19. J. E. Herweh and R. M. Fantazier. Tetrahedron Lett. 2101 (1973).
20. B. T. Gillis and R. Weinkam. J. Org. Chem. **32**, 3321 (1967).
21. E. M. Kosower, B. Pazhenchevsky, and E. Hershkowitz. J. Am. Chem. Soc. **100**, 6516 (1978).
22. R. H. Kent and J.-P. Anselme. Can. J. Chem. **46**, 2322 (1968).
23. C. W. Rees and M. Yelland. J. Chem. Soc. Perkin Trans. I, 221 (1973).
24. B. T. Gillis and J. G. Dain. J. Org. Chem. **36**, 518 (1971).
25. C. J. Michejda. Tetrahedron Lett. 2281 (1968).

26. L. M. CABELKOVA-TAGUCHI. Ph.D. Thesis. Department of Chemistry, McMaster University, Hamilton, Ont. 1977.
27. D. C. FROST, N. P. C. WESTWOOD, N. H. WERSTIUK, L. CABELKOVA-TAGUCHI, and J. WARKENTIN. Can. J. Chem. **55**, 3677 (1977).
28. L. CABELKOVA-TAGUCHI and J. WARKENTIN. Can. J. Chem. **59**, 100 (1981).
29. P. R. WEST. Ph.D. Thesis. Department of Chemistry, McMaster University, Hamilton, Ont. 1967.
30. P. R. WEST and J. WARKENTIN. J. Org. Chem. **34**, 3233 (1969).
31. A. M. CAMERON. Ph.D. Thesis. Department of Chemistry, McMaster University, Hamilton, Ont. 1972.
32. S. L. LEE, A. M. CAMERON, and J. WARKENTIN. Can. J. Chem. **50**, 2326 (1972).
33. A. J. PAINE and J. WARKENTIN. Can. J. Chem. **57**, 2681 (1979).
34. A. J. PAINE. Ph.D. Thesis. Department of Chemistry, McMaster University, Hamilton, Ont. 1979.
35. P. S. ENGEL. J. Am. Chem. Soc. **98**, 1972 (1976).
36. J. F. LIEBMAN and A. GREENBERG. J. Org. Chem. **39**, 123 (1974).
37. M. K. KARAPET'YANTS and M. L. KARAPET'YANTS. Thermodynamic constants of inorganic and organic compounds. Ann Arbor – Humphrey Science Publ., Ann Arbor, MI. 1970.

Can. J. Chem. Downloaded from www.nrcresearchpress.com by 210.87.254.40 on 09/06/12
For personal use only.

Appendix

1. Oxadiazoline **5**; *Scheme 6*

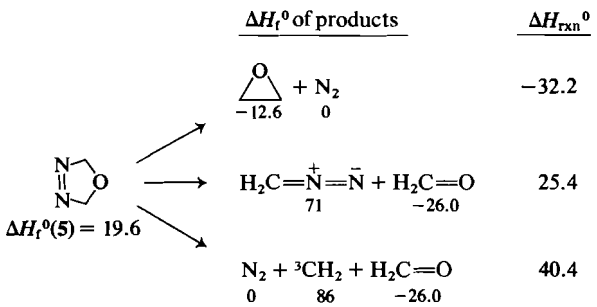

SCHEME 6. Thermochemistry of Δ^3-1,3,4-oxadiazoline

[A 1] ΔH_f^0 (**5**) $\simeq \Delta H_f^0$ (**4**) + ΔH_f^0(C—CH_2—O—CH_2—C) − ΔH_f^0 (C—$CH_2CH_2CH_2$—C)

$= 44.2 + (-39.4) - (-14.79) = 19.6$

2. Thiadiazoline **6**; *Scheme 7*

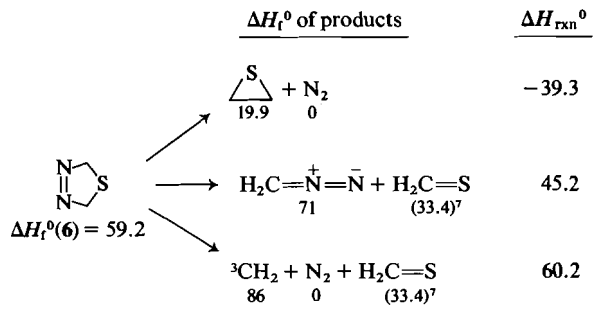

SCHEME 7

[A 2] ΔH_f^0 (**6**) $\simeq \Delta H_f^0$ (**4**) + ΔH_f^0 (C—CH_2—S—CH_2—C) − ΔH_f^0 (C—$CH_2CH_2CH_2$—C)

$= 44.2 + 0.21 - (-14.79) = 59.2$

[7]See footnotes *k* and *i* in Table 1.

*3. 3-*H *Pyrazole 7; Scheme 8*

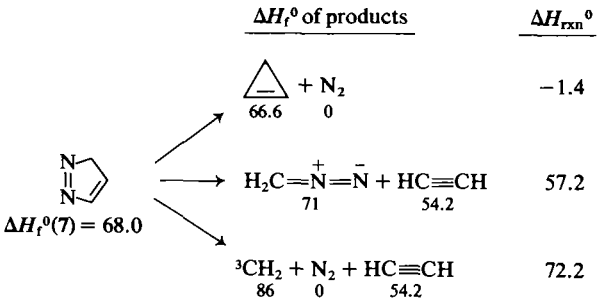

SCHEME 8

[A 3] ΔH_f° (7) $\simeq \Delta H_f^\circ$ (4) + ΔH_f° (C—CH_2—CH=CH—CH_2—C) − ΔH_f° (C—CH_2—CH_2—CH_2—CH_2—C) + ΔH_{int}° (C=C/N=N) = 44.2 + 7.66 − (−19.72) + (−3.6) = 68.0

ΔH_{int}° (C=C/N=N) assumed equal to ΔH_{int}° (C=C/C=C) = −3.6.

4. Pyrazolinone 8; Scheme 9

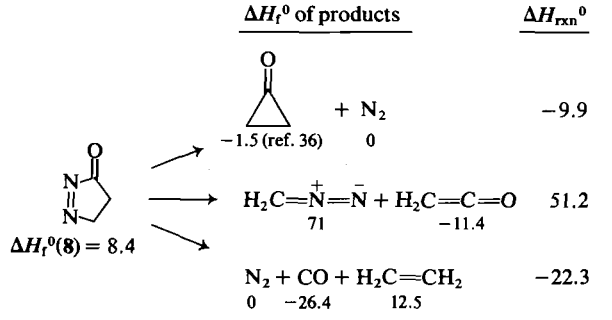

SCHEME 9

[A 4] ΔH_f° (8) $\simeq \Delta H_f^\circ$(4) + ΔH_f° (C—CH_2—CO—CH_2—C) − ΔH_f° (C—CH_2—CH_2—CH_2—C) + ΔH_{int}° (C=O/N=N) = 44.2 + (−41.8) − (−14.79) + (−8.8) = 8.4

ΔH_{int}° (C=O/N=N) assumed equal to ΔH_{int}° (C=O/C=C) = −8.8

5. Pyrazoleninone 9; Scheme 10

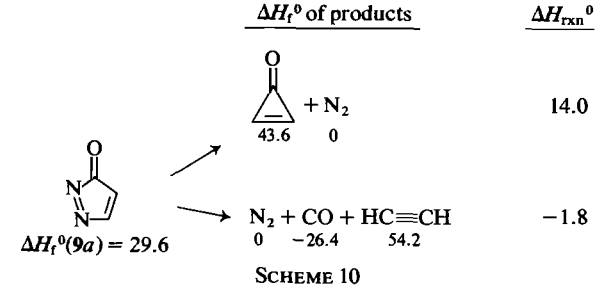

SCHEME 10

[A 5] ΔH_f° (9*a*) = ΔH_f° (8) + ΔH_f° (C—CH_2—CH=CH—CH_2—C) − ΔH_f° (C—$CH_2CH_2CH_2CH_2$—C) + ΔH_{int}° = 8.4 + 7.66 − (−19.72) + (−6.2) = 29.6

The difference between ΔH_{int}° in **9***a* and **8** is assumed to be ½ (ΔH_{int}° (C=C/N=N) + ΔH_{int}° (C=C/C=O)) = ½(−3.6 − 8.8) = −6.2. This gives **9***a* a total of 16 kcal resonance energy. Neglecting the small con-

Can. J. Chem. Downloaded from www.nrcresearchpress.com by 210.87.254.40 on 09/06/12
For personal use only.

tribution due to aromaticity, the heat of formation of cyclopropenone is estimated by eq. [6],[8] and then used in Scheme 10.

[A 6] ΔH_f^0(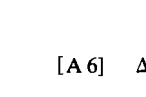) $\simeq \Delta H_f^0$(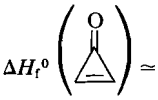) + ΔH_f^0(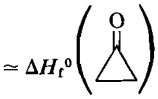) − ΔH_f^0(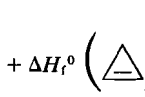) + ΔH_{int}^0(C=C/C=O)

$= -1.5$ (ref. 36) + 66.6 − 12.74 + (−8.8) = 43.6

For **9** itself, phenyl substitution would be expected to have a negligible effect on cyclopropenone formation, but an effect of $2\delta\Delta H_{Ph}^0$ for acetylene extrusion (see Table 1), raising ΔH^0 by 4.0 kcal.

*6. Triazolinone **10***

Here, 3-membered ring formation and resonance energy are assumed to be the same as for **9***a*. Then, the difference between 3-piece extrusion of **10** and **9***a* is equal to the difference between HCN and acetylene extrusion in the Relative Extrusibility Scale:

[A 7] ΔH^0 (3-pce; **10**) $\simeq \Delta H^0$ (3-pce; **9***a*) + ΔH_{ex}^0 (HCN) − ΔH_{ex}^0 (HC≡CH) = −1.8 + 13.8 − 46.5 = −34.5

*7. Methylene Oxadiazoline **11**; Scheme 11*

Assuming ΔH_{int}^0 (N=N/CO_2) $\simeq \Delta H_{int}^0$ (N=N/C=C/O):

[A 8] ΔH_f^0 (**11***a*) $\simeq \Delta H_f^0$ (**16***a*) − ΔH_f^0 (C—CH_2—CMe_2—O—CH_2—C) + ΔH_f^0 (C—CH_2CH_2—O—CH_2—C) − ΔH_f^0 (C—CH_2COOCH_2—C) + ΔH_f^0 (C—CH_2—C(=CH_2)—O—CH_2—C) = −48.0 − (−63.23) + (−44.33) − (−91.5) + (−26.97) = 35.4

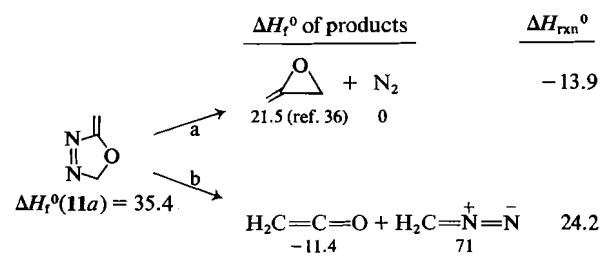

SCHEME 11

Phenyl substitution will have a negligible effect on the 3-membered ring forming reaction (path a) because no new double bonds are formed. On the other hand, phenyl groups will greatly favour 1,3-dipolar cycloreversion (path b), mostly by stabilizing the diazoalkane. Although the absence of necessary group values makes it difficult to quantify this effect, one may compare to carbonyl compounds. In the series H_2CO, PhCHO, Ph_2CO (ΔH_f^0 = −26.0, −6.0, 12.3), the second phenyl group has an effect 1.7 kcal less than the first, due in part to the nonplanarity of the rings. If one combines this fact with an assumption that $\delta\Delta H_{Ph}^0$ for diazoalkane extrusion is the same as that for ketone extrusion, then the two C5 phenyls should lower ΔH_{ex}^0 by 12.7 + 11.0 = 23.7 kcal, in the absence of any steric effect. This yields ΔH_b^0 (**11**) $\simeq$ 0.5 kcal mol^{-1}, which can be rounded down to zero by the steric effect and ketene phenyl effect.

*8. Triazolinone **12**; Scheme 12*

[A 9] ΔH_f^0 (**12**) $\simeq \Delta H_f^0$ (**16***a*) + ΔH_f^0 (C—CH_2—NPh—CH_2—C) − ΔH_f^0 (C—CH_2—O—CH_2—C) + ΔH_{int}^0 (C=O/NPh) − ΔH_{int}^0 (C=C/O) = −48.0 + 29.0 − (−39.4) + (−16.4) − (−23.6) = 27.6

In Scheme 12, ΔH_f^0 (PhNCO) $\simeq \Delta H_f^0$ (PhCHO) − ΔH_f^0 (H_2CO) + ΔH_f^0 (HNCO) = −6.0 − (−26.0) + (−27.90) = −7.9 kcal mol^{-1}. Apparently the α-lactam phenyl group is not coplanar, as in amides (36), so ΔH_{int}^0 (C=O/NPh) is lost on 3-membered ring formation. Equation [10] estimates the heat of formation of **17**.

[8]A referee has suggested that two C=C/C=O interactions should be included in eq. [6]. Although it is difficult to be certain about a unique group like cyclopropenone, interaction energies are generally not additive: ΔH_{int}^0 (C=O/O/C=O) is −23.8 kcal, but may be compared to $2\Delta H_{int}^0$ (C=O/O) = 2 (−23.6) = −47.2; and ΔH_{int}^0 (C=C/C=O/O) is −17.0 kcal, but ΔH_{int}^0 (C=C/C=O) + ΔH_{int}^0 (C=O/O) = −8.8 − 23.6 = −32.4 kcal. (Note that ΔH_{int}^0 (C=C/C=O/O) is not the same as ΔH_{int}^0 (C=C/CO_2): each slash represents a separating ethylene group in a structure analogous to **3**.) Although the interaction of three functional groups is an imperfect model for the situation in cyclopropenone, it is interesting to note that the total interaction is roughly equal to the *mean*, rather than the sum, of the two isolated interactions, apparently legitimizing the assumption made in eq. [6] of the Appendix.

Can. J. Chem. Downloaded from www.nrcresearchpress.com by 210.87.254.40 on 09/06/12
For personal use only.

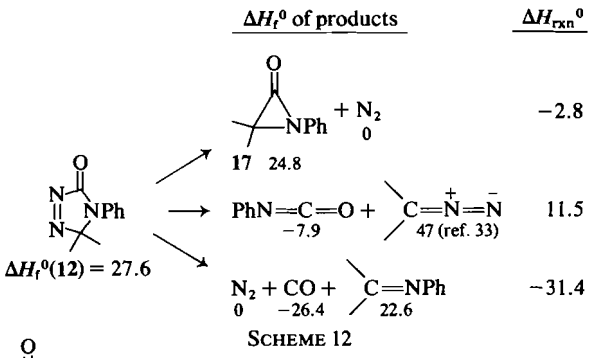

SCHEME 12

[A 10] ΔH_f° (**17**) $\simeq \Delta H_f^\circ$ (H_2C—NH) $- \Delta H_f^\circ$ (C—$CH_2CH_2CH_2$—C) $+ \Delta H_f^\circ$ (C—CH_2—CMe_2—CH_2—C) $- \Delta H_f^\circ$ (C—CH_2NHCH_2—C) $+ \Delta H_f^\circ$ (C—CH_2—NPh—CH_2—C) = 13 (ref. 36) − (−14.79) + (−29.76) − 2.2 + 29.0 = 24.8

9. Triazolinethione 13

[A 11] ΔH° (3-pce; **13**) $\simeq \Delta H^\circ$ (3-pce; **12**) $+ \Delta H_{ex}^\circ$ (CS) $- \Delta H_{ex}^\circ$ (CO) = −31.4 + 38.5 − 15.4 = −8.3

Since the resonance energy in **13** is likely to be less than in **12**, eq. [11] probably represents an upper limit. Without other group equivalents, the 3-membered ring formation and 1,3-dipolar cycloreversion must be equated to system **12**.

10. Iminotriazoline 14

[A 12] ΔH° (3-pce; **14**) $\simeq \Delta H^\circ$ (3-pce; **12**) $+ \Delta H_{ex}^\circ$ (PhN≡C) $- \Delta H_{ex}^\circ$ (CO) = −31.4 + 24.0 − 15.4 = −22.8

Equation [12] assumes that $\delta\Delta H_{Ph}^\circ \simeq 0$ for this triple bond: compare to −2.1 in HCN and +2.0 in HC≡CH. For 1,3-dipolar cycloreversion, eq. [13] proceeds analogously:

[A 13] ΔH° (1,3-dpcr; **14**) $\simeq \Delta H^\circ$ (1,3-dpcr; **12**) $- \Delta H_{ex}^\circ$ (H_2CO) $+ \Delta H_{ex}^\circ$ (H_2C=NH) = 11.5 − 18.3 + 25.3 = 18.5

Finally, 3-membered ring formation is assumed equienergic to system **12**.

*11. Oxadiazolinone 16*a

Reaction enthalpy estimates for 1,3-dipolar cycloreversion and 3-piece fragmentation have been reported earlier (33), as 1 and −30 kcal, respectively. The heat of formation of dimethyl α-lactone (**18**) is estimated in eq. [14],

[A 14] ΔH_f° (**18**) $\simeq \Delta H_f^\circ$ $- \Delta H_f^\circ$(C—$CH_2CH_2CH_2$—C) $+ \Delta H_f^\circ$(C—$CH_2CMe_2CH_2$—C) = −31 (ref. 36) − (−14.79) + (−29.76) = −46.0

leading to a reaction enthalpy of −2 kcal for 3-membered ring formation. The differences between **16***b* and **16***a* were set equal to the difference between **15***b* and **15***a* (next section).

12. Iminooxadiazoline 15

Assuming resonance energies in **15** and **16** are the same, eqs. [15] and [16] estimate reaction enthalpies for **15***a* (dimethyl substituted) and eqs. [17] and [18] for **15***b* (diphenyl substituted). 3-Membered ring formation is assumed equienergic to system **11** at −14 kcal.

[A 15] ΔH° (3-pce; **15***a*) $\simeq \Delta H^\circ$ (3-pce; **16***a*) $- \Delta H_{ex}^\circ$ (CO) $+ \Delta H_{ex}^\circ$ (PhNC) = −30 − 15.4 + 24.0 = −21.4

[A 16] ΔH° (1,3-dpcr; **15***a*) $\simeq \Delta H^\circ$ (1,3-dpcr; **11***a*) $- \Delta H_{ex}^\circ$ (H_2C=C=O) $+ \Delta H_{ex}^\circ$ (HNCO) $+ \delta\Delta H_{Me}^\circ$ = 24.2 − 15.6 − 11.15 − 6.8 = −9.4

[A 17] ΔH° (3-pce; **15***b*) $\simeq \Delta H^\circ$ (3-pce; **15***a*) $+ 2(\delta\Delta H_{Ph}^\circ - \delta\Delta H_{Me}^\circ)$ = −21.4 − 23.7 (see section 7, above) + 6.8 = −38.3

[A 18] ΔH° (1,3-dpcr; **15***b*) $\simeq \Delta H^\circ$ (1,3-dpcr; **15***a*) $+ 2(\delta\Delta H_{Ph}^\circ - \delta\Delta H_{Me}^\circ)$ = −9.4 − 23.7 + 6.8 = −26.3

These calculations illustrate how the Relative Extrusibility Scale, the Table of Interfragment Interactions, and substituent effect corrections can be used to obtain either heats of formation of complicated molecules, or heats of reaction for their decomposition. The latter approach is useful when the heat of formation of one or more of the products is also unknown.

Can. J. Chem. Downloaded from www.nrcresearchpress.com by 210.87.254.40 on 09/06/12
For personal use only.

The absorption spectrum of *trans*-diimide (N_2H_2) in the vacuum ultraviolet region[1]

P. S. NEUDORFL AND R. A. BACK

Division of Chemistry, National Research Council of Canada, Ottawa, Ont., Canada K1A 0R6

AND

A. E. DOUGLAS

Herzberg Institute of Astrophysics, National Research Council of Canada, 100 Sussex Drive, Ottawa, Ont., Canada K1A 0R6

Received August 12, 1980

Can. J. Chem. Downloaded from www.nrcresearchpress.com by 210.87.254.42 on 09/06/12
For personal use only.

P. S. NEUDORFL, R. A. BACK, and A. E. DOUGLAS. Can. J. Chem. **59**, 506 (1981).

The vacuum ultraviolet absorption spectrum of *trans*-diimide (N_2H_2) in the gas phase has been re-examined between 1800 and 1300 Å, using diimide prepared by the thermal decomposition of sodium tosylhydrazide. Two band systems were observed, designated $\tilde{B} \leftarrow \tilde{X}$ and $\tilde{C} \leftarrow \tilde{X}$, with origins at 1727 and 1473 Å, which have been assigned to the Rydberg transitions $3p_\pi(b_u) \leftarrow n_+$ and $4p_\pi(b_u) \leftarrow n_+$ respectively. Both systems show long progressions in ν_2', the N—N—H symmetric bending frequency, and short progressions in ν_3', the symmetric N—N stretching frequency.

The $\tilde{B} \leftarrow \tilde{X}$ system has well-resolved rotational *J* type structure in some bands, and the rotational analysis showed that the ground state is a totally symmetric singlet state of C_{2h} symmetry (planar *trans*-N_2H_2 isomer), and that the system arises from a $^1B_u \leftarrow {}^1A_g$ transition. Rotational constants obtained for the 0–0 band of the $\tilde{B}$-state were $A = 15.63$, $B = 1.32$, and $C = 1.22$ cm^{-1}, and the values of $r_{H—N} = 1.028$ Å, $r_{N—N} = 1.167$ Å, and $\angle$H—N—N = 127.6° were estimated from them assuming a planar *trans* conformation.

P. S. NEUDORFL, R. A. BACK et A. E. DOUGLAS. Can. J. Chem. **59**, 506 (1981).

On a étudié de nouveau le spectre ultraviolet à vide de la *trans*-diimide (N_2H_2) en phase gazeuse entre 1800 et 1300 Å en utilisant une diimide préparée par la décomposition thermique de la tosylhydrazide de sodium. On a observé deux systèmes de bandes que l'on désigne par $\tilde{B} \leftarrow \tilde{X}$ et $\tilde{C} \leftarrow \tilde{X}$ et qui prennent naissance à 1727 et 1473 Å; on les a attribués respectivement aux transitions de Rydberg $3p_\pi(b_u) \leftarrow n_+$ et $4p_\pi(b_u) \leftarrow n_+$. Les deux systèmes montrent de longues progressions pour ν_2', la fréquence de déformation symétrique N—N—H et de courtes progressions pour ν_3' la fréquence d'élongation symétrique N—N.

Le système $\tilde{B} \leftarrow \tilde{X}$ a une structure rotationnelle de type *J* bien résolue dans quelques bandes et l'analyse rotationnelle a montré que l'état fondamental est un état singulet complètement symétrique de symétrie C_{2h} (isomère plan du N_2H_2 *trans*) et que le système provient d'une transition $^1B_u \leftarrow {}^1A_g$. Les constantes de rotation obtenues pour la bande 0–0 de l'état $\tilde{B}$ sont: $A = 15{,}63$, $B = 1{,}32$ et $C = 1{,}22$ cm^{-1} et les valeurs de $r_{H—N} = 1{,}028$ Å, $r_{N—N} = 1{,}167$ Å et $\angle$H—N—N = 127,6° ont été évaluées à partir de ces constantes en admettant une conformation plane *trans*.

[Traduit par le journal]

Introduction

The vacuum ultraviolet spectrum of diimide (N_2H_2) was first studied by Trombetti (1) in 1968, using a microwave discharge through flowing hydrazine vapor as a source of this metastable molecule. The spectrum showed a resolved rotational *J*-structure, and from its apparent intensity alternation it was concluded that the ground electronic state of diimide is not totally symmetric, which by analogy with the isoelectronic molecule O_2, indicated a triplet ground state. Subsequently, however, esr and magnetic susceptibility measurements (2) showed that diimide is not strongly paramagnetic, while analysis of the infrared (3) and near ultraviolet (4) spectra, as well as numerous theoretical calculations (5–7), provided strong evidence against a triplet ground state. It has in fact been established beyond reasonable doubt that the ground state of *trans*-diimide, the most stable N_2H_2 isomer and the only one positively identified experimentally, is a totally symmetric singlet state, ^1A_g. The vacuum ultraviolet spectrum, however, has remained unexplained. It is a strong, reproducible absorption system, and the critical intensity alternation originally observed in a flow system was confirmed in static experiments (2). Suggestions that the spectrum arises from a longlived excited triplet state or from one of the other possible isomers of diimide seem highly improbable (2, 3). The spectrum observed was complicated at some wavelengths by overlapping bands of ammonia, which is unavoidably present in large excess when diimide is prepared by a microwave discharge through hydrazine vapor (2). Wiberg and his colleagues (8) have shown that almost pure diimide can be produced by the thermal decomposition of alkali metal tosylhydrazides, and have also argued that the *cis*-diimide or aminonitrene rather than the *trans* isomer is formed, at least initially, by this method (9). It appeared that a re-examination of the vacuum ultraviolet spectrum using diimide prepared in this way might resolve some of its anoma-

[1]NRCC No. 18694.

0008-4042/81/030506-12$01.00/0

©1981 National Research Council of Canada/Conseil national de recherches du Canada

Can. J. Chem. Downloaded from www.nrcresearchpress.com by 210.87.254.42 on 09/06/12
For personal use only.

lous features, or if indeed other isomers were present, might yield a totally new spectrum. The present paper describes such a re-examination.

Experimental

Diimide, generated continuously by the thermolysis of sodium tosylhydrazide (8) at 70–100°C, was mixed with helium carrier gas at a pressure of 1 to 5 Torr and passed through a trap at −78°C into an 80 cm long absorption tube fitted with LiF windows and cooled at −78°C. Continuous pumping maintained a steady concentration of diimide in the absorption tube, kept at the desired value (of about 0.1 to 0.7 mTorr) by controlling the thermolysis temperature and the helium flowrate.

The absorption spectrum in the wavelength regions 1240–2000 Å and 1370–1550 Å was photographed in the first and seventh orders of a 10 m Eagle spectrograph equipped with gratings with 1200 and 600 lines/mm and reciprocal dispersions of 0.75 and 0.21 Å/mm, using slit widths of 0.10 and 0.02 mm respectively. Third and fourth order iron lines from a hollow cathode source were superimposed on the seventh order spectrum as wavelength standards. A Lyman discharge provided the continuum light source, and spectra were photographed on Ilford Q2 and Kodak SWR plates.

Results

A comparison of the absorption spectra obtained in the present experiments with those of Trombetti (1) and Willis and Back (2) leaves no doubt that the same absorbing species was observed throughout. The virtual absence of ammonia, however, dramatically improves the quality of the spectra, permitting not only measurements of N_2H_2 absorption over a much broader range of wavelengths than before but also much better resolution of the rotational structure. A microdensitometer trace of the absorption spectrum between 1800 and 1350 Å is shown in Fig. 1. The spectrum consists of at least two band systems, one extending from about 1730 to 1520 Å and the other from about 1470 Å to shorter wavelengths. The first system is the one previously described by Trombetti (1), and consists of at least 17 bands, about half of which show a resolved rotational structure. The bands of the 1470 Å system, not previously reported, are much weaker and their rotational structure is not resolved. For convenience, these two systems will be denoted as the $\tilde{B} \leftarrow \tilde{X}$ (following Trombetti (1)) and $\tilde{C} \leftarrow \tilde{X}$ transitions respectively.

In addition to these systems, some rather weak diffuse bands were observed between 1800 and 1730 Å which do not seem to belong to the $\tilde{B} \leftarrow \tilde{X}$ system, whose possible origin will be discussed later. No further absorption was seen up to 2000 Å.

Vibrational Analysis

The $\tilde{B} \leftarrow \tilde{X}$ *System (1730–1520 Å)*

The vibrational assignments, shown in Fig. 1, are the same as Trombetti's (1), although almost twice as many bands were observed in the present spectrum. There are three progressions with $\Delta\nu = 1150 \pm 30\ cm^{-1}$ assigned to the totally symmetric HNN bending vibration, ν_2', in the upper electronic state.[2] The first progression, which consists of seven bands, is the most intense, with the first member at about 1727 Å. The origin of the second progression is blue-shifted by about 1875 cm^{-1} and that of the third progression by another 1845 cm^{-1}. The second progression consists of six bands; the third progression is much weaker, and only four members are observed. The three progressions in ν_2' are assumed to correspond to the excitation of 0, 1, or 2 quanta of the totally symmetric N—N stretching vibration, ν_3'. These progressions account for virtually all the bands of the $\tilde{B} \leftarrow \tilde{X}$ system (with two exceptions, see below), and no further members were observed at longer wavelengths, confirming Trombetti's assignment of the 1727 Å band as the origin. No "hot" bands corresponding to transitions from vibrationally excited levels of the ground state were observed, and because only ν_2' and ν_3' were excited, a simplified band notation, (v_2', v_3'), has been adopted, in which it is implicit that all other vibrational modes in both states are unexcited. The vibrational assignments for the $\tilde{B} \leftarrow \tilde{X}$ band system are given in Table 1; the wavenumbers shown are band origins determined by rotational analysis (see below) or estimated from the gross features of the diffuse bands.

Two additional weak absorption bands were observed in high resolution spectra lying just to the short wavelength side of the (1,1) and (2,1) bands. These showed virtually the same rotational structure as the latter (Table 4, below), but blue-shifted by 58 and 83 cm^{-1} respectively. The weak band adjacent to the (2,1) band shows much sharper rotational structure than the latter, which is quite diffuse, indicating that a different vibrational transition is responsible. The most probable source of these two weak bands, with origins at 61 019 and 62 191 cm^{-1}, would appear to be excitation of the symmetric N—H stretching vibration, ν_1', with the two bands corresponding to $v_1' = 1$, and to $v_1' = 1$, $v_2' = 1$, respectively, with all other vibrations in both states in their zero levels. This assignment leads to values of ν_1' of 3092 and 3085 cm^{-1} in the $\tilde{B}$ state, which may be compared with $\nu_1'' =$

[2]In accordance with the established ground-state frequencies, ν_2 is the symmetric HNN bending vibration, and ν_3 the N—N stretching vibration (3, 4). This is the opposite notation to that used originally by Trombetti (1).

Can. J. Chem. Downloaded from www.nrcresearchpress.com by 210.87.254.42 on 09/06/12
For personal use only.

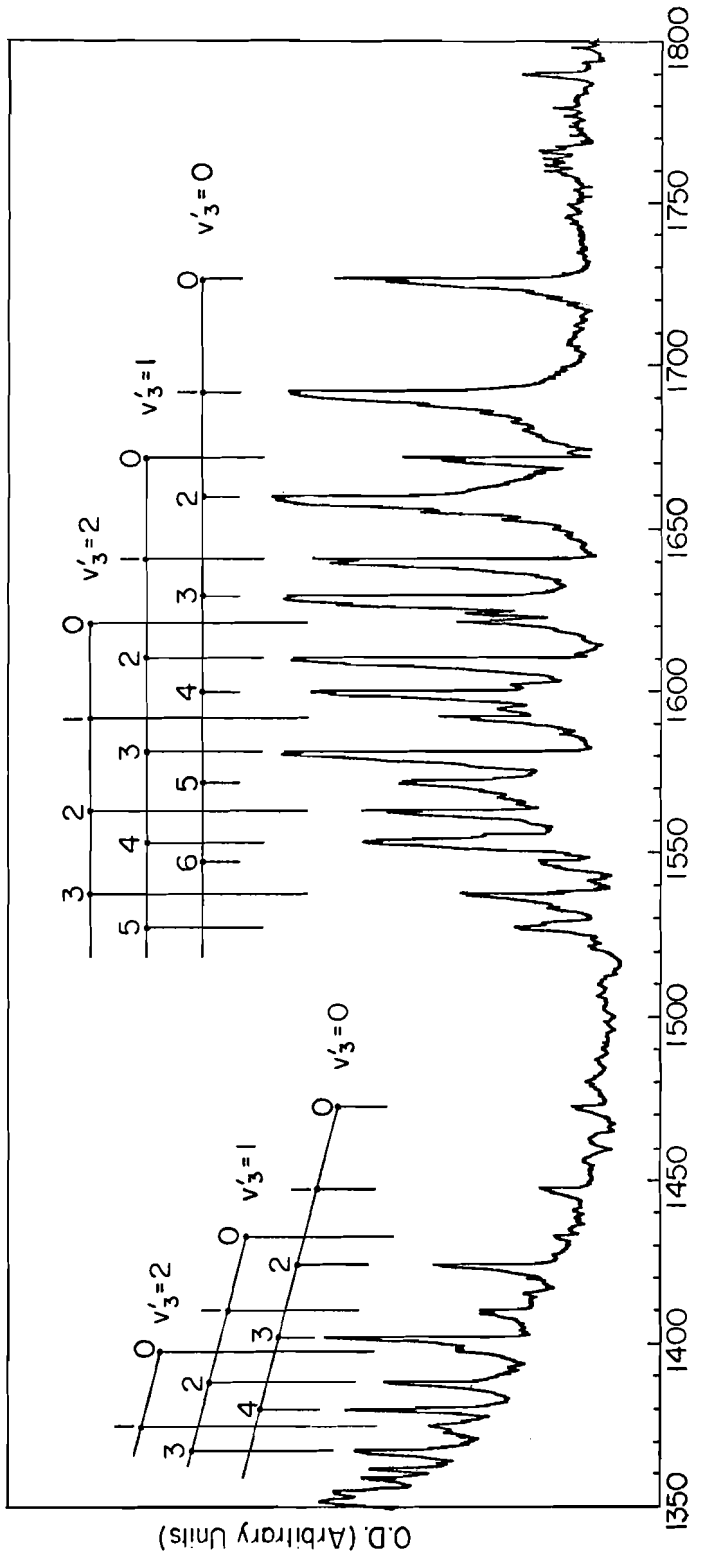

FIG. 1. A low-resolution spectrum of N_2H_2, showing the vibrational assignments. Long progressions belong to ν_2' vibration.

Can. J. Chem. Downloaded from www.nrcresearchpress.com by 210.87.254.42 on 09/06/12
For personal use only.

TABLE 1. Wavenumbers of band origins and vibrational assignments for the $\tilde{B} \leftarrow \tilde{X}$ system of N_2H_2*

	Wavenumber				
v_2'	$v_3' = 0$		$v_3' = 1$		$v_3' = 2$
0	57 926.5	(1 874.6)	59 801.1	(1 845.4)	61 646.5
	(1 180.1)		(1 158.6)		(1 155.4)
1	59 106.6	(1 853.1)	60 959.7	(1 842.2)	62 801.9
	(1 157.5)		(1 148.4)		(1 145.5)
2	60 264.1	(1 844.0)	62 108.1	(1 839.3)	63 947.4
	(1 127.8)		(1 126.1)		(1 127.6)
3	61 391.9	(1 842.3)	63 234.2	(1 840.8)	65 075.0
	(1 118.1)		(1 121.9)		
4	62 510	(1 846.5)	64 356.1		
	(1 073)		(1 064)		
5	63 583	(1 837.1)	65 420		
	(1 038)				
6	64 621				

*All wavenumbers in cm^{-1} *in vacuo*. Wavenumber differences are given in parentheses.

TABLE 2. Wavenumbers of bands and vibrational assignments for the $\tilde{C} \leftarrow \tilde{X}$ system of N_2H_2*

	Wavenumber				
v_2'	$v_3' = 0$		$v_3' = 1$		$v_3' = 2$
0	67 894	(1 849)	69 743	(1 825)	71 568
	(1 180)		(1 179)		(1 172)
1	69 074	(1 848)	70 922	(1 818)	72 740
	(1 168)		(1 154)		(1 206)
2	70 242	(1 834)	72 076	(1 870)	73 946†
	(1 125)		(1 120)		
3	71 367	(1 829)	73 196		
	(1 101)		(1 099)		
4	72 468	(1 827)	74 295†		
	(1 170)				
5	73 638†				

*All wavenumbers in cm^{-1} *in vacuo*. Wavenumber differences are given in parentheses.
†Less certain because of overlap with other bands.

$3128\ cm^{-1}$ for the ground state (10). While these values seem reasonable, the assignment must remain tentative because the bands are weak and partially overlapped.

The $\tilde{C} \leftarrow \tilde{X}$ System (1470–1350 Å)

This band system shows many similarities to the $\tilde{B} \leftarrow \tilde{X}$ system, and very similar vibrational assignments in terms of ν_2' and ν_3' have been made (Fig. 1, Table 2). The bands are weaker and diffuse, with no resolved rotational structure, and the wavenumbers estimated for the band origins in Table 2 are therefore less accurate. Although many more absorption bands can be observed at wavelengths below 1360 Å, they are weak, badly overlapped and diffuse, and no assignments have been attempted.

Table 3 summarizes the fundamental vibrational frequencies measured for the $\tilde{B}$ and $\tilde{C}$ states, together with the values determined previously for the $\tilde{X}$ and $\tilde{A}$ states of diimide, and those for the ground-state $N_2H_2^+$ ion.

Rotational Analysis of the $\tilde{B} \leftarrow \tilde{X}$ System

Typical high-resolution plates are shown in Fig. 2 for the (0,0) and (1,0) bands. It is clear from these spectra that two strong sub-bands are present, and comparison with the previous spectra (1, 2) reveals that the apparent intensity alternation in the latter arose from fortuitous overlap of unresolved lines from these two sub-bands. It will be seen that the rotational structure is in complete accord and only compatible with the ^1A_g ground state of *trans*-diimide whose structure and rotational levels are well established from its infrared spectrum. The molecule of *trans*-N_2H_2 has three different moments of inertia ($I_A \neq I_B \neq I_C$), and as such it should be classified as an asymmetric top; however, since $I_A < I_B \approx I_C$, the molecule is not too far removed from a limiting case of the prolate symmetric top and, with a good approximation, its rotational structure can be described in terms of J and K quantum numbers.

The J-structure

Rotational assignments for the (0,0) and (1,0) bands are shown on the spectra in Fig. 2. In each band two sub-bands are present, one corresponding approximately to a parallel transition with $K' = 0$ and $K'' = 0$, and the other approximately to a perpendicular transition with $K' = 0$ and $K'' = 1$. The assignments of the rotation line can be determined unambiguously from the known rotational structure of the ground state.[3] From the wavenumbers of the lines of the P branch of the $\Delta K = 0$ sub-band those of the R branch were calculated using ground-state combination differences. Since the $\Delta K = -1$ sub-band has the same upper state as the $\Delta K = 0$ sub-band, the line positions for the P, Q, and R branches of the former could be calculated from the measured line positions of the latter and the known combination differences of the ground state. Agreement between calculated and observed line positions for both sub-bands was very good,

[3]We are grateful to Dr. J. W. C. Johns for providing these ground-state data.

TABLE 3. Vibrational fundamentals (cm^{-1}) and geometry of the observed electronic states of diimide

State	ν_1	ν_2	ν_3	Bond length (Å) N—N	Bond length (Å) N—H	∠HNN	Electron configuration	Reference
$\tilde{X}$	3128	1583	1529	1.252	1.028	106.85°	$...n_+(4a_g)^2$	3, 10
$\tilde{A}$	—	1184	1579	1.340	1.022	123°	$...n_+(4a_g)\cdot\pi^*(1b_g)$	4, 18
$\tilde{B}$	3092	1180	1875	1.167	1.028	127.6°	$...n_+(4a_g)\cdot 3p_\pi(5b_u)$	This work
$\tilde{C}$	—	1180	1849	—	—	—	$...n_+(4a_g)\cdot 4p_\pi(nb_u)$	This work
$\tilde{X}(N_2H_2^+)$	—	1180	1860	1.222	1.045	127°	$...n_+(4a_g)$	14

usually within the accuracy of the measurement of the line centres (±0.03 cm^{-1} for the sharpest lines).

Similar rotational analysis was carried out for all bands with resolved *J*-structure, and the wavenumbers (cm^{-1} *in vacuo*) and assignments are given in Table 4. Essentially all the observed lines are accounted for in this analysis or as known lines of ammonia (11) which was still present in low concentration. From the line positions for the P and R branches in Table 4, values for the upper-state rotational constant B_v' were determined for each of the observed vibrational levels. The B_v' values reported in Table 5 are averages, calculated by a simplified formula, $\Delta_2F_v'(J) = R_v(J) - P_v(J) \simeq 4B_v'(J + \frac{1}{2})$, from the lines of the two sub-bands (12*a*).

The K*-structure*

All levels with $K > 0$ in the upper state appear to be greatly broadened by predissociation and no *J* type rotational structure arising from these levels can be observed. Nevertheless in N_2H_2 a weak and diffuse *K*-structure is clearly visible. Table 6 lists approximate positions of several sub-bands in six vibrational bands; wavenumbers were estimated from prints of first-order spectra, and refer to assumed positions of Q branches in a diffuse *K*-structure. To aid in these assignments, comparison was made with spectra of N_2D_2 in which the *K*-structure is better resolved.[4] From the data in Table 6, values of the upper-state rotational constant, A_v', were determined, using the symmetric rotor formulas (12*b*) and the molecular constants for the ground state (3). The values of A_v' are reported in Table 7, and were used to estimate the geometry of the $\tilde{B}$ state, Table 3.

Discussion

The Nature of the Electronic Transitions

The rotational analysis of the $\tilde{B} \leftarrow \tilde{X}$ system has confirmed that the lower state of the transition is the same as that of the infrared spectrum (3), i.e., a totally symmetric singlet state, ^1A_g, with planar *trans* geometry (C_{2h} symmetry). The strength of the absorption indicates that the electronic transition is symmetry allowed. If the $\tilde{B}$ state also has C_{2h} symmetry, it can be shown that it must belong to the ^1B_u species. Thus for C_{2h} symmetry and a ^1A_g ground state, the selection rules allow either ^1B_u or ^1A_u for the upper state; when the symmetry of the rotational levels is considered, only for a ^1B_u upper state is a $\Delta K = 0$ sub-band allowed as was observed. The $\tilde{B} \leftarrow \tilde{X}$ system can therefore be assigned to a $^1B_u \leftarrow {}^1A_g$ electronic transition.

Robin (13) has argued convincingly that the first strong absorption in the vacuum ultraviolet region in diimide and the alkyl azo compounds should come from the $3p \leftarrow n_+$ Rydberg transitions. In Table 8 are listed in order of increasing excitation energy the singlet states that can be derived from the valence-shell and lower Rydberg orbitals of *trans*-diimide. Experimental and theoretical (5) estimates of vertical transition energies are shown in columns 3 and 4, and lend support to Robin's arguments. The $3s \leftarrow n_+$ transition is symmetry forbidden and should be very weak. The 3*p* Rydberg orbitals are split into three components, σ, $\pi(a_u)$, and $\pi(b_u)$, by the geometry of the core molecule, and only two of these, the $3p_\sigma$ and $3p_\pi(b_u)$ components, have the required B_u symmetry. The CI vertical transition energies calculated by Vasudevan *et al.* (5) for the $3p \leftarrow n_+$ states lie well below that observed for the $\tilde{B} \leftarrow \tilde{X}$ system. Their value for the vertical transition energy for the $\tilde{A} \leftarrow \tilde{X}$ system is also lower then the experimental value, by about 0.6 to 0.7 eV, and if their calculated energies for all transitions originating from the n_+ orbital were increased by this amount, the value for the $3p_\pi(b_u) \leftarrow n_+$ transition would become about 7.6 eV, close to the central maximum of the $\tilde{\tilde{B}} \leftarrow \tilde{\tilde{X}}$ band system.[5]

[4]Unpublished spectra, R. A. Back and C. Willis, N_2D_2 generated by microwave discharge in N_2D_4; cf. Trombetti (1).

[5]If the calculated vertical energy for the $3p_\sigma \leftarrow n_+$ transition is similarly adjusted upward by 0.65 eV, an absorption maximum at about 1790 Å is predicted, and it seems possible that the weak diffuse bands observed in this region might be attributed to this transition. Other weak diffuse bands in the 1480–1512 Å region might correspond to the next member, the $4p_\sigma \leftarrow n_+$ transition, in the Rydberg series. Both these assignments are very tentative.

Can. J. Chem. Downloaded from www.nrcresearchpress.com by 210.87.254.42 on 09/06/12
For personal use only.

Can. J. Chem. Downloaded from www.nrcresearchpress.com by 210.87.254.42 on 09/06/12
For personal use only.

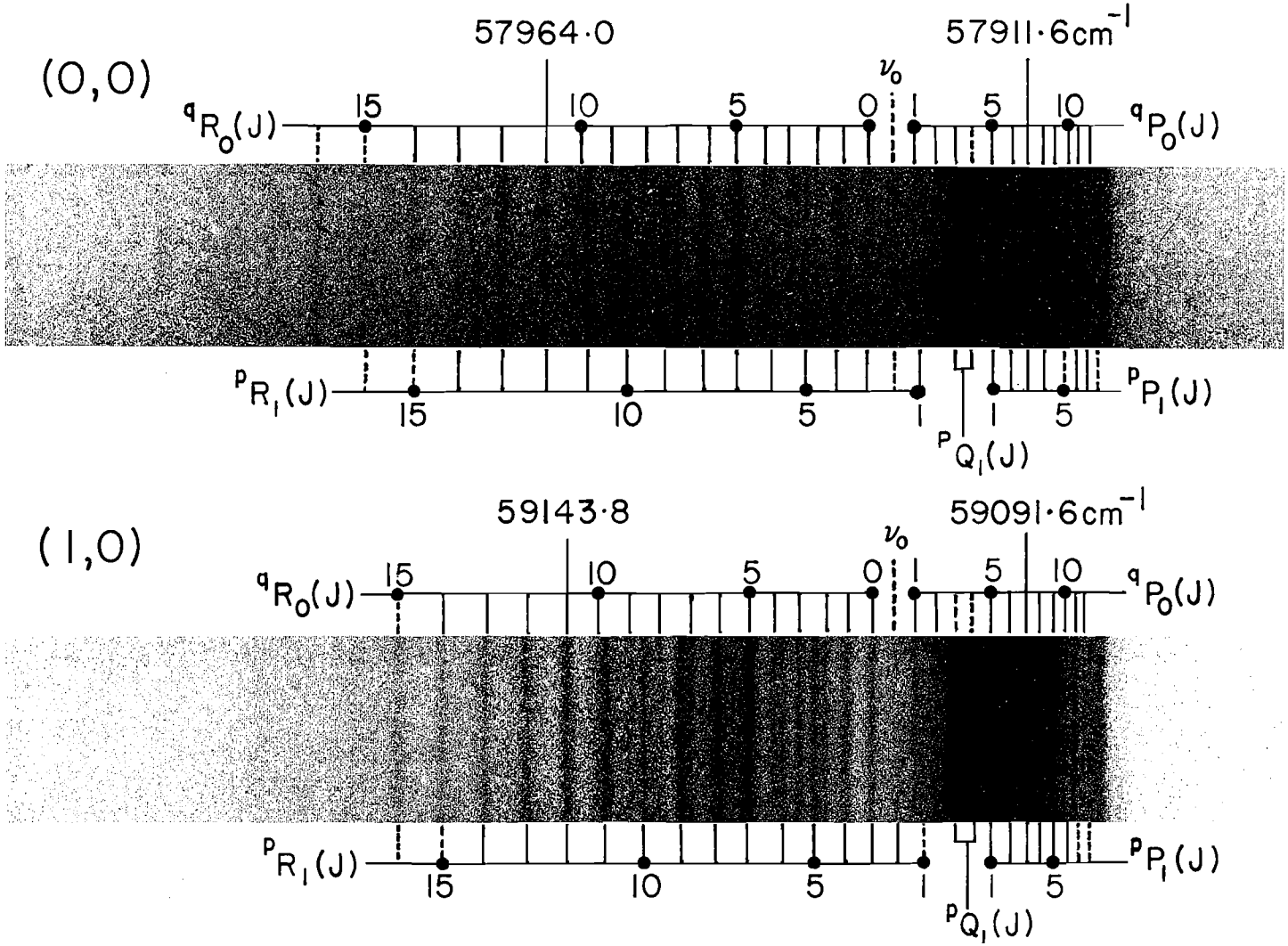

FIG. 2. The 0–0 and $v_2' = 1$–0 bands of *trans*-N_2H_2 (in the present notation called the (0,0) and (1,0) bands respectively) with the rotational assignments shown.

TABLE 4. Vacuum wavenumbers and rotational assignments for the lines of N_2H_2 bands

(*a*) (0,0) and (1,0) bands

	(0,0) band				(1,0) band			
	$K'=0-K''=0$		$K'=0-K''=1$		$K'=0-K''=0$		$K'=0-K''=1$	
J''	R(J)	P(J)	R(J)	P(J)	R(J)	P(J)	R(J)	P(J)
0	57 928.75*				59 108.83*			
1	931.80*	57 924.31	57 922.94	57 915.66*	111.86*	59 104.28		59 095.47*
2	934.56	921.84		913.36*	114.78	101.86	59 106.17	093.21*
3	937.15	918.92*	929.10*	911.63*	117.48		108.83*	091.48*
4	940.44		931.80*	910.08*	120.36		111.86*	089.81*
5	943.26*	915.27*	935.61		122.97*	095.47*	115.77	087.66*
6	946.45*	913.36*	939.00	905.76	126.44*	093.21*	119.25	085.85*
7	949.56	911.63*	943.26*	904.74*	129.90	091.55*	122.97*	
8	952.76	910.08*	946.45*	903.75*	133.35	089.81*	126.44*	083.40*
9	956.88	908.56*	950.76	903.10*	136.47	088.71*	130.53	
10	960.24*	907.06*	955.04		139.40*	087.10*	135.15	
11	964.01*	905.76*	959.70*		143.75*	085.85*	139.11*	
12	968.55*	904.74*	964.01*		148.61*		143.75*	
13	973.66*		968.55*		153.41*		148.61*	
14	978.32*		973.66*		157.97*		153.41*	
15	983.52*		978.32*		163.30*		157.97*	
16	988.58*		983.52*		167.94*		163.30*	
17	994.48*		988.58*		173.58*		167.94*	
18	999.70*				178.64*			
ν_0^{sub}†	57 926.45		57 917.80		59 106.60		59 098.10	

*Overlapped lines.
†Sub-band origin: for the $\Delta K = 0$ it is also a band origin; for the $\Delta K = -1$ it also gives an approximate position of unresolved Q branch.

(*b*) (2,0) and (3,0) bands

	(2,0) band				(3,0) band			
	$K'=0-K''=0$		$K'=0-K''=1$		$K'=0-K''=0$		$K'=0-K''=1$	
J''	R(J)	P(J)	R(J)	P(J)	R(J)	P(J)	R(J)	P(J)
0	60 266.45*				61 393.97*			
1	269.66*	60 261.46		60 252.78*	396.66*	61 389.54	61 388.12	61 380.67*
2	272.48	259.18	60 263.27	250.72*	400.17	387.19	391.33	378.65*
3	274.84	256.77*	266.45*	249.28*	402.39		393.97*	376.74*
4	277.50		269.66*	247.33*	405.48		396.66*	374.85*
5	280.70*	252.78*	273.29	245.77*	408.07*	380.67*	400.57	372.10*
6	283.77	250.72*	276.42	243.12*	411.73*	378.65*	404.36	370.49*
7	286.70	249.28*	280.70*		415.33*	376.74*	407.58	369.70
8	290.26	247.33*	284.25		417.81	374.85*	411.73*	368.91*
9	293.03	245.77*	288.13			373.43*	415.33*	
10	297.30	244.49	292.16	239.48	424.45	372.10*	419.20	
11	301.24*	243.12*	296.83		428.81*	370.49*	423.64	365.20
12	305.52*		301.24*		432.96*	368.91*	428.25*	
13	310.20*		305.52*		437.53*		432.50*	
14	314.84*		310.20*		442.46*	368.07*	437.53*	363.65
15			314.84*		447.17*		442.46*	
16					452.20*		447.17*	
ν_0^{sub}	60 264.05		60 255.55		61 391.90		61 383.15	

*Overlapped lines.

From considerations of orbital overlap, the $3p_\pi(b_u) \leftarrow n_+$ transition, with the Rydberg orbital and the n_+ orbital both in the plane of the molecule, should be much stronger than the transitions involving the $3p_\sigma$ and $3p_\pi(a_u)$ orbitals. It appears reasonable therefore to assign the strong $\tilde{B} \leftarrow \tilde{X}$ absorption system to this transition.

The possible involvement of the $\pi^* \leftarrow n_-$ and $\pi^* \leftarrow \pi$ states in the present absorption spectra requires some comment. The proper positions of

Can. J. Chem. Downloaded from www.nrcresearchpress.com by 210.87.254.42 on 09/06/12
For personal use only.

TABLE 4 (*Continued*)

(*c*) (0,1) and (1,1) bands

	(0,1) band				(1,1) band			
	$K' = 0 - K'' = 0$		$K' = 0 - K'' = 1$		$K' = 0 - K'' = 0$		$K' = 0 - K'' = 1$	
J''	R(J)	P(J)	R(J)	P(J)	R(J)	P(J)	R(J)	P(J)
0	59 803.72*				60 961.84*			
1	806.69*	59 798.77		59 790.03*	964.79*	60 957.43		60 948.52*
2	809.72	796.31	59 799.91	787.85*	968.27*†	954.93	60 958.90†	946.56*
3	811.81	794.01	803.72*	786.09*	970.41		961.84*	944.60*†
4	814.40	792.56*	806.69*	783.83*	973.02*	950.73†	965.07*	942.46*†
5	816.99*	790.03*		782.19*	976.10*†	948.52*	968.27*†	941.17*
6	820.64*	787.85*		781.19*	979.42*	946.56*	972.13	939.00*
7	823.63*	786.09*	816.99*		982.64†	944.60*†	975.79*†	937.57*
8	826.19	783.83*	820.64*		985.65*	942.46*†	979.51*	936.67*
9	830.80	782.19*	824.12*		989.29†	941.17*	983.44	935.55*
10	832.66*	781.19*	828.81	775.35*	991.90*	939.00*	987.24	934.53†
11	836.29*		832.66*		995.79*	937.57*	991.72*	
12	841.84*	777.27*	836.29*		61 000.43*†	936.67*	995.79*	
13	846.00*		841.84*		004.56		61 000.43*†	932.50†
14	850.99*		846.00*		008.76†		005.37	
15	852.72*							
ν_0^{sub}	59 801.10		59 792.50		60 959.73		60 950.55	

*Overlapped N_2H_2 lines.
†Overlapped by NH_3 line.

(*d*) (2,1) and (3,1) bands†

	(2,1) band				(3,1) band			
	$K' = 0 - K'' = 0$		$K' = 0 - K'' = 1$		$K' = 0 - K'' = 0$		$K' = 0 - K'' = 1$	
J''	R(J)	P(J)	R(J)	P(J)	R(J)	P(J)	R(J)	P(J)
0					62 236.13			
1		62 105.23		62 097.00*	239.26	62 231.54*	63 231.54*	
2		103.32		095.00*	242.09	229.67		63 220.88*
3	62 118.80	101.34		092.63*			237.00	219.49*
4		098.71*		090.73*	248.08		240.42	217.69*
5	124.39*	096.99*			251.24*		243.00	215.66*
6	127.98*	095.01*			253.71*	220.88*	246.76	
7	130.75*	092.63*	62 124.39*	085.71	257.75*	219.49*		
8	133.01*	090.73*	127.98*	085.11*	260.06*	217.69*	254.39*	210.87*
9	137.52		130.75*	084.05*	263.98	215.66*	257.75*	
10		086.85*	135.30		267.58	214.47*	262.20	
11	143.75*	086.36*	139.25		270.45*	213.03	266.03	
12		085.11*	143.75*		274.61*		270.45*	
13	152.06	084.05*			278.60*	210.87*	274.61*	
14	156.56							
ν_0^{sub}	62 108.10		62 099.70		63 234.20		63 255.88	

*Overlapped lines.
†All lines are blurred or diffuse.

these states in Table 8 are in some doubt. The CI calculations by Vasudevan *et al.* (5) (column 4) place the former at 7.47 eV and the latter much higher, at 11.67 eV. The photoelectron spectrum reported by Frost *et al.* (14), on the other hand, puts the π-orbital 0.6 eV *below* the n_--orbital, and when combined with the observed value of 3.6 eV for the $\pi^* \leftarrow n_+$ vertical transition (4), leads to estimates of 8.0 and 8.6 eV for the $\pi^* \leftarrow \pi$ and $\pi^* \leftarrow n_-$ states respectively (column 3). These energies are close to those of the $\tilde{B}$ and $\tilde{C}$ states and the $\pi^* \leftarrow \pi$ state has the B_u symmetry observed for the $\tilde{B}$ state. The $\tilde{B} \leftarrow \tilde{X}$ system can nevertheless be safely identified with a Rydberg transition, on the basis of its strength and relative sharpness, and the increase in ν_3 frequency and decrease in N—N bond length relative to the ground state (cf. Table 3); the exact reverse changes would be expected for both $\pi^* \leftarrow$

Can. J. Chem. Downloaded from www.nrcresearchpress.com by 210.87.254.42 on 09/06/12
For personal use only.

TABLE 4 (*Continued*)

(*e*) (0,2) and (1,2) bands

	(0,2) band				(1,2) band			
	$K' = 0 - K'' = 0$		$K' = 0 - K'' = 1$		$K' = 0 - K'' = 0$		$K' = 0 - K'' = 1$	
J''	R(J)	P(J)	R(J)	P(J)	R(J)	P(J)	R(J)	P(J)
0	61 648.51*				62 804.53*			
1	652.18*			61 635.50*	807.63*†	62 799.57		62 790.19
2	654.62*	61 641.40	61 645.53	633.05*	810.20	797.60	62 801.78*	788.54*
3	656.61	639.67	648.51*	631.14*	812.71	795.30	804.53*	786.86*
4	659.64	637.30*	652.18*	628.82*	815.53*	792.54*	807.63*†	785.30*
5	662.90	635.50*	654.62*		818.29*		811.16	782.92*
6	665.70*	633.05*	658.39		821.25*	788.54*	815.53*	
7	668.43*	631.14*	662.05	624.01	824.99*	786.86*	818.29*	779.66*
8	671.15	628.82*	665.70*		827.75†	785.30*	821.25*	
9	675.26	627.47			830.87		824.99*	777.44*
10	678.33	626.05	673.45			782.92*		
11	681.34*		677.30		836.97*		833.08	775.52*
12	685.84*		681.34*		842.88*	779.66*	836.97*	
13	689.67*		685.83*		845.17*		840.41	
14					849.57*	777.44*	845.17*	
ν_0^{sub}	61 646.47		61 637.63		62 801.85		62 793.60	

*Overlapped lines of N_2H_2.
†Overlapped by NH_3 line.

(*f*) (2,2) band‡

	(2,2) band			
	$K' = 0 - K'' = 0$		$K' = 0 - K'' = 1$	
J''	R(J)	P(J)	R(J)	P(J)
0	63 949.82*†			
1	952.87*†			63 936.78†
2	955.00	63 942.10†		936.64*†
3	958.14†	940.31	63 949.82*†	932.32*
4	961.33†	938.79*	952.87*†	930.54*†
5	964.17†	935.84†	956.14†	928.63*
6	967.60*†	934.64†	960.16	
7	970.37*	932.32*	962.99†	
8	973.21†	930.54*†	967.60*†	
9		928.63*	970.37*	923.10*
10			975.32†	
11	983.95*		978.67†	
12	987.93*†	923.73†	983.95*	
13	992.00†	923.10*	986.93*†	
14			993.49†	
ν_0^{sub}	63 947.40		63 938.98	

*Overlapped N_2H_2 lines.
†Overlapped by NH_3 line.
‡This relatively weak band of N_2H_2 is overlapped by strong NH_3 lines.

π and $\pi^* \leftarrow n_-$ transitions (see below). It must be concluded that these valence-shell transitions are probably buried under the stronger $\tilde{B}$ and $\tilde{C}$ systems where they would be difficult to detect photographically, especially if the spectra are diffuse. Some weak diffuse bands are in fact observed between the two systems which cannot be assigned to either, and there is also a maze of unresolved unassigned bands to the blue of the $\tilde{C} \leftarrow \tilde{X}$ system.

The second absorption system observed in the present study, $\tilde{C} \leftarrow \tilde{X}$, shows no resolved rotational fine structure, hence no rigorous information about its electronic configuration or symmetry is available. The vibrational structure, however, and the

Can. J. Chem. Downloaded from www.nrcresearchpress.com by 210.87.254.42 on 09/06/12
For personal use only.

TABLE 4 (*Concluded*)

(*g*) v_1' = 1–0 band and v_1' = 1, v_2' = 1–0 band

	v_1' = 1–0 band‡				v_1' = 1, v_2' = 1–0 band§			
	$K'=0-K''=0$		$K'=0-K''=1$		$K'=0-K''=0$		$K'=0-K''=1$	
J''	R(J)	P(J)	R(J)	P(J)	R(J)	P(J)	R(J)	P(J)
0	61 021.26*†				62 193.71*			
1	024.40*	61 016.71	61 015.91	61 007.14*†	196.77*	62 188.54	62.187.65	62 179.94*
2	026.57†	014.00*†	017.70*†	005.38*	199.01*	186.51‖	190.78	178.05*
3	029.54	011.65†	021.26*†	003.68*†	201.80	184.77	193.71*	176.41*
4	032.08	010.12*	024.40*		204.34‖	182.76*	197.00*	174.00
5	035.37*	007.45*	027.53	000.43*†	208.10‖	179.94*		172.80*
6	038.22*†	005.38*		60 997.94*	211.29*	178.05*		170.37*
7	040.86†	003.68†	035.02*		214.52*	176.41*	207.07	169.29*
8	043.70	000.43*†	038.68*	995.73*†	217.68	174.86	211.29*	167.85*
9	048.18	60 998.22*			220.97‖	172.80*	214.52*	
10	050.64*†	997.94	046.74*†		223.67*‖	171.44*	219.08‖	166.03
11	055.81*†		050.64*†		227.90*‖	170.37*	223.67*‖	165.03
12	059.61*		055.81*†	991.89*	232.13*‖	169.30*	227.08*‖	164.25
13		995.73*†	059.61*		236.23*‖	167.85*	232.62*‖	
ν_0^{sub}	61 018.90		61 010.15		62 191.18		62 182.7	

*Overlapped lines of N_2H_2.
†Overlapped by NH_3 line.
‡A tentative vibrational assignment for a weak series in the (1,1) band (see text).
§A weak series in (2,1) band.
‖Position estimated from the print.

derived frequencies, show much similarity to the $\tilde{B} \leftarrow \tilde{X}$ system, and it can be assigned with some confidence to the next member in the Rydberg series, the $4p_\pi(b_u) \leftarrow n_+$ transition. When the origins of the $\tilde{B}$ and $\tilde{C}$ systems (57 926.45 and 67 893.9 cm^{-1} respectively) are fitted to the well-known Rydberg formula, $\nu = IP - R/(n-\delta)^2$, taking $n = 3$ and 4 and assuming a constant quantum defect, δ, values of IP = 9.62 eV and $\delta = 0.639$ are obtained. The former is in close agreement with recent measurements of the ionization potential of N_2H_2 of 9.65 ± 0.08 eV (15) and 9.7 ± 0.1 eV (16) by mass spectrometry, and 9.59 ± 0.01 eV (14) from its photoelectron spectrum. The quantum defect is of the size expected for *p*-Rydberg orbitals (17), and its value agrees well with estimates by Frost *et al.* (14), who used a term value approach based on the photoelectron spectrum to assign the $\tilde{B} \leftarrow \tilde{X}$ system to a $3p \leftarrow n_+$ Rydberg transition.

TABLE 5. The upper state rotational constants $\bar{B}_v'$ of different vibrational bands*

	$\bar{B}_v'$		
v_2'	$v_3'=0$	$v_3'=1$	$v_3'=2$
0	1.2708	1.261	1.254
1	1.268	1.260	1.253
2	1.265	1.256	1.254
3	1.263	1.258	

*In cm^{-1}; $\bar{B}_v' = \frac{1}{2}(B_v' + C_v')$.

The Geometry of the $\tilde{B}$ *State*

The geometry of the $\tilde{B}$ state was calculated from the rotational constants A_v' and $\bar{B}_v'$ (where $\bar{B}_v' = \frac{1}{2}(B_v' + C_v')$) assuming a planar *trans*-configuration of C_{2h} symmetry, and the same N—H bond length as in the ground state. The latter assumption is supported by the very weak excitation of ν_1', the symmetric N—H stretching vibration, in the spectrum. Table 3 reports values of the N—N bond length and the HNN bond angle obtained for the (0,0) vibrational band. The HNN bond angle is increased by almost 21° from its ground-state value. As in the $\tilde{A} \leftarrow \tilde{X}$ system (4, 18), the long progressions in ν_2' in the spectrum are consistent with a large change in the HNN angle on excitation. The N—N bond distance in the upper state is shorter by about 0.09 Å (i.e., ~7%) than in the ground state; because of its dependence on the assumed N—H bond length, this value is only approximate. A shortening of the N—N bond length is expected from the excitation of one electron from the n_+ orbital, which is considerably N—N antibonding, to a largely nonbonding Rydberg orbital. Associated with this change in bond length, excitation of ν_3' is observed in the spectrum and its frequency increases to 1875 cm^{-1} from 1529 cm^{-1} in the ground state.

In Table 3 are summarized all the available data on the geometry and frequencies of the three symmetric vibrations in the $\tilde{X}$, $\tilde{A}$, $\tilde{B}$, and $\tilde{C}$ states of

Can. J. Chem. Downloaded from www.nrcresearchpress.com by 210.87.254.42 on 09/06/12
For personal use only.

TABLE 6. Sub-bands of N_2H_2*

		Vibrational bands (v_2',v_3')					
K'	K''	(0,0)	(1,0)	(2,0)	(3,0)	(0,1)	(1,1)
0	1	57 917.80	59 098.10	60 255.55	61 383.15	59 792.50	60 950.55
0	0	926.45	106.00	264.05	391.98	801.23	959.73
1	0	941	122	281	412	816	976
2	1	975	162	325	461	851	61 014
3	2	58 021	215	384	534	896	070
4	3	082	285	462	628	956	138
5	4	146	368	556	743	60 026	222
6	5	225	465	667		107	
7	6	320		795		199	
8	7	419					
9	8	526					

*Wavenumbers are in cm^{-1} *in vacuo*; for the $\Delta K = -1$ and $\Delta K = 0$ sub-bands, the values are sub-band origins obtained from the *J*-structure analysis (cf. Table 4); for the $\Delta K = 1$ sub-bands, they refer to approximate positions of unresolved Q branches measured on the prints and their accuracy is not very high, probably ± 2 cm^{-1}.

TABLE 7. Rotational constants of N_2H_2 for different vibrational bands of the $\tilde{B}$ upper state

Vibrational band (v_2',v_3')	Rotational constant (cm^{-1})		
	A_v'	B_v'	C_v'
(0,0)	15.63	1.32	1.22
(1,0)	17.30	1.31	1.22
(2,0)	18.51	1.31	1.26
(3,0)	20.90	1.30	1.26
(0,1)	15.78	1.31	1.26
(1,1)	17.37	1.31	1.26

TABLE 8. Vertical transition energies to the lowest singlet states of *trans*-diimide

		Vertical transition energy, eV		
State	Excitation	Experiment	CI calculation*	Comment
$\tilde{X}\,^1A_g$	None	0.0	0.0	Ground state
$\tilde{A}\,^1B_g$	$\pi^* \leftarrow n_+$	3.6 (3450 Å)†	2.97	Observed: weak g–g forbidden
^1A_g	$3s \leftarrow n_+$	—	6.13	g–g forbidden
^1B_u	$3p_\sigma \leftarrow n_+$	6.9 (1790 Å)?‡	6.26	Weak, diffuse bands between 1735–1793 Å ?
^1A_u	$3p_\pi(a_u) \leftarrow n_+$	—	6.73	3*p* Rydberg transitions; all allowed
$\tilde{B}\,^1B_u$	$3p_\pi(b_u) \leftarrow n_+$	7.6 (1630 Å)‡	6.94	Observed: strong, sharp
^1B_u	$\pi^* \leftarrow \pi$	8.0 (1560 Å)§	11.67	Allowed
^1A_u	$\pi^* \leftarrow n_-$	8.6 (1440 Å)§	7.55	Allowed
$\tilde{C}\,^1B_u$	$4p_\pi(b_u) \leftarrow n_+$	8.8 (1400 Å)‡	—	Observed: strong
^1A_g	$3d_\sigma \leftarrow n_+$	—	—	3*d* Rydberg transitions; g–g forbidden
^1B_g	$3d_\pi \leftarrow n_+$	—	8.03	

*Taken from Table 8 of ref. 5.
†Reference 4.
‡Present work.
§Combining the results of photoelectron (14) and near-uv spectra (4).

Can. J. Chem. Downloaded from www.nrcresearchpress.com by 210.87.254.42 on 09/06/12
For personal use only.

Can. J. Chem. Downloaded from www.nrcresearchpress.com by 210.87.254.42 on 09/06/12
For personal use only.

trans-diimide and the ground state of the $N_2H_2^+$ ion. All the excited species and the ion show large increases in bond angle and decreases in ν_2 arising from removal of one electron from the angle-sensitive n_+ orbital. Such an effect was predicted by Walsh (19) and supported by more recent quantitative calculations of potential energy curves by Vasudevan *et al.* (5), and leads to strong excitation of the ν_2' bending vibration in the spectra.

Both the $\tilde{C}$ state and the ion show increases in ν_3' (and presumably therefore decreases in the N—N bond length) relative to the ground state, very similar to those discussed above for the $\tilde{B}$ state, for similar reasons. The $\tilde{A}$ state, by contrast, shows an *increased* N—N bond length and a little change in ν_3', as expected for excitation of an electron to the N—N antibonding π^* orbital, and the $\pi^* \leftarrow n_-$ and $\pi^* \leftarrow \pi$ states would be expected to show even larger changes in the same direction.

Predissociation in the $\tilde{B}$ *State*

The $\tilde{B} \leftarrow \tilde{X}$ absorption spectrum is very much sharper than the $\tilde{A} \leftarrow \tilde{X}$ system, which showed only a trace of coarse rotational structure at the longest wavelengths. The diffuseness of the latter system has been attributed to a rapid internal conversion to the ground state facilitated by a very low torsional barrier in the excited state (4). The $\tilde{B}$ state, with strong N—N π-bonding, should have a large torsional barrier, and perhaps the lack of an easy torsional route to internal conversion may account for its much greater stability. The $\tilde{B}$ state is nevertheless strongly predissociated, even for the relatively sharp $K' = 0$ levels; for the (0,0) and (1,0) bands very approximate minimum line widths of $\sim 0.8\ cm^{-1}$ can be estimated corresponding to a lifetime of ~ 7 ps (based on the uncertainty principle formula $\Delta\nu\Delta t = 1/2\pi$). With increasing vibrational excitation the bands become progressively more diffuse, with rotational structure barely discernible, for example, in the (4,0) or (3,1) bands. The $\tilde{B} \leftarrow \tilde{X}$ spectrum of N_2D_2 is notably sharper than that of N_2H_2, which was not true for the $\tilde{A} \leftarrow \tilde{X}$ system, suggesting that dissociation of an N—H bond is directly involved in the predissociation.

Summary

(*1*) Rotational analysis of a well-resolved vacuum ultraviolet absorption spectrum of relatively pure diimide produced from the thermolysis of sodium tosylhydrazide has shown that the $\tilde{B} \leftarrow \tilde{X}$ system previously studied by Trombetti arises from the ^1A_g ground state of *trans*-diimide that has been well characterized by its infrared spectrum. No evidence was found for the presence of other isomers or triplet states of diimide. The spectrum is essentially the same as that of diimide produced by a microwave discharge through hydrazine vapor, although almost free of the strong ammonia impurity absorption that obscured much of the latter.

(*2*) The $\tilde{B}(^1B_u) \leftarrow \tilde{X}(^1A_g)$ system and a second new $\tilde{C} \leftarrow \tilde{X}$ system, with origins at 1727 and 1473 Å respectively, are believed to correspond to the Rydberg transitions, $3p_\pi(b_u) \leftarrow n_+$ and $4p_\pi(b_u) \leftarrow n_+$, members of a series converging to an ionization potential of 9.62 eV with a quantum defect of 0.639.

(*3*) Excitation of the $\tilde{B}$ state leads to an increase of 21° in the HNN bond angle and a decrease in the N—N bond length of about 0.09 Å. Associated with these changes in geometry are a decrease in ν_2', the symmetric bending frequency, and an increase in ν_3', the symmetric N—N stretching frequency, in both the $\tilde{B}$ and $\tilde{C}$ states, while both the ν_2' and ν_3' vibrations are excited in the transitions.

Acknowledgement

We are indebted to Mr. F. Alberti for photographing the spectra.

1. A. Trombetti. Can. J. Phys. **46**, 1005 (1968).
2. C. Willis and R. A. Back. Can. J. Chem. **51**, 3605 (1973).
3. M. Carlotti, J. W. C. Johns, and A. Trombetti. Can. J. Phys. **52**, 340 (1974).
4. R. A. Back, C. Willis, and D. A. Ramsay. Can. J. Chem. **52**, 1006 (1974); **56**, 1575 (1978).
5. K. Vasudevan, S. D. Peyerimhoff, R. J. Buenker, W. E. Kammer, and H. -L. Hsu. Chem. Phys. **7**, 187 (1975).
6. R. Ahlrichs and V. Staemmler. Chem. Phys. Lett. **37**, 77 (1976).
7. N. W. Winter and R. M. Pitzer. J. Chem. Phys. **62**, 1269 (1975).
8. N. Wiberg, G. Fisher, and H. Bachhuber. Chem. Ber. **107**, 1456 (1974).
9. N. Wiberg, G. Fisher, and H. Bachhuber. Angew. Chem. Int. Ed. Engl. **15**, 385 (1976); **16**, 780 (1977); G. Fisher. Ph.D. Thesis. L. Maximilians University, Munich. 1977.
10. V. E. Bondybey and J. W. Nibler. J. Chem. Phys. **58**, 2125 (1973).
11. A. E. Douglas and J. M. Hollas. Can. J. Phys. **39**, 479 (1961).
12. G. Herzberg. Infrared and Raman spectra of polyatomic molecules. Van Nostrand Reinhold, New York. 1945. (*a*) p. 390; (*b*) pp. 434–437.
13. M. B. Robin. Higher excited states of polyatomic molecules. Vol. 2. Academic Press, New York. 1975. pp. 68–73.
14. D. C. Frost, S. T. Lee, C. A. McDowell, and N. P. Westwood. J. Chem. Phys. **64**, 4719 (1976).
15. S. N. Foner and R. L. Hudson. J. Chem. Phys. **68**, 3162 (1978).
16. C. Willis, F. P. Lossing, and R. A. Back. Can. J. Chem. **54**, 1 (1976).
17. G. Herzberg. Electronic spectra of polyatomic molecules. Van Nostrand Reinhold, New York. 1966. p. 341.
18. M. Perić, R. J. Buenker, and S. D. Peyerimhoff. Can. J. Chem. **55**, 1533 (1977).
19. A. D. Walsh. J. Chem. Soc. 2288 (1953).

Synthesis, characterization, and X-ray structural analysis of the Cu(I) derivative, $[Me_2Ga(OCH_2CH_2NMe_2)N_2C_5H_7]Cu \cdot PPh_3$

KENNETH S. CHONG, STEVEN J. RETTIG, ALAN STORR, AND JAMES TROTTER

Department of Chemistry, University of British Columbia, 2036 Main Mall, Vancouver, B.C., Canada V6T 1Y6

Received July 28, 1980

KENNETH S. CHONG, STEVEN J. RETTIG, ALAN STORR, and JAMES TROTTER. Can. J. Chem. **59**, 518 (1981).

The Cu(I) complex $[Me_2Ga(OCH_2CH_2NMe_2)N_2C_5H_7]Cu \cdot PPh_3$ has been synthesized and its fluxional behavior in solution probed. Attempts have been made to isolate the analogous Cu(I) carbonyl complex. Crystals of [dimethyl(3,5-dimethyl-1-pyrazolyl)(*N*,*N*-dimethylethanolamino)gallato (*N(2),O,N(3)*)](triphenylphosphine)copper(I) are monoclinic, $a = 18.871(2)$, $b = 9.464(1)$, $c = 18.374(2)$ Å, $\beta = 109.62(1)°$, $Z = 4$, space group $P2_1/c$. The structure was solved by direct methods and was refined by full-matrix least-squares procedures to $R = 0.028$ and $R_w = 0.035$ for 2729 reflections with $I \geq 3\sigma(I)$. The copper atom is bonded to the phosphine and to the tridentate $Me_2Ga(OCH_2CH_2NMe_2)N_2C_5H_7^-$ ligand resulting in a distorted tetrahedral coordination geometry. The Cu—P distance of 2.156(1) Å is unusually short. Other important bond distances (corrected for libration) are: Cu—O, 2.163(2), Cu—N(pyrazolyl), 2.025(3), Cu—N(amino), 2.144(3), Ga—O, 1.896(3), Ga—N, 2.005(3), and Ga—C, 1.972(5) and 1.987(5) Å.

KENNETH S. CHONG, STEVEN J. RETTIG, ALAN STORR et JAMES TROTTER. Can. J. Chem. **59**, 518 (1981).

On a synthétisé le complexe de Cu(I)$[Me_2Ga(OCH_2CH_2NMe_2)N_2C_5H_7]Cu$ et on a prouvé son comportement fluxionnaire en solution. On a essayé d'isoler les complexes carbonylés analogues du Cu(I). Les cristaux de [diméthyl(diméthyl-3,5 pyrazolyl-1)(*N*,*N*-diméthyléthanolamino)gallato(*N(2),O,N(3)*)] triphénylphosphine Cu(I) sont monocliniques et appartiennent au groupe d'espace $P2_1/c$ avec $a = 18,871(2)$, $b = 9,464(1)$, $c = 18,374(2)$ Å, $\beta = 109,62(1)°$, $Z = 4$. On a résolu les structures par les méthodes directes et on les a affinées par la méthode des moindres carrés (matrice entière) jusqu'à des valeurs de $R = 0,28$ et $R_w = 0,035$ pour 2729 réflexions avec $I \geq 3\sigma(I)$. L'atome de Cu est lié à la phosphine et au ligand tridentate $Me_2Ga(OCH_2CH_2NMe_2)N_2C_5H_7^-$ conduisant ainsi une géométrie de coordination tétraédrique déformée. La distance Cu—P de 2,156(1) Å est inhabituellement courte. Les autres longueurs importantes de liaison (corrigée pour la libration) sont: Cu—O, 2,163(2), Cu—N(pyrazolyl), 2,025(3), Cu—N(amino), 2,144(3), Ga—O, 1,896(3), Ga—N, 2,005(3) et Ga—C, 1,972(5) et 1,987(5) Å.

[Traduit par le journal]

Introduction

Tridentate chelating gallate ligands (incorporating pyrazolyl and ethanolamino moieties) that impart an asymmetry in their complexes with metallic species and create electron-rich metal centres have been the subject of a number of recent publications (1). This type of ligand has now been used to stabilize the Cu(I) centre in the complex $[Me_2Ga(OCH_2CH_2NMe_2)N_2C_5H_7]Cu \cdot PPh_3$ and also in attempts to prepare isolable Cu(I) carbonyl derivatives. ^1H nmr results indicate that the title compound is fluxional in solution. In the solid state the title compound has been shown by X-ray structural studies to possess the Cu(I) centre in a tetrahedral environment.

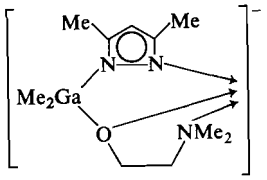

1

Experimental

Starting Materials

Air-sensitive materials were handled in a glove box under an atmosphere of oxygen-free dry nitrogen or in a nitrogen-blanketed apparatus. Tetrahydrofuran (THF) and diethyl ether were dried by refluxing over sodium/benzophenone and were used immediately following distillation. Toluene was dried by refluxing over potassium followed by distillation. The gallium ligand, $Na^+Me_2Ga(OCH_2CH_2NMe_2)N_2C_5H_7^-$, **1**, was prepared as described earlier (2). $Ph_3P \cdot CuBr$ was prepared from Ph_3P and CuBr (3).

Preparation of $[Me_2Ga(OCH_2CH_2NMe_2)N_2C_5H_7]Cu \cdot PPh_3$

A THF solution of the ligand **1** (1.6 mmol) was added to a slurry of $Ph_3P \cdot CuBr$ (0.649 g, 1.6 mmol) in the same solvent. The mixture was stirred overnight and the solvent then removed *in vacuo*. The remaining white solid was extracted with toluene and the extracts filtered. Slow evaporation of the filtrate gave large colorless crystals of the product in approximately 80% yield. *Anal.* calcd. for $[Me_2Ga(OCH_2CH_2NMe_2)N_2C_5H_7]Cu \cdot PPh_3$: C 57.2, H 6.3, N 6.9; found: C 57.6, H 6.4, N 7.0. Room temperature ^1H *nmr* (C_6D_6 solution): τ = 9.97 s ($GaMe_2$), 8.15 s (NMe_2), 7.85 s (pz—Me), 7.66 s (pz—Me), 7.90 t and 5.97 t ($—CH_2—CH_2$) ($J \approx 5$ Hz), 4.01 s (pz—H(4)), 2.95 m and 2.41 m (PPh_3) ($\tau_{C_6H_6} = 2.84$ ppm; s = singlet, t = triplet; pz = pyrazolyl). *Mass spectrum*: the parent ion was not observed, the highest mass signal arising from the ion $[Me_2Ga(OCH_2CH_2NMe_2)N_2C_5H_7]Cu^+$. Other strong signals observed were due to the ions $[MeGa(OCH_2CH_2NMe_2)N_2C_5H_7]Cu^+$, $[MeGa(N_2C_5H_7)O]Cu^+$, PPh_3^+, PPh_2^+, and PPh^+.

Attempted Preparation of $[Me_2Ga(OCH_2CH_2NMe_2)N_2C_5H_7]Cu \cdot CO$

CuCl (0.099 g, 1.00 mmol) was suspended in diethyl ether saturated with carbon monoxide. A solution of the ligand **1** (1.00 mmol) in THF was added dropwise over a period of 30 min. Slowly a flocculent white precipitate formed and after the reac-

0008-4042/81/030518-06$01.00/0

©1981 National Research Council of Canada/Conseil national de recherches du Canada

Can. J. Chem. Downloaded from www.nrcresearchpress.com by 210.87.254.6 on 09/06/12
For personal use only.

Can. J. Chem. Downloaded from www.nrcresearchpress.com by 210.87.254.6 on 09/06/12
For personal use only.

tion mixture had been stirred overnight (under an atmosphere of CO) the mixture was filtered. The ir spectrum of the solution showed a ν_{CO} band at ~2070 cm^{-1} (free CO, ν_{CO} 2143 cm^{-1}). However, after removal of volatiles *in vacuo* the remaining white solid showed no evidence for a Cu—CO moiety in its ir spectrum. When this white solid was treated with CO gas, the ir spectrum of the resulting residue showed a weak ν_{CO} band at ~2078 cm^{-1}. Again this band disappeared when the solid was pumped *in vacuo*. The white solid decomposed slowly to yield in part the previously characterized five-coordinate gallium dimer $(Me_2GaOCH_2CH_2NMe_2)_2$ (4). The propensity of this Cu compound to decomposition and its extreme sensitivity to air curtailed the study of this reaction.

Spectra

The mass spectrum was collected on a Varian MAT CH4 spectrometer at 70 eV with an ion source temperature of 100–180°C and the ^1H nmr spectra on a Varian XL-100 spectrometer using FT techniques.

X-ray Crystallographic Analysis of [Dimethyl(3,5-dimethyl-1-pyrazolyl)(N,N-dimethylethanolamino)gallato-(N(2),O,N(3))](triphenylphosphine)copper(I)

A crystal ca. 0.21 × 0.35 × 0.35 mm in size was mounted in a general orientation. Parameters were refined by least-squares on 2 sin θ/λ values for 25 reflections measured on a diffractometer with Mo K_α radiation (λ = 0.71073 Å). Crystal data at 22°C are:

$C_{29}H_{38}CuGaN_3OP$ fw = 608.89
Monoclinic, a = 18.871(2), b = 9.464(1), c = 18.374(2) Å, β = 109.62(1)°, V = 3091.0(5) Å^3, ρ_m = 1.30 (by flotation in aqueous KI), Z = 4, ρ_c = 1.308 g cm^{-3}, $F(000)$ = 1264, μ(Mo K_α) = 16.3 cm^{-1}. Absent reflections: $h0l$, $l \neq 2n$ and $0k0$, $k \neq 2n$ uniquely indicate the space group $P2_1/c$ (C_{2h}^5, No. 14).

Intensities were measured with graphite-monochromatized Mo K_α radiation on an Enraf-Nonius CAD4-F diffractometer. An ω–2θ scan at 0.96–10.06° min^{-1} over a range of (0.70 + 0.35 tan θ) degrees in ω (extended by 25% on both sides for background measurement) was employed. Data were measured to 2θ = 50°. The intensities of 3 check reflections, measured every 3600 s throughout the data collection, remained constant to within ±4%. After data reduction, an absorption correction was applied using the Gaussian integration method (5, 6). Transmission factors ranged from 0.574 to 0.777 for 190 sampling points. Of the 5415 independent reflections measured, 2729 (50.4%) had intensities greater than $3\sigma(I)$ above background where $\sigma^2(I) = S + 2B + (0.04(S - B))^2$ with S = scan count and B = background count.

The structure was solved by direct methods, the coordinates of the Ga, Cu, and P atoms being determined from an E-map and those of the remaining non-hydrogen atoms from a subsequent Fourier synthesis. After refinement of the non-hydrogen atoms with anisotropic thermal parameters to R = 0.044, a difference map revealed the positions of 35 of the 38 hydrogen atoms. Idealized positions were calculated for all hydrogen atoms which were included as fixed atoms in subsequent calculations (C(sp^3)—H = 0.98, C(sp^2)—H = 0.95 Å, $U_H = xU_C$ where x = 1.25 for methyl H and 1.15 for all others).

The scattering factors of ref. 7 were used for non-hydrogen atoms and those of ref. 8 for hydrogen atoms. Anomalous scattering factors from ref. 9 were used for the Ga, Cu, and P atoms. The weighting scheme, $w = 1/\sigma^2(F)$, where $\sigma^2(F)$ is derived from the previously defined $\sigma^2(I)$ gave uniform average values of $w(|F_o| - |F_c|)^2$ over ranges of $|F_o|$ and was employed in the final stages of refinement. Convergence was reached at R = 0.028 and R_w = 0.035 for 2729 reflections with $I \geq 3\sigma(I)$. For all 5415 reflections R = 0.094 and R_w = 0.035. The function minimized was $\Sigma w(|F_o| - |F_c|)^2$, $R = \Sigma||F_o| - |F_c||/\Sigma|F_o|$ and $R_w = (\Sigma w(|F_o| - |F_c|)^2/\Sigma w|F_o|^2)^{1/2}$.

On the final cycle of refinement the mean and maximum parameter shifts correspond to 0.06 and 0.45σ respectively. The mean error in an observation of unit weight was 1.043. A final difference map showed maximum fluctuations of ±0.28 e Å^{-3}. The final positional and thermal parameters appear in Tables 1 and 2[1] respectively. Measured and calculated structure factors have been placed in the Depository of Unpublished Data.[1]

The ellipsoids of thermal motion for the non-hydrogen atoms are shown in Fig. 1. The thermal motion has been analysed in terms of the rigid-body modes of translation, libration, and screw motion (10) using the computer program MGTLS. The rms standard error in the temperature factors σU_{ij} (derived from the least-squares analysis) is 0.0034 Å^2. Six successful analyses were carried out; three tetrahedra centered at Ga, Cu, and N(3), two PPh moieties and a 12 atom group consisting of the P atom plus the atoms comprising the system of three fused rings (rms ΔU_{ij} = 20, 22, 20, 33, 27, and 70 × 10^{-4} Å^2). Analysis of the phenyl ring containing C(24) and P gave a non-positive-definite libration tensor. The appropriate bond distances have been corrected for libration (11), using shape parameters q^2 of 0.08 for all atoms involved. Corrected bond lengths appear in Table 3 along with the uncorrected values and corrected bond angles are not different from the uncorrected values listed in Table 4 by more than one standard deviation. Intra-annular torsion angles defining the conformations of the chelate rings are listed in Table 5.

Results and Discussion

The compound $[Me_2Ga(OCH_2CH_2NMe_2)N_2C_5H_7]Cu \cdot PPh_3$ was found to be air stable in the solid state and also stable in hydrocarbon solvents under a nitrogen atmosphere. However, on exposure of such solutions to air or on dissolution of the solid in halogenated solvents, decomposition is evidenced by the formation of blue solutions.

The rt ^1H nmr of the title compound in C_6D_6 solvent displayed one signal due to the —$GaMe_2$ protons, one signal due to the —NMe_2 protons, and two pseudo-triplets due to the —CH_2 —CH_2 protons (see Fig. 2). This spectrum is suggestive of a *meridionally* coordinated gallate ligand and consequently a square-planar Cu(I) derivative. A tetrahedral arrangement about the Cu atom in the complex in solution would lead to two signals for each of the —$GaMe_2$ and —NMe_2 groups of protons. However, a square-planar geometry is very unusual for a Cu(I) centre and our previous experience with a related four-coordinate Ni nitrosyl derivative (12) prompted us to investigate the present Cu(I) complex for fluxional behavior in solution.

The —$GaMe_2$ signal was monitored as the temperature of an acetone-d^6 solution was lowered. The sharp singlet at rt gradually broadened at tem-

[1]The structure factor table and Table 2 (thermal parameters) are available, at a nominal charge, from the Depository of Unpublished Data, CISTI, National Research Council of Canada, Ottawa, Ont., Canada K1A 0S2.

Can. J. Chem. Downloaded from www.nrcresearchpress.com by 210.87.254.6 on 09/06/12
For personal use only.

TABLE 1. Final positional parameters (fractional × 10^4; Ga, Cu, and P × 10^5) with estimated standard deviations in parentheses

Atom	x	y	z
Ga	68653(3)	47727(6)	22148(2)
Cu	71334(2)	48756(5)	5639(2)
P	81999(5)	46479(10)	3912(5)
O	7025(1)	6084(3)	1516(1)
N(1)	6389(2)	3258(4)	1453(2)
N(2)	6512(2)	3277(3)	763(2)
N(3)	6315(2)	6352(4)	−106(2)
C(1)	7858(3)	4050(6)	2827(3)
C(2)	6110(4)	5493(7)	2646(3)
C(3)	6035(2)	2047(5)	1504(3)
C(4)	5928(3)	1288(5)	848(4)
C(5)	6231(2)	2080(5)	396(3)
C(6)	6520(3)	7208(5)	1208(3)
C(7)	5964(3)	6829(5)	446(3)
C(8)	5815(3)	1711(6)	2201(3)
C(9)	6278(3)	1777(5)	−383(3)
C(10)	6638(3)	7536(6)	−393(3)
C(11)	5750(3)	5675(6)	−764(3)
C(12)	8198(2)	5346(4)	−537(2)
C(13)	8598(3)	6526(5)	−601(3)
C(14)	8502(3)	7130(5)	−1310(3)
C(15)	8009(3)	6561(6)	−1961(3)
C(16)	7618(3)	5383(6)	−1918(3)
C(17)	7709(2)	4772(5)	−1211(2)
C(18)	9004(2)	5522(4)	1096(2)
C(19)	9745(2)	5278(5)	1154(3)
C(20)	10327(3)	6019(7)	1673(3)
C(21)	10174(3)	7006(6)	2143(3)
C(22)	9447(3)	7234(5)	2106(3)
C(23)	8867(2)	6490(5)	1585(2)
C(24)	8511(2)	2827(4)	393(2)
C(25)	8912(3)	2351(6)	−63(3)
C(26)	9138(5)	921(8)	−9(4)
C(27)	8978(6)	65(7)	511(5)
C(28)	8576(4)	527(6)	952(4)
C(29)	8339(3)	1902(5)	888(3)
H(1a)	7801	3319	3180
H(1b)	8105	3660	2483
H(1c)	8162	4832	3129
H(2a)	6289	5365	3203
H(2b)	6008	6482	2511
H(2c)	5636	4941	2418
H(4)	5691	385	724
H(6a)	6250	7438	1565
H(6b)	6802	8038	1142
H(7a)	5650	7657	232
H(7b)	5640	6067	521
H(8a)	5374	2264	2184
H(8b)	5694	693	2194
H(8c)	6235	1924	2669
H(9a)	5885	1084	−647
H(9b)	6202	2643	−684
H(9c)	6773	1372	−325
H(10a)	7062	7932	31
H(10b)	6815	7219	−808
H(10c)	6254	8276	−591
H(11a)	5304	6278	−955
H(11b)	5961	5507	−1176
H(11c)	5604	4759	−597
H(13)	8950	6928	−151
H(14)	8771	7950	−1347
H(15)	7940	6998	−2467
H(16)	7285	4983	−2376
H(17)	7432	3944	−1188
H(19)	9858	4586	834
H(20)	10833	5857	1716
H(21)	10584	7573	2508
H(22)	9338	7912	2435
H(23)	8363	6661	1566
H(25)	9031	2987	−412
H(26)	9404	578	−332
H(27)	9155	−875	567
H(28)	8460	−96	1294
H(29)	8062	2232	1198

peratures below ~ −40°C, "disappeared", and reappeared as two signals in positions on either side of the position of the original singlet. These two signals were sharp at the lowest temperature attainable (−75°C) and were separated by about 0.2 ppm. This evidence suggests that the Cu(I) centre is indeed tetrahedrally coordinated but that at temperatures above −40°C in solution the molecule undergoes a rapid (on the nmr time scale) fluxional process to give an "average" square-planar environment about the Cu atom.

Two plausible mechanisms might explain the fluxional process. The first possibility involves a simple inversion at the metal centre without dissociation of any of the ligand atoms from the metal. This would give an intermediate square-planar environment about the Cu atom. The second possibility (see Fig. 3) involves a three-coordinate intermediate formed by dissociation of the —NMe_2 part of the gallate ligand from the Cu(I) centre. In this intermediate the —NMe_2 and —$GaMe_2$ groups would also give rise to one signal each in the ^1H nmr spectrum. The expected tetrahedral nature of the Cu(I) complex suggested by these low temperature ^1H nmr studies has been confirmed in the solid state by X-ray crystallographic studies (see below).

At the outset of this study it was thought entirely possible that the compound $[Me_2Ga(OCH_2CH_2NMe_2)N_2C_5H_7]Cu \cdot CO$ should exist and be moderately stable. Effectively in this complex the CO ligand formally replaces the Ph_3P ligand of the title compound. It was thought that the ability of the gallate ligands to create electron-rich metal centres in its complexes (13) would help to stabilize a Cu(I) carbonyl derivative. Thus the only stable Cu(I) carbonyl complexes to have been reported contain ancillary ligands capable of creating increased electron density at the copper centre with

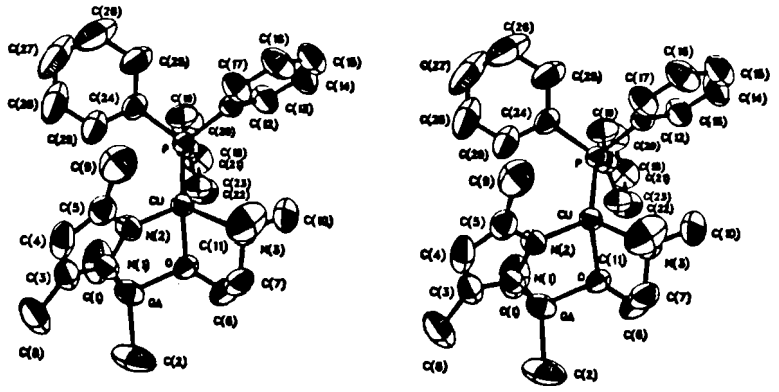

FIG. 1. Stereo view of the [dimethyl(3,5-dimethyl-1-pyrazolyl)(*N,N*-dimethylethanolamino)gallato(*N(2),O,N(3)*)](triphenylphosphine)copper(I) molecule. 50% thermal ellipsoids are shown for the non-hydrogen atoms.

TABLE 3. Bond lengths (Å) with estimated standard deviations in parentheses*

Bond	Length		Bond	Length	
	Uncorr.	Corr.		Uncorr.	Corr.
Ga —O	1.881(3)	1.896	C(5) —C(9)	1.492(6)	1.492
Ga —N(1)	1.994(3)	2.005	C(6) —C(7)	1.485(7)	1.489
Ga —C(1)	1.957(5)	1.972	C(12)—C(13)	1.374(5)	1.390
Ga —C(2)	1.971(5)	1.987	C(12)—C(17)	1.383(5)	1.396
Cu —P	2.151(1)	2.156	C(13)—C(14)	1.378(6)	1.382
Cu —O	2.157(2)	2.163	C(14)—C(15)	1.357(7)	1.369
Cu —N(2)	2.022(3)	2.028	C(15)—C(16)	1.354(7)	1.371
Cu —N(3)	2.139(3)	2.144	C(16)—C(17)	1.380(6)	1.384
P —C(12)	1.828(4)	1.833	C(18)—C(19)	1.384(5)	1.398
P —C(18)	1.829(4)	1.835	C(18)—C(23)	1.369(5)	1.384
P —C(24)	1.820(4)	1.822	C(19)—C(20)	1.381(7)	1.386
O —C(6)	1.414(5)	1.418	C(20)—C(21)	1.367(7)	1.382
N(1)—N(2)	1.364(4)	1.369	C(21)—C(22)	1.369(6)	1.382
N(1)—C(3)	1.347(5)	1.350	C(22)—C(23)	1.382(6)	1.387
N(2)—C(5)	1.334(5)	1.338	C(24)—C(25)	1.379(6)	
N(3)—C(7)	1.458(5)	1.475	C(24)—C(29)	1.378(6)	
N(3)—C(10)	1.455(6)	1.473	C(25)—C(26)	1.412(8)	
N(3)—C(11)	1.464(6)	1.482	C(26)—C(27)	1.362(10)	
C(3)—C(4)	1.358(6)	1.363	C(27)—C(28)	1.355(10)	
C(3)—C(8)	1.506(6)	1.507	C(28)—C(29)	1.368(7)	
C(4)—C(5)	1.377(6)	1.380			

*Corrected distances are referred to throughout the discussion, esd's for these values are assumed to be equal to those for the uncorrected values.

concomitant stronger Cu—CO binding. The first of these incorporated a pyrazolyl borate ligand, viz. $[HB(N_2C_3H_3)_3]Cu \cdot CO$ (14), the complex being air stable with a ν_{CO} ir band at 2083 cm^{-1}. The nature of the tridentate borate ligand necessarily imparts a tetrahedral structure at the Cu(I) centre in this complex, and this was confirmed in a structure determination (15). More recently a number of stable "amine" Cu(I) carbonyl complexes have been reported. These include the diethylenetriamine complex $[Cu(dien)(CO)]^+BPh_4^-$ (16) with a ν_{CO} ir band at 2080 cm^{-1} and a series of ethylenediamine Cu(I) carbonyl complexes (17). In the present study the reaction of $Me_2Ga(OCH_2CH_2NMe_2)N_2C_5H_7^-$ with CuCl in the presence of CO in diethyl ether did generate a species in solution giving an expected low ν_{CO} ir band at ~2070 cm^{-1}. However, isolation of a copper carbonyl complex from solution did not prove feasible. It is evident that only weak coordination of CO occurs in this experiment and although the clear possibility of reversible CO binding exists with this system, the unstable nature of the product from the reaction discouraged any further studies.

Can. J. Chem. Downloaded from www.nrcresearchpress.com by 210.87.254.6 on 09/06/12
For personal use only.

Can. J. Chem. Downloaded from www.nrcresearchpress.com by 210.87.254.6 on 09/06/12
For personal use only.

TABLE 4. Bond angles (deg) with estimated standard deviations in parentheses for non-hydrogen atoms

Bonds	Angle (deg)	Bonds	Angle (deg)
O —Ga —N(1)	97.7(1)	N(1) —C(3) —C(4)	108.5(4)
O —Ga —C(1)	106.3(2)	N(1) —C(3) —C(8)	121.6(5)
O —Ga —C(2)	110.5(2)	C(4) —C(3) —C(8)	129.9(5)
N(1) —Ga —C(1)	105.7(2)	C(3) —C(4) —C(5)	106.3(4)
N(1) —Ga —C(2)	108.3(2)	N(2) —C(5) —C(4)	109.4(4)
C(1) —Ga —C(2)	124.9(3)	N(2) —C(5) —C(9)	120.4(4)
P —Cu —O	121.4(1)	C(4) —C(5) —C(9)	130.2(5)
P —Cu —N(2)	125.5(1)	O —C(6) —C(7)	111.4(4)
P —Cu —N(3)	120.7(1)	N(3) —C(7) —C(6)	112.9(4)
O —Cu —N(2)	91.8(1)	P —C(12)—C(13)	122.9(3)
O —Cu —N(3)	82.8(1)	P —C(12)—C(17)	119.0(3)
N(2) —Cu —N(3)	104.0(1)	C(13)—C(12)—C(17)	117.6(4)
Cu —P —C(12)	113.1(1)	C(12)—C(13)—C(14)	121.1(4)
Cu —P —C(18)	116.5(1)	C(13)—C(14)—C(15)	120.2(5)
Cu —P —C(24)	114.3(2)	C(14)—C(15)—C(16)	120.1(4)
C(12)—P —C(18)	103.8(2)	C(15)—C(16)—C(17)	120.1(5)
C(12)—P —C(24)	104.1(2)	C(12)—C(17)—C(16)	120.9(4)
C(18)—P —C(24)	103.7(2)	P —C(18)—C(19)	123.8(3)
Ga —O —Cu	106.5(1)	P —C(18)—C(23)	118.2(3)
Ga —O —C(6)	121.9(3)	C(19)—C(18)—C(23)	118.0(4)
Cu —O —C(6)	108.0(2)	C(18)—C(19)—C(20)	121.2(4)
Ga —N(1)—N(2)	117.8(2)	C(19)—C(20)—C(21)	119.7(4)
Ga —N(1)—C(3)	132.9(3)	C(20)—C(21)—C(22)	119.9(4)
N(2) —N(1)—C(3)	108.6(4)	C(21)—C(22)—C(23)	120.1(4)
Cu —N(2)—N(1)	117.9(3)	C(18)—C(23)—C(22)	121.0(4)
Cu —N(2)—C(5)	134.5(3)	P —C(24)—C(25)	123.4(4)
N(1) —N(2)—C(5)	107.2(3)	P —C(24)—C(29)	117.1(3)
Cu —N(3)—C(7)	102.2(2)	C(25)—C(24)—C(29)	119.5(4)
Cu —N(3)—C(10)	113.7(3)	C(24)—C(25)—C(26)	119.0(5)
Cu —N(3)—C(11)	112.0(3)	C(25)—C(26)—C(27)	119.1(6)
C(7) —N(3)—C(10)	110.9(4)	C(26)—C(27)—C(28)	121.9(6)
C(7) —N(3)—C(11)	109.5(4)	C(27)—C(28)—C(29)	119.2(7)
C(10)—N(3)—C(11)	108.4(4)	C(24)—C(29)—C(28)	121.2(5)

TABLE 5. Intra-annular torsion angles (deg) chelate rings

Bond	Obs.	Bond	Obs.
Ga —O	−27.2(1)	Cu —O	−2.7(3)
O —Cu	25.9(1)	O —C(6)	28.8(4)
Cu —N(2)	−14.8(2)	C(6)—C(7)	−54.5(4)
N(2)—N(1)	−2.1(2)	C(7)—N(3)	47.2(3)
N(1)—Ga	20.5(2)	N(3)—Cu	−23.2(2)

Crystal Structure of [Dimethyl(3,5-dimethyl-1-pyrazolyl)(N,N-dimethylethanolamino)gallato(N(2),O,N(3))](triphenylphosphine)copper(I)

The crystal structure of $[Me_2Ga(OCH_2CH_2NMe_2)N_2C_5H_7]Cu \cdot PPh_3$ consists of discrete molecular units separated by normal van der Waals distances. The copper atom is bonded to the phosphorus and to the oxygen and two nitrogen atoms of the tridentate $Me_2Ga(OCH_2CH_2NMe_2)N_2C_5H_7^-$ ligand resulting in a distorted tetrahedral coordination geometry. The mean bond angle at copper involving phosphorus is 122.5°, and the remaining bond angles average 92.9°.

The Cu—P distance of 2.156(1) Å is unusually short, the normal range for tetrahedral Cu(I)—P distances being 2.19–2.35 Å with a mean value of 2.270 Å for 61 independent observations. The only known Cu(I)—P bond shorter than that in the present structure is the distance of 2.136(9) Å observed in the pseudotetrahedral complex $(\eta^5\text{-}C_5H_5)Cu \cdot PEt_3$ (18). Two interrelated factors are believed responsible for this short Cu—P distance. Steric constraints of chelation by the ligand **1** cause hybridization changes at the metal which result in increased *s* character of the fourth bond in tetrahedral complexes. This, combined with the enhancement of electron density at the metal centre (13), results in unusually short bond distances, as noted for the tetrahedral complex $[Me_2Ga(OCH_2CH_2NMe_2)N_2C_5H_7]Ni(NO)$ (12). The Cu—O and Cu—N distances are as expected.

The gallium atom has distorted tetrahedral coordination geometry with bond angles ranging from 97.7(1) to 124.9(3)°. The internal geometry of the gallate ligand is in good agreement with that observed in related structures (1) and the ligand conformation is similar to other structures in which the ligand is facially coordinated (12, 19–21). The

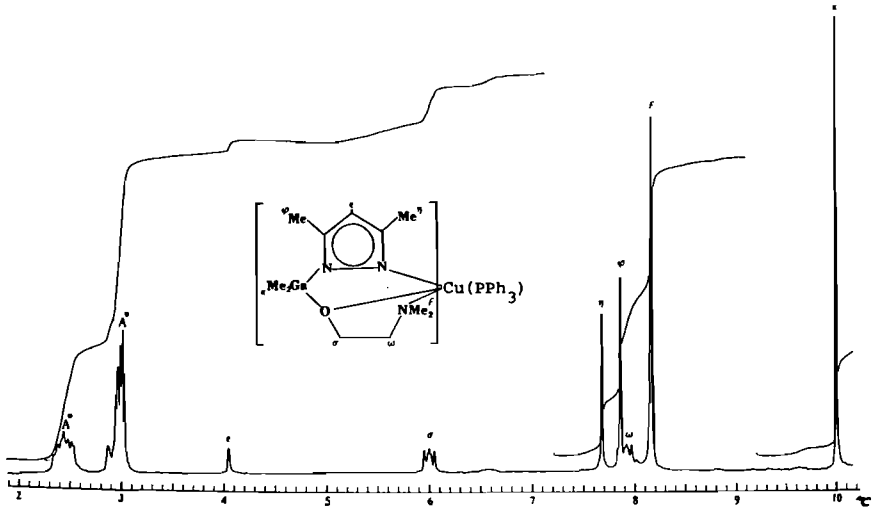

FIG. 2. 100 MHz ^{1}H nmr spectrum of $[Me_2Ga(OCH_2CH_2NMe_2)(N_2C_5H_7)]Cu \cdot PPh_3$ in C_6D_6 solution (A* signals due to PPh_3 ligand).

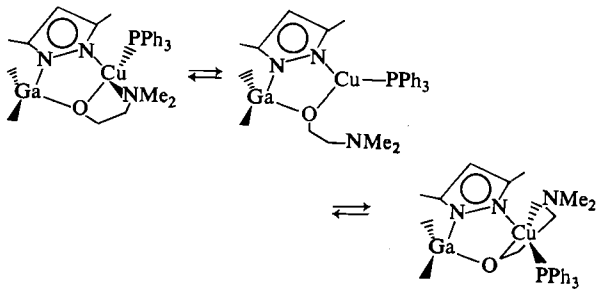

FIG. 3. A possible mechanism for the fluxional process observed for $[Me_2Ga(OCH_2CH_2NMe_2)(N_2C_5H_7)]Cu \cdot PPh_3$ in solution.

pyrazolyl group is planar ($\chi^2 = 0.04$ for N_2C_3) with the metal atoms considerably displaced from the mean plane (Ga by − 0.2540(5) and Cu by −0.1950(5) Å).

The geometry of the phosphine ligand is normal. The phenyl ring containing C(12) is planar within experimental error ($\chi^2 = 8.5$) while the two other phenyl rings are slightly, but significantly, non-planar ($\chi^2 = 19.8$ and 13.7 for rings containing C(18) and C(24), respectively). The phosphorus atom is significantly displaced from each of the three phenyl mean planes (by −0.243(1), 0.087(1), and −0.057(1) Å from the rings containing C(12), C(18), and C(24), respectively). There is a possible weak intramolecular hydrogen bond between the oxygen atom and a phenyl hydrogen (C(23)···O = 3.456(5), H(23)···O = 2.55 Å, C—H···O = 158°).

Acknowledgments

We thank the Natural Sciences and Engineering Research Council of Canada for financial support and the University of British Columbia Computing Centre for assistance. We are grateful to Mr. P. Borda for C, H, N analyses, to Mr. J. Nip for the mass spectrum, and to Ms. M. Tracey for ^{1}H nmr spectra.

1. K. S. CHONG and A. STORR. Can. J. Chem. **58**, 2278 (1980) and references therein.
2. K. S. CHONG, A. STORR, S. J. RETTIG, and J. TROTTER. Can. J. Chem. **55**, 4166 (1977).
3. G. COSTA, E. REISENHOFER, and L. STEFANI. J. Inorg. Nucl. Chem. **27**, 2581 (1965).
4. S. J. RETTIG, A. STORR, and J. TROTTER. Can. J. Chem. **53**, 58 (1975).
5. P. COPPENS, L. LEISEROWITZ, and D. RABINOVICH. Acta Crystallogr. **18**, 1035 (1965).
6. W. R. BUSING and H. A. LEVY. Acta Crystallogr. **22**, 457 (1967).
7. D. T. CROMER and J. B. MANN. Acta Crystallogr. Sect. A, **24**, 321 (1968).
8. R. F. STEWART, E. R. DAVIDSON, and W. T. SIMPSON. J. Chem. Phys. **42**, 3175 (1965).
9. D. T. CROMER and D. LIBERMAN. J. Chem. Phys. **53**, 1891 (1970).
10. V. SCHOMAKER and K. N. TRUEBLOOD. Acta Crystallogr. Sect. B, **24**, 63 (1969).
11. D. W. J. CRUICKSHANK. Acta Crystallogr. **9**, 747 (1956); **9**, 754 (1956); **14**, 896 (1961).
12. K. S. CHONG, S. J. RETTIG, A. STORR, and J. TROTTER. Can. J. Chem. **57**, 3107 (1979).
13. K. S. CHONG and A. STORR. Can. J. Chem. **57**, 167 (1979).
14. M. J. BRUCE and A. P. P. OSTAZEWSKI. J. Chem. Soc. Dalton Trans. 2433 (1973).
15. M. R. CHURCHILL, B. G. DEBOER, F. J. ROTELLA, O. M. A. SALAH, and M. I. BRUCE. Inorg. Chem. **14**, 2051 (1975).
16. M. PASQUALI, F. MARCHETTI, and C. FLORIANI. Inorg. Chem. **17**, 1684 (1978).
17. M. PASQUALI, C. FLORIANI, and A. M. MANFREDOTTI. J. Chèm. Soc. Chem. Commun. 921 (1978).
18. L. T. J. DELBAERE, D. W. MCBRIDE, and R. B. FERGUSON. Acta Crystallogr. Sect. B, **26**, 515 (1970).
19. K. S. CHONG, S. J. RETTIG, A. STORR, and J. TROTTER. Can. J. Chem. **56**, 1212 (1978).
20. K. S. CHONG, S. J. RETTIG, A. STORR, and J. TROTTER. Can. J. Chem. **57**, 1335 (1979).
21. K. S. CHONG, S. J. RETTIG, A. STORR, and J. TROTTER. Can. J. Chem. **58**, 1080 (1980).

Can. J. Chem. Downloaded from www.nrcresearchpress.com by 210.87.254.6 on 09/06/12
For personal use only.

Crystal structure of a stemodin intermediate

RICHARD A. PAUPTIT AND JAMES TROTTER

Department of Chemistry, University of British Columbia, Vancouver, B.C., Canada V6T 1Y6

Received July 25, 1980

RICHARD A. PAUPTIT and JAMES TROTTER. Can. J. Chem. **59**, 524 (1981).

Crystals of the title compound, $C_{22}H_{32}O_3$, are monoclinic, $P2_1/n$, $a = 11.832(1)$, $b = 11.423(1)$, $c = 14.637(1)$ Å, $\beta = 98.71(2)°$, $Z = 4$. The structure was solved by direct methods and was refined to $R = 0.035$ for 2052 reflexions with $I \geq 3\sigma(I)$. The X-ray study was carried out in order to determine the structures of two diastereomeric products obtained from a key step in a projected synthesis of the diterpenoids aphidicolin and stemodin. The product examined is the stemodin intermediate.

RICHARD A. PAUPTIT et JAMES TROTTER. Can. J. Chem. **59**, 524 (1981).

Les cristaux du composé du titre, $C_{22}H_{32}O_3$, sont monocliniques, $P2_1/n$, $a = 11.832(1)$, $b = 11.423(1)$, $c = 14.637(1)$ Å, $\beta = 98.71(2)°$, $Z = 4$. On a résolu la structure par les méthodes directes et on a l'affinée jusqu'à une valeur de $R = 0.035$ pour 2052 réflexions avec $I \geq 3\sigma(I)$. On a fait l'étude par X-rayon pour déterminer les structures de deux produits diastéréomères qu'on a obtenu d'un pas dominant dans une synthèse projetée des diterpenoids aphidicolin et stemodin. Le produit qu'on a examiné est l'intermediaire de stemodin.

Introduction

In connection with a research program directed towards the total synthesis of the tetracyclic diterpenoids aphidicolin and stemodin (**1**), the photochemically-induced cycloaddition of allene to the cyclic enone **2** was investigated (1). Thus, irradiation (4.5 h, low-pressure mercury lamp) of a cold (−72°C) solution of **2** and allene in dry, deoxygenated tetrahydrofuran gave a mixture of two isomeric photoadducts, **3** and **4**, which were separated by column chromatography on silica gel (elution with 10:5:2 cyclohexane – hexane – ethyl acetate). The diastereomer which was eluted from the column first (39% yield) exhibited mp 132–133°C, while the second isomer (42% yield) had mp 134–135°C. In order to determine the structures of these two diastereomeric adducts, prior to continuing the syntheses, the first-eluted isomer has been studied by X-ray methods, and proves to be **3** (and its enantiomorph, since the synthetic materials are racemates).

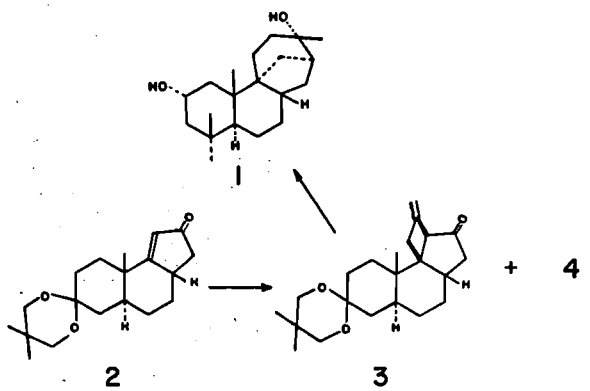

SCHEME 1.

Experimental

Crystal data are as follows:

$C_{22}H_{32}O_3$ fw = 344.5

Monoclinic, $P2_1/n$, $a = 11.832(1)$, $b = 11.423(1)$, $c = 14.637(1)$ Å, $\beta = 98.71(2)°$, $V = 1955.5$ Å^3, $Z = 4$, $\rho_c = 1.17$ g cm^{-3}.

The intensity data were collected on an Enraf-Nonius CAD-4 automatic diffractometer with an ω–θ scan technique and graphite-monochromatized MoKα radiation. The ω-scan angle $\Delta\omega$ was $(1.00 + 0.35 \tan\theta)°$ and was extended by 25% on either side for background counts. The aperture was $(2.50 + \tan\theta)$ mm wide and 4 mm high. The intensities of three standard reflections were measured every 1 h of X-ray exposure time and showed no variation during data collection. The same three reflections were checked for orientation every 100 reflections; automatic reorientation occurred if the scattering vectors differed from the calculated positions by more than 0.05°. Of the 3432 unique reflections collected in the range $0 < \theta \leq 25°$, 2052 (60%) had $I/\sigma(I) \geq 3.0$ ($\sigma^2(I) = S + B + (0.04S)^2$ and S and B are the scan and background counts), and were classified as observed. Only the observed reflections were included in the refinement.

The 500 highest renormalized E's, obtained by using the minimum profile of a K-curve, were input into the MULTAN program (2) and the resulting E-map revealed all the non-H atoms. After three isotropic and three anisotropic full-matrix least-squares refinement cycles a difference map revealed 31 of 32 H's; the position of the remaining H was calculated. Two more refinement cycles with H atoms isotropic, non-H atoms anisotropic, and with use of a polynomial weighting scheme (3) resulted in the final $R = 0.034$ and $R_w = 0.046$, and after several more cycles the H atom parameters had converged. The scattering factors of ref. 4 were used for non-hydrogen atoms and those of ref. 5 for hydrogen atoms. Final atomic positional parameters are given in Table 1.[1]

Discussion

The X-ray study has established that the first-eluted isomer is the β-cyclobutyl species **3**, which

[1]Thermal parameters, bond lengths involving hydrogen atoms, the packing diagram, and the structure factor table are available at a nominal charge from the Depository of Unpublished Data, CISTI, National Research Council of Canada, Ottawa, Ont., Canada K1A 0S2.

0008-4042/81/030524-03$01.00/0

©1981 National Research Council of Canada/Conseil national de recherches du Canada

Can. J. Chem. Downloaded from www.nrcresearchpress.com by 210.87.254.42 on 09/06/12
For personal use only.

Can. J. Chem. Downloaded from www.nrcresearchpress.com by 210.87.254.42 on 09/06/12
For personal use only.

TABLE 1. Final positional parameters (fractional × 10^4, H × 10^3) with estimated standard deviations in parentheses

Atom	*x*	*y*	*z*	Atom	*x*	*y*	*z*
O(1)	3520(2)	−3497(2)	8453(1)	H(041)	138(2)	−25(2)	483(1)
O(2)	3527(1)	−579(1)	4657(1)	H(042)	84(2)	−127(2)	416(2)
O(3)	2338(1)	−455(1)	3236(1)	H(051)	229(2)	−156(2)	587(1)
C(1)	2995(2)	−3078(2)	4720(2)	H(061)	46(2)	−94(2)	607(2)
C(2)	2851(2)	−2282(2)	3875(2)	H(062)	−8(2)	−212(2)	552(2)
C(3)	2542(2)	−1046(2)	4102(1)	H(071)	146(2)	−210(2)	728(2)
C(4)	1500(2)	−1025(2)	4599(1)	H(072)	13(2)	−255(2)	712(2)
C(5)	1635(2)	−1840(2)	5437(1)	H(081)	53(2)	−423(2)	645(1)
C(6)	594(2)	−1791(2)	5940(2)	H(111)	374(2)	−293(2)	673(1)
C(7)	803(2)	−2508(2)	6819(2)	H(131)	179(2)	−515(3)	764(2)
C(8)	1179(2)	−3772(2)	6700(1)	H(132)	134(2)	−394(2)	815(2)
C(9)	2139(2)	−3843(2)	6096(1)	H(141)	218(2)	−573(2)	623(2)
C(10)	1925(2)	−3113(2)	5199(1)	H(142)	257(2)	−535(2)	530(2)
C(11)	3270(2)	−3631(2)	6790(2)	H(161)	542(4)	−478(4)	693(3)
C(12)	2928(2)	−3754(2)	7742(2)	H(162)	473(3)	−603(4)	630(3)
C(13)	1726(2)	−4234(3)	7644(2)	H(171)	23(2)	−384(2)	489(2)
C(14)	2574(2)	−5112(2)	5953(2)	H(172)	67(2)	−320(2)	400(2)
C(15)	3716(2)	−4782(2)	6474(2)	H(173)	119(3)	−438(3)	431(2)
C(16)	4758(3)	−5232(4)	6566(3)	H(181)	289(2)	91(2)	513(1)
C(17)	929(2)	−3683(3)	4554(2)	H(182)	424(2)	85(2)	515(1)
C(18)	3498(2)	659(2)	4782(1)	H(201)	217(2)	105(2)	267(2)
C(19)	3334(2)	1302(2)	3862(1)	H(202)	159(2)	102(2)	360(2)
C(20)	2259(2)	784(2)	3307(2)	H(211)	429(2)	156(2)	281(2)
C(21)	4358(2)	1101(3)	3362(2)	H(212)	506(2)	133(2)	377(2)
C(22)	3149(3)	2597(2)	4022(3)	H(213)	443(2)	25(3)	321(2)
H(011)	366(2)	−282(2)	515(1)	H(221)	304(3)	305(3)	346(3)
H(012)	318(2)	−389(2)	455(2)	H(222)	246(3)	272(3)	434(2)
H(021)	354(2)	−224(2)	360(1)	H(223)	380(3)	290(3)	438(2)
H(022)	224(2)	−258(2)	340(2)				

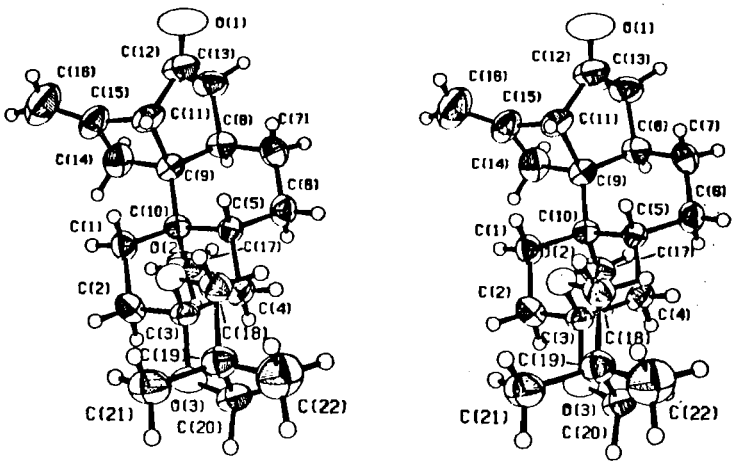

FIG. 1. A stereoview of the molecule (this is the enantiomorph of (3) in Scheme 1).

may prove to be a useful intermediate in a synthesis of stemodin (1). The molecular structure is shown in Fig. 1, and bond lengths and angles are given in Table 2. Bond distances are representative of those expected for C—C, C=C, C—O, and C=O bonds; bond angles are fairly close to those expected for 4-, 5-, and 6-membered rings, with some deviations resulting from strain in the polycyclic molecule. Intermolecular distances[1] are unexceptional.

TABLE 2. Bond lengths (Å) and angles (deg)

Bond	Length (Å)	Bonds	Angle (deg)	Bonds	Angle (deg)
C(1) —C(2)	1.524(3)	C(2) —C(1) —C(10)	112.8(2)	C(9) —C(11)—C(12)	105.1(2)
C(1) —C(10)	1.538(3)	C(1) —C(2) —C(3)	112.4(2)	C(9) —C(11)—C(15)	88.3(2)
C(2) —C(3)	1.509(3)	C(2) —C(3) —C(4)	111.2(2)	C(12)—C(11)—C(15)	110.8(2)
C(3) —C(4)	1.523(3)	C(2) —C(3) —O(2)	105.8(2)	C(11)—C(12)—C(13)	108.9(2)
C(3) —O(2)	1.420(2)	C(2) —C(3) —O(3)	105.1(2)	C(11)—C(12)—O(1)	125.0(2)
C(3) —O(3)	1.424(2)	C(4) —C(3) —O(2)	112.0(2)	C(13)—C(12)—O(1)	126.1(2)
C(4) —C(5)	1.529(3)	C(4) —C(3) —O(3)	112.2(2)	C(8) —C(13)—C(12)	103.0(2)
C(5) —C(6)	1.529(3)	O(2) —C(3) —O(3)	110.2(1)	C(9) —C(14)—C(15)	89.3(2)
C(5) —C(10)	1.546(3)	C(3) —C(4) —C(5)	112.3(2)	C(11)—C(15)—C(14)	92.6(2)
C(6) —C(7)	1.514(3)	C(4) —C(5) —C(6)	111.7(2)	C(11)—C(15)—C(16)	131.9(4)
C(7) —C(8)	1.528(3)	C(4) —C(5) —C(10)	113.0(2)	C(14)—C(15)—C(16)	135.2(4)
C(8) —C(9)	1.544(3)	C(6) —C(5) —C(10)	111.4(2)	O(2) —C(18)—C(19)	111.6(2)
C(8) —C(13)	1.528(3)	C(5) —C(6) —C(7)	110.5(2)	C(18)—C(19)—C(20)	105.6(2)
C(9) —C(10)	1.544(3)	C(6) —C(7) —C(8)	115.3(2)	C(18)—C(19)—C(21)	110.3(2)
C(9) —C(11)	1.571(3)	C(7) —C(8) —C(9)	111.5(2)	C(18)—C(19)—C(22)	109.6(2)
C(9) —C(14)	1.563(3)	C(7) —C(8) —C(13)	108.3(2)	C(20)—C(19)—C(21)	110.3(2)
C(10)—C(17)	1.538(3)	C(9) —C(8) —C(13)	104.6(2)	C(20)—C(19)—C(22)	109.5(2)
C(11)—C(12)	1.515(4)	C(8) —C(9) —C(10)	114.7(2)	C(21)—C(19)—C(22)	111.4(2)
C(11)—C(15)	1.515(4)	C(8) —C(9) —C(11)	104.5(2)	O(3) —C(20)—C(19)	111.5(2)
C(12)—C(13)	1.511(4)	C(8) —C(9) —C(14)	114.3(2)	C(3) —O(2) —C(18)	114.3(1)
C(12)—O(1)	1.199(3)	C(10)—C(9) —C(11)	118.8(2)	C(3) —O(3) —C(20)	114.3(2)
C(14)—C(15)	1.496(4)	C(10)—C(9) —C(14)	113.7(2)		
C(15)—C(16)	1.324(4)	C(11)—C(9) —C(14)	88.0(2)		
C(18)—C(19)	1.521(3)	C(1) —C(10)—C(5)	107.7(2)		
C(18)—O(2)	1.428(3)	C(1) —C(10)—C(9)	111.1(2)		
C(19)—C(20)	1.521(3)	C(1) —C(10)—C(17)	109.7(2)		
C(19)—C(21)	1.525(3)	C(5) —C(10)—C(19)	109.3(2)		
C(19)—C(22)	1.518(4)	C(5) —C(10)—C(17)	111.2(2)		
C(20)—O(3)	1.423(3)	C(9) —C(10)—C(17)	107.8(2)		

Acknowledgements

We thank the Natural Sciences and Engineering Research Council of Canada and the Natural, Applied and Health Sciences Committee, University of British Columbia, for financial support, the University of British Columbia Computing Centre for assistance, and Drs. E. Piers and D. J. Herbert for crystals and helpful discussion.

1. D. J. HERBERT. Ph.D thesis. University of British Columbia, Vancouver, B.C., 1979.
2. G. GERMAIN. P. MAIN, and M. M. WOOLFSON. Acta Crystallogr. A**27**, 368 (1971).
3. D. W. J. CRUICKSHANK. *In* Computing methods in crystallography. *Edited by* J. S. Rollett. Pergamon Press. 1965.
4. D. T. CROMER and J. B. MANN. Acta Crystallogr. A**24**, 321 (1968).
5. R. F. STEWART, E. R. DAVIDSON, and W. T. SIMPSON. J. Chem. Phys. **42**, 3175 (1965).

Can. J. Chem. Downloaded from www.nrcresearchpress.com by 210.87.254.42 on 09/06/12
For personal use only.

Electrochemical reduction of nitroethylenic ketones in hydroorganic medium. Preparation of 4,5-dihydroxy-2-isoxazolines

CHRISTIAN BELLEC AND PIERRE MAITTE

Laboratoire de Chimie des Hétérocycles, Université Pierre et Marie Curie, 4 Place Jussieu, 75230 Paris, France

JOSEPH ARMAND

Laboratoire de Physicochimie des Solutions, Université Pierre et Marie Curie, 4 Place Jussieu, 75230 Paris, France

AND

CLAUDE VIEL

Laboratoire de Pharmacie Chimique II, Faculté de Pharmacie, Rue J. B. Clément, 92290 Chatenay Malabry, France

Received July 15, 1980

CHRISTIAN BELLEC, PIERRE MAITTE, JOSEPH ARMAND, and CLAUDE VIEL. Can. J. Chem. **59**, 527 (1981).

The electrochemical reduction of compounds of the type

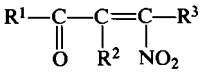

has been investigated in hydroorganic medium between pH 0 and 7. For **3** ($R^1 = R^2 = R^3 = C_6H_5$), the 3,4,5-triphenylisoxazole is obtained at pH 1. **3** in neutral medium, **1** ($R^1 = CH_3$, $R^2 = R^3 = C_6H_5$) and **2** ($R^1 = C_2H_5$, $R^2 = R^3 = C_6H_5$) lead to 4,5-dihydroxy-2-isoxazoline (only one of such compounds is described in the literature). The structure of these compounds has been determined by the usual spectroscopic methods (ir, nmr, mass spectrometry) and by radiocrystallography. A mechanism which accounts for the whole set of our results is proposed: it involves an intermediate α,β-nitrosoethylenic compound which cyclizes into a 4,5-dihydroxy-2-isoxazoline or gives an 1,3-diketone oxime upon reduction; this last compound cyclizes into an isoxazole.

CHRISTIAN BELLEC, PIERRE MAITTE, JOSEPH ARMAND et CLAUDE VIEL. Can. J. Chem. **59**, 527 (1981).

La réduction électrochimique de composés du type

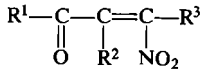

a été étudiée en milieu hydroorganique entre pH = 0 et pH = 7. Pour **3** ($R^1 = R^2 = R^3 = C_6H_5$) on obtient à pH = 1 le triphényl-3,4,5 isoxazole. Dans le cas de **3** en milieu neutre, de **1** ($R^1 = CH_3$, $R^2 = R^3 = C_6H_5$) et de **2** ($R^1 = C_2H_5$, $R^2 = R^3 = C_6H_5$) on isole des dihydroxy-4,5 isoxazolines-2 composés dont un seul est décrit dans la littérature. La structure de ces composés a été déterminée par les méthodes spectroscopiques usuelles (ir, rmn, spectrométrie de masse) et par radiocristallographie. Un mécanisme en accord avec l'ensemble de nos résultats est proposé: il fait intervenir un intermédiaire nitrosé α,β-éthylènique susceptible de se cycliser en dihydroxy-4,5 isoxazoline-2 ou d'être réduit en oxime de dicétone-1,3, celle-ci se transformant ultérieurement en isoxazole.

Introduction

The electrochemical reduction of α,β-ethylenic ketones and α,β-ethylenic nitro derivatives has been the subject of a number of papers (ref. 1, p. 399, ref. 2, p. 81). But, to the best of our knowledge, no investigation of compounds of the type

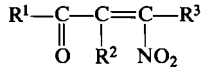

has ever been carried out. We now report the results obtained with **1** ($R^1 = CH_3$, $R^2 = R^3 = C_6H_5$), **2** ($R^1 = C_2H_5$, $R^2 = R^3 = C_6H_5$), and **3** ($R^1 = R^2 = R^3 = C_6H_5$) in hydroorganic medium (CH_3CN 50%). This study is performed at pH < 7 as these compounds decompose rapidly at higher pH values.

Polarography and Electrolysis of 1 and 2

Between pH 1 and 7, both compounds evidence a 2e cathodic wave followed, until pH 4, by a second 4e wave. The $E_{1/2}$ are pH-dependent (Fig. 1).

An electrolysis in dilute solution performed at the potential of the first plateau (pH 1.2, $C = 2 \times 10^{-3}$ *M*, $E = -0.4$ V) consumes 2 electrons per molecule. The polarogram of the electrolyzed solution only shows the second wave of the starting compound. At the same time, the strong uv band of the conjugated system (λ_{max} = 310 nm for **1** and 315 nm for **2**) disappears; the electrolyzed solution evidences another strong band with a λ_{max} at shorter wavelength (λ_{max} = 255 nm for **1** and λ_{max} = 260 nm for **2**).

A preparative electrolysis carried out under similar conditions allows the isolation of the 4,5-dihydroxy-3,4-diphenyl-2-isoxazolines **4** and **5**.

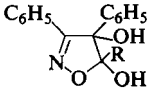

4 R = CH_3
5 R = C_2H_5
7 R = C_6H_5

0008-4042/81/030527-05$01.00/0

©1981 National Research Council of Canada/Conseil national de recherches du Canada

Can. J. Chem. Downloaded from www.nrcresearchpress.com by 210.87.254.5 on 09/06/12
For personal use only.

Can. J. Chem. Downloaded from www.nrcresearchpress.com by 210.87.254.5 on 09/06/12
For personal use only.

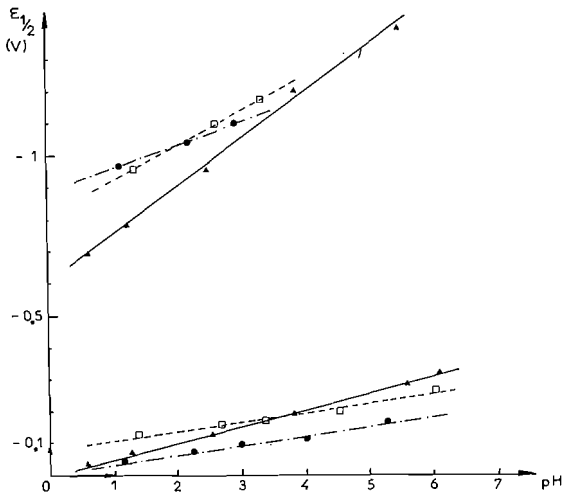

FIG. 1. Plot of $E_{1/2}$ vs. pH: ●, **1**; □, **2**; ▲, **3**.

The usual spectroscopic methods (ir, nmr, mass spectrometry) do not permit assignment of an unambiguous structure to **4** and **5**. However, the spectra clearly show that **4** and **5** are homologous products. The structure of **4** has been determined by radiocrystallography (3) as the *cis*-4,5-dihydroxy-5-methyl-3,4-diphenyl-2-isoxazoline. As for **5**, the nmr spectrum points to a mixture of similar amounts of *cis* and *trans* isomers and not to a single stereoisomer.

Compounds **4** and **5** present a 4 F wave identical to the second wave of **1** and **2**. Preparative electrolysis of **4** and **5** only led to gummy products.

Polarography and Electrolysis of 3

Between pH 1 and 7, **3** shows a first wave, the height of which decreases with increasing pH (Fig. 2) from 4e at pH 1 to 2e at pH 6. Its $E_{1/2}$ is pH-dependent (Fig. 1). It is followed by a second 4e wave.

The consumption of electricity during the electrolysis of a dilute solution at a potential corresponding to the first plateau (pH = 1.4, $c = 2 \times 10^{-3}$ *M*, $E = -0.5$ V) is near 4e per molecule. The height of the second wave decreases during the electrolysis and disappears completely at the completion of the electrolysis. A preparative electrolysis performed under similar conditions gives the 3,4,5-triphenylisoxazole **6**.

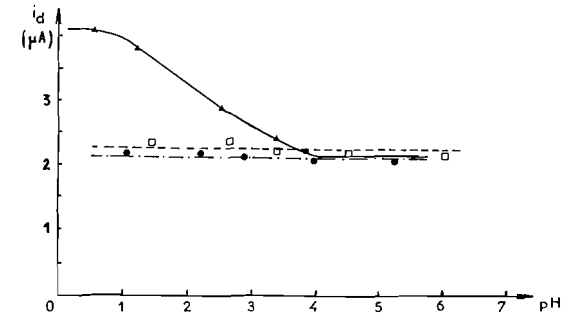

FIG. 2. Plot of i_D vs. pH; ●, **1**; □, **2**; ▲, **3**.

At pH 6.1 ($c = 2 \times 10^{-3}$ *M*, $E = -0.5$ V) coulometry consumes 2e per molecule. The polarogram of the electrolysed solution evidences a single wave identical to the second wave of **3**. A preparative electrolysis leads to the 4,5-dihydroxy-3,4,5-triphenyl-2-isoxazoline, **7**.

Discussion

Reduction of 3 in Acidic Medium

The formation of the isoxazole **6** can be explained by Scheme 1: the

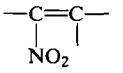

group is reduced into a saturated oxime

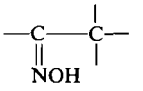

(**8**) according to the classical reduction of α,β-nitroethylenic derivatives (2). The 1,3-diketone monoxime (**8**) obtained cyclizes into a 5-hydroxy-2-isoxazoline (**9**) (4) which then dehydrates spontaneously into the isoxazole **6** (5).

The assignment of the second wave of **3** is more difficult; it can be due to the oxime (**8**) (C_6H_5—C(=NOH)CH_3 gives a 4 F wave with an $E_{1/2}$ near that of **8** (6)) or to isoxazoline **9** as **4** and **5** also present a 4 F wave at similar $E_{1/2}$ (Fig. 1).

A preparative electrolysis at the level of the second waves of **3** (pH 1.20, $E = -1.0$ V) only leads to the trisubstituted isoxazole **6**. We have observed, as it had been noticed before, that the behaviour of unstable compounds may be different by polarography and during an electrolysis: the overall electroreduction of **8** (or **9**) is faster by polarography than the transformation into the isoxazole, while the reverse is true during an electrolysis.

Reduction of 3 in Neutral Medium and of 1 and 2

The nature of the products isolated, the stepwise change with the pH from a 4e to a 2e process in the case of **3** and the absence of discontinuity on $E_{1/2}$ vs. pH plot for **3** point to the existence of a common 2e intermediate for both processes.

This intermediate would be the nitrosoethylenic ketone **10** which, according to the conditions and the nature of R, would be further reduced or would

Can. J. Chem. Downloaded from www.nrcresearchpress.com by 210.87.254.5 on 09/06/12
For personal use only.

cyclize (Scheme 1). In support of this hypothesis, it should be noted that the $E_{1/2}$ of **1**, **2**, and **3** are very near that of nitrostyrene (8): this is in favour of a reduction mechanism involving only the

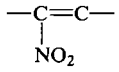

group and not the carbonyl group.

The mechanism for the electrochemical reduction of α,β-nitroethylenic derivatives into saturated oximes is still unknown. However, a mechanism similar to that of nitroaromatics (9) can be considered. It is shown that the electrochemical reduction of nitroaromatics leads to a nitroso derivative after consumption of 2 F per mol; nitrosopyridines have been recently evidenced in the reduction of nitropyridines (10). The nitroso derivative is generally reduced into the corresponding hydroxylamine.

Besides, in the electrochemical reduction of *N*,*N*-disubstituted *o*-nitroanilines, the results can be explained (11) by the intermediacy of a nitroso derivative which undergoes two competitive reactions: a cyclization and an electrochemical reduction.

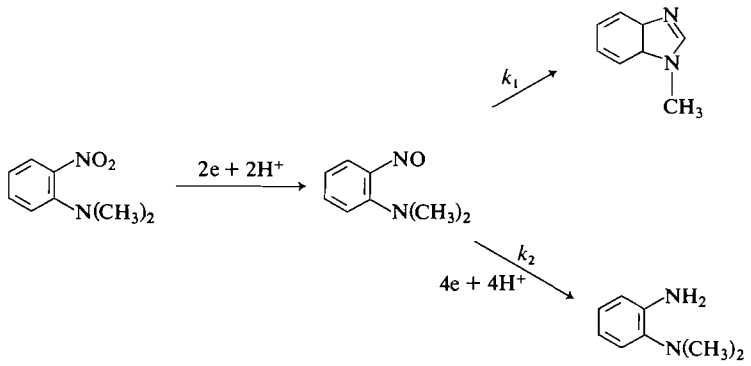

A similar nitroso intermediate undergoing a cyclization has been postulated in the reduction of *o*-nitrobenzoylhydrazide (12).

In the frame of our hypothesis, one can rationalize the different behaviours of **3** and **1**, **2**: the overall rate of the electrochemical reduction of nitroso derivative increases with the acidity of the medium (ref. 2, p. 131); in the case of **3** but not in the case of **1** and **2**, the reduction rate would exceed the cyclization rate at low pH. This can be explained in the following manner: the cyclization takes place through an attack of the N=O group on the carbonyl which is less reactive with an α-phenyl group than with an α-alkyl group.

Conclusion

A mechanism is presented to account for the formation of 4,5-dihydroxy-2-isoxazoline. In a previous study (14) it had been shown that the chemical reduction of **1**, **2**, and **3** leads to different compounds: this, together with the fact that a single 4,5-dihydroxy-2- isoxazoline is described in the literature (15), brings forward the synthetic interest of the electrochemical reduction.

This 4,5-dihydroxy-2-isoxazoline (15) has been prepared by reaction of a nitrile oxide according to:

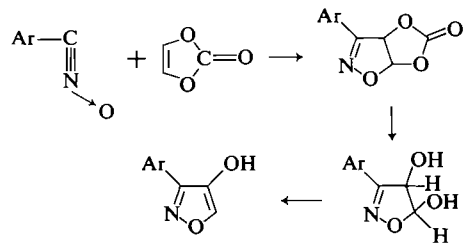

The dehydration of the intermediate 1,2-diols is very easy and it is only in the case where Ar = *p*-NO_2—C_6H_4 that the 4,5-dihydroxy-2-isoxazoline can be isolated.

A general method for the chemical synthesis of 4,5-dihydroxy-2-isoxazoline substituted on the -4 and -5 positions can be designed by reaction of nitrile oxides with disubstituted vinylidene carbonates or with enediol ethers.

Experiments are now in progress to synthesize 4,5-dihydroxy-2-isoxazolines by this route.

Experimental

Techniques

The apparatus and techniques used in hydroorganic medium have been described previously (16, 17). The reference electrode was a saturated calomel electrode. The pH values were measured with a Radiometer model 4 pH-meter equipped with a combined glass–calomel electrode model GK 2302 B standard-

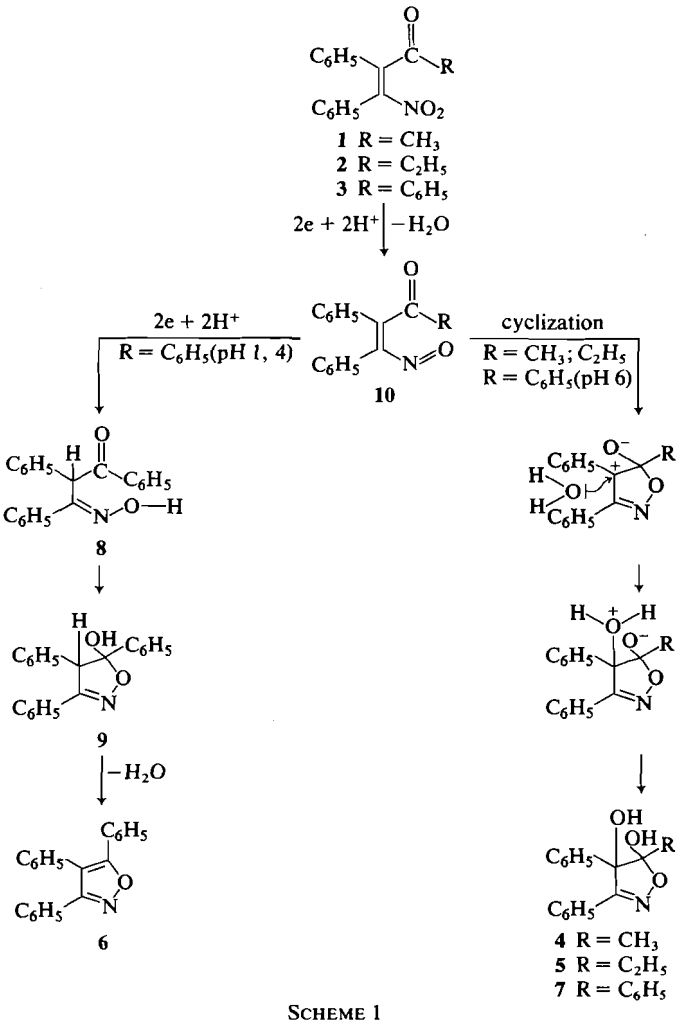

SCHEME 1

ized in aqueous buffer. The microanalyses were performed by the "Service de Microanalyse du CNRS" (Gif sur Yvette). All the compounds described gave correct elemental analysis. The following abbreviations are used in reporting nmr results: s = singlet, d = doublet, t = triplet, q = quadruplet, and m = multiplet.

Preparation of Compounds 1, 2, and 3

Nitroethylenic ketones **1**, **2**, and **3** were prepared according to ref. 14 by reaction of the corresponding ethylenic ketone with dinitrogentetroxide.

Preparative Electrolysis

Electrolysis of 3-Nitro-1,2,3-triphenyl-2-propene-1-one (3) in Acidic Medium

Preparation of 6. Solution (250 mL) is prepared from 125 mL of acetonitrile, 25 mL of a 1 *N* solution of sulfuric acid, and water. This solution (200 mL) and 882 mg (2.5×10^{-3} mol) of **3** are used to fill the cathodic compartment while the remainder is used in the anodic compartment; pH = 1.34, $E = -0.5$ V. During the electrolysis a white solid precipitates in the cell. After consumption of 850 C (4e per mol correspond to 925 C) the current drops to 4 mA. The electrolysis is stopped and the solution is filtered. The precipitate is washed with water and dried over P_2O_5. A white solid, **6**, 560 mg, 76% yield, is obtained; anal. (297) $C_{21}H_{15}NO$; mp 214°C (C_6H_6–ligroïn 50/50) (lit. (18) mp 211–212°C) nmr ($CDCl_3$) 3-Ph + 4-Ph + 5-Ph, m between 6.9 ppm and 7.8 ppm.

Electrolysis of 1-Nitro-1,2-diphenyl-1-butene-3-one (1)

Preparation of 4. The electrolysis was carried out on 200 mL of 0.1 *N* sulfuric acid solution containing 50% of acetonitrile (pH = 1.12) and 1.07 g (4×10^{-3} mol) of **1** at $E = -0.4$ V. After consumption of 835 C (2 F per mol correspond to 775 C) the current decreases to 6 mA. The electrolysis is stopped, and acetonitrile is evaporated to give an oil which crystallizes into a white solid, **4**, 4,5-dihydroxy-3,4-diphenyl-5-methyl-2-isoxazoline, 929 mg, 91% yield, mp 144°C (C_6H_6–ligroïn 75/25). Anal (269) $C_{16}H_{15}NO_3$. The ir spectrum (KBr pellet) ν_{OH} free: 3380 cm^{-1}, $\nu_{OH\ assoc.}$ = 3300 cm^{-1}, $\nu_{C=N}$ = 1600 cm^{-1}; nmr (acetone-d_6)—CH_3, s, 1.1 ppm (3 H); 4-OH + 5-OH, s, 5.3 ppm (2 H) which disappears on the addition of D_2O; 3-Ph + 4-Ph, m between 7.15 and 7.9 ppm (10 H). Nmr ^{13}C ($CDCl_3$)—CH_3, q, 20.63 ppm; 5-C, s, 106.4 ppm; 4-C, s, 90.48 ppm; 3-C, s, 163.12 ppm; phenyl group on 3-C: C bonded to 3-C, s, 136.63 ppm; 3-Ph + 4-Ph, m between 125.4 and 130.5 ppm; mass spectra (10 and 70

Can. J. Chem. Downloaded from www.nrcresearchpress.com by 210.87.254.5 on 09/06/12
For personal use only.

eV) 235, M − 34 (loss of 20H); 220 (loss of CH_3). After these peaks, principal peaks of diphenylisoxazoles are observed (previously reported in the literature (7, 13)).

Electrolysis of 1-Nitro-1,2-diphenyl-1-pentene-3-one (2)

Preparation of 5. A solution is prepared as in the case of **3**. Compound **2** (1.125 g, 4×10^{-3} mol) is reduced in 200 mL of this solution, pH: 1.40, at $E = -0.4$ V. After consumption of 830 C (2e per mol corresponds to 800 C) the current decreases to 3 mA and the electrolysis is stopped. Acetonitrile is evaporated to give a yellow oil which crystallizes into a while solid. A yield of 980 mg of 4,5-dihydroxy-3,4-diphenyl-5-ethyl-2-isoxazoline **5** is obtained (~90%); mp 147–148°C (C_6H_6-ligroïn 60/40); anal. (283) $C_{17}H_{17}NO_3$. Nmr (acetone-d_6)—CH_3, t centered at 0.9 ppm (3H); —CH_2— q centered at 1.42 ppm, (2H); 4-OH + 5-OH, s, 5.05 ppm, s broad, 6.2 ppm (2H) which both disappear upon addition of D_2O; 3-Ph + 4-Ph, m between 7.2 and 7.95 ppm (10H). The ir spectrum (KBr pellet); ν_{OH} 3440 and 3350 cm^{-1}; $\nu_{C=N}$ = 1600 cm^{-1}. Mass spectra (70 eV) 266, M − 17 (loss of OH) 249, M − 34 (loss of 20H), 220 (loss of C_2H_5) and all peaks of diphenylisoxazoles (7, 13).

Electrolysis of 3-Nitro-1,2,3-triphenyl-2-propene-1-one (3) in Neutral Medium

Preparation of 7. Solution (250 mL) is prepared from 125 mL of acetonitrile, 50 mL of a 0.5 *M* solution of phosphoric acid, 30 mL of a 1 *M* solution of sodium hydroxide, and water. This solution (200 mL) and 1.18 g (3.6×10^{-3} mol) of **3** are used to fill the cathodic compartment while the remainder is used in the anodic compartment; pH = 6.10, $E = -0.5$ V. After consumption of 715 C (2 F per mol correspond to 690 C) the current drops to 5 mA. The electrolysis is stopped, acetonitrile is evaporated, and the oil which is formed crystallizes slowly into a white solid. A yield of 1.02 g of 4,5-dihydroxy-3,4,5-triphenyl-2-isoxazoline (**7**) is obtained (87%); mp 159°C (C_6H_6–ligroïn 75/25 vol.). Anal. (331): $C_{21}H_{17}NO_3$. Nmr (acetone-d_6) 4-OH + 5-OH, s broad, 2.95 ppm (2H); 3-Ph + 4-Ph + 5-Ph, m between 7.35 and 8.3 ppm (15H); mass spectra (70 eV): 314, M − 17 (loss of OH); 297, M − 34 (loss of 20H).

1. M. BAIZER. Organic electrochemistry. M. Dekker, New York. 1973.
2. A. J. BARD and H. LUND. Encyclopedia of the electrochemistry of the elements. Vol. XII. M. Dekker, New York. 1979.
3. M. PHILOCHE-LEVISALLES and CH. BELLEC. J. Heterocycl. Chem. To be published.
4. R. ESCALE, R. JACQUIER, B. LY, F. PETRUS, and J. VERDUCCI. Tetrahedron, **32**, 1369 (1976).
5. R. ESCALE, F. PETRUS, and J. VERDUCCI. Bull. Soc. Chim. Fr. 725 (1974).
6. P. SOUCHAY and S. SER. J. Chim. Phys. **49**, 172 (1942).
7. J. H. BOWIE, R. K. KALLURY, and R. G. COOKS. Aust. J. Chem. **22**, 563 (1969).
8. M. MASUI and H. SAYO. Pharm. Bull. **4**, 332 (1956).
9. M. HEYROVSKY and S. VAVRICKA. J. Electroanal. Chem. **28**, 409 (1970).
10. A. DARCHEN and C. MOINET. J. Chem. Soc. Chem. Commun. 487 (1976).
11. M. LE GUYADER and D. PELTIER. Bull. Soc. Chim. Fr. 2695 (1966).
12. H. LUND and L. G. FEOKTISTOV. Unpublished results.
13. A. SELVA and U. VETTORI. Gazz. Chim. Ital. **103**, 223 (1973).
14. CH. BELLEC, D. BERTIN, R. COLAU, S. DESWARTE, P. MAITTE, and C. VIEL. J. Heterocycl. Chem. **16**, 1657 (1979).
15. G. DESMONI, P. GRUNANGER, and S. SERVI. Ann. Chim. Roma, **58**, 1363 (1968).
16. J. ARMAND and L. BOULARES. Bull. Soc. Chim. Fr. 366 (1975).
17. J. PINSON and J. ARMAND. Coll. Czech. Chem. Commun. **36**, 585 (1971).
18. J. F. HANSEN and A. S. STRONG. J. Heterocycl. Chem. **14**, 1289 (1977).

Can. J. Chem. Downloaded from www.nrcresearchpress.com by 210.87.254.5 on 09/06/12
For personal use only.

Fission fragment radiolysis of carbon dioxide

YASUMASA IKEZOE, SHOICHI SATO, AND SABURO SHIMIZU
Japan Atomic Energy Research Institute, Tokai-mura, Ibaraki, Japan

Received April 10, 1980

YASUMASA IKEZOE, SHOICHI SATO, and SABURO SHIMIZU. Can. J. Chem. **59**, 532 (1981).

The fission fragment radiolysis of CO_2 and the CO_2–C_3H_8, CO_2–NO_2 systems is studied in comparison with the γ radiolysis. Two kinds of back reactions (re-oxidation of carbon monoxide to carbon dioxide) are operative in the fission fragment radiolysis. One (a rapid back reaction) is the unidentified ionic chain reaction which proceeds at low CO concentrations, and the other (a slow back reaction) is assigned to a radical reaction ($CO + O + CO_2 \rightarrow 2CO_2$ [3′]). This slow back reaction is a characteristic of the fission fragment radiolysis. The analysis of results gives an upper limit of the radius of fission fragment tracks in the reaction system, $r\rho < 1.04\ \mu g\ cm^{-2}$.

YASUMASA IKEZOE, SHOICHI SATO et SABURO SHIMIZU. Can. J. Chem. **59**, 532 (1981).

On a étudié la radiolyse par fragmentation de fission des systèmes CO_2, CO_2–C_3H_8 et CO_2–NO_2 et on a comparé les résultats à ceux obtenus par radiolyse gamma. Au cours de la radiolyse par fragmentation de fission, il se produit deux sortes de réaction en retour (réoxydation du CO en CO_2). L'une (une réaction en retour rapide) est une réaction ionique en chaîne non identifiée qui a lieu à de faibles concentrations de CO et l'autre (une réaction en retour lente) qui est attribuée à une réaction radicalaire ($CO + O + CO_2 \rightarrow 2CO_2$ [3′]). Cette réaction en retour lente est caractéristique de la radiolyse par fragmentation de fission. L'analyse des résultats donne une limite supérieure du rayon de parcours des fragments de fission dans le milieu réactionnel, $r\rho < 1{,}04\ \mu g\ cm^{-2}$.
[Traduit par le journal]

Introduction

The radiolysis of carbon dioxide has been studied extensively (1) from a variety of viewpoints, such as radiation stability of carbon dioxide as a nuclear reactor coolant (2), radiation energy conversion to chemical energy (3–5), radiation synthesis (6, 7), and ionic reactions in the Martian atmosphere (8). Primary process yields estimated by Willis and Boyd (9) and a numerical model by Kummler *et al.* (10) provide a good understanding of the radiolysis.

In almost all of the preceding papers, an unidentified back reaction, in which the carbon monoxide formed is re-oxidized to carbon dioxide, has been a common subject of interest. It is known that the back reaction is suppressed during the high dose rate irradiation using pulsed electrons (11). There should be a similarity between the fission fragment and the high dose rate radiolysis (12), for the concentration of active species during the irradiation, in either case, reaches a value some orders of magnitude higher than in the γ radiolysis.

The fission fragment radiolysis of carbon dioxide has been studied by several workers (3, 4, 13), and the effects of temperature, pressure, and additives on the yield of carbon monoxide have been examined. But the back reaction in the fission fragments radiolysis has not been reported. In the fission fragment radiolysis, product formation is closely related to the structure of fission fragment tracks in the reaction system. A theoretical track model for water has been proposed by Mozumder and co-workers (14, 15), and fission fragment tracks in the dense gas have been studied experimentally by Meisels *et al.* (16).

In this paper, we attempt to investigate chemical reactions, especially the back reaction, involved in the fission fragment radiolysis of gaseous carbon dioxide. The structure of the fission fragment tracks will be discussed in connection with an LET effect observed experimentally.

Experimental

Reactants and Reaction Vessel

Carbon dioxide (Nihon Sanso, stated purity >99.99%), propane (Takachiho Chemicals, stated purity >99.7%), and nitrogen dioxide (Matheson Co., stated purity 99.5%) were used as reactant gas without purification. The reaction vessel (an inner capsule, 43 mL, stainless steel), which has a needle valve gas inlet at one end and a rupture plate at the other end, was washed with ethanol and with distilled hot water repeatedly, and dried before use.

Fission Fragment Irradiation

A piece of thin uranium–palladium alloy foil[1] was set in an inner capsule which was then filled with reactant gas. Three inner capsules were loaded in an outer capsule, which was irradiated in the Low Temperature Fissiochemical Loop (17) in the Japan Research Reactor 3. The reactant gas in the inner capsule was irradiated by mixed radiations of fission fragments, fast neutrons, and γ rays (FFnγ).

Dosimetry

The absorbed dose was determined by ethylene dosimetry (18) and by calculation (19) using the known thermal neutron

[1]The uranium–palladium alloy foil used in this work was given to our group by the courtesy of Messrs. B. Manowitz and M. Steinberg of the Brookhaven National Laboratory. The foil contained 0.503 mg ^{235}U per 1 cm^2 foil, and the 2.1 μm thick alloy layer was covered on both sides with 0.2 μm thick platinum layers.

0008-4042/81/030532-05$01.00/0
©1981 National Research Council of Canada/Conseil national de recherches du Canada

Can. J. Chem. Downloaded from www.nrcresearchpress.com by 210.87.254.40 on 09/06/12
For personal use only.

Can. J. Chem. Downloaded from www.nrcresearchpress.com by 210.87.254.40 on 09/06/12
For personal use only.

flux. Ethylene was charged in the inner capsule of the same kind and irradiated under the same conditions as the reactant gas. The absorbed dose in ethylene was determined by the yield of hydrogen ($G(H_2) \equiv 1.3$). The absorbed dose in the reactant gas was then obtained by taking into account the stopping power ratio of the secondary electrons and the fast neutrons.

The thermal neutron flux was determined by the activation of ^{59}Co. Two pieces of ^{59}Co metal pellet (7 mg) were attached to the outer capsule. The absorbed dose rate (rad h^{-1}) due to fission fragments was calculated by eq. [1].

$$[1] \qquad (\text{Dose rate})_{FF} = Nf\sigma E\varepsilon_0 K^{-1} W^{-1}$$

where N is the number of ^{235}U atoms in the foil, f the thermal neutron flux (cm^{-2} s^{-1}), σ the cross section of ^{235}U for fission (580×10^{-24} cm^2), E the initial kinetic energy of fission fragments per fission (170 MeV), ε_0 the ratio (0.325) of energy absorbed by the reactant gas to E (19, 20), K is the conversion factor from rad h^{-1} to MeV g^{-1} s^{-1}, and W the weight of the reactant gas in the inner capsule (g).

Absorbed doses determined by the two methods were consistent with each other. Under standard conditons (6 atm CO_2, 1.89 mg ^{235}U); $(\text{dose rate})_{FF} = 6.8$, $(\text{dose rate})_{\gamma} = 3.4$, and $(\text{dose rate})_n < 0.1$ Mrad h^{-1}. Details are described elsewhere (19, 20).

Product Analysis

The inner capsule was punctured at the rupture plate in a vacuum line, and reaction products were analysed by a Toepler pump, a mass spectrometer, or by gas chromatography.

Results and Discussion

CO Formation from CO_2

Formation of carbon monoxide in pure CO_2 by FFnγ and by γ-rays is shown in Fig. 1. Formation of carbon monoxide by γ-rays is saturated at low CO concentrations, and apparent G(CO) at 10 Mrad is less than 0.1. This small G(CO) is explained by the back reaction. On the other hand, formation of carbon monoxide by FFnγ is larger than that by γ-rays. The apparent G(CO) at 10 Mrad, 0.7, lies between the low value for γ-rays (less than 0.1) and a high value reported (7.8) by pulsed electrons (11). With respect to the back reaction, it is less effective under FFnγ irradiation than under γ irradiation, but not suppressed as in the pulsed electron irradiation.

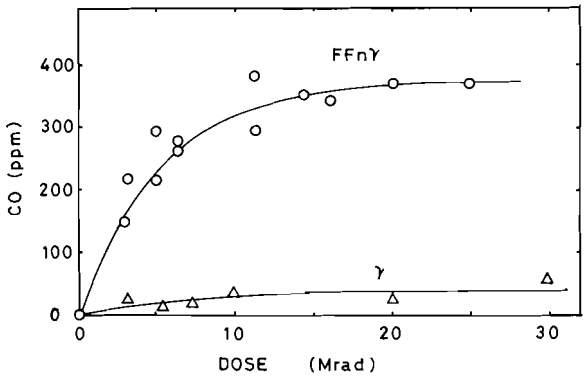

FIG. 1. CO formation from pure CO_2 by FFnγ and by γ. FFnγ: 10.2 Mrad/h (FF; 6.8, $n < 0.1$, and γ; 3.4 Mrad/h), γ: 1.1 Mrad/h. CO_2 6 atm at 298 K in 43 mL stainless steel capsules.

NO_2 Addition

The effect of NO_2 addition on G(CO) and $G(O_2)$ is shown in Fig. 2. G(CO) by FFnγ is higher than by γ-rays in the whole range of NO_2 concentration, 0–1.0%. The difference in G(CO) between the two types of radiation may be attributed to the forward reactions, because the back reaction in the CO_2–NO_2 system (NO_2 1%) may be considered suppressed. Initial decomposition of carbon dioxide by FFnγ is greater than by γ-rays.

The sharp increase in G(CO) with the addition of a small amount of NO_2 (0.2%) is due to the suppression of the back reaction. The increase under irradiation with FFnγ (0.7 to 5.3) was greater than that under γ-irradiation (0.1 to 3.6). This means that the back reaction in pure CO_2 consumes more carbon monoxide under irradiation with FFnγ than under γ-ray irradiation.

The values of $G(O_2)$ were smaller than expected from mass balance, but approached half of G(CO) at low NO_2 concentration.

Pressure Effect

The concentration of active species in fission fragment tracks will increase with the total pressure of the reactant gas, since the range and radius of fission fragment tracks are inversely proportional to the total pressure (14, 15). The pressure depen-

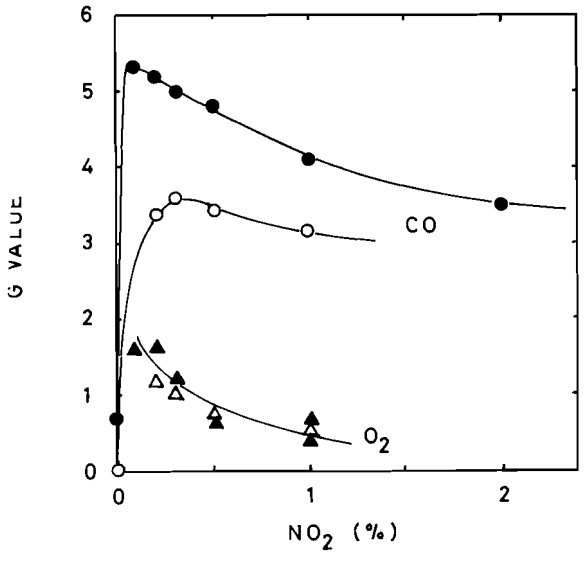

FIG. 2. G(CO) and $G(O_2)$ of CO_2–NO_2 by FFnγ and by γ. Dose rates and CO_2 pressure same as in Fig. 1. G values determined at the absorbed dose of 10 Mrad. ●: CO by FFnγ; ○: CO by γ; ▲: O_2 by FFnγ; △: O_2 by γ.

Can. J. Chem. Downloaded from www.nrcresearchpress.com by 210.87.254.40 on 09/06/12
For personal use only.

dence of G(CO) is shown in Fig. 3. G(CO) in pure CO_2 increased slightly with pressure, and that in the CO_2–NO_2 mixture was constant within experimental error in the pressure range examined, 4–14 atm. This tendency is in qualitative agreement with that observed by Cusack and King (13). They reported an appreciable increase in G(CO) in pure CO_2 and little or no increase in the CO_2–NO_2 mixture.

G(CO) by Fission Fragments

G(CO) by FFnγ, $G_{FFn\gamma}$, is a composite average value due to fission fragments, fast neutrons, and γ-rays. G(CO) attributed solely to fission fragments, G_{FF}, can be estimated by eqs. [2] and [3].

$$[2] \quad G_{FFn\gamma} = \varepsilon_{FF} G_{FF} + \varepsilon_{n\gamma} G_{n\gamma}$$

$$[3] \quad \varepsilon_{FF} + \varepsilon_{n\gamma} = 1$$

where ε_{FF} or $\varepsilon_{n\gamma}$ is the normalized ratio of dose rate of the fission fragments or the fast neutron and the γ dose rate to the total dose rate. The values of ε_{FF} and $\varepsilon_{n\gamma}$ were determined by dosimetry. G_{FF} thus obtained for CO_2–C_3H_8 system is shown in Table 1. It should be mentioned that eq. [2] is correct only when the chemical reactions induced by fission fragments are independent of those by nγ. In the CO_2–C_3H_8 system (21), this condition seems satisfied at low absorbed doses, but in pure CO_2 it is not satisfied as will be shown in the later discussion concerning the rapid back reaction.

The value of G_{FF} in CO_2–C_3H_8, 6.3, is smaller than those found by Cusack and King, 8.7–11.9 (13). The reason for this discrepancy is not clear. It might be attributed to different experimental conditions, such as irradiation temperature, dose rate, and additives. In any event, it is affirmed again that G(CO) by fission fragments is greater than that by γ-rays.

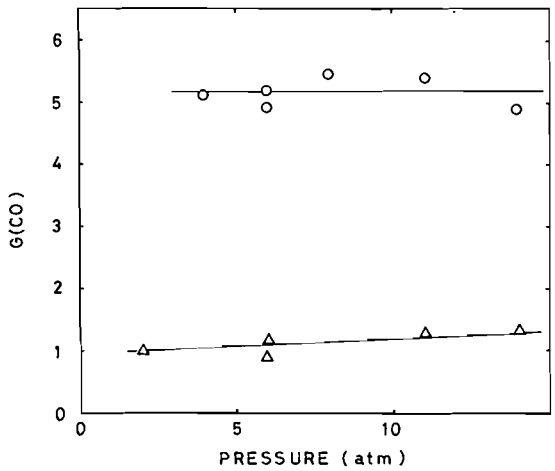

FIG. 3. Pressure dependence of G(CO) of pure CO_2 (△) and of CO_2–NO_2 (0.2%) (○) by FFnγ. Dose rate of FFnγ: 9.9–10.9 Mrad/h. Amounts of ^{235}U controlled to keep the ratio, (dose rate)$_{FF}$/(dose rate)$_{n\gamma}$ = 1.9 ± 0.1. G values determined at the absorbed dose of 5 Mrad.

TABLE 1. G(CO) of pure CO_2 and CO_2–C_3H_8 system and ΔG(CO) by different radiations

Radiations (dose rate)	G(CO)[a] CO_2	G(CO)[a] CO_2–C_3H_8 (0.2%)	ΔG(CO)[b]
γ (1.1 Mrad/h)	0.1	4.7	4.6
nγ (3.4 Mrad/h)	0.3	4.9	4.6
FFnγ (10.2 Mrad/h)	1.5	5.8	4.3
FF (6.8 Mrad/h)	—	6.3[c]	—

[a]Obtained experimentally at the absorbed dose less than 3 Mrad.
[b]Difference between G(CO) in pure CO_2 and in CO_2–C_3H_8 system (0.2%).
[c]Calculated by eq. [2] in text.

Formation and Consumption of CO

Figure 1 shows a saturation curve for the formation of carbon monoxide. At an absorbed dose of more than 10 Mrad, CO formation by reaction [4] and its consumption [5] are balanced.

$$[4] \quad CO_2 \rightsquigarrow CO + \text{others}$$

$$[5] \quad CO + X \rightarrow CO_2 + Y$$

Equation [6] can be written for the formation of carbon monoxide.

$$[6] \quad d[CO]/dt = G(CO)(\text{dose rate}) - k_3[X][CO]$$

CO concentration is expressed as a function of irradiation time by

$$\ln\left\{1 - \frac{[CO]k_3[X]}{G(CO)(\text{dose rate})}\right\} = -k_3[X]t$$

The theoretical curve which best fits the experimental data of Fig. 1 is obtained when G(CO) = 1.47 and $k_3[X] = 5.2 \times 10^{-4}$ s^{-1} for the FFnγ irradiation. G(CO) thus obtained is the initial G value when the back reaction [5] does not contribute. It is notable that Harteck and Dondes have already obtained similar G(CO) values, 0.091–1.26, in the fission fragment radiolysis of carbon dioxide (3). The initial G(CO), 1.47, by our experiments is still smaller than G(CO) in the CO_2–NO_2 or the CO_2–C_3H_8 system. This indicates that there must be another kind of back reaction which operates at a very early stage of FFnγ irradiation when reaction [5] does not take place.

It must be remembered that X in reaction [5] is a complex function of the pressure, dose rate, and impurity level in the reaction system. The initial G(CO) would depend on the irradiation conditions.

Slow and Rapid Back Reactions

Two kinds of back reaction are considered for

Can. J. Chem. Downloaded from www.nrcresearchpress.com by 210.87.254.40 on 09/06/12
For personal use only.

FFnγ irradiation of carbon dioxide; the slow back reaction [5] and the rapid one. For the slow back reaction, reaction [5′] seems plausible, which predominates over reaction [7] under our experimental conditions.

[5′] $CO + O + CO_2 \rightarrow 2CO_2$

where $k = 5.6 \times 10^{-36}$ cm^6 s^{-1} (22).

[7] $O + O + CO_2 \rightarrow O_2 + CO_2$

where $k = 3.0 \times 10^{-33}$ cm^6 s^{-1} (23).

In the extremely high dose rate experiment of Willis, Boyd, and Binder (11), reaction [5′] would become negligible compared with reaction [7] because of high steady state concentration of oxygen atoms. In such a case reaction [5′], as well as the rapid back reaction, will be suppressed. The high CO yield obtained by fission fragments and the comparatively low steady state concentration of oxygen atoms are the reasons why the slow back reaction [5′] is clearly evident in these experiments.

It is commonly presumed that the rapid back reaction is an ionic chain reaction (1, 10). In Table 1, the increase in G(CO), ΔG(CO), with the addition of 0.2% propane to pure CO_2 is ascribed to the suppression of the rapid back reaction. ΔG(CO) values lie in a small range between 4.3 and 4.6 for various radiations.

Considering the chain length, m, of the rapid back reaction, the increase, ΔG(CO), may be expressed as eq. [8].

[8] $\Delta G(CO) = mG(Z)$

where $G(Z)$ is the G value of the unidentified ionic oxidizing species, Z.

In the high dose rate radiolysis (11), the ionic species were destroyed by reaction [9] and they could not initiate the rapid back reaction.[2]

[9] $CO_2^+ + e^- \rightarrow CO + O$

The local concentration of ionic species in the fission fragment tracks is estimated to be higher than their steady state concentration in the high dose rate radiolysis using pulsed electrons. Thus in the fission fragment radiolysis, reaction [9] may be considered fast enough to quench the rapid back reaction in the tracks.

However, from Table 1 it is obvious that by the rapid back reaction a nearly equal amount of carbon monoxide is consumed in the FFnγ radiolysis as in the γ-radiolysis. This may be explained as follows: the ionic species formed outside of fission fragment tracks by nγ have a lifetime sufficient to initiate the rapid back reaction and they consume carbon monoxide which is formed not only outside but also inside of the tracks. This means that radiation chemical reactions induced by FF cannot be separated from those by nγ and eq. [2] becomes invalid.

Ionic Reaction in the Fission Fragment Tracks

The G(CO) by FFnγ was greater than that by γ-rays in every system examined. This is a clear LET effect in the gas phase. This result supports the mechanism inferred previously (4, 21): that is to say, reaction [9] predominates over reaction [10] in the fission fragment tracks.

[10] $CO_2^+ + M \rightarrow CO_2 + M^{+*}$

In the γ-radiolysis, on the other hand, CO_2^+ transfers its charge to additive M (reaction [10]), and does not contribute to the formation of carbon monoxide.

In the γ-radiolysis of the CO_2–C_3H_8 system, reaction [10′] is followed by reactions [11] and [12] (25), and $G(CH_4)$ becomes higher than that by FFnγ.

[10′] $CO_2^+ + C_3H_8 \rightarrow C_3H_8^{+*} + CO_2$

[11] $C_3H_8^{+*} \rightarrow C_2H_5^+, CH_3\cdot, C_2H_4^+, CH_4, \cdots$

[12] $CH_3\cdot + C_3H_8 \rightarrow CH_4 + C_3H_7\cdot$

The constant G(CO) obtained when the total pressure is varied (Fig. 3) may be explained by assuming that, in these experiments, reaction [9] predominates over reaction [10] in the fission fragment tracks.

Fission Fragment Tracks

Reaction [9] being faster than reaction [10], eq. [13] can be written for the reactions in the fission fragment tracks.

[13] $k_9[CO_2^+][e^-] > k_{10}[CO_2^+][M]$

where $[CO_2^+] = [e^-] = n/\pi r^2$ concentration of ions in the tracks, [M] = concentration of additive M (n is the number of ionizations per unit track length ($1.68 \times P \times 10^6$ cm^{-1}, P in atm),[3] and r the average track radius at the time when reaction [9] is taking place). From eq. [13], we obtain an upper limit of the track radius.

[14] $r < (nk_9/\pi k_{10}[M])^{1/2}$

Using appropriate values of k_9 (2×10^{-7} cm^3

[2]The recombining species are probably $CO_2^+(CO_2)_n$ (24) and e^- or $O_2^-(CO_2)_m$ (10). For brevity, $CO_2^+(CO_2)_n$ is represented by CO_2^+, and e^- or $O_2^-(CO_2)_m$ by e^-.

[3]$n = L/W$, where L is the average LET value of fission fragments in carbon dioxide and W the W value (energy required to produce a pair of ions) of carbon dioxide.

s^{-1}),[4] k_{10} (1×10^{-10} cm^3 s^{-1}) (26), and [M] (1.48×10^{18} cm^{-3}; 1% NO_2 in 6 atm CO_2 at 298 K), eq. [15] is obtained.

[15] $r\rho < 1.04$ μg cm^{-2}

This value compares favorably with the range of 100 eV electrons (0.15 ~ 0.51 μg cm^{-2}) (14, 27). Meisels *et al.* gave experimental track radii, 70 ~ 120 nm for ethylene at densities of 0.0795–0.0259 g/cm^3 (16). The corresponding thickness will be 0.56 ~ 0.31 μg cm^{-2}.

This simple estimation for the upper limit of the radius of fission fragment tracks seems qualitatively consistent with Mozumder's track model, in which the track radius is given by the range of 100 eV electrons in the reactant system.

Acknowledgements

The authors thank Messrs. H. Nakajima and T. Kobayashi for their technical assistance in the sample preparation and the operation of the Low Temperature Fissiochemical Loop.

1. A. R. Anderson and D. A. Dominey. Radiat. Res. Rev. **1**, 269 (1976).
2. A. J. Wickham, J. V. Best, and C. J. Wood. Radiat. Phys. Chem. **10**, 107 (1977).
3. P. Harteck and S. Dondes. J. Chem. Phys. **23**, 902 (1955); **26**, 1727 (1957).
4. Y. Ikezoe and S. Sato. J. Nucl. Sci. Technol. **13**, 503 (1976).
5. R. A. Lee. Radiat. Res. **77**, 233 (1979).
6. K. Ishizaki and S. Sato. Chem. Lett. 123 (1979).
7. H. Sakurai, K. Akimoto, S. Toki, and S. Takamuku. Chem. Lett. 467 (1975).
8. D. A. Parkes. Nature, **241**, 110 (1973).
9. C. Willis and A. W. Boyd. Int. J. Radiat. Phys. Chem. **8**, 71 (1976).
10. R. Kummler, C. Leffert, K. Im, R. Piccierelli, L. Kevan, and C. Willis. J. Phys. Chem. **81**, 2451 (1977).
11. C. Willis, A. W. Boyd, and P. E. Binder. Can. J. Chem. **48**, 1951 (1970).
12. W. G. Burns and R. Barker. *In* Progress in reaction kinetics. Vol. 3. *Edited by* G. Porter. Pergamon Press, Oxford. 1965. p. 303.
13. J. H. Cusack and P. A. King. AGN-8196 (1966).
14. A. Mozumder, A. Chatterjee, and J. L. Magee. Adv. Chem. Ser. No. 81, 27 (1968).
15. A. Mozumder. *In* Advances in radiation chemistry. Vol. 1. *Edited by* M. Burton and J. L. Magee. Wiley-Interscience, New York. 1969. p. 1.
16. G. G. Meisels, J. A. LaVerne, Wm. B. Richardson, and T. C. Hsieh. J. Phys. Chem. **82**, 223 (1978); G. G. Meisels, J. P. Freeman, J. P. Gregory, Wm. B. Richardson, and G. J. Sroka. Radiat. Phys. Chem. **11**, 153 (1978); G. G. Meisels, J. P. Gregory, A. A. Siddiki, J. P. Freeman, and Wm. B. Richardson. J. Am. Chem. Soc. **97**, 987 (1975).
17. S. Sato, N. Moriyama, Y. Ikezoe, T. Ishii, M. Hirata, Y. Yamazaki, A. Danno, and K. Oshima. J. Nucl. Sci. Technol. **10**, 379 (1973).
18. Y. Ikezoe, S. Sato, and A. Danno. J. Nucl. Sci. Technol. **8**, 394 (1971); N. Moriyama, Y. Ikezoe, S. Sato, and A. Danno. J. Nucl. Sci. Technol. **11**, 141 (1974).
19. S. Sato, N. Moriyama, Y. Ikezoe, S. Shimizu, T. Kobayashi, Y. Yamazaki, and A. Danno. JAERI-M 4717. 1972.
20. S. Sato, N. Moriyama, Y. Ikezoe, and A. Danno. J. Nucl. Sci. Technol. **10**, 577 (1973).
21. Y. Ikezoe and S. Sato. Bull. Chem. Soc. Jpn. **51**, 33 (1978); **51**, 1016 (1978).
22. E. C. Y. Inn. J. Chem. Phys. **59**, 5431 (1973).
23. R. F. Hampsen and D. Garvin. Natl. Bur. Stand. Technol. Note No. 866, June 1975.
24. L. W. Sieck. Int. J. Chem. Kinet. **10**, 335 (1978).
25. L. I. Bone, L. W. Sieck, and J. H. Futrell. J. Chem. Phys. **44**, 3667 (1966).
26. D. A. Dominey and T. F. Palmer. Discuss. Faraday Soc. **36**, 35 (1963).
27. A. Cole. Radiat. Res. **38**, 7 (1969).

[4]A precise value for k_9 has not been reported. A comparatively low value, 2×10^{-7} cm^3 s^{-1} (10) is adopted tentatively, because recombination of CO_2^+ with O_2^- but not with free electrons is expected in the presence of an appreciable amount of oxygen.

Can. J. Chem. Downloaded from www.nrcresearchpress.com by 210.87.254.40 on 09/06/12
For personal use only.

Vacuum-ultraviolet (147.0 nm and 123.6 nm) photolysis of 1,1-dimethylcyclopropane

JOSEPH B. BINKEWICZ, MICHAEL KAPLAN, AND RICHARD D. DOEPKER
Department of Chemistry, University of Miami, Coral Gables, FL 33124, U.S.A.

Received August 20, 1980

JOSEPH B. BINKEWICZ, MICHAEL KAPLAN, and RICHARD D. DOEPKER. Can. J. Chem. **59**, 537 (1981).

The gas-phase photolysis of 1,1-dimethylcyclopropane has been investigated using xenon (147.0 nm) and krypton (123.6 nm) resonance radiation. Major products observed in order of decreasing importance were isobutene, ethylene, hydrogen, 1,3-butadiene 2-methyl-1,3-butadiene, propylene, allene, methylacetylene, and acetylene. Radical scavengers, NO and O_2, and radical interceptors, H_2S/D_2S and HI, were used to determine the relative importance of radical and molecular processes. CH_3, C_2H_3, C_3H_5, and C_4H_7 radical species were identified and quantified. Ten primary reaction channels were postulated, of which the elimination of methylene was the most predominant, accounting for 34% of the photo-decomposition at 147.0 nm and 39% at 123.6 nm. Although ionization was established at 123.6 nm ($\eta = 0.10$) the nature of a charge transfer or other ion-molecule reaction channel leading to the formation of 2-methyl-1-butene and 2-methyl-2-butene could not be determined.

JOSEPH B. BINKEWICZ, MICHAEL KAPLAN et RICHARD D. DOEPKER. Can. J. Chem. **59**, 537 (1981).

On a étudié la photolyse en phase gazeuse du diméthyl-1,1 cyclopropane en utilisant la radiation de résonance du xénon (147,0 nm) et du krypton (123,6 nm). Les principaux produits observés sont par ordre décroissant d'importance: l'isobutène, l'éthylène, l'hydrogène, le butadiène-1,3 le méthyl-2 butadiène-1,3, le propène, l'allène, le propyne et l'acétylène. On a utilisé les pièges à radicaux NO et O_2 et les intercepteurs de radicaux H_2S/D_2S et HI pour déterminer l'importance relative des processus radicalaire et moléculaire. On a identifié et quantifié les espèces radicalaires CH_3, C_2H_3, C_3H_5 et C_4H_7. On postule la présence de dix chemins réactionnels primaires dans lesquels l'élimination de méthylène prédomine; cette élimination correspond à 34% lors de la photodécomposition à 147,0 nm et de 39% à 123,6 nm. Bien qu'on ait établi la présence d'ionisation à 123,6 nm ($\eta = 0,10$), on ne peut pas déterminer la nature d'un processus de transfert de charge ou d'une autre réaction ion-molécule conduisant à la formation du méthyl-2 butène-1 et du méthyl-2 butène-2.

[Traduit par le journal]

Introduction

Throughout the past years, a series of investigations had been initiated in order to identify the primary and secondary reaction channels for the neutral excited (8.4 eV and 10.0 eV) substituted cyclopropane molecules. The most recent study, the photolysis of *trans*- and *cis*-1,2-dimethylcyclopropane (1) disclosed that the elimination of methylene, reaction [1], was of minor importance

[1] 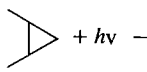 $+ h\nu \longrightarrow CH_2 + C_4H_8$

with a quantum efficiency of 0.10 at 147.0 nm. This is compared to a quantum efficiency of 0.32 for ethylcyclopropane (2*a*) and methylcyclopropane (2*b*). Methylenecyclopropane (2*c*) produced a quantum efficiency of 0.06 for the methylene elimination process. Additional information concerning the photolysis of substituted cyclopropanes has been reported by Collin (3).

An investigation of the photolysis of 1,1-dimethylcyclopropane has been reported recently by Collin *et al.* (4). Their study covered the wavelengths 163.3 nm, 147.0 nm, 123.6 nm, and 106.7–104.8 nm. Although the results reported here closely agree with the investigation of Collin *et al.* at 147.0 nm the 123.6 nm results show considerable important differences.

Experimental Section

Materials

1,1-Dimethylcyclopropane (DMCP), obtained from K and K Laboratories, was purified by vapor phase chromatography using a 12 ft column of 30% squalane on Chromosorb P. at room temperature. Analysis of the resulting DMCP disclosed an impurity of 0.03% *trans*-2-butene. Purification of the other materials used have been described elsewhere (1, 2).

Irradiation and Analysis

The vacuum ultraviolet photolysis of DMCP was investigated at room temperature (25°C) in a standard static system using a 600 cm^3 reaction vessel and a "gettered" xenon (147.0 nm) or krypton (123.6 nm) resonance lamp. Irradiation procedures including photoionization have been reported previously (2, 5). Analysis was performed by vapor chromatography (25 ft, 30% squalane at 60°C, and 6 ft phenyl isocyanate/Porasil C) and mass spectrometry (CEC-21-103 C) as also reported earlier (2, 5).

Actionometry

The chemical actinometers used at 147.0 nm were cyclobutene ($\Phi_{C_4H_4} = 0.23$) (6) and cyclopentene ($\Phi_{C_2H_4} = 0.24$) (5). At 123.6 nm only cyclopentene ($\Phi_{C_2H_4} = 0.19$) (5, 7) was used. The ionization efficiency (η) of 0.16 was assumed for cyclopentene (5, 7) at 123.6 nm. The value was used in order to determine the ionization efficiency of DMCP.

Results

The quantum yields of the major products of the photolysis DMCP at 147.0 nm and 123.6 nm reported in Tables 1–4 are representative data collected under a variety of experimental conditions. In addition to these data, the following observations and controls should be reported.

0008-4042/81/030537-06$01.00/0
©1981 National Research Council of Canada/Conseil national de recherches du Canada

Can. J. Chem. Downloaded from www.nrcresearchpress.com by 210.87.254.105 on 09/05/12
For personal use only.

TABLE 1. Quantum yields; photolysis of 1,1-dimethylcyclopropane at 147.0 nm

	Quantum yield with DMCP in Torr and additives in Torr						
Product	0.2 None	1.0 None	10.0 None	0.2 0.02-NO	1.0 0.1-NO	10.0 1.0-NO	1.0 0.1-NO 105-N_2
CH_4	0.06	0.05	0.06	0.03	0.01	nd[c]	0.01
C_2H_2	0.01	0.02	0.02	0.02	0.02	0.01	0.02
C_2H_4	0.27	0.25	0.27	0.27	0.26	0.25	0.27
C_2H_6	0.17	0.13	0.14	—	—	—	—
C_3H_6	0.07	0.07	0.04	0.05	0.09	0.08	0.09
C_3H_4[a]	0.06	0.07	0.06	0.06	0.05	0.05	0.05
C_3H_4[b]	0.08	0.06	0.07	0.07	0.06	0.09	0.06
1,3-C_4H_6	0.03	0.02	0.02	0.06	0.07	0.07	0.07
i-C_4H_8	0.31	0.34	0.35	0.33	0.34	0.33	0.34
2-Me-1,3-C_4H_5	0.06	0.05	nd	nd	0.09	0.07	0.09
2-Me-1,2-C_4H_5	0.02	0.01	nd	nd	0.03	0.02	0.03
H_2	nd	0.18	0.19	nd	0.17	0.15	nd

[a]Methylacetylene.
[b]Allene.
[c]Not determined.

TABLE 2. Quantum yields; photolysis of 1,1-dimethylcyclopropane at 147.0 nm in the presence of HI/H_2S

	Quantum yield with DMCP in Torr and additive in Torr				
Product	1.0 0.1-HI	1.0 0.1-HI 100-N_2	10.0 1.0-HI	1.0 0.2-H_2S	10.0 2.0-H_2S
CH_4	0.71	0.76	0.75	0.77	0.60
C_2H_2	0.01	0.01	0.01	0.01	0.01
C_2H_4	0.31	0.32	0.33	0.33	0.34
C_2H_6	0.03	0.02	0.03	0.01	0.02
C_3H_6	0.22	0.19	0.21	0.17	0.18
C_3H_4[a]	0.05	0.05	0.06	0.04	0.05
C_3H_4[b]	0.06	0.06	0.06	0.06	0.06
1,3-C_4H_6	0.07	0.07	0.08	0.01	0.01
i-C_4H_8	0.34	0.37	0.37	0.29	0.33
2-Me-1,3-C_4H_5	0.08	0.09	0.06	nd[c]	nd
2-Me-1,2-C_4H_5	0.02	0.03	nd	nd	nd

[a]Methylacetylene.
[b]Allene.
[c]Not determined.

(*1*). Irradiation times were selected as to hold the conversion below 0.05% for the experiments where quantum yields were obtained, except in those cases where hydrogen yields were simultaneously determined through mass spectrometry. Conversions of the order of 0.2% were needed here for sufficient hydrogen production.

(*2*). The quantum yield of ethylene exhibits no pressure sensitivity in the photolysis of DMCP between 0.2 to 4.1 Torr nor was it affected by a tenfold change in irradiation time.

(*3*). Small amounts ($\Phi = 0.02$) of isobutane were observed at both 147.0 nm and 123.6 nm when the photolysis was carried out without scavenger. 1,2-Butadiene was always present to an average quantum yield of 0.02 at 147.0 nm and 0.01 at 123.6 nm.

(*4*). Extensive use of the radical interceptors H_2S/D_2S (8, 9) and HI (10) were employed in this investigation. HI was found to be a more effective radical interceptor than H_2S as suggested by Ausloos *et al.* (10). Increasing the concentration of HI from 3 to 15% revealed that the optimum concentration of HI for radical interception is between 5 and 10% (7% normally used). This corresponds to the maximum in the radical quantum yields vs. HI concentration curve. H_2S, on the other hand, required at least a 10% addition to produce similar effects. Nonradical production was unaffected by the addition of HI, while 1,3-butadiene was reduced in the presence of H_2S. Although the reason for this anomalous result is unclear, it has been observed previously (*2a*, 11). When D_2S (20%) was used, stable products were isolated and determined

Can. J. Chem. Downloaded from www.nrcresearchpress.com by 210.87.254.105 on 09/05/12
For personal use only.

TABLE 3. Quantum yields; photolysis of 1,1-dimethylcyclopropane at 123.6 nm

	Quantum yield with DMCP in Torr and additives in Torr						
Product	1.0 None	8.3 None	10.0 None	1.0 0.1-NO	1.0 0.1-O_2	1.0 1.0-NO	1.0 0.1-NO 100-N_2
CH_4	0.05	0.06	0.06	0.02	0.03	nd[c]	0.01
C_2H_2	0.02	0.01	0.02	0.02	0.01	0.02	0.01
C_2H_4	0.23	0.18	0.21	0.21	0.20	0.21	0.19
C_2H_6	0.18	0.13	0.10	—	—	—	—
C_3H_6	0.08	0.07	0.09	0.05	0.07	0.09	0.10
C_3H_4[a]	0.09	0.05	0.06	0.05	0.06	0.06	0.05
C_3H_4[b]	0.05	0.04	0.05	0.05	0.05	0.04	0.04
1,3-C_4H_6	0.04	0.02	0.04	0.02	0.06	0.05	0.06
i-C_4H_8	0.39	0.36	0.36	0.38	0.41	0.40	0.39
2-Me-1,3-C_4H_5	0.05	nd[c]	nd	0.07	0.10	0.07	0.06
2-Me-1,2-C_4H_5	0.01	nd	nd	0.02	0.02	0.02	0.02
H_2	0.36	nd	0.38	0.33	nd[c]	0.33	nd

[a]Methylacetylene.
[b]Allene.
[c]Not determined.

TABLE 4. Quantum yields; photolysis of 1,1-dimethylcyclopropane at 123.6 nm in the presence of HI/H_2S

	Quantum yield with DMCP in Torr and additive in Torr				
Product	1.0 0.1-HI	10.0 1.0-HI	1.0 0.10-HI 100-N_2	0.5 0.10-H_2S	10.0 2.0-H_2S
CH_4	1.03	0.93	1.01	0.76	0.83
C_2H_2	0.02	0.02	0.02	0.02	0.01
C_2H_4	0.25	0.24	0.24	0.25	0.24
C_2H_6	0.05	0.05	0.03	0.01	—
C_3H_6	0.15	0.15	0.14	0.11	0.13
C_3H_4[a]	0.07	0.08	0.06	0.06	0.05
C_3H_4[b]	0.05	0.04	0.04	0.06	0.06
1,3-C_4H_6	0.09	0.06	0.06	—	—
i-C_4H_8	0.54	0.51	0.48	0.38	0.36
2-Me-1,3-C_4H_5	0.10	0.06	0.09	nd	nd
2-Me-1,2-C_4H_5	0.02	nd[c]	0.02	nd	nd

[a]Methylacetylene.
[b]Allene.
[c]Not determined.

through mass spectrometry. In the 123.6 nm photolysis of DMCP (5.0 Torr) mass spectral analysis of the hydrogen (H_2 = 45, HD = 52, D_2 = 3), methane (CH_4 = 44, CH_3D = 52, CH_2D_2 = 4), propylene (C_3H_6 = 54, C_3H_5D = 46), and butene (C_4H_6 = 82, C_4H_7D = 18) were carried out. Unfortunately, the results obtained when D_2S is used must be considered diagnostic since total radical yields were consistently less than those determined through the use of H_2S or HI addition.

(5). The ionization energy of DMCP, 9.08 eV (12), is below the photoenergy of the krypton (10.0 eV) resonance radiation. The ionization efficiency for DMCP was determined at 123.6 nm and found to be $\eta = 0.10$. Although no product yield vs. applied collector voltage studies were made, the production of 2-methyl-1-butene (Φ = 0.04) and 2-methyl-2-butene (Φ = 0.04) at 123.6 nm is believed to be formed through an ion-molecule pathway (4).

Discussion

147.0 nm

Collin *et al.* (4) reported seven primary processes involving the 147.0 nm photolysis of DMCP. The data presented in Tables 1 and 2 of this work agree within experimental error to that presented by Collin.

Isobutene is clearly the most abundant product produced in the photolysis of 1,1-dimethylcyclopropane. The isobutene yield is unaffected by the presence of nitric oxide or oxygen, although it is slightly increased in the presence of hydrogen iodide. The elimination of methylene from the cy-

Can. J. Chem. Downloaded from www.nrcresearchpress.com by 210.87.254.105 on 09/05/12
For personal use only.

Can. J. Chem. Downloaded from www.nrcresearchpress.com by 210.87.254.105 on 09/05/12
For personal use only.

[2] DMCP + $h\nu \rightarrow CH_2$ + iso-C_4H_8

clopropyl ring (reaction [2]) is the sole reaction channel for isobutene formation, when the photolysis is carried out in the presence of NO or O_2. The quantum efficiency of this pathway is equal to the quantum yield of isobutene (Table 5) $\phi_2 = \Phi_{C_4H_8} = 0.34$. This compares well with a value of 0.35 presented by Collin *et al.* (4).

The formation of 1,3-butadiene and 1,2-butadiene occurs through the elimination of a methyl group and a hydrogen atom (reaction [3]).

[3] DMCP + $h\nu \rightarrow CH_3 + H$ + 1,3/1,2-C_4H_6

This reaction pathway was found to be the sole reaction channel for the production of the butadienes in the photolysis of 1,2-dimethlycyclopropane (1). If the assumption is again made here that reaction [3] is the exclusive pathway for butadiene formation then the quantum efficiency for reaction [3] is equal to the sum of the quantum yields of 1,3- and 1,2-butadiene, $\phi_3 = \Phi_{1,3\text{-}C_4H_6} + \Phi_{1,2\text{-}C_4H_6} = 0.09$. Collin *et al.*'s (4) value was 0.08.

The photolysis (147.0 nm) of *trans*-1,2-dimethylcyclopropane (1) revealed that a portion of the C_4H_7-fragments, resulting from the elimination of a methyl radical, was stable within the pressure range of 0.2 to 25 Torr (1).

[4] 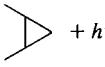 + $h\nu \longrightarrow CH_3 + C_4H_7$

The presence of the C_4H_7 radical species was determined through the use of HI as a radical interceptor (9). The difference in yield of C_4H_8 in the presence of HI with its yield in the presence of NO evaluates the quantum yield of the C_4H_7 radical. For DMCP the quantum efficiency of the parallel reaction pathway is 0.03.

TABLE 5. Photolysis of 1,1-dimethylcyclopropane, a summary of quantum yields

Product	Quantum yield at wavelength 147.0 nm	123.6 nm
C_2H_2	0.02	0.02
C_2H_4	0.26	0.19
C_3H_6	0.08	0.08
C_3H_4[a]	0.05	0.05
C_3H_4[b]	0.06	0.05
1,3-C_4H_6[c]	0.09	0.06
i-C_4H_8	0.34	0.39
2-Me-1,3-C_4H_5	0.09	0.08
2-Me-1,2 C_4H_5	0.02	0.02
2-Me-1-butene	—	0.03
2-Me-2-butene	—	0.05
H_2	0.18	0.33
Radical yields, as determined from H_2S/HI experiments		
CH_3/CH_2	0.74	0.98
C_2H_3	0.07	0.06
C_3H_5	0.13	0.07
C_4H_7	0.03	0.11

[a] Methylacetylene.
[b] Allene.
[c] 1,3-Butadiene + 1,2-butadiene.

[5] DMCP + $h\nu \rightarrow CH_3 + C_4H_7$

This reaction channel was not reported by Collin *et al.* (4).

Methylacetylene and allene are produced through the elimination of two methyl radicals from the photoexcited state of DMCP and is quantified by the sum of the quantum yields of

[6] DMCP + $h\nu \rightarrow 2CH_3 + C_3H_4$

methylacetylene and allene. It must be assumed that isomerization occurred in the formation of methylacetylene. $\phi_6 = 0.06 + 0.05 = 0.11$. A value of 0.10 was reported by Collin *et al.* (4).

The formation of ethylene ($\Phi_{C_2H_4} = 0.26$) may result from the direct cleavage of the 1,2 and 1,3 carbon bonds of the cyclopropane ring, eliminating ethylene and a CH_3CCH_3 species. The CH_3CCH_3 species will rearrange to propylene or decompose to a C_3H_5 radical.

[7] DMCP + $h\nu \rightarrow C_2H_4 + (CH_3CCH_3)^*$

[8] $(CH_3CCH_3)^* \rightarrow CH_3CHCH_2$

[9] $\rightarrow CH_3CCH_2 + H$

The formation of the 2-propenyl radical is demonstrated by the increased formation of propylene in the presence of H_2S (13), since H_2S will intercept the vinyl form but not the allyl structure. HI, on the other hand, will intercept both structures. Isomerization of the C_3H_5 can be demonstrated by the small increase that is observed in the propylene yield when the photolysis is carried out in the presence of HI over that when H_2S is used. The quantum yield of propylene for the DMCP–HI system will dictate the C_3H_5 quantum yield.

Considering reactions [8] and [9], two reaction channels involving the formation of ethylene can be postulated.

[10] DMCP + $h\nu \rightarrow C_2H_4 + C_3H_6$

[11] DMCP + $h\nu \rightarrow C_2H_4 + C_3H_5 + H$

The quantum efficiency of reaction channel 11 may be quantified from the quantum yield of the C_3H_5 radical, which in turn is evaluated through the difference between the quantum yields of propylene with HI and that with NO. $\phi_{11} = \Phi_{C_3H_5} = 0.13$. Collin *et al.* (4) found a value of 0.16 for this pathway.

Although acetylene quantum yields are small its formation reveals a second pathway for the formation of propylene. Reaction [12] is of major impor-

Can. J. Chem. Downloaded from www.nrcresearchpress.com by 210.87.254.105 on 09/05/12
For personal use only.

[12] DMCP + $h\nu \rightarrow C_2H_2 + H_2 + C_3H_6$

tance in the 147.0 nm photolysis of *trans*-1,2-dimethylcyclopropane (1) with a quantum efficiency of 0.24. Here though due to structural changes in the intermediate fragments the quantum efficiency of reaction [12] is greatly reduced. $\phi_{12} = \Phi_{C_2H_2} = 0.02$. If it can be assumed that the formation of propylene is restricted to reactions [10] and [12], the quantum efficiency of reaction channel 10 may thus be evaluated. $\phi_{10} = \Phi_{C_3H_6} - \phi_{12} = 0.06$. Collin *et al.* (4) reported a value of 0.08 for this reaction but did not include reaction channel 12, although their data are consistent with the values reported here.

Ethylene may also be produced through a pathway involving the elimination of a methyl radical and the "splitting" of the resulting C_4H_7 fragment into a vinyl radical and ethylene. This process was reported to have a quantum efficiency of 0.11 for ethylcyclopropane at 147.0 nm (2*a*). Reaction [13]

[13] DMCP + $h\nu \rightarrow CH_3 + C_2H_3 + C_2H_4$

may be evaluated from the quantum yield of vinyl radical formation reported in Table 5. The quantum yield of vinyl radical formation is determined by the difference in ethylene yield when NO is used as a radical interceptor with that when either HI or H_2S is used. $\phi_{13} = \Phi_{C_2H_3} = 0.07$. The formation of ethylene, $\Phi_{C_2H_4} = \phi_{10} + \phi_{11} + \phi_{13} = 0.06 + 0.13 + 0.07 = 0.26$, is indeed consistent with the independent evaluation of reaction channels 10, 11, and 13.

The elimination of two hydrogen atoms or molecular hydrogen from the photoexcited state of

[14] DMCP + $h\nu \rightarrow 2H(H_2) + C_5H_8$

DMCP results in the formation of 2-methyl-1,3-butadiene and 2-methyl-1,2-butadiene depending upon which hydrogen atoms are eliminated. The total quantum efficiency for reaction channel 14 would be the sum of the quantum yield of the two methyl-butadienes. $\phi_{14} = \Phi_{C_5H_{8\text{-}1,3}} + \Phi_{C_5H_{8\text{-}1,2}} = 0.11$. Collin *et al.* (4) reported a value slightly higher at 0.13, which is still within the expected experimental error.

123.6 nm

The primary reaction channels discussed and applied to the 147.0 nm photolysis of 1,1-dimethylcyclopropane are expected to be applicable at 123.6 nm (Tables 3 and 4). The methylene elimination reaction channel 2 again may be evaluated through the scavenged value of isobutene formation, $\phi_2 = \Phi_{C_4H_8} = 0.39$. Similarly, reaction channel 3 is evaluated through the quantum yield of 1,3- and 1,2-butadiene, $\phi_3 = \Phi_{C_4H_{6\text{-}1,3}} + \Phi_{C_4H_{6\text{-}1,2}} = 0.06$, while reaction channel 5 which results in the C_4H_7 radical production has a quantum efficiency of 0.11. It may be noted that the presence of the C_4H_7 radical was further demonstrated at 123.6 nm through the use of D_2S. Here 18% of the resulting butene was mono-deuterated.

The formation of methylacetylene and allene again would be associated with reaction [6], $\phi_6 = 0.05 + 0.05 = 0.10$. As in the lower energy photolyses, propylene is produced through reaction channels 10 and 12, with reaction channel 12 being set equal to the quantum yield of acetylene, $\phi_{12} = \Phi_{C_2H_2} = 0.02$. Reaction channel 10 is quantified through the difference in the quantum yield of propylene and acetylene. $\phi_{10} = 0.08 - 0.02 = 0.06$.

The formation of the 2-propenyl radical again is demonstrated by the increased propylene in the presence of HI/H_2S. Further, when D_2S is used nearly 45% of the propylene was mono-deuterated. This is in good agreement with the quantum efficiency of reaction [11] being assigned a value of 0.07 (47%) and that of the nonradical propylene production of 0.08.

The formation of vinyl radicals at 123.6 nm is again demonstrated through the use of HI/H_2S. The quantum efficiency for the production of vinyl radical at 123.6 nm, reaction [13], was found to be 0.05. Again the check of the quantum yield of ethylene $\Phi_{C_2H_4} = 0.19$ and the sum of the quantum efficiencies for reaction [10] ($\phi_{10} = 0.06$), reaction [11] ($\phi_{11} = 0.07$), and reaction [13] ($\phi_{13} = 0.05$) is within the experimental uncertainty of the method, $\phi_{10} + \phi_{11} + \phi_{13} = 0.18$.

The elimination of two hydrogen atoms or molecular hydrogen again leads to the formation of 2-methyl-1,3-butadiene and 2-methyl-1,2-butadiene (reaction [14]) with a quantum efficiency of 0.10 at 123.6 nm.

At 123.6 nm (10.0 eV) ionization of the parent molecule occurs. The ionization efficiency re-

[15] DMCP + $h\nu \rightarrow (C_5H_{10})^+ + e^-$

ported here was determined to be 0.10 while Collin *et al.* (4) reported a value of 0.28. Collin *et al.* did not report primary reaction channel quantum efficiencies for 123.6 nm but did for the argon (106.7–104.8 nm) resonance study. Although we have also carried out additional experiments with the argon resonance lamp no quantum yields were determined at the time so these results are not reported here. It is assumed that the isomerization of DMCP to the reported methyl butenes directly involve the parent $(C_5H_{10})^+$ ion.

Summary and Conclusion

The vacuum-ultraviolet photolysis of 1,1-dimethylcyclopropane may be described by ten

TABLE 6. Quantum yields for the primary reaction channels of the vacuum-uv photolysis of 1,1-dimethylcyclopropane

Reaction	Quantum yield at wavelength (nm) 147.0	123.6	~106[a]
$\triangle + h\nu \xrightarrow{[2]} CH_2 + i\text{-}C_4H_8$	0.34 (0.35)[b]	0.39	0.22
$\xrightarrow{[3]} CH_3 + H + C_4H_6\text{-}1,3/1,2$	0.09 (0.08)	0.06	0.04
$\xrightarrow{[5]} CH_3 + C_4H_7$	0.03 (—)	0.11	—
$\xrightarrow{[6]} 2CH_3 + C_3H_4$	0.11 (0.10)	0.10	0.15
$\xrightarrow{[13]} CH_3 + C_2H_3 + C_2H_4$	0.07 (0.02)	0.06	≤0.20
$\xrightarrow{[11]} C_2H_4 + H + C_3H_5$	0.13 (0.16)	0.07	
$\xrightarrow{[10]} C_2H_4 + C_3H_6$	0.06 (0.08)	0.06	0.12
$\xrightarrow{[12]} C_2H_2 + H_2 + C_3H_6$	0.02 (—)	0.02	—
$\xrightarrow{[14]} 2H + C_5H_8$	0.11 (0.13)	0.10	0.12
$\xrightarrow{[15]} (C_5H_{10})^{\dagger} + e^-$	0.00 (0.00)	0.10	0.35
	Total 0.97 (0.92)	1.07	1.20

[a] ~106 nm results are by Collin *et al.* (4).
[b] Values reported by Collin *et al.* (4).

primary reaction channels. Quantum efficiencies obtained in this study are reported in Table 6 along with values obtained by Collin *et al.* (4). The product quantum yields summarized in Table 5 were collected with an estimated accuracy of better than 10%, with the exception of hydrogen. Here due to the method required, a 15% error can be expected. Larger error limits might be expected to apply for radical yields, since the resulting quantum yields were obtained as a difference between two quantum values with their own errors limits. Although there were some discrepancies between this work and that of Collin *et al.* (4) with regards to the 123.6 nm photolyses, the 147.0 nm results demonstrated the reproducibility of such studies.

1. T. S. PENDLETON, M. KAPLAN, and R. D. DOEPKER. J. Phys. Chem. **84**, 472 (1980).
2. (*a*) E. LOPEZ and R. D. DOEPKER. J. Phys. Chem. **82**, 752 (1978); (*b*) M. KAPLAN and R. D. DOEPKER. Manuscript in preparation; (*c*) K. L. HILL and R. D. DOEPKER. J. Phys. Chem. **76**, 3153 (1972).
3. G. J. COLLIN. J. Chim. Phys. **74**, 302 (1977).
4. G. J. COLLIN, H. GAGNON-DESLAURIERS, M. SUQUET, K. BUKKA, and J. L. SIMARD. J. Photochem. **9**, 449 (1978).
5. C-K TU and R. D. DOEPKER. J. Photochem. **3**, 13 (1974).
6. A. DELEON and R. D. DOEPKER. J. Phys. Chem. **75**, 3656 (1971).
7. R. LESCLAUX, S. SEARLES, L. W. SIECK, and P. J. AUSLOOS. Chem. Phys. **54**, 3411 (1971).
8. P. AUSLOOS and S. G. LIAS. J. Chem. Phys. **44**, 521 (1966).
9. G. J. COLLIN and P. M. PERRIN. Can. J. Chem. **50**, 2823 (1972).
10. P. AUSLOOS, R. E. REBBERT, and S. G. LIAS. J. Photochem. **2**, 267 (1973).
11. G. J. COLLIN and P. M. PERRIN. Can. J. Chem. **50**, 2400 (1972).
12. F. P. LOSSING. Can. J. Chem. **50**, 3973 (1972).
13. G. J. COLLIN and A. WIECKOWSKI. J. Photochem. **8**, 103 (1978).

Can. J. Chem. Downloaded from www.nrcresearchpress.com by 210.87.254.105 on 09/05/12
For personal use only.

Mass spectral studies of symmetrical and unsymmetrical dialkyl disulfides

DINESH GUPTA, ARTHUR R. KNIGHT, AND PETER J. SMITH[1]

Department of Chemistry and Chemical Engineering, University of Saskatchewan, Saskatoon, Sask., Canada S7N 0W0

Received March 13, 1980

DINESH GUPTA, ARTHUR R. KNIGHT, and PETER J. SMITH. Can. J. Chem. **59**, 543 (1981).

The mass spectra for thirteen symmetrical and thirty-five unsymmetrical dialkyl disulfides have been determined at 70 eV. Carbon–sulfur bond cleavage to give hydrocarbon ions was observed as well as the formation of RS^+ ions. Factors affecting these two processes are discussed. The most favoured decomposition pathway for the molecular ions of most of the dialkyl disulfides (RSSR′) studied was intramolecular hydrogen transfer to give RSSH and R′SSH. The effect of varying the structure of the alkyl groups on this process has been investigated.

DINESH GUPTA, ARTHUR R. KNIGHT et PETER J. SMITH. Can. J. Chem. **59**, 543 (1981).

On a déterminé à 70 eV les spectres de masse de 13 disulfures d'alkyles symétriques et de 35 disulfures non symétriques. On a observé la rupture de la liaison C—S qui conduit aux ions hydrocarbonés ainsi que la formation des ions RS^+. On discute des facteurs qui affectent ces deux processus. Le mode de décomposition le plus favorisé des ions moléculaires de la plupart des disulfures d'alkyles (RSSR′) étudiés est un transfert intramoléculaire d'hydrogène qui donne RSSH et R′SSH. On a étudié l'effet d'un changement de structure des groupes alkyles sur ce mode de fragmentation.

[Traduit par le journal]

Introduction

Organic disulfides have been the subject of extensive investigations (1). This class of compound is found in nature as constituents of essential oils, natural pesticides, and insect pheromones (2, 3). As well, organic disulfides have been studied in considerable detail due to their ability to give protection against ionizing radiation (4).

Several investigations (5–7) of the photochemically induced exchange reactions of aliphatic disulfides have been carried out in our laboratories. Accordingly, it was considered of interest to study the mass spectra of these compounds and, hence, thirty-five unsymmetrical and thirteen symmetrical disulfides were prepared and the results are discussed herein.

Until recently (1) there had been very little reported on the mass spectrometry of aliphatic disulfides. Disulfides which contain sites of unsaturation (e.g., diallyl disulfide and aromatic disulfides) were shown to decompose to a large extent with skeletal rearrangement (8). The major fragmentation pathway for aliphatic disulfides where the alkyl groups are saturated and larger than methyl is the elimination of a neutral alkene molecule. This is the only process considered in detail by other workers (9, 10) and can be represented by either reaction [1*a*] or [1*b*] where sequential loss of two alkene molecules leads to the formation of HSSH.

Block *et al.* (10) considered the detailed mechanism of alkene loss by determining the mass spectrum of bis(ethyl-1,1-d_2)disulfide. It was found

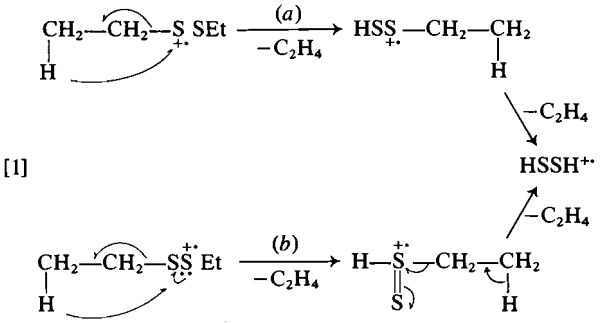

[1]

(reaction [2]) that the molecular ion, *m/z* 126, fragmented by a one-step nonspecific hydrogen transfer to give both *m/z* = 96 and 97. Since *m/z* 96 was the more intense ion (87%), it was concluded that the hydrogen transfers shown in reaction [1] are more favourable than the 1,2 shift presumably responsible for the *m/z* 97 species.

[2] $[CH_3CD_2SSCD_2CH_3]^{+\cdot}$ (*m/z* 126) → $CH_3CD_2SSH^{+\cdot}$ (*m/z* 96) (87%); $CH_3CD_2SSD^{+\cdot}$ (*m/z* 97) (13%)

Alonso *et al.* (11) have recently investigated the fragmentation of a series of unsymmetrical disulfides in order to determine the factors affecting the competing loss of alkene processes taking place in each side of the unsymmetrical system. The fragmentation of unsymmetrical disulfides can lead to two sets of hydrogen transfer derived fragment ions.

It was concluded that the 1,2-H shift is an unfavourable process since $HSSR^{+\cdot}$ was not observed in the mass spectra of the methyl alkyl disulfides studied. Furthermore, the hydrosulfide intermediate, $CH_3SSH^{+\cdot}$, did not fragment to $HSSH^{+\cdot}$

[1]To whom all correspondence should be addressed.

0008-4042/81/030543-06$01.00/0

©1981 National Research Council of Canada/Conseil national de recherches du Canada

Can. J. Chem. Downloaded from www.nrcresearchpress.com by 210.87.254.6 on 09/06/12
For personal use only.

Can. J. Chem. Downloaded from www.nrcresearchpress.com by 210.87.254.6 on 09/06/12
For personal use only.

via a second H transfer. The observation of significant fragment ions from several *t*-butyl alkyl disulfides, formed by transfer of hydrogen from the *t*-butyl group, was concluded to give support to the 1,3-hydrogen migration process observed by Block *et al.* (10).

Alonso *et al.* (11) measured the relative intensity of both RSSH and R′SSH formed from a series of unsymmetrical dialkyl disulfides, RSSR′. A marked preference for RSSH over R′SSH was noted depending on the structure of R and R′ and it was concluded that the position occupied by the migrating hydrogen is very important.

The availability of the large number of both symmetric and unsymmetric alkyl disulfides in the present investigation allows us to quantitatively study the factors associated with the ease of hydrogen transfer to sulfur with loss of the alkene molecule. The intensity ratio $(RSSH)^{+\cdot}/M^{+\cdot}$ was determined and the results discussed in the light of the type and number of hydrogens transferred as well as a consideration of the stability of the resultant alkene molecule. As well, factors affecting various possible competing processes to the alkene loss fragmentation are considered. Such processes have not been discussed previously in the literature.

Results and Discussion

The mass spectra[2] were determined for thirteen symmetrical alkyl disulfides, series 1, at 70 eV and lower ionization energies as well as for thirty-five unsymmetrical alkyl disulfides, series 2–7 (Table 1).

A noteworthy feature of the spectra of the forty-eight disulfides studied is the presence of a significant molecular ion at 70 eV. Only di-*t*-butyldisulfide, **8**, had a molecular ion with relative intensity less than 10% (8%). The significant molecular ions observed for this class of compound, even for high molecular weight disulfides, is useful for both detection and identification.

A favoured decomposition pathway for the molecular ions of thioethers, aliphatic ethers, and aliphatic amines is β-cleavage, reaction [3].

$$[3] \quad [RSCH_2—R']^{+\cdot} \rightarrow RS^+=CH_2 + R'^{\cdot}$$

β-Cleavage, however, was not observed for the disulfides examined in the present study even when there was branching at the α-carbon, e.g., di-*t*-butyldisulfide, **8**. Presumably, the formation of the β-cleavage ion from the disulfides is unfavourable due to the presence of an electronegative sulfur atom adjacent to the positive sulfur in the β-cleavage ion, $RS\overset{+}{S}=CH_2$.[3] This ion does not appear to be stabilized by partial π-bond formation between the two sulfur atoms. The failure of the disulfides to undergo β-cleavage could account to some extent for the relatively intense molecular ions.

A feature of the mass spectrum of aliphatic thioethers (ref. 9, p. 280) is the observation of an ion formed by cleavage of the carbon–sulfur bond with charge retention on sulfur. It has been noted (ref. 9, p. 280) that this process is more favourable for thioethers than for the oxygen analogues. This observation was rationalized as being due to the greater ability of sulfur to stabilize the electron deficiency by participation of its inner shell electrons. However, there was no analogous carbon–sulfur bond rupture observed in the present investigation to give RSS^+. This observation is consistent with the explanation presented for the failure to observe the β-cleavage ions.

Hydrocarbon ions corresponding to R and R′ of both the symmetric and unsymmetric disulfides RSSR and RSSR′ are significant, contrary to ref. 9, p. 292, in the spectra of all the compounds studied except the di-*n*-heptyl and di-*n*-octyl disulfides where hydrocarbon fragments smaller than R are significant. For the symmetric disulfides of series 1 the relative abundance of R varies between 28 and

TABLE 1. List of RSSR′ studied

Series 1	R = R′ = methyl, ethyl, *n*-propyl, *i*-propyl, *n*-butyl, *i*-butyl, *s*-butyl, *t*-butyl, *n*-amyl, *i*-amyl, *n*-hexyl, *n*-heptyl, *n*-octyl; compounds **1–13**, respectively.
Series 2	R = methyl; R′ = ethyl, *n*-propyl, *i*-propyl, *n*-butyl, *i*-butyl, *s*-butyl, *t*-butyl, *n*-amyl, *i*-amyl; compounds **14–22**, respectively.
Series 3	R = ethyl; R′ = *n*-propyl, *i*-propyl, *n*-butyl, *i*-butyl, *s*-butyl, *t*-butyl, *n*-amyl, *i*-amyl, compounds **23–30**, respectively.
Series 4	R = *n*-propyl; R′ = *n*-butyl, *i*-butyl, *s*-butyl, *n*-amyl, *i*-amyl; compounds **31–35**, respectively.
Series 5	R = *i*-propyl; R′ = *n*-butyl, *i*-butyl, *s*-butyl, *n*-amyl, *i*-amyl; compounds **36–40**, respectively.
Series 6	R = *n*-amyl; R′ = *n*-butyl, *i*-butyl, *s*-butyl, *t*-butyl; compounds **41–44**, respectively.
Series 7	R = *i*-amyl; R′ = *n*-butyl, *i*-butyl, *s*-butyl, *t*-butyl; compounds **45–48**, respectively.

[2]A complete listing of the mass spectral peaks for all the compounds down to 3% relative intensity is available, at a nominal charge, from the Depository of Unpublished Data, CISTI, National Research Council of Canada, Ottawa, Ont., Canada K1A 0S2.

[3]This explanation was put forth by Block (12) who studied the solvolysis of chloromethyl methyl disulfide.

TABLE 2. Mass spectral data of hydrocarbon fragment ions (R) derived from dialkyldisulfides at 70 eV

Compound		R^+	$M^{+\cdot}$	$R^+/M^{+\cdot}$ intensity ratio
$CH_3SS(CH_2)_2CH_3$	(**15**)	43(65)	122(75)	0.87
$CH_3SSCHCH_3$ (CH$_3$ branch)	(**16**)	43(57)	122(55)	1.04
$CH_3SS(CH_2)_3CH_3$	(**17**)	57(63)	136(73)	0.86
$CH_3SSCHCH_2CH_3$ (CH$_3$ branch)	(**19**)	57(53)	136(45)	1.18
$CH_3SSCH_2CHCH_3$ (CH$_3$ branch)	(**18**)	57(100)	136(57)	1.75
$CH_3SSC(CH_3)_3$	(**20**)	57(100)	136(32)	3.13
$CH_3SS(CH_2)_4CH_3$	(**21**)	71(14)	150(31)	0.45
$CH_3SSCH_2CH_2CHCH_3$ (CH$_3$ branch)	(**22**)	71(27)	150(28)	0.96

100%. These hydrocarbon ions can be formed directly by simple carbon–sulphur bond cleavage.

Another pathway leading to the hydrocarbon ions R and R′ is decomposition of the odd electron ions $RSSH^{+\cdot}$ and $R'SSH^{+\cdot}$, formed by intramolecular hydrogen transfer, with subsequent loss of $HS_2^{\cdot}$, reaction [4]. The loss of HS_2 has been

$$[4]\quad [RSSR']^{+\cdot} \rightarrow RSSH^{+\cdot} \xrightarrow[*]{-HS_2^{\cdot}} R^+ \qquad [RSSR']^{+\cdot} \rightarrow R'SSH \xrightarrow[*]{-HS_2^{\cdot}} R'^+$$

confirmed in most cases by the observation of a metastable peak. This process, like the simple cleavage process to give R^+, appears to be favoured only when the hydrocarbon ion is reasonably stable; i.e. loss of $HS_2^{\cdot}$ was not observed from RSSH when R = *n*-heptyl and *n*-octyl.

In order to gain a measure of the relative contribution of the two competing processes to give R^+, the ratio $R^+/M^{+\cdot}$ at 70 eV was determined for several dialkyl disulfides, Table 2. Compounds **15–22** cannot give R^+ via decomposition of RSSH since it has recently been shown (11), and confirmed in the present study, that a 1,2-H shift to give RSSH does not occur for methyl alkyl disulfides, CH_3SSR. Consequently, the ratio $R^+/M^{+\cdot}$ should provide a measure of the direct cleavage process to give R^+. It is noted that the ratio increases with increased branching within a series where the size of R is kept constant; i.e., $R^+/M^{+\cdot}$ = 0.86 and 3.13 for CH_3SS-*n*-Bu (**17**) and CH_3SS-*t*-Bu (**20**), respectively. Presumably this increase in ratio reflects a preference for the formation of the branched ion, *t*-butyl as compared with the *n*-butyl cation. Similarly, the ratio increases from 0.45 to 0.96 when R is changed from *n*-amyl (**21**) to isoamyl (**22**).

The hydrocarbon ions R and R′ can be formed by the two competing processes from the compounds shown in Table 3. The intramolecular hydrogen transfer reaction[4] can produce both RSSH and R′SSH which, on loss of $HS_2^{\cdot}$, give R^+ and R'^+. It is noted, however, that for substrates **43** and **47** only R′SSH, *m*/*z* = 136, is formed which fragments to give *m*/*z* 71. The ratios $R^+/M^{+\cdot}$ and $R'^+/M^{+\cdot}$ are similar for both **43** and **47**. This indicates that *m*/*z* 71 is enhanced by decomposition of R′SSH (*m*/*z* 136) since $R^+/M^{+\cdot}$ is significantly greater for **19** than for either **21** or **22**, Table 2.

The ratios are appreciably altered when both RSSH and R′SSH are formed, compounds **41** and **45**. When the relative abundance of RSSH (*m*/*z* 122) is greater than for R′SSH (*m*/*z* 136), compound **41**, the ratio $R^+/M^{+\cdot}$ is greater than $R'^+/M^{+\cdot}$, 3.67 and 1.57, respectively. When, however, RSSH and R′SSH are formed in essentially equal amounts, compound **45**, then $R^+/M^{+\cdot}$ is less than $R'^+/M^{+\cdot}$, 1.43 and 2.43, presumably due to the preference for the formation of the isoamyl cation to that of the

[4]This process will be discussed in more detail in a subsequent section of this manuscript.

Can. J. Chem. Downloaded from www.nrcresearchpress.com by 210.87.254.6 on 09/06/12
For personal use only.

TABLE 3. Mass spectral data of hydrocarbon ions (R and R') derived from RSSR' at 70 eV

Compound		$[RSSH]^{+\cdot}$	$[R'SSH]^{+\cdot}$	R^+	R'^+	$M^{+\cdot}$	$R^+/M^{+\cdot}$ intensity ratio	$R'^+/M^{+\cdot}$ intensity ratio
$CH_3CH_2CH(CH_3)SSCH_2CH_2CH_2CH_2CH_3$	(43)	—	136(81)	57(96)	71(90)	192(53)	1.81	1.70
$CH_3CH_2CH(CH_3)SSCH_2CH_2CH(CH_3)CH_3$	(47)	—	136(61)	57(74)	71(77)	192(35)	2.11	2.20
$CH_3CH_2CH_2CH_2SSCH_2CH_2CH_2CH_2CH_3$	(41)	122(30)	136(12)	57(77)	71(33)	192(21)	3.67	1.57
$CH_3CH_2CH_2CH_2SSCH_2CH_2CH(CH_3)CH_3$	(45)	122(13)	136(11)	57(40)	71(68)	192(28)	1.43	2.43

TABLE 4. Hydrocarbon ions from the symmetrical *n*-alkyl disulfides at 70 eV

RSSR		R^+ *m/z* (rel. int.)	Relative intensities *m/z* 29	*m/z* 43	*m/z* 57	*m/z* 71
R = Ethyl	(2)	29(89)	—	—	—	—
= *n*-Propyl	(3)	43(100)	5	—	—	—
= *n*-Butyl	(5)	57(57)	58	6	—	—
= *n*-Amyl	(9)	71(49)	24	100	—	—
= *n*-Hexyl	(11)	85(28)	17	100	16	—
= *n*-Heptyl	(12)	99(—)	18	34	100	—
= *n*-Octyl	(13)	113(—)	27	74	100	80

n-butyl ion by the direct cleavage process. This is supported by the data for **22** and **17**, Table 2.

Hydrocarbon ions smaller than R and R' are noteworthy in the spectra of all the compounds studied where the alkyl groups of the disulfides were butyl or larger. Table 4 shows the hydrocarbon ions observed when the symmetrical normal alkyl disulfides were examined at 70 eV. Fragmentation of both R and R' by the well established pathway, reaction [5], leads to smaller hydrocarbon ions.

[5] $CH_3CH_2CH_2CH_2{-}\overset{\curvearrowright}{CH_2}{-}\overset{+}{C}H_2 \xrightarrow{m^*} CH_3CH_2CH_2\overset{+}{C}H_2$

However, significant ions smaller than R are observed which cannot be rationalized by the process represented in reaction [5]; i.e. *m/z* 43 with a relative intensity of 100% found in the spectrum of the di-*n*-hexyl substrate (**11**). Similarly, the ions at *m/z* 29 for **9**, *m/z* 57 for **12**, and *m/z* 71 for **13** cannot be accounted for by the loss of ethylene from R. Accordingly, it is suggested that to some degree δ-cleavage occurs with the formation of a cyclic disulfide radical and the hydrocarbon ion, reaction [6].

[6] $[CH_3(CH_2)_5SSCH_2CH_2CH_2CH_2CH_2CH_3]^{+\cdot}$

$$\longrightarrow CH_3CH_2CH_2^+ + CH_3(CH_2)_5{-}\dot{S}{-}S{-}CH_2CH_2CH_2$$

Sulfur–sulfur bond rupture with formation of RS^+ ions has been observed for methyl phenyl disulfide and diphenyl disulfide (ref. 9, p. 292). An examination of the spectra of the symmetric di-*n*-alkyl disulfides in the present study shows also ions resulting from sulfur–sulfur bond cleavage. The relative intensity of the RS^+ ions varies from 16% (di-*n*-octyl disulfide) to 9% (di-*n*-amyl disulfide) and are negligible for the lower molecular weight disulfides. These ions could be formed by a combination of simple sulfur–sulfur bond rupture and decomposition of RSSH ions formed by intramolecular hydrogen transfer, reaction [4]. The loss of $SH^\cdot$ from RSSH to give RS^+ is confirmed by the observation of the appropriate metastable peak. It appears that direct sulfur–sulfur cleavage to give RS^+ is not significant in the case of the dialkyl disulfides, as compared with diphenyl disulfide, since the relative intensity of such ions is negligible for the lower molecular weight disulfides where

Can. J. Chem. Downloaded from www.nrcresearchpress.com by 210.87.254.6 on 09/06/12
For personal use only.

TABLE 5. Mass spectral data of fragment ions derived from 1,3-intramolecular hydrogen transfer*

RSSR′		$M^{+\cdot}$	$[RSSH]^{+\cdot}$	$[R'SSH]^{+\cdot}$	$H_2S_2^{+\cdot}$	$[RSSH]^{+\cdot}/M^{+\cdot}$
$CH_3SSCH_2CH_3$	(**14**)	108(100)	80(100)	—	—	1.00
$CH_3SSCH_2CH_2CH_3$	(**15**)	122(75)	80(100)	—	—	1.33
$CH_3SS(CH_2)_3CH_3$	(**17**)	136(73)	80(100)	—	—	1.37
$CH_3SS(CH_2)_4CH_3$	(**21**)	150(31)	80(44)	—	—	1.42
$CH_3SSCHCH_2CH_3$ (CH$_3$ branch)	(**19**)	136(45)	80(100)	—	—	2.22
$CH_3SSC(CH_3)_3$	(**20**)	136(45)	80(19)	—	—	0.59
$CH_3CH_2SSCH_2CH_2CH_3$	(**23**)	136(59)	94(97)	—	66(54)	1.64
$CH_3CH_2SS(CH_2)_3CH_3$	(**25**)	150(42)	94(100)	—	66(26)	2.38
$CH_3CH_2SS(CH_2)_4CH_3$	(**29**)	164(30)	94(72)	—	66(13)	2.40
$CH_3CH_2SSCHCH_3$ (CH$_3$ branch)	(**24**)	136(68)	94(100)	—	66(60)	1.47
$CH_3CH_2SSCHCH_2CH_3$ (CH$_3$ branch)	(**27**)	150(34)	94(100)	—	66(24)	2.94
$CH_3CH_2SSC(CH_3)_3$	(**28**)	150(32)	94(25)	122(11)	66(19)	0.78
$CH_3CH_2CH_2SS(CH_2)_3CH_3$	(**31**)	164(41)	108(51)	122(13)	66(10)	1.24
$CH_3CH_2CH_2SSCH_2CHCH_3$ (CH$_3$ branch)	(**32**)	164(28)	108(31)	—	66(8)	1.11
$CH_3CH_2CH_2SSCHCH_2CH_3$ (CH$_3$ branch)	(**33**)	164(23)	108(48)	—	66(10)	2.09

*In all cases, this process was confirmed by the observation of the appropriate metastable peak.

decomposition of RSSH leads to HSSH rather than RS^+.

As indicated in reaction [4], odd electron ions $RSSH^{+\cdot}$ and $R'SSH^{+\cdot}$ can be formed from $[RSSR']^{+\cdot}$ by intramolecular hydrogen transfer. Since it has been shown (10, 11) that the process is essentially a 1,3-H transfer (reaction [7]) it was of

[7] 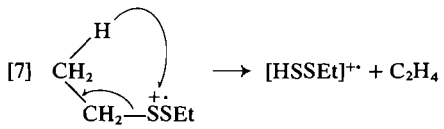 $\longrightarrow [HSSEt]^{+\cdot} + C_2H_4$

interest to determine the factors associated with this process. The mass spectral data of fragment ions derived from 1,3-intramolecular hydrogen transfer for several selected dialkyl disulfides are shown in Table 5 together with the intensity ratio, $[RSSH]^{+\cdot}/M^{+\cdot}$, which provides a measure of the facility of the hydrogen transfer reaction.

It is seen from the data in Table 5 that 1,2-H migration does not occur for the methyl alkyl disulfides, CH_3SSR', **14**, **15**, **17**, **19–21**, to give $R'SSH$. Accordingly, a measure of the ease of hydrogen transfer from R′ to give $RSSH(CH_3SSH)$ can be obtained by considering the ratio, $[RSSH]^{+\cdot}/M^{+\cdot}$. Transfer of a primary hydrogen from **14** appears to be less favourable than transfer of a secondary hydrogen from **15**, **17**, and **21** to give $CH_3SSH^{+\cdot}$ and the terminal alkene; i.e. $[RSSH]^{+\cdot}/M^{+\cdot} = 1.00$ for **14** and 1.33, 1.37, and 1.42 for **15**, **17**, and **21**, respectively. Similarly, transfer of a primary hydrogen from the *t*-butyl group in **20** is not favoured even though there are nine identical hydrogens as $[RSSH]^{+\cdot}/M^{+\cdot} = 0.59$. The stability of the alkene which is formed also must be considered as a factor which determines the ease of hydrogen migration since H-transfer from **19** gives 2-butene whereas 1-butene is obtained from **17**; $[CH_3SSH]^{+\cdot}/M^{+\cdot} = 2.22$ and 1.37 from **19** and **17**, respectively.

Intramolecular hydrogen transfer from the ethyl alkyl disulfides, CH_3CH_2SSR', **23–25**, **27–29**, can lead to both $CH_3CH_2SSH^{+\cdot}$ and $R'SSH^{+\cdot}$. It is

Can. J. Chem. Downloaded from www.nrcresearchpress.com by 210.87.254.6 on 09/06/12
For personal use only.

noted that only **28**, where we have found that H transfer from the *t*-butyl group is not favourable, gave an ion resulting from hydrogen transfer from the ethyl group to sulfur. It appears, therefore, that the initial H migration occurs preferentially from the larger alkyl side chain to give $CH_3CH_2SSH^{+\cdot}$. This can be accounted for by a combination of the ease of H-transfer, secondary preferred over primary, and the stability of the resultant alkene. In all cases, the initially formed $CH_3CH_2SSH^{+\cdot}$ ions underwent a subsequent 1,3-H migration to give $HSSH^{+\cdot}$.

It is seen once again that the ratio $[RSSH]^{+\cdot}/M^{+\cdot}$ depends on the structure of the dialkyl disulfide. Transfer of a secondary hydrogen is preferred over primary; i.e. $[RSSH]^{+\cdot}/M^{+\cdot} = 1.64$ and 1.47 for **23** and **24**, respectively where the alkyl group is changed from *n*-propyl to isopropyl. As well, formation of 2-butene is preferred over 1-butene, $[RSSH]^{+\cdot}/M^{+\cdot} = 2.94$ and 2.38 for **27** and **25**, respectively.

The results obtained for the CH_3CH_2SSR' compounds are similar to those found for $CH_3CH_2CH_2SSR'$. Only in the case of **31**, $CH_3CH_2CH_2SS(CH_2)_3CH_3$, does transfer of a hydrogen occur initially from both alkyl groups to give $RSSH^{+\cdot}$ and $R'SSH^{+\cdot}$. Transfer of hydrogen from the larger alkyl group is preferred. The variation in $[RSSH]^{+\cdot}/M^{+\cdot}$ ratio with structure of the butyl group, **31–33**, can be rationalized by a consideration of the stability of the alkene formed together with the number and type of transferred hydrogen.

Experimental

All symmetrical disulfides were obtained commercially. Unsymmetrical disulfides were prepared by the co-photolysis of two disulfides. Equimolar mixtures of RSSR and R'SSR', using 200–300 μL samples, were irradiated in the liquid phase in quartz cells using a Vycor 7910 filtered low pressure mercury lamp. At the end of the reaction the photolysates were analyzed using a thermal conductivity or flame ionization gas chromatograph. The unsymmetrical disulfides after separation, using a preparative g/c, were directly examined using a MS-12 mass spectrometer at 70 eV with a source temperature of 100°C. All the collected samples were reinjected into the gas chromatograph to establish their purity. As well, there was no variation in the mass spectra when the source temperature was varied between 100°C and 150°C. Consequently, it was established that the disulfides used in the present study are stable under the experimental conditions employed.

Acknowledgements

The authors gratefully acknowledge the financial support of this work by the National Research Council of Canada and the Natural Sciences and Engineering Research Council of Canada.

1. L. FIELD. *In* Organic chemistry of sulfur. *Edited by* S. Oae. Plenum Press, New York, NY. 1977. p. 303.
2. H. C. J. OTTENHEIJM, J. A. M. HULSHOF, and R. J. F. NIVARD. J. Org. Chem. **40**, 2147 (1975).
3. J. A. KLUN, O. L. CHAPMAN, K. C. MATLES, P. W. WOJTKOWSKI, M. BEROZA, and P. E. SONNETT. Science, **181**, 661 (1973).
4. A. PHIL and L. ELDJARN. Pharmacol. Rev. **10**, 437 (1958).
5. D. GUPTA and A. R. KNIGHT. Can. J. Chem. **58**, 1350 (1980).
6. K. SAYAMOL and A. R. KNIGHT. Can. J. Chem. **46**, 999 (1968).
7. D. D. CARLSON and A. R. KNIGHT. Can. J. Chem. **51**, 1410 (1973).
8. J. H. BOWIE, S. O. LAWESSON, C. NOLDE, G. SCHROLL, and D. H. WILLIAMS. J. Chem. Soc. B, 946 (1966).
9. H. BUDZIKIEWICZ, C. DJERASSI, and D. H. WILLIAMS. Mass spectrometry of organic compounds. Holden-Day, San Francisco. 1967.
10. E. BLOCK, M. D. BENTLEY, F. A. DAVIS, I. B. DOUGLASS, and J. A. LACADIE. J. Org. Chem. **40**, 2770 (1975).
11. M. E. ALONSO, H. ARAGONA, A. W. CHITTY, R. COMPAGNONE, and G. MARTIN. J. Org. Chem. **43**, 4491 (1978).
12. E. BLOCK. J. Org. Chem. **39**, 734 (1974).

Can. J. Chem. Downloaded from www.nrcresearchpress.com by 210.87.254.6 on 09/06/12
For personal use only.

Bulk optical properties of phthalocyanine pigment particles

RAFIK O. LOUTFY

Xerox Research Centre of Canada, 2480 Dunwin Drive, Mississauga, Ont., Canada L5L 1J9

Received June 25, 1980

Can. J. Chem. Downloaded from www.nrcresearchpress.com by 210.87.254.6 on 09/06/12
For personal use only.

RAFIK O. LOUTFY. Can. J. Chem. **59**, 549 (1981).

The optical absorption spectra of small particles of α-, β-, and *x*-form of metal-free phthalocyanine (H_2Pc) and vanadyl phthalocyanine (VOPc) surrounded by a dielectric (polymers) have been studied. The true bulk absorption can be obtained by measuring the difference in transmittance of two films of identical composition but different thicknesses. This approach eliminates effectively light reflection losses. Comparison between the absorption spectra measured by direct vs. difference in transmittance revealed a number of differences: shift in the absorption frequencies, change in absorption intensities, and change in peak-to-valley ratio. These differences are due to light scattering which can be significantly minimized by using the differential transmittance method. The true peak absorption of *x*-H_2Pc particles located at 770 and 615 nm had an absorption coefficient of 35.3 and 34.2 μm^{-1}, respectively. The absorption minimum occurs at 477 nm. The peak-to-valley ratio was 27.

The absorption spectra of VOPc particles did not correspond to any one polymorph, but are due to a mixture of two known polymorphs. Some discrepancies between the particle absorption of α-H_2Pc or β-H_2Pc and the corresponding evaporated film absorption were observed. These discrepancies are attributed to the spread in particle size and also to local agglomeration of the particles.

RAFIK O. LOUTFY. Can. J. Chem. **59**, 549 (1981).

On a étudié les spectres d'absorption de petites particules des formes α, β et *x* de la phtalocyanine dépourvue de métal (H_2Pc) et de la vanadyl phtalocyanine (VOPc) entourées d'une substance diélectrique (polymères). On peut évaluer la vraie absorption globale en mesurant la différence de transmission de deux films de composition identique mais d'épaisseur différente. Cette approche élimine effectivement les pertes de lumière par réflexion. La comparaison entre les spectres d'absorption mesurées par transmission directe et par différence de transmission révèlent un certain nombre de différences soit le déplacement des fréquences d'absorption, les variations des intensités d'absorption et les variations du rapport pic-vallée. Ces différences sont dues à la dispersion de la lumière qui peut être minimisée de façon significative en utilisant la méthode de transmission différentielle. Les vrais pics d'absorption des particules *x*-H_2Pc situés à 770 et 615 nm ont respectivement un coefficient d'absorption de 35,3 et 34,2 μm^{-1}. L'absorption minimum se produit à 447 nm. Le rapport picvallée est de 27.

Les spectres d'absorption des particules de VOPc ne correspondent à aucune variété polymorphique, mais ils sont dus à un mélange de deux variétés polymorphiques connues. On observe quelques différences entre les absorptions des particules α-H_2Pc ou β-H_2Pc et l'absorption du film évaporé correspondant. On a attribué ces différences à l'étalement de la dimension de la particule et également à l'agglomération locale des particules.

[Traduit par le journal]

Introduction

It has been recognized for some time that a method of characterizing the optical properties of particulate materials is needed. For example, information about the actual spectral absorption characteristics of metal-free phthalocyanine pigment particles is required to adequately analyze the action spectra of solar cells (1).

Several studies have been carried out in the past to determine the optical characteristics of various organic pigments (2). The most fundamental work is that of Sharp and Lardon (3), where the optical absorption spectra of several phthalocyanines were determined by measuring the transmittance of a series of vacuum deposited thin film of these materials. It is assumed that the absorption characteristics of a pigment in the form of a thin film is the same as that displayed by pigment crystallites. Unfortunately, the pigment properties are frequently changed during the deposition process. Thin films are probably amorphous whereas pigment powders are usually crystalline and thus optically dichroic and bi-refringent (4). Another limitation of this approach is that many pigment materials cannot be successfully vacuum deposited without thermal decomposition or without the occurrence of polymorphic transformation. For instance, the *x*-polymorph of metal-free phthalocyanine (*x*-H_2Pc) cannot be prepared by vacuum deposition. The optical absorption of a thin film of *x*-H_2Pc prepared from a suspension in hydrocarbon or in polymer resin was reported (3). However, no attempts were made to eliminate scattered light contributions. Photoacoustic spectroscopy is emerging as an extremely sensitive detection method which can be applied to study absorption of most kinds of materials including powders, crystals, gels, living biological specimens, gaseous and liquid samples (5). This technique is based on measuring acoustic waves generated when modulated light is absorbed by a sample, rather than observing transmitted or reflected light. This avoids problems that can arise from light scattering. However, a major disadvantage of this technique is the difficulty of quantita-

0008-4042/81/030549-06$01.00/0

©1981 National Research Council of Canada/Conseil national de recherches du Canada

Can. J. Chem. Downloaded from www.nrcresearchpress.com by 210.87.254.6 on 09/06/12
For personal use only.

tion as well as defining standards for spectrometric performance (6). An alternative quantitative method of measuring the optical properties of pigments in particulate form is still needed. Such a technique should account satisfactorily for effects related to light scattering. At the same time, the measurement should not induce modification in the chemistry or crystal structure of the pigment particles and it should be simple.

In this paper, we report the measurements of the optical absorption spectra of particles of α-, β-, and *x*-metal-free phthalocyanine (H_2Pc) and vanadyl phthalocyanine (VOPc). The influence of particle size and shape, and the dielectric constant of the surrounding medium on the absorption frequency and intensity were studied.

Experimental

Materials

β-H_2Pc was obtained from ICI as monolite fast blue GS. It was purified by slurrying and working with hot dimethylformamide. The pigment was milled in isopropanol using stainless steel balls for 72 h in order to reduce the particle size. Acid pasting of β-H_2Pc followed by ice dilution gave a fine powder of α-H_2Pc. This product could be converted to *x*-H_2Pc by neat milling with flintstone for one week (2). Vanadylphthalocyanine was obtained from the reaction of phthalonitrile and vanadyltetrachloride. The deep blue product was acid pasted in sulfuric acid to give submicron size particles.

Sample Preparation

General Procedure

The pigments to be tested were prepared as a series of dilute suspensions in a solution of polyvinylacetate in methylene chloride. The pigment-to-polymer weight ratio was varied from 10 to 60%; the mixture was ball-milled using 1/4 in. stainless steel balls for at least 1/2 h to ensure uniform suspensions. The suspensions were then coated on 2 mil Mylar film using wire wound rods #4, 6, 8, and 16 having a 9, 13.7, 18.3, and 36.6 μm gaps respectively, giving various film thicknesses. The wet coating was allowed to dry and then the apparent film thickness was measured using a Talystep thickness monitoring device. In one experiment, pigment particles suspended in methylene chloride without a polymer binder were used. In this case, the dried film showed excellent uniformity; however, it was mechanically fragile. The dry pigment film was covered with a sheet of Tedlar and then passed through a pressure roller (at 250 lb/sq. in.). This treatment resulted in highly compact, uniform, and mechanically durable films. No transfer of the pigment to Tedlar was observed.

Thin evaporated films of α-, β-H_2Pc, and VOPc were obtained by vacuum depositing onto a glass slide using Balzer vacuum system.

Optical Measurements

The optical absorption spectra of the samples were recorded on a Cary 17 Spectrophotometer at room temperature. The spectra were obtained using the differential technique in order to eliminate reflection and scattering losses. In this technique, a film of the pigment with a thickness $(X - \Delta X)$ was placed in the pass of the reference beam, while another film of the same composition but with a thickness X was placed in the sample compartment. The absorption spectrum is that of a film with thickness ΔX. With this technique, the reflection losses were significantly minimized in particular for pigment samples with particle size < 1 μm such as *x*-H_2Pc, α = H_2Pc, and VOPc. From the absorbance (A) measured at various wavelengths α, the absorption coefficient, was calculated via the following equation:

$$[1] \quad \alpha = 2.303A/NV\Delta Xf$$

In this equation N is the number of particles per unit volume, V is the volume of one particle (NV is the fractional volume concentration of particles), ΔX is the film thickness in cm, and f is a correction factor necessary because the mass density of the film is not equal to the true bulk density. This correction factor was found to relate to the ratio of pigment to polymer as will be discussed later. We have shown that pigment powders can be compressed into dense, mechanically stable films with surfaces having essentially optical quality. In these cases, mass densities in excess of 90% of the true pigment bulk densities are possible. Thus, in absence of agglomeration and when the surface coverage is uniform the absorption coefficient of pigment particles can be obtained using eq. [1] and $f \simeq 1.0$.

The reflectance spectrum of polycrystalline compacts film of *X*-H_2Pc was recorded on Cary 17 Spectrophotometer using the Specular reflectance attachment. Electron micrographs of the pigment samples were made using a Phillips E200 Transmission electron microscope after a proper preparation.

Results and Discussion

Electron micrographs of *x*-H_2Pc, α-H_2Pc, and β-H_2Pc particles are shown in Fig. 1. The particles of *x*-H_2Pc are in the form of needles, the majority of which have a length of ~0.1 μm. α-H_2Pc particles exists as a mixture of needles and flakes. The particle size varies enormously from 0.02 to 0.2 μm. β-H_2Pc particles are large needles varying in length from 2 to 8 μm. Vanadyl phthalocyanine particles are similar to those of *x*-H_2Pc. The variation in particle size and shape is expected to cause a marked effect on the particle absorption. The effective absorption and scattering which accounts for the change in intensity of a light beam passing through the pigment layer is a complicated function of the refractive index of the pigment, the refractive index of the binder, and the particle size. The particle absorption is greatest for small particles when the particle and the medium refractive index match. Also the relative scattering is largest for small particles when the particle and medium indices are matched. Figure 2 shows the specular reflectance spectrum of an *x*-H_2Pc film. A specular reflectance as high as 15% was observed, with maxima at 850, 810, 650, and 480 nm. The reflectance and absorption maxima are quite dissimilar causing the strong dichroic properties of the material.

The Optical Absorption of x-H_2Pc Particles

The problem of determining the fundamental optical properties of pigment materials is difficult because most pigments can only be obtained in particulate form. However, as described above, the absorption of these pigments was measured by preparing a thin film of the particles in a polymer binder

Can. J. Chem. Downloaded from www.nrcresearchpress.com by 210.87.254.6 on 09/06/12
For personal use only.

FIG. 1. Electron micrographs of x-H_2Pc (*A*); α-H_2Pc (*B*); and β-H_2Pc (*C*).

and measuring the difference in transmittance between two films of different thickness. Figure 3 shows the optical absorption spectra of 0.23 μm films of x-H_2Pc particles embedded in polyvinyl

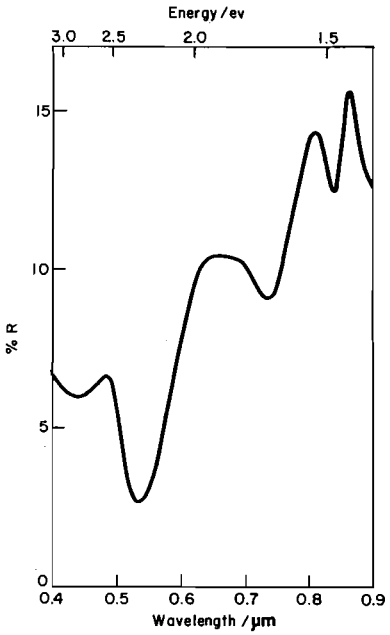

FIG. 2. Reflectance spectrum of a film of polycrystalline x-H_2Pc.

acetate (the pigment concentration corresponds to NV of 0.53). These were obtained by using the direct transmission (curve 1) and by the difference in transmittance (curve 2) technique. A number of differences are apparent: first, a change in intensity of absorption is noticed, particularly in the ir and blue regions of the spectrum. Second, a shift in the absorption frequency, and third a change in the ratio of peak intensities. Curve 1 represents the transmittance and reflectance of the pigmented film, while in curve 2 a significant amount of the reflectance component has been eliminated using the technique of differential transmittance. The success of this technique rests on the high optical quality and uniformity of the x-H_2Pc particulate films.

The absorption coefficient α as defined by eq. [1] was determined for x-H_2Pc films as a function of the volume concentration fraction (NV) and the results are given in Table 1. The assumption that the fraction f is unity for all films gives α's which increase with volume fraction. The dependence of α on the volume fraction must be due to the difference in surface mass density compared to the true material density. The estimated values of f required to give a constant α at any given wavelength as a function of NV are given in Table 1. These values were computed from the ratio of α for a given volume fraction to that at $NV = 1.0$.

Figure 4 shows the absorption spectrum of thin films of x-H_2Pc particles (ΔX = **60 nm**). The ab-

TABLE 1. The dependence of absorption frequency and intensity on x-H_2Pc pigment to polymer (PVA) volume fraction

	Absorption spectral data						
NV	λ (nm)	α (μm^{-1})	λ (nm)	α (μm^{-1})	λ (nm)	α (μm^{-1})	f_{av}[a]
0.079	795.5	11.79	620	9.08	492	0.32	0.29
0.245	786.5	15.66	617	12.65	490	0.90	0.40
0.53	770	16.51	615	15.18	485	0.64	0.46
1.00	770	35.3	615	34.1	477	1.15	1.0

[a] f in eq. [1].

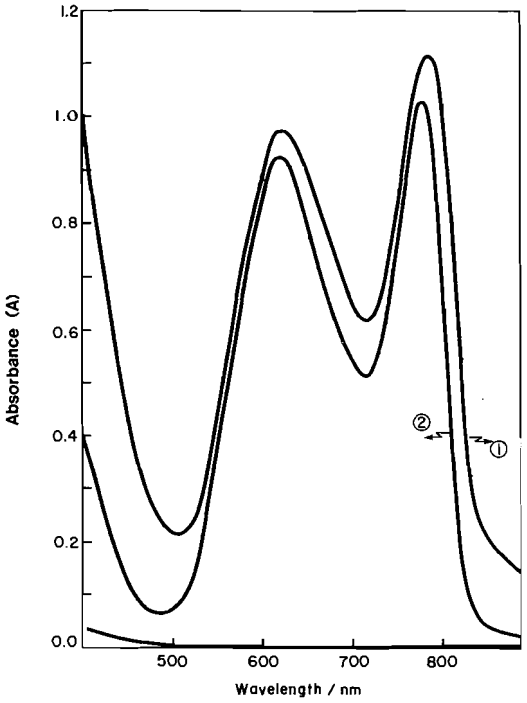

FIG. 3. Optical absorption spectra of x-H_2Pc particles embedded in polyvinylacetate (NV = 0.53): (*1*) a 0.23 μm thick film vs. mylar and (*2*) a 0.46 μm film vs. 0.23 μm films.

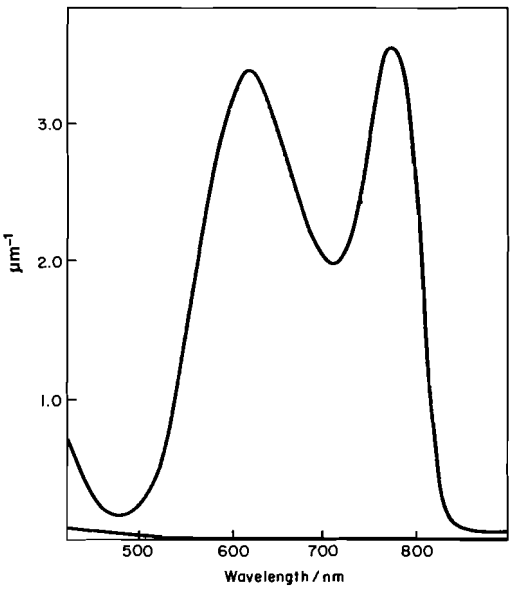

FIG. 4. The absorption spectrum of 60 nm x-H_2Pc particles.

sorption coefficients α corresponding to the absorption maxima at 770 and 615 nm are 35.3 μm^{-1} and 34.1 μm^{-1}, respectively. The absorption minimum in the green occurs at 477 nm. An important aspect of the spectrum is the depth of the absorption minimum at 477 nm. This is best described by the peak-to-valley absorption ratio. This ranges typically from 25 to 35. The α615/α480 ratio for our sample is 27.

Optical Absorption of Vanadyl Phthalocyanine Particles

Vanadyl phthalocyanine (VOPc) exhibited a strong absorption in the ir region of the spectrum at λ = 830 nm, which coincides with the GaAs laser wavelength. Consequently, this material is of considerable interest as a potential infrared photoreceptor material.

The absorption spectra of a number of samples of VOPc particles have been measured using the procedure described in detail in the preceding section. Figure 5 shows the absorption spectrum of compressed thin film of VOPc particles (ΔX = 63 nm) measured using the differential transmittance technique. The absorption coefficient at the absorption maxima 830, 690, 650 nm are 34.4, 31.0, and 31.4 μm^{-1}, respectively. The absorption minimum in the green occurs at 480 nm. The α650/α480 ratio is 21.4. The absorption spectrum of a dispersion of VOPc in polyvinylacetate was quite similar to that of a compressed film with no binder. The estimated fraction, f, for NV = 0.52 was 0.42 which agrees well with that found for similar films of x-H_2Pc.

The absorption of VOPc particles does not correspond to any one of the known polymorphs (see Fig. 6). The peak at 830 nm corresponds to the high

Can. J. Chem. Downloaded from www.nrcresearchpress.com by 210.87.254.6 on 09/06/12
For personal use only.

Can. J. Chem. Downloaded from www.nrcresearchpress.com by 210.87.254.6 on 09/06/12
For personal use only.

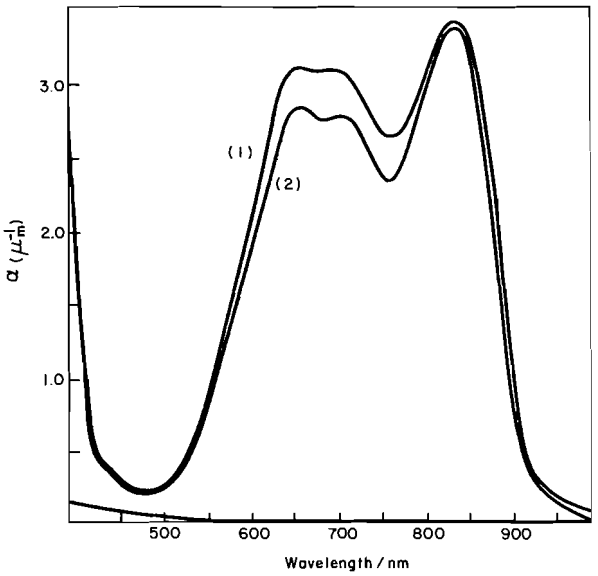

FIG. 5. The absorption of VOPc particles: (*1*) $NV = 1.0$ and (*2*) $NV = 0.51$ in polyvinylacetate ($f = 0.46$).

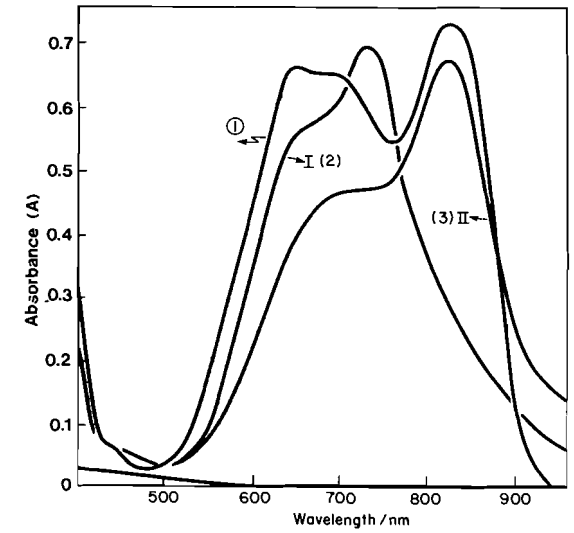

FIG. 6. The absorption spectra of VOPc: (*1*) particles; (*2*) polymorph I, and (*3*) polymorph II.

temperature polymorph II, while the peaks at 650 and 720 nm correspond to the low temperature polymorph I. Therefore, the VOPc particles appear to be a mixture of polymorphs I and II.

The Optical Absorption of α-H_2Pc and β-H_2Pc Particles

The absorption spectra of α-H_2Pc and β-H_2Pc particles were determined by the technique described previously. The peak absorption (620 nm for α-H_2Pc and 645 nm for β-H_2Pc) increased with increasing pigment concentration and ranged from 8 μm^{-1} for a pigment volume fraction of 0.073, 15 μm^{-1} for $NV = 0.53$ to a value of 28 μm^{-1} for a $NV = 1.0$. This corresponds to a ratio of surface mass density to true bulk material density of 0.29 for $NV = 0.073$ and 0.54 for $NV = 0.53$, which are in good agreement with those estimated for x-H_2Pc and VOPc particle/polymer blends.

Comparison of Thin-film Absorption with Particle Absorption Spectra

We have seen that the differential absorption technique minimizes light scattering in the absorption of x-H_2Pc and VOPc particles. It is of interest to compare this technique to that of evaporated thin-film absorption.

Evaporated thin-film absorption and differential particle absorption spectra for α- and β-H_2Pc are shown in Figs. 7 and 8, respectively. Although the shapes of the spectra are similar, there is one major difference. The α-H_2Pc differential particle absorption spectra indicate considerably more absorption in the valley region and less in the peak region than does the evaporated film. The peak-to-valley ratio here is typically 10–15 compared to 31 for the evaporated film. In the case of β-H_2Pc particles there is a general enhanced absorption and softening in the absorption maxima. We have experienced great difficulty in the preparation of β-

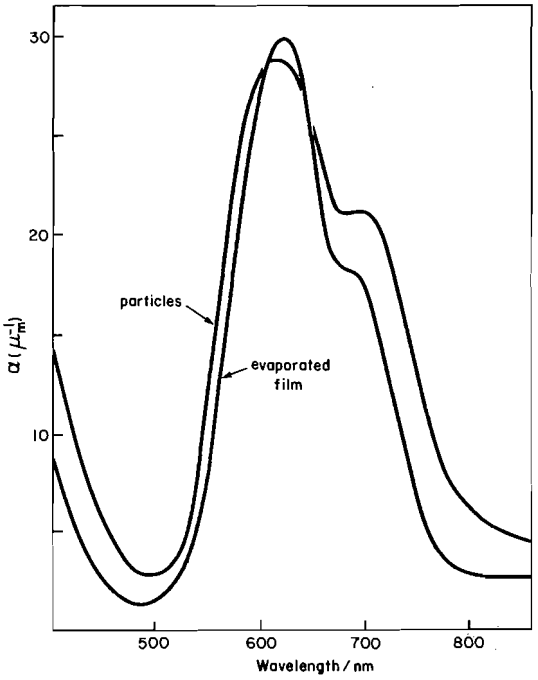

FIG. 7. Comparison of the absorption spectra of α-H_2Pc particles and evaporated film.

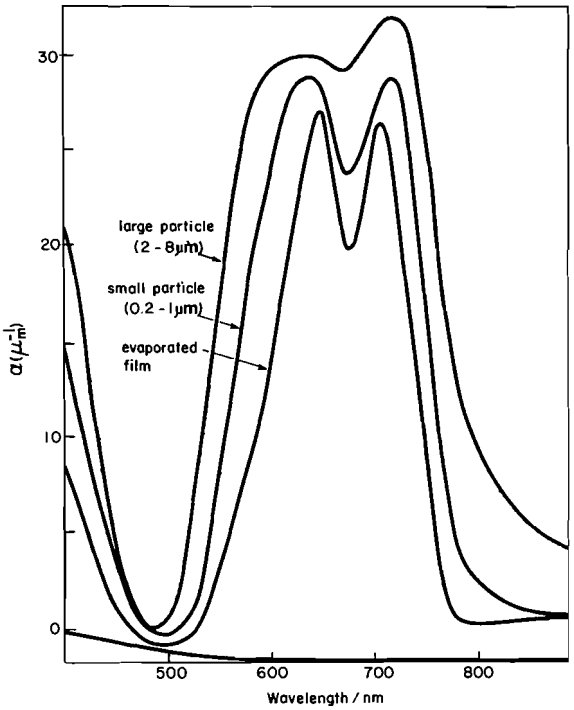

FIG. 8. Comparison of the absorption spectra of β-H_2Pc particles and evaporated film.

H_2Pc particle films due to a strong tendency for agglomeration of the pigment. The fact that the particles are large and are not widely separated due to agglomeration probably leads to a wavelength-dependent scattering which results in additivity failure, particularly in high optical density regions. The agreement between β-H_2Pc particles and evaporated films improves significantly when smaller particles are used, see Fig. 8.

Conclusion

In this work we have attempted to show that the spectroscopic properties of pigment particles are better determined by difference than by direct transmission. This technique minimizes reflection losses and allows the true bulk absorption to be determined. The absorption spectra of *x*-H_2Pc and VOPc particles were successfully determined.

Comparison between the absorption of evaporated and particulate films of α-H_2Pc showed general similarity; although the particle absorption spectra absorbed more strongly in the valley region (480 nm) and less strongly in the peak region (620 nm) than does the evaporated film. A larger discrepancy between the particle and evaporated film absorption of β-H_2Pc was observed. This was attributed to the particle size and also to the local agglomeration of the particles which leads to wavelength-dependent scattering.

Acknowledgements

The author is grateful to L. Marks for many helpful discussions, and to A. Pundsack and J. Zamin for electron micrography.

1. (*a*) R. O. LOUTFY, C. K. HSIAO, and J. H. SHARP. J. Chem. Phys. **71**, 1211 (1979); (*b*) C. K. HSIAO, R. O. LOUTFY, and J. H. SHARP. Proceeding II Solar Energy Conference, Charlottetown, Prince Edward Island, 79–104 (1979).
2. (*a*) R. L. MILLER, M. S. WALKER, C. H. GRIFFITH, and P. C. GOLDSTEIN. Mol. Cryst. Liq. Cryst. **16**, 203 (1972); (*b*) R. O. LOUTFY and J. H. SHARP. J. Phys. Chem. **83**, 1208 (1979); (*c*) F. J. KAMPAS and M. GOUTERMAN. J. Luminesc. **14**, 121 (1976).
3. J. H. SHARP and M. LARDON. J. Phys. Chem. **72**, 3230 (1968).
4. A. R. HANNAM and D. PATTERSON. J. Soc. Dyers Colorists, **79**, 192 (1963).
5. (*a*) W. R. HARSHBARGER and N. B. ROBIN. Acc. Chem. Res. **6**, 329 (1973); (*b*) N. S. NOGAR, M. FISHER, and W. JALENAK. Laser Focus, February, 56 (1979).
6. (*a*) R. E. BLANK, H. PAWLOWSKI, and A. SILVERSMITH. Industrial Research and Development. July 1979, p. 92; (*b*) D. HURSH and T. KUWANA. Anal. Chem. **52**, 646 (1980).

Can. J. Chem. Downloaded from www.nrcresearchpress.com by 210.87.254.6 on 09/06/12
For personal use only.

Apparent stability constants of proton and metal ion complexes of glycine, iminodiacetic acid, nitrilotriacetic acid, and triethylenetetramine in aqueous methanol

TERRENCE B. FIELD[1] AND W. A. E. MCBRYDE

Guelph–Waterloo Centre for Graduate Work in Chemistry, University of Waterloo, Waterloo, Ont., Canada N2L 3G1

Received November 30, 1979[2]

TERRENCE B. FIELD and W. A. E. MCBRYDE. Can. J. Chem. **59**, 555 (1981).

Conditional formation constants were determined at 25°C and with a background electrolyte of 0.1 mol dm^{-3} $NaNO_3$ for the proton, nickel(II), copper(II), and zinc(II) complexes of glycine, iminodiacetic acid, and nitrilotriacetic acid in 0, 20, 50, 80, and 95 volume percent methanol mixed with water. Similar measurements were made for triethylenetetramine in all but 95% methanol, and the formation constants so determined were used to determine K_{MNTA} by a competitive method.

The variation of all constants with solvent composition was examined from the point of view that complex formation is accompanied by solvent displacement. Accordingly it should be possible to correlate the observations by means of an over-all formation constant, valid for any solvent concentration. It was concluded that for two solvents as similar as water and methanol, both of which appear to be involved in solvation or desolvation in the reaction, the correlations sought could not very precisely fix the amounts of solvents displaced or taken up. The goodness of fit to the attempted correlations suggests that they would be useful for interpolations to solvent compositions other than those studied.

TERRENCE B. FIELD et W. A. E. MCBRYDE. Can. J. Chem. **59**, 555 (1981).

Opérant à 25°C et utilisant comme électrolyte de base une solution de $NaNO_3$ à 0,1 mol dm^{-3}, on a déterminé les constantes de formation conditionnelle des complexes du proton, du nickel(II), du cuivre(II) et du zinc avec la glycine, les acides iminodiacétique et nitritotriacétique dans des mélanges méthanol–eau à 0, 20, 50, 70 et 95% en volume. On a fait des déterminations identiques pour la triéthylamine mais sans recourir au mélange méthanol–eau à 95% et on a utilisé les constantes de formation ainsi obtenues pour déterminer K_{MNTA} par une méthode compétitive.

On a examiné la variation de toutes les constantes avec la composition du solvant en tenant compte du fait que la formation des complexes s'accompagne d'un déplacement du solvant. En conséquence il devra être possible de faire concorder les observations au moyen d'une constante globale de formation, valable pour n'importe quelle concentration de solvant. On a conclu que pour deux solvants aussi semblables que l'eau et le méthanol, qui semblent être impliqués dans la solvatation ou la désolvatation au cours de la réaction, les corrélations recherchées ne peuvent pas fixer avec précision les quantités de solvant déplacé ou éliminé. Les meilleurs corrélations obtenues suggèrent qu'elles seraient utiles pour faire des interpolations dans les compositions de solvant différentes de celles étudiées.

[Traduit par le journal]

Introduction

The formation constants of proton and metal ion complexes with organic ligands undergo appreciable changes when measured in mixed solvents containing water compared to their values when measured in solely aqueous solutions. An understanding of this *solvent effect* would be desirable from a purely theoretical standpoint, but also would be of practical value in interpreting or correlating data obtained in solutions other than strictly aqueous. Some success in accounting for the solvent effect has been achieved (1, 2) by adopting the concept of the complete equilibrium constant (3) in which the solvent or solvents associated with the reactant and product molecules is/are included in the complex-forming reaction and its equilibrium constant. Thus in a binary solvent, molecules of one or both components are regarded as excluded or incorporated when an association reaction takes place, and so the activity (concentration) of these participating solvents is included in the equilibrium expression.

The present investigation was planned to test this concept further by examining the progressive effect of added methanol in the solvent upon the formation constants of the complexes of a series of ligands with increasing numbers of donor atoms. In such a series the increase in number of chelate rings formed might be expected to result in a progressively increased rejection of solvent. The essential reaction (omitting charges) is assumed to be

$$\mathrm{M(solv) + Chel(solv) = MChel(solv) \pm solvent}$$

Solvent would probably be displaced in consequence of the direct bonding between metal ion and ligand. Conventional formation constants were measured for the ligands glycine (gly), iminodiacetic acid (IDA), and nitrilotriacetic acid (NTA) reacting with hydrogen ions and the bivalent ions of nickel, copper, and zinc. Additional measurements were made with triethylenetetramine (trien) as a

[1]Present address: Gould Manufacturing of Canada Ltd., Industrial Battery Division, Fort Erie, Ont., Canada.

[2]Revision received September 25, 1980.

0008-4042/81/030555-04$01.00/0

©1981 National Research Council of Canada/Conseil national de recherches du Canada

Can. J. Chem. Downloaded from www.nrcresearchpress.com by 210.87.254.105 on 09/06/12
For personal use only.

competing ligand. The effectiveness of relationships developed previously (1) for interpreting the effect of solvent composition on the apparent stability constants was tested with the results of these determinations.

Experimental

Solvents and Solutions

All solutions were prepared in distilled, deionized water, stored under nitrogen, with addition as indicated of Baker's Analyzed methanol (100%). All salts and acids used to prepare solutions were of reagent grade; alkali solutions were prepared from Baker Dilut-it ampoules (carbonate free) and stored under nitrogen. As necessary, solutions were standardized by published titration methods. The acid content of stock metal ion solutions was determined by means of ion-exchange displacement.

Ligands

Glycine, iminodiacetic acid, and nitrilotriacetic acid were recrystallized from water; solutions prepared from the purified acids were standardized by conductance titration. Triethylenetetramine was prepared as the tetranitrate salt (4), and its purity checked by titration (observed molar mass 398.24 g mol^{-1}).

Titrations

These were carried out in a thermostatted cell (at 25°C), continuously purged with nitrogen, and provided for magnetic stirring of the contents. A Beckman glass electrode (39301) and an Orion solid-state electrode (94-29A) were calibrated and used as concentration probes respectively for hydrogen ions and copper(II) ions. These were used, as appropriate, with various reference electrodes: Leeds and Northrup calomel (117208) filled with saturated KCl or NaCl solution, or Orion single-junction (90-01) filled with Orion solution 90-00-01 or with a home-made filling solution. This last consisted of 0.001 mol dm^{-3} NaCl + 0.099 mol dm^{-3} $NaNO_3$ (or KNO_3) in water, 20% methanol, 50% methanol, etc., and rendered just cloudy by addition of $AgNO_3$. The electrodes were connected through a good-quality switch so that as many as three reference electrodes and two copper-ion electrodes could be used at a time for checks of consistency. The glass – reference electrode pair was applied to an Orion Model 801 digital pH meter, and the solid-state – reference electrode pair to a null-point Radiometer Model 4 pH meter. The solutions to be titrated were of the order of 10^{-3} mol dm^{-3} in ligand or metal ion concentration, and 10^{-1} mol dm^{-3} in background electrolyte in a total volume of 50 cm^3. The titrant was either 1.0 or 2.0 mol dm^{-3} alkali or acid delivered from a micrometer syringe.

Results

The data from the titrations carried out as described were used to calculate the acidity and stability constants for the selected metals and ligands in water–methanol solutions of selected compositions. The large number of results have, for the sake of brevity of this report, been placed with the Depository of Unpublished Data and those for iminodiacetate are plotted in Fig. 1 to illustrate the general trends observed.[3] Unless otherwise noted

[3]Complete set of data may be obtained, at a nominal charge, from the Depository of Unpublished Data, CISTI, National Research Council of Canada, Ottawa, Ont., Canada K1A 0S2.

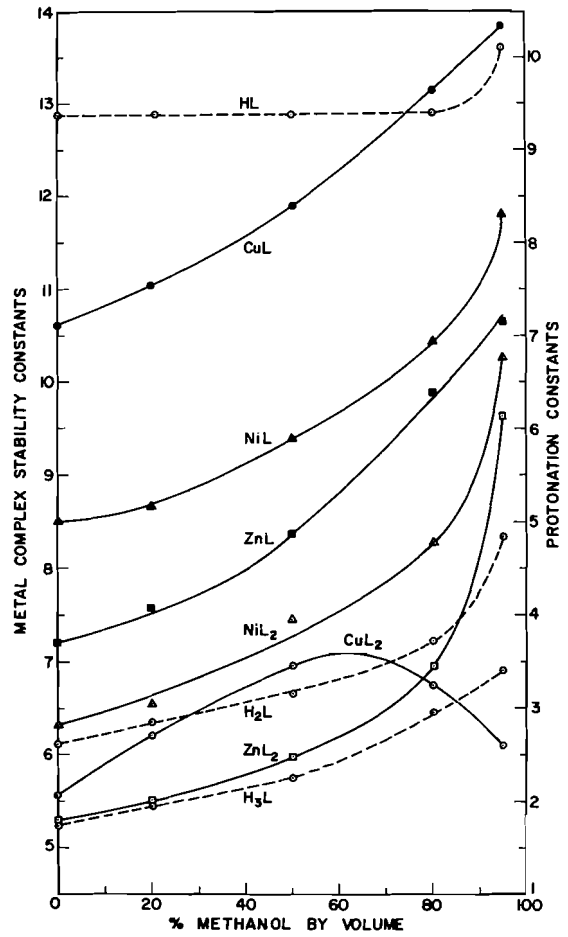

FIG. 1. Metal complex stability constant and protonation constants of iminodiacetate in water–methanol solutions.

all equilibrium constants were calculated from the experimental data by the computer program SCOGS (5), and the various species included for each combination of reactants were those which yielded minimum standard deviations between observed and calculated titers.

Owing to the great stability of some metal–NTA complexes direct determination of their formation constants from pH-titration data is difficult, and is often avoided by carrying out titrations with a competing ligand (6). Both approaches were followed in this study; the second required determinations of stability constants of trien (as competing ligand) in the same media, the values of which are in the Depository of Unpublished Data. There is limited solubility of KNO_3 in aqueous methanol, and of trien$(NO_3)_4$ in methanol-rich solvents, these facts account for the use of $NaNO_3$ as background electrolyte, and for the absence of trien data in 95% methanol. To displace metal ions from a MNTA complex by hydrogen ions requires a high concen-

Can. J. Chem. Downloaded from www.nrcresearchpress.com by 210.87.254.105 on 09/06/12
For personal use only.

Can. J. Chem. Downloaded from www.nrcresearchpress.com by 210.87.254.105 on 09/06/12
For personal use only.

tration of the latter; accurate measurement of this concentration becomes increasingly difficult as pH is lowered below 2, since the emf of the measuring cell is then increasingly affected by liquid junction potentials. Because of this and also because the ionic strength of the analyte may be affected by added electrolyte the relationship between emf and $-\log [H]$ no longer remains linear. There are four protonation constants for NTA, though most authors have only reported three; at low pH the effect of the fourth protonation must be taken into account. Finally, because of the formation of a weak sodium–NTA complex values of K_i^0 for this ligand are somewhat different in sodium salts than in potassium salts as background electrolytes. Regrettably, in spite of having taken all foreseeable precautions, the values of $\log K_1$ for NiNTA obtained by direct determination must be regarded as unsatisfactory. For purposes of all correlations with solvent composition the values calculated from competitive titrations with trien were used.

Discussion

With increasing methanol content in the solvent, amine protonation constants were found first to decrease and then to increase. This effect has been noted for 24 nitrogen bases in methanol–water mixtures as well as numerous other solvents mixed with water (7). All carboxyl protonation constants and the stability constants of most of the metal–ligand complexes increased with the methanol content of the solvent. This regular increase was not found among the formation constants of protonated (MHL) or deprotonated (MOHL) complexes. Also, when the coordination number of the metal was exceeded, with the addition of a second molecule of ligand, $\log K_2$ did not show the same increase with additional methanol in the solvent.

Following an earlier approach to interpretation of the solvent effect in such ionic equilibria (1) an attempt was made to correlate the results from this study in terms of a total equilibrium constant (3). For the reaction

$$aA + bB = A_aB_b + wH_2O + sMeOH$$

$$K_{total} = K_{observed}[H_2O]^w[MeOH]^s$$

In this expression concentrations of water and methanol appear although, strictly speaking, activities of the solvents should have been put in instead. If the total number of solvent molecules displaced is represented by t $(= w + s)$ then it can be shown that

$$[1] \quad \log K_{total} + w \log ([MeOH]/[H_2O]) = \log K_{observed} + t \log [MeOH]$$

a value of t can then be sought which yields the best straight line when the right-hand side of [1] is plotted against $\log ([MeOH]/[H_2O])$. (In this instance only integral values of t were considered, but it is possible to achieve even better fits to the data with fractional values of t.) From the slope and intercept of the straight line, values of w and K_{total} can be found. The results of such correlations for the iminodiacetate complexes are shown in Table 1; corresponding tables giving correlation parameters and total equilibrium constants for the other systems are available from the Depository of Unpublished Data. The quantity R shown in this table is the conventional statistical correlation coefficient.

When all the data are examined this way, it is clear that good to very good correlations (in the sense of R being very close to unity) can be obtained by use of the two-parameter relationship [1]. However, the success of such correlations affords no proof of the validity of the model of solvent exclusion from which [1] was derived. In fact the absence of any consistent pattern among the values of t for some comparatively similar systems (e.g., Table 1) makes it difficult to associate any physical significance with them. Some limited conclusions might be drawn from the correlation parameters. For example, in the protonation of nitrogen centres s values are greater than w values, whereas for oxygen centres the reverse is true; this had previously been found with ethylenediamine and glycine (1). It might be concluded therefore that methanol is preferentially solvated at nitrogen centres; however, equally well this balance of w and s values may simply be an artifact created by the minimum in pK that is typical of nitrogen bases in aqueous methanol. In the case of glycine and IDA the formation of metal complexes, with a single exception, is characterized by negative s values; such values could be interpreted to signify that the metal complexes bind methanol to a greater extent than the reactants. However, that this seeming regular-

TABLE 1. Correlation constants for eq. [1]: IDA complexes

Species formed	t	w	s	K_{total}	R
HL	2	1.07	0.93	11.83	0.994
H_2L	2	1.76	0.24	5.92	1.000
H_3L	1	1.16	−0.16	3.79	0.991
NiL	1	2.04	−1.04	11.25	1.000
NiL_2	3	3.00	0.00	11.56	0.998
CuL	0	1.54	−1.54	12.53	0.992
CuL_2	−5	−2.05	−2.95	0.78	1.000
ZnL	1	2.05	−1.05	10.31	0.989
ZnL_2	5	3.78	1.22	12.72	0.999

Can. J. Chem. Downloaded from www.nrcresearchpress.com by 210.87.254.105 on 09/06/12
For personal use only.

ity is not sustained among metal–NTA complexes places this physical interpretation in doubt. Where $w > t$, values of s are negative and the physical situation corresponding to that would be that the complex binds methanol to a greater extent than the reactants. The solvent exclusion idea, as a basis for explaining the solvent effect on ionic equilibria, was most successfully applied to binary solvents in which one partner exhibited markedly preferential solvation over the other, e.g., water with dioxane (1), or benzene with cyclohexane (2). Methanol is obviously active in solvation, and the simple model used may be incapable of resolving the relative extent to which the two solvents are engaged in the reactions examined. To set a unique value of t for some of these systems is not clear-cut; when experimental variance is taken into account the value of t is often uncertain by 1, and therefore the derived parameters w and s are correspondingly uncertain. Moreover, it is not known whether the solvent molecules postulated to have been displaced or added are from the primary or secondary layer of solvation. It had originally been our supposition that the formation of metal–ligand bonds would liberate solvent molecules from the primary solvation layer. However, in a recent study of partial molar volumes (8), formation of the Ni–EDTA complex in solution was found to be accompanied by a significant increase in volume; this was interpreted to indicate incorporation of electrostricted solvent within the complex.

Finally, we have applied the correlation method based on [1] to data obtained by other workers who have measured some of the same equilibria in aqueous methanol (1, 9–14). The particulars are available in a university thesis (14). It was of some interest to check the correspondence between the present work on glycine and that previously reported from this laboratory. The two lots of values for the equilibrium constants are in reasonably good agreement but did not in a number of cases lead to the same value of t in [1]. As we have said, the goodness of fit of the data is not particularly sensitive to the choice of t value, but the choice of t value can lead to widely differing values of w and s (even to the point of changing sign).

As an example of the uncertainty attending any physical interpretation of the correlation parameters based on [1], we offer in Table 2 the values of these for the stepwise protonation of trien based (*a*) on this work and (*b*) on the measurements of Rohrobacher *et al.* (12). Apart from the fourth-stage protonation constants, the values obtained in the two studies were in reasonable agreement, yet the correlation parameters and complete equilibrium constants differ appreciably.

TABLE 2. Correlation constants for eq. [1]: trien complexes

Species formed	t	w	s	K_{total}	R
HL	1*	0.30	0.70	10.68	1.000
H_2L	1*	0.22	0.78	9.94	0.999
H_3L	1*	0.29	0.71	7.51	1.000
H_4L	3*	1.41	1.59	6.61	1.000
HL	4†	1.44	2.56	14.32	0.999
H_2L	4†	1.43	2.57	13.49	0.999
H_3L	4†	1.30	2.70	10.91	0.999
H_4L	4†	1.11	2.89	7.03	0.999

*This study.
†Data from ref. 12.

In conclusion it must be conceded that while this investigation has added some carefully measured stability constants for the systems examined, it has failed to uphold earlier hopes that the solvent effect might be explained to a large extent on the basis of relative activity of the solvent partners.

Acknowledgement

The authors are grateful for financial support from the National Research Council of Canada.

1. K.-K. MUI, W. A. E. MCBRYDE, and E. NIEBOER. Can. J. Chem. **52**, 1821 (1974).
2. S. H. MEHDI, D. A. BRISBIN, and W. A. E. MCBRYDE. J. Soln. Chem. **4**, 497 (1975).
3. W. M. MARSHALL. J. Phys. Chem. **76**, 720 (1972).
4. W. A. E. MCBRYDE and H. K. J. POWELL. Can. J. Chem. **57**, 1785 (1979).
5. I. G. SAYCE. Talanta, **15**, 1397 (1968).
6. G. SCHWARZENBACH and E. FREITAG. Helv. Chim. Acta, **34**, 1492 (1951).
7. R. BATES. J. Electroanal. Chem. Interfac. Electrochem. **29**, 1 (1971).
8. Y. K. SZE and W. A. E. MCBRYDE. Can. J. Chem. **58**, 1795 (1980).
9. E. ROMANEKO and N. KOSTROMINA. Russ. J. Inorg. Chem. **13**, 958 (1968).
10. G. FARAGLIA, F. J. C. ROSSOTTI, and H. S. ROSSOTTI. Inorg. Chim. Acta, **4**, 488 (1970).
11. D. ROROBACHER, W. J. MCKELLAR, F. R. SHU, and SISTER M. BONAVITA. Anal. Chem. **43**, 561 (1971).
12. D. ROROBACHER, B. J. BLENCOE, and D. W. PARKER. Anal. Chem. **44**, 2339 (1971).
13. A. CHATTOPADHYAY and C. LAHIRI. Ind. J. Chem. **15A**, 930 (1977).
14. T. B. FIELD. Ph.D. Thesis, University of Waterloo, Waterloo. 1978.

Kinetics and mechanism of the thermal decomposition of *N*-nitrosodiphenylmethylimine

MICHAEL T. H. LIU

Department of Chemistry, University of Prince Edward Island, Charlottetown, P.E.I., Canada C1A 4P3

AND

TOSHIKAZU IBATA

Institute of Chemistry, College of General Education, Osaka University, Toyonaka, Osaka, Japan

Received August 17, 1980

This paper was presented at the Symposium in honour of Prof. K. J. Laidler, 63rd Canadian Chemical Conference, Ottawa, June 8–11, 1980, and is dedicated to him on the occasion of his sixty-fifth birthday

MICHAEL T. H. LIU and TOSHIKAZU IBATA. Can. J. Chem. **59**, 559 (1981).

The thermal decomposition of *N*-nitrosodiphenylmethylimine has been investigated in various solvents. The decomposition products are benzophenone and nitrogen. The $\Delta H\dagger$ and $\Delta S\dagger$ parameters for these first-order decompositions have been determined. The experimental evidence is consistent with the hypothesis that the thermolysis of *N*-nitrosodiphenylmethylimine involves the formation of a cyclic transition state via an electrocyclic ring closure mechanism.

MICHAEL T. H. LIU et TOSHIKAZU IBATA. Can. J. Chem. **59**, 559 (1981).

On a étudié dans différents solvants l'effet de la décomposition thermique de la *N*-nitrosodiphénylméthylimine. Les produits de décomposition sont la benzophénone et l'azote. On a déterminé les paramètres $\Delta H\dagger$ et $\Delta S\dagger$ de ces décompositions du premier ordre. La preuve expérimentale concorde avec l'hypothèse qui stipule que la thermolyse de la *N*-nitrosodiphénylméthylimine devrait faire intervenir un état de transition cyclique impliquant un mécanisme électrocyclique d'annellation.

[Traduit par le journal]

Introduction

Since the report of Thoman and Hunsberger on the synthesis and characterization of *N*-nitrosoimines (1), there has been a growing interest in the chemistry of this class of compounds (2–4). These authors reported that the decomposition of *N*-nitroso-2,4′-dimethylbenzophenonimine is first-order and a cyclic mechanism based on observed chemical and spectral properties was suggested for the decomposition of these compounds. However, very little work has been done on the kinetics of reaction of *N*-nitrosoimines. In this paper we wish to report kinetic results for the decomposition of *N*-nitrosodiphenylmethylimine (**1**) in various solvents.

Experimental

Preparation of N-*Nitrosodiphenylmethylimine (1)*

A suspension of anhydrous sodium acetate (14.8 g, 0.18 mol) in 40 mL of dry carbon tetrachloride was cooled to −20°C in a Dry Ice – acetone bath. Nitrosyl chloride (4.0 g, 60 mmol) was added with stirring, followed by a solution of diphenylketimine (7.24 g, 40 mmol) in 15 mL carbon tetrachloride at −20°C.

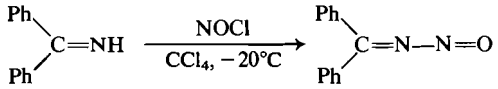

Blue color appeared as soon as the ketimine was added. The mixture was stirred vigorously for 20 min at −20°C and quickly washed with 200 mL of ice cold 10% $NaHCO_3$, followed by 200 mL of ice water. The solution was dried over anhydrous $MgSO_4$, and 30 mL cold *n*-pentane at −20°C was added to the dried CCl_4 solution. The solution was left overnight at −80°C and blue crystal of the *N*-nitrosoimine separated out. **1** was recrystallized from a mixed solvent of ether–*n*-pentane at −70°C, mp 57.5–58.5°C. The melting point (lit. mp 53°C) and spectral data are in good agreement with the reported values (1). Accurate measurements of ε values are difficult because of the rapid decomposition of *N*-nitrosoimine. The values for ε at 0°C in various solvents are the following: CH_3OH, 590 nm (ε54); C_2H_5OH, 590 nm (ε66); and CH_3CN, 596 nm (ε87).

All solvents were distilled before use: C_2H_5OH from $MgOC_2H_5$; CH_3OH from $MgOCH_3$; *i*-PrOH from *i*-PrONa; CH_3CN from P_2O_5 and then K_2CO_3; THF from NaOH and then $LiAlH_4$. Ethyl acetate was washed with saturated NaCl solution, dried, and distilled over $MgSO_4$.

Kinetics Procedure

The kinetics were determined by following the change of absorbance with time at the wavelength of maximum absorption in the visible (590 nm) region. The reaction was monitored by using a Hitachi uv-vis spectrophotometer equipped with a thermostated cell holder. 5–8 mg of **1** were added to the thermostated solvent (4 mL) contained in a 1 cm quartz cell. The cell was shaken vigorously for several seconds and was returned to the cell holder for repetitive scanning. The first-order rate constants were determined graphically from the plot of $\log (A_t - A_\infty)$ against time. Good isosbestic points were observed.

Results and Discussion

The thermal decomposition of *N*-nitrosodiphenylmethylimine, **1**, in various solvents gave benzophenone and nitrogen as the only products. In order to confirm that the oxygen atom in

0008-4042/81/030559-04$01.00/0

©1981 National Research Council of Canada/Conseil national de recherches du Canada

Can. J. Chem. Downloaded from www.nrcresearchpress.com by 210.87.254.42 on 09/05/12
For personal use only.

Can. J. Chem. Downloaded from www.nrcresearchpress.com by 210.87.254.42 on 09/05/12
For personal use only.

benzophenone is not incorporated from an external reagent, we have carried out the following control experiment. Compound **1** was thermolyzed in carbon tetrachloride under a nitrogen atmosphere, once again the products were nitrogen and benzophenone. Although **1** is kinetically stable ($t_{1/2} \sim$ 1/2 h) at ambient temperature, thermodynamically, it is highly unstable. We suggest that this compound is best handled in dilute solution. In all our experiments the concentration of nitrosoimine is approximately 0.01 *M*.

In the temperature range of 25–60°C, **1** undergoes a first-order decomposition in all solvents studied according to the equation:

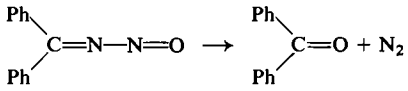

First-order kinetics were obeyed for well over 80% decomposition. Typical first-order plots are given in Fig. 1. The results are shown in Table 1. From the least-squares analysis of the rate constants in Table 1, the activation parameters were determined. The values in various solvents, are summarized in Table 2. A plot given in Fig. 2 of $\Delta H\dagger$ versus $\Delta S\dagger$ shows a linear relationship; this indicates that the same mechanism is operating in various solvents. Nevertheless there is a solvent effect. It is noted in Table 1 that the rate increases with increasing solvent polarity. This effect is also reflected in a lower value for $\Delta H\dagger$ in methanol, as seen in Table 2. The negative entropies of activation in all solvents (Table 2) are indicative of a net loss of rotations in **1** going from ground state to the transition state.

In view of the first-order kinetics, Thoman and Hunsberger (1) suggested that the decomposition of *N*-nitrosoimines might involve an intra- rather than an inter-molecular transition state.

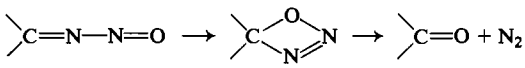

In the light of chemical properties, these authors have also suggested that there is a substantial contribution of the 1,4-dipolar structure (**1′**) to the ground state.

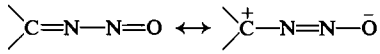

1 **1′**

If, as suggested, the structure of the starting material is a hybrid of **1** and **1′**, then there is double bond character to all of the bonds shown, and hence no free rotation about the CN, NN, and NO bonds. Therefore, no rotational degrees of freedom are lost in proceeding to the cyclic transition state, a feature contrary to our observation. We suggest, therefore, that the contribution of **1′** to the ground state is not significant. Further support for this statement can be seen in the following discussion. The E_t values (5–7) were used as a scale of solvent ionizing power in studying the effect of solvent on the decomposition rate. The solvent parameters and the corresponding calculated rate constants at 30°C are given in Table 3. As illustrated in Fig. 3, the plot of log k against E_t values shows a linear

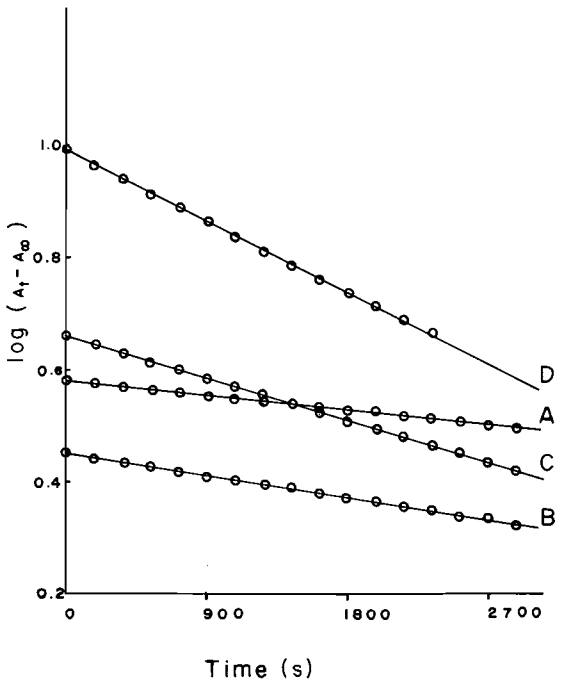

FIG. 1. First-order plots for the decomposition of **1** in THF; *A* = 25°C; *B* = 30°C; *C* = 35°C; *D* = 40°C.

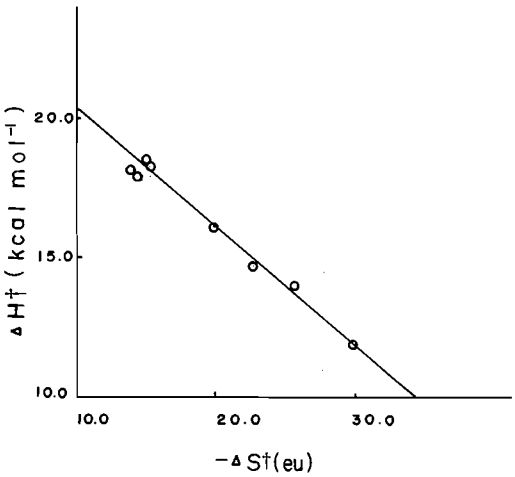

FIG. 2. Plot of $\Delta H\dagger$ against $-\Delta S\dagger$.

Can. J. Chem. Downloaded from www.nrcresearchpress.com by 210.87.254.42 on 09/05/12
For personal use only.

TABLE 1. First-order rate constants for the thermal decomposition of **1** in various solvents

Solvent	10^4k (s^{-1})								
	25.0°C	30.0°C	35.0°C	40.0°C	45.0°C	50.0°C	55.0°C	60.0°C	65.0°C
i-PrOH	3.45	5.86	10.6	18.0	27.5	41.0	58.6		
C_2H_5OH	9.21	13.7	20.8	31.8	46.9	63.7	81.1		
CH_3OH	39.5	56.0	71.9	110	148				
CH_3CN	3.14	5.27	8.80	14.6	23.3	33.9	36.1		
THF	0.68	1.01	1.93	3.22	5.54	8.33	12.4		
$HCONHCH_3$	11.0	15.5	23.3	35.8	54.7	77.7			
$HCON(CH_3)_2$	3.27	5.52	9.47	15.5	25.2	38.4	58.1		
$CH_3COOC_2H_5$	—	1.05 ±0.005	2.40 ±0.01	3.32 ±0.01	5.45 ±0.02	9.08 ±0.03	12.9 ±0.08	21.6 ±0.1	31.0 ±0.1

TABLE 2. Activation parameters for the thermolysis of **1**

Solvent	$\Delta H\dagger$ (kcal mol^{-1})	$\Delta S\dagger$ (eu)
i-PrOH	17.9 ± 0.5	−14.3 ± 1.2
C_2H_5OH	14.0 ± 0.4	−25.5 ± 1.0
CH_3OH	11.9 ± 0.5	−29.7 ± 1.5
CH_3CN	16.2 ± 1.0	−20.4 ± 2.8
THF	18.8 ± 0.5	−14.6 ± 1.1
$HCONHCH_3$	14.7 ± 0.4	−22.9 ± 1.1
$HCON(CH_3)_2$	18.1 ± 0.2	−13.7 ± 0.7
$CH_3COOC_2H_5$	18.4 ± 0.6	−15.6 ± 1.9

TABLE 3. Calculated first-order rate constants at 30°C and solvent parameters

Solvent	$\log k + 4$	E_t (kcal mol^{-1})
i-PrOH	0.77	48.6
C_2H_5OH	1.13	51.9
CH_3OH	1.73	55.5
CH_3CN	0.67	46.0
THF	0.05	37.4
$HCONHCH_3$	1.20	54.1
$HCON(CH_3)_2$	0.76	43.8
$CH_3COOC_2H_5$	0.13	38.1

relationship. From the equation $\log k = aE_t + b$, the value of the slope, a, is 7.5×10^{-2}. Large values of a have been attributed to the formation of an ion-pair in the transition state (8). However, the small value of a in the present case suggests a mechanism in which there is little change in charge separation between the ground state and the transition state. This conclusion further affirms that the contribution of **1′** to the ground state is minimal.

In order for the O atom to migrate to the C atom there must be a cyclic transition state at some stage. To account for the negative $\Delta S\dagger$ values and the small a value in the $\log k$ vs. E_t plot, we would like to consider an electrocyclic ring closure mechanism, which is thermally (and also photochemically) allowed by Woodward–Hoffman rules (9):

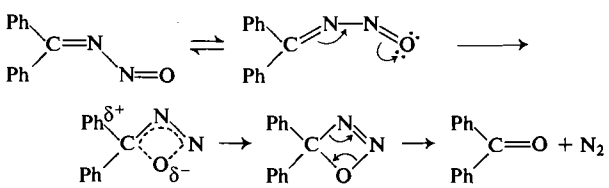

Such a mechanism is in agreement with our results.

It is interesting to note the formation of the four-membered transition state and its similarity to the 1,2-dioxetane system (10–13). The thermochemical data for **1** are unknown. However, an estimate of the heat of reaction from **1** to benzophenone and nitrogen can be made on the basis of bond energy data (14). The reaction is approximately 75 kcal mol^{-1} exothermic. The value of ΔH_f (Ph_2CO) is 12.5 kcal mol^{-1} and the present estimates appear to support the view that ΔH_f (**1**) is of the order of 88 kcal mol^{-1}. Since the combined estimated heat of reaction (~75 kcal) and measured enthalpy of activation (~17 kcal) exceed the energy required for benzophenone excitation, formation of excited states of benzophenone and of nitrogen are possible.

Since the rate of intersystem crossing for the singlet excited benzophenone is fast, no fluorescence should be observed even if the singlet state of benzophenone is produced (15). The benzophenone produced from the thermal reactions of *N*-nitrosodiphenylmethylimine may be in a triplet state. If this is so, then the photoreduction reaction of benzophenone would take place to yield benzopinacol for the thermolysis of **1** in isopropanol. Several attempts were made to detect benzopinacol but it was not found. In addition, solutions of **1** containing a fluorescer such as 9,10-dibromoanthracene were allowed to warm up to room temperature, no luminescence was observed. This means that the branching ratio for energy transfer to the singlet or triplet states of benzophenone is small.

The thermolysis of **1** in acetic acid was also studied. The intense blue color of the *N*-nitrosodiphenylmethylimine disappeared within

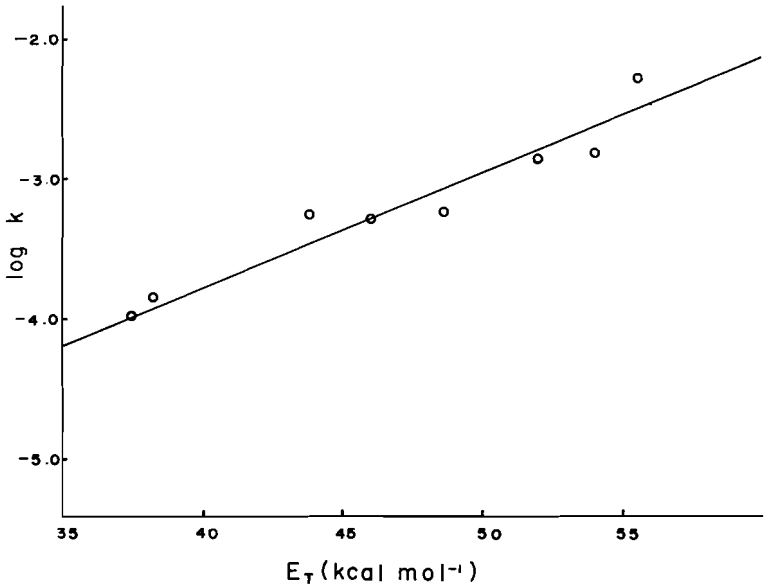

FIG. 3. Plot of log k vs. E_t for the decomposition of **1**.

seconds at room temperature and the products were benzophenone and nitrogen. For this decomposition, the following mechanism is proposed:

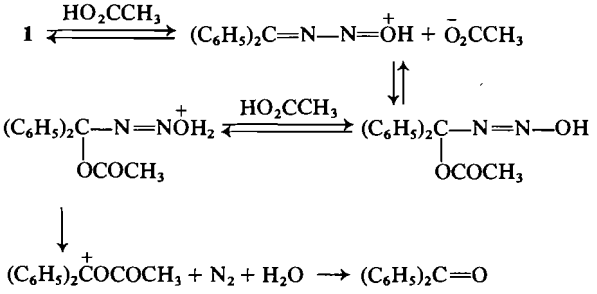

Further investigation of this system is in progress.

Acknowledgements

M.T.H.L. wishes to thank the S.R.C. of U.P.E.I. and the Natural Sciences and Engineering Research Council of Canada for the financial support which made this work possible. The authors also wish to thank Ms. W. Y. Kwan for carrying out some of the experiments. The comments from both referees are much appreciated.

1. S. J. THOMAN and I. M. HUNSBERGER. J. Org. Chem. **33**, 2852 (1968).
2. J. H. VIS and P. MEINCKE. J. Heterocycl. Chem. **7**, 1417 (1970).
3. K. A. AKIBA, S. MATSUNAMI, C. EGUCHI, and N. INAMOTO. Bull. Chem. Soc. Jpn. **47**, 935 (1974).
4. K. A. AKIBA and N. INAMOTO. Heterocycles, **7**, 1131 (1977) and references therein.
5. E. M. KOSOWER. J. Am. Chem. Soc. **80**, 3253 (1958).
6. S. G. SMITH, A. H. FAINBERG, and S. WINSTEIN. J. Am. Chem. Soc. **83**, 618 (1961).
7. C. REICHARDT. Angew. Chem. **77**, 30 (1965).
8. M. YASUDA, K. HARANO, and K. KANEMATSU. J. Org. Chem. **45**, 2368 (1980) and references therein.
9. R. B. WOODWARD and R. HOFFMAN. J. Am. Chem. Soc. **87**, 395 (1965); **87**, 2046 (1965); **87**, 2511 (1965); **87**, 4385 (1965); **87**, 4389 (1965).
10. A. L. BAUMSTARK, T. WILSON, M. E. LANDIS, and P. D. BARTLETT. Tetrahedron Lett. 2397 (1976).
11. K. R. KOPECKY and C. MUMFORD. Can. J. Chem. **47**, 709 (1969).
12. N. J. TURRO, P. LECKTKEN, N. W. SCHORE, G. SCHUSTER, H. C. STEINMETZER, and A. YEKTA. Acc. Chem. Res. **7**, 97 (1974).
13. K. A. HORN, J-Y. KOO, S. P. SCHMIDT, and G. B. SCHUSTER. Mol. Photochem. **9**(1), 1 (1978–1979).
14. J. G. CALVERT and J. N. PITTS, JR. Photochemistry. John Wiley and Sons, Inc., New York. 1966.
15. N. J. TURRO. Modern molecular photochemistry. Benjamin/Cummings, Menlo Park, CA. 1978.

Can. J. Chem. Downloaded from www.nrcresearchpress.com by 210.87.254.42 on 09/05/12
For personal use only.

Thiotungstate isopolyanions: an electrometric study

SHIVA PRASAD

Departamento de Engenharia Química, Centro de Ciências e Tecnologia, Universidade Federal da Paraíba Campina Grande, Paraíba, Brasil

Received July 29, 1980

SHIVA PRASAD. Can. J. Chem. **59**, 563 (1981).

The stoichiometry of the various polyanions formed during the reaction between sodium thiotungstate and sulphuric acid has been investigated by pH and conductance measurements, which have revealed the formation of different polymerized species, viz. $(W_4S_{15})^{6-}$, $(W_2S_7)^{2-}$, and possibly $(W_4S_{13})^{2-}$ in the vicinity of pH 6.2, 4.4, and 2.7 respectively. The formation of $(W_4S_{13})^{2-}$ is, however, not evidenced by the pH investigations. It was observed that at higher hydrogen ion concentration (pH < 2.4), thiotungstate decomposes into hydrated tungsten trisulphide.

SHIVA PRASAD. Can. J. Chem. **59**, 563 (1981).

Faisant appel à des mesures de pH et de conductivité, on a étudié la stoechiométrie des différents polyanions qui se forment au cours de la réaction du thiotungstate de sodium avec l'acide sulfurique. Ces mesures ont permis de mettre en évidence la formation de différentes entités polymérisées comme $(W_4S_{15})^{6-}$, $(W_2S_7)^{2-}$ et possiblement $(W_4S_{13})^{2-}$ respectivement à des pH voisins de 6,2, 4,4 et 2,7. Les études de pH ne prouvent cependant pas qu'il y a formation du polyanion $(W_4S_{13})^{2-}$. On a observé qu'à une concentration plus forte en ions hydrogènes (pH < 2,4), le thiotungstate se décompose en trisulfure de tungstène hydraté.

[Traduit par le journal]

Introduction

There is no reference in the literature to the study of acid–thiotungstate system by electrometric techniques. A few references (1–3) are, however, available concerning the preparation of tungsten trisulphide by the action of acid on thiotungstate, but no light has been thrown by the earlier workers on the constitution of various intermediate species formed during the process of acidification of thiotungstate. With a view to studying in detail the chemistry of the decomposition of sodium thiotungstate on acidification it is considered worthwhile to make a careful and precise study of the acid–thiotungstate system by electrometric techniques, which have provided more conclusive evidences on the condensation processes of oxyanions of tungsten(VI), molybdenum(VI), vanadium(V), arsenic(V), and thioanions of molybdenum(VI) (4–10).

Experimental

Merck's guaranteed extra-pure reagents, tungstic acid, ammonium sulphide, sodium sulphide, and sulphuric acid were used. The sulphide content of the solutions was checked iodometrically by titrating against a standard solution of sodium thiosulphate.

The solution of sodium thiotungstate, was prepared by digesting WS_3 with a solution containing an equivalent amount of Na_2S. Tungsten(VI) contents in WS_3 were determined by 8-hydroxyquinoline as tungsten oxinate (11*a*) and sulphur contents as $BaSO_4$ (11*b*).

pH measurements were carried out on Metrohm Herisau (Switzerland) pH-meter using a wide range glass electrode in conjunction with a sce. Conductance values were recorded by employing a Metrohm Herisau (Switzerland) conductometer. The thiotungstate solution (40 mL) was placed in the cell each time and thermostated at 25 ± 0.1°C.

Job's method of continuous variation was employed for determining the composition of polyanions. This consists of plotting the differences in specific conductivities (the sum of observed specific conductivities of the constituent solutions minus the observed specific conductivities of the mixture) against composition of mixtures.

Results and Discussion

Tungsten trioxide dissolves in sodium hydroxide solution to form sodium tungstate (Na_2WO_4) which, on passage of hydrogen sulphide gas, for a long time acquires a brown colour via yellow and orange. The development of the colour depends on pH, temperature, and time of reaction. The slow development of colour indicates the formation of intermediate thio-oxy compounds by displacement of oxygen by sulphur. The equilibria (12) may be represented as follows:

$$(WO_4)^{2-} \xrightarrow[-H_2O]{H_2S} (WO_3S)^{2-} \xrightarrow[-H_2O]{H_2S} (WO_2S_2)^{2-} \xrightarrow[-H_2O]{H_2S} (WOS_3)^{2-} \xrightarrow[-H_2O]{H_2S} (WS_4)^{2-}$$

The final solution $(WS_4)^{2-}$ on treatment with dilute acid decomposes into tungsten trisulphide with a gradual change in colour intensity and evolution of H_2S. These observations lead us to believe that the addition of the acid to thiotungstate solution causes the formation of different polyanions before

0008-4042/81/030563-03$01.00/0

©1981 National Research Council of Canada/Conseil national de recherches du Canada

Can. J. Chem. Downloaded from www.nrcresearchpress.com by 210.87.254.42 on 09/06/12
For personal use only.

Can. J. Chem. Downloaded from www.nrcresearchpress.com by 210.87.254.42 on 09/06/12
For personal use only.

TABLE 1. Summary of the results of the electrometric titrations: volume of thiotungstate solution taken in the titration cell = 40 mL

Molarity of solutions		Equivalence points (mL) for the formation of								
		$(W_4S_{15})^{6-}$			$(W_2S_7)^{2-}$			$(W_4S_{13})^{2-}$		
H_2SO_4	Na_2WS_4	Calcd	A	B*	Calcd	A	B*	Calcd	A	B*
M/5	*M*/50	1.0	1.0	1.0	2.0	2.0	2.0	3.0	—	3.0
M/10	*M*/80	1.25	1.25	1.25	2.5	2.5	2.45	3.75	—	3.75
M/20	*M*/150	1.33	1.3	1.35	2.67	2.65	2.65	4.0	—	4.05
M/40	*M*/250	1.2	1.15	1.2	2.4	2.4	2.4	3.6	—	3.5

*A and B represent the end-points observed from pH and conductometric titrations respectively.

the final decomposition to WS_3. This phenomenon appears to be identical with polymerisation of alkali tungstate on acidification. The formation of polymerised thiotungstate anions has, therefore, been studied by pH and conductometric titrations, the results of which are summarized in Table 1.

A perusal of the pH titration curves (Fig. 1) indicates that the addition of 1/4 mol of sulphuric acid per mol of sodium thiotungstate yields a pronounced maxima in dpH/dV curves in the region of formation of $(W_4S_{15})^{6-}$. Further action with the acid yields one more inflection in curves shown by the marked change in dpH/dV at the point where the molecular ratio of H_2SO_4:Na_2WS_4 is as 1:2, corresponding to the formation of dithiotungstate anion $(W_2S_7)^{2-}$. It is noted that in the case of higher concentration of solutions the curves are steeper and dpH/dV is more pronounced than for dilute reactants.

Conductometric titrations between sulphuric acid and sodium thiotungstate were also carried out using solutions of the same strengths for the sake of comparison of results. The plots (Fig. 2) of corrected conductance as a function of volume of titrant (H_2SO_4) yielded three defined breaks corresponding to the removal of 0.25, 0.50, and 0.75 mol (as H_2S) of Na_2S per mol of Na_2WS_4. The first two breaks indicate the formation of $(W_4S_{15})^{6-}$ and $(W_2S_7)^{2-}$ as suggested by the preceding pH study. The third break at a WS_4^{2-}:H^+ ratio of 1:1.5 indicated the formation of $(W_4S_{13})^{2-}$. A similar break was, however, not obtained in the pH titration curves, which may be ascribed to the little difference in the pH values of sulphuric acid and of this polyanion.

The decomposition of thiotungstate by sulphuric acid was also followed by Job's method of continuous variation using electrical conductance measurements. Plots of differences in specific conductivity values against composition of the mixture indicated a sharp maximum (Fig. 3) corresponding to a molar ratio for H_2SO_4:Na_2WS_4 of 1:2; this

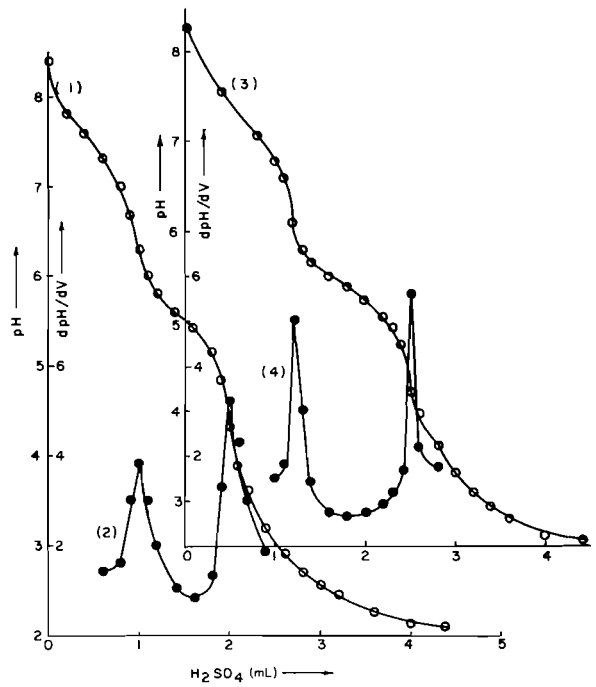

FIG. 1. pH titrations of Na_2WS_4 with H_2SO_4. Curves *1* and *2*: amount of *M*/5 H_2SO_4 (mL) added to 40 mL of *M*/50 Na_2WS_4; curves *3* and *4*: amount of *M*/10 H_2SO_4 (mL) added to 40 mL of *M*/80 Na_2WS_4.

provides further evidence for the formation of dithiotungstate, $(W_2S_7)^{2-}$.

When a basic thiotungstate solution containing WS_4^{2-} and Na^+ is acidified, the thiotungstate ions condense in definite steps, as evidenced by the foregoing electrometric experiments, to form different polythiotungstate anions. The overall condensation process may be considered formally at least to begin with partial neutralization of thiotungstate ions followed by the elimination of H_2S to form a thiobridge in analogy with the oxotungsten(VI) compounds.

$$(WS_4)^{2-} + H^+ \rightarrow [WS_3(SH)]^-$$

$$2[WS_3(SH)]^- \rightarrow (S_3W—S—WS_3)^{2-} + H_2S$$

Can. J. Chem. Downloaded from www.nrcresearchpress.com by 210.87.254.42 on 09/06/12
For personal use only.

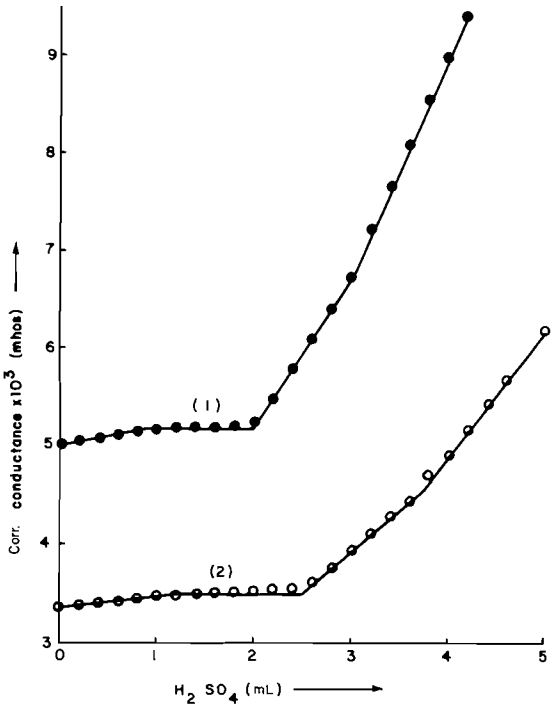

FIG. 2. Conductometric titrations of Na_2WS_4 with H_2SO_4. Curve *1*, amount of *M*/5 H_2SO_4 (mL) added to 40 mL of *M*/50 Na_2WS_4; curve *2*, amount of *M*/10 H_2SO_4 added to 40 mL of *M*/80 Na_2WS_4.

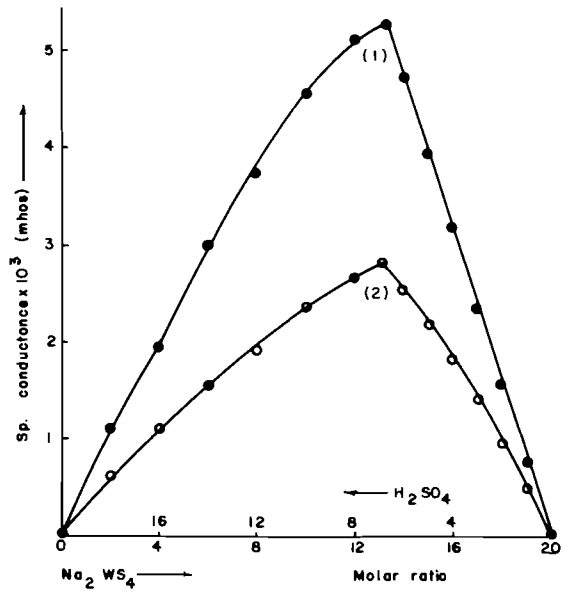

FIG. 3. Continuous variation study by Job's method using equimolar solutions. Curve *1*, *M*/50 H_2SO_4 and *M*/50 Na_2WS_4; curve *2*, *M*/100 H_2SO_4 and *M*/100 Na_2WS_4.

The addition of acid to Na_2WS_4 thus neutralizes 0.25, 0.50, and 0.75 mol of Na_2S per mol of Na_2WS_4, liberating an equivalent amount of H_2S. Further acidification decomposes Na_2WS_4 finally into WS_3, a brown precipitate. The stepwise decomposition of sodium thiotungstate may be represented by the following set of stoichiometric equations:

$$4(Na_2S{\cdot}WS_3) + H_2SO_4 \rightarrow (3Na_2S{\cdot}4WS_3) + Na_2SO_4 + H_2S$$

$$(3Na_2S{\cdot}4WS_3) + H_2SO_4 \rightarrow 2(Na_2S{\cdot}2WS_3) + Na_2SO_4 + H_2S$$

$$2(Na_2S{\cdot}2WS_3) + H_2SO_4 \rightarrow (Na_2S{\cdot}4WS_3) + Na_2SO_4 + H_2S$$

$$(Na_2S{\cdot}4WS_3) + H_2SO_4 \rightarrow 4WS_3 + Na_2SO_4 + H_2S$$

During the preliminary steps of the titrations 2–3 min are required for each pH and conductance value to become steady. This may be due to vigorous evolution of H_2S. A thorough stirring of the cell contents in the vicinity of the end-points has been found necessary.

The results evidently suggest the formation of two different polymerized intermediate species, viz. $(W_4S_{15})^{6-}$ and $(W_2S_7)^{2-}$ in the vicinity of pH 6.2 and 4.4 respectively, before the complete decomposition of thiotungstate into WS_3. The formation of $(W_4S_{13})^{2-}$ at pH 2.7 is indicated by conductometric investigations but could not be evidenced by the pH titrations.

Acknowledgements

The author wishes to express his sincere thanks to CNPq, Brasilia, for the financial assistance to perform this research work and to Professor José Marques de Almeida Júnior, Chief of the Chemical Analysis Laboratory for providing research facilities.

1. A. YA. ZVORYKIN, F. M. PERELMAU, and V. V. TARASOV. Zh. Neorg. Khim. **6**, 1994 (1961).
2. J. C. BERNARD and G. TRIDOT. Bull. Soc. Chim. Fr. 810 (1961).
3. J. W. MELLOR. Comprehensive treatise on inorganic and theoretical chemistry. Vol. II. Longmans, London. 1960. p. 647.
4. R. S. SAXENA and O. P. SHARMA. J. Nucl. Inorg. Chem. **28**, 1881 (1966).
5. R. S. SAXENA and O. P. SHARMA. Z. Anorg. Allg. Chem. **333**, 1 (1964).
6. R. S. SAXENA and G. P. SAXENA. Z. Phys. Chem. **29**, 181 (1961).
7. R. S. SAXENA and M. L. MITTAL. Acta Chim. Hung. **40**, 109 (1964).
8. R. S. SAXENA and M. L. MITTAL. Naturwissenchaften, **51**, 1 (1964).
9. R. S. SAXENA and S. PRASAD. J. Indian Chem. Soc. **45**(10), 940 (1968).
10. S. PRASAD. Ciência e Cultura. In press.
11. A. I. VOGEL. A textbook of quantitative inorganic analysis. Longmans, London. 1968. (*a*) p. 567; (*b*) p. 573.
12. G. TRIDOT and J. C. BERNARD. Acta. Chim. Acad. Sci. Hung. **34**, 179 (1962).

On the existence of intramolecular hydrogen bonds in methyl *o*-mercaptobenzoate and 2-methoxymethylbenzenethiol

TED SCHAEFER, DAVID M. MCKINNON, RUDY SEBASTIAN, AND BERT KRAWCHUK

Department of Chemistry, University of Manitoba, Winnipeg, Man., Canada R3T 2N2

Received July 14, 1980

TED SCHAEFER, DAVID M. MCKINNON, RUDY SEBASTIAN, and BERT KRAWCHUK. Can. J. Chem. **59**, 566 (1981).

Full analyses of the ^1H nmr spectra of methyl *o*-mercaptobenzoate and of 2-methoxymethylbenzenethiol yield spectral parameters suggesting that the *trans* conformer of the former is preferred by 1.6 ± 0.7 kJ/mol in free energy in solution at 305 K. Both *cis* and *trans* conformers can be reasonably discussed in terms of "planar" conformations. The ether displays nearly equal concentrations of *cis* and *trans* conformers. However, these conformers display considerable conformational freedom of the sulfhydryl group. These results are compared to previous infrared data. It is suggested that in the ester the small tendency towards intramolecular hydrogen bonding involves the carbonyl oxygen. Any S—H···O interaction in the ether must surely occur for conformations in which the S—H and C—O bonds are far from the ring plane.

TED SCHAEFER, DAVID M. MCKINNON, RUDY SEBASTIAN et BERT KRAWCHUK. Can. J. Chem. **59**, 566 (1981).

L'analyse détaillée des spectres rmn du *o*-mercaptobenzoate de méthyle et du méthoxyméthyl-2 benzènethiol conduit à des paramètres spectraux suggérant que la différence d'énergie libre en solution à 305 K favorise le conformère *trans* du premier composé de $1,6 \pm 0,7$ kJ/mole. On peut raisonnablement discuter des deux conformères *cis* et *trans* en fonction de conformations "planes". Dans le cas de l'éther les concentrations des conformères *cis* et *trans* sont presqu'égales. Cependant le groupe sulfydryle jouit d'une liberté conformationnelle considérable. On a comparé ces résultats aux données infrarouges obtenues antérieurement. On croit que la faible tendance a former des liaisons hydrogènes intramoléculaire implique l'oxygène du carbone de l'ester. Toute interaction S—H···O dans l'éther doit sûrement se produire dans des conformations où les liaisons S—H et C—O sont éloignées du plan du cycle.

[Traduit par le journal]

Introduction

Because the S—H bond is much less polar than the O—H bond, weaker hydrogen bonding ability is anticipated for thiophenol than for phenol and its derivatives. In particular, *ortho*-substituted thiophenols are discussed in terms of *cis*, **1***a*, and *trans*, **1***b*, conformations (1). Absence of intramolecular hydrogen bonding favors **1***b* on steric grounds, whereas its presence will stabilize **1***a*. Infrared spectroscopy (2, 3) and dipole moment measurements (3) suggest, for example, that when X = NO_2, **1***a* is the predominant form in solution. On the other hand, stereospecific long-range spin–spin coupling constants strongly imply that **1***b* is favored by 2.1 ± 0.8 kJ/mol in $CDCl_3$ and C_6D_6 solutions at 305 K (4). The population ratio of **1***a* and **1***b* is found on the assumption that the long-range coupling constants over five bonds, $^5J_m^{H(3),SH}$ in **1***a* and $^5J_m^{H(5),SH}$ in **1***b*, vanish, and are finite for the all-*trans* arrangement of the intervening bonds, i.e., $^5J_m^{H(5),SH}$ in **1***a*, and $^5J_m^{H(3),SH}$ in **1***b*. This assumption has been investigated (4–7).

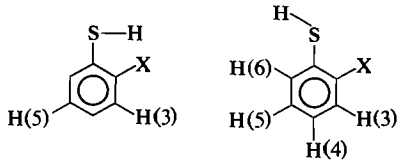

1*a* **1***b*

The twofold barrier to internal rotation in thiophenol (8) is ca. 3 kJ/mol, comparable to thermal energies at ambient temperatures, and much less than the 14.4 kJ/mol in phenol (9). Accordingly, unless the substituent increases the internal barrier substantially by conjugative perturbations, as it does in *para* and *ortho* nitrothiophenol (4, 10), nonplanar conformations should be considered in addition to **1***a* and **1***b*; a complication not encountered with phenol derivatives (6, 11). If the barrier to internal rotation is relatively large, say 12 kJ/mol or more, $^6J_p^{H,SH}$ will be very small (4, 10). For a barrier of 3 kJ/mol, as in thiophenol, $^6J_p^{H,SH}$ is -0.33 Hz (12). In 2-nitrothiophenol, $^6J_p^{H,SH}$ effectively vanishes (4). If the S—H group is held perpendicular to the benzene plane, $^6J_p^{H,SH}$ can become as large in magnitude as 1 Hz (7).

Substantial out-of-plane motion of the S—H group occurs in 2-methoxythiophenol (6) and in some 2-halothiophenol derivatives (5). Indeed, again on the basis of long-range coupling constants, it was shown (7) that 2-hydroxythiophenol in CCl_4 exists mainly as a conformer in which the S—H bond prefers a plane perpendicular to the benzene nucleus; the hydroxyl group hydrogen bonds to the directional lone pair on the sulfur atom.

The stretching frequencies of the S—H bond in the ethyl ester of thiosalicylic acid have been attributed to **2***a* and **2***b* (2). Similarly (2), in dilute solu-

0008-4042/81/030566-06$01.00/0

©1981 National Research Council of Canada/Conseil national de recherches du Canada

Can. J. Chem. Downloaded from www.nrcresearchpress.com by 210.87.254.6 on 09/06/12
For personal use only.

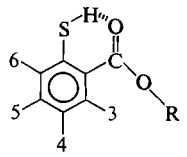

2a

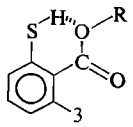

2b

tion in CCl_4, a benzyl ether is thought to exist in conformation **3**.

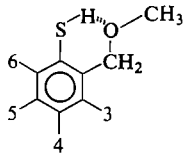

3

In this paper, the long-range coupling constants are determined for **2** (R = CH_3) and **3** in solution. The couplings involving H-3, H-5, and S—H yield information about the relative stability of *cis* and *trans* conformers, while the coupling to H-4, $^6J_p^{H,SH}$, indicates the importance of out-of-plane motion of the mercapto group. The couplings involving the methylene protons in **3** provide a rough measure of the flexibility of the ether fragment.

Experimental

2-Mercaptobenzoic acid (Aldrich) was esterified in acidic methanol containing some acetyl chloride. The product, **2** (R = CH_3), gave the correct mass spectrum and the ^1H nmr spectrum was consistent with **2**.

2-Methoxymethylbenzenethiol, **3**, has previously been prepared from 2-aminobenzyl methyl ether (2). Here **3** was prepared from 2-methylthiobenzyl chloride (13) via 2-methylthiobenzyl methyl ether (14) and oxidation of the latter to the sulfoxide. The sulfoxide was rearranged to the thiohemiacetal acetate with acetic anhydride. Mild basic hydrolysis yielded **3**; bp 75°C/0.2 Torr. *Anal.* calcd. for $C_8H_{10}OS$: C 62.34, H 6.49, S 20.78; found: C 62.09, H 6.58, S 21.02.

Samples of **2** were prepared as ca. 2 mol% solutions in CCl_4 and C_6D_6 and contained some tetramethylsilane (TMS). After transfer to 5 mm od Pyrex tubes, the samples were degassed by five freeze–pump–thaw cycles and were flame-sealed. A similar procedure gave a ca. 3 mol% solution of the ether, **3**, in CCl_4 solution. All solutions contained Linde type 3A sieve.

The ^1H nmr spectra of the three samples were calibrated in the frequency sweep mode at 100.001 MHz (centerband) on an HA100 spectrometer at a probe temperature of 305 K. Markers were placed at ca. 5 Hz intervals, their frequencies relative to the lock frequency were recorded, and the peak frequencies of this procedure yielded peak positions whose rms deviation was $\leq$ 0.02 Hz. The ^1H nmr spectrum of **3** was calibrated under single resonance conditions, as well as in the presence of decoupling fields placed at the S—H band, at the CH_2 band, and at the CH_3 peak.

Results and Discussion

Spectral Analyses

These utilized the computer program LAME (15, 16). The ensuing spectral parameters are given in Tables 1 and 2. The CCl_4 solution of **2** (R = CH_3) gave a spectrum with a chemical shift difference of only 1 Hz between H-5 and H-6, whereas these protons are coupled by 8 Hz. In consequence, there occurs a correlation coefficient of −0.698 between $^4J_o^{H,SH}$ and $^5J_m^{H(5),SH}$, meaning that their individual values are uncertain. For this reason the benzene solution was also examined. As can be seen in Table 1, the chemical shift dispersion of the ring protons is increased and the correlation between $^4J_o^{H,SH}$ and $^5J_m^{H(5),SH}$ decreases, but only to −0.382. Therefore, these parameters are still not as reliably known as their standard deviations would indicate. For **3**, the chemical shifts of H-4 and H-5 differ by 2 Hz and $^6J_p^{H,SH}$ and $^5J_m^{H(5),SH}$ are correlated by −0.399. These facts must be considered in the conformational analysis to follow.

Figure 1 illustrates the spectral quality, displaying the S—H multiplet of **2** in CCl_4 solution. In C_6D_6 the S—H band approximated to a doublet, each component having some structure. The different appearance arose simply from the change in dispersion of the ring proton spectra (see ref. 4 for a similar example).

The Conformational Preference of the S—H Group in the Ester, 2

In CCl_4, the S—H stretching band occurs at 2585 cm^{-1} for benzenethiol (2). In the ethyl ester of 2-mercaptobenzoic acid, the two bands at 2556 and 2523 cm^{-1} (2) were assigned to **2***a* and **2***b*. On the other hand, in the methyl ester one band is tabulated at 2534 cm^{-1} in CCl_4 solution (3). The shifts in frequencies are rather small compared to analogous phenol derivatives but the intensities of the bands are considerably higher than that in thiophenol.

As argued for 2-nitrothiophenol (4), the vanishing $^6J_p^{H,SH}$ in **2** is a strong indication that the S—H conformational preference can be usefully discussed in terms of planar *cis* and *trans* forms. Conjugation with the substituent increases the double-bond character of the C—S bond and raises the internal barrier, perhaps to as much as 10 to 12 kJ/mol (10).

It follows that, because $^5J_m^{H(3),SH}$ is 0.29 ± 0.01 Hz (this coupling does not correlate significantly with any other spectral parameter), a substantial population of the *trans* form exists at 305 K in CCl_4 solution. A similar statement holds for the C_6D_6 solution, in which $^5J_m^{H(3),SH}$ is 0.35 ± 0.02 Hz (the error limits assume that the standard deviations are to be multiplied by three). Now, although $^5J_m^{H(5),SH}$ correlates with $^4J_o^{H,SH}$ in both solutions (but less

Can. J. Chem. Downloaded from www.nrcresearchpress.com by 210.87.254.6 on 09/06/12
For personal use only.

TABLE 1. ^{1}H nmr spectral parameters for methyl *o*-mercaptobenzoate[a] at 100 MHz and 305 K

Parameter	CCl_4[b]	C_6D_6[b]	Parameter	CCl_4[b]	C_6D_6[b]
ν_{SH}	539.435(3)[c,d]	498.897(5)	$^5J_{3,6}$	0.465(10)	0.493(8)
ν_3	794.979(3)	785.583(4)	$^4J_o^{H,SH}$	0.129(8)	−0.041(8)
ν_4	704.220(4)	673.995(6)	$^5J_m^{H(3),SH}$	0.289(4)	0.347(6)
ν_5	721.842(9)	682.334(8)	$^5J_m^{H(5),SH}$	0.163(8)	0.184(10)
ν_6	722.792(7)	689.421(7)	$^6J_p^{H,SH}$	−0.008(4)	−0.032(7)
ν_{CH_3}	386.86	343.0	Root mean square deviation	0.009	0.015
$^3J_{3,4}$	8.024(5)	7.989(8)	Transitions calculated	82	86
$^3J_{4,5}$	7.338(10)	7.308(7)	Peaks observed	45	52
$^3J_{5,6}$	8.020(10)	7.990(7)			
$^4J_{3,5}$	1.584(10)	1.567(12)	Transitions assigned	63	83
$^4J_{4,6}$	1.218(12)	1.203(10)	Largest difference	0.022	0.035

[a]For convenience and consistency with the other compound and structures **1***a* and **1***b*, H-3 is the proton *ortho* to the ester group.
[b]Approximately 2 mol%.
[c]The shifts are given in Hz at 100.001 MHz (centreband) to low field of internal TMS.
[d]The numbers in parentheses are the standard deviations in last one (or two) significant figures.

TABLE 2. ^{1}H nmr spectral parameters for 2-methoxymethylbenzenethiol in CCl_4 at 100 MHz and 305K

Parameter	*a*	*b*	*c*	Parameter	*a*	*b*	*c*
ν_{SH}	—	369.2	369.219(3)	$^4J_o^{H,SH}$	—	−0.300(11)	−0.308(3)
ν_{CH_2}	441.6	—	441.656(3)	$^5J_m^{H(3),SH}$	—	0.293(10)	0.314(3)
$\nu_{CH(_3)}$	—	—	332.20	$^5J_m^{H(5),SH}$	—	0.277(16)	0.266(5)
ν_3	722.134(4)[d]	722.106(7)	722.133(3)	$^6J_p^{H,SH}$	—	−0.342(15)	−0.349(5)
ν_4	706.238(7)	706.245(12)	706.284(5)	$^4J_o^{H,CH_2}$	−0.650(5)	—	−0.642(3)
ν_5	708.303(8)	708.296(12)	708.278(5)	$^5J_m^{H(4),CH_2}$	0.297(7)	—	0.299(4)
ν_6	723.325(4)	723.330(7)	723.348(3)	$^5J_m^{H(6),CH_2}$	0.298(5)	—	0.315(3)
$^3J_{3,4}$	7.598(10)	7.596(16)	7.624(6)	$^6J_p^{H,CH_2}$	−0.438(7)	—	−0.446(4)
$^3J_{4,5}$	7.448(4)	7.449(7)	7.469(2)	$^5J_o^{SH,CH_2}$	—	—	0.320(3)
$^3J_{5,6}$	7.791(10)	7.794(16)	7.763(7)	Root mean square deviation	0.019	0.020	0.018
$^4J_{3,5}$	1.570(12)[e]	1.589(20)[e]	1.503(8)[e]	Transitions calcd.	171	86	495
$^4J_{4,6}$	1.218(15)[e]	1.209(11)[e]	1.270(9)[e]	Transitions assigned	132	68	383
$^5J_{3,6}$	0.478(5)	0.468(8)	0.483(3)	Peaks	75	56	140

[a]Calibrated while decoupling S—H proton.
[b]Calibrated while decoupling CH_2 protons.
[c]Decoupling CH_3.
[d]In Hz at 100.001 MHz to low field of internal TMS; numbers in parentheses are standard deviations in the last one or two places.
[e]These two parameters are correlated by 0.78, accounting for the variation in their values in the different analyses.

strongly in the C_6D_6 solution), the sums of the two ^5J values are close to the sums in 2-methoxythiophenol (6) and in thiophenol itself (12). Furthermore, while the correlations are different in the two solutions, $^5J_m^{H(5),SH}$ does not change significantly. It appears rational, therefore, to attach significance to the $^5J_m^{H(5),SH}$ of 0.17 ± 0.03 Hz in **2** and to deduce a population for the *cis* form. The ratio of *trans* to *cis* populations is then 1.7 to 1 and 2.0 to 1 in CCl_4 and C_6D_6 respectively, yielding a free energy preference for the *trans* conformer of 1.3 ± 0.5 and 1.8 ± 0.5 kJ/mol. In view of the doubt about $^5J_m^{H(5),SH}$ it seems safe to state that the preference is 1.6 ± 0.7 kJ/mol in both solutions.

Can. J. Chem. Downloaded from www.nrcresearchpress.com by 210.87.254.6 on 09/06/12
For personal use only.

Can. J. Chem. Downloaded from www.nrcresearchpress.com by 210.87.254.6 on 09/06/12
For personal use only.

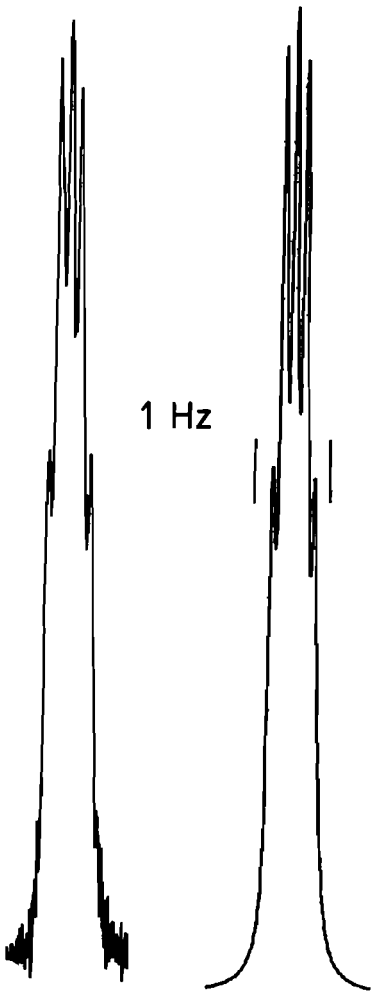

FIG. 1. The ^1H nmr spectrum of the sulfhydryl proton in methyl *o*-mercaptobenzoate as a ca. 2 mol% solution in CCl_4 at 100 MHz and 305 K. The calculated spectrum on the right assumes the parameters in Table 1 and a linewidth at half height of 0.10 Hz. The separation between the midpoints of the outer peaks is 0.58 Hz.

Purely steric interactions might well cause a larger preference for the *trans* conformation (intermolecular association is unimportant (17)). Accordingly, a small degree of hydrogen bonding apparently exists. This conclusion is consistent with the δ_{SH} of 5.39 ppm in the CCl_4 solution, its value being 3.23 ppm for benzenethiol (12). Conjugative electron withdrawal by the ester moiety will increase δ_{SH} somewhat, perhaps by as much as 0.3 ppm (18), leaving ca. 1.9 ppm as a hydrogen-bond shift. The deshielding of the hydroxyl proton in methyl salicylate, relative to phenol in CCl_4, is 6.2 ppm (19, 20). The salicylate exists as the *cis* form to the extent of at least 95%. To a first approximation, if ca. 33% of **2** exists in the *cis* conformation (as indicated by the long-range couplings) and if the deshielding is caused mainly by the time varying electric fields and the large magnetic anisotropy of the ester moiety in this conformer, the observed deshielding of ca. 2 ppm in **2** is rationalized. Of course, the S—H bond is more polarizable than the O—H bond and the geometry will be somewhat different in the *cis* conformers of the two compounds, so that δ_{SH} in **2** can only be said to be roughly consistent with a 2:1 ratio of *trans* to *cis* conformers. (A similar comparison between δ_{OH} and δ_{SH} for 2-methoxyphenol and 2-methoxythiophenol (6) is also consistent with the *cis*/*trans* distribution based on coupling constants.)

These adumbrations imply that the S—H group hydrogen bonds to the carbonyl group in the methylester. Certainly the carbonyl group is a stronger proton acceptor than the ether function in phenol derivatives (6, 21). The two S—H stretching bands reported (2) for the ethyl ester may arise from the *cis* and *trans* forms rather than from **2***a* and **2***b*. Only one stretching frequency was tabulated for the methyl ester (3), yet the reported spectrum apparently consists of two very broad overlapping bands (Fig. 3 of ref. 3), rather similar in appearance to the ethyl ester spectrum (2).

A recent analysis (22) of the ^1H nmr spectrum of **2** in $CDCl_3$ at 360 MHz reports $^5J_m^{H(3),SH}$ as 0.4 Hz and $^5J_m^{H(5),SH}$ as < 0.2 Hz; presumably the latter was not observed as a splitting because of larger linewidths than those in the present analysis. The chemical shifts of H-5 and H-6 were apparently identical (22). The deuterium quadrupole coupling constant (DQCC) in the S—D bond was 133 kHz (22), smaller than the 146 kHz in thiophenol (23). Hydrogen bonding will cause a decrease in the DQCC. If 33% of **2** exists in the *cis* form and if the DQCC of the *trans* form is that in thiophenol, then the *cis* form has a DQCC of ca. 107 kHz. This number also assumes that interconversion of the conformers is faster than about 10^4 Hz but slower than rotational diffusion; a reasonable assumption because the barrier to interconversion must lie in the region of 8 to 12 kJ/mol (10). On the other hand, the observed DQCC in the ester could arise from increased ionicity of the S—D bond caused by electron withdrawal by the ester group, a possibility testable by examination of the *para* isomer.

The Conformational Behaviour of the S—H Bond in 2-Methoxymethylbenzenethiol, 3

In CCl_4 solution, the S—H stretching band at

Can. J. Chem. Downloaded from www.nrcresearchpress.com by 210.87.254.6 on 09/06/12
For personal use only.

2560 cm^{-1} is assigned to the hydrogen bonded S—H group (2). No other band was observed.

The coupling data in Table 2 show that motion of the S—H group in **3** is much less restricted than in **2**, 2-nitrothiophenol (4), or in 2-methoxythiophenol (6). $^6J_p^{H,SH}$ is -0.35 ± 0.02 Hz, hardly different from the -0.33 ± 0.02 Hz in benzenethiol (12). The twofold barrier to out-of-plane rotation in the latter is not below 3.2 kJ/mol (8, 12), implying that **3** cannot be discussed simply in terms of *cis* and *trans* conformers.

Furthermore, $^5J_m^{H,SH}$ values indicate a very slight preference for conformations in which the S—H bonds avoid the other substituent. Their sum is the same to within experimental error as in 4-methylthiophenol (10) and somewhat larger than in thiophenol (12), indicating a $\sigma-\pi$ contribution to $^5J_m^{H,SH}$ (6, 10), in agreement with substantial out-of-plane populations deduced from $^6J_p^{H,SH}$.

The long-range couplings to the sulfhydryl proton are consistent with a relatively weak intramolecular hydrogen bond to the ether oxygen atom. Of course, the structure **3** has an H··O distance of only 1.2 Å, much too short for a stable hydrogen bond. Accordingly, the *cis* conformation would require, say, an out-of-plane twist of about 60° by the S—H and C—O bonds so as to reach the H··O distance of 2.2 Å in the *cis* conformation of 2-methoxythiophenol. In fact, in the latter compound, the *cis* conformer is also slightly less abundant (43%) and δ_{SH} is 3.66 ppm, whereas it is 3.69 ppm in **3**. Naturally, the twist angle of 60° is not meant quantitatively. Nevertheless, the long-range couplings involving the S—H proton are consistent with a skewed *cis* conformation.

The conformational looseness of the S—H bond should be reflected in a similar property of the ether substituent. The barrier to internal rotation of the CH_2OH moiety in benzyl alcohol is very likely less than 1 kJ/mol (24–26) and $^6J_p^{H,CH_2}$ is -0.59 Hz (24). In 2,6-dichlorobenzyl methyl ether (27), where the barrier to rotation about the exocyclic C—C bond must be substantial, $^6J_p^{H,CH_2}$ is -0.20 ± 0.02 Hz; in line with a conformation in which the C—O bond prefers a plane perpendicular to the ring. In **3**, $^6J_p^{H,CH_2}$ is -0.45 ± 0.01 Hz, indicative of an intermediate restriction to motion about the C—C bond. Certainly, if the C—O bond were constrained to the ring plane by a strong hydrogen bond, then $^6J_p^{H,CH_2}$ would be expected (25) to be about -0.85 Hz. It seems unlikely, therefore, that the single stretching band (2) can be identified solely with such a conformer. Furthermore, the two $^5J_m^{H,CH_2}$ numbers are effectively equal, consistent with weak conformational preferences about the exocyclic C—C bond.

The coupling of $+0.32$ Hz between the methylene and sulfhydryl protons (the sign was confirmed by double resonance experiments and simulation with the computer program DOR (28) modified for use with up to 8 spins (29)) has the same magnitude as $^4J_o^{H(6),SH}$, which is -0.31 Hz. This result implies a predominant $\sigma-\pi$ mechanism for $^4J_o^{H,SH}$ (6, 10).

Conclusions

The planar *trans* conformer in methyl *o*-mercaptobenzoate is twice as abundant as the *cis* conformer in solution at 305 K, suggesting only a small degree of intramolecular hydrogen bonding and comparable to that in 2-nitrothiophenol. The *cis* and *trans* conformers in 2-methoxymethylbenzenethiol are equally abundant but display relatively free motion of the sulfhydryl group, comparable to that in benzenethiol itself.

Acknowledgments

We are grateful to the Natural Sciences and Engineering Research Council of Canada for financial assistance.

1. M. R. Crampton. *In* The chemistry of the thiol group. *Edited by* S. Patai. John Wiley and Sons, New York. 1974. Part 1. Chapt. 8.
2. N. Mori, S. Kaido, K. Suzuki, M. Nakamura, and Y. Tsuzuki. Bull. Chem. Soc. Jpn. **44**, 1858 (1971).
3. T. Kobayashi, A. Yamashita, Y. Furuya, R. Horie, and M. Hirota. Bull. Chem. Soc. Jpn. **45**, 1494 (1972).
4. T. Schaefer and W. J. E. Parr. Can. J. Chem. **55**, 3732 (1977).
5. T. Schaefer and W. J. E. Parr. Can. J. Chem. **57**, 1421 (1979).
6. T. Schaefer and T. A. Wildman. Can. J. Chem. **57**, 450 (1979).
7. T. Schaefer, T. A. Wildman, and S. R. Salman. J. Am. Chem. Soc. **102**, 107 (1980).
8. N. W. Larsen and F. M. Nicolaisen. J. Mol. Struct. **22**, 29 (1974).
9. E. Mathier, D. Welti, A. Bauder, and Hs. H. Günthard. J. Mol. Spectrosc. **37**, 63 (1971).
10. T. Schaefer and W. J. E. Parr. Can. J. Chem. **55**, 552 (1977).
11. T. Schaefer and K. Chum. Can. J. Chem. **56**, 1788 (1978).
12. W. J. E. Parr and T. Schaefer. J. Magn. Reson. **25**, 171 (1977).
13. R. Grice and L. N. Owen. J. Chem. Soc. London, 1947 (1963).
14. S. H. Pines, R. Czarja, and N. L. Abramson. J. Org. Chem. **40**, 1920 (1975).
15. S. Castellano and A. A. Bothner-By. J. Chem. Phys. **41**, 3863 (1964).
16. C. W. Haigh and J. M. Williams. J. Mol. Spectrosc. **32**, 398 (1969).
17. S. H. Marcus and S. I. Miller. J. Am. Chem. Soc. **88**, 3719 (1966).
18. S. H. Marcus and S. I. Miller. J. Phys. Chem. **68**, 331 (1964).
19. G. Pala. Nature, **204**, 1190 (1964).

20. A. J. DALE and T. GRAMSTAD. Spectrochim. Acta, Part A, **28**, 639 (1972).
21. G. L. CARLSON and W. G. FATELEY. J. Phys. Chem. **77**, 1157 (1973).
22. L. M. JACKMAN, J. C. TREWELLA, and R. C. HADDON. J. Am. Chem. Soc. **102**, 2519 (1980).
23. B. M. FUNG and I. Y. WIE. J. Am. Chem. Soc. **92**, 1497 (1970).
24. W. J. HEHRE, L. RADOM, and J. A. POPLE. J. Am. Chem. Soc. **94**, 1496 (1972).
25. T. SCHAEFER, W. DANCHURA, W. NIEMCZURA, and W. J. E. PARR. Can. J. Chem. **56**, 1721 (1978).
26. R. J. ABRAHAM and J. M. BAKKE. Tetrahedron, **34**, 2947 (1978).
27. A. F. JANZEN and T. SCHAEFER. Can. J. Chem. **49**, 1818 (1971).
28. G. GOVIL and D. H. WHIFFEN. Mol. Phys. **12**, 449 (1967).
29. T. SCHAEFER, W. DANCHURA, and W. NIEMCZURA. Can. J. Chem. **56**, 2233 (1978).

Can. J. Chem. Downloaded from www.nrcresearchpress.com by 210.87.254.6 on 09/06/12
For personal use only.

Synthèse totale des acides (+) et (−) nonactique à partir de carbohydrates[1]

ROBERT E. IRELAND ET JEAN-PAUL VEVERT

Division of Chemistry and Chemical Engineering, California Institute of Technology, Pasadena, CA 91125, U.S.A.

Reçu le 17 juin 1980

ROBERT E. IRELAND et JEAN-PAUL VEVERT. Can. J. Chem. **59**, 572 (1981).

La synthèse des acides (−) et (+) nonactique **2***a* et **2***b* a été réalisée à partir respectivement de D-mannose (**7**) et de D-gulono-γ-lactone (**22**). Elle fait intervenir comme étape clé le réarrangement [3,3]-sigmatropique de cétène-acétals silylés IV qui permet le contrôle de la configuration du C-2 de l'acide nonactique. Ces cétène-acétals sont préparés à partir d'esters aliphatiques de glycals furanoïques II, qui sont eux même synthétisés en dix étapes à partir du carbohydrate précurseur. Les centres chiraux de ces glycals proviennent de la conservation durant cette suite de transformations des centres correspondants du monosaccharide de départ. Effectué avec ce genre de cétène-acétals le réarrangement de Claisen conduit à des composés comportant l'enchaînement du type aldol désiré. On tire également parti de la connaissance de la configuration absolue des carbones chiraux de l'acide nonactique pour déterminer la conformation (chaise ou bateau?) de l'état de transition du réarrangement [3,3]-sigmatropique.

ROBERT E. IRELAND and JEAN-PAUL VEVERT. Can. J. Chem. **59**, 572 (1981).

The synthesis of (−) and (+) nonactic acids (**2***a*) and (**2***b*) has been achieved starting from D-mannose (**7**) and D-gluono-γ-lactone (**22**) respectively. The key step in the synthesis is the [3,3]-sigmatropic rearrangement of the silylated ketene-acetals IV leading to control of the C-2 configuration of nonactic acid. The ketene-acetals were prepared from aliphatic esters of furanoid-glycals II, which were prepared in ten steps from the carbohydrate precursor. The chiral sites of the glycals arise from the corresponding centres in the starting monosaccharide. This type of ketene-acetal Claisen rearrangement leads to products containing the aldol portion required. At the same time knowledge of the absolute configuration of the chiral carbon atom of nonactic acid allows for the determination of the chair or boat form of the transition state of the [3,3]-sigmatropic rearrangement.

[Journal translation]

Can. J. Chem. Downloaded from www.nrcresearchpress.com by 210.87.254.42 on 09/05/12
For personal use only.

Introduction

La nonactine (**1**) macrotétrolide isolé pour la première fois en 1955 par Prelog, Keller-Schierlein et coll. (1) représente l'homologue le plus simple d'une famille de tétraesters macrocycliques à 32 membres, connus sous le nom de nactines (2) et produits à partir de cultures de streptomyces (3). L'intérêt biologique suscité par ces composés résulte en partie de leurs propriétés antimicrobiennes (G+, fungi) mais surtout de leur capacité à agir comme transporteurs d'ions à travers les membranes biologiques (4). Les nactines forment des complexes 1:1 avec de nombreux ions des métaux alcalins et alcalino-terreux et plus particulièrement avec le potassium (5) qui se trouve littéralement englobé par coordination des huit oxygènes des carbonyles et cycles tétrahydrofuraniques à l'intérieur du squelette carboné (6). Ces propriétés de transporteurs d'ions font entr'autre de ces composés de puissants inhibiteurs de la phosphorilation oxydative de l'ADP en ATP (3). La structure de la nonactine a été élucidée par Prelog, Gerlach et coll. (7). Le macrocycle est formé de quatre subunités d'acides nonactique (**2**) reliés entr'eux par des liaisons ester, avec alternance des énantiomères (−) (**2***a*) et (+) (**2***b*) de telle sorte qu'il présente une configuration *méso*. Son hydrolyse conduit à un mélange racémique d'acides nonactique dont la configuration absolue des quatre carbones chiraux a été déterminée (8). La synthèse de la nonactine a été réalisée par Ger-

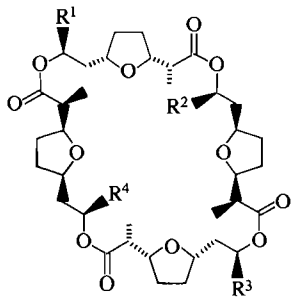

1 $R^1 = R^2 = R^3 = R^4 = CH_3$

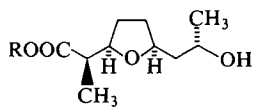

2*a* R = H
3*a* R = CH_3

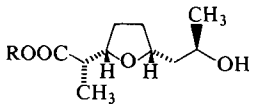

2*b* R = H
3*b* R = CH_3

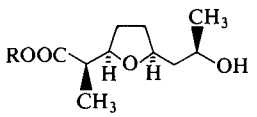

4*a* R = H
5*a* R = CH_3

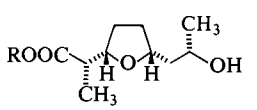

4*b* R = H
5*b* R = CH_3

SCHÉMA 1

[1]CIT Contribution No. 6249.

0008-4042/81/030572-12$01.00/0

©1981 National Research Council of Canada/Conseil national de recherches du Canada

Can. J. Chem. Downloaded from www.nrcresearchpress.com by 210.87.254.42 on 09/05/12
For personal use only.

lach et coll. à partir de l'acide nonactique racémique (9) et par Schmidt et coll. (10) à partir de l'acide (−) nonactique (**2***a*) et de dérivés des épimères (−) (**4***a*) et (+) (**4***b*) en position 8 (Schéma 1). La plupart des synthèses de l'acide nonactique publiées à ce jour conduisent à un mélange racémique (10–14).[2] Elles font généralement intervenir dans l'étape clé pour contrôler la configuration *cis* du tétrahydrofurane-2,5 disubstitué l'hydrogénation catalytique d'un cycle furanique. Seule celle rapportée par Schmidt et coll. permet d'isoler l'acide (−) nonactique (**2***a*) à partir d'un mélange de quatre diastéréoisomères. Par inversion de Walden du C-8 des trois diastéréoisomères restants ces auteurs ont obtenus un mélange duquel l'acide (+) nonactique (**2***b*) a pu être séparé (10, 13). Cette synthèse ne présente toutefois pas un très haut degré de stéréosélectivité. L'oxyde de S (−) propylène, non commercialement disponible, étant d'autre part utilisé comme produit de départ, elle nécessite la préparation de ce composé avec une grande pureté optique à partir d'acide lactique (15).

En raison de l'intérêt grandissant porté aux sucres dans divers laboratoires dont le nôtre (16) en tant que produits de départ chiraux relativement peu onéreux pour la synthèse de produits naturels comportant un nombre élevé de carbones assymétriques, il nous est apparu intéressant d'élaborer une synthèse des énantiomères de l'acide nonactique à partir de cette classe de composés.

Résultats et discussion

Un dérivé du type V (Schéma 2) peut être considéré comme un précurseur intéressant de l'acide nonactique.[3] La synthèse d'un tel composé peut être envisagée par formation de la liaison entre les atomes de carbone chiraux 2 et 3 des deux entités encerclées. De précédents travaux dans notre laboratoire ont démontré que la formation de telles liaisons carbone–carbone, pour l'obtention de dérivés du type aldol apparentés à V, pouvait être réalisée par un réarrangement de Claisen de cétènes-acetals silylés (17). Ceci permet de considérer l'alcool allylique hétérocyclique II comme un intermédiaire clé de cette synthèse. Il permet en effet d'obtenir le cétène-acétal silylé IV devant conduire après le réarrangement [3,3]-sigmatropique au précurseur désiré. Alors que la configuration du carbone 3 de V découle directement de celle du carbone 3 de IV, la configuration du carbone 2 résulte de la géométrie du cétène-acétal silylé et il devient donc important de contrôler celle-ci lors de la formation de IV.

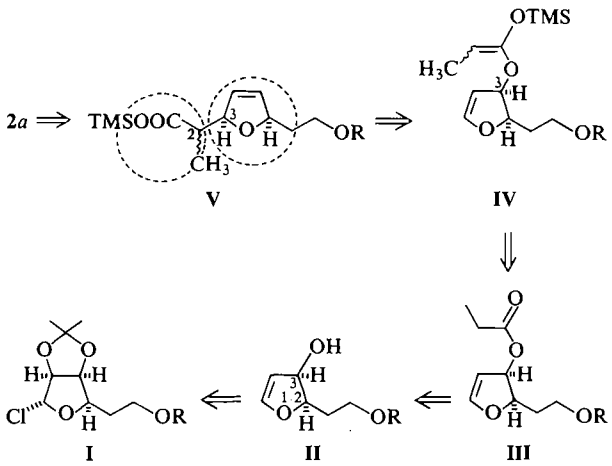

SCHÉMA 2

Des résultats antérieurs obtenus dans ce laboratoire font apparaître que suivant le solvant ou la base employée, la déprotonation à −78°C de l'ester **6** (Schéma 3) conduit à un mélange de proportions variables des énolates *Z* et *E* (17, 18). Ainsi lorsque la déprotonation est effectuée par le diisopropylamidure de lithium (LDA) à −78°C dans le THF l'anion-énolate de type *Z* est formé préférentiellement, tandis que la formation de l'anion-énolate de type *E* est favorisée quand cette déprotonation a lieu dans un mélange de 23% d'hexaméthylphosphotriamide (HMPA) dans le THF.

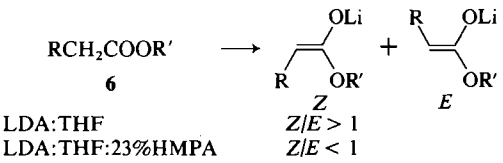

SCHÉMA 3

Le réarrangement de Claisen des cétènes-acétals silylés tels que IV, obtenus par silylation du mélange d'énolates correspondant, conduit à deux esters de silyle γ,δ insaturés diastéréoisomères V. Il a été montré qu'en série acyclique en l'absence d'effets stériques particuliers ce réarrangement s'opérait suivant un état de transition du type chaise (18). La proportion des deux diastéréoisomères formés ne dépend donc que de la proportion relative des deux énolates *E* et *Z* et peut de ce fait être prévue et orientée par un contrôle des conditions dans lesquelles la déprotonation est effectuée. Les résultats préliminaires obtenus en série cy-

[2]Voir aussi P. A. Bartlett et K. K. Jernstedt, cité dans la réf. 2*b*.

[3]Pour des raisons de clarté nous n'avons représenté que les précurseurs de l'énantiomère (−).

Can. J. Chem. Downloaded from www.nrcresearchpress.com by 210.87.254.42 on 09/05/12
For personal use only.

clique semblaient indiquer le passage pour le réarrangement [3,3]-sigmatropique par un intermédiaire du type bateau. L'application de ce réarrangement à la synthèse de produits naturels de configuration connue tels que les deux énantiomères de l'acide nonactique semblait donc devoir de plus fournir des renseignements plus précis quant à la nature de l'état de transition. Les résultats concernant la formation prépondérante de l'énolate *Z* dans le THF et celle prépondérante de l'énolate *E* en présence de HMPA semblant pouvoir être transposés en série cyclique, l'obtention d'une forte proportion de l'un des diastéréoisomères par rapport à l'autre devrait indiquer le passage pratiquement exclusif pour le réarrangement de ce diastéréoisomère majoritaire par un état de transition unique, soit chaise, soit bateau. La comparaison ultérieure de ce diastéréoisomère avec le produit naturel, devrait indiquer par lequel de ces deux états de transition le réarrangement a eu lieu. Par contre l'obtention des deux diastéréoisomères dans des proportions tendant vers 50:50 devrait indiquer le passage compétitif par ces deux états de transition.

L'étape clé de la synthèse proposée devrait donc permettre d'obtenir de façon spécifique la configuration désirée des carbones 3 et 6 et sélectivement celle du carbone 2. Une méthode générale de synthèse de glycals optiquement actifs du type II à partir de sucres a été précédemment mise au point dans notre laboratoire, utilisant la réduction par le lithium dans l'amoniac des chlorures du type I (17*b*, *c*, 19).

Le D-(+)-mannose (**7**) (Schéma 4) a été choisi comme produit de départ pour la synthèse de l'énantiomère (−) (**2***a*). Il est en effet possible d'obtenir pour un prix modique des quantités importantes de l'isomère (+) de ce sucre qui possède la configuration désirée des carbones 4 et 3 appelés à devenir respectivement les carbones 2 et 3 de l'alcool allylique II. Par une série de transformations connues, diacétonisation, benzylation, séparation des deux anomères et hydrolyse sélective de l'un des acétonides, le mélange d'anomères α et β **7** conduit avec un rendement global de 76% à l'α-D-mannofuranoside de benzyle (**8**) (20). En présence de diméthylacétal du diméthylformamide celui-ci est transformé quantitativement en acétal du DMF (**10**) qui par chauffage dans l'anhydride acétique fournit l'oléfine **11***a* (76,5% après chromatographie) et 17,5% d'un composé **9** correspondant à une diacétylation des alcools en position 5 et 6 de **8** (21). La réduction par $LiAlH_4$ de ce diacétate permet de regénérer le diol **8** conduisant à un rendement de 93% en oléfine **11***a* sur la base du diol récupéré.

Une modification de la méthode précédente, introduite par Hanessian et coll. consiste à transformer **10** en iodure d'amonium par traitement par l'iodure de méthyle, et à chauffer le sel obtenu dans le toluène (22). Contrairement à la méthode originale, cette variante appliquée à **10** ne conduit pas à l'oléfine désirée mais à un iodo-formate résultant d'une substitution par l'ion iodure de l'oxygène en position 6 de **10**. Cette réaction est probablement dûe au faible encombrement stérique de cette position et devient la réaction attendue dans le cas des acétals des *N*,*N*-diméthylamides autres que ceux du DMF (28).

L'alcool **12***a* obtenu après hydroboration oxydative de **11***a* par le 9-BBN (96,5% après chromatographie) est protégé quantitativement sous forme de méthoxyméthyléther (MOM) (**13***a*) par réaction de l'alcoolate de potassium correspondant avec l'éther chlorométhylméthylique dans le THF à 0°C. Une tentative de mise en place de ce groupe protecteur suivant un mode opératoire consistant à faire réagir l'alcool et du diméthoxyméthane en présence de P_2O_5 (23) n'a conduit qu'à des rendements médiocres (40% après chromatographie) bien qu'employée avec succés dans notre laboratoire avec des substrats analogues. Le furanoside de benzyle (**13***a*) traité par le lithium dans l'amoniac à −78°C permet d'isoler le lactol **14***a* avec un rendement de 79%. Celui-ci est transformé en chlorure de mannofuranosyle (**15***a*) par le CCl_4 et la PPh_3 dans le THF à reflux (91,5% après distillation). La réduction par le lithium dans l'amoniac à −78°C de ce dernier conduit, comme prévu en série furanique, à un mélange (10:1 d'après le spectre de ^1H rmn du distillat) du glycal **17***a* (70%) et du dérivé **16***a* résultant d'une réduction non suivie de fragmentation de **15***a* (17*c*, 19). Le réarrangement [3,3]-sigmatropique est effectué sur le mélange précédent, le glycal se décomposant partiellement sur gel de silice et Florisil.

Postulant le passage par un intermédiaire du type bateau pour le réarrangement de Claisen, la configuration du carbone 2 de l'acide nonactique nécessite la formation majoritaire de l'énolate de type *Z*. Celui-ci est obtenu par traitement par le diisopropylamidure de lithium dans le THF à −78°C du propionate résultant de l'estérification du chlorure de propionyle par l'alcoolate (*n*-BuLi, THF, −78°C) correspondant de l'alcool allylique **17***a* du mélange précédant. Le mélange d'énolates est piégé a −78°C par le chlorure de triméthylsilyle (TMSCl) et le réarrangement s'opère durant le

Can. J. Chem. Downloaded from www.nrcresearchpress.com by 210.87.254.42 on 09/05/12
For personal use only.

réchauffement jusqu'à la température ambiante. Après hydrolyse des esters de triméthylsilyle, le mélange d'acides traité par le diazométhane conduit aux deux esters γ,δ insaturés diastéréoisomères **18***a*, qui présentent le même R_f en ccm et ne peuvent être séparés à ce stade. L'hydrogénation de la double liaison est réalisée en présence de rhodium sur charbon. Toutefois une faible quantité de produits résultant d'hydrogénolyse et d'isomérisation de la double liaison étant également formés, l'emploi de platine sur charbon lui est préféré. Contrairement à leurs analogues insaturés les deux esters diastéréoisomères **19***a* et **19**′*a* peuvent être séparés par chromatographie sur gel de silice. L'examen du mélange par cpv révèle qu'ils ont été formés dans un rapport de 89:11. Ce rapport élevé semble indiquer d'après le raisonnement précédent le passage par un état de transition unique pour le diastéréoisomère majoritaire et cet état de transition semble avoir été du type bateau. Dans l'attente d'une confirmation univoque par comparaison de l'acide nonactique synthétique avec le composé naturel, différentes constatations semblent soutenir cette hypothèse. Après séparation le spectre de ^{1}H rmn du diastéréoisomère majoritaire présente une résonance du méthyle en position 2 à champ plus élevé (1,11 ppm) que le méthyle correspondant du diastéréoisomère minoritaire (1,20 ppm) et son R_f est d'autre part plus petit. Les différents dérivés et analogues de l'acide nonactique synthétisés ont de même toujours présenté un R_f plus petit et une résonance du méthyle en C-2 à champ plus élevé que les épimères correspondants en C-2 (*7b*, 10*a*, 12). Les probabilités que le diastéréoisomère majoritaire présente comme prévu la même configuration en C-2 que l'acide nonactique étaient donc élevées et semblaient confirmer nos hypothèses. La synthèse a donc été poursuivie avec ce diastéréoisomère, isolé avec un rendement de 48,5% à partir de **17***a*.

La même suite de réactions avait été initialement entreprise à partir de **13**′*a*, l'alcool primaire étant protégé sous forme d'éther de *tert*-butyldiméthylsilyle (TBDMS). Le rendement après le réarrangement de Claisen est toutefois très faible (quelques %). Une explication à ce fait pourrait être l'échange de l'éther de TBDMS avec l'alcoolate de lithium de **17**′*a*, conduisant à des produits se décomposant durant l'hydrolyse. Un argument en faveur de cette explication découle de l'observation suivante. Lors de la formation du glycal **17**′*a* on observe à côté des produits attendus un composé résultant d'un tel échange de l'éther de TBDMS. Voisine de 50% lorsque la réduction est effectuée dans l'amoniac à −33°C, sa formation peut cependant être ramenée à moins de 5% à −78°C. Il semble toutefois que dans le THF cet échange ne puisse être évité.

L'alcool en position 8 de **20***a* est libéré par chauffage de **19***a* dans l'acide chlorhydrique à 2% dans le méthanol anhydre (96,5% après chromatographie) et oxydé en aldéhyde **21***a* avec un rendement de 90% (24). L'introduction du méthyle en position 8 a été effectuée par le diméthylcuprate de lithium à −20°C. Il a été montré que ce réactif, inerte vis-à-vis des cétones et esters carboxyliques, réagit avec les aldéhydes (25). Les deux alcools diastéréoisomères sont obtenus dans des proportions comparables. Le plus polaire devant correspondre à l'ester méthylique de l'acide (−) nonactique (**3***a*) (12) est isolé avec un rendement de 39,5% et son épimère en C-8 (**5***a*) avec un rendement de 45%. L'hydrolyse séparée de ces deux épimères par une solution aqueuse 2 *N* d'hydroxyde de potassium s'effectue en quelques minutes à température ambiante. Elle conduit à l'acide (−) nonactique (**2***a*) et à son épimère en C-8 (**4***a*) avec un rendement de 96% sans qu'aucun produit résultant d'une épimérisation en C-2 ou C-3 ne puisse être détecté par ccm. Les caractéristiques analytiques et spectrales de l'acide (−) nonactique et de son ester méthylique sont en accord avec celles publiées à partir du produit résultant de l'hydrolyse de la dinactine, et plus particulièrement en ^{1}H rmn avec les déplacements chimiques et constantes de couplage du méthyle en C-2 (3, *7b*). Comme prévu (12), des deux épimères en C-8 le plus polaire présente les caractéristiques de l'acide nonactique. Le pouvoir rotatoire négatif obtenu pour **3***a* et **5***a* corrobore les déductions faites après le réarrangement de Claisen, l'épimère en C-2 (*S*,*R*,*S*,*S*) de l'acide nonactique présentant un pouvoir rotatoire positif (*7b*).

L'énantiomère (+) de l'acide nonactique (**2***b*) a été synthétisé suivant le même schéma. Bien que commercialement disponible le L-(−)-mannose n'a pas été choisi comme produit de départ en raison de son prix élevé et la D-gulono-γ-lactone (**22**) (Schéma 5) présentant les configurations désirées des carbones 2, 3 et 4 lui est préférée. Après conversion de **22** en diacétonide et réduction de la lactone par l'hydrure de diisobutyl aluminium (DIBAL) dans l'éther, les deux lactols anomères obtenus sont protégés par benzylation et séparés par chromatographie. L'hydrolyse sélective de l'un des acétonides de l'anomère majoritaire β conduit au diol **24** avec un rendement global de 50%. Celui-ci est diastéréoisomère du diol **8**, la configu-

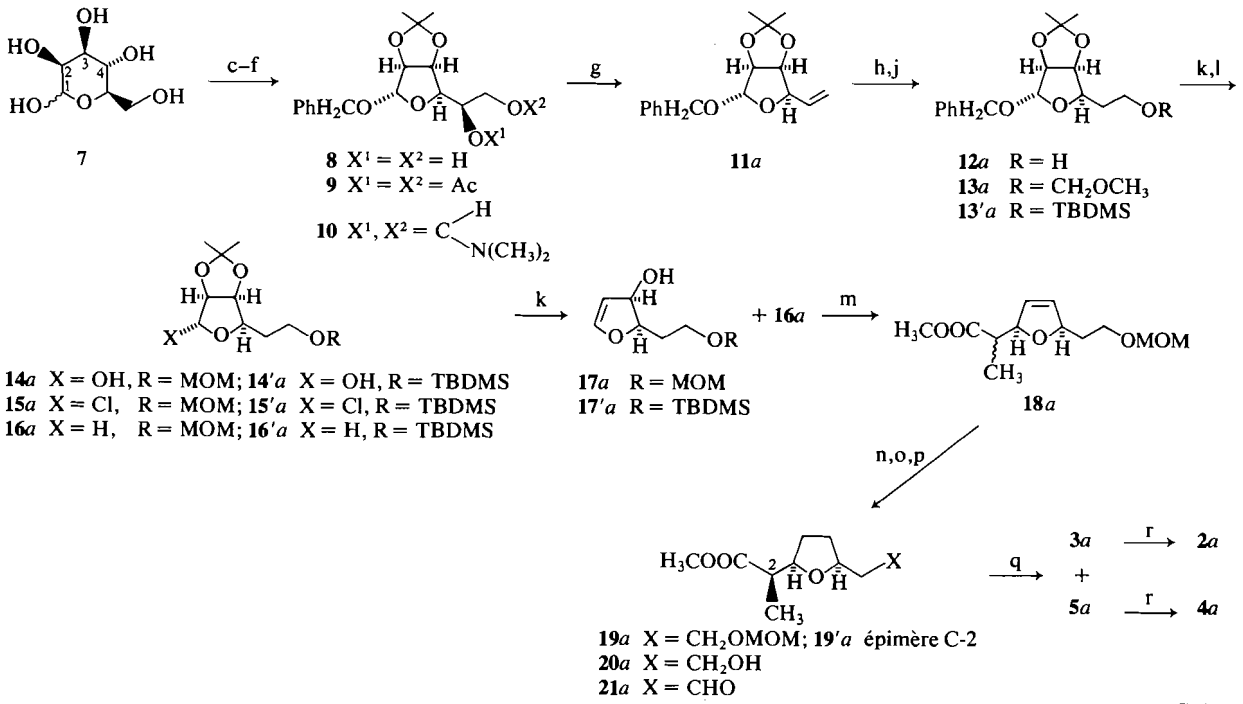

(c) H_3CCOCH_3, H^+; (d) NaH, $PhCH_2Cl$, DMF; (e) HCl conc., CH_3OH; (f) $(CH_3)_2NCH(OCH_3)_2$, CH_2Cl_2; (g) $(H_3CCO)_2O$, 130°C; (h) 9-BBN; NaOH, H_2O_2; (j) KH, $ClCH_2OCH_3$; (k) Li, NH_3, −78°C; (l) Ph_3P, CCl_4; (m) *n*-BuLi; *n*-C_2H_5COCl; LDA, THF, −78°C; TMSCl; 25°C; H_2O, OH^-; CH_2N_2; (n) H_2, Rh/C; (o) 2% HCl, CH_3OH; (p) $(COCl)_2$, DMSO; Et_3N; (q) $Li(CH_3)_2Cu$; (r) 2 *N* KOH, H_2O.

SCHÉMA 4

ration du carbone 5 appelé à perdre sa chiralité lors de l'étape suivante étant la même pour ces deux composés. Sa conversion en oléfine **11***b* énantiomère de **11***a* est effectuée suivant la séquence précédemment décrite. Par une série de réactions identiques à celles utilisées pour obtenir l'énantiomère (−), l'oléfine **11***b* est transformée en aldéhyde **21***b*. L'introduction du méthyle en C-8 par réaction de **21***a* avec le diméthylcuprate de lithium ayant conduit précédemment à un mélange des deux diastéréoisomères légèrement plus riche en l'épimère non désiré (47:53 en produits isolés), nous avons envisagé son incorporation possible par un autre réactif. La réaction de **21***b* avec un équivalent de bromure de méthyl-magnésium dans l'éther à basse température conduit à des rendements en produits isolés aprés chromatographie de 53,5% pour le (+) nonactate de méthyle (**3***b*) et 40% pour son épimère en C-8 (**5***b*). Bien que tendant cette fois encore vers un rapport voisin de 1:1 (57:43 en produits isolés) l'utilisation du réactif de Grignard semble toutefois favoriser légèrement la formation du diastéréoisomère désiré comme le montre l'examen du mélange brut par ccm, et conduire à un rendement sensiblement supérieur (93,5%). Ces résultats font apparaître une stéréoselectivité très faible, et sont en accord avec ceux récemment rapportés par Still et Schneider relatifs à l'addition d'organométalliques sur des β-alkoxyaldéhydes non substitués en α (29). L'hydrolyse comme précédemment de ces deux esters offre l'acide (+) (*S*,*S*,*R*,*R*) nonactique et son épimère en C-8 en tout point équivalents au signe près du pouvoir rotatoire, aux énantiomères précédemment obtenus.

Conclusion

La synthèse des deux énantiomères de l'acide nonactique que nous venons de décrire montre une fois de plus l'intérêt présenté par les sucres comme produits de départ chiraux relativement peu onéreux. D'autre part elle souligne l'intérêt déjà précédemment démontré (18) qui peut être tiré de l'utilisation du réarrangement [3,3]-sigmatropique de cétène-acétals silylés pour la formation de liaisons entre atomes de carbone dont la chiralité peut être présélectionnée. Elle fait également apparaître son application possible à la formation de dérivés du type aldol, déjà intensivement mise à profit lors de la synthèse de l'acide lasalocide A (16). Elle présente en outre un haut degré de stéréosélectivité, le seul centre non contrôlé (C-8)

Can. J. Chem. Downloaded from www.nrcresearchpress.com by 210.87.254.42 on 09/05/12
For personal use only.

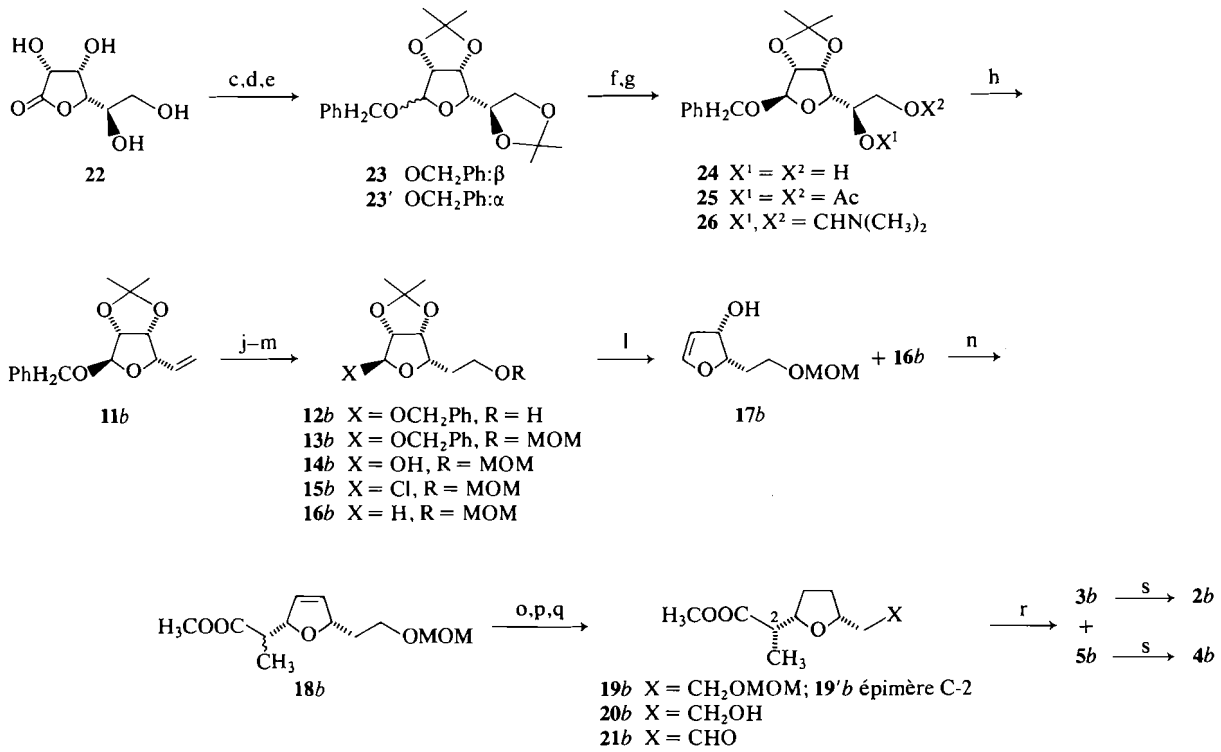

(c) H_3CCOCH_3, H^+; (d) $(i\text{-}C_4H_9)_2AlH$, éther; (e) NaH, $PhCH_2Cl$, DMF; (f) HCl conc., CH_3OH; (g) $(CH_3)_2NCH(OCH_3)_2$, CH_2Cl_2; (h) $(H_3CCO)_2O$, 130°C; (j) 9-BBN; NaOH, H_2O_2; (k) $CH_2(OCH_3)_2$, P_2O_5; (l) Li, NH_3, −78°C; (m) Ph_3P, CCl_4; (n) *n*-BuLi; *n*-C_2H_5COCl; LDA; THF, −78°C; TMSCl; 25°C; H_2O, OH^-; CH_2N_2; (o) H_2, Pt/C, AcOEt; (p) 2% HCl, CH_3OH; (q) $(COCl)_2$, DMSO; Et_3N; (r) CH_3MgBr, −78° → −10°C; (s) 2 *N* KOH, H_2O.

SCHÉMA 5

pouvant être inversé suivant une série de réactions précédemment rapportées (14). D'autre part comme nous l'avons soulignée la forte sélectivité obtenue après le réarrangement [3,3]-sigmatropique et la comparaison de la configuration du C-2 du diastéréoisomère majoritaire obtenu avec l'acide nonactique naturel a permis de confirmer le passage, pour le réarrangement de ce type de cétène-acétals silylés cycliques, par un intermédiaire du type bateau.

Partie expérimentale

Les points de fusion ont été déterminés sur un appareil Hoover à capillaires et ne sont pas corrigés. Les spectres d'absorbtion infrarouge (ir) ont été obtenus avec un spectromètre Perkin-Elmer 727 B et les spectres de résonance magnétique nucléaire ont été enregistrés sur un appareil Varian EM-390 à 90 MHz pour le proton (^1H rmn) et sur un appareil Jeol FX-90 Q pour le carbone (^{13}C rmn). Les solvants utilisés ont été $CDCl_3$ ou CCl_4. Les déplacements chimiques sont exprimés en ppm sur l'échelle δ en prenant le tétraméthylsilane comme référence interne (δMe_4Si = 0,0). Les constantes de couplage sont données en Hz. Les spectres sont décrits de la manière suivante: solvant, δ (multiplicité: s = singulet; d = doublet; t = triplet; q = quadruplet; m = multiplet. Constantes de couplage. Intégration. Interprétation). Les pouvoirs rotatoires ont été mesurés dans une cellule de 1 dm et 1 mL de capacité sur un polarimètre Perkin-Elmer 141.

Les microanalyses ont été effectuées par Spang Microanalytical Laboratory, Ann Arbor, MI. Les échantillons analytiques ont été obtenus, sauf indication contraire, par distillation dans un tube à boules à la pression indiquée.

Les chromatographies en phase vapeur (cpv) ont été effectuées sur un chromatographe Hewlett-Packard 5750 équipé avec un détecteur à ionisation de flamme utilisant l'hélium comme gaz vecteur à un débit de 60 mL/min.

L'avancement des réactions a été suivi sur des prélèvements par spectroscopie de ^1H rmn ou par chromatographie sur couche mince (ccm). Les ccm on été réalisées sur des plaques préparées de gel de silice 60F-254 Merck, de 0,25 mm d'épaisseur. Les chromatographies sur colonne ont été effectuées sur gel de silice Merck "Silica gel 60", 70–230 mesh ASTM, à l'exception de celles réalisées sur gel de silice acide Silicar CC-4 Spécial, Mallinckrodt Chemical Works, St. Louis, MO.

Les solvants et réactifs ont été séchés et distillés avant emploi. L'éther éthylique, le THF et le pentane ont été distillés sur sodium (utilisant la benzophénone comme indicateur pour les deux premiers) et sous une atmosphère d'argon sec. Le méthanol a été distillé sur méthylate de magnésium et le chlorure de méthylène sur pentoxide de phosphore. Le DMSO a été distillé sur hydrure de calcium pulvérisé, sous une pression de 30 Torr. La diisopropylamine et la triéthylamine ont été distillées sur sodium–benzophénone et sous argon juste avant emploi. Le chlorure d'oxalyle a été distillé sous atmosphère d'argon et le chlorure de propionyle sur 10% de quinoléine. Le chlorure

Can. J. Chem. Downloaded from www.nrcresearchpress.com by 210.87.254.42 on 09/05/12
For personal use only.

Can. J. Chem. Downloaded from www.nrcresearchpress.com by 210.87.254.42 on 09/05/12
For personal use only.

d'amonium a été séché sur P_2O_5 à 80°C sous 1 Torr pendant deux jours.

Toutes les réactions ont été réalisées sous atmosphère d'argon sec (à l'exception des hydrogénations et réductions dans l'amoniac) en légère surpression utilisant un système permettant alternativement d'évacuer et d'introduire le gaz inerte. Les réactions (hormis les hydrolyses finales) ont été effectuées avec du matériel (réacteurs, seringues, condenseurs, etc...) préalablement séché 12 h à 140°C et refroidi dans un dessiccateur sur sulfate de calcium anhydre. Les volumes inférieurs à 30 mL ont été introduits à l'aide de seringues à travers des bouchons perforables.

Par traitement habituel on entend: lavage (3 ou 4 fois) par une solution saturée en NaCl de la phase organique, séchage sur $MgSO_4$, filtration, évaporation du solvant sous pression réduite et séchage du résidu plusieurs heures sous une pression de l'ordre de 10^{-2} Torr à température ambiante. Les distillations sur les quantités inférieures à 5 g ont été réalisées dans un tube à boules par chauffage dans un four thermostaté. Les points d'ébulition indiqués se rapportent à ces distillations.

*Phénylméthyl 2,3-*O*-(1-méthyléthylidène)-5,6-*O*-(*N*,*N*-diméthylaminométhylène)-α-*D*-mannofuranoside (**10**)*

A une solution de 51,1 g (164,7 mmol) de phénylméthyl-2,3-*O*-(1-méthyléthylidène)-α-D-mannofuranoside (**8**) (20) dans 600 mL de chlorure de méthylène, on ajoute 96 g (0,8 mol) de *N*,*N*-diméthylformamide diméthylacétal fraîchement redistillé. La solution est maintenue pendant 24 h sous atmosphère d'argon à temperature ambiante. Le solvant est évaporé sous pression réduite à température inférieure à 50°C. Le résidu conservé 12 h supplémentaires sous un vide de 0,01 Torr est utilisé sans autre purification au cours de l'étape suivante: ^{1}H rmn ($CDCl_3$) δ: 1,32 et 1,45 (2s, 2 × 3H, $C(CH_3)_2$); 2,36 (s, 6H, $N(CH_3)_2$); 5,06 (s, 1H, $PhCH_2OCHO$—); 5,40 et 5,46 (2s (diastéréoisomères), 1H, —OCHON<); 7,33 (s, 5H, C_6H_5).

*Phénylméthyl 2,3-*O*-(1-méthyléthylidène)-5,6-didéhydro-5,6-didéoxy-α-*D*-mannofuranoside (**11**a)*

Une solution du produit brut précédent dans 500 mL d'anhydride acétique est chauffée à 130°C pendant 1 heure. L'anhydrique acétique est évaporé sous pression réduite et l'huile résiduelle dissoute dans 500 mL d'éther. Après lavage avec une solution à 5% de $NaHCO_3$ (4 × 75 mL) et traitement habituel on obtient une huile, qui chromatographiée sur gel de silice (éluant: cyclohexane/AcOEt, 85:15) fournit 34,8 g (76,5% à partir de **8**; 96% sur la base du diol **8** régénéré) de **11***a* et 11,34 g (17,5%) de diacétate **9**. La réduction de ce dernier par $LiAlH_4$ permet de régénerer **8** avec un rendement de 93%; Eb: 95–100°C (0,04 Torr); R_f: 0,4 (cyclohexane/AcOEt, 75:25); $[\alpha]_D^{25}$ +56,6° (*c* 1,14, $CHCl_3$); ir ($CHCl_3$): 1020, 1090, 1230, 1385, 1390, 3010, 3030, 3090, 3110 cm^{-1}; ^{1}H rmn ($CDCl_3$) δ: 1,30 et 1,45 (s, 2 × 3H, $2CH_3$); 5,08 (s, 1H, —OCHO—); 5,20–5,53 (m, 2H, C=CH_2); 5,80–6,23 (m, 1H, C=CH); 7,30 (s, 5H, C_6H_5). *Anal.* calc. pour $C_{16}H_{20}O_4$: C 69,55, H 7,29; trouvée: C 69,49, H 7,17.

*Phénylméthyl 2,3-*O*-(1-méthyléthylidène)-5-déoxy-α-*D*-mannofuranoside (**12**a)*

A 250 mL (125 mmol) d'une solution 0,5 *M* de 9-borabicyclo[3.3.1]nonane (9-BBN) dans le THF[4] agitée magnétiquement sous atmosphère d'argon on ajoute à l'aide d'une ampoule à addition 32,5 g (117,6 mmol) de **11***a* en solution dans 130 mL de THF. La solution est maintenue 2 heures et demie à température ambiante. On ajoute successivement par l'ampoule à addition 75 mL d'éthanol, 50 mL d'une solution 6 *M* de NaOH et 25 mL d'une solution à 30% de H_2O_2 et chauffe le mélange 1 heure et demie à 60°C. La phase aqueuse refroidie est saturée en carbonate de potassium. La phase organique est séparée et traitée de manière habituelle. Le résidu chromatographié sur gel de silice (éluant: cyclohexane/AcOEt, 75:25 à 65:35) conduit à l'isolement de 33,4 g (96,5%) d'alcool **12***a* sous forme d'huile; Eb: 120°C (0,05 Torr); R_f: 0,50 (cyclohexane/AcOEt, 50:50); $[\alpha]_D^{25}$ +97° (*c* 1,03, $CHCl_3$); ir ($CHCl_3$): 1010, 1085, 1225, 1385, 1390, 3560, 3640 cm^{-1}; ^{1}H rmn ($CDCl_3$) δ: 1,30 et 1,43 (2s, 2 × 3H, $C(CH_3)_2$); 3,60–3,90 (m, 2H, CCH_2OH); 4,52 (AB, J_{AB} = 12 Hz, ν_{AB} = 13 Hz, 2H, —OCH_2Ph); 5,04 (s, 1H, —OCHO—); 7,32 (s, 5H, C_6H_5); ($CDCl_3$ + D_2O) δ: 3,72 (t, *J* = 6 Hz, 2H, CCH_2OH). *Anal.* calc. pour $C_{16}H_{22}O_5$: C 65,29, H 7,53; trouvée: C 65,19, H 7,66.

*Phénylméthyl 2,3-*O*-(1-méthyléthylidène)-5-déoxy-6-*O*-méthoxyméthyl-α-*D*-mannofuranoside (**13**a)*

Une suspension de KH à 23,6% dans l'huile[5] (16,77 g; 99 mmol) est lavée avec 3 × 100 mL de pentane sous atmosphère d'argon. On ajoute 205 mL de THF, un crystal d'imidazole, refroidit la solution dans un bain de glace et additionne lentement sous agitation magnétique à l'aide d'une ampoule à addition 24,2 g (82,2 mmol) de **12***a* en solution dans 205 mL de THF. A la fin de l'addition le mélange est agité 15 min supplémentaires à 0°C. On ajoute lentement à l'aide d'une seringue 9,43 mL (124 mmol) d'éther chlorométhylméthylique préalablement séché pendant 12 h sur chlorure de calcium, puis 2 h sur carbonate de potassium et filtré. Le bain de glace est enlevé. Le mélange réactionnel maintenu à température ambiante pendant 7 h est alors hydrolysé avec 150 mL d'une solution saturée de bicarbonate de sodium et gardé sous agitation durant la nuit. On ajoute 1 L d'éther et décante la phase organique qui est lavée avec 4 × 250 mL d'une solution saturée de bicarbonate de sodium, puis traitée de façon habituelle. On obtient 27,8 g (100%) de **13***a* (une tache en ccm) qui est utilisé sans autre purification au cours de l'étape suivante. Un échantillon analytique de 1 g est obtenu par chromatographie sur gel de silice (éluant: cyclohexane/AcOEt, 85:15); Eb: 125–127°C (0,01 Torr); R_f: 0,38 (cyclohexane/AcOEt, 75:25); $[\alpha]_D^{25}$ +89,2° (*c* 0,95, $CHCl_3$); ir ($CHCl_3$): 1020, 1050, 1090, 1120, 1165, 1220, 1385, 1390, 2960 cm^{-1}; ^{1}H rmn ($CDCl_3$) δ: 1,30 et 1,43 (2s, 2 × 3H, $C(CH_3)_2$); 2,0 (d de t, J_1 = J_2 = 6 Hz, 2H, —CH_2CH_2OMOM); 3,33 (s, 3H, OCH_3); 3,67 (t, *J* = 6,3 Hz, 2H, —CH_2OMOM); 4,03–4,30 (m, 1H, —$OCHCH_2$—); 4,61 (s large, 4H, —OCH_2O— et —OCHCHO—); 4,53 (AB, J_{AB} = 12 Hz, ν_{AB} = 17 Hz, 2H, —OCH_2Ph); 5,03 (s, 1H, —OCHO—); 7,31 (s, 5H, C_6H_5). *Anal.* calc. pour $C_{18}H_{26}O_6$: C 63,89, H 7,74; trouvée: C 63,93, H 7,68.

*2,3-*O*-(1-Méthyléthylidène)-5-déoxy-6-*O*-méthoxyméthyl-(α et β)-*D*-mannofuranose (**14**a)*

A 1,2 L d'amoniac (redistillé à partir d'une solution bleue de lithium dans l'amoniac) sous agitation à −78°C, on ajoute 1,25 g (180 mmol) de lithium en fil et après 20 min, à l'aide d'une ampoule à addition, une solution de 27,2 g (80,4 mmol) de **13***a* dans 40 mL de THF. Le bain réfrigérant est enlevé et la réaction maintenue sous reflux d'amoniac. Après 2 h, 10,7 g (0,2 mol) de NH_4Cl sec sont ajoutés par portions d'environ 0,5 g. On laisse alors lentement évaporer l'amoniac sous un courant d'argon pendant que 500 mL d'éther anhydre sont ajoutés au milieu réactionnel. Lorsque l'amoniac est totalement évaporé la suspension est filtrée sur verre fritté et l'éther évaporé sous pression réduite. Après chromatographie sur gel de silice (éluant: cyclohexane/AcOEt, 60:40) on isole 15,7 g (79%) de lactol **14***a*. Le spectre de ^{1}H rmn de **14***a* montre la présence d'un seul anomère qui en solution chloroformique s'isomérise en un mélange α et β; Eb: 105°C (0,02 Torr); R_f: 0,30 (cyclo-

[4]Obtenu chez Aldrich.

[5]Obtenu chez Alfa Products.

Can. J. Chem. Downloaded from www.nrcresearchpress.com by 210.87.254.42 on 09/05/12
For personal use only.

hexane/AcOEt, 50:50); ir (film): 1060, 1155, 1210, 1385, 1390, 2940, 3400 cm^{-1}; ^1H rmn ($CDCl_3$) δ: 1,31 et 1,43 (anomère majoritaire), 1,35 et 1,50 (anomère minoritaire) (2 × 2s, 2 × 3H, $C(CH_3)_2$); 1,93 (d de t, $J_1 = J_2 = 6$ Hz, 2H, —CH_2CH_2OMOM); 3,35 (s, 3H, —OCH_3); 3,65 (t, $J = 6$ Hz, 2H, —CH_2OMOM); 4,25 (d de t, $J_1 = 3$ Hz, $J_2 = 6$ Hz, 1H, —$OCHCH_2$—); 4,63 (s, 2H, —OCH_2O—); 5,30 (s, "0,85H", —OCHO-anomère majoritaire). *Anal.* calc. pour $C_{11}H_{20}O_6$: C 53,22, H 8,12; trouvée: C 53,20, H 8,01.

*Chlorure de 5-déoxy-2,3-*O*-(1-méthyléthylidène)-6-*O*-méthoxyméthyl-α-*D*-mannofuranosyle (15*a*)*

On chauffe à 90°C sous agitation magnétique et sous atmosphère d'argon une solution de 993,1 mg (4 mmol) de **14***a*, 2 mL (20 mmol) de tetrachlorure de carbone et 2,1 g (8 mmol) de triphénylphosphine dans 20 mL de THF. Le milieu réactionnel homogène laisse rapidement précipiter de l'oxyde de triphénylphosphine. Après 3 h la solution refroidie est filtrée sur verre fritté et le solvant évaporé sous pression réduite. Le résidu est trituré avec du pentane sec, gardé une demi-heure au réfrigérateur, et l'oxyde de triphénylphosphine qui a cristallisé est filtré. Cette dernière opération est répétée (3 ou 4 fois) jusqu'à élimination complète de l'oxyde de triphénylphosphine. La distillation du produit brut dans un tube à boules permet d'obtenir 976 mg (91,5%) de **15***a*; Eb: 90°C (0,02 Torr); $[\alpha]_D^{25}$ +94,4° (*c* 1,04, $CHCl_3$); ir (film): 1050, 1090, 1160, 1215, 1385, 1390, 2965 cm^{-1}; ^1H rmn ($CDCl_3$) δ: 1,31 et 1,43 (2s, 2 × 3H, $C(CH_3)_2$); 2,0 (d de t, $J_1 = J_2 = 6$ Hz, 2H, —CH_2CH_2OMOM); 3,35 (s, 3H, —OCH_3); 3,63 (t, $J = 6$ Hz, 2H, —CH_2OMOM); 4,25–4,60 (partie X d'un AMX, 1H, —$OCHCH_2$—); 4,60 (s, 2H, —OCH_2O—); 4,70 (partie M d'un AMX, $J_{AM} = 6$ Hz, $J_{MX} = 3$ Hz, 1H, ClCCCH); 4,93 (partie A d'un AMX, $J_{AM} = 6$ Hz, 1H, ClCCH); 6,06 (s, 1H, —OCHCl). *Anal.* calc. pour $C_{11}H_{19}O_5Cl$: C 49,54, H 7,18; trouvée: C 49,62, H 7.29.

*Phénylméthyl 2,3-*O*-(1-méthyléthylidène)-5-déoxy-6-O-[diméthyl-(1,1-diméthyléthyl)-silyl]-α-*D*-mannofuranoside (13′a)*

Une solution de 5,88 g (20 mmol) de **12***a* dans le diméthylformamide anhydre est agitée sous atmosphère d'argon en présence de 5,7 g (84 mmol) d'imidazole préalablement sublimé et 6,33 g (42 mmol) de chlorure de *tert*-butyldiméthylsilane. Après 15 h à température ambiante 200 mL d'eau sont ajoutés au milieu réactionnel qui est extrait par 3 × 100 mL d'éther. Après traitement habituel, l'huile obtenue est chromatographiée sur gel de silice (éluant: cyclohexane/AcOEt, 75:25). On obtient 8,05 g (99%) d'éther silylé **13′***a*; Eb: 140°C (0.07 Torr); R_f: 0,34 (cyclohexane/AcOEt, 75:25); $[\alpha]_D^{25}$ +80,9° (*c* 0,93, $CHCl_3$); ir ($CHCl_3$): 840, 1015, 1095, 1230, 1265, 1385, 1390, 2875, 2950, 2970 cm^{-1}; ^1H rmn ($CDCl_3$) δ: 0,09 (s, 6H, $Si(CH_3)_2$); 0,91 (s, 9H, *t*-C_4H_9 Si); 1,28 et 1,42 (2s, 2 × 3H, $C(CH_3)_2$); 1,91 (d de t, $J_1 = J_2 = 6$ Hz, 2H, $CH_2CH_2OTBDMS$); 3,25 (t, $J = 6,5$ Hz, 2H, $CH_2OTBDMS$); 4,53 (AB, $J_{AB} = 12$ Hz, $\nu_{AB} = 18,6$ Hz, 2H, OCH_2Ar); 5,02 (s, 1H, $OCHOCH_2Ar$); 7,30 (s, 5H, —C_6H_5). *Anal.* calc. pour $C_{22}H_{36}SiO_5$: C 64,67, H 8,88; trouvée: C 64,79, H 9,00.

*2,3-*O*-(1-Méthyléthylidène)-5-déoxy-6-O-[diméthyl-(1,1-diméthyléthyl)-silyl]-α et β-*D*-mannofuranose (14′a)*

Obtenu à partir de 7,96 g (19,5 mmol) de **13′***a* suivant le mode opératoire permettant d'obtenir **14***a* à partir de **13***a*. Après chromatographie sur gel de silice on isole 5,35 g (86%) de **14′***a*; Eb: 97°C (0,02 Torr); R_f: 0,45 (cyclohexane/AcOEt, 50:50); ir ($CHCl_3$): 850, 1015, 1055, 1095, 1230, 1265, 1385, 1390, 2890, 2950, 2970, 3435, 3620 cm^{-1}; ^1H rmn ($CDCl_3$) δ: 0,09 (s, 6H, $Si(CH_3)_2$); 0,93 (s, 9H, *t*-C_4H_9Si); 1,30 et 1,43 (2s, 2 × 3H, $C(CH_3)_2$); 1,93 (d de t, $J_1 = J_2 = 6$ Hz, 2H, $CH_2CH_2OTBDMS$); 3,73 (t, $J = 6$ Hz, 2H, $CH_2OTBDMS$); 5,33 (s, 1H, $OCHOH$). *Anal.* calc. pour $C_{15}H_{30}O_5Si$: C 56,57, H 9,49; trouvée: C 56,49, H 9,36.

*Chlorure de 5-déoxy-2,3-*O*-(1-méthyléthylidène)-6-O-[diméthyl-(1,1-diméthyléthyl)-silyl]-α-*D*-mannofuranosyle (15′a)*

Obtenu à partir de 647 mg (2,03 mmol) de **14′***a* suivant le mode opératoire permettant d'obtenir **15***a* à partir de **14***a*. Obtenu après distillation: 640 mg (94%) Eb: 81°C (0,02 Torr); $[\alpha]_D^{25}$ +82,7° (*c* 0,9, $CHCl_3$); ir ($CHCl_3$): 840, 1095, 1175, 1230, 1265, 1385, 1390, 2875, 2950, 2970 cm^{-1}; ^1H rmn ($CDCl_3$) δ: 0,09 (s, 6H, $Si(CH_3)_2$); 0,93 (s, 9H, *t*-C_4H_9Si); 1,30 et 1,43 (2s, 2 × 3H, $C(CH_3)_2$); 1,96 (d de t, $J_1 = J_2 = 6$ Hz, 2H, $CH_2CH_2OTBDMS$); 3,73 (t, $J = 6$ Hz, 2H, $CH_2OTBDMS$); 4,30–4,53 (partie X d'un AMX, 1H, $OCHCH_2$); 4,73 (partie M d'un AMX, $J_{AM} = 6$ Hz, $J_{MX} = 3$ Hz, 1H, ClCCCH); 4,93 (partie A d'un AMX, $J_{AM} = 6$ Hz, 1H, ClCCH); 6,10 (s, 1H, ClCHO). *Anal.* calc. pour $C_{15}H_{29}O_4SiCl$: C 53,47, H 8,68; trouvée: C 53,35, H 8,49.

2R-cis-2-(β-Méthoxyméthylènoxyéthyl)-2,3-dihydro-3-hydroxyfurane (17a)

A 80 mL d'amoniac (redistillé à partir d'une solution bleue de lithium dans l'amoniac) sous agitation à −78°C on ajoute 110 mg (15,8 mmol; 5 éq.) de lithium en fil, et après une demi-heure à l'aide d'une seringue une solution de 845 mg (3,17 mmol) de **15***a* dans 4 mL de THF. On rince avec 2 × 3 mL de THF et garde sous agitation à −78°C pendant une heure et demie. A la solution bleue est ajouté 1,34 g (25 mmol) de NH_4Cl sec. L'amoniac est évaporé sous courant d'argon et 100 mL d'éther et 2 g de $MgSO_4$ sont ajoutés au milieu réactionnel. Lorsque l'amoniac est évaporé, la suspension est filtrée sur verre fritté et l'éther évaporé sous pression réduite. L'huile résiduelle est triturée avec un mélange d'éther et de pentane (1:1), conservée 1 heure au réfrigérateur et filtrée. La distillation du produit brut conduit à l'obtention de 441 mg d'un mélange de glycal **17***a* et de 1,5-dideoxy-2,3-*O*-(1-méthyléthylidène)-6-*O*-méthoxyméthyl-D-mannofuranose (**16***a*) dans un rapport 10:1 (^1H rmn) correspondant à un rendement de 70% en **17***a*. Différentes tentatives de chromatographie du mélange sur gel de silice ou Florisil ont conduit à une décomposition partielle du glycal; Eb du mélange: 85°C (0,005 Torr); ir (film): 1060, 1115, 1160, 1606, 3450 cm^{-1}; ^1H rmn ($CDCl_3$) δ: 1,90–2,40 (m, 2H, —CH_2CH_2OMOM); 3,35 (s, 3H, —OCH_3); 3,67 (m, 2H, —CH_2OMOM); 4,25 (d de t, $J_1 = J_2 = 7$ Hz, 1H, C=COCH); 4,60 (s, 2H, —OCH_2O—); 4,65–4,73 (m, 1H, $CHOH$); 5,20 (d de d, $J_1 = J_2 = 5,4$ Hz, 1H, —OC=CH—); 6,56 (d, $J = 5,4$ Hz, 1H, —OCH=C—).

[2R[2α(R et S*),5α]]-2,5-Dihydro-5-(2-méthoxyméthylènoxyéthyl)-α-méthyl-2-furanacétate de méthyle (18a)*

A une solution de 441 mg du mélange 10:1 de **17***a* et **16***a* (2,22 mmol de glycal **17***a*) dans 10 mL de THF à −78°C sous atmosphère d'argon, on ajoute sous agitation un crystal de phénantroline et une solution 2,4 *M* de *n*-BuLi dans l'hexane[4] jusqu'à apparition d'une coloration brunâtre (0,96 mL; 2,3 mmol). Après 5 min 0,2 mL (2,33 mmol) de chlorure de propionyle sont ajoutés. On enlève le bain réfrigérant, laisse remonter la température à −10°C et refroidit à nouveau à −78°C. La solution est alors ajoutée à l'aide d'une aiguille à double entrée à une solution 0,5 *N* de 2,33 mmol de diisopropylamidure de lithium dans le THF, maintenue à −78°C sous agitation. Après 15 min on ajoute 1,90 mL (11 mmol) du liquide surnageant obtenu après centrifugation d'un mélange 3:1 (v/v) de chlorure de triméthylsilyle et de triéthylamine, maintient le milieu réactionnel 15 min supplémentaires à −78°C, enlève le bain réfrigérant et garde à température ambiante pendant 20 h. La solution est alors hydrolysée à 0°C avec 50 mL d'une solution 0,5 *N* de NaOH. Les solvants sont évaporés sous pression réduite à température

Can. J. Chem. Downloaded from www.nrcresearchpress.com by 210.87.254.42 on 09/05/12
For personal use only.

inférieure à 30°C, la phase aqueuse extraite par 3 × 50 mL d'éther, acidifiée jusqu à pH 2,5, extraite par 7 × 100 mL d'éther et les phases éthérées réunies traitées de façon habituelle. Un excès d'une solution éthérée de diazométhane est alors ajouté à l'huile obtenue, conduisant à 382 mg de **18***a* brut, qui est directement hydrogéné sans purification ultérieure. Un échantillon analytique est obtenu par chromatographie sur gel de silice (éluant: cyclohexane/AcOEt, 75:25); Eb: 80°C (0,05 Torr); R_f: 0,3 (cyclohexane/AcOEt, 60:40); ir ($CHCl_3$): 1050, 1740 cm^{-1}; ^1H rmn ($CDCl_3$) δ: 1,11 (diastéréoisomère majoritaire) et 1,22 (diastéréoisomère minoritaire) (2 × d, J = 7,2 Hz, 3H, —CH_3); 1,65–1,96 (m, 2H, —CH_2CH_2OMOM); 2,60 (d de q, $J_1 = J_2$ = 7,2 Hz, 1H, —O_2CCH); 3,33 (s, 3H, —OCH_3); 3,63 (t, J = 6,5 Hz, 2H, —CH_2OMOM); 3,68 (s, 3H, —$COOCH_3$); 4,58 (s, 2H, —OCH_2O—); 4,73–5,06 (m, 2H, HCOCH); 5,86 (m, 2H, —HC=CH—). *Anal.* calc. pour $C_{12}H_{20}O_5$: C 59,00, H 8,25; trouvée: C 58,76, H 8,26.

[2R[2α(R),5α]] et [2R[2α(S*),5α]]-Tétrahydro-5-(2-méthoxyméthylènoxyéthyl)-α-méthyl-2-furanacétate de méthyle (19*a*) et (19′a)*

L'ester brut **18***a* en solution dans 20 mL de THF est hydrogéné dans un appareil de Parr en présence de 20 mg de rhodium (5%) sur charbon pendant 4 h sous 4 atm. Après filtration du catalyseur et traitement habituel un échantillon du produit brut est analysé par cpv (SE30 10%; T: 115°C). L'apparition de 2 pics se recouvrant partiellement (t_R: 60 et 63 min) fait apparaître que les 2 diastéréoisomères **19***a* et **19′***a* ont été formés dans une proportion de 89:11. Le produit brut chromatographié sur gel de silice (éluant: cyclohexane/AcOEt, 85:15) conduit à l'isolement de 265 mg de l'ester **19***a* (48,5% à partir du glycal **17***a*); Eb: 75°C (0,05 Torr); R_f: 0,26 (cyclohexane/AcOEt, 60:40); $[\alpha]_D^{25}$ −13,6° (*c* 1,07, $CHCl_3$); ir (film): 1050, 1120, 1160, 1205, 1742, 2970 cm^{-1}; ^1H rmn ($CDCl_3$) δ: 1,11 (d, J = 7,2 Hz, 3H, —CH_3); 2,52 (d de q, $J_1 = J_2$ = 7,2 Hz, 1H, —O_2CCH); 3,33 (s, 3H, —OCH_3); 3,58 (t, J = 6,5 Hz, 2H, —CH_2OMOM); 3,68 (s, 3H, —$COOCH_3$); 3,78–4,13 (m, 2H, —HCOCH—); 4,58 (s, 2H, —OCH_2O—). *Anal.* calc. pour $C_{12}H_{22}O_5$: C 58,52, H 9,00; trouvée: C 58,73, H 8,89.

On isole de même 29,5 mg (5,3% à partir du glycal **17***a*) de l'épimère **19′***a*; R_f: 0,3 (cyclohexane/AcOEt, 60:40); ^1H rmn ($CDCl_3$) δ: 1,20 (d, J = 7,2 Hz, 3H, —CH_3), 2,50 (d de q, $J_1 = J_2$ = 7,2 Hz, 1H, —O_2CCH); 3,33 (s, 3H, —OCH_3); 3,58 (t, J = 6,5 Hz, 2H, —CH_2OMOM); 3,65 (s, 3H, —$COOCH_3$); 3,78–4,13 (m, 2H, —HCOCH—); 4,58 (s, 2H, —OCH_2O—).

[2R[2α(R),5α]]-Tétrahydro-5-(2-hydroxyéthyl)-α-méthyl-2-furanacétate de méthyle (20*a*)*

Une solution de 240 mg (0,97 mmol) de **19***a* dans 50 mL de méthanol anhydre contenant 2,1% d'acide chlorhydrique (préparé à partir de 1,7 mL de chlorure d'acétyle et de 50 mL de méthanol) est chauffée à 45°C pendant 14 h sous atmosphère d'argon. Après évaporation des solvants sous pression réduite, l'huile obtenue est chromatographiée sur gel de silice (éluant: cyclohexane/AcOEt, 65:35). On isole 190 mg (96,5%) d'ester-alcool **20***a*; Eb: 83°C (0,06 Torr); R_f: 0,21 (cyclohexane/AcOEt, 85:15); $[\alpha]_D^{25}$ −26,3° (*c* 1,06, $CHCl_3$); ir ($CHCl_3$): 1080, 1180 1210, 1742, 2875, 3570 cm^{-1}; ^1H rmn ($CDCl_3$) δ: 1,11 (d, J = 7,2 Hz, 3H, —CH_3); 2,52 (d de q, $J_1 = J_2$ = 7,2 Hz, 1H, —O_2CCH—); 3,68 (s, 3H, —$COOCH_3$); 3,71 (t, J = 6,5 Hz, 2H, —CH_2OH); 3,83–4,20 (m, 2H, —HCOCH—). *Anal.* calc. pour $C_{10}H_{18}O_4$: C 59,39, H 8,97; trouvée: C 59,21, H 8,97.

[2R[2α(R),5α]]-Tétrahydro-5-(2-oxoéthyl)-α-méthyl-2-furanacétate de méthyle (21*a*)*

A une solution de 226 mg (0,155 mL; 1,78 mmol) de chlorure d'oxalyle dans 2 mL de chlorure de méthylène agitée à −78°C sous atmosphère d'argon on ajoute 278 mg (0,252 mL; 3,56 mmol) de DMSO et après 5 min une solution de 180 mg (0,89 mmol) de **20***a* dans 8 mL de THF. On maintient à cette température pendant 20 min, ajoute 900 mg (1,23 mL; 8,9 mmol) de triéthylamine, enlève le bain réfrigérant après 5 min et garde sous agitation pendant une heure et demie. Le mélange réactionnel est alors hydrolysé et la phase aqueuse extraite par 3 × 30 mL de chlorure de méthylène. Les phases organiques réunies sont lavées avec respectivement 2 × 20 mL d'une solution à 2% d'HCl et 2 × 20 mL d'une solution à 2% de bicarbonate de sodium, puis traitées de façon habituelle. On isole après chromatographie sur gel de silice (éluant: cyclohexane/AcOEt, 75:25), 160 mg (90%) d'aldéhyde **21***a*; Eb: 70°C (0,03 Torr); R_f: 0,25 (cyclohexane/AcOEt, 50:50); $[\alpha]_D^{25}$ −26,3° (*c* 1,06, $CHCl_3$); ir ($CHCl_3$): 1090, 1730 cm^{-1}; ^1H rmn ($CDCl_3$) δ: 1,11 (d, J = 7,2 Hz, 3H, —CH_3); 3,68 (s, 3H, —$COOCH_3$); 3,9–4,48 (m, 2H, —HCOCH—); 9,82 (t, J = 1,3 Hz, 1H, —CHO).

[2R[2α(R),5α(S*)]] et [2R[2α(R*),5α(R*)]]-Tétrahydro-5-(2-hydroxypropyl)-α-méthyl-2-furanacétate de méthyle (3*a*) et (5*a*)*

A une suspension de 162 mg (0,79 mmol) du complexe $(H_3C)_2S \cdot CuBr$ (26) dans 2 mL de pentane sous agitation à −20°C et sous atmosphère d'argon on ajoute goutte à goutte 0,93 mL (1,5 mmol) d'une solution 1,62 *M* de méthyllithium dans l'éther.[5] Après 20 min à cette température, une solution de 70 mg (0,35 mmol) de **21***a* dans 3 mL d'un mélange 1:1 (v/v) d'éther et de pentane est ajouté au milieu réactionnel qui est alors maintenu pendant 3 h à une température comprise entre −20° et −10°C. La suspension est versée dans 10 mL d'une solution à pH 8 de NH_3/NH_4Cl. La phase aqueuse est extraite par 3 × 20 mL de CH_2Cl_2 et les phases organiques réunies traitées de façon habituelle. Après chromatographie sur gel de silice (éluant: cyclohexane/AcOEt, 70:30) on isole 29,9 mg (39,5%) de **3***a* et 34,2 mg (45%) de **5***a* ainsi que 3 mg d'un mélange de ces deux produits.

(2*R*,3*R*,6*S*,8*S*) Nonactate de méthyle (**3***a*): Eb: 90°C (0,025 Torr); R_f: 0,13 (cyclohexane/AcOEt, 50:50); $[\alpha]_D^{25}$ −20,7° (*c* 0,925, $CHCl_3$); ir ($CHCl_3$): 1090, 1180, 1205, 1285, 1395, 1450, 1475, 1740, 3000, 3535, cm^{-1}; ^1H rmn ($CDCl_3$) δ: 1,11 (d, J = 7,2 Hz, 3H, —O_2CCCH_3); 1,18 (d, J = 6,3 Hz, 3H, HOCCH_3); 2,50 (d de q, $J_1 = J_2$ = 7,2 Hz, 2H, —O_2CCH et OH); 3,67 (s, 3H, —OCH_3); ^1H rmn (CCl_4) δ: 1,08 (d, J = 7,2 Hz, 3H, —O_2CCCH_3); 1,12 (d, J = 6,3 Hz, 3H, HOCCH_3); 2,43 (d de q, $J_1 = J_2$ = 7,2 Hz, 1H, —O_2CCH); 3,60 (s, 3H, —OCH_3); ^{13}C rmn ($CDCl_3$): 175,1; 81,0; 65,2; 51,7; 45,3; 42,9; 30,1; 28,8; 23,2; 13,5. *Anal.* calc. pour $C_{11}H_{20}O_4$: C 61,09, H 9,32; trouvée: C 61,18, H 9,46.

(2*R*,3*R*,6*S*,8*R*) Nonactate de méthyle (**5***a*): Eb: 90°C (0,025 Torr); R_f: 0,17 (cyclohexane/AcOEt, 50:50); $[\alpha]_D^{25}$ −33° (*c* 1,18, $CHCl_3$), ir ($CHCl_3$): identique à **3***a*; ^1H rmn ($CDCl_3$) δ: 1,12 (d, J = 7,2 Hz, 3H, —O_2CCCH_3); 1,15 (d, J = 6,3 Hz, 3H, HOCCH_3); 2,50 (d de q, $J_1 = J_2$ = 7,2 Hz, 1H, —O_2CCH); 3,67 (s, 3H, —OCH_3); ^1H rmn (CCl_4) δ: 1,07 (d, J = 6,3 Hz, 3H, HOCCH_3); 1,09 (d, J = 7,2 Hz, 3H, —O_2CCCH_3); 2,45 (d de q, $J_1 = J_2$ = 7,2 Hz, 1H, —O_2CCH); 3,62 (s, 3H, —OCH_3). *Anal.* calc. pour $C_{11}H_{20}O_4$: C 61,09, H 9,32; trouvée: C 60,94, H 9,20.

Acide [2R[2α(R),5α(S*)]]-tétrahydro-5-(2-hydroxypropyl)-α-méthyl-2-furanacétique (2*a*)*

A 19 mg (0,087 mmol) d'ester **3***a* on ajoute 0,5 mL d'une solution aqueuse 2 *N* de KOH et agite magnétiquement 40 min à température ambiante. La solution est acidifiée jusqu'à pH 1,5 et évaporée à sec à température ambiante sous pression réduite. Le résidu est trituré et filtré sur verre fritté avec 3 × 50 mL de $CHCl_3$. Après évaporation du $CHCl_3$, l'acide brut est

Can. J. Chem. Downloaded from www.nrcresearchpress.com by 210.87.254.42 on 09/05/12
For personal use only.

chromatographié sur gel de silice acide (éluant: cyclohexane/AcOEt, 50:50). On receuille 17 mg (96%) d'acide (−) nonactique (**2***a*); Eb: 130°C (0,003 Torr); R_f: 0,1 (cyclohexane/AcOEt/AcOH, 50:50:2). $[\alpha]_D^{25}$ −9,3°(*c* 1,0, $CHCl_3$); ir ($CHCl_3$): 1090, 1395, 1475, 1720, 2995, 3540 cm^{-1}; ^1H rmn ($CDCl_3$) δ: 1,15 (d, *J* = 7,2 Hz, 3H, —O_2CCCH_3); 1,20 (d, *J* = 6,3 Hz, 3H, HOCCH_3); 2,48 (d de q, $J_1 = J_2$ = 7,2 Hz, 1H, —O_2CCH); 6,39 (2H, OH); ^1H rmn (CCl_4) δ: 1,12 (d, *J* = 7,2 Hz, 3H, —O_2CCCH_3); 1,14 (d, *J* = 6,3 Hz, 3H, HOCCH_3); 2,43 (d de q, $J_1 = J_2$ = 7,2 Hz, 1H, —O_2CCH). *Anal.* calc. pour $C_{10}H_{18}O_4$: C 59,39, H 8,97; trouvée: C 59,23, H 8,98.

Acide [2R[2α(R),5α(R*)]]-tétrahydro-5-(2-hydroxypropyl)-α-méthyl-2-furanacétique (4*a)

On hydrolyse de la même façon 11,5 mg (0,051 mmol) de 8-*épi* nonactate de méthyle (**5***a*) et obtient après chromatographie sur gel de silice acide 10 mg (93%) d'acide (−) 8-*épi* nonactique (**4***a*); R_f: 0,12 (cyclohexane/AcOEt/AcOH, 50:50:2); $[\alpha]_D^{25}$ −50,1° (*c* 1,0, $CHCl_3$); ir ($CHCl_3$): 1090, 1395, 1435, 1475, 1770, 2995, 3350 cm^{-1}; ^1H rmn ($CDCl_3$) δ: 1,12 (d, *J* = 7,2 Hz, 3H, —O_2CCCH_3); 1,18 (d, *J* = 6,3 Hz, 3H, HOCCH_3); 2,47 (d de q, $J_1 = J_2$ = 7,2 Hz, 1H, —O_2CCH); 5,88 (2H, OH); ^1H rmn (CCl_4) δ: 1,09 (d, *J* = 7,2 Hz, 3H, —O_2CCCH_3); 1,14 (d, *J* = 6,3 Hz, 3H, HOCCH_3); 2,42 (d de q, $J_1 = J_2$ = 7,2 Hz, 1H, —O_2CCH). *Anal.* calc. pour $C_{10}H_{18}O_4$: C 59,39, H 8,97; trouvée: C 59,49, H 8,83.

Phénylméthyl 2,3:5,6-di-O-(1-méthyléthylidène)-(α et β)-D-gulofuranoside (23) et (23')

Obtenus à partir de 92 g (0,353 mol) de 2,3:5,6-di-*O*-(1-méthyléthylidène)-(α et β)-D-gulofuranose (27) suivant le mode opératoire permettant d'isoler les mannofuranosides correspondants (20). La chromatographie du mélange brut sur gel de silice (éluant: cyclohexane/AcOEt, 80:20) permet d'isoler 110 g d'anomère β qui recristallisé dans l'éther de pétrole fournit 106,2 g (86%) de **23**; F: 88–89°C (éther de pétrole); R_f: 0,4 (cyclohexane/AcOEt, 80:20); $[\alpha]_D^{25}$ −64,9° (*c* 1,03, acétone); ir ($CHCl_3$): 855, 1015, 1090, 1160, 1230, 1380, 1390, 1465, 2960, 3000 cm^{-1}; ^1H rmn ($CDCl_3$): 1,27; 1,40; 1,43 et 1,45 (4s, 12H, 2 $C(CH_3)_2$); 4,60 (AB, J_{AB} = 12 Hz, ν_{AB} = 20,8 Hz, 2H, —OCH_2Ph); 5,15 (s, 1H, OCHOCH_2Ph); 7,31 (s, 5H, C_6H_5—). *Anal.* calc. pour $C_{19}H_{26}O_6$: C 65,13, H 7,48; trouvée: C 64,99, H 7,38.

On isole de même 6 g (5%) d'α-glycoside **23'**: F: 86–87°C (CH_3OH/H_2O); R_f: 0,17 (cyclohexane/AcOEt, 80:20); $[\alpha]_D^{25}$ −63,4° (*c* 1,08, acétone); ir ($CHCl_3$): 860, 1030, 1080, 1120, 1175, 1230, 1385, 1390, 1465, 2960, 3020 cm^{-1}; ^1H rmn ($CDCl_3$) δ: 1,32; 1,38, 1,45 et 1,50 (4s, 12H, 2 $C(CH_3)_2$); 7,2–7,5 (m, 5H, C_6H_5—). *Anal.* calc. pour $C_{19}H_{26}O_6$: C 65,13, H 7,48; trouvée: C 65,06, H 7,39.

Phénylméthyl 2,3-O-(1-méthyléthylidène)-β-D-gulofuranoside (24)

Obtenu par hydrolyse partielle de 105,8 g (0,302 mol) de **23** suivant le mode opératoire permettant d'isoler l'α-mannofuranoside **8** correspondant (20). Après neutralisation le méthanol est évaporé sous pression réduite et le résidu versé dans 2 L de CH_2Cl_2. La phase organique est séparée et traitée de façon habituelle. On obtient 92,7 g (99%) de **24**. Un échantillon analytique est obtenu par recristallisation dans un mélange AcOEt/éther de pétrole; F: 137–138°C; R_f: 0,43 (EtOAc); $[\alpha]_D^{25}$ −96,3° (*c* 1,12, acétone); ir ($CHCl_3$): 990, 1015, 1095, 1175, 1230, 1385, 1390, 2960, 3030, 3550, 3620 cm^{-1}; ^1H rmn ($CDCl_3$) δ: 1,28 et 1,45 (2s, 6H, $C(CH_3)_2$); 4,58 (AB, J_{AB} = 12 Hz, ν_{AB} = 20,8 Hz, 2H, —OCH_2Ph); 5,15 (s, 1H, —OCHOCH_2Ph); 7,31 (s, 5H, C_6H_5—). *Anal.* calc. pour $C_{16}H_{22}O_6$: C 61,92, H 7,15; trouvée: C 61,89, H 7,09.

Phénylméthyl 2,3-O-(1-méthyléthylidène)-5,6-(N,N-diméthylaminométhylène)-β-D-gulofuranoside (26)

Même mode opératoire que pour le diastéréoisomère **10** à partir de 50,7 g (0,163 mol) de **24**; ^1H rmn ($CDCl_3$) δ: 1,26 et 1,43 (2s, 6H, $C(CH_3)_2$); 2,38 (s, 6H, —$N(CH_3)_2$); 5,13 (s, 1H, —OCHOCH_2Ph); 5,43, (s, 1H, $(H_3C)_2NCH$); 7,30 (s, 5H, C_6H_5).

*Phénylméthyl 2,3-O-(1-méthyléthylidène)-5,6-didéhydro-5,6-didéoxy-β-D-gulofuranoside (11*b)

Même mode opératoire que pour l'énantiomère **11***a* à partir du formamide acétal **26** brut. Obtenu: 34,15 g (75,5% à partir de **24**); F: 36,7–37,5°C (éther de pétrole à −20°C); $[\alpha]_D^{25}$ −54,4° (*c* 0,975, $CHCl_3$). *Anal.* calc. pour $C_{16}H_{20}O_4$: C 69,55, H 7,29; trouvée: C 69,50, H 7,19.

On isole de même 12,2 g (19%) de diacétate **25** qui est recyclé en **24** après réduction par $LiAlH_4$.

*Phénylméthyl 2,3-O-(1-méthyléthylidène)-5-déoxy-β-D-gulofuranoside (12*b)

Même mode opératoire que pour l'énantiomère **12***a*, à partir de 44 g (0,16 mol) de l'oléfine **11***b*. Obtenu: 44,4 g (95%); $[\alpha]_D^{25}$ −99,0° (*c* 1,0, $CHCl_3$). *Anal.* calc. pour $C_{16}H_{22}O_5$: C 65,29, H 7,53; trouvée: C 65,15, H 7,47.

*Phénylméthyl 2,3-O-(1-méthyléthylidène)-5-déoxy-6-O-méthoxyméthyl-β-D-gulofuranoside (13*b)

Le groupe protecteur MOM est plus efficacement introduit par réaction avec l'éther chlorométhylméthylique (cf. **13***a*) et le mode opératoire suivant (23), employé dans notre laboratoire avec succès sur des substrats étroitement apparentés à **12***b*, conduit avec ce composé à des rendements médiocres.

A une solution de 42 g (0,142 mol) de l'alcool **12***b* et 60 mL de $CH_2(OCH_3)_2$ dans 600 mL de CH_2Cl_2 on ajoute sous agitation et sur une période de 20 min 100 g d'un mélange 1:1 de P_2O_5 en poudre et de Celite. Après une heure le milieu réactionnel est versé dans 500 mL d'une solution à 10% de $NaHCO_3$ et extrait par 3 × 500 mL d'éther. Les phases éthérées réunies sont traitées de façon habituelle. Le produit brut chromatographié sur gel de silice (éluant: cyclohexane/AcOEt, 90:10) conduit à l'isolement de 19,3 g (40%) de **13***b*; $[\alpha]_D^{25}$ −88,5° (*c* 1,075, $CHCl_3$). *Anal.* calc. pour $C_{18}H_{26}O_6$: C 63,89, H 7,74; trouvée: C 64,04, H 7,77.

*2,3-O-(1-Méthyléthylidène)-5-déoxy-6-O-méthoxyméthyl-(α et β)-D-gulofuranose (14*b)

Même mode opératoire que pour l'énantiomère **14***a* à partir de 18,45 g (54 mmol) de **13***b*. Obtenu: 11,1 g (82%). *Anal.* calc. pour $C_{11}H_{20}O_6$: C 53,22, H 8,12; trouvée: C 53,24, H 8,10.

*Chlorure de 5-déoxy-2,3-O-(1-méthyléthylidène)-6-O-méthoxyméthyl-β-D-gulofuranosyle (15*b)

Même mode opératoire que pour le chlorure énantiomère **15***a* à partir de 1,97 g (7,93 mmol) de lactol **14***b*. Obtenu: 1,82 g (86%); $[\alpha]_D^{25}$ −92,8° (*c* 0.905, $CHCl_3$). *Anal.* calc. pour $C_{11}H_{19}O_5Cl$: C 49,54, H 7,18; trouvée: C 49,37, H 7,06.

*2S-cis-2-(β-Méthoxyméthylènoxyéthyl)-2,3-dihydro-3-hydroxyfurane (17*b)

Même mode opératoire que pour l'énantiomère **17***a* à partir de 1,8 g (6,75 mmol) du chlorure **15***b*. Obtenu: 1,095 g d'un mélange 10:1 (^1H rmn) de glycal **17***b* et de **16***b*, correspondant à un rendement de 82% en glycal **17***b*.

[2S[2α(R et S*),5α]]-2,5-Dihydro-5-(2-méthoxyméthylènoxyéthyl)-α-méthyl-2-furanacétate de méthyle (18*b)

Même mode opératoire que pour les énantiomères respectifs

Can. J. Chem. Downloaded from www.nrcresearchpress.com by 210.87.254.42 on 09/05/12
For personal use only.

correspondants **18***a* à partir de 1,09 g du mélange 10:1 précédent, correspondant à 5,5 mmol de glycal **17***b*.

[2S[2α(R),5α]] et [2S[2α(S*),5α]]-Tétrahydro-5-(2-méthoxyméthylènoxyéthyl)-α-méthyl-2-furanacétate de méthyle (**19**b) et (**19'**b)*

Obtenu par hydrogénation à pression atmosphérique d'une solution de l'ester insaturé brut précédent **18***b* dans 20 mL d'AcOEt en présence de 100 mg de Pt (5%) sur charbon pendant une demi-heure. Après filtration du catalyseur et traitement habituel de la phase organique, le produit brut est analysé par cpv (SE30 10%; *T*: 118°C). Le même chromatogramme que pour les énantiomères correspondants **19***a* et **19'***a* est obtenu, indiquant que la formation des diastéréoisomères **19***b* et **19'***b* s'est effectuée dans une proportion de 86:14. La chromatographie sur gel de silice (éluant: cyclohexane/AcOEt, 85:15) du produit brut conduit à l'isolement de 596 mg de l'ester **19***b* (44% à partir du glycal **17***b*); $[\alpha]_D^{25}$ +13,8° (*c* 0,995, $CHCl_3$). *Anal.* calc. pour $C_{12}H_{22}O_5$: C 58,52, H 9,00; trouvée: C 58,67, H 9,03.

On isole de même 66,3 mg (4,9% à partir du glycal **17***b*) de l'ester épimère en C-2, **19'***b*; $[\alpha]_D^{25}$ −33,8° (*c* 1,005, $CHCl_3$). *Anal.* calc. pour $C_{12}H_{22}O_5$: C 58,52, H 9,00; trouvée: C 58,27, H 8,90.

[2S[2α(R),5α]]-Tétrahydro-5-(2-hydroxyéthyl)-α-méthyl-2-furanacétate de méthyle (**20**b)*

Même mode opératoire que pour l'alcool énantiomère **19***a* à partir de 230 mg (0,93 mmol) de **19***b*. Obtenu: 179,5 mg (95%); $[\alpha]_D^{25}$ +26,0° (*c* 1,01, $CHCl_3$). *Anal.* calc. pour $C_{10}H_{18}O_4$: C 59,39, H 8,97; trouvée: C 59,47, H 8,86.

[2S[2α(R),5α]]-Tétrahydro-5-(2-oxoéthyl)-α-méthyl-2-furanacétate de méthyle (**21**b)*

Même mode opératoire que pour l'aldéhyde énantiomère **21***a* à partir de 160 mg (0,79 mmol) de l'alcool **20***b*. Obtenu: 144 mg (91%); $[\alpha]_D^{25}$ +28,9° (*c* 1,22, $CHCl_3$). *Anal.* calc. pour $C_{10}H_{16}O_4$: C 59,99, H 8.05; trouvée: C 60,03, H 8,02.

[2S[2α(R),5α(S*)]] et [2S[2α(R*),5α(R*)]]-Tétrahydro-5-(2-hydroxypropyl)-α-méthyl-2-furanacétate de méthyle (**3**b) et (**5**b)*

A une solution de 130 mg (0,65 mmol) d'aldéhyde **21***b* dans 5 mL d'éther anhydre agitée sous atmosphère d'argon à −78°C on ajoute à l'aide d'une seringue 5,5 mL (0,66 mmol) d'une solution 0,12 *M* de CH_3MgBr dans l'éther, préparée par dilution d'une solution commerciale 3 *M* dans l'éther.[4] Le milieu réactionnel est maintenu une demi-heure à −78°C, puis une heure et demie à une température comprise entre −60 et −50°C. On laisse finalement remonter la température jusqu'à −10°C, hydrolyse par une solution saturée de NH_4Cl et extrait la phase aqueuse avec 4 × 50 mL d'éther. Les phases éthérées réunies sont traitées de façon habituelle. La chromatographie du produit brut sur gel de silice (éluant: cyclohexane/AcOEt, 70:30) conduit à l'isolement de 13 mg d'aldéhyde **21***b* n'ayant pas réagi, 67,7 mg d'alcool **3***b* (53,5% calculé à partir de l'aldéhyde recouvré) et 51 mg d'alcool épimère **5***b* (40% calculé à partir de l'aldéhyde recouvré).

(2*S*,3*S*,6*R*,8*R*) Nonactate de méthyle (**3***b*): $[\alpha]_D^{25}$ +22,1° (*c* 0.7, $CHCl_3$). *Anal.* calc. pour $C_{11}H_{20}O_4$: C 61,09, H 9,32; trouvée: C 61,13, H 9,33.

(2*S*,3*S*,6*R*,8*S*) Nonactate de méthyle (**5***b*): $[\alpha]_D^{25}$ +32,9° (*c* 1,07, $CHCl_3$). *Anal.* calc. pour $C_{11}H_{20}O_4$: C 61,09, H 9,32; trouvée: C 61,27, H 9,39.

Acide [2S[2α(R),5α(S*)]]-Tétrahydro-5-(2-hydroxypropyl)-α-méthyl-2-furanacétique (**2**b)*

Même mode opératoire que pour l'acide (−) nonactique (**2***a*) à partir de 19 mg (0,087 mmol) de (+) nonactate de méthyle (**3***b*). Obtenu: 16,9 mg (95%) d'acide (+) nonactique (**2***b*); $[\alpha]_D^{25}$ +10,3° (*c* 1,69, $CHCl_3$). *Anal.* calc. pour $C_{10}H_{18}O_4$: C 59,39, H 8,97; trouvée: C 59,55, H 9.09.

Acide [2S[2α(R),5α(R*)]]-Tétrahydro-5-(2-hydroxypropyl)-α-méthyl-2-furanacétique (**4**b)*

Même mode opératoire que pour l'acide (−) 8-*épi* nonactique (**4***a*) à partir de 25,3 mg (0,117 mmol) de (+) 8-*épi* nonactate de méthyle (**5***b*). Obtenu: 22,6 mg (95,5%) d'acide (+) 8-*épi* nonactique (**4***b*); $[\alpha]_D^{25}$ +51,3° (*c* 1,01, $CHCl_3$). *Anal.* calc. pour $C_{10}H_{18}O_4$: C 59,39, H 8,97; trouvée: C 59,47, H 8,91.

Remerciements

Les auteurs tiennent à remercier l'United States National Science Foundation pour l'attribution d'une bourse (N° CHE 7821066) qui a permis la réalisation de ce travail.

1. R. Corbaz, L. Ettlinger, E. Gäumann, W. Keller-Schierlein, F. Kradoffer, L. Neipp, V. Prelog et H. Zähner. Helv. Chim. Acta, **38**, 1445 (1955).
2. (*a*) K. C. Nicolaou. Tetrahedron, **33**, 683 (1977); (*b*) P. A. Bartlett. Tetrahedron, **36**, 2 (1980).
3. W. Keller-Schierlein et H. Gerlach. Fortschr. Chem. Org. Naturst. **26**, 161 (1968).
4. (*a*) L. A. P. Pioda, H. A. Wachter, R. E. Dohner et W. Simon. Helv. Chim. Acta, **50**, 1373 (1967); (*b*) H. K. Wipf, L. A. P. Pioda, Z. Stefarac et W. Simon. Helv. Chim. Acta, **51**, 377, (1968).
5. J. H. Prestegard et S. I. Chan. J. Am. Chem. Soc. **92**, 4440 (1970).
6. M. Dobler, J. D. Dunitz et B. T. Kilbourn. Helv. Chim. Acta, **52**, 2573 (1969).
7. (*a*) J. Dominguez, J. D. Dunitz, H. Gerlach et V. Prelog. Helv. Chim. Acta, **45**, 129 (1962); (*b*) J. Beck, H. Gerlach, V. Prelog et W. Voser. Helv. Chim. Acta, **45**, 621 (1962).
8. H. Gerlach et V. Prelog. Justus Liebigs Ann. Chem. **669**, 121 (1963).
9. H. Gerlach, K. Oertle, A. Thalmann et S. Servi. Helv. Chim. Acta, **58**, 2836 (1975).
10. (*a*) U. Schmidt, J. Gombos, E. Haslinger et H. Zak. Chem. Ber. **109**, 2628 (1976); (*b*) J. Gombos, E. Haslinger, A. Nikiforov, H. Zak et U. Schmidt. Monatsh. Chem. **106**, 1043 (1975).
11. G. Beck et E. Henseleit. Chem. Ber. **104**, 21 (1971).
12. H. Gerlach et H. Wetter. Helv. Chim. Acta, **57**, 2306 (1974).
13. (*a*) H. Zak et U. Schmidt. Angew. Chem. Int. Ed. Engl. **14**, 432 (1975); (*b*) J. Gombos, E. Haslinger, H. Zak et U. Schmidt. Monatsh. Chem. **106**, 219 (1975); (*c*) J. Gombos, E. Haslinger, H. Zak et U. Schmidt. Tetrahedron Lett. 3391 (1975).
14. M. J. Argo, M. H. Trammell et J. D. White. J. Org. Chem. **41**, 2075 (1976).
15. J. Gombos, E. Haslinger et U. Schmidt. Chem. Ber. **109**, 2645 (1976).
16. R. E. Ireland, S. Thaisrivongs et C. S. Wilcox. J. Am. Chem. Soc. **102**, 1155 (1980).
17. (*a*) R. E. Ireland et C. S. Wilcox. Tetrahedron Lett. 2839 (1977); (*b*) R. E. Ireland, C. S. Wilcox, S. Thaisrivongs et N. Vanier. Can. J. Chem. **57**, 1743 (1979); (*c*) R. E. Ireland, S. Thaisrivongs, N. Vanier et C. S. Wilcox. J. Org. Chem. **45**, 48 (1980).

18. R. E. IRELAND, R. H. MUELLER et A. K. WILLARD. J. Am. Chem. Soc. **98**, 2868 (1976).
19. R. E. IRELAND, C. S. WILCOX et S. THAISRIVONGS. J. Org. Chem. **43**, 786 (1978).
20. J. S. BRIMACOMBE, F. HUNEDY et L. C. N. TUCKER. J. Chem. Soc. C, 1381 (1968).
21. F. W. EASTWOOD, K. J. HARRINGTON, J. S. JOSAN et J. L. PURA. Tetrahedron Lett. 5223 (1970).
22. S. HANESSIAN, A. BARGIOTTI et M. LARUE. Tetrahedron Lett. 737 (1978).
23. K. FUJI, S. NAKANO et F. FUJITE. Synthesis, 276 (1975).
24. A. J. MANCUSO, S. L. HUANG et D. SWERN. J. Org. Chem. **43**, 2480 (1978); K. OMURA et D. SWERN. Tetrahedron, **34**, 1651 (1978).
25. E. BARREIRO, J. L. LUCHE, J. ZWEIG et P. CRABBE. Tetrahedron Lett. 2353 (1975).
26. H. O. HOUSE, CHIA-YEH CHU, J. M. WILKINS et M. J. UMEN. J. Org. Chem. **40**, 1460 (1975).
27. L. M. LERNER, B. D. KOHN et P. KOHN. J. Org. Chem. **33**, 1780 (1968).
28. T. P. CULBERTSON. J. Org. Chem. **38**, 3624 (1973).
29. W. C. STILL et J. A. SCHNEIDER. Tetrahedron Lett. 1035 (1980).

Can. J. Chem. Downloaded from www.nrcresearchpress.com by 210.87.254.42 on 09/05/12
For personal use only.

Ipso nitration. XXII.[1] The stereochemistry of 1,4-dimethyl-4-nitrocyclohexa-2,5-dienols and their acetates and methyl ethers

ALFRED FISCHER, GEORGE N. HENDERSON, AND TREVOR A. SMYTH
Department of Chemistry, University of Victoria, Victoria, B.C., Canada V8W 2Y2
AND
FREDERICK W. B. EINSTEIN AND ROGER E. COBBLEDICK
Department of Chemistry, Simon Fraser University, Burnaby, B.C., Canada V5A 1S6
Received September 16, 1980

ALFRED FISCHER, GEORGE N. HENDERSON, TREVOR A. SMYTH, FREDERICK W. B. EINSTEIN, and ROGER E. COBBLEDICK. Can. J. Chem. **59**, 584 (1981).

The higher melting isomer of 1,4-dimethyl-4-nitrocyclohexa-2,5-dienol has the (*E*)-configuration. The stereospecific interconversion of the dienols and the corresponding acetates and the stereospecific conversion of dienols to methyl ethers allow the assignment of the configurations of the isomeric acetates and ethers. Parallels in physical properties allow the assignment of the stereochemistry of the isomers of 1-alkyl-4-methyl-4-nitrocyclohexa-2,5-dienyl acetates (alkyl = Et, *i*-Pr, *t*-Bu) and of 1-alkyl-4-ethyl-4-nitrocyclohexa-2,5-dienyl acetates (alkyl = Me, Et).

ALFRED FISCHER, GEORGE N. HENDERSON, TREVOR A. SMYTH, FREDERICK W. B. EINSTEIN et ROGER E. COBBLEDICK. Can. J. Chem. **59**, 584 (1981).

L'isomère du diméthyl-1,4 nitro-4 cyclohexanediène-2,5 ol ayant le point de fusion le plus élevé a la configuration (*E*). L'interconversion stéréospécifique des diénols et des acétates correspondants ainsi que la conversion stéréospécifique des diénols en éthers méthyliques permettent d'établir les configurations des acétates et des éthers isomères. En établissant un parallèle entre les propriétés physiques, on peut attribuer la stéréochimie des isomères des acétates d'alkyl-1 méthyl-4 nitro-4 cyclohexadiene-2,5 yles (alkyl = Et, *i*-Pr, *t*-Bu) et des acétates d'alkyl-1 éthyl-4 nitro-4 cyclohexadiene-2,5 yles (alkyl = Me, Et).

[Traduit par le journal]

Introduction

Aromatic compounds containing an activated *ipso* position when nitrated in acetic anhydride give, as major products, nitronium acetate adducts (1–6). The 1,4-adducts are formed as diastereoisomeric pairs. Attempts to assign the configuration of the individual members of such pairs have met with limited success (7–11). In this paper we report the assignment of the configuration of the adducts of *p*-xylene, based on the determination of the structure of (*E*)-1,4-dimethyl-4-nitrocyclohexa-2,5-dienol,[2] by X-ray crystallography.

In our earlier work we attempted to assign the configuration of the adducts through shift-reagent studies. Addition of the shift reagent *tris*-(1,1,1,2,2,3,3-heptafluoro-7,7-[$^2H_6$]dimethyl-4,6-[$^2H_3$]-octanedionato)europium(III)(Eu([$^2H_9$]fod)$_3$), which complexes at the acetate function, might be expected to move the 4-methyl protons in the (*E*)-isomer, with these protons *cis* to europium, more rapidly downfield than in the case of the (*Z*)-isomer. The method is apparently successful in the case of secondary acetate adducts, such as those from toluene, in that there is a significant difference in the relative gradients of proton chemical shifts of the appropriate protons resulting from the addition of Eu([$^2H_9$]fod)$_3$ (7). However, in the case of the *p*-xylene adducts, and more generally for tertiary acetate adducts, the relative shift gradients of the appropriate protons in the diastereoisomers are not significantly different (8–11). Similarly inconclusive results were obtained when the shift study was repeated on the diastereoisomers of 1,4-dimethyl-4-nitrocyclohexa-2,5-dienol. A 23% difference was observed between the relative shift gradients of the 4-CH_3 protons in the diastereoisomers of the 1,4-dimethyl-4-nitrocyclohexadienyl methyl ethers. On this basis the isomer with the higher relative shift gradient[3] was suggested to have the 1-methoxyl group *cis* to the 4-CH_3 (i.e. the (*E*)-diastereoisomer). However, in view of the failure of the method when applied to the corresponding dienols and dienyl acetates, it was suggested that this assignment could only be regarded as tentative (8). In this earlier work the relative configurations of the dienols and acetates were established: ace-

[1]For Part XXI, see ref. 6.

[2]Compound **2***a* in ref. 8, designated in this paper as **8–2***a*. Compounds reported in earlier papers in the series are labelled in this paper as J-K1 where J is the reference to the paper in which the compound is described and K1 is the label of the compound in that paper.

[3]Compound **3***b* in ref. 8. It is most easily distinguished from the diastereoisomer **8–3***a* by the fact that the methoxy protons are at higher field and the other methyl protons are at lower field in **8–3***b* than in **8–3***a*.

0008-4042/81/030584-07$01.00/0
©1981 National Research Council of Canada/Conseil national de recherches du Canada

Can. J. Chem. Downloaded from www.nrcresearchpress.com by 210.87.254.6 on 09/06/12
For personal use only.

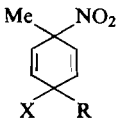

(*E*)

8–1*a* R = Me, X = OAc
10–2*a* R = Et, X = OAc
9–1*a* R = *i*-Pr, X = OAc
11–2*a* R = *t*-Bu, X = OAc
8–2*a* R = Me, X = OH
8–3*b* R = Me, X = OMe

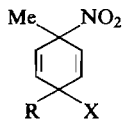

(*Z*)

8–1*b*
10–2*b*
9–1*b*
11–2*b*
8–2*b*
8–3*a*

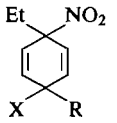

10–1*a* R = Me, X = OAc
10–3*a* R = Et, X = OAc

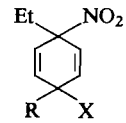

10–1*b*
10–3*b*

tate **8–1***a* and alcohol **8–2***a* have the same configurations, as do their diastereoisomers **8–1***b* and **8–2***b*. However, the configurational relationship between the ethers **8–3***a* and **8–3***b* and the alcohols **8–2***a* and **8–2***b* or acetates **8–1***a* and **8–1***b* was not determined and the tentative assignment of the configurations of the ethers did not provide even a tentative assignment of the configuration of the alcohols and acetates.

Myhre and co-workers have developed a method of synthesis of the 1,4-dialkyl-4-nitrocyclohexadienols by addition of methyllithium to a 4-alkyl-4-nitrocyclohexadienone, and of 4-alkyl-4-nitrocyclohexadienols by reduction of the nitrodienone with sodium borohydride (12). They point out that these reactions are moderately stereoselective and the predominant isomer, assumed to be the (*Z*)-isomer on the basis of an addition *trans* to the nitro group being preferred as a consequence of both steric and field effects of the latter, is the diastereoisomer which, as the acetate, is formed in smaller amount in the nitration reaction. For secondary acetate adducts the assignments based on the shift-reagent studies are in accord with those based on the nitrodienone reduction (12).

Shosenji *et al.* have recently assigned the configurations of the 1,4-dimethyl-4-nitrocyclohexadienyl methyl ethers by infrared spectroscopy (13). They reacted the nitro group in the ethers with methylmagnesium iodide and with methylmagnesium iodide in the presence of cuprous chloride to give the *N*-methylhydroxylamine and the hydroxylamine derivatives, respectively. They observed a band attributed to intramolecular hydrogen bonding between the *cis* hydroxylamine and methoxyl functions in one diastereoisomer (that obtained from compound **3***b* of ref. 8) of each pair.

On this basis they assigned the (*Z*)-configuration to **3***b* (*cis* methoxy and nitro groups) and observed that this was in conflict with the assignment based on shift-reagent studies.

Results and Discussion

Nitration of *p*-xylene in acetic anhydride at −40°C resulted in the formation of the diastereoisomers of 1,4-dimethyl-4-nitrocyclohexa-2,5-dienyl acetate in yields close to 90%. The predominant isomer **8–1***a*, shown below to be the (*E*)-isomer and constituting ca. 70% of the diene component, was crystallized from the crude product and obtained pure. The two diastereoisomers were also separated by low-temperature chromatography, as previously described (8). The nitrocyclohexadienyl acetates were stereospecifically reduced to the corresponding nitrocyclohexadienols with aluminium hydride and the dienols were stereospecifically methylated to the methyl ethers, thus establishing the configurational relationships between the diastereoisomers of the acetates, alcohols, and ethers.[4] In the 2,6-dideuterionitrocyclohexadienols (below) the (*Z*)-diastereoisomer was stereospecifically acetylated to the corresponding acetate and methylated to the corresponding ether, confirming the configurational relationships.

The nmr shift-reagent studies and chemical shift correlations (below) required the unambiguous assignment of the spectra of the adducts. We therefore synthesized the 2,6-dideuterio-1,4-dimethyl-4-nitrocyclohexa-2,5-dienols by addition of methyllithium to 2,6-dideuterio-4-methyl-4-nitrocyclohexa-2,5-dienone. The dienone was itself prepared from 2,6-dideuterio-4-methylphenol via the nitration of the corresponding aryl acetate (cf. refs. 12 and 14). The diastereoisomeric dideuteriocyclohexadienols were separated by high pressure liquid chromatography. In the proton decoupled ^{13}C nmr spectra of the (*E*)- and (*Z*)-deuteriocyclohexadienols, the (*Z*)-acetate, and the (*Z*)-ether, the C-2 and C-6 absorption was readily identified as a triplet, resulting from C–D coupling. In each of the four spectra the (triplet) C-2 and C-6 absorption occurs at lower field than the (singlet) C-3 and C-5 absorption and we assume that this is also the case in the (*E*)-acetate and (*E*)-ether and in other 1,4-dialkyl-

[4]Previously the ethers had been obtained by solvolysis (acid-catalysed methanolysis) of the acetates, a nonstereospecific process (8).

Can. J. Chem. Downloaded from www.nrcresearchpress.com by 210.87.254.6 on 09/06/12
For personal use only.

Can. J. Chem. Downloaded from www.nrcresearchpress.com by 210.87.254.6 on 09/06/12
For personal use only.

4-nitrocyclohexadienyl acetates. In previous work (10, 11) the vinyl carbons closer to the nitro group (C-3 and C-5) have been assumed to absorb at lower field than the vinyl carbons closer to the acetate group (C-2 and C-6). This assumption is clearly incorrect in the case of the dienes derived from *p*-xylene and is most probably incorrect for the dienes derived from other 1,4-dialkylbenzenes.

The ^{1}H nmr absorptions of the vinyl protons adjacent to the nitro group (3-H and 5-H) in the 1,4-dimethyl- 4-nitrocyclohexadiene adducts were also assigned unambiguously from the ^{1}H nmr spectra of the dideuteriodienes. The absorptions of the other vinyl protons (2-H and 6-H) were then assigned from the spectra of the undeuterated compounds. In the dienols, 2-H and 6-H absorb at lower field than 3-H and 5-H. In the dienyl acetates the absorptions are superimposed and in the dienyl methyl ethers 2-H and 6-H absorb at higher field than 3-H and 5-H. The chemical shifts of the vinyl protons of the dienols were incorrectly assigned in the earlier report (8).

A perspective view of the higher melting isomer of 1,4-dimethyl-4-nitrocyclohexa-2,5-dienol, derived from the parameters obtained in the X-ray structure analysis, is shown in Fig. 1. The cyclohexadiene ring is "chemically" planar, the deviations of C-1 and C-4 being 0.03(3) and 0.08(3) Å towards the same side (making the conformation a marginal boat). The methyl groups are *trans*; the molecule has the (*E*)-configuration. The molecules are linked in a spiral fashion along the three-fold screw axis by hydrogen bonding (O.....O 2.75 Å) involving the hydroxyl group. The crystals were of relatively poor quality and we associate this with the disordered diethyl ether molecules of crystallization which lie in channels parallel to *C*.

The configurational relationships previously established between acetate and dienol and confirmed in this paper and those now established between dienol and methyl ether, when combined with the X-ray analysis result, lead to the conclusions that the lower melting acetate with the more widely dispersed 1- and 4-methyl peaks in the ^{1}H nmr spectrum ($\Delta\delta$ = 0.34 ppm) has the (*E*)-configuration, as does the higher melting alcohol and as does the ether with higher field methoxyl group. Thus the compounds **1***a*, **2***a*, and **3***b* of ref. 8 are (*E*)-isomers and correspondingly **1***b*, **2***b*, and **3***a* are (*Z*)-isomers. In the case of the ethers this is the opposite assignment to that made by Shosenji *et al.* (13) but, perhaps fortuitously, it is the same as the tentative assignment based on shift-reagent studies (8). In the case of the dienols it is the same assignment as that suggested by Myhre and co-workers (12). Shosenji *et al.* reported that the photosolvolysis of **8–1***a* in methanol is significantly stereoselective, with 70% **8–3***a* and 30% **8–3***b* being obtained. Similarly **8–1***b* gives 70% **8–3***b* and 30% **8–3***a*, i.e. the photosolvolysis results in predominant inversion (15). They misassigned the stereochemistry of the diastereoisomers of both the acetates and the ethers, thus, fortuitously, making their conclusion valid.

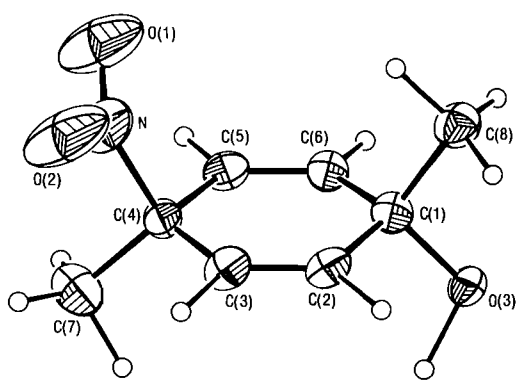

FIG. 1. Perspective view of (*E*)-1,4-dimethyl-4-nitrocyclohexa-2,5-dienol.

We have also made a ^{13}C nmr shift-reagent study, using Eu([$^2H_9$]fod)$_3$, of the 1,4-dimethyl-4-nitrocyclohexa-2,5-dienyl acetates and dienols and some related 1-alkyl-4-methyl-4-nitrocyclohexa-2,5-dienyl acetates. Results are given in Table 1. In the case of the dimethyldienyl acetates the relative shift gradient of the 4-CH_3 carbon atom in the (*E*)-isomer (**8–1***a*) is twice that of the same carbon atom in the (*Z*)-isomer (**8–1***b*), in accord with expectations. The relative shift gradients are less differentiated for the other pairs of corresponding carbon atoms in the two isomers. In the cases of the *a* isomers of 1-ethyl-4-methyl-4-nitrocyclohexadienyl acetate (**10–2**) and 1-isopropyl-4-methyl-4-nitrocyclohexadienyl acetate (**9–1**) the relative shift gradient of the 4-CH_3 carbon atom is likewise twice that of the same carbon in the *b* isomers (for the pairs of diastereoisomeric acetates the *a* isomer is that which is eluted first on chromatography). We therefore conclude that the *a* isomers all have the *E*-configuration. It is also to be noted that the shift gradient of C-4 is consistently smaller in the *a* isomers than in the *b* isomers.

Table 2 shows ^{13}C chemical shifts for the diastereoisomers of the 1-alkyl-4-methyl-4-nitrocyclohexa-2,5-dienyl acetates (**8–1**, **10–2**, **9–1**, and **11–2**) and the 4-ethyl-1-methyl- (**10–1**) and 1,4-diethyl-4-nitrocyclohexa-2,5-dienyl acetates (**10–3**). For each pair of diastereoisomers that diastereoisomer eluted first on chromatography is desig-

TABLE 1. Relative gradients (gradient 1-OCOCH_3 = 1.00) of ^{13}C chemical shifts for diene adducts resulting from the addition of Eu([$^2H_9$]fod)$_3$

Compound	C-1	C-2	C-3	C-4	1-CHCH_3	1-*C*H-	1-O*C*OCH$_3$	4-CH_3
8-1*a*	0.73	0.36	0.29	0.15	—	0.33	1.02	0.16
8-1*b*	0.74	0.35	0.29	0.22	—	0.38	0.84	0.08
10-2*a*	0.72	0.39	0.31	0.18	0.22	0.32	1.10	0.18
10-2*b*	0.71	0.35	0.28	0.22	0.19	0.33	0.93	0.08
9-1*a*	0.76	0.41	0.38	0.25	0.21	0.30	1.11	0.26
9-1*b*	0.76	0.40	0.34	0.30	0.21	0.30	0.93	0.11
8-2*a*	1.00	0.31	0.21	0.17	—	0.48	—	0.07
8-2*b*	1.00	0.29	0.23	0.18	—	0.49	—	0.08

TABLE 2. ^{13}C Chemical shifts (δ_C, ppm) of diene adducts

Compound	C-1	C-2	C-3	C-4	1-CHCH_3	1-*C*H	1-OCOCH$_3$	1-O*C*OCH$_3$	4-*C*H	4-CH*C*H$_3$
8-1*a*	73.4	133.7	126.1	84.9	—	27.1	21.8	169.7	25.4	
8-1*b*	73.1	132.8	126.4	82.5	—	26.9	21.8	169.7	27.8	
10-2*a*	76.5	132.2[a]	127.5[a]	85.0	7.5	32.3	21.8	169.7	25.5	
10-2*b*	76.3	131.4[a]	127.8[a]	82.6	7.7	31.7	21.8	169.7	27.9	
9-1*a*	78.4	130.9	128.1	85.0	16.6	36.0	21.9	169.8	25.5	
9-1*b*	78.2	130.1	128.4	82.8	16.6	35.2	21.8	169.6	27.7	
11-2*a*	79.3	130.8[a]	127.8[a]	84.6	24.8	38.9	21.8	169.7	25.9	
11-2*b*	78.7	129.7	128.2	82.6	24.7	38.3	21.6	169.4	27.1	
10-1*a*	73.7	135.1[a]	124.6[a]	88.1	—	26.9	21.8	169.7	32.2	8.3
10-1*b*	73.2	133.8[a]	125.0[a]	86.4	—	26.9	21.8	169.6	33.6	8.4
10-3*a*	77.0	133.8[a]	126.1[a]	88.3	7.5	32.3[b]	21.6	169.4	32.6[b]	8.2
10-3*b*	76.2	132.5[a]	126.8[a]	86.5	7.8	32.2[b]	21.7	169.3	34.1[b]	8.3

[a]Assignments reversed from those reported earlier (10, 11).[6]
[b]Assignments for 1-CH_2CH_3 and 4-CH_2CH_3 may be reversed.

nated as the *a* isomer. In the *a* isomers of the 1-alkyl-4-methyl series the chemical shift of the 4-methyl group is 25.5 ± 0.4 ppm, 2 ppm less than the chemical shift of the same group in the *b* isomers (27.6 ± 0.5 ppm). The chemical shift of the C-4 atom is 84.9 ± 0.3 ppm in the *a* isomers, 2 ppm larger than that of the same atom in the *b* isomers (82.6 ± 0.2). These differences are certainly significant and are consistent with the existence of a common stereochemical relationship between the *a* isomers, on the one hand, and the *b* isomers, on the other. This conclusion is buttressed by other parallels in the physical properties of *a* isomers versus *b* isomers. In the ^{13}C spectra the chemical shifts of C-1 and C-2 are larger and that of C-3 is smaller in *a* isomers than in *b* isomers. In the ^1H nmr spectrum (Table 3) the chemical shift of the 4-CH_3 protons in the *a* isomers (δ 1.78 ppm) is significantly larger than that of the corresponding protons in the *b* isomers (1.71 ppm). The chemical shift of the acetate methyl group is larger and those of the 2- and 3-protons are smaller in the *a* isomers than in the *b* isomers. The chemical shift of the 1′-H in the alkyl group is smaller in the *a* isomers than in the *b* isomers. The *a* isomers also have lower melting points than the *b* isomers. Some of the individual differences of cited physical properties between *a* and *b* isomers are probably not significant. Collectively the trends are unmistakable. Clearly, all *a* isomers have some fundamental similarity which distinguishes them from *b* isomers and this can only be a common stereochemistry. The *a* isomers must therefore have the *E*-configuration and the *b* isomers must have the *Z*.

The relationships between the physical properties of *a* and *b* isomers identified in the 1-alkyl-4-methyl-4-nitrocyclohexadienyl acetate series also extend to the 1-alkyl-4-ethyl-4-nitrocyclohexadienyl acetate series (**10–1** and **10–3**). Again the *a* isomers are those which are eluted first on chromatography. The 4-ethyl-1-methyl compounds were obtained crystalline and the *a* isomer was the lower melting. In the ^{13}C nmr spectra (Table 2) the chemical shifts of C-1, C-2, and C-4 are larger, and of C-3 and 4-CH_2CH_3 are smaller in the *a* isomers. In addition the chemical shift of 4-CH_2CH_3 is smaller in the *a* isomers. In the ^1H nmr spectra (Table 3) the chemical shifts of 2-H, 3-H, and 1′-H of 1-alkyl, are all smaller and those of the acetate methyl and 4-CH_2CH_3 are larger in the *a* isomers. In addition the shifts of 4-CH_2CH_3 are also larger in the *a* series. The exactly parallel

Can. J. Chem. Downloaded from www.nrcresearchpress.com by 210.87.254.6 on 09/06/12
For personal use only.

TABLE 3. ^{1}H Chemical shifts (δ, ppm) of diene adducts

Compound	2-H	3-H	1-CHCH_3	1-CH	1-OCOCH_3	4-CH	4-CHCH_3	Melting point (°C)
8-1*a*	6.07	6.07	—	1.46	1.99	1.79	—	49
8-1*b*	6.19	6.19	—	1.49	1.97	1.71	—	59
10-2*a*	5.98	6.18	0.79	1.76	1.99	1.79	—	29
10-2*b*	6.07	6.31	0.78	1.83	1.98	1.71	—	54
9-1*a*	5.96	6.22	0.88	2.05	2.00	1.79	—	33
9-1*b*	6.05	6.33	0.89	2.21	1.97	1.71	—	37
11-2*a*	6.03[a]	6.21	0.93	—	1.98	1.75	—	83
11-2*b*	6.04[b]	6.34[c]	0.96	—	1.95	1.70	—	135
10-1*a*	6.09	6.17	—	1.43	1.98	2.16	0.92	20
10-1*b*	6.19	6.19	—	1.47	1.97	2.09	0.86	47
10-3*a*	6.10	6.10	0.77	1.77	1.97	2.14	0.92	
10-3*b*	6.12	6.22	0.84	1.83	1.95	2.05	0.89	

[a]Previously reported as 7.03 (11).
[b]Previously reported as 7.04 (11).
[c]Previously reported as 7.34 (11).

trends of the physical properties in the 4-ethyl series, with that of the 4-methyl series, argues for the same fundamental similarity between *a* isomers in both series, i.e. the *a* isomers in both series have the (*E*)-configuration. For the 4-ethyl compounds this assignment is the same as that made in the previous work on the basis of a shift reagent study of the terminal protons of the 4-ethyl group (10).

In contrast to the situation in the acetates the relative shift gradients for 4-CH_3 in the isomeric dienols **8–2***a* and **8–2***b* are not significantly different (Table 1). We have also examined the ^{13}C and ^{1}H nmr data for the pairs of isomeric 1-alkyl-4-methyl-4-nitrocyclohexa-2,5-dienols, 1-ethyl- and 1-methyl-4-ethyl-4-nitrocyclohexa-2,5-dienols, and some of their methyl ethers. Although there appear to be some systematic differences in the nmr data of diastereoisomers in these series, which can presumably be related to the stereochemistry, these differences appear to be too small to be of value for the assignment of unknown stereochemistry.

Experimental

General experimental methods have been described previously (8, 16). 4-Methylphenol and 1,4-dimethylbenzene were from Aldrich. 4-Methylphenyl acetate was prepared by acetylation of the phenol (17). 4-Methyl-4-nitrocyclohexa-2,5-dienone was prepared by nitration of the acetate in acetic anhydride at −15°C (12, 18) (the reaction mixture was prepared at −78°C and then warmed to −15°C). On slow addition of methanol at −78°C the nitrodienone was precipitated (12). After recrystallization from methanol the colourless crystals had mp 43–45°C; ^{1}H nmr ($CDCl_3$, −20°C) δ: 1.96 (s, 3, CH_3), 6.43 (d, J = 10 Hz, 2-*H* and 6-*H*), 7.19 (d, J = 10 Hz, 3-*H* and 5-*H*) ppm; ^{13}C nmr ($CDCl_3$, −40°C) δ_C: 25.7 (4-*C*H_3), 84.2 (*C*-4), 130.1 (*C*-2 and *C*-6), 143.4 (*C*-3 and *C*-5), 184.1 (*C*-1) ppm. 2,6-Dideuterio-4-methylphenol was obtained by deuteration of 4-methylphenol (10.8 g, 0.1 mol) by refluxing a solution in D_2O (100 g) with PBr_3 (8 cm^3, 0.08 mol) for 5 h (cf. ref. 19). 2,6-Dideuterio-4-methylphenol constituted over 90% of the isolated phenol (nmr) and had mp 31–32°C; ir (KBr): 3310 and 1240 (OH), 2260 (C—D), 2920 (CH_3) cm^{-1}; ^{1}H nmr ($CDCl_3$) δ: 2.24 (s, 3, CH_3), 5.07 (s, 1, O*H*), 7.03 (s, 2, 3-*H* and 5-*H*) ppm; ^{13}C nmr ($CDCl_3$) δ_C: 20.4 (4-*C*H_3), 115.1 (t, J_{CD} = 24.1 Hz, *C*-2 and *C*-6), 130.1 (*C*-3 and C-5), 130.1 (*C*-4), 152.8 (*C*-1) ppm. Acetylation (17) of the dideuteriophenol gave 2,6-dideuterio-4-methylphenyl acetate as an oil, ir (film): 2300 (C—D), 1765, 1220 and 1060 (OCOCH_3) cm^{-1}; ^{1}H nmr ($CDCl_3$) δ: 2.20 (s, 3, 4-CH_3), 2.28 (s, 3, OCOCH_3), 7.14 (s, 2, 3-*H* and 5-*H*) ppm. Nitration of the 2,6-dideuterio-4-methylphenyl acetate gave 2,6-dideuterio-4-methyl-4-nitrocyclohexa-2,5-dienone as colourless crystals, mp 43–45°C; ir ($CDCl_3$): 2340 (C—D), 1670 (C=O), 1555 and 1340 (NO_2) cm^{-1}; ^{1}H nmr ($CDCl_3$, −20°C) δ: 1.96 (s, 3, CH_3), 7.21 (s, 2, 3-*H* and 5-*H*) ppm; ^{13}C nmr ($CDCl_3$, −40°C) δ_C: 25.8 (4-*C*H_3), 84.0 (*C*-4), 129.8 (t, J_{CD} = 26.1 Hz, *C*-2 and *C*-6), 143.0 (*C*-3 and *C*-5), 184.1 (*C*-1) ppm.

Diastereoisomers of 1,4-Dimethyl-4-nitrocyclohexa-2,5-dienyl Acetate

These were prepared by nitration of *p*-xylene in acetic anhydride at −40°C (2, 8). The diene adducts constituted ca. 88% of the nitration products with the (*E*)-isomer (ca. 70% of the diene component) being predominant. Crystallization of the crude nitration product from ether–pentane (1:5 v/v) gave (*E*)-1,4-dimethyl-4-nitrocyclohexa-2,5-dienyl acetate (**8–1***a*). After a second recrystallization the (*E*)-isomer was obtained as colourless crystals and had mp 50–52°C; ir (KBr): 1740, 1250 and 1060 (OCOCH_3), 1535 and 1345 (NO_2) cm^{-1}; ^{1}H nmr ($CDCl_3$, 0°C) δ: 1.43 (s, 3, 1-CH_3), 1.77 (s, 3, 4-CH_3), 1.97 (s, 3, OCOCH_3), 6.07 (s, 4, 2-*H*, 3-*H*, 5-*H*, 6-*H*) ppm; ^{13}C nmr ($CDCl_3$, 0°C) δ_C: 21.7 (OCO*C*H_3), 25.2 (4-*C*H_3), 27.1 (1-*C*H_3), 73.2 (*C*-1), 84.9 (*C*-4), 126.1 (*C*-3 and *C*-5), 133.6 (*C*-2 and *C*-6), 169.6 (O*C*OCH_3) ppm.[5] Chromatography of the crude nitration product at −40°C on 3% deactivated alumina and elution with ether–pentane gave the (*E*)-isomer in the earlier fractions and the (*Z*)-isomer in the later fractions. (*Z*)-1,4-Dimethyl-4-nitrocyclohexa-2,5-dienyl acetate (**8–1***b*) was obtained as colourless crystals on recrystallization from ether–pentane and had mp 57–60°C; ir (KBr): 1725, 1245

[5]The absorptions of the vinyl carbons of the (*Z*)-2,6-dideuterio dienyl acetate (below) could be assigned unambiguously. The carbons at positions 3 and 5 absorb at higher field than those at positions 2 and 6. The same assignment applies to the (*Z*)-dienyl acetate and is assumed to apply to its (*E*)-isomer. In the shift-reagent studies the higher field vinyl carbons move more slowly downfield than the lower field ones. This also suggests that the higher field carbon atoms are there at positions 3 and 5. Assignment of the 1-CH_3 absorptions is based on the assumption that the 1-CH_3 peak is the one which moves downfield more rapidly in the shift-reagent study.

Can. J. Chem. Downloaded from www.nrcresearchpress.com by 210.87.254.6 on 09/06/12
For personal use only.

Can. J. Chem. Downloaded from www.nrcresearchpress.com by 210.87.254.6 on 09/06/12
For personal use only.

and 1065 ($OCOCH_3$), 1535 and 1340 (NO_2) cm^{-1}; ^1H nmr ($CDCl_3$, 0°C) δ: 1.46 (s, 3, 1-CH_3), 1.70 (s, 3, 4-CH_3), 1.96 (s, 3, $OCOCH_3$), 6.19 (s, 4, 2-*H*, 3-*H*, 5-*H*, 6-*H*) ppm; ^{13}C nmr ($CDCl_3$, 0°C) δ_C: 21.8 ($OCOCH_3$), 27.0 (1-CH_3), 27.8 (4-CH_3), 73.0 (*C*-1), 82.4 (*C*-4), 126.3 (*C*-3 and *C*-5), 132.7 (*C*-2 and *C*-6), 169.7 ($OCOCH_3$) ppm.[5]

Diastereoisomers of 1,4-Dimethyl-4-nitrocyclohexa-2,5-dienol and 2,6-Dideuterio-1,4-dimethyl-4-nitrocyclohexa-2,5-dienol

A solution of (*E*)-dienyl acetate (30 g, 0.14 mol) in dry tetrahydrofuran (60 cm^3) was added with stirring to a solution of aluminium hydride (~ 0.28 mol) in tetrahydrofuran (850 cm^3) at −40°C under an argon atmosphere (20). The mixture was warmed to 0°C, then cooled to −40°C and excess hydride decomposed by dropwise addition of water (150 cm^3). After work-up (*E*)-1,4-dimethyl-4-nitrocyclohexa-2,5-dienol (**8–2***a*) was obtained in quantitative yield. After recrystallization (× 2) from ether–pentane a sample was sublimed at 50°C/20 Pa and had mp 107–108°C; ir (KBr): 3270 (OH), 1540 and 1335 (NO_2) cm^{-1}; ^1H nmr ($CDCl_3$) δ: 1.35 (s, 3, 1-CH_3), 1.73 (s, 3, 4-CH_3), 2.06 (s, 1, O*H*), 5.98 (d, 2, *J* = 10 Hz, 3-*H* and 5-*H*), 6.12 (d, 2, *J* = 10 Hz, 2-*H* and 6-*H*) ppm; ^{13}C nmr ($CDCl_3$, 0°C) δ_C: 26.7 (4-CH_3), 27.7 (1-CH_3), 65.4 (*C*-1), 83.8 (*C*-4), 125.0 (*C*-3 and *C*-5), 137.5 (*C*-2 and *C*-6) ppm.[6]

Reduction of the (*Z*)-nitrodienyl acetate gave the (*Z*)-nitrodienol **8–2***b* which after recrystallization from ether–pentane had mp 50–52°C; ir (KBr): 3270 (OH), 1540 and 1340 (NO_2) cm^{-1}; ^1H nmr ($CDCl_3$) δ: 1.30 (s, 3, 1-CH_3), 1.67 (s, 3, 4-CH_3), 2.29 (s, 1, O*H*), 5.99 (d, 2, *J* = 10 Hz, 3-*H* and 5-*H*), 6.07 (d, 2, *J* = 10 Hz, 2-*H* and 6-*H*) ppm; ^{13}C nmr ($CDCl_3$, 0°C) δ_C: 27.1 (4-CH_3), 27.8 (1-CH_3), 64.9 (*C*-1), 83.7 (*C*-4), 125.1 (*C*-3 and *C*-5), 136.7 (*C*-2 and *C*-6) ppm.[6]

The (*E*)- and (*Z*)-nitrodienols were also prepared by addition of methyllithium to 4-nitro-4-methylcyclohexa-2,5-dienone (12). The product mixture contained the (*E*)- and (*Z*)-isomers in a 1:4 ratio and these were separated by high-pressure liquid chromatography at 0°C on silica using ether as eluant. The predominant product, the (*Z*)-isomer, was eluted first.

The 2,6-dideuterionitrodienols were similarly prepared in 95% yield by the addition of methyllithium to 2,6-dideuterio-4-methyl-4-nitrocyclohexa-2,5-dienone. The ratio of (*E*)-isomer: (*Z*)-isomer was ca. 1:3 and the isomers were separated by hplc. (*Z*)-2,6-Dideuterio-1,4-dimethyl-4-nitrocyclohexa-2,5-dienol, eluted first, was recrystallized from ether–pentane as colourless needles, mp 51–52°C; ir (KBr): 3270 (OH), 2260 (C—D), 1540 (NO_2) cm^{-1}; ^1H nmr ($CDCl_3$) δ: 1.27 (s, 3, 1-CH_3), 1.66 (s, 3, 4-CH_3), 3.16 (s, 1, O*H*), 6.01 (s, 2, 3-*H* and 5-*H*) ppm; ^{13}C nmr ($CDCl_3$, 0°C) δ_C: 27.2 (4-CH_3), 27.8 (1-CH_3), 64.7 (*C*-1), 83.5 (*C*-4), 124.6 (*C*-3 and *C*-5), 136.3 (t, J_{CD} = 24.9 Hz, *C*-2 and *C*-6) ppm. (*E*)-2,6-Dideuterio-1,4-dimethyl-4-nitrocyclohex-2,5-dienol was obtained as colourless needles from ether–pentane and had mp 107–109°C; ir (KBr): 3270 (OH), 2260 (C—D), 1535 and 1335 (NO_2) cm^{-1}; ^1H nmr ($CDCl_3$) δ: 1.35 (s, 3, 1-CH_3), 1.73 (s, 3, 4-CH_3), 2.08 (s, 1, O*H*), 5.99 (s, 2, 3-H and 5-H) ppm; ^{13}C nmr ($CDCl_3$, 0°C) δ_C: 26.8 (4-CH_3), 27.8 (1-CH_3), 65.4 (*C*-1), 83.9 (*C*-4), 125.1 (*C*-3 and C-5), 137.2 (t, J_{CD} = 24.4 Hz, *C*-2 and *C*-6) ppm.

Diastereoisomers of 1,4-Dimethyl-4-nitrocyclohexa-2,5-dienyl Methyl Ether; (Z)-2,6-Dideuterio-1,4-dimethyl-4-nitrocyclohexa-2,5-dienyl Methyl Ether

A mixture of (*E*)-nitrodienol (1.7 g, 10 mmol), moist silver oxide (~ 6.8 g, 29 mmol), methyl iodide (27.8 g, 196 mmol), and potassium hydroxide (0.19 g, 3.4 mmol) was stirred at ambient temperature for 5 h (cf. ref. 21). Chloroform was added and the insoluble material filtered off. The filtrate was dried ($MgSO_4$) and refiltered. The chloroform was evaporated under reduced pressure to yield the (*E*)-nitrodienyl methyl ether **8–3***b* as an oil, ir (film): 1545 and 1340 (NO_2), 2825 and 1095 (OCH_3) cm^{-1}; ^1H nmr ($CDCl_3$) δ: 1.32 (s, 3, 1-CH_3), 1.74 (s, 3, 4-CH_3), 3.03 (s, 3, OCH_3), 5.92 (d, 2, *J* = 10 Hz, 2-*H* and 6-*H*), 6.17 (d, 2, *J* = 10 Hz, 3-*H* and 5-*H*) ppm; ^{13}C nmr ($CDCl_3$, 0°C) δ_C: 26.7 and 27.2 (1-$CH_3$and 4-CH_3), 52.0 (1-OCH_3), 70.7 (*C*-1), 84.0 (*C*-4), 128.3 (*C*-3 and *C*-5), 135.7 (*C*2 and *C*-6) ppm.

Methylation of the (*Z*)-nitrodienol by the above procedure afforded the (*Z*)-nitrodienyl methyl ether **8–3***a* as an oil, ir (film): 1545 and 1340 (NO_2), 2830 and 1100 (OCH_3) cm^{-1}; ^1H nmr ($CDCl_3$) δ: 1.28 (s, 3, 1-CH_3), 1.70 (s, 3, 4-CH_3), 3.08 (s, 3, OCH_3), 5.90 (d, 2, *J* = 10 Hz, 2-*H* and 6-*H*), 6.22 (d, 2, *J* = 10 Hz, 3-*H* and 5-*H*) ppm; ^1H nmr (CCl_4) δ: 1.22, 1.67, 3.02, 5.83 (d), 6.17 (d) pm; ^{13}C nmr ($CDCl_3$, 0°C) δ_C: 27.3 and 27.7 (1-CH_3 and 4-CH_3), 52.4 (1-OCH_3), 70.1 (*C*-1), 83.3 (*C*-4), 128.2 (*C*-3 and *C*-5), 135.0 (*C*-2 and *C*-6) ppm.

Methylation of the (*Z*)-2,6-dideuteronitrodienol gave the (*Z*)-dideuteronitrodienyl methyl ether as an oil, ir (film): 2250 (C—D), 1545 and 1340 (NO_2), 2830 and 1100 (OCH_3) cm^{-1}; ^1H nmr ($CDCl_3$) δ: 1.28 (s, 3, 1-CH_3), 1.70 (s, 3, 4-CH_3), 3.08 (s, 3, OCH_3), 6.22 (s, 2, 3-*H* and 5-*H*) ppm; ^{13}C nmr ($CDCl_3$, −5°C) δ_C: 27.3 and 27.7 (1-CH_3 and 4-CH_3), 52.5 (1-OCH_3), 70.0 (*C*-1), 83.3 (*C*-4), 128.2 (*C*-3 and *C*-5), 134.6 (t, J_{CD} = 24.9 Hz, *C*-2 and *C*-6) ppm.

(Z)-2,6-Dideuterio-1,4-dimethyl-4-nitrocyclohexa-2,5-dienyl Acetate

The (*Z*)-dideuteronitrodienol (0.4 g, 2.3 mmol) was stirred for 52 h at 35°C with acetic anhydride (2.4 cm^3) and [$^2H_5$]pyridine (0.27 mm^3, 3.5 mmol). Cold ether (50 cm^3) was added, the organic layer was washed with ice water (5 × 50 cm^3), dried ($MgSO_4$), and the ether evaporated to afford an oil (0.37 g) containing 83 mol% of the acetate. Recrystallization from ether–pentane gave colourless crystals, mp 60–61.5°C; ir (film): 2260 (C—D), 1740, 1245 and 1065 ($OCOCH_3$), 1545 and 1340 (NO_2) cm^{-1}; ^1H nmr ($CDCl_3$) δ: 1.47 (s, 3, 1-CH_3), 1.69 (s, 3, 4-CH_3), 1.94 (s, 3, $OCOCH_3$), 6.21 (s, 2, 3-*H* and 5-*H*) ppm; ^{13}C nmr ($CDCl_3$, 0°C) δ_C: 21.8 ($OCOCH_3$), 26.9 (1-CH_3), 27.8 (4-CH_3), 72.9 (*C*-1), 82.4 (*C*-4), 126.2 (*C*-3 and *C*-5), 132.4 (t, J_{CD} = 24.0 Hz, *C*-2 and *C*-6) ppm.

Structure Determination of (E)*-1,4-Dimethyl-4-nitrocyclohexa-2,5-dienol*

$C_8H_{11}NO_3 \cdot C_4H_{10}O$ f.w. = 243.3

Rhombohedral, space group $R\bar{3}$ (or R3) hexagonal cell *a* = 30.21(1), *c* = 5.848(2) Å, *U* = 4622 $Å^3$, *Z* = 18, ρ_o = 1.57, ρ_c ~ 1.5 (flotation), 18°C, MoKα_1 = 0.70930 Å, μ = 1.4 cm^{-1}.

A crystal of dimensions 0.25 × 0.30 × 0.40 mm was used to collect the 650 independent reflections measured ($2\theta \leq 35°$), of which 463 were observed ($I > 2.3\sigma$), on a Picker FACS-I diffractometer. The structure was determined by direct methods and refined by full-matrix least-squares techniques to $R = 7.0\%$ (assuming space group $R\bar{3}$). ($R = \sum||F_o| - |F_c||/\sum|F_o|$.) The model used did not include hydrogen atoms for the solvent molecule and a final electron-density difference map indicated the major discrepancies were in the solvent area.

1. D. J. Blackstock, A. Fischer, K. E. Richards, J. Vaughan, and G. J. Wright. Chem. Commun. 641 (1970).
2. D. J. Blackstock, J. R. Cretney, A. Fischer, M. P. Hartshorn, K. E. Richards, J. Vaughan, and G. J. Wright. Tetrahedron Lett. 2793 (1970).
3. R. C. Hahn and M. B. Groen. J. Am. Chem. Soc. **95**, 6128 (1973).

[6]Assignments for the vinylic protons and carbons were made by comparison with the deuterated analogue. The chemical shifts of 2-H (6-H) and 3-H (5-H) were wrongly assigned in the earlier report (8).

4. R. B. MOODIE and K. SCHOFIELD. Acc. Chem. Res. **9**, 287 (1976).
5. T. BANWELL, C. S. MORSE, P. C. MYHRE, and A. VOLLMAR. J. Am. Chem. Soc. **99**, 3042 (1977).
6. A. FISCHER, D. R. A. LEONARD, and R. RÖDERER. Can. J. Chem. **57**, 2527 (1979).
7. A. FISCHER and J. N. RAMSAY. J. Chem. Soc. Perkin Trans. II, 237 (1973).
8. A. FISCHER and J. N. RAMSAY. Can. J. Chem. **52**, 3960 (1974).
9. A. FISCHER and R. RÖDERER. Can. J. Chem. **54**, 423 (1976).
10. A. FISCHER, G. N. HENDERSON, and R. J. THOMPSON. Aust. J. Chem. **31**, 1241 (1978).
11. A. FISCHER and R. RÖDERER. Can. J. Chem. **54**, 3978 (1976).
12. C. E. BARNES, K. S. FELDMAN, M. W. JOHNSON, H. W. LEE, and P. C. MYHRE. J. Org. Chem. **44**, 3925 (1979).
13. H. SHOSENJI, A. NAGAYOSHI, T. TAKEMOTO, and K. YAMADA. J. Chem. Soc. Chem. Commun. 770 (1979).
14. C. E. BARNES and P. C. MYHRE. J. Am. Chem. Soc. **100**, 973 (1978); 975 (1978).
15. H. SHOSENJI, K. ESAKI, and K. YAMADA. Tetrahedron Lett. 91 (1980).
16. A. FISCHER and G. N. HENDERSON. Can. J. Chem. **57**, 552 (1979).
17. A. I. VOGEL. Practical organic chemistry. Longmans, London. 1956. p. 669.
18. D. J. BLACKSTOCK, M. P. HARTSHORN, A. J. LEWIS, K. E. RICHARDS, J. VAUGHAN, and G. J. WRIGHT. J. Chem. Soc. B, 1212 (1971).
19. A. A. BOTHNER-BY and E. MOSER. J. Am. Chem. Soc. **90**, 2347 (1968).
20. A. E. FINHOLDT, A. C. BOND, and H. I. SCHLESINGER. J. Am. Chem. Soc. **69**, 1199 (1947); H. C. BROWN and N. M. YOON. J. Am. Chem. Soc. **88**, 1464 (1966); A. FISCHER and K. C. TEO. Can. J. Chem. **56**, 258 (1978).
21. H. BURTON and C. W. SHOPPEE. J. Chem. Soc. 197 (1934).

Erratum: Synthesis and stereochemistry of hydrogenated 1,1,4,4,7a-pentamethylindenes

A. F. THOMAS, M. OZAINNE, AND R. GUNTZ-DUBINI
Research Laboratories, Firmenich SA, Geneva, Switzerland

Ref.: Can. J. Chem. **58**, 1810 (1980)
Received October 30, 1980

On p. 1816, the preparation by method A of 2,6,6-trimethyl-2-(prop-2-ynyl)-cyclohexanone, **13**, is incorrect. Method B is correct, and leads to **13**, which has the spectral properties and microanalysis ascribed to it under method A.

Can. J. Chem. Downloaded from www.nrcresearchpress.com by 210.87.254.6 on 09/06/12
For personal use only.

Silver(I) complexes of 4,6-dimethylpyrimidine-2(1*H*)-thione

RAFFAELE BATTISTUZZI AND GIORGIO PEYRONEL
Istituto di Chimica Generale e Inorganica, University of Modena, 41100 Modena, Italy

Received July 11, 1980

RAFFAELE BATTISTUZZI and GIORGIO PEYRONEL. Can. J. Chem. **59**, 591 (1981).

The following silver(I) complexes of 4,6-dimethylpyrimidine-2(1*H*)-thione (HL) have been prepared and investigated by conductometric, infrared, and Raman methods: $Ag(HL)X$ (X = Cl, Br, I, SCN), $Ag(HL)_2X$ (X = Cl, Br, I, NO_3 (MeOH), ClO_4 ($0.25CHCl_3$), BF_4 ($0.25CHCl_3$)), $Ag_mX_n(H_2L)_{n-m}$ (X = Cl: $m = 6$, $n = 11$; Br: $m = 2$, $n = 3$; I: $m = 5$, $n = 7$), AgL, $AgL \cdot Ag(HL)NO_3$, $AgL \cdot [Ag(HL)X]_2$ (X = ClO_4, BF_4). The HL acts as N,S-chelating ligand in the $Ag(HL)X$ and $Ag(HL)_2X$ (X = NO_3, ClO_4, BF_4) complexes and partially in the $Ag(HL)_2X$ (X = Cl, Br, I) complexes in which the halide ion is still coordinated. In the $Ag_mX_n(H_2L)_{n-m}$ complexes the H_2L^+ ion is at least partially S-coordinated to some silver ions. In AgL, L^- acts as tridentate ligand N,N,S-bridging the silver ions. In the $AgL \cdot Ag(HL)NO_3$ complex the nitrate ion is coordinated.

RAFFAELE BATTISTUZZI et GIORGIO PEYRONEL. Can. J. Chem. **59**, 591 (1981).

On a préparé et étudié par conductimètrie et par la spectroscopie Raman et infrarouge, les complexes suivants de l'argent(I) avec la diméthyl-4,6 1H-pyrimidinethione-2 (HL): $Ag(HL)X$ (X = Cl, Br, I, SCN), $Ag(HL)_2X$ (X = Cl, Br, I, NO_3 (MeOH), ClO_4 ($0.25CHCl_3$), BF_4 ($0.25CHCl_3$)), $Ag_mX_n(H_2L)_{n-m}$ (X = Cl: $m = 6$, $n = 11$; Br: $m = 2$, $n = 3$; I: $m = 5$, $n = 7$), AgL, $AgL \cdot Ag(HL)NO_3$, $AgL \cdot [Ag(HL)X]_2$ (X = ClO_4, BF_4). Le HL agit comme un ligand chélatant N—S dans les complexes $Ag(HL)X$ et $Ag(HL)_2X$ (X = NO_3, ClO_4, BF_4) et partiellement dans les complexes $Ag(HL)_2X$ (X = Cl, Br, I) ou l'ion halogénure est encore coordonné. Dans les complexes de $Ag_mX_n(H_2L)_{n-m}$, l'ion H_2L^+ est au moins coordonné par le soufre à quelques ions d'argent. Dans AgL, L^- agit comme un ligand tridentate dans lequel N,N,S forment un pont entre les ions argent. Dans le complexe $AgL \cdot Ag(HL)NO_3$, l'ion nitrate est coordonné.

[Traduit par le journal]

Introduction

The complexes of 4,6-dimethylpyrimidine-2(1*H*)-thione (Hdmpt = HL)

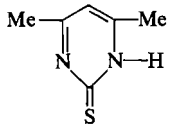

with some divalent metal ions have been previously studied (1, 2) and the crystal structure of the cobalt(III) complexes $Co(dmpt)_3$ has been determined (3). In a previous work (4) we have investigated the copper(I) complexes of the neutral, deprotonated, and protonated ligand. The silver(I) complexes have been prepared now and studied by conductometric methods and infrared and Raman spectra, in order to establish the coordinating sites of the ligand which also depend on the protonation or deprotonation state of the molecule. The coordinating behaviour of this ligand may have an interest in the context of the studies on the coordination of heavy metals to nucleotides and related components of nucleic acids and particularly of the substituted pyrimidines which may have an antitumor activity (refs. 2, 3, and references therein).

Experimental

The ligand and its hydrohalides were prepared by the methods previously described (4). The complexes were prepared as follows:

$Ag(HL)X$ (X = Cl, Br, I, SCN) and $Ag(HL)_2X$ (X = Cl, Br, I)

By refluxing under stirring for 3–4 h the freshly prepared silver salts (3 mmol) in a solution of the ligand (3 or 6 mmol) in 4/1 $CHCl_3$/MeOH (25 cm^3). After standing overnight the complexes were filtered and washed with $CHCl_3$.

$Ag_mX_n(H_2L)_{n-m}$ (X = Cl: m = 6, n = 11; Br: m = 2, n = 3; I: m = 5, n = 7)

By refluxing under stirring for 4 h the freshly prepared silver halide (3 mmol) in a solution of H_2LX (3 or 6 mmol) in 1/1 MeOH/$CHCl_3$ (20 cm^3). The compounds were washed with MeOH and $CHCl_3$.

AgL

A solution of $AgNO_3$ (3 mmol) in H_2O (5 cm^3) was added under stirring to an aqeuous solution (10 cm^3) of the ligand (6 mmol). The instantaneous precipitate was stirred for 2 h and washed with MeOH.

$AgL \cdot Ag(HL)NO_3$ and $AgL \cdot [Ag(HL)X]_2$ (X = ClO_4, BF_4)

A MeOH solution (5 cm^3) of $AgNO_3$, $AgClO_4 \cdot H_2O$, $AgBF_4$ (4 mmol) was added drop by drop under stirring to a hot solution of the ligand (4 mmol) in $CHCl_3$ (20 cm^3). After stirring for 3 h the products were washed with 1/1 MeOH/$CHCl_3$.

$Ag(HL)_2NO_3 \cdot MeOH$ and $Ag(HL)_2X \cdot O.25CHCl_3$ (X = ClO_4, BF_4)

By adding with stirring solid $AgNO_3$, $AgClO_4 \cdot H_2O$, $AgBF_4$ (3 mmol) to a solution of the ligand (6 mmol) in $CHCl_3$ (25 cm^3) for the perchlorate and fluoborate and in $CHCl_3$ + MeOH (17 + 3 cm^3) for the nitrate. After 2 h of stirring the microcrystalline products were washed with $CHCl_3$. All the products were dried *in vacuo* on KOH.

Silver was determined gravimetrically for the halide and thiocyanate complexes and volumetrically by the Volhard's method for the other compounds; carbon, hydrogen, and nitrogen by microanalytical methods (Table 1). Molar conductivities were determined on freshly prepared 10^{-3} *M* DMF solutions at

0008-4042/81/030591-06$01.00/0
©1981 National Research Council of Canada/Conseil national de recherches du Canada

Can. J. Chem. Downloaded from www.nrcresearchpress.com by 210.87.254.6 on 09/06/12
For personal use only.

25°C with a WTW conductivity bridge type LBB. Infrared spectra (Tables 2 and 3) were recorded on the solids in KBr pellets (4000–250 cm^{-1}) and as Nujol mulls on polythene (500–50 cm^{-1}) with a Perkin Elmer 180 spectrophotometer.

Raman spectra (20–600 cm^{-1}) were recorded on the solid samples with a Jobin Yvon Ramanor HG2S spectrophotometer equipped with a Spectra-Physics 165 argon ion laser (514.5 nm line) using a rapidly rotating sample holder. The spectra were calibrated by means of the plasma lines of the laser. Satisfactory Raman spectra could not be obtained for the Ag(HL)I, $Ag_2Br_3(H_2L)$, $Ag_5I_7(H_2L)_2$, $AgL \cdot Ag(HL)NO_3$, and perchlorate complexes because these compounds were unstable or highly fluorescent in the laser beam.

The molecular weights of the compounds could not be determined because of their insolubility or very low solubility (of the order of 10^{-3} *M*) in all the solvents suitable for osmometric or tensimetric determinations. Even in DMF, which seems to be the best solvent for them, some of the compounds as indicated in Table 1 give opalescent solutions, probably with decomposition.

Results and Discussion

In the silver(I) complexes of 4,6-dimethylpyrimidine-2(1*H*)-thione here described, the ligand may be present in the neutral form HL with 1:1 and 1:2 M:HL ratios, in the deprotonated L^- and in the protonated H_2L^+ form.

Copper(I) and silver(I) complexes of Hdmpt show the same stoichiometries only for the compounds M(HL)X (X = Cl, Br, I), $M(HL)_2X$ (X = Cl, Br), ML, and $ML \cdot [M(HL)X]_2$ (X = ClO_4, BF_4).

In DMF solution the complexes Ag(HL)X (X = Cl, Br, I, SCN), $Ag(HL)_2X$ (X = Cl, Br, I), AgL, and $AgL \cdot Ag(HL)NO_3$ behave as non-electrolytes, the complexes $Ag(HL)_2X$ (X = NO_3, ClO_4, BF_4) and $Ag_2Br_3(H_2L)$ as 1:1 electrolytes (Λ_M = 65–90) (5), the complexes $AgL \cdot [Ag(HL)X]_2$ (X = ClO_4, BF_4) as 1:2 electrolytes (Λ_M = 130–170) (5) while the complex $Ag_5I_7(H_2L)_2$ has a molar conductivity intermediate between those of 1:1 and 1:2 electrolytes and the complex $Ag_6Cl_{11}(H_2L)_5$ a molar conductivity of the order or greater than those reported for 1:3 or 1:4 electrolytes (5, 6).

The infrared bands of the ligand HL and its protonated H_2L^+ forms reported and discussed in a previous work (4) were recorded with a Perkin Elmer 521 spectrophotometer. They have been recorded again with a Perkin Elmer 180 spectrophotometer in order to be better compared with the spectra of the new complexes. For this reason some of the wave numbers reported in this work for HL and H_2LCl slightly differ from those given in the previous work (4).

In the silver complexes the ligand bands lying in the ν(C=N) region (Table 2) show only very small frequency decreases which in some cases may be considered as significant for a coordination of the ligand through its ring-nitrogen atom, while for the ligand bands in the 1230–1160 cm^{-1} region, to which a ν(NCN) + ν(NCS) + ν(CS) contribution was previously assigned (4), no significant frequency change is observed. The strong ligand band at 853 cm^{-1} lying in the frequency range in which the ν(C=S) bands of several thioamides were located (7) is substituted in most of the silver(I) Hdmpt complexes by other bands at lower frequencies down to 808 cm^{-1} and this may be a clear indication of the coordination of the ligand through its thiocarbonylic sulphur atom.

In the far ir and Raman spectra (Table 3) some new bands like those in the 320–290 and 200–190 cm^{-1} region are sufficiently distinct from the ligand bands to be safely attributed to metal–ligand vibrations. Other bands like those in the 280–270 cm^{-1} region and 228–224 cm^{-1} regions very near to two strong ligand bands, are only tentatively assigned to metal–ligand bands by considering that they are present only in some complexes. Most of the ν(AgX) bands have been only tentatively assigned as they are not clearly distinct from other bands. Particularly the ν(AgCl) bands at 228–220 cm^{-1} are considered as coincident or coupled with a ν(AgS) mode.

The assignment of the bands in the 320–270 cm^{-1} region to ν(AgN) and in the 230–180 cm^{-1} region to ν(AgS) is in agreement with the assignments given for the Hdmpt complexes of copper(I) (4) ν(CuN) = 317–288 cm^{-1}, ν(CuS) = 223–191 cm^{-1}. For the 2-imino-4-oxo-1,3-thiazolidine complexes ν(AgN) at 290–270 cm^{-1} and ν(AgS) at 235 cm^{-1} were reported (8, 9). For the pyrimidine-2-thione complexes with some bivalent metal halides of the first transition series ν(ML) at 265–231 cm^{-1} were given by attributing to them an appreciable contribution of ν(MN) character (10).

Increased ν(MN) frequencies in the silver(I) Hdmpt complexes with respect to those of the pyrimidine-2-thione complexes of other metals may be due to the electron releasing effect of the 4,6-methyl groups one of which is contiguous to the nitrogen atom.

The chelation ability has been demonstrated for Hdmpt by the X-ray structure of the Co(III) $(dmpt)_3$ complex (3) and admitted for the pyrimidine-2-thione (10) and its 1,4,5-trimethyl derivative (11). The ν(AgX) frequencies reported in Table 3 are in the range of similar values given for bridging halide or for "long" silver–halide bonds (12–15).

With these assumptions and the limitations given by the uncertainty in the identification of some of the metal–ligand and particularly of the metal–halogen stretching bands an interpretation of the complexes may be tentatively done.

The presence of two ν(AgN) and two ν(AgS)

Can. J. Chem. Downloaded from www.nrcresearchpress.com by 210.87.254.6 on 09/06/12
For personal use only.

Can. J. Chem. Downloaded from www.nrcresearchpress.com by 210.87.254.6 on 09/06/12
For personal use only.

TABLE 1. Analytical data, colour, and molar conductivities Λ_M (Ω^{-1} mol^{-1} cm^2) at 25°C in 10^{-3} *M* DMF solution of the 4,6-dimethylpyrimidine-2(1*H*)-thione (HL) complexes

Species	Colour	Ag		C		H		N		Λ_M
		Found	Calcd.	Found	Calcd.	Found	Calcd.	Found	Calcd.	
Ag(HL)Cl	White	38.00	38.04	25.33	25.39	2.83	2.84	9.80	9.87	24
Ag(HL)Br	White	32.85	32.89	21.86	21.95	2.45	2.46	8.50	8.54	22
Ag(HL)I	Light yellow	28.71	28.76	19.11	19.20	2.05	2.15	7.28	7.47	13
Ag(HL)SCN	Ivory	35.18	35.23	27.38	27.43	2.63	2.63	13.64	13.71	39
$Ag(HL)_2Cl$	Ivory	25.00	25.46	34.00	33.98	3.79	3.80	13.19	13.21	19
$Ag(HL)_2Br$	Ivory	23.03	23.04	30.75	30.75	3.44	3.44	11.90	11.96	19
$Ag(HL)_2I$	Ivory	21.03	20.93	27.64	27.95	3.09	3.13	10.73	10.87	14
$Ag(HL)_2NO_3 \cdot MeOH$	Yellowish	22.37	22.37	32.34	32.35	4.13	4.18	14.50	14.51	61
$Ag(HL)_2ClO_4 \cdot \frac{1}{4}CHCl_3$	Light yellow	20.90	20.84	28.50	28.40	3.17	3.16	10.66	10.82	73
$Ag(HL)_2BF_4 \cdot \frac{1}{4}CHCl_3$	Light yellow	21.18	21.36	28.71	29.11	3.24	3.24	10.97	11.09	78
$Ag_6Cl_{11}(H_2L)_5$	Yellowish	37.10	37.13	20.69	20.65	2.60	2.60	8.01	8.03	313
$Ag_2Br_3(H_2L)$	Lemon yellow	36.19	36.16	11.98	12.06	1.49	1.52	4.63	4.69	71
$Ag_5I_7(H_2L)_2$	Yellow	31.54	31.53	8.39	8.42	1.07	1.09	3.22	3.27	111
AgL	White	43.55	43.66	29.08	29.14	2.84	2.85	11.27	11.33	3*
$AgL \cdot Ag(HL)NO_3$	Ivory	38.72	38.72	25.90	25.85	2.71	2.71	12.55	12.56	15*
$AgL \cdot [Ag(HL)ClO_4]_2$	White	34.33	34.35	22.73	22.92	2.45	2.46	8.80	8.91	128*
$AgL \cdot [Ag(HL)BF_4]_2$	White	34.93	35.30	23.44	23.56	2.52	2.53	9.08	9.16	151*

*Opalescent solutions.

Can. J. Chem. Downloaded from www.nrcresearchpress.com by 210.87.254.6 on 09/06/12
For personal use only.

TABLE 2. Principal infrared bands (cm^{-1}) of the neutral (HL) protonated (H_2L^+) and deprotonated-coordinated (AgL) ligand and their complexes

Species	Infrared bands		
HL	1623vs	1567vs 1545sh	853s
Ag(HL)Cl	1613vs	1557vs	860m, 830m
Ag(HL)Br	1615vs	1555vs	838m, 823sm
Ag(HL)I	1615vs	1555vs	843sh, 832wm, 808sm
Ag(HL)SCN	1620vs	1568vs	850sm
$Ag(HL)_2Cl$	1620vs	1558vs	832ms, 810s
$Ag(HL)_2Br$	1620vs	1560vs	840sm, 812s
$Ag(HL)_2I$	1622vs 1613vs	1565vs 1550vs	847m, 835ms, 812vs
$Ag(HL)_2NO_3 \cdot MeOH$	1620vs	1558vs	838sm, 825w, 812s
$Ag(HL)_2ClO_4 \cdot \frac{1}{4}CHCl_3$	1618vs	1560vs	835m
$Ag(HL)_2BF_4 \cdot \frac{1}{4}CHCl_3$	1620vs	1560vs	833wm
H_2LCl	1633vs 1600vs	1555m	849s
$Ag_6Cl_{11}(H_2L)_5$	1625vs 1594vs	1560sh	848ms
$Ag_2Br_3(H_2L)$	1625s 1590vs	1560sh	836w, 820ms
$Ag_5I_7(H_2L)_2$	1613s 1576s	1530sh	835w, 816m
AgL	1574vs	1528s	842m
$AgL \cdot Ag(HL)NO_3$	1625vs 1576vs	1558sm 1528m	824wm
$AgL \cdot [Ag(HL)ClO_4]_2$	1627vs 1593vs	1562sm 1530sm	
$AgL \cdot [Ag(HL)BF_4]_2$	1630vs 1590sh	1562vs 1530sh	

bands, all ir- and Raman-active, and of presumably two ν(AgX) bands ir- and/or Raman-active may indicate for the Ag(HL)X (X = Cl, Br, I) complexes a dimeric structure (**A**)

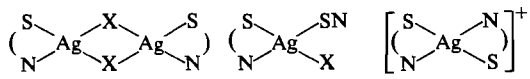

A **B** **C**

in which silver has a pseudo-tetrahedral coordination and the absence of a center of symmetry in the dimer allows the same bands to be ir- and Raman-active.

In the Ag(HL)SCN complex the SCN anion shows the bands ν(CN) at 2075(vs) and 2035(w) cm^{-1} and ν(CS) at 850(sm) cm^{-1} corresponding to a prevalent Ag–NCS coordination (16, 17) which does not exclude a weaker Ag–S secondary interaction. The ν(Ag—NCS) mode may be coupled with the ν(AgN) mode of the ligand in the strong bands at 288 and 271 cm^{-1} while the weaker ν(Ag—SCN) mode may be tentatively identified in the very strong band at 147 cm^{-1}; ν(M—NCS) frequencies in a tetrahedral coordination are given for terminal NCS groups in the range 330–230 cm^{-1} for transition metal complexes while, for bridging SCN groups ν(M—NCS) are given in the same range and ν(M—SCN) in the 230–213 cm^{-1} range (18). Owing to the very weak Ag—SCN bond the coordination may be considered substantially trigonal.

For the $Ag(HL)_2X$ (X = Cl, Br, I) only one strong ν(AgN) band is observed at about 300–290 cm^{-1} while two ν(AgS) bands are present if the band at 228–225 cm^{-1} is assigned to a ν(AgS) mode as for the Ag(HL)X complexes. Also a single ν(AgX) band seems to be recognisable for these complexes. A monomeric tetrahedral structure like **B** may therefore be tentatively proposed with one chelating and one terminally S-bonded ligand molecules and a terminal "long" AgX bond. An ionic structure $[Ag(HL)_2]X$ has to be excluded by the low molar conductivity of these complexes.

This structure, like type **C**, may be admitted for the $Ag(HL)_2X$ (X = NO_3, BF_4, ClO_4) complexes behaving as 1:1 electrolytes in DMF solution, and for which two ν(AgN) and two ν(AgS) (at least for the fluoborate and the perchlorate complexes) are observed. Infrared spectra do not indicate a coor-

Can. J. Chem. Downloaded from www.nrcresearchpress.com by 210.87.254.6 on 09/06/12
For personal use only.

TABLE 3. Far ir and Raman spectra (cm^{-1}) of the neutral (HL), protonated (H_2L^+) and deprotonated-coordinated (AgL) ligand and their complexes

Species	Spectra	ν(AgN)		ν(AgS)		ν(AgX)		δ(AgL)	Ligand and other bands
HL	Ir								286s, 266s, 230vs, 178m, 170m, 90vs, 85vs
	R								268vw, 249ms, 234wm, 183w, 172wm, 120sm, 106sh, 97sm
H_2LCl	Ir								286m, 263ms, 241m, 234sh, 179sb, 140vs, 101s, 94s
Ag(HL)Cl	Ir	322ms	299ms	228s	194s	228s	180vs	137m	286s, 180vs, 145vs, 120s, 112s
	R	323m	295wm	227w	200wm	227w			286wm, 172w, 122w, 115m, 105ms, 87sm
Ag(HL)Br	Ir	317ms	293m	226ms	192mb			136m	285s, 168w, 147sh, 105vs, 97vs
	R	318s	294wm	225w	198mw	159mw	149wm		289m, 237w, 159mw, 149wm, 124sh, 99vs, 84vs
Ag(HL)I	Ir	323w	301m	226sm	199w	115vs		129ms	284s, 183mb, 150ms, 115vs, 90vs
	R	316w	308w	224w	212w	116s	108vs		290w, 259w, 182w, 156mb, 116s, 108vs
Ag(HL)SCN	Ir	288s	271vs		195s	147vs			288s, 240sm, 120m, 98vs, 83ms
	R	284m			204wb			139m	284m, 151wm, 120sh, 105w, 92s
$Ag(HL)_2Cl$	Ir		298s	226s	192s	226s		133sm	284s, 182sh, 148m, 103vs, 98s
	R		291ms	225vw	190mb				280m, 240w, 159wm, 122sh, 110s, 98vs
$Ag(HL)_2Br$	Ir		298sm	226ms	201mb		139vs	139vs	286s, 181mw, 151sh, 92vs
	R		289ms	228w	192mw	160wm		139w	284sb, 236wm, 187mw, 116wm, 99vs, 93s, 88s
$Ag(HL)_2I$	Ir		298sm	227ms	199wm	119m		133wm	286s, 180wm, 170w, 150wm, 91s
	R		294sh		192sh	116wm			288m, 232w, 186w, 159w, 123sh, 96s, 83wm
$Ag(HL)_2NO_3 \cdot MeOH$	Ir	298sh	272w		187ms			133vs	290s, 244sm, 187ms, 146sh, 106vs
	R	300mb	277m		200m				
$Ag(HL)_2BF_4 \cdot \frac{1}{4}CHCl_3$	Ir	298m	276m	228s	185mw				289s, 176mb, 104vs
	R		272mb	229w	180wb				284mb, 244w, 158w, 122w
$Ag(HL)_2ClO_4 \cdot \frac{1}{4}CHCl_3$	Ir	296s	278ms	227s	200w				289vs, 175ms, 121sb, 103vs
$Ag_6Cl_{11}(H_2L)_5$	Ir			220s	200vs	220s		130sh	279s, 169w, 145s, 123vs, 82m
	R				202w			132ms	284ms, 242wm, 141sh, 117wm, 94ms, 88w
$Ag_2Br_3(H_2L)$	Ir				196s	144vs	120vs	128sh	281sm, 231wm, 120vs, 104vs, 83m
$Ag_5I_7(H_2L)_2$	Ir				185s		105vs		283m, 262m, 239ms, 185s, 105vs, 73s
AgL	Ir		288sm	224m	189ms			137s	288sm, 189ms, 167m, 123m, 104m
	R	300wm	293sh		208w				293sh, 155wm, 122vw
$AgL \cdot Ag(HL)NO_3$	Ir	316sm		208vs	180s				287vs, 249mb, 180s, 143vs, 120sb
$AgL \cdot [Ag(HL)BF_4]_2$	Ir	295s	277ms	256ms	177s				295s, 240m, 177s, 160vs, 110vs, 100m
	R	302m	279wm		180mb				294sh, 180mb, 160sh
$AgL \cdot [Ag(HL)ClO_4]_2$	Ir	295s	279m	257m	176sh				295s, 243m, 176sh, 166vs, 140mw, 110s

Can. J. Chem. Downloaded from www.nrcresearchpress.com by 210.87.254.6 on 09/06/12
For personal use only.

dination of these anions in the solid state. The band at 757(m) and 755(ms) cm^{-1} observed for the perchlorate and fluoborate complexes may be assigned to a chloroform deformation mode (ν_5, *E*) (19).

The sequence **A** → **B** → **C** seems to indicate that a second ligand molecule produces a bridge-splitting of the dimer **A** in which the nitrogen atom of the ligand does not overcome the coordinating power of the halide ion in the structure **B** but excludes from the coordination the other anions in the structure **C**.

The complexes $Ag_mX_n(H_2L)_{n-m}$ behave in DMF solution as electrolytes with all or almost all the $(H_2L)^+$ ions not bonded to the anions. The presence of one ν(AgS) band (or two for the chloride) indicate that at least some of these cations should be S-bonded in the solid state. Polymeric anions $Ag_2X_3^-$, AgX_2^-, AgX_3^{2-} have a ribbon structure in which all the silver ions form AgX_4 tetrahedra with doubly or triply bridging halide ions (15). In the present complexes the Ag:X ratio diminishes from the chloride to the iodide down to a value lower than the 1:1.5 ratio. Some of the coordination sites of the silver ions may be occupied by the sulphur atom of some of the H_2L^+ cations.

It is likely that AgL has a polymeric structure in which the tridentate L^- anion bridges several silver ions through both the N-ring atoms and the thiocarbonylic sulphur atom which may itself act as a bridging atom. The band at 167–160 cm^{-1} which appears in the complexes containing the AgL group could be assigned to some weaker AgS bonds of these bridging sulphur atoms.

As shown by the non-electrolyte behaviour of the $AgL \cdot Ag(HL)NO_3$ complex in DMF solution and by the presence of the ir bands at 1290(mb), 824(wm), 742(w), and 710(w) cm^{-1} for this complex the nitrate ion is coordinated in the solid state and this explains the fact that the stoichiometry of this complex is different from that of the $AgL \cdot [Ag(HL)X]_2$ (X = BF_4, ClO_4) complexes. In the ν(C=N) region both the ir bands of the L^- and HL molecules appear separately. For the fluoroborate and perchlorate complexes a band at 256–257 cm^{-1} not present in the other complexes may be assigned to a ν(AgS) mode. The increased frequency of this band with respect to those of the first ν(AgS) band of the other complexes is attributable to the increased AgS bond strength due to the negative charge of the L^- anion.

With silver(I) and copper(I) ions (4) Hdmpt forms $M(HL)X$ and $M(HL)_2X$ complexes in which it behaves as neutral S,N-bonded ligand, ML and mixed $ML \cdot [M(HL)X]_2$ complexes in which it acts as deprotonated N,N,S-bonded ligand and $M_mX_n(H_2L)_{n-m}$ complexes in which it behaves as protonated S-bonded ligand. The ν(MN) and ν(MS) bands have almost the same frequencies for both metals. It seems likely that copper(I) ion has a great tendency to retain a more trigonal coordination with unequivalent Cu—X bonds in the case of bridging halide ions giving one high and one low ν(CuX) frequency while the greater tendency of silver ion to assume a pseudo-tetrahedral coordination makes the Ag—X bonds more equivalent giving two very close low ν(AgX) frequencies. This difference is particularly evident for the $M_mX_n(H_2L)_{n-m}$ complexes which show for the copper(I) ion only the simple $Cu^I(H_2L)X_2$ (X = Cl, Br) stoichiometry, as the Cu^I(8-mercaptopurine)Cl_2 complex with unequivalent Cu^I—Cl bonds (20), while for silver(I) ion they show much more complicated polyanions (15).

Acknowledgments

The infrared and Raman spectra were recorded in the Centro Strumenti of the University of Modena.

1. R. Battistuzzi and G. Peyronel. Spectrochim. Acta, **36A**, 113 (1980).
2. D. M. L. Goodgame, I. Jeeves, and G. A. Leach. Inorg. Chim. Acta, **39**, 247 (1980).
3. B. A. Cartwright, D. M. L. Goodgame, I. Jeeves, P. O. Langguth, and S. Skapski. Inorg. Chim. Acta, **24**, L45 (1977).
4. R. Battistuzzi and G. Peyronel. Transition Met. Chem. **3**, 345 (1978).
5. W. J. Geary. Coord. Chem. Rev. **7**, 81 (1971).
6. J. L. Burmeister, S. D. Patterson, and E. A. Deardorff. Inorg. Chim. Acta, **3**, 105 (1969).
7. K. Jensen and P. Nielsen. Acta Chem. Scand. **20**, 597 (1966).
8. M. R. Udupa and M. Padmanabhan. Inorg. Chim. Acta, **13**, 239 (1975).
9. M. R. Udupa and M. Padmanabhan. J. Inorg. Nucl. Chem. **37**, 1803 (1975).
10. J. Abbot, D. M. L. Goodgame, and I. Jeeves. J. Chem. Soc. Dalton, 880 (1978).
11. D. M. L. Goodgame and G. A. Leach. Inorg. Chim. Acta, **32**, 69 (1979).
12. R. Battistuzzi and G. Peyronel. Transition Met. Chem. **2**, 87 (1977).
13. B. K. Teo and D. M. Barnes. Inorg. Nucl. Chem. Lett. **12**, 681 (1976).
14. B. Gilbert, K. W. Fung, and G. Mamantov. J. Inorg. Nucl. Chem. **37**, 921 (1975).
15. G. L. Bottger and A. L. Geddes. Spectrochim. Acta, **23A**, 1551 (1967).
16. L. C. Nathan. J. Chem. Educ. **51**, 285 (1974).
17. K. Nakamoto. Infrared spectra of inorganic and coordination compounds. Wiley, New York. 1970. p. 188.
18. J. R. Ferraro. Low-frequency vibrations of inorganic and coordination compounds. Plenum Press, New York. 1971. pp. 225, 227.
19. J. C. T. Rendell and L. K. Thompson. Can. J. Chem. **57**, 1 (1979).
20. M. R. Caira and L. R. Nassimbeni. J. Chem. Soc. Dalton, 4 (1976).

Stereochemical studies. IX. Acid-catalyzed rearrangement of δ- to γ-lactones

JOHN T. EDWARD, ELLEN COOKE, AND THEMISTOCLES C. PARADELLIS
Department of Chemistry, McGill University, Montreal, P.Q., Canada H3A 2K6

Received May 13, 1980

JOHN T. EDWARD, ELLEN COOKE, and THEMISTOCLES C. PARADELLIS. Can. J. Chem. **59**, 597 (1981).

Depending on their constitution and stereochemistry, δ-lactones are converted by hot formic acid into pendant or spiro γ-lactones.

JOHN T. EDWARD, ELLEN COOKE et THEMISTOCLES C. PARADELLIS. Can. J. Chem. **59**, 597 (1981).

Sous l'influence de l'acide formique à chaud les δ-lactones se transforment suivant leur constitution et leur stéréochimie soit en lactones ouvertes ou en spiro γ-lactones.

[Traduit par le journal]

Lunn *et al.* (1) reported that treatment of 4-oxa-5β-cholestan-3-one (**1**) with hot formic acid gave a 60% yield of the spiro-γ-lactone **2**; treatment of the less reactive *trans* isomer **3** with hot trifluoroacetic acid gave a small amount of gummy product which appeared, from its spectral properties, to be a mixture of isomeric pendant γ-lactones **4**. (Two isomeric γ-lactones **4** were obtained as crystalline products by a different route.) The different products from the two isomeric δ-lactones **1** and **3** may be rationalized by the mechanism indicated, the bond migrating being anti-periplanar to the O—C bond being broken.

Other cases of acid-catalyzed isomerization of δ-lactones to spiro-γ-lactones have been reported (2, 3) but none (to our knowledge) in which the structure of the γ-lactone, spiro or pendant, depends on the stereochemistry of the starting δ-lactone. Consequently, it became of interest to look at the rearrangement of other δ-lactones, including pairs of isomers, in boiling formic acid. In fact, it was found that all the δ-lactones mentioned below were converted to varying extents into γ-lactones, as well as into small amounts of acidic material. The latter appeared, from its ir spectrum, to be made up of unsaturated acids, and was not investigated further.

The simplest model of the lactones **1** and **3**, was the δ-lactone **5**. In formic acid it gave the γ-lactone **6** (4–7), also synthesized from ethyl levulate (**7**) for comparison. The two most intense peaks in the mass spectrum of the lactone **6** were at *m/e* 99 and 43, corresponding to cleavage of the molecule at the "pendant" bond. This cleavage had been found earlier in a γ-lactone assigned the structure **4**, and serves to distinguish a pendant from its spiro isomer (1).

Cis- (**8**) and *trans*-1-oxa-10-methyldecal-2-one (**10**) offer more complete models of the δ-lactones **1** and **3**, but are available only in 2:1 mixture (8, 9).[1]

[1]Attempts to separate the lactones **8** and **10**, and the lactones **13** and **16** (see below), by vpc under various conditions failed (10).

0008-4042/81/030597-04$01.00/0

©1981 National Research Council of Canada/Conseil national de recherches du Canada

Can. J. Chem. Downloaded from www.nrcresearchpress.com by 210.87.254.40 on 09/06/12
For personal use only.

Can. J. Chem. Downloaded from www.nrcresearchpress.com by 210.87.254.40 on 09/06/12
For personal use only.

This mixture might be expected, on treatment with acid, to yield a large amount of spiro-γ-lactone **9** and a smaller amount of pendant γ-lactone **11**. In fact, the reverse proved true; the main rearrangement product was the pendant γ-lactone **11**, whose structure was established by synthesis from ethyl levulate and cyclopentyl magnesium bromide. Only a small amount of impure product was obtained which had the correct spectral properties for the spiro structure **9**: an ir peak at 1777 cm^{-1} in carbon tetrachloride (γ-lactone); nmr peaks for α and β protons of the γ-lactone ring, but none for γ

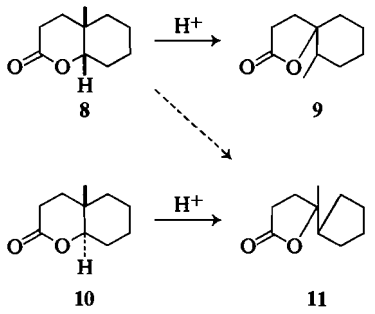

8 **9** **10** **11**

protons; and a methyl doublet (unlike lactones **8**, **10**, and **11**, which have singlet methyl peaks). A small amount of a third rearrangement product was indicated by vaporphase chromatography, but was not obtained pure.

In the mass spectrometer the lactone **11** showed the characteristic pendant-bond cleavage.

The high yield of γ-lactone **11** indicates that it is being formed from the *cis*-lactone **8** as well as the *trans*-lactone **10**. This seems plausible because in its nonsteroid conformation **8***a* the *cis* isomer can undergo antiperiplanar bond migration to give the carbonium ion **12**, the precursor to γ-lactone **11**:

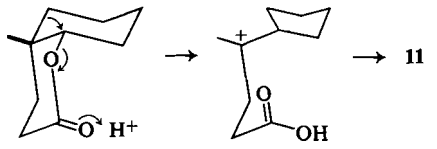

8*a* **12**

Such a possibility is not open to the rigid *cis*-lactone **1**.

The δ-lactones so far considered undergo skeletal rearrangment via tertiary carbonium ions (e.g. **12**). In the absence of an angular methyl group, this rearrangement would have to proceed via a secondary carbonium ion, and so would be less facile. This is illustrated by the effect of formic acid on the isomeric δ-lactones **13** (R = *t*-Bu) and **16** (R = *t*-Bu). Both proved less reactive than the δ-lactones **8** and **10**. The *cis* isomer **13** (R = *t*-Bu) gave a γ-lactone ($\nu_{max}(CCl_4)$: 1778 cm^{-1}) whose nmr spectrum showed peaks for α and β, but no peak for γ protons. This points to the spiro structure **15** (R = *t*-Bu), as does the mass spectrum, which excludes a pendant structure. The more stable *trans* isomer **16** (R = *t*-Bu) also gave a little of the spiro product **15** (R = *t*-Bu). A small amount of *cis* ⇄ *trans* interconversion was observed. This and the formation of the γ-lactone **15** (R = *t*-Bu), may proceed via the unsaturated acid **14** (R = *t*-Bu).

Cis- and *trans*-1-oxadecal-2-one (**13** and **16**; R = H) were available only as 1:2 mixture (10, 11). On treatment with acid this mixture gave a 54% yield of a γ-lactone ($\nu_{max}(CCl_4)$: 1780 cm^{-1}) assigned the spiro structure **15** (R = H) on the basis of spectral evidence similar to that advanced above for **15** (R = *t*-Bu).

In summary, acid-catalyzed rearrangements of δ and γ-lactones seem to be general, and both pendant and spiro structures are formed.

The δ-lactones required as starting materials have all been described previously, except for the lactones **5**, **13** (R = *t*-Bu), and **16** (R = *t*-Bu). The

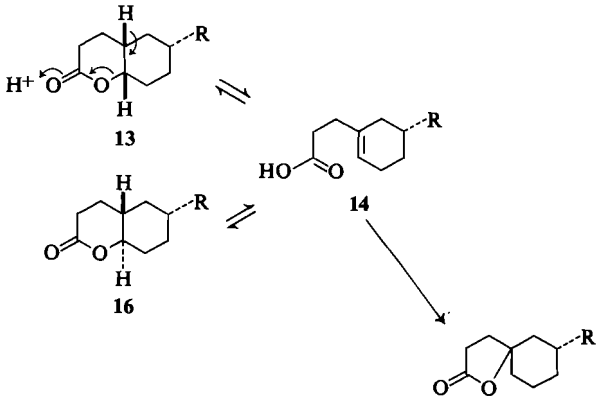

latter two compounds were prepared by reduction of the oily keto-acid **18** obtained by alkaline hydrolysis of the keto-nitrile **17** (11, 12). Under these equilibrating conditions the keto acid should have (to the extent of 96% (13, 14)) the configuration shown in **18**, and hence would be expected (15, 16)

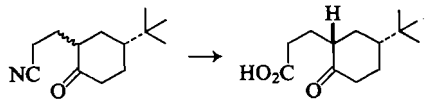

17 **18**

to yield predominantly the *cis* lactone **13** (R = *t*-Bu) when reduced by hydrogen over platinum in acidic solution, and the *trans* lactone **16** (R = *t*-Bu) when reduced by borohydride. In fact, two crystalline lactones were obtained by the two different modes

Can. J. Chem. Downloaded from www.nrcresearchpress.com by 210.87.254.40 on 09/06/12
For personal use only.

of reduction and shown by nmr (16, 17) to have the expected configurations.

Experimental

Melting points were determined on a Kofler hot stage and are corrected. Infrared spectra were obtained with Perkin-Elmer 421, 337, or 257 spectrometers. The nmr spectra were recorded on a Varian A-60 or HA-100 spectrometer. Vapour phase chromatography was done with a Hewlett-Packard F and M 5750 or an Aerograph 705 Autoprep instrument, both equipped with flame ionization detector, and using a Honeywell 10 recorder or a Beckman 10 recorder equipped with a disc integrator. Mass spectra were recorded at 70 eV on a AEI-MS-902 instrument with the sample introduced by a heated probe at the following temperatures: **6**, 35°; **11**, 90°; **15** (R = *t*-Bu), 70°; **15** (R = H), 100°C.

General Procedure for Acid Treatment of δ-Lactones

The δ-lactone (0.5–1.0 g) in anhydrous formic acid (10–20 mL) was heated under reflux, with exclusion of moisture, for 24 h. The solution was concentrated under reduced pressure and the residue taken up in ether and washed with 2% aqueous sodium hydroxide, saturated aqueous NaCl, and dried ($MgSO_4$). The ether was removed and the neutral product purified as described below. The aqueous NaOH washings were acidified and extracted with ether. The ether solution was washed with saturated aqueous NaCl, dried ($MgSO_4$), and concentrated to yield an acid product, typically ν_{max}: 3300–2500, 1710, 1645 cm^{-1}, which was weighed but not examined further.

Treatment of the δ-lactones with trifluoroacetic acid for 24 h at room temperature gave in general the same products but in much smaller amounts.

γ,γ,δ-Trimethyl-δ-valerolactone (5)

A solution of sodium borohydride (0.73 g) and 4,4-dimethyl-5-oxohexanoic acid (6.08 g) (18) in 2*N* aqueous NaOH (19.5 mL) – ethanol (100 mL) was stirred for 24 h at room temperature. Excess sodium borohydride was destroyed with 20% aqueous HCl, and the acidified mixture stirred for 30 min. The solution was saturated with NaCl and extracted with ether. The ether was washed with aqueous $NaHCO_3$, dried ($MgSO_4$), and concentrated, and the residue distilled at reduced pressure to give the δ-lactone **5** (3.4 g; 62%), bp 63°C/0.1 Torr; n_D^{20} 1.4578; $\nu_{max}(CCl_4)$: 2955, 2925, 2860 (C—H), 1740 (C=O) cm^{-1}; $\delta(CCl_4)$: 0.98 (d, 6H, $C(CH_3)_2$), 1.23 (d, 3H, CH—CH_3), 1.66 (m, 2H), 2.46 (m, 2H), 4.21 (q, 1H). *Anal.* calcd. for $C_8H_{14}O_2$: C 67.5, H 9.9; found: C 67.4, H 9.2.

γ-Isopropyl-γ-methyl-γ-butyrolactone (6)

From Reaction of Ethyl Levulate with Isopropyl Magnesium Bromide

Isopropyl magnesium bromide, prepared from magnesium (1.2 g) and isopropyl bromide (6.6 g) in ether (40 mL), was added dropwise to a stirred solution of ethyl levulate (7.2 g) in benzene (50 mL) cooled in ice–salt. The mixture was left overnight and then worked up following Varech *et al.* (19) to yield the γ-lactone **6** (2.4 g; 34%), bp 127–128°C/31 Torr (lit. (5) bp 116°C/16 Torr); $\nu_{max}(CCl_4)$: 2960, 2940, 2880 (C—H), 1787 (C=O) cm^{-1}; $\delta(CCl_4)$: 0.95 (d, J = 4 Hz, 3H), 1.07 (d, J = 4 Hz, 3H), 1.35 (s, 3H), 1.4–2.35 (m, 3H), 2.35–2.8 (m, 2H); mass spectrum *m/e*: 127 (6.1), 99 (100), 98 (6.1), 87 (12.2), 71 (7.6), 56 (7.6), 43 (27.2), 41 (9.1), 39 (6.1). *Anal.* calcd. for $C_8H_{14}O_2$: C 67.5, H 9.9; found: C 67.1, H 9.9.

From Acid Treatment of δ-Lactone 5

The general procedure applied to the lactone **5** gave 26% of acidic material and 62% of neutral product. The latter was shown by vpc (3% OF-1, 6 ft × ¼ in. glass, 130°C, 70 mL/min N_2) to be made up of γ-lactone **6** (95%; 4 min) and recovered **5** (5%). It was distilled at 52–60°C/2 Torr to yield the lactone **6**, identical (ir, nmr, mass spectrum) to synthetic material described above.

γ-Cyclopentyl-γ-methyl-γ-butyrolactone (11)

From Reaction of Methyl Levulate with Cyclopentyl Magnesium Bromide

This was carried out by the procedure described above for the lactone **6**, and the pendant γ-lactone was obtained in 9.1% yield as a colourless oil, bp 72–73°C/1 Torr (lit. (4) bp 135–136°C/10 Torr); ν_{max}(neat): 2950, 2870 (C—H), 1770 (C=O), 1465, 1425, 1385 (C—H), 1292, 1265, 1245, 1220, 1175, 1130, 1105, 1090, 1072, 1015, 945, 918, 815 cm^{-1}; $\delta(CCl_4)$: 1.45 (s, 3H), 1.72 (m, 9H), 1.95–2.40 (m, 2H), 2.40–2.95 (m, 2H); mass spectrum *m/e*: 168 (16.4), 153 (26.2), 113 (29.5), 99 (100.0), 98 (36.1), 71 (14.7), 69 (29.5), 67 (32.8), 56 (9.8), 55 (14.7), 43 (37.8), 41 (50.8). *Anal.* calcd. for $C_{10}H_{16}O_2$: C 71.4, H 9.6; found: C 71.4, H 9.7.

From Acid Treatment of Mixture of δ-Lactones 8 and 10

The standard procedure gave 23% of acidic material and 73% of neutral product. The latter on vpc showed three components having retention times of 7.0 min (16%, A), 8.1 min (53%, B), and 8.8 min (21%, C). Preparative vpc (8% OF-1, 6 ft × ⅜ in. Al, 140°C, 140 mL/min N_2) gave: A (contaminated with some B), tentatively identified as the spiro-γ-lactone **9**, $\nu_{max}(CCl_4)$: 2950, 2880 (C—H), 1777 (C=O), 1469, 1461, 1447, 1421, 1378 (C—H), 1360, 1310, 1272, 1233, 1207, 1180, 1155, 1140, 1128, 1095, 1065, 1055, 1005, 995, 982, 953, 932, 905, 858, 811 cm^{-1}; $\delta(CCl_4)$: 0.93 (d, J = 6 Hz, 3H), 1.65 (m, 9H), 1.5–2.3 (m, 2H), 2.3–2.8 (m, 2H); B, identified (ir, nmr, mass spectrum) with the pendant γ-lactone **11** synthesized above; C (contaminated with B) $\nu_{max}(CCl_4)$: 1777, 1745 cm^{-1}; $\delta(CCl_4)$: 0.57 (s), 0.95 (d, J = 6 Hz), 1.00 (s), 1.75 (s), 1.43 (s), 1.65 (m), 1.9–2.4 (m), not identified.

4-tert-Butyl-2-(2′-hydroxycarbonylethyl) Cyclohexanone (18)

4-*tert*-Butyl-2-(2′-cyanoethyl) cyclohexanone (**17**) (10.3 g) (11, 12) was treated with refluxing 2*N* aqueous NaOH for 9 h. The solution was acidified with 20% hydrochloric acid and extracted with ether. The ether solution was extracted with aqueous sodium bicarbonate, and the latter acidified and extracted with ether. The final ether solution was washed with aqueous NaCl, dried ($MgSO_4$), and concentrated. The residue was distilled and yielded the keto-acid **18** as an oil (10.1 g; 89%), bp 151–155°C/0.5 Torr; ν_{max}(neat): 3400–2500 (bonded OH), 1710 (C=O), 1480, 1473, 1448, 1420, 1397, 1367, 1326, 1283, 1268, 1248, 1228, 1173, 1140, 1113, 1090, 1078, 983, 946, 928 cm^{-1}. *Anal.* calcd. for $C_{13}H_{22}O_2$: C 69.0, H 9.8; found: C 68.7, H 10.0.

6α-tert-Butyl-1-oxa-9β,10β-decal-2-one (13; R = t-Bu)

The keto-acid **18** (4.3 g) was hydrogenated over prereduced platinum oxide (0.5 g) in a mixture of glacial acetic acid (45 mL) and concentrated hydrochloric acid (5 mL). After absorption of one equivalent of hydrogen, the mixture was filtered and the filtrate diluted with ether. The ether solution was washed with water, aqueous sodium bicarbonate, dried ($MgSO_4$), and concentrated. The residue on distillation gave the lactone **13** (R = *t*-Bu) as an oil (2.7 g; 62%), bp 144–146°C/0.65 Torr, crystallizing to a solid. Recrystallization from hexane–ether gave colourless plates, mp 78–80°C (1.8 g), raised to 82–83°C after sublimation; $\nu_{max}(CCl_4)$: 2950, 2870, 2845 (C—H), 1742 (C=O), 1478, 1469, 1457, 1433, 1393, 1363, 1358, 1348, 1333, 1310, 1290, 1198, 1160, 1135, 1105, 1069, 1012, 1001, 935, 925, 850 cm^{-1}; $\delta(CCl_4)$: 0.88 (s, 9H), 1–2.4 (complex m, 12H), 4.38 (m, 1H) (lit. (17) δ 4.52[2]). *Anal.* calcd. for $C_{13}H_{22}O_2$: C 74.2, H 10.5; found: C 74.5, H 10.4.

[2]Value reported for isomer in a *trans–cis* 80:20 mixture (17).

2-tert-Butylcyclohexane-1-spiro-4-butyrolactone (15; R = t-Bu)

The standard procedure applied to the δ-lactone **13** (R = *t*-Bu) gave a 12% yield of acidic material and 86% yield of neutral product showing by vpc (170°C) components at 8.7 min (**15**, R = *t*-Bu; 51%), 15 min (**13**, R = *t*-Bu; 43%), and 18 min (**16**, R = *t*-Bu; 6%).

The crude lactone mixture was distilled at reduced pressure to give, as a first fraction, an oil which solidified on standing. After three recrystallizations from hexane the γ-lactone **15** (R = *t*-Bu) was obtained as colourless crystals, mp 69–72°C; $\nu_{max}(CCl_4)$: 2955, 2875 (C—H), 1778 (C=O), 1475, 1470, 1450, 1423, 1393, 1363, 1295, 1233, 1218, 1195, 1168, 1140, 1125, 1095, 1051, 1012, 960, 913, 840 cm^{-1}; $\delta(CCl_4)$: 0.92 (s, 9H), 1.05–1.95 (m, 9H), 1.95–2.35 (m, 2H), 2.35–2.8 (m, 2H); mass spectrum *m/e*: 210 (8.7), 195 (17.30), 155 (57.7), 154 (81.8), 153 (42.3), 152 (13.5), 139 (7.2), 137 (23.1), 136 (28.8), 135 (12.5), 112 (7.2), 111 (38.4), 109 (7.2), 108 (13.5), 99 (2.2), 98 (7.2), 95 (30.8), 94 (69.3), 93 (19.2), 83 (7.2), 81 (25.0), 79 (14.4), 69 (14.4), 67 (15.4), 57 (100.0), 56 (29.8), 55 (37.5), 53 (9.6), 43 (13.5), 41 (67.4). *Anal.* calcd. for $C_{13}H_{22}O_2$: C 74.2, H 10.5; found: C 74.2, H 10.5

6α-tert-Butyl-1-oxa-9α,10β-decal-2-one (16; R = t-Bu)

Sodium borohydride (0.38 g) was added to a solution of the keto acid **18** (4.5 g) in 2 *N* aqueous NaOH (20 mL) and the solution stirred for 24 h at room temperature. The excess borohydride was destroyed with dilute hydrochloric acid, and the acidified mixture stirred for 30 min to complete lactonization. The mixture was extracted with ether, and the ether solution worked up in the usual way to yield the lactone **16** (R = *t*-Bu) as an oil (3.0 g; 74%) which solidified on standing, and melted unsharply above 45°C. Recrystallization from hexane–ether, followed by sublimation at 35°C/0.2 Torr gave colourless needles, mp 73.5–75°C; $\nu_{max}(CCl_4)$: 2959, 2870 (C—H), 1740 (C=O), 1475, 1469, 1455, 1450, 1419, 1392, 1363, 1330, 1297, 1250, 1240, 1218, 1187, 1128, 1098, 1089, 1045, 990, 965, 925, 905, 862 cm^{-1}; $\delta(CCl_4)$: 0.88 (s, 9H), 0.95–2.5 (complex, 12H), 3.73 (m, 1H) (lit. (17) 3.75[1]). *Anal.* calcd. for $C_{13}H_{22}O_2$: C 74.2, H 10.5; found: C 74.0, H 10.3.

Acid Treatment of δ-Lactone 16 (R = t-Bu)

The standard procedure gave a 13% yield of acidic material and 84% yield of neutral material, shown by vpc (170°C) to be made up of the γ-lactone **15** (R = *t*-Bu) (8.7 min; 3%), an unidentified component (10.5 min; 5%), δ-lactone **13** (R = *t*-Bu) (15 min; 4%) and recovered δ-lactone **16** (R = *t*-Bu) (18 min; 88%).

Acid Treatment of Mixture of δ-Lactones 13 and 16 (R = H)

The standard procedure gave 36% yield of acidic material and 61% yield of neutral product, showing by vpc (150°C) components at 3 min (γ-lactone **15**; R = H; 90%) and at 4.9 min (mixture of δ-lactones **13** and **16**; R = H; 10%). Work-up in the usual way gave the γ-lactone **15** (R = H) as a colourless oil, bp 84°C/2.0 Torr; $\nu_{max}(CCl_4)$: 2960, 2880 (C—H), 1780 (C=O), 1445, 1420, 1368, 1358, 1348, 1333, 1287, 1217, 1190, 1147; 1123, 1043, 1030, 1002, 995, 952, 940, 920, 900, 890, 855, 840 cm^{-1}; $\delta(CCl_4)$: 1.75 (10H), 1.95–2.25 (m, 2H), 2.35–2.88 (m, 2H); mass spectrum *m/e*: 154 (31.2), 125 (9.8), 112 (18.0), 111 (10.0), 99 (14.9), 98 (29.5), 97 (2.4), 83 (9.0), 81 (11.5), 67 (8.2), 56 (12.3), 55 (18.0), 42 (8.2), 41 (14.5). *Anal.* calcd. for $C_9H_{14}O_2$: C 70.1, H 9.2; found: C 69.4, H 9.6.

Acknowledgements

The financial support of the Natural Sciences and Engineering Research Council of Canada is gratefully acknowledged. T.C.P. additionally acknowledges financial assistance from the Institute of State Scholarships, Greece, and the award of a Canadian Industries Ltd. fellowship, and J.T.E. the hospitality of Prof. R. Schaal, Université Pierre et Marie Curie, where this article was written.

1. W. H. Lunn, J. T. Edward, and S. Meyerson. Can. J. Chem. **44**, 279 (1966).
2. P. A. Tardell and G. Di Maio. Tetrahedron, **23**, 2285 (1967).
3. S. B. Kulkarni and S. Dev. Tetrahedron, **24**, 553 (1968).
4. N. Levin, D. Papa, and E. Schwenk. J. Am. Chem. Soc. **69**, 1830 (1947).
5. R. L. Frank, R. Armstrong, J. Kwiatek, and H. A. Price. J. Am. Chem. Soc. **20**, 1379 (1948).
6. R. Rothstein and J. Ficini. C. R. Acad. Sci. **239**, 1694 (1952).
7. S. Obata. J. Pharm. Soc. Jpn. **73**, 1301 (1953).
8. H. O. House and M. Schellenbaum. J. Org. Chem. **28**, 34 (1963).
9. J. T. Edward and J. M. Ferland. Can. J. Chem. **44**, 1317 (1966).
10. T. C. Paradellis. Ph.D. Thesis, McGill University, Montreal, Canada. 1969.
11. H. O. House, H. Babad, R. B. Toothill, and A. W. Noltes. J. Org. Chem. **27**, 4141 (1962).
12. P. Dufëÿ. Bull. Soc. Chim. Fr. 4653 (1969).
13. P. Dufëÿ, J. Delmau, and J. C. Duplan. Bull. Soc. Chim. Fr. 1336 (1967).
14. E. L. Eliel, N. L. Allinger, C. J. Angyal, and G. A. Morrison. Conformational analysis. Interscience Publishers, New York, NY. 1965. p. 11.
15. J. T. Edward and P. F. Morand. Can. J. Chem. **38**, 1325 (1960).
16. J. T. Edward and J. M. Ferland. Can. J. Chem. **44**, 1311 (1966).
17. P. Dufëÿ, J. C. Duplan, and J. Delmau. Bull. Soc. Chim. Fr. 3030 (1968).
18. A. D. Campbell, C. L. Carter, and S. N. Slater. J. Chem. Soc. 1741 (1948).
19. D. Varech, C. Ouannes, and J. Jacques. Bull. Soc. Chim. Fr. 1662 (1965).

Can. J. Chem. Downloaded from www.nrcresearchpress.com by 210.87.254.40 on 09/06/12
For personal use only.

Total synthesis of α- and β-himachalene by an intermolecular Diels–Alder approach

HSING-JANG LIU AND ERIC N. C. BROWNE

Department of Chemistry, University of Alberta, Edmonton, Alta., Canada T6G 2G2

Received September 10, 1980

HSING-JANG LIU and ERIC N. C. BROWNE. Can. J. Chem. **59**, 601 (1981).

A total synthesis of α-himachalene (**2**) and β-himachalene (**3**) has been achieved in eleven steps and in an effective overall yield of 21% from 4,4-dimethyl-2-cyclohexenone (**4**). The synthesis involves keto ester **7** as a key intermediate which is conveniently prepared by the Diels–Alder addition of dienone ester **6** to isoprene.

HSING-JANG LIU et ERIC N. C. BROWNE. Can. J. Chem. **59**, 601 (1981).

Partant de la diméthyl-4,4 cyclohexène-2 one (**4**) on a réalisé, en 11 étapes et avec un rendement global de 21%, une synthèse totale de l'α-himachalène (**2**) et de la β-himachalène (**3**). La synthèse fait appel à un intermédiaire clé, le cétoester **7**, qui est préparé avec facilité par une addition de Diels–Alder de l'ester diénone **6** sur l'isoprène.

[Traduit par le journal]

The himachalane carbon skeleton (**1**) is characteristic of a growing class of sesquiterpenes (1–13). The isolation of two representatives of the class was first reported by Dev and co-workers in 1952 from the essential oil of the Himalayan cedar (*Cedrus deodara Loud*) (1). The gross skeletal structure of the two new hydrocarbons, designated α- and β-himachalene, was reported almost simultaneously in 1961 by Joseph and Dev (2) and by Bredenberg and Erdtman (3) who isolated the two compounds from Atlas cedar (*Cedrus atlantica*) and from *Cedrus libani*. In 1968 Joseph and Dev were able to rigorously establish the structure (4) and the absolute stereochemistry (5) of α-himachalene as **2** and of β-himachalene as **3**. These two natural hydrocarbons have been the subject of considerable synthetic activity and several total syntheses have been accomplished during the last decade (14–17). We wish to report a fundamentally different approach to the synthesis of α- (**2**) and β-himachalene (**3**) in racemic form.

Our synthetic plan called for two critical operations, the construction of a suitably functionalized 4,4-dimethyl-1-decalone derivative (i.e. **16**) and a one-carbon ring enlargement (i.e. **16** → **17**). The former process was facilitated by a Diels–Alder approach using 2-carbomethoxy-4,4-dimethyl-2,5-cyclohexadienone (**6**) as a dienophile. The initial studies (18) on the addition of isoprene to dienone ester **6**, readily prepared from 4,4-dimethyl-2-cyclohexenone (**4**) by carbomethoxylation (**4** → **5**) followed by oxidation with selenium dioxide, employed boron trifluoride etherate as a catalyst. The reaction, carried out at room temperature in ether, resulted in the formation of what appeared to be a single adduct which showed homogeneity on tlc and four methyl singlets in the

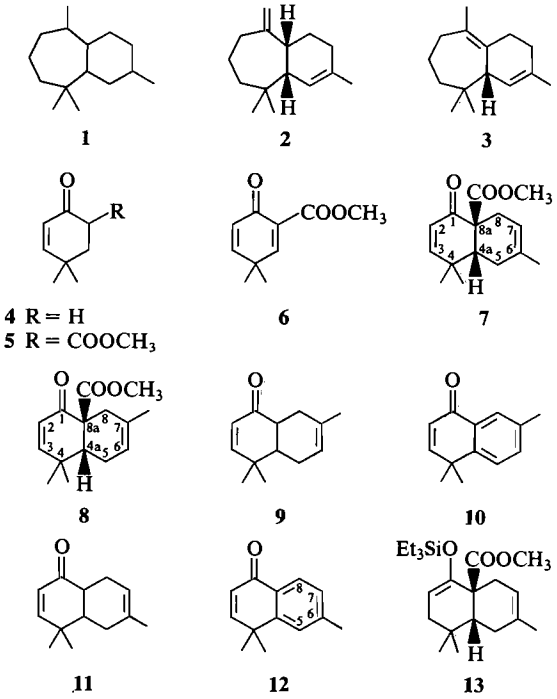

^{1}Hmr spectrum, and to which structure **7** was assigned based on the well established rules governing the Diels–Alder reaction (19). However, further examination of the adduct by ^{13}Cmr revealed that it was in fact a mixture of two compounds (thirty carbon signals). Separation of these two compounds was possible by preparative high-pressure liquid chromatography. Surprisingly, the major component, which amounted to 70% of the mixture, was the undesired *anti-para* adduct **8**. This assignment was confirmed by decarbomethoxylation with lithium iodide dihydrate in refluxing

0008-4042/81/030601-08$01.00/0

©1981 National Research Council of Canada/Conseil national de recherches du Canada

Can. J. Chem. Downloaded from www.nrcresearchpress.com by 210.87.254.105 on 09/06/12
For personal use only.

Can. J. Chem. Downloaded from www.nrcresearchpress.com by 210.87.254.105 on 09/06/12
For personal use only.

2,4,6-collidine (20) to give a mixture of the two known (21) epimeric ketones **9** and oxidation of this mixture with *N*-bromosuccinimide to the known aryl ketone **10** (21). The minor compound was shown spectroscopically to be isomeric with **8** and its structure could be logically deduced as **7**. In further proof of the structure, this compound was subjected to decarbomethoxylation with LiI·2H_2O-collidine. The resulting mixture of the epimeric ketones **11** (ca. 1:1; 97% yield) on oxidation with *N*-bromosuccinimide in carbon tetrachloride gave aryl ketone **12** in 43% yield. The ^{1}Hmr spectrum of **12** showed a signal due to a *peri*-deshielded proton (C-8 H) (22) as a doublet (J = 8 Hz) at δ 7.95. Such a coupling is only compatible with structure **12**.

Examination of a series of Lewis acids as catalyst for the Diels–Alder reaction of dienone ester **6** and isoprene indicated that, whereas BF_3 gave predominantly the undesired isomer **8**, use of stannic chloride resulted in the preferential formation of the desired regioisomer (**7**:**8** = 82:18; 99% total yield). To our knowledge, this is the first example of a Diels–Alder reaction in which the regiochemistry of the product can be reversed solely by choice of an appropriate Lewis acid catalyst.[1]

In the presence of Wilkinson's catalyst (*tris*-triphenylphosphine rhodium(I) chloride) (24) hydrosilanes have been shown (25) to add to α,β-unsaturated ketones exclusively by 1,4-addition to give silyl enol-ethers which readily undergo hydrolysis (26) to give saturated ketones. When keto ester **7** as a 25% solution in benzene was treated with triethylsilane (1 equiv.) and a catalytic amount of Wilkinson's catalyst, only a small amount of addition product was observed after 5 days. However, when finely divided solid keto ester **7** was suspended in triethylsilane in the presence of the catalyst, conversion to product was complete within 24 h. The purified product, obtained in 91% yield was identified as silyl enol-ether **13**. Hydrolysis of **13** with potassium carbonate in aqueous methanol gave the saturated ketone **14** in 88% yield. The crude silyl enol-ether **13** could conveniently be hydrolyzed to give **14** in 94% yield from keto ester **7**.

Keto ester **14** was decarbomethoxylated with LiI·2H_2O-collidine to give *trans*-ketone **15** and its epimer **16**, in 86% yield and in a ratio of ~90:10, which were easily separated by column chromatography on silica gel. In proof of the stereochemical assignment, *cis*-ketone **16** epimerized with sodium

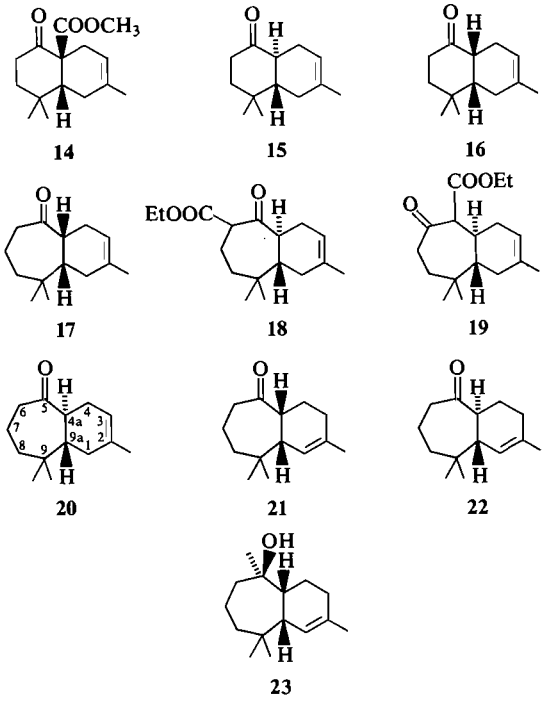

hydroxide in aqueous methanol to give an equilibrium mixture of **15** and **16** in a ratio of 82:18 and in 95% yield.

The most direct approach to α-himachalene (**2**) from this point would appear to require homologation of *cis*-ketone **16** to the ketone **17**. However, since *cis*-ketone **16** was obtained only as a minor product of decarbomethoxylation of **14** and efficient use of the starting materials would require successive epimerizations of **15** followed by chromatographic separation of the minor component **16**, it seemed more expedient to proceed with ring expansion of the major isomer, *trans*-ketone **15** and to correct the ring junction stereochemistry at a later stage.

The ring expansion of ketones with ethyl diazoacetate (27, 28) has been shown (28, 29) to proceed via the selective migration of the less substituted carbon α to the carbonyl group. Treatment of **15** with ethyl diazoacetate and boron trifluoride etherate at 0°C for 1 h gave two chromatographically separable keto esters **18** and **19**. The major product, obtained in 90% yield showed a signal at δ 3.53 in its ^{1}Hmr spectrum characteristic of a methine proton on the α-carbon of a β-keto ester. The signal was a doublet of doublets with coupling constants of 10 Hz and 4 Hz indicating the presence of two adjacent protons. These data were consistent with the assignment of structure **18** to the major product. In the case of the minor product (10%

[1]For an approach to orientation reversal by selection of either thermal or catalytic conditions see ref. 23.

Can. J. Chem. Downloaded from www.nrcresearchpress.com by 210.87.254.105 on 09/06/12
For personal use only.

yield), the nmr signal at δ 3.28 indicating one proton at the α-carbon of a β-keto ester, was a doublet with a coupling constant of 8 Hz indicating the presence of only one adjacent proton. This was consistent with the assignment of structure **19** to the minor product. Both **18** and **19** were single compounds (17 lines in their ^{13}Cmr spectra) existing exclusively in the keto-form. The stereochemistry at the newly introduced chiral center, however, could not be assigned with certainty.

Keto ester **18** was decarbethoxylated with LiI·2H_2O-collidine to give ketone **20** in 85% yield. The ^{1}Hmr spectrum of **20** was identical with previously reported (30) ^{1}Hmr data for **20** obtained by degradation of α-himachalene (**2**).

The synthesis of the key intermediate **21** from ketone **20** requires two operations. In one, the double bond must be moved from the C-2 to the C-1 position. In the other, the stereochemistry of the ring junction must be converted from *trans* to *cis*. Joseph and Dev (30) have reported that ketone **22**, when treated with oxalic acid in aqueous dioxan at reflux for 12 h, produces an equilibrium mixture of **20** and **22** in a ratio of 15:85 (determined by gc analysis). Furthermore it has been reported (16) that the ketone **21**, when subjected to base catalyzed equilibration (conditions unspecified), gives a 50:50 equilibrium distribution with its *trans*-isomer **22**. The sequential application of these two equilibration conditions appeared to offer an acceptable route from **20** to **21**.

It was found, however, that application of oxalic acid equilibrating conditions to ketone **20** produced no detectable (^{1}Hmr, gc) trace of any isomeric ketone and the starting material was recovered quantitatively. The application of more strongly acidic conditions was investigated. In refluxing benzene with *p*-toluenesulfonic acid an equilibrium was rapidly established within 1 h, as determined by gc and ^{1}Hmr analysis. Two peaks were observed by gc in a ratio of 65:35. The minor peak had a retention time identical with that observed for pure ketones **20** and **17**[2] while the major peak had a lower retention time corresponding to ketones **21** and **22**.[3] The product mixture was obtained in quantitative yield and ^{1}Hmr analysis showed the presence of four compounds approximately in the ratio 53:27:14:6. Three of these were identified as the known ketones (16, 30) **22** (53%), **20** (27%), and **21** (14%). The fourth, minor component was shown to be identical with ketone **17**. Flash chromatography of this mixture gave leading fractions of pure *cis*-ketone **21** in approximately 12% yield, and later fractions (in 88% yield) which were a mixture of **17** and **20–22**. In practice this mixture was subjected sequentially to the acid catalyzed equilibration conditions and flash chromatographic removal of the desired *cis*-ketone **21** in order to obtain efficient use of the starting material.

The direct conversion of *cis*-ketone **21** to α-himachalene (**2**) by a Wittig reaction appeared to be straightforward and has been briefly described (16). However, this approach using an excess of methylenetriphenylphosphorane in refluxing ether gave material identifiable as α-himachalene (**2**) (^{1}Hmr) only slowly (74% conversion after 5 days) and in poor yield (~20%) and contaminated with other inseparable hydrocarbon products.

A methylation–dehydration approach proved more effective for the conversion of ketone **21** to himachalenes. As reported (16) the addition of methyl lithium to ketone **21** proceeded smoothly and specifically from the less hindered side of the carbonyl to give 7-*epi*-himachalol (**23**) in 93% yield. The dehydration of alcohol **23** with phosphoryl chloride in refluxing pyridine for 1 h gave a mixture of hydrocarbons in 93% yield composed of α- (**2**) and β-himachalene (**3**) in a ratio of 75:25 by ^{1}Hmr integration. Separation of the two isomeric hydrocarbons by flash chromatography gave pure α-himachalene (**2**) which was identical with the naturally occurring compound by comparison of its ^{1}Hmr, ir, and mass spectra with published values (5, 6). As well, a sample of β-himachalene (**3**) (contaminated by ~20% of the α-isomer **2**) was obtained which showed ^{1}Hmr signals identical with those reported (5, 6) for the natural material.

Experimental

General

Melting points were determined on a Kofler hot stage apparatus and are uncorrected. Elemental analyses were performed by the microanalytical laboratory of this department. Infrared spectra were recorded on a Perkin-Elmer model 457 or Nicolet 7-199 FT-IR spectrophotometer and, except where otherwise stated, were obtained on solutions in chloroform. The ^{1}Hmr spectra were recorded on a Varian HA-100, HA-100/Digilab, or Bruker WH-200 spectrometer and, except where otherwise stated, were obtained on solutions in carbon tetrachloride with tetramethylsilane as internal reference. The ^{13}Cmr spectra were recorded on a Bruker WP-60/Nicolet BNC-12 system or a Bruker HFX-90/Nicolet 1085 system and were obtained on solutions in deuteriochloroform using tetramethylsilane as internal reference. Mass spectra (ms) were recorded using A.E.I. model MS9, MS12, or MS50 mass spectrometers. Gas chromatography (gc) was performed on a Hew-

[2]Ketone **17** was prepared by epimerization of **20** with aqueous sodium hydroxide in refluxing methanol for 48 h. Pure **17** was obtained from the resulting 80:20 (*trans*:*cis*) mixture by flash chromatography (31).

[3]Ketone **22** was obtained by treatment of pure **21** (*vide infra*) with aqueous sodium hydroxide in refluxing methanol to give an 80:20 equilibrium mixture of **22** and **21**.

Can. J. Chem. Downloaded from www.nrcresearchpress.com by 210.87.254.105 on 09/06/12
For personal use only.

lett Packard 5750 research chromatograph using stainless steel columns (8 ft × 1/8 in.) packed with 10% diethylene glycol succinate on 80–100 mesh Chromosorb W, acid washed, and treated with dimethylchlorosilane. Unless stated otherwise, anhydrous magnesium sulfate was used for drying organic solutions. Lithium iodide dihydrate – collidine reagent was prepared as follows. Finely divided anhydrous lithium iodide (514 mg, 3.84 mmol) was suspended in 2,4,6-collidine (3.05 mL) with vigorous stirring. Water (138 μL, 7.68 mmol) was added and the suspension rapidly dissolved. The resulting pale yellow solution had a calculated concentration of 1.28 *N* in lithium iodide dihydrate.

6-Carbomethoxy-4,4-dimethyl-2-cyclohexen-1-one (5)

Sodium hydride (50% oil dispersion, 15.65 g, 0.326 mol) was suspended in 1,2-dimethoxyethane (130 mL, freshly distilled over lithium aluminum hydride) under an atmosphere of nitrogen and dimethyl carbonate (73.4 g, 0.815 mol) was added. The suspension was brought to reflux while stirring with a mechanical stirrer. A solution of 20 g (0.163 mol) of enone **4** (32) in dry 1,2-dimethoxyethane (60 mL) was added dropwise over 1 h. Heating was continued for 4 h and then the mixture was cooled to 0°C. An aqueous 10% solution of acetic acid (200 mL) was added dropwise with stirring and the mixture was extracted with ether. The extracts were washed with water, saturated aqueous sodium bicarbonate, water, and saturated aqueous sodium chloride, dried, filtered, and concentrated. Column chromatography of the residue on silica gel, eluting with 8–20% ether in Skelly B, gave keto ester **5** (18.13 g, 61% yield) as a yellow oil. This compound existed partially (~40% by ^{1}Hmr integration) in the corresponding enol form. The following ^{1}Hmr data were attributed to the keto form: δ: 6.58 (dd, 3/5H, J = 10, J' = 2 Hz, —C*H*=CH—CO—), 5.76 (d, 3/5H, J = 10 Hz, —CH=C*H*—CO—), 3.68 (s, 3 × 3/5H, —O—CH_3), 3.41 (dd, 3/5H, J = 13, J' = 5 Hz, —CH(—CO_2—)—), 2.25 (dd, 3/5H, J = J' = 13 Hz, —CH(—*H*)—), 1.91 (ddd, 3/5H, J = 13, J' = 5, J'' = 2 Hz, —CH(—*H*)—), 1.20 (s, 3 × 3/5H, —CH_3), and 1.06 (s, 3 × 3/5H, —CH_3). The following ^{1}Hmr data were attributed to the enol form: δ: 11.75 (s, 2/5H, =C(—OH)—), 6.00 (d, 2/5H, J = 10 Hz, =C*H*—C(=CH—)—$(CH_3)_2$), 5.76 (d, 2/5H, J = 10 Hz, =C(—CH=)—), 3.72 (s, 3 × 2/5H, —OCH_3), 2.31 (s, 2 × 2/5H, —CH_2—), 1.20 (s, 6 × 2/5H, —CH_3). The following spectral data were recorded for the mixture of keto and enol forms. Infrared (neat): 1744 (ester C=O), 1680 (enone C=O), 1658 (C=C), and 1379 cm^{-1} (CH_3). *Exact Mass* calcd. for $C_{10}H_{14}O_3$: 182.0943; found (ms): 182.0936. *Anal.* calcd. for $C_{10}H_{14}O_3$: C 65.92, H 7.74; found: C 66.13, H 7.74.

2-Carbomethoxy-4,4-dimethyl-2,5-cyclohexadien-1-one (6)

Keto ester **5** (22.04 g, 0.121 mol) was dissolved in 2.204 L of a 5% solution of glacial acetic acid in *tert*-butyl alcohol under an atmosphere of nitrogen. Finely divided selenium dioxide (40.25 g, 0.363 mol) was added. The mixture was stirred with a mechanical stirrer and heated to reflux. After heating for 18 h, the mixture was cooled to room temperature, filtered, and concentrated. The residue was dissolved in ether, washed with water, saturated aqueous sodium bicarbonate and water, dried, filtered, and concentrated. Column chromatography of the residue on silica gel, eluting with 50–100% ether in petroleum ether, gave keto ester **6** which was contaminated with red selenium. Molecular distillation of this material in a Kugelrohr apparatus at 120°C/0.5 Torr gave pure keto ester **6** (17.4 g, 80% yield) as a yellow oil; ir (neat): 1734 (ester C=O), 1660 (ketone C=O), 1398, 1384, and 1360 (CH_3) cm^{-1}; ^{1}Hmr δ: 7.33 (d, 1H, J = 3 Hz, —CH=C(—CO_2—)—), 6.80 (dd, 1H, J = 10, J' = 3 Hz, —C*H*=CH—CO—), 6.06 (d, 1H, J = 10 Hz, —CH=C*H*—CO—), 3.74 (s, 3H, —OCH_3), and 1.33 (s, 6H, 2 × —CH_3). *Exact Mass* calcd. for $C_{10}H_{12}O_3$: 180.07865; found (ms): 180.07834. *Anal.* calcd. for $C_{10}H_{12}O_3$: C 66.65, H 6.71; found: C 66.33, H 6.70.

8aβ-Carbomethoxy-4,4,6-trimethyl-4aβ,5,8,8aβ-tetrahydro-1(4H)-naphthalenone (7)[4] *and 8aβ-Carbomethoxy-4,4,7-trimethyl-4aβ,5,8,8aβ-tetrahydro-1(4H)-naphthalenone (8)*

From BF_3 Catalyzed Reaction

At 0°C, boron trifluoride etherate (0.68 mL, 5.55 mmol) was added to a solution of dienone ester **6** (2 g, 11.1 mmol) and isoprene (22 mL, 0.22 mol) in ether (80 mL). The reaction mixture was stirred at room temperature under an atmosphere of argon for 96 h. Saturated aqueous sodium bicarbonate (40 mL) was added and the resulting mixture was extracted with ether. The extracts were washed with water, dried, filtered, and concentrated. Column chromatography of the residue on silica gel, eluting with 10–12% ether in *n*-hexane, gave a 70:30 mixture (gc analysis) of keto esters **8** and **7** (2.536 g, 92% yield). A 1.70 g sample was separated by preparative high pressure liquid chromatography on a Waters Associates Prep LC/System 500 using one silica gel cartridge and eluting with 50% ether in petroleum ether. Fractions were collected by shaving the leading and trailing edges of the single peak and recycling the central portion. The combined "leading edge" fractions were concentrated to give a sample which was shown by gc analysis to be predominantly keto ester **8** (445 mg, lower gc retention time isomer). This sample crystallized on standing and three recrystallizations from ether gave colourless rhombs of pure keto ester **8**; mp 93–95°C; ir: 1744, 1730 (ester C=O), 1672 (enone C=O), 1384 and 1371 (CH_3) cm^{-1}; ^{1}Hmr δ: 6.43 (d, 1H, J = 10 Hz, —C*H*=CH—CO—), 5.76 (d, 1H, J = 10 Hz, —CH=C*H*—CO—), 5.29 (m, 1H, =CH—), 3.64 (s, 3H, —OCH_3), 2.62 (ddd, 1H, J = 5, J' = 4, J'' = 0.5 Hz, C-4a H), 2.47 (br d, 1H, J = 17 Hz, C-8 H), 2.08 (br d, 1H, J = 17 Hz, C-8 H), 2.01 (m, 2H, C-5 —CH_2—), 1.66 (br s, 3H, =C(—CH_3)—), 1.16 (s, 3H, —CH_3), and 1.00 (s, 3H, —CH_3); ^{13}Cmr δ: 197.4 (C-1), 173.0 (—CO_2—), 158.0 (C-3), 131.1 (C-7), 124.0 (C-2), 119.3 (C-6), 57.5 (C-8a), 52.4 (—OCH_3), 40.4 (C-4a), 36.0 (C-4), 33.1 (C-8), 30.4 (C-4 CH_3), 24.2 (C-5), 23.6 (C-4 or C-7 CH_3), and 23.4 (C-4 or C-7 CH_3). *Exact Mass* calcd. for $C_{15}H_{20}O_3$: 248.1413; found (ms): 248.1410. *Anal.* calcd. for $C_{15}H_{20}O_3$: C 72.55, H 8.12; found: C 72.41, H 8.08. The "trailing edge" fractions were combined and concentrated to give a sample which was shown by gc analysis to be predominantly keto ester **7** (161 mg, higher gc retention time isomer). This sample crystallized on standing and two recrystallizations from ether gave colourless rhombs of pure keto ester **7**; mp 91.5–92.5°C; ir: 1740 (ester C=O), 1667 (enone C=O), 1376 (CH_3), and 828 (C=CH) cm^{-1}; ^{1}Hmr δ: 6.41 (d, 1H, J = 10 Hz, —C*H*=CH—CO—), 5.75 (d, 1H, J = 10 Hz, —CH=C*H*—CO—), 5.34 (br s, 1H, =CH—), 3.67 (s, 3H, —OCH_3), 2.71 (dd, 1H, J = 6, J' = 3 Hz, C-4a H), 2.62 (dm, 1H, J = 19 Hz, C-8 H), 2.14 (dm, 1H, J = 19 Hz, C-8 H), 1.91 (m, 2H, C-5 —CH_2—), 1.67 (br s, 3H, =C(—CH_3)—), 1.19 (s, 3H, —CH_3), and 1.02 (s, 3H, —CH_3); ^{13}Cmr δ: 197.7 (C-1), 173.0 (—CO_2—), 157.9 (C-3), 132.2 (C-6), 123.9 (C-2), 118.5 (C-7), 56.6 (C-8a), 52.4 (—OCH_3), 41.3 (C-4a), 36.2 (C-4), 30.4 (C-4 CH_3), 29.0 (C-5 or C-8), 28.7 (C-5 or C-8), 23.5 (C-4 or C-6 CH_3), and 23.4 (C-4 or C-6 CH_3). *Exact Mass* calcd. for $C_{15}H_{20}O_3$: 248.1412; found

[4]The stereochemical designations used in this and all other chemical names in this section denote relative stereochemistry. All compounds used and obtained were racemic.

Can. J. Chem. Downloaded from www.nrcresearchpress.com by 210.87.254.105 on 09/06/12
For personal use only.

(ms): 248.1412. *Anal.* calcd. for $C_{15}H_{20}O_3$: C 72.55, H 8.12; found: C 72.71, H 8.29. A total of 1.09 g of a mixture of keto esters **7** and **8** was also recovered from the preparative liquid chromatography.

From $SnCl_4$ Catalyzed Reaction

Dienone ester **6** (1.03 g, 5.72 mmol) was dissolved in ether (20 mL) under an atmosphere of nitrogen. Anhydrous stannic chloride (745 mg, 2.86 mmol) was added with stirring followed by addition of isoprene (11.4 mL, 114 mmol). After stirring for 84 h, saturated aqueous sodium bicarbonate (10 mL) was added. The resulting mixture was extracted with ether and the extracts were washed with water, dried, filtered, and concentrated. Column chromatography of the residue on silica gel, eluting with 8–20% ether in petroleum ether, gave a mixture of keto ester **7** and its regioisomer **8** (82:18 by gc analysis, 1.37 g, 97% yield) which crystallized on standing. As an alternative to chromatographic purification the crude residue could be purified by molecular distillation in a Kugelrohr apparatus (~120°C at 0.5 Torr) to give a mixture of keto esters **7** and **8** in 99% yield. One recrystallization of this mixture from ether gave pure keto ester **7** (872 mg) as colourless crystals. Additional keto ester **7** could be obtained either by fractional crystallization from the mother liquor or by preparative high pressure liquid chromatography as described above.

4,4,7-Trimethyl-4aβ,5,8,8aβ-tetrahydro-1(4H)-naphthalenone and 4,4,7-Trimethyl-4aβ,5,8,8aα-tetrahydro-1(4H)-naphthalenone (9)

Keto ester **8** (336 mg, 1.35 mmol) was dissolved in lithium iodide dihydrate – collidine reagent (2.12 mL, 2.70 mmol) under an atmosphere of nitrogen. The mixture was stirred vigorously and heated at reflux for 3 h. The mixture was then cooled to room temperature, poured into cold aqueous 5% hydrochloric acid, and extracted with ether. The extracts were washed with cold 5% aqueous hydrochloric acid and water, dried, filtered, and concentrated. Column chromatography of the residue on silica gel, eluting with 4–8% ether in petroleum ether, gave a mixture of *cis*- and *trans*-enones **9** (50:50 by ^{1}Hmr integration, 195 mg, 76% yield, 97% based on consumed starting material). Further elution with 8–25% ether in petroleum gave recovered keto ester **8** (75 mg, 22% recovery). The ^{1}Hmr spectrum of the product mixture showed two sets of signals identical to those reported for pure compounds (21).

4,4,7-Trimethyl-1(4H)-naphthalenone (10)

The 1:1 mixture of *cis*- and *trans*-enones **9** (120 mg, 0.645 mmol) obtained from the preceding experiment was dissolved in carbon tetrachloride (10 mL). *N*-Bromosuccinimide (230 mg, 1.29 mol) and benzoyl peroxide (5 mg, 0.021 mmol) were added. The mixture was refluxed for 1 h, then cooled to room temperature, filtered, and concentrated. Column chromatography of the residue on silica gel, eluting with 1–2% ether in petroleum ether, gave 44 mg (37% yield) of aryl ketone **10** (21).

4,4,6-Trimethyl-4aβ,5,8,8aβ-tetrahydro-1(4H)-naphthalenone and 4,4,6-Trimethyl-4aβ,5,8,8aα-tetrahydro-1(4H)-naphthalenone (11)

Keto ester **7** (248 mg, 1.00 mmol) was dissolved in the lithium iodide dihydrate – collidine reagent (2.34 mL, 3.00 mmol) and the mixture was brought to reflux. After heating for 3 h the mixture was cooled to room temperature, poured into cold aqueous 5% hydrochloric acid, and extracted with ether. The extracts were washed with cold 5% aqueous hydrochloric acid and water, dried, filtered, and concentrated. Column chromatography of the residue on silica gel, eluting with 4–10% ether in petroleum ether, gave a mixture of *cis*- and *trans*-enones **11** (43:57 by ^{1}Hmr integration, 174 mg, 91% yield, 97% based on consumed starting material). Further elution with 10–15% ether in petroleum ether gave keto ester **7** (18 mg, 7% recovery). The ^{1}Hmr spectrum of the product mixture exhibited two sets of signals. The following ^{1}Hmr data were attributed to the *cis* compound: δ: 6.29 (dd, ~2/5H, J = 10, J' = 2 Hz, —C*H*=CH—CO—), 5.68 (d, ~2/5H, J = 10 Hz, —CH=C*H*—CO—), 5.33 (m, ~2/5H, =CH—), 2.82 (m, ~2/5H, —CO—CH—), 1.58 (br s, 3 × ~2/5H, =C—CH_3), 1.30 (s, 3 × ~2/5H, —CH_3), and 1.10 (s, 3 × ~2/5H, —CH_3). The following ^{1}Hmr data were attributed to the *trans* compound: δ: 6.56 (d, ~3/5H, J = 10 Hz, —C*H*=CH—CO—), 5.72 (d, ~3/5H, J = 10 Hz, —CH=C*H*—CO—), 5.33 (m, ~3/5H, =CH—), 1.66 (br s, 3 × ~3/5H, =C—CH_3), 1.14 (s, 3 × ~3/5H, —CH_3), and 1.04 (s, 3 × ~3/5H, —CH_3). The following spectral data were recorded for the mixture: ir (CCl_4): 1686 (C=O), 1675 (C=O), 1397, 1379, 1367 (CH_3), 790 (C=CH) cm^{-1}. *Exact Mass* calcd. for $C_{13}H_{18}O$: 190.1357; found (ms): 190.1352. *Anal.* calcd. for $C_{13}H_{18}O$: C 82.06, H 9.54; found: C 82.06, H 9.55.

4,4,6-Trimethyl-1(4H)-naphthalenone (12)

A mixture of *cis*- and *trans*-enones **11** (58 mg, 0.31 mmol) obtained from the preceding experiment was dissolved in carbon tetrachloride (10 mL) and *N*-bromosuccinimide (109 mg, 0.61 mmol) and benzoyl peroxide (5 mg, 0.02 mmol) were added. The mixture was stirred vigorously and heated at reflux for 45 min, then cooled to room temperature, filtered, and concentrated. Column chromatography of the residue on silica gel, eluting with 1.5–2% ether in petroleum ether, gave an impure sample of aryl ketone **12** which was subjected to a second chromatographic purification. This provided pure aryl ketone **12** (25 mg, 43% yield); ir 1661 (C=O), 1607, (aromatic C=C), 1395, 1372, 1359 (CH_3), 814 (aromatic CH) cm^{-1}; ^{1}Hmr δ: 7.95 (d, 1H, J = 8 Hz, C-8 H), 7.20 (br s, 1H, C-5 H), 7.09 (dd, 1H, J = 8, J' = 2 Hz, C-7 H), 6.72 (d, 1H, J = 10 Hz, —C*H*=CH—CO—), 6.18 (d, 1H, J = 10 Hz, —CH=C*H*—CO—), 2.40 (s, 3H, —CH=C—C*H*$_3$), and 1.44 (s, 6H, 2 × —CH_3). *Exact Mass* calcd. for $C_{13}H_{14}O$: 186.1045; found (ms): 186.1047.

8aβ-Carbomethoxy-1-triethylsilyloxy-4,4,6-trimethyl-3,4,4aβ,5,8,8a-hexahydronaphthalene (13)

Finely divided keto ester **7** (760 mg, 3.06 mmol) was suspended in triethylsilane (710 mg, 6.12 mmol) and *tris*-triphenylphosphine rhodium(I) chloride (14 mg, 0.015 mmol) was added. The mixture was stirred for 5 h after which additional triethylsilane (710 mg) was added. After a further 19 h the mixture was diluted with petroleum ether, filtered, and concentrated to give crude silyl enol ether **13** (1.28 g). Column chromatography of crude **13** on silica gel, eluting with 3–5% ether in petroleum ether, gave pure silyl enol ether **13** (1.01 g, 91% yield) as a colourless oil; ir: 1743, 1728 (C=O), 1674 (enol C=C), 1387, 1378, 1366 (CH_3), and 820 (C=CH) cm^{-1}; ^{1}Hmr δ: 5.28 (m, 1H, CH_3—C=C*H*—), 4.63 (dd, 1H, J = 6, J' = 3 Hz, —O—C=C*H*—), 3.58 (s, 3H, —O—CH_3), 2.63 (dd, 1H, $J = J'$ = 8 Hz, —CH—), 1.62 (s, 3H, =C—CH_3), 0.96 (s, 6H, —C(CH_3)$_2$), 0.96 (t, 9H, J = 7 Hz, —Si(CH_2CH_3)$_3$), and 0.61 (q, 6H, J = 7 Hz, —Si(CH_2CH_3)$_3$). *Exact Mass* calcd. for $C_{21}H_{36}O_3Si$: 364.2433; found (ms): 364.2433. *Anal.* calcd. for $C_{21}H_{36}O_3Si$: C 69.18, H 9.95; found: C 69.36, H 9.95.

8aβ-Carbomethoxy-4,4,6-trimethyl-3,4,4aβ,5,8,8a-hexahydro-1(2H)-naphthalenone (14)

Pure silyl enol ether **13** (993 mg, 2.72 mmol) was dissolved in

Can. J. Chem. Downloaded from www.nrcresearchpress.com by 210.87.254.105 on 09/06/12
For personal use only.

methanol (50 mL) and a solution of 10% aqueous potassium carbonate (10 mL) was added. The mixture was stirred for 4 h, then poured into water and extracted with methylene chloride. The extracts were washed with water, dried, filtered, and concentrated. Column chromatography of the residue on silica gel, eluting with 3–10% ether in petroleum ether, gave keto ester **14** (598 mg, 88% yield) as a colourless oil; ir: 1743, 1731 (C=O, ester), 1710 (C=O, ketone), 1427 (—CH_2—C=O), 1388, 1367 (CH_3), and 783 (C=CH) cm^{-1}; ^{1}Hmr δ: 5.28 (m, 1H, —CH=), 3.62 (s, 3H, —O—CH_3), 1.60 (s, 3H, =C—CH_3), 1.07 (s, 3H, CH_3) and 0.97 (s, 3H, CH_3); ^{13}Cmr δ: 209.0, 173.7, 131.9, 117.7, 59.5, 52.4, 44.9, 38.4, 35.6, 33.4, 30.7, 29.6, 28.6, 23.8, and 23.5. *Exact Mass* calcd. for $C_{15}H_{22}O_3$: 250.1569; found (ms): 250.1570. *Anal.* calcd. for $C_{15}H_{22}O_3$: C 71.97, H 8.86; found: C 71.83, H 8.73.

Crude silyl enol ether **13** could be hydrolyzed using the procedure above to give keto ester **14** in 94% overall yield from **7**.

4,4,6-Trimethyl-3,4,4aβ,5,8,8aα-hexahydro-1(2H)-naphthalenone (15) and 4,4,6-Trimethyl-3,4,4aβ,5,8,8aβ-hexahydro-1(2H)-naphthalenone (16)

Keto ester **14** (966 mg, 3.86 mmol) was dissolved in 2,4,6-collidine (24 mL) under an atmosphere of nitrogen. Anhydrous lithium iodide (4.14 g, 30.9 mmol) was added to the stirred solution followed by addition of water (556 mg, 30.9 mmol). The mixture was heated under reflux for 2.5 h, then cooled to room temperature, poured into cold 5% aqueous hydrochloric acid, and extracted with ether. The extracts were washed with ice-cold 5% aqueous hydrochloric acid and water, dried, filtered, and concentrated. The gc analysis of the residue showed the presence of *cis*- and *trans*-ketones **16** and **15** in a ratio of ~10:90. Column chromatography of the residue on silica gel, eluting with 4% ether in petroleum ether, gave *trans*-ketone **15** (550 mg, 74% yield) which crystallized on standing. One recrystallization from ether gave colourless crystals of pure *trans*-ketone **15**: mp 71–71.5°C; ir: 1706 (C=O), 1387, 1380 and 1366 (CH_3) cm^{-1}; ^{1}Hmr δ: 5.33 (br s, 1H, =CH—), 1.61 (s, 3H, =C—CH_3), 1.07 (s, 3H, —CH_3), and 0.98 (s, 3H, —CH_3); ^{13}Cmr δ: 212.8, 133.1, 120.2, 48.3, 46.0, 42.2, 38.9, 33.3, 32.5, 29.7, 26.3, 24.2, and 20.0. *Exact Mass* calcd. for $C_{13}H_{20}O$: 192.1514; found (ms): 192.1513. *Anal.* calcd. for $C_{13}H_{20}O$: C 81.20, H 10.48; found: C 80.74, H 10.55. Further elution with 4–5% ether in petroleum ether gave a mixture of *cis*- and *trans*-ketones **16** and **15** (67:33 by gc analysis, 74 mg, 10% yield). Further elution with 5% ether in petroleum ether gave *cis*-ketone **16** (16 mg, 2% yield) which crystallized on standing. One recrystallization from ether gave pure *cis*-ketone **16**; mp 51–53°C; ir: 1709 (C=O), 1390 and 1370 (CH_3) cm^{-1}; ^{1}Hmr δ: 5.22 (br s, 1H, =CH—), 2.81 (dd, 1H, $J = J' = 5$ Hz, —CH—CO—), 1.58 (s, 3H, =C—CH_3), 1.32 (s, 3H, —CH_3), and 0.98 (s, 3H, —CH_3); ^{13}Cmr δ: 211.9, 131.4, 118.9, 46.6, 43.6, 37.9, 35.6, 33.0, 29.3, 27.8, 26.9, 24.1, and 23.7. *Exact Mass* calcd. for $C_{13}H_{20}O$: 192.1514; found (ms): 192.1522. *Anal.* calcd. for $C_{13}H_{20}O$: C 81.20, H 10.48; found: C 80.87, H 10.44.

Equilibration of trans- *and* cis-*Ketones 15 and 16*

A mixture of *trans*- and *cis*-ketones **15** and **16** (50:50 by gc analysis, 618 mg, 3.21 mmol) was dissolved in methanol (25 mL) and 1 *N* aqueous sodium hydroxide (5 mL) was added. After stirring for 1 h the mixture was extracted with methylene chloride. The extracts were washed with water, dried, filtered, and concentrated. Gas chromatographic analysis of the residue showed the presence of *cis*- and *trans*-ketones **16** and **15** in a ratio of 18:82. Column chromatography of the residue on silica gel, eluting with 3% ether in petroleum ether, gave pure *trans*-ketone **15** (401 mg). Continued elution gave a mixture of *cis*- and *trans*-ketones **16** and **15** (50:50 by gc analysis, 160 mg). Further elution with 3–5% ether in petroleum ether gave pure *cis*-ketone **16** (27 mg). The total recovery of ketones **15** and **16** was 95%.

6-Carbethoxy-2,9,9-trimethyl-1,4,4aα,6,7,8,9,9aβ-octahydro-(5H)-benzocyclohepten-5-one (18) and 5-Carbethoxy-2,9,9-trimethyl-1,4,4aα,6,7,8,9,9aβ-octahydro-(5H)-benzocyclohepten-6-one (19)

Ketone **15** (1.69 g, 8.78 mmol) was dissolved in anhydrous ether (25 mL) under an atmosphere of nitrogen in a flask wrapped in aluminum foil to exclude light. The solution was cooled to 0°C and boron trifluoride etherate (2.49 g, 17.6 mmol) was added with stirring. Then ethyl diazoacetate (2.00 g, 17.6 mmol) was added. After 1 h saturated aqueous sodium bicarbonate (5 mL) was added slowly (5 min) and the resulting mixture was extracted with methylene chloride. The extracts were washed with water, dried, filtered, and concentrated. Column chromatography of the residue on silica gel, eluting with 5% ether in petroleum ether, gave keto ester **18** (2.09 g, 86% yield) as a pale yellow oil; ir: 1746 (ester C=O), 1703 (ketone C=O), 1390 and 1368 (CH_3) cm^{-1}; ^{1}Hmr δ: 5.33 (br s, 1H, =CH—), 4.08, 4.06 (each q, total 2H, each $J = 8$ Hz, —O—CH_2—CH_3), 3.53 (dd, 1H, $J = 10$, $J' = 4$ Hz, —CO—CH—CO_2—), 1.65 (s, 3H, =C—CH_3), 1.21 (dd, 3H, $J = J' = 8$ Hz, —O—CH_2—CH_3), 0.95 (s, 3H, —CH_3), and 0.76 (s, 3H, —CH_3); ^{13}Cmr δ: 211.0, 170.3, 134.4, 118.4, 60.9, 54.0, 53.4, 44.1, 43.0, 35.8, 32.0, 30.4 (two carbons), 24.4, 23.5, 19.2, and 14.1. *Exact Mass* calcd. for $C_{17}H_{26}O_3$: 278.1881; found (ms): 278.1883. *Anal.* calcd. for $C_{17}H_{26}O_3$: C 73.35, H 9.41; found: C 73.45, H 9.69.

Continued elution gave a mixture of keto esters **18** and **19** (50:50 by ^{1}Hmr integration, 154 mg, 6% yield). Further elution with 5–30% ether in petroleum ether gave keto ester **19** (195 mg, 8% yield) which crystallized on standing. One recrystallization from ether gave pure white crystals of keto ester **19**: mp 92–96°C; ir: 1750 (ester C=O), 1706 (ketone C=O), 1392, 1369 (CH_3), and 783 (C=CH) cm^{-1}; ^{1}Hmr δ: 5.27 (br s, 1H, =CH—), 4.10 (q, 2H, $J = 8$ Hz, —O—CH_2—CH_3), 3.28 (d, 1H, $J = 8$ Hz, —CO—CH—CO_2—), 2.45 (m, 2H, —CH_2—CO—), 1.63 (s, 3H, =C—CH_3), 1.25 (t, 3H, $J = 8$ Hz, —O—CH_2—CH_3), 1.02 (s, 3H, —CH_3), and 0.81 (s, 3H, —CH_3); ^{13}Cmr δ: 207.5, 169.4, 134.1, 119.3, 63.6, 61.0, 49.8, 40.5, 36.7 (two carbons), 35.9, 33.6, 32.9, 31.7, 23.0, 19.5, and 14.1. *Exact Mass* calcd. for $C_{17}H_{26}O_3$: 278.1882; found (ms): 278.1886. *Anal.* calcd. for $C_{17}H_{26}O_3$: C 73.35, H 9.41; found: C 73.18, H 9.43. The overall yield of keto esters **18** and **19** was 100% and in a ratio of ~90:10 by weight.

2,9,9-Trimethyl-1,4,4aα,6,7,8,9,9aβ-octahydro-(5H)-benzocyclohepten-5-one (20)

Keto ester **18** (307 mg, 1.10 mmol) was dissolved in lithium iodide dihydrate – collidine reagent (5.00 mL, 6.60 mmol) under an atmosphere of nitrogen. The resulting mixture was heated at reflux with stirring for 1 h, then cooled to room temperature, poured into ice-cold 5% aqueous hydrochloric acid and extracted with ether. The extracts were washed with ice-cold aqueous hydrochloric acid and water, dried, filtered, and concentrated. Column chromatography of the residue on silica gel, eluting with 3–5% ether in petroleum ether, gave ketone **20** (192 mg, 85% yield) which crystallized on standing. One recrystallization from ether gave colourless crystals of pure ketone **20**; mp 53–54°C; ir: 1700 (C=O), 1391, 1378, 1368 (CH_3), and 784 (C=CH) cm^{-1}; ^{1}Hmr δ: 5.32 (br s, 1H, =CH—), 2.52 (ddd, 1H, $J = J' = 10$, $J'' = 3$ Hz, —CO—CH—), 1.64 (br s, 3H,

Can. J. Chem. Downloaded from www.nrcresearchpress.com by 210.87.254.105 on 09/06/12
For personal use only.

=C(CH$_3$)—), 0.95 (s, 3H, —CH$_3$), and 0.75 (s, 3H, —CH$_3$); ^{13}Cmr δ: 216.7, 134.4, 118.8, 53.5, 45.8, 43.3, 40.2, 36.1, 32.3, 31.1, 30.7, 23.5, 22.2, and 19.0. *Exact Mass* calcd. for $C_{14}H_{22}O$: 206.1671; found (ms): 206.1676.

2,9,9-Trimethyl-1,4,4aβ,6,7,8,9,9aβ-octahydro-(5H)-benzocyclohepten-5-one (17), 2,9,9-Trimethyl-3,4,4aα,6,7,8,9,9aβ-octahydro-(5H)-benzocyclohepten-5-one (21), and 2,9,9-Trimethyl-3,4,4aα,6,7,8,9,9aβ-octahydro-(5H)-benzocyclohepten-5-one (22)

Ketone **20** (831 mg, 4.03 mmol) was dissolved in dry benzene (25 mL) under an atmosphere of nitrogen. *p*-Toluenesulfonic acid monohydrate (393 mg, 2.02 mmol) was added and the mixture heated at reflux with stirring. After 3 h the mixture was cooled to room temperature and diluted with ether. The resulting solution was washed with saturated aqueous sodium bicarbonate and water, dried, filtered, and concentrated. Flash chromatography of the residue on silica gel eluting with 6% ethyl acetate in petroleum ether gave pure ketone **21** (98 mg, 12% yield) as an oil; ir: 1693 (C=O), 1391, 1378, 1362 (CH$_3$), and 829 (C=CH) cm^{-1}; ^{1}Hmr δ: 5.48 (br s, 1H, =CH—), 2.56 (dd, 1H, J = 8, J' = 4 Hz, —CO—CH—), 1.69 (s, 3H, =C(CH$_3$)—), 1.05 (s, 3H, —CH$_3$), and 0.91 (s, 3H, —CH$_3$); ^{13}Cmr δ: 218.0, 134.5, 122.3, 48.1, 45.3, 44.7, 38.1, 36.5, 31.2, 29.9, 27.2, 25.3, 23.9, and 21.8. *Exact Mass* calcd. for $C_{14}H_{22}O$: 206.1671; found (ms): 206.1675. *Anal.* calcd. for $C_{14}H_{22}O$: C 81.50, H 10.75; found: C 81.34, H 10.40. Continued elution gave a mixture of ketones **17**, **20**, **21**, and **22** (35 mg, 4% yield). Continued elution gave a mixture of ketones **17**, **20**, and **22** (700 mg, 84% yield). The total yield of ketones **17**, **20**, **21**, and **22** obtained was 100%.

The conditions described produced an identical mixture of products in identical yield when applied to a mixture of **17**, **20**, and **22**.

Epimerization of Ketone 20

Ketone **20** (20 mg, 0.097 mmol) was dissolved in methanol (5 mL) under an atmosphere of nitrogen and 1 *N* aqueous sodium hydroxide solution (1 mL) was added. The solution was heated at reflux with stirring for 48 h, then cooled to room temperature, diluted with water, and extracted with ether. The extracts were washed with water, dried, filtered, and concentrated to give a mixture of *cis*- and *trans*-ketones **17** and **20** (20:80 by ^{1}Hmr integration). Flash chromatography of the mixture on silica gel, eluting with 6% ethyl acetate in petroleum ether, gave a mixture of **17** and **20** (16 mg, 80% yield). Continued elution gave pure *cis*-ketone **17** (2 mg, 10% yield) as an oil; ir: 1696 (C=O), 1389, 1377, 1367 (CH$_3$), and 793 (C=CH) cm^{-1}; ^{1}Hmr δ: 5.26 (m, 1H, =CH—), 2.82 (m, 1H, —CO—CH—), 1.70 (s, 3H, =C(CH$_3$)—), 1.12 (s, 3H, —CH$_3$), and 1.00 (s, 3H, —CH$_3$). *Exact Mass* calcd. for $C_{14}H_{22}O$: 206.1670; found (ms): 206.1667.

Epimerization of Ketone 21

Ketone **21** (17 mg, 0.083 mmol) was dissolved in methanol (5 mL) under an atmosphere of nitrogen and 1 *N* aqueous sodium hydroxide (0.5 mL) was added. The mixture was heated at reflux with stirring for 20 h. The reaction mixture was cooled to room temperature, diluted with water, and extracted with ether. The extracts were washed with water, dried, filtered, and concentrated to give a mixture of *cis*- and *trans*-ketones **21** and **22** (20:80 by ^{1}Hmr integration, 13 mg, 77% yield). The ^{1}Hmr of this product mixture showed two sets of signals; a minor set identical with those already reported for *cis*-ketone **21** and a major set attributed to the *trans*-ketone **22**; ^{1}Hmr δ: 5.26 (br s, 1H, =CH—), 1.70 (s, 3H, =C(CH$_3$)—), 1.04 (s, 3H, —CH$_3$), and 0.80 (s, 3H, —CH$_3$); ^{13}Cmr δ: 216.9, 135.7, 122.5, 47.8 (two carbons), 43.0 (two carbons), 37.0, 30.3, 29.8, 26.5, 24.6, 22.4, and 18.0. The following data were also recorded for the mixture of ketones **21** and **22**: ir: 1704 (C=O), 1390, 1365 (CH$_3$), and 828 (C=CH) cm^{-1}. *Exact Mass* calcd. for $C_{14}H_{22}O$: 206.1671; found (ms): 206.1669.

7-Epihimachalol (23)

A 0.25 *N* solution of methyllithium in ether (4.34 mL, 1.08 mmol) was diluted with ether (10 mL). A solution of ketone **21** (149 mg, 0.72 mmol) in dry ether (10 mL) was added dropwise with stirring over 5 min. After stirring for an additional 30 min the reaction mixture was poured into ice and water (~20 mL) and the resulting mixture was extracted with ether. The extracts were washed with water, dried, filtered, and concentrated. Column chromatography of the residue on silica gel, eluting with 5% ether in petroleum ether, gave alcohol **23** (149 mg, 93% yield) which crystallized on standing. One recrystallization from petroleum ether gave white crystals of pure alcohol **23**; mp 66–68°C; ir: 3461 (OH), 1387, 1376, 1363 (CH$_3$), and 856 (C=CH) cm^{-1}; ^{1}Hmr δ: 5.50 (br s, 1H, =CH—), 1.70 (s, 3H, =C(CH$_3$)—), 1.24 (s, 3H, —C(OH)C*H*$_3$), and 0.97 (s, 6H, 2 × —CH$_3$); ms *m/e* ($M^+ - H_2O$): 204.1880 (calcd. for $C_{15}H_{24}$: 204.1878). *Anal.* calcd. for $C_{15}H_{26}O$: C 81.02, H 11.79; found: C 81.14, H 11.55.

α-Himachalene (2) and β-Himachalene (3)

Alcohol **23** (103 mg, 0.464 mmol) was dissolved in dry pyridine (4 mL) under an atmosphere of nitrogen and the resulting solution was heated to reflux. A solution of phosphoryl chloride (142 mg, 0.928 mmol) in pyridine (1 mL) was added and the reaction mixture was refluxed for 1 h. The mixture was cooled to 0°C, poured into ice-cold 5% aqueous hydrochloric acid, and extracted with ether. The extracts were washed with ice-cold aqueous 5% hydrochloric acid and water, dried, filtered, and concentrated. Column chromatography of the residue on neutral alumina (Woelm I), eluting with petroleum ether, gave a mixture of himachalenes **2** and **3** (88 mg, 93% yield) in a ratio of 75:25 by ^{1}Hmr integration. A sample of a similar mixture (130 mg) was purified by flash chromatography on silica gel eluting with petroleum ether. The fractions obtained, in order of elution, contained (*a*) pure α-himachalene (56 mg); (*b*) α- and β-himachalene, 50:50, (40 mg); (*c*) α- and β-himachalene, 40:60, (17 mg); and (*d*) β-himachalene, 80% pure, (4 mg). α-Himachalene (**2**) showed the following spectral data: ir (neat): 3060, 1775, 1626 (C=CH$_2$), 1390, 1379, 1362 (CH$_3$), 885 (C=CH$_2$), 868 (C=CH), and 822 (C=CH$_2$) cm^{-1}; ^{1}Hmr δ: 5.43 (br s, 1H, =CH—), 4.70 (m, 2H, =CH$_2$), 1.68 (d, 3H, J = 1.5 Hz, =C(CH$_3$)—), 1.01 (s, 3H, —CH$_3$), and 0.97 (s, 3H, —CH$_3$). *Exact Mass* calcd. for $C_{15}H_{24}$: 204.1878, found (ms): 204.1874. The sample of β-himachalene (**3**) showed the following spectral data: ^{1}Hmr δ: 5.37 (br s, 1H, =CH—), 2.84 (br s, 1H, =CH—C*H*—C=), 1.74 (s, 3H, =C(CH$_3$)—), 0.99 (s, 3H, —CH$_3$), and 0.75 (s, 3H, —CH$_3$). *Exact Mass* calcd. for $C_{15}H_{24}$: 204.1878; found (ms): 204.1876.

Acknowledgements

We are grateful to the Natural Sciences and Engineering Research Council of Canada and the University of Alberta for financial support.

1. G. S. K. Rao, S. Dev, and P. C. Guha. J. Indian Chem. Soc. **29**, 721 (1952).

2. T. C. JOSEPH and S. DEV. Tetrahedron Lett. 216 (1961).
3. J. B. BREDENBERG and H. ERDTMAN. Acta Chem. Scand. **15**, 685 (1961).
4. T. C. JOSEPH and S. DEV. Tetrahedron, **24**, 3809 (1968).
5. T. C. JOSEPH and S. DEV. Tetrahedron, **24**, 3841 (1968).
6. M. PLATTIER and P. TEISSEIRE. Recherches, **19**, 131 (1974).
7. M. PLATTIER, P. ROUILLIER, and P. TEISSEIRE. Recherches, **19**, 145 (1974).
8. M. PLATTIER and P. TEISSEIRE. Ann. Acad. Bras. Cienc. **44**, 392 (1972).
9. S. C. BISARYA and S. DEV. Tetrahedron, **24**, 3861 (1968).
10. D. R. ADAMS, S. P. BHATNAGAR, and R. C. COOKSON. J. Chem. Soc. Perkin Trans. I, 1502 (1975).
11. R. SHANKARANARAYAN, S. C. BISARYA, and S. DEV. Tetrahedron, **33**, 1207 (1977).
12. D. K. KULSHRESHTHA and R. P. RASTOGI. Phytochemistry, **14**, 2237 (1975).
13. D. K. KULSHRESHTHA and R. P. RASTOGI. Phytochemistry, **15**, 557 (1976).
14. B. D. CHALLAND, G. KORNIS, G. L. LANGE, and P. DE MAYO. Chem. Commun. 704 (1967).
15. B. D. CHALLAND, H. HIKINO, G. KORNIS, G. LANGE, and P. DE MAYO. J. Org. Chem. **34**, 794 (1969).
16. E. WENKERT and K. NAEMURA. Synth. Commun. **3**, 45 (1973).
17. E. PIERS and E. H. RUEDIGER. Chem. Commun. 166 (1979).
18. H. J. LIU and E. N. C. BROWNE. Tetrahedron Lett. 2919 (1977).
19. A. S. ONISHCHENKO. Diene synthesis. Israel Program for Scientific Translation, Jerusalem. 1964.
20. F. ELZINGER. Org. Synth. **45**, 7 (1965).
21. H. J. LIU and E. N. C. BROWNE. Can. J. Chem. **57**, 377 (1979).
22. L. M. JACKMAN and S. STERNHELL. Applications of nuclear magnetic resonance spectroscopy in organic chemistry. 2nd ed. Pergamon Press, Oxford. 1969.
23. Z. STOJANAC, R. A. DICKINSON, N. STOJANAC, R. J. WOZNOW, and Z. VALENTA. Can. J. Chem. **53**, 616 (1975).
24. J. A. OSBORN, F. H. JARDINE, J. F. YOUNG, and G. WILKINSON. J. Chem. Soc. A, 1711 (1966).
25. I. OJIMA, M. NIHONYANAGI, T. KOGURE, M. KUMAGAI, S. HORIUCHI, K. NAKATSUGAWA, and Y. NAGAI. J. Organomet. Chem. **94**, 449 (1975).
26. I. OJIMA, T. KOGURE, M. NIHONYANAGI, and Y. NAGAI. Bull. Chem. Soc. Jpn. **45**, 3506 (1972).
27. W. T. TAI and E. W. WARNHOFF. Can. J. Chem. **42**, 1333 (1964).
28. H. J. LIU and T. OGINO. Tetrahedron Lett. 4937 (1973).
29. H. J. LIU and S. P. MAJUMDAR. Synth. Commun. **5**, 125 (1975).
30. T. C. JOSEPH and S. DEV. Tetrahedron, **24**, 3853 (1968).
31. W. C. STILL, M. KAHN, and A. MITRA. J. Org. Chem. **43**, 2923 (1978).
32. R. L. N. HARRIS, F. KOMITSKY, and C. DJERASSI. J. Am. Chem. Soc. **89**, 4765 (1967).

Can. J. Chem. Downloaded from www.nrcresearchpress.com by 210.87.254.105 on 09/06/12
For personal use only.

Merostabilization in radical ions, triplets, and biradicals. 5. The thermal *cis–trans* isomerization of *para*-substituted tetraphenylethylenes[1]

WILLIAM J. LEIGH AND DONALD R. ARNOLD[2]

Department of Chemistry, Dalhousie University, Halifax, N.S., Canada B3H 4J3

Received July 16, 1980

WILLIAM J. LEIGH and DONALD R. ARNOLD. Can. J. Chem. **59**, 609 (1981).

The *cis*- and *trans*-isomers of four *para*-substituted (three disubstituted and one tetrasubstituted) tetraphenylethylenes have been synthesized, separated, and characterized by either dipole moment or X-ray analysis. The rates of thermal isomerization of the disubstituted derivatives in benzene solution correlate with a substituent parameter reflecting substituent effects on benzylic radical stabilities ($\sigma\cdot$), which reflects the biradical nature of the transition state for thermal isomerization in this system. A significant rate enhancement is observed for the tetrasubstituted derivative, in which merostabilization of the transition state is possible.

The Arrhenius parameters for thermal isomerization in benzene were determined. From the variation observed for the disubstituted derivatives, an estimate of 35.5 kcal mol^{-1} for the rotational barrier in tetraphenylethylene is obtained. The activation energy for thermal isomerization of the tetrasubstituted derivative is 2 kcal mol^{-1} lower than those of the other three; this provides an assessment of the importance of merostabilization in this system.

The thermal isomerization of some related olefins (e.g. bianthrylidenes and indigo derivatives) is discussed in light of these results.

WILLIAM J. LEIGH et DONALD R. ARNOLD. Can. J. Chem. **59**, 609 (1981).

On a synthétisé les isomères *cis* et *trans* de quatre tétraphényléthylènes substitués en positions *para* (trois sont bisubstitués et un est tétrasubstitué) et on les a séparés et caractérisés soit par leur moment dipolaire soit par diffraction des rayons-X. Les vitesses d'isomérisation thermique des dérivés bisubstitués dans une solution de benzène peuvent être reliées à un paramètre de substituant qui est un reflet des effets de substituant sur les stabilités du radical benzyle ($\sigma\cdot$), lesquels sont un reflet de la nature biradicalaire de l'état de transition de l'isomérisation thermique de ce système. On observe une augmentation significative de la vitesse du dérivé tétrasubstitué dans lequel une mérostabilisation de l'état de transition est possible.

On a déterminé les paramètres d'Arrhénius de l'isomérisation thermique dans le benzène. A partir de la variation observée pour les dérivés bisubstitués, on a évalué à 35,5 kcal mol^{-1} la barrière de rotation du tétraphényléthylène. L'énergie d'activation de l'isomérisation thermique du dérivé tétrasubstitué est de 2 kcal mol^{-1} plus faible que celles des trois autres dérivés; ceci donne une appréciation de l'importance de la mérostabilisation dans ce système.

A la lumière de ces résultats, on discute de l'isomérisation thermique de quelques oléfines apparentées (comme les dérivés des bianthrylidènes et de l'indigo).

[Traduit par le journal]

Introduction

It is generally accepted that the ground and first excited states of 90°-twisted ethylene have predominantly biradical character (1). The multiplicities of these states are triplet and singlet, respectively, and they correspond to the first excited triplet state of ethylene in the twisted geometry (the ^3p state (2)) and the transition state for thermal isomerization in the ground state (the ^0p state). This ordering of the p-states is frequently reversed in substituted ethylenes (2).

Substituent effects on the energies of the p-states in ethylene relative to their counterparts in the planar geometry are a result of both steric and electronic factors. Sterically bulky substituents raise the energies of the planar states relative to the p-states. One obvious result of this is the lower activation energies for thermal isomerization generally observed for sterically crowded olefins (3). An illustration of the effect on the triplet state is provided by the stilbenes; the sterically unencumbered *trans*-stilbene triplet is nearly isoenergetic with the twisted ^3p state, while the triplet energy of *cis*-stilbene is about 8 kcal mol^{-1} higher (2). Accordingly, *cis*-stilbene is observed to undergo nonvertical excitation (excitation directly to the ^3p state) while the *trans*-isomer does not (2). In cases where both planar isomers are sterically hindered, nonvertical excitation occurs for both (4).

The relative energies of the planar ground state and the ^0p state are markedly affected by electronic factors. In ethylenes which are symmetrically substituted across the double bond, the general trend observed is that this energy difference decreases the greater the ability of the substituent to stabilize a radical (3*a*, *c*). In other words, the electronic effect of a substituent is much greater on the energy of the ^0p state than on that of the planar ground states. On the other hand, it appears that any difference in stability between planar and twisted triplet states is primarily the result of steric factors (e.g. the stilbenes). Biradical stabilization of the triplet state

[1]A portion of this work was completed at the University of Western Ontario.

[2]Author to whom correspondence may be addressed.

0008-4042/81/030609-12$01.00/0

©1981 National Research Council of Canada/Conseil national de recherches du Canada

Can. J. Chem. Downloaded from www.nrcresearchpress.com by 210.87.254.105 on 09/06/12
For personal use only.

Can. J. Chem. Downloaded from www.nrcresearchpress.com by 210.87.254.105 on 09/06/12
For personal use only.

does appear, however, when one considers the difference in energy between the triplet state and the ground state (i.e. the triplet energy).

The situation is different with ethylenes which are unsymmetrically substituted about the double bond. Since the olefinic carbons are not equivalent, a certain amount of bond polarization will occur in the transition state for thermal isomerization (1). This bond polarization can be stabilized by appropriate substitution of donor and acceptor groups on the double bond. Compounds of this type have characteristically low barriers to thermal isomerization (3*a*, 5) and in extreme cases the most stable ground state conformation is in fact twisted about the double bond (5). These low rotational barriers are alternatively explained as being due to decreased double bond order as a result of the contribution from charge-separated resonance structures (in which the olefinic bond has single bond character) to the resonance hybrid structure describing the ground state of the olefin (3*a*, 5).

The transition state for thermal isomerization and the triplet state of symmetrical (across the double bond) olefins such as stilbene (**1**) and tetraphenylethylene (**2**) are thus expected to have predominantly biradical character. The energies of these states relative to the ground state should therefore be roughly as sensitive to variations in ring-substituents as is the stability of the benzyl or diphenylmethyl radical. Substituent effects on benzyl radical stability are small but clearly significant (6–9); all *para*-substituents with the exception of fluorine stabilize the benzyl radical to a certain extent. It is therefore expected that symmetrically substituted (cf. **1** and **2**) stilbenes and tetraphenylethylenes will exhibit slightly lower triplet energies and activation energies for thermal isomerization than the parent compounds. However, when X and Y in substituted tetraphenylethylenes (**2**) are substituents of opposite electron demand, these quantities may be more significantly affected.

Merostabilization (10) is receiving increased recognition as a factor contributing to the stability of free radicals. This concept accounts for the increased stability imparted to free radicals when

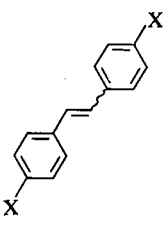

1

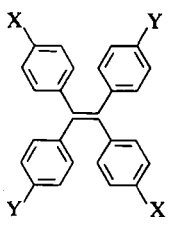

2

simultaneously substituted at the radical site with substituents of opposite electron demand. The effect is most commonly explained in valence bond terminology; the increased stability is a result of the contribution of low energy charge-separated resonance structures to the valence bond hybrid which enables more extensive delocalization of the unpaired electron (10), as is illustrated in [1] with

[1]

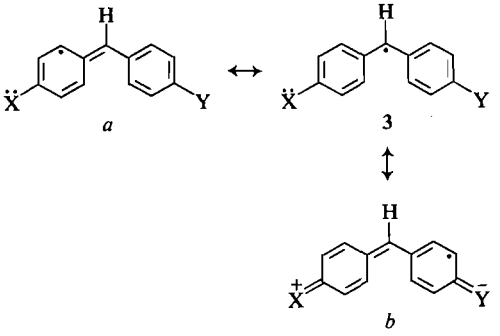

a **3** *b*

the diphenylmethyl radical **3**. The stability of diphenylmethyl is rationalized in terms of resonance structures of type **3***a*, in which unpaired electron density is delocalized onto the *ortho*- and *para*-positions of the rings. Contributions from resonance structures of type **3***b* allow delocalization of the unpaired electron onto *all* carbon atoms in the system. More rigorous explanations have employed molecular orbital theory (11, 12); in fact, the effect was first described in a derivation of a theoretical approach to free radical reactivity (11). A qualitative molecular orbital approach has recently been developed (12).

Although a large number of examples of merostabilized free radicals are now known (10, 12, 13), the effect on other systems containing unpaired electrons has generally not been explored. We have initiated a program designed to assess the importance of merostabilization as a factor contributing to the stability of radical ions, triplet states, and biradical species using the diphenylmethyl radical as the common model system. In our earlier reports in this series, we demonstrated the role of merostabilization in extending electron delocalization in triplet diphenylmethylenes (**4**) (14, 16) and its effect on the stability of benzophenone n,π^* triplets (**5**) (15, 16) and radical anions (**6**) (16).

In this report, we describe the synthesis, separation, and characterization of a series of four *para*-substituted tetraphenylethylenes **2***a–d*, and provide a detailed description of the kinetics of thermal *cis–trans* isomerization. From an analysis of the rates and energetics of the isomerization of the three disubstituted derivatives (**2***a–c*), we obtain an indication of the nature of the "normal" sub-

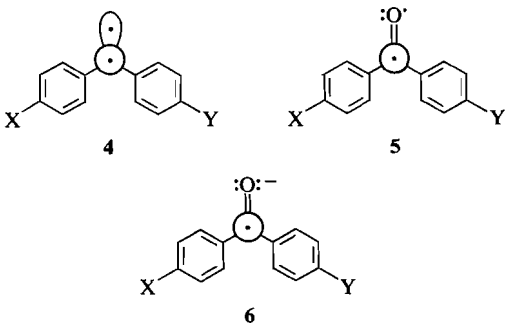

4 5 6

stituent effect (in the absence of merostabilization) on the rotational barrier in tetraphenylethylene. Extrapolation then enables a fairly precise estimate to be made of the rotational barrier in the theoretically important parent compound, tetraphenylethylene. We rationalize the rotational barriers in this and other heavily arylated olefins by considering radical stability arguments, comparing calculated activation energies with experimental values. The effect of merostabilization on the energy of the transition state for thermal isomerization of tetraphenylethylene is demonstrated with the tetrasubstituted derivative **2***d*. With this indication in mind, we offer a different interpretation of the low rotational barriers observed for other important olefinic systems such as indigo derivatives.

Finally, this study provides the first systematic experimental indication of the biradical-like nature of the transition state for thermal *cis–trans* isomerization of symmetrically substituted (across the double bond) olefins.

Results

The tetraarylethylenes (**2***a–d*) were synthesized from the corresponding benzophenones as illustrated in [2] (17), and were obtained as approximately equimolar mixtures of *cis*- and *trans*-isomers. Initial purification by column chromatography removed unreacted ketone and other products. The *cis–trans* isomers were then separated by medium pressure (15–20 psi) column chromatography and/or repeated fractional recrystallization. The olefins were protected as much as possible from unnecessary light, since *cis–trans* isomerization proceeds rapidly and efficiently upon direct irradiation (18*a*). The composition of isomeric mixtures of **2***b–d* could be conveniently determined by high-pressure liquid chromatography (hplc). The *cis*- and *trans*-isomers of **2***a* could not be resolved by hplc under any conditions, so the compositions of mixtures were determined by a combination of ir and ^{1}Hmr spectroscopy (see Experimental).

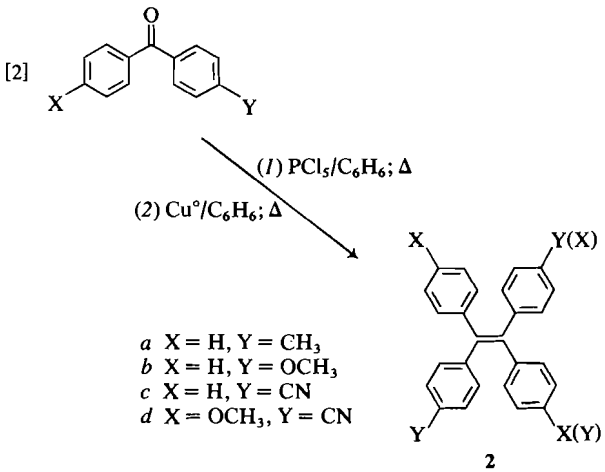

[2]

(*1*) PCl_5/C_6H_6; Δ
(*2*) $Cu°/C_6H_6$; Δ

a X = H, Y = CH_3
b X = H, Y = OCH_3
c X = H, Y = CN
d X = OCH_3, Y = CN

2

The gross structures of **2***a–d* were inferred from their ^{1}Hmr, ir, uv, and mass spectra and elemental analysis; with the exception of *cis*- and *trans*-**2***b* (18) they are all new compounds. The identification of *cis*- and *trans*-isomers of **2***a* was made on the basis of an X-ray crystal structure determination performed on one of the isomers.[3] *Cis*- and *trans*-isomers of **2***b–d* were identified on the basis of their dipole moments. The dipole moments were measured in benzene solution at 25°C by the dielectric constant method (19) and are collected in Table 1. Included in the table for comparison are estimates of the dipole moments calculated by vector addition of standard group moments (20). For ease of calculation, the phenyl groups were assumed to be coplanar, the olefinic bond angles were assumed to be 120°,[4] and methoxy groups were assumed to be freely rotating.[5] The large differences between the dipole moments of the *cis*- and *trans*-isomers of **2***c* and **2***d* allows unambiguous assignments to be made in these cases. The agreement between calculated and observed values is excellent considering the rather gross approximations used in the calculations. The nonzero dipole moment observed for *trans*-**2***c* may be the result of a variety of factors; it is most likely due to the presence of a small

[3] T. S. Cameron, unpublished results. The crystal structures of both *trans*-**2***a* and *trans*-**2***b* are very similar to that found for tetraphenylethylene itself (see ref. 31*a*).

[4] The method of vector analysis used can be best illustrated by pointing out that the calculation of the dipole moment of *cis*-**2***d*, for example, reduces to a calculation of that of 1,2-dicyano-4,5-dimethoxybenzene.

[5] This, though accepted nomenclature (20), is misleading. The notion of "freely rotating" methoxy groups led us to expect calculated dipole moments of zero for *trans*-**2***b* and **2***d*. The calculation, however, gives the average dipole moment of all possible conformations, which is nonzero. The calculated and observed dipole moments of *trans*-4,4′-dimethoxystilbene are 1.70 and 1.69 D, respectively (21).

Can. J. Chem. Downloaded from www.nrcresearchpress.com by 210.87.254.105 on 09/06/12
For personal use only.

Can. J. Chem. Downloaded from www.nrcresearchpress.com by 210.87.254.105 on 09/06/12
For personal use only.

TABLE 1. Calculated and observed dipole moments of tetraphenylethylenes **2***b*–*d*

2[a]		μ_{calc}(debye)[b]	μ_{obs}(debye)[c]
b	*trans*	1.72	1.8
	cis	1.85	2.4
c	*trans*	0.0	1.4
	cis	7.01	7.4
d	*trans*	1.72	2.5
	cis	7.89	8.0

[a]All samples were at least 97% isomerically pure by hplc.
[b]Calculated according to ref. 20.
[c]Benzene solution, 25°C. Error is estimated to be ca. ±0.10.

amount of the *cis*-isomer (a sample of *trans*-**2***c* contaminated with just 2% of the *cis*-isomer would yield a dipole moment of 1.1 D).

We considered our assignment of *cis*- and *trans*-**2***b* to be tentative, though it agrees with that of Olsen and Buckles (18*a*). Their assignment was made primarily on the basis of melting points; they reasoned that the more symmetric *trans*-isomer should pack into a more stable crystalline arrangement and would therefore be the higher melting of the two (18*c*). We note, however, that the higher melting isomers of both **2***c* and **2***d* are in fact the *cis*-isomers. X-ray analysis of *trans*-**2***b* proved the assignment made on the basis of dipole moments to be correct.[3]

The thermal isomerizations of *cis*- and *trans*-**2***a*–*d* were carried out in degassed, sealed ampoules using benzene, benzonitrile, and pyridine (2%) – benzene as solvents. There was no evidence of competing side reactions, leading to other products, in any case. Progress of the isomerization of **2***a* was monitored by ir spectroscopy. Concentration ratios were calculated from the relative absorbances of the 607.9 cm^{-1} band of *trans*-**2***a* and the 630.6 cm^{-1} band of *cis*-**2***a* (in perdeuteriobenzene) and the ratio of the extinction coefficients of these two bands. The concentration ratios were then converted to mole fractions for the kinetic analyses. Progress of the isomerizations of **2***b*–*d* were monitored by hplc. Apparent mole fractions obtained by measurements of peak areas in the hplc trace were converted to true mole fractions with working curves.

For the isomerization of simple olefins (eq. [3]), the sum of the rate constants for forward and reverse reactions can be obtained from concentration vs. time analysis according to eq. [4], which is derived by straightforward manipulation of the standard equation for first order reversible reactions (22*a*). X_0^c, X^c, and X_e^c are mole fractions of the *cis*-isomer at time = 0, t, and equilibrium, respectively. The individual rate constants k_1 and k_2 can

$$[3]\quad \textit{trans}\text{-}\mathbf{2} \underset{k_2}{\overset{k_1}{\rightleftarrows}} \textit{cis}\text{-}\mathbf{2}$$

$$[4]\quad \ln \frac{X_0^c - X_e^c}{X^c - X_e^c} = (k_1 + k_2)t$$

then be obtained from the equilibrium constant:

$$[5]\quad K_e = X_e^c/(1 - X_e^c) = [cis]/[trans] = k_1/k_2$$

Equivalent results are of course obtained irrespective of the direction in which equilibrium is approached.

Rate constants for the isomerization of **2***a*–*d* were obtained by regression analysis of mole fraction – time data according to eq. [4] and are compiled in Table 2. Included in the table are the values of the equilibrium constants measured at each temperature along with recalculated values obtained from regression analysis of the Gibbs equation ($\ln K_e = \Delta H^0/RT$). The individual rate constants k_1 and k_2 can then be calculated from the sums and the recalculated equilibrium constants; for the sake of brevity these are not included, however.

We have used the sum of the rate constants ($k_1 + k_2$) in our analysis of the rates and energetics of *cis*–*trans* isomerization of **2***a*–*d* which follows, and it seems necessary to give some brief justification for this procedure. Although log ($k_1 + k_2$) in fact bears no rigorous thermodynamic significance with regard to the actual rotational barriers in **2***a*–*d*, it does have several advantages over the individual rate constants log k_1 or log k_2. Firstly, the kinetic analysis yields the sum directly, and the added manipulations that are required to obtain the individual rate constants compound the errors. Secondly, the quantity log ($k_1 + k_2$), which defines the activation energy for *approach to equilibrium*, is independent of K_e, and hence is independent of differences in the relative thermodynamic stability of *cis*–*trans* isomers within the series. Variations in the individual activation energies for *cis*→*trans* or *trans*→*cis* isomerization reflect *both* variations in transition state stability and ground state stability. Since the activation energy for approach to equilibrium (E_a) is in fact a *weighted average* of the individual activation energies ($E_a = (k_1E_1 + k_2E_2)/(k_1 + k_2)$) (22*b*), consideration of log ($k_1 + k_2$) provides an indication of the variation in transition state stability only, and effectively excludes the effects of specific interactions which may alter the relative stabilities of *cis*- and *trans*-isomers within the series.

Discussion

An indication of the "normal" substituent effect

TABLE 2. Rates of thermal *cis–trans* isomerization of tetraphenylethylenes **2***a–d*[a]

T(°C)[b]	$10^4(k_1 + k_2)(s^{-1})$	K_e[c]	T(°C)[b]	$10^4(k_1 + k_2)(s^{-1})$	K_e[c]
	2*a*[d]			**2***b*[e]	
195.0	0.54±0.01	0.933(0.937)	191.8	0.52±0.03	0.934(0.942)
205.0	1.20±0.03	0.936(0.938)	198.7	0.92±0.05	0.965(0.943)
216.4	2.95±0.07	0.948(0.939)	206.7	1.76±0.09	0.938(0.945)
225.0	4.96±0.09	0.943(0.940)	216.5	3.64±0.15	0.927(0.947)
235.3	10.41±0.15	0.935(0.941)	226.4	8.51±0.28	0.953(0.949)
242.0	18.09±0.23	0.941(0.942)	232.1	11.11±0.10	0.957(0.950)
216.4[f]	3.12±0.10	0.939	206.7[g]	1.63±0.02	0.938
			207.5[h]	2.64±0.21	0.931
	2*c*[e]			**2***d*	
191.8	0.61±0.01	0.715(0.726)	168.3	0.25±0.01	0.582(0.586)
198.8	1.13±0.02	0.733(0.726)	180.3	0.80±0.05	0.592(0.596)
206.7	1.99±0.03	0.730(0.726)	190.2	1.40±0.05	0.613(0.604)
216.1	3.80±0.17	0.727(0.726)	200.5	3.78±0.01	0.610(0.611)
224.6	7.73±0.10	0.733(0.726)	207.5	5.69±0.32	0.610(0.617)
237.1	18.17±0.23	0.718(0.726)	219.7	13.17±0.22	0.620(0.626)
206.7[g]	1.97±0.01	0.730	207.5[e,g]	5.11±0.30	0.670
207.5[h]	2.17±0.06	0.789	168.3[e,h]	0.35±0.01	0.736
			207.5[e,h]	7.18±0.52	0.689

[a] In degassed benzene solution unless otherwise noted: error limits obtained from least-squares analysis of eq. [4].
[b] ±0.2°C.
[c] $K_e = k_1/k_2 = cis/trans$; error = ±0.005; average of four measurements. The figure in brackets is the recalculated value after least-squares analysis of the Gibbs equation.
[d] In degassed benzene-d_6 solution.
[e] Rate constants are the average of two determinations.
[f] In degassed pyridine-d_5(2%) – benzene-d_6 solution.
[g] In degassed pyridine(2%) – benzene solution.
[h] In degassed benzonitrile solution.

on the rates and energetics of thermal isomerization of tetraphenylethylene, in the absence of merostabilization, is provided by the model compounds **2***a–c*. As the data in Table 2 (205°, 206.7°C) reveal, the rate of isomerization in benzene solution varies slightly (but significantly) with substitution in the *para*-positions of the rings. The rates of isomerization are the same, within experimental error, in pyridine (2%) – benzene as those in benzene, which rules out the possibility of rate enhancements due to adventitious acid catalysis. It is of interest to note that the observed trend in rates (**2***a* < **2***b* < **2***c*) does not correlate with Hammett substituent constants. This is in accord with current notions of substituent effects on benzylic radical stabilities (6–9). We have used the recently measured (9) relative rates of thermal isomerization of *meta*- and *para*-substituted 2-aryl-3,3-dimethylmethylenecyclopropanes to define a scale of substituent parameters reflecting the variation in benzylic radical stability with ring substituent (16):

$$[6] \quad \sigma\cdot = \log k_x/k_H$$

These parameters were found to correlate very well with benzylic proton hyperfine coupling constants from the esr spectra of ring-substituted benzyl radicals (7*a*). To the extent that electron delocalization correlates with radical stability, these parameters appear to accurately represent substituent effects on benzyl radical stabilities.[6]

Using the Arrhenius parameters obtained from our rate constant data for isomerization of **2***a–d* in benzene (*vide infra*), we have calculated the rates of thermal isomerization at one standard temperature (207.5°C) for comparative purposes. These are shown plotted versus $\sum\sigma\cdot$ in Fig. 1.

While the significance of the correlation between $\log(k_1 + k_2)$ and $\sum\sigma\cdot$ in Fig. 1 is admittedly not as great as it could be with the inclusion of more substituents, the trend is clear. The variation in rate within the series **2***a–c* is revealed by the small slope ($\rho\cdot = 0.24$) obtained from least-squares analysis of the three-point plot (c.c. = 0.91). The tetrasubstituted derivative **2***d* deviates significantly from the best line drawn for **2***a–c*, the rate of isomerization being a factor of about two greater than that expected on the basis of the "normal" radical stabilizing effect of the substituents (as predicted by $\sigma\cdot$-values). We attribute this rate enhancement to increased stabilization of the transition state as a result of merostabilization.

[6] As we have pointed out (16), benzylic proton hyperfine constants should provide the most accurate $\sigma\cdot$-scale. Due to the current unavailability of hyperfine data for more than a handful of substituents (7*a*), however, we continue to use the scale derived from Creary's data.

Can. J. Chem. Downloaded from www.nrcresearchpress.com by 210.87.254.105 on 09/06/12
For personal use only.

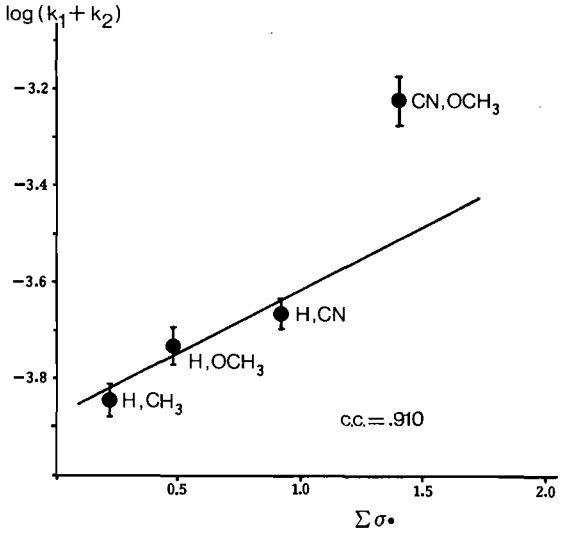

FIG. 1. The rates of thermal isomerization of 2*a*–*d* in benzene solution (207.5°C): log ($k_1 + k_2$) vs. $\Sigma\sigma\cdot$.

Since merostabilization is a result of the ability of the substituents to support charge separation in the free-spin system, the effect should be enhanced in more polar solvents. Koch and co-workers observed a considerable solvent effect on the enthalpy of dissociation of **7**, which exists in equilibrium with the merostabilized radical **8** (13*g*). The enthalpy of dissociation in ethanol (ΔH = 11 kcal mol^{-1}) is 10 kcal mol^{-1} less than the value of 21 kcal mol^{-1} observed in chloroform and benzene.

We therefore measured the rates of isomerization of 2*b*–*d* at 207.5°C in benzonitrile solution (Table 2). The dielectric constants of benzene and benzonitrile at 207.5°C are estimated to be about 2 and 12, respectively (23). The rate of isomerization of 2*d* is indeed enhanced (by ca. 25%) in this solvent relative to the rate in benzene. It seems unlikely, however, that this rate enhancement is attributable entirely to merostabilization: while the dicyano derivative (2*c*) showed no rate enhancement in the more polar solvent, the rate of isomerization of the dimethoxy derivative (2*b*) was significantly faster.

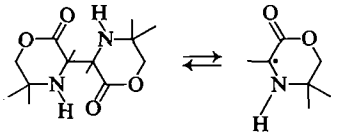

7 **8**

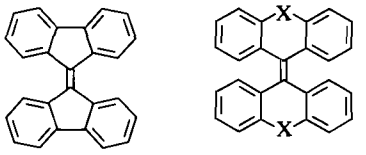

9 **10**

Arrhenius parameters for the thermal isomerization of 2*a*–*d* in benzene solution were determined from the temperature dependence of the rate constants and are compiled in Table 3, along with the ground state enthalpy differences calculated from the temperature dependence of the equilibrium constants according to the Gibbs equation. As expected, the difference in thermodynamic stability between *cis*- and *trans*-isomers is not large, being less than 0.5 kcal mol^{-1}, although the *trans*-isomer is slightly more stable in all cases. Stabilization of the *trans*- relative to the *cis*-isomers may simply be the result of dipole–dipole interactions; the difference in thermodynamic stability increases as the difference in dipole moments between the two isomers increases (2*a*,*b* < 2*c*,*d*). The equilibrium is shifted slightly in favor of the *cis*-isomers in the more polar solvent benzonitrile, though the effect is not large.

Within the series of disubstituted derivatives 2*a*–*c*, the variations in both the activation energies and pre-exponential factors are very small, as the data in Table 3 reveal. "Normal" pre-exponential factors of the order of 10^{12} are observed in each case, which indicates that the isomerization process takes place entirely within the singlet manifold (24). The observation of very low pre-exponential factors and activation energies in early studies of *cis*–*trans* isomerizations were interpreted as being due to the involvement of the triplet state; however, reinvestigation indicated more normal Arrhenius parameters in most cases (25). It is now generally accepted that triplet state involvement is unlikely (24), and that the early indications were the result of catalysis. In any case, the triplet (^3p) energies of 2*a*–*d* appear to be at least 10 kcal mol^{-1} higher than the activation energies for thermal isomerization,[7] so any mechanism for the thermal process involving the triplet state is unlikely.

The activation energies for thermal isomerization of 2*a*–*c* are very similar, varying by not more than 0.2 kcal mol^{-1} within the limits of experimental error. The small variation in activation energy is as expected considering the variation in the rates of isomerization within the series.

It has been pointed out that the difference between the activation energies for thermal isomeri-

[7]W. J. Leigh and D. R. Arnold, unpublished results. The triplet (^3p) energies of 2*a*–*d* have been estimated from a qualitative examination of the relative efficiencies of triplet-sensitized isomerization as a function of sensitizer triplet energy. The triplet energies of 2*a*–*c* are very similar (~48 kcal mol^{-1}) while that of 2*d* is significantly lower (~46 kcal mol^{-1}).

Can. J. Chem. Downloaded from www.nrcresearchpress.com by 210.87.254.105 on 09/06/12
For personal use only.

Can. J. Chem. Downloaded from www.nrcresearchpress.com by 210.87.254.105 on 09/06/12
For personal use only.

TABLE 3. Arrhenius activation energies (E_a) and pre-exponential factors (A) for thermal isomerization[a] and the standard enthalpy differences[b] of **2***a–d* in benzene solution

2	E_a(kcal mol^{-1})[c]	$10^{-12}A$ (s^{-1})[c]	ΔH^0(kcal mol^{-1})[c]
a	35.3±0.6	1.8±1.2	0.1±0.1
b	35.3±0.6	2.3±1.8	0.1±0.2
c	35.1±0.3	2.2±0.8	0.0±0.2
d	32.9±1.2	0.6±0.8	0.5±0.2

[a]Obtained by nonlinear least-squares analysis of the Arrhenius equation, $(k_1 + k_2) = A \exp(-E_a/RT)$.
[b]Obtained by nonlinear least-squares analysis of the equilibrium constants vs. $1/T$.
[c]Error limits obtained from least-squares analyses.

zation (gas phase) of *cis*-stilbene and *cis*-2-butene of 20 kcal mol^{-1} is approximately twice the stabilization energy of the benzyl radical (13 kcal mol^{-1}) (3*c*). The rotational barrier in tetraphenylethylene, which can be estimated to be 35.5 kcal mol^{-1} from the variation in activation energy for **2***a–c*, is therefore similarly expected to reflect the stabilization energy of the diphenylmethyl radical. These results imply additional stabilization of at least 4 kcal mol^{-1} in the diphenylmethyl radical over that in the benzyl radical. Although the bond dissociation energy of diphenylmethane is to our knowledge not available, we can obtain a reasonable estimate of the resonance stabilization energy in diphenylmethyl by considering the spin densities at the benzylic carbon calculated from the α-proton hyperfine constants in the esr spectra of the benzyl radical (ρ = 0.654 (7*a*))[8] and the diphenylmethyl radical (ρ = 0.588 (26)).[8] The spin density at the benzylic carbon decreases by about 30% on going from the ethyl radical (ρ = 0.919 (15)) to the benzyl radical, and a further decrease of about 10% occurs in diphenylmethyl. Taking 13 kcal mol^{-1} as the stabilization energy of the benzyl radical (3*c*, 27*a*), the variation in spin density implies that diphenylmethyl has 1/3 of this, or 4–5 kcal mol^{-1} more stabilization energy than the benzyl radical. This agrees with the value of 4 kcal mol^{-1} calculated from the difference in the activation energies for thermal decomposition of azobis(diphenylmethane) (27*b*) and azobis(phenylmethane) (8*c*). The rotational barrier in tetraphenylethylene is therefore expected to be 8–10 kcal mol^{-1} lower than that for *cis*-stilbene, in agreement with the observed results.

Similar arguments allow estimates of the rotational barriers in related systems such as bisfluorenylidene (**9**) and the bianthrylidenes (**10**). These olefins have been rather extensively studied due to their well-known thermo- and photochromic properties (28). The esr spectra of the 9-fluorenyl and 9-xanthenyl radicals have been determined, and from the α-proton hyperfine constants we can calculate the spin densities at the benzylic carbons to be ρ = 0.52 (29)[8] and ρ = 0.50 (30),[8] respectively. These 20–23% decreases in spin density relative to that in benzyl imply that these radicals each have 8–10 kcal mol^{-1} more stabilization energy than the benzyl radical. Restricting the phenyl rings to a coplanar arrangement effectively doubles the stabilization energy in these radicals compared to diphenylmethyl. This leads to an estimate of 26–30 kcal mol^{-1} for the rotational barriers in **9** and **10**, assuming biradical stabilization to be the major factor contributing to the activation energies for thermal isomerization in these systems.

Figure 2 illustrates the ground state conformations (as determined by X-ray analysis (31)) and the (highest energy) transition states for thermal isomerization in **2**, **9**, and **10**. The larger angle of twist about the double bond in bisfluorenylidene (**9**) compared to that in tetraphenylethylene relieves steric strain due to buttressing of the hydrogens in the 1,1′- and 8,8′-positions. These interactions are relieved in tetraphenylethylene by twisting the phenyl rings relative to one another; the angle of twist about the double bond in tetraphenylethylene is accordingly smaller than in bisfluorenylidene. While these results would imply a smaller degree of double bond order in **9** relative to **2**, it is difficult to quantitatively assess the contribution from these factors to the activation energy for thermal isomerization of **9**.

While 1,1′-substituted derivatives of **9** are known to have free energies of activation in the 20–21 kcal mol^{-1} range (32), an investigation of the thermal isomerization of 2,2′-difluorobisfluorenylidene (by nmr coalescence studies) has led to the suggestion that the rotational barrier in the parent compound is much higher than this (33). Although no indication of $\Delta G^{\ddagger}$ was given in this report, we can estimate a lower limit for the activation energy for isomerization of **9** based on the limited amount of data that

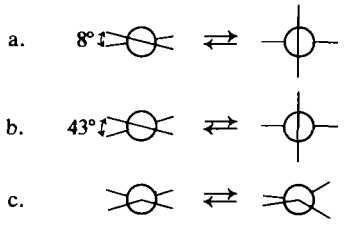

FIG. 2. Newman projections (along the olefinic bond) of the ground state and (highest energy) transition state conformations of (a) tetraphenylethylene (**2**) (31*a*); (b) bisfluorenylidene (**9**) (31*b*); (c) bianthrylidene (**10**) (31*c*).

[8]Calculated according to the McConnell equation; $a = Q\rho$, Q = 25 G.

Can. J. Chem. Downloaded from www.nrcresearchpress.com by 210.87.254.105 on 09/06/12
For personal use only.

was given. The authors indicated that coalescence of the fluorine signals was expected at temperatures "considerably higher than 220°C" (33). Assuming then that $T_c \sim 250$°C, we get an estimate of 26 kcal mol^{-1} for the activation energy in this case.[9] This is in excellent agreement with the value estimated from the spin density argument above, considering that steric destabilization is also expected to contribute to some extent. The importance of biradical stabilization in the bisfluorenylidene system is further demonstrated by the low $\Delta G^{\ddagger}$ observed for thermal isomerization of bis(11*H*-benzo[*b*]fluorenylidene) (23.5 kcal mol^{-1}) (35).

The thermal isomerizations of a wide variety of 2,2′-substituted derivatives of bianthrylidene (**10**) have been studied and are known to have considerably lower activation barriers ($\Delta G^{\ddagger} \sim$ 17–21 kcal mol^{-1}) (36) than the estimate based on radical stability arguments given above. Steric destabilization of the ground state is considerable in this system. Although some of this strain is relieved by puckering of the central rings in the most stable conformer (the A form, see Fig. 2), the highest energy transition state for thermal isomerization is in fact one in which two of the phenyl rings are eclipsed (36). The 90°-twisted form corresponds to the transition state for interconversion of the B forms and is lower in energy.

The small substituent effect on the activation energy for thermal isomerization of tetraphenylethylene is reasonable in view of the known small effect of substituents on benzylic radical stability. These have generally been investigated using relative rate studies; only in a few cases have complete rate–temperature studies been carried out. The activation energies for thermal decomposition of *para*-substituted azocumenes vary by less than 1.5 kcal mol^{-1} over a range of substituents including fluoro, chloro, methyl, and methoxy (8). Activation energies for thermal isomerization of 2-aryl-3,3-dimethylmethylenecyclopropanes were inferred from the rates of isomerization at only two temperatures (37); these vary between 27–30 kcal mol^{-1} for a wide range of substituents. A more reliable estimate can be obtained by calculating the activation energies from the rates of isomerization at 100°C (8), assuming the pre-exponential factor is constant within the series (3×10^{13} s^{-1}). This gives a variation of less than 0.9 kcal mol^{-1} within the entire range of substituents studied. The difference in activation energy between 2-(4-cyanophenyl)- and 2-(4-methylphenyl)-3,3-dimethylmethylenecyclopropane is about 0.5 kcal mol^{-1}. The variation in activation energy for thermal isomerization for **2***a–c* of $\sim$ 0.2 kcal mol^{-1} is thus consistent with the biradical nature of the transition state.

The Arrhenius parameters for thermal isomerization of the tetrasubstituted derivative **2***d* are strikingly different from those observed for **2***a–c*, the activation energy being about 2 kcal mol^{-1} lower than that of **2***c*. We attribute this pronounced lowering of the rotational barrier in **2***d* to additional stabilization of the biradical-like transition state as a result of merostabilization. Simultaneous substitution by both electron-donating and withdrawing groups in the *para*-positions allows an increased contribution from charge-separated resonance structures to the resonance hybrid describing the perpendicular, biradical transition state. The smaller pre-exponential factor observed for **2***d* is also consistent with this explanation. The same interactions which are responsible for lowering the energy of the transition state relative to the ground state also lead to increased rigidity in the transition state, and thus result in a reduction in the entropy of activation. The existence of an isokinetic relationship for thermal olefin isomerizations has been previously noted (24).

It may be argued that the lower activation energy observed for the thermal isomerization of **2***d* may be due to decreased π-bond order in the ground state, as a result of the contribution from polarized resonance structures such as **2***d*′ to the resonance hybrid. Indeed, the exceedingly low barriers to thermal isomerization observed for derivatives of indigo (**11**) have been explained in this way (38). Our data do not allow an estimate of what proportion of the 2 kcal mol^{-1} decrease in activation energy is attributable to such an effect. However, if such bond polarization is in fact important, we

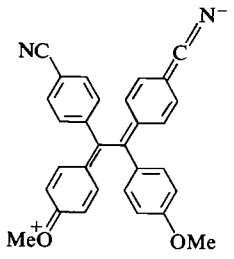

2*d*′

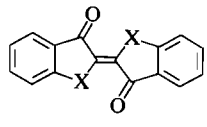

11

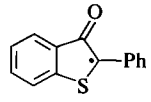

12

[9]Using $\Delta\nu = 34$ Hz (33), we get $k_c \sim 76$ s^{-1} at 250°C (34). E_a is then calculated from the Arrhenius equation assuming $A \sim 10^{13}$ s^{-1}. This corresponds to $\Delta G^{\ddagger} \sim$ 26 kcal mol^{-1}, which is a reasonable lower limit in this case.

Can. J. Chem. Downloaded from www.nrcresearchpress.com by 210.87.254.105 on 09/06/12
For personal use only.

would certainly expect more of a variation in the activation energies for **2***a–c*, since bond polarization should contribute in these derivatives as well, and to different extents depending on substituent. The low rotational barriers observed for indigo derivatives can alternatively be rationalized in terms of a biradical transition state.

The rate of thermal *cis–trans* isomerization (25°C) of **11** as a function of the heteroatom X decreases in the order NMe > NAc > S > Se ≫ O (38, 39), in the same order as the calculated π-bond energies increase (39*a*, 40). This is *not* the sort of trend expected simply on the basis of the ability of the heteroatom to support positive charge.

A biradical transition state, on the other hand, should enjoy considerable stabilization in this system. First of all, both carbonyl groups and heteroatoms adjacent to a radical site are strongly stabilizing (7, 9, 41). Furthermore, heteroatom radical-stabilizing effects increase in the order O < N ≤ S (42). Secondly, merostabilization should have a very pronounced effect in this case as a result of the contribution from resonance structures such as **11***a*, which enable delocalization of the unpaired electrons into the aromatic rings. Katritzky and co-workers have examined the closely analogous radical **12** by esr spectroscopy (10). This stable radical is generated by thermolysis of the dimer at 40–100°C. Analysis of the esr spectrum reveals significant spin density in the benzo-ring.

We believe that merostabilization of radical and radical-like species is a much more prevalent factor than has been recognized in the past. The well studied thermal isomerization of indigo derivatives is offered as an example where merostabilization may contribute to the lowering of the rotational barrier.

Conclusions

The rates of thermal isomerization of a series of *para,para'*-disubstituted tetraphenylethylenes correlate with a set of parameters describing substituent effects on benzylic radical stability, which is consistent with the biradical nature of the transition state. A significant rate enhancement is observed for the tetrasubstituted derivative; this is attributed to the effect of merostabilization on the energy of the transition state for thermal isomerization.

There is only a slight variation in the Arrhenius parameters for isomerization within the series of disubstituted derivatives, which allows an estimate of 35.5 kcal mol^{-1} for the rotational barrier in tetraphenylethylene. The activation energy observed for the tetrasubstituted derivative is about 2 kcal mol^{-1} less than those observed for the three model compounds; this provides an assessment of the contribution from merostabilization to the energy of the transition state for thermal isomerization of tetraphenylethylene derivatives.

Merostabilization may be the dominant factor responsible for the low rotational barriers characteristic of many indigo derivatives.

Experimental

All melting points are corrected. The ^{1}Hmr spectra were recorded on either a Varian T-60 or CFT20 nmr spectrometer and are reported in parts per million (ppm) downfield from TMS. Infrared spectra were recorded on an air-purged Perkin-Elmer 180 grating infrared spectrometer and are reported in wavenumbers, calibrated against the 1601.8 cm^{-1} polystyrene absorption. Ultraviolet–visible absorption spectra were recorded on a Cary-Varian 219 Absorption Spectrometer and are reported in nanometers. Elemental analyses were performed by Chemalytics, Inc. or Canadian Microanalytics, Inc., and agreed to within 0.3% of the calculated values. A Fisher proportional temperature control unit with an insulated silicon oil (Dow Corning 210-H) bath was used in the kinetic studies. Temperatures were recorded using a Hewlett-Packard 2802A thermometer, and did not vary by more than 0.5° during any particular run. Analyses of olefin mixtures (for **2***b–d*) were performed using a Tracor high pressure liquid chromatograph, which consists of a Tracor 995 isochromatographic pump, Model 970 variable wavelength absorbance detector, a Rheodyne model 7120 loop injection valve (20 μL volume), and a Hewlett-Packard Model 7123A strip chart recorder, in conjunction with a Whatman Partisil PXS 10/25 analytical column. The hplc solvents were hexanes (Fisher reagent, distilled) and dichloromethane (Fisher reagent, distilled from phosphorus pentoxide). Peak areas were determined by cutting and weighing, multiplying height by half-width, or planimetry; the three methods were shown to be of equal accuracy. Apparent mole fractions of the *cis*-isomers were obtained by dividing the area of the peak due to the *cis*-isomer by the sum of the areas of both peaks. These were then converted to true mole fractions with working curves, which were simply plots of apparent vs. true mole fractions constructed with ten standard solutions of accurately weighed mixtures of "pure" *cis*- and *trans*-isomers. Where necessary, the true mole fractions of the "pure" isomers were determined by dividing the hplc peak areas by the respective extinction coefficients of the two isomers obtained from their uv spectra in dichloromethane.

Analyses of mixtures of *cis*- and *trans*-**2***a* were performed by ir spectroscopy. The solution (ca. 0.15 *M*) in benzene-d_6 or pyridine-d_5 (2%) – benzene-d_6 was placed in a NaCl solution cell (0.113 mm path length, 60 μL cell volume) and placed in the sample beam of the PE 180 spectrometer. A matched cell containing solvent was placed in the reference beam. The spectrum was then scanned (3 cm^{-1} min^{-1}) through the 645–595 cm^{-1} region under conditions of high sensitivity, high S/N, and linear absorbance. No absorption in this region was evident in spectra of either solvent vs. air or solvent vs. solvent. The ratio of absorbances at 631 cm^{-1} (*cis*-**2***a*) and 608 cm^{-1} (*trans*-**2***a*) was then determined from the ratio of peak heights (average of two determinations), and converted to the concentration ratio using the ratio of extinction coefficients of the two bands. The extinction coefficient ratio ($\varepsilon_{trans}/\varepsilon_{cis}$ = 1.499) was determined by comparing the absorbance ratios of four mixtures of differing compositions with true concentration ratios determined from the integrated intensities of the methyl peaks in the ^{1}Hmr spectra (CFT 20) of the same mixtures in deuterochloroform. Concen-

Can. J. Chem. Downloaded from www.nrcresearchpress.com by 210.87.254.105 on 09/06/12
For personal use only.

tration ratios were then converted to mole fractions for the kinetic analyses.

Benzene used in the dipole moment determinations and kinetic studies was Fisher reagent grade, which had been stirred with concentrated sulfuric acid for 12 h, washed thrice with distilled water, once with saturated aqueous bicarbonate, stirred over sodium for eight hours, and distilled. Pyridine was Eastman reagent grade and was used as received. Benzene-d_6 and pyridine-d_5 were purchased from Merck, Sharpe, and Dohme and used as received. Benzonitrile (Eastman, aniline free) was shaken with silica gel (2 × 100 g), filtered, stirred with calcium hydride for three hours, and decanted. It was then distilled twice from phosphorus pentoxide, taking middle fractions in each case.

The tetraarylethylenes were prepared from the corresponding benzophenones (16) by the method of Buckles and Matlack (17). The benzophenone was refluxed for 24 h with phosphorus pentachloride (1 equiv.) in dry benzene; in most cases, progress of the reaction was followed by ir spectroscopy. Following evaporation of solvent, the crude dichlorides were pumped on under vacuum for 1–3 hours, and then redissolved in fresh, dry benzene. Electrolytic copper dust (10 equiv., dried at 110°C for 12 h) was added and the mixtures refluxed for 24 h. The mixtures were cooled, filtered, and the solvent evaporated to yield the olefins as approximately equimolar mixtures of *cis–trans* isomers contaminated with unreacted benzophenone. The separation, purification, and characterization of each are described in detail below.

1,2-Di(4-methylphenyl)-1,2-diphenylethylene (2a)

The crude product from above (2 g) was chromatographed on a silica gel (65 g) column using hexane as eluant. The olefins (1.1 g, 61%) were eluted first from the column. After evaporation of solvent, the mixture of olefins was dissolved in hot hexane (~15 mL) and allowed to cool slowly in the dark. The two isomers crystallized in different crystalline forms, *needles (cis)* and *spherical clusters (trans)*, which were separated by hand, and recrystallized again. The needles dissolve more readily in warm hexane than do the clusters. A small amount of hexane could therefore be added to *trans*-rich mixtures, warmed slightly to dissolve the needles, and decanted off. A similar treatment was applied to the *cis*-rich mixtures. The *cis*- and *trans*-isomers could be obtained in roughly 90% isomeric purity after three or four careful recrystallizations. Mother liquors were combined and their volumes reduced to afford more material. The *trans*-isomer was finally recrystallized slowly from chloroform–hexane (1:4) to yield colourless plates (mp 171–175°C); ir (KBr): 3020(w), 1511(m), 1490(m), 1442(m), 811(br, m), 759(m), 748(s), 719(m), 700(s), 608(s); uv λ_{max} (ethanol): 242 (26 800), 311 (15 300); ^{1}Hmr ($CDCl_3$) δ: 2.23 (s, 3H), 6.88 (s, 5H), 7.06 (5, 4H). *Anal.* calcd. for $C_{28}H_{24}$: C 93.29, H 6.71; found: C 93.08, H 6.80. The identity of this isomer was inferred from an X-ray analysis. The *cis*-isomer was obtained as colourless needles (mp 130–134°C); ir (KBr): 3020(w), 1511(m), 1490(m), 1442(m), 821(w), 800(m), 785(w), 737(s), 727(w), 696(s), 631(m); uv λ_{max} (ethanol): 242 (25 300), 311 (14 600); ^{1}Hmr ($CDCl_3$) δ: 2.25 (s, 3H), 6.90 (s, 5H), 7.04 (s, 4H).

1,2-Di(4-methoxyphenyl)-1,2-diphenylethylene (2b)

The crude product (oily yellow solid, 33 g) was chromatographed on a silica gel (500 g) column using benzene (60%) – hexane as eluant. Evaporation of the first two material-containing fractions yielded a colourless solid (2.2 g) which was predominantly the *trans*-isomer (by hplc). Evaporation of the next five fractions yielded an oily solid (14.8 g) which was a roughly equimolar mixture of *cis*- and *trans*-isomers. The following six fractions yielded a colourless fluorescent oil (4.0 g) which subsequently crystallized; this was found to consist predominantly of the *cis*-isomer. The combined *trans*-rich mixture was recrystallized from chloroform (10%) – ethanol. A portion of this material (1 g) was chromatographed in the dark on Merck 60 PF-254 preparative layer silica gel (60 g) under a pressure of 8 psi N_2 using cyclohexane (60%) – benzene as the eluant. Fractions (20 mL) were collected and their compositions checked by hplc; those containing less than 5% of the *cis*-isomer were combined and evaporated. One recrystallization from chloroform (10%) – ethanol gave the *trans*-isomer as colourless needles (0.5 g, mp 193–194°C; lit (18*b*) mp 185–187°C).

The *cis*-rich (~75%) mixture isolated from the preliminary column was recrystallized from carbon tetrachloride – methanol, and a portion (1 g) was chromatographed in the dark on preparative layer silica gel (50 g) with cyclohexane (80%) – benzene as eluant (10 psi N_2); 10 mL fractions were collected and monitored by hplc. Those containing less than 5% of the *trans*-isomer were combined and evaporated. The resulting oil was dissolved in chloroform, four times the volume of ethanol was added, and the solution was allowed to crystallize slowly, yielding the *cis*-isomer as colourless needles (mp 134–135°C, lit. (18*a*) mp 135–136°C).

High-pressure Liquid Chromatographic Analysis of 2b

Solvent: dichloromethane (60%) – hexanes, flow rate: 0.95 mL min^{-1}; analytical wavelength: 300 nm; retention times: *trans*-**2***b*, 8 min; *cis*-**2***b*, 10.5 min.

1,2-Di(4-cyanophenyl)-1,2-diphenylethylene (2c)

The crude yellow solid (7.3 g) was dissolved in chloroform–ethanol (1:1, 60 mL), the resulting solution was evaporated to ca. 35 mL and then allowed to cool slowly. The resulting crystals (0.9 g) were collected by vacuum filtration. Ethanol (10 mL) was added to the mother liquors, and this solution was allowed to crystallize slowly. Filtration afforded a further 0.7 g of material which was combined with the first crop of crystals. The mother liquors were evaporated to ca. 30 mL, cooled slowly, and the resulting crystals (1.0 g) collected by filtration; these were shown to be rich in the *trans*-isomer by hplc. This mixture was chromatographed on preparative layer silica gel (50 g) under a pressure of 10 psi N_2 with benzene (60%) – cyclohexane as eluant. The first twenty-five 8 mL fractions contained the *trans*-isomer contaminated with less than 3% of the *cis*-isomer by hplc; these were combined and evaporated to yield a yellowish solid (0.46 g). Two recrystallizations from chloroform–ethanol afforded *trans*-**2***c* as slightly yellow needles, mp 203–204°C; ir (KBr): 2225(s), 1600(m), 1499(m), 1441(m), 859(m), 838(m), 818(m), 767(m), 758(m), 747(w), 701(s), 603(s); uv λ_{max} (ethanol): 247 (34 100), 330 (17 200); ^{1}Hmr ($CDCl_3$) δ: 6.60 (m, 7H), 6.86 (d, 2H). *Anal.* calcd. for $C_{28}H_{18}N_2$: C 87.93, H 4.74; found: C 87.86, H 4.86.

The first two crops of crystals from recrystallization of the crude product (above) consisted of the *cis*-isomer contaminated with small amounts of 4-cyanobenzophenone and the *trans*-isomer (by hplc). Three careful recrystallizations from chloroform–ethanol afforded *cis*-**2***c* as slightly yellow needles, mp 247–249°C; ir (KBr): 2225(s), 1600(m), 1499(m), 1441(m), 858(m), 820(m), 772(m), 733(m), 720(m), 698(s), 628(m); uv λ_{max} (ethanol): 242 (27 200), 294 (14 200), 328 (14 100); ^{1}Hmr ($CDCl_3$) δ: 6.57 (m, 7H), 6.88 (d, 2H). *Anal.* calcd. for $C_{28}H_{18}N_2$: C 87.93, H 4.74; found: C 87.88, H 4.68. The identities of *cis*- and *trans*-**2***c* were inferred from their measured dipole moments (*vide infra*).

High-pressure Liquid Chromatographic Analysis of 2c

Solvent: Dichloromethane; flow rate: 0.95 mL min^{-1}; analytical wavelength: 300 nm; retention times: *trans*-**2***c*, 10 min; *cis*-**2***c*, 18 min.

1,2-Di(4-methoxyphenyl)-1,2-di(4-cyanophenyl)ethylene (2d)

The crude orange solid (38.1 g) was dissolved in hot methanol (400 mL), filtered, and cooled. The resulting yellow solid

Can. J. Chem. Downloaded from www.nrcresearchpress.com by 210.87.254.105 on 09/06/12
For personal use only.

(11.1 g) was collected by vacuum filtration and was shown to contain *cis*- and *trans*-**2***b* in roughly equimolar amounts (by hplc and ^{1}Hmr). A portion of this material (3 g) was chromatographed in the dark on preparative layer silica gel (130 g) under a pressure of 14 psi N_2 using chloroform (25%) – hexanes as eluant. The first three 30 mL fractions contained the *trans*-isomer contaminated with less than 5% of the *cis*. The next seventy-five fractions contained mixtures of the two isomers, and finally the last four were > 95% *cis*-**2***d*.

Evaporation of the first three (combined) fractions from the column yielded a yellow solid (0.32 g). Two recrystallizations from chloroform–hexanes yielded *trans*-**2***d* as bright yellow needles, mp 123–124°C; ir (KBr): 2840(w), 2225(s), 1602(s), 1509(s), 1290(m), 1244(s), 1172(s), 1030(m), 862(w), 830(m), 815(m), 679(w), 574(m); uv λ_{max} (ethanol): 261 (25 800), 353 (12 800); ^{1}Hmr ($CDCl_3$) δ: 3.76 (s, 3H), 6.67 (d, 2H), 6.86 (d, 2H), 7.13 (d, 2H), 7.42 (d, 2H). *Anal.* calcd. for $C_{30}H_{22}N_2O_2$: C 81.43, H 5.01, N 6.33; found: C 81.13, H 5.07, N 6.10.

Evaporation of the last four (combined) fractions yielded a yellowish oil which crystallized (0.23 g). Two recrystallizations from chloroform–methanol yielded *cis*-**2***d* as slightly yellow needles, mp 230–231°C; ir (KBr): 2840(w), 2225(s), 1600(s), 1509(s), 1290(m), 1244(s), 1172(s), 1030(m), 862(w), 828(m), 811(w), 652(w), 585(m); uv λ_{max} (ethanol): 260 (26 900), 279 (19 800), 354 (12 900); ^{1}Hmr ($CDCl_3$) δ: 3.76 (s, 3H), 6.67 (d, 2H), 6.90 (d, 2H), 7.10 (d, 2H), 7.41 (d, 2H). *Anal.* calcd. for $C_{30}H_{22}N_2O_2$: C 81.43, H 5.01, N 6.33; found: C 81.38, H 5.29, N 6.38.

The identities of *cis*- and *trans*-**2***d* were inferred from their measured dipole moments (*vide infra*).

High-pressure Liquid Chromatographic Analysis of 2d

Solvent: dichloromethane; flow rate: 1.5 mL min^{-1}; analytical wavelength: 360 nm; retention times: *trans*-**2***d*, 24 min; *cis*-**2***d*, 28 min.

Samples of *trans*-**2***d* can alternatively be prepared by irradiation of a 0.1 *M* solution of a *cis–trans* mixture of **2***d* in degassed benzene solution with a 1 kW medium pressure mercury lamp (10°, Pyrex filter) for 5–10 min. The resulting mixture (ca. 90% *trans*-**2***d*) can then be chromatographed and/or recrystallized as described above to yield pure samples of *trans*-**2***d*.

Dipole Moment Determinations for cis- *and* trans-2b–d

Preparation of Solutions

A 0.01 *M* solution (100 mL) of the olefin was prepared by dissolving an accurately weighed (±0.2 mg) sample of the olefin in an accurately weighed amount of dry, purified benzene. Weighed amounts of this solution were then diluted with benzene to give a total of five solutions. Concentrations were expressed as mole fractions of the olefin (X_{ol}), and ranged from ca. 2×10^{-4} to 10^{-3}. The solutions were prepared in dry 25 mL volumetric flasks, stoppered, wrapped in parafilm, and stored in the dark until use.

The capacitance of each solution was measured with a Weilheim Dipolemeter DM 01, the temperature of which was held at 25 ± 1°C by means of a thermostatted water bath. The temperature of the water bath did not vary by more than 0.1°C during a run. The cell constant was determined prior to each run by measuring the capacitances of dry air and benzene, and plotting these against dielectric constant (ε); it did not vary significantly throughout the course of the study.

The refractive indices (n) of the solutions were measured with a Fisher refractometer, the temperature of which was also held constant at 25°C with a thermostatted water bath.

A solution was placed in the cell of the dipolemeter and allowed to sit for 15 min to allow temperature equilibration. After measurement of the capacitance (average of six measurements) the cell was drained, rinsed repetitively with benzene, and dried under a stream of nitrogen. The next solution was then placed in the cell and the process was repeated. The capacitances were converted to dielectric constants using the cell constant as determined above.

The slopes obtained from least-squares analysis of plots of ε vs. X_{ol} and n^2 vs. X_{ol} were used to calculate the molecular polarizability at infinite dilution (P_μ°), which was then used to calculate the dipole moment (19). The measured dipole moments, their estimated error limits, and values calculated using standard group moments are compiled in Table 1.

Thermal Isomerization of 2a–d: *Kinetics*

Sample tubes were prepared from 5 or 7 mm Pyrex tubing which had been rinsed once with concentrated nitric acid, thrice with distilled water, soaked in 5% aqueous sodium hydroxide (1 h), rinsed again (three times) with distilled water, and dried in an oven. In the case of **2***a*, the solutions used were ca. 0.15 *M* in benzene-d_6 or pyridine-d_5 (2%) – benzene-d_6, and were degassed by bubbling dry nitrogen through the solution before placing 70 μL aliquots in each of ten tubes. The tubes were then frozen, evacuated, and sealed. In the cases of **2***b–d*, the solutions were ca. 0.001 *M* in benzene, pyridine (2%) – benzene, or benzonitrile and were degassed (three freeze–pump–thaw cycles) and sealed.

Nine tubes were then placed simultaneously in the preset insulated kinetic bath. One tube containing a solution of the other isomer was included to evaluate the equilibrium composition. The temperature of the bath did not fall by more than 0.5° during this procedure and recovered to its original value within 1.5 minutes. Samples were removed after specific time intervals, quenched immediately in an ice bath, opened, and analysed by either ir spectroscopy (**2***a*) or hplc (**2***b–d*). Prior to each run, one tube was used to check the initial composition of the sample to ensure that no accidental heating had occurred during the sealing process. Equilibrium compositions (approached from both directions) were the average of four determinations.

Rate constants were determined by linear regression analysis of the mole fraction vs. time data according to eq. [4], using the Minitab II programme (43*a*). Arrhenius parameters and ΔH^0 values were determined from the temperature dependence of the rate constants for thermal isomerization ($k_1 + k_2$) and the equilibrium constants (K_e) using a nonlinear least-squares programme (43*b*).

Acknowledgements

We wish to express our considerable gratitude to Dr. T. S. Cameron for performing the X-ray analyses. We also gratefully acknowledge the assistance of Dr. D. L. Hooper in obtaining the 80 MHz ^{1}H nmr spectra, and thank Dr. R. K. Chan (University of Western Ontario) for the use of the dipolemeter. We thank Dr. J. Saltiel for an advance copy of the manuscript (2*b*). This work was supported by a grant from the Natural Sciences and Engineering Research Council of Canada.

1. (*a*) L. Salem and C. Rowland. Ang. Chem. Int. Ed. Engl. **11**, 92 (1972); (*b*) L. Salem. Pure Appl. Chem. **33**, 317 (1973).
2. (*a*) J. Saltiel, J. D'Agostino, E. D. Megarity, L. Metts, K. R. Neuberger, M. Wrighton, and O. C. Zafiriou. Organic photochemistry. Vol. 3. *Edited by* O. L. Chapman. Marcel Dekker, Inc., New York. 1973. p. 1, and references therein; (*b*) J. Saltiel and J. L. Charlton. Rearrangements in ground and excited states. Vol. 3. *Edited by* P. de Mayo. Academic Press, Inc. New York. 1980, and references therein.

Can. J. Chem. Downloaded from www.nrcresearchpress.com by 210.87.254.105 on 09/06/12
For personal use only.

3. (*a*) H. O. KALINOWSKI and H. KESSLER. Top. Stereochem. **7**, 295 (1973); (*b*) I. AGRANAT and Y. TAPUHI. J. Am. Chem. Soc. **100**, 5604 (1978); (*c*) S. W. BENSON. Thermochemical kinetics. John Wiley and Sons, Inc., New York. 1968. p. 72.
4. W. G. HERKSTROETER and G. S. HAMMOND. J. Am. Chem. Soc. **88**, 4769 (1966).
5. J. SANDSTRÖM and U. SJÖSTRAND. Tetrahedron, **34**, 371 (1978),and references therein.
6. W. A. PRYOR, T. H. LIN, J. P. STANLEY, and R. W. HENDERSON. J. Am. Chem. Soc. **95**, 6993 (1973), and references therein.
7. (*a*) P. NETA and R. H. SCHULER. J. Phys. Chem. **77**, 1368 (1973); (*b*) E. GEY and N. E. KRUGLYAK. Z. Phys. Chem. Leipzig, **255**, 915 (1974); (*c*) E. GEY and N. E. KRUGLYAK. Z. Phys. Chem. Leipzig, **256**, 737 (1975).
8. (*a*) P. KOVACIC, R. R. FLYNN, J. F. GORMISH, A. H. KAPPELMANN, and J. R. SHELTON. J. Org. Chem. **34**, 3312 (1969); (*b*) J. W. TIMBERLAKE and M. L. HODGES. Tetrahedron Lett. 4147 (1970); (*c*) B. K. BANDLISH, A. W. GARNER, M. L. HODGES, and J. W. TIMBERLAKE. J. Am. Chem. Soc. **97**, 5856 (1975).
9. X. CREARY. J. Org. Chem. **45**, 280 (1980).
10. R. W. BALDOCK, P. HUDSON, A. R. KATRITZKY, and F. SOTI. J. Chem. Soc. Perkin Trans. I, 1422 (1974).
11. M. J. S. DEWAR. J. Am. Chem. Soc. **74**, 3353 (1952).
12. H. G. VIEHE, R. MERENYI, L. STELLA, and Z. JANOUSEK. Angew. Chem. Int. Ed. Engl. **18**, 917 (1979).
13. (*a*) E. M. KOSOWER and E. J. POZIOMEK. J. Am. Chem. Soc. **86**, 5515 (1964); (*b*) A. R. KATRITZKY and F. SOTI. J. Chem. Soc. Perkin Trans I, 1427 (1974); (*c*) A. T. BALABAN, P. T. FRANGOPOL, M. FRANGOPOL, and N. NEGOITA. Tetrahedron, **23**, 4661 (1967); (*d*) A. T. BALABAN. Rev. Roum. Chim. **16**, 725 (1971); (*e*) A. T. BALABAN, M. T. CAPROIU, N. NEGOITA, and R. BAICAN. Tetrahedron, **33**, 2249 (1977); (*f*) K. D. GUNDERMANN and E. ROHRL. Justus Liebigs Ann. Chem. 1661 (1974); (*g*) T. H. KOCH, J. A. OLESEN, and J. DENIRO. J. Am. Chem. Soc. **97**, 7285 (1975); (*h*) L. DE VRIES. J. Am. Chem. Soc. **99**, 1982 (1977); (*i*) L. DE VRIES. J. Am. Chem. Soc. **100**, 926 (1978), (*j*) N. HEIMER. J. Org. Chem. **42**, 3767 (1977); (*k*) L. STELLA, Z. JANOUSEK, R. MERENYI, and H. G. VIEHE. Angew. Chem. Int. Ed. Engl. **17**, 691 (1978); (*l*) H. G. AURICH, E. DEUTSCHLE, and W. WEISS. J. Chem. Res. M, 3455 (1977); (*m*) L. STELLA, R. MERENYI, Z. JANOUSEK, H. G. VIEHE, P. TORDO, and A. MUNOZ. J. Phys. Chem. **84**, 304 (1980).
14. (*a*) D. R. ARNOLD and R. W. R. HUMPHREYS. J. Chem. Soc. Chem. Commun. 181 (1978); (*b*) R. W. R. HUMPHREYS and D. R. ARNOLD. Can. J. Chem. **57**, 2652 (1979).
15. W. J. LEIGH and D. R. ARNOLD. J. Chem. Soc. Chem. Commun. 460 (1980).
16. W. J. LEIGH, D. R. ARNOLD, R. W. R. HUMPHREYS, and P. C. WONG. Can. J. Chem. **58**, 2537 (1980).
17. R. E. BUCKLES and G. M. MATLACK. Org. Synth. Coll. Vol. **4**, 914 (1963).
18. (*a*) R. J. OLSEN and R. E. BUCKLES. J. Photochem. **10**, 215 (1979); (*b*) R. E. BUCKLES and N. A. MEINHARDT. J. Am. Chem. Soc. **74**, 1171 (1952); (*c*) R. E. BUCKLES. Private communication.
19. D. P. SHOEMAKER and C. W. GARLAND. Experiments in physical chemistry. 2nd ed. McGraw-Hill, Inc., New-York. 1967. pp. 298–300.
20. V. I. MINKIN, O. A. OSIPOV, and Y. A. ZHDANOV. Dipole moments in organic chemistry. Plenum Press, New York. 1970. pp. 91, 104.
21. A. E. LUTSKII, L. Y. MALKES, E. M. OBUKHOVA, and A. I. TIMCHENKO. Russ. J. Phys. Chem. **37**, 565 (1963).
22. (*a*) A. A. FROST and R. G. PEARSON. Kinetics and mechanism. 2nd ed. Wiley and Sons, Inc., New York. 1961. p. 196; (*b*) p. 375.
23. A. A. MARYOTT and E. R. SMITH. Table of dielectric constants of pure liquids. U.S. National Bureau of Standards Circular 514. 1951.
24. M. C. LIN and K. J. LAIDLER. Can. J. Chem. **46**, 973 (1968), and references cited therein.
25. R. B. CUNDALL. Prog. React. Kinet. **2**, 165 (1964).
26. A. R. BASSINDALE, A. J. BOWLES, A. HUDSON, and R. A. JACKSON. Tetrahedron Lett. 3185 (1973).
27. (*a*) M. S. CONRADI, H. ZELDES, and R. LIVINGSTON. J. Phys. Chem. **83**, 2160 (1979); (*b*) S. G. COHEN and C. H. WANG. J. Am. Chem. Soc. **77**, 2457 (1955).
28. (*a*) J. H. DAY. Chem. Rev. **63**, 65 (1963); (*b*) T. BERVOCICI, R. KORENSTEIN, K. A. MUSZKAT, and E. FISCHER. Pure Appl. Chem. **24**, 531 (1970); (*c*) R. KORENSTEIN, K. A. MUSZKAT, and S. SHARAFY-OZERI. J. Am. Chem. Soc. **95**, 6177 (1973).
29. E. KOTSCH. Z. Naturforsch. Teil A, **26**, 1836 (1971).
30. M. D. SEVILLA and G. VINCOW. J. Phys. Chem. **72**, 3635 (1968); 3647 (1968).
31. (*a*) A. HOEKSTRA and A. VOS. Acta Crystallogr. Sect. B, **31**, 1716 (1975); 1722 (1975); (*b*) N. A. BAILEY and S. E. HULL. Acta Crystallogr. Sect. B. **34**, 3289 (1978); (*c*) E. HARNIC and G. M. J. SCHMIDT. J. Chem. Soc. 3295 (1954).
32. I. R. GAULT, W. D. OLLIS, and I. O. SUTHERLAND. J. Chem. Soc. Chem. Commun. 269 (1970).
33. I. AGRANAT, M. RABINOVITZ, A. WEITZEN-DAGAN, and I. GOSNAY. J. Chem. Soc. Chem. Commun. 732 (1972).
34. H. KESSLER. Angew. Chem. Int. Ed. Engl. **9**, 219 (1970).
35. M. RABINOVITZ, I. AGRANAT, and A. WEITZEN-DAGAN. Tetrahedron Lett. 1241 (1974).
36. I. AGRANAT and Y. TAPUHI. J. Am. Chem. Soc. **101**, 665 (1979).
37. X. CREARY. J. Org. Chem. **43**, 1777 (1978).
38. (*a*) C. R. GUILIANO, L. D. HESS, and J. D. MARGERUM. J. Am. Chem. Soc. **90**, 587 (1968); (*b*) W. R. BRODE, E. G. PEARSON, and G. M. WYMAN. J. Am. Chem. Soc. **76**, 1034 (1954).
39. (*a*) H. GÜSTEN. J. Chem Soc. Chem. Commun. 133 (1969); (*b*) G. M. WYMAN and W. R. BRODE. J. Am. Chem. Soc. **73**, 1487 (1951); (*c*) R. PUMMERER and G. MARONDEL. Chem. Ber. **93**, 2834 (1960).
40. M. KLESSINGER and W. LÜTTKE. Tetrahedron, **19**, 315 (1963).
41. I. B. AFANAS'EV. Int. J. Chem. Kinet. **7**, 857 (1975).
42. F. BERNARDI, N. D. EPIOTIS, W. CHERRY, H. B. SCHLEGEL, M. WHANGBO, and S. WOLFE. J. Am. Chem. Soc. **98**, 469 (1976).
43. (*a*) T. A. RYAN, JR., B. L. JOINER, and B. F. RYAN. Minitab student handbook. Duxbury Press, N. Scituate, MA. 1976; (*b*) W. E. WENTWORTH. J. Chem. Educ. **42**, 96 (1965); 162 (1965).

Halogenocyclopropanation des éthoxy-alcènes diversement alkylés. Effet *syn*-directeur des groupes éthoxy et alkyles

ROGER BARLET, RAYMOND LE GOALLER ET CLAUDE GEY

Laboratoire de Chimie Organique, Université Scientifique et Médicale de Grenoble, B.P. 53 X, 38041 Grenoble, France

Reçu le 24 avril 1980

ROGER BARLET, RAYMOND LE GOALLER et CLAUDE GEY. Can. J. Chem. **59**, 621 (1981).

Il est montré que des accepteurs faiblement nucléophiles tels que les éthers d'énols subissent pourtant facilement une réaction de cycloaddition avec les monohalogénocarbénoïdes. Les hauts rendements obtenus ainsi que la stéréosélection en faveur des adduits les plus encombrés sont interprétés par une assistance de l'oxygène du substrat auprès du métal du carbénoïde.

ROGER BARLET, RAYMOND LE GOALLER, and CLAUDE GEY. Can. J. Chem. **59**, 621 (1981).

Weakly nucleophilic acceptors such as enol ethers can facilitate cycloaddition reactions with monohalocarbenoids. The high yields and stereoselection towards the more highly hindered adducts are interpreted by complexation of the oxygen atom of the substrate with the metal atom of the carbenoid.

[Journal translation]

Introduction

La méthode d'alkoxycyclopropanation de Schöllkopf et coll. (1, 4), largement utilisée depuis plus de 10 ans, présente un certain nombre de limitations. La plus importante consiste dans le déplacement nucléophile que subit le précurseur carbénique sous l'influence de la base utilisée.

Menée à partir des éthers monochlorés $ROCH_2Cl$ cette méthode ne conduit majoritairement au produit de pontage qu'avec *t*BuLi (1)

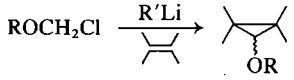

Remarquons cependant que l'utilisation récente de LiTMP (tétraméthyl-2,2,6,6 pipéridinure de lithium), base forte dont l'encombrement réduit l'activité nucléophile (2), permet une limitation sensible de cette réaction secondaire et autorise de bons rendements en éthers cyclopropaniques (3).

Les éthers dichlorés $ROCHCl_2$ présentent un rendement de cyclopropanation amélioré mais les réactions secondaires demeurent importantes (4).

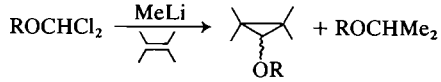

La méthode de Schöllkopf mise en œuvre sur le bromoéthylène a cependant permis l'obtention du méthoxy-1 bromo-2 cyclopropane avec un bon rendement (58%) et une nette *syn*-stéréosélection[1] (*syn*/*anti* = 91:9) (5).

Par ailleurs, quelques alcoxyhalogénocyclopropanes ont déjà été obtenus, par réduction des composés dihalogénés correspondants, avec une nette antistéréosélection que le réducteur soit l'hydrure de tributylétain (6) ou le butyllithium (7, 8).

Désireux de préparer de tels alcoxyhalogénocyclopropanes et de vérifier l'extension possible de la réaction de monohalogénocyclopropanation sur les oléfines fonctionnalisées, telle qu'elle a déjà été développée par l'un d'entre nous (9), nous avons systématiquement soumis les éthoxy-1 éthylènes, diversement alkylés, à l'action du générateur de carbénoïde CH_2Cl_2/MeLi.

Nous présentons, dans ce travail, les résultats de la monohalogénocyclopropanation de ces éthers d'énols substitués. Nous avons obtenu une amélioration sensible des premières chlorocyclopropanations connues de vinyl-éthers non substitués (10) et nous avons pu déterminer la configuration des adduits, par étude rmn, et mettre en évidence la nette stéréosélectivité de la réaction.

Résultats expérimentaux

La réaction de cyclopropanation est pratiquement quantitative et conduit sans sous-produits[2] à la *formation préférentielle des éthoxy-1 chloro-2 cyclopropanes* cis *et* trans *accompagnés minoritairement* des composés bromés correspondants (tableau 1).

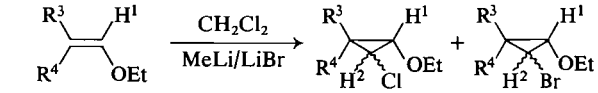

R^3, R^4 = H	**1**	**1***t* + **1***c*	**1**′*t* + **1**′*c*
R^3 = H; R^4 = Me	**2**	**2***t* + **2***c*	**2**′*t* + **2**′*c*
R^3 = Me; R^4 = H	**3**	**3***t* + **3***c*	**3**′*t* + **3**′*c*
R^3, R^4 = Me	**4**	**4***t* + **4***c*	**4**′*t* + **4**′*c*

[1]Les termes *syn* et *anti* (ou *cis* et *trans*) précisent ici et dans la suite du mémoire la position relative du groupement éthoxy et de l'halogène.

[2]Il est cependant nécessaire pour éviter la formation de produits légers d'utiliser un méthyllithium suffisamment concentré (solution dans l'éther de 0,7 à 1,0 *M*).

0008-4042/81/030621-08$01.00/0

©1981 National Research Council of Canada/Conseil national de recherches du Canada

Can. J. Chem. Downloaded from www.nrcresearchpress.com by 210.87.254.40 on 09/05/12
For personal use only.

Can. J. Chem. Downloaded from www.nrcresearchpress.com by 210.87.254.40 on 09/05/12
For personal use only.

TABLEAU 1. Halogenocyclopropanation des éthers α-éthyleniques au moyen de CH_2Cl_2 et MeLi/LiBr (température ordinaire)

Substrats	% Adduits chlorés	% Adduits bromés	Répartition adduits chlorés: No ident. *trans* (*anti*) %	Répartition adduits chlorés: No ident. *cis* (*syn*) %	Répartition adduits bromés: No ident. *trans* (*anti*) %	Répartition adduits bromés: No ident. *cis* (*syn*) %
			1*t*	**1***c*	**1′***t*	**1′***c*
1	76	24	33	66	28	72
			2*t*	**2***c*	**2′***t*	**2′***c*
2	77	23	20	80	5	95
			3*t*	**3***c*	**3′***t*	**3′***c*
3	84	16	47	53	45	55
			4*t*	**4***c*	**4′***t*	**4′***c*
4	93	7	42	58	8	92

TABLEAU 2. Résonance magnétique nucléaire des adduits

ν = 60 MHz, CCl_4, δ, 10^6, J(Hz)

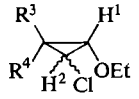

Nature des adduits	δ en ppm ou J en Hz	δ_{H^1}	δ_{H^2}	δ_{R^3}	δ_{R^4}	$\delta_{OCH_2—CH_3}$	$J_{H^1H^2}$	$J_{H^1H^3}$	$J_{H^2H^3}$	$J_{H^2H^4}$
$R^3 = R^4 = H$	**1***t*[a]	3,31	2,95	1,16	0,92	3,56	1,4	7,4	4,8	8,6
	1*c*[b]	3,21	2,89	1,10	0,78	3,63 3,58	5,3	7,4	8	5,3
$R^3 = H$ $R^4 = Me$	**2***t*	3,25	2,52	ind.	1,15	3,60	1,5	7,5	4,5	—
	2*c*	3,00	1,92	ind.	1,07	3,59 3,53	5	8,3	7	—
$R^3 = Me$ $R^4 = H$	**3***t*	2,94	3,10	1,19	ind.	3,63	2,1	—	—	6,5
	3*c*	2,88	2,53	1,12	ind.	3,61 3,55	4,5	—	—	2,5
$R^3 = R^4 = Me$	**4***t*	2,90	2,64	1,13	1,13	3,52	2	—	—	—
	4*c*	2,80	2,57	1,09	1,03	3,57 3,52	5,1	—	—	—

[a]L'analyse des multiplets dus aux protons cyclopropaniques à 100 et 250 MHz a permis de déterminer deux autres couplages de **1***t*, $J_{H^1H^4} = 4$ Hz et $J_{H^3H^4} = 7.4$ Hz.
[b]L'analyse à 100 et 250 MHz a permis de déterminer deux autres couplages de **1***c*, $J_{H^1H^4} = 4.7$ Ha et $J_{H^3H^4} = 7.4$ Hz.

L'addition du méthyllithium sur le mélange éther d'énol – chlorure de méthylène est menée à faible reflux d'éther. Le méthyllithium utilisé est associé à un équivalent de bromure de lithium (lithien préparé par action de MeBr sur Li) et doit être exempt d'ions iodures.

La valeur des déplacements chimiques et des couplages en rmn (tableau 2), l'existence de vibration de valence ν(C—H) en ir comprises entre 3025 et 3040 cm^{-1}, la mise en œuvre d'une réaction de cycloaddition déjà expérimentée sur d'autres substrats faiblement nucléophiles (9) ne laissent

Can. J. Chem. Downloaded from www.nrcresearchpress.com by 210.87.254.40 on 09/05/12
For personal use only.

aucun doute sur la nature cyclopropanique des adduits formés.

Les adduits bromés sont des produits primaires de réaction. En effet *leur formation*, en quantité minoritaire, n'*est pas due à une réaction de substitution nucléophile des adduits chlorés par les ions* Br^- présents dans le milieu (LiBr est associé à MeLi). Nous avons en effet vérifié que, séparés et remis dans les conditions de la réaction (MeLi/LiBr + CH_2Cl_2) mais en l'absence d'éthoxy-alcène accepteur, les adduits chlorés ne conduisent pas à leurs analogues bromés. On peut interpréter cette formation des adduits bromés, comme dans le cas du pontage des dioxolannes ou des cétones éthyléniques (9), par *échange au niveau du complexe carbène–sel intermédiaire*. Ce complexe est sans doute plus probable à température ordinaire ou à reflux d'éther que le chlorométhyllithium ($CHLiCl_2$) stable seulement à basse température et dont l'évolution doit être très rapide après l'échange initial hydrogène–métal.

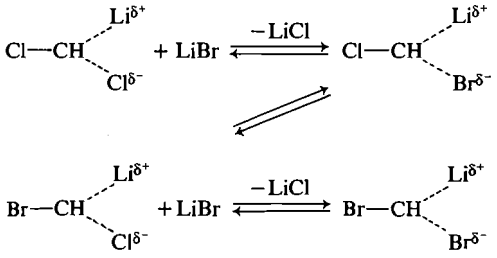

Cet échange est évidemment dû au fait que le lithien utilisé, formé à partir de MeBr, est constitué par une association, équivalent à équivalent, MeLi/LiBr et permet une telle incorporation de Br dans le complexe carbène–sel.

Nous avons d'ailleurs vérifié qu'il suffit d'additionner le méthyllithium à basse température pour bloquer l'échange et observer la formation pratiquement exclusive des adduits chlorés accompagnée cependant d'une chute du rendement.

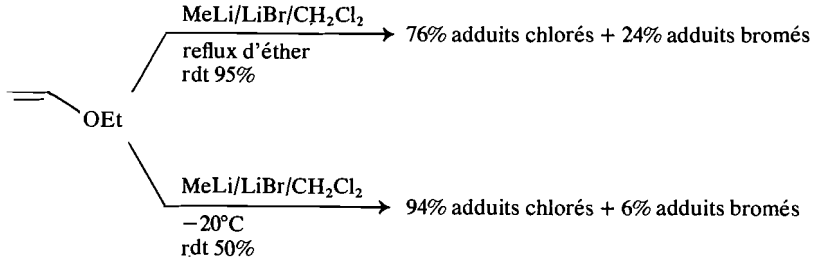

Par contre, nous n'avons pas pu augmenter le pourcentage des adduits bromés par addition d'un équivalent de LiBr au méthyllithium utilisé. Il est vrai que ce bromure de lithium ajouté à la solution lithienne reste insoluble et n'augmente pas la capacité du brome à s'incorporer au complexe carbène–sel.

Stéréochimie des adduits

Nous avons pu élucider la stéréochimie *cis* ou *trans* des adduits au moyen de la résonance magnétique nucléaire (tableau 2) par examen des couplages $^3J(cis)$ et $^3J(trans)$ de H^1 et H^2, des déplacements chimiques de H^1 et H^2 et de l'effet LIS sur ces déplacements. Nous avons pu ajouter à ces critères de configuration d'autres éléments de preuve cohérents dans toute la série.

1. *Valeur des couplages*

L'étude comparée des couplages $^3J(cis)$ et $^3J(trans)$ des hydrogènes vicinaux H^1 et H^2, nettement déblindés par rapport à R^3 et R^4, s'est avérée être le critère déterminant

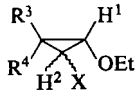

$^3J(cis)_{H^1H^2} > {}^3J(trans)_{H^1H^2}$

Dans le cas de **4***t* et **4***c*, H^1 et H^2 apparaissent sous forme de doublets. La détermination du couplage ^3J est alors directe et permet l'attribution des configurations sans ambiguïté ($^3J(cis)$ = 5,1 Hz, $^3J(trans)$ = 2 Hz).

Les adduits **2***t*, **2***c* (R^3 = H, R^4 = Me) et **3***t*, **3***c* (R^3 = Me, R^4 = H) présentent plusieurs couplages ^3J entre les protons cyclopropaniques et les multiplets, relatifs à H^1 et H^2, ne permettent pas une lecture aussi directe de $^3J_{H^1H^2}$. Il convient alors de recourir soit à des expériences de double résonance lorsque l'écart des fréquences de résonance entre H^1 et H^2 est suffisant pour que l'irradiation d'un des signaux n'affecte pas l'autre (cas de **2***t* et **3***c*), soit à des déterminations approchées liées à un système ABX correspondant à H^1, H^2, H^3 (cas de **2***c*) ou H^1, H^2,

Can. J. Chem. Downloaded from www.nrcresearchpress.com by 210.87.254.40 on 09/05/12
For personal use only.

H^4 (**3***t*). L'obtention conjointe des isomères *cis* et *trans* et leur observation comparée en rmn permet cependant de conclure clairement: **3***t* présente deux multiplets différents (deux $J(trans)$ pour H^1, un $J(trans)$ et un $J(cis)$ pour H^2) alors que **3***c* présente deux multiplets identiques pour H^1 et H^2 (un $J(trans)$ et un $J(cis)$); de même **2***t* présente deux multiplets différents (deux $J(trans)$ pour H^2, un $J(trans)$ et un $J(cis)$ pour H^1) tandis que **2***c* présente deux couplages $J(cis)$.

Les adduits **1***c* et **1***t* présentent des signaux analysables au 1er ordre pour H^1 et H^2. Chaque stéréoisomère montre pour H^1 et H^2 des multiplets identiques avec mise en évidence de 3 couplages vicinaux ^3J. La présence parmi eux d'un couplage $^3J_{H^1H^2}$ de 1,4 Hz dans un cas et 5,3 Hz dans l'autre cas, permet d'attribuer ces multiplets respectivement à **1***t* et **1***c*.

Remarquons que les couplages $^3J_{H^1H^2}$ *des protons cyclopropaniques sont nettement affaiblis par rapport aux valeurs habituelles* respectivement proches de 8 et 4 Hz pour $^3J(cis)$ et $^3J(trans)$ (9). En effet $^3J(cis)$ se trouve être compris entre 4,5 et 5,3 Hz alors que $^3J(trans)$ s'abaisse jusqu'à 1,4 Hz et n'excède pas 2,1 Hz (tableau 2). Seule l'observation simultanée des deux stéréoisomères permet ainsi d'éviter les erreurs d'attribution des configurations puisque $^3J(cis)$ se trouve alors être ici dans la zone de valeur connue de $^3J(trans)$. Un tel abaissement des valeurs de ^3J est d'ailleurs conforme à celui observé par Corey et Ulrich (5) sur le méthoxybromocyclopropane. Notons que ces abaissements n'affectent pas $^3J_{H^1H^3}$, $^3J_{H^2H^3}$ ou $^3J_{H^2H^4}$ et ne concernent que $^3J_{H^1H^2}$ avec la condition que les protons en cause soient l'un et l'autre situés sur des carbones porteurs d'atomes électronégatifs.

2. *Attribution des déplacements chimiques et effet LIS*

(*a*) Il est à noter que ces attributions de configuration fondée sur la valeur des couplages peuvent se faire indépendamment des attributions de déplacements chimiques de H^1 et H^2. *Nous avons cependant généralement attribué au proton* H^1 *le déplacement chimique le plus élevé* conformément aux effets de déblindage supérieur du groupe éthoxy, par rapport aux halogènes, tels qu'ils ressortent des incréments de Shoolery (11) dans les structures RR'—CHX où ces groupes X sont géminés avec le proton observé. En toute rigueur cette attribution n'est valable que dans les cas où la structure cyclopropanique présente une grande symétrie et où l'influence du reste du cycle reste identique.

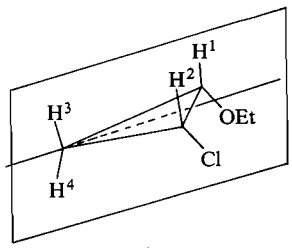

1*c*

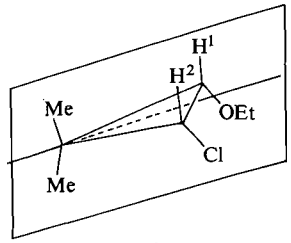

4*c*

Une telle attribution est confirmée par la structure des multiplets et la valeur des couplages dans **2***t*, **2***c* et **3***c*. Par contre pour **3***t* le multiplet le moins large, constitué par deux $J(trans)$, doit être attribué à H^1 bien qu'il soit moins déblindé.

(*b*) L'observation des déplacements chimiques de H^1 et H^2 sur les couples de stéréoisomères **1***c*, **1***t* et **4***c*, **4***t* permet de préciser les *effets de déblindages à travers l'espace de Cl et OEt*. La présence de deux H ou deux Me sur le 3ème carbone cyclopropanique permet d'isoler ces seuls effets sans interférence avec les effets de substituants sur ce carbone.

Le chlore exerce un effet de déblindage de 0,1 ppm sur le proton cyclopropanique vicinal H^1 cis *par rapport au proton* trans. L'estimation de cet effet est obtenue par comparaison, dans le tableau 2, de δH^1 pour les couples **1***c*, **1***t* et **4***c*, **4***t*. *Le groupe éthoxy exerce également un effet de déblindage, réduit à 0,06–0.07 ppm, sur le proton vicinal* H^2 cis *par rapport au proton* trans (comparaison, tableau 2, de δH^2 pour les couples **1***c*, **1***t* et **4***c*, **4***t*).

L'effet du chlore est conforme à celui observé en série cyclopropanique monohalogénée, par contre, l'effet de l'éthoxy est inversé par rapport à la série cyclopropanique monoéthoxylée (12).

(*c*) *L'étude de l'effet LIS* pour les protons H^1 et H^2 sur le couple de stéréoisomères **1***c* et **1***t* nous a permis de vérifier à la fois l'attribution des déplacements chimiques δ_1 et δ_2 ainsi que l'attribution des configurations *cis* et *trans* (Fig. 1). *Cet effet s'avère*, conformément à ce qu'on peut attendre, *plus important pour les isomères* trans *que pour les isomères* cis. L'approche du groupe complexant auprès de l'oxygène de l'éthoxy, siège de la complexation, est en effet rendue plus difficile dans le cas de l'isomère *cis*. L'halogène, situé du même côté que l'éthoxy, ne complexe alors pas, pour son propre compte, le chélate (13) mais le repousse pour des raisons stériques et affaiblit ainsi le degré de complexation c'est-à-dire la valeur des déplacements induits de H^1 et H^2. Il convient cependant de remarquer que le rapport entre les déplacements induits de H^1 et H^2 reste du même ordre quel que soit le stéréoisomère ce qui semble

Can. J. Chem. Downloaded from www.nrcresearchpress.com by 210.87.254.40 on 09/05/12
For personal use only.

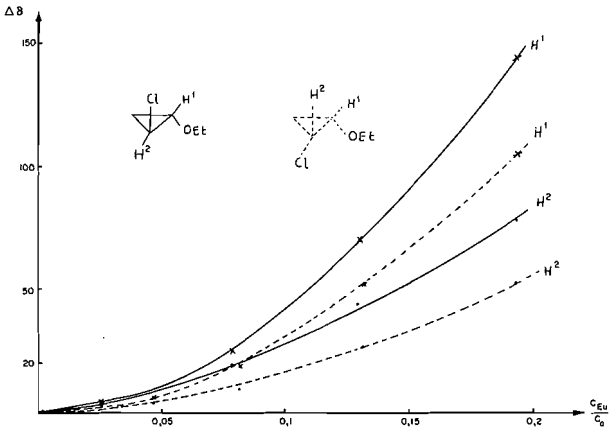

FIG. 1. Effet LIS (complexes de $Eu(dpm)_3$) sur un couple de chloroéthoxycyclopropanes *cis* et *trans*. C_{Eu} = concentration en chélate; C_0 concentration en éther.

indiquer que la position moyenne du complexe d'europium est très proche du plan du cycle. Cette position moyenne implique cependant, aussi bien pour le stéréoisomère *cis* que pour le *trans* un déplacement induit $\Delta\delta_1$ plus élevé que $\Delta\delta_2$. En effet, quelles que soient les contributions respectives des intéractions de contact ou de pseudo contact, H^1, aussi bien à travers les liaisons qu'à travers l'espace, demeure plus proche du site de complexation que H^2.

3. *Autres éléments de détermination des configurations*

Au total, indépendamment de la détermination de configuration précédente fondée sur l'analyse des déplacements chimiques et des couplages des protons cyclopropaniques, nous avons pu mettre en évidence les caractères distinctifs suivants entre les isomères *cis* et *trans*.

Les protons méthyléniques du groupe éthoxy présentent une légère inéquivalence, de l'ordre de 3 Hz, pour les isomères *cis*. Ce doublet de quadruplets fait place à un quadruplet unique pour les isomères *trans*. Cette inéquivalence est conforme à un effet de champ de l'halogène sur les deux hydrogènes voisins OCH_2—CH_3.

Les temps de rétention en chromatographie en phase vapeur sont toujours supérieurs pour les isomères *cis* quelle que soit la nature de la colonne.

Les isomères *trans*, chauffés à reflux de toluène, disparaissent beaucoup plus rapidement que les isomères *cis*, montrant ainsi une aptitude supérieure à l'ouverture disrotatoire, avec formation d'éthoxydiènes conformément aux règles de Woodward–Hoffman (6).

Les isomères *cis* présentent une densité et un indice de réfraction supérieurs (voir Partie expérimentale).

Discussion: effet *syn*-directeur du groupe éthoxy et des groupes méthyles

L'intérêt préparatif de cette réaction d'halogénocyclopropanation réside dans sa facile mise en œuvre et son rendement élevé. Ce rendement est inattendu puisque le groupe éthoxy désactive les doubles liaisons et les rend, à priori, moins aptes à une cycloaddition avec les halogénocarbénoïdes électrophiles. *On peut interpréter cette anomalie apparente par une assistance de l'oxygène* comme dans le cas des dioxolannes éthyléniques (9). Cette assistance serait d'ailleurs accrue dans le cas des éthoxy-alcènes puisque la distance lithium–oxygène dans l'état de transition serait plus faible. Le pouvoir électroattracteur de l'éthoxy pourrait ainsi être largement compensé par cette assistance.

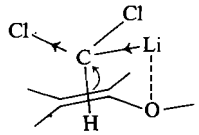

On observe un très net effet syn-*directeur de l'éthoxy et des alkyles de l'accepteur de carbène* (voir tableau 1). La cycloaddition de **1** permet d'isoler l'effet *syn*-directeur de l'éthoxy. La cycloaddition de **2** cumule les effets *syn*-directeurs et entraîne une nette *syn*-stéréosélection. La cycloaddition de **3** ne montre plus qu'une très faible stéréosélection; la compensation des deux effets directeurs semble alors indiquer qu'ils sont du même ordre de grandeur. La *syn*-stéréosélectivité des alkyles par rapport à l'halogénocyclopropanation s'interprète ici de la façon habituelle: *dans l'état de transition, la position* cis *de l'halogène sera favorisée par interaction électrostatique entre l'halogène et les alkyles légèrement positifs* lors du transfert d'électrons de la double liaison vers le carbénoïde (14). Par contre l'effet *syn*-directeur du groupe éthoxy est plus délicat à interpréter. En schématisant le chlorocarbénoïde sous la forme ($LiCHCl_2$) on peut envisager les trois états de transition a, b et c.

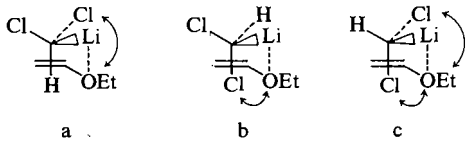

L'état a conduira au composé *trans* tandis que b et c conduiront au composé *cis*; a est, à priori, beaucoup plus probable que b et c. La formation préférentielle du dérivé *cis* peut s'interpréter ainsi:

Can. J. Chem. Downloaded from www.nrcresearchpress.com by 210.87.254.40 on 09/05/12
For personal use only.

la forte interaction Li–O neutralise partiellement le caractère électronégatif de l'oxygène et le groupe éthoxy se rapproche alors du comportement d'un alkyle. Cette forte interaction entraîne une torsion dans l'état de transition avec un éloignement du chlore *syn* dans b et c et un rapprochement du chlore *anti* dans a et c; a sera ainsi déstabilisé par le rapprochement chlore *anti*-oxygène (déstabilisation par effets électronique et stérique) tandis que b sera stabilisé par l'éloignement chlore *syn*-oxygène. b deviendra aussi, sinon plus probable que a. c, destabilisé par le rapprochement chlore *anti*-oxygène et stabilisé par le rapprochement chlore *syn*-oxygène, continuera, malgré la torsion, à jouer un rôle important dans l'état de transition global. Au total le rapport b + c/a deviendra supérieur à 1 et pourra rendre compte de la formation dominante du produit *cis*.

En conformité avec ce que l'on observe dans le cas des dioxolannes α-éthyléniques (9) mais contrairement au cas des oléfines non fonctionnalisées (15), la température ne joue pratiquement aucun rôle vis-à-vis de la stéréosélectivité. Le rapport **1***c*/**1***t* reste inchangé que le pontage soit effectué à reflux d'éther ou à −25°C. On peut également interpréter cette observation par la forte interaction lithium–oxygène dans l'état de transition. La stabilisation additionnelle apportée par les interactions alkyle–halogènes y sera très faible et les énergies d'activation pour la *syn* et l'*anti*-direction seront trop voisines pour que des variations de température de faible ou moyenne amplitude, jouent un rôle sensible.

Conclusion

Ce travail nous a permis d'obtenir des alcoxy halogénocyclopropanes, diversement alkylés, par action du générateur de carbénoïde CH_2Cl_2/MeLi/LiBr sur les alcoxy-alcènes correspondants. La facile mise en œuvre de la réaction à température ordinaire, ses excellents rendements ainsi que l'obtention stéréosélective des adduits complètent et améliorent les premiers résultats observés sur les vinyl-éthers non substitués où la cyclopropanation par CH_2Cl_2/BuLi s'exerçait, à basse température, avec prédominance des isomères chlorés *cis*, à l'exclusion d'isomères bromés et sans précision de rendement (10). La possibilité d'obtenir des adduits bromés, concurremment aux adduits chlorés, constitue effectivement une extension utile de cette réaction puisque de tels adduits ne sont habituellement obtenus en bons rendements que par des réactions difficiles à mettre en œuvre (16) ou peu probables sur des accepteurs faiblement nucléophiles (17).

La stéréochimie des adduits a été établie essentiellement par rmn et nous avons mis en évidence que les couplages $^3J(cis)$ et $^3J(trans)$ des protons cyclopropaniques H^1 et H^2 s'avéraient anormalement faibles.

Nous avons pu montrer et justifier le net effet *syn*-directeur du groupe éthoxy et du groupe méthyle des substrats lors de cette réaction d'halogénocyclopropanation qui conduit ainsi à la formation des adduits les plus encombrés.

Partie expérimentale

Les spectres de rmn ont été enregistrés dans CCl_4, sur appareil fonctionnant, dans la grande généralité des cas, à 60 MHz (Hitachi-Perkin-Elmer R 24) ou pour les composés **1***c* et **1***t* sur HA 100 et Cameca 250.

Les spectres infrarouge ont été réalisé sur un spectrophotomètre Perkin-Elmer 521 à deux réseaux (précision ± 0,5 cm^{-1}).

La cpv analytique a été réalisée sur Aerograph 600 D à ionisation de flamme. La cpv préparative a été effectuée sur Autoprep A 700 et A 705. Les colonnes les plus généralement utilisées ont été des colonnes Ucon Oil de 3 à 10 pieds (1/8 po ou 3/8 po).

Les analyses élémentaires ont été réalisées par le Service Central de Microanalyses du C.N.R.S., Echangeur de Solaize, B.P. 22, 69390 Vernaison, France.

Mode opératoire général

Préparation du méthyllithium associé au bromure de lithium

Dans un ballon à 3 cols on place 21 g (3 at.g) de lithium martelé et découpé en fins morceaux dans 0,5 L d'éther anhydre fraîchement distillé sur $LiAlH_4$. On additionne MeBr gazeux en contrôlant son débit avant et après le ballon réactionnel au moyen de barboteurs. Au début de l'addition l'halogénure se dissout dans l'éther puis la réaction démarre et le lithium prend un éclat métallique très vif. On ajuste le débit d'halogénure de façon à ce qu'il soit totalement consommé (contrôle au barboteur de sortie) et qu'il permette le maintien d'un léger reflux. On additionne en cours de route de l'éther jusqu'à ce que la solution totale soit de 1,5 L. L'addition d'halogénure dure 5 à 6 h. Il est nécessaire de procéder lentement pour éviter la duplication de Wurtz. LiBr reste en solution. MeLi après décantation des produits d'oxydation de Li est dosé par différence (hydrolyse avant et après action du dibromo-1,2 éthane) au moyen de 1*N* HCl. On observe ainsi 10 à 15% de EtOLi formé par rapport à MeLi total. Les quantités de lithium mises en œuvre et la concentration finale de MeLi montrent qu'on ne peut éviter, même avec faible débit d'addition de l'halogénure, 10% de duplication de Wurtz.

Halogénocyclopropanation

Les réactions sont menées sous débit d'azote à partir de 0,025 ou 0,05 mol de MeLi dont la concentration doit être comprise entre 0,7 et 1 mol/L. Le mode opératoire identique sur tous les substrats, se caractérise de la façon suivante: addition goutte à goutte du méthyllithium sur le mélange d'accepteur de carbène en léger excès (éthoxy-alcène)/MeLi ≃ 1,25) et le générateur de carbène en net excès (CH_2Cl_2/MeLi ≃ 3). L'addition est menée de façon à entretenir le reflux d'éther et dure de 1/2 h à 1 h. Après la fin de l'addition on laisse encore sous agitation 1 h à 2 heures. Dès le début de l'addition du méthyllithium le bromure de lithium trouble la solution puis précipite. Le précipité s'épaissit ensuite progressivement. L'hydrolyse est faite sur la glace pilée, la neutralisation de la phase organique par le chlorure d'ammonium en solution saturée et le sèchage par Na_2SO_4 anhydre.

Can. J. Chem. Downloaded from www.nrcresearchpress.com by 210.87.254.40 on 09/05/12
For personal use only.

Les substrats soumis à halogénocyclopropanation sont soit commerciaux (cas de **1** et du mélange **2** + **3**, produits Fluka) soit préparé, dans le cas de **4** selon la méthode de Claisen (18).

Le mélange **2**/**3** (environ 80:20) est séparé en cpv sur SE 30 20 pieds, chargée à 30% (température de colonne 40°C). Le mélange **2** + **3** soumis directement à la cycloaddition carbénique permet de mettre en évidence que **2** réagit plus facilement que **3**.

Caractérisation et identification des adduits

Tous les composés obtenus sont des composés nouveaux à l'exclusion de **1***c* et **1***t* (10). Les analyses élémentaires obtenues sont satisfaisantes (Cl ± 0,3%, Br ± 0,5%) à condition qu'elles soient faites rapidement après les séparations chromatographiques. Si ce n'est pas le cas, bien que les chromatogrammes ou les spectres de rmn restent inchangés, la libération d'halogène altère les analyses.

L'ensemble des composés présente cependant une bonne stabilité en solution. Gardés en solution éthérée les adduits présentent des analyses chromatographiques inchangées après des mois, voire des années pour certains d'entre eux.

Malgré les précautions prises, **1***c*, **2***t*, **3***t*, **3**′*t*, **4***c*, **4**′*c* se décomposent partiellement entre la séparation chromatographique et l'analyse. **1**′*t*, **2**′*t* et **4**′*t* obtenus en faible quantité n'ont pu être collectés et examinés qu'en solution dans le tetrachlorure de carbone. Les analyses que nous avons pu obtenir sont les suivantes.

Composé	Analyse (%)
1*t*	Calc. pour C_5H_9OCl : C 49,81, H 7,47, O 13,28, Cl 29,43
	Trouvée : C 49,56, H 7,63, O 13,53, Cl 29,18
1′*c*	Calc. pour C_5H_9OBr : C 36,36, H 5,45, O 9,70, Br 48,48
	Trouvée : C 36,05, H 5,62, O 9,97, Br 48,03
2*c*	Calc. pour $C_6H_{11}OCl$: C 53,55, H 8,18, O 11,90, Cl 26,37
	Trouvée : C 53,12, H 8,22, O 12,17, Cl 26,07
2′*c*	Calc. pour $C_6H_{11}OBr$: C 40,22, H 6,14, O 8,93, Br 44,69
	Trouvée : C 39,87, H 6,25, O 9,16, Br 44,36
3*c*	Calc. pour $C_6H_{11}OCl$: C 53,55, H 8,18, O 11,90, Cl 26,37
	Trouvée : C 53,39, H 8,31, O 12,11, Cl 26,11
3′*c*	Calc. pour $C_6H_{11}OBr$: C 40,22, H 6,14, O 8,93, Br 44,69
	Trouvée : C 40,01, H 6,31, O 9,07, Br 44,21
4*t*	Calc. pour $C_7H_{13}OCl$: C 56,58, H 8,76, O 10,78, Cl 23,88
	Trouvée : C 56,23, H 8,91, O 10,99, Cl 23,59

Les divers produits n'ont pas été séparés par distillation mais par cpv vu les faibles quantités sur lesquelles nous avons opéré et la complexité des mélanges obtenus. Les stéréoisomères *trans* sont moins retenus en cpv que les stéréoisomères *cis* aussi bien dans le cas des adduits bromés que des adduits chlorés et quelle que soit la colonne utilisée. Les adduits chlorés *cis* et *trans* sortent habituellement tous deux avant les adduits bromés correspondants sauf dans le cas des adduits de **1** ou il y a chevauchement (ordre de sortie **1***t*, **1**′*t*, **1***c*, **1**′*c*).

L'effet LIS a été étudié sur les adduits **1***t* et **1***c*. Le chélate, $Eu(dmp)_3$ est additionné peu à peu sur le substrat dont la concentration est déterminée une fois pour toutes au départ. On mesure les déplacements chimiques induits $\Delta\delta$ et on représente les courbes $\Delta\delta = f(C_{Eu}/C_0)$ (Fig. 1) où C_{Eu} et C_0 sont les concentrations en chélate et en substrat. Les valeurs de $\Delta\delta$ sont données ci-dessous en Hz.

Composé	$\frac{C_{Eu}}{C_0} \times 10^3$	Nature des protons			
		H^1	H^2	$O—CH_2—CH_3$	$O—CH_2—CH_3$
1*t*	30,35	3,5	3	4,5	2
	78,6	25	19	28,5	14,5
	130,4	70	45	68,5	35
	193,8	145	78,5	119	60
1*c*	46,5	6	3,5	5,5	3,5
	81,45	18,5	10	16	8,5
	131,6	53	27	46	23,5
	193,4	106	54	89	47,5

La caractérisation des adduits chlorés en spectrographie de rmn figure dans le tableau 2. Notons que dans le cas de **1***t* et **1***c* l'analyse des spectres enregistrés à 60 MHz permet la détermination des couplages $J_{H^1H^2}$, $J_{H^1H^3}$, $J_{H^2H^3}$, $J_{H^2H^4}$ auxquels il convient d'adjoindre celle des couplages $J_{H^1H^4}$ et $J_{H^3H^4}$ obtenus à 100 et 250 MHz.

Les adduits bromés présentent des spectres identiques à ceux des adduits chlorés; les couplages restent inchangés, les déplacements chimiques sont légèrement réduits (de 1 à 9 Hz). La différence la plus grande est observée pour **1**′*c* qui présente les valeurs suivantes de δ en ppm pour les protons respectifs H^1, H^2, H^3, H^4, $OCH_2—CH_3$: 3,10; 2,72; 1,12; 0,80; 3,61 et 3,59.

La distinction entre les deux types d'adduits au moyen de la densité et de l'indice de réfraction est par contre très nette. Les adduits chlorés présentent une densité légèrement supérieure à 1 et un indice voisin de 1,43 tandis que les adduits bromés présen-

tent une densité voisine de 1,35 et un indice très proche de 1,46. Dans tous les cas les valeurs sont plus élevées pour les stéréoisomères *cis* que pour les stéréoisomères *trans*. Ainsi à titre d'exemple, notons les valeurs suivantes pour les adduits de **2** (d_4^{20}; n_D^{20}): **2***t* (1,054; 1,4252), **2***c* (1,073; 1,4382), **2**′*t* (1,337; 1,4537), **2**′*c* (1,354; 1,4623).

1. U. SCHÖLLKOPF et W. PITTEROFF. Chem. Ber. **97**, 636 (1964).
2. R. A. OLOFSON et C. M. DOUGHERTY. J. Am. Chem. Soc. **95**, 581 (1973).
3. R. A. OLOFSON, K. D. LOTTS et N. BARBER. Tetrahedron Lett. 3779 (1976); 3783 (1976).
4. U. SCHÖLLKOPF et J. PAUST. Chem. Ber. **98**, 2221 (1965); U. SCHÖLLKOPF. Angew. Chem. Int. Ed. Engl. **7**, 588 (1968).
5. E. J. COREY et P. ULRICH. Tetrahedron Lett. 3685 (1975).
6. W. E. PARHAM, F. M. PARHAM, J. F. DOOLEY et M. K. MEILAHN. J. Org. Chem. **33**, 3651 (1968).
7. K. G. TAYLOR, W. E. HOBBS et M. SAQUET. J. Org. Chem. **36**, 369 (1971); K. G. TAYLOR, W. E. HOBBS, M. SCLARK et J. CHAMEY. J. Org. Chem. **37**, 2436 (1972).
8. J. D. WHITE et L. G. WADE. J. Org. Chem. **40**, 118 (1975).
9. R. BARLET et M. VINCENS. Tetrahedron, **33**, 1291 (1977).
10. S. M. SHOSTAKOVSKII, L. N. AKSENOVA, V. I. EROFEEV et V. S. AKSENOV. Chem. Abstr. **79**, 78166j (1973).
11. J. N. SHOOLERY. J. Chem. Phys. **21**, 1899 (1953); J. R. CAVANAUGH et B. P. DAILEY. J. Chem. Phys. **34**, 1099 (1961).
12. J. W. EMSLEY, J. FEENEY et L. H. SUTCLIFFE. Progress in nmr spectroscopy. Vol. 5. Pergamon Press, 1969. p. 168.
13. J. K. M. SANDERS et D. H. WILLIAMS. J. Am. Chem. Soc. **93**, 641 (1971).
14. G. L. CLOSS et J. J. COYLE. J. Org. Chem. **31**, 2759 (1966).
15. G. L. CLOSS et L. E. CLOSS. J. Am. Chem. Soc. **82**, 5723 (1960).
16. S. MIYANO, Y. MATSUMOTO et H. HASHIMOTO. Chem. Commun. 364 (1975).
17. N. KAWABATA, M. TANIMOTO et S. FUJIWARA. Tetrahedron, **35**, 1919 (1979).
18. L. M. CLAISEN. Chem. Ber. **40**, 3903 (1907).

Can. J. Chem. Downloaded from www.nrcresearchpress.com by 210.87.254.40 on 09/05/12
For personal use only.

Nuclear magnetic resonance study of addition–cyclization involving ethyl thioacetoacetate and α-nucleophiles

MICHAEL COCIVERA, SOUMEN BASU,[1] LESLIE COPP,[2] AND VINCENZO MALATESTA[3]

The Guelph–Waterloo Centre for Graduate Work in Chemistry, Department of Chemistry, University of Guelph, Guelph, Ont., Canada N1G 2W1

Received July 9, 1980

MICHAEL COCIVERA, SOUMEN BASU, LESLIE COPP, and VINCENZO MALATESTA. Can. J. Chem. **59**, 629 (1981).

Addition of NH_2NH_2 or NH_2OH to ethyl thioacetoacetate to form the corresponding cyclic product, 3-methylpyrazol-5-one or 3-methylisoxazol-5-one proceeds via cyclization of the carbinolamine formed by addition to the β-keto carbon, i.e., cyclization is faster than dehydration of the carbinolamine to form the imine. In contrast the corresponding carbinolamine derived from ethylacetoacetate undergoes dehydration faster than cyclization. By means of ^1H nuclear magnetic resonance spectroscopy, it is possible to detect the cyclic carbinolamine as well as another transient and measure their rates of decay. Based on these results, a mechanism is proposed.

MICHAEL COCIVERA, SOUMEN BASU, LESLIE COPP et VINCENZO MALATESTA. Can. J. Chem. **59**, 629 (1981).

L'addition du NH_2NH_2 ou du NH_2OH au thioacétoacétate d'éthyle qui conduit au produit cyclique correspondant, la méthyl-3 pyrazolone-5 ou la méthyl-3 isoxazolone-5, se fait via la cyclisation de la carbinolamine obtenue par l'addition du réactif au carbone en β de la cétone; on en déduit que la cyclisation est plus rapide que la déshydratation de la carbinolamine qui conduirait à l'imine. Par opposition, la carbinolamine correspondante provenant de l'acétoacétate d'éthyle se déshydrate plus rapidement qu'elle ne se cyclise, En utilisant la spectroscopie de rmn du ^1H, il est possible de déceler la carbinolamine ainsi que les autres intermédiaires et de mesurer leur vitesse de décomposition. On propose un mécanisme en se basant sur ces résultats.

[Traduit par le journal]

Introduction

Previously (1) we have found that the addition of α-nucleophiles to β-keto esters such as ethyl acetoacetate and diethyl β-ketophosphonate involves an initial addition to the β-keto carbon followed by an intramolecular addition to the ester function. The details of the intramolecular process depend on the nature of the ester and the nucleophile. For ethyl acetoacetate the overall reaction proceeds according to the general mechanism in which X represents either the NH_2 or OH group:

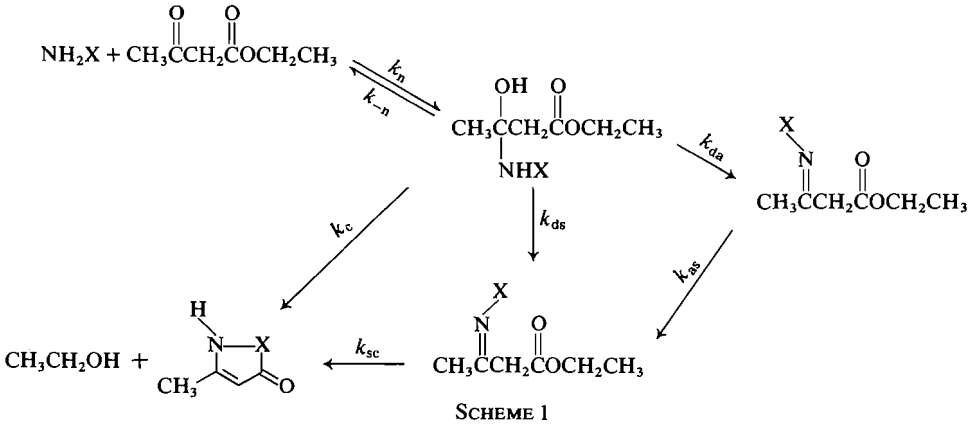

SCHEME 1

For both nucleophiles the equilibrium step is fast relative to the subsequent steps. The relative rates of these steps depend on the nature of the nucleophile. For NH_2OH, k_c is negligible in comparison with k_{ds} and k_{da}. On the other hand, it is commensurate when NH_2NH_2 is the nucleophile.

As a continuation of this study, the reaction of these nucleophiles with ethyl thioacetoacetate is reported in this paper. In contrast with the oxygen ester the thioester undergoes the intramolecular step substantially faster than the dehydration step. Under these conditions, the reaction follows the mechanism:

[1]Present Address: Institute for Aerospace Studies, University of Toronto, Downsview, Ontario.

[2]NSERC Summer Scholar.

[3]Present Address: National Research Council of Canada, Ottawa, Ontario.

0008-4042/81/030629-06$01.00/0

©1981 National Research Council of Canada/Conseil national de recherches du Canada

Can. J. Chem. Downloaded from www.nrcresearchpress.com by 210.87.254.6 on 09/06/12
For personal use only.

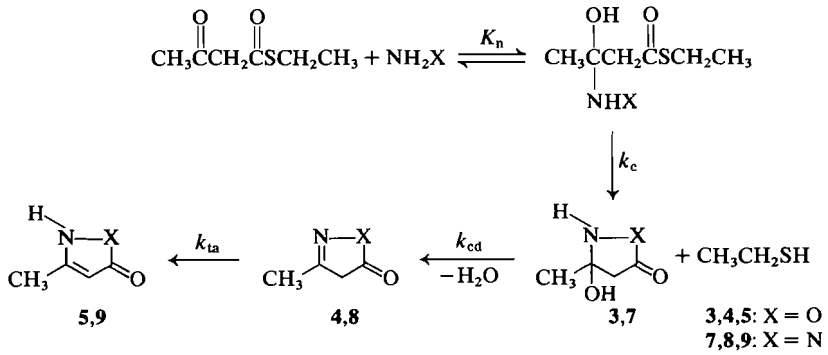

SCHEME 2

The cyclization rate constant has been determined in only a few cases because of limitations placed on the flow system; but k_{cd} and k_{ta} can be determined readily since the steps associated with these rate constants appear to follow pseudo-first order kinetics. For NH_2OH these steps appear to be more complicated since the rate constants depend on the concentration of the nucleophile, and the CH_3-protons of the cyclic imine appear to be involved in an exchange process. A mechanism consistent with these results is suggested.

Experimental

Chemicals

Ethyl thioacetate (Pfaltz and Bauer) was distilled prior to use. Ethyl thioacetoacetate was prepared from ethyl thioacetate by means of a Grignard reaction described previously (2). Sodium phosphate, imidazole, and acetohydroxamic acid were used without purification. In addition, acetohydroxamic acid and *O*-acetylhydroxlamine were prepared *in situ* by reaction of *p*-nitrophenylacetate with hydroxylamine (3) to determine chemical shifts of CH_3-proton resonances under the same conditions of solvent, ionic strength, and temperature as employed in the kinetic studies described below. Diazabicyclooctane (Dabco) was sublimed prior to use. *p*-Nitrophenyl acetate was checked by nmr spectroscopy and used without additional purification.

Solutions

To increase the solubility of ethyl thioacetoacetate, 30:70 (by volume) methanol/water was used as the solvent. To permit comparisons, this solvent was also used for ethyl thioacetate. In these studies, initial concentrations were about 0.06 *M* ethyl thioacetoacetate and 0.1 *M* ethyl thioacetate. The pH of the solution at an ionic strength of 1 *M* (KCl) was determined at 30°C according to the method of Blount and Herman (4) using a Radiometer PHM 63 digital pH meter. The following pK_a values were determined by this technique: NH_2OH, 5.90; NH_2NH_2, 8.23; Dabco, 8.97; and sodium phosphate 6.64.

Kinetic Measurements

All kinetic determinations were made by following the time dependence of the intensities of ^1H nuclear magnetic resonance (nmr) signals obtained at 100 MHz using either static samples or stopped-flow nmr (5). The flow nmr technique differed from that described earlier in that no reservoir was used to equilibrate the nuclei in the magnetic field. This modification was made to reduce the volumes employed and to reduce the chance of leaks of thioethanol into the air. As a result, reliable spectra could be obtained only about 30 s after the flow had been stopped since the internal lock signal intensity fluctuates for about that length of time.

No hydrolysis of either thioester was observed over the period of the kinetic measurements. For ethyl thioacetate the presence of acetohydroxamic acid was confirmed by addition of $FeCl_3$ solution (3, 6*a*, 7).

Results and Discussion

Ethyl Thioacetate

To ascertain the relative importance of intermolecular nucleophilic addition to the acyl carbonyl group of the β-keto thioester, nucleophilic addition to ethyl thioacetate was studied. In general, our results are similar to those obtained previously for *n*-butyl thioacetate (6) using optical spectroscopy. Thus for NH_2NH_2, the observed third order rate constant[4] (k[ester] [NH_2NH_2]^2) is 37, 19, and 21 $M^{-2}min^{-1}$ at pH 8.0, 8.5, and 9.0, respectively. For comparison, values of about 37 and 31 $M^{-2}min^{-1}$ at pH 8.0 and 8.4, respectively, have been reported (6*b*)[5] for *n*-butyl thioacetate. For NH_2OH, the third order rate constant appears to be independent of pH in the range 6.5 to 9.0 (6 pH values), having a value[4] of about 11 $M^{-2}min^{-1}$. Previous results (6*a*) indicate a pH dependence, although the values are close to those obtained in the present study. For example at pH 6.5, 7.0, and 7.5, the values are 10 [15],[6] 10 [11],[6] and 12 [7][6] $M^{-2}min^{-1}$, respectively. In addition, catalysis by phosphate, imidazole, and diazabicyclooctane (Dabco) buffers is not observed whereas imidazole was found to catalyze reaction of NH_2NH_2 with *n*-butyl thioacetate (6*b*). Although the leaving group (*n*-butyl vs. ethyl) and solvent (water/methanol (70:30) vs. water) are somewhat different in the two studies, we suspect that our study is not as precise as the previous one due to the

[4]In most cases the precision is about 15 percent.

[5]Values taken from Fig. 4 of this reference.

[6]Reference 6*a*, for *n*-butyl thioacetate.

Can. J. Chem. Downloaded from www.nrcresearchpress.com by 210.87.254.6 on 09/06/12
For personal use only.

Can. J. Chem. Downloaded from www.nrcresearchpress.com by 210.87.254.6 on 09/06/12
For personal use only.

constraints of the nmr method, i.e., the nucleophile and ester concentrations are comparable. Consequently, k is obtained by means of computer fit (1*c*) of a third order rate equation in contrast with the first order treatment used previously (6).[7]

On the other hand, an advantage of the nmr technique lies in the direct detection of *O*-acetylhydroxylamine,[8] which is produced in competition with acetohydroxamic acid, the thermodynamically favored product. Formation of the former has been inferred from the disparity between the rate of hydroxamic acid formation and the rate of ester decomposition in the pH range 5.4 to 7 (6*a*). The concentration ratio, acetohydroxamic acid/*O*-acetohydroxylamine, appears to depend on pH as well as the nature of the buffer. For Dabco buffer, the pH and ratio are: 8.0, 1.2; 8.5, 0.49; and 9.0, 0.56. At pH 8.0, this ratio is 4.6 and 1.4 for phosphate[9] and imidazole buffers, respectively. Thus, Dabco and imidazole provide the same ratio, which differs substantially from the ratio found for phosphate buffer at the same pH. Although it is possible to speculate about mechanisms consistent with these effects, the number of data do not warrant such discussions. The pH dependence of the ratio indicates that the competition between N and O addition is not altered only by the increase in amount of anion NH_2O^- as the pH is increased. Comparison of the nmr ratios with those obtained kinetically is not meaningful since no buffer other than the nucleophile was employed in the previous study (6*a*).

Ethyl Thioacetoacetate

Figure 1 illustrates the part of the nmr spectrum of ethyl thioacetoacetate that is upfield from the CH_3-proton resonance of methanol at pH 8.0 (0.2 *M* Dabco, μ = 1 *M*) obtained under various conditions. The signal assignments are indicated in the figure caption. Figure 1A illustrates the positions of the two CH_3-proton resonances of ethyl thioacetoacetate. Figure 1B illustrates that not only the thioester (labeled 2) but also a transient (labeled 3) have reacted completely in less than 5 min, in the presence of 0.40 *M* NH_2OH. In fact, the keto CH_3-proton resonance disappears in a time shorter than about 30 s, the shortest time available when the flow system is used without an equilibrating reservoir. The transient species appears to be generated as quickly since its signal intensity is largest at the first scan. We have assigned the cyclic carbinolamine structure **3** to this species because (*a*) its signal has a chemical shift expected for a methyl group that is attached to an sp^3 hybridized carbon atom and differs from that known for the *syn* and *anti* oximes (1*a*), (*b*) its formation is associated with the liberation of thioethanol at a rate that is faster than oxime formation, (*c*) this species converts to a cyclic product rather than the acyclic oxime. The broad signal 4 is not observed on the initial scan but grows to a maximum over the same period as the decay of signal 3, indicating that it is due to species that are generated by the decomposition of species **3**. The width and position of this signal depends on the concentration of NH_2OH free base remaining after the initial reaction of thioester, indicating a proton exchange process associated with a rapid equilibrium reaction involving NH_2OH. A mechanism consistent with these results is the dehydration of **3** to form **4**, which is involved in the equilibrium

[1] 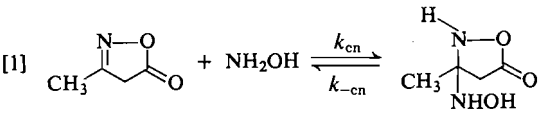

4 **10**

Evidence for the formation of the analogue of **4** is also found when NH_2NH_2 is the nucleophile; however, in this case the equilibrium constant K_{cn} appears smaller than the one for eq. [1] since the line width and chemical shift of the signal do not appear to depend appreciably upon the concentration of NH_2NH_2 (see below). Assuming that the CH_3-proton resonances of **4** and **8** have similar chemical shifts, the [NH_2OH] dependence of the chemical shift of signal 4 has been used to estimate the chemical shift δ_{NN} between the CH_3-proton resonances due to **4** and **10** and the equilibrium constant K_{cn} for eq. [1] (0.95 ppm and 1.3 M^{-1}, respectively).[10] Because only four concentrations of NH_2OH were used, these values should be considered to be semiquantitative. Nevertheless using these data along with line width data, we estimate (1) k_{cn} in eq. [1] to be 1700 $M^{-1}s^{-1}$ and k_{-cn} may be obtained from the expression $K_{cn} = k_{cn}/k_{-cn}$. These values for K_{cn} and k_{cn} are the same order of magnitude as those for the addition of NH_2OH to the keto carbonyl carbon atom of ethyl acetoacetate

[7]For NH_2NH_2, a second order term has also been detected (ref. 6*b*); however, it is sufficiently small relative to the third order term to be neglected in our fit.

[8]The CH_3-proton resonances occur at δ 2.14 and 1.93 for *O*-acetylhydroxylamine and acetohydroxamic acid, respectively.

[9]At pH 7.5, this ratio is 6.0 for phosphate buffer.

[10]Values for δ_{NN} and K_{cn} were estimated using chemical shift data for four NH_2OH concentrations and the equation $\delta - \delta_N = (\delta_{NN} - \delta_N)/K_{cn}[NH_2OH]$ in which δ, δ_{NN}, and δ_N are the chemical shifts of the exchange broadened signal and the CH_3-proton resonances of **10** and **4**, respectively.

Can. J. Chem. Downloaded from www.nrcresearchpress.com by 210.87.254.6 on 09/06/12
For personal use only.

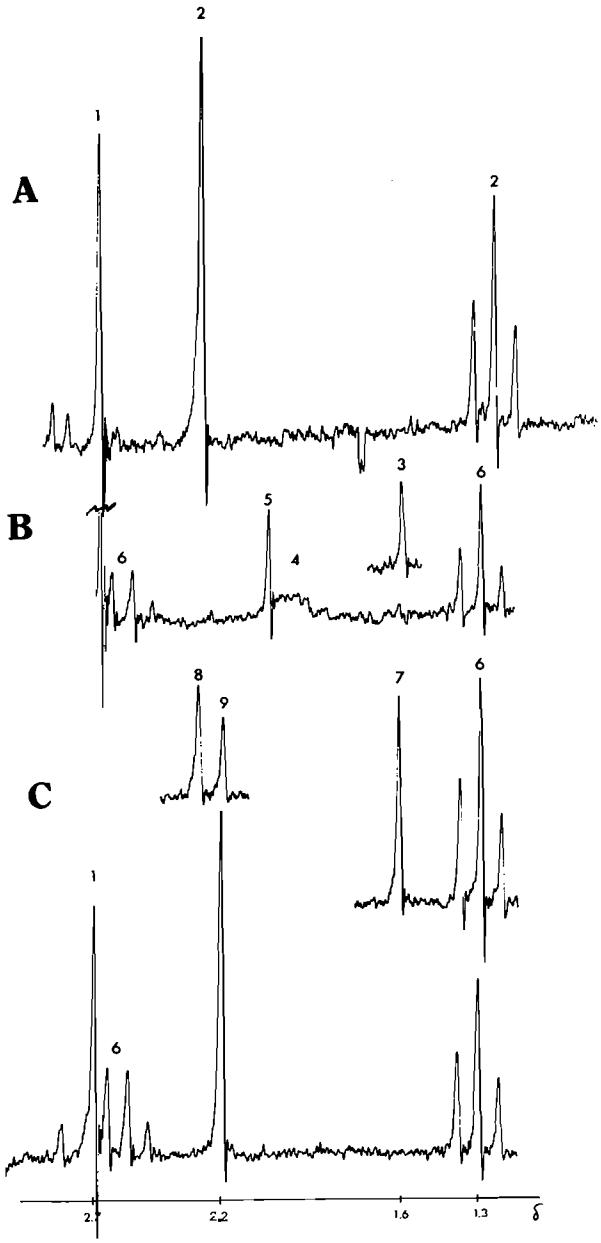

FIG. 1. (A). The upfield portion of the proton nmr spectra at 100 MHz and 30°C in 30% (by volume) aqueous methanol solution of 0.060 *M* ethyl thioacetoacetate at pH 8.0 (0.2 *M* Dabco buffer, $\mu = 1$ *M*). The methylene proton signal is masked by those due to water and methanol. (B). Same as A except that the sweep was started 4.5 min after adding 0.4 *M* NH_2OH. The inset illustrates the intensity and position of a transient signal obtained 1.7 min after mixing. The gain differs from that for A and C. (C). Same as A except that the sweep was started at the end of reaction with 0.2 *M* NH_2NH_2. The inset illustrates the position and intensity of the signals obtained 2.6 min after mixing.

Assignments and chemical shifts in ppm relative to tetramethylsilane: 1. $^{13}CH_3OH$ upfield side band, 2.67; 2. $CH_3COCH_2COSCH_2CH_3$, 2.31 and 1.24; 3. 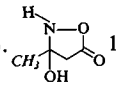 1.58; 4. Coalescence of 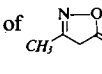 and 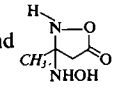 , see text for chemical shifts; 5. 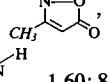 , 2.07; 6. CH_3CH_2SH, 1.29 and 2.60; 7. 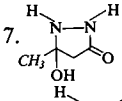 , 1.60; 8. May be due to three compounds, see text; 9. 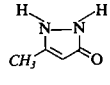 , 2.22.

(1*a*). In contrast, the line width of the oxime of ethyl acetoacetate appears to be independent of NH_2OH concentration in the range 0.1 to 0.3 *M* (1*a*).

Signal 5 is due to the CH_3-proton resonance of the final product, which is assigned structure **5**. This signal is not observed on the first scan and its growth corresponds to the same time-scale as the decay of signal 4. Previously this signal was assumed to be due to the CH_3-proton resonance of **4** (1*a*).

Figure 1C illustrates part of the spectrum obtained at an intermediate time after mixing with NH_2NH_2 (2.6 min) and one obtained at the end of the reaction. Thus, signal 6 indicates that the formation of thioethanol is already complete after 2.6 min. Consequently signals 7, 8, and 9 are not due to compounds containing the thioester group. Because signals 7 and 3 have almost the same chemical shift and 7 is observed with maximum intensity in the first scan, it is assigned to the CH_3-protons of structure **7**. Signal 9 is assigned to the CH_3-protons of **9**, the final product. Signal 8 is more complicated to interpret because it appears to be due to more than one compound, as indicated by the following observations. First, it is observed with maximum intensity in the first scan, and this initial intensity decreases as the concentration of NH_2NH_2 is increased. Simultaneously some of the thioester remains during the first scan. Second, signal 8 remains (at reduced intensity) after the thioester has disappeared (Figure 1C). Consequently, before 2.6 min have elapsed signal 8 may be due to at least two compounds, the thioester[11] and **8**. An additional complication is that NH_2NH_2

[11]The thioester is in equilibrium with acyclic carbinolamine (Scheme 1). However, the expected exchange broadening and shift in the position of the signal is small because pH values of 8.0 or less have been employed and K_n is probably about the same as that for ethyl acetoacetate (0.5 M^{-1}, reference 1*b*).

TABLE 1. Kinetic data for reaction of ethyl thioacetoacetate with NH_2NH_2 in 30:70 (by volume) methanol/water at 30°C, $\mu = 1$

pH	Nucleophile conc. range (M)[a]	[Buffer] M	k_{cd} min^{-1}	k_{ta}[d] min^{-1}
7.0	0.13–0.24	0.10[b]	0.24±0.01	—
7.5	0.14–0.24	0.10[b]	0.28±0.02	0.63±0.05
		0.15[b]	0.30±0.06	0.71±0.04
		0.20[b]	0.39±0.04	1.5 ±0.2
		0.30[b]	0.43±0.04	1.2 ±0.2
8.0	0.14–0.24	0.10[c]	0.15±0.02	0.6 ±0.16
		0.20[c]	0.16±0.04	0.6 ±0.19
		0.30[c]	0.20±0.06	0.6 ±0.15
	0.19–0.34	0.40[c]	0.25±0.04	0.72±0.06

[a]Total concentration after complete decomposition of thioester.
[b]Sodium phosphate.
[c]Dabco.
[d]These values are probably semiquantitative since they are about 3 times the value for k_{cd}. The deviations refer to those obtained upon averaging several k_{ta} values calculated as described in the text.

TABLE 2. Kinetic data for reaction of ethyl thioacetoacetate with NH_2OH in methanol/water (30:70 by volume) at 30°C, $\mu = 1$

pH	Nucleophile conc. range (M)[a]	[Buffer] M	$k_{cd}/[NH_2OH]$[b] M^{-1} min^{-1}	$k_{ta}/[NH_2OH]$[b] M^{-1} min^{-1}
7.0	0.14–0.34	0.10[c]	1.7±0.2	—
	0.14–0.34	0.20[c]	1.9±0.3	10±2[e]
	0.06–0.19	0.30[c]	2.4±0.3	13±2[e]
7.5	0.14–0.34	0.10[c]	2.3±0.3	2.7 ±0.6
	0.14–0.24	0.15[c]	2.1±0.2	2.5 ±0.5
		0.20[c]	3.1±0.6	3.1 ±0.6
8.0	0.14–0.24	0.10[c]	2.7±0.3	0.45±0.2
8.0	0.14–0.34	0.10[d]	1.4±0.2	0.40±0.09
	0.14–0.34	0.20[d]	1.9±0.3	0.20±0.04
	0.24–0.44	0.30[d]	2.0±0.5	0.35±0.02
	0.24–0.44	0.30[d]	2.7±0.4	0.22±0.06
8.5	0.14–0.34	0.10[d]	2.1±0.1	0.30±0.06

[a]Total concentration after complete decomposition of the thioester.
[b]$[NH_2OH]$ refers to concentration of nucleophile free base.
[c]Sodium phosphate.
[d]Dabco.
[e]These values are semiquantitative since they are about 5 times the value for k_{cd}. The deviations refer to those obtained upon averaging several k_{ta} values calculated as described in the text.

addition to the acyl carbonyl of ethyl thioacetoacetate can be appreciable. Thus at pH 8.0 a value of 6 is estimated (see below) for the ratio of the lifetime for addition to the acyl carbonyl vs. that for the process involving addition to the keto carbonyl followed by cyclization. Consequently, roughly a maximum of 14% of the ester may be converted to the hydrazide of acetoacetic acid. The absence of a separate keto CH_3-proton resonance for this compound does not preclude its occurrence since its signal may have a chemical shift that is very close to that for the thioester. Furthermore NH_2NH_2 addition to the keto carbonyl carbon of the hydrazide would be expected to result ultimately in the formation of **9**. Consequently the analysis of the time dependence of signals 7 and 9 appears complicated.

Kinetic Analysis

For both nucleophiles, the time dependence of signals 3 and 7 has been treated as a first order decay.[12] During this period, the concentration of

[12]For cases in which the decay of the thioester was not complete before the first scan of these signals, this analysis was applied to intensity data collected after the thioester had disappeared. This approach was necessary for all the NH_2NH_2 data and for NH_2OH data collected at pH 7.0 and 7.5. For NH_2NH_2, the formation of **7** was assumed to be complete when the thioester was not observed. Consequently since it is possible that **7** may also be formed from the hydrazide of acetoacetic acid, its rate constant may be less accurate.

Can. J. Chem. Downloaded from www.nrcresearchpress.com by 210.87.254.6 on 09/06/12
For personal use only.

Can. J. Chem. Downloaded from www.nrcresearchpress.com by 210.87.254.6 on 09/06/12
For personal use only.

nucleophile is constant, and its effect on the rate constant can be ascertained. Hydroxylamine appears to affect the decay rate of **3** whereas NH_2NH_2 does not appear to affect the decay of **7**. Table 1 lists values for the observed rate constant k_{cd} (Scheme 2) for NH_2NH_2. These data are averages of at least three concentrations of NH_2NH_2. The standard deviations indicate that the apparent dependence upon buffer concentration is within experimental error. In addition, there appears to be no pH dependence over the small range employed.

For NH_2OH, the second order rate constant is listed in Table 2 as $k_{cd}/[NH_2OH]$ in which k_{cd} is the observed first order rate constant. There appears to be no significant dependence upon pH or buffer concentration. The reason for the apparent second order dependence for the decay of **3** can not be decided at this time. One possibility is nucleophilic displacement by NH_2OH to form **10**; however, we are not aware of any precedent for this step.

According to Scheme 2, the formation of **5** and **9** occurs via **4** and **8**, respectively. Consequently the growth of **5** and **9** cannot be considered to obey a simple first order rate law since the time scale is comparable to that for the decay of **3** and **7**, respectively, in most cases. For this reason, k_{ta} has been calculated by means of nonlinear regression (1*b*) to fit the equation

$$[2]\quad C/C_\infty = (k_{ta}\exp -k_{cd}t)/(k_{cd} - k_{ta}) - (k_{cd}\exp -k_{ta}t)/(k_{cd} - k_{ta}) + 1$$

in which C and C_∞ are concentrations at time t and infinity, respectively, for **5** and **9**. For this fit, k_{ta} is the sole unknown.

For NH_2NH_2, k_{ta} does not appear to depend upon nucleophile concentration. The averaged values listed in Table 1 appear to be independent of Dabco concentration. There is an indication of a dependence on the phosphate concentration at pH 7.5.

For NH_2OH, k_{ta} depends on the concentration of nucleophile, and values for the second order rate constant $k_{ta}/[NH_2OH]$ listed in Table 2 appear to be dependent upon pH but independent of buffer concentration. The pH dependence is consistent with the fact that **4** is detectable at high but not low pH in the range employed. The second order nature of the rate would be consistent with a mechanism in which **4** converts to **5** via **10**. The difference in behavior between NH_2OH and NH_2NH_2 is not inconsistent with their relative reactivities for nucleophilic addition to keto carbonyl groups (1*a*, *b*, 8).

Measurement of the rate of formation of **3** and **7** has been restricted because no equilibrating reservoir (5) was employed for the flow nmr measurements (see Experimental), thus preventing intensity measurements prior to about 30 s after mixing. Consequently only approximate rates can be determined based upon the relative intensities of CH_3-triplets of the thioester and thioethanol.[13] The rate constants obtained in this manner are considered to be upper limits since they may involve a contribution from hydrazinolysis or hydroxylaminolysis of the thioester. This rate constant k_c for the formation of **3** or **7** is calculated based on the pre-equilibrium and cyclization steps of Scheme 2 taking into account the fact that the rate is not cleanly first or second order (1*b*). For this purpose, K_n is assumed to be identical to that obtained for ethyl acetoacetate (1*a*, *b*). At pH 7.0, k_c is 5.6 min^{-1} and 6.0 min^{-1} for 0.12 and 0.2 *M* NH_2OH, respectively. For 0.2 *M* NH_2NH_2, k_c is 30 $\pm$ 2 min^{-1} and 63 min^{-1} at pH 8.0 and 7.5, respectively. If it can be assumed that the rate of hydrazinolysis or hydroxylaminolysis of ethyl thioacetoacetate is comparable to that for ethyl thioacetate, the ratios of lifetime for reaction via direct intermolecular nucleophilic addition to the thioester versus that for Scheme 2 are estimated to be 7 for 0.2 *M* NH_2OH at pH 7.0 and 6 for 0.2 *M* NH_2NH_2 at pH 8.0. Consequently these results would suggest that at least 85% of the reaction proceeds via Scheme 2 in these two cases. For NH_2OH, the spectra indicate that this percentage increases with pH.

Acknowledgements

This study has been supported in part by a grant from the Natural Sciences and Engineering Research Council of Canada.

1. (*a*) M. Cocivera, A. Effio, H. Chen, and S. Vaish. J. Am. Chem. Soc. **98**, 7362 (1976); (*b*) M. Cocivera, K. Woo, and P. Livant. Can. J. Chem. **56**, 473 (1978); (*c*) P. Livant and M. Cocivera. J. Org. Chem. **43**, 3011 (1978).
2. M. W. Croyn, M. Chang, and R. A. Wall. J. Am. Chem. Soc. **77**, 3031 (1955).
3. W. P. Jencks. J. Am. Chem. Soc. **80**, 5485 (1958).
4. H. N. Blount and H. B. Herman. J. Phys. Chem. **72**, 3006 (1968).
5. (*a*) M. Cocivera and A. Effio. J. Am. Chem. Soc. **98**, 7371 (1976); (*b*) C. Fyfe, M. Cocivera, S. Damji, T. Hostetter, D. Sproat, and J. O'Brien. J. Magn. Reson. **23**, 377 (1976).
6. (*a*) T. C. Bruice and L. R. Fedor. J. Am. Chem. Soc. **86**, 4886 (1964); (*b*) L. R. Fedor and T. C. Bruice. J. Am. Chem. Soc. **86**, 4117 (1964).
7. F. Lipmann and L. C. Tuttle. J. Biol. Chem. **159**, 21 (1945).
8. V. Malatesta and M. Cocivera. J. Org. Chem. **43**, 1737 (1978).

[13]The triplets must be used because they are not exchange broadened and there is no uncertainty that the intensities are directly related to the relative amounts of the two species.

Bromination–methanolysis of 2,3-disubstituted indoles; effects of side chain structure[1]

EDWARD A. GROSS, SUSAN F. VICE, AND GARY I. DMITRIENKO[2]

Guelph–Waterloo Centre for Graduate Work in Chemistry, Waterloo Campus, Department of Chemistry, University of Waterloo, Waterloo, Ont., Canada N2L 3G1

Received March 10, 1980[3]

EDWARD A. GROSS, SUSAN F. VICE, and GARY I. DMITRIENKO. Can. J. Chem. **59**, 635 (1981).

The bromination–methanolysis of 2,3-dialkylindoles has been shown to lead in some cases to good yields of 3-methoxyindolenines via the corresponding 3-bromoindolenines. However, changes in the structure of the C-2 substituent can cause dramatic changes in the reaction pathway. Structural features expected to stabilize the "enamine" tautomeric form of an indolenine make such methoxyindolenines unstable with respect to acid catalyzed conversion to 2-methoxyalkylindole products.

EDWARD A. GROSS, SUSAN F. VICE et GARY I. DMITRIENKO. Can. J. Chem. **59**, 635 (1981).

On a montré que la réaction de bromation en présence de méthanol des dialkyl-2,3 indoles conduit dans certains cas avec de bons rendements à des méthoxy-3 indolénines par l'intermédiaire des bromo-3 indolénines correspondants. Cependant si l'on modifie la structure du substituant en C-2 il peut se produire des changements majeurs dans le processus réactionnel. Les caractéristiques structurales qui devraient stabiliser la forme tautomère de l'énamine des indolénines rendent instables de telles méthoxyindolénines vis-à-vis de la transformation en méthoxy-2 alkylindoles catalysée par un acide.

[Traduit par le journal]

We have recently reported that the bromination of 2,3-dimethylindole **1** and tetrahydrocarbazole **4** in the presence of triethylamine in methylene chloride or methanol yields the corresponding 3-bromoindolenine **2** or **5** respectively.

The bromoindolenines **2** and **5** represent the first reported 3-bromoindolenines bearing alkyl substituents at C-2 and C-3. They are moderately stable in methanol at room temperature in the presence of triethylamine, but react rapidly upon acidification to yield the corresponding methoxyindolenines **3** and **6** in good yield (1, 2).

The observation that the methanolyses of **2** and **5** were acid catalyzed prompted us to suggest the mechanism illustrated in Scheme 2.

Protonation of the indolenine **2** to give **7** would be expected to catalyze addition of methanol to the C=N bond to give the 2-methoxy-3-bromoindoline **8**. S_N1 reaction of **8** via the carbonium ion **9** would give the 2,3-dimethoxyindoline **10**.

Elimination of methanol would then yield the observed methoxyindolenines **11**. An alternative mechanism involving simple S_N1 displacement of bromide from **7** by methanol would involve creation of a carbonium ion adjacent to the positively charged C=N$^+$—H bond and, as a result, is considered unlikely. Direct S_N2 displacement from **7** was considered unlikely on steric grounds.

In order to explore the generality of this route to methoxy indolenines we have now examined the effect of alterations of C-2 and C-3 substituents on the course of the reaction. Thus 2-phenyl-3-methylindole, upon bromination as described for **1** and **4**, yields a moderately stable 3-bromoindolenine **13** which reacts with methanol to yield the methoxyindolenine **14**.

The fact that **13** undergoes methanolysis (**13** → **14**) in exact analogy with **2** and **5** is of some significance with respect to the mechanism of the methanolysis reaction. A possible mechanism not

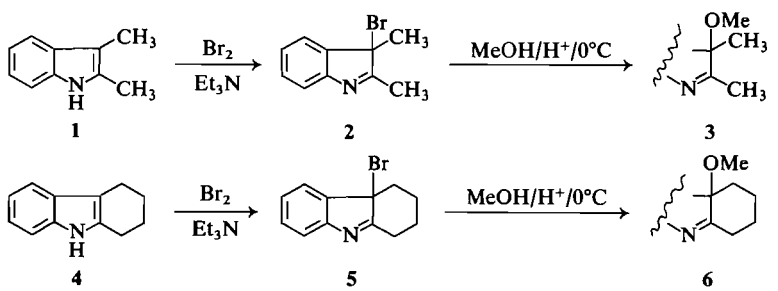

SCHEME 1

[1]Presented in part at the 63rd Annual Conference of the Chemical Institute of Canada, Ottawa, Ont., June 8–11, 1980.

[2]Author to whom all correspondence should be addressed.

[3]Revision received October 17, 1980.

0008-4042/81/030635-06$01.00/0

©1981 National Research Council of Canada/Conseil national de recherches du Canada

Can. J. Chem. Downloaded from www.nrcresearchpress.com by 210.87.254.5 on 09/06/12
For personal use only.

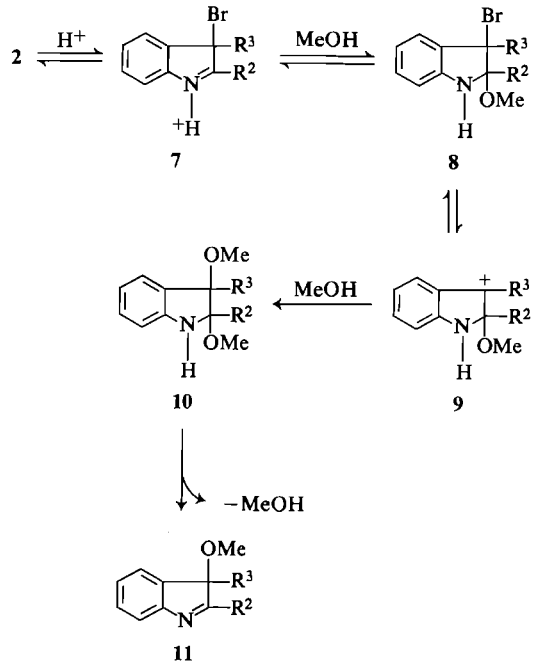

SCHEME 2

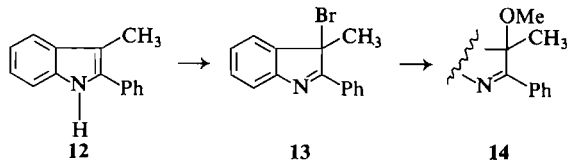

SCHEME 3

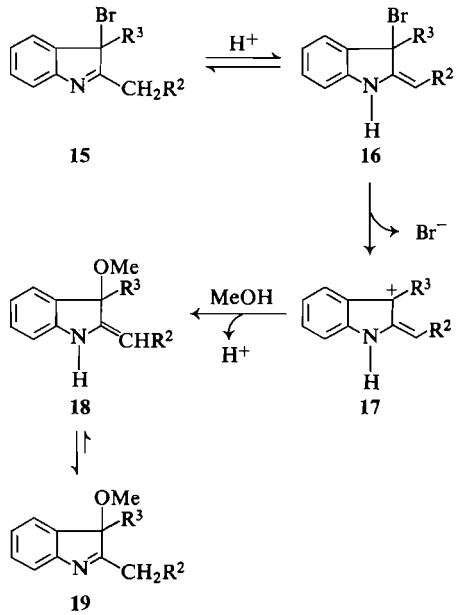

SCHEME 4

previously discussed involves acid catalyzed tautomerism of the bromoindolenine **15** to its enamine form **16**.[4]

Methanolysis of **16** perhaps via an S_N1 process would yield the methoxy analogue **18** which would be expected to rapidly tautomerize to the indolenine form **19**. The fact that **13**, for which such a pathway is not possible, undergoes facile methanolysis suggests that the mechanism of Scheme 4 is unlikely for other bromoindolenines as well.

Bromination–methanolysis of 2-ethyl-3-methylindole under the same conditions yielded none of the corresponding methoxyindolenine **22**, but instead gave a good yield of 2-methoxyethyl-3-methylindole **23**.

That the intermediate produced in the bromination step was the desired bromoindolenine **21** was clearly indicated by its nmr spectrum; δ 1.40 (t, J = 6.5, 3, C-2—CH_2—CH_3), 1.90 (s, 3, C-3—CH_3), 2.63 (q, J = 6.5, 2, C-2—CH_2—CH_3), 6.9–7.5 (m, 4, Ar-H).

It seemed very likely that the formation of **23** occurred via some variation of the general mechanism proposed some time ago by Taylor (3) (see Scheme 6). We initially suspected that the reaction involved tautomerism of the bromoindolenine **21** to the ethylideneindoline **25** ($R^3 = CH_3 = R^2$, X = Br) followed by nucleophilic attack by methanol leading to displacement of bromide, as indicated in Scheme 6 for the general nucleophile Y^-, to give, after deprotonation, the observed product **23**.

Recently, Owellen and Hartke have observed a related phenomenon in the reaction of chloroindolenines of tetrahydrocarbazoles with sodium methoxide (4). Whereas the chloroindolenine **28** (R = H), derived from tetrahydrocarbazole, gives principally the methoxyindolenine **6**, the chloroindolenine **28** (R = CO_2Me), derived from 1-carbomethoxytetrahydrocarbazole **27** (R = CO_2Me), gives the indole **30**. It was proposed that the difference in product types observed with **28** (R = H) and **28** (R = CO_2Me) was due to stabilization of the tautomer **29** of **28** (R = CO_2Me) by the C-1 carbomethoxy group, which could react by Taylor's mechanism to give **30**. A similar stabilization of the tautomer **25** ($R^2 = R^3 = CH_3$, X = Br) of **21** by the methyl substituent would explain the observation that methanolysis of **21** yields **23** whereas methanolysis of **2** gives **3**.

More recent work in our laboratory indicates that **21** in fact does not behave anomalously in the acid

[4]The authors would like to thank Professor E. W. Warnhoff for suggesting this mechanistic possibility.

Can. J. Chem. Downloaded from www.nrcresearchpress.com by 210.87.254.5 on 09/06/12
For personal use only.

Can. J. Chem. Downloaded from www.nrcresearchpress.com by 210.87.254.5 on 09/06/12
For personal use only.

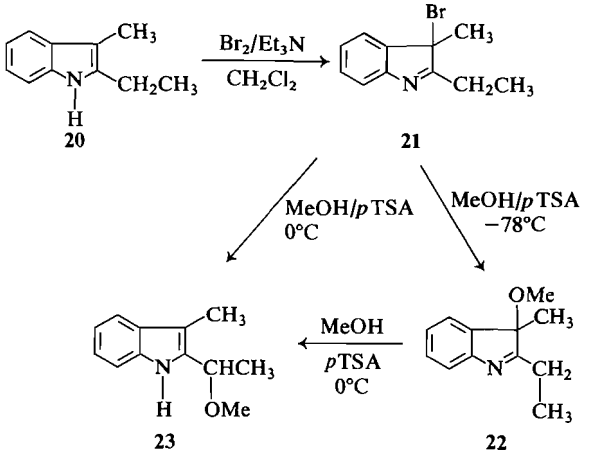

SCHEME 5

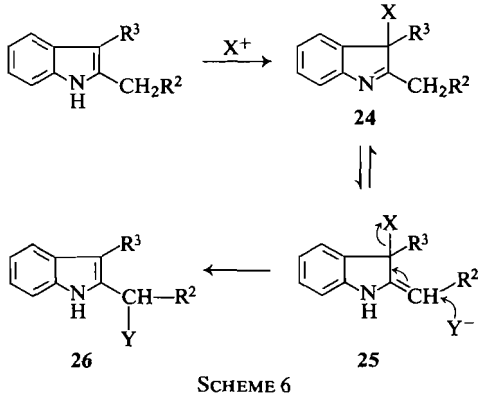

SCHEME 6

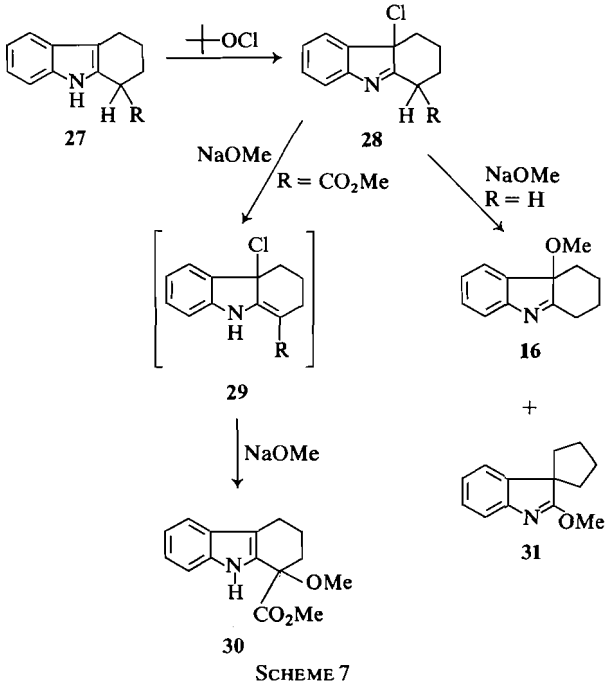

SCHEME 7

catalyzed methanolysis reaction and that under appropriate conditions the desired methoxyindolenine **22** can be isolated. Thus, we have found that acid catalyzed methanolysis of **21** at −78°C occurs rapidly to give, after basic aqueous work-up, a relatively unstable oily product with spectroscopic characteristics compatible with its formulation as 2-ethyl-3-methoxy-3-methylindolenine **22**. Treatment of **22** with acidic methanol at 0°C gave **23** very rapidly and cleanly. The failure to isolate **22** from the methanolysis of **21** at 0°C is thus readily understood.

To further test the generality of the bromination–methanolysis route to methoxyindolenines we examined the effect of ring size in the cycloalkanoindole series **32** on the outcome of the reaction. Our previous study indicated that tetrahydrocarbazole (**32***b*) reacted in the same manner as **1** giving the methoxyindolenine **6** in good yield likely via the sequence **4** → **33***b* → **34***b* → **35***b* → **6**. Bromination–methanolysis of the five-membered ring analogue **32***a* has been found to give a mixture of two products formulated as **35***a* and **36**. Thus **32***a* behaves in the same manner as **1** and **4**, giving a C-3 methoxy substituted system which in this case exists as a stable hydrate **36** or methanol addition product **35***a*. The tendency of indolenines derived from **32***a* to form stable addition products with a number of nucleophiles including alcohols has been noted previously and suggests that there is less ring strain in such a fused ring system when the C-2 carbon is sp^3 hybridized than when it is sp^2 hybridized (5, 6).

In contrast to the 5-membered and 6-membered cycloalkanoindoles, the 7- and 8-membered cycloalkanoindoles **32***c* and **32***d* yielded no detectable products bearing a C-3 methoxy substituent upon bromination–methanolysis at 0°C. Instead the major products were the methoxyindoles **39***c* (60% of the crude product estimated by nmr; 45% isolated yield) and **39***d* (49% of crude product; 28% isolated yield). As was the case with 2-ethyl-3-methylindole **20**, it was possible to isolate the methoxyindolenine **37***c* from the methanolysis of **33***c* at −78°C. The indolenine **37***c* was very labile, decomposing very rapidly in the absence of small amounts of base (triethylamine).

Treatment of crude **37***c* with methanol and acid at 0°C gave **39***c* rapidly and in good yield, presumably via **38***c*. On the other hand no conditions could be found under which **37***d* could be isolated or detected. The brominated intermediate **33***d* derived from **32***d* underwent no reaction with methanol at −78°C. At higher temperatures mixtures of unreacted **33***d* and the indole **39***d* were obtained.

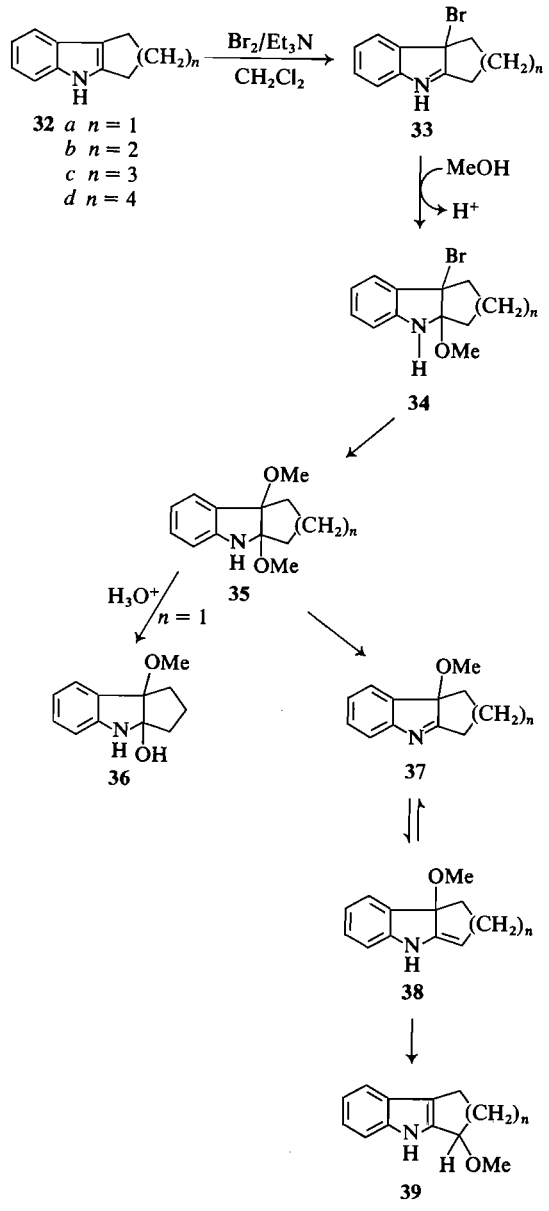

SCHEME 8

There is insufficient evidence with which to formulate a clear explanation for the observed differences in reaction modes of indolenines derived from **32***c* and **32***d* relative to those derived from **1** and **4**.

It should be noted, however, that unfavourable transannular interactions expected in the medium sized ring systems are somewhat relieved by the introduction of sp^2 centers (7). This effect should favour tautomerism of **37** to **38** and thus lead to formation of the indole products **39**. It should also be noted that addition of methanol to **33***d* to give **34***d* involves conversion of an sp^2 center of a medium sized ring to an sp^3 centre. Such a structural change would increase transannular interactions and would thus be unfavourable. The failure of **33***d* to undergo methanolysis at −78°C might well be due to this effect.

It is clear now that, although bromination–methanolysis of 2,3-disubstituted indoles leads in some cases to good yields of 3-methoxyindolenines, subtle structural changes of the C-2 substituent can lead to dramatic changes in the stability of the methoxyindolenines. Methoxyindolenines incorporating structural features which lead to stabilization of the enamine tautomer are relatively unstable and are readily converted to C-2 methoxyalkylindoles on treatment with methanol and acid.

Further reactions of methoxyindolenines which are of potential synthetic utility are currently being studied.

Experimental

General

General experimental details have been described previously (2).

Indoles

2,3-Trimethyleneindole was prepared by the method of Plant and Tomlinson (8). All other indoles used were prepared by the general method of Dave and Warnhoff (9) and had physical characteristics in agreement with literature values.

Bromination of 2-Phenyl-3-methylindole

To a cooled (0°C) solution of 2-phenyl-3-methylindole (1.02 g; 4.91 mmol) in methylene chloride (40 mL) containing triethylamine (2 mL) was added dropwise a solution of bromine (1.1 equivalents) in methylene chloride (7 mL) over a period of 5 min. The solution was stirred in a nitrogen atmosphere at ambient temperature for 10 min. The mixture was washed with 5% aqueous ammonia and water. Removal of solvent from the dried organic phase gave an oily product (1.37 g; 4.79 mmol) formulated as 3-bromo-2-phenyl-3-methylindolenine. Infrared (neat): 1602 (C=N—); uv (0.1% Et_3N/CH_2Cl_2): 330 (22 570); nmr: 2.05 (s, 3), 7.00–7.70 (m, 7), 8.10–8.45.

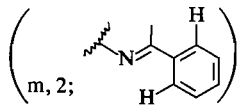

Methanolysis of 3-Bromo-2-phenyl-3-methylindolenine (13)

The bromoindolenine (**13**) was dissolved in methylene chloride (20 mL) and methanol (90 mL) was added at room temperature. After 40 min, the mixture was diluted with water and made basic with 10% aqueous ammonium hydroxide. The mixture was extracted with methylene chloride and the organic extract washed with water, dried, and concentrated to dryness *in vacuo* to give a yellow oil (1.10 g) which consisted principally of 3-methoxy-2-phenyl-3-methylindolenine and minor impurities. A pure sample was obtained by chromatography on silica gel with elution by diethyl ether – petroleum ether (60–80) (15:85) to give **14** as a colourless oil (0.73 g; 3.08 mmol).

Infrared (neat): 1603 (C=N—); uv (0.1% Et_3N/CH_2Cl_2): 335 (27 640); nmr: 1.62 (s, 3), 7.05–7.70 (m, 7), 8.10–8.45. Mass spectra *m/e*: 237 (molecular ion). *Exact Mass* calcd. for $C_{16}H_{15}NO$: 237.1154; found (ms): 237.1143.

Can. J. Chem. Downloaded from www.nrcresearchpress.com by 210.87.254.5 on 09/06/12
For personal use only.

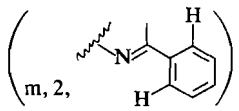

Bromination of 2,3-Dialkylindoles

General. To an ice-cold solution of the indole (approximately 3.1 mmol) in methylene chloride (20 mL) containing triethylamine (1.0 mL) was added a solution of bromine (1 equivalent) in methylene chloride (4 mL) over a period of 5 min. The solution was stirred for 5 min and used directly for isolation of the bromoindolenine or for acid catalyzed methanolysis as described below.

Isolation of 3-Bromo-2-ethyl-3-methylindolenine 21

To the solution of the bromoindolenine prepared as described above was added ice-cold water (75 mL). The mixture was extracted with cold methylene chloride (100 mL). The organic extract was washed with saturated aqueous sodium chloride, dried, and concentrated to give a golden yellow oily product, nmr: 1.40 (t, J = 6.5, 3, C-2—CH_2—CH_3), 1.90 (s, 3, C-3—CH_3), 2.63 (q, J = 6.5, 2, C-2—CH_2—CH_3), 6.9–7.5 (m, 4). Signals due to methylene chloride and triethylamine were also present. Further concentration of the sample *in vacuo* gave a tan coloured crystalline solid which rapidly decomposed to a purple solid with vigorous evolution of HBr upon exposure to a normal atmosphere.

*Isolation of 3-Bromo-2,3-trimethylene Indolenine 33*a

The bromoindolenine **33***a* was isolated as an oil contaminated with methylene chloride and triethylamine by the method described for isolation of **21**; nmr: 1.2–3.4 (m, —$CH_2CH_2CH_2$—, overlapped with CH_2 of triethylamine), 6.9–7.6 (m, Ar-H).

Removal of methylene chloride and triethylamine *in vacuo* led to decomposition as described for **21**.

*Isolation of 3-Bromo-2,3-pentamethylene Indolenine 33*c

The bromoindolenine **33***c* was isolated as an oil contaminated with methylene chloride and triethylamine by the method described for isolation of **21**; nmr: 1.2–2.7 (C-3—$(CH_2)_4$—), 2.8–3.1 (m, 2, C-2—CH_2—), 6.9–7.6 (m, 4, Ar-H).

Removal of the volatile contaminants *in vacuo* led to decomposition as described for **21**.

*Isolation of 3-Bromo-2,3-hexamethylene Indolenine 33*d

The bromoindolenine **33***d* was isolated as an oil contaminated with methylene chloride and triethylamine by the method described for **21**; nmr: 0.7–3.2 (m, —$(CH_2)_6$—, overlapped with —CH_2CH_3 of triethylamine), 6.9–7.6 (m, Ar-H).

Removal of volatile contaminants *in vacuo* led to decomposition.

Methanolysis of 3-Bromo-2-ethyl-3-methylindolenine 21

(a) At 0°C

Anhydrous methanol (20 mL) was added to the solution of the bromoindolenine **21** obtained from the indole **20** (0.490 g; 3.08 mmol) by the general method described above. A solution of *p*-toluenesulfonic acid monohydrate (0.780 g) in methanol (5 mL) was added dropwise over a period of 5 min. The mixture was stirred for 5 min and poured into water (75 mL). The aqueous phase was made basic with 10% aqueous ammonia and the mixture was extracted with methylene chloride (50 mL). The organic phase was washed with saturated aqueous sodium chloride. Removal of solvent *in vacuo* from the dried organic extract yielded the crude product (0.590 g) consisting principally of **23** contaminated with minor impurities as indicated by tlc and nmr. One recrystallization from ether–hexane gave 2-(1′-methoxyethyl)-3-methylindole **23** as small prisms, mp 105–109°C (0.266 g; 1.41 mmol; 46% yield).

Infrared: 3330 (N—H); uv (MeOH): 277 (sh), 282.5 (8380), 291 (6850); nmr: 1.47 (d, J = 7, 3), 2.25 (s, 3), 3.2 (s, 3), 4.58 (q, J = 7, 1), 6.8–7.6 (m, 4), 8.1 (br s, 1); ms *m/e*: 189 (molecular ion). *Anal.* calcd. for $C_{12}H_{15}NO$: C 76.15, H 7.99, N 7.40; found: C 75.82, H 8.00, N 7.31.

(b) At −78°C

A methylene chloride solution of the bromoindolenine **21** (derived from the indole **20** (0.502 g; 3.15 mmol)) was cooled to −78°C and methanol (30 mL) was added. A solution of *p*-toluenesulfonic acid monohydrate (0.79 g) in methanol (5 mL) was added dropwise over a period of 5 min. After 10 min 10% aqueous ammonia was added to the cooled mixture and the reaction was worked up as described in (*a*) above. The product **22** was an oil which contained a small amount of triethylamine. Upon removal of traces of base *in vacuo* the product partially solidified but became relatively unstable decomposing extensively even at 0°C after several hours. Infrared (neat): 1580 (C=N); nmr: 1.38 (t, J = 7, 3, C-2—CH_2—CH_3), 1.47 (s, 3, C-3—CH_3), 2.63 (q, J = 7, 2, C-2—CH_2—CH_3), 2.87 (s, 3, CH_3), 7.2–7.8 (m, 4, ArH); ms *m/e*: 189 (molecule ion).

*Methanolysis of 3-Bromo-2,3-trimethylene Indolenine 33*a *at 0°C*

The crude product obtained by methanolysis of a solution of the bromoindolenine **33***a* (derived from the indole **32***a* (0.490 g; 3.12 mmol)) as described for **21** was chromatographed on silica gel with elution by petroleum ether – diethyl ether (9:1). The major fraction obtained as a white solid, mp 63–68°C (0.320 g; 55% yield), was 2-hydroxy-3-methoxy-2,3-trimethylene indoline **36**. Infrared: 3360 (N—H, O—H); uv (MeOH): 244 (5990), 304 (1762); nmr: 1.1–2.4 (m, 6), 3.30 (s, 3), 3.5 (br, 1), 4.8 (br, 1); 6.3–7.4 (m, 4); ms *m/e*: 205 (molecular ion). *Exact Mass* calcd. for $C_{12}H_{15}NO_2$: 205.1103; found (ms): 205.1079. *Anal.* calcd. for $C_{12}H_{15}NO_2$: C 70.22, H 7.37, N 6.82; found: C 70.78, H 7.45, N 6.83.

Further elution yielded a small amount of an unstable oily product (0.008 g) formulated as 2,3-dimethoxy-2,3-trimethylene indoline **35**. Infrared (neat): 3350 (N—H); uv (MeOH): 243 (8090), 298 (2586); nmr: 1.1–2.4 (m, 6), 3.33 (s, 3), 3.40 (s, 3), 4.2 (br s, 1), 6.3–7.4 (m, 4); ms *m/e*: 219 (molecular ion). *Exact Mass* calcd. for $C_{13}H_{17}NO_2$: 219.1259; found (ms): 219.1245.

*Methanolysis of 3-Bromo-2,3-pentamethylene Indolenine 33*c

(a) At 0°C

The crude product obtained by methanolysis of a solution of the bromoindolenine **33***c* (derived from the indole **32***c* (0.562 g; 3.04 mmol)) as described for **21** was chromatographed on silica gel with elution by diethyl ether – petroleum ether (9:1). The major fraction was a white crystalline solid **39***c* (0.297 g; 1.38 mmol, 45%), mp 84–85.5°C; ir: 3400 (N—H); nmr: 1.1–3.0 (m, 8), 3.3 (s, 3), 4.1–4.4 (m, 1), 6.8–7.6 (m, 4), 8.1 (br s, 1); ms *m/e*: 215 (molecular ion). *Anal.* calcd. for $C_{14}H_{17}NO$: C 78.10, H 7.96, N 6.51; found: C 78.32, H 7.92, N 6.42.

(b) At −78°C

Acid catalyzed methanolysis of the bromoindolenine **33***c* as described for **21** at −78°C gave an oily product, **37***c*, containing traces of methylene chloride and triethylamine. Infrared: 1580 (C=N); nmr: 0.8–3.2 (m, —$(CH_2)_5$—, overlapped with signal from —CH_2CH_3 of triethylamine), 2.87 (s, 3, OCH_3), 7.0–7.6 (m, 4, ArH)). Removal of the last traces of base *in vacuo* led to rapid decomposition to a red gum.

*Methanolysis of 3-Bromo-2,3-hexamethylene Indolenine 33*d

(a) At 0°C

The acid methanolysis of the bromoindolenine **33***d* (derived from the indole **32***d* (6.17 g; 3.10 mmol)) was performed as described for **21** except that acidic methanolysis was performed for 30 min rather than 5 min. Using shorter reaction times gave complex products containing no methoxy groups as indicated by

Can. J. Chem. Downloaded from www.nrcresearchpress.com by 210.87.254.5 on 09/06/12
For personal use only.

nmr analysis. The crude product was chromatographed on silica gel with elution by petroleum ether – diethyl ether (95:5). The major product **39***d* was obtained as a waxy solid (0.20 g; 0.87 mmol). An analytical sample was obtained by recrystallization from petroleum ether – diethyl ether, mp 103.5–105°C. Infrared (Nujol): 3310 (N—H); uv (MeOH): 291 (6308), 299 (sh); nmr: 0.8–3.2 (m, 10), 3.4 (s, 3), 4.70 (dd, $J = 3, J = 5, 1$), 6.9–7.6 (m, 4), 8.5 (br s, 1); ms *m/e*: 229 (molecular ion). *Anal.* calcd. for $C_{15}H_{19}NO$: C 78.56, H 8.35, N 6.11; found: C 78.72, H 8.50, N 6.00.

(b) At −78°C

Acid catalyzed methanolysis of the bromoindolenine **33***d* at −78°C as described for **21** gave only starting material contaminated with very minor impurities. No methoxyindolenine **37***d* could be detected by tlc or nmr analysis.

Acid Catalyzed Methanolysis of the Methoxyindolenine 22

Acid catalyzed methanolysis of the methoxyindolenine **22** as described for the bromoindolenine **21** at 0°C gave a yellow crystalline crude product which was principally **23** as indicated by tlc and nmr analysis. Chromatography of the crude product on silica gel with elution by petroleum ether – diethyl ether (9:1) yielded the pure indole **23** (0.407 g; 2.30 mmol; 73% from the indole **20**) identical in all respects with the indole prepared by methanolysis of **21** at 0°C.

*Acid Catalyzed Methanolysis of the Methoxyindolenine 37*c

Acid catalyzed methanolysis of the methoxyindolenine **37***c* (prepared from the indole **32***c* (0.502 g; 2.71 mmol)) yielded a brown oily product consisting principally of **39***c* and minor unidentified impurities. Chromatography of the crude product on silica gel with elution by petroleum ether – diethyl ether (9:1) gave the pure indole **39***c* (0.411 g; 1.89 mmol; 70% from the indole **32***c*) identical in all respects with the indole obtained by methanolysis of **33***c* at 0°C.

Acknowledgements

We would like to thank the Natural Sciences and Engineering Research Council of Canada and the University of Waterloo for financial support of this work.

1. G. I. DMITRIENKO. Heterocycles, **12**, 1411 (1979).
2. G. I. DMITRIENKO, E. A. GROSS, and S. F. VICE. Can. J. Chem. **58**, 808 (1980).
3. W. I. TAYLOR. Proc. Chem. Soc. 247 (1962).
4. R. J. OWELLEN and C. A. HARTKE. J. Org. Chem. **41**, 102 (1976).
5. P. L. JULIAN, E. W. MEYER, and H. S. PRINTZ. Heterocyclic compounds. Vol. 5. *Edited by* R. E. Elderfield. Wiley, New York. 1952. p. 108.
6. A. S. BAILEY, R. SCATTERGOOD, and W. A. WARR. J. Chem. Soc. C, 3769 (1971).
7. E. L. ELIEL. Steric effects in organic chemistry. *Edited by* M. S. Newman. Wiley, New York. 1956. p. 122.
8. W. H. PERKIN and S. G. P. PLANT. J. Chem. Soc. **123**, 3244 (1923).
9. V. DAVE and E. W. WARNHOFF. Can. J. Chem. **54**, 1015 (1976).

Can. J. Chem. Downloaded from www.nrcresearchpress.com by 210.87.254.5 on 09/06/12
For personal use only.

Structure of condensation products between isonicotinylhydrazine and reducing sugars by ^{13}C nmr spectroscopy

KEITH BAILEY AND ANDREW G. BUTTERFIELD

Drug Research Laboratories, Health Protection Branch, Tunney's Pasture, Ottawa, Ont., Canada K1A 0L2

Received July 8, 1980

KEITH BAILEY and ANDREW G. BUTTERFIELD. Can. J. Chem. **59**, 641 (1981).

The structures of the condensation products of isonicotinylhydrazine (isoniazid) with galactose, glucose, lactose, maltose, glycolaldehyde and glyceraldehyde were investigated by examination of their ^{13}C nmr spectra, determined in D_2O and DMSO-d_6 solution. Spectroscopic data and their interpretation are presented. Spectroscopic and chromatographic (hplc) evidence are combined to show that the products formed with the four sugars exist in solution predominantly as 1-(1β-pyranosyl)-2-isonicotinylhydrazines, and to a lesser extent as the analogous 1α-pyranosyl anomers. The products formed with glycolaldehyde and glyceraldehyde are normal hydrazones.

KEITH BAILEY et ANDREW G. BUTTERFIELD. Can. J. Chem. **59**, 641 (1981).

Nous avons étudié les structures chimiques des produits de condensation entre l'isonicotinyl-hydrazine (isoniazide) et le galactose, le glucose, le maltose, le glyceraldehyde et le glycolaldehyde grâce à leur spectres ^{13}C rmn en solutions dans D_2O et d_6-DMSO. Les données spectroscopiques ainsi que leurs interprétations seront présentées. Ces données spectroscopiques renforcées avec des données chromatographiques (hplc) démontrent que les produits glucidiques se trouvent surtout dans la forme de 1-(1β-pyranosyl)-2-isonicotinyl hydrazine contenant une quantité moindre d'anomères 1α-pyranosyl, tandis que les produits des deux aldéhydes sont des hydrazones ordinaires.

Can. J. Chem. Downloaded from www.nrcresearchpress.com by 210.87.254.40 on 09/06/12
For personal use only.

Introduction

Impurities in isonicotinylhydrazine (isoniazid, isonicotinic acid hydrazide) drug formulations, formed by condensation of the drug with either lactose (1) or glucose (2), have been reported. However, there has been uncertainty about the exact nature of these compounds: they have been referred to as hydrazones (1–3) or as substituted hydrazines (4), the latter implying the absence of an imino carbon at C-1 of the sugar moiety.

During the development of high-performance liquid chromatographic (hplc) methods for the determination of isonicotinylhydrazine (INH) and the lactose and glucose–INH condensation product impurities in INH formulations (5, 6), it was noted that two peaks were obtained for each impurity (6). It was postulated (6) that these two peaks are due to the 1-(1α-pyranosyl) and 1-(1β-pyranosyl)-2-isonicotinylhydrazine anomers, and that their observed interconversion is via the isomeric sugar hydrazone. These observations are to some extent at odds with the hydrazone structure heretofore assumed for these compounds. Knowledge of the structure, and possible isomeric interconversions of these compounds, may help explain their observed physical, chemical, metabolic, and pharmacological characteristics. In an attempt to resolve the uncertainty regarding their structure we studied a series of these compounds obtained from galactose, glucose, lactose, maltose, glyceraldehyde, and glycolaldehyde using carbon-13 nuclear magnetic resonance (^{13}C nmr) spectroscopy and hplc. Shortly after the completion of our work, Takeda (7) reported ^{13}C nmr and other data for the INH-glucose product and some related substances which prompts us to report the results of our studies and our interpretation of the data.

Results and Discussion

Synthesis

Methods for the preparation of various 1-pyranosyl-2-isonicotinylhydrazines have been reported (1, 4, 8). The degree of reaction between INH and the various sugars was monitored by hplc. In all cases, two product peaks were obtained and the earlier-eluting peak, **1***a*–**4***a*, was smaller than the latter, **1***b*–**4***b* (ca. 1:2–1:4). Monitoring of the reaction mixture also showed that monosaccharides reacted with INH much faster than disaccharides, apparently reaching equilibrium at 40°C after 3 and 5 days respectively.

Products obtained in crystalline form were invariably the major reaction products, **1***b*–**4***b*; these were examined by ^{13}C nmr spectroscopy. Attempts to isolate **1***a*–**4***a* using preparative hplc were unsuccessful due to interconversion of the two products in solution. C, H, and N analysis of these products closely matched the theoretical values; however, melting points were generally higher than those previously reported, presumably because of the higher purity of the hydrazines (Table 1).

High Performance Liquid Chromatography

Retention times for compounds **1**–**4**, **9**, and **10** are given in Table 1. The characteristics of the

0008-4042/81/030641-06$01.00/0

©1981 National Research Council of Canada/Conseil national de recherches du Canada

TABLE 1. Retention time (hplc), analytical, and melting point data for isonicotinylhydrazine condensation products

Compound	Retention time[a] (min)	Melting point (°C)	Molecular formula	Analysis (%) found C	found H	found N	calculated C	calculated H	calculated N
1*a*	6.0	NA[h]	$C_{12}H_{17}N_3O_6$	—	—	—	48.15	5.72	14.03
1*b*	8.0	179–181[b]	$C_{12}H_{17}N_3O_6$	47.91	5.74	13.51	48.15	5.72	14.03
2*a*	6.0	NA	$C_{12}H_{17}N_3O_6$	—	—	—	48.15	5.72	14.03
2*b*	7.3	167–168[c]	$C_{12}H_{17}N_3O_6$	48.10	5.84	14.11	48.15	5.72	14.03
3*a*	15.3	NA	$C_{18}H_{27}N_3O_{11}$	—	—	—	46.85	5.90	9.11
3*b*	20.2	204–204.5[d]	$C_{18}H_{27}N_3O_{11}$	46.54	5.98	9.01	46.85	5.90	9.11
4*a*	12.3	NA	$C_{18}H_{27}N_3O_{11}$	—	—	—	46.85	5.90	9.11
4*b*	16.5	NA[e]	$C_{18}H_{27}N_3O_{11}$	46.58	6.10	9.05	46.85	5.90	9.11
9	2.8	168–170[f]	$C_8H_9N_3O_2$	53.51	5.16	23.62	53.63	5.06	23.46
10	3.3	150–151[g]	$C_9H_{11}N_3O_3$	51.87	5.25	20.15	51.56	5.30	20.09

[a]Retention time using hplc system described in text.
[b]From methanol/water (lit. (4) 154.5–154.6°C, dec.).
[c]From water (lit. (4) 160°C, dec.).
[d]From water (lit. (8) 202°C, dec.).
[e]Indistinct.
[f]From aqueous methanol.
[g]From acetone/methanol (lit. (7) 151°C, dec.).
[h]NA = not available.

TABLE 2. ^{13}C chemical shifts of pyranoses[a]

	Galactose		Glucose		Lactose		Maltose	
	D_2O	DMSO-d_6	D_2O	DMSO-d_6	D_2O	DMSO-d_6	D_2O	DMSO-d_6
C-1α	93.97	92.74	94.86	92.37	94.68	92.13	94.80	92.44
C-1β	98.16	97.66	98.75	97.11	98.63	96.81	98.69	96.93
C-1′	—	—	—	—	105.79	103.91	102.51	100.88
C-2α	69.98	68.93	74.21	72.51	74.03	71.42	74.15	72.00
C-2β	73.56	72.27	76.95	75.06	76.70	74.64	76.89	74.46
C-2′	—	—	—	—	73.79	70.69	75.55	73.42
C-3α	70.89	69.05	75.55	73.24	74.27	72.15	76.04	[b]
C-3β	74.47	73.67	78.59	76.89	77.19	74.76	79.01	76.52
C-3′	—	—	—	—	75.43	73.30	75.73	73.42
C-4α	70.95	69.60	72.45	70.81	81.44	81.38	79.98	80.46
C-4β	70.40	68.44	72.45	70.51	81.32	81.02	79.80	79.92
C-4′	—	—	—	—	71.42	68.20	72.21	70.02
C-5α	72.11	70.45	74.21	72.03	72.94	69.84	72.82	[c]
C-5β	76.78	75.12	78.71	76.89	77.61	75.06	77.43	75.12
C-5′	—	—	—	—	78.16	75.55	74.52	72.40
C-6α	62.81	60.73	63.53	61.40	62.98	60.49	63.59	60.91
C-6β	62.63	60.73	63.53	61.40	62.98	60.49	63.59	60.91
C-6′	—	—	—	—	63.83	60.73	63.34	60.91

[a]δ-Values ± 0.03 in ppm from DSS (D_2O) or TMS (DMSO-d_6).
[b]Possibly superimposed with C-2′, 3′ at 73.42 ppm.
[c]Possibly superimposed with C-4′ at 70.02 ppm.

chromatographic system have been described elsewhere (6). Changes in the chromatograms of solutions of the purified hydrazines, **1***b*–**4***b*, on standing, are interpreted as being due to isomerization to equilibrium proportions of the α and β anomers and open-chain (imino) forms and gradual hydrolysis to free INH (and presumably the respective sugar). The ^{13}C nmr spectra for aged solutions of **1***b*–**4***b*, and the results of Takeda (7) for **2***b*, support these conclusions.

^{13}C Nuclear Magnetic Resonance Spectral Assignments

The ^{13}C nmr signals of galactose, glucose, and lactose in D_2O were identified in accordance with the recent literature (9) and of maltose in accordance with the work of Colson *et al.* (10) (Table 2). The tentative assignments of signals presented in Table 2 for DMSO-d_6 solutions have been made on the assumption that the signals will appear in the same order from low to higher field as that observed

Can. J. Chem. Downloaded from www.nrcresearchpress.com by 210.87.254.40 on 09/06/12
For personal use only.

TABLE 3. ^{13}C chemical shifts of isonicotinylhydrazones[a]

		Isonicotinylhydrazine (INH)		INH-glycolaldehyde[b]		INH-glyceraldehyde	
		D_2O	DMSO-d_6	D_2O	DMSO-d_6	D_2O	DMSO-d_6
CH_2OH	t	—	—	63.65	61.10	66.02	64.07
CHOH	d	—	—	—	—	73.91	71.60
C-3,5	d	124.50	121.28	124.92	121.71	124.81	121.77
C-4	s	143.51	140.65	ND	140.78	143.14	140.72
C-2,6	d	152.62	150.49	152.74	150.55	152.68	150.49
HC=N	d	—	—	157.54	153.04	157.23	154.32
C=O	s	170.00	164.34	ND	161.97	167.98	162.28

[a]δ-Values, ± 0.03 in ppm from DSS (D_2O) or TMS (DMSO-d_6); t = triplet, d = doublet, and s = singlet on SFORD; ND = not detected.
[b]Very sparingly soluble in D_2O.

TABLE 4. Assignments of ^{13}C chemical shifts of isonicotinylhydrazinyl pyranoses[a]

	Substrate							
	Galactose		Glucose		Lactose		Maltose	
	D_2O	DMSO-d_6	D_2O	DMSO-d_6	D_2O	DMSO-d_6	D_2O	DMSO-d_6
C-1	93.28	91.83	92.68	91.10	92.55	90.98	92.55	91.04
C-1′	—	—	—	—	105.85	103.91	102.51	101.00
C-2	71.72[b]	68.75[b]	73.67	71.60	73.36	71.42	73.49	71.18
C-2′	—	—	—	—	73.79	70.63	75.55	73.54
C-3	76.16	73.61	79.80	78.04	78.71	76.10	79.56	76.52
C-3′	—	—	—	—	75.43	73.36	75.67	73.54
C-4	71.24[b]	68.38[b]	72.45	70.51	81.32	80.96	79.86	80.04
C-4′	—	—	—	—	71.42	68.26	72.21	70.39
C-5	79.07	76.58	79.19	76.89	77.86	75.00	78.40	76.52
C-5′	—	—	—	—	78.22	75.67	74.52	72.57
C-6	64.19	60.55	63.78	61.46	63.10	60.49	63.71	60.97
C-6′	—	—	—	—	63.83	60.91	63.34	60.97
Isonicotinyl residue								
C=O	171.08	164.40	170.96	164.46	171.28	164.28	170.90	164.34
C-2,6	152.56	150.43	152.56	150.43	152.62	150.37	152.50	150.37
C-4	143.69	140.17	143.63	140.17	143.63	140.05	143.57	140.11
C-3,5	124.80	121.52	124.74	121.52	124.74	121.40	124.68	121.30

[a]δ-Values, ± 0.03 in ppm from DSS (D_2O) or TMS (DMSO-d_6).
[b]These assignments may be reversed.

in D_2O. This assumption is not altogether justified since inspection of the data presented in Table 2 reveals that the signals are not precisely equally affected by the change in solvent. In the case of glucose, the assignments were supported by the observation that signals observed in 1:1 D_2O: DMSO-d_6 appeared at positions intermediate between those in D_2O and DMSO-d_6.

Spectra of hydrazones **9** and **10** clearly showed that single products were formed (Table 3). The product **10**, from glyceraldehyde, had a terminal rather than central imino carbon, since single frequency off-resonance decoupling (SFORD) of the spectrum resulted in the generation of four doublets and a triplet, two singlets remaining. The imino carbons produced signals at about 157 ppm in D_2O and 154 ppm in DMSO-d_6 (Table 3). Signals from C-4 and C=O for **9** in D_2O were not detected, presumably due to the low solubility of this compound under these conditions.

Spectra for the reaction products of INH with galactose, glucose, lactose, and maltose, **1***b*–**4***b*, were recorded in D_2O and DMSO-d_6. Data with tentative assignments are presented in Table 4. Only one signal appears within a 20 ppm-wide window centred on the position of the imino carbon determined above; this is the readily-identifiable signal from the equivalent C-2 and C-6 of the isonicotinyl ring at 152.6 and 150.4 ppm in D_2O and DMSO-d_6, respectively. There is therefore no evidence for an imino carbon in products of this type and open-chain structures **5**–**8** (Fig. 2) can be eliminated from consideration.

Spectra of INH-galactose and INH-glucose displayed only six signals from the sugar moiety in both D_2O and DMSO-d_6 solution and one anomeric

Can. J. Chem. Downloaded from www.nrcresearchpress.com by 210.87.254.40 on 09/06/12
For personal use only.

Can. J. Chem. Downloaded from www.nrcresearchpress.com by 210.87.254.40 on 09/06/12
For personal use only.

TABLE 5. Deshielding effects of INH moiety in INH-pyranoses[a]

	Δ = δ INH-pyranose − δ pyranose (ppm)							
	Galactose		Glucose		Lactose		Maltose	
	D_2O	DMSO-d_6	D_2O	DMSO-d_6	D_2O	DMSO-d_6	D_2O	DMSO-d_6
C-1α	−0.69	−1.09	−2.18	−1.27	−2.13	−1.15	−2.25	−1.40
C-1β	−4.88	−5.83	−6.07	−6.01	−6.08	−5.83	−6.14	−5.89
C-2α	1.74	−0.55	−0.54	−0.91	−0.67	0.00	−0.66	−0.82
C-2β	−1.84	−3.89	−3.28	−3.46	−3.34	−3.22	−3.40	−3.28
C-3α	5.27	4.56	4.25	4.80	4.44	3.95	3.52	3.10[b]
C-3β	1.69	−0.06	1.21	1.15	1.52	1.34	0.55	0.00
C-4α	0.29	−0.85	0.00	−0.30	−0.12	−0.42	−0.12	−0.42
C-4β	−0.84	0.31	0.00	0.00	0.00	0.06	0.06	0.12
C-5α	6.96	6.13	4.98	4.86	4.92	5.16	5.58	6.50[b]
C-5β	2.29	1.46	0.48	0.00	0.25	−0.06	0.97	1.40[b]
C-6α	1.38	−0.18	0.25	−0.06	0.12	0.00	−0.12	0.00
C-6β	1.56	−0.18	0.25	−0.06	0.12	0.00	−0.12	0.00

[a]A negative sign indicates a relative shielding effect at that position; assignments of C-3, C-5 of maltose derivative were uncertain in DMSO-d_6.
[b]Refer to footnotes *b* and *c*, Table 2.

configuration was therefore indicated. The spectra of INH-lactose in D_2O and DMSO-d_6 and of INH-maltose in D_2O displayed 12 signals from the sugar moiety, six of which corresponded in both cases with the chemical shifts of C-1′ – C-6′ in the free sugars (Tables 2 and 4), indicating that the glucopyranosyl rings of these materials have remained intact. Substitution of the INH residue for hydroxyl at C-1 is expected to have minimal effects on the chemical shifts of C-4, C-6, and C-1′ – C-6′ because they are remote from the site of change (11).

The signals from C-4 and C-6 were identified on this basis in all spectra (Table 4). All spectra showed a new signal ascribed to C-1 since it had a chemical shift similar to that of C-1 of the starting sugar in the pyranosyl form.

Very similar chemical shift effects occur at C-1 on formation of the four INH products (Table 5), and since only one C-1 signal was observed in these spectra, it is suggested that all have one and the same configuration at C-1 and that they are 1-pyranosyl-2-isonicotinylhydrazines (Fig. 1). The remaining discussion will be rationalized on these structural premises with an attempt to assign the remaining signals and to define the α- or β-configuration of the products in solution.

In the case of INH-glucose, signals at 72.45 and 70.51 ppm in D_2O and DMSO-d_6, respectively, correspond exactly with signals observed for C-4β in β-glucose. The positions observed in glucose for C-4α are 72.45 (D_2O) and 70.81 ppm (DMSO-d_6) and this signal is therefore assigned to C-4. The following reasoning was employed in an attempt to

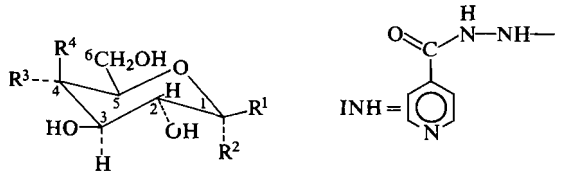

Compound	R^1	R^2	R^3	R^4
β-Galactose	OH	H	H	OH
β-Glucose	OH	H	OH	H
β-Lactose	OH	H	1-β-Galactopyranose	H
β-Maltose	OH	H	1-α-Glucopyranose	H
1a	H	INH	H	OH
1b	INH	H	H	OH
2a	H	INH	OH	H
2b	INH	H	OH	H
3a	H	INH	1-β-Galactopyranose	H
3b	INH	H	1-β-Galactopyranose	H
4a	H	INH	1-α-Glucopyranose	H
4b	INH	H	1-α-Glucopyranose	H

FIG. 1. Structures of 1-pyranosyl-2-isonicotinylhydrazines.

solve the remaining assignments. The effects on chemical shifts at C-3 and C-5 upon formation of the INH-coupled product should be similar in magnitude since they bear the same stereochemical relationship to the anomeric C-1. Therefore, if chemical shift *differences* are measured between C-3 and C-5 of glucose itself, both α and β, and pairs are taken from the three signals which are to be assigned, then one pair should show very similar differences for C-3 and C-5 compared with others. All the possible combinations were worked out, and it was found that the conjecture applies to two combinations, in both of which C-2 is the highest-

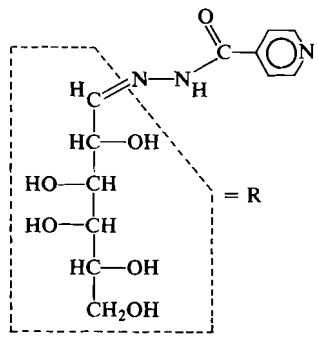

Compound	R
5	Galactosyl (shown)
6	Glucosyl
7	Lactosyl
8	Maltosyl
9	=CH—CH_2OH
10	=CH—CH(OH)—CH_2OH

FIG. 2. Structure of galactose isonicotinylhydrazone (**5**) and related compounds

field of the three signals and its assignment is thereby established (Table 4). The changes in position from the β-series seem to favour slightly the remaining higher-field signal being ascribed to C-3, but in regard to the α-series there is a very marked preference to ascribe the higher-field signal to C-5 in both D_2O and DMSO-d_6. The resulting assignments for INH-glucose (Table 4) agree with those tentatively proposed by Takeda (7) for the D_2O solutions; however, our chemical shifts (relative to DSS) were consistently to lower-field than those published (relative to TMS) by up to 2 ppm.

The spectra of INH-galactose and INH-lactose were interpreted (Table 4) using the same principles as those applied to INH-glucose.

The spectra of maltose in D_2O and DMSO-d_6 indicated that the β:α ratio is approximately 2:1 and 5:1, respectively. The spectrum of INH-maltose in D_2O showed signals which were easily identified as those of the INH moiety, C-1′ – C-6′ and C-1, C-4, and C-6; the C-2, C-3, and C-5 signals were identified as described for glucose. In DMSO-d_6, new C-1 signals appeared at 91.04 and 87.45 ppm with relative intensitives 2.5:1, respectively, in reasonable correspondence with the ratio of peak heights found for the two products on hplc. No imino carbon being apparent, these probably arise from the β and α anomers, respectively, since the chemical shift difference (3.59 ppm) is similar to that of C-1 in maltose (4.49 ppm). The presence of two components led to no difficulties in the identification of C-1′ – C-6′ or C-1, C-4 (partially resolved signals), or C-6, and C-2 of the major component was tentatively assigned to the remaining strong signal positioned between C-5′ and C-4′, as in the D_2O spectrum. Comparisons of chemical shifts with other compounds suggest that C-3 and C-5 of the major component produce the partially resolved signal at 76.52 ppm. A review of the spectrum of INH-maltose, after the solution in D_2O had been kept at ambient temperatures for 3 days, showed a signal at 90.01 ppm of about one tenth the intensity of the major C-1 signal at 92.55 ppm, but other minor signals were poorly resolved from the other pyranoside signals. This higher-field signal is presumably due to C-1 of the minor anomer.

In comparison with the spectra of the pyranoses, those of the INH-pyranoses show consistent effects on the chemical shifts of C-1 – C-6 (Table 5), notably so at C-1, which strongly suggests that the configuration at C-1 is the same in all cases. The chemical shift of C-4 of the INH-pyranoses is close to that in the free β-pyranose, and the shifts of C-3 and C-5 are also much closer to those of the β-pyranoses than the α-pyranoses. It is difficult to explain why the 1α-configuration should lead to de-shielding at C-3 and C-5 of some 4–7 ppm (Table 5); steric shielding might have been anticipated, as observed at C-2. Thus, the ^{13}C chemical shift evidence strongly suggests that the β-INH-pyranoside strongly predominates in both D_2O and DMSO-d_6 solutions. This contention is further supported by the observation of a small amount of the other anomer of INH-maltose in which the minor C-1 signal is upfield of the major C-1 signal; C-1α (minor) is upfield of C-1β (major) of maltose, as with the other free saccharides studied. The relatively bulky INH moiety (as compared with OH) would also be expected to prefer the equatorial 1β-configuration associated with the usual chair conformation of the pyranoses.

Takeda concluded from H-1–H-2 coupling constants that the predominant structure of INH-glucose in D_2O and DMSO-d_6 solutions was that of the 1-(1β-glucopyranosyl)-2-isonicotinylhydrazine (7). We were unable to determine $J_{H\text{-}1\text{-}H\text{-}2}$ of **1–4** in D_2O because the H-1 signal was obscured by the large HDO signal (cf. ref. 7). In DMSO-d_6, H-1 of INH-galactose was not clear but, using Takeda's assignment for INH-glucose, the H-1 signal of the predominant forms **2***b*, **3***b*, and **4***b* was tentatively identified at 3.99 ($J_{H\text{-}1\text{-}H\text{-}2}$ = 8.0 Hz), 4.00 ($J_{H\text{-}1\text{-}H\text{-}2}$ = 7.5 Hz), and 4.00 ($J_{H\text{-}1\text{-}H\text{-}2}$ = 8.0 Hz) ppm, respectively; i.e., having the 1β-configuration. Weak signals in the spectra at 4.7, 4.7, and 4.6 ppm may have been due to small proportions of **2***a*, **3***a*, and **4***a*, respectively. The results of these experiments

Can. J. Chem. Downloaded from www.nrcresearchpress.com by 210.87.254.40 on 09/06/12
For personal use only.

support the conclusion that the structure of INH-sugar products in solution is that of 1-(1β-pyranosyl)-2-isonicotinyl hydrazines.

Experimental

The ^{13}C nmr spectra were determined at 20.1 MHz on a Bruker WP 80 Fourier transform spectrometer. Spectra were recorded at ambient temperature using the deuterium resonance of the solvent as the internal lock. Solution concentration was usually about 100 mg/1.7 mL solvent, in 10 mm tubes. Protons were decoupled by broad-band irradiation (4–5 W, offset 6,000 Hz) except in SFORD experiments (4 W, offset 4,700 Hz). Usually, about 3000–6000 interferograms of 5000 Hz sweep-width were stored for output in 4K data points following transform; this gives a separation in memory addresses of 0.06 ppm. (It was noted that in those instances where spectra were determined more than once, it was very uncommon for chemical shifts to differ by more than one address.) Pulse-widths were 1.5 μs (19.2° tipping angle) with no pulse delay following data acquisition.

Elemental analysis was performed using a Perkin Elmer Model 240 Elemental Analyzer. Melting points were determined on a Thomas Hoover capillary apparatus and are uncorrected.

High performance liquid chromatography was carried out on an instrument consisting of a Beckman 110A single-piston pump, a Rheodyne 7105 injector, a Waters Associates 440 UV (254 nm) detector, and a Perkin-Elmer 56 recorder. A 4.6 × 250 mm Brownlee Laboratories column packed with Merck 10 μm DIOL bonded phase packing was used at ambient temperature. The mobile phase, consisting of pH 4.0, 0.05 *M* aqueous acetate buffer and acetonitrile (12:88), was pumped at 2 mL/min. Samples were dissolved in water (ca. 2 mg/mL) diluted 1:10 with acetonitrile, and 10–25 μL aliquots were chromatographed.

1-(1β-Galactopyranosyl)-2-isonicotinylhydrazine (1b)

Isonicotinylhydrazide (INH) (13.7 g; 0.1 mol) and 18.0 g (0.1 mol) of D (+)-galactose were stirred overnight at ambient temperature in 50 mL of water. The resulting clear solution was maintained at 40°C for 7 days. The solution was concentrated to about 25 mL on a rotary evaporator (40°C), 5 mL of methanol was added, and the solution stored at 4°C for 1 week. The product (2.5 g) was collected, washed with methanol, and dried at 40°C overnight.

1-(1β-Glucopyranosyl)-2-isonicotinylhydrazine (2b)

Compound **2***b* was prepared in a similar manner to **1***b*, except that the crystalline product (3.5 g) was obtained directly from the reaction solution after 1 week at 40°C.

1-(1β-Lactosyl)-2-isonicotinylhydrazine (3b)

Isonicotinylhydrazide (INH) (13.7 g, 0.1 mol) and 34.2 g (0.1 mol) of α-lactose were stirred overnight at ambient temperature in 75 mL of water. The product (5.3 g) was obtained after 7 days at 40°C as described for **2***b*.

1-(1β-Maltosyl)-2-isonicotinylhydrazine (4b)

Isonicotinylhydrazide (INH) (13.7 g, 0.1 mol) and 35.0 g (0.1 mol) of maltose hydrate were heated under reflux in 500 mL of methanol. After 48 h the solution was concentrated to about 100 mL on a rotary evaporator (40°C), 20 mL of acetonitrile was added and the solution stored at −10°C overnight. The crystals obtained were collected, but reverted to a straw coloured oil (2.5 g); hplc showed this liquid to contain about 1.4% INH and **4***a* and **4***b* in the ratio 1:14. ^{13}C nuclear magnetic resonance showed a large peak due to methanol, so the liquid was dried at 40°C *in vacuo* and the residue powdered and dried *in vacuo* at 100°C for 48 h. The semi-crystalline product obtained had an indistinct melting point starting at 110°C and decomposed at 190°C; ^{13}C nmr showed the absence of solvent and hplc showed that the product contained about 4.5% INH and **4***a* and **4***b* in the ratio 1:4.

Glycolaldehyde Isonicotinylhydrazone (9)

Isonicotinylhydrazide (INH) (3.4 g, 0.025 mol) and 1.5 g (0.025 mol) of glycolaldehyde were stirred for 24 h at ambient temperature in 15 mL of methanol. The solution was stored at −10°C overnight. The product was collected, washed with 2-propanol and dried at 40°C overnight.

Glyceraldehyde Isonicotinylhydrazone (10)

Compound **10** was prepared as described for **9**, except that the product was obtained with the addition of acetone prior to storage at −10°C.

Acknowledgements

We would like to thank Mr. H. Avdovich for the ^{13}C nmr spectra, and Mr. H. Séguin for the elemental analyses.

1. L. C. Bailey and H. Abdou. J. Pharm. Sci. **66**, 564 (1977).
2. K. V. N. Rao, S. Kailasam, N. K. Menon, and S. Radhakrishna. Indian J. Med. Res. **59**, 1343 (1971).
3. M. B. Devani, C. J. Shishoo, M. A. Patel, and D. D. Bhalara. J. Pharm. Sci. **67**, 661 (1978).
4. H. H. Fox. J. Org. Chem. **18**, 990 (1953).
5. A. G. Butterfield, E. G. Lovering, and R. W. Sears. J. Pharm. Sci. **69**, 222 (1980).
6. A. G. Butterfield, N. M. Curran, F. F. Matsui, and R. W. Sears. Can. J. Pharm. Sci. In press.
7. Y. Takeda. Carbohydr. Res. **77**, 9 (1979).
8. R. Yamamoto and H. Tanaka. Yakuzaigaku, **17**, 219 (1957).
9. P. E. Pfeffer, K. M. Valentine, and F. W. Parrish. J. Am. Chem. Soc. **101**, 1265 (1979).
10. P. Colson, K. N. Slessor, H. J. Jennings, and I. C. P. Smith. Can. J. Chem. **53**, 1030 (1975).
11. A. S. Perlin. *In* International Review of Science, Organic Chemistry. Series 2. Vol. 7. *Edited by* G. O. Aspinall. Butterworths, London. 1976. pp. 1–35.

Can. J. Chem. Downloaded from www.nrcresearchpress.com by 210.87.254.40 on 09/06/12
For personal use only.

The photochemical reaction of tris(ethylenediamine)cobalt(III) ion with ferrocyanide[1]

COOPER H. LANGFORD[2] AND ROGER L. P. SASSEVILLE

Metal Ions Group, Department of Chemistry, Carleton University, Ottawa, Ont., Canada K1S 5B6

Received April 24, 1980

COOPER H. LANGFORD and ROGER L. P. SASSEVILLE. Can. J. Chem. **59**, 647 (1981).

The photochemical formation of $[Cl(en)_2Co—N{\equiv}C—Fe(CN)_5]^{2-}$ from $Co(en)_3^{3+}$ and $Fe(CN)_6^{4-}$ is explored. Earlier evidence established that the reaction proceeds via electron transfer. Ligand field Co(III) excited states are clearly indicated to be effective. There is evidence that free $Fe(CN)_6^{4-}$ can scavenge these excited states or their successors arising in ion pairs with $Fe(CN)_6^{4-}$. This suggests that the reactive excited state lifetime is at least comparable to the rate of diffusional encounters. However, racemization does not accompany reaction if $(+)_{589}Co(en)_3^{3+}$ is the reactant. Wavelength studies indicate approximate wavelength independence as far as 647.1 nm. These results are in contrast with the behaviour of photosubstitution yields for Co(III) amines.

COOPER H. LANGFORD et ROGER L. P. SASSEVILLE. Can. J. Chem. **59**, 647 (1981).

On étudie la formation photochimique du $[Cl(en)_2Co—N{\equiv}C—Fe(CN)_5]^{2-}$ à partir du $Co(en)_3^{3+}$ et du $Fe(CN)_6^{4-}$. Les données antérieures suggèrent que la réaction se fait par l'intermédiaire d'un transfert d'électron. Il semble clair que les états excités du champ de ligand du Co(III) sont efficaces. Il existe des données à l'effet que le $Fe(CN)_6^{4-}$ libre peut piéger ces états excités ou leurs successeurs apparaissant sous forme de paires d'ions avec $Fe(CN)_6^{4-}$. Ceci suggère que la durée de vie de l'état excité réactif est au moins comparable à la vitesse des rencontres diffusionnelles. Cependant la réaction se fait sans racémisation si le réactif est le $(+)_{589}Co(en)_3^{3+}$. Des études en fonction de la longueur d'onde indiquent que les résultats sont indépendants de la longueur d'onde jusqu'à environ de 647,1 nm. Ces résultats sont contraires au comportement des rendements de photosubstitution des Co(III) amines.

[Traduit par le journal]

Introduction

When the mechanistic step shown in reaction [1]

[1] $$Co(en)_3^{3+} + Fe(CN)_6^{4-} \xrightarrow[\text{L.F.}]{h\nu} Co(en)_3^{2+} + Fe(CN)_6^{3-}$$

was first proposed (1) (en = ethylenediamine), it was an early counter example to the concept that ligand field excited states are reactive only in photochemical ligand substitution or isomerization reactions. It was instead an example of electron transfer to a ligand field excited state. With the discovery of electron transfer quenching of the ^2E state of $Cr(bipy)_3^{3+}$ (bipy = bipyridine) (2), examples of electron transfer to ligand field excited states of Cr(III) and Co(III) coordinated to rigid aromatic ligand systems have multiplied (3) and evidence for redox reactivity of ligand field excited states is no longer rare. On the other hand, cross-over from charge transfer states to ligand field states as the lowest excited state (varying with structure, or medium) often does lead to cross-over to ligand substitution from redox photo-reactivity (4, 5).

The excited states of Cr(III) complexes like $Cr(bipy)_3^{3+}$ which accept electrons from quenchers are long lived and may be regarded as fully vibrationally equilibrated "isomers" of their ground states (6). A Marcus–Hush theory account can be developed for their reactivity. For the same complexes, Stokes shifts are small so that excited states are structurally similar to ground states (7). Moreover, the complexes are resistant to facile substitution reactions (8).

In this frame of reference, the reaction discussed in this paper is different. Luminescence is not observed from the reactive species and the choice of effective reducing agents seems restricted. These facts are somewhat puzzling if the excited state in this case is long lived and can react by diffusional encounter with scavengers as we earlier suggested (1).

Experimental

Materials

Solutions were prepared from redistilled water. Analar grade NaCl was used as is, $K_4Fe(CN)_6 \cdot 3H_2O$ was recrystallized several times (until no perceptible residue remained in the filtration step). $(+)Co(en)_3Cl_3 \cdot H_2O$ was prepared, resolved, and recrystallized several times following a literature method (9).

Reaction Product

The product of photolysis was described (1, 12) as a "cherry red" product but it was not isolated. Nuclear magnetic resonance (1) signals showed it to contain diamagnetic metal centres (presumably d^6Co(III) and d^6Fe(II) as in the reactants). Nuclear magnetic resonance also indicated 2 en molecules bound to Co(III) and one free protonated en in solution (1). An extinction coefficient was estimated (incorrectly!) on the assumption that conversion of $(+)Coen_3^{3+}$ to red product was accompanied by racemization (1). Anion exchange shows the product to be anionic (1).

Samples of red product have now been isolated two ways. (*i*)

[1]Supported under a grant from the Natural Sciences and Engineering Research Council of Canada.

[2]To whom all correspondence should be addressed at Department of Chemistry, Concordia University, Montreal, P.Q., Canada H3G 1M8.

0008-4042/81/040647-05$01.00/0

©1981 National Research Council of Canada/Conseil national de recherches du Canada

Can. J. Chem. Downloaded from www.nrcresearchpress.com by 210.87.254.40 on 09/06/12
For personal use only.

Can. J. Chem. Downloaded from www.nrcresearchpress.com by 210.87.254.40 on 09/06/12
For personal use only.

trans-$Coen_2Cl_2^+$ (9) was allowed to aquate for 0.5 h at room temperature in 50 cm^3 of water, addition of $Fe(CN)_6^{4-}$ dissolved in H_2O produced the red colour. Cooling in ice yielded a red brown solid. On redissolution this gave the familiar visible spectrum: λ_{max} = 440 nm (ε = 300 ± 10 M^{-1} cm^{-1}). The ir spectra in KBr pellets *differed* from a precipitate of $[Coen_3][Fe(CN)_6]$ in the region of CN stretch. The latter compound has a single peak at 2005 cm^{-1}. The red product has a broad CN region with a maximum at 2050 cm^{-1}. Bridging CN has been reported to show a 25–100 cm^{-1} higher frequency than the terminal ligand (10–12). (*ii*) An equivalent material was isolated from photolysis of $Coen_3^{3+}$ with $Fe(CN)_6^{4-}$ by irradiation of 10^{-2} *M* $Fe(CN)_6^{4-}$ plus 10^{-3} *M* $Coen_3^{3+}$ in 4.0 *M* NaCl to about 50% reaction with the 514.5 nm line of an Ar-ion laser ($I \simeq 10^{-7}$ einstein s^{-1}). Gradual evaporation over days yielded red–brown crystals.

The elemental analysis of neither solid was entirely satisfactory. Assuming complete conversion of *trans*-$Coen_2Cl_2^+$ to red product, the spectrum in Fig. 1 is obtained (λ_{max} 440, ε = 305 M^{-1} cm^{-1}). The formulation of the solids as $Na_2[ClCoen_2—NC—Fe(CN)_5]\cdot 5H_2O$ yields ε = 300 ± 10 M^{-1} cm^{-1}. This formulation is closer to the results of elemental analysis than any alternative considered.

Solution Preparations

Stock solutions of $Co(en)_3^{3+}$ and $Fe(CN)_6^{4-}$ were prepared in 2.0 and 4.0 *M* NaCl under dim red light from freshly recrystallized materials and filtered through 0.45 μm millipore filters. A slow thermal reaction which gives rise to a positive error in quantum yields occurred, therefore dilution and mixing was carried out just prior to photolysis to minimize the corrections.

Photolysis Procedure

Irradiations were carried out in a jacketed 10.0 cm Perkin-Elmer micro-polarimeter cell of 5.1 cm^3 capacity (facial area 0.50 cm^2) or in a 5.00 cm cyclindrical quartz spectrophotometer cell (volume = 16.0 cm^3). Irradiations were conducted at 25°C (±1°C) in dim red room light. Light sources were a 1000 W Hg–Xe lamp (Oriel optics) with a Jarrell-Ash 1/4 M monochromator (for λ = 436 nm), a Coherent Radiation 2 W Ar-ion c.w. laser (for λ = 457.9 and 514.5 nm), and a Spectra-Physics 1 W Kr-ion c.w. laser (for λ = 647.1 nm). In all experiments, except those at 647.1 nm, absorbance was adjusted so that greater than 90% of incident light was absorbed. Percent conversions to product were kept low (less than 5%) and light intensities were measured by Reineckate actinometry on *absorbance matched* solution (13). Intensity values ranged from 1–3 × 10^{-8} einstein s^{-1}. Analyses were carried out using Gilford 240 and Cary 14 spectrophotometers as well as a Perkin-Elmer Model 141 automatic polarimeter. The monitoring wavelength for the product

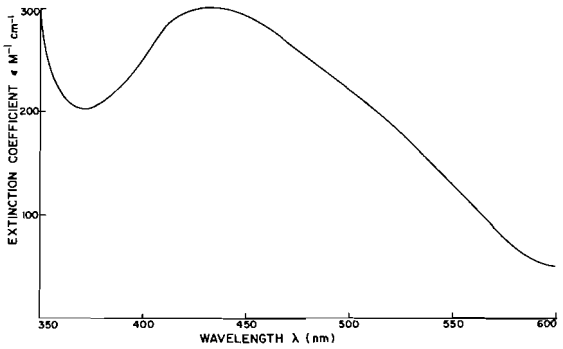

FIG. 1. The visible spectrum of the red product assigned the formulation $[Clen_2Co—N\equiv C—Fe(CN)_5]^{2-}$.

was 440 nm (ε = 300 ± 10 M^{-1} cm^{-1}). The loss of optical activity was followed at 589 nm.

Reaction Stereochemistry

The stereochemical course of the photochemical reaction (eqs. [5]–[10]) of (+)$Co(en)_3^{3+}$ with $Fe(CN)_6^{4-}$ in 2.0 *M* NaCl was investigated. Appropriate solution concentrations of (+)-$Co(en)_3^{3+}$ and $Fe(CN)_6^{4-}$ in 2.0 *M* NaCl were mixed and photolyzed as previously described. The extent of reaction was followed by (*i*) the loss of optical activity at 589 nm and (*ii*) by the spectrophotometric grow-in of product absorption at λ = 440 nm.

Ion Association Measurements

In zero and 2 *M* NaCl media, ion association is extensive. To bring ion pairing constants down to *low enough* values to measure a convenient equilibrium between free ions and pairs, it is necessary to work in media of 4 *M* NaCl. Extensive absorbance and CD measurements reveal that there are NaCl medium effects (14) so that simple interpretation of the decrease in "excess optical absorbance" of the $Coen_3^{3+}$–$Fe(CN)_6^{4-}$ mixtures with increasing NaCl concentration is not a simple guide to ion association. However, measurements in a *swamping and constant medium* are interpretable.

Spectral enhancement at 410 nm was analyzed by the well known Newton–Arcand procedure (15) to obtain ion association constants. Stock solutions of $Coen_3Cl_3$ and $K_4Fe(CN)_6$ were prepared in 4.0 *M* NaCl media filtered (0.45 μm), mixed, and allowed 15 min to come to temperature equilibrium (25.0 ± 0.2°C) in a 10 cm Cary 14 spectrophotometer cell. The molar extinction coefficients (ε) of the free ions (in 4.0 *M* NaCl!) are: $Coen_3^{3-}$, 21.1; $Fe(CN)_6^{4-}$, 2.42 M^{-1} cm^{-1} at 410 nm. Precision of the results is limited by slow thermal reaction. (This is a supplementary reason for not attempting to obtain ion association constants for media lower in NaCl. The thermal reaction correction is large and difficult in these media where thermal reaction is faster.)

Results and Discussion

When solution mixtures of $Co(en)_3^{3+}$ and $Fe(CN)_6^{4-}$ are exposed to visible light it soon becomes apparent to the naked eye that the orange colour of the original mixture is rapidly changed to a "cherry red". This red product is $[Cl(en)_2Co^{III}—NC—Fe(CN)_5]^{2-}$.

(1) Medium Dependence Experiments

Tables 1 and 2 collect quantum yields for appropriate concentrations of $Co(en)_3^{3+}$ and $Fe(CN)_6^{4-}$ mixed and photolyzed with 514.5 nm green laser light at constant intensity in 0 *M* NaCl, 2.0 *M* NaCl, and 4.0 *M* NaCl media. Note that yields are approximately 3 times larger in 0 and 2.0 *M* NaCl media. If only ion paired $Coen_3^{3+}$ excited states entities are reactive, it is easy to account for the lack of dependence of quantum yield on $Fe(CN)_6^{4-}$ concentration in 0 and 2 *M* NaCl media. The unit yield and concentration independence reflect the reactivity of pairs and nearly 100% of Co(III) complexes are ion paired. But this does not provide any test of the capacity of $Fe(CN)_6^{4-}$ to scavenge excited states. This issue is of interest since it could provide an estimate of the lifetime of the reactive

Can. J. Chem. Downloaded from www.nrcresearchpress.com by 210.87.254.40 on 09/06/12
For personal use only.

TABLE 1. Photolysis of $Coen_3^{3+}$–$Fe(CN)_6^{4-}$, λ = 514.5 nm, 0.0 and 2.0 *M* NaCl media[a]

No.	$[Coen_3^{3+}]$ mol dm^{-3} × 10^3	$[Fe(CN)_6^{4-}]$ mol dm^{-3} × 10^2	[NaCl] mol dm^{-3}	Quantum yield, ϕ[b]
[1]	0.97	8.29	0.0	0.88±0.10
[2]	1.32	7.55	0.0	0.90±0.10
[3]	1.62	6.93	0.0	0.92±0.10
[4]	7.17	3.80	2.0	0.88±0.10
[5]	7.17	4.05	2.0	0.91±0.10
[6]	7.17	4.29	2.0	0.97±0.10
[7]	6.40	3.80	2.0	0.99±0.10

[a]Wavelength of irradiation 514.5 nm, T = 25°C.
[b]Average of at least 3 determinations.

TABLE 2. Photolysis of $Coen_3^{3+}$–$Fe(CN)_6^{4-}$, λ = 514.5 nm, 4.0 *M* NaCl

No.	$[Coen_3^{3+}]$ mol dm^{-3} × 10^3	$[Fe(CN)_6^{4-}]$ mol dm^{-3} × 10^2	ϕ_{obs}
[1]	6.39	4.51	0.35±0.02
[2]	6.39	4.27	0.31±0.02
[3]	6.39	4.03	0.30±0.02
[4]	6.39	3.78	0.30±0.02
[5]	9.63	6.20	0.38±0.03
[6]	9.64	5.73	0.32±0.03
[7]	9.59	5.27	0.25±0.02
[8]	9.60	4.04	0.22±0.01
[9]	9.65	2.62	0.17±0.02
[10]	7.08	3.78	0.30±0.03
[11]	7.08	4.03	0.31±0.05
[12]	7.08	4.27	0.32±0.05

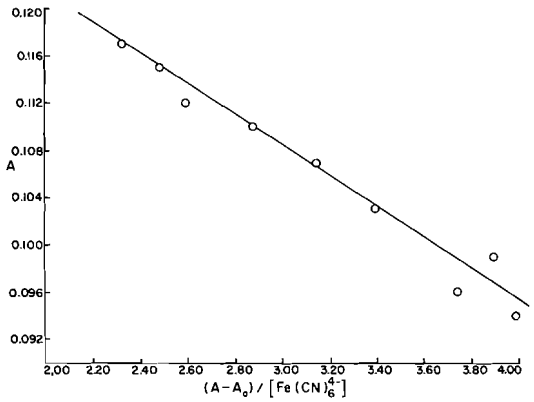

FIG. 2. Newton–Arcand plot for determination of ion association constant between $Coen_3^{3+}$ and $Fe(CN)_6^{4-}$ in the constant ionic strength swamping medium, 4.0 *M* NaCl.

Co(III) excited state. In a preliminary communication (1) on this system, we presented evidence that as ion pairing is suppressed by high ionic strength media, dependence on $Fe(CN)_6^{4-}$ emerges and we suggested an excited state lifetime long enough to permit diffusional encounters with the excited state. Quantitative analysis depends on an estimate of the extent of ion association in 4 *M* NaCl.

A plot of absorbance, A, vs. $(A - A_0)/[Fe(CN)_6^{4-}]$ where A_0 is the absorbance of free $Coen_3^{3+}$ in 4.0 *M* NaCl is shown in Fig. 2. This allows calculations of an ion pairing constant for the medium (K_{eq}) from the slope ($= -1/K_{eq}$) according to the Newton–Arcand procedure (15). The value of 78 ± 5 M^{-1} obtained seems reasonable for the very high ionic strength of the medium.

Returning to Table 2, we recognize that concentrations chosen for photolysis, which must fall between the limits of too low absorbance on the one hand and precipitation on the other, are in a concentration region where 70 ± 15% of the $Coen_3^{3+}$ is ion paired with $Fe(CN)_6^{4-}$. This conclusion is contrary to ref. 1 where it was assumed prior to careful analysis of effects of NaCl on the spectra of $Coen_3^{3+}$ that reduction in the excess absorbance with increasing NaCl implied nearly complete suppression of ion pairing.

If it is assumed that the excited state is too short lived for diffusional encounter, and that all reaction originates in ion pairs, there should be only a weak dependence of quantum yield on concentration of $Fe(CN)_6^{4-}$ in the concentration region that is suitable for photolysis experiments. Figure 3 shows a plot of quantum yields for a constant Co(III) concentration. The dependence is nearly linear in $Fe(CN)_6^{4-}$ with an intercept near zero. This suggests diffusional scavenging. A lifetime for the excited state longer than about 10^{-9} is implied. If the rate of $Fe(CN)_6^{4-}$ scavenging is diffusion-limited ($\sim 10^9$ M^{-1} s^{-1}), the slope in Fig. 3 would imply a lifetime of the order of 10^{-8} s. The effect of Co(III) seen in Table 2 may imply some self quenching. It is possible that the species scavenged is similar to an "exiplex".

(2) Reaction Stereochemistry

When the reaction was first considered (1) it was presumed that the product was racemic and that the

TABLE 3. Reaction stereochemistry,[a] optical activity vs. spectral change

No.	Photolysis time, t (s)	Rotation, $R \pm 0.001$	ΔC_R mol dm^{-3} × 10^4	ϕ_R[b] ±0.05	A_{440} ±0.005	ΔC_S mol dm^{-3} × 10^4	ϕ_S ±0.05
[1]	0.0	0.310	—	—	0.539	—	—
[2]	90.0	0.300	1.8±0.1	0.89	0.594	1.81±0.05	0.89
[3]	180.00	0.291	3.3±0.1	0.81	0.646	3.51±0.05	0.87
[4]	300.0	0.285	4.4±0.1	0.65	0.714	5.74±0.05	0.85
[5]	420.0	0.280	5.2±0.1	0.55	0.796	8.43±0.05	0.89

[a][(+)Coen$_3^{3+}$] = 6.34 × 10^{-3} mol dm^{-3}, [Fe(CN)$_6^{4-}$] = 3.71 × 10^{-2} mol dm^{-3}, [NaCl] = 2.0 mol dm^{-3}, intensity = 1.15 × 10^{-8} einstein s^{-1}, T = 25°C.
[b]Based on the assumption that loss of optical activity measured product disappearance.

TABLE 4. Wavelength dependence experiments

Wavelength (nm)	[Coen$_3^{3+}$] × 10^3 mol dm^{-3}	[Fe(CN)$_6^{4-}$] × 10^2 mol dm^{-3}	[NaCl] mol dm^{-3}	ϕ[a]
436	4.0	3.0	4.0	0.46±0.05
514.5	6.4–7.0	3.8–4.5	4.0	0.31±0.05
514.5	6.4–7.2	3.8–4.3	2.0	0.94±0.10
647.1	2.8	6.1	2.0	1 ±0.2

[a]Individual concentration points are based on a minimum of three replicate runs.

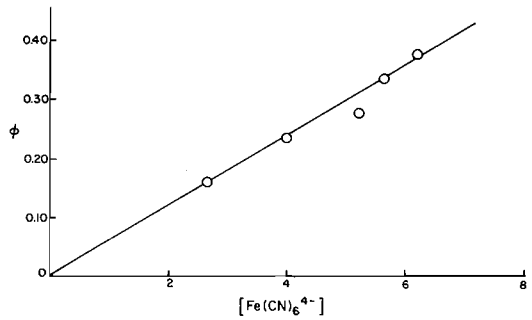

FIG. 3. Dependence of quantum yield on concentration of Fe(CN)$_6^{4-}$ at constant Co(III) concentration. The Fe(CN)$_6^{4-}$ axis is multiplied by 10^2.

course of the reaction could be followed by the loss of optical activity of the chiral reactant (+)-Co(en)$_3^{3+}$. Prior to actual isolation of the product, this assumption was employed to obtain an "incorrect" value of the extinction coefficient of the product. When a solution 6.34 mM (+)Co(en)$_3^{3+}$ and 3.71 mM Fe(CN)$_6^{4-}$ in 2.0 M NaCl is irradiated (λ = 514.5 nm) and the course of the reaction is monitored (*i*) spectrally, λ = 440 nm; ε = 300 M^{-1} cm^{-1} or; (*ii*) polarimetrically, λ = 589 nm ^{d}M = 89°, the results collected in Table 3 are observed. ΔC_R, from loss of optical activity at 589 nm and, ΔC_S, from increase in absorbance at λ = 440 behave differently (ΔC represents a computed concentration change). The quantum yields determined spectrally (ϕ_S) remain constant while the quantum yields (ϕ_R) calculated by assuming that loss of optical activity corresponds to product formation decrease as the extent of reaction increases. This is strong evidence to indicate that the product is not a racemate but rather, at least partially, optically active. Mutarotation appears to take place in the primary step. Ultimate racemization occurs, presumably, in secondary photolytic and/or thermal steps.

(3) Wavelength Dependence Experiments

Since it is possible that the ligand field (L.F.) triplet (or even possibly a quintet) of the Co(III) complex is important, it was desirable to extend photochemical measurements to the red of the spin allowed singlet bands. The Kr-ion laser provided a line at 647.1 nm where absorptivity is low and concentrations must be high. Error is large, but results comparing 647.1 nm behaviour with 514.5 nm are collected in Table 4. Large correction for product absorption, made as described in ref. 16, are mainly responsible for the uncertainty. It was not possible to conduct experiments in 4.0 M NaCl media. For the moment we emphasize only that reactivity *persists* up to 647.1 nm without substantial diminution.

Conclusions

No direct luminescence evidence concerning the lifetimes of Co(III) amine excited states is available against which to check the notion that the reactive state has a lifetime longer than rates of diffusional encounter. However, there is information from the wavelength dependence experiments to suggest some difference between the ligand field redox photochemistry discussed here and the substitutional photochemistry of Co(III) amines. Several authors (4, 16–20) have reported a more or less

Can. J. Chem. Downloaded from www.nrcresearchpress.com by 210.87.254.40 on 09/06/12
For personal use only.

Can. J. Chem. Downloaded from www.nrcresearchpress.com by 210.87.254.40 on 09/06/12
For personal use only.

monotonic decline in substitutional quantum yield as irradiation wavelength is increased. Moreover, the $Co(NH_3)_5Cl^{2-}$ ion shows an increase in the ratio of Cl^- release to NH_3 release as wavelength increases (16). This suggests that substitution reactions occur in competition with rapid relaxation to a lower lying state. Substitution quantum yield from ligand field excited states are small. It has been suggested that the competing process is radiationless return to the $^1A_{1g}$ (approximately O_h symmetry) ground state since both singlet and triplet ligand field excited states are associated with a $t_{2g}^5e_g^1$ electron configuration which is expected to be photolabile. However, the present results and ref. 1 indicate fairly efficient relaxation at all wavelengths between 436 nm to 647 nm to a reactive state. The reactive excited state may be a thermally equilibrated excited state. This longer lived reactive state might be the quintet Co(III) ligand field state which has a configuration ($t_{2g}^4e_g^2$) appropriate for facile reduction to the Co(II) product with the $t_{2g}^5e_g^2$ configuration. Alternately, it might be a change transfer excited state of the ion pair with $Fe(CN)_6^{4-}$ which could be called an *exiplex*. The results do *not* clearly demonstrate reactions of the free $Coen_3^{3+}$ ion as distinct from an ion pair.

1. N. A. P. KANE-MAGUIRE and C. H. LANGFORD. J. Chem. Soc. Chem. Commun. 351 (1973).
2. R. BALLARDINI, G. VARANI, M. T. INDELLI, F. SCANDOLA, and V. BALZANI. J. Am. Chem. Soc. **100**, 7219 (1978).
3. N. SERPONE, M. A. JAMIESON, M. S. HENRY, M. Z. HOFFMAN, J. BOLLETTA, and M. MAESTRI. J. Am. Chem. Soc. **101**, 2907 (1979) and references therein; A. JURIS, M. F. MANFRIN, M. MAESTRI, and N. SERPONE. Inorg. Chem. **17**, 2258 (1978).
4. A. W. ZANELLA, K. H. FORD, and P. C. FORD. Inorg. Chem. **17**, 1051 (1978).
5. J. I. ZINK. Mol. Photochem. **5**, 151 (1973); J. Am. Chem. Soc. **96**, 4464 (1974); Inorg. Chem. **12**, 1018 (1973); M. J. INCORVIA and J. I. ZINK. Inorg. Chem. **13**, 2489 (1974); M. WRIGHTON, H. B. GRAY, and C. S. HAMMOND. Mol. Photochem. **5**, 165 (1973).
6. A. W. ADAMSON. *In* Concepts of inorganic photochemistry. *Edited by* A. W. Adamson and P. D. Fleischauer. Wiley, New York. 1975; A. W. ADAMSON. Proc. Int. Conf. Coord. Chem. **14**, 240 (1972); J. Phys. Chem. **71**, 798 (1967).
7. M. ASANO, D. MONGEAU, D. NICOLLIN, R. SASSEVILLE, and J. A. KONINGSTEIN. Chem. Phys. Lett. **65**, 293 (1979).
8. M. MAESTRI, F. BOLLETTA, L. MAGGI, V. BALZANI, M. S. HENRY, and M. Z. HOFFMAN. J. Am. Chem. Soc. **100**, 2694 (1978).
9. J. A. BROOMHEAD, F. P. DWYER, and J. W. HOGARTH. Inorganic synthesis. Vol. 6. McGraw-Hill, New York. 1969. p. 183; G. G. SCHLESSINGER. Inorganic preparations. Chemical Publishing, New York. 1962.
10. S. BAGGAS and K. GIBSON. Acta Chem. Scand. **27**, 3227 (1973).
11. D. A. DOWS, A. HARRIS, and W. K. WILMARTH. J. Inorg. Nucl. Chem. **21**, 33 (1961).
12. R. A. DECASTELLO, C. P. MACCOLL, and A. HARRIS. J. Org. Chem. **10**, 293 (1971).
13. E. E. WEGNER and A. W. ADAMSON. J. Am. Chem. Soc. **88**, 394 (1966).
14. R. L. P. SASSEVILLE. Unpublished results.
15. T. W. NEWTON and G. M. ARCAND. J. Am. Chem. Soc. **75**, 2449 (1953).
16. C. H. LANGFORD and C. P. J. VUIK. J. Am. Chem. Soc. **98**, 5410 (1976).
17. K. C. CUNNINGHAM and J. F. ENDICOTT. J. Phys. Chem. 1024 (1974).
18. J. D. PETERSEN, R. J. WATTS, and P. C. FORD. J. Am. Chem. Soc. **98**, 3188 (1976); J. F. ENDICOTT and G. J. FERRAUDI. J. Phys. Chem. **80**, 949 (1976).
19. A. W. ADAMSON, A. VOGLER, and I. LANTZKE. J. Phys. Chem. **73**, 4183 (1969).
20. A. VOGLER and A. W. ADAMSON. J. Am. Chem. Soc. **90**, 5943 (1968).

The photovoltaic properties and structure of palladium tetraphenylporphyrin on tin oxide photoelectrochemical cells[1]

COOPER H. LANGFORD,[2] BRYAN R. HOLLEBONE, AND DANIEL NADEZHDIN

Departments of Chemistry, Carleton University, Ottawa, Ont., Canada K1S 5B6 and Department of Chemistry, Concordia University, 1455 de Maisonneuve Blvd. W., Montreal, P.Q., Canada H3G 1M8

Received June 12, 1980

COOPER H. LANGFORD, BRYAN R. HOLLEBONE, and DANIEL NADEZHDIN. Can. J. Chem. **59**, 652 (1981).

The photovoltaic properties of palladium tetraphenylporphyrin films on n-doped SnO_2 transparent electrode in contact with a solution of quinone/hydroquinone are discussed as a function of the preparation of the film and history of its treatment with heat, H_2, or O_2/H_2O. Magnetic circular dichroism (MCD) spectra of the electrodes provide guidance on film structure. There are three important results. First, MCD spectra show that photovoltaic behaviour is *independent* of crystallinity of the film. Second, the evolution of film behaviour as "doping" by O_2/H_2O occurs shows that photoprocesses occur at *both* the interface of the film with SnO_2 and the electrolyte, leading to both photoanodic and photocathodic processes. Third, MCD spectra show that "doping" is not a surface or trace phenomenon but affects the axial ligand sensitive region of the spectra of molecules throughout the film. Transport of charge through the film by successive "redox" reactions appears to provide the simplest qualitative explanation of the results. That is, conduction is by hopping in a non-stoichiometrically oxidized film.

COOPER H. LANGFORD, BRYAN R. HOLLEBONE et DANIEL NADEZHDIN. Can. J. Chem. **59**, 652 (1981).

On discute des propriétés photovoltaiques de films de tétraphénylporphyrine de palladium sur une électrode transparente de SnO_2 dopée au n et qui est en contact avec une solution de quinone/hydroquinone, en fonction de la préparation du film et de l'histoire de son traitement par la chaleur, le H_2 ou le O_2. Les spectres de dichroisme circulaire magnétique (DCM) des électrodes fournissent une indication sur la structure du film. Il y a trois résultats importants. Premièrement, les spectres DCM révèlent que le comportement photovoltaique est indépendant de la cristalinité du film. Deuxièmement, l'évolution du comportement du film quand il se produit un dopage par O_2/H_2O indique que les processus photoélectriques se produisent à la fois à l'interface du film avec SnO_2 et avec l'électrolyte et qu'il en résulte aussi bien des processus photoanodiques que photocathodiques. Troisièmement, les spectres DCM montrent que le dopage n'est pas seulement un phénomène de surface ou de trace, mais qu'il affecte à travers tout le film la région du spectre des molécules sensibles au ligand axial. Le transport de charge à travers le film par des réactions rédox successives semblent fournir la plus simple explication qualitative des résultats. C'est à dire que la conduction se produit par sauts non stoechiométrique dans le film oxydé.

[Traduit par le journal]

Introduction

Recent efforts to develop artificial means of solar energy conversion and storage have led to a renewed interest in the problem of photovoltaic (1, 2) and photoelectrochemical (3, 4) behaviour of prophyrine and phthalocyanine films. In this laboratory, a wide range of structures is being canvassed for use in a cell based on a transparent electrode of n-type SnO_2 on glass (5). One of the more promising compounds in terms of both photovoltaic and photocurrent effects is palladium tetraphenylporphyrin (PdTPP). In this report, we describe the photovoltaic behaviour of PdTPP as a function of mode of film preparation (vacuum sublimation, or spin coating from $CHCl_3$), pretreatment of the film (heating in H_2 or exposure to moist air), and conditions of exposure during electrochemical experimentation in a cell using a quinone/hydroquinone — 1 *M* KCl electrolyte (N_2 or air saturation of the solution).

It has long been recognized that the film electronic properties of porphyrin and phthalocyanine films (which are commonly regarded as p-type organic semiconductors) depend heavily on the history of exposure of the film to oxygen and moisture (1, 6). The origin of the "doping" effects has been associated with surface adsorption and surface states in some discussions. There has also been some tendency to consider "doping" processes to involve low concentrations. In this study, the history of the electrode was recorded in terms of magnetic circular dichroism (MCD) spectra as well as photovoltaic behaviour. These spectra provide a high resolution probe. Film spectra have been assigned previously (7).

It is worth noting at the outset that the MCD probe shows that films may be crystalline or amorphous with little effect on photoelectrochemical properties. The large effects of "doping" on photoelectrochemical behaviour are associated with modification of a sufficient fraction of the film molecules (quite possibly a majority) to radically alter parts of the MCD spectrum. This alteration is similar in *both* crystalline and amorphous films.

[1]Supported by a strategic grant from the Natural Sciences and Engineering Research Council of Canada.

[2]To whom all correspondence should be addressed at Concordia University.

0008-4042/81/040652-06$01.00/0

©1981 National Research Council of Canada/Conseil national de recherches du Canada

Can. J. Chem. Downloaded from www.nrcresearchpress.com by 210.87.254.40 on 09/06/12
For personal use only.

TABLE 1. Absorption spectral features of PdTPP samples

Sample correlation to MCD spectra	Band energies (cm^{-1}) and relative intensities (O.D.)			
1*a*	15 900 (0.08)	18 200 (0.15)	19 500 (0.42)	21 000 (0.16)
1*b*	15 400 (0.8)	16 300 (1.0)	16 800 (1.0)	18 000 (1.5)
	19 100 (>2)	20 600 (>2)		
1c	15 400 (0.3)	16 100 (0.3)	16 600 (0.4)	17 900 (0.9)
	19 100 (1.5)			
2*a*	15 800 (0.04)	18 000 (0.09)	19 400 (0.48)	20 600 (0.07)
2*b*	15 800 (0.04)	18 000 (0.12)	19 400 (0.48)	20 600 (0.14)
	23 400 (1.35)	24 300 (1.35)		
2*c*	15 800 (0.04)	18 000 (0.11)	19 400 (0.43)	21 000 (0.13)
	23 400 (1.26)	24 300 (1.26)		

Experimental

Photoelectrodes consisting of a film of palladium tetraphenylporphyrin deposited on *n*-SnO_2 coated glass plates (O. H. Johns Glass Co.) were prepared in two ways, either by vacuum deposition or by spin coating from chloroform solution.

Palladium tetraphenylporphyrin was prepared by reflux of palladium dichloride with tetraphenylporphyrin in glacial acetic acid and sodium acetate (8). After addition of water and filtration of the crude material final purification was by sublimation *in vacuo* at 350–400°C with rejection of the first fraction below 350°C to eliminate chlorine.

Vacuum deposited films were made by placing the PdTPP in a boat in a tube furnace and after sublimation temperature was achieved, the cleaned (2.5 mm diameter) SnO_2 surface was exposed to the vapour through a shutter for 10 to 30 min depending on the film thickness (~500–1000 Å) desired. After deposition and cooling the coated glass plate was removed from the furnace and stored until needed under dry nitrogen.

In the preparation of the spin coated electrodes the SnO_2 surface was washed successively in nitric acid, detergent, distilled water, and finally dried chloroform. The plate was mounted horizontally with the SnO_2 surface upwards in a high speed rotor, and several drops of a PdTPP solution in dried chloroform (5 m*M*/L) placed on the surface for 10 s. The plate was then spun for 20 s at 3000 rpm, resulting in an evenly spread, dry film (of thickness near 500 Å).

For both films the measurements of photovoltages were carried out in an aqueous solution of 1 *M* KCl, 1 m*M* quinone, and 1 m*M* hydroquinone buffered with a phosphate buffer (pH 5.6–5.7). The electrode was pressed to the wall of a Teflon cell from outside and was sealed with a rubber ring and silicone grease. A brass ring pressed to the dye side of the electrode served for the electrical contact. Dye was removed so that the brass ring contacted the SnO_2 layer. The contact of the light beam to the dye and electrolyte was through a 10 mm hole in the wall of the cell. A fresh portion of the solution of about 30 mL was used for each measurement. Air or purified nitrogen was bubbled through the solution as required during the measurements. A saturated calomel electrode (sce) served as a reference electrode. The cell is the "bubbling gas" cell described previously (9). Open circuit voltage was measured using a "Keithley" electrometer. As a source of illumination a 1000 W Xenon-mercury lamp with yellow uv cutoff filter was used. Light power was approximately equal to 130 mW/cm^2.

The experiments involved obtaining dependences of photovoltage (V_{ph}) upon time (t) under continuous illumination for electrodes treated in various ambients producing different stages of doping depending on the cell aeration conditions.

Absorption spectra of both types of film were measured in a Cary 14 spectrophotometer using uncoated SnO_2 plates as blanks. Magnetic circular dichroism (MCD) spectra were measured in a custom built computer operated spectrophotometer (5) with separately run background spectra again taken from uncoated SnO_2 electrode plates.

The MCD spectra were obtained at room temperature 4.7 T magnetic field in a horizontally mounted superconducting solenoid. The sign and intensity were calibrated with a standard hexaquo cobalt(II) sulphate solution (7) for the solution spectra which also provides the sign convention for the film spectra. The slit was set at 1.0 mm for constant wave number band pass.

The solution spectrum of PdTPP in α-chloronaphthalene could not be obtained beyond 23 000 cm^{-1} because of solvent absorbance.

Results and Discussion

(A) Photoelectrode Structure and Behaviour

The MCD and absorption spectra of the vacuum deposited and spin evaporated films on SnO_2 electrode plates were obtained together with a chloronaphthalene solution spectrum of PdTPP for comparison. While the absorption spectra are very similar (Table 1), the MCD film spectra are radically different as shown in Figs. 1 and 2. The vacuum deposited film (Fig. 1*b* and *c*) display a rich structure in the MCD visible region which could be resolved into a series of strong overlapping *A* terms (Fig. 1*b* and *c*) (7). As in these earlier film studies, none of this structure was observable in the broad absorption spectrum. The detailed *A* term pattern varies from one electrode to another but the same number of bands appear. There are no important changes in these spectra related to storage under nitrogen or air/moisture. On the other hand, the spectrum of the spin coated electrode film is much simpler, consisting of an isolated *A* term in the visible and another in the near-uv (Fig. 2). This pattern resembles the solution spectrum very closely (Fig. 1*a*).

These observations can be interpreted from the structural model developed for vacuum deposited

Can. J. Chem. Downloaded from www.nrcresearchpress.com by 210.87.254.40 on 09/06/12
For personal use only.

Can. J. Chem. Downloaded from www.nrcresearchpress.com by 210.87.254.40 on 09/06/12
For personal use only.

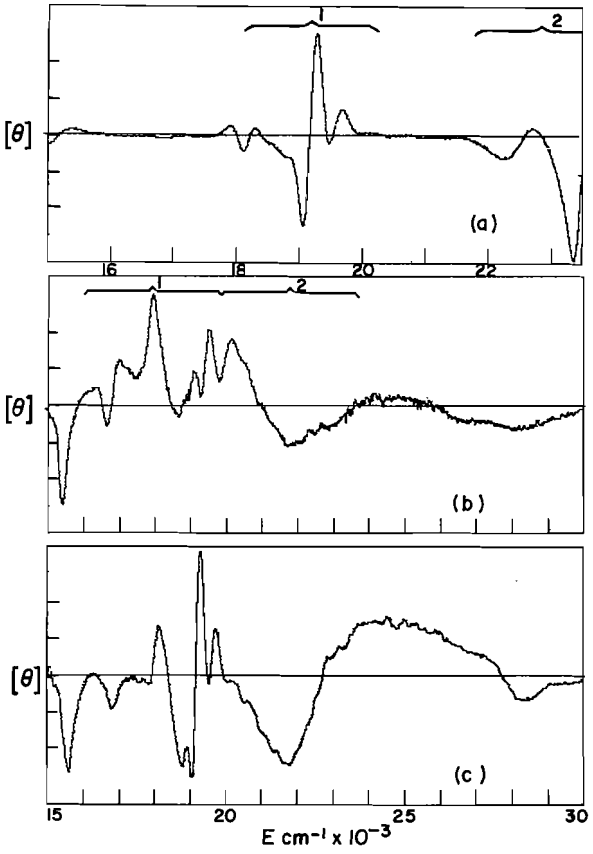

FIG. 1. Magnetic circular dichroism spectra of palladium tetraphenylporphyrin (*a*) in chloroform solution, (*b*) vacuum deposited on SnO_2 treated glass electrode, (*c*) the same PdTPP film electrode after use for 8 h as a photoelectrode in the quinone/hydroquinone bubbled air cell. Ellipticities [θ] are in units of 5×10^{-4} G^{-1}. Region (*1*) is the Q band and region (*2*) is the Soret band of the PdTPP spectrum.

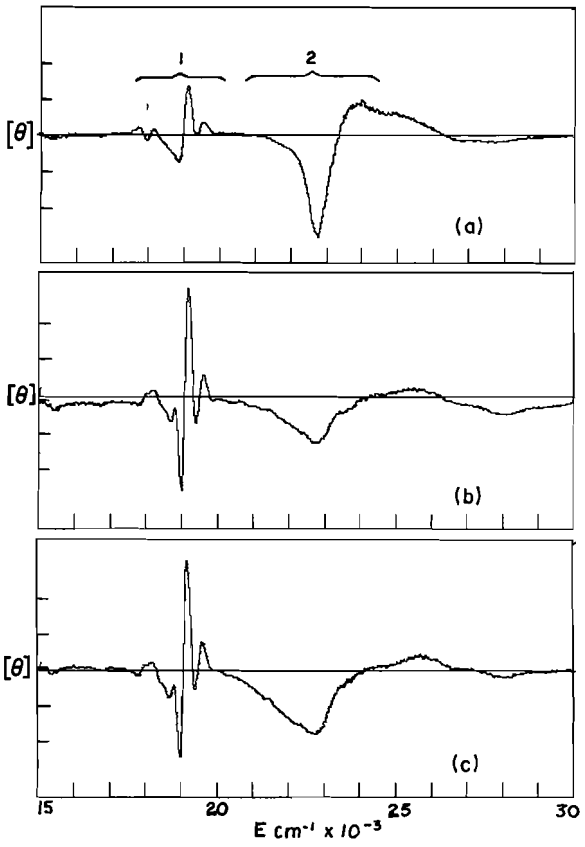

FIG. 2. Magnetic circular dichroism spectra of spin coated palladium tetraphenylporphyrin – SnO_2 electrodes (*a*) after initial preparation from chloroform solution, (*b*) after "hydrogenation" for 24 h at 215°C, (*c*) after use for 8 h as a photoelectrode in the quinone/hydroquinone bubbled air cell. Regions (*1*) and (*2*) as in Fig. 1.

metal phthalocyanine films (7). The visible spectrum of these earlier films was resolved into pairs of *A* and *B* terms which represent the exciton splittings of the electronic origin and the (0–1) vibronic state respectively. In some cases more than one pair of *A* and *B* terms became apparent, indicating that the film consisted of two or more distinct solid phases of the phthalocyanine derivative (α or β) due to the particular conditions of temperature and pressure used during sublimation. The number of MCD bands and the variation of their intensities observable in different individual preparations of the PdTPP films indicates that this compound also forms crystalline films of variable phase composition in the available range of pressure and temperature sublimation conditions.

By contrast the spin evaporated films display no discernable crystalline spectra. Instead the spectrum is nearly superimposible on the solution spectrum in chloroform even after prolonged drying at elevated temperatures. The film appears to be essentially amorphous and any intermolecular interactions must be relatively long range and lacking in regular symmetry.

Turning attention to photovoltaic properties of the films, dependence on history is quite apparent. In all cases, the dark potential settles rapidly to 0.125 V vs. sce, the equilibrium potential of the quinone/hydroquinone couple. Vacuum deposited films which have been stored under dry N_2 but handled in air initially display a *positive* photovoltage vs. sce which decreases fairly rapidly in a manner shown in curve *1* of Fig. 3 finally achieving a *negative* steady state value in 3–4 h. In contrast, both vacuum deposited and spin coated films which were "equilibrated" with moist laboratory air yielded only *negative* photovoltage (Fig. 3, curve *2*). The behaviour is related to the decrease in resistance associated with exposure of films on

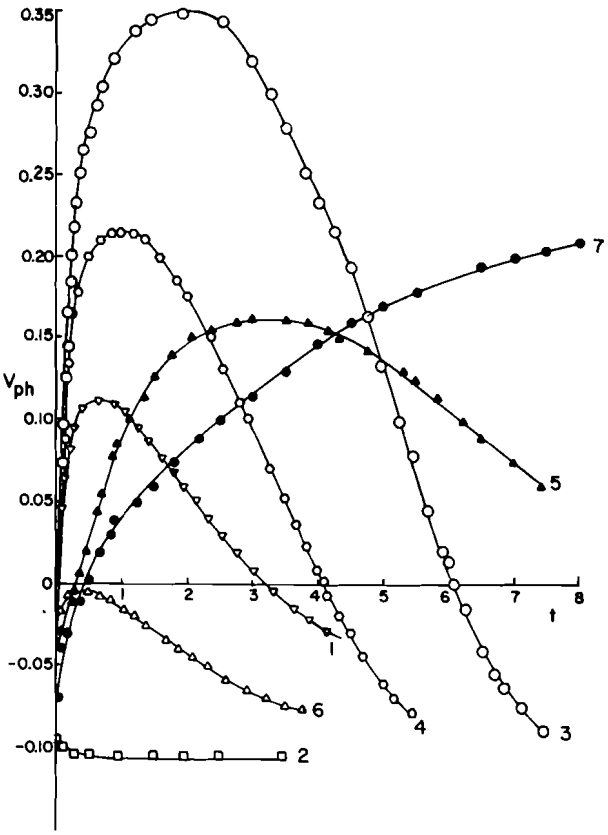

FIG. 3. V_{ph}–time records for SnO_2–PdTPP–electrolyte cell. Curves are for various electrode treatments as follows: *1*, vacuum sublimed electrode with limited exposure to air (stored under N_2 prior to use); *2*, spin coated electrode; *3*, spin coated electrode heated under H_2; *4–7* are all curves for electrodes prepared by spin coating; *4*, H_2 treated then exposed at room temperature to moist air; *5*, H_2 treated and exposed to hot dry air; *6*, H_2 treated, heated, then exposed to moist laboratory air; *7*, H_2 treated then mounted in cell which is N_2 purged to exclude O_2 exposure.

metals to air/moisture (1, 6, 10, 11). The observed photovoltage is strongly influenced by reaction of the film with oxygen and water. The vacuum deposited films have been only briefly exposed to the laboratory atmosphere during transfer from the sublimation apparatus and in mounting the electrochemical cell. They are relatively free of both O_2 and H_2O. However, exposure either to moist air for several hours or to the electrolytic solution itself permits reaction to occur and leads to negative photovoltages essentially the same as observed for the spin evaporation films which were prepared in the presence of humid laboratory air. There is *no evidence, however, of a breakdown in the solid state structure of vacuum deposited films after exposure to moist air, nor of any ordering of the spin deposited films on aging*. Thus the photovoltaic behaviour of the electrodes is *apparently unconnected* to the solid state structure of the film.

In order to more fully characterize these reactions and the accompanying photoelectrochemical behaviour, a series of pretreatments of films were carried out. Attempts to dry and degas films by heat treatments *in vacuo* gave highly variable results and are limited by the temperature of sublimation. Qualitatively, heat treatment produced results related to those described below. A reproducible technique for "drying" and/or removal of O_2 is treatment of the film at 210–215°C under one atmosphere of hydrogen gas, for 24 h. Films from any source treated in this manner yield an initial, but unstable, photovoltage near −0.05 V. This treatment, like the moist air reaction, does not result in any fundamental MCD observable rearrangement of the *film solid state structure*. The series of *A* terms assigned to intermolecular interaction (7) neither appears nor fades. There is, *however*, an increase in the ellipticity of the *visible region* A *term* in the spin deposited film. This is a strong indication of increased delocalization of the ^1E_u state of the ring resulting from removal of an axially coordinated π acid ligand from the Pd^{2+} ion (12). At the same time the first, partially resolved *A* term in the near-uv becomes more intense. This is again a good indication of a ligand change since this band is known experimentally to be sensitive to the axial environment of the metal ion (7, 12) and involves a state with a large metal atom contribution in its basis function (13).

All of these large and easily observed changes in the MCD spectra strongly indicate that reaction of the film with moist air and with hydrogen is an *extensive* phenomenon, *involving a large fraction of available* PdTPP *molecules* and independent of the detailed solid structure. The processes clearly do not represent a minor doping process which could be regarded as the introduction of the small number of defect sites as is frequently associated with production of extrinsic semiconductors.

The hydrogen treated electrodes were then exposed to oxygen and water, either independently or simultaneously, either before or during the course of electrochemical monitoring under controlled conditions. The time evolution of photovoltaic properties was followed and spectra were recorded for various important stages of treatment. The photovoltage for an H_2 treated electrode immersed in air saturated electrolyte rises from its initial negative value very rapidly to a maximum near 0.35 V within 2 h. Later the photovoltage decreases to reach −0.12 V in 8 h (Fig. 3, curve *3*). The original vacuum deposited films (Fig. 3, curve *1*) corre-

Can. J. Chem. Downloaded from www.nrcresearchpress.com by 210.87.254.40 on 09/06/12
For personal use only.

late very closely with the decreasing branch of the hydrogen treated electrode curve, probably indicating a slight but variable degree of reaction with moist air in spite of the storage precautions.

The MCD spectra of initially H_2 treated electrodes (Fig. 2*b*) change considerably after 8 h in the electrochemical cell. The visible region shows a moderate decrease in ellipticity and the near-uv ligand sensitive band narrows again to resemble that in the initially prepared sample (Fig. 2*c*). Both changes strongly indicate recoordination of the axial sites of PdTPP by some oxygen donor ligand. A similar change was seen in the spectrum of a vacuum sublimed film after use in the electrochemical cell (Fig. 1*c*) but the analysis is complicated by overlapping exciton bands.

Curve *4* of Fig. 3 represents the electrode exposed to *wet* air after hydrogen treatment. It has generally the same shape as curve *3*, but the photovoltage maximum value is lower (ca. 0.22 V). Heating the electrode gently in air after the hydrogen treatment results in an appreciable change of shape (curve *5*); the slope of both ascending and descending branches is smaller than in other cases. The maximal value of the photovoltage (ca. 0.16 V) is reached in about 3.5 h. The electrode exposed to wet air after the treatment in hot H_2 and hot air (curve *6*) reaches the maximal value of the photovoltage relatively quickly (in about 30 min) and this value is negative, ca. −0.005 V. The slope of the descending branch is approximately equal to that in curve *5*.

In a nitrogen saturated electrolyte the electrode treated in H_2 shows increase of the photovoltage eventually approaching a limit (curve *7*) but the maximum is not reached even after 48 h of measurements. A supply of air into the electrolyte results in rapid increase of the photovoltage to the maximum and the rapid decrease of the photovoltage to negative values with a slope similar to the initial decay in Fig. 3, curve *3*. This is shown in Fig. 4, curve *1*. Finally, nitrogen purging of the air saturated electrolyte (Fig. 4, curve *2*) results in a rather small and rapid decrease and beyond in a slow increase of the photovoltage.

(B) Photoelectrode Reaction and Charge Transport

The variation of voltage from positive to negative can be given qualitative explanation from the point of view of the reaction process in a PdTPP dye. The system [*n*-SnO_2–PdTPP–electrolyte] has two photosensitive interfaces: I, between electrolyte and PdTPP film with photovoltage V_{ph}^{I}, and II, between PdTPP film and SnO_2 layer with photovoltage V_{ph}^{II}. The measurable open circuit photovoltage V_{ph} is the sum of V_{ph}^{I} and V_{ph}^{II}. We postulate that in a film of "undoped" palladium tetraphenylporphyrin, the photovoltage at the interface I is positive and at the interface II is negative. This is a consequence of electron transfer at each. An increase of axial ligation in the PdTPP film leads to an increase of the positive value of V_{ph}^{I} and the negative value of V_{ph}^{II}. The heating in H_2 results in vigorous removal of water and oxygen from the porphyrin film (6). Contact of the film with the air-saturated electrolyte leads to a reabsorption of oxygen and water by the film, first increasing the extent of coordination in molecules of PdTPP *at interface I* and *later* at *interface II* as well. This successive alteration gives the observed V_{ph} vs. t dependence with the maximum corresponding to the condition $dV_{ph}^{I}/dt = dV_{ph}^{II}/dt$. Thus the time evolution of photovoltages shown in Figs. 3 and 4 shows the diffusion of both water and oxygen from interface I to interface II with a corresponding shift of the dominant photoprocess from reaction of the "minority carrier" (1, 6, 14) (electrons) with the

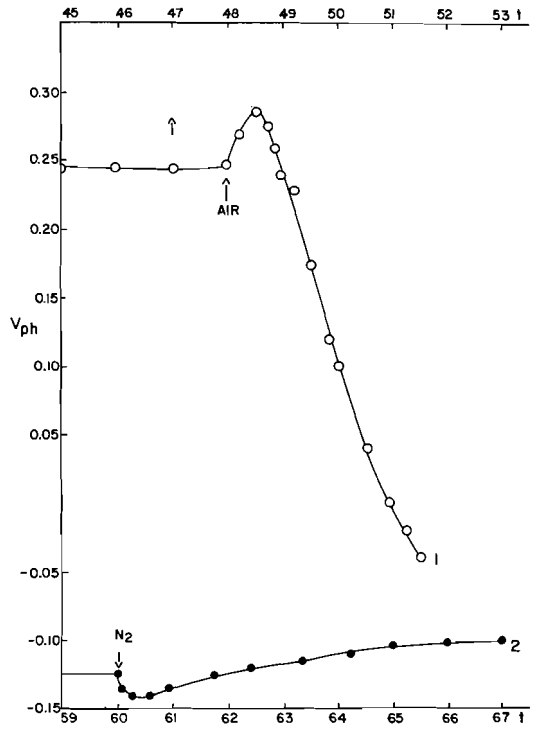

FIG. 4. This figure shows extension of two curves from Fig. 3. Curve *1* shows the effect of admitting air to the cell (curve *3* of Fig. 3) which had been protected from O_2. Curve *2* shows the effect of purging a cell (curve *2* of Fig. 3) with N_2 after it had equilibrated with O_2/H_2O.

Can. J. Chem. Downloaded from www.nrcresearchpress.com by 210.87.254.40 on 09/06/12
For personal use only.

electrolyte to transfer of the same minority carrier (electrons) to the n-SnO_2 layer. This is similar to observations of Fan and Bard (15). As the photoprocess changes, the photoelectrode shifts from a *"photoelectrochemical" cathode to a "photovoltaic" junction driving an electrochemical anode*. This changing process however depends on the presence of both reagents since it is clear from anaerobic experiments (Fig. 3, curve 7) that the second process cannot be achieved by aqueous saturation alone although water does lead to reaction of interface I (with the electrolyte).

The extensive changes in the MCD spectra which accompany the appearance of the anodic behaviour and the observation that crystallinity does not substantially affect the electrochemistry both suggest that electrochemistry of these films is to be treated in terms of individual molecular units. It may even be appropriate to borrow the chemical language of homogeneous electron transfer. Potentially useful theories of electron transfer rate are available. From this point of view, the film appears to act as an activating support for ligand molecules which facilitate electrochemical electron transport by successive redox reactions through the film. This *hopping* mechanism may transfer electrons to quinone at the electrolyte interface with a photopotential V_I from the excited state of the coordinated PdTPP molecules as the initial cathodic process. After film saturation is complete, however, the reverse process by which electrons are transferred to the SnO_2 conduction band from the same excited state is efficient. A very recent study of porphyrin oxidation with iodine suggest partial oxidation and non-stoichiometry is important to efficient electrical processes in such films (16).

In summary, changes in solid state properties which might be expected to affect semiconductor behaviour do not correlate with changes in photovoltaic behaviour. Instead this behaviour is a function of extensive modification of the film by oxygen and water which results in well defined change in the *monomer* MCD spectra of the PdTPP. These changes are similar to those seen in solution coordination studies (12) and are susceptible to interpretation as axial ligation changes. Thus, the anodic behaviour is coupled to *coordination* and probably *activation* of *water* and *oxygen* molecules resulting in a route for successive redox reactions under photoexcitation as the main components of electron transport.

Acknowledgements

We thank Dr. Andre Guillaume for preparations and preliminary electrochemical experiments. This work was supported by a strategic grant from the Natural Sciences and Engineering Research Council of Canada.

1. H. TACHIKAWA and L. R. FAULKNER. J. Am. Chem. Soc. **100**, 4379 (1978).
2. F. R. FAN and L. R. FAULKNER. J. Am. Chem. Soc. **101**, 4779 (1979).
3. I. OKURA and N. KIM-THUAN. J. Mol. Catal. **6**, 227 (1979).
4. J. R. HARBOUR, J. TROMP, and M. L. HAIR. J. Am. Chem. Soc. **102**, 1874 (1980).
5. C. H. LANGFORD, B. R. HOLLEBONE, and T. VANDERNOOT. Adv. Chem. Ser. **184**, 139 (1980).
6. F. GUTMANN and L. E. LYONS. Organic semiconductors. J. Wiley and Sons, New York. 1967. pp. 197–209; 595–598.
7. B. R. HOLLEBONE and M. J. STILLMAN. J. Chem. Soc. Faraday II, **74**, 2107 (1978).
8. D. W. THOMAS and A. E. MARTEL. J. Am. Chem. Soc. **81**, 5111 (1959).
9. C. H. LANGFORD, W. M. SONT, and R. D. BURCH. Inorg. Chim. Acta, **44**, L73 (1980).
10. A. T. VORTANYAN. Sov. Phys. Semicond. **1**, 1261 (1968).
11. S. E. HARRISON and L. H. LUDEWIG. J. Chem. Phys. **45**, 343 (1966).
12. M. J. STILLMAN and A. J. THOMSON. J. Chem. Soc. Faraday II, **70**, 805 (1971).
13. D. A. CASE and M. KARPLUS. J. Am. Chem. Soc. **99**, 6182 (1977).
14. F. J. KAMPAS and M. GOUTERMAN. J. Phys. Chem. **81**, 690 (1977).
15. C. D. JAEGER, F. R. FAN, and A. J. BARD. J. Am. Chem. Soc. **102**, 2592 (1980).
16. T. E. PHILLIPS, R. P. SCARINGE, B. M. HOFFMAN, and J. A. IBERS. J. Am. Chem. Soc. **102**, 3435 (1980).

Can. J. Chem. Downloaded from www.nrcresearchpress.com by 210.87.254.40 on 09/06/12
For personal use only.

The addition of 2,4-dinitrobenzenesulphenyl chloride to 2-methylenebicyclo[2.2.1]hept-5-ene: the crystal structure of 1-chloromethyl-3-*endo*-(2′,4′-dinitrophenylthio)tricyclo[2.2.1.$0^{2,6}$]heptane, $C_{14}H_{13}ClN_2O_4S$[1]

MARIA PRZYBYLSKA

Division of Biological Sciences, National Research Council of Canada, Ottawa, Ont., Canada K1A 0R6

AND

DENNIS G. GARRATT

Division of Chemistry, National Research Council of Canada, Ottawa, Ont., Canada K1A 0R6

Received August 29, 1980

MARIA PRZYBYLSKA and DENNIS G. GARRATT. Can. J. Chem. **59**, 658 (1981).

1-Chloromethyl-3-*endo*-(2′,4′-dinitrophenylthio)tricyclo[2.2.1.$0^{2,6}$]heptane, $C_{14}H_{13}ClN_2O_4S$, crystallizes in space group $P2_1/a$ with unit cell dimensions $a = 12.785(2)$, $b = 10.653(1)$, $c = 11.061(1)$ Å, $\beta = 101.54(1)°$, $Z = 4$.

The structure was solved from Patterson and Fourier maps. The parameters were refined by block-diagonal least-squares to a final $R = 0.038$ for 2063 observed reflections. The structural data provide unequivocal proof for our earlier ascertainment of configurational-specific *exo* attack upon the *endocyclic* double bond of 2-methylenebicyclo[2.2.1]hept-5-ene with homoallylic participation.

The molecule is characterized by the presence of an interaction between oxygen of the 2-nitro group and a sulphur atom, and of a weak bifurcated hydrogen bond system involving C—H···O bonds.

MARIA PRZYBYLSKA et DENNIS G. GARRATT. Can. J. Chem. **59**, 658 (1981).

Le chlorométhyl-1 (dinitro-2′,4′ phénylthio) 3-*endo* tricyclo[2.2.1.$0^{2,6}$] heptane, $C_{14}H_{13}ClN_2O_4S$ cristallise dans le groupe d'espace $P2_1/a$ avec des dimensions de maille de: $a = 12{,}785(2)$, $b = 10{,}653(1)$, $c = 11{,}061(1)$ Å, $\beta = 101{,}54(1)°$, $Z = 4$. La structure a été résolue à partir des diagrammes de Patterson et de Fourier. Les paramètres sont affinés par la méthode des moindres carrés (matrice entière) jusqu'à une valeur finale $R = 0{,}038$ pour les 2063 réflexions observées. Les données de structure confirment d'une façon non ambigue notre conclusion antérieure à l'effet que l'attaque sur la double liaison endocyclique du méthylène-2 bicyclo[2.2.1]heptène-5 se produit d'une façon sétérospécifique par la face *exo* avec une participation homoallylique.

La molécule est caractérisée par une interaction entre l'oxygène du groupe nitro en position 2 et l'atome de soufre et une faible liaison hydrogène bifurquée impliquant des liaisons C—H· · · O.

[Traduit par le journal]

Introduction

In a number of recent publications, Zefirov *et al.* have proposed a mechanistic scenario wherein electrophiles, such as arenesulphenyl halides, undergo addition reactions with carbon–carbon multiple bonds by an ion-pair mechanism with intramolecular attack by the anionoid particle at the cationoid center without full dissociation of the ion-pair (1). In particular, Zefirov *et al.* have used this hypothesis to assign the product derived from the reaction of a sulphenyl chloride with 2-methylenebicyclo[2.2.1]hept-5-ene, **1**, as that of configurationally-specific[2] *endo* attack upon the *endocyclic* double bond with homoallylic participation of the *exocyclic* π system in the product determining step (reaction [1]), to give the *exo*-arylthionortricyclene, **2**.[3]

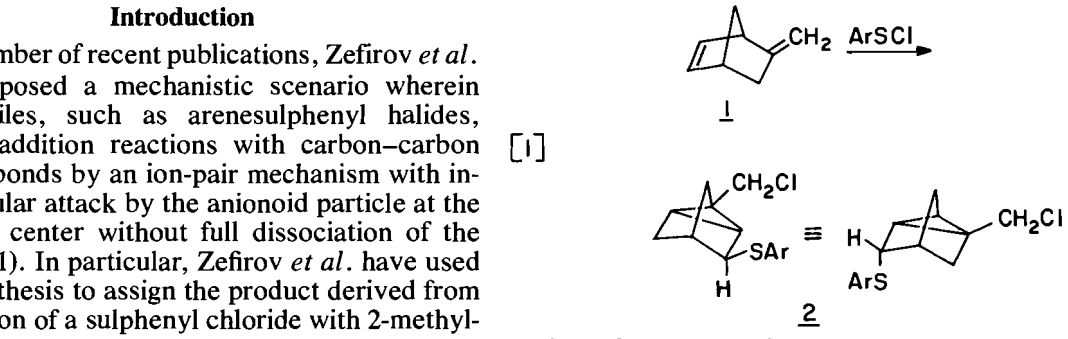

1 [1] 2

[1]NRCC No. 18804.

[2]The term configurational-specificity or -selectivity was originally coined in reference to a problem in allene chemistry in which it became necessary to distinguish which face or faces of the orthogonal π systems was/were being attacked (2). The extension of the use of this term to problems such as *exo* and *endo* attack seems quite reasonable and has been used in this context previously (3).

[3]We have extended the *endo–exo* terminology beyond its original usage in norbornane systems (4) to nortricyclenes in accord with the suggestion of Cristol and Lalonde (5), by referring to configurations with respect to the unsubstituted methano bridge. We agree with Cristol and Lalonde that the use of the terms *endo* and *exo* in these connotations is better than coining new terms, even though the original derivations are not precisely applicable.

0008-4042/81/040658-05$01.00/0

©1981 National Research Council of Canada/Conseil national de recherches du Canada

Can. J. Chem. Downloaded from www.nrcresearchpress.com by 210.87.254.42 on 09/06/12
For personal use only.

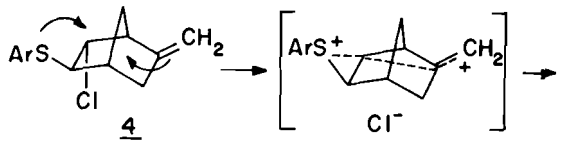

[2]

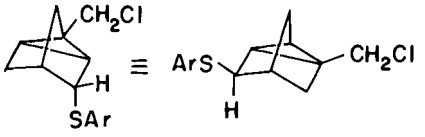

3

This interpretation, however, contrasts with results obtained in these laboratories and elsewhere (6) which predict configurationally-specific *exo* attack upon the *endocyclic* double bond of **1**. In this respect, we and others (7) have recently reported the reaction of **1** with arenesulphenyl chlorides to give the *endo*-arylthionortricyclene, **3**; the product of *exo* attack upon the *endocyclic* double bond with homoallylic participation of the *exocyclic* π system. In support of this assignment, we note the observation that adducts of type **4** isomerize to the nortricyclene, **3**, presumably by way of a thiiranium ion-like intermediate resulting from neighbouring group assistance of carbon–chlorine bond cleavage by the arylthio group (reaction [2]).

In view of the aforementioned differences in interpretation, we felt that it was necessary to unambiguously establish the configurational-specificity of this reaction. We therefore undertook a single crystal X-ray structural determination of the adduct derived from 2,4-dinitrobenzenesulphenyl chloride and diene **1**. As will be seen, the correct structure is that derived from *exo* attack: 1-chloromethyl-3-*endo*-(2′,4′-dinitrophenylthio)tricyclo-[2.2.1.0^{2,6}]heptane.

Experimental

Crystal data are as follows:

$C_{14}H_{13}ClN_2O_4S$ fw = 340.8
Monoclinic, $P2_1/a$, a = 12.785(2), b = 10.653(1), c = 11.061(1) Å, β = 101.54(1)°, V = 1476.0 Å^3, Z = 4, ρ_o = 1.51 (by flotation at 24°C), ρ_c = 1.53 g cm^{-3}, λ(Cu Kᾱ) = 1.54178 Å, μ(Cu Kᾱ) = 38.0 cm^{-1}.

Yellow prisms of mp 101–103°C were obtained from a mixture of cyclohexane and methylene chloride. The space group was established from precession films. The data were collected at room temperature with the Nonius CAD-4 procedures using a crystal of dimensions 0.21 × 0.21 × 0.12 mm and Cu Ni-filtered radiation.

The pertinent details are: ω–2θ scan; 1° < θ < 70°; ω scan angle = (0.7 + 0.2 tan θ)°; SIGPRE (the prescan acceptance parameter) = 0.7; SIGMA = 0.014. ITMAX (the maximam scan time) = 150 s. The prescan speed was 5°/min and two final scans were made in opposite directions with double the variable scan speed. A measurement of two standard reflections every 100 min revealed a decrease in intensity of < 6% during data collection. Three reflections were used as orientation controls and were measured every 60 reflections. Reorientation occurred, if the deviation of any scattering vector in any direction from calculated position was greater than 0.050°.

Out of 2800 measured reflections, 2063 (73.7%) were above threshold of 1.43σ(I_{net}). The net intensities, after scaling, were corrected for Lorentz and polarization effects but not for absorption.

The non-hydrogen atomic coordinates were obtained from Patterson and Fourier maps. Refinement for observed reflections was carried out by block-diagonal least-squares, minimizing $\Sigma w(|F_o| - |F_c|)^2$ with weights.

$$\sqrt{w} = 1/\{1 + [(|F_o| - P_2)/P_1]^2\}^{1/2} \sin^2\theta/P_3$$

where P_1 = 15, P_2 = 10, and P_3 = 0.27.

Hydrogen atoms were located on a difference map carried out when R was 0.073, and which showed no other significant peaks. The non-hydrogen atoms were refined anisotropically and isotropic temperature factors were used for H. Refinement converged at R = 0.038 and R_w = 0.042 for the 2063 observed reflections and the final mean and maximum shifts/esd for all atoms were 0.05 and 0.20, respectively. The scattering factor curves were those of Hanson, Herman, Lea, and Skillman (8) for non-hydrogen atoms and of Stewart, Davidson, and Simpson (9) for H.

All calculations were carried out with the NRCC crystallographic computer programs by Ahmed, Hall, Pippy, and Huber (10).

The final atomic coordinates are presented in Table 1.[4]

Discussion

The projection of the molecule of the nortricyclene derivative is shown in Fig. 1, in which the numbering of the atoms and the bond lengths are also presented. The values of the valency angles, together with their esd's are listed in Table 2. The C—H bonds are in the range 0.92 to 1.05 Å (mean = 0.99 and esd = 0.03 Å).

The C—C bonds of the nortricyclene moiety vary from 1.509 to 1.518 Å with the exception of the bonds to C(4), which are 1.530 to 1.539 Å. They agree well with the values previously reported for 3,5-*endo*,*endo*-dibromotricyclo[2.2.1.0^{2,6}]heptane-7-carboxylic acid (11) with the exception of C(1)—C(7) and C(4)—C(7), which in the latter are 1.541(10) and 1.560(10) Å, respectively, due to the substitution at C(7) by COOH.

The angles of the three-membered ring are 59.8, 60.1, and 60.1°. The endocyclic angles of the five-membered rings vary from 97.2 to 107.6°; the smallest being C(2)—C(3)—C(4) = 97.3°, C(6)—C(5)—C(4) = 97.2°, and C(1)—C(7)—C(4) = 97.4°.

[4]Tables of observed and calculated structure factors and of temperature factors are available, at a nominal charge, from the Depository of Unpublished Data, CISTI, National Research Council of Canada, Ottawa, Ont., Canada K1A 0S2.

Can. J. Chem. Downloaded from www.nrcresearchpress.com by 210.87.254.42 on 09/06/12
For personal use only.

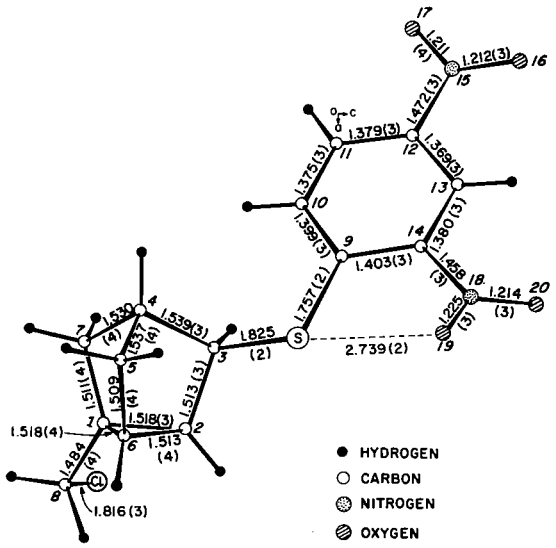

FIG. 1. The projection of the nortricyclene derivative along the *b* axis showing the stereochemistry of the molecule, the numbering scheme, and the bond lengths with their esd values in parentheses.

The S—C(3) and S—C(9) bonds are 1.825(2) and 1.757(2) Å, respectively, and they reflect the difference between S—C(sp^3) and S—C(sp^2) bonds. Similar differences were observed in, for example, dimethyl 3-*endo*-chloro-4-*exo*-phenylthiotricyclo-[4.2.2.$0^{2,5}$]dec-9-ene-7,8-*endo*,*endo*-dicarboxylate (12) (1.819(8) and 1.762(8) Å) and in 2-methylthiobenzothiazole (13) (1.82(3) and 1.77(3) Å).

The nitro groups are rotated about N—C bonds in opposite directions bringing O(16) above and O(20) below the plane of the benzene ring; the distances being 0.09 and −0.50 Å, respectively. The rotation about the C(12)—N(15) bond is ~5° and that about C(14)—N(18) is 28°. The relevant torsion angles are presented in Table 3 and the dihedral angles between the plane of the benzene ring and those of N(15) and N(18) nitro groups are 4.9 and 152.0°, respectively. In *m*-dinitrobenzene (14) both nitro groups are rotated out of the aromatic plane by about 13°, the directions of the rotations being such that the molecular symmetry is *m*. The deviation from symmetry in our structure appears to be caused by the intramolecular interaction between O(19) and S atoms. The O···S distance is 2.739(2) Å, which is considerably smaller than the sum of their van der Waals radii of 3.07 Å (r(O) = 1.42 (15); r(S) = 1.65 Å (16, 17)).

A similar strong intramolecular interaction between S of the $SOCH_3$ group and O(1) of the nitro group was reported by Hamilton and LaPlaca (18) in methyl ester of 2-nitrobenzenesulphenic acid. The structure was characterized by a very short

TABLE 1. Final fractional coordinates with esd's in parentheses (× 10^4 for non-hydrogen atoms and × 10^3 for H) and isotropic temperature factors ($B_{eq} = (8\pi^2/3)\Sigma_i \Sigma_j U_{ij} a_i^* a_j^* a_i \cdot a_j$)

Atom	x	y	z	B_{eq} or B
Cl	4466(1)	1548(1)	−3775(1)	5.1 Å²
S	2982(1)	5298(1)	−570(1)	3.4
C(1)	3698(2)	3917(2)	−3692(2)	3.4
C(2)	3968(2)	4297(2)	−2342(2)	3.4
C(3)	2911(2)	4302(2)	−1927(2)	3.3
C(4)	2217(2)	4763(2)	−3147(2)	3.7
C(5)	2835(2)	5913(3)	−3467(2)	4.3
C(6)	3910(2)	5284(3)	−3338(2)	4.0
C(7)	2500(2)	3766(2)	−4025(2)	3.7
C(8)	4448(2)	3174(3)	−4270(2)	4.3
C(9)	1990(2)	4617(2)	114(2)	3.0
C(10)	1151(2)	3919(2)	−574(2)	3.4
C(11)	398(2)	3342(2)	−35(2)	3.6
C(12)	469(2)	3446(2)	1221(2)	3.4
C(13)	1275(2)	4109(2)	1945(2)	3.3
C(14)	2017(2)	4694(2)	1386(2)	2.9
N(15)	−336(2)	2837(2)	1807(2)	4.6
O(16)	−293(2)	3016(2)	2898(2)	5.9
O(17)	−997(2)	2177(3)	1170(3)	7.7
N(18)	2855(2)	5391(2)	2200(2)	3.7
O(19)	3262(2)	6279(2)	1761(2)	4.8
O(20)	3108(2)	5071(2)	3272(2)	5.8
H(2,1)	464(2)	403(2)	−179(2)	3.4(5)
H(3,1)	270(2)	347(2)	−168(2)	2.9(5)
H(4,1)	143(2)	492(3)	−314(3)	4.3(6)
H(5,1)	285(2)	662(3)	−284(3)	4.4(6)
H(5,2)	257(2)	621(3)	−433(3)	4.5(6)
H(6,1)	458(2)	572(3)	−348(3)	5.0(7)
H(7,1)	223(2)	292(3)	−387(3)	4.2(6)
H(7,2)	222(2)	393(2)	−492(2)	3.8(5)
H(8,1)	422(2)	313(2)	−518(2)	3.8(5)
H(8,2)	523(3)	349(3)	−396(3)	6.0(7)
H(10,1)	107(2)	390(2)	−145(2)	3.1(5)
H(11,1)	−15(2)	289(3)	−51(2)	4.1(6)
H(13,1)	135(2)	421(2)	281(2)	2.9(5)

S···O(1) distance of 2.44 Å and the N—O(1) bond was found to be somewhat longer (1.24 Å) than N—O(2) (1.19 Å). The O—S···O(1) configuration is almost linear, which the authors considered favourable for sulfur *p*- and *d*-orbital participation in the partial bonding. In the title compound C(3)—S···O is also nearly linear. This linearity suggests a trigonal bipyramidal geometry about S, wherein C(3) and O(19) occupy apical sites and C(9) plus the two lone pairs of electrons occupy the three equatorial sites.

A similar interaction between S and O of the *ortho*-nitro group is evident in 3-*endo*-bromo-4-*exo*-(2′-nitrophenylthio)-7,8-*endo*,*endo*-dimethyltricyclo[4.2.2.$0^{2,5}$]dec-7-ene, dimethyl 3-*endo*-chloro-4-*exo*-(2′,4′-dinitrophenylthio) tricyclo-[4.2.2.$0^{2,5}$]dec-9-ene-7,8-*endo*,*endo*-dicarboxylate and in methyl (1*RS*,4*SR*,12*RS*)-4-(2′nitrophenylthio)-9-oxapentacyclo[6.4.0.$0^{2,5}$.$0^{3,7}$.$0^{6,11}$]dodeca-

Can. J. Chem. Downloaded from www.nrcresearchpress.com by 210.87.254.42 on 09/06/12
For personal use only.

Can. J. Chem. Downloaded from www.nrcresearchpress.com by 210.87.254.42 on 09/06/12
For personal use only.

TABLE 2. Bond angles (deg) and esd's

C(3)—S—C(9)	101.1(1)	C(1)—C(7)—C(4)	97.4(2)
C(2)—C(1)—C(6)	59.8(2)	Cl—C(8)—C(1)	110.4(2)
C(2)—C(1)—C(7)	106.8(2)	S—C(9)—C(10)	121.8(2)
C(2)—C(1)—C(8)	121.8(2)	S—C(9)—C(14)	122.2(2)
C(6)—C(1)—C(7)	106.5(2)	C(10)—C(9)—C(14)	116.0(2)
C(6)—C(1)—C(8)	121.7(2)	C(9)—C(10)—C(11)	122.0(2)
C(7)—C(1)—C(8)	123.4(2)	C(10)—C(11)—C(12)	119.4(2)
C(1)—C(2)—C(3)	104.9(2)	C(11)—C(12)—C(13)	121.4(2)
C(1)—C(2)—C(6)	60.1(2)	C(11)—C(12)—N(15)	119.8(2)
C(3)—C(2)—C(6)	107.6(2)	C(13)—C(12)—N(15)	118.8(2)
S—C(3)—C(2)	110.5(2)	C(12)—C(13)—C(14)	118.4(2)
S—C(3)—C(4)	117.4(2)	C(9)—C(14)—C(13)	122.8(2)
C(2)—C(3)—C(4)	97.3(2)	C(9)—C(14)—N(18)	121.1(2)
C(3)—C(4)—C(5)	102.9(2)	C(13)—C(14)—N(18)	116.1(2)
C(3)—C(4)—C(7)	99.6(2)	C(12)—N(15)—O(16)	118.2(2)
C(5)—C(4)—C(7)	102.1(2)	C(12)—N(15)—O(17)	117.9(2)
C(4)—C(5)—C(6)	97.2(2)	O(16)—N(15)—O(17)	123.9(3)
C(1)—C(6)—C(2)	60.1(2)	C(14)—N(18)—O(19)	117.8(2)
C(1)—C(6)—C(5)	106.8(2)	C(14)—N(18)—O(20)	118.6(2)
C(2)—C(6)—C(5)	106.8(2)	O(19)—N(18)—O(20)	123.5(2)

10-one-12-carboxylate (19). The authors did not mention it, but the O···S distances in these structures were found to be 2.630, 2.657, and 2.634 Å, respectively.

Non-bonding interactions of this type are also probably present in two other structures involving the 2-nitrophenylthio moiety (20), as in both cases one of the NO bonds of the nitro group is somewhat longer than the other, and apparently closer to S. Unfortunately the lack of listing of coordinates in both of these publications does not allow the calculation of the O···S distances.

TABLE 3. Selected torsion angles (deg); esd is 0.4°

(*a*) Endocyclic torsion angles of five-membered rings

Ring A: C(1), C(2), C(3), C(4), and C(7)
Ring B: C(2), C(3), C(4), C(5), and C(6)
Ring C: C(1), C(6), C(5), C(4), and C(7)

Bond	A	B	C	Mean	C_s*
C(1)—C(2)	−2.3				
C(2)—C(6)		−2.6		1.7	0.0
C(1)—C(6)			−0.1		
C(2)—C(3)	34.7	−28.1			
C(5)—C(6)		32.1	−30.9	31.4	25.0
C(1)—C(7)	−31.5		31.2		
C(3)—C(4)	−55.4	49.5			
C(5)—C(4)		−51.2	51.8	52.2	40.3
C(7)—C(4)	53.6		−51.9		

*Calculated values for the envelope conformation with a puckering amplitude (q = 0.435 Å) determined from an electron diffraction study of cyclopentane (23).

(*b*) Exocyclic torsion angles

C(7)—C(1)—C(8)—Cl	69.9
C(4)—C(3)—S—C(9)	−95.4
C(3)—S—C(9)—C(10)	23.7
C(9)—C(14)—N(18)—O(19)	−28.4
C(11)—C(12)—N(15)—O(17)	−5.6

The O···S interaction causes the lengthening of N(18)—O(19) to 1.225 from the average for the other three N—O bonds of 1.212 Å. This lengthening combined with the already mentioned shortening of S—C(9) leads to changes in electron density distribution in C(9)—C(14), which is longer than its counterpart C(11)—C(12) (1.403 vs. 1.379 Å) and in C(14)—N(18) which is shorter than C(12)—N(15) (1.458 vs. 1.472 Å). Thus an alternate shortening and lengthening of bonds along the chain S—C(9)—C(14)—N(18)—O(19) is observed. Similar effects were found in, for example, ergotamine (21, 22) in a chain of 5 atoms in which the end oxygens were an acceptor and a donor in hydrogen bond formation. The shortening of C(12)—C(13) is significant and reflects similar alternate changes in electron distribution through the N(15)—C(12) —C(13)—C(14) —N(18) chain.

The endocyclic torsion angles of the nortricyclene moiety (cf. Table 3) show strain. Those involving C(4) deviate most from the calculated values for the envelope conformation with a puckering amplitude (q = 0.435 Å) as determined from an electron diffraction study of cyclopentane (23).

The benzene ring atoms including both nitrogens, but excluding C(13) are planar (χ^2 = 6.8). C(13) lies at 0.012 and S at 0.070 Å above that plane. The puckering of the benzene ring at C(13) may be due to the formation of a weak intramolecular bifurcated hydrogen bond, apparently present between C(13) and one oxygen atom of both nitro groups. Due to the presence of nitro groups the hydrogen at C(13) is relatively acidic and the H(13,1) distances to O(16) and O(20) are 2.48(2) and 2.38(2) Å, respectively. C(13)—H(13,1)···O(16)

and C(13)—H(13,1)···O(20) angles are only 93.6(1.5) and 99.4(1.6)°, but weak asymmetrical bifurcated hydrogen bonds with O—H···O angles as small as 90 and 96° were described by Newton, Jeffrey, and Takagi (24). The interaction of H(13,1) with O(20) appears to be somewhat stronger than with O(16). This difference is probably brought about by the O(19)···S interaction and is supported by the observation that the angle C(14)—C(13)—H(13,1) is smaller than C(12)—C(13)—H(13,1), 117.3(1.4)° vs. 124.3(1.4)°. A similar weak intramolecular C—H···O bond was found in 2,9-diacetyl-9-azabicyclo[4.2.1]non-2,3-ene (25).

The molecules are separated by normal van der Waals contacts. The shortest O(19)···H(3,1′) distance is 2.63(2) Å and the shortest H···H contacts are 2.48(4) and 2.55(3) Å. The shortest Cl···H approach is to H(4,1′) of 2.93(3) Å.

Acknowledgements

The authors wish to thank Mrs. M. E. Pippy and Mrs. H. M. Sheppard for their assistance with the computations.

1. (*a*) N. S. Zefirov, N. K. Sadovaya, R. Sh. Akhmedova, and I. V. Bodrikov. Zh. Org. Khim. **15**, 217 (1979); (*b*) N. S. Zefirov, N. K. Sadovaya, L. A. Novgorodtseva, R. Sh. Akhmedova, S. V. Baranov, and I. V. Bodrikov. Tetrahedron, **35**, 2759 (1979); (*c*) W. A. Smit, N. S. Zefirov, I. V. Bodrikov, and M. Z. Krimer. Acc. Chem. Res. **12**, 282 (1979).
2. (*a*) D. G. Garratt, P. L. Beaulieu, and M. D. Ryan. Tetrahedon, **36**, 1507 (1980); (*b*) D. G. Garratt and P. L. Beaulieu. Can. J. Chem. **58**, 1275 (1980).
3. D. G. Garratt and A. Kabo. Can. J. Chem. **58**, 1030 (1980).
4. J. Bredt. J. Prakt. Chem. **121**, 153 (1929).
5. S. J. Cristol and R. T. Lalonde. J. Am. Chem. Soc. **80**, 4355 (1958).
6. (*a*) G. H. Schmid and D. G. Garratt. *In* The chemistry of double bonded functional groups, Supplement A. Part 2. *Edited by* S. Patai. Wiley and Sons, London. 1977. Chapt. 9; (*b*) T. G. Traylor. Acc. Chem. Res. **2**, 152 (1968); (*c*) A. Hassner, R. P. Hoblitt, C. Heathcock, J. E. Kropp, and M. Lorber. J. Am. Chem. Soc. **92**, 1326 (1970); (*d*) A. Hassner and J. S. Teeter. J. Org. Chem. **35**, 3397 (1970).
7. (*a*) D. G. Garratt, P. L. Beaulieu, and V. M. Morisset. Can. J. Chem. **58**, 1021 (1980); (*b*) D. Heissler and J. J. Riehl. Tetrahedron Lett. 3957 (1979).
8. H. P. Hanson, F. Herman, J. D. Lea, and S. Skillman. Acta Crystallogr. **17**, 1040 (1964).
9. R. F. Stewart, E. R. Davidson, and W. T. Simpson. J. Chem. Phys. **42**, 3175 (1965).
10. F. R. Ahmed, S. R. Hall, M. E. Pippy, and C. P. Huber. NRC Crystallographic Programs for the IBM 360 System, Accession Nos. 133, J. Appl. Crystallogr. **6**, 309 (1973).
11. I. Fleming, P. G. Jones, O. Kennard, and J. P. Michael. J. Chem. Soc. Perkin II, 808 (1979).
12. K. A. Potekhin, E. N. Kurkutova, Yu. T. Struchkov, A. S. Koz'min, V. N. Kirin, N. S. Zefirov, V. V. Ilyukhin, and N. V. Belov. Dokl. Akad. Nauk SSSR, **242**(4), 832 (1978).
13. P. J. Wheatley. J. Chem. Soc. 3636 (1962).
14. J. Trotter and C. S. Williston. Acta Crystallogr. **21**, 285 (1966).
15. A. Bondi. J. Phys. Chem. **68**, 441 (1964).
16. J. Donohue. J. Am. Chem. Soc. **72**, 2701 (1950).
17. J. Donohue. *In* Organic sulfur compounds. Vol. 1. *Edited by* N. Kharasch. Pergamon Press, New York. 1961. p. 1.
18. W. C. Hamilton and S. J. LaPlaca. J. Am. Chem. Soc. **86**, 2289 (1964).
19. (*a*) K. A. Potekhin, E. N. Kurkutova, Yu. T. Struchkov, V. N. Kirin, A. S. Koz'min, N. S. Zefirov, V. V. Ilyukhin, and N. V. Belov. Dokl. Akad. Nauk SSSR, **243**(3), 652 (1978); (*b*) K. A. Potekhin, E. N. Kurkutova, Yu. T. Struchkov, R. Sh. Akhmedova, V. N. Kirin, A. S. Koz'min, and N. S. Zefirov. Dokl. Akad. Nauk SSSR, **242**(2), 341 (1978); (*c*) K. A. Potekhin, E. N. Kurkutova, Yu. T. Struchkov, V. N. Kirin, A. S. Koz'min, N. S. Zefirov, V. V. Ilyukhin, and N. V. Belov. Dokl. Akad. Nauk SSSR, **243**(2), 348 (1978).
20. (*a*) N. S. Zefirov, V. N. Kirin, A. S. Koz'min, I. V. Bodrikov, K. A. Potekhin, and E. N. Kurkutova. Tetrahedron Lett. **17**, 1547 (1979); (*b*) N. S. Zefirov, A. S. Koz'min, V. V. Zhdankin, V. N. Kirin, I. V. Bodrikov, B. B. Sedova, and V. G. Rau. Tetrahedron Lett. 3533 (1979).
21. M. Przybylska and F. R. Ahmed. Acta Crystallogr. Sect. B. In press.
22. H. Hebert. Acta Crystallogr. Sect. B, **35**, 2978 (1979).
23. W. J. Adams, H. J. Geise, and L. S. Bartell. Phys. Inorg. Chem. **92**, 5013 (1970).
24. M. D. Newton, G. A. Jeffrey, and S. Takagi. J. Am. Chem. Soc. **101**, 1997 (1979).
25. C. S. Huber. Acta Crystallogr. Sect. B, **28**, 2577 (1972).

Can. J. Chem. Downloaded from www.nrcresearchpress.com by 210.87.254.42 on 09/06/12
For personal use only.

Static and dynamic phenomena in the quenching of phenanthrene triplets by conjugated dienes in anionic micelles[1]

J. C. SELWYN[2] AND J. C. SCAIANO

Division of Chemistry, National Research Council of Canada, Ottawa, Ont., Canada K1A 0R6

Received August 15, 1980

J. C. SELWYN and J. C. SCAIANO. Can. J. Chem. **59**, 663 (1981).

The photochemistry of phenanthrene in sodium dodecyl sulfate micelles in the presence of conjugated dienes having from five to eight carbon atoms has been examined using laser flash photolysis techniques. The effect of the addition of the diene quenchers on the intensity of the T–T absorptions immediately after singlet decay reflects largely the distribution of the quenchers and can be used to determine micellar properties, e.g. the aggregation number. The effect of quenchers on the lifetime of triplet phenanthrene is largely controlled by the rate constants for quencher entry and exit from the micelles. Typical rates of entry are in the $1–2 \times 10^9\ M^{-1}\ s^{-1}$ range, while the exit rates are strongly dependent on the number of carbon atoms and are different for open and cyclic molecules; for example the exit rate constants are 1.3×10^5 and $3.5 \times 10^5\ s^{-1}$ for 1,3-octadiene and 1,3-cyclooctadiene, respectively.

J. C. SELWYN et J. C. SCAIANO. Can. J. Chem. **59**, 663 (1981).

Utilisant les techniques de la photolyse flash au laser, on a étudié la photochimie du phénanthrène dans des micelles de dodécylsulfate de sodium, en présence de dienes conjugués ayant 5 à 8 atomes de carbone. L'effet de l'addition des pièges de dienes sur l'intensité des absorptions T–T immédiatement après la désintégration du singulet, reflète largement la distribution des pièges, et peut être utilisé pour déterminer les propriétés micellaires, par exemple le nombre d'aggrégation. L'effet des pièges sur la durée de vie du triplet du phénanthrène est largement contrôlé par les constantes de vitesse d'entrée et de sortie des pièges dans les micelles. Les vitesses typiques d'entrée sont de l'ordre de $1–2 \times 10^9\ M^{-1}\ s^{-1}$ tandis que celles de sortie dépendent fortement du nombre d'atomes de carbone et sont différentes selon qu'il s'agit de molécules cyclique ou à chaîne ouverte; par exemple les constantes de vitesse de sortie sont respectivement de $1,3 \times 10^5$ et $3,5 \times 10^5\ s^{-1}$ pour l'octadiène-1,3 et le cyclooctadiène-1,3.

[Traduit par le journal]

Introduction

The kinetics of chemical reactions in micellar systems frequently reflect the distribution of reactants and the kinetics of entry and exit processes, in addition to the interaction between the reagents. Several studies have shown that luminescent probes can be used in the examination of static and dynamic aspects of the behaviour of probes in micelles (1–14). Flash photolysis techniques have also been used to examine kinetic aspects of micellar processes (1, 2, 15, 16) but not to determine micellar properties, such as the aggregation number.

Few rates of exit and entry are known; for example, in the case of ground state probes the values have been determined for several cyclic azoalkanes (5), for nitromethane and diiodomethane (8), and for di-*tert*-butylnitroxide (17). In the case of excited probes, the rates of exit for triplet state probes for a series of arenes were measured by Thomas *et al.* (9) using phosphorescence techniques.

In this paper we examine the quenching of phenanthrene triplets by conjugated dienes in sodium dodecyl sulfate (SDS) micelles. The measurements were carried out by monitoring the T–T absorptions due to phenanthrene triplet using laser flash photolysis techniques.

Results

All the experiments described in this paper have been obtained using laser flash photolysis techniques and employing the pulses (337.1 nm, ~8 ns, up to 10 mJ) of a nitrogen laser for excitation. Most of our experiments have been carried out using phenanthrene as a probe, with the only exception of some runs in which we used 1-methylphenanthrene.

In carefully prepared and deaerated samples one can obtain phenanthrene triplet lifetimes (monitored at 483 nm) in the neighborhood of 300 μs; in our experiments, the quenching by conjugated dienes is always the predominant mode of triplet decay (*vide infra*). Therefore, as long as other modes of triplet decay are much slower, they do not play a role in the kinetic measurements. We have normally regarded as acceptable triplet lifetimes of 100 μs and up in the absence of added quencher.

The type of effects observed by addition of dienes can be clearly divided into two groups: static and dynamic effects. The former refers to those effects which are the result of a probe and a quencher being resident in the same micelle at the time of excitation. Dynamic effects reflect the migration of either the probe or the quencher towards the other.[3] In all our experiments the quenchers are far more mobile than the probe and only the migra-

[1]NRCC No. 18744.

[2]NRCC summer student, 1980.

[3]See also ref. 5 for a similar example.

0008-4042/81/040663-06$01.00/0

©1981 National Research Council of Canada/Conseil national de recherches du Canada

Can. J. Chem. Downloaded from www.nrcresearchpress.com by 210.87.254.105 on 09/06/12
For personal use only.

Can. J. Chem. Downloaded from www.nrcresearchpress.com by 210.87.254.105 on 09/06/12
For personal use only.

tion of the quencher needs to be considered in the time scale of our experiments.

A similar subdivision applies to the analysis of the kinetic data. That is, static phenomena largely reflect the occupancy levels in the micellar phase, while dynamic aspects reflect kinetic processes related to the exit and entry of the quencher from and into the micelle. This subdivision is also used in the rest of this section.

Static Phenomena

The observable yield of phenanthrene triplet (18) decreases upon addition of a conjugated diene. This does not mean that the triplet state is not formed, but rather, that quenching takes place in a time domain shorter than that accessible using nanosecond techniques (~10 ns). We believe that this quenching effect reflects the presence of phenanthrene and quencher in the same micelle at the time of excitation. The analysis for a system of this type is essentially the same as that reported by Turro *et al.* (5, 6) for the quenching of fluorescent probes by cationic quenchers associated to anionic micelles and by partially-solubilized, cyclic azo compounds. If the distribution of the quencher in the micelles is determined by Poisson statistics, then the ratio of the triplet transient absorption in the absence (A^0) and presence (A) of quencher (Q) will be determined by eq. [1].

$$[1] \quad \ln (A^0/A) = [Q_m]\bar{n}/[\text{Det}] - \text{cmc}$$

where $\bar{n}$ is the aggregation number, [Det] the concentration of detergent, cmc the critical micelle concentration and the subscript (e.g. in Q_m) "m" indicates micelle solubilized.

Our experiments (*vide infra*) clearly show that dienes are far from being just static quenchers associated to the micelles, but rather, their exit and entry rates can be quite large. However, in the case of some of the larger molecules, like 1,3-octadiene, one can regard them as fully micellized static probes in the time scale required to measure the yields of triplet phenanthrene. Under these conditions, a plot of ln (A^0/A) vs. [Q] yields, from the slope, $\bar{n}/([\text{Det}] - \text{cmc})$. The data for several concentrations of surfactant can also be plotted using [Q]/([Det] − cmc) in the abscissa. Figure 1 shows the plot obtained in the case of 1,3-octadiene (using cmc = 8.2×10^{-3} *M* (19)) from which we obtained $\bar{n}$ = 63. The method can in principle be utilized in order to determine both aggregation numbers and cmc values (6).

A decrease in the observable yield of phenanthrene triplets is observed upon addition of any of the quenchers used in this study; however, for the

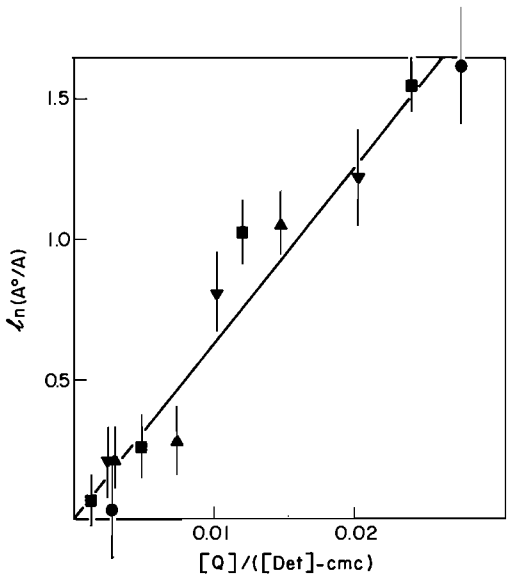

FIG. 1. Plot of the data for 1,3-octadiene according to eq. [1], for the following surfactant concentrations: (●), 0.0762 *M*; (▼), 0.102 *M*; (■), 0.152 *M*; and (▲), 0.254 *M*.

smaller molecules dynamic quenching processes are of considerably greater importance than static effects and the analysis of these is somewhat different, see Discussion.

If sufficient diene is added to a system a point is reached in which all triplets are quenched in static processes and as a result no triplets are observed in the study of transient phenomena. Under these conditions the only detectable species in the singlet state of phenanthrene, which decays with first order kinetics and a lifetime of 60 ns (based on measured values of 58 ns from absorption and 62 ns from fluorescence), and is consistent with literature values (20). Figure 2 shows the absorption spectra of the singlet and triplet states of phenanthrene in SDS micelles. The singlet spectrum has been corrected for fluorescence and measurements at $\lambda <$ 450 nm are subject to considerable error because the magnitude of the correction exceeds that of the absorption signal. Since there is considerable spectral overlap between the singlet and triplet states, it was considered convenient to carry out all experiments under conditions such that the triplet lifetime exceeded 700 ns; under these conditions the role and involvement of the singlet state can be safely ignored.

Dynamic Phenomena

While static phenomena account for quenching events which are controlled by the relative distribution of probes and quenchers (5, 6), dynamic

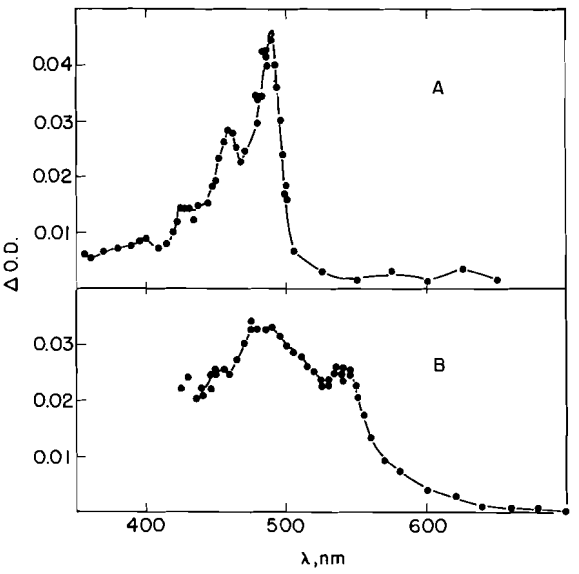

FIG. 2. Transient spectra for phenanthrene in SDS micelles. *A*: triplet state in 0.251 *M* SDS containing 0.001 *M* phenanthrene, recorded between 2 and 20 μs following excitation; *B*: singlet state in 0.30 *M* SDS containing 0.0030 *M* phenanthrene and 0.020 *M* *trans*-1,3-pentadiene, recorded immediately after excitation by the laser pulse.

processes require the migration of the probe and/or quencher, and as a result are a reflection of the mobility of these species. In our experiment the probe has been chosen so that it can be safely assumed that it will not leave the micelle in the time scale of the experiment. There is sufficient evidence in the literature to support this statement (9) and our own experiments are consistent with it.

We will assume that if a diene molecule enters a micelle where an excited phenanthrene resides, quenching occurs with a probability of 1.0. The validity of this assumption can be better understood by combining our own data with those available from the literature (8) and will be dealt with in the Discussion section.

The quenching by dienes can be expected to occur by the mechanism of Scheme 1, where Q represents the quencher and P is a phenanthrene molecule associated to a micelle. The concentrations of P are small enough that only single occupancy needs to be considered and it is important to note that when one uses the concentration term [P], it refers to the concentration of micelles which contain the probe P. The rate of triplet decay is given by:

$$[2] \quad -\partial[^3P]/\partial t = (k_0 + k_+[Q_w])[^3P]$$

That is, the decay of the triplet state of the probe can be expected to occur in a pseudo-first order

$P \xrightarrow{h\nu} {}^1P$ ${}^1P \rightarrow$ decay or $h\nu$ ${}^1P \rightarrow {}^3P$	τ_s^{-1}
${}^3P \rightarrow$ decay or $h\nu'$	$k_0[^3P]$
${}^3P + Q_w \rightarrow {}^3Q_m + P$	$k_+[Q_w][^3P]$
${}^3Q_m \rightarrow$ decay or (exit and decay) $Q_m \rightarrow Q_w$	$k_-[Q_m]$

SCHEME 1

process (k_{expt}) controlled by the concentration of quencher in the aqueous phase ([Q_w]) and the rate of quencher entry into the micelle, k_+.

$$[3] \quad k_{expt} = k_0 + k_+[Q_w]$$

Naturally, [Q_w] is not a convenient variable because what one knows is the total or bulk concentration, not [Q_w]. If the quencher concentration in the aqueous and micellar phase can be regarded as in equilibrium, then

$$[4] \quad K_{eq} = k_+/k_- = [Q_m]/[Q_w][M]$$

where [M] is the concentration of micelles, given by $[M] = ([SDS] - cmc)/\bar{n}$. Substituting in eq. [3]:

$$[5] \quad k_{expt} = k_0 + (k_-/[M])[Q_m]$$

For those molecules which are largely resident in the micellar phase, that is, $[Q_m] \gg [Q_w]$, one can replace [Q_m] for [Q], the bulk quencher concentration, which leads to:

$$[6] \quad k_{expt} \cong k_0 + (k_-/[M])[Q]$$

This equation will apply to the larger molecules, for example, the data for 2,5-dimethyl-2,4-hexadiene are shown in Fig. 3, from which we obtain $k_- = 1.9 \times 10^5\ s^{-1}$.

For those systems where the fraction of

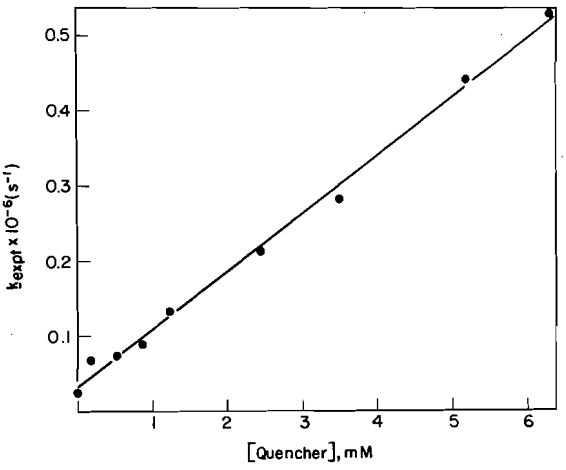

FIG. 3. Plot for the quenching of phenanthrene triplets by 2,5-dimethyl-2,4-hexadiene: [SDS] = 0.165 *M* and [phenanthrene] = 0.001 *M*.

Can. J. Chem. Downloaded from www.nrcresearchpress.com by 210.87.254.105 on 09/06/12
For personal use only.

TABLE 1. Kinetic data for the quenching of phenanthrene triplets by dienes in SDS micelles at room temperature

Quencher (units)	[SDS] range[a] (M)	k_- (s^{-1})	k_+ ($M^{-1}\,s^{-1}$)	K_{eq} (M^{-1})
cis-1,3-Pentadiene	0.051–0.253	8.9×10^6	1.2×10^9	130
trans-1,3-Pentadiene	0.051–0.253	6.9×10^6	9.5×10^8	140
1,3-Hexadiene	0.050–0.254	2.3×10^6	8.3×10^8	360
cis-2-*trans*-4-Hexadiene	0.051–0.253	1.0×10^6	(2.0×10^9)	(1900)[b]
1,3-Cyclohexadiene	0.050–0.249	5.6×10^6	1.3×10^9	240
2,4-Dimethylpentadiene	0.165	3.7×10^5	—	—
1,3-Cycloheptadiene	0.151	1.3×10^6	—	—
1,3-Octadiene	0.076–0.254	1.3×10^5	—	—
2,5-Dimethyl-2,4-hexadiene	0.165	1.9×10^5	—	—
1,3-Cyclooctadiene	0.177	3.5×10^5	—	—

[a]When a range is given the ionic strength was maintained constant at the highest value shown using sodium chloride.
[b]See text for value obtained using eq. [11].

quencher molecules in the aqueous phase cannot be neglected, the values of k_+ and k_- can be derived from a study of the kinetics of triplet decay as a function of quencher *and* surfactant concentration. In this case

$$[7] \quad [Q] = [Q_w] + [Q_m]$$

and

$$[8] \quad K_{eq} = ([Q] - [Q_w])/[Q_w][M]$$

In this case, substituting in eq. [3]

$$[9] \quad k_{expt} = k_0 + \frac{k_+[Q]}{K_{eq}[M] + 1}$$

If we call k_M the slope of plots of k_{expt} vs. [Q], i.e., $k_M = k_+/(K_{eq}[M] + 1)$, then the values of k_+ and k_- can be obtained from a plot of k_M^{-1} vs. [M] according to eq. [10].

$$[10] \quad k_M^{-1} = k_+^{-1} + [M]/k_-$$

Figure 4 shows a plot for 1,3-cyclohexadiene according to eq. [10] (at constant ionic strength), from which the parameters given in Table 1 were obtained. In the case of large molecules, e.g. 1,3-octadiene, only the value of k_- could be obtained. This is due to the fact that the intercept is too small compared with the variation of k_M^{-1} and therefore not significantly different from zero within the experimental error. This observation supports the use of eq. [6] for the larger dienes. In other words, eq. [6] is valid under the conditions where the intercept in eq. [10] can be neglected.

The data obtained applying eq. [10] to several dienes have also been included in Table 1.

In order to confirm that the mobility of phenanthrene could be disregarded we carried out a series of experiments with 1-methylphenanthrene as a probe; the exit rate for 1-methylphenanthrene triplets can be expected to be significantly different from that of phenanthrene triplets (8).[4] As a quencher we have used 1,3-octadiene, which is the slowest example examined; it is reasonable to assume that if the mobility of phenanthrene can be ignored in the case of 1,3-octadiene, the same condition will be met in all the other systems where the mobility of the quencher is considerably greater. The values of k_- for 1,3-octadiene obtained are 1.25×10^5 and 1.32×10^5 s^{-1} using 1-methylphenanthrene and phenanthrene as a probe, respectively.

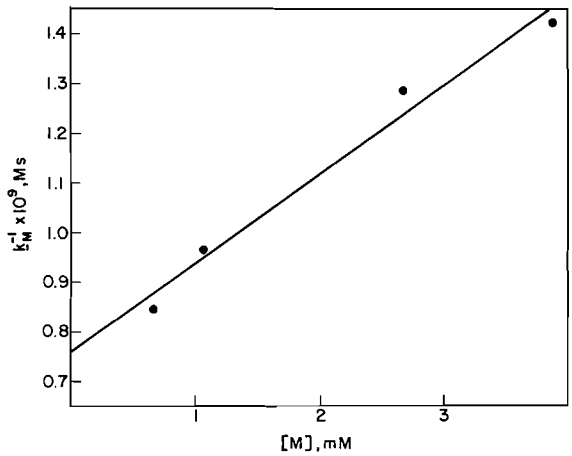

FIG. 4. Plot according to eq. [10] of the data for 1,3-cyclohexadiene.

Discussion

We start this section by noting that the kinetic parameters measured herein all correspond to the ground state of the dienes; by contrast, rate parameters based on phosphorescence quenching (e.g. ref. 8) reflect the behavior of the triplet state. The difference is probably trivial for molecules

[4]Thomas *et al.* (9) have shown that methyl substitution leads to a change of a factor of 2.5 in the rate of exit of naphthalene from SDS micelles.

Can. J. Chem. Downloaded from www.nrcresearchpress.com by 210.87.254.105 on 09/06/12
For personal use only.

Can. J. Chem. Downloaded from www.nrcresearchpress.com by 210.87.254.105 on 09/06/12
For personal use only.

(e.g. arenes) which do not suffer extensive changes upon excitation, but may be substantial where structural or dipolar changes are involved.

The rates of entry could only be determined for C_5 and C_6 dienes, since for the larger molecules the errors would be too large.

Typically we find $k_+ \sim 1\text{–}2 \times 10^9\ M^{-1}\ s^{-1}$. The value is substantially lower than that measured for methylene iodide (8) ($k_+ = 2.5 \times 10^{10}\ M^{-1}\ s^{-1}$, also in SDS micelles), but comparable with the value determined for di-*tert*-butyl nitroxide (17), $k_+ = 1.48 \times 10^9\ M^{-1}\ s^{-1}$. For 1-bromonaphthalene a value of $5\text{–}8 \times 10^9\ M^{-1}\ s^{-1}$ has been estimated (9). In the case of cyclic azoalkanes, Turro *et al.* measured entry rate constants of ca. $4 \times 10^9\ M^{-1}\ s^{-1}$ (5). Clearly small polar molecules (methylene iodide and nitromethane) enter the micelles at substantially faster rates than typical organic molecules, for which the rate constants fall in the $1\text{–}5 \times 10^9\ M^{-1}\ s^{-1}$ range. It is not entirely clear what controls the differences between the various families of substrates, although dipole moment, size, and shape are obvious candidates. More data are clearly necessary in order to reach general conclusions, in addition, it would be desirable to design experiments to test the consistency of the different experimental techniques.

In the previous section we have mentioned that one of the conditions for our kinetic analysis to apply is that if a quencher enters a micelle containing an excited probe, quenching will occur with a probability of 1.0. When a quencher enters a micelle its average residence time will equal k_-^{-1}, that is, it will be in the 0.12 to 10 μs range (Table 1). For reactions with close to diffusion-controlled rate constants in solution, Thomas *et al.* (8) have estimated an intramicellar rate constant of $7.5 \times 10^7\ s^{-1}$; i.e. reaction will occur in ca. 13 ns. Since our residence times are between 10 and 1000 times larger than the mean reaction time, we conclude that the condition mentioned above will be met in all the examples examined.

The rates of exit from the micelles seem to reflect the number of carbon atoms, a parameter that naturally must in turn correlate with the solubility of the dienes in water. In general, we find that for a given number of C-atoms the exit rates are larger for the cyclic quenchers.

In the interpretation of static phenomena we have mentioned before that while eq. [1] can be used for the larger molecules (replacing $[Q_m]$ by the bulk concentration), this approximation does not apply for those cases when a considerable fraction of the quencher molecules are resident in the water phase. In this case the partition equilibrium needs to be taken into consideration (5), which leads to eq. [11].

$$[11] \quad \ln (A^0/A) = \frac{K_{eq}[Q]}{1 + K_{eq}[M]}$$

Therefore, plots of $\ln (A^0/A)$ vs. [Q] are expected to be linear and the reciprocal of the slopes should, in turn, depend linearly on "[Det] − cmc" (replacing [M] by ([Det] − cmc)/$\bar{n}$). The slope of these plots corresponds to $\bar{n}^{-1}$ and the intercept to K_{eq}^{-1}. We find that for small molecules, where $1 \gg K_{eq}[M]$, only K_{eq} can be obtained, the slope being too small for accurate determination; even the values of K_{eq} are subject to considerable errors, reflecting largely that errors in laser flash experiments are more important in static than dynamic phenomena, as well as the logarithmic nature of eq. [11]. For example, for 1,3-cyclohexadiene the values of K_{eq} are $240\ M^{-1}$ from dynamic measurements and $580\ M^{-1}$ using eq. [11]. For large molecules (e.g. C_8), $1 \ll K_{eq}[M]$ and only the aggregation number can be obtained; the treatment being essentially the same as already described. An interesting example is the case of *cis*-2-*trans*-4-hexadiene where the two values in the denominator in eq. [11] are comparable; we obtained $\bar{n} \sim 81$ and $K_{eq} \sim 900\ M^{-1}$. While the errors are relatively large, the data are reasonably consistent with those obtained from dynamic studies or from other techniques.

It is interesting to compare the possibilities of triplet transient spectroscopy with those of fluorescence techniques for the study of micellar properties (i.e. cmc, $\bar{n}$) and kinetic properties (k_+, k_-). We find that while our approach does yield $\bar{n}$ values which are consistent with those obtained by other techniques (e.g. for SDS $\bar{n}$ values are 62 by light scattering (21), 63 by osmometry (22), 71 by fluorescence quenching (5), 60 using the luminescence from $Ru(bipy)_3^{2+}$ (6), 74 by pyrene excimer formation (23), and 63 by quenching T–T absorption in phenanthrene), it is not as simple as, e.g. luminescence quenching. For the determination of dynamic parameters the use of triplet absorption quenching has the advantage that, as a result of the longer time scales involved, it can be used to determine k_- values for quenchers that are largely resident in the micelle (e.g. 1,3-octadiene); it is also important to note that the condition of 100% efficient quenching generally assumed in the study of static phenomena is more likely to be met by triplets than by singlets, again reflecting the longer time scales involved. Also, in the case of dienes which have high energy singlet states, it would be extremely difficult to find a suitable fluorescent probe. In conclusion, both techniques

offer advantages in certain cases: luminescent probes are probably better for the study of micellar properties, while kinetic parameters, in particular for quenchers with high energy singlets, or very low solubility in water can be measured more easily and accurately using triplet transient absorptions.

Finally, it is conceivable that in some cases the *cis* and *trans* isomers of conjugated dienes may show kinetic differences (k_- and k_+) larger than those observed here for 1,3-pentadiene. In such cases it should be possible to design experiments involving the photosensitized isomerization of the dienes which would lead to *cis*/*trans* photostationary ratios substantially different from those obtained in homogeneous solution. This possibility could have considerable synthetic application and deserves further examination.

Experimental Section

Materials

Phenanthrene (Aldrich) was sublimed before the experiment. 1-Methylphenanthrene (ICN) was used as received. Sodium dodecyl sulfate (BDH, specially purified) was also used as received. In those experiments where the concentration of surfactant was changed the ionic strength was kept constant using sodium chloride (Anachemia).

When the isomer used in the case of the quenchers is not specified, it is usually because we used the commercially available isomeric mixture (where applicable). The sources of dienes were as follows: *cis*-1,3-pentadiene from Fluka, 1,3-octadiene from Chem. Samples Co., and all others from Aldrich.

Sample Preparation

The samples were contained in Suprasil cells made of 3 × 7 mm rectangular tubing (Vitro Dynamics), fitted in their upper part with tube of ca. 13 mm id which provided a convenient volume (5–7 mL) to minimize foam losses. In any case, the actual volume of solution (initially 2 mL) to which the quencher or quencher solution was added was determined by weighing the tube after deaerating with oxygen-free nitrogen.

Laser Flash Photolysis

Our facility uses the pulses from a Molectron UV-24 nitrogen laser for excitation. The system has been fully interfaced with a PDP 11-03L computer which processes the data initially acquired by an R-7912 Tektronix transient digitizer. A detailed description of the instrument can be found elsewhere (24).

Acknowledgement

The authors are grateful to Mr. S. E. Sugamori for his technical assistance.

1. J. K. Thomas. Acc. Chem. Res. **10**, 133 (1977).
2. J. K. Thomas, F. Grieser, and M. Wong. Ber. Bunsenges. Phys. Chem. **82**, 937 (1978).
3. N. J. Turro, M. W. Geiger, R. R. Hautala, and N. E. Schore. *In* Micellization, solubilization, and microemulsions. Vol. 1. *Edited by* K. L. Mittal. Plenum, New York. 1977. p. 75.
4. K. Kalyanasundaram. Chem. Soc. Rev. **7**, 453 (1978).
5. A. Yekta, M. Aikawa, and N. J. Turro. Chem. Phys. Lett. **63**, 543 (1979); M. Aikawa, A. Yekta, and N. J. Turro. Chem. Phys. Lett. **68**, 285 (1979).
6. N. J. Turro and A. Yekta. J. Am. Chem. Soc. **100**, 5951 (1978).
7. M. Grätzel and J. K. Thomas. J. Am. Chem. Soc. **95**, 6885 (1973).
8. P. P. Infelta, M. Grätzel, and J. K. Thomas. J. Phys. Chem. **78**, 190 (1974).
9. M. Almgren, F. Grieser, and J. K. Thomas. J. Am. Chem. Soc. **101**, 279 (1979); **101**, 2021 (1979).
10. P. P. Infelta. Chem. Phys. Lett. **61**, 88 (1979).
11. S. S. Atik, M. Nam, and L. A. Singer. Chem. Phys. Lett. **67**, 75 (1979).
12. R. H. Schnehl and D. G. Whitten. J. Am. Chem. Soc. **102**, 1938 (1980) and references therein.
13. M. A. J. Rodgers, M. F. Da Silva, and E. Wheeler. Chem. Phys. Lett. **53**, 165 (1978).
14. J. C. Dederen, M. Van der Auweraer, and F. C. De Schryver. Chem. Phys. Lett. **68**, 451 (1979).
15. K. L. Mittal (*Editor*). Micellization, solubilization and microemulsions. Vol. 2. Plenum, New York. 1977. (*a*) p. 531; (*b*) p. 569.
16. S. C. Wallace and J. K. Thomas. Radiation Res. **54**, 49 (1973); L. Putna, G. Reske, and H. Schmidt. Photochem. Photobiol. **30**, 723 (1979); C. Wolff and M. Grätzel. Chem. Phys. Lett. **52**, 542 (1977); M. Almgren and J. K. Thomas. Photochem. Photobiol. **31**, 329 (1980).
17. N. M. Atherton and S. J. Strach. J. Chem. Soc. Faraday II, **68**, 374 (1972).
18. G. Porter and M. W. Windsor. Proc. R. Soc. Ser. A, **256**, 238 (1958).
19. K. J. Mysels and L. H. Princen. J. Phys. Chem. **63**, 1696 (1959).
20. S. L. Murov. Handbook of photochemistry. Dekker, New York. 1973. Sect. 1.
21. K. Granath. Acta Chem. Scand. **7**, 297 (1953).
22. H. Coll. J. Phys. Chem. **74**, 520 (1970).
23. U. Khuanga, B. K. Selinger, and P. McDonald. Aust. J. Chem. **1**, 29 (1976).
24. J. C. Scaiano. J. Am. Chem. Soc. In press.

Can. J. Chem. Downloaded from www.nrcresearchpress.com by 210.87.254.105 on 09/06/12
For personal use only.

Synthesis and structural studies of iron(II) and iron(III) sulfonates

JOHN S. HAYNES, JOHN R. SAMS, AND ROBERT C. THOMPSON
Department of Chemistry, University of British Columbia, Vancouver, B.C., Canada V6T 1Y6

Received September 9, 1980

Can. J. Chem. Downloaded from www.nrcresearchpress.com by 210.87.254.40 on 09/06/12
For personal use only.

JOHN S. HAYNES, JOHN R. SAMS, and ROBERT C. THOMPSON. Can. J. Chem. **59**, 669 (1981).

The iron(II) sulfonates $Fe(CF_3SO_3)_2$ and $Fe(p\text{-}CH_3C_6H_4SO_3)_2$ have been prepared and on the basis of vibrational and electronic spectra and magnetic and Mössbauer data have been assigned a layer lattice structure involving hexacoordinated iron(II) and terdentate bridging anions. The FeO_6 chromophore in these compounds is distorted by a trigonal elongation along the C_3 axis. $Fe(CH_3SO_3)_2$ has been obtained in two isomeric forms, one having a trigonal elongation of the FeO_6 chromophore, the other a trigonal compression. No structural isomerism has been found for the other iron(II) sulfonates; however, evidence for such isomerism in methanesulfonates of cobalt(II) and zinc(II) is presented. While $Fe(CF_3SO_3)_2$ and $Fe(p\text{-}CH_3C_6H_4SO_3)_2$ appear to be magnetically dilute the presence of antiferromagnetic coupling in both forms of $Fe(CH_3SO_3)_2$ is indicated. The iron(III) sulfonates, $Fe(CF_3SO_3)_3$, $Fe(p\text{-}CH_3C_6H_4SO_3)_3$, and $Fe(CH_3SO_3)_3$, have been prepared and all three are magnetically concentrated exhibiting magnetic moments which are significantly less than 5.92 BM and which decrease with decreasing temperature.

JOHN S. HAYNES, JOHN R. SAMS et ROBERT C. THOMPSON. Can. J. Chem. **59**, 669 (1981).

En se basant sur les spectres de vibration et électronique et sur des données de Mössbauer et magnétiques, on a conclu que les sulfonates de fer(II) $Fe(CF_3SO_3)_2$ et $Fe(p\text{-}CH_3C_6H_4SO_3)_2$ qu'on a préparé, ont une structure cristalline en couches faisant intervenir du fer(II) hexacoordonné et des anions tridentates agissant comme ponts. Le chromophore FeO_6 de ces composés est déformé selon une élongation trigonale le long de l'axe C_3. On a obtenu le $Fe(CH_3SO_3)_2$ sous deux formes isomères, l'une ayant une élongation trigonale du chromophore FeO_6 et l'autre présentant une compression trigonale. On n'a pas trouvé d'isomère de structure des autres sulfonates de Fe(II); cependant on rapporte des données suggérant l'existence d'une telle isomérie dans les méthanesulfonates de cobalt(II) et de zinc(II). On note la présence d'un couplage anti-ferromagnétique des deux formes de $Fe(CH_3SO_3)_2$ même si le $Fe(CF_3SO_3)_2$ et le $Fe(p\text{-}CH_3C_6H_4SO_3)_2$ semblent être magnétiquement dilués. On a préparé les sulfonates de Fe(III), $Fe(CF_3SO_3)_3$, $Fe(p\text{-}CH_3C_6H_4SO_3)_3$ et $Fe(CH_3SO_3)_3$, et tous les trois magnétiquement concentrés ont des moments magnétiques qui sont beaucoup plus faibles que 5,92 BM et qui diminuent avec la température.

[Traduit par le journal]

Introduction

Sulfonate anions, RSO_3^-, have the potential to bond to metal ions as bidentate or terdentate bridging ligands with the consequent formation of highly polymeric materials. Calcium methanesulfonate, $Ca(CH_3SO_3)_2$, has been shown by X-ray diffraction studies to have a structure in which layers of metal atoms are bridged by CH_3SO_3 groups with each anion bridging three different metal centres and each metal ion surrounded by a nearly octahedral array of oxygens from six different anions (1). Analogous structures have been proposed for a number of metal bisfluorosulfates (2) and for the methanesulfonates, trifluoromethanesulfonates, and paratoluenesulfonates of copper(II) and cobalt(II) (3).

The work described here is an extension of our earlier study of iron(II) fluorosulfate (4) and was undertaken to determine whether the structural features exhibited by $Fe(FSO_3)_2$ are common to iron(II) sulfonates in general. This research involves, primarily, the synthesis of iron(II) salts of methane-, trifluoromethane-, and paratoluenesulfonic acids and the structural characterization of these materials using ^{57}Fe Mössbauer, vibrational and electronic spectroscopy, and variable temperature magnetic susceptibility studies.

During the course of this study we discovered that two structural modifications of iron(II) methanesulfonate can be isolated and a preliminary report on this appears elsewhere (5). In an effort to investigate the possibility of structural isomerism in methanesulfonates of other divalent metals we have also prepared and investigated the bismethanesulfonates of calcium, cobalt, copper, and zinc.

Both forms of $Fe(CH_3SO_3)_2$ gave evidence of magnetic concentration and the possibility that magnetic exchange effects might be even stronger in sulfonates of iron(III) prompted a study reported here of the synthesis and magnetic properties of $Fe(CH_3SO_3)_3$, $Fe(p\text{-}CH_3C_6H_4SO_3)_3$, and $Fe(CF_3SO_3)_3$. Previous work showed the magnetic moment of $Fe(FSO_3)_3$ to be significantly below the value expected for high spin d^5 and to be both temperature and field dependent, suggesting the presence of both ferromagnetic and antiferromagnetic coupling in that compound (6).

Experimental

Starting materials and solvents were reagent grade and used without further purification unless otherwise stated. Products were found to be susceptible to atmospheric moisture and, when isolated, required handling in a nitrogen atmosphere dry box or *in vacuo*. C and H analyses were obtained by P. Borda in the

0008-4042/81/040669-10$01.00/0
©1981 National Research Council of Canada/Conseil national de recherches du Canada

Can. J. Chem. Downloaded from www.nrcresearchpress.com by 210.87.254.40 on 09/06/12
For personal use only.

microanalytical laboratory at the University of British Columbia. Iron was determined by redox titration (7).

Preparations

Iron(II) Trifluoromethanesulfonate, $Fe(CF_3SO_3)_2$

Trifluoromethanesulfonic acid (20 mL) was freshly distilled at a pressure of 20 mm Hg at 70°C onto anhydrous iron(II) chloride (12 mmol). The product is insoluble in acid and to ensure complete reaction the reaction mixture was stirred under reflux conditions for approximately 40 h. The white solid product was vacuum filtered, washed with freshly distilled trifluoromethanesulfonic acid, and dried by heating under vacuum at 50°C.

Anal. calcd. for $FeC_2F_6S_2O_6$: C 6.78, H 0.00, Fe 15.8; found: C 6.75, H 0.00, Fe 15.9.

Iron(II) Paratoluenesulfonate, $Fe(p\text{-}CH_3C_6H_4SO_3)_2$

This salt was prepared by the reaction of aqueous solutions of silver(I) paratoluenesulfonate (17 mmol in 50 mL H_2O) with iron(II) chloride tetrahydrate (8.5 mmol in 10 mL H_2O). In order to avoid oxidation of Fe(II) to Fe(III) it was necessary to degas the water prior to use by several freeze–pump–thaw cycles. After combining the aqueous solutions the resulting mixture was stirred under a flow of nitrogen gas and the precipitated silver chloride was removed by filtration under nitrogen. The resulting solution of iron(II) paratoluenesulfonate was evaporated to dryness under vacuum and complete dehydration was accomplished by heating under vacuum at 120°C. The product is a pale green solid.

Anal. calcd. for $FeC_{14}H_{14}S_2O_6$: C 42.22, H 3.55, Fe 14.0; found: C 42.50, H 3.60, Fe 13.9.

α-Iron(II) Methanesulfonate, α-$Fe(CH_3SO_3)_2$

Silver(I) methanesulfonate (9.2 mmol in 30 mL H_2O) and iron(II) chloride tetrahydrate (4.6 mmol in 10 mL H_2O) were combined as described above for the preparation of the paratoluenesulfonate derivative. The product, a white solid, was isolated as described above and dried by heating under vacuum at 130°C.

Anal. calcd. for $FeC_2H_6S_2O_6$: C 9.76, H 2.46, Fe 22.7; found: C 9.93, H 2.48, Fe 22.5.

β-Iron(II) Methanesulfonate, β-$Fe(CH_3SO_3)_2$

An aqueous solution of iron(II) methanesulfonate, prepared as described above, was evaporated to dryness and complete dehydration of the product was obtained by prolonged (about three days) exposure to refluxing 2,2-dimethoxypropane. The product, a white solid, may also be obtained by treating the α-form with 2,2-dimethoxypropane in the same manner.

Anal. found: C 9.59, H 2.60, Fe 22.5.

Iron(II) Methanesulfonate Methanesulfonic Acid Solvate, $Fe(CH_3SO_3)_2 \cdot CH_3SO_3H$

Methanesulfonic acid (20 mL) was distilled at 165°C under pressure of 8.5 mm Hg onto anhydrous iron(II) chloride (15 mmol). A vigorous reaction occurred with the evolution of hydrogen chloride gas. The reaction mixture was heated to approximately 100°C for 8 h; the solid product was removed by vacuum filtration and then washed with several portions of freshly distilled acid. The white solid product was dried in vacuum for 24 h at 150°C. The infrared spectrum correlates well with a superposition of the spectra of α-iron(II) methanesulfonate and methanesulfonic acid (8). The elemental analysis confirms the presence of one molecule of solvent of crystallization.

Anal. calcd. for $FeC_3H_{10}S_3O_9$: C 10.53, H 2.95; found: C 10.37, H 2.86.

Infrared frequencies (cm^{-1}) are as follows: 1323 m, 1190 m sh, 1150 s, 1120 m, 1066 s, 990 s, 920 s, 787 m, 767 m, 566 s, 556 m, 542 m, 506 s, 484 w.

Iron(III) Trifluoromethanesulfonate, $Fe(CF_3SO_3)_3$

This compound was prepared from trifluoromethanesulfonic acid and iron(III) chloride by the method used to prepare the iron(II) derivative. The product, a white solid, was dried at 150°C.

Anal. calcd. for $FeC_3F_9S_3O_9$: C 7.16, H 0.00, Fe 11.1; found: C 7.04, H 0.00, Fe 11.3.

Iron(III) Methanesulfonate, $Fe(CH_3SO_3)_3$

This salt was prepared by the reaction of stoichiometric quantities of silver(I) methanesulfonate and iron(III) chloride hexahydrate as described for the preparation of α-$Fe(CH_3SO_3)_2$. The product, a light yellow solid, was dried by heating at 110°C for 24 h under vacuum.

Anal. calcd. for $FeC_3H_9S_3O_9$: C 10.56, H 2.66, Fe 16.4; found: C 10.50, H 2.80, Fe 16.1.

Iron(III) Paratoluenesulfonate, $Fe(p\text{-}CH_3C_6H_4SO_3)_3$

This salt was prepared by the reaction of silver(I) paratoluenesulfonate with iron(III) chloride hexahydrate as described for the preparation of the iron(II) derivative. The product, an orange solid, was dehydrated by heating under vacuum at 70°C.

Anal. calcd. for $FeC_{21}H_{21}S_3O_9$: C 44.29, H 3.72, Fe 9.8; found: C 44.16, H 3.85, Fe 9.7.

Bismethanesulfonates of Calcium, Cobalt, Copper, and Zinc, $M(CH_3SO_3)_2$

$Co(CH_3SO_3)_2$ and $Cu(CH_3SO_3)_2$ were prepared as described previously (3). The other compounds were prepared by the reaction of silver(I) methanesulfonate with aqueous solutions of the appropriate metal chloride as described for the preparation of α-$Fe(CH_3SO_3)_2$. All compounds were dried under vacuum at 110°C.

Anal. calcd. for $CoC_2H_6S_2O_6$: C 9.63, H 2.43; found: C 9.51, H 2.39. *Anal.* calcd. for $CuC_2H_6S_2O_6$: C 9.46, H 2.38; found: C 9.30, H. 2.48. *Anal.* calcd. for $CaC_2H_6S_2O_6$: C 10.43, H 2.63; found: C 10.52, H 2.71. *Anal.* calcd. for $ZnC_2H_6S_2O_6$: C 9.40, H 2.37; found: C 9.75, H 2.64.

Physical Methods

Infrared and electronic spectra were obtained as before (3). Magnetic susceptibilities were measured at room temperature and three different values of $H dH/dx$ using the Faraday magnetic balance described in the literature (9). The values were found to be field independent for all samples. Variable temperature magnetic susceptibilities were obtained using Gouy equipment (3). The molar magnetic susceptibilities were corrected for the diamagnetism of all atoms; the corrections used were $Fe^{2+} = 13$, $Fe^{3+} = 10$, $CF_3SO_3^- = 46$, $CH_3SO_3^- = 35$, $p\text{-}CH_3C_6H_4SO_3^- = 89$ (all 10^6 cm^3 mol^{-1}). ^{57}Fe Mössbauer spectra were measured as described elsewhere (10). Samples for Mössbauer studies were contained in nylon holders which were sealed with epoxy resin to avoid hydrolysis problems. The Doppler velocity scale was calibrated with a metallic iron foil absorber, and isomer shifts are quoted relative to the centroid of the iron foil spectrum.

Results

Iron(II) Sulfonates

The iron(II) sulfonates, $Fe(CF_3SO_3)_2$, $Fe(p\text{-}CH_3C_6H_4SO_3)_2$, and α-$Fe(CH_3SO_3)_2$, were obtained as hygroscopic powders, the first by reaction of anhydrous iron(II) chloride with trifluoromethanesulfonic acid and the other two by reaction of the silver(I) salt of the appropriate sulfonic acid with iron(II) chloride in aqueous solution followed by dehydration at elevated temperatures. A second form of the methanesulfonate, β-$Fe(CH_3SO_3)_2$, was obtained by prolonged exposure of the α form to refluxing 2,2-dimethoxypropane (DMP). To investigate the possibility of additional structural

Can. J. Chem. Downloaded from www.nrcresearchpress.com by 210.87.254.40 on 09/06/12
For personal use only.

isomers of iron(II) methanesulfonate we attempted to obtain a sample under anhydrous conditions by the reaction of iron(II) chloride with anhydrous methanesulfonic acid. The product obtained was a methanesulfonic acid solvate of composition $Fe(CH_3SO_3)_2 \cdot CH_3SO_3H$. Attempts to remove the solvate molecules by heating were unsuccessful.

Infrared spectra (250 to 1400 cm^{-1}) of the iron(II) sulfonates are given in Table 1 where assignments to vibrations associated with the CSO_3 groups have been made as was done previously for analogous copper and cobalt compounds (3). The two modifications of $Fe(CH_3SO_3)_2$ are clearly distinguished by their distinctive infrared spectra. Figure 1 compares the spectrum of a sample which had been treated for only a few hours with refluxing DMP with the spectra of pure α- and β-forms. The spectrum is clearly a superposition of the spectra of the two forms indicating that α converts directly to β with no other structural isomers present in the system. This is confirmed by the Mössbauer studies.

Mössbauer parameters at two temperatures are given in Table 2. Isomer shift values, δ, are rather high compared to values normally observed for high spin iron(II) (δ normally lies in the range 1.1 to 1.3 mm s^{-1}); the small temperature dependence is presumably a consequence of a second-order Doppler shift. All spectra show quadrupole splitting indicative of some distortion of the FeO_6 octahedra. The ΔE_Q values of $Fe(CF_3SO_3)_2$, $Fe(p\text{-}CH_3C_6H_4SO_3)_2$, and $Fe(FSO_3)_2$ (4) are comparable in magnitude and in temperature dependence; in contrast, the quadrupole splitting values of α-$Fe(CH_3SO_3)_2$ are significantly larger than those of the other derivatives while the ΔE_Q values of β-$Fe(CH_3SO_3)_2$ are significantly smaller. Figure 2 shows the Mössbauer spectra of pure α and β forms of $Fe(CH_3SO_3)_2$ along with the spectrum of a sample of the α form which had been refluxed in DMP for only a few hours (partial conversion to the β form). Consistent with the infrared study, these spectra show the presence of only two structural isomers in the $Fe(CH_3SO_3)_2$ system.

The electronic spectra of the iron(II) sulfonates are all similar in appearance to that reported for $Fe(FSO_3)_2$; they consist of a single broad band centred around 8600–9000 cm^{-1} with a shoulder at lower energy (Table 3).

Magnetic moments have been measured over the range 80 to 300 K and the results are listed in Table 4. The μ_{eff} values for $Fe(CF_3SO_3)_2$ and $Fe(p\text{-}CH_3C_6H_4SO_3)_2$ are in the range normally expected for high spin iron(II) and are comparable to the values shown by $Fe(FSO_3)_2$ while those of α- and particularly β-$Fe(CH_3SO_3)_2$ are anomalously low.

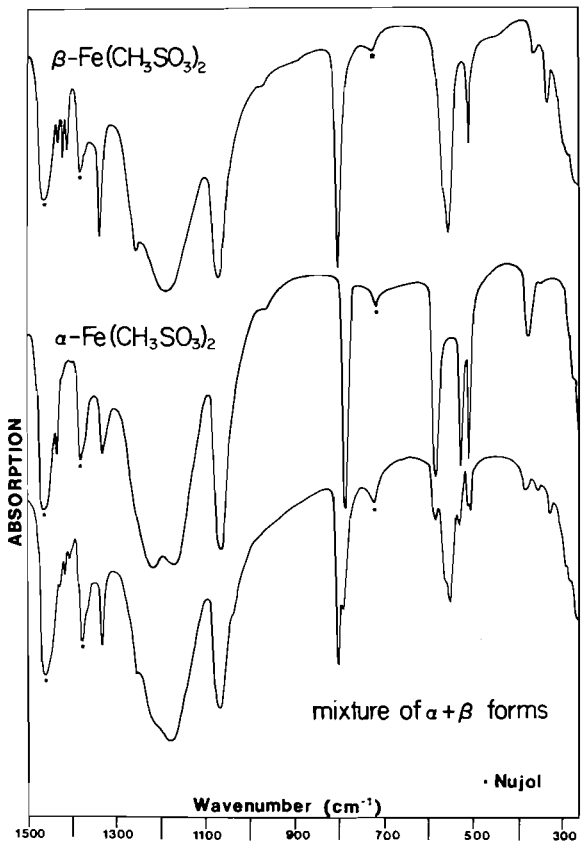

FIG. 1. Infrared spectra of α and β forms of iron(II) methanesulfonate.

The presence of structural isomerism in iron(II) methanesulfonate prompted us to look for evidence for isomerism in other $Fe(XSO_3)_2$ systems. Both $Fe(CF_3SO_3)_2$ and $Fe(p\text{-}CH_3C_6H_4SO_3)_2$ were heated under vacuum and treated with refluxing 2,2-dimethoxypropane for prolonged periods of time. The infrared spectra of different samples so treated remained unchanged, giving no evidence for conversion to isomeric forms. The sample of $Fe(CF_3SO_3)_2$ characterized here was prepared by the reaction of CF_3SO_3H with iron(II) chloride; another sample prepared by the silver salt method (analogous to the method used to obtain α-$Fe(CH_3SO_3)_2$) gave an identical infrared spectrum to that of the first sample indicating the different preparative methods yield the same structural form.

Methanesulfonates of Zn(II), Co(II), Cu(II), and Ca(II)

To pursue the question of isomerism in sulfonate polymers further we prepared methanesulfonates of other divalent metals. $Zn(CH_3SO_3)_2$ prepared by the silver salt method has a very complex infrared spectrum (Table 5 and Fig. 3). Refluxing a sample in

Can. J. Chem. Downloaded from www.nrcresearchpress.com by 210.87.254.40 on 09/06/12
For personal use only.

TABLE 1. Infrared spectra of iron sulfonates[a]

C_{3v} assignment for CSO_3 part	Infrared frequencies (cm^{-1})						
	$Fe(CF_3SO_3)_2$	$Fe(CF_3SO_3)_3$	α-$Fe(CH_3SO_3)_2$	β-$Fe(CH_3SO_3)_2$	$Fe(CH_3SO_3)_3$	$Fe(p\text{-}CH_3C_6H_4SO_3)_2$	$Fe(p\text{-}CH_3C_6H_4SO_3)_3$
$\nu_4(E)SO_3$ as. str.	1239 vs	1230 s 1078 s	1220 s 1175 s	1175 s	1279 s 1050 s br	1195 s	1280 s 1030 s
$\nu_1(A_1)SO_3$ sym. str.	1062 m	1014 s	1066 m	1072 m	980 sh	1145 m	1000 s
$\nu_2(A_1)SC$ str.			790 m	800 m	780 m 760 w	691 m	675 m
$\nu_5(E)SO_3$ as. defn.	647 m	635 m 600 w	587 m 531 m	551 m	565 m sh 530 m	580 m	553 s 540 sh
$\nu_3(A_1)SO_3$ sym. defn.	523 m	515 w 505 m	513 m	507 m	498 m	493 w	481 w
Unassigned	1300 w sh 1201 m 965 w 770 w 592 w 360 m	1370 m 1150 vw 780 w 570 w 428 m 355 w 328 w	1330 w 970 vw 383 m 355 w	1337 m 1260 m 975 vw 360 w 330 w	1340 w sh 410 m br 355 m	1270 vw 1112 vw 1070 m 1040 w 1022 m 822 m 712 w 400 w 370 w 340 w	1375 w sh 1112 m sh 810 s 700 w 420 m br

[a]v = very, s = strong, m = medium, w = weak, sh = shoulder, as. = asymmetric, sym. = symmetric, defn. = deformation, str. = stretch.

Can. J. Chem. Downloaded from www.nrcresearchpress.com by 210.87.254.40 on 09/06/12
For personal use only.

TABLE 2. ^{57}Fe Mössbauer parameters[a]

Compound	T (K)	δ (mm s^{-1})	ΔE_Q (mm s^{-1})	Γ_1 (mm s^{-1})	Γ_2 (mm s^{-1})
$Fe(CF_3SO_3)_2$	293	1.32	1.44	0.28	0.26
	80	1.45	1.84	0.47	0.44
α-$Fe(CH_3SO_3)_2$	293	1.34	2.95	0.41	0.39
	85	1.45	3.37	0.41	0.37
β-$Fe(CH_3SO_3)_2$	293	1.31	0.94	0.28	0.33
	80	1.48	1.41	0.35	0.34
$Fe(p\text{-}CH_3C_6H_4SO_3)_2$	291	1.32	1.39	0.30	0.28
	79	1.42	1.91	0.36	0.35
$Fe(FSO_3)_2$[b]	293	1.37	1.28	0.30	0.28
	84	1.49	1.77	0.32	0.34
$Fe(CF_3SO_3)_3$	293	0.55	0.25	0.78	0.22
	80	0.60	0.33	0.52	0.42
$Fe(CH_3SO_3)_3$	293	0.48	0.34	0.49	0.41
	80	0.59	0.36	0.50	0.46
$Fe(p\text{-}CH_3C_6H_4SO_3)_3$	293	0.49	0.37	0.57	0.44
	80	0.60	0.39	0.59	0.49

[a]Estimated precision of the parameters is ± 0.01 mm s^{-1}.
[b]Data from ref. 4.

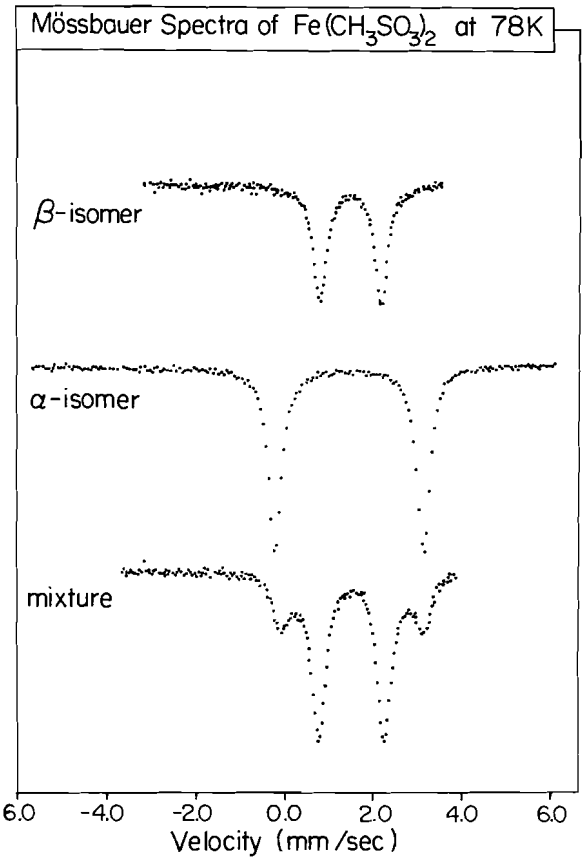

FIG. 2. Mössbauer spectra of α and β forms of iron(II) methanesulfonate.

TABLE 3. Electronic spectra

Compound	Energies of band maxima[a] (cm^{-1})
$Fe(FSO_3)_2$[b]	8800, 7100 sh
$Fe(CF_3SO_3)_2$	8600, 7600 sh
α-$Fe(CH_3SO_3)_2$	9000, 7400 sh
β-$Fe(CH_3SO_3)_2$	9000, 7300 sh
$Fe(p\text{-}CH_3C_6H_4SO_3)_2$	8700, 7300 sh

[a]Samples mulled in Nujol.
[b]Data from ref. 4.

2,2-dimethoxypropane yields a product the infrared spectrum of which is virtually identical to that of β-$Fe(CH_3SO_3)_2$. It seems likely that this sample, identified as β-$Zn(CH_3SO_3)_2$, is structurally similar to the β isomer of iron(II) methanesulfonate and that the original sample is another isomer or mixture of isomers. Inspection of the data in Table 5 shows that the original sample does not contain detectable quantities of β-$Zn(CH_3SO_3)_2$.

$Co(CH_3SO_3)_2$ prepared in the present work has an infrared spectrum identical to that reported previously (3). The spectrum shows reduced symmetry for the CSO_3 moiety and a pattern of lines almost identical to that observed for α-$Fe(CH_3SO_3)_2$. After refluxing this compound, identified as α-$Co(CH_3SO_3)_2$, for several days in DMP, the infrared spectrum of the α modification is replaced by a more complex spectrum indicative of conversion to another form or mixture of forms (Table 5). Interestingly, heating the DMP refluxed

Can. J. Chem. Downloaded from www.nrcresearchpress.com by 210.87.254.40 on 09/06/12
For personal use only.

TABLE 4. Magnetic moment data[a]

Compound	T (K)	μ_{eff} (BM)	T (K)	μ_{eff} (BM)
$Fe(CF_3SO_3)_2$	80	5.38	201	5.46
	82	5.45	203	5.46
	103	5.44	226	5.46
	104	5.48	228	5.45
	126	5.45	250	5.46
	129	5.51	252	5.44
	153	5.45	273	5.43
	153	5.49	277	5.44
	177	5.48	299	5.44
	178	5.47	303	5.44
α-$Fe(CH_3SO_3)_2$	82	5.01	205	5.23
	86	5.02	230	5.25
	106	5.12	254	5.26
	108	5.10	255	5.26
	130	5.15	280	5.27
	131	5.16	305	5.28
	155	5.20	306	5.29
	156	5.21		
	180	5.23		
	205	5.25		
β-$Fe(CH_3SO_3)_2$	77	4.58	180	5.14
	83	4.77	204	5.16
	102	4.86	205	5.17
	106	4.96	230	5.17
	130	5.02	230	5.18
	130	5.03	254	5.19
	154	5.08	255	5.20
	155	5.11	280	5.19
	179	5.13	280	5.20
			306	5.21
$Fe(p\text{-}CH_3C_6H_4SO_3)_2$	80	5.33	224	5.42
	102	5.39	229	5.40
	106	5.40	248	5.40
	127	5.40	254	5.41
	127	5.41	276	5.39
	151	5.42	277	5.38
	153	5.42	298	5.37
	178	5.44	303	5.36
	179	5.44		
	200	5.42		
	204	5.45		
$Fe(CF_3SO_3)_3$	80	5.22	253	5.75
	105	5.43	279	5.73
	130	5.56	306	5.82
	154	5.59		
	179	5.65		
	203	5.68		
	228	5.71		
$Fe(CH_3SO_3)_3$	84	5.09	232	5.52
	101	5.24	255	5.52
	124	5.31	280	5.53
	149	5.39	303	5.51
	182	5.45		
	208	5.50		
$Fe(p\text{-}CH_3C_6H_4SO_3)_3$	85	4.87	230	5.29
	106	4.99	254	5.30
	130	5.08	275	5.29
	156	5.16	304	5.34
	182	5.23		
	207	5.28		

[a]Data for each of the iron(II) compounds were obtained from two separate variable temperature experiments; those for the iron(III) compounds from one variable temperature experiment for each compound.

sample of $Co(CH_3SO_3)_2$ for a few hours at ~150°C results in complete reconversion to the α form as evidenced by the infrared spectra. Similar treatment of β-$Fe(CH_3SO_3)_2$ or β-$Zn(CH_3SO_3)_2$ does not cause reconversion of these materials to their α forms.

The sample of $Cu(CH_3SO_3)_2$ prepared in this work has an infrared spectrum which is identical to that reported previously (3). No amount of prolonged heating at elevated temperatures (~110°C) or treatment with refluxing 2,2-dimethoxypropane effected noticeable change in the spectrum. In view of these observations it seems unlikely that the complex spectrum observed for this material is a consequence of a mixture of different forms. It seems more likely that a single form exists for this compound in which there are non-equivalent methanesulfonate ions as was postulated previously (3).

Calcium(II) methanesulfonate, prepared by the silver salt method, shows a complex infrared spectrum (Table 5) in which more than one absorption is seen in the SO_3 symmetric stretching region. Since this is a non-degenerate A_1 vibration, splitting is not expected even in low symmetry and can be explained only by the presence of non-equivalent anions in the lattice. This is, in fact, consistent with the X-ray structure determination of Charbonnier *et al.* (1). As for copper(II) methanesulfonate, neither prolonged heating at elevated temperatures (~110°C) nor treatment with refluxing 2,2-dimethoxypropane effected noticeable change in the spectrum.

Iron(III) Sulfonates

The compounds $Fe(CF_3SO_3)_3$, $Fe(p\text{-}CH_3C_6H_4SO_3)_3$, and $Fe(CH_3SO_3)_3$ were obtained as hygroscopic powders by substituting iron(III) chloride as the iron source in preparative reactions analogous to those used to obtain the iron(II) sulfonates. The infrared spectra of the iron(III) derivatives are very similar with respect to bands arising from vibrations of the CSO_3 groups. Spectra with assignments are given in Table 1.

Mössbauer parameters are listed in Table 2. The δ values observed here all tend towards the higher limit of values normally observed for high spin iron(III) (δ normally lies in the range 0.1 to 0.6 mm s^{-1}). As for the iron(II) analogues the small temperature dependence of δ is presumably a consequence of a second order Doppler shift. Quadrupole splittings in the range 0.25–0.40 mm s^{-1} are seen for all iron(III) sulfonates studied. The splitting in these compounds shows only a small temperature dependence presumably because no thermally accessible low lying levels are present.

TABLE 5. Infrared spectra of Zn(II), Co(II), and Ca(II) methanesulfonates

C_{3v} assignment for CSO_3 part	Infrared frequencies (cm^{-1})*				
	$Zn(CH_3SO_3)_2$		$Co(CH_3SO_3)_2$		
	(*a*)	(*b*)	(*a*)	(*b*)	$Ca(CH_3SO_3)_2$
$\nu_4(E)SO_3$ as. str.	1288 m 1263 s 1230 s 1200 sh 1170 sh 1135 s	1170 s br	1233 s 1170 s	1180 s br	1200 s br
$\nu_1(A_1)SO_3$ sym. str.	1070 s 1040 s	1063 s	1070 s	1070 s 1035 m	1085 m sh 1070 s
$\nu_2(A_1)SC$ str.	808 m 780 m	800 s	787 s	800 m 780 w	800 s 790 s
$\nu_5(E)SO_3$ as. defn.	580 m 561 m 545 m 524 m	560 sh 550 s	590 m 530 m	563 m 550 m	557 s 542 s
$\nu_3(A_1)SO_3$ sym. defn.	503 w	502 m	512 m	500 w	530 w sh 520 m
Unassigned	1420 w br 1334 w 1288 w 370 w 350 w	1429 w 1419 w 1406 w 1331 m 1259 m 360 w	1330 w 970 w 385 w 373 w 350 w	1330 w 1250 w sh 420 w 390 w	1421 m 1330 m 1260 m 970 w 345 m

*(*a*) Before treatment with 2,2-dimethoxypropane, (*b*) after treatment (see text). See Table 1 for list of abbreviations.

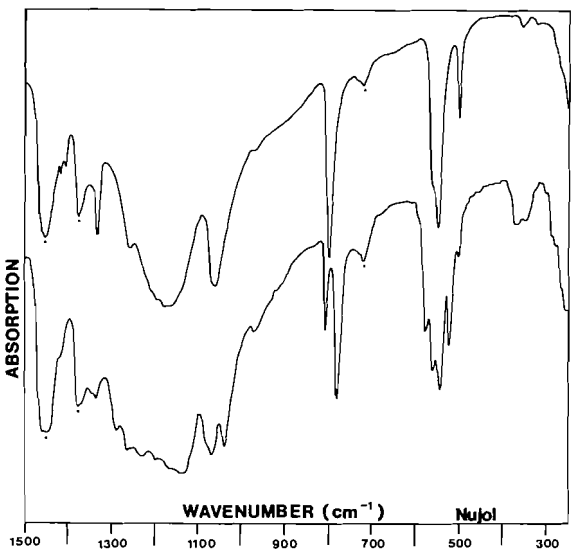

FIG. 3. Infrared spectrum of zinc(II) methanesulfonate. Bottom spectrum is that of initially prepared sample; top spectrum is of a sample after treatment with refluxing 2,2-dimethoxypropane (see text).

The magnetic moments of $Fe(CH_3SO_3)_3$, $Fe(CF_3SO_3)_3$, and $Fe(p\text{-}CH_3C_6H_4SO_3)_3$ measured over the temperature range 80 to 300 K are given in Table 4. The moments are lower than predicted for spin-free d^5 systems (though much higher than expected for spin-paired configurations) and are temperature dependent.

Discussion

Iron(II) Sulfonates

That $Fe(CF_3SO_3)_2$, $Fe(p\text{-}CH_3C_6H_4SO_3)_2$, and $\beta\text{-}Fe(CH_3SO_3)_2$ have basically the same structure as proposed for $Fe(FSO_3)_2$ (4), including a trigonally elongated FeO_6 chromophore, is suggested by the similarities in the infrared and electronic spectra and by the magnitude and temperature dependence of the quadrupole splitting. The CSO_3 groups retain C_{3v} approximate symmetry in all three compounds as evidenced by the fact that, within the limitation of resolution of the infrared spectrometer ($\sim 3\ cm^{-1}$) the $\nu_4(E)$ and $\nu_5(E)$ modes are not split (Table 1). This indicates that, as for $Fe(FSO_3)_2$, all three oxygens must be involved in equivalent coordination to iron. The electronic spectra are consistent with six-coordinate iron(II); the observed splitting of the electronic transition is best explained, as discussed previously (4), in terms of a dynamic Jahn–Teller effect.

Turning to interpretation of the Mössbauer data, a splitting of less than $\sim 2\ mm\ s^{-1}$ as shown by $Fe(CF_3SO_3)_2$, $Fe(p\text{-}CH_3C_6H_4SO_3)_2$, and $\beta\text{-}Fe(CH_3SO_3)_2$ indicates that either the ground state is a singlet and the crystal field splitting is small, or the

Can. J. Chem. Downloaded from www.nrcresearchpress.com by 210.87.254.40 on 09/06/12
For personal use only.

Can. J. Chem. Downloaded from www.nrcresearchpress.com by 210.87.254.40 on 09/06/12
For personal use only.

ground state is a doublet. The former may be obtained by a trigonal or tetragonal compression of the FeO_6 octahedron and the latter by a trigonal or tetragonal elongation. Since the quadrupole coupling constant e^2qQ is positive for tetragonal compression and trigonal elongation stereochemistries and negative for the other two possibilities, determination of the sign of the quadrupole splitting should help establish the form of coordination. Magnetic perturbation Mössbauer studies established that e^2qQ is positive in both $Fe(FSO_3)_2$ (4) and β-$Fe(CH_3SO_3)_2$ (5) and hence that the form of distortion is either trigonal elongation or tetragonal compression. A detailed fitting of the temperature dependence of the quadrupole splitting to a crystal field model for $Fe(FSO_3)_2$ (4) eliminated the possibility of tetragonal symmetry and established the distortion as a trigonal elongation along the C_3 axis of the FeO_6 octahedron and the ground state therefore as

$$[(\sqrt{2/3}|x^2 - y^2\rangle - \sqrt{1/3}|xz\rangle), (\sqrt{2/3}|xy\rangle + \sqrt{1/3}|yz\rangle)]$$

Such a form of distortion then is probable for the other three compounds under discussion and this is supported by more detailed Mössbauer studies including magnetic perturbation Mössbauer work (11). Moreover, a trigonal elongation is consistent with the infrared spectral results which show no observable lowering in the symmetry of the XSO_3 groups below C_{3v}. Anion symmetry would be expected to be lowered in the case of a tetragonally distorted FeO_6 octahedron.

The quadrupole splitting of α-$Fe(CH_3SO_3)_2$ is substantially greater than 2 mm s^{-1} and this is consistent only with an orbital singlet ground state, $|z^2\rangle$ in trigonal symmetry or $|xy\rangle$ in tetragonal symmetry. Magnetic perturbation Mössbauer studies have shown e^2qQ to be negative (5), consistent only with a trigonally compressed FeO_6 octahedron and $|z^2\rangle$ ground state. The infrared spectrum of the compound shows significant splitting of the $\nu_4(E)$ and $\nu_5(E)$ modes (Table 1) indicative of reduction of anion symmetry below C_{3v}. While this would be expected as a consequence of different Fe–O interactions brought about, for example, by a tetragonal distortion of the FeO_6 octahedron, the Mössbauer results show this is not the case here. Other possible causes include a small rhombic component superimposed on the trigonal distortion or a distortion of the $CH_3SO_3^-$ anions of a form in which the CH_3 moiety is displaced from the C_3 axis of the anion brought about, possibly, by intermolecular contacts between anions in adjacent layers of the polymeric lattice.

The high isomer shift values obtained for all the iron(II) compounds (Table 2) indicate a high degree of ionic character in the metal–ligand bonds; using the Walker–Wertheim–Jaccarino model (12) which relates isomer shift values to electron configurations the derived electron configuration for Fe(II) in these compounds is $3d^{6.00}4s^{0.00}$. The differences in isomer shift values are small and, as the isomer shifts are a function of lattice dynamics as well as the *s*-electron density, any attempt at a correlation between the isomer shifts and the base strengths of the anions would be very tenuous.

The magnetic data for $Fe(CF_3SO_3)_2$ and Fe(*p*-$CH_3C_6H_4SO_3)_2$ over the temperature range 80 to 300 K are very similar to those reported earlier for $Fe(FSO_3)_2$ over the same temperature range (4) and support the conclusion that these three compounds have very similar structures. The data could be fitted to the theoretical model described by Figgis *et al.* (13) using the following parameter values (values for $Fe(CF_3SO_3)_2$ given first, values for Fe(*p*-$CH_3C_6H_4SO_3)_2$ given second): orbital reduction factor $k = 0.8$ and 0.75, spin–orbit coupling constant $\lambda = -90$ and $-90\,cm^{-1}$ and axial field splitting paramter $v = 2$ and 3. The accuracy to which these parameters are determined is considered to be no better than ±5% in k and λ and, because of the relative insensitivity of calculated magnetic moments to small distortions, ±2 in the case of v(3). There are no significant differences (except perhaps in the value of k) between the two sets of parameters nor between these parameters and those calculated previously for $Fe(FSO_3)_2$ (4). The magnetic data support the conclusion drawn from the Mössbauer studies that the three compounds under discussion have very similar structures. The orbital reduction factor k decreases as XSO_3 varies from FSO_3 to CF_3SO_3 to *p*-$CH_3C_6H_4SO_3$ and while this may reflect an increase in electron delocalization in this series such an interpretation should be made with caution since a similar variation in λ (the value might also be expected to reflect the degree of electron delocalization) does not occur. Figgis *et al.* have in fact warned that the k values do not provide a good measure of electron delocalization (13).

Attempts to fit the magnetic moment data of α- and β-$Fe(CH_3SO_3)_2$ were less successful. To obtain magnetic moments as low as those observed for α-$Fe(CH_3SO_3)_2$ requires a k value of ~0.7 in the model and an even lower k value of ~0.5 is required for the β-isomer. Even assuming anomalously low k values, agreement between experiment and theory over the entire range of temperatures cannot be obtained with a single set of parameter values. We are forced to conclude that the methanesul-

Can. J. Chem. Downloaded from www.nrcresearchpress.com by 210.87.254.40 on 09/06/12
For personal use only.

fonate compounds are not magnetically dilute but that, particularly in the β-isomer, exchange of an antiferromagnetic nature is taking place between iron centres. In fact, Mössbauer studies have shown β-$Fe(CH_3SO_3)_2$ to undergo an antiferromagnetic phase transition at ~23 K (5). This finding is somewhat surprising not only because of the number of bridging atoms through which such an exchange would have to be transmitted but also because of the highly ionic nature of the iron–sulfonate linkages as indicated by the Mössbauer isomer shift results. It is also not clear why the two methanesulfonate compounds should show magnetic concentration while the paratoluenesulfonate, trifluoromethanesulfonate, and fluorosulfate derivatives appear to be magnetically dilute.

Our studies have generated the following structural model for iron(II) sulfonate polymers. Planes of iron atoms are sandwiched by planes of sulfonate anions; the anions are acting as terdentate ligands, each bridging to three different metal ions; each metal ion is surrounded by oxygen atoms from six different anions. The FeO_6 chromophore is not a regular octahedron and the distortion which is present may be considered as follows. Starting with a regular FeO_6 octahedron this may be distorted by increasing the O—S—O bond angles (compress XSO_3 along its C_3 axis), resulting in a trigonal elongation of FeO_6 along a C_3 axis perpendicular to the plane of iron atoms. This is the form of distortion found in $Fe(CF_3SO_3)_2$, $Fe(p\text{-}CH_3C_6H_4SO_3)_2$, β-$Fe(CH_3SO_3)_2$, and $Fe(FSO_3)_2$. The α form of $Fe(CH_3SO_3)_2$, on the other hand, has a structure in which, relative to the β form, the $CH_3SO_3^-$ anions are elongated along their C_3 axes thus resulting in a trigonal compression of the FeO_6 chromophore.

It is interesting to compare the iron(II) sulfonates with the previously studied cobalt(II) analogues (3). Similarities in their infrared spectra suggest structural similarities in the $M(XSO_3)_2$ (where M = Fe, Co; X = F, CF_3, p-$CH_3C_6H_4$) compounds. They all have C_{3v} anion spectra and any distortion of the MO_6 chromophores from O_h symmetry is likely to be trigonal (proven to be trigonal elongation in the case of the iron compounds). The cobalt(II) methanesulfonate compound identified in the previous section as α-$Co(CH_3SO_3)_2$ has a distorted anion spectrum which is virtually identical to that of α-$Fe(CH_3SO_3)_2$. While it had been suggested earlier (3) that the distortion of the anion might be due to a tetragonal distortion of the CoO_6 octahedron, it is clear from the present work that this is not necessarily the case. It seems more likely that the compound has an octahedral MO_6 chromophore or, as for the iron compound, a trigonally compressed octahedron. Possible causes of reduction in anion symmetry below C_{3v} were discussed previously for α-$Fe(CH_3SO_3)_2$. Another important point of similarity in the iron(II) and cobalt(II) methanesulfonates is that both compounds can be obtained in more than one structural form.

Copper(II) sulfonates have also been studied before; however, direct comparison with the iron(II) analogues is less informative here since the copper salts are all very strongly distorted as expected for a d^9 configuration. One important conclusion based on the present study is that while it had always been assumed previously (3, 6) that $Cu(XSO_3)_2$ compounds contain tetragonally distorted CuO_6 octahedra, it now seems possible that the form of distortion is a trigonal elongation or compression.

Structural Isomerism

Iron(II) methanesulfonate is shown by this work to exist in two distinct structural forms, α-$Fe(CH_3SO_3)_2$ and β-$Fe(CH_3SO_3)_2$. Isomerism in methanesulfonates of this type is not restricted to iron(II). This is demonstrated by the studies on $Co(CH_3SO_3)_2$ which indicate the existence of an α form as well as at least one other isomer and by the studies on $Zn(CH_3SO_3)_2$ which suggest the presence of a β modification and at least one other isomer. Not all metal bismethanesulfonates readily show this structural isomerism, however. $Ca(CH_3SO_3)_2$ and $Cu(CH_3SO_3)_2$, which appear from their infrared spectra to be structurally related (evidence for non-equivalent anions in the lattices of both salts), have been obtained as single forms only.

Considering the proven existence of structural isomers of methanesulfonates, one might expect to find evidence for structural isomerism in other sulfonate derivatives. Thus far, no such evidence has been obtained. As described in the previous section some effort to obtain structural isomers of $Fe(CF_3SO_3)_2$ and $Fe(p\text{-}CH_3C_6H_4SO_3)_2$ has been made but without success. The lack of an α form (trigonally compressed FeO_6 octahedra) of $Fe(CF_3SO_3)_2$ may be a consequence of electronegativity effects. As the electronegativity of X increases, the extent of S—O double bonding in XSO_3^- anions should increase and this should favour larger O—S—O bond angles and therefore trigonally elongated FeO_6 chromophores (β form). For this reason it may prove difficult to obtain any divalent metal fluorosulfate or trifluoromethanesulfonate with the α-$Fe(CH_3SO_3)_2$ structure. On the other hand, one might expect to be able to obtain α isomers of divalent metal paratoluenesulfonates. The fact that we have obtained no evi-

dence for α-Fe(p-$CH_3C_6H_4SO_3)_2$ may simply reflect the lack of a suitable synthetic route to this material.

Iron(III) Sulfonates

The infrared spectra of $Fe(CF_3SO_3)_3$, Fe(p-$CH_3C_6H_4SO_3)_3$, and $Fe(CH_3SO_3)_3$ show significant splitting of the formally doubly degenerate ν_4 and ν_5 modes, consistent with reduction of CSO_3 symmetry below C_{3v} (Table 1). This in turn is consistent with six-coordinate iron(III) since the stoichiometry requires that for FeO_6 chromophores each sulfonate must utilize only two of its oxygen atoms for bonding.

The isomer shifts (Table 2) are consistent with high spin electron configurations for all three compounds with the rather high values indicating, as for the iron(II) derivatives, a rather high degree of ionic character in the iron–oxygen bonds. Again, no correlation between isomer shift and anion basicity seems possible. No quadrupole splitting is expected for octahedral high-spin iron(III) compounds yet small but significant splittings are seen for all three compounds. Any valence contribution to the electric field gradient (i.e. unequal electron distribution in either bonding or non-bonding orbitals) seems difficult to imagine here and a lattice contribution from a non-cubic distribution of charges about the Fe^{3+} ion seems much more likely to account for the observed splitting.

Spin-free iron(III) complexes should have temperature independent magnetic moments of 5.92 BM. All three compounds studied here have moments which are lower than 5.92 BM over the entire range of temperatures (80 to 300 K) and which decrease with decreasing temperature (Table 4). The presence of antiferromagnetic interaction in these compounds seems certain; moreover, the deviation from the expected value of 5.92 BM increases in the series $Fe(CF_3SO_3)_3$ < $Fe(CH_3SO_3)_3$ < Fe(p-$CH_3C_6H_4SO_3)_3$ reflecting perhaps increasing degree of covalent character in the metal–anion bonds along the series.

To summarize the results of the magnetic susceptibility studies, two of the iron(II) sulfonates, the α and β forms of $Fe(CH_3SO_3)_2$, gave evidence for weak magnetic exchange interaction while evidence for significant antiferromagnetic coupling was found for all three iron(III) sulfonates studied. The work has shown that magnetic exchange in iron sulfonate polymers is possible particularly when the metal is in the +3 oxidation state in spite of the fact that iron–sulfonate bonds are highly ionic and the exchange must take place over three atoms in the bridging ligand.

Acknowledgements

Financial support from the Natural Sciences and Engineering Research Council of Canada and the Natural, Applied, and Health Sciences Committee (U.B.C.) is gratefully acknowledged. We thank Mrs. A. Sallos for technical assistance.

1. F. CHARBONNIER, R. FAURE, and H. LOISELEUR. Acta Crystallogr. B33, 1478 (1977).
2. C. S. ALLEYNE, K. O'SULLIVAN MAILER, and R. C. THOMPSON. Can. J. Chem. **52**, 336 (1974).
3. A. L. ARDUINI, M. GARNETT, R. C. THOMPSON, and C. T. C. WONG. Can. J. Chem. **53**, 3812 (1975).
4. J. R. SAMS, R. C. THOMPSON, and T. B. TSIN. Can. J. Chem. **55**, 115 (1977).
5. J. S. HAYNES, J. R. SAMS, and R. C. THOMPSON. Chem. Phys. Lett. **75**, 596 (1980).
6. J. GOUBEAU and J. B. MILNE. Can. J. Chem. **45**, 2321 (1967).
7. G. CHARLOT and D. BÉZIER. Quantitative inorganic analysis. Methuen and Co., London, Engl. 1957. p. 447.
8. S. M. CHACKALACKAL and F. E. STAFFORD. J. Am. Chem. Soc. **88**, 4815 (1966).
9. F. G. HERRING, B. LANDA, R. C. THOMPSON, and C. F. SCHWERDTFEGER. J. Chem. Soc. A, 528 (1971).
10. J. R. SAMS and T. B. TSIN. Inorg. Chem. **14**, 1573 (1975).
11. J. S. HAYNES, J. R. SAMS, and R. C. THOMPSON. To be published.
12. L. R. WALKER, G. K. WERTHEIM, and V. JACCARINO. Phys. Rev. Lett. **6**, 98 (1961).
13. B. N. FIGGIS, M. GERLOCH, J. LEWIS, F. E. MABBS, and G. A. WEBB. J. Chem. Soc. A, 2086 (1968).

Can. J. Chem. Downloaded from www.nrcresearchpress.com by 210.87.254.40 on 09/06/12
For personal use only.

Substituent effects on the spectral behavior and synthesis of mercury 1,5-diarylthiocarbazonates

NORI Y. C. CHU

Materials and Process R and D Laboratory, Vision Care and Safety Products Division, American Optical Corporation, Southbridge, MA 01550, U.S.A.

AND

STEVEN A. GOLDSTEIN[1] AND PHILIP M. KEEHN

Department of Chemistry, Brandeis University, Waltham, MA 02154, U.S.A.

Received June 17, 1980

NORI Y. C. CHU, STEVEN A. GOLDSTEIN, and PHILIP M. KEEHN. Can. J. Chem. **59**, 679 (1981).

Symmetric and unsymmetric substituted 1,5-diarylthiocarbazones, and their mono- and bismercury complexes, were synthesized for spectral analysis. The first singlet–singlet transition of the mercury complexes was determined and the spectral shift produced by trifluoromethyl substitution was compared with that caused by different substituents in similar complexes. The large magnitude of the hypsochromic shift produced by the trifluoromethyl substituent can be explained by concerted steric and inductive effects, while the smaller bathochromic shift induced by the methoxy substituent is a result of opposing steric and electronic effects. In the trifluoromethyl substitution, a hypsochromic shift caused by steric influences was found to be 500 cm^{-1} in the photochromic unactivated state, and 250 cm^{-1} in the photochromic activated state. A similar shift caused by inductive influences was found to be 750 cm^{-1} in the photochromic unactivated state, and 600 cm^{-1} in the photochromic activated state. The smaller spectral shift observed in the photochromic activated state is consistent with the elucidated structure of the unsymmetric 1,5-diarylthiocarbazone, **6***d*, which was shown that the trifluoromethyl substitution was on the phenylazo portion of the molecule by chemical and spectral studies.

NORI Y. C. CHU, STEVEN A. GOLDSTEIN et PHILIP M. KEEHN. Can. J. Chem. **59**, 679 (1981).

En vue d'en faire une analyse spectrale, on a synthétisé des diaryl-1,5 thiocarbazones substituées de façon symétrique et non symétrique ainsi que leurs mono et bis complexes de mercure. On a déterminé la première transition singulet–singulet des complexes de mercure et on a comparé les déplacements produits dans les spectres par le substituant trifluorométhyle avec ceux provoqués par d'autres substituants dans des complexes semblables. On peut expliquer l'ampleur du déplacement hypsochrome provoqué par le substituant trifluorométhyle en se basant sur des effets inductifs et stériques concertés alors que la valeur plus faible du déplacement bathochrome induite par le substituant méthoxy serait le résultat d'effets électronique et stérique opposés. Dans le cas du substituant trifluorométhyle, on a trouvé que le déplacement hypsochrome provoqué par des influences stériques est de 500 cm^{-1} dans l'état photochrome inactivé et de 250 cm^{-1} dans l'état photochrome activé. On a trouvé qu'un déplacement semblable provoqué par des influences inductives est de l'ordre de 750 cm^{-1} dans l'état photochrome inactivé et de 600 cm^{-1} dans l'état photochrome activé. Les déplacements plus faibles observés dans l'état photochrome activé sont en accord avec la structure trouvée pour la diaryl-1,5 thiocarbazone non symétrique (**6***d*) pour laquelle des études chimiques et spectrales on montré que le substituant trifluorométhyle se trouve sur la portion phénylazo de la molécule.

[Traduit par le journal]

Introduction

The photochromic properties of mercury bis-(1,5-diphenylthiocarbazonate) (**1**) were discovered independently by Irving *et al.* (1) and Webb *et al.* (2). Benzene or chloroform solutions of **1** are orange, and show absorption maxima at 485 nm ($\varepsilon \sim 7 \times 10^4$), 320 nm (sh, $\varepsilon \sim 1.5 \times 10^4$), and 270 nm ($\varepsilon \sim 4 \times 10^4$). When irradiated by sunlight, solutions develop an intense blue color which changes back to orange when solutions are placed in the dark. The color change upon irradiation is due to a new absorption centered at 606 nm ($\varepsilon \sim 4 \times 10^4$), and to decreased absorption at 485 nm. The photochromic change is minimized in hydroxylic solvents, organic acids, and bases, and is most dramatic in dry, nonpolar solvents (3).

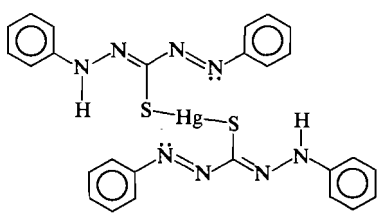

1

The absorption of **1** in the visible region of the spectrum can be attributed to the ligand since a solution of 1,5-diphenylthiocarbazonate ion (**2***b*) exhibits a single strong absorption maximum at 470 nm ($\varepsilon \sim 2 \times 10^4$). 1,5-Diphenylthiocarbazone (**2***a*), however, shows well defined bands at 450 and 620 nm.

The effect of substitution in the benzenoid rings of the ligands on the spectral properties of mercury

[1]Present address: Harvard Medical School, Boston, MA.

0008-4042/81/040679-09$01.00/0

©1981 National Research Council of Canada/Conseil national de recherches du Canada

Can. J. Chem. Downloaded from www.nrcresearchpress.com by 210.87.254.105 on 09/06/12
For personal use only.

TABLE 1. Effect of substituents on the absorption maximum of mercury bis(1,5-diarylthiocarbazonates) in methylene chloride[a]

	Ortho		*Meta*		*Para*	
Substituent	λ_{max} (nm)	ε	λ_{max} (nm)	ε	λ_{max} (nm)	ε
H	485	63 700	485	63 700	485	63 700
C_2H_5	475[b]	44 100	—[c]	—[c]	498	70 700
F	485	52 800	485	63 200	485	56 800
Cl	485	49 000	485	60 900	495	—[e]
CH_3O	510	46 100	490	64 200	510	72 000
CF_3	445	53 000	485[d]	57 000[d]	485[d]	55 900[d]

[a]Data obtained from ref. 5 except as noted.
[b]The adsorption peak for a CH_3 substituent at the *ortho* position is at 475 nm.
[c]Compound not prepared.
[d]Present work.
[e]Sample too insoluble.

bis(1,5-diarylthiocarbazonates) has been documented by Coleman *et al.* (5) (Table 1). They reported that *meta* substituents produced only small effects on the position of the absorption maxima and molar absorptivities, while large spectral changes were produced by *ortho* substituents. They attributed the decrease in the molar absorptivity caused by most *ortho* substituents, and the spectral blue shifts induced by 2-ethyl and 2-trifluoromethyl groups to steric influences.

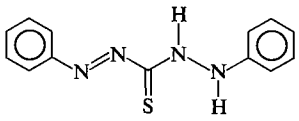

2a

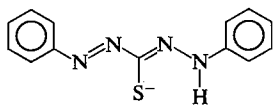

2b

Closer examination of the spectral blue shifts produced by *ortho* substituents reveals that only relatively bulky substituents at this position cause a spectral shift. Steric influences cannot, however, explain the large spectral blue shift produced by 2-trifluoromethyl substituents in comparison with 2-ethyl substituents. This is demonstrated spectrally in mercury bis[1,5-di(2′-methylphenyl)thiocarbazonate], which shows an absorption maximum at 475 nm (as does the 2-ethyl substituted material), since the size of a methyl group is about the same as a trifluoromethyl group.

In order to explain the large spectral shift produced by 2-trifluoromethyl substitution, an investigation of the spectral behavior of symmetric and unsymmetric mercury 1,5-diarylthiocarbazonates with trifluoromethyl substitution has been undertaken.

Synthesis of Diarylthiocarbazones

Methods for synthesis of symmetric 1,5-diarylthiocarbazones have been described by Fischer (6) and Bamberger (7). In the Bamberger method, Scheme 1, 2 mol of aryldiazonium salt are coupled with 1 mol of nitromethane at pH ~ 5 to form nitro(bisarylazo)methane (**4**). Reduction of **4** with ethanolic ammonium sulfate affords 1,5-diarylthiocarbazide (**5**), which is oxidized in alkaline solution to form 1,5-diarylthiocarbazone (**6**).

The coupling of aryldiazonium salts with nitromethane is strongly pH dependent (7). At low pH (~1), 1 mol of aryldiazonium salt couples with 1 mol of nitromethane to form 1-(nitromethylene)-2-arylhydrazine (**3**), while at higher pH (~5), 2 mol of aryldiazonium salt react with 1 mol of nitromethane to form **4**. Pupko and Pelkis (8, 9) have utilized the pH dependence of coupling to synthesize a number of unsymmetric 1,5-diarylthiocarbazones.

Employing the method of Bamberger, with modifications to improve yields, symmetric and unsymmetric trifluoromethyl substituted 1,5-diphenylthiocarbazones were synthesized. We observed that, at low pH (~1), 2-trifluoromethylphenyldiazonium salts predominantly reacted with nitromethane to give 1-(nitromethylene)-2-(2′-trifluoromethylphenyl)hydrazine (**3**, $R_1 = CF_3$), in 90–95% yield. In contrast, the coupling reaction of unsubstituted phenyldiazonium salts (**3**, $R_1 = H$) was not efficient, yields were less than 30%, and obtaining the pure product required numerous recrystallizations.

Structure Determination of 1-(2′-Trifluoromethylphenyl)-5-phenylthiocarbazone

Two isomeric products, **6***d* and **6***e*, could have been obtained in the synthesis of 1-(2′-trifluoromethylphenyl)-5-phenylthiocarbazone from oxidation of **5***d*. The absorption properties of these two isomers, and their mercury complexes, would be different. Therefore, it was important to establish whether the isolated product was a mixture of **6***d* and **6***e*, or one favored product. This was of particular importance since it had previously been demonstrated by X-ray analysis (10) that the azo and hydrazo functions in the symmetric 1,5-

Can. J. Chem. Downloaded from www.nrcresearchpress.com by 210.87.254.105 on 09/06/12
For personal use only.

Can. J. Chem. Downloaded from www.nrcresearchpress.com by 210.87.254.105 on 09/06/12
For personal use only.

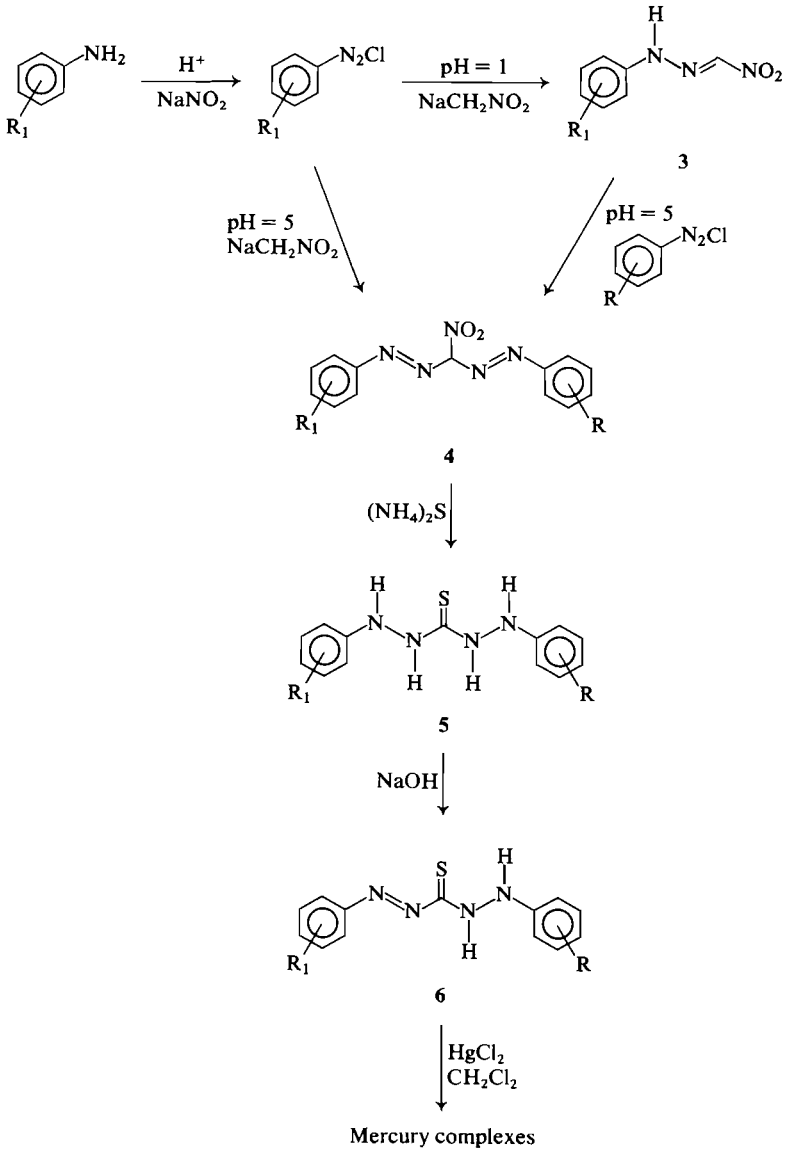

Isomer	R	R_1
a	2′-CF_3	2′-CF_3
b	3′-CF_3	3′-CF_3
c	4′-CF_3	4′-CF_3
d	H	2′-CF_3
e	2′-CF_3	H
f	H	H

SCHEME 1

diphenylthiocarbazone showed no localized single or double bonds in the

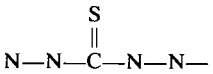

chain and tautomerism would interconvert **6***d* and **6***e* as shown in Scheme 2. Structural analysis identified the product as **6***d*, with the 2-trifluoromethyl substituted aryl ring bound to the azo portion of the thiocarbazone group.

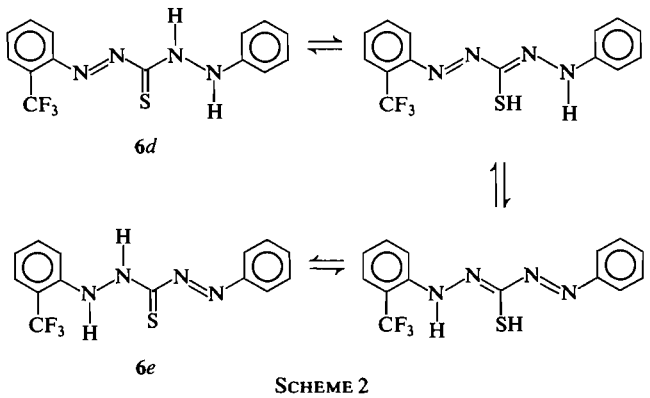

SCHEME 2

The structure determination, Scheme 3, was achieved by employing the reported (11) reaction of thiocarbazones with phosgene to give 1,3,4-thiodiazol-5-ones. Phosgene reacts with the hydrazo portion of thiocarbazone to afford a relatively stable 1,3,4-thiodiazol-5-one (**7***d–f*). Subsequent reduction (12) by zinc of the thiodiazolone produces an aryl amine (**9***d–f*) and a thiosemicarbazide (**10***d–f*). If the isolated thiocarbazone product were a mixture of **6***d* and **6***e*, then this sequence of reactions would yield amines **9***d* and **9***e*, and thiosemicarbazides **10***d* and **10***e* as products of reduction. Isolation of a single amine and thiosemicarbazide pair (**9***d* and **10***d* or **9***e* and **10***e*) would indicate that a single thiocarbazone product had been isolated. Further, if a single amine and thiosemicarbazide pair were produced, the position of the substituted aryl ring relative to the azo or hydrazo function of the thiocarbazone product would be established by the presence of the trifluoromethyl substituent on either the aryl amine (azo portion) or thiosemicarbazide (hydrazo portion).

When the reaction sequence was performed on

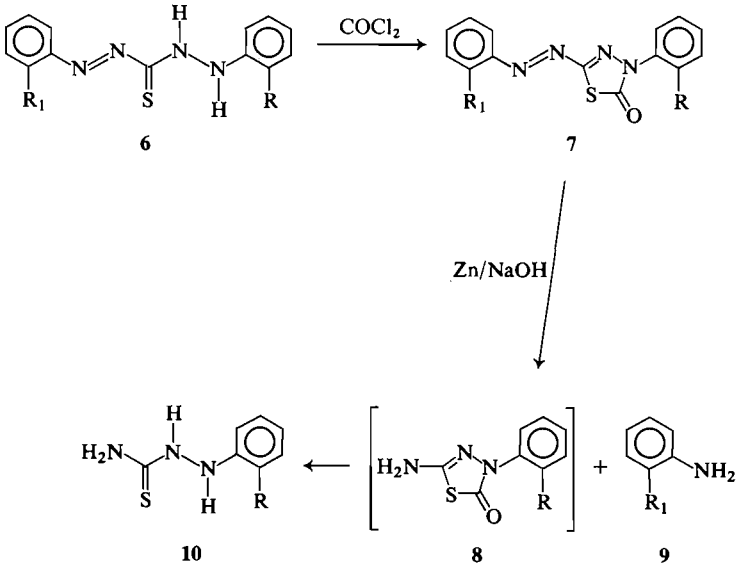

Isomer	R_1	R
d	CF_3	H
e	H	CF_3
f	H	H

SCHEME 3

Can. J. Chem. Downloaded from www.nrcresearchpress.com by 210.87.254.105 on 09/06/12
For personal use only.

Can. J. Chem. Downloaded from www.nrcresearchpress.com by 210.87.254.105 on 09/06/12
For personal use only.

1,5-diphenylthiocarbazone (**6***f*), aniline (**9***f*) was obtained from reduction of 2-phenylazo-4-phenyl-1,3,4-thiodiazol-5-one (**7***f*), as identified by gas chromatographic and infrared spectral analyses (11). Reaction of the isolated thiocarbazone product (**6***d* and/or **6***e*) with phosgene afforded a single orange crystalline product with elemental analysis ($C_{15}H_9F_3N_4OS$) and spectral properties suggesting a thiodiazolone structure. Reduction of the thiodiazolone with zinc and NaOH afforded two major products, a solid and a liquid. Infrared and gas chromatographic analyses of the liquid, when compared with a known standard, demonstrated the presence of 2-trifluoromethylaniline (**9***d*) exclusively; no aniline was observed at the limit of detection sensitivity. The solid product melted at 198–200°C, and its infrared spectrum was identical to 1-phenyl-3-thiosemicarbazide (**10***d*).[2] The isolated thiocarbazone product was therefore a single tautomer, **6***d*, with the 2-trifluoromethyl substituted aryl ring bound to the azo portion of the thiocarbazone group.

Spectral Properties of Mercury Complexes of 1,5-Diarylthiocarbazones

A toluene solution of mercury bis(1,5-diphenylthiocarbazonate) (**1**) shows an intense absorption with a maximum at 485 nm. Upon irradiation the intensity of this band decreases, while a new absorption band appears at 606 nm, Fig. 1. Substitution of the benzenoid rings with 2-trifluoromethyl groups causes a blue shift in these maxima to 445 nm and 560 nm, Fig. 2. No spectral shift is observed when trifluoromethyl substituents are on either the *meta* or *para* positions. These results and the spectral properties of mercury complexes of 1,5-diphenylthiocarbazones with other substituents in the benzenoid rings obtained by Coleman *et al.* (5) are given in Table 1. It is observed that monosubstitution at the *meta* or *para* position does not change the position of the absorption greatly though a large spectral shift is induced by a relatively bulky *ortho* substituent or a trifluoromethyl group.

The spectral shifts produced by *ortho* substituents can be explained by steric and inductive effects. X-ray crystallography (13) shows that the atoms of both ligands in mercury bis(1,5-diphenylthiocarbazonate) exist primarily in a planar configuration. This configuration maximizes the interaction of π-electrons of the benzenoid rings and the

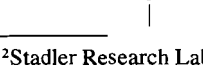

[2]Stadler Research Laboratories, Inc., mp 198–200°C.

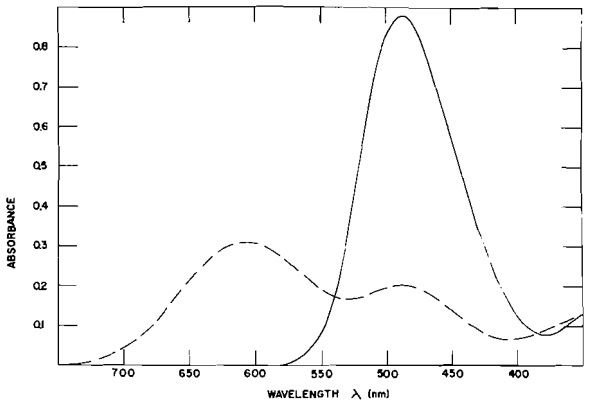

FIG. 1. The absorption spectrum of mercury bis(1,5-diphenylthiocarbazonate) (**1**) in toluene. The solid curve shows the spectrum before and the dashed curve after irradiation.

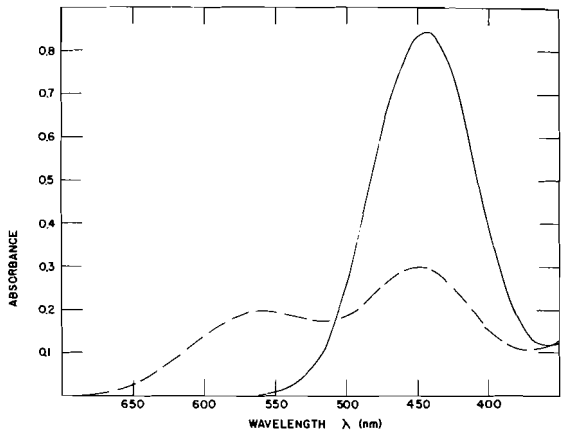

FIG. 2. The absorption spectrum of mercury bis[1,5-di(2-trifluoromethylphenyl)thiocarbazonate] (**14**) in toluene. The solid curve shows the spectrum before and the dashed curve after irradiation.

chain. It seems likely that 2-methyl or 2-ethyl substituents will force the benzenoid rings out of the

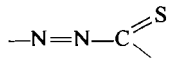

plane and increase the energy required for photochromic activation, causing the observed blue shift. This explanation is consistent with the observation that fluorine or chlorine in the *ortho* position does not cause spectral shifts (while 2-methyl substitution does) since these substituents are smaller than methyl. However, the large spectral shift caused by methoxyl and trifluoromethyl substituents cannot be accounted for by steric effects alone, as asserted by Coleman *et al.* (5).

Mercury complexes with a single 1,5-diphenylthiocarbazone ligand, e.g., phenylmercuric 1,5-diphenylthiocarbazonate (**11**), show absorption maxima at 470–475 nm, which is blue shifted by

TABLE 2. The spectral properties of ϕ HgDZ(1), ϕ HgDZ(2), $Hg[DZ(1)]_2$, $Hg[DZ(2)]_2$, and $Hg[DZ(3)]_2$[a,b]

Compound	Unactivated			Activated		
	λ_{max} (nm)	ν_{max} (cm^{-1})	$\Delta\nu$ (cm^{-1})	λ_{max} (nm)	ν_{max} (cm^{-1})	$\Delta\nu$ (cm^{-1})
$Hg[DZ(1)]_2$ (1)	485	20619	0	606	16502	0
ϕ HgDZ(1) (11)	473	21141	522	596	16778	276
$Hg[DZ(2)]_2$ (12)	467	21413	794	584	17123	621
ϕ HgDZ(2) (13)	457	21882	1263	577	17331	829
$Hg[DZ(3)]_2$ (14)	445	22472	1853	560	17857	1355

[a]HDZ(1) = 1,5-diphenylthiocarbazone (6*f*), HDZ(2) = 1-(2′-trifluoromethylphenyl)-5-phenylthiocarbazone (6*d*), HDZ(3) = 1,5-di(2′-trifluoromethyl)thiocarbazone (6*a*).
[b]Spectra were measured in toluene.

10–15 nm relative to bis-complexes, (e.g., **1**), Table 2. This small hypsochromic shift may result from purely steric effects. Since the Hg—S—C bond angle is likely to be the same as in the bis-complex, the azo-benzenoid ring is twisted out of the chromophoric plane due to the presence of the phenyl group.

In order to assess the individual contributions of the steric and inductive effects, 1,5-diphenylthiocarbazones with a trifluoromethyl substituent in only one of the benzenoid rings, and the mono- and bismercury complexes of these ligands, were studied, Table 2. From these data, one can infer the magnitude of the blue shift produced by steric effects to be about 500 cm^{-1} in the unactivated state, and about 250 cm^{-1} in the activated state, assuming that the blue shift observed in phenylmercuric 1,5-diphenylthiocarbazonate (**11**) is only due to steric effects. The magnitude of the blue shift induced by the inductive effect of the trifluoromethyl group is about 750 cm^{-1} in the unactivated state, and about 600 cm^{-1} in the activated state, if we assume the blue shift observed in mercury bis[1-(2′-trifluoromethylphenyl)-5-phenylthiocarbazonate], **12**, is solely due to inductive effects. The observed blue shift produced by the electron-withdrawing trifluoromethyl group is adequately explained in this manner.

The bathochromic shift, 1000 cm^{-1}, observed in mercury bis[1,5-di-(2′-methoxyphenyl)thiocarbazonate], Table 1, is most likely the result of opposing steric and electronic effects. Assuming steric hindrance is responsible for a blue shift of about 500 cm^{-1}, as above, the actual electronic effect of the two methoxyl groups in this complex can be estimated to be 1500 cm^{-1}. Along these lines, the observed spectrum of mercury bis[1,5-di-(2′-methylphenyl)thiocarbazonate] is consistent with the very weak electron donating power of methyl groups.

It is interesting to note that inductive and steric effects in the activated form, e.g., phenylmercuric 1-(2′-trifluoromethylphenyl)-5-phenylthiocarbazonate (**13**), are smaller than those in the unactivated form. This is consistent with the proposed photochromic mechanism which involves a *cis–trans* isomerization of the azomethine group and a rate determining proton shift (4). Since the main chromophore responsible for absorption is on the phenylazo portion of the molecule which, upon activation, is changed to hydrazo bonding whose contribution to the observed absorption is much smaller. The benzenoid ring with the trifluoromethyl substituent is no longer conjugated with the absorbing chromophore upon activation, and the inductive and steric effects of the trifluoromethyl group are reduced.

Experimental Section

General

The absorption spectra of the mercury complexes were recorded on a Cary 14 spectrophotometer. The infrared source, a General Electric CPR tungsten lamp having a color temperature of 3075 K, of the spectrophotometer was used to irradiate the photochromic solutions and the absorption spectrum of the equilibrium mixture between the activated and unactivated forms was measured. Infrared spectra were recorded on Perkin-Elmer 567 and 180 spectrophotometers. Analytical gas-phase chromatography was performed using a Varian Aerograph Model 920 chromatograph, with a 6 ft by 1/4 in. SS 10% Carbowax 1540, 40% Chromosorb P/W PAW 80–100 mesh column. Melting points were determined on either a Thomas-Hoover capillary or Fischer-Johns melting point apparatus. Elemental analyses were determined by Galbraith Laboratories, Inc., Knoxville, TN.

Trifluoromethylanilines were purchased from Aldrich Chemical Co., Milwaukee, WI. All other chemicals were reagent grade and used without further purification.

Synthesis

(1) Preparation of 1,5-Di(2′-trifluoromethylphenyl)thiocarbazone (6a) and 1-(2′-Trifluoromethylphenyl)-5-phenylthiocarbazone (6d)

(A) Nitrobis(2-trifluoromethylphenylazo)methane (4a)

2-Trifluoromethylaniline (50 g) in concentrated HCl (250 mL) was diazotized with a solution of $NaNO_2$ (23 g) in H_2O (50 mL). NaOAc (100 g) in H_2O (330 mL), and an alkaline solution of nitromethane, prepared by slowly adding nitromethane (10 g) to a stirred cold solution of NaOH (50 g) in H_2O (300 mL) and EtOH (150 mL), were added to the filtered diazotized solution, maintaining $T < 10°C$. The pH of the mixture was about 5.

A maroon precipitate was filtered and purified by two recrys-

Can. J. Chem. Downloaded from www.nrcresearchpress.com by 210.87.254.105 on 09/06/12
For personal use only.

TABLE 3. Melting points and elemental analyses of nitrobis(trifluoromethylphenylazo)-methane derivatives (**4**) $C_{15}H_9F_6N_5O_2$

Compound	Mp (°C)	Experimental[a] (%)				
		C	H	F	N	O[b]
Ortho	152–154	44.39	2.20	28.31	17.22	(7.88)
Meta	149–150	44.37	2.17	28.35	17.06	(8.05)
Para	159–160	44.50	2.13	28.21	17.17	(7.99)

[a]Calculated: C 44.46, H 2.24, F 28.13, N 17.28, O 7.90.
[b]Oxygen cannot be analyzed in the presence of F. The numbers in the parentheses are the difference of 100 and the percentage sum of the other elements.

TABLE 4. The prominent ir bands of nitrobis(trifluoromethylphenylazo)methane derivatives (**4**)

Compound	Infrared bands (KBr), cm^{-1}
Ortho	1584, 1550, 1454, 1372, 1334, 1312, 1270, 1220, 1166, 1132, 1116, 1052, 1032, 996, 850, 790, 766, 753
Meta	1594, 1550, 1464, 1366, 1324, 1294, 1282, 1216, 1194, 1170, 1134, 1094, 1062, 1012, 896, 820, 810, 798
Para	1610, 1554, 1510, 1418, 1354, 1318, 1278, 1226, 1172, 1130, 1100, 1062, 1004, 846, 838

TABLE 5. The melting points and prominent ir bands of 1,5-di(trifluoromethylphenyl)-thiocarbazones, $C_{15}H_{10}F_6N_4S$

Compound	Mp (°C)	Infrared bands (KBr), cm^{-1}
Ortho	>85	3200, 1620, 1580, 1524, 1494, 1462, 1400, 1318, 1280, 1214, 1202, 1178, 1106, 1050, 1032, 754
Meta	113–114	3200, 1618, 1600, 1540, 1502, 1470, 1448, 1332, 1278, 1248, 1208, 1168, 1124, 1092, 1064, 790
Para	121–122	3200, 1620, 1522, 1468, 1426, 1410, 1322, 1252, 1210, 1160, 1120, 1060, 1008, 832

tallizations from 400 mL of boiling EtOH, yielding 60 g **4***a*. *Meta* and *para* derivatives (**4***b*, **4***c*) were prepared in a similar fashion. Elemental analyses and prominent infrared bands are reported in Table 3 and Table 4, respectively.

1-(Nitromethylene)-2-(2′-trifluoromethylphenyl)hydrazine (**3***a*) was similarly prepared, except the pH of the final solution was about 1. For **3***a*: mp 71–72°C; ir(KBr): 3280, 3120, 1620, 1578, 1548, 1480, 1456, 1348, 1325, 1282, 1202, 1150, 1114, 770 cm^{-1}.

Anal. calcd. for $C_8H_6F_3N_3O_2$: C 41.21, H 2.60, F 24.45, N 18.03, O 13.72; found: C 41.09, H 2.63, F 24.65, N 18.03.

*(B) Phenylazo(2′-trifluoromethylphenylazo)nitromethane (4*d*)*

Aniline (40 g) in concentrated HCl (200 mL) was diazotized with $NaNO_2$ (28 g) in H_2O (60 mL). A solution of **3***a* (94 g) in EtOH (600 mL), solid NaOAc (170 g), and the diazotized aniline solution were mixed at $T < 10$°C. The mixture was stirred for 1 h. A maroon precipitate was filtered, washed with H_2O, and purified by recrystallization from boiling EtOH (1 L): mp 131–132°C, ir(KBr): 1590, 1542, 1454, 1354, 1312, 1290, 1264, 1226, 1170, 1156, 1116, 1050, 1030, 774, 760 cm^{-1}.

Anal. calcd. for $C_{14}H_{10}F_3N_5O_2$: C 49.85, H 3.00, F 16.90, N 20.77, O 9.49; found: C 49.70, H 2.98, F 16.73, N 20.86.

(C) Conversion to Thiocarbazone

Nitrobis(2′-trifluoromethylphenylazo)methane (**4***a*) (20 g) was suspended in EtOH (400 mL), treated with $(NH_4)_2S$ solution (60 mL), and stirred until the solid dissolved. The mixture was poured into 2 L of ice water, the light yellow thiocarbazide, **5***a*, was filtered and dissolved in 2% aqueous NaOH (600 mL) with heating. After cooling the solution in an ice-water bath, it was titrated with 1 *N* HCl to pH 5. A green precipitate (**6***a*) was filtered and purified by repeated dissolution and titration. *Meta* and *para* derivatives (**6***b*, **6***c*) were similarly prepared. The prominent infrared bands and melting points are tabulated in Table 5.

Compound **4***d* was converted to unsymmetric thiocarbazone in the same fashion to compound **6***d*: mp 112–114°C; ir(KBr): 3200, 1602, 1586, 1524, 1496, 1464, 1442, 1320, 1276, 1220, 1198, 1166, 1104, 1054, 1032, 752 cm^{-1}.

(2) Preparation of Mercury Complex of Thiocarbazones

The mercury complexes were prepared by reacting thiocarbazone with equal molar amounts of either phenylmercuric chloride or mercuric chloride to form mono- or bis-complex, respectively, in a CH_2Cl_2/H_2O (1:1) mixture. The organic layer was separated and the complex was precipitated out by the addition of MeOH.

The elemental analyses and melting points for the bis-complexes are tabulated in Table 6 with the infrared spectral bands in Table 7. For compound **13**: mp 177–178°C ir(KBr): 3302, 3056, 1606, 1588, 1530, 1460, 1374, 1320, 1282, 1260, 1162, 1150, 1128, 1110, 1050, 1028, 750 cm^{-1}.

Anal. calcd. for $C_{20}H_{15}F_3N_4SHg$: C 39.96, H 2.52, F 9.48, N 9.32, S 5.33, Hg 33.37; found: C 39.86, H 2.63, F 9.28, N 9.19, S 5.61, Hg 33.50.

*(3) 2-Phenylazo-4-phenyl-1,3,4-thiodiazol-5-one (7*f*)*

1,5-Diphenylthiocarbazone (**6***f*) (10 g, 0.039 mol), dissolved in a minimum of benzene, was added to a stirred solution of phosgene (5 g, 0.05 mol) in toluene (25 mL) at 0°C. The reaction mixture was stirred for 1 h, washed with H_2O until no further evolution of HCl gas, and followed with $NaHCO_3$, but kept acidic. After drying with $MgSO_4$ and evaporating the solvent,

Can. J. Chem. Downloaded from www.nrcresearchpress.com by 210.87.254.105 on 09/06/12
For personal use only.

TABLE 6. Melting points and elemental analyses of bismercury complexes of 1,5-di(trifluoromethylphenyl)thiocarbazone (**14**) and of 1-(2′-trifluoromethylphenyl)-5-phenylthiocarbazone (**12**)

Compound	Mp (°C)	Experimental[a] (%) C	H	N	F	S	Hg
Ortho	217–218[b]						
Meta	216–217	36.70	1.95	11.56	22.98	6.58	20.23
Para	248–249[c]						
DZ(2)	254–255	39.74	2.49	13.08	13.32	7.43	23.61

[a]Calculated (*a*) for *ortho*, *meta*, and *para*: C 36.64, H 1.85, N 11.40, F 23.19, S 6.52, Hg 20.40; (*b*) for DZ(2): C 39.69, H 2.38, N 13.23, F 13.45, S 7.57, Hg 23.67.
[b]Literature reported value is 215–216°C (8).
[c]Insufficient material for elemental analysis.

TABLE 7. The prominent ir bands of bismercury complexes of 1,5-di(trifluoromethylphenyl)thiocarbazone (**14**) and of 1-(2′-trifluoromethylphenyl)-5-phenylthiocarbazone (**12**)

Compound	Infrared bands (KBr), cm^{-1}
Ortho	3260, 1608, 1590, 1528, 1462, 1380, 1326, 1322, 1286, 1260, 1170, 1156, 1100, 1052, 1030, 752
Meta	3260, 1616, 1596, 1534, 1486, 1468, 1448, 1366, 1330, 1276, 1170, 1130, 1092, 1062, 898, 794
Para	3260, 1612, 1530, 1502, 1470, 1422, 1364, 1320, 1266, 1164, 1128, 1106, 1062, 1010, 838
DZ(2)	3332, 3064, 1608, 1590, 1532, 1500, 1462, 1380, 1322, 1284, 1264, 1160, 1126, 1054, 1030, 758

10.3 g (92%) of **7***f* was obtained (mp 138–141°C). Trituration with MeOH, and recrystallization from toluene/MeOH, afforded golden needles: mp 142–143°C (lit. mp 140°C) (6); ir($CHCl_3$): 1700, 1679, 1590, 1529, 1489, 1458, 1329, 1257, 1191, 1160, 1149 cm^{-1}.

Compound **7***d* was similarly prepared: mp 128–129°C; ir($CHCl_3$): 1703, 1682, 1598, 1542, 1487, 1457, 1414, 1316, 1270, 1151, 1112, 1092, 1050 cm^{-1}.

Anal. calcd. for $C_{15}H_9F_3N_4OS$: C 51.42, H 2.59, N 16.00, F 16.27, S 9.15, O 4.57; found: C 51.26, H 2.57, N 15.90, F 16.34, S 9.36.

(4) Zinc Reduction of 4-Phenyl-1,3,4-thiodiazol-5-one

2-Phenylazo-4-phenyl-1,3,4-thiodiazol-5-one, **7***f*, (1 g, 0.0034 mol) was dissolved in MeOH/20% NaOH (100 mL v/v). Zinc (0.5 g, 0.0076 mol) was added to the deep red solution and the mixture heated under reflux until no color change on exposure to air (10 min). The reaction mixture was extracted with CH_2Cl_2 and 0.05 μL of the organic extract was injected into the gas chromatograph. Two peaks were observed whose retention times matched that for solvent and aniline **9***f*. The organic layer was evaporated and the residue triturated with ether. The triturate was evaporated, affording a brown oil and an ir spectrum identical to that of commercial aniline.

Similarly, 2-(2′-trifluoromethylphenyl)azo-4-phenyl-1,3,4-thiodiazol-5-one, **7***d*, was dissolved in MeOH/20% NaOH and reduced. Gas chromatograms of the reaction mixture, the mixture with added 2-trifluoromethylaniline (**9***d*), and the mixture with added aniline (**9***f*), are shown respectively in Fig. 3 *a*, *b*, *c*. When the reaction mixture was analyzed, the instrument was set at its highest sensitivity and no aniline was detected. Only 2-trifluoromethylaniline (**9***d*) was observed, identified by a retention time identical to that of supplemented commercial 2-trifluoromethylaniline.

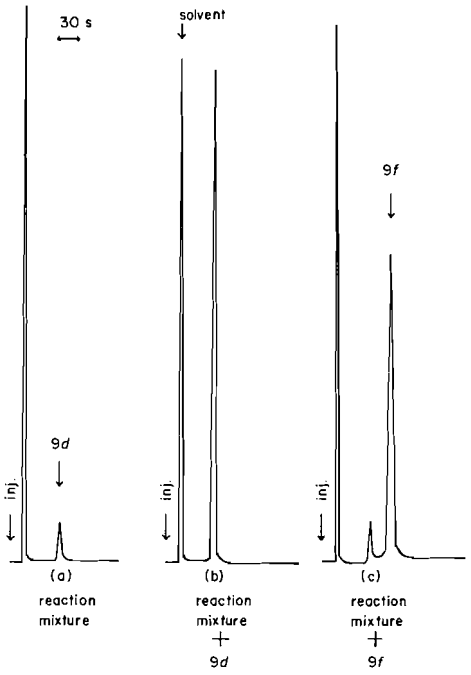

FIG. 3. Gas chromatograms of the organic layer of the zinc reduction of **7***d*. (*a*) Reaction mixture neat, (*b*) reaction mixture with added 2-trifluoromethylaniline (**9***d*), and (*c*) reaction mixture with added aniline (**9***f*).

The organic layer was evaporated and the residue washed with CS_2. The resultant residue was crystallized from benzene/EtOH and afforded white crystalline flakes, mp 198–200°C. The infrared spectrum and the mp were identical to a reported[2] infrared spectrum and mp for 1-phenyl-3-thiosemicarbazide (**10***d*).

Acknowledgements

The authors are grateful to the American Optical Corporation for the support of this work and the permission for publication. The laboratory assistance in synthesizing some of these compounds reported in this work by Mr. Peter G. Piusz is appreciated.

Can. J. Chem. Downloaded from www.nrcresearchpress.com by 210.87.254.105 on 09/06/12
For personal use only.

1. H. IRVING, G. ANDREWS, and E. J. RISDON. J. Chem. Soc. 541 (1949).
2. J. L. A. WEBB, I. S. BHATIA, A. H. CORWIN, and A. G. SHARP. J. Am. Chem. Soc. **72**, 91 (1950).
3. L. S. MERIWETHER, E. C. BREITNER, and C. L. SLOAN. J. Am. Chem. Soc. **87**, 4441 (1965).
4. L. S. MERIWETHER, E. C. BREITNER, and N. B. COLTHUP. J. Am. Chem. Soc. **87**, 4448 (1965).
5. R. A. COLEMAN, W. H. FOSTER, J. KAZAN, and M. MASON. Synthesis of chromotropic colorants. Rept. ANL 66-9-CM, ANL TS-138, Feb. 1966, AD 630908.
6. E. FISCHER. Ann. **190**, 114 (1878); **212**, 320 (1882).
7. E. BAMBERGER. Ber. **27**, 155 (1894).
8. L. A. PUPKO and P. S. PELKIS. J. Org. Chem. USSR, **1**, 115 (1965), Engl. Transl.
9. L. A. PUPKO and P. S. PELKIS. J. Org. Chem. USSR, **1**, 736 (1965), Engl. Transl.
10. H. M. N. H. IRVING. Dithizone, The Chemical Society, Burlington House, London, England, 1977. p. 8.
11. M. FREUND and F. KUH. Ber. **23**, 2824 (1890).
12. E. FISCHER and E. BESTHORN. Ann. **212**, 316 (1882).
13. M. M. HARDING. J. Chem. Soc. 4136 (1958).

Can. J. Chem. Downloaded from www.nrcresearchpress.com by 210.87.254.105 on 09/06/12
For personal use only.

Intramolecular hydride shift in some noncyclic isopropyl ketols

E. W. WARNHOFF, MARGARET Y. H. WONG, and P. SUNDARA RAMAN
Department of Chemistry, University of Western Ontario, London, Ont., Canada N6A 5B7

Received August 19, 1980

E. W. WARNHOFF, MARGARET Y. H. WONG, and P. SUNDARA RAMAN. Can. J. Chem. **59**, 688 (1981).

The acyclic ketols **7** ⇌ **11** and **8** ⇌ **12** have been synthesized by a Reformatsky sequence. Each ketol undergoes intramolecular hydride transfer when refluxed in KOH–H_2O–*t*-BuOH solution. When the procedure was applied to the synthesis of **34**, hydride transfer occurred during the Reformatsky reaction to yield **33** instead. With longer reaction times, **33** underwent self-acylation and β-dicarbonyl cleavage to **37**. Treatment of **33** with aqueous base gave a mixture of ketols **35** and **36** from hydride transfer and β-keto decarboethoxylation. The attempted conversion of the isobutyrate group of the Reformatsky intermediates **21** and **24** to *tert*-butyl was not practicable.

E. W. WARNHOFF, MARGARET Y. H. WONG et P. SUNDARA RAMAN. Can. J. Chem. **59**, 688 (1981).

On a synthétisé les cétols acycliques **7** ⇌ **11** et **8** ⇌ **12** en utilisant une réaction de Reformatsky. Au reflux dans une solution de KOH–H_2O–*t*-BuOH, chaque cétol subit un transfert d'hydrure intramoléculaire. Si on utilise la même méthode pour synthétiser le composé **34**, le transfert d'hydrure se produit pendant la réaction de Reformatsky et conduit de préférence au composé **33**. Si on le soumet à des temps de réaction plus longs le composé **33** subit une autoacylation ainsi qu'un clivage du β-dicarbonyle pour conduire au composé **37**. Le composé **33** réagit avec une base aqueuse et conduit à un mélange de cétols **35** et **36** provenant d'un transfert d'hydrure et d'une β-céto décarboéthoxylation. On n'a pas pu convertir le groupe isobutyrate des intermédiaires **21** et **24** du réactif de Reformatsky en un *tert*-butyle.

[Traduit par le journal]

The increasingly observed phenomenon of base-catalyzed intramolecular hydride shift in ketols (intramolecular Meerwein–Ponndorf–Verley–Oppenauer reactions) has so far only been reported across rings, simple or fused, in which the stereochemical requirements for the transfer are favored by molecular rigidity (e.g. 1–7). To survey the generality of this reaction, we have made and tested some noncyclic ketols, **1** and **2**, whose freedom of rotation and preferred conformations would retard intramolecular hydride transfer.[1]

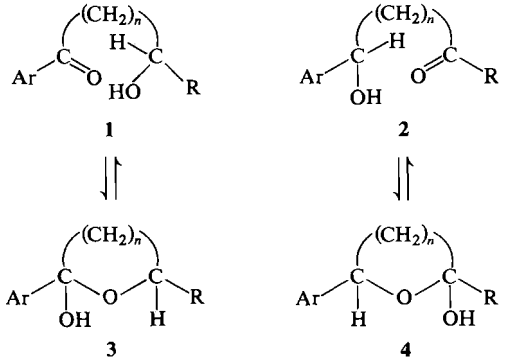

1 ⇌ **3**

2 ⇌ **4**

a R = isopropyl
b R = *tert*-butyl

The first goal was a 1,4-ketol (n = 2), which would have the least rotational freedom in this series, and which could be compared with the previously studied 4-hydroxycyclohexanone **5** (1, 4). The choice of end groups for the ketol chain was governed by two considerations. First, it was desirable to make the equilibrium for any hydride transfer lie to one side for ease of studying rates of hydride transfer. Second, it was feared that carbonyl condensation might be a serious side reaction

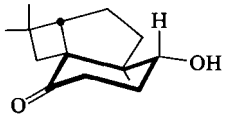

5

during base treatment of the ketols. By making one end group aryl and the other alkyl, it was hoped that the aroyl ketol **1** would predominate at equilibrium;[2] and by making the alkyl group isopropyl or *tert*-butyl, it was hoped to minimize condensation reactions. Unlike the cyclic ketols studied previously, acyclic ketols have the potential disadvantage of existing in equilibrium with their hemiketals **3** and **4**. However, although this factor would complicate product analysis, it could be taken into account.

Initial attempts to synthesize the ketol by alkylation of γ-phenylbutyrolactone with isopropyl Grignard reagent or *tert*-butyllithium, by alkylation of pinacolone and acetophenone with styrene oxide, and by alkylation of acetophenone with bro-

[1]Part of this work was reported at the 62nd Canadian Chemical Conference, Vancouver, B.C., June 3–6, 1979.

[2]On combustion at 25°C in a static bomb, benzyl methyl ketone gives 3 kcal/mol more heat than propiophenone (8). If this value is taken as a measure of the phenyl–carbonyl conjugative stabilization, then **1** should predominate essentially completely over **2**.

0008-4042/81/040688-09$01.00/0
©1981 National Research Council of Canada/Conseil national de recherches du Canada

Can. J. Chem. Downloaded from www.nrcresearchpress.com by 210.87.254.6 on 09/06/12
For personal use only.

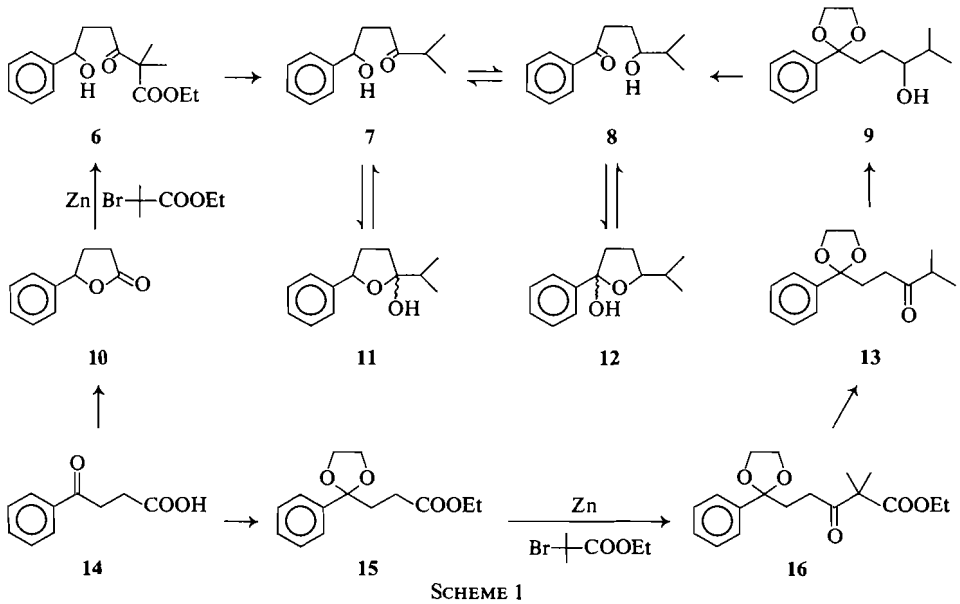

SCHEME 1

mopinacolone were unpromising. Therefore, we turned to the well developed Reformatsky procedure of Lapin and Horeau (9) because it seemed adaptable to preparation of the isopropyl and *tert*-butyl derivatives of a number of homologs (e.g. $n = 2, 3, 4$) of **1** and **2**.

Both ketols **7** and **8** were prepared from the same starting material, β-benzoylpropionic acid **14**, as outlined in Scheme 1. For **8**, the ethylene ketal of ethyl β-benzoylpropionate, **15**, was treated with ethyl α-bromoisobutyrate and zinc to obtain the known keto ester **16**. Base-catalyzed decarboethoxylation of **16** furnished the isopropyl keto ketal **13** which was reduced by $NaBH_4$ to the hydroxy ketal **9**. Acid hydrolysis gave the required phenyl isopropyl ketol **8**.

For the other ketol **7**, β-benzoylpropionic acid was dissolved in aqueous base and then reduced with $NaBH_4$;[3] acidification gave γ-phenylbutyrolactone **10**. The Reformatsky reaction with the lactone **10** and ethyl α-bromoisobutyrate produced a good yield of the hydroxy keto ester **6** which was readily separated from contaminating diethyl tetramethylsuccinate by chromatography. In $CDCl_3$ **6** existed in equilibrium with its cyclic hemiketal **17** in a ratio of ~2:1, respectively. Decarboethoxylation in 2% aqueous ethanolic KOH gave ketol **7**.

As a check on structural and spectroscopic assignments, the ethylene ketal **16** was hydrolyzed to give diketo ester **19** (Scheme 2). Saponification of **19** yielded the diketone **22**. In our hands the acidic hydrolysis of **19** as described in ref. 9 did not lead to **22** but instead gave 2-phenyl-5-isopropylfuran **18** in good yield.

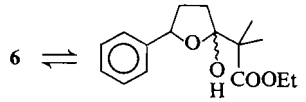

17

Both ketols **7** and **8** existed in equilibrium with minor amounts of their hemiketals which were apparent in the ^{1}Hmr spectra (see Experimental); in $CDCl_3$ at room temperature the ratio of **7**:**11** was 5:1 and that of **8**:**12** was 3:1. For analytical purposes the most useful ^{1}Hmr differences between **7** ⇌ **11** and **8** ⇌ **12** were the positions of the O—C—H proton and the patterns of the aromatic protons. The hydroxymethine proton signal from **7** at δ 4.68 was shifted downfield by the phenyl group relative to the corresponding signal in **8** at δ 3.38. The phenyl protons in **7** ⇌ **11** appeared as a singlet with a broadened base at δ 7.3 and the benzoyl protons in **8** ⇌ **12** as two broad multiplets at δ 7.2–7.6 and 7.9–8.0.

Each ketol **7** ⇌ **11** and **8** ⇌ **12** was subjected to isomerization conditions found earlier to be suitable for **5** (4), KOH–H_2O–*t*-BuOH at reflux. Hydride transfer, **7** ⇌ **8**, did indeed occur[4] and at a rate comparable with that for the cyclic ketone **5**. The

[3]If the acid salt was not preformed, $NaBH_4$ reduction of the keto acid **14** apparently gave some diol from further reduction.

[4]The transfer was judged to be *intra*molecular by the absence of both diketone **22** and the diol corresponding to **22**.

Can. J. Chem. Downloaded from www.nrcresearchpress.com by 210.87.254.6 on 09/06/12
For personal use only.

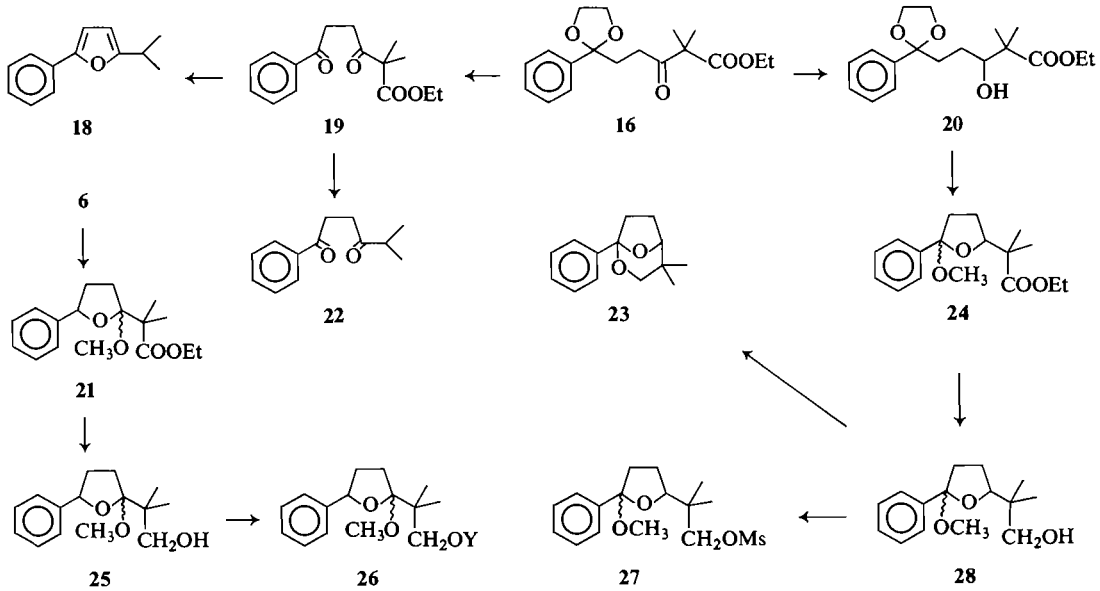

SCHEME 2

reactions were less clean than with **5**, and even under nitrogen some decomposition took place, but after chromatography the ketol fraction from each reaction was found to be a mixture of comparable amounts of **7** ⇌ **11** and **8** ⇌ **12** from glpc analysis (e.g from **7** ⇌ **11** the ratio of **7**:**8** was ~7:3, see Experimental). Although the equilibrium constant was not determined, it was clearly not one-sided. Hence, the conjugation of the carbonyl group with the phenyl group was not sufficient to tip the equilibrium position in favor of **8**,[5] and consequently these compounds were not very suitable for kinetic experiments.

In hope of diminishing hemiketal formation and possibly altering the equilibrium constant for hydride shift, we turned to the preparation of the corresponding *tert*-butyl ketols **1***b* and **2***b* ($n = 2$) by conversion of the carboethoxyl group of the Reformatsky intermediates **6** and **16** into methyl (Scheme 2). The existing ketone group in **6** was protected by formation of the cyclic ketal **21**, which appeared to be a single racemate, in acidic methanol. The isomeric cyclic ketal ester **24** was obtained as a mixture of two diastereomeric racemates by brief borohydride reduction of **16** to **20** which was then treated with acidic methanol. If the reduction mixture from **16** was allowed to stand at room temperature, the ester group began to be reduced to diol **29**, presumably by an intramolecular donation of hydride after the ketone had been reduced (10). $LiAlH_4$ reduction of the cyclic ketal esters **21** and **24** furnished the cyclic ketal alcohols **25**, which was a single crystalline racemate, mp 85°C, and **28**, which was a liquid diastereomeric mixture. Not surprisingly, with the benzylic ketal group and the possibility of intramolecular reaction, compound **28** was very sensitive to acid. Mere standing in $CDCl_3$ resulted in cyclization to the bicyclic ketal **23** with loss of MeOH. However, both ketal alcohols could be converted into the sulfonate esters **26** and **27** in pyridine solution.

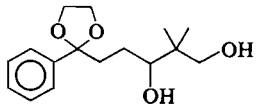

29

Although some difficulty in reducing these hindered neopentyl-like sulfonates to methyl groups was anticipated, it was expected that one of the recently developed procedures (11–14) would work. However, tosylate **26***a* was recovered from the following reductive conditions: NaI/Zn/DME for 1.5 h at reflux (13), NaI/Zn/DMF for 2.5 days at 40°C (13), $NaBH_4$/DMSO for 4 h at 45–50°C (11), and $NaBH_3CN$/HMPT for 18 h at 80°C (12). Two sets of conditions did give reductive removal of tosylate from **26***a*: NaI/Zn/DME for 66 h at 80–95°C (13) and $LiEt_3AlH$/THF at reflux for 3 h (14), but in both cases the product was a mixture of

[5]The failure of carbonyl conjugation to determine the equilibrium position must be linked to the fact that the equilibration also involves the hemiketals **11** and **12**, and the relative stability of these latter would not parallel that of **7** and **8**.

Can. J. Chem. Downloaded from www.nrcresearchpress.com by 210.87.254.6 on 09/06/12
For personal use only.

Can. J. Chem. Downloaded from www.nrcresearchpress.com by 210.87.254.6 on 09/06/12
For personal use only.

at least four components. From similarities in the ^{1}Hmr spectra of these two reduction products and the increase in number of protons on carbon bearing oxygen, it seems likely that rearrangement was occurring via intramolecular attack of the ethereal oxygen atoms followed by oxonium ion cleavage and reduction to give **A** and **B**. In agreement, the methoxyl group was not hydrolyzed by aqueous alcoholic H_2SO_4 at room temperature. After these unpromising results, the replacement of triflate from **26***c* by thiophenoxide was tried, but the yield

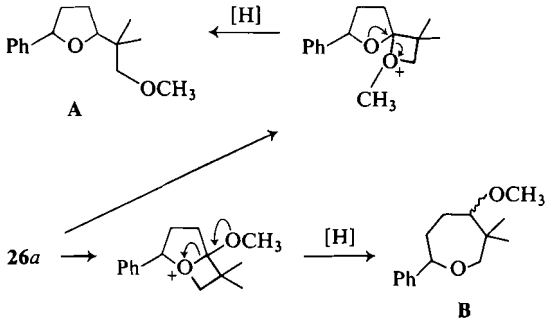

of (possibly rearranged) thioether in the product mixture was too low to be useful for Raney nickel reduction. At this point, the conversion of **26** and **27** into *tert*-butyl ketols was given up.

In spite of the fact that the Reformatsky intermediates were not readily amenable to preparation of *tert*-butyl ketols, the extension of this approach to the next higher isopropyl homolog **2** ($n = 3$) was examined. Surprisingly, the Reformatsky reaction of ethyl α-bromoisobutyrate with δ-phenylvalerolactone **30** (Scheme 3) in refluxing benzene for 2 h did not yield the expected product **34**, but instead the isomeric hydroxy keto ester **33** in which intramolecular hydride transfer had already occurred! Longer reaction time in refluxing benzene led to cyclization of **33** with loss of ethanol to give the rearranged ester **37**. The origin of this product is readily explained by intramolecular acylation of the zinc enolate of **33** (formed from **32**) to yield **38**, followed by intramolecular β-dicarbonyl cleavage to **37** (cf. ref. 15). Attempts to prevent these reactions and to isolate **34** were unsuccessful; at room temperature no reaction occurred, and at reflux for 20 min, although lactone remained, the product that had formed was only the rearranged **33**. With the highly touted trimethyl borate as cosolvent (16) for the Reformatsky synthesis, the only product after 19 h at room temperature was the ring opened methyl ester from δ-phenylvalerolactone.

The contrast between the reaction with δ-phenylvalerolactone and that with γ-phenylbutyrolactone, which gave no evidence of any hydride

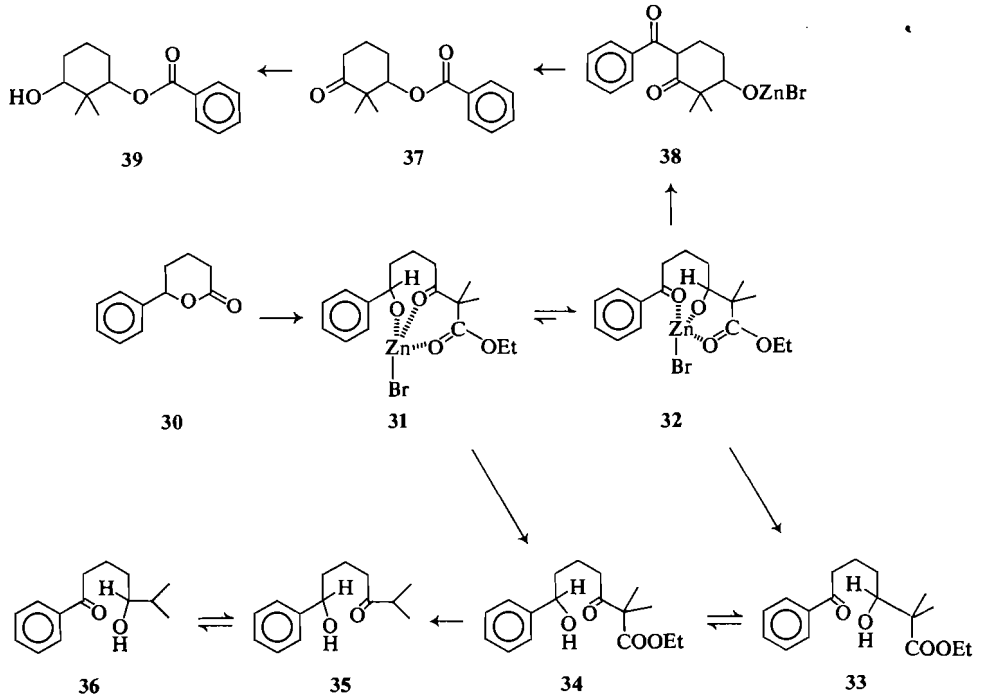

SCHEME 3

Can. J. Chem. Downloaded from www.nrcresearchpress.com by 210.87.254.6 on 09/06/12
For personal use only.

shift during longer reflux periods, must be due to the greater ease of 1,5-hydride transfer in **31**[6] relative to the 1,4-hydride transfer in **6**. This difference is a general phenomenon and is apparently a result of the greater strain imposed on the transition state in order to achieve the required geometry (17, 18) for the 1,4-hydride shift (cf. ref. 2).

Since the Reformatsky product from δ-phenylvalerolactone was pure **33**, the equilibrium between **31** and **32** must lie far toward **32**.[6] Possibly aroyl conjugation is the dominant factor in the **31** ⇌ **32** equilibration, or another possibility from a study of Dreiding models (provided that **31** and **32** are the structures of the zinc alkoxides) is that the zinc complex **32** is less strained than **31** because the quasi 6-membered ring of **32** with two sp^3-carbons is less strained than the quasi 6-membered ring in **31** with only one sp^3-carbon. In a test of the reversibility of the **31** ⇌ **32** hydride shift, ester **33** was heated with KOH–H_2O–*t*-BuOH under the conditions used to equilibrate **7** and **8**. The product was a mixture of decarboethoxylated ketols **35** and **36** in a (presumably equilibrium) ratio of ~1:1. Consequently **33** was converted by hydride shift to the β-keto ester **34** which underwent decarboethoxylation to **35** and further partial hydride shift to **36**.

At this point, although pure ketol **36** could presumably have been made from the next higher homolog of **15**, the Reformatsky reaction had lost much of its original appeal as a synthetic method for these compounds for the several reasons discussed above. Nevertheless, the Reformatsky compounds had served to demonstrate that hydride shift would occur readily in acyclic ketols and to spur the search for more suitable compounds and syntheses for a more detailed study of hydride shift in acyclic ketols. Subsequently, attention has been redirected to the use of *tert*-butyllithium and phenyllithium in a general synthesis of the *tert*-butyl series of **1** and **2** ketols. This approach has been successful and will be reported shortly.

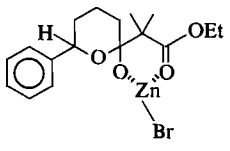

40

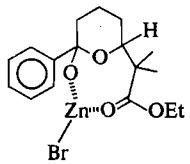

41

Experimental

General

The instruments and chromatographic procedures are the same as in ref. 4. Mass spectra were run at 70 eV unless otherwise specified; only major fragmentation ions are given. For ^{1}Hmr spectra only well resolved signals are reported. Ultraviolet spectra were measured with a Cary Model 219 spectrophotometer. Gas–liquid partition chromatography was done on an Unilab Model 400 all-glass system with a 1.8-m column of 1% DEGS on 60–80 mesh Chromosorb W at 130°C and a hydrogen flame detector. Analyses were done by Chemalytics, Tempe, AZ. The zinc metal used was either granular (20 mesh) or dust from the Fisher Co. and was activated according to ref. 19. Ether extractions included the usual washing with acid and/or base and drying.

Ethyl 6-Hydroxy-6-phenyl-2,2-dimethyl-3-oxo-hexanoate (6)

A mixture of 1.0 g (6.2 mmol) of γ-phenylbutyrolactone (**20**), 0.81 g (12 mmol) of Zn metal, and 25 mL of dry benzene was distilled until 10 mL of benzene had been collected. A solution of 3.0 mL (3.98 g, 20 mmol) of ethyl α-bromoisobutyrate in 10 mL of dry ether was then added, and the reaction mixture was refluxed for 6 h. The Zn had dissolved and a white precipitate of Zn salt had appeared. Cooling, hydrolysis with aqueous H_2SO_4, and extraction with ether furnished 2.20 g of oily liquid. Column chromatography on 50 g of silica gel with $CHCl_3$ eluent gave 1.40 g (81%) of pure liquid hydroxy keto ester **6** which existed in equilibrium with its cyclic hemiketal **17** (**6**:**17** = 2:1 in $CDCl_3$); ir (neat): 3500 (broad strong OH) and 1710 with shoulders at 1725 and 1740 (C=O) cm^{-1}; ^{1}Hmr ($CDCl_3$) δ: 1.18 (3H, t, J = 7 Hz, $CH_3[CH_2]$), 1.32 (6H, s, *gem*-diMe), 1.6–2.7 (5H, m, OH, CH_2CH_2), 4.12 (q, J = 7 Hz, $OCH_2[CH_3]$), 4.18 (q, J = 7 Hz, $OCH_2[CH_3]$), 4.68 (0.65H, varies from bt to m, HC—[OH] of **6**), 4.98 (0.65H, bs, OH of **6**), 5.06 (0.35H, bs, OH of **17**), 5.18 (0.35H, dd, HC—OC of **17**), and 7.32 (5H, s, Ph) ppm; at 220 MHz the signals at 4.68 and 5.18 ppm were clearly resolved dds; ms *m/e*: 260 ($M^+ - H_2O$) and 233 (M^+ − OEt). M^+ calcd. for $C_{16}H_{22}O_4$: 278.1518; found: 278.1518. *Anal.* calcd. for $C_{16}H_{22}O_4$: C 69.04, H 7.97; found: C 69.13, H 7.98.

The less polar impurity eluted first from the column amounted to 460 mg of diethyl tetramethylsuccinate; ir (neat): 1725 (ester C=O) cm^{-1}; ^{1}Hmr ($CDCl_3$) δ: 1.23 (12H, s, Me_2C—CMe_2), 1.25 (6H, t, J = 7 Hz, $2CH_3[CH_2O]$), and 4.10 (4H, q, J = 7 Hz, 2 $OCH_2[CH_3]$) ppm; ms *m/e*: 185 (M^+ − OEt).

6-Hydroxy-6-phenyl-2-methylhexan-3-one (7)

A solution of 70 mg of pure **6** in 5 mL of a 2% solution of KOH in EtOH–H_2O (4:1) was refluxed for 0.5 h. Dilution with water and extraction with ether afforded 52 mg (100%) of colorless liquid ketol **7** which existed in equilibrium with the cyclic hemiketal **11** (**7**:**11** = 5:1 in $CDCl_3$); ir (neat): 3450 (broad intense OH) and 1705 (weak C=O) cm^{-1}; ^{1}Hmr ($CDCl_3$) δ: 1.08 (6H, d, J = 7 Hz, $Me_2[CH]$), 1.9–2.2 (2H, m, CH_2), 2.4–2.8 (2H, m, CH_2C=O), 2.90 (1H, bs, OH), 4.68 (0.85H, t = dd, HC—[OH] of **7**), 5.19 (0.15H, t = dd, HC—OC of **11**), and 7.33 (5H, s, Ph) ppm. At 220 MHz the signals at 4.68 and 5.19 still appeared as triplets; ms *m/e*: 188 ($M^+ - H_2O$), 163 (M^+ − *i*-Pr), and 145 ($M^+ - H_2O$ − *i*-Pr). M^+ calcd. for $C_{13}H_{18}O_2$: 206.1306; found: 206.1297. *Anal.* calcd. for $C_{13}H_{18}O_2$: C 75.69, H 8.80; found: C 75.95, H 8.54.

Ethyl 6,6-Ethylenedioxy-6-phenyl-2,2-dimethyl-3-oxohexanoate (16)

The general procedure of ref. 9 was reduced in scale. A mixture of 1.25 g (5.0 mmol) of ketal ester **15** (9), 0.65 g (10 mmol) of Zn metal, and 25 mL of dry benzene was distilled and stirred (magnetic bar) until 10 mL of benzene had been collected. A solution of 1.95 g (10 mmol) of ethyl α-bromoisobutyrate in 5 mL of dry ether was added dropwise, and the reaction mixture was stirred and refluxed for 6 h. By this time most of the Zn had dissolved and a white turbidity due to Zn salts had appeared. After cooling, the reaction mixture was poured into 50 mL of ice cold aqueous 8 *N* H_2SO_4. The organic layer was separated, washed to neutrality with water, dried, and

[6]The Reformatsky zinc alkoxide products drawn as **31** and **32** might exist as the hemiketal forms **40** and **41** or an equilibrium mixture of all four structures.

Can. J. Chem. Downloaded from www.nrcresearchpress.com by 210.87.254.6 on 09/06/12
For personal use only.

evaporated to leave 1.86 g of crude product which was chromatographed on 50 g of neutral alumina. Benzene–hexane mixtures eluted 1.43 g (89%) of pure liquid **keto ketal ester 16**; ir (neat): 1730 (ester C=O) and 1705 (ketone C=O) cm^{-1}; ^{1}Hmr ($CDCl_3$) δ: 1.20 (3H, t, J = 7 Hz, $CH_3[CH_2]$); 1.34 (6H, s, *gem*-diMe), 2.10–2.30 (2H, m, CH_2), 2.46–2.70 (2H, m, CH_2C=O), 3.7–4.1 (4H, m, OCH_2CH_2O), 4.15 (2H, q, J = 7 Hz, $OCH_2[CH_3]$), and 7.26–7.54 (5H, m, Ph) ppm; ms *m/e*: 320 (M^+), 275 ($M^+ - OEt$), 205 ($M^+ - Me_2CCOOEt$), and 149 (base peak, $PhCH(OCH_2)_2^+$). *Anal.* calcd. for $C_{18}H_{24}O_5$: C 67.48, H 7.55; found: C 67.79, H 7.54.

6,6-Ethylenedioxy-6-phenyl-2-methylhexan-3-one (13)

A solution of 640 mg of keto ketal ester **16** in 10 mL of a 2% solution of KOH in EtOH–H_2O (4:1) was refluxed for 1 h. Dilution with water and extraction with ether yielded 488 mg (98%) of pure colorless liquid **keto ketal 13**; ir (neat): 1710 (C=O) cm^{-1}; ^{1}Hmr ($CDCl_3$) δ: 1.05 (6H, d, J = 7 Hz, $Me_2[CH]$), 2.1–2.3 (2H, m, CH_2), 2.4–2.7 (3H, m, CH_2C=O + $HC[Me_2]$), 3.6–4.1 (4H, m, OCH_2CH_2O), and 7.2–7.5 (5H, m, Ph) ppm; ms *m/e*: no M^+, 205 ($M^+ - i$-Pr), and 149 (base peak, $PhCH(OCH_2)_2^+$). *Anal.* calcd. for $C_{15}H_{20}O_3$: C 72.55, H 8.12; found: C 72.68, H 8.20.

6,6-Ethylenedioxy-6-phenyl-2-methylhexan-3-ol (9)

The above keto ketal **13** sample was dissolved in a few mL of aqueous MeOH and treated with excess $NaBH_4$. Dilution with water and extraction with ether afforded 462 mg (94%) of pure **hydroxy ketal 9**, mp 52–52.5°C after recrystallization from hexanes; ir (neat): 3440 (broad OH) cm^{-1} and no C=O absorption; ^{1}Hmr ($CDCl_3$) δ: 0.88 (6H, d, J = 7 Hz, $Me_2[CH]$), 1.1–2.2 (6H, m, OH, CCH_2CH_2C, $HC[Me_2]$), 3.22–3.50 (1H, m, HC[OH]), 3.64–4.18 (4H, sym m, OCH_2CH_2O), and 7.20–7.56 (5H, m, Ph) ppm; ms *m/e* (20 eV): no M^+, 207 ($M^+ - i$-Pr), and 149 (base peak, $PhCH(OCH_2)_2^+$). *Anal.* calcd. for $C_{15}H_{22}O_3$: C 71.97, H 8.86; found: C 72.26, H 8.81.

4-Hydroxy-1-phenyl-5-methylhexan-1-one (8)

The above hydroxy ketal **9** was dissolved in a few mL of aqueous MeOH containing a drop of 8 N H_2SO_4 and allowed to stand for 15 min. Dilution with water and extraction with ether gave 378 mg of crude liquid product. Chromatography on a 20-g plate of silica gel furnished 298 mg (78%) of pure liquid ketol **8** which existed in equilibrium with the cyclic **hemi ketal 12** (**8**:**12** = 3:1 in $CDCl_3$); uv (MeOH): 242 nm (10 300); ir (neat): 3450 (strong OH) and 1680 (PhC=O) cm^{-1}; ^{1}Hmr ($CDCl_3$) δ: 0.92 (6H, d, J = 7 Hz, $Me_2[CH]$), 1.4–2.1 (4H, bm, CH_2, OH, $HC[Me_2]$), 3.13 (2H, dt, O=CCH_2), 3.38 (0.75H, m, HC—[OH] of **8**), 7.2–7.64 (3.5H, m, *m*- and *p*-H of PhC=O), and 7.88–8.04 (1.5H, m, *o*-H of PhC=O) ppm; ms *m/e*: no M^+, 188 ($M^+ - H_2O$), and 106 (base peak, $PhCOH^+$). *Anal.* calcd. for $C_{13}H_{18}O_2$: C 75.69, H 8.80; found: C 75.13, H 8.90.

Ethyl 6-Phenyl-2,2-dimethyl-3,6-dioxohexanoate (19)

A solution of 1.82 g of keto ketal ester **16** in 10 mL of MeOH plus 0.5 mL of 8 N H_2SO_4 was allowed to stand at room temperature for 30 min. Dilution with water and extraction with ether yielded 1.62 g (100+%) of liquid **diketo ester 19**; ir (neat): 1740 (ester C=O), 1715 (alkyl C=O), and 1690 (PhC=O) cm^{-1}; ^{1}Hmr ($CDCl_3$) δ: 1.26 (3H, t, J = 7 Hz, $CH_3[CH_2]$), 1.46 (6H, s, *gem*-diMe), 2.8–3.5 (4H, m, CH_2CH_2), 4.24 (2H, q, J = 7 Hz, $OCH_2[CH_3]$), 7.3–7.7 (3H, m, *m*- and *p*-ArH), and 7.9–8.1 (2H, m, *o*-ArH); ms *m/e* (25 eV): 185 ($M^+ - H_2O$ – COOEt). *Anal.* calcd. for $C_{16}H_{20}O_4$: C 69.55, H 7.30; found: C 69.91, H 7.59.

1-Phenyl-5-methyl-1,4-hexanedione (22)

A solution of 500 mg of diketo ester **19** in 10 mL of 2% KOH in EtOH–H_2O (4:1) was refluxed for 1 h. Dilution with water and extraction with ether gave 412 mg (100%) of liquid **diketone 22**; uv (MeOH): 242 nm (12 500); ir (neat): 1710 (alkyl C=O) and 1685 (PhC=O) cm^{-1}; ^{1}Hmr ($CDCl_3$) δ: 1.15 (6H, d, J = 7 Hz, $Me_2[CH]$), 2.4–3.4 (5H, m, O=CCH_2CH_2C(=O)CH), 7.0–7.4 (3H, m, *m*- and *p*-ArH), and 7.7–7.9 (2H, m, *o*-ArH) ppm; ms *m/e* (25 eV): 204 (M^+) and 161 (base peak, $M^+ - i$-Pr). M^+ calcd. for $C_{13}H_{16}O_2$: 204.1150; found: 204.1151.

2-Phenyl-5-isopropylfuran (18)

The hydrolysis procedure of Bogavac *et al.* (9) was followed. A solution of 0.5 g of **diketo ester 19** in 2.5 mL of HOAc to which was added 0.5 mL of 10% aqueous H_2SO_4 was refluxed for 1 h. Dilution with water and extraction with ether gave a single compound, the liquid **furan 18**; ir (neat): no OH or C=O absorption; ^{1}Hmr ($CDCl_3$) δ: 1.26 (6H, d, $Me_2[CH]$), 2.98 (1H, septuplet, $HC[Me_2]$), 6.02 (1H, d, J = 3 Hz, furan H), 6.52 (1H, d, J = 3 Hz, furan H), and 7.05–7.70 (5H, m, Ph) ppm; ms *m/e*: 186 (M^+) and 171 (base peak, $M^+ - CH_3$). M^+ calcd. for $C_{13}H_{14}O$: 186.1045; found: 186.1044.

Ethyl 3-Hydroxy-6,6-ethylenedioxy-6-phenyl-2,2-dimethylhexanoate (20)

A solution of 500 mg of keto ketal ester **16** in 10 mL of MeOH was cooled to 0°C and 60 mg of $NaBH_4$ was added in portions. After 15 min, 20 mL of ice water was added, and the product was extracted with ether to yield 508 mg (100+%) of colorless liquid hydroxy ketal ester **20**; ir (neat): 3480 (OH) and 1725 (ester C=O) cm^{-1}; ^{1}Hmr ($CDCl_3$) δ: 1.14 (6H, s, *gem*-diMe), 1.21 (3H, t, J = 7 Hz, $CH_3[CH_2]$), 1.2–2.4 (4H, 2m, CCH_2CH_2C), 2.85 (1H, b, OH), 3.3–4.2 (5H, m, OCH_2CH_2O + HC[OH]), 4.11 (2H, q, J = 7 Hz, $OCH_2[CH_3]$), and 7.26–7.54 (5H, m, Ph) ppm; ms *m/e* (25 eV): no M^+, 277 (M^+ – OEt), 207 ($M^+ - Me_2CCOOEt$), and 149 (base peak, $PhC(OCH_2)_2^+$). *Anal.* calcd. for $C_{18}H_{26}O_5$: C 67.06, H 8.13; found: C 67.19, H 7.91.

If the temperature or time of the reduction was raised, a second more polar product was formed and could be separated by chromatography on alumina. This was the crystalline **diol 29**, mp 133–134°C, from intramolecular reduction of the carboethoxy group after reduction of the ketone (10); ir ($CHCl_3$): 3460 (OH) cm^{-1}, no C=O absorption; ^{1}Hmr ($CDCl_3$) δ: 0.84 (6H, s, *gem*-diMe), 1.0–2.3 (4H, 2m, CCH_2CH_2C), 3.0–3.7 (2H, b, 2OH), 3.43 (3H, m, CH_2[OH] + HC[OH]), 3.7–4.2 (4H, sym dm, OCH_2CH_2O), and 7.26–7.54 (5H, m, Ph) ppm; ms *m/e* (25 eV): no M^+. $M^+ - (CH_3)_2CCH_2OH$ calcd. for $C_{12}H_{15}O_3$: 207.1021; found: 207.1018. $C_6H_5C(OCH_2)_2^+$ calcd. for $C_9H_9O_2$: 149.0603; found: 149.0600. *Anal.* calcd. for $C_{16}H_{24}O_4$: C 68.55, H 8.63; found: C 68.39, H 8.61.

When the ^{1}Hmr solution of **29** in $CDCl_3$ was treated with one drop of concentrated aqueous HCl, the spectrum changed to that of the bicyclic ketal **23**.

Ethyl 2-(2'-Methoxy-5'-phenyl-2'-tetrahydrofuryl)isobutyrate (21)

A solution of 186 mg of hydroxy keto ester **6** in 10 mL of dry MeOH containing two drops of concentrated H_2SO_4 was refluxed for 30 min. The acid was then neutralized by addition of excess solid $NaHCO_3$ before 50 mL of ice cold water was added. Extraction with ether yielded 186 mg of liquid **cyclic ketal ester 21**, which appeared to be a single (±) diastereomer; ir (neat): 1715 (ester C=O) cm^{-1}; ^{1}Hmr ($CDCl_3$) δ: 1.22 (3H, t, J = 7 Hz, $CH_3[CH_2]$), 1.35 (6H, s, *gem*-diMe), 2.01 (2H, 5 lines, $[OCH]CH_2[CH_2]$), 2.48–2.63 (2H, 4 lines, $[CH_2]CH_2[COCH_3]$), 3.19 (3H, s, OCH_3), 4.12 (1H, dd, HC—O), 4.16 (2H, q, J = 7 Hz, $OCH_2[CH_3]$), and 7.32 (5H, s, Ph) ppm; ms *m/e* (20 eV): 292 (M^+), 274 ($M^+ - 18$), 260 (base peak, $M^+ - CH_3OH$), 177 ($M^+ - Me_2CCOOEt$), 134, and 121. *Anal.* calcd. for $C_{17}H_{24}O_4$: C 69.84, H 8.27; found: C 69.71, H 7.93.

2,2-Dimethyl-2-(2'-methoxy-5'-phenyl-2'-tetrahydrofuryl)-ethanol (25)

To a stirred (magnetic bar) suspension of 100 mg of $LiAlH_4$ in

Can. J. Chem. Downloaded from www.nrcresearchpress.com by 210.87.254.6 on 09/06/12
For personal use only.

10 mL of dry ether was added dropwise a solution of 330 mg of cyclic ketal ester **21** in 5 mL of dry ether. After 30 min (or less) at room temperature, excess $LiAlH_4$ was destroyed by the addition of cold water. Extraction with ether gave 284 mg (100%) of white crystalline solid **25**, mp 80–81°C. Recrystallization from hexanes raised the mp to 84–85°C; ir ($CHCl_3$): 3380 (OH) cm^{-1}, no C=O absorption; ^{1}Hmr ($CDCl_3$) δ: 0.85 (6H, s, *gem*-diMe), 1–2 (4H, m, CCH_2CH_2C), 3.20 (3H, s, OCH_3), 3.45 (2H, sym m, CH_2[OH]), 3.3–3.6 (1H, bs, OH), 4.06–4.26 (1H, m, HC—O), and 7.30 (5H, s, Ph) ppm; ms *m/e* (25 eV): no M^+, 219 ($M^+ - OCH_3$), 147, 134, and 121 (base peak). $M^+ - OCH_3$ calcd.: 219.1385; found: 219.1381. *Anal.* calcd. for $C_{15}H_{22}O_3$: C 71.97, H 8.86; found: C 71.32, H 9.41.

Ethyl 2-(5'-Methoxy-5'-phenyl-2'-tetrahydrofuryl)isobutyrate (24)

A solution of 342 mg of hydroxy ketal ester **20** in 10 mL of dry MeOH containing two drops of concentrated H_2SO_4 was refluxed for 30 min. The acid was then neutralized by addition of excess solid $NaHCO_3$. Dilution with 50 mL of ice cold water and extraction with ether gave 330 mg (100+%) of gummy liquid **cyclic ketal ester 24** which was a mixture of two (±) diastereomers in a ratio of ~3:1; ir (neat): 1730 (ester C=O) cm^{-1}, no OH absorption; ^{1}Hmr ($CDCl_3$) δ: 1.26 (3H, t, J = 7 Hz, $CH_3[CH_2]$), 1.24 (s, *gem*-diMe of major isomer), 1.32 (s, *gem*-diMe of minor isomer), 1.6–2.5 (4H, bm, CCH_2CH_2C), 3.00 (s, OCH_3 of major isomer), 3.04 (s, OCH_3 of minor isomer), 4.18 (q, J = 7 Hz, $OCH_2[CH_3]$ of major isomer), 4.21 (q, J = 7 Hz, $OCH_2[CH_3]$ of minor isomer), 4.35–4.60 (1H, m, HC—O of both isomers), and 7.20–7.64 (5H, bm, Ph) ppm. $M^+ - CH_3OH$ calcd. for $C_{16}H_{20}O_3$: 260.1412; found: 260.1417.

Compound **24** decomposes on standing, especially in solvents ($CDCl_3$ or $CHCl_3$) giving rise to acid.

2,2-Dimethyl-2-(5'-methoxy-5'-phenyl-2'-tetrahydrofuryl)-ethanol (28)

To a stirred (magnetic bar) suspension of 60 mg of $LiAlH_4$ in 10 mL of dry ether was added dropwise a solution of 292 mg of cyclic ketal ester **24** in 2 mL of dry ether. After 10 min at room temperature, excess $LiAlH_4$ was destroyed by the addition of cold water. Extraction with ether furnished 258 mg of colorless liquid **hydroxy cyclic ketal 28** which was a mixture of two (±) diastereomers in a ratio of ~3:1; ir (neat): 3400 (strong OH) cm^{-1}, no C=O absorption; ^{1}Hmr (acetone-d_6) δ: 0.96 (3H, s, Me), 1.00 (3H, s, Me), 1.5–2.5 (4H, m, CCH_2CH_2C), 2.97 (s, OCH_3 of major isomer), 3.02 (s, OCH_3 of minor isomer), 3.4–3.7 (3H, m, CH_2OH), 4.06–4.32 (1H, m, HC—O of both isomers), and 7.20–7.62 (5H, m, Ph) ppm; ms *m/e* (18 eV): 250 (M^+), 219 (base peak, $M^+ - OCH_3$), and 177 ($M^+ - Me_2CCH_2OH$). M^+ calcd. for $C_{15}H_{22}O_3$: 250.1569; found: 250.1570.

Although the ^{1}Hmr spectrum of a freshly prepared solution of **28** in $CDCl_3$ could be taken, on standing the compound underwent acid-catalyzed loss of MeOH and formation of the liquid **bicyclic ketal 23**, which was readily purified by thick layer chromatography on silica gel; ir (neat): no OH or C=O absorption; ^{1}Hmr ($CDCl_3$) δ: 0.80 (3H, s, Me), 1.32 (3H, s, Me), 1.5–2.5 (4H, bm, CCH_2CH_2C), 3.45–3.88 (2H, m, CCH_2O) 4.06–4.24 (1H, m, HC—O), and 7.26–7.66 (5H, bm, Ph) ppm; ms *m/e*: 218 (M^+) and 106 (base peak). M^+ calcd. for $C_{14}H_{18}O_2$: 218.1307; found: 218.1309.

2,2-Dimethyl-2-(2'-methoxy-5'-phenyl-2'-tetrahydrofuryl)ethyl p-Toluenesulfonate (26a)

To a solution of 250 mg of the hydroxy ketal **25** in 2 mL of dry pyridine at 5°C was added 200 mg of *p*-TsCl. After standing overnight at 5°C the reaction mixture was diluted with ether and washed with water. Evaporation of the ether left 396 mg (98%) of crude gummy tosylate **26*a*** which was purified by chromatography on alumina; ^{1}Hmr ($CDCl_3$) δ: 0.85 (6H, s, *gem*-diMe), 1–2 (4H, bm, CCH_2CH_2C), 2.42 (3H, s, $ArCH_3$), 3.20 (3H, s, OCH_3), 3.3–4.2 (3H, bm, —CH_2OTs and HC—O), 7.32 (5H, s, Ph), 7.34 and 7.78 (4H, J = 8 Hz, A_2B_2 of *p*-Ts) ppm; ms *m/e* (25 eV): no M^+, 373 ($M^+ - OCH_3$), 147, 134, and 121 (base peak). $M^+ - OCH_3$ calcd. for $C_{21}H_{25}O_4S$: 373.1473; found: 373.1474.

2,2-Dimethyl-2-(2'-methoxy-5'-phenyl-2'-tetrahydrofuryl) ethyl Mesylate (26b)

A solution of 125 mg of hydroxy cyclic ketal **25** and 0.5 mL of dry triethylamine in 5 mL of dry CH_2Cl_2 was cooled to −15°C and treated with 0.04 mL of freshly distilled $MeSO_2Cl$. After 0.5 h the reaction was diluted with cold water and extracted with ether to yield 185 mg of crude product, ^{1}Hmr ($CDCl_3$) δ: 0.90, 0.95, 1.00 (overlapping Me singlets), 2.96 (3H, s, CH_3SO_2), 3.20 (3H, s, CH_3O), 4.0–4.4 (m, CH_2OMs + Ph—CH—O), and 7.23 (5H, s, Ph) ppm; ms *m/e* (25 eV): 296 ($M^+ - CH_3OH$).

2,2-Dimethyl-2-(5'-methoxy-5'-phenyl-2'-tetrahydrofuryl)ethyl Mesylate (27)

A solution of 200 mg of freshly prepared hydroxy cyclic ketal **28** and 0.5 mL of triethylamine in 5 mL of dry CH_2Cl_2 was cooled to −15°C and treated with 0.08 mL of freshly distilled $MeSO_2Cl$. After 0.5 h the reaction mixture was diluted with ether and washed with water. Evaporation of the dried ether solution left 268 mg (100+%) of gummy mesylate **27**, ir (neat): 1350 and 1175 (sulfonate ester) cm^{-1}, no OH or C=O absorption; ^{1}Hmr ($CDCl_3$) δ: 1.03 (6H, s, Me_2C), 3.00 (3H, s, CH_3SO_3), 3.00 (3H, s, OCH_3), 3.3–4.3 (3H, m, —CH_2OMs, HC—O), and 7.1–7.5 (5H, m, Ph) ppm; ms *m/e* (25 eV): 328 (M^+, too weak for precise mass determination) and 296 ($M^+ - CH_3OH$). $M^+ - CH_3OH$ calcd. for $C_{15}H_{20}O_4S$: 296.1082; found: 296.1078.

Reduction of Tosylate 26a

(a) NaI/Zn/DME. A solution of 100 mg of **26*a*** in 20 mL of DME was refluxed with a large excess of NaI and Zn dust for 66 h. Cooling, dilution with ether, and filtration gave a colorless solution which was washed with water, dried, and evaporated to leave 79 mg of crude liquid product. The ^{1}Hmr spectrum indicated the loss of the tosyl group, but tlc analysis revealed several spots. Thick layer chromatography (EtOAc–hexanes, 1:4, development) gave a colorless oil from the major band, ^{1}Hmr ($CDCl_3$) δ: 0.87(s) + 1.07(s) + 1.15(s) + 1.18(s) (total ~7H), 1.4–2.0 (~4H, m, CH_2s), 3.17 (3H, s, OCH_3), 3.93–4.53 (~3H, m, OCH), and 7.17 (5H, s, Ph) ppm.

(b) $LiEt_3BH$. A solution of 86 mg of tosylate **26*a*** in 2 mL of dry THF (freshly distilled from $LiAlH_4$) cooled in an ice bath was treated with 0.42 mL of a 1.0 *M* solution of $LiEt_3BH$ in THF (Aldrich). The reaction mixture was then stirred at reflux temperature for 3 h. After addition of water, 0.2 mL of 3 *N* aqueous NaOH, and 0.2 mL of 30% H_2O_2, the product was extracted with ether to yield 64 mg of crude liquid product. The ^{1}Hmr spectrum verified the absence of the tosyl group and the presence of new peaks in the methyl region, but tlc analysis revealed that the product was a mixture of several compounds. Thick layer chromatography ($CHCl_3$ development) gave a colorless oil from the major band, ir (neat): no OH or C=O absorption; ^{1}Hmr ($CDCl_3$) δ: 1.08(s) + 1.15(s) + 1.20(s) (total ~6H), 1.4–2.0 (~4H, m, CH_2s), 3.18 (3H, s, OCH_3), 3.93–4.53 (3–4H, m, OCH), and 7.16 (5H, s, Ph) ppm.

(c) An authentic specimen of the methoxy ketal of the *tert*-butyl ketol **25** (CH_2OH=CH_3) was prepared by refluxing 85 mg of **2*b*** (Ar = Ph) in 15 mL of dry MeOH with 85 mg of *p*-TsOH for 0.5 h. Quenching with aqueous $NaHCO_3$ and extraction with ether gave 56 mg of pale yellow oily ketal, ^{1}Hmr ($CDCl_3$) δ: 1.07 (9H, s, *t*-Bu), 1.7–2.2 (2H, m, CH_2), 2.4–2.8 (2H, m, CH_2), 3.20 (3H, s, OCH_3), 4.07 (1H, t, PhCHO), and 7.20 (5H, s, Ph) ppm. M^+ calcd. for $C_{15}H_{22}O_2$: 234.1620; found: 234.1623. From the

Can. J. Chem. Downloaded from www.nrcresearchpress.com by 210.87.254.6 on 09/06/12
For personal use only.

t-Bu peak position it seems likely that this ketal was one component of the reduction mixtures described in (*a*) and (*b*).

Preparation and Reaction of 2,2-Dimethyl-2-(2'-methoxy-5'-phenyl-2'-tetrahydrofuryl)ethyl Trifluoromethanesulfonate (26c)

To a solution of 57 mg of hydroxy ketal **25** in 2 mL of CH_2Cl_2 and 0.5 mL of dry pyridine at −15° to −25°C was added 0.05 mL of trifluoromethanesulfonic anhydride. After 45 min the reaction mixture was diluted with CH_2Cl_2 and washed with aqueous $NaHCO_3$. Evaporation of the dried CH_2Cl_2 solution left liquid **26c**; ^{1}Hmr ($CDCl_3$) δ: 1.02 (s, Me), 1.05 (s, Me), 1.4–2.1 (m, CH_2s), 3.67 (s, OCH_3), 4.38 (bs, CH_2—OTrf), 4.48–5.01 (m, PhCH—O), and 7.15 (Ph) ppm.

The crude triflate **26c** was dissolved in a few mL of DMF and stirred (magnetic bar) with 40 mg of NaSPh for 14 h. Neutralization with HOAc and ether extraction afforded the crude thioether which was a mixture of several products from tlc analysis. Thick layer chromatography (EtOAc–hexanes, 1:5, development) gave a colorless liquid from the major band, ^{1}Hmr ($CDCl_3$) δ: 1.02(s) + 1.10(s) + 1.17(s) + 1.20(s) (total ~7H), 1.4–2.2 (m, CH_2s), 3.21 (3H, s, OCH_3), 3.95–4.38 (~3H, m, OCH), and 7.28 (~9H, s, Ph) ppm; ms *m/e* (25 eV): 312 ($M^+ + H - OCH_3$?).

Reformatsky Reaction with δ-Phenylvalerolactone (30)

(*a*) A solution of 377 mg of δ-phenylvalerolactone and 626 mg of ethyl α-bromoisobutyrate in 20 mL of benzene was added dropwise to a refluxing slurry of 210 mg of Zn dust and 10 mL of benzene under N_2. After 2 h the reaction was quenched by the addition of 4 mL of 25% aqueous H_2SO_4. Ether extraction afforded 447 mg (71%) of crude product. Thick layer chromatography in $CHCl_3$–MeOH (98:2) yielded pure liquid **ethyl 2,2-dimethyl-3-hydroxy-7-phenyl-7-oxoheptanoate 33**, uv (MeOH): 240 nm (8950); ir (neat): 3500 (OH), 1725 (ester C=O), and 1690 (PhC=O) cm^{-1}; ^{1}Hmr ($CDCl_3$) δ: 1.18 (6H, s, *gem*-diMe), 1.26 (3H, t, $CH_3[CH_2O]$), 1.34–2.15 (4H, m, CH_2CH_2), 2.84 (1H, bm, OH), 3.02 (2H, t, J = 7 Hz, O=CCH_2), 3.68 (1H, dd (after D_2O), HC[OH]), 4.15 (2H, q, J = 7 Hz, $OCH_2[CH_3]$), 7.2–7.7 (3.65H, m, *m*- + *p*-H of PhC=O), and 7.9–8.1 (1.35H, m, *o*-H of PhC=O) ppm; ms *m/e* (25 eV): 292 (M^+), 274 ($M^+ - H_2O$), 247 (M^+ − OEt), 177 (base peak, $PhCOCH_2CH_2CH_2CHOH^+$), and 105 ($PhC{\equiv}O^+$). $M^+ - H_2O$ calcd. for $C_{17}H_{22}O_3$: 274.1569; found: 274.1567.[7]

(*b*) When the reaction of 0.88 g of lactone **30** and 1.95 g of ethyl α-bromoisobutyrate with 0.65 g of Zn dust in 50 mL of refluxing benzene was conducted for 5 h, the product was a mixture of four compounds. Column chromatography on silica gel with $CHCl_3$–MeOH (99:1) eluted the major, least polar product, **2,2-dimethyl-3-benzoyloxycyclohexanone 37** as a colorless liquid, uv (MeOH): 228 nm (14 850); ir (neat): 1700–1725 (b, ketone + ester C=O) cm^{-1}, no OH absorption; ^{1}Hmr ($CDCl_3$) δ: 1.20 (3H, s, Me), 1.27 (3H, s, Me), 1.65–2.65 (6H, m, $3CH_2$), 5.08 (1H, m, HCOBz), 7.17–7.47 (3H, m, *m*- and *p*-H of PhC=O), and 7.70–7.90 (2H, m, *o*-H of PhC=O) ppm; ms *m/e*: 246 (M^+), 124 ($M^+ - PhCO_2H$), and 105 (base peak, $PhC{\equiv}O^+$). M^+ calcd. for $C_{15}H_{18}O_3$: 246.1256; found: 246.1256.

(*c*) To a stirred (magnetic bar) mixture of 54 mg of Zn dust, 110 mg of lactone **30**, 2 mL of dry THF, and 1.25 mL of dry MeOH-free trimethyl borate (21) at room temperature under N_2 was added 122 mg of ethyl α-bromoisobutyrate. After 19 h when the Zn had apparently been consumed, the reaction was quenched by the addition of 0.65 mL of concentrated NH_4OH and 0.2 mL of glycerol. Dilution with water and extraction with ether gave 82 mg of essentially pure **methyl 5-hydroxy-5-phenylbutyrate**, ^{1}Hmr ($CDCl_3$) δ: 1.4–2.8 (7H, m, $3CH_2$ + OH), 3.53 (3H, s, OCH_3), 4.53 (1H, m, PhCH[OH]), and 7.05 (5H, s, Ph) ppm. M^+ calcd. for $C_{12}H_{16}O_3$: 208.1099; found: 208.1101.

[7]The molecular ion was too weak for exact mass determination.

Structure Proof of Rearrangement Product 37

(*a*) A 50-mg sample of **37** was dissolved in 20 mL of EtOH and treated with 0.1 g of $NaBH_4$ for 2.5 h at room temperature. Dilution with water and extraction with ether gave 32 mg of colorless oily *cis* **39**, uv (MeOH): 228 (16 400); ir ($CHCl_3$): 3615 and 3490 (OH), and 1710 (benzoate C=O) cm^{-1}; ^{1}Hmr ($CDCl_3$) δ: 1.07 (6H, s, *gem*-diMe), 1.1–2.0 (7H, m, 3 CH_2 + OH), 3.37 (1H, m, $w_{1/2}$ = 16 Hz, HC[OH]), 4.67 (1H, m, $w_{1/2}$ = 16 Hz, HCOBz), 7.10–7.47 (3H, m, *m*- and *p*-H of PhC=O), and 7.80–8.00 (2H, m, *o*-H of PhC=O) ppm.

(*b*) A 30-mg sample of the $NaBH_4$ product **39** was refluxed with NaOH–H_2O–THF for 24 h. Ether extraction gave 10 mg of crystalline **2,2-dimethyl-*cis*-1,3-cyclohexanediol**. Recrystallization from hexanes gave 4 mg of needles, mp 110–112°C (lit. (22) mp 110.5°C); ^{1}Hmr ($CDCl_3$) δ: 1.02 (s, *gem*-diMe) and 3.38 (m, 2HC[OH]) ppm; ms *m/e* (25 eV): 143 (M^+ − H) and 126 ($M^+ - H_2O$). $M^+ - H_2O$ calcd. for $C_8H_{14}O$: 126.1045; found: 126.1045. The melting point was not depressed on admixture with an authentic sample of the diol, mp 112–112.5°C, ^{1}Hmr ($CDCl_3$) δ: 1.02 (s, *gem*-diMe) and 3.37 (m, 2HC[OH]) ppm, prepared by $NaBH_4$ reduction of 2,2-dimethyl-1,3-cyclohexanedione obtained by the procedure of Stetter and Sandhagen (23).

Acidification of the basic aqueous saponification solution with aqueous HCl and extraction with ether gave 14 mg of benzoic acid, mp 120–121°C after recrystallization from hexanes, ir ($CHCl_3$) 2700–3400 (broad OH) and 1695 (aryl C=O) cm^{-1}. M^+ calcd. for $C_7H_6O_2$: 122.0368; found: 122.0368. The mixture melting point with an authentic specimen was 120–122°C.

Isomerization Experiments

(*a*) A solution of 80 mg of pure ketol **7** and 6 KOH pellets in 0.2 mL of water and 7 mL of *t*-BuOH was refluxed for 48 h under a N_2 atmosphere.[8] The reddish brown reaction mixture was diluted with water and extracted with ether to yield 70 mg of crude product. Thick layer chromatography gave a colorless liquid mixture of ketols **7** (70%, glpc ret. time 2.0 and 3.2 min)[9] and **8** (30%, glpc ret. time 2.7 min). Peak identities were checked by admixture of authentic **7** and **8**. The ^{1}Hmr spectrum ($CDCl_3$) contained the following characteristic signals: δ 0.92 *i*-Pr d of **8**, 1.08 *i*-Pr d of **7**, 4.68 PhCH[OH] m of 7, and the 7.88–8.04 *o*-benzoyl m of **8**.

(*b*) A 55-mg sample of pure ketol **8** was treated identically as in (*a*) to yield 28 mg of crude product; glpc showed the presence of both ketols **7** and **8** in about the same ratio as in (*a*).

(*c*) A solution of 63 mg of ketol ester **33**, 3 KOH pellets, and 0.2 mL of water in 8 mL of *t*-BuOH was refluxed for 66 h. Dilution with 10 mL of water and extraction with ether gave 42 mg (89%) of neutral material which proved to be an ~1:1 mixture of **35** and **36**; ^{1}Hmr ($CDCl_3$) δ: 0.91 (d, J = 7 Hz, Me_2[CHCHOH] of **36**), 1.07 (d, J = 7 Hz, Me_2[CHC=O] of **35**), 4.63 (m, PhCH[OH] of **35**), 7.17–7.56 (m, ArH of **35** and *m*- + *p*-ArH of **36**), and 7.80–8.00 (m, *o*-ArH of **36**) ppm, no $COOCH_2CH_3$ absorption.

[8]Both ketols **7** and **8** were stable in this reagent at room temperature.

[9]Ketol **7** always gave a characteristic double glpc peak, the origin of which must lie in the ketol ring-chain tautomerism. However, ketol **8** gave only a single peak.

Acknowledgments

We would like to thank the Natural Sciences and Engineering Research Council of Canada for finan-

cial support, Drs. A. A. Grey and A. Lee for some 220 MHz ^{1}Hmr spectra, Heather Schroeder for the 100 MHz ^{1}Hmr spectra, and Doug Hairsine for the mass spectra.

1. E. W. WARNHOFF, P. REYNOLDS-WARNHOFF, and M. Y. H. WONG. J. Am. Chem. Soc. **102**, 5956 (1980).
2. G. A. CRAZE and I. WATT. J. Chem. Soc. Chem. Commun. 147 (1980).
3. I. WATT. Tetrahedron Lett. 4175 (1978).
4. E. W. WARNHOFF. Can. J. Chem. **55**, 1635 (1977).
5. S. DANISHEVSKY and M. HIRAMA. Tetrahedron Lett. 4565 (1977).
6. A. KASAL and A. TRKA. Collect. Czech. Chem. Commun. **42**, 1389 (1977).
7. R. SAKAGUCHI and K. YAMAKAWA. 20th Symp. Chem. Nat. Prod., Sendai, Japan. October 7–10, 1976. pp. 139–146.
8. J. D. COX and G. PILCHER. Thermochemistry of organic and organometallic compounds. Academic Press, London. 1970. p. 216.
9. M. BOGAVAC, H. LAPIN, V. ARSENIJEVIC, and A. HOREAU. Bull. Soc. Chim. Fr. 4437 (1969).
10. J. E. G. BARNETT and P. W. KENT. J. Chem. Soc. 2743 (1963).
11. R. O. HUTCHINS, D. HOKE, J. KEOGH, and D. KOHARSKI. Tetrahedron Lett. 3495 (1969).
12. R. O. HUTCHINS, B. E. MARYANOFF, and C. A. MILEWSKI. J. Chem. Soc. Chem. Commun. 1097 (1971).
13. Y. FUJIMOTO and T. TATSUNO. Tetrahedron Lett. 3325 (1976).
14. S. KRISHNAMURTHY and H. C. BROWN. J. Org. Chem. **41**, 3064 (1976).
15. P. YATES and C. D. ANDERSON. J. Am. Chem. Soc. **80**, 1264 (1958).
16. M. W. RATHKE and A. LINDERT. J. Org. Chem. **35**, 3966 (1970).
17. H. B. BÜRGI, J. D. DUNITZ, and E. SHEFTER. J. Am. Chem. Soc. **95**, 5065 (1973).
18. H. B. BÜRGI, J. M. LEHN, and G. WIPF. J. Am. Chem. Soc. **96**, 1956 (1974).
19. L. F. FIESER and M. FIESER. Reag. Org. Synth. **1**, 1285 (1967).
20. M. JULIA, S. JULIA, and B. BEMONT. Bull. Soc. Chim. Fr. 304 (1960).
21. H. I. SCHLESINGER, H. C. BROWN, D. L. MAYFIELD, and J. R. GILBREATH. J. Am. Chem. Soc. **75**, 213 (1953).
22. V. A. MIRONOV, A. D. FEDOROVICH, and A. A. AKHREM. Izv. Akad. Nauk SSSR, Ser. Khim. 1288 (1973). English translation.
23. H. STETTER and H. J. SANDHAGEN. Chem. Ber. **100**, 2387 (1967).

Can. J. Chem. Downloaded from www.nrcresearchpress.com by 210.87.254.6 on 09/06/12
For personal use only.

Kinetics and mechanism of the oxidation of cyclohexanone by a nickel(III) macrocyclic ligand complex in CH_3CN

WILLIAM A. WELSH,[1] JOHN OTUTAKOWSKI,[2] AND PATRICK M. HENRY

Guelph–Waterloo Centre for Graduate Work in Chemistry, Guelph Campus, Department of Chemistry, University of Guelph, Guelph, Ont., Canada N1G 2W1

Received September 7, 1979[3]

WILLIAM A. WELSH, JOHN OTUTAKOWSKI, and PATRICK M. HENRY. Can. J. Chem. **59**, 697 (1981).

The oxidation of cyclohexanone by the Ni(III) complex of the macrocyclic ligand, 5,5,7,12,12,14-hexamethyl-1,4,8,11-tetraazacyclotetradecane(meso-[14]ane) in acetonitrile solution containing CF_3CO_2H obeyed the rate equation: $-d[Ni(III)]/dt = k[Ni(III)][cyclohexanone]/[CF_3CO_2H]$. Kinetic and spectral studies in the presence of CF_3CO_2Na indicate the inhibition term in CF_3CO_2H is not due to complexation of trifluoroacetate but is a real acid inhibition term. The isotope effect, k_H/k_D using 2,2,6,6-tetradeuterocyclohexanone as substrate, was 3.2. The main product found in greater than 100% yield based on Ni(III) was the non-oxidative product, 2(cyclohexen-1-yl)cyclohexanone, which must have been formed in a radical chain reaction. A mechanism involving deprotonation of one of the coordinated nitrogens followed by rearrangement to a Ni(II) ligand radical intermediate is proposed. The ligand radical extracts a hydrogen from cyclohexanone to give [Ni(II)meso-[14]ane] and a cyclohexanone radical which initiates a radical chain reaction to give the observed dimeric product. Support for the mechanism is provided by recent studies of the base catalyzed decomposition of Ni(III) complexes in aqueous and non-aqueous solvents.

In the presence of CF_3CO_2Na, the Ni(III) complex decomposes rapidly even in the absence of cyclohexanone. This is believed to occur via trifluoroacetoxy radicals, a mechanism which has analogy in other systems.

WILLIAM A. WELSH, JOHN OTUTAKOWSKI et PATRICK M. HENRY. Can. J. Chem. **59**, 697 (1981).

L'oxydation de la cyclohexanone par le complexe de Ni(III) du ligand macrocyclique hexaméthyl-5,5,7,12,12,14 tétraaza-1,4,8,11 cyclotétradécane (mesoane-[14]) dans une solution d'acétonitrile contenant du CF_3CO_2H obéit à l'équation de vitesse: $-d[Ni(III)]/dt = k[Ni(III)][cyclohexanone]/[CF_3CO_2H]$. Des études spectrales et cinétiques en présence de CF_3CO_2Na indiquent que le facteur d'inhibition dans le CF_3CO_2H n'est pas dû à la complexation du trifluoroacétate, mais qu'il est un facteur réel d'inhibition acide. L'effet isotopique k_H/k_D mesuré sur la tétradeutéro-2,2,6,6 cyclohexanone est de 3,2. Le produit principal obtenu avec un rendement supérieur à 100% si l'on se base sur le Ni(III) est un produit qui ne provient pas d'une oxydation, soit la (cyclohexène-1 yl)-2 cyclohexanone, qui a dû se former au cours d'une réaction radicalaire en chaîne. On propose un mécanisme qui fait intervenir la déprotonation d'un des atomes d'azote coordonnés suivie de la transposition en un intermédiaire ligand radicalaire du Ni(II). Le ligand radicalaire arrache un atome d'hydrogène de la cyclohexanone et conduit au [Ni(II)mésoane[14]] et au radical cyclohexanone qui initie la réaction radicalaire en chaîne conduisant aux produits dimères. Ce mécanisme est confirmé par des études récentes sur la décomposition catalysée par une base de complexes de Ni(III) dans des solvants aqueux et non aqueux.

En présence de CF_3CO_2Na, le complexe de Ni(III) se décompose rapidement même en l'absence de cyclohexanone. On pense que cette décomposition a lieu par l'intermédiaire de radicaux fluoroacétoxy, un mécanisme que l'on retrouve dans d'autres systèmes.

[Traduit par le journal]

Introduction

Although transition metal salts catalyze a number of organic oxidation reactions (1–4) there have been few studies on the use of macrocyclic complexes of transition metals for this purpose. In one study the Fe(II), Co(II), and Ni(II) complexes of the saturated Curtius macrocyclic ligand, 5,5,7,12,12,14-hexamethyl-1,4,8,11-tetraazacyclotetradecane(meso-[14]ane), were tested as catalysts for the air oxidation of cyclohexene in acetonitrile (5). The Fe(II) compound was the most active catalyst with the Co(II) compound next and the Ni(II) compound practically inactive. In another study the iron complex of T1M (2,3,9,10-tetramethyl-1,4,8,11-tetraazacyclotetradeca-1,3,8,10-tetraene) was found to catalyze the light promoted oxidation of methanol (6).

In our own studies of the oxidation of organic compounds by iron complexes containing nitrogen donor atoms the question has arisen as to the mode of electron transfer from the organic to the metal oxidant (7–10). With coordinately saturated complexes such as tris(1,10-phenanthroline)iron(III) the electron transfer must occur via an outer sphere mechanism (7, 8). However, with macrocyclic complexes of iron the axial positions are labile so electron transfer could occur after coordination of the organic to the metal center or by transfer of the electron from the organic without prior coordination (9, 10). One intriguing possibility for the latter route is electron transfer of the electron through the nitrogen attached to the Fe(III). An iron(II)–ligand radical intermediate which abstracts a hydrogen from the organic is a likely mechanism. Such an

[1]Present address: W.R. Grace & Co., 7379 Route 32, Columbia, MD 21044, U.S.A.

[2]Undergraduate Summer Research Assistant 1980.

[3]Revision received October 20, 1980.

0008-4042/81/040697-08$01.00/0

©1981 National Research Council of Canada/Conseil national de recherches du Canada

Can. J. Chem. Downloaded from www.nrcresearchpress.com by 210.87.254.6 on 09/06/12
For personal use only.

intermediate, **1**, has been suggested for the self-dehydrogenation of the iron(III) macrocyclic diene complex shown below in acetonitrile solution when water is added in the presence of molecular oxygen (11).

[1] 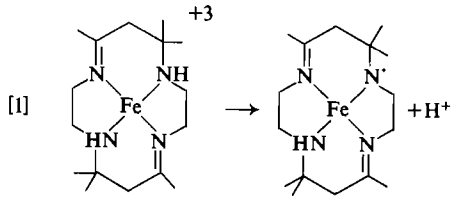

1

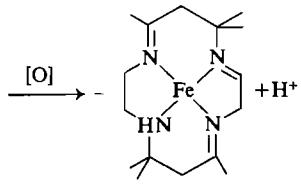

In order to test the possibility of ligand radical intermediates such as **1**, it was decided to study the oxidation of organics by meso-[14]ane complex of Ni(III), **2**, in CH_3CN. **2** and other saturated macrocyclic ligand complexes have been shown to be true compounds of the Ni(III) oxidation state (12–14). Because of the high redox potential of the Ni(III)–Ni(II) couple (E_0 = ca. 1.0 vs. SHE in H_2O containing SO_4^{2-} (15)) this system should favour the ligand radical type intermediate in the oxidation of organics. This paper reports a study of the oxidation of cyclohexanone in acetonitrile by **2**.

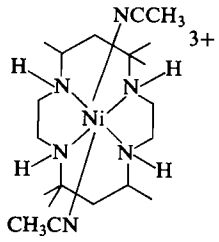

2

After this work was begun Barefield and Mocella reported that the base catalyzed decomposition of the same complex proceeded via a Ni(II)–ligand radical (16). Later several Ni(III) macrocyclic complexes, including **2**, were generated by pulse radiolysis and their decomposition studied (17–20). Although there was some disagreement as to the actual identity of all species detected, an acid inhibition term in the decomposition of the Ni(III) complex was noted and attributed to the equilibrium given by [2], where N–H represents an amino group on the complex (17, 20).

[2] 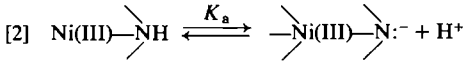

It was suggested (20)[4] that the deprotonated species rearranges to a ligand radical which decomposes by several routes including disproportionation

[3] 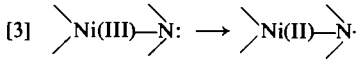

to give the original complex and a complex with an additional imine group; abstraction of hydrogen from an H-donor; or ring fragmentation products.

Complexing in the axial positions with groups such as SO_4^{2-}, OH^-, and Br^- stabilized the Ni(III) complex (15, 17, 18). When Br^- is the ligating group decomposition occurs by formation of $Br^\cdot$ and the Ni(II) complex (17).

Experimental

General

Starting materials were of reagent or comparable grade. Freshly distilled cyclohexanone and CF_3CO_2H were used for the kinetic runs. The CH_3CN solvent was spectroquality and was dried over molecular sieves. The 2,2,6,6-tetradeuterocyclohexanone was prepared by equilibrating ordinary cyclohexanone with D_2O in the presence of a small amount of acid. The nmr spectra indicated that the 2,6 positions contained 95% deuterium. Air-sensitive reactions were carried out with oven-dried glassware using syringe techniques.

Proton nmr spectra were recorded on a Bruker WP-60. Infrared spectra were recorded on a Beckman IR5 while a Cary 118 was used for the visible–uv measurements. Gas chromatographic analyses were carried out with a Hewlett-Packard research chromatograph (model H.P. 5750B) using a 6 ft 20% carbowax 20M column on 60–80 mesh Chromosorb W. Temperature was 200°C and helium flow was 30 mL/min.

Syntheses

The $[Ni(meso\text{-}[14]ane)]^{2+}$ was prepared by reduction of the parent 4,11-diene complex using Raney nickel and base using the procedure described by Curtis (21). The rac and meso forms were then separated using sodium oxalate. The $[Ni(meso\text{-}[14]ane)(CH_3CN)_2](BF_4)_3$ was prepared by the procedure of Barefield and Mocella with the exception $NOBF_4$ was used in place of $NOClO_4$ (16).

Kinetic Runs

The rate of disappearance of the Ni(III) complex was followed by observing the disappearance of the band at 460 nm which is on the shoulder of a charge transfer band. This region of the spectrum is uncluttered by other reactant absorptions and the absorption due to the *d–d* transition of the Ni(II) complex at 460 nm was negligible. The only metal containing product found was the original $[Ni(meso\text{-}[14]ane)]^{2+}$ identified by its nmr spectrum (22). No attempt was made to detect free Ni(II) but the spectra of the final reaction solutions indicated the Ni(II) complex yield was essentially quantitative.

Runs were begun by adding cyclohexanone and/or

[4]Reference 20 proposes this step while ref. 16 does not consider the separate deprotonation equilibria given by [2]. Reference 17 does not consider the detailed pathways for decomposition of the deprotonated complex.

Can. J. Chem. Downloaded from www.nrcresearchpress.com by 210.87.254.6 on 09/06/12
For personal use only.

Can. J. Chem. Downloaded from www.nrcresearchpress.com by 210.87.254.6 on 09/06/12
For personal use only.

CF_3CO_2Na to a solution of the Ni(III) complex in CH_3CN thermostated at 25°C. If CF_3CO_2H is present it was added before the run was started. Good first order plots were obtained for at least two half-lines. Addition of $(CF_3CO)_2O$ to a run containing CF_3CO_2H in order to remove any water which might be present did not affect the rate.

Product Identification

In a typical run a mixture of 25 mL CH_3CN, 1 mL cyclohexanone, and 1.0 g of the Ni(III) complex were stirred for 45 min at which point the colour had changed from deep green to orange. The volume was reduced under vacuum at room temperature to ca. 10 mL. The solution was decanted from a pale green solid and 250 mL of ether was added. After standing in the refrigerator overnight the mixture was again filtered to remove more solid and the volume reduced at room temperature to 5 mL. Thin layer chromatography using CH_3CN as solvent on alumina indicated 3 or 4 minor products which moved with the solvent front and one major product which moved slowly. Gas chromatographic analysis gave only one large peak which had a retention time of about 30 min under the conditions used (see above). Several portions of the solution were injected and this peak was collected in melting point tubes. The nmr and infrared spectra were identical to those for an authentic sample of 2(cyclohexen-1-yl)cyclohexanone.

Control experiments were carried out by stirring 1 g of the Ni(II) complex, 25 mL CH_3CN, and 1 mL cyclohexanone overnight. After workup the concentrated reaction mixture was analysed by gc using the conditions described previously. No 2(cyclohexen-1-yl)cyclohexanone was detected.

Results

All kinetic and equilibrium studies were made at 25°C in dry acetonitrile solvent.

Kinetics

The kinetics were first determined in acid-free acetonitrile. The data are presented in Table 1. The fact that the value of k_2 calculated assuming the reaction is first order in each reactant is constant indicates the rate expression under these conditions is given by [4] with average value of 4.2×10^{-3} M^{-1} s^{-1} for k_2.

$$[4] \quad \text{Rate} = k_2[\mathbf{2}][\text{cyclohexanone}]$$

The average value of k_2 for the runs with 2,2,6,6-tetradeuterocyclohexanone is 1.3×10^{-3} M^{-1} s^{-1}. Thus the isotope effect k_H/k_D is 3.2.

Addition of trifluoroacetic or methanesulfonic acids caused a yellowing of the green solution and a lowering of the rate of cyclohexanone oxidation. The kinetics of the acid inhibition were studied using CF_3CO_2H. Results are listed in Table 2. A plot of k_2 vs. $1/[CF_3CO_2H]$ gives a linear plot with an intercept of zero and a slope of 1.24×10^{-5} s^{-1}. Thus the rate expression in the presence of CF_3CO_2H is given by [5] where k' is 1.24×10^{-5} s^{-1}.

$$[5] \quad \frac{-d[\mathbf{2}]}{dt} = \frac{k'[\mathbf{2}][\text{cyclohexanone}]}{[CF_3CO_2H]}$$

TABLE 1. Effect of Ni(meso-[14]ane)$(CH_3CN)_2^{3+}$ and cyclohexanone concentrations on rate in acid free acetonitrile at 25°C

[Ni(III)] ($M \times 10^3$)	Cyclohexanone ($M \times 10$)	k_2[a] (M^{-1} $s^{-1} \times 10^3$)
4.0	0.51	4.3
4.0	1.27	4.5
4.0	2.54	4.2
4.0	3.81	4.2
4.0	5.08	4.4
1.6	2.54	4.3
2.3	2.54	4.2
3.1	2.54	4.0
3.9	2.54	4.2
3.0	2.65[b]	1.4
3.0	2.65[b]	1.3
3.4	2.65[b]	1.2
3.4	2.65[b]	1.4

[a] k_2 defined by [1].
[b] 2,2,6,6-Tetradeuterocyclohexanone is organic reactant.

TABLE 2. Effect of trifluoroacetic acid concentration on rate of oxidation of cyclohexanone by Ni(meso-[14]ane)$(CH_3CN)_2^{3+}$ in CH_3CN at 25°C[a]

$[CF_3COOH]$ ($M \times 10^2$)	k_{obs} ($s^{-1} \times 10^5$)
3.25	36.0
6.50	20.7
13.0	9.22
19.5	6.46

[a] [Ni(meso-[14]ane)$(CH_3CN)_2^{3+}$] = 3.8×10^{-3} M; [cyclohexanone] = 2.54×10^{-1} M.

The effect of sodium trifluoroacetate on rates of oxidation of cyclohexanone was also studied. These systems did not give accurate results since the disappearance of the Ni(III) was only about 25% faster in the presence of cyclohexanone than it is in its absence. However, trifluoroacetic acid inhibited the rates of Ni(III) in both the presence and absence of cyclohexanone. Data are listed in Table 3.

Oxidation Products

Identification of oxidation products was not entirely successful. Thin layer chromatography indicated the presence of 3 or 4 minor products, none of which was 2-hydroxycyclohexanone, and one major product. The major product, present in greater than 100% yield based on Ni(III), was found to be 2(cyclohexen-1-yl)cyclohexanone but the minor products could not be separated and identified. The 2(cyclohexen-1-yl)cyclohexanone is not an actual oxidation product and could have been formed by an aldol condensation followed by

TABLE 3. Effect of sodium acetate concentration on rate of Ni(meso-[14]ane)$(CH_3CN)_2^{3+}$ disappearance in presence and absence of cyclohexanone at 25°C[a]

$[CF_3O_2Na]$ ($M \times 10^2$)	$[CF_3CO_2H]$ ($M \times 10^2$)	k_{obs}[b] ($s^{-1} \times 10^5$)	Blank k_{obs}[c] ($s^{-1} \times 10^5$)	Net k_{obs}[d] ($s^{-1} \times 10^5$)
0.20	0	31.0	23.0	7.0
0	2.5	58.6	0.7	57.9
5.0	2.5	12.2	8.1	4.1
10.0	2.5	15.3	12.0	3.3
20.0	2.5	18.7	14.0	4.7
5.0	10.0	1.4	1.1	0.3
10.0	10.0	3.1	2.4	0.7
20.0	10.0	6.7	5.3	1.4

[a] $[Ni(meso\text{-}[14]ane)(CH_3CN)_2^{3+}] = 3.8 \times 10^{-3}$ *M*.
[b] [Cyclohexanone] = 2.5×10^{-1} *M*.
[c] No cyclohexanone present.
[d] The value of k_{obs} in presence of cyclohexanone minus blank k_{obs}.

dehydration (23). However, control experiments with all reactants but the Ni(III) demonstrated that the aldol condensation does not occur under the reaction conditions.

Spectral Studies

In the absence of acid the Ni(III) macrocycle gave a spectra identical to that reported previously (12). The effect of CF_3CO_2H concentration on the spectra was studied in the range of $[CF_3CO_2H]$ used in the determination of acid dependence. Spectra are shown in Fig. 1. As the concentration of CF_3CO_2H increased the absorption in the 410 nm region decreased and the absorption in the 290 nm region increased giving an isosbestic point at 316 nm. The absorption due to CF_3CO_2H is observed at 210 nm. However the change in absorbancies is small and attempts to fit the data to reasonable equilibria using non-linear regression analysis gave no consistent sets of equilibrium constants.

The oxidation of cyclohexanone is also inhibited by methanesulfonic acid. However the changes in spectra upon addition of CH_3SO_3H were quite different from those obtained from the addition of CF_3CO_2H. The absorbance in both the 410 nm region and 325 nm region decreased with increase in absorbance at 280 nm and an isosbestic point at 299 nm.

The effect of added sodium trifluoroacetate on the spectra was also determined. Since the reduction of the Ni(III) was fast in the absence of CF_3CO_2H, some acid was also added. The spectra in the absence of acid, however, were qualitatively the same. Spectra are shown in Fig. 2.

Discussion

Before discussing possible mechanisms it is necessary to discuss the nature of the acid inhibition. It is possible that the acid itself is merely a source of trifluoroacetate ion which is coordinating to the Ni(III) and slowing the rate by lowering the redox potential (15, 17, 18). Thus the changes in spectra shown in Fig. 1 could result from ligation of trifluoroacetate although the changes could not be explained by any simple equilibria scheme. However, as shown in Fig. 2, addition of sodium trifluoroacetate changes the spectra considerably, suggesting that acid alone causes little complexing although the hump in spectra 5, in which there is only acid, suggests the possibility of some complexing. The fact that the spectra change little as the trifluoroacetate concentration increases indicates complexing is almost complete at the lowest $[CF_3CO_2Na]$.

The effect of sodium trifluoroacetate on rate is fairly definitive. The data are not very accurate because of the high rate of reduction of the Ni(III) complex in the absence of cyclohexanone. However the data in Table 3 indicate that both the trifluoroacetate and cyclohexanone induced re-

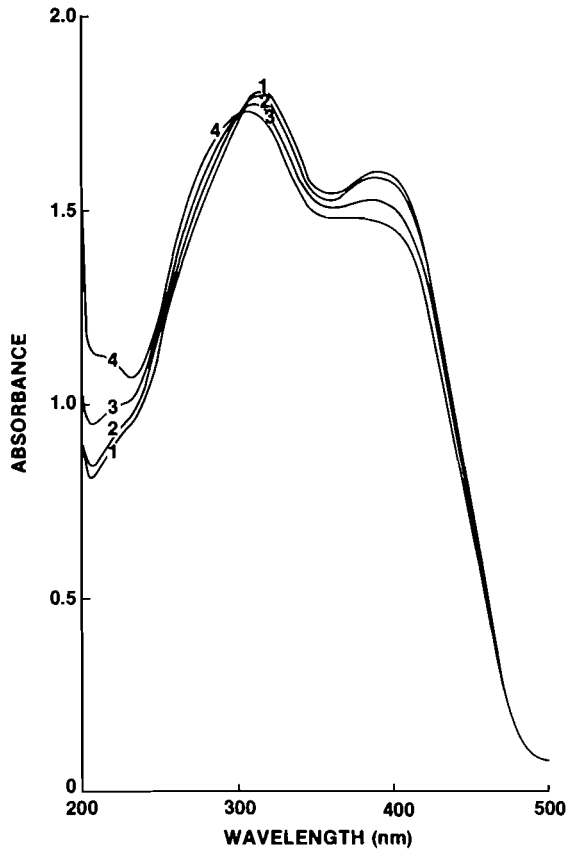

FIG. 1. Spectra of **2** in CH_3CN at various $[CF_3CO_2H]$. [**2**] = 3×10^{-3} *M*. $[CF_3CO_2H] = 0.013$ *M* (*1*); 0.025 *M* (*2*); 0.065 *M* (*3*); 0.13 *M* (*4*).

Can. J. Chem. Downloaded from www.nrcresearchpress.com by 210.87.254.6 on 09/06/12
For personal use only.

Can. J. Chem. Downloaded from www.nrcresearchpress.com by 210.87.254.6 on 09/06/12
For personal use only.

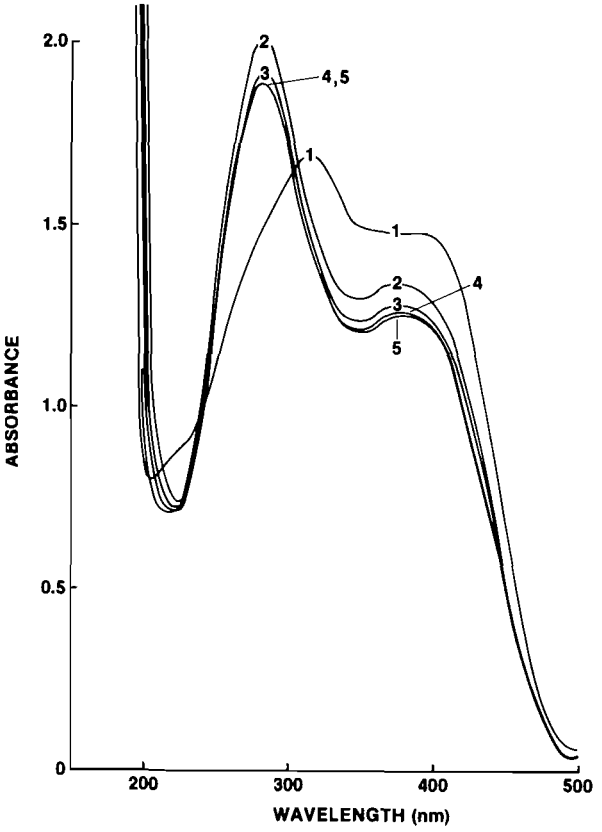

FIG. 2. Effect of CF_3CO_2Na on spectra at $[CF_3CO_2H] = 0.25\,M$. [2] = $3 \times 10^{-3}\,M$. $[CF_3CO_2Na] = 0\,M$ (*1*); $0.025\,M$ (*2*); $0.050\,M$ (*3*); $0.10\,M$ (*4*); $0.20\,M$ (*5*).

duction of Ni(III) are inhibited by acid. Thus the acid inhibition cannot be due to trifluoroacetate ligation since the acid inhibition would have disappeared if that were so.

In light of the recent work on the base catalysed decomposition of Ni(III) macrocycles (16–20) the results of the present work can best be explained by the following general mechanism.[5]

[6] $2 \underset{}{\overset{K_1}{\rightleftharpoons}}$ 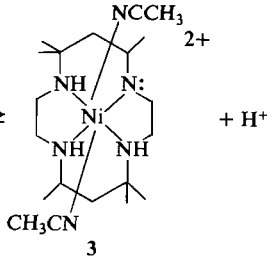 $+ H^+$

3

[7] $3 \overset{K_2}{\rightleftharpoons}$ 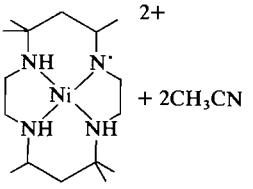 $+ 2CH_3CN$

4

[8] 4 + 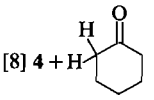 $\xrightarrow{\text{slow}}$ 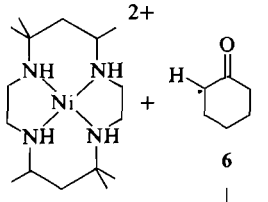 +

5 6

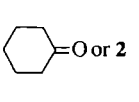

Organic products

Barefield and Mocella (16) proposed that one typical reaction of the radical, **4**, is hydrogen extraction from a H atom donor which in this case is cyclohexanone. The acid inhibition term in the rate expression indicates deprotonation of the ligand is a reversible process and the isotope effect with 2,2,6,6-tetradeuterocyclohexanone indicates [8] is the slow step. Thus radical formation ([7]) must also be an equilibrium process. This is the first evidence for the reversibility of ligand radical formation.

Although the general reaction scheme is consistent with the experimental results and previous work, the detailed pathways for some of the steps are not clearly defined. Thus the initial step of the organic reaction is written as H atom extraction to give the radical **5**. However another possibility involves electron transfer from the enol form of the ketone.

[9] 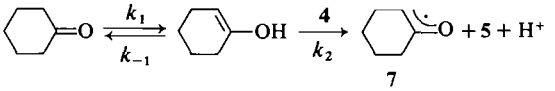

7

Oxidation of cyclohexanone by one electron oxidants apparently usually proceeds the keto form although at least one such oxidant, tris(1,10-phenanthroline)iron(III) ($[Fe(III)phen_3]^{3+}$) which had been previously assumed to attack the keto form (24), has been shown to proceed via the enol tautomer (**7**). The probability of each path can be discussed in terms of the isotope effects.

There is little work on isotope effects in H extraction from C—H bonds by nitrogen radicals (25) but an isotope of k_H/k_D of 4 was reported for the extraction of benzylic hydrogens from toluene and

[5]The proton could also be lost from the nitrogen next to the carbon containing 2 methyl groups to give another isomer of **3**. Likewise the radical in **4** could, and very likely is, also on the other nitrogen. For simplicity only one isomer of **3** and **4** is shown.

Can. J. Chem. Downloaded from www.nrcresearchpress.com by 210.87.254.6 on 09/06/12
For personal use only.

deuterated toluene by the dimethylamino radical (26) and a value, k_K/k_D, of 16 was found for extraction of H from cyclohexane and cyclohexane-d_8 by the 2,2,6,6-tetramethylpiperidyl radical (27). The latter value is probably high because of the hindered nature of the radical but the former falls in range (k_H/k_D = 2–7 for H extraction by carbon radicals (24, 25)). Thus the isotope effect of 3.2 found in the present study is in the expected range. It is even more difficult to predict the isotope effect on [9]. Since the reaction is first order in **2** the reaction of **2** with the enol would have to be rate determining and an equilibrium isotope effect for formation of the enol would be operative.[6] Since cleavage of O—H bonds has a higher isotope effect than cleavage of C—H bonds (28*a*), the isotope effect on k_{-1} would be greater than on k_1, and deuteration of the cyclohexanone would increase the content of enol and contribute to a negative isotope effect. Thus in the oxidation of cyclohexanone by $[Fe(III)phen_3]^{3+}$, a reaction known to proceed via the enol tautomer, a negative isotope effect, k_D/k_H of 2.7 was observed when the reaction was run in D_2O with non-deuterated cyclohexanone (7). The net isotope effect will depend on the value of k_H/k_D for k_2 which in turn will depend on whether the O—H bond is broken in the course of electron transfer of **4**. If it is broken the net isotope could easily be the 3.2. However if this bond is not broken a small or negative isotope effect would be expected. Previous work on the $[Fe(III)phen_3]^{3+}$ system mentioned above (7) suggested the O—H is not broken during electron transfer so the appreciable isotope effect of 3.2 would appear to favour [8].

[10] **6** + $Fe(III)(phen)_3$ + H_2O → 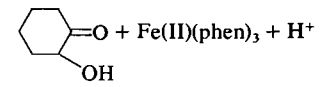 + $Fe(II)(phen)_3$ + H^+

The exact mode of oxidation of cyclohexanone is also not well defined. In the aqueous oxidation by $Fe(III)(phen)_3$ the only initial oxidation product is 2-hydroxycyclohexanone which must result from further oxidation of the initial radical by more $Fe(III)(phen)_3$ in the presence of water. In the present system the actual oxidation is overshadowed by a non-oxidative chain reaction to give 2-(cyclohexen-1-yl)cyclohexanone. One possible scheme is given below:

[11] **6** + 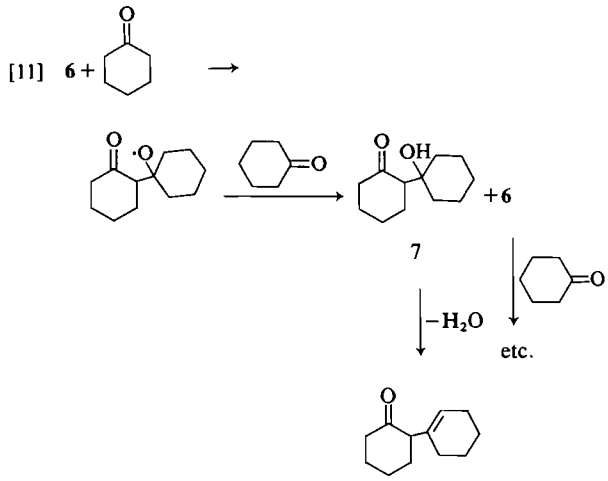

Although radicals do not usually add to carbonyl compounds there are a few examples of addition (29–32), the closest analogy being the addition of cyclohexyl radicals to formaldehye to eventually give a product analogous to **7** (30).

The form of the acid inhibition in the rate expression deserves brief comment. If the acid base equilibrium in [5] is as written then a first order inhibition in $[CF_3CO_2H]$ would not be expected unless CF_3CO_2H is a strong acid in CH_3CN. If it is a weak acid the inhibition term would be a square root term since $[H^+] = \sqrt{CF_3CO_2H}\sqrt{K_a}$ where K_a is the acid dissociation constant of CF_3CO_2H in CH_3CN. Although the authors are aware of no determinations of the pK_a of CF_3CO_2H in CH_3CN, methanesulfonic acid, which is a stronger acid than CF_3CO_2H in water (28*b*), has a pK_a of 10 in CH_3CN (34). Thus CF_3CO_2H is almost certainly a weak acid in CH_3CN. The first order term means that the molecular acid rather than the free proton is causing the inhibition. This is not surprising for a non-hydroxylic solvent such as CH_3CN.

The rates in the presence of trifluoroacetate, shown in Table 3, are, as expected, lower than in the presence of acid alone because of change of redox potential by ligation (15, 17, 18). One curious result is the fact that at $[CF_3CO_2H] = 0.025\,M$ the values of blank and net k_{obs}'s increase little, if at all, with increase in $[CF_3CO_2Na]$ while at $[CF_3CO_2H] = 0.1\,M$, both increase almost linearly. However, detailed speculation in such a complicated system does not seem warranted.

The CF_3CO_2Na induced reduction of the Ni(III) complex probably involves electron transfer from a coordinated $CF_3CO_2^-$ to give a trifluoroacetate

[6]Of course if the reaction were run in a hydroxyl solvent such as water an equilibrium isotope effect would not be observed since the deuteriums would rapidly exchange with the protons of the solvent to produce non-deuterated cyclohexanone. However with CH_3CN as solvent no exchange can occur.

radical by a mechanism similar to that previously proposed for coordinated bromide (17).

The trifluoroacetate radical likely decomposes by decarboxylation to give the $CF_3\cdot$ radical, a reaction the acetoxy radical undergoes (35). The $CF_3\cdot$ can then extract hydrogen from solvent, cyclohexanone, or Ni(III) complex to give a variety of products.

[12] 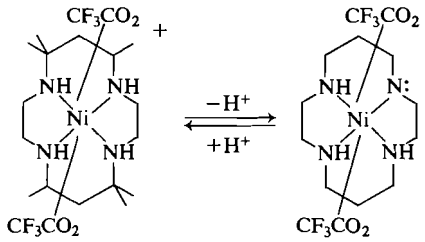

8

[13] 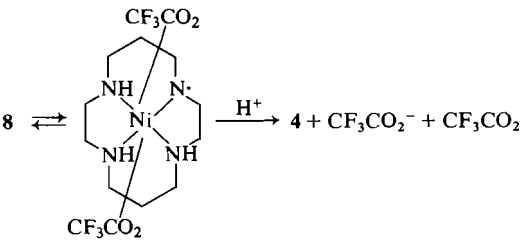

Assuming that K_1 in [6] is small the rate expression for cyclohexanone oxidation is given by [14].

$$[14]\quad \text{Rate} = \frac{kK_1K_2[\mathbf{2}][\text{cyclohexanone}]}{[CF_3CO_2H](1 + K_2)}$$

The value of pK_1 in water has been estimated to be above 11 (17) and must be above 9 to explain the kinetic data (20). The value of pK_1 should be considerably higher in CH_3CN. Using the value of 10^{-11} for K_1 and the value of 1.24×10^{-5} for k' in [5] a value of $kK_2/(1 + K_2) \simeq 10^6$ can be calculated. There is little precedent on which to base an estimate of K_2 but for purposes of comparison it can be arbitrarily assigned a value of one. This gives a value of k in [8] of about 10^6. Dialkyl amino radicals have been reported to be poor H abstractors (26, 27, 33, 36, 37). However they undergo competitive decomposition reactions such as disproportionation very rapidly ($k \simeq 10^9\ M^{-1}\ s^{-1}$) so abstraction is masked. One case where the hydrogen abstraction rates have been measured is with the sterically hindered 2,2,6,6-tetramethylpiperidyl radical (27). With cyclohexane the second order rate constant for abstraction is $0.08\ M^{-1}\ s^{-1}$. Thus even taking into account the fact that this radical is hindered and cyclohexanone is probably more reactive than cyclohexane the value of $10^6\ M^{-1}\ s^{-1}$, which must be considered a minimum value, seems high. However **4** is likely to have very different reactivity from neutral organic nitrogen radicals. Thus it is possible it coordinates the organic substrate prior to electron transfer, thus making the reaction more facile. A study of the organic oxidation in aqueous solution using fast reaction techniques would probably provide further information on the detailed steps of the oxidation.

In spite of the uncertainties regarding detailed pathways this work does demonstrate that ligand radicals can be an important pathway in oxidation of organic compounds by macrocyclic ligand complexes.

Acknowledgement

The authors thank the Natural Sciences and Engineering Research Council of Canada for financial support.

1. R. STEWARD. Oxidation mechanisms. W. A. Benjamin, New York, NY. 1964.
2. Oxidation in organic chemistry. Part A. *Edited by* K. B. Wiberg; Part B. *Edited by* W. S. Trahanovsky. Academic Press, New York, NY. 1973.
3. P. M. MAITLIS. The organic chemistry of palladium. Vol. II. Academic Press, New York, NY. 1971.
4. P. M. HENRY and G. L. LANGE. Oxidation of C=C and C=N groups. *In* The chemistry of the functional groups. *Edited by* S. Patai. Supplement A, Double bonded functional groups, Part 2. John Wiley and Sons, New York, NY. 1977. Chapt. 11.
5. L. H. GALE, D. C. OLSON, and J. VASILEVSKIS. J. Catal. **24**, 548 (1972).
6. D. W. REICHGOTT and N. J. ROSE. J. Am. Chem. Soc. **99**, 1813 (1977).
7. F. T. T. NG and P. M. HENRY. J. Am. Chem. Soc. **98**, 3606 (1976).
8. F. T. T. NG and P. M. HENRY. Can. J. Chem. **55**, 2900 (1977).
9. W. WELSH. Unpublished data.
10. F. T. T. NG and P. M. HENRY. Abstracts of Papers, ACJ/CSJ Chemical Congress, Honolulu, Hawaii, April 1979; American Chemical Society, Washington, DC. 1979. INOR 272.
11. V. L. GOEDKEN and D. H. BUSCH. J. Am. Chem. Soc. **94**, 7355 (1972).
12. D. C. OLSON and J. VASILEVSKIS. Inorg. Chem. **8**, 1611 (1969).
13. E. K. BAREFIELD and D. H. BUSCH. J. Chem. Soc. D, 522 (1970).
14. E. J. GORE and D. H. BUSCH. Inorg. Chem. **12**, 1 (1973).
15. E. ZEIGERSON, G. GINZBURG, N. SCHWARTZ, Z. LUZ, and D. MEYERSTEIN. Chem. Commun. 241 (1979).
16. E. K. BAREFIELD and M. T. MOCELLA. J. Am. Chem. Soc. **97**, 4238 (1975).
17. M. JAACOBI, D. MEYERSTEIN, and J. LILIE. Inorg. Chem. **18**, 429 (1979).
18. H. COHEN, L. J. KIRSCHENBAUM, E. ZEIGERSON, M. JAACOBI, E. FUCHS, G. GINZBURG, and D. MEYERSTEIN. Inorg. Chem. **18**, 2763 (1979).
19. G. FERRAUDI and L. PATTERSON. Chem. Commun. 755 (1977).
20. P. MARUTHAMUTHU, L. K. PATTERSON, and G. FERRAUDI. Inorg. Chem. **17**, 3157 (1978).

Can. J. Chem. Downloaded from www.nrcresearchpress.com by 210.87.254.6 on 09/06/12
For personal use only.

21. N. F. CURTIS. J. Chem. Soc. C, 1979 (1967).
22. Z. G. WARNER and D. H. BUSCH. J. Am. Chem. Soc. **91**, 4092 (1969).
23. A. V. IOGANSEV, G. A. KURKCHI, V. B. BAEVA, Z. N. RASSKAZOVA, and G. A. SALAMATIVA. Zh. Org. Khim. **7**, 2509 (1971).
24. R. STEWARD. *In* Isotopes in organic chemistry. Vol. 2. *Edited by* E. Buncel and C. C. Lee. Elsevier Scientific Publishing Company, Amsterdam. 1967. Chapt. 7, p. 297.
25. E. S. LEWIS. *In* Isotopes in organic chemistry. Vol. 2. *Edited by* E. Buncel and C. C. Lee. Elsevier Scientific Publishing Company, Amsterdam. 1967. Chapt. 4, pp. 144–145.
26. C. J. MICHEJDA and W. P. HOSS. J. Am. Chem. Soc. **92**, 6298 (1970).
27. J. R. ROBERTS and K. U. INGOLD. J. Am. Chem. Soc. **95**, 3228 (1973).
28. R. P. BELL. The proton in chemistry. 2nd ed. Cornell University Press, Ithaca, NY. 1973. (*a*) p. 227; (*b*) p. 29.
29. F. F. RUST, F. H. SEUBOLD, and W. E. WAUGHAM. J. Am. Chem. Soc. **70**, 3258 (1948).
30. G. FULLER and F. F. RUST. J. Am. Chem. Soc. **80**, 6148 (1958).
31. W. H. URRY, M. H. PAI, and C. Y. CHEN. J. Am. Chem. Soc. **86**, 5343 (1964).
32. W. G. BENTRUDE and K. R. DARNELL. Chem. Commun. 810 (1968); J. Am. Chem. Soc. **90**, 3588 (1968).
33. K. M. JOHNSTON, G. H. WILLIAMS, and H. J. WILLIAMS. J. Chem. Soc. B, 1114 (1966).
34. J. F. COETZEE. *In* Advances in physical organic chemistry. Vol. 4. *Edited by* A. Streitwieser, Jr. and R. W. Taft. Interscience, New York, NY. 1967. p. 76.
35. C. WALLING. Free radicals in solution. John Wiley and Sons, Inc., New York, NY. 1963. p. 493.
36. B. R. COWLEY and W. A. WATERS. J. Chem. Soc. 1228 (1961).
37. D. MACKAY and W. A. WATERS. J. Chem. Soc. C, 813 (1966).

Can. J. Chem. Downloaded from www.nrcresearchpress.com by 210.87.254.6 on 09/06/12
For personal use only.

^{13}C shieldings in *syn* and *anti* aldimines and ketimines

ROBERT R. FRASER, JACQUES BANVILLE, FUMINORI AKIYAMA, AND NOEMI CHUAQUI-OFFERMANNS
Department of Chemistry, University of Ottawa, Ottawa, Ont., Canada K1N 9B4

Received August 19, 1980

ROBERT R. FRASER, JACQUES BANVILLE, FUMINORI AKIYAMA, and NOEMI CHUAQUI-OFFERMANNS. Can. J. Chem. **59**, 705 (1981).

The ^{13}C chemical shifts in a variety of aldimines and in both acyclic and cyclic ketimines have been examined. A comparison of the shieldings at the α carbons in *syn* versus *anti* stereoisomers shows a consistent upfield shift of 8–11 ppm in the *syn* isomer. The greater magnitude found in imines vs. oximes or hydrazones is a clear indication of a steric origin for the differential shieldings. The shifts in the imines of cyclohexanones exhibited stereochemically dependent effects of methyl substitution, very similar to those in analogous oxime and hydrazone derivatives. Chemical shift differences in the *syn* isomers of the α-phenethylimines of chiral aldimines and ketimines allow a facile measurement of diastereomer ratios for such compounds.

ROBERT R. FRASER, JACQUES BANVILLE, FUMINORI AKIYAMA et NOEMI CHUAQUI-OFFERMANNS. Can. J. Chem. **59**, 705 (1981).

On a examiné les déplacements chimiques du ^{13}C de diverses aldimines et des cétimines acycliques et cycliques. En comparant le blindage au niveau des carbones en positions α des stéréoisomères *syn* et *anti*, on constante un déplacement vers les champs forts de 8–11 ppm en faveur de l'isomère *syn*. La valeur plus forte observée pour les imines par rapport à celle des oximes ou des hydrazones est une nette indication de l'origine stérique des blindages différentiels. Les déplacements observés dans les imines de cyclohexanones ont des effets qui dépendent stéréochimiquement de la substitution par les méthyles et qui sont très semblables à ceux des dérivés analogues d'oximes et d'hydrazones. Les différences de déplacement chimique des isomères *syn* des α-phénéthylimines d'aldimines et de cétimines chirales permettent de mesurer facilement les rapports de diastéréoisomères dans de tels composés.
[Traduit par le journal]

The ^{13}C spectral characteristics of aldehydes and ketones have been thoroughly studied (1, 2) and more recently many of their carbonyl derivatives including oximes (3–5), hydrazones (5, 6), and oxime ethers (6) have received considerable attention. Another class of nitrogen-containing carbonyl derivatives which has not been studied to any significant extent is the imines, data on only a few aryl (7) and a few *anti* aldimine derivatives (8) having been reported. During the course of our studies on the alkylation of ketimines (9, 10) and aldimines (11, 12) we have had the opportunity to record a large number of spectra of both the *syn* and *anti* isomers. In this paper we wish to describe the spectral characteristics of a number of representative examples in order to demonstrate the capability of ^{13}C nmr to reveal both configurational and conformational information for this class of compounds. In addition, the comparison of configurational effects with those previously observed in other species provides clear evidence for the dominance of steric factors in causing the large differential *syn–anti* shifts.

Experimental

The imines described herein have all been synthesized either from the parent ketone or aldehyde and amine or by alkylation of the lithiated intermediate. A typical procedure, the preparation of imine **34** and its *syn* alkylation product, **35**, follows.

A solution of 20 mmol of 4-*tert*-butylcyclohexanone in 15 mL of dry ether containing 8 g of 4A molecular sieves was treated with 30 mmol of isopropylamine. After stirring for 5 h the solution was filtered, the sieves washed with three 3-mL portions of ether, and the combined ether solutions concentrated. Bulb-to-bulb distillation of the residue gave an 82% yield of imine, **34**, bp 65–70°C (0.1 Torr). A solution of lithium diisopropylamide was prepared in a serum-capped flask under an atmosphere of nitrogen by the addition of 12.6 mmol of butyllithium (2 *M* in hexane, Alfa Inorganics) to 12.6 mmol of diisopropyl amine in 20 mL of dry tetrahydrofuran (THF) at −20°C. After stirring for 10 min 12 mmol of imine, **34**, was added. The resultant solution was stirred for 1 h at 25°C, cooled to −78°C, and then 12.6 mmol of methyl iodide was added. After stirring for 1 h the solvent was removed under reduced pressure at −20°C. The residue was extracted with ether and the ether extracts were washed with sodium carbonate (5%) and sodium chloride (5%) solutions, then dried. The residue after removal of solvent was dissolved in $CDCl_3$ (−20°C) and examined immediately by ^{13}C nmr at −20°C. The spectrum showed the product to consist of a 90:7:3 ratio of **35**:**36**:**37**. Hydrolysis of this mixture in 5 mL THF and 15 mL of 1 *M* oxalic acid for 1 h at 25°C gave, after extraction, drying, and distillation, a mixture of *cis* and *trans* 4-*tert*-butyl-2-methylcyclohexanone (13) in a ratio of 1:3. The yield was 81%.

Compounds **30** (14) and **31** (15) have been prepared previously. Compounds **32** and **33** were prepared by the method used to prepare **30** (14). Their proofs of structure rest with the method of preparation and their ^1H and ^{13}C nmr spectral properties.

The proof of structure for all the intermediate *syn* methylation products rests on (*a*) ^1H and ^{13}C spectra, (*b*) observed isomerization to the *anti* form which was synthesized independently, when possible, and (*c*) cleavage of the *anti* imine to the corresponding aldehyde or ketone of known structure as confirmed by ^1H nmr, ir, and vpc.

The chemical shifts in the ^{13}C spectra are reported in δ units (ppm from TMS) as measured on a Varian FT-80 nmr spectrometer (sweep width 4000 Hz, 8000 data points, acquisition time 1 s, pulse width 25°) operating at either 27°C or, for the purpose of observing the somewhat transient *syn* intermediate, at −20 to −40°C. The solvent used was normally $CDCl_3$ con-

0008-4042/81/040705-05$01.00/0
©1981 National Research Council of Canada/Conseil national de recherches du Canada

Can. J. Chem. Downloaded from www.nrcresearchpress.com by 210.87.254.105 on 09/06/12
For personal use only.

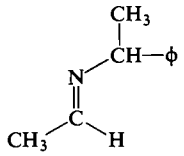

1

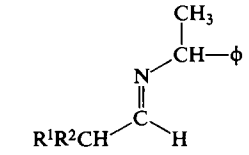

2 $R^1 = CH_3, R^2 = H$
4 $R^1 = CH_3, R^2 = CH_2\phi$
6 $R^1 = CH_3, R^2 = CH_3$
8 $R^1 = CH_3, R^2 = C_2H_5$
10 $R^1 = CH_3, R^2 = CH(CH_3)_2$

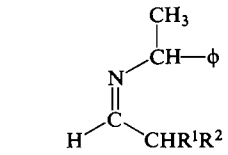

3 $R^1 = CH_3, R^2 = H$
5 $R^1 = CH_3, R^2 = CH_2\phi$
7 $R^1 = CH_3, R^2 = CH_3$
9 $R^1 = CH_3, R^2 = C_2H_5$
11 $R^1 = CH_3, R^2 = CH(CH_3)_2$

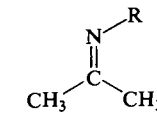

12 $R = CH(CH_3)_2$
13 $R = CH_2\phi$
14 $R = C(CH_3)_3$

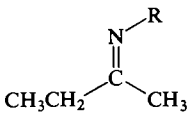

15 $R = CH_2\phi$
17 $R = CH(CH_3)\phi$
19 $R = C(CH_3)_3$

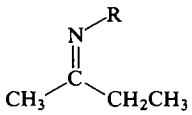

16 $R = CH_2\phi$
18 $R = CH(CH_3)\phi$
20 $R = C(CH_3)_3$

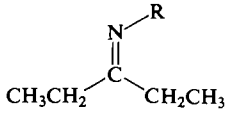

21 $R = CH_2\phi$
22 $R = CH(CH_3)_2$
23 $R = CH(CH_3)\phi$

taining 5 to 15% of residual THF. It was shown independently that the effect of adding 15% of THF to a chloroform solution of an imine resulted in less than 0.2 ppm change in any of the signals. The shift data are therefore reliable to better than 0.2 ppm. The assignments of signals were made on the basis of off-resonance decoupling experiments, known substituent effects, and, for the cyclohexanones reported in Table 4, in analogy with the closely related derivatives studied previously (6). Signals for carbons having the same multiplicity and differing by less than two ppm may therefore be of reverse assignment.

Results and Discussion

A. Acyclic Aldimines and Ketimines

Table 1 presents the chemical shift data for eleven aldimines and twelve ketimines. One important feature in the chemical shift data is particularly noteworthy. As previously observed (3–6) in oximes, oxime ethers, and hydrazones, there is a very pronounced upfield shift for a carbon *syn* to the *N*-substituent in comparison with the shift for the same carbon when *anti* (hereafter referred to as Δ_{sa}). Previously, upfield shifts have been attributed in the main to steric interactions although the possibility that the field effect of a polar N—OR or N—NR_2 group contributed to the shielding difference has frequently been proposed. In an interesting study of cyclic ketoximes, Geneste *et al.* (4) demonstrated a remarkable dependence of Δ_{sa} on

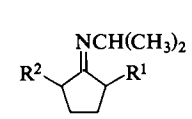

24 $R^1 = R^2 = H$
28 $R^1 = CH_3, R^2 = H$
29 $R^1 = H, R^2 = CH_3$

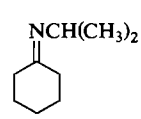

25

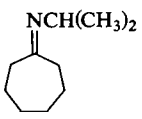

26

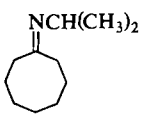

27

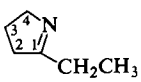

30

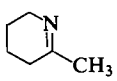

31

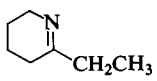

32

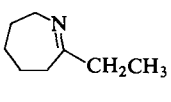

33

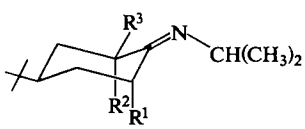

34 $R^1 = R^2 = R^3 = H$
35 $R^1 = CH_3, R^2 = R^3 = H$
36 $R^1 = R^3 = H, R^2 = CH_3$
37 $R^1 = R^2 = H, R^3 = CH_3$
38 $R^1 = R^2 = CH_3, R^3 = H$
39 $R^1 = R^3 = CH_3, R^2 = H$

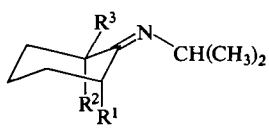

40 $R^1 = R^2 = R^3 = H$
41 $R^1 = CH_3, R^2 = R^3 = H$
42 $R^1 = H, R^2(\text{or } R^3) = CH_3$
43 $R^1 = R^2 = CH_3, R^3 = H$
44 $R^1 = R^3 = CH_3, R^2 = H$

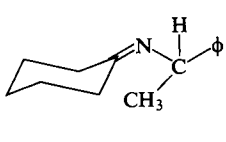

45

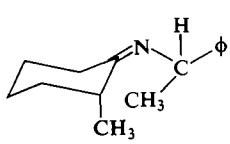

46

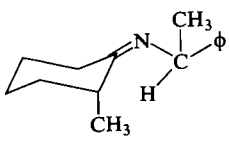

47

Can. J. Chem. Downloaded from www.nrcresearchpress.com by 210.87.254.105 on 09/06/12
For personal use only.

Can. J. Chem. Downloaded from www.nrcresearchpress.com by 210.87.254.105 on 09/06/12
For personal use only.

TABLE 1. ^{13}C shifts in acyclic aldimines and ketimines[a]

Compound	1s	2s	3s	1a	2a	3a	N-α	N-β	C=N
1				22.0			69.8	24.4	159.2
2				29.1	10.3		69.6	24.8	164.1
3	23.2	10.4					58.5	23.4	172.2
4				41.05	17.3		69.4	24.7	166.9
				41.13	40.6		69.5	24.9	167.1
5	36.0	17.5					58.8	23.3	170.6
	36.4	40.2, 40.8					59.0	23.5	170.9
6				34.0	19.4		69.4	24.9	168.3
7	27.5	19.4, 19.0					58.2	24.1	170.3
8				40.9	27.1	11.5	69.6	24.9	167.8
					17.1				
9	35.2	27.3, 17.6	12.2				58.4	25.7	172.5
	35.1	17.2	12.0						
10				45.4	31.2	20.3	69.4	24.7	167.5
					14.2	19.7			
11	40.0	31.6, 15.3	20.8				58.7	24.1	170.5
	39.8	14.8	19.4					23.3	
12	17.8			29.4			50.5	23.6	163.6
13	18.7			29.4			55.5		167.9
14	22.0			31.4			54.5	30.5	164.3
15	18.3			36.7	11.5		56.2		[c]
16	27.1	11.7		24.5			55.2		[c]
17	16.9			35.8	10.9		58.2	25.0	169.1
18	25.4	11.1		26.5			58.2	25.1	169.8
19	21.5			38.2	12.1		55.6	31.8	166.2
20	29.8	12.9		[b]			55.6	32.3	167.5
21	26.0	11.6		33.6	11.9		54.2		174.3
22	23.2	11.7		33.0	11.8		49.5	24.0	172.2
23	24.0	11.2		32.7	11.4		58.1	25.4	[c]

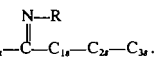

[a] The numbering for this table only is $C_{3a}—C_{2a}—C_{1a}—C(=N—R)—C_{1s}—C_{2s}—C_{3s}$.
[b] Not assignable.
[c] Quaternary C signal was not observed.

TABLE 2. Differential α-shieldings

	N—R	Carbon group	Δsa (ppm)
Aldimines			
2 vs. **3**	$CH(CH_3)\phi$	CH_2	5.9
4 vs. **5**	$CH(CH_3)\phi$	CH	5.1
6 vs. **7**	$CH(CH_3)\phi$	CH	6.5
8 vs. **9**	$CH(CH_3)\phi$	CH	5.7
10 vs. **11**	$CH(CH_3)\phi$	CH	5.4
Ketimines			
12	$CH(CH_3)_2$	CH_3	11.6
13	$CH_2\phi$	CH_3	10.7
14	$C(CH_3)_3$	CH_3	9.4
15 vs. **16**	$CH_2\phi$	CH_3	6.2
		CH_2	9.6
17 vs. **18**	$CH(CH_3)\phi$	CH_3	9.6
		CH_2	10.4
19 vs. **20**	$C(CH_3)_3$		
		CH_2	8.4
21	$CH_2\phi$	CH_2	7.6
22	$CH(CH_3)_2$	CH_2	9.8
23	$CH(CH_3)\phi$	CH_2	8.7
24	$CH(CH_3)_2$	CH_2	8.6
25	$CH(CH_3)_2$	CH_2	11.4
26	$CH(CH_3)_2$	CH_2	10.4

the dihedral angle between the αCH bond and the N—O bond. In assessing the role of the electric field effect these authors concluded that it makes a significant contribution along with steric factors. The magnitude of Δ_{sa} values which we have listed in Table 2 does not seem to be explicable on the basis of an electric field effect since the polarity of the N—C bond in all imines is the reverse of an NO bond, yet the Δ_{sa} values are invariably larger in the imines than in analogous oximes (3) or other derivatives (5, 6). Furthermore, there appears to be at least a trend for the larger Δ_{sa} values to appear in the sterically more congested cases, e.g. ketimines > aldimines and *N*-isopropyl > *N*-benzyl. In addition the well-documented 5 to 8 ppm high yield shift in *Z* versus *E* alkenes (16) cannot result from field effects.

B. Cyclic Ketimines

As already noted for the acyclic compounds, the data in Table 3 show much larger Δ_{sa} values for ketimines than for ketoximes (4) of the same ring size. For example, the respective Δ_{sa} values for the

TABLE 3. ^{13}C shifts in cyclic ketimines

Compound	C-1	C-2	C-3	C-4	C-5	C-6	C-7	N-α	N-β
24	176.5	28.0	24.1	25.1	36.6			53.2	23.5
25		28.9	27.4	26.2	27.9	40.3		48.9	24.0
26	171.5	30.2	[a]	[a]	[a]	40.6		48.7	23.1
27	172.7	29.5	[a]	[a]	[a]	[a]	40.3	49.4	23.5
28	[b]	34.3	33.0	21.0	34.9	(17.8C—CH_3)		52.8	23.5
29	[b]	28.2	21.9	32.2	40.5	(17.5C—CH_3)			

							Side chain		
							α	β	
30	179.2	37.0	26.9	60.9			32.7	10.7	
31	[b]	30.3	19.7	21.8	49.3		27.5		
32	171.8	28.8	19.7	22.1	50.0		33.9	10.6	
33	179.0	33.1	31.6	26.7	23.8	51.9	35.7	10.5	
							N-α	N-β	CH_3
45	172.0	29.6	27.2	26.1	27.9	40.3	57.8	25.1	
46 (*S*,*R*)	176.4	31.8	32.7	20.2	27.7	35.8	57.0	24.8	17.1
47 (*S*,*S*)	175.9	31.5	33.2	20.2	27.7	35.8	57.4	24.8	16.8

[a] Not assigned.
[b] Not observed.

cyclopentanone derivatives are 8.6 vs. 3.5 and for the cyclohexanones 11.4 vs. 6.5. It is also interesting to note a parallel behavior for the shift of the methine carbon attached to nitrogen in that it shows a pronounced high field shift in **25** and **26** relative to **24**. This is also consistent with a reciprocal steric shielding effect on that carbon. Methyl substitution effects in the five-membered ring are consistent with those observed in cyclopentanone itself (2). The data for the endocyclic systems **30–33** appear unexceptional, resembling qualitatively those in cyclopentene, cyclohexene, and cycloheptene (1).

C. Cyclohexanone Imines, 34–44

The *N*-isopropyl imines of 4-*tert*-butylcyclohexanone and cyclohexanone and their monomethyl and dimethyl derivatives have been synthesized by a method which provides both the *syn* and *anti*-stereoisomers (8). Their ^{13}C chemical shifts have been measured and are presented in Table 4. We have previously described the ^{13}C shifts of methylation products for the oxime ethers and hydrazones of the same ketones (6) as well as of the structurally related *N*-nitrosopiperidines and 4-phenyl-*N*-nitrosopiperidines (17). The most notable feature of the data in Table 4 is that they reveal almost identical effects of methyl substitution in compounds **34** to **44** as those observed earlier for the oxime ethers and hydrazones of the same parent ketones, reflecting the same conformational properties for all three classes of carbonyl derivatives.

Thus the conformation of the potentially mobile *syn*-2-methylation compound **41** can be concluded to have the 2-methyl substituent axial (from the value of the shielding at C-4). The same conclusion applies to *cis*-2,6-dimethylcyclohexanone-*N*-isopropyl imine (i.e. only a diaxial arrangement of the two methyl groups can account for the shielding at C-4). By comparison, *anti*-2-methylcyclohexanone *N*-isopropyl imine appears to be an approximately equal blend of axial and equatorial conformers, while the *trans*-2,6-dimethyl derivative exists in the conformation having the *syn*-methyl axial and the *anti*-methyl equatorial. The steric factors responsible for these conformational properties are presumably the same as those discussed in detail in our two previous papers on the oxime ethers, hydrazones, and nitrosamines (6, 17).

D. Differential Shieldings on Diastereomeric α-Phenethyl Imines

In Table 1, entries for 5, 9, and 11 show how readily ^{13}C can detect the presence of two diastereomers in these *syn*-aldimines. The differences in chemical shifts for the two diastereomers are usually observable at those carbons closest to the site of steric compression. Thus the *anti*-isomers of the same aldimines showed either reduced or unobservable shielding differences. The same ability to observe separate signals in *syn*-2-substituted cyclohexanone-*N*-α-phenethyl imines is illustrated by entries **45**, **46**, and **47**, the assignment of stereochemistry for the two isomers being that earlier elucidated by the studies by Yamada and coworkers (18).

Can. J. Chem. Downloaded from www.nrcresearchpress.com by 210.87.254.105 on 09/06/12
For personal use only.

TABLE 4. ^{13}C shieldings in cyclohexanone derivatives

Compound	C-2	C-3	C-4	C-5	C-6	CH_3 *syn*	CH_3 *anti*
34	27.9	28.2	47.8	28.2	39.6		
35	31.1	34.2	41.1	28.3	35.7	18.1	
36[a]	41.7	34.4	41.3	28.2	24.2		18.9
37[a]	41.3	37.9	47.8	28.7	28.3		17.4
38	30.7	33.4	36.5	33.6	40.9	20.0 and	21.3
39	30.1	34.6	41.0	35.9	38.0	17.1 and	18.4
40	28.9	27.4	26.2	27.9	40.2		
41	30.8	32.9	20.1	27.4	35.2	17.1	
42[a]	42.1	35.3	23.6	27.8	26.9		17.6
43	30.3	31.5	15.2	31.9	40.3	18.9	20.7
44	30.8	33.1	20.0	36.5	35.9	16.7	17.4

[a]For **36**, **37**, and **42**, C-2 represents the carbon bearing the methyl group which is *anti* to the imine's alkyl group. In all other compounds C-2 is *syn*. The shifts for C-1 all fall in the range 170 to 175 while the *tert*-butyl signals appear at 32.2 ± 0.2 and 27.5 ± 0.3. *N*-isopropyl signals appear in the range 48.1–49.1 and 23.5 to 24.4.

The fact that the two diastereomers exhibit resolvable shift differences for those carbons close to or on the *N*-alkyl substituent makes ^{13}C a very convenient method of determining the ratio of diastereomers, which in turn will reflect the degree of asymmetric induction in the alkylation reaction (12). This use of ^{13}C for quantitative measurements assumes equal relaxation times for each pair of diastereomer signals.[1] To be sure that this is so, we have measured the peak height ratios using repetition rates of 1 and 10 s for three different diastereomeric mixtures and could detect less than a 5% difference in intensity ratios in every case. We can therefore be sure that the intensity ratio for a pair of signals representing the two diastereomers will have its accuracy determined by the S/N ratio unless this exceeds 20:1.

Acknowledgement

We wish to thank the Natural Sciences and Engineering Research Council of Canada for their financial support.

1. J. B. STOTHERS. Carbon-13 nmr spectroscopy. Academic Press, New York. 1972.
2. J. B. STOTHERS and C. T. TAN. Can. J. Chem. **52**, 308 (1974).
3. G. E. HAWKES, K. HERWIG, and J. D. ROBERTS. J. Org. Chem. **39**, 1017 (1974).
4. P. GENESTE, R. DURAND, J.-M. KAMENKA, H. BEIERBECK, R. MARTINO, and J. K. SAUNDERS. Can. J. Chem. **56**, 1940 (1978).
5. C. A. BUNNELL and P. L. FUCHS. J. Org. Chem. **42**, 2614 (1977).
6. R. R. FRASER, K. L. DHAWAN, and K. TAYMAZ. Org. Magn. Reson. **11**, 269 (1978).
7. G. W. BUCHANAN and B. A. DAWSON. Org. Magn. Reson. **13**, 293 (1980).
8. M. NAULET, M. L. FILLEUX, G. J. MARTIN, and J. PORNET. Org. Magn. Reson. **7**, 326 (1975).
9. R. R. FRASER, J. BANVILLE, and K. L. DHAWAN. J. Am. Chem. Soc. **100**, 7999 (1978).
10. K. N. HOUK, R. W. STROZIER, N. G. RONDAN, R. R. FRASER, and N. CHUAQUI-OFFERMANNS. J. Am. Chem. Soc. **102**, 1426 (1980).
11. R. R. FRASER and J. BANVILLE. J. Chem. Soc. Chem. Commun. 47 (1979).
12. R. R. FRASER, F. AKIYAMA, and J. BANVILLE. Tetrahedron Lett. 3929 (1979).
13. B. J. L. HUFF, F. N. TULLER, and D. CAINE. J. Org. Chem. **34**, 3070 (1969); J. M. CONIA and P. BRIET. Bull. Soc. Chim. Fr. 3881 (1966).
14. A. ETIENNE and Y. CORREIA. Bull. Soc. Chim. Fr. 3704 (1969).
15. M. F. GRUNDON and B. E. REYNOLDS. J. Chem. Soc. 2445 (1964).
16. J. B. STOTHERS and N. K. WILSON. Top. Stereochem. **8**, 48 (1974).
17. R. R. FRASER and T. B. GRINDLEY. Can. J. Chem. **53**, 2465 (1975).
18. M. KITAMOTO, K. HIROI, S. TERASHIMA, and S. YAMADA. Chem. Pharm. Bull. Jpn. **22**, 459 (1974).
19. G. C. LEVY and G. L. NELSON. J. Am. Chem. Soc. **94**, 4897 (1972).

[1]This assumption applies only to signals arising from the same carbon in a pair of diastereomers, e.g., a pair of *syn* methyl signals. Differential nOe's for *syn* and *anti* carbons are normally seen as in oximes (19).

Can. J. Chem. Downloaded from www.nrcresearchpress.com by 210.87.254.105 on 09/06/12
For personal use only.

Double layer structure at the mercury/methanol solution interface

ZOFIA BORKOWSKA[1] AND W. RONALD FAWCETT

The Guelph–Waterloo Centre for Graduate Work in Chemistry (Guelph Campus), Department of Chemistry, University of Guelph, Guelph, Ont., Canada N1G 2W1

Received May 28, 1980

ZOFIA BORKOWSKA and W. RONALD FAWCETT. Can. J. Chem. **59**, 710 (1981).

Differential capacity against electrode potential data are presented for the mercury/methanol interface for a variety of salts at 25°C and for $NaClO_4$ solutions as a function of temperature. Ionic specific adsorption from solutions of KF, $NaClO_4$, and $LiBF_4$ was shown to be absent on the basis of the usual criteria. The dielectric properties of the inner layer are discussed on the basis of the three-state model for solvent structure from which it is deduced that the majority of solvent molecules are adsorbed at mercury with their dipole vectors parallel to the interface. The deep minimum in inner layer differential capacity, which occurs at the same electrode charge density independent of the nature of the salt (-0.05 C m^{-2}), corresponds to conditions for which the surface concentrations of the minority components, dipoles oriented with the field or against it, are equal. The experimental temperature coefficient of the inner layer capacity is a maximum at this charge density in agreement with the predictions of the three-state model.

ZOFIA BORKOWSKA et W. RONALD FAWCETT. Can. J. Chem. **59**, 710 (1981).

On présente des données de capacité différentielle versus potentiel d'électrode à l'interface mercure/méthanol pour divers sels à 25°C et pour des solutions de $NaClO_4$ à diverses températures. L'adsorption ionique spécifique à partir de solutions de KF, de $NaClO_4$ et de $LiBF_4$ est inexistante si on se base sur les critères usuels. On discute des propriétés diélectriques de la couche interne en s'appuyant sur un modèle de structure du solvant à trois états à partir duquel on déduit que la plupart des molécules du solvant sont adsorbées sur le mercure avec leurs dipoles orientés parallèlement à l'interface. La profondeur minimale de la capacité différentielle de la couche interne, qui se produit pour la même densité de charge à l'électrode indépendamment de la nature du sel ($-0{,}05$ C m^{-2}), correspond aux conditions pour lesquelles les concentrations de surface des composants secondaires (orientation des dipoles avec ou contre le champ) sont égales. Le coefficient expérimental de température de la capacité de la couche interne atteint son maximum pour cette densité de charge en accord avec les prévisions de la modèle de trois états.

[Traduit par le journal]

Introduction

The differential capacity of the Hg/methanolic (MeOH) solution interface was studied by Grahame (1) who showed that capacity data obtained in the presence of KF could be analyzed on the basis of the dual capacitor model of the double layer with no evidence of ionic specific adsorption. Inner layer capacity curves in systems where specific adsorption is negligible all display a deep minimum at small negative charge densities, no other extrema being visible in the polarizable range even at lower temperatures (for a review, see ref. 2).

It was recently shown that the inner layer capacity against charge density curve for the Hg/MeOH interface can be successfully described on the basis of a three-state model which assumes that solvent molecules are not significantly associated at the surface (3). This model predicts that when the inner layer capacity curves exhibit a minimum, one should also observe maxima if the electrode can be polarized sufficiently far in the positive and negative directions from the minimum. Capacity maxima at positive charge densities have been observed for several aprotic solvents such as dimethylformamide (4), acetone (5), dimethylsulphoxide (6), and nitromethane (7); however, it is not clear whether these are due to solvent reorientation, anionic adsorption, or a combination of both phenomena (8).

The purpose of the present study was to obtain capacity data with a variety of electrolytes, the ions of which were anticipated to not adsorb strongly at mercury. The intention was also to extend the measurements as far as possible in the positive range to see whether a capacity maximum could indeed be observed. Finally, it was desirable to obtain inner layer capacity data as a function of temperature and to examine these data within the context of the three-state model (3).

Experimental

The differential capacity against electrode potential curves were measured at a frequency of 335 Hz on the ac bridge described previously (9) which was modified with operational amplifiers to provide potentiostatic control of the dropping mercury electrode (10). The potential of zero charge (pzc) was determined for each solution using a streaming mercury electrode in the absence of oxygen. All potentials were measured against a saturated KCl calomel refereńce electrode in methanol on a null voltameter of high input impedance with a precision of ± 0.1 mV. The reference electrode compartment was separated from the main body of the cell, the liquid junction being established in a solution wetted stopcock. The counter electrode was a cylinder of Pt (~3 cm^2 area) surrounding the dropping mercury elec-

[1]On leave from the Institute of Physical Chemistry, Polish Academy of Sciences, Warsaw, Poland.

0008-4042/81/040710-08$01.00/0

©1981 National Research Council of Canada/Conseil national de recherches du Canada

Can. J. Chem. Downloaded from www.nrcresearchpress.com by 210.87.254.105 on 09/06/12
For personal use only.

Can. J. Chem. Downloaded from www.nrcresearchpress.com by 210.87.254.105 on 09/06/12
For personal use only.

trode. The whole cell was surrounded by an outer jacket through which methanol at a fixed temperature was pumped; the temperature of the methanol was established in Brinkman thermostat with a precision of ±0.2°.

Spectroscopic grade methanol was dried over 3 Å molecular sieves and distilled twice under a nitrogen atmosphere. The water content determined by Karl Fischer titration was ~0.01%. All salts were twice recrystallized, $NaClO_4$ from methanol, KF from triply distilled water, and $LiBF_4$ from acetone. The KF was dried in a Pt dish at very high temperatures. The other salts were dried at 100°C over P_2O_5 under vacuum. All measurements and solution preparation were carried out in a controlled atmosphere chamber under purified N_2. The solutions were deaerated with purified N_2 which had been presaturated with the vapour of the solution under study.

Results and Discussion

$NaClO_4$ as Electrolyte

Curves of differential capacity C against electrode potential E measured for $NaClO_4$ solutions in MeOH in the concentration range 0.01 to 0.2 mol dm^{-3} at 25°C are presented in Fig. 1. An inflection on the capacity curves is visible at the most positive potentials and a diffuse layer minimum, at the lower concentrations. The dependence of the pzc on salt concentration (Table 1) is rather small and within the limits expected because of the change in liquid junction potential between the main cell and reference electrode compartments. This result suggests that ionic specific adsorption is negligible at the pzc.

The presence of ionic specific adsorption was tested on the basis of plots of the reciprocal of the experimental capacity $1/C$ against the reciprocal of the diffuse layer capacity $1/C_d$ as estimated by the Gouy–Chapman model for constant electrode charge density σ and varying electrolyte concentration (11). These plots are linear with unit slope in the range $-0.04 \leq \sigma \leq 0.04$ C m^{-2}, suggesting that specific adsorption is absent. An adaptation of this plot at the pzc (12) involves plotting $1/C$ against the reciprocal of the square root of the electrolyte concentration $1/c^{1/2}$, the slope being $(RT/2F^2\varepsilon\varepsilon_0)^{1/2}$ according to the Gouy–Chapman model, where ε is the dielectric constant of the solvent, ε_0, the permittivity of free space, and the other symbols have their usual meaning. In the present case, when the electrolyte concentration is expressed in mol m^{-3}, the resulting straight line has a slope of 22.2 $mol^{1/2}$ $m^{1/2}$ F^{-1} corresponding to a solvent dielectric constant equal to 30.5. This value is somewhat smaller than that quoted for pure methanol (32.7) and may indicate some degree of dielectric saturation due to the electrolyte (13).

Esin and Markov plots were also constructed using the present data and values of activity coefficients reported elsewhere (14). Although this method of testing for ionic specific adsorption is not as sensitive as that discussed above, the plots have the appearance expected of a system without specific adsorption in the range $-0.15 \leq \sigma \leq 0.04$ C m^{-2} (Fig. 2). A similar conclusion was reached by Taraszewska (15) who attributed it to good solvation of the constituent ions in $NaClO_4$ by MeOH.

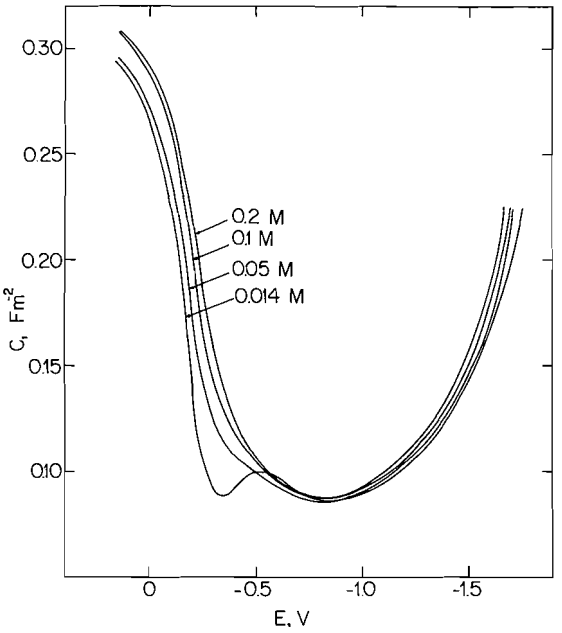

FIG. 1. Differential capacity C against electrode potential E for the Hg/methanol interface with various concentrations of $NaClO_4$ as indicated.

TABLE 1. Values of the differential capacity and electrode potential* for the interface, Hg/$NaClO_4$ in methanol at the point of zero charge

Salt concentration (mol dm^{-3})	Electrode potential, E_0 (V)	Differential capacity, C_0 (F m^{-2})
0.014	-0.326_6	0.0890
0.05	-0.327_9	0.1160
0.1	-0.330_4	0.1320
0.2	-0.333_1	0.1460

*Measured with respect to a calomel electrode in methanol saturated with KCl.

Values of the differential and integral capacity of the Hg/MeOH interface in the presence of $NaClO_4$ are given in Table 2.

The Influence of the Counter Ion on the Inner Layer Capacity

In order to assess the influence of counter ion nature on the shape of the capacity against potential curves, measurements were also made with 0.1 M solutions of KF and $LiBF_4$ as electrolytes. The

Can. J. Chem. Downloaded from www.nrcresearchpress.com by 210.87.254.105 on 09/06/12
For personal use only.

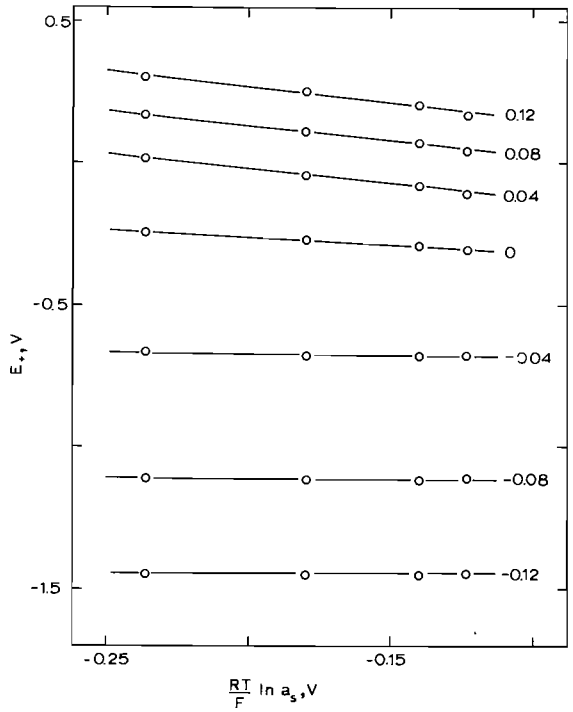

FIG. 2. Esin–Markov plots for the Hg/methanol interface with $NaClO_4$ as electrolyte. E_+ is the potential of the Hg electrode with respect to a reference electrode reversible to the sodium ion ($E_+ = E - RT \ln a_s/2F$) and a_s is the salt activity. The charge density for each plot is indicated in C m^{-2}.

TABLE 2. Differential capacity C_i and integral capacity K_i of the inner layer as a function of electrode charge density σ for the Hg/methanol interface with $NaClO_4$ as electrolyte at 25°C

σ (C m^{-2})	C_i (F m^{-2})	K_i (F m^{-2})	σ (C m^{-2})	C_i (F m^{-2})	K_i (F m^{-2})
0.08	0.347	0.303	−0.06	0.096	0.114
0.06	0.349	0.292	−0.08	0.108	0.111
0.04	0.341	0.269	−0.10	0.129	0.112
0.02	0.288	0.232	−0.12	0.157	0.116
0	0.183	0.183	−0.14	0.193	0.122
−0.02	0.126	0.150	−0.16	0.245	0.129
−0.04	0.099	0.126			

present data for the KF system agree well with those obtained earlier by Grahame (1) who concluded that ionic specific adsorption was absent for this system in MeOH. On the basis of the results obtained (Fig. 3), it seems reasonable to assume that ionic specific adsorption is also not important for the $LiBF_4$ system. It is interesting to note that the minimum capacity (0.087 F m^{-2}) which occurs at negative potentials is independent of the nature of the electrolyte.

At more negative potentials, the capacity increases in the order

$$C(Li^+) < C(Na^+) < C(K^+)$$

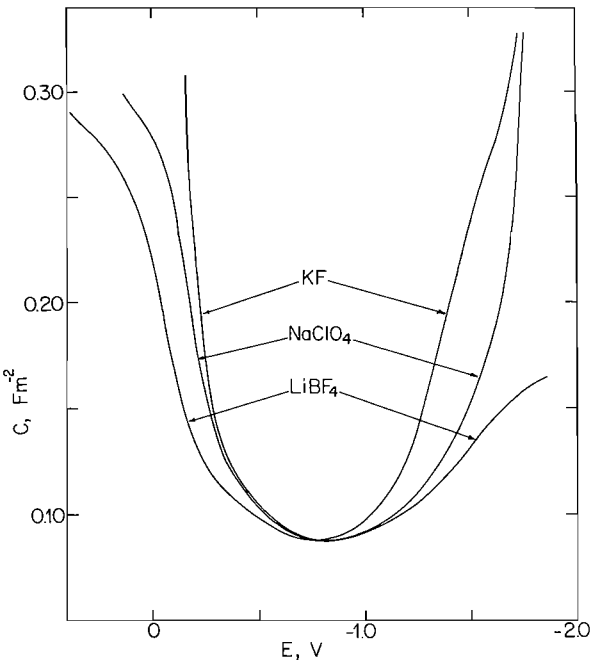

FIG. 3. Differential capacity C against electrode potential E for the Hg/methanol interface with 0.1 M solutions of KF, $NaClO_4$, and $LiBF_4$ as indicated.

Similar observations were made earlier for the alkali metal chlorides in methanol (16) and water (17) and for the alkali metal perchlorates in ethylene carbonate (9). This effect has been attributed to a corresponding decrease in the average thickness of the inner layer due to the generally recognized decrease in alkali metal cation solvation in the order (18)

$$Li^+ > Na^+ > K^+$$

On the other hand, it has also been explained by weak cation specific adsorption which cannot be detected on the basis of the usual criteria (19). A third explanation is that the dielectric constant of the inner layer is affected by the nature of the cation at the outer Helmholtz plane (oHp). This explanation is discussed in more detail below.

A marked dependence of the interfacial capacity on the nature of the anion is apparent at more positive potentials (Fig. 3). Comparison of inner layer capacity against charge density curves for KF, $NaClO_4$, $LiBF_4$, and KPF_6, calculated assuming that ionic specific adsorption is absent, reveals that C_i increases in the order

$$C_i(PF_6^-) < C_i(BF_4^-) < C_i(ClO_4^-) < C_i(F^-)$$

for positive values of σ. MeOH is one of the few non-aqueous solvents in which fluoride salts are soluble. The fact that the inner layer capacity is

Can. J. Chem. Downloaded from www.nrcresearchpress.com by 210.87.254.105 on 09/06/12
For personal use only.

highest in the presence of this anion suggests that it may be weakly specifically adsorbed from methanol. The solvation of small non-polarizable anions like F^- depends greatly on hydrogen bonding which is much weaker in MeOH than in H_2O. The ordering of differential capacity observed for the other anions is similar to that observed in other solvents including dimethylsulphoxide (6), propylene carbonate (21), ethylene carbonate (9), acetone (5), and nitromethane (7). To the extent that these anions are not specifically adsorbed, the ordering of capacities can be attributed to variation in ionic size and the effects of the anions on dipole–dipole interactions in the solvent monolayer solvating the electrode.

The Temperature Dependence of the Inner Layer Capacity

The differential capacity of the Hg/MeOH interface was determined with 0.1 *M* $NaClO_4$ as electrolyte in the temperature range 0 to 54°C. Inner layer capacity against charge density curves estimated using the Gouy–Chapman model for the diffuse layer are shown in Fig. 4. The curves are characterized by a minimum whose position is independent of temperature at -0.05 C m^{-2}. The value of the capacity at the minimum increases with temperature, the temperature coefficient dC_i/dT being 1.5×10^{-4} F m^{-2} °C^{-1}. This result is similar to that obtained by Payne for NH_4NO_3 solutions in MeOH (2). At charge densities more negative than -0.1 C m^{-2}, C_i is approximately independent of temperature whereas at sufficiently positive values of σ, dC_i/dT becomes negative. At 0°C, a maximum is clearly visible on the inner layer capacity curve at 0.05 C m^{-2}, the position of the maximum shifting to higher charge densities with increase in temperature. Finally, at sufficiently far positive charge densities, the temperature coefficient of C_i falls to very low values. The variation in inner layer capacity with temperature is illustrated in Fig. 5 where the coefficient $d(1/C_i)/dT$ is plotted against electrode charge density. In assessing the data obtained here, it should be kept in mind that the observed temperature variation is considerably less than that obtained for the Hg/aqueous solution interface (22).

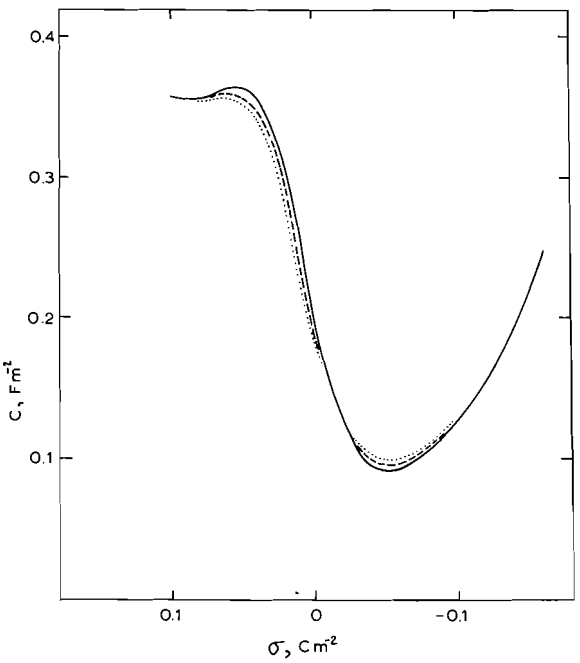

FIG. 4. Differential capacity of the inner layer C_i against electrode charge density σ for the Hg/methanol interface in the presence of $NaClO_4$ at three temperatures: (—) 0°C, (---) 25°C, and (· · ·) 54°C.

Molecular Models for the Dielectric Properties of the Inner Layer

A variety of models for the dielectric properties of the solvent in the inner layer have been developed in which the solvent is represented as a monolayer of dipolar spheres (23). Parsons (24) derived a four-state model for protic solvents in which molecular clusters are an important component of the monolayer. The four states considered are solvent monomers and clusters, each of which may occupy two positions with the dipole vector pointing towards ("up") or away from the metal electrode ("down"). When this model was used to describe the inner layer capacity data for the Hg/MeOH interface in the presence of KF (1), a good fit was obtained in the region of the minimum over a range of approximately 0.1 C m^{-2} but at more extreme positive and negative charge densities, the calculated curve lay above the experi-

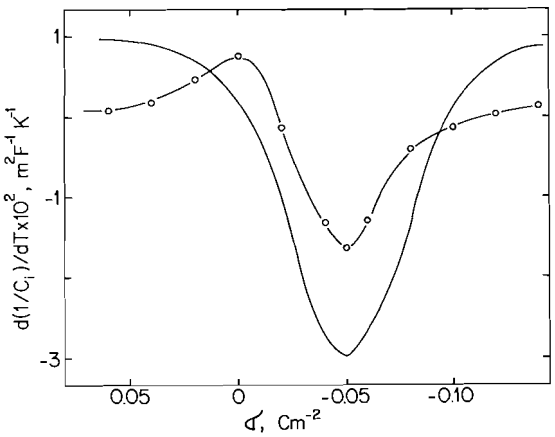

FIG. 5. The temperature coefficient $d(1/C_i)/dT$ against electrode charge density σ for the Hg/methanol interface in the presence of $NaClO_4$ (○) and according to the three-state model on the basis of the parameters for Na^+ (Table 3) (—).

Can. J. Chem. Downloaded from www.nrcresearchpress.com by 210.87.254.105 on 09/06/12
For personal use only.

mental points (25). Alternatively, a three-state model with solvent monomers having their dipole vectors in the "up" and "down" directions, and in a third direction with the vector "parallel" to the interface has been proposed for unassociated or weakly associated solvents in which molecular clusters are not an important component at the surface (3). This model is able to describe the same data over a wider range of electrode charge densities (~ 0.2 C m^{-2}); however, the calculated curve falls below the experimental points at positive charge densities (3, 23). In its simplest form, that is, when anisotropy of the polarizability is ignored, the three-state model predicts that the capacity curve is symmetrical with respect to the minimum value and that the minimum corresponds to the charge density where the surface concentrations of dipoles in the "up" and "down" orientations are equal.

Inner layer capacity curves for the three salts KF, $NaClO_4$, and $LiBF_4$ from which ionic specific adsorption was found to be either absent or negligible are presented in Fig. 6. It is readily apparent that one set of parameters is not able to describe any of the curves due to their lack of symmetry. Consideration of these data together with those

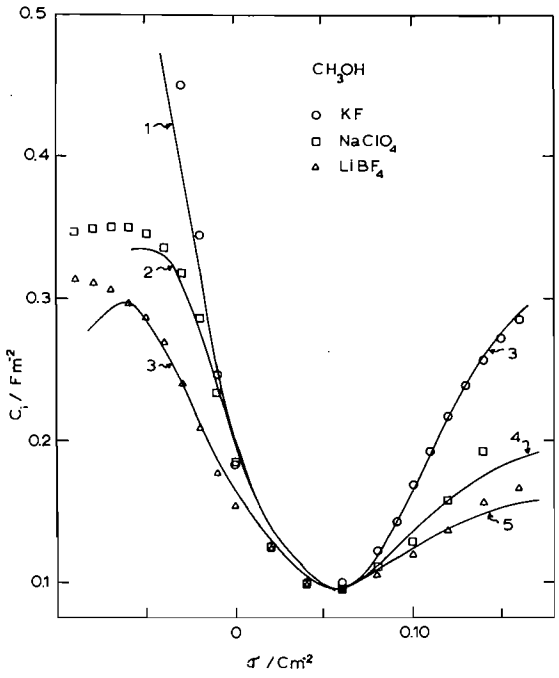

FIG. 6. Inner layer capacity C_i against electrode charge density σ for the Hg/methanol interface with KF (○), $NaClO_4$ (□), and $LiBF_4$ (△) as electrolytes. The curves *1–5* were calculated from the three-state model using the parameters summarized in Table 3. The curves are shown at charge densities positive or negative of the minimum on the curve, a point at which C_i is independent of the nature of the salt.

obtained in other solvents (2, 23, 26) suggests that one or more of the parameters characterizing the solvent molecules in the inner layer may depend on the nature of the counter ion at the oHp. One of these parameters is the effective thickness of the inner layer, d. Although the diameter of the solvent molecule represented as a sphere is a constant, the effective thickness depends on the size of the counter ion and the degree to which it retains its solvation sheath in the direction of the electrode/solution interface. Secondly, the effective coordination number c_e, which is very important in estimating the magnitude of the dipole–dipole interaction energy, may depend on the counter ion nature; since c_e is a reflection of the effectiveness of dipole imaging in the metal phase and the double layer beyond the initial monolayer which solvates the electrode, its value should depend on the "local" dielectric constant of the double layer which itself depends on the nature and concentration of ions at the oHp (27). Finally, it is interesting to note that the minimum value of C_i occurs at the same charge density for the three salts and that it is independent of the nature of the salt within experimental error.

Theoretical curves which best describe the experimental ones in regions positive and negative of the capacity minimum were constructed on the basis of the three-state model by varying d and c_e, the values of the dipole moment p (1.66 D) and polarizability (3.26×10^{-3} nm^3) being the experimental values reported in the literature (23). The equations defining the fractions of the surface covered by "up", "down", and "parallel" dipoles in the monolayer are (3)

$$[1] \quad f_1 + f_2 + f_3 = 1$$

$$[2] \quad kT \ln (f_1/f_2) = U_{20} - U_{10} - 2p(E + X)$$

and

$$[3] \quad kT \ln (f_1/f_3) = U_{30} - U_{10} - p(E + X)$$

f_1, f_2, and f_3 are the fractions of molecules in the "up", "down", and "parallel" orientations, respectively; U_{10}, U_{20}, and U_{30} are the corresponding residual energies; E is the field due to the charge on the electrode; and X is the reaction field at an average dipole due to surrounding dipoles. The reaction field is given by

$$[4] \quad X = c_e[p(f_1 - f_2) - \alpha E]/(d^3 + c_e\alpha)$$

Having assumed values for d and c_e these equations are solved for the fractions f_1, f_2, and f_3 and the potential drop across the monolayer $\Delta\phi$ is calculated:

Can. J. Chem. Downloaded from www.nrcresearchpress.com by 210.87.254.105 on 09/06/12
For personal use only.

[5] $\Delta\phi = 4\pi\sigma d + (4\pi N_T d^3/c_e)X$

On differentiating eqs. [1]–[3] with respect to surface charge density, one obtains

[6] $x_1 + x_2 + x_3 = 0$

[7] $$kT\frac{x_1}{f_1} - kT\frac{x_2}{f_2} = -2p\left(4\pi + \frac{dX}{d\sigma}\right)$$

and

[8] $$kT\frac{x_1}{f_1} - kT\frac{x_3}{f_3} = -p\left(4\pi + \frac{dX}{d\sigma}\right)$$

where x_1, x_2, and x_3 are the derivatives $df_1/d\sigma$, $df_2/d\sigma$, and $df_3/d\sigma$, respectively, and

[9] $$\frac{dX}{d\sigma} = \frac{c_e}{(d^3 + c_e\alpha)}[p(x_1 - x_2) - 4\pi\alpha]$$

Having solved eqs. [6]–[8] for x_1, x_2, and x_3 the differential capacity of the inner layer is calculated according to the relationship

[10] $$\frac{1}{C_i} = \frac{d\Delta\phi}{d\sigma} = 4\pi d + \frac{4\pi N_T d^3}{c_e}\frac{dX}{d\sigma}$$

After choosing the parameters d and c_e, the residual energy differences, $U_{20} - U_{10}$ and $U_{30} - U_{10}$ were calculated from the experimental values of the charge density and inner layer capacity at the minimum on the capacity against charge density curve (3).

The theoretical curves generated for the negative segments of the inner layer capacity curves with Li^+, Na^+, and K^+ as counter ions, and for the positive segments with BF_4^-, F^-, and ClO_4^- as counter ions are shown in Fig. 6. The parameters chosen for each of these curves are summarized in Table 3. It is interesting to note that the assumed diameter of the methanol molecule represented as a sphere is constant for all of the curves except that with ClO_4^- as counter ion. The value chosen (0.335 nm) is reasonable on the basis of the Courtauld model for the molecule (23). As the effective coordination number c_e increases, the rate of increase of C_i from its minimum value decreases. If it is assumed that the distance of closest approach of the alkali metal cations is determined by their unsolvated radii, then the smallest cation, Li^+, would have the greatest influence on dipole orientation in the solvent monolayer. This is apparently reflected in the present model by an increase in the effective number of nearest neighbours for each dipole in the monolayer. The influence of anions is more difficult to assess since anion solvation reflects both ion–dipole interaction and hydrogen bonding in the case of methanol (20). In any case, the above analysis suggests that a more detailed model for the solvent monolayer should reflect the asymmetry in the capacity curves due to the influence of the counter ion at the oHp. Because of the variation in c_e and d with counter ion nature, the residual energy differences $U_{20} - U_{10}$ and $U_{30} - U_{10}$ also vary. The average value for $U_{20} - U_{10}$ is -17.4 kJ mol^{-1}; this reflects the fact that dipoles with their negative ends towards the metal are more stable than dipoles with positive orientation at the pzc. The average value for $U_{30} - U_{10}$ is -17.7 kJ mol^{-1}. Thus dipoles in the parallel orientation are the most stable at an uncharged surface and predominate in the monolayer over most of the polarizable range of the electrode (23). The average value of the surface potential ($\Delta\phi_0$ at the pzc) is -0.42 V. The assumption that minimum orientation in the monolayer occurs at negative charge densities which leads to the negative value of $\Delta\phi_0$ is supported by the observation that the maximum adsorption of aliphatic organic compounds occurs at a negatively charged Hg surface (28). It is also interesting to note that the surface potential at the methanol/air interface is negative (~ -0.2 V) (29).

TABLE 3. Parameters used in the three-state model to calculate inner layer capacity curves at the mercury/methanol interface in the presence of various counter ions

Curve*	Counter ion	Molecular diameter d (nm)	Effective coordination number, c_e
1	F^-	0.335	13.2
2	ClO_4^-	0.365	13.2
3	BF_4^-	0.335	13.95
	K^+		
4	Na^+	0.335	14.9
5	Li^+	0.335	15.5

*The integers in the table refer to the curves illustrated in Fig. 6. In all cases, the dipole moment of methanol was assumed to be 1.66 D (5.54×10^{-30} C m) and the polarizability, 3.26×10^{-3} nm^3.

According to the three-state model, the potential drop across the monolayer at the principal extremum is independent of temperature (4). If this feature of the theory is correct, one may estimate the temperature coefficient of the surface potential from the present data. Defining a rational potential scale with respect to the pzc, ϕ^m, the potential drop across the inner layer may be written as

[11] $\phi^m - \phi^d = \Delta\phi - \Delta\phi_0$

where ϕ^d is the potential drop across the diffuse layer and $\Delta\phi_0$, the potential drop across the solvent monolayer at the pzc. At the principal extremum, $d\Delta\phi_m/dT = 0$, and therefore

[12] $$\frac{d(\phi^m - \phi^d)_m}{dT} = -\frac{d\Delta\phi_0}{dT}$$

where the subscript m signifies the principal extremum. On the basis of the data obtained for the $NaClO_4$ system in MeOH, the value of $d\Delta\phi_0/dT$ is -0.2 mV K^{-1}. This value agrees well with those estimated on the basis of the temperature dependence of the potential of the pzc (14). The average value of $d\Delta\phi_0/dT$ estimated according to the three-state model on the basis of the parameters used to generate the curves in Fig. 6 is -0.12 mV K^{-1}. The sign of the temperature coefficient of the surface potential is easily explained on the basis of the three-state model. At the pzc, dipoles in the parallel orientation are the major component of the monolayer with the concentration of negatively oriented dipoles greater than that of positively oriented ones (3, 23). As the temperature increases, the number of dipoles in the parallel orientation decreases with a corresponding increase in the number of "down" (negatively oriented) dipoles.

It is also interesting to examine the predictions of the three-state model with respect to the temperature dependence of the inner-layer capacity. The variation in $d(1/C_i)/dT$ with electrode charge density on the basis of the parameters for Na^+ ion (Table 3) is illustrated in Fig. 5. The most striking feature of this curve is that a minimum in $d(1/C_i)/dT$ occurs at the same charge density where it is observed experimentally. The magnitude of the calculated coefficient is considerably greater than the experimental value at this extremum; however, the temperature dependence itself is small in comparison with the magnitude of the capacity. A maximum is observed on the experimental curve just positive of the principal extremum; on the other hand, the maximum on the calculated curve is much less pronounced and occurs at more positive charge densities. Because of the asymmetric character of the experimental capacity curves, it is clear that the simple three-state model cannot describe the temperature dependence of C_i in all its details. However, the fact that a minimum in $d(1/C_i)/dT$ is observed experimentally at the charge density where it is predicted to be according to the theory is striking.

The variation in the temperature coefficients of the inner layer capacity, potential drop, and free energy with temperature according to the three-state model is illustrated in Fig. 7 on the basis of the parameters for the Na^+ ion (Table 3). As pointed out above $d\Delta\phi/dT$ is zero at the principal extremum; it is also zero at charge densities corresponding to maxima on the calculated capacity curve. The potential drop $\Delta\phi$ cannot be measured experimentally. However, the temperature coefficient $d\Delta\phi/dT$ could be estimated on the basis

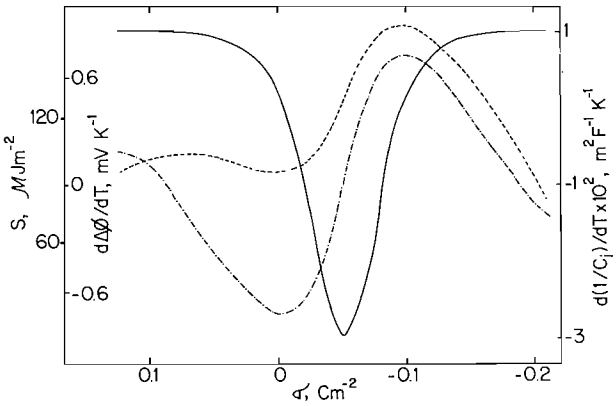

FIG. 7. Entropy of the solvent monolayer, S (---), and the temperature coefficients $d\Delta\phi/dT$ (- · · · -) and $d(1/C_i)/dT$ (—) as a function of electrode charge density σ according to the three-state model assuming $d = 0.335$ nm, $c_e = 14.9$, $p = 1.66$ D, and $\alpha = 3.26 \times 10^{-3}$ nm. The corresponding inner layer capacity is illustrated by curve *3* in Fig. 6.

of the temperature dependence of the potential drop across the inner layer, $\phi^m - \phi^d$, and the experimental estimate of $d\Delta\phi/dT$ at the pzc. The entropy of the monolayer obtained from the dependence of the free energy on temperature possesses a sharp maximum at charge densities negative of the principal extremum. The asymmetric nature of this curve is due to the fact that both the configurational entropy and dipole–dipole interaction energy are complex functions of the electrode field. This feature of the theory could be tested by studying the temperature dependence of the interfacial tension at the Hg/MeOH interface. Experiments to study this aspect of the Hg/non-aqueous solution interface are currently in progress.

In conclusion, the three-state model provides an acceptable description of the dielectric properties of the Hg/MeOH interface on the basis of available data. This model could be refined if some account is made of the effect of specific ions in the double layer on the thickness of the inner layer and on the magnitude of dipole–dipole interactions between solvent molecules which solvate the electrode. On the other hand, weak ionic specific adsorption is difficult to detect experimentally, and therefore, could account for part of the observed effect of specific ions. It is clear that an improved experimental technique for assessing ionic adsorption is required before the effect of ions on interfacial solvent structure can be asssessed further. It should be noted that in the three-state model it is not necessary to consider dipole–dipole interactions and the reaction field parallel to the electrode's field. Parsons has pointed out (30) that considerable ordering of dipole vectors parallel to the electrode is ex-

Can. J. Chem. Downloaded from www.nrcresearchpress.com by 210.87.254.105 on 09/06/12
For personal use only.

pected. In the case of methanol, hydrogen bonding would be expected to play a role in this ordering since in the "parallel" orientation the —OH bond is approximately parallel to the interface.

Acknowledgement

The financial assistance of the Natural Sciences and Engineering Research Council of Canada is gratefully acknowledged.

1. D. C. GRAHAME. Z. Elektrochem. **59**, 740 (1955).
2. R. PAYNE. Adv. Electrochem. Electrochem. Eng. **7**, 1 (1970).
3. W. R. FAWCETT. J. Phys. Chem. **82**, 1385 (1978).
4. W. R. FAWCETT, B. M. IKEDA, and J. B. SELLAN. Can. J. Chem. **57**, 2268 (1979).
5. Z. BORKOWSKA. J. Electroanal. Chem. **79**, 206 (1977).
6. R. PAYNE. J. Am. Chem. Soc. **89**, 489 (1967).
7. M. JURKIEWICZ-HERBICH. J. Electroanal. Chem. **92**, 221 (1978).
8. R. M. REEVES. Mod. Aspects Electrochem. **9**, 239 (1974).
9. W. R. FAWCETT and M. D. MACKEY. J. Chem. Soc. Faraday Trans. I, **69**, 634 (1973).
10. R. D. ARMSTRONG and G. D. WEST. J. Electroanal. Chem. **30**, 385 (1971).
11. R. PARSONS and F. G. R. ZOBEL. J. Electroanal. Chem. **9**, 333 (1965).
12. W. R. FAWCETT and R. O. LOUTFY. J. Electroanal. Chem. **39**, 185 (1972).
13. H. BEHRET, F. SCHMITHALS, and J. BARTHEL. Z. Phys. Chem. N. F. **96**, 73 (1975).
14. Z. BORKOWSKA, W. R. FAWCETT, and S. ANANTAWAN. J. Phys. Chem. **84**, 2769 (1980).
15. J. TARASZEWSKA. J. Electroanal. Chem. **49**, 443 (1974).
16. S. MINC and J. JASTRZEBSKA. Dokl. Akad. Nauk SSSR, **120**, 114 (1958); S. MINC and M. BRZOSTOWSKA. Rocz. Chem. **34**, 1109 (1960).
17. D. C. GRAHAME. J. Electrochem. Soc. **98**, 343 (1951).
18. W. R. FAWCETT. J. Electroanal. Chem. **39**, 474 (1972).
19. B. B. DAMASKIN. J. Electroanal. Chem. **65**, 799 (1975).
20. A. J. PARKER. Chem. Rev. **69**, 1 (1969).
21. G. J. HILLS and R. M. REEVES. J. Electroanal. Chem. **38**, 1 (1972).
22. D. C. GRAHAME. J. Am. Chem. Soc. **79**, 2093 (1957).
23. W. R. FAWCETT. Israel J. Chem. **18**, 3 (1979).
24. R. PARSONS. J. Electroanal. Chem. **59**, 229 (1975).
25. R. PARSONS. Electrochim. Acta, **21**, 681 (1976).
26. Z. BORKOWSKA and W. R. FAWCETT. Elektrokhimiya. In press.
27. H. D. HURWITZ, A. SANFELD, and A. STEINCHEN-SANFELD. Electrochim. Acta, **9**, 929 (1964).
28. J. D. GARNISH and R. PARSONS. Trans. Faraday Soc. **63**, 1754 (1967).
29. B. CASE and R. PARSONS. Trans. Faraday Soc. **63**, 1224 (1967).
30. R. PARSONS. J. Electroanal. Chem. **109**, 369 (1980).

Can. J. Chem. Downloaded from www.nrcresearchpress.com by 210.87.254.105 on 09/06/12
For personal use only.

Kinetics of the oxidation of dimethyl sulfoxide with aqueous hydrogen peroxide catalyzed by sodium tungstate[1]

YOSHIRO OGATA[2] AND KAZUSHIGE TANAKA

Department of Applied Chemistry, Faculty of Engineering, Nagoya University, Chikusa-ku, Nagoya, Japan

Received July 2, 1980

YOSHIRO OGATA and KAZUSHIGE TANAKA. Can. J. Chem. **59**, 718 (1981).

The oxidation of dimethyl sulfoxide (DMSO) by hydrogen peroxide in the presence of a catalytic amount of sodium tungstate (Na_2WO_4) has been studied kinetically by means of iodometry of hydrogen peroxide. The reaction is first-order with respect to the substrate and the catalyst, but independent of the concentration of hydrogen peroxide which is present in excess of the catalyst. The polarographic study implies that in solutions two main kinds of peroxytungstic acids (H_2WO_5 and H_2WO_8) are formed which contain active oxygen in ratios (active oxygen):(Na_2WO_4) of 1:1 and 4:1, respectively. The effect of acidity on the oxidation rate and a probable mechanism involving a rate-determining attack of peroxytungstic acids are discussed.

YOSHIRO OGATA et KAZUSHIGE TANAKA. Can. J. Chem. **59**, 718 (1981).

Faisant appel à l'iodométrie du peroxyde d'hydrogène, on a étudié l'oxydation du diméthylsulfoxyde (DMSO) par le peroxyde d'hydrogène, en présence d'une quantité catalytique de tungstate de sodium (Na_2WO_4). La réaction est du premier ordre par rapport au substrat et au catalyseur, mais elle est indépendante de la concentration du peroxyde d'hydrogène qui est en excès par rapport au catalyseur. Les études polarographiques indiquent qu'il se forme en solution deux types principaux d'acides peroxytungstiques (H_2WO_5 et H_2WO_8) qui contiennent respectivement des rapports d'oxygène actif (oxygène actif) (Na_2WO_4) de 1:1 et 4:1. On discute de l'effet de l'acidité sur la vitesse d'oxydation ainsi que d'une mécanisme probable faisant intervenir l'attaque des acides peroxytungstiques dans l'étape déterminante.

[Traduit par le journal]

Introduction

It is well known that molybdic and tungstic acids are converted to peroxy acids on treatment with aqueous hydrogen peroxide. Kinetic studies on the tungstic acid-catalyzed epoxidation of allyl alcohol (1) and fumaric acid (2) with H_2O_2 have been reported. However, details of the structure and behavior of peroxytungstic acid remain equivocal. The present paper describes the rate data, the effect of acidity, and a probable mechanism of the Na_2WO_4-catalyzed oxidation of DMSO by hydrogen peroxide in aqueous buffers.

Results and Discussion

Polarography

Before carrying out the kinetic studies, we intended to clarify the constituents of a mixture of sodium tungstate and hydrogen peroxide in an acetate buffer (pH 4.0) by the polarographic method (3). Firstly, the dependence of the kinetic current[3] of peroxytungstates upon reaction time was studied with an equimolar (each 2×10^{-3} *M*) mixture of Na_2WO_4 and H_2O_2 in the acetate buffer at 25°C. Although the decomposition of H_2O_2 in the presence of Na_2WO_4 at pH over 4.0 was appreciable in the kinetics as shown later, this effect is negligible in the polarography, since H_2O_2 decomposition is slow at pH 4.0–5.1 and H_2O_2 concentrations in the polarography are smaller than those in the kinetic study. The result is shown in Fig. 1. The observed kinetic current is a measure for the concentration of peroxytungstates (probably Na_2WO_5 and Na_2WO_8). The kinetic current at pH 4.0 increases with time and after ca. 3 h it reaches a constant value, 2.98 μA/m*M*.

[1] $\mathrm{ST} \overset{H_2O_2}{\rightleftharpoons} \mathrm{PeT}$

[2] $\mathrm{PT} \underset{a}{\overset{H_2O_2}{\rightleftharpoons}} \mathrm{PePT} \xrightarrow[b]{} \mathrm{PeT}$

This phenomenon suggests that depolymerization of peroxypolytungstates (PePT) is slow (step *b* in reaction [2]). Even if concentration of H_2O_2 is increased to four times that of Na_2WO_4, the kinetic current at pH 4.0 reaches a constant value, 8.87 μA/m*M*, only after ca. 2.5 h. But at pH 5.1, the

[1]Contribution No. 273.

[2]To whom all correspondence should be addressed.

[3]The kinetic current is the current produced by the reduction of peroxy compound which is continuously reformed at the surface of the cathode. For simplification, we considered only WO_4^{2-} and WO_5^{2-} as shown in the following reactions.

$$WO_4^{2-} + H_2O_2 \rightarrow WO_5^{2-} + H_2O$$
$$WO_5^{2-} + 2H^+ + 2e \rightarrow WO_4^{2-} + H_2O$$

Since the kinetic current is proportional to the concentration of peroxy compound, the concentration of H_2O_2 which reacted with the tungstate can be measured from the ratio of $[H_2O_2]_0/[Na_2WO_4]_0$ at inflection, thus the structure of the peroxide can be deduced.

0008-4042/81/040718-05$01.00/0

©1981 National Research Council of Canada/Conseil national de recherches du Canada

Can. J. Chem. Downloaded from www.nrcresearchpress.com by 210.87.254.6 on 09/06/12
For personal use only.

Can. J. Chem. Downloaded from www.nrcresearchpress.com by 210.87.254.6 on 09/06/12
For personal use only.

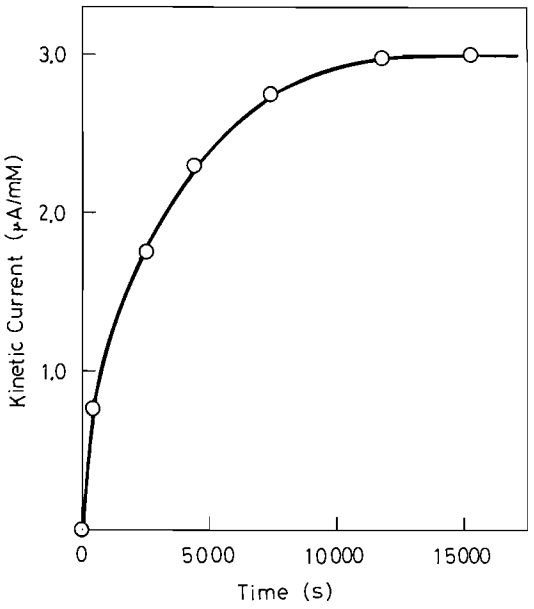

FIG. 1. The kinetic current of peroxytungstates in an acetate buffer (pH 4.0) at 25°C as a function of time. $[Na_2WO_4]_0 = [H_2O_2] = 2 \times 10^{-3}$ *M*.

kinetic current of a Na_2WO_4–H_2O_2 equimolar mixture (each 2×10^{-3} *M*) reaches a value of 3.63 μA/m*M* immediately and does not increase with time, which is ascribed to the absence of polytungstates (PT). Simple tungstate (ST) is totally converted immediately to peroxytungstates (PeT) (eq. [1]). Tungstate (WO_4^{2-}) has a tendency to polymerize to $[HW_6O_{21}]^{5-}$ and $[(HW_6O_{20})_n]^{3n-}$ with decreasing pH at 5.5–3.5 (4) and PT reacts rapidly with H_2O_2 (step *a* in reaction [2]) in view of our kinetic study as shown later, so that the above phenomena suggest that step *b* in reaction [2] is slower than reaction [1] at pH 4.0–3.5. Accordingly, reactions [1] and [2] occur simultaneously at pH 4.0, while only reaction [1] occurs at pH 5.1. Thus the rate of formation of PeT from PePT at pH 4.0 was rather slow; hence most of the kinetic current measurements by means of polarography were made after standing at 25°C for 4 h.

Some workers (1, 2, 5) have reported on the structures of peroxytungstic acids, but their structures are still ambiguous. Hence, the dependence of the kinetic current of PeT at various ratios of $[H_2O_2]_0/[Na_2WO_4]_0$ was studied (Fig. 2). The current is proportional to concentrations of PeT, e.g., 2.94 μA/m*M* with an equimolar (each 2×10^{-3} *M*) mixture. As seen in Fig. 2, the kinetic current increases with the ratio $[H_2O_2]_0/[Na_2WO_4]_0$ until the ratio reaches 4:1 and there is also an inflection at the ratio of 1:1. These results suggest that there are two

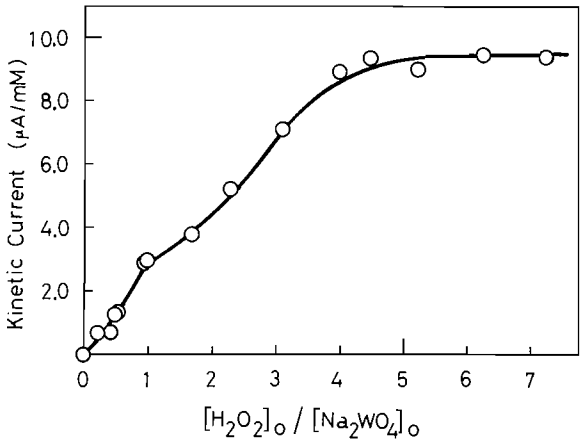

FIG. 2. The kinetic current of peroxytungstates in an acetate buffer (pH 4.0) at 25°C as a function of $[H_2O_2]_0/[Na_2WO_4]_0$.

principal PeT, presumably Na_2WO_5 and Na_2WO_8, whereas little Na_2WO_6 and Na_2WO_7 exist, if any, since there are no inflections at the ratio $[H_2O_2]_0/[Na_2WO_4]_0$ of 2:1 and 3:1. Though Richardson (5) postulated that an H_2O_2–H_2WO_4 mixture in the molar ratio of 4:1 contains polymeric acid $H_2W_2O_{15}$ besides H_2WO_8, $H_2W_2O_{15}$ does not seem to exist, because the second-order rate constant does not decrease with increasing concentration of tungstate as shown in our kinetics.

Kinetics

The kinetics of the oxidation of DMSO in a mixture of Na_2WO_4 and H_2O_2 were measured iodometrically in aqueous buffers of various pH values. Since the decomposition of H_2O_2 in the presence of Na_2WO_4 at pH over 4.0 was appreciable, the rate of oxidation of DMSO was calculated by subtracting the rate of the decomposition of H_2O_2 from the measured rate. The decomposition rate was faster than the oxidation rate at pH values greater than 7, thus the kinetics at these pH values were not reliable.

The rate thus corrected is first-order with respect to DMSO and the catalyst, but independent of the concentration of hydrogen peroxide which is present in excess of the catalyst (Table 1). Accordingly, the rate equation is expressed as:

$$v = k_2 w[\text{DMSO}]$$

Here w is the initial stoichiometric concentration of sodium tungstate and k_2 the second-order rate constant. Also, the rate calculated by the decrease of [DMSO] using nmr gave the same expression and analogous rate constant, e.g., 3.24×10^{-2} M^{-1} s^{-1} with 1×10^{-3} *M* Na_2WO_4 and 3.0×10^{-2} *M*

Can. J. Chem. Downloaded from www.nrcresearchpress.com by 210.87.254.6 on 09/06/12
For personal use only.

TABLE 1. Rate data[a] for the Na_2WO_4-catalyzed oxidation of DMSO with aqueous H_2O_2 at pH 4.0 (AcOH–AcONa) at 25°C

Initial concentration × 10^3 M			
$[Na_2WO_4]_0$	$[H_2O_2]_0$	$[DMSO]_0$	$k_2 \times 10^2$ M^{-1} s^{-1}
2.0	35.6	15.0	2.84
2.0	34.9	20.0	2.55
2.0	36.6	25.0	2.71
2.0	36.0	30.0	2.62
2.0	35.2	35.0	2.87
2.0	50.4	25.0	2.57
2.0	39.2	25.0	2.68
2.0	19.2	25.0	2.58
2.0	10.9	25.0	2.86
1.6	44.2	25.0	2.85
1.0	47.3	25.0	2.74
1.0	32.0	25.0	2.67
1.0	19.7	25.0	2.35

[a] $v = k_2[Na_2WO_4]_0[DMSO]$; rates were derived by subtracting the rate of the decomposition of H_2O_2 from the measured rate. The reaction was started by addition of DMSO to a Na_2WO_4–H_2O_2 mixture which was kept standing for 4 h.

H_2O_2 at pH 4.0, although the constancy of k_2 is rather poor.

The above rate data suggest that H_2O_2 alone cannot oxidize DMSO directly under these conditions. Actually, H_2O_2 (2.95×10^{-2} M) and DMSO (2.50×10^{-2} M) do not react at 25°C in the absence of tungstate. Hence H_2O_2 should oxidize tungstic acid to peroxytungstic acids which react with DMSO in a rate-determining step. If the oxidation of tungstic acid to peroxytungstic acids determined the rate, then the rate of DMSO oxidation would be proportional to $w[H_2O_2]$ and independent of [DMSO]. Also the polyperoxytungstic acids (PPeT),[4] which has been postulated by Richardson, should exist only in small amounts, if any, under these conditions in view of the rate data, because the rate constants change little with changing concentration of Na_2WO_4 while holding the concentrations of DMSO and H_2O_2 constant; e.g., at 2.50×10^{-2} M DMSO, k_2 values were 2.35×10^{-2} M^{-1} s^{-1} with 1×10^{-3} M Na_2WO_4 and 1.97×10^{-2} M H_2O_2 and 2.58×10^{-2} M^{-1} s^{-1} with 2×10^{-3} M Na_2WO_4 and 1.92×10^{-2} M H_2O_2. PPeT should have less reactivity than simple PeT because of their lower content of active oxygen and their coiled structure.

The above kinetic results seem to be in conflict, since the reaction of Na_2WO_4 with H_2O_2 was rather slow at pH 4.0 on the basis of our polarographic studies. But this apparent slow formation of PeT at pH 4.0 may be due to the slow depolymerization of PePT. Tungstate reacts with H_2O_2 rapidly at pH 5.1, where PT and hence PePT hardly exist as is obvious in the polarography. Csányi (6) reported that no peroxypolymolybdate, but only monomeric dihydroperoxy-1-molybdate $MoO_2(OOH)(OO^-)$, was formed when H_2O_2 was added to polymolybdate. However, in the case of tungstate, PePT may be formed very rapidly from PT, since the oxidation rate constants for the reaction of DMSO with a Na_2WO_4–H_2O_2 mixture kept standing for only 2 min were similar (slightly smaller) to those for 4 h, e.g., k_2 values were 2.67×10^{-2} M^{-1} s^{-1} with a 4 h Na_2WO_4–H_2O_2 mixture and 2.46×10^{-2} M^{-1} s^{-1} with a 2 min Na_2WO_4–H_2O_2 mixture. These results imply that Na_2WO_5, Na_2WO_8, and PePT are formed immediately after mixing Na_2WO_4 with aqueous H_2O_2 in an acetate buffer (at pH 4.0) and PePT are gradually converted into Na_2WO_5 and Na_2WO_8. Furthermore, the oxidation rate of Na_2WO_8 may be slightly faster than that of Na_2WO_5 because of the higher electrophilicity of Na_2WO_8, while the oxidation rate per unit tungsten of PePT may be slightly lower than that of Na_2WO_5 because of the steric hindrance. But the difference between their rates seems to be small, since the rate constants for a Na_2WO_4–H_2O_2 mixture at 2 min are similar to those at 4 h.

Effect of Acidity

The effect of acidity of the solution on the second-order rate constant k_2 is shown in Fig. 3. The decrease of k_2 at high acidity (at $-H_0 > 1.5$) may be ascribed to the protonation of DMSO, forming $(CH_3)_2SOH^+$, in view of the observed partial protonation of DMSO in concentrated H_2SO_4

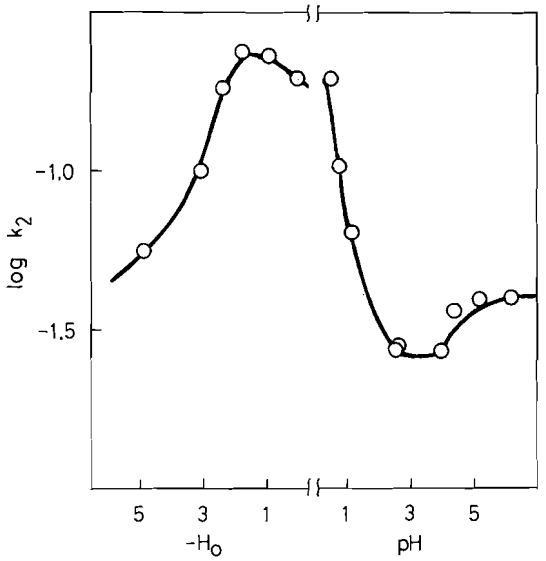

FIG. 3. Effect of acidity of solution on the second-order rate constant k_2 for the H_2O_2 oxidation of DMSO at 25°C. $[Na_2WO_4]_0 = 1 \times 10^{-3}$ M, $[H_2O_2]_0 = 3.0 \times 10^{-2}$ M, $[DMSO]_0 = 2.5 \times 10^{-2}$ M.

[4] PPeT are polymers of peroxytungstates, while PePT are peroxides of polytungstates.

Can. J. Chem. Downloaded from www.nrcresearchpress.com by 210.87.254.6 on 09/06/12
For personal use only.

(7). Since the oxidation by peracids involves an electrophilic attack, the reaction is inhibited by the protonation of substrate. The observed decrease of the rate constant with increasing pH at 0–2.5 suggests that the oxidation is retarded by increasing concentration of the anions (T—OO^-) of the peroxytungstic acids (T—OOH), since there are two distinct active species, i.e., T—OOH at pH < 0 and T—OO^- at pH > 2.5, where T—OOH means H_2WO_5 and H_2WO_8, etc. The curve is similar to that observed in Na_2MoO_4-catalyzed oxidation of DMSO by H_2O_2.[5] Both H_2WO_5 and H_2WO_8 may be main attacking species[6] for this oxidation. The free acids T—OOH should be more active than T—OO^-. The above reasoning assumes that the first ionization of peroxytungstic acids occurs at pH 0–2.5, because the second ionization constant for H_2WO_8 measured by Dedman by a direct and reliable way using pH and spectrophotometric measurements was 1.4×10^{-7} mol L^{-1} at 0.056 *M* H_2O_2 (8), and also the first ionization constant of peroxymolybdate H_2MoO_6, which gave a log k_2: pH curve analogous to that of peroxytungstic acids,[5] was reported to be 3×10^{-3} mol L^{-1} and its second ionization constant 7×10^{-10} mol L^{-1} (6). On the other hand, Raciszewski (1) assumed on the basis of his kinetics of allyl alcohol that the first ionization constant of H_2WO_5 was 4.5×10^{-7} mol L^{-1}, but his value, which was estimated by the acidity effect, is ambiguous as to whether it is the first or second ionization constant.

The observed minimum of log k_2 at pH ca. 4 may be explained by the polymerization of tungstate WO_4^{2-}, which has a tendency (4) to polymerize with decreasing pH at 5.5–3.0. This tendency toward polymerization is supported by our polarographic studies, in which the kinetic current of a Na_2WO_4–H_2O_2 mixture at pH 5.1 does not increase with time, while the current at pH 4.0 increases with time as stated above. These results suggest that PT may be present at pH 4.0. Since PePT seems to exist, as stated in the discussion of the kinetics, the stoichiometric initial concentration at pH 4.0 of tungstate is approximately expressed as:

$$w \cong [HWO_5^-] + [HWO_8^-] + [PT] + [PePT] + [HWO_4^-]$$

[PT] and $[HWO_4^-]$ can be neglected, assuming that PT and HWO_4^- react with H_2O_2 rapidly and completely to form their peroxides as described above; hence

$$[3] \quad w \cong [HWO_5^-] + [HWO_8^-] + [PePT]$$

Since [PePT] decreases with increasing pH at 5.5–3.5 because of the decrease of PT and thus the content of $[HWO_8^-]$ increases with pH, the rate increases with increasing pH.

Mechanism

These facts suggest the following mechanism for the oxidation at pH 3.5–5.0.

$$[4] \quad Na_2WO_4 \overset{\text{fast}}{\rightleftharpoons} 2Na^+ + WO_4^{2-}$$

$$[5] \quad WO_4^{2-} + H_2O \overset{\text{fast}}{\rightleftharpoons} HWO_4^- + OH^-$$

$$[6] \quad (a+b)HWO_4^- + (a+4b)H_2O_2 \overset{\text{fast}}{\rightleftharpoons} aHWO_5^- + bHWO_8^- + (a+4b)H_2O$$

$$[7] \quad HWO_5^- + (CH_3)_2SO \xrightarrow[k_1]{\text{slow}} (CH_3)_2SO_2 + HWO_4^-$$

$$[8] \quad HWO_8^- + (CH_3)_2SO \xrightarrow[k_2]{\text{slow}} (CH_3)_2SO_2 + HWO_7^-$$

$$[9] \quad HWO_7^- + H_2O_2 \overset{\text{fast}}{\rightleftharpoons} HWO_8^- + H_2O$$

In aqueous solution of pH 4.0, WO_4^{2-} is converted mostly into HWO_4^- (reaction [5]).[7] This acid anion reacts rapidly with H_2O_2 to give HWO_5^- and HWO_8^- (reaction [6]); PT also reacts with H_2O_2 to give PePT, which depolymerizes slowly in the presence of H_2O_2 to give HWO_5^- and HWO_8^-, as stated in the polarographic study. Since there is no polarographic evidence for the presence of HWO_7^- which contains active oxygen in a ratio (active oxygen):(Na_2WO_4) = 3:1, HWO_7^- may be unstable, changing rapidly to HWO_8^- by H_2O_2 (reaction [9]).

Thus the rate is expressed as

$$v = \{k_1[HWO_5^-] + k_2[HWO_8^-] + k_3[PePT]\}[DMSO]$$

Here k_1, k_2, and k_3 represent the rate constants of HWO_5^-, HWO_8^-, and PePT, respectively. Assuming $k_1 \cong k_2 \cong k_3$ as stated above

$$v \cong k_2\{[HWO_5^-] + [HWO_8^-] + [PePT]\}[DMSO]$$

or

$$v = k_2 w[DMSO]$$

This expression is consistent with the experimental results, and supports the mechanism.

Experimental

Materials

DMSO was purified by vacuum distillation (bp 86°C, 21 mm). Sodium tungstate was of commercial guaranteed reagent grade.

[5]This work was carried out in part by Mr. H. Shimizu, Nagoya University, 1979.

[6]PeT with the ratio of (active oxygen):$(Na_2WO_4)_t$ = 2:1 (i.e., H_2WO_6 or $H_2W_2O_{11}$) was reported to be formed in strong acid solutions (9), but PeT with ratio $[H_2O_2]_0$:$[Na_2WO_4]_0$ of 2:1 was not observed in our polarography at pH 4.0, hence they would be unstable, their concentrations being negligible.

[7]Dissociation constant for HWO_4^- (pK_2) is 6.9 (2).

Product

Oxidation of DMSO gave dimethyl sulfone ($DMSO_2$) in 91.5% isolated yield, when a mixture of DMSO (1×10^{-2} *M*), H_2O_2 (1×10^{-2} *M*), and Na_2WO_4 (1×10^{-3} *M*) was reacted at 25°C for 24 h in an acetate buffer (pH 4.0).

Polarography

The kinetic current was determined by the method described by Kolthoff (3), and measured with a Na_2WO_4–H_2O_2 system to obtain information on active species in the Na_2WO_4-catalyzed oxidation by H_2O_2. A mixture of Na_2WO_4 and H_2O_2 in an acetate buffer (pH 4.0) was kept standing at 25°C for 4 h, and then aliquots were taken out and analyzed on a Yanagimoto Model P8-D and P8-PT of direct polarography.

Kinetics

A mixture of Na_2WO_4 and H_2O_2 in an acetate buffer was kept standing at 25°C for 4 h (or 2 min in some cases), then the reaction was started by addition of DMSO. Aliquots (each 5 mL) were taken out at appropriate intervals of time, and their peroxide contents were determined iodometrically. The concentrations of DMSO were calculated from peroxide concentrations, since the oxidation product of DMSO was only dimethyl sulfone. At higher pH, where the marked decomposition of H_2O_2 was observed, the rate of oxidation of DMSO was corrected by subtracting the rate of the decomposition of H_2O_2 from the measured rate. In order to follow the rate of consumption of DMSO by nmr (δ 3.2) the oxidation was conducted at pH 4.0. The reaction was quenched by addition of aqueous $Na_2S_2O_3$ for nmr analysis.

The effect of acidity on the oxidation rate was studied in aqueous media using acetate – acetic acid buffers at pH 3.2–6.2, acetate – hydrochloric acid buffers at pH 0.8–3.2, and sulfuric acid at pH below 0.8.

Acknowledgements

The authors are grateful to Mr. H. Shimizu for his helpful preliminary study and to Dr. J. P. Schirmann for his advice on the structure of peroxytungstic acids.

1. Z. Raciszewski. J. Am. Chem. Soc. **82**, 1267 (1960).
2. M. A. Beg and I. Ahmad. J. Catal. **39**, 260 (1975).
3. I. M. Kolthoff and E. P. Parry. J. Am. Chem. Soc. **73**, 5315 (1951).
4. D. L. Kepert and J. H. Kyle. J. Chem. Soc. Dalton, 133 (1978).
5. E. Richardson. J. Less-Common Met. **2**, 360 (1960).
6. L. H. Csányi. Acta Chim. Acad. Sci. Hung. **14**, 79 (1958); Chem. Abstr. **52**, 19647 (1958).
7. R. C. Paul, D. S. Dhillon, D. Konwer, and J. K. Puri. J. Inorg. Nucl. Chem. **39**, 1011 (1977).
8. A. J. Dedman, T. J. Lewis, and D. H. Richards. J. Chem. Soc. 5020 (1963).
9. W. P. Griffith. J. Chem. Soc. 5345 (1963).

Can. J. Chem. Downloaded from www.nrcresearchpress.com by 210.87.254.6 on 09/06/12
For personal use only.

Analysis of generalized two-dimensional homonuclear nmr spectra[1]

ALEX D. BAIN[2]
Department of Chemistry, Scarborough College, University of Toronto, Toronto, Ont., Canada
AND
JACQUES BORNAIS AND SYDNEY BROWNSTEIN
Division of Chemistry, National Research Council of Canada, Ottawa, Ont., Canada K1A 0R9

Received June 23, 1980

ALEX D. BAIN, JACQUES BORNAIS, and SYDNEY BROWNSTEIN. Can. J. Chem. **59**, 723 (1981).

Analysis of the free induction decays from 90°–90° two-dimensional homonuclear pulse sequences gives complete spectral information from each transition in the f_2 dimension. Theoretical intensities and frequencies are illustrated for the common cases AX, A_2X, AMX, A_2X_2, AA'XX', and A_2X_3 along with experimental examples of each. An analysis of intensities is given. From these examples it should be possible to determine chemical shift and spin-coupling values even when many lines in the f_2 dimension are obscured by other spectral features.

ALEX D. BAIN, JACQUES BORNAIS et SYDNEY BROWNSTEIN. Can. J. Chem. **59**, 723 (1981).

L'analyse des désintégrations par induction libre obtenues à partir de séquences pulsées homonucléaires bi-dimensionnelles 90°–90° fournit une information spectrale complète de chaque état de transition dans la dimension f_2. On a illustré les intensités théoriques et les fréquences dans les cas usuels: AX, A_2X, AMX, AA', XX' et A_2X_3 de concert avec des exemples expérimentaux de chacun d'eux. On donne une analyse des intensités. A partir de ces exemples, il devrait être possible de déterminer les déplacements chimiques et les valeurs du couplage de spin même quand plusieurs pics de la dimension f_2 sont masqués par d'autres caractéristiques spectrales.

[Traduit par le journal]

Introduction

Two-dimensional homonuclear nmr spectroscopy is now well established as a technique for the nmr spectroscopist (1, 2). The basic principle is that we allow a spin system to evolve for some time t_1 before collecting the free induction decay (FID). Fourier transformation of the FID gives a spectrum whose frequency scale is conventionally called f_2. The experiment is repeated for a series of values of t_1, so that Fourier transformation of each point in the spectrum with respect to t_1 yields a second frequency dimension f_1. Our purpose here is to explore some of the details of chemical shift-correlated two-dimensional spin echo nmr spectroscopy (3, 4), which is closely related to the SECSY technique (5).

The most common pulse sequence used on homonuclear systems is the 90°–t_1/2–180°–t_1/2–FID sequence which spreads homonuclear couplings out in f_1 (1) while not affecting chemical shifts or heteronuclear couplings (6). This can help untangle complicated spectra with overlapped multiplets, but no new information is contained in such a spectrum.

By changing the second pulse in the sequence to a 90° pulse we can also discover the connectivity of the spin system. Any line in the 1D spectrum represents a transition of a particular nucleus. In the 90°–t_1/2–180°–t_1/2–FID sequence the f_1 spectrum of that transition shows only a single line (although the data are often "tilted" to collect members of a multiplet along one axis (7)). In the 90°–t_1/2–90°–t_1/2–FID experiment, the f_1 spectrum of a transition contains several lines. There are lines due not only to other members of the multiplet but also lines due to other nuclei that cause the spin–spin splitting. Therefore the f_1 spectrum corresponding to this transition is essentially a copy of the subspectrum to which the transition belongs. This allows us to obtain relative chemical shifts of nuclei which are coupled and hence the connectivity.

The price to be paid for this information is that the f_1 frequency range must be larger so that either more data must be collected or the digital resolution must be sacrificed. The original 90°–t_1–90°–FID (2) sequence produced a copy of the subspectrum in f_1 for each line in the 1D spectrum but required an f_1 sweep width equal to that in f_2. Changing the sequence to 90°–t_1/2–90°–t_1/2–FID produces two copies of the subspectrum in f_1 called the additive and subtractive spectrum (3) with the important feature that the subtractive spectrum is based at zero frequency in f_1. The additive spectrum is suppressed by the SECSY pulse sequence (5) so that the f_1 range needed is determined by the largest

[1]Issued as NRCC No. 18815.

[2]Present address: Bruker Spectrospin (Canada) Ltd., 2410 Dunwin Dr., Unit 4, Mississauga, Ont., Canada L5L 1J9.

0008-4042/81/040723-08$01.00/0
©1981 National Research Council of Canada/Conseil national de recherches du Canada

Can. J. Chem. Downloaded from www.nrcresearchpress.com by 210.87.254.5 on 09/06/12
For personal use only.

chemical shift difference which can lead to substantial savings in digitization.

In this paper we apply the 90°–t_1/2–90°–t_1/2–FID sequence to most spin systems of common interest to the chemist. We analyse the positions and intensities of the lines in f_1 so that more complex spectra, beyond the reach of normal techniques, may be analysed using 2D nmr.

Line Intensities in Homonuclear 2D nmr

Unlike normal nmr, the relative line intensities in two-dimensional nmr are quite sensitive to experimental parameters; two major ones are the homogeneity of the static magnetic field and the flip angle of the second pulse. Field homogeneity is important because the experiment relies on the transfer of x–y magnetization at time t_1 after it has been created. Dephasing during t_1 decreases this magnetization and leads to broader and less intense lines in f_1, an effect which is only partly counteracted by the formation of a spin echo (8, 9). Since field inhomogeneities are not reproducible, no explicit formula can be given but, generally speaking, lines with higher f_1 frequencies will be most strongly affected. Furthermore, lines that are close together in f_1 are affected to a similar extent by this mechanism.

Within a multiplet, the intensity ratios familiar from 1D nmr are less frequently seen in 2D nmr. For a given transition of a particular nucleus, the f_1 spectrum contains two types of lines. The first type is lines that are due to the mixing of the given transition with other transitions of the same nucleus. For these lines in f_1 the intensities are "normal" when exact 90° pulses are used in the absolute value display, doublets have two equally intense lines, triplets are in the ratio 1:2:1, and quartets are in the ratio 1:3:3:1. The second type of line is that which arises from the mixing of the given transition with transitions of other nuclei, i.e. when coherence has been transferred between nuclei. In this case, for exact 90° pulses, the absolute value display gives doublets with two equally intense lines but triplets have their central lines missing and quartets appear in the ratio 1:1:1:1. These intensities are characteristic of coherence transfer (10, 11).

All these intensities are distorted if the second pulse is not exactly 90°, although these distortions can be suppressed by cycling the phase of pulses (12). By a generalization of the superspin description of 2D nmr (11, 13) we can derive an explicit formula for the flip angle dependence for the lines in the 2D spectrum of a weakly coupled system subjected to a 90°–t_1/2–α–t_1/2–FID experiment.

The magnetization corresponding to each line in the spectrum is represented by a vector in Liouville space which has the following form (14)

$$[1] \quad x = \mu\sqrt{n}|1^s_{+1}, 1) \sum_M f_{M,l}|M_0, l)$$

The notation used is as follows. The quantity μ^3 is the transition moment of the line (13) whose square is proportional to the normal intensity of the line. We assume that the transition belongs to a group of n equivalent spins, which are represented by the Liouville space ket $|1^s_{+1}, 1)$. The sum

$$\sum_M f_{M,l}|M_0, l)$$

characterizes the spins coupled to the group that we are observing. For instance, $n = 2$ for the components of the quartet part of the proton spectrum of an ethyl group, and

$$\sum_M f_{M,l}|M_0, l)$$

characterizes the spin combination of protons in the methyl group corresponding to each component. These coefficients, μ and $f_{M,l}$ are given in Tables 1 and 2 of ref. 14.

The transition defined by eq. [1] can mix, in either an additive or subtractive fashion, with itself, with another transition of the same nucleus, or with a transition of a different nucleus that is connected by scalar coupling to the nucleus we are considering. By the method in ref. 11 it can be shown that the intensity of the line in f_1, due to mixing of the transition in eq. [1] with another transition of the same nucleus (denoted by primes), is given by eq. [2a] and [2b]

$$[2a] \quad \text{subtractive intensity} = n\,\mu\mu'\,d^1_{1-1}(\alpha) \times \sum_M f_{Ml}\,f'_{Ml}\,d^M_{00}(\alpha)$$

$$[2b] \quad \text{additive intensity} = n\,\mu\mu'\,d^1_{11}(\alpha) \times \sum_M f_{Ml}\,f'_{Ml}\,d^M_{00}(\alpha)$$

where the $d^M_{mn}(\alpha)$ are Wigner matrix elements. In this case, they are simple; $d^1_{1-1}(\alpha) = (\sin^2\alpha/2)$, $d^1_{11}(\alpha) = (\cos^2\alpha/2)$ and $d^M_{00}(\alpha) = P_M(\cos\alpha)$, the Mth order Legendre polynomial, where α is the flip angle. Therefore for additive and subtractive mixing within the same multiplet, the dependence on flip angle is a sum of Legendre polynomials. For $\alpha = 90°$, all these formulae give "normal" intensities,

[3]The transition moment μ (13) is referred to in earlier work (14) as $-C_{1,1}$. Equations [7] and [8] in (14) are, respectively, missing factors of $\sqrt{m}$ and $\sqrt{n}$.

Can. J. Chem. Downloaded from www.nrcresearchpress.com by 210.87.254.5 on 09/06/12
For personal use only.

Can. J. Chem. Downloaded from www.nrcresearchpress.com by 210.87.254.5 on 09/06/12
For personal use only.

triplets have intensities in the ratio 1:2:1, etc. For larger flip angles, one peak becomes dominant (the only one that remains for $\alpha = 180°$) (3) and for small flip angles it is relatively less intense. Also, for $\alpha = 180°$, the additive spectrum disappears because $(\cos^2 \alpha/2) = 0$.

When the transition we are considering turns up in the f_1 spectrum of a line belonging to another nucleus, then coherence transfer (10, 11) has occurred. This happens via a particular part of the density matrix that is shared by the two nuclei (11) and gives "anomalous" intensities. The general formulae for the intensity in the subtractive and additive spectra are

$$[3a] \quad \text{subtractive intensity} = \mu\,\mu'\sqrt{n'}\sqrt{n}\, d^1_{10}(\alpha) \times d^1_{0-1}(\alpha)\, f_{1,1}\, f'_{1,1}$$

$$[3b] \quad \text{additive intensity} = \mu\,\mu'\sqrt{n'}\sqrt{n}\, d^1_{10}(\alpha) \times d^1_{01}(\alpha)\, f_{1,1}\, f'_{1,1}$$

In this case, $d^1_{10}(\alpha) = d^1_{0-1}(\alpha) = -d^1_{01}(\alpha) = -(\sin \alpha/\sqrt{2})$ and the coefficients $f_{1,1}$ are obtained from Table 2 of ref. 12. The flip angle dependence is simple; they are proportional to $(\sin^2 \alpha)/2$, which can be factored into $(\sin^2 \alpha/2)(1 + \cos \alpha) = (\sin^2 \alpha/2)(1 + P_1)$ or into $(\cos^2 \alpha/2)(1 - P_1)$. For $\alpha = 90°$, these formulae give the "anomalous" intensities: in the absolute value mode, doublets look normal, triplets have their central line missing, and quartets appear as four equally intense lines. This is illustrated in Fig. 1, where the subtractive part of the 2D ^{1}H nmr spectrum of an ethyl group subjected to a $90°$–$t_1/2$–$90°$–$t_1/2$–FID experiment is schematically illustrated. The symmetry of these intensities is a reflection of the symmetry of eqs. [2] and [3]. For instance, the two blocks in Fig. 1 which represent lines due to coherence transfer between nuclei are identical except in position. The central lines of the triplet are missing from the f_1 spectra of the quartet, and the f_1 spectrum of the central line of the triplet shows no quartet lines. These theoretical intensities are to be compared with the observed intensities in Fig. 2 where both the additive and subtractive lines are shown. Fig. 2*a* includes the slice along f_1 of the fourth column in Fig. 1, and 2*b* the fifth column. As the flip angle of the second pulse is increased, the intensity of the lines in f_1 due to coherence transfer decreases until it vanishes at 180°. Table 1 gives the explicit formulae for the full flip angle dependence in the AX system.

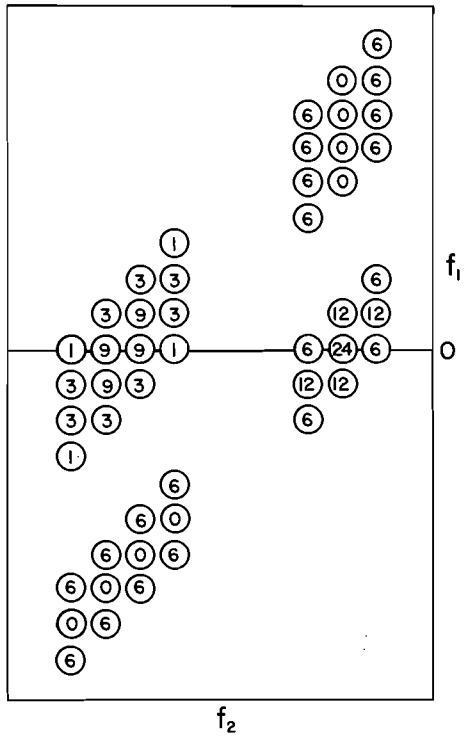

FIG. 1. Schematic plot of the subtractive part of a 2D nmr spectrum of an ethyl group subjected to the $90°$–$t_1/2$–$90°$–$t_1/2$–FID experiment. Circles represent line positions and the numbers represent intensities in the absolute value mode.

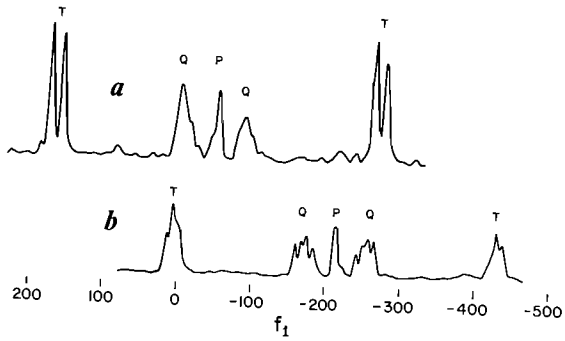

FIG. 2. Traces in f_1 space for the system ethylbromide. Lines Q arise from the quartet, lines T from the triplet, and lines P are phantom; (*a*) transition $\omega_A - 3J/2$; (*b*) transition $\omega_X + J$. The vertical scales in (*a*) and (*b*) are different.

Experimental

Samples were prepared by dissolving the compounds in deuterochloroform or dimethylsulfoxide without any precautions. Spin echo FID's were accumulated at room temperature for ^{1}H at 100.1 MHz on a Varian XL-100 spectrometer equipped with a Nicolet TT100 Fourier Transform System and a Nicolet 1180 computer. Peak positions in f_2 are relative to the carrier frequency and are not referenced to a chemical standard. A 90° pulse required 10 μs. The pulse sequence used was $90°$–$t_1/2$–$90°$–$t_1/2$–FID, with all timing under software control. Quadrature phase detection (QPD) was employed with the carrier in the center of the lines of interest in each case except vinyl acetate and the results of Fig. 2. For the vinyl acetate sample the carrier was placed to the low frequency side of the AMX system

TABLE 1. Flip angle dependence of intensity for the system AX[a]

Transition	Line $\omega_A + J/2$	$\omega_A - J/2$	$\omega_X + J/2$	$\omega_X - J/2$
	Subtractive spectra (times $\sin^2 \alpha/2$)			
$\omega_A + J/2$	$\frac{1+P}{2}$	$\frac{1-P}{2}$	$\frac{1+P}{2}$	$-\frac{1+P}{2}$
$\omega_A - J/2$	$\frac{1-P}{2}$	$\frac{1+P}{2}$	$-\frac{1+P}{2}$	$\frac{1+P}{2}$
$\omega_X + J/2$	$\frac{1+P}{2}$	$-\frac{1+P}{2}$	$\frac{1+P}{2}$	$\frac{1-P}{2}$
$\omega_X - J/2$	$-\frac{1+P}{2}$	$\frac{1+P}{2}$	$\frac{1-P}{2}$	$\frac{1+P}{2}$
	Additive spectra (times $\cos^2 \alpha/2$)			
$\omega_A + J/2$	$\frac{1+P}{2}$	$\frac{1-P}{2}$	$-\frac{1-P}{2}$	$\frac{1-P}{2}$
$\omega_A - J/2$	$\frac{1-P}{2}$	$\frac{1+P}{2}$	$\frac{1-P}{2}$	$-\frac{1-P}{2}$
$\omega_X + J/2$	$-\frac{1-P}{2}$	$\frac{1-P}{2}$	$\frac{1+P}{2}$	$\frac{1-P}{2}$
$\omega_X - J/2$	$\frac{1-P}{2}$	$-\frac{1-P}{2}$	$\frac{1-P}{2}$	$\frac{1+P}{2}$

[a]Where $P = \cos \alpha$.

to prevent folding into the spectral region of the signal from the methyl protons. For Fig. 2 it was important to ensure that the phase alteration scheme of our QPD software would not perturb line intensities. Spectral widths and the number of data points were varied for optimum presentation of the spectra within the limits imposed by the memory size of the magnetic disk system. When QPD was employed the spectral width would be slightly greater than the total spread of the lines in f_2. Without QPD it would be twice this value. The bandwidth of the receiver was adjusted by a filter to equal or slightly exceed the spectral width. The magnitudes of the increments in t_1 were chosen to give a sufficient spectral width in f_1 space to prevent folding of the signals in every case except vinyl acetate. Normally 256 increments were used, frequently followed by zero filling to improve the fineness of digitization. The FID data were collected and processed using Nicolet software. The fineness of digitization, Hz per data point, in the f_2 and f_1 dimensions respectively, are for the systems AX 0.31 and 0.20, for A_2X 0.23 and 0.25, for AMX 0.78 and 1.95, for A_2X_2 0.39 and 0.65, for AA'XX' 0.049 and 0.39, and for A_2X_3 0.49 and 1.95. The line widths are unlikely to be less than three times these numbers. Narrower lines could be obtained by finer digitization. All frequencies are in Hz.

Results

Calculated and observed peak positions in f_1 space, along with the expression for the calculation of peak positions, are presented for each transition in f_2 space in the tables. Frequencies in f_1, obtained directly from the traces, have been doubled to compare them with those calculated from f_2 values. Tables 2, 3, 4, 6, and 7 are deposited as unpublished data[4] and Table 5 is included herein as an example of the agreement between calculated and observed frequencies. It also indicates, by transition, the lines expected to have zero intensity for the A_2X_2 system. Table 2 is for the AX system of the aromatic protons of 3-bromo-4,5-dimethoxybenzoic acid dissolved in deuterodimethylsulfoxide. All 36 predicted signals are observed. The average deviation between observed and calculated frequencies is 0.24 Hz in a total spectral range of 35.97 Hz. For each of the four transitions the central signal is taken to be 0.00 Hz.

Table 3 has the results for the A_2X system of the aromatic protons of 2,6-dimethylaniline. Forty of the 47 signals with non-zero intensity are observed with an average deviation of 0.88 Hz in a range of 83.01 Hz. The lines in f_2 are perturbed from the ideal A_2X system since the ratio J/δ is rather large and also because of small couplings to the methyl protons. These effects are minor compared to the coarseness of digitization.

In Table 4, for the AMX system of the olefinic protons of vinyl acetate, 255 of a possible 300 signals are observed with an average deviation of 5.1 Hz in 1009.8 Hz. Similarly Table 5 for the A_2X_2 system of methoxyethylacetate lists 57 of 58 possible values with an average deviation of 0.6 Hz in a range of 149.8 Hz. Table 6 lists the theoretical and experimental values for the A_2X_3 system of ethyl bromide. Of the 89 possible lines 79 are observed with an average deviation of 0.7 Hz in a range of 394.9 Hz. There are 16 prominent lines in the nor-

[4]These tables can be obtained, at a nominal charge, from the Depository of Unpublished Data, CISTI, National Research Council of Canada, Ottawa, Ont., Canada K1A 0S2.

Can. J. Chem. Downloaded from www.nrcresearchpress.com by 210.87.254.5 on 09/06/12
For personal use only.

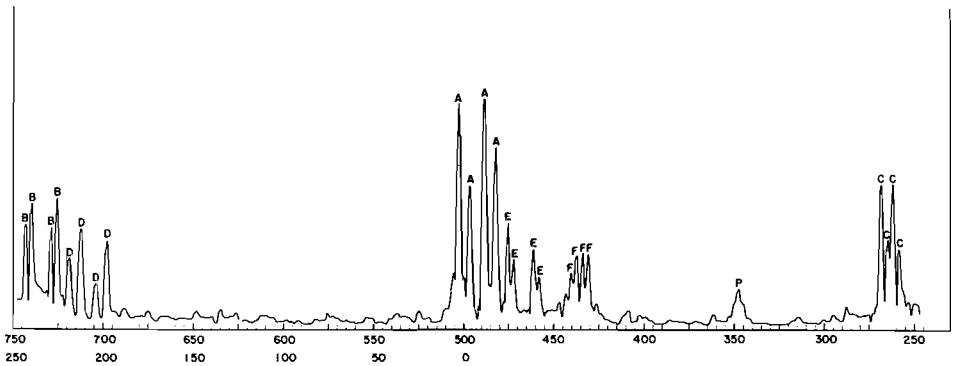

FIG. 3. The traces in f_1 space for the transition ($\omega_A - JA/2 - JX/2$) from the two dimensional proton spectrum of vinylacetate.

mal proton spectrum of *o*-dichlorobenzene, an AA'XX' system. This should give a total of 528 signals in the two-dimensional spectrum. The entire spectrum was recorded but only those lines corresponding to the 1st, 5th, and 11th lines, from the high frequency end, were analyzed. These were analyzed for the subtractive components to give 48 possible signals of which 34 were observed with an average deviation of 0.8 Hz in a range of 56.6 Hz. The results are listed in Table 7.

Discussion

In each of the six different types of nuclear spin systems investigated it is possible to explain all the observations by a relatively simple procedure (3). The frequency of each line in f_2 space is assigned as its separation from the carrier, due regard being taken of sign. For a given transition in f_2 space the line positions in f_1 space are given by the difference (subtractive) and sum (additive) of the frequency of that transition with the frequencies of all the other transitions in f_2 space. In addition there is one line (phantom) whose position in f_1 space is equal to the frequency of the transition in f_2 space. As a result a 1D spectrum containing N lines in a coupled spin system may yield up to $N(2N + 1)$ lines in the two-dimensional spectrum.

As an example of this analysis the trace in f_1 space for the transition ($\omega_A - JA/2 - JX/2$) is shown in Fig. 3. Since the lines for the three nuclear species A, M, and X are well separated compared to the coupling constants, groups of four closely spaced lines are observed for the subtraction or addition of the frequencies around that of A, M, or X. Two sets (additive and subtractive) for each of the three nuclei give six groups of four lines each. These groups are labelled A to F in the figure. In addition the phantom line, labelled P, is also observed. Groups C to F are folded and the frequency scale in Fig. 3 is also folded.

When the frequency of a line in f_1 space is greater than the spectral width used in that dimension there is folding back into the spectrum in the same manner as is found in one-dimensional Fourier Transform nmr. Although this folding can normally be identified it is preferable to avoid folding and therefore minimize the danger of overlap. At the same time it is desirable to use as small a spectral width as possible in f_1 space so that fine digitization may be employed without an excessive number of increments to t_1. The minimum spectral width in f_1 space is required when the carrier frequency is set in the center of the spectral region containing the signals of interest. This necessitates the use of QPD for the spectrometer. A consequence of obtaining the two-dimensional spectrum with quadrature phase detection and with the carrier in the center of the spectral region is a characteristic appearance for the spectrum. The lines to high frequency of the carrier in f_2 space will primarily also be to positive frequency in f_1 space. Under these conditions the phantom lines can be clearly distinguished about halfway between the subtractive and additive lines. This is illustrated in Fig. 4 for the proton resonance spectrum of ethyl bromide. Despite the absolute nature of the line positions when QPD is employed, no additional spectral information may be obtained. It has been shown that the lines in f_1 space from the additive spectra may be removed by the appropriate phase angle changes of the transmitter along with additive and subtractive accumulation of the FID's (5). There is some similarity between this sequence and that normally employed to remove instrumental imbalance during quadrature phase detection. It therefore follows that QPD is not necessarily "transparent" in two-dimensional nmr experiments. This is illustrated in Table 8 where the additive spectrum is more intense without QPD and with a smaller carrier offset. When employing QPD, additional weak lines are sometimes observed in f_1 space on both sides of zero at multiples of the offset frequency.

Can. J. Chem. Downloaded from www.nrcresearchpress.com by 210.87.254.5 on 09/06/12
For personal use only.

TABLE 5. Expressions and results for the system A2X2

Transition	Expression	F_1 Predicted[a]	F_1 Observed[a]	Intensity observed
$\omega_A + J$	$(\omega_A + J) - (\omega_A + J)$	0.00	0.00	vs
	$(\omega_A + J) - \omega_A$	4.69	4.49	s
	$(\omega_A + J) - (\omega_A - J)$	9.38	9.69	m
	$(\omega_A + J) - (\omega_X + J)$	62.78	63.05	s
	$(\omega_A + J) - \omega_X$	67.47[b]		
	$(\omega_A + J) - (\omega_X - J)$	72.16	72.32	s
	$(\omega_A + J) + (\omega_A + J)$	66.66	66.66	w
	$(\omega_A + J) + \omega_A$	61.98	58.89	s
	$(\omega_A + J) + (\omega_A - J)$	57.32	51.66	s
	$(\omega_A + J) + (\omega_X + J)$	3.88	4.49	s
	$(\omega_A + J) + \omega_X$	−0.81[b]		
	$(\omega_A + J) + (\omega_X - J)$	−5.50	−4.67	w
	$(\omega_A + J)$	33.33	33.33	m
ω_A	$\omega_A - (\omega_A + J)$	−4.69	−4.67	m
	$\omega_A - \omega_A$	0.00	0.00	s
	$\omega_A - (\omega_A - J)$	4.69	3.66	m
	$\omega_A - (\omega_X + J)$	58.10[b]		
	$\omega_A - \omega_X$	62.79[b]		
	$\omega_A - (\omega_X - J)$	67.48[b]		
	$\omega_A + (\omega_A + J)$	61.98	61.89	m
	$\omega_A + \omega_A$	57.30	58.84	m
	$\omega_A + (\omega_A - J)$	52.64	54.56	w
	$\omega_A + (\omega_X + J)$	−0.80[b]		
	$\omega_A + \omega_X$	−5.49[b]		
	$\omega_A + (\omega_X - J)$	−10.18[b]		
	ω_A	28.65	28.66	m
$\omega_A - J$	$(\omega_A - J) - (\omega_A + J)$	−9.38	−9.34	m
	$(\omega_A - J) - \omega_A$	−4.69	−4.17	s
	$(\omega_A - J) - (\omega_A - J)$	0.00	0.00	s
	$(\omega_A - J) - (\omega_X + J)$	53.44	53.66	s
	$(\omega_A - J) - \omega_X$	58.13[b]		
	$(\omega_A - J) - (\omega_X - J)$	62.82	63.00	s
	$(\omega_A - J) + (\omega_A + J)$	57.32	58.00	w
	$(\omega_A - J) + \omega_A$	52.64		
	$(\omega_A - J) + (\omega_A - J)$	47.98	45.49	m
	$(\omega_A - J) + (\omega_X + J)$	−5.46	−5.17	m
	$(\omega_A - J) + \omega_X$	−10.15[b]		
	$(\omega_A - J) + (\omega_X - J)$	−14.84	−13.84	m
	$(\omega_A - J)$	23.99	23.99	s
$\omega_X + J$	$(\omega_X + J) - (\omega_A + J)$	−62.78	−62.76	s
	$(\omega_X + J) - \omega_A$	−58.10[b]		
	$(\omega_X + J) - (\omega_A - J)$	−53.44	−53.34	s
	$(\omega_X + J) - (\omega_X + J)$	0.00	0.00	vs
	$(\omega_X + J) - \omega_X$	4.69	5.32	m
	$(\omega_X + J) - (\omega_X - J)$	9.32	9.92	m
	$(\omega_X + J) + (\omega_A + J)$	3.88	4.42	s
	$(\omega_X + J) + \omega_A$	−0.80[b]		
	$(\omega_X + J) + (\omega_A - J)$	−5.46	−4.34	m
	$(\omega_X + J) + (\omega_X + J)$	−58.90	−58.43	m
	$(\omega_X + J) + \omega_X$	−63.59	−62.76	s
	$(\omega_X + J) + (\omega_X - J)$	−68.28	−67.50	w
	$(\omega_A + J)$	−29.45	−29.32	s
ω_X	$\omega_X - (\omega_A + J)$	−67.47[b]		
	$\omega_X - \omega_A$	−62.79[b]		
	$\omega_X - (\omega_A - J)$	−58.13[b]		
	$\omega_X - (\omega_X + J)$	−4.69	−4.34	m
	$\omega_X - \omega_X$	0.00	0.00	s
	$\omega_X - (\omega_X - J)$	4.69	4.49	s
	$\omega_X + (\omega_A + J)$	−0.81[b]		

Can. J. Chem. Downloaded from www.nrcresearchpress.com by 210.87.254.5 on 09/06/12
For personal use only.

TABLE 5 (*Concluded*)

Transition	Expression	F_1 Predicted[a]	F_1 Observed[a]	Intensity observed
	$\omega_X + \omega_A$	−5.49[b]		
	$\omega_X + (\omega_A - J)$	−10.15[b]		
	$\omega_X + (\omega_X + J)$	−63.59	−63.01	w
	$\omega_X + \omega_X$	−68.28	−68.01	w
	$\omega_X + (\omega_X - J)$	−72.97	−72.67	m
	ω_X	−34.14	−34.67	m
$\omega_X - J$	$(\omega_X - J) - (\omega_A + J)$	−72.16	−72.33	s
	$(\omega_X - J) - \omega_A$	−67.48[b]		
	$(\omega_X - J) - (\omega_A - J)$	−62.82	−63.00	s
	$(\omega_X - J) - (\omega_X + J)$	−9.38	−9.00	w
	$(\omega_X - J) - \omega_X$	−4.69	−4.53	s
	$(\omega_X - J) - (\omega_X - J)$	0.00	0.00	s
	$(\omega_X - J) + (\omega_A + J)$	−5.50	−5.77	w
	$(\omega_X - J) + \omega_A$	−10.18[b]		
	$(\omega_X - J) + (\omega_A - J)$	−14.84	−15.33	m
	$(\omega_X - J) + (\omega_X + J)$	−68.28	−67.34	w
	$(\omega_X - J) + \omega_X$	−72.97	−72.33	s
	$(\omega_X - J) + (\omega_X - J)$	−77.66	−77.26	w
	$(\omega_X - J)$	−38.83	−38.87	s

[a]For the methylene protons of 2-methoxyethyl acetate.
[b]These lines should have zero intensity.

In the first five spin systems illustrated it is possible to assign an explicit transition to each line observed in the one-dimensional spectrum. In these cases the theory is straightforward for calculation of the line positions in f_1 space (3). For the spin system AA′XX′ of *ortho*-dichlorobenzene it is not possible to describe all the lines explicitly (15). Nevertheless it is proven by this work that the approach of taking frequency differences between line positions in the one-dimensional spectrum, as dictated by theory, adequately predicts the line positions in f_1 space. Some lines in these cases may have zero intensity. It is to be noted that for this system only subtractive lines were observed.

The chief sources of error in obtaining line positions in f_1 space appears to be due to errors in timing and incrementing the t_1 intervals, and coarseness of digitization. The first error can be partially corrected by assigning a frequency of 0.0 to the zero position line and adjusting the values for

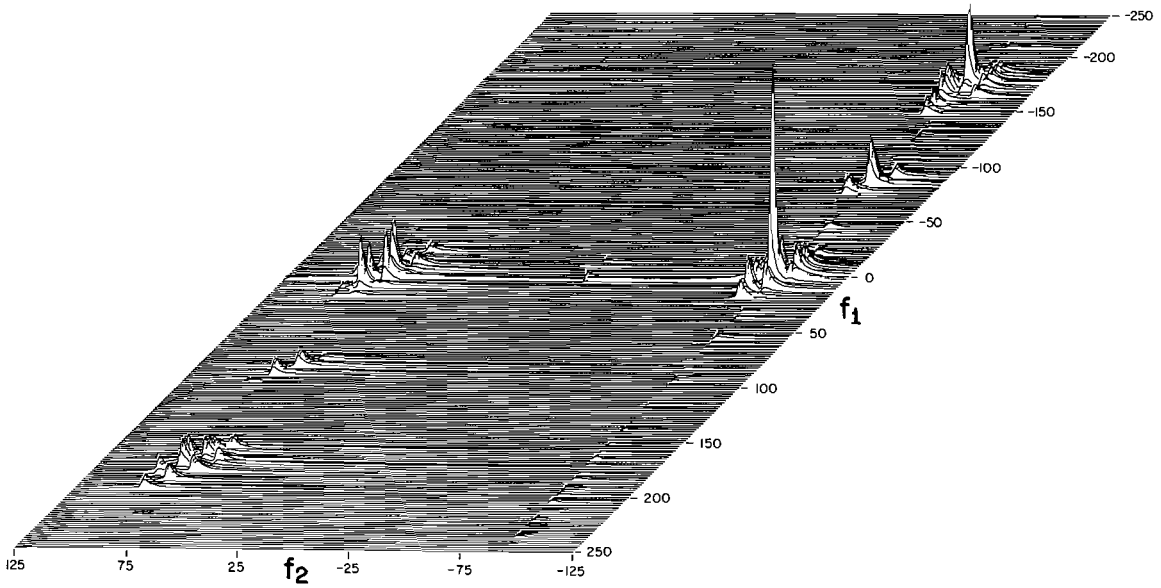

FIG. 4. The two dimensional proton resonance spectrum of ethyl bromide.

Can. J. Chem. Downloaded from www.nrcresearchpress.com by 210.87.254.5 on 09/06/12
For personal use only.

TABLE 8. Intensity ratio of subtractive to additive spectra for the system AX as a function of carrier offset and quadrature phase detection

Carrier offset, Hz	QPD	Ratio
60	Off	2.6
60	On	7.4
20	Off	2.3
20	On	16

the other lines according to their deviation from the actual zero. This procedure was employed in the present investigation. It is not adequate when employed for folded lines.

It is clear from the present studies that all the information in the spectrum is contained in f_1 space for each transition in f_2 space as previously illustrated for an AX system (3). Although the intensities are often distorted, the causes of these distortions are understood.

Acknowledgement

A.D.B. would like to thank the National Research Council of Canada for its hospitality.

1. R. FREEMAN and G. A. MORRIS. Bull. Magn. Reson. **1**, 5 (1979).
2. W. P. AUE, E. BARTHOLDI, and R. R. ERNST. J. Chem. Phys. **64**, 2229 (1976).
3. A. D. BAIN, R. A. BELL, J. R. EVERETT, and D. W. HUGHES. J. Chem. Soc. Chem. Commun. 256 (1980).
4. A. D. BAIN, R. A. BELL, J. R. EVERETT, and D. W. HUGHES. Can. J. Chem. **58**, 1947 (1980).
5. K. NAGAYAMA, K. WÜTHRICH, and R. R. ERNST. Biochem. Biophys. Res. Commun. **90**, 305 (1979).
6. J. R. EVERETT, D. W. HUGHES, A. D. BAIN, and R. A. BELL. J. Am. Chem. Soc. **101**, 6776 (1979).
7. K. NAGAYAMA, P. BACHMANN, K. WÜTHRICH, and R. R. ERNST. J. Magn. Reson. **31**, 133 (1978).
8. A. A. MAUDSLEY, A. WOKAUN, and R. R. ERNST. Chem. Phys. Lett. **55**, 9 (1978).
9. A. D. BAIN. Chem. Phys. Lett. **57**, 281 (1978).
10. A. A. MAUDSLEY, L. MÜLLER, and R. R. ERNST. J. Magn. Reson. **28**, 463 (1977).
11. A. D. BAIN. J. Magn. Reson. **39**, 335 (1980).
12. G. BODENHAUSEN, R. FREEMAN, and D. L. TURNER. J. Magn. Reson. **27**, 511 (1977).
13. A. D. BAIN. J. Magn. Reson. **37**, 209 (1980).
14. A. D. BAIN and J. S. MARTIN. J. Magn. Reson. **29**, 137 (1978).
15. D. R. WHITMAN. J. Chem. Phys. **36**, 2085 (1962).

Can. J. Chem. Downloaded from www.nrcresearchpress.com by 210.87.254.5 on 09/06/12
For personal use only.

Medium effect on acidity constants of some 2-styryl- 4-phenylthiazole ethiodide derivatives

HUSSEIN S. EL-KASHEF, REFAT ABDEL-HAMIDE, MOHAMED R. MAHMOUD,[1] AND MAHER M. HAMED
Chemistry Department, Faculty of Science, Assiut University, Assiut, Egypt

Received July 10, 1980

HUSSEIN S. EL-KASHEF, REFAT ABDEL-HAMIDE, MOHAMED R. MAHMOUD, and MAHER M. HAMED. Can. J. Chem. **59**, 731 (1981).

The pK values of some 2-styryl-4-phenylthiazole ethiodide derivatives in different organic solvent – water mixtures were determined. It is observed that as the amount of the organic solvent in the medium increases the pK of the dimethylamino derivative is decreased while that of the hydroxy derivatives is increased. It is concluded that the major important effects responsible for this behaviour are the difference in the stabilization of the base by dispersion forces in case of the amino derivative and by donor hydrogen bonds from solvent molecules in the case of the hydroxy derivatives. The effect of the molecular structure of the compound on pK is also discussed.

HUSSEIN S. EL-KASHEF, REFAT ABDEL-HAMIDE, MOHAMED R. MAHMOUD et MAHER M. HAMED. Can. J. Chem. **59**, 731 (1981).

Opérant dans divers mélanges de solvants organiques et d'eau, on a déterminé les valeurs du pK de quelques dérivés de styril-2 phényl-4 thiazoles avec l'idoure d'éthyle. Lorsque la quantité de solvant organique du milieu augmente on observe d'une part que le pK du dérivé diméthylamine diminue alors que d'autre part le pK du dérivé hydroxylé augmente. On en conclut que les principaux facteurs responsables de ce comportement sont la différence de stabilisation de la base par des forces de dispersion dans le cas du dérivé aminé et par les donneurs de liaisons hydrogènes à partir des molécules de solvant dans le cas des dérivés hydroxylés. On discute également de l'effet de la structure moléculaire du composé sur la valeur du pK.

[Traduit par le journal]

Introduction

Recently we have reported the medium effect on the ionisation constants of some 2-styryl pyridine and quinoline ethiodide derivatives (1, 2). However, it is known that the styryl cyanine derivatives are quite interesting compounds because of their application as photosensitizers (3, 4) as well as in many biological aspects (5–8). Furthermore, 2-styryl-4-phenylthiazole ethiodide derivatives are recognized as useful indicators in many nonaqueous titrations of weak acids (9).

Since no work has been reported on the medium effect on the ionisation process of 2-styryl-4-phenylthiazole ethiodide derivatives, this paper reports the pK values of some 2-styryl-4-phenylthiazole ethiodide derivatives in water – organic solvent mixtures. The organic solvents used are methanol, ethanol, acetone, *N*,*N*-dimethylformamide, and dimethyl sulfoxide. The 2-styryl-4-phenylthiazole ethiodide derivatives used in this investigation are

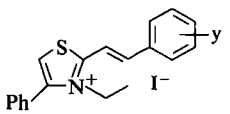

I y = *p*-NMe_2
II y = *o*-OH
III y = *p*-OH
IV y = *m*-OMe, *p*-OH

[1]To whom all correspondence should be addressed.

Experimental

Materials and Methods

Compounds **I–IV** were prepared following the method of Mills and Smith (10); where equimolar amounts of 2-methyl-4-phenylthiazole ethiodide (11) and the appropriate aldehyde were refluxed in ethanol for 3 h in the presence of two drops of piperidine as a catalyst. The reaction mixture was concentrated and the solid product was recrystallized from ethanol. The results of analysis as well as the melting points of the compounds prepared are given in Table 1. All chemicals used in this investigation for preparation of the derivatives and the organic solvents used were of BDH (AR) grade. Stock solutions 10^{-3} M of the compounds were prepared by dissolving the solid in the organic solvent. More dilute solutions were prepared by accurate dilution.

pH control was achieved by using acetate buffer solutions and a modified universal buffer solution (12). The pH of the solutions was checked at 25°C using a WG PYE model 290 pH-meter, reading to ±0.005 pH units.

TABLE 1. Analytical and melting points data of the compounds **I–IV**

Compound	Melting point (°C)	Found (calcd) % C	H	N	S
I	110	54.25 (54.55)	5.16 (5.01)	6.10 (6.06)	6.82 (6.93)
II	90	52.55 (52.42)	4.10 (4.17)	3.18 (3.22)	7.28 (7.36)
III	130	52.52 (52.42)	4.10 (4.17)	3.16 (3.22)	7.25 (7.36)
IV	145	51.85 (51.62)	4.40 (4.34)	3.06 (3.01)	6.80 (6.89)

0008-4042/81/040731-06$01.00/0
©1981 National Research Council of Canada/Conseil national de recherches du Canada

Can. J. Chem. Downloaded from www.nrcresearchpress.com by 210.87.254.105 on 09/06/12
For personal use only.

Can. J. Chem. Downloaded from www.nrcresearchpress.com by 210.87.254.105 on 09/06/12
For personal use only.

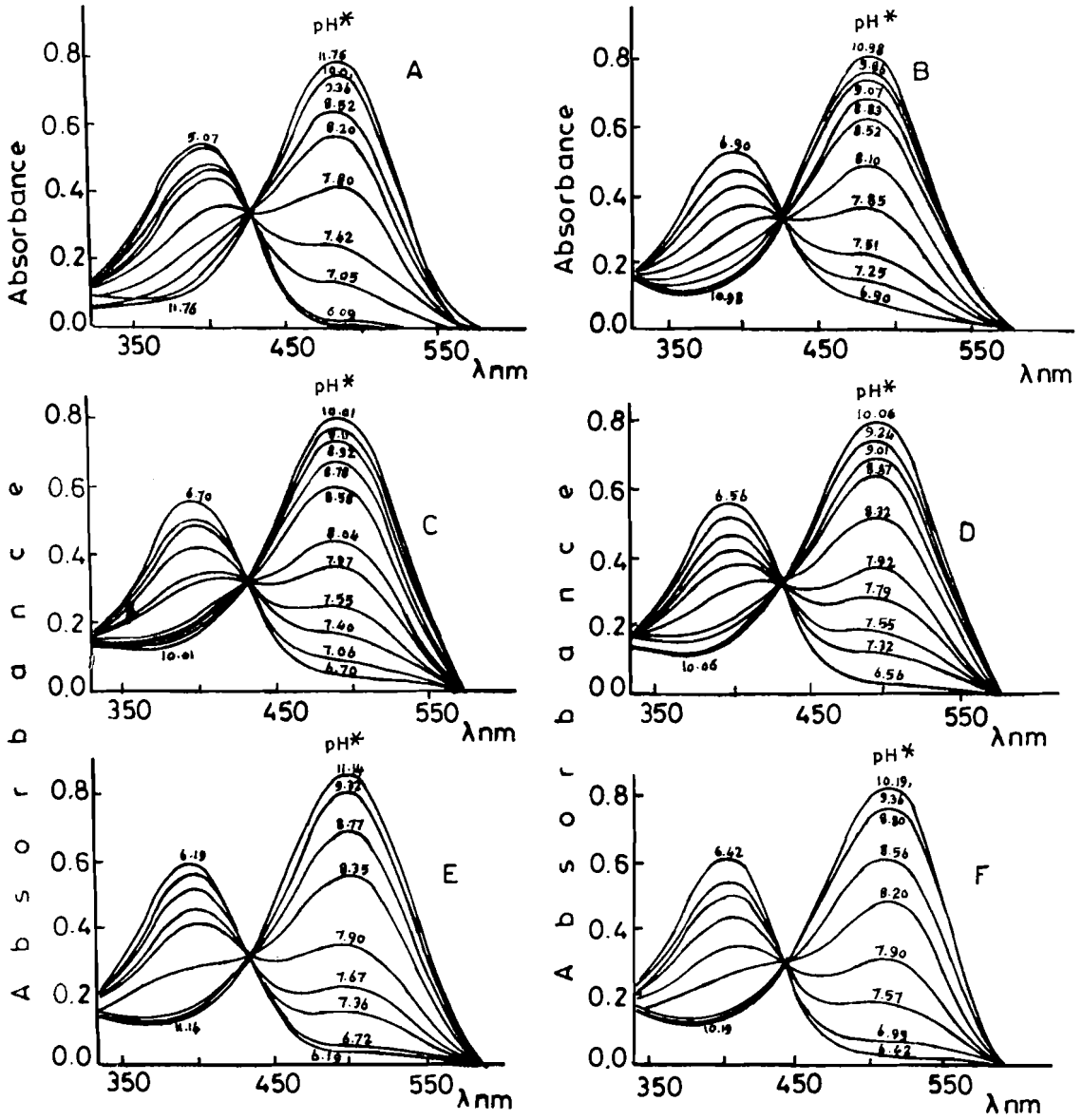

FIG. 1. Absorption spectra of 3×10^{-5} *M* of compound **IV** solution containing different percentages of methanol. By wt.% MeOH: *A*, 0.0; *B*, 8.08; *C*, 16.52; *D*, 25.35; *E*, 34.54; *F*, 44.18.

To account for the difference in properties for partially aqueous solutions relative to pure aqueous ones, the pH values of the former solutions were corrected making use of the procedure described by Douheret (13). If the pH-meter is standardized using aqueous buffers, the meter reading pH(R) obtained in a partially aqueous medium differs by an amount δ from the corrected reading pH* which refers to the standard state in the partially aqueous medium,

$$pH^* = pH(R) - \delta$$

The values of δ of the aqueous buffer solutions containing varying proportions of each of the organic solvents used were determined by Douheret (13, 14).

The absorption spectra were measured on a UNICAM SP 8000 spectrophotometer within the wavelength range 300–700 nm using 1 cm matched silica cells. All measurements were carried out at 25°C.

Results and Discussion

The visible absorption spectra of the compounds **I–IV** either in pure aqueous buffer solutions or in those containing different proportions of an organic solvent (methanol, ethanol, acetone, DMF, and DMSO) were recorded (Fig. 1). It is worth noting that acetate buffer solutions were used in the case of compound **I** due to the low p*K* value of

Can. J. Chem. Downloaded from www.nrcresearchpress.com by 210.87.254.105 on 09/06/12
For personal use only.

this compound relative to the lower limit pH value of the universal buffer series. Generally, the spectra of solutions with low pH (< 2 in the case of compound **I** and <7 in the case of compounds **II–IV**) represent the absorption by the protonated or non-ionic species of compounds **I** and **II–IV** respectively, whereas those at higher pH of the medium are due to the non-protonated or ionic species. On increasing the pH of the medium, the absorbance of the band due to the protonated or non-ionic form decreases, whereas that of the non-protonated or ionic form increases.

The high red shift observed in the λ_{max} of the band in solutions of high pH's relative to that observed in solutions of low pH's is convincing evidence for the charge transfer nature of this band (1, 2).

The spectra of the compounds **I–IV** in all media studied are characterised by a clear isosbestic point denoting the existence of an acid–base equilibrium.

$H^+A^+ \rightleftharpoons A^+ + H^+$ Compound **I**
$HA^+ \rightleftharpoons A + H^+$ Compounds **II–IV**

The absorbance–pH* curves (Fig. 2) are of typical dissociation or association types, confirming the acid–base equilibrium.

The acid dissociation constant, pK_a, of the compounds was determined from the variation of the absorbance with pH* taking advantage of three different spectrophotometer methods, viz. the half-height (15), limiting absorbance (15), and Colleter methods (16). The results obtained are given in Tables 2 and 3.

The results listed in these tables reveal the fact that pK_a values of all compounds are largely dependent on both the proportion and the nature of the organic co-solvent used. The ionisation constant of the dimethylamino derivative (compound **I**) increases with increase in the amount of the organic solvent in the medium while that of the hydroxy derivatives (compounds **II–IV**) decreases in the same direction.

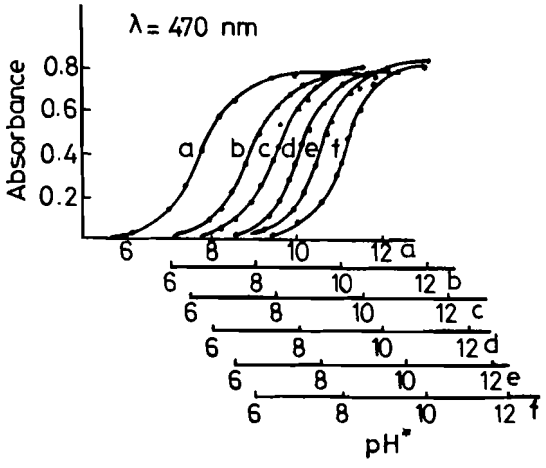

FIG. 2. Absorbance–pH* curves for compound **IV** in universal buffer solutions containing different percentages of methanol. By wt.% MeOH: *a*, 0.0; *b*, 8.08; *c*, 16.52; *d*, 25.35; *e*, 34.54; *f*, 44.18.

The acidity constant in aqueous medium (K_1) may be related to that in partially aqueous medium (K_2) by means of equations (17)

[1] $K_{(1)} = K_{(2)}\gamma_{H^+}\gamma_{A^+}/\gamma_{H^+A^+}$

[2] $K_{(1)} = K_{(2)}\gamma_{H^+}\gamma_{A}/\gamma_{HA^+}$

where γ is the activity coefficient of the subscripted species in a partially aqueous medium relative to that in a pure one. Since it is known that the electrostatic effects of solvents will operate only on the activity coefficients of any charged species (17), in the case of compound **I** the electrostatic effect on the activity coefficient of the proton (H^+), free base (A^+), and on that of the acid (H^+A^+) will cancel to a large extent. Consequently the electrostatic effect is expected to have a relatively small influence on the deprotonation constant of this compound. On the other hand, for the hydroxy derivatives the magnitude of this effect on the proton exceeds that on the acid (HA^+). Thus the ionisation constant of these compounds is expected to decrease with increase in the percentage of the organic solvent in the medium, which is in line with the results given in Tables 2 and 3.

Furthermore, it is recognized that effects such as hydrogen bonding, solvent basicity, dispersion forces, and proton–solvent interaction act as important factors influencing the ionisation constants of acids in the presence of organic solvent. Accordingly, the observed decrease in pK_a of compound **I** can be mainly ascribed to the high stabilization of the base of this compound by dispersion forces rather than by hydrogen bonding in partially aqueous media. This dispersion interaction is established between the delocalized oscillator dipole of the conjugated base and the localized oscillator dipole of the solvent. The high stabilization of the base by dispersion forces in partially aqueous media relative to those in pure aqueous media is due to the fact that the effective density of dispersion centers of any of the solvents under study is higher than that of water (18). Furthermore, the observed decrease in pK_a of the compound **I** as the amount of organic solvent in the medium is increased can be attributed also to the expected high stabilization of the proton by its interaction with organic solvent and water molecules in the mixture than that with water molecules alone (17).

TABLE 2. Mean pK_a values for compounds **I** (2.0×10^{-5} *M*) and **II** (2.0×10^{-5} *M*) and the λ_{max} values of the different forms in water – organic solvent mixtures

% (w/w) of organic solvent	Dielectric constant of the medium at 25°C	Compound I			Compound II		
			λ_{max} (nm)			λ_{max} (nm)	
		pK_a	Protonated form	Non-protonated form	pK_a	Non-ionic form	Ionic form
0.00	78.40	2.61	342	468	7.85	384	458
			Methanol				
8.08	76.24	2.58	345	475	7.96	380	470
16.52	73.81	2.34	345	478	8.05	382	474
25.35	71.06	2.25	345	482	8.16	384	478
34.54	67.92	1.82	345	485	8.24	386	485
44.18	64.29	1.52	345	486	8.37	387	490
			Ethanol				
8.06	76.61	2.51	348	476	8.09	378	473
16.48	74.52	2.31	348	482	8.19	382	478
25.28	72.07	1.95	348	485	8.33	386	485
34.48	69.15	1.73	348	488	8.43	388	490
44.11	65.64	1.41	348	489	8.49	390	498
			Acetone				
8.07	76.85	2.40	347	478	8.10	380	475
16.49	75.05	2.09	347	480	8.25	385	485
25.29	72.90	1.88	347	484	8.42	385	490
34.49	70.28	1.62	347	486	8.54	386	498
44.13	67.02	1.39	348	487	8.73	388	504
			DMF				
9.54	77.34	2.36	347	478	8.05	380	475
19.17	76.09	1.87	347	484	8.12	384	485
28.91	74.60	1.56	347	485	8.19	386	490
34.50	72.77	1.38	348	486	8.22	386	496
			DMSO				
10.90	77.53	2.56	347	475	8.00	378	474
21.59	76.50	2.24	347	480	8.12	380	480
34.06	75.28	1.75	348	482	8.18	382	485
42.34	73.80	1.43	348	484	8.24	386	495

Careful examination of the pK_a values of compound **I** in the different organic solvent – water media studied reveals the fact that in the presence of the same amount of the organic solvent in the medium, the pK_a values of this compound vary with the nature of the organic solvent used according to the following sequence

$$\text{DMSO} \leq \text{DMF} < \text{acetone} < \text{ethanol} < \text{methanol}$$

However, this is expected as a result of the decrease in the solvent polarizability on going from DMSO to methanol within the above sequence (18). This behaviour can be considered as convincing evidence for the fact that the high stabilization of the base by dispersion forces and of the proton by its interaction with solvent are the two important factors responsible for the decrease in pK_a of the compound **I** as the amount of the solvent in the medium is increased.

On the other hand, the increase in pK_a of each of compounds **II–IV** as the amount of the organic solvent in the medium is increased can be ascribed to the high stabilization of the ionic form by solvent donor hydrogen bonding in pure aqueous medium relative to that in partially aqueous medium. This is presumably due to the greater tendency of water molecules to donate hydrogen bonds as compared with the other solvent molecules (17).

The results given in Tables 1 and 2 for compounds **II–IV** indicate that the variation of pK_a value in the media containing the same percentage of alcohol or acetone appears to be in the order:

$$\text{methanol} < \text{ethanol} < \text{acetone}$$

This is presumably due to the decrease in tendency of the solvent molecules to donate hydrogen bonds to the ionic form on going from methanol to acetone (17, 19).

Can. J. Chem. Downloaded from www.nrcresearchpress.com by 210.87.254.105 on 09/06/12
For personal use only.

TABLE 3. Mean pK_a values for compounds **III** (1.0×10^{-5} *M*) and **IV** (3×10^{-5} *M*) and the λ_{max} values of the different forms in water – organic solvent mixtures

%(w/w) of organic solvent	Dielectric constant of the medium at 25°C	Compound III			Compound IV		
			λ_{max} (nm)			λ_{max} (nm)	
		pK_a	Non-ionic form	Ionic form	pK_a	Non-ionic form	Ionic form
0.00	78.40	7.94	385	456	7.76	394	480
			Methanol				
8.08	76.24	8.01	385	462	7.91	394	485
16.52	73.81	8.14	396	466	8.05	396	490
25.35	71.06	8.19	388	470	8.08	398	495
34.54	67.92	8.27	390	475	8.13	400	500
44.18	64.29	8.39	392	480	8.17	403	510
			Ethanol				
8.06	76.61	8.14	385	462	7.94	395	488
16.48	74.52	8.22	387	478	8.06	398	496
25.28	72.07	8.34	390	478	8.14	400	505
34.48	69.15	8.46	392	485	8.24	403	516
44.11	65.64	8.49	394	493	8.28	406	525
			Acetone				
8.07	76.85	8.18	385	466	8.06	398	490
16.49	75.05	8.31	386	470	8.17	400	500
25.29	72.90	8.54	390	484	8.34	402	510
34.49	70.28	8.79	391	488	8.49	404	520
44.13	67.02	8.88	395	496	8.70	406	528
			DMF				
9.54	77.34	8.06	384	468	7.87	396	494
19.17	76.09	8.13	388	478	8.04	398	504
28.91	74.60	8.30	390	485	8.09	400	512
34.50	72.77	8.43	394	495	8.18	404	522
			DMSO				
10.90	77.53	8.09	384	467	7.87	394	490
21.59	76.50	8.20	386	474	8.11	398	500
34.06	75.28	8.27	390	483	8.25	400	509
42.34	73.80	8.35	392	490	8.33	401	518

This behaviour can be considered as evidence for the fact that the difference in the stabilization of ionic forms by donor-hydrogen bond from solvent molecules is a major factor responsible for the increase in pK_a as the amount of the organic solvent in the medium is increased.

Careful examination of the results reveals that the pK_a value in the presence of the poorer hydrogen bond donors DMF or DMSO is less than the one obtained in the presence of the same amount of acetone or ethanol (Tables 2 and 3). This can be ascribed to the high basic character of the former solvents, reflecting itself in the construction of a strong acceptor hydrogen bond from the OH group of the non-ionised form and thus facilitating the ionisation process of the OH group (i.e. low pK_a).

The red shift observed in the λ_{max} of the band responsible for the absorption of the base of compound **I** and the ionic form of each compound **II–IV** as the amount of the solvent in the medium increases (Tables 2 and 3) can be interpreted as follows. In the case of compound **I**, as the concentration of the organic solvent in the medium increases the extent of dispersion forces between the base and the solvent molecules is expected to increase. This in turn will increase the proportion of the polarized structure of the base in solution and consequently an easy intramolecular charge transfer is expected to occur. On the other hand, in the case of compounds **II–IV** as the amount of the non-aqueous component in the medium increases, the free negative charge on the oxygen atom of the base is increased. This is due to the weak tendency of the molecules of the solvent to form donor hydrogen bonds with the oxygen atom relative to water molecules. This in turn will reflect itself in the increase of the intramolecular charge transfer from the oxygen atom to the delocalized molecular orbital of the

Can. J. Chem. Downloaded from www.nrcresearchpress.com by 210.87.254.105 on 09/06/12
For personal use only.

thiazolium cation and thus a lower excitation energy is required.

Effect of Molecular Structure on pK_a

It is evident that the pK_a value of each of the compounds under investigation in the presence of the same amount of organic solvent is lower than that of the corresponding derivative of 2-styryl pyridine or quinoline ethiodides (1, 2). This can be interpreted as follows. Since the thiazole ring belonging to the compounds under investigation contains two hetero atoms, one should expect that this ring is characterized by high electron-withdrawing character relative to the pyridine or quinoline rings. This leads to an increase in the intramolecular CT from the aryl moiety in case of the compounds under investigation, affording a lower negative charge density on the aromatic system. This in turn results in weaker bonding of the proton (low pK_a value).

1. M. R. MAHMOUD and R. ABDEL-HAMIDE. Indian J. Chem. **17**(A), 70 (1979).
2. M. R. MAHMOUD, R. ABDEL-HAMIDE, and K. A. IDRISS. Bull. Chem. Soc. Jpn. **52**(2), 574 (1979).
3. J. M. EDER and L. LUPPOCRAMER. Ausfurliches Handbuch der Photographie. 1932. Band II, Teil 3.
4. T. TAKAHASHI and K. SATO. Yokugaku Zasshi, 467 (1958).
5. M. BANNO. Kanko Shikiso, **34**, 1 (1955).
6. L. K. MUSHKALO. Zh. Obshch. Khim. **29**, 1030 (1959); **29**, 1034 (1959).
7. C. BAHNER, C. COOK, J. DALE, J. FAIN, E. FRANKLIN, J. GOAN, W. STUMP, and J. WILSON. J. Org. Chem. **22**, 682 (1957).
8. C. BAHNER, J. DALE, J. FAIN, E. FRANKLIN, J. GOAN, W. STUMP, M. WEST, and J. WILSON. J. Org. Chem. **22**, 1110 (1957).
9. A. BLAZSCK-BODA, A. SZURKOS, and M. VERNES. Proc. Conf. Appl. Phys. Chem. 2*nd*, **1**, 25 (1972).
10. WM. H. MILLS and J. L. B. SMITH. J. Chem. Soc. **121**, 2724 (1922).
11. HANZSCH. Annalen, **250**, 269 (1889).
12. H. T. S. BRITTON. Hydrogen ions. Chapman Hall, London. 1952. pp. 313, 364.
13. G. DOUHERET. Bull. Soc. Chim. Fr. 1412 (1967).
14. G. DOUHERET. Bull. Soc. Chim. Fr. 3122 (1968).
15. R. M. ISSA, H. SADEK, and I. I. IZZAT. Z. Phys. Chem. N.F. **74**, 17 (1971).
16. J. C. COLLETER. Ann. Chem. Paris, 415 (1960).
17. J. F. COETZEE and C. D. RITCHIE. Solute–solvent interactions. Marcel Dekker Ltd., New York, London. 1969. pp. 64, 78, 221.
18. M. ALFENAAR and G. L. DELIGNY. Rev. Trav. Chim. **86**, 292 (1967).
19. F. FRANK and D. J. G. IVES. Q. Rev. **20**, 1 (1966).

Can. J. Chem. Downloaded from www.nrcresearchpress.com by 210.87.254.105 on 09/06/12
For personal use only.

Graphical rules of steady-state reaction systems

CHOU KUO-CHEN[1]

Shanghai Institute of Biochemistry, Chinese Academy of Sciences, 320 Yo-Yang Road, Shanghai 200031, China

AND

STURE FORSEN

Physical Chemistry 2, Chemical Center, P.O.B. 740, S-220 07 Lund 7, Sweden

Received July 25, 1980

CHOU KUO-CHEN and STURE FORSEN. Can. J. Chem. **59**, 737 (1981).

Four rules to deal with first-order or pseudo-first-order steady-state reaction systems are presented.

By means of Rule 1, we can immediately write down the apparent rate constants of consecutive reaction systems. This rule is actually the same as the "Rule of Thumb" proposed by Gilbert, but here its mathematical proof is given.

Rule 2 and Rule 3 may serve to derive the apparent rate constants of various complex reaction systems. In comparison with the general algebraic methods, these two rules can simplify laborious calculations that would otherwise be tedious and liable to errors.

Rule 4 presents a new schematic method to calculate the concentrations of the reactants. The new method, in simplifying the calculation of complex problems, is extraordinarily efficacious in comparison with the existing schematic methods. For complex mechanisms which are too complicated to be treated with the general manual calculation method, the practical calculations show that we can easily write down the desired results by means of Rule 4.

In addition, Rules 2, 3, and 4 include corresponding check formulae, by use of which we can avoid missing subgraphs to be counted. Their advantages will be manifested particularly in dealing with complex mechanisms.

The mathematical proofs of these rules are given in the Appendices.

CHOU KUO-CHEN et STURE FORSEN. Can. J. Chem. **59**, 737 (1981).

On présente quatre règles permettant de traiter des systèmes réactionnels où l'état stationnaire est du premier ordre et du pseudo premier ordre. A l'aide de la règle 1, on peut immédiatement décrire les constantes de vitesse apparentes pour des systèmes de réactions consécutives. Cette règle est de fait la même que l'approximation proposée par Gilbert mais on en fournit ici une preuve mathématique.

Les règles 2 et 3 peuvent servir à déduire les constantes de vitesse apparentes de plusieurs systèmes réactionnels complexes. Par comparaison avec les méthodes algébriques générales, ces deux règles permettent de simplifier les calculs laborieux qui seraient par ailleurs pénibles et susceptibles d'erreurs.

Dans la règle 4, on présente une nouvelle méthode schématique de calcul des concentrations des réactifs. La nouvelle méthode, en simplifiant la solution de problèmes complexes, est extraordinairement efficace par rapport aux méthodes schématiques existantes. Dans les cas des méchanismes complexes qui sont trop compliqués pour être traités par la méthode générale de calcul manuel, les calculs pratiques montrent que nous pouvons facilement aboutir aux résultats désirés à l'aide de la règle 4.

De plus les règles 2, 3 et 4 comprennent des formules de vérification qui permettent, lorsqu'elles sont utilisées, de s'assurer que tous les sous graphes sont comptés. Leurs avantages se manifestent particulièrement dans le traitement des méchanismes complexes.

On donne en Appendice les preuves mathématiques de ces règles.

[Traduit par le journal]

I. Introduction

In chemical kinetics, the following two categories of steady-state reaction systems are often encountered.

(*i*) It is assumed that in this category of reaction system the absolute rates of change of the concentrations of all intermediates are zero, and all individual rate constants can be treated as first-order or pseudo-first-order rate constants. For this kind of reaction system, it frequently becomes desirable or necessary to derive the apparent rate constant in terms of individual rate constants. Previous investigators (1–4) have accordingly suggested various algebraic methods for this purpose. However, as pointed out by Gilbert (5), this kind of derivation is laborious and error-prone for any but trivally simple mechanisms. Thus, he presented the "Rule of Thumb" (5), which is very effective for the consecutive reaction mechanisms whose common expression is as in [3]. However, Gilbert did not give the mathematical proof in his article (5). Besides, the "Rule of Thumb" cannot be used to deal with general mechanisms of the first category, such as mechanism [9] and mechanism [15]. For these mechanisms, the ordinary algebraic methods would involve more labour and be more error-prone. Hence, three schematic rules are presented here. Rule 1 is actually the same as the "Rule of Thumb", but the mathematical principle of this rule is given in Appendix 1 as a special case

[1]Visiting Professor in Chemical Center of Lund of Sweden where this paper was accomplished, and now Visiting Professor in Baker Laboratory of Chemistry, Cornell University, USA.

0008-4042/81/040737-19$01.00/0

©1981 National Research Council of Canada/Conseil national de recherches du Canada

Can. J. Chem. Downloaded from www.nrcresearchpress.com by 210.87.254.42 on 09/06/12
For personal use only.

of the proof of Rule 2. Rule 2 and Rule 3 can be used to derive the apparent rate constants for general mechanisms of the first category.

(*ii*) Reaction systems of the second category are often encountered in enzyme kinetics. The fundamental assumption here is that the absolute rates of change of the concentrations of all enzyme species in the reaction system are zero, and the conversion rate constant between any two enzyme species can be treated as first-order or pseudo-first-order. Laidler (6) has given a thorough discussion of the validity of this assumption. In general, for this kind of reaction system, concentrations of various enzyme species are to be calculated. But such calculations are extremely tedious and liable to error for any but simple mechanisms of little interest if one uses the ordinary algebraic methods. King and Altman (7) thus first suggested the use of the schematic method. Their method has been widely welcomed and adopted due to its simplicity and appeal to intuition. Since then, several investigators (8–14) have successively developed and modified the King–Altman method. Nonetheless, the calculation procedure still becomes unwieldy with complex mechanisms (15). Thus, Indge and Childs (15) and Cornish-Bowden (16) suggested approaches suitable for implementation on a computer. From another viewpoint, in this paper we shall present a new schematic method (Rule 4). This method is very efficacious in simplifying the calculation of complex problems. Practical calculations show that for complex mechanisms which are too complicated to be treated with the existing manual calculation methods, we can easily write out the desired results by means of Rule 4.

II. The Graphical Rules Concerning the First Category of Steady-state Reaction Systems

This kind of reaction system can be illustrated as follows:

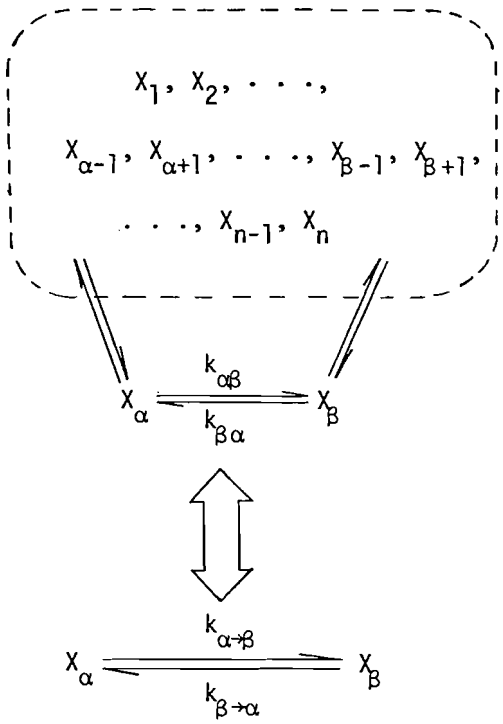

The symbols enclosed by the broken line denote the intermediates. According to the previous assumption, we have[2] $dx_\gamma/dt = 0$ ($\gamma \neq \alpha, \beta$). In order to be general as far as possible, we suppose that reversible reactions are possible between each pair of reactants in [1], and let the rate constant for $X_i \rightarrow X_j$ be k_{ij}, and that for $X_j \rightarrow X_i$ be k_{ji} ($i, j = 1, 2, ..., n$). Here, k_{ij} is the first-order or the pseudo-first-order rate constant. For the sake of simplicity in formulation, we may specify $k_{ii} = 0$ by definition of k_{ij}. Now, let us see how to express the apparent rate constants $k_{\alpha\rightarrow\beta}$ and $k_{\beta\rightarrow\alpha}$ in terms of the individual kinetic constants k_{ij}.

First of all, consider the following simple case:

[2] In this paper, the reactants are represented by capital letters and their concentrations by the corresponding lower-case letters.

Can. J. Chem. Downloaded from www.nrcresearchpress.com by 210.87.254.42 on 09/06/12
For personal use only.

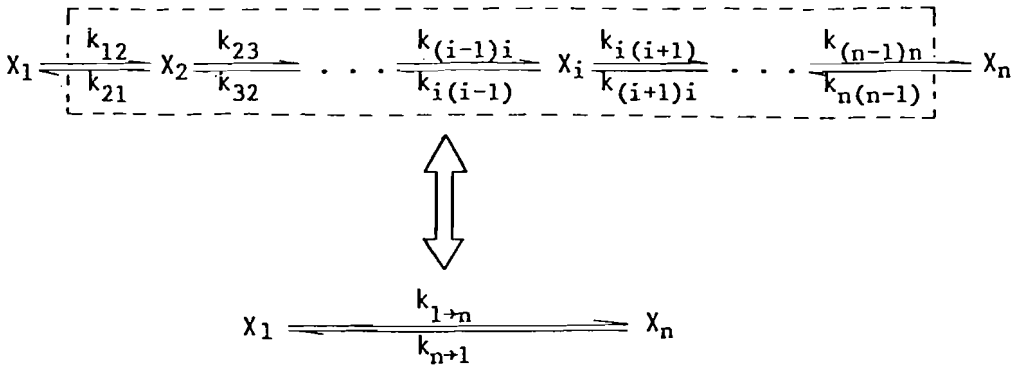

[3]

Obviously, [3] is a special case of [1] when $\alpha = 1$, $\beta = n$, and $k_{ij} = 0$ if $j \neq i \pm 1$. For this kind of consecutive reaction mechanisms, we have Rule 1 as follows.

Rule 1

(*a*) The numerator of $k_{1\to n}$ is equal to the product of all the individual rate constants in [3] whose arrows are towards the right, while the opposite is true for the numerator of $k_{n\to 1}$.

(*b*) The denominator of $k_{1\to n}$ and that of $k_{n\to 1}$ are the same, and both are equal to a sum of $n - 1$ items, in which the ith item can be obtained in the following way: cut the arrows between X_i and X_{i+1} ($i = 1, 2, \ldots, n - 1$) in [3], and then take the product of all rate constants whose arrows point in either direction away from the cut.

Example 1. Calculate the apparent rate constants of the following steady-state reaction system

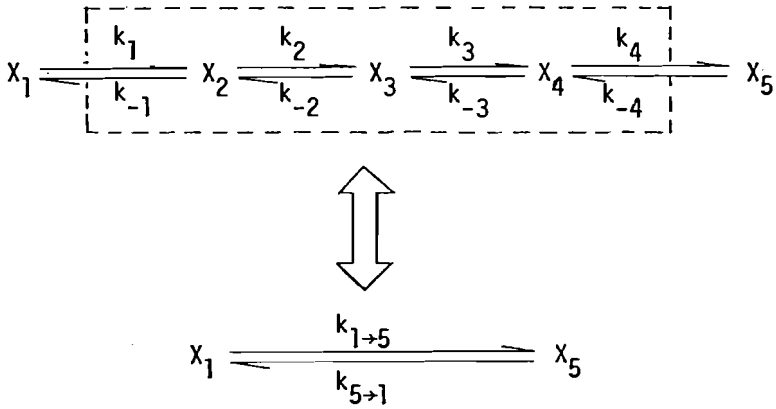

By Rule 1, we immediately obtain

$$k_{1\to 5} = \frac{k_1k_2k_3k_4}{k_2k_3k_4 + k_{-1}k_3k_4 + k_{-1}k_{-2}k_4 + k_{-1}k_{-2}k_{-3}}$$

$$k_{5\to 1} = \frac{k_{-1}k_{-2}k_{-3}k_{-4}}{k_2k_3k_4 + k_{-1}k_3k_4 + k_{-1}k_{-2}k_4 + k_{-1}k_{-2}k_{-3}}$$

Although Rule 1 is very easy and intuitive, it cannot be used to derive the apparent rate constants of mechanisms like [9] and [15]. Therefore, more general rules are needed.

Rule 2

(*a*) Draw a directed graph $\mathscr{D}$ to express the reaction system [1]. The method is as follows: depict n points and label them with $X_1, X_2, \ldots, X_n$, respectively; if there is a directed reaction for $X_i \to X_j$, namely, $k_{ij} \neq 0$, then draw an arc from X_i to X_j (with an arrow towards X_j), and weight the arc with k_{ij}; if there is no directed reaction for $X_i \to X_j$, namely, $k_{ij} = 0$, then do not depict such an arc.

(*b*) The desired rate constants $k_{\alpha\to\beta}$ and $k_{\beta\to\alpha}$ can then be expressed as

Can. J. Chem. Downloaded from www.nrcresearchpress.com by 210.87.254.42 on 09/06/12
For personal use only.

Can. J. Chem. Downloaded from www.nrcresearchpress.com by 210.87.254.42 on 09/06/12
For personal use only.

$$[4]\quad \begin{aligned} k_{\alpha\to\beta} &= N_\beta/N_{\alpha,\beta} \\ k_{\beta\to\alpha} &= N_\alpha/N_{\alpha,\beta} \end{aligned}$$

Here, N_β can be obtained in the following way: find all subgraphs in $\mathscr{D}$, each of which possesses $n-1$ arcs (n is the number of points in $\mathscr{D}$), but contains no cycle, no two or more than two arcs coming out of one point, and no arc coming out of X_β (the point denotes the βth reactant). Then, for each of these subgraphs, take the product of all its weights. On taking a sum of these results, we immediately obtain N_β.

In a completely analogous way, we can get N_α.

$N_{\alpha,\beta}$ in eq. [4] can be obtained as follows: find all subgraphs in $\mathscr{D}$, each of which possesses $n-2$ arcs, but contains no cycle, no two or more than two arcs coming out of one point, and also no arc coming out of X_α and X_β (the points denote the αth and βth reactants, respectively). Then for each of these subgraphs, take the product of all its weights. The sum of these results will directly yield $N_{\alpha,\beta}$.

(*c*) In order to facilitate checking, and to avoid missing any subgraphs in the calculations, we can also calculate the numbers of subgraphs to be counted, beforehand. The method is as follows: construct a matrix $\mathbf{A}(\mathscr{D}) = [a_{ij}]$, where

$$[5]\quad a_{ij} = \begin{cases} 1 & \text{if there is a connecting line from } X_i \text{ to } X_j \text{ in } \mathscr{D} \\ 0 & \text{if there is no connecting line from } X_i \text{ to } X_j \text{ in } \mathscr{D} \end{cases}$$

Reconstruct a matrix $\mathbf{B}(\mathbf{A}) = [b_{ij}]$, where

$$[6]\quad b_{ij} = \begin{cases} \sum_{t=1}^{n} a_{it} & \text{if } i = j \\ -a_{ij} & \text{if } i \neq j \end{cases}$$

then we have

$$[7]\quad P_\alpha = \det \mathbf{B}_{\bar{\alpha},\bar{\alpha}},\quad P_\beta = \det \mathbf{B}_{\bar{\beta},\bar{\beta}}$$

$$[8]\quad P_{\alpha,\beta} = \det \mathbf{B}_{\bar{\alpha},\bar{\alpha};\bar{\beta},\bar{\beta}}$$

where P_α, P_β, and $P_{\alpha,\beta}$ are the numbers of subgraphs to be counted in the calculation of N_α, N_β, and $N_{\alpha,\beta}$, respectively; $\mathbf{B}_{\bar{\alpha},\bar{\alpha}}$ denotes the submatrix obtained by removing the αth row and αth column from $\mathbf{B}$; $\mathbf{B}_{\bar{\alpha},\bar{\alpha};\bar{\beta},\bar{\beta}}$ denotes the submatrix obtained by removing both the αth row, αth column and the βth row, βth column; and so on. The symbol det means taking the determinant value of the following matrix.

For the mathematical proof of Rule 2, refer to Appendix 1.

Example 2. Calculate the apparent rate constants $k_{1\to4}$ and $k_{4\to1}$ for the following mechanism

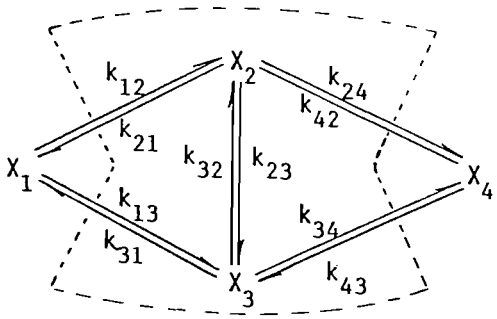

[9]

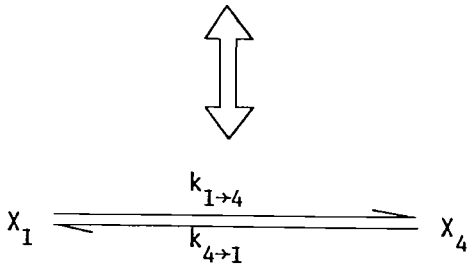

Can. J. Chem. Downloaded from www.nrcresearchpress.com by 210.87.254.42 on 09/06/12
For personal use only.

First of all, depict the corresponding directed graph as shown in Fig. 1. Then, following part *b* of Rule 2, we immediately obtain

[10] $N_4 =$ 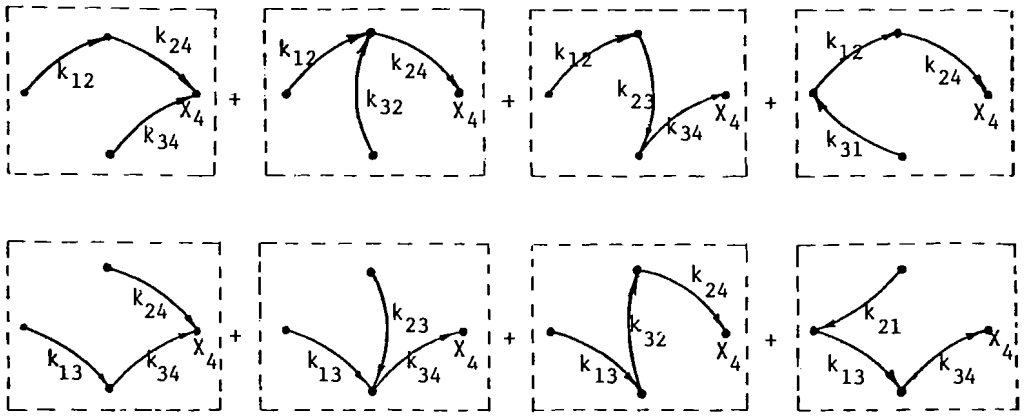

$$= k_{12}k_{24}k_{34} + k_{12}k_{32}k_{24} + k_{12}k_{23}k_{34} + k_{31}k_{12}k_{24} + k_{13}k_{34}k_{24} + k_{13}k_{23}k_{34} + k_{13}k_{32}k_{24} + k_{21}k_{13}k_{34}$$

[11] $$N_1 = k_{42}k_{21}k_{31} + k_{42}k_{32}k_{21} + k_{42}k_{23}k_{31} + k_{34}k_{42}k_{21} + k_{43}k_{31}k_{21} + k_{43}k_{23}k_{31} + k_{43}k_{32}k_{21} + k_{24}k_{43}k_{31}$$

[12] $N_{1,4} =$ 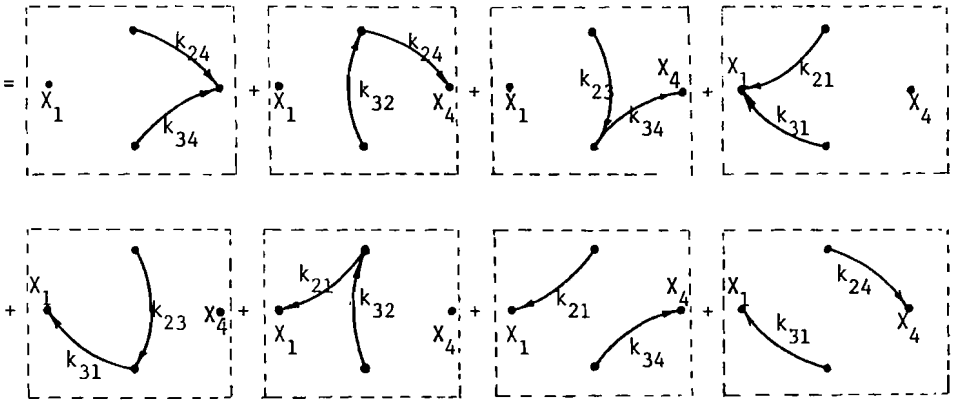

$$= k_{24}k_{34} + k_{32}k_{24} + k_{23}k_{34} + k_{21}k_{31} + k_{23}k_{31} + k_{32}k_{21} + k_{21}k_{34} + k_{31}k_{24}$$

Substituting [10]–[12] into [4], we immediately obtain the desired results $k_{1\to4}$ and $k_{4\to1}$.

Check: From Fig. 1 and eqs. [5] and [6], we have

$$\mathbf{A} = \begin{bmatrix} 0 & 1 & 1 & 0 \\ 1 & 0 & 1 & 1 \\ 1 & 1 & 0 & 1 \\ 0 & 1 & 1 & 0 \end{bmatrix} \qquad \mathbf{B} = \begin{bmatrix} 2 & -1 & -1 & 0 \\ -1 & 3 & -1 & -1 \\ -1 & -1 & 3 & -1 \\ 0 & -1 & -1 & 2 \end{bmatrix}$$

Then from eqs. [7] and [8], we have[3]

[3]It can easily be proved that for a symmetric directed graph like Fig. 1 (i.e. the one in which whenever there is an arc from X_i to X_j there must exist an arc from X_j to X_i), the value of P_α is always the same no matter which number in 1, 2, ..., n is taken for α; and in such a case we also have $n^{\gamma\to\alpha} = n^{\alpha\to\gamma}$, $n^{\gamma\to m} = n^{m\to\gamma}$, and so on.

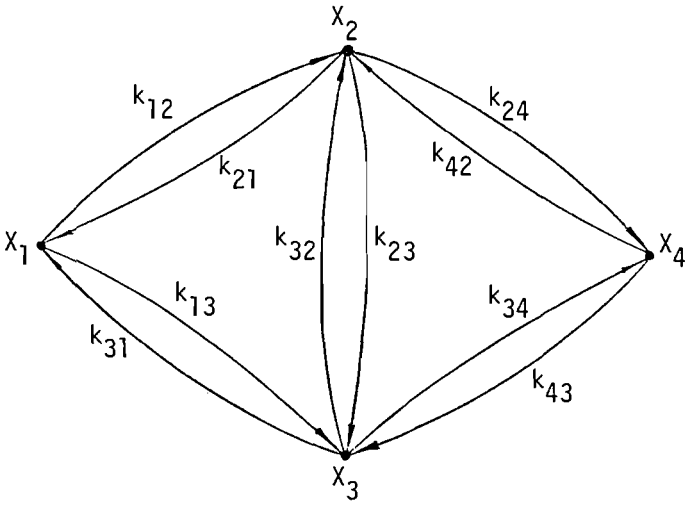

FIG. 1. The directed graph $\mathscr{D}$ of mechanism [9].

$$P_1 = \begin{vmatrix} 3 & -1 & -1 \\ -1 & 3 & -1 \\ -1 & -1 & 2 \end{vmatrix} = 8 \qquad P_4 = \begin{vmatrix} 2 & -1 & -1 \\ -1 & 3 & -1 \\ -1 & -1 & 3 \end{vmatrix} = 8 \qquad P_{1,4} = \begin{vmatrix} 3 & -1 \\ -1 & 3 \end{vmatrix} = 8$$

This means that no subgraph is omitted during the above calculations for N_1, N_4, and $N_{1,4}$.

This example tells us that the apparent rate constants for general mechanisms belonging to [1] can be easily derived by Rule 2. The calculational labor is much less than that by the general algebraic methods. However, when the mechanisms are more complex, the number of subgraphs to be counted will increase and confusion will ensue. In such a case, we suggest using Rule 3, as follows:

Rule 3

(*a*) Draw a directed graph $\mathscr{D}$ to express the reaction system [1].

(*b*) Add a loop with the weight $\sum_{i=1}^{n} k_{it}$ to each point X_i ($i = 1, 2, ..., n$), and alter the sign of the weight for each arc in $\mathscr{D}$, i.e., change k_{ij} to $-k_{ij}$ ($i \neq j$). The graph thus obtained is denoted by $\mathscr{D}^\dagger$. For instance, the $\mathscr{D}$ in Fig. 2 is in this way transformed to $\mathscr{D}^\dagger$ in Fig. 3.

(*c*) N_β in eq. [4] can then be obtained as follows: select any point in $\mathscr{D}^\dagger$, say X_γ, as a starting reference point.[4] Find all subgraphs in $\mathscr{D}^\dagger$, each of which possesses a path from X_γ to X_β, and all cycles that neither intersect with each other nor with the path. For each such subgraph, take the product of all of its weights and multiply by the sign of $(-1)^{n+c+1}$, where c is the number of cycles in the respective subgraph. On taking the sum of these results, we immediately obtain N_β.

N_α can be obtained in a completely analogous way.

(*d*) $N_{\alpha,\beta}$ in eq. [4] can be obtained in the following way: remove both the point X_α and the point X_β from $\mathscr{D}^\dagger$. (The arcs linked with the two points are of course also removed.) The graph thus obtained is denoted by $\mathscr{D}^\dagger_{\alpha,\beta}$. Find all subgraphs in $\mathscr{D}^\dagger_{\alpha,\beta}$, each of which possesses all those cycles that do not intersect with each other. Then, for each of these subgraphs, take the product of all its weights and multiply with a sign factor of $(-1)^{c_0}$, where c_0 is the number of cycles with arcs of even number in the respective subgraphs. Taking a sum of these results, we immediately obtain $N_{\alpha,\beta}$.

(*e*) In order to facilitate checking, we can also estimate the number of subgraphs to be counted. The method is as follows: if matrices $\mathbf{A}(\mathscr{D}^\dagger)$ and $\mathbf{A}(\mathscr{D}^\dagger_{\alpha,\beta})$ are constructed in accordance with eq. [5], then we have

$$[13] \quad n^{\gamma\to\alpha} = \text{per } [\mathbf{A}(\mathscr{D}^\dagger)]_{\bar{\alpha},\bar{\gamma}} \quad - n^{\gamma\to\beta} = \text{per } [\mathbf{A}(\mathscr{D}^\dagger)]_{\bar{\beta},\bar{\gamma}}$$

$$[14] \quad n_{\alpha,\beta} = \text{per } \mathbf{A}(\mathscr{D}^\dagger_{\alpha,\beta})$$

where $n^{\gamma\to\alpha}$ and $n^{\gamma\to\beta}$ are the numbers of subgraphs to be counted when X_γ is taken as the starting reference point to calculate N_α and N_β, respectively. $n_{\alpha,\beta}$ is the number of subgraphs when $N_{\alpha,\beta}$ is calculated; per

[4]The result is independent of the point that is selected as the starting reference point. However, we generally prefer to choose the reference point as far from the specified point as possible, so that fewer subgraphs will have to be counted.

Can. J. Chem. Downloaded from www.nrcresearchpress.com by 210.87.254.42 on 09/06/12
For personal use only.

Can. J. Chem. Downloaded from www.nrcresearchpress.com by 210.87.254.42 on 09/06/12
For personal use only.

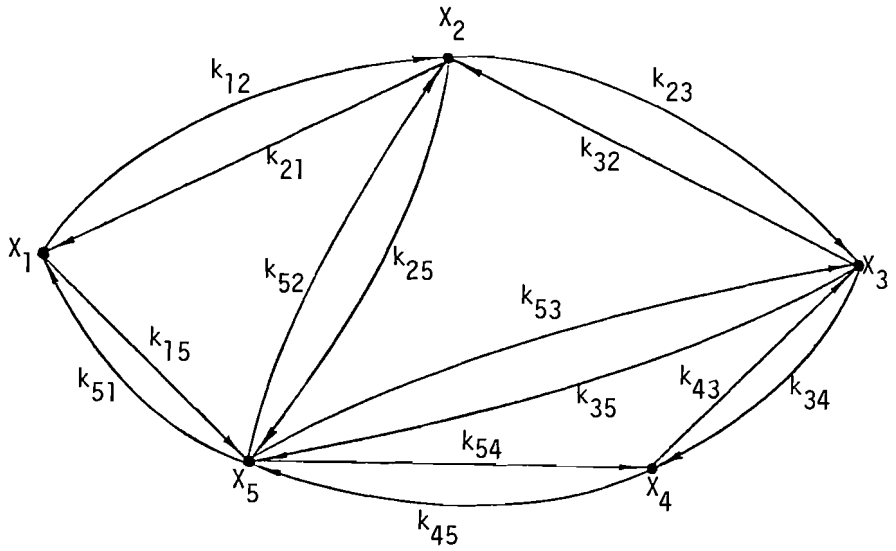

FIG. 2. The directed graph $\mathscr{D}$ of mechanism [15].

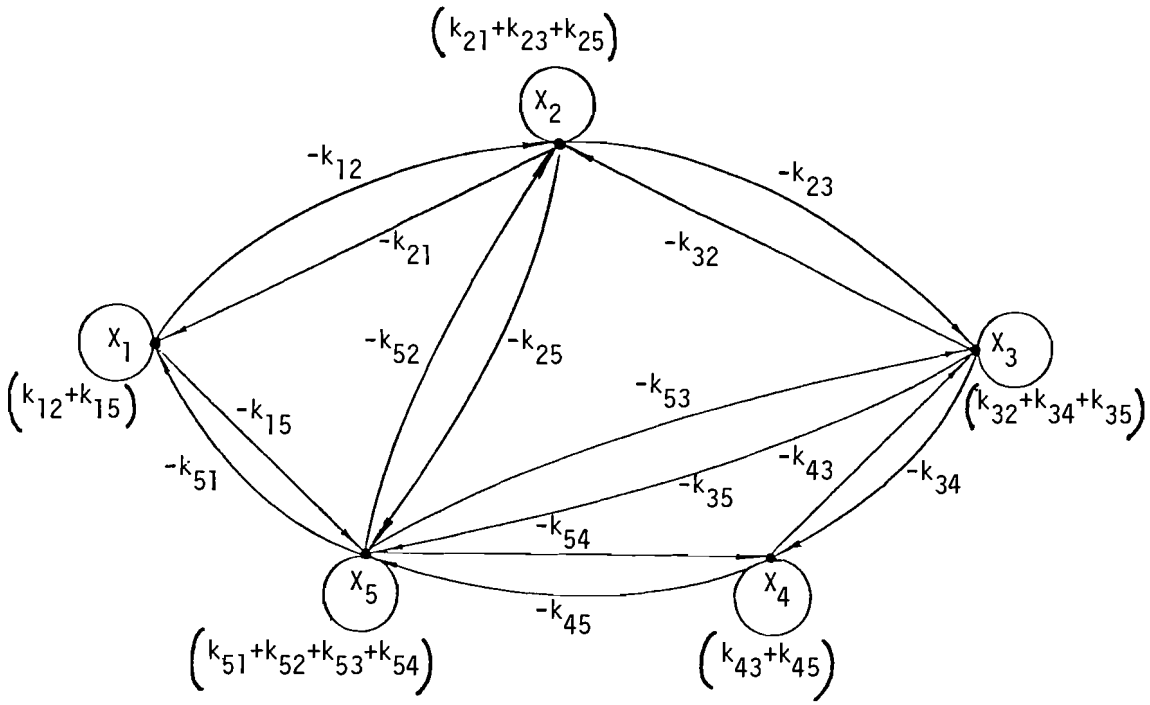

FIG. 3. The transformed graph $\mathscr{D}^{\dagger}$ obtained from Fig. 2 according to (*b*) of Rule 3.

denotes taking the permanent value of a matrix. *The so-called permanent of a matrix is a sum of all terms obtained by expanding the corresponding determinant but discarding the sign sgn σ which appears in each term of the determinant expansion.* Thus, it is very easy to calculate the permanent value of a matrix defined by [5] where the elements are either 1 or 0. For instance, we have

$$\text{per}\begin{bmatrix}1 & 1\\ 1 & 1\end{bmatrix} = 2 \qquad \text{per}\begin{bmatrix}1 & 1 & 0\\ 1 & 1 & 1\\ 1 & 1 & 1\end{bmatrix} = 4 \qquad \text{per}\begin{bmatrix}1 & 1 & 1\\ 1 & 1 & 1\\ 1 & 1 & 1\end{bmatrix} = 6$$

and so on. The permanent of a matrix is discussed in more detail in Appendix 2 and ref. 14.

The mathematical proof of Rule 3 is given in Appendix 3.

Example 3. Calculate the apparent rate constants $k_{1\to3}$ and $k_{3\to1}$ for the following mechanism

[15]

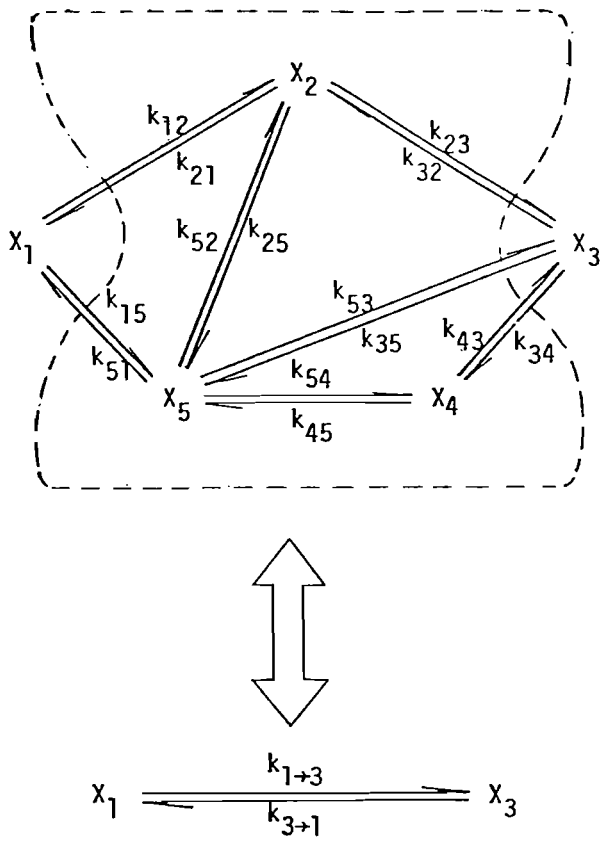

whose corresponding directed graph $\mathscr{D}$ is drawn in Fig. 2. For this mechanism, from [7] and [8] we have[3]

$$P_1 = P_3 = 21 \qquad P_{1,3} = 19$$

which indicates that if we use Rule 2 to calculate $k_{1\to3}$ (or $k_{3\to1}$), there are 21 and 19 subgraphs to be counted in deriving its numerator and denominator, respectively.

Now, let us use Rule 3. First, transform $\mathscr{D}$ of Fig. 2 into $\mathscr{D}^\dagger$ of Fig. 3 and $\mathscr{D}^\dagger_{1,3}$ of Fig. 4 according to part *b* and part *d*, respectively, of Rule 3. Then, from [13] and [14] we have

$$n^{1\to3} = \text{per}\,[\mathbf{A}(\mathscr{D}^\dagger)]_{\bar{3},\bar{1}} = \text{per}\begin{bmatrix}1&0&0&1\\1&1&0&1\\0&1&1&1\\1&1&1&1\end{bmatrix} = 7$$

$$n_{1,3} = \text{per}\,\mathbf{A}(\mathscr{D}^\dagger_{1,3}) = \text{per}\begin{bmatrix}1&0&1\\0&1&1\\1&1&1\end{bmatrix} = 3$$

which means that only 7 subgraphs are to be counted if we choose $\mathbf{X}_1$ as the starting reference point to calculate the numerator N_3, and only 3 subgraphs are enough for the denominator $N_{1,3}$. (Note that diagonal elements in the above matrices $\mathbf{A}(\mathscr{D}^\dagger)$ and $\mathbf{A}(\mathscr{D}^\dagger_{1,3})$ are 1's because each $\mathbf{X}_i$ is involved in an arc to itself.) Owing to the remarkable decrease in the numbers of counted subgraphs, we can directly write down the desired results according to part *c* and part *d* of Rule 3, respectively:

Can. J. Chem. Downloaded from www.nrcresearchpress.com by 210.87.254.42 on 09/06/12
For personal use only.

Can. J. Chem. Downloaded from www.nrcresearchpress.com by 210.87.254.42 on 09/06/12
For personal use only.

[16] $N_3 =$ 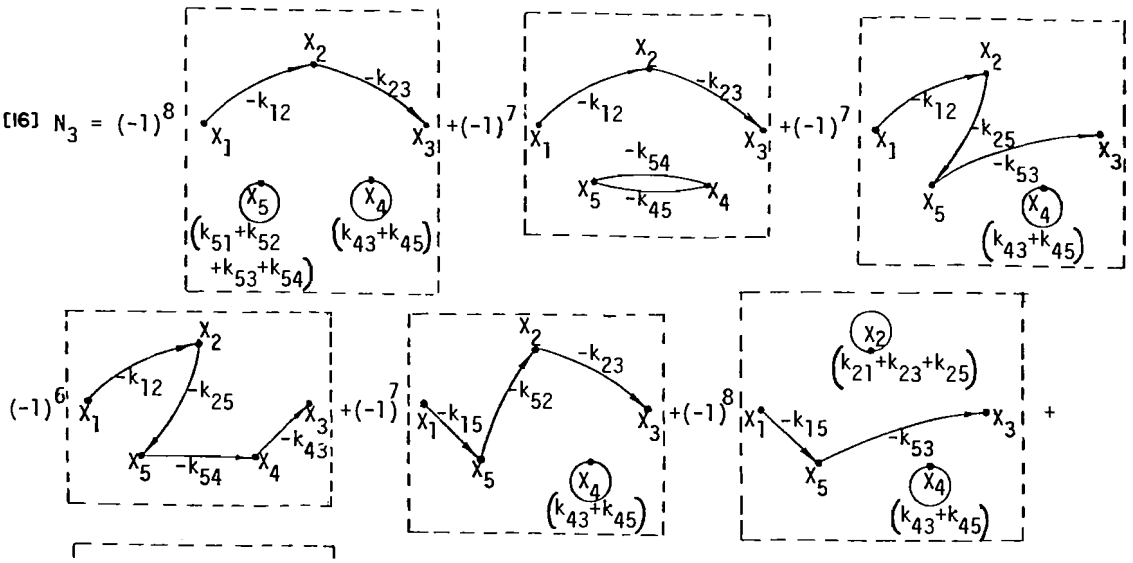

$$= k_{12}k_{23}(k_{43}+k_{45})(k_{51}+k_{52}+k_{53}+k_{54}) - k_{12}k_{23}k_{45}k_{54} + k_{12}k_{25}k_{53}(k_{43}+k_{45}) + k_{12}k_{25}k_{54}k_{43} + k_{15}k_{52}k_{23}(k_{43}+k_{45}) + k_{15}k_{53}(k_{21}+k_{23}+k_{25})(k_{43}+k_{45}) + k_{15}k_{54}k_{43}(k_{21}+k_{23}+k_{25})$$

$$= k_{12}k_{23}k_{43}(k_{51}+k_{52}+k_{53}+k_{54}) + k_{12}k_{23}k_{45}(k_{51}+k_{52}+k_{53}) + k_{12}k_{25}k_{53}(k_{43}+k_{45}) + k_{12}k_{25}k_{54}k_{43} + k_{15}k_{52}k_{23}(k_{43}+k_{45}) + k_{15}k_{53}(k_{21}+k_{23}+k_{25})(k_{43}+k_{45}) + k_{15}k_{54}k_{43}(k_{21}+k_{23}+k_{25})$$

[17] $N_{1,3} =$ 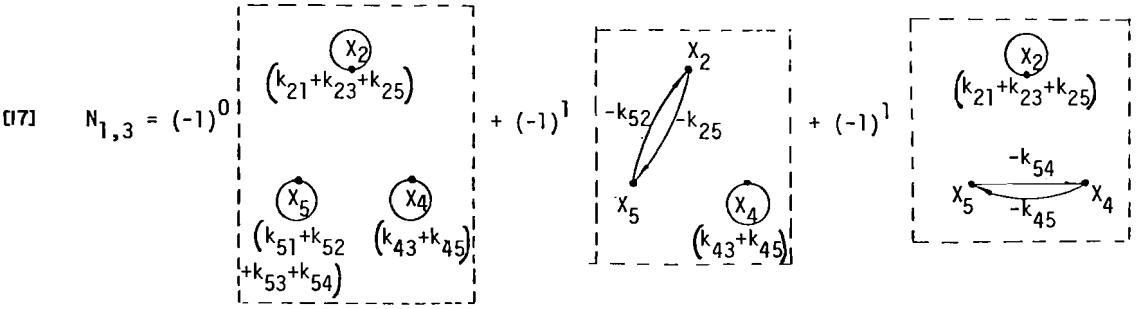

$$= (k_{21}+k_{23}+k_{25})(k_{43}+k_{45})(k_{51}+k_{52}+k_{53}+k_{54}) - k_{25}k_{52}(k_{43}+k_{45}) - k_{45}k_{54}(k_{21}+k_{23}+k_{25})$$

$$= (k_{21}+k_{23})k_{43}(k_{51}+k_{52}+k_{53}+k_{54}) + (k_{21}+k_{23})k_{45}(k_{51}+k_{52}+k_{53}) + k_{25}k_{43}(k_{51}+k_{53}+k_{54}) + k_{25}k_{45}(k_{51}+k_{53})$$

Substituting [16] and [17] into eq. [4], we immediately obtain $k_{1\to3}$. In a completely similar way, we can get $k_{3\to1}$.

From the above example we can see that for more complex mechanisms, it is more convenient to use Rule 3. But for simple mechanisms, Rule 2 is more intuitive, and furthermore it can naturally lead to Rule 1 (the "Rule of Thumb" (5)) when Rule 2 is applied to the consecutive reaction mechanisms whose common expression is illustrated by [3]. Of course, calculations with either rule will always lead to the same result.

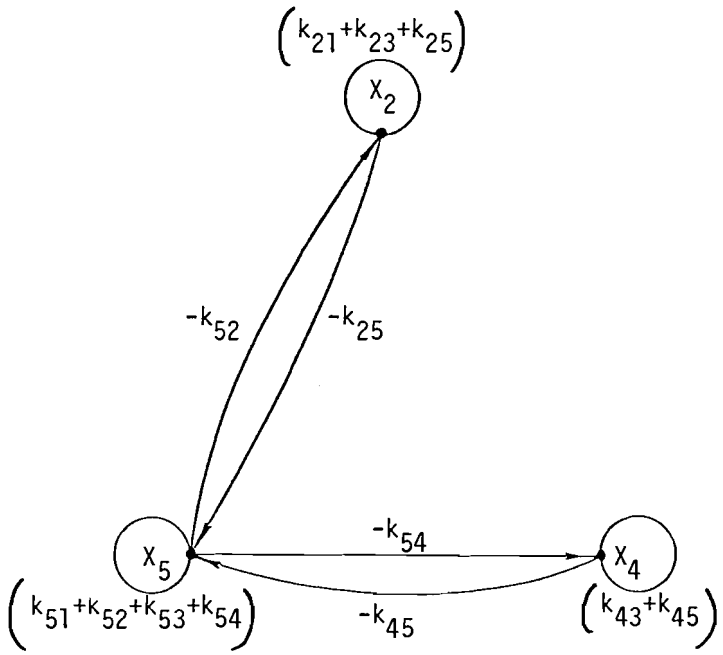

FIG. 4. The transformed graph $\mathscr{D}^{\dagger}_{1,3}$ obtained from Fig. 3 according to (*d*) of Rule 3.

III. The Graphical Rules Concerning the Second Category of Steady-state Reaction Systems

This kind of reaction system can be summarily illustrated as follows:

[18]

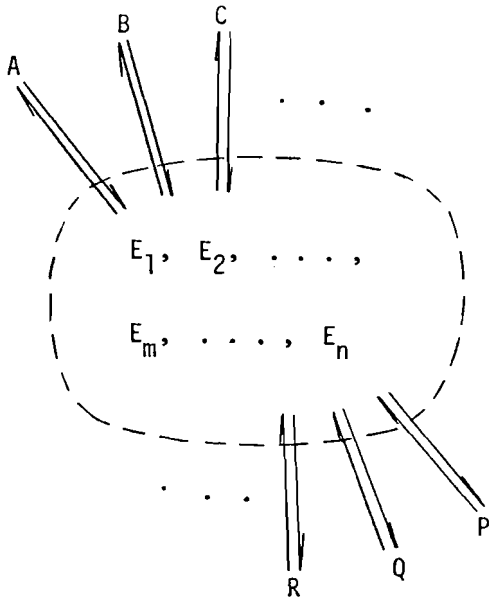

E_m ($m = 1, 2, \ldots, n$) enclosed by the dotted line represents various enzyme species; A, B, C, ... and P, Q, R, ... represent substrates and products, respectively. Likewise, let the rate constant for $E_i \rightarrow E_j$ be k_{ij}, and that for $E_j \rightarrow E_i$ be k_{ji}. Here, k_{ij} and k_{ji} are first-order or pseudo-first-order rate constants. For reaction systems of this category, the steady-state assumption requires $de_m/dt = 0$.[2] Below, we shall present a new graphical rule to derive e_m, the concentration of the mth enzyme species.

Rule 4

(*a*) Draw a directed graph $\mathscr{D}$ to express mechanism [18]. As a special example, let us consider the following

Can. J. Chem. Downloaded from www.nrcresearchpress.com by 210.87.254.42 on 09/06/12
For personal use only.

three-state single substrate, single product reaction

$$[19]\quad E + A \underset{k_{-1}}{\overset{k_1}{\rightleftharpoons}} EA \qquad EA \underset{k_{-2}}{\overset{k_2}{\rightleftharpoons}} EP \qquad EP \underset{k_{-3}}{\overset{k_3}{\rightleftharpoons}} E + P$$

which was employed by King and Altman (7) as a model, and obviously belongs to the category of [18]. If we suppose $E_1 = E$, $E_2 = EA$, $E_3 = EP$, and $k_{12} = k_1 a$, $k_{21} = k_{-1}$, $k_{23} = k_2$, $k_{32} = k_{-2}$, $k_{31} = k_3$, $k_{13} = k_{-3}p$, then the directed graph $\mathscr{D}$ of mechanism [19] is as shown in Fig. 5.

(*b*) Add a loop with weight $\sum_{t=1}^{n} k_{it}$ to each point E_i ($i = 1, 2, \ldots, n$), and alter the sign of the weight for each arc in $\mathscr{D}$. The new graph thus obtained is denoted by $\mathscr{D}^\dagger$. For instance, the $\mathscr{D}$ in Fig. 5 is accordingly transformed to $\mathscr{D}^\dagger$ in Fig. 6.

(*c*) Then we have

$$[20]\quad e_m = \frac{N_m}{\sum_{i=1}^{n} N_i} e_0$$

where e_0 is the total enzyme concentration. N_m can be obtained in a completely analogous way as given in part *c* of Rule 3 for calculating N_β. (X and β in Rule 3 are replaced by E and *m*, respectively.) For instance, following this procedure, for $\mathscr{D}^\dagger$ of Fig. 6, we at once have:

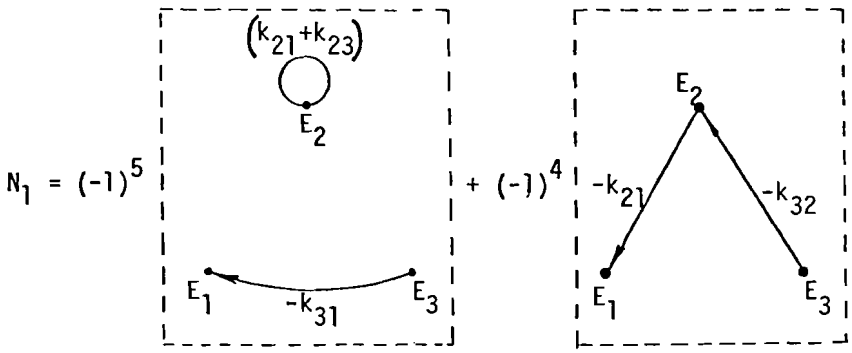

$$= k_{31}(k_{21}+k_{23}) + k_{32}k_{21}$$

$$N_2 = k_{32}(k_{12}+k_{13}) + k_{31}k_{12}$$

$$N_3 = k_{13}(k_{21}+k_{23}) + k_{12}k_{23}$$

Substituting N_1, N_2, N_3 into [20], we immediately obtain the concentrations of the enzyme species in mechanism [19].

(*d*) Likewise, we have the check formula

$$[21]\quad n^{\gamma \to m} = \text{per } \mathbf{A}(\mathscr{D}^\dagger)_{\bar{m},\bar{\gamma}}$$

to estimate the number of subgraphs being counted when E_γ in $\mathscr{D}^\dagger$ is taken as the reference point to derive N_m. For instance, for Fig. 6 we have

$$\mathbf{A}(\mathscr{D}^\dagger) = \begin{bmatrix} 1 & 1 & 1 \\ 1 & 1 & 1 \\ 1 & 1 & 1 \end{bmatrix}$$

Can. J. Chem. Downloaded from www.nrcresearchpress.com by 210.87.254.42 on 09/06/12
For personal use only.

Can. J. Chem. Downloaded from www.nrcresearchpress.com by 210.87.254.42 on 09/06/12
For personal use only.

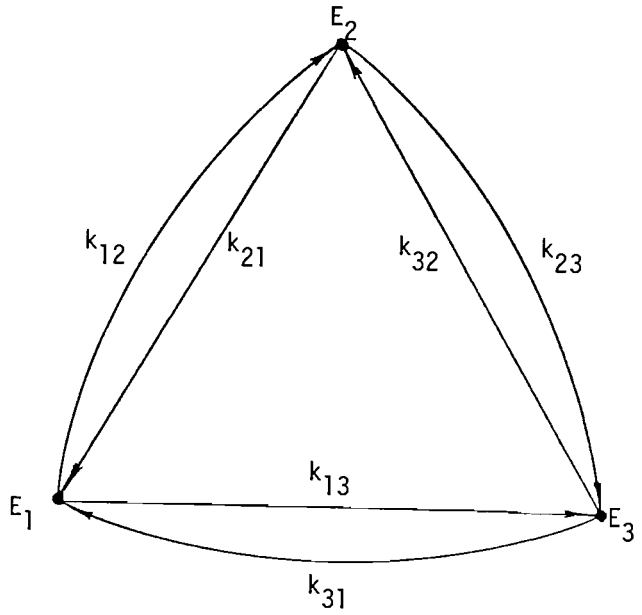

FIG. 5. The directed graph $\mathscr{D}$ of mechanism [19].

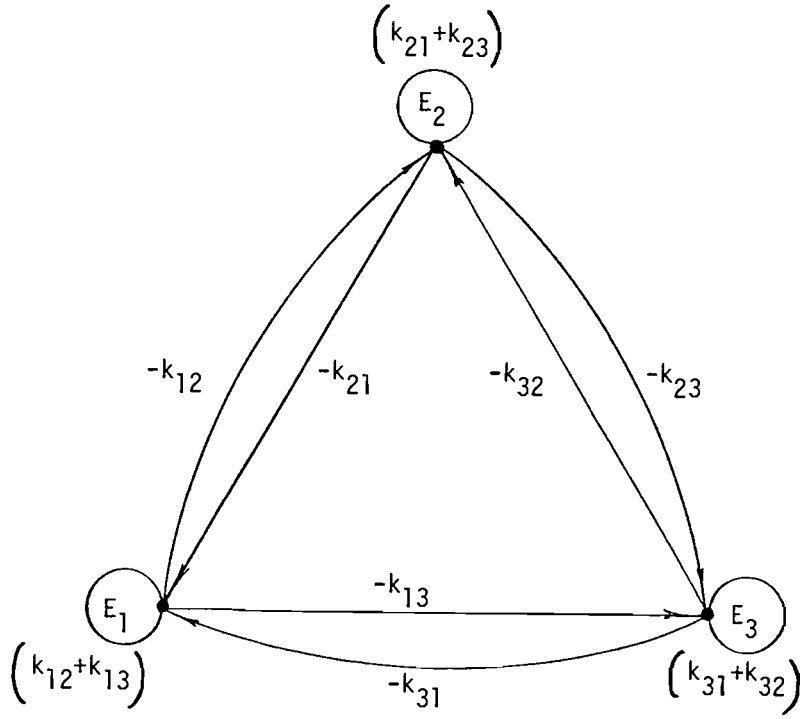

FIG. 6. The transformed graph $\mathscr{D}^{\dagger}$ obtained from Fig. 5 according to (*b*) of Rule 4.

and

$$n^{3\to 1} = \text{per}\begin{bmatrix} 1 & 1 \\ 1 & 1 \end{bmatrix} = 2$$

which indicate that no subgraph was lost in the above calculation of N_1.

Can. J. Chem. Downloaded from www.nrcresearchpress.com by 210.87.254.42 on 09/06/12
For personal use only.

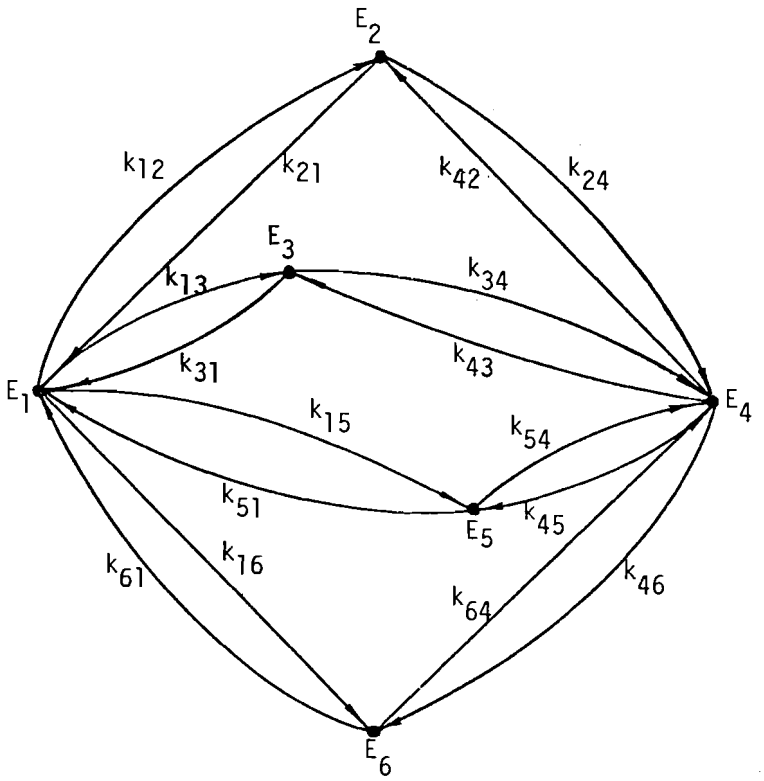

FIG. 7. The directed graph $\mathscr{D}$ of mechanism [22].

The mathematical principle of Rule 4 is given in Appendix 4.

Example 4. Consider the following Bi Bi random mechanism (17)

[22]

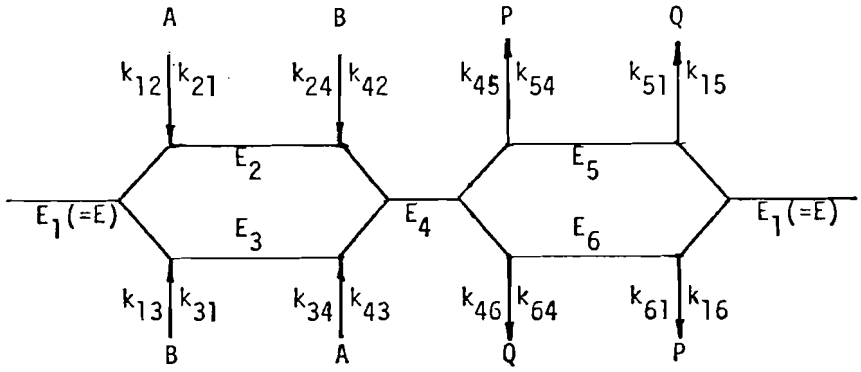

The corresponding directed graph $\mathscr{D}$ is drawn in Fig. 7. For such a mechanism, if the King–Altman method is used, 32 subgraphs (18)[5] must be counted to calculate each N_m ($m = 1, 2, ..., 6$). It is too laborious to be practical, as the probability of committing errors is great. It is also very difficult (18) to use the existing manual calculation methods to obtain the desired results. Now, let us use Rule 4. First, transform $\mathscr{D}$ of

[5]The number of subgraphs to be counted for the King–Altman method can be easily estimated with a rule presented by Chou *et al.* in ref. 14.

Fig. 7 into $\mathscr{D}^{\dagger}$ of Fig. 8 according to (*b*) of Rule 4. By [21] we then have

$$n^{4\to 1} = \text{per}\begin{bmatrix}1&1&0&0&0\\1&0&1&0&0\\0&1&1&1&1\\1&0&0&1&0\\1&0&0&0&1\end{bmatrix} = \text{per}\begin{bmatrix}0&1&0&0\\1&1&1&1\\0&0&1&0\\0&0&0&1\end{bmatrix} + \text{per}\begin{bmatrix}1&1&0&0\\0&1&1&1\\1&0&1&0\\1&0&0&1\end{bmatrix}$$

$$= \text{per}\begin{bmatrix}1&1&1\\0&1&0\\0&0&1\end{bmatrix} + \text{per}\begin{bmatrix}1&1&1\\0&1&0\\0&0&1\end{bmatrix} + \text{per}\begin{bmatrix}0&1&1\\1&1&0\\1&0&1\end{bmatrix}$$

$$= 1 + 1 + 2 = 4$$

$$n^{1\to 4} = n^{4\to 1} = 4 \text{ (see footnote 3)}$$

$$n^{1\to 2} = n^{1\to 3} = n^{1\to 5} = n^{1\to 6} = 7$$

The above results tell us that only 4 subgraphs need to be counted in calculating N_1 (taking E_4 as the reference point) and N_4 (taking E_1 as the reference point), and only 7 subgraphs need to be counted in calculating N_2, N_3, N_5, N_6 (all taking E_1 as the reference point). Due to the evident decrease in the number of subgraphs, it is very easy by following part *c* of Rule 4 to obtain the desired result:

[23] $N_1 = (-1)^{10}$ 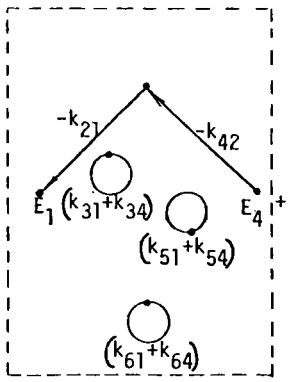

$+(-1)^{10}$ 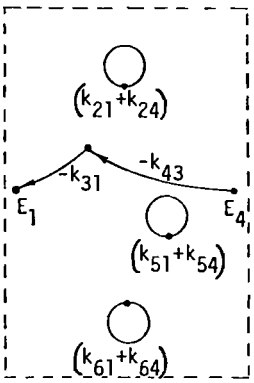

$+(-1)^{10}$ 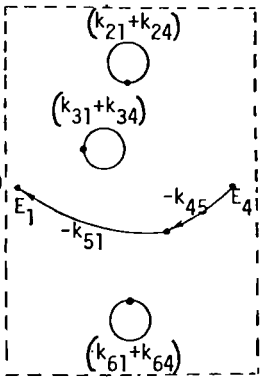

$+ (-1)^{10}$ 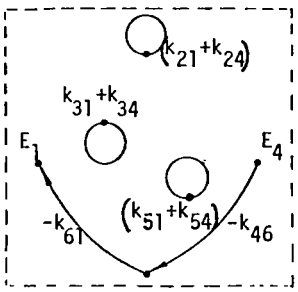

$$= k_{42}k_{21}(k_{31}+k_{34})(k_{51}+k_{54})(k_{61}+k_{64}) + k_{43}k_{31}(k_{21}+k_{24})(k_{51}+k_{54})(k_{61}+k_{64}) + k_{46}k_{61}(k_{21}+k_{24})(k_{31}+k_{34})(k_{51}+k_{54} + k_{45}k_{51}(k_{21}+k_{24})(k_{31}+k_{34})(k_{61}+k_{64})$$

From the symmetry concerning E_1 and E_4 in Fig. 8, we readily see

N_4 = The result obtained from eq. [23] through exchanging subscripts 1 and 4

In a similar way, we can also get the expressions for N_2, N_3, N_5, and N_6. In fact, however, when this method becomes familiar, it is quite unnecessary to depict the decomposed subgraphs one by one as done above; very often we can directly write down the desired results according to the graph $\mathscr{D}^{\dagger}$ or even $\mathscr{D}$, as follows:

Can. J. Chem. Downloaded from www.nrcresearchpress.com by 210.87.254.42 on 09/06/12
For personal use only.

Can. J. Chem. Downloaded from www.nrcresearchpress.com by 210.87.254.42 on 09/06/12
For personal use only.

[24] $$N_2 = k_{12}(k_{31}+k_{34})(k_{42}+k_{43}+k_{45}+k_{46})(k_{51}+k_{54})(k_{61}+k_{64}) - k_{12}k_{34}k_{43}(k_{51}+k_{54})(k_{61}+k_{64}) - k_{12}k_{45}k_{54}(k_{31}+k_{34})(k_{61}+k_{64}) - k_{12}k_{46}k_{64}(k_{31}+k_{34})(k_{51}+k_{54}) + k_{13}k_{34}k_{42}(k_{51}+k_{54})(k_{61}+k_{64}) + k_{15}k_{54}k_{42}(k_{31}+k_{34})(k_{61}+k_{64}) + k_{16}k_{64}k_{42}(k_{31}+k_{34})(k_{51}+k_{54})$$

$$= k_{12}k_{31}k_{51}k_{61}(k_{42}+k_{43}+k_{45}+k_{46}) + k_{12}k_{31}k_{51}k_{64}(k_{42}+k_{43}+k_{45}) + k_{12}k_{31}k_{54}k_{61}(k_{42}+k_{43}+k_{46}) + k_{12}k_{31}k_{54}k_{64}(k_{42}+k_{43}) + k_{12}k_{34}k_{51}k_{61}(k_{42}+k_{45}+k_{46}) + k_{12}k_{34}k_{51}k_{64}(k_{42}+k_{45}) + k_{12}k_{34}k_{54}k_{61}(k_{42}+k_{46}) + k_{12}k_{34}k_{54}k_{64}k_{42} + k_{13}k_{34}k_{42}(k_{51}+k_{54})(k_{61}+k_{64}) + k_{15}k_{54}k_{42}(k_{31}+k_{34})(k_{61}+k_{64}) + k_{16}k_{64}k_{42}(k_{31}+k_{34})(k_{51}+k_{54})$$

Likewise, with the help of the symmetry in Fig. 8 between E_2 and E_3, E_2 and E_5, and E_2 and E_6, we at once have

N_3 = The result obtained from eq. [24] through exchanging the subscripts 2 and 3

N_5 = The result obtained from eq. [24] through exchanging the subscripts 2 and 5

N_6 = The result obtained from eq. [24] through exchanging the subscripts 2 and 6

Substituting the above results into eq. [20], we immediately obtain e_m ($m = 1, 2, ..., 6$), the concentrations of all enzyme species in mechanism [22].

In addition, Rule 4 has been successfully used to deal with a Bi Uni Uni Bi Ping Pong Mechanism (19*a*, 20), and we obtained the result that the concentration of each enzyme species contains 64 terms in the numerator and 512 terms in the denominator (21). Such a complicated result could hardly be derived if the ordinary manual calculation methods are employed. Rule 4 has also been used to derive the concentrations of the enzyme species of a mechanism with branched catalytic cycles such as

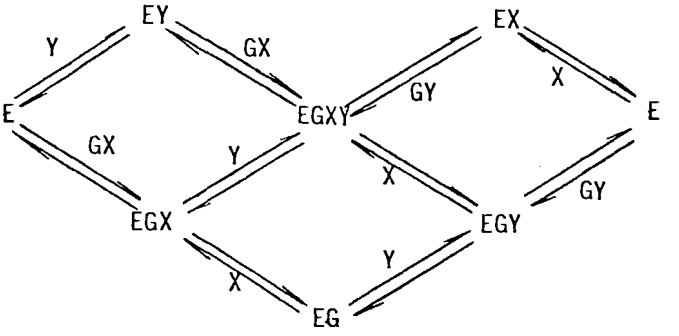

Ainsworth (19*b*) pointed out that the derivation of the rate equation of this mechanism is a formidable task if a computer would not be employed because there are 672 terms in the denominator for the concentration of each enzyme species, and 96 terms in the corresponding numerator. However, by means of Rule 4, we could easily write down the rather involved result (22), which is exactly the same as that obtained by Kinderlerer and Ainsworth (23) with a computer.

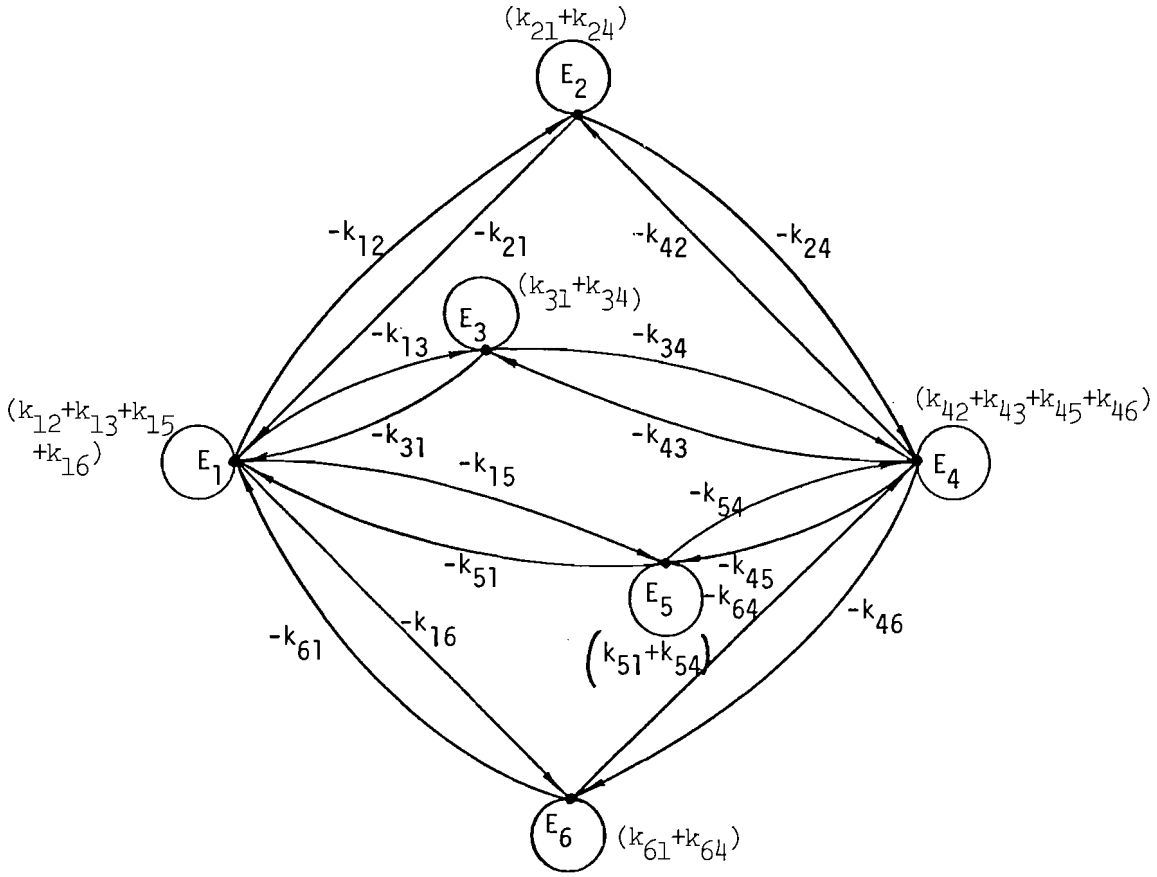

FIG. 8. The transformed graph $\mathscr{D}^{\dagger}$ obtained from Fig. 7 according to (*b*) of Rule 4.

Acknowledgments

The authors are much indebted to Dr. Robert E. Carter for his very valuable suggestions. Illuminative discussion with Professor Manfred Eigen is also gratefully acknowledged.

1. W. JOST. Z. Naturforsch. **2***a*, 159 (1947).
2. J. Z. HEARON. Bull. Math. Biophys. **15**, 121 (1953).
3. A. A. FROST and R. G. PEARSON. Kinetics and mechanism. 2nd ed. Wiley, New York and London. 1961.
4. J. WEI and C. D. PRATER. Adv. Catal. **13**, 203 (1962).
5. H. F. GILBERT. J. Chem. Educ. **54**, 492 (1977).
6. K. J. LAIDLER. Can. J. Chem. **33**, 1614 (1955).
7. E. L. KING and C. ALTMAN. J. Phys. Chem. **60**, 1375 (1956).
8. M. V. VOLKENSTEIN and B. N. GOLDSTEIN. Biochim. Biophys. Acta, **115**, 471 (1966).
9. S. CHA. J. Biol. Chem. **243**, 820 (1968).
10. H. J. FROMM. Biochem. Biophys. Res. Commun. **40**, 682 (1970).
11. B. A. ORSI. Biochim. Biophys. Acta, **258**, 4 (1972).
12. N. SESHAGIRI. J. Theor. Biol. **34**, 469 (1972).
13. S. AINSWORTH. J. Theor. Biol. **44**, 161 (1974).
14. K. C. CHOU, S. P. JIANG, W. M. LIU, and C. H. FEE. Sci. Sin. **22**, 341 (1979).
15. K. J. INDGE and R. E. CHILDS. Biochem. J. **155**, 567 (1976).
16. A. CORNISH-BOWDEN. Biochem. J. **165**, 55 (1977).
17. W. W. CLELAND. Biochim. Biophys. Acta, **67**, 104 (1963).
18. A. CORNISH-BOWDEN. Principles of enzyme kinetics. Butterworths, London–Boston. 1976. Chapt. 3.
19. S. AINSWORTH. Steady-state enzyme kinetics. The Macmillan Press Ltd., London–Basingstoke. 1977. (*a*) p. 26, eq. 1.46; (*b*) p. 145.
20. H. CEDAR and J. H. SCHWARZ. J. Biol. Chem. **244**, 4122 (1969).
21. K. C. CHOU, R. E. CARTER, and S. FORSEN. Chem. Scr. In press.
22. Y. N. LIAN. Personal communication.
23. J. KINDERLERER and S. AINSWORTH. Int. J. Biomed. Comput. **7**, 1 (1976).
24. F. HARARY. Graph theory. Addison-Wesley. 1966. pp. 203, 204.
25. W. K. CHEN. Applied graph theory. North-Holland. 1971. Chapt. 2.

Can. J. Chem. Downloaded from www.nrcresearchpress.com by 210.87.254.42 on 09/06/12
For personal use only.

Can. J. Chem. Downloaded from www.nrcresearchpress.com by 210.87.254.42 on 09/06/12
For personal use only.

Appendix 1. The Mathematical Principles of Rule 1 and Rule 2

Let us first prove Rule 2. Since Rule 1 is a special case of Rule 2, if the latter is proved, the former will automatically be valid. For the general mechanism [1] of the first category of steady-state reaction systems, without lossing generality, we may prescribe $\alpha = 1$, and $\beta = n$. Now, in order to derive the apparent rate constant $k_{1\to n}$, according to the steady-state assumption, we have the following system of equations:

$$[A.1]\quad \begin{cases} -\dfrac{dx_1}{dt} = \displaystyle\sum_{i=1}^{n} k_{1i}x_1 - k_{21}x_2 - \cdots - k_{(n-1)1}x_{n-1} = v \\ -\dfrac{dx_2}{dt} = -k_{12}x_1 + \displaystyle\sum_{i=1}^{n} k_{2i}x_2 - \cdots - k_{(n-1)2}x_{n-1} = 0 \\ \cdots\cdots\cdots\cdots\cdots\cdots\cdots\cdots \\ -\dfrac{dx_{n-1}}{dt} = -k_{1(n-1)}x_1 - k_{2(n-1)}x_2 - \cdots + \displaystyle\sum_{i=1}^{n} k_{(n-1)i}x_{n-1} = 0 \\ -\dfrac{dx_n}{dt} = -k_{1n}x_1 - k_{2n}x_2 \cdots - k_{(n-1)n}x_{n-1} = -v \end{cases}$$

where x_i ($i = 1, 2, \ldots, n$) is the concentration of the reactant X_i, v is the steady-state reaction rate, and k_{ij} is the conversion rate constant for $X_i \to X_j$. For simplification, we can prescribe $k_{ii} = 0$ by the definition of k_{ij}. In the above n equations, the negative sum of the preceding $n - 1$ equations will yield the nth equation, hence these n equations are linearly dependent. Discarding the nth equation, we have (in accordance with Cramer's rule):

$$[A.2]\quad x_1 = \frac{\det \mathbf{K}_{\bar{1},\bar{1},\bar{n},\bar{n}}}{\det \mathbf{K}_{\bar{n},\bar{n}}} v$$

where $\mathbf{K}_{\bar{n},\bar{n}}$ is the $n - 1$ order matrix obtained by removing the nth row and nth column from the matrix

$$[A.3]\quad \mathbf{K} = \begin{bmatrix} \displaystyle\sum_{i=1}^{n} k_{1i} & -k_{12} & \cdots & -k_{1n} \\ -k_{21} & \displaystyle\sum_{i=1}^{n} k_{2i} & \cdots & -k_{2n} \\ \cdots & \cdots & \cdots & \cdots \\ -k_{n1} & -k_{n2} & \cdots & \displaystyle\sum_{i=1}^{n} k_{ni} \end{bmatrix}$$

and $\mathbf{K}_{\bar{1},\bar{1},\bar{n},\bar{n}}$ is the $n - 2$ order matrix obtained by removing both the 1st row, 1st column, and the nth row, nth column from K. It is obvious that det $\mathbf{K}_{\bar{n},\bar{n}}$ is just the same as N_n in refs. 14 and 18, so it is profitable to let

$$[A.4]\quad \begin{cases} N_n = \det \mathbf{K}_{\bar{n},\bar{n}} \\ N_{1,n} = \det \mathbf{K}_{\bar{1},\bar{1},\bar{n},\bar{n}} \end{cases}$$

On the other hand, by definition of the apparent rate constant, we have

$$[A.5]\quad v = dx_n/dt = k_{1\to n}x_1$$

Substituting [A.4] and [A.5] into [A.2], we obtain

$$[A.6]\quad k_{1\to n} = N_n/N_{1,n}$$

It has been proved in ref. 14 that the numerator N_n in eq. [A.6] can be calculated with the schematic method as described in Rule 2. Moreover, according to Tutte's theorem (24), it is readily seen that the number of subgraphs involved in such a way can be calculated by eq. [7].

As for the denominator $N_{1,n}$ in [A.6], following the analysis given by Cornish-Bowden (18), we learn that the expansion of the determinant $N_{1,n} = \det \mathbf{K}_{\bar{1},\bar{1};\bar{n},\bar{n}}$ will be a sum of products of $n - 2$ rate constants, in each of which: 1 and n do not occur as first subscript, while 2, ..., $n - 1$ occur once only as first subscript; no cycles of subscripts (such as $k_{23}k_{34}k_{42}$...) occur; each product has a positive sign; all allowed products occur. If the above conclusions are expressed in the schematic terminology, we get at once the calculation method for $N_{1,n}$ as given in Rule 2. Furthermore, in terms of Tutte's theorem, it is also evident that the number of subgraphs thus involved can be calculated by eq. [8].

Likewise, the corresponding conclusions can be obtained for $k_{n\to 1}$.

This completes the proof of Rule 2. Obviously, it will naturally lead to Rule 1 if Rule 2 is applied to the reaction mechanisms whose common expression is written as [3].

Appendix 2. The Permanent of a Matrix and Its Principal Properties

By the definition given in Rule 3 for a permanent, the following fundamental properties are obvious.

Property 1. A matrix **C** has the same permanent value as its transposed matrix; i.e.

$$\text{per } \mathbf{C} = \text{per } \mathbf{C}^{\mathrm{T}}$$

Property 2. The permanent value remains the same on exchanging any two rows (or columns) of a matrix.

Property 3. The permanent of a matrix can be expanded along any of its rows (or columns), e.g.,

$$\text{per}\begin{bmatrix} c_{11} & c_{12} & \cdots & c_{1n} \\ c_{21} & c_{22} & \cdots & c_{2n} \\ \cdot & & & \cdot \\ \cdot & & & \cdot \\ \cdot & & & \cdot \\ c_{n1} & c_{n2} & \cdots & c_{nn} \end{bmatrix} = c_{11}\,\text{per}\begin{bmatrix} c_{22} & \cdots & c_{2n} \\ \cdot & & \\ \cdot & & \\ \cdot & & \\ c_{n2} & \cdots & c_{nn} \end{bmatrix} + c_{12}\,\text{per}\begin{bmatrix} c_{21} & c_{23} & \cdots & c_{2n} \\ \cdot & \cdot & & \cdot \\ \cdot & \cdot & & \cdot \\ \cdot & \cdot & & \cdot \\ c_{n1} & c_{n2} & \cdots & c_{nn} \end{bmatrix}$$

$$+ \cdots + c_{1n}\,\text{per}\begin{bmatrix} c_{21} & \cdots & c_{2(n-1)} \\ \cdot & & \cdot \\ \cdot & & \cdot \\ \cdot & & \cdot \\ c_{n1} & \cdots & c_{n(n-1)} \end{bmatrix}$$

By means of this property, for a matrix whose elements are either 1 or 0 as defined by eq. [5], the permanent can be easily calculated.

Corollary 1. If **J** is an $n \times n$ matrix with all of its elements equal to 1, we then have

$$\text{per } \mathbf{J} = n!$$

Corollary 2. If $\mathbf{J}_n^{(m)}$ is an $n \times n$ matrix in which there are m independent zero elements (i.e., any two of these zero elements are in different rows and columns) and all the other elements are equal to 1, then we have

$$\text{per } \mathbf{J}_n^{(m)} = n! - (n-1)!C_m^{\,1} + (n-2)!C_m^{\,2} + \ldots + (-1)^m(n-m)!C_m^{\,m}$$

Corollary 3. The permanent of a matrix with any zero row (or column) is equal to zero.

Remark. Owing to Property 2, which reflects an essential difference between permanent and determinant, it is usually forbidden during the operation of taking the permanent to add a multiple of one row (or column) to another as done in the calculation of a determinant.

Appendix 3. The Mathematical Principles of Rule 3

In fact, Rule 3 is another schematic method for calculating N_α, N_β, and $N_{\alpha,\beta}$. As in Appendix 1, we may assume $\alpha = 1$ and $\beta = n$ without losing generality.

We know that an $n \times n$ matrix $\mathbf{C} = [c_{ij}]$ can be expressed by a weighted directed graph with n points $(C_1, C_2, \ldots, C_n)$. The method is as follows: If $c_{ij} \neq 0$, draw an arc from point C_i to point C_j, and label it

Can. J. Chem. Downloaded from www.nrcresearchpress.com by 210.87.254.42 on 09/06/12
For personal use only.

with weight c_{ij}; if $c_{ij} = 0$, do not depict an arc from C_i to C_j. In this way, a one-to-one correspondence between the matrix and the directed graph is established.

Now, it is obvious that the matrix corresponding to the directed graph $\mathscr{D}^{\dagger}_{1,n}$ obtained through steps (*a*), (*b*), and (*d*) is exactly $\mathbf{K}_{\bar{1},\bar{1};\bar{n},\bar{n}}$. Consequently, we can use the graphical method as given in part *d* of Rule 3 and the check formula [14] to calculate $N_{1,n} = \det \mathbf{K}_{\bar{1},\bar{1};\bar{n},\bar{n}}$ of eq. [A.6]. Proof concerning the last step involves more terminology of graph theory and hence is omitted. The interested reader can find the details of the proof in ref. 14.

As for N_1 and N_n, let us consider the following hypothetical equations:

$$\text{[A.7]} \quad \begin{cases} \sum_{i=1}^{n} k_{1i}x_1 - k_{21}x_2 - \cdots - k_{n1}x_n = 0 \\ -k_{12}x_1 + \sum_{i=1}^{n} k_{2i}x_2 - \cdots - k_{n2}x_n = 0 \\ \quad\vdots \qquad\quad \vdots \qquad\qquad\quad \vdots \\ -k_{1n}x_1 - k_{2n}x_2 - \cdots \sum_{i=1}^{n} k_{ni}x_n = 0 \end{cases}$$

$$\text{[A.8]} \quad x_1 + x_2 + \cdots + x_n = 1$$

The n equations in [A.7] are linearly dependent since their sum is always equal to zero (note that $k_{ii} = 0$ according to the previous prescription). In order to get the definite solutions, we can replace any one of [A.7] with eq. [A.8].

If we use eq. [A.8] to replace the nth equation in [A.7], then from Cramer's rule and the properties of determinants, we can obtain

$$\text{[A.9]} \quad x_n = N_n \Big/ \sum_{i=1}^{n} N_i$$

where

$$\text{[A.10]} \quad N_i = \det \mathbf{K}_{\bar{i},\bar{i}} \quad (i = 1, 2, \ldots, n)$$

Therefore, N_n in [A.9] is just the same as that given in [A.4].

On the other hand, if we use [A.8] to replace the γth ($\gamma \neq n$) equation in [A.7], the result of x_n thus derived should remain the same, and can also be written as [A.9]. But for these n equations, according to ref. 25, N_n, the numerator of the root x_n, can also be calculated with the schematic method as given in part *c* of Rule 3 and with eq. [13] as a check formula. Obviously, such a conclusion can be extended to cover any of N_i ($i = 1, 2, \ldots, n$).

This completes the proof of Rule 3.

Appendix 4. The Mathematical Principles of Rule 4

Actually, the equations describing the second-category steady-state reaction system, whose common expression is given in [18], can be directly obtained from the hypothetical eqs. [A.7] and [A.8] by replacing $x_1, x_2, \ldots, x_n, 1$ with $e_1, e_2, \ldots, e_n, e_0$, respectively.

Likewise, according to Cramer's rule and the properties of determinants, we have

$$e_m = \left(N_m \Big/ \sum_{i=1}^{n} N_i\right) e_0 \quad (m = 1, 2, \ldots, n)$$

where the N_i are exactly the same as those in [A.10]. Therefore, the proof given in Appendix 3 has already covered the remaining part of the mathematical principles of Rule 4.

Can. J. Chem. Downloaded from www.nrcresearchpress.com by 210.87.254.42 on 09/06/12
For personal use only.

Can. J. Chem. Downloaded from www.nrcresearchpress.com by 210.87.254.105 on 09/06/12
For personal use only.

COMMUNICATION

Spin trapping chemistry of 3,3,5,5-tetramethylpyrroline-*N*-oxide: an improved cyclic spin trap

EDWARD G. JANZEN, RAGHAV V. SHETTY, AND SUSAN M. KUNANEC

Department of Chemistry, Guelph–Waterloo Centre for Graduate Work in Chemistry, University of Guelph, Guelph, Ont., Canada N1G 2W1

Received November 17, 1980

EDWARD G. JANZEN, RAGHAV V. SHETTY, and SUSAN M. KUNANEC. Can. J. Chem. **59**, 756 (1981).

The use of 3,3,5,5-tetramethylpyrroline-*N*-oxide as a spin trap has been investigated. Spin adducts are found to be more persistent than for 5,5-dimethylpyrroline-*N*-oxide (DMPO) although the esr spectra are quite similar.

EDWARD G. JANZEN, RAGHAV V. SHETTY et SUSAN M. KUNANEC. Can. J. Chem. **59**, 756 (1981).

On a étudié la possibilité d'utiliser le *N*-oxyde de la tétraméthyl-3,3,5,5 pyrroline comme capteur de spin. On a trouvé que les adduits de spin qui en découlent sont plus persistants que ceux qui proviennent du *N*-oxyde de diméthyl-5,5 pyrroline (ODMP); ceci en dépit du fait que les spectres rpe sont tout à fait semblables dans les deux cas.

[Traduit par le journal]

Introduction

Many applications of the use of 5,5-dimethylpyrroline-*N*-oxide, **1**, (DMPO) as a spin trap have been published since the first esr study appeared in the literature (1–3). The β-hydrogen hyperfine splitting constants (β-H hfsc's) of the spin adducts vary markedly with the nature of the radical trapped, and the rate constant of spin trapping is very fast (4–7). DMPO has been particularly useful in trapping hydroxyl radicals in the presence of hydrogen peroxide or superoxide because the spectra of the spin adducts of the hydroxy and hydroperoxy/peroxy anion are easily distinguishable (8, 9). Both adducts appear to be reasonably persistent in a number of solvents (10–12).

However, other DMPO adducts have relatively short lifetimes and sometimes cannot be detected under normal spin trapping conditions, e.g. alkyl, aryl, benzoyloxy adducts. Since disproportionation of cyclic nitrones with β-methine hydrogens is probably relatively fast (13) it seems reasonable to expect that steric hindrance could slow down this reaction and thus make the spin adducts more persistent. The nitrone desired would be 3,3,5,5-tetramethylpyrroline-*N*-oxide (**3**).[1] This compound was synthesized by a literature procedure (14) and the spin trapping chemistry investigated. Preliminary results are reported here.

Since the acronym TMPO has already been used for **2** (2, 11) we suggest 3,3,5,5-M_4PO for **3** (or M_4PO) and hence 5,5-M_2PO for **1** and 2,5,5-M_3PO for **2**.

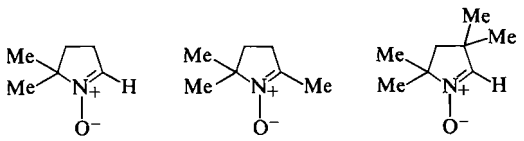

1 5,5-M_2PO

2 2,5,5-M_3PO

3 3,3,5,5-M_4PO

Results

The spin adduct spectra of M_4PO consist of doublets of triplets or triplets of doublets depending on the radical trapped (see Table 1). As was found for DMPO adducts, nonpolar substituents give spectra with relatively large β-H hfsc's, e.g. alkyl or aryl. The β-H must be in a pseudo-axial position if $a_\beta^H \simeq 26$–30 G. However, for electron-withdrawing polar groups the β-H hfsc is much smaller, indicating that the polar substituent prefers the pseudo-axial position regardless of bulk. For DMPO only the hydroxy and azidyl adducts have $a_N = a_\beta^H$ (8, 16). In the M_4PO adducts $a_N \neq a_\beta^H$ for the hydroxy adduct but $a_N = a_\beta^H$ for azidyl and acyl adducts. This coincidence of hfsc's seems fortuitous. It should be noted that no γ-H hfs is

[1]Compound **3** is a colorless, crystalline solid at room temperature (mp 33–35°C) and easier to handle than DMPO. Compound **3** is purified by recrystallization from pentane and is soluble in a wide range of polar and nonpolar solvents.

0008-4042/81/040756-03$01.00/0

©1981 National Research Council of Canada/Conseil national de recherches du Canada

TABLE 1. Hyperfine splitting constants for spin adducts of 3,3,5,5-tetramethylpyrroline-*N*-oxide[a]

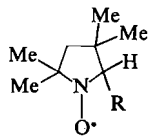

Radical (R·)	Source and solvent	a_N (G)	a_β^H (G)
CH_3·	30% H_2O_2, DMSO, H_2O, *hν*	16.60	27.00
C_6H_5·	Phenylazotriphenylmethane, benzene	14.41	23.86
$HOCH_2$·	CH_3OH, Ph_2CO, *hν*	15.12	21.99
HOO·[b]	1% H_2O_2, buffer pH 6, *hν*	15.67	20.02
·CO_2^-	HCO_2Na, DBPO,[c] H_2O	15.71	19.85
H·	*n*-Bu_3SnH, benzene[d]	14.61	18.29 (2H)
	n-Bu_3SnH, methanol[d]	15.56	19.8 (2H)
HO·	10% H_2O_2, buffer[e] pH 6, *hν*	15.30	16.88
	1% H_2O_2, buffer[e] pH 6, *hν*	15.28	16.73
	$Na_2S_2O_8$, buffer[e] pH 6	15.29	16.81
	$Na_2S_2O_8$, buffer[f] pH 2	15.29	16.82
N_3·	NaN_3,[g] $Na_2S_2O_8$, H_2O	14.88	14.88[h]
$C_6H_5\dot{C}$=O	PhCHO, DBPO	14.18	14.18
$(CH_3)_2N\dot{C}$=O	DMF, DBPO	13.59	13.59
$SO_4^{\cdot-}$	$Na_2S_2O_8$, buffer[e] pH 6	14.04	8.34
	$Na_2S_2O_8$, buffer[f] pH 2	13.99	8.33
$C_6H_5CO_2$·	$(PhCO)_2$, benzene	12.53	7.97
$O_2^{\cdot-}$	KO_2, benzene, dch-18-crown-6[i]	13.38	7.95
$(CH_3)_3CO$·	DBPO, benzene	13.31	5.81

[a] At room temperature.
[b] Tentative assignment.
[c] DBPO = di-*tert*-butylperoxalate.
[d] Spontaneous spin adduct formation.
[e] Commercial potassium phosphate monobasic – sodium hydroxide buffer containing formalin as inhibitor.
[f] Commercial potassium chloride – hydrochloric acid buffer containing formalin as inhibitor.
[g] Additional lines due to other spin adducts and nitroxyl radicals; see ref. 15.
[h] a_β^N = 2.98 G; see ref. 16.
[i] 0.1 *M* Dicyclohexyl-18-crown-6 ether.

found for M_4PO adducts, indicating that in DMPO adducts this splitting comes from the 3-position.

Of interest is the observation that spin adducts of M_4PO are much more persistent than those of DMPO. Thus the phenyl and benzoyloxy adducts of M_4PO still give strong esr spectra even after 2 or 3 days, whereas with DMPO the former is very weak after one hour, while the latter cannot be detected at all using phenylazotriphenylmethane and benzoyl peroxide in benzene at room temperature, respectively. In competition experiments using 0.05 *M* of both phenyl *tert*-butyl nitrone (PBN) and M_4PO in the same solution and 0.003 *M* di-*tert*-butylperoxalate as a *tert*-butoxyl radical source the ratio of the initial slopes of the intensities of the spin adduct spectra is 16:5 for M_4PO:PBN, i.e. the rate constant for spin trapping *tert*-butoxyl radicals is about 3× faster for M_4PO than for PBN. Based on earlier data (4) it can be estimated that the rate constant for trapping *tert*-butoxyl radicals is only 3× slower for M_4PO than for DMPO. It thus appears that by introducing two methyl groups in the 3-position of a 5-membered ring nitrone the usefulness as a spin trap can be greatly enhanced because the relatively small loss in rate of the spin trapping reaction due to steric hindrance is more than made up for by the large gain in spin adduct persistence.

Acknowledgements

The suggestion that 3,3,5,5-tetramethylpyrroline-*N*-oxide was the spin trap to study came from Dr.

Can. J. Chem. Downloaded from www.nrcresearchpress.com by 210.87.254.105 on 09/06/12
For personal use only.

K. U. Ingold on the occasion of the International symposium on Electron Spin Resonance in Chemistry in Thessaloniki, Greece on Sept. 23–29, 1979. This work is being supported by the Natural Sciences and Engineering Research Council of Canada. Grateful acknowledgement is hereby made.

1. M. IWAMURA and N. INAMOTO. Bull. Chem. Soc. Jpn. **40**, 702 (1967).
2. E. G. JANZEN and J. I.-P. LIU. J. Magn. Reson. **9**, 510 (1973); E. G. JANZEN, C. A. EVANS, and J. I.-P. LIU. J. Magn. Reson. **9**, 511 (1973).
3. E. G. JANZEN. *In* Free radicals in biology. Vol. IV. *Edited by* W. A. Pryor. 1980. p. 115.
4. E. G. JANZEN and C. A. EVANS. J. Am. Chem. Soc. **95**, 8205 (1973).
5. E. G. JANZEN, C. A. EVANS, and E. R. DAVIS. *In* Organic free radicals. *Edited by* W. A. Pryor. ACS Symposium Series, **69**, 433 (1978).
6. Y. MAEDA, P. SCHMID, D. GRILLER, and K. U. INGOLD. Chem. Commun. 525 (1978).
7. Y. MAEDA and K. U. INGOLD. J. Am. Chem. Soc. **101**, 4975 (1979).
8. J. R. HARBOUR, V. CHOW, and J. R. BOLTON. Can. J. Chem. **52**, 3549 (1974).
9. E. G. JANZEN, D. E. NUTTER, JR., E. R. DAVIS, B. J. BLACKBURN, J. L. POYER, and P. B. MCCAY. Can. J. Chem. **56**, 2237 (1978).
10. J. R. HARBOUR and M. L. HAIR. J. Phys. Chem. **82**, 1397 (1978).
11. E. FINKELSTEIN, G. M. ROSEN, and E. J. RAUCKMAN. J. Am. Chem. Soc. **102**, 4994 (1980).
12. P. R. MARRIOTT, M. J. PERKINS, and D. GRILLER. Can. J. Chem. **58**, 803 (1980).
13. K. U. INGOLD. *In* Free radicals. Vol. I. *Edited by* J. K. Kochi. 1973. p. 63.
14. R. BONNETT, R. F. C. BROWN, V. M. CLARK, I. O. SUTHERLAND, and A. TODD. J. Chem. Soc. 2094 (1959).
15. E. G. JANZEN, H. J. STRONKS, D. E. NUTTER, JR., E. R. DAVIS, H. N. BLOUNT, J. L. POYER, and P. B. MCCAY. Can. J. Chem. **58**, 1596 (1980).
16. W. KREMERS and A. SINGH. Can. J. Chem. **58**, 1592 (1980).

Can. J. Chem. Downloaded from www.nrcresearchpress.com by 210.87.254.105 on 09/06/12
For personal use only.

Constantes d'ionisation de dérivés de la pyrazolidine-3,5-dione dans l'éthanol. Relation avec l'électroactivité

CLAIRE GUEUTIN-PELINARD, ELISABETH NIVAUD, PATRICK BOUCLY ET MICHEL GUERNET

Laboratoire de Chimie Analytique, Centre d'Etudes Pharmaceutiques, Rue J. B. Clement, 92290 Chatenay Malabry, France

Reçu le 21 mars 1980[1]

CLAIRE GUEUTIN-PELINARD, ELISABETH NIVAUD, PATRICK BOUCLY et MICHEL GUERNET. Can. J. Chem. **59**, 759 (1981).

Les constantes d'ionisation de dérivés pharmacologiquement actifs de la pyrazolidine-3,5-dione ont été déterminées dans l'éthanol par potentiométrie et spectrophotométrie. L'électroactivité de ces composés est sous la dépendance de l'équilibre entre les formes énolique et dicétonique existant dans ce solvant.

CLAIRE GUEUTIN-PELINARD, ELISABETH NIVAUD, PATRICK BOUCLY, and MICHEL GUERNET. Can. J. Chem. **59**, 759 (1981).

Ionisation constants of some pyrazolidine-3,5-dione derivatives were measured in ethanol by potentiometric and spectrophotometric methods. The electroactivity of these compounds is in relation to the enolic and diketonic equilibrium in this medium.

Introduction

La réduction électrochimique dans l'éthanol de quelques dérivés de la pyrazolidine-3,5-dione a été précédemment étudiée (1). En voltampérométrie linéaire à une électrode de mercure, la phénylbutazone, l'oxyphenbutazone, la cétophénylbutazone, la prénazone et la sulfinpyrazone, se réduisent à des potentiels de demi-vague très voisins. Cependant, les intensités limites pour des concentrations et des conditions expérimentales identiques varient considérablement de l'un à l'autre de ces composés.

La présente étude a pour but de préciser les réactions mises en jeu lors des réductions électrochimiques et d'expliquer les variations de courant observées. Les déterminations potentiométrique et spectrale des pK_a apparents des différents dérivés et l'étude de leur électroactivité en fonction de l'acidité du milieu permettent de proposer une relation entre l'électroactivité et les équilibres entre les différentes formes tautomères présentes en solution.

Résultats

Les composés étudiés existent sous deux formes moléculaires tautomères, énolique et dicétonique, et sous une forme anionique, énolate; les constantes d'acidité apparentes globales mesurées correspondent à l'ensemble des équilibres en solution (éq. [1]).

L'expression des constantes d'acidité apparentes K_a peut s'écrire:

$$K_a = \frac{[\text{énolate}][H^+]}{[\text{moléculaire}]}$$

[1]

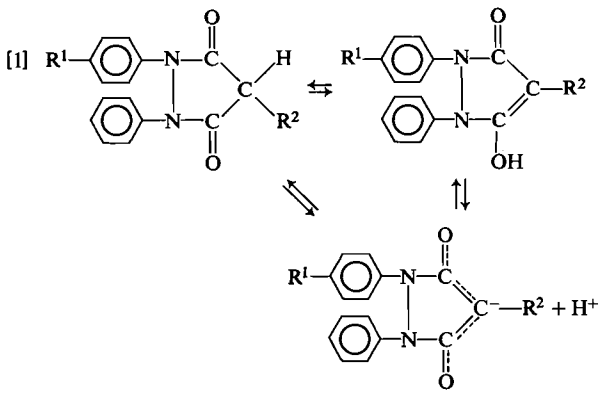

Composé	R^1	R^2
Phénylbutazone	H	C_4H_9
Oxyphenbutazone	OH	C_4H_9
Cétophénylbutazone	H	$CH_2-CH_2-C(=O)-CH_3$
Sulfinpyrazone	H	$CH_2-CH_2-S(=O)-C_6H_5$
Prénazone	H	$CH_2-CH=C(CH_3)_2$

La forme moléculaire est constituée de la forme énol et de la forme dicétone, il en résulte que l'égalité suivante est toujours vérifiée: [moléculaire] = [dicétone] + [énol].

La méthode de détermination spectrophotométrique de ces constantes K_a met à profit le fait qu'en milieu très acide ces dérivés existent uni-

[1]Révision reçue le 5 novembre 1980.

0008-4042/81/050759-04$01.00/0

©1981 National Research Council of Canada/Conseil national de recherches du Canada

Can. J. Chem. Downloaded from www.nrcresearchpress.com by 210.87.254.6 on 09/06/12
For personal use only.

TABLEAU 1. Longueurs d'onde (λ_m) et coefficients d'extinction moléculaire (ε) déterminés au maximum d'absorption de chaque composé en milieux neutre, acide et basique

Composé	Milieu neutre		Milieu acide		Milieu alcalin	
	λ_m (nm)	ε	λ_m (nm)	ε	λ_m (nm)	ε
Phénylbutazone	245	14010	240	14960	266	23930
Cétophénylbutazone	253	16370	242	16040	263	24110
Sulfinpyrazone	246	24570	242	19850	261	28890
Oxyphenbutazone	242	17400	240	17790	265	23770
Prénazone	241	15460	241	15640	269	24460

TABLEAU 2. Constantes d'ionisation et charactéristiques électrochimiques

Paramètres	Composés				
	Phénylbutazone	Cétophénylbutazone	Oxyphenbutazone	Sulfinpyrazone	Prénazone
pK_a (potentiométrie)	8,26 ± 0,04	7,60 ±0,06	8,87 ±0,06	6,89 ± 0,04	8,53 ± 0,06
pK_a (spectrophotométrie)	8,27 ± 0,05	7,62 ± 0,03	9,05 ± 0,03	6,84 ± 0,06	8,56 ± 0,02
$E_{\frac{1}{2}}$ (en volt) (F_c/F_c^+)	−1,835	−1,905	−1,930	−1,910 −1,630	−1,855
I_1 (en nA)	400	600	280	320 480	200

quement sous forme moléculaire dicétonique (2) et absorbent dans l'ultra-violet; en milieu basique la forme ionisée (énolate) qui prédomine absorbe également mais la longueur d'onde du maximum d'absorption est différente de celle de la forme moléculaire dicétonique. Les valeurs des différents paramètres spectraux déterminés en milieu neutre, perchlorique (1 *M*) et en présence d'éthylate de sodium (1 *M*) sont reportés dans le tableau 1.

Les pK_a sont déterminés selon la méthode décrite par Albert et Serjeant (3); les variations d'absorbance *A* en fonction du pH tamponné de la solution éthanolique, déterminées au maximum d'absorption de la forme énolate permettent d'atteindre les constantes d'acidité apparentes en utilisant la relation:

$$pK_a = pH_i + \log \frac{(A\ pH_b - A\ pH_i)}{(A\ pH_i - A\ pH_a)}$$

ou pH_i = pH du tampon utilisé, $A\ pH_i$ = absorbance de la solution tamponnée, $A\ pH_b$ = absorbance en milieu éthylate de sodium 0,1 *N* et $A\ pH_a$ = absorbance en milieu perchlorique 0,1 *N*.

Les tampons sont choisis de telle manière que le pH soit proche du pK_a apparent à déterminer; le couple acide dichloroacétique/dichloroacétate de sodium, pK_a = 6,89 (4) est employé pour la cétophénylbutazone et la sulfinpyrazone; le couple acide monochloracétique/monochloracétate de sodium, pK_a = 8,51 (4) est utilisé pour la phénylbutazone, l'oxyphenbutazone et la prénazone. Les valeurs obtenues et leurs limites de confiance, calculées pour un risque d'erreur à 5% sont reportées dans le tableau 2.

Dans le double but de confirmer ces valeurs et d'étudier l'influence de la concentration sur l'équilibre dicétoénolique, une détermination de ces mêmes constantes a été effectuée par potentiométrie avec une électrode à hydrogène. Le domaine de concentration utilisable pour ces déterminations est alors trois cents fois supérieur à celui des déterminations spectrales. En effet il n'était pas exclu que la dilution ait une influence sur cet équilibre, entraînant une variation du pK_a apparent.

Les pK_a sont déterminés par mesure du pH d'une solution éthanolique de concentration équimoléculaire (10^{-2} *M*) en forme moléculaire et en base conjuguée. Le pH est mesuré à l'aide d'une électrode à hydrogène préalablement étalonnée. L'expression du pH de la solution est donnée par la relation (5):

$$pH_x = pH_s + \frac{(E_x - E_s)F}{2{,}303\ RT}$$

ou pH_x = pH à déterminer, pH_s = pH du tampon standard utilisé, E_x = potentiel de la solution de la substance à étudier, E_s = potentiel de la solution tampon standard, F = 96 487 C mol^{-1}, R = 8,3143 J K^{-1} mol^{-1} et T = température en degré K.

Les valeurs des pK_a obtenus sont résumées dans le tableau 2. Une étude statistique de comparaison des moyennes obtenues pour chaque composé par l'une ou l'autre méthode montre que celles-ci ne sont pas significativement différentes pour un risque d'erreur inférieur à 5% à l'exception de l'oxyphenbutazone pour lequel l'écart entre les deux méthodes atteint 0,18 unité pH.

Can. J. Chem. Downloaded from www.nrcresearchpress.com by 210.87.254.6 on 09/06/12
For personal use only.

Can. J. Chem. Downloaded from www.nrcresearchpress.com by 210.87.254.6 on 09/06/12
For personal use only.

Une bonne concordance est donc observée entre les déterminations spectrophotométriques et potentiométriques.

Les potentiels de demi-vague ($E_{\frac{1}{2}}$) mesurés par rapport à celui du système ferrocène–ferrocinium et les intensités limites (I_l) observées en solution éthanolique en milieu neutre en présence de perchlorate de lithium sont reportés dans le tableau 2. Les voltampérogrammes réalisés dans l'éthanol en milieu acide ($HClO_4$ $2 \cdot 10^{-3}$ *M*) et basique (EtONa $2 \cdot 10^{-3}$ *M*) ne présentent pas de vague de réduction correspondant au composé étudié. Dans le dichlorométhane en présence de perchlorate de tétrabutylammonium, les composés étudiés ne sont pas électroréductibles.

Discussion

La valeur du courant limite I_l est reliée à la concentration de la forme électroactive C_s selon la loi de Fick $I_l = -n \cdot d \cdot C_s$ (*n* étant le nombre d'électrons échangés, *d* le coefficient de proportionalité). L'électrolyse à potentiel imposé (1) montre que ces composés se réduisent tous selon un processus monoélectronique; en admettant que pour ces dérivés de structure voisine, les coefficients de diffusion sont très peu différents, les intensités observées I_l, sont directement fonction de la concentration de la forme électroactive présente en solution. Il apparaît à l'exception de la sulfinpyrazone qui se réduit en deux étapes en raison de la présence d'un groupement sulfoxyde et qui de ce fait doit être considérée à part, que plus le pK_a est petit, plus le courant limite est important. Les mesures voltampérométriques étant effectuées en milieu non tamponné, il est exclu que les valeurs de courant observées soient imputables à l'autodissociation (acide/base conjuguée) en solution; en effet, compte tenu des valeurs des pK_a, le pourcentage infime de ces composés sous forme énolate dans les conditions de la voltampérométrie est indécelable. Les différences de courant observées ne peuvent s'expliquer que par la possibilité pour ces dérivés d'exister sous plusieurs formes dont une seule serait électroactive.

La forme énolique étant plus acide que la forme dicétonique, l'augmentation du rapport [énol]/[cétone] entraîne une diminution du pK_a apparent. Comme l'acidité apparente des composés évolue dans le même sens que les intensités limites de diffusion, il apparaît vraisemblable que seule la forme énolique est électroréductible. Notons que les constantes d'ionisation apparentes ne sont pas liées uniquement à l'équilibre cétoénolique mais aussi à la nature des différents substituants R^1 et R^2; la constante d'ionisation globale ne permet pas de déterminer la part qui revient à chacun des facteurs.

Cependant, l'hypothèse de la corrélation entre le pK_a, l'équilibre dicétoénolique et le courant limite de diffusion est confirmée par l'étude de l'électroactivité en fonction du pH dans l'éthanol. En effet, l'étude voltampérométrique montre que l'électroactivité disparaît lors de l'addition de protons: celle-ci entraîne une prédominance de la forme dicétonique par déplacement de l'équilibre [1]. De même, dans un milieu alcalinisé par l'éthylate de sodium il n'existe pas de vague de diffusion correspondant à la réduction du composé; l'énolate n'est donc pas électroactif.

Dans le dichlorométhane, solvant dans lequel seule la forme dicétonique est présente (2), aucune réduction électrochimique n'a été mise en évidence.

La forme énolique peut donc seule être responsable de l'électroactivité de ces molécules; ceci est confirmé par le fait que les dérivés de la pyrazolidine-3,5-dione disubstitués en 4 qui ne peuvent exister sous forme énol ne sont pas réductibles dans les conditions décrites (1).

La réaction électrochimique peut être schématisée:

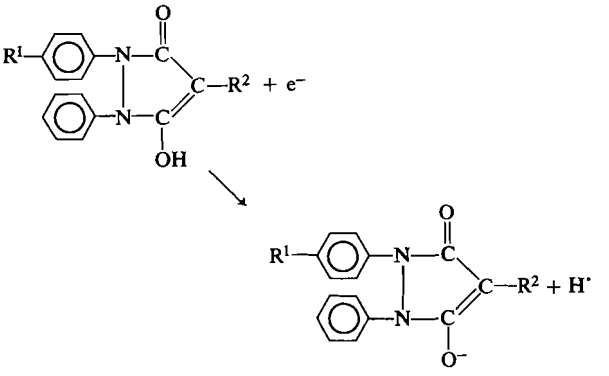

Conclusions

Les formes énoliques de la phénylbutazone, de la prénazone, de la cétophénylbutazone et de l'oxyphenbutazone sont responsables de l'électroactivité de ces molécules. Les intensités limites correspondant aux vagues de réduction observées en voltampérométrie linéaire augmentent lorsque la constante d'ionisation augmente; l'exploitation des courbes intensité–potentiel apporte des renseignements précieux sur la structure des composés en solution.

Partie expérimentale

Réactifs

Ethanol Merck deshydraté par la méthode de Lund et Bjerrum (6). La teneur en eau déterminée par la méthode de Karl Fischer est inférieure à 0,025%. Acide glycolique cristallisé dans

l'acétone. Acide monochloracétique cristallisé dans le benzène. Acide dichloracétique purifié par distillation fractionnée. Acide salicylique et barbital: Fluka. Phénylbutazone, oxyphenbutazone, cétophénylbutazone, prénazone et sulfinpyrazone: leur pureté est vérifiée par ccm sur plaque de silicagel fluorescent en utilisant comme solvant, soit cyclohexane/méthylisobutylcétone/acide acétique glacial (80:35:5) (phénylbutazone R_f 0,77, oxyphenbutazone R_f 0,40, cétophénylbutazone R_f 0,25); soit cyclohexane/chloroforme/méthanol/acide acétique glacial (60:30:5:5) (sulfinpyrazone R_f 0,34, prénazone R_f 0,50). La migration est effectuée sous atmosphère d'azote, à l'abri de la lumière. La teneur en eau déterminée par la méthode de Karl Fischer est inférieure à 0,2%.

Matériel et technique

Les pK_a sont déterminés par spectrophotométrie (3) en solution $3 \cdot 10^{-5}$ M au maximum d'absorption de la forme anionique (spectrophotomètre Varian type 635) à 25° ± 0,1°C. Pour chaque produit 7 déterminations sont effectuées à l'aide de 7 tampons de pH correspondant à $pK_a \pm 0{,}6$, $pK_a \pm 0{,}4$, $pK_a \pm 0{,}2$ et pK_a (valeur approximative déterminée lors d'un essai préliminaire).

Les déterminations potentiométriques sont réalisées en solution éthanolique 10^{-2} M neutralisées à 50% par addition d'éthanolate de sodium, à l'aide de la cellule: Pt/H_2 (1 atmosphère) solution tampon//LiCl (0,1 M) AgCl/Ag. L'électrode à hydrogène est à plaque de platine platiné Tacussel type Pt151. L'électrode de référence est une électrode Ag/AgCl. Quatre mesures indépendantes sont réalisées pour chaque composé. L'étalonnage est réalisé à l'aide de 2 solutions tampons (5), acide salicylique 10^{-2} M/salicylate de Li 10^{-2} M et acide diéthylbarbiturique 10^{-2} M/diéthylbarbiturate de Na 10^{-2} M. Les mesures de potentiel sont effectuées à 25°C ± 0,1° sur un millivoltmètre Tacussel S70AS/N.

Les mesures voltampérométriques sont réalisées en solution éthanolique $2 \cdot 10^{-3}$ M en présence de perchlorate de lithium 0,2 M (Merck pour analyse). Les potentiels sont imposés à l'aide d'un potentiostat Tacussel type PRG 5. Les électrodes utilisées sont les suivantes. Electrode de travail: électrode à goutte de mercure à temps de goutte imposé Tacussel type MPO; électrode de référence: électrode au calomel aqueux; électrode auxiliaire: électrode de platine poli.

1. C. Pelinard, E. Nivaud et P. Boucly. Talanta, **25**, 119 (1978).
2. V. J. Stella et J. D. Pipkin. J. Pharm. Sci. **65**, 1161 (1976).
3. A. Albert et E. P. Serjeant. Ionisation constants of acids and bases. Chapman and Hall, London. 1971.
4. L. J. Minnick et M. Kilpatrick. J. Phys. Chem. **43**, 259 (1939).
5. R. G. Bates. Determination of pH. 2ième éd. John Wiley and Sons, New York. 1973.
6. H. Lund et J. Bjerrum. Ber. B, **64**, 210 (1931).

Can. J. Chem. Downloaded from www.nrcresearchpress.com by 210.87.254.6 on 09/06/12
For personal use only.

Chemistry of chelocardin. V.[1] Condensation with amino reagents

DANIEL T. W. CHU,[2,3] STUART N. HUCKIN,[4] EDITH BERNSTEIN, AND DAVID L. GARMAISE[3]
Abbott Laboratories, Montreal, P.Q., Canada H3C 3K6
AND
RICHARD S. EGAN[5] AND RUTH S. STANASZEK
Abbott Laboratories, North Chicago, IL 60064, U.S.A.

Received August 22, 1980

DANIEL T. W. CHU, STUART N. HUCKIN, EDITH BERNSTEIN, DAVID L. GARMAISE, RICHARD S. EGAN, and RUTH S. STANASZEK. Can. J. Chem. **59**, 763 (1981).

The nature of the products obtained from the reaction of chelocardin (**1**) and the model compound 2-acetyldimedone (**5**) with a variety of amines was investigated. It was observed that amines react with β-triketones having an exocyclic carbonyl side-chain to give exclusively β,β′-diketoenamines with substitution at the side-chain carbonyl.

DANIEL T. W. CHU, STUART N. HUCKIN, EDITH BERNSTEIN, DAVID L. GARMAISE, RICHARD S. EGAN et RUTH S. STANASZEK. Can. J. Chem. **59**, 763 (1981).

On a étudié la nature des produits provenant de la réaction de la chélocardine (**1**) et du composé type l'acétyl-2 dimédone (**5**) avec différentes amines. On a observé que les amines réagissent avec les β tricétones ayant sur la chaîne latérale un groupe carbonyle exocyclique pour conduire exclusivement aux β,β′-dicétoénamines portant le substituant au niveau du carbonyle de la chaîne latérale.

[Traduit par le journal]

Chelocardin, a broad spectrum antibiotic that was first described in 1962 (1) and subsequently shown to be **1** (2), possesses a β-triketone system in ring A. During the course of our chemical investigation on the modifications of chelocardin, it was found that the ring A β-triketone is the most reactive center in the molecule and is highly susceptible to chemical modification.

We have reported that chelocardin hydrochloride (**1**) reacted with a variety of amino compounds (amines, hydrazines, hydrazides, and aromatic amines) to yield 2a-substituted derivatives (**2**)[6] having antibacterial spectra similar to the parent antibiotic (3) as illustrated in Scheme 1.

The same reaction course was observed with *N*-carbobenzoxychelocardin (**3**) (4). Condensation of **3** with amino compounds also yielded 2a-substituted derivatives **4**. This exclusive substitution reaction represents a preferential attack of the side chain carbonyl to provide a novel β,β′-diketoenamine structure. An analogous condensation of the exocyclic carbonyl in the β-tricarbonyl system of usnic acid has recently been reported (5). However, the spectroscopic data were not sufficient to establish the substitution at the exocyclic carbonyl instead of the other two carbonyl groups. The correctness of the structural assignments was only established by X-ray analysis.

This article presents our results on further chemical studies with model β-triketones designed to provide spectroscopic evidence to firmly establish the position of amino substitution.

The nmr spectra of chelocardin and its derivatives (other than a few 4-*N*-acyl derivatives) are poorly resolved. Hence, their nmr spectra offer little clue as to which carbonyl in ring A has undergone substitution. However, the ^{13}C nmr spectrum shows one resonance for each carbon in the molecule, and the structural assignments of these derivatives were based on extensive analyses of the ^{13}C nmr data.

The three carbonyl carbons of the A-ring β-triketone system and the C(12) carbonyl make up the four most downfield resonances of chelocardin hydrochloride and its derivatives in the ^{13}C nmr spectra. These resonances are all generally found between 170 ppm and 210 ppm. Comparison of the chemical shifts of 2-acetyldimedone (**5**) with ring A resonances of chelocardin hydrochloride (1) and *N*-carbobenzoxychelocardin (**3**) permits assignments of the corresponding carbons (Table 1).

[1]For Part IV of this series, see ref. 8.

[2]Author to whom correspondence concerning this paper should be addressed.

[3]Present address: Abbott Laboratories, D-482, North Chicago, IL 60064, U.S.A.

[4]Present address: Agassiz Research Station, P.O. Box 1000, Agassiz, B.C., Canada V0M 1A0.

[5]Present address: McNeil Laboratories, Fort Washington, PA 19034, U.S.A.

[6]In this paper structures are given as tautomer (I) for simplicity but an equilibrium with other tautomeric forms II and III and the geometric isomer IV is not excluded.

0008-4042/81/050763-05$01.00/0
©1981 National Research Council of Canada/Conseil national de recherches du Canada

Can. J. Chem. Downloaded from www.nrcresearchpress.com by 210.87.254.42 on 09/06/12
For personal use only.

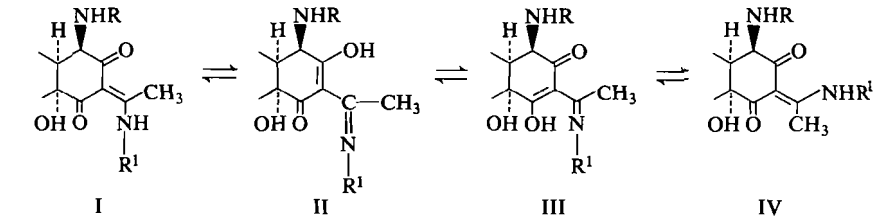

I II III IV

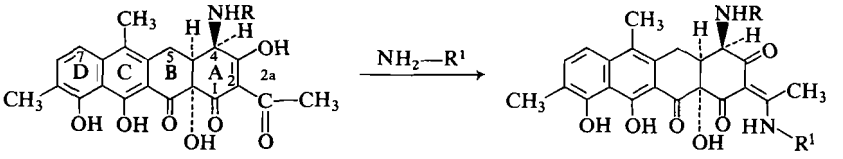

1 R = H·HCl
3 R = $COOCH_2C_6H_5$

2 R = H·HCl
4 R = $COOCH_2C_6H_5$

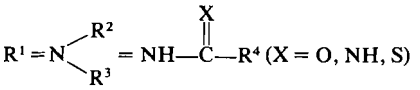

R^2, R^3, R^4 = alkyl or aromatic or H

SCHEME 1

TABLE 1. Comparative ring A ^{13}C nmr chemical shift data[a] of chelocardin (**1**), *N*-carbobenzoxychelocardin (**3**), and 2-acetyldimedone (**5**)

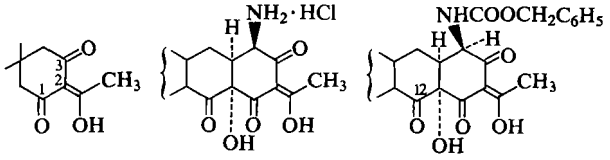

5 **1** **3**

Assignments	5	1	3
C(1)	196.3	190.6	190.6
C(3)	196.3	191.1	196.0
C(2)	112.0	110.7	111.2
C(2a)	201.6	200.0	200.5
C(2a)CH_3	28	26.5	26.3
C(12)	—	199.6	200.8

[a]Chemical shift data are given in ppm downfield from internal Me_4Si and spectra taken in Me_2SO.

The specific C(1) and C(3) assignments were made on the basis of relative insensitivity of C(1) to changes in the substituent at C(4). Differentiation between C(2a) and C(12) in *N*-carbobenzoxychelocardin (**3**) was made on the basis of long range couplings visible in coupled spectra; the 200.5 ppm resonance is clearly split into a quartet as a consequence of coupling with the methyl protons. Excellent agreement for C(2), C(2a), and C(2a)-methyl resonances was also observed. Hence a positive correlation with known derivatives of 2-acetyldimedone with respect to their ^{13}C nmr chemical shifts would firmly establish the position of substitution by the amino reagents.

2-Acetyl-5,5-dimethyl-3-*N*-pyrrolidylcyclohex-2-en-1-one (**8**) was prepared according to the method of Alt and Speziale (6) as shown in Scheme 2. Its structure was shown by nmr analysis to have no vinyl proton, and to possess two sets of nonequivalent methylene protons at δ 2.07 and δ 2.56 ppm.

Reaction of acetyldimedone (**5**) with pyrrolidine under similar experimental conditions as those for the preparation of aminochelocardin derivatives gave the pyrrolidylacetyldimedone (**9**). This compound is different from compound **8**, having a different R_f value in the thin-layer chromatographic analysis. Its nmr spectrum shows the presence of a singlet at δ 2.12 corresponding to four methylene protons. On the basis of symmetry considerations, the presence of the pyrrolidyl group at the side chain was fully established. This represents the first time a complete structure proof for the product of condensation of amines with a β-triketone sys-

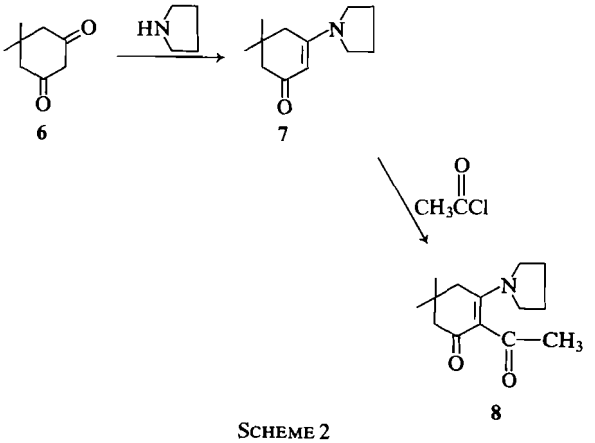

6 **7** **8**

SCHEME 2

Can. J. Chem. Downloaded from www.nrcresearchpress.com by 210.87.254.42 on 09/06/12
For personal use only.

TABLE 2. Comparative ^{13}C nmr chemical shift data[a] of 2-acetyldimedone (**5**) and substituted 2-acetyldimedones

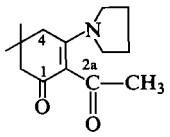

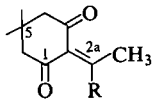

Assignments	**8**	**5** (R = OH)	**9** R =	**10** (R = NH_2)
C(1)	192.8	196.3	189.7	196.5
C(3)	164.8	196.3	189.7	196.5
(C2)	112.3	112.0	110.3	106.5
C(2a)[b]	198.1	201.6	176.0	173.2
C(2a)CH_3[b]	32.2	28	23.5	24
C(4)	43.1	48.8	51.6	52.3
C(6)	51.0	48.8	51.6	52.3
2C(5)CH_3	27.7	27.5	28.1	27.8

[a]See corresponding footnote to Table 1.
[b]Substantial changes occurred with substitution.

tem having an exocyclic carbonyl side chain was obtained by spectroscopic methods.

Aminoacetyldimedone (**10**) prepared by treatment of acetyldimedone (**5**) and hexamethyldisilazane or ammonium acetate (7) shows the presence of a singlet at δ 2.54 ppm corresponding to four methylene protons in its nmr spectrum. Its structure was established based on symmetry and off-resonance single frequency decoupling (ORSFD) considerations.

The nmr chemical shift data of 2-acetyldimedone (**5**) as well as the amino substituted 2-acetyldimedone derivatives **8**, **9**, and **10** are given in Fig. 1. No significant change in chemical shift for the 2a-methyl group is observed. Their comparative ^{13}C nmr chemical shift data are shown in Table 2. The ^{13}C nmr chemical shifts of the three carbonyl carbons of the β-triketone system and also the 2a-methyl of the 2-acetyldimedone (**5**) are profoundly affected by substitutions of amino functions on the 2a carbonyl as well as the 1 or 3 carbonyl as illustrated in Table 2.

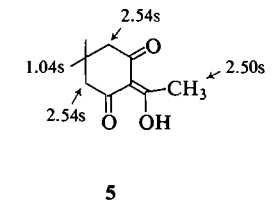

5

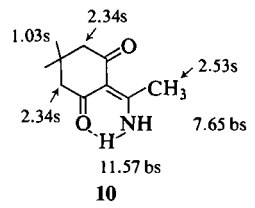

10

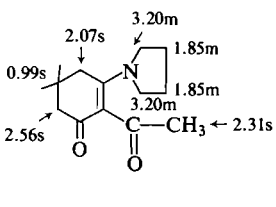

8

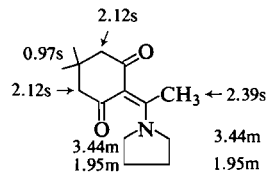

9

FIG. 1. Comparative nmr chemical shift data (given in ppm with spectra taken in DMSO-d_6) of 2-acetyldimedone (**5**) and substituted 2-acetyldimedones.

When the substitution of the amino group is on the 2a carbonyl (e.g. **9** and **10**), the C(2a) and C(2a)-methyl carbon resonances undergo substantial *upfield* shifts. On the other hand, when the substitution of the amino group is on the 1 or 3 carbonyl, the C(2a)-methyl carbon resonance undergoes substantial *downfield* shift. This observation in chemical shifts in ^{13}C nmr is extremely useful in the determination of the location of the substitution of amino reagents to chelocardin (**1**) or its *N*-protected derivatives.

All the amino-chelocardin derivatives obtained according to the route described (3) show an additional absorption at approximately 307–312 nm in their uv spectra, indicating the formation of a vinylogous imide system (6). Their mass spectra show the presence of several fragments normally found in the mass spectrum of chelocardin; the most important and prominent ion can be assigned to structure B shown in Fig. 2 (*m/e* 270, $C_{16}H_{14}O_6$) (2). This suggests that substitution of the amino group is not located in the B, C, and D rings.

In order to establish the position of the substitution, an analysis of the ^{13}C nmr spectra of the amino-chelocardin derivatives and also those of 2-acetyldimedone and its amino analogues was studied. The comparative ring A ^{13}C nmr chemical shift data of chelocardin hydrochloride (**1**), *N*-carbobenzoxychelocardin (**3**), and their amino derivatives **11**, **12**, **13**, **14**, **15**, and **16** are shown in Table 3. An excellent correlation was observed when their

Can. J. Chem. Downloaded from www.nrcresearchpress.com by 210.87.254.42 on 09/06/12
For personal use only.

Can. J. Chem. Downloaded from www.nrcresearchpress.com by 210.87.254.42 on 09/06/12
For personal use only.

TABLE 3. Comparative ring A ^{13}C nmr chemical shift data[a] of chelocardin (**1**), *N*-carbobenzoxychelocardin (**3**), and their derivatives

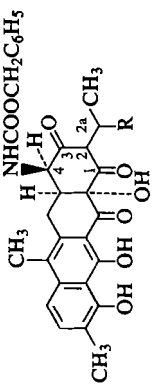

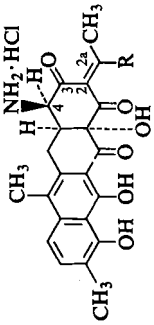

Assignments	1	11	12	3	13	14	15	16
	R = OH	R = *p*-NHC$_6$H$_4$—SO$_2$NH$_2$	R = NH—	R = OH	R = NH$_2$	R = N	R = NHCH$_2$C$_6$H$_5$	R = NHNHAc
C(1)	190.6	189.2	189.0	190.6	190.8	184.1	191.3	190.8
C(3)	191.1	191.1	191.0	196.0	192.0	185.6	191.3	192.1
C(2)	110.7	106.7	106.4	111.2	105.0	109.0	106.4	104.7
C(2a)[b]	200.0	173.9	174.1	200.5	174.5	176.6	173.8	169.4
C(2a)CH_3[b]	26.5	20.3	19.8	26.3	23.8	23.6	17.8	16.5

[a]See corresponding footnote to Table 1.
[b]Substantial upfield shift observed.

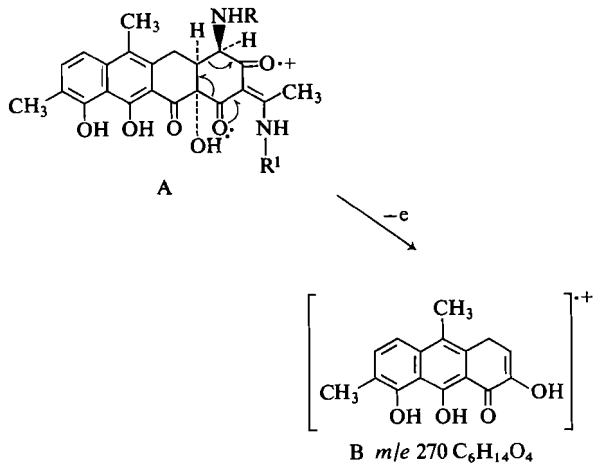

FIG. 2. Major fragmentation of chelocardin and analogues.

^{13}C nmr chemical shift values were compared with those of aminoacetyldimedones. (**13** vs. **10** and **14** vs. **9**). All the derivatives show substantial *upfield* shifts for their corresponding C(2a) and C(2a)-methyl carbon resonances. Using the previous observations with 2-acetyldimedone (**5**) and its amino analogues, all the amino-chelocardin analogues would have their amino substitutions at the 2a-carbonyl group. This confirms our previous finding that reaction of chelocardin hydrochloride (**1**) or *N*-carbobenzoxychelocardin (**3**) with amino reagents always gives rise to 2a-amino substituted chelocardin derivatives **2** or **4**.

In summary, we have provided a confirmation of the structures of the chemical reaction products obtained with the highly functionalized and reactive chelocardin and various amines. It further establishes a general reaction that a β-triketone having an exocyclic carbonyl function reacts with amines to give β,β′-diketoenamines having substitution exclusively on the exocyclic carbonyl.

Experimental

Melting points were determined on a Fisher-Johns melting point apparatus and are uncorrected. The infrared spectra were recorded on a Beckman Model IR8 infrared spectrophotometer. The nmr spectra were recorded on Varian Associates EM-360 and HA-100 spectrometers in deuterated solvents; resonance positions are given on the δ scale (ppm) relative to internal tetramethylsilane. The mass spectra were recorded on an AEI MS-902 double-focussing mass spectrometer. The uv spectra were recorded on a Unican SP-800A spectrometer in 0.1 *N* methanolic hydrogen chloride solution. The ^{13}C nmr spectra were recorded on a Varian Associates XL-100-15/TT-100 spectrometer system in Me_2SO; resonance positions are given in ppm relative to internal tetramethylsilane. Parameters used were pulse width (30°) 3.5/μs, pulse delay 0.5–1.0, 6K sweep width, and 8K data table.

Preparation of Amino Derivatives of Chelocardin

2a-Amino-substituted analogues of chelocardin were prepared according to the procedure reported previously (3, 4). The general procedure for the preparation of these analogues was to add a slight excess of 1 mole equivalent of the corresponding hydrazine, hydrazide, or aniline to a solution of chelocardin hydrochloride (**1**) or its free base or *N*-carbobenzoxychelocardin (**3**) in 98% aqueous tetrahydrofuran or methanol. (In the case of anilines, one to two mole equivalents of acetic acid was also added.) The reaction mixture was allowed to stand for at least 1 h at room temperature (a few compounds required a longer reaction time). The product was isolated by precipitation, filtration, and recrystallization.

Amino Derivatives of 2-Acetyldimedone

The 2-acetyl-5,5-dimethyl-3-*N*-pyrrolidylcyclohex-2-en-1-one (**8**) was prepared according to the method of Alt and Speziale (6). The preparation of 2-aminoacetyldimedone (**10**) was reported recently (7).

Pyrrolidylacetyldimedone (9)

Pyrrolidylacetyldimedone was prepared as follows. Pyrrolidine (71 mg, 1 mmol) was added to a solution of 2-acetyldimedone (182 mg, 1 mmol) in benzene (25 mL). After it was refluxed with removal of water for 8 h, the benzene was removed to give a yellow solid. Column chromatography on silica gel using chloroform/methanol (9:1) as eluent yielded 210 mg pure product **9** (90% yield). The nmr and ^{13}C nmr data are given in the text. *Anal.* calcd. for $C_{14}H_{21}NO_2$: C 71.45, H 8.99, N 5.95; found: C 71.15, H 9.10, N 5.91.

Acknowledgements

We thank the staff of the microanalytical department of Abbott Laboratories for the elemental analyses and Sandra L. Mueller for recording the mass spectra.

1. T. J. Oliver, J. F. Prokop, R. R. Bower, and R. H. Otto. Antimicrob. Agents Chemother. 583 (1962); A. C. Sinclair, J. R. Schenck, G. C. Post, E. V. Cardinal, S. Burokas, and H. H. Fricke. Antimicrob. Agents Chemother. 592 (1962).
2. L. A. Mitscher, W. Rosenbrook, Jr., W. W. Andres, R. S. Egan, J. Schenck, and J. V. Juvarkar. Antimicrob. Agents Chemother. 38 (1970); L. A. Mitscher, J. V. Juvarkar, W. Rosenbrook, Jr., W. W. Andres, J. Schenck, and R. S. Egan. J. Am. Chem. Soc. **92**, 6070 (1970).
3. (*a*) M. Inaba, E. Bernstein, and D. L. Garmaise. U.S. Patent No. 3, 907, 889 (1975); (*b*) E. Bernstein, M. Inaba, and D. L. Garmaise. U.S. Patent No. 3, 910, 906 (1975); (*c*) D. Chu and D. L. Garmaise. U.S. Patent No. 3, 894, 061 (1975); (*d*) D. L. Garmaise, D. T. W. Chu, E. Bernstein, M. Inaba, and J. M. Stamm. J. Med. Chem. **22**, 559 (1979).
4. D. T. W. Chu, S. N. Huckin, and E. Bernstein. Can. J. Chem. **55**, 3341 (1977).
5. J. P. Kutney and I. H. Sanchez. Can. J. Chem. **54**, 2795 (1976).
6. G. H. Alt and A. J. Speziale. J. Org. Chem. **29**, 798 (1964).
7. D. T. W. Chu and S. N. Huckin. Can. J. Chem. **58**, 138 (1980).
8. D. T. W. Chu, E. Bernstein, and S. N. Huckin. Can. J. Chem. **56**, 1059 (1978).

Can. J. Chem. Downloaded from www.nrcresearchpress.com by 210.87.254.42 on 09/06/12
For personal use only.

Solubility of water in vinyl chloride

E. COLIN CLARKE, DAVID N. GLEW, AND DENIS J. MAISONNEUVE

Corporate Research and Development, Dow Chemical of Canada, Limited, Sarnia, Ont., Canada N7T 7K7

Received August 12, 1980

E. COLIN CLARKE, DAVID N. GLEW, and DENIS J. MAISONNEUVE. Can. J. Chem. **59**, 768 (1981).

The solubility of water in liquid vinyl chloride has been measured over the temperature range −17° to 60°C by a classical water absorption method. Solubility equations for water in vinyl chloride have been derived and the standard thermodynamic function changes for water transfer have been evaluated.

E. COLIN CLARKE, DAVID N. GLEW et DENIS J. MAISONNEUVE. Can. J. Chem. **59**, 768 (1981).

Utilisant la méthode classique d'absorption d'eau, on a mesuré la solubilité de l'eau dans le chlorure de vinyle liquide dans un intervalle de température allant de −17° à 60°C. On a déduit les équations de solubilité de l'eau dans le chlorure de vinyle et on a évalué les variations de la fonction thermodynamique standard du transfert de l'eau.

[Traduit par le journal]

Introduction

Although the solubility of vinyl chloride in water has been measured recently (2) there are apparently no measurements reported in the literature for the solubility of water in liquid vinyl chloride. This work describes such solubility measurements which define the vinyl chloride – water system between −17° and 60°C.

The solubility of water in liquid vinyl chloride is determined by a classical weighing method. Water and vinyl chloride liquid are equilibrated at constant temperature. Part of the water-saturated vinyl chloride phase is vaporized completely and passed through a preweighed drying tower. The increase in weight of the drying tower is attributed to the water in the vinyl chloride.

Experimental

A 500 cm^3 stainless steel cylinder, fitted with short dip-tube and Nupro stainless steel bellows valve, was evacuated, plugged, and weighed. All weights were corrected for the buoyancy of air. About three grams of water, injected by syringe into a 200 cm^3 roundbottomed flask, were vacuum distilled into the cylinder cooled by a Dry Ice – acetone mixture. The cylinder was plugged, brought to ambient temperature, and reweighed. About 350 g of vinyl chloride were charged by gravity into the recooled cylinder from a sample cylinder. The cylinder was plugged, warmed to ambient temperature, and reweighed.

The cylinder was inverted carefully to avoid getting water into the dip-tube and was fitted, as shown in Fig. 1, with capped exit tube a, with aluminum ring bearing b, and with aluminum drive collar c. The cylinder was immersed with its axis 35° from the vertical in a large thermostat bath and located by gripping collar c in the chuck of a slow-drive electric motor with ring b bearing on a stationary Teflon® seat. The thermostat temperature was maintained within 0.01°C and measured by platinum resistance thermometer and Müller bridge. The vinyl chloride liquid was saturated with water by rotating the cylinder once per second for a period of 20 h; equilibration for 72 h proved that full saturation was attained within 20 h. After rotation was stopped, the cylinder was left for one hour to permit settling of dispersed water, if any.

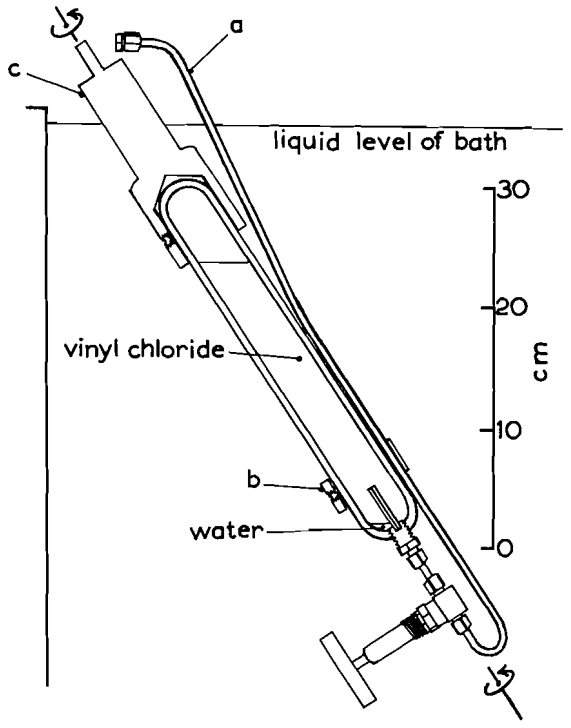

FIG. 1. Assembly for cylinder rotation.

A dry nitrogen stream of 700 cm^3/min was passed for five minutes through a needle control valve, the drying tower, and a Gilmont No. 2 flowmeter connected in series. The nitrogen flow was stopped and the pressure dropped to atmospheric, the Teflon® stopcocks on the tower were closed, the tower was disconnected and weighed full of nitrogen. The tower weight was corrected for the weight of nitrogen and the buoyancy of air.

The needle valve, drying tower, and flowmeter were reconnected and the closed needle valve was attached to the freshly uncapped exit tube a from the cylinder. A miniature thermocouple was taped to the underside of tube a 5 cm from the needle valve and two infrared lamps were positioned to heat the airborne section of tube a. The cylinder valve below the thermostat liquid was opened and the infrared lamps switched on to

0008-4042/81/050768-04$01.00/0

©1981 National Research Council of Canada/Conseil national de recherches du Canada

Can. J. Chem. Downloaded from www.nrcresearchpress.com by 210.87.254.42 on 09/06/12
For personal use only.

Can. J. Chem. Downloaded from www.nrcresearchpress.com by 210.87.254.42 on 09/06/12
For personal use only.

maintain tube a about 15°C above thermostat temperature. Vinyl chloride liquid saturated with water was vaporized completely in heated tube a and the vapour controlled by the needle valve to give a flow of 370 cm^3/min through the drying tower. The flow was continued for 3–4 h until 120–180 g vinyl chloride had passed through the drying tower, after which the cylinder valve was closed. Residual vinyl chloride liquid in tube a was allowed to evaporate after which the needle valve was closed and tube a was disconnected and capped. A nitrogen flow of 700 cm^3/min was passed for five minutes through the drying tower to displace vinyl chloride vapour, and the drying tower full of nitrogen was weighed as before. The final weight of the drying tower minus its initial weight gave the weight of water removed from the vaporized vinyl chloride.

The cylinder still contained 170–230 g vinyl chloride which was sufficient to cover the dip-tube and ensure that only liquid vinyl chloride had left the cylinder. The cylinder assembly, shown in Fig. 1, was removed from the thermostat, fittings b and c removed, the cylinder and valve washed with acetone and dried, tube a was disconnected from the valve, and the valve plugged. To remove thermostat liquor from within the valve bonnet, the stem, handle, and bonnet were disassembled from the body-bellows, all were washed with acetone and dried, and the valve was reassembled. The cylinder was reweighed. The cylinder weight minus its initial weight full of vinyl chloride gave the weight of vinyl chloride saturated with water that passed into the drying tower. The small weight of vinyl chloride vapour at atmospheric pressure remaining in tube a that did not pass into the drying tower was neglected.

The drying tower containing a cylindrical bed of solid desiccant 4.5 cm diameter and 5 cm deep weighed about 600 g. Many experiments were carried out to find suitable drying agents for vinyl chloride. Molecular sieves and activated alumina were unsuitable because of strong vinyl chloride adsorption and possible polymerization. Potassium hydroxide (5 mm pellets) and calcium oxide (5 mm lumps) were insufficiently fine to remove all water from the vinyl chloride. The desiccant finally chosen for use in the drying tower was a 5 cm bed of 2 mm barium oxide granules having equilibrium water pressure about 10^{-19} atm.

All experiments were conducted with the drying tower backed-up in series by a second and similar drying tower which was weighed and invariably confirmed that no significant water escaped with the vinyl chloride from the first tower.

Because of the known long-term toxic effects of vinyl chloride, care was taken to ensure that none was released into the laboratory workspace and that all was vented via an efficient fume-hood system directly into the atmosphere where degradation was fast.

Results and Discussion

Results for the solubility S (mg H_2O/kg solution) of water in liquid vinyl chloride between −17° and 60°C are presented in Table 1. The solubility between 0° and 60°C in equilibrium with liquid water is best represented by the equation

$$[1] \quad \log_{10} S = 7.1666 - 1246.7/T$$

which was evaluated by a weighted least-squares method (1) with $T(K) = 273.15 + t(°C)$. The weights were assessed on the basis that the errors derived entirely from the two weighings of the drying tower. The standard error shown in Table 1 is the experimental uncertainty of the solubility determination.

TABLE 1. Solubility of water in vinyl chloride

t (°C)	S (mg H_2O/kg solution)	Standard error
−16.75	178*	18
−12.13	230*	20
4.51	475	17
5.00	470	18
5.00	483	19
5.01	490	19
5.04	511	20
24.99	942	21
25.00	949	24
44.98	1757	25
44.98	1793	28
59.92	2695	25
59.94	2622	22

*Equilibrium with ice.

TABLE 2. Solubility of water in vinyl chloride from [1]

t (°C)	S (mg H_2O/kg solution)	σ
0	400	6
10	580	7
20	820	7
25	966	8
30	1132	8
40	1532	8
50	2035	10
60	2657	15
70	3415	25
80	4328	38

Table 2 presents calculated S values together with their standard errors as derived from [1] and the error matrix for temperatures between 0°C and 80°C.

Liquid Water – Liquid Vinyl Chloride – Gas System

The liquid water (l_1) – liquid vinyl chloride (l_2) – gas (g) three-phase system attains equilibrium at constant temperature according to the equation

$$[2] \quad \underset{\substack{x_1^{l_1} \\ x_2^{l_1}}}{H_2O\,(l_1)} + \underset{\substack{x_1^{l_2} \\ x_2^{l_2}}}{C_2H_3Cl\,(l_2)} \rightleftharpoons \underset{p_1}{H_2O\,(g)} + \underset{p_2}{C_2H_3Cl\,(g)}$$

in which $x_1^{l_1}$ and $x_1^{l_2}$ are the mole fractions of component 1, water, in phases l_1 and l_2; $x_2^{l_1}$ and $x_2^{l_2}$ are the mole fractions of component 2, vinyl chloride, in l_1 and l_2; and p_1 and p_2 are the water and vinyl chloride saturation partial pressures for equilibrium.

Table 3 presents values of the equilibrium phase compositions for the water – vinyl chloride system between −17°C and 60°C. The second column gives our solubility results expressed as mole fractions. The third column gives $x_2^{l_1}$ values calculated from

Can. J. Chem. Downloaded from www.nrcresearchpress.com by 210.87.254.42 on 09/06/12
For personal use only.

TABLE 3. Phase compositions for water – vinyl chloride system

t (°C)	$x_1^{l_2}$ × 10^3	$x_2^{l_1}$ × 10^3	p_1 (atm) × 10^3
−16.75	0.618	—	1.388*
−12.13	0.797	—	2.122*
4.51	1.646	3.28	8.294
5.00	1.627	3.27	8.582
5.00	1.672	3.27	8.583
5.01	1.697	3.27	8.586
5.04	1.771	3.27	8.603
24.99	3.259	3.03	31.14
25.00	3.283	3.03	31.16
44.98	6.068	3.04	94.19
44.98	6.193	3.04	94.20
59.92	9.287	3.18	195.2
59.94	9.038	3.18	195.4

*Equilibrium with ice.

TABLE 4. Equilibrium constant and standard thermodynamic function changes for water transfer into vinyl chloride

t (°C)	K_1 × 10^3	ΔG_1^0 ($l_1 \rightarrow l_2$) (J mol^{-1})
−20	0.61 ± 0.01	15 585 ± 46
−10	0.93 0.02	15 261 40
0	1.39 0.02	14 937 34
10	2.02 0.02	14 612 28
20	2.85 0.03	14 288 22
25	3.35 0.03	14 126 19
30	3.93 0.03	13 963 17
40	5.31 0.03	13 639 14
50	7.04 0.03	13 315 13
60	9.19 0.05	12 990 16
70	11.80 0.08	12 666 20
80	14.95 0.13	12 342 26

$\Delta H_1^0(l_1 \rightarrow l_2) = 23\,796 \pm 213$ J mol^{-1}
$\Delta S_1^0(l_1 \rightarrow l_2) = 32.44 \pm 0.67$ J K^{-1} mol^{-1}
$R = 8.31434$ J K^{-1} mol^{-1} (6)

the solubility measurements of Hayduk and Laudie (2), together with the vapour pressure of vinyl chloride (3). The water partial pressure, p_1, is given in the fourth column of Table 3. Above 0°C p_1 is evaluated from the vapour pressure of water (4) using Raoult's Law. Below 0°C p_1 is the vapour pressure of ice (4).

Consider the equilibrium of water between phases l_1 and l_2 represented by the equation

$$[3] \quad \underset{x_1^{l_1}}{H_2O\,(l_1)} \rightleftharpoons \underset{x_1^{l_2}}{H_2O\,(l_2)}$$

with equilibrium constant K_1 defined by

$$[4] \quad K_1 = x_1^{l_2}/x_1^{l_1}$$

In order to include our solubilities in equilibrium with ice we use an equivalent definition of K_1 given by

$$[5] \quad K_1 = x_1^{l_2}/a_1$$

where a_1 is the water activity, evaluated as the vapour pressure of ice divided by that of supercooled water (4).

Over the temperature range of our measurements K_1 is well represented by

$$[6] \quad \log_{10} K_1 = 1.6943 - 1243.0/T$$

which was determined by a weighted least-squares method (1). The weight assigned to the $\log_{10} K_1$ value for each solubility measurement was proportional to the square of the mass of water absorbed in the drying tower. From the fit of the measurements by [6], the standard error on a single solubility was equivalent to 3.3 mg H_2O on the two weighings of the drying tower.

The least-squares analysis gives the calculated values and associated standard errors at 25°C, $K_1 = 3.352 \pm 0.026 \times 10^{-3}$, ΔG_1^0 ($l_1 \rightarrow l_2$) = 14 126 ± 19 J mol^{-1}, ΔH_1^0 ($l_1 \rightarrow l_2$) = 23 796 ± 213 J mol^{-1}, ΔS_1^0 ($l_1 \rightarrow l_2$) = 32.44 ± 0.67 J K^{-1} mol^{-1}. These standard thermodynamic function changes refer to eq. [3] for the molar transfer of water at unit mole fraction from a liquid water phase into a liquid vinyl chloride phase. The water transfer into vinyl chloride is seen to be limited by the high enthalpy change but promoted by the positive entropy change; this corresponds with hydrogen bonded water at low enthalpy and orientationally constrained in the liquid water phase, giving weakly bonded water with more orientational freedom in the liquid vinyl chloride phase.

Table 4 presents calculated values and standard errors for the equilibrium constant and standard thermodynamic function changes for water transfer into vinyl chloride between −20° and 80°C.

Consider the equilibrium of water between phases l_2 and g represented by the equation

$$[7] \quad \underset{x_1^{l_2}}{H_2O\,(l_2)} \rightleftharpoons \underset{p_1}{H_2O\,(g)}$$

with equilibrium Henry Law constant H_1 defined by

$$[8] \quad H_1 = p_1/x_1^{l_2}$$

Between −17° and 60°C H_1 is well represented by

$$[9] \quad \log_{10} H_1 = 25.8846 - 2016.1/T - 7.335 \log_{10} T$$

which was determined by least squares (1) using the same weights as before. From the fit of the measurements by [9] the standard error on a single

TABLE 5. Henry Law constant and standard thermodynamic function changes for water transfer from vinyl chloride into gas phase

t (°C)	H_1 (atm)	ΔG_1^0 ($l_2 \rightarrow g$) (J mol^{-1})	ΔH_1^0 ($l_2 \rightarrow g$) (J mol^{-1})	ΔS_1^0 ($l_2 \rightarrow g$) (J K^{-1} mol^{-1})
−20	1.96 ± 0.10	−1414 ± 107	23 159 ± 1272	97.07 ± 4.62
−10	2.96 0.09	−2373 69	22 549 1037	94.71 3.70
0	4.29 0.08	−3308 41	21 939 804	92.43 2.83
10	6.01 0.07	−4222 28	21 329 577	90.24 2.01
20	8.15 0.09	−5113 26	20 719 366	88.12 1.25
25	9.39 0.10	−5551 27	20 414 278	87.09 0.94
30	10.74 0.11	−5984 27	20 110 223	86.08 0.72
40	13.81 0.13	−6835 24	19 500 282	84.10 0.85
50	17.35 0.11	−7667 17	18 890 474	82.18 1.44
60	21.35 0.13	−8479 17	18 280 695	80.32 2.11
70	25.80 0.33	−9273 36	17 670 926	78.52 2.79
80	30.65 0.69	−10050 66	17 060 1160	76.77 3.46

ΔCp_1^0 ($l_2 \rightarrow g$) = −60.99 ± 23.94 J K^{-1} mol^{-1}
R = 8.31434 J K^{-1} mol^{-1} (6)

solubility measurement was again found to be equivalent to 3.3 mg H_2O for the two drying-tower weighings. Student's t-test shows that the coefficient of $\log_{10} T$ in [9] is significant at the 2.9% level (5).

The above analysis gives calculated values and their standard errors at 25°C, H_1 = 9.388 ± 0.102 atm, ΔG_1^0 ($l_2 \rightarrow g$) = −5551 ± 27 J mol^{-1}, ΔH_1^0 ($l_2 \rightarrow g$) = 20 414 ± 278 J mol^{-1}, ΔS_1^0 ($l_2 \rightarrow g$) = 87.09 ± 0.94 J K^{-1} mol^{-1}, ΔCp_1^0 ($l_2 \rightarrow g$) = −61.0 ± 23.9 J K^{-1} mol^{-1}. These standard thermodynamic function changes refer to [7] for the molar transfer of water from a liquid vinyl chloride phase at unit water mole fraction into an ideal gas phase at one atmosphere pressure. These values show that in its vaporization from liquid vinyl chloride water behaves like a normal nonassociated liquid with a standard vaporization entropy of 87 J K^{-1} mol^{-1}, near to the characteristic Trouton value 88. Our results indicate a heat capacity for water dissolved in vinyl chloride of 95 ± 24 J K^{-1} mol^{-1}.

Table 5 presents calculated values and standard errors for the Henry Law constant and standard thermodynamic function changes for water transfer from liquid vinyl chloride into the gas phase between −20° and 80°C.

1. E. C. W. CLARKE and D. N. GLEW. Trans. Faraday Soc. **62**, 539 (1966).
2. W. HAYDUK and H. LAUDIE. J. Chem. Eng. Data, **19**, 253 (1974).
3. Kirk-Othmer Encyclopedia of Chemical Technology. 2nd ed. Vol. 5. John Wiley and Sons Inc., New York. 1964. p. 172.
4. N. E. DORSEY. Properties of ordinary water-substance. Reinhold Publishing Corporation, New York. 1940.
5. R. A. FISHER. Statistical methods for research workers. 13th ed. Oliver and Boyd, Edinburgh. 1958. p. 160.
6. National Bureau of Standards Technical News Bulletin, March 1971.

Can. J. Chem. Downloaded from www.nrcresearchpress.com by 210.87.254.42 on 09/06/12
For personal use only.

Solution of the strong-collision master equation for unimolecular reaction

S. R. VATSYA[1] AND H. O. PRITCHARD

Centre for Research in Experimental Space Science, York University, Downsview, Ont., Canada M3J 1P3

Received September 10, 1980

S. R. VATSYA and H. O. PRITCHARD. Can. J. Chem. **59**, 772 (1981).

A complete solution of the strong-collision master equation for unimolecular reaction is derived, for any number of distinct reaction products. This solution provides exact results for any chemical activation process under the strong-collision assumption.

S. R. VATSYA et H. O. PRITCHARD. Can. J. Chem. **59**, 772 (1981).

On a trouvé une solution complète, quelque soit le nombre de réactifs impliqués, de l'équation fondamentale dérivant des réactions unimoléculaires impliquant des collisions fortes. Cette solution fournit des résultats exacts pour tout processus d'activation chimique pour lequel on fait l'hypothèse d'une collision forte.

[Traduit par le journal]

Can. J. Chem. Downloaded from www.nrcresearchpress.com by 210.87.254.40 on 09/06/12
For personal use only.

Introduction

The purpose of this paper is to provide a complete solution of the strong-collision unimolecular reaction problem using the master-equation formulation; systems considered include thermal reaction to give a single product or to give any number of distinct products, and also the complementary chemical activation problems, but all in the absence of electromagnetic radiation. We summarise briefly here the key results of this dissertation. (*i*) An extremely accurate approximation for the shape of the unimolecular fall-off in strong-collision systems is given by eq. [23], and rarely will a practising kineticist want to go beyond this approximation; if however, it is necessary to do so, the exact rate constant can be found by using eq. [11]. (*ii*) Equation [25] gives an equally accurate representation of the different fall-off shapes when there are two (or more) distinct reaction products; again, an exact solution is available through the use of eq. [22]. (*iii*) Equation [17], together with eq. [15], gives the population evolution as a function of time, and this, via eq. [26], yields a complete solution to the chemical activation problem within this approximation.

In establishing these conclusions, the complete eigenvalue spectrum for the strong-collision case is required for all pressures, and many of these results will be used later in a treatment of the weak-collision problem.

The Master Equation for Unimolecular Reaction

We divide the energy-level spectrum of the reactant molecule into n grains having fractional populations $\tilde{n}_i$ at thermal equilibrium. Transitions between the grains are induced by collision with the heat bath molecules M, with rate constants q_{ij} for transition from grain i to grain j. In the absence of any reaction, the thermal relaxation of the reactant molecule is described by the set of equations

$$[1] \qquad \mathrm{d}\boldsymbol{n}(t)/\mathrm{d}t = \mathbf{A}\boldsymbol{n}(t)$$

where $\boldsymbol{n}(t)$ is the population vector and $\mathbf{A}$ is a matrix whose elements are

$$a_{ij} = q_{ji}[\mathrm{M}], \quad a_{ii} = -\sum_{j \neq i} a_{ji}$$

The matrix $\mathbf{A}$ is symmetrised by the transformation

$$[2] \qquad \mathbf{B} = -\mathbf{E}^{-1/2}\mathbf{A}\mathbf{E}^{1/2}$$

with $e_{ij} = \delta_{ij}\tilde{n}_i$; $\mathbf{B}$ has one eigenvalue which is zero, with corresponding eigenvector $\mathbf{S}_0$ having elements $S_{0j} = \tilde{n}_j{}^{1/2}$, $j = 0, 1, \ldots, n-1$, and the remainder of the eigenvalues are positive and, in general, distinct.

We may choose a special form of $\mathbf{A}$, viz.

$$[3] \qquad a_{ij} = \mu\{(1 - \delta_{ij})\tilde{n}_i - \delta_{ij}(1 - \tilde{n}_i)\}$$

which has a single eigenvalue equal to zero, and an $(n-1)$-fold degenerate eigenvalue of numerical magnitude μ, the relaxation rate (1). The matrix $\mathbf{A}$ corresponds to the strong-collision assumption usually made in the description of unimolecular reactions, except that it is somewhat more general (2, 3) — in the sense that μ does not have to be equated to the collision rate, but can take any appropriate value, viz. $\mu = -\lambda[\mathrm{M}]Z$ in the usual terminology (1); many properties of this relaxation matrix have already been given (1, 3).

When unimolecular decay of the molecule from within certain grains is allowed, the evolution of the population vector now becomes (in the absence of any back-reaction)

$$[4] \qquad \mathrm{d}\boldsymbol{\eta}(t)/\mathrm{d}t = (\mathbf{A} - \mathbf{D})\boldsymbol{\eta}(t)$$

[1]Formerly S. R. Singh.

0008-4042/81/050772-07$01.00/0

©1981 National Research Council of Canada/Conseil national de recherches du Canada

Can. J. Chem. Downloaded from www.nrcresearchpress.com by 210.87.254.40 on 09/06/12
For personal use only.

where $\eta_i(t)$ is the fraction of the original population remaining in grain i at time t, and $\mathbf{D}$ is a diagonal matrix whose elements $d_{ij} = \delta_{ij}d_i$ are the specific rate constants for decay from the grain i to products. Usually, in the reactive region, d_i will differ from grain to grain, but in the non-reactive region, there will be many grains having $d_i = 0$; in what follows, we will treat the general case where the multiplicity of any d_i is arbitrary.

The matrix $(\mathbf{A} - \mathbf{D})$ in [4] may be symmetrised in the same way as [2] to give $(\mathbf{B} + \mathbf{D})$, and we now derive the complete eigenvalue spectrum of this matrix, together with the corresponding eigenvectors. The following definitions will be useful: (,) represents the scalar product of two vectors, and $p_0 = \mathbf{S}_0(\mathbf{S}_0,)$ is the eigenprojection corresponding to the zero eigenvalue of the matrix $\mathbf{B}$.

The Eigenvalues of $(\boldsymbol{B} + \boldsymbol{D})$

Let the distinct diagonal elements of $\mathbf{D}$ be d_j, each with multiplicity m_j, $j = 0, 1, 2, ..., M$. We order the set $\{d_j\}$ in an increasing manner. Also, let the eigenvalues γ_{ji} of $(\mathbf{B} + \mathbf{D}) = [\mu(1 - p_0) + \mathbf{D}]$ be organised in $(M + 1)$ groups, the jth group defined by $(\mu + d_{j-1}) < \gamma_{ji} \leq (\mu + d_j)$, $i = 0, 1, ...$; and we arbitrarily set $d_{-1} = -\infty$. Since $0 \leq [\mu(1 - p_0) + \mathbf{D}] \leq (\mu + \mathbf{D})$, all of the eigenvalues are covered by this definition. We shall also assume that the distinct eigenvalues $\{\gamma_{ji}\}$ of the jth group are ordered in an increasing manner with i.

The eigenvalue equation for a particular (ji) takes the following form

$$[5] \qquad (\mu - \gamma_{ji} + \mathbf{D})\rho_{ji} = \mu p_0 \rho_{ji}$$

If $\gamma_{ji} \neq \mu + d_j$, then

$$[6] \qquad \rho_{ji} = \mu(\mu - \gamma_{ji} + \mathbf{D})^{-1} p_0 \rho_{ji}$$

From [6] it follows that the range of ρ_{ji} is spanned by the single vector $(\mu - \gamma_{ji} + \mathbf{D})^{-1}\mathbf{S}_0$ and hence the multiplicity of γ_{ji} is one, i.e. γ_{ji} is a simple eigenvalue. Equation [6] now yields that γ_{ji} is a solution of

$$[7] \qquad 1 = \mu(\mathbf{S}_0,(\mu - \gamma + \mathbf{D})^{-1}\mathbf{S}_0) = \mu \sum_{k=0}^{M} \frac{\tilde{n}^k}{(\mu - \gamma + d_k)}$$

where

$$\tilde{n}^k = \sum_{l=1}^{m_k} \tilde{n}_{v(k,l)}$$

and $v(k,l)$ is defined by $(\mathbf{D})_{vv} = d_k$, $l = 1, 2, ..., m_k$; note that whenever the degeneracy m_k of d_k is 1, $\tilde{n}^k$ becomes $\tilde{n}_k$, the fractional equilibrium population for the grain k. Each of the solutions of [7] is easily seen to be some eigenvalue γ_{ji} with an eigenvector being equal to $(\mu - \gamma_{ji} + \mathbf{D})^{-1}\mathbf{S}_0$.

Consider a solution $\bar{\gamma}$ of [7]. Since $(\mu - \bar{\gamma} + \mathbf{D})^{-1}$ exists, we have

$$(\mu - \bar{\gamma})(\mu - \bar{\gamma} + \mathbf{D})^{-1} = 1 - (\mu - \bar{\gamma} + \mathbf{D})^{-1}\mathbf{D}$$

and hence $\bar{\gamma}$ is a solution of

$$[8] \qquad \gamma = \mu(\mathbf{S}_0,(\mu - \gamma + \mathbf{D})^{-1}\mathbf{D}\,\mathbf{S}_0) = \mu \sum_{k=0}^{M} \frac{\tilde{n}^k d_k}{(\mu - \gamma + d_k)}$$

Conversely, a solution $\bar{\gamma} \neq \mu$ of [8] is a solution of [7], by the same argument. Thus [8] may have a spurious solution equal to μ, which will happen if and only if $d_0 \neq 0$, which follows from the following: if $d_0 \neq 0$, $\mathbf{D}^{-1}$ exists and hence μ is clearly a solution of [8]; if $d_0 = 0$, then the right side of [8] is easily seen to be less than μ for each $\gamma \leq \mu$. It is clear that [7] cannot have μ as a solution for all μ; thus, if $d_0 = 0$, then [7] and [8] are equivalent. Further, it is clear that an eigenvalue in the jth group which is not a solution of [7] is equal to $(\mu + d_j)$. With the appropriate transcription of symbols, [8] is the same as eq. [20] derived by Nordholm in ref. 2. The solutions of [7] are easily seen to be the zeros of a polynomial, as expected. The degree of the polynomial is $(M + 1)$ and therefore it has $(M + 1)$ zeros. All of these zeros will be distinct, otherwise there will be at least one simple eigenvalue having multiplicity greater than one. Further

$$\delta(x) = \mathrm{d}/\mathrm{d}x[(\mathbf{S}_0,(\mu - x + \mathbf{D})^{-1}\mathbf{S}_0)] = (\mathbf{S}_0,(\mu - x + \mathbf{D})^{-2}\mathbf{S}_0) \geq 0$$

and

$$\delta(x) \neq 0$$

for that would imply that $\mathbf{S}_0 = 0$. Thus, $(\mathbf{S}_0,(\mu - x + \mathbf{D})^{-1}\mathbf{S}_0)$ is a strictly increasing function for

$$(\mu + d_{j-1}) < x < (\mu + d_j)$$

and each j; and

$$\lim_{x \to \mu + d_{j-1}, \mu + d_j} (\mathbf{S}_0,(\mu - x + \mathbf{D})^{-1}\,\mathbf{S}_0) = -\infty, +\infty \qquad j = 1, 2, ..., M$$

For $j = 0$, $(\mathbf{S}_0,(\mu - x + \mathbf{D})^{-1}\mathbf{S}_0)$ is a positive increasing function on $(-\infty,\mu + d_0)$ and while it approaches infinity at $(\mu + d_0)$, at $-\infty$ it is zero. Consequently, there is at least one solution of [7] in each of the $(M + 1)$ groups.

Now consider a typical degenerate eigenvalue, i.e. $(\mu + d_j)$ for some j. The eigenvalue equation reads as

Can. J. Chem. Downloaded from www.nrcresearchpress.com by 210.87.254.40 on 09/06/12
For personal use only.

[9] $(\mathbf{D} - d_j)\rho_j' = \mu p_0 \rho_j'$

where we denote by ρ_j' the eigenprojection corresponding to the eigenvalue $(\mu + d_j)$. For an arbitrary vector ϕ we have that $(\mathbf{S}_0,\rho_j'\phi)\tilde{n}_k^{1/2} = 0$ for each $k = \nu(j,l)$, $l = 1, 2, ..., m_j$; and hence $(\mathbf{S}_0,\rho_j'\phi) = 0$ for each ϕ. This, together with [9], implies that $(\rho_j'\phi)_k = 0$ for $k \neq \nu(j,l)$. The range of ρ_j' is, therefore, the set of vectors ϕ such that $(\mathbf{S}_0,\phi) = 0$ with $\phi_k = 0$ for $k \neq \nu(j,l)$, which is clearly $(m_j - 1)$ dimensional. Thus, the multiplicity of the degenerate eigenvalue of the jth group is $(m_j - 1)$.

It is clear now that in the jth group there are two distinct eigenvalues, one $(\mu + d_j)$ with multiplicity $(m_j - 1)$ and one strictly less than $(\mu + d_j)$ with multiplicity one. If $m_j = 1$, then the matrix has no eigenvalue equal to $(\mu + d_j)$ which is implied by the fact that the multiplicity of $(\mu + d_j)$ is zero; if $m_j = 2$, $(\mu + d_j)$ is a simple eigenvalue. However, for the present, we reserve the term simple for the solutions of [7] and degenerate for the others; the eigenprojection corresponding to the degenerate eigenvalues is already determined. In the following, we obtain approximations to the simple eigenvalues; the corresponding eigenvectors are clearly determined by [6]. For a further convenience of writing, the simple eigenvalue of the jth group will now be denoted by γ_j.

Let

[10] $\gamma_j = \mu + d_j - \gamma_j'$

and rearrange [7] to read

[10a] $\gamma_j' = \dfrac{\mu\tilde{n}^j}{1 - \mu\beta(\gamma_j')} = \chi(\gamma_j')$

where

$$\beta(x) = \sum_{j \neq k=0}^{M} \tilde{n}^k/(x + d_k - d_j)$$

The correction γ_j', thus, is the unique fixed point of $\chi(x)$ in $(0,d_j - d_{j-1})$. Since $\gamma_j' + d_k - d_j \neq 0$ for all j and $k \neq j$, we have

$$\lim_{\mu \to 0} \gamma_j'/\mu = \tilde{n}^j$$

i.e.

$$\gamma_j \simeq d_j + \mu(1 - \tilde{n}^j)$$

for small μ; this is consistent with the pattern of behaviour observed numerically, i.e. eqs. [15] and [16] of ref. 3.

If $d_0 = 0$, then

$$\gamma_0 \simeq \mu \sum_i{}' \tilde{n}_i$$

where the summation is over all *reactive* states, denoted by $\sum'$. In two other recent articles we have shown that (4) the approximation

$$\gamma_{ap} \simeq \mu \sum_i{}' \tilde{n}_i \Big/ \left(1 - \sum_i{}' \tilde{n}_i\right)$$

and that (5) $\gamma_{ap} \geq \gamma_0$; in both these treatments we had assumed that $\gamma_0 < \mu$, which is true for all μ if and only if $d_0 = 0$. This we show in the following.

The *if* part is already established from the fact that $\gamma_0 < \mu + d_0$. For the *only if* part we notice that γ_0 is the smallest eigenvalue of $[\mu(1 - p_0) + \mathbf{D}]$ and $\mu(1 - p_0) \geq 0$; therefore $\gamma_0 \geq d_0$. If $\gamma_0 < \mu$ and $d_0 \neq 0$, then for small enough μ we shall have $\gamma_0 < d_0$.

It should be remarked here that for moderate values of μ, γ_0 does not have to be greater than μ even if $d_0 \neq 0$. In fact for large enough μ, $\gamma_0 < \mu$ for any value of d_0 as we shall see shortly.

For $j \geq 1$ we have that

$$\lim_{\mu \to \infty} \gamma_j'/\mu = 0$$

for $0 < \gamma_j' < (d_j - d_{j-1})$. Now the trace of

$$[\mu(1 - p_0) + \mathbf{D}] = (n - 1)\mu + \sum_{j=0}^{M} m_j d_j$$

must be equal to the sum of its eigenvalues which is

$$n\mu + \sum_{j=0}^{M} (m_j d_j - \gamma_j')$$

Hence

[10b] $\sum_{j=0}^{M} \gamma_j' = \mu$

Therefore

$$\lim_{\mu \to \infty} \gamma_0'/\mu = 1$$

i.e.

$$\lim_{\mu \to \infty} \gamma_0/\mu = 0$$

Re-writing eq. [8] for γ_0, we get

[11] $\gamma_0 = \mu \sum_{k=0}^{M} \dfrac{\tilde{n}^k d_k}{(\mu - \gamma_0 + d_k)} = \bar{\phi}(\gamma_0)$

It follows that

$$\lim_{\mu\to\infty}\gamma_0 = \lim_{\mu\to\infty}\sum_{k=0}^{M}\tilde{n}^k d_k \Big/ \left(1 - \frac{\gamma_0}{\mu} + \frac{d_k}{\mu}\right)$$

$$= \sum_{k=0}^{M}\tilde{n}^k d_k$$

$$= \lim_{\mu\to\infty}\gamma_{ap} \quad (4)$$

In order to obtain

$$\gamma_j'(\infty) = \lim_{\mu\to\infty}\gamma_j'$$

for $j \geq 1$, we notice that

$$\lim_{\mu\to\infty}(1 - \mu\beta(\gamma_j')) > 0$$

otherwise $\gamma_j' < 0$ or ∞ for some μ. Also

$$\lim_{\mu\to\infty}(1 - \mu\beta(\gamma_j')) = \infty$$

otherwise

$$\lim_{\mu\to\infty}\gamma_j' = \infty$$

and

$$\gamma_j' < d_j - d_{j-1}$$

Thus

$$\mu\beta(\gamma_j') \xrightarrow[\mu\to\infty]{} -\infty$$

and hence

$$[12]\quad \gamma_j'(\infty) = -\frac{\tilde{n}^j}{\beta(\gamma_j'(\infty))}$$

$$= \frac{\tilde{n}^j}{\sum_{j\neq k=0}^{M}\tilde{n}^k/(d_j - d_k - \gamma_j'(\infty))} = \bar{\chi}(\gamma_j'(\infty))$$

Equation [12] does not appear to have any simple solution even though

$$[12a]\quad \sum_{j=1}^{M}\gamma_j'(\infty) = \lim_{\mu\to\infty}(\mu - \gamma_0') = \sum_{i=0}^{M}\tilde{n}^i d_i - d_0$$

is a rather simple relation. Rather, therefore, than obtaining approximations to $\gamma_j'(\infty)$, $j \geq 1$, separately, we will obtain approximations to $\gamma_j'(\mu)$ for all μ. In fact the properties of $\chi(x)$ and $\bar{\chi}(x)$ are similar; therefore, treating [10*a*] and [12] separately is unnecessary.

For each μ there must be an interval U_j containing γ_j' such that $1 - \mu\beta(x) > 0$ for x in U_j; otherwise since $\beta(x)$ is continuous $\mu\beta(\gamma_j') \geq 1$ and hence $\gamma_j' < 0$ or ∞. The function $\beta(x)$ is a decreasing function of x in $(0, d_j - d_{j-1})$ taking a maximum (finite) value at zero, the minimum being $-\infty$ at $d_j - d_{j-1}$. If the set $\{d_k,\tilde{n}_k\}$ is such that $\beta(0) \leq 0$ then clearly U_j may be taken to be $[0,d_j - d_{j-1}]$ for all μ. However, if $\beta(0) > 0$, which certainly can happen for some choices of $\{d_k,\tilde{n}_k\}$, then there is a maximum value of μ up to which $[0,d_j - d_{j-1}]$ may be taken for U_j and above which U_j is properly contained in $[0,d_j - d_{j-1}]$.

Let x_0 be in U_j and $x_{m+1} = \chi(x_m)$, $m = 0, 1, 2, \ldots$. We now consider the convergence properties of $\{x_m\}$. First, we have that

$$\chi(x) > 0; \quad \lim_{x\to d_j - d_{j-1}}\chi(x) = 0$$

and

$$\frac{d\chi(x)}{dx} = -\frac{\mu^2\tilde{n}^j\delta(x)}{(1 - \mu\beta(x))^2} \leq 0, \quad x \text{ in } U_j$$

where

$$\delta(x) = \sum_{j\neq k=0}^{M}\tilde{n}^k/(x + d_k - d_j)^2$$

In fact, $d\chi(x)/dx < 0$, for the equality would imply that $\delta(x) = 0$. Thus, $\chi(x)$ is a strictly decreasing function of x in U_j. These remarks apply also to $\bar{\chi}(x)$ of [12] with obvious modifications. Following the argument of Theorem 1, ref. 5, it is now easy to establish the following result.

Let x_0 be in U_j and $\chi(\chi(x_0)) \geq x_0$; then $x_{2m+1} \downarrow y_1 \geq \gamma_j'$ and $x_{2m} \uparrow y_2 \leq \gamma_j'$. If the inequality in the assumption is reversed, the bound property and the inequalities in the result are also reversed. If $x_0 = 0$ is in U_j and $\chi(x_0) < d_j - d_{j-1}$, $\chi(\chi(x_0)) > 0$ and hence the condition is satisfied.

It is well known that if $|d\chi(x)/dx| < 1$ for all x in U_j, and $\{x_m\}$ as defined above are in U_j, then $x_{m\xrightarrow{m\to\infty}}\gamma_j'$. It is easy to check that this will be true for small μ, but for arbitrary choice of $\{d_k,\tilde{n}_k\}$ and μ, this condition may not be satisfied even at γ_j'. (If the condition is satisfied at γ_j', then it is clearly satisfied in some interval about γ_j' which may be smaller than U_j.) However, for a large class of $\{d_k,\tilde{n}_k\}$ we expect that $|d\chi(x)/dx| < 1$ for all μ; in fact, the leading term in $-d\chi(x)/dx$ is easily seen to be $\tilde{n}^j/\tilde{n}^{j-1}$ which is usually less than one in most unimolecular applications.[2] An approximation to γ_j' is given by $\chi(x_0)$ for some x_0 in U_j: in that case, an

[2]We refrain from reproducing the derivation here: it is available upon request, at a nominal charge, from the Depository of Unpublished Data, CISTI, National Research Council of Canada, Ottawa, Ont., Canada K1A 0S2.

Can. J. Chem. Downloaded from www.nrcresearchpress.com by 210.87.254.40 on 09/06/12
For personal use only.

Can. J. Chem. Downloaded from www.nrcresearchpress.com by 210.87.254.40 on 09/06/12
For personal use only.

error bound is given by

$$[13]\quad \chi(x_0) - \chi(\gamma_j') = \frac{\mu^2 \tilde{n}^j(\beta(x_0) - \beta(\gamma_j'))}{(1 - \mu\beta(x_0))(1 - \mu\beta(\gamma_j'))}$$

$$= \frac{\mu\gamma_j'(\gamma_j' - x_0)}{(1 - \mu\beta(x_0))} \times \sum_{j\neq k=0}^{M} \tilde{n}^k/[(x_0 + d_k - d_j)(\gamma_j + d_k - d_j)]$$

It is clear that if μ is small, the error is small; the error may also be small if $|d_k - d_j|$ are large and γ_j', x_0 are small in comparison with $d_j - d_{j-1}$. All of these results remain valid for $\gamma_j'(\infty)$ if the limiting value is taken as μ becomes large.

The Convergence of Approximations to γ_0

In the following, we produce an alternative scheme to approximate γ_0 under the assumption that $d_0 = 0$, which is always true in the unimolecular reaction problem. We recall in this case that γ_0 is the unique fixed point of $\bar{\phi}(x)$ in $(0,\mu)$.

We observe that $\bar{\phi}(x) > 0$ for x in $(-\infty, \mu + d_1)$, $\bar{\phi}(-\infty) = 0$, $\bar{\phi}(\mu + d_1) = \infty$, and all of the fixed points of $\bar{\phi}(x)$ are simple eigenvalues. Thus, there must be precisely two fixed points of $\bar{\phi}(x)$ in $(0,\mu + d_1)$, one of them being $\gamma_0 < \mu$, and the other being $\gamma_1 > \mu$. Let $\bar{x}_0 \leq \gamma_0$ and $\bar{x}_{m+1} = \bar{\phi}(\bar{x}_m)$, $m = 0, 1, 2, \ldots$; then $\bar{x}_m \uparrow \gamma_0$ from the following argument: Since $\bar{x}_0 \leq \gamma_0$, we have that $\bar{x}_1 = \bar{\phi}(\bar{x}_0) \geq \bar{x}_0$. Further, if $\bar{x}_{m+1} \geq \bar{x}_m$, then $\bar{x}_{m+2} = \bar{\phi}(\bar{x}_{m+1}) \geq \bar{\phi}(\bar{x}_m) = \bar{x}_{m+1}$, and therefore, by induction, $\{\bar{x}_m\}$ is a non-decreasing sequence. Now, since

$$\gamma_0 - \bar{x}_{m+1} = \int_{\bar{x}_m}^{\gamma_0} \frac{d\bar{\phi}(x)}{dx}\, dx$$

$\bar{x}_m \leq \gamma_0$ implies that $\bar{x}_{m+1} \leq \gamma_0$. This together with the fact that $\bar{x}_0 \leq \gamma_0$ implies that $\{\bar{x}_m\}$ is bounded by γ_0 and hence must converge from below to $y_0 \leq \gamma_0 < \mu$. It is trivial to check that y_0 is a fixed point of $\bar{\phi}(x)$ and in view of the uniqueness of the fixed point in $(0,\mu)$, $y_0 = \gamma_0$. It is obvious that x_0 may be taken to be zero.

A similar argument shows that if $\bar{x}_0$ is such that $\gamma_1 > \bar{x}_0 \geq \gamma_0$ then $\bar{x}_m \downarrow \gamma_0$. Thus it is possible to produce lower and upper bounds to γ_0 using the present procedure, provided that $d_0 = 0$. However, if $\bar{x}_0 > \gamma_1$, the above argument may be modified to show that $\{\bar{x}_m\}$ will exhibit rather uncontrollable behaviour; this could arise in practice if the original reaction matrix contains some rather small values $d_1, d_2, \ldots$, whence γ_1 will lie rather close to γ_0 in the region of low pressure, and could account for some of the convergence difficulties noted by Nordholm (2).

It is pertinent to remark here that in ref. 5 a function $\phi(x)$ was obtained with the properties that $\phi(\gamma_0) = \gamma_0$ and if $\bar{x}_m \lessgtr \gamma_0$, then $x_m = \phi(\bar{x}_m) \lessgtr \gamma_0$. The present bound $\bar{x}_m$ may therefore be used to produce an opposite bound x_{m+1}. Further, all of the above results remain valid for $d_0 \neq 0$ for μ not too small so that $\gamma_0 < \mu$ if γ_1 in the discussion is replaced by μ and d_1, by d_0.

Calculation of Population Distribution $\boldsymbol{\eta}$(t)

The evolution of the system is described by

$$[14]\quad \boldsymbol{\eta}(t) = \mathbf{E}^{1/2} \exp\{-[\mu(1 - p_0) + \mathbf{D}]t\}\mathbf{E}^{-1/2}\boldsymbol{\eta}(0)$$

$$= \mathbf{E}^{1/2}\Big\{\sum_{j=0}^{M} \rho_j \exp(-\gamma_j t) + \sum_{j=0}^{M} \rho_j' \exp[-(\mu + d_j)t]\Big\}\mathbf{E}^{-1/2}\boldsymbol{\eta}(0)$$

where γ_j, ρ_j are the simple eigenvalues and the corresponding eigenprojections, and ρ_j' is the eigenprojection corresponding to $(\mu + d_j)$ which could have multiplicity $(m_j - 1) \geq 0$; in the case that $(\mu + d_j)$ has multiplicity zero, $\rho_j' = 0$. Let ψ_j be the normalised eigenvector corresponding to γ_j, i.e.

$$[15]\quad \psi_j = \frac{(\mu - \gamma_j + \mathbf{D})^{-1}\mathbf{S}_0}{||(\mu - \gamma_j + \mathbf{D})^{-1}\mathbf{S}_0||} = \frac{(\mu - \gamma_j + \mathbf{D})^{-1}\mathbf{S}_0}{\left[\sum_{i=0}^{n-1} (\mu - \gamma_j + (\mathbf{D})_{ii})^{-2}\tilde{n}_i\right]^{1/2}}$$

We have $\rho_j = \psi_j(\psi_j,)$. Let I_j be the projection defined by $\mathbf{D}I_j = d_j I_j$; the projection ρ_j' is given by

$$[16]\quad \rho_j' = I_j - \frac{I_j\mathbf{S}_0(I_j\mathbf{S}_0, \quad)}{(\mathbf{S}_0, I_j\mathbf{S}_0)} = I_j - \frac{I_j\mathbf{S}_0(I_j\mathbf{S}_0, \quad)}{\sum_{i=1}^{m_j} \tilde{n}_{\nu(j,i)}}$$

The ith component $\eta_i(t)$ of the vector $\boldsymbol{\eta}(t)$ is now given by

$$[17]\quad \eta_i(t) = \tilde{n}_i^{1/2} \sum_{j=0}^{M} (\psi_j)_i \exp(-\gamma_j t) \sum_{k=0}^{n-1} (\psi_j)_k \tilde{n}_k^{1/2}\eta_k(0) + \tilde{n}_i^{1/2} \sum_{j=0}^{M} \exp[-(\mu + d_j)t] \sum_{k=1}^{m_j} \delta_{i\nu(j,k)} \times \left[\tilde{n}^{-1/2}{}_{\nu(j,k)}\eta_{\nu(j,k)}(0) - \tilde{n}^{1/2}{}_{\nu(j,k)} \frac{\sum_{l=1}^{m_j} \eta_{\nu(j,l)}(0)}{\sum_{l=1}^{m_j} \tilde{n}_{\nu(j,l)}}\right]$$

The first term in [17] is similar to the expression

Can. J. Chem. Downloaded from www.nrcresearchpress.com by 210.87.254.40 on 09/06/12
For personal use only.

usually given for the evolution of the population (1); the second term allows for the contribution to the relaxation from any groups of degenerate eigenvalues, whose existence was not fully appreciated previously.

Reaction to Two or More Products

Many unimolecular reactions give two or more distinguishable products and, in general, the fall-off behaviour for the formation of each product will be different (6–8). Let d_i^1 and d_i^2 be the respective rate constants for formation of products 1 and 2 from grain i, and assume that these two processes do not interfere with each other except in so far as the occurrence of each depletes the population of the grain itself, and of the neighbouring grains: thus $d_i^1 + d_i^2 = d_i$. Now

$$[18] \quad \gamma_0 = -\lim_{t\to\infty} \frac{1}{N(t)} \frac{dN(t)}{dt}$$

where

$$[19] \quad N(t) = \sum_{i=0}^{n-1} \eta_i(t) \sim [\exp(-\gamma_0 t)] \times (\mathbf{S}_0,\psi_0)(\psi_0,\mathbf{E}^{-1/2}\boldsymbol{\eta}(0)) \text{ for large } t$$

Further

$$[20] \quad \frac{dN(t)}{dt} = -\sum_{i=0}^{n-1} d_i\eta_i(t) \sim [\exp(-\gamma_0 t)] \times (\mathbf{S}_0,\mathbf{D}\psi_0)(\psi_0,\mathbf{E}^{-1/2}\boldsymbol{\eta}(0))$$

and thus $\gamma_0 = (\mathbf{S}_0,\mathbf{D}\psi_0)/(\mathbf{S}_0,\psi_0)$ as expected. The decomposition we need is

$$\gamma_0 = \gamma_0^1 + \gamma_0^2$$

where

$$[21] \quad \gamma_0^{1,2} = \lim_{t\to\infty} \sum_{i=0}^{n-1} d_i^{1,2}\eta_i(t) \Big/ \sum_{i=0}^{n-1} \eta_i(t) = (\mathbf{S}_0,\mathbf{D}^{1,2}\psi_0)/(\mathbf{S}_0,\psi_0)$$

$$[22] \quad = \mu(\mathbf{S}_0,(\mu - \gamma_0 + \mathbf{D})^{-1}\mathbf{D}^{1,2}\mathbf{S}_0)$$

This solution is exact provided that $t \gg \mu^{-1}$.

Approximate values for $\gamma_0^{1,2}$ can be obtained by substituting approximate values for γ_0. Suppose one substitutes $x_m \simeq \gamma_0$ for γ_0 in [22]: it is clear that the approximate values $\bar{\gamma}_0^{1,2}$ of $\gamma_0^{1,2}$ satisfy the relation

$$\bar{\gamma}_0^1 + \bar{\gamma}_0^2 = \bar{\Phi}(x_m) = x_{m+1} \simeq \gamma_0$$

Approximate expressions for $\gamma_0^{1,2}$ may also be obtained by using [21] directly, which is valid for an arbitrary eigenvector ψ_0 rather than the normalised one. Approximate expressions γ_{ap} and ψ_{ap} for γ_0 and ψ_0 respectively were obtained in ref. 4 which satisfy

$$\gamma_{ap} \geq \gamma_0$$

$$(\mathbf{S}_0, \psi_{ap}) = 1$$

and

$$(\mathbf{S}_0,\mathbf{D}\psi_{ap}) = \gamma_{ap}$$

These expressions are

$$[23] \quad \gamma_{ap} = (\mathbf{D}^{1/2}\mathbf{S}_0,[1 + \mu^{-1}\mathbf{D}^{1/2}(1 - p_0)\mathbf{D}^{1/2}]^{-1} \times \mathbf{D}^{1/2}\mathbf{S}_0) = (\mathbf{J}\mathbf{S}_0,(1 - \mu^{-1}\mathbf{J}p_0\mathbf{J})^{-1}\mathbf{J}\mathbf{S}_0) = \frac{\mu \sum_{i=0}^{n-1} \tilde{n}_i d_i(\mu + d_i)^{-1}}{\left[1 - \sum_{i=0}^{n-1} \tilde{n}_i d_i(\mu + d_i)^{-1}\right]}$$

where

$$\mathbf{J} = (1 + \mu^{-1}\mathbf{D})^{-1/2}\mathbf{D}^{1/2}$$

Also, for ψ_{ap}, we have

$$[24] \quad \psi_{ap} = \mathbf{S}_0 - \mu^{-1}(1 - p_0)\mathbf{D}^{1/2} \times [1 + \mu^{-1}\mathbf{D}^{1/2}(1 - p_0)\mathbf{D}^{1/2}]^{-1}\mathbf{D}^{1/2}\mathbf{S}_0 = \mathbf{S}_0 - \mu^{-1}(1 - p_0)\mathbf{J}^2 \times \mathbf{S}_0/[1 - \mu^{-1}(\mathbf{S}_0, \mathbf{J}^2\mathbf{S}_0)] = (1 + \mu^{-1}\mathbf{D})^{-1}\mathbf{S}_0/[1 - \mu^{-1}(\mathbf{S}_0, \mathbf{J}^2\mathbf{S}_0)]$$

An approximation to $\gamma_0^{1,2}$ is now clearly given by

$$[25] \quad \gamma_0^{1,2} \simeq \bar{\gamma}_0^{1,2} = \frac{\mu \sum_{i=0}^{n-1} \tilde{n}_i d_i^{1,2}(\mu + d_i)^{-1}}{1 - \sum_{i=0}^{n-1} \tilde{n}_i d_i(\mu + d_i)^{-1}}$$

which satisfies the relation $\bar{\gamma}_0^1 + \bar{\gamma}_0^2 = \gamma_{ap}$ as expected. The extension to more than two product channels is obvious.

Discussion

For a simple unimolecular reaction yielding only one product, a good approximation to the strong-collision rate constant is given by eq. [23], as we have shown previously (4). If there are two products, equivalent approximations to the partial rates are given by eq. [25], and so on.

However, if we wish to know the evolution of the population distribution or, alternatively, wish to treat a chemical activation problem which implicitly requires this information, then we need to know all the eigenvalues and eigenvectors of the reaction matrix. Moreover, since there is a strong tendency for inconsistencies between the reaction matrix, its eigenvalues, and its eigenvectors to become magnified

Can. J. Chem. Downloaded from www.nrcresearchpress.com by 210.87.254.40 on 09/06/12
For personal use only.

in such calculations, it is necessary to know these quantities with reasonable precision.

From our examination of the properties of the reaction matrix and its eigenvalues, we come to the following conclusions. The general topology of the eigenvalues is as we have already described it (1, 3–5, 9). However, if there are m_j entries in the reaction matrix having identical values of the decay rate constant d_j, then there is an eigenvalue of exactly $(\mu + d_j)$ with degeneracy $(m_j - 1)$. Only one member of each such group is shifted in value to $\gamma_j = \mu + d_j - \gamma_j'$, eq. [10]. If the quantity d_j appears only once, then the eigenvalue γ_j is also given by this same expression, [10]. Now, provided that the graining can be achieved in such a way that $\tilde{n}^j > \tilde{n}^{j-1}$, the iterative scheme [10*a*] should converge extremely quickly to give the small correction γ_j', thus yielding γ_j itself very easily. This scheme is also valid for γ_0, and it will be perfectly satisfactory at low pressures. However, at high pressures, since $\gamma_0'(\mu) \to \mu$, it will be preferable to use the alternative scheme based on eq. [11], which is in fact that used by Nordholm (2). We note that, assuming $d_0 = 0$, a sure way to achieve convergence is to start with a point x_0 in $[0,\mu]$ in the iteration procedure. If $x_0 \geq \gamma_0$, a non-increasing sequence will result while $x_0 \leq \gamma_0$ will yield a non-decreasing sequence, both converging from above and below respectively. Zero or γ_{ap} (if $\gamma_{ap} \leq \mu$) are of course acceptable starting points, which will clearly yield lower and upper bounds respectively. These remarks apply to $\gamma_0^{1,2}$ in [22] as well.

Note that in the low pressure limit

$$\gamma_{ap} = \mu\sum'\tilde{n}_i/(1 - \sum'\tilde{n}_i)$$

whereas the *exact* solution is

$$\gamma_0 = \mu\sum'\tilde{n}_i$$

on the other hand, $\gamma_{ap} \to \gamma_0$ as $\mu \to \infty$, the high pressure limit.

Having obtained all the eigenvalues to the required accuracy, the non-degenerate eigenvectors are given by [15]; for the degenerate eigenvalues, the eigenvectors are not unique and are best handled through the corresponding eigenprojection [16] as in the general expression [17] for the population evolution.

Complete solution of the chemical activation problem follows once the evolution of the populations is known. We start with an initial population vector $\boldsymbol{\eta}(0)$ representing the distribution formed from reactants in the initial act. The rate of formation of the rth dissociation product is simply

$$[26] \quad \int_0^\infty \sum' d_i^r \eta_i(t) \mathrm{d}t$$

where $\sum'$ denotes summation over only reactive states, and r runs over all open reaction channels, *including* redissociation to reactants. The extent of stabilisation is obtainable either by difference, or by calculation of the total non-reactive populations at long time. Notice that it is necessary to use the full expression [17] for $\eta_i(t)$ in [26] (rather than some long-time approximation such as we used in [19] or [20]), since it is only through the contributions from the second term in [17] for which $d_i = 0$ that significant non-linearity of the stabilisation to dissociation ratios at low pressures, i.e. the so-called "low pressure turn-up" (10), will arise.

1. A. W. YAU and H. O. PRITCHARD. Can. J. Chem. **56**, 1389 (1978).
2. S. NORDHOLM. Chem. Phys. **29**, 55 (1978).
3. H. O. PRITCHARD and A. LAKSHMI. Can. J. Chem. **57**, 2793 (1979).
4. S. R. SINGH and H. O. PRITCHARD. Chem. Phys. Lett. **73**, 191 (1980).
5. S. R. VATSYA and H. O. PRITCHARD. Proc. R. Soc. London, A. In press.
6. M. H. B. VAYJOOEE, A. W. YAU, and H. O. PRITCHARD. Can. J. Chem. **55**, 1595 (1977).
7. M. C. FLOWERS. Can. J. Chem. **56**, 29 (1978).
8. K. D. KING, B. J. GAYNOR, and R. G. GILBERT. Int. J. Chem. Kinet. **11**, 11 (1979).
9. H. O. PRITCHARD. Can. J. Chem. **55**, 284 (1977).
10. G. H. KOHLMAIER and B. S. RABINOVITCH. J. Chem. Phys. **38**, 1692 (1963); **38**, 1709 (1963).

The preparation of porphyrin S-411 (dehydrocoproporphyrin) and harderoporphyrin from protoporphyrin IX

DAVID DOLPHIN AND RAMANI SIVASOTHY

Department of Chemistry, The University of British Columbia, Vancouver, B.C., Canada V6T 1Y6

Received August 22, 1980

DAVID DOLPHIN and RAMANI SIVASOTHY. Can. J. Chem. **59**, 779 (1981).

Protoporphyrin IX dimethyl ester has been converted into the two 2,4-positional isomers bearing hydroxyethyl and methoxycarbonylvinyl side chains. The 4-(2-hydroxyethyl) group was extended to a methoxycarbonylethyl group to give the tetramethyl ester of porphyrin S-411 (2-methoxycarbonylvinyl-4-methoxycarbonylethyldeuteroporphyrin dimethyl ester). On the other hand reduction of the 4-methoxycarbonylvinyl to the corresponding methoxycarbonylethyl group and dehydration of the 2-(2-hydroxyethyl) to a vinyl side chain gave the trimethyl ester of harderoporphyrin (2-vinyl-4-methoxycarbonylethyldeuteroporphyrin dimethyl ester).

DAVID DOLPHIN et RAMANI SIVASOTHY. Can. J. Chem. **59**, 779 (1981).

On a transformé l'ester diméthylique de la protoporphyrine IX en ses isomères de positions en 2 et 4 ayant des chaînes latérales hydroxyéthyle et méthoxycarbonylvinyle. On a allongé le groupe (hydroxy-2 éthyl)-4 de façon à obtenir l'ester tétraméthylique de la porphyrine S-411 (ester diméthylique de la méthoxycarbonylvinyl-2 méthoxycarbonyléthyl-4 deutéroporphyrine). D'autre part, la réduction du groupe méthoxycarbonylvinyl-4 en groupe méthoxycarbonyléthyle correspondant et la déshydratation subséquente du groupe (hydroxy-2 éthyl)-2 en une chaîne latérale vinylique conduisent à l'ester triméthylique de la hardéroporphyrine (ester diméthylique de la vinyl-2 méthoxycarbonyléthyl-4 deutéroporphyrine).

[Traduit par le journal]

During studies on porphyrin biosynthesis and metabolism two previously unknown porphyrins have been recently identified. Harderoporphyrin **1** (R^1 = —CH=CH_2, R^2 = —$CH_2CH_2CO_2H$), an intermediate between the copro and proto ring systems, was first isolated from the Harderian gland of rodents (1) and its structure confirmed by synthesis (1–6). Meconium is accumulated in the bowel during human fetal development; it is discharged shortly after birth and has been found to be rich in bile pigments and porphyrins (7). Investigation, by counter current distribution techniques, of ether soluble porphyrins obtained from meconium detected a porphyrin having a Soret absorption band at 410–411 nm in 5% w/v hydrochloric acid. This porphyrin was called porphyrin S-411 (8); it is also known as dehydrocoproporphyrin. Its structure was assigned (9) as **1** (with R^1 and R^2 as —CH=$CHCO_2H$ and $CH_2CH_2CO_2H$), and this was confirmed by synthesis of both isomers via *b*-oxobilanes (10). Porphyrin S-411 is also found in normal bone marrow and feces (11). Finally *Spirographis* porphyrin **1** (R^1 = CHO, R^2 = —CH=CH_2), also known as chlorocruoroporphyrin, has been isolated from various polychete worms (12) where it functions as an oxygen carrying pigment.

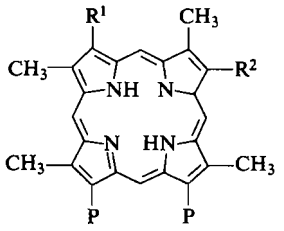

1

Syntheses of harderoporphyrin (1–6), porphyrin S-411 (5, 10), and *Spirographis* porphyrin (3) have been reported. We report here the preparation of these porphyrins, as their methyl esters, from protoporphyrin IX dimethyl ester. Protoporphyrin IX has two peripheral vinyl groups at the 2- and 4-positions. Although it has been reported (13) that the 2-vinyl group is more reactive than the 4-vinyl, subsequent studies (3, 14–16) have not substantiated the initial claim. Consequently partial derivatization of the vinyl groups results in a mixture of the 2,4-isomeric porphyrins. Therefore, if such intermediates are to be synthetically attractive, an efficient method for their separation is essential. Reports on the partial syntheses from protoporphyrin IX of *Spirographis* porphyrin (3, 15–18), and harderoporphyrins (3) have appeared. The most novel of these is from Inhoffen *et al.* (18), where the mono-derivatization of protoporphyrin was effected via the photoprotoporphyrins **4**, and we chose this as our starting point. Exposure of protoporphyrin IX to oxygen and light gives the isomeric (2 and 4) photoprotoporphyrins (**4**) in a yield of 75%. The reaction involves the 1,4-addition of singlet oxygen, whose formation is photosensitized by porphyrin, to either of the vinyl substituted pyrrolenine rings (A or B) followed by de-

0008-4042/81/050779-07$01.00/0

©1981 National Research Council of Canada/Conseil national de recherches du Canada

Can. J. Chem. Downloaded from www.nrcresearchpress.com by 210.87.254.105 on 09/06/12
For personal use only.

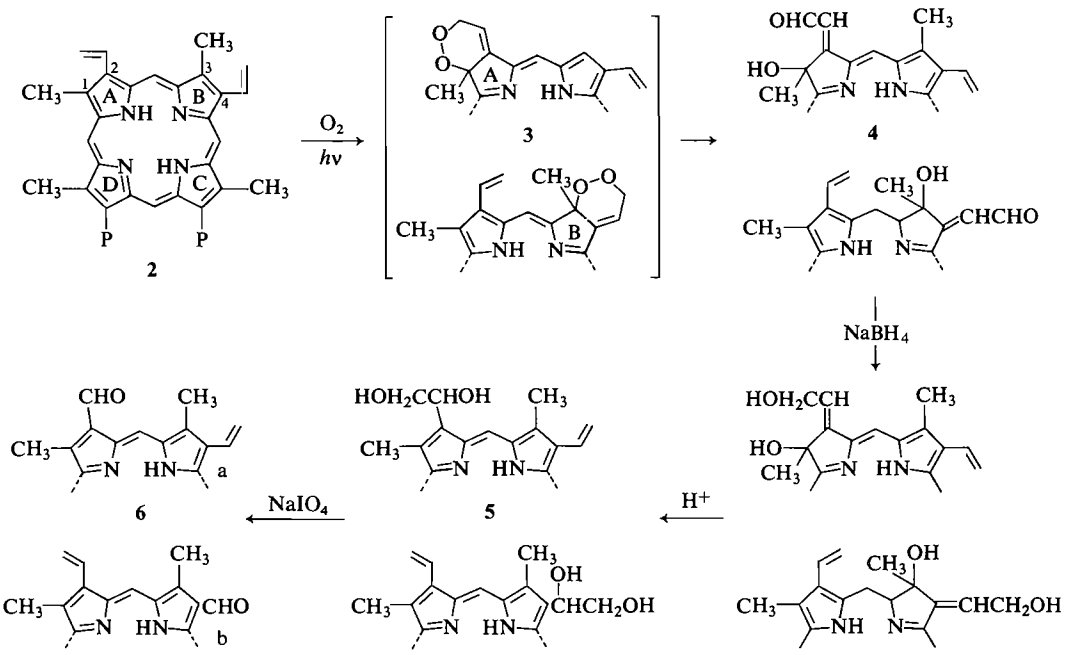

SCHEME 1

composition of the peroxide (**3**) (18) (Scheme 1). Mono-derivatization is achieved through the inhibitory electron-withdrawing effect of the formylethylidene group (**4**) towards an additional Diels–Alder reaction. This procedure, after chromatography of the isomeric photoprotoporphyrins, gave a 35% yield of each isomer. Isomeric porphyrins are, in general, difficult to separate chromatographically since the small differences in mobility exerted by the different disposition of the peripheral groups are overwhelmed by the flat porphyrin. This is not the case with the nonplanar "chlorins", such as the photoprotoporphyrins, and their chromatographic behaviours are usually sufficiently different to make separation routine. This proved to be the case where the compound of higher mobility (silica gel/dichloromethane) was identified as 4-photoprotoporphyrin (ring B). Borohydride reduction of the photoprotoporphyrins followed by rearrangement and cleavage of the resulting glycols (**5**) gave the corresponding formyl-vinyl derivative **6** (*Spirographis* porphyrins) in an 80% yield. The high yields reported by Inhoffen *et al.* (18) for the synthesis of the isomeric formyl-vinyl porphyrins **6** could not be reproduced using the cited reaction conditions (19, 20). Clezy and Fookes (19) obtained a yield of 25% from the photoprotoporphryin dimethyl ester by changing the solvent from dichloromethane–benzene to dioxane. A 60% yield was reported by Hamilton (21), who used a modification of Clezy's method. In the present study, a procedure similar to that of Hamilton's was employed to give a 75% yield.

While chromatographic separation of the photoprotoporphyrin isomers (**4**) is routine it is nevertheless tedious. Thus the mixed isomers were used to develop the chemistry described below, after which the pure isomers were used to synthesize the final products.

The condensation of the formylvinyldeuteroporphyrins **6** with malonic acid was achieved in pyridine using piperidine as the base catalyst to give the acrylic side chain of **7**.

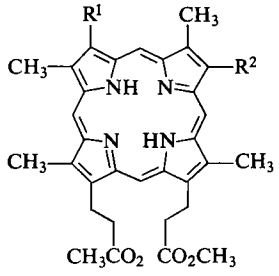

7

a $R^1 = -CH{=}CHCO_2H$, $R^2 = -CH{=}CH_2$

b $R^1 = -CH{=}CH_2$, $R^2 = -CH{=}CHCO_2H$

Conversion of the vinyl group of **7** into a propionate side chain would provide porphyrin S-411. A sequence of reactions to effect this conversion is outlined in Scheme 2. The scheme relies on a preferential oxidation of the vinyl over the acrylate group and if the photooxidation is a Diels–Alder

Can. J. Chem. Downloaded from www.nrcresearchpress.com by 210.87.254.105 on 09/06/12
For personal use only.

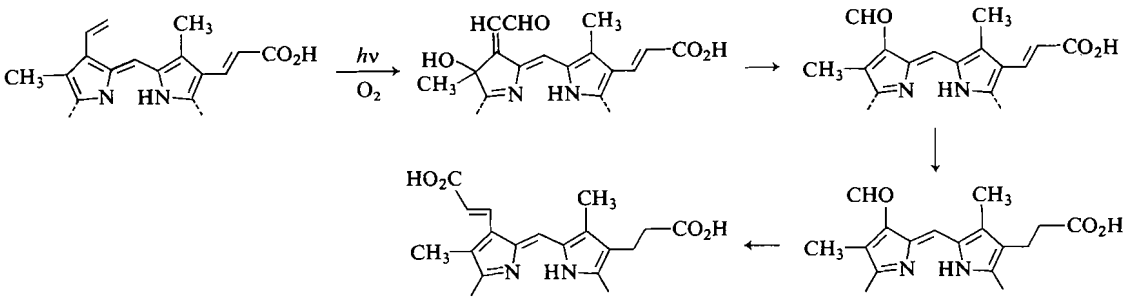

SCHEME 2

type of reaction, as has been suggested, the acrylic acid diene component should be deactivated by the electronegative carboxylic acid. Consequently, a preferential oxidation of the vinyl group was anticipated. When the mono-acrylic acid mono-vinyl-deuteroporphyrin **7** in dichloromethane containing 10% pyridine was exposed to direct sunlight a color change from red to green was observed over a period of three days. Thin-layer chromatography of the green solution revealed four (two pairs) and not, as expected, only one pair of products. Clearly the acrylic acid and the vinyl-containing dienes can both participate in the photooxidation. Since separation of these components proved impractical, as did prior reduction of the acrylate double bond in the presence of the vinyl group, this route was abandoned.

Kenner *et al.* (22) converted the two vinyl groups of protoporphyrin IX to propionic acid groups to give coproporphyrin III. Using a similar approach, as outlined in Scheme 3, conversion of the vinyl group of **6** to a propionic acid group gave porphyrin S-411. Treatment of **6** with two equivalents of thallium(III) nitrate (TTN) in methanol gave the 2,2-dimethyoxyethyl derivative **8** (3, 22). Strict adherence to the literature procedure (3) resulted in a 70% yield, whereas a modified procedure consistently gave a yield of 90%. Condensation of **8** with malonic acid as described above gave **9**. Hydrolysis of the acetal in THF followed by sodium borohydride reduction and re-esterification gave the 2-hydroxyethyl derivative **10**. Conversion of **10** to **11** may be effected with either thionyl bromide in dichloromethane–DMF (22) or carbon tetrabromide–triphenylphosphine (3). The former method was found unsatisfactory in the presence of alkenes whereas the latter method proved satisfactory in our hands. Treatment of **11** with cyanide in 1-methylpyrrolidone gave the nitrile **12** which upon methanolysis gave the porphyrin S-411 which was identical to an authentic sample with respect to melting point, mixture melting point, spectral properties (nmr, ir, uv–vis, ms), and tlc mobility.

The conversion of a 2-hydroxyethyl to a vinyl

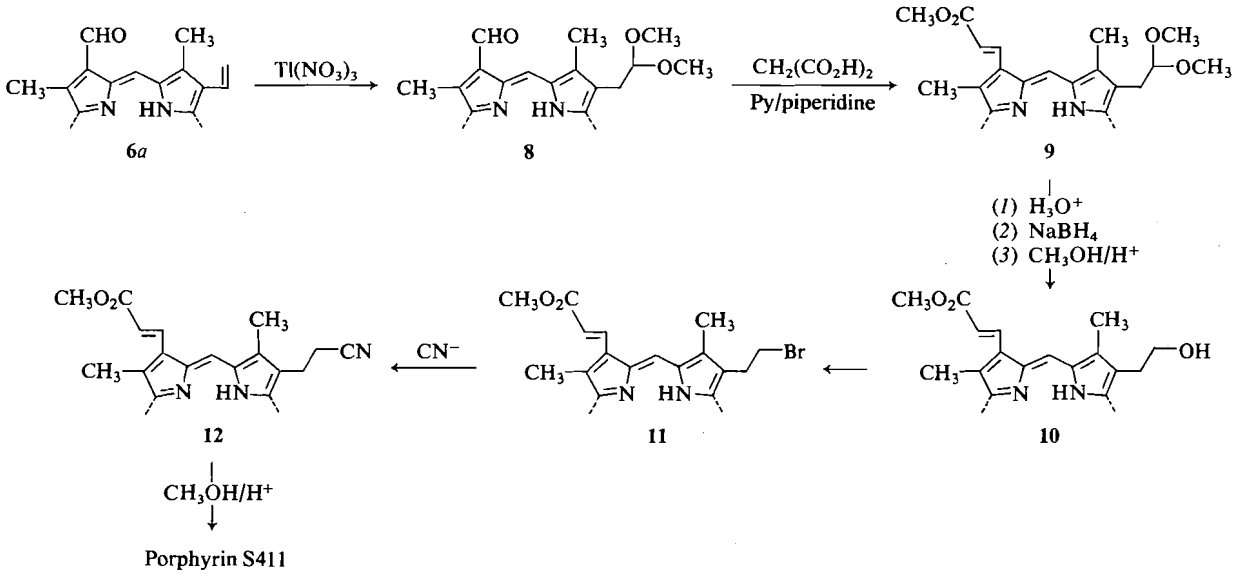

SCHEME 3

Can. J. Chem. Downloaded from www.nrcresearchpress.com by 210.87.254.105 on 09/06/12
For personal use only.

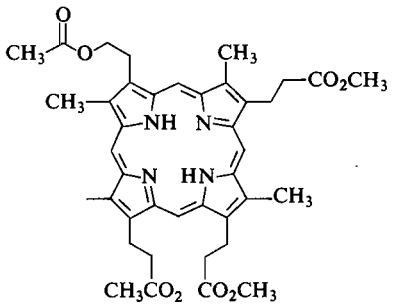

13

side chain is well established in porphyrin chemistry where the need arises for a vinyl precursor which is stable to the conditions employed for the condensations of pyrroles to porphyrins. Thus conversion of the 2-hydroxy to the 2-chloroethyl derivative and dehydrohalogenation of the porphyrin zinc complex with potassium *tert*-butoxide generates the vinyl group (23). More recently Clezy *et al.* (24) have generated the vinyl group from either the 2-chloroethyl or methanesulfonate derivative using sodium hydroxide in aqueous pyridine. These reactions suggest how the other photoprotoporphyrin isomer (**4***b*) which was not used in the synthesis of S-411 would provide an intermediate suitable for the synthesis of harderoporphyrin (**1**; $R^1 = —CH=CH_2$, $R^2 = —CH_2CH_2CO_2H$).

Indeed conversion of **4***b* (as outlined in Schemes 1 and 3) to the corresponding 2,4-positional isomer of **10** gave 2-(hydroxyethyl)-4-methoxycarbonylvinyldeuteroporphyrin dimethyl ester (**7**; $R^1 = —CH_2CH_2OH$, $R^2 = —CH{:}CHCO_2CH_3$) via the corresponding 2-(2,2-dimethoxyethyl)-4-formyl (**7**; $R^1 = (CH_3O)_2CHCH_2—$, $R^2 = —CHO$), 2-(2,2-dimethoxyethyl) - 4 - methoxycarbonylvinyldeuteroporphyrin dimethyl ester (**7**; $R^1 = (CH_3O)_2CHCH_2—$, $R^2 = —CH{:}CHCO_2CH_3$). Acetylation of **7** ($R^1 = —CH_2CH_2OH$, $R^2 = —CH{:}CHCO_2CH_3$) gave 2-(2-acetoxyethyl)-4-methoxycarbonylvinyldeuteroporphyrin dimethyl ester (**7**; $R^1 = —CH_2CH_2OCOCH_3$, $R^2 = —CH{:}CHCO_2CH_3$) and catalytic reduction of the acrylate side chain gave the corresponding propionate side chain of 2-(2-acetoxyethyl-4-methoxycarbonylethyldeuteroporphyrin dimethyl ester (**13**). Compound **20** was a key intermediate in the total synthesis of harderoporphyrin (**10**), and its conversion by the same route gave, in our hands, harderoporphyrin which was identical to an authentic sample.

Experimental

Visible spectra were obtained on a Cary 17 spectrophotometer using Spectro grade dichloromethane unless otherwise specified. The ^1H nmr were obtained in the FT mode at either 100 or 270 MHz with a Varian XL-100 or Nicolet Model MC-80 spectrometer using $CDCl_3$. Mass spectra (ms) were recorded using Atlas CH-4 and A.E.I. MS-902 spectrometers. Column chromatography was performed using silica gel (Woelm-activity IV). Thin layer chromatography was carried out on Silica Gel GF precoated plates (Analtech-Uniplate 250 μ).

*Photoprotoporphyrin Dimethyl Esters (4*a, b)

Photoprotoporphyrins were prepared from protoporphyrin IX dimethyl ester according to the method of DiNello and Dolphin (25) in a combined yield of 72%. The average yield of each pure crystalline isomer after chromatography was 22%.

*Isomer I (4*a)

An analytical sample was recrystallized from dichloromethane–methanol mp 220–222°C (lit. (18) mp 222–223°C); λ_{max}(nm): 388, 436, 568, 613, 671; ^1H nmr: 1.26 (s, 3H, aliphatic CH_3), 3.26 (m, 4H, propionate, βCH_2), 3.36, 3.42, 3.62 (s, each 3H, ring methyls), 3.71 (d, 6H, methyl ester CH_3), 4.28 (m, 4H, propionate αCH_2), 6.14 (m, 2H, vinyl CH_2), 6.54 (d, 1H, olefinic CH), 7.60 (m, 1H, vinyl CH), 7.60, 8.42, 9.66, 9.76 (s, each 1H, *meso*-H), 9.97 (s, 1H, aldehyde H); ms: 622 (100), 579 (48), 549 (19).

*Isomer II (4*a)

An analytical sample was recrystallized from dichloromethane–methanol mp 241–243°C (lit. (18) mp 244°C); λ_{max}(nm): 393, 422, 566, 610, 668; ^1H nmr: 1.38 (s, 3H, aliphatic CH_3), 2.72, 3.27, 3.39 (s, each 3H, ring methyls), 3.27 (m, 4H, propionate βCH_2), 3.73 (s, 6H, methyl ester CH_3), 4.24 (m, 4H, propionate αCH_2), 5.91 (d, 1H, olefinic CH), 6.17 (m, 2H, vinyl CH_2), 7.93 (m, 1H, vinyl CH), 7.49, 8.19, 9.59, 9.62 (s, each 1H, *meso*-H), 10.06 (s, 1H, aldehyde H); ms: 622 (100), 579 (44), 549 (15).

*2-(4)-Formyl-(2)-vinyldeuteroporphyrin Dimethyl Esters (6*a, b)

The procedure used is a modification of Hamilton's method (21). To a solution of **4***a* or **4***b* (250 mg) in dry dichloromethane (125 mL) was added sodium borohydride (250 mg) in dry methanol (10 mL). The reaction mixture was stirred at room temperature for one hour. Thin-layer chromatography at the end of this reaction period, methyl acetate – heptane 1:1 v/v, R_f starting material 0.46, product 0.25, indicated the completion of the reaction. Excess sodium borohydride was destroyed by the dropwise addition of acetic acid. The reaction mixture was washed with water (200 mL × 2), dried over sodium sulfate, filtered, and the solvent removed *in vacuo*.

The dark brown residue was dissolved in dioxane (125 mL) and sodium periodate (400 mg) in boiling water (0.75 mL) was added, followed by concentrated sulfuric acid (0.5 mL). The reaction was monitored by tlc, methyl acetate – heptane 1:1 v/v, R_f starting material 0.25, product 0.75. The reaction was complete in one hour. The purple solution was diluted with water (600 mL) and extracted with dichloromethane (100 mL). The organic phase was washed with 5% $NaHCO_3$ and water, dried over sodium sulfate, filtered, and evaporated to dryness. The solid was dissolved in a minimum volume of chloroform and chromatographed on silica gel (methanol–chloroform 1:20 v/v). The first fraction was the desired product.

*Isomer I (6*a)

An analytical sample was recrystallized from dichloromethane – petroleum ether (30–60°C), mp 275–278°C (lit. (18) mp 278–279°C); λ_{max}(nm): 418, 518, 558, 583, 642; ^1H nmr 3.26 (t, 4H, propionate βCH_2), 3.52, 3.58, 3.70, 3.76 (s, 12H, ring methyls), 3.66 (s, 6H, methyl ester CH_3), 4.35 (m, 4H, propionate αCH_2), 6.32 (m, 2H, vinyl CH_2), 8.21 (dd, 1H, vinyl CH), 9.78, 9.86, 9.92, 10.66 (s, each 1H, *meso*-H), 11.32 (s, 1H, aldehyde H); ms: 592 (100), 519 (81), 446 (18).

Can. J. Chem. Downloaded from www.nrcresearchpress.com by 210.87.254.105 on 09/06/12
For personal use only.

Can. J. Chem. Downloaded from www.nrcresearchpress.com by 210.87.254.105 on 09/06/12
For personal use only.

Isomer II (6b)

An analytical sample was recrystallized from dichloromethane – petroleum ether (30–60°C); mp 223°C (lit. (18) mp 225°C); λ_{max}(nm): 420, 518, 558, 583, 642; ^{1}H nmr: 3.20 (m, 4H, propionate βCH_2), 3.30, 3.42, 3.48, 3.58 (s, each 3H, ring methyls), 3.69 (d, 6H, methyl ester CH_3), 4.26 (m, 4H, propionate αCH_2), 6.12 (dd, 2H, vinyl CH_2), 7.84 (q, 1H, vinyl CH), 9.19, 9.52, 9.60, 10.28 (s, each 1H, *meso*-H), 11.06 (s, 1H, aldehyde H); ms: 592 (100), 519 (57), 446 (18).

2-(4)-Acrylic Acid-4-(2)-vinyldeuteroporphyrin Dimethyl Esters (7a, b)

A solution of the mixed isomers **6***a* and **6***b* (100 mg) was dissolved in pyridine (50 mL), and malonic acid (2 g) in pyridine (10 mL) was added. The mixture was heated to 50°C, with stirring, and piperidine (0.75 mL) was added. The temperature of the reaction mixture was then raised to 80°C and maintained there for five hours.

After cooling the reaction mixture to room temperature it was poured into dilute hydrochloric acid (100 mL, 5% v/v). The porphyrin was extracted into chloroform and the organic layer washed with water, dried over sodium sulfate, filtered, and the solvent removed *in vacuo*. The residue was chromatographed on a silica gel preparative layer plate with chloroform–methanol 20:1 v/v as eluent. The slow moving band was removed from the silica gel with a chloroform–methanol solution and the solvent removed *in vacuo*. The residue was crystallized from dichloromethane–methanol in a yield of 72%; λ_{max}(nm): 418, 512, 552, 581, 637; ^{1}H nmr: 3.26 (m, 4H, propionate βCH_2), 3.52–3.66 (m, 18H, ring methyls, methyl ester CH_3), 4.38 (m, 4H, propionate αCH_2), 6.24 (m, 2H, vinyl CH_2), 6.88 (m, 1H, acrylic acid βCH), 8.16 (m, 1H, vinyl CH), 9.18 (m, 1H, acrylic acid αCH), 9.84 (s, 4H, *meso*-H).

Photooxidation of 7

A solution of 7*a*, *b* (20 mg) in dichloromethane containing 10% pyridine in a 100 mL measuring cylinder was exposed to direct sunlight. A colour change from red to green was observed after a day. The reaction was monitored by tlc using dichloromethane–ether 20:1 v/v. The completion of the reaction was gauged by the disappearance of the starting material on tlc. The reaction mixture was successively washed with 1 *N* hydrochloric acid, 5% sodium bicarbonate solution, and finally with water. The organic phase was dried over sodium sulfate and the solvent removed *in vacuo*.

The thin-layer chromatogram of the reaction mixture revealed two pairs of bands which could not be separated by tlc.

2-(4)-Formyl-4-(2)-(2,2-dimethoxyethyl)deuteroporphyrins

To a solution of **6***a* (or **6***b*) (100 mg) in dichloromethane (30 mL) and methanol (5 mL), was added thallium(III) nitrate trihydrate (300 mg, 3.2 mmol) in methanol (10 mL). The solution was stirred at room temperature for 45 min. Concentrated HCl (0.5 mL) was added and SO_2 was passed through the solution for 10 min. The mixture was extracted with dichloromethane (100 mL). The organic phase was washed with water, dried over sodium sulfate, filtered, and taken down to dryness *in vacuo*. The residue was dissolved in a minimum volume of dichloromethane and chromatographed on silica gel (dichloromethane–ether 20:1 v/v). The main fraction was taken down to dryness and the residue crystallized from dichloromethane – petroleum ether to give 96 mg (90%) of deep red needles.

2-Formyl-4-(2,2-dimethoxyethyl)deuteroporphyrin Dimethyl Ester (8)

An analytical sample was recrystallized from dichloromethane – petroleum ether (30–60°C), mp 167–169°C; λ_{max}(nm) (ε mM): 413 (251), 515 (10.9), 555 (19.1), 578 (11.7), 640 (2.00); ^{1}H nmr: 3.24 (t, 4H, propionate βCH_2), 3.42 (s, 6H, acetal CH_3), 3.48, 3.53, 3.56, 3.59 (s, each 3H, ring methyls), 3.66 (d, 6H, methyl ester CH_3), 4.24 (m, 4H, propionate αCH_2), 4.38 (d, 2H, acetal CH_2), 5.05 (t, 1H, acetal CH), 9.62, 9.85, 10.59 (s, 4H, *meso*-H), 11.22 (s, 1H, aldehyde H); ms: 654 (44), 622 (100), 549 (44). *Anal.* calcd. for $C_{37}H_{42}N_4O_7$: C 67.87, H 6.47, N 8.56; found: C 67.76, H 6.27, N 8.34.

2-(2,2-Dimethoxyethyl)-4-formyldeuteroporphyrin Dimethyl Ester (7; $R^1 = (CH_3O)_2CHCH_2$—, $R^2 = CHO$)

An analytical sample was recrystallized from dichloromethane – petroleum ether (30–60°C), mp 174–176°C; λ_{max}(nm) (ε mM): 413 (186.2), 515 (8.5), 555 (13.8), 578 (6.03), 639 (1.41); ^{1}H nmr: 3.22 (t, 4H, propionate βCH_2), 3.36 (s, 6H, acetal CH_3), 3.48, 3.52, 3.58, 3.61 (s, each 3H, ring methyls), 3.64, 3.68 (s, each 3H, methyl ester CH_3), 4.06 (d, 2H, acetal CH_2), 4.24, 4.32 (two t, each 2H, propionate αCH_2), 4.9 (t, 1H, acetal CH), 9.60 (s, 1H), 9.74 (s, 2H), 10.6 (s, 1H, *meso*-H), 11.24 (s, 1H, aldehyde H); ms: 654 (15), 622 (100), 549 (44). *Anal.* calcd. for $C_{37}H_{42}N_4O_7$: C 67.87, H 6.47, N 8.56; found: C 68.17, H 6.00, N 8.14.

2-Methoxycarbonylvinyl-4-(2,2-dimethoxyethyl)deuteroporphyrin Dimethyl Ester (9)

A solution of **8** (100 mg) and malonic acid (3 g) in pyridine (100 mL) was heated to 50°C. To this solution piperidine (0.2 mL) was added and the temperature raised to 80°C. The progress of the reaction was monitored by tlc using dichloromethane–methanol 20:1 v/v, R_f starting material 0.88, product 0.12. After five hours the reaction mixture was cooled and poured into 1 *N* hydrochloric acid (400 mL) and extracted into chloroform (200 mL). The chloroform layer was washed with 5% sodium bicarbonate solution and repeatedly with water. The organic phase was dried over sodium sulfate, filtered, and the solvent evaporated under reduced pressure.

The porphyrin residue was treated with 5% sulfuric acid in methanol (100 mL) overnight in the cold (refrigerator). The porphyrin ester was extracted into chloroform and the organic phase washed first with 5% sodium bicarbonate solution and then with water; it was dried over sodium sulfate, filtered, and the solvent removed *in vacuo*.

The residue was chromatographed on 100 g silica gel using chloroform–acetone 30:1 v/v as eluent. The desired porphyrin was eluted as the second fraction. The eluate was evaporated and the residue crystallized from dichloromethane – petroleum ether (30–60°C) in a yield of 78 mg (72%). An analytical sample was recrystallized from dichloromethane – petroleum ether (30–60°C), mp 192–194°C; λ_{max}(nm) (ε mM): 412 (218.8), 509 (14.5), 549 (20.9), 574 (12.3), 635 (3.55); ^{1}H nmr: 3.26 (t, 4H, propionate βCH_2), 3.43 (s, 6H, acetal CH_3), 3.56 (s, 6H, methyl ester CH_3), 3.56, 3.63, 3.68 (s, 12H, ring methyls), 4.08 (s, 3H, acrylic ester CH_3), 4.34 (m, 6H, propionate αCH_2, acetal αCH), 5.06 (t, 1H, acetal βCH), 6.99 (d, 1H, acrylic acid βCH), 9.22 (d, 1H, acrylic acid αCH), 9.87, 9.94, 9.98 (s, 4H, *meso*-H); ms: 710 (44), 678 (100), 605 (44). *Anal.* calcd. for $C_{40}H_{46}N_4O_4$: C 67.69, H 6.52, N 7.88; found: C 67.26, H 6.25, N 7.75.

2-Methoxycarbonylvinyl-4-(2-hydroxyethyl)deuteroporphyrin Dimethyl Ester (10)

A solution of **9** (53 mg) in tetrahydrofuran (30 mL) containing water (0.6 mL) was refluxed with concentrated hydrochloric acid (0.2 mL) for five minutes. The reaction mixture was cooled and the porphyrin extracted into dichloromethane (30 mL) containing pyridine (10 mL). The organic phase was washed with water, dried over sodium sulfate, and the solvent removed *in vacuo*. The residue in dichloromethane (30 mL) at 0°C was treated with a cold (0°C) solution of borohydride (250 mg) in methanol (10 mL). While stirring, the reaction mixture was allowed to attain room temperature. The excess sodium borohy-

Can. J. Chem. Downloaded from www.nrcresearchpress.com by 210.87.254.105 on 09/06/12
For personal use only.

dride was then destroyed by the dropwise addition of acetic acid. The organic phase was washed with water, dried over sodium sulphate, filtered, and the solvent evaporated under reduced pressure. The residue was re-esterified with 5% sulphuric acid in methanol and chromatographed using dichloromethane–ether 20:1 (v/v) as eluent. The major band was collected, the solvent evaporated, and the residue crystallized from dichloromethane–methanol to give 30 mg (70%). An analytical sample was recrystallized from dichloromethane–methanol; λ_{max}(nm) (ε mM): 412 (275), 508 (20.0), 548 (26.3), 574 (16.6), 636 (5.0); ^{1}H nmr: 3.28 (m, 4H, propionate βCH_2), 3.50, 3.95, 4.06 (m, 18H, ring methyls, propionate ester CH_3), 4.08 (s, 3H, acrylic ester CH_3), 4.42 (m, 6H, propionate αCH_2, hydroxyethyl αCH_2), 7.07 (d, 1H, acrylic βCH), 9.35 (d, 1H, acrylic αCH), 10.04 (s, 2H), 10.10 (s, 1H), 10.14 (s, 1H, *meso*-H); ms: 666 (100), 635 (26), 607 (10), 593 (21). *Anal.* calcd. for $C_{38}H_{42}N_4O_7$: C 68.45, H 6.35, N 8.40; found: C 68.08, H 6.72, N 8.16.

2-Methoxycarbonylvinyl-4-(2-bromoethyl)deuteroporphyrin Dimethyl Ester (11)

Method 1

Compound **11** was prepared from **10** according to the method of Kenner *et al.* (22). The reaction was carried out at room temperature to give a 55% yield.

Method 2

A solution of carbon tetrabromide (100 mg) and triphenyl phosphine (80 mg) in dry dichloromethane (2 mL) was added to a stirred solution of **10** (30 mg) in dry dichloromethane (10 mL) and refluxed for 20 min. The cooled reaction mixture was diluted with dichloromethane (20 mL) and washed with water. The organic phase was dried over sodium sulfate, filtered, and the solvent removed *in vacuo*. The residue was chromatographed using dichloromethane–ether 20:1 v/v. The major band which eluted first was collected and taken to dryness. The residue was crystallized from dichloromethane – petroleum ether to give compound **11** in a yield of 72%.

An analytical sample was recrystallized from dichloromethane – petroleum ether (30–60°C), mp 196–200°C; λ_{max}(nm) (ε mM): 413 (467), 508 (33.1), 548 (41.7), 576 (25.1), 635 (9.1); ^{1}H nmr: 3.24 (m, 4H, propionate βCH_2), 3.50 (m, 12H, ring methyls), 3.64 (s, 3H, 3.66 and s, 3H, propionate ester CH_3), 4.08 (m, 5H, acrylic ester CH_3, bromoethyl βCH_2), 4.34 (m, 6H, propionate αCH_2, bromoethyl αCH_2), 6.93 (d, 1H, acrylic βCH), 9.12 (d, 1H, acrylic αCH), 9.74 (s, 2H), 9.80 (s, 1H), 9.92 (s, 1H, *meso*-H); ms: 730 (100), 728 (100), 657 (21), 655 (21), 648 (46). *Anal.* calcd. for $C_{38}N_{41}N_4O_6Br$: C 62.55, H 5.66, N 7.68, Br 10.95; found: C 62.50, H 5.54, N 7.44, Br 10.68.

2-Methoxycarbonylvinyl-4-(2-cyanoethyl)deuteroporphyrin Dimethyl Ester 12

To a solution of **11** (10 mg) in *N*-methylpyrrolidone (10 mL) was added, with stirring, a solution of sodium cyanide (10 mg) in *N*-methylpyrrolidone (5 mL). The reaction mixture was stirred at room temperature and the progress of the reaction was monitored by tlc using dichloromethane–ether 20:1 v/v; R_f starting material 0.58, product 0.29. On completion of the reaction, the reaction mixture was diluted with dichloromethane. The organic phase was repeatedly washed with water, dried over sodium sulfate, filtered, and taken to dryness. The residue was chromatographed on silica gel using dichloromethane–ether 20:1 v/v as eluent. The major band was collected, the solvent evaporated, and the residue crystallized from dichloromethane – petroleum ether in a yield of 70%. An analytical sample was recrystallized from dichloromethane – petroleum ether, mp 242–244°C; λ_{max}(nm) (ε mM): 412 (389), 507 (33.1), 547 (37.2), 576 (240), 634 (9.33); ^{1}H nmr: 3.26 (m, 6H, propionate βCH_2, cyanoethyl βCH_2), 3.60 (s, 9H), 3.67 (s, 9H, ring methyls, propionate ester CH_3), 4.09 (s, 3H, acrylic ester CH_3), 4.36 (m, 6H, propionate αCH_2), 7.04 (d, 1H, acrylic acid βCH), 9.28 (d, 1H, acrylic ester αCH), 9.81 (s, 1H), 9.98 (s, 1H), 10.02 (s, 2H, *meso*-H); ms: 675 (100), 602 (30), 635 (50).

Porphyrin S-411 Tetramethyl Ester

(1; R^1 = —CH=CHCO$_2$CH$_3$, R^2 = —CH$_2$CH$_2$CO$_2$CH$_3$)

Compound **12** (10 mg) was dissolved in methanol (10 mL) saturated with hydrogen chloride and left overnight in the refrigerator. The porphyrin was extracted into dichloromethane and the organic layer washed with 5% sodium bicarbonate solution and water. After the solvent was removed *in vacuo* the residue was chromatographed with dichloromethane–ether 20:1 v/v as eluent. The first eluted compound was collected, the solvent removed *in vacuo*, and the residue crystallized from dichloromethane – petroleum ether, in almost quantitative yield to give a product, mp 237–239°C (lit. (10) mp 236–238°C), which was identical to an authentic sample of porphyrin S-411; λ_{max}(nm): 413, 509, 549, 576, 635; ^{1}H nmr: 3.26 (m, 6H, propionate βCH_2), 3.48 (s, 9H), 3.60 (s, 3H), 3.64 (s, 3H), 3.68 (s, 6H), 4.08 (s, 3H, ring methyls, acrylic ester CH_3, and propionate ester CH_3), 4.38 (m, 6H, propionate αCH_2), 7.04 (d, 1H, acrylic βCH), 9.30 (d, 1H, acrylic αCH), 9.96 (s, 1H), 10.00 (s, 2H), 10.04 (s, 1H, *meso*-H); ms: 708 (100), 677 (7), 649 (14), 635 (34).

2-(2-Hydroxyethyl)-4-methoxycarbonylvinyldeuteroporphyrin Dimethyl Ester (7; R^1 = —CH$_2$CH$_2$OH, R^2 = —CH:CHCO$_2$CH$_3$)

2-(2,2-Dimethoxyethyl)-4-methoxycarbonylvinyldeuteroporphyrin dimethyl ester (**7**; R^1 = $(CH_3O)_2CHCH_2$—, R^2 = $—CH_2CHCO_2CH_3$) (prepared from **7**; R^1 = $(CH_3O)_2CHCH_2$—, R^2 = CHO as described above for the isomer **9**) was reacted in a manner identical to that described above for the preparation of **10** to give the product in 70% yield. An analytical sample was recrystallized from dichloromethane–methanol; λ_{max}(nm) (ε mM): 410 (274), 507 (16.2), 548 (26.7), 573 (15.2), 635 (6.6). *Anal.* calcd. for $C_{38}H_{42}N_4O_7 \cdot 1/2H_2O$: C 67.53, H 6.42, N 8.29; found: C 67.66, H 6.83, N 7.79.

2-(2-Acetoxyethyl)-4-methoxycarbonylvinyldeuteroporphyrin Dimethyl Ester (7; R^1 = —CH$_2$CH$_2$OCOCH$_3$, R^2 = —CH:CHCO$_2$CH$_3$)

2-(2-Hydroxyethyl)-4-methoxycarbonylvinyldeuteroporphyrin dimethyl ester was dissolved in pyridine (10 mL) containing acetic anhydride (1 mL) and allowed to stand overnight. The reaction mixture was poured into 1% hydrochloric acid (50 mL) and the porphyrin extracted into ether. The organic layer was washed with 5% sodium bicarbonate solution followed by water. After drying over sodium sulfate the solvent was removed *in vacuo*. The residue was purified by chromatography using dichloromethane–ether 20:1 v/v. The major band was collected, the solvent removed, and the residue crystallized from dichloromethane – petroleum ether in a yield of 72%; λ_{max}(nm): 411, 508, 548, 575, 635; ^{1}H nmr: 2.10 (s, 3H, acetoxyethyl CH_3), 3.16 (m, 4H, propionate βCH_2), 3.56, 3.62, 3.64 (all s, 18H, ring methyls, propionate CH_3), 4.90 (m, 2H, acetoxyethyl βCH_2), 4.02 (s, 3H, acrylic ester CH_3), 4.34 (m, 6H, propionate αCH_2, acetoxyethyl αCH_2), 7.02 (d, 1H, acrylic βCH), 9.34 (d, 1H, acrylic αCH), 10.12 (s, 2H), 10.20 (s, 1H), 10.24 (s, 1H, *meso*-H).

2-(2-Acetoxyethyl)-4-methoxycarbonylethyldeuteroporphyrin (13)

2-(2-Acetoxyethyl)-4-methoxycarbonylvinyldeuteroporphyrin dimethyl ester (5 mg) in tetrahydrofuran (5 mL) was hydrogenated over 10% palladium–charcoal at room temperature until the solution turned colourless. The catalyst was filtered off and the solution was stirred while air was bubbled through until the visible spectrum indicated the complete oxidation of the porphyrinogen. The solvent was removed *in vacuo* and the

residue chromatographed using dichloromethane–ether 20:1 v/v as eluent. The major band was collected, the solvent evaporated under reduced pressure, and the residue crystallized from dichloromethane – petroleum ether to give **13** (3.3 mg, 65%), mp 155–157°C (lit. (10) mp 155–156°C), which had identical spectral properties to those previously reported (10); λ_{max}(nm): 399, 500, 531, 567, 621; ^{1}H nmr: 2.08 (s, 3H, acetoxyethyl CH_3), 3.20 (m, 6H, propionate βCH_2), 3.67, 3.69 (d, 21H, ring methyls, methyl ester CH_3), 4.24 (m, 8H, propionate αCH_2, acetoxyethyl αCH_2), 4.88 (t, 2H, acetoxyethyl βCH_2), 10.10 (s, 2H), 10.12 (s, 2H, *meso*-H).

Harderoporphyrin Trimethyl Ester (1; R^1 = —CH=CH_2, R^2 = —$CH_2CH_2CO_2CH_3$)

2-(2-Acetoxyethyl)-4-methoxycarbonylethyldeuteroporphyrin (**13**) (5 mg) was converted to harderoporphyrin trimethyl ester in the manner reported by Couch *et al.* (10) via the intermediacy of 2-(2-hydroxyethyl)- and 2-(2-chloroethyl)-4-methoxyethylcarbonyldeuteroporphyrins to give 2 mg (35%) of a product identical to an authentic sample of harderoporphyrin trimethyl ester, mp 201–202°C (lit. (10) mp 203–204°C); a mixture melting point showed no depression with an authentic sample.

Acknowledgements

We wish to thank Professors A. H. Jackson and K. M. Smith for generous gifts of porphyrin S-411 and harderoporphyrin. This work was supported by the Natural Sciences and Engineering Research Council of Canada and the United States National Institutes of Health (AM 17989). D.D. wishes to express his thanks to the Harvard Chemistry Department for its assistance in the preparation of this manuscript during his stay as a Visiting Professor, fall 1980.

1. G. Y. Kennedy, A. H. Jackson, G. W. Kenner, and C. J. Suckling. FEBS Lett. **6**, 9 (1970).
2. J. A. S. Caveleiro, G. W. Kenner, and K. M. Smith. Chem. Commun. 183 (1973).
3. G. W. Kenner, J. M. E. Quirke, and K. M. Smith. Tetrahedron, **32**, 2753 (1976).
4. A. H. Jackson, G. W. Kenner, K. M. Smith, and C. J. Suckling. Tetrahedron, **32**, 2757 (1976).
5. I. A. Chaudhry, P. S. Clezy, and V. Diakiw. Aust. J. Chem. **30**, 879 (1977).
6. K. M. Smith and K. C. Langry. Chem. Commun. 217 (1980).
7. J. Waldenstrom. Z. Physiol. Chem. **239**, 111 (1936).
8. J. W. French and E. Thonger. Clin. Sci. **31**, 337 (1966).
9. J. M. French, D. C. Nicholson, and C. Rimmington. Biochem. J. **120**, 393 (1970).
10. P. W. Couch, D. E. Games, and A. H. Jackson. J. Chem. Soc. Perkin Trans. I, 2492 (1976).
11. L. Eales. Clinical chemistry of the porphyrin. *In* The porphyrins. Vol. VI. *Edited by* D. Dolphin. Academic Press, New York. 1979.
12. H. Fischer and C. V. Seeman. Z. Physiol. Chem. **242**, 133 (1936).
13. J. Barrett and P. S. Clezy. Nature, **184**, 1988 (1959).
14. W. S. Caugey, J. O. Alben, W. J. Fujimoto, and J. L. York. J. Org. Chem. **31**, 2631 (1966).
15. M. Sono and T. Asakura. Biochemistry, **13**, 4387 (1974).
16. H. Fischer and K. O. Deilman. Hoppe-Zeyler's Z. Physiol. Chem. **280**, 186 (1944).
17. R. Lemberg and J. E. Falk. Biochem. J. **41**, 674 (1951).
18. H. H. Inhoffen, H. Brockman, Jr., and K. M. Bleisner. Justus Liebigs Ann. Chem. **730**, 173 (1969).
19. P. S. Clezy and C. J. R. Fookes. Aust. J. Chem. **27**, 371 (1974).
20. D. H. O'Keefe. Ph.D. Dissertation, University of Arizona. 1974.
21. A. D. Hamilton. M.Sc. Dissertation, University of British Columbia. 1976.
22. G. W. Kenner, S. W. McCombie, and K. M. Smith. Justus Liebigs Ann. Chem. 1329 (1973).
23. R. P. Carr, A. H. Jackson, G. W. Kenner, and G. S. Sach. J. Chem. Soc. C, 487 (1971).
24. P. S. Clezy and C. J. R. Fookes. Aust. J. Chem. **30**, 217 (1977).
25. R. K. DiNello and D. Dolphin. J. Org. Chem. **45**, 5196 (1980).

Can. J. Chem. Downloaded from www.nrcresearchpress.com by 210.87.254.105 on 09/06/12
For personal use only.

Influence of stereochemistry, screening, and deuteration of long and short intramolecular easily polarizable hydrogen bonds on their infrared continua

BOGUMIL BRZEZINSKI

Institute of Chemistry, A. Mickiewicz University, 60780 Poznań, Poland

AND

GEORG ZUNDEL

Institute of Physical Chemistry, Universität München, 8000 München 2, Theresienstr. 41, West Germany

Received July 31, 1980

BOGUMIL BRZEZINSKI and GEORG ZUNDEL. Can. J. Chem. **59**, 786 (1981).

$HClO_4$ salts of *N,N'*-tetramethylalkanes (compounds **1–6**) and of *N,N'*-tetraalkyl-*o*-xylildiamines (compounds **7–11**) and $HAuCl_4$ salts of *N,N'*-tetramethyl-*o*-xylildiamine-di-*N*-oxide (compound **12**) and of *o*-xylildipiperidyl-di-*N*-oxides (compounds **13–14**) were studied by nmr and ir spectroscopy. It is shown that in the compounds **3**, **4**, **5**, and **7–11**, long intramolecular $N^+H\cdots N \rightleftharpoons N\cdots H^+N$ hydrogen bonds with large proton polarizability and in compounds **12–14**, short intramolecular $O^+H\cdots O \rightleftharpoons O\cdots H^+O$ hydrogen bonds with large proton polarizability are formed. The study of the compounds **1–6** shows that the most favorable conditions for the formation of the intramolecular easily polarizable hydrogen bonds occur with compound **4**, i.e., if these hydrogen bonds are present in the 7-membered rings. In the case of compounds **7–14** it is shown that the continua usually observed with easily polarizable hydrogen bonds vanish when these bonds become screened from their solvent environments. Then, instead of continua only bands of the fundamental transitions are observed, with the long $N^+H\cdots N \rightleftharpoons N\cdots H^+N$ bonds in the region 2800–1800 cm^{-1} and with the short $O^+H\cdots O \rightleftharpoons O\cdots H^+O$ bonds in the region 1200–850 cm^{-1}. This result demonstrates that for the occurrence of the ir continua, the interaction of the easily polarizable hydrogen bonds with their solvent environments is absolutely necessary. Furthermore, it is shown with the long as well as the short hydrogen bonds that the intensity of the continua decreases strongly with deuteration, demonstrating that in both cases the deuteron polarizabilities are much smaller than the proton polarizabilities of the hydrogen or deuterium bonds, respectively. From this observation it is concluded that the proton potentials of these structurally symmetrical hydrogen bonds are considerably deformed by their molecular surroundings.

BOGUMIL BRZEZINSKI et GEORG ZUNDEL. Can. J. Chem. **59**, 786 (1981).

On a étudié, par spectroscopie ir et nmr, les perchlorate de *N,N'*-tétraméthylalcanes (composés **1** à **6**) et de *N,N'*-tétraalkyl *o*-xylildiamines (composés **7** à **11**) et les sels de $HAuCl_4$ du di-*N*-oxyde de la *N,N'*-tétraméthyl *o*-xylildiamine (composé **12**) et des di-*N*-oxydes de *o*-xylildipipéridyle (composés **13**, **14**). Dans le cas des composés **3**, **4**, **5** et **7–11** on montre qu'il se forme de longues liaisons hydrogène intramoléculaires $N^+H\cdots N \rightleftharpoons N\cdots H^+N$ avec polarisabilité forte alors que dans les composés **12** à **14**, il se forme de courtes liaisons hydrogène intramoléculaires $O^+H\cdots O \rightleftharpoons O\cdots H^+O$ avec polarisabilité forte. L'étude des composés **1** à **6** révèle que les conditions les plus favorables à la formation de liaisons hydrogène intramoléculaires facilement polarisables sont réalisées dans le composé **4**, i.e. si ces liaisons hydrogène se retrouvent dans des cycles à 7 chaînons. On montre, dans le cas des composés **7** à **14**, que les continus habituellement observés avec les liaisons hydrogènes facilement polarisables, disparaissent quand ces liaisons deviennent blindées de l'environnement du solvant. On n'observe alors que des bandes des transitions fondamentales, au lieu des continus avec les longues liaisons $N^+H\cdots N \rightleftharpoons N\cdots H^+N$ dans la région de 2800–1800 et avec les courtes liaisons $O^+H\cdots O \rightleftharpoons O\cdots H^+O$ dans la région de 1200–850 cm^{-1}. Ce résultat démontre que l'interaction des liaisons hydrogène facilement polarisables avec l'environnement de leur solvant est absolument nécessaire à l'existence des continus en ir. De plus on montre qu'avec les longues, aussi bien qu'avec les courtes liaisons hydrogène, l'intensité des continus diminue fortement avec la deutériation, démontrant que dans les deux cas les polarisabilités du deutéron sont respectivement beaucoup plus faibles que celles du proton ou du deutérium des liaisons hydrogène. A partir de ces observations, on a conclu que les potentiels du proton de ces liaisons hydrogène structurallement symétriques sont considérablement déformés par leur environnement moléculaire.

[Traduit par le journal]

Introduction

The proton polarizabilities of hydrogen bonds with double minimum proton potential or with a broad flat proton potential well, i.e., hydrogen bonds in which the protons may fluctuate, are extremely large (1–4*a*). Intramolecular hydrogen bonds show some advantages for studies of hydrogen bonded systems, for instance, they form, usually quantitatively, if the steric conditions are appropriate. Various types of intramolecular hydrogen bonds with large proton polarizabilities of the type $B^+H\cdots B \rightleftharpoons B\cdots H^+B$ (5, 6), of the type $B_1{}^+H\cdots B_2 \rightleftharpoons B_1\cdots H^+B_2$ (7) and of the type $B_1H\cdots B_2 \rightleftharpoons B_1{}^-\cdots H^+B_2$ (8–10) have already been studied from this point of view. In this paper, various properties of such bonds are investigated systematically with long and short, positively charged, structurally symmetrical hydrogen bonds.

Due to their large proton polarizabilities and dipole moments, these hydrogen bonds usually interact strongly with their environments (4*a*). Firstly, the local electrical fields in solutions polarize these hydrogen bonds (induced dipole interaction). Secondly, due to the large proton polarizability, transitions in the hydrogen bonds couple with transitions in their environments, whereby the coupling with

0008-4042/81/050786-09$01.00/0

©1981 National Research Council of Canada/Conseil national de recherches du Canada

Can. J. Chem. Downloaded from www.nrcresearchpress.com by 210.87.254.40 on 09/06/12
For personal use only.

Can. J. Chem. Downloaded from www.nrcresearchpress.com by 210.87.254.40 on 09/06/12
For personal use only.

low wave number vibrations is probably of particular significance. Both interaction effects are important for the occurrence of ir continua in systems with easily polarizable hydrogen bonds. Thus, these continua should vanish if these hydrogen bonds are screened from their solvent environments (4*a*). This effect of screening has already been demonstrated with the $HClO_4$ salts of *N*,*N*′-dipiperidylalkanes (5).

Easily polarizable hydrogen bonds of medium length cause continua extending from about 3200 cm^{-1} toward smaller wave numbers over the whole ir region. Easily polarizable hydrogen bonds which are relatively long cause continua which are particularly intense in the region 2800–1800 cm^{-1} and extend with less intensity toward smaller wave numbers, whereas easily polarizable hydrogen bonds which are relatively short absorb preferentially in the region 1600–600 cm^{-1}. This relation between bond length and wave number distribution has already been studied with various systems (4, 11) and was confirmed theoretically (3, 13). If these easily polarizable bonds are considered isolated, the proton polarizability is greatest with the long hydrogen bonds and decreases with the bond length (2–4*a*). In this paper, examples of long and short structurally symmetrical, easily polarizable hydrogen bonds will be discussed.

From a theoretical study (12) it is known that when the hydrogen or deuterium bonds have a symmetrical double minimum potential, the deuteron polarizabilities are much larger than the proton polarizabilities, whereas with asymmetrical double minimum potentials the deuteron polarizabilities are smaller than the proton polarizabilities.

Results and Discussion

Structurally symmetrical intramolecular hydrogen bonds are investigated with respect to the following parameters: *1*, the influence of stereochemical condition on the formation of these intramolecular bonds; *2*, the influence of screening; and *3*, the influence of deuteration on the infrared absorbance.

1. Stereochemistry and Formation of Hydrogen Bonds

The $HClO_4$ salts of *N*,*N*′-tetramethylalkanes were studied. The structural formulas are as follows:

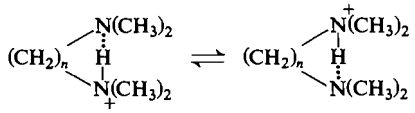

1–6: $n = 1–6$

The formation of the intramolecular hydrogen bonds was studied in solutions as a function of *n*, i.e., the number of CH_2 groups in the molecules. The nmr data are given in Tables 1 and 2. The chemical shift of the NH^+ protons in the case of the $HClO_4$ salts of compounds **3**, **4**, and **5**, and especially the comparison of this chemical shift with the value of the 1:2 complexes (1 *M* base: 2 *M* $HClO_4$) shows that the NH^+ groups in the $HClO_4$ salts of these compounds form hydrogen bonds. This is in contrast to the finding with the $HClO_4$ salts of compounds **1**, **2**, and **6**. With the $HClO_4$ salts of the compounds **3**, **4**, and **5**, these chemical shifts of the NH^+ protons are completely independent of concentration (Table 1), and excess of base has no influence on the NH^+ proton signal with compounds **4** and **5** and only a very weak influence with compound **3** (Table 2). All these results taken together demonstrate that the hydrogen bonds formed are intramolecular.

In the case of the $HClO_4$ salt of compound **3**, the chemical shift of the NH^+ proton is smaller than with the compounds **4** and **5** (Table 1), and only a very weak shift is observed when an excess of base is added (Table 2). This finding can be explained by incomplete formation of the hydrogen bonds as well as by the fact that the hydrogen bonds formed are weaker intramolecular hydrogen bonds. The ir results presented later show that both effects together are responsible for the smaller chemical shift.

With the $HClO_4$ salts of compounds **1** and **2** and especially with that of compound **6**, small shifts of the NH^+ proton signals towards lower fields are observed (Table 1). Furthermore, additional base also shifts these signals a little toward lower fields (Table 2). These findings can be explained by the formation of a small number of intermolecular hydrogen bonds.

Figure 1 shows the ir spectra of the $HClO_4$ salt solutions of compounds **2–6** and, for comparison, the spectra of the free bases. The spectrum of the $HClO_4$ salt of compound **1** is very similar to that of compound **2**. In the cases of the $HClO_4$ salts of compounds **3**, **4**, and **5** (Fig. 1 *b*, *c*, and *d*), intense continua are observed. These continua are much more intense in the region 2800–1800 cm^{-1}, showing a band-like structure with one maximum, and extend with less intensity toward smaller wave numbers over the whole region studied. This spectral feature is characteristic for long, easily polarizable hydrogen bonds (13). Thus, the intramolecular $N^+H\cdots N \rightleftharpoons N\cdots H^+N$ bonds are relatively long hydrogen bonds with large proton polarizability.

Can. J. Chem. Downloaded from www.nrcresearchpress.com by 210.87.254.40 on 09/06/12
For personal use only.

TABLE 1. Chemical shifts (ppm) of the NH^+, OH^+, CH_2, and CH_3 protons in the $HClO_4$ salts of the bases **1–11** and in $HAuCl_4$ salts **12–14***

	Concentration (mol/dm³)									
	1:1 complex							1:2 complex		
Base	0.1	0.2	0.3	0.4	0.5	CH_3	CH_2	0.1	CH_2	CH_3
1	7.23	7.27	7.29	7.34	7.35	2.56 d		7.19		2.57 d
2	7.38	7.38	7.37	7.41	7.46	2.57 d		7.21		2.58 d
3	11.46	11.47	11.48	11.48	11.49	2.58 s		7.20		2.59 d
4	14.12	14.10	14.12	14.11	14.12	2.57 s		7.19		2.58 d
5	13.89	13.90	13.90	13.91	13.91	2.56 s		7.18		2.57 d
6	7.77	7.79	7.85	7.88	7.89	2.52 d		7.20		2.54 d
7	14.15	14.14	14.15	14.16	14.16		4.00 s	7.17	4.35 d	
8	14.04	14.04	14.05	14.05	14.05		4.00 s	7.16	4.35 d	
9	14.00	13.99	13.99	14.00	14.01		4.10 s	7.16	4.37 d	
10	13.96	13.96	13.97	13.97	13.97		4.10 s	7.16	4.38 d	
11	13.92	13.93	13.92	13.94	13.93		4.10 s	7.15	4.40 d	
12	18.55	18.55	18.54	18.55	18.56					
13	17.89	17.88	17.89	17.89	17.89					
14	17.75	17.76	17.76	17.77	17.76					

*d, doublet; s, singlet.

TABLE 2. Chemical shifts (ppm) of the proton in the hydrogen bond, as influenced by the base concentration

		Chemical shift at concentration of the additional base (mol/dm³)				
Base	Concentration of the 1:1 complex (mol/dm³)	0.1	0.2	0.3	0.4	0.5
1	0.1	7.54	7.76	7.98	8.15	8.29
2	0.1	7.38	7.53	7.63	7.72	7.79
3	0.1	11.47	11.47	11.45	11.45	11.44
4	0.1	14.12	14.12	14.13	14.13	14.13
5	0.1	13.90	13.89	13.90	13.89	13.89
6	0.1	7.98	8.17	8.35	8.50	8.62
7	0.1	14.15	14.15	14.16	—	—
8	0.1	14.05	14.05	—	—	—
9	0.1	14.00	—	—	—	—
10	0.1	13.96	—	—	—	—
11	0.1	13.92	—	—	—	—
12	0.1	18.55	18.55	18.55	—	—
13	0.1	17.89	17.89	17.89	—	—
14	0.1	17.77	17.76	17.76	—	—

This result is confirmed by nmr data. Table 1 shows that the CH_3 proton signal is a doublet for the $HClO_4$ salts of compounds **1**, **2**, and **6**, as well as for all 1:2 complexes (1 *M* base: 2 *M* $HClO_4$). This splitting is caused by the spin–spin coupling of the CH_3 protons with the NH^+ proton. In contrast to this finding, for the $HClO_4$ salts of compounds **3**, **4**, and **5** only a singlet CH_3 proton signal is observed. This result demonstrates that the NH^+ proton is delocalized in the $N^+H\cdots N \rightleftharpoons N\cdots H^+N$ bonds, as expected, in light of the ir results.

In the case of the $HClO_4$ salt of compound **3**, the continuum is a little less intense, and the broad maximum is shifted considerably toward higher wave numbers. The nmr data have already suggested that the intramolecular hydrogen bonds are not formed quantitatively with the $HClO_4$ salt of compound **3**. This result is confirmed by the broad shoulder of the stretching vibration of non-hydrogen bonded NH^+ groups at about 3100 cm^{-1}. In the $HClO_4$ salts forming no intramolecular hydrogen bond, this vibration is observed as an intense band with maximum at 3100 cm^{-1}. Thus, the finding that the continuum is less intense with compound **3** is explained by incomplete formation of the intramolecular hydrogen bonds. The broad band-like structure of the continuum is mainly caused by the fundamental transitions. Thus, the shift of the

Can. J. Chem. Downloaded from www.nrcresearchpress.com by 210.87.254.40 on 09/06/12
For personal use only.

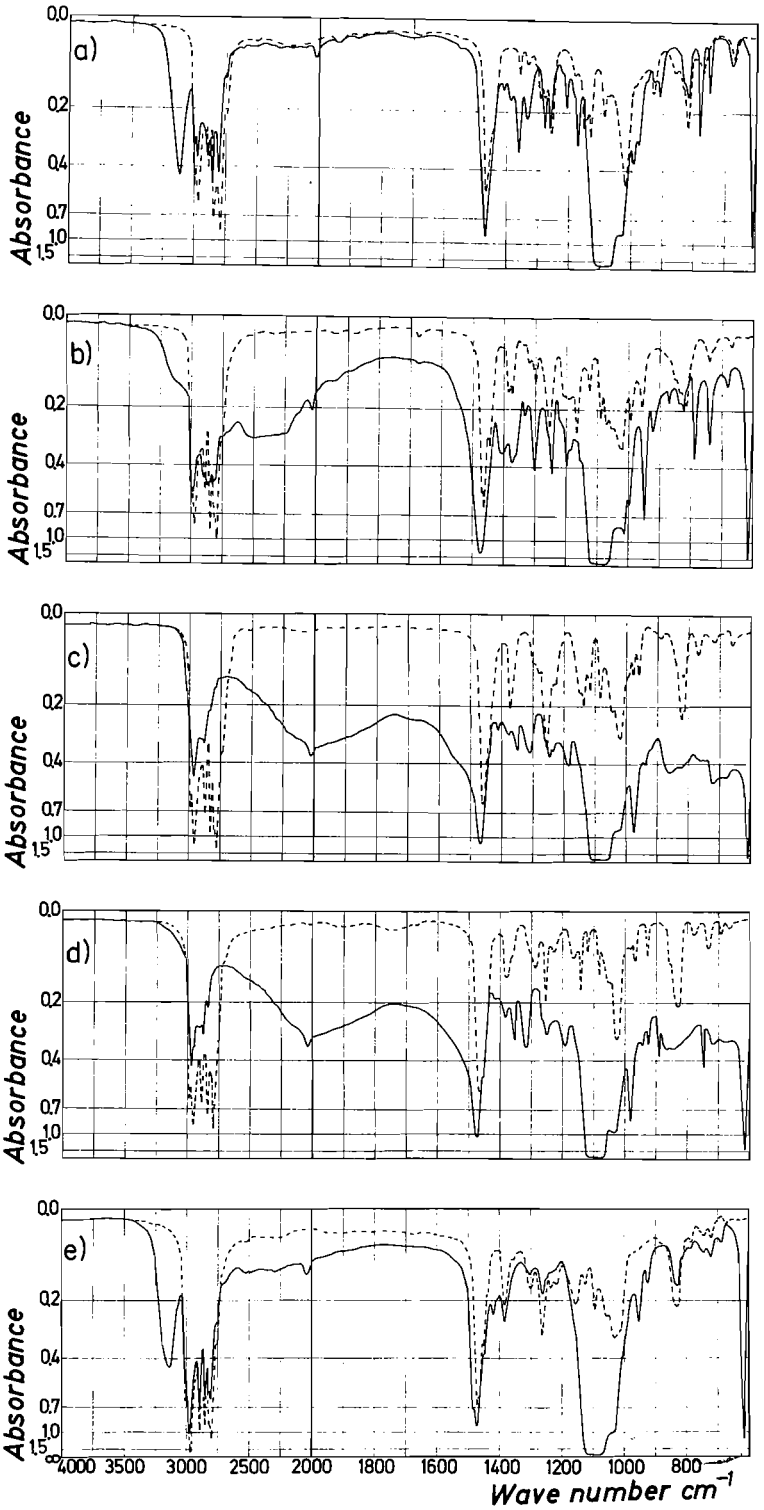

FIG. 1. Infrared spectra of bases (---) and of their $HClO_4$ salts (—) of compounds **2–6**.

maximum of the continuum toward larger wave numbers, observed with the $HClO_4$ salt of compound **3**, demonstrates that the intramolecular bonds are weaker. This result is in good agreement with the non-complete formation of these hydrogen bonds with this compound.

The very weak continuum observed with compound **6** may be caused by an intermolecular $N^+H\cdots N \rightleftharpoons N\cdots H^+N$ bond. The presence of a few such bonds was suggested by nmr data.

In summary we can state that in contrast to the results with the $HClO_4$ salts of compounds **1**, **2**, and **6**, with the $HClO_4$ salts of compounds **3**, **4**, and **5** intramolecular easily polarizable $N^+H\cdots N \rightleftharpoons N\cdots H^+N$ hydrogen bonds are formed. With the $HClO_4$ salt of compound **3**, these hydrogen bonds are a little weaker and not formed quantitatively. With the $HClO_4$ salt of compound **5**, these hydrogen bonds are a little weaker than with the $HClO_4$ salt of compound **4**, but the hydrogen bonds are also formed quantitatively.

All these results can be understood by considering the steric conditions. Molecular models show that with the $HClO_4$ salts of compounds **1** and **2**, the formation of an intramolecular hydrogen bond is impossible due to sterical constraint and the formation of intermolecular hydrogen bonds is hindered by the bulky CH_3 groupings and the rest of the molecule. With the $HClO_4$ salt of compound **3**, the steric constraint is smaller, therefore, a bent intramolecular hydrogen bond can be formed which is weaker than that in the $HClO_4$ salt of compound **4**. In the case of this $HClO_4$ salt, the steric conditions for the formation of the intramolecular $N^+H\cdots N \rightleftharpoons N\cdots H^+N$ bonds are most favorable, and decrease a little in the case of the $HClO_4$ salt of compound **5**. In the $HClO_4$ salt of compound **6**, the steric constraint is again so great that no intramolecular hydrogen bonds can be formed.

2. *Screening of the Hydrogen Bonds from their Environments*

The influence of screening against their solvent environment was studied with long, structurally symmetrical intramolecular $N^+H\cdots N \rightleftharpoons N\cdots H^+N$ bonds in $HClO_4$ salts of *N,N'*-tetraalkyl-*o*-xylildiamines (compounds **7–11**), and with short structural symmetrical intramolecular $O^+H\cdots O \rightleftharpoons O\cdots H^+O$ bonds in $HAuCl_4$ salts of *N,N'*-tetramethyl-*o*-xylildiamine-di-*N*-oxide (compound **12**) and *o*-xylildipiperidyl-di-*N*-oxides (compounds **13–14**). These compounds were chosen for these studies because the sterical conditions are very favorable for the formation of intramolecular hydrogen bonds. With the compounds **12–14** the salts were formed with $HAuCl_4$ instead of $HClO_4$, since with these compounds the formation of short intramolecular hydrogen bonds is expected (14, 15). Such hydrogen bonds cause continua which are most intense at smaller wave numbers (4*a*, 13, 16). Studies of $HClO_4$ salts in this region are strongly hindered by the very intense stretching vibration of the ClO_4^- ions masking the spectrum between 1000 and 1150 cm^{-1}.

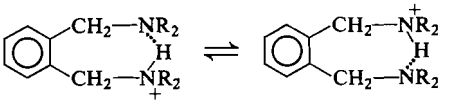

7, R = C_2H_5; **8**, R = C_3H_7; **9**, R = C_4H_9
10, R = C_5H_{11}; **11**, R = C_6H_{13}

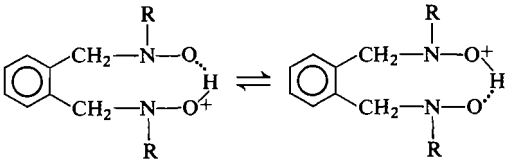

12, R = $(CH_3)_2$

13, R =

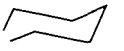

14, R =

The chemical shift of the NH^+ protons (compounds **7–11**) and that of the OH^+ protons (compounds **12–14**), and especially the comparison of these chemical shifts with the value of the 1:2 complexes (1 *M* base: 2 *M* $HClO_4$) in Table 1, shows that these NH^+ or OH^+ groups in their respective salts form hydrogen bonds. These signals are completely independent of the concentration and of the presence of excess base (Table 2), if their solubility allows these compounds to be studied with excess base.

These results together demonstrate that the hydrogen bonds are intramolecular and formed quantitatively.

The position of the NH^+ proton signals is almost the same with compounds **7–11**, demonstrating that the intramolecular $N^+H\cdots N \rightleftharpoons N\cdots H^+N$ bonds are of comparable strength in all these compounds. The position of the OH^+ proton signal differs a little with compound **11**, where R = $(CH_3)_2$, and with compounds **12** and **13**. This difference of the shifts is, however, so small that these hydrogen bonds are also of comparable strength.

In view of the fact that all these hydrogen bonds are structurally symmetrical, the proton potentials must also be symmetrical if these hydrogen bonds are considered isolated from their environment. Hydrogen bonds with such proton potentials are

Can. J. Chem. Downloaded from www.nrcresearchpress.com by 210.87.254.40 on 09/06/12
For personal use only.

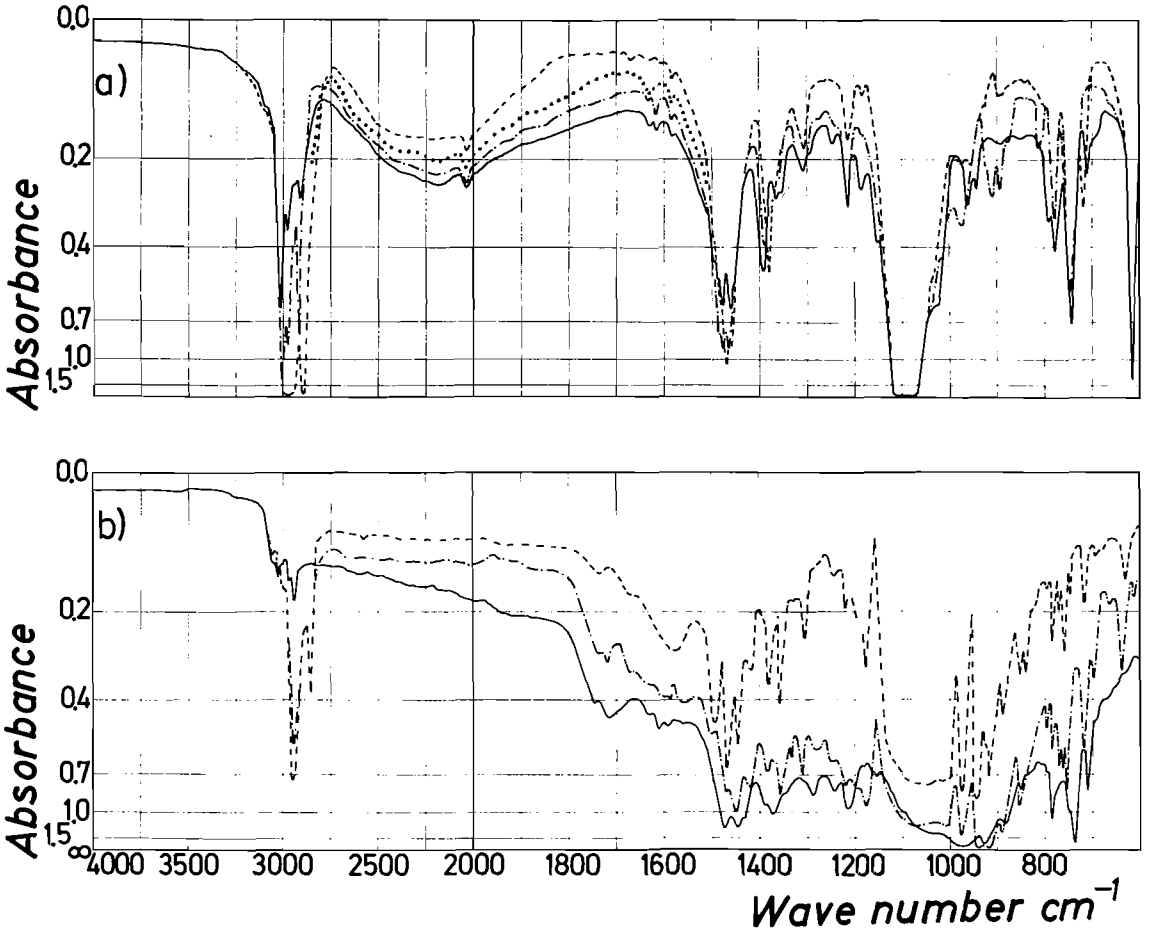

FIG. 2. Infrared spectra of *N*,*N*′-tetra-R-*o*-xylildiamine $HClO_4$ salts. (*a*) — R = C_2H_5 (**7**); ----- R = C_3H_7 (**8**); ··· R = C_4H_9 (**9**); --- R = C_6H_{13} (**11**). (*b*) $HAuCl_4$ salts of compounds **12**–**14**: —, **12**; -----, **13**; ---, **14**.

usually easily polarizable (1–4*a*). The proton within easily polarizable hydrogen bonds is delocalized. This result is confirmed by the nmr data in Table 1. The CH_2 proton signals of the 1:2 complexes (1 *M* base: 2 *M* acid), if they can be studied (solubility), are doublets, indicating spin–spin coupling of the CH_2 proton. When hydrogen bonds are formed, the CH_2 signals are singlets in all cases, indicating that such coupling no longer occurs, because the protons in these intramolecular hydrogen bonds are delocalized.

The ir spectra of these compounds are shown in Fig. 2, in Fig. 2*a* are shown compounds with $N^+H\cdots N \rightleftharpoons N\cdots H^+N$ bonds and in Fig. 2*b* those with $O^+H\cdots O \rightleftharpoons O\cdots H^+O$ bonds. Let us first consider compound **7** (solid line in Fig. 2*a*) and compound **12** (solid line in Fig. 2*b*). With these compounds, the substituents are relatively small, and, therefore, the intramolecular hydrogen bonds may interact with their environments. With compound **7**, a continuum is observed. It shows an intense band-like structure in the region 2800–1800 cm^{-1}, with maximum at about 2100 cm^{-1}, and extends with less intensity towards smaller wave numbers over the whole region. This spectral feature is characteristic of long hydrogen bonds with large proton polarizability (4*b*, 11, 13). With compound **12**, a continuum is found which is most intense in the region 1800–700 cm^{-1}. This spectral feature is characteristic of short hydrogen bonds with large proton polarizability (4*a*, 13). Thus the intramolecular $N^+H\cdots N \rightleftharpoons N\cdots H^+N$ bonds are relatively long and the intramolecular $O^+H\cdots O \rightleftharpoons O\cdots H^+O$ bonds relatively short, easily polarizable hydrogen bonds.

In the series of compounds **7**–**11**, the substituents become increasingly bulky and thus, the intramolecular $N^+H\cdots N \rightleftharpoons N\cdots H^+N$ bonds increasingly screened from their solvent environments. The same is true in the series of compounds **12**–**14**

Can. J. Chem. Downloaded from www.nrcresearchpress.com by 210.87.254.40 on 09/06/12
For personal use only.

Can. J. Chem. Downloaded from www.nrcresearchpress.com by 210.87.254.40 on 09/06/12
For personal use only.

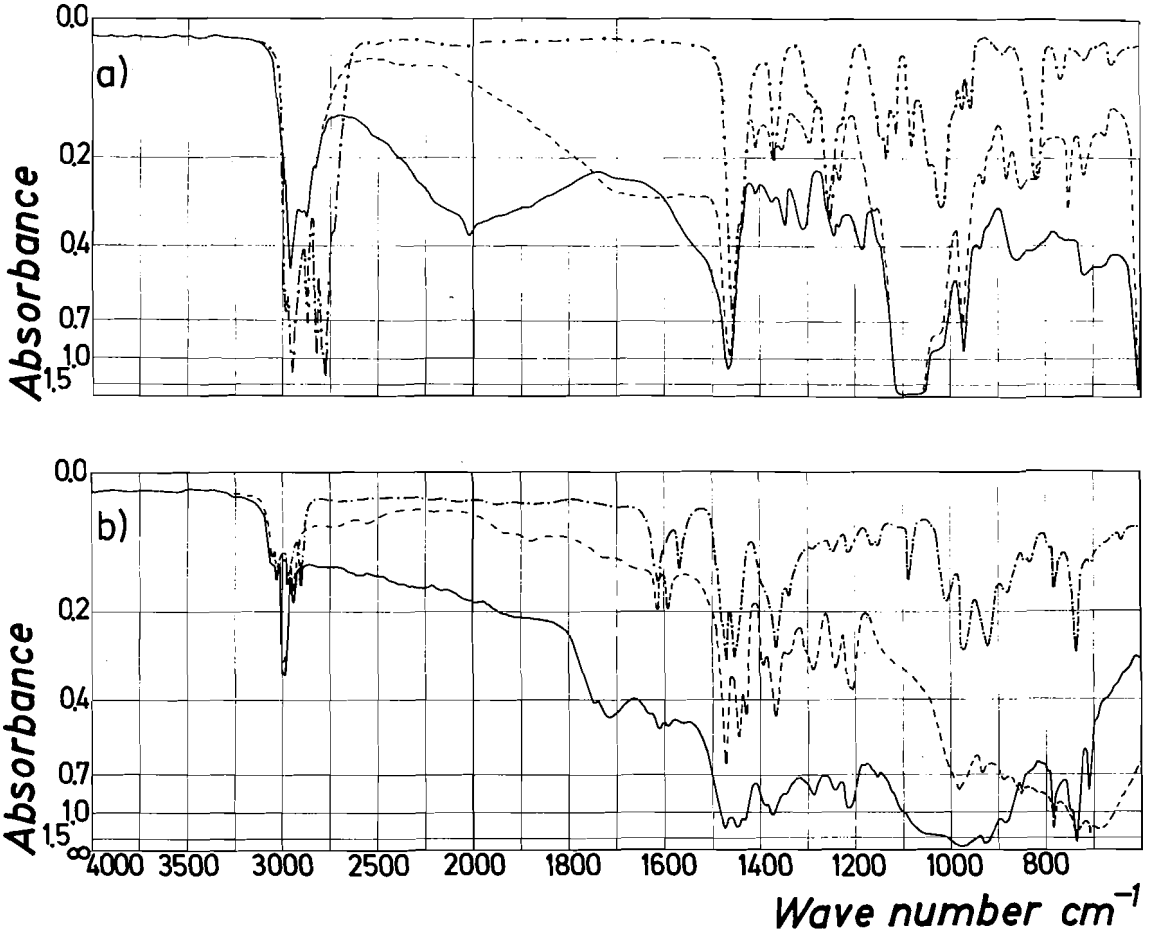

FIG. 3. Infrared spectra of (*a*) compound **3**: —, $HClO_4$ salt; ---, $DClO_4$ salt; -·-·-, free base; (*b*) compound **12**: —, $HAuCl_4$ salt; ---, $DAuCl_4$ salt; -·-·-, free base.

with the intramolecular $O^+H\cdots O \rightleftharpoons O\cdots H^+O$ bonds.

With increasing screening of the $N^+H\cdots N \rightleftharpoons N\cdots H^+N$ bonds (Fig. 2*a*), the continuum vanishes almost completely and a band remains. This band is found in the same position (region 2800–1800 cm^{-1}) where the continuum has shown its band-like structure, which was mainly caused by the fundamental transition of the hydrogen bonds.

With increasing screening of the $O^+H\cdots O \rightleftharpoons O\cdots H^+O$ bonds, as can be seen in Fig. 2*b*, the continuum vanishes and an intense broad band remains in the region 1200–850 cm^{-1}, and a much less intense band is found in the region 1700–1400 cm^{-1}. In analogy to the assignment in ref. 15, the intense band at smaller wave numbers is assigned to the fundamental transition of the hydrogen bonds and the relatively weak band at higher wave numbers to the bending vibration. When with increasing screening the continuum draws back to the band in the region 1200–850 cm^{-1}, various pronounced Evans holes (17–19) arise within this band at 1157, 990, 954, and 930 cm^{-1}.

In summary we can state that with increasing screening of the easily polarizable hydrogen bonds against their solvent environment the ir continua vanish and bands of the usual fundamental transitions of the hydrogen bonds are observed. Thus, for the occurrence of the continua the interaction of the easily polarizable hydrogen bonds with their solvent environments is absolutely necessary. This confirms the theory that the continuity of energy level differences observed as ir continua arises due to the interaction of the easily polarizable hydrogen bonds with local fields in their environment, and due to coupling of transitions in the easily polarizable hydrogen bond with vibrations in their solvent environment.

3. *Change of the Polarizability with Deuteration*

Figure 3 shows spectra of the $HClO_4$ salts and their deuterated analogues, and for comparison the

Can. J. Chem. Downloaded from www.nrcresearchpress.com by 210.87.254.40 on 09/06/12
For personal use only.

spectra of the free bases. As an example of long hydrogen bonds, spectra of compound **3** are shown, and as an example of short hydrogen bonds, spectra of compound **12**.

These figures show that with long hydrogen bonds the continuum decreases strongly with deuteration. The band-like structure caused by the fundamental transitions of the deuterium bonds is found with maximum at 1650 cm^{-1}. With short hydrogen bonds the continuum also decreases strongly with deuteration and a band of the fundamental transition of the deuterium bond appears with maximum at about 710 cm^{-1}.[1] These results demonstrate that with these long and short intramolecular hydrogen bonds, the deuteron polarizabilities are much less than the proton polarizabilities of the respective hydrogen bonds. This shows (see Introduction) that the potentials in these structurally symmetrical hydrogen or deuterium bonds, respectively, are already so strongly deformed that the deuteron is largely localized at one side of the bonds, whereas this is not the case with the protons, since the levels of the proton have a little higher energy than those of the deuteron. Thus the protons may have much larger fluctuation amplitudes within the potential well than the deuterons.

These results together demonstrate that the potentials, of easily polarizable hydrogen bonds, even structurally symmetrical ones are strongly deformed by interaction with the solvent.

Conclusions

It is shown that the most favorable conditions for the formation of intramolecular, easily polarizable $NH^+\cdots N \rightleftharpoons N\cdots H^+N$ bonds in the $HClO_4$ salts of compounds **1–6** occur when these hydrogen bonds are present within the 7-membered rings.

When easily polarizable hydrogen bonds are screened from their solvent environments the continua, usually observed when easily polarizable hydrogen bonds are present in amorphous media, vanish. Then, with the long $N^+H\cdots N \rightleftharpoons N\cdots H^+N$ bonds, the band of the fundamental transitions is found in the region 2800–1800 cm^{-1}, whereas with the short $O^+H\cdots O \rightleftharpoons O\cdots H^+O$ bonds, this band is observed in the region 1200–850 cm^{-1}. Thus, for the occurrence of the continua, interaction of the easily polarizable hydrogen bonds with their solvent environments is absolutely necessary. This confirms that the continuity of energy level differences, observed as ir continuum, arises only due to the interaction of the easily polarizable hydrogen bonds with local electrical fields in their environments, and due to coupling of transitions in the easily polarizable hydrogen bonds with vibrations in their environments.

With long as well as with short, structurally symmetrical hydrogen bonds, the continuum decreases strongly with deuteration, demonstrating that the deuteron polarizabilities are much less than the proton polarizabilities. This becomes understandable, if one also assumes that with the structurally symmetrical hydrogen bonds, the potentials are strongly deformed due to interaction effects with their solvent environment.

The reason for this great deformation of the proton potentials due to their molecular surroundings is the large proton polarizability these hydrogen bonds have if isolated from their environment.

The result that the proton potentials of easily polarizable hydrogen bonds are strongly deformed by interaction with their solvent environments is in good agreement with other theoretical as well as experimental findings. In ref. 21, the interaction of a structurally symmetrical hydrogen bond with a polar environment was treated theoretically with the result that if the proton is in the ground state, the proton potentials usually become more and more asymmetrical due to polar environments. The intensity of the Rayleigh scattering in the Raman spectra near the excitation line is a direct measure of the anisotropy of the proton or deuteron polarizabilities and thus, since these polarizabilities occur only in bond direction, of the polarizabilities. It was shown (22) that this scattering is much more intense with easily polarizable hydrogen bonds than with deuterium bonds.

Materials and Methods

The preparation of the substances as well as the analytical data are given in ref. 23. The substances were deuterated by triple recrystallisation from methanol-d_1. All handling of these substances must be done in a very carefully dried glove box.

All spectra were recorded in 0.5 *M* CD_3CN solutions. CD_3CN was stored over 3 Å molecular sieve. The nmr spectra were recorded with a Varian HA 100 spectrometer. All these spectra were calibrated against TMS as internal standard. To record the ir spectra a cell with NaCl windows was used (layer thickness 0.1 mm). The bands of acetonitrile-d_3 were compensated by a cell with pure acetonitrile-d_3 in the reference beam. All ir spectra were obtained with a spectrophotometer 325 (Bodenseewerk Perkin-Elmer, Überlingen) (program 6.5, time response 2).

Acknowledgement

Our thanks are due to the Deutsche Forschungsgemeinschaft and the Fonds der Chemischen Industrie for their support of this work.

[1] It is known from literature data (ref. 12, ref. 20, Fig. 1*c* and *d*) that with medium length, easily polarizable hydrogen or deuterium bonds, the intensity of the continua also decreases but not so strongly.

1. E. G. WEIDEMANN and G. ZUNDEL. Z. Naturforsch. **25**a, 617 (1970).

2. R. JANOSCHEK, E. G. WEIDEMANN, H. PFEIFFER, and G. ZUNDEL. J. Am. Chem. Soc. **94**, 2387 (1972).
3. R. JANOSCHEK, E. G. WEIDEMANN, and G. ZUNDEL. J. Chem. Soc. Faraday II, **69**, 505 (1973).
4. (*a*) G. ZUNDEL. *In* The hydrogen bond – recent developments in theory and experiments. Vol. II. *Edited by* P. Schuster, G. Zundel, and C. Sandorfy. North Holland Publ. Co., Amsterdam. 1976; (*b*) B. BRZEZINSKI and G. ZUNDEL. J. Mol. Struct. In press.
5. B. BRZEZINSKI and G. ZUNDEL. J. Chem. Soc. Faraday Trans. II, **75**, 661 (1979).
6. B. BRZEZINSKI and G. ZUNDEL. Chem. Phys. Lett. **70**, 55 (1980).
7. B. BRZEZINSKI and G. ZUNDEL. Chem. Phys. Lett. **61**, 315 (1979).
8. B. BRZEZINSKI and G. ZUNDEL. Chem. Phys. Lett. **44**, 521 (1976).
9. B. BRZEZINSKI and G. ZUNDEL. Z. Phys. Chem. Frankfurt, **111**, 31 (1978).
10. B. BRZEZINSKI and G. ZUNDEL. J. Mol. Struct. **68**, 315 (1980).
11. B. BRZEZINSKI and G. ZUNDEL. J. Chem. Soc. Faraday Trans. II, **72**, 2127 (1976).
12. R. JANOSCHEK, A. HAYD, E. G. WEIDEMANN, M. LEUCHS, and G. ZUNDEL. J. Chem. Soc. Faraday Trans. II, **74**, 1238 (1978).
13. A. HAYD, E. G. WEIDEMANN, and G. ZUNDEL. J. Chem. Phys. **70**, 86 (1979).
14. M. SZAFRAN. Pol. J. Chem. **52**, 249 (1978).
15. D. HADŽI. *In* The hydrogen bond – recent developments in theory and experiments. Vol. II. *Edited by* P. Schuster, G. Zundel, and C. Sandorfy. North Holland Publ. Co., Amsterdam. 1976.
16. Z. PAWLAK and L. SOBCZYK. Advances in molecular relaxation interaction processes. Vol. 5. Elsevier Publishing Co., Amsterdam. 1973. p. 99*ff*.
17. J. C. EVANS and N. WRIGHT. Spectrochim. Acta, **16**, 352 (1960).
18. J. C. EVANS. Spectrochim. Acta, **16**, 994 (1960).
19. A. HAYD and E. G. WEIDEMANN. J. Chem. Phys. **70**, 86 (1979).
20. G. ZUNDEL. Hydration and intermolecular interaction. Academic Press, New York. 1969. p. 116*ff*; Mir Moscov, 1972.
21. H. PFEIFFER, G. ZUNDEL, and E. G. WEIDEMANN. J. Phys. Chem. **83**, 2544 (1979).
22. W. DANNINGER and G. ZUNDEL. J. Chem. Phys. To be published.
23. B. BRZEZINSKI. To be published.

Can. J. Chem. Downloaded from www.nrcresearchpress.com by 210.87.254.40 on 09/06/12
For personal use only.

N-Picrylethylenediamine – methoxide ion interactions: *N*-deprotonation and σ-complex formation reactions

ERWIN BUNCEL,[1] MASASHI HAMAGUCHI,[2] AND ALBERT R. NORRIS[1]

Department of Chemistry, Queen's University, Kingston, Ont., Canada K7L 3N6

Received August 18, 1980

ERWIN BUNCEL, MASASHI HAMAGUCHI, and ALBERT R. NORRIS. Can. J. Chem. **59**, 795 (1981).

The interactions of *N*-picrylethylenediamine as the HCl salt (PED) with methoxide ion in dimethyl sulfoxide – methanol (DMSO/MeOH) media and with 1,4-diazabicyclooctane in dimethyl sulfoxide have been investigated spectrophotometrically at 25.0°C. Evidence is presented to show that, in solvent mixtures rich in dimethyl sulfoxide (e.g. 95/5, V/V, DMSO/MeOH), deprotonation reactions at the nitrogen centres on the ethylenediamine occur in preference to reactions in which σ-complexes are formed via addition of CH_3O^- to one or more ring carbon atoms. The initial 1:1 interaction of CH_3O^- and PED results in the rapid, reversible deprotonation of the NH centre while the 2:1 interaction is associated with rapid, reversible abstraction of H^+ from the NH_3^+ centre. At mole ratios of CH_3O^- to PED > 3 a σ-complex is formed as a result of the addition of CH_3O^- ion to a C-3 ring carbon atom of the di-deprotonated PED. The uv–visible absorption properties of these various species are reported and compared to the properties of corresponding species formed in related systems.

ERWIN BUNCEL, MASASHI HAMAGUCHI et ALBERT R. NORRIS. Can. J. Chem. **59**, 795 (1981).

On a étudié, par spectrophotométrie à 25°C, les interactions du chlorhydrate de *N*-picryléthylènediamine (PED) avec l'ion méthylate dans un mélange de diméthylsulfoxide – méthanol (DMSO/MeOH) et avec le diaza-1,4 bicyclooctane dans le diméthylsulfoxyde. On prouve que dans des mélanges de solvant riches en diméthylsulfoxyde (i.e. 95/5, V/V, DMSO/MeOH) les réactions de déprotonation ont lieu au niveau de l'azote central de l'éthylènediamine de préférence aux réactions dans lesquelles les complexes σ se forment via l'addition de CH_3O^- à l'un ou plusieurs des atomes de carbone du cycle. L'interaction initiale 1:1 du CH_3O^- et du PED conduit à une déprotonation rapide, réversible du NH central tandis que l'interaction 2:1 est associée à une élimination rapide, réversible de H^+ à partir du NH_3^+ central. Pour des rapports molaires de CH_3O^- à PED > 3 il se forme un complexe σ par suite de l'addition de CH_3O^- au carbone en position 3 du cycle de PED bidéprotoné. On rapporte les spectres d'absorption dans le visible et l'uv de ces différentes espèces et on les compare à celles des espèces correspondantes formées dans les système apparentées.

[Traduit par le journal]

Introduction

We have reported previously (1, 2) that, in dimethyl sulfoxide – methanol (DMSO/MeOH) solvent mixtures, the interaction of methoxide ion (CH_3O^-) with *N*-methylpicramide (NMP) leads to the formation of species **1**, **2** (R = H), and **3**, while *N*,*N*-dimethylpicramide (DMP) gives rise to species **2** (R = CH_3) and **4**.

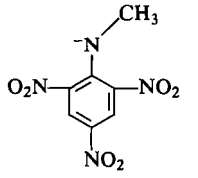

1

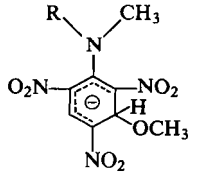

2

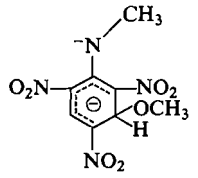

3

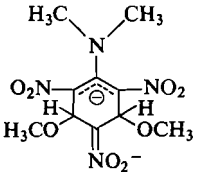

4

A particularly important observation which emerged from these studies was that DMSO stabilizes the conjugate base of NMP, **1**, with respect to the σ-complex **2** (R = H). As a result, DMSO/MeOH solutions rich in DMSO, e.g. 95 volume % DMSO, in which the mole ratio of CH_3O^- to NMP was < 1, contained **1** as the major product of the interaction of CH_3O^- and NMP. This fact enabled us to obtain, for the first time, good uv–visible absorption data for species **1** and **3**.

As part of a continuing study of the reactions of *N*-substituted picramides with CH_3O^-, we now report on the species formed in the reactions of the HCl salt of *N*-picrylethylenediamine, **5**, with methoxide ion in DMSO/MeOH media and with 1,4-diazabicyclooctane (DABCO) in dimethyl sulfoxide.

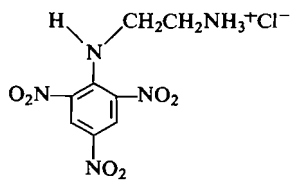

5

Results

In the uv–visible region *N*-picrylethylenedi-

[1]To whom all correspondence should be addressed.

[2]Permanent address: Department of Chemistry, College of General Education, Osaka University, Osaka 560, Japan.

0008-4042/81/050795-07$01.00/0

©1981 National Research Council of Canada/Conseil national de recherches du Canada

Can. J. Chem. Downloaded from www.nrcresearchpress.com by 210.87.254.105 on 09/06/12
For personal use only.

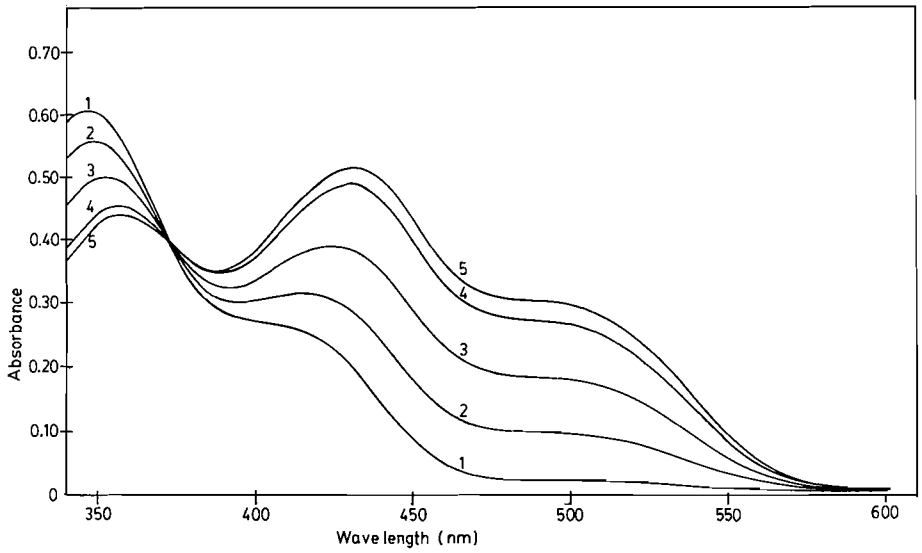

FIG. 1. Initial absorption spectra of the HCl salt of *N*-picrylethylenediamine (4.26×10^{-4} *M*) in dimethyl sulfoxide – methanol (95/5, V/V) containing various concentrations of sodium methoxide ($NaOCH_3$). $[CH_3O^-]$ (*M*): *1*, 0; *2*, 1.04×10^{-4}; *3*, 2.21×10^{-4}; *4*, 3.29×10^{-4} *M*; *5*, 4.08×10^{-4}; 0.10 cm cell; 25.0°C.

amine as the HCl salt (**5**) shows, in dimethyl sulfoxide – methanol (95/5, V/V) as solvent, an absorption maximum at 347 nm ($\varepsilon = 1.44 \times 10^4\ M^{-1}\ cm^{-1}$) and a broad shoulder with midpoint at 405 nm ($\varepsilon = 0.64 \times 10^4\ M^{-1}\ cm^{-1}$).

The addition of progressively larger amounts of sodium methoxide ($NaOCH_3$) to a solution of **5** in dimethyl sulfoxide – methanol (95/5, V/V) results in the simultaneous disappearance of the absorption band due to **5** and the appearance of a new band characterized by an absorption maximum at 430 nm and a broad shoulder whose mid-point occurs at 490 nm (Fig. 1). Conversion of starting material to this new absorbing species, **M**, is essentially complete upon the addition of 1 mol-equiv. of base to the solution containing **5**. The equilibrium constant (K_1) associated with the formation of **M** according to the reaction

[1] $\mathbf{5} + CH_3O^- \rightleftharpoons \mathbf{M}$

is accordingly estimated to be $\geq 5 \times 10^5\ M^{-1}$ at 25.0°C. Solutions containing only **5** and **M** exhibit an isosbestic point at 374 nm (Fig. 1). Both the conversion of **5** to **M** and the conversion of **M** to **5**, via the addition of trifluoroacetic acid (TFA), occur within the time required to mix the reagents and record the spectrum of the resulting solution (< 20 s). Assuming complete conversion of **5** to **M** as the result of the addition of 1 mol-equiv. of $NaOCH_3$ to **5**, we calculate molar absorptivity (ε) values of 1.38×10^4 and $0.81 \times 10^4\ M^{-1}\ cm^{-1}$ at 430 and 490 nm, respectively, for species **M** (Table 1).

The addition of progressively increasing amounts of $NaOCH_3$ to a solution containing species **M** leads to the replacement of the absorption band due to **M** by a new absorption band possessing an absorption maximum at 443 nm and a shoulder with mid-point at 490 nm (Fig. 2). Conversion of **M** to this new absorbing species, **N**, is essentially complete upon the addition of a further 1 mol-equiv. of base to the solution containing **M** (2 mol-equiv. of $NaOCH_3$, in total, added to **5**). The equilibrium constant (K_2) characterizing the formation of **N** from **M** and $NaOCH_3$ is once again estimated to be $\geq 5 \times 10^5\ M^{-1}$ at 25.0°C. The spectra of solutions containing only **M** and **N** are characterized by an isosbestic point at 391 nm (Fig. 2). The addition of TFA rapidly and quantitatively converts **N** to **M** and, with the addition of excess acid, **N** to **5**. Assuming complete conversion of **M** to **N** as the result of the addition of 2 mol of $NaOCH_3$ per mol of **5** originally present in solution, we calculate ε values of $1.72 \times 10^4\ M^{-1}\ cm^{-1}$ and $1.29 \times$

TABLE 1. Values of molar absorptivities, ε, at selected wavelengths for *N*-picrylethylenediamine as the HCl salt and species **M**, **N**, and **O**; 95/5 (V/V) dimethyl sulfoxide – methanol as solvent; $T = 25.0$°C

	$\varepsilon\ (M^{-1}\ cm^{-1} \times 10^{-4})$ at $\lambda_{(nm)}$					
Compound	335	347	430	443	490	506
5	1.32	1.44	0.48	0.30	0.0	0.0
M	0.66	0.93	1.38	0.81	0.82	0.78
N	0.38	0.52	1.61	1.72	1.29	1.24
O	1.13	1.16	0.43	0.62	2.90	3.37

Can. J. Chem. Downloaded from www.nrcresearchpress.com by 210.87.254.105 on 09/06/12
For personal use only.

Can. J. Chem. Downloaded from www.nrcresearchpress.com by 210.87.254.105 on 09/06/12
For personal use only.

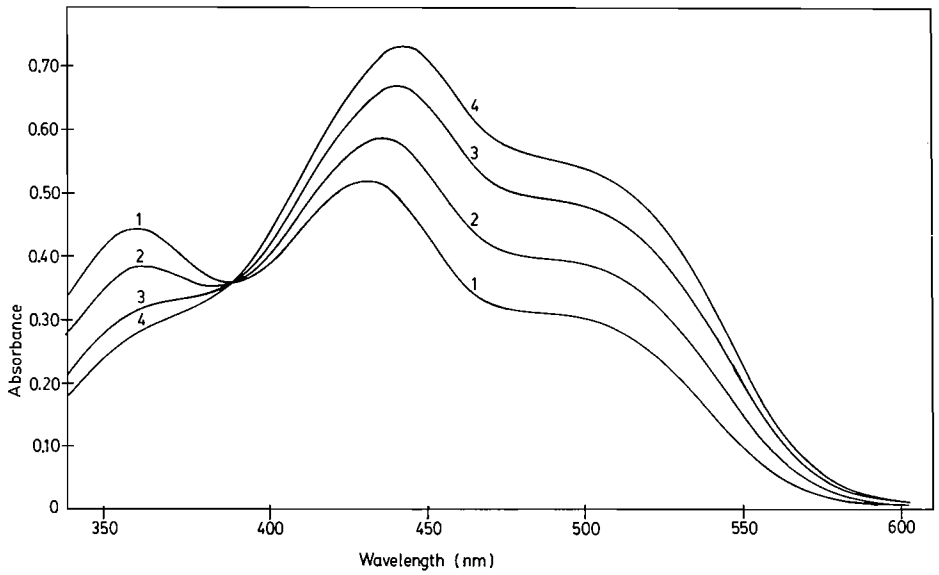

FIG. 2. Initial absorption spectra of the HCl salt of *N*-picrylethylenediamine (4.26×10^{-4} *M*) in dimethyl sulfoxide – methanol (95/5, V/V) containing various concentrations of sodium methoxide ($NaOCH_3$). $[CH_3O^-]$ (*M*): *1*, 4.26×10^{-4}; *2*, 5.56×10^{-4}; *3*, 7.02×10^{-4}; *4*, 8.41×10^{-4}; 0.10 cm cell; 25.0°C.

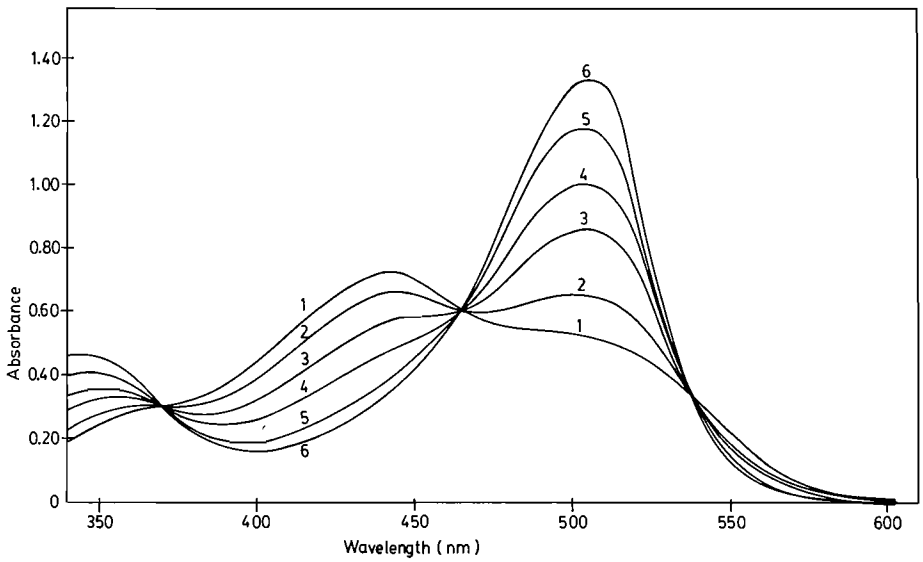

FIG. 3. Initial absorption spectra of the HCl salt of *N*-picrylethylenediamine (4.38×10^{-4} *M*) in dimethyl sulfoxide – methanol (95/5, V/V) containing various concentrations of sodium methoxide ($NaOCH_3$). $[CH_3O^-]$ (*M*): *1*, 8.76×10^{-4}; *2*, 11.3×10^{-4}; *3*, 14.4×10^{-4}; *4*, 16.9×10^{-4}; *5*, 29.3×10^{-4}; *6*, 42.8×10^{-4}; 0.10 cm cell; 25.0°C.

10^4 M^{-1} cm^{-1} at 443 and 490 nm, respectively, for species **N**.

The addition of sodium methoxide to a solution containing species **N** results in the simultaneous disappearance of the absorption band due to **N** and the appearance of a new absorption band with maxima at 344 and 506 nm (Fig. 3). The new maxima are attributed to the production of a single new absorbing species, **O**, in solution. Solutions containing only the absorbing species **N** and **O** are characterized by isosbestic points at 370, 466, and 538 nm (Fig. 3). The conversion of **N** to **O** is rapid and is quantitatively reversed by the addition of TFA; TFA in excess of total base added to the original solution regenerates **5** from **O**. Utilizing the limiting absorbance values obtained at high concentrations of $NaOCH_3$ and, assuming complete conversion of **5** to **O** under these conditions, we

Can. J. Chem. Downloaded from www.nrcresearchpress.com by 210.87.254.105 on 09/06/12
For personal use only.

calculate ε values of 1.16×10^4 and 3.37×10^4 M^{-1} cm^{-1} at 344 and 506 nm, respectively, for species **O**. The value of the equilibrium constant (K_3) associated with the reaction

[2] $N + CH_3O^- \rightleftharpoons O$

is calculated to be $1.8 \pm 0.1 \times 10^3$ M^{-1} at 25.0°C.

The rapid ($t_{1/2} < 1$ s) conversion of **N** to **O** described above is followed by a much slower process ($t_{1/2} \sim 30$ min) as a result of which the absorption maximum in the visible region shifts from 506 to 503 nm and the value of the absorbance at the absorption maximum increases very slightly (<5%). During this time the peak at 345 remains constant in position and the value of the absorbance at 345 nm remains unchanged. An isosbestic point at 464 nm is associated with the spectra of the solution throughout the course of this slow conversion of **O** to the new absorbing species. The addition of TFA, in excess of total base, to a solution containing the species absorbing at 503 and 345 nm rapidly regenerates the original reactant **5**.

Discussion

It has been shown that the reaction of **5** with CH_3O^- in dimethyl sulfoxide – methanol (95/5, V/V) leads to the rapid, reversible formation of at least three and possibly four new absorbing species in solution. What are the composition and structure of each of these species?

Species **M** is generated as a result of a 1:1 interaction of **5** and CH_3O^-. This interaction may involve either proton abstraction by CH_3O^- or the addition of CH_3O^- to a ring carbon atom to form a σ-complex. If the reaction is one of proton abstraction, at what point in the molecule is the proton being abstracted? Based on the results obtained in earlier studies (1–4), reasonable formulations of **M** would include the following:

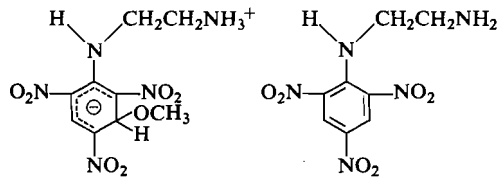

6

7

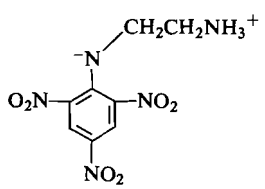

8

The addition reaction to form σ-complex **6** may be ruled out by noting that, by analogy with the spectra observed for other related σ-complexes (4), e.g. **4**, one might expect **6** to show two distinct absorption maxima in the visible region with an ε value at the lower wavelength maximum of $\sim 3 \times 10^4$ M^{-1} cm^{-1}. Species **M** clearly does not display these absorption characteristics (Fig. 1) and formulation of **M** as the σ-complex **6** may be tentatively ruled out on this basis. A much stronger argument ruling against the formulation of **M** as **6** is the observation that in dry dimethyl sulfoxide, 1,4-diazabicyclooctane (DABCO), which cannot form a σ-complex (5) but can deprotonate the N-centres, also reacts with **5** to generate a species whose absorption characteristics are identical (λ_{max} and ε) to those of **M**.

Given that the initial interaction of **5** and CH_3O^- involves deprotonation and not σ-complex formation, which N-centre is being deprotonated? It would seem that **7** should possess absorption characteristics little different from those of the related compounds picramide and *N*-methylpicramide, the uv–visible absorption characteristics of which are very similar to those of the starting compound **5**. Thus, in that case, conversion of **5** to species **7** should be accompanied by only minor spectral changes. However, as noted in Fig. 1, there is a marked change in spectral features accompanying the conversion of **5** to **M** and, for this reason, we believe that **M** is not likely to be correctly formulated as species **7**.

This leaves us with **8** as the remaining plausible formulation for **M**. The absorption properties (λ_{max} and ε) for species **M** are not inconsistent with this suggestion; values of λ_{max} and ε at λ_{max} for species closely related to **8** are listed in Table 2. We note that the ε for species **M** at its absorption maximum (1.38×10^4 M^{-1} cm^{-1}) is somewhat lower than the ε values quoted for the related species **1**, **9**, and **10** (6,

TABLE 2. Values of absorption maxima and molar absorptivities (ε) at the absorption maxima for some selected anions and σ-complexes

Compound	Absorption maximum (nm)	ε (M^{-1} cm^{-1} × 10^{-4}) at λ_{max}
9	520	1.7
1	442	1.71
10	380	1.5
8 (M)	430	1.38
11 (N)	443	1.72
3	508	4.00
	335	1.23
14 (O)	506	3.37
	344	1.16

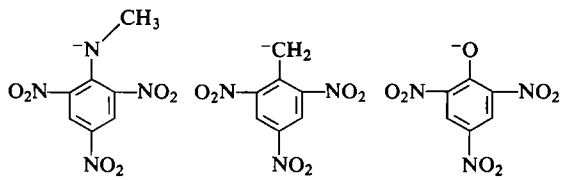

1 9 10

7). This may possibly be the result of one of the *ortho* nitro groups in **8** being somewhat out of the plane of the ring as a consequence of strong H-bonding between a hydrogen on the NH_3^+ group and an oxygen atom of the *ortho* nitro group (8).

A possible alternative explanation of the lower than expected value of ε at 430 nm is that species **M** consists of an equilibrium mixture of **7** and **8**. Rapid equilibration of **7** and **8** (reaction [3]) characterized

[3] $7 \rightleftharpoons 8$

by an equilibrium constant K' would then yield a weighted average value of ε_{430} given by eq. [4] (9).

[4] $$\varepsilon_{430} = \left(\frac{1}{K' + 1}\right)\varepsilon_8 + \left(\frac{K'}{K' + 1}\right)\varepsilon_7$$

In this case, an $\varepsilon_7 = 0$ and an $\varepsilon_8 = 1.42 \times 10^4\ M^{-1}\ cm^{-1}$ at 430 nm yield a K' of 34, i.e. the predominant reaction product is species **8**. However, the position of equilibrium in the interconversion of **7** and **8**, and as a result ε_{430}, would be expected to be strongly solvent dependent. Since the same value of ε_{430} for species **M** is obtained in experiments involving the reaction of DABCO with **5** in dry DMSO and in the reaction of CH_3O^- with **5** in DMSO/MeOH (95/5, V/V), it seems unlikely that the somewhat lower value of ε_{430} for **8** can be explained in this way.

The equilibrium constant of $\geq 5 \times 10^5\ M^{-1}$ associated with the formation of **8** from **5** and CH_3O^- seems reasonable when compared to the equilibrium constant of $2 \pm 1 \times 10^5\ M^{-1}$ associated with the formation of **1** via reaction of *N*-methylpicramide and CH_3O^- under comparable reaction conditions (1).

Given that **M** is correctly formulated as **8**, the reaction of **M** with a further molecule of CH_3O^- to form **N** could conceivably result in either **11** or **12** being formed.

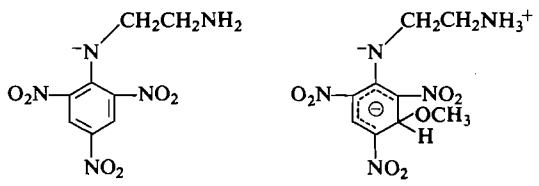

11 12

The differences in the spectral properties of **N** and related σ-complex **3** conclusively rules against formulating **N** as **12**. In accord with this conclusion is the observation that, in dry dimethyl sulfoxide, the addition of excess DABCO to a solution of **5** results in a species whose spectral properties are identical to those of **N**. Further, the spectral properties of **N** and **1** are almost identical in terms of λ_{max} values and values of ε at λ_{max} (Table 2). Species **N** is therefore formulated as **11**.

We note that in the closely related species **9**, **1**, and **10** the more electronegative the atom bearing the formal negative charge, the higher the energy required to bring about the lowest energy electronic transition. The promotion of an electron in **8** must be rendered somewhat more difficult than in **11** (or **1**) by virtue of the positive charge on the NH_3^+ group in **8**. In agreement with this, the absorption maximum of **8** is at 430 nm, while the absorption maxima of **1** and **11** are at 442 and 443 nm, respectively.

We conclude, therefore, that in dimethyl sulfoxide – methanol (95/5, V/V) the addition of 2 mol of CH_3O^- per mol of **5** results in successive reversible deprotonation reactions according to the sequence:

[5] $5 \rightleftarrows 8\,(M) \rightleftharpoons 11\,(N)$

This order must reflect, on the one hand, higher solvation energies associated with **8** as compared to **7** and, on the other, a higher solvation energy for the deprotonated species **8** and **11** as compared to the anionic σ-complexes **6** and **12**. The preferential solvation of **8** over **7** is perhaps somewhat unexpected (10, 11). It could conceivably result from the possibility in **8** of delocalizing negative charge from the N centre over the ring and the ability of the NH_3^+ function to H-bond to the partially negatively charged oxygen of an *ortho* nitro group as depicted in **13**. Alternatively, both the negatively charged

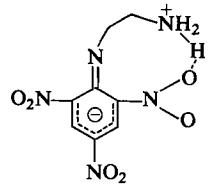

13

trinitrocyclohexadienate portion of the molecule and the NH_3^+ group may each be strongly solvated by hydrogen bonding to DMSO. The preferential formation of deprotonated species **1** over σ-complex **2** (R = H) in solvents rich in dimethyl sulfoxide (e.g. 95/5, V/V) has been observed previously (1) in the reactions of *N*-methylpicramide and

Can. J. Chem. Downloaded from www.nrcresearchpress.com by 210.87.254.105 on 09/06/12
For personal use only.

Can. J. Chem. Downloaded from www.nrcresearchpress.com by 210.87.254.105 on 09/06/12
For personal use only.

CH_3O^- in mixed dimethyl sulfoxide – methanol solutions.

Further reaction of N with CH_3O^- is postulated to result in the formation of **14** (species **O**).

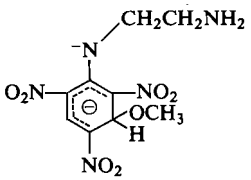

14

The similarities in the absorption properties of species **O** and compound **3** (Table 1) offers excellent support for the formulation of species **O** as **14**. Also in agreement with this conclusion is the observation that the addition of a large excess of DABCO to dry dimethyl sulfoxide solutions containing species **N** does not result in any further spectral change, i.e. there is no evidence for the formation of species **O** under these reaction conditions.

The equilibrium constant of $1.8 \pm 0.1 \times 10^3\ M^{-1}$ characterizing the conversion of **N** to **O**, i.e. **8** to **14**, is very similar to the equilibrium constant characterizing the conversion of **1** to **3** ($1.5 \pm 0.2 \times 10^3\ M^{-1}$) under comparable reaction conditions (1). This observation lends further support to our conclusions regarding asssignment of the structures of **8** and **14**.

The rather slow conversion of species **O** to species **P** remains to be considered. It is possible that species such as **15** and **16** are formed via the

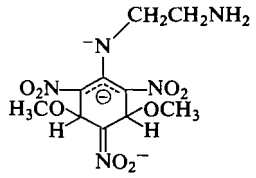

15

16

reaction of **14** (**O**) with CH_3O^-. However, the very slight changes in absorption noted in going from **O** to **P** together with the observation that species of general structure **15** and **16** possess markedly different spectra (3, 4, 10) than does a species such as **14** argues against formulating species **P** as **15** or **16**. In view of the similarities in their spectra, it seems more likely that **O** and **P** differ but slightly in their structures. One possibility is that **14** exists in two isomeric forms in which the $CH_2CH_2NH_2$ group attached to N-1 is either *syn*- or *anti*- to the CH_3O group attached at C-3 (4, 12, 13). If one isomeric form is kinetically preferred in the reaction of **11** with CH_3O^- but is thermodynamically unstable with respect to the second, more slowly generated isomer, the slow conversion of **O** to **P** might then be associated with the establishment of the equilibrium mixture of isomers in solution.

It is of interest that at no time was there evidence for the formation of the spiro species **17** (R = H) or **18** (R = H). These species would be isomeric with **11** and **14**, respectively.

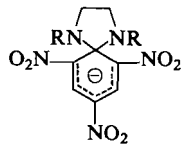

17

18

The corresponding methyl substituted species, **17** (R = CH_3), is readily formed in the reaction of *N*,*N*′-dimethyl-*N*-picrylethylenediamine with CH_3O^- under comparable reaction conditions (14, 15) and its spectrum is characteristically different from the spectra of the species observed in the present study.

One reason that **17** (R = H) is not observed is clearly that deprotonation of **7** to form **11** is kinetically more favorable than formation of **17** (R = H) by reaction of **7** and CH_3O^-. Steric factors (relief of strain in formation of **17** (R = CH_3) from its precursor) might also be important in determining the stability of **17** (R = CH_3) as compared to **17** (R = H).

Experimental

N-Picrylethylenediamine hydrochloride (**5**) was prepared by a modification of the procedure given by Bernasconi and Gehriger (14). A solution of picryl chloride (2.50 g, 0.010 mol) in benzene (50 mL) was added dropwise during 20 min to a stirred mixture of ethylenediamine (1.21 g, 0.020 mol) in benzene (15 mL) and 2 *N* KOH solution (15 mL). After 1 h the benzene layer was separated and the residue acidified with dilute HCl until 1 *N*. The aqueous solution after heating with activated carbon, filtering, and cooling yielded 1.2 g (40%) of crude product. This was twice recrystallized from 1 *N* HCl to yield white crystals mp 250°C (decomposed). *Anal.* calcd. for $C_8H_{10}O_6N_5Cl$: C 31.23, H 3.28, N 22.76; found: C 31.26, H 3.39, N 22.35. Use of the two-phase system, as described above, minimizes the formation of dipicrated ethylenediamine which leads to the rather low yields obtained when C_2H_5OH is used as a reaction medium. Dimethyl sulfoxide, methanol, and 1,4-diazabicyclooctane were purified as described previously (1, 2).

The procedures used in preparing stock solutions of the above reagents and in carrying out the spectrophotometric measurements were as described previously (1, 2).

1. E. Buncel, M. Hamaguchi, and A. R. Norris. Can. J. Chem. **58**, 1609 (1980).
2. E. Buncel, M. Hamaguchi, and A. R. Norris. Can. J. Chem. **58**, 1615 (1980).
3. E. Buncel, A. R. Norris, and K. E. Russell. Q. Rev. Chem. Soc. **22**, 123 (1968) and references therein.
4. M. J. Strauss. Chem. Rev. **70**, 667 (1970) and references therein.

5. E. BUNCEL and W. EGGIMANN. J. Am. Chem. Soc. **99**, 5958 (1977).
6. E. BUNCEL, A. R. NORRIS, K. E. RUSSELL, and R. TUCKER. J. Am. Chem. Soc. **94**, 1646 (1972).
7. V. GOLD and C. H. ROCHESTER. J. Chem. Soc. 1722 (1964).
8. E. BUNCEL, A. R. NORRIS, K. E. RUSSELL, and P. J. SHERIDAN. Can. J. Chem. **52**, 25 (1974).
9. L. E. ORGEL and R. S. MULLIKEN. J. Am. Chem. Soc. **79**, 4839 (1957).
10. M. R. CRAMPTON. Adv. Phys. Org. Chem. **7**, 211 (1969).
11. E. BUNCEL and H. WILSON. Adv. Phys. Org. Chem. **14**, 133 (1977) and references therein.
12. C. F. BERNASCONI and R. G. BERGSTROM. J. Am. Chem. Soc. **95**, 3603 (1973).
13. N. MARENDIC and A. R. NORRIS. Can. J. Chem. **51**, 3927 (1973).
14. C. F. BERNASCONI and C. L. GEHRIGER. J. Am. Chem. Soc. **96**, 1092 (1974).
15. E. BUNCEL, M. HAMAGUCHI, and A. R. NORRIS. J. Chem. Soc. Perkin I, 2205 (1980).

Can. J. Chem. Downloaded from www.nrcresearchpress.com by 210.87.254.105 on 09/06/12
For personal use only.

Acylation du (cyclopropylméthyl)triméthylsilane. Une nouvelle voie d'accès aux énones non conjuguées

M. GRIGNON-DUBOIS, J. DUNOGUÈS ET R. CALAS

Laboratoire de Chimie Organique et Laboratoire de Chimie des Composés Organiques du Silicium et de l'Etain associé au C.N.R.S. (No 35), Université de Bordeaux I, 351, Cours de la Libération 33405 Talence, France

Reçu le 24 juillet 1980

M. GRIGNON-DUBOIS, J. DUNOGUÈS et R. CALAS. Can. J. Chem. **59**, 802 (1981).

L'acylation du (cyclopropylméthyl)triméthylsilane par $RCOCl/AlCl_3$ (R: groupe hydrocarboné saturé) constitue une voie douce d'accès aux cétones β,γ-éthyléniques exemptes d'isomères conjugués. Avec les chlorures d'acides α,β-éthyléniques, on observe une compétition entre la scission C—H et C—Si en position allylique alors que le chlorure de chloracétyle conduit essentiellement à la cétone γ,δ-éthylénique. Une interprétation de l'ensemble de ces résultats est proposée: elle met en jeu le rôle catalytique d'HCl dans la formation des cétones β,γ-éthyléniques et des chlorocétones.

M. GRIGNON-DUBOIS, J. DUNOGUÈS, and R. CALAS. Can. J. Chem. **59**, 802 (1981).

Acylation of (cyclopropylmethyl)trimethylsilane using $RCOCl/AlCl_3$ (R: saturated hydrocarbon group) constitutes a mild, convenient route to β,γ-unsaturated ketones free from the conjugated isomers. With α,β-unsaturated acyl chlorides a competitive reaction between the C—H and C—Si allylic cleavage is observed whereas chloroacetyl chloride affords the γ,δ-ethylenic corresponding ketone. A mechanism involving the catalytic role of HCl in the formation of β,γ-unsaturated and chloroketones is proposed.

Introduction

Au cours de travaux antérieurs, nous avons montré que le (cyclopropylméthyl)triméthylsilane **1**, facilement obtenu par cyclopropanation de l'allyltriméthylsilane (rdt: 70%) (1), réagissait avec les électrophiles par ouverture du cycle conduisant à des butènes fonctionnels. Ainsi, avec le chlorosulfonate de triméthylsilyle (1), la réaction est univoque et l'on isole l'ester sulfonique γ,δ-éthylénique $CH_2{=}CH{-}(CH_2)_2SO_3SiMe_3$ résultant de la scission de la liaison $C{-}SiMe_3$ et avec le brome, électrophile plus faible, la réaction conduit au mélange de dibromo-1,2 et tribromo-1,2,4 butanes, résultant de l'addition de Br_2 respectivement au butène-1 et au bromo-1 butène-3 formés dans un premier stade (2). Nous avions alors invoqué, pour interpréter ces resultats, une compétition entre l'élimination du groupe $SiMe_3$ et celle d'un proton.

La mise en évidence d'une telle compétition, alors qu'habituellement c'est la liaison C—Si allylique qui est scindée, nous a encouragés à approfondir notre étude dans ce domaine. De plus, les cétones β,γ- et γ,δ-éthyléniques étant des composés recherchés et souvent difficiles à obtenir à l'état pur, nous avons entrepris d'étudier l'acylation du (cyclopropylméthyl)triméthylsilane catalysée par $AlCl_3$. Nous avons analysé la composition du mélange réactionnel en fonction de la nature du chlorure d'acide utilisé.

Résultats

Le composé **1** a été mis à réagir avec une série de chlorures d'acides en présence d'une quantité stœchiométrique de chlorure d'aluminium. Selon les cas, nous avons obtenu, après hydrolyse, des cétones γ,δ- ou β,γ-éthyléniques parfois accompagnées de dérivés chlorés. Ces résultats sont résumés dans le tableau 1.

Notons qu'avec le chlorure de chloracétyle (exemple *h*) la réaction conduit essentiellement à la cétone γ,δ-éthylénique, alors qu'avec le chlorure d'isobutyryle ou de pivaloyle, électrophiles plus faibles, on isole la cétone β,γ-éthylénique exempte de son isomère γ,δ-insaturé. Les chlorures d'acides α,β-insaturés occupent une position intermédiaire puisque, moins réactifs que le chlorure d'acétyle par exemple, ils permettent néanmoins d'isoler les dérivés à double liaison terminale.

D'un point de vue synthétique, cette réaction constitue une nouvelle méthode de préparation des cétones β,γ-éthyléniques exemptes d'isomères conjugués, ce qui confère à notre méthode une valeur synthétique réelle. En outre, les composés **4, 5, 6, 11, 14** et **16** n'avaient jamais été décrits à notre connaissance.

Discussion

L'obtention de cétones γ,δ-éthyléniques s'interprète aisément par un mécanisme comparable à

0008-4042/81/050802-05$01.00/0
©1981 National Research Council of Canada/Conseil national de recherches du Canada

Can. J. Chem. Downloaded from www.nrcresearchpress.com by 210.87.254.5 on 09/06/12
For personal use only.

TABLEAU 1. Acylation du (cyclopropylméthyl)triméthylsilane

	RCOCl R—	Composition du mélange réactionnel (%)						Rendement global en cétones éthyléniques (%)
				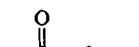				
a	CH_3—			**2**	70	**3**	30	60
b	*i*Pr—			**4**	~100		Traces	80
c	*t*Bu—			**5**	100			75
d	C_6H_{11}—			**6**	55	**7**	45	40
e	C_6H_5—			**8**	50	**9**	33	30
f	$CH_3CH{=}CH$—	**10**	17	**11**	50	**12**	33	60
g	$CH_3{-}C(CH_3){=}CH$—	**13**	60	**14**	25	**15**	15	50
h	$ClCH_2$—	**16**	30	**17**	5	**18**	5	35

celui précédemment proposé dans le cas de la sulfonation (1).

Notons que la forme protonée (a) a souvent été invoquée en série cyclopropanique (3). Cependant, il a été montré par le calcul, que le silicium pouvait également donner lieu à un "pontage" (forme b) (4) et de telles espèces ont été depuis fréquemment invoquées (5).

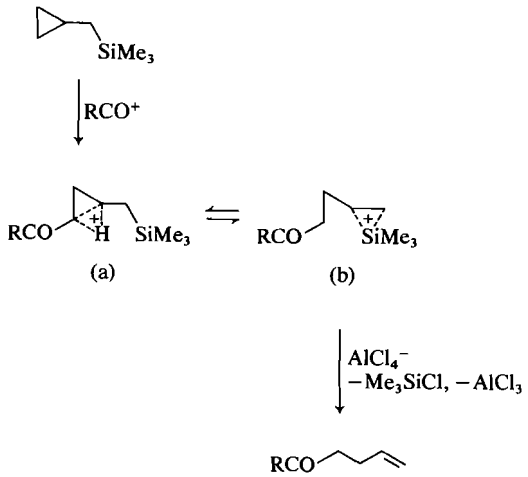

Par contre, la formation de cétones β,γ-éthyléniques et de chlorocétones ne peut s'interpréter directement à partir du substrat. Nous avons vérifié que ces composés ne provenaient pas d'une altération de la cétone γ,δ-éthylénique. Cette dernière est parfaitement stable dans les conditions où l'on opère et même en présence de deux équivalents d'$AlCl_3$.

Par ailleurs, nous avons synthétisé la cyclopropylacétone **19**. En effet on peut supposer que **19** pourrait se former par scission de la liaison C—Si selon:

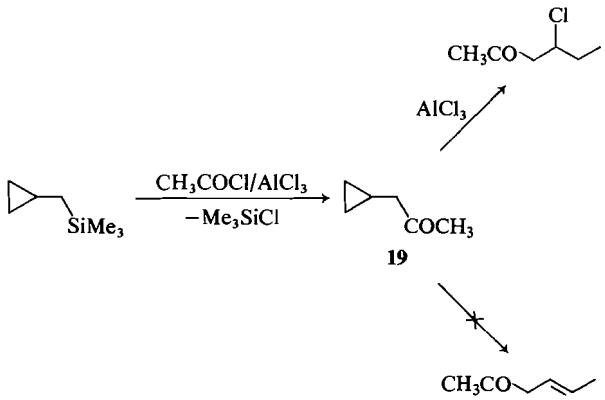

En présence d'$AlCl_3$ ce composé se transforme partiellement en chlorocétone. Toutefois, nous n'avons pas retenu un tel mécanisme, puisqu'il ne rend pas compte de l'obtention de la cétone β,γ-éthylénique.

Enfin, une éventuelle isomérisation de **1** en triméthylsilyl-4 butène-1 est également à rejeter. En effet, Sakurai *et al.* (6) ont montré que l'acétylation de ce composé conduisait essentiellement à **19**.

A partir de ces résultats, nous pensons que la formation de cétones β,γ-éthyléniques et de chlorocétones est due à la présence d'HCl. Il se formerait en cours de réaction et entraînerait la scission de **1** avec libération de butène-1, dont l'acylation permet de rendre compte de nos résultats. Effectivement **1** réagit avec HCl gazeux selon:

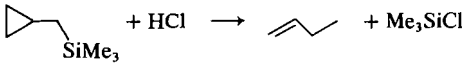

L'acétylation du butène-1 à −15°C, conduit à un mélange de **2** et **3** (proportions en poids **2:3** = 70:30). Cette réaction, relativement lente en l'ab-

Can. J. Chem. Downloaded from www.nrcresearchpress.com by 210.87.254.5 on 09/06/12
For personal use only.

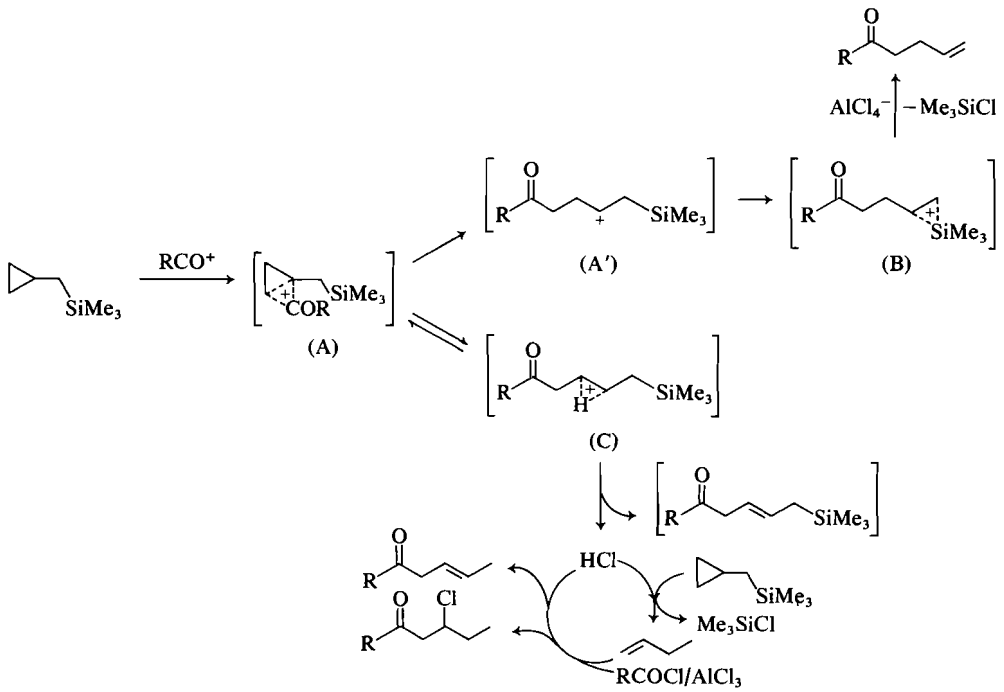

SCHÉMA 1. Interprétation proposée pour l'acylation du (cyclopropylméthyl)triméthylsilane.

sence de catalyseur, est très rapide en présence d'$AlCl_3$. De plus, l'acétylation de **1** réalisée en présence d'un équivalent de *N*-chlorosuccinimide (NCS)[1] conduit à un mélange complexe ne contenant pas de produit d'acétylation, mais dans lequel nous avons décelé (spectrométrie de masse) la présence de dérivés chlorés. En opérant en présence de triéthylamine, on favorise l'apparition de cétone γ,δ-éthylénique.[2]

La formation d'HCl au sein du milieu réactionnel semble donc bien réelle et est à rapprocher des résultats obtenus lors de la bromuration de **1** (2). Ces observations nous amènent à proposer le schéma réactionnel ci-après (Schéma 1).

En fonction de la nature du réactif, il interviendrait une compétition entre la scission de la liaison C—Si conduisant à un dérivé à double liaison terminale et celle d'une liaison C—H. En effet, on peut penser que l'espèce intermédiaire A évoluera différemment en fonction de l'importance de sa charge positive: plus cette charge sera grande et plus le silicium aura tendance à la stabiliser conduisant ainsi à l'intermédiaire B qui évoluera ensuite vers la cétone γ,δ-éthylénique. C'est effectivement ce que l'on observe avec le chlorure de chloracétyle qui est un électrophile puissant. Par contre, si cette charge est faible, le caractère cyclopropanique restera marqué dans l'état de transition qui évoluera plutôt vers la forme C, susceptible de se stabiliser par perte d'un proton, conduisant ainsi à une cétone éthylénique siliciée et à HCl. Ce dernier, en présence d'$AlCl_3$, réagit instantanément avec **1** pour donner du butène-1 beaucoup plus réactif que **1** en acylation électrophile. Celle-ci va donc venir concurrencer la réaction étudiée et conduira à la cétone β,γ-éthylénique et à la chlorocétone. C'est ce qui intervient par exemple avec les chlorures d'acétyle ou de pivaloyle qui sont des électrophiles relativement faibles.

Notons que la formation de cétone β,γ-éthylénique s'accompagne de la libération d'HCl qui est ainsi régénéré. Il suffit donc d'une trace d'acide (et par conséquent de cétone siliciée)[3] pour que la réaction puisse évoluer totalement vers la formation de butène-1.

Le cas des chlorures d'acides α,β-éthyléniques est apparemment en contradiction avec les autres résultats puisqu'ils conduisent à la formation de

[1]Le NCS réagit avec HCl avec formation de succinimide et libération de chlore (7).

[2]L'adjonction de quantités croissantes d'Et_3N abaisse considérablement les rendements et les cétones γ,δ-éthyléniques n'ont pu être obtenues exemptes des isomères β,γ- par cette méthode.

[3]Ceci explique que nous n'ayons pas trouvé trace de ce composé qui doit, de plus, être très instable dans le milieu réactionnel.

Can. J. Chem. Downloaded from www.nrcresearchpress.com by 210.87.254.5 on 09/06/12
For personal use only.

Can. J. Chem. Downloaded from www.nrcresearchpress.com by 210.87.254.5 on 09/06/12
For personal use only.

cétones γ,δ-éthyléniques. En fait nous avons ici des composés peu réactifs et si l'on peut admettre que la forme C est défavorisée lorsque l'électrophilie du complexe $RCOCl/AlCl_3$ diminue, il faut aussi considérer que la facilité d'acylation du butène diminue et donc que le mécanisme faisant appel à HCl pourrait être défavorisé. La compétition serait alors favorable à la formation de la cétone γ,δ-éthylénique.

Avec PhCOCl, électrophile beaucoup plus faible, on peut admettre que B serait trop défavorisé par rapport à C et qu'en dépit d'une faible réactivité de PhCOCl vis-à-vis du butène, la formation de la cétone β,γ-éthylénique et de la chlorocétone serait favorisée. Cette observation est corroborée par les faibles rendements observés.

Rappelons que nous avons déjà signalé une telle compétition en fonction du réactif lors de l'acétylation de sila-3 cyclopentènes-1 (7), et en fonction de la structure du substrat lors de la sulfonation des sila-3 cyclopentènes-1 et silabicyclo[3.1.0] hexanes (8), ainsi que lors de l'acétylation de ces derniers.

Remarque

L'acétylation de **1** par $CH_3CO^+BF_4^-$ a conduit à la cétone β,γ-éthylénique alors que cet électrophile réputé puissant aurait dû conduire à l'isomère γ,δ-éthylénique. Ceci n'est pas en contradiction avec notre interprétation puisque le cycle catalytique fait alors intervenir HF, beaucoup plus réactif que HCl vis-à-vis de **1**.

Conclusion

De même que la sulfonation et la bromuration, l'acylation électrophile du (cyclopropylméthyl)-triméthylsilane s'effectue avec ouverture du cycle à 3 chaînons. L'attaque du noyau cyclopropanique conduit au développement d'une charge positive qui, en fonction du réactif, évolue par perte d'un proton ou du groupe $SiMe_3$.

Cette compétition entre la scission d'une liaison C—H et celle d'une liaison C—Si en β d'une charge positive, non pas au stade de l'attaque mais à celui de l'élimination, n'avait pas été signalée sur ces substrats. Ces résultats constituent un nouvel exemple de la réactivité de ces liaisons C—H que nous avions mise par ailleurs en évidence (8, 9) et viennent confirmer l'interprétation que nous avions alors donnée.

Sur le plan synthétique, nous proposons une nouvelle méthode de préparation de cétones β,γ-éthyléniques particulièrement intéressante dans le cas où R = *i*Pr ou *t*Bu, puisque les produits correspondants, qui n'étaient pas connus, sont obtenus avec de bons rendements.

Partie expérimentale

Préparation du (cyclopropylméthyl)triméthylsilane

Nous l'avons obtenu par cyclopropanation de l'allyltriméthylsilane. Nous avons utilisé la méthode de Simmons-Smith modifiée selon Rawson et Harrison (10) en utilisant une durée de chauffage de 24 h. Le composé **1** est ainsi obtenu avec 70% de rendement, pé = 113°C/760 Torr; rmn (CCl_4, $HCCl_3$ à 7,27 ppm comme réf. int.) δ (s: singulet, d: doublet, m: massif ou multiplet): 0,3 (s, 9H, $SiMe_3$), 0,3 à 0,7 (m, $3CH_2$ et 1 CH) ppm.

Réactions d'acylation

Elles sont effectuées à la rampe à vide sous atmosphère d'argon. Le chlorure d'aluminium est préalablement dégazé à la pompe à palettes.[4] Les chlorures d'acides sont distillés sur magnésium puis conservés sous argon.

Dans un ballon à tubulure latérale, on place 0,02 mol d'$AlCl_3$ que l'on recouvre par 20 cm^3 de CH_2Cl_2. L'ensemble étant refroidi à 0°C, on additionne 0,02 mol de chlorure d'acide. Au bout d'une heure à 0°C la solution de complexe est rapidement dégazée. Le (cyclopropylméthyl)triméthylsilane (0,019 mol), en solution dans 10 cm^3 de CH_2Cl_2, est alors additionné à −90°C. Cette température est maintenue pendant 15 min puis on la laisse remonter jusqu'à −15°C (durée 2 h); CH_2Cl_2 et Me_3SiCl formé sont alors en partie éliminés sous pression réduite (trompe à eau). La solution résiduelle est ensuite versée sur un mélange eau glacée/NaCl/pentane (100 cm^3 d'eau pour 50 cm^3 de pentane environ) vigoureusement agité. Cette technique permet d'opérer à −10°C et de soustraire les cétones formées à la solution aqueuse fortement acide. Celle-ci est ensuite extraite au pentane et l'ensemble des phases organiques est lavé avec une solution saturée de $NaHCO_3$, puis à l'eau et enfin séché.

Le mélange réactionnel obtenu après élimination du solvant est filtré sur une petite colonne de SiO_2 (Silice 60 Merck, 70–230 mesh). Par élution au pentane, on sépare l'hexaméthyldisiloxane et le substrat n'ayant pas réagi, des dérivés carbonylés. Ces derniers sont analysés en cpg et purifiés par chromatographie liquide–solide ou par cpg préparative.

Description des produits obtenus

Les spectres de rmn (^1H) ont été enregistrés sur un appareil fonctionnant à 60 MHz (Perkin-Elmer R 24) (δ ppm, solvant CCl_4, réf. int. TMS à 0,0).

Tous les produits nouveaux ont des microanalyses C, H, O en accord avec les formules proposées (voir le tableau 2).

Cétones β,γ-éthyléniques

A l'exception de **8, 11** et **14**, elles présentent toutes en ir (film NaCl) une bande ν(C=O) vers 1715 cm^{-1}.

Le composé **2**, rmn: 1,6 (massif large, CH_3), 2,0 (s, CH_3CO), 3,0 (pseudo t, CH_2), 5,5 (m, 2H, CH=CH).

Le composé **4**, rmn: 0,9 (t, CH_3), 1,7 (massif large, 3H, CH_3—C=), 2,5 (q, 2H, CH_2—CH_3), 3,1 (pseudo t, CH_2CO), 5,5 (m, 2H, CH=CH).

Le composé **5**, rmn: 1,1 (d, 6H, $2CH_3$), 1,8 (massif large, 3H, CH_3—C=), 2,3 (sept, CH), 3,1 (pseudo t, CH_2CO), 5,4 (m, 2H, CH=CH).

Le composé **6**, rmn: 1,3 à 2 (massif, 10H, 5 CH_2 du cycle), 2 à 2,3 (massif 1H, CH—CO), 3,1 (pseudo t, CH_2CO), 5,4 (m, 2H, CH=CH).

Le composé **8**, ir: ν: 1680 (C=O), 1600 et 1580 (C=C, aromatiques) cm^{-1}; rmn: 1,7 (d élargi, 3H, CH_3), 3,5 (pseudo t, CH_2CO), 5,5 (m, 2H, CH=CH), 7,1 à 7,5 (m, 3H aromatiques), 7,8 à 8,1 (m, 2H aromatiques).

Le composé **11**, rmn: 1,6 (d élargi, 3H, CH_3CH—), 1,8 (d élargi, 3H, CH_3CH=), 3,05 (pseudo t, CH_2CO), 5,3 (m, 2H,

[4]L'utilisation d'$AlCl_3$ fraîchement sublimé ne modifie pas les résultats obtenus.

TABLEAU 2. Résultats de microanalyse des composés nouveaux

	Analyse (%)					
	calc.			trouvée		
Composé	C	H	Cl	C	H	Cl
4	76,19	11,11	—	76,34	10,85	—
5	77,14	11,42	—	77,01	11,19	—
6	79,51	10,84	—	79,69	10,71	—
11	77,41	9,67	—	77,59	9,41	—
14	78,26	10,14	—	78,02	9,99	—
16	54,54	6,81	26,89	54,82	6,97	25,96

CH=CH), 5,7 et 6,0 (2 m, 1H, =C*H*—CH_3), 6,2 à 6,8 (2q, J = 6,5 Hz, 1H, =CH—CH_3).

Le composé **14**, rmn: 1,8 (d élargi, 3H, CH_3C=), 2,1 (d, 6H, $(CH_3)_2C$=), 3,0 (pseudo t, CH_2CO), 5,5 (m, 2H, CH=CH), 6,0 (signal large, 1H, =CH—CO).

Cétones γ,δ-éthyléniques

Elles sont caractérisées en ir par la fréquence de vibration ν(C=C) vers 1650 cm^{-1} et ν(C=O) vers 1720 cm^{-1}. En rmn les protons éthyléniques donnent un spectre ABC (X_2) caractéristique.

Le composé **10**, ir: ν: 1680 (C=O), 1650 (C=C) cm^{-1}; rmn: 1,7 (d élargi, 3H, CH_3—C=), 2 à 2,5 (m, 4H, CH_2CH_2), 4,8, 4,9 et 4,95 (3m, 2H, CH_2=CH), 5,2 à 5,7 (m, 1H, C*H*=CH_2), 5,8 et 6 (2m, 1H, =CH—CO), 6,5 à 7 (m, 1H, CH_3*C*H=).

Le composé **13**, rmn: 1,8 (s, 3H, CH_3), 2,0 (s, 3H, CH_3), 2,2 (signal large 2H, CH_2—C=), 3,0 (massif, 2H, CH_2CO), 4,85, 5,0 et 5,1 (3m, 2H, CH_2=CH), 5,3 à 6 (m, 1H, C*H*=CH_2), 6 (signal large, 1H, =CH—CO).

Le composé **16**, ir: ν: 1710 (C=O), 1620 (C=C) cm^{-1}; rmn: 1,5 à 3 (m, 4H, CH_2—CH_2), 4,0 (s, 2H, CH_2CO), 4,8, 4,9 et 5,1 (3m, 2H, CH_2=CH), 5,3 à 6 (m, 1H, C*H*=CH_2).

Cétones β-chlorées

En rmn (^{1}H), ces cétones se caractérisent notamment par un multiplet (^{1}H) centré vers 4 ppm attribuable au proton de —CHCl— et un spectre AB dédoublé (2H) (—CO—CH_2—) où n'apparaissent nettement que les 4 raies principales. Signalons que ces cétones sont instables même à température ambiante (perte de HCl).

Acétylation du butène-1

Dans 20 cm^3 de CH_2Cl_2 refroidi à −15°C, on dissout 5 g de butène-1 (0,09 mol) puis on additionne 0,02 équivalent du complexe $CH_3COCl/AlCl_3$ préparé comme précédemment. Les réactifs sont laissés en contact pendant 1 h à cette température puis après hydrolyse, extraction à l'éther, séchage et filtration sur silice, on récupère 1 g d'un mélange **2** + **3** dans les proportions ~70:30.

Obtention de 19

Le butène-3 ol-1 (0,4 mol) et Me_6Si_2NH (0,2 mol) sont chauffés 2 h au reflux après addition de quelques gouttes de Me_3SiCl. Le produit ainsi obtenu est alors soumis à la cyclopropanation (mode opératoire précédemment décrit pour **1**, rdt: 60%). La fonction OH est ensuite restituée par méthanolyse en présence de quelques gouttes d'HCl puis oxydée par le réactif de Corey et Suggs (11). On isole ainsi la cyclopropylacétone **19** avec un rendement global de 48%; ir: ν(C=O) à 1716 cm^{-1}; rmn: 0,15 (m, 2H, cyclopropyl), 0,6 (m, 2H, cyclopropyl), 1,04 (m, 1H, cyclopropyl), 2,2 (s, 3H, CH_3CO), 2,3 (d, 2H, CH_2—CO).

1. M. GRIGNON-DUBOIS, J.-P. PILLOT, J. DUNOGUÈS, N. DUFFAUT et R. CALAS. J. Organomet. Chem. **124**, 135 (1977).
2. M. GRIGNON-DUBOIS, J. DUNOGUÈS et R. CALAS. J. Chem. Res. S, 6 (1979).
3. H. HART et R. SCHLOSBERG. J. Am. Chem. Soc. **90**, 5189 (1968).
4. C. EABORN, F. FEICHTMEYR, M. HORN et J. N. MURREL. J. Organomet. Chem. **77**, 39 (1974).
5. T. H. CHAN et I. FLEMING. Synthesis, 761 (1979).
6. H. SAKURAI, T. IMAI et A. HOSOMI. Tetrahedron Lett. 4045 (1977).
7. M. GRIGNON-DUBOIS, J. DUNOGUÈS et R. CALAS. J. Organomet. Chem. **97**, 31 (1975).
8. M. GRIGNON-DUBOIS, J. DUNOGUÈS, N. DUFFAUT et R. CALAS. J. Organomet. Chem. **188**, 311 (1980).
9. M. GRIGNON-DUBOIS, J. DUNOGUÈS et R. CALAS. J. Organomet. Chem. **181**, 285 (1979).
10. R. J. RAWSON et I. T. HARRISON. J. Org. Chem. **35**, 2057 (1970).
11. E. J. COREY et J. W. SUGGS. Tetrahedron Lett. 2647 (1975).

Can. J. Chem. Downloaded from www.nrcresearchpress.com by 210.87.254.5 on 09/06/12
For personal use only.

Some comments on Linnett Double Quartet theory

WILLIAM B. JENSEN

Department of Chemistry, University of Wisconsin, Madison, WI 53706, U.S.A.

Received July 22, 1980

WILLIAM B. JENSEN. Can. J. Chem. **59**, 807 (1981).

The recent critical evaluation of Linnett Double Quartet theory by Langler, Trenholm, and Wasson is critically examined and found to be based on misrepresentations of the theory's basic postulates and its use in predicting chemical reactivity. Various ways in which Linnett's original work can be profitably extended are suggested and briefly discussed.

WILLIAM B. JENSEN. Can. J. Chem. **59**, 807 (1981).

Un examen approfondi révèle que la critique récente de la théorie du double quartet de Linnet faite par Langler, Trenholm et Wasson est le reflet d'une mauvaise interprétation des postulats de base de la théorie et de leur utilisation dans la prévision de la réactivité chimique. On suggère différents moyens d'utiliser avec profit le travail original de Linnet et on en discute brièvement.

[Traduit par le journal]

Can. J. Chem. Downloaded from www.nrcresearchpress.com by 210.87.254.42 on 09/06/12
For personal use only.

The April 15, 1980, issue of this journal carried an article by Langler, Trenholm, and Wasson (1) which purports to be a critical reexamination and evaluation of the application of Linnett Double Quartet (LDQ) theory to problems of structure, reactivity, and resonance in organic chemistry. This article presents an interpretation of LDQ theory which is, in the present writer's opinion, incorrect and potentially misleading for those readers who are only superficially acquainted with Linnett's work. Consequently, it is felt that some comments on this interpretation are in order. On the other hand, the article does call attention to a number of situations which, though far from invalidating LDQ theory as the authors contend, do point to a need for a more explicit consideration of nuclear–nuclear repulsions in certain qualitative applications of the theory. Such a treatment is made in the present paper and is shown both to resolve the problems raised by Langler *et al.* and to point to a new area of application for Firestone's theory of Linnett or L strain (2, 3).

The Role of the Nuclei in LDQ Theory

The major source of difficulty with the authors' interpretation of LDQ theory stems from their misconceptions about its primary postulates. After first describing the concept of two tetrahedral spin sets, the authors summarize the theory as follows: "Molecular structures are elaborated by maximizing electronic separations and minimizing electronic repulsions. Priority, it is assumed, must be given to maximizing the separation of electrons having the same spin." This is correct as far as it goes, but appended to this statement is a footnote which reads, "The role of the nuclei is ignored." In other words, the authors claim that LDQ theory is based on the premise that electron correlation is the *sole* determinant of both molecular structure and reactivity. This is simply not true. Thus, for example, Dale (4) in his summary of LDQ theory lists, in addition to the postulates dealing with electronic charge and spin correlation, the following two additional postulates. (*1*) "The attraction between electrons and atomic nuclei tends to draw a maximum number of electrons to regions between atoms." (*2*) "Two electrons of opposite spin may occur together as a pair (coincidence) when more electrons can thereby be concentrated between two atoms to form a bond." Likewise, Lawless and Smith (5) state the underlying principles of LDQ theory to be that "electrons are electrostatically attracted by the nuclei, are mutually repelled by other electrons, and have a tendency to achieve a fairly uniform charge distribution in a given chemical species, as limited by the effect of the spin wave function and relative electronegativities of the atoms involved."

In both statements the nuclei are assigned a key role. Structures are a result of the dynamic interplay between the desire of the electrons, on the one hand, to reduce their mutual repulsions by maintaining their spin sets and as much anticoincidence between the sets as possible, and the desire of the nuclei, on the other hand, to increase their electron attractions and reduce nuclear–nuclear repulsions by concentrating as many electrons as possible along the internuclear axes. Indeed, the role of the nuclei is assumed to be so apparent from traditional bonding concepts that the two standard books on LDQ theory by Luder (6) and Linnett (7) do not even explicitly state postulates dealing with these effects, the authors concentrating instead on the novelty which the postulate of spin correlation introduces into the treatment of the electron repulsions. Nevertheless, a reading of these books quickly shows that the nuclei play the roles outlined by Dale, and by Lawless and Smith.

0008-4042/81/050807-07$01.00/0

©1981 National Research Council of Canada/Conseil national de recherches du Canada

Can. J. Chem. Downloaded from www.nrcresearchpress.com by 210.87.254.42 on 09/06/12
For personal use only.

Linnett himself originally presented LDQ theory as a simple modification of Lewis' original bonding concepts (8). Like both the two-dimensional topological Lewis structures themselves, and their three-dimensional extensions in terms of the tangent sphere model (9–14) and the VSEPR rules (15), LDQ theory makes use of such concepts as the octet rule (for period 2 elements), the electroneutrality principle (in terms of favorable formal charge distributions), and the isoelectronic principle, as well as assorted electrostatic arguments common to all such localized bonding models. Its sole innovation is its use of the postulate of the two tetrahedral spin sets to account for the effects of the Pauli principle and its attempt to maximize their degree of correlation within the bounds set by the other electrostatic energy components. The practical consequences of this are the appearance of valence electrons which are not close-paired and the possibility of one, three, and five electron bonds in addition to the close-paired two, four, and six electron bonds of the conventional Lewis – tangent sphere – VSEPR model. As Serratosa has succinctly put it, "All fundamental principles of chemical bonding are preserved in Linnett's theory, except the 'idolatry' for the Lewis *doublet*" (16).

It is true, however, that writers on LDQ theory, while always emphasizing the role of the nuclei in forcing the spin sets into coincidence, have often had little or nothing to say about the relative efficiency of various electron configurations in reducing nuclear–nuclear repulsions or about the relative efficiency of various kernels, as expressed by their charges and sizes (i.e., electronegativities), in forcing the electrons into coincidence and in distorting the spin sets due to inequalities in their relative attractions for the electrons. This emphasis (or lack thereof) is in fact consistent with the origins of LDQ theory as, like the Lewis – tangent sphere – VSEPR model, it assumes that electronic repulsions and electron–nuclear attractions are the two major determinants of molecular structure in the case of primarily covalent species. However, in so doing, LDQ theory does not deny the existence of nuclear–nuclear repulsions nor that they play a role in determining the finer details of structure and reactivity (or, indeed, a major role in the case of ionic species). Bent, for example, has made a number of specific applications of nuclear–nuclear repulsions within the context of LDQ theory in order to rationalize certain trends in bond angles and bond lengths (9–14), and Firestone has called attention to a number of situations in which it is not possible to arrive at a satisfactory disposition of the tetrahedral spin sets without simultaneously moving bonding electrons away from the regions of the nuclear–nuclear axes (2, 3). This frequently occurs in the case of transition state species and the resulting destabilization, due to the increase in nuclear–nuclear repulsions and the decrease in electron–nuclear attractions, has been termed Linnett or L strain by Firestone and has been used by him to analyze the origin of activation energies in the case of E2, S_H2, and S_N2 reactions (17). A similar explicit treatment of nuclear–nuclear repulsions quickly resolves a number of the problems discussed by Langler *et al.*

A case in point is the authors' treatment of the excited states of oxygen. The Linnett structures of the ground state ($^3\Sigma_g^-$) and first two excited states ($^1\Delta_g$) and ($^1\Sigma_g^+$) are given by structures **1–3**. The authors point out that the ground state **1** and the first excited state **2** differ very little in the degree of electron close-pairing and yet have an energy separation of 22.6 kcal/mol, whereas the first excited state **2** and second excited state **3** differ a great deal in the amount of electron repulsion, all six electron pairs having become close-paired in the $^1\Sigma_g^+$ state, and yet differ in energy by only 15.1 kcal/mol. They conclude that while an "analysis of apparent electronic separations is qualitatively helpful ... (it) ... can be somewhat misleading quantitatively." However, an examination of structures **1** and **2** shows that while both exhibit similar degrees of electron correlation and both place four electrons in the bond region, structure **1** concentrates at least one of these electrons directly on the nuclear–nuclear axis, whereas structure **2** does not. The resulting difference in the efficiency of screening the nuclear–nuclear repulsions, as well as the greater electron–nuclear attraction for the electron so placed, should account for most of the 22.6 kcal/mol separation. Structures **2** and **3**, on the other hand, do not differ significantly in the degree to which they concentrate electrons on the nuclear–nuclear axis and their somewhat lower energy separation of 15.1 kcal/mol should be largely due to differences in electron repulsion energy resulting from the increased close-pairing in structure **3**.

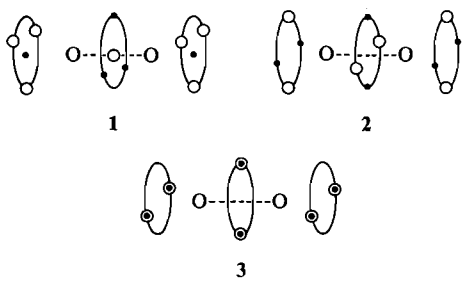

1 **2** **3**

Can. J. Chem. Downloaded from www.nrcresearchpress.com by 210.87.254.42 on 09/06/12
For personal use only.

A similar analysis resolves the anomalies in the average bond energies per CC bonding pair discussed by the authors later in the paper (where we are again reminded in a footnote that the nuclei are neglected). Using Linnett structures **4–6** for

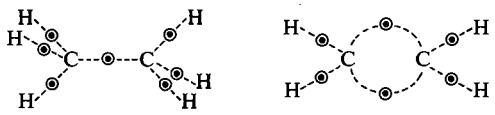

4

5

6

ethane, ethene, and ethyne, the authors argue that LDQ theory would predict a similar average energy per CC bond pair in ethane and ethene, as both contain close pairs, but a much higher energy per pair in ethyne where the pairs have achieved a degree of anticoincidence. They then point out that the observed energies per pair are exactly the opposite, being 83.1 kcal/mol for ethane, 73.5 kcal/mol for ethene, and 64.6 kcal/mol for ethyne. Again, as with the simplest possible electrostatic model, LDQ theory would not predict a double bond to be twice as strong as a single bond. The close pairs in ethene are not localized directly on the nuclear–nuclear axis like the pair in ethane and the resulting increase in nuclear–nuclear repulsion (and decrease in electron–nuclear attraction) should lead to a lower average energy per bond pair in ethene. In ethyne the nuclear–nuclear repulsions would be even greater as the spin set polyhedra now share common faces rather than common edges, drawing the nuclei even closer together without at the same time increasing the degree to which the electron density is directly concentrated on the nuclear–nuclear axis. However, the decrease in electron repulsion in ethyne should partly offset this increase and, if anything, the drop in energy per CC pair on going from ethene to ethyne should be somewhat less than the drop on going from ethane to ethene, as is in fact observed.

Molecular Structure

Given the authors' premise that LDQ theory denies the role of the nuclei in structure formation, it is difficult to imagine how they account for the electrons ever forming close pairs; indeed, in the case of simple hydrides they assume that the electrons don't. Any attempt to invoke close-pairing of the electrons due to electron–nuclear attractions is labeled as inconsistent. Instead the authors postulate that the central atoms in CH_4, NH_3, and H_2O maintain the completely correlated spin sets of Ne and they place the protons on lines connecting electrons of opposite spin with no electron density whatsoever directly between the proton and central kernel. The completely correlated electrons of Ne lie at the corners of a cube formed by the interpenetration of the two tetrahedral spin sets, electrons of like spin being separated by the face diagonals of the cube and electrons of opposite spin by the cube edges. Needless to say, given 12 edges and only four to two protons, several alternatives are equally likely, leading to the authors' claim that LDQ theory "may be ambiguous" in predicting molecular geometry. In the case of CH_4, for example, they conclude that, on the basis of electronic correlation alone, square planar and tetrahedral methane are equally likely, but by invoking proton–proton repulsions arrive at the tetrahedral structure. A similar procedure in the case of NH_3, however, leads to the incorrect conclusion that it is trigonal planar.

Surely, given the proton's size, no nucleus or kernel could be expected to be more effective in inducing close pair formation. Only such small highly-charged kernels as F^{7+} and O^{6+} would be capable of combating this tendency, as is postulated in the case of hydrogen-bonded species such as HF_2^-. These are the only cases in which Linnett appears to propose structures for stable long-lived species in which the electrons bonded to H are not close paired and even here at least one electron per bond is placed directly between the proton and the other kernel. Though the authors' treatment of hydride geometries may be viewed as an unsuccessful attempt on their part to try new variations of Linnett's postulates in which electron repulsions and nuclear–nuclear repulsions are considered as the major determinants of structure, rather than electron repulsions and electron–nuclear attractions, this treatment does not correspond to that of standard LDQ theory, which correctly predicts that NH_3 is pyramidal (6, 7).

However, the authors do call attention to a number of interesting problems relating to the structures of hydrocarbon anions. They point out, for example, that it is impossible to write a LDQ structure for the allyl anion in which one has both resonance stabilized CC bonds (i.e., two non-close-paired, three-electron CC bonds rather than one close-paired double and one close-paired single bond) and close-paired CH bonds at the same time. Using Linnett's more condensed symbolism, in which a thin line represents an anticoincident pair and a thick line a coincident or close pair, the struc-

ture for the allyl anion (which is isoelectronic with O_3) may be written as

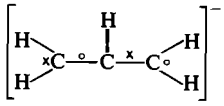

7

The authors also propose a LDQ structure for the ethene anion which suffers from the even graver problem of simultaneously forcing three electrons into spatial coincidence, two of which have the same spin

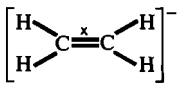

8

and they imply that this result casts severe doubts on the validity of standard LDQ theory. However, this proposed structure is incorrect on several counts. Not only does it violate the octet rule for carbon, it incorrectly predicts a bond order of $2\frac{1}{2}$ for the CC bond. Addition of an electron to the π^* LUMO of ethene should in fact reduce the CC bond order to $1\frac{1}{2}$. The proper Linnett structure for $C_2H_4^-$ (which is isoelectronic with O_2^-) should be:

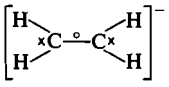

9

Unlike structure **8**, this structure does not require the spatial coincidence of three electrons and gives the proper CC bond order. However, like the structure for the allyl anion, it leads to a lack of close-pairing in the CH bonds.[1]

What both the allyl and ethene anion structures appear to represent is, in fact, a previously unrecognized example of the application of Firestone's concept of Linnett or L strain (2, 3). Because it is not possible to reduce the electron repulsions in the CC bonds without simultaneously increasing the nuclear–nuclear repulsions in the CH bonds, these species suffer, like the transition states discussed by Firestone, from L strain. Consequently, LDQ theory would predict that they should be highly reactive, particularly with respect to oxidation, as is indeed the case.

Reactivity

The authors' treatment of the application of LDQ theory to reactivity is even more misleading. An analysis of this treatment is simplified by first defining some vocabulary. By *kind* of bond we will mean the kind of nuclei involved in the bond (e.g., H—H vs. O—H); by bond *multiplicity* we will mean the total number of valence electrons in the bond, and by bond *electron correlation*, the arrangement of these electrons. This latter factor is unique to LDQ theory and affects the bond energy both through changes in electron repulsion energies and changes in the relative screening of the nuclear–nuclear repulsions.

All of these factors affect the energy of a species and hence the energy of a reaction. Only in the case of a reaction in which the number, kind, and multiplicities of the bonds in the products and reactants are identical can one expect a correlation between ΔH of the reaction and the change in electron correlation. In cases in which one or more of the other factors also change, we can also expect a correlation if we compare two reactions such that the changes in all the factors, save the electron correlation, are the same for both reactions. In this case the correlation will involve the sign of the relative ΔH values (i.e., $\Delta\Delta H$) and the relative changes in the correlation energies for the two reactions; that is, it will tell us which of the two reactions is the more endothermic, but will tell us nothing about the absolute values or signs of the individual ΔH changes of each reaction.

A third situation in which LDQ theory may be applied is in predicting whether the experimental ΔH of a reaction will be more exothermic or more endothermic than the theoretical value calculated be means of simple Lewis structures and tabulated bond energies. This requires that LDQ theory predict the structure of either a single reactant or product to differ significantly from that given by its close-paired Lewis structure. This difference may involve both bond multiplicities and electron correlation. The situation is exactly similar to that used to evaluate resonance energies, the classic example being the difference between the experimental ΔH for the hydrogenation of benzene and that calculated for a single Kekulé structure. This analogy is more than formal as both resonance in VB theory and configuration interaction in MO theory are attempts, like the double-quartet hy-

[1]It should be noted that the authors themselves also suggest a resolution of the ethene and allyl anion structures which involves separation of the electrons in the σ bonds. However, they introduce a new symbolism into their formulas at this point and never explain what it means. That is, from their proposed formulas, one cannot tell whether they are postulating an angular splitting or a radial splitting of the σ bonds. If their proposed structures are identical with LDQ structures **7** and **9**, then it is difficult to understand why they bring up structure **8** in the first place and why they fail to cite Firestone's work for a proper interpretation of the result within the context of standard LDQ theory.

Can. J. Chem. Downloaded from www.nrcresearchpress.com by 210.87.254.42 on 09/06/12
For personal use only.

Can. J. Chem. Downloaded from www.nrcresearchpress.com by 210.87.254.42 on 09/06/12
For personal use only.

pothesis, to account for electron correlation effects.

On the other hand, Langler *et al.*, consistent with their denial of the role of the nuclei, put forward the claim that LDQ theory pretends to be able to predict the sign of the enthalpy change for a reaction by simply evaluating the change in electron correlation, irrespective of the number, kind, and multiplicities of the bonds made or broken in the reaction. The procedure they adopt is to evaluate the change in the number of close pairs on going from reactants to products. If this change is positive (loss of correlation), ΔH is assumed to be positive; if it is negative (gain of correlation), ΔH is assumed to be negative. This procedure is then applied to ten reactions and shown to give an incorrect result for virtually all of them, allowing the authors to conclude that LDQ theory "does not provide a guide to chemical reactivity, in contrast to claims made for it." An examination of these reactions shows that eight of them involve the making and breaking of different kinds of bonds (mostly H—H bonds converted into O—H, N—H, and C—H bonds or vice versa) and that the remaining two involve changes in bond multiplicities. In short, none of them conform to the circumstances under which LDQ theory (in contrast to the authors) would postulate a correlation between ΔH and change in electron correlation.

It is instructive in this regard to examine the three reactions (not included in the table of ten just mentioned) which the authors quote[2] from Linnett's original paper (8) and book (7) in order to justify their procedure:

[1] $2(CH_3)_2CO \rightarrow C(CH_3)_4 + CO_2$ $\Delta H < 0$

[2] $3(^1\Sigma_g^+O_2) \rightarrow 2O_3$ $\Delta H < 0$

[3] $2NO \rightarrow ONNO$ $\Delta H > 0$

Again making use of Linnett's condensed symbolism,[3] the first of these reactions may be written as

[4] 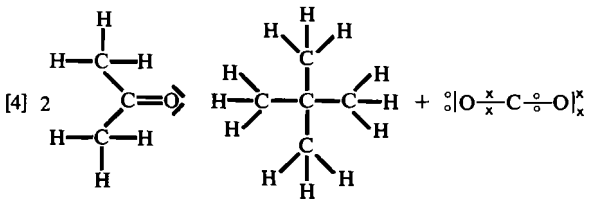

[2]See ref. 7, pp. 45–46 and ref. 8, p. 2647 and footnote 14 on the same page.

[3]Here we have positioned the lines for nonbonding pairs in a manner similar to conventional Lewis structures in order to avoid the appearance of dangling bonds conveyed by Linnett's original formulas.

As can be seen, the number, kind, and multiplicities of the bonds are the same on both sides. The correlation of the CC and CH bonds is also the same, only that of the CO bonds changing. In other words, unlike the ten reactions tested by the authors, this reaction conforms to the conditions under which there should be a correlation between ΔH and change in electron correlation. Interestingly, Linnett's purpose in quoting this reaction was not to explicitly predict the sign of its enthalpy change but to use its known ΔH value to estimate the energy involved per electron pair in close pairing.

The second reaction may be formulated as

[5] 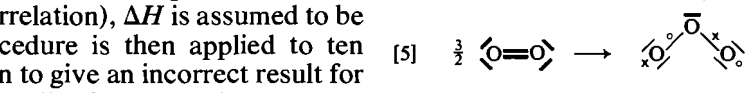

It fails to conform to the necessary conditions as there is a change in both bond multiplicity and electron correlation. However, Linnett does not pretend to predict the sign of ΔH for this reaction as the authors claim, but rather the sign of $\Delta\Delta H$ relative to the same reaction using the $^3\Sigma_g^-$ ground state of O_2

[6] 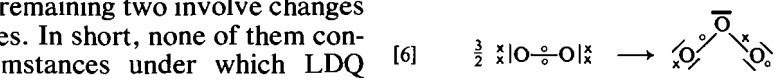

The change in bond multiplicity is the same for both reactions so $\Delta\Delta H$ must reflect the relative changes in the electron correlation energies for the two reactions. In keeping with the predictions of LDQ theory, reaction [5] is in fact found to be more exothermic than [6] by 57 kcal/mol. The fact that the ΔH of reaction [5] happens to be exothermic and that of [6] endothermic is an accident of the example used, and Linnett's correlation deals only with the sign of $\Delta\Delta H$ and not the signs of the individual ΔH values.

Finally, we have the third example, which involves changes in bond multiplicities, electron correlation, and kind of bond.

[7] 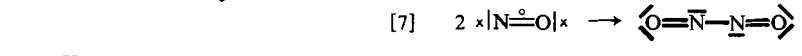

Here again Linnett is not predicting the sign of ΔH as the authors claim, but rather that it must be more endothermic than would have been predicted by the classically formulated version given by simple Lewis structures:

[8] 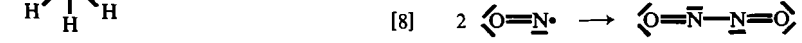

In other words, it is an example of the third situation discussed earlier.[4] Reaction [8] must be inherently exothermic as, like all simple radical dimeri-

[4]A comparison of this type is also given for O_3 in ref. 7, pp. 61–62.

Can. J. Chem. Downloaded from www.nrcresearchpress.com by 210.87.254.42 on 09/06/12
For personal use only.

zations, it merely involves the formation of a new bond without any old bonds being broken in the process. In contrast, the Linnett structure in eq. [7] predicts that the N—N bond can only be formed at the expense of the multiplicity of the NO bonds and with loss of the electron correlation in the monomer. In other words, LDQ theory predicts that the experimental ΔH should be more endothermic than that predicted by eq. [8]. Linnett does not quantitatively test this prediction by comparing the experimental and calculated ΔH values, but instead remains content with the fact that NO doesn't dimerize to any great extent under ambient conditions, indicating that the endothermic shift ($\Delta\Delta H$) relative to the necessarily exothermic ΔH predicted by [8] is so large as to either make the real reaction inherently endothermic or the exothermic value so small that is is unable to offset the unfavorable entropy change expected for dimerization reactions in general.

Curiously, in their discussion of reactivity, the authors let pass without comment one of the few explicit attempts to apply LDQ theory to problems of reactivity, namely Firestone's (2, 3, 17) analysis of E2, S_H2, and S_N2 transition states in terms of Linnett or L-strain, even though they reference his papers on the subject. Finally, the authors' bibliography of the literature dealing with LDQ theory is far from complete, a number of major references being conspicuously absent (4, 5, 9–14, 18–39).

In conclusion, the paper by Langler *et al.* is anything but a critical evaluation of the application of LDQ theory to problems of structure and reactivity in organic chemistry. By denying the role of the nuclei and applying only the postulates dealing with electron repulsion, they produce a misleading picture of LDQ theory and then proceed to demonstrate that it leads to unsatisfactory results in predicting structure and reactivity. Indirectly, however, the Langler article points to the need for a greater development and refinement of Linnett's original work. One area of refinement, briefly touched on here, is a comparison of the relative efficiency of the electrons in bonds of the same kind and multiplicity, but differing correlation, in screening kernel–kernel repulsions.

A second area of refinement would be in assessing the relative efficiency of various nuclei or kernels in inducing close pairing. Other things being equal, one would expect this ability to increase with increasing kernel charge and decreasing kernel size. When kernels of identical charge but differing size act as central atoms in isoelectronic species, there will also be a tendency to resist ligand-induced close-pairing as the central kernel increases in size. This is because the same number of valence electrons must screen a proportionately larger surface area in the case of a large kernel, or, conversely, close pairing for a large kernel will be more strongly resisted because it results in the descreening of a proportionately larger amount of surface area. Likewise, distortions of the shared spin sets due to differences in the electronegativities of the kernels, or even due to differences in the relative attraction of a kernel for the bonding versus the nonbonding electrons in a given spin set, can lead to a decrease in electron repulsion because of the resulting *radial* electron correlation, thereby supplementing the *angular* correlation which LDQ theory currently emphasizes.[5]

Considerations of this kind could easily provide a qualitative rationale for the discontinuity in structures and bonding properties shown on passing from period 2 species to their heavier group analogs (e.g., H_2O vs. H_2S, H_2Se, H_2Te; NH_3 vs. PH_3, AsH_3, SbH_3, etc.), accounting for the differences in bond angles, the inert pair effect, the reluctance of these elements to form multiple bonds among themselves, etc. Another area of application would be in assessing the relative amounts of L-strain to be expected in a series of S_N2 displacement reactions in which the donor species and acceptor atom are kept constant but the substituents on the acceptor atom are varied.

1. R. F. LANGLER, J. E. TRENHOLM, and J. S. WASSON. Can. J. Chem. **58**, 780 (1980).
2. R. A. FIRESTONE. Tetrahedron Lett. 971 (1968).
3. R. A. FIRESTONE. J. Org. Chem. **34**, 2621 (1969).
4. J. DALE. *In* Chemistry of acetylenes. *Edited by* H. G. Viehe. Dekker, New York, NY. 1969. pp. 82–92.
5. E. W. LAWLESS and I. C. SMITH. Inorganic high-energy oxidizers. Dekker, New York, NY. 1968. pp. 221–233.
6. W. F. LUDER. The electron-repulsion theory of the chemical bond. Reinhold, New York, NY. 1967.
7. J. W. LINNETT. The electronic structure of molecules. Methuen, London. 1964.
8. J. W. LINNETT. J. Am. Chem. Soc. **83**, 2643 (1961).
9. H. A. BENT. J. Chem. Educ. **42**, 302 (1965); **42**, 348 (1965).
10. H. A. BENT. *In* The chemistry of organic sulfur compounds. Vol. 2. *Edited by* N. Kharasch and C. Y. Meyers. Pergamon, New York, NY. 1966. Chapt. 1.
11. H. A. BENT. Chemistry, **40**(1), 8 (1967).
12. H. A. BENT. Chem. Rev. **68**, 587 (1968).
13. H. A. BENT. J. Chem. Educ. **45**, 768 (1968).
14. H. A. BENT. Fortschr. Chem. Forsch. **14**, 1 (1970).
15. R. J. GILLESPIE. Molecular geometry. Van Nostrand Reinhold, New York, NY. 1972.
16. F. SERRATOSA. J. Chem. Educ. **50**, 402 (1973).
17. R. A. FIRESTONE. J. Org. Chem. **36**, 702 (1971).
18. J. LENNARD-JONES. Adv. Sci. 136 (1954).
19. P. G. DICKENS and J. W. LINNETT. Rev. Chem. Soc. **11**, 291 (1957).

[5]Some progress in this direction has been made by Luder. See ref. 6, Chapt. 6, and ref. 33.

20. J. W. LINNETT. Nature, **187**, 859 (1960).
21. D. M. HIRST and J. W. LINNETT. Proc. Chem. Soc. 427 (1961).
22. H. A. BENT. Inorg. Chem. **2**, 747 (1963).
23. J. W. LINNETT. Am. Sci. **52**, 459 (1964).
24. J. W. LINNETT and R. M. ROSENBERG. Tetrahedron, **20**, 53 (1964).
25. A. P. ZIPP. J. Chem. Educ. **44**, 494 (1967).
26. C. L. BUMGARDNER and G. H. WAHL. J. Chem. Educ. **45**, 347 (1968).
27. W. F. LUDER. Chemistry, **42**(6), 16 (1969).
28. J. W. LINNETT. *In* Essays in structural chemistry. *Edited by* A. J. Downs, D. A. Long, and L. A. Stavley. Plenum, New York, NY. 1971. Chapt. 1.
29. S. ZUFFANTI. Chemistry, **43**(5), 8 (1970).
30. W. F. LUDER. Can. Chem. Educ. **5**(3), 13 (1970).
31. W. F. LUDER. Am. Sci. **58**, 259 (1970).
32. W. F. LUDER. Can. Chem. Educ. **6**(1), 19 (1971).
33. W. F. LUDER. Can. Chem. Educ. **7**(1), 14 (1972).
34. W. F. LUDER. Can. Chem. Educ. **7**(10), 9 (1972).
35. B. E. DOUGLAS and D. H. MCDANIEL. Concepts and models of inorganic chemistry. Blaisdell, Waltham, MA. 1965. pp. 67–70.
36. M. C. DAY and J. SELBIN. Theoretical inorganic chemistry. 2nd ed. Reinhold, New York, NY. 1969. pp. 201–205.
37. G. DEMITRAS, C. R. RUSS, J. SALMON, J. H. WEBER, and G. WEISS. Inorganic chemistry. Prentice-Hall, Englewood Cliffs, NJ. 1972. pp. 130–136.
38. R. RICH. Periodic correlations. Benjamin, New York, NY. 1965. pp. 19–25.
39. G. C. PIMENTAL and R. D. SPRATELY. Chemical bonding clarified through quantum mechanics. Holden-Day, San Francisco, CA. 1969. pp. 148–153.

Can. J. Chem. Downloaded from www.nrcresearchpress.com by 210.87.254.42 on 09/06/12
For personal use only.

Ab initio molecular orbital calculations for SF_4, SOF_2, and SO_2F_2 [1]

N. COLIN BAIRD AND KATHLEEN F. TAYLOR

Department of Chemistry, University of Western Ontario, London, Ont., Canada N6A 5B7

Received September 9, 1980

N. COLIN BAIRD and KATHLEEN F. TAYLOR. Can. J. Chem. **59**, 814 (1981).

Ab initio molecular orbital calculations are reported for SF_4 (both C_{2v} and C_{4v} symmetries), SOF_2, and SO_2F_2. Geometry searches were conducted using the STO-3G* basis set; the energies were recalculated at the predicted equilibrium structures also using STO-3G and 44-31G, and the latter basis set with the addition of five real *d* Gaussian orbitals on the sulfur atom. The predicted geometries agree well with experiment, although S=O bonds are consistently predicted too long by ~0.03 Å, and the variation in S—F bond lengths among different environments is underestimated. The energy stabilization associated with the addition of *d* orbitals is generally consistent with our previous calculations, i.e. it is a constant amount per bond in hypervalent sulfur compounds in extended basis calculations. Replacement of F by OH is predicted to be more exothermic in SO_2F_2 than in SOF_2, and the relevance of this prediction to estimated heats of formation for SOF_2 and $SO(OH)_2$ is discussed.

N. COLIN BAIRD et KATHLEEN F. TAYLOR. Can. J. Chem. **59**, 814 (1981).

On rapporte des calculs *ab initio* des orbitales moléculaires du SF_4 (symétries C_{2v} ainsi que C_{4v}) du SOF_2 et du SO_2F_2. On a étudié la géométrie en utilisant la base STO-3G*; faisant appel à des bases STO-3G et 44-31G, on a calculé de nouveau les énergies au niveau d'équilibre prédit pour les structures; on a aussi effectué des calculs utilisant la base 44-31G à laquelle on a ajouté 5 orbitales de Gauss réelles sur l'atome de soufre. Les géométries prévues sont en accord avec les résultats expérimentaux en dépit du fait que les liaisons S=O soient surestimées d'environ 0,03 Å et les variations des longueurs de liaison S—F dans des environnements différents soient sous-évaluées. L'énergie de stabilisation associée à l'addition des orbitales *d* est généralement en accord avec nos calculs antérieurs, c'est à dire qu'elle correspond à une quantité constante par liaison dans les composés de soufre hypervalents lors de calculs sur des bases larges. On prédit que le remplacement de F par OH doit être plus exothermique dans SO_2F_2 que dans SOF_2 et on discute de l'importance de cette prévision dans l'évaluation des chaleurs de formation du SOF_2 et du $SO(OH)_2$.

[Traduit par le journal]

Introduction

Recently we reported *ab initio* MO calculations for a series of oxides, oxyacids, and oxyanions of sulfur in its +4 and +6 oxidation states (1). The predicted geometries, obtained using the STO-3G* basis set (i.e. with five real 3*d* Gaussian orbitals on the sulfur atom) agreed fairly well with experiment, consistent with the experience of Collins *et al.* for hypervalent systems (2). The energy lowering associated with the addition of sulfur 3*d* orbitals to the basis set was found to be approximately constant per bond for S(IV) and S(VI). We extended the 44-31G basis set for sulfur also to include *d* orbitals, and established that while the effect of the *d* orbital addition was less, the gain per bond varies little from an average of 28 kcal mol^{-1}.

In this report, these calculations are extended to some interesting molecules containing sulfur–fluorine bonds, namely the tetrafluoride SF_4 and the oxyfluorides SOF_2 and SO_2F_2. Our main interest was to establish whether the STO-3G* basis would predict accurate geometries for these systems, and whether the energetic stabilization upon *d* orbital addition to the STO-3G and to the 44-31G basis sets held to the constant values established previously for S—O and S—O—H systems. The tetrafluoride is of particular interest, given the calculations reported for it by Radom and Schaefer (3). They found that whereas the 44-31G basis set correctly predicts a C_{2v} structure for the molecule, the STO-3G basis incorrectly predicts that the C_{4v} (square pyramid) geometry is much more stable.

Method of Calculation

All computations reported herein were obtained using the "Gaussian 76" program (4) on a CDC Cyber 73 computer. Details concerning the STO-3G, STO-3G*, and 44-31G basis sets are discussed in papers by Pople and co-workers (2). The 44-31G* basis set corresponds to the addition of five real 3*d* Gaussian orbitals, each of exponent 0.60, to sulfur. (This value is the average of optimized exponents for SO_2 and SO_3, as established previously (1).) Bond lengths and angles were consecutively varied and reoptimized until the variations were less than 0.01 Å and 0.5°, respectively. In each case, the initial geometry chosen was close to that reported experimentally (except of course for the C_{4v} structure of SF_4).

Once the optimum structure for each molecule had been obtained at the STO-3G* level, its energy was recalculated using the STO-3G, 44-31G, and 44-31G* basis sets. The total energies obtained

[1]Research supported by the Natural Sciences and Engineering Research Council of Canada.

0008-4042/81/050814-03$01.00/0

©1981 National Research Council of Canada/Conseil national de recherches du Canada

TABLE 1. Calculated energies of sulfur–fluorine molecules

Name and formula	Total energy (au)		Energy improvement (kcal mol^{-1}) by addition of d orbitals	
	STO-3G*	44-31G*	STO-3G*	44-31G*
Sulfur tetrafluoride C_{2v} SF_4	−785.4374	−794.2550	266.2	110.3
C_{4v}	−785.4311	−794.2366	249.4	103.3
Thionyl fluoride SOF_2	−663.2037	−670.4227	225.4	110.3
Sulfuryl fluoride SO_2F_2	−737.0526	−745.1542	357.2	179.7

using the bases with d orbitals, and their differences compared to the STO-3G and 44-31G bases, are reported in Table 1. The optimized STO-3G* structures are shown in Fig. 1; experimental values are given in parentheses.

Results and Discussion

The geometries computed for thionyl fluoride and for sulfuryl fluoride both agree fairly well with the modern electron-diffraction results (see Fig. 1). The O=S=O angle in SO_2F_2 is correctly predicted to be significantly larger than tetrahedral, although the effect is exaggerated slightly. (The same value for this angle was predicted for sulfuric acid.) The O=S—F and F—S—F angles in both SOF_2 and SO_2F_2 agree well with experiment. The sulfur–oxygen bond lengths in these molecules are overestimated by 0.03 Å and 0.04 Å respectively, an effect previously established from our study of sulfur–oxygen systems.

The sulfur–fluorine bond lengths predicted for SOF_2, SO_2F_2, and SF_4 (C_{2v} structure) agree well with the experimental results, the average deviation being 0.026 Å. This latter value is somewhat misleading, however, since the differences are not consistently positive or negative; the net spread in the calculated S—F distances (1.56 to 1.61 Å) is rather less than for the experimental values (1.530 to 1.646 Å). Although the "in-plane" bonds in sulfur tetrafluoride are predicted correctly to be shorter than those out of plane, the differential is only half that observed. In their study of the isoelectronic molecule ClF_3 also using the STO-3G* basis set, Collins *et al.* also established that the differential between the equatorial and the axial bonds was underestimated (0.012 Å calculated versus 0.100 Å experimental). They found that the difference was reproduced accurately using the 44-31G basis set, although the Cl—F bond lengths were seriously overestimated. The same holds true for

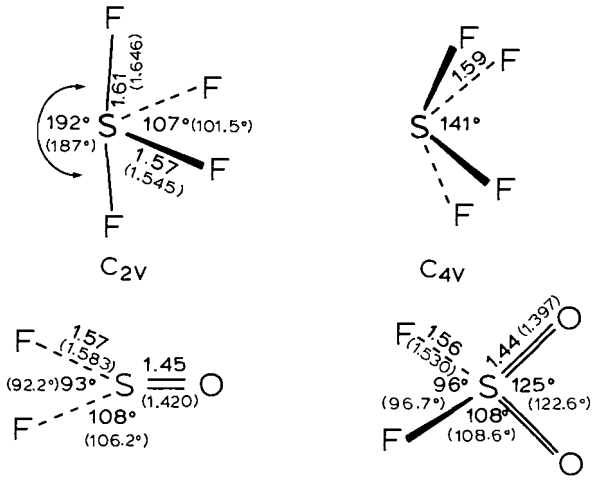

FIG. 1. Calculated STO-3G* geometries for SF_4 (C_{2v} and C_{4v}), SOF_2, and SO_2F_2. All distances are in Å. Experimental values (in parentheses) for SF_4 are from Tolles and Gwinn (8), for SOF_2 are from Hargittai and Mijlhoff (9), and for SO_2F_2 are from Hagen *et al.* (10).

SF_4, since the S—F length differential was well predicted (0.092 Å versus 0.101 Å experimental), but the absolute values were too large (by ~0.09 Å), in the 44-31G calculations reported by Radom and Schaefer (3). The conclusion that d orbitals are required to obtain realistic geometry predictions is consistent with the work of several authors (1, 5, 6) who found that the lengths of S=O bonds are not predicted even semiquantitatively without the addition of such functions to sulfur.

For SF_4, the STO-3G* basis set predicts the C_{2v} structure to be that of lowest energy, in agreement with the experimental geometry (see Table 1 and Fig. 1). Both the F_{axial}—S—F_{axial} and the $F_{equatorial}$—S—$F_{equatorial}$ angles are somewhat greater than observed (Fig. 1). The optimum C_{4v} structure lies only 3.9 kcal mol^{-1} above the C_{2v} form at the STO-3G* level; we have not investigated

whether any barrier exists to prevent the collapse of the C_{4v} form to the C_{2v} form. The energetic advantage of the C_{2v} form over the C_{4v} form rises to 11.5 kcal mol^{-1} at the 44-31G* level, compared to 4.5 kcal with the extended basis set minus the *d* functions on sulfur. With the STO-3G* basis, the C_{4v} structure is preferred, by 12.8 kcal mol^{-1}, compared to the 22.4 kcal preference found by Radom and Schaefer; the difference presumably is due to the use of experimental bond angles for the C_{2v} structure in the earlier calculations. We conclude that the incorrect C_{4v} structure for sulfur tetrafluoride is obtained only with the minimal basis set, and that improvement of the wavefunction either by addition of *d* orbitals to the sulfur (as in the present calculations) or by use of an extended basis set (as in the present calculations and also in the 44-31G geometry optimization by Radom and Schaefer) leads to the correct prediction that the C_{2v} geometry is optimum.

The calculated improvements in the total energies upon addition of sulfur *d* orbitals (see Table 1) for the three fluorine-containing molecules are similar to those found for the S(IV) and S(VI) oxides and oxyacids, when comparisons are made on a per bond basis (1). The stabilization energies with the extended basis for SF_4 (C_{2v} structure) and SOF_2 both are 27.6 $kcal^{-1}$, close to the average established previously. The corresponding improvement in SO_2F_2 is 30.0 kcal mol^{-1} per bond for a total of 179.7 kcal, slightly above the range in the oxides and oxyacids. In contrast, the *d* orbital stabilization for the C_{4v} structure of sulfur tetrafluoride of 25.8 kcal mol^{-1} per bond falls at the low end of the scale. The energy improvements calculated upon addition of *d* orbitals to sulfur at the minimal basis set level, as expected, are larger than with the extended basis; however only the value for SF_4 (C_{2v}) falls outside (slightly above) the rather wide ranges found in the sulfur–oxygen systems.

A comparison of the total energies reported previously for $SO_2(OH)_2$ and $SO(OH)_2$ with those for the isoelectronic molecules SO_2F_2 and SOF_2 reveals that the replacement of fluorine by hydroxyl is predicted to be more favourable by 6.1 kcal mol^{-1} at the 44-31G* level (and 7.5 at STO-3G*) for SO_2F_2 than it is for SOF_2. If valid, this implies that Benson's predicted heat of formation ΔH_f (7) of -127 ± 3 kcal mol^{-1} for $SO(OH)_2$ is about 7 kcal mol^{-1} too negative, or that the experimental ΔH_f of -130 ± 5 kcal mol^{-1} for SOF_2 is 7 kcal too positive, or some combination of the two effects. The lesser stabilization of fluorine replacement by hydroxyl in SOF_2 than in SO_2F_2 is consistent with Benson's rule (7) that such replacements become increasingly favourable as the electronegativity of the central atom or group increases, since presumably the $\diagdown\!\!\diagup SO_2$ group is more electronegative than is the $\diagdown\!\!\diagup SO$ unit.

1. N. C. Baird and K. F. Taylor. J. Comput. Chem. In press.
2. J. B. Collins, P. von R. Schleyer, J. S. Binkley, and J. A. Pople. J. Chem. Phys. **64**, 5142 (1976).
3. L. Radom and H. F. Schaefer III. Aust. J. Chem. **28**, 2069 (1975).
4. J. A. Pople. Quantum Chemistry Program Exchange, **11**, 368 (1978).
5. S. Huzinaga and M. Yoshimine. J. Chem. Phys. **68**, 4486 (1978).
6. P. G. Mezey and A. Kapur. Can. J. Chem. **58**, 559 (1980).
7. S. W. Benson. Chem. Rev. **78**, 23 (1978).
8. W. M. Tolles and W. D. Gwinn. J. Chem. Phys. **36**, 1119 (1962).
9. I. Hargittai and F. C. Mijlhoff. J. Mol. Struct. **16**, 69 (1973).
10. K. Hagen, V. R. Cross, and K. Hedberg. J. Mol. Struct. **44**, 187 (1970).

Application of the Hancock steric constants to interpretation of heat of solution of benzamide in aliphatic alcohols

STEFANIA TANIEWSKA-OSIŃSKA, LEOKADIA KAMIŃSKA-BARTEL, AND HENRYK PIEKARSKI
Department of Chemistry, University of Lodz, Lodz 91416, Poland
AND
TADEUSZ M. KRYGOWSKI
Department of Chemistry, University of Warsaw, Warsaw 02093, Poland

Received December 16, 1979[1]

STEFANIA TANIEWSKA-OSIŃSKA, LEOKADIA KAMIŃSKA-BARTEL, HENRYK PIEKARSKI, and TADEUSZ M. KRYGOWSKI. Can. J. Chem. **59**, 817 (1981).

The enthalpies of solution of benzamide in several aliphatic alcohols and of benzoic acid in *n*-hexanol have been measured. A linear correlation has been found between standard enthalpies of solution of benzamide and benzoic acid and Hancock steric constants.

STEFANIA TANIEWSKA-OSIŃSKA, LEOKADIA KAMIŃSKA-BARTEL, HENRYK PIEKARSKI et TADEUSZ M. KRYGOWSKI. Can. J. Chem. **59**, 817 (1981).

Les enthalpies de solution du benzamide dans divers alcools aliphatiques et de l'acide benzoique dans le *n*-hexanol ont été mesurés. On a démontré qu'il existe une corrélation linéaire entre les enthalpies standards de solution et les constantes stériques de Hancock pour le benzamide et l'acide benzoique.

[Traduit par le journal]

Introduction

Calorimetric and spectrometric investigations of benzoic acid solutions in aliphatic alcohols (1, 2) suggested that this compound forms mixed associates in alcohol solutions, probably of the type AB_2 (A = acid, B = alcohol).

In the earlier work (3) calorimetric measurements of benzamide solutions in methanol, 1-propanol, and 2-propanol were carried out. These results also led to the conclusion that benzamide occurs in alcohols at infinite dilution in the form of mixed associates.

The present work is concerned with the effect of the size and the shape of alcohol molecules on the thermochemical properties of benzamide solutions in alcohols.

We have also attempted here to correlate standard enthalpies of solution of benzamide with Hancock steric constants.

Experimental

Benzamide (by POCh-Gliwice, reagent grade) was crystallized twice from twice distilled water and dried in a vacuum dryer at 70°C. Benzoic acid was sublimed and dried under vacuum at 56°C. Alcohols: ethanol, isobutanol, *n*-pentanol, *n*-hexanol, *t*-butanol, and *t*-pentanol, were initially dried by means of molecular sieve (type 4A, Fluka AG) and then distilled (4). Alcohols purified in this way were again stored over the molecular sieves and redistilled directly before use.

Water content in the investigated alcohols, determined by spectroscopic methods, did not exceed 0.05%. To observe the influence of water present in the solvent on the investigated effects we measured the heat of solution of benzamide in the solvent with additional small amount of water. The results did not change within the experimental error limits.

The solution enthalpy measurements were performed by an "Isoperibol" calorimeter described in the literature (5).

The measurements of heat of solution of benzamide in *t*-butanol were performed at 299.15 K (mp 298.85 K), for other alcohols at 298.15 K.

Results and Discussion

The experimental values of integral enthalpies of solution, ΔH_m, of benzamide in the investigated alcohols and of benzoic acid in *n*-hexanol are summarized in Table 1.

The integral enthalpy of solution is, within the limits of experimental error, a linear function of concentration in all investigated solutions. The ΔH^0 values were determined by calculating the parameters of a straight line

$$\Delta H_m = \Delta H^0 + Am$$

by the method of least squares and extrapolation to $m = 0$.

Standard enthalpies of solution $\Delta H^0(BzNH_2)$ of benzamide are given in Table 2. The values of standard enthalpies of solution of benzoic acid ΔH^0(HBz) taken from earlier works (1, 2, 6, 7) are also included in Table 2.

In order to compare the enthalpies of solvation of benzoic acid and benzamide in alcohols one must know the enthalpies of sublimation of both compounds. According to Davies and Jones (8) the enthalpy of sublimation of benzoic acid is

[1]Revision received June 3, 1980.

0008-4042/81/050817-04$01.00/0
©1981 National Research Council of Canada/Conseil national de recherches du Canada

Can. J. Chem. Downloaded from www.nrcresearchpress.com by 210.87.254.5 on 09/06/12
For personal use only.

Can. J. Chem. Downloaded from www.nrcresearchpress.com by 210.87.254.5 on 09/06/12
For personal use only.

TABLE 1. ΔH_m values for benzamide and benzoic acid in aliphatic alcohols at 298.15 K (1 kcal = 4.184 kJ)

(*a*) Benzamide

Ethanol		*i*-Butanol	
m (mol kg^{-1})	ΔH_m (kcal mol^{-1})	m (mol kg^{-1})	ΔH_m (kcal mol^{-1})
0	4.53	0	5.52
0.0119	4.53	0.00694	5.50
0.0136	4.53	0.00755	5.52
0.019	4.51	0.00897	5.53
0.029	4.57	0.020	5.52
0.039	4.58	0.025	5.56
0.062	4.54	0.041	5.50
0.082	4.52	0.048	5.54
0.105	4.50	0.078	5.50
		0.092	5.50
		0.100	5.52

t-Pentanol		*n*-Pentanol	
m (mol kg^{-1})	ΔH_m (kcal mol^{-1})	m (mol kg^{-1})	ΔH_m (kcal mol^{-1})
0	4.64	0	4.97
0.00864	4.62	0.00704	4.95
0.00876	4.65	0.00719	4.97
0.023	4.64	0.00766	4.98
0.024	4.61	0.0187	5.02
0.046	4.64	0.0190	4.87
0.049	4.68	0.039	4.85
0.071	4.59	0.058	4.90
0.077	4.67	0.076	4.90
0.105	4.60	0.100	4.97

n-Hexanol		*t*-Butanol	
m (mol kg^{-1})	ΔH_m (kcal mol^{-1})	m (mol kg^{-1})	ΔH_m (kcal mol^{-1})
0	5.04	0	4.75
0.00429	5.04	0.00452	4.76
0.01161	5.02	0.00911	4.77
0.02019	5.00	0.01351	4.78
0.02978	4.99	0.01874	4.79
0.04099	4.98		
0.05262	4.97		

(*b*) Benzoic acid in *n*-hexanol

m (mol kg^{-1})	ΔH_m (kcal mol^{-1})
0	3.59
0.00443	3.57
0.01060	3.55
0.01678	3.52
0.02289	3.51

21 850 cal/mol. We did not find in the literature the value of the sublimation enthalpy of benzamide. Then we calculated this quantity by means of approximate methods (9–11). The evaluated sublimation enthalpy of benzamide was 20.00 kcal/mol.

From the comparison of the enthalpies of solvation of benzamide $\Delta H_{sol}(BzNH_2)$ and benzoic acid $\Delta H_{sol}(HBz)$, which in the case of methanol solutions are: −16.02 kcal/mol and −18.87 kcal/mol, respectively, it can be noted that the effect of the solvation of benzamide in alcohols is less negative than in the case of benzoic acid. The observation can probably be explained by the difference of the energy of the bonds O—H···O and N—H···O both in the crystalline state and in solution (3).

The more endothermic effect of the dissolution of benzamide in alcohols may also be explained by the non-planar structure of the benzamide molecules (12, 13) which makes their penetration into the structure of the alcohol more difficult than in the case of the planar molecules of benzoic acid. The increase of ΔH^0 with the growth of both the length of the alkyl chain of the alcohol and its branching seems to be caused by non-specific interactions (1, 3).

We tried to correlate the obtained standard enthalpies of solution of benzamide in alcohols with Taft steric constants E_s.

The solution enthalpies of benzamide $\Delta H^0(BzNH_2)$ as well as of benzoic acid $\Delta H^0(HBz)$ in nine aliphatic alcohols (Table 2) are described according to the relation given by Taft (14) by means of the equations:

$$\Delta H^0(BzNH_2) = -1.40E_s + 4.36, \quad r = 0.937$$

and

$$\Delta H^0(HBz) = -1.20E_s + 3.09, \quad r = 0.937$$

However, in the case of benzoic acid it was found that the steric constants calculated according to Palm, taking hyperconjugation into consideration, correlate standard enthalpies of benzoic acid solutions much better (15). In this work we applied Hancock steric constants E_s^* (16) calculated from the equation

$$E_s^* = E_s + 0.36(n - 3)$$

in which n is the number of C—H bonds. For the same set of $\Delta H^0(BzNH_2)$ values in nine alcohols we found a linear regression of the type

[1] $$\Delta H^0(BzNH_2) = -1.12E_s^* + 4.12$$

with regression coefficient $r = 0.983$. In the case of benzoic acid solutions we obtained the equation

[2] $$\Delta H^0(HBz) = -0.95E_s^* + 2.89$$

for which the linear regression coefficient was $r = 0.989$. The improvement of linear regression caused by the change of Taft constants from E_s to Hancock constants E_s^* is significant at C.L. = 0.95.

The functions calculated according to equations

TABLE 2. $\Delta H^0(BzNH_2)$, $\Delta H^0(HBz)$ values in aliphatic alcohols and Hancock constants E_s^* used in correlation analysis (1 kcal = 4.184 kJ)

Alcohol	E_s^*	$\Delta H^0(BzNH_2)$ (kcal mol^{-1})	Reference	$\Delta H^0(HBz)$ (kcal mol^{-1})	Reference
1. Methanol	0	3.98	3	2.98	7
2. Ethanol	−0.376	4.53	This paper	3.10	1
3. *n*-Propanol	−0.666	4.82	3	3.52	1
4. *i*-Propanol	−1.082	5.27	3	3.94	1
5. *n*-Butanol	−0.696	4.92	6	3.55	6
6. *i*-Butanol	−1.236	5.52	This paper	4.03	6
7. *s*-Butanol	−1.632	5.87	6	4.47	6
8. *n*-Pentanol	−0.706	4.97	This paper	3.53	2
9. *n*-Hexanol	−0.636	5.04	This paper	3.59	This paper
10. *t*-Butanol	−2.458	4.75	This paper	4.34	6
11. *t*-Pentanol	−2.658	4.64	This paper	3.65	2

with Hancock's steric constants (solid lines) and the experimental points are presented in Fig. 1.

It follows from Fig. 1, both in the case of benzamide and benzoic acid, that there are two alcohol solutions, *t*-butanol and *t*-pentanol, which do not satisfy the linear correlation. The magnitudes of these deviations, endothermic in nature, are as follows: 0.89 kcal/mol and 1.76 kcal/mol for benzoic acid and 2.12 kcal/mol and 2.45 kcal/mol respectively for benzamide solutions. For two systems not obeying the linear correlation the most probable explanation is that the solvation mechanism from the other systems under investigation becomes different. In this case, because of the branched alkyl groups of *t*-butanol and *t*-pentanol probably a lower number of alcohol molecules takes part in the solvation. This results in a more endothermic shift of the heat of solution in comparison to the heats for the alcohols obeying relations [1]and [2].

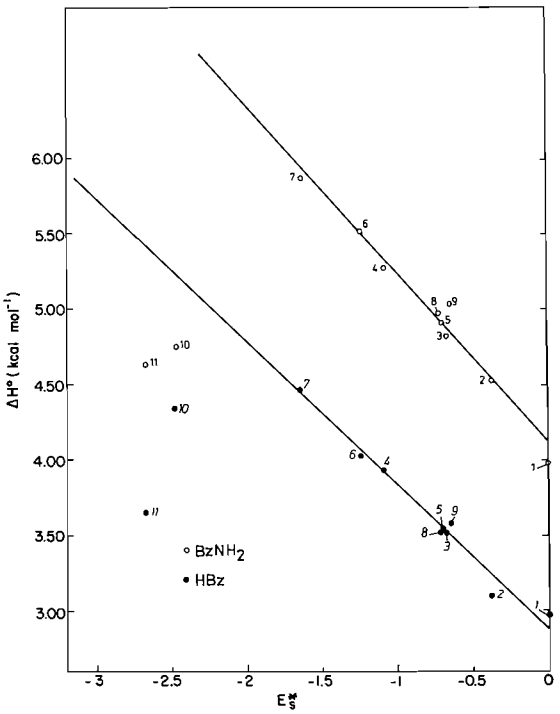

FIG. 1. Correlation of standard enthalpies of solution and Hancock's steric constants.

Linear dependence of standard enthalpies of solution of benzamide and benzoic acid on steric effects, and thus on size and shape of alkyl radicals of alcohols, seems to confirm the conclusion that nonspecific interactions are responsible for the differences among the heats of solution in particular alcohols.

It is well known that steric constants refer usually to changes of free enthalpy of some process. In our case they are linear functions of the solution enthalpy of solvation processes. Thus it can be supposed that in the investigated systems the entropy of solution, ΔS^0, is a linear function of the enthalpy, ΔH^0, or is constant within the limits of the experimental errors.

Confirmation of this suggestion would demand further investigations of changes of free enthalpy of benzamide and benzoic acid solutions in alcohols.

1. S. TANIEWSKA-OSIŃSKA, R. GROCHOWSKI, and H. PIEKARSKI. Proceedings of the Ist International Conference on Calorimetry and Thermodynamics, Warsaw. 1969. p. 875.
2. H. PIEKARSKI, S. TANIEWSKA-OSIŃSKA, and R. GROCHOWSKI. Soc. Sci. Lodz Acta Chim. **18**, 31 (1973).
3. S. TANIEWSKA-OSIŃSKA and H. PIEKARSKI. Soc. Sci. Lodz Acta Chim. **16**, 61 (1971).
4. A. WEISBERGER, E. S. PROSKAUER, J. A. RIDDICK, and E. E. TOOPS, JR. Organic solvents. Interscience Publishers, New York. 1955.
5. S. TANIEWSKA-OSIŃSKA and H. PIEKARSKI. J. Solution Chem. 7, 891 (1978).
6. H. PIEKARSKI. Doctoral Thesis, University of Lodz. 1975.
7. S. TANIEWSKA-OSIŃSKA. Dissertation, University of Lodz. 1965.
8. M. DAVIES and J. G. JONES. Trans. Faraday Soc. **50**, 1042 (1954).

Can. J. Chem. Downloaded from www.nrcresearchpress.com by 210.87.254.5 on 09/06/12
For personal use only.

9. K. M. WATSON. Ind. Eng. Chem. **35**, 398 (1943).
10. R. C. REID and T. K. SHERWOOD. *In* The properties of gases and liquids. New York. 1958.
11. L. RIEDEL. Z. Elektrochem. **53**, 222 (1949); Chem. Eng. Tech. **24**, 353 (1952); **26**, 259 (1954); **28**, 419 (1956).
12. B. R. PENFOLD and J. C. B. WHITE. Acta Crystallogr. **12**, 130 (1959).
13. M. J. ARONEY, R. J. W. LE FEVRE, and A. N. SINGH. J. Chem. Soc. **31**, 79 (1965).
14. R. W. TAFT. *In* Steric effects in organic chemistry. *Edited by* M. S. Newman. Wiley, New York. 1956. p. 556.
15. S. TANIEWSKA-OSIŃSKA, H. PIEKARSKI, and J. KRUSZEWSKI. Bull. Acad. Polon. Sci. Ser. Sci. Chim. **22**, 789 (1974).
16. C. K. HANCOCK, E. A. MEYERS, and J. YAGER. J. Am. Chem. Soc. **83**, 4211 (1961).

Can. J. Chem. Downloaded from www.nrcresearchpress.com by 210.87.254.5 on 09/06/12
For personal use only.

Spectroscopic and electrochemical properties of intramolecularly hydrogen-bonded compounds. *Ortho*-hydroxyazobenzenes

SALVATORE MILLEFIORI AND ARCANGELO MILLEFIORI

Istituto Dipartimentale di Chimica e Chimica Industriale, Università di Catania, viale A. Doria 8, 95125 Catania, Italy

Received April 18, 1980

SALVATORE MILLEFIORI and ARCANGELO MILLEFIORI. Can. J. Chem. **59**, 821 (1981).

The gas-phase uv photoelectron spectra and the half-wave polarographic reduction potentials in acetonitrile solutions of a series of 2-hydroxy-5-methylazobenzene have been determined. The first three IP's and the $E_{1/2}$ values were linearly correlated with σ^+ and σ constants, respectively. $E_{1/2}$ can also be linearly related to the energy of the lowest unoccupied molecular orbital. Effects of the intramolecular hydrogen bonding on the pe spectra and on the polarographic reduction of the title compounds were evaluated by comparing the experimental findings in 2-hydroxy-5-methylazobenzene, 2-methoxy-5-methylazobenzene, and *p*-hydroxyazobenzene. On H-bond formation, the antibonding combination of the two nitrogen lone-pairs, n_-, and the oxygen lone-pair is ionized at a slightly higher energy and at a lower energy, respectively, than in the non H-bonded compound. The first π-ionization band is slightly lowered in energy in the non H-bonded structure, probably owing to a normal substituent effect. These features are not maintained in the 4′-nitro derivative, where the band encompassing the n_- ionization remains at the same potential in both structures, while the first π band in the non H-bonded compound moves toward higher IP. Spectral differences between the bonded and nonbonded structures are the result of a balance of substituent effects, and of both hydrogen bond and orbital interactions. The solution electron affinity of the studied compounds increases on H-bond formation by an amount comparable with the experimental strength of the H-bonding. INDO/S-CI calculations are in qualitative agreement with the experimental results.

SALVATORE MILLEFIORI et ARCANGELO MILLEFIORI. Can. J. Chem. **59**, 821 (1981).

On a déterminé les spectres photoélectroniques uv en phase gazeuse et la demi-onde des potentiels de réduction polarographique, dans des solutions d'acétonitriles, d'une série d'hydroxy-2 méthyl-5 azobenzènes. Les trois premières valeurs des PI et la valeur $E_{1/2}$ sont respectivement reliées d'une façon linéraire aux constantes σ^+ et σ. La valeur $E_{1/2}$ peut également être reliée d'une façon linéaire à l'énergie de la plus basse orbitale moléculaire vacante. On a évalué les effets de la liaison hydrogène intramoléculaire sur les spectres pe et sur la réduction polarographique des composés mentionnés dans le titre, en comparant les résultats expérimentaux obtenus pour l'hydroxy-2 méthyl-5 azobenzène, le méthoxy-2 méthyl-5 azobenzène et le *p*-hydroxyazobenzène. Lors de la formation de la liaison hydrogène, la combinaison anti-liante du doublet électronique libre de l'azote, n_-, et le doublet électronique libre de l'oxygène est ionisé respectivement à une énergie légèrement supérieure et à une plus faible énergie que dans le cas des composés n'ayant pas de liaison hydrogène. La première bande d'ionisation π a une énergie légèrement plus faible dans la structure ne comportant pas de liaison hydrogène à cause d'un effect normal de substituant. Ces caractéristiques ne se maintiennent pas dans le dérivé nitré en position 4′, où la bande englobant l'ionisation n_- reste au même potentiel dans les deux structures, alors que la première bande π dans le composé sans liaison hydrogène, se déplace vers des valeurs de PI plus élevées. Les différences spectrales entre les deux structures liée et non liée sont le résultat d'un équilibre des effets de substituant, et des interactions de liaison hydrogène et d'orbitale. L'affinité électronique de la solution des composés étudiés augmente lors de la formation d'une liaison hydrogène, d'une quantité comparable à la force expérimentale de la liaison hydrogène. Les calculs INDO/S-CI s'accordent qualitativement avec les résultats expérimentaux.

[Traduit par le journal]

Introduction

Hydrogen bonds induce physically and chemically significant electronic perturbations within a molecule. Ultraviolet and X-ray photoelectron (pe) spectroscopy have proved that on H-bond formation the molecular orbital (MO) localized on the proton-acceptor atom is stabilized, while the MO localized on the proton-donor atom moves in the opposite direction (1). These results are supported by theoretical calculations (2). The effects of the H-bonding on the electron affinity (EA) of the molecule are less known. The H-bonding effects can mix with those arising from orbital interactions. In spite of the fact that the available experimental data, to our knowledge, are all in line with the above findings, a different behaviour cannot a priori be excluded. In fact *ab initio* calculations on β-hydroxyacrolein have shown (2*b*) that the *n* orbital energy of the H-bonded C_{2v} form is raised by 0.14 eV relative to the non H-bonded C_s (*trans*) form. CNDO/2 calculations on the intramolecular H-bonding in *ortho*-hydroxyazobenzenes (3) have also predicted a destabilization, following H-bonding, of both the MO's localized on the proton-acceptor center (the azo group) and on the lowest unoccupied MO (LUMO), together with a lowering of the energy of the highest π MO (HO-π-MO). The present work is undertaken to study the effects of the intramolecular H-bonding on the electronic structure of *ortho*-hydroxyazobenzenes by means of gas-phase uv pe spectroscopy and polarographic experiments. In addition some INDO/S-CI calcu-

0008-4042/81/050821-07$01.00/0

©1981 National Research Council of Canada/Conseil national de recherches du Canada

Can. J. Chem. Downloaded from www.nrcresearchpress.com by 210.87.254.105 on 09/06/12
For personal use only.

lations were carried out. This theoretical approach has proved to be valuable in studying spectroscopic properties of azo compounds (4).

Experimental

Ultraviolet pe spectra were recorded on a Perkin-Elmer PS 18 spectrophotometer with He(I) and He(II) excitations. Xe and Ar have been used for calibration. Polarographic half-wave reduction potentials were obtained using a three-electrode Amel polarograph model 563. Spectrograde acetonitrile was used as solvent. It was dried over neutral alumina and distilled at constant boiling point. Polarographic-grade tetrabutylammonium iodide (TBAI) was used as supporting electrolyte. It was dried under reduced pressure at 90°C before use. The depolarizer's concentration was about 5×10^{-4} *M*. The concentration of TBAI was 0.1 *M* throughout the experiments. Solutions were deoxygenated by H_2. The potentials, uncorrected for IR drop, are referred to a saturated calomel electrode. Polarograms were recorded at 25 ± 0.5°C. 2-Methoxy-5-methylazobenzene **1**, not previously reported in the literature, was obtained from 2-hydroxy-5-methylazobenzene **2** by methylation with $(CH_3)_2SO_4$ in sodium ethoxide solution: red oil bp 180°C at 10 Torr. Its identity was checked by means of nmr spectroscopy. In particular, no trace of a hydroxyl proton peak was detected. 2-Hydroxy-5-methylazobenzene and derivatives were synthesized by means of the familar diazo-coupling reactions, following standard procedures, from *p*-cresol and the appropriate amine. The presence of the CH_3 group in the *p*-position with respect to the OH group allows us to obtain exclusively the *ortho*-hydroxy azo derivative. INDO/S-CI calculations have been carried out using the parameterization reported in ref. 5.

Results and Discussion

Photoelectron Spectroscopy

In the 7.5–10.5 eV spectral region of azobenzene derivatives five ionization events are expected. They should correspond to those observed in azobenzene (6), which arise (*1*) from the $a_u(\pi_1)$ MO delocalized on the whole molecule; (*2*) from the $a_g(n_-)$ MO (the antibonding combination of the two nitrogen lone-pairs) localized in the azo group; (*3*, *4*) from two degenerate MO's (π_2 and π_3) which have nodes in 1–4 positions; and (*5*) from the $b_g(\pi_4)$ MO delocalized on the whole molecule. It was shown that electron-donor substituents make the $a_u(\pi_1)$ MO shift above the $a_g(n_-)$ MO (7). Actually the pe spectrum of 2-methoxy-5-methylazobenzene shows, in the low-energy spectral region, three bands (Fig. 1). However, their relative intensities are roughly in the ratio 1:2:2. On the basis of previous work (7), the first band at 7.87 eV can be attributed to a π ionization (corresponding to the a_u ionization in the C_{2h} point group). The second band should encompass the n_- and π_2 ionizations, and the third band the π_3 and π_4 ionizations. The spectrum of 2-hydroxy-5-methylazobenzene (Fig. 1) shows the same three band system in the 7–10 eV range, the higher-energy band now being split. The spectra of 4'-derivatives of **2** are similar; they are exemplified by

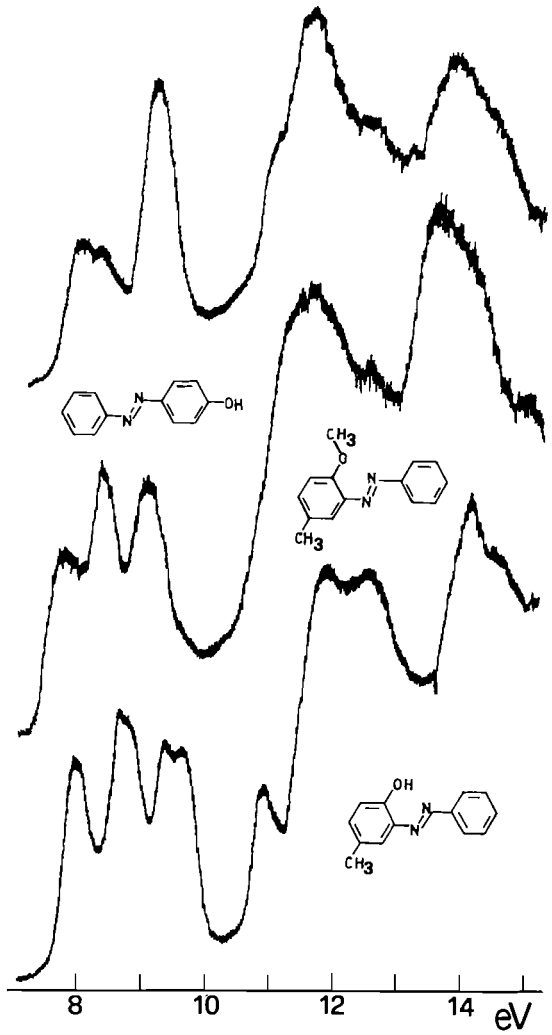

FIG. 1. He(I) photoelectron spectra of 2-hydroxy-5-methylazobenzene (**2**), 2-methoxy-5-methylazobenzene (**1**), and 4-hydroxyazobenzene.

the spectrum of 2-hydroxy-5-methyl-4'-chloroazobenzene (Fig. 2). This compound is also chosen to illustrate the effect of the energy radiation on the band intensity. It is evident that under He(II) radiation (Fig. 2) the intensity of the second band increases slightly relative to the first and third bands. Moreover the intensity of the band centered at 11.52 eV is weaker in the He(II) spectrum. This band very probably includes the Cl_{3p} ionization.

The above results support the tentative inference that the second band includes the n_- ionization, given that the proposed cross-section order of 2*p* orbitals at He(II) radiation is C < N (8).

The pe spectra of 3' derivatives of **2** are exemplified by the spectrum of 2-hydroxy-5-methyl-3'-chloroazobenzene, Fig. 2. Now the relative in-

Can. J. Chem. Downloaded from www.nrcresearchpress.com by 210.87.254.105 on 09/06/12
For personal use only.

Can. J. Chem. Downloaded from www.nrcresearchpress.com by 210.87.254.105 on 09/06/12
For personal use only.

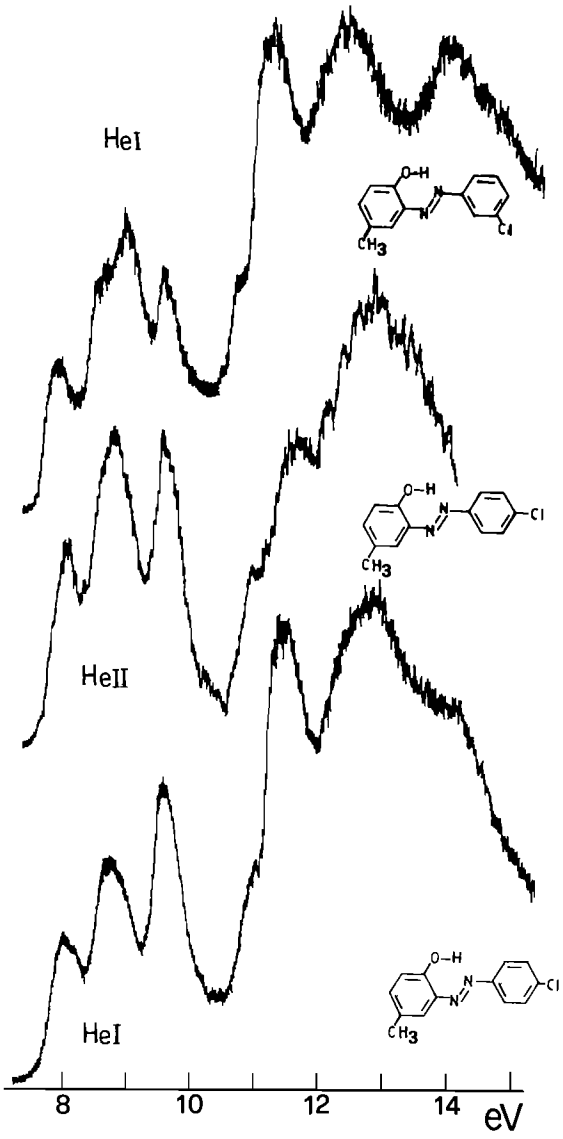

FIG. 2. Photoelectron spectra of 2-hydroxy-5-methyl-4'-chloroazobenzene, He(I); 2-hydroxy-5-methyl-4'-chloroazobenzene, He(II); and 2-hydroxy-5-methyl-3'-chloroazobenzene, He(I).

tensity within the three-band system is roughly 1:3:1. The second band is split and it very likely includes, besides the n_- and π_2 ionizations, the π_3 ionization, which is shifted towards a lower IP relative to **2**, owing to its marked sensitivity to the *meta* substitution. INDO/S-CI calculations, in fact, predict that the π_3 MO is entirely localized on the *ortho* and *meta* positions of the non H-bonded ring.

The measured IP's of the studied compounds are reported in Table 1, together with the proposed assignment. This is supported by the INDO/S-CI calculations, whose predicted ionization energies are also included in Table 1.

Polarographic Reduction

The pertinent polarographic data for the present azo compounds are summarized in Table 2. In acetonitrile solution all compounds are reduced in two one-electron steps. The first wave of the two non H-bonded compounds is reversible. It is slightly less reversible for the H-bonded compounds as can be deduced from the potential index $E_{1/4} - E_{3/4}$, which is somewhat higher than the theoretical value of 56 mV (9). The second wave is irreversible. This behaviour is typical of the electroreduction of azocompounds in aprotic media (10–13).

Correlation of Substituent Effects

The evolution of the first three ionization bands in the present series is followed by means of a σ^+ type (14) correlation, to have data comparable with previous ones (4, 7). However, the use of the Hammett σ constant (15) gives comparable results. The regression lines are:

$$IP_1 = 7.94 \pm 0.02 + (0.24 \pm 0.04)\sigma^+$$

$$IP_2 = 8.65 \pm 0.02 + (0.32 \pm 0.04)\sigma^+$$

$$IP_3 = 9.53 \pm 0.02 + (0.51 \pm 0.05)\sigma^+$$

There is no cross-over between equivalent bands, thus the nature of the band can be considered the same along the series. As found previously (4, 7, 16, 17) the n_- ionization (IP_2) is markedly dependent on substituent. The slope of the plot is equal to that found (0.33 eV) in a corresponding series of disubstituted non H-bonded azo compounds (*p*-methoxyazobenzenes) (4). Therefore the H-bonding (which involves the nitrogen lone-pairs) does not apparently affect the sensitivity of the n_- ionization towards the substituent.

A linear relationship is also obtained between the first reduction potential of the azocompound and the Hammett σ constant (15)

$$E_{1/2} = -1.12 \pm 0.003 + (0.27 \pm 0.01)\sigma$$

The use of the σ^+ constant in electrode reduction processes is not well defined and limited to a few particular cases (18). We are not aware of recent applications of σ^+ type correlation in polarographic experiments. The $E_{1/2}$ vs. σ correlation ensures that the electrode reduction mechanism relative to the first electron transfer is the same through the series, so that correlations between $E_{1/2}$ and structural indexes are meaningful. The *p*-NO_2 derivative is very far off the general trend. The use of σ^- (1.04–1.27) (18) for this compound much improves

Can. J. Chem. Downloaded from www.nrcresearchpress.com by 210.87.254.105 on 09/06/12
For personal use only.

TABLE 1. Vertical ionization potentials (eV) of 2-hydroxy-5-methylazobenzene derivatives[a] and INDO/S-CI[b] ionization energies (eV) for the parent compounds **1** and **2**

Substituent	Vertical ionization potentials (eV) Band 1 π_1	Band 2 n_-,π_2	Band 3 π_3,π_4	Band 4 O_{2p}
None (**2**)	7.95	8.65	9.36,9.67	10.95
IE(INDO/S-CI) **2**	8.3(π_1)	8.8(n_-),8.9(π_2)	9.5(π_3),9.9(π_4)	
4′-OCH_3	7.76	8.43	9.34	(10.8),(11.2)
4′-CH_3	7.88	8.48	9.37	10.82
4′-Cl	8.01	8.71	9.58	11.00
4′-NO_2	8.14	8.92	9.90	11.16
3′-OCH_3	7.85	(8.4),8.71	9.53	(10.9),(11.2)
3′-CH_3	7.88	(8.6),8.93	9.54	10.85
3′-Cl	7.99	(8.7),9.10	9.66	10.93
3′-NO_2	8.19	9.03	9.94	11.16
2-Methoxy-5-methylazobenzene (**1**)				
	7.87	8.48	9.26	
IE(INDO/S-CI) **1**	8.2(π_1)	8.7(n_-),8.9(π_2)	9.3(π_3),9.8(π_4)	
2-Methoxy-5-methyl-4′-nitroazobenzene				
	(8.3)	8.96	9.87	10.91
4-Hydroxyazobenzene				
	8.18	8.49	9.33	11.20

[a]Figures in brackets are unresolved peaks.
[b]In the INDO/S-CI calculations the structure of the non H-bonded compound **1** was generated from **2** by a 180° rotation of the OH group around the C—O bond.

TABLE 2. Polarographic data of 2-hydroxy-5-methylazobenzene derivatives in acetonitrile

Substituent	First wave $E_{1/2}$ V	I_d $\mu A \cdot mol^{-1}$ $m^{-2/3}\,t^{1/2}$	$E_{1/4}-E_{3/4}$ mV	Second wave $E_{1/2}$ V	I_d $\mu A \cdot mol^{-1}$ $m^{-2/3}\,t^{1/2}$	$E_{1/4}-E_{3/4}$ mV
None	−1.112	3.00	70	−1.79	2.50	90
4′-OCH_3	−1.200	2.98	70	−1.88	2.10	80
4′-CH_3	−1.153	2.95	71	−1.85	2.40	80
4′-Cl	−1.065	2.98	72	−1.73	2.70	80
4′-NO_2	−0.710	3.20	80			
3′-OCH_3	−1.090	3.08	72	−1.74	2.38	74
3′-CH_3	−1.125	2.76	68	−1.80	2.38	75
3′-Cl	−1.030	2.58	60	−1.68	2.46	74
3′-NO_2	−0.930	2.64	74			
2-Methoxy-5-methylazobenzene						
	−1.445	3.00	60	−1.88	2.47	80
2-Methoxy-5-methyl-4′-nitroazobenzene						
	−1.025	3.30	60			

its position on the correlation and gives indication of considerable participation of mesomeric interactions. $E_{1/2}$ can also be related to the energy of the LUMO (Fig. 3), thus indicating that it can be taken as a measure of the solution EA of the azocompound. The regression line is

$$E_{1/2} = -2.15 \pm 0.07 + (0.56 \pm 0.04)\mathrm{EA}$$

Effects of Hydrogen Bond

The electronic perturbations induced by the intramolecular H-bonding can be evaluated by comparing the pe spectra of **1**, **2**, and 4-hydroxyazobenzene, Fig. 1. Although band shifts are relatively small, on passing from **1** to **2** we may note (*a*) a small shift (ca. 0.1 eV) towards a higher IP of the first band, which can probably be associated with the substitution of H for CH_3, (*b*) a shift of ca. 0.2 eV towards a higher IP of the second band encompassing the n_- ionization, (*c*) the appearance at 10.95 eV of a band, not evident in the spectrum of **1**,

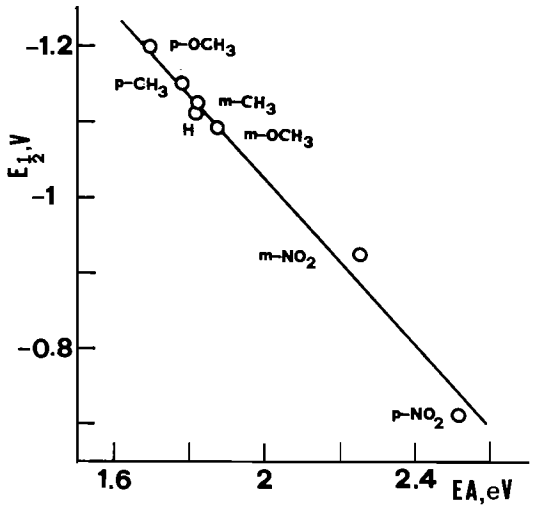

FIG. 3. Plot of the first half-wave reduction potential of 2-hydroxy-5-methylazobenzenes vs. the calculated INDO/S-CI electron affinity.

probably because it is hidden under the intense band centered at about 12.1 eV. This ionization is absent in the pe spectrum of azobenzene, but it appears at ca. 11.2 eV in 4-hydroxyazobenzene. It can reasonably be assigned to the O_{2p} ionization. In fact the corresponding event is observed at ca. 11.5 eV in the phenol (19), at 11.1 eV in 2-methoxy-*N*-benzylidenemethylamine (20) and at 10.79 eV in *p*-methoxyazobenzene (4).

These results seem to point out a slight stabilization of the n_- MO on H-bond formation, and the expected destabilization (ca. 0.3 eV) of the MO localized on the proton-donor atom.

The INDO/S-CI calculations, while rightly predicting a slightly higher ionization energy of the n_- MO, do not, however, show a MO clearly localized on O_{2p} atomic basis owing to heavy mixing, so that the inferred destabilization of the O_{2p} MO cannot be settled by the calculations.

The observed stabilization of the n_- orbital in **2** with respect to **1** is less than that obtained in other intramolecularly H-bonded systems (1). In particular it is much less than that observed (0.6 eV) in 2-hydroxy-*N*-benzylidenemethylamine (20), where an intramolecular H-bonding of comparable energy is present (21, 22). This can very probably be traced back to the correlation diagram of Fig. 4. In the non H-bonded conformation the two N lone-pairs are nearly degenerate and the n_- level is raised by **a** above the N_1 level because of n–n interactions. In the H-bonded conformation the N_2 lone-pair is stabilized owing to the H-bonding. Consequently (23) the destabilization of the n_- orbital is **b** < **a**. Experimentally we observe, on H-bonding formation, a decrease in the n_- MO energy by an amount

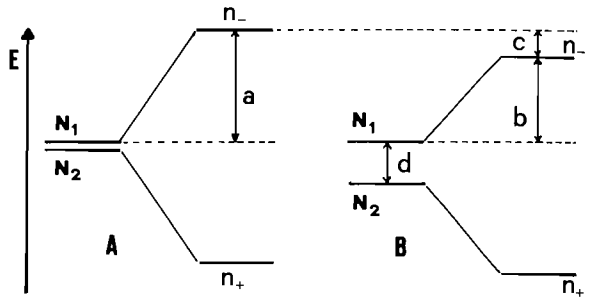

FIG. 4. Correlation diagram for the two nitrogen lone-pairs interaction; (A) non H-bonded structure, (B) H-bonded structure.

c, which is likely to be less than **d**. In addition, through-space interactions (23) between n_- and the O_{2p} lone-pair, which would contribute in raising the energy of the n_- level, may be operative. In fact, INDO/S-CI calculations show that the n_- orbital mixes with the O_{2p} σ-MO in an antibonding way, while contributions to this orbital from the O_{2p} lone-pair are vanishing in the nonbonded structure. Through-bond interactions (23) can also operate in both structures and they are expected to lower the IP_{n_-}. Notice that orbital interactions are conformation-dependent (24) and cannot be quantitatively assessed without a precise knowledge of the molecular geometry.

The sum of substituent, H-bonding, and MO interactions lead in the 4′-nitro derivatives to the situation illustrated in Fig. 5. Now the first two bands in the nonbonded compound are poorly resolved owing to the shift of the first band to a higher IP, while the second band, encompassing the n_- ionization, appears to rest at the same potential in both compounds. Thus in this case we note a different behaviour than in the parent compounds **1** and **2**. These results indicate that the electronic structure of the present azo-compounds, as inferred from their pe spectra, results from a delicate balance among substituent, H-bonding, and orbital interaction effects. Therefore they point out the difficulty in relating electronic effects to the presence of intramolecular H-bonding when many perturbation factors are operative, even if the observed trends are in the expected direction. No attempt has been made to extend the above analysis to the other members of the series.

The effects of the intramolecular H-bonding on the solution EA of the title compounds were evaluated by comparing the effects of the OH and OCH_3 groups on $E_{1/2}$.

The first reduction potential of **1** $E^1_{1/2}$ (**1**) (−1.1445 V) is 0.039 V more negative than $E^1_{1/2}$ of 5-methylazobenzene (−1.406 V) (11), obtained under the same experimental conditions. This is a

Can. J. Chem. Downloaded from www.nrcresearchpress.com by 210.87.254.105 on 09/06/12
For personal use only.

Can. J. Chem. Downloaded from www.nrcresearchpress.com by 210.87.254.105 on 09/06/12
For personal use only.

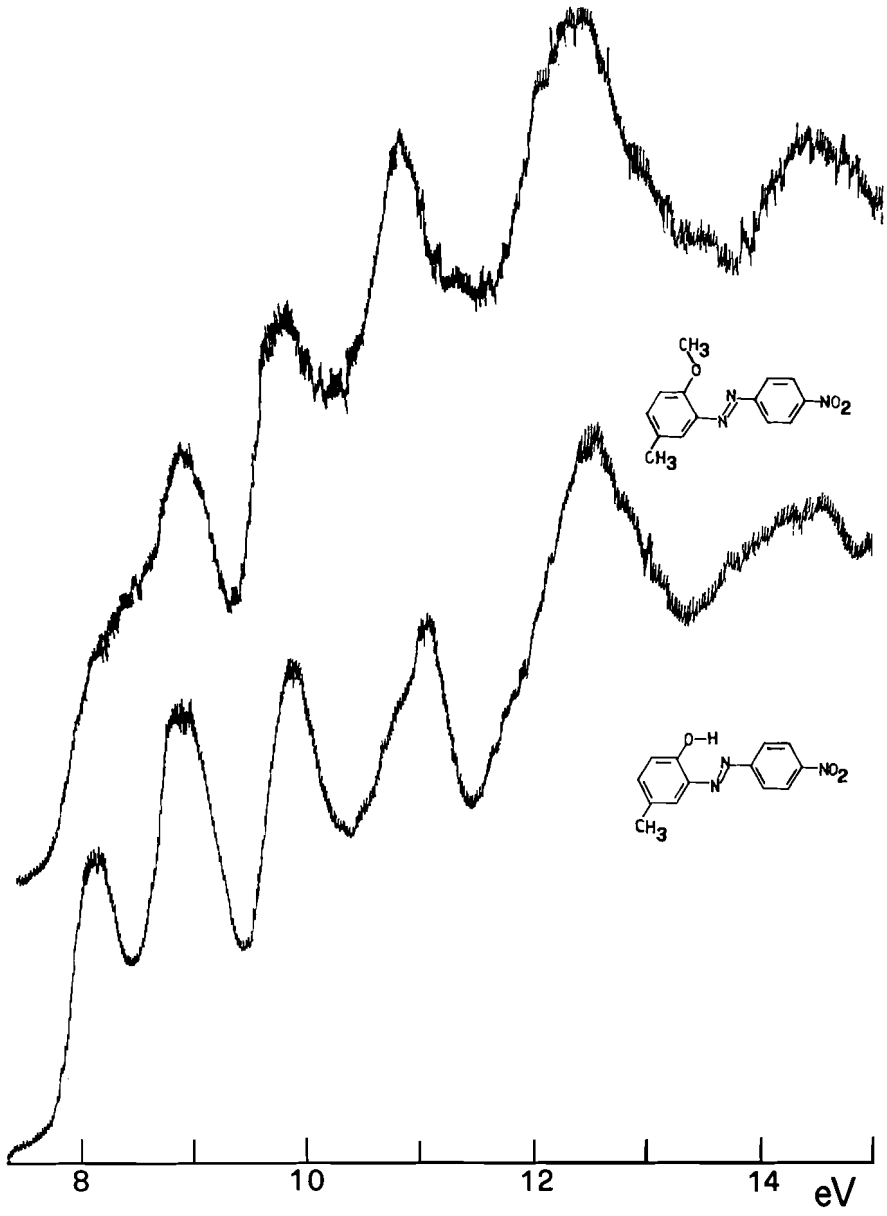

FIG. 5. He(I) photoelectron spectra of 2-hydroxy-5-methyl-4′-nitroazobenzene and 2-methoxy-5-methyl-4′-nitroazobenzene.

normal effect of the OCH_3 group on $E_{1/2}$, since electron-donor groups make the electrode reduction more difficult. In the absence of specific interactions, a similar effect is expected on replacing the OCH_3 with the OH group. Actually $E^1_{1/2}$ (**2**) (−1.112 V) is more positive than that of 5-methylazobenzene. Therefore, under the reasonable assumption that OH and OCH_3 groups display the same "normal" substituent effect on $E_{1/2}$, the energy difference $E^1_{1/2}$ (**2**) − $E^1_{1/2}$(**1**) of 0.333 V is very likely to be the consequence of the H-bonding on EA. The corresponding figure in 4′-nitro derivatives of **1** and **2** is 0.315 V. Orbital interactions between the LUMO and occupied MO's should operate in the opposite direction, i.e. they should decrease the EA value. On the basis of INDO/S-CI calculations it is probable that they do not contribute to the difference between the π^* levels of **1** and **2**, given the same MO composition in both compounds. The calculated INDO/S-CI EA values (within the Koopmans' approximation) for **1** and **2** are 1.52 and 1.83 eV respectively, i.e. EA(**2**) − EA(**1**) = 0.31 eV, in excellent agreement with the experimental results. The polarographic half-wave

reduction potentials may reveal themselves useful for investigating electronic perturbations arising from H-bonding interactions. Accordingly $E_{1/2}$ values may be used for a relative evaluation of the H-bonding energy (3, 25). In the present case $E_{1/2}$ values compared well with the experimental H-bonding strength of 2-hydroxy-5-methylazobenzene (0.38 eV) and 2-hydroxy-5-methyl-4′-nitroazobenzene (0.37 eV), obtained by means of ^{1}H nmr measurements (21).

Acknowledgements

This work was partially supported by C.N.R., Rome. Susan M. Whitehouse is gratefully acknowledged for having revised the manuscript.

1. (*a*) R. S. Brown and D. A. Allison. J. Am. Chem. Soc. **99**, 3568 (1977); (*b*) R. S. Brown and W. Marcinko. J. Am. Chem. Soc. **99**, 6500 (1977), and references therein; (*c*) S. Leawell, J. Steiken, and J. L. Franlin. J. Chem. Phys. **59**, 4343 (1973); (*d*) J. S. Wieczorek, T. Koenig, and T. Balle. J. Electron Spectrosc. Relat. Phenom. **6**, 215 (1975); (*e*) R. K. Thomas. Proc. R. Soc. London, **331**, 249 (1972).
2. (*a*) A. Johanson, P. Kollman, and S. Rothemberg. Chem. Phys. Lett. **18**, 276 (1973); (*b*) J. E. Del Bene. Chem. Phys. Lett. **44**, 512 (1976); (*c*) P. A. Kollman and L. C. Allen. J. Am. Chem. Soc. **93**, 4991 (1971); (*d*) S. W. Dietrich, E. C. Jorgensen, P. A. Kollman, and S. Rothemberg. J. Am. Chem. Soc. **98**, 8310 (1976).
3. S. Millefiori and A. Millefiori. J. Chem. Soc. Faraday Trans. II, **76**, 827 (1980).
4. S. Millefiori and A. Millefiori. J. Chem. Soc. Faraday Trans. II. In press.
5. V. Galasso and G. C. Pappalardo. J. Chem. Soc. Perkin Trans. II, 574 (1976).
6. T. Kobayashi, K. Yokota, and S. Nagakura. J. Electron Spectrosc. Relat. Phenom. **6**, 167 (1975).
7. S. Millefiori, A. Millefiori, S. Pignataro, G. Di Stefano, and F. P. Colonna. Z. Naturforsch. Teil A, **34**, 1496 (1979).
8. U. Gelius. J. Electron Spectrosc. Relat. Phenom. **5**, 985 (1975).
9. J. Tomes. Collect. Czech. Chem. Commun. **9**, 12 (1937).
10. J. L. Sadler and A. J. Bard. J. Am. Chem. Soc. **99**, 1979 (1968).
11. S. Millefiori and G. Favini. Z. Phys. Chem. N.F. **75**, 23 (1971).
12. S. Klopman and N. Doddapaneni. J. Phys. Chem. **78**, 1825 (1974).
13. P. J. Cressman, G. C. Hartman, J. E. Kuder, F. D. Saeva, and D. Wychick. J. Chem. Phys. **61**, 2740 (1974).
14. H. C. Brown and Y. Okamoto. J. Am. Chem. Soc. **80**, 4979 (1958).
15. D. H. McDaniel and H. C. Brown. J. Org. Chem. **23**, 420 (1958).
16. R. Egdell, J. C. Green, and C. N. R. Rao. Chem. Phys. Lett. **33**, 600 (1975).
17. C. N. R. Rao. Tetrahedron, **32**, 1561 (1976).
18. P. Zuman. Substituent effects in organic polarography. Plenum Press, New York. 1967.
19. J. W. Rabalais. Principles of ultraviolet photoelectron spectroscopy. Wiley, New York. 1977.
20. I. Fragala', S. Millefiori, and A. Recca. J. Chem. Res. S, 28 (1980).
21. S. Millefiori, S. Raudino, and A. Millefiori. J. Chem. Res. S, 274 (1979).
22. S. Millefiori and A. Millefiori. J. Chim. Phys. In press.
23. R. Hoffmann. Acc. Chem. Res. **4**, 1 (1971).
24. M. Klessinger and P. Rademaker. Angew. Chem. Int. Ed. Engl. **18**, 826 (1979).
25. M. Uehara and J. Nakaya. Bull. Soc. Chem. Jpn. **43**, 3136 (1970).

Can. J. Chem. Downloaded from www.nrcresearchpress.com by 210.87.254.105 on 09/06/12
For personal use only.

The biosynthesis of cyclopropane fatty acids. I. Feeding experiments with oleic acid-9,10-d_2, oleic acid-8,8,11,11-d_4, and L-methionine-methyl-d_3

PETER H. BUIST AND DAVID B. MACLEAN
Department of Chemistry, McMaster University, Hamilton, Ont., Canada L8S 4M1

Received September 8, 1980

PETER H. BUIST and DAVID B. MACLEAN. Can. J. Chem. **59**, 828 (1981).

cis-9-Octadecenoic acid-9,10-d_2 and *cis*-9-octadecenoic acid-8,8,11,11-d_4 and L-methionine-methyl-d_3 were administered to cultures of *Lactobacillus plantarum* and converted by the organism to the corresponding cyclopropyl compounds. The first experiment showed that no scrambling or loss of label occurred when a methylene unit was added across the double bond of the labelled substrate. In the second experiment, again, no loss or scrambling of label occurred, a result which ruled out any mechanism for biological cyclopropanation involving allylic activation of the double bond. The third experiment yielded a biosynthetic cyclopropane fatty acid containing deuterium located exclusively at the methylene group of the cyclopropane ring. Up to 17% of a d_1-species accompanied the major dideuterated compound. The lone deuterium in the d_1-cyclopropane fatty acid occupies both positions of the methylene group to the same extent. It has been shown that the extent to which d_1-cyclopropane fatty acid is produced increases with cell growth. The extent of exchange was similar in the cyclopropanation of both the 9,10- and 11,12-isomers of *cis*-octadecenoic acid.

PETER H. BUIST ET DAVID B. MACLEAN. Can. J. Chem. **59**, 828 (1981).

Les acides octadécen-9 *cis* oique 9,10-d_2 et octadécèn-9 *cis* oique 8,8,11,11-d_4 ainsi que la L-méthionine-méthyl-d_3 injectés dans des cultures de *Lactobacillus plantarum* sont transformées en composés cyclopropaniques correspondants. La première expérience a montré qu'il n'y a pas de mélange ou de perte du marqueur lorsqu'on ajoute un méthylène à travers la double liaison du substrat marqué. Une deuxième expérience confirme la première; ces résultats écartent tout mécanisme de cyclopropanation biologique impliquant une activation allylique de la double liaison. La troisième expérience a provoqué la biosynthèse d'un acide gras contenant un cyclopropane portant un deutérium exclusivement sur le méthylène du cyclopropane. Dans le composé principal bideutéré, on trouve jusqu'à 17% d'unités monodeutérés. Le deutérium de l'acide gras comportant un cyclopropane monodeutéré est réparti également entre les deux positions du méthylène. On a montré que le taux de production d'acide gras marqué comportant un cyclopropane-d_1 augmente avec la croissance de la cellule. Les taux d'échange sont très voisins lors de la cyclopropanation des deux isomères 9,10 et 11,12 de l'acide octadécènoique *cis*.

[Traduit par le journal]

Cyclopropane fatty acids such as lactobacillic acid, **1**, and dihydrosterculic acid, **2**, occur as phospholipid esters in many bacterial cell membranes (1). From the biosynthetic studies of Hofmann, O'Leary, and Law, it was determined that the cyclopropane ring in these compounds was formed by the addition of a C_1 unit, derived from methionine, across the double bond of the corresponding olefinic fatty acid. Thus, the alkylation of *cis*-vaccenic acid, **3**, yielded lactobacillic acid, **1**, and the alkylation of oleic acid, **4**, gave rise to dihydrosterculic acid, **2** (2). Later, using partially purified enzyme preparations, Law and co-workers established, by in vitro studies, that the cyclopropanation reaction involved *S*-adenosyl-L-methionine (SAM) as the alkylating agent, and olefinic fatty acid phospholipids, in the correct micellar state, as the substrate (2), Fig. 1. The precise mechanistic details of this unique biochemical reaction have not been elucidated, primarily because of difficulties in purifying the enzyme(s) responsible for this transformation. Only very recently has any substantial progress been made in this direction (3).

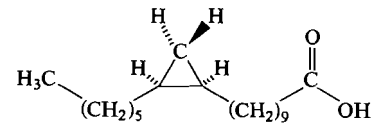

1

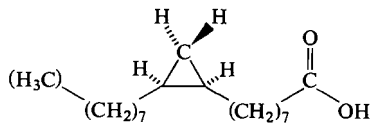

2

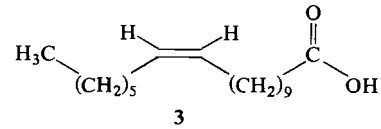

3

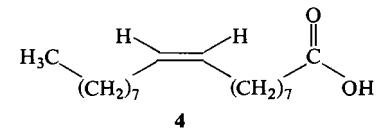

4

The crucial mechanistic point to be clarified is whether proton abstraction to form the methylene unit occurs before or after carbon–carbon bond

0008-4042/81/050828-11$01.00/0
©1981 National Research Council of Canada/Conseil national de recherches du Canada

Can. J. Chem. Downloaded from www.nrcresearchpress.com by 210.87.254.105 on 09/06/12
For personal use only.

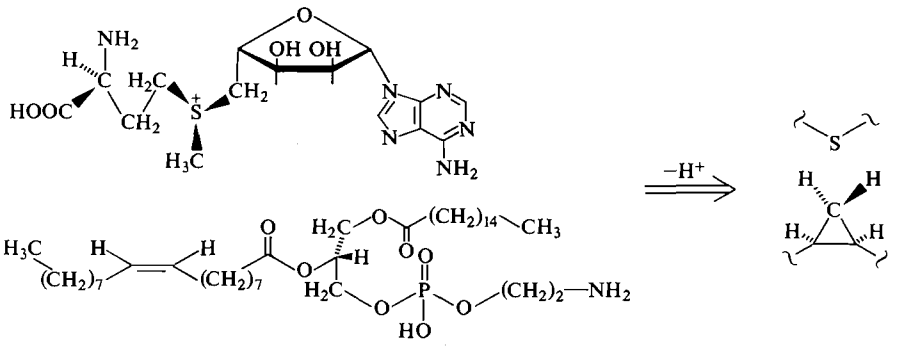

FIG. 1.

formation. Reasonable chemical mechanisms can be written for both alternatives.

Cohen *et al.* have proposed that the cyclopropanation reaction may proceed via a sulfur ylid which donates its methylene unit to a metal such as copper (4). Methylenation of a double bond by this metal–carbenoid species would lead to cyclopropane ring formation (Scheme 1).

Lederer, in his review of *C*-alkylation reactions (5), proposed that the cyclopropane ring might be formed by direct methylation of a double bond by SAM, followed by a 1,3-elimination of a proton. He linked cyclopropane ring formation with biological exomethylene group formation. Compounds containing the latter group are considered to be derived from the same intermediate carbonium ion, which then undergoes a 1,2-hydride shift followed by 1,2-elimination of a proton (Scheme 2).

In previous studies the involvement of allylic protons in the cyclopropanation reaction was not investigated. In order to test for any reaction at the allylic positions, such as that shown in a general way in Scheme 3, allylically deuterated oleic acid was prepared and administered in lieu of biotin to *Lactobacillus plantarum*. The use of this microorganism in these studies was convenient since *L. plantarum* will grow in the absence of biotin (a vitamin required for fatty acid biosynthesis) if olefinic fatty acids, such as oleic acid, are supplied in the medium. Under these conditions, very high (ca. 100%) incorporation of labelled oleic acid into dihydrosterculic acid can be achieved (6).

Vinylically deuterated oleic acid was also pre-

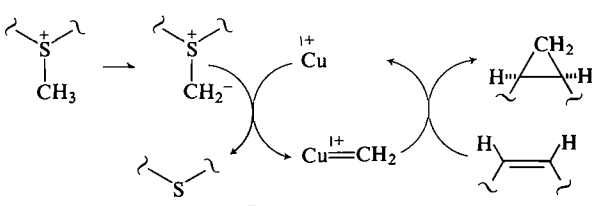

SCHEME 1

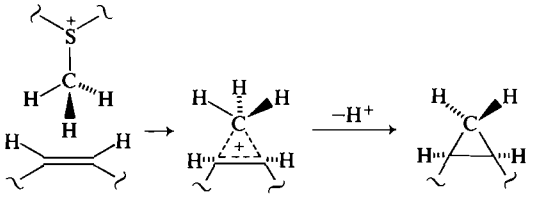

SCHEME 2

pared and administered to the same organism. Although this experiment had already been reported by Polacheck *et al.* (6), its repetition at this time was appropriate for two reasons. Firstly, we were able to prepare oleic acid-9,10-d_2 of better isotopic and stereochemical purity than the previous workers, and secondly, we were able to locate the label unambiguously both in the precursor and in the biosynthetic product through ^2H, ^1H, and ^{13}C nmr spectroscopy. In fact, nmr methods, along with ms, were used routinely throughout this work to locate and to quantitate the label, respectively.

Methyl oleate-9,10-d_2 was prepared by catalytic reduction of the corresponding alkyne using D_2 and Lindlar's catalyst (7) (Scheme 4). Only traces of the *trans* isomer were formed when hexane was used as solvent (up to 8% was formed when ethyl acetate or ethanol-O-*d* was used as solvent). This method also gave methyl oleate-9,10-d_2 with very high deuterium content (>95% d_2) in contrast with other procedures in the literature (e.g. ref. 8). Examination of the ^1H, ^2H, and ^{13}C nmr spectra of the product showed that essentially all the label was at the vinylic positions.

Methyl oleate-8,8,11,11-d_4 was prepared by the route outlined in Scheme 5. The 9,10-diketone, obtained by permanganate oxidation of oleic acid (9), was treated with a mixture of D_2O, DCl, and acetic acid-O-*d*. Catalytic reduction of the exchanged diketone gave predominantly the *erythro* diol which could be freed from the *threo* isomer by recrystallization from ethyl acetate. The *erythro* diol was treated with methyl orthoformate and the

Can. J. Chem. Downloaded from www.nrcresearchpress.com by 210.87.254.105 on 09/06/12
For personal use only.

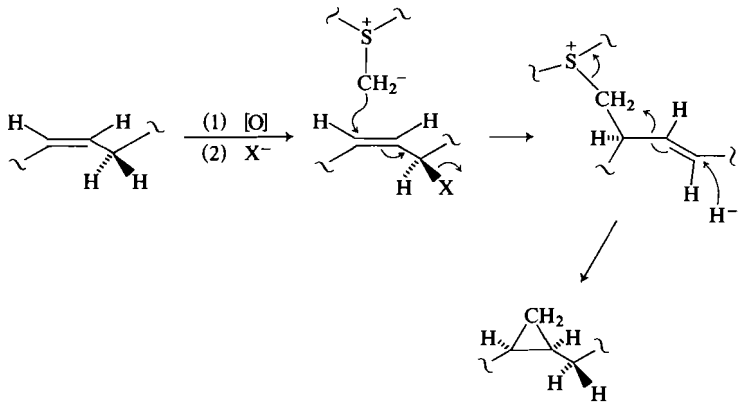

SCHEME 3

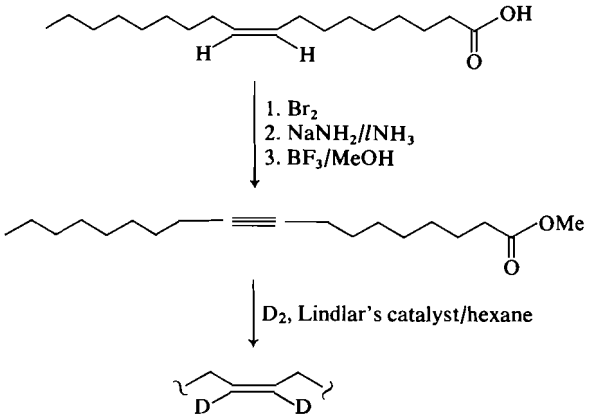

SCHEME 4

resulting 1,3-dioxalan was heated to yield a mixture of methyl oleate and oleic acid, by elimination of CO_2 and methanol. No *trans* olefin was detected in the product. The crude mixture was treated with diazomethane to convert all of the fatty acid to its methyl ester.

L-Methionine-methyl-d_3 was obtained commercially.

The two deuterated fatty acids were fed to the microorganism at a concentration of 0.07 m*M* on a 10 L scale. Approximately 5 mg of cyclopropane fatty acid were isolated in each experiment (representing a 2.5% conversion). For comparison purposes, the Simmons–Smith reaction (10) was employed to prepare deuterated cyclopropanes from the corresponding deuterated olefins. Examination of the synthetic and biosynthetic samples by ms indicated that label was not lost in either feeding experiment (Table 1). The presence of small amounts (2–3%) of unlabelled cyclopropane fatty acid in the biosynthetic products was probably caused by residual olefin fatty acid biosynthesis.

The label in the biosynthetic product from both feeding experiments was located by nmr methods. The cyclopropyl protons in the ^{1}H nmr of methyl dihydrosterculate appear as multiplets at δ 0.66 (3H) and at δ −0.26 (1H). These resonances have been assigned by Longone and Miller (11). The *cis* protons at C-9 and C-10 and the methylene proton *trans* to the two alkyl substituents resonate together at ca. δ 0.6 while the methylene proton *cis* to the 2 alkyl substituents is observed at ca. δ −0.3. Specific deuterium labelling at the methylene would be necessary in order to check these assignments. In the ^{1}H nmr spectrum of the biosynthetic cyclopropane derived from oleic acid-9,10-d_2, a pair of doublets (J_{gem} = ca. 4 Hz) at δ 0.55 (1H) and δ −0.36 (1H) was observed as expected. The ^{2}H nmr spectrum of the above compound featured one signal at δ 0.93. (Errors of ± δ 0.5 are not uncommon when an external reference is used.) Comparison of the ^{13}C nmr spectrum of the nonlabelled and biosynthetic cyclopropane (compounds 1 and 2, Table 2) showed that the spectrum of the latter compound lacked a signal at 16.2 ppm (previously assigned by Batchelor *et al.* (12) to C-9 and C-10). Also, β isotope shifts were observed for the signals of the adjacent methylenes at C-8 and C-12 (0.2 ppm) and of the bridging carbon atom at C-19 (0.2 ppm). On the basis of the above evidence, it was concluded that scrambling or loss of deuterium had not occurred on biological cyclopropanation of oleic acid-9,10-d_2.

That no scrambling of label had occurred in the oleic acid-8,8,11,11-d_4 feeding was clear from the following spectroscopic data. The ^{1}H nmr spectrum of the biosynthetic cyclopropane revealed that the signals of the cyclopropyl protons were not reduced in intensity and further that the multiplet at δ 0.66 was sharpened because of the absence of hydrogen at C-8 and C-11. The ^{2}H nmr spectrum showed one peak at δ 1.3, as might be expected for deuterons located at C-8 and C-11. The ^{13}C nmr

Can. J. Chem. Downloaded from www.nrcresearchpress.com by 210.87.254.105 on 09/06/12
For personal use only.

TABLE 1. Deuterium content* of synthetic and biosynthetic cyclopropane fatty acids derived from oleic acid-9,10-d_2 and oleic acid-8,8,11,11-d_4

	Synthetic 9,10 d_2-cyclopropane acid	Biosynthetic 9,10 d_2-cyclopropane acid	Synthetic 8,8,11,11 d_4-cyclopropane acid	Biosynthetic 8,8,11,11 d_4-cyclopropane acid
% d_0	1.0	3.0	0.4	3.4
% d_1	3.5	4.0	1.4	1.4
% d_2	95.5	93.0	4.0	4.1
% d_3			15.1	14.7
% d_4			79.1	76.4

*The experimental error was estimated to be ±1% for each isotopic species expressed as a percentage.

spectrum of the biosynthetic sample was identical with that of a synthetic sample prepared by a Simmons–Smith reaction on methyl oleate-8,8,11,11-d_4 (compounds 3 and 4, Table 2).

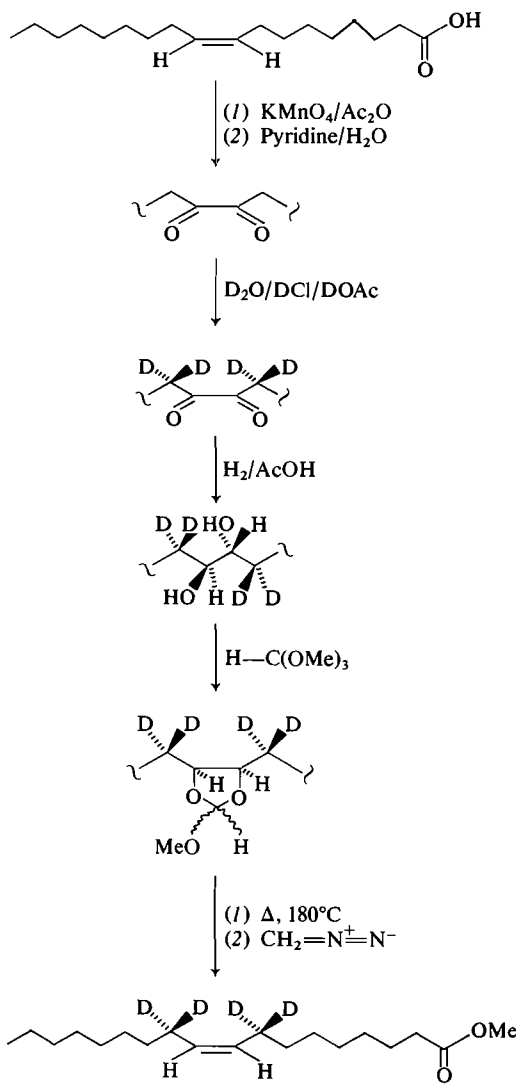

SCHEME 5

The results with allylically deuterated methyl oleate rule out any mechanism for biological cyclopropanation involving allylic protons and the results of the oleic acid-9,10-d_2 feeding confirm those obtained by Polacheck *et al.* (6). One may also conclude that if the carbonium ion mechanism (Scheme 2) is correct, then the intermediate from which a proton is abstracted might be considered to be an edge-protonated cyclopropane. The fact that scrambling and loss of label did not occur in the oleic acid-9,10-d_2 feeding, suggests that no equili-

TABLE 2. ^{13}C chemical shifts of deuterium labelled and unlabelled cyclopropane fatty acid

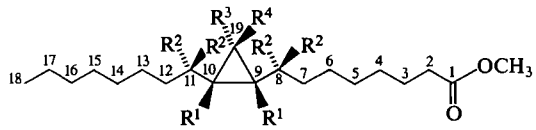

1 $R^1 = R^2 = R^3 = R^4 = H$ (synthetic)
2 $R^1 = D, R^2 = R^3 = R^4 = H$ (biosynthetic)
3 $R^1 = H, R^2 = D, R^3 = R^4 = H$ (synthetic)
4 $R^1 = H, R^2 = D, R^3 = R^4 = H$ (biosynthetic)

	Compound			
Carbon No.	**1**	**2**	**3**	**4**
1	173.3	(—)	173.3	173.3
2	34.1	34.1	34.1	34.1
3	25.3	25.3	25.3	25.3
4	29.5	29.8	29.6	29.5
5	29.8	29.8	29.8	29.7
6	30.1	30.1	30.2	30.1
7	30.6	30.6	30.4	30.3
8	29.2	29.0	Absent	Absent
9	16.2	Absent	16.0	16.0
10	16.2	Absent	16.0	16.0
11	29.2	29.0	Absent	Absent
12	30.6	30.6	30.4	30.3
13	30.1	30.1	30.2	30.1
14	29.8	29.8	29.8	29.7
15	29.8	29.8	29.8	29.7
16	32.3	32.3	32.3	32.3
17	23.1	23.0	23.1	23.0
18	14.3	14.2	14.3	14.3
CO_2CH_3	50.9	50.8	50.9	50.9
19	11.3	11.1	11.3	11.2

Can. J. Chem. Downloaded from www.nrcresearchpress.com by 210.87.254.105 on 09/06/12
For personal use only.

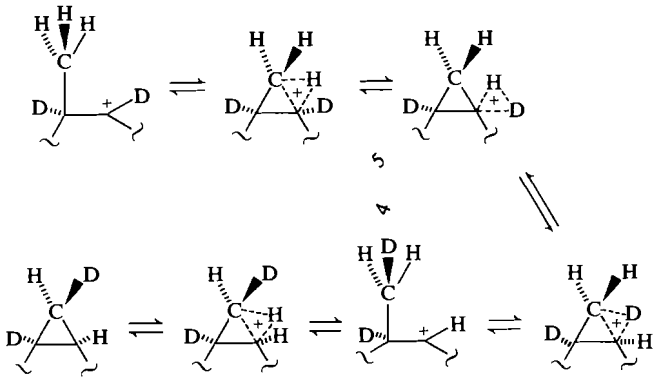

SCHEME 6

bration of edge and various corner-protonated cyclopropyl species had occurred (13) (Scheme 6).

We also carried out feeding experiments with methionine-methyl-d_3, in which the label in the biosynthetic cyclopropyl product was again located and measured by nmr and ms methods, respectively. Earlier workers showed that a cyclopropane fatty acid derived from methionine-methyl-d_3 contained two deuterium atoms; however, it was not stated whether any d_1 species was present, nor was the label in the biosynthetic product located (14).

In this study, methionine-methyl-d_3 (d_3, 95.8%; d_2, 1.4%; d_1; 0.9%; d_0, 1.9%) was administered to *L. plantarum* under a variety of culture conditions. The results of the mass spectral examination of the biosynthetic cyclopropyl product obtained in each experiment are shown in Table 3. It can be seen that a significant amount of d_1-cyclopropyl fatty acid accompanies the d_2-species in each case. The reasons for the variation in d_1-content will be discussed (see below). To check the reliability of the ms analysis, methyl dihydrosterculate-19-d_2 was prepared by treating methyl oleate with CD_2I_2 in a Simmons–Smith reaction; its deuterium content was shown to be identical with that found for the CD_2I_2 from which it was prepared.

Various nmr methods were used to locate the deuterium label in the biosynthetic product. The ^1H nmr spectrum of the cyclopropyl product obtained in Experiment 1 (see Table 3) showed that the signal at δ −0.3, assigned to the methylene proton *syn* to the two alkyl substituents in the nonlabelled material (11) had disappeared. The signal at δ 0.6, assigned to H-9, H-10, and the methylene proton *anti* to the two alkyl substituents was two-thirds as intense as the signal in the nondeuterated analogue. The ^2H nmr spectrum of the biosynthetic cyclopropyl fatty acid from Experiment 5 (Table 3) had two peaks of equal intensity at δ 0.42 and δ −0.5.

TABLE 3. Deuterium content of biosynthetic cyclopropane fatty acids derived from methionine-methyl-d_3

Experiment*	Deuterium content (%) d_0	d_1	d_2	$d_1/d_1 + d_2$
1. (Biotin) 36 h	3.9	9.7	86.4	9.7
2. (Oleic acid)	0.8	7.3	91.9	7.4
3. (*a*) (Biotin)	1.5	13.8	84.7	14.1
(*b*) (Biotin) 64 h	1.9	13.8	84.3	14.1
4. (*a*) (Biotin)	4.1	16.0	79.9	16.7
(*b*) (Oleic acid)	3.3	5.6	91.1	5.8
(*c*) (Vaccenic acid)	5.6	7.2	87.2	7.6
5. (Biotin) 48 h	15.7†	12.2	72.0	14.5

*Either biotin (10 μg/L) or the fatty acid (0.07 m*M*) indicated was added to the basal medium of Henderson and Snell (26) along with methionine-methyl-d_3 (0.67 m*M*). Unless otherwise stated cells were harvested after 24 h. Experiment 5 was carried out under anaerobic conditions but otherwise conditions were similar to 3(*a*). Deuterium contents were determined by ms (see Experimental).

†The high d_0 content was due to d_0-methionine in the methionine-methyl-d_3 used for this feeding.

Curve fitting and integration showed the peak intensities to be in the ratio of 49.4 ± 2 to 50.5 ± 2, indicating that the monodeuterated species contributing 14.5% of the total signal intensity was equally labelled at both methylene positions. Inspection of the ^{13}C nmr spectrum of the dihydrosterculic acid obtained in Experiment 2 (Table 3) showed that deuterium label had not shifted to C-9 or C-10, since the signal attributed to these carbon atoms, although showing a β isotope shift of 0.2 ppm, was not reduced in intensity. The signal assigned by Batchelor *et al.* (12) to the methylene carbon atom in the undeuterated compound was absent. From the above data, it can be seen that the deuterium label from methionine-methyl-d_3 was located at the two methylene positions of the cyclopropane.

Support for this conclusion was obtained by closer mass spectrometric examination of the

Can. J. Chem. Downloaded from www.nrcresearchpress.com by 210.87.254.105 on 09/06/12
For personal use only.

Can. J. Chem. Downloaded from www.nrcresearchpress.com by 210.87.254.105 on 09/06/12
For personal use only.

TABLE 4. Search for d_3 species in biosynthetic methyl lactobacillate from experiment 4(*a*)*

Gas chromatography – mass spectra Run No.	Synthetic methyl lactobacillate-19-d_2	Biosynthetic methyl lactobacillate-19-d_2
1	0.233 ± 0.01	0.232 ± 0.01
2	0.236 ± 0.01	0.237 ± 0.01
3	0.234 ± 0.01	0.233 ± 0.01
Average	0.234 ± 0.02	0.234 ± 0.02
Corrected for M + 1, M + 2 contribution from d_1-species	0.234 ± 0.02	0.230 ± 0.02

*The numbers in the table represent the ratio, $(M + 1)^+/M^+$ for methyl lactobacillate-d_2.

biosynthetic cyclopropyl fatty acid from Experiment 4(a), in order to determine if any d_3 species were present. The $(M + 1)^+/M^+$ ratio for synthetic methyl lactobacillate-19-d_2 was compared with that of the methyl lactobacillate derived from methioninemethyl-d_3. The results of these gc–ms runs are shown in Table 4. A d_3-species might have arisen by the mechanism shown in Scheme 7. The fact that such a species was not found is consistent with the nmr results (see above) and the observation that scrambling or loss of deuterium label was not detected in the oleic acid-9,10-d_2 feeding experiment.

The formation of d_1-cyclopropane fatty acid in the methionine-methyl-d_3 feedings (Table 3) indicates that exchange of a d_3-methyl species had occurred at some stage in the biosynthetic pathway. Examination of Table 3 (Experiments 2, 4 (b), (c)) shows that the extent to which this exchange process occurs is independent of the nature of the fatty acid administered to the organism. *cis*-Vaccenic and oleic acids, when added in lieu of biotin to the medium, gave products that had similar d_1-contents. It is also apparent that the acids reduced the extent of d_1-species formation markedly. Since growth on the fatty acid medium was rather poor, it was thought that the extent of exchange increased with cell growth. Comparison of the d_1 content obtained in Experiment 1, where for some undetermined reason the cells did not grow out properly, and the d_1 content obtained in Experiments 3 and 5, where growth was normal, further substantiated this hypothesis. A feeding experiment, using methionine-methyl-d_3 was performed in which the cells were isolated at early exponential phase (13 h) and late exponential phase (24 h) and the d_1 content of the biosynthetic cyclopropane fatty acid determined by ms. The results are shown in Table 5. As anticipated, the ratio $\% d_1/(\% d_1 + \% d_2)$ of the cyclopropane fatty acid isolated at 13 h was substantially (50%) lower than that isolated at 24 h. One factor which might control the extent of exchange is the pH of the medium, which drops at a rate proportional to cell growth. If the exchange is occurring at the active site of cyclopropane synthetase, then it might be expected that the rate of exchange would be sensitive to pH, since it is thought that the cyclopropanation reaction takes place on the cell membrane phospholipids, in close proximity to the external medium (15).

The observation of exchange in cyclopropane fatty acid biosynthesis is important because it establishes a possible mechanistic link between biological cyclopropyl and exomethylene group formation. In 1965, Jauréguiberry *et al.* (16) showed that significant quantities of d_1-tuberculostearic acid (11%) and d_1-ergosterol (16%) accompanied the d_2 species in feeding experiments using methionine-methyl-d_3 (Scheme 8). (The $\% d_1$ val-

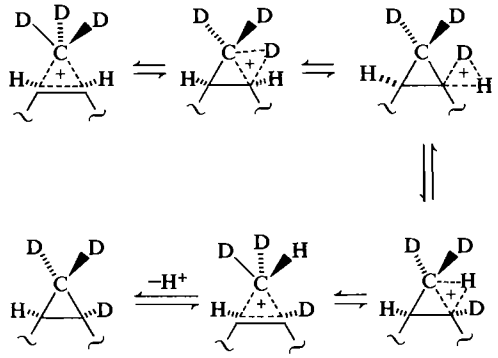

SCHEME 7

TABLE 5. Analytical data* obtained for cells isolated at 13.5 and 24 h

		Cells isolated at 13.5 h	Cells isolated at 24 h
pH of medium at time of isolation		5.9	4.4
Average turbidity at time of isolation		21.0	40.1
Cell yield (mg/100 mL of culture)		5.2	12.4
Fatty acid content (mg)		4.7	20.7
% Cyclopropane fatty acid		13	32
Deuterium content of cyclopropane fatty acid	$\% d_0$	8.8	4.4
	$\% d_1$	7.3	11.3
	$\% d_2$	83.0	84.3
$\% d_1/(\% d_1 + \% d_2)$		8.0	11.8

*Essentially the same culture conditions employed in experiment 3 were used here.

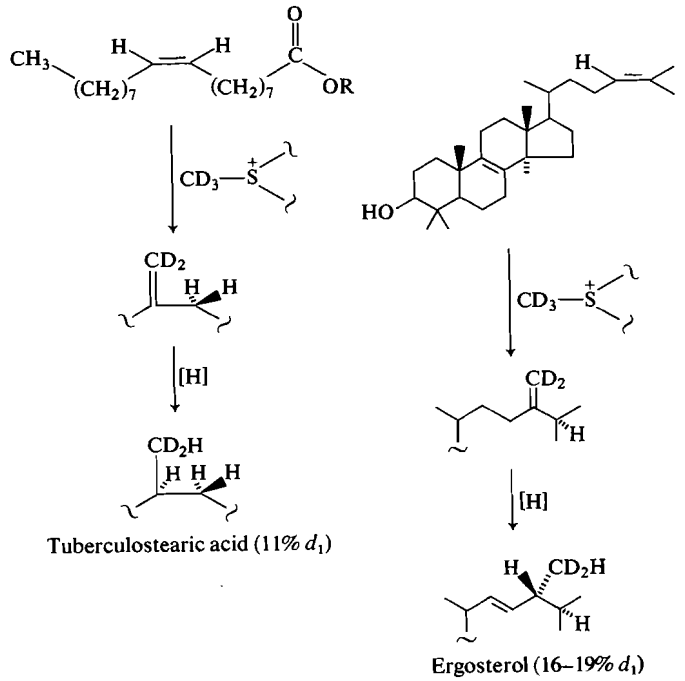

SCHEME 8

ues quoted in this discussion have been recalculated as $\% d_1/(\% d_1 + \% d_2)$ values in order to allow better comparison of the data.) Because the exomethylene intermediates leading to the above two compounds had not been examined for d_1-content, some confusion existed as to the stage at which the exchange had occurred (5). That the methyl group of methionine had not exchanged prior to the alkylation step was shown by the isolation of aurantiogliocladin and ergosterol from the same methionine-methyl-d_3 feeding experiment; the former compound was shown to contain d_3-methyl groups without any appreciable exchanged species, while the ergosterol contained 17% of a d_1-species (5). More recently, Mercer and Russell (17) have determined the deuterium contents of three intermediate 24-exomethylene sterols as well as that of ergosterol, isolated from a methionine-methyl-d_3 feeding experiment. When the d_1-contents of these compounds are expressed as $\% d_1/(\% d_1 + \% d_2)$, it is clear that both the exomethylene intermediates and ergosterol contain the same amount of monodeuterated species (20–24%). One possible interpretation of these data is that exchange is taking place at the initial carbonium ion stage in the formation of the exomethylene group. In view of our findings, the mechanism for this exchange might be explained by reversible cyclopropane group formation, prior to the 1,2-hydride shift, as originally suggested by de Mayo (as quoted in ref. 5) (Scheme 9). Exchange in cyclopropane group biosynthesis might thus be occurring by a similarly reversible 1,3-proton elimination process. This explanation for the exchange process assumes that the cyclopropanation reaction is, in fact, proceeding by a carbonium ion mechanism similar to that proposed for exomethylene group formation. Support for this assumption comes from the enzymological studies of Law and co-workers (2, 18). Both processes require SAM as the alkylating agent. The olefinic substrate must be present as a phospholipid in an appropriate micellar state (the precise structure of the required micelle is not known). Both reactions occur at the 9,10-position of a *cis*-monounsaturated C_{18} fatty acid, although C_{16} substrates are also alkylated. Sulfhydryl reagents such as *p*-hydroxymercuribenzoate inhibit both enzymes, indicating that thiol groups may be important in catalysis (19, 20). Both enzymes are water soluble and thus not membrane bound. As in the case of cyclopropane fatty acid biosynthesis, tuberculostearic acid production increases as the cells enter the stationary growth phase. These observations indicate that the two processes, cyclopropanation and exomethylene group formation, have much in common and suggest that the enzymes in both cases operate on phospholipids present in the cell membrane.

The above arguments do not, however, rule out

Can. J. Chem. Downloaded from www.nrcresearchpress.com by 210.87.254.105 on 09/06/12
For personal use only.

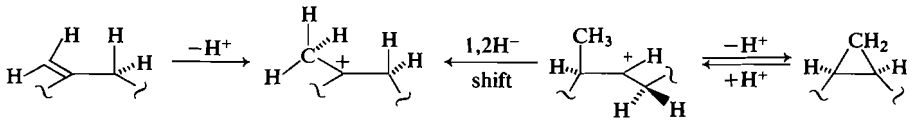

SCHEME 9

Cohen's carbenoid mechanism for the biological cyclopropanation reaction. Reversible sulfur ylid formation (Scheme 1) prior to methylene transfer would also account for the exchange process. However, it has never been proved that cyclopropane synthetase is a metalloenzyme. In order to do this, extensive purification of the enzyme would be required and only recently has any progress been made in this direction (3). Early studies with crude enzyme preparations showed that cyclopropane synthetase was not inhibited by cyanide ion, a reagent known to inhibit metalloenzymes (19, 21). This fact tends to militate against the carbenoid mechanism.

It has been assumed that the exchange process is, in fact, intimately connected with the mechanism of the cyclopropanation reaction. Yet it is possible that exchange of the methyl group is occurring via a process totally unrelated to the alkylation reaction. Mercer and Russell, for example, have suggested that degradation and resynthesis of methionine could, at least partially, account for the observed d_1 content in biosynthetic 24-exomethylene sterols isolated from a methionine-methyl-d_3 feeding (17). In a future paper, experiments will be described which test this explanation for the exchange observed in the biosynthesis of cyclopropane fatty acids.

Experimental

Apparatus, Methods, and Materials

Melting points were determined on a Kofler micro hot stage apparatus and are uncorrected. Infrared spectra were obtained on a Perkin Elmer 238 spectrophotometer. The ^{1}H nmr spectra were run at 90 MHz on a Varian EM 390 spectrometer or on a Bruker WH 90 FT spectrometer. The ^{13}C nmr and ^{2}H nmr spectra were obtained on the latter instrument. The ^{13}C nmr spectra were recorded at 22.62 MHz, at a probe temperature of 30°C. Samples were 0.3 *M* in C_6D_6 using the solvent resonance at 128.05 ppm as reference. A microprobe was used for small samples (≤ 10 mg). The ^{2}H nmr was performed at 13.8 MHz at a probe temperature of 35°C. Samples were 0.02 *M* in CCl_4 using acetone-d_6 as external reference or C_6D_6 as internal reference. All chemical shifts are reported with reference to TMS and are quoted in δ (ppm) values.

Methionine-methyl-d_3 and methylene iodide-d_2 were purchased from Merck, Sharp and Dohme Canada, Limited, Isotope Division, Pointe Claire–Dorval, P.Q.

Silica gel 60F-254 (Merck) was used for tlc and open column chromatography. A Waters A.L.C. 100 liquid chromatograph, equipped with a refractive index detector, was used for the hplc of fatty acid methyl esters. A reverse phase column (Partisil-ODS-2 Magnum 9, 50 cm × 9.4 mm id) was used in both the preparative and analytical mode. The mobile phase was acetonitrile – ethyl acetate 70:30 at a flow rate of 1.6 mL/min. Gas–liquid chromatography of the fatty acid methyl esters was performed, using a Pye Unicam Series 104 gas chromatograph, equipped with a flame ionization detector. A stainless steel column (20 ft × ⅛ in. id), packed with 15% OV-275 on Chromosorb P, A.W. DCMS (100/120) was used with helium as the mobile phase at a flow rate of 7 mL/min and at a temperature of 220°C.

The microorganism used in this study was *Lactobacillus plantarum*, ATCC 8014, obtained from the American Type Culture Collection, Rockville, MD, U.S.A. The organism was grown at 37°C in a Precision Thelco hot air incubator and maintained as a stab culture at 4°C in a nutrient agar medium prepared by adding 2% agar to Lactobacilli M.R.S. broth (Difco). The biochemical and morphological characteristics of the organism were checked at the outset of this study and were found to be in accord with those described in the literature. Cells were isolated by centrifugation either at 3500 rpm on an International Clinical desk-top centrifuge for small scale experiments or at 5000 rpm on a Beckman Model J-21 centrifuge equipped with a JA10 or JA20 centrifuge head. Cells were dried in a New Brunswick Sci. Co. Freezer dryer.

Deuterium contents of the fatty acid methyl esters were determined by ms using either a CEC No. 21-110B mass spectrometer at 70 eV and a source temperature of 100–150°C and a direct introduction probe or a VG Micromass 7070F instrument, at a source temperature of 190°C, coupled to a Varian model 3700 gas chromatograph. When the CEC instrument was used, approximately 0.5 mg of sample was needed to allow scanning of the M^+ and $(M-32)^+$ ions. (The $M-32$ ion resulted from the loss of methanol from the fatty acid methyl esters.) The distribution of deuterium was calculated from both sets of data; good agreement between the two calculated results was always observed to within experimental error. The ion intensities were arrived at by taking the average of 5–10 measurements. The standard deviation was ±1 for each ion intensity. The precision of the calculated deuterium content was ±1% for each isotopic species expressed as a percentage. In the gc–ms method, the entire gc peak was scanned repetitively, once per second, and the intensities integrated. This procedure eliminated errors caused by isotopic fractionation on the gc column. An independent check on the validity of this method was made by running the same compound on the CEC and VG mass spectrometers. The calculated deuterium content was as follows; on the CEC: d_2, 79.9%; d_1, 16.0%; d_0, 4.1%; on the VG: d_2, 79.9%; d_1, 15.9%; d_0, 4.2%.

Methyl cis*-9-Octadecenoate-9,10-*d_2

9-Octadecynoic acid was prepared from oleic acid by the method of Khan *et al.* (22). The corresponding methyl ester was used to prepare the title compound by a modification of a literature procedure (7).

Lindlar's catalyst was prepared in the following manner. Calcium carbonate (1.25 g) was placed in a two-necked 50 mL round bottomed flask, followed by D_2O (10 mL, 99.95% deuterated), and the flask attached to a hydrogenation apparatus via a reflux condenser. The apparatus was flushed with argon. Palladium dichloride (105 mg) was dissolved in D_2O (1.1 mL) containing DCl (0.1 mL) and the red solution added via syringe to the calcium carbonate suspension. The mixture was stirred for

Can. J. Chem. Downloaded from www.nrcresearchpress.com by 210.87.254.105 on 09/06/12
For personal use only.

Can. J. Chem. Downloaded from www.nrcresearchpress.com by 210.87.254.105 on 09/06/12
For personal use only.

5 min at room temperature and 10 min at 80°C, whereupon the apparatus was evacuated and filled with deuterium gas (D_2). The flushing procedure was repeated twice, after which the solution was stirred and the absorption of D_2 at atmospheric pressure was monitored. When D_2 absorption had stopped (20 mL), the now grey suspension was filtered and resuspended in D_2O (12.5 mL) and a solution of lead diacetate (125 mg) in D_2O (2.0 mL) was added under argon. The mixture was stirred at room temperature for 10 min and at 100°C for 40 min. The catalyst was then filtered, washed with D_2O, and dried over P_2O_5 *in vacuo*.

The reduction of methyl 9-octadecynoate (0.5 mmol) was performed using deuterium gas at room temperature, over Lindlar's catalyst (12 mg) at atmospheric pressure, in hexane (5 mL). After 15 min, the theoretical amount of D_2 had been absorbed. The distribution of deuterium was determined by ms to be: d_2, 96%; d_1, 3%; d_0, 1%. ^1H nuclear magnetic resonance of the product showed that the vinyl proton absorption at δ 5.3 in the unlabelled analogue had disappeared. Also in the ^{13}C nmr spectrum, the signals at 130 ppm attributed to the vinyl carbon atoms of the d_0-material were absent. The ^2H nmr of the product showed only traces of deuterium at carbon atoms other than the vinylic (δ 5.3).

9,10-Dioxooctadecanoic Acid-8,8,11,11-d_4

Acetic anhydride, distilled through glass helices (102 g), was placed in a three-necked, 500 mL, round bottomed flask fitted with a reflux condenser and an addition funnel. Deuterium oxide (99.7% D, 40.0 g) was added and the reaction mixture stirred and heated until an exothermic reaction set in, at which point heating was halted. When the hydrolysis was complete, the flask was cooled in ice and acetyl chloride (19.6 g) was added slowly. The final mixture contained acetic acid-O-*d* (2.25 mol), D_2O (0.75 mol), DCl (0.25 mol). 9,10-Dioxooctadecanoic acid (7.8 g), prepared by the method of Jensen and Sharpless (9), was added and the mixture heated to 65°C for 0.5 h. The solvent was removed *in vacuo* and the exchange repeated once more with fresh medium. After work-up, ^1H nmr showed that the intensity of the signal at 2.7 ppm had been greatly reduced. The sample (7.8 g) was dried *in vacuo* to remove traces of DCl and D_2O, and used directly in the next step.

9,10-Dihydroxyoctadecanoic Acid

Platinum oxide (500 mg), suspended in acetic acid (10 mL) in a 250 mL round bottomed flask, was prehydrogenated, after which the tetradeutero diketone (7.8 g) prepared above was added in acetic acid (50 mL) and the hydrogenation allowed to proceed over 22 h; 1090 mL of hydrogen was absorbed (97% of theoretical). The white solid which had precipitated out of solution was dissolved by adding acetone and the solution was filtered from the catalyst. The solvents were removed *in vacuo* and an aliquot of the residue (mp 115°C) was methylated with diazomethane and analyzed via boric acid impregnated silica gel tlc (mobile phase 60:40 ether – petroleum ether; the tlc plates were prepared by spraying Merck silica gel plates with a saturated methanolic boric acid solution). Comparison with an authentic sample prepared by $KMnO_4$ oxidation of oleic acid showed that the major product was the *erythro* diol. Two recrystallizations from ethyl acetate yielded pure *erythro* diol, 5 g, mp 126–128°C (lit. 23 mp 132°C).

Methyl cis-*9-Octadecenoate-8,8,11,11-*d_4

Erythro-9,10-dihydroxyoctadecanoic acid-8,8,11,11-d_4 (5 g) was heated with methyl orthoformate (6 mL) under argon at 90°C for 0.5 h. Excess methyl orthoformate was evaporated and the resulting 1,3-dioxalan heated at 160°C for 4.75 h, at which time the evolution of carbon dioxide had ceased. The product was shown by tlc to be mainly oleic acid accompanied by some methyl oleate. The product was treated with diazomethane to convert the acid to its methyl ester which was isolated by dissolving the crude product in chilled hexane and centrifuging to remove a large amount of gelatinous precipitate. Removal of the solvent gave a residue of 3.9 g. Open column chromatography using Merck T.L.C. silica gel (100 g) and elution with ether–hexane (2:23) yielded the pure title compound; glc analysis showed the product to be the stereochemically pure *cis*-olefin. Analysis of the ^1H, ^2H, and ^{13}C nmr spectra showed that the label was exclusively at the allylic positions. In the ^1H nmr spectrum, the signal at δ 2.0, present in the unlabelled compound, was absent. The signal assigned to the allylic carbon atoms at 27.4 ppm in the unlabelled compound had disappeared in the ^{13}C nmr spectrum of the labelled material. Only 1 peak at δ 1.8 was present in the ^2H nmr spectrum, as expected. Analysis of the product by ms showed that it had the following deuterium content: d_4, 79.1%; d_3, 15.1%; d_2, 4.0%; d_1, 1.4%; d_0, 0.4%.

Preparation of Methyl cis-*9,10-Methyleneoctadecanoate-9,10-*d_2(10)

Zinc dust (400 mg, AnalaR B.D.H.) was suspended in boiling acetic acid in a 10 mL round bottomed flask. The mixture was stirred for 1 min, cupric diacetate (80 mg) in boiling acetic acid (2 mL) was added, and stirring continued for ca. 3 min until the blue solution had been completely decolorized. The red-brown zinc–copper couple was washed with acetic acid (5 × 3 mL) and ether (5 × 3 mL). Ether (1 mL) was then added, followed by diiodomethane (2.5 g) and methyl *cis*-9-octadecenoate-9,10-d_2 (100 mg) in ether (4 mL). A reflux condenser was fitted to the flask and the system flushed with argon. The ether solution was warmed to initiate the reaction and after an initial exothermic reaction had subsided, the solution was heated under reflux for 24 h, under argon, at an oil bath temperature of 55°C. (After 12 h, ether (2 mL) was added to replace that lost by evaporation.) Pyridine and ether were added to the cooled reaction mixture until a white precipitate ceased to form. The mixture was filtered and the solids washed with ether. The yellow residue, obtained by evaporation of the ether, was placed under high vacuum (0.01 Torr) and excess pyridine and diiodomethane removed. The residual oil was taken up in hexane and filtered through glass wool to remove an orange solid. Reverse phase hplc analysis (acetonitrile – ethyl acetate, 75:25) showed essentially one peak assigned to the cyclopropane compound. Preparative separation of an aliquot of the crude product gave a sample which was subjected to ms analysis.

Preparation of Methyl cis-*9,10-Methyleneoctadecanoate-8,8,11,11-*d_4

Methyl oleate-8,8,11,11-d_4 was converted to the title compound by a method identical with that used for the preparation of methyl *cis*-9,10-methyleneoctadecanoate-9,10-d_2.

Feeding Experiments with cis-*9-Octadecenoic Acid-9,10-*d_2 *and* cis-*9-Octadecenoic Acid-8,8,11,11-*d_4

The same protocol was used for both feeding experiments.

The labelled fatty acids (200 mg) in 95% ethanol (1 mL) were added to an autoclaved basal medium (10 L) containing Tween 40 (10 g). The basal medium (1 L) contained Bacto-Biotin Assay medium (Difco) (37.5 g) and a vitamin free casein hydrolysate solution (50.0 mL). Two culture tubes containing the complete medium (10 mL) were inoculated with a saline cell suspension[1] (0.05 mL), and the cultures allowed to grow for 24 h. The result-

[1]A freshly grown inoculum was used. A culture tube containing M.R.S. Broth (Difco, 10 mL) was inoculated from a stock stab culture. After 24 h of growth, the cells were harvested, washed with 0.85% saline several times, and resuspended in saline (10 mL).

Can. J. Chem. Downloaded from www.nrcresearchpress.com by 210.87.254.105 on 09/06/12
For personal use only.

ing culture (4 mL) was used to inoculate 3 × 500 mL Erlenmeyer flasks containing identical media (150 mL). After 24 h of growth, each culture was used to inoculate identical media (3.25 L), each contained in 3 × 5 L culture flasks. Growth was allowed to continue for 36 h, after which the cells were harvested and the fatty acids extracted according to the method of Hofmann *et al.* (24). The methyl esters were separated by preparative hplc (see Apparatus, Methods, and Materials). The total amount of fatty acids obtained in the oleic acid-9,10-d_2 feeding was 18 mg. The relative proportions of the three major fatty acids were: oleic acid (C_{18}), 8%; palmitic acid (C_{16}), 58%; dihydrosterculic acid (C_{19}), 34%. The total fatty acids amounted to 10 mg in the oleic acid-8,8,11,11-d_4 feeding. The relative proportions of the three fatty acids were: C_{18}, 12%; C_{16}, 43%; C_{19}, 45%.

Methionine-methyl-d_3 *and Biotin Feeding (Experiment 1, Table 3)*

A filter sterilized solution of methionine-methyl-d_3 was added along with biotin to autoclaved basal medium to make a final concentration of 100 mg/L (methionine) and 10 μg/L (biotin). The complete medium (10 mL) was inoculated from a stab culture. After 24 h of growth, aliquots of this culture (0.1 mL) were used to inoculate the same medium (5 × 10 mL). After 24 h of growth, each culture was used to inoculate identical media in 5 × 500 mL Erlenmeyer flasks (200 mL each). After 36 h, only 2 flasks had grown out properly. The reason for this was not determined. The cells from all flasks were harvested and the fatty acids extracted by the procedure of Hofmann *et al.* (24). The total fatty acids amounted to 5.0 mg. The relative proportions of each fatty acid were *cis*-vaccenic (C_{18}), 11%; palmitic (C_{16}), 48%; lactobacillic (C_{19}), 41%.

Methionine-methyl-d_3 *and Oleic Acid Feeding (Experiment 2, Table 3)*

Methionine-methyl-d_3 (120 mg, filter sterilized) was added to autoclaved basal medium (1.26 L) containing oleic acid (24 mg and Tween 40 (2.2 g)). The complete medium (16 × 10 mL) was inoculated with a saline cell suspension (0.05 mL). After 24 h, these cultures (2 × 10 mL) were used to inoculate each of 8 × 500 mL Erlenmeyer flasks containing identical media (125 mL each). The cells were harvested after 24 h of growth and the fatty acids extracted.

The total fatty acid content of the cells was 20 mg. The relative proportion of each fatty acid was: C_{18}, 17%; C_{16}, 54%; C_{19}, 39%.

Methionine-methyl-d_3 *and Biotin Feeding (Experiment 3*(a),(b), *Table 3)*

Methionine-methyl-d_3 (100 mg) was added to basal medium (1015 mL) along with biotin (10 μg). After filter sterilization, the complete medium (14 × 10 mL) was inoculated with a saline cell suspension (0.05 mL) and allowed to grow for 24 h. The resulting cultures (2 × 10 mL) were used to inoculate 7 × 250 mL Erlenmeyer flasks containing identical media (125 mL). Twenty-four hours later, 3 flasks were harvested and after 64 h, the remaining flasks were harvested and the fatty acids extracted. The cells from the 24 h culture contained 5.3 mg of total fatty acid. The relative proportion of each fatty acid was C_{18}, 8%; C_{16}, 38%; C_{19}, 54%. The cells from the 64 h culture contained 9.6 mg of total fatty acid. The relative proportion of each fatty acid was: C_{18}, 7%; C_{16}, 36%; C_{19}, 57%.

Feeding Experiments Using Methionine-methyl-d_3 *and Either Biotin, Oleic Acid, or* cis-*Vaccenic Acid (Experiment 4* (a),(b),(c), *Table 3)*

Basal medium (2 L) was prepared and to 1600 mL was added Tween 40 (1.6 g) (Medium A) and to the remaining 400 mL was added biotin (4.0 mg) (Medium B). Medium A was distributed among 160 culture tubes and Medium B among 40 culture tubes. The media were then autoclaved. *cis*-Vaccenic acid (16 mg) in 95% ethanol (1 mL) was added in equal portions to 80 culture tubes containing Medium A. The same procedure was carried out using oleic acid. L-Methionine-methyl-d_3 (120 mg in 21 mL of water) was filter sterilized separately and 0.1 mL aliquots were added aseptically to each of the 200 culture tubes. Each culture tube was then inoculated with a saline cell suspension (0.05 mL, a Klett reading of 360 was recorded for this inoculum). After 24 h, good growth was obtained in the biotin-containing medium, but only poor growth resulted in both fatty acid-containing media. The cells were harvested and the fatty acids extracted. The total amount of fatty acids obtained from the cells grown in biotin was 9.7 mg (C_{18}, 40%; C_{16}, 37%; C_{19}, 23%); from the cells grown on oleic acid, 5.0 mg (C_{18}, 21%; C_{16}, 53%; C_{19}, 26%); from the cells grown on vaccenic acid, 10.3 mg (C_{18}, 35%; C_{16}, 53%; C_{19}, 12%).

Methionine-methyl-d_3 *Feeding (Isolation of Cells at 13.5 and 24 h)*

Methionine-methyl-d_3 (145 mg) and biotin (14.5 μg) were added to basal medium (1.45 L). After filter sterilization, the medium was distributed in 145 mL portions among 15 250 mL Erlenmeyer flasks. The flasks were inoculated with a saline cell suspension (1 mL, Klett reading of 490). At 13.5 h, 6 flasks were harvested, after measuring pH and turbidity. The cells were dried and weighed (598 mg) and the fatty acids extracted (by the procedure of Ohlrogge *et al.* (25)). The total fatty acid content was 4.7 mg (C_{18}, 51%; C_{16}, 37%; C_{19}, 21%). At 24 h, the same procedure was carried out with another 4 flasks. The total fatty acid content was 20.7 mg from 721 mg of cells (C_{18}, 27%; C_{16}, 41%; C_{19}, 32%).

Methyl Dihydrosterculate-19-d_2

Methyl oleate was converted to the title compound using CD_2I_2 by the methods described for the preparation of methyl *cis*-9,10-methyleneoctadecanoate-9,10-d_2.

Acknowledgements

We thank the Natural Sciences and Engineering Research Council of Canada for financial support. One of us (P.H.B.) gratefully acknowledges the award of an N.S.E.R.C. postgraduate scholarship.

We also wish to thank Dr. J. J. Miller for the use of his laboratory facilities for growing and harvesting the microbial cultures and Dr. J. B. Stothers for running the ^2H nmr spectrum of methyl oleate-9,10-d_2.

1. W. W. CHRISTIE. *In* Topics in lipid chemistry. Vol. 1. *Edited by* F. D. Gunstone. John Wiley and Sons, New York. 1970. p. 1.
2. J. H. LAW. Acc. Chem. Res. **4**, 199 (1971), and references cited therein.
3. F. R. TAYLOR and J. E. CRONAN, JR. Biochemistry, **18**, 3292 (1979).
4. T. COHEN, G. HERMAN, T. M. CHAPMAN, and D. KUHN. J. Am. Chem. Soc. **96**, 5627 (1974).
5. E. LEDERER. Q. Rev. **23**, 453 (1969).
6. J. W. POLACHECK, B. E. TROPP, J. H. LAW, and J. A. MCCLOSKEY. J. Biol. Chem. **241**, 3362 (1966).
7. R. RAPHAEL. Acetylenic compounds in organic chemistry. Academic Press, Inc., New York. 1955. p. 200.
8. E. A. EMKEN. Fatty acids and glycerides. *Edited by* A. Kuksis. Plenum Press, New York. 1978. p. 83.

9. H. P. JENSEN and K. B. SHARPLESS. J. Org. Chem. **39**, 2314 (1974).
10. W. W. CHRISTIE and R. T. HOLMAN. Lipids, **1**, 176 (1966).
11. D. T. LONGONE and A. H. MILLER. J. Chem. Soc. Chem. Commun. 447 (1967).
12. J. G. BATCHELOR, R. J. CUSHLEY, and J. H. PRESTEGARD. J. Org. Chem. **39**, 1698 (1974).
13. M. SAUNDERS, P. VOGEL, E. L. HAGEN, and J. ROSENFELD. Acc. Chem. Res. **6**, 53 (1973).
14. S. POHL, J. H. LAW, and R. RYHAGE. Biochem. Biophys. Acta, **70**, 583 (1963).
15. G. S. COX, E. THOMAS, H. R. KABACK, and H. WEISSBACH. Arch. Biochem. Biophys. **158**, 667 (1973).
16. G. JAURÉGUIBERRY, J. H. LAW, J. A. MCCLOSKEY, and E. LEDERER. Biochemistry, **4**, 347 (1965).
17. E. I. MERCER and S. M. RUSSELL. Phytochemistry, **14**, 445 (1975).
18. Y. AKAMATSU and J. H. LAW. J. Biol. Chem. **245**, 701 (1970).
19. H. ZALKIN, J. H. LAW, and H. GOLDFINE. J. Biol. Chem. **238**, 1242 (1963).
20. Z. EL HACHIMI, R. AZERAD, R. ELLOUZ, and E. LEDERER. C.R. Acad. Sci. Ser. C, **272**, 1169 (1971).
21. B. L. VALLEE and W. E. C. WACKER. The proteins, composition, structure and function. 2nd ed. Vol. 5. *Edited by* Hans Neurath. Academic Press, New York. 1970. p. 133.
22. N. A. KHAN, F. E. DEATHERAGE, and J. B. BROWN. Organic syntheses. Vol. XXXVII. *Edited by* J. Cason. J. Wiley and Sons, New York. 1957. p. 77.
23. J. C. TRAYNARD. Bull. Soc. Chim. Fr. 323 (1952).
24. K. HOFMANN, D. B. HENIS, and C. PANOS. J. Biol. Chem. **228**, 349 (1957).
25. J. B. OHLROGGE, F. D. GUNSTONE, I. A. ISMAIL, and W. E. M. LANDS. Biochem. Biophys. Acta, **431**, 257 (1976).
26. L. M. HENDERSON and E. E. SNELL. J. Biol. Chem. **172**, 15 (1948).

Can. J. Chem. Downloaded from www.nrcresearchpress.com by 210.87.254.105 on 09/06/12
For personal use only.

The Orton rearrangement in aprotic solvents. Part IV.[1] An examination of the kinetics of the rearrangement of *N*-bromo-4-chloroacetanilide and *N*-bromoacetanilide catalyzed by trifluoroacetic acid and trifluoroacetic acid-*d*

PETER DAVID GOLDING, SETHU REDDY, JOHN MARSHALL WILLIAM SCOTT,[2] VALERIE ANN WHITE, AND JUNE GERTRUDE WINTER

Chemistry Department, Memorial University of Newfoundland, St. John's, Nfld., Canada A1B 3X7

Received July 25, 1979[3]

PETER DAVID GOLDING, SETHU REDDY, JOHN MARSHALL WILLIAM SCOTT, VALERIE ANN WHITE, and JUNE GERTRUDE WINTER. Can. J. Chem. **59**, 839 (1981).

The rates of rearrangement of *N*-bromo-4-chloroacetanilide to 2-bromo-4-chloroacetanilide catalyzed by trifluoroacetic acid and trifluoroacetic acid-*d* have been measured as a function of acid concentration in chlorobenzene at $T = 323$ K. Similar experiments have been carried out with *N*-bromoacetanilide and *N*-bromo-4-chloro-2,6-dideuterioacetanilide. A comprehensive analysis of the observed rates for each substrate as a function of acid concentration reveals that the rearrangements involve at least three mechanistic steps when trifluoroacetic acid is the catalyst. In contrast, the rate of rearrangement of *N*-bromoacetanilide catalyzed by trichloroacetic acid at $T = 288$ K appears to follow a limiting form of the same rate law. Earlier observations are assessed in the light of the proposed mechanism, and it is concluded that both present and past work can be satisfactorily rationalized in terms of an intramolecular migration of bromine.

PETER DAVID GOLDING, SETHU REDDY, JOHN MARSHALL WILLIAM SCOTT, VALERIE ANN WHITE et JUNE GERTRUDE WINTER. Can. J. Chem. **59**, 839 (1981).

On a mesuré les vitesses de transposition de la *N*-bromochloro-4 acétanilide en bromo-2 chloro-4 acétanilide catalysée par les acides trifluoroacétiques normaux et deutérés, en fonction de la concentration de l'acide dans le chlorobenzène à 323 K. On a réalisé des expériences identiques avec la *N*-bromoacétanilide et la *N*-bromo chloro-4 dideutéro-2,6 acétanilide. Une analyse complète des vitesses observées, pour chaque substrat en fonction de la concentration de l'acide, révèle que les transpositions font intervenir au moins trois étapes mécanistiques quand le catalyseur est l'acide trifluoroacétique. A l'opposé, la vitesse de transposition de la *N*-bromoacétanilide catalysée par l'acide trichloroacétique à 288 K semble suivre une forme limite de la même loi de vitesse. A la lumière du mécanisme proposé, on a évalué les observations antérieures et on a conclu que le présent travail ainsi que le précédent peuvent être rationalisés en fonction d'une migration intramoléculaire du brome.

[Traduit par le journal]

Introduction

The rearrangement of *N*-halogenoanilides to their corresponding ring halogenated isomers has attracted much attention since the early days of a more physical approach to the behaviour of organic molecules (2). The details of the rearrangement in aqueous systems with hydrohalic acids as catalysts are well established, but mechanistic descriptions of the rearrangement in aprotic solvents catalyzed by carboxylic acids and phenols present a less satisfactory picture. In the most recent review of the rearrangement, Shine (3) states that the role of the acid catalyst in aprotic media is not yet understood.

The study of proton transfer reactions, of which the Orton rearrangement is an example, constitutes an important and significant part of modern chemical theory (4–6). Catalyses by acids and bases have been extensively examined in hydroxylic or protic solvents, whereas the same phenomena in aprotic solvents have received less comment (4, 7). Indeed, the current situation with respect to acid–base catalysis in aprotic media is virtually identical to an account offered by Bell (7) over thirty years ago. The reluctance of chemists to examine acid–base catalysis in aprotic media may be associated with the view that ionogenic or nominally ionogenic reactions in aprotic media tend to be complex (cf. ref. 8). There is no real difference in principle, however, between protic and aprotic solvents with respect to the fundamental problem, namely, the specification of the catalytic species and their relative reactivities. In the present communication we attempt to solve this problem for the rearrangements of *N*-bromo-4-chloroacetanilide (NBCA) to 2-bromo-4-chloroacetanilide and *N*-bromoacetanilide (NBA) to 4-bromoacetanilide catalyzed by trifluoroacetic acid (TFA) in chlorobenzene. The kinetics of the rearrangements of NBCA and *N*-bromo-4-chloro-2,6-dideuterioacetanilide (NBCA-2,6-d_2) in chlorobenzene with TFA-*d* and TFA as the respective catalysts have also been investigated.

[1]For Part III, see ref. 1.

[2]Author to whom all correspondence should be directed.

[3]Revision received November 17, 1980.

0008-4042/81/050839-12$01.00/0

©1981 National Research Council of Canada/Conseil national de recherches du Canada

Can. J. Chem. Downloaded from www.nrcresearchpress.com by 210.87.254.105 on 09/06/12
For personal use only.

Can. J. Chem. Downloaded from www.nrcresearchpress.com by 210.87.254.105 on 09/06/12
For personal use only.

The variation of these rates of rearrangement as a function of acid concentration shows interesting and marked differences from those of the NBA/trichloroacetic acid (TCA) system reported by Bell (9). We regard these differences to be of considerable mechanistic significance when related to earlier observations (1, 10–14) and the details of these matters form the substance of the present contribution.

Experimental

Materials

The preparation and purification of NBA and NBCA, and the purification of commercial chlorobenzene were accomplished by methods described previously (11). The hydrogen atoms attached to the 2,6-carbons of *p*-chloroaniline were exchanged for deuterium under acidic conditions, and the resulting 4-chloro-2,6-dideuterioaniline was acylated and *N*-brominated in the usual way (11) to produce NBCA-2,6-d_2.The reaction of deuterium oxide with a slight excess of trifluoroacetic anhydride was used to prepare TFA-*d* which was then purified by distillation. The physical and analytical properties of the above compounds were in satisfactory agreement with literature values. The concentrations of acids and substrates in chlorobenzene were determined by titration, and all materials and solutions were stored in the absence of light over anhydrous Drierite.

Kinetic Measurements

Kinetic measurements were carried out using conventional methods (9, 11) at $T = (323.15 \pm 0.02)$ K with a single concentration (ca. 0.01 *M*) of substrate (NBCA, NBCA-2,6-d_2, or NBA) and several acid concentrations (TFA or TFA-*d*). In all cases the stoichiometric concentration of acid (c_a) was never less than three times that of the substrate. Pseudo-first order rate constants were obtained via a linear least-squares treatment of the concentration–time data, and these observed rate constants (k_{obs}) were at worst reproducible to 5%. The results of these measurements are summarized in Tables 1 to 3, and Table 4 provides similar quantities related to the NBA/TCA system measured by Bell (ref. 9, see Table II, p. 384). The tables also include the quantity $k_{obs}/c_a = \alpha$, which represents the apparent second order rate constants (see ref. 9, p. 387).[4]

The data for the NBCA/TFA system are a combination of the results of two different investigators[5] working in periods separated by a year. The two separate studies employed different, freshly prepared samples of all substances. That the results of the two studies were in excellent agreement strongly supports the observation of the unusual acid dependence of the pseudo-first order rate constants (see below).

Results and Discussion

A Comparison with Earlier Work

The most extensive investigation prior to the present study was Bell's (9) in which the rate of rearrangement of NBA was examined as a function of temperature, solvent, and the strength and concentration of phenolic and carboxylic acid

[4]The meaning of α here should not be confused with the more common usage as a Brönsted exponent. The continued use of α in the present text is prompted only by our fidelity to Bell's original notation.

[5]S.R. and V.A.W.

TABLE 1. The rates of rearrangement for NBCA (and NBCA-2,6-d_2)[a] catalyzed by TFA in chlorobenzene at $T = (323.15 \pm 0.02)$ K

$c_a \times 10^2$, mol·L^{-1}	$k_{obs} \times 10^5$, s^{-1} (runs)[b]	$\alpha \times 10^4$, L·mol^{-1}·s^{-1}
2.01	2.11 ± 0.06 (4)	10.5 ± 0.3
3.92	5.02 ± 0.31 (3)	12.8 ± 0.8
5.45	7.93 ± 0.24 (4)	14.6 ± 0.4
10.6	18.0 ± 0.3 (4)	17.0 ± 0.3
13.9	24.9 ± 0.3 (4)	17.9 ± 0.2
20.2	36.1 ± 0.4 (4)	17.9 ± 0.2
24.6	43.4 ± 1.3 (5)	17.6 ± 0.5
25.9	42.8 ± 1.2 (4)	16.5 ± 0.4
31.4	54.7 ± 1.4 (4)	17.4 ± 0.5

[a]At 323 K and the same TFA concentration, the rates of rearrangement for NBCA-2,6-d_2 and NBCA are not appreciably different. For example, at a TFA concentration of 0.246 mol·L^{-1} the rate for NBCA-2,6-d_2 is $(44.1 \pm 0.56) \times 10^{-5}$ s^{-1}.
[b]The rates here and in Tables 2 and 3 are mean values (± standard deviation) weighted with respect to the reciprocal variance of each of the kinetic runs at the various acid concentrations.

TABLE 2. The rates of rearrangement for NBCA catalyzed by TFA-*d* in chlorobenzene at $T = (323.15 \pm 0.02)$ K

$c_a \times 10^2$, mol·L^{-1}	$k_{obs} \times 10^5$, s^{-1} (runs)	$\alpha \times 10^4$, L·mol^{-1}·s^{-1}
4.86	4.21 ± 0.05 (4)	9.5 ± 0.2
9.59	9.41 ± 0.10 (3)	10.1 ± 0.1
14.3	14.7 ± 0.1 (4)	10.3 ± 0.1
20.1	20.3 ± 0.1 (4)	9.8 ± 0.1
25.1	23.9 ± 0.4 (4)	8.7 ± 0.1

TABLE 3. The rates of rearrangement for NBA catalyzed by TFA in chlorobenzene at $T = (323.15 \pm 0.02)$ K

$c_a \times 10^2$, mol·L^{-1}	$k_{obs} \times 10^5$, s^{-1} (runs)	$\alpha \times 10^4$, L·mol^{-1}·s^{-1}
2.09	3.93 ± 0.19 (4)	18.8 ± 0.9
5.06	13.7 ± 0.4 (4)	27.1 ± 0.8
10.7	32.9 ± 0.5 (4)	30.7 ± 0.5
15.5	50.2 ± 0.5 (4)	32.4 ± 0.3
20.8	67.5 ± 1.6 (4)	32.5 ± 0.8
29.0	92.5 ± 0.8 (3)	31.9 ± 0.3

TABLE 4. The rates of rearrangement for NBA catalyzed by TCA in chlorobenzene at $T = 288$ K[a]

$c_a \times 10^2$, mol·L^{-1}	$k_{obs} \times 10^6$, s^{-1}	$\alpha \times 10^4$, L·mol^{-1}·s^{-1}
0.359	0.889	2.48
0.520	1.30	2.50
0.780	2.07	2.65
1.30	3.53	2.72
1.56	3.76	2.41
1.82	4.76	2.62
2.35	5.24	2.23
2.60	6.65	2.56
3.25	7.55	2.32
3.90	8.95	2.29
5.20	11.4	2.19
7.80	16.2	2.08
10.4	19.4	1.87
13.0	23.2	1.78
18.2	30.4	1.67
26.0	37.9	1.46

[a]These rate data taken from Bell's work (9) are recalculated in units of s^{-1}.

Can. J. Chem. Downloaded from www.nrcresearchpress.com by 210.87.254.105 on 09/06/12
For personal use only.

catalysts. In chlorobenzene the pseudo-first order rate constants (k_{obs}) for various acid concentrations (c_a), when reduced to unit acid concentration (α) and subsequently plotted against c_a, gave shallow curves with negative slopes which are concave in shape from $c_a = 0$ (cf. Fig. 1). Under favorable circumstances these curves could be extrapolated graphically to yield k_{obs}/c_a at infinite dilution (α_0), the value of which was considered to be a measure of the catalytic power of the *monomeric* acid. Values of α_0 estimated in this way for various phenols and carboxylic acids provided an excellent Brönsted linear free energy relationship (ref. 9, p. 389).

Bell explained the form of the α versus c_a curves in the following manner. It was assumed (9) that the carboxylic acid catalysts (RCOOH) were present in monomeric (M) and dimeric (D) forms, the result of the dimerization

$$[1] \quad 2\text{RCOOH} \overset{K_d}{\rightleftharpoons} (\text{RCOOH})_2$$

where K_d is the dimerization constant, and that the respective rate constants k_M and k_D were related to the observed rate by

$$[2] \quad k_{obs} = k_M[M] + k_D[D]$$

Bell also tacitly assumed that the rate was first order with respect to both the monomeric and dimeric forms of the acid catalyst, i.e., k_M and k_D were second order rate constants. The concentration–rate data, however, were not analyzed in such a way so as to confirm this crucial, yet perhaps unwarranted, assumption. Indeed, Bell apparently relegated the observed rates to be entirely functions of monomeric acid catalysis inasmuch as the abscissa of his Brönsted linear free energy relationship is the pK_a of the aqueous monomeric acid.

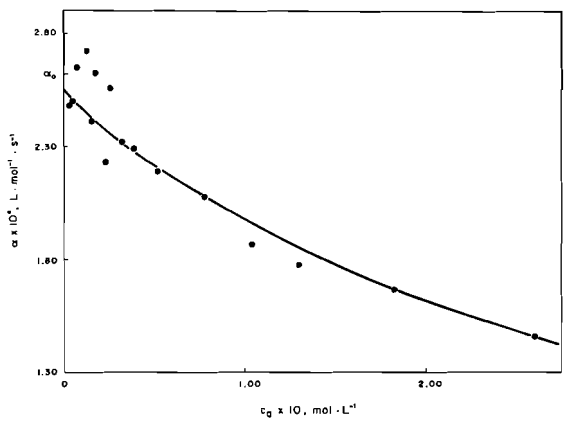

FIG. 1. The α versus c_a profile for the rearrangement of NBA catalyzed by TCA in chlorobenzene at $T = 288$ K. The value of k_{obs}/c_a at infinite dilution reported by Bell (9) is shown as α_0.

Nevertheless, if we develop Bell's original hypothesis from the equilibrium given by eq. [1]

$$[3] \quad K_d = [D]/[M]^2$$

Mass balance requires that the stoichiometric concentration of the catalyst be related to the concentrations of M and D such that

$$[4] \quad c_a = [M] + 2[D]$$

which, in conjunction with eq. [3], gives

$$[5] \quad c_a = [M] + 2K_d[M]^2$$

Combining eqs. [2], [3], and [5] yields

$$[6] \quad k_{obs} = k_M c_a - K_d(2k_M - k_D)[M]^2$$

and division by c_a leads to

$$[7] \quad \frac{k_{obs}}{c_a} = k_M - \frac{K_d(2k_M - k_D)[M]}{1 + 2K_d[M]}$$

As $c_a \rightarrow 0$, $[M] \rightarrow 0$; thus the negative term on the right hand side of eq. [7] is well behaved mathematically at infinite dilution, and the intercept of the α versus c_a curve may be correctly identified with the second order rate constant appropriate to the monomeric catalyst.[6] Within the framework of the major portion of Bell's experimental findings the above analysis is satisfactory, but in some solvents (e.g., benzene) the steep rise of the curve precluded extrapolation to α_0.

Nevertheless, Bell's treatment does not satisfactorily accommodate our observations. Firstly, since α depends on c_a for all the systems investigated (see also refs. 9, 11), none of the reactions are of unit order with respect to the catalysts. Further confirmation of this is provided by plots of $\log_{10} k_{obs}$ versus $\log_{10} c_a$ which give slopes considerably in excess of unity. This observation implies that the isotope effect for NBCA rearrangement cannot be calculated from the ratio of the respective rate constants, $k_{obs}(H)/k_{obs}(D)$, at identical concentrations of TFA and TFA-*d*.

Secondly, and more fundamental, the behaviour of the α versus c_a correlations for NBCA/TFA, NBCA/TFA-*d*, and NBA/TFA differs from that observed by Bell (9) for NBA/TCA (see Figs. 1 and 2). For all the phenolic and carboxylic acid catalysts employed by this author, α is assumed to extrapolate to a finite, positive, limiting value (α_0) as $c_a \rightarrow 0$ (cf. Fig. 1). In the present work, how-

[6]It should be noted that since c_a, not [M], is the independent variable in the α versus c_a correlation, the graphical extrapolation procedure employed by Bell to estimate α_0 corresponds to the limiting form of eq. [7] at infinite dilution. Ultimately, no confirmation of eq. [2] was offered since Bell did not develop eq. [7] to evaluate the magnitude of k_D.

Can. J. Chem. Downloaded from www.nrcresearchpress.com by 210.87.254.105 on 09/06/12
For personal use only.

ever, the α versus c_a curves for the NBA/TFA, NBCA/TFA, and NBCA/TFA-*d* systems have *positive* slopes and are *convex* in shape from $c_a = 0$, and the curves also appear to extrapolate to the *origin* of the α, c_a coordinate system rather than to a positive, upper limiting value (see Fig. 2). Furthermore, there is a strong indication in the present work that the α's may go through maxima at various c_a values, although these maxima are not sharply defined,[7] but eq. [7], which embodies the formalities of Bell's treatment, will not support a concentration dependent maximum in the α,c_a coordinate system. In consequence, the validity of Bell's extrapolation procedure (9) of α to α_0 at infinite dilution must now be considered suspect, since it is certainly inappropriate in the case of our own observations (see Fig. 2); moreover, any evaluation of the isotope effect for NBCA rearrangement from $\alpha_0(H)/\alpha_0(D)$ is precluded. In an effort to resolve these differences we first find it necessary to reinterpret some results of another study which also have a contradictory bearing on Bell's original assumptions.

Evidence for Two Intermediates in the Rearrangement

Some years ago Dewar and Couzens (13) conducted a series of experiments designed to distinguish between an intermolecular or an intramolecular mechanism for the rearrangement. The first of these experiments involved the "rearrangement" of NBA in the presence of acetanilide uniformly labelled with ^{14}C.

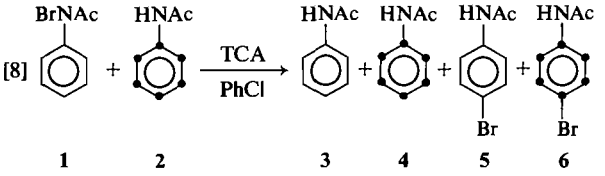

Dewar and Couzens reasonably assumed that products **3** and **6** would be absent if the rearrangement is intramolecular. While the presence of all four products indicated the mechanism to be complex, in the present context the more important fact is that **3** and **6** arose from an acid catalyzed, bromine "scrambling" reaction between **1** and **2** *which was faster than the loss of "active" bromine from nitrogen to the ring*. Dewar and Couzens also demonstrated that bromine exchange between nitrogens did not involve the intermediate production of trichloroacetyl hypobromite (CCl_3COOBr).

[7]There is a hint of a similar maximum in the plot of α versus c_a for the NBA/TCA data (see Table 4 and Fig. 1), but this maximum was ignored in the original presentation and perhaps considered the result of experimental error.

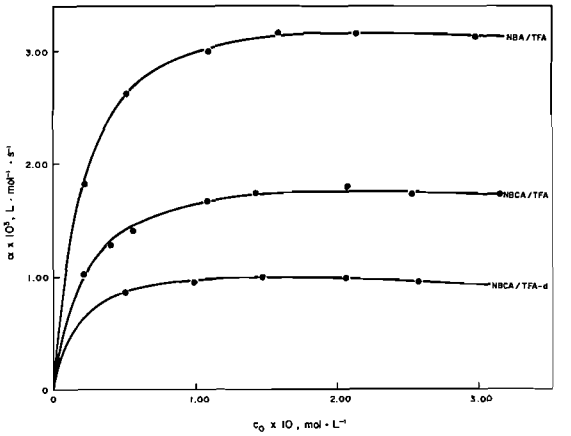

FIG. 2. The α versus c_a profiles for the rearrangement of NBA catalyzed by TFA and the rearrangement of NBCA catalyzed by TFA and by TFA-*d* in chlorobenzene at $T = 323.15$ K.

The reality of the bromine scrambling reaction was elegantly confirmed by examining the rate of loss of active bromine from (*a*) **1** in the presence of an equimolar amount of **7**, and (*b*) **3** in the presence of an equimolar amount of **8**, where **7** and **8** are

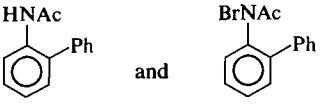

7 8

It was observed that in both (*a*) and (*b*) the mixtures gave *identical* rates of loss of active bromine despite the fact that separately the rate of loss of active bromine from **1** is ca. *a factor of ten faster* than that from **8**. An acid catalyzed scrambling reaction of bromine between the species provides a satisfactory explanation of these observations, i.e., whether one starts with **1** and **7** or with **3** and **8**, equimolar amounts of **1**, **7**, **3**, and **8** are rapidly produced via the scrambling reaction.

Mechanistic discussions of the Orton rearrangement in aprotic solvents have invariably assumed that the slow step in the rearrangement is proton transfer to nitrogen (or oxygen) and that the migration of bromine to its terminal location subsequent to protonation is rapid and irreversible (cf. ref. 15). This mechanistic description, however, must be revised since it fails to accommodate both our own results and those of the Dewar, Couzens investigation. Clearly, the rate of proton attack on nitrogen (or oxygen) must be faster than the observed rate for rearrangement, since the rate of proton transfer exceeds the overall rate of bromine scrambling, which in turn is faster than the observed rate for rearrangement. Thus, proton transfer to the acetanilides cannot be entirely rate determining.

Initially, proton attack by carboxylic acid

Can. J. Chem. Downloaded from www.nrcresearchpress.com by 210.87.254.105 on 09/06/12
For personal use only.

catalysts in aprotic media undoubtedly will take the form of hydrogen bonding, a process known to be both rapid and reversible between oxygen and nitrogen (cf. ref. 16). Consequently, while hydrogen bonding between the acetanilides and acid catalysts is unlikely to be rate determining, it is followed by the slower, formal transfer of a proton to the substrate. The resulting pre-equilibrium mechanism then requires that both the hydrogen bonded and the protonated *N*-bromo compounds be considered as intermediates. Thus, the simplest mechanistic description for rearrangement is

$$[9] \quad S + \Sigma A_n \overset{K_1}{\rightleftharpoons} \Sigma SA_n \underset{k_2}{\overset{k_1}{\rightleftharpoons}} \Sigma I_n \xrightarrow{k_3} \text{products}$$

where S represents the substrate (*N*-bromo compound), A_n are the various catalytic species (monomeric and higher polymeric forms of the acid catalyst), SA_n are the associated hydrogen bonded intermediates and I_n are the corresponding protonated *N*-bromo intermediates. How many of the acid species (A_n) contribute to k_{obs}? Does the acid catalyst participate in reaction steps subsequent to the protonation of substrate? What is the simplest rate law which accommodates the differences between the variations of α with c_a reported by Bell and those observed in the present work? The answers to these important questions and an explanation for our observations in which TFA and TFA-*d* are catalysts are contingent upon an interpretation of other significant observations related to rearrangement in anisole and chlorobenzene.

Evidence for a Third Intermediate

The mechanism for the rearrangements of *N*-bromo- and *N*-chloroacetanilides[8] catalyzed by phenols and carboxylic acids has consistently resisted several probing investigations into the nature of its details (see particularly ref. 13). These rearrangements are typified by

[10] 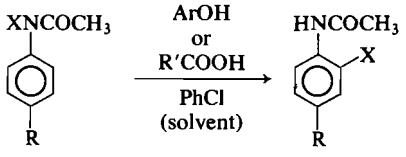

and

[11] 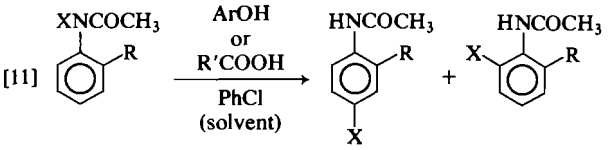

where R = H, Ph, CH_3, Cl, Br, NO_2, etc. and X = Cl, Br. While all of the data examined above suggest that reversible protonation is the first step in the advance towards product, the nature of the intermediate arising from protonation has not been specified. The intermediate is perhaps best considered as a tight ammonium ion pair, and its fate under various conditions is an important mechanistic step for which two alternate paths have been proposed.

Soper and co-workers (14) examined the reaction of *N*-bromoacetanilide with acetic acid in anisole/chloroform mixtures and found 4-bromoanisole to be the major product. They also observed that the rate of disappearance of bromine bonded to nitrogen was independent of the anisole concentration. To explain these observations they postulated that the protonated substrate gave acetyl hypobromite in a slow step

[12] 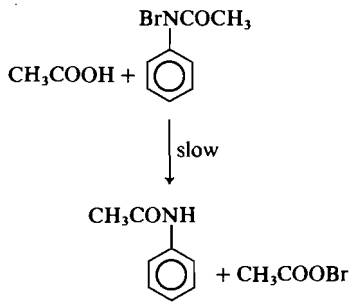

followed by the rapid bromination of anisole

[13] 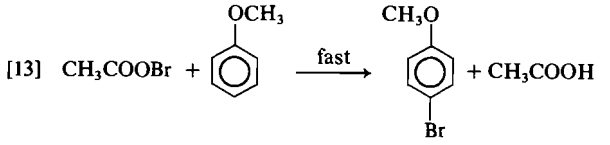

to give 4-bromoanisole and acetic acid, the catalyst. The postulated intermediacy of the hypobromite is superfluous, however, in the sense that bromine transfer to anisole could take place directly from nitrogen. Hence, the production of hypobromite may be an unwarranted hypothesis both for the rearrangement itself and for halogen migration to a more reactive aromatic system. The latter forms the gist of Dewar's criticism (15) of the Soper mechanism. The alternative proposed by Dewar was that halogen migration is intramolecular and proceeds via a π-complex subsequent to proto-

[8]The only iodo compound about which there is information is *N*-iodoformanilide. The rearrangement of this compound in anisole appears to occur in the same fashion as the rearrangements of *N*-bromo- and *N*-chloroacylanilides in chlorobenzene. This is unusual inasmuch as the *N*-bromo and *N*-chloro compounds halogenate anisole under similar conditions (1, 12–14, 17).

Can. J. Chem. Downloaded from www.nrcresearchpress.com by 210.87.254.105 on 09/06/12
For personal use only.

nation, and that all steps following protonation are rapid and irreversible.

In 1957 Dewar and Scott (10) reported that *N*-bromo-2-nitroacetanilide failed to rearrange when treated with TCA in chlorobenzene (see reaction [11]; R = NO_2, X = Br), and that the products from this particular process were 4-bromochlorobenzene and 2-nitroacetanilide. Other 2-substituents with electron attracting properties inferior to that of the 2-nitro group, namely, R = CH_3, F, Cl, Br, and Ph, gave the normal rearrangement products in chlorobenzene. In carbon tetrachloride, however, *N*-bromo-2-nitroacetanilide rearranged in the presence of TCA to give 4-bromo-2-nitroacetanilide, the expected product. Scott (11) subsequently demonstrated that a series of similar 4-substituted *N*-bromo compounds in reaction [10] behaved like those in reaction [11], i.e., a nitro group in the 4-position also led to the production of 4-bromochlorobenzene. A kinetic investigation of the reactions summarized by eq. [10] was consistent with bromine migration in the 4-nitro compound occurring subsequent to protonation. Dewar and Scott (10) and Scott (11) speculated that the exceptional behaviour of the 2-nitro and 4-nitro substrates was a consequence of the increased electrophilic character of the bromine at some stage along the reaction coordinate, and this was attributed to the strong electron withdrawing properties of the nitro group relative to the other substituents investigated.

In 1957 Dewar (13) reconsidered his earlier proposals with respect to the mechanism of the rearrangement on the basis of his work with Couzens (see eq. [8] and related discussion). We may usefully add that the scrambling reaction discovered by these workers exceeds the rate of rearrangement only when the carboxylic acid catalyst is strong. This suggests that the electrophilic character of the bromine in the exchange between nitrogens also depends on the ease or extent of proton transfer. Although acid hypobromites were specifically excluded in Dewar's explanation for the nitrogen to nitrogen migration of bromine, these were retained as "complexed" rather than "kinetically free" intermediates. Further comment as to their role in the rearrangement itself, however, was apparently left in abeyance.

A further study by Scott and Martin (12) of the reaction investigated by Soper and co-workers (see reactions [12] and [13] above) and the related reaction involving *N*-chloroacylanilides (1) revealed that the reactions afforded both the 2-halogeno- and 4-halogenoanisoles. The scope of these experiments is summarized in the following equations.

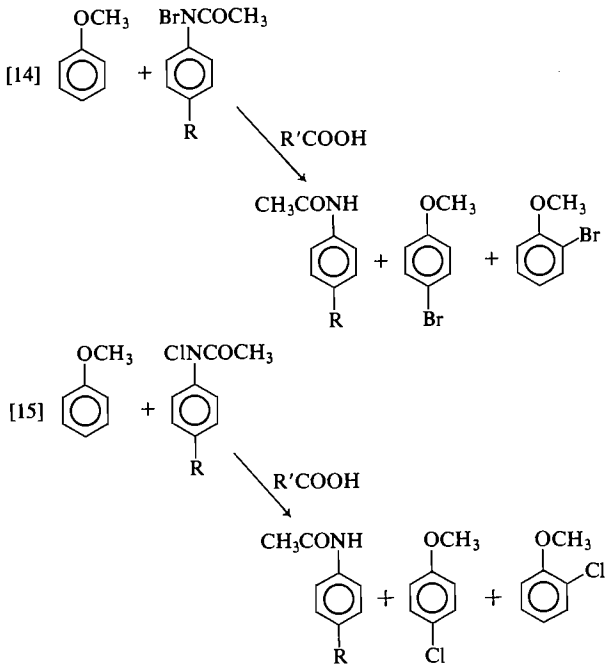

The observed *ortho*/*para* product ratios related to each *N*-bromoacylanilide/carboxylic acid system (eq. [14]; 16 ratios) and each *N*-chloroacylanilide/carboxylic acid system (eq. [15]; 12 ratios) are pertinent to the present discussion.

Firstly, we wish to draw attention to the fact that the ratios from the bromination reactions are a function of both the bromine source and the acid catalyst. As noted earlier, this observation is inconsistent with the intermediate production of kinetically free hypobromites (12). Secondly, we also note that the reactivity of the bromine, as measured by the selectivity of the bromination, increases with the basic strength of the amine related to the *N*-bromoacylanilide and the acidic strength of the catalyst. Alternatively, it may be stated that the electrophilic character of the bromine is increased by factors in the reactants which facilitate proton transfer. The same factors appear to be operative in the case of the *N*-chloroacylanilides, although the ratios are less sensitive to structural alterations in the chlorine source. This reduction in sensitivity is due to the replacement of bromine by the more electronegative chlorine, a case analogous to that shown by *N*-bromo-4-nitroacetanilide where the basicity of the *N*-halogenoacylanilide is reduced as a consequence of the electron withdrawing properties of the 4-substituent.

As we noted earlier, bromine migration to solvent is not confined to anisole but also occurs in

Can. J. Chem. Downloaded from www.nrcresearchpress.com by 210.87.254.105 on 09/06/12
For personal use only.

chlorobenzene with *N*-bromo-2-nitroacetanilide and *N*-bromo-4-nitroacetanilide. In contrast to the anisole brominations, however, the less strongly electron withdrawing substituents, i.e., F, Cl, Br, CH_3, and Ph, give the anticipated rearranged products in chlorobenzene. Clearly, two possibilities exist for the bromination of chlorobenzene and anisole. Either bromine migration occurs at the same position along the reaction coordinate for both solvents or the migrations of bromine to each solvent involve different intermediates. All the evidence presented above is consistent only with the *direct transfer of bromine from nitrogen to solvent* in the anisole brominations. If the same situation existed in chlorobenzene, then since the nitro group produces the *least reactive* bromine in anisole, i.e., the *most selective* anisole brominations, the other substituents, namely, F, Cl, Br, CH_3, and Ph, should also induce bromination of the chlorobenzene. This is *not* what is observed. We can only conclude that the bromination of chlorobenzene by the 2-nitro and 4-nitro substrates takes place by a different mechanism, one involving a further distinct intermediate, namely, the π-complex. Thus, the bifurcation of products which occurs in chlorobenzene is a consequence of the differing reactivity of bromine at the π-complex stage where the reactivity of the incipient bromine cation is enhanced by electron withdrawing substituents and diminished by electron donating substituents. In anisole, on the other hand, the extent or ease of proton transfer to form the protonated substrates will be increased by electron donating substituents and decreased by electron withdrawing substituents. Hence, the effect of the substituents is entirely in the *opposite sense* in anisole and depends solely on how efficiently the substituents facilitate proton transfer.

While the intervention of acyl hypobromites in the chlorobenzene reactions would lead to the same results, we exclude this possibility because the products obtained by Dewar and Couzens (13) in reaction [8] cannot be accounted for by the invocation of kinetically free hypobromite intermediates. We take these latter results to mean that bromine scrambling occurs from the protonated substrate, while rearrangement proceeds via a π-complex.

Finally, we wish to draw attention to one further interesting fact concerning the Orton rearrangement which has thus far been neglected. Bell and Brown (17) reported some time ago that *N*-iodoformanilide rearranges in anisole when treated with carboxylic acids and phenols. The 4-position in anilides is approximately a factor of 10 *less* reactive towards electrophiles than the same position in anisole (18), and hence, if rearrangement occurred via a kinetically free hypoiodite, substitution would not favour the anilide. Indeed, since the molar concentration of anisole is ca. 10 $mol \cdot L^{-1}$ while the concentration of *N*-iodoformanilide in the anisole varied from about 0.01 to 0.1 $mol \cdot L^{-1}$, the effective competition factor, which is a function of both concentration and reactivity, will favour the anisole by at least three orders of magnitude. In spite of this large "reactivity gradient", *N*-iodoformanilide *rearranges* in the presence of anisole. This, together with all the evidence presented above, is strongly indicative of an intramolecular rearrangement for the acid catalyzed component of the reaction in which the halogenating species never becomes kinetically free.

The Role of the Carboxylic Acid Catalysts

The association of carboxylic acids in nonaqueous solvents is well documented (cf. refs. 19, 20), but recent studies (21, 22) of these hydrogen bonding phenomena and the polymeric aggregates which result reveal that monomeric association is not limited to cyclic dimers for acid concentrations above 10^{-3} $mol \cdot L^{-1}$. In general, however, the trend of increasing association with decreasing acid strength is evident (19–21), and the contention that TFA in chlorobenzene at 323 K is likely to be present predominately as monomer in equilibrium with a small amount of dimer, even for acid concentrations exceeding 10^{-3} $mol \cdot L^{-1}$, is supported by Stevens (19) in his study of the self-association of TFA in nonaqueous solvents.

With reference to Fig. 2, the variation of α with c_a at lower TFA concentrations requires that at least a term in $[M]^2$ be present in the expression for the observed rates since the shape of the curves cannot be accommodated solely by a term in [M]. Furthermore, since the concentration–rate data for the TFA systems are not amenable to treatment according to Bell's rate law (see eq. [2]), in which terms in both [M] and $[M]^2$ are present, we can only surmise that the substrate is not catalyzed to product by a single monomeric species. The kinetic meaning of a term in $[M]^2$ in the rate expression is equivocal; such a term can be interpreted as the attack of dimer on substrate, a termolecular reaction between substrate and two monomers, or the sequential attack of two monomers, first on substrate and then on an intermediate. A further examination of k_{obs} as a function of c_a, however, shows that the observed rates cannot be interpreted simply as a function of $[M]^2$ at lower TFA concentrations. This observation leads to the conclusion that the successive attack of two monomeric

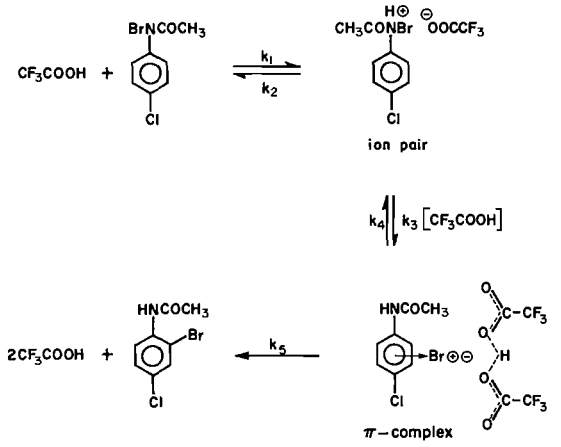

FIG. 3. A simplified mechanistic description for the rearrangement of NBCA catalyzed by TFA in chlorobenzene.

species on the substrate must account for the major portion of catalytic activity in the TFA systems.

In the light of the foregoing, we propose a general mechanism like that shown in Fig. 3 for monomeric TFA catalysis of NBCA to rearranged product. This mechanism is summarized by

$$[16]\quad S + M \underset{k_2}{\overset{k_1}{\rightleftharpoons}} I_1 \underset{k_4}{\overset{k_3[M]}{\rightleftharpoons}} I_2 \xrightarrow{k_5} \text{products}$$

In view of the previous observations related to both intermolecular bromine scrambling between substrate nitrogens (13) and bromine transfer reactions from substrate to solvent (1, 10–12, 15), we envisage I_1 as a tight ammonium ion pair. The k_1 step then initially involves a hydrogen bonding preequilibrium between monomeric acid and substrate followed by the slower, formal transfer of a proton to the substrate. While it is generally accepted that hydrogen bonding between oxygen and oxygen or nitrogen is rapid and reversible, and that proton transfer subsequent to hydrogen bonding is relatively slower, such a description may be oversimplified (cf. ref. 23). To avoid such complexity at this stage and any conjecture regarding the initial site of hydrogen bonding in the substrate (oxygen or nitrogen), we prefer to simply consider the hydrogen bonding and proton transfer processes as a single reaction step.

While the solvation, separation, and reaction of the ions in aqueous protonated substrate is likely to be rapid, a similar demise of the ion pair in chlorobenzene is not apt to occur since the solvent is unlikely to separate and support the resulting solvated, free ions. Clearly the necessary reorganization of charge for further reaction must occur within the species in some other manner. We view the attack of a second acid monomer on I_1 as electrophilic catalysis, wherein the acid monomer hydrogen bonds to the anionic moiety of the tight ammonium ion pair. In concert with this wider distribution of negative charge over the resulting "dimeric anion", the positive charge of the tight ion pair migrates to bromine, formally producing a brominium ion which may participate in a scrambling reaction, transfer to solvent, or, by intramolecular migration, form the π-complex I_2.[9] Reaction from I_2 to products is represented for convenience as a single reaction step, but this advance presumably occurs via the usual series of aromatic substitution equilibria and intermediates, namely, from the $Br^{(+)}$ π-complex to the σ-complex to the $H^{(+)}$ π-complex, from which a final, irreversible proton transfer to the dimeric anion occurs, thus rendering the rearranged product.

To test the fidelity of the foregoing description, application of the steady state theorem to eq. [16] leads to a rate law given by

$$[17]\quad k_{obs} = \frac{k_1 k_3 k_5 [M]^2}{k_2(k_4 + k_5) + k_3 k_5 [M]} = \frac{k_1 [M]^2}{k_2(k_4 + k_5)/k_3 k_5 + [M]}$$

Our data for the NBA/TFA, NBCA/TFA, NBCA/TFA-*d* systems and those for the NBA/TCA system reported by Bell (9) have been regressed in compliance with eq. [17] using the method suggested by Wentworth (24) for nonlinear regression. The regression results, quoted in Table 5 and illustrated in linear form ($[M]^2/k_{obs}$ vs. [M]) in Figs. 4 and 5, satisfactorily accommodate both our own results and those of Bell for the NBA/TCA system.

The magnitude and reproducibility of the K_d values quoted in Table 5 should reflect primarily on the validity of the data treatment and ultimately on the justification for the assumption which constrains catalytic reactivity to the monomeric species in the simple monomer–dimer acid equilibrium. While thermodynamic data apparently are unavailable for the self-association of TCA or TFA in chlorobenzene, some comparisons can be made. Bulmer and Shurvell (21) have summarized some K_d values reported for TCA/C_6H_6 based on a monomer–dimer model, 1.1 L·mol^{-1} at 293 K (25), 6.7 and 5 L·mol^{-1} at 298 K (26, 27), which are in reasonable agreement with K_d (TCA/PhCl/288 K)

[9]We have described the k_3 step here as a concerted process more for the sake of brevity than to deny the existence of a second ion pair intermediate between I_1 and the π-complex. The existence of such an intermediate will not significantly alter the present mechanistic argument.

Can. J. Chem. Downloaded from www.nrcresearchpress.com by 210.87.254.105 on 09/06/12
For personal use only.

TABLE 5. Carboxylic acid dimerization constants and rate constants for some acid catalyzed rearrangements of NBA and NBCA in chlorobenzene[a]

Substrate/acid	K_d, L·mol^{-1}	$k_1 \times 10^4$, L·mol^{-1}·s^{-1}	$[k_2(k_4+k_5)/k_3k_5] \times 10^4$, L·mol^{-1}
NBA/TFA	0.387 ± 0.104	42.0 ± 1. 7	246 ± 18
NBCA/TFA	0.362 ± 0.053	22.5 ± 0.5	230 ± 10
NBCA/TFA-*d*	0.749 ± 0.206	14.4 ± 0.9	235 ± 17
NBA/TCA[b]	3.57 ± 0.31	2.86 ± 0.06	4.27 ± 1.19

[a] These results are obtained by treating the entire concentration–rate data sets using the weighted, nonlinear regression technique suggested by Wentworth (24).

[b] These data are computed from Bell's work (9) at 288 K, a temperature different from T = 323 K for the other substrate/acid systems reported here.

= 3.57 L·mol^{-1} found here. There are also favourable comparisons between the values of K_d(TFA/PhCl) = 0.387 and 0.362 L·mol^{-1} quoted in Table 5 and K_d(TFA/C_6H_6) < 1 L·mol^{-1} and K_d(TFA/$ClCH_2CH_2Cl$) ≃ 0.6 L·mol^{-1} calculated for 323 K from data estimated by Stevens (19). In view of these comparisons, the K_d values determined here appear to be of the correct order of magnitude.

The internal consistency of the data treatment is also good, inasmuch as K_d(TFA/PhCl) is reproducible from the kinetic results of two different systems, NBA/TFA and NBCA/TFA (see Table 5). Indeed, the two K_d values are much closer than might be reasonably expected since they represent the indirect determination of a parameter which is entirely dependent on the precision of a different primary observable, i.e., the kinetics of the systems. Hence, both the magnitude and reproducibility of the K_d values lend some credence to the approximations implicit in the rate law of eq. [17] when taken in conjunction with the monomer–dimer self-association model of eq. [1]. The large standard errors associated with the K_d values reported in Table 5 perhaps reflect the fact that carboxylic acid self-association is not confined to cyclic dimerization but that higher, "linear" polymers are also present (cf. refs. 21, 22). Nevertheless, while the concentrations of such species are apt to be appreciable for weaker carboxylic acids in chlorobenzene, concentrations of these linear polymers are likely to be much lower at comparable acid concentrations of stronger carboxylic acids, e.g., TFA and TCA (19, 21). Another consideration which might adversely influence the constancy of the K_d values is the association of catalytic acid with product. This effect, however, is likely to be

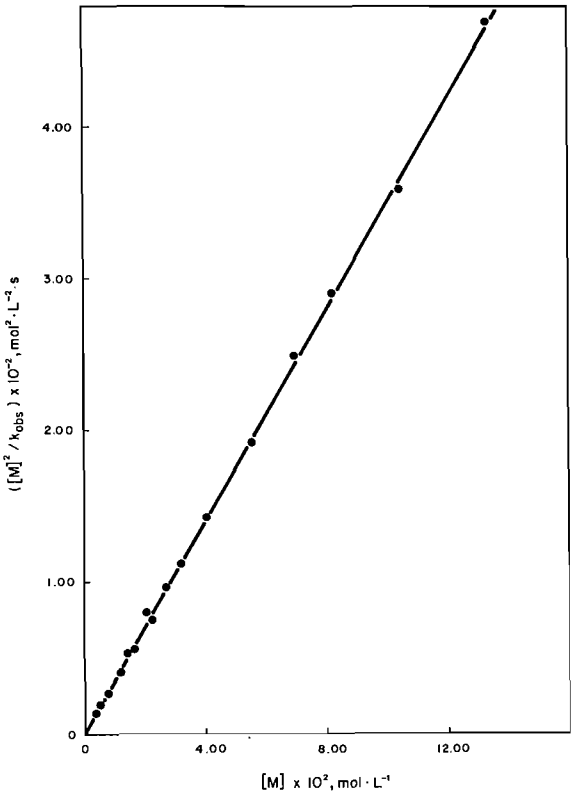

FIG. 4. The linear correlation of $[M]^2/k_{obs}$ versus [M] for the rearrangement of NBA catalyzed by TCA in chlorobenzene at T = 288 K.

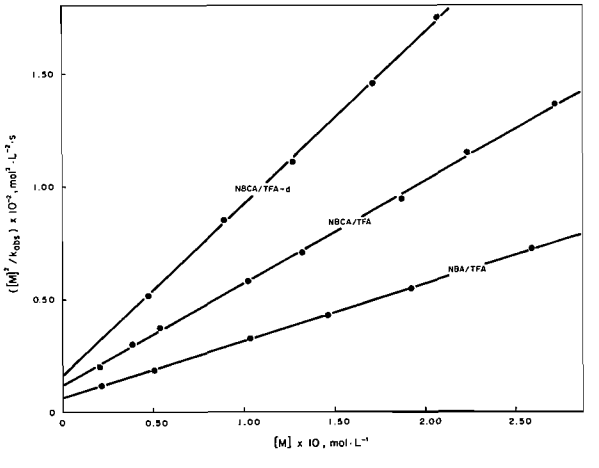

FIG. 5. The linear correlations of $[M]^2/k_{obs}$ versus [M] for the rearrangement of NBA catalyzed by TFA and the rearrangement of NBCA catalyzed by TFA and by TFA-*d* in chlorobenzene at 323.15 K.

Can. J. Chem. Downloaded from www.nrcresearchpress.com by 210.87.254.105 on 09/06/12
For personal use only.

Can. J. Chem. Downloaded from www.nrcresearchpress.com by 210.87.254.105 on 09/06/12
For personal use only.

minimized since the reactions were carried out under pseudo-first order conditions.

The standard errors associated with the rate constants quoted in Table 5 are much lower than those for the K_d values, indicating the values of k_1 and $k_2(k_4 + k_5)/k_3k_5$ are less sensitive to the acid self-association model. The k_1 values support the hypothesis that the first overall reaction step involves proton transfer in that k_1(NBA/TFA/323 K) > k_1(NBA/TCA/288 K) and k_1(NBCA/TFA/323 K) > k_1(NBCA/TFA-*d*/323 K), i.e., the rate of proton transfer diminishes with decreasing aqueous acid strength. Further, from a simple inductive consideration NBA is likely to be a better proton acceptor than NBCA. If the initial mechanistic step is proton transfer, this should and does result in k_1(NBA) > k_1(NBCA) for TFA/PhCl at the same temperature.

Within their standard errors, the rate constant ratios $k_2(k_4 + k_5)/k_3k_5$ are the same for the NBA/TFA, NBCA/TFA, and NBCA/TFA-*d* systems. This implies that these ratios are not very sensitive to substrate structure, with one inference being that participation of the second acid monomer is largely independent of substrate, a feature expected for our proposed mechanism. In view of this result it also seems plausible to assume that $k_5 \gg k_4$ in our mechanistic scheme, such that $k_2(k_4 + k_5)/k_3k_5 \simeq k_2/k_3$. This simplification seems to be in accord with the notion that a second acid monomer hydrogen bonds to the anionic moiety of the ion pair in the electrophilic catalysis of the species to π-complex. Since association via hydrogen bonding is apparently more favourable for weaker than for stronger carboxylic acids, the k_2/k_3 ratio might be expected to diminish with the increases in k_3 which accompany decreasing strength in the acid catalyst. This is apparently the case, viz. k_2/k_3(NBA/TFA/323 K) > k_2/k_3(NBA/TCA/288 K), where TCA, the weaker acid at a lower temperature, is likely to associate with the ion pair more readily than TFA in the k_3 reaction step.

In the present study the deviation of the order of reaction from unity with respect to TFA concentration clearly centers on the magnitude of $k_2(k_4 + k_5)/k_3k_5$. If, however, k_3 increases more rapidly than k_2 as the strength of the catalytic acid decreases and $k_5 >> k_4$, such that $k_2/k_3 << [M]$, the rate law will take the limiting form

$$[18] \quad k_{obs} = k_1[M]$$

for weaker carboxylic acid catalysts. Some support for these limiting simplifications in the rate law is forthcoming from an examination of the results for NBA/TCA/PhCl/288 K in Table 5 wherein $k_2(k_4 + k_5)/k_3k_5$ is small compared to the lowest [M]. The concentration–rate data for this system then should be amenable to treatment according to eq. [18] and this is indeed the case, with $K_d = 3.57$ and $k_1 = 2.86 \times 10^{-4}$ L·mol^{-1}·s^{-1}. The observation that the empirical rate law for catalysis by weaker carboxylic acids will take the limiting form of eq. [18] puts Bell's (9) contention that proton transfer is rate determining in the rearrangement into perspective. Since Bell's work centered mainly on the catalysis of NBA rearrangement by several carboxylic acids which are considerably weaker than TFA, the bulk of his results would be more or less empirically consistent with eq. [18]. Despite the fact that Bell's work suggests the participation of only a single acid monomer in the rearrangement and that proton transfer is entirely rate determining, we emphasize here that such a proposal is not consistent with our results for catalysis by TFA. Moreover, the simplest mechanism which will accommodate our observations is one which requires the successive participation of two monomeric acid species.

A further point with respect to the influence of $k_2(k_4 + k_5)/k_3k_5$ and K_d on the α,c_a profiles may be usefully added. Division of eq. [17] by eq. [5] gives

$$[19] \quad \alpha = \frac{k_1k_3k_5[M]}{\{k_2(k_4 + k_5) + k_3k_5[M]\}\{1 + 2K_d[M]\}}$$

Differentiation of eq. [19] with respect to c_a leads to the conclusion that the rate law given by eq. [17], when taken in conjunction with the concentration expression of eq. [5], will yield a maximum in the α,c_a coordinate system. The differentiation itself is lengthy, and for brevity we omit its entire description save to quote the result, namely,

$$[20] \quad c_{a\,max} = (2K_d)^{-\frac{1}{2}}(r)^{\frac{1}{2}} + r$$

where $r = k_2(k_4 + k_5)/k_3k_5$, the ratio of rate constants in the denominator of the rate law. In view of this result, eq. [17] is clearly the simplest rate law which can accommodate concentration dependent maxima in the α versus c_a plots for the NBCA/TFA, NBCA/TFA-*d*, and NBA/TFA systems (see Fig. 2). We reiterate that the same procedure, when applied to a simpler, single intermediate mechanism (see eq. [18]) or to Bell's rate law (see eq. [2]), will not yield a concentration dependent maximum in the α,c_a coordinate system. In consequence, these mechanistic schemes cannot accommodate our data for the stronger catalytic acids if the shallow maxima observed in the α,c_a plots for these acids are indeed real.

For a weaker carboxylic acid K_d will be larger than for a stronger one, and $c_{a\,max}$, the concentration at which the maximum occurs in the α,c_a coor-

Can. J. Chem. Downloaded from www.nrcresearchpress.com by 210.87.254.105 on 09/06/12
For personal use only.

dinate system, will tend to be lower for a weaker acid, with the maximum lying closer to the α-axis. This effect is further enhanced since $k_2(k_4 + k_5)/k_3k_5 \simeq k_2/k_3$ is smaller for a weaker acid (see above). This point allows the resolution of a question outstanding in the previous discussion as to whether or not the apparent maximum in the α,c_a profile for the NBA/TCA system is real or spurious (see Fig. 1). From the data in Table 5, eq. [20] predicts a maximum at $c_{a\,max} = 1.56 \times 10^{-3}$ mol·L^{-1}, a concentration below the TCA concentration range examined by Bell (see Table 4). On this basis we can only conclude that the apparent maximum at $c_a = 1.3 \times 10^{-2}$ mol·L^{-1} in the α,c_a curve is indeed spurious. Even though a real maximum was not observed for this system at 288 K, maxima are evident for several substrates catalyzed by TCA at 318 K in chlorobenzene (11). Since only three acid concentrations were examined for these substrates, however, analysis of these data is limited to qualitative comment.

Isotope Effects

The fact that NBCA-2,6-d_2/TFA demonstrated no measurable isotope effect when compared with NBCA/TFA (see Table 1) would seem to support our contention that k_5 is large compared to the other rate constants (e.g., $k_5 >> k_4$, see above) and that the reaction steps from the first π-complex to product are relatively rapid. This observation, however, does not necessarily confirm (nor invalidate) the mechanistic considerations related to the final stages of the rearrangement, i.e., whether proton (or deuteron) loss with strong carboxylic acids may or may not become part of the rate determining step of the rearrangement.[10] Wolfsberg and co-workers (28–30) have argued on numerous occasions that the observation of isotope effects is a consequence of force constant changes between the ground and transition states. This is a necessary but not a sufficient condition for isotope effects to be observed since, as Streitweiser *et al.* (31) have pointed out, if there is no net change in the frequency sums of the vibrations between the two states, the isotope effect arising from other "non-zero point" sources is likely to be small. They specifically consider the problem of aromatically bonded hydrogen/deuterium and the behaviour of such systems in aromatic substitution. They explain the small isotope effects (31) by a cancellation in the frequency sums between reactants and transition states.

The small, normal isotope effect associated with proton/deuteron transfer for NBCA/TFA and NBCA/TFA-*d*, $k_1(H)/k_1(D) = 1.6$, is consistent with other observations for these processes between oxygen and nitrogen. The large, inverse isotope effect $K_d(H)/K_d(D) = 0.48$ for the association of TFA versus TFA-*d* is puzzling, however, since the gas phase dimerization does not appear to show any appreciable isotope effect (ref. 20, p. 367). Nevertheless, one might generally anticipate deuterated acids to display more association in solution than the related hydrogen acids since the deuterated acids are weaker.[11] By way of qualitative rationalization we again offer the Streitwieser zero point energy treatment which considers only the vibrations of the protium compound. The dimerization of an "*n* atom" carboxylic acid must give rise to six new vibrations since the reactants are characterized by $2(3n - 6)$ vibrations whereas the product is characterized by $6n - 6$ vibrations. The new vibrations generated in the dimerization involve hydrogen in an important way since the new links are through hydrogen. The frequency sum related to the six new motions may increase even if some of the force constants are reduced relative to the monomeric acid.[12] Such an increase would lead to an inverse effect.

Final Comments

The rates of rearrangement of the *N*-bromoacylanilides demonstrate a further complexity, namely, that in some cases the pseudo-first order rates at a fixed acid concentration are functions of the substrate concentration. This is well established for NBA/TCA in chlorobenzene (33), but the phenomenon is absent in the case of *N*-bromo-2-methylacetanilide/TCA in the same solvent (10). While the origins of these observations remain obscure, the rationalization of their behaviour proposed by Bell and Levinge (33) may be valid. Rearrangements of the *N*-chloro and *N*-iodo analogues are kinetically complex, and in some instances show drastic departures from pseudo-first order kinetics. This is in marked contrast to the *N*-bromoacylanilides, which are invariably well behaved in this respect (see, however, the *N*-bromobenzanilide/TCA system (34)). The erratic

[10]It should be noted that at any given acid concentration the simple ratio of the observed rate constants for NBCA/TFA and NBCA-2,6-d_2/TFA, $k_{obs}(H)/k_{obs}(D)$, does not provide $k_5(H)/k_5(D)$, the ratio required to establish the isotope effect for this final step.

[11]This is evident, for instance, in the case of D_2O and H_2O wherein D_2O is the more associated (32) and is also the weaker acid.

[12]Since the force constants are related to the motions of all of the atoms, force constants in the dimer cannot be compared rigorously with those originally present in the monomer. The qualitative nature of this argument is appreciated.

behaviour of the *N*-chloro and *N*-iodo compounds has been attributed to side reactions between substrate and product, and also to a reaction involving two substrate molecules. Unfortunately, these complexities prohibit clarification of the acid catalyzed mechanism since it is doubtful whether the carboxylic acid catalyzed component of the rearrangement can be quantitatively isolated from the other processes which contribute to the diminution of substrate.

The present communication strongly suggests that the Orton rearrangement in aprotic solvents is intramolecular and that the mechanistically significant steps in the advance to product are protonation of the substrate, heterolytic fission of the nitrogen–halogen bond, and rearrangement of the resulting ion pair to π-complex.

Acknowledgements

The authors are grateful to Dr. S. H. Morris and Mr. F. J. P. Steele for their helpful advice and assistance, and one of the authors (J.M.W.S.) wishes to thank the National Research Council of Canada for financial support.

1. J. M. W. Scott and J. G. Martin. Can. J. Chem. **44**, 2901 (1966).
2. C. K. Ingold. Structure and mechanism in organic chemistry. Cornell University Press, Ithaca, NY. 1953. Chapt. 11. pp. 604–610.
3. H. J. Shine. Aromatic rearrangements. Elsevier Publishing Co., New York. 1967. Chapt. 8(b). pp. 228–230.
4. R.P. Bell. The proton in chemistry. 2nd ed. Cornell University Press, Ithaca, NY. 1973.
5. W. P. Jencks. Catalysis in chemistry and biochemistry. McGraw-Hill Book Co., New York. 1969.
6. M. L. Bender. Mechanism of homogeneous catalysis from protons to proteins. Wiley–Interscience, New York. 1971.
7. R. P. Bell. Acid–base catalysis. Oxford University Press, Oxford. 1941.
8. C. K. Ingold. Proc. Chem. Soc. London, 279 (1957).
9. R. P. Bell. Proc. R. Soc. London, Ser. A, **143**, 377 (1934).
10. M. J. S. Dewar and J. M. W. Scott. J. Chem. Soc. 2676 (1957).
11. J. M. W. Scott. Can. J. Chem. **38**, 2441 (1960), and references therein.
12. J. M. W. Scott and J. G. Martin. Can. J. Chem. **43**, 732 (1965).
13. M. J. S. Dewar. Aromatic rearrangements. Kekulé symposium, IUPAC. Butterworths, London. 1959. p. 179.
14. G. C. Israel, A. N. W. Tuck, and F. G. Soper. J. Chem. Soc. 547 (1945).
15. M. J. S. Dewar. The electronic theory of organic chemistry. Oxford University Press, Oxford. 1949. Chapt. 11. pp. 225–229.
16. C. G. Swain, D. A. Kuhn, and R. L. Schowen. J. Am. Chem. Soc. **87**, 1553 (1965).
17. R. P. Bell and J. F. Brown. J. Chem. Soc. 1520 (1936).
18. H. C. Brown and L. M. Stock. *In* Advances in physical organic chemistry. *Edited by* V. Gold. Academic Press, Inc., New York. 1963.
19. T. L. Stevens. The self-association of trifluoroacetic acid in organic solvents. Ph.D. thesis, University of Oklahoma. 1968. pp. 65, 67.
20. G. Pimentel and A. L. McClellan. The hydrogen bond. W. H. Freeman and Co., San Francisco. 1960.
21. J. T. Bulmer and H. F. Shurvell. J. Phys. Chem. **77**, 256 (1973).
22. J. T. Bulmer and H. F. Shurvell. Can. J. Chem. **53**, 1251 (1975).
23. G. D. Burfoot, E. F. Caldin, and H. Goodman. J. Chem. Soc. Faraday Trans. I, **70**, 105 (1974).
24. W. E. Wentworth. J. Chem. Educ. **42**, 96 (1965).
25. Y. Nagai and O. Simamura. Bull. Chem. Soc. Jpn. **35**, 132 (1962).
26. J. Steigman and W. Cronkright. Spectrochim. Acta, Part A, **26**, 1805 (1970).
27. S. Bruckenstein and A. Saito. J. Am. Chem. Soc. **87**, 698 (1965).
28. J. Bigeleisen and M. Wolfsberg. *In* Advances in chemical physics. Vol. 1. *Edited by* I. Prigogine. Interscience Publishers, Inc., New York. 1958. pp. 15–76.
29. M. J. Stern and M. Wolfsberg. Pure Appl. Chem. **8**, 225 (1964).
30. M. J. Stern and M. Wolfsberg. Pure Appl. Chem. **8**, 325 (1964).
31. A. J. Streitwieser, Jr., R. H. Jagow, R. C. Fahey, and S. Suzuki. J. Am. Chem. Soc. **80**, 2326 (1958).
32. P. M. Laughton and R. E. Robertson. *In* Solute–solvent interactions. *Edited by* J. F. Coetzee and C. D. Ritchie. Marcel Dekker, New York. 1969. pp. 401–403.
33. R. P. Bell and R. V. H. Levinge. Proc. R. Soc. London, Ser. A, **151**, 211 (1935).
34. R. P. Bell and O. M. Lidwell. J. Chem. Soc. 1096 (1939).

Can. J. Chem. Downloaded from www.nrcresearchpress.com by 210.87.254.105 on 09/06/12
For personal use only.

Thermolysis of the tricyclic 1,2-dioxetanes 3,4:3,4-dipropano-, 3,4-pentano-3,4-propano-, and 3,4-butano-3,4-propano-1,2-dioxetane[1]

KARL R. KOPECKY, PETER A. LOCKWOOD,[2] RODRIGO RICO GOMEZ,[3] AND JAN-YIH DING
Department of Chemistry, University of Alberta, Edmonton, Alta., Canada T6G 2E1

Received September 3, 1980

KARL R. KOPECKY, PETER A. LOCKWOOD, RODRIGO RICO GOMEZ, and JAN-YIH DING. Can. J. Chem. **59**, 851 (1981).

The title compounds have been isolated in crystalline form by cyclization of the corresponding bromo- or iodohydroperoxides. The activation parameters for thermolysis are, respectively (E_a, kcal/mol, ΔS^*, eu): 25.6 ± 0.6, 4 ± 2; 29.8 ± 0.4, 4 ± 2; 26.3 ± 0.5, 1 ± 2. The singlet $^1\phi$ and triplet $^3\phi$ excited state product yields produced on thermolysis of these compounds are, respectively: 0.011, 0.10; 0.0019, 0.18; 0.0013, 0.11. These yields are relative to a value of 0.31 for $^3\phi$ of tetramethyl-1,2-dioxetane. The cyclic 1,5-diones from thermolysis of the last two title compounds cyclized before isolation to give the bicyclic hydroxyketones.

KARL R. KOPECKY, PETER A. LOCKWOOD, RODRIGO RICO GOMEZ et JAN-YIH DING. Can. J. Chem. **59**, 851 (1981).

La cyclisation des bromo- ou iodo-hydroperoxydes correspondants permet d'isoler les composés mentionnés dans le titre, sous forme cristallisée. Les paramètres d'activation de thermolyse sont respectivement: (E_a kcal/mol, ΔS^*, u.e.): 25,6 ± 0,6, 4 ± 2; 29,8 ± 0,4, 4 ± 2; 26,3 ± 0,5, 1 ± 2. Les rendements en produits de l'état singulet $^1\phi$ et triplet $^3\phi$ excité, obtenus lors de la thermolyse de ces composés, sont respectivement de 0,011, 0,10; 0,0019, 0,18; 0,0013, 0,11. Ces rendements sont exprimés en fonction d'une valeur de 0,31 pour le $^3\phi$ du tétraméthyl-dioxétane-1,2. Les diones-1,5 cycliques provenant de la thermolyse des deux derniers composés mentionnés dans le titre se cyclisent avant d'être isolées en donnant les hydroxycétones bicycliques.
[Ttraduit par le journal]

Thermolysis of 1,2-dioxetanes results in the formation of carbonyl cleavage products in quantitative yield and in light emission (1), eq. [1]. Both

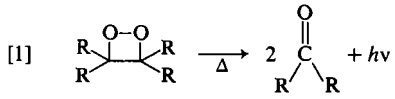

singlet and triplet excited states are formed directly in the primary step of the reaction and the triplet almost always predominates by a large factor in the examples studied to date; for reviews see ref. 2. The factors which affect the yield of excited states and the triplet–singlet ratio are the subject of considerable investigation (3). The tricyclic dioxetane 3,4:3,4-dibutano-1,2-dioxetane **1**, prepared in order to study the effect of the rigidity of its structure on the rate of its thermolysis and the yield of excited states produced, was found to produce much smaller amounts of excited state products than were formed from the mono- and bicyclic dioxetanes trimethyl-, **2**, tetramethyl-, **3**, and *cis*-3,4-butano-3,4-dimethyl-1,2-dioxetane, **4** (4).

The present paper reports the preparation and thermolysis of three other tricyclic dioxetanes, 3,4:3,4-dipropano-1,2-dioxetane **5**, 3,4-butano-3,4-propano-1,2-dioxetane **6**, and 3,4-pentano-3,4-propano-1,2-dioxetane **7** in a test to determine whether the behaviour of **1** is general for dioxetanes of this structural type.

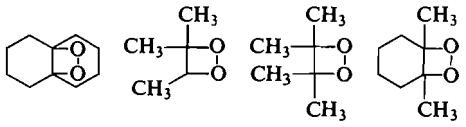

1 **2** **3** **4**

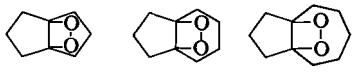

5 **6** **7**

Results

The preparation and chemical characterization of **5**, **6**, and **7** are shown in Schemes 1, 2, and 3, respectively. The route shown appears to be more convenient than previous methods (5) for the preparation of the alkene **8** on a large scale. The silver ion assisted cyclization (1*f*) of the corresponding β-halohydroperoxides was used to prepare the 1,2-dioxetanes. These products were characterized chemically by low temperature reduction with lithium aluminum hydride to the corresponding diols and by thermolysis to the diketones. The diketones **9** and **11** from **6** and **7** could not be isolated. They cyclized spontaneously to the corresponding ketols **10** and **12** (6). These were the only products that could be detected from ozonolysis of the corresponding alkenes and from the manganese dioxide oxidation of the corresponding diols. All three 1,2-

[1]This research was supported by the National Research Council of Canada and was presented in part at the 174th National Meeting of the American Chemical Society, Chicago, IL, Aug. 29–Sept. 2, 1977. Abstracts ORGN 016.

[2]Holder of a National Research Council of Canada Scholarship, 1970–1974.

[3]Present address: Departamento de Quimica Organica, Facultad de Ciencias, Universidad de Malaga, Malaga, Spain.

0008-4042/81/050851-08$01.00/0
©1981 National Research Council of Canada/Conseil national de recherches du Canada

Can. J. Chem. Downloaded from www.nrcresearchpress.com by 210.87.254.105 on 09/06/12
For personal use only.

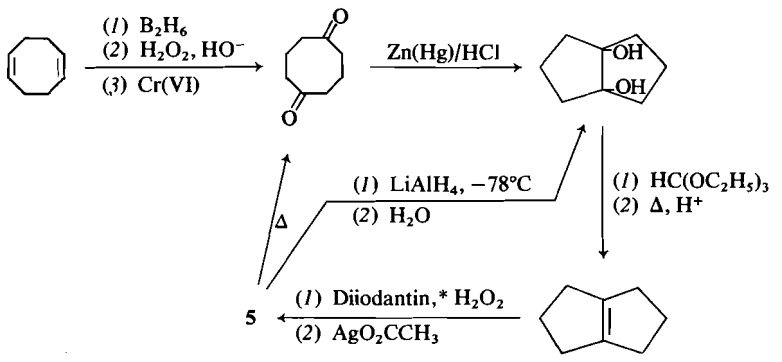

*1,3-Diiodo-5,5-dimethylhydantoin

SCHEME 1

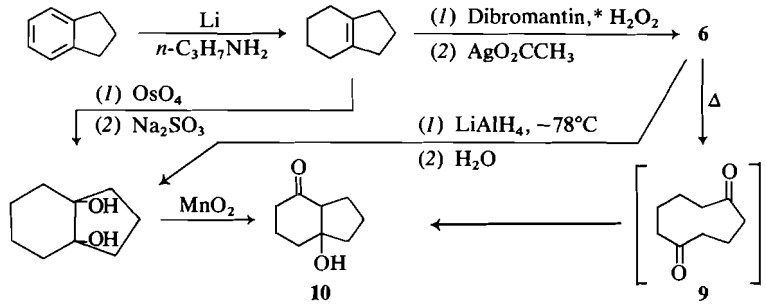

*1,3-Dibromo-5,5-dimethylhydantoin

SCHEME 2

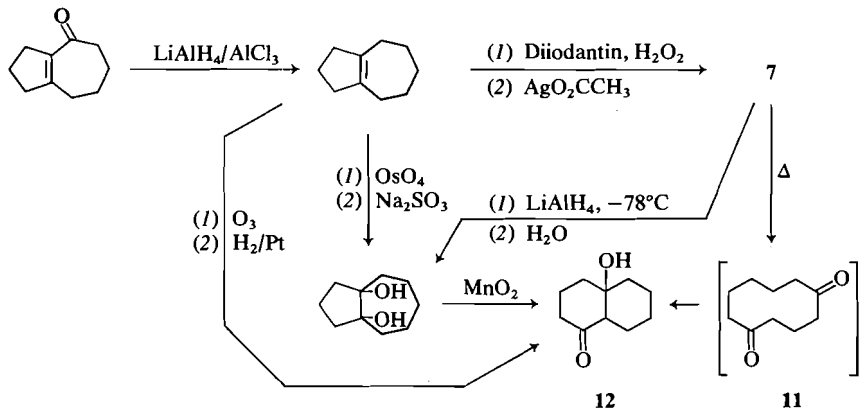

SCHEME 3

dioxetanes were crystallized from 2-methylbutane at −78°C to give yellow crystals. Solutions of **5** were stable, but crystalline material, freed of solvent, 92% active oxygen, always decomposed rapidly and completely, even at 0°C. Crystalline **7**, 99% active oxygen, was quite stable and **6**, 98% active oxygen, melted below room temperature to give a relatively stable yellow oil.

The rates of thermolysis, Table 1, of the 1,2-dioxetanes were measured by following the decay of luminescence of their aerated benzene or toluene solutions containing added 9,10-dibromoanthracene DBA (1*e*, 4). First order kinetics were obeyed for at least three half-lives of decomposition. Activation parameters were calculated (7) from the rate constants. Yields of excited singlet $^1\phi$ and triplet $^3\phi$ products formed on thermolysis of the 1,2-dioxetanes, Table 2, were determined from

Can. J. Chem. Downloaded from www.nrcresearchpress.com by 210.87.254.105 on 09/06/12
For personal use only.

Can. J. Chem. Downloaded from www.nrcresearchpress.com by 210.87.254.105 on 09/06/12
For personal use only.

TABLE 1. Kinetic parameters for thermolysis of some 1,2-dioxetanes

Dioxetane	Concentration, 10^3 M	Temperature, °C	10^5 k, s^{-1}	E_a, kcal/mol	$\Delta S^{\ddagger}$, eu
5[a]	2.5	45.1	32.6 ± 0.7	25.6 ± 0.6	4 ± 2[b]
	6	25.0	2.13 ± 0.05		
6[c]	4.5	64.8	38.3 ± 0.02	26.3 ± 0.5	1 ± 2[d]
		46.1	3.85 ± 0.15		
7[e]	8	93.7	27.3 ± 0.1	29.8 ± 0.4	4 ± 2[f]
	14	75.0	3.04 ± 0.05		
1				22.7 ± 0.9[g]	
3				25.8 ± 0.5[g,h]	

[a] In benzene with 10^{-2} M DPA. A run at 45.1°C with 10^{-2} M DBA gave $k = 33.6 \times 10^{-5}$ s^{-1}.
[b] At 25°C.
[c] In toluene with 10^{-3} M DBA.
[d] At 46°C.
[e] In toluene with 10^{-2} M DBA.
[f] At 75°C.
[g] Reference 1*f*.
[h] Other workers have obtained higher values: 27.6 ± 1 kcal/mol (3*a*).

TABLE 2. Yields of excited products[a]

Dioxetane	Temperature, °C	$^3\phi$	$^1\phi \times 10^4$
1[b]	24	0.011	0.048
3[b]	45	0.31	4.4
5[c]	25	0.10[d]	110
6	45	0.11	13
7[c]	69	0.18	19

[a] In toluene except as indicated.
[b] From ref. 4.
[c] In benzene.
[d] Corrected for contribution from singlet carbonyl by factor obtained by multiplying intercept from 1/DPA plot by ϕ_F^{DBA} at 45°C (~0.065).

plots of the reciprocal of the light intensity vs. the reciprocal of the 9,10-diphenylanthracene, DPA, and 9,10-dibromoanthracene, DBA, concentrations, respectively (1*e*, 6). The spectrofluorimeter was calibrated using DBA solutions of **3** as a light standard. A value of 0.31 was used for the yield of excited triplet acetone formed from thermolysis of **3** (6).[4]

Discussion

Kinetics

The four tricyclic 1,2-dioxetanes **1**, **5**, **6**, and **7** undergo thermolysis with energies of activation that span a range of 7 kcal/mol. The rapid thermolysis of **1** is not at all general for tricyclic 1,2-dioxetanes. Neither is a somewhat decreased stability restricted to **1**, for two other 1,2-dioxetanes with 3,4-butano substituents are less stable than expected: **13**, E_a = 22.5 kcal/mol, is less stable than **14**, E_a = 24.5 kcal/mol (11); and **15**, E_a = 23.7 kcal/mol, is less stable than **16**, E_a = 25.2 kcal/mol, or **17**, E_a = 25.9 kcal/mol (12). However, the 1,2-dioxetanes **4** and **6**, which also have 3,4-dibutano substituents, have stabilities similar to that of **3** and are more stable than **1**, **13**, and **15**. Also, the 1,2-dioxetane **18** is as stable as **19** (3*a*), so that rather subtle effects appear to be involved in these thermolyses.

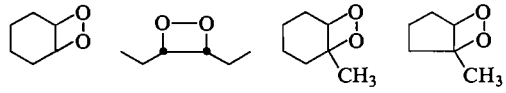

13 **14** **15** **16**

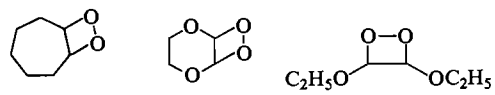

17 **18** **19**

The energies of activation for thermolysis of these bi- and tricyclic 1,2-dioxetanes could be calculated in principle with the assumption that the rate determining step is cleavage of the O—O bond to form a diradical, eq. [2] (13). The fusion of a

[2] 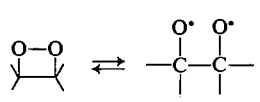

1,2-dioxetane ring to a mono- or bicyclic ring system most likely will introduce a strain in addition to the sum of the strain energies of the component rings. There are no experimental values for the

[4] This value is based on the luminol light standard (8). The use of the luminol standard should yield apparent excited state yields that are smaller by a factor of ~2.5 (9) than those determined on the basis of the radioactive light standard (10) which is often used (1*e*, 2*a*). The value of 0.31 obtained for the yield of excited triplet acetone formed from **3** (4) compares well with the value of 0.3 which was based on the radioactive light standard (3*a*). A fortuitous combination of errors in our determination of this value (4) must have accumulated in order to make it equal to that obtained by using the radioactive standard. The excited state yields determined by us previously (4) and in the present paper of all the other dioxetanes can be compared directly relative to **3** even without regard to the correctness of the absolute values.

Can. J. Chem. Downloaded from www.nrcresearchpress.com by 210.87.254.105 on 09/06/12
For personal use only.

heats of formation of bi- or tricyclic hydrocarbon molecules analogous to any of the above 1,2-dioxetanes from which one could estimate the magnitude of the extra strain energies. The extra strain energies probably vary from structure to structure since all the tricyclic 1,2-dioxetanes are calculated to have the same energies of activation for thermolysis if it is assumed that there is no extra strain energy or if all have the same extra strain energy.

Although a quantitative calculation of the energetics of the thermolysis of the various 1,2-dioxetanes cannot be made yet, some of the structural effects can be accounted for in a qualitative way. The cyclohexane ring in *cis*-bicyclo[4.2.0]octane is flattened at the side of the bridge and twisted at the other side (14). The distortion in the 1,2-dioxetane analogue should be similar. If the O—O stretching is accompanied by a twisting motion during decomposition (11), eq. [3],

[3] 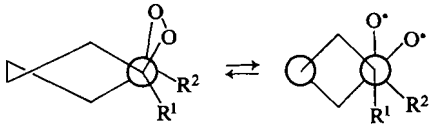

20 21

the extra strain energy will decrease as the diradical is formed. This might account for the lesser stability of **13** as compared with **14** and of **1** as compared with the other tricyclic 1,2-dioxetanes. The other tricyclic 1,2-dioxetanes all contain at least one five-membered ring. In cyclopentane the dihedral angle between the adjacent *cis*-bonds is smaller than in cyclohexane and the fusion of a 1,2-dioxetane ring to the corresponding bicyclic hydrocarbon ring systems to produce **5**, **6**, and **7** may not introduce as much extra strain energy as is present in **1**, **13**, and **15**. This would result in a higher energy of activation for decomposition of **5**, **6**, and **7**. There will be little, if any, twisting motion on opening of the 1,2-dioxetane ring in **5**, **6**, and **7** to the corresponding diradicals. Since **5** and **6** have stabilities similar to that of **3**, the twisting motion is not a required one for 1,2-dioxetane decomposition.

The 1,2-dioxetane **7** is extremely stable. Inspection of molecular models indicates that the "inside" hydrogen atoms on the carbon atoms adjacent to the bridgehead carbon atoms of the seven membered ring of **7** are forced closer together as the O—O bond is stretched. No such transannular interaction occurs when the O—O bonds of **1**, **5**, or **6** are stretched, and this may account, at least in part, for the much greater stability of **7**. A twisting motion can accompany the O—O stretch in decomposition of the bicyclic dioxetane **17** and the transannular H—H interaction can be much less than in **7**.

In comparing **4** (**20**, $R^1 = R^2 = CH_3$) with **15** (**20**, $R^1 = H$, $R^2 = CH_3$) there is relief of CH_3—CH_3 interaction by the twisting motion but an increase in this interaction as the O—O bond stretches in **4**. As well, the axial CH_3 interaction with CH_2 is increased as the twisting motion occurs. None of these interactions occurs in **15**, but it is not clear that the balance of these interactions should cause **4** to decompose with the higher energy of activation.

The 1,4-dioxane and cyclohexane rings have nearly the same shape (15) so that the extra strain energy in **18** and in **13** might be about the same. The diradical corresponding to **21** which is derived from **18** will be destabilized relative to that derived from **13** because of the anomeric effect (16) of an axial oxygen atom. However, the magnitude (17) of this effect is not large enough to account for all the greater stability of **18** over that of **13**, $\Delta E_a = 1.9$ kcal/mol (3*a*).[5]

Excited State Yields

The unusually low yield of excited state product found (4) to be produced on thermolysis of **1** is not general for tricyclic 1,2-dioxetanes. The yields of excited states formed from **5**, **6**, and **7** are greater than those from **1** by a factor of 10 to 20, although they are somewhat smaller than those, $^3\phi = \sim 0.25$ to ~ 0.5, from monocyclic 1,2-dioxetanes containing four alkyl substituents (3*b*). As has been found for mono- and bicyclic 1,2-dioxetanes, the yield of triplet products is much greater than that of excited singlet state products on thermolysis of all the tricyclic 1,2-dioxetanes. There is a large variation in yield of excited singlet state formed from the tricyclic 1,2-dioxetanes. These yields from **1** and **5** vary by a factor of about 2000. The rate of thermolysis of **5** in the presence of 10^{-2} *M* DPA was

[5] A referee has pointed out that an empirical correlation results by assuming that the ring strain correction for bicyclic dioxetanes can be obtained from the differences in ring strain between the cycloalkane and the cycloalkene. As shown below, the correlation places the energy of activation for decomposition of **13** and **17** within experimental error of that for the model **14** and places those for **15** and **16** within experimental error of each other:

Compound	E_a (exp.)[a]	Ring strain correction[a,b]	Corrected E_a[a]
14	24.5	0	24.5
13	22.5	1.4	23.9
17	25.9	−1.0	24.9
15	23.7	1.4	25.1
16	25.2	−0.4	24.8

[a] In kcal/mol.
[b] Cycloalkane–cycloalkene ring strain.

Can. J. Chem. Downloaded from www.nrcresearchpress.com by 210.87.254.105 on 09/06/12
For personal use only.

within experimental error the same as that in the presence of 10^{-2} *M* DBA. This makes it unlikely that luminescence initiated by an electron transfer (18) from DPA to **5** contributes to the light emitted from solutions of **5** containing DPA. Thus, the yield of excited singlet state given in Table 2 for **5** is likely the true yield. The varying yields of excited singlet state formed to not appear to correlate with any structural factor.

In order to assess whether the low excitation yields from **1** were due to a lack of sufficient energy from the decomposition, the energies available for excitation of the carbonyl products from the tricyclic 1,2-dioxetanes were calculated, Table 3. The values of ΔH_r for reaction of **1**, **5**, **6**, and **7** will be maximum values, and therefore the values of the energy available for excitation, $E_a - \Delta H_r$, will be minimum values, as the calculations were made with the assumption that there is no extra strain energy in these molecules. These values of ΔH_r were obtained by adding the individual hydrocarbon ring strains (13*a*) to ΔH_r for **3**. In fact, as indicated above, there is likely to be extra strain energy in these molecules and its magnitude will vary from structure to structure. Another assumption that was made is that there is no strain energy in the product diketones (implying that they are born in their most stable conformation). This is likely to be so. The strain energies of cyclooctanone, cyclononanone, and cyclodecanone are 1.5, 4.6, and 3.6 kcal/mol, respectively (13*c*, 19). These strain energies are much smaller than those of the corresponding cycloalkanes. Molecular mechanics calculations show that introduction of a second carbonyl group into cyclodecanone reduces the strain energy by another 3 kcal/mole (20) so that the cyclic diones derived from **1**, **5**, and **7** must be nearly strain-free and that from **6** will have little more than 2 kcal/mol of strain energy at most.

The low yields of excited states produced from **1** are not caused by insufficient exothermicity, as the energy available, at least 93 kcal/mol, is sufficient to populate even the singlet, ~85–87 kcal/mol, as well as the triplet, ~77 kcal/mol, excited states. If **1** contains some extra strain energy, then there will be as much or more energy available from it as from **3**, which produces 30 times as much triplet excited state as does **1**. Thus it appears that the total energy available from thermolysis is not a factor in the amounts of excited states that are formed. Even **7**, from which there is at least 17 kcal/mol more energy available than from **3**, produces less excited triplet state product than does **3**.

It has been noted (3*c*) that there is a correlation between excited state yield and the energy of activation for a considerable number of 1,2-dioxetanes. This trend is obeyed by the tricyclic 1,2-dioxetanes studied here, with the compounds having the lowest and highest energies of activation for thermolysis producing respectively the lowest and highest yields of excited states.

TABLE 3. Calculated energies available for excitation

Dioxetane	$\Delta H_r^{a,b}$	$E_a - \Delta H_r^a$
1	−69	92
3	−69[c]	95
5	−83	108
6	−76	102
7	−83	113

[a] In kcal/mol.
[b] $\Delta H_r = \Delta H_f^\circ$ (carbonyl products) − ΔH_f° (dioxetane).
[c] A value of ~65 has been obtained experimentally (13*b*).

Mono- and bicyclic 1,2-dioxetanes have available to them a twisting motion that may accompany the opening of the ring to form the diradical. Any such motion must be quite restricted in the tricyclic 1,2-dioxetanes **5**, **6**, and **7**, yet this has little effect on excited state yields. The results show that a twisting motion is not necessary for the efficient production of excited states.

Experimental

Melting points and boiling points are uncorrected. Nuclear magnetic resonance spectra were recorded with Varian analytical spectrometers models HA-100, A-60, and A-56/60 (^{1}H spectra) using tetramethyl silane as internal standard and with a Brucker HFX 10 spectrometer (^{13}C spectra). Gas chromatography analyses were carried out on Aerograph 202 and A-90-P3 gas chromatographs. Infrared spectra were recorded on Perkin-Elmer Model 421 and Model 337 spectrophotometers. Refractive indexes were measured with a Bausch and Lomb Abbe-3L refractometer.

Anhydrous magnesium sulfate was used as drying agent and solvents were removed with a rotary evaporator unless otherwise noted. Iodometric analyses were carried out using the method of Organic Synthesis (21).

1(5)-Bicyclo[3.3.0]octene **8**

Hydroboration–oxidation of 1,5-cyclooctadiene produced 1,5-cyclooctanediol (22) which was oxidized (23) to 1,5-cyclooctanedione which was in turn cyclized with zinc amalgam in hydrochloric acid (5*e*, 24) to give *cis*-1,5-bicyclo[3.3.0]octanediol in 93% yield, mp 64.5–65.5°C (lit. (24*a*) mp 61.5–62°C). A mixture of 10.3 g (0.07 mol) of this diol and 10 g (0.07 mol) of triethyl orthoformate was placed in a bath at 130°C (25). Ethanol began to distill (through a short path distillation apparatus) after 10 min. This distillation was complete after 30 min, a small chip of sodium metal was added, and the residue was distilled to give 12.0 g (85%) of a clear oil, bp 74–76°C/3 Torr, n_D^{20} 1.4590. This reaction was very sluggish, even with added acetic acid, unless the diol had been recrystallized from carbon tetrachloride.

The mixed ortho ester was placed in a short path distillation apparatus, a few crystals of benzoic acid were added, and the mixture was heated to 180°C. After 5 h distillation was complete,

Can. J. Chem. Downloaded from www.nrcresearchpress.com by 210.87.254.105 on 09/06/12
For personal use only.

the distillate was washed with water, dried ($CaCl_2$), and chromatographed through silica gel using pentane as the eluent to produce 5.6 g (86%) of **8**, a clear oil, bp 141–142°C/707 Torr, n_D^{20} 1.4836 (lit. (5*e*) bp 141°C/760 Torr, n_D^{20} 1.4832).

1(7)-Bicyclo[5.3.0]decene

A mixture of 1(2)- and 1(6)-bicyclo[4.4.0]decene obtained by reduction of tetralin with lithium in ethyl- and dimethylamine (26) was treated with performic acid (27) and from the reaction mixture *trans*-1,6-bicyclo[4.4.0]decanediol was isolated. The crude diol was converted with lead tetraacetate (27) to 1,6-cyclodecanedione which was in turn heated with hot aqueous sodium bicarbonate to give 1(7)-bicyclo[5.3.0]decen-2-one (28). This material decomposed on standing so unless it was used immediately it was reduced to the corresponding allylic alcohol with sodium borohydride (28).

A solution of 10 g (0.067 mol) of the ketone in 100 mL ether was added very slowly to a slurry made up from 30.6 g (0.29 mol) of aluminum chloride and 4.4 g (0.116 mol) lithium aluminum hydride and which had been stirred at 10°C for 15 min (29). After the addition was complete the reaction mixture was heated under reflux for one hour, then cooled and diluted with 200 mL ether. Sodium sulfate was added in small portions until gas evolution ceased. The pure white precipitate was filtered, washed with ether, and the combined filtrates were shaken with water and then dried. Solvent was removed and the residual yellow oil was distilled in a Kugelrohr apparatus to give a colorless oil. This was chromatographed on alumina using pentane as an eluent. Pentane was removed and the residue distilled to give 5.2 g (57%) of an oil, bp 193°C/700 Torr, n_D^{20} 1.4937 (lit. (30) bp 95°C/27 Torr, n_D^{20} 1.4935); ^{13}C nmr ($CDCl_3$): 137.16, 40.03, 30.75, 30.16, 27.76, and 22.39 ppm. *Anal.* calcd. for $C_{10}H_{16}$: C 88.16, H 11.84; found: C 88.41, H 11.71.

Either the ketone or the allylic alcohol could be used in this reduction. Attempts to convert the allylic alcohol to **9** using sodium in liquid ammonia, a procedure found to be useful for reduction of other allylic alcohols (31), always resulted in recovered starting material.

1(6)-Bicyclo[4.3.0]nonene

A mixture of 13 g indane, 9.0 g of lithium metal, and 350 mL of 1-propylamine was stirred under argon for 4.8 h (32). Ammonium chloride was then added until the reaction mixture remained colorless after which 200 mL ether and 200 mL water were added. The aqueous layer was extracted with ether and the combined ether layers were dried and concentrated. The residual oil was distilled (bad foaming) through a 10 cm Vigreux column to give 7.8 g (63%) of colorless oil, bp 165°C/710 Torr (lit. (33) bp 168–169°C/760 Torr).

3,4:3,4-Dipropano-1,2-dioxetane 5

To 4 mL ether at −40°C was added very slowly 1.7 g 98% hydrogen peroxide, then 1.0 g (9.2 mmol) **8**, and then in small portions over 1.5 h 1.75 g (4.6 mmol) 1,3-diiodo-5,5-dimethylhydantoin. The dark mixture was then stirred 15 min at −40°C, allowed to warm to −25°C over 20 min, and then poured into a mixture of 30 mL ice-water and 20 mL ether. The organic layer was washed quickly with cold water (2 × 20 mL), with small portions of cold 5% sodium thiosulfate solution until the iodine color was just discharged, with cold water, and dried at −20°C. It was then concentrated at 0°C to one-fourth its volume and 30 mL cold dichloromethane was added. The concentration and addition of dichloromethane was repeated twice more. The final solution was added to a stirred slurry of 5.5 g silver acetate in 30 mL dichloromethane. The resulting mixture was stirred at 0°C for 15 min, filtered through Celite, and the filtrate was washed with water, aqueous sodium bicarbonate, water, and then dried. Solvent was removed at 0°C to give a light yellow oil which was allowed to warm to 20°C under 0.01 Torr. The volatile material was trapped at −70°C to give a bright yellow oil which was stored at −70°C. The combined products of five such preparations were chromatographed at −40°C. The product was eluted as a yellow band with 95:5 pentane–ether. Solvent was removed at 0°C and the resulting bright yellow oil was recrystallized three times from 2-methylbutane at −70°C to give 0.27 g (4%) of pale yellow crystals of **5**, 92% active oxygen, which melted below room temperature.

Use of the bromohydroperoxide gave poorer yields of product. Neither the bromo- nor the iodohydroperoxide of **8** could be purified by chromatography or low temperature crystallization.

Solutions of **5** could be stored in aerated 2-methylbutane or benzene solution for many weeks but decomposed within a few seconds at room temperature when freed of solvent.

1-Bromo-6-hydroperoxybicyclo[4.3.0]nonane

Addition of 3.7 g (12.9 mmol) of 1,3-dibromo-5,5-dimethylhydantoin to a mixture of 3.0 g (25 mmol) of 1(6)-bicyclo[4.3.0]nonene and 3.75 mL (110 mmol) of 98% hydrogen peroxide in 25 mL ether at −5°C was carried out and the resulting reaction mixture worked up in the usual way (1*f*). After drying ($CaCl_2$) most of the solvent was removed at −10°C and the residual liquid was kept at −78°C overnight. Solvent was decanted from the crystals which formed. These were washed with cold ether and solvent was removed under 0.5 Torr at −10°C to give 2.8 g (47%) of crystals that decomposed within 60 s at room temperature, mp 43–46°C (dec., preheated bath). A satisfactory analysis was not obtained. This material was used directly for the preparation of the 1,2-dioxetane.

3:4-Butano-3:4-propano-1,2-dioxetane 6

A solution of 2.8 g (12 mmol) of the above product in 20 mL dichloromethane was added quickly to a suspension of 18 g (110 mmol) of silver acetate in 160 mL dichloromethane at 0°C. The reaction mixture became red during the addition and then rapidly turned pale yellow. It was stirred a further 20 min and filtered through Celite. The filtrate was shaken with water and with bicarbonate solution, dried, and concentrated at 0°C to give 1.9 g yellow liquid. This was applied to a 4 × 20 cm column of silica gel at −30°C and the column was eluted with 95:5 pentane–ether. The fractions (20 mL) were monitored by tlc and those containing only **6** were pooled and concentrated at 0°C to give 0.19 g (11%) of yellow oil which was taken up in 2 mL isopentane. Beautiful yellow crystals of **6** were deposited at −78°C which melted below 20°C after removal of solvent at −78°C to give a yellow liquid, 98.4% active oxygen. The stability of pure **6** at 20°C is much greater than that of **5**.

Later fractions of the chromatography contained a single compound which was tentatively identified from its infrared and nmr spectra as an allylic hydroperoxide, 0.8 g (47%).

3:4-Pentano-3:4-propano-1,2-dioxetane 7

This 1,2-dioxetane was prepared from the iodohydroperoxide using the procedure described above for the preparation of **5**, except that the crude product obtained from the silver acetate reaction was not subjected to low pressure distillation. From 2.0 g of 1(7)bicyclo[5.3.0]decene there was obtained 2 g yellow oil which was adsorbed in four portions on a 1 × 20 cm column of silica gel at −40°C. The column was eluted with 4:1 pentane–ether. The fractions containing the yellow bands from the four chromatographies were combined and rechromatographed as before. The product was recrystallized four times from 2-methylbutane at −78°C to give 0.65 g (26%) of yellow needles, mp 57–59°C, 99.5% active oxygen, which appeared to be quite stable at 20°C.

Can. J. Chem. Downloaded from www.nrcresearchpress.com by 210.87.254.105 on 09/06/12
For personal use only.

Characterization of 5

Solvent was removed at 0°C from a sample of **5** in pentane. After about 30 s at 20°C the residual yellow liquid had turned into white crystals (50 mg) which consisted (tlc) of a major and a minor component. Column chromatography on silica gel using ether as eluent gave 42 mg (84%) of 1,5-cyclooctanedione, mp and mixture mp 71–72°C.

A solution of 46 mg **5** in 5 mL pentane was added to a stirred slurry of 90 mg lithium aluminum hydride in 20 mL ether at −78°C. Sodium sulfate decahydrate was then added to the reaction mixture until no more hydrogen was evolved. The precipitate was filtered, washed with ether, and the combined filtrates dried and concentrated to an oil which was taken up in 10 mL benzene. The benzene was evaporated. The evaporation with benzene was repeated once more and left 41 mg (87%) of white crystals, mp and mixture mp with authentic *cis*-1,5-bicyclo[3.3.0]octanediol 64–65.5°C.

cis-*1,6-Bicyclo[4.3.0]nonanediol*

A mixture of 0.55 g (3.5 mmol) of 1(6)-bicyclo[4.3.0]nonene and 1.0 g (3.9 mmol) of osmium tetroxide in 25 mL ether was stirred at 20°C for 24 h. The reaction mixture was filtered and the precipitate was boiled with a solution of 5 g sodium bisulfite in 25 mL ethanol and 100 mL water for 14 h. The reaction mixture was filtered, the filtrate was concentrated to half its volume and extracted with methylene chloride. The organic layer was dried, and concentrated to yield 0.35 g (61%) of white crystals, mp 64–66°C (lit. (33) mp 67–67.5°C).

6-Hydroxybicyclo[4.3.0]nonan-2-one

A mixture of 0.12 g of the above diol and 1.1 g of manganese dioxide (34) in 5 mL methylene chloride was stirred at 22°C for 3 h and then filtered. Removal of the solvent left a viscous oil, homogeneous on tlc with a different R_f from starting material, which showed strong absorption in the infrared spectrum at 3500 and 1700 cm^{-1}. This was presumably 6-hydroxybicyclo[4.3.0]nonan-2-one. Yellow crystals were initially deposited on preparation of the 2,4-dinitrophenylhydrazone. These quickly turned red when the reaction mixture was warmed. The product was recrystallized from methanol–chloroform to give red needles, mp 248–250°C (lit. (35) mp 250°C for the 2,4-dinitrophenylhydrazone of 1(6)-bicyclo[4.3.0]nonen-2-one).

Ozonolysis of 1(6)-Bicyclo[4.3.0]nonene

Ozone was passed through a solution of 2 g of the alkene in 50 mL methylene chloride at −78°C (until the blue color persisted). A solution of dimethyl sulfide in methylene chloride was added. The reaction mixture was allowed to warm to 22°C and washed several times with water. The solvent was removed to give a white solid which was recrystallized from ether to give 0.3 g of a white powder, mp 180°C (lit. (33) mp 180°C for

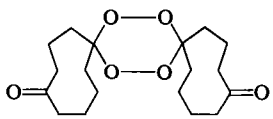

A mixture of 170 mg of this material and 50 mg platinum dioxide in 30 mL dioxane was stirred under hydrogen for 18 h. Removal of catalyst and solvent left an oily solid which gave 50 mg white powder on crystallization from ether, mp 190°C; ms(CH_5^+) *m/e*: 341.1976 ($M^+ + 1$, $C_{18}H_{24}O_6 + H^+$ required 341.1964). *Anal.* calcd. for $C_{18}H_{24}O_6$: C 63.51, H 8.23; found: C 63.33, H 8.43. It has not been possible yet to isolate 1,5-cyclononanedione (33, 35, 36).

Characterization of 6

Reduction of 9 mg of **6** with lithium aluminum hydride as described for **5** gave a trace of an oil which was homogeneous on tlc and had the same R_f value as that of *cis*-1,6-bicyclo[4.3.0]nonanediol.

A solution of toluene containing 2 mg of **6** was heated at 80°C for 4 h; tlc of resulting solution revealed one product with R_f the same as that of 6-hydroxybicyclo[4.3.0]nonan-2-one.

cis-*1,7-Bicyclo[5.3.0]decanediol*

A mixture of 0.53 g (3.9 mmol) of 1(7)-bicyclo[5.3.0]decane and 1.0 g (3.9 mmol) of osmium tetroxide in 40 mL ether was allowed to react and the mixture worked up as described for the preparation of *cis*-1,6-bicyclo[4.3.0]nonanediol to give a yellow oil. This was chromatographed on silica gel using ether as eluent. The product was colorless oil, 0.45 g (68%), ir ν_{max} (neat): 3460; ^{13}C nmr ($CDCl_3$): 82.21, 43.43, 39.27, 30.53, 22.82, and 21.01 ppm. *Anal.* calcd. for $C_{10}H_{18}O_2$: C 70.55, H 10.66; found: C 70.56, H 10.62.

1(6)-Bicyclo[4.4.0]decen-2-one

Ozone in an argon stream (37) was passed through a solution of 0.25 g 1(7)-bicyclo[5.3.0]decene in 40 mL ethyl acetate at −78°C until a blue color just persisted. The resulting solution was allowed to warm to 0°C while passing through a stream of argon. Platinum black, 200 mg, was then added and the mixture was stirred under an atmosphere of hydrogen for several hours. Removal of the catalyst and solvent gave 0.29 g (94%) of a colorless oil which showed strong absorption at 3480 as well as at 1705 in the infrared spectrum and was presumably the cyclized ketol *cis*-6-hydroxybicyclo[4.4.0]decan-2-one **12** (6). The oil was warmed a few minutes with 25 mL methanolic 1% potassium hydroxide. Work-up and removal of solvent gave 0.24 g (92%) of a light yellow oil, n_D^{20} 1.500, semicarbazone mp 243–245°C, oxime mp 147–148°C (lit. (38) for 1(6)-bicyclo[4.4.0]decen-2-one, n_D^{20} 1.4931, semicarbazone mp, 246–247°C, oxime 148–149°C).

Attempts to isolate the diketone **11** from oxidation of *cis*-1,7-bicyclo[5.3.0[decanediol with active manganese dioxide (37) were also unsuccessful. Only the oily cyclic ketol **12** was obtained.

Characterization of 7

Reduction of 50 mg of **7** with lithium aluminum hydride as described for **5** gave 46 mg (91%) of an oil which was identical (tlc and infrared) with the *cis*-1,7- bicyclo[5.3.0]decanediol prepared as described above.

A 100 mg sample of **7** in 5 mL benzene was heated at 100°C for 15 h in a sealed tube. Removal of benzene gave 100 mg of an oil whose infrared spectrum was very similar to that of the ketol **12** prepared as described above.

Kinetic Studies

The rates of decay of luminescence of solutions of the 1,2-dioxetanes containing DBA or DPA were measured using the apparatus previously described (1*f*). The results are presented in Table 1.

Excited State Yields

The apparatus and methods used have been described (4). Plots of the reciprocal of the light intensity vs. the reciprocal of the fluorescer concentration for solutions of the dioxetanes were made and light intensities at infinite fluorescer concentration (DBA for triplet yields, DPA for singlet yields) determined from the intercepts of the plots. The apparatus was calibrated with a toluene solution of **3** containing DBA (4) at 44.8°C. The yield of triplet acetone formed from **3** was taken to be 31% and the efficiency of energy transfer from the triplet excited ketones to give singlet excited DBA was taken as 0.2 (2*a*). The fluorescence efficiency of DPA was taken to be 1 at all temperatures

studied and the fluorescence efficiences of DBA at 25, 45, and 69°C were calculated to be 0.093, 0.065, and 0.036, respectively (3*a*).

1. (*a*) K. R. KOPECKY and C. MUMFORD. Can. J. Chem. **47**, 709 (1969); (*b*) P. D. BARTLETT and A. P. SCHAAP. J. Am. Chem. Soc. **92**, 3223 (1970); (*c*) C. S. FOOTE and S. MAZUR. J. Am. Chem. Soc. **92**, 3225 (1970); (*d*) W. H. RICHARDSON and V. F. HODGE. J. Am. Chem. Soc. **93**, 3996 (1971); (*e*) T. WILSON and A. P. SCHAAP. J. Am. Chem. Soc. **93**, 4126 (1971); (*f*) K. R. KOPECKY, J. E. FILBY, C. MUMFORD, P. A. LOCKWOOD, and J.-Y. DING. Can. J. Chem. **53**, 1103 (1975).
2. (*a*) T. WILSON. *In* MPT Int. Rev. Sci., Chem. Kinet. Ser. Two. Vol. 9. *Edited by* D. R. Herschbach. Butterworths, London. 1976. p. 265; (*b*) P. D. BARTLETT and M. E. LANDIS. *In* Singlet oxygen. *Edited by* H. H. Wasserman and R. W. Murray. Academic Press, New York. 1979. p. 243.
3. (*a*) T. WILSON, D. F. GOLAN, M. S. HARRIS, and A. L. BAUMSTARK. J. Am. Chem. Soc. **98**, 1086 (1976); (*b*) E. J. H. BECHARA, A. L. BAUMSTARK, and T. WILSON. J. Am. Chem. Soc. **98**, 4648 (1976); (*c*) W. H. RICHARDSON, J. H. BURNS, M. E. PRICE, R. CRAWFORD, M. FOSTER, P. SLUSSER, and J. H. ANDEREGG. J. Am. Chem. Soc. **100**, 7596 (1978).
4. K. R. KOPECKY and J. E. FILBY. Can. J. Chem. **57**, 283 (1979).
5. (*a*) E. VOGEL. Chem. Ber. **85**, 25 (1952); (*b*) A. C. COPE, J. M. GRISAR, and P. E. PETERSON. J. Am. Chem. Soc. **82**, 4306 (1960); (*c*) E. J. COREY and E. BLOCK. J. Org. Chem. **34**, 1233 (1969); (*d*) L. A. PAQUETTE and R. W. HOUSER. J. Am. Chem. Soc. **91**, 3870 (1969); (*e*) W. T. BORDEN and T. RAVINDRANTHAN. J. Org. Chem. **36**, 4125 (1971); (*f*) W. T. BORDEN, P. W. CONCANNON, and D. I. PHILLIPS. Tetrahedron Lett. 3161 (1973).
6. P. S. WHARTON and G. A. HIEGEL. J. Org. Chem. **30**, 3254 (1965).
7. J. F. BUNNETT. *In* Rates and mechanisms of reactions. Vol. 8, Part 1 of Technique of organic chemistry. 2nd ed. *Edited by* A. Weissberger. Interscience, New York. 1961. p. 199.
8. J. LEE and H. H. SELIGER. Photochem. Photobiol. **4**, 1015 (1965).
9. (*a*) J. W. HASTINGS and G. T. REYNOLDS. *In* Bioluminescence in progress. *Edited by* F. H. Johnson and Y. Haneda. Princeton University Press, Princeton, NJ. 1966. p. 45; (*b*) D. K. DUNN, G. A. MICHALISZYN, I. G. BOGACKI, and E. A. MEIGHEN. Biochemistry, **12**, 4911 (1973); (*c*) P. R. MICHAEL and L. R. FAULKNER. Anal. Chem. **48**, 1188 (1976).
10. (*a*) J. W. HASTINGS and G. WEBER. J. Opt. Soc. Am. **53**, 1410 (1963); (*b*) J. W. HASTINGS and G. WEBER. Photochem. Photobiol. **4**, 1049 (1965).
11. A. L. BAUMSTARK and C. E. WILSON. Tetrahedron Lett. 2569 (1979).
12. P. LECHTKEN, G. REISSENWEBER, and P. GRUBMÜLLER. Tetrahedron Lett. 2881 (1977).
13. (*a*) S. W. BENSON. Thermochemical kinetics. 2nd ed. John Wiley and Sons, New York, NY. 1976; (*b*) H.-C. STEINMETZER, A. YEKTA, and N. J. TURRO. J. Am. Chem. Soc. **96**, 282 (1974).
14. A. SPELBOS, F. C. MIJLHOFF, W. H. BAKKER, R. BADEN, and L. VAN DEN ENDEN. J. Mol. Struct. **38**, 155 (1977).
15. M. DAVIS and O. HASSEL. Acta Chem. Scand. **17**, 1181 (1963).
16. R. U. LEMIEUX and N. J. CHU. Abstracts of the 133rd National Meeting of the American Chemical Society. San Francisco, CA. April 1958. p. 31N.
17. E. L. ELIEL and C. A. GIZA. J. Org. Chem. **33**, 3754 (1966).
18. (*a*) J.-Y. KOO and G. B. SCHUSTER. J. Am. Chem. Soc. **100**, 4496 (1978); (*b*) G. B. SCHUSTER. Acc. Chem. Res. **12**, 366 (1979).
19. G. WOLFF. Helv. Chim. Acta, **55**, 1446 (1972).
20. N. L. ALLINGER, M. T. TRIBBLE, and M. A. MILLER. Tetrahedron, **28**, 1173 (1972).
21. H. B. KNIGHT and D. SWERN. *In* Org. Synth. Coll. Vol. **4**. *Edited by* N. Rabjohn. John Wiley and Sons, Inc., New York. 1963. p. 895.
22. F. F. KNIGHTS and H. C. BROWN. J. Am. Chem. Soc. **90**, 5280 (1968).
23. G. I. GLOVER, R. B. SMITH, and H. RAPOPORT. J. Am. Chem. Soc. **87**, 2003 (1965).
24. E. W. ENKERT and J. E. VODER. J. Org. Chem. **35**, 2896 (1970).
25. G. CRANCK and F. W. EASTWOOD. Aust. J. Chem. **17**, 1392 (1964).
26. R. A. BENKESER and E. M. KAISER. J. Org. Chem. **29**, 955 (1964).
27. S. DEV. J. Indian Chem. Soc. **31**, 1 (1954).
28. A. G. ANDERSON and J. A. NELSON. J. Am. Chem. Soc. **73**, 232 (1951).
29. (*a*) B. R. BROWN and A. M. S. WHITE. J. Chem. Soc. 3755 (1957); (*b*) J. BROOME, B. R. BROWN, A. ROBERTS, and A. M. S. WHITE. J. Chem. Soc. 1406 (1960).
30. E. KOVATS, A. FÜRST, and H. GÜNTHARD. Helv. Chim. Acta, **37**, 534 (1954).
31. K. R. KOPECKY, W. A. SCOTT, P. A. LOCKWOOD, and C. MUMFORD. Can. J. Chem. **56**, 1114 (1978).
32. J. E. STARR and F. H. EASTMAN. J. Org. Chem. **31**, 1393 (1966).
33. R. CRIEGEE and H. ZOGEL. Chem. Ber. **84**, 215 (1951).
34. J. ATTENBURROW, A. B. F. CAMERON, and J. H. CHAPMAN. J. Chem. Soc. 1094 (1952).
35. V. PRELOG, K. SCHENKER, and W. KÜNIG. Helv. Chim. Acta, **36**, 471 (1953).
36. G. L. BUCHANAN, J. G. HAMILTON, and R. A. RAPHAEL. J. Chem. Soc. 4606 (1963).
37. G. A. COOK, A. D. KIFFER, C. V. KUMPP, A. H. MALICK, and L. A. SPENCE. Adv. Chem. Ser. **21**, 44 (1959).
38. M. F. ANSELL and J. W. DUCKER. J. Chem. Soc. 5219 (1960).

Can. J. Chem. Downloaded from www.nrcresearchpress.com by 210.87.254.105 on 09/06/12
For personal use only.

Interactions gauches et chemins réactionnels. Etudes conformationnelles d'hydroxyalkyl-4 cyclohexènes contraints

JEANINE BOUTEILLER-PRATI, JEAN-CLAUDE BOUTEILLER ET JEAN-PIERRE AYCARD[1]

Laboratoire de Chimie Organique Structurale, Université de Provence, 13, Rue Henri Poincaré, 13397 Marseille, Cedex 13, France

Reçu le 11 février 1980[2]

JEANINE BOUTEILLER-PRATI, JEAN-CLAUDE BOUTEILLER et JEAN-PIERRE AYCARD. Can. J. Chem. **59**, 859 (1981).

L'étude par rmn des alcools obtenus par addition de CH_3Li ou $AlLiH_4$ au carbonyle exocyclique des alkyl-3 méthoxycarbonyl-4 (acétyl-4) cyclohexènes *cis* et *trans* (alkyl = H, CH_3 ou $C(CH_3)_3$), permet d'accéder aux paramètres J et δ. A partir des valeurs des constantes de couplage expérimentales, on détermine les enthalpies libres conformationnelles (ΔG^0_X) des substituants méthylcarbinol et diméthylcarbinol (−0,62 et 2,08 kcal mol^{-1} respectivement) ainsi que les équilibres conformationnels des différents alcools. Pour R = *tert*-butyle, la nette prépondérance du conformère diaxial des isomères *trans* permet d'envisager une addition à partir des conformères de plus haute énergie.

JEANINE BOUTEILLER-PRATI, JEAN-CLAUDE BOUTEILLER, and JEAN-PIERRE AYCARD. Can. J. Chem. **59**, 859 (1981).

From J and δ values determined by the nmr study of alcohols obtained by addition of CH_3Li and $LiAlH_4$ to the exocyclic carbonyl of *cis* and *trans* 3-alkyl 4-carbomethoxy (or acetyl) cyclohexenes (alkyl = H, CH_3, $C(CH_3)_3$), we have deduced the conformational free energy values (ΔG^0_X) of the $CH(CH_3)OH$ and $C(CH_3)_2OH$ substituents (0.62 and 2.08 kcal mol^{-1} respectively) as well as the values for some related conformational equilibria. For *trans tert*-butyl derivatives the stability of the diaxial conformer agrees with a reaction path involving high energy conformers.

Introduction

S'il est bien connu que la proportion et la nature des produits de réaction ne dépend que de la différence d'énergie libre des états de transition (1), pour des structures présentant un équilibre conformationnel, il existe peu d'exemples dans la littérature d'intervention préférentielle des conformères de haute énergie (2, 3).

Ayant mis en évidence un tel comportement dans des dérivés substitués en position 4 du *tert*-butyl-3 cyclohexène (3) nous avons essayé dans le présent travail de relier l'intervention de ces conformères "peu stables" au développement des contraintes stériques dans l'état de transition.

Pour ce, nous avons entrepris une étude structurale et conformationnelle par rmn d'alcools résultants d'une addition nucléophile sur la fonction carbonyle exocyclique d'alkyl-3 acétyl-4 ou méthoxycarbonyl-4 cyclohexènes (alkyl = H, méthyl, *tert*-butyl). En effet, pour ce type de réaction, nous pouvons envisager que dans l'état de transition, l'accroissement des contraintes stériques entre les substituants vicinaux, provenant du passage d'un carbone hybridé sp^2 à un carbone de type sp^3, va se traduire par d'importantes modifications conformationnelles et qu'il sera possible de favoriser des chemins impliquant des conformères de haute énergie qui seront moins contraints dans l'état de transition.

Résultats expérimentaux

Les différents alcools (cf. Schéma 1) sont obtenus (cf. Partie expérimentale) par addition de CH_3Li ou des hydrures $LiAlH_4$ et Sélectride sur la fonction carbonyle d'alkyl-3 acétyl-4 ou méthoxycarbonyl-4 cyclohexènes (alkyl = H, CH_3, $(CH_3)_3C$). D'une manière générale et malgré l'utilisation de molécules deutériées en position allylique (4), les spectres de rmn relatifs au protons H_1, H_2 et H_3 (cf. Schéma 1) sont de type ABC partiellement masqués par les signaux des groupements alkyles.

SCHÉMA 1. Numérotation des composés*

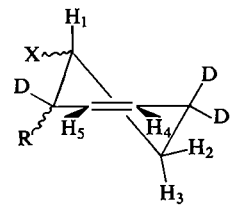

	R		
X	H	CH_3	$C(CH_3)_3$
$CHCH_3OH$	**10**		**30***t*
$C(CH_3)_2OH$	**11**	**21***c*	**31***t*
		21*t*	
CH_2OH	**12**	**22***c*	**32***c*
		22*t*	**32***t*

*L'indice *c* ou *t* est relatif α la position respectivement *cis* ou *trans* des substituants. Pour faciliter les comparaisons nous avons utilisé la même numérotation que dans les réferences 4 et 10, les protons exocycliques sont numérotés H_6 et H_7.

[1]Auteur à qui toute correspondance doit être adressée.

[2]Revision reçue le 7 juillet 1980.

0008-4042/81/050859-06$01.00/0

©1981 National Research Council of Canada/Conseil national de recherches du Canada

Can. J. Chem. Downloaded from www.nrcresearchpress.com by 210.87.254.5 on 09/06/12
For personal use only.

TABLEAU 1. Paramètres rmn des alcools*

	Composé						
	10	**30*t***	**11**	**21*t***	**31*t***	**32*c***	**32*t***
δR		1,0		1 à 1,2	0,95	0,90	0,90
δMe—COH	1,24	1,55	1,80	1 à 1,2	1,10		
δ_1	1,48	2,58	2,45	4,00	3,02	1,96	3,01
δ_2	1,91	2 à 2,15	2,27	3,11	2,78	1,55	1,97
δ_3	1,28	2 à 2,15	1,67	3,00	2,15	1,43	3,00
δ_4	5,60	5,65	5,70	5,62	5,72	5,76	5,55
δ_5	5,60	5,65	5,70	5,49	5,65	5,69	5,67
δ_6	3,46	4,96				3,35	{3,47
δ_7						3,35	{3,78
J_{12}	2,9	3,4	2,3	3,5	2,4	3,2	2,9
J_{13}	9,4	4,2	11,7	8,4	5,8	5,5	3,8
J_{15}	—	—	—	—	—	0,8	—
J_{16}	6,4	7,8	—	—	—	7,4	{10,2
J_{17}	—	—	—	—	—	7,4	{ 4,2
J_{23}	−13,0	−14,5	−12,0	−13,9	−14,5	−13,4	−13,3
J_{45}		−10		−9,8	−10,5	−10,4	−10,3
$J_{6—Me}$	6,7						
J_{6-7}							−10,2

*Solvant: CCl_4, T = 303 K, δ en ppm par rapport au TMS, *J* en Hz.

Afin de pouvoir les analyser nous avons utilisé un réactif de déplacement l'Eu(FOD)$_3$-D-27; les paramètres ainsi déterminés sont regroupés dans le Tableau 1.

Analyse des spectres de rmn

Lors de l'attaque d'un ion hydrure sur les alkyl-3 acétyl-4 cyclohexènes, il peut se former *a priori* deux diastéréoisomères suivant l'entrée du réactif par l'une ou l'autre des faces du carbonyle.

Dans ce cas, les spectres rmn des produits se compliquent par la superposition des signaux des deux isomères *thréo* et *érythro*, et seuls les paramètres du diastéréoisomère majoritaire de **10** et **30*t*** obtenu par action du Sélectride ont pu être déterminé. L'utilisation de cet hydrure encombré permet en effet d'augmenter la diastéréosélectivité de la réaction qui passe de 50% à 90%. Cependant, malgré cette préférence (5) et contrairement aux résultats observés en série cyclique (6), l'existence dans nos composés de trois conformères acycliques (7) pour chacune des deux conformations cycliques possibles (4) empêche toute prévision suivant l'un des modèles de Cram et Abd Elhafez (8) ou de Felkin et coll. (9); il est donc impossible d'attribuer à ce diastéréoisomère la stéréochimie *thréo* ou *érythro*.

Le spectre du composé **10** présente à δ = 5,10 et δ = 2,92 ppm deux singulets correspondant respectivement aux protons éthyléniques et au proton du groupement hydroxyle; à δ = 1,24 ppm on observe un doublet (*J* = 6,7 Hz) attribué aux protons du groupement méthyle. Le reste du spectre se compose d'un multiplet à 3,46 ppm facilement identifiable au proton H_6 du groupement méthylcarbinol, de quatre raies attribuables au signal du proton H_2, ainsi qu'à δ = 1,48 ppm d'un système complexe qui peut être attribué au signal du proton H_1 couplé par trois autres protons. Le signal du proton H_3 en partie recouvert par celui du groupement méthyle apparait sous la forme de quatre raies centrées à δ = 1,28 ppm dont l'attribution est confirmée par l'existence de deux grandes constantes de couplage (−13 et 9,4 Hz).

Sans réactif de déplacement, le diastéréoisomère majoritaire (90%) **30*t***, obtenu par réduction à l'aide du Sélectride du *trans tert*-butyl-3 trideutérioacétyl-4 cyclohexène D_3-3,6,6, présente essentiellement un spectre de type AB centré à 5,75 ppm correspondant au signal des protons éthyléniques et un doublet à δ = 3,50 ppm identifiable au proton exocyclique H_6. Les autres protons et le signal du *tert*-butyle compris entre 0,80 et 1,80 ppm ne peuvent être résolus. Après addition d'Eu(FOD)$_3$-D-27, tous les protons du cycle sont différenciés: à δ = 2,58 ppm, on observe un massif composé de cinq raies attribuable au proton H_1 couplé à trois autres protons; centrés à 2,0 et 2,15 ppm apparaissent deux massifs composés de quatre raies présentant une grande constante de couplage (*J* = 14,5 Hz) correspondant vraisemblablement à la constante *gem* et deux petites constantes (*J* = 4,2 et 3,4 Hz respectivement) qui indiquent malgré l'ambiguité d'attribution une position préférentiellement axiale du substituant méthylcarbinol.

Can. J. Chem. Downloaded from www.nrcresearchpress.com by 210.87.254.5 on 09/06/12
For personal use only.

Can. J. Chem. Downloaded from www.nrcresearchpress.com by 210.87.254.5 on 09/06/12
For personal use only.

TABLEAU 2. Equilibres conformationnels des alcools

Composé	$\langle {}^3J_{13} \rangle$	x_e*	$\Delta G^0 = G_e - G_a$ kcal mol^{-1}
10	9,4	0,74	$-0,62 \pm 0,02$
30*t*	4,2	0,22	$+0,77 \pm 0,06$
	3,4	0,14	$+1,10 \pm 0,07$
11	11,7	0,97	$-2,08 \pm 0,02$
21*t*	8,4	0,64	$-0,34 \pm 0,03$
31*t*	5,8	0,38	$+0,29 \pm 0,04$
12			$-0,9$ (7)
22*t*		0,92	$-1,5$ (6)
22*c*	10,4		$-0,9$ (6)
32*c*	5,5	0,35	$+0,37 \pm 0,04$
32*t*	3,8	0,18	$+0,92 \pm 0,06$
	2,9	0,09	$+1,40 \pm 0,08$

*x_e = Fraction molaire du conformère à substituant équatorial en position 4 sur le cyclohexène calculée à partir des paramètres J_{ee} = 2 Hz et J_{aa} = 12 Hz.

En présence de réactif de déplacement, le spectre du composé **11** présente à $\delta = 5,70$ ppm un singulet correspondant aux protons éthyléniques et trois massifs distincts entre 1 et 3 ppm. Le proton H_3 est facilement attribuable au triplet centré à 1,67 ppm, l'observation de deux grandes constantes de couplage (J = 12 Hz et J = 11,7 Hz) indiquant une position équatoriale préférentielle du groupement diméthylcarbinol. Les protons H_1 et H_2 se présentent sous forme de deux massifs de quatre raies chacun, centrés respectivement à 2,45 ppm et 2,27 ppm. L'attribution de ces protons a été effectuée en considérant leurs constantes de couplage avec H_3 et en prenant ${}^2J_{23} = -12$ Hz.

Le spectre du composé **21***t* obtenu en présence de sel de lanthanide présente pour les protons du cycle un système de type ABX, partiellement recouvert par les signaux des deux groupements méthyles du carbinol, et dont les massifs de quatre raies centrés à δ = 4,00, 3,00 et 3,11 ppm sont facilement attribuables respectivement aux protons H_1, H_3 et H_2. Les protons éthyléniques apparaissent sous forme d'un système AB.

Pour le composé **21***c*, l'addition d'Eu(FOD)$_3$-D-27 conduit à un déplacement simultané des signaux des protons du cycle et des groupements méthyles sans qu'il soit possible d'en éliminer la superposition et seule la partie du spectre correspondant aux protons éthyléniques ($\delta_4 = 5,56$ ppm, $\delta_5 = 5,48$ ppm, $J_{45} = -10,4$ Hz) peut être exploitée.

L'analyse du spectre de **31***t*, analogue à celui de **21***t* ne présente pas de difficulté. L'existence des deux petites constantes de couplage entre les protons H_1H_2 et H_1H_3 semble indiquer, dans l'hypothèse d'une conformation demi-chaise, une préférence axiale du substituant diméthylcarbinol.

Pour le composé **31***c* comme pour **21***c* l'utilisation d'Europium ne permet pas d'exploiter le spectre de rmn car les signaux de groupements méthyles du diméthyl carbinol se déplacent en même temps que ceux des protons du cycle.

Dans le cas des composés **32***c* et **32***t* l'ensemble des paramètres de rmn (cf. Tableau 1) sont obtenus à partir des modifications isotopiques D_3 et D_5 provenant de la réduction des *tert*-butyl-3 méthoxycarbonyl-4 cyclohexènes D_3-3,6,6 *cis* et *trans* par $LiAlH_4$ et $LiAlD_4$ respectivement. En présence de réactif de déplacement les spectres de type AMX et ABX ne présentent pas de difficultés particulières. Au niveau du substituant exocyclique le spectre de **32***c* se compose d'un doublet correspondant aux deux protons H_6 et H_7 couplés à H_1 avec une constante de 7,4 Hz. Pour **32***t*, on observe un spectre de type ABX composé d'un triplet à δ = 3,47 ppm (J = 10,2 Hz) et de quatre raies centrées à δ = 3,78 ppm correspondant à des couplages de 10,2 et 4,2 Hz.

Conformation cyclique (cf. Tableau 2)

A partir des constantes expérimentales $\langle {}^3J_{13} \rangle$[3] entre les protons *trans* portés par les carbones C-4 et C-5 et les constantes spécifiques estimées dans un travail précédent (10), $2 < J_{ee} < 5$ Hz et J_{aa} = 12 Hz, il est possible de déterminer les populations des différents conformères en équilibre, ainsi que les différences d'énthalpie libre qui leur sont associées. Ces valeurs sont regroupées dans le Tableau 2, nous y avons joint celles obtenues par Mackay (11) sur l'hydroxyméthyl-4 cyclohexène **12**, ainsi que celles relatives aux méthyl-3 hydroxyméthyl-4 cyclohexènes **22***c* et **22***t* (10).

Pour les dérivés monosubstitués **10** et **11** les valeurs obtenues correspondant aux enthalpies libres conformationnelles des substituants en position 4 sur le cyclohexène, $\Delta G^0_{CHCH_3OH} = -0,62 \pm 0,02$ kcal mol^{-1}; $\Delta G^0_{C(CH_3)_2OH} = -2,08 \pm 0,02$ kcal mol^{-1} ($-2,18$ kcal mol^{-1}) (11).

Ces résultats confirment la préférence équatoriale des substituants en position 4 sur le cyclohexène. Il faut noter toutefois la préférence équatoriale très marquée du groupement diméthylcarbinol homomorphe d'un groupement *tert*-butyle.

Pour le composé **32***c*, la faible valeur de J (5,5 Hz, cf. Tableau 1) implique une préférence axiale du substituant en position 4, analogue à celle observée pour le *tert*-butyl-3 méthoxycarbonyl-4 cyclohexène (ΔG^0 = 0,3 kcal mol^{-1}) (4*a*).

[3]Nous avons montré dans un travail cristallographique récent (cf. réf. 13*b*) que pour ce type de dérivés la valeur de l'angle dièdre ϕ_{45} était peu soumise à variation (cf. Table 1, réf. 13*b*). Cette variation maximum $\Delta\phi \simeq 4°$ correspondrait à un $\Delta J \simeq$ 0,7 Hz trop faible pour influencer notablement la valeur de ΔG^0.

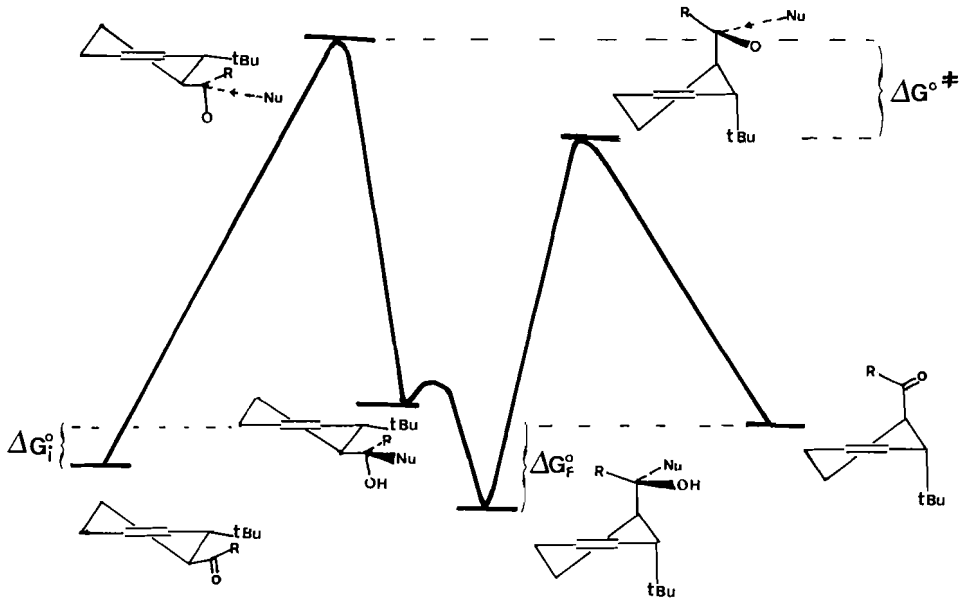

SCHÉMA 2

Dans le cas des alcools tertiaires **11**, **21***t*, **31***t* on observe une augmentation de la valeur du ΔG^0 avec la taille du substituant R (de $\Delta G^0 = -2{,}1$ kcal mol^{-1} pour R = H à $\Delta G^0 = +0{,}29$ kcal mol^{-1} pour R = *tert*-butyle). Ce résultat illustre bien la déstabilisation des conformères diéquatoriaux sous l'effet d'une interaction diéquatoriale entre un groupement encombrant $C(CH_3)_2OH$ homomorphe d'un *tert*-butyle et un groupement R vicinal.

La dernière remarque que nous pouvons faire est relative à l'ensemble des dérivés *tert*-butylés **30***t*, **31***t*, **32***t*. Pour ces dérivés analogues aux di-*tert*-butyl-3,4 cyclohexènes *trans*, nous obtenons de petites constantes de couplage J_{13} (4,2 ou 3,4, 5,8 et 3,8 ou 2,9 Hz), qui dans l'hypothèse d'une conformation demi-chaise ou sofa (12), indiquent une nette préférence pour des conformères à groupement *tert*-butyle pseudo-axial.[4] Cette valeur élevée des populations de conformères diaxiaux (≥ 60%) supérieure à celle observée pour les homologues *tert*-butyl-3 cyano-4 ou méthoxycarbonyl-4 cyclohexènes (4) est vraisemblablement due à l'augmentation de l'encombrement stérique du substituant exocyclique,[5] qui dans nos composés, est équivalent à un groupement méthyle ou *tert*-butyle.

Interactions gauches et chemins réactionnels

A partir des résultats obtenus dans le paragraphe précédent, nous pouvons envisager une hypothèse quant à la nature du conformère impliqué dans l'attaque du nucléophile. En effet, conformément au principe de Hamond (1), celle-ci aura lieu sur le conformère conduisant à l'état de transition de plus basse énergie, c'est-à-dire sur celui dans lequel les contraintes stériques seront minimales.

Si pour les dérivés monosubstitués, l'approche du réactif se traduit par une augmentation de l'encombrement stérique qui n'affecte pas la plus grande stabilité des conformères équatoriaux (cf. Tableau 2, composés **10**, **11**, **12**). Pour les dérivés disubstitués en 3,4, et particulièrement pour les isomères *trans*, le passage du carbone sp^2 du carbonyle à une hybridation sp^3 conduit à une déstabilisation importante des conformères diéquatoriaux.[6]

Dans ces conditions, nous pouvons envisager

[4]Pour ces composés, l'évolution de la valeur ΔG^0 qui conduit à une diminution de la fraction molaire des conformères diaxiaux en passant de **30***t* à **32***t* peut s'expliquer par l'existence de deux phénomènes antagonistes: d'une part, la déstabilisation du conformère diéquatorial sous l'effet de l'interaction entre les substituants *tert*-butyle et CR_2OH, et d'autre part une stabilisation de celui-ci due à la préference conformationnelle du substituant CR_2OH.

[5]Dans un travail récent (13) il a été montré que l'une des causes possibles de l'existence d'une hétérogénéité conformationnelle dans cette série, était la courte distance existant entre le carbone central du substituant en position 4 et les carbones du groupement *tert*-butyle.

[6]Alors que pour les *t*-Bu-3 méthoxycarbonyl-4 ou acétyl-4 cyclohexènes *trans* (4) la fraction molaire de l'isomère diéquatorial est de l'ordre de 0,75 pour les composés **30***t*, **31***t* et **32***t* elle est inférieure à 0,40.

Can. J. Chem. Downloaded from www.nrcresearchpress.com by 210.87.254.5 on 09/06/12
For personal use only.

Can. J. Chem. Downloaded from www.nrcresearchpress.com by 210.87.254.5 on 09/06/12
For personal use only.

pour ces dérivés (cf. Schéma 2) un chemin réactionnel issu du conformère de haute énergie à substituants diaxiaux, énergétiquement favorisé dans l'état de transition.

Conclusion

Ce travail nous a permis de déterminer les équilibres conformationnels d'une série de carbinol, méthylcarbinol et diméthylcarbinol-4- cyclohexènes diversement substitués en position 3. Les résultats obtenus pour les stéréoisomères *trans tert* -butylés en 3 permettent d'envisager une addition sur le conformère diaxial.

Partie expérimentale

Toutes les synthèses ont été effectuées sur des stéréoisomères purs préalablement séparés par chromatographie en phase vapeur préparative. La synthèse des cétones et des esters utilisés a déjà été décrite (4).

Les alcools primaires et secondaires ont été préparés suivant la méthode générale indiquée ci-dessous.

Dans un ballon équipé d'un réfrigérant muni d'un piège à chlorure de calcium, d'une ampoule à verser et d'une agitation magnétique, on introduit $LiAlH_4$ en suspension dans de l'éther anhydre. On verse ensuite goutte à goutte la cétone ou l'ester en solution éthérée ($LiAlH_4$ est en excès). Lorsque l'addition est terminée, on porte à reflux pendant une heure tout en maintenant l'agitation. On effectue ensuite une hydrolyse basique du mélange réactionnel (14). L'alumine formée est filtrée sur verre fritté. On lave ensuite le mélange réactionnel avec une solution saturée en chlorure de sodium, puis on sèche sur $MgSO_4$ anhydre. Le mélange réactionnel est analysé par chromatographie en phase vapeur (cpv) dans les conditions suivantes: Chromatographe Girdel Série 3000 équipé d'un détecteur à ionisation de flamme; gaz vecteur: azote, débit $\simeq$ 10 cm³/min; température injecteur 200°C; température détecteur: 215°C; colonne en acier inoxydable de 1/8 po de diamètre et de 3 m de long, remplie de Chromosorb W(NAW) 60/80 mesh, imprégné de polyéthylèneglycol 4000 à 20% en poids.

tert-*Butyl-3 méthylcarbinol-4 cyclohexène* trans ***30***t

On fait réagir 0.25 g ($1.4 \cdot 10^{-3}$ mol) de *tert*-butyl-3 acétyl-4 cyclohexène *trans* (*4b*) et 0.014 g ($3.5 \cdot 10^{-3}$ mol) de $AlLiH_4$. Le rendement est de 98%; cpv: température 140°C; tr: 50,0 min; ir (CCl_4) ν_{max}: 3630 et 3450 (—OH), 3030 (=C—H), 1650 (C=C) cm^{-1}.

On synthétise de la même manière le *tert*-butyl-3 méthylcarbinol-4 cyclohexène (D_3-3,6,6) *trans* et le *tert*-butyl-3 [méthyl (D_3) carbinol]-4 cyclohexène (D_3-3,6,6) *trans* à partir des cétones correspondantes.

tert-*Butyl-3 carbinol-4 cyclohexène* cis ***32***c

On l'obtient par action de 0.5 g ($1.3 \cdot 10^{-2}$ mol) de $AlLiH_4$ sur 0.5 g ($2.4 \cdot 10^{-3}$ mol) de *tert*-butyl-3 méthoxycarbonyl-4 cyclohexène *cis* (*4a*). Le rendement est de 98%; pé: 98°C/2 Torr; cpv: température 170°C; tr: 39,5 min; ir (CCl_4) ν_{max}: 3630 et 3400 (—OH), 3020 (=C—H) cm^{-1}.

tert-*Butyl-3 carbinol-4 cyclohexène* trans ***32***t

On opère comme précédemment; pf: 67–70°C; cpv: température 170°C; tr: 48.1 min; ir (CCl_4) ν_{max}: 3630 et 3410 (—OH), 3020 (=C—H), 1650 (C=C) cm^{-1}.

On a préparé de la même manière les *tert*-butyl-3 carbinol-4 cyclohexènes (D_3-3,6,6) *cis* et *trans* à partir des esters correspondants. Par action de $AlLiD_4$ sur ces esters, nous avons obtenu les *tert*-butyl-3 [carbinol (D_2)]-4 cyclohexène (D_3-3,6,6) *cis* et *trans*.

Méthylcarbinol-4 cyclohexène (D₄-3,3,6,6) ***10***

On utilise 0.65 g d'acétyl-4 cyclohexène (D_4-3,3,6,6) et 0.05 g de $AlLiH_4$; cpv: température 120°C; tr: 36 min; ir (CCl_4) ν_{max}: 3620 et 3510 (—OH), 3030 (=C—H), 1650 (C=C) cm^{-1}.

Réduction par le Li-Sélectride (5)

Dans un ballon muni d'un réfrigérant surmonté d'un piège à chlorure de calcium, d'une ampoule à verser, d'une arrivée d'azote et d'une agitation magnétique, on effectue un balayage d'azote durant une heure tout en refroidissant à −78°C. On verse ensuite 3.75 cm³ ($3.75 \cdot 10^{-3}$ mol) d'une solution commerciale 1 *M* de tri-(*sec* butyl) borohydrure de lithium (Li-Sélectride) (Aldrich) et 20 cm³ de THF anhydre. Puis on ajoute goutte à goutte $1.5 \cdot 10^{-3}$ mol de cétone en solution dans du THF anhydre. Lorsque l'addition est terminée, on laisse revenir le mélange reactionnel à température ambiante. L'excès d'hydrure est détruit par quelques cm³ d'eau que l'on ajoute tout en maintenant le ballon à 0°C. Après avoir alcalinisé avec 1.5 cm³ de solution de soude 3 *N* et chauffé à 35°C quelques instants, on ajoute 2.5 cm³ de H_2O_2 (110 volumes) tout en refroidissant le ballon à l'aide d'un mélange eau/glace. On verse ensuite le mélange réactionnel sur de la glace, on ajoute une petite quantité de chlorure de sodium solide et on extrait au pentane. Rendement 88%.

tert-*Butyl-3 [méthyl(D_3) carbinol]-4 cyclohexène (D_3-3,6,6)* trans ***30***t D_6

On l'obtient par action du Li-Sélectride sur le *tert*-butyl-3 trideutérioacétyl-4 cyclohexène (D_3-3,6,6) *trans*; ir (CCl_4) ν_{max}: 3630 et 3450 (—OH), 3030 (=C—H), 2100 à 2220 (C—D), 1650 (C=C) cm^{-1}.

Les alcools tertiaires sont obtenus par l'addition du méthyl lithium en solution dans l'éther (solution commerciale 2 *M*, Aldrich) sur les cétones ou esters correspondants, selon le mode opératoire suivant.

Dans un ballon refroidi par un bain de glace, on fait réagir le méthyl lithium sur l'ester ou la cétone en solution dans l'éther anhydre, tout en maintenant le mélange réactionnel sous atmosphère d'azote. Lorsque l'addition est terminée on porte à reflux pendant une dizaine de minutes, puis on hydrolyse à froid avec une solution saturée en NH_4Cl. La phase aqueuse est extraite à l'éther puis cette solution éthérée est séchée sur sulfate de magnésium anhydre. Après évaporation du solvant, on obtient l'alcool tertiaire.

Les conditions d'analyse en chromatographie en phase vapeur sont les mêmes que précédemment.

Diméthylcarbinol-4 cyclohexène (D₄-3,3,6,6) ***11***

On additionne à 0.6 g d'acétyl-4 cyclohexène (D_4-3,3,6,6), 4 cm³ de la solution de méthyl lithium. Le rendement est de 98%; cpv: température 120°C; tr: 33.2 min; ir (CCl_4) ν_{max}: 3620 et 3500 (—OH), 2100 à 2200 (C—D) cm^{-1}.

Méthyl-3 diméthylcarbinol-4 cyclohexène cis ***21***c

Chromatographie en phase vapeur: température 130°C; tr: 24.5 min; ir (CCl_4) ν_{max}: 3620 et 3500 (—OH), 3020 (=C—H) cm^{-1}.

Méthyl-3 diméthylcarbinol-4 cyclohexène trans ***21***t

Chromatographic en phase vapeur: température 130°C; tr: 19.9 min; ir (CCl_4) ν_{max}: 3620 et 3500 (—OH), 3020 (=C—H) cm^{-1}.

*tert-Butyl-3 diméthylcarbinol-4 cyclohexène (D_3-3,3,6,6) 31*t

On fait réagir 0.50 g de *tert*-butyl-3 acétyl-4 cyclohexène (D_3-3,3,6,6) avec 3 cm³ de la solution de méthyl lithium. Rendement de 99%; cpv: température 140°C; tr: 51 min; ir (CCl_4) ν_{max}: 3610 et 3480 (—OH), 3030 (=C—H), 2100 à 2200 (C—D) cm^{-1}.

Spectres de rmn

Les spectres de rmn ont été enregistrés sur un appareil Varian XL 100 équipé d'un découpleur hétéronucléaire du deutérium, en utilisant des solution d'alcool (10% dans CCl_4 sec) préalablement dégazées. L'Eu(FOD)$_3$-D-27 est ajouté par fractions de 10 mg environ jusqu'à l'obtention de spectres simples. Les spectres sont simulés sur un ordinateur HP 2100 à l'aide du programme LAOCON III (15). Les paramètres affinés par itérations successives du même programme sont regroupés dans le Tableau 1.

1. (*a*) E. L. ELIEL. Stereochemistry of carbon compounds. McGraw Hill, New York. 1962. pp. 151 et 237; (*b*) N. S. ZEFIROV. Tetrahedron, **33**, 2719 (1977).
2. D. C. WIGFIELD, S. FEINER et D. J. PHELPS. J. Org. Chem. **40**, 2533 (1975).
3. (*a*) L. PIZZALA, J. P. AYCARD et H. BODOT. J. Org. Chem. **43**, 1013 (1978); (*b*) R. C. CAMBIE, P. S. RUTLEDGE, T. SMITH-PALMER et P. D. WOODGATE. J. Chem. Soc. Perkin Trans. I, 997 (1978); (*c*) J. BOUTEILLER-PRATI. Thèse de Doctorat de Spécialité, Marseille. 1979.
4. (*a*) J. P. AYCARD et H. BODOT. Org. Magn. Reson. **7**, 226 (1975); (*b*) J. PRATI, J. C. BOUTEILLER et J. P. AYCARD. C. R. Acad. Sci. Ser. C, **283**, 617 (1976).
5. H. C. BROWN et S. KRISHNAMURTY. J. Am. Chem. Soc. **94**, 7159 (1972).
6. R. O. HUTCHINS. J. Org. Chem. **42**, 920 (1977).
7. M. HIROTA, T. HAGIWARA et H. SATONAKA. Bull. Chem. Soc. Jpn. **40**, 2439 (1967).
8. D. J. CRAM et F. A. ABD ELHAFEZ. J. Am. Chem. Soc. **74**, 5828 (1952).
9. M. CHEREST, H. FELKIN et N. PRUDENT. Tetrahedron Lett. 2201 (1968).
10. J. P. AYCARD, R. GEUSS, J. BERGER et H. BODOT. Org. Magn. Reson. **5**, 473 (1973).
11. K. D. MACKAY. Ph.D. Dissertation, University of Minnesota. 1969.
12. R. BUCOURT. Top. Stereochem. **8**, 159 (1974).
13. (*a*) R. VIANI. Thèse de Doctorat ès Sciences Physiques, Université de Provence, Marseille. 1978; (*b*) R. VIANI, J. LAPASSET, J. P. AYCARD et H. BODOT. J. Org. Chem. **44**, 899 (1979).
14. L. F. FIESER et M. FIESER. Reagents for organic synthesis. Vol. 1. John Wiley and Sons, New York. 1967. p. 583.
15. A. A. BOTHNER-BY et S. M. CASTELLANO. J. Chem. Phys. **41**, 3863 (1964).

Can. J. Chem. Downloaded from www.nrcresearchpress.com by 210.87.254.5 on 09/06/12
For personal use only.

Catalytic oxidation of *n*-propane and methyl alcohol over nickel(II) oxide

I. M. HOODLESS, R. A. ROSS, AND R. SWAMINATHAN

Department of Chemistry, Lakehead University, Thunder Bay, Ont., Canada P7B 5E1

Received July 28, 1980

I. M. HOODLESS, R. A. ROSS, and R. SWAMINATHAN. Can. J. Chem. **59**, 865 (1981).

The catalytic oxidation of propane over nickel(II) oxide has been studied in the temperature range 280 to 490°C. Complete oxidation to carbon dioxide and water occurred. Fractional rate order dependencies were obtained for propane and oxygen and the reaction was inhibited by water vapour but not by carbon dioxide. It is suggested that the interaction of the adsorbed hydrocarbon with the adsorbed oxygen species, O^-, is the rate-limiting step in the reaction at the lower temperature.

Preliminary measurements of the oxidation of propane–methanol mixtures indicated that the alcohol supressed carbon dioxide formation. Conductivity studies have shown that, in these mixtures, methanol strongly interacts with the catalyst resulting in surface reduction.

I. M. HOODLESS, R. A. ROSS et R. SWAMINATHAN. Can. J. Chem. **59**, 865 (1981).

On a étudié l'oxydation catalytique du propane par l'oxyde de Ni(II) dans l'intervalle de température allant de 280 à 490°C. On a observé une oxydation complète en dioxyde de carbone et en eau. On a déterminé pour le propane et l'eau, les facteurs qui influencent l'ordre de vitesse fractionnaire et on a trouvé que la réaction est inhibée par la vapeur d'eau mais non par le bioxyde de carbone. On suggère que l'interaction entre l'hydrocarbure adsorbé et les espèces adsorbées d'oxygène, O^-, est l'étape déterminante de la réaction aux températures les plus basses.

Des mesures préliminaires sur l'oxydation de mélanges propane/méthanol indiquent que l'alcool élimine la formation de CO_2. Des mesures de conductivité ont montré que dans ces mélanges le méthanol interagit fortement avec le catalyseur formé par réduction de la surface.

[Traduit par le journal]

Introduction

Transition metal oxides are widely used as oxidation catalysts. The variation in their catalytic activity for redox reactions has been correlated with properties such as metal–oxygen bond strengths and oxygen lability (1–3). In determining the oxide activity, one standard reaction employed is the complete oxidation of methane (4, 5). Considering the importance of the catalytic oxidation of hydrocarbons it is surprising that relatively few studies of this type have been made on higher alkanes. Moro-Oka *et al.* (6) measured the catalytic activity of various oxides for the oxidation of isobutene, acetylene, ethylene, and propane and found a correlation of the activity with the heat of formation of the oxide. Yu Yao *et al.* (7, 8) have also carried out a detailed study of the oxidation of hydrocarbons on NiO and Cr_2O_3 microcrystals while Anshits *et al.* (9, 10) investigated the relative reactivity in oxidation of C_1 to C_8 alkanes on copper oxide catalysts.

One feature of the previous work is that the reactions were carried out in an excess of oxygen and complete oxidation occurred. The present paper reports on a kinetics study of propane oxidation on a NiO catalyst and, in this case, the hydrocarbon is present in excess. Some preliminary studies of the oxidation of propane–methanol mixtures are also reported.

Experimental Section

Apparatus and Method

The design and operation of the flow system has been described (11). High-purity helium was used as the carrier gas at atmospheric pressure in the flow system and in the Beckman GC-5 gas chromatograph which was operated as previously described (11). The catalyst reactor was used in a differential mode and constructed from stainless steel, 30 cm × 3.14 cm id. Temperature was maintained to within ± 0.5°C by a "Thermoelectric 400" proportional controller. "Blank" runs with reacting gas mixtures showed no measurable catalysis on the reactor walls until >430°C; at 480°C this accounted for 5% reaction using the standard propane/oxygen mixture.

All reaction rate measurements were recorded after steady catalytic activity was achieved, for example, after 3 h at 280°C. The standard inlet reacting gas mixture contained *n*-propane and oxygen at respective partial pressures of 45.6 and 15.2 Torr (6.08 and 2.03 kPa). The experiments were conducted up to 490°C where a maximum conversion level of 15% was recorded. Details of experiments with other gas mixtures are included in the Results section.

The conductivity cell, constructed in Pyrex, was of the flow-through type. The NiO compact, 1.3 cm diameter and 0.2 cm in thickness, was clamped under slight pressure between platinum electrodes. The temperature of the sample was determined by an iron–constantan thermocouple in contact with the lower electrode. The compact was maintained in a constant flow of helium (26 mL min^{-1}) and reactant gases were introduced at a flow rate of 3–4 mL min^{-1}. The conductivity was measured on a Wayne-Kerr B641 universal bridge operating at 1592 Hz.

Surface areas were determined by low-temperature krypton adsorption (BET; −196°C; $\sigma = 21.5$ Å^2). The NiO had a surface area of 2.5 $m^2\ g^{-1}$ and in the catalysis experiments a 1 g sample was used.

Materials

Nickel(II) oxide was prepared from nickel carbonate as noted earlier (12). No changes in color or in the X-ray powder diffraction patterns were detected in samples before and after catalysis.

n-Propane (I.G.; 99.5% minimum), carbon dioxide (Coleman; 99.99%), carbon monoxide (C.P.; 99.5% minimum), oxygen

0008-4042/81/050865-05$01.00/0

©1981 National Research Council of Canada/Conseil national de recherches du Canada

Can. J. Chem. Downloaded from www.nrcresearchpress.com by 210.87.254.40 on 09/06/12
For personal use only.

Can. J. Chem. Downloaded from www.nrcresearchpress.com by 210.87.254.40 on 09/06/12
For personal use only.

(super-pure; 99.99%), helium (high purity; 99.995%), and A.C.S. reagent grade methanol were used as supplied.

Results

Kinetics of Propane Oxidation

The reaction rate was determined from 280 to 490°C. Kinetics measurements were made in the region of less than 15% total reaction and under these conditions the rate of reaction was essentially independent of the flow rate, Fig. 1. A standard flow rate of 250 mL min^{-1} (N.T.P.) was employed in subsequent studies. In all cases the only products of catalysis detected were carbon dioxide and water.

The reaction orders were investigated from 280 to 320°C and from 450 to 490°C by varying the partial pressures of propane (15.5–60.2 Torr) and oxygen (3.04–15.2 Torr), Fig. 2. The orders of reaction for propane and oxygen were 0.50 ± 0.06 and 0.25 ± 0.07 respectively from 280 to 320°C and 0.37 ± 0.02 and 0.43 ± 0.06 respectively from 450 to 490°C. As noted in the Experimental section, the results at the higher temperatures are slightly complicated by the fact that a small amount of oxidation occurs in the absence of the catalysts. The effect of additions of the products on the reaction rate is shown in Fig. 3; carbon dioxide has no effect on the rate, while water appears to inhibit the reaction. The reaction order for water in both temperature ranges was -0.35 ± 0.04.

Conductivity Studies

The effects of individual reactants and mixtures of reactants on the conductivity of an NiO compact were investigated in the reaction temperature range (345 to 350°C). Some of the results are shown in Fig. 4. Oxygen and mixtures of oxygen and propane always increase the catalyst conductivity while methanol and mixtures of methanol, propane, and oxygen always decrease the conductivity. The influence of propane on the catalyst conductivity is more variable; admission of propane to the catalyst, pre-treated in oxygen, reduces its conductivity while if the catalyst is pre-reduced in methanol the effect of propane is to produce a limited increase in the conductivity.

Competitive Oxidation Studies

A number of preliminary studies have been made of the oxidation of propane in the presence of methanol, Fig. 5(*a*). The only products detected in gas chromatographic analysis were carbon dioxide, water, and formaldehyde although trace quantities of ethylene were detected by mass spectrographic analysis. The rates of disappearance of methanol

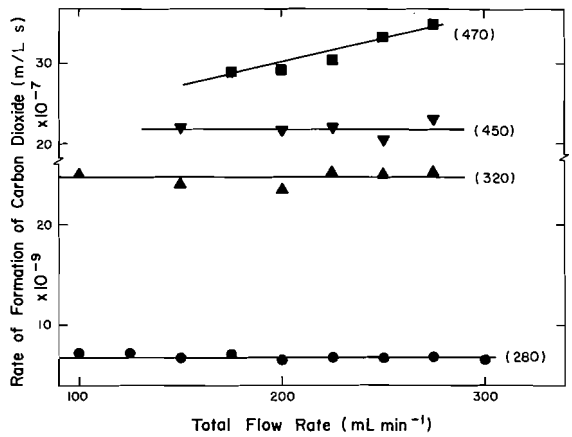

FIG. 1. Effect of flow rate on the rate of formation of carbon dioxide; partial pressure of propane 45.2 Torr, oxygen partial pressure 15.2 Torr. Reaction temperatures (°C) are in parentheses.

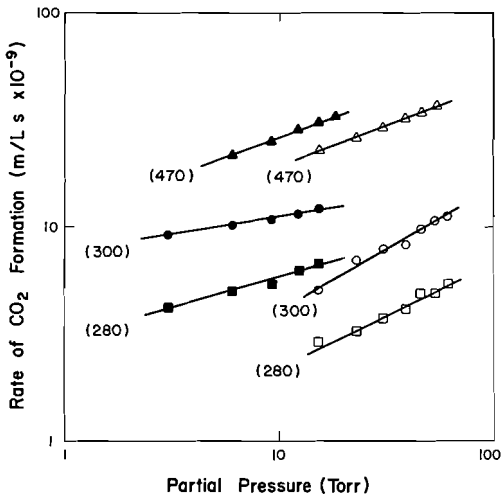

FIG. 2. Rate of formation of carbon dioxide as a function of partial pressures of reactants. ■, ●, ▲, varying partial pressure of oxygen with constant partial pressure of propane (45.6 Torr); □, ○, △, varying partial pressure of propane with constant partial pressure of oxygen (15.2 Torr). Rates at 470°C have been divided by 100. Reaction temperature (°C) are in parentheses.

and propane exceeded the amounts of carbon dioxide and formaldehyde formed but there was no evidence for the formation of significant amounts of carbon monoxide or C_1 to C_4 hydrocarbons to account for this discrepancy.

In the oxidation of mixtures of propane and carbon monoxide, the latter is rapidly oxidised to carbon dioxide, Fig. 5(*b*). At partial pressures above 20 Torr carbon monoxide, the rate of propane oxidation also increases while at lower pressures it appears likely that the carbon monoxide has either

Can. J. Chem. Downloaded from www.nrcresearchpress.com by 210.87.254.40 on 09/06/12
For personal use only.

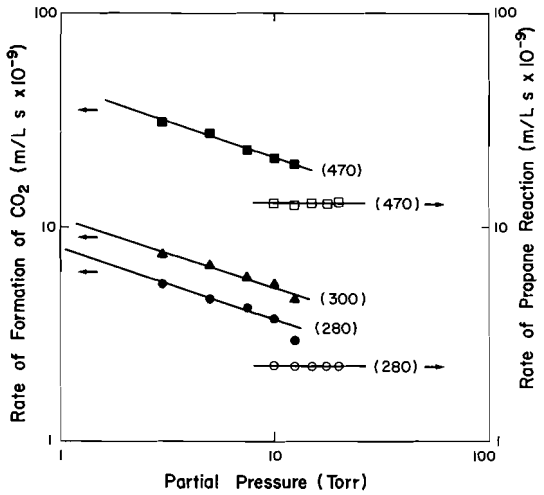

FIG. 3. Rate of oxidation of propane as a function of partial pressures of products. ●, ▲, ■, varying partial pressure of water with constant partial pressures of propane (45.6 Torr) and oxygen (15.2 Torr); ○, □, varying partial pressure of carbon dioxide with partial pressures of propane and oxygen as above. Rates at 470°C have been divided by 100. Reaction temperatures (°C) are in parentheses.

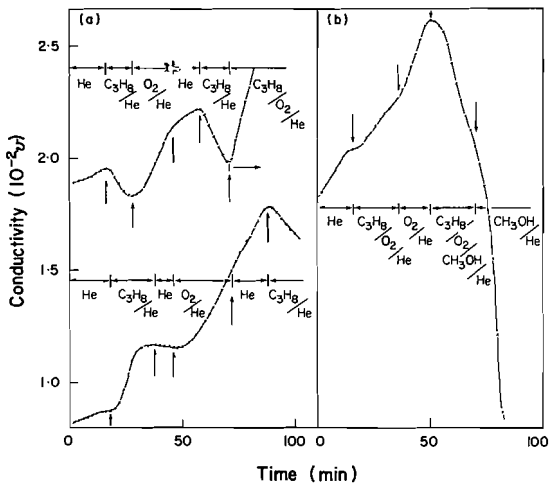

FIG. 4. Effect of reactants and mixtures of reactants on the conductivity of NiO at reaction temperature of 348 ± 2°C. (*a*) Upper curve: NiO compact pre-treated in oxygen, lower curve: NiO compact pre-treated in methanol, (*b*) NiO compact pre-treated in oxygen.

no effect or suppresses the rate of propane oxidation. The results indicate that carbon monoxide oxidation, if it is an intermediate step in the oxidation of propane, is not rate limiting.

Discussion

The rate of carbon dioxide formation, r, as a function of the partial pressures, p, can be described by an empirical expression of the form:

$$[1] \quad r = k \frac{P_{O_2}{}^m P_{C_3H_8}{}^n P_{CO_2}{}^o}{P_{H_2O}{}^l}$$

The temperature dependence of the rate of formation of carbon dioxide is shown in Fig. 6, from which an apparent activation energy of 106.9 kJ mol^{-1} has been determined. Moro-Oka *et al.* (6) and

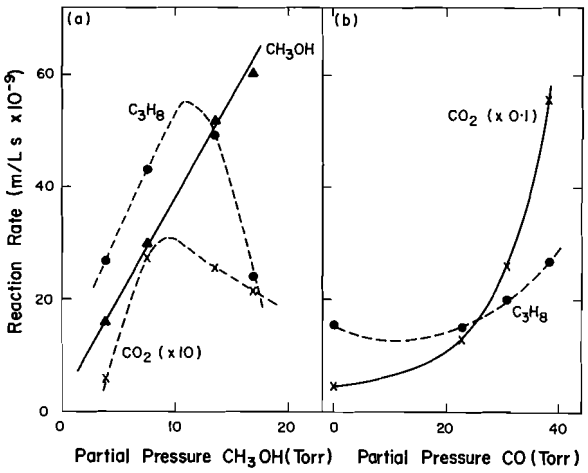

FIG. 5. (*a*) The effect of varying methanol partial pressures on the rate of formation of carbon dioxide and the rate of disappearance of the reactants at 320°C ($P_{C_3H_8}$ = 28.4 Torr, P_{O_2} = 14.3 Torr). (*b*) The effect of varying partial pressures of carbon monoxide on the rate of formation of carbon dioxide and the rate of reaction of propane at 320°C ($P_{C_3H_8}$ = 45.6 Torr, P_{O_2} = 15.2 Torr).

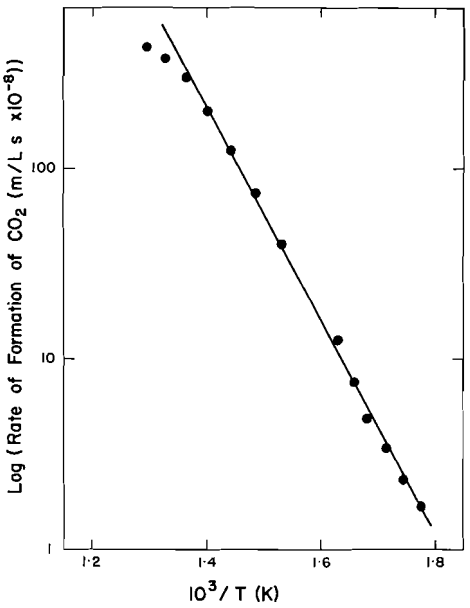

FIG. 6. Temperature dependence of the rate of formation of carbon dioxide ($P_{C_3H_8}$ = 45.6 Torr, P_{O_2} = 15.2 Torr).

TABLE 1. Kinetic orders and activation energy for propane oxidation, $r = kP_{O_2}{}^m P_{C_3H_8}{}^n P_{CO_2}{}^o / P_{H_2O}{}^l$

Reference	Temperature range (°C)	l	m	n	Activation energy (kJ mol^{-1})
Moro-Oka *et al.* (6)	350–416		0.40	0.89	109.5
Yao and Kummer (7)	230–400	0.26	0.29	0.53	87.8
Present work	280–320	0.35	0.25	0.50	106.9
	450–490	0.35	0.43	0.37	

Yu Yao and Kummer (7) have also investigated the oxidation of hydrocarbons on a number of metal oxides. Their results for the oxidation of propane on NiO are compared with the present work in Table 1.

Since the reaction orders for propane and oxygen are less than unity a Langmuir–Hinshelwood type mechanism may be inferred with competition between the hydrocarbon and oxygen for adsorption sites. Both adsorption of oxygen and of propane (on a reduced surface) led to increase in the conductivity of the sample indicating electron transfer from the catalyst to the adsorbate. It is evident that the oxygen was the more abundant species on the surface since only complete oxidation of the hydrocarbon was detected.

A number of mechanisms have been proposed for the catalytic oxidation of alkanes. On the basis of their studies on a Cu_2O catalyst, Anshits *et al.* (10) suggested that, at lower temperatures, complete oxidation occurred by an associative mechanism, i.e., the interaction of molecular oxygen with the adsorbed form of the hydrocarbon. In terms of the present work on NiO, the observed reaction orders appear to be inconsistent with this mechanism and, in addition, the conductivity results show that oxygen is readily absorbed on the catalyst in an anionic form. A second mechanism proposed (10) for the reaction at higher temperatures was that the rate-limiting step involved the reaction of the hydrocarbon with the catalysts with the formation of carboxylate and formate-type groups at the surface. Additionally kinetic isotope effect measurements (6) indicate that fission of a C—H bond is involved in the rate-determining step. This reaction of the hydrocarbon with the surface could involve either lattice oxygen or adsorbed oxygen. In the present work on NiO there is some evidence that the adsorbed oxygen species plays a direct role in the reaction rather than acting as a reservoir for the reduction–oxidation cycle of the catalyst. When propane alone is admitted to the catalyst no oxidation products are detected. Additionally the opposite changes in conductivity when propane is introduced to an oxygen-covered and a reduced surface, Fig. 4, would suggest that the propane is undergoing reaction with the adsorbed oxygen.

The experimental rate order in oxygen partial pressure increased from 0.25 between 280 and 320°C to 0.43 between 450 and 490°C. This phenomenon is probably related to the nature, lability, and amount of adsorbed oxygen on the catalyst surface. The rate order in the higher temperature range would be close to that expected from a simple dissociative reaction where catalytically active $O^-(a)$ species are formed on oxygen adsorption:

$$[2] \quad \tfrac{1}{2}O_2(g) + Ni^{2+}(c) \rightleftharpoons Ni^{2+\oplus}(c) + O^-(a)$$

$Ni^{2+\oplus}$ is a positive hole which can be equated to $O^-(a)$ at the steady state if the intrinsic positive hole concentration is negligible.

Numerous studies of oxygen chemisorption on oxides have indicated that the anionic adsorbed species may be O_2^- or O^{2-} as well as O^- (13–15). Adsorbed O^- has been suggested as the reactive species for a number of oxidation reactions on NiO (16, 17) including previous investigations of alkane oxidations at 279°C on NiO/Al_2O_3 catalysts (18). It is, however, surprising that only products of complete oxidation, CO_2 and H_2O, were observed in the present work.

While the surface will be predominantly covered by adsorbed oxygen, as shown by the effect of propane–oxygen mixtures on the conductivity (Fig. 4), it might be expected that in the decomposition of the carboxylate-type compounds, formed by the interaction of the hydrocarbon, some C_2 products would be produced. Either the C_2 fragments must be rapidly readsorbed and undergo oxidation or, possibly, the hydrocarbon initially adsorbs "planar" to the catalysts surface so that interaction with adsorbed oxygen and fission of C—H bonds on more than one carbon atom occurs without the necessity for readsorption. The inhibiting effect of water can be ascribed to its competing with oxygen and the hydrocarbon for the reactive adsorption sites on the surface.

The oxidation of mixtures of propane and methanol has not yet been studied in such detail. The initial results indicate that the presence of

Can. J. Chem. Downloaded from www.nrcresearchpress.com by 210.87.254.40 on 09/06/12
For personal use only.

methanol supresses the rate of carbon dioxide formation but the rate of propane disappearance is increased. Additionally both the rate of carbon dioxide production and the rate of propane disappearance go through a maximum with increase in the partial pressure of methanol, Fig. 5. Additional experiments have shown that the position of the maximum is a function of the propane and oxygen partial pressures. The major product detected in the reaction is formaldehyde and one obvious route for its formation is through the dehydrogenation of methanol. Previously O^-(a) has been sugggested as the active species in alcohol dehydrogenation on oxides (19). The appearance of a maximum in the hydrocarbon curve is consistent with competition between propane and methanol for O^-(a) sites. However, the disappearance of propane is greatly in excess of the appearance of carbon dioxide and possibly some polymerization may occur on the surface under these conditions. The conductivity measurements (Fig. 4) show that in mixtures of propane, methanol, and oxygen, it is methanol which has the dominent influence on the surface and the rapid decrease in conductivity in the presence of methanol alone indicates that it can also react with lattice oxygen causing reduction at the surface.

Acknowledgments

We wish to thank the Natural Sciences and Engineering Council of Canada for financial support of this work.

1. G. K. Boreskov. Adv. Catal. **15**, 285 (1964).
2. D. G. Klissurski. Proc. 4th Int. Congr. Catal. Moscow 1968, Vol. 1, Ed. Akad. Kiado, Budapest. 1970. p. 477.
3. E. F. McCaffrey, D. G. Klissurski, and R. A. Ross. Proc. 5th Int. Congr. Catal. Miami Beach, 1972. Elsevier Publishing Co., Amsterdam. 1973. p. 151.
4. T. V. Andruskevich, V. V. Popovskii, and G. K. Boreskov. Kinet. Katal. **6**, 860 (1965).
5. J. E. Germain, P. Spender, and J. P. Beaufils. Mém. Soc. Chim., 5e série, 203 (1965).
6. Y. Moro-Oka, Y. Morikawa, and A. Ozaki. J. Catal. **7**, 23 (1967).
7. Y-F. Yu Yao and J. T. Kummer. J. Catal. **28**, 124 (1973).
8. Y-F. Yu Yao. J. Catal. **28**, 139 (1973).
9. A. G. Anshits, V. D. Sokolovskii, G. K. Boreskov, and A. A. Davydov. Dokl. Akad. Nauk SSSR, **213**, 607 (1973).
10. A. G. Anshits, V. D. Sokolovskii, G. K. Boreskov, A. A. Davydov, A. A. Budneva, T. A. Avdeev, and I. I. Zakharov. Kinet. Catal. **16**, 74 (1975).
11. B. W. Krupay and R. A. Ross. J. Catal. **39**, 369 (1975).
12. B. W. Krupay and R. A. Ross. Z. Phys. Chem. N.F. **106**, 83 (1977).
13. H. B. Charman, R. M. Dell, and S. S. Teale. Trans. Faraday Soc. **59**, 453 (1963).
14. E. R. S. Winter. J. Catal. **6**, 35 (1965).
15. M. Iwamoto, Y. Yoda, M. Egashira, and T. Seiyama. J. Phys. Chem. **80**, 1989 (1976).
16. K. Aika and J. H. Lunsford. J. Phys. Chem. **81**, 1393 (1977).
17. A. Bielanski and J. Haber. Catal. Rev.-Sci. Eng. **19**(1), 38 (1979).
18. G. Matis, F. Juillet, and S. J. Teichner. Bull. Soc. Chim. 1633 (1976); 1637 (1976).
19. A. J. Tench, T. Lawson, and J. F. J. Kibblewhite. J. Chem. Soc. Faraday Trans. 1, **68**, 1169 (1972).

Can. J. Chem. Downloaded from www.nrcresearchpress.com by 210.87.254.40 on 09/06/12
For personal use only.

Total synthesis of (+)-thromboxane B_2 from D-glucose. A detailed account[1]

STEPHEN HANESSIAN AND PIERRE LAVALLEE[2]
Department of Chemistry, University of Montreal, Montreal, P.Q., Canada H3C 3V1
Received August 13, 1980

This paper is dedicated to Prof. Raymond U. Lemieux on the occasion of his 60th birthday

STEPHEN HANESSIAN and PIERRE LAVALLEE. Can. J. Chem. **59**, 870 (1981).

The total synthesis of thromboxane B_2 from D-glucose is described, based on the recognition of hidden carbohydrate-type symmetry in the molecule. Methyl 2-deoxy-α-D-*ribo*-hexopyranoside was prepared from D-glucose and manipulated in such a way as to introduce C-branching at C-4 in a stereocontrolled manner. This crucial intermediate was then transformed into the target compound by adaptations of established methodology in the field.

STEPHEN HANESSIAN et PIERRE LAVALLEE. Can. J. Chem. **59**, 870 (1981).

La synthèse totale du thromboxane B_2 à partir du D-glucose est décrite. La stratégie est basée sur la reconnaissance d'une symétrie type carbohydrate dans le squelette carboné de la molécule. Le méthyl 2-deoxy-α-D-*ribo*-hexopyrannoside préparé à partir du D-glucose a été manipulé afin d'introduire les substituants requis de façon régio- et stéréocontrôllée. Un intermédiaire crucial a été ainsi obtenu, qui, après modifications systématiques a donné accès au produit désiré.

The field of prostaglandin biosynthesis has been recently crowned by two landmark events, namely, the discovery of the thromboxanes (TXA_2 and TXB_2), and prostacyclin (PGI_2) (1). Pioneering studies have shown that PGI_2, the predominant product formed from endoperoxides in blood vessel linings, is capable of preventing the blood clotting process, while the same endoperoxides in platelets can be converted into TXA_2 which causes platelets to clump and aggregate. Thus, a common biosynthetic intermediate appears to be leading to two unique substances. A critical balance in the production of PGI_2 and TXA_2 appears to be a vital biological condition, and further knowledge gained from research on these naturally-occurring and structurally related bioregulatory agents will undoubtedly expand our understanding of the factors responsible for atherosclerosis and related disease states. Samuelsson and co-workers (2) have shown that TXA_2 is transformed rather rapidly into TXB_2, which unlike its precursor, is biologically inert as a platelet aggregating agent. Nevertheless, it is a valuable substrate for the study of a variety of biochemical processes.

The first syntheses of TXB_2 were reported by the Upjohn group (3) where $PGF_{2\alpha}$ and two of its synthetic intermediates were individually utilized as starting materials. Shortly thereafter, we announced our synthesis of TXB_2 from D-glucose (4), which was followed by a direct total synthesis of the racemic material (5) and other syntheses (6) leading to optically active intermediates of TXB_2.

In this paper, we disclose the details of our original stereocontrolled synthesis of (+)-TXB_2 which is also adaptable to the preparation of analogs. Examination of the structure of TXB_2 shows the presence of a 6-membered lactol which can be related to a 2,4,6-trideoxy-D-*ribo*-hexopyranose (Scheme 1). Viewed in this perspective (7) it becomes apparent that the major synthetic challenge in attaining the intended objective is the regio- and stereocontrolled introduction of chain-branching at C-4 utilizing an appropriate carbohydrate precursor. The judicious choice of protecting groups compatible with otherwise well known operations in prostaglandin chemistry (8) becomes an important parameter in finalizing the general synthetic blueprint for such a structure.

Methyl 4,6-*O*-benzylidene-2-deoxy-α-D-*ribo*-hexopyranose **2**, which is readily available in high yield from α-D-glucose (9), was an ideal starting material since it already contains a deoxy function as required in the tetrahydropyran portion of the target (Scheme 2). The corresponding crystalline benzoate **3** was subjected to hydrogenolysis and the resulting crystalline diol **4** was transformed into the highly crystalline *tert*-butyldiphenylsilyl ether **5** by treatment with *tert*-butyldiphenylsilyl chloride (10). The choice of protecting group for the primary

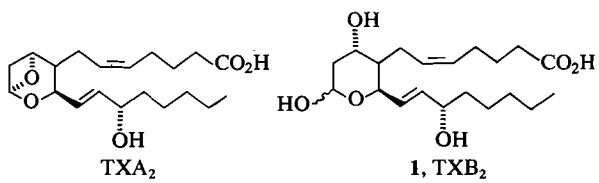

SCHEME 1

[1]For a preliminary account, see ref. 4.
[2]NRCC predoctoral fellow 1972–1976.

0008-4042/81/050870-08$01.00/0
©1981 National Research Council of Canada/Conseil national de recherches du Canada

Can. J. Chem. Downloaded from www.nrcresearchpress.com by 210.87.254.42 on 09/06/12
For personal use only.

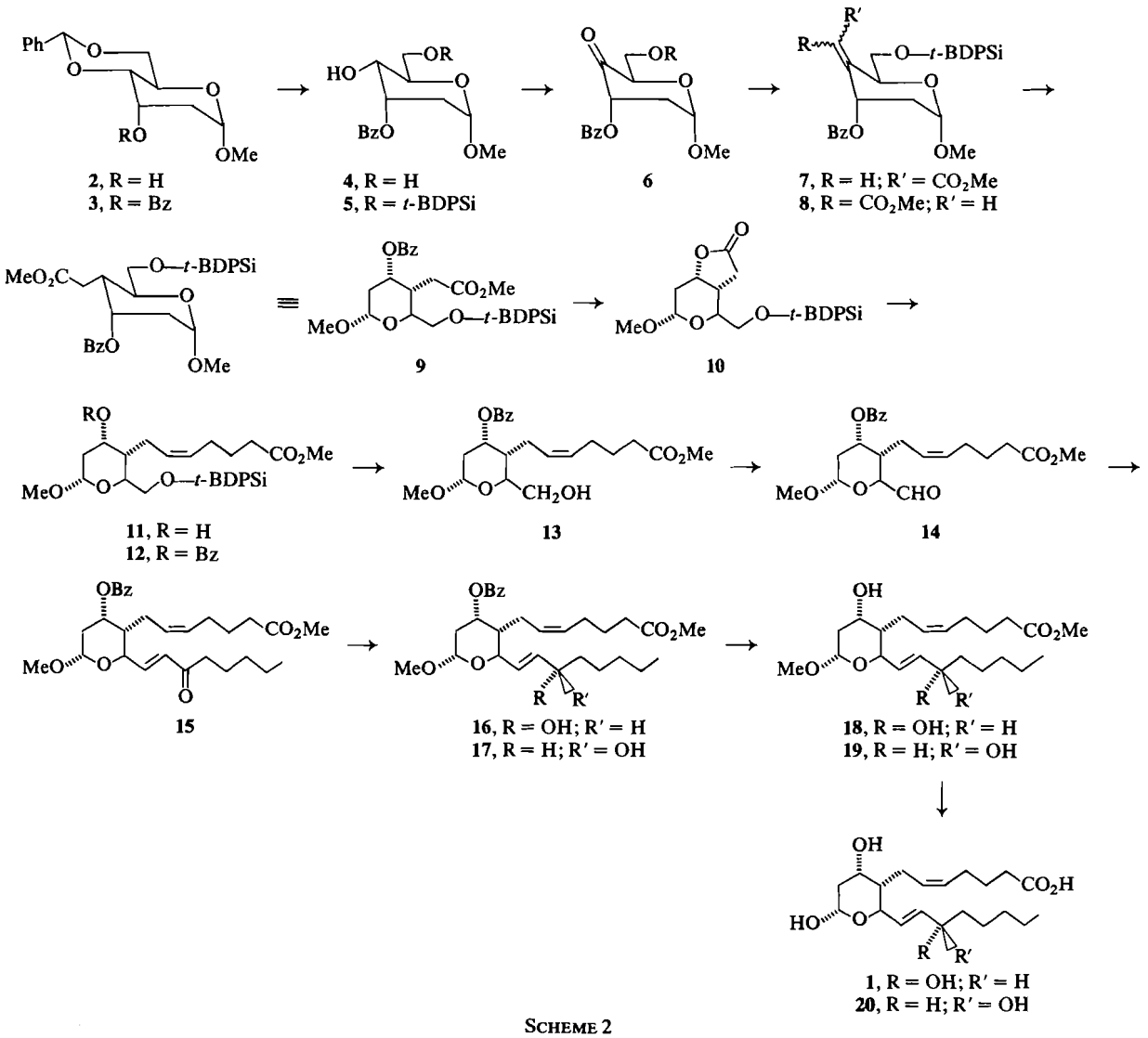

SCHEME 2

hydroxyl function was critical, since alternative options such as the commonly used trityl and *tert*-butyldimethylsilyl group (11) would not have been compatible with subsequent transformations envisaged in our synthetic scheme. Oxidation of the C-4 hydroxyl group in **5** could be effected with a variety of oxidants including DMSO – acetic anhydride. This led to the expected ketone **6** in 80% yield but contamination of the mother liquors with the methylthiomethyl ether derivative of **5** rendered the recovery of additional product somewhat lengthy. Oxidation of **5** in DMSO in the presence of 1-ethyl-3-(3-dimethylaminopropyl)carbodiimide hydrochloride (12) and pyridinium trifluoroacetate led to the crystalline ketone derivative **6** in 94% yield without resorting to chromatography. That no epimerization at C-3 had taken place was evident from ^{1}Hmr data and from the chemistry that was to follow. Although this carbodiimide is better known as a reagent for peptide coupling (12), we have found it to be an excellent substitute for dicyclohexylcarbodiimide in Pfitzner–Moffatt oxidations (13), particularly in that the hydrochloride salt of the corresponding urea derivative is water soluble. Our initial attempts at chain-branching by treatment of **6** with (ethoxycarbonyl)methylenetriphenylphosphorane were unsuccessful and the ketone was recovered unchanged, even when the reaction was attempted in refluxing THF. With the more reactive tributylphosphine analog, a complex

Can. J. Chem. Downloaded from www.nrcresearchpress.com by 210.87.254.42 on 09/06/12
For personal use only.

Can. J. Chem. Downloaded from www.nrcresearchpress.com by 210.87.254.42 on 09/06/12
For personal use only.

mixture of products was obtained which was difficult to resolve by chromatography. Application of the phosphonate modification of the Wittig reaction proved much more practical, although the choice of base and solvent was critical. Thus, treatment of **6** with dimethyl(methoxycarbonyl)-methylphosphonate in the presence of sodium hydride in 1,2-dimethoxyethane, THF, or toluene, and at different temperatures, gave in all cases the expected exocyclic olefinic product (as a mixture of *E* and *Z* isomers), contaminated with another unknown olefinic product. However, adopting a published procedure (14) in which the carbanion was generated with potassium *tert*-butoxide in anhydrous toluene proved highly efficient in our case and led to the formation of a 1:1 mixture of the olefins **7** and **8** as the sole products in a combined yield of 90% after chromatographic purification. Based on spectroscopic data and literature precedents (9), the two products thus obtained were assigned as *E* and *Z* isomers respectively. In the *E* isomer, H-3 is found at δ 6.16 ppm ($J_{3,2a}$ = 10 Hz), downfield from the same signal in the parent ketone **6** by only 0.29 ppm, while in the *Z* isomer **8** H-3 is strongly deshielded, Δδ 0.98, due to the effect of the carbomethoxy group. By the same reasoning the deshielding patterns of H-5 in the respective isomers are reversed. The olefins **7** and **8** were individually oxidized with ozone and each was converted into the starting ketone **6** in high yield, thus providing chemical proof for their structures. The presence of an axial group at C-3 and the original choice of an α-glycoside were considered to be dominant factors in controlling the outcome of the catalytic hydrogenation of the exocyclic olefinic linkage. Not too surprisingly, however, there were substantial differences in the hydrogenation rates, although the product was the expected branched-chain derivative **9** in either case. Thus, whereas the *Z* isomer **8** was converted into **9** in the presence of 10% palladium-on-charcoal within 8 h, the *E* isomer **7** required 20% palladium hydroxide-on-charcoal and a 24 h exposure. The reasons for this are not immediately apparent, although inspection of molecular models reveals that in the *E* isomer, an interaction could exist between the methoxycarbonyl and the bulky *tert*-butydiphenylsilyl group, thus rendering the β-side somewhat less readily accessible to a weaker catalyst. Definitive proof for the orientation of the acetic acid side-chain was secured from spectroscopic data and chemical transformations. Having thus introduced the crucial branch-point at C-4, attention was next turned to the elaboration of the carboxyl-containing side chain of TXB_2. Treatment of the ester **9** with 1.4 equivalents of DIBAH in toluene at −78°C led to a mixture of the desired aldehyde and starting material. Using a large excess of reagent led to a mixture of several products. A practical recourse was to generate a lactone intermediate such as **10**. Thus, treatment of **9** with 0.3 equivalents of sodium methoxide in methanol led, after 4 days, to the crystalline lactone **10** in 76% yield. A more efficient procedure was to subject the ester **9** to methanolysis in the presence of anhydrous potassium carbonate, which led to the lactone **10** in higher yield (85%). Alkoxide mediated alcoholysis of diesters of the type **9** is expected to produce the corresponding hydroxy ester; however, using quasi-stoichiometric quantities of alkoxide the intramolecularly formed *cis*-lactone is apparently the thermodynamically more stable entity compared to the corresponding *cis*-hydroxy ester from which it is derived. Treatment of the lactone **10** with DIBAH following known methodology gave the corresponding lactol which was treated with the Wittig reagent generated from (4-carboxybutyl)-triphenylphosphonium bromide in the presence of lithium hexamethyldisilazane in HMPT (15). This led to the expected *cis*-olefin **11** in good yield after esterification. The prostaglandin literature (8) is replete with syntheses in which the *cis*-olefinic linkage of the carboxyl side chain has been introduced using the above mentioned phosphonium salt and dimsylsodium in DMSO as solvent. Until recently, however, few experimental details were available in the literature for this method (16). In our hands, we have found the Rosen procedure (15) to be convenient and highly reproducible from run to run and have used it in this as well as other instances, particularly when small quantities of materials were available for the Wittig reaction.

At this juncture, we deemed it necessary to secure chemical evidence concerning the correct orientation of substituents at C-3 and C-4, since epimerization at C-3 in **6** and a subsequent reduction of the products **7** and **8** from the α-side could have conceivably led to a *cis*-lactone with the opposite stereochemistry relative to **10**. Accordingly, **11** was oxidized with 1-ethyl-3-(3-dimethylaminopropyl)carbodiimide hydrochloride in DMSO to the corresponding 3-keto derivative **21** (Scheme 3) in 86% yield. This was treated in methanol with

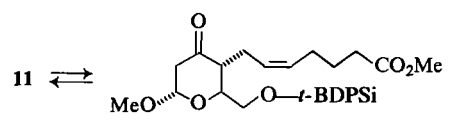

21

SCHEME 3

TABLE 1. ^{13}C magnetic resonance data of compounds **4–9** (ppm from TMS)

Carbon atom	4	5	6	7	8	9	10
1	97.2	97.0	97.5	97.4	97.7	97.5	96.7
2	33.3	33.2	34.1	38.2	35.6	33.3	32.8
3	68.0	68.3[a]	71.7	69.3	65.1	68.4[a]	75.1
4	66.9	68.1[a]	204.7	[b]	[b]	36.8	34.9
5	69.9	69.7	77.2	72.5	66.4	68.8[a]	68.2
6	62.5	64.8	63.5	66.1	63.5	65.3	65.4
C(1)—O*Me*	55.2	55.0	55.1	55.4	55.1	54.9	55.2
CO_2Me				51.2	51.7	51.5	
Me_3—*C*		19.3	19.2	19.2	19.2	19.3	19.2
Ph=O	167.0	166.7	165.1	164.7	165.4	166.0	
				165.8	165.9		
CO_2R				157.9[c]	148.5[c]	172.2[c]	175.8
C(4)=*C*—*H*				111.3	117.6		
C(4)—CH_2						32.4	31.0

[a] These numbers can be reversed within the same column.
[b] Unresolved signal.
[c] R = Me.

potassium carbonate during 5 h after which chromatographic examination revealed the presence of the original ketone and a small quantity of a product arising from elimination. The ketone **21** was subsequently isolated from such a mixture (72.5%) and was found to be identical to the original material. Had the olefinic side-chain been in the axial orientation, it would have undergone base-catalyzed epimerization to the equatorial isomer. Reduction of **21** with sodium borohydride in methanol at 0°C led to **11** in 74% yield. From the experiments, it was clear that the stereochemical integrity at C-3 had been maintained during the oxidation and subsequent phosphonate condensation reaction, and that the reduction of the olefins **7** and **8** led, as expected, to the acetate side-chain with an α-orientation (D-*ribo* configuration as in **9**). The ^{13}Cmr spectral parameters for compounds **4–10** are listed in Table 1 and the assignments are based on correlations with known compounds and from literature data (17). Pursuing our synthetic scheme towards TXB_2, the hydroxyl group in **11** was protected by benzoylation to give **12** as a syrup, which was desilylated with fluoride ion (11) to the alcohol **13** and the latter was oxidized to the aldehyde **14** with the Collins reagent according to its adaptation to carbohydrates (18). The yields of these individual steps were high and the products were characterized by spectroscopic data. Chain extension of the aldehyde **14** was effected with *n*-tributylphosphoranylidene-2-heptanone (19) in the usual manner to give the α,β-unsaturated ketone derivative **15** in 79% yield after chromatography. In view of their modes of formation and genesis, all the intermediates to this point in the synthesis are optically pure. Reduction of **10** was effected with zinc borohydride in a mixture of 1,2-dimethoxyethane and ether, whereby two epimeric alcohols were formed in high yield and separated by thick layer chromatography. A slight preponderance (40%) of the "15-*S*" epimer **16** (later to be related to the natural product) was observed over the 15-*R* epimer **17** (33%). These compounds were individually transformed into TXB_2 and its "15-*R*" isomer by carefully executed deprotection techniques. Debenzoylation of **16** in the presence of potassium carbonate in methanol under a nitrogen atmosphere afforded the corresponding alcohol **18** as a syrup in 80% yield. The corresponding *O*-trimethylsilyl derivative showed a mass spectrum that was in complete accord with the expected structure and with the results published by Samuelsson and co-workers (2). The ester **18** was hydrolyzed with dilute alkali and the resulting sodium salt was treated with excess Dowex-50 (H^+) giving first the methyl glycoside derivative of TXB_2, which on longer contact with the acidic resin was hydrolyzed to TXB_2. The material crystallized from a mixture of ethyl acetate, ether, and petroleum ether to give beautiful plates, identical with an authentic sample. Similar treatment of the epimeric **17** gave the ester **19** and finally "15-epi" TXB_2, **20**, a syrup. The ^{13}Cmr data for compounds **11–18** in the natural series are listed in Table 2 and the assignments have been made based on literature precedents in the PG area. Since the Wittig reagent that provides the C-15 side-chain is available in optically pure form from malic acid (20), the sequence **14** → **16** can provide material with the natural "15-*S*" configuration directly, or indirectly by inversion of configuration of **17** as in the PG series (21). Thus, the entire synthesis of (+)-TXB_2 can be considered to be stereospecific. An X-ray crystallographic study of TXB_2 has shown that the unit

Can. J. Chem. Downloaded from www.nrcresearchpress.com by 210.87.254.42 on 09/06/12
For personal use only.

Can. J. Chem. Downloaded from www.nrcresearchpress.com by 210.87.254.42 on 09/06/12
For personal use only.

TABLE 2. ^{13}C magnetic resonance data of compounds **11, 12, 13, 18, 19**

Carbon atom	11	12	13	18	19
1	174.0	173.7	173.9	174.2	[b]
2	33.5	33.5	33.3	33.5	33.3
3	24.2	24.7	24.6	24.8	24.8
4	26.6	26.7[a]	26.7	26.6	26.5
5	[b]	[b]	[b]	129.2	128.9[a]
6	[b]	[b]	[b]	127.9	128.1[a]
7	25.3	26.3[a]	24.6	25.2	25.2
"8"	41.1	39.5	39.1	45.1	45.2
"9"	65.3	68.0	67.7	64.4	64.5
"10"	36.1	33.3	33.3	35.8	35.9
"11"	99.0	97.5	97.6	99.1	99.1
"12"	69.3	69.2	68.8	69.4	69.4
"13"	65.3	65.0	63.1	130.6	130.4
"14"				138.0	138.1
"15"				72.3	72.1
"16"				37.1	37.2
"17"				25.2	25.2
"18"				31.8	31.8
"19"				22.6	22.6
"20"				14.0	14.0
CO_2Me	51.3	51.2	51.3	51.5	51.5
C("11")—O*Me*	54.8	54.7	54.9	55.2	55.1
Ph*C*=O		165.9	166.0		
Me_3—*C*	19.4	19.4			
Me$_3$—C	26.9	26.9[a]			

[a] These numbers can be interchanged within the same column.
[b] Unresolved signal.

cell consists of α,β-anomers in the ratio of 35:65 (22).

Experimental

Melting points are uncorrected. Optical rotations were measured on a Perkin-Elmer automatic spectropolarimeter, model 141. The ^{1}Hmr spectra were recorded on a Jeol instrument at 60 MHz unless otherwise stated, with tetramethylsilane as internal standard, in deuterochloroform as solvent. The ^{13}C nmr spectra were recorded on a Bruker WH-90 instrument at 22.6 MHz. Mass spectra were recorded on an AEI-902 mass spectrometer at low resolution. Column chromatography was done using silica gel G254, with application of moderate suction. Solvents for tlc are as follows; solvent A: benzene–EtOAc, 10:1; solvent B: benzene–EtOAc, 10:3; solvent C: benzene–EtOAc, 10:6; solvent D: benzene–EtOAc, 1:1; solvent E: ethyl acetate – acetic acid, 99:1; solvent F: $CHCl_3$–MeOH, 10:1.

*Methyl 3-*O*-Benzoyl-4,6-*O*-benzylidene-2-deoxy-*α*-*D*-ribo-hexopyranoside (3)*

A solution containing 8 g (30 mmol) of **2** (9) in 60 mL of dry pyridine was treated with 4.2 mL (36 mmol) of benzoyl chloride at 0°C. The solution was stirred overnight at room temperature, then it was poured in a mixture of water, ice, and ether. Processing the organic layer in the usual way gave a syrup that crystallized from ether – petroleum ether to give the title compound in three crops (10.34 g, 93%). Recrystallization gave a pure sample, mp 100–101°C; $[\alpha]_D^{25}$ +182.9° (*c* 1.18, $CHCl_3$); λ_{max}(KBr): 1715 cm^{-1}; nmr data, δ (ppm): 2.08 (H_{2a}, $J_{2a,2e}$ = 15.7 Hz, $J_{2a,1}$ = 4 Hz, $J_{2a,3}$ = 3.5 Hz), 2.39 (H_{2e}, $J_{2e,2a}$ = 15.7 Hz; $J_{2e,3}$ = 3 Hz; $J_{2e,1}$ = 0.75 Hz), 3.37 (s, OCH_3), 4.75 (H_1, dd, $J_{1,2a}$ = 4 Hz, $J_{1,2e}$ = 0.75 Hz), etc. *Anal.* calcd. for $C_{21}H_{22}O_6$: C 68.10, H 5.99; found: C 68.58, H 6.15.

*Methyl 3-*O*-Benzoyl-2-deoxy-α-*D*-ribo-hexopyranoside (4)*

A solution of **3** (11 g, 30.5 mmol) in a mixture of ethyl acetate (150 mL) and methanol (75 mL) was hydrogenated in the presence of 20% palladium hydroxide on charcoal (1.5 g) (23). After 18 h, the catalyst was filtered and the filtrate was evaporated to dryness. The residue was crystallized from a mixture of dichloromethane, ether, and petroleum ether to give the title compound (7.93 g, 94%). An analytical sample was obtained, after two recrystallizations, from a mixture of hexanes and pentane, mp 112–114°C; $[\alpha]_D$ +158° (*c* 1.06, $CHCl_3$); R_f 0.57 (solvent F); λ_{max}(KBr): 3340 (OH), 1720 (C=O) cm^{-1}. *Anal.* calcd. for $C_{14}H_{18}O_6$: C 59.56, H 6.43; found: C 59.60, H 6.78.

*Methyl 3-*O*-Benzoyl-6-*O*-(tert-butyldiphenylsilyl)-2-deoxy-α-*D*-ribo-hexopyranoside (5)*

A solution containing **4** (7.48 g, 26.5 mmol) and imidazole (4.1 g, 59 mmol) in 53 mL of dry DMF was treated at 0°C with a 0.5 *M* solution of *tert*-butyldiphenylsilyl chloride (10) (58 mL, 29 mmol) in the same solvent. After stirring at room temperature for 20 h, the solution was diluted with water and ether. Processing the organic layer gave a crystalline residue that was recrystallized from ether – petroleum ether to give the title compound, mp 114–116°C (11.7 g, 85%). An analytical sample showed mp 116–118°C (hexanes); $[\alpha]_D$ +90.2° (*c* 1.1, $CHCl_3$); R_f 0.41 (solvent A); ms *m/e*: 489 (M^+ – Me_3C), etc. *Anal.* calcd. for $C_{30}H_{36}O_6Si$: C 69.20, H 6.97; found: C 69.05, H 6.76.

*Methyl 3-*O*-Benzoyl-6-*O*-(tert-butyldiphenylsilyl)-2-deoxy-α-*D*-erythro-hexopyranosid-4-ulose (6)*

To a cooled solution containing **5** (20.8 g, 40 mmol) and 1-ethyl-3-(3-dimethylaminopropyl)carbodiimide hydrochloride (EDAC·HCl) (4, 12) (23.04 g, 120 mmol) in 300 mL of dry DMSO was added successively 4.9 mL (60 mmol) of pyridine and 3.6 mL (50 mmol) of trifluoracetic acid and the solution was diluted with ether and ice-water; the organic layer was pro-

Can. J. Chem. Downloaded from www.nrcresearchpress.com by 210.87.254.42 on 09/06/12
For personal use only.

cessed as usual to give a viscous syrup which crystallized from a mixture of ether – petroleum ether to give compound **6** (19.94 g, 94%). Two recrystallizations gave an analytical sample, mp 86–88°C; $[\alpha]_D$ +148° (*c* 1.22, $CHCl_3$); R_f 0.68 (solvent A); λ_{max}(KBr): 1760 (C=O) cm^{-1}; ms *m/e*: 461 ($M^+ - Me_3C$), 429 ($M^+ - Me_4C - MeOH$), etc; *Anal.* calcd. for $C_{30}H_{34}O_6$ Si: C 69.47, H 6.61; found: C 69.97, H 7.07.

*Synthesis of Methyl 3-O-Benzoyl-6-O-(*tert*-butyldiphenylsilyl)-2,4-dideoxy-4-C-[E-(methoxycarbonyl)methylene]-*α*-D-erythro-hexopyranoside 7, and the Z Isomer, 8*

To a cooled suspension of potassium *tert*-butoxide (0.8 g, 7.2 mmol) in 100 mL of toluene was added dimethyl (methoxycarbonyl)methylphosphonate dropwise and with stirring. After 1 h, ketone **6** (3.1 g, 6.0 mmol) was added in one portion and the solution was stirred at room temperature for 8 h. The solution was diluted with ether, then treated with 10% dihydrogen sodium phosphate. Processing the organic layer gave a mixture of the *E* and *Z* isomers (3.26 g, 94%). Chromatographic separation (solvent A) gave the *Z* isomer **8** (1.68 g, 48.6%) and the *E* isomer **7** (1.46 g, 42.8%) in that order of elution. For **7**, $[\alpha]_D$ +199.3° (*c* 1.16, $CHCl_3$); nmr data, at 100 MHz, δ (ppm): 1.70 (m, H_{2a}, $J_{2a,2e}$ = 14 Hz, $J_{2a,3}$ = 10 Hz, $J_{2a,1}$ = 3.75 Hz), 2.90 (dd, H_{2e}, $J_{2e,2a}$ = 14 Hz, $J_{2e,1}$ = 7.0 Hz), 3.40 (s, OMe), 3.63 (s, CO_2Me), 5.0 (dd, H_1, $J_{1,2e}$ = 7.0 Hz, $J_{1,2a}$ = 3.75 Hz), 6.0 (s, C=CH), 6.15 (d, H_3, $J_{3,2a}$ = 10 Hz), etc; M^+ 574, ms *m/e*: 543 ($M^+ - MeO$), etc; for **8**, $[\alpha]_D$ +162.5° (*c* 1.0, $CHCl_3$); nmr data at 100 MHz, δ(ppm): 2.25 (m, H_{2a}, H_{2e}), 3.3 (s, OMe), 3.75 (s, CO_2Me), 6.0 (s, C=CH), 6.85 (m, H_3), etc; M^+ 543; ms *m/e*: 517 ($M^+ - Me_3C$), etc.

Ozonolysis of 7 and 8

A solution containing **7** (50 mg, 0.87 mmol) in 10 mL of methanol was treated with a stream of ozone (0.12 mmol/min) at −78°C. After 5 min of stirring (0.88 mmol ozone uptake; ~1 equivalent), nitrogen gas was passed through the solution, then 4 drops of dimethylsulfide were added. After standing at room temperature overnight, the solution was evaporated to dryness and the residue was purified by preparative tlc (solvent A, R_f 0.68) to give 36 mg (80%) of **6** as a homogeneous syrup. Crystallization was effected from petroleum ether to give 17 mg of **6**, mp and mixture mp 86–88°C; $[\alpha]_D$ +147.3°. Ozone treatment of the other isomer **8** gave essentially the same results.

*Methyl 3-O-Benzoyl-6-O-(*tert*-butyldiphenylsilyl)-2,4-dideoxy-4-C-[(methoxycarbonyl)methyl]-*α*-D-ribo-hexopyranoside, (9)*

From **7**: A solution containing 1.46 g (2.54 mmol) of **7** in a mixture of ethyl acetate and methanol (120:50 mL) was hydrogenated in the presence of 20% palladium hydroxide on charcoal (23) (0.5 g). After 24 h, the catalyst was filtered and the filtrate was processed as usual to give a syrup. Chromatography (solvent A, R_f 0.48) gave 1.11 g (70%) of the title compound as a viscous syrup, $[\alpha]_D$ +100.4° (*c* 1.17, $CHCl_3$); λ_{max}(film): 1737 (CO_2Me) cm^{-1}; nmr data, δ(ppm): 3.3 (s, OMe), 3.55 (s, CO_2Me), 4.85 (m, H_1), 5.4 (m, H_3), etc; ms *m/e*: 545 ($M^+ - MeO$), 519 ($M^+ - Me_3C$), etc. From **8**: hydrogenation of this isomer for 8 h gave the title compound (92%) having the physical constants described above.

*Methyl 6-O-(*tert*-Butyldiphenylsilyl)-4-C-(carboxymethyl)-2,4-dideoxy-*α*-D-ribo-hexopyranoside,γ-Lactone, (10)*

A solution containing **9** (0.836 g, 1.45 mmol) in 35 mL of dry methanol was treated with 0.2 g (1.45 mmol) of dry potassium carbonate and the suspension was stirred under nitrogen for 60 h. Neutralization with Rexyn 102 (H^+), and processing of the filtered suspension gave a colorless syrup which was purified by preparative tlc (solvent B, R_f 0.52) to give 0.518 g (85%) of the lactone **10**. Crystallization from petroleum ether gave 0.43 g of material with mp 80.5–81.5°C; $[\alpha]_D$ +41.8° (*c* 1.05, $CHCl_3$). An additional 70 mg was obtained from the mother liquors but remained as a syrup; λ_{max}(KBr): 1780 (C=O) cm^{-1}; ms *m/e*: 409 ($M^+ - MeO$), 383 ($M^+ - Me_3C$), 351 ($M^+ - Me_3C - MeOH$), etc. *Anal.* calcd. for $C_{25}H_{32}O_6$ Si: C 68.15, H 7.32; found: C 68.46, H 8.00.

Synthesis of 11

A solution of DIBAH (3.65 mL, 5.1 mmol) in hexanes was added to a solution containing the lactone **10** (1.5 g, 3.4 mmol) in anhydrous toluene at −78°C under nitrogen. After stirring for 30 min at −78°C, the solution was diluted with ether (25 mL) and saturated aqueous ammonium chloride (20 mL) while gradually allowing it to warm to room temperature after the additions. The solution was filtered over Celite and the latter was washed successively with water (30 mL) and ethyl acetate (100 mL). The organic phase was processed as usual to give the lactol derivative corresponding to **10**.

A solution of 1.58 *M* *n*-butyl lithium (17.2 mL, 27 mmol) in pentane was added to bis(trimethylsilyl)amine (3.16 g, 27.2 mmol) in 30 mL of dry ether at 0°C, under nitrogen. The solvents were evaporated under a current of dry nitrogen during 1 h and the resulting crystalline lithium bis(trimethylsilyl)amide was dissolved in 30 mL of dry HMPT. The solution was transferred into a solution of (4-carboxybutyl)triphenylphosphonium bromide (6.03 g, 13.6 mmol dried at 110°C, 0.02 Torr, 6 h) in 15 mL of HMPT. The *dark red* solution of the corresponding ylid was stirred under nitrogen for 1 h, then slowly transferred (25 min) into a cooled (0°C) solution containing the lactol (1.5 g, 3.4 mmol) in 15 mL of HMPT using a double tip needle under nitrogen pressure. After stirring at room temperature for 20 min, the solution was diluted with ether (250 mL) and ice-water and was acidified to pH ~ 2 with a 0.2 *M* solution of sodium bisulfate (250 mL). The organic phase was processed as usual to give an oil (3.57 g) which was dissolved in 10 mL of dichloromethane and 5 mL of methanol and treated with an excess of diazomethane in ether. Unreacted reagent was destroyed by addition of small portions of silica gel and the solution was filtered and the filtrate was evaporated to a syrup. Purification by preparative tlc (solvent A, R_f 0.34) gave 1.27 g (67%) of the title compound as a syrup; $[\alpha]_D$ +62.5° (*c* 1.09, $CHCl_3$); λ_{max}(film): 1738 (C=O) cm^{-1}; ms *m/e*: 509 ($M^+ - MeO$), 508 ($M^+ - MeOH$), etc.

Synthesis of 12

To a cooled solution of **11** (0.92 g, 1.7 mmol) in 15 mL of dry pyridine was added benzoyl chloride (0.42 g, 3 mmol) dropwise and with stirring. After stirring at room temperature overnight, the solution was poured into ice-water and ether, and the organic layer was processed as usual to give, after preparative tlc (solvent A, R_f 0.5) the title compound (0.91 g, 89%) as a colorless syrup; $[\alpha]_D$ +92.6° (*c* 1.04, $CHCl_3$); λ_{max}(film): 1736 (CO_2Me), 1715 (OBz) cm^{-1}; ms *m/e*: 612 ($M^+ - MeOH$), 587 ($M^+ - Me_3C$), 555 ($M^+ - Me_3C - MeOH$), 491 ($M^+ - MeOH - PhCO_2$) etc.

Synthesis of 13

A solution containing **12** (0.885 g, 1.37 mmol) in 5 mL of dry tetrahydrofuran was treated with a 1 *M* solution of tetra-*n*-butylammonium fluoride (3 mL). After stirring at room temperature for 3 h, the solution was evaporated to dryness and the residue was purified by preparative tlc (solvent B, R_f 0.20) to give the title compound **12** as a syrup (0.5 g, 89.5%); $[\alpha]_D$ +130° (*c* 1.02, $CHCl_3$); λ_{max}(film): 1735 (CO_2Me), 1715 (OBz) cm^{-1}; M^+ 406; ms *m/e*: 375 ($M^+ - MeO$), 343 ($M^+ - MeO - MeOH$), etc.

Synthesis of 14

A solution containing **13** (0.5 g, 1.22 mmol) in 15 mL of dry

Can. J. Chem. Downloaded from www.nrcresearchpress.com by 210.87.254.42 on 09/06/12
For personal use only.

dichloromethane was added rapidly to a solution of the Collins reagent prepared from chromium trioxide (1.46 g, 14.6 mmol) in pyridine (2.36 mL, 29.3 mmol) and dichloromethane (100 mL), under nitrogen. After stirring vigorously for 30 min the mixture was poured into ice-water and dichloromethane; the organic layer was processed as usual to give a syrup. The latter was dissolved in toluene (50 mL), the solution evaporated to dryness, the residue was taken up in ether, filtered, and the filtrate was evaporated to a syrup (0.446 g, 91%) which was used as such in the next step. The chromatographically homogeneous material showed λ_{max}(film): 1738 (CO_2Me, CHO), 1718 (OBz) cm^{-1}; R_f 0.4 (solvent B).

Synthesis of 15

A solution containing 1-tributylphosphoranylidene 2-heptanone (19) (0.42 g, 1.32 mmol) in dry ether (5 mL) was added to the aldehyde **14** (0.446 g, 1.1 mmol) in 20 mL of ether. The solution was stirred at room temperature for 3 h, it was then evaporated to dryness and the residue was purified by preparative tlc (solvent B, R_f 0.68) to give the title compound as a syrup (0.438 g, 79%); $[\alpha]_D$ +153.0° (*c* 1.14, $CHCl_3$); λ_{max}(film): 1736 (CO_2Me), 1718 (OBz), 1637 (C=C—*C*=*O*), 1636 (*C*=*C*—C=O) cm^{-1}; nmr data at 100 MHz, δ ppm: 2.26 ($H_{"16"}$, t, J = 7.5 Hz), 3.32 (s, OMe), 3.58 (s, CO_2Me), 4.68 ($H_{"12"}$, dd, $J_{"12,8"}$ = 10 Hz, $J_{"12,13"}$ = 6.25 Hz), 4.83 ($H_{"11"}$, d, $J_{"11"}$ = 3.73 Hz), 6.45 ($H_{"14"}$, d, $J_{"14,13"}$ = 15.6 Hz), 6.89 ($H_{"13"}$, dd, $J_{"13,14"}$ = 15.6 Hz, $J_{"13,12"}$ = 6.25 Hz), etc; M^+ 500; ms *m/e*: 468 (M^+ − MeOH), 437 (M^+ − MeOH − MeO), 399 (M^+ − $(CH_2)_3$ CO_2Me), 378 M^+ − $PhCO_2H$), 347 (M^+ − MeOH − $PhCO_2$), 315 (M^+ − 2MeOH − $PhCO_2$), 279 (M^+ − $PhCO_2H$ − $C_5H_{11}C$), etc.

Zinc Borohydride Reduction of 15. Isolation of the "C-15" Epimeric Alcohols 16 and 17

A 0.5 *M* solution of zinc borohydride (3 mL) in 1,2-dimethoxyethane was added to the enone **15** (0.37 g, 0.74 mmol) in 15 mL of anhydrous ether under nitrogen. The mixture was stirred for 3 h at room temperature, then it was diluted with ether (20 mL) and saturated ammonium chloride (20 mL). Processing the organic phase gave a 1:1 mixture of the epimeric alcohols **16** and **17** (0.354 g). Separation by preparative tlc (solvent C) gave the two products as syrups.

For the "15*S*" alcohol **16**: 0.15 g (40%), R_f 0.43; $[\alpha]_D$ +137.8° (*c* 1.19, $CHCl_3$); nmr data at 100 MHz, δ ppm: 3.34 (OMe), 3.60 (CO_2Me), 4.18 ($H_{"15"}$, m), 4.44 ($H_{"12"}$, dd, $J_{"12,8"}$ = 9.5 Hz, $J_{"12,13"}$ = 7.0 Hz), 4.79 ($H_{"11"}$, d, J = 3.75), 5.70 ($H_{"13"}$, dd, $J_{"13,14"}$ = 15.6 Hz, $J_{"13,12"}$ = 7.0 Hz), 6.08 ($H_{"14"}$, dd, $J_{"14,13"}$ = 15.6 Hz, $J_{"14,15"}$ = 5.6 Hz), etc; M^+ 502; ms *m/e*: 484 (M^+ − H_2O), 470 (M^+ − MeOH), 399 (M^+ − MeOH − C_5H_{11}), 348 (M^+ − MeOH − $PhCO_2H$), 330 (M^+ − $(CH_2)_3CO_2Me$ − C_5H_{11}), 304 (M^+ − C_5H_{11} − CH=CH$(CH_2)_3CO_2Me$), 227 (M^+ − MeOH − $PhCO_2H$ − C_5H_{11}), etc.

For the "15 *R*" isomer **17**: 0.125 g (33.7%); R_f 0.50; $[\alpha]_D$ +132.0° (*c* 0.91, $CHCl_3$); nmr data at 100 MHz, δ ppm: 3.36 (s, OMe), 3.60 (s, CO_2Me), 4.10 ($H_{"15"}$, m), 4.46 ($H_{"12"}$, dd, $J_{"12,8"}$ = 9.5 Hz, $J_{"12,13"}$ = 7 Hz), 4.70 ($H_{"11"}$, d, J = 3.75 Hz), 5.72 ($H_{"13"}$, dd, $J_{"13,14"}$ = 15.6 Hz, $J_{"13,12"}$ = 7 Hz), 5.92 ($H_{"14"}$, dd, $J_{"14,13"}$ = 15.6 Hz, $J_{"14,15"}$ = 5.6 Hz), etc; M^+ 502; ms *m/e*: 484 (M^+ − H_2O), 470 (M^+ − MeOH), 399 (M^+ − MeOH − C_5H_{11}), 348 (M^+ − MeOH − $PhCO_2H$). For the M^+ − MeOH fragment ($C_{27}H_{50}O_5Si_2$): calcd. 510.3197; observed, 510.3214.

Synthesis of 18

A solution of the ester **16** (0.15 g, 0.3 mmol) in anhydrous methanol (15 mL) containing potassium carbonate (0.14 g, 1 mmol) was stirred at room temperature in a nitrogen atmosphere for 96 h. The solution was then neutralized with Rexyn-102 (H^+) and processed in the usual way to give a residue which was chromatographed on silica gel (solvent D, R_f 0.38) to give **18** (0.094 g, 80%) as a colorless syrup; $[\alpha]_D$ +95.8° (*c* 1.09, $CHCl_3$); for the M^+ − MeOH − H_2O fragment ($C_{21}H_{32}O_4$): calcd. 348.2249; found 348.2246; ms *m/e*: 366 (M^+ − MeOH), etc; R_f 0.68 (solvent E). The corresponding bis-trimethylsilyl derivative (R_f 0.8, solvent C) had a mass spectral fragmentation pattern identical to the published report (2). For the M^+ − MeOH fragment ($C_{27}H_{50}O_9Si_2$): calcd. 510.3197; found 510.3214.

Synthesis of 19

A solution of the ester **17** (0.125 g, 9.25 mmol) was treated as described for the preceding compound to give **19** as a syrup (0.071 g, 71.5%); $[\alpha]_D$ +93.8° (*c* 1.1, $CHCl_3$); ms *m/e*: 380 (M^+ − H_2O), 366 (M^+ − MeOH), 348 (M^+ − MeOH − H_2O), etc; R_f 0.73 (solvent E).

(+)-Thromboxane B_2, (1): {2R-[2α(1E, 3S), 3β(Z), 4β, 6(α, β)]}-7-[tetrahydro-4,6-dihydroxy-2-(3-hydroxy-1-octenyl)-2H-pyran-3-yl]-5-heptenoic Acid

A solution of **18** (0.032 g, 0.08 mmol) in 1 mL of 0.1 *M* NaOH and 1 mL of methanol was stirred at room temperature for 8 h. The solution was evaporated to dryness below 35°C, the residue was dissolved in 4 mL of water and treated with Dowex-50 (H^+) (5 mL). After a few minutes the solution became somewhat opalescent, then gradually cleared during the course of 1 h. The formation of the "methyl glycoside" derivative of thromboxane B_2 could be easily monitored by tlc (solvent D or E). The resin was removed by filtration, the filtrate was extracted with a 2:1 mixture of ethyl acetate and ether (150 mL, total), and the extracts were processed as usual to give a syrup (0.025 g, 85%). Crystallization was effected by dissolving the syrup (0.025 g) in 4 drops of ethyl acetate, adding 2 mL of ether followed by 4 mL of petroleum ether or hexanes to give a turbid solution. After standing overnight, crystals of thromboxane B_2 were obtained (0.016 g), mp 91–93°C (lit. (3), mp 92–94°C). Recrystallization from the same solvent mixture gave material with mp 95–96°C, undepressed upon admixture with an authentic sample;[3] R_f 0.40 (solvent E); $[\alpha]_D$ +57.4° (*c* 0.26, EtOAc); λ_{max}(film): 1705 (C=O); ms *m/e*: 335 (M^+ − H_2O − HO), 317 (M^+ − $2H_2O$ − HO), 272 (M^+ − $3H_2O$ − CO_2), 246 (M^+ − $2H_2O$ − HO − C_5H_{11}), etc.

"15"-Epi Thromboxane B_2, 20

A solution of the "15 *R*" derivative **19** (0.03 g, 0.075 mmol) was treated as described for the preparation of **1** to give the title epi-derivative as a syrup (0.024 g, 86%); R_f 0.44 (solvent E); $[\alpha]_D$ +50.2° (*c* 1.0, EtOAc).

Oxidation and Reduction of Intermediate 11

To a solution containing **11** (0.061 g, 0.113 mmol) in 1 mL of DMSO were added successively 0.013 g of pyridine, 0.017 g of trifluoroacetic anhydride, and 0.067 g (0.37 mmol) of 1-ethyl-3-(3-dimethylaminopropyl)carbodiimide hydrochloride (EDAC·HCl). After 3 h of stirring under nitrogen, the solution was diluted with ether (50 mL) and water. Processing the organic phase as usual gave a syrup which was purified by preparative tlc to give the ketone **21** as a syrup (0.052 g, 86%); R_f 0.43 (solvent A); $[\alpha]_D$ +51.4° (*c* 1.0, $CHCl_3$); λ_{max}(film): 1738 (CO_2Me), 1720 (C=O) cm^{-1}; M^+ 538; ms *m/e*: 507 (M^+ − MeO), 481 (M^+ − Me_3C), 450 (M^+ − Me_3C − MeO), 449 (M^+ − Me_3C − MeOH), 379 (M^+ − MeOH − CH=CH$(CH_2)_3CO_2Me$), etc.

Attempted epimerization of **21** (K_2CO_3, MeOH, pH 10, 5 h, N_2) showed some elimination (5–10%). Neutralization with Rexyn-102 (H^+) and processing gave a syrup which was identical to the starting ketone **21**; $[\alpha]_D$ +50.8°; ir, nmr, R_f.

[3]We thank Drs. N. A. Nelson, R. C. Kelly, and W. P. Schneider of the Upjohn Co. for a sample of thromboxane B_2.

Reduction of the above obtained material (0.036 g) with sodium borohydride (0.02 g) in methanol at 0°C gave, after work-up and preparative tlc, the alcohol **11** (0.027 g, 74%), identical with material obtained previously according to the synthetic scheme ($[\alpha]_D$, nmr, ir, R_f).

Acknowledgments

We thank the National Research Council of Canada and le Ministère de l'éducation du Québec for financial support and for a fellowship to P.L.

1. K. H. GIBSON. Chem. Soc. Rev. **6**, 489 (1977); Science, **196**, 1072 (1977).
2. M. HAMBERG, J. SVENSSON, and B. SAMUELSSON. Proc. Natl. Acad. Sci. U.S.A. **72**, 2994 (1975); M. HAMBERG and B. SAMUELSSON. Proc. Natl. Acad. Sci. U.S.A. **71**, 3400 (1974); M. HAMBERG, J. SVENSSON, and B. SAMUELSSON. Proc. Natl. Acad. Sci. U.S.A. **71**, 3824 (1974); Science, **190**, 770 (1975).
3. N. A. NELSON and R. W. JACKSON. Tetrahedron Lett. 3275 (1976); R. C. KELLY, I. SCHLETTER, and S. J. STEIN. Tetrahedron Lett. 3279 (1976); W. P. SCHNEIDER and R. A. MORGE. Tetrahedron Lett. 3283 (1976).
4. S. HANESSIAN and P. LAVALLEE. Can. J. Chem. **55**, 562 (1977).
5. E. J. COREY, M. SHIBASAKI, J. KNOLLE, and T. SUGAHARA. Tetrahedron Lett. 785 (1977).
6. E. J. COREY, M. SHIBASAKI, and J. KNOLLE. Tetrahedron Lett. 1625 (1977); H. OHRUI and S. EMOTO. Agric. Biol. Chem. **41**, 1773 (1977); O. HERNANDEZ. Tetrahedron Lett. 219 (1978); A. G. KELLY and J. S. ROBERTS. Chem. Commun. 228 (1980).
7. S. HANESSIAN. Acc. Chem. Res. **12**, 159 (1979); B. FRASER-REID and R. ANDERSON. Prog. Chem. Org. Nat. Prod. **39**, 1 (1979), and references cited therein.
8. K. C. NICOLAOU, G. P. GASIC, and W. E. BARNETTE. Angew. Chem. Int. Ed. Engl. **17**, 293 (1978), and references cited therein.
9. A. ROSENTHAL and P. CATSOULACOS. Can. J. Chem. **46**, 2868 (1968); L. F. WIGGINS. Methods Carbohydr. Chem. **2**, 188 (1963).
10. S. HANESSIAN and P. LAVALLEE. Can. J. Chem. **53**, 2975 (1975).
11. E. J. COREY and A. VENKATESWARLU. J. Am. Chem. Soc. **94**, 6190 (1972).
12. J. C. SHEEHAN, P. A. CRUICKSHANK, and G. L. BOSHART. J. Org. Chem. **26**, 2525 (1961); J. C. SHEEHAN and P. A. CRUICKSHANK. Org. Synth. **48**, 83 (1968).
13. K. E. PFITZNER and J. G. MOFFATT. J. Am. Chem. Soc. **85**, 3027 (1963); **87**, 5661 (1965); G. H. JONES and J. G. MOFFATT. Methods Carbohyd. Chem. **6**, 315 (1972).
14. A. ROSENTHAL and L. B. NGUYEN. J. Org. Chem. **34**, 1029 (1969).
15. P. ROSEN, G. W. HOLLAND, J. L. JERNOW, F. KIENZLE, and S. KWOH. 9th IUPAC Conference on Natural Products, Ottawa, Ont., June 24–28, 1974. Abstr. p. 5A.
16. E. W. YANKEE, U. AXEN, and G. L. BUNDY. J. Am. Chem. Soc. **96**, 5865 (1974).
17. (*a*) J. D. ROBERTS, F. J. WEIGERT, J. I. KROSCHWITZ, and H. J. REICH. J. Am. Chem. Soc. **92**, 1338 (1970); (*b*) F. J. WEIGERT and J. D. ROBERTS. J. Am. Chem. Soc. **92**, 1347 (1970); (*c*) D. E. DORMAN and J. D. ROBERTS. J. Am. Chem. Soc. **92**, 1355 (1970); (*d*) D. E. DORMAN, M. JOUTELAT, and J. D. ROBERTS. J. Org. Chem. **36**, 2757 (1971); (*e*) A. S. PERLIN, B. CASU, and H. J. KOCH. Can. J. Chem. **48**, 2596 (1970); (*f*) J. B. STOTHERS and P. C. LAUTERBUR. Can. J. Chem. **42**, 1563 (1964); (*g*) G. LUKACS, F. PIRIOU, S. D. GERO, D. A. VAN DORP, E. W. HAGAMAN, and E. WENKERT. Tetrahedron Lett. 515 (1973); G. F. COOPER and J. FRIED. Proc. Natl. Acad. Sci. U.S.A. **70**, 1579 (1973).
18. R. E. ARRICK, D. C. BAKER, and D. HORTON. Carbohydr. Res. **26**, 441 (1973).
19. N. FINCH, L. DELLA VECCHIA, J. J. FITT, R. STEPHANI, and I. VLATTAS. J. Org. Chem. **38**, 4412 (1973).
20. E. J. COREY, T. K. SCHAFF, W. HUBER, U. KOELLIKER, and N. M. WEINSHENKER. J. Am. Chem. Soc. **92**, 397 (1970).
21. E. J. COREY, K. C. NICOLAOU, M. SHIBASAKI, Y. MACHIDA, and C. S. SHINER. Tetrahedron Lett. 3183 (1975); E. J. COREY, K. C. NICOLAOU, and M. SHIBASAKI. Chem. Commun. 658 (1975).
22. S. FORTIER, M. GERMAN, D. A. LANGS, and G. DETITA. Acta Crystallogr. Sect. B, **36**, 1099 (1980).
23. W. M. PEARLMAN. Tetrahedron Lett. 1663 (1967).

Can. J. Chem. Downloaded from www.nrcresearchpress.com by 210.87.254.42 on 09/06/12
For personal use only.

Synthesis of 3′,7′-anhydrooctose nucleosides related to the ezomycins and the octosyl acids

KWAN SOO KIM AND WALTER A. SZAREK

Carbohydrate Research Institute and Department of Chemistry, Queen's University, Kingston, Ont., Canada K7L 3N6

Received September 8, 1980

This paper is dedicated to Prof. Raymond U. Lemieux on the occasion of his 60th birthday

KWAN SOO KIM and WALTER A. SZAREK. Can. J. Chem. **59**, 878 (1981).

Several novel 3′,7′-anhydrooctose nucleosides, including a 3′,7′-anhydroocturonic acid nucleoside, namely 1-(3,7-anhydro-5,6-dideoxy-β-D-*allo*-octofuranosyluronic acid)-3-methyluracil (**40**), have been synthesized. The synthetic sequence leading to **40** consists of three key steps: preparation of an octose nucleoside by a chain extension of an uridine derivative using a Wittig reaction, conversion of the octose nucleoside into a bicyclic-octose nucleoside by an intramolecular cyclization, and elaboration of a carboxylic acid function at the C-8′ position of the bicyclic-octose nucleoside. The structures of the 3′,7′-anhydrooctose nucleosides have been established by their uv, ^{1}Hmr, ^{13}Cmr, and mass spectral data.

KWAN SOO KIM et WALTER A. SZAREK. Can. J. Chem. **59**, 878 (1981).

On a synthétisé plusieurs nucléosides du type anhydro-3′,7′ octose dont le nucléoside de l'acide anhydro-3′,7′ octuronique, soit (l'acide anhydro-3,7 didéoxy-5,6 β-D-*allo*-octofurannosyluronique)-1 méthyl-3 uracil (**40**). La synthèse comprend 3 étapes principales; la première étape consiste à préparer un nucléoside de type octose par élongation de la chaîne d'un dérivé de l'uridine en utilisant une réaction de Wittig. Dans la deuxième étape, on transforme l'octose en un nucléoside bicyclique en faisant appel à une cyclisation intramoléculaire. La troisième étape permet de fixer une fonction acide carboxylique en position C′-8 du nucléoside octose bicyclique. On a établi les structures des nucléosides anhydro-3′,7′ octose en se basant sur les données des spectres uv, rmn du ^{1}H et du ^{13}C et de la spectrométrie de masse.

[Traduit par le journal]

Introduction

The synthesis of carbohydrates containing carbon chains composed of more than six carbon atoms, carbohydrates which have been called higher-carbon sugars (1), has posed a considerable challenge. Such syntheses require the creation of C—C bonds together with control of the absolute stereochemistry at every carbon center. It is noteworthy that the concept of asymmetric synthesis was first realized by Emil Fischer's cyanohydrin reaction with carbohydrates (2). Added impetus has, in recent years, been given to this area of carbohydrate chemistry, by the development of new methods of chain extension (3) and by the discovery of various important antibiotics containing highly complex, higher-carbon sugars, such as lincomycin (4), celesticetin (5), apramycin (6), oxyapramycin (7), the ezomycins (8), mildiomycin (9), tunicamycin (10), and hikizimycin (11).

A major program in this laboratory has been concerned with the development of new methods of chain extension and with the synthesis of antibiotics containing higher-carbon sugars and of related systems; some methods (12) and the synthesis of lincomycin (13) were reported several years ago, and, recently, the synthesis of the octodiose related to apramycin has been also accomplished in this laboratory (14).

The present study is concerned with the ezomycins (15, 16) and the octosyl acids (17) which were obtained from two different strains of *Streptomyces* and which contain a unique type of higher-carbon sugar.

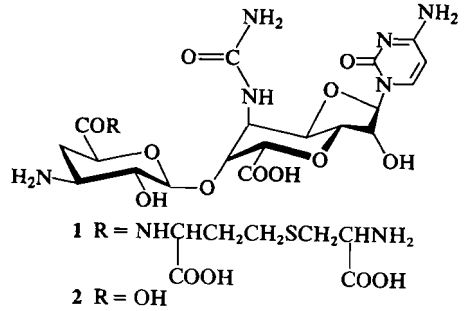

1 R = NHCHCH$_2$CH$_2$SCH$_2$CHNH$_2$ (COOH, COOH)

2 R = OH

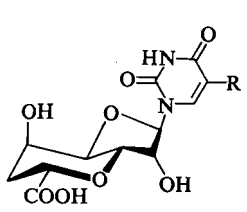

3 R = COOH

4 R = CH$_2$OH

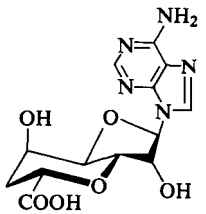

5

The sugar, a 3,7-anhydrooctonic acid in ezomycins A_1 (**1**), A_2 (**2**), B_1, B_2, C_1, and C_2 (**8**) and in octosyl acids A (**3**) and B (**4**) (17), is the first octose derivative containing a rigid bicyclic system in which a furanoid ring is *trans*-fused to a pyranoid ring. In spite of their structural similarities, the ezomycins and octosyl acids show marked differences in biological activities. Thus, whereas the

0008-4042/81/050878-11$01.00/0

©1981 National Research Council of Canada/Conseil national de recherches du Canada

Can. J. Chem. Downloaded from www.nrcresearchpress.com by 210.87.254.5 on 09/06/12
For personal use only.

Can. J. Chem. Downloaded from www.nrcresearchpress.com by 210.87.254.5 on 09/06/12
For personal use only.

ezomycins are antifungal antibiotics (16), the octosyl acids are devoid of any such activity.

However, the adenine analog (**5**) of the octosyl acids, readily obtained from **3** by transglycosylation (18, 19), was found to be an inhibitor of cyclic-AMP phosphodiesterases from various animal tissues (19). In fact, octosyl acids **3** and **4** may be regarded as carboanalogs of 3′,5′-cyclic nucleotides. The unique structures and the biological activities of the ezomycins and the octosyl acids have inspired various studies related to these compounds during the last few years. For example, a biosynthesis of octosyl acid A has been accomplished by Sato *et al.* (20), and a synthesis of an octose derivative related to the octosyl acids has been attempted (21). A ^{13}Cmr spectroscopic study of the ezomycins has been also reported (22).

The present article describes the first synthesis of 3′,7′-anhydrooctose nucleosides and of a 3′,7′-anhydrooctonic acid nucleoside.

Results and Discussion

On the basis of a retrosynthetic analysis, it seemed most appropriate to prepare an octose nucleoside from a ribonucleoside by a three-carbon chain extension followed by cyclization of the octose nucleoside to afford a 3′,7′-anhydrooctose nucleoside. As the starting material, the readily available 2′,3′-isopropylidene-3-methyluridine (**6**) (23) was chosen. This compound could be prepared from 2′,3′-*O*-isopropylideneuridine in large quantities more easily by methylation with *N*,*N*-dimethylformamide dimethyl acetal. For the chain extension of **6**, the three Wittig reagents **7**, **8**, and **9** were chosen. Although the Wittig reagent **7** would not provide functionality at C-8′ of the 3′,7′-anhydrooctose nucleoside, nevertheless, because of its ready availability (24) and simple structure, **7** was employed, prior to the use of Wittig reagents **8** and **9**, for the synthesis of prototype compounds, especially in order to examine the formation of the *trans*-fused, bicyclic ring system.

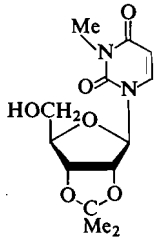

6

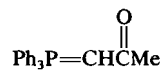

7

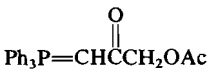

8

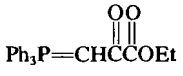

9

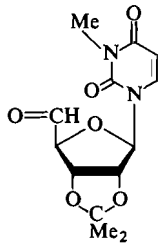

10

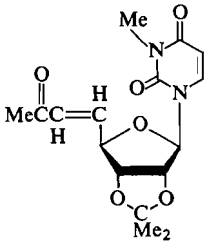

11

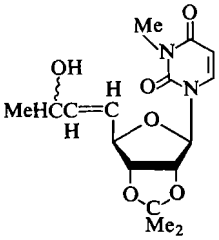

12

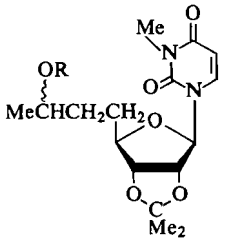

13 R = H
14 R = Ts

The aldehyde **10**, obtained by oxidation of **6** and employed without isolation from the reaction mixture, was allowed to react with the Wittig reagent **7**. Chromatographic purification afforded the α,β-(*E*)-unsaturated ketone **11** in 77% yield from **6**. The ^{1}Hmr spectrum of **11** showed a doublet of doublets ($J_{5',6'}$ = 16 Hz, $J_{4',5'}$ = 6 Hz) at δ 6.89 for H-5′ and a singlet at δ 2.29 for H-8′. Compound **11** was reduced with sodium borohydride to give a chromatographically homogeneous, epimeric mixture, namely 1-[(*E*)-5,6,8-trideoxy-2,3-*O*-isopropylidene-β-D-*allo* (and α-L-*talo*)-oct-5-enofuranosyl]-3-methyluracil (**12**). The ^{1}Hmr spectrum of **12**, however, indicated that small amounts of the saturated alcohols **13**, which are the desired products of the next step, were also generated during the borohydride reduction of **11**. Catalytic hydrogenation of the allylic alcohols **12** in the presence of 10% palladium-on-charcoal afforded the saturated alcohols **13**. Treatment of **13** with *p*-toluenesulfonyl chloride gave **14**. The isopropylidene groups in **14** were cleaved using 90% formic acid at 0°C to afford the diols **15** in 78% yield. Cyclization was accomplished by treatment of the *p*-tolylsulfonates **15** with sodium hydride in *N*,*N*-dimethylformamide at room temperature. Two epimeric 3′,7′-anhydrooctose nucleosides were separated by column chromatography. The crystalline, faster-moving

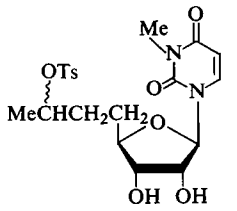

15

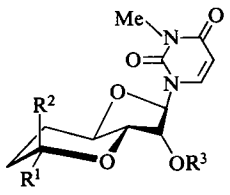

16 R^1 = Me, R^2 = R^3 = H
17 R^1 = R^3 = H, R^2 = Me
18 R^1 = Me, R^2 = H, R^3 = Ac
19 R^1 = H, R^2 = Me, R^3 = Ac

isomer was identified as being 1-(3,7-anhydro-5,6,8-trideoxy-β-D-*allo*-octofuranosyl)-3-methyluracil (**16**) (25%). The slower-moving isomer, namely 1-(3,7-anhydro-5,6,8-trideoxy-α-L-*talo*-octofuranosyl)-3-methyluracil (**17**), was obtained as a syrup in 21% yield. Acetylation of **16** and **17** afforded monoacetates **18** and **19**, respectively.

The *trans*-fused bicyclic system of compounds **16** and **17** is supported by a sharp singlet ($J_{1',2'}$ = 0 Hz) owing to H-1′ protons in their ^{1}Hmr spectra. Usually the ^{1}Hmr spectra of uridine derivatives show a doublet for the anomeric proton. The $J_{1',2'}$ value of **15**, which is the immediate precursor of **16** and **17**, is 3.5 Hz. The zero value of $J_{1',2'}$ of **16** and **17** corresponds to a C-3′ *endo* conformation of the furanose ring and a *trans* relationship between H-1′ and H-2′. Small or zero values of $J_{1',2'}$ have been observed in the cases of 3′,5′-cyclic nucleotides (25), the ezomycins (8), and the octosyl acids (17). The mass spectra of **16** and **17** reflect very clearly the bicyclic nature of the molecules. The mass spectrum of **16** shows characteristic nucleoside-base peaks at *m/e* 155 (b + 30), *m/e* 127 (b + 2H), and *m/e* 126 (b + H) (26). In addition to these prominent ions, a major mode of fragmentation, not observed in other nucleoside spectra, is represented by the most intense peak at *m/e* 128, owing to the species formed from the molecular ion by the opening of the ribose ring, and a peak at *m/e* 98 owing to further decomposition of this species (see Scheme 1). Comparable fragmentation patterns have been observed in the spectra of 3′,5′-cyclic nucleotides (27). The intact sugar fragment is absent in this mass spectrum; however, the ion (*m/e* 139), formed from the molecular ion by the elimination of H_2O and subsequent cleavage of the glycosidic bond, is comprised of the entire bicyclic-sugar carbon skeleton.

The stereochemistry at C-7′ of **16** and **17** was assigned on the basis of their ^{13}Cmr and ^{1}Hmr chemical-shift data. The epimer, whose C-8′ signal resonated at δ 21.0 in its ^{13}Cmr spectrum, was assigned as being compound **16** bearing an equatorial methyl group, whereas the compound whose C-8′ signal was at δ 17.5 in its ^{13}Cmr spectrum was assigned as being compound **17** bearing an axial methyl group. In their ^{1}Hmr spectra, the resonance for the H-8′ protons of **16** (δ 1.32) appears at slightly higher field than that of **17** (δ 1.36). It has been well established that, whereas the carbon resonance of an equatorial methyl group in cyclohexane and 1,3-dioxane systems (28) shifts downfield relative to that of the corresponding axial one, the protons of an equatorial methyl group in cyclohexane, 1,3-dioxane, and 1,3,5-trioxane systems (29) resonate at higher field than do those of the corresponding axial one.

The initial studies established the feasibility of the synthesis of a 3′,7′-anhydrooctose nucleoside

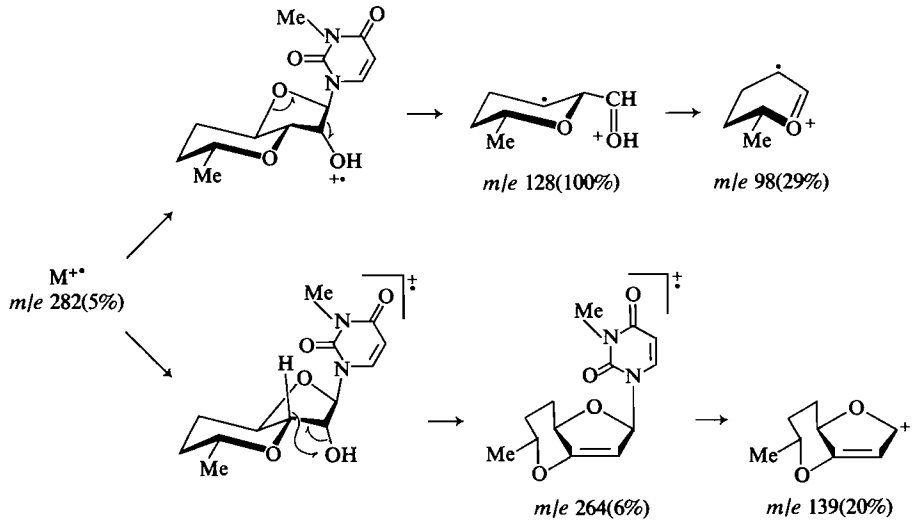

SCHEME 1

Can. J. Chem. Downloaded from www.nrcresearchpress.com by 210.87.254.5 on 09/06/12
For personal use only.

Can. J. Chem. Downloaded from www.nrcresearchpress.com by 210.87.254.5 on 09/06/12
For personal use only.

by the approach described above. Attention was then directed to the functionalization of the C-5′, C-6′, and C-8′ positions, a process which is required for the eventual total synthesis of the ezomycins and the octosyl acids. Although the C-5′—C-6′ double bond in compounds **11** and **12** can be easily functionalized, the introduction of functionality at C-8′ is not feasible at any stage of the above synthetic sequence. This problem was solved by employing another Wittig reagent, namely **8** (30), which could be prepared in a reasonable quantity relatively easily using a modified procedure. Wittig reagent **9** (31) would be more suitable than **8** for the introduction of the carboxylic acid function at C-8′, however, the product of a Wittig reaction of **9** and **10** decomposed during the course of the reaction and subsequent processing.

A Wittig reaction of **8** and **10** afforded after chromatography the syrupy α,β-(*E*)-unsaturated ketone **20** in 72% yield from **6**. The ^{1}Hmr spectrum of **20** showed a large *trans*-ethylenic coupling constant ($J_{5',6'}$ = 16 Hz). Compound **20** was reduced with sodium borohydride in absolute ethanol at −20°C to afford a chromatographically homogeneous, epimeric mixture, namely 1-[(*E*)-8-*O*-acetyl-5,6-dideoxy-2,3-*O*-isopropylidene-β-D-*allo* (and α-L-*talo*)-oct-5-enofuranosyl]-3-methyluracil (**21**). The allylic alcohols **21** were converted by catalytic hydrogenation into the saturated alcohols **22**. The reaction of **22** with *p*-toluenesulfonyl chloride afforded **23**. Cleavage of the isopropylidene groups of **23** was accomplished with 90% formic acid at 0°C to give **24** in 75% yield.

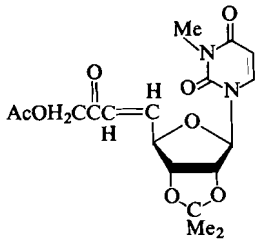

20

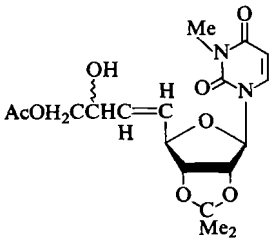

21

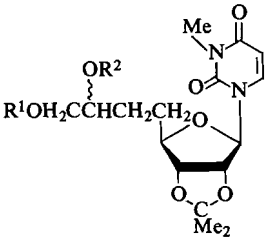

22 R^1 = Ac, R^2 = H
23 R^1 = Ac, R^2 = Ts
27 R^1 = $CH_2CH{=}CH_2$, R^2 = H
28 R^1 = $CH_2CH{=}CH_2$, R^2 = Ts

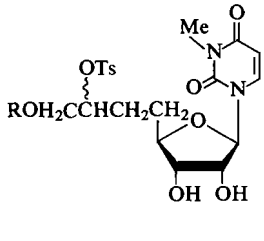

24 R = Ac
29 R = $CH_2CH{=}CH_2$

Treatment of **24** with sodium hydride in dry 1,2-dimethoxyethane or *N*,*N*-dimethylformamide unexpectedly gave a complex multiplicity of products. One of the major products was identified as being an oxirane derivative (**25**). However, the desired 3′,7′-anhydrooctose nucleoside was not detected. Although this attempted cyclization reaction was not fully investigated, the complication of the reaction might be attributable to the lability of the acetyl group under the reaction conditions. The acetyl groups in **23** were replaced by allyl groups (32) by a sequence of three steps: (*i*) conversion of **23** into a mixture of oxiranes using sodium methoxide in chloroform; (*ii*) ring opening of the oxiranes **26** with sodium alloxide in allyl alcohol at room temperature; (*iii*) treatment of the resulting secondary alcohols **27** with *p*-toluenesulfonyl chloride. The oxirane ring opening of **26** with alloxide was regioselective and provided the expected secondary alcohol **27** exclusively in 88% yield. The ^{1}Hmr spectrum of **27** showed a two-proton multiplet at δ 5.03–5.34 owing to two terminal vinylic protons and an one-proton multiplet at δ 5.58–6.39 attributable to another vinylic proton of the allyl group. The *p*-tolylsulfonates **28** obtained in this way were converted into **29** in 89% yield by treatment with 90% formic acid at 0°C.

The stage was again set for the elaboration of the bicyclic ring system. Cyclization was accomplished by treatment of **29** with sodium hydride in 1,2-dimethoxyethane at room temperature to afford a chromatographically homogeneous, epimeric mixture (**30**) in 50% yield. A sharp singlet at δ 5.65 owing to anomeric protons in the ^{1}Hmr spectrum of **30** indicated the *trans*-fused bicyclic structure. The allyl groups in **30** were isomerized to prop-1-enyl groups by treatment with $RhCl(PPh_3)_3$ in refluxing aqueous ethanol (33). At this stage the two epimers could be separated by careful column chromatography to afford pure **31** in 45% and **32** in 42% yield. The ^{1}Hmr spectrum of **31** showed a three-proton doublet of doublets at δ 1.56 attributable to the allylic-methyl protons of the prop-1-enyl group and a one-proton multiplet at δ 5.86–6.30 attributable to a vinylic proton on the carbon next to the oxygen atom of the prop-1-enyl group. The ^{1}Hmr spectrum of **32** also showed similar patterns of signals at δ 1.58 and at δ 5.91–6.32. The stereochemistry at C-7′ of the two epimers **31** and **32** was not assigned at this stage; however, it could be established later by the structural assignment of the two epimers **35** and **36** which were derived from **31** and **32**, respectively. Benzoylation of **31** and **32** gave monobenzoates **33** and **34**, respectively. Removal of the prop-1-enyl groups in **33** and **34** was

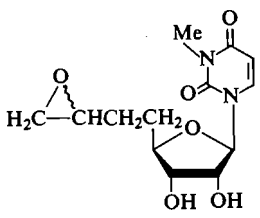

25

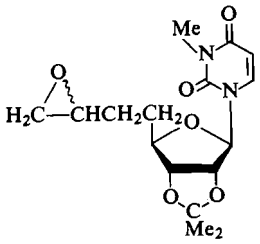

26

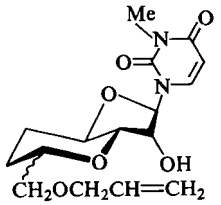

30

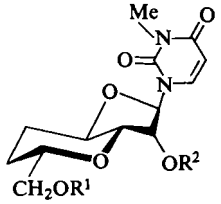

31 R^1 = CH=CHCH$_3$, R^2 = H
33 R^1 = CH=CHCH$_3$, R^2 = Bz
35 R^1 = H, R^2 = Bz
37 R^1 = R^2 = H

accomplished with 0.1 *N* hydrochloric acid in aqueous methanol at room temperature (32) to afford 1-(3,7-anhydro-2-*O*-benzoyl-5,6-dideoxy-β-D-*allo*-octofuranosyl)-3-methyluracil (**35**) and 1-(3,7-anhydro-2-*O*-benzoyl-5,6-dideoxy-α-L-*talo*-octofuranosyl)-3-methyluracil (**36**), respectively. Hydrolysis of the prop-1-enyl groups in **33** and **34** with mercuric chloride in the presence of mercuric oxide (34) resulted in the partial decomposition of products **35** and **36**. The stereochemistry at C-7′ of compounds **35** and **36** was readily assigned in a manner similar to that used for the assignments in the cases of the bicyclic octose nucleosides **16** and **17**. Thus, the C-8′ signal in the ^{13}Cmr spectrum of one epimer appeared at δ 65.0 and that of another epimer appeared at δ 60.9. The former was assigned as being compound **35** bearing an equatorial hydroxymethyl group and the latter as being compound **36**. The stereochemistry at C-7′ of compounds **31–34**, thereby, could be correctly assigned.

Thus, the synthesis of a 3′,7′-anhydrooctose nucleoside with a functional group at C-8′ has been accomplished. Finally, the hydroxymethyl group of compound **35** was further transformed into a carboxylic acid function. Oxidation of **35** with chromium(VI) reagents was not very satisfactory, mainly because the isolation of the product from the reaction mixture was difficult or very tedious owing to the solubility of the product. Better results could be obtained by employing catalytic oxidation. Thus, compound **37**, obtained from **35** by debenzoylation, was oxidized in the presence of 10% platinum-on-charcoal at pH 8–9 at 70°C to give 1-(3,7-anhydro-5,6-dideoxy-β-D-*allo*-octofuranosyluronic acid)-3-methyluracil (**39**) in 74% yield. Treatment of **39** with 3% hydrogen chloride in methanol afforded the methyl ester **40**. The ^{1}Hmr spectrum of **40** showed a three-proton singlet at δ 3.75 attributable to the methyl ester at C-8′. The ir spectrum of **40** showed a broad band at 3430 cm^{-1}.

The sequence leading to the 3′,7′-anhydroocturonic acid nucleoside as described in this paper can be adapted to the synthesis of the ezomycins, the octosyl acids, and their analogs. Further investigations into the functionalization at C-5′ and C-6′ of the 3′,7′-anhydrooctose nucleoside are currently underway, and a different approach to the synthesis of 3′,7′-anhydrooctose nucleosides will be reported separately.

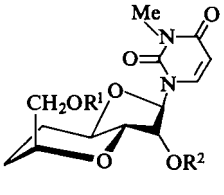

32 R^1 = CH=CHCH$_3$, R^2 = H
34 R^1 = CH=CHCH$_3$, R^2 = Bz
36 R^1 = H, R^2 = Bz
38 R^1 = R^2 = H

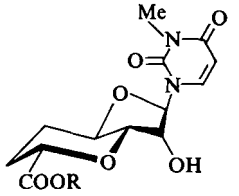

39 R = H
40 R = Me

Experimental

Evaporations were performed under reduced pressure at or below 40°C (bath temperature). Melting points were determined on a Fisher–Johns apparatus and are uncorrected. Optical rotations were measured with a Perkin–Elmer model 141 automatic polarimeter at 23 ± 3°C. Infrared spectra were recorded with a Perkin–Elmer 180 or a Perkin–Elmer 598 infrared spectrophotometer. Ultraviolet spectra were measured with a Unicam SP 800B or a Perkin–Elmer 552 spectrophotometer. The ^{1}Hmr spectra were determined with a Varian EM-360 or Bruker HX-60 spectrometer in chloroform-*d* with tetramethylsilane (TMS) as the internal standard, unless otherwise stated. The ^{13}Cmr were recorded in chloroform-*d* solution on a Bruker HX-60 spectrometer equipped with an FT60M Fourier transform accessory at 15.09 MHz; chemical shifts are given in parts per million downfield from TMS. Mass spectra were taken on a Jeolco model JMS-015C spectrometer using the direct-sample inlet system with a 70 eV ionization energy. Microanalyses were performed by Guelph Chemical Laboratories Ltd., Guelph, Ont. Thin-layer chromatography (tlc) was performed on precoated glass plates (silica gel 60 F-254, 0.25 mm thickness) from EM Laboratories Inc., using the following solvent systems (v/v): (*A*) toluene–acetone, 1:1; (*B*) toluene – ethyl acetate, 1:1; (*C*) toluene–acetone, 2:1; (*D*) toluene – ethyl acetate, 2:1; (*E*) ethyl acetate; (*F*) ethyl acetate – methanol, 2:1; (*G*) *n*-butanol – methanol–water, 8:1:1. The developed plates were air dried and compounds located by irradiation of the plates with uv light and by heating the plates at 150°C after they had been sprayed with 10% aqueous sulfuric acid containing 1% cerium sulfate and 1.5% molybdic acid. Column chromatography was performed on Brinkmann silica gel 60 (70–230 mesh, E. Merck). E. Merck precoated glass plates (silica gel F-254, 20 × 20 cm, 2 mm thickness) were used for preparative tlc chromatography.

Can. J. Chem. Downloaded from www.nrcresearchpress.com by 210.87.254.5 on 09/06/12
For personal use only.

Can. J. Chem. Downloaded from www.nrcresearchpress.com by 210.87.254.5 on 09/06/12
For personal use only.

2',3'-O-Isopropylidene-3-methyluridine (6)

A suspension of 2',3'-*O*-isopropylideneuridine (35) (7.1 g, 20 mmol) and *N,N*-dimethylformamide dimethyl acetal (9.5 g, 80 mmol) in chloroform (80 mL) was heated at reflux temperature with vigorous stirring. The mixture became homogeneous within 30 min. After 8 h the solvent was evaporated to give a reddish syrup which slowly crystallized on standing. Recrystallization from ethanol–ether gave compound **6** (6.5 g, 87%) having R_f 0.57 (solvent *A*), mp 133–134°C (lit. (10) mp 133.5–134°C); ^{1}Hmr δ: 1.38 (3H, s, Me), 1.60 (3H, s, Me), 3.33 (3H, s, NMe), 3.55–3.92 (3H, m, H-4', 2(H-5')'s), 4.29 (1H, bs, OH, exchanged in D_2O), 4.74–5.02 (2H, m, H-2', H-3'), 5.73 (1H, d, $J_{1',2'}$ = 1.2 Hz, H-1'), 5.74 (1H, d, $J_{5,6}$ = 8 Hz, H-5), 7.60 (1H, d, H-6).

1-[(E)-5,6,8-Trideoxy-2,3-O-isopropylidene-β-D-ribo-oct-5-eno-1,4-furanosid-7-ulosyl]-3-methyluracil (11)

To a solution of **6** (2.39 g, 8 mmol) in dimethylsulfoxide (40 mL), stirred at room temperature under nitrogen, pyridine (0.64 mL), trifluoroacetic acid (0.30 mL), and *N,N'*-dicyclohexylcarbodiimide (4.96 g, 24 mmol) were added. After 12 h, the Wittig reagent **7** (3.31 g, 10.4 mmol) was added and stirring was continued for a further 24 h at room temperature. Oxalic acid dihydrate (2.9 g) and ethyl acetate (200 mL) were then added and the mixture was stirred for 10 min. This mixture was poured into saturated sodium chloride solution (100 mL), stirred for a few min, and filtered. The separated aqueous layer was extracted once more with ethyl acetate (80 mL). The combined ethyl acetate solutions were washed with dilute aqueous sodium hydrogen carbonate, saturated aqueous sodium chloride, and cold water, dried ($MgSO_4$), and evaporated to give a dark red syrup. The thick syrup was dissolved again in ethyl acetate and insoluble *N,N'*-dicyclohexylurea was removed by filtration. This procedure was repeated a few more times to remove *N,N'*-dicyclohexylurea. The resulting red syrup (5.5 g) was chromatographed on a column of silica gel by elution with toluene – ethyl acetate, 7:5 (v/v), to afford **11** as a colorless syrup (2.07 g, 77%) having R_f 0.23 (solvent *B*); $[\alpha]_D$ +54.8° (*c* 0.062, $CHCl_3$); ir (film) ν_{max}: 1710, 1680, 1665, 1630 cm^{-1}; uv λ_{max} (EtOH): 217 (ε 13 000), 259 (6800) nm; ^{1}Hmr δ: 1.38 (3H, s, isopropylidene-Me), 1.59 (3H, s, isopropylidene-Me), 2.29 (3H, s, H-8''s), 3.32 (3H, s, NMe), 4.51–5.17 (3H, m, H-2'–H-4'), 5.61 (1H, d, $J_{1',2'}$ = 1.2 Hz, H-1'), 5.78 (1H, d, $J_{5,6}$ = 8.0 Hz, H-5), 6.22 (1H, d, $J_{5',6'}$ = 16.0 Hz, H-6'), 6.89 (1H, dd, $J_{4',5'}$ = 6.0 Hz, H-5'), 7.27 (1H, d, H-6). *Anal.* calcd. for $C_{16}H_{20}N_2O_6$: C 57.14, H 5.99, N 8.33; found: C 57.33, H 6.24, N 7.73.

1-[(E)-5,6,8-Trideoxy-2,3-O-isopropylidene-β-D-allo (and α-L-talo)-oct-5-enofuranosyl]-3-methyluracil (12)

To a stirred solution of **11** (1.62 g, 4.8 mmol) in ethanol (30 mL) was added sodium borohydride (0.19 g, 5.0 mmol) at 0°C in the dark. Thin-layer chromatography (solvent *C*) showed that after 5 min the reaction mixture contained only one component (R_f 0.33) but no starting material. The reaction mixture was carefully neutralized with 1 *N* hydrochloric acid and the neutral mixture was evaporated to a residue which was concentrated several times with methanol. The residue was extracted with hot ethyl acetate (4 × 30 mL) and the extract was filtered through a small amount of silica gel. Evaporation of the solvent gave **12** as a chromatographically homogeneous white foam (1.60 g, 98%). An analytical sample was obtained by preparative tlc using toluene–acetone, 1:1 (v/v), as eluent; ir (film) ν_{max}: 3430, 1710, 1670, 1630 cm^{-1}; uv λ_{max} (EtOH): 212 (ε 6800), 258 (9800) nm; ^{1}Hmr δ: 1.26 (3H, d, $J_{7',8'}$ = 6.0 Hz), 1.34 (3H, s, isopropylidene-Me), 1.58 (3H, s, isopropylidene-Me), 2.67 (1H, bs, OH, exchanged in D_2O), 3.30 (3H, s, NMe), 3.67–5.02 (4H, H-2'–H-4', H-7'), 5.49–5.90 (2H, m, H-5', H-6'), 5.64 (1H, d, $J_{1',2'}$ = 1.2 Hz, H-1'), 5.73 (1H, d, $J_{5,6}$ = 8.0 Hz, H-5), 7.26 (1H, d, H-6).

1-[5,6,8-Trideoxy-2,3-O-isopropylidene-β-D-allo (and α-L-talo)-octofuranosyl]-3-methyluracil (13)

A solution of **12** (2.15 g, 6.3 mmol) in ethanol (150 mL) was shaken in a standard Paar bottle together with 10% palladium-on-charcoal catalyst (0.35 g) under a 1-atm hydrogen pressure at room temperature. As soon as the shaking was started, hydrogen was consumed very rapidly. After 10 min the hydrogen uptake had almost ceased. Thin-layer chromatography (solvent *C*) showed that the R_f value of the product was the same as that of the starting material. The reaction mixture was filtered through Celite twice and the filtrate was concentrated to a white foam which was chromatographed on a column of silica gel by elution with toluene – ethyl acetate, 5:6 (v/v), to give **13** as a white foam (1.81 g, 84%); ir (film) ν_{max}: 3430, 1710, 1670, 1640 cm^{-1}; uv λ_{max} (EtOH): 214 (ε 8000), 259 (12 600) nm; ^{1}Hmr δ: 1.21 (3H, d, $J_{7',8'}$ = 6.0 Hz, H-8'), 1.34 (3H, s, isopropylidene-Me), 1.43–2.03 (4H, m, 2(H-5')'s, 2(H-6')'s), 1.57 (3H, s, isopropylidene-Me), 2.45 (1H, bs, OH, exchanged in D_2O), 3.28 (3H, s, NMe), 3.64–4.61 (4H, H-3'–H-5', H-7'), 4.84 (1H, dd, $J_{2',3'}$ = 6.5 Hz, $J_{1',2'}$ = 2.0 Hz, H-2'), 5.58 (1H, d, H-1'), 5.72 (1H, d, $J_{5,6}$ = 8.0 Hz, H-5), 7.19 (1H, d, H-6). *Anal.* calcd. for $C_{16}H_{24}N_2O_6$: C 56.46, H 7.11, N 8.23; found: C 56.06, H 7.42, N 7.97.

1-[5,6,8-Trideoxy-2,3-O-isopropylidene-7-O-p-tolylsulfonyl-β-D-allo (and α-L-talo)-octofuranosyl]-3-methyluracil (14)

To a solution of **13** (0.86 g, 2.5 mmol) in pyridine (4 mL) was added at 0°C *p*-toluenesulfonyl chloride (0.52 g, 2.8 mmol). The reaction mixture was kept at 0°C overnight to give only one product (R_f 0.21, solvent *D*). The reaction mixture was poured with vigorous stirring into ice-water (40 mL). The aqueous mixture was extracted with dichloromethane; the dichloromethane extract was washed successively with cold 1 *N* sulfuric acid, saturated aqueous sodium hydrogen carbonate, and cold water. Evaporation of the dried ($MgSO_4$) solution afforded **14** as a chromatographically homogeneous syrup (1.07 g, 85%). An analytical sample was obtained by preparative tlc using toluene–acetone, 2:1 (v/v), as eluent; ir (film) ν_{max}: 1710, 1670, 1630, 1360, 1180 cm^{-1}; uv λ_{max} (EtOH): 227 (ε 12 000), 259 (10 500) nm; ^{1}Hmr δ: 1.22 (3H, d, $J_{7',8'}$ = 6.0 Hz, H-8'), 1.32 (3H, s, isopropylidene-Me), 1.56 (3H, s, isopropylidene-Me), 1.65–1.84 (4H, m, 2(H-5')'s, 2(H-6')'s), 2.42 (3H, s, PhMe), 3.28 (3H, s, NMe), 3.82–4.76 (3H, H-3', H-4', H-7'), 4.80 (1H, dd, $J_{2',3'}$ = 6.5 Hz, $J_{1',2'}$ = 2.0 Hz, H-2'), 5.56 (1H, d, H-1'), 5.71 (1H, d, $J_{5,6}$ = 8.0 Hz, H-5), 7.15 (1H, d, H-6), 7.17–7.78 (5H, m, aromatic H's). *Anal.* calcd. for $C_{23}H_{30}N_2O_8S$: C 55.86, H 6.11, N 5.67, S 6.48; found: C 55.49, H 6.34, N 5.48, S 6.19.

1-[5,6,8-Trideoxy-7-O-p-tolylsulfonyl-β-D-allo (and α-L-talo)-octofuranosyl]-3-methyluracil (15)

The product **14** (0.90 g, 1.8 mmol) was dissolved in cold 90% formic acid (5 mL) and the solution was kept at 0°C overnight. Cold water (15 mL) was added to the reaction mixture and evaporated. Addition of more water and evaporation were repeated to afford a pale yellow, solid residue which was fractionated on a column of silica gel by elution with toluene–acetone, 3:2 (v/v), to give **15** as a colorless glass (0.65 g, 78%) having R_f 0.10 (solvent *C*); ir (film) ν_{max}: 3420, 1710, 1660, 1630, 1360, 1180 cm^{-1}; uv λ_{max} (EtOH): 226 (ε 13 000), 259 (12 600) nm; ^{1}Hmr δ: 1.20 (3H, d, $J_{7',8'}$ = 6.0 Hz, H-8'), 1.69–1.89 (4H, m, 2(H-5')'s, 2(H-6')'s), 2.42 (3H, s, PhMe), 3.27 (3H, s, NMe), 3.87 (2H, bs, 2 OH), 4.02–4.78 (4H, H-2'–H-4', H-7'), 5.67 (1H, d, $J_{1',2'}$ = 3.5 Hz, H-1'), 5.77 (1H, d, $J_{5,6}$ = 8.0 Hz, H-5), 7.15–7.81 (6H, H-6, aromatic H's).

Cyclization of 15

The product **15** (0.6 g, 1.3 mmol) in *N,N*-dimethylformamide

TABLE 1. Carbon-13 chemical-shift data[a] for 3′,7′-anhydrooctose nucleosides **16**, **17**, **35**, and **36**

Compound	C-2	C-4	C-5	C-6	C-1′	C-2′	C-3′	C-4′	C-5′	C-6′	C-7′	C-8′	NMe
16	150.8	162.7	101.6	137.6	94.2	75.6[b]	80.3[b]	75.9[b]	31.5	29.5	73.5[b]	21.0	27.6
17	150.9	162.8	101.7	137.6	93.8	72.7[b]	73.9[b]	76.2[b]	25.0	27.9	70.9[b]	17.5	27.6
35	150.6	162.3	102.3	138.6	93.3	74.2[b]	79.8[b]	79.1[b]	28.5	25.5	76.2[b]	65.0	27.6
36	150.7	162.3	102.3	138.4	92.3	72.5[b]	74.6[b]	76.2[b]	23.4	26.1	73.8[b]	60.9	27.6

[a]In ppm downfield from tetramethylsilane in chloroform-*d*.
[b]Assignments may be changed.

(10 mL) was vigorously stirred with sodium hydride (0.13 g, 5.2 mmol, 50% oil dispersion) at room temperature for 3 h, after which time tlc (solvent *C*) showed the absence of starting material. The reaction mixture was poured with stirring into ice-water (100 mL) and the mixture was extracted exhaustively with dichloromethane. The combined organic solutions were washed with a small amount of cold water, dried ($MgSO_4$), and concentrated to a syrup. Column chromatography on silica gel (toluene–acetone, 5:2 (v/v)) gave crystalline 1-(3,7-anhydro-5,6,8-trideoxy-β-D-*allo*-octofuranosyl)-3-methyluracil (**16**) (0.095 g, 25%). Recrystallization from toluene afforded white crystalline **16** having R_f 0.30 (solvent *C*), mp 219.5–220°C; $[\alpha]_D$ +25.0° (*c* 0.14, $CHCl_3$); ir (KBr) ν_{max}: 3410, 1700, 1650, 1620 cm^{-1}; uv λ_{max} (EtOH): 214 (ε 7800), 261 (13 300) nm: ^{1}Hmr δ: 1.26 (3H, d, $J_{7',8'}$ = 6.0 Hz, H-8′), 1.56–2.31 (4H, m, 2(H-5′)'s, 2(H-6′)'s), 2.85 (1H, bs, OH, exchanged in D_2O), 3.07–4.29 (4H, H-2′–H-4′, H-7′), 3.30 (3H, s, NMe), 5.56 (1H, s, H-1′), 5.70 (1H, d, $J_{5,6}$ = 8.0 Hz, H-5), 7.25 (1H, d, H-6). See Table 1 for ^{13}Cmr data. Mass spectrum *m/e*: 282 (M^+, 14%), 264 ($M^+ - H_2O$, 6), 155 (b + 30, 42), 139 (264 − b, 20), 128 [M^+ − (b + CHO), 100], 127 (b + 2H, 62), 126 (b + H, 16), 98 (128 − CHOH, 29), 69 [(b + H) − MeNCO, 31]. *Anal.* calcd. for $C_{13}H_{18}N_2O_5$: C 55.31, H 6.43, N 9.92; found: C 55.22, H 6.39, N 9.73.

1-(3,7-Anhydro-5,6,8-trideoxy-α-L-*talo*-octofuranosyl)-3-methyluracil (**17**) was isolated as a colorless syrup (0.082 g, 21%) having R_f 0.26; $[\alpha]_D$ +31.7° (*c* 0.30, $CHCl_3$); ir (film) ν_{max}: 3410, 1700, 1650, 1620 cm^{-1}; uv λ_{max} (EtOH): 214 (ε 7400), 261 (13 300) nm; ^{1}Hmr δ: 1.32 (3H, d, $J_{7',8'}$ = 6.0 Hz, H-8′), 1.67–2.39 (4H, m, 2(H-5′)'s, 2(H-6′)'s), 3.02 (1H, bs, OH, exchanged in D_2O), 3.28–4.51 (4H, H-2′–H-4′, H-7′), 3.30 (3H, s, NMe), 5.56 (1H, s, H-1′), 5.72 (1H, d, $J_{5,6}$ = 8.0 Hz, H-5), 7.27 (1H, d, H-6). See Table 1 for ^{13}Cmr data. Mass spectrum *m/e*: 282 (M^+, 10%), 264 ($M^+ - H_2O$, 5), 155 (b + 30, 50), 139 (264 − b, 18), 128 [M^+ − (b + CHO), 100], 127 (b + 2H, 65), 126 (b + H, 22), 98 (128 − CHOH, 32), 69 [(b + H) − MeNCO, 33]. *Anal.* calcd. for $C_{13}H_{18}N_2O_5$: C 55.31, H 6.43, N 9.92; found: C 55.46, H 6.30, N 9.80.

[(Acetoxymethyl)carbonyl]methylenetriphenylphosphorane (8)

To a cold solution of 1,3-dichloro-2-propanone (5 g, 39 mmol) (**36**) in acetone (150 mL) was added powdered lithium bromide (50 g) with vigorous stirring using a mechanical stirrer. The reaction mixture was stirred at 18–20°C for 3 days. Evaporation of the solvent gave a brownish solid which was partitioned between water and dichloromethane. The aqueous solution was extracted once more with a small amount of dichloromethane. The combined dichloromethane solutions were washed with cold water, dried ($MgSO_4$), and evaporated to afford crude 1,3-dibromo-2-propanone as a syrup.

A solution of the crude 1,3-dibromo-2-propanone in toluene (25 mL) was added dropwise to a stirred solution of triphenylphosphine (10.2 g, 39 mmol) in toluene (30 mL) at room temperature. Stirring was continued overnight at room temperature. The solid was collected by filtration, washed with toluene, and dried. To a stirred solution of the dried salt in 60% aqueous methanol (250 mL) was added an excess of powdered sodium carbonate. Stirring was continued for 30 min and more water (50 mL) was added to the reaction mixture. After being stirred for another 30 min, the solid was collected by filtration, washed thoroughly with water, and dried in a desiccator to afford crude (bromoacetyl)methylenetriphenylphosphorane (7.5 g) as a white solid having R_f 0.18 (solvent *E*).

A mixture of the crude (bromoacetyl)methylenetriphenylphosphorane (7.5 g) and powdered sodium acetate (18 g) in *N,N*-dimethylformamide (200 mL) was stirred vigorously using a mechanical stirrer at 50°C for 3 days. The reaction mixture was poured into water and the mixture was extracted with dichloromethane a few times. The combined dichloromethane extracts were washed with water, dried ($MgSO_4$), and concentrated to a dark brownish solid. A solution of this solid in ethyl acetate was filtered through silica gel. Evaporation of the solvent afforded **8** as a yellow solid (4.1 g, 28% from 1,3-dichloro-2-propanone) having R_f 0.16 (solvent *E*); ^{1}Hmr δ: 2.12 (3H, s, OAc), 4.58 (2H, s, $COCH_2O$), 7.24–7.71 (16H, PCH, 15 aromatic H's). This material was suitable for use in the subsequent reaction.

1-[(E)-8-O-Acetyl-5,6-dideoxy-2,3-O-isopropylidene-β-D-ribo-oct-5-eno-1,4-furanosid-7-ulosyl]-3-methyluracil (20)

To a solution of **6** (1.79 g, 6.0 mmol) in dimethylsulfoxide (30 mL), stirred at room temperature under nitrogen, pyridine (0.48 mL), trifluoroacetic acid (0.23 mL), and *N,N′*-dicyclohexylcarbodiimide (3.72 g, 18 mmol) were added. After 18 h, the Wittig reagent **8** (2.94 g, 7.8 mmol) was added and stirring was continued for a further 24 h at room temperature. The product was isolated by the procedure which was used for **11** to give, after column chromatography (toluene–acetone, 6:1 (v/v)), **20** as a colorless syrup (1.7 g, 72%) having R_f 0.36 (solvent *B*); ir (film) ν_{max}: 1735, 1700, 1660, 1630 cm^{-1}; uv λ_{max} (EtOH) 226 (ε 10 100), 255 (8500) nm; ^{1}Hmr δ: 1.36 (3H, s, isopropylidene-Me), 1.57 (3H, s, isopropylidene-Me), 2.16 (3H, s, OAc), 3.28 (3H, s, NMe), 4.56–5.01 (4H, H-3′, H-4′, 2(H-8′)'s), 5.08 (1H, dd, $J_{2',3'}$ = 6.0 Hz, $J_{1',2'}$ = 1.2 Hz, H-2′), 5.56 (1H, d, H-1′), 5.76 (1H, d, $J_{5,6}$ = 8.0 Hz, H-5), 6.27 (1H, d, $J_{5',6'}$ = 16.0 Hz, H-6′), 6.99 (1H, dd, $J_{4',5'}$ = 5.5 Hz, H-5′), 7.16 (1H, d, H-6).

1-[(E)-8-O-Acetyl-5,6-dideoxy-2,3-O-isopropylidene-β-D-allo (and α-L-talo)-oct-5-enofuranosyl]-3-methyluracil (21)

To a stirred solution of **20** (1.46 g, 3.7 mmol) in ethanol (20 mL) was added sodium borohydride (0.15 g, 3.9 mmol) at −20°C in the dark. Thin-layer chromatography (solvent *A*) showed that after 5 min the reaction mixture contained one major component (R_f 0.51) but no starting material. The product was isolated by the procedure which was used for **12** to give, after column chromatography (toluene–acetone, 5:2 (v/v)), **21** as a colorless syrup (1.25 g, 85%); ir (film) ν_{max}: 3430, 1735, 1710, 1660, 1630 cm^{-1}; uv λ_{max} (EtOH): 212 (ε 6700), 259 (9100) nm; ^{1}Hmr δ: 1.35 (3H, s, isopropylidene-Me), 1.57 (3H, s, isopropylidene-Me), 2.08 (3H, s, COMe), 3.29 (3H, s, NMe), 3.63–4.80

Can. J. Chem. Downloaded from www.nrcresearchpress.com by 210.87.254.5 on 09/06/12
For personal use only.

Can. J. Chem. Downloaded from www.nrcresearchpress.com by 210.87.254.5 on 09/06/12
For personal use only.

(5H, H-3′, H-4′, H-7′, 2(H-8′)'s), 4.99 (1H, dd, $J_{2',3'}$ = 6.0 Hz, $J_{1',2'}$ = 1.5 Hz, H-2′), 5.60 (1H, d, H-1′), 5.74 (1H, d, $J_{5,6}$ = 8.0 Hz, H-5), 5.76–5.97 (2H, m, H-5′, H-6′), 7.21 (1H, d, H-6).

*1-[8-*O*-Acetyl-5,6-dideoxy-2,3-*O*-isopropylidene-*β*-D-*allo *(and α-L-talo)-octofuranosyl]-3-methyluracil (22)*

Catalytic hydrogenation of the allylic alcohols **21** (1.25 g, 3.4 mmol) was performed as described above for **12** and afforded, after column chromatography (toluene–acetone, 5:2 (v/v)), **22** as a glass (1.2 g, 90%) having R_f 0.51 (solvent *A*); ir (film) ν_{max}: 3430, 1730, 1710, 1665, 1630 cm^{-1}; uv λ_{max} (EtOH): 212 (ε 7600), 259 (11 800) nm; ^{1}Hmr δ: 1.36 (3H, s, isopropylidene-Me), 1.58 (3H, s, isopropylidene-Me), 1.48–1.95 (4H, m, 2(H-5′)'s, 2(H-6′)'s), 2.08 (3H, s, OAc), 2.89 (1H, bs, OH, exchanged in D_2O), 3.30 (3H, s, NMe), 3.63–4.67 (5H, H-3′, H-4′, H-7′, 2(H-8′)'s), 4.94 (1H, dd, $J_{2',3'}$ = 6.0 Hz, $J_{1',2'}$ = 2.0 Hz, H-2′), 5.67 (1H, d, H-1′), 5.78 (1H, d, $J_{5,6}$ = 8.0 Hz, H-5), 7.30 (1H, d, H-6). *Anal.* calcd. for $C_{18}H_{26}N_2O_8$: C 54.26, H 6.58, N 7.03; found: C 54.57, H 6.87, N 6.88.

*1-[8-*O*-Acetyl-5,6-dideoxy-2,3-*O*-isopropylidene-7-*O*-p-tolylsulfonyl-*β*-D-*allo *(and α-L-talo)-octofuranosyl]-3-methyluracil (23)*

To a solution of **22** (1.1 g, 2.8 mmol) in pyridine (5 mL) was added at 0°C *p*-toluenesulfonyl chloride (0.58 g, 3.1 mmol). The product was isolated by the procedure which was used for **14** to give, after column chromatography (toluene – ethyl acetate, 5:2 (v/v)), **23** as a white foam (1.27 g, 83%) having R_f 0.51 (solvent *C*); ir (film) ν_{max}: 1710, 1670, 1630, 1360, 1180 cm^{-1}; uv λ_{max} (EtOH): 228 (ε 14 000), 259 (11 800) nm; ^{1}Hmr δ: 1.35 (3H, s, isopropylidene-Me), 1.56 (3H, s, isopropylidene-Me), 1.64–1.98 (4H, m, 2(H-5′)'s, 2(H-6′)'s), 1.90 (3H, s, OAc), 2.43 (3H, s, PhMe), 3.29 (3H, s, NMe), 3.78–4.92 (6H, H-2′–H-4′, H-7′ 2(H-8′)'s), 5.60 (1H, d, $J_{1',2'}$ = 2.0 Hz, H-1′), 5.73 (1H, d, $J_{5,6}$ = 8.0 Hz, H-5), 7.15 (1H, d, H-6), 7.20–7.80 (5H, m, aromatic H's).

*1-[8-*O*-Acetyl-5,6-dideoxy-7-*O*-p-tolylsulfonyl-*β*-D-*allo *(and α-L-talo)-octofuranosyl]-3-methyluracil (24)*

Hydrolysis of **23** (0.18 g, 0.33 mmol) was performed as described above for **14** and afforded, after preparative tlc (toluene–acetone, 2:3 (v/v)), **24** as a glass (0.13 g, 75%) having R_f 0.36 (solvent *A*); ir (film) ν_{max}: 3410, 1710, 1670, 1630, 1360, 1180 cm^{-1}; uv λ_{max} (EtOH): 227 (ε 13 000), 259 (12 000) nm; ^{1}Hmr δ: 1.66–2.01 (4H, m, 2(H-5′)'s, 2(H-6′)s), 2.46 (3H, s, PhMe), 3.29 (3H, s, NMe), 3.60–5.11 (8H, H-2′–H-4, H-7′, 2(H-8′)'s, 2 OH's), 5.64 (1H, d, $J_{1',2'}$ = 3.5 Hz, H-1′), 5.82 (1H, d, $J_{5,6}$ = 8.0 Hz, H-5), 7.27 (1H, d, H-6), 7.28–7.84 (5H, m, aromatic H's).

Treatment of 24 with Sodium Hydride

To a solution of **24** (0.101 g, 0.20 mmol) in dry 1,2-dimethoxyethane, stirred at room temperature under nitrogen, sodium hydride (0.014 g, 0.59 mmol) was added. Thin-layer chromatography (solvent *A*) showed that after 10 min the reaction mixture contained five new components (R_f 0.27, 0.48, 0.51, 0.66, and 0.78) and the starting material (R_f 0.36). After the reaction mixture had been stirred overnight tlc showed that three new components (R_f 0, 0.08, and 0.23) had been formed and that two of the components formed earlier (R_f 0.48 and 0.66) had almost disappeared. Cold water was added to the reaction mixture and the solution was carefully neutralized with 0.1 *N* hydrochloric acid. The neutralized solution was evaporated to dryness. The residue was extracted with methanol and the extract was evaporated to give a white solid which was fractionated on preparative tlc using toluene–acetone, 2:3 (v/v), as eluent. One (R_f 0.27) of the major components was identified as being 1-[7,8-anhydro-5,6-dideoxy-β-D-*allo* (and α-L-*talo*)-octofuranosyl]-3-methyluracil (**25**) (0.015 g, 25%); ir (film) ν_{max}: 3440, 1710, 1670, 1630 cm^{-1}; uv λ_{max} (EtOH): 212 (ε 7800), 259 (13 000) nm; ^{1}Hmr δ: 1.57–2.02 (4H, m, 2(H-5′)'s, 2(H-6′)'s), 2.45–3.08 (3H, m, H-7′, 2(H-8′)'s), 3.27 (3H, s, NMe), 3.65–4.38 (5H, H-2′–H-4′, 2 OH's), 5.66 (1H, d, $J_{1',2'}$ = 3.5 Hz, H-1′), 5.75 (1H, d, $J_{5,6}$ = 8.0 Hz, H-5), 7.34 (1H, d, H-6).

When **24** was treated with sodium methoxide in chloroform only one product was obtained (92%), which was identical to the material (**25**) isolated in the above experiment.

*1-[7,8-Anhydro-5,6-dideoxy-2,3-*O*-isopropylidene-*β*-D-*allo *(and α-L-talo)-octofuranosyl]-3-methyluracil (26)*

To a solution of **23** (0.94 g, 1.7 mmol) in chloroform (25 mL) was added sodium methoxide (0.114 g, 2.0 mmol) with stirring at 0°C. After the reaction mixture had been stirred overnight at 0°C, tlc (solvent *C*) showed that the reaction mixture contained only one component (R_f 0.46) but no starting material. The reaction mixture was carefully neutralized with cold 1 *N* hydrochloric acid, diluted with water (15 mL), and extracted with dichloromethane (2 × 10 mL). The combined extracts were washed with water, dried ($MgSO_4$), and evaporated to give **26** as a syrup (0.57 g, 97%). An analytical sample was obtained by preparative tlc using toluene–acetone, 2:1 (v/v), as eluent; ir (film) ν_{max}: 1710, 1670, 1630 cm^{-1}; uv λ_{max} (EtOH): 212 (ε 7800), 259 (13 000) nm; ^{1}Hmr δ: 1.28 (3H, s, isopropylidene-Me), 1.52 (3H, s, isopropylidene-Me), 1.45–1.97 (4H, m, 2(H-5′)'s, 2(H-6′)'s), 2.38–2.99 (3H, m, H-7′, 2(H-8′)'s), 3.27 (3H, s, NMe), 3.81–4.63 (2H, m, H-3′, H-4′), 4.84 (1H, dd, $J_{2',3'}$ = 6.0 Hz, $J_{1',2'}$ = 2.0 Hz, H-2′), 5.56 (1H, d, H-1′), 5.70 (1H, d, $J_{5,6}$ = 8.0 Hz, H-5), 7.17 (1H, d, H-6).

*1-[8-*O*-Allyl-5,6-dideoxy-2,3-*O*-isopropylidene-*β*-D-*allo *(and α-L-talo)-octofuranosyl]-3-methyluracil (27)*

To a stirred solution of **26** (0.57 g, 1.7 mmol) in allyl alcohol (7 mL) was added sodium alloxide (0.20 g, 2.5 mmol) at 0°C. The reaction mixture was stirred at 45–50°C. After 8 h tlc (solvent *C*) showed that the reaction mixture contained only one component (R_f 0.29) but no starting material. The reaction mixture was carefully neutralized with cold 1 *N* hydrochloric acid. The neutralized solution was diluted with water (10 mL) and the solution was extracted with dichloromethane (3 × 10 mL). The combined extracts were washed with cold water, dried ($MgSO_4$), and concentrated to a brownish syrup which was purified by column chromatography (toluene–acetone, 3:1 (v/v)) to afford pure **27** as a colorless syrup (0.61 g, 88%); ir (film) ν_{max}: 3480, 1710, 1660, 1630 cm^{-1}; uv λ_{max} (EtOH): 211 (ε 6800), 259 (9300) nm; ^{1}Hmr δ: 1.32 (3H, s, isopropylidene-Me), 1.50–1.90 (4H, m, 2(H-5′)'s, 2(H-6′)'s), 1.54 (3H, s, isopropylidene-Me), 2.66 (1H, bs, OH), 3.27–4.64 (7H, H-3′, H-4′, H-7′, 2(H-8′)'s, 2 vinylic H's), 3.30 (3H, s, NMe), 4.85 (1H, dd, $J_{2',3'}$ = 6.0 Hz, $J_{1',2'}$ = 2.0 Hz, H-2′), 5.03–5.34 (2H, m, terminal vinylic H's) 5.58–6.39 (1H, m, vinylic H), 5.64 (1H, d, H-1′), 5.75 (1H, d, $J_{5,6}$ = 8.0 Hz, H-5), 7.23 (1H, d, H-6).

*1-[8-*O*-Allyl-5,6-dideoxy-2,3-*O*-isopropylidene-7-*O*-p-tolylsulfonyl-*β*-D-*allo *(and α-L-talo)-octofuranosyl]-3-methyluracil (28)*

To a solution of **27** (0.58 g, 1.4 mmol) in pyridine (3 mL) was added at 0°C *p*-toluenesulfonyl chloride (0.33 g, 1.7 mmol). Thin-layer chromatography (solvent *C*) showed that after the reaction mixture had been kept overnight it contained only one component (R_f 0.56) but no starting material. The product was isolated by the procedure which was used for **14** to give **28** as a syrup (0.75 g, 94%). An analytical sample was obtained by preparative tlc using toluene–acetone, 2:1 (v/v) as eluent; ir (film) ν_{max}: 1710, 1670, 1630, 1360, 1180 cm^{-1}; uv λ_{max} (EtOH): 227 (ε

Can. J. Chem. Downloaded from www.nrcresearchpress.com by 210.87.254.5 on 09/06/12
For personal use only.

15 000), 259 (13 500) nm; ^{1}Hmr δ: 1.26 (3H, s, isopropylidene-Me), 1.48 (3H, s, isopropylidene-Me), 1.60–1.78 (4H, m, 2(H-5')'s, 2(H-6')'s), 2.45 (3H, s, PhMe), 3.23 (3H, s, NMe), 3.32–5.18 (10H, H-2'–H-4', H-7', 2(H-8')'s, 2 allylic H's, 2 terminal vinylic H's), 5.38–5.99 (1H, m, vinylic H), 5.54 (1H, d, $J_{1',2'}$ = 2.0 Hz, H-1'), 5.68 (1H, d, $J_{5,6}$ = 8.0 Hz, H-5), 7.05–7.79 (6H, aromatic H's, H-6).

*1-[8-*O*-Allyl-5,6-dideoxy-7-*O*-p-tolylsulfonyl-β-D-allo (and α-L-talo)-octofuranosyl]-3-methyluracil (29)*

Deblocking of the isopropylidene groups of **28** (0.7 g, 1.2 mmol) was performed as described above for **14** and afforded, after column chromatography (toluene–acetone, 7:3 (v/v)), **29** as a colorless syrup (0.58 g, 89%) having R_f 0.17 (solvent *C*); ir (film) ν_{max}: 3430, 1710, 1660, 1355, 1180 cm^{-1}; uv λ_{max} (EtOH): 227 (ε 15 500), 259 (13 500) nm; ^{1}Hmr δ: 1.69–2.02 (4H, m, 2(H-5')'s, 2(H-6')'s), 2.44 (3H, s, PhMe), 3.30 (3H, s, NMe), 3.28–5.39 (10H, H-2'–H-4', H-7', 2(H-8')'s, 2 allylic H's, 2 terminal vinylic H's), 5.62 (1H, d, $J_{1',2'}$ = 3.5 Hz), 5.48–6.34 (1H, m, vinylic H), 5.76 (1H, d, $J_{5,6}$ = 8.0 Hz, H-5), 7.08–7.83 (6H, H-6, 5 aromatic H's).

*1-[8-*O*-Allyl-3,7-anhydro-5,6-dideoxy-β-D-allo (and α-L-talo)-octofuranosyl]-3-methyluracil (30)*

Product **28** (0.57 g, 1.1 mmol) in 1,2-dimethoxyethane (20 mL) was stirred with sodium hydride (0.11 g, 4.4 mmol, 50% oil dispersion) at room temperature for 8 h. The reaction mixture was poured into ice-water (40 mL) and the mixture was exhaustively extracted with dichloromethane. The combined extracts were washed with a small amount of water, dried ($MgSO_4$), and concentrated to a syrup which was chromatographed on a column of silica gel (toluene–acetone, 5:2 (v/v)) to give **30** as a colorless syrup (0.22 g, 54%) having R_f 0.49 (solvent *A*); ir (film) ν_{max}: 3420, 1710, 1660, 1630 cm^{-1}; uv λ_{max} (EtOH): 214 (ε 6400), 262 (9850) nm; ^{1}Hmr δ: 1.55–2.05 (4H, m, 2(H-5')'s, 2(H-6')'s), 3.30 (3H, s, NMe), 3.14–4.40 (9H, H-2'–H-4', H-7', 2(H-8')'s, 2 allylic H's, OH), 5.02–5.39 (2H, m, 2 terminal vinylic H's), 5.65 (1H, s, H-1'), 5.59–6.23 (1H, m, vinylic H), 6.77 (1H, d, $J_{5,6}$ = 8.0 Hz, H-5), 7.34 (1H, d, H-6).

Isomerization of the Allyl Groups in 30 with $RhCl(PPh_3)_3$

A mixture of **30** (210 mg, 0.56 mmol), 1,4-diazabicyclo[2.2.2]-octane (18 mg), and $RhCl(PPh_3)_3$ (52 mg, 0.056 mmol) in 60% aqueous ethanol was heated at reflux temperature. After 1.5 h tlc (solvent *A*) showed that the reaction mixture contained two components (R_f 0.55, 0.58) but no starting material. The reaction mixture was filtered, and the filtrate was concentrated to half-volume and then partitioned between water and dichloromethane. The aqueous layer was further extracted with dichloromethane a few times. The dried (K_2CO_3) organic solution was concentrated to a brownish foam which was fractionated on a column of silica gel (toluene–acetone, 3:1 (v/v)) to give 1-[3,7-anhydro-5,6-dideoxy-8-*O*-(prop-1-enyl)-β-D-*allo*-octofuranosyl]-3-methyluracil (**31**) as a colorless syrup (94 mg, 45%) having R_f 0.58, $[\alpha]_D$ +32.7° (*c* 0.26, CH_2Cl_2); ir (film) ν_{max}: 3430, 1710, 1660, 1630 cm^{-1}; uv λ_{max} (EtOH): 212 (ε 6500), 261 (12 500) nm; ^{1}Hmr δ: 1.56 (3H, dd, ^1J = 6.5 Hz, ^2J = 1.5 Hz, allylic Me), 1.58–2.02 (4H, m, 2(H-5')'s, 2(H-6')'s), 3.15–5.01 (8H, H-2'–H-4', H-7', 2(H-8')'s, =CH, OH), 3.29 (3H, s, NMe), 5.61 (1H, s, H-1'), 5.71 (1H, d, $J_{5,6}$ = 8.0 Hz, H-5), 5.86–6.30 (1H, m, =HCO), 7.30 (1H, d, H-6).

1-[3,7-Anhydro-5,6-dideoxy-8-*O*-(prop-1-enyl)-α-L-*talo*-octofuranosyl]-3-methyluracil (**32**) was isolated as a colorless syrup (88 mg, 42%) having R_f 0.55; $[\alpha]_D$ +35.4° (*c* 0.26, CH_2Cl_2); ir (film) ν_{max}: 3430, 1710, 1660, 1630 cm^{-1}; uv λ_{max} (EtOH): 212 (ε 7000), 261 (12 500) nm; ^{1}Hmr δ: 1.58 (3H, dd, ^1J = 6.5 Hz, ^2J = 1.5 Hz, allylic Me), 1.58–2.02 (4H, m, 2(H-5')'s, 2(H-6')'s), 3.19–4.94 (8H, H-2'–H-4', H-7', 2(H-8')'s, =CH, OH), 3.30 (3H, s, NMe), 5.62 (1H, s, H-1'), 5.76 (1H, d, $J_{5,6}$ = 8.0 Hz, H-5), 5.91–6.32 (1H, m, =HCO), 7.38 (1H, d, H-6).

1-(3,7-Anhydro-2-O-benzoyl-5,6-dideoxy-β-D-allo-octofuranosyl)-3-methyluracil (35)

To a cooled solution of **31** (92 mg, 0.25 mmol) in pyridine (2 mL) was added benzoyl chloride (42 mg, 0.30 mmol). The reaction mixture was kept at room temperature for 30 min and then poured into cold water (20 mL), and the mixture was extracted with dichloromethane (2 × 20 mL). Concentration and then co-evaporation with toluene of the dried ($MgSO_4$) dichloromethane solution afforded crude 1-[3,7-anhydro-2-*O*-benzoyl-8-*O*-(prop-1-enyl)-β-D-*allo*-octofuranosyl]-3-methyluracil (**33**) as a colorless syrup having R_f 0.72 (solvent *A*). To a solution of crude **33** in 60% aqueous methanol (8 mL) was added 0.1 *N* hydrochloric acid in 80% aqueous methanol (8 mL). The reaction mixture was stirred at room temperature for 8 h and then neutralized by addition of silver carbonate. The silver salts were removed by filtration. The filtrate was concentrated to half-volume and then extracted with dichloromethane several times. The dried ($MgSO_4$) organic solution was concentrated to a yellow solid which was fractionated by preparative tlc (toluene–acetone, 2:1 (v/v)) to afford **35** as a colorless syrup (87 mg, 88% from **31**) having R_f 0.46 (solvent *C*); $[\alpha]_D$ +28.8° (*c* 0.07, CH_2Cl_2); ir (film) ν_{max}: 3430, 1710, 1660, 1630 cm^{-1}; uv λ_{max} (EtOH): 231 (ε 15 100), 258 (10 300) nm; ^{1}Hmr δ: 1.54–1.88 (4H, m, 2(H-5')'s, 2(H-6')'s), 3.28 (3H, s, NMe), 3.52–3.86 (6H, H-3', H-4', H-7', 2(H-8')'s, OH), 5.62 (1H, d, $J_{2',3'}$ = 4.0 Hz, H-2'), 5.72 (1H, s, H-1'), 5.78 (1H, d, $J_{5,6}$ = 8.0 Hz, H-5), 7.21–8.23 (6H, H-6, aromatic H's). See Table 1 for ^{13}Cmr data.

1-(3,7-Anhydro-2-O-benzoyl-5,6-dideoxy-α-L-talo-octofuranosyl)-3-methyluracil (36)

Compound **32** (85 mg, 0.23 mmol) was benzoylated as described above for compound **31** to give crude 1-[3,7-anhydro-2-*O*-benzoyl-5,6-dideoxy-8-*O*-(prop-1-enyl)-α-L-*talo*-octofuranosyl]-3-methyluracil (**34**) as a colorless syrup having R_f 0.72 (solvent *A*). Removal of the prop-1-enyl group of **34** was performed as described above for **33** to afford, after the preparative tlc (toluene–acetone, 2:1 (v/v)), **36** as a colorless syrup (80 mg, 88% from **32**) having R_f 0.43 (solvent *C*); $[\alpha]_D$ +32.7° (*c* 0.09, CH_2Cl_2); ir (film) ν_{max}: 3430, 1710, 1660, 1630 cm^{-1}; uv λ_{max} (EtOH): 230 (ε 14 000), 258 (10 000) nm; ^{1}Hmr δ: 1.75–1.96 (4H, m, 2(H-5')'s, 2(H-6')'s), 3.28 (3H, s, NMe), 3.66–4.15 (6H, H-3', H-4', H-7', 2(H-8')'s, OH), 5.62 (1H, d, $J_{2',3'}$ = 4.0 Hz, H-2'), 5.77 (1H, d, $J_{5,6}$ = 8.0 Hz, H-5), 5.78 (1H, s, H-1'), 7.20–8.15 (6H, H-6, aromatic H's). See Table 1 for ^{13}Cmr data.

1-(3,7-Anhydro-5,6-dideoxy-β-D-allo-octofuranosyl)-3-methyluracil (37)

To a solution of **35** (80 mg, 0.20 mmol) in methanol (2 mL) was added 1 *N* sodium methoxide in methanol (0.07 mL) at room temperature. The reaction was complete almost immediately. The reaction mixture was filtered through ion-exchange resin (H^+) and the resin was washed with a small amount of methanol. Evaporation of the methanol solution afforded a brownish residue which was purified by preparative tlc (ethyl acetate–acetone, 3:1 (v/v)) to give **37** as an amorphous solid (58 mg, 98%) having R_f 0.63 (solvent *F*); $[\alpha]_D$ +21.2° (*c* 0.05, MeOH); ir (KBr) ν_{max}: 3350, 1700, 1660, 1620 cm^{-1}; uv λ_{max} (MeOH): 214 (ε 7500), 262 (12 800) nm; ^{1}Hmr δ (DMSO-d_6): 1.66–2.12 (4H, m, 2(H-5')'s, 2(H-6')'s), 3.27 (3H, s, NMe), 3.11–4.28 (6H, H-2'–H-4', H-7', 2(H-8')'s), 5.72 (1H, s, H-1'), 5.80 (1H, d, $J_{5,6}$ = 8.0 Hz, H-5), 7.66 (1H, d, H-6). *Anal.* calcd. for $C_{13}H_8N_2O_6$: C 52.35, H 6.08, N 9.39; found: C 52.39, H 6.23, N 9.47.

1-(3,7-Anhydro-5,6-dideoxy-α-L-talo-octofuranosyl)-3-methyluracil (38)

Compound **36** (29 mg, 0.072 mmol) was debenzoylated in a

Can. J. Chem. Downloaded from www.nrcresearchpress.com by 210.87.254.5 on 09/06/12
For personal use only.

manner similar to that used for compound **35** to afford, after preparative tlc (ethyl acetate – acetone, 3:1 (v/v)), **38** as an amorphous solid (21 mg, 98%) having R_f 0.61 (solvent *F*); $[\alpha]_D$ +25.6° (*c* 0.06, MeOH); ir (film) ν_{max}: 3350, 1700, 1650, 1620 cm^{-1}; uv λ_{max} (MeOH): 214 (ε 7500), 262 (13 000) nm; ^{1}Hmr δ (DMSO-d_6): 1.75–2.21 (4H, m, 2(H-5′)'s, 2(H-6′)'s), 3.27 (3H, s, NMe), 3.18–4.23 (6H, H-2′–H-4′, H-7′, 2(H-8′)'s), 5.72 (1H, s, H-1′), 5.82 (1H, d, $J_{5,6}$ = 8.0 Hz, H-5), 7.71 (1H, d, H-6). *Anal.* calcd. for $C_{13}H_{18}N_2O_6$: C 52.35, H 6.08, N 9.39; found: C 52.59, H 6.08, N 9.20.

*1-(3,7-Anhydro-5,6-dideoxy-*β*-D-*allo*-octofuranosyluronic acid)-3-methyluracil (39)*

A mixture of **37** (50 mg, 0.17 mmol) in water (5 mL) and 10% platinum-on-charcoal catalyst (13 mg) were placed in a 30-mL test tube. The pH of the solution was adjusted to ~8.5 by addition of saturated aqueous sodium hydrogen carbonate solution. Oxygen was vigorously bubbled through the reaction mixture to provide sufficient agitation. The temperature of the reaction mixture was maintained at 70°C by means of a water bath throughout the course of the reaction. Every 30 min the pH of the reaction mixture was checked and adjusted to 8.5. The reaction was complete in 3 h. The reaction mixture was filtered through Celite twice and the filtrate was washed with dichloromethane. The aqueous solution was eluted through ion-exchange resin (H^+) and then freeze-dried to give a brownish foam which was carefully purified by preparative tlc (*n*-butanol – methanol–water, 8:1:1 (v/v)) to afford **39** as a colorless glass (39 mg, 74%) having R_f 0.18 (solvent *G*); $[\alpha]_D$ +14.4° (*c* 0.3, 0.1 *N* aqueous sodium hydroxide); ir (film) ν_{max}: 3420, 1710, 1660, 1620 cm^{-1}; uv λ_{max} (H_2O): 213 (ε 7800), 262 (13 500) nm; ^{1}Hmr δ (D_2O): 1.78–2.29 (4H, m, 2(H-5′)'s, 2(H-6′)'s), 2.97–4.45 (4H, H-2′–H-4′, H-7′), 3.26 (3H, s, NMe), 5.71 (1H, s, H-1′), 5.88 (1H, d, $J_{5,6}$ = 8.0 Hz, H-5), 7.62 (1H, d, H-6). *Anal.* calcd. for $C_{13}H_{16}N_2O_7$: C 50.00, H 5.17, N 8.97; found: C 50.13, H 5.23, N 9.11.

*3-Methyl-1-(methyl 3,7-anhydro-5,6-dideoxy-*β*-D-*allo*-octofuranosyluronate)uracil (40)*

To a stirred solution of compound **39** (37 mg, 0.12 mmol) in methanol (1 mL) was added 5% hydrogen chloride in methanol (2 mL) at °C. After 2 h, the reaction mixture was neutralized with silver carbonate. Silver salts were removed by filtration and the filtrate was concentrated to a pale yellow syrup which was purified by preparative tlc (toluene–acetone, 1:1 (v/v)) to afford **40** as a colorless syrup (31 mg, 81%) having R_f 0.38 (solvent *A*); $[\alpha]_D$ +25.7° (*c* 0.05, $CHCl_3$); ir (film) ν_{max}: 3430, 1710, 1660, 1630 cm^{-1}; uv λ_{max} (MeOH): 214 (ε 7500), 262 (14 000) nm; ^{1}Hmr δ: 1.75–2.23 (4H, m, 2(H-5′)'s, 2(H-6′)'s), 3.27 (3H, s, NMe), 3.75 (3H, s, COOMe), 3.02–4.51 (4H, H-2′–H-4′, H-7′), 5.72 (1H, s, H-1′), 5.86 (1H, d, $J_{5,6}$ = 8.0 Hz, H-5), 7.62 (1H, d, H-6).

Acknowledgements

The authors are grateful to the Natural Sciences and Engineering Research Council of Canada for its support of this work in the form of a grant (to W.A.S.) and to Queen's University for its award of fellowships (to K.S.K.).

1. J. M. Webber. Adv. Carbohydr. Chem. **17**, 15 (1962); C. S. Hudson. Adv. Carbohydr. Chem. **1**, 1 (1945).
2. K. Freudenberg. Adv. Carbohydr. Chem. **21**, 1 (1960).
3. H. Paulsen, K. Roden, V. Sinnwell, and W. Koebernick. Angew. Chem. Int. Ed. Engl. **15**, 439 (1976); H. Paulsen. Pure Appl. Chem. **49**, 1169 (1977); J. A. Secrist III and S.-R. Wu. J. Org. Chem. **44**, 1434 (1979).
4. R. R. Herr and G. Slomp. J. Am. Chem. Soc. **89**, 2444 (1967); W. Schroeder, B. Bannister, and H. Hoeksema. J. Am. Chem. Soc. **89**, 2448 (1967); G. Slomp and F. A. Mackeller. J. Am. Chem. Soc. **89**, 2454 (1967); B. J. Margerlein, R. D. Birkenmeyer, R. R. Herr, and F. Kagan. J. Am. Chem. Soc. **89**, 2459 (1967).
5. H. Hoeksema. J. Am. Chem. Soc. **86**, 4224 (1964); H. Hoeksema and J. W. Hinman. J. Am. Chem. Soc. **86**, 4979 (1964); H. Hoeksema. J. Am. Chem. Soc. **90**, 755 (1968).
6. S. O'Connor, L. K. T. Lam, N. D. Jones, and M. O. Chaney. J. Org. Chem. **41**, 2087 (1976).
7. D. E. Dorman, J. W. Paschal, and K. E. Merkel. J. Am. Chem. Soc. **98**, 6885 (1976).
8. K. Sakata, A. Sakurai, and S. Tamura. Tetrahedron Lett. 4327 (1974); Agric. Biol. Chem. **39**, 885 (1975); Tetrahedron Lett. 3191 (1975); Agric. Biol. Chem. **40**, 1993 (1976).
9. S. Harada, E. Mizuta, and T. Kishi. J. Am. Chem. Soc. **100**, 4895 (1978).
10. T. Ito, Y. Kodama, K. Kawamura, K. Suzuki, A. Takatsuki, and G. Tamura. Agric. Biol. Chem. **41**, 2303 (1977).
11. B. C. Das, J. D. Defaye, and K. Uchida. Carbohydr. Res. **22**, 293 (1972); K. Uchida and B. C. Das. Biochimie, **55**, 635 (1973); K. Uchida. Agric. Biol. Chem. **40**, 395 (1976); K. Uchida, E. Breitmair, and W. A. Koenig. Tetrahedron, **31**, 2315 (1975); S. Ennifar, B. C. Das, S. M. Nash, and R. Nagarajan. J. Chem. Soc. Chem. Commun. 41 (1977); M. Vuilhorgne, S. Ennifar, B. C. Das, J. W. Paschal, R. Nagarajan, E. W. Hagaman, and E. Wenkert. J. Org. Chem. **42**, 3289 (1977).
12. G. B. Howarth, D. G. Lance, W. A. Szarek, and J. K. N. Jones. Can. J. Chem. **47**, 75 (1969); D. G. Lance and W. A. Szarek. Carbohydr. Res. **10**, 306 (1969); G. B. Howarth, W. A. Szarek, and J. K. N. Jones. Chem. Commun. 1339 (1969); D. G. Lance, W. A. Szarek, J. K. N. Jones, and G. B. Howarth. Can. J. Chem. **47**, 2871 (1969).
13. G. B. Howarth, W. A. Szarek, and J. K. N. Jones. J. Chem. Soc. C, 2218 (1970); G. R. Woolard, E. B. Rathbone, W. A. Szarek, and J. K. N. Jones. J. Chem. Soc. Perkin Trans. I, 950 (1976).
14. H. C. Jarrell and W. A. Szarek. Carbohydr. Res. **67**, 43 (1978); Can. J. Chem. **56**, 144 (1978); **57**, 924 (1979).
15. K. Sakata, A. Sakurai, and S. Tamura. Agric. Biol. Chem. **37**, 697 (1973).
16. K. Sakata, A. Sakurai, and S. Tamura. Agric. Biol. Chem. **38**, 1883 (1974).
17. K. Isono, P. F. Crain, and J. A. McCloskey. J. Am. Chem. Soc. **97**, 943 (1975).
18. T. Azuma, K. Isono, P. F. Crain, and J. A. McCloskey. Tetrahedron Lett. 1687 (1976).
19. T. Azuma and K. Isono. Chem. Pharm. Bull. **25**, 3347 (1977).
20. T. Sato, K. Hirasawa, J. Uzawa, T. Inaba, and K. Isono. Tetrahedron Lett. 3441 (1979).
21. K. Anzai and T. Saita. J. Chem. Soc. Chem. Commun. 681 (1976); Bull. Chem. Soc. Jpn. **50**, 169 (1977).
22. K. Sakata and J. Uzawa. Agric. Biol. Chem. **41**, 413 (1977); K. Sakata, J. Uzawa, and A. Sakurai. Org. Magn. Reson. **10**, 230 (1977).
23. N. K. Kochetkov, E. I. Budowsky, and V. N. Shibaev. *In* Synthetic procedures in nucleic acid chemistry. Vol. 1. *Edited by* W. W. Zorbach and R. S. Tipson. Interscience, New York, NY. 1968. p. 498.
24. Y. A. Zhdanov, G. N. Dorofeenko, and L. A. Uslova. Zh. Obshch. Khim. **35**, 181 (1965); F. Ramierz, A. V. Domvrovsky, and M. I. Shevchuk. J. Org. Chem. **22**, 41 (1957).

25. C. D. JARDETZKY. J. Am. Chem. Soc. **84**, 62 (1962); F. E. HRUSKA, A. A. GREY, and I. C. P. SMITH. J. Am. Chem. Soc. **92**, 4088 (1970); M. KAINOSHO and K. AJISAKA. J. Am. Chem. Soc. **97**, 6839 (1975).
26. K. BIEMANN and J. A. MCCLOSKEY. J. Am. Chem. Soc. **84**, 2005 (1962).
27. A. M. LAWSON, R. N. STILLWALL, M. M. TACKER, K. TSUBOYAMA, and J. A. MCCLOSKEY. J. Am. Chem. Soc. **93**, 1014 (1971).
28. D. K. DALLING and D. M. GRANT. J. Am. Chem. Soc. **89**, 6612 (1967); A. J. JONES, E. L. ELIEL, D. M. GRANT, M. C. KNOEBER, and W. F. BAILEY. J. Am. Chem. Soc. **93**, 4772 (1971).
29. F. JOHNSON, W. D. GUROWITZ, and N. A. STARKOVSKY. Tetrahedron Lett. 1173 (1962); F. JOHNSON, N. A. STARKOVSKY, and W. D. GUROWITZ. J. Am. Chem. Soc. **87**, 3492 (1965); E. L. ELIEL and M. C. KNOEBER. J. Am. Chem. Soc. **90**, 3444 (1968); J. L. JUNGNICKEL and C. A. REILLY. J. Mol. Spectrosc. **16**, 135 (1965); M. BARON and D. P. HOLLIS. Recl. Trav. Chim. Pays-Bas, **83**, 391 (1964).
30. D. E. BERGSTROM and W. C. AGOSTA. Tetrahedron Lett. 1087 (1974).
31. Y. A. ZHDANOV and L. A. USLOVA. Zh. Obshch. Khim. **36**, 1211 (1966).
32. J. CUNNINGHAM, R. GIGG, and C. D. WARREN. Tetrahedron Lett. 1191 (1964); J. GIGG and R. GIGG. J. Chem. Soc. C, 82 (1966); R. GIGG and C. D. WARREN. J. Chem. Soc. 2205 (1965).
33. E. J. COREY and J. W. SUGGS. J. Org. Chem. **38**, 3224 (1973).
34. R. GIGG and C. D. WARREN. J. Chem. Soc. C, 1903 (1968).
35. R. S. TIPSON. *In* Synthetic procedures in nucleic acid chemistry. Vol. 1. *Edited by* W. W. Zorbach and R. S. Tipson. Interscience, New York, NY. 1968. p. 431.
36. J. B. CONANT and O. R. QUAYLE. Org. Synth. Coll. Vol. **1**, 211 (1932).

Can. J. Chem. Downloaded from www.nrcresearchpress.com by 210.87.254.5 on 09/06/12
For personal use only.

The preparation of amino sugars and branched-chain sugars by palladium-catalyzed, allylic substitution of alkyl hex-2-enopyranosides

HANS H. BAER AND ZAHER S. HANNA
Department of Chemistry, University of Ottawa, Ottawa, Ont., Canada K1N 9B4
Received August 11, 1980

This paper is dedicated to Prof. Raymond U. Lemieux on the occasion of his 60th birthday

HANS H. BAER and ZAHER S. HANNA. Can. J. Chem. **59**, 889 (1981).

Ethyl 4,6-di-*O*-acetyl-2,3-dideoxy-α-D-*erythro*-hex-2-enopyranoside (**1**) in the presence of triphenylphosphine and a catalytic amount of tetrakis(triphenylphosphine)palladium(0) reacted with a variety of amines or with reactive methylene compounds to give high yields of products aminated or *C*-alkylated, respectively, in an allylic position. Some analogous experiments were performed using the β-D-*erythro* anomer (**2**) and the α-D-*threo* epimer (**3**) of **1**. The constitutions and configurations of the new products were established by means of mass spectra, ^{13}C- and ^{1}H-nmr spectra, and optical rotation data. The reactions of **1** were found to be highly regio- and stereoselective, giving almost exclusively 4-substituted 2-enopyranosides with retention of configuration, except in the case of dibenzylamine which produced a mixture of the corresponding enoside and its 2-substituted, 3,4-unsaturated isomer having the α-D-*threo* configuration. The reactions of **2** appeared slightly less selective although they, too, furnished mainly 4-substituted 2-enopyranosides with retention of configuration. Regioselectivity was low or lacking in two *C*-alkylations performed with **3**, which gave mixtures of 4-substituted 2-enosides and 2-substituted 3-enosides. Some aspects of conformation and optical rotation in enopyranosides are discussed.

HANS H. BAER et ZAHER S. HANNA. Can. J. Chem. **59**, 889 (1981).

Le composé éthyl-4,6-di-*O*-acétyl-2,3-didésoxy-α-D-*érythro*-hex-2-énopyranoside (**1**) en présence de triphénylphosphine et d'une quantité catalytique de tétrakis(triphénylphosphine)palladium(0) réagit avec différentes amines ou des composés ayant un groupement méthylène réactif et conduit avec d'excellents rendements aux produits aminés ainsi qu'aux dérivés *C*-alkylés en position allylique. On a réalisé des expériences similaires en utilisant l'anomère β-D-*erythro* (**2**) et l'épimère α-D-*thréo* (**3**) de **1**. Les spectres de masse et de rmn du ^{1}H et du ^{13}C ainsi que les données de rotation optique ont permis d'établir les structures et les configurations des nouveaux produits. Les réactions impliquant le composé **1** sont fortement régio- et stéréosélectives et donnent presqu'exclusivement les 2-énopyranosides substitués en position 4 avec rétention de configuration; la réaction avec la dibenzylamine fait exception puisqu'elle conduit a un mélange de l'énoside correspondant et de son isomère substitué en position **2**, insaturé en 3,4 et possédant la configuration α-D-*thréo*. Les réactions du composé **2** semblent être moins sélectives bien qu'elles conduisent principalement aux 2-énopyranosides substitués en position 4 avec rétention de configuration. La régiosélectivité est faible ou inexistante lors des deux *C*-alkylations réalisées avec le composé **3**; ces réactions donnent des mélanges de 2-énosides et 3-énosides substitués en position 4 et 2, réspectivement. Quelques aspects de la conformation et de la rotation optique des énopyranosides sont discutés.

Introduction

Recently we communicated (1) the first results of a study concerning the potential utility of organopalladium reagents for the functionalization of carbohydrates. The present article reports full details of the work and includes some additional results which have since been elaborated. In connection with our current interest in the development of methods for the synthesis of unusual amino, deoxy, unsaturated, and branched-chain sugars (2), we decided to examine whether the palladium-catalyzed substitution of allylic acetates by amines or reactive methylene compounds (3–6) might be employed to advantage in carbohydrate chemistry. In this reaction, which represents one of the numerous applications of organopalladium chemistry (7) that are currently in widespread use, an allylic acetate in the presence of a catalyst such as tetrakis(triphenylphosphine)palladium forms an intermediate π-allylpalladium complex that is then attacked by an added nucleophile, to give an allylically substituted product. The palladium species liberated upon collapse of the intermediary complex is reconverted into a catalytically active form by the action of the excess of triphenylphosphine which is provided. A high degree of regioselectivity and stereocontrol is normally observed in these substitutions (6), although certain exceptions to this welcome trend have been noted and discussed.

As our chief substrate for an evaluation of the utility of the method in the carbohydrate field,[1] we chose the crystalline ethyl 4,6-di-*O*-acetyl-2,3-dideoxy-α-D-*erythro*-hex-2-enopyranoside (**1**). This compound is readily prepared (9) from commercially available D-glucal triacetate. For some ancillary experiments, to be performed in the hope of

[1]To our knowledge, only one organopalladium reaction (of a different kind) with carbohydrates has been previously studied. Arai and Daves (8) effected regiospecific addition of a 1,3-dimethyl-2,4-pyrimidinedion-5-ylpalladium salt across the double bond of the enol ethers D-glucal triacetate and D-arabinal diacetate.

0008-4042/81/050889-18$01.00/0
©1981 National Research Council of Canada/Conseil national de recherches du Canada

Can. J. Chem. Downloaded from www.nrcresearchpress.com by 210.87.254.105 on 09/06/12
For personal use only.

Can. J. Chem. Downloaded from www.nrcresearchpress.com by 210.87.254.105 on 09/06/12
For personal use only.

shedding light on stereochemical implications, the β-D-*erythro* anomer **2** and the α-D-*threo* epimer **3** of the pseudoglycal **1** were desired. Although the methyl glycoside analog (**2***a*) of **2** was known (10, 11), and was used in the present work for a confirmatory experiment, the ethyl glycoside **2** could not be found in the literature. However, we were able to synthesize it readily, also from D-glucal triacetate, by way of ethoxymercuration followed by elimination of the elements of mercuric acetate with sodium iodide, in a manner analogous to that described (11, 12) for the synthesis of **2***a*. The intermediate encountered in this synthesis, ethyl 2-acetoxymercuri-3,4,6-tri-*O*-acetyl-2-deoxy-β-D-glucopyranoside, was a highly crystalline compound (see Experimental). The α-D-*threo* epimer **3** was obtained by acetylation of the corresponding, crystalline diol.[2] A high-yielding procedure for its preparation from tri-*O*-acetyl-D-galactal has recently been described (14).

Results and Discussion

Formation of Unsaturated Amino and Branched-chain Sugars

The enopyranoside **1** was allowed to react, in tetrahydrofuran solution at reflux temperature, with a variety of nucleophiles in the presence of triphenylphosphine (0.7 molar equiv.) and a catalytic amount (0.07 molar equiv.) of tetrakis(triphenylphosphine)palladium. The use of diethylamine, piperidine, cyclohexylmethylamine, and benzylmethylamine led to the 4-aminated glycosides **4–7**, respectively, in yields of 70–87% after chromatographic purification. According to tlc and nmr spectroscopic evidence, the compounds **4–6** were formed as single isomers accompanied, at most, by traces of slow-moving impurities. In the case of **7**, a second but minor compound was seen to be present in the crude reaction mixture; it was removed by preparative tlc and could not be identified. By contrast, the reaction of **1** with dibenzylamine was less selective. It gave in 83% yield a separable mixture of two products that were present in a ratio of approximately 3:7 (by nmr). The minor component crystallized after chromatographic separation and proved to be the 4-aminated glycoside **8** whereas the major component failed to crystallize and was found to be the 2-aminated, 3,4-unsaturated isomer **9**.

[2]For a gift of a sample of this diol we are indebted to Professor B. Fraser-Reid who informed us privately that it was prepared from the corresponding α-D-*erythro* diol by C-4 inversion through benzoylation in the presence of dialkyl azodicarboxylate and triphenylphosphine (13), followed by saponification.

Reaction of **1** with the primary amine, benzylamine, produced a more complex result. The expected 6-*O*-acetyl-4-benzylamino glycoside **10** could be isolated in only 31% yield, and the bulk of the reaction product was a chromatographically slow-moving mixture of two components which were difficult to separate. The nmr spectrum of this mixture suggested that the components were partially *O*-deacetylated **1** and the *O*-deacetylated derivative (**11**) of **10**. Acetylation of the mixture followed by chromatography led to the recovery of **1** (50%) and, in addition, furnished the syrupy but homogeneous *N*-acetyl-*O*-acetyl derivative **12** (15%) whereby the joint yield of isolated, aminated products (**10** + **12**) was raised to 46%. When syrupy **10** was stored for an extended period in the refrigerator, hydroxyl and amide bands developed in its ir spectrum, at the expense of the ester band. A sample stored at room temperature slowly crystallized in the course of a few weeks, and the crystals exhibited amide but no ester carbonyl bands. Although this transformation was not investigated further, it seems obvious that **10** underwent O → N acetyl migration to give **13**.

A preliminary examination of the reaction between **1** and some primary, aromatic amines has led to the conclusion, based on nmr spectra of the products obtained, that *p*-aminobenzophenone, *p*-aminoacetophenone, and 2,6-dimethylaniline are also incorporated into the glycoside. However, analysis of these reactions is still incomplete.

No amination was achieved with diisopropylamine, presumably because of the steric hindrance associated with this molecule. Instead, acetate elimination occurred to give the diene **14***a* which rearranged to **14***b*. The same happened on prolonged heating of **1** and catalyst in the presence of triethylamine or, indeed, in the absence of any amine. Details on the formation and properties of these dienic products are reserved for publication elsewhere.

C-Alkylations of **1** were performed in full analogy to the aminations just described, by use of several reactive methylene compounds that were administered as their sodio derivatives in tetrahydrofuran solution. Reactions with dimethyl malonate, diethyl malonate, and methyl phenylsulfonylacetate proceeded well, furnishing the branched-chain glycosides **15–17** in yields of 87, 83, and about 60%. Whereas **15** and **16** showed no evidence for isomeric inhomogeneity, crude **17** contained a small proportion of an unidentified by-product. However, **17** was obtained as a chromatographically and nmr-spectroscopically homogeneous

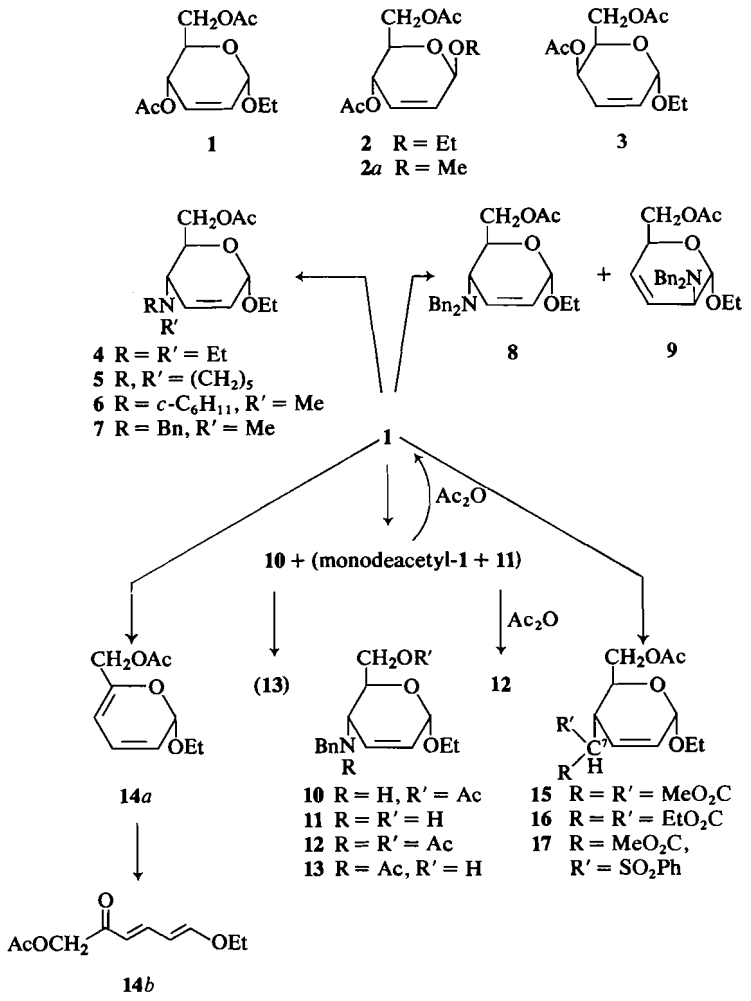

product by crystallization. Its configuration at C-7 in the side-chain remained unknown. Also tested with **1** were malononitrile and ethyl cyanoacetate. They too gave *C*-alkylated products, but the yields were poor in these instances and the products have not as yet been characterized definitively, nor have attempts been made to optimize reaction conditions.

In view of the high regioselectivity which was observed in all those aminations and alkylations of **1** that proceeded with good yields, with the noteworthy exception of the reaction with dibenzylamine, it appeared interesting to supplement the findings by some comparative experiments using stereoisomers of **1** as substrates. The β-enopyranoside **2** reacted equally well with diethylamine and benzylmethylamine, giving the aminated glycosides **18** and **19** in excellent yields. As was the case in the α-series (cf. **7**), a very small proportion of an unidentified by-product (presumably an isomer) was present in **19** as revealed by the nmr spectrum. The reaction of dibenzylamine with **2** gave a result even more abnormal than the reversal of regioselectivity encountered in its reaction with **1**. Apparently, no aminated ethyl glycoside was formed; instead, we found a major product that possessed a dibenzylamino group but had lost the glycosidic ethoxyl group. The exceptional behavior of dibenzylamine is the subject of ongoing studies.

The β-enopyranoside **2** and, likewise, its methyl analog **2***a* reacted with dimethylmalonate to give high yields of *C*-alkylated products. Although these appeared as single spots in tlc, they were revealed by nmr spectroscopy to be composed of strongly preponderant, major components and minor isomers. The chief components were the 4-substituted, 2-enosides **20** and **20***a*, respectively, whereas the

Can. J. Chem. Downloaded from www.nrcresearchpress.com by 210.87.254.105 on 09/06/12
For personal use only.

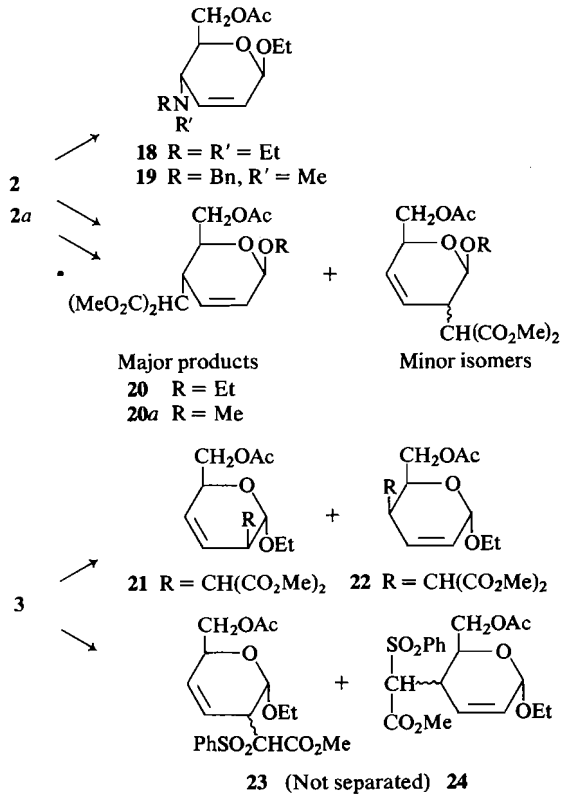

accompanying isomers were indicated by mass-spectral data to have the constitution of 2-substituted 3-enosides (*vide infra*).

For the α-D-*threo* enoside **3**, only two palladium-catalyzed substitutions have thus far been examined; in both instances, regioselectivity was found to be lower than in the analogous reactions with **1** or **2**. With dimethyl malonate, **3** gave in 66% yield an approximately 3:1 mixture of the 2-alkylated, 3,4-unsaturated α-D-*threo* glycoside **21** and its 4-alkylated, 2,3-unsaturated isomer **22**. In addition, small proportions of two chromatographically slow-moving products were isolated. Both of them originated from *C*-alkylation as they contained methyl ester groups of an incorporated malonate residue. However, they had lost both *O*-acetyl groups. Reacetylation of one of these minor fractions gave **21**, spectroscopically identified with the major component in the aforementioned mixture of main products. The other slow-moving by-product remained unaffected by acetylation and its ^{1}H nmr spectrum suggested the presence of three methyl ester groups. Hence the product had probably arisen from *O*-deacetylated **21** or **22** by transesterification with dimethyl malonate.

With methyl phenylsulfonylacetate, **3** gave also a mixture of two isomeric substitution products. Although separation could not be achieved, the ^{1}H nmr spectrum indicated a ratio of ~1:1. Formulas **23** and **24** are suggested as likely structures of these compounds. No information regarding the C-7 configuration is available.

Assignment of Structure

The gross structures of new compounds were supported by elemental analysis, fitting infrared spectra, the molecular ion peak present in the mass spectrum in most cases (Table 1), and the requisite substituent resonances displayed in the proton and carbon-13 nmr spectra. More detailed constitutional and configurational information was derived from spectral data and from optical rotations, as follows.

Mass Spectra

First of all, it was necessary to ascertain the position of the olefinic double bond in the pyranoside rings. This was made possible by mass spectrometry, which permits one to distinguish between 2,3- and 3,4-unsaturated hexopyranosides on the basis of different fragmentation patterns (15–17). For the former type of enosides, retrodienic fragmentation leads to two fragments (a and b) according to Scheme 1. In our compounds, since R″ = CH_3CO, M_b = 102 and hence $M_a = M - 102$. On the other hand, enopyranosides of the latter type are fragmented to give a diene (c) and alkyl formate (d) (Scheme 1). For ethyl glycosides, with M_d = 74, a fragment c having $M_c = M - 74$ is therefore diagnostic for 3,4-unsaturation. Table 1 shows that the amino glycosides **4–8**, **12**, **18**, and **19** gave prominent peaks of m/e $M - 102$, indicative of their 2,3-unsaturated structures. There were also peaks of m/e $M - 74$, but their intensities were only 1–6% of those of the $M - 102$ peaks. Although these minor peaks possibly may signify the presence of minute proportions of 3,4-unsaturated isomers that had escaped detection by tlc or nmr spectroscopy, they could well have resulted from thermal rearrange-

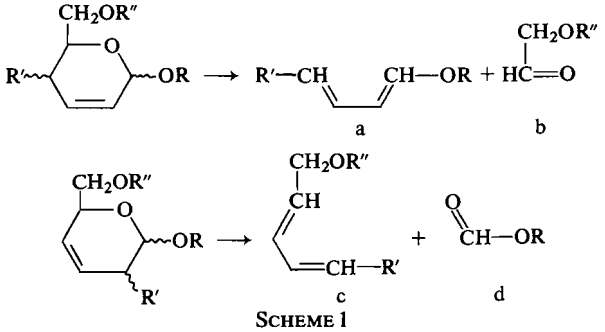

SCHEME 1

Can. J. Chem. Downloaded from www.nrcresearchpress.com by 210.87.254.105 on 09/06/12
For personal use only.

Can. J. Chem. Downloaded from www.nrcresearchpress.com by 210.87.254.105 on 09/06/12
For personal use only.

TABLE 1. Selected mass spectral data[a]

Compound	Mass spectra *m/e* (in parentheses, intensity in % of base peak)			
	M^+	$M^+ - 102$	$M^+ - 74$	Others [assignment]
4	271 (1)	169 (74)	197 (1.1)	
5	283 (1.1)	181 (85.5)	209 (1.3)	
6	311 (0.2)	209 (91.4)	237 (2)	
7	319 (0.1)	217 (53)	245 (1.3)	
8	395 (0.1)	293 (38.4)	321 (2.1)	264 (24.7) [293 − Et]
9	Not observed	293 (1)	321 (12)	262 (23) [321 − OAc]
12	347 (1.7)	245 (43)	273 (0.4)	
15	330 (1.2)	228 (22.8)	256 (1)	169 (53.1) [228 − OAc], 197 (6.2) [256 − OAc]
16	358 (0.5)	256 (10)	Not observed	183 (25) [256 − EtO_2C], 211 (4.2) [$M^+ - 74 - EtO_2C$]
17	Not observed	Not observed	Not observed	411 (1.2) [$M^+ - 1$], 169 (49) [$M^+ - 102 - PhSO_2$], 141 (31.8) [$PhSO_2$]
18	271 (1.7)	169 (87.6)	197 (5.1)	
19	319 (0.7)	217 (46.7)	245 (2.9)	
20	330 (2.1)	228 (9)	256 (2)	169 (27) [228 − OAc], 197 (7.5) [256 − OAc]
20*a*	316 (0.4)	214 (12.1)	256[b] (1.7)	155 (38.8) [214 − OAc], 197 (4) [256 − OAc]
21	330 (0.3)	228 (3)	256 (4)	197 (11) [256 − OAc], 169 (16) [228 − OAc]

[a]The spectra were obtained with an A.E.I. MS 902 mass spectrometer fitted with a direct-inlet probe, at an ionizing potential of 50–55 eV. A full analysis of the fragmentation paths is in preparation for publication (J. Krause, Z. S. Hanna, and H. H. Baer).
[b]$M^+ - 60$ (loss of *methyl* formate).

ment of the compounds in the mass spectrometer prior to electron impact (17). On the other hand, the amine **9** gave only a feeble peak of *m/e* $M - 102$ but a peak 12 times as strong at *m/e* $M - 74$. Furthermore, **9** gave an intense daughter peak at *m/e* 262, believed to result from loss of OAc from the $M - 74$ fragment. By contrast, the positional isomer **8** showed only a weak peak at *m/e* 262 (with 12% of the intensity seen in **9**), whereas it produced a strong daughter peak at *m/e* 264 attributable to loss of C_2H_5 from its $M - 102$ fragment. Conversely, in **9**, this peak had an intensity of only 8% relative to that in **8**. These features clearly permitted allocation of the double bond positions as shown.

The *C*-alkylated compounds **15**, **16**, **20**, and **20*a*** were similarly revealed to possess 2,3-unsaturated structures, on account of the strong dominance of $M - 102$ over $M - 74$ peaks (or the analogous $M - 60$ peak in the case of the methyl glycoside **20*a***). It is noteworthy, though, that the $M - 102$ peaks generally were markedly lower in intensity relative to the base peak than in the cases of the aminated analogs, presumably because of a high instability associated with fragments that contain a malonic ester moiety. In support of this explanation, strong daughter peaks were observed, which arose from loss of CH_3CO_2 from the $M - 102$ fragments of **15**, **20**, and **20*a***, and from loss of $C_2H_5CO_2$ in the case of **16**.

As already mentioned, the β-glycosides **20** and **20*a*** were revealed by their ^{13}C nmr spectra to contain minor proportions of isomers that could not be isolated. The mass spectra exhibited minor peaks at *m/e* $M - 74$ and $M - 60$, respectively, whose intensities were somewhat greater (22 and 14%) relative to the major, $M - 102$ peaks, than in the preceding compounds where these intensities ranged from 1–6% (see above). These findings corroborated the assumption that the by-products accompanying **20** and **20*a*** were 2-substituted, 3,4-unsaturated analogs.

The mass spectrum of the phenylsulfonyl derivative **17** did not display peaks attributable to $M - 102$ or $M - 74$, such fragments apparently being too unstable to survive in this instance. Indeed, loss of $C_6H_5SO_2^+$ (*m/e* 141) was conspicuous, with concomitant formation of an intense ion peak at *m/e* 169 attributable to $M - 102 - 141$. The spectrum thus provided at least indirect evidence for the structure of **17**.

The spectrum of **21** failed to yield information to allocate the olefinic bond. Peaks for $M - 102$ and $M - 74$ were both weak and quite similar in intensity, and the same applied to daughter peaks expected to originate from loss of CH_3CO_2. However, the spectrum was useful at least insofar as it established the non-identity of **21** with the α-D-*erythro* isomer **15**. Furthermore, the spectrum of *isolated* **21** ($[\alpha]_D$ +100°) was extremely similar to that of the *mixture* ($[\alpha]_D$ +24°) of **21** and **22** originally obtained from **3**. This observation together with the ambiguous fragmentation pattern suggests that **21** is particularly prone to sigmatropic rearrangement which may occur in the spectrometer to some consider-

TABLE 2. Selected ^{13}C chemical shifts (ppm from TMS)[a]

Compound	C-1	C-2	C-3	C-4	C-5	C-6	Others[b]
1[c]	94.3	128.1	129.0	65.4	67.0	64.3	
2	95.0	126.2	130.7	64.5	72.9	63.7	
3	93.8	125.2	130.8	62.9	66.7	64.0	
4	94.3	127.4	130.5	54.7	67.1	64.8	44.9 (*N*—CH_2)
5	93.8			59.0	66.3	64.7	50.7 (*N*—CH_2)
6	94.2	127.3	132.9	53.8	66.9	64.9	33.6 (*N*—CH_3), 62.9 (*N*—C—C_2)
7	94.3	128.1	128.3	56.5	66.3	64.5	38.2 (*N*—CH_3), 58.7 (*N*—CH_2-*Ph*)
8	94.3	128.6	128.9	52.4	66.2	64.0	55.0 (*N*—CH_2-*Ph*)
9	97.4	54.6	126.2, 128.7		65.7	63.3	54.3 (*N*—CH_2-*Ph*)
10	94.2	126.1	131.7	50.8	69.1	64.3	50.4 (*NH*—CH_2-*Ph*)
12	93.9	126.1	128.9[d]	49.9	67.0	64.1	49.0 (*AcN*—CH_2-*Ph*)
15	94.2	126.7	129.4	35.6	66.8	64.2	51.3 (C-7)
16	94.2	126.5	129.5	35.5	66.7	64.3	51.3 (C-7)
17	94.2	126.7	129.3	33.8	66.6	63.9	
18	95.6	129.0	129.0	53.8	72.3	65.1	44.5 (*N*—CH_2)
19	95.0	127.1	129.3	55.5	71.1	65.1	38.2 (*N*—CH_3), 58.3 (*N*—CH_2-*Ph*)
20	93.0	126.1	128.1	34.1	70.0	64.7	
[e]	96.1	39.8	126.3, 126.7		72.3	66.0	
20*a*	94.4	126.3	127.8	34.0	70.0	64.6	
[f]	100.7	39.7	126.3, 126.6		72.1	65.9	
21	97.4	38.4	124.6, 127.3		67.4	65.3	54.5 (C-7)
22	94.6	128.1	129.1	35.1	66.8	63.4	50.2 (C-7)
23	96.5	37.2					
24	94.3			33.7			

[a]Spectra were taken from chloroform solutions with a Varian CFT-20 instrument.
[b]In addition to the resonances listed, all compounds showed resonances as expected for the carbon atoms in the various substituents.
[c]The values for **1** are in good agreement with published (20) data.
[d]The signal was difficult to differentiate from nearby Ph signals; an alternative value is 129.3.
[e]The minor by-product present in **20**, believed to be a 3-enoside.
[f]The minor by-product present in **20***a*, believed to be a 3-enoside.

able degree. Ferrier *et al.* (16) have found such rearrangements to be especially facile when the migrating substituent was attached quasi-axially as in **21** and **22**, rather than quasi-equatorially as in **15** and most of the other compounds here considered. The mass-spectral peculiarity of **21** therefore tends to support its formulation as a *threo* compound. Finally, the spectrum of the mixture of phenylsulfonyl derivatives tentatively designated as **23** and **24** furnished little structural information other than admitting that one of the components (**24**) may have been identical with **17**.

^{13}C *Nuclear Magnetic Resonance Spectra*

The ^{13}C nmr signals were assigned to individual nuclei on the basis of multiplicities observed in proton-coupled spectra and in accordance with known chemical shift regularities (ref. 18 and literature cited therein). The chemical shifts of the pyranose carbon and some selected substituent carbon atoms are assembled in Table 2. It is seen that all of the compounds to which was assigned the 2,3-unsaturated α-D-*erythro* structure (**4–8**, **10**, **12**, and **15–17**) show the C-1 resonance in the narrow range of 93.8–94.3 ppm (relative to tetramethylsilane). The δ-effect upon C-1 associated with a configurational inversion at C-4 is expected to be small, and this is borne out in the starting compounds **1** and **3** whose C-1 resonances both occur in the same range. In the mixture of the two *C*-bis-(methoxycarbonyl)methyl derivatives obtained from **3**, only the minor component (**22**) showed a reasonably similar C-1 shift (94.6 ppm), and so did one of the components (provisionally termed **24**) of the mixture of methoxycarbonyl(phenylsulfonyl)methyl derivatives (94.3 ppm). These data appear consistent with the assignment of a 2,3-unsaturated constitution to **22** and **24**. By contrast, C-1 experienced a noticeable downfield shift, to 97.4 ppm, in the α-glycosides **9** and **21** for which the mass spectra had provided positive (**9**) or circumstantial (**21**) evidence for 3,4-unsaturation. By analogy it may be assumed that **23**, showing its C-1 resonance at 96.5 ppm, is 3,4-unsaturated also. Some further consistencies supporting the assignments may be noted. Thus, in each of the three pairs of regioisomers (**8/9**, **21/22**, and **23/24**), the carbon bearing the newly-introduced substituent resonates at lower field by 2.2 – 3.5 ppm when it is in position 2 than when it is in position 4. The pair of 4-epimers **15/22** shows a shielding difference in the expected direction for a quasi-equatorially vs. a quasi-axially substituted C-4, although the effect is quite small in this instance (0.5 ppm). A similar

Can. J. Chem. Downloaded from www.nrcresearchpress.com by 210.87.254.105 on 09/06/12
For personal use only.

Can. J. Chem. Downloaded from www.nrcresearchpress.com by 210.87.254.105 on 09/06/12
For personal use only.

insensitivity of the C-4 shift cannot be excluded for **17** and its 4-epimer; for this reason it was not possible to decide whether the non-isolated, mixture component **24** was identical with one or the other of the α-D-*erythro* compounds having the structure **17** (two C-7 epimers being possible), or whether it was an α-D-*threo* stereoisomer. As regards **9**, **21**, and **23**, the near coincidence of their C-1 shifts would obviously be consistent with an assumption that these compounds possess an identical configuration. However, it does not represent proof since the change from an axial C-2 substituent (α-D-*threo* configuration) to an equatorial one (α-D-*erythro* configuration) replaces one shielding factor by another one of similar magnitude, with little if any net effect upon the C-1 shift to be expected. This is exemplified in methyl α-D-mannopyranoside → α-D-glucopyranoside and other pairs of epimers having comparable features (18). On the basis of their optical rotations (*vide infra*), **9** and **21** could be assigned the α-D-*threo* configuration, and it is noteworthy in this context that the constitutionally analogous, α-D-*erythro* glycoside **35***a* also shows (19) a similar C-1 resonance (97.0 ppm).

In ordinary methyl β-hexopyranosides, excepting the mannosides, C-1 is generally deshielded by ca. 2–5 ppm relative to the corresponding α-anomers (18). The methyl 4,6-*O*-benzylidene-2,3-dideoxy-α- and -β-D-*erythro*-hex-2-enopyranosides, which are comparable to our compounds but for their rigid conformation due to the *trans*-fused acetal ring, were found (20) to obey this rule (Δδ −3.1 ppm). The difference is somewhat smaller (−1.5 to −1.8 ppm) in the 4,6-di-*O*-acetyl-2,3-dideoxy-D-hex-2-enopyranosyl dimethylphosphonates (**1–3** and β-D-*threo* isomer, with $P(O)(OMe)_2$ replacing OEt) recently studied by Paulsen and co-workers (21). The data in Table 2 indicate that the β-glycosides **2**, **18**, and **19** also give C-1 resonances to slightly lower field than do their α-anomers **1**, **4**, and **7** (Δδ −0.7, −1.3, and −0.7, respectively). The γ-effect of anomerization upon C-5, on the other hand, was distinctly larger in these pairs (Δδ −5.9, −5.2, and −4.9 ppm, respectively), exceeding the values observed (21) in the phosphonates just mentioned (−2.5 and −3.3 ppm) and coming closer to the value (−6.6 ppm) reported (20) for the benzylidene acetals. Summation of the chemical shifts for C-1 to C-6 in **4** and **7** (Σ_{1-6} 538.8 and 538.0 ppm) and their β-anomers **18** and **19** (Σ_{1-6} 544.7 and 543.1 ppm), and juxtaposition of these values with the sums for **1** (Σ_{1-6} 548.1 ppm) and **2** (Σ_{1-6} 553.0 ppm), respectively, is taken as a good indication (18) for structural equivalence. A similar exercise comparing Σ_{1-6} for the *C*-alkylated α-glycoside **15** (516.7 ppm) with the values for the β-glycosidic analogs **20** (516.0 ppm) and **20***a* (517.1 ppm) surprisingly did not yield any such difference of 5–6 ppm for anomerism. A possible reason for this apparent discrepancy may lie in differing conformational features as will be discussed below. As regards the minor by-products that accompanied **20** and **20***a*, their carbon atoms showed chemical shift relations, to the structurally analogous atoms in **20** and **20***a*, that were qualitatively similar to the relations seen in the pair of positional isomers **21/22**. Thus, C-1 and the alkyl-substituted carbon in particular, and to a lesser degree C-5 and C-6, all were significantly deshielded relative to their counterparts in **20** and **20***a*. These comparisons reinforced the suggestion, already intimated by the mass spectra, that the by-products were 2-substituted, 3,4-unsaturated isomers of **20** and **20***a*. Unfortunately, the configuration at C-2 could not be established definitively since the optical rotations of these products are unavailable for confirmation. From the ^{13}C nmr data alone it might tentatively be concluded that the β-D-*threo* configuration obtains, i.e., a 1,2-*cis* equatorial – axial substituent orientation. The C-1 and C-2 shifts in such an arrangement should differ little, for reasons discussed previously, from those in an α-D-*threo* arrangement, i.e., 1,2-*trans* diaxial, whereas deshielding by several ppm in C-1 and C-2 is expected for the β-D-*erythro* configuration (1,2-*trans* diequatorial). A comparison of the data for the by-product of **20** with those of the α-D-*threo* isomer **21** points to the former alternative, the relevant shift differences being only −1.3 and +1.4 ppm.

^1H *Nuclear Magnetic Resonance Spectra*

The ^1H nmr parameters are listed in Table 3. The spectra of the aminated, α-glycosidic derivatives **4–8** and **10**, as well as those of the *C*-alkylated derivatives **15–17**, were sufficiently resolved to permit first-order analysis which established the D-*erythro* configuration of these 2-enosides. The olefinic protons resonated in the δ 6.0 region and gave AB quartets showing $^3J_{2,3}$ = 10.0–10.5 Hz; each constituent part was split further, by small vicinal and allylic couplings with H-1 and H-4. The anomeric proton produced a broadened singlet or narrow multiplet near δ 5.0. Of diagnostic significance was the H-4 signal, which occurred at highest field as far as ring protons were concerned. It was a doublet ($J_{4,5}$ = 10 Hz) of narrowly-spaced multiplets. The large vicinal coupling constant required H-4 and H-5 to have an *anti* orientation and therefore proved the D-*erythro* configuration. The individual multiplets composing the H-4 doublet

Can. J. Chem. Downloaded from www.nrcresearchpress.com by 210.87.254.105 on 09/06/12
For personal use only.

TABLE 3. The ^1H nuclear magnetic resonance data[a]

Compound	Chemical shifts[b] (δ)							Coupling constants[c] (Hz)									
	H-1	H-2	H-3	H-4	H-5	H-6,6′	H-7	$J_{1,2}$	$J_{1,3}$	$J_{1,4}$	$J_{2,3}$	$J_{2,4}$	$J_{3,4}$	$J_{4,5}$	$J_{5,6}$	$J_{5,6'}$	$J_{4,7}$
1	5.05nm	5.86nm		5.31dq	4.08ddd	4.2m		2.7[d]	−1[d]	2[d]		−2[d]	2[d]	9.2	~2.5,	5.0[e]	
2	5.13q	5.94s		5.21dq	4.02dt	4.25d, 4.26d		See footnote 4 in the text						5.0	4.8	6.3	
3	5.06d	6.00dd	6.12dd	5.02dq	4.36o	4.23q		2.5	~0	~0	10.0	< −0.5	4.5	2.5	6.5		
4	4.98nm	5.83ddd	6.05ddd	3.31dtd	3.96ddd	4.35dq		2.7	−1.2	1.8	10.5	−2.0	2.0	10.5	2.7	5.5	
5	4.96nm	5.82ddd	6.11ddd	3.08dm	4.0–4.6m			2.5	−1.0	~2	10.5	−2.0	2.0	10			
6	4.97nm	5.79ddd	6.03ddd	3.36dm	3.99ddd	4.30dq		2.7	−1.2	1.8	10.5	−2.0	2.0	10	3.0	5.0	
7	4.98nm	5.89ddd	6.15ddd	3.26dtd	4.06ddd	4.32dq		2.5	−1	1.7	10.7	−2.1	2.0	10	2.7	5.5	
8	4.97nm	5.93dt	6.24ddd	3.41dm	4.0–4.4m			2.5	~−1		10.5	−2.5	~2	10			
9	5.08t	3.13nm	5.87s		4.0–4.4m			< 1	~−1				0				
10	4.99nm	5.76ddd	6.10ddd	3.14dtd		4.35d		2.5	−1	1.7	10.0	−2.0	~2	10			
15	5.00nm	5.77ddd	6.00ddd	3.00cm	4.06ddd	4.16q, 4.37q	3.61d	2.8	−1	1.5	10.0	−2.4	2.0	10.5	3.0	5.0	4.0
16	5.00nm	5.76ddd	6.03ddd	3.01cm	4.11ddd	4.17q, 4.39q	3.58d	2.7	−1	1.5	10.0	−2.5	2.0	10.5	3.0	5.0	4.0
17	5.00nm	5.77dt	6.33ddd	3.27cm	4.0–4.5m	4.0–4.5m	4.0–4.5m	2.7	~−1		10.5	−2.5	~2	10			
18	5.09nm	5.91m		3.26cm	3.92q	4.31d								5.5	5.5		
19	5.05nm	5.97m		3.16cm	4.0–4.4m									4.7			
20	4.92s	5.87m		2.84ddd	4.0–4.5m		3.56d							4.0			9.0
20*a*	4.81s	5.87m		2.85ddd	3.9–4.5m		3.57d							4.3			9.0
21	4.88nm	2.85dm	5.77nm		4.36cm	4.09q, 4.27q	3.51d	< 1					0		1.5	2.0	9.5
22	4.93dd	5.83ddd	6.09ddd					2.5	−1	~0.5	10.0	< −1	5.2				

[a]From 100 MHz spectra of solutions in $CDCl_3$ containing tetramethylsilane as standard. In addition to the signals listed, all compounds showed substituent resonances as required by the structures.
[b]Signal multiplicities are indicated as cm (complex multiplet), d (doublet), nm (narrow multiplet), m (multiplet), o (octet), q (quartet), s (singlet), and t (triplet). Values refer to signal midpoints.
[c]Measured at 250 Hz sweep width.
[d]Estimated from observed splittings; see footnote 4 in the text.
[e]Splittings observed in the H-5 multiplet; these may not equal the coupling constants because of the proximity of the H-6,6′ signal.

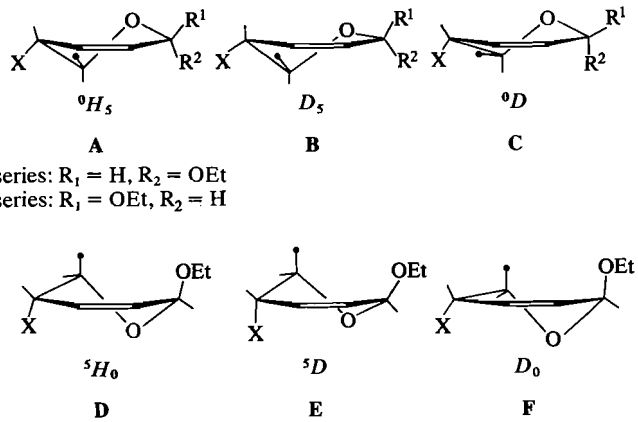

contained small (1–2 Hz) vicinal ($J_{3,4}$), allylic ($J_{2,4}$), and homoallylic ($J_{1,4}$) couplings that were mirrored in the corresponding, downfield proton signals. An additional splitting of 4 Hz discernible in the H-4 signals of **15** and **16** was due to vicinal coupling with H-7, the methine proton in the side-chain.

A more detailed analysis of the signal fine-structure should make possible a correlation of the various small vicinal and allylic couplings just mentioned with the conformational shape of the molecules. It appeared reasonable to assume that the products would in this regard resemble the parent glycoside **1**, for which the $^0H_5$ half-chair conformation (formula **A**) had been proposed (9). Upon detailed spectral analysis of related molecules, Paulsen and co-workers (21) and Thiem *et al.* (22) recently came to the conclusion that α-D-*erythro*-hex-2-enopyranosides tend to adopt a noticeably flattened version of this half-chair, approaching the corresponding "sofa form" in which C-5 protrudes below the plane defined by C-1 to C-4 and the ring oxygen atom (formula **B**);[3] this geometry has been confirmed by X-ray crystallography in three cases (21–23). The spectra of our α-D-*erythro* products generally supported a similar molecular shape, rather than the alternate ^0D sofa form (formula **C**) advocated by Watanabe *et al.* (24) for some 4-amino hex-2-enosides closely related to our derivatives, which they synthesized by different methods. Thus, the allylic couplings $^4J_{1,3}$ and $^4J_{2,4}$ of −1 to −1.2 and −2 to −2.5 Hz, respectively, implied dihedral angles $\Phi_{1,2}$ and $\Phi_{3,4}$ in the ranges of 50–55 and 67–80°, according to Garbisch's relationship (25) given in eq.[1]

[1] $^4J = 1.3 \cos^2 \Phi - 2.6 \sin^2 \Phi \ (0° \leq \Phi \leq 90°)$

[2] $^3J = 6.6 \cos^2 \Phi + 2.6 \sin^2 \Phi \ (0° \leq \Phi \leq 90°)$

In an ideal D_5 sofa form, these angles are 60 and 90°, respectively; very small ring torsions in the direction towards a flattened $^0H_5$ form moves them into the indicated ranges. The homoallylic couplings, $^5J_{1,4}$ = 1.5–1.8 Hz, were in accord with those found (22, 26, 27) in other 2-enosides featuring comparable, mutual dispositions of H-1 and H-4. The vicinal couplings through sp^2 hybridized carbon ($^3J_{1,2}$ and $^3J_{3,4}$) require special comment. The relationship provided by Garbisch (25) for this situation (eq. [2]) fails to predict accurate values in the case of enopyranosides. It was first noted by Anet (28) that the parameter of +2.6 may be too large, and couplings smaller than the minimum value derivable from eq. [2], namely 2.6 Hz for Φ = 90°, have since been observed on numerous occasions (20–22, 24, 26, 27, 29–32). However, qualitatively the small coupling $J_{3,4}$ = 2 Hz, consistently shown by our products (Table 3), certainly was in line with a large dihedral angle $\Phi_{3,4}$ as required by the conformation discussed. For an angle $\Phi_{1,2}$ of 50–55°, eq. [2] predicts $^3J_{1,2}$ values of 3.9–4.3 Hz; taking into account the well-known weakening of vicinal coupling at the anomeric center, in addition to an inherent inaccuracy of the equation, the observed values of 2.5–2.8 Hz do appear reasonable. Finally it may be noted that, for all of the new 4-substituted α-D-*erythro*-2-enopyranosides, the vinylic proton signal occurring at higher field was assigned to H-2, while that at lower field was assigned to H-3. The same chemical shift relation was observed by Lemieux *et al.* (26, 27) in the 4,6-acetals **25**, **26**, **29**, and **30**, and in the methyl pent-2-enopyranosides **31** and **32**; corresponding assignments have since been made for numerous hex-2-enopyranose derivatives (14, 24, 30, 32). On the other hand, the relation is the *reverse* in pent-2-enofuranosides (27), in some of the aforementioned enopyranosyl phosphonates (21), and in certain disaccharidic analogs of **1** (22,

[3]The symbol *SO* has been used for sofa conformations, e.g., SO_5 for **B** (22). Inasmuch as single-letter conformational symbols are now in general use and *S* is already reserved for skew forms, we propose the letter *D* (from divan) for such conformations.

Can. J. Chem. Downloaded from www.nrcresearchpress.com by 210.87.254.105 on 09/06/12
For personal use only.

Can. J. Chem. Downloaded from www.nrcresearchpress.com by 210.87.254.105 on 09/06/12
For personal use only.

31, 33*a*). In compound **1** itself (and also in **2**) the vinylic signals happen to coincide,[4] a phenomenon encountered not infrequently in this series (Table 3 and refs. 20 and 29), and its is therefore clear that such shift differences as may be observable are quite sensitive to structural differences. A justification for our mode of assignment derives from the fact that the signal attributed to H-2 (δ 5.8 ± 0.1) incurred little change from the resonance position in **1** (δ 5.86), whereas a downfield shift to 6.15 ± 0.15 was evident for the other signal, which could therefore be allocated to H-3, the proton vicinal to the site of chemical modification.

An evaluation of the spectra of the β-glycosides **18**–**20***a* obtained from the β-D-*erythro* enoside **2** (or **2***a* in the case of **20***a*) must begin with a consideration of **2** itself. This deserves to be done in some detail as it is pertinent also to the discussion of optical rotations that will be presented in a subsequent section. For some 2-substituted analogs of **2**, namely, certain β-linked D-*erythro*-hex-2-enopyranose derivatives bearing an acetoxy group at C-2, the inverted, $^5H_0$ half-chair conformation (33*b*, 34) or a flattened version approaching the closely related ^5D sofa conformation (22) have been deduced from nmr data. No doubt the nonbonded interaction existing in such compounds, between the vinylic substituent and the neighboring, quasi-equatorial β-anomeric group (the $A^{(1,2)}$ strain (35)) contributes jointly with the anomeric effect to destabilization of the normal $^0H_5$ half-chair and favors inversion, overcoming opposition by a C-1,5 *syn*-diaxial-type substituent interaction (which in half-chair conformations is diminished anyway). No such opposing interaction is present in alkyl 4-*O*-acetyl-2,3-dideoxypent-2-enopyranosides, e.g. **28** and **32**, which on the strength of the anomeric effect alone prefer a conformation wherein the anomeric group is pseudoaxial rather than one wherein it is pseudoequatorial (**28′** and **32′**) (27, 29). Although in **2** the anomeric effect could be anticipated to favor a similar conformation, it was more difficult to predict whether 1,5-substituent interaction would significantly counteract. The spectrum of **2** showed the H-4 signal as a doublet of narrow multiplets at δ 5.21. The largest spacing (5.0 Hz) was mirrored in the upfield multiplet given by H-5 and hence represented $J_{4,5}$. This coupling immediately revealed a substantial deviation from the $^0H_5$ or D_5 forms (formulas **A** and **B**) in which the α-glycosides were found to reside, and for which $J_{4,5}$ = 9–10.5 Hz. On the other hand, the value appeared too large to be compatible with the inverted conformations $^5H_0$, ^5D, and D_0 (formulas **D**–**F**) where $\Phi_{4,5}$ is in the range 60–90° and $J_{4,5}$ should therefore be only 1–3 Hz. A possibility is the ^0D sofa form (formula **C**) with $\Phi_{4,5}$ = 150° but, as the sole representation of **2**, this is deemed unlikely for it does not have the benefit of the anomeric effect. Unfortunately, the small additional splittings observed in the H-4 signal and those present in the H-1 signal could not be used to decide the matter. However, the data were consistent with the assumption that **2** exists as a conformational equilibrium to which an inverted form such as $^5H_0$ or ^5D makes a large contribution.[4]

Now, the spectra of the β-glycosides **18**–**20***a* paralleled that of **2** in that they all displayed similar $J_{4,5}$ values, with those of the *C*-alkyl derivatives **20** and **20***a* being even somewhat smaller (~ 4 Hz). In view of the foregoing discussion this feature was compatible with the β-D-*erythro* configuration and suggested conformational similarity to **2**, with perhaps an increased preference for an inverted form in **20** and **20***a*. The assigned configuration was supported by the optical rotation of the products (see later), but definitive proof to exclude the β-D-*threo* configuration could not be obtained from the nmr data alone, mainly because the olefinic proton signals were ill resolved and pertinent *J* values could not be determined. However, one noteworthy observation relates to a comparison of the *C*-alkyl derivatives in the two anomeric series (**15** and **16** vs. **20** and **20***a*) with regard to the vicinal $J_{4,7}$ couplings found in the H-4 and sidechain methine proton signals. The most favored torsional orientation of the C-4 substituent about the C-4,7

[4]Because of this coincidence in **1**, the protons H-3, H-2, and H-1 constitute an AA′X system, as do H-2, H-3, and H-4. Hence, H-1 and H-4 are expected to give multiplets with splittings arising from averaging of the coupling constants involved. The two narrow parts of the wide H-4 doublet ($J_{4,5}$ = 9.2 Hz) each appeared as crude quartets with a line separation of ~0.7 Hz. Line separation in the H-1 multiplet (W_H = 3.6 Hz) was ~1.2 Hz. Calculation shows that these patterns can arise from estimated coupling constants as given in Table 3. These constants are compatible with the geometry of a flattened $^0H_5$ conformation approaching the D_5 form.

In compound **2**, the vinylic protons also coincided and the situation is, therefore, analogous. The two constituent parts of the H-4 doublet were quartets with a line separation of ~1.2 Hz, whereas H-1 gave a quartet with a line separation of 0.8 Hz. We have calculated approximate splittings as may be expected for the six conformations **A** – **F**, using estimated coupling constants that seemed reasonable for the respective, dihedral angles; eq, [1] was used for calculating $J_{1,3}$ and $J_{2,4}$, and values reported in this paper and elsewhere (14, 22, 26, 27, 33) were taken into account for choosing $J_{1,2}$, $J_{1,4}$, and $J_{3,4}$. The resultant splittings ranged from 0.3 to 1.7 Hz for H-1 and from 0.5 to 1.9 Hz for H-4, but none of the sets of values so derived for each individual conformation corresponded well with the actually observed pattern. However, the data were accommodated by a 1:1 equilibrium of the ^5D form (calculated splittings: H-1, 0.5; H-4, 1.9 Hz) and the D_5 form (calculated splittings: H-1, 1.0 Hz; H-4, 0.5 Hz).

Can. J. Chem. Downloaded from www.nrcresearchpress.com by 210.87.254.105 on 09/06/12
For personal use only.

bond should place H-7 antiperiplanar to H-4, allowing the bulky alkoxycarbonyl groups to point away from the sugar ring. In **15** and **16**, however, such an arrangement would imply a *syn*-parallel orientation of one of these groups with the acetoxymethyl group at C-5. To alleviate this, some rotation about the C-4,7 bond appears to take place, resulting in a diminished $J_{4,7}$ value (4 Hz). By contrast, there is no such steric encumbrance to be expected for **20** and **20***a* if indeed they are D-*erythro* compounds residing in an inverted conformation. In keeping with this assumption, their $J_{4,7}$ values of 9.0 Hz indicated a more nearly antiperiplanar orientation of H-4 and H-7.

The 3,4-unsaturated glycosides **9** and **21** displayed closely similar overall patterns of their respective ring proton signals, although H-1 to H-4 were slightly more deshielded in **9**. Specifically, they showed nearly identical patterns in their very narrow H-1 signals, their virtually coinciding olefinic proton signals (H-3 and H-4), and their complex multiplets for H-5. Also very similar in shape and width were the complex multiplets given by H-2, except that in **21** the multiplet was doubled by coupling with H-7. A splitting of 9.5 Hz indicated here, too, an H-2,7 *anti* situation. Very weak H-1,2 coupling ($\leq$ 1 Hz) as observed in **9** and **21** is characteristic for 3-enopyranosides having the α-D-*threo* configuration whereas corresponding α-D-*erythro* epimers show values of 3.5–4 Hz (36, 37, and refs. in Table 5). The optical rotations confirmed the assignment.

The parameters for **3** (Table 3) were in fair agreement with data recently given (14) for the same compound (but measured in a different solvent). They bear out a flattened $^0H_5$ half-chair conformation, which is in harmony with previous observations (33*b*) of similar conformational behavior in α-D-*threo* and α-D-*erythro*-hex-2-enopyranose systems. Finally, the data for compound **22**, whose H-1, H-2, and H-3 signals were clearly separated and visible in the spectrum of the crude mixture of **21** and **22**, allowed allocation of the α-D-*threo*-2-enoside structure to this minor product.

Optical Rotations

The configurational assignments made by spectroscopy were corroborated, and questions that remained open were settled, by the inclusion of arguments derived from comparison of optical rotations, with due consideration of conformational aspects (38) of optical superposition. Table 4 lists the molar rotations, $[M]_D = [\alpha]_D \times$ mol. wt./100, for chloroform solutions unless indicated otherwise. It

TABLE 4. Molecular rotations of enopyranosides in chloroform

2-Enosides	Configuration	$[M]_D$ (°)
1	α-D-*erythro*	+303; +276[a]
4		+460
5		+465
6		+466
7		+527
8		+678
10		+350
12		+448
15		+309
16		+334
17		+305
2	β-D-*erythro*	+285; +383[a]
18		+362
19		+376
20[b]		+173
20*a*[b]		+139
3	α-D-*threo*	−442
22		−600
3-Enosides	**Configuration**	$[M]_D$ (°)
9	α-D-*threo*	+614
21		+330

[a]In benzene.
[b]Containing small proportion of isomer (see text).

is seen that all of the α-D-*erythro* 2-enopyranosides, whose configurations are secure, are strongly dextrorotatory. This is fully in line with abundant data on analogous molecules found in the literature and conforms to a generality first stressed by Ferrier and co-workers (39). As has also been noted previously, it is apparent that the magnitude of $[M]_D$ depends to a considerable degree on the nature and size of the 4-substituent (compare, for example, ref. 27). The relatively low value of the primary amine **10**, as compared to the other amines, may perhaps be due to special effects of solvation or hydrogen bonding.

The β-glycosides **18**–**20***a* are less dextrorotatory than their α-linked counterparts; in either series the rotations are lower for *C*-alkylated than for aminated derivatives. However, in the parent diacetates **2** and **1** the difference is very small, and in benzene solution **2** is even *more* dextrorotatory than **1** (+383 vs. +276°), an anomaly that has been suspected (40) before. Deviations from Hudson's rule of isorotation have also been recognized in (nonacetylated) pairs of anomeric alkyl 2,3-dideoxypent-2-enopyranosides (27, 29) and in 2-acetylated 3-deoxy-hex-2-enopyranosides (33*b*). Likewise, the anomeric assignments for the aforementioned hexenopyranosyl phosphonates, originally made on the basis of optical rotations,

Can. J. Chem. Downloaded from www.nrcresearchpress.com by 210.87.254.105 on 09/06/12
For personal use only.

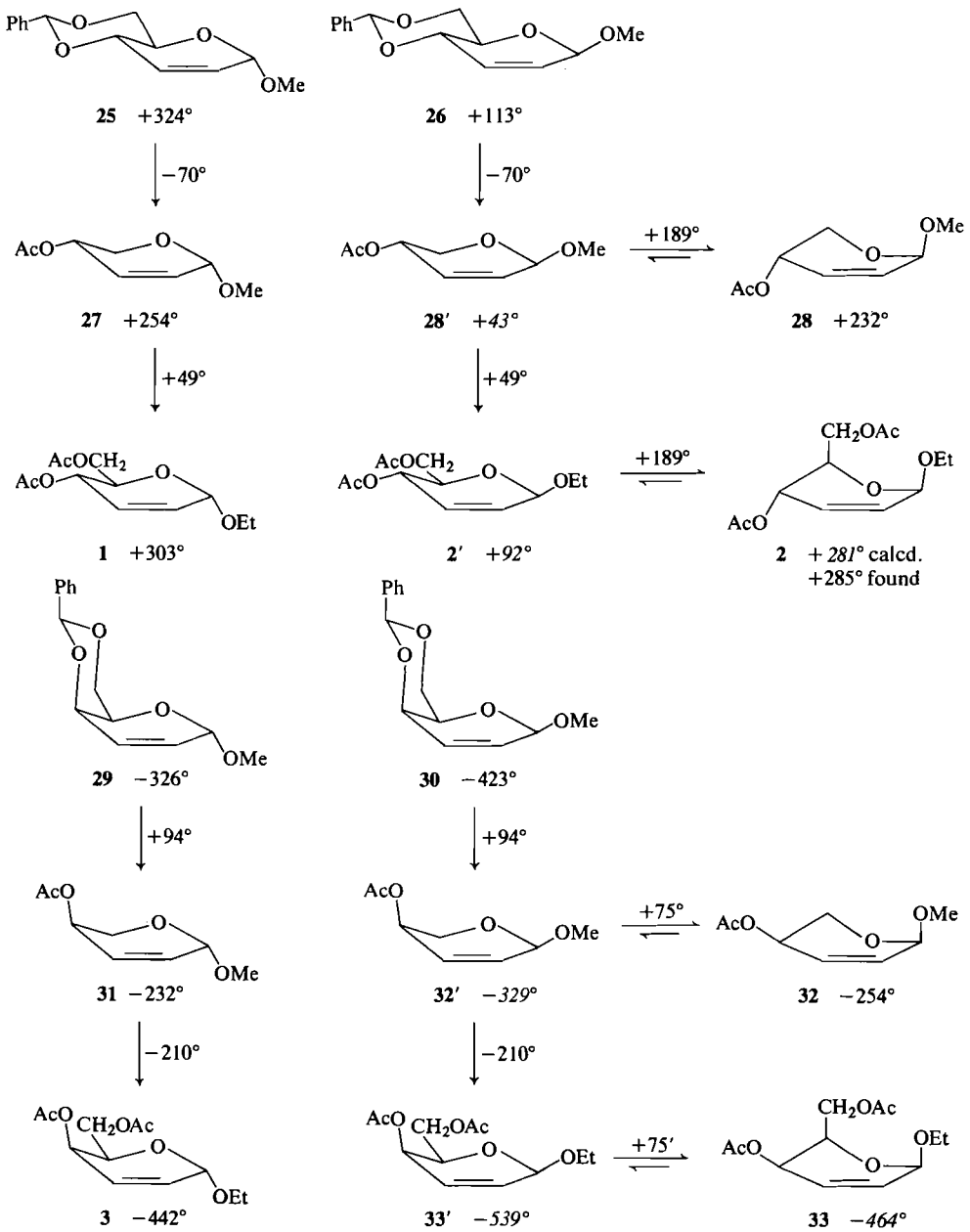

Values based on calculation are shown in italics.

SCHEME 2

later had to be revised (21, 41). The anomalies doubtless are rooted in the conformational behavior of β-D-glycosides in the enoside family (*vide supra*). In order to put the choice between the 4-epimeric alternatives for **18–20***a* on firm ground, and because there is a paucity of analogous β-D-*threo* derivatives for comparison, it became desirable to examine what sign and range of rotation could be predicted for each of the two configurational possibilities. Fortunately, this could be done with the aid of data, provided by Lemieux *et al.* (26, 27), on six securely characterized compounds (the benzylidene derivatives **25**, **26**, **29**, and **30**, and the pentosides **31** and **32**) in conjunction with our own data on **1**, **2**, and **3**. The argument is illustrated in Scheme 2. Compare the conformationally fixed acetal **25** with the 4-acetate **27** (the enantiomer of **32**) that is known to exist in the same, or nearly the same, conformation. The structural alteration entails a rotatory shift of −70° ($[M]_D$ values). An identical structural change in the conformationally rigid, β-anomeric acetal **26** may be expected to

TABLE 5. Specific rotations of some alkyl hex-3-enopyranosides in chloroform

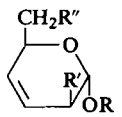

34*a–c*
α-D-*threo*

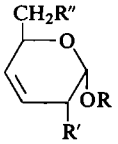

35*a–e*
α-D-*erythro*

Compound	R	R′	R″	$[\alpha]_D$	(Ref.)
9				+155.3	(a)
21				+100	(a)
34*a*	Me	OBn	OBn	+44	(13*b*)
34*b*	Me	OH	$OCPh_3$	+38	(42)
34*c*	Et	SCSMe ‖ O	OCSMe ‖ S	+50	(43)

Compound	R	R′	R″	$[\alpha]_D$	(Ref.)
35*a*	Me	OBn	OBn	−30	(19)
35*b*	Me	*p*NO_2BzO	*p*NO_2BzO	−57.7	(42)
35*c*	Me	OH	$OCPh_3$	−11.3	(42)
35*d*	Me	OMs	$OCPh_3$	−28.5	(42)
35*e*	Et	SCSMe ‖ O	OCSMe ‖ S	−100	(43)

[a]This work.

cause the same shift, which leads to a *calculated* rotation of 43° for the conformer **28′** of **28**. However, compound **28** (the enantiomer of **31**) is known to exist predominantly in the conformation having pseudoaxial substituents as depicted, and the difference to its actual rotation of +232°, namely 189°, therefore represents the sum total of optical changes associated with this conformational equilibration. Now consider the structural alteration **27** → **1**, disregarding the optically insignificant replacement of OMe by OEt. Introduction of the 5-acetoxymethyl substituent increases the rotation by 49°. Use of this increment in applying the same manoeuvre to **28′** leads to a calculated rotation of +92° for **2′**, a conformer of **2** deduced by nmr spectroscopy to be unstable (*vide supra*). If one now makes the assumption that the equilibration **2′** ⇌ **2** is attended by a similar optical contribution as the process **28′** ⇌ **28**, and consequently uses the same value (+189°) for it, a calculated rotation of +281° in indicated for **2**, in remarkably good agreement[5] with the measured value of 285°. Performance of the same exercise starting with the D-*threo* acetals **29** and **30** involves the pentosides **31** and **32** as well as the hexenoside **3** and should lead to a good indication of the rotation to be expected for the latter's unknown β-anomer **33**. As the scheme shows, different parameters apply here for the various transformations. Thus, in **29** → **31**, replacement of the fused ring by 4-acetoxy, and in **31** → **3**, the introduction of a 5-acetoxymethyl group, produce rotatory changes opposite in sign and different in degree compared to the preceding series. The increment for conformational inversion (+75°) is also different. The final result of the exercise is the prediction that β-D-*threo* compounds of type **33** will be *highly levorotatory regardless of conformational preference*, and it is therefore evident that **18–20***a* must be β-D-*erythro* compounds. As an ancillary bonus, the calculations contribute to an understanding why it is inadvisable to rely on Hudson's rule of isorotation for anomeric (as opposed to epimeric) assignments in enopyranoside pairs which are not constrained in the same rigid conformation. Although the rotational differences in such pairs can be fairly large and in the expected direction (Table 4), substituent and solvent influences may cause them to become quite small (even reversed), as exemplified by **27**/**28**, **1**/**2**, and **3**/**33**.

For the 3,4-unsaturated α-D-glycosides **9** and **21** the *threo* configuration was buttressed, and the *erythro* configuration rejected, by comparing their specific rotations with those of model compounds found in the literature (Table 5). The product which was formed together with **21** and judged on the basis of ^{13}C nmr data to be a positional isomer rather than a stereoisomer, but differed from **15** and was therefore assigned formula **22**, showed strong levorotation as expected for an α-D-*threo* 2-enoside.

Summary

In summary, the palladium-catalyzed substitution of allylic acetates has proved to be a useful method for the preparation of unsaturated amino and branched-chain sugars. With the hex-2-enopyranoside 4,6-diacetates thus far employed as substrates, it leads chiefly, but not in every case exclusively, to 4-substituted 2-enopyranosides. As far as

[5]There may be an element of coincidence in this, since the equilibrium constants for **28′**⇌**28** and **2′**⇌**2** are not necessarily the same and, furthermore, application of the same increment (+189°) to both equilibrations may not be entirely sound. Nevertheless, a reasonable agreement was to be expected.

Can. J. Chem. Downloaded from www.nrcresearchpress.com by 210.87.254.105 on 09/06/12
For personal use only.

Can. J. Chem. Downloaded from www.nrcresearchpress.com by 210.87.254.105 on 09/06/12
For personal use only.

can be judged from present results, this substitution occurs essentially stereospecifically with retention of configuration at C-4. Evidently the palladium catalyst species, in forming the π-allyl complex, prefers to place itself on the side of the pyranose ring opposite to the acetoxy group it is displacing, which is in accord with the general understanding of this interaction (6, 7). The palladium is then in turn displaced by the nucleophile approaching from the opposite direction, with resultant net retention of configuration. As regards the regioselectivity of the nucleophilic attack, the preference for C-4 may in part be due to polarisation of the π-allyl complex by the electron-withdrawing effect of the anomeric center. For the reactions with **1**, steric hindrance to nucleophile approach at C-2 by the neighboring, quasi-axial glycosidic group can probably be invoked as a contributing factor since selectivity was indeed most pronounced in that series. However, selectivity was similar in the aminations of the β-glycoside **2**, although it was noticeably diminished in *C*-alkylations of **2** and **2***a*. The apparent lack or reversal of regioselectivity in the two reactions thus far studied with **3** is interesting, as is the exception provided by dibenzylamine in its reaction with **1**. As far as the latter is concerned, thermodynamic factors may play a role since allylic amination (but not *C*-alkylation) is believed to be reversible (7). However, it would clearly be premature to attempt, at this stage, an exhaustive assessment of the factors which govern the stereochemistry of these substitutions in enopyranoside systems.

From a practical point of view it may be noted that the aminations here described offer an attractive approach to syntheses of 4-aminopolydeoxy sugars related to such antibiotics constituents as forosamine (2,3,4,6-tetradeoxy-4-dimethylamino-D-*erythro*-hexose, ossamine (its D-*threo* epimer), tolyposamine (4-amino-2,3,4,6-tetradeoxy-L-*erythro*-hexose), and the sugar moiety (4-amino-2,3,4-trideoxy-D-*erythro*-hex-2-enopyranuronic acid) of blasticidin S (44).

Experimental

Optical rotations were measured at room temperature in a Perkin-Elmer 141 automatic polarimeter and refer to chloroform solutions unless otherwise stated. Infrared spectra of syrupy compounds were obtained from liquid films, and those of crystalline compounds from Nujol mulls. For tlc, precoated silica gel plates SIL G-25 UV_{254} were used, and for preparative tlc, glass plates were coated with MN-Kieselgel G/UV_{254} (both products of Macherey-Nagel and Co., West Germany). Spots were made visible by inspection under uv light and/or by use of a spray with 5% sulfuric acid in ethanol and subsequent heating. Column chromatography was performed with Silica Gel 60 (E. Merck AG, West Germany). Unless otherwise indicated, solvent systems employed for development were mixtures of ethyl acetate and petroleum ether in the proportions (A) 1:2, (B) 1:3, (C) 1:4, and (D) 1:10. Here and elsewhere in the text, petroleum ether refers to the fraction having bp 30–60°C.

Preparation of the Unsaturated Glycoside Diacetates 1, 2, and 3

Ethyl 4,6-di-*O*-acetyl-2,3-dideoxy-α-D-*erythro*-hex-2-enopyranoside (**1**) was prepared from 3,4,6-tri-*O*-acetyl-1,5-anhydro-2-deoxy-D-*arabino*-hex-1-enitol (tri-*O*-acetyl-D-glucal) by the method of Ferrier (9); it showed mp 79°C and $[\alpha]_D$ +107° (*c* 1, benzene) as reported; $[\alpha]_D$ +117.3° (*c* 2.2, chloroform).

For the preparation of the β-anomer **2**, tri-*O*-acetyl-D-glucal was first ethoxymercurated, in analogy to its methoxymercuration described by Inglis *et al.* (12). A solution of the glycal (5.0 g, 18.4 mmol) in absolute ethanol (20 mL, dried over and distilled from magnesium) was added to a stirred suspension of mercuric acetate (6.14 g, 19.2 mmol) in absolute ethanol (70 mL) whereupon the salt dissolved rapidly. Ethyl 3,4,6-tri-*O*-acetyl-2-acetoxymercuri-2-deoxy-β-D-glucopyranoside began to crystallize after an hour and was collected after overnight storage of the reaction mixture. (It thus proved unnecessary to convert the product into the chloromercuri compound as had been done in the methoxymercuration just cited.) The crystals (3.50 g, 33%) had mp 177°C after recrystallization from ethyl acetate; $[\alpha]_D$ −15.5° (*c* 2.3); ν_{max} (Nujol): 1735 and 1240 (OAc), 1620–1600 (AcO^-), 1300, 1140–1000, and 920 cm^{-1}. Two sharp, medium strong bands at 755 and 690 cm^{-1} were possibly due to Hg-O vibrations (45). Nuclear magnetic resonance (100 MHz, $CDCl_3$) δ: 5.17 (dd, $J_{2,3}$ = 11.3, $J_{3,4}$ = 9.3 Hz, H-3), 4.95 (t, J = 9.3 Hz, H-4), 4.71 (d, $J_{1,2}$ = 10 Hz, H-1), 4.34 (dd, $J_{5,6}$ = 4.7, $J_{6,6'}$ = 12 Hz, H-6), 4.09 (dd, $J_{5,6'}$ = 2.7, $J_{6,6'}$ = 12 Hz, H-6′), 3.95–3.4 (m, 3H, *Me*—CH_2 and H-5), 2.62 (dd, J = 10 and 11.3 Hz, H-2), 2.15, 2.06, 2.02 (3 s, total intensity 12H, 4 OAc), 1.22 (t, J = 7 Hz, ethyl CH_3). *Anal.* calcd. for $C_{16}H_{24}HgO_{10}$ (577): C 33.31, H 4.19; found: C 33.51, H 4.36.

A solution of this acetoxymercuri derivative (1.0 g) in aqueous, 75% ethanol (25 mL) was mixed with a solution of sodium iodide (1.5 g) in 25 mL of the same solvent. Complete conversion of the mercurial (R_f 0.0) into **2** (R_f 0.6) was indicated by tlc (solvent A) after 30 min. The mixture was concentrated *in vacuo* to one-third of its volume and then diluted with water to 50 mL. The organic product was transferred into ether by several extractions, and the extract was washed successively with sodium thiosulfate solution and water, dried over $MgSO_4$, and evaporated to give **2** as a colorless syrup (0.38 g, 85%); $[\alpha]_D$ +148.5° (*c* 3.6, benzene); ν_{max}: 1750 and 1240 (OAc), 1130–970, 910, 815, and 750 cm^{-1}. *Anal.* calcd. for $C_{12}H_{18}O_6$ (258.3): C 55.80, H 7.02; found: C 55.82, H 7.00.

The known (12, 40) *methyl* glycoside analog (**2***a*) of **2** was prepared by analogous methoxymercuration (11) followed by elimination (12). The nmr data (100 MHz, $CDCl_3$) of the intermediate methyl 3,4,6-tri-*O*-acetyl-2-chloromercuri-2-deoxy-β-D-glucopyranoside δ: 5.18 (dd, $J_{2,3}$ = 11.5, $J_{3,4}$ = 9 Hz, H-3), 4.93 (t, J = 9 and 9.5 Hz, H-4), 4.65 (d, $J_{1,2}$ = 9.7 Hz, H-1), 4.32 (dd, $J_{5,6}$ = 5, $J_{6,6'}$ = 12.5 Hz, H-6), 4.09 ($J_{5,6'}$ = 2.5, $J_{6,6'}$ = 12.5 Hz, H-6′), 3.67 (o, H-5), 3.52 (s, 3H, OMe), 2.55 (dd, J = 9.7 and 11.5 Hz, H-2), 2.08 and 2.04 (s, 6 and 3H, 3 OAc).

Ethyl 4,6-di-*O*-acetyl-2,3-dideoxy-α-D-*threo*-hex-2-enopyranoside (**3**) (14) was obtained by conventional acetylation with acetic anhydride in pyridine (1 h at 25°C), of a crystalline sample of ethyl 2,3-dideoxy-α-D-*threo*-hex-2-enopyranoside[2] kindly donated by Professor B. Fraser-Reid. The diacetate was a colorless syrup, R_f 0.8 (solvent A), $[\alpha]_D$ −171.5° (*c* 1.5, chloroform) (lit. (14) $[\alpha]_D$ −171° (dichloromethane); ν_{max}: 1750 and 1240 (OAc), 1110, 1050, 1020–970, 915, 850, 760 and 600 cm^{-1}.

Can. J. Chem. Downloaded from www.nrcresearchpress.com by 210.87.254.105 on 09/06/12
For personal use only.

General Procedure for Allylic Substitution

For Amination

The catalyst, tetrakis(triphenylphosphine)palladium(0), may be prepared according to Coulson (46) or purchased from Aldrich Chemical Company, Inc. Tetrahydrofuran used as a solvent was reagent grade and was purified further by drying over, and distillation from, lithium aluminum hydride. The other reactants were also reagent grade but used without pretreatment unless specially noted. Reactions were normally performed on a 0.5 mmol scale with respect to the glycoside employed (0.13 g). Deviations from this amount of starting glycoside are specifically indicated and imply proportionate changes in the amounts of solvent and other reactants. Typically the glycoside (0.13 g, 0.5 mmol), triphenylphosphine (93 mg, 0.35 mmol), and the catalyst (41 mg, 0.035 mmol) were stirred in tetrahydrofuran (10 mL) for 30 min at room temperature, under nitrogen, in a flask equipped with reflux condenser and gas inlet. An excess of the amine (3.3–3.5 mmol) was then added by syringe, and the mixture was boiled under reflux until monitoring by tlc indicated absence of the starting glycoside. (See individual sections for the various reaction times.) The cooled reaction mixture was then partitioned between ether and water. The aqueous phase was extracted with ether (4 × 30 mL), and the combined extracts and organic phase were dried ($MgSO_4$) and evaporated to give a yellow residue which contained the aminated sugar together with triphenylphosphine oxide, residual amine, and other impurities. Column chromatography or preparative tlc of the material, as indicated in the individual sections, furnished the desired product in homogeneous form, usually as a colorless, analytically pure oil.

For Alkylation

The mixture of glycoside, triphenylphosphine, and catalyst was prepared as described above, except that only 5 mL of tetrahydrofuran was used as the solvent. Separately and simultaneously, a solution of the sodio derivative of the reactive methylene component was prepared. For this purpose, sodium hydride (130 mg of a 61% dispersion in mineral oil; ca. 3.3 mmol) was washed twice with hexane and once with tetrahydrofuran by decantation and was then suspended in 5 mL of tetrahydrofuran. The methylene component (3.35 mmol or slightly more) was added dropwise with stirring, which caused the hydride to dissolve completely in the course of 15 min. The solution was added, in one portion, to the aforementioned solution of reactants when the latter had interacted for 30 min, and the mixture was then heated at reflux until tlc indicated completion of the reaction. The precautions and processing modes applied were the same as those in the aminations.

*Ethyl 6-O-Acetyl-2,3,4-trideoxy-4-diethylamino-α-D-*erythro-*hex-2-enopyranoside (4)*

Compound **4** was obtained from **1** and diethylamine (0.35 mL) after a reaction time of 48 h and preparative tlc (solvent C). The colorless oil (110 mg, 80%) showed R_f 0.9 (tlc with solvent A); $[\alpha]_D$ +169.8° (*c* 1); ν_{max}: 1745 and 1260 (OAc), 1150–1000 (C—N, C—O—C), and 730 (*cis* alkene) cm^{-1}. *Anal.* calcd. for $C_{14}H_{25}NO_4$ (271.4): C 61.97, H 9.29, N 5.16; found: C 62.11, H 9.18, N 4.97.

*Ethyl 6-O-Acetyl-2,3,4-trideoxy-4-piperidino-α-D-*erythro-*hex-2-enopyranoside (5)*

Prepared exactly like the preceding compound, but with piperidine (0.33 mL), **5** was a colorless oil (100 mg, 70%), R_f 0.9 (tlc in solvent A); $[\alpha]_D$ +164.3° (*c* 1); ν_{max}: 1745 and 1240 (OAc), 1160–1000 (C—N, C—O—C), and 730 (*cis* alkene) cm^{-1}. *Anal.* calcd. for $C_{15}H_{25}NO_4$ (283.4): C 63.58, H 8.89, N 4.94; found: C 63.41, H 8.97, N 4.67.

*Ethyl 6-O-Acetyl-4-(N-cyclohexyl)methylamino-2,3,4-trideoxy-α-D-*erythro-*hex-2-enopyranoside (6)*

From **1** (200 mg) and cyclohexylmethylamine (0.44 mL), compound **6** was obtained after a reaction time of 5 days; it was accompanied by traces of 2 slow-moving by-products (tlc with solvent A) which were readily removed by preparative tlc (solvent C). The colorless, homogeneous product (180 mg, 75%) had $[\alpha]_D$ +149.7° (*c* 1); ν_{max}: 1745 and 1240 (OAc), 1120–1000 (C—N, C—O—C), and 730 (*cis* alkene) cm^{-1}. *Anal.* calcd. for $C_{17}H_{29}NO_4$ (311.4): C 65.56, H 9.39, N 4.50; found: C 65.53, H 9.27, N 4.51.

*Ethyl 6-O-Acetyl-4-(N-benzyl)methylamino-2,3,4-trideoxy-α-D-*erythro-*hex-2-enopyranoside (7)*

Reaction of **1** with benzylmethylamine (0.5 mL) was complete after 24 h, and tlc (solvent A) showed a main spot (R_f 0.8) accompanied by a minor spot (R_f 0.7) which was presumably due to an isomer. Isolated by preparative tlc (solvent C), the major product **7** was a colorless syrup (140 mg, 87%) that tended to crystallize on strong cooling (mp below 0°C); $[\alpha]_D$ +165.4° (*c* 1); ν_{max}: 3100–3050, 1600, 1500, and 700 (Ph), 1745 and 1240 (OAc), 1120–970 (C—N, C—O—C), and 740 (*cis* alkene) cm^{-1}. *Anal.* calcd. for $C_{18}H_{25}NO_4$ (319.4): C 67.69, H 7.89, N 4.39; found: C 67.53, H 7.83, N 4.51.

*Ethyl 6-O-Acetyl-4-dibenzylamino-2,3,4-trideoxy-α-D-*erythro-*hex-2-enopyranoside (8) and Ethyl 6-O-Acetyl-2-dibenzylamino-2,3,4-trideoxy-α-D-*threo-*hex-3-enopyranoside (9)*

The reaction of **1** with dibenzylamine (0.64 mL) was nearly complete after 30 h. The tlc (solvent B) indicated the presence of 2 main products having $R_f \sim 0.8$ (major product) and ~ 0.7 (minor product), together with traces of slow-moving by-products. Integration of the sufficiently separated acetoxyl group signals in the nmr spectrum of the crude mixture (166 mg, 83%) suggested that the two main components were present in the ratio 7:3. The components were separated by preparative tlc using multiple irrigation with solvent D, which furnished either product free from the other (according to nmr spectra).

The syrupy, slower-moving, minor product proved to be the isomer **8**. It crystallized on storage in the refrigerator. Collected after trituration with petroleum ether and recrystallized from that solvent, it showed mp 78–79°C; $[\alpha]_D$ +171.4° (*c* 1.4); ν_{max}: 3100–3040, 1600, 1500, and 700 (Ph), 1745 and 1240 (OAc), 1120–975 (C—N, C—O—C), and 755–735 (*cis* alkene) cm^{-1}. *Anal.* calcd. for $C_{24}H_{29}NO_4$ (395.5): C 72.89, H 7.39, N 3.54; found: C 72.69, H 7.56, N 3.54.

The faster-moving, major product (**9**) failed to crystallize; $[\alpha]_D$ +155.3° (*c* 1.2). Its infrared spectrum was very similar to that of **8**, showing only minor differences in the fingerprint region. *Anal.* calcd. as for **8**; found: C 72.57, H 7.83, N 3.68.

*Ethyl 6-O-Acetyl-4-benzylamino-2,3,4-trideoxy-α-D-*erythro-*hex-2-enopyranoside (10) and Ethyl 6-O-Acetyl-4-(N-benzylacetamido)-2,3,4-trideoxy-α-D-*erythro-*hex-2-enopyranoside (12)*

After the reaction of **1** with benzylamine (0.36 mL) for 24 h, tlc with solvent A indicated the presence of 3 products ($R_f \sim 0.6$, 0.25, and 0.2) together with some remnant **1** ($R_f \sim 0.75$). An additional 10 mg of catalyst and 0.1 mL of benzylamine were introduced and refluxing was continued for another 9 h, which caused **1** to disappear completely. Upon processing, the mixture of products was applied to a silica gel column that was irrigated with solvent C. The fast-moving product (**10**) was isolated as a colorless oil (48 mg, 31%); $[\alpha]_D$ +115.5° (*c* 1.1); ν_{max}: 3200 (broad, NH), 3100–3050, 1600 and 1500 (weak), and 700 (Ph),

Can. J. Chem. Downloaded from www.nrcresearchpress.com by 210.87.254.105 on 09/06/12
For personal use only.

1740 and 1240 (OAc), 1100–1000 (C—N, C—O—C), and 730 (*cis* alkene) cm^{-1}. On aging of the sample, an amide band at 1650 cm^{-1} developed owing to O→N acetyl migration.

The 2 slow-moving products were subsequently eluted from the column as a mixture. An attempt was made to separate this mixture by preparative tlc (solvent D), but separation was unsatisfactory in that each of the 2 bands isolated contained a substantial proportion of the other component (~ ⅓ according to nmr spectra). The spectra suggested that the components were the *O*-deacetylated derivative (**11**, R_f 0.25) of **10**, and partially *O*-deacetylated **1** (R_f 0.2). The fractions were individually acetylated with acetic anhydride and pyridine (16 h at room temperature), whereupon they gave similar tlc patterns showing a fast-moving spot (**1**) and a slow-moving spot (the *N*-acetyl-*O*-acetyl derivative **12**). Preparative tlc (solvent D) of these mixtures gave a total of 65 mg (50% recovery) of **1**, identified by its nmr spectrum and an undepressed mixture mp of 79–81°C; and oily but homogeneous **12** (27 mg, 15%) showing $[\alpha]_D$ +129° (*c* 1.1); ν_{max}: 3100–3050, 1610 and 1500 (weak), and 700 (Ph), 1740 (ester CO), 1650 (amide CO), 1250–970 (multiple bands), 900, and 735 cm^{-1}. *Anal.* calcd. for $C_{19}H_{25}NO_5$ (347.4): C 65.69, H 7.25, N 4.03; found: C 65.53, H 7.41, N 3.83.

Ethyl 6-O-*Acetyl-2,3,4-trideoxy-4-[bis(methoxycarbonyl)-methyl]*-α-D-erythro-*hex-2-enopyranoside (15)*

Reaction (10 h) of **1** and dimethyl malonate (0.40 mL) gave **15** as the sole product, according to tlc (R_f ~ 0.4, solvent A). The colorless syrup (145 mg, 87%) obtained after processing showed $[\alpha]_D$ +93.5° (*c* 1.3); ν_{max}: 1740 (ester CO), 1250–970 (C—O—C), and 730 (*cis* alkene) cm^{-1}. *Anal.* calcd. for $C_{15}H_{22}O_8$ (330.3): C 54.54, H 6.71; found: C 54.72, H 6.89.

Ethyl 6-O-*Acetyl-2,3,4-trideoxy-4-[bis(ethoxycarbonyl)-methyl]*-α-D-erythro-*hex-2-enopyranoside (16)*

Compound **1** and diethyl malonate (0.50 mL) were allowed to react for 24 h. In this instance, the product **16** had the same R_f value (0.8) as **1** and could only be distinguished by the light brown color of its spot, which differed from the black spot given by **1** (tlc with solvent A). Possibly the reaction was finished earlier. Processing gave **16** (150 mg, 83%) as a colorless syrup, $[\alpha]_D$ +93.4° (*c* 1.1); ν_{max}: 1750, 1730 (ester CO), 1250–1000 (C—O—C), and 730 (*cis* alkene) cm^{-1}. *Anal.* calcd. for $C_{17}H_{26}O_8$ (358.4): C 56.97, H 7.31; found: C 56.81, H 7.57.

Ethyl 6-O-*Acetyl-2,3,4-trideoxy-4-[methoxycarbonyl-(phenylsulfonyl)methyl]*-α-D-erythro-*hex-2-enopyranoside (17)*

Compound **1** (300 mg, 1.16 mmol) was allowed to react with a 0.117 *M* solution (65 mL) of methyl phenylsulfonylacetate sodium in tetrahydrofuran. Incomplete consumption of **1** was noted by tlc (solvent A) after 48 h; an additional 30 mg of catalyst and 4 mL of the solution of the sodio ester solution were introduced, whereupon **1** disappeared completely after a further 24 h of refluxing. There was formed one major product (R_f ~ 0.45) which was accompanied by a minor, slightly faster moving product. Column chromatography using solvent C as eluent gave 300 mg (63%) of the product as a syrup that still contained the minor by-product. Crystallization from ethyl acetate – petroleum ether furnished chromatographically pure **17**, mp 100–102°C; $[\alpha]_D$ +74° (*c* 2.8); ν_{max} (Nujol): 3100–3050, 1600, and 700 (Ph), 1750–1730 (ester CO), 1320 (S—O), 1250–950 (multiple bands, S=O, C—O—C), and 730 (*cis* alkene) cm^{-1}. *Anal.* calcd. for $C_{19}H_{24}O_8S$ (412.4): C 55.33, H 5.87, S 7.77; found: C 55.08, H 5.77, S 7.62.

Ethyl 6-O-*Acetyl-2,3,4-trideoxy-4-[bis(methoxycarbonyl)-methyl]*-β-D-erythro-*hex-2-enopyranoside (20)*

Reaction of **2** with dimethyl malonate (0.40 mL) was complete after 10 h; a single spot having R_f 0.55 was seen in tlc (solvent A). The product was isolated by use of a column which was eluted, first, with petroleum ether, and then with solvent D. Even though the oily product so obtained (145 mg, 87%) appeared chromatographically homogeneous, the presence of a small proportion (probably not more than 10%) of an isomer was revealed by the ^{13}C nmr spectrum; $[\alpha]_D$ +52.5° (*c* 3); ν_{max}: 1750–1730 (ester CO), 1300–1010 (multiple bands), 880–800, and 735 cm^{-1}. *Anal.* calcd. for $C_{15}H_{22}O_8$ (330.3): C 54.54, H 6.71; found: C 54.63, H 6.76.

Methyl 6-O-*Acetyl-2,3,4-trideoxy-4-[bis(methoxycarbonyl)-methyl]*-β-D-erythro-*hex-2-enopyranoside (20a)*

Compound **20***a* was obtained from **2***a* (120 mg) exactly as just detailed for **20**, after a reaction time of 20 h. The pale yellow syrup (125 mg, 83%) gave a single spot in tlc (R_f 0.6, solvent A) but contained, nevertheless, a small proportion of an isomer, according to the ^{13}C nmr spectrum; $[\alpha]_D$ +44° (*c* 0.5); ν_{max}: 1750 (ester CO), 1300–1050 (multiple bands), 970, 870–810, and 740 cm^{-1}. *Anal.* calcd. for $C_{14}H_{20}O_8$ (316.3): C 53.16, H 6.37; found: C 53.16, H 6.47.

Ethyl 6-O-*Acetyl-2,3,4-trideoxy-4-diethylamino*-β-D-erythro-*hex-2-enopyranoside (18)*

The reaction of **2** (130 mg) with diethylamine (0.85 mL) was not entirely complete after 20 h (tlc with solvent A); it was completed by adding further amounts of diethylamine (0.4 mL) and catalyst (20 mg) and continued refluxing for another 6 h. Processing included the passage of the crude product through a silica gel column which was eluted, first with petroleum ether and then with solvent D. Compound **18** was obtained as a colorless syrup (90 mg, 66%), R_f 0.3 (solvent A); $[\alpha]_D$ +133.6° (*c* 1.1); ν_{max}: 1745 and 1250 (OAc), 1200, 1120–1020 (C—N, C—O—C), 980, 900, 835, 800, 730, and 700 cm^{-1}.

Ethyl 6-O-*Acetyl-4-(*N-*benzyl)methylamino-2,3,4-trideoxy*-β-D-erythro-*hex-2-enopyranoside (19)*

The reaction between **2** (195 mg) and benzylmethylamine (0.75 mL) showed, after 24 h, a product that differed from **2** only in the color (light brown vs. black) of its tlc spot, but not in the R_f value (0.6 in solvent A). Refluxing was continued for another 24 h, which caused no change in the tlc picture. After processing (with use of dichloromethane instead of ether for extraction of the aqueous phase) and column chromatographic purification (elution with petroleum ether followed by solvent D), compound **19** was obtained as a colorless syrup (220 mg, 91%), $[\alpha]_D$ +118.2° (*c* 1.3); ν_{max}: 3100–3050, 1600, 1500, and 700 (Ph), 1745 and 1240 (OAc), 1120–970 (C—N, C—O—C), 900 and 810, and 755–730 (*cis* alkene) cm^{-1}. *Anal.* calcd. for $C_{18}H_{25}NO_4$ (319.4): C 67.69, H 7.89, N 4.39; found: C 67.47, H 8.13, N 4.26.

Ethyl 6-O-*Acetyl-2,3,4-trideoxy-2-[bis(methoxycarbonyl)-methyl]*-α-D-threo-*hex-3-enopyranoside (21) and Ethyl* 6-O-*Acetyl-2,3,4-trideoxy-4-[bis(methoxycarbonyl)methyl]-hex-2-enopyranoside (22)*

The reaction was performed with **3** (347 mg), triphenylphosphine (246 mg), and palladium catalyst (108 mg) in tetrahydrofuran (15 mL), to which was added dimethyl malonate (1.32 mL) and sodium hydride (61%; 343 mg) in tetrahydrofuran (10 mL). All of **3** had disappeared after 15 h of heating at reflux temperature. Thin-layer chromatography with solvent A showed a strong spot (R_f 0.6) together with a second, fairly strong, double spot (R_f ~ 0.1) and an intermediate trace spot. Column chromatography produced the fast-moving material (295 mg, 66%) which, although homogeneous in tlc, proved to be a ~3:1 mixture of **21** and **22**, according to ^1H and ^{13}C nmr spectra. This mixture of isomers showed $[\alpha]_D$ +24° (*c* 1.3) and an infrared

Can. J. Chem. Downloaded from www.nrcresearchpress.com by 210.87.254.105 on 09/06/12
For personal use only.

spectrum that agreed with expectations. *Anal.* calcd. for $C_{15}H_{22}O_8$ (330.3): C 54.54, H 6.71; found: C 54.37, H 6.65.

The slow-moving material emerged from the column on continued elution with solvent D. There were obtained 2 fractions (55 and 65 mg), both of which showed methyl ester but lacked acetyl group resonances in the nmr spectrum. Acetylation with acetic anhydride and pyridine at room temperature left the first fraction unchanged whereas it converted the second fraction into a syrupy monoacetate, $[\alpha]_D$ +100° (*c* 0.24), whose ^{1}H nmr spectrum matched the signals belonging to the major component (**21**) in the spectrum of the aforementioned mixture of **21** and **22**. The infrared spectrum was also closely similar to that of the mixture; ν_{max}: 1750 and 1250 (ester), 1200–1000 (C—O—C), 930, 820, and 730 cm^{-1}.

*Mixture of Ethyl 6-O-Acetyl-2,3,4-trideoxy-2-[methoxycarbonyl(phenylsulfonyl)methyl]-α-D-hex-3-enopyranoside (**23**) and Ethyl 6-O-Acetyl-2,3,4-trideoxy-4-[methoxycarbonyl-(phenylsulfonyl)methyl]-α-D-hex-2-enopyranoside (**24**)*

Compound **3** (200 mg) was allowed to react with a 0.177 *M* solution (40 mL) of methyl phenylsulfonylacetate sodium in tetrahydrofuran. All of **3** was consumed after 5 days, and two product spots of comparable strength and similar mobilities (R_f ~ 0.4–0.5) were seen in tlc (solvent A). The products could not be separated; their presence in a ratio of ~ 1:1 was indicated by ^{1}H and ^{13}C nmr spectra. The mixture of **23** and **24** showed $[\alpha]_D$ +39.4° (*c* 2.8). *Anal.* calcd. for $C_{19}H_{24}O_8S$ (412.4): C 55.33, H 5.87, S 7.77; found: C 55.25, H 5.83, S 7.74.

Acknowledgments

This work was supported by the Natural Sciences and Engineering Research Council of Canada. We are indebted to Professor H. Alper for a gift of palladium catalyst.

1. H. H. Baer and Z. S. Hanna. Carbohydr. Res. **78**, c11 (1980).
2. H. H. Baer and Z. S. Hanna. Carbohydr. Res. **85**, 136 (1980); H. H. Baer and H. R. Hanna. (*a*) Carbohydr. Res. **77**, c12 (1979); (*b*) Can. J. Chem. **58**, 1751 (1980); H. H. Baer and A. J. Bell. (*a*) Carbohydr. Res. **75**, 175 (1979); (*b*) Can. J. Chem. **56**, 2872 (1978); H. H. Baer and C. B. Madumelu. (*a*) Carbohydr. Res. **67**, 329 (1978); (*b*) Can. J. Chem. **56**, 1177 (1978); H. H. Baer, F. Linhart, and H. R. Hanna. Can. J. Chem. **56**, 3087 (1978); H. H. Baer and F. F. Z. Georges. (*a*) Can. J. Chem. **55**, 1100 (1977); **55**, 1348 (1977); (*b*) Carbohydr. Res. **55**, 253 (1977).
3. T. S. Shryne, E. J. Smutny, and D. P. Stevenson. U. S. Pat. No. 3,493,617 (1970).
4. W. E. Walker, R. M. Manyk, K. E. Atkins, and M. L. Farmer. Tetrahedron Lett. 3817 (1970); K. E. Atkins, W. E. Walker, and R. M. Manyk. Tetrahedron Lett. 3821 (1970).
5. G. Hata, K. Takahashi, and A. Miyako. Chem. Commun. 1392 (1970); K. Takahashi, A. Miyako, and G. Hata. Bull. Chem. Soc. Jpn. **45**, 230 (1972).
6. B. M. Trost and J. P. Genet. J. Am. Chem. Soc. **98**, 8516 (1976); B. M. Trost and T. R. Verhoeven. (*a*) J. Am. Chem. Soc. **98**, 630 (1976); (*b*) J. Am. Chem. Soc. **99**, 3867 (1977); (*c*) J. Am. Chem. Soc. **100**, 3435 (1978); (*d*) J. Am. Chem. Soc. **101**, 1595 (1979); (*e*) J. Org. Chem. **41**, 3215 (1976); B. M. Trost and P. E. Strege. J. Am. Chem. Soc. **99**, 1649 (1977); B. M. Trost, S. A. Godleski, and J. P. Genet. J. Am. Chem. Soc. **100**, 3930 (1978); B. M. Trost and E. Keinan. J. Am. Chem. Soc. **100**, 7779 (1978); B. M. Trost, T. R. Verhoeven, and J. M. Fortunak. Tetrahedron Lett. 2301 (1979); B. M. Trost and T. R. Verhoeven. J. Am. Chem. Soc. **102**, 4730 (1980).
7. B. M. Trost. Tetrahedron, **33**, 2615 (1977); R. F. Heck. Acc. Chem. Res. **12**, 146 (1979); J. Tsuji. Organic synthesis with palladium compounds. Springer-Verlag, New York. 1980.
8. I. Arai and G. D. Daves, Jr. J. Am. Chem. Soc. **100**, 287 (1978).
9. R. J. Ferrier. Methods Carbohydr. Chem. **6**, 307 (1972); R. J. Ferrier and N. Prasad. J. Chem. Soc. C, 571 (1969).
10. A. Rosenthal and J. N. C. Whyte. Can. J. Chem. **46**, 2245 (1968).
11. A. DeBoer, C. J. Thanel, and G. A. Wilson. Tetrahedron Lett. 5137 (1972).
12. G. L. Inglis, J. C. P. Schwarz, and L. McLaren. J. Chem. Soc. 1014 (1962).
13. (*a*) D. Mitsunobu and M. Eguchi. Bull. Chem. Soc. Jpn. **44**, 3427 (1971); (*b*) G. Alfredsson and P. J. Garegg. Acta Chem. Scand. **27**, 724 (1973); (*c*) G. Grynkiewicz and H. Burzynska. Tetrahedron, **32**, 2109 (1976).
14. G. Grynkiewicz, W. Priebe, and A. Zamojski. Carbohydr. Res. **68**, 33 (1979).
15. A. Rosenthal. Carbohydr. Res. **8**, 61 (1968).
16. R. J. Ferrier, N. Vethaviyasar, O. S. Chizhov, V. I. Kadentsev, and B. M. Zolotarev. Carbohydr. Res. **13**, 269 (1970).
17. G. Descotes, P. Boullanger, Tachi-Dung, and J.-C. Martin. Carbohydr. Res. **71**, 305 (1979).
18. A. S. Perlin. Int. Rev. Sci., Org. Chem. Ser. 2, **7**, 1 (1975); R. G. S. Ritchie, N. Cyr, and A. S. Perlin. Can. J. Chem. **54**, 2301 (1976); H. Paulsen, V. Sinnwell, and W. Greve. Carbohydr. Res. **49**, 27 (1976).
19. P. J. Garegg and B. Samuelsson. Synthesis, 813 (1979).
20. D. E. Iley and B. Fraser-Reid. Can. J. Chem. **57**, 653 (1979).
21. G. Adiwidjaja, B. Meyer, H. Paulsen, and J. Thiem. Tetrahedron, **35**, 373 (1979).
22. J. Thiem, J. Schwentner, E. Schüttpelz, and J. Kopf. Chem. Ber. **112**, 1023 (1979).
23. R. Stokhuyzen and C. Chieh. J. Chem. Soc. Perkin Trans. II, 481 (1976).
24. K. A. Watanabe, R. S. Goody, and J. J. Fox. Tetrahedron, **26**, 3883 (1970).
25. E. W. Garbisch, Jr. J. Am. Chem. Soc. **86**, 5561 (1964).
26. R. U. Lemieux, E. Fraga, and K. A. Watanabe. Can. J. Chem. **46**, 61 (1968).
27. R. U. Lemieux, K. A. Watanabe, and A. A. Pavia. Can. J. Chem. **47**, 4413 (1969).
28. E. F. L. J. Anet. Carbohydr. Res. **1**, 348 (1966).
29. B. Fraser-Reid, B. J. Carthy, N. L. Holder, and M. Yunker. Can. J. Chem. **49**, 3038 (1971).
30. B. Fraser-Reid, S. Y.-K. Tam, and B. Radatus. Can. J. Chem. **53**, 2005 (1975).
31. K. Heyns and J. I. Park. Chem. Ber. **109**, 3262 (1976).
32. R. R. Schmidt and R. Angerbauer. Carbohydr. Res. **72**, 272 (1979).
33. (*a*) R. J. Ferrier and N. Prasad. J. Chem. Soc. C, 581 (1969); (*b*) R. J. Ferrier and C. H. Sankey. J. Chem. Soc. 2339 (1966); 2345 (1966).
34. R. U. Lemieux and R. J. Bose. Can. J. Chem. **44**, 1855 (1966).
35. F. Johnson and S. K. Malhotra. J. Am. Chem. Soc. **87**, 5492 (1965).
36. R. J. Ferrier and N. Vethaviyasar. J. Chem. Soc. C, 1907 (1971).

37. J. C. FLORENT, C. MONNERET, and Q. KHUONG-HUU. Carbohydr. Res. **56**, 301 (1977).
38. D. H. WHIFFEN. Chem. Ind. London, 964 (1956); J. H. BREWSTER. J. Am. Chem. Soc. **81**, 5483 (1959); **81**, 5493 (1959); R. U. LEMIEUX and J. C. MARTIN. Carbohydr. Res. **13**, 139 (1970).
39. D. M. CIMENT and R. J. FERRIER. J. Chem. Soc. C, 441 (1966); D. M. CIMENT, R. J. FERRIER, and W. G. OVEREND. J. Chem. Soc. C, 447 (1966).
40. R. J. FERRIER. J. Chem. Soc. 5443 (1964).
41. H. PAULSEN and J. THIEM. Chem. Ber. **106**, 3850 (1973); J. THIEM, B. MEYER, and H. PAULSEN. Chem. Ber. **111**, 3325 (1978).
42. N. L. HOLDER and B. FRASER-REID. Can. J. Chem. **51**, 3357 (1973).
43. R. J. FERRIER and N. VETHAVIYASAR. Carbohydr. Res. **58**, 481 (1977).
44. S. HANESSIAN and T. HASKELL. *In* The carbohydrates. Vol. IIA. *Edited by* W. Pigman and D. Horton. Academic Press, New York. 1970. p. 139.
45. E. MASLOWSKY, JR. Vibrational spectra of organometallic compounds. John Wiley and Sons, New York. 1977.
46. D. R. COULSON. Inorg. Synth. **13**, 121 (1974).

Can. J. Chem. Downloaded from www.nrcresearchpress.com by 210.87.254.105 on 09/06/12
For personal use only.

Rotation optique et structure moléculaire. I. Cas des cyclitols et anhydro-1,6 sucres

MAURICE CHASTRETTE ET JEAN-CLAUDE MARTIN[1]

Université de Lyon I, Ecole Supérieure de Chimie Industrielle de Lyon, ERA 689 du C.N.R.S., BP 2002, 69603 Villeurbanne, France

Reçu le 28 mai, 1980

Ce papier est dédié au Prof. Raymond U. Lemieux à l'occasion de son 60ème anniversaire

MAURICE CHASTRETTE et JEAN-CLAUDE MARTIN. Can. J. Chem. **59**, 907 (1981).

Les relations entre rotation moléculaire et structure de composés à géométrie rigide (cyclitols et anhydro-1,6 sucres) sont étudiées en fonction des interactions entre les dipoles des liaisons carbone–oxygène et des contributions du cycle ou du squelette hydrocarboné. L'influence des interactions à longue distance (à travers 2 ou 3 atomes de carbones) n'est pas négligeable et un jeu de paramètres est proposé pour chacune des familles étudiées.

MAURICE CHASTRETTE and JEAN-CLAUDE MARTIN. Can. J. Chem. **59**, 907 (1981).

The relationships between molecular rotation and the structure of the rigid cyclitols and anhydro-1,6 sugars are studied as a function of the interactions between the carbon–oxygen bond dipoles and contributions from the ring or the hydrocarbon skeleton. The influence of long distance interactions (through 2 or 3 carbon atoms) is not negligible and a variety of parameters is suggested for each of the families of compounds studied.

[Journal translation]

La relation entre la structure d'un composé organique et son activité optique a fait l'objet d'études nombreuses notamment dans le domaine des sucres, depuis que Whiffen (1) a proposé le principe d'additivité des contributions de chaque élément conformationnel d'asymétrie. Ce principe a été repris dans un certain nombre de travaux (2–7) qui ont mis en évidence des corrélations empiriques pour différentes familles de dérivés. Ces travaux sont basés sur la définition d'un certain nombre d'interactions dipolaires simples à faible distance (une seule liaison entre les dipoles) et éventuellement sur la contribution globale d'un cycle ou d'un squelette hydrocarboné.

L'approche proposée dans ce mémoire consiste à envisager dans deux séries de composés bien connus et de structure rigide (cyclitols et anhydro-1,6 hexopyranoses) l'ensemble des interactions possibles dans la molécule sans faire aucune hypothèse ni sur leur valeur, ni sur leurs combinaisons mathématiques et à déterminer ensuite par une méthode de calcul par régression les paramètres nuls ou sans signification statistique.

Les dérivés choisis pour cette étude ont des structures déterminées par spectroscopie rmn, ir et par cristallographie aux rayons X (8–13). Leurs rotations moléculaires ont été plusieurs fois déterminées. Par ailleurs, la rigidité structurale de ces composés n'est pas affectée par les substitutions des cycles dans les exemples choisis.

La procédure utilisée consiste à envisager deux types d'interactions; la première concerne l'interaction du squelette avec un substituant. Elle est nulle dans le cas des cyclitols; dans le cas des anhydro-1,6 sucres, elle est désignée par $R/_nO_{ax}$ ou $R/_nO_{eq}$; n désignant le nombre de liaisons carbone–carbone séparant les supports des dipoles (n = 1, 2 ou 3). Les autres interactions caractérisent les substituants des cycles et sont désignées conventionnellement par $O_i/_nO_j$, les positions axiales ou équatoriales étant repérées par les indices i et j et n ayant la même signification que précédemment. Il faut remarquer cependant que les interactions du 3ème ordre (n = 3) $O_i///O_j$ sont nulles (substituants dans le plan de symétrie) pour les cyclitols et absentes dans le cas des anhydro-1,6 hexopyranoses. Le nombre maximum total de paramètres servant à décrire l'ensemble des structures est donc de douze.

Type d'interaction	n = 1 (1e ordre)	n = 2 (2e ordre)	n = 3 (3e ordre)
Squelette/ substituant	R/O_{ax}	$R//O_{ax}$	$R///O_{ax}$
	R/O_{eq}	$R//O_{eq}$	$R///O_{eq}$
Substituant/ substituant	O_{ax}/O_{ax}	$O_{ax}//O_{ax}$	—
	O_{ax}/O_{eq}	$O_{ax}//O_{eq}$	—
	O_{eq}/O_{eq}	$O_{eq}//O_{eq}$	—

Le calcul est réalisé avec un programme classique de régression multiple faisant intervenir au départ toutes les variables. On élimine ensuite les variables non significatives.

Résultats et discussion

Il est important de noter que notre objectif a été de rechercher dans chaque famille de dérivés, dont la structure et la géométrie sont bien connues, des relations permettant de prévoir au sein de ce groupe

[1]Auteur à qui toute correspondance doit être adressée.

0008-4042/81/050907-04$01.00/0

©1981 National Research Council of Canada/Conseil national de recherches du Canada

TABLEAU 1. Rotations moléculaires des cyclitols

Cyclitol	O_{eq}/O_{eq}	O_{eq}/O_{ax}	$O_{ax}//O_{eq}$	Obs. (1)	Litt. (5) Calc.	Litt. (5) Ecart	Méthode 1 Calc.	Méthode 1 Ecart	Méthode 2 Calc.	Méthode 2 Ecart
1/2 Diol 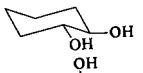	−1	0	0	−48	−45	+3	−44,2	3,8	−43,8	4,2
1,2/3 Triol 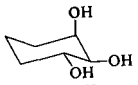	−1	−1	−1	−92	−90	+2	−94,8	2,8	−92,3	0,3
1,2,3/4 Tetrol 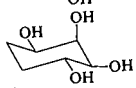	−1	0	−1	−49	−45	+4	−53,3	4,3	−52,6	3,6
1,2,4/3 Tetrol 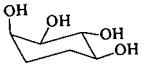	0	−1	−1	−54	−45	+9	−53,9	0,1	−48,5	5,5
1,3/2,4 Tetrol 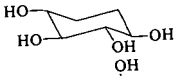	−1	0	0	−43	−45	−2	−44,2	1,2	−43,8	0,8
1,2,4/3,5 Pentol 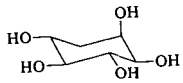	−1	−1	0	−91	−90	+1	−85,7	5,3	−83,4	7,6
1,2,3/4,5 Pentol 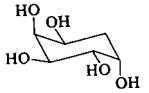	1	1	2	+100	+90	+10	97,3	2,7	101,1	1,1
1,3,4/2,5 Pentol 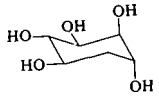	0	1	1	+49	+45	+4	47,3	1,7	48,5	0,5
1,2,4/3,5,6 Hexol 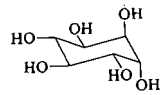	1	2	0	+117	135	−18	120,5	3,5	123,1	6,1
Ecart moyen ē						5,88		2,83		3,30

de composés la valeur des rotations moléculaires. Il serait difficile de faire des comparaisons entre deux séries de produits différents, dont la géométrie et la conformation ne sont pas identiques.

Cyclitols

Les calculs préliminaires de régression montrent que les interactions $O_{eq}//O_{eq}$ pour le second ordre et O_{ax}/O_{ax} pour le premier ordre sont négligeables. Une régression linéaire sur les interactions restantes donne l'équation suivante

$$[M] = -3{,}31 + (40{,}88)n\,[O_{eq}/O_{eq}] + (41{,}47)n\,[O_{eq}/O_{ax}] + (9{,}14)n\,[O_{ax}//O_{eq}]$$

avec un coefficient de corrélation de $r = 0{,}999$ et un écart moyen de 2,83; n désigne le nombre d'interactions du type présentes dans la molécule et les incertitudes absolues pour les trois coefficients de l'équation précédente sont respectivement 2,68, 2,23 et 1,97.

Cette équation fournit un excellent accord entre les résultats calculés et les valeurs expérimentales (Tableau 1, Méthode 1).

Un second calcul, réalisé en imposant une condition supplémentaire (contribution nulle du cycle) conduit à l'équation suivante:

$$[M] = 43{,}76\,n\,[O_{eq}/O_{eq}] + 39{,}68\,n\,[O_{eq}/O_{ax}] + 8{,}82\,n\,[O_{ax}//O_{eq}]$$

Le coefficient de corrélation est de $r = 0{,}998$ et l'écart moyen de 3,30 (Tableau 1, Méthode 2).

On peut remarquer que dans ces deux calculs, les valeurs obtenues restent en accord avec celles proposées par Lemieux et Martin (5). Le calcul effectué par ces auteurs ne considérait qu'une seule interaction au premier ordre et négligeait celles du second ordre. Un calcul de régression effectué selon ces hypothèses conduit à un écart moyen de 5,88, nettement supérieur à ceux indiqués ci-dessus.

Les interactions qui n'ont pas d'influence marquante d'après le résultat du calcul sont celles qui font intervenir des liaisons coplanaires. Il nous a cependant paru préférable de ne pas les éliminer a priori.

TABLEAU 2. Rotations moléculaires des anhydro-1,6 sucres

Anhydro-1,6 hexopyranoses	Obs*	Litt. (17) Calc.	Ecart	Calc.	Ecart
Tridésoxy-2,3,4	−120	−127,3	7,3	−117,1	2,9
Didésoxy-2,3 *érythro*	−155	−164,2	9,2	−166,1	11,1
Didésoxy-2,3 *thréo*	−75	−90,4	15,4	−65,3	9,7
Didésoxy-2,4 *érythro*	−118	−134,1	16,1	−125,3	7,3
Didésoxy-2,4 *thréo*	−105	−121	16	−108,9	3,9
Didésoxy-3,4 *érythro*	−75	−78,5	3,5	−69,0	6,0
Didésoxy-3,4 *thréo*	−173	−176,1	3,1	−185,4	12,4
Désoxy-2 *xylo*	−31	−34,1	3,1	−31,6	0,6
Désoxy-2 *lyxo*	−102	−83,6	18,4	−116,3	14,3
Désoxy-2 *arabino*	−172	−157,4	14,6	−157,9	14,1
Désoxy-2 *ribo*	−244	−234,1	9,9	−233,6	10,4
Désoxy-3 *ribo*	−117,0	−115,4	1,6	−118,1	1,1
Désoxy-3 *xylo*	−12	−41,6	29,6	−17,2	5,2
Désoxy-3 *arabino*	−228	−213	15	−234,5	6,5
Désoxy-3 *lyxo*	−126	−139,2	13,2	−133,6	7,6
Désoxy-4 *ribo*	−23	−20,5	2,5	−18,0	5,0
Désoxy-4 *arabino*	−240	−247,7	7,7	−235,6	4,4
Désoxy-4 *xylo*	−57	−71,7	14,7	−60,8	3,8
Désoxy-4 *lyxo*	−127	−169,3	42,3	−117,9	9,1
β-*gluco*	−108	−108,6	0,6	−109,8	1,8
β-*gulo*	81	79,5	1,5	+75,7	5,3
β-*altro*	−345	−347,7	2,7	−343,8	1,2
β-*galacto*	−36	−34,8	1,2	−26,4	9,6
β-*manno*	−207	−206,2	0,8	−208,9	1,9
β-*allo*	−123	−120,5	2,5	−126,3	3,3
β-*ido*	−150	−147,7	2,3	−141,9	8,1
β-*talo*	−131	−134,1	3,1	−125,4	5,6
Ecart moyen			9,41		6,4

*Voir réfs. 15 à 19.

Anhydro-1,6 hexopyranoses

Le problème posé faisait intervenir l'ensemble des douze paramètres proposés ci dessus. Il fallait donc tenter de simplifier le jeu des paramètres considérés. Une première approche a consisté à examiner si certaines interactions du squelette avec les substituants pouvaient être négligées. Aucun résultat acceptable n'a pu être obtenu selon cette hypothèse. Cependant, ces calculs ont montré que les interactions $R//O_{ax}$ et $R//O_{eq}$ étaient beaucoup plus faibles que les autres, de signes opposés et de valeurs absolues très proches (9 et 7 approximativement). Un calcul préliminaire considérant ces deux valeurs comme opposées peut alors être réalisé et montre que, de plus, comme dans le cas des cyclitols, l'interaction O_{ax}/O_{ax} est également négligeable. Un second calcul faisant intervenir les huit paramètres restants montre que la variable $O_{ax}//O_{eq}$ n'est pas significative; la valeur obtenue pour cette variable est en effet égale à −3,4 avec un écart type de ±6,7. On remarquera que dans le cas du *trans*-cyclohexane diol-1,3 une telle interaction a été estimée à environ 19 (14, 15) alors que dans les cyclitols, elle est de 9,1 (voir ci-dessus). Ces différences peuvent être provoquées par une modification conformationnelle d'une série à l'autre. Le présent travail ne prétend pas rationaliser dans une même corrélation l'ensemble des deux séries.

Le calcul définitif avec 7 variables seulement aboutit aux résultats consignés dans le tableau 2. Les valeurs calculées sont obtenues à partir de l'équation:

$$[M] = -117{,}1 - (49{,}0)n\,[R///O_{ax}] + (51{,}8)n\,[R///O_{eq}] + (8{,}2)n\,[R//O_{ax}]\ (\text{ou} - n\,R//O_{eq}) + (48{,}0)n\,[R/O_{ax}] - (68{,}4)n\,[R/O_{eq}] + 41{,}9\,n\,[O_{eq}/O_{eq}] + 59{,}3\,n\,[O_{ax}/O_{eq}]$$

Les écarts-types observés sur les coefficients des variables sont respectivement 4,4 pour $R///O_{ax}$; 5,0 pour $R///O_{eq}$; 2,1 pour $R//O_{ax}$; 4,4 pour R/O_{ax}; 5,0 pour R/O_{eq}; 5,3 pour O_{eq}/O_{eq} et 3,5 pour O_{ax}/O_{eq}.

Les valeurs prises par les différentes interactions sont rassemblées dans le tableau 3. On voit que les hypothèses retenues dans les calculs précédents (16, 17) ne sont pas toutes vérifiées.

TABLEAU 3. Paramètres calculés pour les diverses interactions présentes dans les anhydro-1,6 sucres

Interaction	Valeur calculée	Valeurs proposées (réf. 17)	
$R///O_{ax}$	−49,0	−36,9	−100
		ou	
$R///O_{eq}$	51,8	+36,9	+100
$R//O_{ax}$	8,2	+6,8	—
$R//O_{eq}$	−8,2	—	−6,8
R/O_{ax}	48,0	48,8	+113,6
R/O_{eq}	−68,4	−48,8	−113,6
O_{eq}/O_{eq}	41,9 (40,9)*	—	—
O_{ax}/O_{eq}	59,3 (41,5)*	—	—

*Valeurs obtenues pour les cyclitols.

En effet si on constate que l'hypothèse d'interactions égales et opposées est vérifiée pour $R///O_{ax}$ et $R///O_{eq}$ d'une part et $R//O_{ax}$ et $R//O_{eq}$ d'autre part, elle ne l'est pas pour le couple R/O_{ax} et R/O_{eq} dont les valeurs sont respectivement 48,0 et −68,4.

Nous avons donc montré qu'il est possible à l'intérieur d'une même famille, de géométrie et de conformation fixées, de n'utiliser qu'un seul jeu de paramètres et d'obtenir un écart moyen satisfaisant tant pour les dérivés substitués que pour les dérivés désoxy.

Néanmoins, il est possible de faire quelques remarques comparatives dans les deux séries cyclitols et anhydro-1,6 sucres. (*a*) La valeur O_{eq}/O_{eq} reste inchangée (41,9 et 40,9) et semble donc liée directement à la relation spatiale entre deux substituants équatoriaux. (*b*) La valeur O_{ax}/O_{eq} est en revanche nettement modifiée d'une série à l'autre, de même que la valeur $O_{ax}//O_{eq}$ précédemment discutée.

Le principe même de l'analyse de ces interactions et de leur calcul est de déterminer les paramètres importants qui lient dans chaque famille l'activité optique et la relation spatiale des substituants, sans chercher pour l'instant la généralisation et la rationalisation de l'ensemble des paramètres obtenus.

1. D. H. WHIFFEN. Chem. Ind. London, 964 (1956).
2. J. H. BREWSTER. J. Am. Chem. Soc. **81**, 5483 (1959).
3. S. YAMANA. Bull. Soc. Chem. Jpn. **33**, 1741 (1960).
4. S. YAMANA. Experientia, **21**, 305 (1965).
5. R. U. LEMIEUX et J. C. MARTIN. Carbohydr. Res. **13**, 139 (1970).
6. D. HORTON et J. D. WANDER. Carbohydr. Res. **14**, 83 (1970).
7. J. APPLEQUIST. J. Am. Chem. Soc. **95**, 8258 (1973).
8. J. DOLEZALOVA, M. CERNY, T. TRNKA et J. PACAK. Collect. Czech. Chem. Commun. **41**, 1944 (1976).
9. L. D. HALL et L. HOUGH. Proc. Chem. Soc. 382 (1962).
10. E. R. RUCKEL et C. SCHUERCH. J. Org. Chem. **31**, 2233 (1966).
11. F. SWEET et R. K. BROWN. Can. J. Chem. **46**, 2289 (1968).
12. K. HEYNS et J. WEYER. Ann. **718**, 2289 (1968).
13. Y. J. PARK, H. S. KIM et G. A. JEFFREY. Acta Crystallogr. Sect. A, **25**, 197 (1969).
14. W. RIGBY. J. Chem. Soc. 1586 (1949); 1588 (1949).
15. J. PECKA, J. STANEK, JR. et M. CERNY. Collect. Czech. Chem. Commun. **39**, 1192 (1974).
16. M. CERNY, J. PACAK et J. STANEK. Chem. Ind. London, 1559 (1966).
17. M. CERNY et J. STANEK, JR. Adv. Carbohydr. Chem. Biochem. **34**, 23 (1977).
18. M. CERNY, J. STANEK et J. PACAK. Collect. Czech. Chem. Commun. **34**, 1750 (1969).
19. T. TRNKA et M. CERNY. Collect. Czech. Chem. Commun. **37**, 3632 (1972).

Can. J. Chem. Downloaded from www.nrcresearchpress.com by 210.87.254.6 on 09/06/12
For personal use only.

COMMUNICATION

Solvolysis of 9-(*ortho*-substituted benzyl)fluorene-9-trimethylammonium ions. The effect of steric crowding

JYOTSNA PRADHAN AND PETER JAMES SMITH[1]

Department of Chemistry and Chemical Engineering, University of Saskatchewan, Saskatoon, Sask., Canada S7N 0W0

Received November 3, 1980

JYOTSNA PRADHAN and PETER JAMES SMITH. Can. J. Chem. **59**, 911 (1981).

The solvolytic reaction of several 9-(*ortho*-substituted benzyl)fluorene-9-trimethylammonium salts in ethanol at 57.3°C has been found to give both the substitution and elimination products. The observed rate constant for alkene formation increases when both *ortho* positions have substituents, $k_{obs}(s^{-1}) = 2.35 \times 10^{-5}$ and 268×10^{-5} for 2-Me and 2,6-diMe compounds, respectively. As well, the magnitude of the observed hydrogen–deuterium isotope effect is dependent on ring substituents, $k_{obs}^{H}/k_{obs}^{D} = 1.22$ and 2.35 for 2-Me and 2,6-diMe substrates, respectively. The results are discussed in the light of steric acceleration favouring loss of the poor leaving group, which leads to only the second example of a trimethylammonium salt reacting via the E1 mechanism.

JYOTSNA PRADHAN et PETER JAMES SMITH. Can. J. Chem. **59**, 911 (1981).

On a trouvé que la réaction de solvolyse de plusieurs sels de (benzyl *ortho* substitués)-9 fluorényl triméthylammonium-9 dans l'éthanol à 57,3°C donne à la fois des produits de substitution et des produits d'élimination. La constante de vitesse observée pour la formation de l'alcène augmente quand les deux positions *ortho* sont substituées $k_{obs}(s^{-1}) = 2{,}35 \times 10^{-5}$ et 268×10^{-5} respectivement pour les composés méthyl-2 et diméthyl-2,6. L'importance de l'effet isotopique observé pour le deutérium dépend également des substituants sur le cycle, $k_{obs}^{H}/k_{obs}^{D} = 1{,}22$ et 2,35 respectivement pour les composés méthyl-2 et diméthyl-2,6. On discute des résultats en fonction d'une légère accélération stérique favorisant la perte d'un mauvais groupe nucléofuge; ceci constituerait seulement le second exemple de sels de triméthylammonium réagissant selon un mécanisme E1.

[Traduit par le journal]

Studies on the concerted one-step elimination from quaternary ammonium salts (1) and organic nitrate esters (2) have shown that electron-withdrawing substituents on the phenyl ring increase the rate of reaction with the corresponding transition state becoming more reactant-like, having decreased C—H and C—N (O—N) bond weakening. The effect of the substituent on the transition state geometry is in accord with Hammond's postulate (3) and also Thornton's (4) and More O'Ferrall's (5) theories.

In a recent investigation (6, 7) on the E2 reaction of 9-(4-substituted benzyl)fluorene-9-trimethylammonium ions (**1**) with ethoxide ion in ethanol, however, it was found that the variation of both the primary hydrogen–deuterium and nitrogen isotope effects with the 4-substituent on the phenyl ring were the opposite to those found in the earlier studies. As well, the Hammett ρ value of 1.33 for the reaction of **1** was very much less than 3.77 found for the reaction of the 2-arylethyl quaternary ammonium ions with ethoxide (8). It was concluded that for reactions in which the 4-substituent increases the rate of reaction, both the carbon–hydrogen and carbon–nitrogen bond rupture is more advanced in the transition state. This variance with Hammond's postulate was discussed in the light of a possible steric crowding at the transition state.

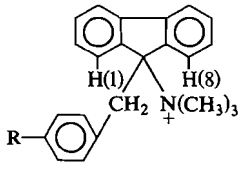

1

In order to test the proposal that interaction of the *ortho*-hydrogens on the phenyl ring with the 1,8 hydrogens of the fluorene nucleus results in the anti-Hammond behaviour, a series of *ortho*-substituted quaternary ammonium salts were prepared. These salts, unlike the 4-substituted compounds which were unreactive in ethanol, reacted in absolute ethanol in the absence of base to give both the alkene and ether products. The observed rate constants for the formation of the alkene from several *ortho*-substituted salts, k_{obs}, and their β,β-d_2 analogues, as well as the percent alkene, are given in Table 1. As well, the ratio k_E/k_S (Scheme 1) calculated from the percent alkene, together with the hydrogen–deuterium isotope effect, k_{obs}^{H}/k_{obs}^{D}, are included.

The observed rate constants for the formation of the alkene from the 2-Me and 2,4-diMe salts are similar and are approximately one hundred times less than the corresponding rate constants for the 2,6-diMe and 2,4,6-triMe substrates. It appears,

[1]Author to whom correspondence should be addressed.

0008-4042/81/050911-02$01.00/0

©1981 National Research Council of Canada/Conseil national de recherches du Canada

TABLE 1. Rate constants, percent alkene, and hydrogen–deuterium isotope effects for reaction of 9-(*ortho*-substituted benzyl)fluorene-9-trimethylammonium salts in absolute ethanol at 57.3°C

Substrate	$10^5 k_{obs}$ (s^{-1})	% alkene	$k_E/k_S = \frac{[alkene]}{[ether]}$	(k_E^H/k_E^D)*	k_{obs}^H/k_{obs}^D
2-Me	2.35	56.2	1.28	1.54	1.22
2-Me-β,β-d_2	1.92	42.8	0.748		
2,4-diMe	2.85	56.8	1.31	1.76	1.16
2,4-diMe-β,β-d_2	2.45	40.1	0.669		
2,6-diCl	9.60	28.6	0.401	2.10	1.45
2,6-diCl-β,β-d_2	6.60	14.7	0.172		
2,6-diMe	268.0	28.8	0.404	2.78	2.35
2,6-diMe-β,β-d_2	114.0	11.6	0.131		
2,4,6-triMe	248.0	25.4	0.340		

*Calculated with the assumption that $k_S^H/k_S^D = 0.9$.

therefore, that since *ortho*-methyl groups accelerate the reaction[2] and the *para*-substituent has very little effect, the rate enhancement is due to steric acceleration. Dreiding stereomodels indicate considerable interaction between the *ortho*-methyl groups and the 1,8-hydrogens on the fluorene ring and, as well, the methyl groups of the trimethylammonium group. To our knowledge, this is only the second example (9) of a trimethylammonium salt (poor leaving group) undergoing solvolysis to give an alkene in an E1 process. The reaction is promoted by a relief of steric interactions and not only by the formation of a favourable carbocation.

The reaction of the 2,6-diCl substrate with ethanol is slower than the 2,6-diMe process, but is faster than the reaction of the 2,4-diMe compound. These observations can be accommodated by the steric argument since chlorine is smaller than methyl (Taft E_s values). As well, it is seen that the percent alkene decreases when both *ortho*-positions bear a substituent; e.g., % alkene = 56.2 and 28.8 for the 2-Me and 2,6-diMe compounds, respectively. This is also consistent since the presence of the *ortho*-substituents leads to an increase in the nonplanarity of the alkene due to interactions with the 1,8-hydrogens on the fluorene ring. As well, the presence of the *ortho*-groups provides steric hindrance to ethanol which acts as base to remove the β-hydrogen from the carbocation.

The carbocation mechanism for the formation of the alkene and ether products can be represented by Scheme 1. If it is assumed that all steps are irreversible then it can be shown that the observed rate constant for alkene formation is given by $k_{obs} = k_1 k_E/k_E + k_S$. If $k_E > k_S$ then $k_{obs}^H/k_{obs}^D \simeq k_1^H/k_1^D$ and the observed isotope effects will mainly be secondary β-deuterium effects, i.e. when $k_E/k_S = 1.28$ then $k_{obs}^H/k_{obs}^D = 1.22$ for the 2-Me substrate. When, however, $k_E < k_S$ then

$$k_{obs}^H/k_{obs}^D = (k_1^H/k_1^D)(k_E^H/k_E^D)$$

and a larger observed isotope effect is expected since the loss of a proton from the carbocation (k_E) is a primary effect; i.e. when $k_E/k_S = 0.404$ then $k_{obs}^H/k_{obs}^D = 2.35$ for the 2,5-diMe salt. The isotope effects for loss of hydrogen from the carbocation can be calculated from the observed percent alkene. The values for k_E^H/k_E^D ranging from 1.54 to 2.78 are reasonable primary effects. To our knowledge this is the first observation of a variable hydrogen–deuterium isotope effect for elimination under solvolytic conditions where substituents on a single substrate are varied. It is a consequence of steric interactions rather than electronic factors.

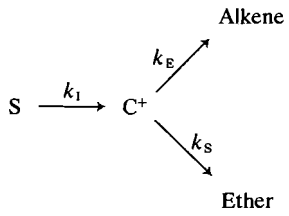

SCHEME 1

[2]The salts are completely stable in EtOH when there are no *ortho*-substituents.

Acknowledgement

The authors gratefully acknowledge the financial support of this work by the Natural Sciences and Engineering Research Council of Canada.

1. P. J. SMITH and A. N. BOURNS. Can. J. Chem. **52**, 749 (1974).
2. P. J. SMITH, C. A. POLLOCK, and A. N. BOURNS. Can. J. Chem. **53**, 1319 (1975).
3. G. S. HAMMOND. J. Am. Chem. Soc. **77**, 334 (1955).
4. D. A. WINEY and E. R. THORNTON. J. Am. Chem. Soc. **97**, 3102 (1975).
5. R. A. MORE O'FERRALL. J. Chem. Soc. B, 274 (1970).
6. P. J. SMITH and S. K. TSUI. J. Am. Chem. Soc. **95**, 4760 (1973).
7. G. S. DYSON and P. J. SMITH. Can. J. Chem. **54**, 2339 (1976).
8. W. H. SAUNDERS, JR., D. G. BUSHMAN, and A. F. COCKERILL. J. Am. Chem. Soc. **90**, 1775 (1968).
9. E. D. HUGHES and J. WILBY. J. Chem. Soc. 4094 (1960).

Can. J. Chem. Downloaded from www.nrcresearchpress.com by 210.87.254.6 on 09/06/12
For personal use only.

A ^{125}Te Mössbauer study of hexahalotellurates, pentahalotellurates, and tetrahaloaryltellurates

NIGEL S. DANCE, PABLO DOBUD, AND COLIN H. W. JONES

Chemistry Department, Simon Fraser University, Burnaby, B.C., Canada V5A 1S6

Received August 26, 1980

NIGEL S. DANCE, PABLO DOBUD, and COLIN H. W. JONES. Can. J. Chem. **59**, 913 (1981).

The ^{125}Te Mössbauer spectra of a number of hexahalotellurates have been measured and no significant effects of the size or symmetry of the cation on the Mössbauer parameters were observed. The mixed hexahalotellurates, $M_2TeX_4Y_2$ (X, Y = Cl, Br, or I), do not exhibit a quadrupole splitting, Δ, and the trends in δ with variation in X and Y are discussed. The pentahalotellurates $MTeCl_5$, $MTeBr_5$, and $MTeBr_4Cl$ also yield single line spectra and this is interpreted as evidence of intermolecular bridging. The tetrahaloaryl tellurates $MArTeX_4$ and $MArTeX_3Y$ (X, Y = Cl, Br, or I) have been studied and the trends in Δ with variation X and Y are consistent with an additive model. The trends in δ are more complex.

NIGEL S. DANCE, PABLO DOBUD et COLIN H. W. JONES. Can. J. Chem. **59**, 913 (1981).

On a mesuré les spectres Mössbauer du ^{125}Te d'une série d'hexahalotellurates et on n'a pas observé d'effets significatifs de la taille ou de la symétrie du cation sur les paramètres de Mössbauer. Les hexahalotellurates mixtes $M_2TeX_4Y_2$ (X, Y = Cl, Br ou I) ne présentent pas de couplage quadrupolaire, Δ, et on discute des variations de δ en fonction de X ou Y. Les pentahalotellurates $MTeCl_5$, $MTeBr_5$ et $MTeBr_4Cl$ donnent également des spectres de raies simples et on interprète ceci comme une preuve de l'existence d'un pont intermoléculaire. On a étudié les tétrahalotellurates $MArTeX_4$ et $MArTeX_3Y$ (X, Y = Cl, Br ou I) et les variations de Δ avec celles de X et de Y sont en accord avec un modèle additif. Les variations de δ sont plus complexes.

[Traduit par le journal]

Introduction

Among the first tellurium compounds to be studied by ^{125}Te Mössbauer spectroscopy were the hexahalotellurates (1). In these compounds the TeX_6^{2-} anion is octahedral, as evidenced by vibrational, X-ray, and nqr spectroscopy, and the lone-pair on the tellurium appears to be $5s^2$ in character. The bonding to the tellurium may then be viewed as involving $3c$–$4e$ bonds in which only the tellurium $5p$ orbitals participate. The ^{125}Te Mössbauer parameters for these compounds are quite consistent with this interpretation (1, 2). Thus the hexahalotellurates do not exhibit a quadrupole splitting, while the isomer shifts are positive and increase in the series $TeI_6^{2-} < TeBr_6^{2-} < TeCl_6^{2-}$. This suggests that the number of p-electrons removed in bonding from the tellurium increases with increasing electronegativity of the halogen and that the $5s^2$ electrons become increasingly deshielded from the nucleus. This would lead to an increase in the nuclear s-electron density and a more positive isomer shift (1, 2).

In a recent ^{35}Cl nqr study of the $TeCl_6^{2-}$, $SnCl_6^{2-}$, and $PbCl_6^{2-}$ salts (3), the effect on the anion of varying the size and symmetry of the cation was studied. While it might have been expected that for large cations of low symmetry significant distortion of the anion may have been observed, no evidence for such distortions in the form of inequivalent chlorine ligands was found for the hexachlorotellurates. Small changes in the ionicity of the Te—Cl bond were observed, although they did not appear to correlate with the size of the cation. In the present study we have re-examined this question using ^{125}Te Mössbauer spectroscopy to probe the lone-pair character of the $5s^2$ electrons as the size and symmetry of the cation is varied. It may be noted that the Mössbauer spectra of a number of hexahalides with large cations have been reported previously but that the reproducibility in the isomer shifts reported for those compounds was not very good (1, 4).

The above study was also of interest in another context. Donaldson and co-workers (5, 6) have proposed that in $CsSnBr_3$ and in the hexachlorides M_2EX_6 (M = K, Rb, Cs; E = Se, Te, Po; X = Cl, Br) there is a delocalisation of the ns^2 non-bonding lone-pair into delocalised low-energy bands in the solid involving halogen d orbitals. The population of such bands might be expected to vary as the size of the cation and the lattice parameters are changed and it was of interest to determine whether or not evidence for such changes were observed in the Mössbauer isomer shifts.

Mixed halotellurates of the kind $TeCl_nBr_{5-n}^-$ and $TeX_4Y_2^{2-}$ (X, Y = F, Cl, Br, or I) have been prepared by Ozin and Vander Voet (7) and characterised by ir and Raman spectroscopy. A number of these mixed halide anions have been prepared in this work and their Mössbauer spectra recorded. The objective here was to determine whether or not the five co-ordinate species $TeCl_nBr_{5-n}^-$ or the 6

0008-4042/81/060913-05$01.00/0

©1981 National Research Council of Canada/Conseil national de recherches du Canada

Can. J. Chem. Downloaded from www.nrcresearchpress.com by 210.87.254.6 on 09/06/12
For personal use only.

Can. J. Chem. Downloaded from www.nrcresearchpress.com by 210.87.254.6 on 09/06/12
For personal use only.

TABLE 1. ^{125}Te Mössbauer parameters of the hexahalo- and pentahalotellurates

Compound	δ* ($\pm$0.08 mm s^{-1})	Γ ($\pm$0.1 mm s^{-1})
$(NH_4)_2TeCl_6$	1.72	6.8
$(Et_4N)_2TeCl_6$	1.74	5.2
$(n\text{-}Bu_4N)_2TeCl_6$	1.70	6.6
$(Ph_4As)_2TeCl_6$	1.72	6.4
$(Ph_3Se)_2TeCl_6$	1.72	5.7
$(PyH)_2TeCl_6$	1.63	7.1
$(picH)_2TeCl_6$†	1.65	6.9
$(Et_4N)_2TeBr_6$	1.47	6.6
$(Ph_4As)_2TeBr_6$	1.56	5.0
$(n\text{-}Bu_4N)_2TeCl_4Br_2$	1.54	6.5
$(n\text{-}Bu_4N)_2TeCl_4I_2$	1.51	7.1
$(Et_4N)_2TeCl_4Br_2$	1.46	7.6
$(Et_4N)_2TeCl_4I_2$	1.55	6.9
$(Et_4N)_2TeCl_4F_2$	1.55	7.1
$(Et_4N)_2TeBr_4Cl_2$	1.54	6.7
$(n\text{-}Bu_4N)_2TeBr_4I_2$	1.43	5.8
$(Et_4N)_2TeBr_4F_2$	1.27	8.3
$(Et_4N)TeCl_5$	1.49	7.7
$(Et_4N)TeBr_4Cl$	1.44	7.0
$(Et_4N)TeBr_5$	1.41	7.2

*Isomer shift with respect to I/Cu, source, and absorbers at 4.2 K. All spectra were single lines.

†pic is 4-picolinium 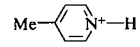

TABLE 2. ^{125}Te Mössbauer parameters of the tetrahaloaryltellurates

Compound†	δ* ($\pm$0.08 mm s^{-1})	Δ ($\pm$0.01 mm s^{-1})	Γ (mm s^{-1})
$(Ph_3PCH_2Ph^+)(RTeCl_4^-)$	1.10	8.5	5.7
$(Ph_3PCH_3^+)(RTeCl_3Br^-)$	0.88	8.2	5.6
$(Ph_3PCH_3^+)(RTeCl_3I^-)$	0.90	7.6	6.1
$(Ph_3PCH_2Ph^+)(RTeBr_3Cl^-)$	0.94	7.7	5.5
$(Ph_3PCH_3^+)(RTeBr_4^-)$	1.04	7.5	4.7
$(Ph_3PCH_3^+)(RTeBr_3I^+)$	0.83	6.4	6.0
$(Ph_3PCH_2Ph^+)(RTeI_3Cl^-)$	0.72	6.2	6.4
$(Ph_3PCH_3^+)(RTeI_3Br^-)$	0.91	5.7	6.9
$(Ph_3PCH_3^+)(RTeI_4^-)$	0.90	4.9	5.1

*δ isomer shift with respect to I/Cu, source, and absorbers at 4.2 K.
†R = p-$C_2H_5OC_6H_4$.

co-ordinate anions would exhibit a quadrupole splitting or a significant diminution in isomer shift resulting from stereochemical activity of the lone-pair.

Finally, as an extension of the above and of our previous studies of organotellurium halides, we have studied the tetrahaloaryltellurates $RTeX_4^-$ and $RTeX_3Y^-$ (X, Y = Cl, Br, or I; R = p-$EtOC_6H_4$). These measurements provide an interesting comparison with the data for the mixed hexahalotellurates and also provide a further test of the applicability of a simple additive model in interpreting ^{125}Te quadrupole splittings in such molecules.

Results and Discussion

The ^{125}Te Mössbauer parameters are reported in Tables 1 and 2. Excellent spectra were obtained for these compounds at 4.2 K, with percent resonance absorptions of 5 to 10% being observed.

Hexahalotellurates, M_2TeX_6

The Mössbauer spectra of all the hexahalotellurates were single lines of relatively narrow linewidth. The absence of a quadrupole splitting, together with the fact that the isomer shifts for the hexachlorides, or for the hexabromides, were very similar, regardless of the size or symmetry of the cation, is further evidence of a lack of any appreci-

able distortion of the hexahalotellurate anion in these compounds. Such distortion would have been expected to result in an electric field gradient at the tellurium or, at least, in a diminution in the *s*-electron density at the nucleus and hence a smaller isomer shift. Thus this work supports the findings of Brill and Welsh (3) that the anion remains octahedral even in the presence of large unsymmetrical cations.

It must be noted, however, that $(Ph_4As)_2TeCl_6$, when prepared from TeO_2/HCl and $Ph_4As^+Cl^-$, yielded an isomer shift of 1.43 mm s^{-1}, significantly smaller than that for the same compound when prepared from $TeCl_4$ and $Ph_4As^+Cl^-$ in CH_2Cl_2 or benzene. The two samples also yielded different X-ray powder diffraction patterns (8). The two preparations may correspond to different polymorphic forms of the same compound and in the one of smaller isomer shift there may be some small distortion from regular octahedral symmetry.

Returning to the discussion of the main body of the data, the small change in the Te—Cl bond ionicity with change in the cation observed in the ^{35}Cl nqr experiments (3) by Brill and Welsh was not reflected in any significant change in the Mössbauer isomer shift. We have previously established an expression for the isomer shift in terms of the number of *p*-holes on tellurium, using the nqr data to estimate the tellurium *p*-orbital population in the hexahalotellurates (2):

$$\delta = 0.44hp - 0.14$$

where δ is the isomer shift in mm s^{-1} relative to an ^{125}I/Cu source and *hp* is the number of holes in the tellurium 5*p* shell.

Thus in $(NH_4)_2TeCl_6$, the ^{35}Cl coupling constant was 29.98 MHz, corresponding to a *p*-orbital imbalance on the chlorine of 0.3. In each Te—Cl bond, assuming that the bonding is predominantly *p* in character, there would be $1.7e^-$ on Cl and $0.3e^-$ on Te. The tellurium *p*-orbital occupancy would then be 1.8 and *hp* would be 6.0 − 1.8 = 4.2. This corresponds to an isomer shift of 1.7 mm s^{-1}. In $(4\text{-picH})_2TeCl_6$ and $(pyH)_2TeCl_6$ the ^{35}Cl coupling constants were 33.36 and 32.98 MHz, respectively, corresponding to a chlorine *p*-orbital imbalance of ca. 0.33, a tellurium *hp* value of 4.0 and an isomer shift of 1.62 mm s^{-1}. The experimentally observed δ's for these compounds were indeed a little lower than that for $(NH_4)_2TeCl_6$, although the agreement between the predicted and observed values is probably fortuitous given the large errors in δ. Certainly the Mössbauer isomer shifts are consistent with the explanation that the small variations in ^{35}Cl coupling constants arise from small differences in the tellurium *p*-orbital populations rather than through variations in the stereochemical activity of the lone-pair.

In connection with the work of Donaldson and co-workers (5, 6), there is no evidence from the Mössbauer data for any delocalisation of the $5s^2$ lone-pair into bands in the solid, at least at 4.2 K, in either the chlorides or bromides, since such delocalisation would have been expected to lead to variations in the isomer shift with changes in the size of the cation.

Mixed Hexahalotellurates, $M_2TeX_4Y_2$

In the series $M_2TeCl_4Y_2$, where Y = F, Cl, Br, or I, there is no resolvable quadrupole splitting in the Mössbauer spectra. The isomer shift for $TeCl_6^{2-}$ is observed to be the most positive in the series (1.74 mm s^{-1}), while $\delta \simeq 1.5$ mm s^{-1} when Y = F, Br, or I. The same results were observed for both the tetrabutyl- and tetraethylammonium compounds. In the bromide series, $M_2TeBr_4Y_2$, where Y = F, Cl, Br, or I, the spectra were again single lines and a δ value of 1.27 cm s^{-1} was observed for $TeBr_4F_2^{2-}$.

Two factors may be identified as influencing the Mössbauer parameters in these anions. Firstly, as the electronegativity of the halogen bonded to tellurium increases, there will be an increased removal of electron density from the tellurium and, where such electron density is predominantly *p* in character, as appears to be the case in the parent hexahalide anions, this would lead to an increased deshielding of the tellurium $5s^2$ electrons and, hence, an increase in the Mössbauer isomer shift. It is noted, however, that $TeCl_4F_2^{2-}$ and $TeBr_4F_2^{2-}$ have δ values smaller than the parent hexachloride or hexabromide, respectively. Secondly, on replacing two chlorine ligands in $TeCl_6^{2-}$ by two F, Br, or I ligands (and from ir and Raman studies this replacement appears to be *cis* in nature), this will necessarily lead to some distortion from regular octahedral geometry about the tellurium. Such distortion would imply that the $5s^2$ electrons are no longer stereochemically inactive and this would result in a decrease in the nuclear *s*-electron density and, hence a decrease in the isomer shift.

The relative insensitivity of δ to the nature of Y for $TeCl_4Y_2^{2-}$, and for $TeBr_4Y_2^{2-}$, Y = Cl, Br, or I, suggests that both the above effects are operative to some extent and that when Y = F the second factor appears to be more important. The effects are, in any event, small, as evidenced by the small changes in isomer shift. The direct removal of 5*s* electrons

Can. J. Chem. Downloaded from www.nrcresearchpress.com by 210.87.254.6 on 09/06/12
For personal use only.

Can. J. Chem. Downloaded from www.nrcresearchpress.com by 210.87.254.6 on 09/06/12
For personal use only.

from tellurium has a much larger effect on δ than the removal of *p*-electrons, since the latter only influences δ through the second order deshielding effect. Thus, even in $TeCl_4F_2^{2-}$ and $TeBr_4F_2^{2-}$, the stereochemical activity of the $5s^2$ electrons will only be small, consistent with the fact that there is no observable quadrupole splitting. In $TeBr_4F_2^{2-}$ the experimental linewidth was significantly broader than that for the other compounds and this could be explained by the presence of a very small, unresolved electric quadrupole interaction.

Pentahalotellurates, $MTeX_5$

The $TeCl_5^-$, $TeBr_5^-$, and $TeBr_4Cl^-$ tetraalkylammonium compounds were prepared as described in ref. 7 and in the Experimental section and gave ir spectra in good agreement with those of ref. 7.

The Mössbauer spectra did not exhibit a quadrupole splitting, although $[Et_4N][TeCl_5]$ had a significantly smaller isomer shift than $[Et_4N][TeCl_6]$. The absence of a quadrupole splitting here contrasts with the case of $KTeF_5$, where a quadrupole splitting of ca. 6.0 mm s^{-1} was observed (1). The latter compound is known to contain the discrete square pyramidal anion TeF_5^- (9). The vibrational spectra of $[Et_4N][TeCl_5]$ and $[Et_4N][TeBr_5]$ were interpreted by Ozin and Vander Voet (7) assuming that these compounds also contain TeX_5^- anions and that the Te—X bond lengths are the same as those in the parent TeX_6^{2-} anions, although in TeF_5^- the Te—F bond lengths for the apical and basal fluorines are 1.84 and 1.96 Å, respectively. The crystal structure (10) of $TeCl_4 \cdot PCl_5$, however, shows the presence of PCl_4^+ cations and chain-like polymeric $[TeCl_5^-]_n$ anions with distorted octahedral co-ordination about the tellurium. The polymeric chains consist of $TeCl_4$ groups with two short Te—$Cl_{equatorial}$ and two long Te—Cl_{axial} bonds, the $TeCl_4$ units being linked by two bridging chlorine atoms in *cis* position with the Te—Cl bridging contacts being somewhat longer than the Te—Cl_{axial} bonds. The ir and Raman spectra of the $[TeCl_5^-]_n$ polymeric anion in $TeCl_4 \cdot PCl_5$ show similarities to the spectra of $[Et_4N][TeCl_5]$, suggesting a similar environment about the tellurium in the two cases. The absence of a ^{125}Te quadrupole splitting in $[Et_4N][TeCl_5]$ is certainly consistent with a high co-ordination number and the presence of halogen bridges about the tellurium.

The fact that the isomer shift is smaller in $[Et_4N][TeCl_5]$ than in $[Et_4N]_2[TeCl_6]$ may be explained by the small amount of stereochemical activity associated with the lone-pair that would be expected in a distorted octahedral structure.

Tetrahaloaryltellurates, $RTeX_4^-$ and $RTeX_3Y^-$

In previous studies (11, 12) we have investigated the Mössbauer parameters of a wide range of organotellurium compounds, including tellurides R_2Te, dihalides R_2TeX_2, trihalides $RTeX_3$, and telluronium salts $R_3Te^+X^-$. We have also previously reported Mössbauer parameters for $RTeCl_4^-$. In the present work we have extended these studies to include $RTeBr_4^-$ and $RTeI_4^-$ and a number of mixed tetrahaloaryltellurates (Table 2).

The parent tetrahalotellurate anions $RTeX_4^-$ (X = Cl, Br, or I; R = *p*-$C_2H_5OC_6H_4$—) all exhibit a significant quadrupole splitting. These ions are square pyramidal with the organic ligand occupying the axial position (11). The bonding to the halogen ligands would again be viewed as $3c$–$4e$ involving only tellurium $5p$ orbitals. The electric field gradient derives from *p*-orbital imbalance between the *z*-axis, as defined by the Te—C bond, and the *x*–*y* plane in which the four halogen ligands lie. This *p*-orbital imbalance arises because of the difference in the ionicity of the Te—C and Te—halogen bonds and also because of the significant tellurium *s*-character associated with the Te—C bond, which confers significant *p*-character on the lone-pair. The stereochemically active lone-pair is then viewed as occupying the sixth co-ordinate position *trans* to the aryl group. The fact that the Te—C bond has significant *s*-character associated with it has been recognised in our previous Mössbauer studies (11, 12).

The above interpretation is supported by the observation that the quadrupole splittings decrease in the order $RTeCl_4^- > RTeBr_4^- > RTeI_4^-$. As the electronegativity of the halogen ligands decreases, the removal of *p*-electron density from the tellurium in the *x*–*y* plane decreases and the quadrupole splittings likewise decrease. The isomer shift of $RTeCl_4^-$ is significantly smaller than that of $TeCl_6^{2-}$ or $TeCl_5^-$, and this reflects the marked decrease in nuclear *s*-electron density as a result of removal of tellurium $5s$ electrons into the Te—C bond.

In the mixed tetrahaloaryltellurates $RTeX_3Y$, when X = Cl and Y = Cl, Br, or I, it is observed that Δ decreases in the series Y = Cl > Br > I. For the bromide series, i.e. X = Br, Y = Cl, Br, or I, the Δ values again decrease in the series Y = Cl > Br > I and a similar trend is again observed for the iodides, i.e., $RTeI_3Cl^- > RTeI_3Br^- > RTeI_4^-$ (Fig. 1). These trends again reflect a decrease in the removal of *p*-orbital electron density from the tellurium in the *x*–*y* plane as the electronegativity of the halogen ligand, Y, decreases. It would appear that in these compounds Δ is a simple additive property of

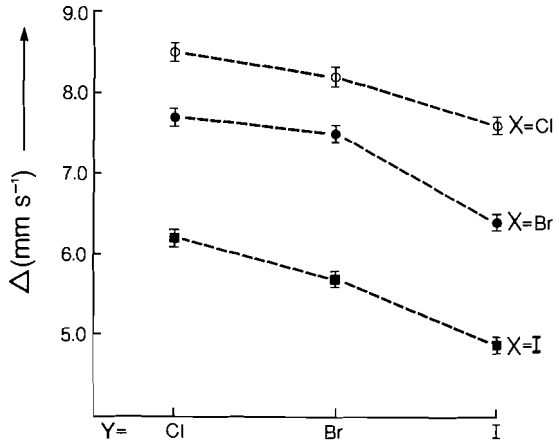

FIG. 1. Quadrupole splittings for ⊕ $RTeCl_3Y$, ● $RTeBr_3Y$, and ■ $RTeI_3Y$ where Y = Cl, Br, or I.

the ligands attached to the tellurium. To a first approximation, and ignoring any asymmetry in the $RTeX_3Y$ anions, the difference in quadrupole splitting between $RTeCl_4^-$ and $RTeBr_4^-$ should then just be twice that between $RTeCl_3Br^-$ and $RTeClBr_3^-$, and indeed that is the case. The agreement is not as good when comparing the chlorides and iodides or the bromides and iodides, but the trends are certainly in the right direction.

These findings are consistent with the previous work on the organotellurides, dihalides, and trihalides, where an additive model also appeared to work quite well in rationalising the Δ values (11, 12).

In contrast with the quadrupole splittings, the isomer shifts do not show any simple trends. This in part must reflect the fact that the range of δ values is small, while the errors in δ are large and, therefore, trends in δ are difficult to discern. However $RTeI_3Cl^-$ has a significantly smaller δ value than $RTeI_4^-$ while, on the basis of electronegativities and the removal of *p*-electron density from the tellurium, just the opposite would have been expected. Small changes in the *s*–*p* character of the lone-pair on Te may be important here and these would have a more marked effect on δ than on Δ.

Experimental

All compounds were prepared following literature procedures. Thus the hexahalotellurates were prepared by dissolving TeO_2 in 12 *M* HCl and adding the appropriate cation chloride salt in a minimum amount of water (3). In the case of $(Ph_4As)_2TeBr_6$ this produced an amorphous powder of anomalously low isomer shift. When the compound was prepared from $TeCl_4$ and Ph_4AsCl in CH_2Cl_2, a crystalline product was observed with the tellurium Mössbauer parameters shown in Table 1.

The mixed hexahalotellurates were prepared (7) by direct trituration in dry CH_2Cl_2 of $TeCl_4$ and $TeBr_4$ with the appropriate cation salt in the stoichiometry 1:2. The pentahalide salts were prepared in a similar way (7) employing a 1:1 stoichiometry. These preparations were carried out in a dry box using vacuum sublimed $TeCl_4$ and $TeBr_4$. The compounds were characterised by ir and Raman spectroscopy and by chemical analysis.

The tetrahaloaryltellurates were prepared (13) by reacting *p*-ethoxyphenyltellurium trihalides with the phosphium salts $(Ph_3{\cdot}PCH_2Ph^+)X^-$, where X = Cl, Br, and I, in chloroform and acetonitrile as solvents. The compounds were identified by chemical analysis and by melting points; in the latter case good agreement was found with the literature values except for $[p\text{-}EtOC_6H_4TeBr_3Cl][Ph_3PCH_2Ph]$, where a value of 171–173°C was found, in comparison with the literature value of 122–124°C.

The Mössbauer spectra were recorded (11) at 4.2 K on naturally abundant 100–200 mg cm^{-2} samples using an $^{125}Sb/Cu$ source (New England Nuclear). Both the source and absorber were immersed in liquid helium in a Harwell Instruments Dewar. A Harwell Instruments 200 series wave-form generator, attenuator, and transducer were used to drive the absorbers with constant acceleration. Spectra were accumulated in 256 channels of a Nuclear Data 2200 series 1024 channel analyser. A NaI(Tl) detector was used and the 35.56 keV Mössbauer γ-ray was monitored through the iodine escape peak. The spectrometer was routinely monitored at 4.2 K using internal tellurium standards, e.g. TeO_2 and $[Et_4N]_2TeCl_6$, and was calibrated using an iron foil and $^{57}Co/Pd$ source at room temperature. The spectra were computer fitted to independent Lorentzians (11).

Acknowledgement

The authors wish to acknowledge a grant in support of this research from the Natural Sciences and Engineering Research Council of Canada.

1. T. C. GIBB, R. GREATREX, N. N. GREENWOOD, and A. C. SARMA. J. Chem. Soc. A, 212 (1970).
2. B. M. CHEYNE, J. J. JOHNSTONE, and C. H. W. JONES. Chem. Phys. Lett. **14**, 545 (1972).
3. T. B. BRILL and W. A. WELSH. J. Chem. Soc. Dalton, 357 (1973).
4. M. L. UNLAND. J. Chem. Phys. **49**, 4514 (1968).
5. J. D. DONALDSON and J. SILVER. Inorg. Nucl. Chem. Lett. **10**, 537 (1974).
6. J. D. DONALDSON, J. SILVER, S. HADJIMINOLIS, and S. D. ROSS. J. Chem. Soc. Dalton, 1500 (1975).
7. G. A. OZIN and A. VANDER VOET. J. Mol. Struct. **13**, 435 (1972).
8. E. R. CLARK, N. S. DANCE, C. H. W. JONES, W. R. MCWHINNIE, and J. MALLAKI. Unpublished results.
9. A. J. EDWARDS and M. A. MOUTY. J. Chem. Soc. A, 703 (1969).
10. B. KREBS, B. BUSS, and W. BURGER. Z. Anorg. Chem. **397**, 1 (1973).
11. N. S. DANCE and C. H. W. JONES. Can. J. Chem. **56**, 1745 (1978).
12. C. H. W. JONES, W. R. MCWHINNIE, and F. J. BERRY. Mössbauer effect methodology, **10**, 227 (1976).
13. N. PETRAGNANI, L. T. CASTELLANOS, K. J. WYNNE, and W. MAXWELL. J. Organomet. Chem. **55**, 295 (1973).

Can. J. Chem. Downloaded from www.nrcresearchpress.com by 210.87.254.6 on 09/06/12
For personal use only.

^{129}I Mössbauer spectra of tellurium iodides. Part II

NIGEL S. DANCE AND COLIN H. W. JONES

Chemistry Department, Simon Fraser University, Burnaby, B.C., Canada V5A 1S6

Received August 26, 1980

NIGEL S. DANCE and COLIN H. W. JONES. Can. J. Chem. **59**, 918 (1981).

The ^{129}I Mössbauer spectra of PhTeI, p-EtOPhTeI$_2^-$, p-EtOPhTeI$_4^-$, Ph_3TeI, $(Me_2TeI_2)_2{\cdot}Ph_2Hg$, and Na_2HgI_4 have been measured and the data interpreted in terms of the bonding to tellurium in these compounds and ions. Evidence is presented that PhTeI is polymeric. The ^{129}I coupling constants in p-EtOPhTeI$_2^-$ and p-EtOPhTeI$_4^-$ are very similar and are the same as those observed in other compounds containing linear I—Te—I linkages, lending support to the use of an additive model in interpreting ^{125}Te quadrupole splittings. The compound Ph_3TeI is best formulated as an ionic species. The compound formed on reaction of α-Me_2TeI_2 with Ph_2Hg is concluded to be $(Me_2PhTe^+)_2HgI_4^{2-}$.

NIGEL S. DANCE et COLIN H. W. JONES. Can. J. Chem. **59**, 918 (1981).

On a mesuré les spectres de Mossbauer de ^{129}I des composés suivants: PhTeI, p-EtOPhTeI$_2^-$, p-EtOPhTeI$_4^-$, Ph_3TeI, $(Me_2TeI_2)_2{\cdot}Ph_2Hg$ et Na_2HgI_4, et on a interprété les résultats en fonction de la liaison du tellure dans ces composés et dans ces ions. On présente des données suggérant que le PhTeI existe sous forme de polymère. Les constantes de couplage de ^{129}I des ions p-EtOPhTeI$_2^-$ et p-EtOPhTeI$_4^-$ sont très semblables et sont identiques à celles observées dans d'autres composés où la liaison I—Te—I est linéaire; ce résultat tend à confirmer l'utilité d'une modèle additif pour interpréter les découplages quadrupolaires du ^{125}Te. La meilleure façon de représenter le composé Ph_3TeI est de le considérer comme étant un composé ionique. On conclut que le composé obtenu par la réaction de α-Me_2TeI_2 avec Ph_2Hg est le $(Me_2PhTe^+)_2HgI_4^{2-}$.

[Traduit par le journal]

Introduction

In an earlier paper (1) we reported the ^{129}I Mössbauer spectra of Cs_2TeI_6, α-Me_2TeI_2, α-TeI, TeI_4, and $PhTeI_3$. As a continuation of that work, and as part of an ongoing related study of the ^{125}Te Mössbauer spectra of organotellurium compounds (2), we have measured the ^{129}I Mössbauer spectra of PhTeI, $(Ph_3MeP^+)(p$-EtOPhTeI$_2^-)$, (Ph_3MeP^+)-$(p$-EtOPhTeI$_4^-)$, Ph_3TeI, and the adduct formed by reaction of α-Me_2TeI_2 with Ph_2Hg.

These compounds provide a measure of the ionicity of the Te—I bond in a number of different environments. In part they also provide a useful independent check of the basic assumptions, used in interpreting the ^{125}Te Mössbauer data of a number of organotellurium halides, that in a range of compounds a simple additive model may be used in interpreting ^{125}Te quadrupole splittings (2).

The adduct formed by reaction of Me_2TeI_2 with Ph_2Hg was of some interest since the nature of the bonding in this compound has been open to question (3).

Results and Discussion

The parameters computed from the ^{129}I spectra are given in Table 1 and the ^{125}Te parameters for these compounds are given in Table 2. A sample ^{129}I Mössbauer spectrum, that for PhTeI, is illustrated in Fig. 1.

PhTeI

Petragnani *et al.* (4) have reported that tellurenyl halides may be prepared by reaction of halogen with the ditelluride in solution in benzene at 0°C and that on further reaction with a phosphonium salt, $ArTeX_2^-$ salts can be isolated. We have used this route to prepare PhTeI, p-EtOPhTeI, and p-EtOPhTeI$_2^-$. While Petragnani *et al.* (4) did not attempt to isolate the tellurenyl halides, Schulz and Klar (5) have demonstrated that PhTeI can indeed be prepared this way. The black solid that precipitates on reaction of Ph_2Te_2 with I_2 in benzene analysed as PhTeI and no evidence for $PhTeI_3$, the other likely product of this reaction, was obtained.

The ^{125}Te and ^{129}I Mössbauer spectra of PhTeI indicated the presence of only one tellurium and one iodine site. The ^{129}I Mössbauer spectrum was clean and well resolved (Fig. 1) in contrast with that of $PhTeI_3$ which we have previously studied (1) and which gave a complex spectrum consistent with the presence of a number of inequivalent iodine sites.

The ^{125}Te quadrupole splitting for PhTeI of 6.5 mm s^{-1} is significantly smaller than that generally observed for Te(II) compounds, where Δ values of 10–15 mm s^{-1} are normally found (6). Thus, for example, Ph_2Te and $C_6H_5N{=}NC_6H_4TeCl$ have Δ values of 10.5 and 11.8 mm s^{-1} respectively (Table 2). The latter compound, a tellurenyl chloride, has the structure shown in Fig. 2 in which there is an intramolecular contact, the environment about the tellurium being essentially planar (7). The origin of the large quadrupole splitting lies in the considerable p-orbital imbalance between the p_z lone pair directed out of the bonding (xy) plane and the p_x and p_y orbitals.

0008-4042/81/060918-05$01.00/0

©1981 National Research Council of Canada/Conseil national de recherches du Canada

Can. J. Chem. Downloaded from www.nrcresearchpress.com by 210.87.254.5 on 09/06/12
For personal use only.

Can. J. Chem. Downloaded from www.nrcresearchpress.com by 210.87.254.5 on 09/06/12
For personal use only.

TABLE 1. ^{129}I Mössbauer parameters

Compound	^{129}I δ* (mm s^{-1})	^{129}I e^2qQ† (MHz)	
PhTeI	0.38	−894.2	
p-EtOPhTeI$_2^-$	0.16	−585.2	
α-Me_2TeI_2	0.17	−672.7	
p-EtOPhTeI$_4^-$	0.19	−730.6	($\eta = 0.11 \pm 0.03$)
Ph_3TeI	−0.23	0	
$Me_2TeI_2 \cdot Ph_2Hg$	−0.13	−504.8	
Na_2HgI_4 (frozen solution)	−0.10	−510.0	
I_2	0.84	−1495.4	($\eta = 0.16 \pm 0.01$)
NaI	−0.48	0	

*δ with respect to Zn^{129}Te, source and absorbers at 4.2 K.
†η = 0 except where noted.

TABLE 2. ^{125}Te Mössbauer parameters

Compound	^{125}Te δ† (mm s^{-1}) (±0.10)	^{125}Te Δ (mm s^{-1}) (±0.2)	Reference*
PhTeI	0.42	6.5	
p-EtOPhTeI	0.53	7.1	
$C_6H_5N{=}NC_6H_4TeCl$	0.63	11.8	
p-EtOPhTeI$_2^-$	0.46	13.9	
α-Me_2TeI_2	0.52	7.6	
p-EtOPhTeI$_3$	1.0	5.2	1
p-EtOPhTeI$_4^-$	0.90	4.9	
Ph_3TeI	0.38	5.6	
$(Me_2TeI_2)_2 \cdot Ph_2Hg$	0.14	5.5	3

*This work except where noted.
†δ with respect to I/Cu, source and absorbers at 4.2 K.

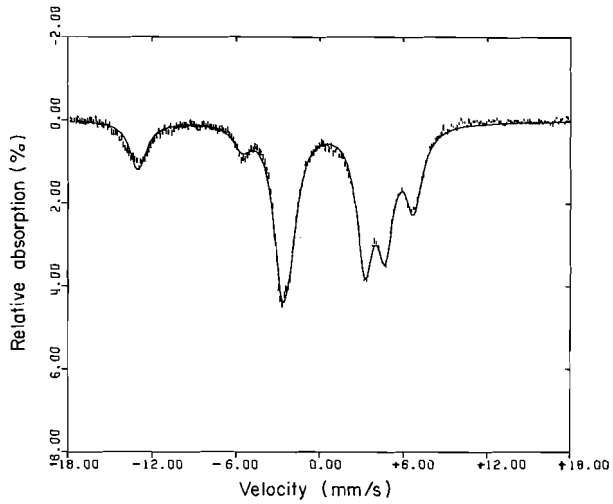

FIG. 1. The ^{129}I Mössbauer spectrum of PhTeI.

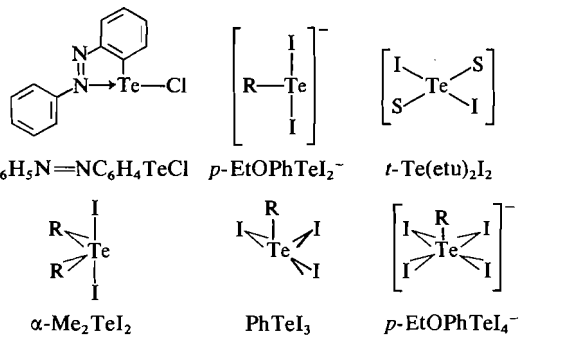

FIG. 2. A representation of the structures of a number of the compounds of interest.

The ^{129}I Mössbauer parameters for PhTeI are also somewhat unusual. The coupling constant of −894 MHz compares with those of −1308 and −1190 MHz for terminal iodine atoms in a α-TeI and TeI_4 respectively (1). The small ^{125}Te and ^{129}I quadrupole couplings suggest that PhTeI is polymeric. The presence of Te---I intermolecular contacts could lead to an increased co-ordination about the tellurium and hence a Δ value smaller than that observed in Ph_2Te, for example. Such bridging could also lead to a longer primary Te—I bond and a smaller iodine coupling constant than that observed for terminal Te—I bonds.

The ^{129}I Mössbauer data may be interpreted in terms of valence orbital populations on the iodine (1). The use of such a simple, valence bond approach must only be considered an approximation. However, its success in interpreting a large body of ^{129}I Mössbauer data in the past suggests that this approach has some validity. Thus, this isomer shift allows an estimation of h_p, the number of holes in the 5*p* shell of the iodine (Table 3) while the coupling constant allows an estimation of U_p, the *p*-orbital imbalance (1). The fact that h_p and U_p are the same in magnitude and that $\eta = 0$ for ^{129}I in PhTeI suggests that the iodine is utilising only a *p*-orbital in bonding to the tellurium and that any I---Te—I bridging units must be linear.

Can. J. Chem. Downloaded from www.nrcresearchpress.com by 210.87.254.5 on 09/06/12
For personal use only.

The observation that PhTeI appears to be polymeric is not unexpected, given that α-TeI and TeI_4 are both polymeric (8, 9) and that intermolecular contacts are often observed in organotellurium iodides (10). Free tellurenyl halide molecules have only been observed in those cases where there is an intramolecular contact between the organic ligand and the tellurium as in the chloride noted above.

p-EtOPhTeI$_2^-$ *and p-EtOPhTeI*$_4^-$

The ^{129}I Mössbauer spectra of α-Me_2TeI_2 and Cs_2TeI_6 were reported previously and the present results for α-Me_2TeI_2 (Table 1) are in good agreement with that work. The tellurium in α-Me_2TeI_2 may be viewed as being in a distorted octahedral environment with bridging iodine atoms, although the bridging contacts are relatively long and weak (11). The I—Te—I linkage is nearly linear. The ^{129}I coupling constants in α-Me_2TeI_2 and Cs_2TeI_6 were found to be very similar. It was of some interest to measure the ^{129}I spectra of *p*-EtOPhTeI_2^- and *p*-EtOPhTeI_4^- and to compare the iodine coupling constants in these molecules with those in α-Me_2TeI_6 and Cs_2TeI_6. The *p*-EtOPhTeI_2^- anion will be T-shaped (Fig. 2) with the I—Te—I linkage again essentially linear. The crystal structure of the related compound C_6H_5Te-(ethylenethiourea)I shows this molecule to have this geometry with an essentially linear S—Te—I linkage (12). In contrast, the *p*-EtOPhTeI_4^- anion will be square based pyramidal (Fig. 2) with the organic ligand occupying the axial position and the TeI_4 grouping lying in a plane with linear I—Te—I bonds. Thus these two ions represent rather different geometries about the tellurium than those observed in Cs_2TeI_6 or α-Me_2TeI_2, yet all contain the linear I—Te—I linkage.

The compound (*p*-EtOPhTeI_2^-)(Ph_3MeP^+) was prepared (4) by adding Ph_3MePI to *p*-EtOPhTeI. The anion *p*-EtOPhTeI_2^- yields a large ^{125}Te quadrupole splitting consistent with the presence of a planar Te(II) species in which the p_z lone pair is directed out of the bonding plane. The ^{129}I coupling constant of *p*-EtOPhTeI_2^- is comparable with, although somewhat smaller than, that of α-Me_2TeI_2. Moreover, it compares very well with that of another Te(II) iodide which we studied sometime ago, namely *trans*-Te(ethylenethiourea)$_2$-$^{129}I_2$, in which the environment about tellurium is again planar (6) and the I—Te—I linkage is linear (Fig. 2).

The compound (*p*-EtOPhTeI_4^-)(Ph_2MeP^+) was made by addition of Ph_3MePI to *p*-EtOPhTeI_3. The *p*-EtOPhTeI_4^- anion yields a small ^{125}Te Mössbauer quadrupole splitting of 5.2 mm s^{-1} consistent with the presence of a square based pyramidal structure. The ^{129}I Mössbauer data indicated the presence of only one iodine site, in comparison with that of the triiodide, $PhTeI_3$, studied previously, which yields a complex spectrum arising from at least three inequivalent iodine sites (1, 10) (Fig. 2). The iodine coupling constant of −730 MHz in a *p*-EtOPhTeI_4^- is comparable with, but a little greater than, that of α-Me_2TeI_2.

Thus for the species *trans*-Te(ethylenethiourea)$_2I_2$, *p*-EtOPhTeI_2^-, TeI_6^{2-}, α-Me_2TeI_2, and *p*-EtOPh-TeI_4^- the iodine coupling constants span a small range from −585 to −731 MHz (Table 3). The I—Te—I linkage appears to remain relatively constant in bonding character in all of these compounds and ions as the number and character of the other ligands bonded to the tellurium changes and as the charge on the molecular species changes. There appears to be a small increase in the iodine coupling constant for iodine bonded to Te(IV) in comparison with that for iodine bonded to Te(II).

While the above discussion focussed attention on the ^{129}I coupling constants the isomer shifts are also reasonably constant for these compounds (Table 1). The h_p and U_p values estimated from δ and e^2qQ are given in Table 4 and are consistent with the bonding occurring to the iodine exclusively through an iodine *p*-orbital. The presence of any iodine *s*-character in the bond would lead to a value of U_p greater than the apparent h_p value.

The linear I—Te—I linkages in the molecules and ions listed in Table 3 may be viewed as three-centre bonds in which a single *p*-orbital on the tellurium atom overlaps with *p*-orbitals on the two iodine ligands, the bonds being relatively long and ionic. The iodine coupling constants are roughly one-half that observed for a terminal iodine atom bonded to tellurium in, for example, α-TeI, where the coupling constant is −1308 Hz, corresponding to a 2c—2e bond.

The constancy of the bonding character of the I—Te—I linkages for the compounds and ions of Table 3 is of some interest. In studying a wide range of organotellurium compounds of Te(II) and Te(IV)

TABLE 3. Coupling constants for iodine in different tellurium compounds

Compound	e^2qQ(129) (MHz)	Reference
Cs_2TeI_6	−725	1
α-Me_2TeI_2	−673	
p-EtOPhTeI_4^-	−731	
trans-Te(etu)$_2I_2$*	−598	6
p-EtOPhTeI_2^-	−585	

*etu = ethylenethiourea.

Can. J. Chem. Downloaded from www.nrcresearchpress.com by 210.87.254.5 on 09/06/12
For personal use only.

TABLE 4. h_p and U_p values calculated from δ and e^2qQ

Compound	^{129}I	
	h_p*	U_p†
PhTeI	0.55	0.55
p-EtOPhTeI$_2^-$	0.40	0.37
α-Me$_2$TeI$_2$	0.41	0.42
p-EtOPhTeI$_4^-$	0.42	0.46
Ph$_3$TeI	0.20	0

*Assuming no s-character in the bond and that $\delta = 1.5\ h_p - 0.44$ (mm s^{-1}).
†Where $U_p = -e^2q_{mol}Q/e^2q_0Q$ and e^2q_0Q is +1607 MHz for ^{129}I.

it has been found that a simple additive rule can be used to rationalise the ^{125}Te quadrupole splittings. The present ^{129}I Mössbauer data further support the use of such a model since the I—Te—I linkage certainly remains relatively constant in bonding character.

Ph_3TeI

Here, no resolvable quadrupole coupling was observed in the iodine Mössbauer spectrum, while the isomer shift was found to lie in the range of the ionic iodides. There has been some discussion in the past of interionic interactions in the tellurium salts in the solid state (13). For example, in the structure of Ph$_3$Te(NCO)·½CHCl$_3$, Te---N and Te---O contacts were observed which, while significantly longer than those expected of single bonds, were shorter than the sums of the Van der Waal's radii. However, the ^{129}I isomer shift and the absence of measurable ^{129}I quadrupole coupling constant in Ph$_3$TeI suggests that there are no significant bonding interactions between tellurium and iodine and that the compound can be formulated as being ionic, i.e. Ph$_3$Te$^+$I$^-$.

$Me_2TeI_2 \cdot Ph_2Hg$

We have previously studied the product of the reaction of α-Me$_2$TeI$_2$ with Ph$_2$Hg (3) and proposed that the compound could be formulated as (Me$_2$PhTe$^+$)$_2$HgI$_4^{2-}$. The ^{125}Te Mössbauer parameters are consistent with the presence of a telluronium cation (3) and here we report the ^{129}I Mössbauer data. The ^{129}I Mössbauer parameters are reported in Table 1 and are compared with those of the HgI$_4^{2-}$ anion, prepared in aqueous solution by reacting Na^{129}I with HgI$_2$. It can be seen that Me$_2$TeI$_2$·Ph$_2$Hg has essentially the same ^{129}I Mössbauer parameters as HgI$_4^{2-}$, lending further support to the formulation of the former compound as (Me$_2$PhTe$^+$)$_2$HgI$_4^{2-}$.

The present ^{129}I data for (Me$_2$PhTe)$_2$HgI$_4$ and Na$_2$HgI$_4$ may be compared with that previously reported by Sakai *et al.* for HgI$_2$ as a crystalline solid and in frozen solution in dioxane (14). In HgI$_2$ the iodine is in a bridging environment and e^2qQ is positive in sign, η is 0.54, and consistent with some 4% s-character in the bonding to iodine. In the complex formed with dioxane it is assumed that HgI$_2$ is present as essentially isolated linear HgI$_2$ units with dioxane molecules forming distant contacts to the mercury in the plane at right angles to the bonding axis (15). The iodine coupling constant and isomer shift in this instance are −770 MHz and +0.18 mm s^{-1} respectively. In comparison, in HgI$_4^{2-}$ which is tetrahedral e^2qQ is −500 MHz and δ = −0.1 mm s^{-1}. Thus, not unexpectedly, the Hg—I bond is more ionic in the tetrahedral sp^3 complex ion HgI$_4^{2-}$ than in the linear sp HgI$_2$ isolated species.

Experimental

All compounds were prepared using literature methods with the exception of α-Me$_2$TeI$_2$ which was prepared directly from Me$_2$Te and elemental ^{129}I$_2$ in chloroform solution. Thus, PhTeI was prepared by reaction of Ph$_2$Te$_2$ with ^{129}I$_2$ in benzene (5). In a second preparation p-EtOPhTe^{129}I in benzene was treated with Ph$_3$MeP$^+$I$^-$ with the formation of p-EtOPhTeI$_2^-$·Ph$_3$MeP$^+$ (4). The compound p-EtOPhTeI$_4^-$ was prepared by first reacting p-EtOPh$_2$Te$_2$ with a small stoichiometric excess of ^{129}I$_2$ to form p-EtOPhTe^{129}I$_3$ (16) and then reaction with Ph$_3$MeP$^+$I$^-$ (17). The telluronium iodide Ph$_3$TeI was prepared by reaction of Ph$_3$TeCl with ^{129}I$_2$ in ethanol (18). The reaction of α-MeTe^{129}I$_2$ with Ph$_2$Hg in chloroform yielded (Me$_2$PhTe$^+$)$_2$Hg^{129}I$_4^{2-}$ (19). The sample of Na$_2$Hg^{129}I$_4$ was prepared by reacting Na^{129}I with HgI$_2$ in stoichiometric quantity in aqueous solution.

The ^{129}I used in these preparations was obtained from Oak Ridge National Laboratories as Na^{129}I in sodium sulphite solution and from this it was possible to prepare ^{129}I$_2$ and Na^{129}I to be used in the preparation noted above. The samples prepared contained 10–20 mg cm^{-2} of ^{129}I. Samples containing ^{129}I were not chemically analysed but non-active samples prepared using the same methods were identified by elemental analysis and, where appropriate, melting points, and ir spectra.

The general methods used in recording the ^{129}I and ^{125}Te Mössbauer spectra and in computer fitting the data have been described previously (1, 2). In brief, the ^{125}Te spectra were recorded on 100 mg naturally abundant samples at 4.2 K using an ^{125}Sb/Cu source (New England Nuclear). The ^{129}I spectra were recorded on ^{129}I labelled compounds, again at 4.2 K, using a Zn^{129m}Te source prepared in our laboratory from ^{129m}Te obtained from New England Nuclear as tellurite ion in aqueous solution. The tellurite was reduced to elemental tellurium and the dried powder heated with zinc under vacuum in a quartz capsule at 500°C.

Spectra were recorded using a Harwell Instruments 200 series drive and a Nuclear Data 2200 series analyser. The spectrometer was routinely calibrated using a ^{57}Co/Pd source and iron foil absorber at room temperature.

Spectra were computed to independent Lorentzians and in the analysis of ^{129}I spectra the approach taken by Pasternak (20) was used, taking Q^*/Q = 1.238 for ^{129}I (21).

Acknowledgement

The authors wish to acknowledge a grant in

support of this research from the Natural Sciences and Engineering Research Council of Canada.

1. C. H. W. JONES and M. MAUGUIN. J. Chem. Phys. **68**, 3067 (1978).
2. C. H. W. JONES, R. SCHULTZ, W. R. MCWHINNIE, and N. S. DANCE. Can. J. Chem. **54**, 3234 (1976).
3. N. S. DANCE and C. H. W. JONES. J. Organomet. Chem. **152**, 175 (1978).
4. N. PETRAGNANI, L. TORRES, K. J. WYNNE, and D. J. WILLIAMS. J. Organomet. Chem. **76**, 241 (1974).
5. P. SCHULZ and G. KLAR. Z. Naturforsch. **30B**, 40 (1975).
6. B. M. CHEYNE, C. H. W. JONES, and P. VASUDEV. Can. J. Chem. **50**, 3677 (1972).
7. R. E. COBBLEDICK, F. W. B. EINSTEIN, W. R. MCWHINNIE, and F. H. MUSA. J. Chem. Res. (M), 1901 (1979).
8. R. KNIEP, D. MOOTZ, and A. RABENAU. Z. Anorg. Allg. Chem. **442**, 17 (1976).
9. V. PAULAT and B. KREBS. Angew. Chem. Int. Ed. **15**, 39 (1976).
10. J. D. MCCULLOUGH and C. KNOBLER. Inorg. Chem. **15**, 2728 (1976).
11. L. Y. Y. CHAN and F. W. B. EINSTEIN. J. Chem. Soc. Dalton, 316 (1972).
12. O. VIKANE. Acta Chem. Scand. A**29**, 787 (1975).
13. D. D. TITUS, J. LEE, and R. F. ZIOLO. J. Organomet. Chem. **120**, 381 (1976).
14. H. SAKAI, Y. MAEDA, S. ICHIBA, and H. NEGITA. Chem. Phys. Lett. **27**, 27 (1974).
15. T. B. BRILL. J. Inorg. Nucl. Chem. **32**, 1869 (1970).
16. N. PETRAGNANI. Tetrahedron, **11**, 15 (1960).
17. N. PETRAGNANI, L. T. CASTELLANOR, K. J. WYNNE, and W. MAXWELL. J. Organomet. Chem. **55**, 295 (1973).
18. K. LEDERER. Ber. **536**, 1430 (1920).
19. F. L. GILBERT and T. M. LOWRY. J. Chem. Soc. 3179 (1928).
20. M. PASTERNAK. Symp. Faraday Soc. No. 1, 119 (1967).
21. H. DEWAARD. *In* Mössbauer effect data index. *Edited by* J. G. Stevens and V. E. Stevens. Plenum, New York. 1973. p. 447.

Can. J. Chem. Downloaded from www.nrcresearchpress.com by 210.87.254.5 on 09/06/12
For personal use only.

Kinetics and mechanism of unimolecular decomposition of 3-methyl-1-*p*-tolyltriazene

KEITH VAUGHAN
Department of Chemistry, Saint Mary's University, Halifax, N.S., Canada B3H 3C3
AND
MICHAEL T. H. LIU
Department of Chemistry, University of Prince Edward Island, Charlottetown, P.E.I., Canada C1A 4P3

Received June 23, 1980

KEITH VAUGHAN and MICHAEL T. H. LIU. Can. J. Chem. **59**, 923 (1981).

Kinetic parameters (E_a and ΔS^+) for the thermolysis of 3-methyl-1-*p*-tolyltriazene (**1**) in tetrachloroethylene have been determined. The near-zero value for ΔS^+ suggests a transition state with minimal stretching of the N—N bonds in tautomers **1***a* or **1***b*. The activation energy (E_a = 29.2 kcal/mol) and ΔS^+ for the decomposition of **1** are very similar to those of the azoarylalkanes (Ar—N=N—R), suggesting a similar mechanism of degradation. The major products of the thermolysis of **1** are *p*-toluidine, *N*-methyl-*p*-toluidine, and *p*-chlorotoluene, which are rationalized in terms of homolytic breakdown of both tautomers.

KEITH VAUGHAN et MICHAEL T. H. LIU. Can. J. Chem. **59**, 923 (1981).

On a déterminé les paramètres cinétiques (E_a et ΔS^+) de la thermolyse du méthyl-3 *p*-tolyl-1 triazène (**1**) dans le chlorure de méthylène. La valeur du ΔS^+ qui est voisine de zéro suggère un état de transition avec une élongation minimale des liaisons N—N des tautomères **1***a* ou **1***b*. L'énergie d'activation (E_a = 29,2 kcal/mol) et le ΔS^+ de la décomposition de **1** sont très voisines de celles des azoarylalkanes (Ar—N=N—R) suggérant ainsi que leurs mécanismes de dégradation sont analogues. Les produits principaux de la thermolyse du composé **1** sont la *p*-toluidine, la *N*-méthyl *p*-toluidine et le *p*-chlorotoluène dont on peut rationnaliser la formation en fonction d'un clivage homolytique des deux tautomères.

[Traduit par le journal]

Introduction

Alkyl aryl triazenes (Ar—N=N—NHR) have been widely studied and their synthesis, tautomerism, degradation, and biological properties have recently been reviewed (1). These monoalkyltriazenes exist as a tautomeric mixture of forms **A** and **B** (2, 3):

$$\underset{\mathbf{A}}{\text{R—NH—N=N—Ar}} \rightleftarrows \underset{\mathbf{B}}{\text{R—N=N—NHAr}}$$

The kinetics of the benzoic acid-catalyzed decomposition of 3-alkyl-1-aryltriazenes in aprotic solvents has been studied (3, 4) and it has been suggested that proton transfer and departure of the alkyl cation are synchronous and rate determining during the decomposition to give $ArNH_2$, N_2, and products from the alkyl fragment. The thermal decomposition of methylphenyltriazene in apolar hydrocarbon solvents follows first order kinetics (5), and the formation of methyl radicals was clearly demonstrated. In addition, a CIDNP investigation of the thermolysis of monoalkyltriazenes has demonstrated the formation of the aminyl radical pair ($\dot{A}rNH$ $\dot{R}$), which is presumed to arise via homolysis of the unconjugated tautomeric form **B** (6). The analogous tautomeric form has also been implicated in the decomposition of monoalkyltriazenes in aqueous solution; when Ar contains electron-withdrawing groups, a simple unimolecular heterolysis occurs involving the alkane diazonium ion (7):

$$\text{R—N=N—NHAr} \rightarrow \text{R—}\overset{+}{\text{N}}\equiv\text{N} + {}^-\text{NHAr}$$

We report here the measurement of the kinetic parameters for the unimolecular decomposition of 3-methyl-1-*p*-tolyltriazene (**1**) in tetrachloroethylene and an interpretation of the elementary processes involved in the degradation of this class of compounds.

Experimental

Materials

3-Methyl-1-*p*-tolyltriazene (**1**), obtained from Aldrich Chemical Company, was recrystallized from petroleum ether before use, and had mp 81–82°C. Tetrachloroethylene was spectroscopic grade.

Kinetics

Kinetic measurements were carried out by following the characteristic absorption of the triazene (**1**) with a Unicam SP 800A uv spectrophotometer. In all experiments, the decompositions were conducted in sealed Pyrex tubes containing an 0.1 *M* solution of **1** in tetrachloroethylene. Kinetic parameters were determined by following the change of absorbance with time at the wavelength of maximum absorption (337 nm in C_2Cl_4). First-order rate constants were determined graphically from the plot of log ($A_t - A_\infty$) against time.

Product Analysis

3-Methyl-1-*p*-tolyltriazene (**1**) in tetrachloroethylene (0.1 *M* solution) was heated at 100°C until starting material could not be detected (after approximately 2 h) by tlc on silica gel F-254 (Merck) with chloroform as eluent (the triazene **1** had R_f 0.32).

0008-4042/81/060923-04$01.00/0
©1981 National Research Council of Canada/Conseil national de recherches du Canada

Can. J. Chem. Downloaded from www.nrcresearchpress.com by 210.87.254.105 on 09/06/12
For personal use only.

Can. J. Chem. Downloaded from www.nrcresearchpress.com by 210.87.254.105 on 09/06/12
For personal use only.

The solution was evaporated *in vacuo* to afford a dark red oil. The 60 MHz ^{1}H nmr spectrum of this residue was recorded in deuteriochloroform solution with a Varian EM360 spectrometer; assignments of ^{1}H signals were made by comparison with spectra of pure, authentic compounds and with published chemical shift data (6).

The product analysis was further refined by column chromatography on silica gel 30–70 mesh (Merck–Brinkman) with carbon tetrachloride as the initial eluent, followed successively by ether/CCl_4 (1:1), ether alone, chloroform, and finally 95% ethanol.

Results and Discussion

Table 1 lists the first-order rate constants for the decomposition of 3-methyl-1-*p*-tolyltriazene (1) in tetrachloroethylene. These data gave an excellent Arrhenius plot from which eq. [1] was obtained by least-squares analysis. R is taken as 0.00198 kcal mol^{-1} K^{-1}.

$$[1] \quad k = 10^{13.8 \mp 0.8} \exp(-29.2 \mp 1.4/RT)\ s^{-1}$$

An A factor of $10^{13.8}$ corresponds to a $\Delta S^{\ddagger}$ of 2.2 cal mol^{-1} K^{-1} at 104°C, the mean of the temperature range over which these measurements were made. The activation energy (E_a) and $\Delta S^{\ddagger}$ for the decomposition of the triazene (**1**) are very similar to those of the arylazoalkanes (Ar—N=N—R) (8) (see Table 2), suggesting a similar mechanism of degradation of these compounds. Unsymmetrical azoalkanes decompose with unequal stretching of the two C—N bonds; in the extreme case of arylazoalkanes the evidence (9) is overwhelmingly in favour of one-bond scission to give the radical pair Ar—N=N$^{\cdot}$ R$^{\cdot}$ (10). Lorand and co-workers (11) have shown that Ar—N=N$^{\cdot}$ is longer lived than the solvent cage. The similarity in the kinetic parameters of triazene and azo-compounds suggests that triazene fragmentation occurs by one-bond scission to give either of the radical pairs ArN=N$^{\cdot}$ $^{\cdot}$NHCH$_3$ or ArNH$^{\cdot}$ N$^{\cdot}$=N—CH$_3$ (Scheme 1). However, the kinetic parameters do not distinguish the pathways of decomposition from tautomer **1***a* or tautomer **1***b*.

TABLE 1. First-order rate constants for the decomposition of **1** in tetrachloroethylene

t (°C)	$k \times 10^4$ (s^{-1})
91.8	1.83
94.0	2.25
95.4	3.27
98.0	4.92
100.7	5.75
104.0	9.27
108.2	10.8
112.1	18.3
116.0	24.3

TABLE 2. Comparison of kinetic parameters of the triazene (**1**) and the azoarylalkanes (Ar—N=N—R)

	E_a (kcal/mol)	$\Delta S^{\ddagger}$ (cal/mol^{-1} K^{-1})
Triazene (**1**)	29.2 ± 1.4	2.2 ± 3.0
Azoarylalkanes* (Ar—N=N—R)	27.0–34.0	3.9–5.2

*Reference 8.

The near zero $\Delta S^{\ddagger}$ value for the decomposition of **1** may indicate that the stretching of the N—N bond in **1***a* or **1***b* is minimal in the transition state. However, there may be other reasons for the small $\Delta S^{\ddagger}$, which may contain a contribution from loss of rotational freedom. For example, resonance stabilization of ArNH$^{\cdot}$ (from **1***b*) may freeze rotation about the C—N bond more fully than in the reactant; this may also be a factor in arylazoalkane decomposition.

Analysis of the product mixture suggests that decomposition of triazene (**1**) proceeds mainly via homolysis of **1***b*. The major component of the product mixture had *C*-methyl chemical shift at δ 2.18 and was identified as *p*-toluidine by comparison with authentic material; the yield of *p*-toluidine from the thermolysis of **1** was estimated to be 42%. A second component of the product mixture had *C*-methyl δ 2.33 as well as *N*-methyl chemical shift δ 2.68; these chemical shifts correlate with those reported for *N*-methyltoluidine (6). However, the yield of *N*-methyltoluidine from **1** was only 5%. A third component, which was the major compound in the first fraction from column chromatography, had a *C*-methyl chemical shift at δ 2.28; this component has a typical aromatic AA′BB′ pattern for a *p*-disubstituted benzene. The coupling constant (J = 8 Hz) in the AA′BB′ pattern is identical with that in authentic *p*-chlorotoluene, which has a measured *C*-methyl chemical shift of δ 2.27. The yield of *p*-chlorotoluene from the decomposition of **1** was less than 10%. These nmr assignments agree entirely with those made by Albert *et al.* (6). The moderate material balance (57% total recovery) in the product analysis reflects considerable tar formation in the reaction mixture. The 43% of radicals not accounted for probably underwent addition to tetrachloroethylene leading to some polymerization.

Scheme 1 shows the most probable mechanistic pathways consistent with these observations. One-bond scission of tautomer **1***b* gives the radical pair **3**, which can give rise to the major product,

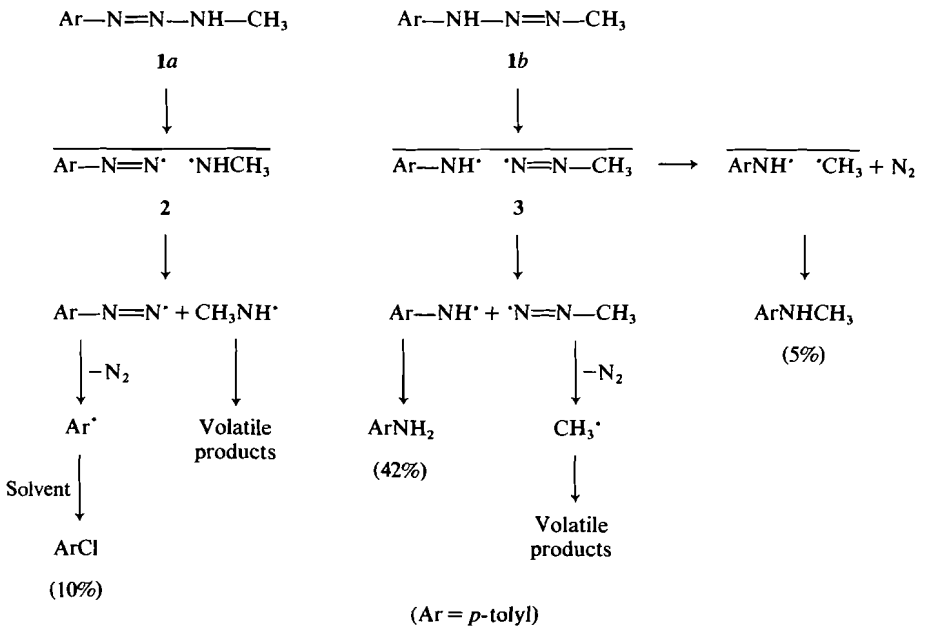

(Ar = *p*-tolyl)

SCHEME 1

p-toluidine, after cage dissociation and H-abstraction by the arylaminyl radical, ArṄH. Alternatively, loss of nitrogen from the methyl diazenyl radical MeN=N· within the cage affords the pair ArṄH ĊH$_3$ which combine to give the observed minor product *N*-methyl-*p*-toluidine. Similar one-bond scission of tautomer **1***a* gives the radical pair **2**; since the aryldiazenyl radical ArN=Ṅ is relatively long-lived (11), dissociation of the radical pair will likely precede loss of N_2 to give the aryl radical Ar·. Abstraction of chlorine from the solvent by Ar· accounts for the formation of the observed product, *p*-chlorotoluene. Since ArN=Ṅ is long-lived, the pair Ar· ṄHCH$_3$ is unlikely to form and cannot be the source of *p*-toluidine.

Unless the relative amounts of the products are a reflection of the efficiency of H-abstraction by aminyl-radical over Cl-abstraction from the solvent by *p*-tolyl radical, the ratio of *p*-toluidine to *p*-chlorotoluene (>4:1) suggests that the major pathway of homolysis of **1** involves tautomer **1***b*. This preference probably reflects a greater reactivity associated with the unconjugated tautomer (**1***b*) rather than a greater concentration of **1***b* in the tautomeric mixture in accordance with the Curtin–Hammett principle (12). Indeed the tautomerism in **1** has been shown, by variable temperature nmr (2, 13), to favour the conjugated form **1***a*. The CIDNP investigation of monoalkyltriazene thermolysis (6) also showed the preferred fragmentation of the unconjugated tautomer and the formation of the arylaminyl–alkyl pair ArṄH ĊH$_3$.

Further studies of the thermolysis of monoalkyl triazenes will be aimed at the elucidation of the effect of substituents in the aryl group on the kinetics and course of the reaction. Tautomerism of the type (**1***a* ⇄ **1***b*) is greatly influenced by the nature of the aryl substituent and the latter might have a substantial effect on the thermal degradation. A preliminary study of a comparison of the *p*-tolyltriazene (**1**) with the *p*-nitrophenyl analogue suggests that the nitro-compound is much more stable to thermolysis. However, the determination of kinetic parameters for the nitrophenyltriazene by the spectrophotometric method proved impossible, due to the intense interference in the uv spectrum by the product of degradation, *p*-nitroaniline. Alternative methods of kinetic measurement are being examined.

Acknowledgements

The authors gratefully acknowledge the financial support of the Natural Sciences and Engineering Research Council of Canada. We are also grateful for technical assistance to C. Hinman, P. Godreau, W. Y. Kwan, and J. Szabo.

1. K. VAUGHAN and M. F. G. STEVENS. Chem. Soc. Rev. 377 (1978).
2. K. VAUGHAN. J. Chem. Soc. Perkin Trans. II, 17 (1977).
3. N. S. ISAACS and E. RANNALA. J. Chem. Soc. Perkin Trans. II, 899 (1974).

Can. J. Chem. Downloaded from www.nrcresearchpress.com by 210.87.254.105 on 09/06/12
For personal use only.

4. N. S. ISAACS and E. RANNALA. J. Chem. Soc. Perkin Trans. II, 902 (1974).
5. A. CSERHEGYI, G. SZENTGYORGYI, and O. DOBIS. Magy. Chem. Foly. **77**, 607 (1971).
6. K. ALBERT, K.-M. DANGEL, A. RIEKER, H. IWAMURA, and Y. IMAHASHI. Bull. Chem. Soc. Jpn. **49**, 2537 (1976).
7. C. C. JONES, M. A. KELLY, M. L. SINNOTT, and P. J. SMITH. J. Chem. Soc. Chem. Commun. 322 (1980).
8. G. L. DAVIES, D. H. HEY, and G. H. WILLIAMS. J. Chem. Soc. 4397 (1956); Comprehensive chemical kinetics. Vol. 5. *Edited by* C. H. Bamford and C. F. H. Tipper. Elsevier, New York. 1972. p. 582.
9. P. S. ENGEL. Chem. Rev. **80**, 102 (1980), and references therein.
10. W. A. PRYOR and K. SMITH. J. Am. Chem. Soc. **92**, 5403 (1970).
11. R. G. KRYGER, J. P. LORAND, N. R. STEVENS, and N. R. HERRON. J. Am. Chem. Soc. **99**, 7589 (1977).
12. J. I. SEEMAN and W. A. FARONE. J. Org. Chem. **43**, 1854 (1978).
13. R. CURCI and V. LUCCHINI. Spectrosc. Lett. **6**, 293 (1973).

Can. J. Chem. Downloaded from www.nrcresearchpress.com by 210.87.254.105 on 09/06/12
For personal use only.

The reaction of some propargyl alcohols with benzeneselenenyl chloride[1]

DENNIS G. GARRATT[2]

Department of Chemistry, University of Ottawa, Ottawa, Ont., Canada K1N 9B4 and the Division of Chemistry, National Research Council of Canada, Ottawa, Ont., Canada K1A 0R6

AND

PIERRE L. BEAULIEU,[3] AND VERONIQUE M. MORISSET[3]

Department of Chemistry, University of Ottawa, Ottawa, Ont., Canada K1N 9B4

Received July 22, 1980

DENNIS G. GARRATT, PIERRE L. BEAULIEU, and VERONIQUE M. MORISSET. Can. J. Chem. **59**, 927 (1981).

The reaction of benzeneselenenyl chloride with twenty-two propargyl alcohols in methylene chloride solution is reported. Products of both Markownikoff and anti-Markownikoff regiochemistry are formed in an *anti* stereospecific manner. The regioselectivity or specificity is found to be very dependent upon the nature of the substituents geminal to the alcoholic moiety. In general the presence of bulky substituents geminal to the alcoholic moiety tend to favour formation of the anti-Markownikoff adduct under conditions of kinetic control. The Markownikoff adducts are found to be favoured thermodynamically.

DENNIS G. GARRATT, PIERRE L. BEAULIEU et VERONIQUE M. MORISSET. Can. J. Chem. **59**, 927 (1981).

On rapporte la réaction du chlorure de benzènesélénenyle avec vingt-deux alcools propargyliques en solution dans le chlorure de méthylène. Des produits d'addition de type Markownikoff et anti-Markownikoff se forment d'une manière *anti* stéréospécifique. On a trouvé que la régiosélectivité ou la spécificité dépendent fortement de la nature des substituants géminaux de l'unité alcoolique. En général la présence de substituants géminaux encombrants sur la portion alcoolique tend à favoriser cinétiquement la formation d'adduits anti-Markownikoff. Les adduits du type Markownikoff sont thermodynamiquement favorisés.

[Traduit par le journal]

Can. J. Chem. Downloaded from www.nrcresearchpress.com by 210.87.254.42 on 09/06/12
For personal use only.

Many investigators during the last few years have studied the utility of organoselenium compounds as reagents for cyclofunctionalizations (1–14). Our interest in allene chemistry had led us during this period to study electrophilically-induced cyclizations of α-allenic alcohols as a stereospecific synthesis of 2,5-dihydrofurans (15).

[1] $H_2C{=}C{=}CHCH_2OH \longrightarrow$ 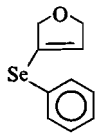

As precursors to these allenic alcohols and allenes in general, it was necessary for us to prepare a large number of propargyl alcohols. The very facile nature of the allenic cyclization reactions suggested to us that we might be able to force a cyclization of our propargyl alcohols (eq. [2]) to either oxacyclobutenes or methyleneepoxides. These experiments were, however, unsuccessful. Simultaneously, Filer and co-workers arrived at similar conclusions (16).[4] The only products observed and isolable were those of simple 1,2-addition. Several differences are, however, to be noted between our individual studies. Because of our prior interest in electrophilic additions to alkynes (17–21), we decided to complete our initial investigation. The results of this study are reported herein.

[2] 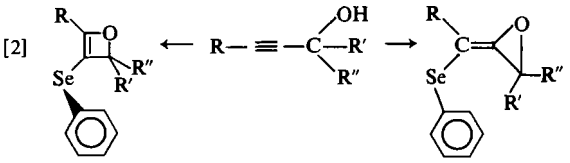

Results and Discussion

The reaction of benzeneselenenyl chloride with propargyl alcohols, **1–22**, gives one or both of the two possible regioisomers of *anti* stereospecific addition (eq. [3]). Reaction times were found to vary greatly, from a few seconds or minutes for species **1–3** to a few weeks for species **4**, **21**, and **22**, when the reactions were carried out in methylene chloride solution at ambient temperatures (20–24°C). Isolated yields are normally essentially quantitative, although some adducts proved unstable after a few days. The initially observed product distributions are given in Table 1.

Assignment of alkene configuration as *E* has been made on the basis of vicinal carbon-13 –

[1] Issued as NRCC No. 18898.

[2] Author to whom correspondence may be addressed at the Division of Chemistry, National Research Council of Canada, Ottawa, Ont., Canada K1A 0R6.

[3] Current address: Department of Chemistry, University of Alberta, Edmonton, Alta., Canada T6G 2G2.

[4] C. Filer, private communication.

0008-4042/81/060927-08$01.00/0

©1981 National Research Council of Canada/Conseil national de recherches du Canada

Can. J. Chem. Downloaded from www.nrcresearchpress.com by 210.87.254.42 on 09/06/12
For personal use only.

[3] 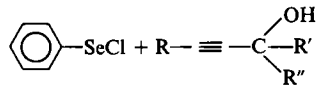

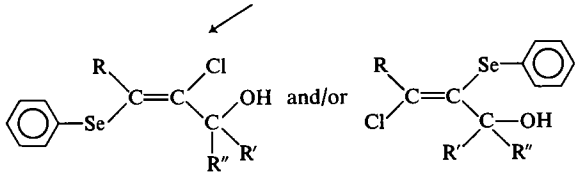

Markownikoff adduct anti-Markownikoff adduct

	R	R′	R″
1	H	CH_3	CH_3
2	H	C_2H_5	C_2H_5
3	H	i-C_3H_7	i-C_3H_7
4	H	t-C_4H_9	t-C_4H_9
5	H	C_6H_5	C_6H_5
6	H	CH_3	C_2H_5
7	H	CH_3	t-C_4H_9
8	H	CH_3	C_6H_5
9	H	H	C_6H_5
10	H	H	i-$C_{10}H_7$
11	c-C_6H_{11}	H	i-C_3H_7
12	i-C_4H_9	i-C_4H_9	i-C_4H_9
13	C_2H_5	C_2H_5	C_2H_5
14	C_2H_5	CH_3	t-C_4H_9
15	t-C_4H_9	CH_3	i-C_3H_7

proton coupling constants, $^3J_{CC=CH}$. Previous studies in these laboratories and elsewhere (22–25) have shown that $^3J_{CC=CH}(trans)$ is greater than or equal to $^3J_{CC=CH}(cis)$ and that the *trans* couplings are normally in the range of 8 to 11 Hz, as observed during this study. Also of some diagnostic utility were vicinal selenium-77 – proton, $^3J_{SeC=CH}$, and selenium-77 – carbon-13, $^3J_{CC=CSe}$, couplings and allylic carbon-13 – proton couplings, $^4J_{HC=CCH}$ (26, 27).

Assignment of adduct regiochemistry as Markownikoff, M, or anti-Markownikoff, aM, follows from an examination of their respective ^1H and ^{13}C nmr chemical shifts. In particular, it is noted that adducts derived from terminal propargyl alcohols, **1–10** and **16–21** have very diagnostic ^1H nmr spectra. The vinyl protons of the Markownikoff adducts are observed to resonate in the range δ 5.70–5.92 ppm, whereas the vinyl protons of the anti-Markownikoff adducts resonate in the range δ 6.20–6.47 ppm. Confirmation of these assignments is found in the analogous ^{13}C nmr chemical shifts for the olefinic methine carbon. For the Markownikoff adducts these carbons resonate between δ 110.1 and 116.1, whereas in the case of the anti-Markownikoff adducts the carbons resonate in the region 119.1–127.7.

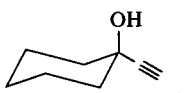

16

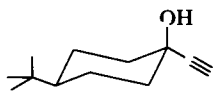

17

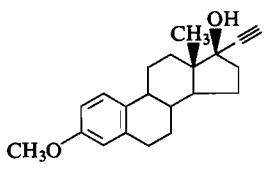

18

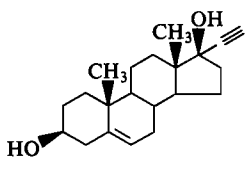

19

In making the assignments given in Table 1, we note that we have reversed the regiochemistry originally assigned by Filer *et al.* for the adduct of benzeneselenenyl chloride and alkyne **16**. Full spectral data are given in the Experimental.

An examination of Table 1 shows the rather surprising result that twelve out of twenty-two of the propargyl alcohols give products of regiospecific Markownikoff addition, and that eight of the remaining ten give products of regiospecific anti-Markownikoff addition. ^1H nuclear magnetic resonance studies over a period of five to six months further showed that those adducts initially formed with the anti-Markownikoff orientation, isomerize slowly and stereospecifically to the corresponding Markownikoff isomer of *E* configuration. The Markownikoff species, in contrast, show no tendency to isomerize. These data therefore suggest that the anti-Markownikoff adducts are formed under conditions of kinetic control, and that the Markownikoff adducts are products of thermodynamic control.

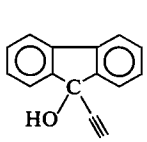

20

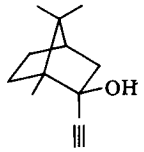

21

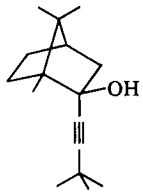

22

Mechanistically such a scenario is readily interpretable. The observation of anti-Markownikoff addition under conditions of kinetic control clearly indicates that the alkyl groups exert a strong steric effect in the product determining transition state. If one assumes that the selenenylation of propargyl alcohols follows a reaction hypersurface similar to that proposed for simple alkynes (20), it is clear that

Can. J. Chem. Downloaded from www.nrcresearchpress.com by 210.87.254.42 on 09/06/12
For personal use only.

TABLE 1. Initially observed product distributions for the addition of benzeneselenenyl chloride to some propargyl alcohols in methylene chloride solution at ambient temperature

Propargyl alcohol	% Composition	
	Markownikoff	anti-Markownikoff
1	100	0
2	100	0
3	100	0
4	32*	68*
5	100	0
6	100	0
7	0	100
8	100	0
9	0	100
10	0	100
11	20	80
12	100	0
13	100	0
14	100	0
15	100	0
16	100	0
17	0	100
18	0	100
19	0	100
20	100	0
21	0	100
22	0	100

*Product composition determined when reaction reached 85% completion. This is neither a kinetic nor a thermodynamic product distribution.

the carbon of the substituent, the selenirenium ring, and the entering chloride ion must all lie in the same plane. Consequently the steric hindrance to attack at the terminal position is less than attack at the most substituted center, thus leading to the preferential formation of the anti-Markownikoff species.

Our hypothesis suggests that in those cases where regiospecific Markownikoff addition is observed, the observation of regiospecific addition might arise from a very fast isomerization of the form: aM → M. In order to test this concept we initially carried out nmr experiments using alkynes **1**, **3**, and **16**, wherein we were able to monitor the course of the reaction as a function of time. In all three cases only the Markownikoff adducts were observable. If one, at this point, makes the assumption that the products of kinetic control are indeed of the anti-Markownikoff regiochemistry, we are left with the conclusion that in these cases the rates of isomerization, aM → M, are much faster than the rates of addition.

In contrast to the above, a similar experiment using alkyne **4** showed, at approximately 5% reaction, only the presence of the anti-Markownikoff adduct. However, when the reaction had reached 85% completion, the ratio M:aM had increased to 32:68. While our data, in this case, are inconclusive due to the poor sensitivity of the ^{1}H nmr technique, it seems possible that the rate of isomerization of the anti-Markownikoff adduct is competitive with the initial rate of addition. A direct comparison of rates, however, is difficult since the first step (the addition reaction) is almost certainly a second-order process (eq. [4]), first-order in alkyne and first-order in selenenyl chloride (20), whereas the second step (the isomerization) is most likely a first-order process (eq. [5]). The formation of a single isomer of *E* configuration from this latter process suggests that the isomerization occurs with neighbouring group assistance by selenium, passing by way of a selenirenium ion-like intermediate, **23** (20, 21, 28).

A third situation is found in the additions to the steroidal alkynes, **18** and **19**. In these cases, the rates of isomerization are much slower than the rates of addition. For example, the reaction of 5-androsten-17α-ethynyl-3β,17β-diol, **19**, with benzeneselenenyl chloride under standard conditions (temperature, concentration) reaches completion after approximately 30 h. The subsequent isomerization, however, has a half-life of approximately 3 months.

Perhaps the most surprising observation, as seen on examination of Table 1, concerns the two cyclohexylethynes, **16** and **17**. 1-Ethynylcyclohexanol, **16**, is observed to give the Markownikoff adduct regiospecifically, whereas its 4-*tert*-butyl derivative gives the anti-Markownikoff adduct regiospecifically. Two factors may be important in this situation. From a semi-quantitative point of view we note that $k_1' \ll k_1(\text{eq}) + k_1(\text{ax})$ and

[4] $C_6H_5SeCl + H{-}{\equiv}{-}C(OH)(C_4H_9) \rightarrow$ Cl, H, OH, SeC_6H_5

[5] Cl, OH, H, SeC_6H_5 → HO, H, Se^+, C_6H_5, Cl^- (**23**) → H, Cl, C_6H_5Se, HO

Can. J. Chem. Downloaded from www.nrcresearchpress.com by 210.87.254.42 on 09/06/12
For personal use only.

[6]

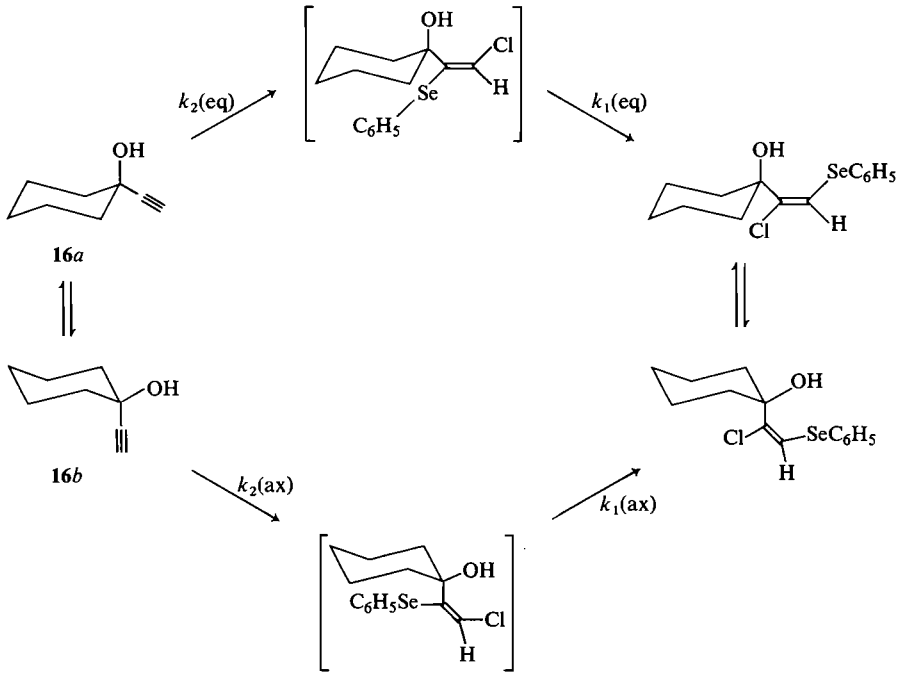

that $k_2' < k_2(\text{eq}) + k_2(\text{ax})$ (see eqs. [6] and [7]). For example, the reaction with **16** reaches completion within 2–3 min under conditions wherein the analogous reaction with **17** requires 12–15 h. Furthermore, while **16** yields immediately the Markownikoff isomer as the only observable product, **17** gives the anti-Markownikoff adduct which subsequently isomerizes completely to the Markownikoff species over a period of 3–4 weeks.

The only physical difference between the two systems is the presence of a *tert*-butyl group on C4 of alkyne **17**, a position which must be considered remote relative to the reaction site. The differences in reactivity must therefore be related to either a long range inductive effect or to conformation. In the case of **17**, the ethynyl group is held in an equatorial conformer by virtue of its *trans* relationship to the *tert*-butyl group (29). For **16**, however, it seems reasonable that an equilibrium exists between the two possible chair conformers, **16***a* and **16***b*. Clearly the ethynyl groups in **16***a* and **16***b* may have different reactivities (30). Since axial substituents are generally considered to be in a more crowded environment than equatorial substituents, and since the steric requirements of the transition state for this addition reaction may be considered greater than the steric requirements of the ground states, the conclusion is drawn that the axial ethynyl group in **16***b* should react more slowly than its equatorial analogue in **16***a*. On this basis one predicts that **17** will react faster than **16**, since **16** is a mixture of both conformers. Our results, however, show the opposite. We find that **16** reacts faster than **17**. Clearly some other factor is responsible.

One possibility is that selenirenium ion formation is stabilized by means of the adjacent hydroxy group by donation of an electron lone-pair from oxygen, **24** (31, 32). In support of this scenario, model studies using Dreiding molecular models indicate that an equatorial hydroxy group is better situated to interact with the developing selenirenium ion than its axial counterpart.

A stabilizing effect on the part of the hydroxy group may also account for the somewhat unprecedented regiochemical isomerizations (20). For example, the reaction of benzeneselenenyl chloride with ethynylcyclohexane under equivalent conditions to those used during this study leads to a 89:11 mixture of the respective anti-Markownikoff

[7]

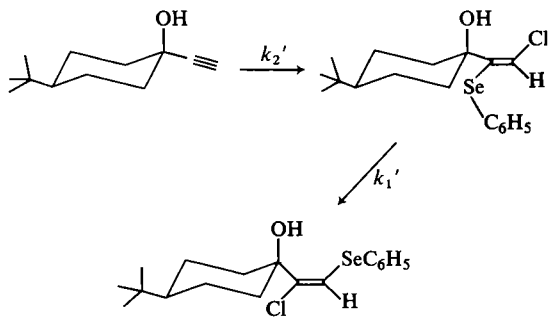

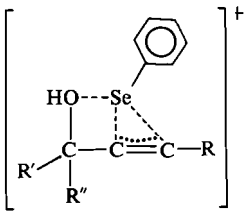

24

25, and Markownikoff, 26, adducts (eq. [8]). These adducts, in contrast to those derived from 16 and 17, show no tendency, even after four months in methylene chloride solution at ambient temperature, to isomerize!

[8] 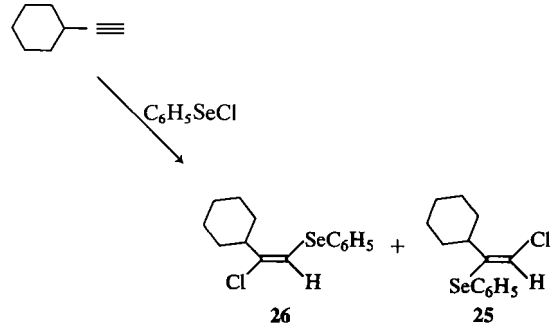

If our hypothesis of a stabilizing interaction between oxygen and selenium is correct, the absence of products of internal cyclization, which both we and Filer *et al.* (16) sought, is readily explained. Additional studies are in progress in an effort to further ascertain the mechanism of this reaction.

Experimental

General

The ^1H and ^{13}C nmr spectra were run on Varian HA-100, T-60, and FT80-16K spectrometers and on a Bruker WP-80 spectrometer. Chloroform-*d* was used as an internal lock and reference for ^{13}C nmr experiments. All spectral parameters are referenced to TMS. Determination of carbon-13 – proton coupling constants and selenium – carbon-13 coupling constants is based upon first-order analysis of the fully coupled spectra, and may not thus represent true *J* values. Infrared spectra were recorded on a Unicam SP1100 spectrometer using neat liquid films or CCl_4 solutions in NaCl cavity cells. Melting points were recorded on a Fisher-Johns block and are reported uncorrected.

Terminal Propargyl Alcohols

General Procedure

Terminal propargyl alcohols were isolated from the reaction of ethynylmagnesium bromide with various ketones and aldehydes in THF solutions. Simple aldehydes and ketones were commercially available from Aldrich, Chemical Samples, and Eastman Kodak. 3-Methyl-2-pentanone was prepared according to known methods (33). 2,2-Dimethyl-3-propanal was obtained by alkylation of isobutyraldehyde using solid–liquid phase transfer catalysis according to the method of Purohit and Subramanium (34). Ethynylmagnesium bromide was prepared by the slow addition of ethylmagnesium bromide to a saturated solution of purified acetylene in THF under a vigorous stream of acetylene. The ketone or aldehyde was subsequently added and the mixture refluxed overnight. Hydrolysis with dilute aqueous HCl, extraction with ether, drying over $MgSO_4$, and distillation or recrystallization yielded the alcohols in 40–50% yields.

3-Isopropyl-2-methyl-4-pentyn-3-ol

Acetylene was purified by passing through a trap at −50°C, concentrated H_2SO_4, NaOH pellets, and anhydrous $CaSO_4$. It was then bubbled for 10 min in 200 mL of dried THF before the addition of 0.5 mol of ethylmagnesium bromide in 250 mL of THF. The Grignard reagent was added very slowly while a vigorous stream of acetylene was passed through the reaction mixture. The solution turned dark brown during the addition. Subsequently, 2,4-dimethyl-3-pentanone, 0.3 mol, was added and the mixture refluxed overnight. Normal acidic work-up and distillation at atmospheric pressure yielded the desired alcohol in 62% yield, bp 168–169°C.

Disubstituted Propargyl Alcohols

Monosubstituted acetylenes were treated with a 10% excess of *n*-butyllithium in THF at 0°C under nitrogen. The resulting mixture was stirred for 2 h and subsequently a 10% excess of an aldehyde or ketone in THF was added to the reaction mixture which was then refluxed for a further 2 h. Saturated aqueous NH_4Cl hydrolysis, extraction with ether, and distillation yielded the pure alcohols.

5-Cyclohexyl-2-methyl-4-pentyn-3-ol

Cyclohexylethyne (Chemical Samples Co.), 0.1 mol, was dissolved in 25 mL of dried THF under a nitrogen atmosphere. A 10% excess of 1.6 *M n*-BuLi in hexane was added at 0°C. The mixture was stirred for 2 h. Isobutyraldehyde, 0.11 mol, was added at room temperature and the mixture refluxed for 2 h. Normal work-up and distillation under reduced pressure gave the pure alcohol in 81% yield, bp 120–122°C/14 Torr.

Spectral Parameters and Physical Data for the Propargyl Alcohols

2-Methyl-3-butyn-2-ol, 1: bp 110–112°C/760 Torr, yield 47%; ir (cm^{-1}): 3370 (s, C≡CH), 3500 (mb, OH) 3680 (m, free OH); ^{13}C nmr δ: 64.6 (s), 89.2 (s), 69.9 (d), 31.4 (q).

3-Ethyl-1-pentyn-3-ol, 2: bp 50–55°C/10 Torr, yield 44%; ir (cm^{-1}): 3380 (s, C≡CH), 3500 (sb, OH), 3690 (m, free OH); ^{13}C nmr δ: 72.0 (s), 86.8 (s), 72.4 (d), 34.2 (t), 8.5 (q).

3-Isopropyl-4-methyl-1-pentyn-3-ol, 3: bp 168–169°C/760 Torr, yield 62%; ir (cm^{-1}): 3370 (s, C≡CH), 2140 (w, C≡C), 3550 (sb, OH), 3700 (m, free OH); ^{13}C nmr δ: 77.3 (s), 85.1 (s), 73.2 (d), 34.1 (d), 17.77 (q), 16.00 (q).

3-tert-Butyl-4,4-dimethyl-1-pentyn-3-ol, 4: bp 76–80°C/11 Torr, yield 17%; ir (cm^{-1}): 3370 (s, C≡CH), 2140 (w, C≡C), 3700 (s, free OH), no band for H-bonded OH was observed in this case; ^{13}C nmr δ: 80.9 (s, *C*OH), 87.1 (s, *C*≡CH), 73.4 (d, C≡*C*H), 41.1 (s, *t*Bu), 28.5 (q, *t*Bu).

1,1-Diphenyl-2-propyn-1-ol, 5: bp 150–160°C/0.25 Torr, yield 75%; ir (cm^{-1}): 3370 (s, C≡CH), 2145 (w, C≡C), 3600 (mb, OH), 3750 (m, free OH); ^{13}C nmr δ: 74.2 (s, *C*OH), 86.4 (s, *C*≡CH), 75.5 (d, C≡*C*H), 144.4 (s, C_x), 128.2 (d), 126.0 (d), 127.7 (d).

3-Methyl-1-pentyn-3-ol, 6: bp 120°C/760 Torr, yield 52%; ir (cm^{-1}): 3375 (s, C≡CH), 3500 (sb, OH), 3690 (m, free OH); ^{13}C nmr δ: 68.4 (s, *C*OH), 87.9 (s, *C*≡CH), 71.1 (d, C≡*C*H), 36.4 (t, Et), 8.9 (q, Et), 29.1 (q, Me).

3,4,4-Trimethyl-1-pentyn-3-ol, 7: bp 145–148°C/760 Torr, yield 62%; ir (cm^{-1}): 3365 (s, C≡CH), 3550 (mb, OH), 3690 (m, free OH); ^{13}C nmr δ: 73.6 (s, *C*OH), 87.6 (s, *C*≡CH), 71.7 (d, C≡*C*H), 37.8 (s, *t*Bu), 24.9 (q, *t*Bu), 24.7 (q, Me).

Can. J. Chem. Downloaded from www.nrcresearchpress.com by 210.87.254.42 on 09/06/12
For personal use only.

Can. J. Chem. Downloaded from www.nrcresearchpress.com by 210.87.254.42 on 09/06/12
For personal use only.

2-Phenyl-3-butyn-1-ol, 8: bp 108–111°C/7 Torr, yield 41%; ir (cm^{-1}): 3370 (s, C≡CH), 2140 (w, C≡C), 3500 (sb, OH); ^{13}C nmr δ: 69.8 (s, *C*OH), 87.3 (s, *C*≡CH), 73.1 (d, C≡*C*H), 33.1 (q, Me), 145.1 (s, Ph), 128.3 (d, Ph), 124.9 (d, Ph), 127.7 (d, Ph).

1-Phenyl-2-propyn-1-ol, 9: bp 117–120°C/10 Torr, yield 61%; ir (cm^{-1}): 3375 (s, C≡CH), 2150 (w, C≡C), 3500 (sb, OH), 3700 (m, free OH); ^{13}C nmr δ: 63.9 (d, *C*OH), 83.7 (s, *C*≡CH), 74.8 (d, C≡*C*H), 140.1 (s, Ph), 128.5 (d, Ph), 126.7 (d, Ph), 128.3 (d, Ph).

1-(1'-Naphthyl)-2-propyn-1-ol, 10: bp 180–186°C/0.35 Torr, yield 35%; ir (cm^{-1}): 3375 (s, C≡CH), 3400–3600 (sb, OH), 3700 (m, free OH).

1-Cyclohexyl-4-methyl-1-pentyn-3-ol, 11: bp 120–121°C/12 Torr, yield 81%; ir (cm^{-1}): 3300–3600 (sb, OH), 3700 (m, free OH); ^{13}C nmr δ: 68.0 (d, *C*OH), 80.0 (s), 90.1 (s), 29.0 (d), 32.8 (t), 24.8 (t), 26.0 (t), 34.7 (d, *i*Pr), 18.28 (q, *i*Pr), 17.43 (q, *i*Pr).

3-Ethyl-4-heptyn-3-ol, 13: bp 172–176°C/760 Torr, yield 45%; ir (cm^{-1}): 2265 (w, C≡C), 3400–3600 (sb, OH), 3700 (m, free OH).

3,4,4-Trimethyl-4-heptyn-3-ol, 14: bp 78–80°C/13 Torr, yield 62%; ir (cm^{-1}): 2270 (w, C≡C), 3450–3650 (sb, OH), 3710 (m, free OH); ^{13}C nmr δ: 73.7 (s, *C*OH), 83.2 (s, C≡C), 85.1 (s, C≡C), 13.8 (t, Et), 12.1 (q, Et), 38.0 (s, *t*Bu), 25.0 (q, *t*Bu, Me).

2,3,6,6-Tetramethyl-4-heptyn-3-ol, 15: bp 72–77°C/10 Torr, yield 75%; ir (cm^{-1}): 2280 (w, C≡C), 3400–3600 (sb, OH), 3705 (m, free OH).

1-Ethynylcyclohexanol, 16: bp 81–83°C/10 Torr, yield 61%; ir (cm^{-1}): 3375 (s, C≡CH), 2140 (w, C≡C), 3400 (sb, OH), 3680 (m, free OH); ^{13}C nmr δ: 68.5 (s, *C*OH), 87.9 (s, *C*≡CH), 72.1 (d, C≡*C*H), 39.8 (t), 23.1 (t), 25.1 (t).

Trans-*1-Ethynyl-4-*tert*-butylcyclohexanol, 17*: recrystallized from 40–60° pet. ether, mp 98–99°C, yield 67%; ir (cm^{-1}): 3370 (s, C≡CH), 3500 (wb, OH), 3670 (m, free OH); ^{13}C nmr δ: 27.7 (q, *t*Bu), 32.3 (s, *t*Bu), 47.2 (d, C4), 24.8 (t, C3, 5), 40.3 (t, C2, 6), 69.5 (s, *C*OH), 87.2 (s, *C*≡CH), 72.8 (d, C≡*C*H).

1,3,5(10)-Estratrien-17α-ethynyl-3β,17β-diol 3-Methyl Ether (Aldrich), **18**: ^{13}C nmr δ: 126.3 (C1), 111.5 (C2), 157.5 (C3), 113.9 (C4), 137.9 (C5), 29.8 (C6), 27.6 (C7), 39.0 (C8), 43.5 (C9), 132.6 (C10), 26.4 (C11), 39.5 (C12), 47.1 (C13), 49.5 (C14), 22.8 (C15), 32.8 (C16), 79.9 (C17), 12.8 (C18), 55.2 (q, MeO), 87.6 (s, *C*≡CH), 74.0 (d, C≡*C*H).

5-Androsten-17α-ethynyl-3β,17β-diol (Steraloids, Inc.), **19**: mp 242–245°C, rot. −124° (dioxane, 25°C); ^{13}C nmr δ: 39.0 (C1), 31.5 (C2), 71.8 (C3), 46.7 (C4), 140.9 (C5), 121.4 (C6), 32.6 (C7), 31.7 (C8), 50.8 (C9), 42.3 (C10), 20.8 (C11), 37.3 (C12), 50.7 (C13), 49.8 (C14), 23.2 (C15), 36.6 (C16), 80.0 (C17), 12.7 (C18), 19.5 (C19), 88.1 (s, *C*≡CH), 74.0 (d, C≡*C*H).

endo-*2-Ethynyl-1,7,7-trimethylbicyclo[2.2.1]heptan-2-ol*, prepared from *d*-camphor, **21**: mp 207.5–209°C, yield 47%; ir (cm^{-1}): 3375 (s, C≡CH), 3500 (wb, OH), 3690 (m, free OH); ^{13}C nmr δ: 53.7 (s, C1), 77.9 (s, C2), 48.5 (t, C3), 45.4 (d, C4), 32.6 (t, C5), 27.0 (t, C6), 47.9 (s, C7), 21.4 (q, MeC7), 21.0 (q, MeC7), 10.4 (q, MeC1), 87.6 (s, *C*≡CH), 77.9 (d, C≡*C*H).

endo-*3',3'-Dimethylbutynyl-1,7,7-trimethylbicyclo[2.2.1]-heptan-2-ol*, prepared from *d*-camphor, **22**: ^{13}C nmr δ: 53.1 (s, C1), 77.9 (s, C2), 48.6 (t, C3), 45.6 (d, C4), 32.7 (t, C5), 26.9 (t, C6), 47.8 (s, C7), 21.5 (q, MeC7), 21.1 (q, MeC7), 10.3 (q, MeC1), 92.0 (s, *C*≡C*t*Bu), 82.9 (s, C≡*C*t*Bu*), 27.4 (s, *t*Bu), 31.2 (q, *t*Bu).

Benzeneselenenyl chloride was purchased from Aldrich and recrystallized prior to use, mp 64.3°C.

Product Studies

General Procedure

To a solution of the respective propargyl alcohol (6.00 mmol) in 25 mL of anhydrous CH_2Cl_2 was added an equivalent (6 mmol) of benzeneselenenyl chloride as a solution in 5 mL of anhydrous CH_2Cl_2. The additions were carried out such that the propargyl alcohol was always retained in excess. After the solutions had become colourless or pale yellow the solvent was evaporated, and the residual oils analyzed by ^1H and ^{13}C nmr. Samples were further analyzed after purification on silica gel plates and/or columns. Control experiments run in CD_2Cl_2 and subjected to immediate ^1H nmr analysis showed the same product distributions as those found above, Table 1.

Anti-Markownikoff Adducts

*1,3,5(10)-Estratrien-17α-(*E*-1'-phenylseleno-2'-chloroethenyl)-3β,17β-diol 3-Methyl Ether*: prepared from **18** in 88% yield; ^1H nmr δ: 6.62 (s, 1H), 2.8 (bs, 1H, CO*H*), 0.97 (s, 3H, Me at C17), 3.72 (s, 3H, Me at C3); ^{13}C nmr δ: 141.0 (s, =*C*Se), 121.7 (d, =*C*HCl), 132.2 (s, C_{Se}), 132.0 (d, C_o), 129.5 (d, C_m), 127.6 (d, C_p), 126.1 (d, C1), 111.4 (d, C2), 157.5 (s, C3), 113.8 (d, C4), 137.9 (s, C5), 29.7 (t, C6), 27.5 (t, C7), 39.7 (d, C8), 43.3 (d, C9), 132.5 (s, C10), 26.5 (t, C11), 35.4 (t, C12), 50.6 (s, C13), 50.1 (d, C14), 23.8 (t, C15), 33.9 (t, C16), 87.9 (s, C17), 14.7 (q, C18), 55.1 (q, MeO at C3). *Anal.* calcd. for $C_{27}H_{31}O_2SeCl$: C 64.61, H 6.23, Cl 7.06, Se 15.73; found: C 64.64, H 6.41, Cl 7.28, Se 15.94.

*5-Androsten-17α-(*E*-1'-phenylseleno-2'-chloroethenyl)-3β,17β-diol*: prepared from **19** in 95% yield, ^1H nmr δ: 6.52 (s, 1H), 2.53 (bs, 2H, CO*H* at C17 and C3), 1.00 (s, 3H, Me at C17), 0.93 (s, 3H, Me at C10), 5.32 (m, 1H, =C*H* at C6); ^{13}C nmr δ: 141.4 (s, =*C*Se), 121.3 (d, =*C*HCl), 132.1 (s, C_{Se}), 132.1 (d, C_o), 129.5 (d, C_m), 127.6 (d, C_p), 37.2 (t, C1), 31.6 (t, C2), 71.6 (d, C3), 42.2 (t, C4), 140.8 (s, C5), 121.3 (d, C6), 32.8 (t, C7), 31.6 (d, C8), 50.0 (d, C9), 35.1 (s, C10), 21.0 (t, C11), 36.5 (t, C12), 49.7 (s, C13), 51.3 (d, C14), 24.2 (t, C15), 33.7 (t, C16), 87.8 (s, C17), 14.6 (q, C18), 19.5 (q, C19). *Anal.* calcd. for $C_{27}H_{35}O_2SeCl$: C 64.09, H 6.97, Cl 7.01, Se 15.61; found: C 64.32, H 7.04, Cl 6.88, Se 15.64.

E-*1-Cyclohexyl-1-chloro-2-phenylseleno-4-methyl-1-penten-3-ol*: prepared from **11**: ^1H nmr δ: 2.3 (bs, 1H), 7.0–7.7 (m, 5H), 0.98 (d, 3H), 1.12 (d, 3H); ^{13}C nmr δ: 147.7 (s), 127.2 (s), 132.9 (s, Ph), 131.9 (d, Ph), 129.9 (d, Ph), 127.7 (d, Ph), 78.0 (d, *C*HOH), 47.5 (d, c-hex), 35.1 (d, *i*Pr), 31.6 (t, c-hex), 30.3 (t, c-hex), 26.6 (t, c-hex), 19.6 (q, *i*Pr), 19.4 (q, *i*Pr). *Anal.* calcd. for $C_{18}H_{25}OSeCl$: C 58.15, H 6.78, Cl 9.54, Se 21.24; found: C 58.37, H 7.01, Cl 9.57, Se 21.20.

E-*1-Chloro-2-phenylseleno-3-*tert*-butyl-4,4-dimethyl-1-penten-3-ol*: prepared from **4**: ^1H nmr δ: 6.3 (s, 1H), 2.3 (bs, 1H), 1.17 (s, 9H), 1.26 (s, 9H); ^{13}C nmr δ: 119.2 (d, =*C*HCl), 136.5 (s, =*C*Se), 89.5 (s, *C*OH), 42.8 (s, *t*Bu), 29.7 (q, *t*Bu). *Anal.* calcd. for $C_{17}H_{25}OSeCl$: C 56.75, H 7.00, Cl 9.85, Se 21.95; found: C 56.59, H 7.06, Cl 9.69, Se 22.16.

E-*1-Chloro-2-phenylseleno-3,4,4-trimethyl-1-penten-3-ol*: prepared from **7** in 97% yield: ^1H nmr δ: 6.47 (s, 1H), 2.8 (bs, 1H, CO*H*), 1.67 (s, 3H), 1.02 (s, 9H), 7.0–7.6 (m, 5H); ^{13}C nmr δ: 142.3 (s, =CSe), 120.0 (d, $^1J_{CH}$ = 203.0 Hz, =*C*HCl), 80.6 (s, *C*OH), 41.1 (s, *t*Bu), 26.2 (q(h), $^1J_{CH}$ ≈ 125.3 Hz, $^3J_{CH}$ = 4.7 Hz, *t*Bu), 23.7 (q, $^1J_{CH}$ = 127.9 Hz, Me), 132.5 (d, Ph), 132.0 (s, Ph), 129.5 (d, Ph), 127.7 (d, Ph). *Anal.* calcd. for $C_{14}H_{19}OSeCl$: C 52.93, H 6.03, Cl 11.16, Se 24.85; found: C 53.01, H 6.17, Cl 11.09, Se 24.99.

E-*1-(1'-Naphthyl)-2-phenylseleno-3-chloro-2-propen-1-ol*: prepared from **10** in 95% yield: ^1H nmr δ: 6.20 (s, 1H), 6.57 (s, 1H), 2.7 (bs, 1H, CO*H*), 7.0–7.8 (12H); ^{13}C nmr δ: 138.3 (s, =*C*Se), 119.2 (d, =*C*HCl), 68.5 (d, *C*HOH), 133.6 (d), 128.9 (d), 126.0 (d), 135.4 (s), 133.3 (s), 130.4 (s), 128.6 (d), 128.3 (s), 127.7 (d), 125.3 (d), 124.9 (d), 124.0 (d), 122.9 (d). *Anal.* calcd. for $C_{19}H_{15}OSeCl$: C 61.06, H 4.05, Cl 9.49, Se 21.13; found: C 60.96, H 4.99, Cl 9.81, Se 21.06.

E-*1-Phenyl-2-phenylseleno-3-chloro-2-propen-1-ol*: prepared from **9** in 86% yield: ^1H nmr δ: 6.25 (s, 1H), 6.00 (s, 1H), 2.8 (bs,

Can. J. Chem. Downloaded from www.nrcresearchpress.com by 210.87.254.42 on 09/06/12
For personal use only.

1H, CO*H*), 6.9–7.7 (m, 10H); ^{13}C nmr δ: 140.4 (s, =*C*Se), 119.1 (d, *C*HCl), 71.2 (d, *C*HOH), 138.8 (s), 133.5 (d), 129.3 (d), 129.0 (d), 128.2 (d), 127.8 (d), 126.5 (s), 125.8 (d). *Anal.* calcd. for $C_{15}H_{13}OSeCl$: C 55.66, H 4.05, Cl 10.95, Se 24.39; found: C 55.58, H 4.11, Cl 10.78, Se 24.57.

trans-*1-(*E-*1'-Phenylseleno-2'-chloroethenyl)-4-*tert-*butylcyclohexanol*: prepared from **17** in 99% yield; ^{1}H nmr δ: 6.42 (s, 1H, =C*H*Cl), 3.6 (bs, 1H), 0.98 (s, 9H), 2.8 (bd, 1H), 1.0–2.5 (m, 8H); ^{13}C nmr δ: 121.1 (d, =*C*HCl), 139.9 (s, =*C*Se), 76.2 (s, *C*OH), 38.7 (t, c-hex), 24.5 (t, c-hex), 46,4 (d, c-hex), 32.2 (s, *t*Bu), 27.5 (q, *t*Bu), 131.4 (s, Ph), 132.6 (d, Ph), 129.5 (d, Ph), 127.6 (d, Ph). *Anal.* calcd. for $C_{18}H_{25}OSeCl$: C 58.15, H 6.78, Cl 9.54, Se 21.24; found: C 57.93, H 6.89, Cl 9.80, Se 21.00.

Markownikoff Adducts

E-*2-Methyl-3-chloro-4-phenylseleno-3-buten-2-ol*: prepared from **1** in quantitative yield, ^{1}H nmr δ: 5.83 (s, 1H), 2.78 (bs, 1H), 1.62 (s, 6H), 7.2–7.7 (m, 5H); ^{13}C nmr δ: 144.7 (s(m), =*C*Cl), 112.5 (d, $^1J_{CH}$ = 203.1 Hz, =*C*HSe), 134.4 (d(m), $^1J_{CH}$ = 163.6 Hz, C_o), 129.5 (d(m), $^1J_{CH}$ = 162.1 Hz, C_m), 129.2 (s, C_{Se}), 128.2 (d(t), $^1J_{CH}$ = 161.3 Hz, $^3J_{CH}$ = 7.2 Hz, C_p), 74.4 (s(dq'), $^2J_{CH}$ = 4.0 Hz, $^3J_{CH}$ = 8.0 Hz, *C*OH), 28.2 (q(q), $^1J_{CH}$ = 127.6 Hz, $^3J_{CH}$ = 4.0 Hz, Me). *Anal.* calcd. for $C_{11}H_{13}OSeCl$: C 47.93, H 4.75, Cl 12.86, Se 28.65; found: C 47.91, H 4.67, Cl 12.92, Se 28.53.

E-*1-Phenylseleno-2-chloro-3-ethyl-1-penten-3-ol*: prepared from **2** in 99% yield; ^{1}H nmr δ: 5.72 (s, 1H), 2.53 (bs, 1H), 1.88 (m, 4H), 0.95 (t, 6H), 7.1–7.5 (m, 5H); ^{13}C nmr δ: 143.4 (s, =*C*Cl), 110.7 (d, =*C*HSe), 79.7 (s, *C*OH), 31.8 (t, Et), 7.7 (q, Et), 135.6 (d, Ph), 129.5 (d, Ph), 128.6 (d, Ph), 131.4 (s, Ph). *Anal.* calcd. for $C_{13}H_{17}OSeCl$: C 51.42, H 5.64, Cl 11.67, Se 26.00; found: C 51.36, H 5.55, Cl 11.76, Se 26.32.

E-*1-Phenylseleno-2-chloro-3-isopropyl-4-methyl-1-penten-3-ol*: prepared from **3** in 99% yield; ^{1}H nmr δ: 5.92 (s, 1H), 2.43 (bs, 1H), 2.52 (m, 2H), 1.00 (d, 6H), 1.05 (d, 6H), 7.1–7.6 (m, 5H); ^{13}C nmr δ: 142.5 (s, =*C*Cl), 112.9 (d, $^1J_{CH}$ = 201.2 Hz, =*C*HSe), 83.9 (s(dt), $^3J_{CH}$ = 10.3 Hz, *C*OH), 34.5 (d, $^1J_{CH}$ = 126.9 Hz, *i*Pr), 18.2 (q(h), $^1J_{CH}$ = 125.3 Hz, $^3J_{CH}$ = 5.5 Hz, *i*Pr), 17.3 (q(h), $^1J_{CH}$ = 125.6 Hz, $^3J_{CH}$ = 4.8 Hz, *i*Pr), 135.5 (d, Ph), 129.8 (s, Ph), 129.6 (d, Ph), 128.6 (d, Ph). *Anal.* calcd. for $C_{15}H_{21}OSeCl$: C 54.31, H 6.38, Cl 10.69, Se 23.80; found: C 54.22, H 6.22, Cl 10.80, Se 23.62.

E-*1-Phenylseleno-2-chloro-3-*tert-*butyl-4,4-dimethyl-1-penten-3-ol*: prepared from **4** via the isomerization of the first formed aM adduct; ^{1}H nmr δ: 5.86 (s, 1H), 2.5 (bs, 1H), 1.21 (s, 18H); ^{13}C nmr δ: 137.8 (s, =*C*Cl), 110.1 (d, =*C*HSe), 87.1 (s, *C*OH), 41.2 (s, *t*Bu), 29.5 (q, *t*Bu).

E-*2-Chloro-3-phenylseleno-1,1-diphenyl-2-propen-1-ol*: prepared from **5** in 95% yield; ^{1}H nmr δ: 5.91 (s, 1H), 3.6 (bs, 1H), 7.07–7.8 (m, 15H); ^{13}C nmr δ: 143.5 (s, =*C*Cl), 116.1 (d, =*C*HSe), 82.2 (s, *C*OH), 135.0 (d), 129.6 (d), 128.6 (d), 129.3 (s). *Anal.* calcd. for $C_{21}H_{17}OSeCl$: C 63.09, H 4.29, Cl 8.87, Se 19.75; found: C 62.78, H 4.01, Cl 8.99,Se 19.59.

E-*1-Phenylseleno-2-chloro-3-methyl-1-penten-3-ol*: prepared from **6** in 97% yield; ^{1}H nmr δ: 5.73 (s, 1H), 0.93 (t, 3H), 2.60 (bs, 1H, CO*H*), 2.0 (m, 2H), 1.57 (s, 3H), 7.1–7.5 (m, 5H); ^{13}C nmr δ: 144.3 (s, =*C*Cl), 111.7 (d, $^1J_{CH}$ = 202.4 Hz, =*C*HSe), 76.9 (s, *C*OH), 32.9 (t, $^1J_{CH}$ = 125.2 Hz, Et), 7.9 (q, $^1J_{CH}$ = 125 Hz, Et), 26.4 (q, $^1J_{CH}$ = 127.1 Hz, Me), 134.9 (d(m), $^1J_{CH}$ = 164 Hz, C_o), 129.5 (d, $^1J_{CH}$ = 161 Hz, C_m), 129.1 (s, C_{Se}), 128.4 (d(t), $^1J_{CH}$ = 161.1 Hz, $^3J_{CH}$ = 7.8 Hz, C_p). *Anal.* calcd. for $C_{12}H_{15}OSeCl$: C 49.76, H 5.22, Cl 12.24, Se 27.26; found: C 50.01, H 5.32, Cl 12.16, Se 27.31.

E-*1-Methyl-1-phenyl-2-chloro-3-phenylseleno-2-propen-1-ol*: prepared from **8** in 99% yield; ^{1}H nmr δ: 5.87 (s, 1H), 2.98 (bs, 1H), 1.93 (s, 3H), 7.0–8.0 (m, 10H); ^{13}C nmr δ: 145.1 (s, =*C*Cl), 114.2 (d, =*C*HSe), 77.5 (s, *C*OH), 27.4 (q, Me), 134.9 (d), 129.6 (d), 128.4 (d), 129.0 (s), 144.1 (s), 128.2 (d), 125.5 (d), 127.5 (d). *Anal.* calcd. for $C_{16}H_{15}OSeCl$: C 56.91, H 4.48, Cl 10.50, Se 23.38; found: C 57.02, H 4.53, Cl 10.54, Se 23.28.

E-*2,8-Dimethyl-4-phenylseleno-5-chloro-6-isobutyl-4-nonen-6-ol*: prepared from **12** in 91% yield; ^{1}H nmr δ: 7.0–7.6 (m, 5H), 2.8 (d, 2H), 1.4–2.2 (m, 7H), 0.7–1.3 (m, 36H); ^{13}C nmr δ: 138.5 (s, C4), 138.3 (s, C5), 131.4 (s, Ph), 131.1 (d, Ph), 129.2 (d, Ph), 127.2 (d, Ph), 81.0 (s, *C*OH, C6), 51.5 (t, C3), 48.3 (t, C7), 27.8 (d, C2), 24.9 (d, C8), 24.6 (q, C9), 24.5 (q, C9'), 21.9 (q, C1). *Anal.* calcd. for $C_{21}H_{33}OSeCl$: C 60.65, H 8.00, Cl 8.52, Se 18.98; found: C 60.69, H 8.04, Cl 8.44, Se 19.03.

E-*3-Phenylseleno-4-chloro-5-ethyl-3-hepten-5-ol*: prepared from **13** in 88% yield; ^{1}H nmr δ: 2.9 (bs, 1H), 7.0–7.6 (m, 5H), 2.9 (q, 2H), 1.0 (t, 3H), 0.83 (t, 6H), 1.5–2.3 (m, 4H); ^{13}C nmr δ: 140.8 (s, C4), 134.7 (s, C3), 131.5 (s, Ph), 130.9 (d, Ph), 129.2 (d, Ph), 127.1 (d, Ph), 79.6 (s, *C*OH, C5), 37.1 (t, C2), 31.9 (t C6), 12.9 (q, C1), 8.3 (q, C7). *Anal.* calcd. for $C_{15}H_{21}OSeCl$: C 54.31, H 6.38, Cl 10.69, Se 23.80; found: C 54.42, H 6.48, Cl 10.37, Se 24.03.

E-*2,2,3-Trimethyl-4-chloro-5-phenylseleno-4-hepten-3-ol*: prepared from **14** in 96% yield; ^{13}C nmr δ: 143.4 (s, C4), 133.7 (s, C5), 130.8 (s, Ph), 129.3 (d, Ph), 128.9 (d, Ph), 126.4 (d, Ph), 75.4 (s, *C*OH, C3), 41.6 (s, *t*Bu, C2), 38.2 (t, Et, C6) 26.3 (q, *t*Bu, C1), 24.6 (q, Me), 12.6 (q, Et, C7). *Anal.* calcd. for $C_{16}H_{23}OSeCl$: C 55.58, H 6.70,Cl 10.25, Se 22.84; found: C 55.71, H 6.61, Cl 10.32, Se 22.97.

E-*2,3,6,6-Tetramethyl-4-chloro-5-phenylseleno-4-hepten-3-ol*: prepared from **15** in 93% yield; ^{13}C nmr δ: 131.8 (s, C5), 134.4 (s, C4), 131.3 (s, Ph), 131.5 (d, Ph), 129.2 (d, Ph), 127.7 (d, Ph), 71.6 (*C*OH, C3), 39.1 (d, *i*Pr, C2), 31.1 (q, *t*Bu, C7), 29.8 (s, *t*Bu, C6), 27.5 (q, Me), 18.0 (q, *i*Pr, C1), 17.5 (q, *i*Pr, C1'). *Anal.* calcd. for $C_{17}J_{25}OSeCl$: C 56.75, H 7.00, Cl 9.85, Se 21.95; found: C 56.69, H 7.31, Cl 9.99, Se 22.02.

*1-(*E-*2'-Phenylseleno-1'-chloroethenyl)cyclohexanol*: prepared from **16** in 99% yield; ^{1}H nmr δ: 5.83 (s, 1H), 2.5 (bs, 1H), 1.0–2.3 (m, 10H), 7.1–7.6 (m, 5H); ^{13}C nmr δ: 144.9 (s, =*C*Cl), 112.7 (d, $^1J_{CH}$ = 203.1 Hz, =*C*HSe), 75.8 (s, *C*OH), 34.5 (t, c-hex), 25.0 (t, c-hex), 21.5 (t, c-hex), 134.3 (d, Ph), 129.5 (d, Ph), 128.1 (d, Ph), 129.5 (s, Ph). *Anal.* calcd. for $C_{14}H_{17}OSeCl$: C 53.26, H 5.43, Cl 11.23, Se 25.01; found: C 53.18, H 5.39, Cl 11.06, Se 25.28.

trans-*1-(*E-*2'-phenylseleno-1'-chloroethenyl)-4-*tert-*butylcyclohexanol*: prepared from **17** by the isomerization of the first formed aM adduct in methylene chloride solution; ^{1}H nmr δ: 5.42 (s, 1H), 0.98 (s, 9H), 7.0–7.7 (m, 5H), 2.6 (bs, 1H), 1.0–3.2 (m, 9H); ^{13}C nmr δ: 114.3 (d, =*C*HSe), 146.5 (s, =*C*Cl), 74.8 (s, *C*OH), 36.6 (t, c-hex), 24.4 (t, c-hex), 47.4 (d, c-hex), 32.3 (s, *t*Bu), 27.5 (q, *t*Bu). *Anal.* found: C 58.21, H 6.81, Cl 9.86, Se 21.39.

E-*2-Chloro-3-phenylseleno-1,1-dibenzobutamethylene)-2-propen-1-ol ((9-Hydroxy-9-(*E-*1'-chloro-2'-phenylseleneoethenyl)fluorene))*: prepared from **20** in 99% yield; ^{1}H nmr δ: 5.70 (s, 1H), 2.88 (bs, 1H), 7.0–8.0 (m, 13H); ^{13}C nmr δ: 147.2 (s, =*C*Cl), 114.2 (d, =*C*HSe), 83.5 (s, *C*OH), 135.4 (d), 129.6 (d), 128.3 (d), 129.0 (s), 140.4 (s), 139.3 (s), 120.0 (d), 123.8 (d), 129.4 (d), 128.7 (d). *Anal.* calcd. for $C_{21}H_{15}OSeCl$: C 63.41, H 3.80, Cl 8.91, Se 19.85; found: C 63.35, H 3.88, Cl 8.79, Se 19.86.

Acknowledgements

The financial support of the Natural Sciences and Engineering Research Council of Canada for the portion of this work carried out at the University of Ottawa is greatfully acknowledged, as is the aid of Mr. H. Séguin in carrying out the elemental analyses.

1. D. L. J. CLIVE, G. CHITTATTU, and C. K. WONG. Can. J. Chem. **55**, 3894 (1977).
2. D. L. J. CLIVE, C. K. WONG, W. A. KIEL, and S. M. MENCHEN. J. Chem. Soc. Chem. Commun. 379 (1978).
3. P. A. GRIECO, Y. YOKOYAMS, S. GILMAN, and M. NISHIZAWA. J. Org. Chem. **42**, 2034 (1977).
4. R. M. SCARBOROUGH, JR., A. B. SMITH III, W. E. BARNETTE, and K. C. NICOLAOU. J. Org. Chem. **44**, 1742 (1979).
5. C. L. PEDERSEN. J. Chem. Soc. Chem. Commun. 704 (1974).
6. K.C. NICOLAOU, W. E. BARNETTE, and R. L. MAGOLDA. J. Am. Chem. Soc. **100**, 2567 (1978).
7. D. L. J. CLIVE, G. CHITTATTU, N. J. CURTIS, W. A. KIEL, and C. K. WONG, J. Chem. Soc. Chem. Commun. 725 (1977).
8. K. C. NICOLAOU, W. J. SIPIO, R. L. MAGOLDA, and D. A. CLAREMON. J. Chem. Soc. Chem. Commun. 83 (1979).
9. A. TOSHIMITAU, S. UEMURA, and M. OKANO. J. Chem. Soc. Perkin Trans. I, 1206 (1979).
10. D. L. J. CLIVE. Aldrichimica Acta, **11**, 43 (1978).
11. D. L. J. CLIVE and G. CHITTATTU. J. Chem. Soc. Chem. Commun. 484 (1977).
12. K. C. NICOLAOU and Z. LYSENKO. J. Am. Chem. Soc. **99**, 3185 (1977).
13. K. C. NICOLAOU and Z. LYSENKO. Tetrahedron Lett. 1257 (1977).
14. D. L. J. CLIVE, G. CHITTATTU, and C. K. WONG. J. Chem. Soc. Chem. Commun. 441 (1978).
15. P. L. BEAULIEU, V. M. MORISSET, and D. G. GARRATT. Tetrahedron Lett. **21**, 129 (1980).
16. C. N. FILER, D. AHERN, R. FAZIO, and E. J. SHELTON. J. Org. Chem. **45**, 1313 (1980).
17. K. YATES, G. H. SCHMID, T. W. REGULSKI, D. G. GARRATT, H.-W. LEUNG, and R. S. MCDONALD. J. Am. Chem. Soc. **95**, 160 (1973).
18. G. H. SCHMID, A. MODRO, F. LENZ, D. G. GARRATT, and K. YATES. J. Org. Chem. **41**, 2331 (1976).
19. G. H. SCHMID, A. MODRO, D. G. GARRATT, and K. YATES. Can. J. Chem. **54**, 3045 (1976).
20. G. H. SCHMID and D. G. GARRATT. Chem. Scr. **10**, 76 (1976).
21. D. G. GARRATT and G. H. SCHMID. Chem. Scr. **11**, 170 (1977).
22. D. G. GARRATT and P. BEAULIEU. Can. J. Chem. **57**, 119 (1979).
23. J. E. ANDERSON. Tetrahedron Lett. 4079 (1975).
24. G. L. KARABATSOS, J. D. GRAHAM, and F. M. VANE. J. Am. Chem. Soc. **84**, 37 (1962).
25. C. A. KINGSBURY, D. DRANEY, A. SOPCHIK, W. RISSLER, and D. DURHAM. J. Org. Chem. **41**, 3863 (1976).
26. M. BARFIELD and S. STERNHELL. J. Am. Chem. Soc. **94**, 1905 (1972).
27. P. L. BEAULIEU and D. G. GARRATT. Can. J. Chem. Submitted.
28. G. H. SCHMID and D. G. GARRATT. Tetrahedron Lett. 3991 (1975).
29. S. WINSTEIN and N. J. HOLNESS. J. Am. Chem. Soc. **77**, 5562 (1955).
30. D. H. R. BARTON. Experientia, **6**, 316 (1950).
31. M. SHIMIZU, R. TAKEDA, and I. KUWAJIMA. Tetrahedron Lett. 3461 (1979).
32. M. SHIMIZU, R. TAKEDA, and I. KUWAJIMA. Tetrahedron Lett. 419 (1979).
33. F. C. WHITMORE, W. L. EVERS, and H. S. ROTHROCK. Org. Synthesis, Coll. Vol. II, Wiley, New York. 1965. p. 408.
34. V. G. PUROHIT and R. SUBRAMANIAN. Chem. Ind. 731 (1978).

Can. J. Chem. Downloaded from www.nrcresearchpress.com by 210.87.254.42 on 09/06/12
For personal use only.

The selective cleavage of permethylated glycopyranosiduronic acid linkages by oxidative decarboxylation with lead tetraacetate[1]

GERALD OLIVER ASPINALL,[2] HANY KAMAL FANOUS, NIMAL SAVITRI KUMAR,[3] AND VELUPILLAI PUVANESARAJAH

Department of Chemistry, York University, Downsview, Toronto, Ont., Canada M3J 1P3

Reveived October 21, 1980

GERALD OLIVER ASPINALL, HANY KAMAL FANOUS, NIMAL SAVITRI KUMAR, and VELUPILLAI PUVANESARAJAH. Can. J. Chem. **59**, 935 (1981).

Reaction of permethylated glycopyranosiduronic acids with lead tetraacetate furnishes epimeric 5-acetoxypentopyranosides as products of oxidative decarboxylation. Glycoside cleavage then occurs on treatment with sodium borohydride which affords the corresponding pentitols with exposure of aglyconic hydroxyl groups. The reaction sequence has been performed with permethylated derivatives of methyl β-melibiosiduronic acid, methyl β-gentiobiosiduronic acid, gum arabic, leiocarpan A, *Sterculia urens* gum, and citrus pectic acid. The scope of the reaction sequence in polysaccharide studies is discussed.

GERALD OLIVER ASPINALL, HANY KAMAL FANOUS, NIMAL SAVITRI KUMAR et VELUPILLAI PUVANESARAJAH. Can. J. Chem. **59**, 935 (1981).

Les acides glycopyrannosiduronique perméthylés réagissent avec le tétraacétate de plomb et conduisent par décarboxylation oxydante aux acéto-5 pentopyrannosides épimères. Un clivage du glycoside se produit lors de son traitement par le borohydrure de sodium et il se forme des pentitols correspondants avec une libération des groupes hydroxyles de l'acide aglyconique. On a réalisé cette série de réaction sur les dérivés perméthylés des composés suivants: l'acide méthyle β-mélibiosiduronique, l'acide méthyl β-gentiobiosiduronique, la gomme arabique, le leiocarpane A, la gomme du *Sterculia urens* et l'acide pectique des citrus. On discute des possibilités qu'offre cette série de réaction dans l'étude des polysaccharides.

[Traduit par le journal]

Kitagawa and his collaborators (1, 2) have studied several methods for the selective cleavage of glycosiduronic acid linkages in saponin derivatives and related model compounds. In one procedure oxidative decarboxylation of permethylated glycosiduronic acids with lead tetraacetate was shown to furnish an epimeric mixture of the corresponding 5-acetoxypentopyranosides. Treatment of these substances with sodium methoxide to effect deacetylation led to liberation of the aglyconic component in high yield. However, attempts to characterize the pentodialdose component which would be expected to be produced at the same time showed that the conditions for its liberation caused eliminations to occur, and acetylation of the products led to formation of a crystalline unsaturated compound which retained none of the chiral centres of the parent hexuronic acid residue. Nevertheless the intermediacy of pentodialdoses in the above reaction sequence was demonstrated by the formation of diastereomeric nitrocyclitols, each of which retained the stereochemistry of C-2, C-3, and C-4 of the parent glycosiduronic acid, when the 5-acetoxypentopyranosides were treated with sodium methoxide in the presence of nitromethane (2). Kitagawa *et al.* (1, 2) commented on the obvious application of this type of reaction to polysaccharide investigations. In continuation of our studies on the controlled depolymerization of acidic polysaccharides (3, 4) we now describe experiments on the selective cleavage by oxidative decarboxylation of glycosiduronic acid linkages in permethylated polysaccharides and related model compounds.

Model substrates for the oxidative decarboxylation reaction sequence were permethylated derivatives (**2** and **6**) of methyl β-melibiosiduronic acid (**1**) (5) and methyl β-gentiobiosiduronic acid (**4**). Compounds in the latter series were prepared by standard methods involving (*a*) condensation of (methyl 2,3,4-tri-*O*-acetyl-α-D-glucopyranosyluronate)bromide and methyl 2,3,4-tri-*O*-acetyl-β-D-glucopyranoside to give the peracetylated glycoside (**3**), (*b*) deacetylation and saponification, (*c*) permethylation by the Hakomori procedure (6) to give the fully methylated ester glycoside (**5**), and (*d*) saponification.

The permethylated aldobiouronic acids (**2** and **6**) with added internal reference compounds were each reacted with lead tetraacetate. Treatment of the reaction products with sodium borohydride caused deacetylation of the 5-acetoxypentopyrano-

[1]Presented in part at the 10th International Symposium on Carbohydrate Chemistry, Sydney, New South Wales, Australia, July 7–11, 1980.

[2]Author to whom enquiries should be addressed.

[3]On leave from the University of Sri Lanka, Peradeniya Campus (1977–1978).

0008-4042/81/060935-06$01.00/0

©1981 National Research Council of Canada/Conseil national de recherches du Canada

Can. J. Chem. Downloaded from www.nrcresearchpress.com by 210.87.254.105 on 09/06/12
For personal use only.

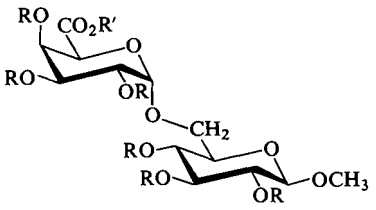

1 R = H, R′ = H
2 R = CH_3, R′ = H

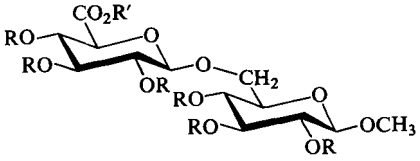

3 R = Ac, R′ = CH_3
4 R = H, R′ = H
5 R = CH_3, R′ = CH_3
6 R = CH_3, R′ = H

sides and thence, after ring opening of the resulting hemiacetal with liberation of the aglyconic component, reduction of the pentodialdose without detectable base-catalyzed elimination. Acetylation of these reaction mixtures afforded in each case methyl 6-*O*-acetyl-2,3,4-tri-*O*-methyl-β-D-glucopyranoside in at least 90% yield (based on the internal reference compound) and the 1,5-di-*O*-acetyl-2,3,4-tri-*O*-methylpentitol (the arabinitol derivative from **2** and the xylitol derivative from **6**) in only slightly lower yield (~80%, possibly due to the volatility of these compounds). The identities of these compounds were confirmed by glc – mass spectrometry.

In order to show that the degradation could be performed with polysaccharide substrates (see Scheme 1), permethylated gum arabic was carefully saponified, methylated arabic acid (**7**) was reacted with lead tetraacetate, the resulting modified polysaccharide was treated with sodium borohydride, and the products were acetylated. The products from the net cleavage of glycosiduronic acid linkages were separated into fractions of low and high molecular weight. The fraction of low molecular weight was further fractionated to give a minor component identified as 1,5-di-*O*-acetyl-2,3,4-tri-*O*-methylxylitol by glc – mass spectrometry, and a major component, whose ^1H and mass spectra were indistinguishable from those of 1,5-di-*O*-acetyl-2,3-di-*O*-methyl-4-*O*-(2,3,4-tri-*O*-methyl-α-L-rhamnopyranosyl)-D-xylitol (**8**) (4). The fraction of high molecular weight was a degraded methylated polysaccharide. Gas–liquid chromatographic examination of the mixture of methyl glycosides formed on methanolysis showed, within the limits of detection, that reaction had resulted in complete removal of methylated glucuronic acid residues and of the terminal rhamnose residues attached to some of them. Quantitative analysis of the constituent sugars in the methylated degraded polysaccharide by glc of the partially methylated alditol acetates formed on hydrolysis, reduction, and acetylation showed that the proportions of other sugar residues, namely, those of arabinose and galactose methyl ethers, were unaltered (Table 1).

Attention was next directed to the degradation of methylated leiocarpan A (7) which contains a main chain with alternating D-glucuronic acid and D-mannose residues with the latter carrying a variety of side-chains. Reaction of the permethylated polysaccharide with lead tetraacetate followed by treatment with sodium borohydride furnished a mixture of partially methylated oligosaccharide alditols. Although the components have yet to be separated and individually characterized, analysis of the sugar constituents in the oligosaccharide alditol mixture by glc of the products formed on methanolysis and acetylation showed that ~90% of the original 2,3-di-*O*-methylglucuronic acid residues had been modified and replaced by those of 2,3-di-*O*-methylxylitol.

In contrast to the degradation of β-D-glucopyranosiduronic acid residues, reactions of α-D-galactopyranosiduronic acid residues may proceed with difficulty. Kitagawa *et al.* (2) observed incomplete reaction when methyl 2,3,4-tri-*O*-methyl-α-

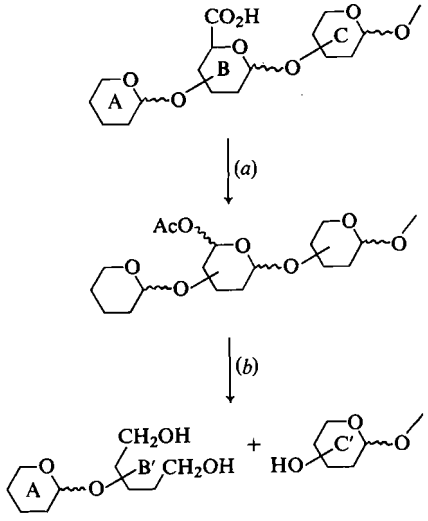

SCHEME 1. Selective fragmentation of glycosiduronic acid (B) linkages by (*a*) reaction with lead tetraacetate followed by (*b*) treatment with sodium borohydride to give pentitol units (B′) with attached substituents (A), when present, and exposure of aglyconic hydroxyl groups in the next inner residue (C′). (For simplicity other substituents are omitted.)

Can. J. Chem. Downloaded from www.nrcresearchpress.com by 210.87.254.105 on 09/06/12
For personal use only.

TABLE 1. Methylation analyses of neutral sugar components of methylated gum arabic and degraded methylated arabic acid

			Derived alditol acetates[c] (mol%)			
	T^a	T^b	(A)	(B)	(C)	(D)
2,3,4-Me_3 Rha[d]	0.44	0.47	8	6	0	0
2,3,5-Me_3 Ara[d]	0.44	0.47	17	14	18	14
2,3,4-Me_3 Ara	0.55	0.63	2	2	3	2
2,5-Me_2 Ara	0.87	1.04	17	13	16	12
2,3,4,6-Me_4 Gal	1.10	1.19	13	10	12	9
2,4,6-Me_3 Gal	1.95	2.18	3	2	5	4
2,3,4-Me_3 Gal	3.04	3.49	4	4	6	4
2,4-Me_2 Gal	4.83	6.10	23	19	26	20
2-Me Gal	6.02	7.74	13	11	14	11

[a,b]Retention times of partially methylated alditol acetates relative to those of 1,5-di-*O*-acetyl-2,3,4,6-tetra-*O*-methyl-D-glucitol on columns *A* and *B*.
[c](A) Neutral sugar constituents only from methylated gum arabic; (B) calculated from (A) allowing for 19% of uronic acid residues; (C) neutral sugar constituents from degraded methylated arabic acid; (D) calculated from (C) allowing for loss of all glucuronic acid and rhamnose residues.
[d]The relative proportions of these two sugars were estimated separately by glc of the methyl glycosides formed on methanolysis of the methylated polysaccharides.

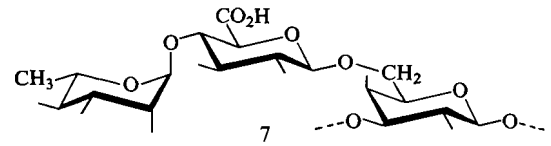

7

Terminal residues in methylated arabic acid: unless otherwise specified substituents are OCH_3.

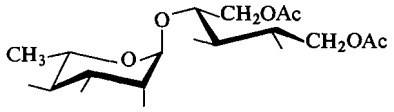

8

D-galactopyranosiduronic acid was treated with lead tetraacetate, although in our hands reaction of the permethylated disaccharide (**2**) containing a configurationally similar α-D-galactopyranosiduronic acid residue had proceeded satisfactorily. However, reaction of such residues in permethylated polysaccharides was very slow, and repeated additions of lead tetraacetate were necessary in order to achieve substantial, but not yet complete, modification. *Sterculia urens* gum (**8**) contains terminal β-D-glucopyranosiduronic acid together with internal 2,4- and 3,4-di-*O*-substituted α-D-galactopyranosiduronic acid residues at branch points. The progress of reaction of the permethylated polysaccharide with lead tetraacetate was monitored by treatment of samples with sodium borohydride followed by glc analysis in the following ways: (*a*) direct acetylation to furnish 2,3,4-tri-*O*-methylxylitol diacetate liberated from terminal glucuronic acid residues; (*b*) methanolysis and acetylation to afford also *inter alia* partially methylated alditol acetates from modified glycosylically substituted uronic acid units and methyl ester methyl glycoside derivatives from unmodified uronic acid units; and (*c*) hydrolysis, reduction, and acetylation to give partially methylated alditol acetates from neutral sugar residues and modified uronic acid units. Using similar proportions of reagent to substrate to those used for methylated leiocarpan A, almost complete reaction of terminal glucuronic acid residues took place. After extended reaction with repeated additions of reagent the partially methylated alditol acetates derived from the modified methylated gum were examined by glc and the identities of the newly formed 2,3,4-tri-*O*-methylxylitol, and 2- and 3-*O*-methylarabinitol peracetates were confirmed by mass spectrometry. Comparison of the relative proportions of these partially methylated alditol acetates with those formed directly from the parent methylated gum (Table 2) showed in addition increases in the relative proportions of derivatives from 2,3,6-

TABLE 2. Analysis of partially methylated alditol acetates from methylated *Sterculia urens* gum and modified methylated polysaccharide

		Relative proportions of derived alditol acetates[b]	
	T^a	(A)	(B)
2,3,4-Me_3 Rha	0.45	1.00	1.00
3,4-Me_2 Rha	0.87	0.50	1.25
3-Me Rha	1.62	0.31	1.13
2,3,4,6-Me_4 Gal	1.17	1.55	1.59
2,3,6-Me_3 Gal	2.10	0.62	0.91
2,3,4-Me_3 Xyl	0.58	—	0.92
2-Me Ara	1.76	—	0.31
3-Me Ara	1.95	—	0.69

[a]Retention times of partially methylated alditol acetates relative to those of 1,5-di-*O*-acetyl-2,3,4,6-tetra-*O*-methyl-D-glucitol on column *A* at 170°C.
[b](A) Neutral sugar constituents only from methylated *Sterculia urens* gum; (B) neutral sugar and modified uronic acid constituents after treatment of methylated gum acid with lead tetraacetate followed by sodium borohydride.

Can. J. Chem. Downloaded from www.nrcresearchpress.com by 210.87.254.105 on 09/06/12
For personal use only.

Can. J. Chem. Downloaded from www.nrcresearchpress.com by 210.87.254.105 on 09/06/12
For personal use only.

tri-*O*-methylgalactose and 3-*O*-methylrhamnose, which components would be only partially liberated whilst carrying unmodified galactopyranosyluronic acid substituents.

Methylated citrus pectic acid (9) with added 1,6-anhydro-2,3,4-tri-*O*-methyl-β-D-galactopyranose as internal reference was reacted with lead tetraacetate, and subsequent treatment with sodium borohydride followed by acetylation gave 2,3-di-*O*-methylarabinitol triacetate in 25% yield. This figure represents less than the actual extent of uronic acid transformed since the neutral sugar residues in the parent pectic acid would furnish glycosylically substituted *O*-methylarabinitol derivatives. Furthermore, modification of one of a pair of galacturonic acid residues in the galacturonan portion of the chain would give rise to a disaccharide derivative containing a di-*O*-methylarabinitol residue. Qualitative comparison of the relative proportions of 2,3-di-*O*-methylgalacturonic acid derivatives formed on methanolysis and acetylation of the original and modified methylated pectic acids indicated that more than 50% of the galacturonic acid residues had been transformed.

Two general approaches have been used in the fragmentation of uronic acid-containing polysaccharides, namely, base-catalyzed β-eliminations from esterified hexuronic acids and those involving the net cleavage of glycosiduronic acid linkages (for further discussion see ref. 3). The former approach as developed by Lindberg and his collaborators (10), which has been widely used for methylated derivatives and may be extended to acetal-protected polysaccharides (11), has the great advantages of speed and ease of monitoring by methylated sugar analysis, but the reaction results in total loss of uronic acid residues and further degradation may take place from liberated reducing groups. In contrast, net cleavage of glycosiduronic acid linkages followed by reduction of the derived pentodialdoses results in product formation in which complete structural information is retained except for the configurations at the anomeric centers and C-5 of the uronic acid residues. This approach was first developed by Kochetkov *et al.* (12) in applying the Hofmann degradation of glycosiduronamides and was then extended to the cleavage of nonterminal linkages in methylated polysaccharides (3). The present studies show that similar results may be achieved by oxidative decarboxylation of per-*O*-methylated derivatives with lead tetraacetate followed by reductive scission with sodium borohydride (see Scheme 1) to give pentitol residues as recognizable derivatives from the parent hexuronic acid residues. Similar structural conclusions regarding the glucuronic acid units in gum arabic were drawn previously from the results of the Hofmann degradation of glucosiduronamide residues (3) and of the selective hydrolysis of hex-5-enopyranoside residues formed on modification of glucuronic acid residues (4) in the permethylated polysaccharide. Our results to date on the oxidative decarboxylation of polysaccharides containing α-D-galactopyranosiduronic acid residues have shown that prolonged reaction with repeated additions of reagent will be necessary to achieve complete modification of these hexuronic acid residues. Nevertheless, this sequence of reactions is the most direct procedure yet available for this selective cleavage of internal and external glucopyranosiduronic acid linkages with no detectable fragmentation of residues vulnerable to other reagents. The procedure has an advantage over the Hofmann glycosiduronamide degradation in avoidance of strongly basic conditions. It should therefore be possible to extend the procedure to the degradation of polysaccharides carrying removable protecting (e.g. acyl) groups and to distinguish between esterified (invulnerable to lead tetraacetate) and nonesterified uronic acid units, as in pectins.

Experimental

Evaporations were carried out under diminished pressure at temperatures of 40°C or less. Optical rotations were measured with a Perkin-Elmer model 141 polarimeter at 20 ± 2°. The ir spectra were measured on a Unicam SP 200 spectrophotometer. Unless otherwise stated, ^{1}H nmr spectra were recorded on a Varian EM 360 spectrophotometer in deuteriochloroform with tetramethylsilane as internal standard. Gas–liquid chromatography was performed with a Tracor 560 chromatograph using columns of Gas-Chrom Q coated with (*A*) 3% of silicone gum OV-225 or (*B*) 3% of silicone–polyester copolymer ECNSS-M; on a Pye 204 chromatograph using (*C*) a column of Superpak 20M (Analab) or (*D*) a W.C.O.T. column coated with silicone gum SE-30; or (*E*) on a Perkin-Elmer Sigma 3B chromatograph using a S.C.O.T. column coated with silicone gum OV-225. For glc – mass spectrometry, columns in a Pye 204 chromatograph were attached by a jet separator to a VG Micromass 16F mass spectrometer operated with an inlet temperature of 250°C, an ionization potential of 70 eV, and an ion-source temperature of ~250°C.

Methyl (Methyl Hexa-O-acetyl-β-gentiobiosid)uronate (3)

Methyl (2,3,4-tri-*O*-acetyl-α-D-glucopyranosyl)uronate bromide (13) (5.4 g, 13.6 mmol) and methyl 2,3,4-tri-*O*-acetyl-β-D-glucopyranoside (2.9 g, 9 mmol) were condensed in nitromethane (100 mL) and benzene (20 mL) containing mercuric cyanide (3.5 g, 14 mmol), and the mixture was stirred at 40°C for 24 h with exclusion of moisture. Further mercuric cyanide (3.5 g, 14 mmol) was added and stirring was continued for an additional 24 h at 40°C. The cooled solution was diluted with benzene, washed several times with cold aqueous sodium hydrogen carbonate and then with water, dried, and concentrated. The resulting syrup (4.7 g) was chromatographed on

Can. J. Chem. Downloaded from www.nrcresearchpress.com by 210.87.254.105 on 09/06/12
For personal use only.

silica gel with dichloromethane–chloroform–acetone (10:10:1) as eluant. The major product was recrystallized from ethanol to give the acetylated glycoside ester (**3**) (3.4 g), mp 174–175°C; $[\alpha]_D$ −23.8° (*c*, 3.2 in chloroform); nmr ($CDCl_3$) δ: 2.03 (18H, 6 × OAc), 3.53 (s, 3H, OCH_3), 3.77 (s, 3H, CO_2CH_3). *Anal.* calcd. for $C_{26}H_{36}O_{18}$: C 49.06, H 5.70; found: C 48.93, H 5.66.

Methyl (Methyl Hexa-O-methyl-β-gentiobiosid)uronate (5) and the Derived Acid (6)

0.2 *M* Sodium methoxide in methanol (8 mL) was added to the acetylated glycoside ester (**3**) (2.55 g, 4 mmol) in methanol (30 mL) and the solution was stirred at room temperature for 20 min. The solution was stirred with Amberlite resin IR-120(H) to remove sodium ions and the filtrate was concentrated to give syrupy methyl (methyl β-gentiobiosid)uronate (1.3 g); nmr (D_2O) δ: 3.57 (s, 3H, OCH_3), 3.83 (s, 3H, CO_2CH_3). 1*M* Sodium hydroxide was added to the foregoing ester glycoside (1.32 g, 4 mmol) in water (50 mL) at 0°C to bring the solution to pH 12. The solution was kept at 0°C for 1 h with addition of further sodium hydroxide to maintain a pH of 12. The solution was treated with Amberlite resin IR-120(H) to remove sodium ions, and concentration of the filtrate afforded acid glycoside (**4**) (1.25 g), mp 128°C; nmr (D_2O) δ: 3.55 (s, 3H, OCH_3). The foregoing methyl β-gentiobiosiduronic acid (1 g) was dissolved in 0.67 *M* sodium methylsulfinylmethanide in methyl sulfoxide (75 mL), and methyl iodide (50 mL) was added to the cooled solution and the solution was stirred at room temperature for 1 h. Excess methyl iodide was removed under diminished pressure, the reaction mixture was poured into water (50 mL), and the aqueous solution was extracted 4 times with dichloromethane. The combined extracts were washed with water, dried, and concentrated to a syrup which was chromatographed on silica gel with dichloromethane–acetone (5:1) as eluant to give methyl (methyl hex-*O*-methyl-β-gentiobiosid)uronate (**5**) (1.23 g) mp (after recrystallization from ether – light petroleum) 174–175°C; $[\alpha]_D$ −44° (*c*, 0.85 in chloroform); ir ν_{max} (film): 1745 (ester C=O) cm^{-1}; nmr ($CDCl_3$) δ: 3.48–3.60 (m, 21H, ether and glycosidic OCH_3), 3.77 (s, 3H, CO_2CH_3). *Anal.* calcd. for $C_{20}H_{36}O_{12}$: C 51.27, H 7.75; found: C 51.27, H 7.73.

The methylated ester glycoside (**5**) (300 mg) was saponified in aqueous solution at pH 12 as described previously to methylated acid glycoside (**6**) (260 mg), mp 123–124°C (after recrystallization from ether – light petroleum); ir $\nu_{max}(H_2O)$: 1765 cm^{-1}; nmr ($CDCl_3$) δ: 3.43–3.56 (m, 21H, ether and glycosidic OCH_3), 7.83 (broad, 1H, CO_2H, exchanged with D_2O). *Anal.* calcd. for $C_{19}H_{34}O_{12}$: C 50.21, H 7.54; found: C 50.48, H 7.81.

Degradations of Permethylated Aldobiouronic Acids 2 and 6 with Lead Tetraacetate

Lead tetraacetate (100 mg) was added to methyl hexa-*O*-methyl-β-melibiosiduronic acid (**2**, formed on saponification of the ester **1** (5) as described for **6**) (29 mg) and 1,6-anhydro-2,3,4-tri-*O*-methyl-β-D-galactopyranose (**14**) (7 mg) in benzene (30 mL) containing pyridine (0.2 mL) and the solution was heated under reflux for 4 h. The cooled solution was diluted with benzene and filtered, the filtrate was washed with water, the aqueous solution was extracted with ether, and the combined extracts were dried and concentrated. Sodium borohydride (50 mg) was added to the residue in water (5 mL) and after 5 h at room temperature the solution was treated with Amberlite resin IR-120(H) to destroy excess of hydride and remove sodium ions, filtered, and concentrated by co-distillation with toluene and then methanol. The residue was acetylated in acetic anhydride – pyridine (1:1) (1 mL) and glc examination of the products on column *A* (150°C) showed the formation of compounds with the retention times of methyl 6-*O*-acetyl-2,3,4-tri-*O*-methyl-β-D-glucopyranoside (92%, based on the internal standard) and 1,5-di-*O*-acetyl-2,3,4-tri-*O*-methyl-L-arabinitol (80%). Separate examination of the products by glc – mass spectrometry using column *C* (150°C) showed that the products gave mass spectra in conformity with the assigned structures.

In similar fashion methyl hexa-*O*-methyl-β-gentiobiosiduronic acid (25 mg) with added 1,6-anhydro-2,3,4-tri-*O*-methyl-β-D-galactopyranose (10 mg) was reacted with lead tetraacetate (100 mg) in benzene (30 mL) containing pyridine (0.2 mL). Analysis of the products after treatment with sodium borohydride and acetylation showed the formation of compounds with the retention times of methyl 6-*O*-acetyl-2,3,4-tri-*O*-methyl-β-D-glucopyranoside (96%) and 1,5-di-*O*-acetyl-2,3,4-tri-*O*-methylxylitol (92%), whose identities were confirmed by glc – mass spectrometry.

Lead Tetraacetate Degradation of Methylated Arabic Acid

Methylated gum arabic (**4**) (300 mg) was saponified in water (30 mL) at 0°C by the dropwise addition of 1 *M* sodium hydroxide to maintain a pH of 12 and the solution was kept for 2 h with further addition of base as required. Sodium ions were removed by treatment with Amberlite resin IR-120(H) and concentration of the filtrate afforded methylated arabic acid (280 mg), whose ir spectrum showed absence of absorption at 1750 cm^{-1} (ester C=O) indicating completeness of reaction.

Methylated arabic acid (150 mg) in benzene (30 mL) containing pyridine (2 mL) and lead tetraacetate (500 mg) was heated under reflux for 4 h and, after addition of further lead tetraacetate (200 mg), for an additional 16 h. The cooled solution was diluted with benzene and filtered, the filtrate was washed with water, the aqueous solution was extracted with ether, and the combined extracts were dried and concentrated. Completeness of reaction was shown (*a*) by ir absorption at 1750 cm^{-1} (acetate C=O) but none at 1600 cm^{-1} (hexuronate —CO_2^-) on treatment with triethylamine, and (*b*) by the absence of peaks with retention times of methyl ester methyl glycosides of 2,3,4-tri- and 2,3-di-*O*-methylglucuronic acid on glc examination of the methanolysis products on column *A* (150°C). Sodium borohydride (50 mg) was added to the residue in water–methanol (3:2) (5 mL) and the solution was kept overnight, treated with Amberlite resin IR-120(H) to destroy excess of hydride and remove sodium ions, filtered, and concentrated by co-distillation with toluene and then methanol. The residue was acetylated with acetic anhydride – pyridine (1:1) (1 mL). After normal work-up, addition of light petroleum to the products in ether afforded degraded methylated arabic acid (115 mg), which was washed thoroughly until free of products of low molecular weight (detected by tlc) and then purified by chromatography on Sephadex LH-20 using dichloromethane as eluant.

The sugar components of methylated gum arabic and of the degraded methylated arabic acid were analyzed as partially methylated alditol acetates formed on hydrolysis, followed by reduction with sodium borohydride and acetylation, by glc on columns *A* and *B*, and average values from the two determinations are shown in Table 1. For separation of derivatives of 2,3,4-tri-*O*-methylrhamnose and 2,3,5-tri-*O*-methylarabinose, methylated polysaccharides were heated under reflux with methanolic 5% hydrogen chloride and the resulting methyl glycosides were examined by glc on column *A* (100°C, 5°/min to 180°C).

The supernatant liquid from the above precipitation of degraded methylated polysaccharide was chromatographed on silica gel using dichloromethane–methanol (10:1) as eluant. The main component of the minor fraction (5 mg) was identified as 1,5-di-*O*-acetyl-2,3,4-tri-*O*-methylxylitol by glc – mass spectrometry on column *A* (150°C). The major fraction (16 mg) was identified as the partially methylated disaccharide alditol acetate (**8**) from the nmr spectrum ($CDCl_3$) (δ 1.27 (d, 3H $J_{5,6}$ = 6 Hz, H-6 of Me_3 rhamnopyranose residue), 2.10 (s, 6H, 2 × OAc),

Can. J. Chem. Downloaded from www.nrcresearchpress.com by 210.87.254.105 on 09/06/12
For personal use only.

and 3.53 (m, 15H, 5 × OCH_3)) and by glc – mass spectrometry on column *C* (180°C), which showed a single component whose mass spectrum was indistinguishable from that previously reported (3) and included peaks of the same relative abundance at *m/e* 307, 247, 189, 157, and 117.

Lead Tetraacetate Degradation of Methylated Leiocarpan A

Methylated leiocarpan A (150 mg) was saponified as described for methylated gum arabic to give methylated gum acid (120 mg); ir ν_{max} (NaCl): 1740 cm^{-1} (shifted completely to 1600 cm^{-1} on treatment with triethylamine). Methylated gum acid (100 mg) in benzene (8 mL) containing pyridine (0.2 mL) and lead tetraacetate (400 mg) was heated under reflux for 15 h. The product, isolated as above, was treated with sodium borohydride (200 mg) in tetrahydrofuran–water (1:1) and normal work-up afforded a mixture of partially methylated oligosaccharide alditols. A portion of this material was methanolyzed and the products were acetylated. These products were compared with those similarly derived from the parent methylated polysaccharide by glc on column *A* (120°C, 10 min, 5°/min to 180°C and hold). The results showed that the methylated oligosaccharide alditols afforded the same derivatives of the neutral methylated sugar components, less than 10% of the quantity of the methyl ester methyl glycoside acetates of 2,3-di-*O*-methylglucuronic acid, but as a major new product, 2,3-di-*O*-methylxylitol triacetate, whose identity was confirmed by glc – mass spectrometry.

Lead Tetraacetate Degradation of Methylated Sterculia uren *Gum*

Methylated gum acid (100 mg), prepared by saponification of the methylated gum, was heated under reflux in benzene (8 mL) containing pyridine (0.2 mL) and lead tetraacetate (300 mg) for 5 h. Further lead tetraacetate (5 × 100 mg) was added at intervals during another 10 h. Precipitated lead salts were removed by centrifugation and a portion of the combined supernatant liquid and washings was withdrawn and treated with sodium borohydride. The products were analyzed by glc on column *A* (120°C, 10 min, 5°/min to 180°C) after (*a*) direct acetylation and (*b*) methanolysis and acetylation. The results indicated that ~90% of the 2,3,4-tri-*O*-methylglucuronic acid residues had been converted into 2,3,4-tri-*O*-methylxylitol diacetate but that only a small proportion of the *O*-methylgalacturonic acid residues had been modified. Lead tetraacetate (300 mg) was added to the remaining benzene solution which was heated under reflux for 15 h with periodic additions (5 × 100 mg) of further reagent. The cooled solution was filtered, and the filtrate was washed with water, dried, and concentrated to a syrup which was treated with sodium borohydride and analyzed as above (*a* and *b*). The results indicated that all of the 2,3,4-tri-*O*-methylglucuronic acid residues had been modified and that some of the *O*-methylgalacturonic acid residues had been converted into 2- and 3-*O*-methylarabinitol peracetates. A further portion of the reaction mixture was hydrolyzed, reduced with sodium borohydride, and acetylated. The resulting mixture of partially methylated alditol acetates was compared with that similarly formed from the parent methylated gum by glc on column *A* (170°C) (Table 2). The identities of 2,3,4-tri-*O*-methylxylitol, and 2- and 3-*O*-methylarabinitol peracetates were confirmed by co-chromatography with authentic samples on columns *A* and *E*, and by glc – mass spectrometry.

Lead Tetraacetate Degradation of Methylated Citrus Pectic Acid

Methylated pectic acid (100 mg), from saponification of methylated citrus pectin (9), with added 1,6-anhydro-2,3,4-tri-*O*-methyl-β-D-galactopyranose (20 mg) (11) was heated under reflux in benzene (10 mL) containing pyridine (0.2 mL), and lead tetraacetate (4 × 100 mg) was added at intervals during 5 h. Precipitated lead salts were removed by filtration and two further sets of addition of reagent were carried out. The reaction mixture was worked up as described for modified methylated *S. urens* gum and treated with sodium borohydride. A portion of the product was acetylated and glc on column *A* showed the formation of 2,3-di-*O*-methylarabinitol triacetate (25%) whose identity was confirmed by glc – ms. A further portion of the product was methanolyzed and acetylated and comparison of the derivatives with those formed from the parent methylated pectic acid by glc on column *A* showed that more than 50% of the 2,3-di-*O*-methylgalacturonic acid residues had undergone modification.

Acknowledgements

The authors are grateful for financial support from the Natural Sciences and Engineering Research Council of Canada, for the award of a Royal Society Commonwealth Bursary (to N.S.K.), and for the recording of mass spectra by Dr. B. H. Khouw.

1. I. KITAGAWA and M. YOSHIKAWA. Heterocycles, **8**, 783 (1977).
2. I. KITAGAWA, M. YOSHIKAWA, and A. KADOTA. Chem. Pharm. Bull. **26**, 484 (1978).
3. G. O. ASPINALL and K.-G. ROSELL. Can. J. Chem. **56**, 685 (1978).
4. G. O. ASPINALL and K.-G. ROSELL. Can. J. Chem. **56**, 680 (1978).
5. G. O. ASPINALL, T. N. KRISHNAMURTHY, W. MITURA, and M. FUNABASHI. Can. J. Chem. **53**, 2182 (1975).
6. S. HAKOMORI, J. Biochem. Tokyo, **55**, 205 (1964).
7. G. O. ASPINALL and J. J. CARLYLE. J. Chem. Soc. C, 851 (1969), and previous papers.
8. G. O. ASPINALL and NASIR-UD-DIN. J. Chem. Soc. 2710 (1965).
9. G. O. ASPINALL and K.-S. JIANG. Carbohydr. Res. **38**, 247 (1974).
10. B.LINDBERG, J. LÖNNGREN, and J. L. THOMPSON. Carbohydr. Res. **28**, 351 (1973).
11. M. CURVALL, B. LINDBERG, and J. LÖNNGREN. Carbohydr. Res. **41**, 235 (1975).
12. N. K. KOCHETKOV, O. S. CHIZHOV, and A. F. SVIRIDOV. Carbohydr. Res. **14**, 277 (1970).
13. G. N. BOLLENBACK, J. W. LONG, D. G. BENJAMIN, and J. A. LINDQUIST. J. Am. Chem. Soc. **77**, 3310 (1955).
14. D. MCCREATH and F. SMITH. J. Chem. Soc. 387 (1939).

β-Lactams. VIII. The synthesis of iso-oxapenams from *N*-substituted-4-hydroxymethylazetidinones

GHOLAM HOSEIN HAKIMELAHI AND GEORGE JUST

Department of Chemistry, McGill University, Montreal, P.Q., Canada H3A 2K6

Received August 22, 1980

GHOLAM HOSEIN HAKIMELAHI and GEORGE JUST. Can. J. Chem. **59**, 941 (1981).

The synthesis of 3,3-disubstituted iso-oxapenams is described.

GHOLAM HOSEIN HAKIMELAHI et GEORGE JUST. Can. J. Chem. **59**, 941 (1981).

On décrit la synthèse d'iso-oxapenam 3,3-disubstitués.

Can. J. Chem. Downloaded from www.nrcresearchpress.com by 210.87.254.40 on 09/06/12
For personal use only.

We have recently shown (1) that 2,2-disubstituted tetrahydrofurans can be prepared from the corresponding 1,1-disubstituted butan-4-ols by reaction with trifluoromethanesulfonyl chloride – triethylamine, provided that the substituents stabilize an incipient carbanion ($pK_A = 11 \simeq 15$). In this paper, we describe the application of this method to the synthesis of iso-oxapenams of type **2** and **9**.

The cyclization reaction had originally been observed on the benzyl ester **1***b* (1) and its course elucidated using methyl ester **1***a* (1), where products obtained gave unambiguous mass spectra; *p*-nitrobenzyl ester **1***c*, prepared by adaptation of literature procedures (2), was eventually used to prepare free acid **2***f* since it could be cleaved in the presence of the highly labile (3) iso-oxapenam ring system.

Treatment of either diastereomer of hydroxymethylazetidinone **1***a* with trifluoromethanesulfonyl chloride (1 equiv.) and triethylamine (2 equiv.) in methylene chloride at 0°C gave, in 69% yield, the formal oxidation product of **1***a* having structure **2***a*. The nmr spectrum of **2***a* indicated the loss of two hydrogen atoms, and was consistent with the structure proposed, as were the ^{13}C nmr, uv, and the ir spectra. The latter showed the presence of azide (2105 cm^{-1}), ester (1730 cm^{-1}), and highly strained β-lactam (1790 cm^{-1}) functions. The C.I.-mass spectrum showed M + 1, M + 1 – $N_3CH{=}C{=}O$, and $PhCO^+$, and the E.I.-mass spectrum significant fragments for $M^+ - COOMe$, $M^+ - COOMe - N_2$, $M^+ - COOMe - N_3CH{=}C{=}O$, and $PhCO^+$ (100%). β-Lactam **2***a* could not be obtained in totally pure form and was extremely labile to acid, giving ketoester **10** (4), characterized as its dinitrophenylhydrazone.

The formation of an intermediate triflate **1***d* in the conversion of alcohol **1***a* to iso-oxapenam **2***a* could be ruled out by preparing triflate **1***d* from alcohol **1***a* with trifluoromethanesulfonic anhydride, and showing that triflate **1***d* was stable to triethylamine in methylene chloride. The most likely explanation for the cyclization is a sequence where trifluoromethanesulfonyl chloride acts as a chlorinating agent at the potential carbanionic site, followed by a replacement of the chlorine by the alcohol function (5). This hypothesis is further supported by the fact that treatment of either triflate **1***d* or styrylazetidinone **3***a* (3) with trifluoromethanesulfonyl chloride – triethylamine in methylene chloride at 0°C, followed by standard aqueous work-up, gave ketoester **10**, presumably via the highly labile chloroazetidinones of type **3***b*.

Iso-oxapenams **2***b* and **2***c* were prepared from alcohols **1***b* and **1***c* in a similar manner.

Catalytic reduction for one hour of azide **2***a* in ethyl acetate using palladium on charcoal as catalyst gave the very unstable amino β-lactam **2***d* in 20% yield only. Its instability was probably due to a bimolecular reaction of the amine function with a β-lactam group, since the β-lactam absorption at 1790 cm^{-1} disappeared over a period of a few hours, and was accompanied by the appearance of an amide absorption band at 1680 cm^{-1}.

The catalytic reduction was, therefore, carried out in the presence of acetic anhydride, and the relatively stable acetamido-β-lactam **2***e* was obtained in 47% yield. Having established a methodology for the conversion of the azide function to an amide group, the catalytic reduction in the presence of acetic anhydride was applied to azido *p*-nitrobenzyl oxapenam **2***c*, permitting the isolation of the free acid **2***f* in 35% yield. Its structure was proven by treatment with diazomethane, which gave **2***e* described above.

The stereochemistry of the phenyl group and the carbonyl function in compounds **2** was not determined. However, ^{13}C nmr and other spectroscopic data seemed to indicate that only one isomer was present.

We next studied the cyclization reaction using dialkyl aminomalonates as starting materials. Pre-

0008-4042/81/060941-04$01.00/0

©1981 National Research Council of Canada/Conseil national de recherches du Canada

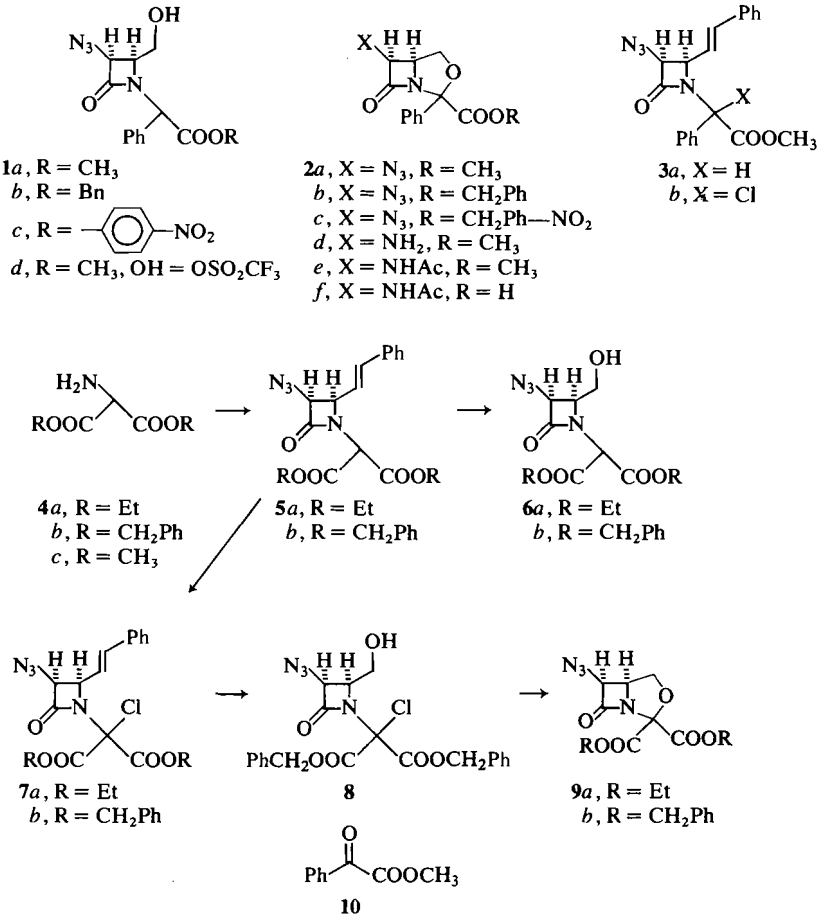

liminary studies were carried out on the commercially available diethyl aminomalonate **4***a*. Under precisely defined conditions, it was transformed to its cinnamylidene Schiff base, which could not be characterized, but was immediately transformed to azido β-lactam **5***a* in 24% yield only by the action of azidoacetyl chloride. Similarly, dibenzyl aminomalonate, prepared in good yield by a modification of the literature procedure (6), was converted to β-lactam **5***b* in 20% yield. It should be noted that dimethyl aminomalonate, when submitted to the same reaction conditions, gave no detectable β-lactam **5**. Di-*tert*-butyl aminomalonate, the most desirable starting material, could not be prepared using appropriate adaptations of literature (7) procedures. Ozonolysis of **5***a* or **5***b*, followed by sodium borohydride reduction (8), gave alcohols **6***a* and **6***b* in approximately 25% yield only, perhaps because of oxidation of the enolic form of **5**. Addition of acetic or trifluoroacetic acid to the ozonolysis solvent did not increase the yields. Treatment of **6***a* or **6***b* with one equivalent of trifluoromethanesulfonyl chloride and two equivalents of triethylamine gave iso-oxapenam **9***a* and **9***b* in approximately 60% yield.

Because of the extremely poor yields observed in most steps of this sequence, styryl lactam **5***b* was first chlorinated with CF_3SO_2Cl/NEt_3, and the mixture immediately submitted to the ozonolysis – borohydride reduction sequence described. Alcohol **8**, obtained in 57.6% yield, was cyclized quantitatively with triethylamine to iso-oxapenam **9***b*, identical to **9***b* obtained above. Attempts to transform the azide function to an amine or amide group by reaction with hydrogen sulfide – triethylamine (9), followed by quenching of the amine with phenylacetyl chloride, or by catalytic hydrogenation in the presence or absence of acetic anhydride failed, giving products which did not show the presence of a β-lactam function as evidenced by the disappearance of the 1780–1790 cm^{-1} band in the infrared.

We therefore introduced the amide group at an earlier stage by reducing the azide group of **5***b*, and acylating the resulting amine with phenylacetyl chloride – pyridine (9). Styryl amide **11** was then

Can. J. Chem. Downloaded from www.nrcresearchpress.com by 210.87.254.40 on 09/06/12
For personal use only.

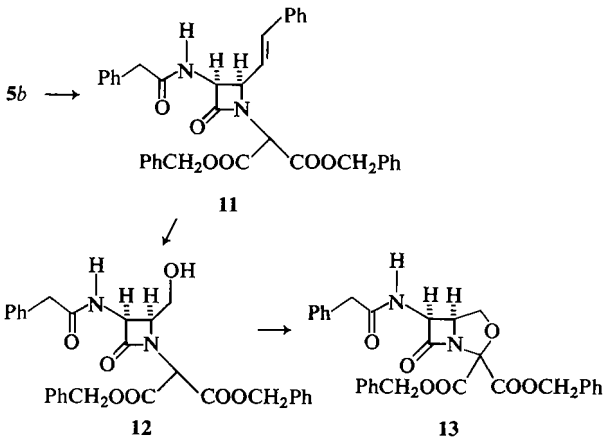

submitted to ozonolysis, followed by sodium borohydride reduction, and the resulting alcohol **12** was cyclized to **13** with trifluoromethanesulfonyl chloride – triethylamine. All attempts to hydrogenolyse the benzyl groups of **13** failed, and resulted in the destruction of the β-lactam ring.

Experimental

For general procedures, see (2).

Iso-oxapenams 2a, 2b, *and* 2c

Each diastereomer of **1***a*, **1***b*, and **1***c* was submitted to identical reaction conditions and purification procedures, which will be described for **1***a* only. Their spectra were similar except for their ester variations.

β-Lactam **1***a* (0.290 g, 1 mmol) was dissolved in 15 mL dry CH_2Cl_2. Triethylamine (0.202 g, 2 mmol) was added. Trifluoromethanesulfonyl chloride (0.169 g, 1 mmol) in 5 mL dry CH_2Cl_2 was added dropwise while the reaction mixture was stirring at room temperature. After 1 h, the solution was washed with water, dried, and evaporated to give the crude product, which was chromatographed on silica gel. Elution with CH_2Cl_2 gave 0.2 g (69%) **2***a* as an oil. Ultraviolet λ_{max} (EtOH): 255 nm (ε 220); ir (CH_2Cl_2): 2105 (N_3), 1790 (β-lactam), 1730 (ester) cm^{-1}; nmr ($CDCl_3$) δ: 3.90 (s, 3H, CH_3), 4.00–4.60 (m, 4H, $CHCHCH_2O$), 7.30–7.80 (m, 5H, Ph); ^{13}C nmr ($CDCl_3$ at 77.10 ppm) 171.50 (C=O), 164.77 (N—C=O), 135.04–127.90 (Ph), 69.23 (C(3)), 65.12 (CH_2O), 63.53 ($CHCH_2O$), 52.74 (CHN_3), 52.61 (OCH_3) ppm; ms E.I. 260 ($M^+ - N_2$), 229 (M^+ – COOMe), 201 (M^+ – COOMe – N_2), 146 (M^+ – COOMe – $N_3CH{=}C{=}O$), 105 (Ph^+CO), 77 (Ph^+); C.I. 289 ($M^+ + 1$), 261 ($M^+ + 1 - N_2$), 206 ($M^+ + 1 - N_3CH{=}C{=}O$) and Ph^+CO. *Anal.* calcd. for $C_{13}H_{12}N_4O_4$: C 54.16, H 4.20, N 19.44; found: C 53.65, H 4.01, N 19.18.

Acetamido β-*Lactam* 2e

Azido β-lactam **2***a* (0.2 g, 0.69 mmol) was dissolved in 30 mL dry ethyl acetate containing 5 mL acetic anhydride, and 10% Pd/C (0.05 g) was added. The mixture was hydrogenated at room temperature and 30 psi for 1.5 h. The solution was then filtered and evaporated, and the residue was chromatographed on silica gel using $CHCl_3$ as eluent to give **2***e* (0.1 g) in 47% yield. Infrared: 3410 (NH), 1789 (β-lactam), 1735 (ester), 1675 (amide) cm^{-1}; nmr ($CDCl_3$) δ: 2.22 (s, 3H, CH_3CO), 3.78 (s, 3H, CH_3), 3.82–4.63 (m, 4H, $CHCHCH_2O$), 6.50 (d, 1H, NH), 7.21–7.42 (m, 5H, Ph); ms C.I. 305 ($M^+ + 1$), 205 ($M^+ - CH_3CONHCH{=}C{=}O$). *Anal.* calcd. for $C_{15}H_{16}N_2O_5$: C 59.21, H 5.26, N 9.21; found: C 58.98, H 5.45, N 9.38.

β-*Lactam* 2f

β-Lactam **2***c* (0.2 g, 0.48 mmol) was dissolved in 30 mL ethyl acetate containing 10 mL acetic anhydride. 10% Pd/C (0.1 g) was added. The reaction mixture was hydrogenated at room temperature and 40 psi for 2 h. The solution was filtered and evaporated to dryness, 20 mL water was added, and the organic material was extracted with ethyl acetate, dried, and the solvent evaporated to give the crude product as a foam. Crystallization from diethyl ether gave 0.05 g (35%) β-lactam **2***f*, mp 101–104°C. Infrared (CH_2Cl_2): 3200–3500 (COOH, NH), 1780 (β-lactam), 1710 (acid), 1665 (amide) cm^{-1}; nmr ($CDCl_3$–D_2O) δ: 2.19 (s, 3H, CH_3), 3.82–4.2 (m, 3H, $CHCH_2O$), 4.41 (d, 1H, CHND, J = 5 Hz), 7.22–7.41 (m, 5H, Ph). Treatment of **2***f* with ethereal diazomethane gave the corresponding methyl ester **2***e* which was identical to that obtained before.

Azido-β-*lactams* 5a *and* 5b

Both β-lactams were prepared in an identical manner. Their spectra were similar except for their ester variations. Their chemical ionization mass spectra show $M^+ + 1$ and other appropriate fragments.

The following is a representative procedure.

To a solution of **4***a* (4 g, 0.022 mol) in 40 mL of dry CH_2Cl_2 was added cinnamaldehyde (3.1 g, 0.023 mol). Magnesium sulfate was added and the solution was stirred at room temperature for 6 h. The solution was filtered and triethylamine (2.5 g, 0.024 mol) was added. A solution of azidoacetyl chloride (3.6 g, 0.03 mol) in 30 mL dry CH_2Cl_2 was added dropwise over 10 min. The solution was stirred for 5 h and evaporated to dryness. The residue was dissolved in ether, treated with charcoal, filtered, and evaporated to give an oily product, which was chromatographed on silica gel. Elution with CH_2Cl_2 gave azido β-lactam **5***a* (2 g) in 24% overall yield. Infrared (CH_2Cl_2): 2100 (N_3), 1770 (β-lactam), 1750 (ester) cm^{-1}; nmr ($CDCl_3$) δ: 1.21 (t, 6H, $2CH_3$, J = 8 Hz), 4.21 (q, 4H, $2CH_2$, J = 8 Hz), 4.60–4.81 (m, 2H, $CHCHN_3$), 5.08 (s, 1H, CH), 5.91–6.81 (m, 2H, CH=CH), 7.19–7.41 (m, 5H, Ph); nmr (C_6D_6) δ: 0.50–1.11 (m, 6H, $2CH_3$), 3.51–4.12 (m, 4H, $2CH_2$), 4.38–4.60 (m, 1H, CHC=C), 4.64 (d, 1H, CHN_3, J = 5 Hz), 5.10 (s, 1H, CH), 5.90–6.71 (m, 2H, CH=CH), 7.01–7.21 (m, 5H, Ph); ms C.I. 373 ($M^+ + 1$), 345 ($M^+ + 1 - N_2$), 290 ($M^+ + 1 - N_3CH{=}C{=}O$), 328 ($M^+ + 1$ – OEt), 202 ($M^+ + 1 - \phi CH{=}CHCH{=}CHN_3$). *Anal.* calcd. for $C_{18}H_{20}N_4O_5$: C 58.06, H 5.37, N 15.05; found: C 58.12, H 5.29, N 15.10.

4-Hydroxy-azido-β-*lactams* 6a *and* 6b

Both β-lactams **5***a* and **5***b* were submitted to identical reaction conditions and separation procedures, which will be described for **5***a* only. Their spectra were similar, except for their ester variations. Their chemical ionization mass spectra showed ($M^+ + 1$) and appropriate fragments.

β-Lactam **5***a* (2 g, 5.4 mmol) in 50 mL dry CH_2Cl_2 was saturated with nitrogen gas at −78°C. Then a mixture of O_3–N_2 gas was bubbled in until KI starch paper showed excess ozone. The excess ozone was removed by a stream of nitrogen. Then 5 equiv. dimethyl sulfide was added. After 1 h, $NaBH_4/Al_2O_3$ (1 g:10 g, (8)) was added, and the reaction mixture was stirred for 1 h at room temperature. Filtration and evaporation gave the crude product, which was purified on silica gel using $CHCl_3$ as eluent to give 0.6 g (37%) hydroxy β-lactam **6***a*. Infrared (CH_2Cl_2): 2100 (N_3), 1760 (β-lactam), 1740 (ester) cm^{-1}; nmr ($CDCl_3$) δ: 1.25 (t, 6H, $2CH_3$, J = 6 Hz), 3.31 (b, 1H, OH), 3.61–3.80 (m, 3H, $CHCH_2O$), 4.20 (q, 4H, $2CH_2$, J = 6 Hz), 4.77 (d, 1H, CHN_3, J = 5 Hz), 5.20 (s, 1H, CH); ms C.I. 301 ($M^+ + 1$), 273 ($M^+ + 1 - N_2$), 218 ($M^+ + 1 - N_3CH{=}C{=}O$), 228 ($M^+ + 1$ – COOEt), 256 ($M^+ + 1$ – OEt). *Anal.* calcd. for $C_{11}H_{16}N_4O_6$: C 44.00, H 5.33, N 18.66; found: C 44.12, H 5.42, N 18.39.

Can. J. Chem. Downloaded from www.nrcresearchpress.com by 210.87.254.40 on 09/06/12
For personal use only.

Can. J. Chem. Downloaded from www.nrcresearchpress.com by 210.87.254.40 on 09/06/12
For personal use only.

Chloro-β-lactams 7a *and* 7b

Both β-lactams **5***a* and **5***b* were submitted to identical reaction conditions which will be described for **5***a* only. Their spectra were similar except for their ester variations.

β-Lactam **5***a* (1 g, 2.7 mmol) was dissolved in 50 mL dry CH_2Cl_2. Triethylamine (0.3 g, 2.9 mmol) was added. Trifluoromethanesulfonyl chloride (0.5 g, 2.9 mmol) in 5 mL dry CH_2Cl_2 was added dropwise over 5 min at 0°C. The reaction mixture was allowed to warm to room temperature while stirring (1 h). The solution was evaporated to dryness and diethyl ether was added. The ethereal solution was washed with water, dried, and treated with charcoal. Filtration and evaporation gave a quantitative yield of chloro-β-lactam **7***a* as an oil. Infrared: 2105 (N_3), 1790 (β-lactam), 1760 (ester) cm^{-1}; nmr ($CDCl_3$) δ: 1.01–1.30 (m, 6H, $2CH_3$), 3.93–4.39 (m, 4H, CH_2), 4.77 (dd, 1H, CHC=C, J_1 = 5 Hz, J_2 = 7 Hz), 5.05 (d, 1H, CHN_3, J = 5 Hz), 6.05 (dd, 1H, PhCH=*CH*, J_1 = 8 Hz, J_2 = 16 Hz), 6.61 (d, 1H, PhCH, J = 16 Hz), 7.20–7.31 (m, 5H, Ph); ms C.I. 407 ($M^+ + 1$, Cl-cluster).

Hydroxy-β-lactam 8

β-Lactam **7***b* (1.4 g, 2.6 mmol) in 40 mL dry CH_2Cl_2 was submitted to the identical reaction conditions which were described for the preparation of β-lactam **6***a*, except that $MgSO_4$ was used to dry the solution before adding the $NaBH_4/Al_2O_3$ complex. Chromatography on silica gel and elution with $CHCl_3$ gave 0.7 g (57.6%) β-lactam **8**. Infrared (CH_2Cl_2): 2100 (N_3), 1790 (β-lactam), 1750 (ester) cm^{-1}; nmr ($CDCl_3$) δ: 2.42 (b, 1H, OH, exchangeable with D_2O), 3.81 (b, 2H, *CH*$_2$OH), 4.20–4.51 (m, 1H, CH), 4.65 (d, 1H, CHN_3, J = 5 Hz), 5.10 (s, 4H, CH_2), 7.19 (s, 10H, Ph). *Anal.* calcd. for $C_{21}H_{19}N_4O_6Cl$: C 54.96, H 4.14, N 12.21, Cl 7.74; found: C 55.07, H 4.03, N 12.35, Cl 7.85.

Iso-oxapenams 9a *and* 9b

Both β-lactams **9***a* and **9***b* were prepared in the same manner, which will be described for **9***b* only. Their spectra were similar except for their ester variations.

(*a*) β-Lactam **6***b* (0.2 g, 0.47 mmol) was dissolved in 30 mL dry CH_2Cl_2. Triethylamine (0.101 g, 1 mmol) was added. A solution of trifluoromethanesulfonyl chloride (0.085 g, 0.5 mmol) in 5 mL dry CH_2Cl_2 was added dropwise at 5°C, during a period of 5 min. The temperature was permitted to rise to 30°C in 1 h. The solution was washed with water, dried, and evaporated to give an oily product, which was chromatographed on silica gel. Elution with CH_2Cl_2 gave 0.12 g (59.5%) of **9***b* as an oil. Infrared (CH_2Cl_2): 2105 (N_3), 1795 (β-lactam), 1750 (ester) cm^{-1}; nmr ($CDCl_3$) δ: 4.21–4.80 (m, 4H, $CHCHCH_2O$), 5.10 (s, 4H, $2CH_2$), 7.20 (s, 10H, Ph). *Anal.* calcd. for $C_{21}H_{18}N_4O_6$: C 59.71, H 4.26, N 13.27; found: C 60.01, H 4.20, N 13.19.

(*b*) Chloro-β-lactam **8** (0.5 g, 1.09 mmol) was dissolved in 20 mL dry CH_2Cl_2. Triethylamine (0.12 g, 1.2 mmol) was added, and the solution was stirred at room temperature for 1 h. The solution was washed with water, dried, and evaporated to give an oily product. Chromatography on silica gel and elution with CH_2Cl_2 gave 0.4 g (86%) β-lactam **9***b* which was identical to **9***b* obtained before.

Phenylacetamido-β-lactam 11

To a solution of azido β-lactam **5***b* (2.48 g, 0.005 mol) in 70 mL dry CH_2Cl_2 at 0°C was added triethylamine (0.6 g, 0.006 mol). A stream of H_2S gas was bubbled in for 20 min. The solution was allowed to stand for 2 h at room temperature. Evolution of nitrogen gas was observed. A stream of nitrogen gas was bubbled in for 30 min, then was added 1.5 g (0.018 mol) pyridine, followed by dropwise addition of 0.9 g (0.006 mol) phenylacetyl chloride in 10 mL CH_2Cl_2. The solution was stirred for 2 h at 25°C, then was washed with 5% HCl solution, 10% $NaHCO_3$ solution, and brine. It was then dried over $MgSO_4$, and evaporated to give impure amide, which was chromatographed on silica gel. CH_2Cl_2 eluted impurities, and $CHCl_3$ gave 2.5 g (84%) of β-lactam **11** as an oil. Infrared (CH_2Cl_2): 3400 (NH), 1770 (β-lactam), 1750 (ester), 1680 (amide) cm^{-1}; nmr ($CDCl_3$) δ: 3.41 (s, 2H, CH_2), 4.75 (dd, 1H, *CH*CH=C, J_1 = 5 Hz, J_2 = 8 Hz), 5.00–5.21 (m, 5H, $2CH_2O$ and CH), 5.5 (dd, 1H, C*H*NH, J_1 = 5 Hz, J_2 = 8 Hz), 5.85 (dd, 1H, *CH*=CHPh, J_1 = 8 Hz, J_2 = 16 Hz), 6.45 (d, 1H, CHPh, J = 16 Hz), 6.61 (d, 1H, NH, J = 8 Hz), 7.00–7.40 (m, 20H, Ph); ms C.I. 589 ($M^+ + 1$), 454 ($M^+ + 1$ − COOBn), 414 ($M^+ + 1$ − $PhCH_2CONHCH$=C=O). *Anal.* calcd. for $C_{36}H_{32}N_2O_6$: C 73.46, H 5.44, N 4.76; found: C 73.41, H 5.41, N 4.81.

4-Hydroxymethyl-β-lactams 12

β-Lactam **11** (2.94 g, 0.005 mol) in 50 mL dry CH_2Cl_2 was saturated with nitrogen gas at −78°C. Then a mixture of O_3/N_2 gas was bubbled in until KI starch paper showed excess ozone (16 min). The excess ozone was removed by passing a stream of N_2 for 10 min. Then dimethylsulfide (1.6 g, 5 equiv.) was added. The temperature of the solution was permitted to rise to 25°C over 1 h, following which 4 g $MgSO_4$ was added. After a few minutes, $NaBH_4/Al_2O_3$ (1 g:10 g) was added while stirring. After 1 h the solution was filtered and evaporated to give the impure product, which was chromatographed on silica gel. CH_2Cl_2 eluted impurities and 4-hydroxy-β-lactam **12** was eluted with $CHCl_3$, 2 g (76%). Infrared (CH_2Cl_2): 3250–3550 (NH, OH), 1769 (β-lactam), 1735 (ester), 1685 (amide) cm^{-1}; nmr ($CDCl_3$) δ: 3.50 (s, 2H, CH_2), 5.60–4.18 (bm, 4H, $CHCH_2OH$), 5.10 (s, 4H, CH_2O), 5.38 (s, 1H, CH), 5.58 (dd, 1H, *CH*NH, J_1 = 5 Hz, J_2 = 9 Hz), 7.00 (b, 1H, NH), 7.20 (s, 15H, Ph). *Anal.* calcd. for $C_{29}H_{28}N_2O_7$: C 67.44, H 5.42, N 5.42; found: C 67.34, H 5.49, N 5.44.

Iso-oxapenam 13

Preparation of β-lactam **13** from acetamide-β-lactam **12** was achieved by the same method which was described for preparation of **9***b* from **6***b*. Iso-oxapenam **13** was obtained in 70% yield. Infrared (CH_2Cl_2): 3410 (NH), 1790 (β-lactam), 1756 (ester), 1685 (amide) cm^{-1}; nmr ($CDCl_3$) δ: 3.52 (s, 2H, $COCH_2$), 4.31–4.82 (m, 4H, $CHCHCH_2O$), 5.20 (s, 4H, $2CH_2$), 7.30 (bs, 16H, Ph and NH).

Acknowledgements

We wish to thank the Natural Sciences and Engineering Research Council of Canada for financial support, the Ministry of Science and Higher Education of Iran and University of Shiraz for a scholarship (G.H.H.), and Dr. O. Mamer and Ms. J. Montgomery for recording the mass spectra.

1. G. H. HAKIMELAHI and G. JUST. Tetrahedron Lett. 3645 (1979).
2. G. H. HAKIMELAHI and G. JUST. Can. J. Chem. **57**, 1932 (1979).
3. J. BRENNAN, G. RICHARDSON, and R. J. STOODLEY. J. Chem. Soc. Chem. Commun. 49 (1980).
4. C. F. H. ALLEN. J. Am. Chem. Soc. **52**, 2955 (1930).
5. G. H. HAKIMELAHI and G. JUST. Tetrahedron Lett. 3643 (1979).
6. H. M. KISSMAN and B. WITKOP. J. Am. Chem. Soc. **75**, 1970 (1953).
7. R. LOCQUIN and V. CERCHEZ. C. R. Acad. Sci. **186**, 1360 (1928).
8. E. SANTANIELLO, F. PONTI, and A. MANZUCCHI. Synthesis, 891 (1978).
9. T. W. DOYLE, B. BELLEAU, B. YULUH, C. F. FERRARI, and M. P. CUNNINGHAM. Can. J. Chem. **55**, 468 (1977).

Oxydation anodique de β-cétocarboxylates en milieu aqueux ou hydroorganique. Application à la synthèse de γ-dicétones, de cétones éthyléniques et de cétoamides

MONCEF CHKIR

Laboratoire de Chimie Organique, Ecole Normale Supérieure, 43 rue de la liberté, Le Bardo, Tunisie

ET

DANIEL LELANDAIS[1] ET CATHY BACQUET

Laboratoire de Chimie Organique Structurale, Bâtiment F, 4 Place Jussieu, 75230 Paris, France

Reçu le 18 juin, 1980

Can. J. Chem. Downloaded from www.nrcresearchpress.com by 210.87.254.105 on 09/06/12
For personal use only.

MONCEF CHKIR, DANIEL LELANDAIS et CATHY BACQUET. Can. J. Chem. **59**, 945 (1981).

L'étude systématique de l'oxydation anodique d'ions β cétocarboxylates en milieu aqueux ou hydroorganique a permis de dégager les conditions dirigeant l'orientation de cette réaction. Il est ainsi possible, par le choix du milieu réactionnel et de la structure de l'ion de départ de synthétiser des produits aussi différents que les γ-dicétones, les cétones éthyléniques et les cétoamides.

Le schéma de formation de ces deux derniers composés fait intervenir un ion α-cétocarbénium habituellement difficile à obtenir.

MONCEF CHKIR, DANIEL LELANDAIS, and CATHY BACQUET. Can. J. Chem. **59**, 945 (1981).

A systematic study of the anodic oxidation of β-ketocarboxylate anions in aqueous or hydroorganic solvents allows to distinguish the factors directing this reaction. Thus, it is possible by the appropriate choice of reaction medium and the structure of the starting ion to synthesize products such as γ diketones, ethylenic ketones and ketoamides.

The mode of formation of these last two classes of compound involves an α-ketocarbonium ion which is usually difficult to obtain.

[Journal translation]

L'utilisation de l'oxydation anodique de carboxylates ω-fonctionnalisés pour l'obtention de composés de couplage suivant le schéma 1 est l'une des applications les plus importantes de la réaction de Kolbe.

L'analyse des cas où X est un groupement oxo a été envisagée par de nombreux auteurs. Cependant si les α-céto carboxylates ont donné lieu à un début d'étude systématique (1), la littérature, avant publication de nos notes préliminaires (2, 3, 4), ne relevait rien de tel pour les β-cétocarboxylates. Tout au plus Willstätter et Pfannenstiel (5) avaient utilisé une réaction de ce type pour la synthèse du dioxa-3,6 octanedioate-1,8 d'éthyle, réaction qu'ils avaient menée à bien avec un rendement de 12%.

Pourtant les deux principaux types d'évolution de la réaction de Kolbe, dimérisation du radical formé ou oxydation ultérieure de celui-ci en carbocation, laissaient espérer l'obtention de γ-dicétones d'une part, et la formation d'ions α-cétocarbénium, d'accès *à priori* difficile, d'autre part (Schéma 2).

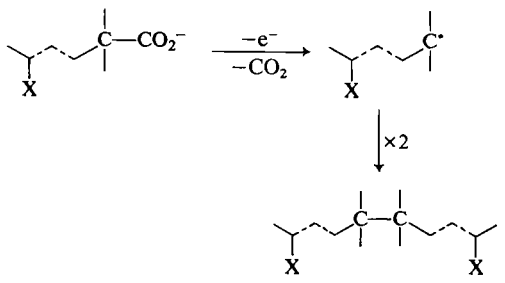

SCHÉMA 1

Nous avons donc entrepris ce travail en nous limitant dans un premier temps à l'électrolyse des β-cétocarboxylates en milieux aqueux ou hydroorganique. La solubilité de ces sels dans de tels solvants permet d'envisager la synthèse de produits en quantités acceptables en laboratoire.

Par ailleurs la littérature offre des méthodes faciles pour préparer des β-cétocarboxylates de structure très variée.

Cependant l'utilisation de β-cétocarboxylates impose certaines contraintes dans le choix des conditions expérimentales. En effet l'instabilité des β-céto-acides correspondants interdit l'emploi des milieux d'électrolyse acides habituellement utilisés dans les réactions de couplage radicalaire (6). De plus, la dégradation facile des sels sous l'effet de la chaleur, nécessite dans tous les cas le maintien de la solution d'électrolyse à une température inférieure à 30°C. Enfin notre but était la synthèse de composés organiques intéressants ou nouveaux avec une sélectivité et des rendements qui fassent de la méthode proposée un véritable mode de préparation de ces produits.

Il fallait donc choisir des conditions opératoires telles que l'oxydation anodique s'oriente vers la formation du radical suivie soit de la dimérisation, soit d'une oxydation électrochimique conduisant à

[1]Auteur à qui adresser toute correspondance.

0008-4042/81/060945-07$01.00/0

©1981 National Research Council of Canada/Conseil national de recherches du Canada

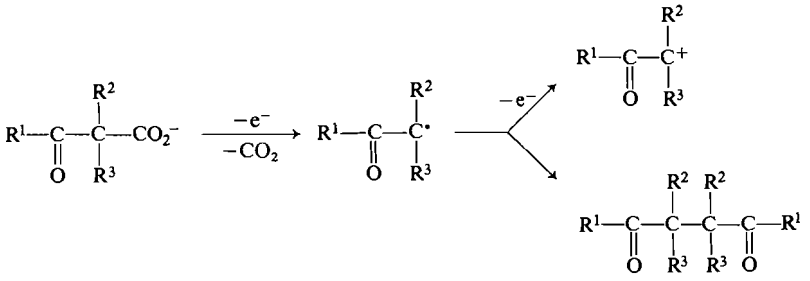

SCHÉMA 2

l'ion α-cétocarbénium susceptible de subir diverses réactions chimiques. Pour cela nous nous sommes basés sur les règles empiriques proposées classiquement (6), ainsi que sur des résultats que nous avons obtenus antérieurement (2).

Résultats

1. Orientation vers la voie radicalaire. Synthèse de γ-dicétones

Des études effectuées au laboratoire nous ont amenés à choisir un milieu eau–dioxanne (5:3) contenant environ une mole de β-cétocarboxylate de potassium; ce milieu s'est, en effet, révélé favorable à la duplication radicalaire. L'oxydation est réalisée sur une électrode de platine portée à une tension qui permette d'avoir une densité de courant supérieure à 0,25 A/cm². Dans tous les cas le potentiel a été supérieur à 2,2 V par rapport à l'électrode au calomel. Les produits de départ et les produits d'arrivée n'étant pas réductibles, l'électrolyse est conduite dans une cellule à compartiments non séparés. La réaction est arrêtée après consommation d'un Faraday par mole. Dans ces conditions, les résultats obtenus sont consignés dans le tableau 1.

Les γ-dicétones sont des éléments de base en synthèse, qu'il s'agisse par exemple de la préparation d'hétérocycles ou de cyclopenténones (7, 8), en témoignent le grand nombre de publications dont elles font l'objet (9 à 12).

Le tableau 1 permet de constater que ces composés sont obtenus aussi bien quand $R^2 = R^3 = H$, quand seul un groupement est un alkyle ou encore quand R^2 et R^3 sont tous les deux des alkyles. Lorsque R^2 est différent de R^3 il se forme une quantité égale de deux diastéréoisomères (*méso* et *dl*) que nous avons généralement pu séparer. L'attribution de la configuration résulte d'une étude développée par ailleurs.[2]

Les rendements de la réaction sont toujours de l'ordre de 30 à 40%. Ces rendements peuvent paraître modestes; néanmoins comparée aux autre méthodes d'obtention de γ-dicétones (13 à 15) cette réaction reste compétitive. Elle présente en particulier quelques avantages. Ainsi le seul produit secondaire observé est la cétone saturée R^1—CO—CHR^2R^3 ce qui rend la séparation des γ-dicétones particulièrement aisée. Par ailleurs, le mode de synthèse des sels de départ permet une grande variété de groupements R^1, R^2, R^3 d'où la possibilité de préparer un large éventail de γ-dicétones. Une application particulière a été faite pour la synthèse d'un composé deutérié difficilement accessible par deutériation directe.

2. Orientation vers la voie cationique. Obtention de cétones α,β-éthyléniques

L'eau pure étant connue pour être favorable à la voie cationique, de même qu'un milieu basique (6), nous avons électrolysé des solutions aqueuses de concentration environ molaire en carboxylate de potassium et en potasse. La facile électroréduction des cétones α,β-éthyléniques obtenues nécessite l'emploi d'une cellule à compartiments séparés. La libération d'un proton lors de la réaction:

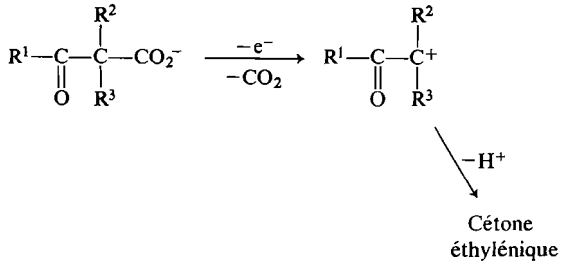

SCHÉMA 3

peut entraîner une acidification du milieu réactionnel ce qui risque d'une part, de favoriser la cétone saturée (voir 1), d'autre part de créer des conditions de pH défavorables à la voie cationique. Pour pallier cet inconvénient le pH du compartiment anodique est maintenu constant par addition de potasse.

L'anode utilisée est en platine; une anode en graphite, censée favoriser la formation du carbocation (6), n'a pas amélioré les résultats. Le potentiel imposé à l'anode est toujours supérieur à 2,2 V, la densité de courant est maintenue à 0,10–

[2]Résultats à paraître.

Can. J. Chem. Downloaded from www.nrcresearchpress.com by 210.87.254.105 on 09/06/12
For personal use only.

Can. J. Chem. Downloaded from www.nrcresearchpress.com by 210.87.254.105 on 09/06/12
For personal use only.

TABLEAU 1. Synthèse de γ-dicétones

Anion	γ-Dicétone	Rdt (%)
$CH_3—CO—CH_2—CO_2^-$	$(CH_3—CO—CH_2)_2$	38
$iPr—CO—CH_2—CO_2^-$	$(iPr—CO—CH_2)_2$	40
$tBu—CO—CH_2—CO_2^-$	$(tBu—CO—CH_2)_2$	38
$Me—CO—CHMe—CO_2^-$	$(Me—CO—CHMe)_2$	39
$Me—CO—CHEt—CO_2^-$	$(Me—CO—CHEt)_2$	36
$Me—CO—CMe_2—CO_2^-$	$(Me—CO—CMe_2)_2$	37
$Me—CO—CMeEt—CO_2^-$	$(Me—CO—CMeEt)_2$	34
$iPr—CO—CMe_2—CO^-$	$(iPr—CO—CMe_2)_2$	33
$tBu—CO—CHEt—CO_2^-$	$(tBu—CO—CHEt)_2$	32
$tBu—CO—CDEt—CO_2^-$	$(tBu—CO—CDEt)_2$	32

TABLEAU 2. Synthèse de cétones α,β-éthyléniques

Anion	Cétone éthylénique	Rdt (%)
$Me—CO—CMe_2—CO_2^-$	$Me—CO—CMe=CH_2$	90
$iPr—CO—CMe_2—CO_2^-$	$iPr—CO—CMe=CH_2$	90
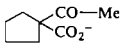	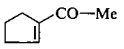	60
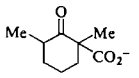	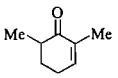	55
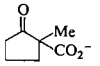		80
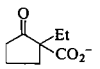		70
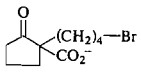	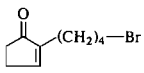	50

0,15 A/cm² et l'électrolyse est arrêtée après passage de deux Faradays par mole.

Le tableau 2 résume les résultats obtenus lorsque R^2 et R^3 sont des groupements alkyles. Il apparait que, lorsque l'un des groupements R^2 ou R^3 (ou les deux) est un hydrogène, le seul produit isolé est la cétone saturée $R^1COCH_2R^2$. Les rendements observés font de cette réaction un bon mode de préparation de cétones éthyléniques, d'autant plus qu'elle présente l'avantage d'être simple et rapide à mettre en œuvre. En outre cette méthode permet dans certains cas, le passage en deux réactions, l'une chimique (16) l'autre électrochimique de la cétone saturée à la cétone éthylénique. Notons que la réaction de Kolbe, en ne modifiant pas d'autres fonctions présentes dans la molécule, rend possible l'obtention de composés telle la bromobutyl-2 cyclopentène-2 one, susceptible d'être utilisée dans les réactions ultérieures.

3. Orientation vers la voie cationique. Obtention de cétoamides

Ayant vérifié par cette synthèse de cétones α,β-éthyléniques qu'il est possible de créer des carbo-

TABLEAU 3. Synthèse de cétoamides

Solvant	Anion: $Me-CO-C(Me)(Me)-CO_2^-$	Anion: $Me-CO-C(Et)(Me)-CO_2^-$	Anion: $iPr-CO-C(Me)(Me)-CO_2^-$
MeCN	$Me-CO-C(Me)(Me)-NH-CO-Me$ 50%	$Me-CO-C(Et)(Me)-NH-CO-Me$ 48%	$iPr-CO-C(Me)(Me)-NH-CO-Me$ 45%
EtCN	$Me-CO-C(Me)(Me)-NH-CO-Et$ 42%	$Me-CO-C(Et)(Me)-NH-CO-Et$ 37%	$iPr-CO-C(Me)(Me)-NH-CO-Et$ 33%
*i*PrCN	$Me-CO-C(Me)(Me)-NH-CO-iPr$ 21%	$Me-CO-C(Et)(Me)-NH-CO-iPr$ 20%	$iPr-CO-C(Me)(Me)-NH-CO-iPr$ 18%

cations $R^1COC^+R^2R^3$, nous avons pensé les faire réagir sur des nitriles RCN. Cette réaction analogue à celle de Ritter et Minieri (17) conduirait à des cétoamides selon:

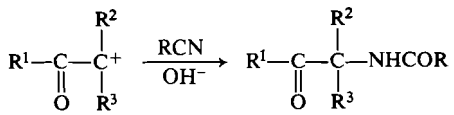

SCHÉMA 4

Ces cétoamides constituent en effet une famille originale d'amides *N*-substitués qui restent très recherchés en fonction de leurs applications diverses (18 à 22). Il est difficile de travailler en milieu nitrile pur à cause, en particulier, de la mauvaise solubilité des carboxylates dans ce solvant. Nous avons donc utilisé un milieu nitrile contenant un minimum d'eau. Ces conditions sont connues pour être assez favorables à l'obtention d'amides *N*-alcoylés par électrochimie (23, 24).

Les ions intermédiaires formés lors de la réaction étant susceptibles d'être réduits à la cathode, nous avons mené les électrolyses dans une cellule à compartiments séparés. L'anode utilisée est une lame de platine. Comme dans le cas des cétones α,β-éthyléniques, l'emploi d'une anode en graphite n'a pas amélioré les rendements. Les résultats obtenus sont rassemblés dans le tableau 3.

Les cétoamides n'ont été obtenus que lorsque R^2 et R^3 sont des groupements alkyles. Si l'un des deux est un hydrogène seule la cétone saturée $R^1COCH_2R^2$ se forme. Les rendements de la réaction décroissent de l'acétonitrile (50%) à l'isobutyronitrile (20%). Dans ce dernier cas se pose le problème de la solubilité dans l'eau, d'où la diminution du rendement. Par ailleurs, il apparait progressivement comme produit secondaire un peu de γ-dicétone $(R^1COR^2R^3)_2$. Enfin il faut signaler que ces produits sont dans leur grande majorité des produits nouveaux. L'un d'entre eux[3] a été soumis sous contrôle de l'ANVAR à des tests pharmacologiques préliminaires. Il ressort de cette étude que ce produit devrait être classé parmi les tranquillisants bien qu'il augmente, dans un certain intervalle des doses administrées, les phases motrices et exploratrices. Deux tranquillisants connus, le chlordiazépoxide et le diazépam présentent cette même dualité.

Ces premiers résultats montrent bien l'intérêt de synthétiser ce type de composé. En effet la substitution sur l'azote par un groupement carbonylé semble accroître l'activité psychotrope des produits ce qui n'est pas évident si la fonction carbonylée est introduite sur la chaîne carbonée.

Discussion

Cette étude montre l'importance de deux facteurs influant sur le déroulement de la réaction: (*1*) la structure de l'ion carboxylate; (*2*) la nature du milieu d'électrolyse .

Structure de l'ion carboxylate

Nous n'avons pas observé, même dans des

[3] *i*PrCOCMe$_2$NHCOMe.

Can. J. Chem. Downloaded from www.nrcresearchpress.com by 210.87.254.105 on 09/06/12
For personal use only.

Can. J. Chem. Downloaded from www.nrcresearchpress.com by 210.87.254.105 on 09/06/12
For personal use only.

milieux très favorables, de produits d'origine cationique dans les cas où R^2 et R^3 ne sont pas tous deux des alkyles. Nous retrouvons ainsi une règle empirique énoncée par Eberson: "les radicaux dont le potentiel d'ionisation est supérieur à 8 eV résistent généralement à une oxydation ultérieure en cation" (voir réf. 23).

Pour les radicaux α-carbonylés nous ne disposons que du potentiel d'ionisation du radical $^{\cdot}CH_2—COCH_3$ qui est de 7,95 eV. Mais par ailleurs, nous savons que le potentiel d'ionisation des radicaux α-cyanés varient de la façon suivante: $^{\cdot}CH_2CN$, 10,87 eV; $CH_3\dot{C}H—CN$, 9,76 eV et $(CH_3)_2\dot{C}—CN$: 9,15 eV (25, 26), Une évolution parallèle conduirait à environ 6,85 eV pour le radical carbonylé monométhylé et 6,25 eV pour le diméthylé.

Ces valeurs paraissent éloignées de la frontière des 8 eV proposée dans la règle d'Eberson. Cependant celle-ci ne peut s'appliquer rigoureusement puisque les potentiels d'ionisation sont déterminés en phase gazeuse par impact électronique ou photoionisation, alors que nous avons effectué les électrolyses en solution. De plus la règle d'Eberson avait été établie pour des radicaux alkylés électrolysés dans le méthanol. Nos résultats montrent néanmoins que la facilité d'oxydation du radical en carbocation va de pair avec un faible potentiel d'ionisation de ce radical.

Dans le cas des radicaux carbonylés électrolysés en milieu aqueux basique, nous remarquons un changement de comportement brutal: les β-cétocarboxylates monoalkylés conduisent uniquement à des produits issus d'une réaction radicalaire, alors que les composés dialkylés ne fournissent que des produits d'origine cationique. Ces résultats montrent néanmoins qu'il est facile de créer, par voie électrochimique, un ion α-cétocarbénium d'accès *à priori* difficile.

Milieu réactionnel

L'étude présentée met aussi en évidence l'importance du choix du milieu réactionnel pour orienter la réaction.

En effet, le milieu va non seulement déterminer le type d'intermédiaire qui va se former par électrolyse de β-cétocarboxylates dialcoylés (un radical en milieu dioxanne-eau, un carbocation en milieu basique aqueux, ou un mélange des deux espèces en milieu basique hydroorganique), mais encore orienter la réaction de l'intermédiaire (obtention de cétones éthyléniques en milieu aqueux ou obtention de cétoamides en milieu eau–acétonitrile). Le principal intérêt de ce travail, à côté des problèmes théoriques qu'il soulève, réside dans l'élaboration de composés aussi différents que les γ-dicétones, les cétones éthyléniques et les cétoamides à partir de matières premières d'accès aisé.

Partie expérimentale

Les spectres ir ont été effectués sur un appareil Perkin-Elmer 457G, les spectres rmn sur un appareil Varian EM360 en solution dans le tétrachlorure de carbone (référence interne hexaméthyldisiloxane).

Préparation des esters-β cétoniques

Plusieurs méthodes ont été utilisées pour préparer les β-cétocarboxylates suivants (Schéma 5); alcoylation de l'acétyl acétate d'éthyle selon Cournot (27) cas **1, 4, 5, 6, 7, 10**; alcoylation de la carbéthoxy-2 cyclopentanone selon la réf. 28, cas **13, 14**; double condensation du dibromo-1,4 butane sur l'acétyl acétate d'éthyle selon la réf. 16, cas **10**; condensation de cétones sur le diéthylcarbonate selon la réf. 29, cas **2, 3, 9**; condensation du dibromo-1,4 butane sur le sel de potassium de la carbéthoxycyclopentanone selon la réf. 30, cas 15.

Synthèse des carboxylates β-cétoniques

1. Saponification des esters β-cétoniques (mode opératoire général)

Une solution de 5,6 g de potasse en solution dans 50 mL d'eau est ajoutée à température ambiante à 0,1 mole d'ester β-cétonique; une agitation magnétique est maintenue pendant 16 h. Après extraction à l'éther, la phase aqueuse contenant le sel β-cétonique est électrolysée.

2. Synthèse directe de sels β-cétoniques

La synthèse des composés **8, 11** et **12** s'effectue par condensation des cétones saturées correspondantes sur le bioxyde de carbone (29).

Appareillage

Conditions d'électrolyse (mode opératoire général)

Les électrolyses sont menées à l'aide d'un potentiostat Tacussel modèle ASA 10A permettant d'imposer un potentiel fixe à l'anode. Les mesures coulométriques ont été faites sur un intégrateur Tacussel IG 4100 monté en série sur le circuit. L'in-

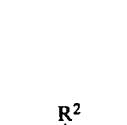

No	R^1	R^2	R^3
1	Me	H	H
2	*i*Pr	H	H
3	*t*Bu	H	H
4	Me	Me	H
5	Me	H	Et
6	Me	Me	Me
7	Me	Me	Et
8	*i*Pr	Me	Me
9	*t*Bu	H	Et

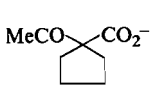

10

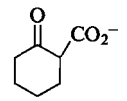

11

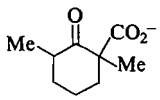

12

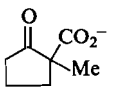

13

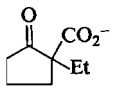

14

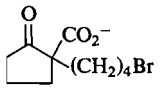

15

SCHÉMA 5

Can. J. Chem. Downloaded from www.nrcresearchpress.com by 210.87.254.105 on 09/06/12
For personal use only.

tensité du courant est mesurée par un ampèremètre monté sur le circuit de la cathode.

La cellule d'électrolyse est constituée par une cuve servant de compartiment cathodique au fond de laquelle se trouve une nappe de mercure (cathode). Un verre fritté servant de compartiment anodique est ajusté à l'intérieur de la cuve dans le cas d'électrolyse en compartiments séparés. L'anode est une lame de platine. Une agitation magnétique est maintenue au cours de la réaction et la tension imposée est toujours supérieure à 2,2 V par rapport à l'électrode de référence au calomel, de façon à obtenir une densité de courant de l'ordre de 0,10 à 0,15 A/cm^2 pour les réactions par voie cationiques et de 0,25 A/cm^2 pour les réactions par voie radicalaire. A la fin de l'électrolyse la solution est recueillie, neutralisée par une solution diluée d'acide chlorhydrique puis extraite plusieurs fois à l'éther. Les solvants et produits légers sont distillés sous pression ordinaire. Les résidus sont fractionnés sous pression réduite et analysés par chromatographie en phase vapeur. Nous avons utilisé trois types de colonne: silicone SE30, cyanosilicone XE60 et Carbowax 20M. La colonne de Carbowax donne généralement les meilleurs résultats et permet notamment de séparer les diastéréoisomères des composés bifonctionnels. Nous avons le plus souvent doublé la chromatographie en phase vapeur par une séparation des produits sur couche mince. Nous avons utilisé un support de silice légèrement platrée GF25H et un éluant composé de 50% d'éther de pétrole, 25% d'éther et 25% de chloroforme. Les produits sont révélés avec une lampe à ultraviolet puis fixés à l'aide d'une solution sulfurique de sulfate de cérium.

Obtention des γ-dicétones

1. Conditions d'électrolyse (mode opératoire général)

Dans une cellule non divisée, 50 mL d'une solution aqueuse contenant 0,1 mole de sel β-cétonique sont ajoutés à 30 mL de dioxanne. Une agitation magnétique est maintenue. L'électrolyse est arrêtée après consommation d'un Faraday par mole. La solution est traitée selon le mode opératoire général.

2. Produits isolés

Tous les rendements ont été calculés par rapport au β-cétocarboxylate de départ.

Hexanedione-2,5. Séparée en cpv sur colonne Carbowax à 150°C; rendement 38%. Identique à un échantillon commercial.

Diméthyl-2,7 octanedione-3,6 (31). Séparée en cpv sur colonne Carbowax à 180°C; rendement 40%; $Eb_{0,9}$ 100–102°C; dioxime F 172–173°C (litt (31) F 174–175°C); rmn (CCl_4): 2,6 (s, 2H), 2,5 (hept, 1H), 1,1 (d, 6H) ppm.

Tétraméthyl-2,2,7,7 octanedione-3,6 (32). Séparée en cpv sur colonne de silicone à 160°C; rendement 38%; Eb_{18} 106–107°C (litt. (32) Eb_{10} 106–107°C); rmn (CCl_4): 2,5 (s, 2H), 1,0 (s, 9H) ppm.

Diméthyl-3,4 hexanedione-2,5 (33). Séparée en cpv sur colonne Carbowax à 135°C; rendement 39%; rmn (CCl_4): 2,8 (m, 1H), 2,1 (s, 3H), 1,1 (m, 3H) ppm. Il s'agit d'un mélange de deux isomères.

Diéthyl-3,4-hexanedione-2,5 (34). Rendement 36%; Eb_{20} 112–115°C (litt. (34) Eb_{20} 112–115°C); rmn (CCl_4), isomère 1: 2,85 (m, 1H), 2,1 (s, 3H), 1,6 (m, 2H), 0,8 (t, 3H) ppm; isomère 2: 2,70 (m, 1H), 2,1 (s, 3H), 1,45 (m, 2H), 0,8 (t, 3H) ppm.

Tétraméthyl-3,3,4,4 hexanedione-2,5 (35). Séparée en cpv sur colonne de Carbowax à 135°C; rendement 37%; $Eb_{0,5}$ 40°C (litt. (35) $Eb_{0,5}$ 40°C); rmn (CCl_4): 2,1 (s, 3H), 1,2 (s, 6H) ppm.

Diéthyl-3,4 diméthyl-3,4 hexanedione-2,5 (36). Rendement 34%; Eb_1 95–97°C; rmn (CCl_4), isomère 1: 2,0 (s, 3H), 1,17 (s, 3H), 1,35 (q, 2H), 0,8 (t, 3H) ppm; isomère 2: 2,05 (s, 3H), 1,20 (s, 3H), 1,13 (q, 2H), 0,8 (t, 3H) ppm.

Hexaméthyl-2,4,4,5,5,7 octanedione-3,6 (37). Séparée en cpv sur colonne de silicone à 180°C. Rendement 33%; $Eb_{1,5}$ 75–77°C (litt. (37) $Eb_{5,5}$ 108–111°C); rmn (CCl_4): 3,1 (hept, 1H), 1,3 (s, 6H), 1,1 (d, 6H) ppm.

Tétraméthyl-2,2,7,7 diéthyl-4,5 octanedione-3,6. Séparée en cpv sur colonne de cyanosilicone à 160°C; rendement 32%; $Eb_{0,5}$ 105–107°C; F 44–45°C; ir v: 1720 cm^{-1}; rmn (CCl_4): 3,4 (m, 1H), 1,5 (m, 2H), 1,2 (s, 9H), 0,8 (m, 3H) ppm. Il s'agit d'un mélange de deux isomères. *Anal.* calc. pour $C_{16}H_{30}O_2$: C 75,53, H 11,89; trouvée: C 75,71, H 11,84.

Deutéro-4,5 tétraméthyl-2,2,7,7 diéthyl-4,5 octanedione-3,6. Séparée en cpv sur colonne de cyanosilicone à 160°C; rendement 32%; $Eb_{0,5}$ 105–107°C; ir v: 1720 cm^{-1}; rmn ($CDCl_3$), isomère 1: 1,6 (m, 2H), 1,15 (s, 9H), 0,8 (t, 3H) ppm; isomère 2: 1,4 (m, 2H), 1,15 (s, 9H), 0,8 (t, 3H) ppm.

Obtention des cétones éthyléniques

1. Conditions d'électrolyse (mode opératoire général)

Une solution contenant 0,1 mole de sel β-cétonique et 0,1 mole de potasse dans 50 mL d'eau est introduite dans le compartiment anodique. Dans le compartiment cathodique, une solution aqueuse de potasse de même concentration est versée de façon à égaliser les niveaux des deux compartiments. L'électrolyse est arrêtée après consommation de deux Faradays par mole. La solution est traitée selon le mode opératoire général.

2. Produits isolés

Méthyl-3 butène-3 one-2. Rendement 90%. Identique à un échantillon commercial.

Diméthyl-2,4 pentène-1 one-3 (38). Séparé en cpv sur colonne de Carbowax à 95°C. Rendement 90%; Eb_{40} 52–54°C (litt. (38) Eb_{60} 55°C); rmn (CCl_4): 5,9 (2m, 2H), 3,3 (hept, 1H), 1,9 (m, 3H), 1,1 (d, 6H) ppm.

Acétyl-1 cyclopentène (39). Séparé sur colonne de Carbowax à 160°C. Rendement 60%; F 206–208°C; rmn (CCl_4): 6,6 (m, 1H), 2,5 à 2 (m, 6H), 2,2 (s, 3H) ppm.

Diméthyl-2,6 cyclohexène-2 one-1 (40). Séparé sur colonne de Carbowax à 185°C. Rendement 55%; rmn (CCl_4): 6,7 (m, 1H), 2,6 à 1,9 (m, 5H), 1,8 (m, 3H), 1,15 (d, 3H) ppm.

Méthyl-2 cyclopentène-2 one-1 (41). Séparé sur colonne de Carbowax à 165°C. Rendement 80%; rmn (CCl_4): 7,3 (m, 1H), 2,7 à 2 (m, 4H), 1,8 (m, 3H) ppm.

Ethyl-2 cyclopentène-2 one-1 (42). Séparé sur colonne de Carbowax à 175°C. Rendement 70%; rmn (CCl_4): 7,2 (m, 1H), 2,7 à 1,9 (m, 6H), 1,1 (t, 3H) ppm.

Bromobutyl-2 cyclopentène-2 one-1. Séparée sur colonne de silicone à 200°C. Rendement 50%; ir v: 1710, 1630 cm^{-1}; rmn (CCl_4): 7,2 (m, 1H), 3,35 (t, 2H), 2,7 à 1,5 (m, 10H) ppm. *Anal.* calc. pour $C_9H_{13}OBr$: C 49,79, H 6,04, Br 36,81; trouvée: C 49,83, H 6,00, Br 36,78.

Obtention des cétoamides

1. Conditions d'électrolyse (mode opératoire général)

Une solution de 0,1 mole de sel β-cétonique dans 50 mL d'eau est introduite dans le compartiment anodique puis 30 mL d'acétonitrile, de propionitrile ou d'isobutyronitrile sont ajoutés. Dans le compartiment cathodique une solution de potasse de même concentration est versée de façon à égaliser les niveaux des deux compartiments. Les électrolyses sont conduites à pH légèrement alcalin, une solution de potasse est ajoutée au fur et à mesure que la réaction se poursuit. L'électrolyse est arrêtée après consommation de deux Faradays par mole. La solution anodique est traitée selon le mode opératoire général. Après évaporation des solvants, le résidu est abondonné au réfrigérateur. Les céto-amides cristallisent généralement au bout de quelques jours. Un lavage à zéro degré permet une première purification des produits.

Can. J. Chem. Downloaded from www.nrcresearchpress.com by 210.87.254.105 on 09/06/12
For personal use only.

2. Produits isolés

N(*diméthyl-1,1 oxo-2 propyl) acétamide* (43). Rendement: 50%; F 108–110°C; ir ν: 3450, 3400, 1715, 1670 cm^{-1}; rmn ($CDCl_3$): 6,6 (s, 1H), 2,2 (s, 3H), 2,0 (s, 3H), 1,5 (s, 6H) ppm.

N(*diméthyl-1,1, oxo-2 propyl) propionamide*. Rendement: 42%; F 74–75°C; ir ν: 3450, 3400, 1715, 1650 cm^{-1}; rmn ($CDCl_3$): 6,4 (s, 1H), 2,2 (q, 2H), 2,1 (s, 3H), 1,4 (s, 6H), 1,15 (t, 3H) ppm. *Anal.* calc. pour $C_8H_{15}NO_2$: C 61,12, H 9,62, N 8,91; trouvée: C 61,06, H 9,68, N 8,95.

N(*diméthyl-1,1 oxo-2 propyl) isobutyramide*. Rendement 21%; F 96–98°C; ir ν: 3440, 3400, 1720, 1670 cm^{-1}; rmn ($CDCl_3$): 6,4 (s, 1H), 2,4 (hept, 1H), 2,2 (s, 3H), 1,5 (s, 6H), 1,1 (d, 6H) ppm. *Anal.* calc. pour $C_9H_{17}NO_2$: C 63,13, H 10,00, N 8,18; trouvée: C 63,17, H 9,89, N 8,21.

N(*éthyl-1 méthyl-1 oxo-2 propyl) acétamide*. Rendement: 48%; F 58–60°C; ir ν: 3500, 3470, 1715, 1665 cm^{-1}; rmn ($CDCl_3$): 7,2 (s, 1H), 2,1 (s, 3H), 1,9 (s, 3H), 1,5 (s, 3H), 1,3 (q, 2H), 0,8 (t, 3H) ppm. *Anal.* calc. pour $C_8H_{15}NO_2$: C 61,12, H 9,62, N 8,91; trouvée: C 61,13, H 9,53, N 8,84.

N(*éthyl-1 méthyl-1 oxo-2 propyl) propionamide*. Rendement 37%; F 64–66°C; ir ν: 3440, 3400, 1715, 1670 cm^{-1}; rmn ($CDCl_3$): 6,4 (s, 1H), 2,25 (q, 2H), 2,2 (s, 3H), 1,6 (q, 2H), 1,5 (s, 3H), 1,1 (t, 3H), 0,7 (t, 3H) ppm. *Anal.* calc. pour $C_9H_{17}NO_2$: C 63,13, H 10,00, N 8,18; trouvée: C 63,09, H 10,06, N 8,16.

N(*éthyl-1 méthyl-1 oxo-2 propyl) isobutyramide*. Rendement: 20%; $Eb_{0,5}$ 115–120°C; ir ν: 3450, 3400, 1715, 1670 cm^{-1}; rmn ($CDCl_3$): 6,4 (s, 1H), 2,4 (hept, 1H), 2,2 (s, 3H), 1,6 (q, 2H), 1,5 (s, 3H), 1,2 (d, 6H), 0,7 (t, 3H). *Anal.* calc. pour $C_{10}H_{19}NO_2$: C 64,83, H 10,34, N 7,56; trouvée: C 64,87, H 10,30, N 7,54.

N(*triméthyl-1,1,3 oxo-2 butyl) acétamide* (43). Rendement: 45%; F 98–100°C; ir ν: 3450, 3400, 1715, 1665 cm^{-1}; rmn ($CDCl_3$): 7,4 (s, 1H), 3,1 (hept, 1H), 1,95 (s, 3H), 1,4 (s, 6H), 1,1 (d, 6H) ppm.

N(*triméthyl-1,1,3 oxo-2 butyl) isobutyramide*. Rendement 33%; $Eb_{0,5}$ 120–125°C; ir ν: 3450, 3400, 1720, 1670 cm^{-1}; rmn ($CDCl_3$): 6,7 (s, 1H), 3,2 (hept, 1H), 2,2 (q, 2H), 1,6 (s, 6H), 1,17 (t, 3H), 1,1 (d, 6H) ppm. *Anal.* calc. pour $C_9H_{17}NO_2$: C 63,13, H 10,00, N 8,18; trouvée: C 63,20, H 10,05, N 8,03.

N(*triméthyl-1,1,3 oxo-2 butyl) isobutyramide*. Rendement 18%; F 104–106°C; ir ν: 3450, 3400, 1715, 1670 cm^{-1}; rmn ($CDCl_3$): 6,7 (s, 1H), 3,1 (hept, 1H), 2,4 (hept, 1H), 1,5 (s, 6H), 1,12 (d, 6H), 1,1 (d, 6H) ppm. *Anal.* calc. pour $C_{11}H_{21}NO_2$: C 66,29, H 11,62, N 7,03; trouvée: C 66,20, H 11,66, N 7,08.

1. B. Wladislaw et J.-P. Zimermann. J. Chem. Soc. B, 290 (1970).
2. M. Chkir et D. Lelandais. Chem. Commun. 1369 (1971).
3. D. Lelandais et M. Chkir. Tetrahedron Lett. 3113 (1974).
4. D. Lelandais et M. Chkir. C. R. Acad. Sci. Ser. C, **281**, 721 (1975).
5. R. Willstätter et A. Pfannenstiel. Ann. **422**, 11 (1920).
6. M. Baizer. Organic electrochemistry. M. Dekker, New York. 1973. p. 476.
7. J. E. McMurry et J. Melton. J. Am. Chem. Soc. **93**, 5309 (1971).
8. J. E. McMurry et T. E. Glass. Tetrahedron Lett. 2575 (1971).
9. J. L. Hermann, J. E. Richman et R. H. Schlessinger. Tetrahedron Lett. 3271 (1973).
10. A. Pelter, C. R. Harrisson et D. Kirkpatrick. Tetrahedron Lett. 4497 (1973).
11. L. C. Blaszczak et J. E. Mc.Murry. J. Org. Chem. **39**, 258 (1974).
12. Y. Kobayashi, T. Taguchi et E. Tokuno. Tetrahedron Lett. 3741 (1977).
13. D. Koch, H. Schäfer et E. Steckhan. Chem. Ber. **107**, 3640 (1974).
14. M. Covello et E. Abignente. Ann. Chem. Rome, **52**, 92325 (1962).
15. Y. Ito, T. Konoike et T. Saegusa. J. Am. Chem. Soc. **97**, 649 (1975).
16. L. J. Goldsworthy. J. Chem. Soc. 377 (1934).
17. J. J. Ritter et P. P. Minieri. J. Am. Chem. Soc. **70**, 4045 (1948).
18. S. Hideo, K. Kenj et Y. Shunichi. Chem. Pharm. Bull. **20**, 361 (1972).
19. Lion Dentifrice Co. Ltd., Br. Patent No. 1,233,072. (Chem. Abstr. **75**, 6315x (1971)).
20. K. Tetsu, Y. Yutaka et S. Takao. Yakugaku Zasshi, **90**, 1400 (1970); Chem. Abstr. **74**, 5343d (1971).
21. S. Minoru, K. Jiro et H. Akira. Chem. Pharm. Bull. **18**, 2074 (1974).
22. M. Benoit-Guyot, J. L. Benoit-Guyot et A. Boucherle. Chimie Thérapeutique **4**, 412 (1973).
23. L. Eberson et K. Nyberg. Acta Chem. Scand. **18**, 1567 (1968).
24. A. Laurent, E. Laurent et R. Tardivel. Tetrahedron Lett. 4861 (1973).
25. R. I. Reed. Ion production by electron impact. Academic Press, New York. 1962.
26. N. L. Weinberg et H. R. Weinberg. Chem. Rev. **68**, 448 (1968).
27. A. Cournot. Bull. Soc. Chim. Fr. **35**, 98 (1906).
28. G. Vavon et H. Horeau. Bull. Soc. Chim. Fr. **1**, 1703 (1934).
29. R. Levine et C. R. Hauser. J. Am. Chem. Soc. **66**, 1768 (1934).
30. P. S. Mariano, R. B. Steitle, D. G. Watson, M. J. Peters et E. Bay. J. Am. Chem. Soc. **98**, 5899 (1976).
31. L. F. Deemer, L. Lutwak et F. Strong. J. Am. Chem. Soc. **70**, 154 (1948).
32. W. H. Brown et G. F. Wright. Can. J. Chem. **35**, 236 (1957).
33. R. Criegee et K. Nool. Ann. **627**, 1 (1959).
34. E. Wolthuis, B. Brossenbroeh, G. De. Wall, E. Geels et A. Leegwater. J. Org. Chem. **28**, 148 (1963).
35. M. S. Kharash, H. C. McBray et W. H. Hurry. J. Am. Chem. Soc. **70**, 1269 (1948).
36. A. Harris. U.S. Patent No. 3,466,349. 9 Sept. 1969. Chem. Abstr. **71**, 92228x (1969).
37. M. F. Ansell, W. I. Hickinbottom et P. G. Holton. J. Chem. Soc. 349 (1955).
38. J. Colonge et J. C. Dubin. Bull. Soc. Chim. Fr. 1180 (1960).
39. J. R. Hawthorne et R. Robinson. J. Chem. Soc. 763 (1936).
40. M. Mousseron, R. Jacquier et F. Winternitz. C. R. Acad. Sci. **224**, 1230 (1947).
41. M. Gaddis et W. Butz. J. Am. Chem. Soc. **69**, 1203 (1947).
42. M. F. Ansell et S. S. Brown. J. Chem. Soc. 2955 (1958).
43. J. Y. Becker, L. L. Miller et T. M. Siegel. J. Am. Chem. Soc. **97**, 849 (1975).

Rydberg and valence-shell transitions in the quartz ultraviolet spectra of aliphatic thiones

A. E. BRUNO, D. J. CLOUTHIER, P. G. MEZEY, AND R. P. STEER[1]

Department of Chemistry and Chemical Engineering, University of Saskatchewan, Saskatoon, Sask., Canada S7N 0W0

Received July 28, 1980

A. E. BRUNO, D. J. CLOUTHIER, P. G. MEZEY, and R. P. STEER. Can. J. Chem. **59**, 952 (1981).

The electronic absorption spectra of 3,3-dimethylbutane-2-thione and 3-methylbutane-2-thione in the gas phase have been measured and the observed transitions assigned with the aid of *ab initio* and semi-empirical calculations. In the quartz ultraviolet region four transitions are observed. A strong, broad, structureless band is assigned to the $\pi \rightarrow \pi^*$ transition and three weaker, narrower bands are assigned to Rydberg $n \rightarrow 4s$, $n \rightarrow 4p_y$ and $n \rightarrow 4p_z$ transitions on sulfur.

A. E. BRUNO, D. J. CLOUTHIER, P. G. MEZEY et R. P. STEER. Can. J. Chem. **59**, 952 (1981).

On a mesuré les spectres électroniques d'absorption de la diméthyl-3,3 butanethione-2 et de la méthyl-3 butanethione-2 en phase gazeuse et on a identifié les transitions à l'aide de calculs *ab initio* et semi-empiriques. Dans la région ultraviolette du quartz, on a observé 4 transitions: une bande large et intense non structurée que l'on attribue à la transition $\pi \rightarrow \pi^*$ et trois bandes plus faibles et plus étroites que l'on attribue aux transitions de Rydberg du soufre $n \rightarrow 4s$, $n \rightarrow 4p_y$ et $n \rightarrow 4p_z$.

[Traduit par le journal]

Introduction

Although clear distinctions have been made between Rydberg and valence-shell electronic transitions in organic molecules containing a wide variety of chromophores (1), the aliphatic thiones have not been examined from this point of view. The existing assignments (2–6) of higher energy absorption bands in the uv–visible spectra of aliphatic thiones are inconsistent and may be incorrect, in part, in light of recent work on thioformaldehyde (7–9). The photochemistry of the higher excited states of the thiones (10, 11) has been of great interest in recent years and a re-examination of thione uv spectra is also warranted from this standpoint.

Aliphatic thiones exhibit two weak, overlapping band systems in the visible which are unmistakably assignable to transitions involving $n \rightarrow \pi^*$ electron promotions which produce the lowest triplet and lowest excited singlet states of the molecule (12). The interpretation of the spectra in the quartz ultraviolet is less straightforward, however, since several band systems of comparable intensity overlap. Two strong, broad unstructured absorptions at $210\,nm < \lambda_{max} < 320\,nm$ have been observed previously in solution and have been assigned to $\pi \rightarrow \pi^*$ and $n \rightarrow \sigma^*$ transitions (2–5). Rydberg transitions in these solution spectra have not been identified but would tend to be obscured by solvent absorption in the expected absorption region. Moreover, the electronic spectra may be complicated by tautomerization which can occur in thiones possessing labile α-hydrogen atoms (13). Further difficulties are associated with the instability of many aliphatic thiones. No electronic spectra of aliphatic thiones in the gas phase have been reported.

In this paper we report the quartz ultraviolet spectra of two aliphatic thiones, 3,3-dimethylbutane-2-thione (**I**) and 3-methylbutane-2-thione (**II**), in the gas phase and assign the observed band systems to Rydberg and valence shell transitions with the aid of *ab initio* and semi-empirical calculations.

Experimental and Calculational Techniques

I and **II** were prepared by the acid-catalyzed reaction of H_2S with the corresponding ketones according to the method of Paquer and Vaille (14). After vacuum distillation the thiones were purified by preparative gas chromatography using a 3 m glass column containing 30% SE 30 on 60/80 acid-washed Chromosorb W. Samples were stored under vacuum in the dark at 77 K.

Absorption spectra were taken on a Cary 118 uv–visible spectrophotometer which had been flushed for 24 h with dry nitrogen. Matched 10 cm cells with Suprasil windows were used to obtain gas phase spectra using an evacuated cell as a reference. All measurements were made at a room temperature of 23 ± 2°C.

Because experimental structures of these thiones have not been reported, their ground state geometries were estimated by *ab initio* calculations using a modified version of the Gaussian 70 program in which an STO-3G minimal basis set is employed (15). This program is known to reproduce the measured ground state geometries of smaller thiocarbonyls with good accuracy (16). The most important bond angles and lengths were sequentially optimized in several iterations to obtain a final geometry. CNDO/2 calculations based upon these estimations were then used to obtain values of the oscillator strengths of the valence-shell transitions. The thiones were assumed to exhibit C_{2v} local symmetry about the $>C{=}S$ moiety in the ground electronic state. The z axis of the coordinate system was chosen to be coincident with the C—S bond axis, with the x axis perpendicu-

[1]To whom all correspondence should be addressed.

0008-4042/81/060952-05$01.00/0

©1981 National Research Council of Canada/Conseil national de recherches du Canada

Can. J. Chem. Downloaded from www.nrcresearchpress.com by 210.87.254.6 on 09/06/12
For personal use only.

Can. J. Chem. Downloaded from www.nrcresearchpress.com by 210.87.254.6 on 09/06/12
For personal use only.

lar to the C—CS—C plane, in accordance with Mulliken's recommendation (17).

Results and Discussion

The gas phase spectra of **I** and **II** in the quartz ultraviolet are shown in Fig. 1. A weak, broad, structureless band with maximum intensity at 500 nm and a weaker shoulder to the red was found in the visible gas phase spectra of both compounds. The main band is assigned to the $\tilde{A} \leftarrow \tilde{X}$, $^1(n \rightarrow \pi^*)$ transition and the shoulder to the red to the corresponding triplet, in complete agreement with previous interpretations of similar aliphatic thione spectra in solution (2–5, 12). The quartz ultraviolet spectra of these and similar compounds in solution are poorly defined but provide evidence of the existence of at least two transitions. The gas phase spectra are much clearer. The spectrum of **I** at a pressure of 0.18 Torr is seen to consist of four overlapping but clearly resolvable bands in the 185 nm $< \lambda <$ 270 nm region. The spectrum of **II** is less well resolved in the $\lambda <$ 200 nm region and may be complicated by the presence of an unknown amount of enethiol (13). Nevertheless, the spectra of **I** and **II** are very similar, as expected. Because **I** is the simplest aliphatic thione which neither polymerizes nor tautomerizes significantly on the time scale of these experiments, it was chosen as a model compound for spectral assignment.

The strongest of the four overlapping bands in the uv spectrum of **I** is broad (fwhm ~ 5800 cm^{-1}) and structureless, is centered at 220 nm, and underlies a weaker, sharper band with maximum at 224 nm. Assuming that the broader band is Gaussian in shape, deconvolution of these two absorptions yields oscillator strengths of 0.15 and 0.016 for the two transitions. The broad, strong transition thus has features which are very similar to those of the well-documented $\pi \rightarrow \pi^*$ valence-shell transitions of smaller thiocarbonyl halides (18, 19) and of thioformaldehyde (8). Thiophosgene, for example, exhibits a strong (f = 0.059), broad (fwhm ~ 4000 cm^{-1}) transition with λ_{max} at 254 nm, assigned to a $\pi \rightarrow \pi^*$ electron promotion, whereas CF_3CSF has a similar band (20) with λ_{max} at 211 nm and fwhm of 5300 cm^{-1}. The intensity of this band in **I** is entirely consistent with an allowed ($\tilde{B}(^1A_1) \leftarrow \tilde{X}(^1A_1)$ in C_{2v} symmetry) transition involving a $\pi \rightarrow \pi^*$ intravalence electron promotion localized on the thiocarbonyl moiety. The breadth of the band is also consistent with the substantial elongation of the C—S bond associated with a reduction in the nominal C—S bond order from two to one and with the change in geometry from planar to pyramidal (about the C—CS—C linkage) on excitation. Equilibrium bond length increases of ca. 0.5 Å and excited state out-of-plane angles of up to 30° have been determined from the $\tilde{B} \leftrightarrow \tilde{X}$ spectra of those tetraatomic thiocarbonyls (18, 19, 21) which exhibit sufficient structure to permit detailed vibrational analysis. By analogy with the thiocarbonyl halides, the origin of this $\pi \rightarrow \pi^*$ transition likely lies near the long wavelength onset of measurable absorption near 270 nm.

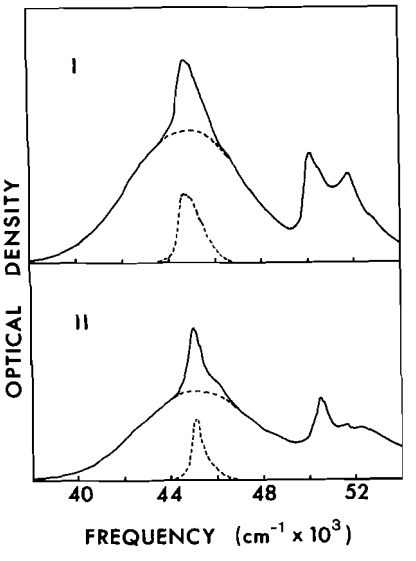

FIG. 1. Gas phase quartz ultraviolet spectra of **I** (3,3-dimethylbutane-2-thione) and **II** (3-methylbutane-2-thione). Dotted lines show the deconvolution of the overlapping $\pi \rightarrow \pi^*$ and $n \rightarrow 4s$ transitions.

These assignments are confirmed by measured solvent shifts. The visible band exhibits a hypsochromic shift with increasing solvent polarity which is characteristic of $n \rightarrow \pi^*$ transitions. The strong, broad band in the ultraviolet exhibits a small bathochromic shift, characteristic of $\pi \rightarrow \pi^*$ transitions.

The remainder of the quartz ultraviolet spectrum consists of three bands of about equal, moderate ($f \sim 0.02$) intensity and of the same general shape. In **I** these bands occur with λ_{max} at 224 nm (5.59 eV), 200 nm (6.21 eV), and 193 nm (6.42 eV). Each has a width of ca. 1200 cm^{-1} (fwhm) and exhibits some faint evidence of unresolved vibrational structure. All three bands are assigned to Rydberg transitions on the basis of the following evidence. First, in the parent thiocarbonyl, thioformaldehyde, three band systems assigned to $n \rightarrow 4s$, $n \rightarrow 4p_y$, and $n \rightarrow 4p_z$ Rydberg transitions, have been observed in the quartz ultraviolet (8). The aforementioned three transitions in **I** are observed in the same spectral region

TABLE 1. Comparisons of observed and calculated transition energies in several thiocarbonyls

State	Excitation	Polarization	E_{exp} (eV) I	E_{exp} (eV) II	Thioacetone E_{calcd}[a] (eV)	Thioformaldehyde E_{exp}[b] (eV)	Thioformaldehyde E_{calcd}[c] (eV)
$\tilde{X}(^1A_1)$	—	—	0.00	0.00	0.00	0.00	0.00
$\tilde{a}(^3A_2)$	$n \rightarrow \pi^*$	—	~2.2	—	2.18	1.80	1.84
$\tilde{A}(^1A_1)$	$n \rightarrow \pi^*$	—	2.53	—	2.53	2.03	2.17
$\tilde{B}(^1A_1)$	$\pi \rightarrow \pi^*$	z	4.71[d]	4.83[d]	6.80	5.72	7.92
$\tilde{C}(^1B_2)$	$n \rightarrow 4s$	y	5.54	5.59	5.23	5.83	5.83
$^1A_1$	$n \rightarrow 4p_y$	z	6.21	6.27	6.04	6.59	6.62
$^1B_2$	$n \rightarrow 4p_z$	y	6.42	~6.4	5.93	6.83	—
$^1A_2$	$n \rightarrow 4p_x$	—	—	—	5.90	—	7.78

[a]Reference 23.
[b]Reference 8.
[c]Reference 24.
[d]Onset of absorption (see text). All others from band maxima.

and with comparable spacing and intensity. The comparison is illustrated in Table 1. The thioformaldehyde Rydberg band systems are narrow and are about a factor of 10 less intense compared to the $\pi \rightarrow \pi^*$ valence-shell absorption. The present gas phase spectra of **I** and **II** exhibit similar properties.

The lowest energy of these Rydberg transitions has been observed previously at ca. 215 nm in hydrocarbon solution spectra of similar aliphatic thiones, but has been misassigned as $n \rightarrow \sigma^*$. The corresponding transitions in the gas phase spectra of **I** and **II** occur at 224 and 222 nm, respectively. Thus, the substantial increase in energy expected of a Rydberg transition on going from vapor to solution is observed (22).

Support for the assignment of these three bands to Rydberg transitions is also found in the *ab initio* SCF-CI calculations of the electronic spectrum of thioacetone by Bruna, Buenker, and Peyerimhoff (23) (cf. Table 1). Three allowed Rydberg transitions are predicted at 5.23, 5.93, and 6.04 eV for this molecule. The Rydberg transition of lowest energy in **I** and **II** (at 5.54 eV and 5.59 eV, respectively) corresponds well to the calculated lowest energy Rydberg state in thioacetone at 5.23 eV and is assigned as sulfur $n \rightarrow 4s$ ($^1B_2 \leftarrow {}^1A_1$ in C_{2v}) on this basis. This transition is also accurately predicted by a similar calculation on thioformaldehyde (24) (cf. Table 1). The two other allowed Rydberg transitions, which are calculated to lie at 5.93 eV and 6.04 eV in thioacetone, correspond to sulfur $n \rightarrow 4p_z$ and $n \rightarrow 4p_y$ electron promotions respectively. Two narrow, closely-spaced absorptions which lie within 0.5 eV of these predicted energies are found in the spectrum of **I**. It is impossible to distinguish between the $n \rightarrow 4p_y$ and $n \rightarrow 4p_z$ transitions in the absence of polarization data. However, by analogy with H_2CS, we tentatively assign the lower energy of these two to the $^1A_1 \leftarrow \tilde{X}(^1A_1)$ ($n \rightarrow 4p_y$) Rydberg transition and the one of higher energy to the $^1B_2 \leftarrow \tilde{X}(^1A_1)$ ($n \rightarrow 4p_z$) Rydberg transition. The $n \rightarrow 4p_x$ transition is predicted to occur at 5.90 eV in thioacetone but is electric-dipole forbidden and is therefore anticipated to be of much lower intensity than the three allowed transitions which are actually observed.

The quantum defect, Δ, for each Rydberg transition was calculated using the expression

$$[1] \quad E = I_p - R/(n - \Delta)^2$$

where E (eV) is the experimental transition energy, R is the Rydberg constant, n is the principal quantum number of the excited electron, and I_p is the ionization potential of the compound of interest. Ionization potentials of **I** and **II** have not been measured. However, using the value of I_p = 8.60 eV for thioacetone, determined from its photoelectron spectrum (25) and assuming $n = 4$, values of Δ given in Table 2 are obtained. Since **I** and **II** will likely have slightly lower ionization potentials than thioacetone, the values of Δ calculated in this way are probably slightly high. Nevertheless, reasonable correspondence is found with the quantum defects reported by Price *et al.* (26, 27) for H_2S and by McDiarmid (28) for $(CH_3)_2S$, particularly in view of the tendency of Δ for transitions to *ns* Rydberg states to decrease with increasing alkylation of the chromophoric group. The data are shown in Table 2. Such a comparison may not be unreasonable in view of the atomic-like nature of Rydberg transitions.

It has been argued that it is more appropriate to use a value of $n = 3$ than $n = 4$ to describe the lowest energy Rydberg transitions in H_2CS (29). There is theoretical evidence (30) that in formaldehyde the lowest energy Rydberg orbital centroids lie in the CH_2 region of that molecule. Use of $n = 3$ for H_2CS results in values of Δ which are similar to those of H_2CO. The implication of using $n = 3$ to describe these transitions in thiocarbonyls is that

Can. J. Chem. Downloaded from www.nrcresearchpress.com by 210.87.254.6 on 09/06/12
For personal use only.

TABLE 2. Quantum defects of Rydberg transitions of I and II

Series	E (eV) I	E (eV) II	I_p (eV)	Δ I	Δ II	Δ_{H_2S}[a]	$\Delta_{(CH_3)_2S}$[b]
$n \rightarrow 4s$	5.54	5.59	8.60	1.89	1.87	2.04	2.00
$n \rightarrow 4p_y$	6.21	6.27	8.60	1.61	1.58	1.57	1.55
$n \rightarrow 4p_z$	6.42	~6.4	8.60	1.50	~1.5	1.57	1.55

[a]References 26 and 27.
[b]Reference 28.

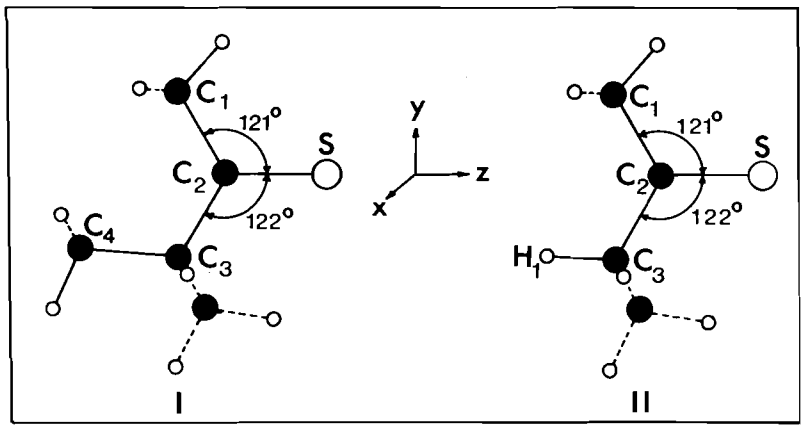

FIG. 2. Calculated geometry of ground state I and II. In both molecules C_2—S, C_1—C_2, C_2—C_3, and C_3—C_4 bond lengths are 1.60 Å, 1.54 Å, 1.54 Å, and 1.56 Å respectively. In II, the C_3—H_1 bond length is 1.086 Å. All C—C—H bond angles and all C—C_3—C bond angles are 109.5°. The two CH_3 groups attached to C_3 are located above and below the plane of the figure and are superimposed in the perspective shown.

the lowest energy Rydberg orbitals assume large measures of carbon 3*s* or 3*p* character. If a value of $n = 3$ is used in the present work, values of Δ are obtained for **I** and **II** which are substantially smaller than those determined for the corresponding transitions in H_2CS (29), but which nevertheless do not differ greatly from those of the lowest energy Rydberg transitions in the aldehydes and ketones. However, in view of the experimental uncertainties in Δ in the present work and the absence of orbital electron density calculations for these molecules, further speculation on the choice of *n* is unwarranted.

The calculated ground state geometries of **I** and **II** are shown in Fig. 2. The lowest energy conformation is one in which the C_1, C_2, C_3, C_4, and S atoms in **I** or the C_1, C_2, C_3, H_1, and S atoms in **II** are coplanar. The C—S bond length of 1.60 Å is nearly identical to both the calculated and experimentally measured C—S bond lengths in the ground states of several tetraatomic thiocarbonyl halides (16). The C_1—C_2 and C_2—C_3 bond lengths and the C—C—S bond angles are unremarkable. There is no evidence in these calculations which would indicate that **I** and **II** are atypical aliphatic thiones.

The results of CNDO/2 calculations of the oscillator strengths of the valence-shell transitions also support the above assignments. These calculations are based on the geometries given above and follow the method outlined by McGlynn *et al.* (31). A similar method was used successfully in the analysis of the electronic spectra of F_2CS, Cl_2CS, and H_2CS by Farnworth *et al.* (32). The results are shown in Table 3. In this calculation the one-center integrals were computed analytically using CNDO/2 molecular orbitals, the important (involving C_1, C_2, C_3, and S) two-center integrals were computed by the method of Yaranos (33), and the experimental transition energies were employed. The calculated oscillator strengths of the valence-shell transitions agree moderately well with those observed experimentally in the present study. Only lower limits are given for the measured oscillator strengths of **II** because of the unknown extent of tautomerization to the corresponding enethiol at the time of spectral measurement.

Conclusions

Four electronic transitions are observed in the quartz ultraviolet spectra of aliphatic thiones in the gas phase. The strongest transition is very broad

Can. J. Chem. Downloaded from www.nrcresearchpress.com by 210.87.254.6 on 09/06/12
For personal use only.

TABLE 3. Calculated and measured oscillator strengths and some thiocarbonyls

	I		II		CH_2S	
Transition	f_{exp}	f_{calcd}	f_{exp}	f_{calcd}	f_{exp}[a]	f_{calcd}[b]
$n \rightarrow \pi^*$	2.2×10^{-5}	0.000	2×10^{-4}	0.000	4×10^{-5}	0.000
$\pi \rightarrow \pi^*$	0.15	0.68	>0.1	0.57	0.38[c]	0.40
$n \rightarrow 4s$	0.016	—	>0.005	—	0.038	—
$n \rightarrow 4p_y$	0.023	—	>0.01	—	—	—
$n \rightarrow 4p_z$	0.030	—	>0.009	—	—	—

[a]Reference 7.
[b]Reference 32.
[c]Estimate based on comparison with H_2CO. See ref. 8.

and unstructured and is assigned to a $\pi \rightarrow \pi^*$ valence-shell electron promotion. This assignment is supported by CNDO/2 calculations of the oscillator strength and by comparisons with several other thiocarbonyl-containing molecules. Three weaker and narrower Rydberg transitions, one of which ($n \rightarrow 4s$) overlaps the broad $\pi \rightarrow \pi^*$ band, are also observed. The two highest energy of these Rydberg bands have not been observed previously in aliphatic thiones. The lowest energy Rydberg transition had been misassigned as an $n \rightarrow \sigma^*$ electron promotion in previous solution spectra.

Acknowledgement

The continuing financial assistance of the Natural Sciences and Engineering Research Council of Canada is gratefully acknowledged.

1. C. SANDORFY. Top. Curr. Chem. **86**, 92 (1979).
2. M.J. JANSSEN. Recl. Trav. Chim. Pays-Bas, **79**, 464 (1960).
3. C. N. R. RAO, A. BALASUBRAMANIAM, and J. RAMACHANDRAN. J. Sci. Ind. Res. **20B**, 382 (1961).
4. J. FABIAN and R. MAYER. Spectrochim. Acta, **20**, 299 (1964).
5. J. FABIAN, H. VIOLA, and R. MAYER. Tetrahedron, **23**, 4323 (1967).
6. J. BARRETT and F. S. DEGHAIDY. Spectrochim. Acta, **31A**, 707 (1975).
7. R. H. JUDGE and G. W. KING. Can. J. Phys. **53**, 1927 (1975).
8. R. H. JUDGE, C. R. DRURY-LESSARD, and D. C. MOULE. Chem. Phys. Lett. **53**, 82 (1978).
9. R. H. JUDGE and G. W. KING. J. Mol. Spectrosc. **74**, 175 (1979); **78**, 51 (1979).
10. P. DEMAYO. Acc. Chem. Res. **9**, 52 (1975).
11. N. J. TURRO, V. RAMAMURTHY, W. CHERRY, and W. FARNETH. Chem. Rev. **78**, 125 (1978).
12. R. P. STEER. Rev. Chem. Intermed. In press.
13. D. PAQUER. Int. J. Sulfur Chem. **7B**, 269 (1972).
14. D. PAQUER and J. VIALLE. Bull. Soc. Chim. Fr. 3595 (1963).
15. W. J. HEHRE, W. A. LATHAN, R. DITCHFIELD, M. D. POPLE, and J. A. NEWTON. Gaussian 70, Quantum Chemistry Program Exchange, Indiana University, Bloomington, IN.
16. A. KAPUR, R. P. STEER, and P. G. MEZEY. J. Chem. Phys. **69**, 968 (1978); **70**, 745 (1979); **71**, 588 (1979).
17. R. S. MULLIKEN and C. A. RIEKE. Rep. Progr. Phys. **8**, 136 (1941).
18. D. J. CLOUTHIER, A. R. KNIGHT, R. P. STEER, R. H. JUDGE, and D. C. MOULE. J. Mol. Spectrosc. **83**, 148 (1980).
19. R. H. JUDGE and D. C. MOULE. J. Mol. Spectrosc. **80**, 363 (1980).
20. D. J. CLOUTHIER. Ph.D. Thesis, University of Saskatchewan. 1979.
21. D. J. CLOUTHIER, A. R. KNIGHT, R. P. STEER, and P. A. HACKETT. Chem. Phys. **48**, 1 (1980); **48**, 13 (1980).
22. M. B. ROBIN. Higher excited states of polyatomic molecules. Vol. 1. Academic Press, New York. 1974.
23. P. J. BRUNA, R. J. BEUNKER, and S. D. PEYERIMHOFF. Chem. Phys. **22**, 375 (1977).
24. P. J. BRUNA, S. D. PEYERIMHOFF, and R. J. BUENKER. Chem. Phys. **3**, 35 (1974).
25. H. W. KROTO, B. M. LANDSBERG, R. J. SUFFOLK, and A. VODDEN. Chem. Phys. Lett. **29**, 265 (1974).
26. W. C. PRICE. J. Chem. Phys. **4**, 147 (1936).
27. W. C. PRICE, J. P. TEEGAN, and A. D. WALSH. Proc. R. Soc. London, **201A**, 600 (1950).
28. R. MCDIARMID. J. Chem. Phys. **61**, 274 (1974).
29. C. R. DRURY-LESSARD. Ph.D. Thesis, McMaster University. 1980.
30. L. B. HARDING and W. A. GODDARD III. J. Am. Chem. Soc. **99**, 677 (1977).
31. S. P. MCGLYNN, L. G. VANQUICKENBORNE, M. KINOSHITA, and D. G. CARROLL. Introduction to applied quantum chemistry. Holt, Rinehart and Winston, Inc., New York. 1972. p. 299*ff*.
32. E. R. FARNWORTH, G. W. KING, and D. C. MOULE. Chem. Phys. **1**, 82 (1973).
33. W. A. YARANOS. Z. Naturforsch., **21A**, 1869 (1966). Program #158, Quantum Chemistry Program Exchange, Indiana University, Bloomington, IN.

Can. J. Chem. Downloaded from www.nrcresearchpress.com by 210.87.254.6 on 09/06/12
For personal use only.

Studies in general acid and general base catalysis. Rate–acidity profiles for prototropic processes[1]

ROSS STEWART AND R. SRINIVASAN

Department of Chemistry, University of British Columbia, Vancouver, B.C., Canada V6T 1Y6

Received August 1, 1980

ROSS STEWART and R. SRINIVASAN. Can. J. Chem. **59**, 957 (1981).

A theoretical study has been made of the effect of changing acidity on the rate of aqueous prototropic reactions. These processes, typified by ketone enolization, are catalyzed by general acids and bases and their log rate – pH profiles may take a number of different shapes. In the absence of buffer catalysis there are four reaction paths available to a substrate Z: $ZH^+ + HO^-$, $Z + HO^-$, $ZH^+ + H_2O$, and $Z + H_2O$. Equations have been derived that express the contributions each of these paths makes to the observed rate in terms of the experimental catalytic constants, the proton activating factor (*paf*), the deprotonating factor (*dpf*), and the basicity of the substrate as expressed by K_{ZH^+}. For ideal systems the relative rates of the kinetically equivalent paths $Z + H_2O$ and $ZH^+ + HO^-$ (though one does not know which is the larger) is given by the quantity $3.0 \times 10^{17}\, k^2_{H_2O}/(k_{H^+}k_{HO^-})$ where k_{H^+}, k_{HO^-}, and k_{H_2O} are the experimental catalytic constants. It is argued in the case of the real substrate acetone that (*a*) this quantity underestimates the rate difference, and (*b*) the more important path is $Z + H_2O$. Where *paf* is available from rate data determined in buffers an unequivocal choice can be made between the kinetically equivalent paths, provided *paf* is a constant for the particular substrate.

ROSS STEWART et R. SRINIVASAN. Can. J. Chem. **59**, 957 (1981).

On a étudié l'effet du changement d'acidité sur la vitesse des réactions prototropiques en solutions aqueuses. Ces réactions, dont l'exemple typique est l'énolisation d'une cétone, sont en général catalysées par les acides et les bases et leurs courbes de log de vitesse en fonction du pH peuvent être de formes différentes. En l'absence d'une catalyse tamponnée, il y a 4 chemins réactionnels probables pour un substrat Z: $ZH^+ + HO^-$, $Z + HO^-$, $ZH^+ + H_2O$ et $Z + H_2O$. On en a déduit des équations qui expriment les contributions de chacune de ces voies à la vitesse observée en fonction des constantes catalytiques expérimentales, du facteur activant du proton (*fap*), du facteur de déprotonation (*fdp*) et de la basicité du substrat tel qu'exprimé par K_{ZH^+}. Dans les systèmes idéaux, les vitesses relatives des voies cinétiquement équivalentes $Z + H_2O$ et $ZH^+ + HO^-$ sont données par la quantité $3{,}0 \times 10^{17} \times k^2_{H_2O}/(k_{H^+}k_{HO^-})$ ou k_{H^+}, k_{HO^-} et k_{H_2O} sont les constantes catalytiques expérimentales. Dans le cas d'un substrat réel, tel l'acétone, on pense que (*a*) cette quantité sous-estime la différence de vitesse et (*b*) la voie la plus importante est $Z + H_2O$. Quand le *fap* est disponible à partir des données de vitesse déterminées dans les tampons on peut faire un choix univoque entre les chemins réactionnels cinétiquement équivalents en admettant que le *fap* est constant pour un substrat particulier.

[Traduit par le journal]

The effect of changing acidity on the rates of acid and base catalyzed reactions is obviously a matter of great practical importance in organic chemistry. Early work in acid and base catalysis was concerned chiefly with establishing rate laws. Later as mechanistic studies begin to be pursued, the various steps in such reactions came to be described in some detail (1).

The activated forms of organic compounds are usually the protonated or deprotonated entities and studies over the past two decades have established p*K* values for such species for most kinds of organic compound. While our mechanistic understanding of the steps in most acid or base catalyzed reactions is now quite good (1), there has been lacking a general treatment of acid and base catalysis that would relate structural and other features to overall rate effects, particularly to rate–acidity profiles. The latter can assume a number of shapes (Fig. 1), even for simple prototropic reactions in the absence of buffer catalysis, as has been shown particularly by the work of Jones *et al.* (2, 4, 5). We have recently examined the effect on reactivity of protonating organic compounds and deprotonating reagent bases in terms of the quantities *paf* (proton activating factor) and *dpf* (deprotonating factor) (6). In this paper we develop the equations for the various routes that can lead from reactant to product in acid and base catalyzed processes, the sums of which give the rate–acidity profile. To simplify the treatment we consider only aqueous solution and only prototropic reactions, those in which a proton is relocated in the substrate – a not inconsequential set of reactions since these are the rate-controlling steps of many oxidation, condensation, and other processes. Furthermore, we consider only catalysis by H^+, H_2O, and HO^-. That is, we neglect the effect of buffers, which, in the case of general acid and general base catalyzed reactions, can significantly change the shapes of rate–acidity profiles, particularly in the regions near neutrality (1, 3). Finally, we ignore, as seems reasonable for aqueous solution (1), the possibility of proton loss and proton gain being simultaneous.

[1]Presented in part at the International Symposium on Physical Organic Chemistry, Toronto, August 1979.

Backgound

Consider an organic compound Z that undergoes

0008-4042/81/060957-07$01.00/0

©1981 National Research Council of Canada/Conseil national de recherches du Canada

Can. J. Chem. Downloaded from www.nrcresearchpress.com by 210.87.254.6 on 09/06/12
For personal use only.

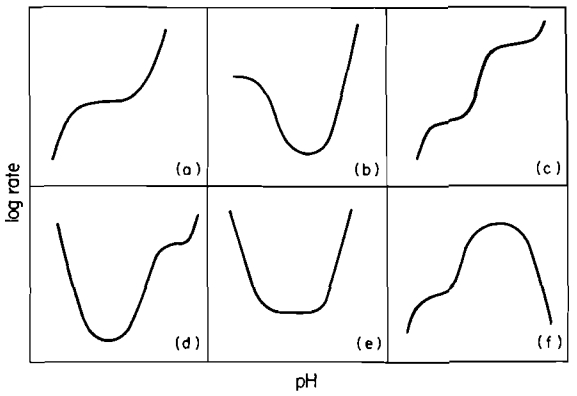

FIG. 1. A schematic portrayal of the rate–pH profiles for ionization or enolization of six selected compounds. In all cases water is the solvent and there is no buffer catalysis. The compounds, with literature references in parentheses, are (*a*) caffeine (2), (*b*) 1,4-dimethyl-2-pyrimidone (corrected for self-catalysis) (3), (*c*) paraxanthine (2), (*d*) 2-imino-1,4-dimethyl-1,2-dihydropyrimidine (3), (*e*) acetophenone (4), (*f*) xanthine (2). Only the curves in *a*, *b*, and *e* can be represented by the four terms [4]–[7] given herein; in *c*, *d*, and *f* additional protonation states intrude.

reaction via either its anion or a tautomeric form Z′. When a carbon–hydrogen bond is broken in forming the anion or tautomer the rate-controlling step involves attack on Z or ZH^+ by base, either water, hydroxide ion, or the basic component of any buffer that is present. The activating effect of protonating Z to give ZH^+ is expressed by the term *paf* (eq. [1]), which, when buffer systems are used can be determined (eq. [2]) from the catalytic constants k_{HA} and k_{A^-} of the buffer components determined in the standard way, and from the acidity constants K_{ZH^+} and K_{HA} of the substrate and the buffer acid (6, 7).

[1] $paf = k_{ZH^+ + B}/k_{Z+B}$

where B = H_2O, HO^-, or A^-

[2] $paf = k_{HA}K_{ZH^+}/k_{A^-}K_{HA}$

Activation by base is expressed in terms of *dpf*, in which the relative proton abstracting abilities of HO^- and H_2O are compared (eq. [3]) (6) (in most cases these are the only base pairs for which data are available).

[3] $dpf = k_{Z+HO^-}/k_{Z+H_2O}$

The magnitude of *paf* varies enormously depending on the structure of the substrate, but always seems to be less than *dpf*. Thus removing a proton from water, the base, is more effective than adding a proton to Z, the substrate.

Rate–Acidity Profiles

For the reaction of Z or ZH^+ with H_2O or HO^- there are four paths that contribute to reaction (reactions [4]–[7]). (The reactive intermediate might be, for example, the enol or enolate anion of a ketone.)

[4] $ZH^+ + HO^- \rightarrow$ reactive intermediate

[5] $Z + HO^- \rightarrow$ reactive intermediate

[6] $ZH^+ + H_2O \rightarrow$ reactive intermediate

[7] $Z + H_2O \rightarrow$ reactive intermediate

The rate contribution, V, of each of these paths is given by eqs. [8] to [11],

[8] $V_{ZH^+ + HO^-} = k_{ZH^+ + HO^-}[ZH^+][HO^-]$

[9] $V_{Z+HO^-} = k_{Z+HO^-}[Z][HO^-]$

[10] $V_{ZH^+ + H_2O} = k_{ZH^+ + H_2O}[ZH^+][H_2O]$

[11] $V_{Z+H_2O} = k_{Z+H_2O}[Z][H_2O]$

The rate–acidity profile, which is determined by the way the sum of the four rate contributions varies with acidity, turns out to depend on the magnitude of three variables: *paf*, *dpf*, and K_{ZH^+}. This point is illustrated for one of these variables in Fig. 2 where K_{ZH^+} is allowed to vary, while for simplicity's sake *paf* and *dpf* are kept fixed at 10^7 and 10^{10}, respectively.

The curves in Fig. 2, shown as log V_{rel} – pH rate profiles, have been generated by computer using the techniques described in the calculations section of this paper and the equations derived therein. V_{rel} is the relative rate of a pathway based on the rate constant k_{Z+HO^-} and the total substrate concentration being unity.

It can be seen in Fig. 2 that the way in which the observed rate responds to changing acidity depends on the basicity assigned to the substrate, the patterns of the three rate–acidity profiles being quite distinct.

A fourth pattern shown in Fig. 3 appears when pK_{ZH^+} is assigned a value of 5.7, with *dpf* being kept fixed at 10^{10}. Under these conditions the rate profile appears to consist of only two linear sections, one pH-dependent and the other pH-independent. The significance of the number 5.7 (15.7 − log *dpf*) arises as follows.

It can be seen from an examination of the curves in Fig. 2 that a profile of the type considered here can only arise when $V^{max}_{ZH^+ + HO^-} = V^{max}_{ZH^+ + H_2O}$ and it can be easily shown that under these conditions the quantities $V_{ZH^+ + HO^-}$ and $V_{ZH^+ + H_2O}$ become equal when the pH equals the pK_{ZH^+} of the substrate.

Referring to eqs. [8] and [9], it is clear that at the pK

$$k_{ZH^+ + HO^-}[ZH^+][HO^-] = k_{ZH^+ + H_2O}[ZH^+][H_2O]$$

and $k_{ZH^+ + HO^-}/k_{ZH^+ + H_2O}$, which is equal to *dpf*, becomes equal to $[H_2O]/[HO^-]$ or $[H^+]/K_{H_2O}$, where

Can. J. Chem. Downloaded from www.nrcresearchpress.com by 210.87.254.6 on 09/06/12
For personal use only.

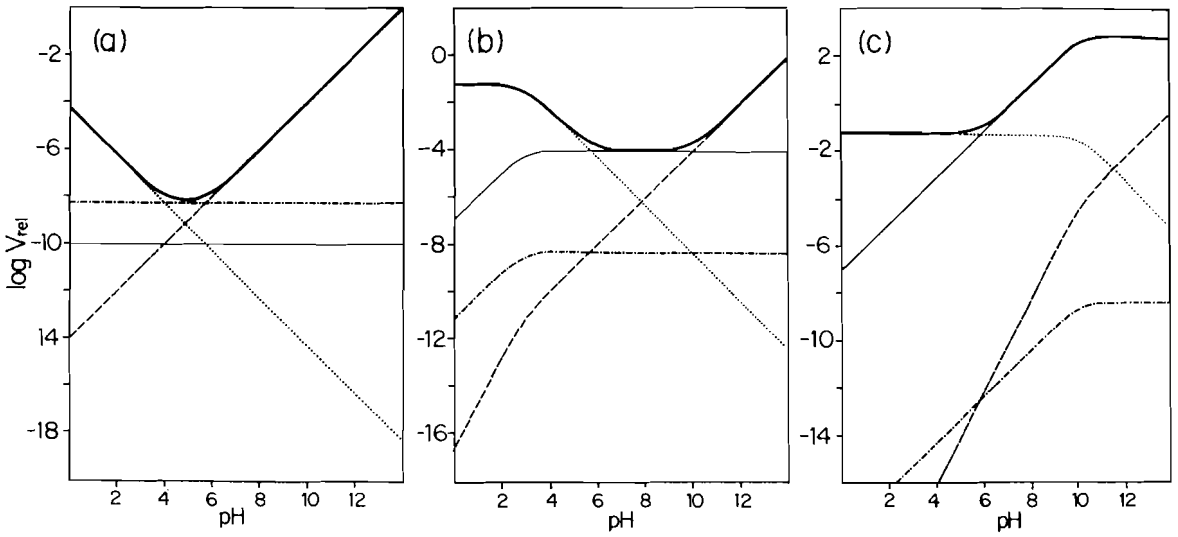

FIG. 2. Plots of logarithm of relative rate against pH showing the contribution of the four pathways that lead to reactive intermediates of a substrate Z. The heavy line represents the observed rate; the light solid line represents $V_{ZH^+ + HO^-}$; the dashed line represents V_{Z+HO^-}; the dotted line represents $V_{ZH^+ + H_2O}$; the dashed and dotted line represents V_{Z+H_2O}. (*a*) $paf = 10^7$, $dpf = 10^{10}$, $pK_{ZH^+} = -3.0$; (*b*) $paf = 10^7$, $dpf = 10^{10}$, $pK_{ZH^+} = +3.0$; (*c*) $paf = 10^7$, $dpf = 10^{10}$, $pK_{ZH^+} = 10.0$.

$$K_{H_2O} = [H^+][HO^-]/[H_2O] = 1.8 \times 10^{-16}$$

and $pK_{H_2O} = 15.7$.

Since $[H^+] = K_{ZH^+}$ at the pK,

$$dpf = K_{ZH^+}/K_{H_2O}$$

Therefore, eq. [12] holds for those reactions which show the simple rate–acidity profile given in Fig. 3.

[12] $$\log dpf + pK_{ZH^+} = 15.7$$

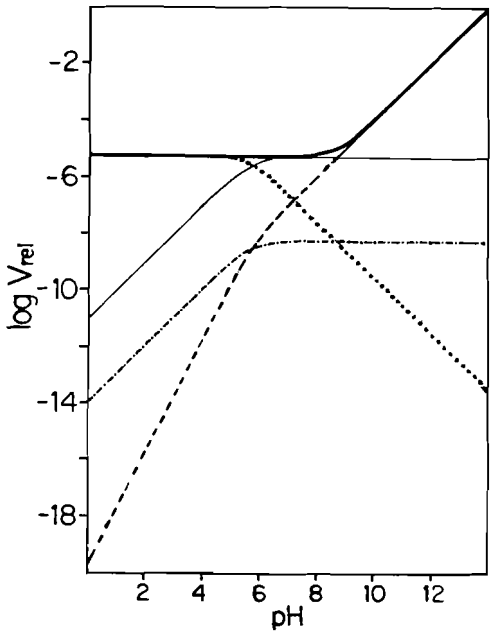

FIG. 3. Plot of logarithm of relative rate as a function of pH for a reaction identical to those shown in Fig. 2, except that the substrate has a pK_{ZH^+} of 5.7.

The magnitude of *paf* is of no importance in determining conditions for which such a curve will appear (provided that *paf* is greater than unity, which it must necessarily be). Thus, though Fig. 3 has been constructed by setting $\log paf = 3$, $\log dpf = 10$, and $pK_{ZH^+} = 5.7$, any value of *paf* greater than unity could be used to produce the same shape of curve. When $\log dpf$ and pK_{ZH^+} are varied but their sums kept equal to 15.7 the curves shown in Fig. 4 are generated.

Kinetically Equivalent Routes

The two reaction paths shown in reactions [4] and [7] represent kinetically equivalent paths. The difference in magnitude between their rates (though not which is the greater) can be calculated, providing the catalytic coefficients k_{H^+}, k_{HO^-}, and k_{H_2O} have been experimentally determined. Provided that the true values of *paf*, *dpf*, and K_{ZH^+} are known the difference in magnitude *and* which is the greater can be determined. There is an inherent ambiguity in the latter method, however, since only apparent *dpf* values can be determined from experimental data. These points will become clear as the pertinent equations are developed below.

The ratio of the two rates is given by eq. [13].

[13] $$\frac{V_{ZH^+ + HO^-}}{V_{Z+H_2O}} = \frac{k_{ZH^+ + HO^-}}{k_{Z+H_2O}} \frac{[ZH^+][HO^-]}{[Z][H_2O]}$$

Can. J. Chem. Downloaded from www.nrcresearchpress.com by 210.87.254.6 on 09/06/12
For personal use only.

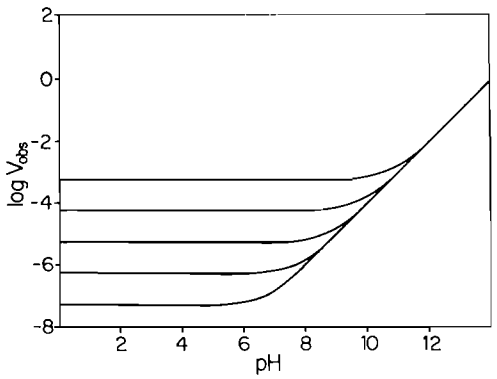

FIG. 4. Plots of logarithm of observed rate as a function of pH for various values of log *dpf* and pK_{ZH^+}, which in each case sum to 15.7. The respective values of log *dpf* and pK_{ZH^+} are from top to bottom, above: 8.0, 7.7; 9.0, 6.7; 10.0, 5.7; 11.0, 4.7; 12.0, 3.7. The *paf* is 10^3 in all cases.

Since

$$paf \cdot dpf = \frac{k_{ZH^+ + HO^-}}{k_{Z+HO^-}} \frac{k_{Z+HO^-}}{k_{Z+H_2O}} = \frac{k_{ZH^+ + HO^-}}{k_{Z+H_2O}}$$

then eq. [14] holds.

$$[14] \quad \frac{V_{ZH^+ + HO^-}}{V_{Z+H_2O}} = \frac{paf \cdot dpf \cdot K_{H_2O}}{K_{ZH^+}}$$

where $K_{H_2O} = 1.8 \times 10^{-16}$ as before. Equation [14] has been derived on the assumption that

$$dpf = k_{Z+HO^-}/k_{Z+H_2O}$$

That is, the more important pathway is assumed to be that shown in eq. [7], with the experimental catalytic constant k_{H_2O} being identical to the hidden rate constant k_{Z+H_2O}. An identical equation to [14], except for the left-hand term being inverted, can be derived by assuming the predominance of the path shown in eq. [4].

The acid HA and base A^- in eq. [2] can be taken as H^+ and H_2O, respectively, giving eq. [15].

$$[15] \quad paf = k_{H^+}K_{ZH^+}/k_{H_2O}K_{H^+}$$

where

$$K_{H^+} = [H_2O] = 55.5\ M$$

Furthermore,

$$dpf = k_{Z+HO^-}/k_{Z+H_2O} = k_{HO^-}/k_{H_2O}$$

Therefore eq. [14] becomes, after substitution and inversion, eq. [16].

$$[16] \quad \frac{V_{Z+H_2O}}{V_{ZH^+ + HO^-}} = \frac{k^2_{H_2O}(55.5)}{k_{H^+}k_{HO^-}(1.8 \times 10^{-16})}$$

$$= 3.0 \times 10^{17}\left(\frac{k^2_{H_2O}}{k_{H^+}k_{HO^-}}\right)$$

Again, an identical equation except for the left-hand term being inverted can be derived by assuming that $V_{ZH^+ + HO^-}$ is greater than V_{Z+H_2O}. Equations [14] and [16] and their analogs are useful only for assessing the relative importance of the two paths, not for distinguishing between them. This is as expected since a kinetic analysis cannot be expected to distinguish between kinetically equivalent pathways.

The theoretical treatment presented to this point is for ideal systems, those in which *paf* is independent of the base (H_2O or HO^-), and those in which *dpf* is independent of the ionic state of the substrate (Z or ZH^+). Indeed, if one of these conditions obtains, the other must do so also: if

$$(k_{ZH^+ + H_2O}/k_{Z+H_2O}) = (k_{ZH^+ + HO^-}/k_{Z+HO^-}) = paf$$

then

$$(k_{ZH^+ + HO^-}/k_{ZH^+ + H_2O}) = (k_{Z+HO^-}/k_{Z+H_2O}) = dpf$$

The application of the above ideas to the special case of acetone is considered in the next section.

Acetone

Acetone is an unusual ketone in that water catalysis, as expressed by the experimental catalytic coefficient k_{H_2O}, is significant over only a very narrow region of the pH spectrum. This can be seen in Fig. 5 where the acid and base catalyzed processes (undoubtedly $V_{ZH^+ + H_2O}$ and V_{Z+HO^-}) will make comparable contributions under such circumstances (see also Fig. 2*a*, in which the values

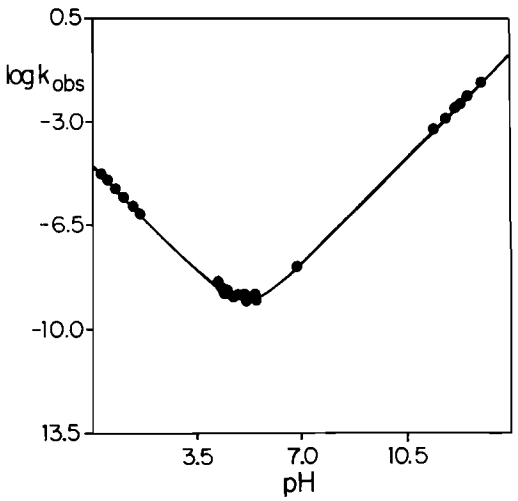

FIG. 5. Plot of logarithm of the rate of enolization of acetone in water in the absence of buffer catalysis at 25°C. The experimental points have been obtained by extrapolating to zero buffer concentration the rate data given in refs. 8, 9, and 10. The line was drawn by computer using the value of k_{H^+}, k_{HO^-}, and k_{H_2O} given in the text.

Can. J. Chem. Downloaded from www.nrcresearchpress.com by 210.87.254.6 on 09/06/12
For personal use only.

TABLE 1. Catalytic coefficients for enolization of acetone and derivatives[a]

Reagent	k_{H^+} 10^5 M^{-1} s^{-1}	k_{HO^-} M^{-1} s^{-1}	k_{H_2O} 10^{12} M^{-1} s^{-1}	log *dpf*
Acetone	2.84	0.166	8.33	10.3
Acetonylacetone	2.52	1.67	41.7	10.6
Chloroacetone	6.32	9.3	967	10.0
Bromoacetone	—	200	4830	10.6
1,1-Dichloroacetone	—	450	13200	10.5

[a]Rate data of Bell and Lidwell (8) except for k_{H^+} and k_{HO^-} values for acetone, which come from ref. 9, $T = 25°C$.

there assigned to *paf*, *dpf*, and K_{ZH^+} are very close to those for acetone). The experimental values of Bell and Lidwell (8) and Hine, Kaufman, and Cholod (9) for k_{H_2O}, k_{H^+}, and k_{HO^-} are 8.3×10^{-12} M^{-1} s^{-1}, 2.54×10^{-5} M^{-1} s^{-1}, and 0.166 M^{-1} s^{-1}, respectively. When these values are substituted in eq. [16] a value of 4.4 is obtained for the ratio V_{Z+H_2O} and $V_{ZH^+ + HO^-}$.

As has been pointed out earlier, eq. [16] does not indicate which of the kinetically equivalent paths is the more important. We shall argue that for acetone and most other Type 1 compounds (6) V_{Z+H_2O} is greater than $V_{ZH^+ + HO^-}$. Furthermore, we believe that the rate ratio is actually greater for acetone than the theoretical value of 4.4, since eq. [16] is based on ideal behaviour, specifically that *paf* and *dpf* are independent of the ionic state of the base (H_2O or HO^-) and the substrate (Z or ZH^+).

Table 1 lists the catalytic constants for a number of ketones and it can be seen that both k_{HO^-} and k_{H_2O} are sensitive to changes in structure of the ketone. Indeed, when log k_{HO^-} is plotted against log k_{H_2O} for these compounds a straight line of close to unit slope is obtained (slope = 1.03, correlation coefficient 0.983). The catalytic constant k_{H^+}, on the other hand, changes only slightly as the ketone structure is changed, presumably because of opposing substituent effects on the protonation of the substrate and on the rate-controlling deprotonation of its conjugate acid (11). Since the catalytic constants k_{HO^-} and k_{H_2O} are linearly related it is reasonable to assume that it is V_{Z+H_2O} rather than $V_{ZH^+ + HO^-}$ that is the major contributor to the water-catalyzed rate. Were $V_{ZH^+ + HO^-}$ the major component some correlation would have been expected between k_{H^+} and k_{H_2O}. (Earls and Jones have used a similar argument in the case of acetophenone (4).)

The slope of unity found for the plot of log k_{HO^-} against log k_{H_2O} indicates that the inductive effect of substituents modifies the rate of proton abstraction by HO^- and H_2O equally. Stated differently, the *dpf* values are little affected by substituents that influence the rate of enolization by the inductive effect. We regard this as a general principle in closely related systems. The *dpf* values, however, differ when the substituent is in conjugation with the reaction site. For example, acetylacetone, discussed below, has a *dpf* of 10^8 (12).

If $V_{ZH^+ + HO^-}$ is, indeed, the lesser of the two kinetically equivalent rates can we estimate its magnitude independently and then check the rate ratio that has been calculated using eq. [16]? It turns out that acetylacetone is a reasonable model for protonated acetone, as can be seen by comparing the reaction parameters given in Table 2. Taking 4.0×10^4 M^{-1} s^{-1} as the value of $k_{ZH^+ + HO^-}$ for acetone leads to a value of 600 for $V_{Z+H_2O}/V_{ZH^+ + HO^-}$, considerably greater than that calculated using eq. [16]. This discrepancy probably arises from the operation of the Reactivity–Selectivity Principle (RSP) (15), which predicts that $k_{ZH^+ + H_2O}/k_{Z+H_2O}$ will be greater than $k_{ZH^+ + HO^-}/k_{Z+HO^-}$. Equation [16], which was derived on the assumption that these two quantities are equal, gave a value of 4 for the reactivity ratio and we have argued that V_{Z+H_2O} is, indeed, greater than $V_{ZH^+ + HO^-}$. The RSP will operate in the direction to *increase* this factor, possibly to a value as high as the 600 estimated here. A second approach to resolving the ambiguity of the kinetically equivalent routes is considered in the next section.

Type I and Type II Systems: Buffer Catalysis

We have previously used the terms Type I and Type II to distinguish reactions in which deprotonation of the conjugate acid gives a neutral species, such as an enol (Type I), from those which give a mesoionic intermediate (Type II), such as that shown below (6).

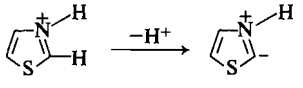

Type II reactions frequently have rate–acidity profiles of the chair type (Fig. 1*a*) and this is a result of reaction $ZH^+ + HO^-$ being more important than

Can. J. Chem. Downloaded from www.nrcresearchpress.com by 210.87.254.6 on 09/06/12
For personal use only.

TABLE 2. Comparison of reactivity parameters for acetylacetone and protonated acetone; $T = 25°C$

Compound	Brönsted coefficient	k_{AcO^-} M^{-1} s^{-1}	k_{H_2O} M^{-1} s^{-1}	k_{HO^-} M^{-1} s^{-1}	Reference
$CH_3—\overset{O}{\overset{\|}{C}}—CH_2—\overset{O}{\overset{\|}{C}}—CH_3$	0.52	3.6	3.0×10^{-4}	4.0×10^4	8, 12
$CH_3—\overset{+OH}{\overset{\|}{C}}—CH_3$	0.45	3.1[a]	2.6×10^{-4} [a]	?	8

[a]Based on a pK_{ZH^+} value of −2.72 for acetone (13). Should this value, which has not been universally accepted (14), be found to be in error the individual rate constants would have to be changed, but all by the same amount and so the argument given in the text would be unaffected.

reaction $Z + H_2O$, unlike the situation with acetone and other Type I compounds. With such a log rate – pH profile there is no ambiguity, the ratio $V_{ZH^+ + HO^-}/V_{Z+H_2O}$ must be greater than unity and, indeed, it may be enormous. For example, in the case of thiazole it is roughly 10^{12} (6, 16).

Most Type I compounds exhibit concave-upward curves such as those shown in Fig. 1 *b*, *d*, and *e*, and for such compounds the ambiguities regarding the mechanism of the plateau were discussed in a previous section of this paper. For such compounds buffer catalysis can usually be measured and *paf* determined using eq. [2]. Provided the same *paf* holds for the two acid–base pairs, H^+/H_2O and HA/A^-, the log rate – pH profile would tell us which is the dominant path and to what extent. Consider the curve in Fig. 6. The right-hand side of the curve represents reaction of $Z + HO^-$, the left-hand side $ZH^+ + H_2O$. The plateau can represent either $Z + H_2O$, or $ZH^+ + HO^-$. It can be readily shown that hydroxide ion catalysis becomes manifest when $pH = pK_{H_2O} - \log dpf$; at this pH the dominant path changes from one in which water is the base to one in which hydroxide ion is the base.* This pH will correspond to one or the other termini of the plateau, $pH_{(a)}$ or $pH_{(b)}$ provided *paf* is not a function of the acid–base pair used but only of the substrate.[2] Thus in Fig. 6, if $pH_{(a)} = pK_{ZH^+} + \log paf$ then the dominant pathway at the plateau is $ZH^+ + HO^-$; if $pH_{(b)} = pK_{ZH^+} + \log paf$ then $Z + H_2O$ dominates. Furthermore, the length of the plateau, $pH_{(a)} - pH_{(b)}$, gives the logarithm of the ratio of the two rates, $V_{ZH^+ + HO^-}$ and V_{Z+H_2O}.

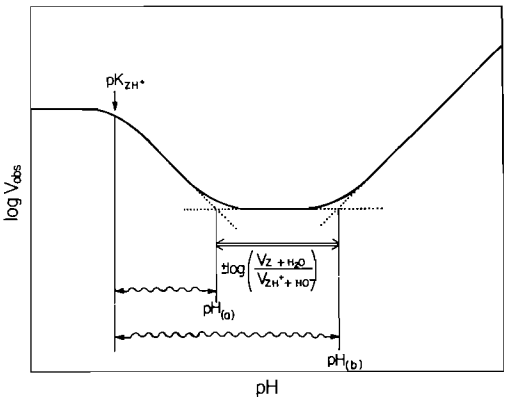

FIG. 6. A log rate – pH profile showing the relation between pK_{ZH^+}, log *paf*, and the length of the plateau. *One* of the two wavy lines represents log *paf*.

Calculations

The rate of ionization, V, of a carbon acid Z in water at any pH in the absence of buffers is given by eq. [17].

$$[17] \quad V = k_{ZH^+ + HO^-}[ZH^+][HO^-] + k_{Z+HO^-}[Z][HO^-] + k_{ZH^+ + H_2O}[ZH^+][H_2O] + k_{Z+H_2O}[Z][H_2O]$$

where [Z] and $[ZH^+]$ represent equilibrium concentrations. These concentrations can be expressed in terms of the total concentration of the substrate, $[Z]_t$ as follows

$$[Z] = \frac{[Z]_t K_{ZH^+}}{K_{ZH^+} + [H^+]}$$

$$[ZH^+] = \frac{[Z]_t [H^+]}{K_{ZH^+} + [H^+]}$$

The relative rate V_{rel} is thus determined by eq. [18], where the numerical value of $[Z]_t$ and k_{Z+OH^-} are arbitrarily kept at unity

$$[18] \quad V_{rel} = \{(k_{ZH^+ + HO^-} K_{H_2O}[H_2O]) + (K_{ZH^+} K_{H_2O}[H_2O]) + (k_{ZH^+ + H_2O}[H_2O][H^+]) + (k_{Z+H_2O} K_{ZH^+}[H_2O])\}/(K_{ZH^+} + [H^+])$$

Equation [18] can be expressed in terms of *paf* and *dpf*, since when k_{Z+HO^-} is unity, $paf = k_{ZH^+ + HO^-}$, $dpf = 1/k_{Z+H_2O}$, and $paf/dpf = k_{ZH^+ + H_2O}$.

[2]Use of an incorrect value of pK_{ZH^+} does not affect this determination since the error is cancelled by that in the determination of *paf* using eq. [2].

* Furthermore, when $pH = pK_{ZH^+} + \log paf$ the dominant path changes from one in which ZH^+ is the substrate to one in which Z is the substrate."

FOR ERRATA SEE v 59 #24 19 81 p 3318...

ERRATA ERRATA

Can. J. Chem. Downloaded from www.nrcresearchpress.com by 210.87.254.6 on 09/06/12
For personal use only.

$$[19]\quad V_{rel} = \left\{(paf\,K_{H_2O}[H_2O]) + \frac{K_{ZH^+}K_{H_2O}[H_2O]}{[H^+]} + \frac{paf\,[H^+][H_2O]}{dpf} + \frac{K_{ZH^+}[H_2O]}{dpf}\right\} \Big/ \left\{K_{ZH^+} + [H^+]\right\}$$

The four terms in parentheses in eq. [19] correspond to catalysis by mechanisms [4], [5], [6], and [7] respectively. The plot of log V_{rel} against pH was generated from the above equation for various values of *paf*, *dpf*, and K_{ZH^+} with the aid of a computer employing a value of 55.5 *M* for $[H_2O]$ and 1.8×10^{-16} for K_{H_2O}. The curves were drawn by connecting 500 data points distributed evenly over the pH range 0–14. The plot for any specific mechanism was likewise obtained by neglecting the three terms that do not pertain to the mechanism considered.

In the case of the plot shown in Fig. 6 the pH values at which the horizontal line (water catalysis) intersects the straight line of negative slope (H^+ catalysis) and that of positive slope (HO^- catalysis) in the plot of log V_{obs} against pH are given by $pH_{(a)}$ and $pH_{(b)}$ respectively. It is apparent that at $pH_{(a)}$ the rates of water-catalyzed and H^+-catalyzed reactions are equal, while at $pH_{(b)}$ the rates of water-catalyzed and HO^--catalyzed reactions are equal. The following equations, therefore, hold, where k_{H^+}, k_{HO^-}, and k_{H_2O} are the observed catalytic constants.

$$pH_{(a)} = \log k_{H^+} - \log k_{H_2O}[H_2O]$$

$$pH_{(b)} = \log k_{H_2O}[H_2O] - \log k_{HO^-}K_{HA}[H_2O]$$

Therefore

$$[20]\quad \frac{[H^+]_a}{[H^+]_b} = 3.0 \times 10^{17}\left(\frac{k^2_{H_2O}}{k_{H^+}k_{HO^-}}\right)$$

The right-hand side of eq. [20] is, in fact, the ratio of $V_{ZH^+ + HO^-}$ and V_{Z+H_2O}, or vice versa (see eq. [16]). Consequently, the relative importance of the two kinetically equivalent paths for water catalysis is given by the antilog of $pH_{(b)} - pH_{(a)}$.

Acknowledgement

The financial support of the Natural Sciences and Engineering Research Council of Canada is gratefully acknowledged.

1. R. P. Bell. The proton in chemistry. 2nd ed. University Press, Ithaca, New York. 1973; M. L. Bender. Mechanisms of homogeneous catalysis from protons to proteins. Wiley, New York. 1971; W. P. Jencks. Catalysis in chemistry and enzymology. McGraw-Hill, New York. 1969.
2. J. R. Jones and S. E. Taylor. J. Chem. Soc. Perkin Trans. II, 1253 (1979).
3. R. Stewart, S. J. Gumbley, and R. Srinivasan. Can. J. Chem. **57**, 2783 (1979).
4. D. W. Earls and J. R. Jones. J. Chem. Soc. Faraday Trans. **1**, 2186 (1975).
5. J. A. Elvidge, J. R. Jones, C. O'Brien, E. A. Evans, and H. C. Sheppard. J. Chem. Soc. Perkin Trans. II, 174 (1974).
6. R. Stewart and R. Srinivasan. Acc. Chem. Res. **11**, 271 (1978).
7. R. Stewart and J. M. McAndless. J. Chem. Soc. Perkin Trans II, 376 (1972).
8. R. P. Bell and O. M. Lidwell. Proc. R. Soc. London, Ser. A. **176**, 88 (1940).
9. J. Hine, J. C. Kaufman, and M. S. Cholod. J. Am. Chem. Soc. **94**, 4590 (1972).
10. D. P. N. Satchell. J. Chem. Soc. 2878 (1957); R. P. Bell and K. Yates. J. Chem. Soc. 1927 (1962); C. F. Cullis and M. H. Hashmi. J. Chem. Soc. 2512 (1956); J. R. Jones. Trans. Faraday Soc. **65**, 2138 (1969); J. R. Jones. Trans. Faraday Soc. **61**, 95 (1965); R. P. Bell and H. C. Longuet-Higgins. J. Chem. Soc. 636 (1946).
11. R. P. Bell and G. A. Wright. J. Chem. Soc. Trans. Faraday Soc. **57**, 1386 (1961).
12. M. L. Ahrens, M. Eigen, W. Kruse, and G. Maass. Ber. Bunsenges. Phys. Chem. **74**, 380 (1970).
13. R. A. McClelland and W. F. Reynolds. Can. J. Chem. **54**, 718 (1976); G. Perdoncin and G. Scorrano. J. Am. Chem. Soc. **99**, 6983 (1977); A. Levi, G. Modena, and G. Scorrano. J. Am. Chem. Soc. **96**, 6585 (1974).
14. R. A. Cox, C. R. Smith, and K. Yates. Can. J. Chem. **57**, 2952 (1979).
15. C. D. Johnson. Chem. Rev. **75**, 755 (1975); D. J. McLellan. Tetrahedron, **34**, 2331 (1978).
16. R. A. Coburn, J. M. Landesberg, D. S. Kemp, and R. A. Olofson. Tetrahedron, **34**, 2331 (1978).

Can. J. Chem. Downloaded from www.nrcresearchpress.com by 210.87.254.6 on 09/06/12
For personal use only.

Resonance Raman spectrum of a deuterated crystal violet: $[p(CH_3)_2N{\cdot}C_6D_4]_3C^+Cl^-$

S. SUNDER

Whiteshell Nuclear Research Establishment, Atomic Energy of Canada Ltd., Pinawa, Man., Canada R0E 1L0

AND

H. J. BERNSTEIN

Division of Chemistry, National Research Council of Canada, Ottawa, Ontario, Canada K1A 0R6

Received October 21, 1980

S. SUNDER and H. J. BERNSTEIN. Can. J. Chem. **59**, 964 (1981).

Resonance Raman spectra have been obtained for a deuterated crystal violet $[p(CH_3)_2N{\cdot}C_6D_4]_3C^+Cl^-$, as a dilute aqueous solution. The assignment of some of the strong features seen in the spectra of crystal violet and deuterated crystal violet is discussed.

S. SUNDER et H. J. BERNSTEIN. Can. J. Chem. **59**, 964 (1981).

On a obtenu les spectres Raman du cristal de violet deutéré $[p(CH_3)_2N{\cdot}C_6D_4]_3C^+Cl^-$ sous forme de solution aqueuse diluée. On discute de l'identification de quelques unes des caractéristiques marquantes observées dans les spectres du cristal de violet deutéré et non deutéré.

[Traduit par le journal]

Introduction

Crystal violet (CV) is an important analytical reagent in chemical and biological studies. It is used in the analysis of uranium (1, 2), thorium (2, 3) and other heavy metals and ions (4, 5) and has numerous applications in biological studies (6, 7). These applications of crystal violet result from its ability to exhibit characteristic spectral changes in the presence of other macromolecules and ions. Therefore, there is much interest in studying the spectral properties of crystal violet including its resonance Raman spectrum. Resonance Raman spectroscopy, due to its ability to give detailed molecular information at very low concentration of the sample, is being increasingly used to investigate systems with chromophoric moieties. Spectra of CV have been reported previously (8–14). All of these communications deal with the normal crystal violet and there is no published report on the resonance Raman spectrum of any of its deuterated derivatives according to the information available to us. Here we report the resonance Raman spectra of one of its deuterated derivatives $[p(CH_3)_2N{\cdot}C_6D_4]_3C^+Cl^-$ i.e., crystal violet-d_{12} or CV-d_{12}.

Experimental

Crystal violet-d_{12} was synthesized and generously supplied by Dr. L. Leitch of the National Research Council of Canada. The isotopic purity of the CV-d_{12} is better than 98% as indicated by its proton magnetic resonance spectrum. Raman spectra were obtained using a Spex-1400 double monochromator equipped with an EMI 6256 photomultiplier and photon counting electronics (15). An argon ion laser, Coherent Radiation model 52GA, was used to obtain the exciting radiation of 488 nm and 514.5 nm respectively. The laser output was filtered using a narrow band-pass spike filter and the laser power was adjusted so that the power of the exciting radiation was ~100 mW at the sample. The sample solution was contained in a rotating cell (16). Spectra were recorded using a 90° scattering geometry. The polarization of the scattered light going into the monochromator was selected by a polaroid analyzer placed between the collecting lens and the entrance slit and a polarization scrambler was placed between the polaroid analyzer and the entrance slit.

Visible absorption spectra were recorded using a Carey 14 spectrophotometer (15).

Results

The visible and uv absorption spectrum of CV-d_{12} as a dilute aqueous solution is very similar to that reported for the normal crystal violet (8, 13, 17) with a strong maximum around 590 nm in the visible region. The resonance Raman spectrum of CV-d_{12} is shown in Fig. 1. The Raman spectrum was excited using 488 nm radiation and the concentration of the CV-d_{12} in the aqueous solution was about 5×10^{-5} M. The frequency values of the observed features are listed in Table 1 and the frequency accuracy is estimated to be $\pm 2\,cm^{-1}$. The spectra were recorded at a resolution of $\sim 3\,cm^{-1}$. Table 1 also contains the depolarization ratio and the qualitative relative intensities of the observed spectral features. The spectra shown in Fig. 1 are photocopies of the original spectra. Here it may be mentioned that the monochromator employed was linear in wavelength and not in frequency. The spectra reported here are uncorrected for the frequency dependence of the instrumental response.

We have included in Fig. 1 the spectrum of normal crystal violet recorded under similar experimental conditions for the purpose of comparison. The spectrum of normal CV shown in Fig. 1

[1]NRCC No. 19011.

0008-4042/81/060964-04$01.00/0

©1981 National Research Council of Canada/Conseil national de recherches du Canada

Can. J. Chem. Downloaded from www.nrcresearchpress.com by 210.87.254.105 on 09/06/12
For personal use only.

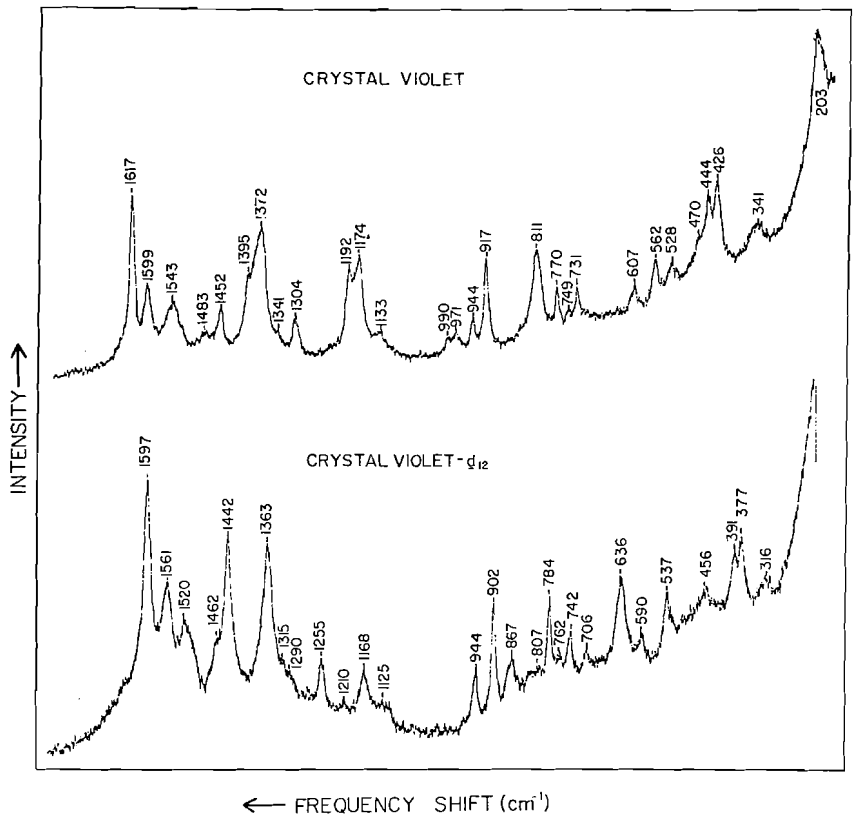

FIG. 1. Resonance Raman spectra of $\sim 5 \times 10^{-5} M$ aqueous solution of crystal violet (upper spectrum) and crystal violet-d_{12} (bottom spectrum) using 488 nm radiation from Ar^+ laser as the exciting line.

basically agrees with that reported in literature for this molecule (8, 13, 14). The spectrum of normal CV shown in Fig. 1 contains many well resolved doublets which were not clearly resolved in some of the earlier reports (9, 12). The notable examples of this are the doublets at about (*a*) 1174 cm^{-1} and 1192 cm^{-1}, (*b*) 426 cm^{-1} and 444 cm^{-1}, and (*c*) 971 cm^{-1} and 990 cm^{-1}.

Discussion

X-Ray data for the triphenyl carbonium ion suggest a propeller shaped structure with molecular symmetry D_3 (18). Analysis of the magnetic circular dichroism of the visible–uv absorption spectra also suggests a D_3 symmetry for crystal violet and related triphenyl carbonium derivatives (19). In this structure the phenyl rings of the molecule are at a dihedral angle of $\sim 30°$ with the central C_3C^+ plane and are symmetrically oriented with respect to each other. Resonance Raman spectra of crystal violet also suggest a D_3 symmetry for the molecule, as discussed by Angeloni *et al.* (13) and it turns out that no evidence from the resonance Raman spectra of CV-d_{12} described here is against this conclusion. The majority of the bands seen in the resonance Raman spectrum of CV have been assigned to the vibrations of the phenyl part of the molecule (9, 12, 13). Angeloni *et al.* have discussed the effect of lowering of symmetry on the vibrations arising from the phenyl rings. We studied the molecule with deuteration at the phenyl rings due to the predominance of the bands in the resonance Raman spectra arising from this part of the molecule.

Our tentative assignment for some of the strong bands seen in the spectrum of CV-d_{12} is given in Table 1. Before discussing the assignment of the deuterated crystal violet we would like to make a few brief comments on the literature assignments for normal CV. Three different groups of workers have suggested the assignments for the spectrum of CV (9, 12, 13). The strong Raman band seen around 1372 cm^{-1} has been assigned to the ^+C—C stretching vibration in ref. 12 while in refs. 9 and 13 it is assigned to the phenyl—N stretching vibrations. We agree with the latter assignments as the Raman

Can. J. Chem. Downloaded from www.nrcresearchpress.com by 210.87.254.105 on 09/06/12
For personal use only.

Can. J. Chem. Downloaded from www.nrcresearchpress.com by 210.87.254.105 on 09/06/12
For personal use only.

TABLE 1. Resonance Raman spectrum of crystal violet-d_{12}[a]

Raman shift[b]	Polarization[c]	Assignment[d]
1597 vs	p	ω_9
1561 ms	dp	
1520 m, br	pp	
1462 sh	pp	ω_{19}
1442 s	dp	
1363 s	dp	$\nu_{(N-\phi)}$
1315 sh, w	p	ω_{14}
1290 sh, vw	dp	
1255 w	dp	
1210 vvw	—	
1168 w	p	Combination (537 + 636)?
1125 sh, vw	p	Combination (537 + 590)?
944 w	p	ω_{12}
902 s	dp	
867 w	dp	ω_9
807 vw, br		
784 m	p	ω_{17}
762 vw, br	dp	
742 w	p	
706 vw	dp	
636 s	pp	ω_{10}
590 w	p	ω_6
537 m	pp	
456 w, br	dp	
391 m	p	ω_{16}
377 m	dp	
316 w, br	dp	$\delta(\phi-c-\phi)$

[a]As 5×10^{-5} *M* aqueous solution.
[b]Frequency in cm^{-1}, s, m, w, v, br, sh stand for strong, medium, weak, very, broad and shoulder, respectively.
[c]Polarization study done here using 514.5 nm exciting line; p, dp, and pp stand for polarized, depolarized, and partially polarized, respectively.
[d]Assignment of the bands is in terms of Wilson's notation (20, 21) for the benzene vibrations as used by previous workers for normal CV (9, 12, 13).

spectrum of dimethylaniline also shows a strong band around 1350 cm^{-1} (9). Although we agree with Angeloni *et al.* about the assignment of the 1372 cm^{-1} band to the ϕ—N stretch, the spectrum of CV-d_{12} reported here does not support their assignment of the polarized feature around 1395 cm^{-1} to the second vibration arising from the ϕ—N stretching. This feature is absent in the spectrum of CV-d_{12}, Fig. 1, which suggests that the vibration responsible for this band most probably involves the hydrogen atoms attached to the benzene ring. The suggested assignments for the strong depolarized band around 917 cm^{-1} also differ from one another as given in the three published papers (9, 12, 13). Gicquel *et al.* (12) have attributed this band to the C—H bending vibrations while Aleksandrov *et al.* (9) have attributed it to the benzene ring breathing (vibration ω_1 in Wilson's nomenclature), and Angeloni *et al.* have attributed it to the ring deformation vibration (i.e., vibration ω_{12} in Wilson's notation). A comparison of the spectra of CV and CV-d_{12} (Fig. 1) suggests that the band ~917 cm^{-1} in the spectrum of CV most probably corresponds to the band seen ~902 cm^{-1} in the spectrum of the deuterated derivative. Both are strong, depolarized, and appear similar in shape. If one accepts the suggestion that these two bands are due to similar vibrations in CV and CV-d_{12} respectively, then the absence of the expected deuterium shift, i.e., frequency ratio of 917/902 = 1.016, indicates that the normal mode responsible for these bands does not involve CH bends of benzene rings as suggested in ref. 12.

The assignment of the deuterated crystal violet given in Table 1 is based on the assignment of normal crystal violet, taking into account the lowering of the frequency for the modes involving hydrogen atoms attached to the benzene ring on deuteration. The strong band seen at about 811 cm^{-1} in the spectrum of CV can be readily correlated with the band at ~636 cm^{-1} in the spectrum of CV-d_{12}. The high frequency band is absent in the spectrum of CV-d_{12} and the low frequency band is absent in normal CV. Both bands appear with relatively strong intensity in their respective spectrum and are polarized. If one accepts the suggestion that the vibrations responsible for these two bands have nearly the same internal coordinate description, then the frequency ratio of the two bands, i.e., 811/636 = 1.275, suggests a strong involvement of the phenyl hydrogen atoms. This assignment is supported by the fact that the ω_{10} is seen at 849 cm^{-1} and 663 cm^{-1} in C_6H_6 and C_6D_6, respectively (22). Similar arguments can be used to correlate the depolarized band at ~1192 cm^{-1} in the spectrum of CV with the band at ~867 cm^{-1} in the spectrum of CV-d_{12}. The frequency ratio of these two bands is 1192/867 ~ 1.375, which suggests the involvement of the phenyl hydrogen atoms. In benzene and benzene-d_6 the ω_9 mode is seen at 1178 and 868 cm^{-1} respectively (22), which supports the correlation and assignment suggested above for the 1192 and 867 bands in CV and CV-d_{12} respectively. Table 1 also contains the assignment of a few strong bands based mainly on the spectra of normal CV and related molecules.

Acknowledgement

We are grateful to Dr. L. Leach for synthesizing and supplying the CV-d_{12} used in this work.

1. N. B. S. SINGH, S. V. MOHAN, and G. R. BALASUBRAMONIAN. J. Radioanal. Chem. **52**, 319 (1979).
2. G. G. SCHEMELEVA, K. N. BAGDASAROV, O. K. RUBTSOVA, S. V. MALYGINA, L. I. MININA, YU. V. STEPANENKO, and

R. I. KOLESNIK. Izv. Sev. Kavk Nauchn. Tsentra Vyssh. Skh. Estestv. Nauk. **6**, 43 (1978).
3. R. I. KOLESNIK, G. G. SHCHEMELEVA, and K. N. BAGDASAROV. *In* Fiz.-Khim. Metody Anal. Kontrolya Proizvod. *Edited by* O. A. Talaev; Dagest. Gos. Univ. Makhachkala, U.S.S.R. 1975. p. 94.
4. Z. MARCOZENKO and J. MARUSZAK. Chem. Anal. Warsaw, **24**, 341 (1979).
5. E. L. KOTHNY. Analyst, London, **94**, 198 (1969).
6. N. BENGET, T. FOLKE, and P. ERICA. Biophys. Chem. **8**, 1 (1978).
7. Y. KIWAMU and H. HIDEKO. Chem. Lett. **5**, 465 (1976).
8. H. J. BERNSTEIN. Advances in Raman spectroscopy. Vol. 1. *Edited by* J. P. Mathieu. Heyden, London. 1973. p. 305.
9. I. V. ALEKSANDROV, YA S. BOBOVICH, A. T. VAZTANYAN, and A. N. SIDOTOV. Opt. Spectrosk. **42**, 64 (1977); Engl. Transl. Opt. Spectrosc. **42**, 35 (1977).
10. K. L. JEANMAIRE and R. P. VAN DUYNE. J. Electroanal. Chem. **84**, 1 (1977).
11. R. P. VAN DUYNE. In Chemical and biochemical applications of lasers. *Edited by* C. B. Moore. Academic Press. 1979. p. 179.
12. J. GICQUEL, M. CARLES, and H. BODOT. J. Phys. Chem. **83**, 699 (1979).
13. L. ANGELONI, G. SMULEVICH, and M. P. MARZOCCHI. J. Raman Spectrosc. **8**, 305 (1979).
14. L. ANGELONI, G. SMULEVICH, and M. P. MARZOCCHI. J. Mol. Struct. **61**, 331 (1978).
15. S. SUNDER and H. J. BERNSTEIN. Can. J. Chem. **52**, 2851 (1974).
16. W. KEIFER and H. J. BERNSTEIN. Appl. Spectrosc. **25**, 500 (1971).
17. J. GRIFFITHS. *In* Colour and constitution of organic molecules. Academic Press, London. 1976. pp. 8, 254.
18. A. H. GOME DE MESQUITA, C. H. MACGILLAVRY, and K. ERIKS. Acta Crystallogr. **18**, 437 (1965).
19. H. P. J. M. DECKKERS and E. C. M. KIELMAN-VAN LUYT. Mol. Phys. **31**, 1001 (1976).
20. E. B. WILSON JR., J. C. DECIUS, and P. C. CROSS. Molecular vibrations, McGraw-Hill Book Co. Inc., New York. 1955. Chapt. 10. pp. 240–272.
21. F. R. DOLLISH, W. F. FATELEY, and F. F. BENTLEY. Characteristic Raman frequencies of organic compounds. John Wiley and Sons, New York. 1974. Chapt. 13. pp. 162–181.
22. J. FAVROT, P. CAILLET, and M. T. FOREL. J. Chim. Phys. **71**, 1337 (1974).

Can. J. Chem. Downloaded from www.nrcresearchpress.com by 210.87.254.105 on 09/06/12
For personal use only.

Isomérisation de l'ion phényl-2 oxétane protoné avant sa fragmentation en spectrométrie de masse

HENRI EDOUARD AUDIER, ARIELLE MILLIET ET MARGARET MRUZEK
Laboratoire de Synthèse Organique, Ecole Polytechnique, 91128 Palaiseau Cedex, France
ET
JEAN PIERRE DENHEZ, PIERRE DIZABO ET CATHERINE SCHAAL
Laboratoire de Spectrométrie Moléculaire, Université Pierre et Marie Curie, 75230 Paris Cedex 05, France
Reçu le 25 juillet 1980

HENRI EDOUARD AUDIER, ARIELLE MILLIET, MARGARET MRUZEK, JEAN PIERRE DENHEZ, PIERRE DIZABO et CATHERINE SCHAAL. Can. J. Chem. **59**, 968 (1981).

Les fragmentations de l'ion phényl-2 oxétane protoné dans un spectromètre de masse par ionisation chimique et de certains ions isomères ont été étudiées à l'aide de composés deutériés ou marqués au carbone 13. Avant sa fragmentation, l'ion phényl-2 oxétane protoné s'ouvre pour donner un carbocation hydroxylé susceptible de s'isomériser par transfert 1–2 ou 1–3 d'hydrures. L'ion phényl-3 propanal protoné ainsi formé élimine une molécule d'eau et donne un ion indène protoné. Le profil réactionnel et le mécanisme proposés sont en accord avec les résultats expérimentaux.

HENRI EDOUARD AUDIER, ARIELLE MILLIET, MARGARET MRUZEK, JEAN PIERRE DENHEZ, PIERRE DIZABO, and CATHERINE SCHAAL. Can. J. Chem. **59**, 968 (1981).

Fragmentations of the phenyl-2 oxetane ion by chemical ionization mass spectrometry, and of some isomeric ions, have been studied using deuterated and ^{13}C labelled compounds. The heterocyclic system of the protonated phenyl-2 oxetane ion is broken before fragmentation giving a hydroxylated carbocation which can isomerize by 1–2 or 1–3 hydride transfers. The protonated phenyl-3 propanal thus obtained eliminates a molecule of water and yields a protonated indene ion. The potential energy profile and the mechanism proposed are in agreement with the experimental results.

Introduction

L'étude de la fragmentation des éthers cycliques protonés (1) par ionisation chimique a montré que la première étape de cette fragmentation consiste en une isomérisation de l'ion moléculaire en carbocation hydroxylé (Schéma 1). Par transfert 1–2 d'hydrures (2–6) ou par transfert de méthylures (4–6), les ions aldéhydes ou cétones protonés conduisent à des carbocations du même type. Inversement de tels carbocations sont susceptibles de se cycliser en éthers protonés, qu'ils proviennent de composés carbonylés protonés ou qu'ils découlent de la perte d'eau d'un diol protoné (7, 8) (Schéma 1).

Dans tous ces dérivés, les compétitions entre les réactions de fragmentation et celles d'isomérisation dépendent non seulement des ΔH_f des états initiaux et finals, mais également des ΔH_f des formes isomères et des énergies d'activation nécessaires aux transferts 1–*n* d'hydrures.

La similitude des spectres ic (ionisation chimique) de phényl-2 oxétane **I**, du phényl-3 propane diol 1–3 **II**, du phényl-3 époxy 1–2 propane **III** et du phényl-3 propanal **IV** protonés avec du méthane, laisse présager que ces processus d'isomérisation interviennent aussi quand la chaîne est substituée par un noyau benzénique (Tableau 1).

Dans ce travail, l'examen des spectres des dérivés

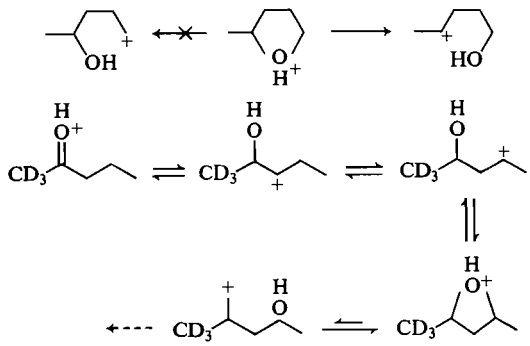

SCHÉMA 1

marqués par du deutérium du phényl-2 oxétane **I** a conduit à proposer un mécanisme de fragmentation qui a été confronté au profil réactionnel correspondant.

Résultats et discussion

Les spectres ic du phényl-2 oxétane protoné par du méthane ou de l'isobutane montrent, outre le pic moléculaire $[MH]^+$, trois fragments principaux $m/z = 117$ $[A]^+$, $m/z = 105$ $[B]^+$ et $m/z = 91$ $[C]^+$. Dans l'isobutane on peut détecter de plus un fragment mineur $m/z = 107$ et dans le méthane, un fragment $m/z = 57$.

L'intensité des pics dépend considérablement des conditions expérimentales, gaz protonant et

0008-4042/81/060968-06$01.00/0
©1981 National Research Council of Canada/Conseil national de recherches du Canada

Can. J. Chem. Downloaded from www.nrcresearchpress.com by 210.87.254.40 on 09/06/12
For personal use only.

Can. J. Chem. Downloaded from www.nrcresearchpress.com by 210.87.254.40 on 09/06/12
For personal use only.

TABLEAU 1. Spectres ic des composés **1** à **4** (décomposition des ions dans la source; gaz protonant: méthane; rep. 6 V·cm^{-1}; T = 150°C)

Composé étudié		$[MH]^+$ m/z 135	$[A]^+$ m/z 117	$[B]^+$ m/z 105	$[C]^+$ m/z 91	m/z 57
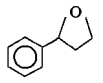	**I**	40	14	25	17	4
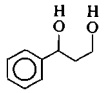	**II**	55	18	14	11	2
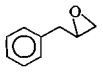	**III**	15	59	7	17	2
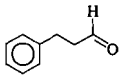	**IV**	21	53	4	20	2

repousseur d'ions, donc de la distribution d'énergie interne de $[MH]^+$. A chacune de ces principales fragmentations en compétition est associé un pic métastable. Celui-ci est "applati" pour la transition $[MH]^+ \rightarrow [A]^+$ et "gaussien" pour les deux autres transitions. De ce fait la comparaison des hauteurs relatives de ces pics n'a que peu de sens. La comparaison des surfaces de ces pics métastables montre que la réaction $[MH]^+ \rightarrow [A]^+$ nécessite la plus faible énergie d'activation, la transition $[MH]^+ \rightarrow [B]^+$, a besoin de plus d'énergie, son pic métastable ayant une surface inférieure au précédent.

Les spectres d'ions métastables des composés marqués permettent de préciser le mécanisme et indiquent que l'ion $[A]^+$ m/z = 117 formé à basse énergie interne par perte d'eau a sans doute une structure bicyclique: (*i*) les hydrogènes portés par les carbones 2, 3 et 4 n'interviennent pas dans cette fragmentation à basse énergie; ils ne sont échangés ni avec l'hydrogène protonant, ni avec les hydrogènes du noyau aromatique (Tableau 3); (*ii*) la perte d'eau est précédée d'un échange de l'hydrogène protonant avec ceux du noyau benzénique (dérivé **1***a*, Tableau 3); (*iii*) un hydrogène du cycle aromatique est éliminé lors de la fragmentation. En effet, le spectre du dérivé **1***f* pentadeutérié sur le cycle aromatique présente des pics $[MH - D_2O]^+$ et $[MH - HDO]^+$ confirmant par ailleurs l'échange de l'hydrogène protonant.

TABLEAU 2. Spectres ic du composé **1** (décomposition des ions dans la source; gaz protonant: isobutane; T = 150°C)

	m/z				
Repousseur d'ions	135	117	107	105	91
6 V cm^{-1}	57	29	2	9	3
16 V cm^{-1}	26	32	2	13	27

La structure indanique **5** de l'ion m/z = 117 suggérée par les spectres des composés marqués est confirmée par les spectres d'activation par collision (ca); le spectre ca de cet ion provenant de la fragmentation de l'ion **1** est indentique à celui de l'indène protoné (8).

Le mécanisme de fragmentation proposé est en accord avec les résultats expérimentaux et le profil réactionnel (Fig. 1).

(*a*) La protonation s'effectue, soit sur le noyau aromatique, soit sur l'oxygène; les affinités protoniques (ap) de ces deux centres sont en effet très proches (toluène: ap = 193 kcal·mol^{-1}; oxétane: ap = 197 kcal·mol^{-1} (9)).

(*b*) La forme protonée sur le noyau benzénique peut s'isomériser en forme protonée sur l'oxygène. Cette dernière forme s'ouvre pour donner le carbocation hydroxylé le plus stable: l'ion **6** (1). Cette réaction est rapide dans la mesure où le ΔH_f de **6** est bien inférieur au ΔH_f de l'ion **1**.

(*c*) Le carbocation **6** s'isomérise par transferts

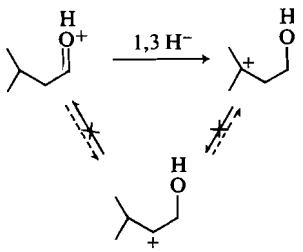

SCHÉMA 2

TABLEAU 3. Déplacements des différents pics métastables observés dans les composés marqués (ic isobutane, rep. 6 V cm^{-1})

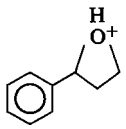

		91	92	93	94	95	96	105	106	107	108	109	110	117	118	119	120	121
1*a*	$0d_1$	25	75	—	—	—	—	—	>95	—	—	—	—	30	70	—	—	—
1*b*	$2d_1$	5	95	—	—	—	—	—	>95	—	—	—	—	—	>95	—	—	—
1*c*	$4,4d_2$	45	55	—	—	—	—	>95	—	—	—	—	—	—	—	95	—	—
1*d*	$2,4,4d_3$	—	55	45	—	—	—	—	>95	—	—	—	—	—	—	—	>95	—
1*e*	$3,3d_2$	—	60	40	—	—	—	—	—	>95	—	—	—	—	—	>95	—	—
1*f*	ϕd_5	—	—	—	—	75	25	—	—	—	—	—	>95	—	—	—	35	65
1*g*	$2,^{13}C$	—	>95	—	—	—	—	—	>95	—	—	—	—	—	>95	—	—	—

d'hydrure en ions **7** (ou **7**′) et **4** (2–4). La structure de l'ion **6** a été considérée comme "benzylique" et non "tropylique" à cause de la forte barrière d'isomérisation qui existe entre ces deux formes (10, 11). Par contre, il a été proposé, compte tenu des travaux relatifs à la stabilisation d'un carbocation en β d'un noyau benzénique (12, 13), que l'ion **7** pouvait s'isomériser en ion bicyclique **7**′. La réaction d'isomérisation de **6** en **4** par deux transferts successifs 1–2 d'hydrure et par l'intermédiaire de la forme **7**′ a une énergie d'activation maximale de 12 kcal·mol^{-1}. Le passage par l'intermédiaire **7** est très improbable. En effet, le passage direct de l'ion **6** à l'ion **4** par un transfert 1–3 d'hydrure est également possible; de tels transferts exigent des énergies d'activation de l'ordre de 6 à 8 kcal·mol^{-1} (6, 14) (Schéma 2).

(*d*) L'élimination d'eau s'effectue par attaque du carbocation **4** sur le cycle aromatique donnant le complexe intermédiaire **8** qui perd une molécule d'eau et donne l'ion indène protoné **5** (Fig. 1). Cet ion a un ΔH_f inférieur de 25 kcal·mol^{-1} environ à celui de l'ion phénylallyl isomère susceptible cependant de se former pour les ions $[MH]^+$ de plus haute énergie interne. La largeur du pic métastable de la transition $[MH]^+ \rightarrow [A]^+$ permet d'affirmer que le ΔH_f de l'état de transition de cette réaction est bien supérieur à celui de l'état final; la perte en énergie cinétique, calculée à partir de la largeur du pic métastable, est de 400 meV, soit 9,3 kcal·mol^{-1}. Cet état de transition ne peut être l'indanol protoné, puisque pour ce composé la largeur du pic métastable correspondant à la perte d'eau est bien inférieure (perte en énergie cinétique 70 meV, soit 1,6 kcal·mol^{-1}).

(*e*) Les ΔH_f des formes moléculaires protonées, soit sur le noyau aromatique, soit sur l'oxygène, étant très voisines, les échanges entre l'hydrogène protonant l'oxygène et les hydrogènes du noyau aromatique sont importants.

L'étude des fragments $[B]^+$ $m/z = 105$ et $[C]^+$ $m/z = 91$ permet de préciser plusieurs aspects du mécanisme. Tout d'abord le Tableau 3 montre que les ions $[B]^+$ et $[C]^+$ qui proviennent de $[MH]^+$ par élimination respectivement de CH_2O et de C_2H_4O contiennent intégralement le carbone 2 (dérivé **1***g*); il n'y a ni isomérisation, ni transposition de la chaîne conduisant à permuter les carbones 2 et 4.

Par ailleurs, l'hydrogène en position 2 se retrouve dans les ions $[B]^+$ et $[C]^+$ pour plus de 95%, par contre le groupement CH_2 en position 4 est totalement éliminé au cours de la formation du fragment $[B]^+$ (dérivés **1***c* et **1***d*, Tableau 3).

Les hydrogènes de l'hétérocycle ne s'échangent donc, ni entre eux, ni avec ceux du cycle aromatique, ni avec l'hydrogène protonant. Les réactions d'isomérisation des carbocations hydroxylés **6** → **7**′ → **4** ne sont donc pas réversibles dans les conditions expérimentales de cette étude.

La formation de l'ion $[B]^+$ s'accompagnant de l'élimination des deux hydrogènes portés par le carbone 4, nécessite le transfert de l'hydrogène protonant sur le carbone 2 (Fig. 1). De ce fait, l'échange préalable de l'hydrogène protonant avec ceux du cycle aromatique ne peut être décelé. L'ion $[B]^+$ $m/z = 105$ est déplacé à $m/z = 106$ pour le dérivé **1***a* et à $m/z = 110$ pour le composé **1***f*.

La participation de l'hydrogène protonant à la formation de l'ion $[C]^+$ est essentiellement liée à son échange préalable avec les hydrogènes benzéniques (comparaison des spectres de **1***a* et de **1***f*, Tableau 3).

Il ressort du Tableau 3 que l'hydrogène transféré contribuant à la formation de l'ion $[C]^+$ provient pour moitié de la position 3 et pour moitié de la position 4.

L'ion $[C]^+$ semble, comme le laisse prévoir le profil réactionnel, être le résultat soit d'un double transfert 1–2 d'hydrures (**6** → **7**′ → **4**) amenant un hydrogène du carbone 3 sur le carbone 2, soit d'un simple transfert 1–3 d'hydrure plaçant un hydrogène du carbone 4 sur le carbone 2.

Can. J. Chem. Downloaded from www.nrcresearchpress.com by 210.87.254.40 on 09/06/12
For personal use only.

Can. J. Chem. Downloaded from www.nrcresearchpress.com by 210.87.254.40 on 09/06/12
For personal use only.

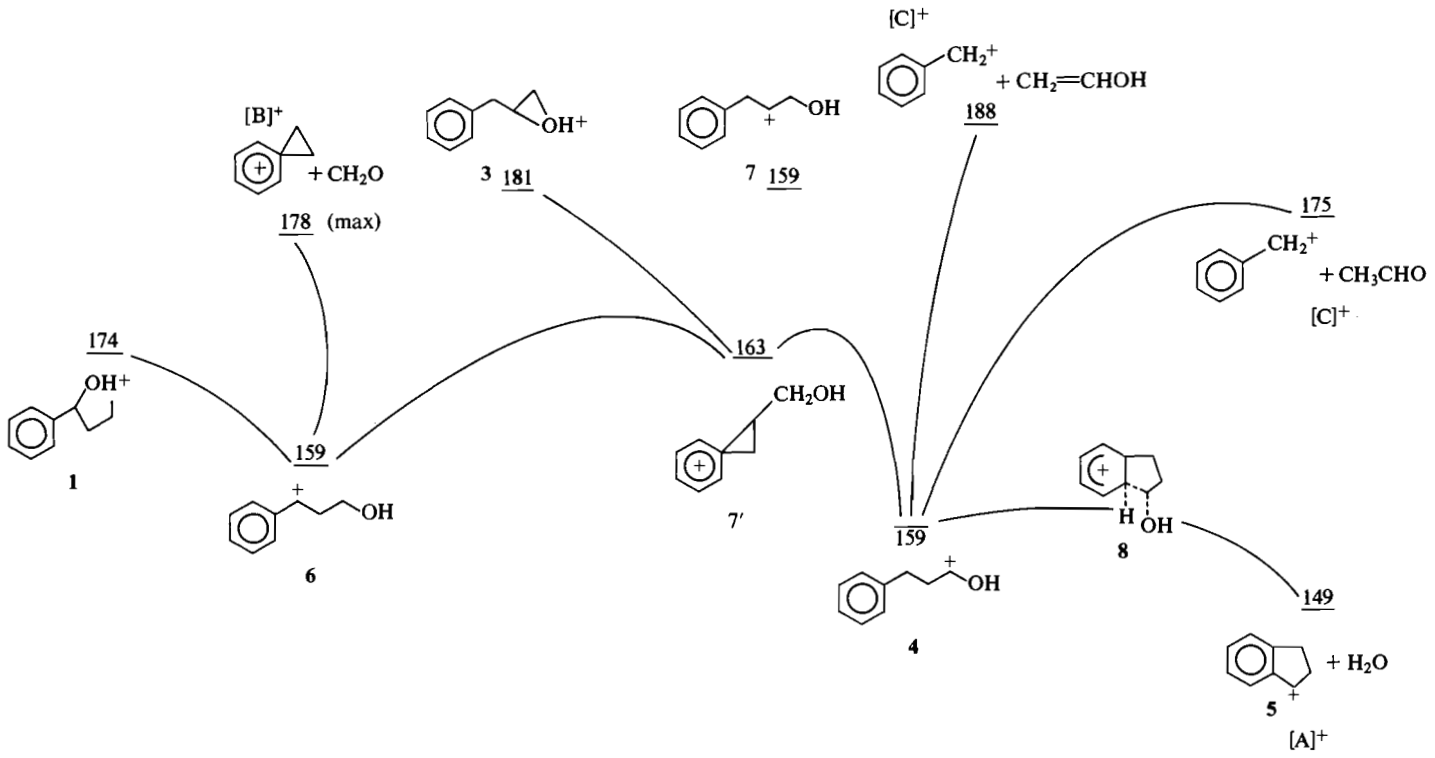

FIG. 1. Profil réactionnel; les ΔH^{0}_{f298} des niveaux sont donnés en kcal·mol^{-1}.

Can. J. Chem. Downloaded from www.nrcresearchpress.com by 210.87.254.40 on 09/06/12
For personal use only.

Suivant la nature du fragment neutre formé, deux mécanismes peuvent être proposés pour former l'ion $[C]^+$ à partir de l'ion **4**: (*i*) rupture directe conduisant à la formation d'un énol; (*ii*) rupture accompagnée du transfert de l'hydrogène hydroxylique sur le carbone 3, donnant une molécule d'acétaldéhyde.

Ces données expérimentales montrent que les ΔH_f des états de transition des réactions **6** → **4** par transferts 1–2 ou 1–3 d'hydrures sont voisins.

La comparaison des spectres des composés **I**, **II**, **III** et **IV** est en accord avec les mécanismes et le profil réactionnel proposés.

Le Tableau 1 montre que, si les mêmes pics se retrouvent pour les 4 composés étudiés, l'intensité du pic $m/z = 105$ est toutefois plus faible pour les composés **III** et **IV**. Ce phénomène est plus accentué à basse énergie. En effet, alors que pour les composés **I** et **II** les surfaces des pics métastables $[MH]^+ \rightarrow [A]^+$ et $[MH]^+ \rightarrow [B]^+$ sont du même ordre de grandeur, pour les composés **III** et **IV** les pics métastables correspondant à la formation de l'ion $[B]^+$ ne peuvent être détectés.

La réaction **4** → **6** ne s'effectue donc pas plus pour ces dérivés que pour le phényl-2 oxétane protoné, pour lequel il a été montré que la réaction **6** → **4** n'était pas réversible. Par ailleurs, le Tableau 1 indique que les intensités des ions $[MH]^+$ correspondant aux composés **III** et **IV**, sont très voisines alors que leurs ΔH_f sont très différents.

En fait l'ion **3** s'isomérise très rapidement dans la source pour conduire à l'ion **4** plutôt qu'à l'ion **6**.

Le noyau aromatique favorise probablement un passage concerté direct à la forme **7'** qui s'isomérise ensuite en ion **4**. Cette isomérisation ayant lieu dans la source, les ions **4** formés, soit directement par protonation du phényl-3 propanal **IV**, soit par isomérisation du phényl-3 époxy 1–2 propane **III**, sont désactivés par chocs et ont des énergies internes comparables quelle que soit leur provenance; c'est pourquoi leurs spectres ic sont très voisins.

Par ailleurs, les données expérimentales montrent que le mécanisme de perte d'eau $[MH]^+ \rightarrow m/z = 117$ est identique pour tous les composés étudiés: (*a*) les spectres d'activation par collisions des ions m/z 117 sont identiques quel que soit le composé de départ (8). Ils sont superposables à celui de l'indène protoné; (*b*) les transitions $[MH]^+ \rightarrow m/z$ 117 sont accompagnées d'un pic métastable de même largeur (énergie cinétique 400 MeV ± 10).

Ces données sont en accord avec le mécanisme de perte d'eau proposé pour le phényl-2 oxétane protoné: **1** → **6** → **4** → $[MH - H_2O]^+$.

Conclusion

Les études relatives à la perte d'eau des aldéhydes et cétones protonés acycliques ont montré que les transferts 1–2 d'hydrure sont réversibles (6) lorsque ces réactions d'isomérisation ont des états de transition dont le ΔH_f est très inférieur à celui du dernier état de transition conduisant à la perte d'eau. Elles ne sont pas réversibles dans le cas contraire.

Dans l'exemple étudié ici, la barrière due à la réaction **4** → **6** est à l'origine de la non-réversibilité observée. Ce phénomène est à rapprocher de celui qui est observé pour le méthyl-3 butanal protoné (6), pour lequel la perte d'eau s'effectue avec un transfert d'hydrogène sélectif et sans échange préalable de l'hydrogène protonant: une énergie d'activation est nécessaire à l'isomérisation du carbocation stable initial en un carbocation tertiaire également stable (Schéma 2).

Par rapport au comportement des aldéhydes éthers ou diols alicycliques, l'introduction d'un cycle aromatique dans la chaîne influence considérablement les processus de rupture: (*a*) en modifiant les valeurs relatives des ΔH_f des différents carbocations formés, en particulier en stabilisant la charge positive sur le carbone adjacent au noyau; et (*b*) en induisant une réaction de cyclisation qui formellement s'apparente à la réaction de Friedel et Craft.

Partie expérimentale et calculs

Tous les ΔH_f cités sont des ΔH_{f298}^0.

Les ΔH_f des ions $[MH]^+$ provenant de la protonation d'une molécule neutre sont obtenus suivant la réaction [1]:

$$[1] \quad MH^+ \xrightarrow{ap} M + H^+$$

à partir du ΔH_f du proton, 366 kcal·mol^{-1}, du ΔH_f de la molécule neutre que l'on calcule en utilisant les incréments de Benson (15) et des affinités protoniques (ap) trouvées dans la littérature.

Toutes les valeurs sont données en kcal·mol^{-1}. Phényloxétane protoné **1**, $\Delta H_f = 174$, $\Delta H_{f_I} = 5{,}5$; ap (oxétane) = 197 (9); ap (toluène) = 193 (9). Phényl-3 époxy 1–2 propane protoné **3** $\Delta H_f = 181$, $\Delta H_{f_{III}} = 5{,}5$; ap (oxirane) = 190 (9). Phényl-3 propanal protoné **4**, $\Delta H_f = 155$, ΔH_f $CH_3CH_2\overset{+}{C}HOH = 132$ (16–18).[1] Indanol protoné $\Delta H_f = 144$, $\Delta H_{f_{indanol}} = -25$; ap (2-butanol) = 197 (19). Indène protoné **5**, $\Delta H_f = 206$, $\Delta H_{f_{indène}} = 40$; ap (styrène) = 202 (9).

Le ΔH_f de l'ion $[C]^+$ a été trouvé dans la littérature. Les ΔH_f des autres ions sont obtenus à partir des ΔH_f d'ions de structure voisine auxquels on fait subir une substitution isodesmique (20) dont l'incrément est calculé par la méthode de Benson (15). Ces valeurs ne sont qu'indicatives dans la mesure où le rôle d'un noyau benzénique dans la stabilisation de la charge positive portée par une chaîne n'a pas encore été étudié. Le ΔH_f de **6** = 159 est obtenu à partir du ΔH_f du styrène protoné = 200 auquel

[1]Une valeur de 130 kcal·mol^{-1} basée sur l'affinité protonique du propionaldéhyde a été attribuée à cet ion (4).

on ajoute l'incrément de substitution isodesmique − 41. Le ΔH_f de **7** est calculé à partir du ΔH_f de $C_6H_5CH_2\overset{+}{C}HCH_3$ (20): $\Delta H_f = 215$, l'incrément est −36. Le ΔH_f de l'ion $[B]^+$ est obtenu à partir du PA (potentiel d'apparition) d'un ion supposé identique obtenu, soit par perte de brome du 1-bromophényléthane, soit par perte d'un radical CH_3CO de la phényl-4 butanone 2, on obtient ainsi deux valeurs limites $205 < \Delta H_f < 217$. (21). Le ΔH_f de l'ion **7'** est obtenu par substitution isodesmique sur l'ion précédent, l'incrément étant −43.

Les spectres ont été effectués à l'I.C.S.N.–C.N.R.S. de Gif-sur-Yvette sur un appareil AEI MS 9 dont la source a été modifiée (22).

Les mesures relatives à la perte en énergie cinétique ont été effectuées sur l'appareil ZAB-2F de l'Ecole Polytechnique Fédérale de Lausanne avec un système AGHIS, $T = 180°C$, le gaz réactif étant l'isobutane (≃0,5 Torr). Les déterminations ont été faites dans la deuxième région libre de champ en mesurant la largeur à mi-hauteur du pic métastable et en effectuant la moyenne de trois mesures.

Nous remercions l'I.C.S.N. et Monsieur Pierre Varenne pour sa collaboration.

La préparation des composés étudiés a été décrite précédemment (23).

1. H. E. AUDIER, A. MILLIET, C. PERRET et P. VARENNE. Org. Mass Spectrom. **14**, 129 (1979).
2. R. D. BOWEN et D. H. WILLIAMS. J. Am. Chem. Soc. **99**, 6822 (1977).
3. R. D. BOWEN, D. H. WILLIAMS, G. HVISTENDAHL et J. R. KALMAN. Org. Mass Spectrom. **13**, 721 (1978).
4. R. D. BOWEN et D. H. WILLIAMS. J. Am. Chem. Soc. **100**, 7454 (1978).
5. F. W. MCLAFFERTY et I. SAKAI. Org. Mass Spectrom. **11**, 669 (1976).
6. H. E. AUDIER, A. MILLIET et J. C. TABET. Helv. Chim. Acta, **63**, 344 (1980).
7. H. E. AUDIER, A. MILLIET, C. PERRET et P. VARENNE. Org. Mass Spectrom. **14**, 132 (1979).
8. H. E. AUDIER, A. MILLIET, M. MRUZEK et J. C. TABET. Bull. Soc. Chim. Belg. **89**, 157 (1980).
9. D. H. AUE, et M. T. BOWERS. Gas phase ion chemistry. Vol. 2. *Edité par* M. T. Bowers. Academic Press, New York. 1979.
10. P. KUCK, et H. FR. GRÜTZMACHER. Org. Mass Spectrom. **13**, 81 (1978).
11. F. W. MCLAFFERTY et F. M. BOCKHOFF. Org. Mass Spectrom. **14**, 181 (1979).
12. H. F. GRÜTZMACHER. Org. Mass Spectrom. **3**, 131 (1970).
13. J. L. OCCOLOWITZ. Aust. J. Chem. **20**, 2387 (1967).
14. M. SAUNDERS et J. J. STOFKO. J. Am. Chem. Soc. **95**, 252 (1973).
15. S. W. BENSON. Thermochemical kinetics. John Wiley, New York. 1968.
16. R. YAMDAGNI et P. KEBARLE. J. Am. Chem. Soc. **98**, 1320 (1976).
17. J. F. WOLF, R. H. STALEY, I. KOPPEL, M. TAAGEPERA, R. T. MCIVER, JR., J. L. BEAUCHAMP et R. W. TAFT. J. Am. Chem. Soc. **99**, 5417 (1977).
18. F. P. LOSSING. J. Am. Chem. Soc. **99**, 7526 (1977).
19. J. L. BEAUCHAMP, et M. C. CASERIO. J. Am. Chem. Soc. **94**, 2638 (1972).
20. R. D. BOWEN et D. H. WILLIAMS. Org. Mass Spectrom. **12**, 475 (1977).
21. H. M. ROSENSTOCK, K. DRAXL, B. W. STEINER et J. T. HERRON. J. Phys. Chem. Ref. Data, **6** (1977).
22. P. VARENNE. Thèse d'université, Orsay, France. 1976.
23. C. SCHAAL et M. RICARD. J. Labelled Compd. Radiopharmaceut. **16**, 727 (1978).

Can. J. Chem. Downloaded from www.nrcresearchpress.com by 210.87.254.40 on 09/06/12
For personal use only.

Photochemical reactions of charge-transfer complexes. III. Molecular orbital studies of the charge-transfer complexes between 1,2-dimethoxyethylenes and 1,2-dicyanoethylenes

PO CHEONG WONG[1] AND RUSSELL J. BOYD[2]

Department of Chemistry, Dalhousie University, Halifax, N.S., Canada, B3H 4J3

Received August 19, 1980

PO CHEONG WONG and RUSSELL J. BOYD. Can. J. Chem. **59**, 974 (1981).

Ab initio and PCILO molecular orbital (MO) calculations for the four $\pi-\pi^*$ charge-transfer complexes formed between maleonitrile (MN) and fumaronitrile (FN), and *cis* (CS) and *trans*-1,2-dimethoxyethylene (TR) are reported. The donor and the acceptor molecules are stacked in parallel planes. *Trans* and *cis*-1,2-dihydroxyethylene are used as the model compounds for TR and CS in the determination of the optimum geometries of the complexes. Both types of MO calculations indicate that the eclipsed geometry (with the two central double bonds parallel and the centres of the double bonds centred over one another) is relatively unstable. With limited geometry searching, we find that the slipped geometry (with the two central double bonds parallel but separated at a projected distance of 2.2 Å and the oxygen atoms above the cyanocarbon atoms) is the preferred structure. According to the *ab initio* calculations the relative order of the calculated heats of formation (ΔH^{θ}'s) for these complexes is: MN–CS > FN–CS > FN–TR > MN–TR.

PO CHEONG WONG et RUSSELL J. BOYD. Can. J. Chem. **59**, 974 (1981).

On rapport des calculs *ab initio* et PCILO d'orbitales moléculaires (OM) de quatre complexes $\pi-\pi^*$ de transfert de charge entre le maléonitrile (MN) et le fumaronitrile (FN) et les diméthoxy-1,2 éthylènes *cis* (CS) et *trans* (TR). Les molécules acceptrices et donneuses sont entassées dans des plans paralelles. On a utilisé les dihydroxy-1,2 éthylènes *cis* et *trans* comme composés modèles pour déterminer les géométries optimales des complexes de TR et de CS. Les deux types de calculs OM indiquent que la géométrie éclipsée (avec les deux doubles liaisons centrales paralelles et les centres des doubles liaisons centrées l'une sur l'autre) est relativement instable. A partir de recherches limitées sur la géométrie, nous avons trouvé que la structure préférée est la géométrie décalée (avec les deux doubles liaisons centrales paralelles mais séparées d'une distance projetée de 2,2 Å et les atomes d'oxygène au-dessus des atomes de carbone du groupement cyano). Selon les calculs *ab initio*, l'ordre relatif des chaleurs de formation calculées (ΔH^{θ}'s) de ces complexes est le suivant: MN–CS > FN–CS > FN–TR > MN–TR.

[Traduit par le journal]

Introduction

In spite of the fact that the binding energy of a charge-transfer (ct) complex in solution is of the order of a few kcal mol^{-1} (1), it has been very difficult to predict experimentally or theoretically the exact orientation of the donor and the acceptor in the complex. X-ray crystallographic structures provide the only reliable experimental information for ct complexes. However, caution must be taken in applying these solid phase results to the solution phase since there is uncertainty about the importance of crystal packing forces for the individual complex (2). Orientation effects in ct complexes have not been fully investigated by theoretical methods. Here, we define orientation effects as the effects of the orientation of the substituents on the geometry and stability of the ct complex. Several theoretical studies of the most stable geometries of ct complexes have been reported (see the references in later sections). However, the effects of the substituents of the subsystems on the geometry of the $\pi-\pi^*$ complexes have not been systematically investigated so far. It would be interesting to know how the substituents of the donor molecule align with those of the acceptor molecule in the complex in solution. A basic understanding of the orientation effects would help us to predict the geometry of the ct complex which in turn will be useful in (*1*) the rationalization of the 3-D structure of some biological macromolecules where ct interactions are important (1*c*), and (*2*) the selection of suitable donors and acceptors for the study of photochemical isomerization of olefins through the irradiation of the ct complexes. The latter is a potentially useful synthetic method for preparing stereospecific olefins (3). Selective irradiation of the ct complex formed by one olefin isomer with a proper donor (or acceptor) would lead to enrichment of the alternative olefin isomer. A successful example has been demonstrated in the irradiation of the ct complex between *trans*-stilbene (*t*-ST) and fumaronitrile (FN) where *cis*-stilbene (*c*-ST) can be obtained in up to 86% yield (3). Of course in this particular example, the difference in the absorption spectra and the stability of the *trans* and *cis*-stilbene complexes can be accounted for by merely considering the difference in their oxidation potentials ($E_{1/2}^{ox}$(Ag/$AgNO_3$) being 1.10 V[3] and 1.40 V[4] respec-

[1]Current address: Chemistry Division, National Research Council, 100 Sussex Drive, Ottawa, Ont., Canada K1A 0R6.

[2]Author to whom correspondence should be addressed.

[3]Corrected value from J. E. Kuder *et al.* (30).

[4]Estimated from a relationship between ct transition energies and oxidation potentials of the donors (31).

0008-4042/81/060974-08$01.00/0

©1981 National Research Council of Canada/Conseil national de recherches du Canada

Can. J. Chem. Downloaded from www.nrcresearchpress.com by 210.87.254.105 on 09/06/12
For personal use only.

Can. J. Chem. Downloaded from www.nrcresearchpress.com by 210.87.254.105 on 09/06/12
For personal use only.

tively). The orientation effects in this case may in fact be overwhelmed by this major effect. Orientation effects are important in the case *t*-ST–FN and *t*-ST–MN complexes, where the equilibrium constant (K) of the former is larger (K = 1.7 and 1.0 M^{-1}, respectively) even though the acceptors have the same reduction potentials.

In the present study, we try to predict theoretically the most stable geometries as well as the heats of formation (ΔH^{θ}'s) of the four ct complexes formed between *trans* and *cis*-1,2-dimethoxyethylene (TR and CS), and fumaronitrile (FN) and maleonitrile (MN). These four complexes represent the smallest system for the study of orientation effects. This is because the ionization potentials (adiabatic) of the two donors are very similar (7.40 and 7.38 eV for *trans* and *cis*-1,2-diethoxyethylene respectively (4)), while the reduction potentials for the two acceptors are the same. According to the Mulliken theory (1), the difference in the strength of the complex will reflect the orientation effects for structurally similar systems.

In this paper *ab initio* molecular orbital (MO) calculations and Perturbation Configuration Interaction using Localized Orbitals (PCILO) (5) calculations have been used to predict the geometries and the heats of formation (ΔH^{θ}'s) of the π–π^* ct complexes. A comparison of the results from these two MO methods will be discussed in detail.

Method

All computations were performed on a Control Data CYBER 170-720 system. Two computational methods within the supermolecule approximation (6) were employed in this work to calculate the stabilization energies (ΔE equivalent to ΔH^{θ}) for the formation of charge-transfer complexes (eq. [1]).

$$[1] \quad \Delta E = E_C - (E_D + E_A)$$

E_D and E_A are the energies of the isolated donor and acceptor molecules respectively and E_C is the energy of the complex.

The standard single determinant *ab initio* calculations were performed using the GAUSSIAN 76 (G76) program (7) with the spin-restricted Hartree-Fock (RHF) procedure. The geometries of the subsystems employed in the complexes were assumed to be the same as the isolated molecules. This assumption is justified by the fact that there is no significant change in bond length of the central double bonds upon complex formation according to both X-ray crystallographic analysis on solid state ct complexes (2) and our calculations. The

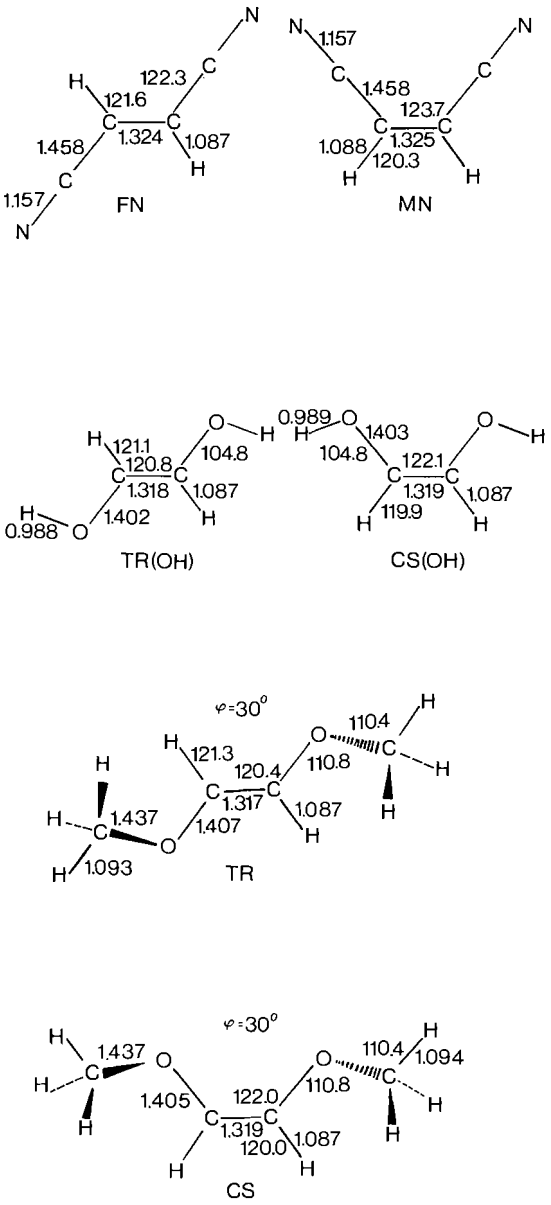

FIG. 1. STO-3G geometries of the olefins (bond lengths in Å, angles in degrees). ϕ refers to the $H_{Me}COC$ dihedral angles of TR (*trans*-1,2-dimethoxyethylene) and CS (*cis*-1,2-dimethoxyethylene).

geometries of the isolated donors and acceptors (Fig. 1) were fully optimized using the minimal STO-3G basis set.[5] The initial search for an optimum geometry used the models *trans* and *cis*-1,2-

[5]At the STO-3G level, the *trans* isomer of the olefins R—CH=CH—R is predicted to be more stable by 0.63 and 1.26 kcal/mol, whereas PCILO with third-order Epstein-Nesbet partitioning predicts the *cis* isomer to be more stable by 0.34 and 0.91 kcal/mol where R is CN and OCH_3, respectively.

TABLE 1. Calculated ΔH^{θ} (kcal mol^{-1}) of the charge-transfer complexes

Complex	Structure[a]	STO-3G	STO-3G[b]	3-21G[b]	4-31G[b]	PCILO[b]	($\bar{c}$ d = 2.5Å)
	3*a*	−0.15	−0.08	−0.49	—	−0.37	
MN–TR	**3***b*	—	−0.53	−1.14	—	−0.54	
	3*c*	−0.27	−0.73	−1.97	—	−13.70	(−5.90)
FN–TR	**2***a*	+0.13	+0.31	+0.06	—	−0.47	
	2*b*	−0.99	−1.06	−2.11	−2.53	−1.87	
	2*c*	−0.43	−0.71	−1.89	−1.94	−6.87	(−3.65)
MN–CS	**1***a*	+0.73	+0.78	—	+2.19	−0.31	
	1*b*	−1.02	−1.06	—	−2.79	−0.67	
	1*c*	−1.83	−2.03	−5.00	—	−14.24	(−7.90)
FN–CS	**4***a*	−0.13	−0.13	−0.49	—	−0.45	
	4*b*	−0.93	−1.00	−2.06	—	−1.72	
	4*c*	−1.31	−1.56	−3.16	—	−8.16	(−4.85)

[a]The structures are shown in Figs. 2–5.
[b]Using the model dihydroxymethylenes.

dihydroxyethylene as the donors. For computational convenience, the planar structures for both the dihydroxy and the dimethoxyethylene were used throughout although the optimized geometries of the latter (both *cis* and *trans*) have the methyl groups 30° off the molecular plane. The donor and the acceptor olefins were constrained to parallel planes in the search for the most stable geometry. The validity of this assumption is supported by both X-ray crystallographic analysis on $\pi-\pi^*$ ct complexes (2) and our calculations; that is, the complex becomes less stable when one of the planes is tilted in either direction. Calculations with larger split-valence basis sets, 3-21G and 4-31G, were performed for the dihydroxy complexes at selected geometries with an expanded version of the GAUSSIAN 76 program. Only one of the complexes with the 4-31G basis set was calculated due to limitations on high speed memory storage space.

The Cullen-Zerner version[6] which is a modified Daudey version (8) of the PCILO program was used in this work. Initial geometries for the complexes were taken from the STO-3G optimization results. The intermolecular distances were further optimized accordingly. The bond polarities of the subsystems and the complexes were optimized. The third order Epstein-Nesbet partitioning (EN) of the Hamiltonian has been used throughout. In some cases a comparison has also been made with the results obtained from the Møller-Plesset partitioning to third and fourth order.

Results

For the sake of brevity only selected results of the geometry searching are summarized in Table 1. A similar set of optimum structures is included for each complex, although it should be stressed that in all cases other structures less stable than the preferred ones were considered.

MN–CS Complex

According to the G76 calculation with the STO-3G basis set, the complex is not stable (repulsive) when the donor and acceptor are arranged as in structure **1***a* (Fig. 2), where the two central double bonds are parallel and the centres of the double bonds are centred over one another. The complex gains stability when the double bond of CS is rotated around the centre. A local minimum is obtained at $\phi = 150°$, structure **1***b* (ϕ is defined as the projected angle between the two double bonds with the zero taken to be the eclipsed geometry **1***a*). The optimum intermolecular distance (d) of **1***b* is $d = 3.8$ Å.

When the centre of CS is moved away from the centre over centre arrangement with $\phi = 180°$, ΔE becomes more negative (i.e. the complex becomes more stable). A minimum is found at $a = 2.2$ Å, structure **1***c* with ϕ being 180° and $d = 3.35$ Å where a is defined as the projected perpendicular distance between the two centres of the double bonds. The results for the dimethoxy complexes are essentially the same although the magnitude of ΔE is smaller. With the 3-21G calculations, ΔE becomes more negative in an analogous manner (Table 1).

The PCILO results are rather different as far as intermolecular distance and ΔE are concerned (Fig. 2). Nevertheless, the relative stabilities of **1***a*, **1***b* and **1***c* are consistent with the *ab initio* results.

FN–TR Complex

There are two possible arrangements for the centre over centre structures; the OH group can be placed either over the CN group, as in structure **2***a*, or on the other side of the double bond (Fig. 3). In either case, the G76 results for this complex are similar to the MN–CS complex in that the eclipsed

[6]J. M. Cullen and M. C. Zerner. Unpublished work.

Can. J. Chem. Downloaded from www.nrcresearchpress.com by 210.87.254.105 on 09/06/12
For personal use only.

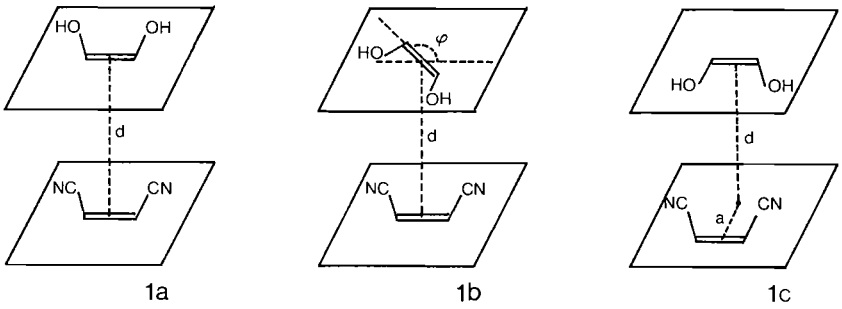

ΔH°_{calcd} (kcal mol^{-1})

G76(STO-3G)	+0.78 (d=3.8)	−1.06 (d=3.8, φ=150°)	−2.03 (d=3.35, a=2.2)
PCILO(EN)	−0.31 (d=2.8)	−0.67 (d=2.8, φ=150°)	−14.25 (d=2.0, a=2.2)

FIG. 2. The optimum structures of the MN–CS (OH) complex.

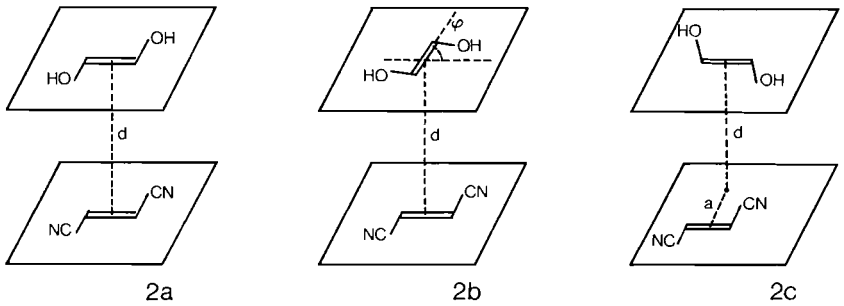

ΔH°_{calcd} (kcal mol^{-1})

G76(STO-3G)	+0.31 (d=3.8)	−1.06 (d=3.8, φ=45°)	−0.71 (d=3.35, a=2.2)
PCILO(EN)	−0.47 (d=2.8)	−1.87 (d=2.6, φ=60°)	−6.87 (d=2.0, a=2.2)

FIG. 3. The optimum structures of the FN–TR (OH) complex.

structure **2***a* is the least stable. A minimum can be obtained by rotating the double bond of TR about the centre with $\phi = 45°$ at $d = 3.8$ Å, structure **2***b*. Moving the centre of TR along the axes of the double bonds of both FN and TR (structure **2***b*) leads to a less negative ΔE. In contrast to the MN–CS complex, structure **2***c* is only a local minimum with $\phi = 0°$, $d = 3.35$,and $a = 2.2$ Å. The PCILO results, however, still favour structure **2***c* over structures **2***a* and **2***b*.

MN–TR Complex

As shown in Fig. 4, structure **3***a* is somewhat less stable than the other structures at the STO-3G level. Structure **3***b* represents a local minimum since moving the centre of TR of this structure off the centre along the direction of the double bonds of either TR or MN results in decreased stability. Structure **3***c*, which is similar to **1***c*, is the minimum. The PCILO results again support the relative stability of **3***a*, **3***b*, and **3***c*.

FN–CS Complex

As shown in Fig. 5, structure **4***a* is the least stable at the STO-3G level. Structure **4***b* corresponds to a local minimum while structure **4***c* is the minimum. The PCILO results again support the relative stability of the three structures of the FN–CS complex.

Discussion

Since the introduction of the classical theory for charge-transfer complex formation by Mulliken,

Can. J. Chem. Downloaded from www.nrcresearchpress.com by 210.87.254.105 on 09/06/12
For personal use only.

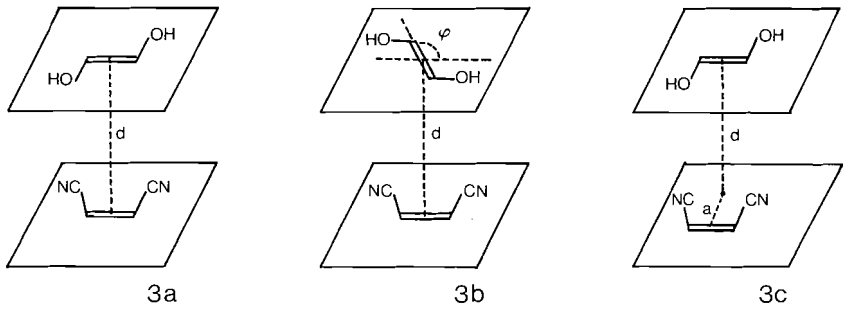

3a 3b 3c

ΔH°_{calcd} (kcal mol^{-1})

G76 (STO-3G)	-0.08 (d=3.8)	-0.53 (d=3.8, φ=113°)	-0.73 (d=3.35, a=2.2)
PCILO (EN)	-0.37 (d=2.8)	-0.54 (d=2.8, φ=150°)	-13.70 (d=2.0, a=2.2)

FIG. 4. The optimum structures of the MN–TR (OH) complex.

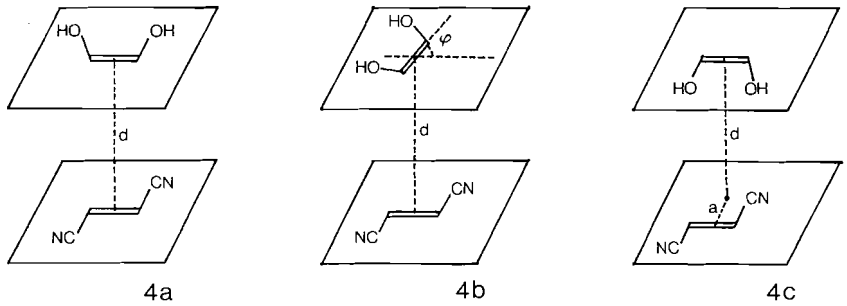

4a 4b 4c

ΔH°_{calcd} (kcal mol^{-1})

G76 (STO-3G)	-0.13 (d=3.8)	-1.00 (d=3.8, φ=52.5°)	-1.56 (d=3.35, a=2.2)
PCILO (EN)	-0.45 (d=2.8)	-1.72 (d=2.6, φ=30°)	-8.16 (d=2.0, a=2.2)

FIG. 5. The optimum structures of the FN–CS (OH) complex.

using a two-determinant charge-transfer resonance formalism (1*a*), several approaches have been developed to estimate the heat of formation (ΔH^{θ}) and the geometries of ct complexes (6, 9). Among these theories, there are two which have lead to considerable success: (*1*) the electrostatic-perturbation theory developed by Murrell *et al.* (9*d*) accounting for intermolecular forces, in the region of small overlap, by an extension of the theory for long range intermolecular interactions, and (*2*) the supermolecule approach, first introduced by Chesnut and Moseley (6), taking the whole complex as one molecular moiety for which general molecular orbital theories are applicable.

Using the electrostatic-perturbation approach, Lippert *et al.* (10) were able to calculate ΔH^{θ}'s for a number of ct complexes within close agreement with the observed values. Their calculations also predict the existence of rotational isomers for benzene–tetracyanoethylene (TCNE) and *p*-xylene–TCNE complexes, however, the relative stability to the two isomeric complexes of the latter was the opposite to that observed by Voigt and co-workers (11).

With the availability of large-scale computational facilities and advances in computational MO methods, the supermolecule approach has become significantly more popular and convenient for studying the properties of ct complexes. MO studies employing Extended Huckel Theory (EHT) (6, 12)

Can. J. Chem. Downloaded from www.nrcresearchpress.com by 210.87.254.105 on 09/06/12
For personal use only.

Can. J. Chem. Downloaded from www.nrcresearchpress.com by 210.87.254.105 on 09/06/12
For personal use only.

and semiempirical SCF methods (Pariser-Parr-Pople (13), CNDO and INDO (14)) demonstrated the potential of the supermolecule approach for predicting the most stable geometry of $\pi-\pi^*$ ct complexes. However, the quantitative values of ΔH^0's and interplane distances are generally poor. EHT calculations on some complexes failed to find any stable arrangement (15). The CNDO/2 and INDO methods overestimate ΔE while the minima are generally at too small a separation between the complex components (14). On the other hand, the MINDO/2 calculations have failed to find energy minima for some $\pi-\pi^*$ ct complexes (16).

There are three factors which cause the semiempirical methods to overestimate the binding energy: (*1*) the neglect of basis set superposition error (BSSE) (17), (*2*) underestimation of the electronic repulsion due to the neglect of differential overlap (14*b*), and (*3*) omission of geometry optimization. The first two factors are probably more important. The BSSE is more important in calculations using small basis sets. Improvements can be made by (*i*) increasing the basis set to the Hartree-Fock limit, or (*ii*) the introduction of configuration interaction (CI) with a reasonably large basis set, or (*iii*) the use of the counterpoise method (18). The PCILO method is therefore better, for calculating ΔE, than any of the other semiempirical methods since it does include CI over the localized molecular orbitals (19). The computing time for PCILO is almost the same as CNDO/2 even though all the single and double excited configurations are included. There are limitations to this method, however, since it starts with the minimal basis set and uses the CNDO approximations for evaluating the integrals. Therefore, uncertainties due to the BSSE and the underestimated electronic repulsion still exist. Generally speaking, PCILO normally gives good ΔE although there are exceptional cases (19). The intercomponent distance is also too short at minima as in the CNDO cases.

The *ab initio* MO method is the best choice although it requires substantially larger computing facilities and longer computational times. The improvement of the *ab initio* method is partly due to a better description of the electronic repulsion and partly due to smaller BSSE upon employing larger basis sets. In order to estimate the BSSE in our systems at the STO-3G level (see refs. 18 and 20 for relevant discussions) we have applied the counterpoise method (18). Our calculations suggest that the BSSE for the MN–CS complex is only -0.11 kcal mol^{-1} for structures **1***a* and **1***b*, and zero for **1***c*. In practice, the ΔE's calculated by use of the smaller basis sets are generally too small (21). The use of a larger basis set would improve ΔE relative to the observed value, but the theoretical value would still be too low since the single determinant SCF procedure does not account for the dispersion energy due to electron correlation (21*b*). A few procedures have recently been established to retrieve the dispersion energy (18*c*, 21*b*, 22), although this has not been included in the present study.

As shown in Table 1 and Figs. 2 to 5, the *ab initio* interplane distance for structures *a* and *b* is 3.8 Å which is somewhat longer than that usually observed from X-ray crystallographic analysis (2) of complexes in the solid state (3.1 to 3.6 Å). This result is consistent with the only two $\pi-\pi^*$ ct complexes (formaldehyde–ethylene and carbonyl cyanide – benzene complexes) studied previously by *ab initio* MO methods (18*c*, 21). The eclipsed geometry is relatively unstable. The instability is probably due to the unsubstituted ethylene–ethylene interaction which is repulsive according to the *ab initio* and valence-bond calculations on the ethylene dimer (20). Studies on the benzene–benzene system also support this conclusion. For instance, PCILO calculations (19*b*, *d*) suggest that the eclipsed benzene dimer is repulsive. This conclusion is easily visualized in terms of the Orientation and Overlap Principle (HOMO–LUMO interaction) introduced by Mulliken (9*a*). Moreover, CNDO/INDO calculations on the *p*-benzoquinone–aniline (toluene) complex (14*b*) favour the staggered form of both the benzenes and the substituents. The importance of steric effects and hydrogen bonding is, however, uncertain. The stability of the **1–4***c* and **2***b* structures may be explained in terms of electrostatic attraction between the oxygen atom and the cyanocarbon, at the same time avoiding overlap of the ethylene moieties. This explanation gains support from the study of the intramolecular ct complex (fixed geometries) of paracyclophanes with two e-donating substituents on one of the benzene rings and two e-withdrawing substituents on the other (23). The elipsed isomer is more stabilized by ct interaction than the anti isomer due to the closer proximity of the e-donating and e-withdrawing substituents.

The ΔE's calculated with the 4-31G basis are generally greater than those obtained at the STO-3G level. This tendency is probably due to an overestimation of charge effects with the 4-31G basis (21*a*, *b*, 24). The addition of d functions would be expected to move ΔE downward from the 4-31G values towards the STO-3G results (21*c*). However, this would be time consuming even with the decreased size of the model dihydroxyethylene complexes. Table 1 reveals that the split-valence 3-21G basis recently introduced by Binkley *et al.*

Can. J. Chem. Downloaded from www.nrcresearchpress.com by 210.87.254.105 on 09/06/12
For personal use only.

(25) would be a better choice to calculate the SCF ΔE. The computational time with the 3-21G basis is about 15% less than with the 4-31G basis. According to Morokuma's calculation on the formaldehyde–ethylene system (21*b*), the dispersion energy would be about the same magnitude as the SCF ΔE's. Therefore, an estimate for the gas phase ΔH^{θ}'s can be made by doubling the ΔE's calculated at 3-21G level (i.e., ΔH^{θ}_{calc} would be -3.9, -4.2, -10.0, and -6.4 kcal mol^{-1} for the MN–TR(OH), FN–TR(OH), MN–CS(OH), and FN–CS(OH) complexes, respectively). The magnitude of the ΔH^{θ}'s for the corresponding dimethoxy complexes will be slightly smaller (see Table 1 for the comparison of the ΔH^{θ}'s at the STO-3G level). The small ΔH^{θ}'s for the dimethoxy complexes are probably due to the steric effect of the methyl groups.

Another way to estimate the ΔH^{θ}'s is to use an empirical relation between the ΔH^{θ}'s and the difference in the oxidation potential of the donor and the reduction potential of the acceptor. A straight line can be obtained by plotting the ΔH^{θ}'s (gas) of a series of π–π^* complexes between tetracyanoethylene (TCNE) and methyl substituted benzenes (26) versus ($E^{ox}_{1/2}$(D) $-$ $E^{red}_{1/2}$(A)). The reduction potential of TCNE is -0.06 V vs. Ag/AgNO$_3$ (0.1 *M*) (27). The oxidation potentials of the methyl substituted benzenes have been summarized elsewhere (28). The oxidation potentials of *trans* and *cis*-1,2-dimethoxyethylene are 0.72 and 0.70 V[7] respectively. The reduction potentials of FN and MN are -1.63 V (3). From this relation, the ΔH^{θ}'s (gas) for all four of our complexes are predicted to be about 5 kcal mol^{-1} (Fig. 6).

The STO-3G minimum geometry is usually a good estimate for ct complexes (21). In our cases, assignment of the most stable geometry may be sensitive to the corresponding dispersion energies. Using a point charge model, structures **1**–**4***c* would possess smaller dispersion than **1**–**4***a*,*b* since the intercomponent distances for structure **1**–**4***c* are longer than for the others. Nevertheless, the PCILO results (containing a certain amount of dispersion energy) support the *ab initio* SCF results.

The PCILO energies calculated through to third order with Epstein-Nesbet partitioning are reasonably good for structures **1**–**4***a*,*b*. With structures **1**–**4***c* the equilibrium interplane distances appear to be too short (2.0 Å). Therefore, the ΔE's are probably overestimated. It has been suggested that a better estimate for ΔE would be at 2.5 Å (19*c*) (Table 1). The geometries from PCILO are comparable to those of the *ab initio* results although the

[7]Estimated from a relationship between IP and $E^{ox}_{1/2}$ ($E^{ox}_{1/2}$ = 0.827 IP $-$ 5.40 V) (see ref. 32).

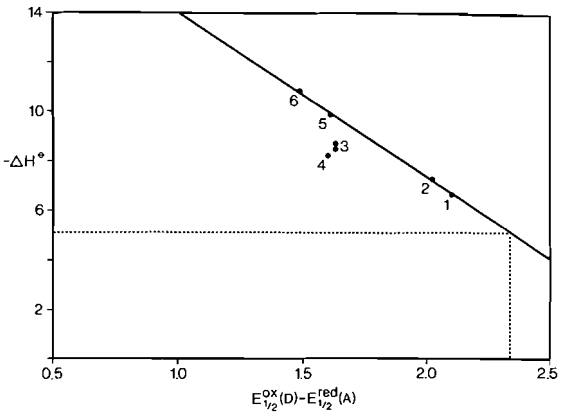

FIG. 6. The relation between ΔH^{θ} (gas)$_{expt}$ (in kcal/mol) and the redox potentials (in volts) of the acceptor (TCNE) and donor (methyl substituted benzenes). The donors represented are: (1) benzene; (2) toluene; (3) *o*-xylene; (4) *p*-xylene; (5) mesitylene; (6) durene.

TABLE 2. The calculated ΔH^{θ} (kcal mol^{-1}) of the MN–CS complex from the PCILO method[a]

Structure	EN (3°) $-\Delta H^{\theta}$ (*d*, Å)	MP (3°) $-\Delta H^{\theta}$ (*d*, Å)	MP (4°) $-\Delta H^{\theta}$ (*d*, Å)
1*a*	0.31 (2.8)	4.16 (2.4)	9.89 (2.2)
1*b*	0.67 (2.8)	3.66 (2.4)	7.14 (2.2)
1*c*[b]	14.25 (2.0)	28.11 (2.0)	43.11 (1.8)

[a]The notation is as follows: EN (3°), MP (3°), and MP (4°) refer to third-order Epstein-Nesbet partitioning, third-order Møller-Plesset, and fourth-order Møller-Plesset partitioning, respectively.
[b]*a* = 2.2 Å.

ΔE's appear to be overestimated. There are two situations where significant differences are found between the two methods: (*1*) ΔE for the MN–TR(OH) complex is too high, and (*2*) structure **1**–**4***c* seems significantly more stable than the other structures. These differences are probably due to the fact that PCILO underestimates the electronic repulsion to a lesser extent. Furthermore the geometries have not been optimized by the PCILO method in this work.

The ΔE's calculated through to 3rd and 4th order, especially to 4th order with Møller-Plesset partitioning, are generally larger (probably overestimated) than those of the 3rd order Epstein-Nesbet partitioning (Table 2). Therefore, the latter should be preferred for evaluating intermolecular forces.

Conclusion

The *ab initio* and PCILO MO calculations carried out on four ct complexes (FN–CS, FN–TR, MN–CS, MN–TR) indicate that the eclipsed geometries are relatively unstable. Since we feel that the PCILO method overestimates ΔE due to the use of the CNDO approximations, we have more confidence in the results from the *ab initio* calcula-

tions. The order of stability of the four complexes according to the *ab initio* calculations is MN–CS > FN–CS > FN–TR > MN–TR. Comparison of these predictions with the experimental results is reported in the following paper in this journal (29). And finally we wish to emphasize that this paper reports the first *ab initio* study of π–π^* ct complexes for which experimental heats of formation are available.

Acknowledgments

We are grateful for the assistance of Mr. K. W. Ling in expanding the G76 program to handle up to 127 basis functions. We also want to thank Dr. M. C. Zerner of the University of Guelph for providing us with an unpublished version of the PCILO program. The financial support of the Natural Sciences and Engineering Research Council of Canada in the form of a Postdoctoral Fellowship to P.C.W. and an Operating Grant to R.J.B. is gratefully acknowledged.

1. (*a*) R. S. MULLIKEN. J. Am. Chem. Soc. **74**, 811 (1952); (*b*) R. S. MULLIKEN and W. B. PERSON. Molecular complexes. Wiley, New York, NY. 1969; (*c*) R. FOSTER. Organic charge-transfer complexes. Academic Press, New York, NY. 1969.
2. C. K. PROUT and B. KAMENAR. *In* Molecular complexes. Vol. 1. *Edited by* R. Foster. Crane, Russak & Co., Inc., New York, NY. 1973.
3. (*a*) D. R. ARNOLD and P. C. WONG. J. Am. Chem. Soc. **101**, 1894 (1979); (*b*) P. C. WONG and D. R. ARNOLD. Can. J. Chem. **58**, 918 (1980); (*c*) Can. J. Chem. **57**, 1037 (1979).
4. C.-G. LEE. Ph.D. thesis, Columbia University, New York. 1973.
5. (*a*) S. J. DINER, J. P. MALRIEU, and P. CLAVERIE. Theor. Chim. Acta, **13**, 1 (1969); (*b*) Theor. Chim. Acta, **13**, 18 (1969); (*c*) S. DINER, J. P. MALRIEU, F. JORDAN, and M. GILBERT. Theor. Chim. Acta, **15**, 100 (1969).
6. D. B. CHESNUT and R. W. MOSELEY. Theor. Chim. Acta, **13**, 230 (1969).
7. J. S. BINKLEY, R. A. WHITEHEAD, P. C. HARIHARAN, R. SEEGER, and J. A. POPLE. QCPE, **11**, 368 (1978).
8. P. CLAVERIE, J. P. DAUDEY, S. DINER, CL. GIESSNER-PRETTRE, M. GILBERT, J. LANGLET, J. P. MALRIEU, and U. PINCELLI. QCPE, **11**, 220 (1979).
9. (*a*) R. S. MULLIKEN. Recl. Trav. Chim. Pays-Bas, **75**, 845 (1956); (*b*) B. MAYOH and C. K. PROUT. J. Chem. Soc. Faraday Trans. II, 1072 (1972); (*c*) W. H. HERNDON and J. FEUER. J. Am. Chem. Soc. **90**, 5914 (1968); (*d*) J. N. MURRELL, M. RANDIC, and D. R. WILLAMS. Proc. R. Soc. Ser. A, **284**, 566 (1965); (*e*) R. L. FURRY, JR. J. Phys. Chem. **65**, 1927 (1965); (*f*) H. KURODA, I. IKEMOTO, and H. AKAMATU. Bull. Chem. Soc. Jpn. **39**, 1842 (1966).
10. J. L. LIPPERT, M. W. HANNA, and P. J. TROTTER. J. Am. Chem. Soc. **91**, 4035 (1969).
11. M. J. MOBLEY, K. E. RIECKOFF, and E.-M. VOIGT. J. Phys. Chem. **82**, 2005 (1978).
12. (*a*) J. P. LOWE. J. Am. Chem. Soc. **102**, 1262 (1980); (*b*) D. F. EATON and D. A. PENSAK. J. Am. Chem. Soc. **100**, 7428 (1978).
13. Z. YOSHIDA and T. KOBAYASHI. Theor. Chem. Acta, **23**, 67 (1971).
14. (*a*) D. B. CHESNUT and P. E. S. WORMER. Theor. Chim. Acta, **20**, 250 (1971); (*b*) O. MO, M. YANEZ, and J. I. FERNANDEZ ALSONO. J. Phys. Chem. **79**, 137 (1975); (*c*) B. D. SILVERMAN. J. Chem. Phys. **70**, 1614 (1979).
15. (*a*) P. BIRNER and H.-J. HOFFMANN. Z. Chem. **13**, 186 (1973); (*b*) S. WORD. Acta Chem. Scand. **20**, 2377 (1966); (*c*) R. ARNAND, D. FARAMOND-BAUD, and M. GELUS. Theor. Chim. Acta, **31**, 335 (1973).
16. T. OHTA, T. FUJIKAWA, and H. KURODA. Bull. Chem. Soc. Jpn. **47**, 2115 (1974).
17. (*a*) E. CLEMENTI. J. Chem. Phys. **46**, 3851 (1967); (*b*) N. R. KESTNER. J. Chem. Phys. **48**, 252 (1968).
18. (*a*) S. F. BOYS and F. BERNARDI. Mol. Phys. **19**, 553 (1970); (*b*) M. BULSKI and G. CHALASINSKI. Theor. Chim. Acta, **44**, 399 (1977); (*c*) W. KOLOS. Theor. Chim. Acta, **51**, 219 (1979).
19. (*a*) R. ARNAUD, D. FARAMOND-BAUD, and M. GELUS. Theor. Chim. Acta, **31**, 335 (1973); (*b*) J. M. CULLEN. M.Sc. thesis, University of Guelph, Guelph, Ont. 1976; (*c*) R. LOCHMAN and H.-J. HOFFMANN. Int. J. Quant. Chem. **11**, 427 (1977); (*d*) R. LOCHMAN. Int. J. Quant. Chem. **12**, 795 (1977); (*e*) Int. J. Quant. Chem. **12**, 841 (1977); (*f*) R. LOCHMAN and P. HOBZA. Int. J. Quant. Chem. **15**, 73 (1979).
20. P. E. S.WORMER and A. VAN DER AVOIRD. J. Chem. Phys. **62**, 3326 (1975).
21. (*a*) W. A. LATHAN and K. MOROKUMA. J. Am. Chem. Soc. **97**, 3615 (1975); (*b*) W. A. LATHAN, G. R. PACK, and K. MOROKUMA. J. Am. Chem. Soc. **97**, 6624 (1975); (*c*) H. UMEYAMA, K. MOROKUMA, and S. YAMABE. J. Am. Chem. Soc. **99**, 330 (1977); (*d*) R. R. LUCCHESE and H. F. SCHAEFER III. J. Am. Chem. Soc. **97**, 7205 (1975); (*e*) R. R. LUCCHESE, K. HABER, and H. F. SCHAEFER. III. J. Am. Chem. Soc. **98**, 7617 (1976); (*f*) P. KOLLMAN. J. Am. Chem. Soc. **99**, 4875 (1977).
22. F. MULDER, M. V. HEMERT, P. E. S. WORMER, and A. VAN DER AVOIRD. Theor. Chim. Acta, **46**, 39 (1977).
23. H. VOGLER, G. EGE, and H. A. STAAB. Tetrahedron, 2441 (1975).
24. P. A. KOLLMAN and L. C. ALLEN. Chem. Rev. **72**, 283 (1972).
25. J. S. BINKLEY, J. A. POPLE, and W. H. HEHRE. J. Am. Chem. Soc. **102**, 940 (1980).
26. (*a*) M. KROLL. J. Am. Chem. Soc. **90**, 1097 (1968); (*b*) I. HANAZAKI. J. Phys. Chem. **76**, 1982 (1972).
27. M. E. PEOVER. Trans. Faraday Soc. **58**, 2370 (1962).
28. D. R. ARNOLD and P. C. WONG. Can. J. Chem. **57**, 2098 (1979).
29. P. C. WONG and D. R. ARNOLD. Can. J. Chem. **59**, 982 (1981).
30. J. E. KUDER, H. W. GIBSON, and D. WYCHICK. J. Org. Chem. **40**, 875 (1975).
31. D. R. ARNOLD and P. C. WONG. Can. J. Chem. **57**, 2098 (1979); H. W. LAANHOVEN and R. J. F. NIVAROL. Recl. Trav. Chim. Pays-Bas, **86**, 1478 (1965).
32. W. C. NEIKAM, G. R. DIMELER, and M. M. DESMOND. J. Electrochem. Soc. **111**, 1190 (1964).

Can. J. Chem. Downloaded from www.nrcresearchpress.com by 210.87.254.105 on 09/06/12
For personal use only.

Photochemical reactions of charge-transfer complexes. IV. The orientation effects of charge-transfer complexes: theory and experiment

PO CHEONG WONG[1] AND DONALD R. ARNOLD[2]

Department of Chemistry, Dalhousie University, Halifax, N.S., Canada B3H 4J3

Received September 9, 1980

PO CHEONG WONG and DONALD R. ARNOLD. Can. J. Chem. **59**, 982 (1981).

In paper number III of this series (2) *ab initio* and PCILO molecular orbital calculations for the four $\pi-\pi^*$ charge-transfer (ct) complexes formed between maleonitrile (MN) and fumaronitrile (FN), and *cis* (CS) and *trans*-1,2-dimethoxyethylene (TR) were reported. This paper reports the ct transition absorption characteristics and association constants of these complexes as a function of temperature. From this data the heats of formation of the complexes are determined and these experimental results are then compared with the theoretical values; good agreement is obtained. The order of complex stability ($-\Delta H^\theta$ (kcal mol)) measured in chloroform solution is: MN–TR (0.55) < FN–TR (0.65) < MN–CS (0.78) < FN–CS (1.25).

We reach the conclusion that, for these complexes, orientation effects of the substituents are quite small in magnitude and that the dominant factor influencing complex stability follows the redox potential difference. The structures of the complexes are discussed in view of these results.

PO CHEONG WONG et DONALD R. ARNOLD. Can. J. Chem. **59**, 982 (1981).

Dans la troisième publication de cette série (2) on a rapporté les calculs d'orbitales moléculaires *ab initio* et PCILO des quatre complexes $\pi-\pi^*$ de transfert de charge (tc) entre la maléonitrile (MN), la fumaronitrile (FM) et les diméthoxy-1,2 éthylène *cis* (CS) et *trans* (TR). Dans cette publication on rapporte les caractéristiques de l'absorption de transition tc et les constantes d'association de ces complexes en fonction de la température. On a déterminé, à partir de ces données, les chaleurs de formation des complexes et on a comparé ces résultats expérimentaux aux valeurs théoriques; on a obtenu un parfait accord. L'ordre de stabilité du complexe ($-\Delta H^\theta$ (kcal mol)) mesuré dans une solution de chloroforme est le suivant: MN–TR (0,55) < FN–TR (0,65) < MN–CS (0,78) < FN–CS (1,25).

Nous avons conclu dans le cas de ces complexes que les effets d'orientation des substituants sont négligeables et que le facteur principal influençant la stabilité du complexe suit la différence de potentiel redox. On discute de la structure de ces complexes à la lumière de ces résultats.

[Traduit par le journal]

Introduction

We have recently reported a potentially useful photochromic system based upon the irradiation of charge-transfer (ct) complexes of olefins in solution (1). For example, the ct absorption band of the *trans*-stilbene – fumaronitrile (*t*-ST–FN) complex extends out to longer wavelengths than the ct absorption band of the *cis*-stilbene – fumaronitrile (*c*-ST–FN) complex. Irradiation of the *t*-ST–FN complex results in up to an 86% enrichment in *cis*-stilbene (1*a*). The position and absorption intensity of the ct absorption band is related to the strength of the complex. For structurally similar compounds, Mulliken has demonstrated that the strength of the complex depends mainly on the ionization potential (or oxidation potential $E_{1/2}^{ox}$ (D)) of the donor and electron affinity (or reduction potential $E_{1/2}^{red}$ (A)) of the acceptor. Therefore, the differences in the ct equilibrium constants (K) between the *t*-ST–FN complex and the *c*-ST–FN complex can be explained in terms of the difference between $E_{1/2}^{ox}$ (D) of *c* and *t*-ST. However, the contribution due to the differences in the geometries of the donor may also be important. For example, if the complex favours a geometry where the two central double bonds are parallel and the substituents are projected over one another (eclipsed form), then one might expect the *t*-ST–FN complex to have a higher binding energy than the *c*-ST–FN complex. Evidence supporting this hypothesis is obtained from the difference in the equilibrium constants of the *t*-ST–FN complex and the *t*-ST–MN complex (K being 0.17 and 0.10 M^{-1}, respectively) (1*b*). Since FN and MN have essentially the same reduction potentials (1*b*), the larger equilibrium constant for the *t*-FN complex may be due to orientation effects which arise from a favourable alignment of the olefin substituents.

Employing FN and MN as a probe for orientation effects in ct complexes, we have previously examined a series of dimethoxynaphthalene (DMN) donors where the methoxy substituents would presumably align better with either FN or MN (1*b*). For example, if the most favourable geometry is eclipsed, then MN would be expected to form stronger ct complexes with 2,3- and 1,4-DMN, while FN would form a stronger complex with 1,5-DMN. However, the observed association

[1]Current address: Division of Chemistry, National Research Council of Canada, 100 Sussex Drive, Ottawa, Ont., Canada K1A 0R6.

[2]Author to whom correspondence should be addressed.

0008-4042/81/060982-08$01.00/0

©1981 National Research Council of Canada/Conseil national de recherches du Canada

Can. J. Chem. Downloaded from www.nrcresearchpress.com by 210.87.254.5 on 09/06/12
For personal use only.

Can. J. Chem. Downloaded from www.nrcresearchpress.com by 210.87.254.5 on 09/06/12
For personal use only.

constants and the heats of formation of these ct complexes are not consistent with this hypothesis. We found that maleonitrile complexes more strongly with 1,4- and 1,5-DMN than FN but not with 2,3-DMN. These results were interpreted in terms of there being more than one favourable geometry for the small π-acceptors to complex with the relatively larger π-donors. The observed stability of these complexes would then be a composite for all contributing geometries.

In this account, we examine orientation effects more closely by comparing the experimental K and the ΔH^0 of the ct complexes formed between FN and MN with three smaller π-donors i.e., 1,3-benzodioxole, and *trans*- and *cis*-1,2-dimethoxyethylene (TR and CS). It is important to emphasize that the 1,2-dicyanoethylene – 1,2-dimethoxyethylene system is one of the best systems for examining these orientation effects since (*i*) the sizes of the π-donors and the π-acceptors are small and comparable, (*ii*) the *trans*- and *cis*-donors have very similar oxidation potentials (0.72 and 0.70 V, respectively), and (*iii*) the *trans*- and *cis*-acceptors have essentially identical reduction potentials (−1.63 V) (1*b*).

Another interesting acceptor, bicyclo[2.2.2]-oct-2-ene-2,3-dinitrile, which we naively predicted would complex more strongly with CS than TR as the result of steric hindrance, was also examined.

Theoretical calculations of the optimum geometry and ΔH^0 for the four 1,2-dicyanoethylene – 1,2-dimethoxyethylene complexes have been carried out using two different molecular orbital (MO) methods (*ab initio* and PCILO). Details of the calculations are reported in a separate paper (2). The results from both the experimental and the theoretical work will be discussed here.

We have also investigated the photochemistry of the 1,2-dicyanoethylene – 1,2-dimethoxyethylene complexes. A preliminary account of this study will also be given.

Results

The ultraviolet–visible spectrophotometric (uv–vis) method (3) was used to measure the association constant (K) for the objective ct complexes. Determination of the K and ct extinction coefficient (ε_λ at wavelength λ) was performed using two methods, the Foster–Hammick–Wardley (F–H–W) method (4) and the Seal–Mukherjee–Mukherjee (S–M–M) method (5). There was good agreement between the two methods in all cases.

In the F–H–W method, a plot of $OD/[A]_0$ versus OD gives a straight line, of which the slope and the y-intercept correspond to $-K$ and $K.\varepsilon_\lambda\ [D]_0$ respectively; OD is the optical density (absorbance), and $[D]_0$ and $[A]_0$ refer to the total concentration of complexed and free donor and acceptor, respectively. A typical F–H–W plot is shown in Fig. 1.

The S–M–M method is an alternative method of solving the Rose–Drago equation (6). Taking $x = [D]_0 + [A]_0$, $y = [D]_0[A]_0/OD$ and $z = OD$, the plot of z versus x yields a straight line with the y-intercept = n and the slope = m. The plot of y versus x yields another straight line with the y-intercept = $M - M^2m$ and the slope = $L - M^2 - n$, where L and M are defined as $1/\varepsilon_\lambda$ and $1/(K.\varepsilon_\lambda)$. Figures 2 and 3 are typical plots of z vs. x and y vs. x.

For the 1,2-dicyanoethylene – 1,3-benzodioxole

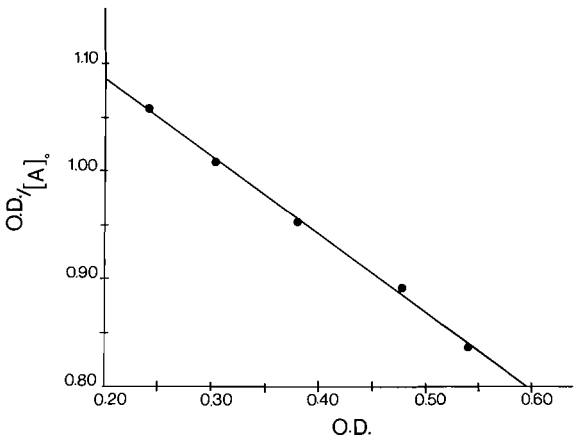

FIG. 1. F–H–W plot for the MN–CS complex in $CHCl_3$ at 2.2°C (λ = 315 nm).

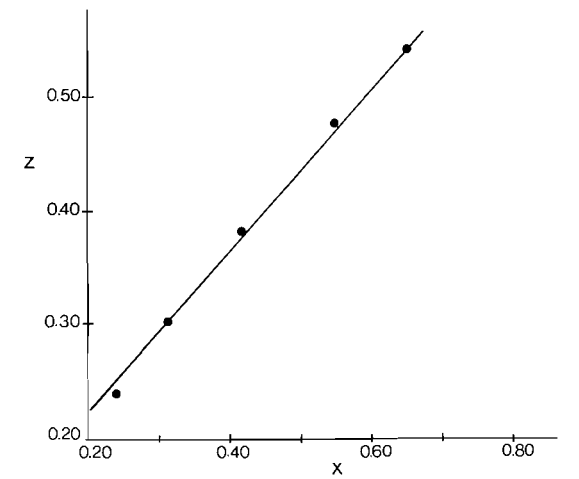

FIG. 2. S–M–M plot of z vs. x for the MN–CS complex in $CHCl_3$ at 2.2°C (λ = 315 nm).

Can. J. Chem. Downloaded from www.nrcresearchpress.com by 210.87.254.5 on 09/06/12
For personal use only.

TABLE 1. Spectroscopic constants for charge-transfer complexes in chloroform solution

Complex	ε_{315}[a]	K (M^{-1})[b] 2.2°C	17.2°C	32.8°C	47.8°C	$-\Delta H^{\theta}$[c] (kcal mol^{-1})	$-\Delta S^{\theta}$[d] (eu)
MN–TR	166	0.51	0.49	0.46	0.45	0.55	3.3
FN–TR	180	0.35	0.32	0.32	0.29	0.65	4.6
MN–CS	146	0.71	0.67	0.63	0.58	0.78	3.5
FN–CS	189	0.58	0.51	0.45	0.42	1.25	5.7

[a]Average values essentially independent of temperature.
[b]±0.03 M^{-1}.
[c]±0.09 kcal mol^{-1}.
[d]±0.4 eu.

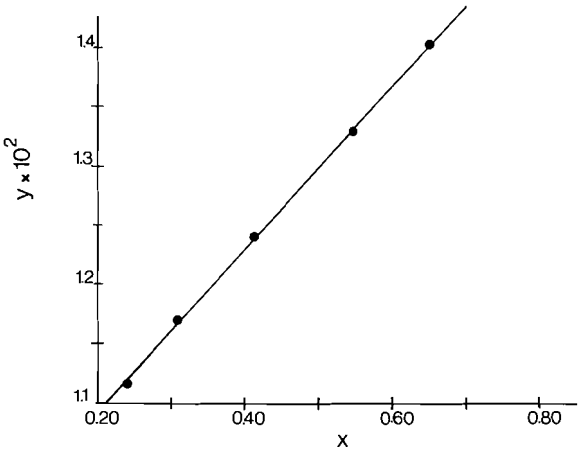

FIG. 3. S–M–M plot of y vs. x for the MN–CS complex in $CHCl_3$ at 2.2°C (λ = 315 nm).

(1,3-BDO) system, the K for the FN and MN complexes are identical (0.15 M^{-1}) while ε_{325} for the FN complex is slightly larger (500 and 455 for the FN and MN complex, respectively).

The experimental results for the 1,2-dicyanoethylene – 1,2-dimethoxyethylene system are listed in Table 1. It is well known that accurate separation of K and ε_{λ} from the spectrophotometric measurement is very difficult. Since ε_{λ} is nearly temperature-independent, evaluation of the ΔH^{θ} and ΔS^{θ} is possible from plots of log ($K.\varepsilon_{\lambda}$) versus $1/T$ (3). These results are shown in Fig. 4. The experimental heats of formation (ΔH^{θ}) are listed in Table 1 (the larger negative values correspond to more stable complexes). To our surprise, the most stable complex is the FN–CS complex while the least stable complex is the MN–TR complex.

Bicyclo[2.2.2]-oct-2-ene-2,3-dinitrile (BODN) forms very weak complexes with both TR and CS. The values of K and ε_{360} for the BODN complex are 0.06 M^{-1} and 50, respectively.

Irradiation of the MN–CS complex in acetonitrile solution leads to isomerization of both olefins. An accurate photostationary state composition was not obtained due to relatively rapid, competing consumption of the olefins through polymerization.

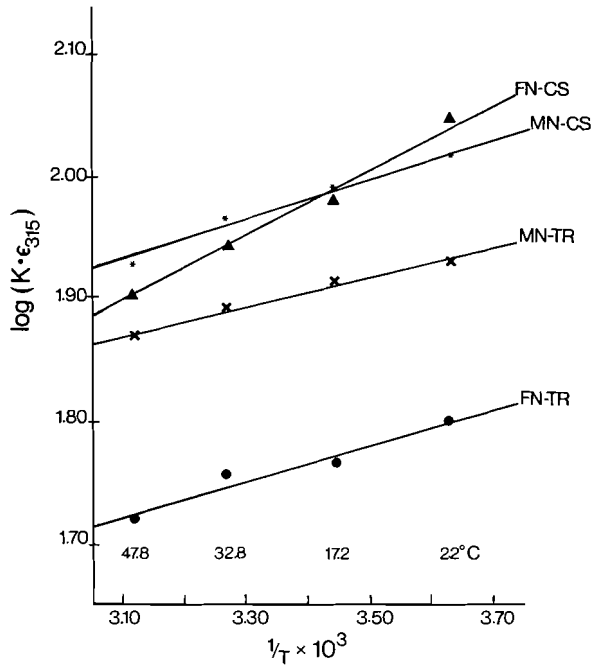

FIG. 4. Van't Hoff plots for the ct complexes.

Our preliminary results from the triplet-sensitized isomerization of *cis*- and *trans*-1,2-dimethoxyethylene indicate that the triplet energies for these two olefins are quite low. In fact, triplet sensitized isomerization proceeds at a reasonable rate even when acridine (E_T = 45.3 kcal mol^{-1}) is used as the sensitizer.

Molecular Orbital Calculations

Details of the molecular orbital calculations are reported elsewhere (2). A brief summary will be given here since these results are so important to the discussion that follows. Two computational methods (*ab initio* and PCILO (7)) were employed to calculate the heats of formation (ΔH^{θ}) for the 1,2-dicyanoethylene – 1,2-dimethoxyethylene ct complexes using the supermolecule approximation (8). The donor and the acceptor molecules are situated in parallel planes. Assuming that no

TABLE 2. Calculated $-\Delta H^\theta$'s of the charge-transfer complexes at optimum geometries

Complex	G76 (kcal mol^{-1}) STO-3G	STO-3G[a]	3-21G[a]	4-31G[a]	PCILO(NE)[a] (kcal mol^{-1})
MN–TR	0.27	0.73	1.97	—	13.70
FN–TR	0.99[b]	1.06[b]	2.11[b]	2.53[b]	6.87
MN–CS	1.83	2.03	5.00	—	14.25
FN–CS	1.31	1.56	3.16	—	8.16

[a]Using the models *cis*- and *trans*-dihydroxyethylene.
[b]The optimum geometries are the rotated geometries while all others are the slipped geometries (see text).

structural change in the components accompanies complex formation, the optimized geometry for each complex is obtained starting from the optimized geometries (STO-3G) of the individual components. The standard single determinant *ab initio* calculations were performed using the GAUSSIAN 76 program (G76) (9) with the spin-restricted Hartree–Fock (RHF) procedure. The initial search for the optimum geometries of ct complexes used the models *trans*- and *cis*-1,2-dihydroxyethylene as the donors. Calculations using the split valence basis sets, 3-21G (10) and 4-31G, were also performed for the model complexes at selected geometries. The calculated ΔH^θ of the ct complexes at optimum geometries[3] are listed in Table 2. At the STO-3G level, the calculated ΔH^θ values for the dimethoxy complexes are slightly smaller than for the corresponding dihydroxy complexes. This was attributed to steric effects due to the presence of the methyl groups.

The interplane distances (d's) calculated from G-76 at STO-3G level are reasonable. The optimum d's are 3.8 Å for the eclipsed and the rotated geometries, and 3.35 Å for the slipped geometries. These are quite close to the observed d's from X-ray crystallographic analysis for solid state ct complexes which are normally between 3.2 to 3.6 Å (11). The PCILO optimum d's, on the other hand, are too short (with the optimum d's equal to 2.6 Å for the eclipsed and rotated geometries and 2.0 Å for the slipped geometries) for the systems studied.

Discussion

Listed in Table 3 is a summary of the experimental spectroscopic constants for the series of ct complexes we have so far examined. The magnitude of the ct equilibrium constants is more or less inversely related to the donor oxidation potential. Donors having lower values of $E^{ox}_{1/2}$ generally form stronger ct complexes. There is no obvious way to predict which 1,2-dicyanoethylene isomer will form a stronger ct complex with a given donor. The relationships between K, ε_λ, ΔH^θ and ΔS^θ are not monotonic as has been peviously reported (12). A large value of K may not necessarily correspond to large values of ε_λ, ΔH^θ or ΔS^θ.

The ε_λ for the FN complexes tend to be larger than those for the corresponding MN complexes with only one exception (t-ST complexes). This behaviour was also observed in the benzene – 1,2-dicyanoethylene system (13). The magnitude of ε_λ also varies with the donor structures. Our results indicate that ε_λ should be larger for more highly conjugated donors.

ΔS^θ and ΔH^θ are linearly related within series of complexes which share a common component (D or A). The variation for the relationship between ΔH^θ and K can then be explained in terms of the difference due to the entropy term.

The best way to discuss the stability of ct complexes uses ΔH^θ since these values can be calculated theoretically. The calculated ΔH^θ of course corresponds to gas phase values which, experimentally, are quite close to those obtained in inert nonpolar solvents (3). In the following discussion, we will therefore concentrate on the ΔH^θ results.

As shown in Table 3, the stability of the complexes, in increasing order is: MN–TR < FN–TR < MN–CS < FN–CS. According to Mulliken theory, the first two complexes are expected to be less stable than the last two since TR has the higher $E^{ox}_{1/2}$. It is difficult to predict which of the complexes within the pairs would be more stable. Assuming that the eclipsed geometry would be the more stable structure, we would have predicted the relative stability of the complexes to be MN–TR < FN–TR and FN–CS < MN–CS. Since the ΔH^θ of the FN–CS complex is distinctly larger than those of the other complexes, the validity of this assumption is obviously questionable. Evidence against

[3]The rotated geometry is one with the two olefins in parallel planes and center over center, while the two central double bonds are separated at a rotational angle (4). The slipped geometry is one with the two olefins in parallel planes with the two central double bonds parallel and separated at a projected distance of 2.2 Å. Details of these geometries are shown in ref. 2.

Can. J. Chem. Downloaded from www.nrcresearchpress.com by 210.87.254.5 on 09/06/12
For personal use only.

Can. J. Chem. Downloaded from www.nrcresearchpress.com by 210.87.254.5 on 09/06/12
For personal use only.

TABLE 3. Spectroscopic constants for charge-transfer complex formation

Complex (A–D)	K (M^{-1})	ε_λ (λ nm)	$-\Delta H^\theta$ (kcal mol^{-1})	$-\Delta S^\theta$ (eu)	$E^{ox}_{1/2}$(D)[a] (V)
MN–TR	0.49[b]	166(315)	0.55	3.3	0.72[e]
FN–TR	0.32[b]	180(315)	0.65	4.6	0.72
MN–CS	0.67[b]	146(315)	0.78	3.5	0.70[e]
FN–CS	0.51[b]	189(315)	1.25	5.7	0.70
FN–1,4-DMN	0.40[c] (0.54)[i]	519(380)	0.89[i]	4.2[i]	0.75[f]
MN–1,4-DMN	0.86[c] (0.67)[i]	302(380)	1.14[i]	4.5[i]	0.75
FN–1,5-DMN	0.57[c]	413(380)	—	—	0.93[f]
MN–1,5-DMN	0.83[c]	297(380)	—	—	0.93
FN–2,3-DMN	0.59[c] (0.66)[i]	465(350)	—	—	1.04[f]
MN–2,3-DMN	0.56[c] (0.61)[i]	367(350)	—	—	1.04
FN–*t*-ST	0.17[d]	657(350)	—	—	1.10[g]
MN–*t*-ST	0.10[d]	833(350)	—	—	1.10
FN–*c*-ST	0.04[d]	250(350)	—	—	1.40[h]
FN–1,3-BDO	0.15[d]	500(325)	—	—	1.09[e]
MN–1,3-BDO	0.15[d]	455(325)	—	—	1.09

[a]Refers to $Ag/AgNO_3$ (0.1 M) in acetonitrile.
[b]17.2 ± 0.1°C.
[c]23 ± 1°C.
[d]Measured in benzene solution at 23 ± 1°C. All other measurements were performed in chloroform solutions.
[e]This work.
[f]See ref. 29.
[g]See ref. 30.
[h]Estimated value. See ref. 1*a*.
[i]Hmr results. All the other results are from spectrophotometric measurements.

the eclipsed structures being the most stable can also be inferred from the 1,2-dicyanoethylene – dimethoxynaphthalene system (1*b*), although the effect of the relative size of D and A is difficult to assess in this system.

According to both the *ab initio* and PCILO MO calculations, the eclipsed geometries for all four 1,2-dicyanoethylene–1,2-dimethoxyethylene complexes *are* relatively unstable. While there are some minor discrepancies between the results from these two MO methods and it is difficult to judge which method gives the more accurate estimates, we have more faith in the *ab initio* results since self consistent field (SCF) procedures are employed in this method.

The most stable (optimum) STO-3G geometries for the MN–CS, MN–TR, and FN–CS complexes are the slipped geometries, while the rotated geometry is preferred in the FN–TR complex. In the slipped geometries of all four complexes as well as the rotated geometry of the FN–TR complex, the oxygen atoms and the cyanocarbons are almost projected over each other. The reasons why the slipped and rotated geometries are preferred are probably: (*i*) the parent ethylene–dimer is repulsive in the eclipsed geometry (14) which is presumably due mainly to HOMO–LUMO interactions (15); (*ii*) the electrostatic attraction between the oxygen atoms (δ^-) and the cyanocarbons (δ^+) is relatively important.

The comparison of the experimental and the theoretical heats of formation of ct complexes is not a straightforward problem. There are some important considerations: (*i*) the experimental ΔH^θ should be obtained for the gas phase; (*ii*) in the *ab initio* calculation, one has to consider the effects of the choice of the basis set and the electron–electron correlation; and, (*iii*) the experimental ΔH^θ is an average value for all the geometries of the ct complex following the Boltzmann distribution, while the theoretical value is obtained from only a single pair of D and A at the optimum geometry.

Since the evaluation of gas phase ΔH^θ is not convenient, most of the experimental values in the literature (and all of the values in this study) have been obtained in inert, relatively nonpolar solvents. The ΔH^θ measured in hexane solution is, in general, reasonably close to that in the gas phase (3). In methylene chloride solution, the ΔH^θ is about one-half as large as in the gas phase (16). Therefore, in order to get an estimate of the gas phase ΔH^θ from our chloroform solution data, we can multiply our ΔH^θ (Table 1) by a factor of two which would give values at the upper limit. The ΔH^θ_{gas} would than be 1.10, 1.30, 1.56, and 2.5° kcal mol^{-1} for the MN–TR, FN–TR, MN–CS, and FN–CS complexes, respectively.

As shown in Table 2, the *ab initio* SCF ΔH^θ are consistently larger with larger basis sets. According to many authors (17), the 4-31G calculation

Can. J. Chem. Downloaded from www.nrcresearchpress.com by 210.87.254.5 on 09/06/12
For personal use only.

tends to give high SCF ΔH^θ values. The use of polarization functions would bring ΔH^θ's down from 4-31G results (18). However, our complexes are too large for such calculations, even with the model dihydroxy derivative. In the single determinant *ab initio* SCF calculations, the electron correlation energies (representing dispersion energies in ct complexes) are neglected even when larger basis sets are employed (17*b*, 19). The contribution from dispersion energies in conjugated systems such as $\pi-\pi^*$ complexes is relatively important; it could be of the same order of magnitude as the SCF ΔH^θ's according to the only two $\pi-\pi^*$ ct complexes calculated using the *ab initio* method (17*b*). Verification of the accuracy of these two calculations is difficult due to the dearth of experimental data. The results reported here provide the first comparison of experimental and theoretical results for $\pi-\pi^*$ ct complexes.

A comparison of the ΔH^θ values from Tables 1 and 2 indicates that the STO-3G results will be the closest if one also includes the dispersion energies (multiply the calculated ΔH^θ by a factor of two) (17*b*). It appears now that the *ab initio* calculations with large basis sets and the PCILO calculations give values larger than the experimental ΔH^θ's. One possible source of the overestimation of the ΔH^θ's may come from the basis set superposition error (BSSE). We have examined this possibility at the STO-3G level using the counterpoise method (19*a*, 20). Our results for the MN–CS (OH) complex indicate that BSSE is relatively unimportant. We can rule out the BSSE as an error source here, since the calculations using larger basis sets than the STO-3G basis would presumably contain smaller BSSE. As we pointed out earlier, the comparison of the experimental and theoretical ΔH^θ's is not straightforward, and the results from calculations using large basis sets may in fact be valid since they correspond only to the optimum geometries of the ct complexes. Following the same argument, one can also explain why the calculated ΔH^θ of the MN–CS complex is larger than that of the FN–CS complex, which is the opposite of that observed (compare Tables 1 and 2).

We considered the possibility of observing a difference in stability between the bicyclo[2.2.2]oct-2-ene-2,3-dinitrile (BODN) – FN and the BODN–MN complexes due to possible steric hindrance in forming the former complex. Unfortunately, the additional carbon chain raises the reduction potential of BODN ($E^{red}_{1/2} = -2.02$ V, vs. $Ag/AgNO_3$ (0.1 *M*) in acetonitrile) significantly higher than MN so that BODN complexes are too weak to be accurately measured using the spectrophotometric method.

The irradiation of the MN–CS complex in acetonitrile results in isomerization of both olefins. The mechanism for the isomerization is probably the same as that reported for the stilbene and dimethoxynaphthalene systems (1*b*): (*i*) electron transfer from donor to acceptor within the excited complex to form a singlet radical ion pair; (*ii*) intersystem crossing to the triplet radical ion pair through hyperfine interaction; (*iii*) back electron transfer within the triplet radical ion pair to give the triplet excited donor or acceptor; (*iv*) the triplet olefins decaying to the ground state *trans*- and *cis*-olefins. We have not further investigated the detailed mechanism in this system since it would have limited applicability as a photochromic system due to the relatively fast rate of polymer formation. In any event, the first step (electron transfer) should be favourable (ΔG is negative) (21).

Since the rate of formation of TR is about one-third of that for FN, following our mechanism, the triplet energy of CS could be higher than that of MN by only a very small amount (~ 1 kcal mol^{-1}). This appears to be surprisingly low for dimethoxyethylene since the triplet energies of ethylene and *cis*-2-butene are 82 and 78.2 kcal mol^{-1}, respectively. However, our preliminary study of the triplet sensitized isomerization of CS indicates that the triplet energy is, in fact, quite low (efficient isomerization can be observed when acridine, $E_T =$ 45.3 kcal mol^{-1} (22) is used as the triplet sensitizer).

Conclusion

From the experimental ΔH^θ's measured for the ct complexes of MN and FN with a series of isomeric donors, we find that the orientation effects of the substituents are quite small in magnitude and the relative stabilities of the complexes are not always predictable by our present theoretical calculations.

Molecular orbital calculations using the *ab initio* method and the PCILO method indicate that the most stable geometries for the 1,2-dicyanoethylene – 1,2-dimethoxyethylene ct complexes are the slipped and the rotated geometries, which are presumably the result of electrostatic attraction between the oxygen atoms and the cyanocarbons, and the instability of the eclipsed geometries. The eclipsed geometries are relatively unstable, presumably because of the same repulsive forces which destabilize two of the parent molecules when they are in this orientation.

Experimental

General

1,3-Benzodioxole (Aldrich Chemical Co.) was distilled twice before use. Fumaronitrile (Aldrich Chemical Co.) was freshly sublimed under vacuum before use. Maleonitrile was prepared by the iodine-catalyzed thermal isomerization of fumaronitrile

Can. J. Chem. Downloaded from www.nrcresearchpress.com by 210.87.254.5 on 09/06/12
For personal use only.

(23), and was purified by column chromatography on neutral alumina (Fisher) eluting with benzene–hexanes (1:1), followed by recrystallization from ether–pentane. Chloroform, benzene, and acetonitrile were purified as previously described (1*b*).

The ^{1}Hmr spectra were recorded on either a Varian T-60 or CFT-20 instrument with tetramethylsilane as the internal reference. The infrared spectra were run on a Perkin-Elmer 180 infrared spectrometer and calibrated against the 1602 cm^{-1} polystyrene absorption. Mass spectra were obtained from a Consolidated Electrodynamics Corporation 21-104 mass spectrometer. Half-wave oxidation and reduction potentials were measured by cyclic voltammetry as described elsewhere (24).

All irradiations were performed using a General Electric Co. 1 kW medium pressure mercury vapour arc lamp (unless otherwise specified) with a quartz cooling jacket (Photochemical Research Associates) at 10°C.

Bicyclo[2.2.2]oct-2-ene-2,3-dinitrile was prepared using a procedure modified from that reported by Scheiner *et al.* (25). Details are given below.

Dimethyl Bicyclo[2.2.2]oct-2-ene-2,3-dicarboxylate (I)

1,3-Cyclohexadiene (26) (3.2 g, 0.04 mol) was mixed with freshly distilled dimethyl acetylenedicarboxylate (4.55 g, 0.032 mol) and the solution was stirred at 60–65°C for 18 h, until all the acetylenedicarboxylate had reacted. The viscous liquid was dissolved in methanol (100 mL), 5% Pd/C powder (0.25 g) was added, and the mixture was stirred at room temperature. Hydrogen gas was bubbled through this solution at a slow rate and the progress of the reaction was monitored by the disappearance of the vinyl protons in the ^{1}Hmr. After the reaction was complete (ca. 6 h), the solution was filtered and concentrated. The solid product was recrystallized from hexanes to colourless needles, 6.45 g (90%); mp 45°C; ir (KBr): 2950 (m), 1720 (s), 1630 (w), 1430 (w), 1275 (w), and 1080 (w) cm^{-1}; ^{1}Hmr ($CDCl_3$) δ: 1.52 (m, 8H), 3.02 (br s, 2H), 3.80 (s, 6H).

Bicyclo[2.2.2]oct-2-ene-diamide (II)

Sodium methoxide (0.35 g) was dissolved in methanol (300 mL) and the solution was saturated with ammonia at −10°C. A solution of I (4.48 g, 0.04 mol) in 50 mL methanol was added dropwise to the above solution. The mixture was stirred at −10°C for 20 min and then kept at room temperature in a stoppered flask for 4 days. The crystals which separated were filtered, washed with methanol, and dried. The mother liquid was concentrated and saturated with ammonia. This solution was kept at room temperature for 3 more days and the solid product isolated as before. The total yield of II was 2.50 g (64%); mp 238–240°C; ir (KBr): 3350 (s), 3300 (m), 3180 (s), 1635 (s), 1600 (s), 1430 (w), 1415 (w), 1380 (m), 1100 (w), 820 (w), 690 (m) and 650 (m) cm^{-1}; ^{1}Hmr (DMSO-d_6) δ: 1.25 (m, 8H), 3.20 (br s, 2H), 7.14 (br s, 2H), 7.50 (br s, 2H); ms *m/e*: 194.

Bicyclo[2.2.2]oct-2-ene-2,3-dinitrile

Bicyclo[2.2.2]oct-2-ene-2,3-diamide (II) (2.33 g, 0.012 mol) was mixed with an excess amount of freshly distilled phosphorous oxychloride (15 mL) and stirred at reflux temperature for 5 h. The resulting brown solution was cooled in an ice bath. The cold solution was then transferred to a beaker containing 30 g of crushed ice. The mixture was stirred well and then extracted with benzene (50 mL). The benzene layer was washed with ice-cold distilled water (5 × 20 mL) and 10% sodium bicarbonate solution (10 mL), followed by distilled water (3 × 20 mL). The solution was dried over anhydrous $MgSO_4$ and concentrated on a rotary evaporator. The resulting cream colored solid was sublimed under vacuum (95°C) to give a colorless solid which was recrystallized from benzene–hexanes (1:3) to needles, 1.2 g (63%); mp 120°C; ir (KBr): 2960 (s), 2875 (m), 2215 (m), 1458 (w), 1325 (w), 1240 (w), 1160 (w), 1120 (w) and 860 (m) cm^{-1}; ^{1}Hmr ($CDCl_3$) δ: 1.20 (m, 8H), 3.04 (br s, 2H); ms *m/e*: 158.

cis-*1,2-Dimethoxyethylene (27)*

Alumina (38 g, 8–14 mesh) was packed in a pyrolysis tube and preheated at 300°C in a tube furnace under a constant flow of nitrogen (90 mL/min) for 5 h to remove water. 1,1,2-Trimethoxyethane (20 g), prepared from vinyl acetate according to reported procedure (28), was introduced dropwise from an addition funnel into the nitrogen stream and the product mixture was collected in a receiving flask cooled in a Dry Ice – isopropanol bath. The reaction mixture was dried over 4A molecular sieves, filtered, and the *cis* isomer was isolated by preparative vapour phase chromatography (vpc) (10 ft × 1/2 in. column of 25% Theed on Chromosorb W at 90°C, He flow rate 70 mL/min, retention time 32 min). ^{1}Hmr ($CDCl_3$) δ: 3.52 (s, 6H), 5.12 (s, 2H).

trans-*1,2-Dimethoxyethylene*

A nitrogen purged solution of *cis*-1,2-dimethoxyethylene (300 mg) and acetophenone (80 mg) in *n*-hexane (600 mL) was irradiated in a Pyrex vessel for 48 h, yielding a photostationary state mixture of *trans–cis*, 65:35. A 450-W medium pressure mercury vapor lamp (Hanovia) was used in this case. The *trans*-isomer was isolated by preparative vpc using the same conditions as for the *cis*-isomer (retention time 21 min); ^{1}Hmr (CCl_4) δ: 3.40 (s, 6H), 6.15 (s, 2H).

*Determination of Association Constants (*K*) of Charge-transfer Complexes by the Uv–vis Method*

A chloroform solution of the donor (ca. 10 m*M*) was prepared. Then a series of five solutions were prepared by weighing various amounts of the acceptor (ca. 0.2 to 0.6 *M*) in 5 mL volumetric flasks before introducing 3 mL of the above solution through a pipette. The optical densities (OD) at selected wavelengths were recorded on a Cary 219 spectrophotometer equipped with a direct digital temperature readout device. The temperature of the solutions was maintained (±0.05°) by circulating coolant from a Polyscience 90 thermostated bath. In all cases studied, no chemical change of the solutions was encountered during the time required to make the measurements.

K and ε_λ were determined by both the FHW and SMM methods. The slopes and y-intercepts of the plots were computed using a standard linear least-squares program. The correlation coefficients were generally better than 0.96.

Irradiation of the Maleonitrile – cis-*1,2-Dimethoxyethylene Charge-transfer Complex*

An acetonitrile-d_3 solution of MN (0.3 *M*) and CS (0.3 *M*) was irradiated through a 1 cm filter solution composed of sodium bromide (120 g) and lead nitrate (0.75 g) in 250 mL water ($\lambda >$ 330 nm). After irradiating for 65 h, the reaction mixture contained MN (71%), FN (18%), CS (33%), TR (6%), and (presumably) polymeric material. Irradiation for a longer period (144 h) resulted in further consumption of the olefins; the solution contained MN (22%), FN (13%), CS (9%), and TR (2%). There was no change in either of the control experiments, irradiating MN or CS alone under the same conditions.

The Triplet-sensitized Isomerization of cis-*1,2-Dimethoxyethylene*

Nitrogen purged *n*-hexane solutions of *cis*-1,2-dimethoxyethylene (0.05 *M*) and the triplet sensitizer (< 0.01 *M*) were irradiated in Pyrex vessels. Progress of the isomerizations were monitored by vpc (10 ft 25% Theed on Chromosorb W at 90°C). Reasonably fast rates of isomerization were observed when the following sensitizers (triplet energies in kcal mol^{-1}) were employed: 1,3,5-triacetylbenzene (74.0), xanthen-9-one (74.0), thioxanthen-9-one (65.5), 2-acetonaphthone (59), fluoren-9-one (53), 3.3′-carbonyl-bis(7-diethylaminocoumarin) (52.0), phenanthrenequinone (49), and acridine (45.3).

Acknowledgements

This work was supported by a grant from the Natural Sciences and Engineering Research Council of Canada. We gratefully acknowledge the assistance of Dr. K. Ramakrishnan who prepared pure samples of the required known compounds.

1. (*a*) D. R. ARNOLD and P. C. WONG. J. Am. Chem. Soc. **101**, 1894 (1979); (*b*) P. C. WONG and D. R. ARNOLD. Can. J. Chem. **58**, 918 (1980).
2. P. C. WONG and R. J. BOYD. Can. J. Chem. **59**, 974 (1981).
3. R. FOSTER. Organic charge-transfer complexes. Academic Press, New York, NY. 1969.
4. R. FOSTER, D. L. HAMMICK, and A. A. WARDLEY. J. Am. Chem. Soc. 3817 (1953).
5. B. K. SEAL, A. K. MUKHERJEE, and D. C. MUKHERJEE. Bull. Chem. Soc. Jpn. **52**, 2088 (1979).
6. (*a*) N. J. ROSE and R. S. DRAGO. J. Am. Chem. Soc. **81**, 6138 (1959); (*b*) **81**, 6141 (1959).
7. (*a*) J. M. CULLEN and M. C. ZERNER. An unpublished version of the PCILO program; (*b*) S. J. DINER, J. P. MALRIEU, and P. CLAVERIE. Theor. Chim. Acta, **13**, 1 (1969); (*c*) **13**, 18 (1969); (*d*) S. DINER, J. P. MALRIEU, F. JORDAN, and M. GILBERT. Theor. Chim. Acta, **15**, 100 (1969).
8. D. B. CHESNUT and R. W. MOSELEY. Theor. Chim. Acta, **13**, 230 (1969).
9. J. S. BINKLEY, R. A. WHITEHEAD, P. C. HARIHARAN, R. SEEGER, and J. A. POPLE. QCPE, **11**, 368 (1978).
10. J. S. BINKLEY, J. A. POPLE, and W. H. HEHRE. J. Am. Chem. Soc. **102**, 940 (1980).
11. C. K. PROUT and B. KAMENAR. *In* Molecular complexes. Vol. 1. *Edited by* R. Foster. Crane, Russak and Co., Inc., New York, NY. 1973.
12. G. BRIEGLEB. Electronen-Donator-Acceptor-Komplexe. Springer Verlag, Berlin. 1961.
13. P. SCHULER and H. HEUSINGER. J. Mol. Struct. **28**, 25 (1975).
14. P. E. S. WORMER and A. VAN DER AVOIRD. J. Chem. Phys. **62**, 3326 (1975).
15. R. S. MULLIKEN. Recl. Trav. Chim. Pays-Bas, **75**, 845 (1956).
16. MILTON TAMRES. *In* Molecular complexes. Vol. 1. *Edited by* R. Foster. Crane, Russak and Co., Inc., New York, NY. 1973.
17. (*a*) W. A. LATHAN and K. MOROKUMA. J. Am. Chem. Soc. **97**, 3615 (1975); (*b*) W. A. LATHAN, G. R. PACK, and K. MOROKUMA. J. Am. Chem. Soc. **97**, 6624 (1975); (*c*) P. A. KOLLMAN and L. C. ALLEN. Chem. Rev. **72**, 283 (1972).
18. H. UMEYAMA, K. MOROKUMA, and S. YAMABE. J. Am. Chem. Soc. **99**, 330 (1977).
19. (*a*) W. KOLOS. Theor. Chim. Acta, **51**, 219 (1979); (*b*) F. MULDER, M. V. HEMERT, P. E. S. WORMER, and A. VAN DER AVOIRD. Theor. Chim. Acta, **46**, 39 (1977).
20. (*a*) S. F. BOYS and F. BERNARDI. Mol. Phys. **19**, 553 (1970); (*b*) M. BULSKI and G. CHALASINSKI. Theor. Chim. Acta, **44**, 399 (1977).
21. D. REHM and A. WELLER. Isr. J. Chem. **8**, 259 (1970).
22. P. S. ENGEL and B. M. MONROE. Adv. Photochem. **8**, 245 (1971).
23. G. E. FICKEN, R. P. LINSTEAD, E. STEPHEN, and M. WHALLEY. J. Chem. Soc. 3879 (1958).
24. W. J. LEIGH, D. R. ARNOLD, R. W. R. HUMPHREYS, and P. C. WONG. Can. J. Chem. **58**, 2537 (1980).
25. P. SCHEINER, K. K. SCHMIEGEL, G. SMITH, and W. R. VAUGHAM. J. Org. Chem. **28**, 2960 (1963).
26. (*a*) H. R. SNYDER and L. A. BROOK. Org. Synth. Coll. Vol. **2**, 171 (1963); (*b*) J. P. SCHAEFER and L. ENDERS. Org. Synth. Coll. Vol. **5**, 285 (1973).
27. J. T. WALDRON and W. H. SNYDER. J. Chem. Eng. Data, **18**, 441 (1973).
28. T. KOKUBO, S. IWATSUKI, and Y. YAMASHITA. Macromolecules, 482 (1968).
29. A. ZWEIG, L. H. MAURER, and B. G. ROBERTS. J. Org. Chem. **32**, 1322 (1967).
30. J. E. KUDER, H. W. GIBSON, and D. WYCHICK. J. Org. Chem. **40**, 875 (1975).

Can. J. Chem. Downloaded from www.nrcresearchpress.com by 210.87.254.5 on 09/06/12
For personal use only.

Equilibrium decomposition pressures of the compounds Na_2ZrCl_6 and Na_2HfCl_6

G. J. KIPOUROS AND S. N. FLENGAS

Department of Metallurgy and Materials Science, University of Toronto, Toronto, Ont., M5S 1A4

Received August 5, 1980

G. J. KIPOUROS and S. N. FLENGAS. Can. J. Chem. **59**, 990 (1981).

The chemical equilibria representing the reactions

$$Na_2ZrCl_6(s \text{ or } l) \geq 2NaCl\ (s \text{ or } l) + ZrCl_4\ (vap, P, T)$$

and

$$Na_2HfCl_6\ (s \text{ or } l) \geq 2NaCl\ (s \text{ or } l) + HfCl_4\ (vap, P,T)$$

were investigated by direct vapour pressure measurements and thermodynamic data such as free energies and enthalpies of reaction have been calculated.

With reference to the separation of Hf from Zr by a recently developed process based on the selective reactivity of $ZrCl_4$ and $HfCl_4$ vapours with alkali chlorides, it is shown that the efficiency of alkali chlorides as separating agents increases in the order of LiCl → NaCl → KCl.

G. J. KIPOUROS et S. N. FLENGAS. Can. J. Chem. **59**, 990 (1981).

En utilisant des mesures directes de pression de vapeur, on a étudié les équilibres chimiques suivants:

$$Na_2ZrCl_6\ (s \text{ ou } l) \geq 2NaCl\ (s \text{ ou } l) + ZrCl_4\ (vap, P,T)$$

et

$$Na_2HfCl_6\ (s \text{ ou } l) \geq 2NaCl\ (s \text{ ou } l) + HfCl_4\ (vap, P,T)$$

et on a calculé les énergies libres et les enthalpies de réaction.

En relation avec la méthode récemment mise au point pour séparer le Hf du Zr qui est basée sur la réactivité sélective des vapeurs de $ZrCl_4$ et de $HfCl_4$ avec les chlorures alcalins, on a montré que l'efficacité des chlorures alcalins en tant qu'agents séparateurs augmente dans l'ordre suivant LiCl → NaCl → KCl.

[Traduit par le journal]

Introduction

In previous publications from this laboratory the vapour pressures of $ZrCl_4$ in equilibrium with its solutions containing alkali chlorides such as LiCl (3), NaCl, KCl (1, 2, 5), and CsCl (4), and of $HfCl_4$ in equilibrium with its solutions containing alkali chlorides such as LiCl (3), KCl (5), and CsCl (4), have been determined by direct experimental techniques involving the use of a spoon type Bourdon gauge (1, 2), a molten tin isoteniscope (3, 4) or a quartz spiral type Bourdon gauge (5).

In the present investigation, a quartz spiral type Bourdon gauge has been applied to the determination of the vapour pressures of $ZrCl_4$ and $HfCl_4$ in equilibrium with the two pure compounds Na_2ZrCl_6 and Na_2HfCl_6, respectively, over a temperature range extending below and above their melting points.

From the results of this study, the equilibrium dissociation constants, free energies, and enthalpies for the reactions

[1] $Na_2MCl_6\ (s) \rightleftharpoons 2NaCl\ (s) + MCl_4\ (vap)$

where M represents Zr or Hf, have been calculated.

The equilibrium constant for the exchange reaction

[2] Na_2ZrCl_6 (in solid solution) + $HfCl_4$ (vapour) $\rightleftharpoons$ Na_2HfCl_6 (in solid solution) + $ZrCl_4$ (vapour)

was also calculated.

From the above data, the theoretical efficiency for the separation of hafnium from zirconium by a previously developed process based on the selective reactivity of $ZrCl_4$ and $HfCl_4$ vapours with alkali halides (6, 7), has been calculated.

Experimental

At specific partial pressure and temperature pure $ZrCl_4$ and $HfCl_4$ vapours react with solid NaCl to form the stoichiometric solid complex compounds Na_2ZrCl_6 and Na_2HfCl_6 respectively. The corresponding reactions may be written as:

[3] $2NaCl\ (s) + ZrCl_4\ (v) \rightarrow Na_2ZrCl_6\ (s)$
at P,T P,T

and

[4] $2NaCl\ (s) + HfCl_4\ (v) \rightarrow Na_2HfCl_6\ (s)$
at P,T P,T

The $NaCl–Na_2ZrCl_6$ (1) and $NaCl–Na_2HfCl_6$ (8) binary systems are related by simple eutectic type phase diagrams which clearly indicate the stability of these congruently melting complex compounds.

The general method applied for the preparation of the pure stoichiometric compounds was developed in this laboratory earlier (1, 2) and involves the reaction of finely ground NaCl,

0008-4042/81/060990-06$01.00/0

©1981 National Research Council of Canada/Conseil national de recherches du Canada

Can. J. Chem. Downloaded from www.nrcresearchpress.com by 210.87.254.40 on 09/06/12
For personal use only.

Can. J. Chem. Downloaded from www.nrcresearchpress.com by 210.87.254.40 on 09/06/12
For personal use only.

having a particle size of less than 325 mesh, with $ZrCl_4$ or $HfCl_4$ vapours at 1 atm pressure.

When the formation of the complex compounds is completed, the weight gain of NaCl, which is converted to either Na_2ZrCl_6 or Na_2HfCl_6, remains constant with time and it indicates mole ratios of NaCl to $ZrCl_4$ or NaCl to $HfCl_4$, respectively, equal to 2.

The optimum reaction temperature for both Na_2ZrCl_6 and Na_2HfCl_6 has been found to be 485°C. Reaction time was of the order of 80 to 100 h.

The $ZrCl_4$ and $HfCl_4$ salts were purchased from the Wah Chang Corporation of America, Albany, New York. As they were always received in a partially hydrolyzed condition, they were purified by repeated sublimations in vacuum through a molten tin plug, as reported earlier (3).

The NaCl used in the present investigation was reagent grade containing less than 0.01% total impurities, and supplied by Fisher Scientific. It was dried under vacuum, at 500°C.

Handling of materials, preparation of samples, and transfer to the reaction cells were conducted in a dry box filled with argon gas.

The apparatus for measuring the equilibrium vapour pressures of $ZrCl_4$ and $HfCl_4$ over the pure complex compounds Na_2ZrCl_6 and Na_2HfCl_6 respectively consisted of a hollow fused quartz Bourdon spiral pressure gauge connected to a quartz reaction cell as it has been described elsewhere (5).

For these measurements the temperature of the sample container was varied between 360 and 660°C while the upper part of the apparatus containing the Bourdon spiral was maintained at temperatures about 30°C higher than the corresponding normal sublimation points of pure $ZrCl_4$ and $HfCl_4$.

Specimens were introduced into the sample container of the apparatus in the form of powders. It was found that large quantities of absorbed gas were released from the salt upon heating. This introduced a systematic error into the measurements. Accordingly, an elaborate degassing procedure was employed in which the cell was repeatedly heated, cooled, reopened, and evacuated. When the residual gas was no longer present upon cooling, equilibrium vapor pressures were measured.

Experimental Results

The vapour pressures of $ZrCl_4$ and $HfCl_4$, in equilibrium with the pure compounds Na_2ZrCl_6 and Na_2HfCl_6 respectively, were determined. Pressures were measured in mm Hg, and corrections were made for mercury expansion and for gravity effects (9, 10) to convert to standard conditions, i.e. at 273.15 K and an acceleration of free fall of 9.80665 m/s^2. These corrected pressures are given in Table 1. Temperatures reported herein are based on the IPTS-68 (11). In Fig. 1 these data are plotted as $\ln P_{MCl_4}$ vs. $1/T$. The lines shown on the graphs are calculated by the least-squares method, while the points are experimental.

Some experimental points for the equilibrium decomposition pressures of Na_2ZrCl_6 obtained previously in the laboratory (1) using a quartz type spoon gauge are also shown in Fig. 1 and are in good agreement with the present work. These previous data were obtained only at higher temperatures near the melting temperature of Na_2ZrCl_6 as at lower temperatures the measurements became irreversible due to gases absorbed by the sample.

TABLE 1. Measured vapour pressures of $ZrCl_4$ and $HfCl_4$ over the pure compounds Na_2ZrCl_6 and Na_2HfCl_6, respectively.

$ZrCl_4$		$HfCl_4$	
T (°C)	P (mm Hg)	T (°C)	P (mm Hg)
399	19.0	380	12.9
420	22.9	415	13.9
459	26.8	449	16.9
490	32.8	507	28.8
517	41.0	530	34.8
541	58.7	561	51.7
546	62.7	590	112.4
574	112.4	616	241.8
601	261.6	644	562.3
625	629.2	659	1,021.0
638	799.4	562	59.7
652	928.7	541	35.8
658	985.3	534	35.0
650	913.7	509	30.8
647	759.1	498	24.8
610	307.3		
597	204.8		
576	151.0		
570	110.4		
531	45.8		
494	36.0		
460	27.0		
437	23.8		

As it was pointed out above the spiral type gauge used in the present work can withstand large pressure gradients and sudden decompression and is well suited for extensive degassing procedures, thus making possible accurate measurements at low pressures.

Also shown in Fig. 1 are equilibrium pressures reported by Morozoy and Sun-In-Chzhu (12) and Korshunov and Gregory (13) which are in disagreement with the values measured in the present study. In these studies transportation techniques have been employed and no mention was made of the problem of depleting $ZrCl_4$ or $HfCl_4$ from the condensed Na_2ZrCl_6 or Na_2HfCl_6 phases during the course of an experiment. The quantitative determination of transported $ZrCl_4$ and $HfCl_4$ was done colorimetrically and by flame photometry. Furthermore, the data of Morozov and Sun-In-Chzhu (12), which have been obtained at temperatures for which both solid and molten Na_2ZrCl_6 are present, have been represented by a single least-squares line (13).

The corresponding equations for the temperature dependence of the equilibrium pressures within the characteristic temperature ranges were calculated and are given in Table 2.

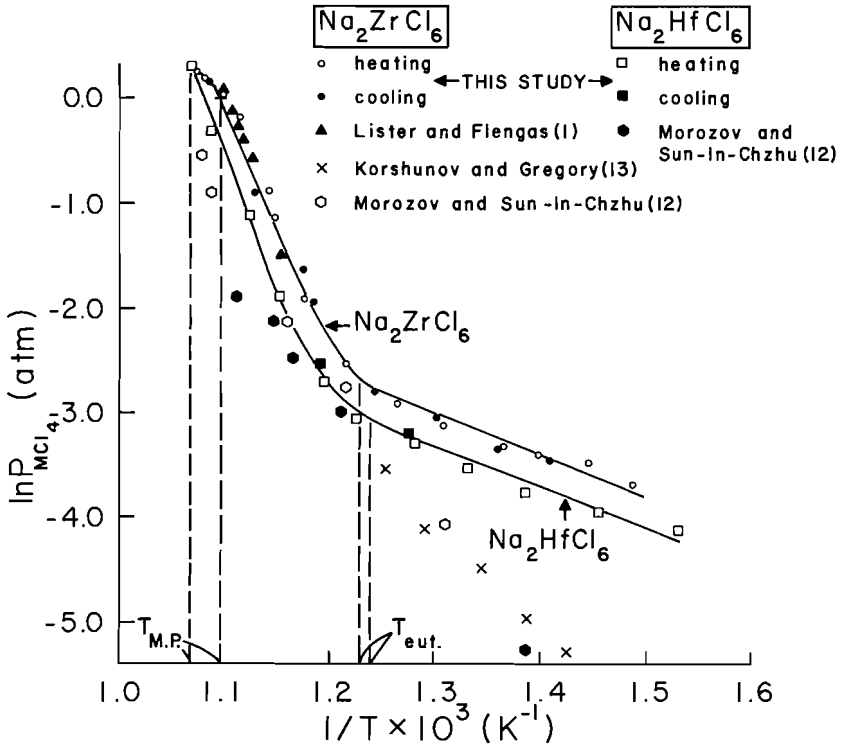

FIG. 1. $\ln P_{MCl_4}$ versus $1/T$ diagram for the pure complex compounds Na_2ZrCl_6 and Na_2HfCl_6.

TABLE 2. Equilibrium vapour pressures of $ZrCl_4$ and $HfCl_4$ over the pure compounds Na_2ZrCl_6 and Na_2HfCl_6 respectively

Equilibrium reactions	Na_2MCl_6 (mol%)	Temperature range (K)	$\ln P_{MCl_4}^{(atm)} = A + B/T$		
			A	B	St. error
[1] Na_2ZrCl_6 (solid) $\rightleftharpoons$ 2NaCl (solid) + $ZrCl_4$ (vap)	100	672–821	2.0259	−3 880	0.0691
[2] Na_2ZrCl_6 (solid) $\rightleftharpoons$ 2NaCl (in solution) + $ZrCl_4$ (vap)	100	821–919		Non-linear	
[3] Na_2ZrCl_6 (liquid) $\rightleftharpoons$ 2NaCl (in solution) + $ZrCl_4$ (vap)	100	919–931	11.5270	−10 538	0.0646
[4] Na_2HfCl_6 (solid) $\rightleftharpoons$ 2NaCl (solid) + $HfCl_4$ (vap)	100	653–813	1.5305	−3 749	0.0842
[5] Na_2HfCl_6 (solid) $\rightleftharpoons$ 2NaCl (in solution) + $HfCl_4$ (vap)	100	813–933		Non-linear	
[6] Na_2HfCl_6 (liquid) $\rightleftharpoons$ 2NaCl (in solution) + $HfCl_4$ (vap)	100	933–		High pressures	

Reaction [1] in Table 2 defines the equilibrium pressure of $ZrCl_4$ over pure solid Na_2ZrCl_6 and solid NaCl at temperatures lower than the eutectic temperature shown in Fig. 1.

Reaction [2] in Table 2 represents the equilibrium pressure of $ZrCl_4$ over pure solid Na_2ZrCl_6 at temperatures higher than the eutectic temperature and in the presence of a solution of NaCl and Na_2ZrCl_6 of liquidus composition, as given by the phase diagram (1). Due to the temperature and composition dependence of the activity of NaCl in this region, the $\ln P_{ZrCl_4}$ vs. $1/T$ plot exhibits the curvature shown.

Reaction [3] in Table 2 represents the equilibrium pressure of $ZrCl_4$ over pure molten Na_2ZrCl_6 at temperatures higher than its melting point.

Similar considerations apply to reactions [4], [5], and [6] for Na_2HfCl_6 given in Table 2. It should be noted that the non-linear and upper linear portions of the pressure curves for Na_2ZrCl_6 in Fig. 1 intercept at a temperature which is in agreement with the melting point of the compound Na_2ZrCl_6. As it is shown in Tables 1 and 2 vapour pressure measurements over pure liquid Na_2HfCl_6 have not been conducted since the pressures involved were too high to be measured safely with the pressure gauge.

Discussion

Below the corresponding eutectic temperatures of the pseudobinary systems NaCl–Na_2ZrCl_6 and NaCl–Na_2HfCl_6 respectively, the thermal decomposition of the chlorozirconate and chlorohafnate

Can. J. Chem. Downloaded from www.nrcresearchpress.com by 210.87.254.40 on 09/06/12
For personal use only.

Can. J. Chem. Downloaded from www.nrcresearchpress.com by 210.87.254.40 on 09/06/12
For personal use only.

complex compounds are described by the reactions:

[5] Na_2ZrCl_6 (s) $\rightleftharpoons$ 2NaCl (s) + $ZrCl_4$ (vap)

[6] Na_2HfCl_6 (s) $\rightleftharpoons$ 2NaCl (s) + $HfCl_4$ (vap)

By choosing the standard states for the condensed phases as the pure solids at all temperatures and for the vapour phases, the pure vapours at 1 atm, the thermodynamic equilibrium constants for the decomposition reactions [5] and [6] can be written as:

[7] $K_5 = P_{ZrCl_4}$(vap)

[8] $K_6 = P_{HfCl_4}$(vap)

Actual pressures have been used, in these equations, instead of fugacities as the zirconium tetrachloride vapour is known to be unimolecular and ideal (14, 15), and hafnium tetrachloride vapour would be expected to be quite similar.

The standard heat ΔH_R^0 for the decomposition reactions may be obtained from the van't Hoff equation, written as:

[9] $d \ln K/dT = -\Delta H_R^0/RT^2$

while the standard free energy and the average standard entropy can be determined from the well known equations

[10] $\Delta G^0 = -RT \ln K$

[11] $\Delta G_R^0 = \Delta H_R^0 - T\Delta S_R^0$

The results of these calculations for pure Na_2ZrCl_6 and Na_2HfCl_6 are given in Table 3. From these data the equilibrium constant of the exchange reaction:

[12] $HfCl_4$ (vap) + Na_2ZrCl_6 (as a solid solution of Na_2ZrCl_6 in Na_2HfCl_6) = $ZrCl_4$ (vap) + Na_2HfCl_6 (as a solid solution of Na_2HfCl_6 in Na_2ZrCl_6)

is calculated as

[13] $$K_{ex} = \left(\frac{P_{ZrCl_4}}{P_{HfCl_4}}\right)_{\text{vapour}} \left(\frac{X_{Na_2HfCl_6}}{X_{Na_2ZrCl_6}}\right)_{\text{in solid solution}}$$

In this equation, mole fractions (X's) have been substituted for activities, because of the suggested ideal behaviour of the solid solutions (16).

Since [12] was derived by subtracting [5] from [6] given in Table 2, the temperature dependence of the equilibrium constant given by [13] may be calculated by combining [7] and [8] as:

[14] $\ln K_{ex} = 0.4954 - 131/T$

TABLE 3. Thermodynamic values for the decomposition of the pure compounds Na_2ZrCl_6 and Na_2HfCl_6

Compound	Temperature range (K)	ΔH_R^0 (dec.) (cal/mol)	ΔS_R^0 (dec.) (eu)
Na_2ZrCl_6	672–821	7 709	4.025
Na_2HfCl_6	653–813	7 449	3.041

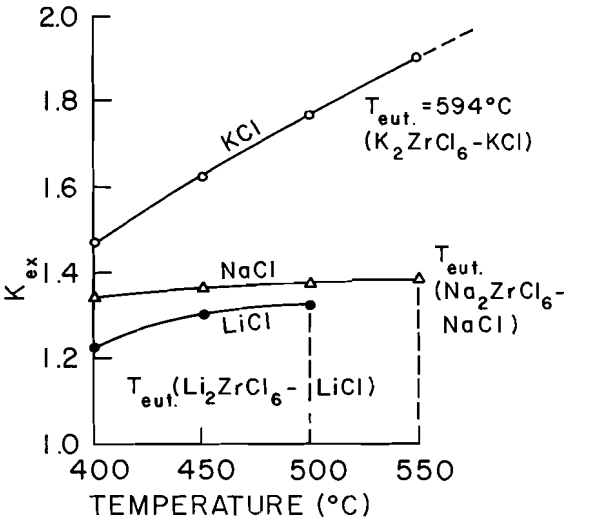

FIG. 2. Temperature dependence of the equilibrium constants K_{ex} for the exchange reactions:

$HfCl_4$(vap) + A_2ZrCl_6 (solid solution) $\rightleftharpoons$ A_2HfCl_6 (solid solution) + $ZrCl_4$(vap)

where A = Li^+, Na^+, or K^+.

A plot of K_{ex} vs T (in °C) is shown in Fig. 2. Data for the previously investigated systems employing LiCl (3) and KCl (5), respectively, are also included in this figure for comparison purposes.

It has been shown in a previous publication (6) that impure $ZrCl_4$ containing $HfCl_4$ may be purified in a closed two-compartment reaction cell in which the impure Zr(Hf)Cl_4 mixture is placed in the first compartment, which is kept at a temperature T_1 while the alkali chloride ACl is placed in the second compartment, which is kept at a temperature T_2.

The separation proceeds through the formation of the complex compounds A_2ZrCl_6 and A_2HfCl_6 which appear in the second compartment as a solid solution. The efficiency of the separation process depends upon the magnitude of the equilibrium constant for the exchange reaction [12].

The efficiency of separation η defined as:

[15] $$\eta = \frac{(\text{Wt\%HfCl}_4)_{\text{initial}} - (\text{Wt\%HfCl}_4)_{\text{final}}}{(\text{Wt\%HfCl}_4)_{\text{initial}}} \times 100$$

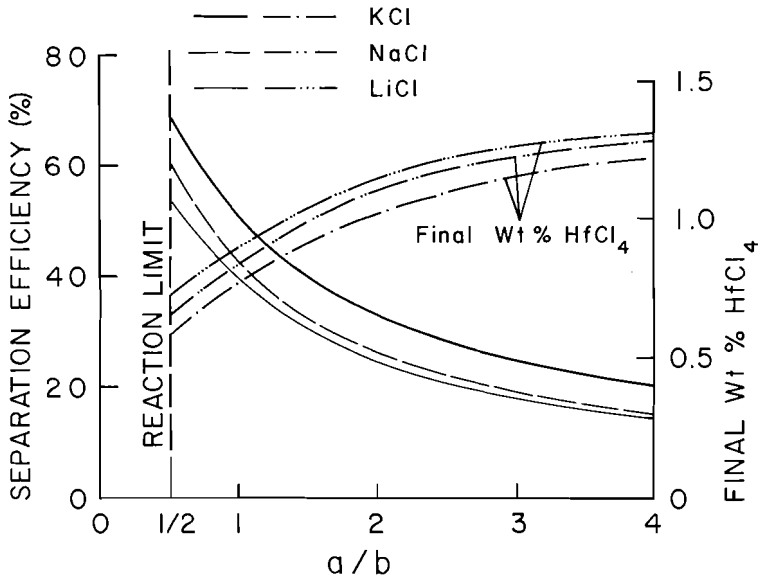

FIG. 3. Variation of the separation efficiency factor "η" and of the final wt% $HfCl_4$, with the molar ratio a/b of $Zr(Hf)Cl_4$ to LiCl, NaCl, or KCl, respectively. Calculations are based on $Zr(Hf)Cl_4$ initially containing 1.54 wt% $HfCl_4$. T_1 and T_2 temperatures are respectively 330°C and 450°C.

may be calculated from the previously derived relationship (7)

$$[16] \qquad K_{ex} = \frac{2(X'_{ZrCl_4})a - b + 2Z}{2(X'_{HfCl_4})a - 2Z} \cdot \left(\frac{P_{ZrCl_4}{}^0}{P_{HfCl_4}{}^0}\right)_{(T_1)} \cdot \frac{2Z}{b - 2Z}$$

where X'_{ZrCl_4} and X'_{HfCl_4} are the mole fractions of $ZrCl_4$ and $HfCl_4$ respectively in the $Zr(Hf)Cl_4$ mixture initially present in the first compartment of the separation cell prior to reaction; a represents the total number of moles of $Zr(Hf)Cl_4$ present in the first compartment of the reactor, prior to separation; b represents the number of moles of ACl present in the second compartment of the reactor; Z is the number of moles of $HfCl_4$ which have reacted with ACl and are retained in the second compartment of the reactor after equilibrium has been reached; $P_{ZrCl_4}{}^0$ and $P_{HfCl_4}{}^0$ are the sublimation pressures (17) of pure $ZrCl_4$ and $HfCl_4$ respectively, at the temperature T_1.

Considering a reactor containing NaCl and T_1 and T_2 temperatures of 330 and 450°C respectively the separation efficiency factor η may be calculated from the determined values of K_{ex} and for various ratios of a/b.

Figure 3 illustrates the variation of η with the a/b ratio for LiCl, NaCl, and KCl. As is seen, η increases as the a/b ratio decreases. Hence the separation becomes more efficient when the amount of the $Zr(Hf)Cl_4$ mixture placed in compartment I is close to that required by the stoichiometry for the formation of Na_2ZrCl_6 and Na_2HfCl_6. The reaction limit is reached at $a/b = 0.5$, at which point all the added tetrachloride vapours react with the NaCl. On the other hand, as the a/b ratio approaches the value of 0.5, most of the $Zr(Hf)Cl_4$ is present as a Na_2ZrCl_6–Na_2HfCl_6 solid solution in compartment II. Hence for practical purposes, the a/b ratio must be larger than 0.5, and a value of about 0.8 to 1.0 appears optimum. At $a/b = 0.8$ the calculated separation efficiency is about 52%.

By comparing LiCl, NaCl, and KCl as separating agents for Hf, it is evident that at 450°C the separation efficiency increases in the order LiCl → NaCl → KCl.

1. R. L. LISTER and S. N. FLENGAS. Can. J. Chem. **43**, 2947 (1965).
2. R. L. LISTER and S. N. FLENGAS. J. Electrochem. Soc. **111**, 343 (1964).
3. J. E. DUTRIZAC and S. N. FLENGAS. Advances in Extractive Metallurgy Symposium, paper 24, April 17–20. The Institution of Mining and Metallurgy, London, England, 1967.
4. D. A. ASVESTAS, P. PINT, and S. N. FLENGAS. Can. J. Chem. **55**, 1154 (1977).
5. G. J. KIPOUROS and S. N. FLENGAS. Can. J. Chem. **56**, 1549 (1978).
6. J. E. DUTRIZAC and S. N. FLENGAS. Canadian patent No. 863,258 (February 9, 1971).

Can. J. Chem. Downloaded from www.nrcresearchpress.com by 210.87.254.40 on 09/06/12
For personal use only.

7. S. N. FLENGAS and J. E. DUTRIZAC. Metall. Trans. B, 8B, 377 (1977).
8. I. S. MOROZOV and SUN-IN-CHZHU. Russ. J. Inorg. Chem. **4**, 307 (1959).
9. D. AMBROSE. Vapour pressures. *In* Chemical thermodynamics, Vol. I. *Edited by* M. L. McGlashan. The Chemical Society, 1973. Chapt. 7.
10. W. G. BROMBACHER, D. R. JOHNSON, and J. L. CROSS. Mercury barometers and manometers. National Bureau of Standards, Washington, DC. Monograph 8. 1960.
11. R. L. POWELL *et al.* Thermocouple reference tables based on the IPTS-68. National Bureau of Standards, Washington, DC. Monograph 125. 1974.
12. I. S. MOROZOV and SUN-IN-CHZHU. Russ. J. Inorg. Chem. **4**, 1176 (1959).
13. B. G. KORSHUNOV and N. W. GREGORY. Inorg. Chem. **3**, 451 (1964).
14. O. RAHLES and W. SISCHER. Z. Anorg. Allg. Chem. **21**, 349 (1933).
15. J. A. N. FRIEND, A. T. W. COLLEY and R. S. HAYES. J. Chem. Soc. 494 (1930).
16. S. N. FLENGAS and P. PINT. Can. Metall. Q. **8**, 151, (1969).
17. A. A. PALKO, A. D. RYON, and D. W. KUHN. J. Phys. Chem. **62**, 319 (1958).

Can. J. Chem. Downloaded from www.nrcresearchpress.com by 210.87.254.40 on 09/06/12
For personal use only.

Allylic derivatives of nickel and palladium

KENNETH S. CHONG, STEVEN J. RETTIG, ALAN STORR, AND JAMES TROTTER

Department of Chemistry, University of British Columbia, 2036 Main Mall, Vancouver, B.C., Canada V6T 1Y6

Received September 10, 1980

KENNETH S. CHONG, STEVEN J. RETTIG, ALAN STORR, and JAMES TROTTER. Can. J. Chem. **59**, 996 (1981).

The synthesis of novel allylic derivatives of Ni and Pd incorporating the bispyrazolylgallate ligand $Me_2Ga(N_2C_5H_7)_2^-$ is described. Pyrazolyl-bridged homobinuclear and trinuclear nickel allyl systems are also presented. Crystal structures of $[Me_2Ga(N_2C_5H_7)_2]Ni(\eta^3\text{-}C_3H_5)$ and $[(\eta^3\text{-}C_3H_5)Ni(N_2C_5H_7)_2]_2Ni$ are described. Crystals of the former are triclinic, $a = 8.265(1)$, $b = 10.487(1)$, $c = 11.755(2)$ Å, $\alpha = 72.60(1)$, $\beta = 87.28(1)$, $\gamma = 67.58(1)°$, $Z = 2$, space group $P\bar{1}$ and crystals of the latter are monoclinic, $a = 7.9172(3)$, $b = 10.6929(1)$, $c = 16.9118(6)$ Å, $\beta = 102.887(2)°$, $Z = 2$, space group $P2_1/c$. Both structures were solved by Patterson and Fourier syntheses and were refined by full-matrix least-squares procedures to $R = 0.026$ and 0.025 for 3329 and 2914 reflections with $I \geq 3\sigma(I)$ respectively. In both structures the M—(N—N)$_2$—M rings are in the boat conformation and the allyl groups display twofold orientational disorder. In $[Me_2Ga(N_2C_5H_7)_2]Ni(\eta^3\text{-}C_3H_5)$ the nickel coordination may be regarded as square-planar with the allyl ligand occupying two coordination sites and the coordination about the gallium is distorted tetrahedral. Important bond lengths (corrected for libration) are: Ni—N, 1.926(2) and 1.929(2), Ni—C, 1.971(5)–2.025(3), Ga—N, 1.994(2) and 1.996(2), Ga—C, 1.966(3) and 1.988(3) Å. The trinuclear complex $[(\eta^3\text{-}C_3H_5)Ni(N_2C_5H_7)_2]_2Ni$ is centrosymmetric with the central Ni(1) atom bonded to four pyrazolyl nitrogen atoms in square-planar fashion. The outer Ni(2) atom is bonded to two pyrazolyl nitrogens and to an allyl group and also has square-planar coordination geometry. Important bond distances in this complex are: Ni(1)—N, 1.897(1) and 1.901(1), Ni(2)—N, 1.908(2) and 1.912(2), Ni(2)—C, 1.97(1)–2.022(3) Å.

KENNETH S. CHONG, STEVEN J. RETTIG, ALAN STORR et JAMES TROTTER. Can. J. Chem. **59**, 996 (1981).

On décrit la synthèse de nouveaux dérivés allyliques du Ni et du Pd dans lesquels on a incorporé le ligand bispyrazolylgallate, $Me_2Ga(N_2C_5H_7)_2^-$. On a aussi obtenu les systèmes allyliques homobinucléaire et trinucléaire du nickel ayant un pyrazolyle en position de pont. On décrit les structures du cristal de $[Me_2Ga(N_2C_5H_7)_2]Ni(\eta^3\text{-}C_3H_5)$ et du $[(\eta^3\text{-}C_3H_5)Ni(N_2C_5H_7)_2]_2Ni$. Les cristaux du premier composé sont tricliniques avec $a = 8{,}265(1)$, $b = 10{,}487(1)$, $c = 11{,}755(2)$ Å, $\alpha = 72{,}60(1)$, $\beta = 87{,}28(1)$, $\gamma = 67{,}58(1)°$, $Z = 2$, groupe d'espace $P\bar{1}$ et les cristaux du deuxième composé sont monocliniques avec $a = 7{,}9172(3)$, $b = 10{,}6929(1)$, $c = 16{,}9118(6)$ Å, $\beta = 102{,}887(2)°$, $Z = 2$, groupe d'espace $P2_1/c$. On a résolu les deux structures par les synthèses de Patterson et de Fourier et on les a affinées par la méthode des moindres carrés (matrice entière) jusqu'à des valeurs respectives de R de 0,026 et 0,025 pour 3329 et 2914 réflexions avec $I \geq 3\sigma(I)$. Dans les deux structures, les cycles M—(N—N)$_2$—M ont une conformation bateau et les groupes allyles montrent un double désordre d'orientation. On peut considérer la coordination du Ni du composé $[Me_2Ga(N_2C_5H_7)_2]Ni(\eta^3\text{-}C_3H_5)$ comme plan carré avec le ligand allyle occupant deux sites de coordination alors que la coordination autour du gallium est tétraédrique déformée. Les longueurs de liaisons importantes (corrigées pour la libration) sont: Ni—N, 1,926(2), et 1,929(2), Ni—C, 1,971(1)–2,025(3), Ga—N, 1,994(2) et 1,996(2), Ga—C 1,966(3) et 1,988(3) Å. Le complexe trinucléaire $[(\eta^3\text{-}C_3H_5)Ni(N_2C_5H_7)_2]_2Ni$ est centrosymétrique avec l'atome de nickel central lié à 4 atomes d'azote du pyrazolyle de manière plan carré. L'atome de nickel extérieur est lié à deux atomes d'azote du pyrazolyle et à un groupe allyle et a également une géométrie de coordination plan carré. Les distances de liaison importantes de ce complexe sont: Ni(1)—N, 1,897(1) et 1,901(1), Ni(2)—N, 1,908(2) et 1,912, Ni(2)—C, 1,97(1)–2,022(3)Å.

[Traduit par le journal]

Introduction

Earlier reports have described the synthesis of bidentate chelating anionic pyrazolyl gallate ligands of the type $Me_2Ga(N_2C_3H_3)_2^-$ and their complexation with divalent transition metal ions (1–4). More recent studies have extended this work to include both symmetrical tridentate chelating ligands of the type $MeGa(N_2C_3H_3)_3^-$ (5), and unsymmetrical tridentate chelating ligands of the type $[Me_2Ga(N_2C_3H_3)(OCH_2CH_2NMe_2)]^-$ (ref. 6 and references therein). The present account describes the use of the above bidentate ligands in the preparation of some allylic derivatives of both Ni and Pd and also our attempts to complex the unsymmetrical tridentate gallate ligands to the Ni(allyl) moiety. The crystal structure determinations of the complexes $[Me_2Ga(N_2C_5H_7)_2]Ni(\eta^3\text{-}C_3H_3)$ and $[(\eta^3\text{-}C_3H_3)Ni(N_2C_5H_7)_2]_2Ni$ are described.

Experimental

Starting Materials

Air-sensitive materials were handled in a glove box under an atmosphere of oxygen-free dry nitrogen or in a nitrogen-blanketed apparatus. Tetrahydrofuran (THF) was dried by refluxing over sodium/benzophenone and was used immediately following distillation. Benzene was dried by refluxing over potassium followed by distillation. The bidentate gallium ligand $Na^+Me_2Ga(N_2C_5H_7)_2^-$ was prepared as described previously (4) and used as a THF solution. The tridentate ligand $Na^+[Me_2Ga(N_2C_5H_7)(OCH_2CH_2NMe_2)]^-$ was prepared as a THF solution as described earlier (7). $(C_3H_5)_2Ni$ was prepared from $(C_3H_5)MgCl$ and $NiBr_2$ and subsequently converted to $[(C_3H_5)NiBr]_2$ by reaction with HBr (8). The $[(\text{"allyl"})PdCl]_2$ compounds ("allyl" = $\eta^3\text{-}C_3H_5$ and $\eta^3\text{-}C_4H_7$) were prepared via reaction of $PdCl_2$ with the appropriate "allyl"Cl in the presence of CO and MeOH (9).

Preparation of $[Me_2Ga(N_2C_5H_7)_2]Pd$"allyl" Compounds

$[(C_4H_7)PdCl]_2$ (0.394 g, 1.5 mmol) was dissolved in THF and $Na^+Me_2Ga(N_2C_5H_7)_2^-$ (3.0 mmol) in the same solvent added. The yellow solution slowly turned colorless and after stirring for

0008-4042/81/060996-11$01.00/0

©1981 National Research Council of Canada/Conseil national de recherches du Canada

Can. J. Chem. Downloaded from www.nrcresearchpress.com by 210.87.254.6 on 09/06/12
For personal use only.

Can. J. Chem. Downloaded from www.nrcresearchpress.com by 210.87.254.6 on 09/06/12
For personal use only.

1 h, solvent was removed *in vacuo* and the residue extracted with benzene. Filtration of the extracts followed by slow evaporation of the filtrate gave white crystals of the product. Yield ~60%. *Anal.* calcd. for $Me_2Ga(N_2C_5H_7)_2Pd(C_4H_7)$: C 42.6, H 6.0, N 12.4; found: C 42.8, H 6.0, N 12.4. ^1H nmr (C_6D_6 solution): τ = 9.65s, 9.55s ($GaMe_2$), 8.28s (*Me* allyl), 7.92s, 7.78s, (pz-Me), 7.51s (*anti*-H), 6.71s (*syn*-H), 4.21s (pz-H(4)) ($\tau_{C_6H_6}$ = 2.84 ppm; s = singlet; pz = pyrazolyl).

The compound $[Me_2Ga(N_2C_5H_7)_2]Pd(C_3H_5)$ was prepared in an identical manner from $[(C_3H_5)PdCl]_2$ starting material. Yield ~75%. *Anal.* calcd. for $[Me_2Ga(N_2C_5H_7)_2]Pd(C_3H_5)$: C 41.2, H 5.8, N 12.8; found: C 41.3, H 5.8, N 13.2. ^1H nmr (C_6D_6 solution): τ = 9.67s, 9.62s ($GaMe_2$), 7.96s, 7.80s (pz-Me), 7.53d (J = 12 Hz, *anti*-H), 6.22d (J = 7 Hz, *syn*-H), 5.02tt (J = 7, 12 Hz, unique-H) 4.22s (pz-H(4)) (d = doublet, tt = triplet of triplets).

Preparation of $[Me_2Ga(N_2C_5H_7)_2]Ni(\eta^3\text{-}C_3H_5)$

A THF solution of $[(C_3H_5)NiBr]_2$ (0.287 g, 0.8 mmol) was cooled to −78°C and a solution of the ligand $Na^+Me_2Ga(N_2C_5H_7)_2^-$ (1.6 mmol) in the same solvent added dropwise over 30 min. The color of the solution gradually changed from red to yellow and after stirring for a further 30 min at 0°C, $MgSO_4$ (~5 g) was added and the mixture filtered. Removal of solvent from the filtrate gave yellow–brown crystals of the product in approximately 70% yield. *Anal.* calcd. for $[Me_2Ga(N_2C_5H_7)_2]Ni(\eta^3\text{-}C_3H_5)$: C 46.2, H 6.5, N 14.4; found: C 46.0, H 6.5, N 14.4. ^1H nmr (C_6D_6 solution): 9.66s, br, 9.19s, br ($GaMe_2$), 7.99d (J = 12 Hz, *anti*-H), 7.89s, 7.81s (pz-Me), 7.29d, br (J = 7 Hz, *syn*-H), 4.70tt, br (J = 7, 12 Hz, unique-H), 4.36s (pz-H(4)) (br = broad).

Reaction of Na^+L^- with $[(C_3H_5)NiBr]_2$

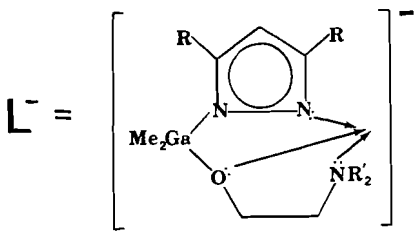

A THF solution of $[(C_3H_5)NiBr]_2$ was cooled to −78°C and a double molar amount of the ligand Na^+L^-, in the same solvent, was added dropwise. Slowly the red solution became yellow and a white precipitate formed. After stirring the reaction mixture for 1 h at 0°C, volatiles were removed *in vacuo*. In some cases, a yellow solid co-condensed in the cold trap and this material was identified as $(C_3H_5)_2Ni$ by mass spectrometry. The remaining yellow–brown residue was extracted with heptane to leave a green or blue residue (the color of the residue depended on the substituents on the ligand L). The heptane extracts were filtered and evaporation of the filtrate gave red crystals of $[Ni(N_2C_5H_7)(C_3H_5)]_2$ or $[Ni(N_2C_3H_3)(C_3H_5)]_2$. Finally, the green or blue residue was extracted with benzene. Filtration followed by evaporation of the filtrate gave crystals of the complexes L_2Ni (10, 11), $[LNi(N_2C_3H_3)]_2$ (7), or $LNi[(N_2C_5H_7)_2GaMe_2]$ (11) depending on the ligand L^-. These complexes have all been described previously.

Preparation of $[Ni(N_2C_5H_7)(C_3H_5)]_2$

$[(C_3H_5)NiBr]_2$ (0.180 g, 0.5 mmol) was dissolved in THF and a solution of $Na^+N_2C_5H_7^-$ (0.118 g, 1.0 mmol) in the same solvent added. The color of the solution changed from red to yellow and after the reaction mixture had been stirred for 24 h, the solvent was removed *in vacuo*. The remaining yellow residue was extracted with benzene and slow evaporation of the filtered extracts yielded a red crystalline product in approximately 40% yield. *Anal.* calcd. for $[Ni(N_2C_5H_7)(C_3H_5)]_2$: C 49.3, H 6.2, N 14.4; found: C 49.1, H 6.3, N 14.1. ^1H nmr (C_6D_6 solution): 7.89s, 7.89s, 7.81s, 7.64s (pz-Me), 7.71d, 7.79d (J = 14 Hz, *anti*-H), 7.18d, 6.96d ($J \approx$ 7 Hz, *syn*-H), 4.58m (unique-H), 4.21s (pz-H(4)) (m = multiplet).

Spectra

The mass spectra were collected on a Varian MAT CH4 spectrometer at 70 eV with an ion source temperature of 100–180°C and the ^1H nmr spectra on a Varian XL-100 spectrometer using FT techniques.

X-ray Crystallographic Analyses

[Dimethylbis(3,5-dimethyl-1-pyrazolyl)gallato(N',N')](η³-allyl)-nickel(II)

The crystal chosen was mounted in a general orientation and had dimensions of ca. 0.11 × 0.32 × 0.65 mm. Unit-cell parameters were refined by least-squares on 2 sin θ/λ values for 25 reflections measured on a diffractometer with Mo K_α radiation (λ = 0.71073 Å). Crystal data (at 22°C) are:

$C_{15}H_{25}GaN_4Ni$ f.w. = 389.82

Triclinic, a = 8.265(1), b = 10.487(1), c = 11.755(2) Å, α = 72.60(1), β = 87.28(1), γ = 67.58(1)°, V = 896.2(2) Å³, Z = 2, ρ_c = 1.445 gcm⁻³, $F(000)$ = 404, μ(Mo K_α) = 25.5 cm⁻¹. Absent reflections: none, space group $P\bar{1}$ (C_i^1, No. 2) from structure analysis.

Intensities were measured with graphite monochromatized Mo K_α radiation on an Enraf-Nonius CAD4-F diffractometer. An ω–2θ scan at 0.91–10.06° min⁻¹ over a range of (0.65 + 0.35 tan θ) degrees in ω (extended by 25% on both sides for background measurement) was employed. Data were measured to 2θ = 55°. The intensities of 3 check reflections, measured every 3600 s throughout the data collection, remained constant to within ±1.5%. After data reduction, an absorption correction was applied using the Gaussian integration method (12, 13). Transmission factors ranged from 0.429 to 0.769 for 224 sampling points. Of the 5199 independent reflections measured, 3329 (64%) had intensities greater than 3σ(I) above background where $\sigma^2(I) = S + 2B + (0.04(S - B))^2$ with S = scan count and B = background count.

Analysis was initiated in the centrosymmetric space group $P\bar{1}$ on the basis of the E-statistics. The coordinates of the Ga and Ni atoms were determined from the Patterson function and those of the remaining non-hydrogen atoms from a subsequent difference map. Refinement of the non-hydrogen atoms with anisotropic thermal parameters gave R = 0.040. A difference map at this point indicated twofold disordering of the central allyl carbon atom. The C(4) and C(4′) atoms were included in the refinement with isotropic thermal parameters and fixed occupancy factors of 0.5 for each site. The resulting isotropic thermal parameters were employed to estimate the site occupancies at 0.6 for C(4) and 0.4 for C(4′). These atoms were then assigned anisotropic thermal parameters and the structure refined to R = 0.037. All hydrogen atoms (including disordered allyl hydrogens) were located from a subsequent difference map and were included in the refinement with isotropic thermal parameters. The occupancy factors for the disordered atoms were kept fixed at the previously determined values. The scattering factors of ref. 14 were used for non-hydrogen atoms and those of ref. 15 for hydrogen atoms. Anomalous scattering factors from ref. 16 were used for the Ni atoms. The weighting scheme, $w = 1/\sigma^2(F)$

Can. J. Chem. Downloaded from www.nrcresearchpress.com by 210.87.254.6 on 09/06/12
For personal use only.

TABLE 1. Final positional parameters (fractional N and C × 10^4, Ga and Ni × 10^5, H × 10^3) with estimated standard deviations in parentheses

Atom*	*x*	*y*	*z*
	$[Me_2Ga(N_2C_5H_7)_2]Ni(\eta^3\text{-}C_3H_5)$		
Ga	61733(3)	36083(2)	32000(2)
Ni	63000(4)	7143(3)	26070(3)
N(1)	6919(2)	3342(2)	1623(2)
N(2)	6922(2)	2122(2)	1412(2)
N(3)	3978(2)	3259(2)	3161(2)
N(4)	4060(2)	2108(2)	2793(2)
C(1)	5684(5)	5597(3)	3185(3)
C(2)	7817(4)	1983(4)	4490(3)
C(3)	8581(6)	−962(4)	2717(4)
C(4)′	7297(8)	−1412(5)	3004(7)
C(4′)″	7706(13)	−1226(8)	3725(11)
C(5)	6130(6)	−1037(3)	3846(4)
C(6)	7361(3)	4147(3)	618(2)
C(7)	7656(4)	3440(3)	−226(2)
C(8)	7360(3)	2186(3)	289(2)
C(9)	2282(3)	4010(2)	3299(2)
C(10)	1283(3)	3353(3)	3002(2)
C(11)	2418(3)	2181(3)	2689(2)
C(12)	7463(5)	5570(4)	506(3)
C(13)	7378(6)	1061(5)	−255(3)
C(14)	1719(5)	5303(3)	3733(3)
C(15)	2008(5)	1138(4)	2249(4)
H(1a)	491(5)	628(4)	256(3)
H(1b)	543(5)	563(4)	396(4)
H(1c)	672(5)	567(4)	320(3)
H(2a)	755(7)	221(5)	502(5)
H(2b)	795(6)	134(5)	446(4)
H(2c)	881(8)	190(5)	441(5)
H(3a)	910(8)	−109(6)	218(5)
H(3b)′	931(8)	−87(6)	350(6)
H(3c)″	736(20)	−94(15)	195(14)
H(4)′	682(9)	−190(8)	239(6)
H(4′)″	828(12)	−118(9)	426(8)
H(5a)	528(7)	−101(6)	426(5)
H(5b)′	665(8)	−73(6)	456(5)
H(5c)″	564(11)	−122(8)	325(8)
H(7)	790(4)	381(3)	−100(3)
H(10)	14(4)	363(3)	301(3)
H(12a)	842(7)	551(5)	102(4)
H(12b)	647(6)	625(5)	65(4)
H(12c)	798(5)	577(4)	−10(4)
H(13a)	828(6)	8(5)	5(4)
H(13b)	735(6)	162(5)	−122(5)
H(13c)	646(6)	82(5)	−4(4)
H(14a)	220(6)	509(5)	451(5)
H(14b)	61(5)	559(4)	382(3)
H(14c)	201(4)	616(4)	314(3)
H(15a)	290(5)	51(4)	201(3)
H(15b)	87(6)	149(4)	198(4)
H(15c)	200(6)	34(5)	285(4)
	$[(\eta^3\text{-}C_3H_5)Ni(N_2C_5H_7)_2]_2Ni$ (coordinates × 10^5, C(2′) × 10^4, H × 10^3)		
Ni(1)	50000	50000	50000
Ni(2)	28443(3)	27245(2)	39919(1)
N(1)	29954(18)	43876(13)	53075(8)
N(2)	20827(19)	34155(14)	48903(9)
N(3)	36640(18)	52993(13)	39370(8)

TABLE 1. (*Concluded*)

Atom*	*x*	*y*	*z*
N(4)	27961(20)	43288(14)	34912(8)
C(1)	30203(41)	9387(21)	43608(18)
C(2)′	41387(48)	11834(26)	38783(22)
C(3)	35486(48)	16929(26)	31163(18)
C(4)	22556(24)	47052(18)	59209(11)
C(5)	8256(26)	39384(20)	58938(13)
C(6)	7706(24)	31464(20)	52476(12)
C(7)	34594(23)	63301(17)	34714(10)
C(8)	24413(26)	60325(19)	27180(11)
C(9)	20552(25)	47735(18)	27502(11)
C(10)	29298(35)	57207(21)	65079(14)
C(11)	−5005(37)	21297(31)	49422(17)
C(12)	42283(33)	75599(19)	37716(15)
C(13)	9954(42)	39611(28)	21085(15)
C(2′)″	2812(20)	1061(13)	3489(9)
H(1a)′	339(5)	78(3)	496(2)
H(1b)′	175(5)	78(4)	413(2)
H(1c)″	214	55	441
H(1d)″	406	82	473
H(2)′	540(6)	131(4)	411(3)
H(2′)″	181	67	318
H(3a)′	418(4)	199(3)	279(2)
H(3b)′	228(5)	143(3)	288(2)
H(3c)″	305	152	250
H(3d)″	485	196	334
H(5)	8(4)	396(2)	620(2)
H(8)	209(3)	662(2)	227(2)
H(10a)	334(4)	641(2)	628(2)
H(10b)	384(4)	549(3)	692(2)
H(10c)	192(4)	606(3)	668(2)
H(11a)	−73(3)	199(3)	437(2)
H(11b)	−19(4)	135(3)	516(2)
H(11c)	−146(6)	238(3)	504(2)
H(12a)	364(4)	816(3)	348(2)
H(12b)	553(5)	753(3)	385(2)
H(12c)	433(4)	766(3)	435(2)
H(13a)	25(5)	432(3)	178(2)
H(13b)	167(5)	341(3)	192(2)
H(13c)	35(5)	323(4)	232(2)

*Prime denotes occupancy 0.6 or 0.8, double primes denote occupancy 0.4 or 0.2 (see text).

where $\sigma^2(F)$ is derived from the previously defined $\sigma^2(I)$ gave uniform average values of $w(|F_o| - |F_c|)^2$ over ranges of $|F_o|$ and was employed in the final stages of refinement. Convergence was reached at $R = 0.026$ and $R_w = 0.031$ for 3329 reflections with $I \geq 3\sigma(I)$. For all 5199 reflections $R = 0.061$ and $R_w = 0.036$. The function minimized was $\Sigma w(|F_o| - |F_c|)^2$, $R = \Sigma||F_o| - |F_c||/\Sigma|F_o|$ and $R_w = (\Sigma w(|F_o| - |F_c|)^2/\Sigma w|F_o|^2)^{1/2}$.

On the final cycle of refinement the mean and maximum parameter shifts corresponded to 0.13 and 2.5σ (oscillating *x* for H(3c)) respectively. The mean error in an observation of unit weight was 0.9715. A final difference map showed no unusual features. The final positional and thermal parameters appear in Tables 1 and 2,[1] respectively. Measured and calculated structure factors have been placed in the Depository of Unpublished Data.[1]

[1]The structure factor table and Table 2 (thermal parameters) are available, at a nominal charge, from the Depository of Unpublished Data, CISTI, National Research Council of Canada, Ottawa, Ont., Canada K1A 0S2.

Bis[bis(3,5-dimethylpyrazolyl)(η³-allyl)niccolato(II)(N′,N′)]-nickel(II)

Details of the structure analysis are the same as for $[Me_2Ga(N_2C_5H_7)_2]Ni(\eta^3\text{-}C_3H_5)$ except where noted. Crystal dimensions were ca. 0.20 × 0.35 × 0.70 mm. Crystal data are:

$C_{26}H_{38}N_8Ni_3$ f.w. = 638.78

Monoclinic, $a = 7.9172(3)$, $b = 10.6929(1)$, $c = 16.9118(6)$ Å, $\beta = 102.887(2)°$, $V = 1395.65(7)$ Å^3, $Z = 2$, $\rho_c = 1.520$ gcm^{-3}, $F(000) = 668$, μ(Mo K$_\alpha$) = 20.4 cm^{-1}. Absent reflections: $h0l$, $l \neq 2n$ and $0k0$, $k \neq 2n$ define uniquely the space group $P2_1/c$ (C_{2h}^5, No. 14).

An ω–2θ scan at 1.06–10.06° min^{-1} over a range of (0.70 + 0.35 tan θ)° in ω was employed. Of 4030 reflections measured (to $2\theta = 60°$), 2914(72%) had intensities greater than $3\sigma(I)$ above background. An absorption correction was applied, transmission factors ranging from 0.503 to 0.663 for 264 sampling points.

The coordinates of the Ni atoms were determined from the Patterson function and those of the remaining non-hydrogen atoms from a subsequent difference map. Refinement of the

Can. J. Chem. Downloaded from www.nrcresearchpress.com by 210.87.254.6 on 09/06/12
For personal use only.

Can. J. Chem. Downloaded from www.nrcresearchpress.com by 210.87.254.6 on 09/06/12
For personal use only.

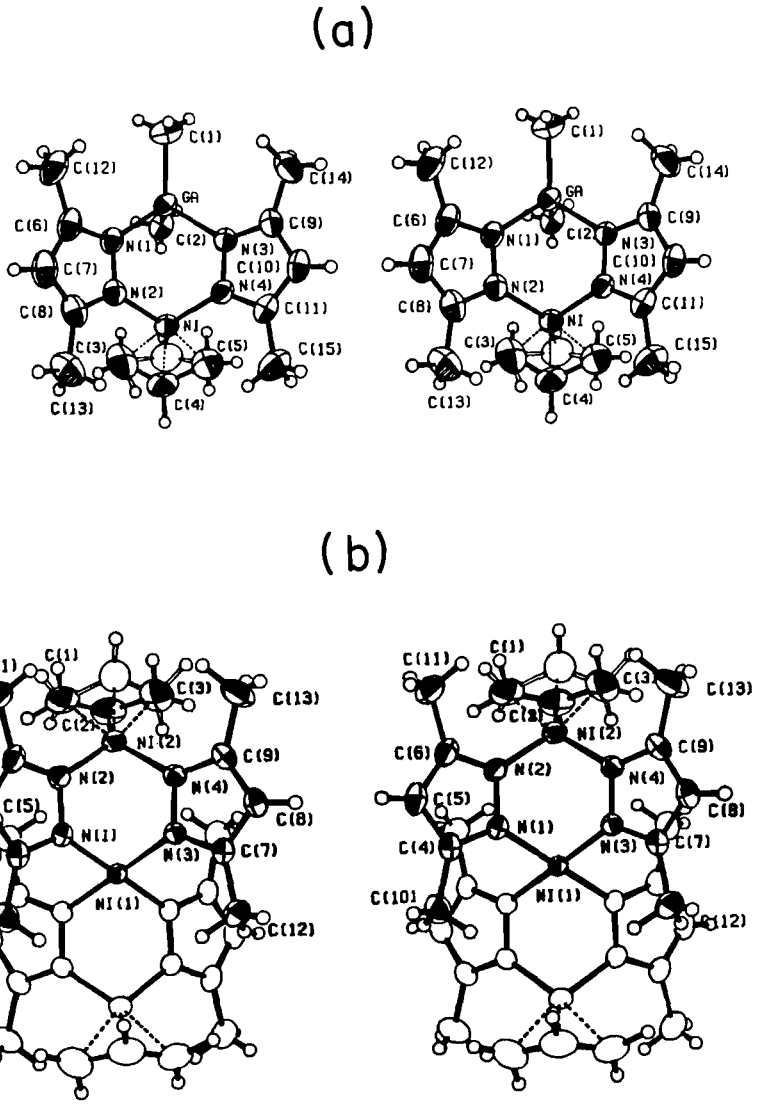

FIG. 1. Stereo views of [dimethylbis(3,5-dimethyl-1-pyrazolyl)gallato(N',N')](η^3-allyl)nickel(II) (*a*) and bis[bis(3,5-dimethylpyrazolyl)(η^3-allyl)niccolato(II) (N',N')]nickel(II) (*b*). 50% thermal ellipsoids are shown for the non-hydrogen atoms.

non-hydrogen atoms with anisotropic thermal parameters gave $R = 0.040$. The central allyl carbon atom was again disordered, this time the second site having a lower occupancy. The allyl disorder was treated as before, starting with occupancies of 0.75 for C(2) and 0.25 for C(2′) and adjusting to final values of 0.80 and 0.20. All hydrogen atoms except those associated with the 20% occupied allyl group were located from a difference map and were refined with isotropic thermal parameters. The hydrogen atom positions for the 20% occupied allyl were calculated and kept fixed in subsequent cycles of refinement. Convergence was reached at $R = 0.025$ and $R_w = 0.031$ for 2914 reflections with $I \geq 3\sigma(I)$, $R = 0.047$ and $R_w = 0.034$ for all 4030 reflections. The mean and maximum parameter shifts on the final cycle of refinement corresponded to 0.09 and 1.1σ respectively. The mean error in an observation of unit weight was 1.023. A final difference map showed maximum fluctuations of -0.47 to 0.36 e Å^{-3} near the metal atoms and ± 0.2 e Å^{-3} elsewhere.

The thermal motion in both molecules (shown in Fig. 1) has been analysed in terms of the rigid-body modes of translation, libration, and screw motion (17). For $[Me_2Ga(N_2C_5H_7)_2]Ni(\eta^3\text{-}C_3H_5)$ (rms $\sigma U_{ij} = 0.0018$ Å^2) analysis of all non-hydrogen atoms except the terminal allyl carbons, C(3) and C(5), gave physically reasonable results and rms $\Delta U_{ij} = 0.0031$ Å^2. For $[(\eta^3\text{-}C_3H_5)Ni(N_2C_5H_7)_2]_2Ni$ (rms $\sigma U_{ij} = 0.0010$ Å^2) analysis was successful for all non-hydrogen atoms except the allyl and methyl carbon atoms (rms $\Delta U_{ij} = 0.0020$ and 0.0015 Å^2 with and without constraint to $\bar{1}$ symmetry, bond distances being essentially identical for both cases). The appropriate bond distances have been corrected for libration (18), using shape parameters q^2 of 0.08 for all atoms involved. Corrected bond lengths appear in Table 3 along with the uncorrected values and corrected bond angles are within one standard deviation of the uncorrected values given in Table 4. Intra-annular torsion angles defining the conformations of the six-membered M_2N_4 rings are given in Table 5.

TABLE 3. Bond lengths (Å) with estimated standard deviations in parentheses
(*a*) Non-hydrogen atoms

Bond	Length		Bond	Length	
	Uncorr.	Corr.		Uncorr.	Corr.
			$[Me_2Ga(N_2C_5H_7)_2]Ni(\eta^3\text{-}C_3H_5)$		
Ga —N(1)	1.990(2)	1.996	N(3) —C(9)	1.351(3)	1.352
Ga —N(3)	1.988(2)	1.994	N(4) —C(11)	1.340(3)	1.341
Ga —C(1)	1.962(3)	1.966	C(3) —C(4)	1.310(7)	1.311
Ga —C(2)	1.983(3)	1.988	C(3) —C(4′)	1.371(11)	1.373
Ni —N(2)	1.920(2)	1.926	C(4) —C(5)	1.384(8)	1.386
Ni —N(4)	1.923(2)	1.929	C(4′) —C(5)	1.248(11)	1.250
Ni —C(3)	2.005(3)	2.007	C(6) —C(7)	1.369(4)	1.373
Ni —C(4)	1.970(5)	1.971	C(6) —C(12)	1.492(4)	1.493
Ni —C(4′)	1.990(8)	1.992	C(7) —C(8)	1.383(4)	1.387
Ni —C(5)	2.023(2)	2.025	C(8) —C(13)	1.496(4)	1.498
N(1)—N(2)	1.374(3)	1.379	C(9) —C(10)	1.372(4)	1.374
N(1)—C(6)	1.357(3)	1.360	C(9) —C(14)	1.492(4)	1.493
N(2)—C(8)	1.341(3)	1.342	C(10)—C(11)	1.373(4)	1.376
N(3)—N(4)	1.376(2)	1.381	C(11)—C(15)	1.488(4)	1.490
			$[(\eta^3\text{-}C_3H_5)Ni(N_2C_5H_7)_2]_2Ni$		
Ni(1)—N(1)	1.894(1)	1.897	N(4) —C(9)	1.346(2)	1.346
Ni(1)—N(3)	1.899(1)	1.901	C(1) —C(2)	1.357(5)	1.358
Ni(2)—N(2)	1.905(2)	1.908	C(1) —C(2′)	1.453(15)	
Ni(2)—N(4)	1.910(2)	1.912	C(2) —C(3)	1.381(5)	1.382
Ni(2)—C(1)	2.004(2)	2.004	C(2′) —C(3)	1.165(15)	
Ni(2)—C(2)	1.972(3)	1.973	C(4) —C(5)	1.390(3)	1.392
Ni(2)—C(2′)	1.969(14)		C(4) —C(10)	1.488(3)	1.489
Ni(2)—C(3)	2.022(3)	2.022	C(5) —C(6)	1.376(3)	1.377
N(1) —N(2)	1.369(2)	1.371	C(6) —C(11)	1.493(3)	1.494
N(1) —C(4)	1.344(2)	1.346	C(7) —C(8)	1.384(3)	1.386
N(2) —C(6)	1.344(2)	1.344	C(7) —C(12)	1.490(3)	1.492
N(3) —N(4)	1.373(2)	1.376	C(8) —C(9)	1.384(3)	1.385
N(3) —C(7)	1.343(2)	1.344	C(9) —C(13)	1.493(3)	1.494

Results and Discussion

In a previous publication the preparation of several compounds of the general type DNi(NO) (where D is a tridentate pyrazolyl gallate ligand) were discussed (19). The formal replacement of the three electron NO ligand by the three electron "allyl" ligand leads to a marked difference in the stability of the resulting compounds. Thus when Na^+L^- was reacted with $[(C_3H_5)NiBr]_2$, the isolated gallium containing product was inevitably the same Ni(II) product obtained from the reaction of Na^+L^- with $NiBr_2$ (7, 10, 11). In addition when Na^+L^- (R = R′ = Me) was reacted with ["allyl"-$PdCl]_2$ (allyl = C_3H_5 or C_4H_7) the only "allyl" product isolated was $[Pd(N_2C_5H_7)$ "allyl"$]_2$. Thus with neither the nickel allyl nor the palladium allyl systems were we able to isolate complexes incorporating a tridentate gallate ligand. It is perhaps noteworthy that using the cyclopentadienyl ligand in this area the compounds $CpPd(C_3H_5)$ (9) and $CpNi(C_3H_5)$ (20) have both been prepared and the former compound has been structurally characterized (21). In addition the pyrazolyl borate compound $[HB(N_2C_3H_3)_3]Pd(C_3H_5)$ has also been prepared but ^1H nmr data for this compound suggest a bidentate pyrazolylborate ligand (22). In sharp contrast the reactions of $[(C_3H_5)NiBr]_2$ and ["allyl"$PdCl]_2$ with bidentate pyrazolyl gallate ligands did give the expected compounds. In the case of the Ni derivative the stability of the resulting compound (it can be sublimed under vacuum at 60°C without change) is again in marked contrast to the nickel nitrosyl system where compounds containing a bispyrazolyl gallate ligand could not be isolated.

The compounds $[Me_2Ga(N_2C_5H_7)_2]$Pd"allyl" and $[Me_2Ga(N_2C_5H_7)_2]Ni(\eta^3\text{-}C_3H_5)$ were prepared by the reaction of $Na^+[Me_2Ga(N_2C_5H_7)_2]^-$ with ["allyl"$PdCl]_2$ and $[(C_3H_5)NiBr]_2$ respectively. The mass spectra of all three complexes showed weak signals due to the parent ions (~5%) with other strong signals due to the ions P—Me^+ (60%) and P—Me—"allyl"-H^+ (100%) (where P = parent).

The ^1H nmr spectra of the two palladium compounds $[Me_2Ga(N_2C_5H_7)_2]Pd(C_4H_7)$ and $[Me_2Ga$-

Can. J. Chem. Downloaded from www.nrcresearchpress.com by 210.87.254.6 on 09/06/12
For personal use only.

Can. J. Chem. Downloaded from www.nrcresearchpress.com by 210.87.254.6 on 09/06/12
For personal use only.

TABLE 4. Bond angles (deg) with estimated standard deviations in parentheses, non-hydrogen atoms

Bonds	Angle (deg)	Bonds	Angle (deg)
	$[Me_2Ga(N_2C_5H_7)_2]Ni(\eta^3\text{-}C_3H_5)$		
N(1) —Ga —N(3)	96.63(7)	N(4) —N(3) —C(9)	108.2(2)
N(1) —Ga —C(1)	110.8(1)	Ni —N(4) —N(3)	120.0(1)
N(1) —Ga —C(2)	109.2(1)	Ni —N(4) —C(11)	132.3(2)
N(3) —Ga —C(1)	111.7(1)	N(3) —N(4) —C(11)	107.6(2)
N(3) —Ga —C(2)	107.7(1)	Ni —C(3) —C(4)	69.3(3)
C(1) —Ga —C(2)	118.6(2)	Ni —C(3) —C(4′)	69.4(3)
N(2) —Ni —N(4)	93.82(7)	Ni —C(4) —C(3)	72.2(2)
N(2) —Ni —C(3)	96.2(1)	Ni —C(4) —C(5)	71.8(2)
N(2) —Ni —C(4)	129.3(2)	C(3) —C(4) —C(5)	124.3(6)
N(2) —Ni —C(4′)	133.0(3)	Ni —C(4′) —C(3)	70.5(4)
N(2) —Ni —C(5)	168.7(1)	Ni —C(4′) —C(5)	73.3(4)
N(4) —Ni —C(3)	169.3(1)	C(3) —C(4′) —C(5)	130.8(10)
N(4) —Ni —C(4)	133.8(2)	Ni —C(5) —C(4)	67.7(2)
N(4) —Ni —C(4′)	129.1(3)	Ni —C(5) —C(4′)	70.5(4)
N(4) —Ni —C(5)	97.4(1)	N(1) —C(6) —C(7)	108.6(2)
C(3) —Ni —C(4)	38.5(2)	N(1) —C(6) —C(12)	123.4(3)
C(3) —Ni —C(4′)	40.1(3)	C(7) —C(6) —C(12)	128.0(3)
C(3) —Ni —C(5)	72.5(2)	C(6) —C(7) —C(8)	106.4(2)
C(4) —Ni —C(5)	40.5(2)	N(2) —C(8) —C(7)	109.1(2)
C(4′)—Ni —C(5)	36.2(3)	N(2) —C(8) —C(13)	121.5(3)
Ga —N(1)—N(2)	117.0(1)	C(7) —C(8) —C(13)	129.2(2)
Ga —N(1)—C(6)	134.8(2)	N(3) —C(9) —C(10)	108.2(2)
N(2) —N(1)—C(6)	108.1(2)	N(3) —C(9) —C(14)	122.6(2)
Ni —N(2)—N(1)	121.2(1)	C(10)—C(9) —C(14)	129.1(2)
Ni —N(2)—C(8)	131.0(2)	C(9) —C(10) —C(11)	106.8(2)
N(1) —N(2)—C(8)	107.8(2)	N(4) —C(11) —C(10)	109.1(2)
Ga —N(3)—N(4)	117.6(1)	N(4) —C(11) —C(15)	122.1(3)
Ga —N(3)—C(9)	133.8(2)	C(10)—C(11) —C(15)	128.7(3)
	$[(\eta^3\text{-}C_3H_5)Ni(N_2C_5H_7)_2]_2Ni$		
N(1) —Ni(1)—N(3)	89.67(6)	Ni(2)—N(4) —C(9)	133.7(1)
N(1) —Ni(1)—N(3)*	90.33(6)	N(3) —N(4) —C(9)	107.7(1)
N(2) —Ni(2)—N(4)	91.53(6)	Ni(2)—C(1) —C(2)	68.8(2)
N(2) —Ni(2)—C(1)	97.7(1)	Ni(2)—C(1) —C(2′)	67.3(6)
N(2) —Ni(2)—C(2)	131.7(1)	Ni(2)—C(2) —C(1)	71.3(2)
N(2) —Ni(2)—C(2′)	136.0(4)	Ni(2)—C(2) —C(3)	71.7(2)
N(2) —Ni(2)—C(3)	169.7(1)	C(1) —C(2) —C(3)	120.5(3)
N(4) —Ni(2)—C(1)	170.8(1)	Ni(2)—C(2′)—C(1)	69.8(6)
N(4) —Ni(2)—C(2)	131.8(1)	Ni(2)—C(2′)—C(3)	75.5(7)
N(4) —Ni(2)—C(2′)	128.5(4)	C(1) —C(2′)—C(3)	130.1(12)
N(4) —Ni(2)—C(3)	98.4(1)	Ni(2)—C(3) —C(2)	67.9(2)
C(1) —Ni(2)—C(2)	39.9(1)	Ni(2)—C(3) —C(2′)	70.6(7)
C(1) —Ni(2)—C(2′)	42.9(4)	N(1) —C(4) —C(5)	108.5(2)
C(1) —Ni(2)—C(3)	72.4(1)	N(1) —C(4) —C(10)	123.1(2)
C(2) —Ni(2)—C(3)	40.4(1)	C(5) —C(4) —C(10)	128.4(2)
C(2′) —Ni(2)—C(3)	33.9(4)	C(4) —C(5) —C(6)	105.7(2)
Ni(1) —N(1) —N(2)	120.0(1)	N(2) —C(6) —C(5)	109.6(2)
Ni(1) —N(1) —C(4)	131.4(1)	N(2) —C(6) —C(11)	121.9(2)
N(2) —N(1) —C(4)	108.6(1)	C(5) —C(6) —C(11)	128.5(2)
Ni(2) —N(2) —N(1)	118.8(1)	N(3) —C(7) —C(8)	108.7(2)
Ni(2) —N(2) —C(6)	133.6(1)	N(3) —C(7) —C(12)	122.5(2)
N(1) —N(2) —C(6)	107.6(2)	C(8) —C(7) —C(12)	128.8(2)
Ni(1) —N(3) —N(4)	119.8(1)	C(7) —C(8) —C(9)	106.0(2)
Ni(1) —N(3) —C(7)	131.5(1)	N(4) —C(9) —C(8)	109.0(2)
N(4) —N(3) —C(7)	108.5(1)	N(4) —C(9) —C(13)	121.9(2)
Ni(2) —N(4) —N(3)	118.5(1)	C(8) —C(9) —C(13)	129.1(2)

*Coordinates related to those in Table 1 by $1-x, 1-y, 1-z$.

TABLE 5. Intra-annular torsion angles (deg) in chelate rings

$[Me_2Ga(N_2C_5H_7)_2]Ni(\eta^3\text{-}C_3H_5)$		$[(\eta^3\text{-}C_3H_5)Ni(N_2C_5H_7)_2]_2Ni$	
Bond	Obs.	Bond	Obs.
Ga —N(1)	−49.5(1)	Ni(1)—N(1)	56.7(1)
N(1)—N(2)	−1.8(1)	N(1) —N(2)	−1.2(1)
N(2)—Ni	55.2(1)	N(2) —Ni(2)	−54.4(1)
Ni —N(4)	−60.5(1)	Ni(2)—N(4)	52.5(1)
N(4)—N(3)	10.7(1)	N(4) —N(3)	4.2(1)
N(3)—Ga	44.5(1)	N(3) —Ni(1)	−58.4(1)

$(N_2C_5H_7)_2]Pd(C_3H_5)$ are shown in Fig. 2. In each case only one signal is observed for each of the *syn* and *anti* protons of the "allyl" group and this is indicative of either a rapidly rotating or symmetrically coordinated (with respect to the gallate ligand) "allyl" group. The observation of two signals for the Ga—Me protons is consistent with a boat conformation for the Ga—(N—N)$_2$—Pd ring, a configuration demonstrated for the nickel derivative $[Me_2Ga(N_2C_5H_7)_2]Ni(\eta^3\text{-}C_3H_5)$ in the solid state through a crystal structure determination (see below).

The rt ^{1}H nmr spectrum of $[Me_2Ga(N_2C_5H_7)_2]$-$Ni(\eta^3\text{-}C_3H_5)$ was similar to that of the analogous Pd derivative shown in Fig. 2*b* but the signals due to the $GaMe_2$ and the allyl *syn* protons were fairly broad. Variable temperature ^{1}H nmr spectra for this Ni complex confirmed our expectations of a fluxional species in solution. On cooling an acetone-d_6 solution the $GaMe_2$ signals gradually sharpened until at 0°C the low temperature limiting spectrum was reached. Conversely, on warming the sample solution, the original broad $GaMe_2$ signals disappeared to be replaced by a single signal at ~60°C. A probable explanation for these observations is that at low temperatures the boat conformation for the Ga—(N—N)$_2$—Ni ring is static but at high temperatures this six-membered ring is rapidly inverting (see Fig. 3). A similar mechanism has been proposed for the fluxional behavior of the complex $[Me_2Ga(N_2C_3H_3)_2]_2Ni$ in solution. Two GaMe signals were again observed at low temperature but only one GaMe signal was observed at high temperature (2). In the present mechanism it has been assumed that the allyl group is rapidly rotating at higher temperatures.

The nickel compound was also found to undergo a novel disproportionation reaction in solution:

$$2[Me_2Ga(N_2C_5H_7)_2]Ni(\eta^3\text{-}C_3H_5) \rightleftharpoons [Me_2Ga(N_2C_5H_7)]_2 + [Ni(N_2C_5H_7)(C_3H_5)]_2$$

The extent of this reaction was monitored by ^{1}H nmr spectroscopy. Freshly prepared solutions of $[Me_2Ga(N_2C_5H_7)_2]Ni(\eta^3\text{-}C_3H_5)$ showed no extraneous signals. However, after 1 day at room temperature, substantial amounts of $[Me_2Ga(N_2C_5H_7)]_2$ and $[Ni(N_2C_5H_7)(C_3H_5)]_2$ were evident in the sample solution. (These were identified by comparison of the new signals with the ^{1}H nmr spectra of the pure materials.) The extent of the disproportionation increased gradually over approximately one week after which time the relative amounts of the three species appeared constant.

The compound $[Ni(N_2C_5H_7)(C_3H_5)]_2$ was readily prepared directly by the reaction of $Na^+(N_2C_5H_7)^-$ with $[(C_3H_5)NiBr]_2$. The predicted dimeric nature of this compound was confirmed by mass spectrometry and the ^{1}H nmr spectrum was found to be similar to that reported for the palladium analog $[Pd(N_2C_5H_7)(C_3H_5)]_2$ (23). The observation of four signals for the pyrazolyl methyl protons and fairly complicated patterns for the allyl protons suggest that a number of conformational isomers may exist in solutions of this Ni complex, a phenomenon invoked by Trofimenko to rationalize the ^{1}H nmr spectrum of the Pd analog (23). This conformational isomerism may also have thwarted our numerous attempts to produce high quality single crystals suitable for X-ray diffraction studies. An incomplete structure analysis of this compound[2] has provided some important information (see below). In our attempts to produce good quality crystals of $[Ni(N_2C_5H_7)(C_3H_5)]_2$ we inadvertantly produced very small quantities of excellent crystals of the trimetallic nickel complex $[(\eta^3\text{-}C_3H_5)Ni(N_2C_5H_7)_2]_2Ni$. The structure of this complex is described below and consists of the same type of double boat conformation about the central square-planar Ni atom observed in related molecules (1, 3, 24).

[2]Crystals of $[Ni(N_2C_5H_7)(C_3H_5)]_2$ are monoclinic, a = 6.677(1), b = 15.846(2), c = 8.870(1) Å, β = 107.01(1)°, Z = 2, space group $C2/m$, Cm or $C2$ (the noncentrosymmetric space groups being strongly indicated by the E-statistics). The nickel and pyrazolyl positions have been determined in both Cm and $C2$ but the allyl group appears to be severely disordered. No satisfactory solution has yet been found.

Can. J. Chem. Downloaded from www.nrcresearchpress.com by 210.87.254.6 on 09/06/12
For personal use only.

Can. J. Chem. Downloaded from www.nrcresearchpress.com by 210.87.254.6 on 09/06/12
For personal use only.

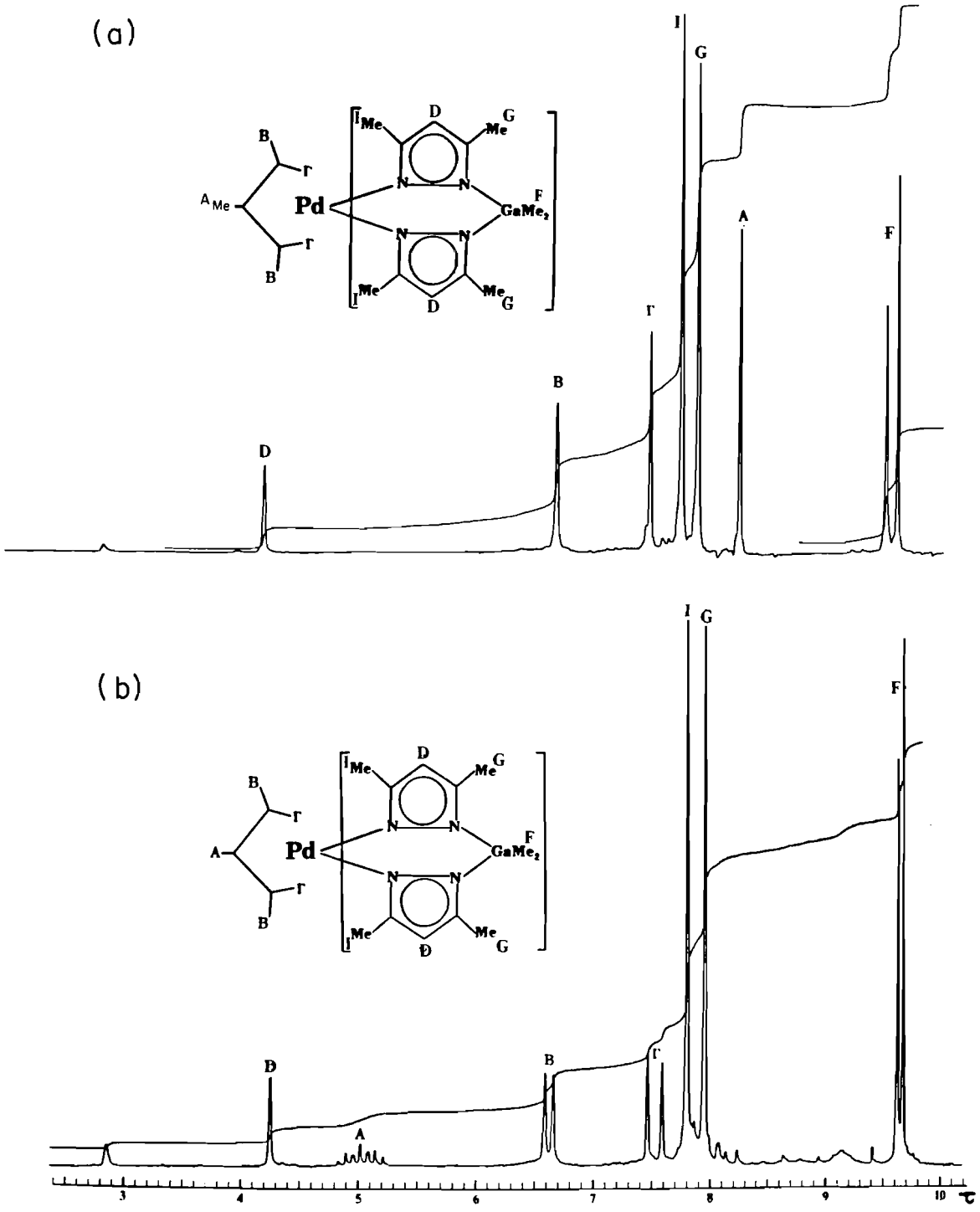

FIG. 2. 100 MHz ^{1}H nmr spectrum of (*a*) $[Me_2Ga(N_2C_5H_7)_2]Pd(C_4H_7)$ and (*b*) $[Me_2Ga(N_2C_5H_7)_2]Pd(C_3H_5)$ in C_6D_6 solution.

X-ray Crystallographic Analyses of $[Me_2Ga(N_2C_5H_7)_2]Ni(\eta^3\text{-}C_3H_5)$ and $[(\eta^3\text{-}C_3H_5)Ni(N_2C_5H_7)_2]_2Ni$

Both crystal structures consist of discrete molecules separated by normal van der Waals distances. In both complexes the allyl groups display twofold orientational disorder. In $[Me_2Ga(N_2C_5H_7)_2]Ni(\eta^3\text{-}C_3H_5)$, the preferred orientation (60% to 40%) has the central allyl CH moiety directed toward the "outside" of the molecule (see Fig. 1)

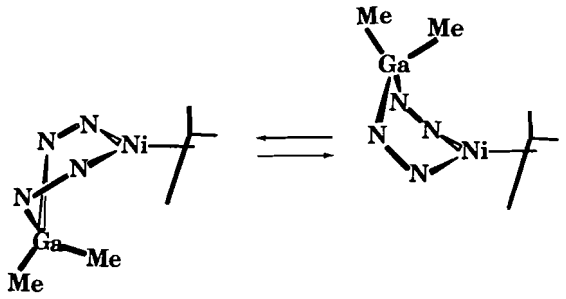

FIG. 3. Proposed conformational equilibrium for $[Me_2Ga(N_2C_5H_7)_2]Ni(\eta^3\text{-}C_3H_5)$ in acetone-d_6 solution (C_3H_3 fragments of pyrazolyl groups omitted for clarity).

while in $[(\eta^3\text{-}C_3H_5)Ni(N_2C_5H_7)_2]_2Ni$, the opposite orientation is strongly preferred (80% to 20%). In the solid state the predominance of one orientation of the allyl group over the other results from steric interactions between the terminal CH_2 moieties of the allyl ligand and the pyrazolyl methyl groups, two of which are close to the allyl ligand in $[Me_2Ga(N_2C_5H_7)_2]Ni(\eta^3\text{-}C_3H_5)$ and four in $[(\eta^3\text{-}C_3H_5)Ni(N_2C_5H_7)_2]_2Ni$. The disordering of the allyl groups is consistent with the ^1H nmr results for $[Me_2Ga(N_2C_5H_7)_2]Ni(\eta^3\text{-}C_3H_5)$ discussed above and corresponds to the coexistence in the solid state at room temperature of both isomers depicted in Fig. 3. An analogous situation exists for $[(\eta^3\text{-}C_3H_5)Ni(N_2C_5H_7)_2]_2Ni$, for which there are four possible isomers.

The $[Me_2Ga(N_2C_5H_7)_2]Ni(\eta^3\text{-}C_3H_5)$ molecule possesses approximate mirror symmetry; the mirror plane containing both metal atoms, the central allyl CH and the methyl carbon atoms bonded to gallium. With the exception of bonds involving the allyl ligand, all bond lengths related by the mirror plane agree within experimental error while mirror related bond and torsion angles are generally close but there are some statistically (but not chemically) significant differences. The central Ga—(N—N)$_2$—Ni ring has a distorted boat conformation with a Ga...Ni separation of 3.2748(4) Å and a dihedral angle of 111.3° between the pyrazolyl mean planes, the boat being steeper than those in $[Me_2Ga(N_2C_3H_3)_2]_2Ni$ (1) where the corresponding parameters are 3.432 Å and 116.4°. The N—Ni—N angle of 93.87(7)° is consistent with pseudosquare-planar coordination geometry about the Ni atom. The mean Ni—N distance is 1.928(2) Å and the Ni—C(allyl) distances are in the range 1.971(5)–2.025(3) Å (see below for further discussion). The gallium atom has distorted tetrahedral coordination geometry with bond angles ranging from 96.63(7) to 118.6(2)°. The mean Ga—N distance of 1.995(1) Å and the Ga—C bond lengths of 1.966(3) and 1.988(3) Å are normal.

Each centrosymmetric molecule of $[(\eta^3\text{-}C_3H_5)Ni(N_2C_5H_7)_2]_2Ni$ contains a square-planar central Ni(II) coordinated by four pyrazolyl nitrogen atoms and two pseudosquare-planar outer Ni(II) centres each coordinated by two pyrazolyl nitrogen atoms and an allyl group. The molecule has approximate C_{2h} symmetry, the mirror plane containing the three nickel atoms and the central allyl CH moieties. As for $[Me_2Ga(N_2C_5H_7)_2]Ni(\eta^3\text{-}C_3H_5)$ there are no chemically significant deviations from the noncrystallographic symmetry. The slightly distorted boat conformation observed for the Ni—(N—N)$_2$—Ni rings (torsion angles in Table 5) and the overall molecular shape are similar to those observed in the related molecules $[Me_2Ga(N_2C_3H_3)_2]_2Ni$ (1), $[Me_2Ga(N_2C_3H_3)_2]_2Cu$ (3) and $[(NO)Ni(N_2C_5H_7)_2]_2Ni$ (24). There is a large variance in M...M cross-ring distances and torsion angles in the M_2N_4 rings (1, 3, 24), these parameters depending on the coordination geometry of both metal atoms as well as on steric factors arising from the ligands. The cross-ring distance in $[(\eta^3\text{-}C_3H_5)Ni(N_2C_5H_7)_2]_2Ni$ is 3.2314(2) Å and the dihedral angle between the pyrazolyl mean planes is 112.5°, similar to the corresponding values for $[Me_2Ga(N_2C_5H_7)_2]Ni(\eta^3\text{-}C_3H_5)$ (see above). The M...M distances in the present structure are significantly shorter than those observed in related structures which range from 3.3770(3) Å in $[(NO)Ni(N_2C_5H_7)_2]_2Ni$ (24) to 3.790 for the nearly planar M_2N_4 ring in $[Me_2Ga(N_2C_5H_7)_2]_2Cu$ (3). The compound $[Ni(N_2C_5H_7)(C_3H_5)]_2$ has a very steep boat conformation for the central Ni_2N_4 ring with a Ni...Ni separation of only 3.00 Å^2. This is in sharp contrast to the Ni...Ni distance of 3.673(1) Å observed for the planar Ni_2N_4 ring in the closely related molecule $[(NO)Ni(N_2C_5H_7)]_2$ (24).

The central Ni(1) atom has nearly ideal square-planar coordination geometry with N—Ni—N angles of 89.67(6) and 90.33(6)°. The mean Ni(1)—N distance of 1.899(2) Å is intermediate between the corresponding values of 1.895(4) Å in $[Me_2Ga(N_2C_3H_3)_2]_2Ni$ (1) and 1.905(1) Å in $[(NO)Ni(N_2C_5H_7)_2]_2Ni$ (24). The mean Ni(2)—N distance of 1.910(2) Å is significantly shorter than the value of 1.928(2) Å observed in $[Me_2Ga(N_2C_5H_7)_2]Ni(\eta^3\text{-}C_3H_5)$. These values may be compared to the mean value observed for the trigonal planar Ni(I) in $[(NO)Ni(N_2C_5H_7)_2]_2Ni$ (24) of 1.922(3) Å. The Ni—C(allyl) distances of 1.97(1)–2.022(3) Å are in excellent agreement with those in $[Me_2Ga(N_2C_5H_7)_2]Ni(\eta^3\text{-}C_3H_5)$ and in other Ni(II) allyls (21, 25).

As was noted previously (24), in each of the present structures one of the pyrazolyl groups is rigorously planar within experimental error while

Can. J. Chem. Downloaded from www.nrcresearchpress.com by 210.87.254.6 on 09/06/12
For personal use only.

the other is slightly, but significantly, non-planar (χ^2 = 4.8, 24.9, 18.6, and 4.4 for the N_2C_3 rings containing N(1) and N(3) for $[Me_2Ga(N_2C_5H_7)_2]$-$Ni(\eta^3\text{-}C_3H_5)$ and $[(\eta^3\text{-}C_3H_5)Ni(N_2C_5H_7)_2]_2Ni$ respectively). The metal atoms are significantly displaced from the pyrazolyl mean planes ($[Me_2Ga(N_2C_5H_7)_2]Ni(\eta^3\text{-}C_3H_5)$: Ga 0.1019(3), 0.2293(2); Ni 0.0429(3), −0.1166(3) Å for rings containing N(1) and N(3) respectively and for $[(\eta^3\text{-}C_3H_5)Ni(N_2C_5H_7)_2]_2Ni$: Ni(1) −0.0522(3), 0.1118(2); Ni(2) −0.0297(2), 0.0052(2) Å as above). All other bond distances in the ordered parts of both molecules assume expected values.

Acknowledgments

We thank the Natural Sciences and Engineering Research Council of Canada for financial support and the University of British Columbia Computing Centre for assistance. We are grateful to Mr. P. Borda for C, H, N analyses, to Mr. J. Nip for mass spectra, and to Ms. M. Tracey for ^{1}H nmr spectra.

1. D. F. RENDLE, A. STORR, and J. TROTTER. J. Chem. Soc. Dalton Trans. 176 (1975).
2. F. G. HERRING, D. J. PATMORE, and A. STORR. J. Chem. Soc. Dalton Trans. 711 (1975).
3. D. J. PATMORE, D. F. RENDLE, A. STORR, and J. TROTTER. J. Chem. Soc. Dalton Trans. 718 (1975).
4. K. R. BREAKELL, D. J. PATMORE, and A. STORR. J. Chem. Soc. Dalton Trans. 749 (1975).
5. K. R. BREAKELL, S. J. RETTIG, D. L. SINGBEIL, A. STORR, and J. TROTTER. Can. J. Chem. **56**, 2099 (1978).
6. K. S. CHONG and A. STORR. Can. J. Chem. **58**, 2278 (1980).
7. K. S. CHONG, S. J. RETTIG, A. STORR, and J. TROTTER. Can. J. Chem. **55**, 4166 (1977).
8. G. WILKE, B. BOGDANOVIC, P. HARDT, P. HEINBACH, W. KEIM, M. KRONER, W. OBERKIRCH, K. TANAKA, E. STEINRUCKE, D. WALLER, and H. ZIMMERMAN. Angew. Chem. Int. Ed. **5**, 151 (1966).
9. B. L. SHAW. Proc. Chem. Soc. 247 (1960).
10. K. S. CHONG, S. J. RETTIG, A. STORR, and J. TROTTER. Can. J. Chem. **56**, 1212 (1978).
11. K. S. CHONG, S. J. RETTIG, A. STORR and J. TROTTER. Can. J. Chem. **58**, 1091 (1980).
12. P. COPPENS, L. LEISEROWITZ, and D. RABINOVICH. Acta Crystallogr. **18**, 1035 (1965).
13. W. R. BUSING and H. A. LEVY. Acta Crystallogr. **22**, 457 (1967).
14. D. T. CROMER and J. B. MANN. Acta Crystallogr. Sect. A, **24**, 321 (1968).
15. R. F. STEWART, E. R. DAVIDSON, and W. T. SIMPSON. J. Chem. Phys. **42**, 3175 (1965).
16. D. T. CROMER and D. LIBERMAN. J. Chem. Phys. **53**, 1891 (1970).
17. V. SCHOMAKER and K. N. TRUEBLOOD. Acta Crystallogr. Sect. B, **24**, 63 (1969).
18. D. W. J. CRUICKSHANK. Acta Crystallogr. **9**, 747 (1956); **9**, 754 (1956); **14**, 896 (1961).
19. K. S. CHONG, S. J. RETTIG, A. STORR, and J. TROTTER. Can. J. Chem. **57**, 3107 (1979).
20. W. R. MCCLELLAN, H. H. HUEHN, H. N. CRIPPS, E. L. MUETTERTIES, and B. W. HOWK. J. Am. Chem. Soc. **83**, 1601 (1961).
21. M. KH. MINASYANTS and YU. T. STRUCHKOV. Zh. Strukt. Khim. **9**, 481 (1968).
22. S. TROFIMENKO. J. Am. Chem. Soc. **91**, 588 (1969).
23. S. TROFIMENKO. Inorg. Chem. **10**, 1372 (1971).
24. K. S. CHONG, S. J. RETTIG, A. STORR, and J. TROTTER. Can. J. Chem. **57**, 3090 (1979).
25. A. SIRIGU. Inorg. Chem. **9**, 2245 (1970).

Can. J. Chem. Downloaded from www.nrcresearchpress.com by 210.87.254.6 on 09/06/12
For personal use only.

Crystal structure of raucubaine

RICHARD A. PAUPTIT AND JAMES TROTTER

Department of Chemistry, University of British Columbia, Vancouver, B.C., Canada V6T 1Y6

Received August 14, 1980

RICHARD A. PAUPTIT and JAMES TROTTER. Can. J. Chem. **59**, 1007 (1981).

Crystals of raucubaine, isolated from *Rauwolfia salicifolia*, $C_{20}H_{24}N_2O_3$, m.w. = 340.4, are monoclinic, $P2_1$, $a = 7.2179(3)$, $b = 12.8169(7)$, $c = 9.1996(2)$ Å, $\beta = 93.040(3)°$, $V = 849.87$ Å^3, $\rho_c = 1.33$ g cm^{-3}, $Z = 2$, $R = 0.046$ for 1699 reflections. The previously-unknown structure of this alkaloid was determined.

RICHARD A. PAUPTIT et JAMES TROTTER. Can. J. Chem. **59**, 1007 (1981).

Les cristaux de raucubaine, isolées de *Rauwolfia salicifolia*, $C_{20}H_{24}N_2O_3$, m.w. = 340.4, sont monocliniques, $P2_1$, $a = 7.2179(3)$, $b = 12.8169(7)$, $c = 9.1996(2)$ Å, $\beta = 93.040(3)°$, $V = 849.87$ Å^3, $\rho_c = 1.33$ g cm^{-3}, $Z = 2$, $R = 0.046$ pour 1699 réflexions. La structure auparavant inconnue de cet alcoloide a été determinée.

Introduction

The leaves of the plant *Rauwolfia salicifolia griseb.*, a species endemic to Cuba, yield a new alkaloid, raucubaine (1). Spectroscopic data suggested structures for various fragments, but did not allow elucidation of the complete structure, which has now been determined by X-ray crystal analysis.

Experimental

Crystal data as in the abstract. The intensity data were collected on an automatic Enraf-Nonius CAD-4 diffractometer using nickel-filtered CuKα radiation (λ = 1.54188 Å). An ω–2θ scan was used with an ω scan angle of $(0.90 + 0.15 \tan\theta)°$ extended on either side by 25% for background counts. The horizontal aperture width was $(2.00 + 0.5 \tan\theta)$ mm. The intensities of three standard reflections were measured every 1 h and used to scale the data. Three additional reflections were used as orientation control; reorientation occurred if the difference between observed and calculated scattering vectors was greater than 0.05°. In the θ range $2° < \theta \leq 75°$, 1700 out of 1822 reflections (93.3%) had $I/\sigma(I) \geq 3.00$, where $\sigma^2(I) = S + B + (0.04S)^2$ and S and B are the scan and time-corrected background counts, and were considered observed.

The structure was solved by direct methods. The E's were obtained by following the minimum profile of a K-curve and input into the MULTAN program (2). Considerable difficulty was encountered in trying to obtain a solution until four symbols in addition to the three origin-determining reflections were forced into MULTAN's symbolic addition routine. The resulting E-map revealed the positions of all 25 non-hydrogen atoms. After three isotropic full-matrix least-squares refinement cycles the atoms could easily be identified as C, N, or O from their temperature factors (all atoms were initially considered as carbons). Three more isotropic cycles and a difference map showed the number and atom-type of the non-hydrogen atoms to be correct. After an anisotropic refinement cycle a difference map produced all the hydrogen positions, and on refining all atoms (H isotropic; C, N, O anisotropic) the need for an extinction correction became apparent. R dropped from 0.054 to 0.049 on four least-squares cycles refining only an isotropic extinction parameter and the scale factor. The scattering factors of ref. 3 were used for non-hydrogens and those of ref. 4 for hydrogen atoms. The structure was refined to convergence using a polynomial weighting scheme updated after every cycle (5). The final isotropic extinction parameter g was 1.627×10^{-3} and the final R and R_w were 0.046 and 0.066, respectively. The atomic positional parameters of the non-hydrogen atoms are presented in Table 1.[1]

TABLE 1. Atomic positional parameters*

Atom	x	y	z
O(1)	1116(4)	4770	5140(3)
O(2)	−1156(4)	5339(3)	6484(3)
O(3)	3684(6)	6299(4)	4579(4)
N(1)	2470(5)	2341(4)	9816(4)
N(2)	3488(5)	2647(4)	6267(4)
C(1)	−1066(6)	4300(5)	10212(5)
C(2)	−1807(8)	4045(7)	11553(6)
C(3)	−1200(8)	3173(7)	12299(6)
C(4)	202(8)	2559(5)	11811(5)
C(5)	972(6)	2813(4)	10507(4)
C(6)	289(6)	3677(4)	9696(4)
C(7)	1326(5)	3681(4)	8302(4)
C(8)	3134(5)	3189(4)	8898(4)
C(9)	3906(9)	1854(5)	10774(6)
C(10)	1795(5)	4769(4)	7657(4)
C(11)	3664(5)	4822(4)	6884(4)
C(12)	5235(6)	4104(5)	7421(5)
C(13)	4449(5)	3015(4)	7658(4)
C(14)	1704(7)	2160(4)	6513(5)
C(15)	334(6)	2897(4)	7205(4)
C(16)	3473(6)	3382(4)	5020(5)
C(17)	3089(5)	4547(4)	5306(4)
C(18)	409(5)	5021(4)	6415(4)
C(19)	4037(6)	5244(4)	4204(5)
C(20)	3340(9)	5037(6)	2640(6)

*Estimated standard deviations are given in parentheses and correspond to the least significant digits.

Discussion

The molecular structure (Fig. 1) is of a new type, with interesting biosynthetic aspects. Figure 2 shows a stereoview of the molecule which illus-

[1]Anisotropic thermal parameters, hydrogen positional and thermal parameters, bond angles involving hydrogens, the packing diagram, and the structure factor table are available, at a nominal charge, from the Depository of Unpublished Data, CISTI, National Research Council of Canada, Ottawa, Ont., Canada K1A 0S2.

0008-4042/81/061007-03$01.00/0

©1981 National Research Council of Canada/Conseil national de recherches du Canada

Can. J. Chem. Downloaded from www.nrcresearchpress.com by 210.87.254.5 on 09/06/12
For personal use only.

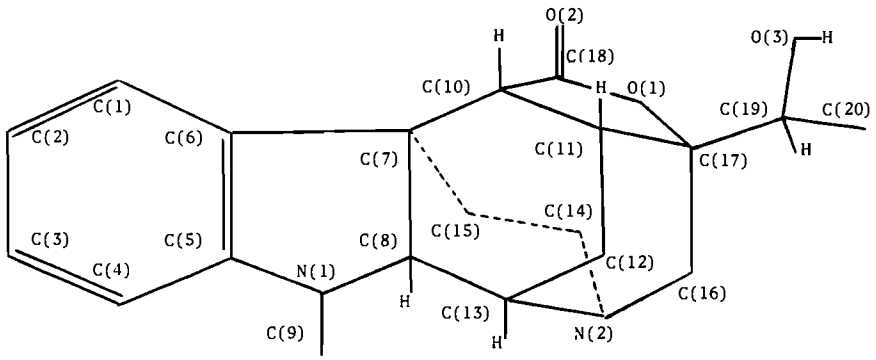

FIG. 1. Atomic labelling scheme.

TABLE 2. Bond lengths (Å)

Bond	Length (Å)	Bond	Length (Å)
C(1) — C(2)	1.409(7)	C(10) — C(18)	1.513(5)
C(1) — C(6)	1.366(7)	C(11) — C(12)	1.522(6)
C(2) — C(3)	1.37(1)	C(11) — C(17)	1.530(5)
C(3) — C(4)	1.38(1)	C(12) — C(13)	1.527(7)
C(4) — C(5)	1.387(7)	C(13) — N(2)	1.499(5)
C(5) — C(6)	1.410(6)	C(14) — N(2)	1.460(6)
C(5) — N(1)	1.419(7)	C(14) — C(15)	1.531(6)
C(6) — C(7)	1.519(5)	C(16) — N(2)	1.484(6)
C(7) — C(8)	1.526(5)	C(16) — C(17)	1.544(6)
C(7) — C(10)	1.559(5)	C(17) — C(19)	1.539(6)
C(7) — C(15)	1.570(5)	C(17) — O(1)	1.453(4)
C(8) — N(1)	1.472(6)	C(18) — O(1)	1.343(5)
C(8) — C(13)	1.538(6)	C(18) — O(2)	1.206(5)
C(9) — N(1)	1.464(6)	C(19) — O(3)	1.422(6)
C(10)—C(11)	1.559(5)	C(19) — C(20)	1.521(7)
C(1) — H(1)	0.99(6)	C(13) — H(13)	0.96(6)
C(2) — H(2)	1.10(9)	C(14) — H(141)	0.97(6)
C(3) — H(3)	1.01(7)	C(14) — H(142)	0.94(6)
C(4) — H(4)	0.97(8)	C(15) — H(151)	0.89(6)
C(8) — H(8)	0.99(5)	C(15) — H(152)	0.98(6)
C(9) — H(91)	1.08(8)	C(16) — H(161)	0.93(6)
C(9) — H(92)	0.92(8)	C(16) — H(162)	1.02(6)
C(9) — H(93)	0.97(9)	C(19) — H(19)	0.98(6)
C(10) — H(10)	0.99(4)	C(20) — H(201)	1.02(6)
C(11) — H(11)	0.98(5)	C(20) — H(202)	1.0(1)
C(12) — H(121)	0.96(6)	C(20) — H(203)	0.93(7)
C(12) — H(122)	1.03(7)	O(3) — H(O3)	0.9(1)

trates the cage-like framework. The central cage (i.e. not including the dihydroindole group) consists of three six-membered rings and a five-membered ring so connected as to form a "bowl" of which the open face is the nine-membered ring C(7)—C(15)—C(14)—N(2)—C(16)—C(17)—O(1)—C(18)—C(10). The C(10)—C(11)—C(12)—C(13)—C(8)—C(7) ring has a slightly distorted chair conformation, while the other two six-membered rings have slightly skewed boat conformations.

The five-membered ring has a skew conformation; C(10) and C(11) are both 0.24 Å away from the mean plane of the ring (including O(2)), but on opposite sides. The dihydroindole group is planar if C(8) and C(9) are not included. In this way the greatest deviation of any atom in the plane (C(1) to C(7), N(1)) from mean plane is 0.057 Å for C(4), whereas C(8) and C(9) are 0.66 and 0.73 Å away from the plane on the same side; i.e. the envelope of the dihydroindole five-membered ring is C(8).

All bond distances (Table 2) are within normal ranges, and bond angles[1] (Table 3) are as reasonable as could be expected given the constraints of

Can. J. Chem. Downloaded from www.nrcresearchpress.com by 210.87.254.5 on 09/06/12
For personal use only.

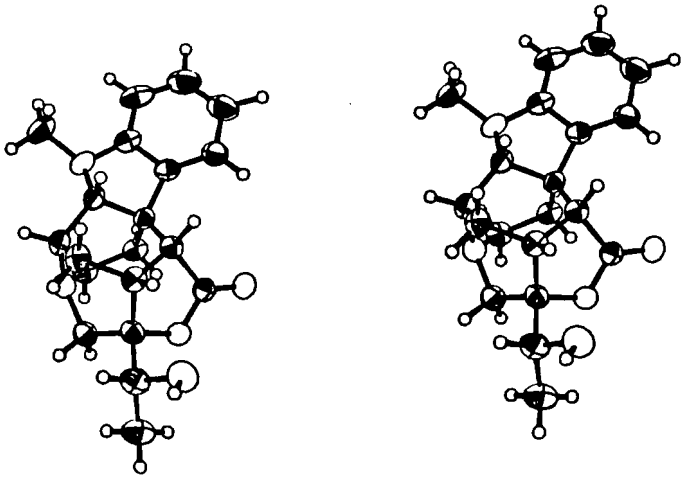

FIG. 2. A stereoview of the molecule, with 50% thermal ellipsoids.

TABLE 3. Bond angles between non-hydrogen atoms

Bonds	Angle (deg)	Bonds	Angle (deg)
C(6) — C(1) — C(2)	118.7(5)	C(12) — C(11) — C(17)	109.2(3)
C(1) — C(2) — C(3)	120.1(6)	C(11) — C(12) — C(13)	108.8(3)
C(2) — C(3) — C(4)	121.6(5)	C(8) — C(13) — C(12)	102.8(4)
C(3) — C(4) — C(5)	118.9(5)	C(8) — C(13) — N(2)	113.8(3)
C(4) — C(5) — C(6)	119.8(5)	N(2) — C(13) — C(12)	109.0(3)
C(4) — C(5) — N(1)	129.6(4)	C(13) — N(2) — C(14)	112.0(3)
N(1) — C(5) — C(6)	110.6(4)	C(13) — N(2) — C(16)	116.3(3)
C(1) — C(6) — C(5)	120.8(4)	C(14) — N(2) — C(16)	114.9(3)
C(1) — C(6) — C(7)	133.2(4)	N(2) — C(14) — C(15)	113.3(3)
C(5) — C(6) — C(7)	106.0(4)	C(14) — C(15) — C(7)	112.3(3)
C(6) — C(7) — C(8)	98.4(3)	N(2) — C(16) — C(17)	118.5(3)
C(6) — C(7) — C(10)	116.8(3)	C(16) — C(17) — C(11)	110.0(3)
C(6) — C(7) — C(15)	108.2(3)	C(16) — C(17) — C(19)	111.0(3)
C(8) — C(7) — C(10)	107.9(3)	C(16) — C(17) — O(1)	110.9(3)
C(8) — C(7) — C(15)	108.6(3)	C(11) — C(17) — C(19)	112.6(3)
C(10) — C(7) — C(15)	115.4(3)	C(11) — C(17) — O(1)	105.6(3)
C(7) — C(8) — N(1)	102.3(3)	C(19) — C(17) — O(1)	106.5(3)
C(7) — C(8) — C(13)	110.0(3)	C(10) — C(18) — O(1)	110.0(3)
N(1) — C(8) — C(13)	123.5(4)	C(10) — C(18) — O(2)	128.1(4)
C(5) — N(1) — C(8)	102.8(3)	O(1) — C(18) — O(2)	121.8(3)
C(5) — N(1) — C(9)	116.4(4)	C(17) — C(19) — C(20)	112.7(4)
C(8) — N(1) — C(9)	114.7(4)	C(17) — C(19) — O(3)	107.5(4)
C(7) — C(10) — C(11)	115.1(3)	O(3) — C(19) — C(20)	109.9(4)
C(7) — C(10) — C(18)	109.2(3)	C(17) — O(1) — C(18)	111.8(3)
C(11) — C(10) — C(18)	101.5(3)		
C(10) — C(11) — C(12)	118.2(3)		
C(10) — C(11) — C(17)	103.0(3)		

the cage. Figure 3 shows a stereo-packing diagram;[1] the molecules are strung together along the two-fold axis (i.e. along *b*) by O(3)—H···N(2) hydrogen bonds, O(3)···N(2) = 2.815(5) Å.

Acknowledgements

We thank the Natural Sciences and Engineering Research Council of Canada and the Natural, Applied, and Health Sciences Committee, University of British Columbia, for financial support, the University of British Columbia Computing Centre for assistance, and Drs. James P. Kutney and Patricia Sierra for crystals and helpful discussion.

1. J. P. KUTNEY, J. TROTTER, R. A. PAUPTIT, B. R. WORTH, and P. SIERRA. Heterocycles, **14**, 1309 (1980).
2. G. GERMAIN, P. MAIN, and M. M. WOOLFSON. Acta Crystallogr. A**27**, 368 (1971).
3. D. T. CROMER and J. B. MANN. Acta Crystallogr. A**24**, 321 (1968).
4. R. F. STEWART, E. R. DAVIDSON, and W. T. SIMPSON. J. Chem. Phys. **42**, 3175 (1965).
5. D. W. J. CRUICKSHANK. *In* Computing methods in Crystallography. *Edited by* J. S. Rollett. Pergamon Press. 1965.

Can. J. Chem. Downloaded from www.nrcresearchpress.com by 210.87.254.5 on 09/06/12
For personal use only.

Approaches to the synthesis of triterpenoids. VI. The synthesis of 3,3,10aβ-trimethyl-1,2,3,4,4aβ,5,8,9,10,10a-decahydrophenanthren-7(6*H*)-one, a potential intermediate for pentacyclic triterpene synthesis[1]

JOHN W. APSIMON,[2] DAVID MOIR, AND KAZUYUKI YAMASAKI
Department of Chemistry, Carleton University, Ottawa, Ont., Canada K1S 5B6
Received October 17, 1980

JOHN W. APSIMON, DAVID MOIR, and KAZUYUKI YAMASAKI. Can. J. Chem. **59**, 1010 (1981).

Investigations of the CDE ring construction of naturally occurring triterpenoids are described. The efficient synthesis of 3,3,10aβ-trimethyl-1,2,3,4,4aβ,5,8,9,10,10a-decahydrophenanthren-7(6*H*)-one (**25**) has been achieved. The D/E ring junction of the molecule, as well as that of related compounds, has been established by the use of ^{13}C nmr spectra. The synthetic intermediate **25** can be considered as a key substance for a synthetic entry to friedelin (**1**) in addition to β-amyrin (**23**).

JOHN W. APSIMON, DAVID MOIR et KAZUYUKI YAMASAKI. Can. J. Chem. **59**, 1010 (1981).

On décrit les recherches sur la synthèse des cycles CD et E des triterpènes naturels. On a réalisé une synthèse appropriée de la 6*H* triméthyl-3,3,10aβ décahydro-1,2,3,4,4aβ,5,8,9,10,10a phénantrénone-7 (**25**). En utilisant la rmn du ^{13}C, on a identifié la stéréochimie de la jonction des cycles D/E de cette molécule ainsi que celle des composés apparentés. On peut considérer l'intermédiaire **25** comme une substance de base permettant d'accéder à la friedeline (**1**) ainsi qu'à la β-amyrine (**23**).

[Traduit par le journal]

Synthesis of pentacyclic triterpenoids is complicated by their structural complexity arising from the presence of a considerable number of contiguous asymmetric centres including a beautifully arranged array of angular methyl groups. During recent years several laboratories have made significant contributions in this area,[3] one of which is the first total synthesis of friedelin (**1**) by Ireland's group (2), and some progress related to the total synthesis of triterpenoids has also been reported from these laboratories.[4]

In particular, in the preceding papers (3) in this series we have discussed a synthetic strategy based on ABC + E ring construction (**2**) that has led us to the pentacyclic species **3** and **4**.

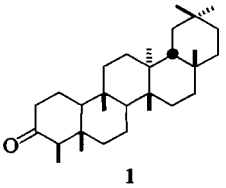

1

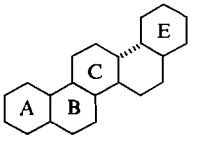

2

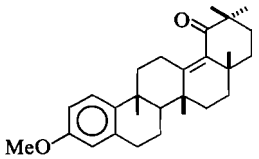

3

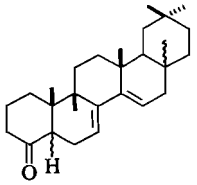

4

Among several different approaches currently being investigated in these laboratories, we now wish to report the completion of the first subgoal of an investigation concerning a variation on the above strategy, that is, a CDE + A ring construction as outlined in **5**. Since the bond formation indicated by the dotted line in **5** has been successfully demonstrated to generate the desired *trans*-fused B/C ring system present in friedelin when a proper ACDE ring unit is subjected to cycloalkylation (4), the foreseeable synthetic complexity associated with the approach is apparently reduced to the problem of construction of an appropriate CDE ring unit. Thus, the preparation of such a unit corresponding to that of the naturally occurring triterpenoids became our immediate concern, and tricyclic compound **6** was chosen as our prime synthetic objective since it provides not only the correct stereochemistry at the D/E ring junction but also the opportunity for further elaboration of the C ring to suitable precursors for pentacyclic species.

The initial phases of the synthetic route were

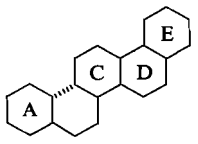

5

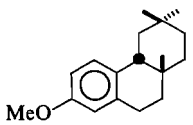

6

[1]Taken in part from the Ph.D. Dissertation of K.Y. (Carleton University, Ottawa, Canada, 1978). For Part V see ref. 3*b*.

[2]Author to whom inquiries should be directed.

[3]For successful triterpene syntheses and promising approaches see refs. 4–14 in Part III of this series (1).

[4]See Part I–V of this series.

0008-4042/81/061010-08$01.00/0
©1981 National Research Council of Canada/Conseil national de recherches du Canada

Can. J. Chem. Downloaded from www.nrcresearchpress.com by 210.87.254.5 on 09/06/12
For personal use only.

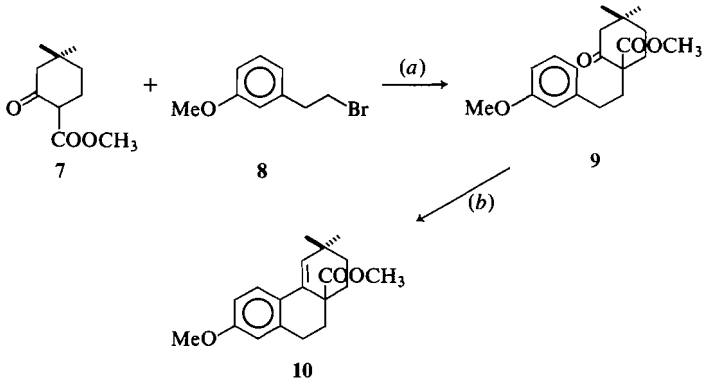

Reagent: (*a*) *t*-BuOK; (*b*) *p*-TSA, benzene.

SCHEME 1

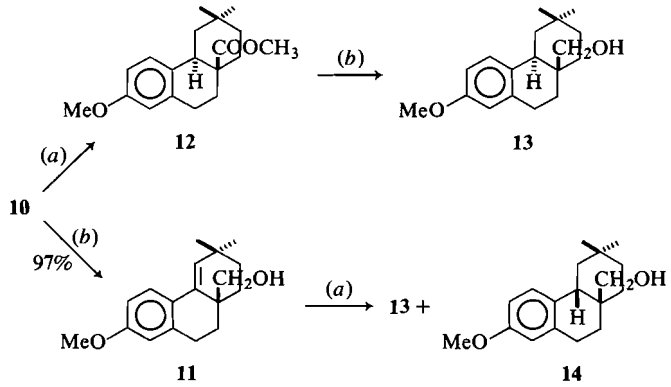

Reagents: (*a*) 10% Pd–C, H_2; (*b*) $LiAlH_4$

SCHEME 2

accomplished by alkylation of keto ester **7** (1) with **8**, using potassium *tert*-butoxide as a base to give **9** in 31% yield. Cyclization of this material was effected by refluxing in benzene containing a catalytic amount of *p*-toluenesulfonic acid, yielding the tricyclic ester **10** in 83% yield (Scheme 1). Next we attempted to reduce the double bond in **10** by catalytic hydrogenation. Previous studies from these laboratories (1) as well as literature precedents (5) suggest the strong directive effect of an angular hydroxymethyl group in catalytic hydrogenation. Therefore we predicted, a priori, that the catalytic hydrogenation of **10** with a carbomethoxy group at its angular position would produce a *trans*-D/E ring junction, whereas hydrogenation of the corresponding alcohol **11** could provide a *cis*-D/E ring junction predominantly by virtue of the attractive interaction between the catalyst surface and the hydroxyl group. Experimentally, the tricyclic alcohol **11** was prepared by lithium aluminium hydride reduction of **10** (97%), and hydrogenation of both tricyclic compounds **10** and **11** was investigated. Ester **10**, upon hydrogenation, (10% Pd–C, toluene), gave what appeared to be a single reduced ester **12** in 98% yield, and this ester was further reduced with lithium aluminum hydride to alcohol **13** (94%) to which we later assigned the *trans*-stereochemistry. By contrast, hydrogenation of **11** gave the alcohol of ambiguous stereochemical purity **14** which proved to be a mixture of the *cis*- and *trans*-alcohols (64% *trans*, 36% *cis* estimated by glc). These sequences are outlined in Scheme 2.

Although our surmise turned out to be at least partially true, the directive effect of a hydroxymethyl group in the hydrogenation of **11** was not as discriminating as we wished and certainly could not reverse the stereochemical course of hydrogenation. Furthermore, hydrogenation in a number of different solvents did not appreciably change the composition of the *cis*- and *trans*-isomers mixture.[5]

[5]The only exception was found when hydrogenation was conducted in acetonitrile, in which case a *very slow* formation of the *cis*-isomer only was noted. This route did not prove to be synthetically useful.

Can. J. Chem. Downloaded from www.nrcresearchpress.com by 210.87.254.5 on 09/06/12
For personal use only.

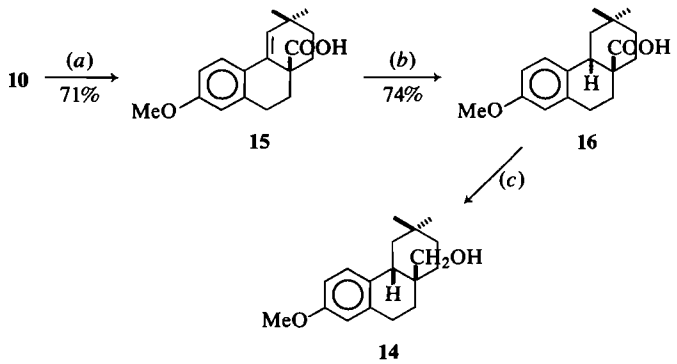

Reagents: (*a*) KOH, $CH_3OCH_2CH_2OH$, (*b*) Li, liq. NH_3, (*c*) $LiAlH_4$.

SCHEME 3

Following the observations of Thompson *et al.* (6), we then decided to investigate the metal–ammonia reduction of the unsaturated carboxylic acid **15** which would be expected, by analogy to their results, to produce the *cis*-ring junction. The required acid **15** was prepared by hydrolysis of ester **10** with potassium hydroxide in refluxing methoxyethanol. Acid **15** was reduced with lithium in liquid ammonia to give a single saturated carboxylic acid **16** in 74% yield, which was in turn converted to an alcohol **14** by lithium aluminum hydride reduction (see Scheme 3). This alcohol proved not to be identical with **13** obtainable from lithium aluminum hydride reduction of **12**.

Stereochemical assignments for **13** and **14**, and hence for **12** and **16**, are based on the following evidence. The ^{13}C chemical shift for the angular carbon atom bearing a hydroxyl group in **13** appears at 59.2 ppm, while the corresponding shift for **14** is at 69.2 ppm. If we assume that **13** possessed a *trans*-junction and **14** is the *cis* isomer, then the above ^{13}C chemical shifts are in complete agreement with the generalization that the angular methyl group in a *trans*-decalin is always shielded significantly when it is compared to its counterpart in a *cis*-decalin (7). The ^1H nmr spectra of a pair of alcohols **13** and **14** display a marked difference in the spectral pattern due to their C(10)-hydroxymethyl protons. The signals in **13** appear at δ 3.20 and 3.61 as a pair of doublets (J = 11 Hz), on the other hand the corresponding pair in **14** is located at δ 3.30 and 3.42 (J = 11 Hz).[6]

Dreiding models of both isomers show that the *trans*-alcohol can probably be conformationally described as **17** and the *cis*-alcohol as either **18** or **19**.[7] Considering the fact that one of the geminal dimethyl groups (δ 0.89) in **14** is shielded substantially more than either of those in **13** (δ 1.04, 1.07), it appears that the preferred configuration for **14** is probably **18** because in this configuration the methyl group is located in the shielding region of the benzene ring. It is also evident from the two projections **17** and **18** that one of the two protons belonging to the *cis*-hydroxymethyl group in the *trans*-isomer **17** experiences the anisotropic effect of the benzene ring by which the proton closer to the benzene ring is shielded considerably relative to the other one, while in **18** no such effect is clear. On this basis, the observed larger difference in the chemical shifts of the doublets in **13** (δ 3.20, 3.61, Δδ = 0.41) as opposed to the difference in **14** (δ 3.30, 3.42, Δδ = 0.12) can be explained. As the foregoing arguments imply, our stereochemical assignments, the *trans*-junction for **13** and *cis*- for **14**, seemed quite reasonable at this stage and were

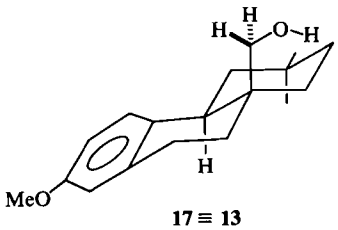

17 ≡ 13

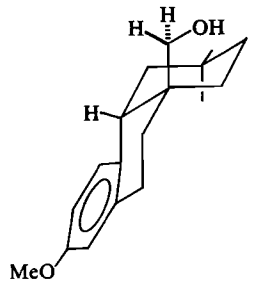

18 ≡ 14

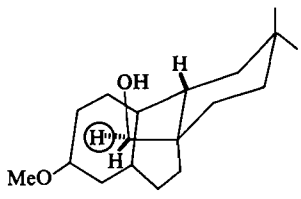

19 ≡ 14

[6]Thompson *et al.* (6) have reported similar spectral patterns for their *cis*- and *trans*-alcohols without further comment.

[7]This is only one of the possible rotamers.

Can. J. Chem. Downloaded from www.nrcresearchpress.com by 210.87.254.5 on 09/06/12
For personal use only.

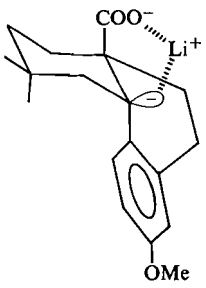

20

later confirmed when the ^{13}C data for a pair of hydrocarbons derived respectively from **13** and **14** became available.

The stereochemical outcome of the lithium–ammonia reduction of **15**, leading to the generation of a *cis*-ring junction, is of particular interest and worthy of further comments. A number of examples in which a carboxyl grouping in the vicinity of a reducible double bond would probably be responsible for stereocontrolled reductions have been reported (6, 8) and McMurry *et al.* have commented on the role of the carboxylic acid function in this type of reduction. We believe that this role is general and are of the opinion that the carboxylic acid function would either direct the approach of a proton donor from its side of a reducible molecule or contribute to lowering of the energy level of an anionic intermediate such as **20** where the *cis*-relationship between the carboxyl group and the anionic center is maintained.

We have briefly investigated the role of angular substituents in directing the stereochemistry of the lithium–ammonia reduction in these cases. Thus, reduction of ester **10** yielded a mixture of 47% *cis* and 53% *trans* reduction products and alcohol **11** provided 82% *cis* (**14**) and 18% *trans* (**13**) reduction products. Comparing these data to the above highly stereoselective (>98%) formation of the *cis* compound **16** from acid **15** it is evident that acidic functional groups (CH_2OH or COOH) play a vital role in deciding the direction of protonation of intermediates analogous to **20** or are involved in stabilizing a particular conformation as already suggested.

Having thus established the routes to both alcohols **13** and **14**, we turned our attention to the preparation of the target molecule **6**. First, the tricyclic alcohol **13** was oxidized to the aldehyde **21** by Corey oxidation, which was then subjected to Wolff–Kishner reduction. During this reduction the consistent formation of phenol **22** was observed, besides the production of ethers **23**. Therefore, from a practical point of view, a mixture of **22** and **23** was treated with methyl iodide in the presence of sodium hydride at room temperature, and this remethylation procedure afforded only ether **23**. Analogously, alcohol **14** was transformed into the desired tricycle **6** via the aldehyde **24** (Scheme 4).

The obtention of both ethers **23** and **6** has provided us with further conclusive information regarding the stereochemistry of their ring junctions. Thus, upon comparison of the ^{13}C nmr spectra of both materials, it is seen that the angular methyl group in **23** appears at 27.5 ppm while the corresponding signal for **6** is at 15.2 ppm. These chemical shifts indicate that **23** has the *trans*-ring junction and **25** is *cis*-fused, and that our assignments for the structures of the parent alcohols **13** and **14** are correct. The synthetic objective **6** is thus available quite efficiently (overall yield from **10** = 39%).

Preliminary experiments on further elaboration of **6** have so far been encouraging. Reduction of the aromatic ring of **6** in lithium – liquid ammonia and direct mild acid treatment of the product provided the title compound, β,γ-enone **25** in 89% yield. This tricyclic compound appears to be a versatile synthon convertible to the CDE ring of friedelin **1** as

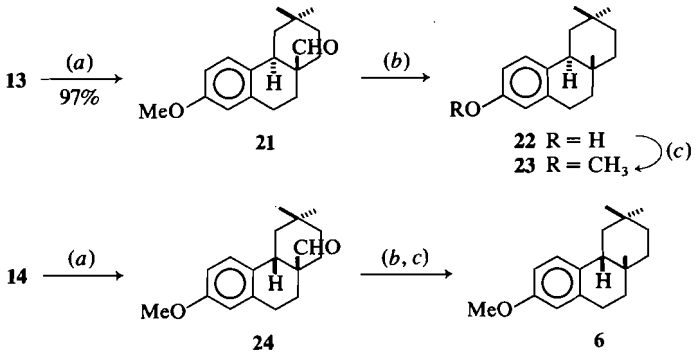

Reagents: (*a*) PCC; (*b*) Wolff–Kishner reduction, (*c*) NaH, CH_3I, THF.

SCHEME 4

Can. J. Chem. Downloaded from www.nrcresearchpress.com by 210.87.254.5 on 09/06/12
For personal use only.

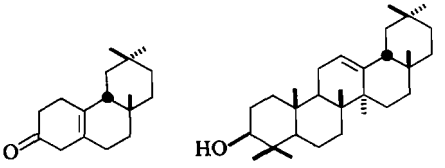

25 26

well as that of β-amyrin **26**, since it is endowed with the requisite functionalities to incorporate (9) the variety of methyl groups and double bond isomers found in a variety of triterpenoids.

Experimental

General

All melting points were determined on a Fisher-Johns apparatus and are uncorrected. Boiling points are not corrected. Infrared spectra were recorded on a Perkin-Elmer Model 237B infrared spectrometer, ultraviolet spectra on a Perkin-Elmer 202 ultraviolet–visible spectrophotometer. Mass spectra were obtained on an AE1 MS12 instrument at Trent University. Nuclear magnetic resonance spectra were measured on a Varian T-60 (Carleton University) or Varian HA-100 (University of Ottawa), using tetramethylsilane as an internal standard. Chemical shifts are expressed in the δ scale with the following designations; s, singlet; d, doublet; t, triplet; m, multiplet, br, broadened. Combustion analyses were performed by Spang Microanalytical Laboratory, Ann Arbor, MI.

All reactions and chromatograms were routinely monitored by thin-layer chromatography (tlc) (Merck 60 PF-254 plates, 0.25 mm), using 1:5 hexane – ethyl acetate as eluent. Spots were developed by exposing to iodine vapour. Preparative thin-layer chromatography was carried out on Merck 60 F-254 precoated silica gel plates of 2.0 mm thickness. Bands were visualized by viewing under an ultraviolet source. Silica gel (Davison Chemical Co., grade 923, 100–200 mesh) was used for column chromatography.

The terms "dry benzene" and "dry toluene" refer to benzene or toluene which was distilled and stored over sodium. "Dry tetrahydrofuran" was obtained by distillation from lithium aluminum hydride. "Anhydrous ether" was available from Mallinckrodt Canada Ltd. Petroleum ether refers to the fraction boiling at 30–60°C.

2-Methoxycarbonyl-5,5-dimethylcyclohexanone (7)

Dry methyl carbonate (270 g, 3.00 mol) and sodium hydride (72 g, 3.00 mol) in 500 mL of dry tetrahydrofuran were heated at reflux temperature with mechanical stirring. To this suspension (1) was added dropwise 125 g (1.03 mol) of 3,3-dimethylcyclohexanone (1) in 200 mL of dry THF. Two minutes after the addition, about 1 g of potassium hydride was added to initiate the reaction. The solution was refluxed for an additional 1½ h. The mixture was then cooled in an ice bath for 30 min and hydrolyzed by the careful addition of 3 *M* aqueous acetic acid solution. The organic material was extracted with chloroform, then washed with saturated sodium bicarbonate solution and brine. Drying over anhydrous sodium sulphate and removal of solvent under reduced pressure gave a yellow oil from which the title keto ester **7** (115 g, 65%) was distilled under vacuum, bp 78–83°C/1.0 Torr; ir (neat): 1746, 1723, 1657, and 1623 (α-ketoester) cm^{-1}; nmr (CCl_4) δ: 0.97 (s, 6H, *gem*-dimethyl) and 3.70 (s, 3H, —COO-CH_3).

2-Methoxycarbonyl-5,5-dimethyl-2-(m-methoxyphenethyl)-cyclohexanone (9)

(*a*) The procedure of Daum *et al.* (10) was followed. Potassium (11.7 g, 0.30 mol) was dissolved in 250 mL of dry *tert*-butanol. To this was added dropwise 50.6 g (0.03 mol) of the above ketoester (**7**) diluted with 100 mL of *tert*-butanol. An additional 100 mL of *tert*-butanol was added, followed by the addition of 2-(*m*-methoxyphenyl)-ethyl bromide (**8**) diluted with 100 mL of *tert*-butanol. The reaction mixture was refluxed with mechanical stirring for 80 h. The cooled reaction mixture was poured into ice-water. Ether was added and the organic layer was separated. The ether layer was washed with dilute (3 *N*) hydrochloric acid, saturated sodium bicarbonate solution, and brine. After drying over sodium sulphate, the solvent was removed *in vacuo* to leave a yellow oil. This oil was distilled under high vacuum; the first fraction (13.2 g) contained the starting ketoester **7** and *m*-methoxystyrene; the second fraction (10.2 g) which boiled at 63–83°C contained the ester and the bromide **8**; the third fraction that boiled at 83–85°C was chiefly the bromide **8**, the final fraction that boiled at 168–172°C (0.3 Torr) was collected (a yellow viscous oil, 27.2 g, 31%); ir (neat): 1734 (ester), and 1712 (carbonyl) cm^{-1}; nmr ($CDCl_3$) δ: 0.89 (s, 3H, C-5 CH_3), 1.03 (s, 3H, C-5 CH_3), 3.70 (s, 3H, —COOCH_3), 3.76 (s, 3H, —OCH_3), and 6.62–7.30 (m, 4H, aromatics); ms *m/e* (relative intensity): 318 (M^+, 6), 184 (33), 152 (21), 135 (27), 134 (100), and 121 (23). *Anal.* calcd. for $C_{19}H_{26}O_3$: C 75.46, H 8.67; found: C 75.32, H 8.58.

(*b*) Potassium (5.0 g, 0.13 mol) was dissolved in 200 mL of dry benzene containing 20 mL of *tert*-pentyl alcohol under reflux. To the solution was added 19.5 g (0.106 mol) of the keto ester **7** diluted with 50 mL of dry benzene while ca. 50 mL of benzene was being removed through a Dean-Stark trap. Then, a solution of *m*-methoxyphenylethyl tosylate (32.7 g, 0.107 mol) in 100 mL of benzene was added dropwise with stirring under reflux. Reflux was continued for 24 h. The cooled reaction mixture was poured into ice-water and benzene was added. The benzene layer was separated and the aqueous layer was extracted with benzene (×2). The combined benzene extracts were washed with water, dilute (3 *N*) hydrochloric acid, saturated sodium bicarbonate solution, and brine. The solvent was removed *in vacuo* to leave a yellow oil. This oil was chromatographed on silica gel. Elution with hexane – ethyl acetate (10:1) separated the starting ketoester **7** (7.1 g) and yielded 10.2 g (30%) of **9** as a yellow viscous oil.

7-Methoxy-10a-methoxycarbonyl-3,3-dimethyl-1,2,3,9,10,10a-hexahydrophenanthrene (10)

Compound **9** (10 g, 0.31 mol) and 2.5 g of *p*-toluenesulphonic acid in 400 mL of dry benzene were refluxed under nitrogen for 12 h. Upon cooling, the reaction mixture was passed through a short column packed with neutral aluminium oxide (Woelm). Concentration of the solution under reduced pressure yielded the cyclized material (**10**) (7.8 g, 83%) as a yellow solid. An analytical sample of **10** was obtained by recrystallization from hexane as colourless crystals, mp 74–75°C; ir (KBr): 1712 (ester) cm^{-1}; nmr ($CDCl_3$) δ: 1.05 (s, 3H, C-3 CH_3), 1.10 (s, 3H, C-3 CH_3), 3.54 (s, 3H, COOCH_3), 3.72 (s, 3H, OCH_3), 5.94 (s, 1H, C-4 H), and 6.50–7.57 (m, 3H, aromatic); ms *m/e* (relative intensity): 300 (M^+, 100), 285 (100), 241 (31), and 225 (42). *Anal.* calcd. for $C_{19}H_{24}O_3$: C 75.97, H 8.05; found: C 75.98, H 8.08.

7-Methoxy-10aβ-methoxycarbonyl-3,3-dimethyl-1,2,3,4,4aα,9,10,10a-octahydrophenanthrene (12)

Ester **10** (382 mg, 1.27 mmol) was hydrogenated over 70 mg of 10% Pd/C in 50 mL of toluene. After 12 h, palladium–carbon was removed by filtration through a pad of Celite and the solution was concentrated to yield 376 mg (98%) of the hydrogenated product (**12**) as a white powder. A sample was recrystallized from hexane – ethyl acetate (3:1), mp 91–92°C; ir (KBr): 1739 (ester) cm^{-1}; nmr ($CDCl_3$) δ: 1.02 (s, 6H, C-3 *gem*-dimethyl), 3.54 (s, 3H, COOCH_3), 3.75 (s, 3H, OCH_3), and 6.50–7.23 (m, 3H, aromatic); ms *m/e* (relative intensity): 302 (M^+, 100), 242 (100), 186 (19), and 171 (19). *Anal.* calcd. for $C_{19}H_{26}O_3$: C 75.46, H 8.67; found: C 75.48, H 8.60.

Can. J. Chem. Downloaded from www.nrcresearchpress.com by 210.87.254.5 on 09/06/12
For personal use only.

Can. J. Chem. Downloaded from www.nrcresearchpress.com by 210.87.254.5 on 09/06/12
For personal use only.

10aβ-Hydroxymethyl-7-methoxy-3,3-dimethyl-1,2,3,4,4aα,9,10,10a-octahydrophenanthrene (13)

A slurry of 100 mg (2.50 mmol) of lithium aluminium hydride in 40 mL of dry ether was stirred under nitrogen while the ester **12** (670 mg, 2.22 mmol) in 50 mL of dry ether was added dropwise. The mixture was then refluxed for 4 h. Excess lithium aluminum hydride was destroyed by adding saturated sodium sulphate solution. The resulting suspension was diluted with dilute (3 *N*) hydrochloric acid and the ether layer was separated. The ether layer was washed with water (×2) and dried over sodium sulphate. Removal of ether under reduced pressure gave 569 mg (94%) of the alcohol **13** as a white powder. Recrystallization twice from hexane – ethyl acetate (4:1) afforded a sample of analytical purity: mp 119–120°C; ir (Nujol): 3270 (hydroxyl) cm^{-1}; nmr ($CDCl_3$) δ: 1.04 (s, 3H, C-3 CH_3), 1.07 (s, 3H, C-3 CH_3), 3.20 (d, 1H, J = 11 Hz, C-10a CH_2—OH), 3.61 (d, 1 H, J = 11 Hz, C-10a—OH), 3.79 (s, 3H, OCH_3), and 6.60–7.14 (m, 3H, aromatic); ms *m/e* (relative intensity): 274 (M^+, 100), 243 (34), 173 (19), and 147 (21). *Anal.* calcd. for $C_{18}H_{26}O_2$: C 78.79, H 9.55; found: C 78.84, H 9.48.

10a-Hydroxymethyl-7-methoxy-3,3-dimethyl-1,2,3,9,10,10a-hexahydrophenanthrene (11)

A slurry of 352 mg (8.8 mmol) of lithium aluminium hydride in 50 mL of dry ether was stirred under nitrogen during addition of a solution containing 2.80 g (9.3 mmol) of the ester **10** in 50 mL of dry ether. After addition was completed, the mixture was refluxed for 4 h and stirred overnight at room temperature. Excess lithium aluminium hydride was destroyed by adding saturated sodium sulphate solution. The resulting suspension was diluted with dilute (3 *N*) hydrochloric acid. The organic layer was separated, then washed with sodium bicarbonate solution and brine. Drying over sodium sulphate and removal of solvent *in vacuo* gave 2.55 g of semi-solids. The solids were purified by column chromatography (silica gel, eluted with hexane – ethyl acetate) to afford 2.49 g (97%) of the title alcohol (**11**) as a white powder. The material was recrystallized from hexane to give a sample of analytical purity, mp 55–56°C; ir (KBr): 3400 cm^{-1}; nmr ($CDCl_3$) δ: 1.03 (s, 3H, C-3 CH_3), 1.07 (s, 3H, C-3 CH_3), 3.46 (s, 2H, C-10a —CH_2—OH), 3.76 (s, 3H, OCH_3), 5.84 (s, 1H, C-4 H), and 6.50–7.42 (m, 3H, aromatic). *Anal.* calcd. for $C_{18}H_{24}O_2$: C 79.37, H 8.88; found: C 79.41, H 8.90.

Catalytic Hydrogenation of 11

A solution of 550 mg (2.00 mmol) of the alcohol **11** in 50 mL of toluene was hydrogenated at room temperature over 50 mg of 10% Pd/C for 20 h. Palladium–carbon was removed by filtration through Celite. Concentration of the solvent provided 564 mg of a white solid. Some material was recrystallized to give a sample that melted at 59–61°C. The mass spectrum of the sample showed a molecular ion peak at *m/e* 274. The nmr spectrum of this solid showed a complex pattern of peaks at 3.10–3.70 which was analyzed to be composed of two pairs of doublets, and on this basis the product was found to be a mixture of **13** and **14**.

The hydrogenation was repeated in the following solvents: ethanol, ethanol – 10% aqueous sodium hydroxide, acetic acid, and acetonitrile. After work-up, the residue was examined by nmr. The *cis*- and *trans*-mixtures were obtained in these solvents except acetonitrile, in which the *cis*-product (**14**) was produced predominantly, but the time for hydrogenation of 30 mg of **11** was ca. 150 h.

10a-Carboxy-7-methoxy-3,3-dimethyl-1,2,3,9,10,10a-hexahydrophenanthrene (15)

Ester **10** (1.03 g, 4.44 mmol) in 70 mL of methoxyethanol was refluxed with 2 g (36 mmol) of potassium hydroxide for 48 h under nitrogen. The cooled reaction mixture was acidified with dilute (3 *N*) hydrochloric acid and extracted with ether. The ether extract was washed with water (×2) and brine, and dried over sodium sulphate. Removal of ether under reduced pressure gave 695 mg (71%) of acid **15**. A sample was recrystallized twice from ethanol to afford a white powder, mp 180°C (dec.); ir (KBr): 3300–2400, 1735, and 1690 (carboxylic acid) cm^{-1}; nmr ($CDCl_3$) δ: 1.03 (s, 3H, C-3 CH_3), 1.10 (s, 3H, C-3, CH_3), 3.75 (s, 3H, OCH_3), 5.90 (s, 1H, C-4 H), 6.45–7.50 (m, 3H, aromatic), and 7.91 (s, 1H, COO*H*); ms *m/e* (relative intensity): 286 (M^+, 64), 271 (100), and 241 (15). *Exact Mass* calcd. for $C_{18}H_{22}O_3$: 286.1569; found: 286.1524.

10aβ-Carboxy-7-methoxy-3,3-dimethyl-1,2,3,4,4aβ,9,10,10a-octahydrophenanthrene (16)

The procedure of Thompson *et al.* (6) was followed. A solution of 300 mg (1.05 mmol) of the acid (**15**) in 20 mL of dry 1:1 tetrahydrofuran–ether was added to a stirred solution of 100 mg (19 mg-atoms) of lithium in 60 mL of distilled liquid ammonia. After 30 min the blue reaction mixture was quenched by adding solid ammonium chloride, and ammonia was allowed to evaporate. To this, dilute (3 *N*) hydrochloric acid was added and the organic substance was extracted with ether. The ether extract was washed with water (×2) and brine, and dried over sodium sulphate. Removal of the solvent under reduced pressure provided 274 mg of crude solid which was recrystallized from ethanol to give 222 mg (74%) of the title acid **16** as fine needles. The material was further recrystallized from ethanol to afford a sample for combustion analysis, mp 175–182°C with partial sublimation; ir (KBr): 3450, 3200, and 1723 (carboxylic acid) cm^{-1}; nmr ($CDCl_3$) δ: 0.90 (s, 3H, C-3 CH_3), 1.03 (s, 3H, C-3 CH_3), 3.74 (s, 3H, OCH_3), and 6.50–7.06 (m, 3H, aromatic); ms *m/e*: 288 (M^+, 100), 242 (63), and 186 (11). *Anal.* calcd. for $C_{18}H_{24}O_3$: C 74.97, H 8.39; found: C 74.79, H 8.46.

10aβ-Hydroxymethyl-7-methoxy-3,3-dimethyl-1,2,3,4,4aβ,9,10,10a-octahydrophenanthrene (14)

A slurry of 68 mg (1.7 mmol) of lithium aluminium hydride in 20 mL of dry tetrahydrofuran was stirred under nitrogen during dropwise addition of a solution containing 555 mg (1.9 mmol) of the acid (**16**) in 50 mL of dry THF. Upon completion of addition, the mixture was refluxed for 2 h. The cooled reaction mixture was titrated with saturated sodium sulphate solution and the solids formed were removed by filtration through Celite. The filtered solution was dried over sodium sulphate and the solvent was removed at reduced pressure to leave 498 mg (96%) of the alcohol (**14**) as an amorphous solid. Two recrystallizations from hexane afforded an analytical sample, mp 97–98°C; ir (KBr): 3350 (hydroxyl) cm^{-1}; nmr ($CDCl_3$) δ: 0.87 (s, 3H, C-3 CH_3), 1.00 (s, 3H, C-3 CH_3), 3.30 (d, 1H, J = 11 Hz, —CH_2—OH), 3.42 (d, 1H, J = 11 Hz, —CH_2—OH), 3.74 (s, 3H, OCH_3), and 6.54–6.96 (m, 3H, aromatic); ms *m/e* (relative intensity): 274 (M^+, 100), 256 (22), and 243 (22). *Anal.* calcd. for $C_{18}H_{26}O_2$: C 78.79, H 9.55; found: C 78.80, H 9.59.

10aβ-Formyl-7-methoxy-3,3-dimethyl-1,2,3,4,4aα,9,10,10a-octahydrophenanthrene (21)

Pyridinium chlorochromate (213 mg, 0.98 mmol) was suspended in 20 mL of dry methylene chloride, and the *trans*-alcohol **13** (181 mg, 0.66 mmol) was added rapidly at room temperature. The reaction mixture was stirred for 3 h. The resulting solution was diluted with ether, the solvent was decanted from the black mass, and the mass was washed with ether. The combined ether solutions were passed through a Florisil column and the solvent was removed at reduced pressure to give 174 mg (97%) of the aldehyde **21** as fine white crystals. Recrystallization of the material from aqueous methanol afforded a sample of analytical purity as fine needles, mp 86–87°C; ir (KBr) (CCl_4): 1714 (aldehyde) cm^{-1}; nmr ($CDCl_3$) δ: 1.03 (s, 6H, C-3 *gem*-dimethyl), 3.74 (s, 3H, OCH_3), 6.54–7.30 (m, 3H, aromatic), and 9.57 (s, 1H, aldehyde). *Anal.* calcd. for $C_{18}H_{24}O_2$: C 79.37, H 8.88; found: C 79.40, H 8.86.

Can. J. Chem. Downloaded from www.nrcresearchpress.com by 210.87.254.5 on 09/06/12
For personal use only.

7-Hydroxy-3,3,10aβ-trimethyl-1,2,3,4,4aα,9,10,10a-octahydrophenanthrene (22) and 7-Methoxy-3,3,10aβ-trimethyl-1,2,3,4,4aα,9,10,10a-octahydrophenanthrene (23)

Aldehyde **21** (1.10 g, 4.05 mmol), 50 mL of distilled diethylene glycol, and 7.5 mL (0.15 mol) of hydrazine hydrate were warmed to 120°C over a 1 h period and maintained at this temperature for 2 h. Upon cooling, 2.8 g (0.05 mol) of potassium hydroxide was added, and the mixture was brought to boiling point with concurrent removal of water by distillation over a period of 3 h. Reflux was continued for a further 6 h. After cooling, the mixture was acidified with dilute hydrochloric acid (3 *N*) and extracted with ether. The ether extract was washed with water (×5), then brine, and dried over magnesium sulphate. Concentration at reduced pressure left 894 mg of crystalline material that showed two spots on tlc. Some material (200 mg) was chromatographed on preparative tlc (hexane – 25% ethyl acetate) to separate 98 mg of less polar substance (R_f = 0.84, hexane – 10% ethyl acetate) and 75 mg of more polar substance (R_f = 0.64).

The more polar substance was recrystallized from methanol (twice) to afford a sample of the phenol **22** as an amorphous solid, mp 92–94°C; ir (CCl_4): 3640 (phenol) and 1510 (aromatic) cm^{-1}; nmr ($CDCl_3$) δ: 0.65 (s, 3H, C-10a CH_3), 0.98 (s, 3H, C-3 CH_3), 1.03 (s, 3H, C-3 CH_3), 5.74 (br, 1H, —O*H*), and 6.33–7.00 (m, 3H, aromatic). *Anal.* calcd. for $C_{17}H_{24}O$: C 83.55, H 9.90; found: C 83.49, H 9.90.

Recrystallization of the less polar substance from methylene chloride – methanol (1:3) gave a sample of the ether **23** as prisms with a yellow tinge, mp 43–44°C; ir (KBr): 1612 and 1501 (aromatic ring) cm^{-1}; uv_{max} (CH_3OH): 218 (ε = 7940), 278 (2340), and 287 nm (2060); nmr ($CDCl_3$) δ: 0.67 (s, 3H, C-10a CH_3), 0.97 (s, 3H, C-3 CH_3), 3.76 (s, 3H, OCH_3), and 6.55–7.20 (m, 3H, aromatic); ms *m/e* (relative intensity): 258 (M^+, 100). *Anal.* calcd. for $C_{18}H_{26}O$: C 83.67, H 10.14; found: C 82.60, H 10.06.

Phenol **22** was methylated according to the method of Stoochnoff and Benoiton (11). Thus, the phenol (50 mg, 0.2 mmol) was dissolved in 50 mL of dry tetrahydrofuran containing 10 mg (0.4 mmol) of suspended sodium hydride (98% dry). To this, was added 230 mg (0.9 mmol) of methyl iodide and the mixture was stirred at room temperature overnight. Water was added to destroy the remaining sodium hydride and the organic substance was extracted with ether. The ether extract was washed with water and brine, and dried over magnesium sulphate. Removal of the solvent at reduced pressure left 45 mg (85%) of chromatographically pure ether **23**.

Similarly, the remaining mixtures of the phenol **22** and the ether **23** were treated with 100 mg (4.2 mmol) of sodium hydride (98% dry) and 2.4 g (10 mmol) of methyl iodide. The solution was left at room temperature overnight with stirring. Work-up as above gave 667 mg of ether **23**. The combined yield of the two step WolfKishner methylation was 75%.

10aβ-Formyl-7-methoxy-3,3-dimethyl-1,2,3,4,4aβ,9,10,10a-octahydrophenanthrene (24)

Pyridinium chlorochromate (1.47 g, 6.80 mmol) was suspended in 70 mL of dry methylene chloride, and the *cis*-alcohol **14** (1.25 g, 4.53 mmol) was added quickly. The reaction mixture was stirred at room temperature for 5 h. The resulting black solution was diluted with ether, the solvent was decanted, and the black solid was washed with ether. The combined ether solutions were passed through a Florisil column and the solvent was removed under reduced pressure to leave 1.19 g (96%) of the aldehyde **24**. Recrystallization of the material twice from aqueous methanol afforded a sample of analytical purity as fine needles with a yellow tinge, mp 100–102°C; ir (CCl_4): 1718 (aldehyde) cm^{-1}; nmr ($CDCl_3$) δ: 0.93 (s, 3H, C-3 CH_3), 1.03 (s, 3H, C-3 CH_3), 3.74 (s, 3H, OCH_3), 6.50–7.10 (m, 3H, aromatic), and 9.40 (s, 1H, aldehyde proton). *Anal.* calcd. for $C_{18}H_{24}O_2$: C 79.37, H 8.88; found: C 79.30, H 8.86.

7-Methoxy-3,3,10aβ-trimethyl-1,2,3,4,4aβ,9,10,10a-octahydrophenanthrene (6)

Aldehyde **24** (2.88 g, 10.5 mmol), 70 mL of distilled diethylene glycol, and 25 mL (0.49 mol) of hydrazine hydrate (100%) were warmed to 100°C over a 2 h period and maintained at this temperature for 2 h. Upon cooling, potassium hydroxide (5.6 g, 0.10 mol) was added, and the mixture was boiled with concurrent removal of water by distillation over a period of 3 h. The solution was refluxed for a further 12 h. After cooling, the mixture was acidified with dilute (3 *N*) hydrochloric acid and extracted with ether. The ether extract was washed with water and brine, and dried over magnesium sulphate. Concentration at reduced pressure gave 2.38 g of crystalline material. This material was methylated in 50 mL of dry tetrahydrofuran using sodium hydride (200 mg, 8.33 mmol) and methyl iodide (4.00 g, 16.5 mmol). Work-up with ether afforded ether **6** (2.02 g, 75%). A sample of the material was twice recrystallized from methanol to give the ether as colourless needles, mp 65–66°C; ir (KBr): 1600 and 1510 (aromatic ring) cm^{-1}; uv_{max} (CH_3OH): 220 (ε = 5210), 280 (1740), and 285 (1610) nm; nmr ($CDCl_3$) δ: 0.89 (s, 6H, C-3 *gem*-dimethyl), 1.00 (s, 3H, C-10a CH_3), 3.76 (s, 3H, OCH_3), and 6.57–7.06 (m, 3H, aromatic); ms *m/e* (relative intensity): 258 (M^+, 100). *Anal.* calcd. for $C_{18}H_{26}O$: C 83.67, H 10.14; found: C 83.55, H 10.15.

3,3,10aβ-Trimethyl-1,2,3,4,4aβ,5,8,9,10,10a-decahydrophenanthren-7(6H)-one (25)

This procedure of Wiesner *et al.* (12) was followed. A solution of 600 mg (2.32 mmol) of the *cis*-ether (**6**) in 50 mL of dry 1:1 tetrahydrofuran – *tert*-butanol was added over 15 min to a stirred solution of lithium (320 mg, 45.7 mg-atoms) in distilled ammonia (ca. 100 mL). The mixture was stirred at acetone – Dry Ice temperature for 1 h. The blue reaction mixture was quenched by adding absolute methanol, and ammonia was allowed to evaporate. The residue was dissolved in water (100 mL) and extracted with ether (×4). The ether extract was dried by passing through a pad of magnesium sulphate and concentrated to afford a colourless oil. This oil was immediately dissolved in cold absolute ethanol (100 mL) and treated with 1 *M* aqueous oxalic acid solution (30 mL) for 30 min at 0°C. The mixture was neutralized by dropwise addition of saturated sodium carbonate solution. Normal work-up with ether gave 512 mg (89%) of the ketone **25** as a yellow oil which solidified upon refrigeration, but melted at room temperature. The material was distilled under vacuum to afford a colourless oil, bp 95–100°C/1.0 Torr; ir (neat): 1718 (carbonyl) cm^{-1}; uv_{max} (CH_3OH): transparent beyond 210 nm; nmr ($CDCl_3$) δ: 0.87 (s, 3H, C-10a CH_3) and 0.90 (s, 6H, C-3 *gem*-dimethyl); ms *m/e* (relative intensity): 246 (M^+, 100), 231 (100), 217 (86), 105 (38), 91 (41), 79 (31), 69 (31), and 55 (34). *Anal.* calcd. for $C_{17}H_{26}O$: C 82.87, H 10.64; found: C 82.90, H 10.68.

Acknowledgements

We thank the Natural Sciences and Engineering Research Council of Canada and Carleton University for generous financial assistance of our research program.

1. J. W. ApSimon, S. Badripersaud, T. T. T. Nguyen, and R. Pike. Can. J. Chem. **56**, 1646 (1978).
2. (*a*) R. E. Ireland and D. M. Walba. Tetrahedron Lett.

1071 (1976); (*b*) D. M. WALBA. Ph.D. dissertation, California Institute of Technology, 1976.
3. (*a*) J. W. ApSIMON, S. BADRIPERSAUD, J. W. HOOPER, R. PIKE, G. I. BIRNBAUM, C. HUBER, and M. L. POST. Can. J. Chem. **56**, 2139 (1978); (*b*) J. W. ApSIMON and I. TOTH. J. Chem. Soc. Chem. Commun. 67, (1979).
4. R. E. IRELAND, M. I. DAWSON, C. J. KOWALSKI, C. A. LIPIUSKI, D. R. MARSHALL, J. W. TILLEY, J. BORDNER, and B. L. TRUS. J. Org. Chem. **40**, 973 (1975).
5. H. W. THOMPSON and R. E. NAIPAWER. J. Am. Chem. Soc. **95**, 6379 (1973).
6. H. W. THOMPSON, E. MCPHERSON, and B. L. LEUCES. J. Org. Chem. **41**, 2903 (1976).
7. D. CAINE and T. L. SMITH, JR. J. Org. Chem. **43**, 755 (1978).
8. J. E. MCMURRY, Z. C. BLASZCZAK, and M. A. JOHNSON. Tetrahedron Lett. 1633 (1978).
9. R. GINSING and A. D. CROSS. J. Am. Chem. Soc. **87**, 4629 (1965).
10. S. J. DAUM, P. E. SHAW, and R. L. CLARKE. J. Org. Chem. **32**, 1430 (1967).
11. B. A. STOOCHNOFF and N. L. BENOITON. Tetrahedron Lett. 21 (1973).
12. K. WIESNER, I. H. SANCHEZ, K. S. ATURAL, and S. J. LEE. Can. J. Chem. **55**, 1091 (1977).

Can. J. Chem. Downloaded from www.nrcresearchpress.com by 210.87.254.5 on 09/06/12
For personal use only.

Can. J. Chem. Downloaded from www.nrcresearchpress.com by 210.87.254.40 on 09/06/12
For personal use only.

The iodination of azetidinone thio compounds. A convenient synthesis of 2-iodomethylpenams

RONALD G. MICETICH,[1] ROBERT A. FORTIER, AND PETER WOLFERT
Raylo Chemicals Limited, 8045 Argyll Road, Edmonton, Alta., Canada T6C 4A9

Received November 21, 1980

This paper is dedicated to Prof. Raymond U. Lemieux on the occasion of his 60th birthday

RONALD G. MICETICH, ROBERT A. FORTIER, and PETER WOLFERT. Can. J. Chem. **59**, 1018 (1981).

A practical method for the synthesis of 2β-iodomethyl-2α-methylpenams is described. These compounds undergo facile isomerization to the 3β-iodo-3α-methylcephams. A preliminary kinetic study of these reactions is reported. The isomerization of the 2β-iodomethylpenams to the 3β-iodocephams can be prevented by oxidation to the sulfoxide.

RONALD G. MICETICH, ROBERT A. FORTIER et PETER WOLFERT. Can. J. Chem. **59**, 1018 (1981).

On décrit une méthode pratique de synthèse des iodométhyl-2β méthyl-2α pénames. Ces composés s'isomérisent facilement en iodo-3β méthyl-3α céphames. On rapporte une étude cinétique préliminaire de ces réactions. L'isomérisation des iodométhyl-2β pénames en iodo-3β céphames peut être évitée par le biais d'une oxydation en sulfoxyde.

[Traduit par le journal]

The conversion of thiazolineazetidinones, **1**, and azetidinone disulfides, **2**, to 3-iodocephams, **4**, in high yields, with *trace* amounts of the corresponding 2-iodomethylpenams, **5**, has been reported (1, 2). Further studies have shown that with appropriate changes in reaction conditions the 2-iodomethylpenams, **5**, become the *major* products.

Compounds **1**, in a suitable organic solvent, react with iodine in the presence of moisture to give a mixture of **4** and **5**. The overall yield and the relative ratio of **4** and **5** depend on factors such as the purity of **1**, the nature of the group R, the presence or absence of air or oxygen, and on the reaction time. Convenient solvents for this reaction are methylene chloride, chloroform, or toluene. A reaction using purified (chromatographed and recrystallized from ether to constant mp, 85°C) **1***a*, showed only about 20% (from ^{1}Hmr spectral analysis) overall reaction after 7 h. By comparison, crude **1***a*, under otherwise identical conditions, underwent 90% conversion after 5 h. The iodination of **1** proceeded smoothly, under the conditions used, when R was phenoxymethyl (reactions employing commercial penicillin V as precursor), but when R was phenylmethyl (penicillin G as precursor), this reaction was slow and incomplete.[2] The reaction was catalyzed by air or oxygen, or by the presence of metal salts such as ferric chloride.

The reaction time is one of the most important factors in determining the yield of products and the ratio of **5** to **4** formed. A typical reaction (see Experimental) was monitored by removing aliquots from the reaction mixture at suitable intervals of time, and after work-up, analyzing the resulting product by its ^{1}Hmr spectrum in $CDCl_3$. The 3-iodocepham, **4**, C(3)—CH_3 singlet at about δ 1.99, the thiazolineazetidinone, **1**, CH_3 singlet at about δ 1.72, and the 2-iodomethylpenam **5**, C(2)—CH_3 singlet at about δ 1.38, are well separated, so that the integration of these signals provides a convenient measure of these three compounds in the product (no other compounds being detected in the reaction).

The results of this kinetic study can be summarized as follows.

1. The concentration of **1** drops rapidly to about 18% of its original value after 2 h, and then tapers off slowly to 15% in 5 h, 3.5% in 22 h, and 1.5% in 30 h.

2. The concentration of the 2-iodomethylpenam, **5**, rises rapidly and reaches a maximum of about 80% of the total material present in 1 to 3 h, and thereafter drops to about 12% in 22 h, and 9% in 30 h.

3. The concentration of the 3-iodocepham, **4**, increases fairly slowly to about 40% in 5 h, 84.5% in 22 h, and 89.5% in 30 h.

It is evident that the 2-iodomethylpenam, **5**, is the initial product of the reaction and is then slowly converted to the 3-iodocepham, **4**, via the thiiran-

[1]Author to whom correspondence may be addressed.

[2]H. Tanino *et al.* (5) report on anomalous behaviour of compounds **1** to oxidation.

0008-4042/81/061018-03$01.00/0

©1981 National Research Council of Canada/Conseil national de recherches du Canada

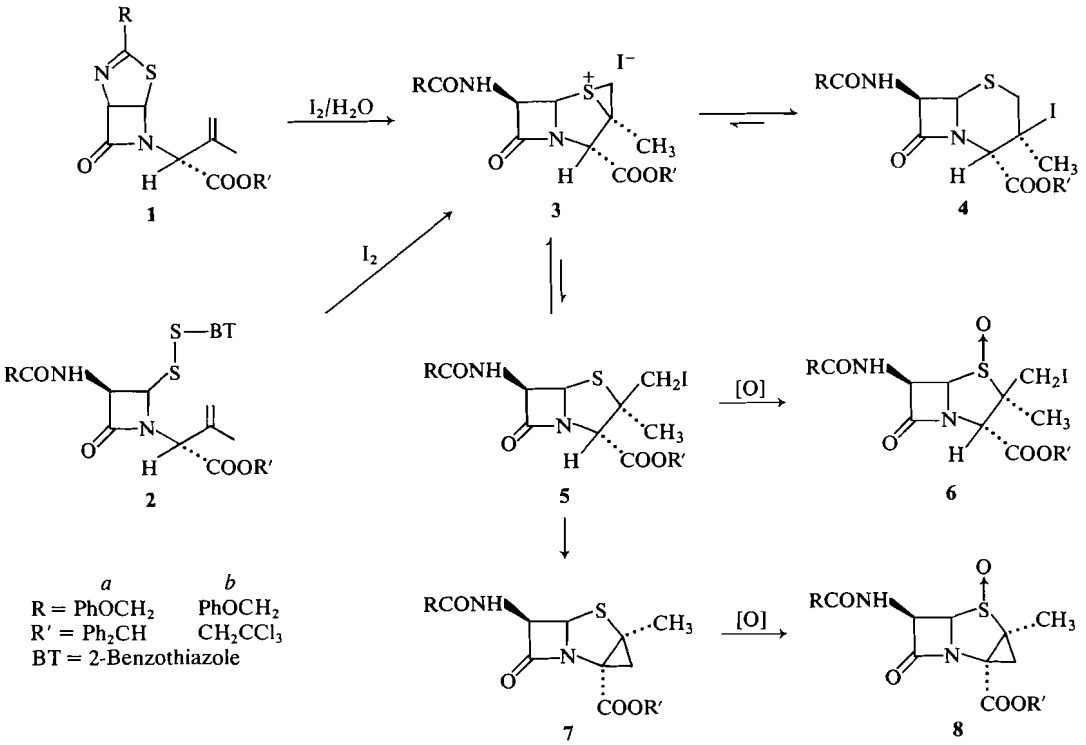

ium intermediate, **3**.[3] Compounds **5** were in fact converted to **4** on storage (in solution or even in the solid state).[3] The concentration of **5***a* in a solid sample left at 23°C changed from 71% to 35% in 4 days, and to 14% in 2 weeks. Purification of **5** could be effected by rapid chromatography using silica gel, the compounds being obtained as amorphous white powders[4] which contained trace amounts of **4** (the amount of **4** increasing with time). The configuration of C(2) in **5** is as indicated.[5]

The reactions of compounds **2** with iodine were similar, in that the 2-iodomethylpenams, **5**, were the initial products and then underwent transformation to the 3-iodocephams, **4**.[3,6] These reactions did *not* require moisture, and proceeded easily and reproducibly at temperatures of about 25°C. A further advantage of this alternate route to **5** is that the reactions were independent of the nature of R. The ^{1}Hmr ($CDCl_3$) spectra (3) of the 2-iodomethylpenams, **5**, showed sharp singlets at δ 1.38 (3H, C(2)—CH_3) and 3.80 (2H, C(2)—CH_2I), while the 3-iodocephams, **4**, showed a singlet at δ 1.99 (3H, C(3)—CH_3) and a quartet (J = 14 Hz) at about 2.80 (2H, C(2)—CH_2).

Oxidation of **5** by peracids produced the 2β-iodomethyl-2α-methylpenicillin-1β-sulfoxides, **6**,[5] which are stable, since the formation of the thiiranium intermediate is now prevented. These compounds were purified by gradient elution chromatography on silica gel using methylene chloride – ether as eluant and were obtained as off-white amorphous solids[4] in over 70% yield (after chromatography) from **1**. The ^{1}Hmr ($CDCl_3$) spectra were, for **5***a*, δ: 1.00 (s, 3H, C(2)—CH_3), 3.77 (q, J = 10 Hz, 2H, C(2)—CH_2I), 4.5 (s, 2H, —OCH_2CO), 4.88 (s, 1H, C(3)—*H*), 4.93 (d, 1H, C(5)—*H*), 6.03 (dd, 1H, C(6)—*H*), 6.8 to 7.4 (m, 16H, $3C_6H_5$ and $CH\phi_2$), 8.10 (d, 1H, N*H*); for **5***b*, δ: 1.50 (s, 3H, C(2)—CH_3), 3.85 (s, 2H, C(2)—CH_2I), 4.50 (s, 2H, OCH_2CO), 4.7 to 5.2 (m, 4H, CH_2CCl_3, C(3)—*H*, and C(5)—*H*), 6.0 (dd, 1H, C(6)—*H*), 6.8 to 7.35 (m, 5H, C_6H_5), and 8.15 (d, 1H, N*H*).

[3]S. Kukolja *et al.* (see ref. 6 and earlier papers) have discussed the mechanism and stereochemistry of similar reactions involving thiiranium ions, and have also noted the spontaneous rearrangement of a 2-chloromethylpenam to a 3-chlorocepham.

[4]The analysis (elemental or high resolution mass spectral) of all new compounds described were within acceptable limits.

[5]The configuration is assigned on the basis of mechanistic considerations, from analogy with related reactions to produce the 2-halomethylpenams from **2**,[6] and from the results of thermolytic reactions of 2-substituted methylpenam sulfoxides to be described in publications to follow.

[6]T. Kamiya *et al.* (7) describe the preparation of 2-chloromethylpenams and 2-bromomethylpenams by a similar process. These compounds are reported to be relatively stable in the solid state.

Can. J. Chem. Downloaded from www.nrcresearchpress.com by 210.87.254.40 on 09/06/12
For personal use only.

Compounds **5**, and their sulfoxides, **6**, were readily converted by bases such as DBN or DBU, or even by sodium acetate into the 2,3-methylene-penams, **7**, or their sulfoxides, **8**, respectively (4).

Experimental

A typical reaction to convert **1***a* to **6***a* is described.

Crude **1***a* (20 g, 40 mmol) and iodine (17 g, 66 mmol) were dissolved in CH_2Cl_2 (300 mL) and stirred vigorously with water (300 mL) that had been previously saturated with air, the reaction being done with free access to air. After 35 min, the organic layer was separated and shaken with aqueous sodium thiosulfate (twice), and brine, and then dried ($MgSO_4$). (If **5** is required, concentration and rapid chromatography on silica gel will provide **5**. A ^{1}Hmr spectrum on the residue from an aliquot of the solution obtained above indicated a 78% overall yield of **5**.) The filtrate was cooled in an ice-bath and *m*-chloroperbenzoic acid (9.6 g of 85%, 48 mmol) added to the stirred solution. After 0.5 h at 0°C and 1 h at ambient temperature, the reaction mixture was extracted with aqueous sodium bicarbonate (twice), then brine, dried ($MgSO_4$), and concentrated to give 26.3 g (theoretical) of a yellow foam. Gradient elution chromatography on silica gel using methylene chloride to methylene chloride (20% ether) gave 18.6 g (71%) of **6***a*, as an off-white foam, and 4.6 g (17.5%) of the 3-iodocepham sulfoxide. Compound **6***a* precipitated from cold ether–hexane as an off-white amorphous powder with the ^{1}Hmr spectral characteristics reported above.

Acknowledgements

The authors thank the National Research Council of Canada (Industrial Research Assistance Program) for the research grant, and Connlab Holdings Limited, for their support.

1. R. G. MICETICH and R. B. MORIN. Tetrahedron Lett. 979 (1976).
2. (*a*) R. G. MICETICH and R. B. MORIN. *In* Recent advances in the chemistry of β-lactam antibiotics. *Edited by* J. Elks. The Chemical Society, U.K. 1977. Chapt. 23; (*b*) M. FOGLIS, G. FRANCESCHI, P. MASI, and A. SUARATO. Ger. Patent No. 2534811.
3. (*a*) S. KUKOLJA, N. D. JONES, M. O. CHANEY, T. K. ELZEY, M. R. GLEISSNER, J. N. PASCHAL, and D. E. DORMAN. J. Org. Chem. **40**, 2388 (1975); (*b*) H. TANIDA, T. TSUSHIMA, H. ISHITOBI, T. IRIE, T. YANO, H. MATSUMURA, and K. TORI. Tetrahedron Lett. 3303 (1975).
4. T. KAMIYA, T. TERAJI, M. HASHIMOTO, O. NAKAGUCHI, and T. OKU. J. Am. Chem. Soc. **97**, 5020 (1975).
5. H. TANINO, S. NATSUKA, and Y. KISHI. Tetrahedron Lett. 581 (1976).
6. S. KUKOLJA, S. R. LAMMERTS, M. R. GLEISSNER, and A. I. ELLIS. J. Am. Chem. Soc. **97**, 3192 (1975).
7. T. KAMIYA, T. TERAJI, Y. SAITO, M. HASHIMOTO, O. NAKAGUCHI, and T. OKU. Tetrahedron Lett. 3001 (1973).

Can. J. Chem. Downloaded from www.nrcresearchpress.com by 210.87.254.40 on 09/06/12
For personal use only.

The iodination of azetidinone thio compounds. *unsym*-Azetidinone disulfides from thiazolineazetidinones

RONALD G. MICETICH, ROBERT A. FORTIER, AND JENNIFER LIEW
Raylo Chemicals Limited, 8045 Argyll Road, Edmonton, Alta., Canada T6C 4A9

Received November 21, 1980

This paper is dedicated to Prof. Raymond U. Lemieux on the occasion of his 60th birthday

RONALD G. MICETICH, ROBERT A. FORTIER, and JENNIFER LIEW. Can. J. Chem. **59**, 1020 (1981).

The products of the reaction of thiazolineazetidinones with alkyl and aralkyl sulfenyl iodides (generated *in situ*) are hydrolysed to *unsym*-azetidinone disulfides.

RONALD G. MICETICH, ROBERT A. FORTIER et JENNIFER LIEW. Can. J. Chem. **59**, 1020 (1981).

Les produits de la réaction des thiazolineazétidinones avec les iodures d'alkyles et les iodures d'aralkyles sulfényles (produits *in situ*) sont transformés par hydrolyse en disulfures d'azétidinones *non symétriques*.

[Traduit par le journal]

The conversion of thiazolineazetidinones, **1**, to 3-iodocephams (1, 2) and 2-iodomethylpenams (3) by reaction with iodine in the presence of moisture has been reported. A useful process modification involves the reaction of **1** with a sulfenyl iodide in the presence of moisture, the sulfenyl iodide being generated *in situ* by the action of iodine on a mercaptan, a disulfide, a thiol acid, or a thioamide (including thiourea) (1, 2).

A possible mechanism for the reaction when a sulfenyl iodide is employed is summarized in Scheme 1. Reaction of **1** with a sulfenyl iodide

0008-4042/81/061020-03$01.00/0
©1981 National Research Council of Canada/Conseil national de recherches du Canada

Compounds **5**, and their sulfoxides, **6**, were readily converted by bases such as DBN or DBU, or even by sodium acetate into the 2,3-methylene-penams, **7**, or their sulfoxides, **8**, respectively (4).

Experimental

A typical reaction to convert **1***a* to **6***a* is described.

Crude **1***a* (20 g, 40 mmol) and iodine (17 g, 66 mmol) were dissolved in CH_2Cl_2 (300 mL) and stirred vigorously with water (300 mL) that had been previously saturated with air, the reaction being done with free access to air. After 35 min, the organic layer was separated and shaken with aqueous sodium thiosulfate (twice), and brine, and then dried ($MgSO_4$). (If **5** is required, concentration and rapid chromatography on silica gel will provide **5**. A ^{1}Hmr spectrum on the residue from an aliquot of the solution obtained above indicated a 78% overall yield of **5**.) The filtrate was cooled in an ice-bath and *m*-chloroperbenzoic acid (9.6 g of 85%, 48 mmol) added to the stirred solution. After 0.5 h at 0°C and 1 h at ambient temperature, the reaction mixture was extracted with aqueous sodium bicarbonate (twice), then brine, dried ($MgSO_4$), and concentrated to give 26.3 g (theoretical) of a yellow foam. Gradient elution chromatography on silica gel using methylene chloride to methylene chloride (20% ether) gave 18.6 g (71%) of **6***a*, as an off-white foam, and 4.6 g (17.5%) of the 3-iodocepham sulfoxide. Compound **6***a* precipitated from cold ether–hexane as an off-white amorphous powder with the ^{1}Hmr spectral characteristics reported above.

Acknowledgements

The authors thank the National Research Council of Canada (Industrial Research Assistance Program) for the research grant, and Connlab Holdings Limited, for their support.

1. R. G. MICETICH and R. B. MORIN. Tetrahedron Lett. 979 (1976).
2. (*a*) R. G. MICETICH and R. B. MORIN. *In* Recent advances in the chemistry of β-lactam antibiotics. *Edited by* J. Elks. The Chemical Society, U.K. 1977. Chapt. 23; (*b*) M. FOGLIS, G. FRANCESCHI, P. MASI, and A. SUARATO. Ger. Patent No. 2534811.
3. (*a*) S. KUKOLJA, N. D. JONES, M. O. CHANEY, T. K. ELZEY, M. R. GLEISSNER, J. N. PASCHAL, and D. E. DORMAN. J. Org. Chem. **40**, 2388 (1975); (*b*) H. TANIDA, T. TSUSHIMA, H. ISHITOBI, T. IRIE, T. YANO, H. MATSUMURA, and K. TORI. Tetrahedron Lett. 3303 (1975).
4. T. KAMIYA, T. TERAJI, M. HASHIMOTO, O. NAKAGUCHI, and T. OKU. J. Am. Chem. Soc. **97**, 5020 (1975).
5. H. TANINO, S. NATSUKA, and Y. KISHI. Tetrahedron Lett. 581 (1976).
6. S. KUKOLJA, S. R. LAMMERTS, M. R. GLEISSNER, and A. I. ELLIS. J. Am. Chem. Soc. **97**, 3192 (1975).
7. T. KAMIYA, T. TERAJI, Y. SAITO, M. HASHIMOTO, O. NAKAGUCHI, and T. OKU. Tetrahedron Lett. 3001 (1973).

Can. J. Chem. Downloaded from www.nrcresearchpress.com by 210.87.254.5 on 09/06/12
For personal use only.

The iodination of azetidinone thio compounds. *unsym*-Azetidinone disulfides from thiazolineazetidinones

RONALD G. MICETICH, ROBERT A. FORTIER, AND JENNIFER LIEW
Raylo Chemicals Limited, 8045 Argyll Road, Edmonton, Alta., Canada T6C 4A9

Received November 21, 1980

This paper is dedicated to Prof. Raymond U. Lemieux on the occasion of his 60th birthday

RONALD G. MICETICH, ROBERT A. FORTIER, and JENNIFER LIEW. Can. J. Chem. **59**, 1020 (1981).

The products of the reaction of thiazolineazetidinones with alkyl and aralkyl sulfenyl iodides (generated *in situ*) are hydrolysed to *unsym*-azetidinone disulfides.

RONALD G. MICETICH, ROBERT A. FORTIER et JENNIFER LIEW. Can. J. Chem. **59**, 1020 (1981).

Les produits de la réaction des thiazolineazétidinones avec les iodures d'alkyles et les iodures d'aralkyles sulfényles (produits *in situ*) sont transformés par hydrolyse en disulfures d'azétidinones *non symétriques*.

[Traduit par le journal]

The conversion of thiazolineazetidinones, **1**, to 3-iodocephams (1, 2) and 2-iodomethylpenams (3) by reaction with iodine in the presence of moisture has been reported. A useful process modification involves the reaction of **1** with a sulfenyl iodide in the presence of moisture, the sulfenyl iodide being generated *in situ* by the action of iodine on a mercaptan, a disulfide, a thiol acid, or a thioamide (including thiourea) (1, 2).

A possible mechanism for the reaction when a sulfenyl iodide is employed is summarized in Scheme 1. Reaction of **1** with a sulfenyl iodide

0008-4042/81/061020-03$01.00/0
©1981 National Research Council of Canada/Conseil national de recherches du Canada

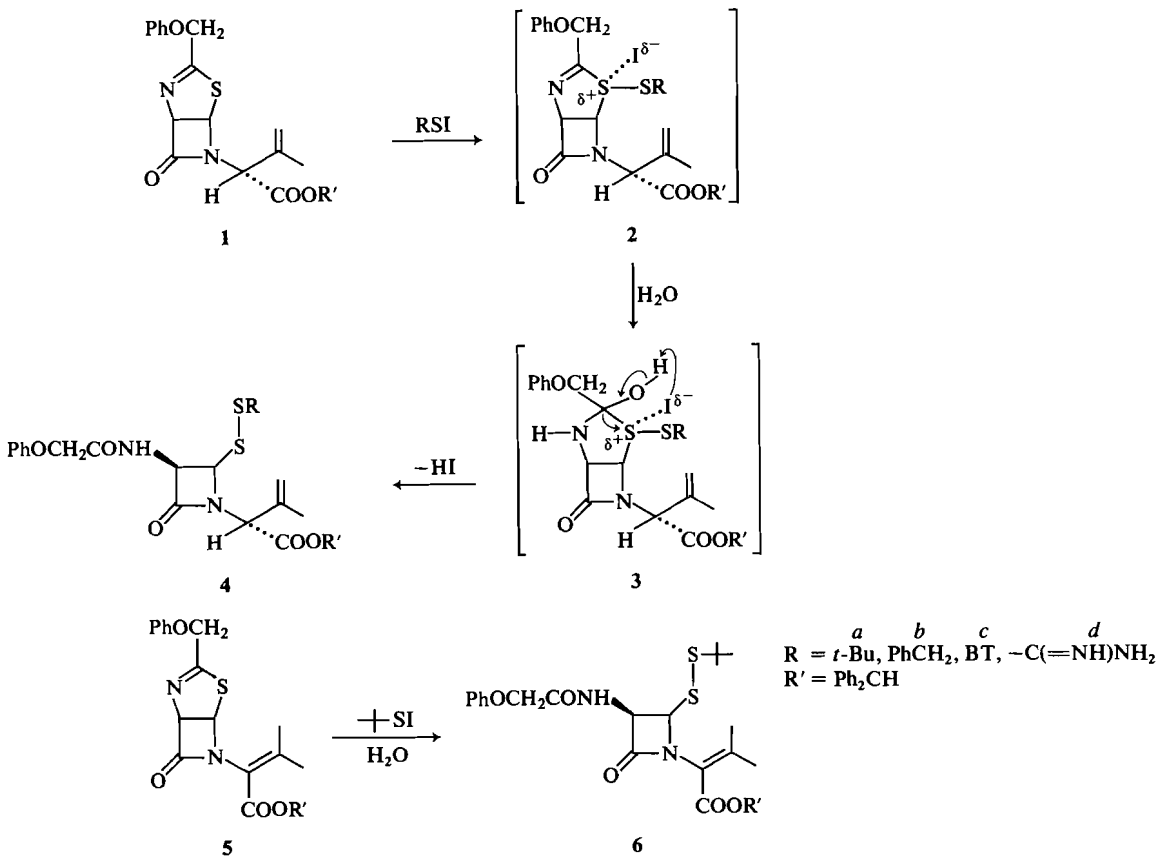

SCHEME 1

generates the thiosulfonium iodide, **2**, resulting in activation of the —C=N— bond to hydrolysis, **2** → **3** → **4**, which then reacts with excess iodine or sulfenyl iodide to form the 3-iodocepham as previously reported (1, 2).

In accordance with this suggested mechanism it is possible, by using the proper stoichiometry and reaction conditions (see Experimental), to prepare **4***a* (77%) and **4***b* (25%) by this reaction. Attempts to isolate **4***c* (BT = 2-benzothiazolyl) (4) and **4***d* (5), using 2-mercaptobenzothiazole and thiourea respectively as the sulfenyl iodide precursor, gave only trace amounts of these compounds. The products in these two cases were the 3-iodocepham and the thiazolineazetidinone, **1**. The data would suggest that the reactivity of the disulfide bond of **4** to iodination (and possibly other halogenation reactions) is dependent on the nature of the "R" group. When "R" is an aromatic (such as 2-benzothiazolyl), or an amidino (from thiourea) moiety, the disulfide bond in **4** is susceptible to halogenation, so that compounds **4** compete favourably with **1** in reactions with iodine or sulfenyl iodides. When "R" is an alkyl (such as *tert*-butyl), or an aralkyl (benzyl) group, the disulfide bond is deactivated and compounds **4***a* and **4***b* are hence isolated. In a recent patent, Underwood (6) has described the conversion of **1** to **4** utilizing isolated sulfenyl chlorides. In every example the "R" group was an alkyl moiety.

This novel method of opening the thiazoline ring can also be applied to other systems such as the α,β-double bond isomer, **5**. Reaction with *tert*-butylsulfenyl iodide (produced *in situ*) produces the *unsym*-azetidinone disulfide, **6**, in about 50% yield after chromatography.

Compounds **4** have been produced by the thermolysis of a penicillin sulfoxide in the presence of a suitable mercaptan. The sulfenic acid formed by heating the penicillin sulfoxide is trapped by the mercaptan to give **4**. Kamiya *et al.* (4) found that when stoichiometric amounts of heteroaromatic mercaptans such as 2-mercaptobenzothiazole were used high yields of **4** were obtained. Barton and co-workers (7) report that when excess of an alkylmercaptan was used the product was the α,β-

Can. J. Chem. Downloaded from www.nrcresearchpress.com by 210.87.254.5 on 09/06/12
For personal use only.

unsaturated isomer of **4**, none of the β,γ-isomer, **4**, being isolated. In this case, double bond isomerization occurred during the reaction. The present method permits the preparation of the β,γ-isomers of these compounds. Compounds of type **4** are important synthetic intermediates for the preparation of modified cephalosporins (see for example refs. 4, 8, and 9).

Experimental

Iodine (2.60 g, 0.0102 mol) was added to an ice-cold, stirred solution of the thiazolineazetidinone, **1** (R′ = $CH\phi_2$, 5.0066 g, 0.0101 mol) and *tert*-butylmercaptan (1.2 mL, 0.0106 mol) in methylene chloride (40 mL) and the mixture stirred in an ice-bath for 30 min. Water (40 mL) was added, and stirring continued for 24 h at ambient temperature. The separated orange-red colored organic layer was extracted with aqueous sodium thiosulfate solution, then water, dried ($MgSO_4$), filtered, and concentrated to give 6.13 g of a green-yellow foam. Chromatography on silica gel using 5% ether in methylene chloride as eluant gave 4.7 g (77%) of **4***a* as a white foam; nmr ($CDCl_3$) spectrum, δ: 1.27 (s, 9H, $C(CH_3)_3$), 1.92 (s, 3H, —C—CH_3), 4.57 (s, 2H, —OCH_2—), 4.94 (d, 2H, —C=CH_2), 5.11 (s, 1H, —CHCOO—), 5.27 (d, 1H, C(4)—*H*), 5.52 and 5.67 (dd, 1H, C(3)—*H*), 6.87 to 7.49 (m, 17H, C_6H_5, $CHC\phi_2$, and N*H*).

When benzylmercaptan was used in place of *tert*-butylmercaptan, **4***b* (25%) was obtained as white foam after chromatography. The nmr ($CDCl_3$) spectrum, δ: 1.83 (s, 3H, —C—CH_3), 4.83 (s, 2H, $CH_2\phi$), 4.56 (s, 2H, —OCH_2—), 4.87 to 5.38 (m, 5H, —C=CH_2, —CHCOO, β-lactam *H*'s), 6.78 to 7.56 (m, 22H, C_6H_5, $CH\phi_2$, N*H*).

When *tert*-butyl mercaptan was reacted in a similar manner with compound **5** and iodine and water, **6** (50%) was obtained as a white foam after chromatography. The nmr ($CDCl_3$) spectrum, δ: 1.1 (s, 9H, $C(CH_3)_3$), 2.1 and 2.2 (ss, 6H, $=C(CH_3)_2$), 4.5 (s, 2H, OCH_2), 5.03 to 5.4 (m, 2H, β-lactam *H*'s), 6.8 to 7.4 (m, 16H, —$CH\phi_2$ and C_6H_5).

High resolution mass spectral data were consistent with the structures.

Acknowledgements

The authors thank the National Research Council of Canada (Industrial Research Assistance Program) for the research grant, and Connlab Holdings Limited for their support.

1. R. G. Micetich and R. B. Morin. Tetrahedron Lett. 979 (1976).
2. R. G. Micetich and R. B. Morin. *In* Recent advances in the chemistry of β-lactam antibiotics. *Edited by* J. Elks. The Chemical Society, U.K. 1977. Chapt. 23.
3. R. G. Micetich, R. A. Fortier, and P. Wolfert. Can. J. Chem. **59**, 1018 (1981).
4. T. Kamiya, T. Teraji, Y. Saito, M. Hashimoto, O. Nakaguchi, and T. Oku. Tetrahedron Lett. 3001 (1973).
5. R. G. Micetich and R. B. Morin. U.S. Patent No. 4,039,530. 2 Aug. 1977.
6. W. G. E. Underwood. Glaxo Labs. Ger. Patent No. 2,303,889. 2 Aug. 1973.
7. R. D. Allan, D. H. R. Barton, N. Girijavallabhan, P. G. Sammes, and M. V. Taylor. J. Chem. Soc. 1182 (1973).
8. Y. Hamashima, K. Ishikura, H. Ishitobi, H. Itani, T. Kubota, K. Minami, M. Murakami, W. Nagata, M. Narisada, Y. Nishitani, T. Okada, H. Onoue, H. Satoh, Y. Sendo, T. Tsuji, and M. Yoshioka. *In* Recent advances in the chemistry of β-lactam antibiotics. *Edited by* J. Elks. The Chemical Society, U.K. 1977. Chapt. 24.
9. R. B. Woodward. *In* Recent advances in the chemistry of β-lactam antibiotics. *Edited by* J. Elks. The Chemical Society, U.K. 1977. Chapt. 18.

Hydrogen–deuterium exchange of heteroaromatics in neutral D_2O at elevated temperatures

Nick Henry Werstiuk and George Timmins

Department of Chemistry, McMaster University, Hamilton, Ont., Canada L8S 4M1

Received December 2, 1980

Nick Henry Werstiuk and George Timmins. Can. J. Chem. **59**, 1022 (1981).

Pyridine (**1**), 2-methylpyridine (**2**), 3-methylpyridine (**3**), 4-methylpyridine (**4**), and 1,10-phenanthroline undergo H—D exchange in neutral D_2O at elevated temperatures (180–300°C). With a suitable choice of temperature and reaction time it is possible to prepare selectively deuterated or perdeuterated substrates in good yield.

Nick Henry Werstiuk et George Timmins. Can. J. Chem. **59**, 1022 (1981).

La pyridine (**1**), la méthyl-2 pyridine (**2**), la méthyl-3 pyridine (**3**), la méthyl-4 pyridine (**4**) et la phénantroline-1,10 subissent un échange H—D dans du D_2O neutre à des températures élevées (180–300°C). En choisissant judicieusement la température et le temps de réaction, il est possible de préparer sélectivement et avec un excellent rendement des produits deutérés et perdeutérés.

[Traduit par le journal]

0008-4042/81/061022-03$01.00/0

©1981 National Research Council of Canada/Conseil national de recherches du Canada

Can. J. Chem. Downloaded from www.nrcresearchpress.com by 210.87.254.5 on 09/06/12
For personal use only.

unsaturated isomer of **4**, none of the β,γ-isomer, **4**, being isolated. In this case, double bond isomerization occurred during the reaction. The present method permits the preparation of the β,γ-isomers of these compounds. Compounds of type **4** are important synthetic intermediates for the preparation of modified cephalosporins (see for example refs. 4, 8, and 9).

Experimental

Iodine (2.60 g, 0.0102 mol) was added to an ice-cold, stirred solution of the thiazolineazetidinone, **1** (R′ = $CH\phi_2$, 5.0066 g, 0.0101 mol) and *tert*-butylmercaptan (1.2 mL, 0.0106 mol) in methylene chloride (40 mL) and the mixture stirred in an ice-bath for 30 min. Water (40 mL) was added, and stirring continued for 24 h at ambient temperature. The separated orange-red colored organic layer was extracted with aqueous sodium thiosulfate solution, then water, dried ($MgSO_4$), filtered, and concentrated to give 6.13 g of a green-yellow foam. Chromatography on silica gel using 5% ether in methylene chloride as eluant gave 4.7 g (77%) of **4***a* as a white foam; nmr ($CDCl_3$) spectrum, δ: 1.27 (s, 9H, $C(CH_3)_3$), 1.92 (s, 3H, —C—CH_3), 4.57 (s, 2H, —OCH_2—), 4.94 (d, 2H, —C=CH_2), 5.11 (s, 1H, —CHCOO—), 5.27 (d, 1H, C(4)—*H*), 5.52 and 5.67 (dd, 1H, C(3)—*H*), 6.87 to 7.49 (m, 17H, C_6H_5, $CHC\phi_2$, and N*H*).

When benzylmercaptan was used in place of *tert*-butylmercaptan, **4***b* (25%) was obtained as white foam after chromatography. The nmr ($CDCl_3$) spectrum, δ: 1.83 (s, 3H, —C—CH_3), 4.83 (s, 2H, $CH_2\phi$), 4.56 (s, 2H, —OCH_2—), 4.87 to 5.38 (m, 5H, —C=CH_2, —CHCOO, β-lactam *H*'s), 6.78 to 7.56 (m, 22H, C_6H_5, $CH\phi_2$, N*H*).

When *tert*-butyl mercaptan was reacted in a similar manner with compound **5** and iodine and water, **6** (50%) was obtained as a white foam after chromatography. The nmr ($CDCl_3$) spectrum, δ: 1.1 (s, 9H, $C(CH_3)_3$), 2.1 and 2.2 (ss, 6H, $=C(CH_3)_2$), 4.5 (s, 2H, OCH_2), 5.03 to 5.4 (m, 2H, β-lactam *H*'s), 6.8 to 7.4 (m, 16H, —$CH\phi_2$ and C_6H_5).

High resolution mass spectral data were consistent with the structures.

Acknowledgements

The authors thank the National Research Council of Canada (Industrial Research Assistance Program) for the research grant, and Connlab Holdings Limited for their support.

1. R. G. Micetich and R. B. Morin. Tetrahedron Lett. 979 (1976).
2. R. G. Micetich and R. B. Morin. *In* Recent advances in the chemistry of β-lactam antibiotics. *Edited by* J. Elks. The Chemical Society, U.K. 1977. Chapt. 23.
3. R. G. Micetich, R. A. Fortier, and P. Wolfert. Can. J. Chem. **59**, 1018 (1981).
4. T. Kamiya, T. Teraji, Y. Saito, M. Hashimoto, O. Nakaguchi, and T. Oku. Tetrahedron Lett. 3001 (1973).
5. R. G. Micetich and R. B. Morin. U.S. Patent No. 4,039,530. 2 Aug. 1977.
6. W. G. E. Underwood. Glaxo Labs. Ger. Patent No. 2,303,889. 2 Aug. 1973.
7. R. D. Allan, D. H. R. Barton, N. Girijavallabhan, P. G. Sammes, and M. V. Taylor. J. Chem. Soc. 1182 (1973).
8. Y. Hamashima, K. Ishikura, H. Ishitobi, H. Itani, T. Kubota, K. Minami, M. Murakami, W. Nagata, M. Narisada, Y. Nishitani, T. Okada, H. Onoue, H. Satoh, Y. Sendo, T. Tsuji, and M. Yoshioka. *In* Recent advances in the chemistry of β-lactam antibiotics. *Edited by* J. Elks. The Chemical Society, U.K. 1977. Chapt. 24.
9. R. B. Woodward. *In* Recent advances in the chemistry of β-lactam antibiotics. *Edited by* J. Elks. The Chemical Society, U.K. 1977. Chapt. 18.

Hydrogen–deuterium exchange of heteroaromatics in neutral D_2O at elevated temperatures

Nick Henry Werstiuk and George Timmins

Department of Chemistry, McMaster University, Hamilton, Ont., Canada L8S 4M1

Received December 2, 1980

Nick Henry Werstiuk and George Timmins. Can. J. Chem. **59**, 1022 (1981).

Pyridine (**1**), 2-methylpyridine (**2**), 3-methylpyridine (**3**), 4-methylpyridine (**4**), and 1,10-phenanthroline undergo H—D exchange in neutral D_2O at elevated temperatures (180–300°C). With a suitable choice of temperature and reaction time it is possible to prepare selectively deuterated or perdeuterated substrates in good yield.

Nick Henry Werstiuk et George Timmins. Can. J. Chem. **59**, 1022 (1981).

La pyridine (**1**), la méthyl-2 pyridine (**2**), la méthyl-3 pyridine (**3**), la méthyl-4 pyridine (**4**) et la phénantroline-1,10 subissent un échange H—D dans du D_2O neutre à des températures élevées (180–300°C). En choisissant judicieusement la température et le temps de réaction, il est possible de préparer sélectivement et avec un excellent rendement des produits deutérés et perdeutérés.

[Traduit par le journal]

0008-4042/81/061022-03$01.00/0

©1981 National Research Council of Canada/Conseil national de recherches du Canada

Can. J. Chem. Downloaded from www.nrcresearchpress.com by 210.87.254.5 on 09/06/12
For personal use only.

Digitoxigenin-3-alkyl ethers[1]

ROBERT GREENHOUSE
Syntex, S. A., Division de Investigacion, Apartado Postal 10-820, Mexico 10, D.F.
AND
JOSEPH M. MUCHOWSKI
Syntex Research, Institute of Organic Chemistry, 3401 Hillview Ave., Palo Alto, CA 94304, U.S.A.

Received November 4, 1980

ROBERT GREENHOUSE and JOSEPH M. MUCHOWSKI. Can. J. Chem. **59**, 1025 (1981).

The synthesis of the title compounds was accomplished by (*i*) boron trifluoride etherate catalysed alkylation of digitoxigenin with diazoalkanes, (*ii*) silver tetrafluoroborate assisted solvolysis of 3-desoxy-3α-iododigitoxigen **2***d* in an alcoholic medium, and (*iii*) *m*-chloroperbenzoic acid induced oxidative solvolytic displacement on the iodo compound **2***d* in the presence of alcohols. The third process was the most useful for the preparation of the mono ethers **2***e* and **2***f* of ethylene glycol and glycerol, respectively.

ROBERT GREENHOUSE et JOSEPH M. MUCHOWSKI. Can. J. Chem. **59**, 1025 (1981).

On a synthétisé les composés mentionnés dans le titre de la façon suivante: (*i*) une alkylation de la digitoxigénine par les diazoalcanes en présence de l'éthérate de trifluorure de bore, (*ii*) une solvolyse, assistée par le tétrafluoroborate d'argent, du désoxy-3 iodo-3*a* digitoxigène (**2***d*) en milieu alcoolique, et (*iii*) un déplacement solvolytique oxydant, induit par l'acide *m*-chloroperbenzoique, du composé iodé **2***d* en présence d'alcools. Cette trosième étape est la plus utile dans la préparation, par exemple, des mono éthers **2***e* et **2***f* de l'éthylène glycol et du glycérol.

[Traduit par le journal]

Digitoxigenin-3-alkyl ethers were required in connection with our interest in modified cardenolides with a therapeutic ratio superior to that found in the cardiac glycosides currently in use.

Simple 3-alkyl ethers of digitoxigenin have heretofore not been described in the literature. Indeed, 3,16-di-*O*-methylgitoxigenin **1***b*, prepared by the boron trifluoride etherate catalysed alkylation of gitoxigenin **1***a* with diazomethane, appears to be the only example of a 3-alkoxy cardenolide which has been reported to date (1).

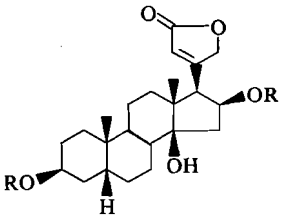

1*a* R = H
1*b* R = CH_3

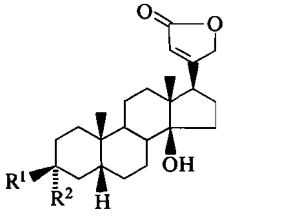

2*a* R^1 = OH; R^2 = H
2*b* R^1 = OCH_3; R^2 = H
2*c* R^1 = $OCH_2C_6H_5$; R^2 = H
2*d* R^1 = H; R^2 = I
2*e* R^1 = $HOCH_2CH_2O$; R^2 = H
2*f* R^1 = $HOCH_2CHCH_2O$; R^2 = H
OH

The conversion of digitoxigenin **2***a* into the corresponding 3-alkyl ethers, a seemingly simple chemical operation, could not be accomplished using the more common methods of effecting such transformations. For example, the Williamson ether synthesis with various alkyl halides (methyl iodide, allyl bromide, benzyl bromide, or epibromohydrin) in the presence of a variety of bases (sodium hydride (2), barium oxide, sodium hydroxide under phase transfer conditions (3), thallium(I) ethoxide (4), proton sponge, 1,5-diazabicyclo[4.3.0]non-5-ene, 2,6-lutidine, etc.) in diverse solvents, consistently failed to give the expected products. In addition, the reaction of digitoxigenin with a large excess of an alkyl halide (see above), in the presence of silver tetrafluoroborate or mercuric perchlorate, in solvents such as acetonitrile, dimethylformamide, etc., did not occur in the desired sense. Of the large number of methods examined using digitoxigenin as the substrate, only the boron trifluoride etherate catalysed reaction of diazoalkanes (e.g. diazomethane and phenyldiazomethane) was successful, but this process did not take place with more complicated diazo compounds such as ethyl diazoacetate.

A much more useful point of embarkation for the synthesis of the desired compounds was 3-desoxy-3α-iododigitoxigenin **2***d*. This substance, which was prepared from digitoxigenin and triphenylphosphine diiodide (5),[2] gave the methyl ether **2***b*, in 55% yield, when solvolysed in methanol containing silver tetrafluoroborate.

[1]Contribution no. 566 from the Syntex Institute of Organic Chemistry.

[2]This compound, mp 175–177°C, was first prepared (and fully characterized) by E. Prisbe, Syntex Research, Palo Alto, CA.

0008-4042/81/071025-03$01.00/0
©1981 National Research Council of Canada/Conseil national de recherches du Canada

Can. J. Chem. Downloaded from www.nrcresearchpress.com by 210.87.254.5 on 09/06/12
For personal use only.

Can. J. Chem. Downloaded from www.nrcresearchpress.com by 210.87.254.5 on 09/06/12
For personal use only.

Similarly, the l-glyceryl ether **2***f* was obtained in 25% and 28% yields when the reaction was effected in glycerol–tetrahydrofuran–dimethylformamide or glycerol – *tert*-butanol solutions, respectively. In all of these reactions an olefinic material, probably a mixture of the Δ^3- and Δ^4-isomers of anhydrodigitoxigenin, was formed as the principal by-product.

The most successful approach to the synthesis of the title compounds was based on the oxidative solvolytic displacement of hypervalent iodine (6) from the α-iodo compound **2***d*. Thus, the reaction of **2***d* with *m*-chloroperbenzoic acid in the presence of methanol, ethylene glycol, or glycerol, at room temperature, gave the ethers **2***b*, **2***e*, and **2***f*, respectively. Compound **2***f* was synthesized unambiguously, and in much better yield, by the acidic hydrolysis of the product derived from the oxidative displacement reaction using glycerol acetonide.

This ether synthesis obviously is of considerable utility. The mildness of the conditions under which the reaction is conducted suggest several other areas where it could be used advantageously.

The cardiotonic activities of the ethers of digitoxigen were evaluated in driven left atria of the guinea pig (7). In this assay compounds **2***e* and **2***f* were equipotent with digitoxigenin whereas the methyl and benzyl ethers, **2***b* and **2***c*, were ca. 0.3 and 0.1 times as active as digitoxigenin. The separation of cardiotonic activity and toxicity (arrhythmias, negative inotropic effects) was in no case, however, better than that observed for digitoxigenin.

Experimental

The melting points were determined in a Mel-Temp apparatus and are corrected. The infrared spectra were measured with a Perkin-Elmer Model 237 grating infrared spectrophotometer. The ultraviolet spectra were recorded with a Perkin-Elmer Model 402 ultraviolet visible spectrophotometer. The nmr spectra were taken with a Varian T-60 nmr spectrometer and are expressed as parts per million (δ) from internal tetramethylsilane. The mass spectra were measured with an Atlas CH-4 spectrometer. The high pressure liquid chromatographic separations were effected using a Dupont Model 841 apparatus equipped with a Waters Associates refractive index detector.

3β-Methoxy-14β-hydroxy-5β-card-20(22)-enolide 2(b)

(a) From Digitoxigenin and Diazomethane

Ethereal diazomethane (prepared from nitrosomethylurea (5 g)) was added in portions with stirring at 0°C to a solution of digitoxigenin (0.500 g) in dry dichloromethane (80 mL) containing boron trifluoride etherate (2 drops). If nitrogen evolution did not begin shortly after the addition of the first portion of the diazomethane solution an additional one drop of boron trifluoride etherate was added. When the addition was completed (ca. 50 min) the solution was stirred at 0°C until the yellow colour of the diazomethane had disappeared. The solution was diluted with an equal volume of ether and washed successively with 10% sodium carbonate solution and water; the organic phase was dried over sodium sulfate and evaporated *in vacuo*. The residue was subjected to thin layer chromatography (tlc) on silica gel (ethyl acetate – hexane, 2:3) to give a crystalline solid (0.345 g, 66%) which had mp 165.5°C after crystallization from dichloromethane–hexane; $[\alpha]_D$ +24.4° (*c* 0.242, $CHCl_3$), ir ($CHCl_3$) ν_{max}: 3520, 3490, 1792, 1749, 1625 cm^{-1}; uv (MeOH) λ_{max}: 223 nm (ε 12 600); nmr ($CDCl_3$)δ: 0.86 (s, 3H), 0.91 (s, 3H), 1.00–3.00(m, 23H), 3.23 (s, 3H), 3.45 (m, 1H), 4.88 (m, 2H), 5.83 (m, 1H); ms *m/e*: 388 (M^+). *Anal.* calcd. for $C_{24}H_{36}O_4$: C 74.19, H 9.34; found: C 73.90, H 8.96.

(b) By the Silver Tetrafluoroborate Assisted Solvolysis of 2d *in Methanol*

Silver tetrafluoroborate (0.025 g) was added to a stirred solution of the 3α-iodo compound **2***d* (0.050 g) in dry methanol (7 mL). After 40 min at room temperature the mixture was diluted with ether, the ether phase was washed with 5% sodium bicarbonate solution, dried, and evaporated. Thin-layer chromatographic analysis (silica gel, ethyl acetate – hexane, 3:7) of the residue showed that starting material was still present and therefore the mixture was resubmitted to the solvolysis conditions described above. After 2 h, the usual work-up gave a mixture which was subjected to tlc on silica gel using the above solvent system. A less polar product (0.018 g, presumably a mixture of Δ^{-3} and Δ^{-4} anhydrodigitoxigenin) and the more polar ether (0.023 g, 55%) were obtained. After crystallization from dichloromethane–hexane, it has mp 165–165.5°C, undepressed on admixture with a sample synthesized by method (*a*).

(c) By Oxidative Solvolysis of 2d

meta-Chloroperbenzoic acid (0.183 g) was added, in one portion, to a solution of the 3α-iodo compound **2***d* (0.200 g) in anhydrous methanol (15 mL) containing dry dichloromethane (5 mL). After 1 h at room temperature, the mixture was poured into ether (175 mL), the solution was washed with 5% sodium bicarbonate solution, dried, and evaporated *in vacuo*. The residue was filtered through a short column of silica gel using ether as the solvent. The mixture thus obtained was separated by high pressure liquid chromatography (hplc) on a 50 cm × ⅜ in. Lichrosorb column using ethyl acetate – hexane (1:3) as the developing solvent (flow rate 9 mL/min at 1100 psig). The major product (0.072 g, 45%) had a retention time of 26.5 min and was identical to the methyl ether obtained by methods (*a*) or (*b*).

3β-Benzyloxy-14β-hydroxy-5β-card-20(22)-enolide 2e

A solution of phenyldiazomethane, prepared from *N*(*N*^{1}-nitrosobenzylaminomethyl)benzamide (3.80 g) according to the method of Sekiya *et al.* (8), in dry dichloromethane (15 mL) was added in portions (0.5 mL) at 0°C, to a stirred solution of digitoxigenin (0.500 g) in dry dichloromethane (30 mL) containing boron trifluoride etherate solution (5 drops, prepared from boron trifluoride etherate (1 mL) and anhydrous dichloromethane (9 mL)). When the addition was completed, stirring was continued for an additional 10 min and the solution was diluted with dichloromethane. The mixture was washed with water, dried, and evaporated *in vacuo*. The oily residue was subjected to tlc on silica gel (ethyl acetate – hexane, 3:2) to give a solid (0.356 g, 57%). Crystallization of this material from hexane–dichloromethane followed by hexane–acetone gave the analytical specimen mp 145.5–146°C; $[\alpha]_D$ +24.6° (*c* 0.245, $CHCl_3$); ir (KBr) ν_{max}: 3530, 1785, 1755, 1740 sh, 1720 sh, 1627 cm^{-1}; uv (MeOH) λ_{max}: 219 nm (ε 15 100); nmr ($CDCl_3$) δ: 0.86 (s, 3H), 0.93 (s, 3H), 1.00–3.00 (m, 23H), 3.68 (m, 1H), 4.44 (s, 2H), 4.84 (m, 2H), 5.81 (s, 1H), 7.26 (s, 5H); ms *m/e*: 464 (M^+). *Anal.* calcd. for $C_{30}H_{40}O_4$: C 77.55, H 8.68; found: C 77.24, H 8.49.

3β-(2-Hydroxyethoxy)-14β-hydroxy-5β- card-20(22)-enolide **2e**

meta-Chloroperbenzoic acid (0.177 g) was added, in one portion, to a stirred solution of the iodo compound (0.196 g) in dioxan (9 mL) to which ethylene glycol (6 mL) had been added. After 1.5 h the reaction mixture was poured into water and the product was extracted with ether. The extract was washed successively with water and 5% sodium bicarbonate solution, dried over sodium sulfate, and evaporated *in vacuo*. The residue was subjected to tlc (hexane–acetone, 7:3) to give the major product (0.093 g, 55%) as a crystalline solid. Crystallization of this material from a small volume of ethyl acetate gave a powder, mp 174.5–182.5°C. On occasion, a solid, mp 165–166°C, was obtained, but the higher melting modification was the more stable one; $[\alpha]_D$ +25° (*c* 0.145, $CHCl_3$); ir ($CHCl_3$) ν_{max}: 3625, 3490, 1791, 1749, 1723 cm^{-1}, uv (MeOH) λ_{max}: 219 nm (ε 14 500); nmr ($CDCl_3$) δ: 0.90 (s, 3H), 0.94 (s, 3H), 1.15–2.96 (m, 24H), 3.40–3.80 (m, 5H), 4.90 (s, 2H), 5.87 (s, 1H). *Anal.* calcd. for $C_{25}H_{38}O_5$: C 71.74, H 9.15; found: C 71.74, H 9.20.

3β-(2,3-Dihydroxypropoxy)-14β-hydroxy 5β-card- 20(22)-enolide **2f**

meta-Chloroperbenzoic acid (0.900 g) was added, all at once, to a stirred solution of the iodo compound **2*d*** (1.00 g) in dry dichloromethane (25 mL) and glycerol acetonide (25 mL). After 1 h, methanol (100 mL) and 0.1 *N* sulfuric acid (50 mL) were added and the mixture was stirred for 3.25 h. The mixture was made neutral by the addition of solid sodium bicarbonate and was then concentrated *in vacuo* to remove most of the methanol. The mixture thus obtained was partitioned between water and ethyl acetate. The organic phase was washed with water, dried over sodium sulfate, and evaporated *in vacuo*. The residue (1.31 g) was taken up in dichloromethane (25 mL) and applied to a column of silica gel (50 g). Elution with ether (500 mL) removed nonpolar material and elution with ethyl acetate (500 mL) removed the partially purified product. This material was purified by hplc in the manner described above using ethyl acetate – hexane (8:1) as the eluting solvent at a flow rate of 12 mL/min at 1500 psig. The pure material (0.310 g, 36%), presumably a mixture of stereoisomers, on crystallization from ethyl acetate had mp 197°C; $[\alpha]_D$ +22.3 (*c* 0.274, $CHCl_3$); ir (KBr) ν_{max}: 3420, 1775, 1747, 1615 cm^{-1}; uv (MeOH) λ_{max}: 220 nm (ε 14 800); nmr ($CDCl_3$)δ: 0.88 (s, 3H), 0.93 (s, 3H), 1.00–3.00 (m, 25H), 3.66 (m, 6H), 4.88 (m, 2H), 5.85 (s, 1H); ms *m/e*: 430 ($M^+ - H_2O$). *Anal.* calcd. for $C_{26}H_{30}O_6$: C 69.61, H 8.99; found: C 69.47. H 8.96.

Acknowledgements

We thank Mr. E. Prisbe, Syntex Research, Institute of Organic Chemistry, for providing us with the experimental details for the preparation of the α-iodo compound **2*d***. We also thank Dr. A. Strosberg, Institute of Pharmacology, for the evaluation of the cardiotonic activities of the title compounds.

1. C. Lindig, H. J. Schmidt, and K. Repke. East German Patent No. 100,263 (1974).
2. U. E. Diner, F. Sweet, and R. K. Brown. Can. J. Chem. **44**, 1591 (1966); B. A. Stoochnoff and N. L. Benoitin. Tetrahedron Lett. 21 (1973); C. A. Brown and D. Barton. Synthesis, 434 (1974).
3. A. Menz. Angew. Chem. Int. Ed. Engl. **12**, 846 (1973); H. H. Freedman and R. A. Dubois. Tetrahedron Lett. 3251 (1975).
4. H. Kalinowski, D. Seebach, and G. Crass. Angew. Chem. Int. Ed. Engl. **14**, 1379 (1975).
5. E. J. Prisbe, J. Smejkal, J. P. H. Verheyden, and J. G. Moffat. J. Org. Chem. **41**, 1836 (1976).
6. H. J. Reich and S. L. Peake. J. Am. Chem. Soc. **100**, 4888 (1978); R. C. Cambie, B. G. Lindsay, P. S. Rutledge, and P. D. Woodgate. J. Chem. Soc. Chem. Commun. 919 (1978); R. C. Cambie, D. Chambers, B. G. Lindsay, P. S. Rutledge, and P. D. Woodgate. J. Chem. Soc. Perkin Trans. I, 822 (1980).
7. R. Thomas, J. Boutagy, and A. Gelbart. J. Pharmacol. Exp. Ther. **191**, 219 (1974).
8. M. Sekiya, Y. Ohashi, Y. Terao, and R. Ito. Chem. Pharm. Bull. **24**, 369 (1976).

Can. J. Chem. Downloaded from www.nrcresearchpress.com by 210.87.254.5 on 09/06/12
For personal use only.

Lignin and related compounds. VIII. Lignin monomers and dimers from hydrogenolysis of aspen poplar wood using rhodium-on-charcoal catalyst

KENICHI SUDO,[1] DONALD J. MULLORD, AND JAMES M. PEPPER

Department of Chemistry and Chemical Engineering, University of Saskatchewan, Saskatoon, Sask., Canada S7N 0W0

Received October 14, 1980

KENICHI SUDO, DONALD J. MULLORD, and JAMES M. PEPPER. Can. J. Chem. **59**, 1028 (1981).

Aspen poplar wood meal has been subjected to catalytic hydrogenolysis in dioxane–water (9:1) at 500 psig initial pressure of hydrogen over a 5% rhodium-on-charcoal catalyst for five hours at 195 ± 5°C. The resulting chloroform-soluble lignin degradation products were separated by cellulose and silica gel column chromatography. The following compounds were isolated and identified: 4-hydroxybenzoic acid (**5**), 1-(4-hydroxy-3,5-dimethoxyphenyl)-1-propanone (propiosyringone) (**6**), 2,2′-dihydroxy-3,3′-dimethoxy-5,5′-dipropylbiphenyl (**7**), 2,3-bis(4-hydroxy-3,5-dimethoxyphenyl)-1-propanol (**11**), and a mixture of 3-(4-hydroxy-3,5-dimethoxyphenyl)-2-(4-hydroxy-3-methoxyphenyl)-1-propanol (**9**) and 3-(4-hydroxy-3-methoxyphenyl)-2-(4-hydroxy-3,5-dimethoxyphenyl)-1-propanol (**10**).

KENICHI SUDO, DONALD J. MULLORD et JAMES M. PEPPER. Can. J. Chem. **59**, 1028 (1981).

On a soumis de la sciure de bois de peuplier en suspension dans un mélange de dioxanne–eau (9:1) à une hydrogénolyse catalytique effectuée en utilisant une pression initiale d'hydrogène de 500 psig, du rhodium sur charbon à 5% comme catalyseur et une température de 195 ± 5°C pendant 5 heures. On a fait appel à la chromatographie sur colonne de cellulose et de silice pour séparér les produits de dégradation de la lignine qui sont solubles dans le chloroforme. On a isolé et identifié les composés suivants: l'acide hydroxy-4 benzoique (**5**), la (hydroxy-4 diméthoxy-3,5 phényl)-1 propanone-1 (propiosyringone) (**6**), le dihydroxy-2,2′ diméthoxy-3,3′ dipropyl-5,5′ biphényle (**7**), le bis(hydroxy-4 diméthoxy-3,5 phényl)-2,3 propanol-1 (**11**) et un mélange des (hydroxy-4 diméthoxy-3,5 phényl)-3 (hydroxy-4 méthoxy-3 phényl)-2 propanol-1 (**9**) et (hydroxy-4 méthoxy-3 phényl)-3 (hydroxy-4 diméthoxy-3,5 phényl)-2 propanol-1 (**10**).

[Traduit par le journal]

Introduction

In earlier publications (1, 2) the suitability of using a 5% rhodium-on-charcoal catalyst for the hydrogenolysis of wood was described. From the chloroform-soluble fractions high yields of the following monomeric lignin degradation products were obtained: compounds **1** and **3** from spruce wood and compounds **1–4** from aspen wood.

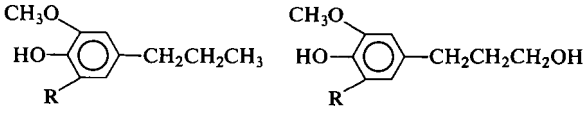

1 R = H
2 R = OCH_3

3 R = H
4 R = OCH_3

At that time attention was drawn to the significance of such a major potential source of phenolic chemicals. However, by the same procedure, other monomeric and oligomeric lignin products, whose identification would add to the knowledge of lignin structure, are produced in lesser amounts. We wish to report the isolation and characterization of compounds **5**, **6**, **7**, **11**, and a mixture of **9** and **10**.

Discussion

The same procedure for wood hydrogenolysis and lignin extraction as reported earlier (1, 2) was used but with a dioxane–water ratio of 9:1 instead of 1:1. Under these conditions only 75.5% of the original lignin was isolated as a chloroform-soluble fraction as compared to complete extraction in the earlier experiments. Under these modified conditions some selective bond cleavage may have occurred as is reflected in the nature of the isolated products. The chloroform extract was separated on a silica gel column using cyclohexane – ethyl acetate as the eluant, initially in a 3:1 ratio but with gradually increasing proportions of ethyl acetate

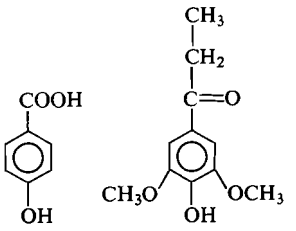

5

6

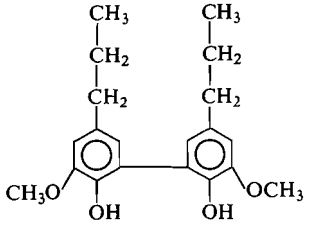

7

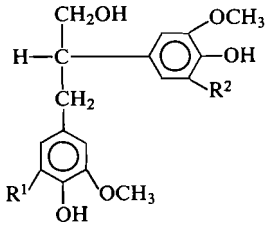

8 $R^1 = R^2 = H$
9 $R^1 = OCH_3$, $R^2 = H$
10 $R^1 = H$, $R^2 = OCH_3$
11 $R^1 = R^2 = OCH_3$

[1]Present address: Forestry and Forest Products Research Institute, P.O. Box 16, Tsukuba Norin Kenkyu, Danchi-Nai, Ibaraki, Japan 305.

0008-4042/81/071028-04$01.00/0

©1981 National Research Council of Canada/Conseil national de recherches du Canada

Can. J. Chem. Downloaded from www.nrcresearchpress.com by 210.87.254.6 on 09/06/12
For personal use only.

Can. J. Chem. Downloaded from www.nrcresearchpress.com by 210.87.254.6 on 09/06/12
For personal use only.

until a ratio of 1:1 was attained. A final elution (fraction P) was made using acetone. By this process, starting from 400 g of wood meal, the chloroform-soluble lignin degradation products (51.6 g) were divided among sixteen fractions (A–P) with recoveries of 0.259, 18.7, 1.62, 1.39, 3.20, 1.28, 1.24, 2.18, 0.687, 0.576, 0.796, 1.08, 1.91, 0.360, 0.990, and 8.61 g, respectively, for a total of 44.9 g (87%). Fraction B contained the monomeric lignin degradation products (**1–4**) whose isolation and characterization had been studied earlier (1, 2). Each other fraction was further separated using silica gel and/or cellulose column chromatography. Only from C, D, E, J, K, L, M, and P were amounts of pure compounds obtained that were adequate for characterization. Fractions C, D, and L are discussed herein; the others will be reported later. 4-Hydroxybenzoic acid (**5**) and 1-(4-hydroxy-3,5-dimethoxyphenyl)-1-propanone (**6**) isolated from fraction D, and 2,2′-dihydroxy-3,3′-dimethoxy-5,5′-dipropylbiphenyl (**7**) from fraction C were each identified by ir, ms, and by comparison with an authentic sample. Aspen lignin has been reported to contain large amounts of 4-hydroxybenzoate groups (3) so it is not surprising to find **5** in the products of this reaction. The isolation of **6** is more unusual under the hydrogenation conditions. It represents evidence for either the presence of an α-carbonyl group in the protolignin or possibly for the generation of 1-(4-hydroxy-3,5-dimethoxyphenyl)-1,2-propanediol (by alkyl – alkyl ether or glycosidic bond cleavage), followed by dehydration and tautomerization to give **6**. Considerable evidence is available for the 5–5 biphenyl linkage in lignin (3) and compound **7** was first isolated by Nahum in 1965 (4).

All available evidence suggests that a chromatographically "pure" substance obtained from fraction L was a mixture of compounds 3-(4-hydroxy-3,5-dimethoxyphenyl)-2-(4-hydroxy-3-methoxyphenyl)-1-propanol (**9**) and 3-(4-hydroxy-3-methoxyphenyl)-2-(4-hydroxy-3,5-dimethoxyphenyl)-1-propanol (**10**).[2] The mass spectrum showed

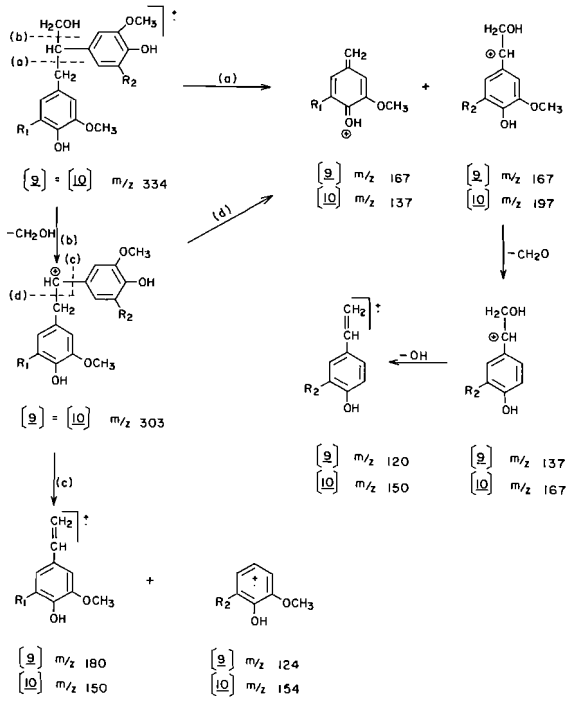

FIG. 1. Suggested fragmentation pattern of compounds **9** and **10**.

the molecular ion peak at *m/z* 334, a prominent base peak at *m/z* 167, and other main peaks at *m/z* 303, 197, 180, 167, 150, 137, and 122. The suggested fragmentation pattern as given in Fig. 1 shows that all the main peaks can only be accounted for on the basis of a mixture of **9** and **10**. Mass spectral patterns of pure **8** and **11** as reported by Sakakibara (5, 6), if considered additively, show a similar fragmentation pattern with the exception of the molecular ion peaks. Further support for the composition of the isolated fraction was provided by an examination of the ^{1}Hmr spectrum (Fig. 2) of the acetylated product and its comparison with the separate ^{1}Hmr spectra of compounds **8** and **11** as reported by Sakakibara and co-workers (5, 6). By this comparison the following assignments can be made: δ: 2.02 (s, 3H, alc-OAc), 2.28 (s, 3H, aryl-OAc), 2.29 (s, 3H, aryl-OAc), 2.70–3.02 (m, 2H, C_α—H), 3.02–3.33 (m, 1H, C_β—H), 3.69(s) and 3.74(s) (9H, aryl-OCH_3), 4.22 (d, 2H, C_α—H, J = 6.5 Hz), 6.17(s) and 6.28(s), (2H, aryl-H (syringyl)), and 6.40–7.03 (m, 3H, aryl-H (guaiacyl)). By comparing the relative peak areas of the two singlets at δ 6.17 and 6.28, corresponding to the syringyl ring protons, it was determined that the relative abundance of **9** to **10** was in the approximate molar ratio of 45:55.

[2]In earlier experiments (DJM) part of the dimeric lignin fraction from a Rh-C catalyzed hydrogenolysis of aspen poplar was converted into the trimethylsilyl ethers and separated on a 6 ft, 1/8 in. od stainless steel column packed with 15% SE-30 on Chromosorb W (AW-SMCS treated, 100/120 mesh) and temperature programmed from 200–300°C at 4°/min. Three fractions were collected at retention times of 18.5, 20.5, and 22.6 min. Mass spectral analysis showed molecular ion peaks at *m/z* 520, 550, and 580, respectively. Analysis of these spectra indicated that these fractions were the trimethylsilyl ethers of **8**, of a mixture of **9** and **10**, and of **11**, respectively.

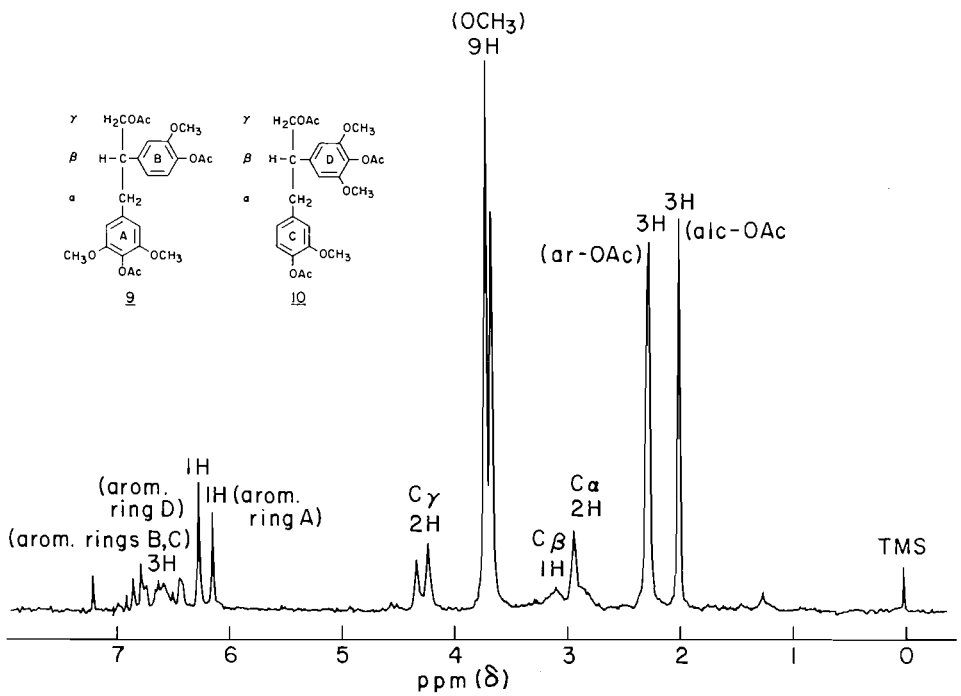

FIG. 2. ^{1}Hmr spectrum of mixture of compounds **9** and **10** (acetates).

2,3-Bis-(4-hydroxy-3,5-dimethoxyphenyl)-1-propanol (**11**), isolated from fraction M, was characterized by ir, ms, and ^{1}Hmr. The mass spectrum showed a molecular ion peak at *m/z* 364, the base peak at *m/z* 167, and other prominent peaks at *m/z* 194, 180, and 137. The mechanism of fragmentation for this molecule would be similar to that illustrated in Fig. 1. The ^{1}Hmr pattern of the diacetate was similar to that reported for this compound by Sudo and Sakakibara (6).

Evidence for the existence of the C_β—C_1 type of linkage in lignin has been reported previously. From the hydrolysis products of beech wood, Nimz *et al.* (7, 8) isolated compounds analogous to **8**, **10**, and **11**, but retaining the α-hydroxy function. Using catalytic hydrogenation over a copper chromite catalyst, Sakakibara and co-workers (5, 6) obtained **8** from Ezomatsu wood and **11** from Yachidamo wood. The work reported here on the isolation of the mixed type of dimers, **9** and **10** (containing both guaiacyl and syringyl nuclei), along with **11** (two syringyl nuclei), is of particular significance and is most readily explained by Freudenberg's free radical theory of lignin formation (9).

Experimental

Aspen poplar (*Populus tremuloides*, Michx.) sapwood (20 mesh) was extracted in a Soxhlet extractor for 48 h with ethanol–benzene (1:1), then under reflux with acetone–water (9:1) for 24 h and air dried. Found: Klason lignin, 18.9%; moisture, 4.04%. The catalyst, 5% rhodium-on-charcoal was obtained from K & K Laboratories Inc., silica gel (Bio-sil A, 100–200 mesh) from BIO-RAD Laboratories, and cellulose powder from W & R Balston, Ltd.

General Reaction Procedure

A typical hydrogenolysis was as follows: wood meal (20 g), 5% Rh-C (2 g), dioxane–water (9:1) (300 mL) were placed in a 500 mL beaker inside a one litre Parr pressure reactor. After flushing twice with hydrogen, it was filled to an initial pressure of 500 psig. The temperature was raised and controlled at 195 ± 5°C for 5 h during which time the mixture was stirred using a magnetic stirrer. After cooling, the reactor contents were filtered, the pulp and catalyst washed with dioxane–water (9:1), and the combined filtrates extracted exhaustively with chloroform. After drying, the solvent was removed to leave the chloroform-soluble extract which, from a total of 400 g wood meal, weighed 51.6 g (68.3% of Klason lignin).

Separation of Lignin Degradation Products

Using a silica gel column (67 mm × 500 mm), the total chloroform-soluble material was separated by a gradient development technique. The column was eluted initially with cyclohexane – ethyl acetate (3:1) and then with gradually increasing proportions of ethyl acetate until a ratio of 1:1 was achieved. As a result fifteen fractions (A → O) were obtained. Residual material on the column was removed using acetone (fraction P). Total recovery was 44.9 g (87%). Further column chromatographic separation of each fraction was monitored using thin layer chromatography (developed with toluene – formic acid – ethyl formate (5:1:4), followed by spraying with 50% sulfuric acid and heating to 105°C).

Isolation of Compounds 5 and 6

Fraction D (1.38 g) was separated using a silica gel column (15 mm × 600 mm). Elution with cyclohexane–acetone (7:1) gave rise to two crude, separate, crystalline products. Recrystallization of one product from xylene–ethanol gave colourless

Can. J. Chem. Downloaded from www.nrcresearchpress.com by 210.87.254.6 on 09/06/12
For personal use only.

needles (21.2 mg), mp 213–214°C, no mp depression on mixing with authentic 4-hydroxybenzoic acid, **5**. The second product, after recrystallization from methylene chloride – petroleum ether (40–60°C), gave colourless needles (12.2 mg), mp 107–109°C, no mp depression on mixing with authentic 1-(4-hydroxy-3,5-dimethoxyphenyl)-1-propanone, **6**.

Isolation of Compound 7

Fraction C (1.62 g) was separated using a silica gel column (25 mm × 700 mm). Elution with cyclohexane–acetone (8:1) first removed some monomeric compounds, followed by a fraction which, after further chromatographic separation using a cellulose column (15 mm × 650 mm) and xylene–dimethylformamide (15:1) gave rise to a crude solid. Recrystallization from methylene chloride – petroleum ether (40–60°C) gave colourless crystals (5.2 mg), mp 147–150°C.

Isolation of Mixture of Compounds 9 and 10

Fraction L (1.08 g) was separated using a cellulose column (15 mm × 650 mm). Elution with xylene–dimethylformamide (10:1) yielded a component (87.5 mg) which required further purification using a silica gel column, eluting first with benzene–acetone (8:1) and rechromatographing using chloroform–methanol (100:1). This liquid product (49.4 mg) was used for mass spectral analysis. Acetylation of part of this material gave a product which was finally purified using a silica gel column (10 mm × 300 mm) and cyclohexane – ethyl acetate (5:1) as the eluting solvent. The product (32.1 mg) could not be crystallized. *Anal.* calcd. for $C_{24}H_{28}O_9$: C 62.60, H 6.13; found: C 62.49, H 6.15%.

Isolation of Compound 11

Fraction M (1.91 g) was separated using a cellulose column (20 mm × 600 mm) and gradient development elution starting with xylene and dimethyl formamide (10:1) with increasing dimethylformamide. A compound which gave a purple spot if monitored by tlc was collected and rechromatographed twice using silica gel columns (15 mm × 600 mm), first with benzene–acetone (7:1) and then with cyclohexane–acetone (3:1). After recrystallization from ethanol–water, compound **11** was obtained (45.2 mg), mp 169–171°C (lit. (6) mp 170–172°C).

Acknowledgements

The authors wish to acknowledge the financial assistance provided by the Natural Sciences and Engineering Research Council of Canada and the University of Saskatchewan.

1. J. M. Pepper and Y. W. Lee. Can. J. Chem. **47**, 723 (1969).
2. J. M. Pepper and R. W. Fleming. Can. J. Chem. **56**, 896 (1978).
3. K. V. Sarkanen and C. H. Ludwig (*Editors*). Lignins: Occurrence, formation, structure and reactions. Wiley-Interscience, New York, NY. 1971.
4. L. Nahum. Ind. Eng. Chem. **4**, 71 (1965).
5. M. Ohta and A. Sakakibara. Mokuzai Gakkaishi, **15**, 247 (1969).
6. K. Sudo and A. Sakakibara. Mokuzai Gakkaishi, **19**, 165 (1973).
7. H. Nimz and K. Das. Chem. Ber. **104**, 2359 (1971).
8. H. Nimz. Chem. Ber. **99**, 469 (1966).
9. K. Freudenberg and A. C. Neish. Constitution and biosynthesis of lignin. Springer Verlag, New York, 1968.

Can. J. Chem. Downloaded from www.nrcresearchpress.com by 210.87.254.6 on 09/06/12
For personal use only.

Interaction électron–solvant dans la radiolyse-γ du *N*-methylacétamide et de ses mélanges à l'eau. Effet d'intercepteurs sélectifs

T. H. TRAN-THI, A. M. KOULKÈS-PUJO[1] ET J. SUTTON

CNRS et DPC/SCM, Centre d'Etudes Nucléaires de Saclay, 91190 Gif sur Yvette, France

Reçu le 18 septembre 1980

T. H. TRAN-THI, A. M. KOULKÈS-PUJO et J. SUTTON. Can. J. Chem. **59**, 1032 (1981).

L'étude des mécanismes de réactions de la radiolyse-γ du *N*-méthylacétamide (NMA) à 30°C (constante diélectrique 178) en présence d'intercepteurs d'électrons (N_2O; HCl,2NMA; $(CH_3)_2CO$) a permis de montrer que l'attachement d'un électron pré-solvaté sur NMA correspond à une réaction lente comparativement à celle de N_2O avec la même espèce. Cet attachement serait probablement dissociatif. Les constantes de vitesse de l'électron "sec" avec N_2O, $(CH_3)_2CO$, et NMA seraient dans l'ordre suivant:

$$k_{e^-+N_2O} \geq 70k_{e^-+(CH_3)_2CO} \geq 110k_{e^-+NMA}$$

T. H. TRAN-THI, A. M. KOULKÈS-PUJO, and J. SUTTON. Can. J. Chem. **59**, 1032 (1981).

A study of the reaction mechanism of the γ-radiolysis of *N*-methyl acetamide (NMA) at 30°C (dielectric constant 178) in the presence of various electron scavengers (N_2O; HCl·2NMA; $(CH_3)_2CO$) has shown that the attachment of a presolvated electron to NMA is a slow reaction compared to that of N_2O with the same species. This attachment probably is dissociative. The rate constants of the "dry" electron with N_2O, acetone (Ac), and NMA are in the following order

$$k_{e^-+N_2O} \geq 70k_{e^-+Ac} \geq 110k_{e^-+NMA}$$

1. Introduction

L'étude systématique du comportement des amides sous l'effet des rayonnements a été peu développée malgré l'importance de ces composés dans les réactions des biopolymères tels que les protéines et les polypeptides. En effet, les groupements amidiques dans les molécules de polypeptides semblent conserver dans une large mesure leur caractère de groupement amide isolé (1), ce qui justifie le développement actuel des recherches sur les amides à l'état monomère et en tant que solvant.

Le NMA à cet effet devrait permettre d'atteindre des rendements en ions libres élevés. Or nos résultats de radiolyse pulsée (2) ont permis de montrer que les électrons ne sont pas solvatés par les molécules de NMA dans le solvant pur. Dans les milieux mixtes NMA–H_2O une concentration 5,3 *M* en eau soit 10% en poids, est suffisante pour que le spectre d'absorption du mélange désaéré et irradié corresponde à celui de l'électron hydraté.

L'absence d'électron solvaté dans le NMA pur nous a amenés à suggérer que l'électron s'attache sur cette molécule selon un processus éventuellement dissociatif. La technique de radiolyse pulsée ne nous ayant pas permis de mettre en évidence de bande d'absorption pouvant être attribuée à l'anion NMA^- dans le domaine de l'uv et du visible (250–750 nm), nous avons poursuivi cette étude par la technique de radiolyse-γ continue, complémentaire de la radiolyse pulsée. En effet, le dosage des produits finals et l'utilisation d'intercepteurs sélectifs pourraient fournir des idées sur l'identité des espèces transitoires mises en jeu dans les mécanismes radiolytiques. Ainsi le protoxyde d'azote N_2O intercepteur connu d'électrons solvatés, d'anions, mais également d'électrons présolvatés pourrait réagir avec l'anion NMA^- ou l'électron présolvaté pour former de l'azote. La mesure du rendement en azote formé au cours de la radiolyse du système NMA + N_2O et sa variation avec l'addition de divers intercepteurs secondaires susceptibles de réagir différemment avec les électrons présolvatés ou NMA^- pourraient contribuer à élucider l'hypothèse de l'existence de l'anion NMA^-.

2. Partie expérimentale

A. Conditions opératoires

Irradiation

Des cellules de 6 mL contenant le solvant pur (NMA) désaéré, saturé de gaz (N_2O ou N_2O + Ar) ou en mélange avec d'autres solutés et cosolvants sont maintenues à 38 ± 1°C afin de conserver le NMA à l'état liquide. Les différents mélanges de gaz (N_2O + Ar) fournis par l'Air Liquide ont été utilisés afin d'avoir plusieurs concentrations de N_2O dans le NMA. La solubilité de N_2O dans le NMA déterminée à 38°C et à pression atmosphérique est de $7{,}2 \times 10^{-2}$ *M*. Nous avons contrôlé que la loi de Henry est vérifiée pour différentes pressions partielles de N_2O. Nous avons ainsi pu faire varier la concentration de N_2O dans le NMA de $7{,}2 \times 10^{-4}$ *M* à $7{,}2 \times 10^{-2}$ *M*.

Dosimétrie

Les échantillons sont irradiés à une source de ^{60}Co de 100 Ci. Le débit de la dose mesuré avec le dosimètre Fricke est $I_E = 2{,}84 \times 10^{18}$ eV h^{-1} cm^{-3} pour l'eau pure. On suppose que les rayonnements γ ou les électrons accélérés interréagissent avec tous les électrons du milieu, de sorte que le débit de dose I_{NMA} absorbée par le solvant peut être calculé à partir de

[1]A qui les demandes de tirés à part doivent être adressées.

0008-4042/81/071032-05$01.00/0

©1981 National Research Council of Canada/Conseil national de recherches du Canada

Can. J. Chem. Downloaded from www.nrcresearchpress.com by 210.87.254.105 on 09/06/12
For personal use only.

Can. J. Chem. Downloaded from www.nrcresearchpress.com by 210.87.254.105 on 09/06/12
For personal use only.

TABLEAU 1. Rendements en produits finals

NMA (M)	N_2O (M)	2é soluté ou co-solvant (M)		$G(N_2)$	$G(H_2)$	$G(CH_4)$	$G(CH_2O)$
13	0	0		0	0,90±0,05	0,33±0,06	—
	$7,2 \times 10^{-4}$	0		1,65±0,2	0,80±0,05	0,43±0,06	—
13	$7,2 \times 10^{-3}$	0		1,80±0,2	0,80±0,05	0,38±0,06	—
	$2,7 \times 10^{-2}$	0		2,5 ±0,3	0,78±0,05	0,38±0,06	—
	$7,2 \times 10^{-2}$	0		3,3 ±0,3	0,93±0,05	0,39±0,06	1,4±0,5
	$7,2 \times 10^{-3}$		0,10	1,6 ±0,3	0,86±0,05	0,37±0,10	
13	$7,2 \times 10^{-2}$	HCl,2NMA	0,10	3,1 ±0,4	0,78±0,05	0,40±0,06	
	$7,2 \times 10^{-2}$		0,50	3,4 ±0,4	0,88±0,05	0,35±0,06	
12,02	$7,2 \times 10^{-4}$		1,02	3?	0,96±0,05	0,14±0,06	
12,02	$7,2 \times 10^{-3}$		1,02	3,3 ±0,3	0,83±0,05	0,44±0,06	
10,62	$7,2 \times 10^{-3}$		2,50	2,2 ±0,3	0,83±0,05	0,49±0,06	
8,25	$7,2 \times 10^{-3}$		5,00	2,5 ±0,3	0,78±0,05	0,48±0,06	
		$(CH_3)_2CO$					
12,02	$7,2 \times 10^{-2}$		1,02	3,2 ±0,3	0,78±0,05	0,39±0,06	
10,62	$7,2 \times 10^{-2}$		2,50	3,4 ±0,3	0,86±0,05	0,45±0,10	
8,25	$7,2 \times 10^{-2}$		5,00	3,3 ±0,3	0,78±0,05	0,42±0,08	
0	$7,2 \times 10^{-2}$		13,70	2,2 ±0,2	0,58±0,05	1,30±0,10	
12,98			0,14	3,3 ±0,3	0,90±0,10	0,44±0,06	
12,78			1,00	2,9 ±0,3	0,88±0,10	0,26±0,10	
11,84	$7,2 \times 10^{-2}$	H_2O	5,00	2,7 ±0,3	0,85±0,05	0,16±0,06	
8,98			17,22	2,5 ±0,3	0,93±0,05	Négligeable	
6,51			27,80				0,8±0,5
11,83	$7,2 \times 10^{-2}$	$(CH_2)_2CO$ 1,00 + H_2O 1,01		3,45±0,3	0,86±0,05	0,42±0,06	

I_E en tenant compte des densités électroniques relatives de l'eau et du NMA.

Purification des solvants

Le NMA, produit Merck, a été purifié selon le procédé mis au point par Pucci, Vedel et Trémillon (3) qui consiste à éliminer les trois impuretés connues CH_3NH_2, CH_3COOH et H_2O, successivement par addition de H_2SO_4, K_2CO_3 et CaO, chacun de ces traitements étant suivi d'une distillation sous pression réduite. La principale impureté résiduelle demeure l'eau dont la concentration est de 63 ppm soit $3,9 \times 10^{-3}$ M. Le distillat recueilli est conservé sous atmosphère inerte dans une boîte à gants.

L'acétone R. P. Merck a été utilisé tel quel. L'eau est tridistillée. L'acide HCl,2NMA synthétisé suivant la réaction de Mannich et Heilner (4)[2] a été purifié par dissolution dans l'éther et par recristallisation dans l'acétone.

Analyse des produits finals

Les produits finals gazeux sont isolés par la technique du vide et analysés par chromatographie en phase gazeuse à l'aide d'un chromatographe Perkin-Elmer modèle F_6 à catharomètre. Les colonnes de 3 m de long remplies de tamis moléculaire 5 Å sont maintenues à 80°C. Le gaz vecteur est l'argon.

Le formaldéhyde a été dosé suivant la méthode colorimétrique et spectrophotométrique de Bricker et Vail (5), que nous avons adaptée à nos conditions opératoires (6).

B. Résultats expérimentaux

Les rendements en produits finals (H_2, CH_4, N_2 et CH_2O) formés au cours de la radiolyse des différents systèmes étudiés sont reportés dans le tableau 1.

NMA pur

Le NMA pur désaéré et irradié produit de l'hydrogène et du méthane avec les rendements respectifs:

$$G(H_2) = 0,90 \pm 0,05$$

$$G(CH_4) = 0,33 \pm 0,06$$

La valeur du $G(H_2)$ est à comparer à celle obtenue par irradiation du formamide par Matsumoto et coll. (7), $G(H_2) = 0,87$, et par Head et Walker (8), $G(H_2) = 0,94$. Elle est de beaucoup supérieure à celle trouvée pour le diméthylformamide $G(H_2) = 0,4$ par Kroh et Burzynska (9). De plus, le rendement en méthane que ces auteurs indiquent pour le formamide est négligeable ($G(CH_4) < 0,01$) et $G(CH_4) = 0$ pour le diméthylformamide. En revanche dans le cas du NMA, nous n'avons pas mis en évidence de CO contrairement aux deux autres amides.

NMA + N_2O

Les rendements en hydrogène et méthane ne sont pas affectés par la présence de N_2O quelle que soit sa concentration de 10^{-4} M à 10^{-2} M (tableau 1). Pour la concentration en N_2O la plus élevée, le rendement $G(N_2)$ égal à $3,3 \pm 0,3$ est encore loin de la valeur du rendement correspondant à l'ionisation totale estimée pour les liquides à $4,5 \pm 0,5$.

Effets de divers intercepteurs secondaires (HCl,2NMA; $(CH_3)_2CO$; H_2O)

Les résultats obtenus avec les différents intercepteurs secondaires laissent apparaître plusieurs points importants:

(*a*) L'acide HCl,2NMA entièrement dissocié dans le NMA (10) n'a pas d'effet sur les rendements initiaux en hydrogène, méthane et azote, quelle que soit la concentration en N_2O, malgré la grande réactivité connue du proton H^+ avec les anions et les électrons solvatés.

(*b*) L'effet de l'acétone (Ac) est plus complexe. En effet la présence de l'acétone dans les solutions NMA $7,2 \times 10^{-3}$ en N_2O, fait croître le rendement initial en azote. Ainsi pour le mélange NMA + Ac 1 M, $G(N_2) = 3,3 \pm 0,3$ au lieu de $1,8 \pm 0,2$

[2]Nous remercions J. C. Hallé qui a bien voulu nous fournir des échantillons de ce produit.

Can. J. Chem. Downloaded from www.nrcresearchpress.com by 210.87.254.105 on 09/06/12
For personal use only.

en absence d'acétone. Cependant l'augmentation de la concentration en acétone à 2,5 *M* et à 5 *M* fait également croître $G(N_2)$ mais à des valeurs respectives plus faibles de 2,2 ± 0,3 et 2,5 ± 0,3.

En revanche, en présence de N_2O $7{,}2 \times 10^{-2}$ *M*, $G(N_2)$ reste constant et égal à 3,3 quelle que soit la concentration en acétone variant de 1 à 5 *M*. L'addition d'un second intercepteur secondaire (H_2O) au système NMA + N_2O $7{,}2 \times 10^{-2}$ *M* + Ac 1 *M* n'affecte pas le rendement initial en N_2 qui reste égal à 3,45 ± 0,3. Les variations complexes du rendement initial en N_2 suivant les concentrations de N_2O et des intercepteurs secondaires seront discutées ultérieurement, mais nous pouvons d'ores et déjà remarquer que le rendement en N_2 dans le milieu acétone seul est plus faible que celui obtenu pour ses divers mélanges au NMA.

D'autre part, pour les concentrations en N_2O supérieures à $7{,}2 \times 10^{-4}$ *M*, les rendements en H_2 et CH_4 ne sont pratiquement pas affectés par la présence de l'acétone.

(*c*) L'addition d'eau (de $3{,}9 \times 10^{-3}$ *M* à 17,22 *M*) au système NMA + N_2O provoque un abaissement lent du rendement en N_2, indiquant ainsi une action effective de l'eau sur les précurseurs conduisant à la formation de N_2. Ceci est également vrai pour le méthane dont le rendement diminue rapidement et devient négligeable pour H_2O 17,22 *M*. En revanche, l'hydrogène est formé avec un rendement à peu près constant ce qui laisserait supposer que son origine est moléculaire.

3. Discussion

Les nombreux termes employés dans la littérature pour distinguer les différents états de l'électron (électrons secs, piégés, présolvatés, solvatés), nous amènent à préciser le sens des termes que nous allons utiliser.

Le terme d'électron sec ou présolvaté (noté e^-) introduit par Hamill (11), désigne l'électron mobile, délocalisé, capable (avant de réorienter les molécules du solvant) de se recombiner avec l'ion positif ou de réagir soit avec le solvant lui-même en conduisant à un attachement électronique, soit avec certains intercepteurs à concentration suffisante.

L'absence d'électrons solvatés par NMA dans le milieu NMA pur ainsi que dans les mélanges avec l'eau (12) nous ont permis d'envisager l'hypothèse de l'attachement de l'électron présolvaté sur la molécule de NMA conduisant à un anion NMA^- transitoire dans un état fondamental ou excité, pouvant se dissocier. On aurait:

[1] $NMA \rightsquigarrow NMA^+ + e^-$

[2] $NMA + e^- \rightarrow NMA^-$
$\searrow$
$NMA^{-*} \rightarrow$ produits

Les intercepteurs pourraient alors réagir soit avec l'électron présolvaté soit avec les anions-radicaux du solvant. Par exemple dans le cas de N_2O, la formation d'azote pourrait provenir de l'une des réactions suivantes:

[3] $NMA^- + N_2O \rightarrow N_2 + O^- + NMA$

[4] $e^- + N_2O \rightarrow N_2 + O^-$

N_2O est connu d'ailleurs comme un bon capteur d'électrons tant solvatés que présolvatés (11, 13). Si la réaction [2] est rapide devant la réaction [4], l'azote proviendrait principalement de la réaction [3]. Un intercepteur efficace d'anion tel que le proton H^+, devrait avoir pour effet de faire décroître fortement le rendement en azote. En effet tous les anions organiques sont connus pour réagir rapidement avec H^+. Nous ne citerons pour mémoire que le cas de la benzophénone dont l'anion $(C_6H_5)_2\dot{C}O^-$ est rapidement transformé en radical $(C_6H_5)_2\dot{C}OH$ (14). En revanche le rendement en azote devrait demeurer inchangé s'il provenait des électrons présolvatés puisque ces derniers sont connus pour ne pas réagir avec H^+ (13). L'invariance du rendement en N_2 semble montrer que si l'attachement d'un électron présolvaté sur NMA est possible, cette réaction est plutôt lente comparativement à celle de l'attachement électronique sur N_2O. L'azote se forme principalement par la réaction [4] avec une constante de vitesse de réaction k_4 très grande devant k_2 étant donné le rapport de concentration des deux intercepteurs [NMA] = $\sim$200[N_2O].

Head et Walker (8) dans leur étude sur la radiolyse-γ du formamide (FA) saturé en N_2O ont trouvé un rendement en N_2 semblable au nôtre $G(N_2) = 3{,}2 \pm 0{,}3$. Contrairement au cas du NMA, ce rendement diminue rapidement en présence de H_2SO_4 ajouté comme intercepteur secondaire. L'absence d'électron solvaté dans ce milieu a amené ces auteurs à suggérer la présence d'anions FA^- formés par attachement des électrons secs sur les molécules de FA et à attribuer la diminution du $G(N_2)$ à une compétition entre H^+ et N_2O pour cet anion.

Dans le cas du NMA, la non réactivité de l'ion H^+ laisse supposer que l'attachement électronique s'il existe, est dissociatif. On aurait alors les réactions possibles suivantes:

[5] $NMA + e^- \rightarrow CH_3CO^{\cdot} + CH_3NH^-$ ou
$\searrow$ $CH_3CO^- + CH_3NH^{\cdot}$ ou
$\searrow$ autres produits

La réaction [5] en compétition avec la réaction [4] permettrait d'expliquer l'absence de plateau à la courbe de dilution que l'on pourrait tracer à partir des résultats portés dans le tableau 1. Le rendement en N_2 ne proviendrait donc que d'une partie des électrons formés au cours de la radiolyse.

Un autre intercepteur secondaire l'acétone (Ac) a été utilisé car il réagit tant avec les électrons secs que solvatés (15, 16). Son anion Ac^- est très réactif envers N_2O (17). L'addition de Ac pourrait entraîner une augmentation du rendement en azote

Can. J. Chem. Downloaded from www.nrcresearchpress.com by 210.87.254.105 on 09/06/12
For personal use only.

par compétition avec la réaction [5]. $G(N_2)$ devrait alors tendre vers le rendement total d'ionisation du solvant par le truchement des réactions suivantes:

[6] $e^- + Ac \rightarrow Ac^-$

[7] $Ac^- + N_2O \rightarrow N_2 + O^- + Ac$

L'augmentation du rendement en N_2 de $1,8 \pm 0,2$ à $3,3 \pm 0,3$ respectivement en absence et en présence d'acétone 1 *M* dans les solutions $7,2 \times 10^{-3}$ *M* en N_2O dans NMA, indique bien une compétition réelle entre N_2O, Ac et NMA pour l'électron sec en faveur de l'acétone. Cependant une augmentation de la concentration en acétone à 2,5 *M* et 5 *M* dans ce même milieu fait diminuer $G(N_2)$ respectivement à $2,2 \pm 0,3$ et $2,5 \pm 0,3$.

L'augmentation de la concentration d'acétone déplace bien la compétition entre les réactions [4]–[6] en faveur de [6], mais elle entraîne également une modification non négligeable des propriétés diélectriques du milieu. En effet nous avons déterminé les constantes diélectriques des mélanges NMA et Ac, et nous avons constaté qu'elle diminue de moitié quand la concentration en acétone augmente de 1 *M* à 5 *M* (tableau 2). L'abaissement de la constante diélectrique ne peut que favoriser les réactions de recombinaisons géminées de l'anion Ac^- entraînant ainsi une diminution du rendement en ions libres.

D'ailleurs pour l'acétone pur ($\varepsilon_{Ac}^{35°} = 20,7$), Chaudhri et Asmus (18) en utilisant la technique de radiolyse pulsée couplée à la conductimétrie, ont déterminé un rendement en ions libres $G(Ac^-) = 1,20 \pm 0,2$. En présence de solutés (acide perchlorique ($HClO_4$) anthracène (An) ou tétranitrométhane ($C(NO_2)_4$)), les rendements en ions libres secondaires, formés par transfert de la charge négative provenant de $(CH_3)_2CO^-$ tels que $G(Cl^-) = 1,4 \pm 0,1$; $G(An^-) = 1,7 \pm 0,2$ ou $G(C(NO_2)_3^-) = (2,15 \pm 0,10)$ sont tous supérieurs à celui de $(CH_3)_2CO^-$ lui-même. Cette différence est attribuée à la possibilité de ces anions d'échapper pendant une durée plus longue que l'anion Ac^- à la recombinaison géminée. Robinson et Rodgers (19) proposent pour ce même solvant une valeur encore plus faible du rendement en ions libres $G_{fi} = 0,75 \pm 0,05$ comparativement à celui des géminés $G_{gi} = 2,3 \pm 0,2$. L'étude en radiolyse pulsée de la cinétique de disparition de l'anion Ac^- absorbant à 550 nm et du cation Ac^+ à 860 nm les ont amenés à conclure à deux modes différents de disparition de l'anion: la première par recombinasion géminée avec Ac^+, et la seconde par réaction avec d'autres espèces transitoires formées au cours de la radiolyse. La valeur du rendement d'azote que nous avons déterminé par radiolyse-γ de l'acétone en présence de N_2O est $G(N_2) = 2,2 \pm 0,3$. Ce rendement n'est pas forcément égal à celui des ions libres si la réaction [7] intervient aussi dans les zones à forte densité d'ionisation et d'excitation. Cependant cette valeur est faible pour un rendement d'ionisation totale et on peut admettre que l'anion Ac^- disparait partiellement par une réaction de recombinaison géminée, cette dernière étant en partie inhibée par la présence de NMA. Cependant, la présence d'acétone ne joue plus pour une concentration en N_2O de $7,2 \times 10^{-2}$ *M*. $G(N_2)$ reste invariant et égal à $3,3 \pm 0,3$ quelle que soit la concentration en acétone de 1 *M* à 5 *M*. Ce résultat montre que dans ce cas, la vitesse de la réaction de l'électron sec avec N_2O est supérieur à celle avec l'acétone. En tenant compte des concentrations respectives de N_2O, Ac et NMA, on peut estimer que les constantes de vitesse varient suivant cet ordre

$$k_{e^-+N_2O} \geq 70k_{e^-+Ac} \geq 110k_{e^-+NMA}$$

En résumé, aussi bien dans les milieux NMA + N_2O que NMA + N_2O + HCl,2NMA la formation d'azote semble provenir exclusivement de la dissociation de l'anion N_2O^- formé à partir de l'attachement d'un électron sec sur N_2O.

En présence d'acétone elle peut cependant trouver une partie de son origine dans la réaction de l'anion Ac^- avec N_2O.

TABLEAU 2. Valeurs de la constante diélectrique des mélanges NMA–Ac

Milieu	*t* (°C)	ε	Réf.
NMA 13 *M*	31,4	178,9	24
NMA 12,02 *M* + $(CH_3)_2CO$ 1,00 *M*	25	162,2	*a*
NMA 10,62 *M* + $(CH_3)_2CO$ 2,50 *M*	25	127,65	*a*
NMA 8,25 *M* + $(CH_3)_2CO$ 5,00 *M*	25	86,45	*a*
$(CH_3)_2CO$ 13,7 *M*	25	20,7	24

[a]S. Blanchard. Communication personnelle.

Effet de l'eau

Dans les systèmes NMA + H_2O + N_2O où l'électron a une probabilité non négligeable de se solvater (par exemple à partir d'une concentration en eau de 5,3 *M* soit 10% en poids (2)) la présence d'eau fait abaisser le rendement en N_2. La constante diélectrique des mélanges eau–NMA (tableau 3) est toujours supérieure a celle de l'eau pur. Les différentes réactions possibles des électrons sont les suivantes:

[4] $e^- + N_2O \rightarrow N_2 + O^-$

[5] $e^- + NMA \rightarrow$ Produits

[8] $e^- + nH_2O \rightarrow e_{aq}^-$

[9] $e_{aq}^- + N_2O \rightarrow N_2 + O^-$ $\quad k_9 = 8,7 \times 10^9\ M^{-1}\ s^{-1}$ (20)

Can. J. Chem. Downloaded from www.nrcresearchpress.com by 210.87.254.105 on 09/06/12
For personal use only.

TABLEAU 3. Valeurs de la constante diélectrique des mélanges NMA–H_2O

Milieu	ε	Réf.
NMA 13 *M*	183,0	25
NMA 12,98 *M* + H_2O 0,138 *M*	181,0	
NMA 12,78 *M* + H_2O 1,00 *M*	170,0	
NMA 11,84 *M* + H_2O 5,00 *M*	136,5	
NMA 8,98 *M* + H_2O 17,22 *M*	100,0	
NMA 6,51 *M* + H_2O 27,8 *M*	91,0	

[10] $e_{aq}^- + H^+ \rightarrow H^\cdot$ $k_{10} = 2{,}3 \times 10^{10}\ M^{-1}\ s^{-1}$ (15)

[11] $e_{aq}^- + e_{aq}^- \rightarrow H_2 + 2OH^-$ $k_{11} = 6 \times 10^9\ M^{-1}\ s^{-1}$ (21)

[12] $e_{aq}^- + NMA \rightarrow$ Produits $k_{12} = 2{,}6 \pm 0{,}2 \times 10^6\ M^{-1}\ s^{-1}$[3]

[13] $e_{aq}^- + H_2O \rightarrow$ Produits $k_{13} = 1{,}0 \pm 0{,}2 \times 10^4\ M^{-1}\ s^{-1}$[3]

Nous suggérons que la baisse du rendement en N_2 provient de différentes compétitions possibles.

(*a*) Entre N_2O et H_2O pour l'électron sec (réactions [4] et [8]), le temps de solvatation de l'e^- a été estimée par Rentzepis et coll. (22) à 4 ps.

(*b*) Entre N_2O et H^+ pour l'électron hydraté e_{aq}^- par les réactions [9] et [10].

(*c*) Entre N_2O et e_{aq}^- selon [9] et [11].

La valeur de la constante de vitesse de réaction de l'e_{aq}^- avec H_2O ($k_{13} = 1{,}0 \times 10^4\ M^{-1}\ s^{-1}$) et celle que nous avons déterminée pour la réaction de e_{aq}^- avec NMA ($k_{12} = 2{,}6 \times 10^6\ M^{-1}\ s^{-1}$) nous permettent de négliger les réactions [12] et [13] devant les réactions [9]–[11].

Head et Walker (8) dans leur étude de la radiolyse du formamide (FA) ont également étudié l'effet de l'eau sur le rendement en azote dans les solutions de FA saturées en N_2O et n'ont pas trouvé d'effet jusqu'à une concentration en eau 0,19 *M* soit 0,86% en poids. Ce résultat n'est pas surprenant si l'on tient compte du fait que pour les mélanges H_2O–FA, la bande d'absorption correspondant à l'e_{aq}^- n'apparaît qu'à partir d'une concentration en eau égale à 20% en poids soit 11,1 *M* (23); pour le NMA, il suffit de 10% en eau (soit 5,3 *M*) pour que le spectre d'absorption de l'e_{aq}^- soit visible (2). D'ailleurs le rendement d'azote baisse déjà pour une concentration en eau de 1 *M*.

L'addition d'acétone 1 *M* au mélange NMA(11,8 *M*) + H_2O (1 *M*) + N_2O($7{,}2 \times 10^{-2}$ *M*) a permis par ailleurs de montrer que le rendement en azote dans ce mélange reste égal à celui déterminé en absence d'eau $G(N_2) = 3{,}45 \pm 0{,}3$. Il est supérieur à celui déterminé pour le même mélange exempt d'acétone ($G(N_2) = 2{,}9$). Ce résultat laisse présumer: soit que Ac^- formé à partir des électrons hydratés selon $e_{aq}^- + Ac \rightarrow Ac^-$ réagit avec N_2O pour augmenter le rendement de l'azote en favorisant une compétition avec les réactions de destruction de l'e_{aq}^- (réactions [10], [11]); soit que la vitesse de réaction de l'électron sec avec Ac est supérieure à celle de la solvatation de l'e^- avec H_2O de l'ordre de $2{,}5 \times 10^{11}\ s^{-1}$ (21) ce qui nous permettrait d'avoir une évaluation de k_{e^-+Ac} connaissant la concentration en Ac(1 *M*) $k_{e^-+Ac} \geq k = 2{,}5 \times 10^{11}\ M^{-1}\ s^{-1}$.

[3]Valeurs déterminées dans nos conditions expérimentales par radiolyse pulsée. Comme suggéré par l'un des referees, la vitesse de la réaction [13] est en fait la somme des vitesses des différentes réactions de disparition de e_{aq}^-.

1. J. ZABICKY. The chemistry of amides. Wiley Interscience. 1970.
2. A. M. KOULKÈS-PUJO, L. GILLES, J. C. HALLÉ et J. SUTTON. Radiat. Phys. Chem. **10**, 73 (1977).
3. A. E. PUCCI, J. VEDEL et B. TRÉMILLON. J. Electroanal. Chem. **22**, 253 (1969).
4. C. MANNICH et G. HEILNER. Ber. 5SB, 36 (1922).
5. C. E. BRICKER et W. A. VAIL. Anal. Chem. **22**, n° 5720 (1960).
6. T. H. TRAN THI et A. M. KOULKÈS-PUJO. Analusis, **8**, 163 (1980).
7. A. MATSUMOTO, N. HAYASHI et N. N. LICHTIN. Radiat. Res. **41**, 299 (1970).
8. D. A. HEAD et D. C. WALKER. Can. J. Chem. **48**, 1657 (1970).
9. J. KROH et E. BURZYNSKA. Radiochem. Radioanal. Lett. **27**, 101 (1976).
10. J. C. HALLÉ, R. SCHALL, A. M. KOULKÈS-PUJO, J. SUTTON et T. H. TRAN THI. J. Chem. Res. **3**, 86 (1979).
11. W. H. HAMILL. J. Phys. Chem. **73**, 1341 (1969).
12. T. H. TRAN THI. Thèse 3ème cycle, Orsay, 1978.
13. T. SAWAI et W. H. HAMILL. J. Phys. Chem. **74**, 3914 (1970).
14. G. E. ADAMS, J. H. BAXENDALE et J. W. BOAG. Proc. R. Soc. A, **277**, 549 (1964).
15. S. GORDON, E. J. HART, M. S. MATHESON, J. RABANI et J. K. THOMAS. Discuss. Faraday Soc. **36**, 193 (1963).
16. E. J. HART, S. GORDON et J. K. THOMAS. J. Phys. Chem. **68**, 1271 (1964).
17. M. A. J. RODGERS. J. Chem. Soc. Faraday Trans. **68**, 1278 (1976).
18. S. A. CHAUDHRI et K. D. ASMUS. J. Phys. Chem. **76**, 26 (1972).
19. A. J. ROBINSON et M. A. J. RODGERS. J. Chem. Soc. Faraday Trans. I. **69**, 2036 (1973).
20. S. GORDON, E. J. HART, M. S. MATHESON, J. RABANI et J. K. THOMAS. J. Am. Chem. Soc. **85**, 1375 (1963).
21. E. J. HART. The hydrated electron. Wiley Interscience. 1970. p. 76.
22. P. M. RENTZEPIS, P. P. JONES et J. JORTNER. J. Chem. Phys. **59**, 2 (1973).
23. D. C. WALKER et S. C. WALLACE. Can. J. Chem. **49**, 3399 (1971).
24. J. A. RIDDICK et W. B. BUNGER. Organic solvents: physical properties and methods of purification. Vol. 2. 3è ed. Wiley Interscience. 1970.
25. R. REYNAUD. Bull. Soc. Chim. Fr. 3945 (1968).

The tryptophan fluorescence lifetime puzzle. A study of decay times in aqueous solution as a function of pH and buffer composition[1]

EVA GUDGIN, RICARDO LOPEZ-DELGADO,[2] AND WILLIAM R. WARE

Photochemistry Unit, Department of Chemistry, University of Western Ontario, London, Ont., Canada N6A 5B7

Received April 23, 1980

EVA GUDGIN, RICARDO LOPEZ-DELGADO, and WILLIAM R. WARE. Can. J. Chem. **59**, 1037 (1981).

Tryptophan fluorescence decay kinetics have been systematically investigated in aqueous solutions as a function of pH as well as in a variety of buffer solutions. Below pH 7.0, the decay appears to be double exponential with a subnanosecond component confirming the previous findings of Rayner and Szabo (3). In the low pH region, where the proton concentration becomes kinetically significant, tryptophan fluorescence is collisionally quenched by $[H^+]$ with diffusion controlled rate and no experimental evidence is found regarding the appearance at low pH of a new tryptophan molecular species, namely the cationic form. At pH $\geq$ 7.0, the decay becomes triple-exponential with the appearance of a long component whose contribution to the total emission intensity increases rapidly with increasing pH at the expense of the other two. Lifetimes and relative intensities of each decay component depend in a complex way on pH and on the buffer chemical composition.

EVA GUDGIN, RICARDO LOPEZ-DELGADO et WILLIAM R. WARE. Can. J. Chem. **59**, 1037 (1981).

La cinétique du déclin de la fluorescence du tryptophane a été étudiée dans des solutions aqueuses en fonction du pH dans une serie de solutions tampons. En dessous du pH 7.0 le déclin est bi-exponentiel avec une composante de courte durée de vie, dans le domaine de temps de la subnanoseconde, ce qui confirme les resultats préalables de Rayner et Szabo (3). Dans la region du bas pH, où la concentration des protons commence à devenir importante du point de vue cinétique, la fluorescence du tryptophane est eteinte par $[H^+]$ avec une constante de vitesse controllée par la diffusion, et on ne trouve pas d'evidence expérimentale concernant l'apparition à pH bas d'une nouvelle espèce moléculaire du tryptophane, c'est-à-dire, de la forme cationique. Pour des pH $\geq$ 7.0 le déclin devient tri-exponentiel et on observe l'apparition d'une composante de longue durée de vie et dont la contribution à l'intensité totale d'emission augmente très rapidement avec le pH au détriment des deux autres composantes. Les durées de vie de fluorescence aussi bien que les intensitée relatives de chaque composante dépendent d'une manière complexe et du pH et de la composition chimique de la solution tampon.

"The short fluorescence lifetimes encountered for aqueous solutions of aromatic amino-acids lead to relatively large uncertainties in the values obtained. Within these limits the emission lifetimes for tryptophan ... from different laboratories are in satisfactory agreement" (2.6–3.0 ns; single exponential decay). This statement appeared in a review article by Weinryb and Steiner (1) in 1971.

However, from 1976 until very recently, a number of published reports (2–5) have introduced an amazing confusion into this particular subject, which has a certain interest since aromatic amino-acids have been extensively used as intrinsic fluorescent tags for protein structural and dynamical studies by spectrofluorometric methods. In all but one (5) of the above-mentioned publications, a double exponential decay is reported, which favours, according to the authors, the appealing model of two electronic excited states (^1L_a and ^1L_b) uncoupled to each other but independently coupled to the ground state through the radiation field (dual fluorescence). Nevertheless, in ref. 4, an idea, which is not essentially new (6, 7), of two different ground state conformers is cautiously advanced; also Rayner and Szabo in a very recent paper (8) have abandoned the idea of simultaneous $^1L_a \rightarrow {}^1A$ and $^1L_b \rightarrow {}^1A$ radiative transitions in favour of the coexistence of different populations of rotational conformers (rotamers) in the ground state. On the other hand, de Lauder and Wahl (9) studied the fluorescence decay of tryptophan as a function of pH and explained the observed variations of lifetimes in terms of mixtures of different ionic species present.

Although previous results of one of the authors (5) compare quite well (taking into account the fact (5) that only the red part of the emission was analyzed) with those of Rayner and Szabo (3), as well as with "classic" lifetime values (1), the bulk of the reported data is in strong contradiction; therefore, we think it is necessary to carefully reinvestigate the problem as a function of a number of pertinent experimental parameters in order to properly understand the tryptophan excited state relaxation mechanism.

In this preliminary work, we have re-examined the problem of the existence of a subnanosecond component in the tryptophan decay (3) as well as

[1]Publication No. 256 from the Photochemistry Unit, Department of Chemistry, University of Western Ontario, London, Ontario.

[2]Permanent address: CNRS – Laboratoire de Photophysique Moléculaire, Bâtiment 213, Université de Paris Sud, 91405 Orsay, France.

0008-4042/81/071037-08$01.00/0

©1981 National Research Council of Canada/Conseil national de recherches du Canada

Can. J. Chem. Downloaded from www.nrcresearchpress.com by 210.87.254.5 on 09/06/12
For personal use only.

Can. J. Chem. Downloaded from www.nrcresearchpress.com by 210.87.254.5 on 09/06/12
For personal use only.

the effect of pH on the molecular absorption and emission spectra and on the fluorescence decay parameters.

L-Tryptophan (Aldrich, 99%) was recrystallized from water–ethanol solutions and dried under vacuum. We have used three different kinds of buffer solutions made up in triple-distilled water in order to cover the pH region of interest: (*1*) 0.1 *M* citric acid – 0.2 *M* Na_2HPO_4 (2.5–7.6 pH region); (*2*) 0.2 *M* NaH_2PO_4 – 0.2 *M* Na_2HPO_4 (6.8–8.0 pH region); (*3*) sodium tetraborate (8.0–11.0 pH region). The ionic strength has been kept roughly constant.

Buffer solutions as well as tryptophan solutions were prepared immediately before each run in order to avoid as much as possible any unwanted aging effect. It has also been verified that the presence or absence of oxygen in the solutions does not, in the limit of our precision, show any noticeable effect on the measured lifetimes.

Absorption spectra were recorded in a Cary-219 spectrophotometer; fluorescence spectra were obtained by means of a Perkin-Elmer MPF-4 spectrofluorometer.

Fluorescence lifetime measurements were performed with a commerical PRA-3000 "Nanosecond Spectrofluorimeter". The system is directly interfaced to a DEC MINK-II computer allowing for fast data treatment. The Nanosecond Spectrofluorimeter is composed of three main elements: (*i*) PRA-510B low pressure thyratron triggered H_2 flash lamp with 10–45 kHz repetition rate; (*ii*) Jobin-et-Yvon H-10 type (high aperture, extremely high transmission power, very low optical noise, 8 nm/mm dispersion) excitation and emission monochromators; (*iii*) a Seven Stage (PRA model 1551) photomultiplier, cooled by Peltier Effect down to −30°C and coupled to an Elscint STD-N1 Snap-Off Timing Discriminator. This tube has less than one count per second dark counting rate.

The experimental decay data $I(t)$, stored in the Multichannel Analyzer, are the convolution

$$[1] \quad I(t) = g(t)*F(t)$$

where $F(t)$ is the true fluorescence decay profile. For the simplicity of the discussion, we have not taken into account parasitic effects such as scattered light or the dark counting background, that pertinent *blank* experiments easily check for.

$$[2] \quad g(t) = I_0(\lambda_{Ex},t)*R_{PM}(\lambda_{Em},t)$$

is a certain instrumental function; $I_0(\lambda_{Ex},t)$ represents the flash profile at the excitation wavelength λ_{Ex}, which is convoluted by the response function of the photodetector $R_{PM}(\lambda_{Em},t)$ at the fluorescence wavelength λ_{Em}. In general, R_{PM} is wavelength dependent (10) and we necessarily have to record another instrumental function

$$[3] \quad g'(t) = I_0(\lambda_{Em},t)*R_{PM}(\lambda_{Em},t)$$

with the lamp profile $I_0(\lambda_{Em},t)$ now measured at the fluorescence wavelength for the mathematical treatment of data in order to recover $F(t)$. However, in general, for conventional flash lamps

$$[4] \quad \frac{g(t)}{g'(t)} = \frac{I_0(\lambda_{Ex},t)}{I_0(\lambda_{Em},t)} = K(\lambda,t) \neq 1$$

and consequently a certain type of calibration is needed.

A flash lamp similar to the one used in the present work has been calibrated (11) using Synchrotron Radiation as a Standard of Excitation (12), in the 170–220 nm spectral region. It was found (11) that the lamp plasma decay is superexponential during the first two decades, with a fwmh ~ 1.8 ns and *wavelength independent*.

The light pulse profile of the lamp used in this work was studied in two different ways.

(*i*) A standard solution of anthracene in *n*-hexane has been excited with $I_0(\lambda,t)$, λ being varied systematically between 220 and 350 nm; $g'(t)$, eq. [3], has been recorded every time at constant λ_{Em} = 450 nm. After iterative convolution (see below) the lifetimes recovered for every excitation wavelength are identical within statistical error.

(*ii*) $g'(t)$ has been recorded every 10 nm in the 220–450 nm spectral range, with the surprising result that it is *wavelength invariant* within statistical error in the entire spectral region of interest. It is difficult to understand how $I_0(\lambda,t)$ could show a variance with λ that continuously cancels a concomitant variance with λ of $R_{PM}(\lambda,t)$, (see eq. [3]) in order to generate the observed λ-invariance of $g'(t)$. A plausible answer could be that both $I_0(t)$ and $R_{PM}(t)$ for this particular instrument are wavelength independent. This hypothesis could be easily checked using Synchrotron Radiation as a standard (11, 12). However, all we need for the purpose of this work is that

$$[5] \quad g(t) = g'(t) = \text{constant}$$

The true fluorescence decay is then recovered by iterative convolution of $g(t)$ by one, two, or three exponential decays with a weighted least-squares convolution procedure until the best fit is obtained with $I(t)$, as defined by a minimum χ^2 value and residuals randomly distributed at better than the 95% confidence limit. The entire decay curve has been analyzed in each case, paying particular attention to the leading edge, where contributions

TABLE 1. Tryptophan fluorescence lifetimes and relative emission intensities in aqueous solution in function of pH: citric acid – sodium phosphate buffer. $\lambda_{Exc} \sim 280$ nm; emission through 350 nm cut-off filter, $T = 20°C$

pH	τ_1 (ns)	I_1	τ_2 (ns)	I_2	[Citric acid] ($M \times 10^2$)
2.55	2.33±0.15	0.89	0.38±0.15	0.11	8.86
3.0	2.57±0.13	0.92	0.44±0.15	0.08	7.95
3.5	2.65±0.12	0.94	0.49±0.15	0.06	6.97
4.0	2.76±0.1	0.93	0.45±0.15	0.07	6.15
4.5	2.87±0.1	0.93	0.50±0.15	0.07	5.46
5.0	2.95±0.1	0.94	0.52±0.15	0.06	4.85
5.5	2.98±0.1	0.93	0.40±0.15	0.07	4.30
6.0	3.07±0.1	0.94	0.55±0.15	0.06	3.68
6.8	3.16±0.1	0.93	0.59±0.15	0.07	2.27

from very short components are likely to be most important.

Concerning the anomalously high lifetime values reported in ref. 2, it is plausible that the authors were simply measuring "electric noise" from the excitation source, for we have verified the appearance of long components in the fluorescence time distribution when the lifetime experiment is performed in the presence of strong "parasitic" radio-frequency fields.

Lifetime values of ref. 4 were obtained by powerful solid state laser excitation of aqueous solutions. Assuming the laser beam is focussed into 0.1 mm², the density of excitation will be of the order of a T W/cm²! If one assumes the likely appearance of self-focussing effects, then the result would be even more catastrophic. In these experimental conditions, with such a high density electric field, one is no longer probing the relaxation of a weakly dense population of excited species. On the one hand, it has already been shown (13) that high power solid state laser excitation of condensed media leads to quite different relaxation kinetics as compared to that obtained by relatively weak excitation. Also, we have verified in this laboratory that a few hours irradiation of fresh aqueous solutions of tryptophan at neutral pH, with a 150 W xenon lamp, leads to strong photodecomposition of the molecule. Very recently, Phillips and coworkers (14) have reached similar conclusions concerning the work reported in ref. 4.

We have recorded absorption and emission spectra that look very similar for all samples and compare quite well with those reported in the literature; however, a small monotonous red shift is observed in both emission and absorption with increasing pH.

In buffered aqueous solutions with pH < 7.0, we find (see Table 1) systematically a double exponential decay with lifetime values τ_1 and τ_2 which compare quite well with those of Rayner and Szabo (3). When fluorescence at all wavelengths (excitation at 280 nm; emission through 305 nm cut-off filter) is collected, the 3.1 ns component (τ_1) contributes (I_1) nearly 95% to the total intensity at neutral pH, in good agreement with "classic" data (1). When fluorescence lifetimes are measured as a function of emission wavelength, our results confirm the general trends already reported (3): the contribution (I_2) of the subnanosecond component (τ_2) increases with decreasing wavelength. However, we measure pre-exponential factor ratios rather smaller than those reported in ref. 3.

We have carefully investigated the possibility of an experimental artifact (such as Raman scattering from water or direct scattering of the exciting flash) being the origin of this subnanosecond component with negative results. Another possibility would be the contribution of rotational depolarization of the fluorescence during the lifetime of the excited state. This explanation was ruled out by the following experiment: fluorescence lifetimes were measured with a polarizer on the excitation side producing vertically polarized light and another on the emission side set at the "magic" angle. No changes either on τ_1 and I_1 or τ_2 and I_2 were observed within statistical error.

Also indicated in the right hand column of Table 1 is the total concentration of citric acid (as the neutral molecule and citrate anion) at the pH studied. There is an equilibrium between the two species depending on buffer composition, however it can be seen generally that increasing the total concentration of both species over $0.02M$ quenches τ_1 significantly.

We have also studied the tryptophan fluorescence decay behaviour in the low pH region under the same experimental conditions as those reported in ref. 9, i.e., aqueous solution where the pH is adjusted by adding increasing quantities of concentrated HCl.

Our results (see Table 2) do not compare well

Can. J. Chem. Downloaded from www.nrcresearchpress.com by 210.87.254.5 on 09/06/12
For personal use only.

TABLE 2. Tryptophan fluorescence lifetimes and relative emission intensities in HCl–water solutions as a function of pH. $\lambda_{Exc} \sim 280$ nm; emission through 305 nm cut-off filter, $T = 20°C$

pH	$[H^+]$ (M/L)	τ_1 (ns)	I_1	τ_2 (ns)	I_2
3.5	3.2×10^{-4}	3.2 ±0.1	0.94	0.52±0.15	0.06
2.0	10^{-2}	1.70±0.1	0.80	0.43±0.15	0.20
1.6	2.5×10^{-2}	1.20±0.15	0.65	0.40±0.15	0.35
1.45	3.5×10^{-2}	1.05±0.15	0.70	0.37±0.20	0.30
1.28	5.25×10^{-2}	0.80±0.15	0.80	0.31±0.25	0.20
1.21	6.2×10^{-2}	0.75±0.2	0.85	0.13±0.4	0.15
1.1	7.9×10^{-2}	0.51±0.2	1.00	—	—
1.0	10^{-1}	0.49±0.2	1.00	—	—
0.84	0.145	0.34±0.25	1.00	—	—

with de Lauder and Wahl's (9) data. Again, we find a two component decay, with lifetime values and relative emission intensities very similar to the ones observed in the citric acid – phosphate buffer at neutral pH (see Table 1). A plot of $1/\tau_1$ versus the proton concentration (see Fig. 1) yields an almost straight line; from the slope we found $K_q \sim 1.8 \times 10^{10} M^{-1}\,s^{-1}$, showing that protons quench one of the fluorescence components with a diffusion-controlled rate. The behaviour of the shortest component τ_2 is more difficult to describe because of the much lower precision of the lifetime values; the apparent increase in its relative intensity I_2 above pH $\sim$ 1.5 could be simply due to a differential quenching of τ_1 by protons. Around pH $\sim$ 1.25, τ_2 seems to be catastrophically quenched by the acid and below pH $\sim$ 1.2 the fluorescence decay becomes single exponential within our precision.

When pH is increased, beginning around pH = 7.0, a third longer component is observed whose lifetime τ_3 depends on the buffer composition (see Table 4); its contribution, I_3, to the total emission strongly increases with pH and is already overwhelming at pH $\geq$ 10.0 (see Table 3 and Fig. 2). A concomitant decrease in the contributions of the other two components (I_1 and I_2) is also observed. However, the striking observation is that in a large range (7.0–10.0) the pH does not seem to have an important effect on any of the three lifetime values, but only influences their relative contribution to the total intensity. It is also interesting to note that the buffer composition does not seem to affect the lifetimes of the two shorter components, τ_1 and τ_2, in this pH range.

In Fig. 3 we give a graphical demonstration of our method of fluorescence decay analysis showing that above pH 7.0 double exponential fits are not adequate. Table 5 gives the results of the analyses. Figure 3*a* illustrates the double-exponential analysis of early times where the influence of a subnano-

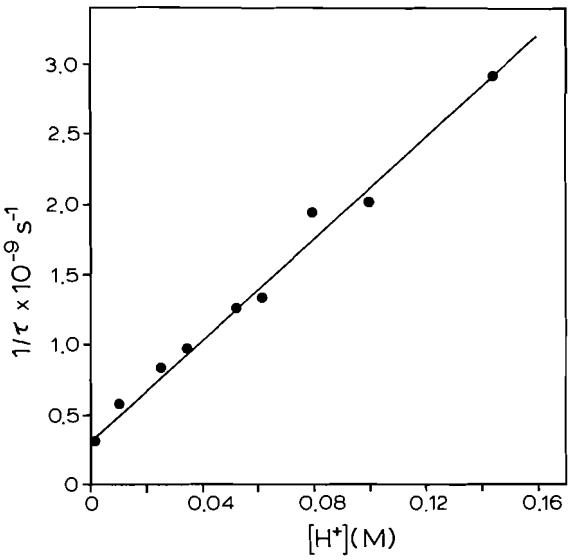

FIG. 1. Effect of HCl concentration on the tryptophan intermediate lifetime (τ_1) component (see Table 2); $[H^+]$ is the proton concentration. The slope yields a quenching rate constant $K_q \sim 1.8 \times 10^{10} M^{-1}\,s^{-1}$.

second component should be greatest; Fig. 3*d* through *f* show double-exponential analyses of the late time distribution where the contribution of long-lived components should be greatest; Fig. 3*c* shows the best double-exponential fit of the entire time distribution. The χ^2 value indicated in Table 5 for Fig. 3*c* is already relatively very large and the residuals are definitely not random, particularly around the early times (see also Fig. 4*a*); also the decay parameters are some sort of weighted average of those values found in analyses 3*a* and 3*f*. The last column of Table 5 shows that the computer has rejected analyses 3*b* and *c* as not meeting the requirement of random residuals within a 95% confidence limit. Using a triple-exponential analysis program in the PDP-11 computer we obtain a

Can. J. Chem. Downloaded from www.nrcresearchpress.com by 210.87.254.5 on 09/06/12
For personal use only.

Can. J. Chem. Downloaded from www.nrcresearchpress.com by 210.87.254.5 on 09/06/12
For personal use only.

TABLE 3. Tryptophan fluorescence lifetime values and relative emission intensities in sodium tetraborate buffer solutions as a function of pH. $\lambda_{Exc} \sim 280$; emission through 305 nm cut-off filter, $T = 20°C$

pH	τ_1 (ns)	I_1	τ_2 (ns)	I_2	τ_3 (ns)	I_3
7.0	3.19±0.1	0.94	0.60±0.15	0.06	9.1 ±0.5	<0.01
7.5	3.08±0.1	0.91	0.55±0.15	0.05	9.1 ±0.3	~0.03
8.0	3.16±0.1	0.855	0.55±0.15	0.045	9.0 ±0.2	0.10
8.5	3.20±0.1	0.735	0.50±0.20	0.035	9.2 ±0.1	0.23
9.0	3.15±0.1	0.495	0.47±0.30	0.025	9.2 ±0.1	0.485
9.5	3.16±0.1	0.255	(0.5 ±0.5)[a]	~0.015	9.1 ±0.1	0.73
10.0	3.15±0.2	0.10	(0.5 ±0.5)[a]	<0.01	9.18±0.1	0.89
10.5	3.11±0.4	0.03	(0.5 ±0.5)[a]	<0.01	9.0 ±0.1	0.96

[a]Because of the increasing activity of τ_3, the precision on the τ_2 measurement becomes very poor.

TABLE 4. Tryptophan fluorescence lifetimes as a function of the buffer composition: Buffer I = citric acid – sodium phosphate; Buffer II = sodium monophosphate – sodium diphosphate; Buffer III = sodium tetraborate (see text). $\lambda_{Exc} = 280$ nm; emission is observed through 305 nm cut-off filter; $T = 20°C$

Solvent	τ_1/ns	τ_2/ns	τ_3/ns
H_2O (NaOH)	3.15±0.1	0.6±0.15	9.4±0.1
H_2O (Buffer I)	3.15±0.1	0.5±0.15	7.0±0.1
H_2O (Buffer II)	3.15±0.1	0.5±0.15	7.8±0.1
H_2O (Buffer III)	3.15±0.1	0.5±0.15	9.2±0.1

convolution through the entire time distribution with a much lower χ^2 and randomly distributed residuals (see Fig. 4*b* and Table 5). The same three lifetimes are consistently retrieved in all our triple-exponential analyses between pH 7 and 10.5. We would like to point out that in this particular system the analysis is helped by the fact that the three fluorescence lifetimes are very different and therefore it is easy to differentiate between them.

We have, at the same time, reinvestigated the excitation wavelength effect; our results confirm the findings already reported by one of us (5): in aqueous solutions, for a given pH, tryptophan fluorescence lifetimes are independent of the excitation wavelength; moreover, at pH < 7.0, relative intensities I_1 and I_2 seem to remain constant with λ_{Exc} in the 240–300 nm spectral region. However, at pH ≃ 8.5, the relative intensity I_3 of the long component is very sensitive to λ_{Exc}: it contributes 24% to the total intensity when exciting at 280 nm; this contribution jumps to ~50%, when exciting at 310 nm.

In this preliminary communication, we have restricted ourselves to a phenomenological description of experimental results; nevertheless, on the basis of these results, we believe we can arrive at certain conclusions:

(*i*) It is necessary to conclude that the tryptophan fluorescence decay is double exponential below pH 7.0, with a subnanosecond component (3), although its contribution to the total intensity is only a few percent above pH 2.5, in good agreement with "classic" data (1). Since it contributes mainly to the leading edge of the fluorescence time distribution, it only becomes apparent with modern sophisticated methods of mathematical data treatment.

(*ii*) Our results in the low pH range are in contradiction with the data reported by de Lauder and Wahl (9) and they do not support their conclusion of the appearance of a new ionic species,

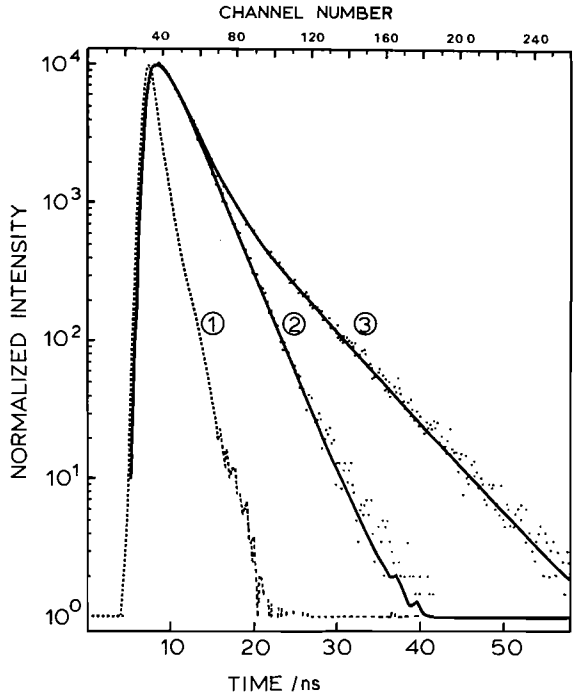

FIG. 2. Experimental decay curves. (*1*) Instrumental function $g'(t) = g(t)$. (*2*) Tryptophan in citric acid – sodium phosphate buffer pH = 6.8; double exponential decay (see Table 1): $\chi^2 = 1.155$. (*3*) Tryptophan in sodium tetraborate buffer, pH = 8.5; triple-exponential decay (see Table 3): $\chi^2 = 1.09$; $\lambda_{Exc} \simeq 280$ nm; fluorescence through 305 nm cut-off filter. $T = 20°C$.

Can. J. Chem. Downloaded from www.nrcresearchpress.com by 210.87.254.5 on 09/06/12
For personal use only.

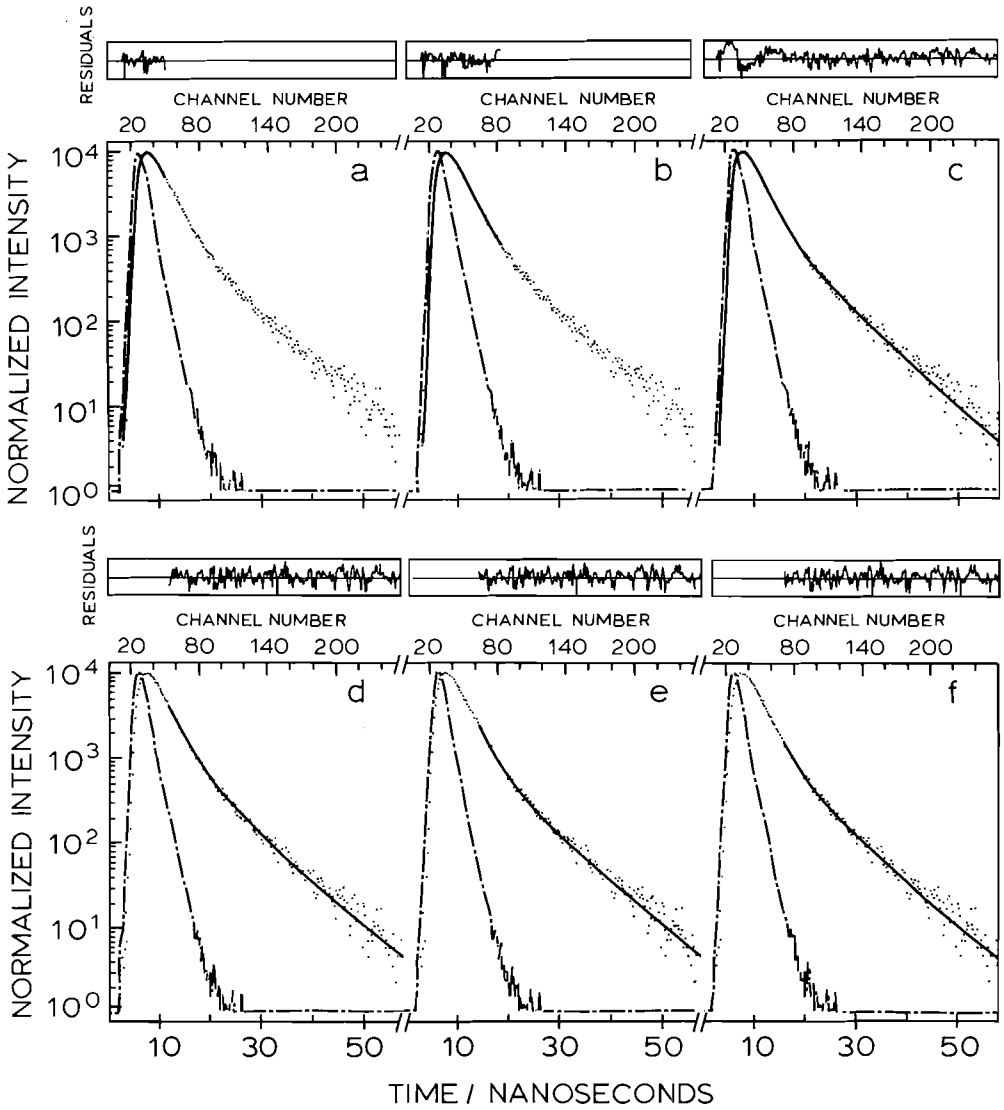

FIG. 3. Analysis of fluorescence–time distribution for tryptophan in sodium tetraborate buffer at pH 8.5 as a function of time. Residuals of each convolution are shown above the decay profile. For results of analyses see Table 5.

TABLE 5. Analysis of fluorescence–time distribution for tryptophan in sodium tetraborate buffer at pH 8.5

Channels	τ_1/ns	τ_2/ns	τ_3/ns	χ^2	Accepted?
		Results from dual-exponential analysis			
(*a*) 13–50	0.51±0.18	3.72±0.17		1.24	Yes
(*b*) 13–80	1.04±0.11	4.18±0.06		1.27	No
(*c*) 13–255	1.84±0.03	8.49±0.13		1.79	No
(*d*) 53–255	3.13±0.08	9.11±0.17		1.06	Yes
(*e*) 63–255	3.05±0.13	9.02±0.19		1.07	Yes
(*f*) 70–255	3.28±0.21	9.19±0.25		1.09	Yes
		Results from the triple-exponential analysis			
13–255	0.44±0.11	3.19±0.05	9.21±0.15	1.09	Yes

Can. J. Chem. Downloaded from www.nrcresearchpress.com by 210.87.254.5 on 09/06/12
For personal use only.

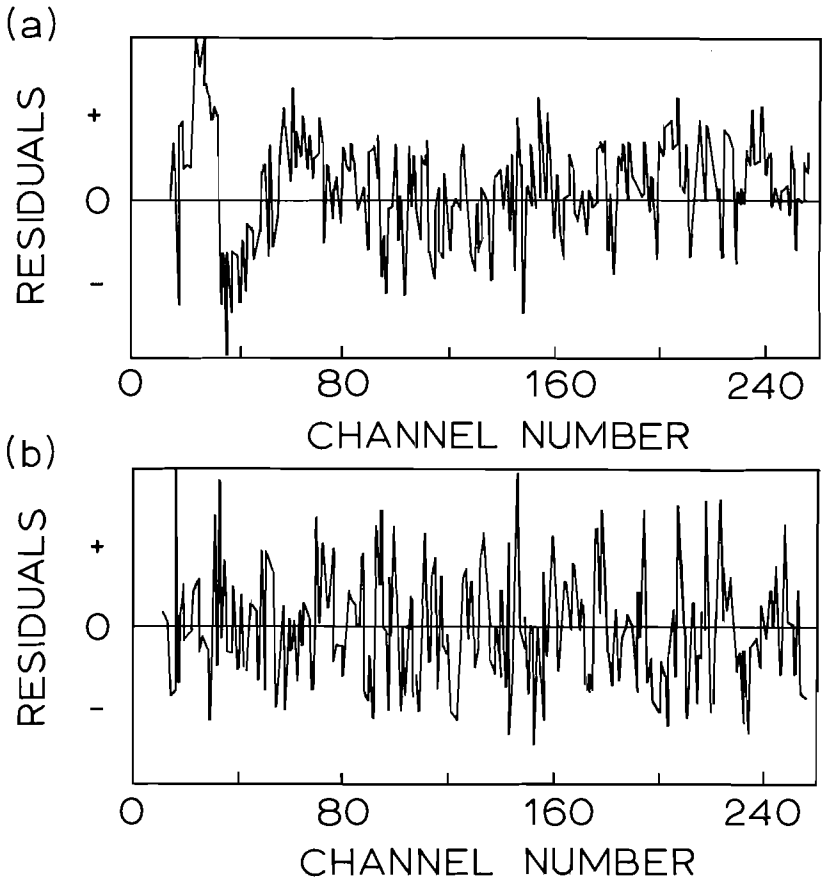

FIG. 4. (*a*) Residuals from double-exponential analysis from channels 13 to 255 yielding values shown in Table 5. Rejected on the basis of non-random distribution of residuals. (*b*) Residuals from triple-exponential analysis from channels 13 to 255 yielding values shown in Table 5. Distribution of residuals is now random.

namely the cationic form of tryptophan $R(NH_3^+)\cdot COOH$, induced by the pH. Our results are better understood in terms of a collisional quenching by H^+ with a diffusion controlled rate.

(*iii*) At pH $\geq$ 7.0, the tryptophan fluorescence decay becomes triple-exponential, increasing apparently the magnitude of the puzzle! This result, mainly the fact that the long component contribution I_3 becomes very quickly preponderant with increasing pH, jeopardizes the very recent tentative rationalization by Szabo and Rayner (8) of the tryptophan fluorescence lifetime puzzle in terms of rotational isomers, since their arguments to explain their decay times measured at pH $\sim$ 7.0 are based upon rotational isomer populations measured by nmr experiments in tryptophan in alkaline solutions (15). Our results show clearly that tryptophan decay kinetics are very different in the two media.

(*iv*) From our work, we have clear experimental evidence that tryptophan decay kinetics are strongly dependent upon the buffer composition; consequently, we firmly believe that any report on tryptophan fluorescence lifetimes should clearly describe the chemical composition of the solution, which is not the case most of the time.

(*v*) Finally, the triple-exponential decay we find at pH > 7.0 does not support the model (3) of dual fluorescence from two independent (^1L_a, ^1L_b) excited states.

In order to acquire more insight into the tryptophan fluorescence lifetime puzzle, more systematic research work is clearly needed, and mainly on solvent, temperature, and isotopic substitution effects. Also, a study of tryptophan pure crystal decay kinetics would be very helpful in the understanding of the problem of molecular conformations in the ground state. Work on these lines is presently in progress in this laboratory.

Acknowledgements

The authors wish to acknowledge the financial assistance of the Natural Sciences and Engineering Research Council of Canada, the Centre for Chemical Physics, University of Western Ontario, and ARO-Durham. The authors also wish to thank Dr. Arthur Szabo for providing a preprint of his latest work and for useful discussions.

1. I. WEINRYB and R. F. STEINER. *In* Excited states of proteins and nucleic acids. *Edited by* R. F. Steiner and I. Weinryb. Plenum Press, New York, NY. 1971. p. 293.
2. W. X. BALCAVAGE and T. ALVAGER. Mol. Photochem. **7**, 309 (1976).
3. D. M. RAYNER and A. G. SZABO. Can. J. Chem. **56**, 743 (1978).
4. G. R. FLEMING, J. M. MORRIS, R. J. ROBBINS, G. J. WOOLFE, P. J. THISTLETHWAITE, and G. W. ROBINSON. Proc. Natl. Acad. Sci. U.S.A. **75**, 4652 (1978).
5. B. ALPERT, D. M. JAMESON, R. LÓPEZ-DELGADO, and R. SCHOOLEY. Photochem. Photobiol. **30**, 479 (1979).
6. B. DONZEL, P. GAUDUCHON, and PH. WAHL. J. Am. Chem. Soc. **96**, 801 (1974).
7. P. GAUDUCHON and PH. WAHL. Biophys. Chem. **8**, 87 (1978).
8. A. G. SZABO and D. M. RAYNER. J. Am. Chem. Soc. **102**, 554 (1980).
9. W. B. DE LAUDER and PH. WAHL. Biochemistry, **9**, 2750 (1970).
10. B. SIPP, J. A. MIEHÉ, and R. LÓPEZ-DELGADO. Opt. Commun. **16**, 202 (1976).
11. J. C. ANDRÉ, R. LÓPEZ-DELGADO, R. L. LYKE, and W. R. WARE. Appl. Opt. **18**, 1355 (1979).
12. R. LÓPEZ-DELGADO. Opt. Commun. **27**, 195 (1978).
13. R. LÓPEZ-DELGADO, J. A. MIEHÉ, and B. SIPP. Opt. Commun. **19**, 79 (1976).
14. K. P. CHIGGINO, G. R. MANT, D. PHILLIPS, and A. J. ROBERTS. J. Photochem. **11**, 297 (1979).
15. J. R. CAVANAUGH. J. Am. Chem. Soc. **92**, 1488 (1970).

Can. J. Chem. Downloaded from www.nrcresearchpress.com by 210.87.254.5 on 09/06/12
For personal use only.

Synthesis of inorganic multilayers on chromatographic supports[1]

PALITHA P. WICKRAMANAYAKE, AMARES CHATT, and WALTER A. AUE[2]
Trace Analysis Research Centre, Dalhousie University, Halifax, N.S., Canada B3H 4J3

Received February 4, 1980[3]

PALITHA P. WICKRAMANAYAKE, AMARES CHATT, and WALTER A. AUE. Can. J. Chem. **59**, 1045 (1981).

Multilayers of various metal oxides have been produced on typical chromatographic supports such as diatomaceous earth and silica gel. The layer thickness was characterized for phases based on iron and chromium. These data, as well as chromatographic evidence obtained on chromium oxide, suggest that the layers are homogeneous. Similar, but less well characterized layers of aluminum and titanium oxides have been obtained.

PALITHA P. WICKRAMANAYAKE, AMARES CHATT et WALTER A. AUE. Can. J. Chem. **59**, 1045 (1981).

On a préparé des couches multiples d'oxydes métalliques sur des supports chromatographiques usuels tels la terre diatomée et le gel de silice. On a caractérisé l'épaisseur des couches dans le cas des phases préparées avec le chrome et le fer. Ces données ainsi que les preuves chromatographiques obtenues pour l'oxyde de chrome, suggèrent que les couches sont homogènes. On a obtenu des phases identiques, mais moins bien caractérisées avec les oxydes de titane et d'aluminium.

[Traduit par le journal]

Introduction

Gas–solid chromatography on inorganic surfaces is well known; in fact, this technique preceded the much more popular gas–liquid chromatography by a few years.

Gas–solid chromatography, however, is generally limited to the separation of gases and low-boiling liquids. Its application for purposes other than this straightforward one had therefore to contribute a large part of its current appeal for scientists. Nowadays it is often used to characterize various equilibria and to obtain kinetic information in catalysis research.

The chemical activity of a chromatographic surface may be a drawback for analytical purposes, but it has led to numerous studies in which such materials were used as catalysts and separation media at the same time. (For a review of this area, see ref. 1.)

Besides silica and alumina, a number of metal oxides – e.g. those of chromium, titanium, and iron (2–4) — have been used directly as adsorbents in gas–solid chromatography. Unsuitable pore structures or inferior mechanical stability may restrict such uses.

Hence, from early on, many attempts were made to coat metal oxides or salts on supports better suited to chromatographic use. For instance, aluminas modified by iron oxide (5–8) or chromia (9) have successfully separated hydrogen isotopes.

As pointed out by Aigner *et al.* (10), loading chromatographically active inorganics onto typical supports such as alumina or silica may lead to heterogeneous layers. One approach that would seem reasonable for obtaining homogeneous ones is the derivatization of amply present surface groups, e.g. the silanols. Such reactions are well known; they have been used most often to characterize the physical and chemical properties of various surfaces (for a review see ref. 11).

It should be noted here that the terms "homogeneous" and "heterogeneous" can have different meanings. A pure silica surface, for instance, is homogeneous in that only silicon is present (besides oxygen and hydrogen). But it is heterogeneous in that it contains a variety of surface features, for instance, different types of silanol groups. For the purpose of this paper, we shall use the former classification. In other words, a homogeneous layer of chromia on silica will be one that completely covers the silica support, on the inside of the pores as well as on the outside of the particle. Quite obviously, this "physical" homogeneity is not identical with "chromatographic" homogeneity (linear isotherm, symmetrical peaks, etc.).

Our group has recently attempted to investigate the chromatographic potential as well as the possibly detrimental effects, of various metal-containing surface species. Oxide and reduced-type structures were used by themselves and as carriers for "bonded" organic layers. Good gas chromatographic performance was obtained on several of these phases based on diatomaceous earth (12). A liquid-chromatography type silica gel was used to show that metal oxides bonded to its surface could drastically change lc retention patterns (13).

The main purpose of such prior studies was to define chromatographic utility. Multiple applica-

[1]Material taken from Ph.D. thesis of first author.
[2]To whom all correspondence should be addressed.
[3]Revision received October 29, 1980.

0008-4042/81/071045-06$01.00/0
©1981 National Research Council of Canada/Conseil national de recherches du Canada

Can. J. Chem. Downloaded from www.nrcresearchpress.com by 210.87.254.5 on 09/06/12
For personal use only.

Can. J. Chem. Downloaded from www.nrcresearchpress.com by 210.87.254.5 on 09/06/12
For personal use only.

tions of metal-containing reagents were used in several cases. Yet it was not established whether such usage did in fact bring about the formation of multiple layers. It would appear interesting indeed, for chromatography as well as for surface chemistry, to know for a variety of select cases whether layers can be built on top of each other at will, or whether a "monomolecular" layer represents the limit. If multiple layers could be achieved, and if such layers were indeed "homogeneous" (cf. ref. 21), then chromatographic properties would be expected to stay reasonably constant once the monomolecular range had been exceeded. The current study was devised along these lines of interest.

Experimental

Figure 1 shows a schematic cross section of the set-up used to coat diatomaceous earth or silica gel support particles. These were filled into the vertical Pyrex tube which had Clearseal terminals and a fine frit located about 2/3 down its heated section.

The surrounding furnace was lab-made by drilling a block of aluminum. The block was heated by two cartridges (Watlow) and insulated by Marinite (Johns-Manville). Two sections of 1/4 in. copper tubing were used to pass tap water through the aluminum block for rapid cool-down.

Reagents were introduced from a little borosilicate vessel dangling inside the tube on a wire leading through a septum. This allowed positioning the reagent outside or inside the heated zone. Liquid reagents could also be introduced by injecting directly into the reagent vessel through another septum located on the side of the tube.

Synthesis of Multiple Layers

All supports were initially dried in vacuum at 110°C for 6 h.

Iron

About 4 g of Chromosorb W, NAW, 45/60 mesh, cleaned of metal contamination as described earlier (14), was filled into the reaction tube and covered by a quartz wool plug. An excess of anhydrous $FeCl_3$ was quickly filled into the reagent vessel and the apparatus assembled.

Then a 60 mL/min stream of dry nitrogen was turned on by opening valve A. Thirty minutes later the furnace was turned on and took another 30 min to reach the desired temperature of 280°C. After a further 30 min at 280°C, the cup containing $FeCl_3$ was lowered into the heated zone. The reaction was allowed to proceed for 90 min, during which excess $FeCl_3$ collected at the cold bottom outlet of the reaction tube.

Then the reagent vessel was raised and filled with 0.5 mL of water injected through the side port. Lowering the vessel into the heated zone introduced water vapor to the coated support; in addition, all of the nitrogen stream was bubbled through the "water doping tube" by closing valve A and opening valves B and C.

After 30 min in this condition, the apparatus was switched back to dry nitrogen. Traces of moisture that had condensed on the colder parts were driven off with a hot-air gun. The nitrogen purge was continued for 15 min; then the heater was turned off and the furnace cooled down by passing cold water through the copper tubing. This procedure was presumed to produce the "first layer"; it was precisely repeated for each additional "layer".

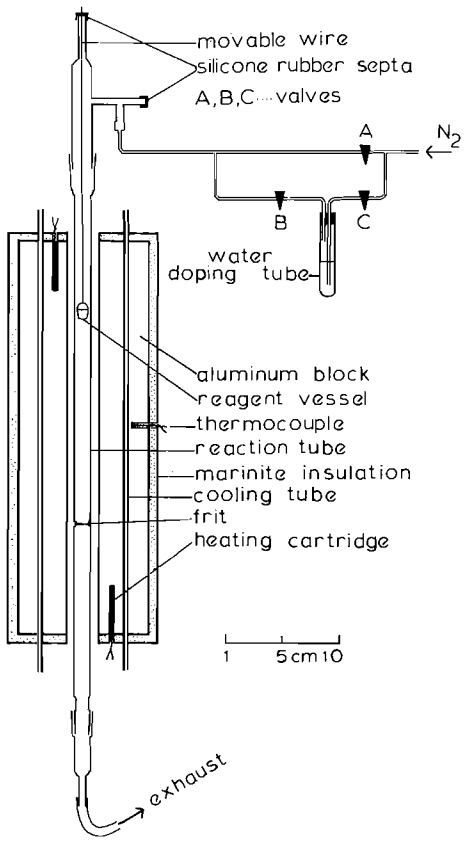

FIG. 1. Schematic of reaction tube, introduction system, and furnace.

Chromium

The coating of chromium was similar to that of iron with three exceptions. First, both Chromosorb W and silica gel 62, 80/100 mesh, were used. Second, the reagent CrO_2Cl_2 was introduced by injecting through the side port into the reagent vessel; ~0.2 mL for Chromosorb, ~0.5 mL for silica gel. Opening the reaction tube thus became unnecessary and the cool-down step was consequently omitted. Third, the reaction between support and chromyl chloride was allowed to proceed for 45 min.

Aluminum

The reagent was anhydrous $AlCl_3$, the support silica gel 62, 80/100 mesh. Otherwise the procedure was similar to that used for iron.

Titanium

Here the support was Chromosorb W, the reagent $TiCl_4$. Otherwise the procedure conformed to that given for chromium.

Analyses

Iron was extracted by boiling 6 *N* HCl and determined by atomic absorption flame spectrometry. Chromium was similarly extracted, but showed some resistance to complete extraction especially when multiple layers — and, consequently, longer heating periods — were involved. The extract was analysed by atomic absorption.

In addition, neutron activation analysis was used on the complete phases containing Cr, Al and Ti. The samples were

Can. J. Chem. Downloaded from www.nrcresearchpress.com by 210.87.254.5 on 09/06/12
For personal use only.

placed into pre-cleaned polyethylene vials, which were heat-sealed and irradiated at the Dalhousie University SLOWPOKE reactor at a flux of 5×10^{11} n cm^{-2} s^{-1}. A high resolution Ge(Li) detector was used to record the γ-ray spectra.

Results and Discussion

The synthesis of chromatographic "bonded phases" via the presumed reaction of silanol groups has some controversial aspects; whether viewed from the organic side as now popular in liquid chromatography, or from the inorganic side as done in this study. To start with, the number and nature of silanol groups is usually in doubt. Full agreement is lacking even on the number of silanol groups on a "fully hydroxylated" silica surface.

When these silanol groups react, circular arguments easily arise. For instance, the stoichiometry of a particular reagent may be judged by the assumed number of silanol groups it is offered to react with. In other experiments, in turn, this or a similar reagent, with now assumed stoichiometry, may be used to determine the number of silanol groups. Aside from the potential involvement of such a circular argument, the choice of reagents and reaction conditions has a strong influence on the apparent result.

The difficulties inherent in this area are clearly illustrated, for instance, by an early publication of Boehm and co-workers (15). In the work of Peri *et al.* (16), who proposed a surface structure for silica based on its reaction with aluminum trichloride and silicon tetrachloride, it is suggested that often two silanol groups react with one halide molecule. Obviously, such stoichiometries strongly influence expectations of how thick a nominally monomolecular layer ought to be.

The situation becomes even more complicated with multiple reagent exposures. For instance, Hair and Hertl (17) reacted silica with PCl_3 and BCl_3 and subsequently hydrolysed the products to produce P—OH and B—OH groups for their ir study. In order to maximize the concentration of these surface groups, they had to repeat the reaction with halide and water as often as four and five times. (From the fact that they had to do this one would assume that, there, homogeneous multilayers were *not* produced by multiple reactions; however, such was also not the objective of their study.) A few of the variables involved in producing a particular layer thickness in multi-reaction experiments have been discussed in a previous paper (12).

Here, the nominal "number of layers", i.e., the number of reactions with metal halide and subsequent hydrolyses, is correlated with the number of metal atoms per 100 Å^2 of the original support. This is shown in Fig. 2 for iron. The number of iron atoms after the first coating corresponds approximately to the (most commonly assumed) number of available hydroxyl groups.

In the case of chromium shown in Fig. 3, however, the number of chromium atoms in the first coating is between two to three times that of the iron atoms in the case above. Chromium forms multilayers with apparent ease and even though the two methods of analysis, AA and NA, differ considerably in the higher concentration range, this trend nevertheless emerges clearly from the graph.

Why chromium should form heavier layers than iron is not immediately apparent. However, the presumed initial reaction with silanol groups is just one of a variety of processes that can occur on the surface. For instance, a reagent may not only "bond" but also "decompose" there. The former reaction is likely dependent on the presence of silanols, the latter likely not. Furthermore, deposition of a layer may start with the former but continue with the latter process.

This would complicate a mechanistic description of the synthesis, but in terms of the final product it may be an advantage. To wit, the problem here is

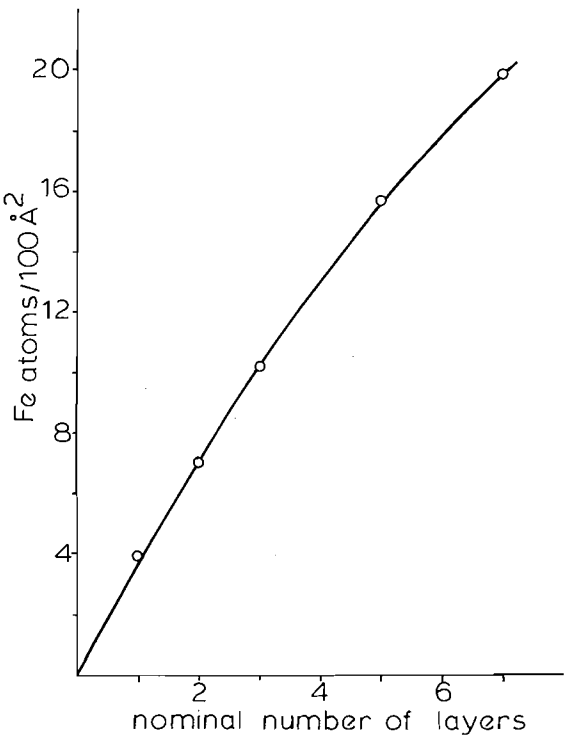

FIG. 2. Iron content of Chromosorb W treated with $FeCl_3$ and H_2O; as determined by AA. See text for details.

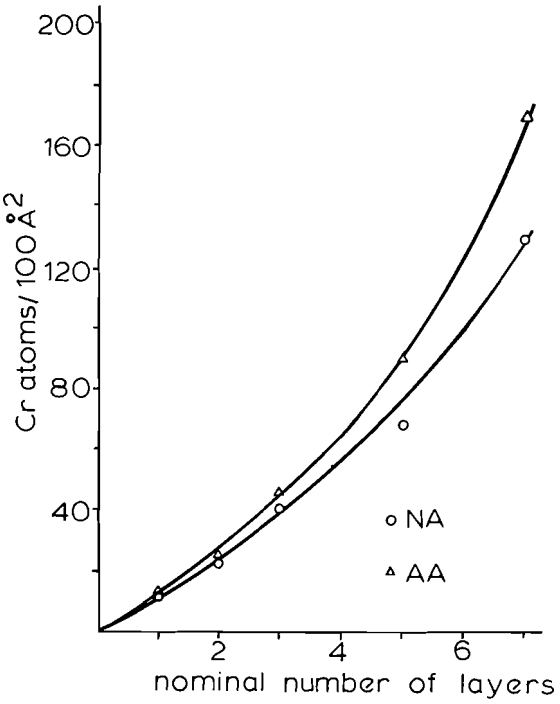

FIG. 3. Chromium content of Chromosorb W treated with CrO_2Cl_2 and H_2O; as determined by AA and NA. See text for details.

to produce a *homogeneous* layer — and a starting reaction involving densely and evenly distributed surface groups (the silanols) would be a helpful first step. Once a monolayer has been formed in this manner, reagent degradation may help to thicken it.

This scenario compares favorably with one in which a decomposing reagent would be the *lone* contributor. More likely than not, such a process would result in isolated agglomerations of metal oxide on a partially covered silica surface — in other words, in a heterogeneous layer.

Aside from tests of layer homogeneity, the question of mechanism could be resolved by experimental means. For instance, the kinetics of "surface reaction" and "reagent decomposition" are different. Once the accessible silanol groups have reacted in the former manner, the reaction should cease. The latter process, however, should be characterized by a fairly constant deposition rate (after, perhaps, a differently behaved initial phase). Other tests could involve the presumably larger contribution of a reagent decomposition process at higher temperatures or longer exposure times.

A further possible test of deposition mechanism utilizes the introduction of water between applications of metal halide (see Experimental). Water is presumably necessary to hydrolyze halide and provide bound hydroxyl groups to form the next layer.

If this presumption were entirely correct (and if the first application of metal halide were to saturate all available silanol groups), then the second and any further halide treatment *without* intermittent introduction of water should not significantly increase layer thickness. If, on the other hand, reagent decomposition were the prevailing mechanism, then the layers should build up in regular fashion with or without water treatment.

On a rather superficial basis, we have done some experiments that indicate the presence of both mechanisms. For instance, four applications of ferric chloride with intermittent water treatments lay down 13 Fe atoms on 100 Å^2 (Fig. 2). The same procedure but *without* water yields about 8 iron atoms on the same area. What is achieved by the second application of $FeCl_3$ after exposure to water vapor, requires (roughly) a second, third, and fourth halide treatment in its absence. The assumption of more than one mechanism seems therefore justified in the case of iron.

However, the evidence is far from making an ironclad case. A variety of questions would still need to be investigated. These include adsorption vs. reaction of halide and water molecules, the effects of temperature and time of exposure, and the behavior of different metal species. Desirable as such investigations may be, they were beyond the limited framework of this study. Questions other than of a mechanistic nature needed attention.

The chromium layers of Fig. 3 are bonded to a diatomaceous earth support with average pore size well above 10^3 Å. In analogy to the "bonding" of organic polymers (18) or organosilicon monomers (19) to the surface of supports of different pore sizes, one could have suspected that the number of chromium atoms bonded to 100 Å^2 of a silica gel like grade 62 with a surface area of approximately 300 m^2/g, would turn out to be less than those bonded to the diatomaceous earth of nominally 1 m^2/g.

This was indeed the case — as can be seen, for instance, from the analytical data for one and three layers. Instead of holding 12 and 40 Cr atoms as the Chromosorb did, the silica gel held only 4 and 10 chromium atoms per 100 Å^2, respectively. Silica gel 62 as a support was interesting for us to investigate; not only because of the potential extension to liquid chromatography but also because this material produces efficient gas–solid chromatography with aliphatics and aromatics.

Can. J. Chem. Downloaded from www.nrcresearchpress.com by 210.87.254.5 on 09/06/12
For personal use only.

TABLE 1. Retention temperatures t_R in °C of various gas chromatographic solutes in a standard program

Solute	Silica gel	Silica gel + 4 Cr/100 Å²	Silica gel + 10 Cr/100 Å²
Benzene	140	125	120
Naphthalene	225	212	210
Toluene	162	155	150
m-Xylene	185	178	173
n-Heptane	109	125	130
n-Undecane	173	200	210
Cyclohexane	88	105	108
Decalin	155	185	190
Average of absolute differences[a]	16.5	5	

[a] $\Sigma|\Delta t_R|/8$, where Δt_R is the difference in retention temperature for each of the eight solutes on silica gel and one-layer chromia, and on one-layer and three-layer chromia, respectively.

Thus we had the chance to test chromia homogeneity in a gas chromatographic experiment, using a one-layer material that was close to "monomolecular", and a three-layer one definitely beyond this ill-defined state.

What is one to expect from chromatographic retention experiments on these two materials of 4 and 10 Cr/100 Å²? If the layers are non-homogeneous (isolated chromia deposits strewn about the silica surface), then solute interactions involve both chromia and silica in both cases. That would suggest greater differences between the one- and three-layer phases. If the layers, on the other hand, are homogeneous, then there should be relatively little difference between the 4 and 10 Cr/100 Å² materials, since the former should be already close to covering the silica surface. What is presumed here, of course, is that the precise nature (really the chromatographic behavior) of "chromia" is the same in both cases, and that one can find chromatographic solutes that interact differently, though still on a comparable scale, with chromia and silica.

Fortunately, the chromatographic behavior of a chromium oxide layer differs distinctly from that of silica. On chromia, aliphatics are more and aromatics are less retained than on silica gel — the best possible situation for a test of surface homogeneity. Table 1 lists the results, and they are similar both for solutes that increase and for solutes that decrease in retention with the introduction of chromia. Once the first layer has been laid down, most of the change in retention has been accomplished. Thus both chromatographic and analytical data suggest (though neither of them proves) that it is possible in this case to synthesize successive, homogeneous metal oxide layers.

It can be added that the general performance of chromia layers, in gas as well as in liquid chromatography, is equivalent to that of silica in terms of efficiency (HETP) and peak symmetry, but that the retention characteristics of the two materials, fortunately, are different. A short chromatographic characterization of chromia layers has just appeared (20).

It would come as no surprise if the chromia layer were to exhibit catalytic activity — as, in fact, most chromatographic supports do. A typical catalysis study was never performed on the bonded inorganics, even though that could be interesting in its own right. Most chromatographers experience only the undesirable effect of a catalytic surface: its detrimental influence on solute integrity. In this context, and under our conditions and with our test compounds, overt degradation of migrating molecules was never apparent.

Thus the primary test of catalytic activity as well as of layer homogeneity was chromatographic in nature. This appeared to make sense, since our main interest is in chromatography and the synthesis of bonded phases for use by that technique. However, as one of the reviewers of this manuscript has pointed out, chromatographic testing alone is a bit unusual from the general viewpoint of surface characterization. To discuss the situation, we are adding the following few comments.

Chromatographic separation depends on the sorption of solute molecules on available surfaces. These surfaces are formally of two types: the outside of particles (in contact with the fast-flowing mobile phase) and the inside (in contact with slow-flowing or stagnant carrier). A rough calculation may help to appreciate the relative contributions of these two types of surfaces.

Typical silica gel 62 has a surface area of 300 m^2/g; as a gc packing its average particle diameter may be, say, 150 μm. If we consider the particles as spheres for purposes of calculation, and assume an apparent density of 0.2 g/cm^3, then the outside

Can. J. Chem. Downloaded from www.nrcresearchpress.com by 210.87.254.5 on 09/06/12
For personal use only.

surface is close to one tenth of one percent of the totally available one. Or, if we think in terms of a surface technique like ESCA, which would sample, say, about 50 Å deep, then, again, a volume negligible in terms of the total particle would be scrutinized. When extrapolating the results of such a technique to the chromatographic behavior of a particular packing, one has therefore to assume that the particle outside resembles the porous interior in terms of surface chemistry.

Unfortunately, this did not seem to have been the case with our materials covered by iron or chromium oxide. When sent for ESCA to Hewlett-Packard in Palo Alto, CA, the values for iron and chromium came back much lower than presumed from the overall content of these metals. Why the values were low has not been established. The effect could arise from synthesis conditions but, more likely, simply represents abrasion during handling, and transport across the continent. After all, the layers are only a few angstroms thick. Chromatographically, abrasion of the particle periphery is of course unimportant, since retention is essentially accomplished by the protected interior surfaces. A correlation of ESCA data with chromatographic characteristics would thus have been misleading. It is realized, of course, that particles can be treated with more caution — but we like to mention this disappointing attempt as a case-in-point for the difficulties and potential pitfalls that can arise in analyzing chromatographic packings.

The problem of porous particles surfaced again in infrared spectroscopy. For transmission ir spectroscopy, the sample has to be brought at least to a translucent form. Although plain silica becomes translucent when suspended in solvents such as chloroform, it turned out that the modified materials did not. This attempt having failed, other ir approaches were considered not more likely to succeed. A thin disc, reacted in analogy to a support with metal halide, may have turned out translucent — but, even then, it would have been extremely difficult to ascertain the surface homogeneity by transmission ir spectroscopy as some of the disc interior, closed to the metal halide, could have interfered. The other option, reflectance ir spectroscopy, was beyond the scope of this work.

To return to the synthesis of inorganic layers, the coating of one and three layers of alumina and titania was attempted on silica gel 62 and Chromosorb W, respectively. Neutron activation analysis showed that, for one layer, five aluminum atoms and nine titanium atoms were held onto 100 Å^2. These numbers increased to 9 and 24, respectively, after three coatings. These results are in essential accord with earlier data obtained on Porasil (13) and follow similar trends as those of Fe and Cr. Even though gas chromatography on alumina or titania turned out to be much poorer than on bare silica, it appears that here, too, multilayer formation was possible.

Acknowledgments

This research was supported by Natural Sciences and Engineering Research Council of Canada grant A-9604. Thanks are due to R. Myatt for the aluminum oven, and to J. Müller for the reaction tube. We appreciate the early experiments on iron coating by T. Tsuda.

1. S. H. Langer, J. Y. Yurchak, and J. E. Patton. Ind. Eng. Chem. **61**, 11 (1969).
2. E van der Vlist and J. M. de Jong. J. Chromatogr. **52**, 486 (1970).
3. M. J. O'Brien and R. L. Grob. J. Chromatogr. **155**, 129 (1978).
4. A. Betti, G. Loddi, C. Bighi, and F. Dondi. J. Chromatogr. **106**, 291 (1975).
5. D. L. West and A. L. Marston. J. Am. Chem. Soc. **86**, 4731 (1964).
6. J. King Jr. J. Phys. Chem. **67**, 1397 (1963).
7. G. F. Shipman. Anal. Chem. **34**, 877 (1962).
8. W. R. Moore and H. R. Ward. J. Phys. Chem. **64**, 832 (1960).
9. H. A. Smith and P. P. Hunt. J. Phys. Chem. **64**, 383 (1960).
10. R. Aigner, H. Spitzy, and R. W. Frei. Anal. Chem. **48**, 2 (1976).
11. H.-P. Boehm. Angew. Chem. Int. Ed. Engl. **5**, 533 (1966).
12. W. A. Aue, M. M. Daniewski, and E. E. Pickett. J. Chromatogr. **189**, 13 (1980).
13. R. Aigner-Held, W. A. Aue, and E. E. Pickett. J. Chromatogr. **189**, 139 (1980).
14. W. A. Aue, M. M. Daniewski, E. E. Pickett, and P. R. McCullough. J. Chromatogr. **111**, 37 (1975).
15. H.-P. Boehm, M. Schneider, and F. Arendt. Z. Anorg. Allg. Chem. **320**, 43 (1963).
16. J. B. Peri and A. L. Hensley Jr. J. Phys. Chem. **72**, 2926 (1968).
17. M. L. Hair and W. Hertl. J. Phys. Chem. **74**, 91 (1970).
18. C. R. Vogt and W. A. Aue. J. Chromatogr. Sci. **16**, 268 (1978).
19. P. P. Wickramanayake and W. A. Aue. J. Chromatogr. **195**, 25 (1980).
20. W. A. Aue and P. P. Wickramanayake. J. Chromatogr. **197**, 21 (1980).
21. B. Camara, P. Fink, G. Pforr, and B. Rackow. Z. Chem. **12**, 451 (1972).

Can. J. Chem. Downloaded from www.nrcresearchpress.com by 210.87.254.5 on 09/06/12
For personal use only.

Dielectric relaxation of lithium and sodium perchlorates in 1,2-dimethoxyethane and propylene carbonate

HUBERT CACHET, MOHAMED FEKIR, AND JEAN-CLAUDE LESTRADE

Groupe de Recherche n°4 du C.N.R.S., Physique des Liquides et Electrochimie, associé à l'Université Pierre et Marie Curie, 4 place Jussieu, 75230 Paris Cedex 05, France

Received May 5, 1980

HUBERT CACHET, MOHAMED FEKIR, and JEAN-CLAUDE LESTRADE. Can. J. Chem. **59**, 1051 (1981).

The complex permittivity of $LiClO_4$ and $NaClO_4$ solutions in 1,2-dimethoxyethane (DME) has been measured in the frequency range 0.140–123.2 GHz. The data have been analysed according to a model for the reorientation of ion pairs given in a previous paper. The dielectric data are supplemented by conductivity measurements in a broad concentration range (10^{-4}–1 mol/L) which evidence the large extent of salt association. The main result is that the solvation of Li^+ and Na^+ by DME cannot be described as simply as in the case of other solvents, such as tetrahydrofuran or ethyl acetate, as far as the dielectric properties are concerned: while the assumption of rigidly bound solvating molecules was acceptable for the latter solvents, some freedom in the reorientation of these molecules has to be taken into account for the case of DME. $LiClO_4$ solutions in propylene carbonate (PC) + benzene and PC + DME mixtures have also been studied. The data, for the latter, can be qualitatively interpreted under the assumption that PC molecules take the place of DME molecules in the solvation sheath, even at low PC concentration.

HUBERT CACHET, MOHAMED FEKIR et JEAN-CLAUDE LESTRADE. Can. J. Chem. **59**, 1051 (1981).

La permittivité complexe de solutions de $LiClO_4$ et $NaClO_4$ dans le 1,2-diméthoxyéthane a été mesurée entre 0,140 et 123,2 GHz. Les résultats ont été analysés selon un modèle de réorientation de paires d'ions exposé dans un précédent article.

Les données diélectriques sont complétées par des mesures de conductivité dans un large domaine de concentration (10^{-4}–10 mol/L) qui mettent en évidence l'importance de l'association du sel. Le principal résultat est que la solvatation de Li^+ et Na^+ par le DME ne peut pas être décrite de manière aussi simple que dans le cas d'autres solvants, tels le tétrahydrofuranne et l'acétate d'éthyle, en ce qui concerne les propriétés diélectriques: tandis que l'hypothèse de molécules solvatantes rigidement liées était acceptable pour ces derniers solvants, il faut tenir compte d'une certaine liberté d'orientation de ces molécules dans le cas du DME. Des solutions de $LiClO_4$ dans les mélanges carbonate de propylène (PC) + benzène et PC + DME ont aussi été étudiées. Pour ces derniers, les données expérimentales peuvent être expliquées qualitativement en supposant que des molécules de PC prennent la place de molécules de DME dans la couche de solvatation même aux basses concentrations de PC.

Introduction

In a recent paper (1), we have shown that the dielectric relaxation of $LiClO_4$ in tetrahydrofuran (THF) and ethyl acetate solutions could be interpreted by a model in which the salt is assumed to be associated into ion pairs. The ion pairs are simultaneously the rotating dipoles and the diffusing defects which perturb the rotation of the dipoles; this model is derived from Glarum's (2) and Hunt and Powles' (3) theory, with a new feature consisting of the assumption that the ion pairs can be considered as a hard sphere fluid when calculating their radial distribution function. A parallel study of the conductivity vs. concentration curves, up to about 1 *M*, yielded (1) an anion–cation closest distance of approach, not very different from the radius of the ion pair deduced from the dielectric study. The dipole moment of the ion pair was also discussed in terms of this radius, and the discussion showed that Li^+ was solvated. A solvation number was also deduced from that part of the overall relaxation spectrum which can be assigned to the reorientation of the solvent molecules.

In this work, we present data about $LiClO_4$ solutions in 1,2-dimethoxyethane (DME) and propylene carbonate (PC). These solvents are used as components of the electrolyte solutions in high energy density batteries with lithium as anode. The data are analysed in the same way as those previously reported (1), but it will be shown that the solvation of Li^+ (and Na^+) by DME has to be taken into account in a different way.

Experimental

Conductivity measurements have been performed exactly in the same way as previously described (1), using a parallel-plate cell and the General Radio 1608-A impedance bridge between 10^3 and 2×10^4 Hz, and a coaxial cell with the General Radio 1615-A transformer ratio bridge between 10^3 and 10^5 Hz, for the less conducting systems. The complex permittivity measurements have been performed (4) with a slotted line and a coaxial cell between 0.15 and 3 GHz, with waveguide interferometers at 9.4 and 34 GHz. Additional measurements at 123.2 GHz, using a Michelson interferometer (5), have been performed in the Centre Hyperfréquence et Semi-Conducteurs (Université des Sciences et Techniques de Lille, France) by courtesy of Professor Constant.

The perchlorates are dried in vacuum, at 240°C for at least 36 h. The solvents are dried by contact on molecular sieves. The water content of the solutions, determined by coulometric titration, is typically 50 ppm before use, 200 ppm after use in the dielectric cells. All experiments have been performed at 25°C.

0008-4042/81/071051-10$01.00/0

©1981 National Research Council of Canada/Conseil national de recherches du Canada

Can. J. Chem. Downloaded from www.nrcresearchpress.com by 210.87.254.6 on 09/06/12
For personal use only.

Can. J. Chem. Downloaded from www.nrcresearchpress.com by 210.87.254.6 on 09/06/12
For personal use only.

Conductivity

As previously explained (1), the salt is assumed to be in the form of single ions ($\alpha_1 c$), ion-pairs ($\alpha_2 c$), triple ions ($\alpha_3 c$), and quadrupoles ($\alpha_4 c$), where c is the overall concentration. The formations of ion-pairs, triple ions, and quadrupoles are governed by chemical equilibria with constants K_2, K_3, and K_4:

$$[1]\quad \begin{aligned} A^+ + B^- &\rightleftarrows AB & K_2\\ A^+ + AB &\rightleftarrows ABA^+ & K_3\\ AB + B^- &\rightleftarrows BAB^- & K_3\\ AB + AB &\rightleftarrows ABBA & K_4 \end{aligned}$$

where K_2 and K_3 depend on the dielectric constant ε_s of the solution (higher than that of the solvent) through the following equations

$$[2]\quad K_2 = (4\pi N_A a_2^3/3000) \exp (e^2/a_2\varepsilon_s kT - 1/2)$$

$$[3]\quad K_3 = (\pi N_A a_3^3/1000] \exp (e^2/2a_3\varepsilon_s kT - 3/2)$$

N_A is Avogadro's number, e the charge of the ions, k Boltzmann's constant, T the absolute temperature, a_2 the closest distance of approach of A^+ and B^-, a_3 a characteristic distance for the formation of triple ions. The equivalent conductivity Λ is assumed to depend only on α_1 and α_3:

$$[4]\quad \Lambda = \Lambda_0(\alpha_1 + \alpha_3/3)$$

where Λ_0 is the limiting equivalent conductivity of the salt in the form of single ions. Previously (1), we had corrected this equation by multiplying Λ_0 by η/η_0 where η is the viscosity of the solution and η_0 the viscosity of the solvent. Such a correction is active in the high concentration region, and it yielded a maximum in the theoretical Λ vs. c curve of $LiClO_4$ in ethyl acetate solutions. The same was found with $NaClO_4$ solutions in DME, which are about to be discussed in the present paper. Repeating the calculations without this corrective term, i.e. with eq. [4], showed the data were better reproduced and the maximum disappeared. The best values of the parameters (a_2, a_3, K_4) were changed, but this change was important only for K_4, moderate for a_3, and negligible for a_2. This reinforces the opinion that in such an analysis, K_4 strongly depends on the model, so that we cannot rely on the distinction between "free" ion pairs AB and ion-pairs engaged in a quadrupole ABBA; on the other hand a_2 does not depend too much on the model. In what follows, we thus adopt eq. [4] without any correction for the change of viscosity with concentration.

The data for $LiClO_4$ and $NaClO_4$ solutions in DME are shown in Fig. 1. The solid and dashed lines are the Λ vs. c curves calculated with the following sets of parameters.

$$LiClO_4 \begin{cases} a_2 = 4.70 \times 10^{-8}\,\text{cm} \\ a_3 = 11.0 \times 10^{-8}\,\text{cm} \end{cases} \quad K_4 = 8.8\,M^{-1}$$

$$NaClO_4 \begin{cases} a_2 = 4.70 \times 10^{-8}\,\text{cm} \\ a_3 = 11.8 \times 10^{-8}\,\text{cm} \end{cases} \quad K_4 = 8.7\,M^{-1}$$

Λ_0 is chosen as 176.4 ohm^{-1} cm^2 mol^{-1} for $LiClO_4$, 189.5 ohm^{-1} cm^2 mol^{-1} for $NaClO_4$. These values are derived from the values found in tetrahydrofuran (156.1 ohm^{-1} cm^2 mol^{-1} for $LiClO_4$ (6), 167.7 ohm^{-1} cm^2 mol^{-1} for $NaClO_4$ (7)) and application of the Walden rule which states the product $\Lambda_0\eta_0$ is constant.

The more striking feature of this result is that nearly the same set of parameters is found for both series of solutions. It can be seen in the raw data since at any concentration Λ does not depend very much on which salt ($LiClO_4$ or $NaClO_4$) is in solution. This fact is in contrast with the difference in the solubilities: $LiClO_4$ is not soluble in DME at a concentration higher than 0.2–0.25 M at 25°C. This is true in a dry solvent, because this solubility increases rapidly if a small amount of water is added. For instance, we had already given dielectric data on a 0.5 M solution of $LiClO_4$ in DME (8), with a water content of 6.3 g/L, i.e. 0.35 M. The second point to be noticed about these data is that the distance a_2 is significantly higher than for the solutions in tetrahydrofuran and ethyl acetate: the values 3.95 and 3.92 $\times$ 10^{-8} cm found with the viscosity correction

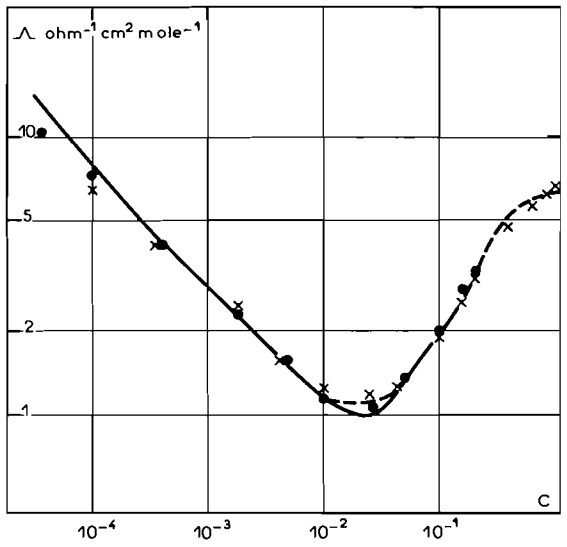

FIG. 1. Equivalent conductivity of $LiClO_4$ (●) and $NaClO_4$ (×) solutions in DME vs. salt concentration (mol/L). The solid ($LiClO_4$) and dashed lines ($NaClO_4$) have been drawn according to the model given in the text, with fitted values of a_2, a_3, and K_4.

Can. J. Chem. Downloaded from www.nrcresearchpress.com by 210.87.254.6 on 09/06/12
For personal use only.

(1) are changed into 3.97 and 3.93 $\times$ 10^{-8} cm with eq. [4].

Dielectric Relaxation

The overall measured complex permittivity can be written as:

$$\varepsilon(\omega) = \varepsilon_m(\omega) + \Delta\varepsilon(\omega) + \sigma/i\omega\varepsilon_0$$

where $\varepsilon_m(\omega)$ is the contribution of the solvent molecules and σ the static conductivity; $\Delta\varepsilon(\omega)$ is thus the contribution of the ions apart from the losses arising from the frequency independent conductivity σ. This splitting of $\varepsilon(\omega)$ into different terms has been discussed elsewhere (9), the discussion being summarized in ref. 1, where expressions are also given for the calculation of $\Delta\varepsilon(\omega)$. The latter read:

$$[5] \quad \Delta\varepsilon(\omega) = \frac{\varepsilon_s - \varepsilon_m}{1 + i\omega\tau_0}\left\{1 + i\omega\tau_0 \int_0^\infty 3r(x + r) \times \exp\left[-(x + r)^3 + r^3 - \lambda x\right] dx\right\}$$

where

$$[6] \quad r = R_s/L_0; \qquad (4\pi/3)\rho L_0{}^3 g(R_s) = 1$$

$$[7] \quad \lambda^2 = (L_0{}^2/D\tau_0)(1 + i\omega\tau_0)$$

These expressions correspond to a model of ion-pairs, whose numerical density is ρ, which reorient with a characteristic time τ_0 and which diffuse with a coefficient D. Their radial distribution function is that of hard spheres with a diameter R_s. Upon a collision, the time correlation function of the dipole moment vanishes instantly. The diffusion coefficient D can be related to the viscosity η of the solution and to a characteristic diameter R_0 through the Stokes–Einstein formula:

$$[8] \quad D = kT/6\pi\eta(R_0/2)$$

The (macroscopic) relaxation time τ_0 can be related to the same quantities by the Debye formula with the Powles–Glarum equation (10) for a micro/macroscopic correction:

$$[9] \quad \tau_0 = (3\varepsilon_s/(2\varepsilon_s + \varepsilon_m))4\pi(R_0/2)^3\eta/kT$$

In eqs. [5] and [9], ε_s is the low frequency limit of ε', the real part of $\varepsilon(\omega)$; ε_m is the same quantity for $\varepsilon_m(\omega)$, i.e. the contribution of the solvent molecules to the static permittivity. More details on the model and the calculations are given in ref. 1.

Solvation can be dealt with through a discussion of $\varepsilon_m(\omega)$. In ref. 1, as in previous papers, we had considered that $\varepsilon_m(\omega)$ could be deduced from the spectrum of the pure solvent, $\varepsilon_{m0}(\omega)$ with the transformation

$$[10] \quad (\varepsilon_m(\omega) - \varepsilon_\infty)/(\varepsilon_m - \varepsilon_\infty) = (\varepsilon_{m0}(\omega) - \varepsilon_\infty)/(\varepsilon_{m0} - \varepsilon_\infty)$$

the only change being in the static permittivity (ε_{m0} for the pure solvent, ε_m for the solvent contribution in the solution). The formula is deduced from the following model of solvation: a part of the solvent molecules reorients freely, i.e. in the same way, with the same characteristic time, in the pure solvent and in the solution; another part of the molecules does not reorient at all because they belong to a rigid solvation sheath built in such a way that the overall dipole moment of this aggregate is zero. Let qc be the concentration of the latter, $\rho_{ms} = \rho_m - qc$ the concentration of the former; ρ_m is the overall concentration of the solvent molecules in the solution, c the salt concentration; ρ_{ms}, hence q, can be deduced from the Fröhlich–Kirkwood formula written as:

$$[11] \quad \frac{(\varepsilon_m - \varepsilon_\infty)(2\varepsilon_m + \varepsilon_\infty)}{q\varepsilon_m} = \frac{N_A\rho_{ms}}{9000\varepsilon_0 kT} \times g_m\mu_m{}^2\left(\frac{\varepsilon_\infty + 2}{3}\right)^2$$

where the product $g_m\mu_m{}^2$ (Kirkwood correlation factor multiplied by the square of the dipole moment of the solvent molecules) can be deduced from the same formula applied to the pure solvent.

As shown further, this model does not apply to the DME solutions studied in the present work. In order to make the comparison of these solutions with previous ones easier, we performed the calculations on THF and ethyl acetate solutions of $LiClO_4$ solutions in a slightly different way, without any assumption on the value of q, formerly supposed to be equal to 4. In fact, this value is not very well determined by experiment and 4 is not significantly better than, say, 6 for a dilute solution. In the present case, a first run was performed without any constraint upon ε_m, then the function $\varepsilon_m(c)$ was smoothed and the calculations performed a second time with these smoothed values for ε_m; the fitting is not significantly worse for any system, and the result is given in Fig. 2 as a $q(c)$ curve. We have also reported the change in R_0 and R_s with c, because we dropped the condition $R_s \leq R_0$, used in ref. 1. The limiting values of q, for $c = 0$, are 5.9 $\pm$ 1.3 for THF solutions and 5.8 $\pm$ 1.1 for ethyl acetate solutions. Though higher than 4, these values remain small enough for a model involving a rigid solvation sheath to be acceptable. Moreover, the apparent dipole moment of $LiClO_4$ deduced from the difference $\varepsilon_s - \varepsilon_m$ leads to μ = 11.4 $\pm$ 0.4 D for both series,

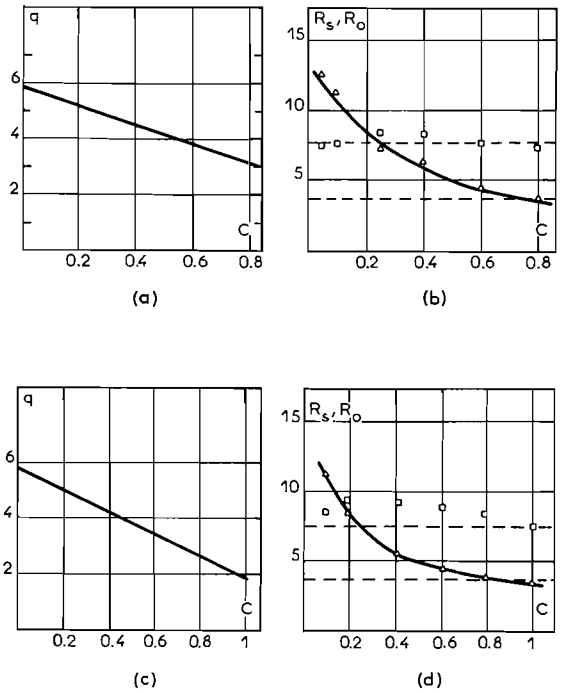

FIG. 2. $LiClO_4$ solutions in THF (upper part) and ethyl acetate (lower part). Salt concentration c in mol/L. Left (a and c), solvation number q in a rigid solvation sheath model defined in text. Right (b and d), collision distance R_s (△) and diameter R_0 (□) of the equivalent diffusion and rotation sphere, in the model of ion pairs. These lengths are given in Angströms. The horizontal dashed lines in b and d correspond to a_2 and $2a_2$ (characteristic distance of ion-pairing from conductivity data).

as a low concentration limit of μ_a; this value is slightly higher than in ref. 1 (10.5 ± 0.5 D) but the discussion remains unchanged, because the value of μ cannot be predicted with accuracy (it is difficult to take into account the solvating molecules in this calculation).

Solutions in DME

We have already reported dielectric measurements with $LiClO_4$ solutions in DME and dioxolane (8). The water content of these solutions was too large to be negligible, as shown by more recent measurements reported in the present paper. Though a correction can be made on the spectra to take water into account (11), we shall limit our study in the present case to the dried samples already considered above in the discussion of conductivity. The complex permittivity data are given in Table 1. Two samples of solvent have been used, with slightly different results. The difference can probably be ascribed to a difference in the residual water content. Anyway, each solution, in what follows, is compared to the appropriate sample of solvent. The dielectric relaxation of DME can be described by the Cole–Cole formula (12):

$$[12]\quad \varepsilon_{m0}(\omega) = \varepsilon_\infty + (\varepsilon_{m0} - \varepsilon_\infty)/(1 + (i\omega\tau)^{1-h})$$

with $0 < h < 1$. The infinite frequency permittivity has been estimated as 2.16, adding 20% to the electronic polarization α_e deduced from the optical refractive index $n_D = 1.38$, using the Clausius Mosotti formula. The set of equations reads:

$$[13]\quad (\varepsilon_\infty - 1)/(\varepsilon_\infty + 2) = (4\pi/3)\rho_m\alpha \qquad \alpha = 1.20\,\alpha_e$$
$$(n_D^2 - 1)/(n_D^2 + 2) = (4\pi/3)\rho_m\alpha_e$$

The parameters ε_{m0}, τ, and h which describe the relaxation of the solvents are given in Table 2 for both samples together with their water content. The influence of water can be seen from the difference with the same analysis performed on a third sample; the corresponding data of the latter, which had not been dried but used as received, have already been published (8). The autoassociation of DME can be discussed from the variations of the dielectric constant with temperature and dilution in a nonpolar component; the conclusion was that DME is not an associated liquid, as far as its dielectric properties are concerned (11).

A first analysis of the dielectric data of the solutions has been performed in exactly the same conditions as for the solutions in THF and ethyl acetate, i.e. with the assumption of a rigid, nonpolar aggregate of solvent molecules around the cation. As can be seen from Fig. 3, the value of q extrapolated at zero concentration is higher than 30 for both salts. So high a value had been observed only for associated solvents such as ethanol or methanol ($q = 25$ to 35) (13), whereas in nonassociated solvents, it is always lower than 6 to 8, whatever the analysis may be (9). In the present case, it can hardly be accepted that an ion could freeze so large a number of solvent molecules in their freedom of reorientation, when these molecules are able to reorient independently one from another. This difficulty can be circumvented if we drop the assumption that solvating molecules are rigidly bound to an ion, and if we accept that they are able to rotate with a characteristic time τ_p, longer than the reorientation time τ in pure solvent. The complex permittivity $\varepsilon_m(\omega)$ which originates from the solvent, in a solution, can thus be written as:

$$[14]\quad \varepsilon_m(\omega) = (\varepsilon_m - \varepsilon_p)/(1 + i\omega\tau_p) + \varepsilon_p(\omega)$$
$$(\varepsilon_p(\omega) - \varepsilon_\infty)/(\varepsilon_p - \varepsilon_\infty)$$
$$= (\varepsilon_{m0}(\omega) - \varepsilon_\infty)/(\varepsilon_{m0} - \varepsilon_\infty)$$

where ε_m is equal to ε_{m0} corrected for the change in the overall number of solvent molecules from pure solvent to the solution. The difference with the other model is that every molecule present in the solution con-

Can. J. Chem. Downloaded from www.nrcresearchpress.com by 210.87.254.6 on 09/06/12
For personal use only.

Can. J. Chem. Downloaded from www.nrcresearchpress.com by 210.87.254.6 on 09/06/12
For personal use only.

TABLE 1. Complex permittivity of DME and perchlorate solutions in DME. All $NaClO_4$ solutions are in DME (sample 2)

(*a*) DME and $LiClO_4$ + DME

	DME (sample 1)		DME (sample 2)		$LiClO_4$ (0.05 *M*) + DME (sample 2)		$LiClO_4$ (0.10 *M*) + DME (sample 2)	
f (GHz)	ε′	ε″	ε′	ε″	ε′	ε″	ε′	ε″
0.140	7.02	0.02	6.98	0.02	8.29	1.14	9.47	3.16
0.265	7.04	0.04	6.97	0.03	8.22	0.75	9.37	1.95
0.375	7.06	0.06	7.07	0.06	8.24	0.65	9.28	1.62
0.385	7.04	0.05	6.98	0.05	8.19	0.64	9.27	1.60
0.625	7.06	0.09	7.05	0.09	8.16	0.62	9.08	1.40
1.061	7.05	0.14	7.03	0.14	8.02	0.68	8.81	1.35
1.667	7.06	0.21	6.98	0.22	7.83	0.80	8.45	1.43
2.825	6.96	0.33	7.00	0.35	7.56	0.94	7.97	1.51
9.335	6.64	1.02	6.64	1.02	6.80	1.44	6.79	1.73
34.715	5.17	2.23	5.17	2.23	5.15	2.35	5.22	2.38
123.219	2.83	1.52	—	—	—	—	—	—

	$LiClO_4$ (0.10 *M*) + DME (sample 1)		$LiClO_4$ (0.15 *M*) + DME (sample 2)		$LiClO_4$ (0.2 *M*) + DME (sample 1)		$LiClO_4$ (0.25 *M*) + DME (sample 2)	
f (GHz)	ε′	ε″	ε′	ε″	ε′	ε″	ε′	ε″
0.140	9.32	2.88	10.44	5.79	11.37	9.70	12.03	13.42
0.265	9.19	1.81	10.31	3.49	11.27	5.67	12.07	7.77
0.375	9.44	1.67	10.21	2.82	11.12	4.59	11.96	6.05
0.385	9.09	1.50	10.15	2.77	11.03	4.37	11.79	5.96
0.625	9.27	1.46	9.91	2.29	10.69	3.50	11.53	4.76
1.061	8.92	1.42	9.47	2.10	10.14	3.00	10.70	3.84
1.667	8.52	1.50	8.95	2.09	9.53	2.89	9.92	3.49
2.825	7.99	1.58	8.28	2.04	8.53	2.53	8.81	3.02
9.335	6.80	1.68	6.86	1.97	6.91	2.25	6.94	2.43
34.715	5.10	2.34	5.11	2.47	5.10	2.46	5.04	2.49

(*b*) $NaClO_4$ + DME

	$NaClO_4$ (0.1 *M*) + DME		$NaClO_4$ (0.2 *M*) + DME		$NaClO_4$ (0.4 *M*) + DME	
f (GHz)	ε′	ε″	ε′	ε″	ε′	ε″
0.140	9.25	2.82	10.96	8.43	12.71	26.54
0.265	9.15	1.77	10.88	4.96	13.36	14.73
0.375	9.24	1.63	10.86	4.16	12.94	11.06
0.385	9.06	1.46	10.66	3.89	12.85	11.14
0.625	9.05	1.38	10.43	3.26	12.24	7.87
1.061	8.71	1.35	9.86	2.85	11.33	6.06
1.667	8.31	1.44	9.15	2.69	10.16	5.09
2.825	7.92	1.49	8.41	2.47	8.99	4.16
9.335	6.69	1.61	6.80	2.06	6.87	2.84
34.715	5.03	2.29	5.05	2.40	5.02	2.55

	$NaClO_4$ (0.6 *M*) + DME		$NaClO_4$ (0.8 *M*) + DME		$NaClO_4$ (1 *M*) + DME	
f (GHz)	ε′	ε″	ε′	ε″	ε′	ε″
0.140	13.25	46.00	12.86	67.03	12.62	85.50
0.265	14.26	25.45	14.87	36.98	15.13	46.62
0.375	14.28	19.03	14.90	26.37	15.32	34.19
0.385	14.20	18.67	15.06	26.73	14.96	33.79
0.625	13.52	12.99	14.22	17.47	14.71	22.34
1.061	12.30	9.41	12.77	12.28	12.91	15.38
1.667	10.76	7.47	11.03	9.37	11.19	11.42
2.825	9.33	5.74	9.43	6.87	9.51	8.18
9.335	6.88	3.40	6.86	3.93	6.84	4.28
34.715	5.07	2.77	5.04	2.79	5.03	2.85

TABLE 2. Dielectric relaxation of DME

Sample	Water content (ppm)	ε_{m0}	ε_∞	$10^{12}\tau$ (s)	h
1	250	7.050±0.005	2.16	3.65±0.04	0.045±0.008
2	200	7.000±0.005	2.16	3.57±0.07	0.049±0.010

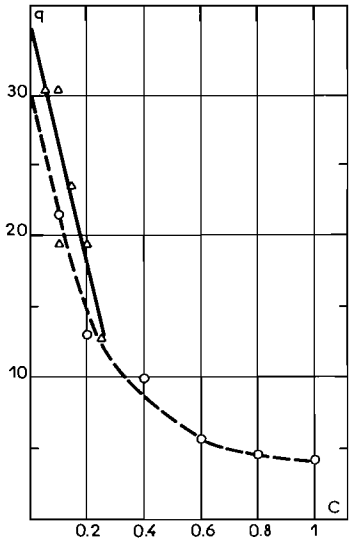

FIG. 3 $LiClO_4$ (△, solid line) and $NaClO_4$ (○, dashed line) in DME: solvation number in a rigid solvation sheath model.

tributes to the polarization since it reorients, though very slowly. The solvation number $q = (\rho_m - \rho_p)/c$ is then the number of molecules which interact with an ion in such a way that it reorients slower than in pure solvent. Of course such a splitting of the solvent molecules in two classes is arbitrary; ρ_p can be calculated from ε_p, using the Fröhlich–Kirkwood formula (eq. [11]) where ε_{ms} is changed into ε_p, ρ_{ms} into ρ_p. A common value of τ_p can be used in the analysis for each salt. The best choice is 350×10^{-12} s for $LiClO_4$, 300×10^{-12} s for $NaClO_4$, about 100 times as long as in pure solvent. The results of the analysis are given in Table 3. A smoothing over ε_p vs. c has also been performed, as above over ε_m vs. c The q values thus found can be given as

$$q = 8.54 - 6.47c \qquad \text{for } LiClO_4$$

$$q = 11.2 - 15.6c + 8.1c^2 \qquad \text{for } NaClO_4$$

In this model, there is no reason for the limiting (zero concentration) values of q to be lower than 6–8, but they are actually lower than in the first analysis. However the main point which is evidenced is that solvation in DME is qualitatively different from what it is in THF, ethyl acetate, and other non-associated solvents previously studied (9) since the simple model used before cannot apply.

The μ_a values of Table 3 can also be extrapolated to zero concentration and yield the dipole moment of the ion pair: 12.5 D for $LiClO_4$, 12.2 D for $NaClO_4$. The polarisability α_+ of the solvated cation can be deduced from the cation–anion distance $r = 2a_2$ using the Böttcher formula which gives the dipole moment μ of two polarisable charge points

$$[15] \quad \mu = er\,\frac{1 - (\alpha_+ + \alpha_-)/r^3 - 8\alpha_+\alpha_-/r^6}{1 - 4\alpha_+\alpha_-/r^6}$$

with $\alpha_- = 5.30 \times 10^{-24}$ cm^3 for ClO_4, under the assumption that the anion is not solvated. The value of α_+ thus found is 32×10^{-24} cm^3, much higher than the value found in THF or ethyl acetate, which was about 13×10^{-24} cm^3. This reinforces the idea that a larger number of molecules interact with the cation in DME than in other solvents, since the molecular polarisability of these solvents is not so different (about 10×10^{-24} cm^3 for THF, 14×10^{-24} cm^3 for DME).

The values of R_s decrease with increasing concentration of salt, but always remain larger than a_2, as in THF solutions. As previously discussed in the latter case (1), this can be explained by the fact that considering the ion-pairs as hard spheres is too crude an approximation, and that nevertheless, their closest distance of approach is always larger than the corresponding distance for two ions. But, whereas for THF solutions R_0 was about twice a_2, we find here $R_0 < 2a_2$; this might be taken as an argument in favor of a solvating sheath which is not made of tightly bound molecules, in agreement with the model: the reorientation and the diffusion of the ion pair are faster, and thus correspond to smaller equivalent spheres.

An open question is the difference between $LiClO_4$ and $NaClO_4$ since their solubilities in DME are quite different, whereas no difference can be observed for the dielectric properties of the solutions.

Solutions in PC + Benzene Mixtures

$LiClO_4$ solutions in pure PC solutions are highly conducting, but information about ion–solvent molecule and ion–ion interaction can be obtained if such solutions are diluted in a nonpolar solvent. Complex permittivity data of 0.2 M $LiClO_4$ solutions in PC + benzene mixtures are given in Table 4, along with the data for the corresponding solvents.

Can. J. Chem. Downloaded from www.nrcresearchpress.com by 210.87.254.6 on 09/06/12
For personal use only.

TABLE 3. Dielectric relaxation of $LiClO_4$ ($\tau_p = 350 \times 10^{-12}$ s) and $NaClO_4$ ($\tau_p = 300 \times 10^{-12}$ s) solutions in DME

Salt	Solvent sample	c (mol/L)	ε_p	q	ε_m	ε_s	μ_a (D)	$10^8 R_s$ (cm)	$10^8 R_0$ (cm)
$LiClO_4$	2	0.050	6.77	8.2	7.00	8.3	12.4	14.9	6.6
	2	0.099	6.55	7.9	6.99	9.5	12.2	13.0	7.4
	1	0.100	6.60	7.9	7.04	9.4	11.8	12.2	7.3
	2	0.152	6.35	7.55	6.99	10.5	11.7	10.9	7.5
	1	0.200	6.22	7.25	7.03	11.5	11.4	9.3	7.4
	1	0.250	6.06	6.9	7.03	12.4	11.2	8.8	7.6
$NaClO_4$	2	0.10	6.44	9.7	7.00	9.3	11.6	13.3	7.4
		0.20	6.05	8.4	6.98	11.1	11.0	10.3	7.6
		0.40	5.57	6.2	6.95	13.6	9.8	7.5	7.4
		0.60	5.36	4.7	6.92	15.2	8.9	6.2	7.2
		0.80	5.19	3.9	6.90	15.9	8.1	5.3	6.6
		1.00	4.81	3.8	6.87	16.8	7.6	5.3	6.5

TABLE 4. $LiClO_4$ (0.2 M) solutions in PC + benzene mixtures and corresponding solvents. Complex permittivity data

	PC (3.00 M) + benzene		PC (4.50 M) + benzene		PC (5.99 M) + benzene	
f (GHz)	ε'	ε''	ε'	ε''	ε'	ε''
0.140	14.12	0.29	21.58	0.50	29.85	0.81
0.265	14.07	0.51	21.48	0.91	29.77	1.44
0.375	14.01	0.70	21.61	1.32	29.71	1.97
0.385	14.05	0.72	21.40	1.30	29.73	2.05
0.625	13.89	1.13	21.42	2.13	29.53	3.24
1.061	13.68	1.87	21.07	3.54	28.57	5.24
1.667	13.22	2.78	20.25	5.31	26.76	7.42
2.825	11.69	3.86	17.44	7.28	21.92	9.82
9.335	6.52	4.83	8.22	7.70	9.96	10.52
34.715	3.74	2.29	4.33	3.38	4.77	4.32
123.219	3.06	1.33	3.12	1.66	3.13	2.53
	$LiClO_4$ + PC (2.99 M) + benzene		$LiClO_4$ + PC (4.46 M) + benzene		$LiClO_4$ + PC (5.96 M) + benzene	
f (GHz)	ε'	ε''	ε'	ε''	ε'	ε''
0.140	14.04	18.71	19.38	34.18	26.02	44.58
0.265	13.78	11.00	19.78	19.50	26.83	24.92
0.375	13.25	8.53	19.51	14.56	26.83	18.83
0.385	13.19	8.60	19.48	14.69	26.58	18.49
0.625	12.49	6.35	18.63	10.61	25.87	13.50
1.061	11.65	5.18	17.63	8.58	24.51	11.18
1.667	10.89	4.81	16.46	8.11	22.51	10.56
2.825	9.44	4.55	13.86	7.76	17.92	9.56
9.335	5.59	3.82	7.08	6.29	8.56	9.16
34.715	3.70	1.84	4.22	2.83	4.82	3.95
123.219	2.99	0.93	3.59	1.64	3.90	1.92

The dielectric property of pure PC has been studied up to 34 GHz by Cavell (14). His data have been supplemented in this work by a measurement at 125 GHz ($\varepsilon = 4.05 - i2.84$). These data have been analysed according to the Cole–Davidson formula (15).

$$[16] \quad \varepsilon_{m0}(\omega) = \varepsilon_\infty + (\varepsilon_{m0} - \varepsilon_\infty)/(1 + i\omega\tau)^\beta$$

with $0 < \beta < 1$. The same equation has been used for the PC + benzene mixtures. The data have been analysed with the condition that the polarization $(\varepsilon_\infty - 1)/(\varepsilon_\infty + 2)$ is a linear function of the corres-

Can. J. Chem. Downloaded from www.nrcresearchpress.com by 210.87.254.6 on 09/06/12
For personal use only.

TABLE 5. Dielectric relaxation of PC and PC + benzene mixtures

PC (mol/L)	ε_{m0}	ε_∞	$10^{12}\tau$ (s)	β	$10^6\sigma$ (Ω^{-1} cm^{-1})	g
Pure PC	65.5±0.1	2.92	52±2	0.83±0.01	0	0.90
5.99	29.9±0.1	2.59	40.1±0.8	0.78±0.01	4±3	0.91
4.50	21.61±0.06	2.51	37.8±0.8	0.76±0.01	2±1	0.89
3.00	14.11±0.02	2.43	34.3±0.7	0.74±0.01	2.3±0.5	0.86

TABLE 6. Dielectric relaxation of $LiClO_4$ (0.2 mol/L) solutions in PC + benzene mixtures

PC (mol/L)	ε_m	q	$10^3\sigma$ (Ω^{-1} cm^{-1})	ε_s	μ_a	$10^8 R_s$ (cm)	$10^8 R_0$ (cm)
5.96	20.4	9.8	3.40	27.1	12.5	12.0	6.3
4.46	14.0	8.3	2.60	20.3	12.4	12.3	8.1
2.99	8.78	6.4	1.36	14.6	12.2	11.8	10.0

ponding quantity for each component:

$$[17]\quad (\varepsilon_\infty - 1)/(\varepsilon_\infty + 2) = \frac{\rho_b\,\varepsilon_b - 1}{\rho_{b_0}\,\varepsilon_b + 2} + \frac{\rho_{PC}\;\varepsilon_{\infty,PC} - 1}{\rho_{0,PC}\,\varepsilon_{\infty,PC} + 2}$$

where the subscript b refers to benzene, ρ_b and ρ_{PC} are the partial densities of each component in the solution, as opposed to ρ_{0b} and $\rho_{0,PC}$ which refer to the pure liquid. The parameters of the dielectric relaxation of pure PC and mixed solvents are given in Table 5. This table also gives the Kirkwood correlation factor g of PC, calculated from the Fröhlich–Kirkwood formula (eq. [11]) with μ_{PC} = 4.94 D (16). The g factor can also be calculated at various temperatures from the data of Gores (17) between −45°C and 40°C. The Clausius Mosotti formula is used to evaluate ε_∞ at each temperature, the density being given in ref. 17; g increases from 0.79 to 0.92 in the above temperature range These values indicate that PC is not a highly associated liquid, as far as the dielectric properties are concerned.

The solutions themselves have been analysed with the same model of association as above. Solvation has been dealt with as in THF solutions, i.e. with the assumption of a nonpolar rigid aggregate of q molecules around each cation. The number thus found, as shown in Table 6, is higher than in THF, but lower than in DME with the same assumption and at the same concentration. In the present case, it can probably be explained by the high dipole moment of PC which probably strongly interacts through electrostatic forces with Li^+. This high solvation number is in agreement with the high value found for R_s and R_0, especially at the lower PC content.

Solutions in PC + DME Mixtures

The complex permittivity data for each solvent and each solution are given in Table 7. The salt concentration is kept constant, at the highest value possible in pure dry DME (0.2 *M*, $LiClO_4$); the concentration of PC corresponds to 1–2–4–6 molecules of PC per cation. The spectra of the solvents can be analysed with the assumption that the contribution of PC is a simple Debye relaxation, while that of DME is the same as in pure DME apart from a change of magnitude $(\varepsilon_{DME} - \varepsilon_\infty)$ related to the change in the partial density of DME from $\rho_{DME,0}$ (pure liquid) to ρ_{DME} (mixture). The complex permittivity of the mixed solvent thus reads:

$$[18]\quad \varepsilon_m(\omega) = \varepsilon_{DME}(\omega) + \Delta\varepsilon_{PC}/(1 + i\omega\tau_{PC})$$

where $\varepsilon_{DME}(\omega)$ results from eqs. [10] and [11] where the subscript m should be changed into the subscript DME. Table 8 gives the parameters of the spectra. The relaxation time of PC is about 4 times as long as that of DME, so that the decomposition just performed is not meaningless. Because of the high dipole moment of PC, its dielectric contribution is about the same as that of DME at the highest concentration used (1.2 *M*).

The spectra of the solutions involve many parameters if we adopt the model of non-rigid solvation sheath which we found necessary to develop for the case of pure DME as solvent. It is not a problem of numerical analysis, as the program used proved to be able to find out these parameters. The difficulty comes from the fact that the data themselves are not accurate enough for such information to be extracted. The analysis has then been performed under the assumption that only the magnitudes $(\varepsilon_{DME} - \varepsilon_\infty)$ and $\Delta\varepsilon_{PC}$ change in the presence of salt. The latter is assumed to contribute as in pure DME, according to eqs. [5] to [9]. Two solvation numbers

Can. J. Chem. Downloaded from www.nrcresearchpress.com by 210.87.254.6 on 09/06/12
For personal use only.

Can. J. Chem. Downloaded from www.nrcresearchpress.com by 210.87.254.6 on 09/06/12
For personal use only.

TABLE 7. $LiClO_4$ solutions in PC + DME mixtures and corresponding solvents. Complex permittivity data

	PC (0.2 *M*) + DME		PC (0.4 *M*) + DME		PC (0.8 *M*) + DME		PC (1.2 *M*) + DME	
f (GHz)	ε′	ε″	ε′	ε″	ε′	ε″	ε′	ε″
0.140	8.07	0.04	9.19	0.08	11.15	0.11	13.13	0.14
0.265	8.06	0.06	9.17	0.12	11.13	0.17	13.12	0.24
0.375	8.10	0.09	9.16	0.15	11.22	0.25	13.17	0.36
0.385	8.06	0.09	9.17	0.15	11.13	0.24	13.12	0.34
0.625	8.08	0.15	9.14	0.22	11.20	0.39	13.11	0.57
1.061	8.08	0.25	9.11	0.35	11.15	0.62	13.06	0.93
1.667	8.10	0.39	9.10	0.57	11.10	0.95	12.95	1.42
2.825	7.89	0.59	8.85	0.87	10.59	1.43	12.18	2.10
9.335	7.21	1.58	7.76	2.11	8.62	3.15	9.27	4.14
34.715	5.12	2.44	5.24	2.68	5.32	3.13	5.44	3.53
123.219	2.92	1.53	3.02	1.72	2.99	2.00	2.31	1.69
	$LiClO_4$ + PC (0.2 *M*) + DME		$LiClO_4$ + PC (0.4 *M*) + DME		$LiClO_4$ + PC (0.8 *M*) + DME		$LiClO_4$ + PC (1.2 *M*) + DME	
f (GHz)	ε′	ε″	ε′	ε″	ε′	ε″	ε′	ε″
0.140	12.19	15.20	12.63	22.75	13.38	33.57	14.69	46.20
0.265	12.22	8.57	13.10	12.51	14.44	18.36	15.59	24.91
0.375	12.08	6.68	12.90	9.31	14.31	13.72	15.62	18.32
0.385	11.97	6.49	12.91	9.31	14.18	13.45	15.67	18.14
0.625	11.61	4.87	12.52	6.57	13.91	9.09	15.24	12.07
1.061	10.96	3.98	11.77	5.05	13.11	6.82	14.53	8.62
1.667	10.29	3.60	11.06	4.31	12.29	5.65	13.67	7.04
2.825	9.11	3.02	9.89	3.63	10.89	4.53	12.17	5.53
9.335	7.29	2.70	7.65	3.14	8.25	4.01	8.88	4.92
34.715	5.14	2.69	5.18	2.92	5.27	3.21	5.39	3.61
123.219	3.23	1.73			2.68	1.70		

are thus found,

$$q_{DME} = (\rho_{DME} - \rho_{DME,s})/c$$

and

$$q_{PC} = (\rho_{PC} - \rho_{PC,s})/c$$

where the second subscript, s, refers to the concentration, in the electrolyte solutions, of the molecules which contribute the relaxation. For the case of DME, this concentration results from eq. [11], with m standing for "DME". For the case of PC, the Fröhlich–Kirkwood equation is written for a mixture of PC and DME so that, taking into account eq. [11], $\rho_{PC,s}$ is deduced from:

$$[19]\quad \frac{(\varepsilon_M - \varepsilon_\infty)(2\varepsilon_M + \varepsilon_\infty)}{9\varepsilon_M} = \frac{N_A \rho_{PC,s}}{9000\varepsilon_0 kT} q_{PC}\mu_{PC}^2 \times \left(\frac{\varepsilon_\infty + 2}{3}\right)^2 + \frac{(\varepsilon_{DME} - \varepsilon_\infty)(2\varepsilon_{DME} + \varepsilon_\infty)}{9\varepsilon_{DME}}$$

where $q_{PC}\mu_{PC}^2$ corresponds to the quantity given in Table 9, which refers to PC in the mixed solvent. The results of the analysis are given in Table 9, along with the same analysis (corresponding to a rigid solvation sheath) for the case of the 0.2 *M* $LiClO_4$ solution in pure DME. The solvation numbers thus found have no real physical significance themselves, as they have for the solutions in pure DME, but the interesting point demonstrated by these experiments is the drastic decrease in q_{DME} when PC is added to the solution. This is accompanied by an increase in q_{PC}, and can be taken as indicating a strong influence of PC, even at low concentration with respect to the salt concentration, in the solvation phenomenon of Li^+ by DME.

TABLE 8. Dielectric relaxation of PC + DME mixtures

ρ_{PC} (mol/L)	ρ_{DME} (mol/L)	$\Delta\varepsilon_{PC}$	$10^{12}\tau_{PC}$ (s)	ε_{DME}
0.20	9.40	1.11	14.9	6.975
0.40	9.24	2.30	15.8	6.886
0.80	8.92	4.46	17.0	6.706
1.20	8.62	6.62	18.5	6.536

Conclusion

Complex permittivity data of $LiClO_4$ and $NaClO_4$ solutions in DME have been analysed according to a model for the reorientation of ion-pairs, which had been shown to apply to a variety of systems in a previous work (1). In contrast with the case of

TABLE 9. Dielectric relaxation of $LiClO_4$ (0.2 mol/L) in PC + DME mixtures

ρ_{PC} (mol/L)	ε_{DME}	q_{DME}	$\Delta\varepsilon_{PC}$	q_{PC}	ε_s	μ_a (D)	$10^3\sigma$ (ohm^{-1} cm^{-1})	$10^8 R_s$ (cm)	$10^8 R_0$ (cm)
0	4.87	19.5	—	—	11.4	13.9	0.72	13.6	9.5
0.2	5.88	9.6	1.09	0	12.4	12.5	1.15	11.1	9.1
0.4	6.32	4.9	2.14	0.1	13.2	11.7	1.72	8.1	8.5
0.8	6.31	3.5	3.62	0.7	14.5	11.5	2.58	6.5	8.1
1.2	6.33	1.7	5.33	1.1	15.9	11.1	3.56	6.7	8.1

$LiClO_4$ in other solvents, such as THF and ethyl acetate, the assumption of tightly linked solvating molecules leads to unrealistic values of the solvating number, so that the data have been analysed with the assumption that these molecules retain some freedom of reorientation. This assumption is also supported by the fact that the radius of the equivalent rotating and diffusing sphere which represents the ion-pair in the model is smaller than the closest distance of approach between cation and anion, as deduced from the conductivity data. $LiClO_4$ solutions in PC + benzene and PC + DME mixtures have also been investigated, and analysed according to the same model of ionic relaxation. While PC + benzene solutions exhibit trivial behaviour, some qualitative information can be drawn from PC + DME solutions: it seems that PC takes the place of DME in the solvation sheath, even at low PC concentration. This might explain why the solubility of $LiClO_4$ in DME drastically increases when a small amount of PC is added to the solvent.

1. H. CACHET, A. CYROT, M. FEKIR, and J. C. LESTRADE. J. Phys. Chem. **83**, 2419 (1979).
2. S. GLARUM. J. Chem. Phys. **33**, 639 (1960).
3. B. I. HUNT and J. G. POWLES. Proc. Phys. Soc. **88**, 513 (1966).
4. H. CACHET, J. C. LESTRADE, and J. P. BADIALI. *In* High frequency dielectric measurement. *Edited by* J. C. Chamberlain and G. W. Chantry. IPC Science and Technology Press, Guildford, Engl. 1974. p. 38.
5. Y. LEROY. Thesis, Lille. 1967.
6. J. C. JUSTICE and C. TREINER. C.R. Acad. Sci. **269**, 1364 (1969).
7. H. FARBER and S. PETRUCCI. J. Phys. Chem. **80**, 327 (1976).
8. P. BEUZELIN, H. CACHET, A. CYROT, and J. C. LESTRADE. J. Chim. Phys. **74**, 1131 (1977).
9. J. C. LESTRADE, J. P. BADIALI, and H. CACHET. *In* Dielectric and related molecular processes. Vol. 2. *Edited by* M. Davies. The Chemical Society, London, Engl. 1975. Chapt. 3; J. P. BADIALI, H. CACHET, A. CYROT, and J. C. LESTRADE. *In* Molecular motions in liquids. *Edited by* J. Lascombe. D. Reidel, Dordrecht, Holland. 1974. p. 179.
10. J. G. POWLES. J. Chem. Phys. **21**, 633 (1853); S. H. GLARUM. J. Chem. Phys. **33**, 1371 (1960).
11. M. FEKIR. Thèse de 3e cycle, Paris XI University. 1971.
12. R. H. COLE and K. S. COLE. J. Chem. Phys. **9**, 341 (1941).
13. J. P. BADIALI, H. CACHET, and J. C. LESTRADE. J. Chim. Phys. **64**, 1350 (1967).
14. E. A. S. CAVELL. J. Chem. Soc. Faraday Trans. II, **70**, 78 (1974).
15. D. W. DAVIDSON and R. H. COLE. J. Chem. Phys. **19**, 1484 (1951).
16. R. F. KEMPA and W. H. LEE. J. Chem. Soc. 1936 (1958).
17. H. J. GORES. Thesis, Saarbrücken, West Germany. 1974.

Can. J. Chem. Downloaded from www.nrcresearchpress.com by 210.87.254.6 on 09/06/12
For personal use only.

The intramolecular Cannizzaro reaction of phthalaldehyde

ROBERT S. MCDONALD[1] AND CHRISTINE E. SIBLEY[2]

Department of Chemistry, Mount Saint Vincent University, Halifax, N.S., Canada B3M 2J6

Received August 6, 1980

ROBERT S. MCDONALD and CHRISTINE E. SIBLEY. Can. J. Chem. **59**, 1061 (1981).

Phthalaldehyde undergoes an intramolecular Cannizzaro reaction in aqueous base to produce the *o*-hydroxymethylbenzoate ion. The kinetics of the reaction have been measured over a range of sodium hydroxide concentration at 40°C. The reaction is considerably slower than that of the analogous reaction of phenylglyoxal since it proceeds exclusively via the cyclic hydrate dianion which must undergo a very unfavorable ring opening before internal hydride transfer can occur.

ROBERT S. MCDONALD et CHRISTINE E. SIBLEY. Can. J. Chem. **59**, 1061 (1981).

La phtaldéhyde subit une réaction de Cannizzaro intramoléculaire en présence d'une base en solution aqueuse et produit l'ion *o*-hydroxyméthylbenzoate. On a mesuré la cinétique de la réaction en faisant varier la concentration en hydroxyde de sodium à 40°C. La réaction est considérablement plus lente que la réaction analogue du phénylglyoxale puisqu'elle se fait exclusivement par l'intermédiaire d'un dianion hydraté cyclique qui doit subir une ouverture de cycle très défavorable avant que le transfert interne d'hydrure ne se produise.

[Traduit par le journal]

Introduction

Intramolecular reactions have been frequently studied as models for reactions occurring within an enzyme–substrate complex (1, 2). Thus systems have been investigated which mimic the chemistry at the active site of several proteases and lysozyme and which involve amide, ester, or acetal hydrolysis catalyzed by various proximate functional groups. However, few model systems have been proposed to mimic the behavior of the oxidoreductases which catalyze hydride transfer between substrate and coenzyme. An intramolecular Cannizzaro reaction might provide such a model.

The Cannizzaro reaction of aldehydes with no α-H has been extensively studied and reviewed (3) and the mechanism of the reaction is now well understood (4).[3] Kinetic studies of the homogeneous reaction (usually in mixed aqueous–organic solvents) show the reaction to be second order in aldehyde and may be both first and second order in hydroxide. These latter kinetic terms have been taken (7) to represent rate-determining hydride transfer from the hydrate monoanion and dianion, respectively, to a second aldehyde molecule.

Although several intramolecular Cannizzaro reactions have been reported (6, 8, 9) only that of phenylglyoxal has been investigated in any mechanistic detail (6, 10, 11). We chose initially to investigate the behavior of the *o*-dialdehyde, phthalaldehyde (**1**), in aqueous base to see if it also undergoes this intramolecular hydride transfer (to produce *o*-hydroxymethylbenzoate ion). This reaction has not been reported previously and we hoped, if reaction did occur, to extend investigation of catalysis to a series of amine-thiols as Franzen (12) has done for phenylglyoxal. This paper reports only the results of the base-catalyzed reaction.

Experimental

General

Routine ultraviolet spectra were recorded on a Beckman 24 spectrophotometer. Kinetic runs were carried out on a Hitachi (Perkin-Elmer) 139 instrument equipped with a Haake FG circulating thermoregulator. An Orion 601A pH meter with a combination electrode was used to measure all pH values. The meter was standardized with Fisher certified buffers at pH 7.00 and 10.00. Routine nuclear magnetic resonance spectra were recorded on a Varian EM 360A 60 MHz spectrometer. Peak positions were measured in ppm (δ) relative to tetramethylsilane (TMS) as internal reference in $CDCl_3$.

Materials

The purification of phthalaldehyde and the preparation of buffer solutions has been described previously (13). Water distilled through an all-glass apparatus (Corning Mega-Pure) was used in the preparation of all solutions. Stock 1.0 and 0.10 *M* NaOH solutions were prepared by diluting the appropriate Fisher concentrate with boiled, then cooled, distilled water (in the case of the 0.10 *M* solution, KCl was added to maintain an ionic strength of 1.0). All dilutions of these stock solutions were made with 1.0 *M* KCl. The 1.0 and 0.2 *M* NaOH solutions were standardized against primary standard potassium acid phthalate and found to be 0.9957 and 0.1983 *M* in NaOH respectively. The concentrations of all other base solutions were assumed to be within 1% of the specified value and no corrections to rate constants were made. The 2.0 *M* NaOH solution was prepared by diluting the 1.0 *M* concentrate to half the specified volume with water. The 1.50 *M* solution was prepared by dilution of this solution with water.

[1]Author to whom correspondence should be addressed.

[2]Summer research assistant.

[3]An alternative mechanism involving benzyl benzoate as an intermediate in the Cannizzaro reaction of benzaldehyde has received some support (5, 6) but more recent evidence (4) has cast doubt on this proposal.

0008-4042/81/071061-07$01.00/0

©1981 National Research Council of Canada/Conseil national de recherches du Canada

Can. J. Chem. Downloaded from www.nrcresearchpress.com by 210.87.254.6 on 09/06/12
For personal use only.

Can. J. Chem. Downloaded from www.nrcresearchpress.com by 210.87.254.6 on 09/06/12
For personal use only.

For comparison with the uv spectrum of **1** under conditions in which it is present primarily in one of the cyclic forms (see Scheme 1), the cyclic acetal, 1,3-dimethoxyphthalan, was prepared.

Phthalaldehyde (5.0 g) was refluxed for three hours in 40 mL methanol (a large excess) in the presence of a catalytic amount of *p*-toluene sulfonic acid. The cooled solution was poured into 100 mL of 5% Na_2CO_3 and extracted (4 × 50 mL) with ether. The combined ether extracts were dried ($MgSO_4$), filtered, and concentrated to yield a colourless liquid (6.4 g, 93%) which by nmr analysis proved to be a mixture of *cis*- (54%) and *trans*- (33%) 1,3-dimethoxyphthalan accompanied by 13% of the noncyclic *bis*-acetal. Simple distillation (bp 59–61°C at 1 Torr) reduced to 6% the amount of *bis*-acetal, leaving the *cis*- and *trans*-isomers in the unchanged ratio 1.7:1. This method provides a much simpler route to the acetals than that previously reported (14) and the *cis*:*trans* ratio observed is similar to that (1.5) measured by Aso and Tagami (15). This product was used directly for the uv spectral measurements.

Kinetics

Kinetic runs were initiated by injecting 10–20 μL of a 0.03 *M* stock solution of phthalaldehyde in dioxane into 3.0 mL of the aqueous base solution which had been temperature pre-equilibrated for at least 30 min in the cell compartment of the Hitachi instrument. The reaction was monitored at 230 nm on the high wavelength shoulder of the λ_{max} of the product which appears to be near 200 nm. Typically, for a 1.50×10^{-4} *M* solution of substrate, the absorbance changed from 0.18 to 0.67 at this wavelength during a kinetic run. Normally, 25 absorbance readings were made over the extent of 90% reaction and an "infinity" value taken after at least ten half-lives. Pseudo-first-order rate constants (k_{obs}) were calculated from the slopes of the semi-logarithmic plots of $(A_\infty - A)$ vs. time using a standard linear regression analysis on a computer. All kinetic plots were strictly linear ($r \geq 0.999$) over at least three half-lives of the reaction. The quoted rate constants are the average of at least duplicate determinations; agreement between replicate runs was normally within 3%.

Product

The final uv spectrum of the reaction mixture after a kinetic run was virtually superimposable on that of an equal concentration of phthalide in aqueous base. The ring opening of phthalide with hydroxide producing *o*-hydroxymethylbenzoate is known to be a very rapid reaction under these conditions (k_{OH} = 0.87 $M^{-1}s^{-1}$ at 25°C (16)).

Product isolation was carried out as follows. A solution of phthalaldehyde (317 mg; 2.36 mmol) in 25 mL of 0.25 *M* NaOH (6.25 mmol) was stirred for 8 h at 40°C. The solution was acidified with HCl to pH 2 and stirred for a further three hours at room temperature. The aqueous solution was then poured into an equal volume of saturated NaCl and extracted with CH_2Cl_2 (3 × 75 mL). The combined extracts were dried ($MgSO_4$), filtered, and concentrated to yield 295 mg (93% yield) of a white crystalline solid which proved to be pure phthalide by nmr analysis and mp after recrystallization (73–74°C; lit. (17) mp 75°C). We chose to isolate the lactone rather than the hydroxy-acid since preliminary product runs gave mixtures of the two compounds (the acid-catalyzed lactonization reaction has been studied (18)).

To determine whether the base-catalyzed reaction indeed involves an intramolecular hydride transfer, a product isolation run was carried out as above but using 0.25 *M* NaOD in D_2O. The solution was acidified with DCl and extracted with CH_2Cl_2. After removal of solvent, the solid was taken up in $CDCl_3$ for nmr analysis. On our machine, the relative integral of the aromatic to methylene protons of a commercial phthalide sample was in the ratio 4.0:1.95. The ratios for two separate product runs in D_2O were 4.0:1.94 and 4.0:1.96. Clearly no deuterium (< 1%) is incorporated into product from solvent and hydride transfer is intramolecular.

Results and Discussion

pK_a Measurement of Hydrate (2)[4]

The uv spectrum of **1** in dioxane is that expected for an aromatic aldehyde (λ_{max} nm (ε): 222(26 700), 256(8460), 297(2190)). However, spectra in aqueous solution show significantly weaker absorptions in this region indicative of extensive hydration to form **2**; K_{H_2O} is 7.7 at 25°C and 4.0 at 40°C (13). These absorptions remain essentially constant in intensity in a series of phosphate buffers over the pH range 5.7–10 but become progressively weaker as the pH increases further. This is illustrated in Fig. 1(a) where the extinction coefficient at 259 nm (the apparent λ_{max} values for aqueous solutions of **1** occur at 259 and 299 nm) is plotted as a function of the pH of the solution (phosphate buffer or sodium hydroxide). Much of the absorption in the neutral or weakly basic solutions at this wavelength is due to the 11–12% of **1** which is not hydrated under these conditions. However, as the pH increases above 10, the absorption intensity decreases as remaining **1** is siphoned out via **2** to monoanion **3** and eventually to dianion **4** (see Scheme 1). The spectrum in 1.0 *M* NaOH (λ_{max} nm (ε): 259 (448)) is reminiscent of that for a nonconjugated benzenoid system and is similar to that observed for 1,3-dimethoxyphthalan (in 1.0 *M* KCl at 25°C, λ_{max} nm (ε): 251(423), 256(419), sh 280(65)).

The inflection point of the sigmoidal curve in Fig. 1(a) reveals the pK_a of the hydrate to be in the range 11.5–11.6. Alternatively (and rather more accurately), a plot of $\log(\varepsilon - \varepsilon_\infty)/(\varepsilon_0 - \varepsilon)$ vs. pH where ε_0 and ε_∞ are limiting values[5] of the extinction coefficients at low and high pH respectively, should be linear with an intercept at $\log(\varepsilon - \varepsilon_\infty)/(\varepsilon_0 - \varepsilon) = 0$ of pH = pK_a. This plot is illustrated in Fig. 1(b); least-squares analysis yields a value of the pK_a of 11.44(±0.05); slope = −0.91 ± 0.04, r = 0.993. The data at 299 nm gave plots of similar shape and yielded a pK_a value of 11.56(±0.06); slope = −0.91 ± 0.06, r = 0.985. Thus, we assign a value of 11.50(±0.10) to the first pK_a of **2** at 25°C, μ = 1.0. This value may be compared to that (12.2) observed by McClelland and co-workers[6] for 1-phthalanol. Apart from the statistical correction to the pK_a for the two identical acidic centres in **2** (0.3), the

[4]The structures of all compounds referred to by numbers are shown in Scheme 1.

[5]Limiting values for the extinction coefficients used to construct Fig. 1(*b*) were: at low pH (ε_0), 1163; at high pH (ε_∞), 437.

[6]R. A. McClelland, private communication.

Can. J. Chem. Downloaded from www.nrcresearchpress.com by 210.87.254.6 on 09/06/12
For personal use only.

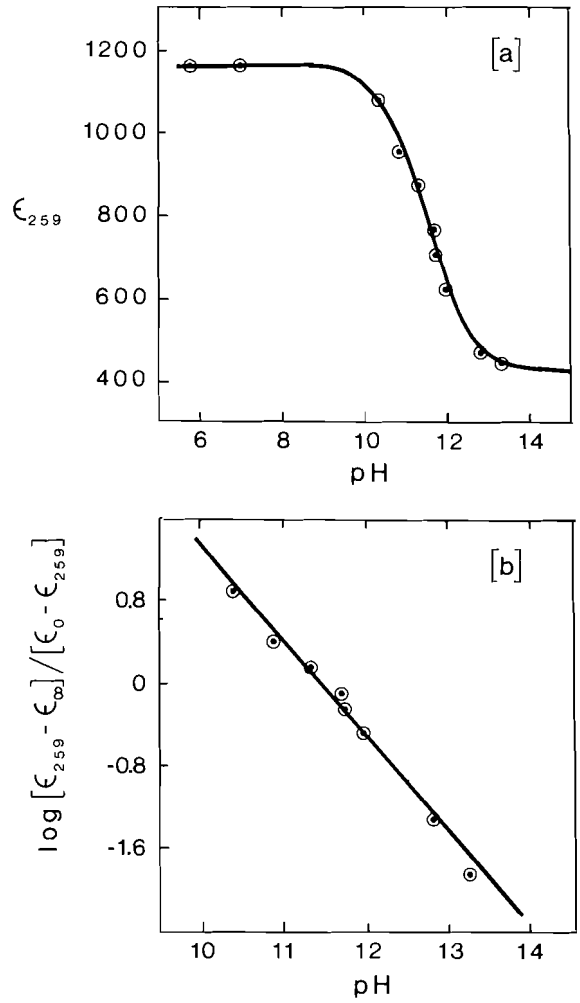

FIG. 1. (*a*) The pH dependence of the extinction coefficients at 259 nm of aqueous solutions of **1** at 25°C, μ = 1.0; (*b*) The plot for the graphical determination of the pK_a of **2** at 25°C, μ = 1.0. The intercept of this plot at Y = 0 gives the pK_a.

effective acid-strengthening inductive effects of both the aromatic and ethereal substituents in **2** should be larger than those in 1-phthalanol. Thus our value for the first pK_a of **2** is quite reasonable.

The Cannizzaro Reaction

It is clear from uv spectral and product isolation results (see Experimental) that **1** undergoes a base-catalyzed intramolecular hydride transfer to form the *o*-hydroxymethylbenzoate ion. The product contains no deuterium when the reaction is carried out in NaOD–D_2O.

The pseudo-first-order rate constants (k_{obs}) for appearance of product under various conditions are collected in Table 1 and the data at 40.3°C are plotted vs. [NaOH] in Fig. 2.

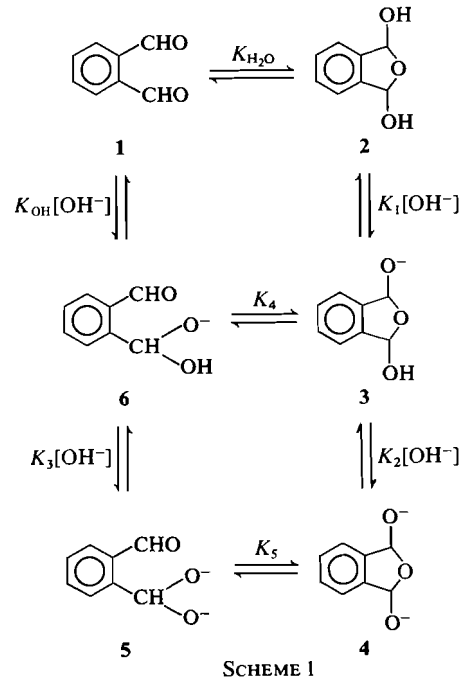

SCHEME 1

Kinetic runs carried out in NaOH solutions greater than 1.0 *M* are no longer at an ionic strength of 1.0. However, the k_{obs} value in 1.0 *M* NaOH which is also 1.0 *M* in KCl (μ = 2.0) is identical within experimental error to that observed in the absence of KCl (μ = 1.0) illustrating that these kinetic data have negligible rate contributions due to variable ionic strength over this range. These results have been analyzed with the rest of the kinetic data.

A change of solvent from water to 50% by volume methanol–water caused an 8.8-fold rate reduction in 0.20 *M* NaOH, a result not unexpected for the polar reaction. However, this particular solvent mixture was chosen to allow calculation of the "effective concentration" of the second aldehyde group in the substrate acting as an internal hydride acceptor. This is done by dividing the second-order rate constant, k_2, for our reaction ($1.33 \times 10^{-4} M^{-1}s^{-1}$) by the third-order rate constant for the intermolecular Cannizzaro reaction of benzaldehyde under identical conditions of solvent and temperature. This latter value at 40.3°C in 50% methanol–water can be calculated from the data of Tommila (5*b*) to be $1.03 \times 10^{-5} M^{-2}s^{-1}$ which leads to an "effective concentration" of the second CHO group in **1** of 13 *M*.

Also collected in Table 1 are the second-order rate constants k_2 (= k_{obs}/[NaOH]), for the reaction. It is clear that k_2 is reasonably constant at 40.3°C ($1.19 \pm 0.03 \times 10^{-3} M^{-1}s^{-1}$) up to 0.25 *M* NaOH

Can. J. Chem. Downloaded from www.nrcresearchpress.com by 210.87.254.6 on 09/06/12
For personal use only.

TABLE 1. Collected kinetic data for the intramolecular Cannizzaro reaction of **1** in aqueous NaOH

[NaOH] (M)	Conditions[a]	k_{obs} ($\times 10^4$ s^{-1})[b]	k_2 ($\times 10^3$ M^{-1} s^{-1})[c]
0.05		0.586(±0.008)	1.17
0.10		1.205(±0.008)	1.21
0.15		1.84 (±0.02)	1.23
0.20		2.34 (±0.08)	1.17
	50% (v/v)CH_3OH/H_2O	0.266(±0.005)	0.133
	30.5°C	0.906(±0.013)	0.453
	46.5°C	4.49 (±0.04)	2.24
	52.0°C	7.83 (±0.08)	3.92
0.25		2.90 (±0.02)	1.16
0.50		4.61 (±0.03)	0.922
0.75		5.63 (±0.07)	0.751
1.00		6.78 (±0.10)	0.678
	1.0 M KCl (μ = 2.0)	6.85 (±0.07)	0.685
1.50	μ = 1.50	8.16 (±0.08)	0.544
2.00	μ = 2.00	9.38 (±0.08)	0.469

[a] Unless noted otherwise, the conditions are 40.3 (±0.5)°C, ionic strength = 1.0 with KCl in aqueous solution.
[b] Average of 2–4 runs; the errors quoted are standard deviations.
[c] $k_2 = k_{obs}/[NaOH]$.

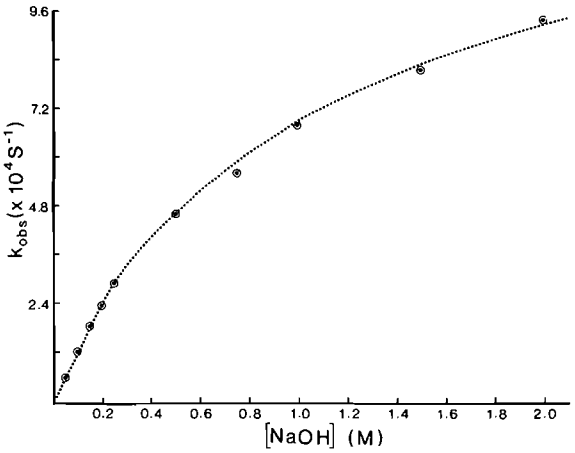

FIG. 2. The hydroxide ion-dependence of the pseudo-first-order rate constants for appearance of product in aqueous solutions of **1** at 40.3°C, μ = 1.0. (Data from Table 1).

(Fig. 2 is essentially linear over this range with a zero intercept) but decreases considerably at higher concentrations. Since we believed initially that k_2 was a true second-order (bimolecular) rate constant, the effect of temperature on k_2 was examined over the range 30–52°C at a base concentration where Fig. 2 is essentially linear (0.20 M NaOH). The activation parameter plot (of ln k_2T^{-1} vs. T^{-1}) yielded values for $\Delta H^{\ddagger}$ and $\Delta S^{\ddagger}$ of 19.0 ± 0.5 kcal mol^{-1} and −11.4 ± 1.6 cal K^{-1} mol^{-1}, respectively. We hesitate to interpret these data since it is now clear that k_2 is a composite of rate and equilibrium constants which will be variously affected by temperature (see Scheme 1 and Appendix).

The data in Table 1 and Fig. 2 at 40.3°C fit an equation of the form [1] from 0.05 to 2.0 M NaOH.

A weighted nonlinear regression

$$[1] \quad k_{obs} = \frac{a[OH^-]}{1 + b[OH^-]}$$

of the data to eq. [1] yields values for a and b of 1.38 ± 0.02 × 10^{-3} M^{-1}s^{-1} and 0.99 ± 0.02 M^{-1}, respectively. The solid curve in Fig. 2 is a graph of this equation and predicts the k_{obs} values with an overall standard deviation of 5.1%. At sufficiently high [OH^-], k_{obs} should reach a limiting value, k_∞ (= a/b) of 1.39 × 10^{-3} s^{-1}.

We propose the mechanism found in eqs. [2] and [3] for the Cannizzaro reaction of **1** leading to

$$[2] \quad \mathbf{3} \underset{}{\overset{K_2[OH^-]}{\rightleftharpoons}} \mathbf{4} \overset{K_{-5}}{\rightleftharpoons} \mathbf{5}$$

$$[3] \quad \mathbf{5} \xrightarrow[\text{Slow}]{k} \text{o-}C_6H_4(CH_2O^-)(CO_2^-) \xrightarrow[\text{Fast}]{H_2O} \text{o-}C_6H_4(CH_2OH)(CO_2^-)$$

o-hydroxymethylbenzoate. The initial hydration of **1** and subsequent ionization of **2** to **3** should be very rapid and essentially complete within a few milliseconds of mixing **1** with any of the base solutions used in this study (13). The effective starting point for the subsequent reaction then is **3**. We assume that essentially all unreacted **1** is present as **3** or **4** over the range of [NaOH] used here (i.e. $[\mathbf{1}]_s$ = [**3**] + [**4**]).[7] No significant reaction of the monoanion

[7] Inspection of the equilibrium constants relating these species in aqueous base (see Appendix) reveals that even in 0.05 M NaOH about 92% of the substrate is immediately converted to **3** and **4**. This proportion increases to 97% in 0.1 M NaOH and to 99% in 0.20 M base. Above 0.20 M NaOH, only the relative proportions of **3** and **4** vary significantly; the ratio [**3**]/[**4**] being given by K_2[OH^-]. No significant amounts (≤1%) of **1**, **5**, or **6** are present at any base concentration used in this study.

Can. J. Chem. Downloaded from www.nrcresearchpress.com by 210.87.254.6 on 09/06/12
For personal use only.

(see Scheme 1) can be detected under our conditions.[8] If the internal hydride transfer step in **5** is rate-limiting (with a first-order rate constant, k), then the rate of appearance of product is given by eq. [4] where K_{-5} is the equilibrium constant for the very unfavorable ring opening of the cyclic hydrate

[4] $\text{Rate} = d[P]/dt = k[\mathbf{5}] = kK_{-5}[\mathbf{4}]$

dianion. The rate is also given by equation [5] where k_{obs} is the pseudo-first-order rate constant

[5] $\text{Rate} = k_{obs}[\mathbf{1}]_s$

and since $[\mathbf{1}]_s = [\mathbf{3}] + [\mathbf{4}]$, the expression for k_{obs} becomes:

[6] $k_{obs} = kK_{-5}K_2[OH^-]/(1 + K_2[OH^-])$

where $K_2[OH^-] = [\mathbf{3}]/[\mathbf{4}]$. Equation [6] has the form required for k_{obs} (see eq. [1]) and thus values for K_2, k_2, and kK_{-5} are 0.99 M^{-1}, 1.38×10^{-3} M^{-1} s^{-1}, and 1.39×10^{-3} s^{-1}, respectively.

The K_2 value gives rise to a value of 13.53 for the second pK_a of the cyclic hydrate at 40°C and if we make no temperature correction to K_2 (11, 19), a value for pK_{a_2} for **2** at 25°C of 14.00 can be calculated. It is interesting to note that the difference between successive pK_a values for **2** at 25°C of 2.50 is similar to that observed for malonic acid ($\Delta pK_a = 2.86$ (20)) in which the acidic hydrogens are the same number of atoms apart.

In the Appendix estimates for many of the equilibrium constants relating species derived from **1** in aqueous base have been collected. These include a value for K_5 (1.2×10^5) which allows calculation of K_{-5} to be 8.3×10^{-6}. Now k, the rate constant for internal hydride transfer in **5**, may be estimated to be 170 s^{-1}. Considering the number of calculations and approximations required in the estimation of K_5 in the Appendix, the cumulative error in K_5 (and therefore k) may be considerable (up to several hundred percent).

For comparison purposes, the kinetics of the analogous intramolecular Cannizzaro reaction of phenylglyoxal were reinvestigated under conditions similar to those of the above study (in aqueous solution at 40°C, ionic strength 1.0, and over the range of [NaOH] from 0.05 to 1.0 M). From 0.05 to 0.50 M NaOH, the rate of disappearance of starting material is strictly first-order in substrate and first-order in hydroxide, the second-order rate constant, k_2', being 0.211 ± 0.006 M^{-1} s^{-1} at 40°C, $\mu = 1.0$.[9] The predominant form of phenylglyoxal under these conditions is the monoanion of the aldehyde hydrate and the reaction proceeds almost entirely via the dianion (11). We are unable to effect any significant ionization to the dianion even up to 1.0 M NaOH in contrast to the behavior of **1**.[10] This is not unexpected since the second pK_a of the hydrate can be estimated to be 16.0 at 40°C (see below). The rate constant, k_2', is a composite of the equilibrium constant for dianion formation from monoanion, K_2', and the first-order rate constant, k', for intramolecular hydride transfer. Hine and Koser (11) have determined the equilibrium constant for monoanion formation from the hydrate (K_1') for phenylglyoxal to be 276 M^{-1} at 35°C. Making no temperature correction to 40°C, and assuming the relation: $K_2' = 10^{-5} \times K_1'$ used by Hine and Koser (19) for *gem*-diols of this type, K_2' may be estimated to be 2.76×10^{-3} M^{-1} (corresponding to a pK_{a_2} of 16.0 at this temperature). This then allows calculation of k' ($= k_2'/K_2'$) on the phenylglyoxal pathway to be 76 s^{-1} at 40°C.

Thus, although the rate of product formation in the Cannizzaro reaction of phenylglyoxal is at least 150-fold that for the phthalaldehyde reaction, the actual hydride transfer steps are quite similar in rate (within a factor of 3 by our calculations). This is clearly attributable to the very unfavorable ring opening of the cyclic hydrate dianion (**4**) to **5** which must precede hydride transfer in the reaction of **1**. The similarity in rate for the elementary hydride transfer steps in the two pathways is somewhat surprising since one might expect the three-membered cyclic transition state required in the phenylglyoxal pathway to be energetically (and entropically) more favorable than the five-membered one required in the reaction of **1**. In this latter reaction, the formyl acceptor group must also be rotated out of coplanarity with the aromatic ring as hydride transfer occurs. Nevertheless, the free energy barriers for the hydride transfer steps must be within 1 kcal mol^{-1} of one another.

Although the study of hydride transfer mechanisms which require hydroxide-catalysis provides limited information concerning such mechanisms in biological systems, the chemist working on model systems for enzymic catalysis often finds such background information on the chemical behavior of these models useful. Current studies in this laboratory are concerned with the collection of

[8]Hine and Koser (11) were able to detect a small contribution to the rate due to reaction of the monoanion for the intramolecular Cannizzaro reaction of phenylglyoxal only by working in very dilute (down to 0.001 M) NaOH solutions. The predominant reaction pathway above 0.003 M base is via the dianion.

[9]Average of 13 runs; the error quoted is the standard deviation.

[10]In fact at [NaOH] greater than 0.50 M, k_2' actually increases, to 0.236 M^{-1} s^{-1} in 0.75 M base and to 0.245 M^{-1} s^{-1} in 1.0 M base. This is presumably a small specific salt effect.

detailed kinetic data for the internal hydride transfer of phenylglyoxal in the presence of amine-thiols of general structure: $HSCH_2CH_2NR_2$ (12). These compounds promote formal hydride transfer in aqueous solution in a pH region of some biological relevance (from 6–9).

Acknowledgements

We are pleased to thank Mr. E. V. Martin for carrying out the kinetic work on phenylglyoxal and Dr. O. S. Tee for valuable discussions. We also wish to thank the Natural Sciences and Engineering Research Council of Canada for continued financial support in the form of an operating grant (to R.S.M.).

1. A. J. KIRBY and A. R. FERSHT. Prog. Bioorg. Chem. **1**, 1 (1972).
2. T. H. FIFE. Adv. Phys. Org. Chem. **11**, 1 (1975).
3. T. A. GEISSMAN. Organic reactions. Vol. 2. John Wiley and Sons, Inc., New York, NY. 1944. p. 94.
4. D. LUTHER and H. KOCH. Chem. Ber. **99**, 2227 (1966); C. G. SWAIN, A. L. POWELL, W. A. SHEPPARD, and C. R. MORGAN. J. Am. Chem. Soc. **101**, 3576 (1979).
5. (*a*) A. LACHMAN. J. Am. Chem. Soc. **45**, 2356 (1923); (*b*) E. TOMMILA. Ann. Acad. Sci. Fenn. Ser. A, **59**, 3 (1942); Chem. Abstr. **38**, 6175_3 (1944).
6. E. R. ALEXANDER. J. Am. Chem. Soc. **69**, 289 (1947).
7. J. HINE. Physical organic chemistry. 2nd ed. McGraw-Hill, New York, NY. 1962. p. 267–268.
8. A. R. GRAY and R. C. FUSON. J. Am. Chem. Soc. **56**, 739 (1934).
9. E. M. FRY, E. J. WILSON, and C. S. HUDSON. J. Am. Chem. Soc. **64**, 872 (1942).
10. W. v. E. DOERING, T. I. TAYLOR, and E. F. SCHOENEWALDT. J. Am. Chem. Soc. **70**, 455 (1948); O. K. NEVILLE. J. Am. Chem. Soc. **70**, 3499 (1948).
11. J. HINE and G. F. KOSER. J. Org. Chem. **36**, 3591 (1971); J. HINE and C. D. FISCHER, JR. J. Am. Chem. Soc. **97**, 6513 (1975).
12. V. FRANZEN. Chem. Ber. **88**, 1361 (1955); **90**, 623 (1957).
13. R. S. MCDONALD and E. V. MARTIN. Can. J. Chem. **57**, 506 (1979).
14. E. SCHMITZ. Chem. Ber. **91**, 410 (1958).
15. C. ASO and S. TAGAMI. Macromolecules, **2**, 414 (1969).
16. D. R. STORM and D. E. KOSHLAND, JR. J. Am. Chem. Soc. **94**, 5805 (1972).
17. R. C. WEAST (*Editor*). Handbook of chemistry and physics. 59th ed. The Chemical Rubber Co., Cleveland, OH. 1978. p. C-438.
18. J. F. BUNNETT and C. F. HAUSER. J. Am. Chem. Soc. **87**, 2214 (1965).
19. J. HINE and G. F. KOSER. J. Org. Chem. **36**, 1348 (1971).
20. W. P. JENCKS and J. REGENSTEIN. *In* Handbook of biochemistry. *Edited by* H. A. Sober. The Chemical Rubber Company, Cleveland, OH. 1968. p. J-193.
21. P. GREENZAID. J. Org. Chem. **38**, 3164 (1973).
22. J. H. SEDON and P. ZUMAN. J. Org. Chem. **41**, 1957 (1976).
23. J. TIROUFLET and M. DELEPINE. C. R. Acad. Sci. **236**, 1426 (1953).
24. R. P. BELL and P. E. SORENSEN. J. Chem. Soc. Perkin Trans. II, 1594 (1976).

Appendix

Equilibrium Involving 1 in Aqueous Base

Species derived from **1** in aqueous base are related by the equilibria shown in Scheme 1 in the Results and Discussion.

Equilibria on the horizontal involve formation of the five-membered ring and should progressively favor the cyclic form as one proceeds from the neutral species through the monoanion to the dianion. Equilibria on the vertical all involve hydroxide (addition or ionization); K_1, K_2, and K_3 can be related to pK_a values using the relation: $pK_a = pK + pK_w$.

In the preceding discussion, a value for K_5 (actually K_{-5}) was required to separate a composite rate–equilibrium constant. The following represents an attempt to evaluate it. The data used refer to 25°C where most of the measurements or estimates are based.

The hydration equilibrium constant, K_{H_2O} is 7.7 at 25°C (13). The first pK_a of **2** is 11.50 at this temperature which corresponds to a value for K_1 of $320\,M^{-1}$. Estimation of K_{OH} for hydroxide addition to **1** is more difficult since it cannot be observed directly (the predominant forms of **1** in aqueous base are **3** and **4**). However, Greenzaid (21) and Sedon and Zuman (22) have observed a linear correlation between log K_{OH} for a series of *o*-substituted benzaldehydes and the pK_a of the corresponding benzoic acid (log $K_{OH} = 4.0 - 1.25\ pK_a$). A value for the pK_a of *o*-formylbenzoic acid has been reported to be 4.56 (23) but this value does appear to be anomalous since the pK_a of benzoic acid is 4.20 (ref. 20, p. J-194) and an *o*-formyl substituent should be acid-strengthening. It is now clear from the ^1H nmr spectrum in D_2O that *o*-formylbenzoic acid exists predominantly (≥95%) as 3-hydroxyphthalide in aqueous solution. However, an examination of the pK_a values of a series of benzoic acids bearing *o*-substituents of similar electronic and steric effects to a formyl group (i.e. the halogens, cyano, carboxyl, nitro) lead us to assign a pK_a of 2.84 (±0.3) to *o*-formylbenzoic acid. This leads to a K_{OH} value of $5.6\,M^{-1}$ after statistical correction for the two identical aldehyde groups. This value may be compared to values observed for the 2-chloro, 2,4-dichloro, and 2-nitro substituted benzaldehydes of 2.5, 6.8, and $10.0\,M^{-1}$, respectively (24). This now permits calculation of K_4 ($K_{H_2O} \cdot K_1/K_{OH}$) to be 440.

Our kinetic results have yielded a value for K_2 of $0.99\,M^{-1}$ at 40°C and we make no temperature correction at 25°C. The second ionization constant for the *gem*-diol hydrate of *o*-formylbenzaldehyde

Can. J. Chem. Downloaded from www.nrcresearchpress.com by 210.87.254.6 on 09/06/12
For personal use only.

(K_3) is now required. Hine and Koser (19) have estimated that the second pK_a of a *gem*-diol of this type is related to the first by the equation: $pK_{a_2} = pK_{a_1} + 5.0$. The first p$K_a$ of the hydrate of benzaldehyde has been estimated to be 12.8 (21) and we assume that the *o*-formyl group will have the same effect on the pK_a of this hydrate as it does on the pK_a of benzoic acid (i.e. acid-strengthening by 1.36 pK_a units). This leads to successive pK_a values for *o*-formylbenzaldehyde hydrate of 11.44 and 16.44. Thus K_3 is 3.6×10^{-3} ($10^{14-16.44}$) M^{-1} at 25°C and K_5 ($= K_2 \cdot K_4/K_3$) can be estimated to be 1.2×10^5. Clearly the cyclization equilibria are in the expected order: K_5 (1.2×10^5) > K_4 (440) > K_{H_2O} (7.7).

Can. J. Chem. Downloaded from www.nrcresearchpress.com by 210.87.254.6 on 09/06/12
For personal use only.

Thermodynamics of acid dissociation of aqueous bisulfite ion: ΔH^0, $\Delta C_p{}^0$, and ΔV^0 at 298.15 K

GREGORY C. ALLRED, JOHN W. LARSON,[1] AND LOREN G. HEPLER

Department of Chemistry and Oil Sands Research Laboratory, University of Lethbridge, Lethbridge, Alta., Canada T1K 3M4

Received September 8, 1980

GREGORY C. ALLRED, JOHN W. LARSON, and LOREN G. HEPLER. Can. J. Chem. **59**, 1068 (1981).

Calorimetric measurements of the enthalpy of protonation of sulfite ion and the enthalpy of proton transfer from bisulfite ion to carbonate ion have led to two independent values for the standard enthalpy of the acid dissociation reaction represented by $HSO_3^-(aq) = H^+(aq) + SO_3^{2-}(aq)$. Further calorimetric and density measurements have led to apparent and partial molar heat capacities and volumes for sulfite and bisulfite ions. Results of all of these measurements are summarized by $\Delta H^0 = -3.59 \pm 0.10$ kJ mol^{-1}, $\Delta C_p{}^0 = -262 \pm 7$ J K^{-1} mol^{-1}, and $\Delta V^0 = -28.7 \pm 1.0$ cm^3 mol^{-1} for the acid dissociation of $HSO_3^-(aq)$ at 298.15 K. These results are used for thermodynamic calculations of the temperature and pressure dependence of the equilibrium constant for acid dissociation of $HSO_3^-(aq)$.

GREGORY C. ALLRED, JOHN W. LARSON et LOREN G. HEPLER. Can. J. Chem. **59**, 1068 (1981).

Des mesures calorimétriques de l'enthalpie de protonation de l'ion sulfite et de l'enthalpie du transfert du proton de l'ion bisulfite à l'ion carbonate ont permis d'obtenir deux valeurs indépendantes de l'enthalpie standard de la réaction de dissociation acide représentée par l'équation $HSO_3^-(aq) = H^+(aq) + SO_3^{2-}(aq)$. Des mesures additionnelles de calorimétrie et de densité ont conduit aux capacités calorifiques et aux volumes molaires partiels apparents des ions sulfites et bisulfites. On peut résumer les résultats de toutes ces mesures par: $\Delta H^0 = -3{,}59 \pm 0{,}10$ kJ mol^{-1}, $\Delta C_p{}^0 = -262 \pm 7$ J K^{-1} mol^{-1} et $\Delta V^0 = -28{,}7 \pm 1{,}0$ cm^3 mol^{-1} pour la dissociation de l'acide $HSO_3^-(aq)$ à 298,15 K. On a utilisé ces résultats pour les calculs thermodynamiques de l'effet de la température et de la pression sur la constante d'équilibre de dissociation de $HSO_3^-(aq)$.

[Traduit par le journal]

Introduction

Although aqueous solutions of sulfur dioxide and the related bisulfite and sulfite ions are of considerable general scientific interest and also have substantial technological importance, useful thermodynamic properties are either unavailable or are of unsatisfactory accuracy. We have therefore undertaken the calorimetric and density measurements to be described here.

The first acid ionization or dissociation of "sulfurous acid" can be represented by

[1] $H_2SO_3(aq) = H^+(aq) + HSO_3^-(aq)$

where we use $H_2SO_3(aq)$ to represent all of the un-ionized species formed in aqueous solutions of sulfur dioxide. The second acid dissociation is represented by

[2] $HSO_3^-(aq) = H^+(aq) + SO_3^{2-}(aq)$

In this paper our particular focus is on the thermodynamics of this second acid dissociation reaction. More specifically, we have made calorimetric measurements leading to values for $\Delta H_2{}^0$ and $\Delta C_{p,2}{}^0$ for this reaction at 298.15 K. Measurements of densities have led to $\Delta V_2{}^0$ for this same reaction, also at 298.15 K. All of these values have been used for thermodynamic calculations of the effects of temperature and pressure on the equilibrium constant (K_2) for this reaction.

[1]Visiting Scientist from Marshall University, Huntington, WV, U.S.A.

Experimental

Enthalpy measurements were made using an LKB 8700 Precision Calorimetry System and a modified LKB 8721 titration calorimeter. Our modified glass calorimetric vessel (~100 cm^3) is a combination of the standard LKB 8721-1 (ampoule) and LKB 8721-2 (titration) vessels that permits us to make both ampoule and titration measurements. The titrant delivery system is a Metrohm E-415 automatic piston buret with a 10 cm^3 buret, operated in the fixed increment mode. The temperature of the thermostatted bath, and therefore of the titrant solution entering the calorimeter, was monitored with a quartz crystal thermometer. Electrical calibrations were made after each calorimetric titration.

Heat capacity measurements were made with a Picker flow calorimeter of a type that has been described previously (1). A small systematic error in the heat capacity measurements made with this calorimeter has been identified and corrected as also described previously (2, 3).

Densities were measured with a Picker flow densimeter of a kind that has been described before (4).

Results of all measurements refer to 298.15 K.

Perchloric acid solution was prepared from reagent grade 70% perchloric acid and freshly boiled double distilled water. For the first set of enthalpimetric titrations, calibration of the buret and standardization of the perchloric acid solution were performed together, using Fisher primary standard tris(hydroxymethyl)-aminomethane (TRIS), which had been crushed and then dried at 363 K for 2 h. A weighed sample of TRIS was partially neutralized with 4.00 cm^3 of perchloric acid titrant delivered from the piston buret under conditions similar to those of an enthalpimetric titration. The portion of TRIS remaining (about 10%) was then further titrated to the endpoint with a more dilute solution of $HClO_4$, which had been standardized previously. Combination of results of these titrations with the density permitted calculation of both the molality and molarity of the stock solution of perchloric acid. Duplicate experiments established that the quantity of acid delivered was constant to 0.03%.

0008-4042/81/071068-06$01.00/0

©1981 National Research Council of Canada/Conseil national de recherches du Canada

Can. J. Chem. Downloaded from www.nrcresearchpress.com by 210.87.254.40 on 09/06/12
For personal use only.

Can. J. Chem. Downloaded from www.nrcresearchpress.com by 210.87.254.40 on 09/06/12
For personal use only.

Fisher certified reagent grade anhydrous sodium sulfite was used without further treatment in the enthalpimetric titrations with perchloric acid. This material was weighed into glass ampoules (1.0 cm^3), which were sealed with silicone rubber stoppers and wax. Each ampoule contained 1.060 ± 0.002 g of Na_2SO_3. Iodometric titration of material in three ampoules taken at random showed that the contents were 99.2 ± 0.2% by mass sodium sulfite.

One of the difficulties encountered in any attempt to determine ΔH_2 is that of oxidation of sulfite to sulfate by dissolved oxygen, which proceeds at an appreciable rate (5). In order to minimize oxidation, sodium sulfite solutions were prepared in the calorimetric reaction vessel by breaking an ampoule into 89.70 cm^3 of freshly boiled double distilled water, which had been cooled under and saturated with N_2. Nitrogen gas, saturated with water vapor, was bled into the vapor space of the calorimetric vessel during the course of each run.

Following dissolution of Na_2SO_3 in the reaction vessel, 0.5 cm^3 of $HClO_4$ solution was injected to protonate about 10% of the sulfite present. After thermal equilibration and an initial rating period, the main titration, comprising a single injection of 4.00 cm^3 of 1.696$_4$ *M* $HClO_4$ titrant, was begun when the temperature of the vessel matched that of the bath in such a way as would produce no detectable thermal effect when the titrant was the same as the solution in the vessel.

To evaluate the corrected temperature change, all measured thermistor resistances were converted to temperatures and the data for the initial and final rating periods were fitted by least squares analysis to the integrated form of Newton's cooling law. The corrections for heat exchange with the surroundings and thermal contributions from stirring and Joule heating of the thermistor were evaluated by computer assisted integration of the time–temperature curves according to the Regnault–Pfaundler method.

The chemicals used in the second approach to the enthalpy determination were reagent grade sodium carbonate (BDH AnalaR) dried at 543 K for 1 h, Baker analyzed reagent grade sodium bicarbonate, recrystallized Fisher certified sodium sulfite, and Fisher certified sodium bisulfite ($Na_2S_2O_5$). Titration of all compounds with either HCl or NaOH indicated high purity. Both the Na_2SO_3 and the $Na_2S_2O_5$ gave negative sulfate spot tests with acidic $BaCl_2$.

Buffer solutions were made by dissolving known masses of these solutes in a known mass of degassed distilled water. The decrease in mass of the water due to hydration of $Na_2S_2O_5$ to form $NaHSO_3$ was allowed for in the calculation of molalities. The solutions were prepared just prior to the calorimetric runs and were kept under a nitrogen atmosphere. Water-saturated nitrogen gas was bled into the vapor space of the calorimeter during the runs.

The temperature rises in the enthalpimetric titrations involving carbonate/bicarbonate and sulfite/bisulfite solutions were evaluated according to Dickinson's method.

Stock solutions used in the determination of the apparent molar heat capacities and volumes were prepared in the same way and from the same sodium sulfite and sodium bisulfite used in the second set of enthalpy measurements. The solutions contained molalities of Na_2SO_3 and $NaHSO_3$ in the ratios 9:1, 1:1, and 1:9.

Results

We represent the reaction between sulfite/bisulfite buffer solutions and perchloric acid by

[3] $HClO_4(aq, I = 1.696) + Na_2SO_3(aq, I = 0.269) = NaHSO_3(aq, I = 0.186) + NaClO_4(aq, I = 0.186)$

The average result of 7 determinations of the enthalpy of this reaction, ΔH_3, is given in Table 1. In order to obtain the desired ΔH_2^0, the enthalpies of the following reactions must also be evaluated:

[4] $HClO_4(aq, I = 1.696) = HClO_4(aq)$

[5] $Na_2SO_3(aq, I = 0.269) = Na_2SO_3(aq)$

[6] $NaHSO_3(aq, I = 0.186) = NaHSO_3(aq)$

[7] $NaClO_4(aq, I = 0.186) = NaClO_4(aq)$

In order to reduce the uncertainty in the corrections applied to ΔH_3 to derive ΔH_2^0, the enthalpy of dilution of perchloric acid to 0.0725 molal was determined under conditions similar to those used to determine ΔH_3. The enthalpy of dilution from 0.0725 molal to infinite dilution was taken from the compilation by Parker (6) to give the value of ΔH_4 reported in Table 1. It was necessary to estimate values for ΔH_5 and ΔH_6 as these do not appear in the literature.

The enthalpy of dilution of Na_2SO_4 has been determined over a range of concentrations by Wallace and Robinson (7). We estimate ΔH_5 by making the assumption that the enthalpies of dilution of Na_2SO_3 in the buffer solution where hydrolysis is nearly completely suppressed, and of Na_2SO_4, which does not hydrolyze to an appreciable extent, will be similar.

To estimate the value of ΔH_6 we assume that the enthalpy of dilution of sodium bisulfite in the buffer solution will be similar to that of some other strong 1:1 electrolytes at the same ionic strength. We chose as model electrolytes $NaClO_3$, $NaNO_3$, and $NaBrO_3$, for which enthalpies of dilution have been tabulated (6); ΔH_6 was taken as the average of the heats of dilution for these three model electrolytes.

The enthalpy of dilution of $NaClO_4$ in the product mixture is assumed to be equal to the value for a pure $NaClO_4$ solution of the same ionic strength, and was taken from Parker's compilation (6).

All of these values were combined according to

[8] $$\Delta H_2^0 = -\Delta H_3 + \Delta H_4 + \Delta H_5 - \Delta H_6 - \Delta H_7$$

to give $\Delta H_2^0 = -3.52\ kJ\ mol^{-1}$. We estimate the total uncertainty in this result, due to chemicals,

TABLE 1. Measured enthalpies of reactions [3] and [4] and estimated enthalpies of dilution

Reaction	ΔH / kJ mol^{-1}	Estimated uncertainty / kJ mol^{-1}
[3]	3.122	0.044
[4]	0.564	0.025
[5]	−0.982	0.060
[6]	−0.003	0.020
[7]	−0.017	0.020

TABLE 2. Enthalpies of reaction of aqueous sodium bisulfite with excess aqueous sodium carbonate[a]

Addition number	Ionic strength	Q / J	Q_h / J	α	$-\Delta H_9$ / kJ mol^{-1}
1	0.200	30.45	2.71	0.999	18.10
2	0.200	28.74	0.44	0.997	18.51
3	0.200	27.67	0.20	0.959	18.68
1	0.400	58.88	2.09	0.999	18.50
2	0.400	56.71	0.35	0.997	18.41
3	0.400	54.60	0.17	0.958	18.50
1	0.600	85.68	2.03	0.999	18.24
2	0.600	84.34	0.34	0.997	18.36
3	0.600	81.65	0.16	0.957	18.55

[a]See text following eq. [9] for information about compositions and quantities of solutions.

calorimetric measurements, and enthalpies of dilution, to be less than 0.10 kJ mol^{-1}.

In the second set of measurements the enthalpy of the reaction

[9] $$NaHSO_3(aq) + Na_2CO_3(aq) = Na_2SO_3(aq) + NaHCO_3(aq)$$

was determined by titrating an aqueous sodium bicarbonate/carbonate buffer with an aqueous sodium bisulfite/sulfite buffer. In order to minimize the corrections for heats of dilution, hydrolysis, and extent of reaction, buffer solutions of equal ionic strength with a 9:1 ratio of Na_2CO_3 to $NaHCO_3$ and a 1:9 ratio of Na_2SO_3 to $NaHSO_3$ were used. The heat evolved with each of three successive additions of 10.22 cm^3 of the sulfite buffer to 75.0 cm^3 of the carbonate buffer was determined, with results given in Table 2. The enthalpy of reaction [9], ΔH_9, is that calculated from the equation

[10] $$\Delta H_9 = -(Q + Q_h)/\alpha n$$

where Q is the measured heat evolved, Q_h is the heat due to the hydrolysis of the carbonate, α is the fraction of the added bisulfite reacting according to eq. [9], and n is the number of moles of $NaHSO_3$ added. The values of Q_h were calculated by multiplying the enthalpy of hydrolysis of CO_3^{2-}(ΔH_h^0 = 41.12 kJ mol^{-1}) (8) by the calculated change in the number of moles of OH^-(aq) present in the solution. The latter values were calculated using $K_h = 2.13 \times 10^{-4}$, and Davies' modification (9) of the extended Debye–Hückel equation for calculating the activity coefficients. Values of K_a for HSO_3^-(aq) and HCO_3^-(aq) were combined to give $K_9 = 1.17 \times 10^3$. This value was used to calculate the extent of reaction, α.

A linear extrapolation of these results to $I = 0$ yields $\Delta H_9^0 = -18.50$ kJ mol^{-1}, which is then combined with $\Delta H^0 = 14.70$ kJ mol^{-1} for the dissociation of HCO_3^-(aq) (8) to give $\Delta H_2^0 = -3.80$ kJ mol^{-1} for the dissociation of HSO_3^-(aq). The total estimated uncertainty in this value is about 0.30 kJ mol^{-1}.

We take as a best value for ΔH_2^0 a weighted average of the two experimentally determined quantities, the weighting factors being proportional to the reciprocals of the uncertainties quoted. This procedure leads to $\Delta H_2^0 = -3.59 \pm 0.10$ kJ mol^{-1}.

Results of measurements with the Picker flow calorimeter are heat capacities per unit volume of solution. Combination of these heat capacities with the densities that we have also measured leads to heat capacities per unit mass of solution. Further combination of these latter heat capacities with the already known (10) heat capacity of pure water (4.1793 J K^{-1} g^{-1}) leads to apparent molar heat capacities. Similarly, densities of solutions in combination with the already known density of pure water (0.997044 g cm^{-3}) leads to apparent molar volumes. Because the measurements of heat capacities and densities to be reported here were made on buffer solutions, it is useful to define our apparent molar properties according to

[11] $$\phi_Y = [Y(\text{solution}) - n_1 Y_1^0]/(n_2 + n_3)$$

in which Y is the extensive property (heat capacity or volume) of a specified quantity of solution, n_1 is the number of moles of water in the specified quantity of solution, Y_1^0 is the molar property of the pure solvent water, and n_2 and n_3 represent the numbers of moles of $NaHSO_3$ and Na_2SO_3 in this specified quantity of solution.

Apparent molar properties of reasonably dilute solutions of electrolytes are accurately represented by equations of the form

[12] $$\phi_Y = \phi_Y^0 + A_Y(d_1^0)^{1/2}\omega^{3/2}m^{1/2} + B_Y\omega m$$

in which A_Y values come from the Debye–Hückel theory and B_Y values are adjustable parameters. The "valence factor" ω is defined as

Can. J. Chem. Downloaded from www.nrcresearchpress.com by 210.87.254.40 on 09/06/12
For personal use only.

TABLE 3. Parameters for eq. [12] applied to apparent molar heat capacities and volumes of $NaHSO_3/Na_2SO_3$ buffer solutions

F_2	ϕ_C^0 / J K^{-1} mol^{-1}	B_C / J K^{-1} mol^{-2} kg	ϕ_V^0 / cm^3 mol^{-1}	B_V / cm^3 mol^{-2} kg
0.1	−154.6	36.8	6.5	1.9
0.5	−70.2	30.5	18.0	2.2
0.9	20.6	20.3	30.4	0.8

[13] $\omega = I/m = 0.5 \Sigma \nu_i z_i^2 m_i/m$

in which I is the ionic strength, m_i is the molality of a particular solute, and m is the total molality.

For application of eq. [12] to apparent molar volumes we use $A_V(d_1^0)^{1/2} = 1.865\,\text{cm}^3\,\text{mol}^{-3/2}\,\text{kg}^{1/2}$ from Millero (11) and for application to apparent molar heat capacities we use $A_C(d_1^0)^{1/2} = 28.95\,\text{J K}^{-1}\,\text{mol}^{-3/2}\,\text{kg}^{1/2}$ from Desnoyers (12). In connection with our use of this latter value, which is adopted here partly for consistency with some related earlier investigations, we note that there is some evidence (13, 14) for a slightly larger value for $A_C(d_1^0)^{1/2}$. We also define solute mole fractions according to

[14] $F_2 = n_2/(n_2 + n_3)$ and $F_3 = n_3/(n_2 + n_3)$

in which subscripts 2 and 3 refer to $NaHSO_3$ and Na_2SO_3, respectively. For F_2 values of 0.9, 0.5, and 0.1 (corresponding to compositions of buffer solutions we have investigated) we have ω values of 1.2, 2.0, and 2.8, respectively.

Following application of small corrections for hydrolysis, ionization, and (in the case of heat capacities) chemical relaxation as described elsewhere (15–18) in detail, we have obtained desired ϕ_Y^0 values by way of linear least-squares fitting of $\phi_Y - A_Y(d_1^0)^{1/2}\omega^{3/2}m^{1/2}$ against ωm, with results that are summarized in Table 3.

The apparent molar properties at infinite dilution of the buffer solutions are related to the corresponding apparent molar properties of the constituent electrolytes by

[15] $\phi_Y^0 = F_2\phi_Y^0(NaHSO_3) + F_3\phi_Y^0(Na_2SO_3)$

Using $F_2 + F_3 = 1$ and least-squares fitting of eq. [15] to the results in Table 3 we have obtained the following:

$$\phi_C^0(NaHSO_3) = 41.2\,\text{J K}^{-1}\,\text{mol}^{-1}$$
$$\phi_V^0(NaHSO_3) = 33.2\,\text{cm}^3\,\text{mol}^{-1}$$
$$\phi_C^0(Na_2SO_3) = -177.8\,\text{J K}^{-1}\,\text{mol}^{-1}$$

and

$$\phi_V^0(Na_2SO_3) = 3.3\,\text{cm}^3\,\text{mol}^{-1}$$

As previously demonstrated in many investigations, it is useful to assign values for the thermodynamic properties of individual ions in aqueous solution at infinite dilution. The customary procedure for doing so is based on $\phi_Y^0(H^+) = 0$, which leads (11, 19) to $\phi_C^0(Na^+) = 43\,\text{J K}^{-1}\,\text{mol}^{-1}$ and to $\phi_V^0(Na^+) = -1.2\,\text{cm}^3\,\text{mol}^{-1}$. We now combine these values for Na^+(aq) with those given in the paragraph above for $NaHSO_3$(aq) and Na_2SO_3(aq) to obtain the following:

$$\phi_C^0(HSO_3^-) = -2\,\text{J K}^{-1}\,\text{mol}^{-1}$$
$$\phi_V^0(HSO_3^-) = 34.4\,\text{cm}^3\,\text{mol}^{-1}$$
$$\phi_C^0(SO_3^{2-}) = -264\,\text{J K}^{-1}\,\text{mol}^{-1}$$

and

$$\phi_V^0(SO_3^{2-}) = 5.7\,\text{cm}^3\,\text{mol}^{-1}$$

Discussion and Thermodynamic Calculations

Selections of several earlier reviews (10, 20–22) are in accord with $K_2 = 5.6 \times 10^{-8}$ and $\Delta G^0 = 41.4\,\text{kJ mol}^{-1}$ for the acid dissociation of HSO_3^-(aq) at 298.15 K. We accept (Table 4) and use these values for further calculations.

The first two groups of reviewers (10, 20) chose $\Delta H_2^0 = -9.3$ and $-12.1\,\text{kJ mol}^{-1}$, with large uncertainties in both values. The two more recent reviews (21, 22) have both chosen $\Delta H_2^0 = -5.2\,\text{kJ mol}^{-1}$, based on the calorimetric enthalpy of neutralization reported by Zambonin and Jordan (23). Although this latter value is almost certainly better than the earlier values just cited, it is not in good agreement with $\Delta H_2^0 = -3.59\,\text{kJ mol}^{-1}$ based on our measurements and therefore requires further consideration as follows.

The ΔH_2^0 from Zambonin and Jordan (23) differs from our value by 44%, but this is not a meaningful indication of the difference between results of the calorimetric measurements made in the two labora-

TABLE 4. Thermodynamics of acid dissociation of HSO_3^-(aq) as in eq. [2] at 298.15 K

$K_2 = 5.6 \times 10^{-8}$	Refs. 10, 20–22
$\Delta G_2^0 = 41.4\,\text{kJ mol}^{-1}$	Refs. 10, 20–22
$\Delta H_2^0 = -3.59\,\text{kJ mol}^{-1}$	This work
$\Delta S_2^0 = -150.9\,\text{J K}^{-1}\,\text{mol}^{-1}$	From ΔG_2^0 and ΔH_2^0 above
$\Delta C_{p,2}^0 = -262\,\text{J K}^{-1}\,\text{mol}^{-1}$	This work
$\Delta V_2^0 = -28.7\,\text{cm}^3\,\text{mol}^{-1}$	This work

Can. J. Chem. Downloaded from www.nrcresearchpress.com by 210.87.254.40 on 09/06/12
For personal use only.

Can. J. Chem. Downloaded from www.nrcresearchpress.com by 210.87.254.40 on 09/06/12
For personal use only.

tories. Zambonin and Jordan (23) measured the enthalpy of neutralization (-61.0 kJ mol^{-1}), which must be combined with the enthalpy of ionization of water (55.8 kJ mol^{-1}) to yield the desired ΔH_2^0. We can bring the results of Zambonin and Jordan (23) into perfect accord with our present result by assuming that their measured enthalpy of neutralization was too exothermic by only 2.6%. On the other hand, our measured enthalpy of protonation of SO_3^{2-} would have to be in error by 44% to make our derived ΔH_2^0 be in agreement with the value from Zambonin and Jordan (23). We also note that any air oxidation to sulfate that might have occurred in connection with the measurements by Zambonin and Jordan (23) would have had the effect of making their derived ΔH_2^0 be too exothermic, which is in the right direction to account for the difference between their $\Delta H_2^0 = -5.2$ kJ mol^{-1} and our $\Delta H_2^0 = -3.59$ kJ mol^{-1}. On the basis of all of these considerations and also because we have obtained nearly the same values for ΔH_2^0 by two independent routes (direct protonation of SO_3^{2-} and proton transfer from HSO_3^- to CO_3^{2-}), we select (Table 4) our ΔH_2^0 as the best available value and use it for subsequent calculations.

Changes in heat capacity ($\Delta C_{p,2}^0$) and volume (ΔV_2^0) for the acid dissociation of HSO_3^-(aq) as in reaction [2] can be calculated from conventional ionic heat capacities and volumes by way of

$$[16] \quad \Delta Y_2^0 = \phi_Y^0(SO_3^{2-}) - \phi_Y^0(HSO_3^-)$$

Using the ionic ϕ_C^0 and ϕ_V^0 values for HSO_3^-(aq) and SO_3^{2-}(aq) from our investigations as reported earlier in this paper in equation [16] leads to $\Delta C_{p,2}^0 = -262$ J K^{-1} mol^{-1} and to $\Delta V_2^0 = -28.7$ cm^3 mol^{-1}, both referring to 298.15 K.

We do not know of any earlier results that permit us to make any useful comparisons with our $\Delta C_{p,2}^0$, $\phi_C^0(HSO_3^-)$, or $\phi_C^0(SO_3^{2-})$. We can, however, compare our $\phi_V^0(SO_3^{2-}) = 5.7$ cm^3 mol^{-1} with $\phi_V^0(SO_3^{2-}) = 8.9$ cm^3 mol^{-1} selected by Millero (11) and also compare our $\Delta V_2^0 = -28.7$ cm^3 mol^{-1} with $\Delta V_2^0 = -22.7$ cm^3 mol^{-1} selected by Hamann (24) in his thorough review of effects of pressure on acid–base reactions in aqueous solutions. Both of these earlier values appear to be less accurate than our values; we list our ΔV_2^0 in Table 4 and use it for subsequent thermodynamic calculations.

Before going on with some thermodynamic calculations based on quantities listed in Table 4, we discuss and estimate uncertainties to be associated with our results that have been reported in this paper. We have already explained and cited ± 0.1 kJ mol^{-1} as our estimate of the total uncertainty to be associated with ΔH_2^0. Further considerations of uncertainties related to our measurements of heat capacities and densities, compositions of solutions, and data treatment (hydrolysis and ionization corrections, and values used for $A_Y(d_1^0)^{1/2}$ in eq. [12]) lead us to estimate that total uncertainties in our values for $\Delta C_{p,2}^0$ and ΔV_2^0 are about ± 7 J K^{-1} mol^{-1} and ± 1.0 cm^3 mol^{-1}, respectively.

Integration of the van't Hoff equation

$$[17] \quad d \ln K/dT = \Delta H^0/RT^2$$

with ΔH^0 taken to be independent of temperature leads to

$$[18] \quad \ln K_2 = 432/T - 18.146$$

for the acid dissociation of HSO_3^-(aq) as in eq. [2]. A better approach is to allow for the temperature dependence of ΔH^0 by way of

$$[19] \quad d\Delta H^0/dT = \Delta C_p^0$$

Integration of eq. [19] with $\Delta C_{p,2}^0$ taken to be independent of temperature leads to

$$[20] \quad \Delta H_2^0 = -262T + 74530 \qquad (\text{kJ mol}^{-1})$$

Further integration of [17] with [20] leads to

$$[21] \quad \ln K_2 = -8964/T - 31.51 \ln T + 192.899$$

for the acid dissociation of HSO_3^-(aq). Equations [18] and [21] are both illustrated in Fig. 1, which clearly shows the value of considering $\Delta C_{p,2}^0$ as well as ΔH_2^0 (at 298.15 K) in relation to the temperature dependence of K_2. Equation [20] shows that $\Delta H_2^0 = 0$ at 284 K, which is consistent with the maximum in $\ln K_2$ calculated from eq. [21] and

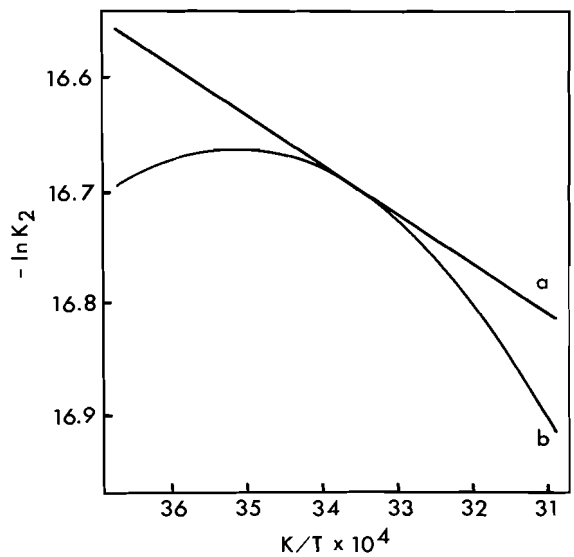

FIG. 1. Plot of $-\ln K_2$ vs. K/T for reaction [2]: (*a*), eq. [18]; (*b*), eq. [21].

displayed in Fig. 1. Equation [21] can be improved and made applicable over a still wider range of temperature by consideration of the temperature dependence of $\Delta C_{p,2}^0$ in equation [19], but these further heat capacities are not now available.

Integration of

$$[22] \quad \mathrm{d} \ln K/\mathrm{d}P = -\Delta V^0/RT$$

with ΔV_2^0 taken to be independent of pressure leads to

$$[23] \quad \ln K_2 = 0.001173P - 16.697$$

for the acid dissociation of HSO_3^-(aq) at 298.15 K, when P is expressed in atmospheres. Equation [23] could be improved and made applicable to a wider range of pressures by consideration of compressibilities and thence of the pressure dependence of ΔV_2^0, but this additional information is not now available.

Acknowledgments

We thank the Natural Sciences and Engineering Research Council and the Alberta Oil Sands Technology and Research Authority for support of this research.

1. P. Picker, P.-A. Leduc, P. R. Philip, and J. E. Desnoyers. J. Chem. Thermodyn. **3**, 631 (1971).
2. G. Perron, N. Desrosiers, and J. E. Desnoyers. Can. J. Chem. **54**, 2163 (1976).
3. J. E. Desnoyers, C. de Visser, G. Perron, and P. Picker. J. Solution Chem. **5**, 605 (1976).
4. P. Picker, E. Tremblay, and C. Jolicoeur. J. Solution Chem. **3**, 377 (1974).
5. D. A. Hegg and P. V. Hobbs. Atm. Environ. **12**, 241 (1978).
6. V. B. Parker. Thermal properties of aqueous uni-univalent electrolytes. NSRDS NBS-2. U.S. Government Printing Office, Washington, DC. 1965.
7. W. E. Wallace and A. L. Robinson. J. Am. Chem. Soc. **63**, 958 (1941).
8. R. L. Berg and C. E. Vanderzee. J. Chem. Thermodyn. **10**, 1049 (1978).
9. R. A. Robinson and R. H. Stokes. Electrolyte solutions. 2nd ed. Rev. Butterworths, London. 1959.
10. D. D. Wagman, W. H. Evans, V. B. Parker, I. Halow, S. M. Bailey, and R. H. Schumm. National Bureau of Standards Technical Note 270-3. U.S. Government Printing Office, Washington, DC. 1968.
11. F. J. Millero. *In* Water and aqueous solutions: structure, thermodynamics, and transport properties. *Edited by* R. A. Horne. Wiley-Interscience, New York. 1972. Chapt. 13.
12. P. R. Philip and J. E. Desnoyers. J. Solution Chem. **1**, 353 (1972); P.-A. Leduc, J.-L. Fortier, and J. E. Desnoyers. J. Phys. Chem. **78**, 1217 (1974).
13. D. J. Bradley and K. S. Pitzer. J. Phys. Chem. **83**, 1599 (1979).
14. J. J. Spitzer, I. V. Olofsson, P. P. Singh, and L. G. Hepler. Can. J. Chem. **57**, 2798 (1979).
15. E. M. Woolley and L. G. Hepler. Can. J. Chem. **55**, 158 (1977).
16. C. Jolicoeur, L.-L. Lemelin, and R. Lapalme. J. Phys. Chem. **83**, 2806 (1979).
17. J. W. Larson, K. G. Zeeb, and L. G. Hepler. To be published.
18. J. W. Larson and L. G. Hepler. To be published.
19. A. Roux, G. M. Musbally, G. Perron, J. E. Desnoyers, P. P. Singh, E. M. Woolley, and L. G. Hepler. Can. J. Chem. **56**, 24 (1978).
20. J. W. Larson and L. G. Hepler. *In* Solute–solvent interactions. *Edited by* J. F. Coetzee and C. D. Ritchie, Marcel Dekker, NY. 1969. Chapt. 1.
21. J. W. Cobble, H. P. Stephens, I. R. McKinnon, and E. F. Westrum, Jr. Inorg. Chem. **11**, 1669 (1972).
22. L. G. Hepler and H. P. Hopkins, Jr. Rev. Inorg. Chem. **1**, 303 (1979).
23. P. G. Zambonin and J. Jordan. Anal. Chem. **41**, 437 (1969).
24. S. D. Hamann. *In* Modern aspects of electrochemistry, No. 9. *Edited by* B. E. Conway and J. O'M. Bockris, Plenum, NY. 1974. Chapt. 2.

Can. J. Chem. Downloaded from www.nrcresearchpress.com by 210.87.254.40 on 09/06/12
For personal use only.

Charge distributions and chemical effects. XXV. On the homogeneity of total molecular energies and the relationships between electronic, orbital, and total energies[1]

SÁNDOR FLISZÁR, MARIELLE FOUCRAULT, MARIE-THÉRÈSE BÉRALDIN, AND JACQUES BRIDET

Department of Chemistry, University of Montreal, Montreal, P.Q., Canada H3C 3V1

Received November 21, 1980

SÁNDOR FLISZÁR, MARIELLE FOUCRAULT, MARIE-THÉRÈSE BÉRALDIN, and JACQUES BRIDET. Can. J. Chem. **59**, 1074 (1981).

With the definition of a "screening factor" σ_k transforming the nuclear charge Z_k of an atom k into an "effective" nuclear charge $Z_k^* = Z_k\sigma_k$, the total energy $E = E(Z_k^*, Z_l^*, \ldots)$ of a molecule at equilibrium can be expressed as a homogeneous function of degree γ/α in $Z_k^*, Z_l^*, \ldots$, i.e. $E = -\Sigma_k Z_k^{*\gamma/\alpha}$, where α is the average of the α_k's ($\alpha_k = \partial \ln Z_k\sigma_k/\partial \ln Z_k$) and $\gamma = (V_{ne} + 2V_{nn})/E$ is a function of the nuclear–electronic, nuclear–nuclear, and total energies. Molecular energies calculated in this manner agree within 0.045% (average deviation) with their SCF counterparts. The sums of the orbital energies are correctly predicted from the equation $\Sigma_i \nu_i \varepsilon_i^{orb} = (3 - \gamma)E$. A separation of the individual nuclear–electronic and nuclear–nuclear contributions to the total potential energy $V(k, \text{mol})$ of each nucleus k indicates that the K_k^{mol} factors of the energy formula $E = \Sigma_k K_k^{mol} V(k, \text{mol})$ are constant for each type of atom, thus stressing the basic homogeneity of the total energy rather than of the electronic energy only. The γ function, which is the inverse of the molecular average of the K_k^{mol}'s, can be estimated in a simple way from atomic data.

SÁNDOR FLISZÁR, MARIELLE FOUCRAULT, MARIE-THÉRÈSE BÉRALDIN et JACQUES BRIDET. Can. J. Chem. **59**, 1074 (1981).

L'utilisation d'un "facteur d'écran" σ_k pour définir une charge nucléaire "effective" $Z_k^* = Z_k\sigma_k$ à partir de la charge nucléaire Z_k d'un atome k permet d'exprimer l'énergie totale $E = E(Z_k^*, Z_l^*, \ldots)$ d'une molécule à l'équilibre comme une fonction homogène de degré γ/α en $Z_k^*, Z_l^*, \ldots$, c'est-à-dire $E = -\Sigma_k Z_k^{*\gamma/\alpha}$, où α est la moyenne des α_k atomiques ($\alpha_k = \partial \ln Z_k\sigma_k/\partial \ln Z_k$) et où $\gamma = (V_{ne} + 2V_{nn})/E$ dépend de E ainsi que des énergies potentielles noyau–électron et noyau–noyau. Les énergies moléculaires calculées ainsi diffèrent de 0.045% (en moyenne) des valeurs SCF. La somme des énergies d'orbitales est correctement déduite de l'équation $\Sigma_i \nu_i \varepsilon_i^{orb} = (3 - \gamma)E$. La séparation des contributions noyau–électron et noyau–noyau à l'énergie potentielle totale $V(k, \text{mol})$ de chaque noyau k révèle que les facteurs K_k^{mol} de la formule $E = \Sigma_k K_k^{mol} V(k, \text{mol})$ sont des constantes pour chaque espèce atomique, en confirmant ainsi l'hommogénéité de l'énergie totale plutôt que celle de l'énergie électronique seulement. La fonction γ, qui est l'inverse de la moyenne moléculaire des facteurs K_k^{mol}, peut être facilement déduite à partir de données atomiques.

Introduction. Basic Formulas

The relationships between the various contributions to the total molecular energy which are investigated here play a major role in local density functional theory, which is of interest because the exact functional (1) would appear to contain a substantial local component (2). The local contribution involved in a description of molecular energies is conveniently introduced by means of the derivative $(\partial E/\partial Z_k)_{Z_l \neq k}$ of the total (kinetic + potential) energy E with respect to the nuclear charge Z_k of the kth atom. For atom k, the nuclear–electronic attraction energy $V_{ne}(k, \text{mol})$ arises from all electrons in the molecule and the total potential energy involving nucleus Z_k is

$$[1] \quad V(k, \text{mol}) = V_{ne}(k, \text{mol}) + Z_k \Sigma_{l \neq k} Z_l / r_{lk}$$

where the sum over l runs over all nuclei but k and r_{lk} is the distance from nucleus k to nucleus l. This quantity is central in the present theory because, applying the Hellmann–Feynman theorem, it results that[2]

$$[2] \quad Z_k(\partial E/\partial Z_k) = V(k, \text{mol})$$

and

$$[3] \quad \Sigma_k Z_k(\partial E/\partial Z_k) = V_{ne} + 2V_{nn}$$

On the other hand, the total energy E of a molecule in its equilibrium geometry can be expressed in terms of the electron–nucleus attraction energy V_{ne}, the electron–electron repulsion energy V_{ee}, and the nucleus–nucleus repulsion energy V_{nn} by applying the virial theorem, i.e.

$$[4] \quad 2E = V_{ne} + V_{ee} + V_{nn}$$

Consequently, one obtains from eqs. [3] and [4] that

$$[5] \quad 2E - \Sigma_k Z_k(\partial E/\partial Z_k) = V_{ee} - V_{nn}$$

Next, if the ε_i^{orb} are Hartree–Fock orbital energies with occupations ν_i, we obtain from the Hartree–Fock formula

$$E = \Sigma_i \nu_i \varepsilon_i^{orb} - (V_{ee} - V_{nn})$$

and from eq. [5] that

$$[6] \quad 3E - \Sigma_k Z_k(\partial E/\partial Z_k) = \Sigma_i \nu_i \varepsilon_i^{orb}$$

which is an identity in Hartree–Fock theory provided, of course, that all quantities are evaluated at equilibrium geometry. Equation [6] led Parr and

[1] Extracted from the M.Sc. thesis of M.F., Université de Montréal, 1981.

[2] For simplicity, we do not repeat the subscript indications referring to the variables which are obviously kept constant in these partial derivatives.

0008-4042/81/071074-09$01.00/0

©1981 National Research Council of Canada/Conseil national de recherches du Canada

Can. J. Chem. Downloaded from www.nrcresearchpress.com by 210.87.254.6 on 09/06/12
For personal use only.

TABLE 1. Comparison of SCF $E/\sum_i \nu_i \varepsilon_i^{orb}$ ratios with those given by eq. [7], using the γ's of eq. [8]

Molecule	E (au)	$\sum_i \nu_i \varepsilon_i^{orb}$ (au)	$-V/T$	γ	$E/\sum_i \nu_i \varepsilon_i^{orb}$ SCF	$E/\sum_i \nu_i \varepsilon_i^{orb}$ eq. [7]
CH_4	−40.1873	−27.6090	1.9991	2.3139	1.4556	1.4571
c-C_3H_6	−117.0236	−79.3177	1.9994	2.3229	1.4754	1.4769
C_2H_2	−76.8097	−51.6582	2.0009	2.3267	1.4869	1.4852
CO	−112.6971	−72.5298	2.0005	2.3557	1.5538	1.5521
CO_2	−187.5628	−120.0562	1.9998	2.3602	1.5623	1.5630
O_2	−149.5115	−93.8435	2.0002	2.3719	1.5932	1.5921
H_2O	−76.0134	−47.4388	1.9997	2.3763	1.6023	1.6033
NH_3	−56.1753	−36.7448	2.0015	2.3447	1.5288	1.5260
HCN	−92.8466	−61.1872	2.0004	2.3408	1.5174	1.5170
HCNO	−167.7063	−108.3997	2.0009	2.3529	1.5471	1.5454

Gadre to formulate the theorem (3) that "a necessary and sufficient condition for the validity of the equality

$$[7] \quad (3-\gamma)E = \sum_i \nu_i \varepsilon_i^{orb}$$

is that $E(Z_k, Z_l, ...)$ is a homogeneous function of degree γ in Z_k, Z_l, ...". This theorem provides an interesting basis for the understanding of approximate energy formulas of the form

$$E = \text{constant} \times \sum_i \nu_i \varepsilon_i^{orb}$$

which are implied in Hückel and extended Hückel descriptions of molecular energies. Indeed, for $\gamma = 7/3$, which is the characteristic homogeneity of both Thomas–Fermi (4) and local density functional theory (2), eq. [7] yields the Ruedenberg approximation (5)

$$E = (3/2)\sum_i \nu_i \varepsilon_i^{orb}$$

Finally, it is readily deduced from eqs. [3], [6], and [7] that

$$[8] \quad E = (1/\gamma)(V_{ne} + 2V_{nn})$$

which gives the original Politzer equation (6)

$$E = (3/7)(V_{ne} + 2V_{nn})$$

if γ is taken at its Thomas–Fermi value of 7/3. Equation [8] is instrumental in the forthcoming calculations of γ.

The object of the present work is to investigate the nature of the homogeneity parameter γ defined by eq. [7] and to study energy formulas derived in the spirit of the Parr–Gadre theorem.

Numerical Applications of Equations [7] and [8]

Present GTO $(9s5p|6s) \rightarrow [5s3p|3s]$ calculations, using Dunning's exponents (7) and optimum contraction vectors (8), are in satisfactory agreement with eq. [7], in which the γ values are those given by eq. [8], notwithstanding the fact that the virial $-V/T$ ratios slightly differ from the theoretical value of 2. The $E/\sum_i \nu_i \varepsilon_i^{orb}$ ratios, which are very sensitive to small changes in γ, clearly vary too widely from case to case to be replaced by an "average" constant value, at least for the accuracy required in this type of energy calculations (Table 1).

Postponing temporarily the detailed discussion concerning the variations of γ, the point which is now made numerically clear is that the homogeneity parameter γ cannot be regarded as a constant when going from one molecule to another.

In the following, we use the γ values given by eq. [8] and, to begin with, examine an interesting aspect related to the Parr–Gadre theorem mentioned above. Indeed, the total molecular energy

$$E = E(Z_k, Z_l, ...)$$

can be written[3]

$$[9] \quad E = \text{"constant"} \times \sum_k Z_k^{\gamma}$$

(This can be shown simply by differentiating eq. [9], assuming that the "constant" and γ are not functions of Z_k, Z_l, ..., and using eq. [8] to give eq. [3].) Now, of course, the consistency of eqs. [3] and [8] with

[3] A more general solution satisfying the equation

$$\gamma E = \sum_k Z_k(\partial E/\partial Z_k)$$

implied in writing eq. [7] is

$$E = \text{constant} \times \sum_k Z_k^{\gamma}(1 + \sum_l a_{kl} Z_k^{-\omega(k,l)} Z_l^{\omega(k,l)})$$

where a_{kl} and $\omega(k,l)$ are Z-independent parameters. The neglect of the

$$\sum_k Z_k^{\gamma} \sum_l a_{kl} Z_k^{-\omega(k,l)} Z_l^{\omega(k,l)}$$

terms represents a simplification which does not obscure the main conclusions resulting from this study. Quite on the contrary, the use of the present approximation ultimately reveals both the relative smallness of the neglected part and its physical importance at levels of numerical accuracy which, however, are beyond what can be reached within the limits of precision set by the present type of analysis.

Can. J. Chem. Downloaded from www.nrcresearchpress.com by 210.87.254.6 on 09/06/12
For personal use only.

Can. J. Chem. Downloaded from www.nrcresearchpress.com by 210.87.254.6 on 09/06/12
For personal use only.

TABLE 2. SCF calculations of γ and $E/\sum_k Z_k^{\gamma}$ for selected molecules (au)*

Molecule	E	$V_{ne} + 2V_{nn}$	γ	$-E/\sum_k Z_k^{\gamma}$
CH_4	−40.1873	−92.9890	2.3139	0.5982
C_2H_6	−79.2096	−183.6590	2.3186	0.5936
c-C_3H_6	−117.0236	−271.8287	2.3229	0.5892
C_2H_4	−78.0166	−181.2153	2.3228	0.5893
C_3H_6	−117.0454	−271.8560	2.3227	0.5895
i-C_4H_8	−156.0745	−362.5377	2.3229	0.5894
C_2H_2	−76.8097	−178.7001	2.3265	0.5853
C_6H_6	−230.6508	−536.5871	2.3264	0.5859
C_2	−75.3621	−175.6068	2.3302	0.5793
CO	−112.6971	−265.5034	2.3559	0.5572
CO_2	−187.5628	−442.6726	2.3601	0.5528
O_2	−149.5115	−354.6622	2.3721	0.5388
N_2	−108.8826	−255.3503	2.3452	0.5676
NH_3	−56.1754	−131.6974	2.3444	0.5687
N_2O	−183.5996	−431.9101	2.3525	0.5602

*Additional examples can be extracted from the compilation of our SCF results (Table 5).

eq. [9], i.e., ultimately, the validity of the Parr–Gadre theorem, does not require that the "constant" in eq. [9] be necessarily the same for all molecules. This point is examined by means of the $E/\sum_k Z_k^{\gamma}$ results presented in Table 2.

The answer is clear: the value of the $E/\sum_k Z_k^{\gamma}$ ratio differs from molecule to molecule (within extreme limits of the order of $\sim 12\%$) when the γ values given by eq. [8] are used. It is also true, on the other hand, that with an appropriate empirical choice of a single γ for all molecules, and of an accordingly determined constant $E/\sum_k Z_k^{\gamma}$ ratio, it still remains possible to use eq. [9] as a reasonable simple first approximation. The merits of such an approach are discussed elsewhere (3). In this work, however, we prefer to carry on with the γ's of eq. [8] and submit the following argument for treating the variable $E/\sum_k Z_k^{\gamma}$ ratio.

An examination of the results given in Table 2 reveals, indeed, that the hydrocarbons having the same H:C (atom:atom) ratio (e.g. 2 for the ethylenes and cyclopropane) also exhibit nearly the same $E/\sum_k Z_k^{\gamma}$ ratio and, moreover, that this ratio varies regularly with the H:C composition. This observation suggests that the "constant" of eq. [9] possibly represents in each case an appropriate "average" depending on the composition of the molecule, an idea which is exploited as follows in a simple way.

New Energy Formulas

Let us define a "screening factor" σ_k for each atom k of the molecule which transforms the nuclear charge Z_k to give an "effective" nuclear charge Z_k^*, i.e.

$$[10] \quad Z_k^* = Z_k\sigma_k$$

and examine, to begin with, the consequences of introducing this multiplier. Using

$$\partial Z_k = (1/\sigma_k)\partial Z_k^* + Z_k^*\partial(1/\sigma_k)$$

(from eq. [10]) for calculating $Z_k(\partial E/\partial Z_k)$ it is found that

$$[11] \quad Z_k(\partial E/\partial Z_k) = \alpha_k Z_k^*(\partial E/\partial Z_k^*)$$

where

$$[12] \quad \alpha_k = 1 + Z_k(\partial \ln \sigma_k/\partial Z_k) = \partial \ln Z_k\sigma_k/\partial \ln Z_k$$

In carrying out the sum over all k's of the terms given in eq. [11], we use the weighted molecular average of all atomic α_k's, i.e.

$$[13] \quad \alpha(\text{average}) = \frac{\sum_k \alpha_k Z_k^*(\partial E/\partial Z_k^*)}{\sum_k Z_k^*(\partial E/\partial Z_k^*)}$$

and obtain, from eqs. [11] and [13],

$$[14] \quad \sum_k Z_k(\partial E/\partial Z_k) = \alpha\sum_k Z_k^*(\partial E/\partial Z_k^*)$$

Finally, we deduce from the equation

$$\gamma E = \sum_k Z_k(\partial E/\partial Z_k)$$

(see eqs. [6] and [7]), which does not imply constancy of γ, and from eq. [14] that

$$[15] \quad (\gamma/\alpha)E = \sum_k Z_k^*(\partial E/\partial Z_k^*)$$

This equation does not imply any approximations and remains consistent with eq. [7] for molecules in their equilibrium geometry. Applying now the argument developed by Parr and Gadre on the basis of the equation

$$\gamma E = \sum_k Z_k(\partial E/\partial Z_k)$$

it appears from eq. [15] that the total molecular energy

$$E = E(Z_k^*, Z_l^*, \ldots)$$

Can. J. Chem. Downloaded from www.nrcresearchpress.com by 210.87.254.6 on 09/06/12
For personal use only.

is a homogeneous function of degree γ/α in Z_k^*, Z_l^*, ..., i.e.[3]

[16] $E = -\sum_k Z_k^{*\gamma/\alpha}$

In this approach, the quantity corresponding to the absolute value of the "constant" appearing in eq. [9] is given by the weighted average

$$\langle \sigma_k^{\gamma/\alpha} \rangle = \sum_k \sigma_k^{\gamma/\alpha} Z_k^{\gamma/\alpha} / \sum_k Z_k^{\gamma/\alpha}$$

of the individual atomic $\sigma_k^{\gamma/\alpha}$'s. Indeed, eq. [16] can also be written as follows:

[17] $E = -\langle \sigma_k^{\gamma/\alpha} \rangle \sum_k Z_k^{\gamma/\alpha}$

This is the type of equation which has been successfully applied by Parr and Gadre to the study of diatomics. In terms of the present equations, the Parr–Gadre calculations correspond to an approximation implying constancy of $\langle \sigma_k^{\gamma/\alpha} \rangle$ (evaluated at 0.51130). Moreover, γ/α (identified as γ) was taken at an empirically determined constant value of 2.40073 suggesting that, just like γ, α remains fairly constant from molecule to molecule. Equation [7], however, is not satisfied in this approach. Our formalism now permits us to evaluate E and $\sum_i \nu_i \varepsilon_i^{orb}$ at more refined levels of approximation. In a first approximation, dropping the constraint of constant γ and $\langle \sigma_k^{\gamma/\alpha} \rangle$ parameters, we have examined a number of polyatomic molecules tentatively assuming that each chemical species can be adequately described by a constant $Z_k^{*1/\alpha}$ value. Using the appropriate γ's (eq. [8]), a fit of eq. [16] with our SCF results gives $Z_H^{*1/\alpha} = 0.94715$, $Z_C^{*1/\alpha} = 4.75059$, $Z_N^{*1/\alpha} = 5.48845$, and $Z_O^{*1/\alpha} = 6.17329$. The back-calculation of the molecular energies by means of eq. [16] agrees, in this approximation, within 0.087% (average deviation) with the corresponding SCF energies. Similar calculations using an extended GTO(9*s*5*p*2*d*|6*s*2*p*) → [5*s*3*p*1*d*|3*s*1*p*] basis set yield $Z_H^{*1/\alpha} = 0.95333$ and $Z_C^{*1/\alpha} = 4.74756$ and a satisfactory agreement with the SCF energies of methane, ethane, ethylene, acetylene, cyclopropane, and C_2 (0.087% average deviation).

While these results are certainly encouraging, we shall now examine in what way the constraint of a constant average α can be dropped and, moreover, how γ can be estimated without having recourse to eq. [8].

The γ Function

At this stage we introduce the defining equation (9–11)

[18] $E_k(\text{mol}) = K_k^{\text{mol}} V(k, \text{mol})$

for the energy E_k(mol) of an atom k being part of a molecule, without making any a priori assumption regarding the possible value(s) of the K_k^{mol} factors of the individual atoms. With eq. [18] the total molecular energy becomes

[19] $E = \sum_k K_k^{\text{mol}} V(k, \text{mol})$

i.e., noting that $\sum_k K_k^{\text{mol}} V(k, \text{mol}) / \sum_k V(k, \text{mol}) = K_{Av}^{\text{mol}}$ is just a weighted average of the individual K_k^{mol}'s,

[20] $E = K_{Av}^{\text{mol}} \sum_k V(k, \text{mol}) = K_{Av}^{\text{mol}} (V_{ne} + 2V_{nn})$

Consequently, comparing this result with eq. [8], it appears that

[21] $\gamma = 1/K_{Av}^{\text{mol}}$

We examine now the K_k^{mol} coefficients of eq. [18]. Indeed, K_k^{mol} multiplies a total potential energy which consists of two distinct contributions, i.e. (see eq. [1]) a nuclear–electronic and a nuclear–nuclear part. It may be regarded questionable that the same factor should apply to these two distinct parts. The answer is that one can always consider two independent multipliers, K_k^{el} and K_k^{nucl}, so that

[22] $E_k(\text{mol}) = K_k^{el} V_{ne}(k, \text{mol}) + K_k^{nucl} Z_k \sum_{l \neq k} Z_l / r_{lk}$

In doing so, eq. [18] remains valid provided that

[23] $K_k^{\text{mol}} = [K_k^{el} V_{ne}(k, \text{mol}) + K_k^{nucl} Z_k \sum_{l \neq k} Z_l / r_{lk}] / V(k, \text{mol})$

which is simply the weighted average of K_k^{el} (for the nuclear–electronic part) and K_k^{nucl} (for the nuclear–nuclear part).

Let us now study a number of molecules containing C, H, N, and O in order to determine the appropriate independent coefficients K_k^{el} and K_k^{nucl} for each of these atoms. This is done, firstly, by calculating the potential energies appearing in eq. [22] for each individual atom in the molecule. Secondly, we add separately the nuclear–electronic and the nuclear–nuclear terms to give sub-sums which collect only the contributions of atoms of the same chemical species. For example, V_{ne}(C) represents the sum of all the $V_{ne}(k, \text{mol})$ terms where the k's refer to carbon nuclei. Similarly, V_{nn}(C) is the sum of all the $Z_k \sum Z_l / r_{lk}$ terms in which the k's are carbon nuclei. Similar sub-sums, e.g. V_{ne}(H), V_{nn}(H), etc., are calculated for each chemical species which is present in the molecule and the total molecular energy is written, according to eq. [19], as

[24] $E = K_C^{el} V_{ne}(C) + K_C^{nucl} V_{nn}(C) + K_H^{el} V_{ne}(H) + K_H^{nucl} V_{nn}(H) +$ similar terms for all other atoms

Can. J. Chem. Downloaded from www.nrcresearchpress.com by 210.87.254.6 on 09/06/12
For personal use only.

TABLE 3. Total nuclear–electronic and nuclear–nuclear potential energies at the H, C, N, and O atoms (au)

Molecule	E	V_{ne}(C)	V_{nn}(C)	V_{ne}(H)	V_{nn}(H)	V_{ne}(N)	V_{nn}(N)	V_{ne}(O)	V_{nn}(O)
CH_4	−40.1873	−100.2656	11.7289	−19.7718	15.3201				
C_2H_6	−79.2096	−228.1297	51.1972	−40.0624	33.3354				
C_3H_8	−118.2337	−374.4720	109.0946	−65.0052	56.0248				
i-C_4H_{10}	−157.2587	−539.6236	185.7761	−94.5820	83.3626				
c-C_3H_6	−117.0236	−376.3293	111.1690	−47.5990	40.9305				
C_2H_4	−78.0166	−223.5607	46.7265	−24.9011	20.5200				
C_3H_6	−117.0454	−367.4661	102.2346	−45.4778	38.8526				
i-C_4H_8	−156.0745	−530.1119	176.4405	−71.3979	62.5316				
C_3H_4	−115.8401	−360.5592	95.5614	−28.2598	23.9482				
C_2H_2	−76.8097	−217.0177	40.3486	−11.1428	9.1113				
C_6H_6	−230.6508	−880.8391	350.8043	−62.4695	55.9172				
C_2	−75.3621	−205.7492	30.1424						
O_2	−149.5115							−410.0160	55.3542
CO	−112.6971	−109.8135	22.1348					−199.9595	22.1348
CO_2	−187.5628	−130.7283	43.8118					−428.7758	73.0197
HCHO	−113.8358	−114.2367	26.5331	−12.5863	10.4877			−203.4122	24.9173
CH_2CO	−151.6824	−245.7894	70.0738	−14.2701	12.1892			−212.9322	34.8350
CH_3OH	−115.0196	−116.1844	28.1106	−28.2037	23.9217			−207.0799	28.3463
$(CH_3)_2O$	−154.0298	−252.6870	76.4858	−49.6558	43.0449			−226.7787	48.0917
$(C_2H_5)_2$	−232.0913	−566.1524	213.0260	−104.2653	93.1150			−253.0217	74.2742
H_2O	−76.0134			−11.4907	9.5445			−187.5284	8.8454
N_2	−108.8826					−301.0867	45.7365		
NH_3	−56.1754			−15.8140	12.6917	−139.3205	10.7452		
N_2H_2	−109.9529			−13.5987	11.5861	−309.5363	53.3495		
N_2H_4	−111.1507			−28.7378	24.5660	−314.3405	57.5796		
HCN	−92.8466	−110.3062	22.2444	−5.5838	4.6337	−149.2453	20.9435		
CH_2N_2	−147.7922	−119.9192	21.8256	−14.5698	12.4575	−333.4445	78.2786		
NH_2CN	−147.8677	−126.6993	38.8213	−16.0989	14.1607	−323.1644	66.5878		
CH_3CN	−131.8884	−242.4038	66.3117	−21.6591	18.5128	−159.4134	30.9515		
N_2O	−183.5996					−334.1089	80.2627	−213.5334	35.4652
HCNO	−167.7063	−128.7459	41.5189	−7.3236	6.4249	−163.0884	35.0321	−213.3403	34.9326

Equation [24] enables thus a separation of the nuclear–electronic from the nuclear–nuclear contributions for each chemical species contained in the molecule. The results are presented in Table 3.

A multiple regression analysis was carried out using the potential energy terms of Table 3. The individual multipliers derived in this fashion from eq. [24] for the nuclear–electronic and nuclear–nuclear contributions are given in Table 4.

The present results indicating that $K_k^{el} = K_k^{nucl}$ now settle an important question, namely that of the constancy of the K_k^{mol} factor introduced in the defining of eq. [18]. Indeed, had it been $K_k^{el} \neq K_k^{nucl}$, then K_k^{mol} would have changed to some extent from molecule to molecule, depending on the relative weights of $V_{ne}(k, \text{mol})$ and $Z_k\sum_{l\neq k}Z_l/r_{lk}$ (eq. [23]). The observed constancy of K_k^{mol} for each chemical species, at least within the limits set by the accuracy of the present type of analysis, adds considerable support to earlier work (10, 11) in which this constancy has been postulated, namely in applications of eq. [19] (13). Finally, this result discriminates in favor of homogeneity of the total energy, as opposed to homogeneity of the electronic energy only,[4] i.e., ultimately, fully supports the arguments based on the Parr–Gadre theorem leading to eq. [16].

TABLE 4. The K_k^{el}, K_k^{nucl}, and K_k^{mol} coefficients of eqs. [22]–[24]*

Atom	K_k^{el}	K_k^{nucl}	K_k^{mol}
H	0.500	0.500	0.500
C	0.429	0.429	0.429
N	0.423	0.413	0.426
O	0.422	0.423	0.4216

*Alternatively, by means of eqs. [7] and [21], using the Hartree–Fock ε_i values and the equilibrium geometries given in ref. 12, we find for the diatomics C_2, N_2, and O_2 that $K_k^{mol} = 0.4291$, 0.4260, and 0.4211, respectively. Similarly, one obtains $K_k^{mol} = 0.4318$ (Li), 0.4321 (B), and 0.4169 (F).

The constancy of K_k^{mol} for each chemical species now enables us to derive approximate but still accurate molecular γ values. Let us examine the energy of atomization, ΔE_a^*, of a vibrationless molecule at 0 K, i.e.

$$\Delta E_a^* = \sum_k \langle\psi_k|H_k|\psi_k\rangle - \langle\psi_{mol}|H_{mol}|\psi_{mol}\rangle$$

where H_k and H_{mol} are the appropriate Hamiltonians

[4]A detailed discussion of related questions is offered in ref. 3.

Can. J. Chem. Downloaded from www.nrcresearchpress.com by 210.87.254.6 on 09/06/12
For personal use only.

and ψ_k and ψ_{mol} the corresponding ground-state wave functions. Applying the Hellmann–Feynman theorem, it is

[25] $V(k, \text{mol}) = V_{ne}(\text{free atom } k) - Z_k(\partial \Delta E_a^*/\partial Z_k)$

It is well known (9) that

$$Z_k(\partial \Delta E_a^*/\partial Z_k) \ll V(k, \text{mol})$$

Consequently, we may write, to a good approximation,

[26] $V(k, \text{mol}) \simeq V_{ne}(\text{free atom } k)$

Therefore, applying this approximation in the exact definition of K_{Av}^{mol} and using eq. [21]

$$\gamma = 1/K_{Av}^{mol}$$

it is

[27] $$\gamma \simeq \frac{\sum_k V_{ne}(\text{free atom } k)}{\sum_k K_k^{mol} V_{ne}(\text{free atom } k)}$$

from which γ can be deduced from the composition of the molecule and the appropriate K_k^{mol} values indicated in Table 4. The V_{ne}(free atom k) values are conveniently derived from experimental ground-state atomic energies and calculated E/V_{ne} ratios for the isolated atoms, giving V_{ne}(free atom) = −1.0000 (H), −88.4879 (C), −128.6872 (N), and −178.7457 au (O). The precision of these V_{ne}(free atom k) values is not too critical in the evaluation of γ by means of eq. [27].

Discussion and Numerical Tests of Equation [16]

In writing eq. [16] on the basis of eq. [15], the new homogeneity parameter γ/α is treated as a constant. It follows from eq. [16] that

$$Z_k^*(\partial E/\partial Z_k^*) = -(\gamma/\alpha)Z_k^{*\gamma/\alpha}$$

This expression, combined with eqs. [2] and [11], gives

$$-Z_k^{*\gamma/\alpha} = (\alpha/\gamma\alpha_k)V(k, \text{mol})$$

From a comparison of this result with those expressed by eqs. [16] and [19] it appears that

$$K_k^{mol} = \alpha/\gamma\alpha_k$$

and, consequently, that

[28] $$-Z_k^{*\gamma/\alpha} = K_k^{mol} V(k, \text{mol})$$

Finally, using the defining equation

$$Z_k^* = Z_k\sigma_k$$

it is concluded that

[29] $$\sigma_k^{\gamma/\alpha} = -K_k^{mol} Z_k^{-\gamma/\alpha} V(\text{k, mol})$$

Concerning eq. [28], which unifies the energy formulas [16] and [19], it is noteworthy that its validity is not linked to any particular choice for γ/α as long as the σ_k's are adjusted to give the $Z_k^{*\gamma/\alpha}$ values required by this expression. The following numerical tests are therefore made directly on the basis of the best possible $Z_k^{*\gamma/\alpha}$ values. Equation [29], on the other hand, is instructive because it reveals something about the "constancy" of the σ_k factors. It is now clear that these multipliers differ slightly, but significantly, from atom to atom and, moreover, that they are not strictly constant for each type of atom. Indeed, eqs. [25] and [29] show that

$$\sigma_k^{\gamma/\alpha} = -K_k^{mol} Z_k^{-\gamma/\alpha}[V_{ne}(\text{free atom } k) - Z_k(\partial \Delta E_a^*/\partial Z_k)]$$

meaning that $\sigma_k^{\gamma/\alpha}$ depends in part on a "local" portion of the molecular binding energy, a problem which has been thoroughly studied elsewhere (11) in terms of local electron densities affecting chemical binding.[5] Energy differences between isomers are reflected in subtle changes of $\sigma_k^{\gamma/\alpha}$ and, hence, of $Z_k^{*\gamma/\alpha}$. Our choice of a set of constant $Z_k^{*\gamma/\alpha}$'s remains nevertheless a valid first approximation because of the relatively narrow range of variation of $V(k, \text{mol})$ (eqs. [25], [26]).

With these premises, we have calculated total energies from eq. [16] with $Z_k^{*\gamma/\alpha}$ = 0.60309 (H), 37.79858 (C), 54.40009 (N), and 74.82589 (O), parameters which best satisfy eq. [28] when used with our SCF potential energies. The calculated total energies (eq. [16]) agree within 0.045% (average error) with their SCF counterparts. Moreover, it is also interesting to use these $Z_k^{*\gamma/\alpha}$ parameters for a numerical evaluation of the derivative

[30] $$\partial \ln Z_k^{*\gamma/\alpha}/\partial \ln Z_k = 1/K_k^{mol}$$

which follows from eqs. [10], [12], and

$$\gamma\alpha_k/\alpha = 1/K_k^{mol}$$

Using the power series

$$a_0 + a_1 \ln Z_k + a_2(\ln Z_k)^2$$

for a numerical fit of the $\ln Z_k^{*\gamma/\alpha}$ results for C, N, and O (which is a reasonable approximation in this short range of variations),[6] we find from eq. [30] that K_k^{mol} = 0.493 (H), 0.432 (B), 0.426 (C), 0.421 (N), 0.417 (O), and 0.413 (F), values which are systematically about ~1% smaller than those given in

[5] At this level, one should also consider the terms described in footnote 3 which were neglected in writing the approximations [9] and [16].

[6] The coefficients are $a_0 = -0.290676$, $a_1 = 2.030605$, and $a_2 = 0.088647$.

TABLE 5. Comparison between SCF energies and those derived from the approximations described in the text (au)

		E		V_{ne}		V_{ee}		$\sum_i \nu_i \varepsilon_i^{orb}$	
Molecule	V_{nn}	Approx.	SCF	Approx.	SCF	Approx.	SCF	Approx.	SCF
CH_4	13.5245	−40.2109	−40.1873	−120.1147	−120.0380	26.1684	26.1028	−27.5670	−27.6090
C_2H_6	42.2663	−79.2156	−79.2096	−268.1876	−268.1916	67.4901	67.4967	−53.9918	−53.9792
C_3H_8	82.5597	−118.2204	−118.2337	−439.3635	−439.4772	120.3630	120.4354	−80.4171	−80.3580
i-C_4H_{10}	134.5693	−157.2251	−157.2587	−633.9717	−634.2056	184.9521	185.0717	−106.8423	−106.7563
c-C_3H_6	76.0498	−117.0142	−117.0236	−423.8662	−423.9282	113.7880	113.7557	−79.2760	−79.3177
C_2H_4	33.6233	−78.0095	−78.0166	−248.4244	−248.4619	58.7821	58.7434	−52.8507	−52.8965
C_3H_6	70.6974	−117.0142	−117.0454	−413.1614	−413.2508	108.4356	108.4521	−79.2760	−79.2907
i-C_4H_8	119.4861	−156.0189	−156.0745	−601.3277	−601.5098	169.8038	169.8565	−105.7012	−105.7040
C_3H_4	59.7548	−115.8080	−115.8401	−388.7968	−388.8190	97.4260	97.2864	−78.1368	−78.3085
C_2H_2	24.7300	−76.8033	−76.8097	−228.1582	−228.1600	49.8216	49.8815	−51.7117	−51.6582
C_6H_6	203.3607	−230.4099	−230.6508	−942.8161	−943.3086	278.6356	278.6600	−155.1350	−155.3515
C_2	15.0712	−75.5971	−75.3621	−206.3592	−205.7492	40.0938	39.9114	−50.5745	−50.5219
O_2	27.6771	−149.6518	−149.5115	−410.3163	−410.0164	83.3356	83.3451	−93.9933	−93.8435
CO	22.1348	−112.6244	−112.6971	−309.8616	−309.7730	62.4780	62.3021	−72.2812	−72.5298
CO_2	58.4157	−187.4503	−187.5628	−559.9039	−559.5041	126.5876	125.9223	−119.2784	−120.0562
H_2CO	30.9690	−113.8306	−113.8358	−330.0182	−330.2353	71.3880	71.6379	−73.4116	−73.1669
CH_2CO	58.5490	−151.6292	−151.6824	−473.2871	−472.9917	111.4797	111.0803	−98.6985	−99.1512
CH_3OH	40.1893	−115.0368	−115.0196	−350.9452	−351.4679	80.6823	81.2289	−74.5438	−73.9800
$(CH_3)_2O$	83.8112	−154.0415	−154.0298	−528.7804	−529.1215	136.8862	137.2420	−100.9665	−100.5990
$(C_2H_5)_2O$	190.2076	−232.0510	−232.0913	−922.7532	−923.4393	268.4436	268.9402	−153.8150	−153.3587
H_2O	9.1950	−76.0321	−76.0134	−198.3618	−199.0175	37.1026	37.7695	−48.1245	−47.4388
N_2	22.8683	−108.8002	−108.8826	−301.1364	−301.0868	60.6677	60.6493	−71.0008	−71.1016
NH_3	11.7185	−56.2094	−56.1754	−154.8641	−155.1344	30.7268	31.1491	−37.2011	−36.7448
N_2H_2	32.4678	−110.0064	−109.9529	−322.8214	−323.1350	70.3408	70.6841	−72.1334	−71.7366
N_2H_4	41.0728	−111.2125	−111.1507	−342.5152	−343.0782	79.0174	79.8553	−73.2679	−72.3681
HCN	23.9108	−92.8017	−92.8466	−264.8736	−265.1352	55.3594	55.5702	−61.3531	−61.1872
CH_2N_2	61.2808	−147.8049	−147.7922	−468.5566	−467.9334	111.6660	111.0531	−77.4197	−98.0200
NH_2CN	59.7849	−147.8049	−147.8677	−465.5648	−465.9627	110.1701	110.2927	−97.4197	−97.3599
CH_3CN	57.8880	−131.8065	−131.8884	−423.4190	−423.4763	101.9180	101.9253	−87.7765	−87.8511
N_2O	57.8640	−183.6261	−183.5996	−548.6082	−547.6381	123.4920	122.9064	−117.9981	−118.5573
HCNO	58.9543	−167.6276	−167.7063	−512.4436	−513.4983	118.2341	118.2741	−108.3478	−108.3866

Table 4. These results certainly justify our approximate energy partitioning in terms of atomic-like contributions which is reflected by eqs. [16] and [18].

There is another point deserving attention. The σ_k's of the individual atoms k, which are likely not to be the same for H, C, etc., depend to some extent on the molecular environment (eq. [29]), although an approximation implying their constancy is certainly a good one (eq. [26]). On the other hand, if eq. [16] is used with fixed atomic σ_k's, its validity is linked to that of the assumed "constancy" of the σ_k's. Here we submit that if some value of γ/α minimizes the differences between the σ_k's of different atoms (C, N, etc.), the range of variation of the σ_k's of each type of atom would also be minimized, thus approaching the requirements for internal consistency of eq. [16] involving constant atomic σ_k values. By means of the $Z_k^{*\gamma/\alpha} = (\sigma_k Z_k)^{\gamma/\alpha}$ values given above, it is found that the differences between σ_C, σ_N, and σ_O are minimized for $\gamma/\alpha = 2.3733$, giving

$$\sigma_C = 0.7701,\ \sigma_N = 0.7695,\ \sigma_O = 0.7701,$$
$$\text{and } \sigma_H = 0.8081$$

Including H in this analysis, it appears that

$$\sigma_H = 0.8038,\ \sigma_C = 0.8004,\ \sigma_N = 0.8029,$$
$$\text{and } \sigma_O = 0.8063$$

for $\gamma/\alpha = 2.3149$. Finally, assuming now $\gamma/\alpha = 7/3$, it results that

$$\sigma_H = 0.8052,\ \sigma_C = 0.7905,\ \sigma_N = 0.7920,$$
$$\text{and } \sigma_O = 0.7945$$

Can. J. Chem. Downloaded from www.nrcresearchpress.com by 210.87.254.6 on 09/06/12
For personal use only.

Can. J. Chem. Downloaded from www.nrcresearchpress.com by 210.87.254.6 on 09/06/12
For personal use only.

While this type of analysis does not provide a clear-cut answer about the "true" value of γ/α, it is clear that the Thomas–Fermi or local density functional homogeneity constraint of $\sim 7/3$ corresponds to a situation in which the σ_k's of the various atoms are quite similar one to another.

The fact that γ/α is taken at a constant value does not imply that γ itself is a constant. Hence, using the γ values given by our approximation (eq. [27]) and the K_k^{mol} values of Table 4, we obtain an estimate of the sum $\sum_i \nu_i \varepsilon_i^{\text{orb}}$ of the orbital energies (eq. [7]). Finally, using the appropriate V_{nn} values, we obtain V_{ne} from eq. [8] and V_{ee} (eq. [4]). The results are given in Table 5, together with their SCF counterparts.

The results are self-explanatory and vividly support the views having led to eq. [16] as well as the approximations used for estimating γ. They suggest the following conclusions.

Conclusions

The proportionality relationship

$$E \propto \sum_k Z_k^{\gamma}$$

in which γ is a characteristic constant for the molecule under study and where the proportionality factor is left undetermined, satisfies the equation

$$\gamma E = \sum_k Z_k (\partial E/\partial Z_k)$$

This expression describes an energy partitioning in terms of atomic-like contributions. Introducing a multiplier σ_k for defining an "effective" nuclear charge

$$Z_k^* = Z_k \sigma_k$$

we find that

$$(\gamma/\alpha)E = \sum_k Z_k^* (\partial E/\partial Z_k^*)$$

(in which γ/α is now a new characteristic constant) and, moreover, that

$$E = -\sum_k Z_k^{*\gamma/\alpha} = -\langle \sigma_k^{\gamma/\alpha} \rangle \sum_k Z_k^{\gamma/\alpha}$$

The ratio $E/\sum_k Z_k^{\gamma/\alpha}$ is thus defined in terms of the multipliers σ_k which differ from atom to atom. A first approximation with

$$\langle \sigma_k^{\gamma/\alpha} \rangle = 0.51130 \text{ and } \gamma/\alpha = 2.40073$$

is known to give reasonable results in calculations of total energies (3). This type of approach, which has the merits of its simplicity, meets, however, with a major difficulty. The constant γ/α exponent, simply identified as γ, fails, indeed, to satisfy the equation

$$(3 - \gamma)E = \sum_i \nu_i \varepsilon_i^{\text{orb}}$$

Our approach, on the contrary, not only satisfies the approximation

$$E = -\sum_k Z_k^{*\gamma/\alpha}$$

but equally well that giving the sum $\sum_i \nu_i \varepsilon_i^{\text{orb}}$ of the orbital energies. The reason is that even though γ/α is constant, it is γ itself which determines the relationship between total and orbital energies. It is seen that the use of the σ_k multipliers restores in a simple way the required internal consistency among energy formulas which play a central role not only in Hartree–Fock theory but also in exact and local density functional theory.

The calculation of γ, using either the appropriate $V(k, \text{mol})$ values or valid approximations thereof, rests on the validity of the energy formula

$$E = \sum_k K_k^{\text{mol}} V(k, \text{mol})$$

This equation, which has been thoroughly tested on previous occasions (10, 11, 13), reproduces the present SCF energies (Table 5) with an average error of 0.106%. We feel presently unable to go beyond this level of accuracy, partly because the SCF virial $-V/T$ ratio is usually not exactly 2 and, moreover, because it is uncertain whether the present GTO basis set describes the molecules containing nitrogen and oxygen with the same degree of accuracy as the hydrocarbons. Our analysis which has explicitly considered a separation of the individual nuclear–electronic and nuclear–nuclear contributions to the potential energies, rather than merely forcing a fit of the sum $\sum_k K_k^{\text{mol}} V(k, \text{mol})$ with SCF total energies, concludes that the K_k^{mol}'s are, indeed, constants for the individual atoms. This result, as well as the way it has been deduced, is important not only because it lends strong support to earlier work which was based on this energy formula but also because it discriminates in favor of homogeneity of the total energy over that of the electronic energy only. Homogeneity of the total energy is a basic aspect in the present theory.

The assumption of a constant σ_k for each type of atom is supported, as a first approximation, by the present results which also suggest that $\gamma/\alpha \sim 7/3$. The K_k^{mol} coefficients are now defined in terms of the σ_k's and of γ/α by the formula

$$1/K_k^{\text{mol}} = (\gamma/\alpha)\partial \ln (Z_k \sigma_k)/\partial \ln Z_k$$

which provides the link between the two alternate descriptions of molecular energies which have been analysed in this work. While the present results illustrate the merits and the limitations of the description of molecular energies in terms of atomic-like $Z_k^{*\gamma/\alpha}$ contributions, they leave room for refine-

ments by a consideration of the subtle influence of local properties on σ_k, thus creating a bridge between the present views and the concept of a molecule regarded as a collection of "atoms" or, alternatively, of "chemical bonds" (11).

Acknowledgements

We express our gratitude to Dr. B. N. McMaster for helpful discussions, to the National Research Council of Canada for financial assistance, and to "Le Centre de Calcul de l'Université de Montréal" for generous computer time.

1. P. HOHENBERG and W. KOHN. Phys. Rev. Sect. B, **136**, 864 (1964).
2. R. G. PARR, S. R. GADRE, and L. J. BARTOLOTTI. Proc. Natl. Acad. Sci. USA, **76**, 2522 (1979).
3. R. G. PARR and S. R. GADRE. J. Chem. Phys. **72**, 3669 (1980).
4. N. H. MARCH. Adv. Phys. **6**, 1 (1957).
5. K. RUEDENBERG. J. Chem. Phys. **66**, 375 (1977).
6. P. POLITZER. J. Chem. Phys. **64**, 4239 (1976); **69**, 491 (1978).
7. T. H. DUNNING. J. Chem. Phys. **53**, 2823 (1970).
8. G. KEAN. M.Sc. Thesis, Université de Montréal, Montréal. 1974.
9. S. FLISZÁR and M. T. BÉRALDIN. J. Chem. Phys. **72**, 1013 (1980).
10. P. POLITZER. J. Chem. Phys. **70**, 1067 (1979).
11. S. FLISZÁR. J. Am. Chem. Soc. **102**, 6946 (1980).
12. P. E. CADE and W. HUO. At. Data Nucl. Data Tables, **12**, 415 (1973); **15**, 1 (1975); P. E. CADE and A. C. WAHL. At. Data Nucl. Data Tables, **13**, 339 (1974) and references therein.
13. T. ANNO. J. Chem. Phys. **72**, 782 (1980).

Can. J. Chem. Downloaded from www.nrcresearchpress.com by 210.87.254.6 on 09/06/12
For personal use only.

Etude rmn (^{1}H et ^{13}C) des interactions entre les nucléosides et les bleus de platine obtenus à partir du méthyle-1 nicotinamide

JEAN-PIERRE LAURENT ET PAULE LEPAGE

Laboratoire de Chimie de Coordination du CNRS associé à l'Université Paul Sabatier, 205 route de Narbonne, 31400 Toulouse, France

Reçu le 29 février 1980[1]

JEAN-PIERRE LAURENT et PAULE LEPAGE. Can. J. Chem. **59**, 1083 (1981).

Les interactions entre deux "bleus de platine" obtenus à partir du méthyle-1 nicotinamide et divers nucléosides (guanosine, cytidine, uridine et adénosine) ont été étudiées à l'aide de la spectrographie de rmn (^{1}H et ^{13}C). Les résultats obtenus montrent que les sites d'interaction sont identiques à ceux qui sont généralement observés pour les complexes "classiques" du platine(II), le *cis*-$Pt(NH_3)_2Cl_2$ par exemple.

JEAN-PIERRE LAURENT and PAULE LEPAGE. Can. J. Chem. **59**, 1083 (1981).

The interactions between two "platinum blues", obtained from 1-methylnicotinamide, and various nucleoside (guanosine, cytidine, uridine, and adenosine) have been studied by ^{1}H and ^{13}C nmr spectroscopy. The results obtained show that the interaction sites are identical to those usually observed for normal Pt(II) complexes, e.g. *cis*-$Pt(NH_3)_2Cl_2$.

[Journal translation]

Can. J. Chem. Downloaded from www.nrcresearchpress.com by 210.87.254.40 on 09/06/12
For personal use only.

De nombreux travaux ont été consacrés à l'étude des interactions entre les ions des métaux lourds et les constituants des acides nucléiques (1, 2). Les études en solution ont ainsi fait largement appel à la spectrographie de résonance protonique mais le petit nombre de protons non échangeables, intervenant dans la structure des bases purines ou pyrimidiques, limite la portée des résultats obtenus. La résonance du noyau ^{13}C, au contraire, permet d'atteindre des informations plus précises sur la localisation des sites d'interaction par suite du nombre important de carbones observables.

L'intérêt de tels travaux s'est accru dans le cas du platine à la suite de la découverte des propriétés antitumorales de certains complexes de type classique (tel *cis*-$Pt(NH_3)_2Cl_2$) ou appartenant au groupe des espèces dites "bleus de platine" (3–5). Ces derniers composés, dont la coloration bleue est la caractéristique commune la plus évidente, ont donné lieu, depuis leur découverte, à un nombre important de travaux (cf. par exemple les réfs 6 à 13). Ils posent encore de nombreux problèmes, en particulier pour ce qui est de leur mode d'action. Disposant de deux espèces originales (14), nous avons entrepris d'étudier leur réaction avec quelques nucléosides, dans la perspective retenue par de nombreux auteurs (15–19) et suivant laquelle l'activité antitumorale de ces produits serait liée à des interactions spécifiques avec l'ADN. Si par suite de leur caractère polymère et de la présence d'un certain paramagnétisme, la résonance nucléaire n'est pas l'outil de choix pour étudier les complexes bleus eux-mêmes, cette technique permet cependant de préciser la nature des sites d'interaction avec les nucléosides.

Résultats et discussions

1. Les complexes bleus

Les complexes bleus du platine sont généralement obtenus à partir des produits d'hydrolyse[2] du complexe *cis*-$Pt(NH_3)_2Cl_2$ et d'un ligand présentant une fonction amide ou lactame. La classe la plus étudiée actuellement fait intervenir l'uracile et ses dérivés (4, 5). Nous avons pu obtenir une espèce originale en utilisant K_2PtCl_4 comme précurseur et le méthyle-1 nicotinamide (cf. fig. 1) comme ligand (14). La réaction conduit à une espèce neutre de type chloro (A) qui, par action du nitrate d'argent en milieu aqueux permet d'atteindre une espèce cationique de type aquo ou hydroxo (B).

Ces espèces sont amorphes et, de ce fait, difficiles à caractériser. Sur la base des seules données analytiques, il n'est pas possible de proposer une formulation entièrement satisfaisante mais ce résultat peut être atteint en envisageant l'ensemble des propriétés physico-chimiques de ces espèces. A partir des résultats d'analyse, il apparaît que dans (A) et (B), une seule molécule de méthyle-1 nicotinamide intervient par atome de platine et que, dans (A), le rapport atomique Cl/Pt est toujours légèrement supérieur à 2. La solubilité de (B) dans l'eau a permis la mise en œuvre d'un dosage oxydant (20) réalisé en milieu sulfurique dilué à l'aide de sulfate cérique et suivi par la décroissance de la bande d'absorption caractéristique à 715 nm. Dans l'hypothèse où le produit final

[1]La revision reçue le 19 octobre 1980.

[2]Sur la nature de ces produits d'hydrolyse, cf. réf. 16.

0008-4042/81/071083-06$01.00/0

©1981 National Research Council of Canada/Conseil national de recherches du Canada

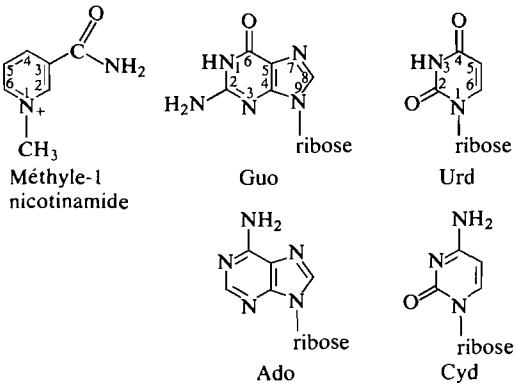

FIG. 1. Les composés étudiés: numérotation retenue pour la présentation des données rmn.

serait du platine(IV), ce dosage accorde au platine présent dans (B) un degré d'oxydation formel égal à $2{,}2_5 \pm 0{,}0_5$.

Ce résultat est en quelque sorte confirmé par l'observation de signaux RPE, faibles mais parfaitement discernables. Les spectres obtenus sont de symétrie axiale ($g_{\|} = 1{,}98$; $g_{\perp} = 2{,}40$) et présentent de très grandes analogies avec le spectre du complexe bleu obtenu à partir de 1′ α-pyridone (13).

La spectrographie infra-rouge enfin établit que le ligand intervient, dans les deux espèces, sous forme déprotonée et que la coordination se ferait à la fois par l'oxygène et le groupement NH de la fonction amide. Dans ces conditions, il semble raisonnable de représenter les espèces (A) et (B) par les formules respectives:

$$Pt_n(L\text{–}H)_nCl_{2n+1}(H_2O)_m$$

et

$$Pt_n(L\text{–}H)_n(NO_3)_{2n+1}(H_2O)_{2n}$$

avec $n = 4$ ou 5. m est variable suivant les échantillons mais reste compris entre 5 et 7. (L–H) désigne la forme déprotonée du méthyle-1 nicotinamide.

En définitive on peut dire que les complexes (A) et (B) présentent les caractéristiques habituelles des "bleus de platine": absorption dans le visible, production de signaux RPE. Ceci, joint aux faits que le platine se trouve dans un état d'oxydation fractionnaire et que le ligand se coordine par la fonction amide déprotonée, suggère que la structure de (A) et (B) doit présenter de nombreuses analogies avec celles qui ont été déjà proposées ou établies pour certains complexes de ce type (11–13).

Les spectres de résonance nucléaire confirment bien ces données, mais n'apportent que peu de renseignements supplémentaires. L'espèce (A), pratiquement insoluble dans l'eau, n'est que peu soluble dans le diméthylsulfoxyde et il n'a pas été possible d'obtenir de spectre de résonance ^{13}C. D'une façon générale, les spectres obtenus présentent des pics larges, mais dont il est possible d'évaluer la position. Les résultats sont rassemblés dans le tableau 1. Ils permettent de conclure que, dans les espèces (A) et (B), l'identité du ligand n'est pas altérée, si ce n'est que le groupement amide est déprotoné. Dans les spectres ^1H obtenus sur des solutions dans le DMSO, on observe en effet à la complexation un déplacement important du signal NH (de 8,6 à 4,4 ppm), cohérent avec la déprotonation du motif NH_2, alors que les autres signaux ne sont que très peu affectés. Au niveau des spectres ^{13}C, le passage du ligand libre à l'espèce (B) s'accompagne de modifications faibles sauf pour les noyaux C(3) et C(7) qui se trouveraient ainsi au voisinage du site de complexation.

2. *Interaction des complexes bleus avec les nucléosides*

D'une façon très générale, nous avons considéré les spectres de résonance (^1H et ^{13}C) de plusieurs mélanges présentant des proportions variées de complexe et de nucléoside en solution aqueuse. Les nucléosides envisagés sont la guanosine (guo), la cytidine (Cyd), l'uridine (Uri) et l'adénosine (Ado) (cf. fig. 1). Les mélanges sont examinés après une période de repos (12 h à 40°C, pD = 6) au terme de laquelle une filtration permet d'écarter l'excès éventuel de réactifs qui apparaît généralement quand le rapport [Nucl]/[Pt] est différent de deux.

Pour un rapport égal à deux, on obtient une dissolution totale des deux constituants, même si, pris séparément, ceux-ci sont insolubles (ou très faiblement solubles) dans l'eau au voisinage de la neutralité (cas de la guanosine et de l'espèce A par exemple). Cette observation suggère qu'une interaction privilégiée correspondrait à une stoechiométrie mettant en jeu deux molécules de nucléoside par atome de platine. En fait, l'examen des spectres de résonance confirme cette conclusion, sauf dans le cas de l'adénosine.

En ce qui concerne les signaux du méthyle-1 nicotinamide, un seul ensemble a pu être détecté dans tous les échantillons examinés de composition [Nucl]/[Pt] = 2/1.[3] Ces signaux sont facilement repérables, à l'exception de ceux qui correspondent aux carbones C(3) et C(7) qui, dans certains cas, n'ont pas été décelés. Quoi qu'il en soit, les signaux observés apparaissent toujours à ces posi-

[3]La largeur des pics de résonance ne permettrait pas de distinguer deux signaux présentant des déplacements différant de moins de 1 ppm.

Can. J. Chem. Downloaded from www.nrcresearchpress.com by 210.87.254.40 on 09/06/12
For personal use only.

Can. J. Chem. Downloaded from www.nrcresearchpress.com by 210.87.254.40 on 09/06/12
For personal use only.

TABLEAU 1. Déplacements chimiques δ^1H et $\delta^{13}C$ en ppm par rapport au TMS (solution aqueuse, pH 6)

	H(2)	H(4),H(5)	H(6)	CH_3
Ligand libre	9,22	8,11	8,89	4,33
Espèce (A)	9,6	8,3	9,1	4,3
Espèce (B)	9,5	8,2	9,0	4,3

	C(2)	C(3)	C(4)	C(5)	C(6)	C(7)	CH_3
Ligand libre	148,0	133,9	145,8	128,9	150,5	166,1	52,3
Espèce (B)	147,5	137,4	146,2	128,9	150,9	169,3	52,2

TABLEAU 2. Déplacements chimiques δ^1H dans les mélanges 2/1 (solution aqueuse, pH 6)

	H(2)	H(5)	H(6)	H(8)	H(1′)
Guo	—	—	—	8,00	5,94
Guo/(A)	—	—	—	8,72	5,96
Cyd	—	6,02	7,83	—	5,76
Cyd/(A)	—	6,14	7,95	—	5,82
Cyd/(B)	—	6,12	7,89	—	5,81
Uri	—	5,78	7,79	—	5,94
Uri/(B)	—	5,67	7,61	—	5,92
Ado	8,11	—	—	8,28	6,11
Ado/(A)	8,26 (8,66;8,59)[a]	—	—	8,71 (8,94;8,78)[a]	6,15 (m)[b]
Ado/(B)	8,22 (8,52;8,45)[a]	—	—	8,59 (8,81;8,66)[a]	6,12 (m)[b]

[a] Voir texte.
[b] Multiplets centrés sur 6,15 et 6,12 ppm.

tions extrêmement voisines de celles qu'ils ont dans les complexes bleus initiaux, soit: 169 pour C(7), 151 C(6), 148 C(2), 146 C(4), 137 C(3), 129 C(5) et 52 ppm. Il en est de même pour les spectres de résonance ^1H.

Au niveau des noyaux ^1H et ^{13}C des nucléosides, nous considérerons tout d'abord le cas des échantillons de composition 2/1. Les résultats obtenus sont rassemblés dans les tableaux 2 et 3. Les valeurs retenues pour les déplacements (δ^1H et $\delta^{13}C$) des nucléosides résultent de nos propres déterminations; elles sont en accord avec les données de la littérature (10, 18, 19, 21–27). Les déplacements des noyaux ^{13}C de l'ose ne sont pas rapportés ici, les modifications liées à l'introduction des espèces bleues restant inférieures ou au plus égales à 1,2 ppm.

A pH 6, la guanosine est sous forme neutre et la base présente un seul proton, H(8), non échangeable et nettement décelable dans le spectre (δ = 8,00 ppm) ainsi que le proton H(1′) de l'ose. Ce dernier n'est que peu affecté par l'addition du complexe (A), contrairement à H(8) dont le déplacement évolue fortement (0,72 ppm). Si le mélange réactionnel (2/1) est évaporé sous vide puis repris dans le diméthylsulfoxyde, on obtient un spectre d'aspect semblable à celui de la guanosine libre mais faisant apparaître un déplacement important de H(8) (8,64 pour 8,00 ppm dans la guanosine isolée) et des variations faibles pour les autres noyaux; H(1′) (5,82 pour 5,92), NH_2 (6,43 pour 6,31) et NH (10,05 pour 9,88 ppm). Il faut noter ici que ces solutions dans le diméthylsulfoxyde s'altèrent très rapidement, les spectres comportant plusieurs types de signaux attribuables au solvant. Les résultats obtenus à partir des spectres ^1H tendent à localiser l'interaction platine–guanosine au niveau de l'azote N(7), ce qui semble confirmé par l'étude de la résonance ^{13}C qui crédite le carbone C(8) de la plus forte perturbation.

Pour ce qui est de la cytidine, la base présente deux protons non échangeables H(5) et H(6), qui sont affectés dans des proportions très voisines par l'addition de (A) ou de (B). Les modifications enregistrées dans les spectres ^{13}C sont plus significatives. Elles privilégient très nettement les carbones C(2) et C(4) et désignent ainsi l'azote N(3) comme site d'interaction.

A pH 6, l'uridine se trouve essentiellement sous la forme déprotonée en N(3). Comme dans le cas de

TABLEAU 3. Déplacements chimiques $\delta^{13}C$ dans les mélanges 2/1 (solutions aqueuses, pH 6)

	C(2)	C(4)	C(5)	C(6)	C(8)
Guo	154,6	152,4	117,6	157,8	137,0
Guo/(A)	155,2	151,2	119,7	156,6	142,2
Cyd	158,0	166,8	96,3	142,2	
Cyd/(A) (2/1)	153,3	162,9	97,1	142,9	
Cyd/(B) (2/1)	154,8	163,7	96,8	142,5	
Uri	152,4	164,3	102,6	142,2	
Uri/(B) (2/1)	157,8	174,7	101,4	139,6	
Ado	153,0	150,1	120,4	156,8	140,7
Ado/(A)	156,1 (158,5;154,3)	150,1 (n.o.)	129,9 (n.o.)	160,8 (n.o.)	149,8 (146,7;142,2)
Ado/(B)	155,4	150,3	127,1	158,2	145,6

la cytidine, la base possède deux protons non échangeables H(5) et H(6). Aucune réaction n'a pu être mise en évidence à partir des spectres (^1H et ^{13}C) caractérisant des mélanges 2/1 et 1/1 d'uridine et de l'espèce chlorée (A). Au contraire, les mélanges 2/1 formés par l'espèce (B) sont le siège d'une forte baisse de pH (jusqu'à la valeur 1,5). Les spectres obtenus après avoir ramené le pH à la valeur 6 présentent des modifications significatives. Ceci est particulièrement net pour les spectres ^{13}C dans lesquels les noyaux C(4) et C(2) sont le plus fortement affectés. Ces effets désignent l'azote N(3) comme site d'interaction.

Dans le cas de l'adénosine, les spectres ^1H ne conduisent pas à des résultats totalement dépourvus d'ambiguïté. Sous forme neutre, ce nucléoside présente, au niveau de la base, deux protons non échangeables H(2) et H(8) dont les déplacements sont voisins (8,11 et 8,28 ppm). Cette proximité rend délicat l'établissement d'une filiation entre les spectres du ligand libre et complexé, et ce d'autant plus que plusieurs jeux de signaux se manifestent dans les spectres des mélanges. Pour les mélanges 2/1 constitués à partir de l'espèce (A), un de ces jeux (8,26; 8,71 ppm) se distingue des deux autres (8,94; 8,78 et 8,66; 8,59 ppm) par une intensité nettement plus marquée.On observe également plusieurs signaux aux environs de 6,16 ppm. Ces remarques peuvent être étendues aux spectres ^1H des mélanges formés par l'espèce (B) et aux spectres ^{13}C. Pour ces derniers, l'ensemble principal de signaux fait apparaître des perturbations maximales pour les noyaux C(5) et C(8). Ces effets seraient cohérents avec l'existence d'une interaction en N(7).

En définitive, les résultats obtenus pour des mélanges 2/1 permettent de penser que, vis-à-vis du platine engagé dans les espèces bleues (A) et (B), les nucléosides se comportent préférentiellement comme des ligands monodentates par l'intermédiaire des sites N(7) (Guo et Ado) et N(3) (Cyd et Uri).

Ces sites d'interaction sont ceux qui sont le plus généralement retenus dans la littérature (10, 18, 19, 21–28). Des interactions secondaires sont suggérées dans le cas de l'adénosine. Nous les envisagerons plus loin.

Les spectres correspondant à des mélanges de compositions différentes de 2/1 sont, le plus souvent, identiques à ceux des mélanges 2/1.

Les constituants en excès n'apparaissent pas dans les spectres (cas des constituants insolubles ou peu solubles tels que l'espèce (A) ou la guanosine) ou donnent des signaux facilement repérables (constituants solubles comme, par exemple, l'espèce (B)).

Dans deux cas cependant les modifications de composition se traduisent par des changements significatifs dans l'allure des spectres: apparition de nouveaux signaux (guanosine et défaut de (A)) ou variation des intensités relatives des différents ensembles de signaux (adénosine et excès ou défaut de (A) ou (B)).

C'est ainsi que, dans le premier cas, on note dans les spectres ^1H l'apparition, à côté du pic principal précédemment observé (8,72 ppm), d'un pic secondaire à 8,51 ppm. De la même façon, les spectres ^{13}C présentent de nouveaux signaux à 128,5;186,8 et 155,5 ppm. Ces nouveaux signaux pourraient correspondre à une interaction secondaire mettant en jeu les sites O(6) et N(7) de la guanosine (26, 29, 30).

Dans le cas de l'adénosine, les modifications du rapport [Nucl]/[Pt] provoquent des changements dans les intensités relatives des trois ensembles de signaux qui sont déjà présents dans les spectres des mélanges 2/1.

Il faut noter ici qu'en résonance de ^{13}C, on n'observe qu'une partie des signaux attendus dans l'hypothèse de la coexistence de trois formes. Ceci

Can. J. Chem. Downloaded from www.nrcresearchpress.com by 210.87.254.40 on 09/06/12
For personal use only.

Can. J. Chem. Downloaded from www.nrcresearchpress.com by 210.87.254.40 on 09/06/12
For personal use only.

peut être dû au fait que deux de ces formes sont toujours présentes en faibles quantités et que, dans ces conditions, certains signaux, ceux des carbones quaternaires en particulier, ont une intensité très faible. En effet, l'espèce majoritaire dans les spectres des mélanges 2/1 l'emporte toujours sur les deux autres. L'observation de plusieurs ensembles de signaux peut être rapprochée des remarques déjà formulées (21, 25, 31) et concernant les possibilités d'interaction de l'ion métallique avec l'adénosine au niveau de N(7), mais aussi de N(1) et même, simultanément, de N(1) et N(7), le nucléoside jouant alors le rôle de pont entre deux centres métalliques pour conduire à un complexe dinucléaire. Ces hypothèses seraient compatibles avec les valeurs des déplacements observés ici, ainsi qu'avec les modifications d'intensité des signaux en fonction de la composition des mélanges étudiés.

Conclusions

Pour conclure cette étude, nous retiendrons tout d'abord que si la rmn (^1H et ^{13}C) n'est pas un outil de choix pour étudier les complexes bleus du platine, cette spectroscopie peut être utilisée pour préciser la nature des sites d'interaction des nucléosides avec ces espèces bleues. Dans les conditions expérimentales utilisées (pD = 6, solutions aqueuses relativement concentrées (de l'ordre de 0,1 M)) les espèces bleues (A) et (B) obtenues à partir du méthyle-1 nicotinamide réagissent avec les nucléosides suivant des processus extrêmement voisins de ceux observés pour les complexes plus "classiques" du platine(II) ou du palladium(II). Il apparaît en effet que les interactions se situent essentiellement au niveau des sites N(7) (Guo et Ado) et N(3) (Cyd et Uri), les nucléosides se comportant en ligands monodentates et l'uridine réagissant sous forme déprotonée.

L'intervention d'interactions secondaires au niveau des sites O(6) (Guo) et N(1) (Ado) pourrait être également envisagée, en particulier quant le rapport des concentrations [Nucl]/[Pt] devient inférieur à 2. L'intensité des signaux qui leur correspondent reste cependant toujours faible.

Il est intéressant de noter qu'aucune modification importante de la position ou de la largeur des signaux attribuables au méthyle-1 nicotinamide n'intervient quand on passe des espèces bleues initiales (A) et (B) aux mélanges renfermant les nucléosides. Par ailleurs, ces mélanges conservent, pendant un certain laps de temps (de l'ordre de plusieurs jours) après leur préparation, une coloration bleue et continuent à donner des signaux RPE complexes mais décelables. Ces deux observations suggèrent que la structure des espèces (A) et (B) n'est pas profondément modifiée par l'interaction avec les nucléosides. Dans la mesure où les propriétés de (A) et de (B) permettent de les rapprocher des autres bleus connus et de leur attribuer une structure semblable, il semblerait que l'enchaînement d'atomes de platine dans un état d'oxydation fractionnaire soit conservé et que l'interaction avec les nucléosides ne fasse pas intervenir une forme mononucléaire comme cela a été suggéré pour les systèmes bleus de platine – protéines (32).

Partie expérimentale

La préparation des espèces bleues (A) et (B) a été décrite par ailleurs (14). Les nucléosides utilisés sont des produits commerciaux.

Les mélanges réalisés dans l'eau lourde à partir des constituants en proportions variables ne sont étudiés qu'après une période de repos (12 h à 40°C, pH = 6) à l'obscurité.

Les spectres rmn ont été réalisés sur un appareil Bruker WH 90 opérant à 90,00 MHz pour ^1H et à 22,62 MHz pour ^{13}C en mode pulsé avec transformation de Fourier. De 30 000 à 50 000 signaux de libre précession ont été accumulés dans 8K mémoire pour la résonance de ^{13}C. On a utilisé un temps de répétition de 3 s et une impulsion voisine de 60°.

1. R. PHILLIPS. Chem. Rev. **66**, 501 (1966).
2. R. M. IZATT, J. J. CHRISTENSEN et J. H. RYTTING. Chem. Rev. **71**, 439 (1971).
3. B. ROSENBERG. Naturwissenschaften, **60**, 399 (1973).
4. J. P. DAVIDSON, P. J. FABER, R. G. FISHER, JR., D. MANSY, H. J. PERESIE, B. ROSENBERG et L. VAN CAMP. Cancer Chemother. Rep. **59**, 287 (1975).
5. B. ROSENBERG. Cancer Chemother. Rep. **59**, 589 (1975).
6. K. A. HOFMANN et G. BUGGE. Chem. Ber. **41**, 312 (1908).
7. R. D. GILLARD et G. WILKINSON. J. Chem. Soc. 2835 (1964).
8. B. B. BROWN, R. D. BURBANK et M. B. ROBIN. J. Am. Chem. Soc. **90**, 5621 (1968); **91**, 2895 (1969).
9. J. K. BARTON, H. N. RABINOWITZ, D. J. SZALDA et S. J. LIPPARD. J. Am. Chem. Soc. **97**, 5305 (1975).
10. G. Y. H. CHU, R. E. DUNCAN et R. S. TOBIAS. Inorg. Chem. **16**, 2625 (1977).
11. J. K. BARTON, S. A. BEST, S. J. LIPPARD et R. A. WALTON. J. Am. Chem. Soc. **100**, 3785 (1978).
12. J. K. BARTON, D. J. SZALDA, H. N. RABINOWITZ, J. V. WASZCZAK et S. J. LIPPARD. J. Am. Chem. Soc. **101**, 1434 (1979).
13. J. K. BARTON, C. CARAVANA et S. J. LIPPARD. J. Am. Chem. Soc. **101**, 7269 (1979).
14. J.-P. LAURENT, P. LEPAGE et F. GALLAIS. C.R. Acad. Sci. **287**C, 543 (1978).
15. K. V. SHOOTER, R. HOWSE, R. K. MERRIFIELD et A. B. ROBINS. Chem. Biol. Inter. **5**, 289 (1972).
16. J. J. ROBERTS et J. M. PASCOE. Nature, **235**, 282 (1972).
17. I. A. G. ROOS, A. J. THOMSON et S. MANSEY. J. Am. Chem. Soc. **96**, 6484 (1974).
18. R. W. GELLERT et R. BAU. J. Am. Chem. Soc. **97**, 7379 (1975).
19. J.-P. MACQUET et TH. THEOPHANIDES. Biopolymers, **5**, 51 (1975).
20. A. J. THOMSON, I. A. G. ROOS et R. D. GRAHAM. J. Clin. Hemat. Oncol. **7**, 242 (1977).

21. M. C. LIM et R. B. MARTIN. J. Inorg. Nucl. Chem. **38**, 1911 (1976).
22. M. T. CHENON, P. J. PUGMIRE, D. M. GRANT et R. P. PAUZICA. J. Am. Chem. Soc. **97**, 4627 (1975).
23. J. B. STOTHERS. Carbon-13 NMR spectroscopy. Academic Press, New York, NY. 1972.
24. D. J. NELSON, PH. L. YEAGLE, TH. L. MILLER et R. B. MARTIN. Bioinorg. Chem. **5**, 353 (1976).
25. N. HADJILIADIS et TH. THEOPHANIDES. Inorg. Chim. Acta, **16**, 67 (1976).
26. N. HADJILIADIS et TH. THEOPHANIDES. Inorg. Chim. Acta, **16**, 77 (1976).
27. J. DEHAND et J. JORDANOV. J. Chem. Soc. Dalton Trans. 1588 (1977).
28. W. M. SCOVELL et T. O'CONNOR. J. Am. Chem. Soc. **99**, 120 (1977).
29. G. PNEUMATIKIS, N. HADJILIADIS et TH. THEOPHANIDES. Inorg. Chim. Acta, **22**, L1 (1977).
30. J. DEHAND et J. JORDANOV. J. Chem. Soc. Chem. Commun. 598 (1976).
31. N. HADJILIADIS, P. KOUKOURANIS et TH. THEOPHANIDES. Inorg. Chim. Acta, **7**, 226 (1973).
32. C. C. F. BLAKE, S. J. OATLEY et R. J. P. WILLIAMS. J. Chem. Soc. Chem. Commun. 1043 (1976).

Can. J. Chem. Downloaded from www.nrcresearchpress.com by 210.87.254.40 on 09/06/12
For personal use only.

Hydrolyse des dérivés de cyclopropylidène-3 propyle. Structure et stéréochimie des alcools précurseurs et des produits résultant de l'hydrolyse

ROBERT FAURE

Laboratoire de Chimie Organique Physique, Université d'Aix-Marseille III, Rue H. Poincaré, 13397 Marseille Cedex 4, France

ET

GILBERT LEANDRI ET ALAIN MEOU

Laboratoire Associé au C.N.R.S. no 109, Université d'Aix-Marseille III, Rue H. Poincaré, 13397 Marseille Cedex 4, France

Reçu le 3 octobre 1980

ROBERT FAURE, GILBERT LEANDRI et ALAIN MEOU. Can. J. Chem. **59**, 1089 (1981).

Nous avons enregistré les spectres de rmn du carbone-13 de 14 alcools β-cyclopropylidéniques **1**, de structure

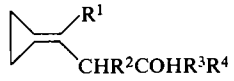

(R¹, R², R³ et R⁴ = H ou CH_3)

Tous les déplacements chimiques ont été attribués et les effets de substituant sont discutés en fonction de la conformation moléculaire. La stéréochimie des deux diastéréoisomères des alcools **1***e* ($R^1 = R^3 = H$; $R^2 = R^4 = CH_3$) et **1***k* ($R^3 = H$; $R^1 = R^2 = R^4 = CH_3$) a été établie à partir des résultats de spectroscopie infrarouge et de résonance magnétique nucléaire du proton.

Nous avons également enregistré les spectres de carbone-13 des produits résultant de l'hydrolyse des tosylates de cyclopropylidène-3 propanol **1***a* et de cyclopropylidène-4 butanol-2 **1***b*. L'analyse de ces données permet d'établir sans ambiguité la structure et la stéréochimie des produits d'hydrolyse.

ROBERT FAURE, GILBERT LEANDRI, and ALAIN MEOU. Can. J. Chem. **59**, 1089 (1981).

The ^{13}C nmr spectra of 14 β-cyclopropylidenic alcohols **1** have been determined:

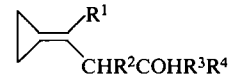

(R¹, R², R³ and R⁴ = H or CH_3)

All the chemical shifts were assigned and the substituent effects are discussed as a function of molecular conformation. The stereochemistry of two diastereoisomers of alcohols **1***e* ($R^1 = R^3 = H$; $R^2 = R^4 = CH_3$) and **1***k* ($R^3 = H$; $R^1 = R^2 = R^4 = CH_3$) was established from ir spectroscopy and ^1H nmr results.

The ^{13}C nmr spectra of products arising from hydrolysis of 3-cyclopropylidene propanol **1***a* and 4-cyclopropylidene 2-butanol **1***b* tosylates have been also recorded. The analysis of these data enables us to establish unambiguously the structure and the stereochemistry of the hydrolysis products.

Introduction

Dans un récent travail (1), nous avons montré l'aptitude qu'avaient les tosylates de cyclopropylidène-3 propyle **I** à se réarranger au cours de réactions de solvolyse. Les premiers résultats expérimentaux sont en faveur d'une participation du doublet π de la liaison éthylénique au départ du groupement partant, le cation cyclopropyl-cyclopropyle ainsi formé pouvant évoluer et conduire aux composés **2** à **4** (figure 1). Les structures de ces composés ont été déduites des résultats de spectroscopie infrarouge et de résonance magnétique nucléaire du proton à 60 MHz. Ces méthodes analytiques n'ont toutefois pas permis de déterminer la stéréochimie des dérivés de la série *b* (R = CH_3).

Pour confirmer l'hypothèse d'une participation du doublet π au départ du processus d'hydrolyse, les études cinétiques et stéréochimiques sont actuellement en cours;[1] de telles études nécessitent une connaissance précise de la stéréochimie des produits d'hydrolyse et des alcools β-cyclopropylidéniques **1** précurseurs des tosylates **I**. La résonance magnétique nucléaire du carbone-13 qui est une méthode dont les avantages en analyse conformationnelle sont reconnus (2, 3), convient tout à fait à ce genre d'études. En associant à ces résultats de ^{13}C d'autres données spectroscopiques, infrarouge ou rmn du proton à haut champ, nous allons montrer qu'il est possible d'une part de confirmer ou d'infirmer les structures précédemment proposées pour les composés **2** à **4** (1), d'autre part de déterminer la stéréochimie des alcools β-cyclopropylidéniques **1** et des différents produits d'hydrolyse de la série *b*.

Partie expérimentale

Les spectres de carbone-13 ont été enregistrés sur un spectromètre Varian FT-80 à la température de 28 ± 2°C. Les déplacements chimiques mesurés sur les spectres totalement découplés par bruit sont rapportés au signal du TMS pris comme référence interne. Pour chacun des composés un spectre en découplage partiel a été enregistré afin de déterminer la multipli-

[1] M. Bertrand, G. Leandri et A. Meou. Travaux non publiés.

0008-4042/81/071089-07$01.00/0

©1981 National Research Council of Canada/Conseil national de recherches du Canada

Can. J. Chem. Downloaded from www.nrcresearchpress.com by 210.87.254.6 on 09/06/12
For personal use only.

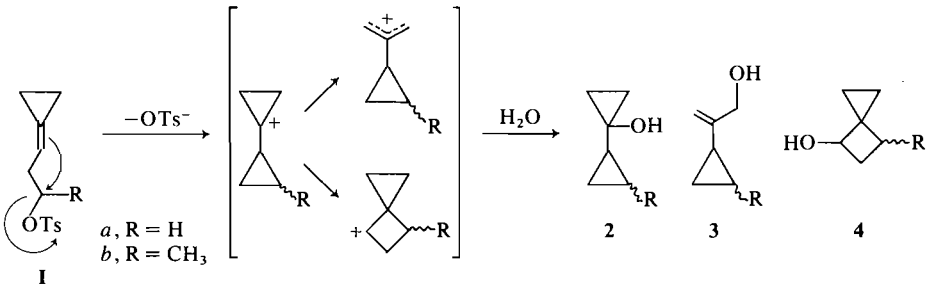

FIG. 1. Structure des produits résultant de l'hydrolyse des tosylates de cyclopropylidène-3 propyle **I** (1).

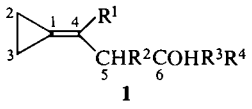

1

R^1, R^2, R^3 et R^4 = H ou CH_3

cité des différents signaux de résonance. Les spectres de proton ont été obtenus en balayage de fréquence sur un spectromètre Cameca opérant à 250 MHz (T = 20°C). Ces différentes études spectroscopiques ont été réalisées en solution dans le chloroforme deutérié à l'exception des spectres de ^{13}C des composés **1***a* à **1***c* qui ont été enregistrés dans l'acétone deutériée. Enfin les diverses méthodes utilisées pour la préparation des alcools β-cyclopropylidéniques **1** ont déjà été décrites dans un récent mémoire (4).

Structure et stéréochimie des alcools β-cyclopropylidéniques

Les déplacements chimiques du carbone-13 des alcools β-cyclopropylidéniques **1** sont présentés dans le tableau 1.

Stéréochimie des alcools **1***e et* **1***k*

Les alcools secondaires **1***e* et **1***k* qui possèdent deux centres asymétriques sont obtenus sous forme de couples de diastéréoisomères (**A** et **B**); l'isomère **A**, élué le premier en chromatographie en phase vapeur sur colonne polaire, est toujours majoritaire: 56% dans le cas de **1***e* et 79% dans le cas de **1***k* (4). La stéréochimie de ces alcools peut aisément être établie par spectroscopie infrarouge; en effet, comme cela a déjà été mis en évidence dans le cas des alcools β-éthyléniques (5, 6) dans les alcools du type **1** le groupement hydroxyle doit être lié intramoléculairement avec les électrons π de la liaison éthylénique pour former une liaison hydrogène. Puisque la bande d'absorption $\nu_{(OH)}$ relative à cette chélation est insensible aux effets de dilution (7), une étude en fonction de la concentration permet alors de déterminer la force d'une telle liaison et, par conséquent, d'accéder à la stéréochimie des alcools étudiés.

En ce qui concerne **1***e* et **1***k*, l'examen des spectres infrarouge (4) montre que cette association intramoléculaire est plus importante pour l'isomère **A**. Si l'on considère les différents rotamères des formes *érythro* et *thréo* des alcools **1***e* et **1***k* (figure 2), on constate que, compte tenu des interactions *gauches* déstabilisantes entre groupements volumineux, l'association par liaison hydrogène est particulièrement favorisée pour le rotamère T1. On peut donc affirmer que **A** est l'isomère *thréo*.

Cette chélation est beaucoup plus intense pour **1***k***A** que pour **1***e***A**; cela s'explique, d'une part par une nucléophilie accrue du système π (effet donneur du méthyle), et, d'autre part, par une déstabilisation plus importante des rotamères T2 et T3 (perturbations supplémentaires apportées par le groupement méthyle).

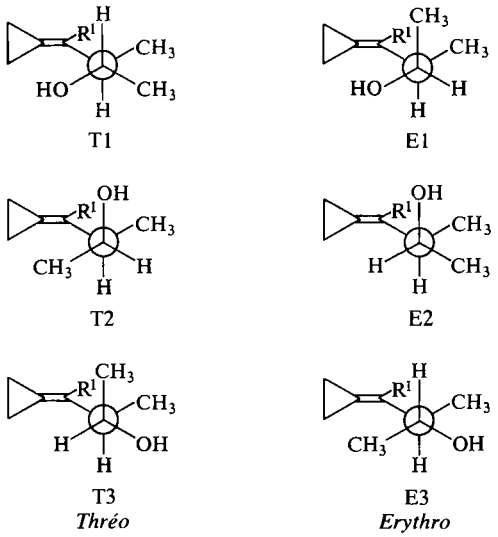

FIG. 2. Représentation de Newman des différents rotamères des formes *érythro* et *thréo* de **1***e* (R^1 = H) et de **1***k* (R^1 = CH_3).

La mesure de la constante de couplage[2] entre les deux protons portés par les carbones asymétriques confirme en partie les conclusions précédentes. Selon Karplus (8), le couplage entre protons vicinaux doit être plus élevé pour les rotamères dont les liaisons CH se trouvent en position antipériplanaire. Dans ces conditions on devrait observer une

[2]Cette valeur est déterminée par une analyse de la figure de couplage du proton H(6); on simplifie cette analyse par une irradiation des protons du groupement méthyle R^3 (ou R^4).

Can. J. Chem. Downloaded from www.nrcresearchpress.com by 210.87.254.6 on 09/06/12
For personal use only.

Can. J. Chem. Downloaded from www.nrcresearchpress.com by 210.87.254.6 on 09/06/12
For personal use only.

TABLEAU 1. Déplacements chimiques du ^{13}C. Alcools β-cyclopropylidéniques

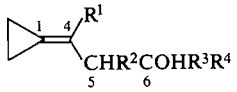

1

No	R^1	R^2	R^3	R^4	C-1	C-2	C-3	C-4	C-5	C-6	Autres
1*a***	H	H	H	H	123.2	2.5	1.9	115.7	36.2	62.2	
1*b***	H	H	CH_3	H	123.4	2.6	1.8_5	115.8	42.4	67.6	$R^3 = 23.3$
1*c***	H	H	CH_3	CH_3	124.1	2.9	1.8	115.5	46.9	70.9	$R^3 = R^4 = 29.3$
1*d*	H	CH_3	H	H	121.6	2.6	1.7	121.0	39.4	67.4	$R^2 = 16.9$
1*e***A**†	H	CH_3	CH_3	H	122.7	2.5	2.0_5	120.5	44.2	71.4	$R^2 = 16.1$; $R^3 = 20.0$
1*e***B**†	H	CH_3	H	CH_3	122.1	2.6	1.9	120.6	44.1	71.6	$R^2 = 15.9$; $R^4 = 20.4$
1*f*	H	CH_3	CH_3	CH_3	122.7	2.4‡	2.3‡	120.3	47.8	73.1	$R^2 = 15.4$; $R^3 = R^4 = 26.8$
1*g*	CH_3	H	H	H	117.2	1.8	3.0	121.2_5	39.9	60.6	$R^1 = 20.9$
1*h*	CH_3	H	CH_3	H	117.9	2.1	3.0_5	121.9	46.8	66.1	$R^1 = 21.1$; $R^3 = 23.1$
1*i*	CH_3	H	CH_3	CH_3	119.5	2.6_5	3.5	122.2	50.4	72.1	$R^1 = 23.0$; $R^3 = R^4 = 29.9$
1*j*	CH_3	CH_3	H	H	116.5	0.9	3.5	125.8	42.9	66.0	$R^1 = 18.7$; $R^2 = 15.7$
1*k***A**†	CH_3	CH_3	CH_3	H	117.3	1.3	3.5	126.4	48.3	69.7_5	$R^1 = 18.6$; $R^2 = 14.9$; $R^3 = 20.2$
1*k***B**†	CH_3	CH_3	H	CH_3	116.5	1.0	3.8	127.8	47.6	70.2	$R^1 = 19.5$; $R^2 = 13.9$; $R^4 = 21.2$
1*l*	CH_3	CH_3	CH_3	CH_3	118.1	1.8	4.2	127.0	50.4_5	73.8	$R^1 = 20.5$; $R^2 = 14.0$; R^3‡ = 28.3; R^4‡ = 28.0

*Ces composés ont été étudies en solution dans l'acétone deutériée.
†La stéréochimie de ces structures sera précisée par ailleurs (voir texte).
‡Déplacements dont l'attribution peut être inversée.

valeur plus grande pour l'isomère *thréo* du fait de la stabilité préférentielle du rotamère T1. Cette proposition est vérifiée pour **1***k* (**A**, $J_{H(5)H(6)} = 9.7_5$ Hz; **B**, $J_{H(5)H(6)} = 7.2_5$ Hz). Par contre, en ce qui concerne **1***e*, les deux couplages sont identiques (6 Hz), ce qui empêche toute conclusion sur la stéréochimie des deux diastéréoisomères. Cependant ces résultats traduisent la grande stabilité du rotamère E3, qui est, notons le, le plus apte à donner des associations intermoléculaires.

Enfin, compte tenu du mode de préparation de ces alcools (4), la prépondérance de l'isomère *thréo* est conforme à la règle de Cram et Abd Alhafez (9) qui prévoit une attaque privilégiée sur la face la moins encombrée du carbonyle.

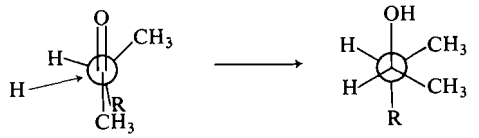

Isomère *thréo*

Attribution des déplacements chimiques et analyse des effets de substituant

En tenant compte de la multiplicité des différents signaux de résonance et des résultats de la littérature (2, 10) concernant des molécules de structure voisine, nous pouvons attribuer sans ambiguité les déplacements chimiques des différents carbones exceptés ceux relatifs aux carbones C-2 et C-3. Cette dernière attribution, qui dépend de la substitution de la position 4, nécessite de ce fait une discussion plus détaillée.

Dans le cas des composés **1***a* à **1***f* ($R^1 = H$), le carbone C-3 résonne à champ plus fort que C-2 (effet γ gauche (11)). Toutefois, en ce qui concerne **1***f*, il n'en est plus ainsi puisque les raies de résonance de ces deux atomes sont pratiquement confondues. Nous proposerons ultérieurement une explication à ce phénomène. Considérons maintenant les dérivés **1***g* à **1***k* ($R^1 = CH_3$): la méthylation en position 4 est à l'origine de nouvelles interactions qui n'étaient pas prises en compte dans la première série. En conséquence certaines conformations, moins encombrées d'un point de vue stérique, vont être favorisées, en particulier celles dans lesquelles le carbone C-6 se trouve à proximité de C-3, et ce comme le montre la figure suivante:

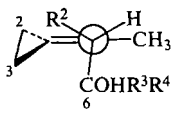

Notons que ce type de conformation est également stabilisé par la liaison hydrogène existant entre ce groupement hydroxyle et les électrons de la liaison éthylénique (voir le précédent chapitre). De l'interaction entre les carbones C-3 et C-6 (interaction δ stérique (12)) il s'ensuit un déblindage de C-3. L'ordre des déplacements chimiques est alors inversé par rapport à la première série d'alcools. Dans le cas de **1***k* on peut également invoquer l'existence de conformations privilégiées dans lesquelles C-6 se trouve dans le voisinage de C-3. Toutefois l'effet de déblindage est moins prononcé, compte tenu des plus faibles interactions stériques ($R^1 = H$).

Structure et stéréochimie des produits d'hydrolyse

Les alcools **1***a* et **1***b* sont convertis en tosylates puis hydrolysés. Les produits formés et présents en quantité suffisante pour pouvoir être séparés par chromatographie en phase vapeur sont alors analysés.

*Cas du cyclopropylidène-3 propanol 1*a

En plus de **1***a* non transposé, on isole deux alcools **2***a* et **3***a* (figure 3) dont les structures respectives ont été déduites des résultats de spectroscopie infrarouge et de résonance magnétique nucléaire du proton (1). En ce qui concerne l'hydroxy-1 cyclopropyl-1 cyclopropane **2***a* et le cyclopropyl-2 propène-2 ol-1 **3***a*, leurs données spectroscopiques sont cohérentes avec celles de la littérature (13–15). Les structures proposées pour **2***a* et **3***a* sont confirmées par les résultats de la rmn du ^{13}C. Les déplacements chimiques de ces composés sont donnés dans le tableau 2.

*Cas du cyclopropylidène-4 butanol-2 1*b

Les structures des différents produits isolés sont présentées en figure 4. Dans notre précédent travail, la stéréochimie de ces composés n'avait pas été précisée; seul le pourcentage global des différents isomères avait été donné, excepté pour **3***b* où les formes *cis* et *trans* avaient été séparées par

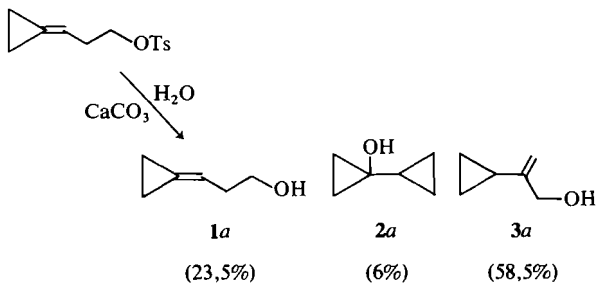

FIG. 3. Structure des produits d'hydrolyse du tosylate de cyclopropylidène-3 propanol **1***a*.

Can. J. Chem. Downloaded from www.nrcresearchpress.com by 210.87.254.6 on 09/06/12
For personal use only.

TABLEAU 2. Déplacements chimiques du ^{13}C. Composés **2** et **3**

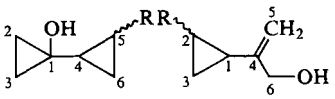

2*a* R = H **3***a* R = H
2*b* R = CH_3 **3***b* R = CH_3

Composés	C-1	C-2	C-3	C-4	C-5	C-6	R
2*a*	57.2	11.6	11.6	16.5	2.7_5	2.7_5	
2*b cis*	54.8	11.4*	13.7*	29.4	10.4	12.9*	21.8
2*b trans*	56.7	11.1_5*	12.0*	25.3	10.9	11.8*	18.6_5
3*a*	13.3_5	6.0_5	6.0_5	150.5	106.3	65.5	
3*b cis*	18.9	11.8	9.4	146.6	109.3	66.8	12.6
3*b trans*	22.1_5	15.0	14.5	150.4	105.6	65.5	19.0

*Déplacements dont l'attribution peut être inversée.

TABLEAU 3. Comparaison entre déplacements chimiques théoriques et expérimentaux. Structures **2***b* et **3***b*

		Forme *cis*			Forme *trans*		
Composés	Atome	obs.	calc.	écart*	obs.	calc.	écart*
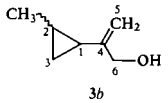 **3***b*	1	18.9	22.2_5	3.3_5	22.1_5	22.2_5	0.1
	2	11.8	14.2_5	2.4_5	15.0	14.2_5	-0.7_5
	3	9.4	14.9_5	5.5_5	14.5	14.9_5	0.4_5
	CH_3	12.6	19.6	7.0	19.0	19.6	0.6
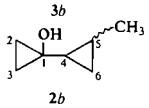 **2***b*	4	29.4	25.4	−4.0	25.3	25.4	0.1
	5	10.4	11.6_5	1.2_5	10.9	11.6_5	0.7_5
	6	12.9	10.9_5	-2.0_5	11.8	10.9_5	-0.8_5
	CH_3	21.8	19.6	−2.2	18.6_5	19.6	0.9_5

*Ecart = δcalc. − δobs.

chromatographie préparative en phase vapeur mais non identifiées.

Détermination de la stéréochimie de **2**b *et* **3**b

Stothers *et al.* (16) ont montré que la stéréochimie de systèmes rigides peut être simplement déterminée par comparaison entre les déplacements chimiques expérimentaux et ceux calculés par additivité des effets de substituant. En ce qui concerne des substituants vicinaux, les écarts à l'additivité sont plus importants pour l'isomère *cis* (effets stériques) que pour l'isomère *trans*. Ces déviations représentent des interactions de second ordre (interactions croisées) qui ne sont pas prises en compte dans le cas des dérivés monosubstitués. En série cyclopropanique nous avons déjà montré l'importance de telles interactions dans le cas des isomères *cis* (17).

Les déplacements chimiques des formes *cis* et *trans* des composés **2***b* et **3***b* sont présentés dans le tableau 2. Dans le tableau 3 sont rassemblées les valeurs théoriques et expérimentales des déplacements chimiques des carbones cyclopropaniques

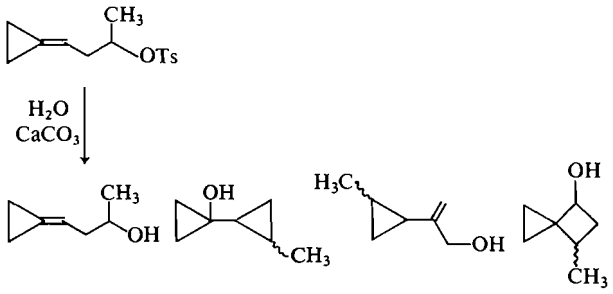

FIG. 4. Produits isolés lors de l'hydrolyse du tosylate de cyclopropylidène-4 butanol-2 **1***b*.

de **2***b* et **3***b* ainsi que les valeurs des déviations. Les données relatives au méthyl cyclopropane sont issues de la référence 17.

En ce qui concerne **2***b*, le pourcentage de forme *trans*, calculé par intégration de pics devant présenter une relaxation similaire est d'environ 15%.

Can. J. Chem. Downloaded from www.nrcresearchpress.com by 210.87.254.6 on 09/06/12
For personal use only.

Can. J. Chem. Downloaded from www.nrcresearchpress.com by 210.87.254.6 on 09/06/12
For personal use only.

TABLEAU 4. Déplacements chimiques du ^{13}C. Dérivés du spiro [2,3] hexane

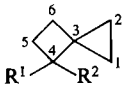

Composé	R^1	R^2	C-1	C-2	C-3	C-4	C-5	C-6	Autres
6*	H	H	12.4	12.4	20.2	31.2	17.3	31.2	
7	H	OH	7.2	9.3	28.1	71.0	30.4_5	23.5	
8	CH_3	OH	7.6	8.9	31.3	74.1	36.2	23.1	CH_3 : 24.6

*Valeurs de la référence 18.

Contrairement à **3***b* (pour lequel la forme *trans* est prépondérante) le groupement méthyle est plus blindé en position *trans* qu'en position *gauche*. De plus la non-équivalence des méthylènes cyclopropaniques (carbones C-2 et C-3) des formes *cis* et *trans* de **2***b* suggère une rotation empêchée autour de la liaison C1—C4; ce phénomène n'est pas observé pour le dérivé non substitué **2***a*.

Détermination de la structure de **4**b

L'analyse du spectre de ^{13}C de ce composé montre l'existence de deux formes, présentes en proportions équivalentes, et de déplacements chimiques très proches. La structure précédemment proposée (1) pour **4***b*, à savoir l'hydroxy-4 méthyl-6 spiro [2,3] hexane n'est pas compatible avec les données de ^{13}C. En effet, d'une part les méthyles sont équivalents dans chacune de ces deux formes, alors qu'on s'attendrait à des valeurs différentes des déplacements chimiques si les structures étaient du type ci-dessous (*trans* ou *cis*); d'autre part, les

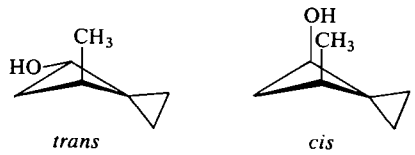

trans *cis*

déplacements chimiques de **4***b* ne sont pas en accord avec les valeurs observées pour le spiro [2,3] hexane **6** (18) et ses dérivés **7** et **8**. Ces deux derniers composés ont été spécialement synthétisés pour cette étude selon des méthodes déjà décrites dans la littérature (19). Les déplacements chimiques des composés **6** à **8** sont présentés dans le tableau 4.

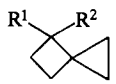

6 $R^1 = R^2 = H$
7 $R^1 = H; R^2 = OH$
8 $R^1 = CH_3; R^2 = OH$

Compte tenu des remarques précédentes il est nécessaire de considérer une évolution différente du cation cyclopropyl-cyclopropyle (cf. figure 1) primitivement formé lors de l'hydrolyse. On peut ainsi envisager la formation d'un composé possédant la structure **5***b*: la présence de deux centres asymétriques expliquant l'existence des deux formes, en l'occurrence des diastéréoisomères, précédemment mises en évidence par rmn du carbone-13.

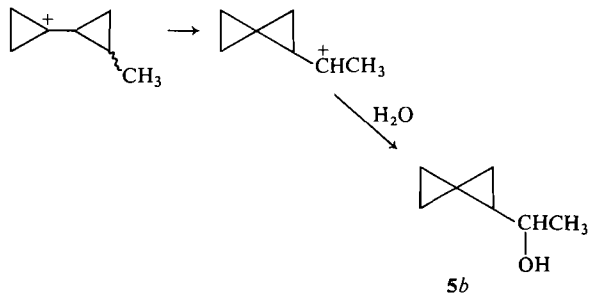

5*b*

Une manière élégante de vérifier notre hypothèse, et, dans le même temps, de réaliser une attribution univoque des déplacements chimiques des deux diastéréoisomères, consiste en une synthèse stéréospécifique de **5***b*. Il a déjà été montré (20, 21) que la cyclopropanation d'alcools allyliques[3] selon la méthode de Simmons-Smith conduit à un seul diastéréoisomère.

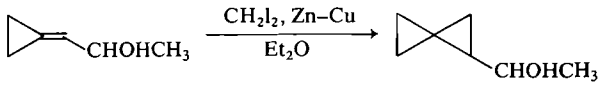

Racémique Un seul diastéréoisomère

Le conformère le plus apte à réagir est celui dont le groupement cyclopropylidénique est éclipsé par le proton du carbone fonctionnel, ce qui permet

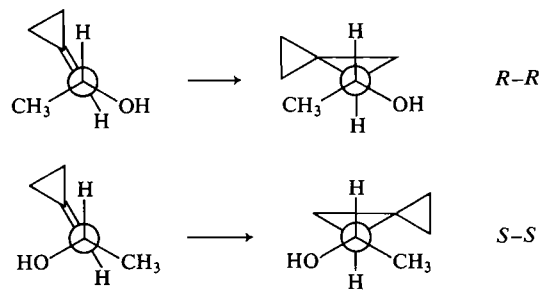

R–R

S–S

[3]Ces alcools doivent nécessairement posséder un groupement en *cis* de la chaîne portant l'hydroxyle.

TABLEAU 5. Déplacements chimiques du ^{13}C. Spiro [2,2]pentyl-1 éthanol

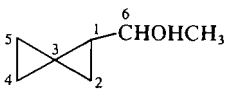

	Composés		
	S–R ou *R–S*	*R–R* ou *S–S*	
Atomes	Solvolyse	Solvolyse	Simmons-Smith
C-1	25.3	25.1	25.1
C-2	10.9_5	10.0	10.0
C-3	12.7	13.8	13.9
C-4	3.3	3.7	3.7
C-5	5.1	5.8	5.8
C-6	72.0	71.8	71.8
CH_3	22.6	22.6	22.7

l'attaque du réactif iodozincique et sa complexation par le groupement hydroxyle. Deux conformères présentent cette disposition et conduisent aux deux énantiomères *R–R* ou *S–S*.

La formation de l'autre diastéréoisomère (*R–S* ou *S–R*) est empêchée par l'encombrement stérique dû au groupement méthyle. Notons toutefois que les résultats de rmn du carbone-13 mettent en évidence sa présence à l'état de traces (~1 à 2%).

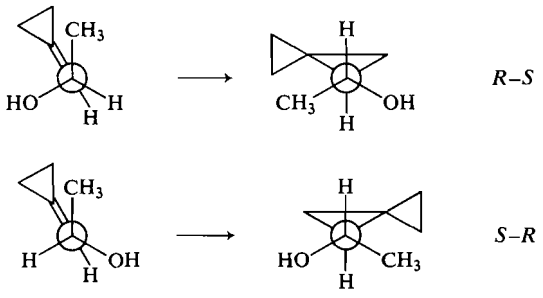

Les déplacements chimiques du ^{13}C du produit formé dans cette réaction (tableau 5) confirment d'une part l'hypothèse faite sur la structure de **5***b* et, d'autre part, permettent une attribution univoque des déplacements des deux diastéréoisomères. Notons enfin que les constantes physiques de ce produit sont cohérentes avec les données de la littérature (22).

1. M. BERTRAND, G. LEANDRI et A. MEOU. Tetrahedron Lett. 1841 (1979).
2. J. B. STOTHERS. ^{13}C nmr spectroscopy. Academic Press, New York. 1972.
3. N. K. WILSON et J. B. STOTHERS. Stereochemical aspects of ^{13}C nmr spectroscopy. Topics in stereochemistry. Vol. 8. *Edité par* N. L. Allinger et E. L. Eliel. Interscience, New York. 1974.
4. M. BERTRAND, G. LEANDRI et A. MEOU. Tetrahedron, sous presse.
5. G. C. PIMENTEL et A. L. MCCLELLAN. The hydrogen bond. W. H. Freeman and Company, San Francisco, London. 1960.
6. M. D. JOESTEN et L. J. SHAAD. Hydrogen bonding. M. Dekker Inc., New York. 1974
7. L. J. BELLAMY. Advances in infrared group frequencies. Chapman and Hall, London. 1975.
8. M. KARPLUS. J. Chem. Phys. **30**, 11 (1959).
9. D. J. CRAM et F. A. ABD ALHAFEZ. J. Am. Chem. Soc. **74**, 5828 (1952).
10. R. J. CRAWFORD, H. TOKUNAGA, L. M. H. C. SCHRIJVER, J. C. GODARD et T. NAKASHIMA. Can. J. Chem. **56**, 992 (1978).
11. D. M. GRANT et B. V. CHENEY. J. Am. Chem. Soc. **89**, 5315 (1967).
12. S. H. GROVER, J. P. GUTHRIE, J. B. STOTHERS et C. T. TAN. J. Magn. Reson. **10**, 227 (1973).
13. C. GIRARD et J. M. CONIA. J. Chem. Research (M), 2351 (1978).
14. J. A. LANDGREBE et L. W. BECKER. J. Am. Chem. Soc. **90**, 395 (1968).
15. J. SALAUN. J. Org. Chem. **43**, 2809 (1978).
16. J. B. STOTHERS, C. T. TAN et K. C. TEO. J. Magn. Reson. **20**, 570 (1975).
17. J. P. MONTI, R. FAURE et E. J. VINCENT. Org. Magn. Reson. **8**, 611 (1976).
18. K. C. RAMEY, D. C. LINI et G. KROW. General review of nmr. Annual reports on nmr spectroscopy. Vol. 6A. *Edité par* E. F. Mooney. 1975. p. 207.
19. W. KIRMSE et S. SCHNEIDER. Chem. Ber. **102**, 2440 (1969).
20. M. RATIER, M. CASTAING, J. P. GODET et M. PEREYRE. J. Chem. Research (M), 2306 (1978).
21. P. A. BARTLETT. Tetrahedron, **36**, 3 (1980).
22. R. MAURIN. Thèse, Marseille. 1971.

Can. J. Chem. Downloaded from www.nrcresearchpress.com by 210.87.254.6 on 09/06/12
For personal use only.

The transfer of alkanoic acids from dodecane to water[1,2]

NORMAN H. SAGERT, MICHAEL J. QUINN, AND ROBERT S. DIXON

Research Chemistry Branch, Atomic Energy of Canada Research Company, Whiteshell Nuclear Research Establishment, Pinawa, Man., Canada R0E 1L0

Received July 17, 1980

NORMAN H. SAGERT, MICHAEL J. QUINN, and ROBERT S. DIXON. Can. J. Chem. **59**, 1096 (1981).

A rotating diffusion cell was used to study the transfer of five alkanoic acids from dodecane to water under conditions of known interfacial area and hydrodynamics. The acids studied were acetic, butanoic, hexanoic, 2-methylbutanoic and 2,2-dimethylpropanoic acids. Small interfacial resistances to mass transfer were noted, the mass transfer coefficients for interfacial transfer being in the range 2.6 to 4.7 μm/s at 25°C. This small range means that the effects of the length and structure of the alkane chain on the resistance to mass transfer are minimal. A study of the temperature dependence of the resistance to mass transfer at the interface showed that the resistance is largely entropic rather than enthalpic.

NORMAN H. SAGERT, MICHAEL J. QUINN et ROBERT S. DIXON. Can. J. Chem. **59**, 1096 (1981).

On a utilisé une cellule de diffusion rotative pour étudier le transfert de cinq acides alcanoiques, du dodécane à l'eau dans des conditions où la surface interfaciale et l'hydrodynamique sont connus; on a étudié les acides suivants: butanoique, hexanoique, méthyl-2 butanoique et diméthyl-2,2 propanoique. On a noté de faibles résistances interfaciales au transfert de masse; les coefficients de transfert de masse lors du transfert interfacial sont de l'ordre de 2,6 à 4,7 μm/s à 25°C. Ce faible écart signifie que les effets de la longueur des chaînes et la structure de l'alcane influencent très faiblement la résistance au transfert de masse. Une étude de l'effet de la température sur la résistance au transfert de masse à l'interface à montré que la résistance est plutôt de nature entropique que de nature enthalpique.

[Traduit par le journal]

Introduction

In separating the components of irradiated nuclear fuel, solvent extraction processes are usually involved (1). In such processes, species are transferred between aqueous and organic phases across the aqueous–organic interface. It would be useful to be able to study the chemical processes occurring at the interface but to do this, the hydrodynamics must be known exactly (2).

The rotating disc has been an invaluable tool for studying kinetics, electrochemical and otherwise, at solid–liquid interfaces (3). The thickness of the boundary layer is constant over the surface of the disc and this thickness can be calculated exactly (3, 4). Unfortunately a liquid–liquid interface cannot support the shear stress necessary to allow it to be rotated in isolation and thus to establish rotating disc hydrodynamics at both sides of the interface. Albery *et al.* (5, 6) have partially solved this problem by introducing a porous filter disc into the interface. The filter disc is filled with one of the two fluids, and the fluid interface is located at one of its surfaces. The filter disc can then be rotated to establish rotating disc hydrodynamics at both surfaces of the disc. Although the mass transfer resistance in the disc must now be allowed for, Albery *et al.* (5) used thin Millipore filters (~150 μm) of high porosity (~80%) to ensure small resistances. They used this method to investigate mass transfer for a number of systems, and carried out some studies of the transfer of hexanoic acid across the hexane–water interface.

The purpose of this work is to extend the studies of the transfer of alkanoic acids at the alkane–water interface. First, dodecane was used as the alkane since it is a relatively non-volatile solvent. Secondly, the transfer was studied as a function of temperature to distinguish between enthalpic and entropic effects. Finally a number of alkanoic acids were examined to determine whether the structure of the alkane chain played any role in the rate of transfer.

Experimental

Apparatus

The diffusion cell was built according to the design of Albery *et al.* (5). For the experiments described here, dodecane containing dissolved alkanoic acids was placed in a rotating cylinder whose end was closed with a porous filter disc. The acids diffused through the disc and into the aqueous phase. This aqueous phase was kept at a constant pH (generally 8.0) with a Mettler Titration System operating as a pH stat, and the volume of base required to maintain the set pH was displayed as a function of time on an X–Y recorder.

Details of the cell are shown in Fig. 1. The outer aqueous phase, A, was contained in a thermostatted water bath whose temperature was controlled to ±0.1°C. The air space above the aqueous phase was purged with purified nitrogen, N, to eliminate absorption of atmospheric CO_2. The pH of the aqueous phase was monitored using the glass electrode, E, and a sodium

[1]AECL No. 6922.

[2]Presented in part at 63rd Chemical Conference of the Chemical Institute of Canada, Ottawa, Ont., June 1980.

0008-4042/81/071096-05$01.00/0

©1981 National Research Council of Canada/Conseil national de recherches du Canada

Can. J. Chem. Downloaded from www.nrcresearchpress.com by 210.87.254.40 on 09/06/12
For personal use only.

Can. J. Chem. Downloaded from www.nrcresearchpress.com by 210.87.254.40 on 09/06/12
For personal use only.

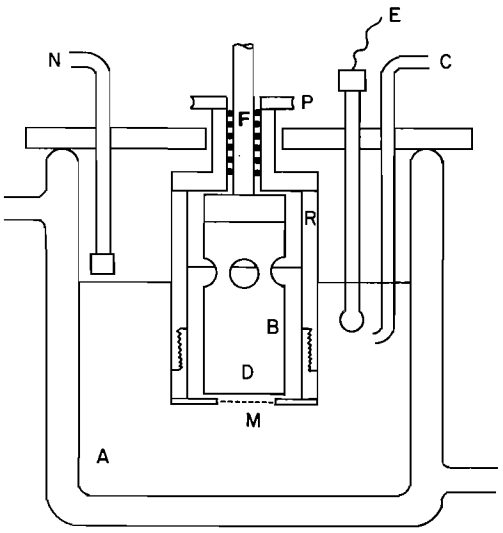

FIG. 1. Schematic diagram of rotating diffusion cell. A, aqueous phase; B, stationary baffle; C, inlet for base; D, dodecane phase; E, glass electrode; F, fixed inlet supporting stationary baffle; M, filter; N, nitrogen purge inlet; P, pulley system; R, rotating perspex reservoir.

hydroxide solution was introduced through the inlet C under the control of the pH stat.

The dodecane phase, D, usually with 0.1 mol/dm^3 of alkanoic acid, was contained in a perspex reservoir R, which was rotated on the hollow fixed rod F. A pulley system P, connected to a DC servomotor was geared to allow rotation speeds up to 16 Hz. The bottom of the reservoir was a thin perspex plate with provision for cementing a 25 mm diameter filter flush with the bottom of the plate. For convenience the bottom third of the reservoir was detachable. The filter, a Millipore RAWP, with pores of 1.2 μm diameter, was rendered hydrophobic with Fisher "Dricote" preparation.

Rotation of this reservoir would have given good rotating disc hydrodynamics only at the bottom surface of the filter disc. The innovation of Albery *et al.* (5) was to provide good rotating disc hydrodynamics at the inner surface of the filter by introducing a stationary hollow cylindrical baffle B. This stationary baffle protects the organic liquid inside it from the shear of the rotating reservoir. The baffle extends to within 2 mm of the bottom of the reservoir, a distance large enough not to affect centrifugal flow across the filter face. The organic liquid returns to the center region of the baffle through large holes drilled in the side at the top of the liquid level.

Methods

To begin a run, the filter was impregnated with the dodecane solution and the apparatus was assembled. The aqueous solution of 10^{-3} mol/dm^3 KCl was added until it almost reached the filter. Then dodecane solution and the aqueous solution were added simultaneously, keeping the level of the dodecane a little higher than that of the water. About 55 cm^3 of dodecane solution was added, and a record of elapsed time was started when the water first reached the filter. At this point the filling equipment was removed, rotation started, and the volumes of base necessary to keep the pH constant were recorded continuously.

Distribution coefficients were obtained by equilibrating aqueous and dodecane phases for several hours, separating, and analyzing both phases by titration. The aqueous phase was titrated with standard alkali. For the dodecane phase, an excess of aqueous alkali was equilibrated with this phase, and this was back-titrated with standard acid.

Materials

The dodecane was Phillips Pure Grade which was passed through a column of activated alumina, and the water was triple distilled from Pyrex. Its conductivity was 190 μS/m. The alkanoic acids were all reagent grade and were used without further purification. The acetic acid was Fisher reagent grade, butanoic and hexanoic acids were from Matheson, Coleman and Bell, and the isomeric pentanoic acids were from Aldrich.

Results and Discussion

The rate constant for the transfer of an alkanoic acid to water, k, may be defined (6, 7) by eq. [1]

$$[1] \quad J = kA\Delta C$$

where J is the flux in mol/s, A is the area of the filter over which transfer takes place, and ΔC is the effective concentration difference of alkanoic acid between dodecane and water. Since the acid concentration in the water is very small (pH = 8.0), ΔC is given by the concentration of acid in the dodecane, C_β, the dodecane phase being designated the β phase and the aqueous phase the α phase. In these experiments, the number of moles of base added to maintain the pH at 8.0 is equal to the number of moles of acid crossing the interface. Thus the flux is given by the slope of the experimental plot of base solution added against time. These plots were linear over the time scales used. Figure 2 shows a typical example, using hexanoic acid at various rotation speeds. From the measured fluxes, rate constants can be calculated. Corrections were made to ΔC (C_β) to allow for the decrease in ΔC with time as the experiment progressed.

Mass transfer resistances (total resistance, $1/k$)

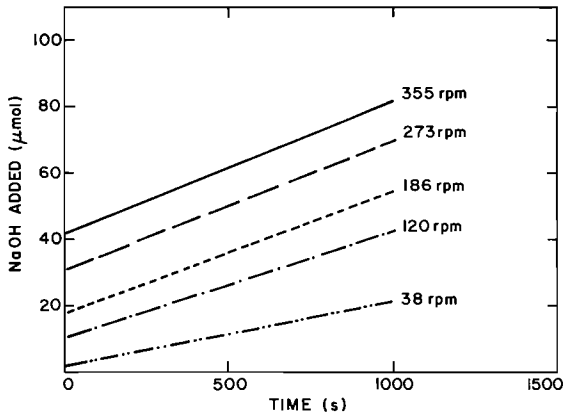

FIG. 2. Flux measurements for transfer of 0.1 mol/dm^3 hexanoic acid from dodecane to water at the indicated rotation speeds. T = 25°C.

Can. J. Chem. Downloaded from www.nrcresearchpress.com by 210.87.254.40 on 09/06/12
For personal use only.

add linearly (7). Thus it is advantageous to describe the separate resistances encountered by the acid as it is transferred from the dodecane to the water, bearing in mind that the filter contains dodecane and the dodecane–water interface is located at the bottom surface of the filter. Distribution coefficients, K, are defined by the ratio C_β/C_α as required by IUPAC convention. The acid first crosses the laminar diffusion layer in the dodecane and encounters a resistance δ_β/D_β where δ_β and D_β are the thickness of the diffusion layer in dodecane and the diffusion coefficient of the acid in dodecane, respectively. A further resistance is encountered in the dodecane-filled pores of the filter and this is given by l/aD_β where l is the effective path length and a the porosity of the filter. Any resistance to mass transfer at the interface will be given by $1/ak_i$ where k_i is the rate constant for interfacial transfer. Finally the resistance to mass transfer across the diffusion layer in the water would be given by $K\delta_\alpha/D_\alpha$. The total resistance to mass transfer would thus be given by eq. [2]

$$[2]\quad \frac{1}{k} = \frac{\delta_\beta}{D_\beta} + \frac{l}{aD_\beta} + \frac{1}{ak_i} + \frac{K\delta_\alpha}{D_\alpha}$$

The thickness of the diffusion layer is given by the Levich equation, eq. [3] (3, 4), where W is the rotation speed in Hz and v the kinematic viscosity in m^2/s.

$$[3]\quad \delta = 0.643\, \nu^{1/6} D^{1/3} W^{-1/2}$$

Thus, combining eq. [2] with eq. [3], a relationship between k and W is obtained.

$$[4]\quad \frac{1}{k} = \frac{l}{aD_\beta} + \frac{1}{ak_i} + 0.643\left(\frac{\nu_\beta^{1/6}}{D_\beta^{2/3}} + \frac{K\nu_\alpha^{1/6}}{D_\alpha^{2/3}}\right)\frac{1}{W^{1/2}}$$

A plot of $1/k$ against $1/W^{1/2}$ should be linear with an intercept of $l/aD_\beta + 1/ak_i$ and with a theoretically predictable slope, provided distribution, diffusion, density, and viscosity data are available.

Viscosity and density data for water up to 100°C are readily available. Viscosities for dodecane were taken from Hogenboom *et al.* (8). With some exceptions (9, 10), diffusion coefficients were not generally available. They were therefore calculated by the Wilke–Chang method using the molal volume increments listed by Sherwood, Pigford, and Wilke (11) and an association parameter for water of 2.60 (12). Allowance was made for dimerization in the dodecane. Distribution coefficients for butanoic and hexanoic acids were taken from Aveyard and Mitchell (12) and those for acetic, 2,2-dimethylpropanoic, and 2-methylbutanoic acids were measured. The values applicable for 0.1 mol/dm^3 in dodecane were used. Values of the distribution coefficients and diffusion coefficients used are shown in Table 1.

Plots of $1/k$ against $1/W^{1/2}$ are shown in Figs. 3 and 4 for hexanoic and butanoic acids respectively. The slopes shown are calculated from eq. [4]. These theoretical slopes fit the data reasonably well except at the lowest rotation speeds and lowest temperatures. At the lowest speeds, it is possible that the conditions for the derivation of eq. [3] are not obeyed, as the thickness of the hydrodynamic layer approaches the radius of the disc (3, 4).

Finally, it is necessary to correct for the effect of dimerization of the alkanoic acids in the dodecane. Albery *et al.* (5) have considered this problem and have set up and solved the transport equations. If K_2 is the equilibrium constant for dimerization in the organic phase, their analysis shows that the flux is given by eq. [5]

$$[5]\quad J = \frac{D_1(C_1 + 2C_2)_{x=\delta}}{\delta}\left(\frac{1 + 2D_2K_2C_1/D_1}{1 + 2K_2C_1}\right)_{x=\delta}$$

where x is the distance from the interface, C is the concentration, as before, and subscripts 1 and 2 refer to monomer and dimer respectively. For a simple dimerization $K_2C_1 = C_2/C_1$. In this case, where dimerization is highly favoured (13), the bracketed last term in eq. [5] is nearly equal to D_2/D_1 which, in turn, from the Wilke–Chang expression (11), is given by 0.660.

From the intercepts in plots such as those shown in Figs. 3 and 4, k_i may be evaluated if l, a, and D_β are known (eq. [4]). Values of D_β were, of course, calculated from the Wilke–Chang expression. Thus it is necessary to know only the effective path length, l, and the porosity, a, of the filter. In their original paper, Albery *et al.* (5) chose the effective path length as the measured thickness of the filter and obtained a porosity of 82% from the manufacturer's data and from a study of the electrochemical reduction of *p*-nitrophenol at a filter-covered electrode by Chien *et al.* (14). Later electrochemical work by Albery, in which the rotating reservoir was filled with mercury and the reduction of Cu(II) was followed, showed that an effective porosity of 78% was more appropriate.[3] The measured filter thickness of 140 μm was used as the effective path length.

The values obtained for k_i at 25°C are shown in Table 2. Also shown are the rate constants for transfer in the reverse direction, k_{-i}, calculated from the distribution coefficients. The values of k_i are quite constant, being in the range 3.8 ± 1.2

[3]W. J. Albery. Private communication.

Can. J. Chem. Downloaded from www.nrcresearchpress.com by 210.87.254.40 on 09/06/12
For personal use only.

TABLE 1. Distribution coefficients and diffusion coefficients $T = 25°C$

Alkanoic acid	$K = C_\beta/C_\alpha$	D_β (10^{-9} m²/s)	D_α (10^{-9} m²/s)
Acetic	0.022	1.11	1.34
Butanoic	0.355	0.82	0.99
2-Methylbutanoic	1.35	0.74	0.89
2,2-Dimethylpropanoic	2.60	0.74	0.89
Hexanoic	5.75	0.68	0.82

TABLE 2. Kinetic parameters for alkanoic acid transfer between dodecane and water at 25°C

Alkanoic acid	$\Delta^\alpha_\beta G°$ (kJ/mol)	k_i (μm/s)	$\Delta G_i^{\ddagger}$ (kJ/mol)	k_{-i} (μm/s)	$\Delta G_{-i}^{\ddagger}$ (kJ/mol)
Acetic	−9.3	3.8	42.4	0.086	51.7
Butanoic	−2.6	2.6	43.3	0.92	45.9
2-Methylbutanoic	0.74	4.0	42.2	5.4	41.5
2,2-Dimethylpropanoic	2.8	3.8	42.4	9.7	40.0
Hexanoic	4.3	4.6	41.8	26.9	37.5

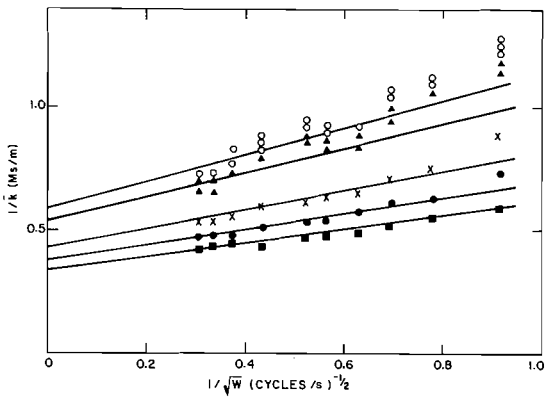

FIG. 3. Levich plots for the transfer of 0.1 mol/dm³ hexanoic acid from dodecane to water. $T = 20°C$ (○); 25°C (▲); 40°C (×); 50°C (●); and 60°C (■).

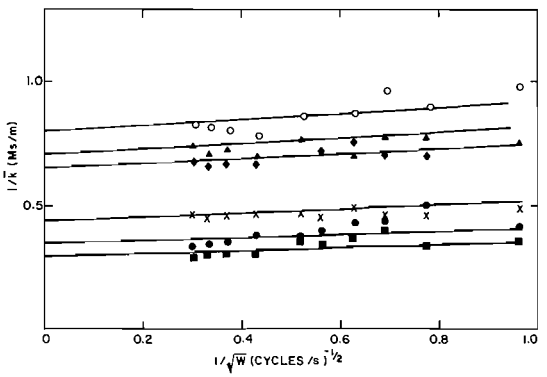

FIG. 4. Levich plots for the transfer of 0.1 mol/dm³ butanoic acid from dodecane to water. The legend for temperatures is as in Fig. 3.

μm/s. On the other hand the rate constants in the reverse direction vary by a factor of about 300.

The rate constant k_i may be expressed by eq. [6]

$$[6] \quad k_i = Z \exp(\Delta G_i^{\ddagger}/RT)$$

where $\Delta G_i^{\ddagger}$ is the free energy of activation and Z is a frequency factor, usually taken as $(RT/2\pi m)^{1/2}$ where m is the reduced mass (15, 16). Thus Z has a value close to 100 m/s at 25°C. Free energies of activation can thus be calculated from eq. [6]; these are shown in Table 2. The free energies for the complete transfer process, $\Delta^\alpha_\beta G^{\ominus}$, can, of course, be calculated from the distribution coefficients, and thus the free energies of activation for the reverse reaction, $\Delta G_{-i}^{\ddagger}$, can be calculated. These values are also given in Table 2. The energy barriers in the forward direction are very similar, suggesting a common transfer process. It is tempting to suggest that the peak of the barrier occurs in splitting the dimer and ionizing the acid group before the acid passes into the aqueous phase. Dimerization has been postulated as the rate determining step in the transfer of alkanoic acids from water to carbon tetrachloride in a series of experiments using the rising drop technique (17–19). Certainly, the length and degree of branching of the alkane chain of the acid has little effect on the height of the free energy barrier.

Equation [6] may be expressed in a slightly expanded form

$$[7] \quad k_i = Z \exp(\Delta S_i^{\ddagger}/R) \exp(-\Delta H_i^{\ddagger}/RT)$$

The frequency factor, Z, taken as 100 m/s at 25°C is assumed proportional to $\sqrt{T}$ (15). Thus, follow-

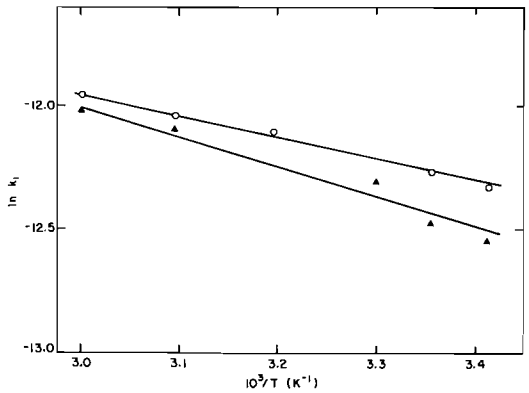

FIG. 5. Arrhenius plots of rate constant for interfacial transfer for acetic (▲) and hexanoic acids (○).

ing Laidler (20), the experimental Arrhenius activation energy E_a, is given by $\Delta H_i^{\ddagger} + (1/2)RT$.

Studies of the interfacial resistance to transfer were made as a function of temperature for all systems. Some typical results are shown in Fig. 5, plotted in the Arrhenius fashion with $\ln k_i$ plotted against the reciprocal of the absolute temperature. From the slope of the line the experimental activation energy, E_a, and thus the enthalpy of activation, $\Delta H_i^{\ddagger}$, can be obtained. Entropies of activation may then be calculated. The enthalpies and entropies of activation so obtained are listed in Table 3.

The free energies of activation are independent of the concentration units of the standard states used for defining the distribution coefficient since this coefficient is taken as a simple ratio of concentrations. The assignment of $Z = 100$ m/s allows the free energy of activation to be calculated independent of the choice of the standard states. Thus, from Table 3, it is apparent that entropic effects are much more important in defining the height of the free energy barrier. With the possible exception of butanoic acid, the entropies of activation are all large and negative. Their similarity suggests again that we are dealing primarily with effects of the carboxylic acid group, and that the size and structure of the hydrocarbon chain has relatively little effect on the kinetics of transfer. Albery *et al.* (5) reported an entropic barrier for the hydrolysis of methyl nicotinate, where a carboxylate group is involved, whereas they reported an enthalpic barrier for the hydrolysis of *p*-methylbenzyl chloride. It is interesting to note that the entropy barrier we obtained is roughly equal to the entropy of ionization of carboxylic acids (21), suggesting a charge separation in the transition state. Further speculation is probably unwarranted at the present time.

TABLE 3. Entropies and enthalpies of activation for the transfer of alkanoic acids from dodecane to water at 25°C

Alkanoic acid	E_a (kJ/mol)	$\Delta H_i^{\ddagger}$ (kJ/mol)	$\Delta S_i^{\ddagger}$ (J/mol·K)
Acetic	10.0	8.8	−112
Butanoic	23.9	22.7	−69
2-Methylbutanoic	12.9	11.7	−102
2,2-Dimethylpropanoic	15.8	14.0	−95
Hexanoic	7.3	6.1	−120

Acknowledgements

We would like to express our thanks to Professor W. J. Albery and Dr. J. Hadgraft for their interest in this work and for sharing results with us prior to publication. Mr. V. J. Lopata and Mr. R. Watchman obtained some of the preliminary data.

1. W. P. BEBBINGTON. Sci. Am. **235** (6), 30 (1976).
2. G. ASTARITA. Mass transfer with chemical reaction. Elsevier Publishing Co., Amsterdam. 1967.
3. A. C. RIDDIFORD. *In* Advances in electrochemistry and electrochemical engineering. Vol. 4. *Edited by* P. Delahay. Interscience, New York. 1966. pp. 47–116.
4. V. G. LEVICH. Physicochemical hydrodynamics. Prentice-Hall, Englewood Cliffs, NJ. 1962. pp. 60–78.
5. W. J. ALBERY, J. F. BURKE, E. B. LEFFLER, and J. HADGRAFT. J. Chem. Soc. Faraday I, **72**, 1618 (1976).
6. W. J. ALBERY, A. M. COUPER, J. HADGRAFT, and C. RYAN. J. Chem. Soc. Faraday I, **70**, 1124 (1974).
7. J. T. DAVIES and E. K. RIDEAL. Interfacial phenomena. Academic Press, London. 1963. pp. 301–342.
8. D. L. HOGENBOOM, W. WEBB, and J. A. DIXON. J. Chem. Phys. **46**, 2586 (1967).
9. D. E. BIDSTRUP and C. J. GEANKOPLIS. J. Chem. Eng. Data, **8**, 170 (1963).
10. W. J. ALBERY, A. R. GREENWOOD, and R. F. KIBBLE. Trans. Faraday Soc. **63**, 360 (1966).
11. T. K. SHERWOOD, R. L. PIGFORD, and C. R. WILKE. Mass transfer. McGraw-Hill, New York. 1975. pp. 25–31.
12. R. AVEYARD and R. W. MITCHELL. Trans. Faraday Soc. **66**, 37 (1970).
13. Y. MARCUS, E. YANIR, and A. S. KERTES. Equilibrium constants of liquid–liquid distribution reactions. Part III. Compound forming extractants, solvating solvents and inert solvents. Pergamon Press, Oxford. 1977.
14. Y. W. CHIEN, C. L. OLSEN, and T. D. SOKOLOSKI. J. Pharm. Sci. **62**, 435 (1973).
15. R. A. MARCUS. J. Chem. Phys. **43**, 679 (1965).
16. R. A. MARCUS. J. Phys. Chem. **67**, 853 (1963).
17. W. NITSCH. Kolloid-Z. **197**, 122 (1964).
18. W. NITSCH. Chem. Ing.-Tech. **38**, 525 (1966).
19. W. NITSCH and H. HOLZER. Tenside, **4**, 97 (1967).
20. K. J. LAIDLER. Theories of chemical reaction rates. McGraw-Hill, New York. 1969. pp. 52–55.
21. J. J. CHRISTENSEN, R. M. IZATT, and L. D. HANSEN. J. Am. Chem. Soc. **89**, 213 (1967).

Can. J. Chem. Downloaded from www.nrcresearchpress.com by 210.87.254.40 on 09/06/12
For personal use only.

Stereospecific total synthesis of (±)-cassipurine, an alkaloid from rhizophoraceae

JERZY TADEUSZ WRÓBEL AND JAN ADAM GLIŃSKI
Department of Chemistry, University of Warsaw, 02-093 Warsaw, Pasteura 1, Poland

Received June 9, 1980

JERZY TADEUSZ WRÓBEL and JAN ADAM GLIŃSKI. Can. J. Chem. **59**, 1101 (1981).

Two isomeric 1α,2α-epoxy- and 1β,2β-epoxypyrrolizidines have been obtained from 1,2-dehydropyrrolizidine. The structure of both isomers has been determined enabling a study of the stereochemistry of their reactions with a number of sulfur-containing nucleophilic reagents. The BzS^- anion has been shown to stereospecifically attack the C2 carbon atom of both compounds. In the three-stage process 1β,2β-epoxypyrrolizidine was transformed into 1α,2α-epithiopyrrolizidine, which reacts stereospecifically with benzylthiol to yield 1α-(2β-thiobenzylpyrrolizidine)-thiol. This, in turn, oxidizes in air to give a mixture of three diastereomeric 1α,1′α-dithio-2β,2′β-dithiobenzyldipyrrolizidines. These diastereomers were chromatographically separated into the racemic mixture and the *meso* diastereomer. Treatment of the racemic mixture with Na/liquid NH_3 induced debenzylation without cleavage of the disulfide bond. The resulting enantiomeric 1α,1′α-dithio-2β,2′β-dimercaptodipyrrolizidines were oxidized in air to give racemic cassipurine.

JERZY TADEUSZ WRÓBEL et JAN ADAM GLIŃSKI. Can. J. Chem. **59**, 1101 (1981).

A partir de la déhydro-1,2 pyrrolizidine, on a obtenu les époxy-1α,2α et -1β,2β pyrrolizidines isomères. On a déterminé la structure des deux isomères par l'étude de la stéréochimie de leurs réactions avec une série de réactifs nucléophiles contenant du soufre. L'anion BzS^- attaque de façon stéréospécifique l'atome de carbone en position 2 des deux composés. On a transformé, par une série de 3 réactions l'époxy-1β,2β pyrrolizidine en époxy-1α,2α pyrrolizidine qui réagit de façon stéréospécifique avec le benzylthiol en donnant le (thiobenzyl-2β pyrrolizidine)-1α thiol. Ce dernier composé à son tour par oxydation à l'air donne un mélange de trois diastéréoisomères des dithio-1α,1′α 2β,2′β-benzyldipyrrolizidines. On a séparé ces diastéréoisomères par chromatographie en un mélange racémique et le diastéréoisomère *méso*. Le mélange racémique traité par du Na/NH_3 liq. est débenzylé sans clivage de la liaison disulfure. Les dithio-1α,1′α 2β,2′β-dimercaptodipyrrolizidines ainsi obtenues donnent, par oxydation à l'air, la cassipurine racémique.

[Traduit par le journal]

Alkaloid cassipurine, **1**, has been isolated by Wright and Warren (1), and chemically studied by Cooks *et al.* (2). The X-ray study carried out by Gafner and Admiraal (3) has shown that the stereochemistry of cassipurine corresponds to the 1α,1′α:2β,2′β-(bisdithiodipyrrolizidine) isomer. They have reported the absolute configuration of the naturally occuring enantiomer to be "very probably" (3) of the type S,S′ as referred to the N atoms.

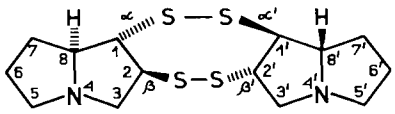

1

In the present paper the total synthesis of racemic cassipurine is described. The basic approach involves the synthesis of the 1α,2β-dithio-substituted pyrrolizidine skeleton under conditions of full stereochemical control followed by coupling two such disulfide bonds bridging C1 with C1′ and C2 with C2′ carbon atoms. The procedure leading to the desired 1α,2β configuration of sulfur atoms in the pyrrolizidine skeleton has been developed by studying the stereochemistry of the oxirane ring cleavage in both isomeric 1,2-epoxypyrrolizidines. 1α,2α-Epoxypyrrolizidine, **2**, and 1β,2β-epoxypyrrolizidine, **3**, have been obtained from racemic 1,2-dehydropyrrolizidine (4), and then examined in reactions with sulfur nucleophilic reagents. Benzylthiol, thiolacetic acid, and sodium hydrosulfide have been found to attack isomer **2** exclusively at the C2 carbon atom. The mechanism of the reaction with isomer **3** depends on the size of the attacking reagent. Relatively small molecules of thiolacetic acid and SH^- anions preferentially attack the C2 carbon atom, but the product of the attack at the C1 carbon atom also has been observed.

Reactions with benzylthiol were stereospecific:

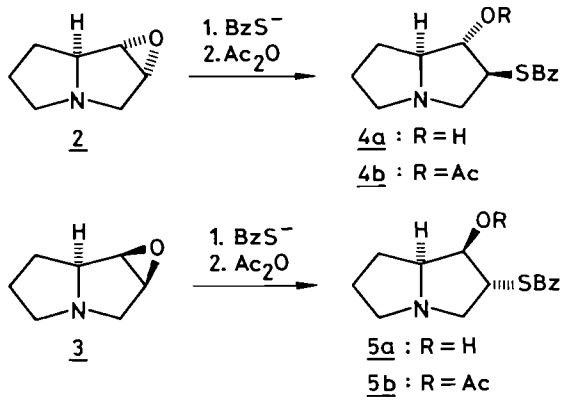

2 **3**

0008-4042/81/071101-04$01.00/0

©1981 National Research Council of Canada/Conseil national de recherches du Canada

Can. J. Chem. Downloaded from www.nrcresearchpress.com by 210.87.254.5 on 09/06/12
For personal use only.

Can. J. Chem. Downloaded from www.nrcresearchpress.com by 210.87.254.5 on 09/06/12
For personal use only.

1α-hydroxy-2β-thiobenzylpyrrolizidine, **4***a*, and 1β-hydroxy-2α-thiobenzylpyrrolizidine, **5***a*, were obtained from epoxides **2** and **3** respectively. This has been shown by the ^{1}Hmr spectra of the acetylated derivatives **4***b* and **5***b*. Analysis of the proton signal of the diagnostic hydrogen atom linked to the same carbon atom as the acetyl group indicates that in both products the attack of the thiobenzyl group occurs at the C2 carbon atom.

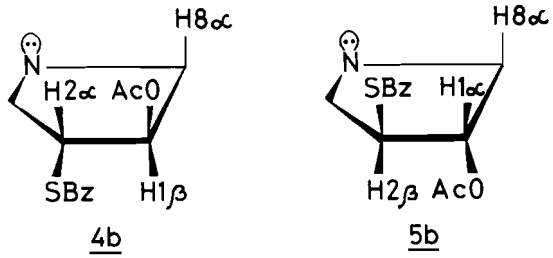

The ^{1}Hmr spectrum of the derivative **4***b* shows a triplet at δ = 4.86 ppm attributed to the H1β proton. The equality of both coupling constants is due to the two symmetrically situated vicinal protons. Hence, $J_{1\beta,2\alpha}$ = 2.5 Hz and $J_{1\beta,8\alpha}$ = 2.5 Hz. In the spectrum of the **5***b* derivatives the doublet of doublets corresponding to the H1α proton appears at δ = 5.06 ppm. The coupling constant of 5 Hz results from H1α—H8α protons coupling. The out-of-plane H1α and H2β protons have a coupling constant of 2.5 Hz. The larger chemical shift of the H1β proton results from the fact that the C—H1α hydrogen bond is situated in a plane in a position parallel to the free electron pair on the nitrogen atom.

In analogy to the reaction of 1,2-epoxypyrrolizidines with sulfur nucleophilic reagents, 1α,2α-epithiopyrrolizidine, **6**, (of epoxide **3** configuration) was reacted with benzylthiol. The reaction product, 1α-(2β-thiobenzylpyrrolizidine)-thiol, **9**, has the same configuration of sulfur atoms as cassipurine.

1α,2α-Epithiopyrrolizidine, **6**, was obtained in three steps from 1β,2β-epoxypyrrolizidine, **3**, (with an overall yield of 65%) using the method of Goodman *et al.* (5). A stereoselective reaction of **3** with thiolbenzoic acid yields 1β-hydroxy-2α-thiobenzoylpyrrolizidine, **7**, and 2β-hydroxy-1α-thiobenzoylpyrrolizidine, **7***a*, in a 9:1 ratio. The hydroxyl groups in compounds **7** and **7***a* were esterified with $MeSO_2Cl$ to give 1β-(2α-thiobenzoylpyrrolizidine)-methanesulfonate, **8**, and 2β-(1α-thiobenzoylpyrrolizidine)-methanesulfonate, **8***a*, which were equally good precursors of **6**. Compounds **7***a* and **8***a* have not been separated but they were detected by tlc and by the characteristic H2α signals in ^{1}Hmr spectra (**7***a*: δH2α = 4.40 ppm, **8***a*: δH2α = 5.00 ppm). Nucleophilic cleavage of the thiirane ring in episulfide **6** was stereospecific. In addition to 1α-mercapto-2β-thiobenzoylpyrrolizidine, **9**, adduct **10** has also been obtained (about 15%).

Coupling the two pyrrolizidine skeletons by two disulfide bridges between C1—C1′ and C2—C2′ carbon atoms, respectively, was carried out using 1-hydroxy-2-benzylthiopyrrolizidines **4***a* and **5***a*.

Compound **5***a* was reduced with sodium in liquid ammonia. Under these conditions the S—C bond cleavage occurs exclusively between the sulfur atom and the benzyl group, to yield 1β-hydroxy-

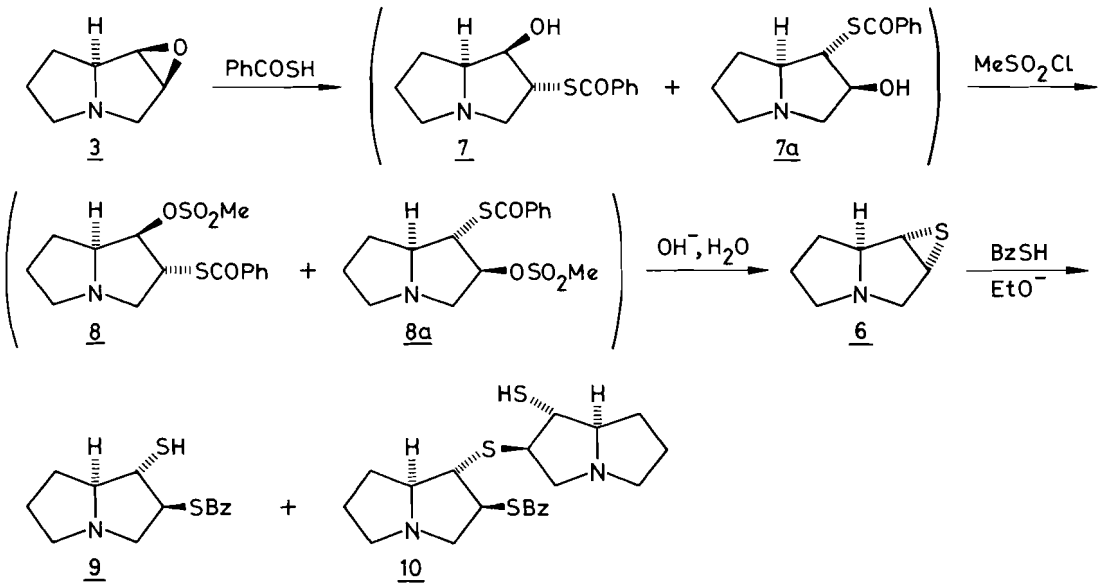

Can. J. Chem. Downloaded from www.nrcresearchpress.com by 210.87.254.5 on 09/06/12
For personal use only.

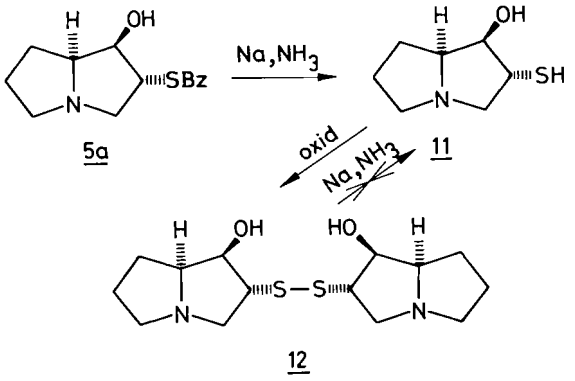

2α-mercaptopyrrolizidine, **11**. Iodine oxidation of the latter results in three diastereomers of 2α,2′α-dithio-1β,1′β-dihydroxydipyrrolizidine, **12**, obtained in excellent yield. It has been shown that the S—S bond joining two pyrrolizidine skeletons is resistant to sodium in liquid ammonia. This very unusual behavior of the disulfide bond has been known hitherto only in the case of cassipurine. The selective removal of the benzyl group using sodium in liquid ammonia leaves the disulfide bond intact and enables the reduction of 1α,1′α-dithio-2β,2′β-dithiobenzyldipyrrolizidines, **13**.

The diastereomeric 1α,1′α-disulfides **13** were obtained by oxidation in air of the racemic thiol **9**. The mixture of the diastereomers **13** was chromatographically separated into two fractions of equal weight. One of these fractions contains a racemic mixture of the two enantiomers. The second fraction consists of the *meso* diastereomer. The racemic mixture of the enantiomers **13** was debenzylated with Na/liquid NH_3 to give a racemic mixture of 1α,1′α-dithio-2β,2′β-dimercaptodipyrrolizidines, **14**, which without isolation were oxidized by bubbled oxygen. From the resulting mixture thin white crystals were obtained. Their molecular weight as determined by high resolution mass spectroscopy is 346.0660 (calcd. 346.0664). The mass fragmentation ions coincide with data reported for cassipurine.

The *meso* diastereomer **13** treated in a similar way yields no product of the same (346) molecular weight.

Experimental

All melting and boiling points are uncorrected. Spectra were obtained as follows: ^{1}Hmr at 100 MHz on a Jeol JNM-4H-100 spectrometer in $CDCl_3$ using TMS as internal standard (δ = 0.0 ppm); symbols s, d, t, q, m stand for singlet, doublet, triplet, quartet, multiplet, respectively; ms on a LKB-2091 gc–ms low resolution instrument with a direct inlet system operating at 70 eV. High resolution and FD (field desorption) measurements were performed using a Varian MAT-771 instrument. Merck Al_2O_3 plates type E were used for tlc and preparative chromatography. For column chromatography Merck Al_2O_3-60 Activ was used.

1α,2α-Epoxypyrrolizidine, 2, and 1β,2β-Epoxypyrrolizidine, 3

A solution of 1,2-dehydropyrrolizidine (0.14 mol) in 250 mL of sulfuric acid 1:4 was treated with sucessive portions of *N*-bromoacetamide (0.16 mol). The solution was stirred for 4 h, then made alkaline with K_2CO_3 and stirred for another hour. Precipitated KCl was filtered off and the solution was extracted with $CHCl_3$ (8 × 100 mL) to finally yield 9 g of the mixture of the epoxides **2** and **3**. Stereomers **2** and **3** were separated on an alumina column; **3** was eluted with Et_2O + 5% MeOH, then Et_2O + 30% MeOH was used to elute compound **2**. Upon distillation 0.025 mol of **2** and 0.044 mol of **3** were obtained. Total yield of **2** + **3** was 44%.

Compound **2**, a colourless oil, bp 70°C/10 Torr; ^{1}Hmr: 3.5–3.9 (m, 3p), 2.9–3.5 (m, 3p), 2.7 (m, 1p), 1.8–2.1 (m, 4p); ms: 41(100), 68(66), 80(12), 96(90), 108(18), 125(67). *Anal.* calcd. for $C_7H_{11}NO$: C 67.2, H 8.9, N 11.2%; found: C 66.6, H 9.0, N 11.2%.

Compound **3**, a colourless oil, bp 66°C/10 Torr; ^{1}Hmr: 3.3–4.0 (m, 4p), 2.4–3.3 (m, 3p), 1.5–2.3 (m, 4p); ms: 41(100) 68(57), 70(30), 96(82), 108(16), 125(51). *Anal.* found: C 66.5, H 8.7, N 11.0%.

*1α-Hydroxy-2β-thiobenzylpyrrolizidine, 4*a

An ethanolic solution of **2** (10 mmol), benzylthiol (11 mmol), and a catalytic amount of KOH was kept for 36 h at room temperature to complete the reaction. After a routine processing of the solution, crude **4***a* was obtained. Crystallization from acetone resulted in white needles (75% yield), mp 124°C; ^{1}Hmr ($CDCl_3$ + D_2O): 7.3 (C_6H_5), 3.8 (s, $C_6H_5CH_2$), 3.57 (t, 1p), 2.2–3.4 (m, 6p), 1.5–2.0 (m, 4p); ms: 70(97), 83(21), 91(27), 126(100), 158(11), 249(1). *Anal.* calcd. for $C_{14}H_{19}NOS$: C 67.4, H 7.7, N 5.6%; found: C 67.2, H 7.80, N 5.7%.

*1β-Hydroxy-2α-thiobenzylpyrrolizidine, 5*a

Compound **5***a* was obtained from **3** similarly to compound **4***a* from **2**. White crystals (from acetone), mp 103°C, 75% yield; ^{1}Hmr ($CDCl_3$ + D_2O): 7.3 (C_6H_5), 3.98 (t, 1p), 3.77 (s, $C_6H_5CH_2$), 3.63 (m, 1p), 3.1–3.2 (m, 4p), 2.4 (m, 1p), 1.6–2.0 (m, 4p); ms: 70(100), 83(15), 91(25), 126(75), 158(25), 249(1). *Anal.* found: C 67.1, H 7.5, N 5.5%.

*1α-Acetoxy-2β-thiobenzylpyrrolizidine, 4*b

Compound **4***b* was obtained from **4***a* using an excess of Ac_2O in $CHCl_3$. The mixture was stored at room temperature for 36 h.

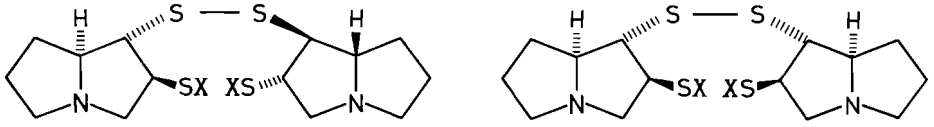

One of the enantiomers

13 : X = Bz
14 : X = H

(meso) Diastereomer

Can. J. Chem. Downloaded from www.nrcresearchpress.com by 210.87.254.5 on 09/06/12
For personal use only.

After routine processing compound **5***b* was isolated from solution as a viscous colourless oil (95% yield); ^{1}Hmr: 7.3 (C_6H_5), 4.86 (t, H1β), 3.80 (s, $C_6H_5CH_2$), 3.15–3.5 (m, H8α, H2β, H3α), 2.95 (m, H5α), 2.5–2.8 (m, H3β, H5β), 2.05 (s, CH_3CO), 1.65–2.03 (m, H6α, H6β, H7α, H7β); ms: 43(60), 7(100), 83(25), 91(49), 108(40), 168(99), 200(7), 291(3). *Anal.* found: C 67.1, H 7.5, N 5.7%.

1β-Acetoxy-2α-thiobenzylpyrrolizidine, **5**b

Compound **5***b* was obtained from **5***a* similarly to compound **4***b* from **4***a* with a 95% yield of noncrystallizing oil; ^{1}Hmr: 7.3 (C_6H_5): 5.06 (dd, H1α), 3.97 (t, H8α), 3.83 (s, $C_6H_5CH_2$), 3.2 (m, H2β), 2.7–3.2 (m, H3α, H3β, H5α), 2.46 (m, H5β), 2.08 (s, CH_3CO), 1.5–2.0 (m, H6α, H6β, H7α, H7β); ms: 43(58), 70(100), 91(48), 108(16), 168(90), 200(14), 291(6). *Anal.* found: C 67.0, H 7.5, N 5.5%.

1α,2α-Epithiopyrrolizidine, **6**

A three-necked flask was connected with a dropping funnel containing 3.8 mmol of **8** dissolved in 30 mL of an Et_2O–MeOH mixture. To the flask was added 8.5 mmol KOH dissolved in 60 mL of water. Argon was bubbled through the magnetically stirred solution. The bubbling was periodically interrupted and a water vacuum pump was connected to the reaction flask in order to evaporate the ethereal layer. After dropping was completed (about 20 min), the solution was stirred for an additional 15 min. Residual Et_2O and MeOH were evaporated *in vacuo*. The aqueous solution was filtered and extracted with $CHCl_3$. The extract was dried and evaporated to give pure **6** as a light yellow oil (98%) yield), which did not require distillation; ^{1}Hmr: 3.68 (t, 1p), 3.35–3.55 (m, 3p), 2.6–3.32 (m, 3p), 1.4–2.3 (m, 4p); ms: 41(23), 80(36), 81(13), 108(100), 141(25). *Anal.* calcd. for $C_7H_{11}NS$: C 59.5, H 7.9, N 9.9%; found: C 59.2, H 7.7, N 9.8%.

1β-Hydroxy-2α-thiobenzylpyrrolizidine, **7**

In a stoppered flask a mixture of epoxide **3** (16 mmol) and thiobenzoic acid (24 mmol) in $CHCl_3$ solution was stored at room temperature for 36 h. Then the mixture was processed to give crude **7**, which after crystallization from acetone gave 72% of pure compound **7**. White crystals had mp 133°C; ^{1}Hmr ($CDCl_3 + D_2O$): 7.95 (2p), 7.4 (3p), 4.02–4.3 (H1α, H2β), 3.75 (dt, H8α), 2.9–3.4 (m, H3α, H3β, H5α), 3.65 (m, H5β), 1.5–2.2 (m, H6α, H6β, H7α, H7β); ms: 70(10), 75(10), 77(18), 83(9), 105(15), 126(89), 158(1), 263(0.2). *Anal.* calcd. for $C_{14}H_{17}NO_2S$: C 63.8, H 6.5, N 5.3%; found: C 63.6, H 6.5, N 5.3%.

1β-(2α-Thiobenzoylpyrrolizidine)-methanesulfonate, **8**

Methanesulfonic chloride (6.7 mmol) was added to a solution of 5.7 mmol of **7** in 20 mL of dry pyridine. The mixture was kept for 36 h at 10°C and then pyridine was removed *in vacuo*. After routine processing the dry residue gave a viscous oil, which crystallized after a few days in a refrigerator. Recrystallization from acetone gave 91% of pure **8** as colourless plates having mp 83°C; ^{1}Hmr: 7.9 (2p), 7.48 (3p), 4.85 (dd, H1α), 4.27 (t, H2β), 3.95 (dt, H8α), 3.3 (CH_3), 3.16–3.3 (m, 2p), 2.9–3.17 (m, 1p), 2.45–2.8 (m, 1p), 1.7–2.1 (m, 4p); ms: 105(100), 108(63), 135(12), 140(9), 148(9), 204(64), 262(13), 341(0.2). *Anal.* calcd. for $C_{15}H_{19}NO_4S_2$: C 52.7, H 5.6, N 4.1%; found: C 52.5, H 5.6, N 4.0%.

1β-Hydroxy-2α-mercaptopyrrolizidine, **11**

Compound **5***a* (5.6 mmol) was dissolved in 50 mL of liquid ammonia and then 24 mmol of sodium were added. After a few seconds the reaction was completed and only a light blue colour of the solution remained. Ammonia was allowed to evaporate and the dry residue was dissolved in a small amount of water. The aqueous solution was extracted with benzene. The organic layer was discarded, the aqueous layer was evaporated, and the residue was extracted with $CHCl_3$ + 10% MeOH mixture. Colourless crystals, readily oxidizable to compound **12**, were obtained from the extract with 94% yield. The crystals decomposed above 120°C. Mass spectra: 41(13), 55(15), 70(100), 83(12), 126(37), 159(0.8).

2α,2′α-Dithio-1β,1′β-dihydroxydipyrrolizidine, **12**

The thiole **11** was oxidized by air bubbled through the MeOH solution. White crystals were recrystallized from Et_2O + 5% MeOH mixture to give 80% of **12**, mp 187°C; ^{1}Hmr ($CDCl_3 + D_2O$): 4.47 (dd, H1α), 3.92 (q, H8α), 3.76 (m, H2β), 3.0–3.25 (m, H3α, H3β, H5α), 2.6 (m, H5β), 1.6–2.3 (m, H6α, H6β, H7α, H7β); ms: 55(15), 70(100), 108(9), 126(35), 158(8), 191(9), 317(0.3). *Anal.* calcd. for $C_{14}H_{24}N_2O_2$: C 53.8, H 7.8, N 17.9%; found: C 53.6, H 7.6, N 17.7%.

1α,1′α-Dithio-2β,2′β-dithiobenzylpyrrolizidine, **13**

An ethanolic solution of episulfide **6** (6 mmol) and benzylthiol (12 mmol) was refluxed with a catalytic amount of EtONa. Argon was passed through the solution. After 75 min the reaction was completed. Ethanol was evaporated and then aqueous H_2SO_4 was added to the residue. An excess of benzylthiol was removed with C_6H_6 and the aqueous layer was made alkaline and extracted with $CHCl_3$. The resulting mixture of 1α-mercapto-2β-thiobenzylpyrrolizidine, **9**, and 1α,2′β-(1′α-mercaptopyrrolizidine-2β-thiobenzylpyrrolizidine)-sulfide, **10**, was oxidized in air to give a mixture of disulfides. After preparative chromatography on alumina (Et_2O + 4% MeOH + 2% H_2O) two fractions were obtained. One of them contained a racemic mixture of the enantiomers **13** (17% yield, R_f 0.81), while the other consisted of the **13** *meso* diastereomer (17% yield, R_f 0.85). The two fractions were noncrystallizing viscous oils.

For the racemic mixture, ^{1}Hmr ($CDCl_3$–C_6D_6, 1:1): 7.26 (C_6H_5), 3.75 (s, $C_6H_5CH_2$), 3.05–3.65 (m, 3p), 2.65–3.04 (m, 2p), 2.21–2.63 (m, 2p), 1.39–2.14 (m, 4p); ms: 70(56), 91(100), 108(77), 142(58), 174(3), 232(50), 264(16), 297(10), 298(14), 406(3), 528(0.1), 529(0.8); FD: M + 1 = 529. *Anal.* calcd. for $C_{28}H_{36}N_2S_4$: C 63.6, H 6.9, N 5.3%; found: C 63.1, H 6.7, N 5.1%.

For the *meso* diastereomer, ^{1}Hmr ($CDCl_3$– C_6D_6, 1:1): 7.27 (s, C_6H_5), 3.68 (s, $C_6H_5CH_2$), 3.48 (m, 1p), 3.05–3.38 (m, 2p), 2.62–2.98 (m, 2p), 2.18–2.58 (m, 2p), 1.37–2.02 (m, 4p); ms: 70(13), 91(100), 108(20), 142(43), 174(6), 232(37), 264(10), 297(17), 298(8), 406(2), 528(0.3), 529(1.2); FD: M + 1 = 529. *Anal.* found: C 63.0, H 6.6, N 5.2%.

(±)-Cassipurine

To a flask 50 mL of liquid NH_3, 0.2 mmol of **13** (racemic mixture), and 0.5 mmol of sodium wee added. After a few seconds the reaction was completed and NH_3 was allowed to evaporate. The dry residue was extracted with a mixture of $CHCl_3$ + 5% MeOH. The resulting solution of the racemic 1α,1′α-dithio-2β,2′β-dimercaptodipyrrolizidine, **14**, was oxidized (without separation of pure compound **14**) in air. After routine processing, the solution gave crystals of racemic cassipurine (10% yield). Recrystallization from acetone resulted in white thin needles, mp 191°C; ms: 41(15), 70(25), 80(13), 106(8), 108(100), 140(25), 141(41), 173(17), 174(45), 205(6), 346(22); FD: M^+ = 346. *Exact Mass* calcd.: 346.0664; found: 346.0660.

1. W. Wright and F. L. Warren. J. Chem. Soc. 284 (1967).
2. R. G. Cooks, F. L. Warren, and D. H. Williams. J. Chem. Soc. 286 (1967).
3. G. Gafner and L. J. Admiraal. Acta Crystallogr. Sect. B, **25**, 2114 (1969).
4. J. H. Williams. Diss. Abstr. Int. B, **34**, 1952 (1973).
5. L. Goodman, A. Benitez, and B. R. Baker. J. Am. Chem. Soc. **80**, 1680 (1951).

FOR ERRATA SEE
v.59 #12 1981 p.1744

1,7-Dioxaspiro[5.5]undecanes. An excellent system for the study of stereoelectronic effects (anomeric and *exo*-anomeric effects) in acetals[1] ERRATA

PIERRE DESLONGCHAMPS, DARYL D. ROWAN, NORMAND POTHIER, GILLES SAUVÉ, AND JOHN K. SAUNDERS

Laboratoire de Synthèse Organique, Département de Chimie, Faculté des Sciences, Université de Sherbrooke, Sherbrooke (Qué.), Canada J1K 2R1

Received September 3, 1980

PIERRE DESLONGCHAMPS, DARYL D. ROWAN, NORMAND POTHIER, TILLES SAUVÉ, and JOHN K. SAUNDERS. Can. J. Chem. **59**, 1105 (1981).

Several isomeric compounds derived from the spiro systems **5** to **9** (Scheme 4) were obtained from the acid cyclization of the appropriate dihydroxy ketone precursor.

The configuration and the conformation of the products obtained was determined by ^{13}C nmr analysis and equilibration studies. The experimental results can be rationalized by taking into account the anomeric and the *exo*-anomeric effects and the usual steric interactions.

PIERRE DESLONGCHAMPS, DARYL D. ROWAN, NORMAND POTHIER, TILLES SAUVÉ et JOHN K. SAUNDERS. Can. J. Chem. **59**, 1105 (1981).

Plusieurs composés isomères dérivés des systèmes spiranniques **5** à **9** (Schéma 4) furent obtenus par cyclisation en milieu acide des précurseurs dihydroxycétoniques appropriés.

La configuration et la conformation des produits obtenus ont été déterminées par la rmn du ^{13}C et par des études d'équilibration. Les résultats expérimentaux sont expliqués en tenant compte de l'effet anomère, de l'effet *exo*-anomère et des interactions stériques habituelles.

Stereoelectronic effects have been recognized for a long time to influence the configuration and the conformation of acetals, particularly in carbohydrates where these effects were first discovered and discussed in terms of the anomeric and *exo*-anomeric effects (1).[2,3]

α- And β-glycosides can theoretically take conformations A_1, A_2, A_3 and E_1, E_2, E_3 respectively (Scheme 1). The relative proportions of these various conformers in α and β-glycosides should be influenced by the usual steric interactions and by stereoelectronic effects. For instance, if stereoelectronic effects (anomeric and *exo*-anomeric effects) are important, the following predictions can be made: (*a*) conformer A_2 has only one anomeric effect and conformers A_1 and A_3 have two each,[4] and since A_3 must be eliminated because of strong steric interactions, A_1 must correspond to the most stable conformer of an α-glycoside; (*b*) conformer E_3 has no anomeric effect whereas E_1 and E_2 have one each, and since E_2 has an extra steric interaction (one *gauche* form of butane ≈0.9 kcal/mol) by comparison with E_1, β-glycosides should exist as a mixture of conformers E_1 and E_2 in which E_1 should predominate.

The validity of the above conclusion depends on the importance of the anomeric effect. Efforts have been made to evaluate the anomeric effect by undertaking equilibration studies between equatorial and axial isomers at the anomeric center in carbohydrates (4), and in monosubstituted 2-alkoxytetrahydropyrans (5) as well as in more rigid systems (6). The anomeric effect has been evaluated to be of the order of 1.2 to 1.8 kcal/mol from these studies. These evaluations cannot, however, be very precise because the orientation of the OR group in the axial and in the equatorial isomer was not considered, and the influence of the *exo*-anomeric effect was consequently neglected.

The evaluation of the anomeric effect could be achieved by determining the relative proportions of conformers in equatorial (E_1, E_2, and E_3) and axial (A_1 and A_2) 2-alkoxytetrahydropyrans respectively. This analysis, which could be done in principle by a study at low temperature by nmr spectroscopy, does not seem to be realizable because the energy barrier of rotation between conformers is presumably too small.[5]

[1]This work has been presented at the 8th Natural Products Symposium, University of West Indies, Mona, Jamaica, January 1980, and at the 1st International Symposium on Stereoelectronic Effects, University of St. Andrews, Scotland, July 1980.

[2]The preference for an alkoxy group to be axially oriented is due to the anomeric effect, whereas the preference for the R group of the side chain at the anomeric center to be in the A_1 or the E_1 conformation in α and β-glycosides respectively is due to the *exo*-anomeric effect (Scheme 1).

[3]The anomeric (or the *exo*-anomeric) effect is considered to be a stabilizing effect which occurs when an electron pair of an oxygen atom is oriented antiperiplanar to a C—OR bond. The stabilization would be gained through an electronic delocalization due to the overlap of an electron lone pair orbital of an oxygen with the antibonding orbital of a C—OR sigma bond (2, 3).

[4]In this article, we use the term anomeric effect to describe either an anomeric or an *exo*-anomeric effect, assuming that both effects are of the same order of magnitude.

[5]This analysis is also impossible if equatorial and axial isomers exist in only one preferred conformation.

0008-4042/81/071105-17$01.00/0

©1981 National Research Council of Canada/Conseil national de recherches du Canada

Can. J. Chem. Downloaded from www.nrcresearchpress.com by 210.87.254.5 on 09/06/12
For personal use only.

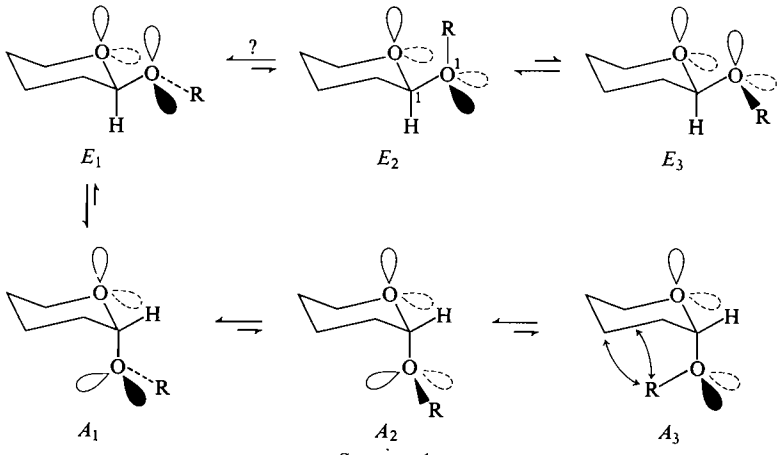

SCHEME 1

The analysis could also be done by nmr at room temperature provided that the various conformers have sufficiently different coupling constants. This method has the disadvantage that small percentages of some conformers will be difficult to detect. Using this method, in an attempt to assess the relative abundance of conformers E_1 and E_2 in β-glycosides, Lemieux (7) was unable to detect conformer E_2. Thus, E_1 and E_2 would be separated by over 2 kcal/mol. It was suggested that this rather unexpected situation would be mainly the result of a short C(1)—O(1) bond which would amplify the steric interaction in E_2. Also, by comparison of bond length (X-ray) in α and β-glycosides, Lemieux *et al.* (8) further suggested that the *exo*-anomeric effect would be stronger in the β-anomer. The fact remains that there exists no experimental evidence, including X-ray (9) and dipole moment studies (10), that α and β-glycosides exist in conformations other than A_1 and E_2 respectively.

The above results indicate that 2-alkoxytetrahydropyrans are not very appropriate models for a precise evaluation of the anomeric and the *exo*-anomeric effect. There is, however, a very interesting experiment on the evaluation of the anomeric effect which has been described by Descotes *et al.* (11). They have studied the acid catalyzed isomerization of *cis* and *trans* bicyclic acetals **1** and **2** (Scheme 2) and found, at equilibrium, a mixture of 57% *cis* and 43% *trans*. The *cis* isomer **1** corresponds to conformer E_2 (or A_2) which has one anomeric effect, whereas the *trans* isomer **2** corresponds to conformer E_3 which has none. It was possible to estimate the steric effects in *cis* acetal **1** (one *gauche* interaction = 0.85 kcal/mol and one interaction for an axial OR group to cyclohexane = 0.8 kcal/mol) and, by taking into account an entropy factor (0.42 kcal/mol at 80°C) caused by the fact that *cis* acetal **1** exists as a mixture of two conformations (*cis* decalin system), they arrived at

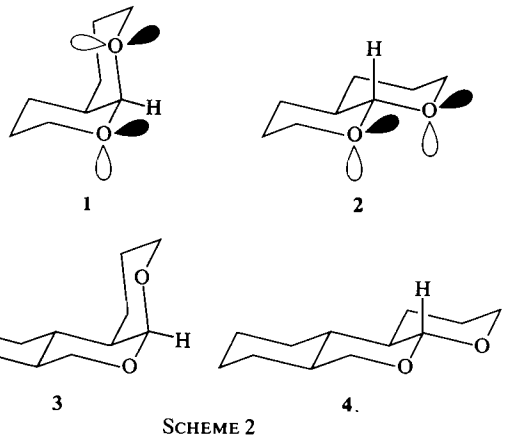

SCHEME 2

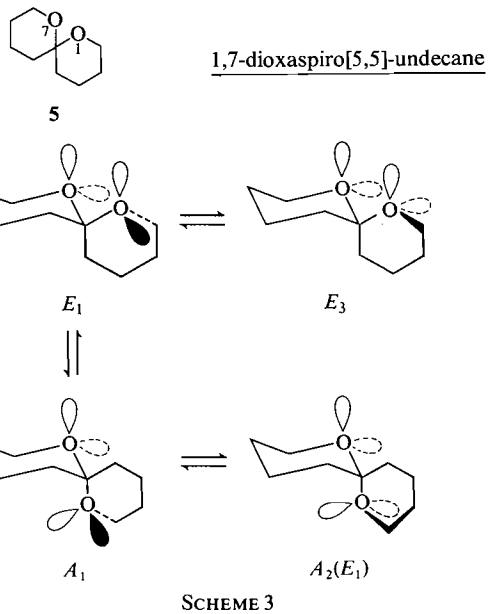

SCHEME 3

Can. J. Chem. Downloaded from www.nrcresearchpress.com by 210.87.254.5 on 09/06/12
For personal use only.

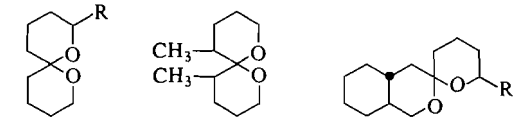

5 R = H
6 R = CH_3

7

8 R = H
9 R = CH_3

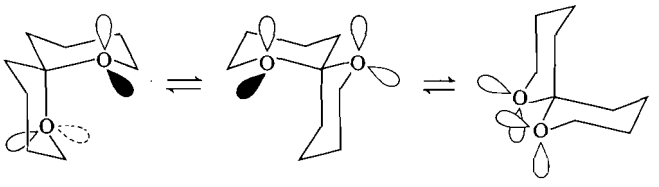

5*a* (0 kcal/mol) 5*b* (2.4 kcal/mol) 5*c* (4.8 kcal/mol)

SCHEME 4

a value of 1.4 kcal/mol for the anomeric effect. We have recently studied the equilibration of *cis* and *trans* tricyclic acetals **3** and **4** and have arrived at a value of 1.5 kcal/mol (12), which confirms the result of Descotes *et al.* The value of 1.4–1.5 kcal mol must, however, be considered a minimum value because, as suggested by Lemieux *et al.* (8), the value for the steric interactions might be larger, being amplified by a shortened C—O bond.[6]

We have undertaken a study on the conformational analysis and on the acid hydrolysis of the 1,7-dioxaspiro[5.5]-undecane system **5** (Scheme 3) in order to obtain results on the evaluation of both the anomeric and the *exo*-anomeric effects. We wish to report these results.

We envisaged that the spiro system **5** would be a very convenient one for the study of stereoelectronic effects in the acetal function for the following reasons: (*a*) **5** can take three different conformations which correspond to either conformer E_1 (or A_2), E_3, or A_1 of α and β-2-alkoxytetrahydropyrans; (*b*) with **5**, it appeared possible to undertake a conformational analysis by low temperature nmr spectroscopy, because the energy barrier for each conformational change which involves a chair inversion should be high enough; (*c*) analogously to the system of Descotes *et al.*, the steric effects should also be easily evaluated; and (*d*) by adding appropriate alkyl substituents to the spiro system **5**, it appeared possible to isolate isomeric compounds which would differ by existing in one of the above conformations.

We have studied the parent compound **5**, the methyl substituted derivatives **6** and **7**, the tricyclic system **8**, as well as the corresponding methyl substituted derivatives **9** (Scheme 4).

[6]Jeffrey *et al.* (13) were the first to carry out molecular orbital calculations on the anomeric effect, and suggested that as much as 4 to 6 kcal/mol of stabilization can be involved.

Results and Discussion

Spiro System 5

Compound **5** can exist theoretically in the three conformations **5***a*, **5***b*, and **5***c* (Scheme 4). Conformation **5***a* has two oxygens having each an electron pair oriented antiperiplanar to a polar C—O bond, conformation **5***b* has only one, whereas conformation **5***c* has none. Consequently, **5***a* has two anomeric effects, **5***b* has only one, whereas **5***c* has none. Accepting the value of 1.4 kcal/mol for one anomeric effect, conformations **5***a* and **5***b* should be more stable than conformation **5***c* by 2.8 and 1.4 kcal/mol respectively on that basis.[7]

The next task concerns the evaluation of steric effects in these three conformations. In conformation **5***a*, the two oxygens are oriented axial to a ring. In conformation **5***c*, there are two methylene groups oriented axial to a ring. In conformation **5***b*, there are one oxygen and one methylene group axially oriented to a ring. When a methylene group is axially oriented, it corresponds to two *gauche* forms of butane evaluated at 0.9 kcal/mol each (14). When an oxygen is axially oriented, it corresponds to two *gauche* forms of *n*-propylether ($O—CH_2—CH_2—CH_2$) which we have evaluated at 0.4 kcal/mol each (15). On that basis, the steric effect for conformations **5***a*, **5***b*, and **5***c* should correspond to 1.6 (4 × 0.4), 2.6 (2 × 0.4 + 2 × 0.9), and 3.6 (4 × 0.9) kcal/mol respectively (Table 1).

If the stabilizing anomeric and the destabilizing steric effects are taken together, conformation **5***a* should be more stable than conformations **5***b* and **5***c* by 2.4 and 4.8 kcal/mol respectively (Table 1). *This analysis leads to the prediction that the spiro compound 5 must exist essentially in conformation* 5a *only.*

[7]We make the assumption that when there are two anomeric effects in the same conformation, they are additive.

Can. J. Chem. Downloaded from www.nrcresearchpress.com by 210.87.254.5 on 09/06/12
For personal use only.

TABLE 1. Evaluation of steric and stereoelectronic effects*

	Effects, compound **5**		
	5*a*	**5***b*	**5***c*
	2 *ae* = −2.8	1 *ae* = −1.4	
	4 *co* = 1.6	2 *co* = 0.8	
		2 *cc* = 1.8	4 *cc* = 3.6
Total	−1.2	1.2	3.6
Relative to **5***a*	0	2.4	4.8

	Effects, compound **14**			
	14*a*	**14***b*	**14***c*	**14***d*
	2 *ae* = −2.8	1 *ae* = −1.4		1 *ae* = −1.4
	4 *co* = 1.6	2 *co* = 0.8		2 *co* = 0.8
		2 *cc* = 1.8	4 *cc* = 3.6	2 *cc* = 1.8
			1 δ*cc* = 4.0	1 δ*cc* = 4.0
Total	−1.2	1.2	7.6	5.2
Relative to **14***a*	0	2.4	8.8	6.4

	Effects, compound **15**			
	15*a*	**15***b*	**15***c*	**15***d*
	2 *ae* = −2.8	1 *ae* = −1.4		1 *ae* = −1.4
	3 *co* = 1.2	1 *co* = 0.4		2 *co* = 0.8
	1 *cc* = 0.9	3 *cc* = 2.7	4 *cc* = 3.6	2 *cc* = 1.8
	1 δ*co* = 2.4	1 δ*co* = 2.4		
Total	1.7	4.1	3.6	1.2
Relative to **14***a*	2.9	5.3	4.8	2.4

	Effects, compound **21**		
	21*a*	**21***b*	**21***c*
	2 *ae* = −2.8	1 *ae* = −1.4	
	6 *co* = 2.4	4 *co* = 1.6	4 *co* = 1.6
	2 *cc* = 1.8	1 *cc* = 0.9	6 *cc* = 5.4
		2 δ*cc* = 8.0	
Total	1.4	9.1	7.0
Relative to **21***a*	0	7.7	5.6

	Effects, compound **22**		
	22*a*	**22***b*	**22***c*
	2 *ae* = −2.8	1 *ae* = −1.4	
	6 *co* = 2.4	4 *co* = 1.6	
	4 *cc* = 3.6	3 *cc* = 2.7	
		1 δ*cc* = 4.0	4 δ*cc* = 16.0
Total	3.2	6.9	16.0
Relative to **21***a*	1.8	5.5	14.6

Can. J. Chem. Downloaded from www.nrcresearchpress.com by 210.87.254.5 on 09/06/12
For personal use only.

TABLE 1. (*Continued*)

	Effects, compound **23**			
	23*a*	**23***b*	**23***c*	**23***d*
	2 *ae* = −2.8 6 *co* = 2.4 1 *cc* = 0.9 1 δ*cc* = 4.0	1 *ae* = −1.4 5 *co* = 2.0 5 *cc* = 4.5	2 *co* = 0.8 3 *cc* = 2.7 2 δ*cc* = 8.0	1 *ae* = −1.4 3 *co* = 1.2 1 *cc* = 0.9 2 δ*cc* = 8.0
Total	4.5	5.1	11.5	8.7
Relative to **21***a*	3.1	3.7	10.1	7.3

	Effects, compound **34**	
	34*a*	**34***b*
	2 *ae* = −2.8 4 *co* = 1.6	1 *ae* = −1.4 2 *co* = 0.8 2 *cc* = 1.8
Total	−1.2	1.2
Relative to **34***a*	0	2.4

	Effects, compound **35**	
	35*a*	**35***b*
	1 *ae* = −1.4 2 *co* = 0.8 2 *cc* = 1.8	4 *cc* = 3.6
Total	1.2	3.6
Relative to **34***a*	2.4	4.8

	Effects, compound **43**	
	43*a*	**43***b*
	2 *ae* = −2.8 3 *co* = 1.2 1 *cc* = 0.9 1 δ*co* = 2.4	1 *ae* = −1.4 2 *co* = 0.8 2 *cc* = 1.8
Total	1.7	1.2
Relative to **43***b*	0.5	0

	Effects, compound **44**	
	44*a*	**44***b*
	1 *ae* = −1.4 2 *co* = 0.8 2 *cc* = 1.8	4 *cc* = 3.6 1 δ*cc* = 4.0
Total	1.2	7.6
Relative to **43***b*	0	6.4

Can. J. Chem. Downloaded from www.nrcresearchpress.com by 210.87.254.5 on 09/06/12
For personal use only.

TABLE 1. (*Concluded*)

	Effects, compound **46**	
	46*a*	**46***b*
	2 *ae* = −2.8 4 *co* = 1.6	1 *ae* = −1.4 2 *co* = 0.8 2 *cc* = 1.8 1 δ*cc* = 4.0
Total	−1.2	5.2
Relative to **46***a*	0	6.4

	Effects, compound **47**	
	47*a*	**47***b*
	1 *ae* = −1.4 1 *co* = 0.4 3 *cc* = 2.7 1 δ*cc* = 4.0	4 *cc* = 3.6
Total	5.7	3.6
Relative to **46***a*	6.9	4.8

* 1 *ae* = one anomeric effect; 1 *co* = one *gauche* form of $OCH_2CH_2CH_2$; 1 *cc* = one *gauche* form of *n*-butane; 1 δ*co* = CH_3 and oxygen in a 1,3 diaxial arrangement; 1 δ*cc* = two CH_3's in a 1,3 diaxial arrangement.

The spiro compound **5** was prepared by the method (**10** + **11** → **12** → **13** → **5**) described in Scheme 5.[8] The ^{13}C nmr spectra of **5** at room temperature or at low temperature (≃ −130°C, $CHFCl_2$) are virtually identical and they show five peaks only.[9] This result indicates that **5** exists in only one conformation which can either be **5***a* or **5***c*. Due to symmetry, conformations **5***a* and **5***c* should show five peaks only, whereas conformation **5***b* should exhibit eleven peaks. Conformation **5***b* is therefore eliminated. Conformation **5***a* has two anomeric effects whereas **5***c* has none, and on that basis, **5***c* must be eliminated. Rigorous evidence confirming this conclusion has been obtained by X-ray analysis (*vide infra*). Consequently, **5***a* corresponds to the stable conformation of **5** as predicted.

Interestingly, compound **5** does not yield the corresponding dihydroxyketone precursor upon acid hydrolysis; however, in the presence of deuterated water, it incorporated four deuterium atoms (at C(5) and C(11)). This result shows that **5** undergoes hydrolysis, but the equilibrium lies toward the spiro ketal **5** in preference to the dihydroxyketone precursor.

Spiro System **6**

The spiro system **6** was considered next. With **6**, two isomers, **14** and **15** (Scheme 6), are possible and each can exist in principle in four different conformations (**14***a*–*d* and **15***a*–*d* respectively). Furthermore, the two isomers **14** and **15** are theoretically interconvertible under acidic conditions (**14** can be converted into the mirror image of **15** by opening and reclosure of the acetal function).

The evaluation of the anomeric and the steric effects in the eight conformations of isomers **14** and **15** is described in Table 1. When a methyl group was found to be in a 1,3-diaxial arrangement with another methyl (or methylene) group (δ C, C) or with an oxygen atom (δ C, O) we have taken the values of 4.0 and 2.4 kcal/mol respectively for the corresponding steric interactions (17, 18).

The relative stability of the four conformers (**14***a*–*d* and **15***a*–*d*) for each of the two isomers **14** and **15** is shown in Scheme 6. This analysis shows that isomer **14** should exist in conformation **14***a* (0 kcal/mol) only, whereas isomer **15** should exist as a mixture of a major (**15***d*, 2.4 kcal/mol) and a minor (**15***a*, 2.9 kcal/mol) conformer. However, since isomers **14** and **15** are interconvertible, and since conformer **14***a* is more stable than conformer **15***d* by 2.4 kcal/mol, this analysis leads to the prediction that under thermodynamically controlled conditions, only isomer **14** should be formed and that it should exist in conformation **14***a* only.

The preparation of the spiro system **6** (**10** + **16** → **17** → **18** → **6**) is described in Scheme 5. We have isolated only one isomer (**14**) and analysis by ^{13}C nmr shows that **14** exists in only one conforma-

[8] A shorter synthesis of **5** has been recently published, see ref. 16.

[9] A detailed account of the ^{13}C nmr spectral analysis is reported in the accompanying publication.

Can. J. Chem. Downloaded from www.nrcresearchpress.com by 210.87.254.5 on 09/06/12
For personal use only.

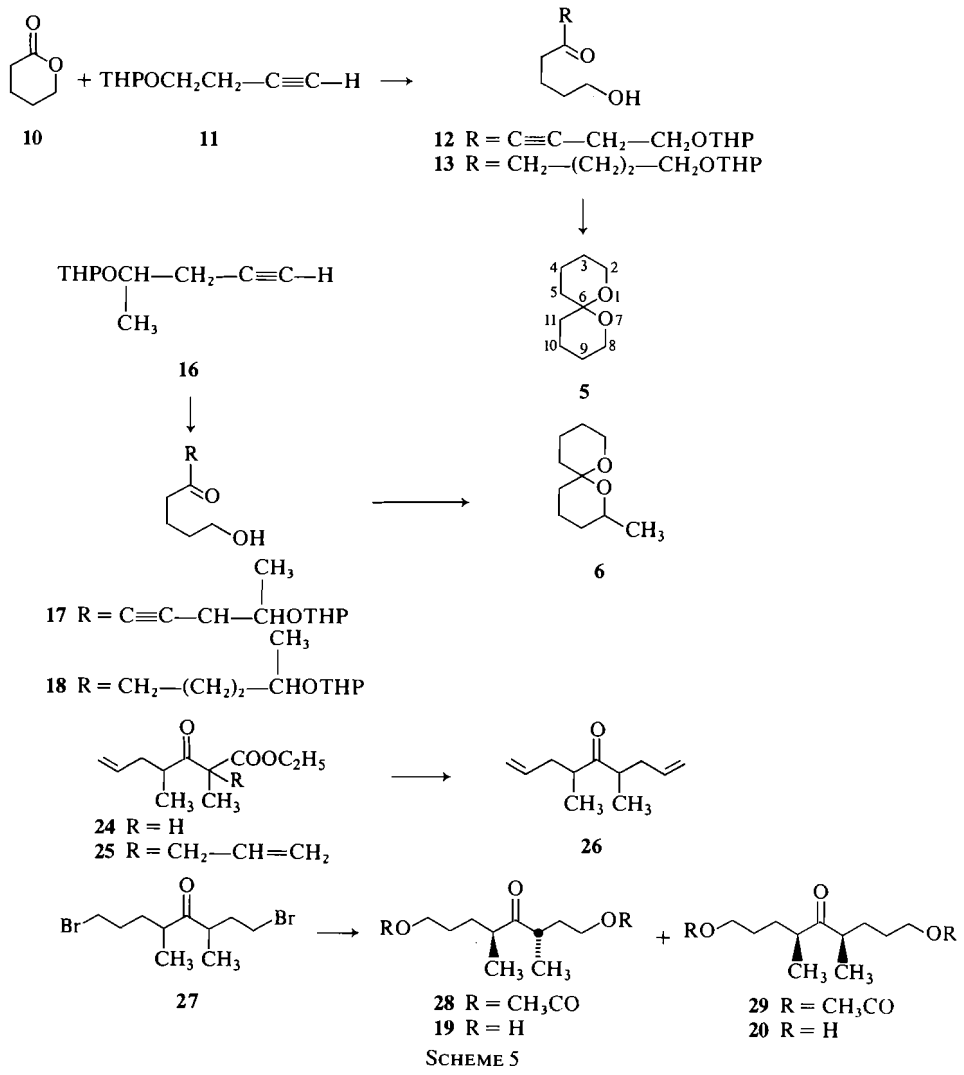

SCHEME 5

tion which corresponds to **14***a*.[9] Upon hydrolysis (2.3 *M* DCl in 60% D_2O/DME), compound **14** did not hydrolyse but incorporated four deuterium atoms. This result shows that hydrolysis of **14** takes place but the equilibrium lies toward the cyclic form **14** in preference to the corresponding dihydroxyketone. This result further proves that under thermodynamic conditions, the isomer **15** should not be observed, a result in accord with our prediction.

Spiro System 7

We will now consider the spiro system **7** which has two methyl groups. With this system, there are three possible isomers; two of them, **21** and **22**, are formed from the cyclization of the *dl* dihydroxyketone **19** (Scheme 7), whereas the third isomer **23** comes from the cyclization of the isomeric *meso* dihydroxyketone **20**. Under acidic conditions, **21** and **22** should be readily interconvertible and if these acidic conditions are strong enough to allow epimerization of the two dihydroxyketones **19** and **20**, the three isomeric compounds **21**, **22**, and **23** should be interconvertible.

Molecular models show that isomer **21** can exist in the three conformations, **21***a–c* (Scheme 8), isomer **22** in the three conformations, **22***a–c*, and isomer **23** in the four conformations, **23***a–d*. The relative stabilities of these various conformers of the three isomers **21**, **22**, and **23** are indicated in Scheme 8 and the detailed analysis is described in Table 1.

Isomer **21** should therefore exist in conformation **21***a* only (0 kcal/mol), isomer **22** should also exist in only one conformation (**22***a*, 1.8 kcal/mol), whereas isomer **23** should exist as a mixture of a

Can. J. Chem. Downloaded from www.nrcresearchpress.com by 210.87.254.5 on 09/06/12
For personal use only.

Can. J. Chem. Downloaded from www.nrcresearchpress.com by 210.87.254.5 on 09/06/12
For personal use only.

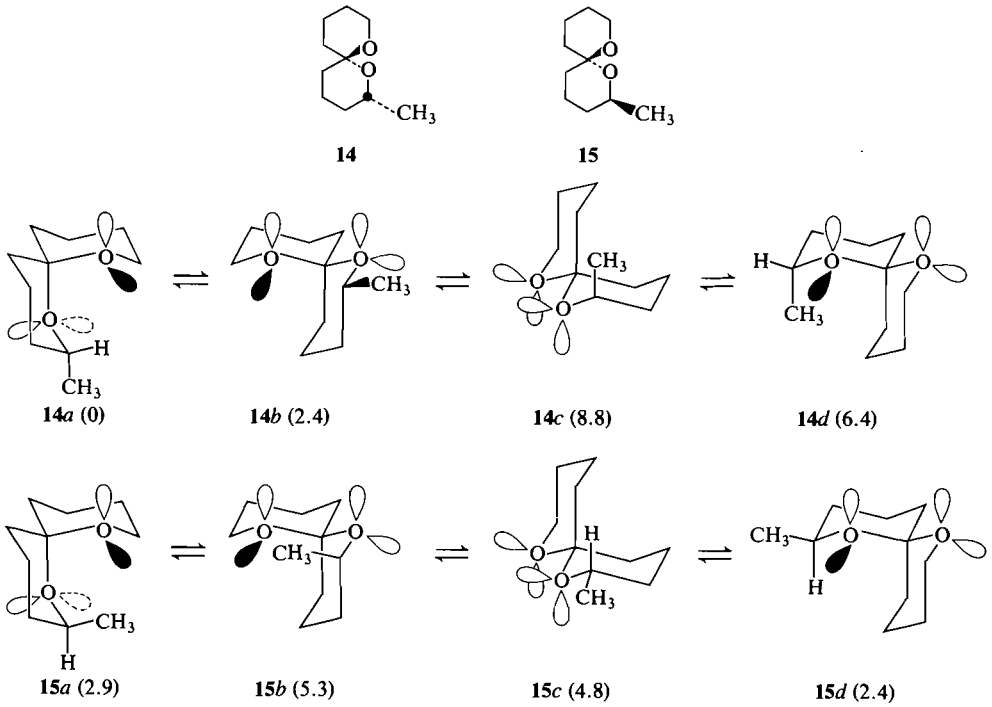

SCHEME 6

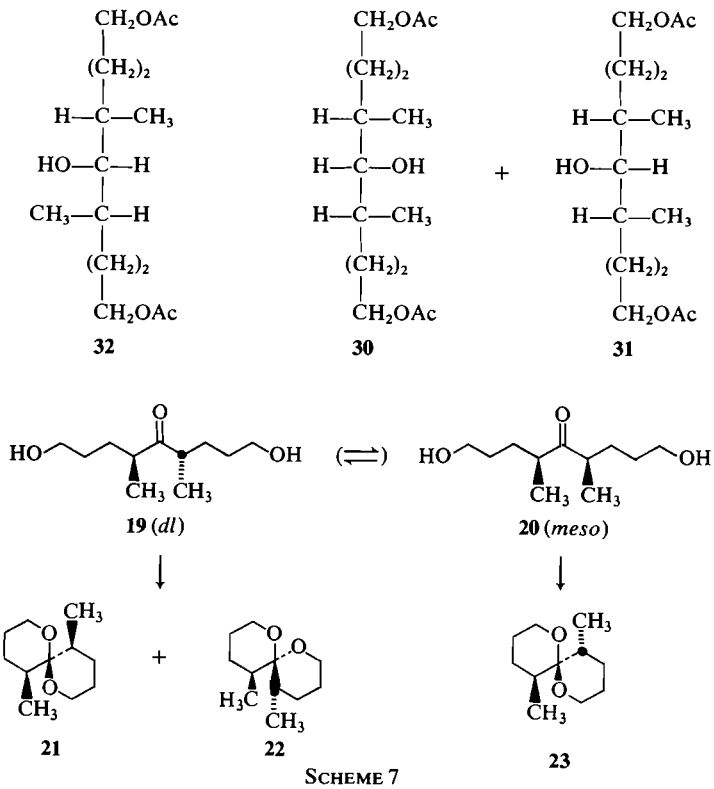

SCHEME 7

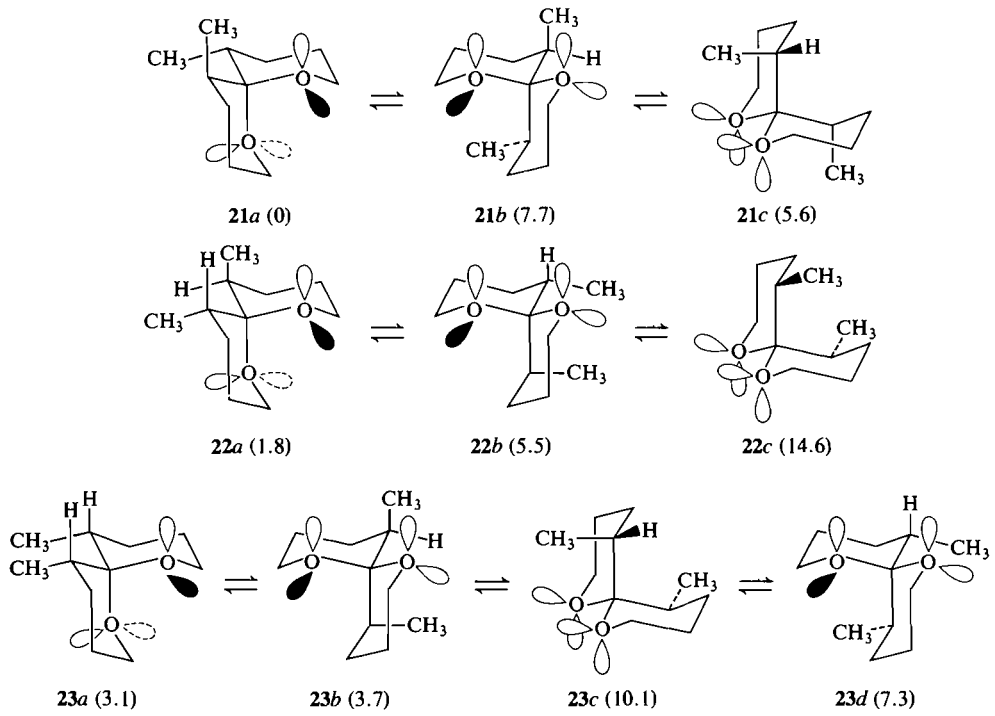

SCHEME 8

major (**23***a*, 3.1 kcal/mol) and a minor (**23***b*, 3.7 kcal/mol) conformer. This analysis leads to the prediction that, under thermodynamic conditions, the *dl* precursor **19** should yield a ≃97:3 mixture of isomers **21** and **22** which will exist in conformations **21***a* and **22***a* respectively, whereas the *meso* precursor **20** should yield **23** existing as a mixture of conformers **23***a* and **23***b*.

However, if the acidic conditions used allow the equilibration of the isomeric precursors **19** and **20**, isomer **23** which is at least 3.1 kcal/mol less stable than isomer **21** should not be observed, and a ≃97:3 mixture of isomers **21** and **22** should be isolated.

The preparation of a mixture of *dl* and *meso* dihydroxyketones **19** and **20** (**24** → **25** → **26** → **27** → **28** + **29** → **19** + **20**) is described in Scheme 5. Cyclization of this mixture under mild acidic conditions (PTSA/$CHCl_3$) gave a mixture of the three isomeric spiroketals **21**, **22**, and **23** which were separated. These products were identified by their spectral data, equilibration experiments, and behavior under hydrolysis conditions; ^{13}C nmr spectroscopy further showed that **21** and **22** exist in conformations **21***a* and **22***a* respectively. We have also been able to show by low temperature study ($CHFCl_2$, 160 K, 250 MHz), that **23** exists as a mixture of conformations **23***a* and **23***b*, as predicted.[9]

Treatment of **21** under aqueous acid conditions (0.1 *N* HCl in H_2O/acetone) did not yield the precursor *dl* dihydroxyketone **19**, but gave a ≃97:3 mixture of **21** and **22**. Repeating the above experiment with deuterated water, compound **21** was shown to incorporate two deuterium atoms. Treatment of **23** under the same acidic conditions gave also a 97:3 mixture of **21** and **22**. Under milder acidic conditions (0.01 *N* HCl in 20% H_2O/acetone) **23** produced a mixture of **21**, **22**, and the *meso* dihydroxyketone **20**, which was isolated as the corresponding *meso* ketodiacetate **29**.[10]

These results are again completely consistent with our predictions based on the evaluation of the steric and the anomeric effects.

Spiro System 8

With the tricyclic spiro system **8**, two isomers, **34** and **35**, are possible from the cyclization of the dihydroxyketone **33** (Scheme 9) and they can exist

[10]The structure of *meso* ketodiacetate **29** was proven in the following way. Upon reduction of the ketone function, **29** can give the two isomers **30** and **31** whereas the *dl* ketodiacetate **28** can give the isomer **32** only. The ketodiacetate obtained (**29**) was reduced ($NaBH_4$, MeOH); ^{13}C nmr analysis showed the presence of two signals for a carbon bearing a secondary alcohol indicating that a mixture of **30** and **31** was obtained. The product of the reduction of a 1:1 mixture of **28** and **29** showed three different signals for a carbon bearing a secondary alcohol, indicating that a mixture of **30**, **31**, and **32** was obtained.

Can. J. Chem. Downloaded from www.nrcresearchpress.com by 210.87.254.5 on 09/06/12
For personal use only.

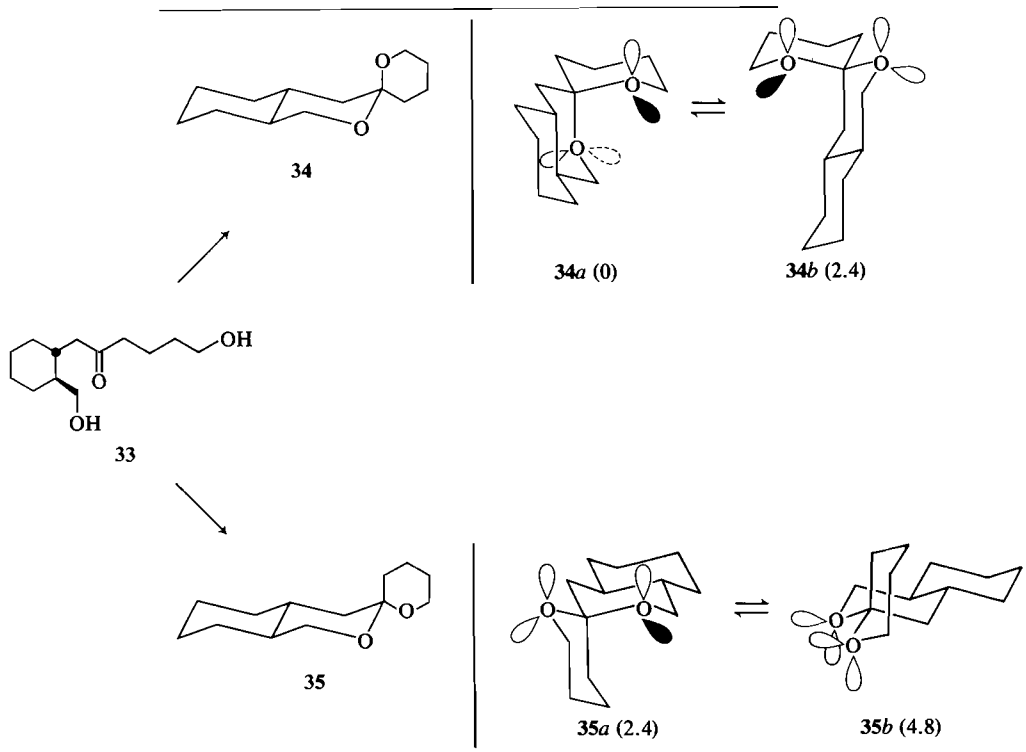

SCHEME 9

in two conformations each, which are **34***a*–*b* and **35***a*–*b* respectively. The detailed analysis of the relative stability of these four structures is described in Table 1. Conformer **34***a* (0 kcal/mol) is more stable than **34***b* (2.4 kcal/mol); isomer **34** should therefore exist in conformation **34***a* only. Similarly, conformer **35***a* (2.4 kcal/mol) is more stable than **35***b* (4.8 kcal/mol); isomer **35** should exist in conformation **35***a* only. However, since conformer **34***a* is more stable than conformer **35***a* by 2.4 kcal/mol, and since the isomers **34** and **35** can be interconverted by equilibration under acidic conditions, only isomer **34** should be observed under thermodynamically controlled conditions.

The preparation of the tetrahydropyranyl derivative **38** of monocyclic dihydroxyketone **33** (**36** + **11** → **37** → **38**) is described in Scheme 10. Treatment of **38** under acidic conditions (0.1 *N* HCl/CH_3OH) gave only the tricyclic ketal product **34** which was shown by ^{13}C nmr to exist in conformation **34***a* only.[9] Under aqueous acidic conditions (1 *N* DCl, acetone), compound **34** did not hydrolyse or equilibrate with **35** but incorporated four deuterium atoms. We have also prepared the monocyclic dihydroxyketone **33** (**38** → **39** → **40** → **41** → **33**, Scheme 10) and this product was cyclized under mild acid conditions (catalyst *p*-TSOH in $CHCl_3$); the reaction was stopped before completion and the reaction mixture was acetylated ($(CH_3CO)_2O$, pyridine) before isolation. This procedure gave a mixture of tricyclic acetal **34** and ketodiacetate **41** as well as a very small quantity of tricyclic acetal **35**. Compound **35** was obtained pure (≃1.5 mg) and characterized by infrared, ^1H nmr, and mass spectrometry. Upon treatment under acidic conditions (1 *N* HCl in acetone), tricyclic acetal **35** was irreversibly transformed into the more stable isomer **34**. These results are again in complete agreement with our prediction.

Spiro System 9

This spiro system can theoretically give the four isomers **43**, **44**, **46**, and **47** (Scheme 11). The two isomers **43** and **44** come from the cyclization of the dihydroxyketone precursor **42**, whereas the two isomers **46** and **47** come from the cyclization of the isomeric dihydroxyketone precursor **45**. In this case, **42** and **45** cannot be interconverted by epimerization. The isomers **43** and **44** which are interconvertible under acidic conditions can exist in two conformations each, which are **43***a*, *b* and **44***a*, *b*, respectively (Scheme 12). Similarly, the isomers **46** and **47** which are also interconvertible under acidic conditions can exist in two conformations each which are **46***a*, *b* and **47***a*, *b*, respectively.

Can. J. Chem. Downloaded from www.nrcresearchpress.com by 210.87.254.5 on 09/06/12
For personal use only.

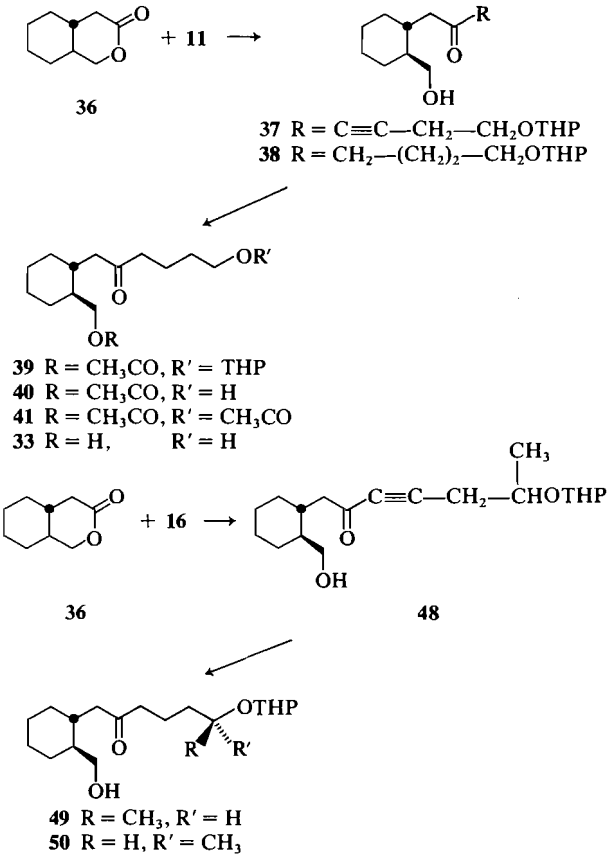

SCHEME 10

The analysis of the relative stabilities of the eight conformers of the four isomeric compounds **43**, **44**, **46**, and **47** is described in detail in Table 1 and shown in Scheme 12.

Isomer **43** should exist as a mixture of a major (**43***b* 0 kcal/mol) and a minor conformer (**43***a*, 0.5 kcal/mol). Isomer **44** should exist only in conformation **44***a* (0 kcal/mol). However, isomers **43** and **44** are interconvertible under acid conditions; a $\simeq 1:1$ mixture of isomers **43** and **44** should therefore be isolated from the cyclization of the precursor **42**. The isomer **43** should, however, slightly predominate at equilibrium due to an entropy factor, because **43** can exist in two conformations (**43***a* and **43***b*) whereas **44** can exist in only one (**44***a*).

Isomer **46** should exist in conformation **46***a* (0 kcal/mol) only, whereas isomer **47** should exist as a mixture of conformers **47***a* (6.9 kcal/mol) and **47***b* (4.8 kcal/mol). However, since isomers **46** and **47** are interconvertible under acidic conditions, only isomer **46** existing in conformation **46***a* should be isolated under thermodynamically controlled conditions.

Thus, under thermodynamically controlled conditions, the acid cyclization of a mixture of the isomeric dihydroxyketones **42** and **45** should yield a mixture of the three isomers **43**, **44**, and **46**. The preparation of a mixture of the tetrahydropyranyl derivatives **49** and **50** of the dihydroxyketones **42** and **45** (**36** + **16** → **48** → **49** + **50**) is described in Scheme 10. Cyclization of **49** and **50** under acidic conditions (1 *N* HCl, acetone), yielded as expected a mixture of **43**, **44**, and **46** which were separated by chromatography. Low temperature ^{13}C nmr study confirms that isomers **44** and **46** are conformationally rigid and exist in conformations **44***a* and **46***a* respectively.[9] Contrary to our analysis, isomer **43** exists in conformation **43***b* only; steric effects might have been underestimated in **43***a*, especially the 1,3 diaxial interaction between the oxygen and the methyl group.

Furthermore, under acidic conditions, isomer **43** (or **44**) was converted into a $\simeq 1:1$ mixture of isomers **43** and **44**. It was also shown that isomer **46** does not isomerize under acidic conditions, indicating that under thermodynamically controlled conditions the formation of **47** cannot compete with that of **46**.

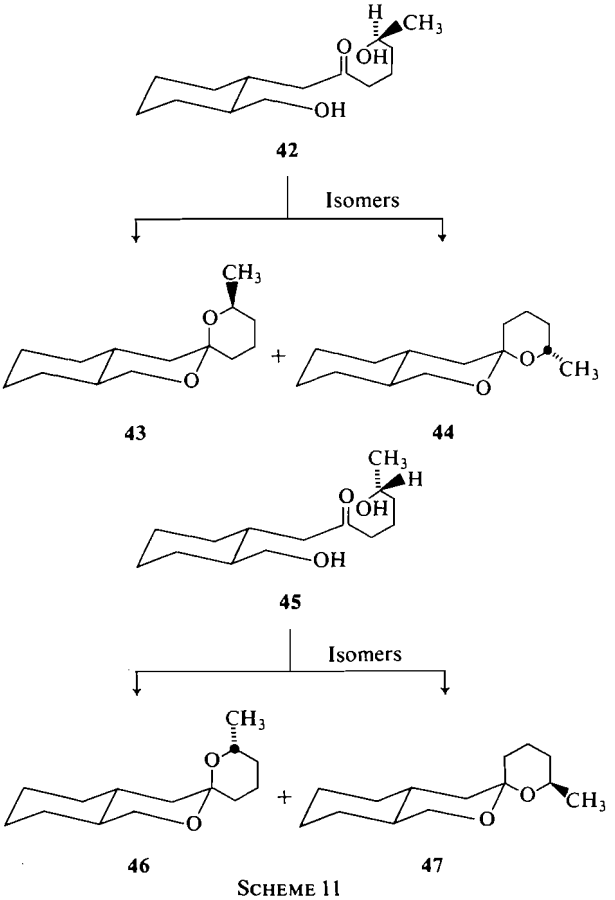

SCHEME 11

Can. J. Chem. Downloaded from www.nrcresearchpress.com by 210.87.254.5 on 09/06/12
For personal use only.

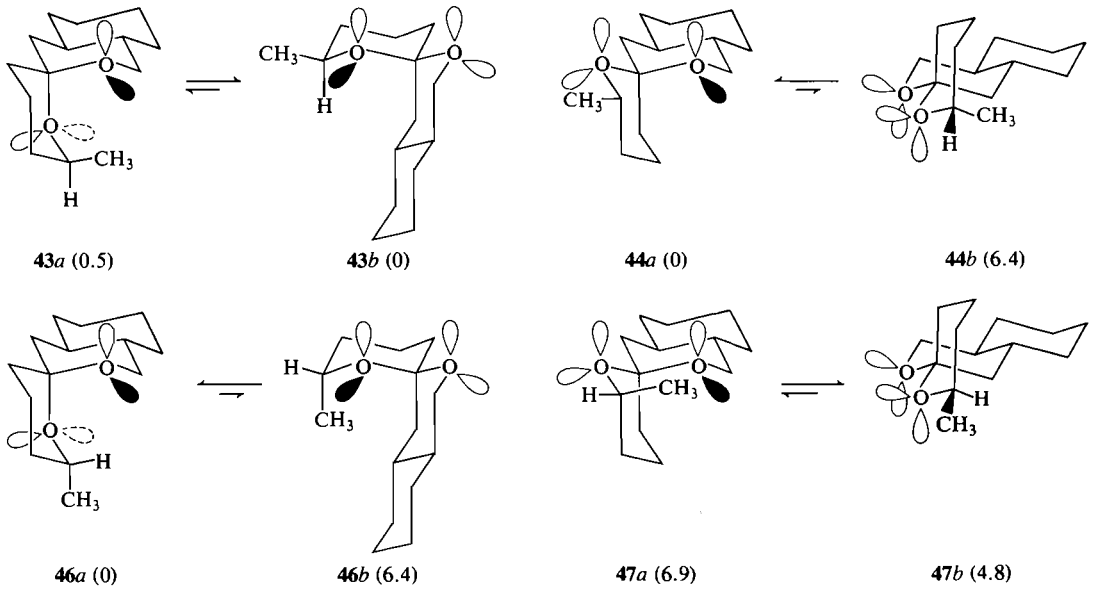

SCHEME 12

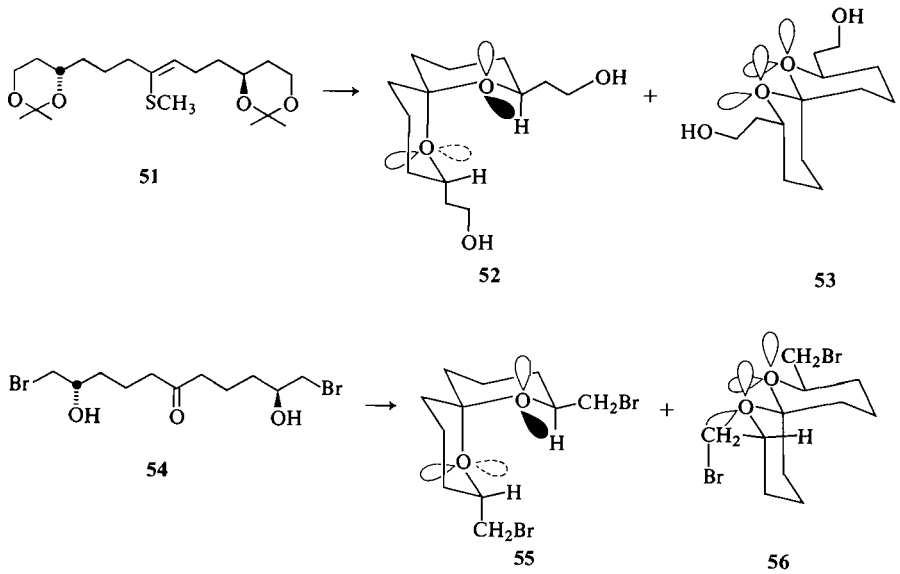

SCHEME 13

Results from the Literature

Compound **51**, a masked tetrahydroxyketone (Scheme 13), which can theoretically give the isomers **52** and **53**, was found to yield the isomer **52** exclusively (19). The structure of **52** was proven by X-ray analysis. Similarly, dibromodihydroxyketone **54** can theoretically give either isomer **55** or **56**. Upon cyclization, the isomer **55** was the product formed (20), and its structure was also established by X-ray analysis (21). The recently reported total synthesis of ionophore A-23187 (22), a polyether antibiotic which can be considered as a substituted 1,7-dioxaspiro[5.5]undecane system, i.e. **5**, confirms these results. Thus, these results described in the literature rigorously established that conformer **5***c* of **5** is much less stable than conformer **5***a*, as predicted.

Conclusion

These results constitute very strong evidence concerning the importance of the anomeric (and the *exo*-anomeric) effect. The value of 1.4 kcal/mol for

Can. J. Chem. Downloaded from www.nrcresearchpress.com by 210.87.254.5 on 09/06/12
For personal use only.

Can. J. Chem. Downloaded from www.nrcresearchpress.com by 210.87.254.5 on 09/06/12
For personal use only.

an anomeric effect must, however, be considered as a minimum value, because the steric interactions might be larger than those observed in a simple cyclohexane (8).

These results demonstrate clearly that the basic spiro system **5** exists in conformation **5***a* only; **5** can therefore be considered as a conformationally rigid system.[11]

Experimental

Vapor-phase chromatographic (vpc) analyses and separations were carried out on a Varian Aerograph instrument, model 2800 equipped with a thermal conductivity detector. The infrared (ir) spectra were recorded in chloroform on a Perkin-Elmer 257 spectrophotometer. Proton nuclear magnetic resonance (^{1}H nmr) spectra were recorded in deuterochloroform on a Bruker WP-60 instrument with TMS as an internal standard. The ^{13}C nmr spectra were recorded on a Bruker HX-90 spectrometer equipped with a Nicolet 1083 computer (8K memory for data) operating in the Fourier transform mode. Spectra were recorded in deuterochloroform with a sweep width of 5000 Hz. Mass spectra were obtained on Hitachi-Perkin-Elmer RMU-6-A and Micromass ZAB-2F machines. Microanalyses were carried out by Guelph Chemical Laboratories Ltd., Guelph, Ontario. Bicyclic lactone **36** was obtained by Baeyer–Villiger oxidation (23) of *trans*-hydrindanone (24).

The abbreviation plc (x% E/H) refers to preparative thin layer chromatography eluting with x% ether in hexane. The following abbreviations are also used: RT (room temperature); s (singlet); bs (broad singlet); d (doublet); t (triplet); q (quartet); quin (quintet); m (multiplet); $W/2$ (peak width at half peak height).

*Acetylene **11***

To dihydropyran (84 g, 1.0 mol) cooled in an ice bath was added 3-butyn-1-ol (50 g, 0.70 mol) and then concentrated hydrochloric acid (2 drops). After 3 h at RT, potassium carbonate (1 g) was added and after 15 min stirring the solution was filtered and distilled to give pure compound **11** (99 g, 90%); bp 72–78°C/20 Torr; ir: 3280, 1124, 1108, 1053, and 1017 cm^{-1}; ^{1}H nmr δ: 1.63 (6H, m), 1.95 (1H, t, J = 2.5 Hz, HC≡C), 2.48 (2H, t of d, J = 7.0 Hz, 2.5 Hz, CH_2C≡C), 3.30–4.15 (4H, m, CH_2O), 4.64 (1H, bs, OCHO).

*Acetylene **16***

A small quantity of propargyl bromide was added to magnesium (9.2 g, 0.38 mol) and mercuric chloride (catalytic quantity) under ether (50 mL). Once the reaction had been initiated by gentle heating, the solution was cooled to 0°C and the remainder of the propargyl bromide (47.6 g, 0.40 mol) in ether (100 mL) was slowly added. After 30 min, acetaldehyde (19.8 g, 0.45 mol) in ether (100 mL) was slowly added and the reaction stirred at room temperature for a further 30 min. The solution was acidified with 1 *N* hydrochloric acid and the organic phase was removed. The aqueous phase was extracted with ether (3 × 50 mL) and the combined ether phases were then washed with brine (1×), dried (Na_2SO_4), and evaporated. The residue was added to dihydropyran (42 g, 0.50 mol) maintained at 0°C. Two drops of concentrated hydrochloric acid were then added and the solution was left at RT for 3 h. Potassium carbonate (1 g) was added and after 15 min stirring, the reaction was filtered and distilled to give pure compound **16** (19 g, 30%); bp 90–95°C/20 Torr; ir: 3310, 1110, 1053, 1000, and 973 cm^{-1}; ^{1}H nmr δ: 1.24 and 1.32 (3H, d, J = 10.5 Hz, isomeric CH_3), 1.62 (6H, m), 2.00 (1H, m, HC≡C), 2.20–2.60 (2H, m, CH_2C≡C), 3.30–4.20 (3H, m, CHOR), 4.75 (1H, bs, OCHO).

*1,7-Dioxaspiro[5.5]undecane (**5**)*

To a solution of compound **11** (3.08 g, 20 mmol) in tetrahydrofuran (25 mL) at −78°C was added slowly *n*-butyllithium (1.6 *M* in hexane, 20 mmol). After 30 min, δ-valerolactone (2.00 g, 20 mmol) in tetrahydrofuran (25 mL) was rapidly added and the reaction was allowed to warm to RT. The solution was poured into water (50 mL) and the organic phase was separated. The aqueous phase was extracted with ether (3 × 50 mL) and the combined organic phases were then dried (Na_2SO_4) and evaporated. The oily residue was taken up in dry methanol (50 mL) and hydrogenated (40 psi over PtO_2). After filtration through silica gel, concentrated hydrochloric acid (2 drops) was added and the solution was left at RT overnight. Evaporation of the methanol gave a residue which was taken up in ether and dried (Na_2SO_4 and some K_2CO_3). Evaporation, followed by chromatography on silica gel gave, on elution with 5% E/H, spiroketal **5** (1.10 g, 33%) as a clear oil; ir: 1164, 1076, 1046, and 966 cm^{-1}; ^{1}H nmr δ: 1.60 (12H, m), 3.3–4.0 (4H, m, CH_2O); ^{13}C nmr δ: 18.6 (t), 25.4 (t), 35.8 (t), 60.3 (t), 94.9 (s); ms *m/e*: 156 (M^+).

*2-Methyl-1,7-dioxaspiro[5.5]undecane **14** (**6**)*

To a solution of acetylene **16** (3.53 g, 20 mmol) in tetrahydrofuran (20 mL), cooled to −78°C, was slowly added *n*-butyllithium (21 mmol of 1.6 *M* solution in hexane). After 30 min, a solution of δ-valerolactone (2.0 g, 20 mmol) in tetrahydrofuran (40 mL) was rapidly added and the solution was then allowed to warm to RT. The reaction was quenched in water (50 mL), the organic phase was removed, and the aqueous phase was ether extracted (3×). The combined organic phases were dried (Na_2SO_4) and evaporated to give an oily residue which was hydrogenated (40 psi) over platinum oxide in methanol (50 mL). The catalyst was removed by filtration through silica gel, concentrated hydrochloric acid (2 drops) was added and the solution was left at RT overnight. The solvent was removed under reduced pressure and the residue was taken up in ether and dried ($MgSO_4/K_2CO_3$). Evaporation and chromatography on silica gel gave, on elution with 5% E/H, methyl spiroketal **14** (900 mg, 26%) as a clear oil; ir: 1384, 1216, 1093, 1064, and 994 cm^{-1}; ^{1}H nmr δ: 1.14 (3H, d, J = 10.5 Hz, CH_3), 1.54 (12 H, m), 3.60 (3H, m, CHOR); ^{13}C nmr δ: 18.6 (t), 19.0 (t), 21.8 (q), 25.4 (t), 32.7 (t), 35.1 (t), 35.9 (t), 60.2 (t), 65.1 (d), 95.5 (s); ms *m/e*: 170 (M^+).

*Deuteration of Spiroketals **5** and **14***

The spiroketals (100–300 mg) in dimethoxyethane (3.0 mL), deuterium oxide (3.0 mL), and 35% deuterium chloride/D_2O (1.5 mL) were maintained at RT overnight. The reaction was diluted with water (10 mL) and ether extracted (3 × 20 mL). Drying ($MgSO_4$) and evaporation of solvent gave the deuterated ketals; d_4-acetal **5**: ^{13}C nmr δ: 18.3, 25.3, 60.4, anomeric carbon not observed; d_4-acetal **14**: ^{13}C nmr δ: 18.4, 18.7, 21.8, 25.4, 32.7, 60.3, 65.2, anomeric carbon not observed.

*Keto-ester **24***

A suspension of sodium hydride (4.22 g, 50% dispersion, 88 mol, washed with pentane (2×)) in tetrahydrofuran (200 mL) was cooled in an ice/salt bath under nitrogen and ethyl-α-propionyl propionate (12.6 g, 9.64 mL, 80 mmol) was added dropwise with rapid stirring. Ten minutes after gas evolution ceased, *n*-butyllithium (81 mmol, 1.6 *M* in hexane) was added and, after a further 10 min, allyl bromide (8.0 mL, 92 mmol). The

[11] The basic spiro system **5** can therefore be used to develop a new strategy for the synthesis of aliphatic chains containing several asymmetric centers and functional groups. Work is now in progress in our laboratory to demonstrate the validity of this new strategy.

Can. J. Chem. Downloaded from www.nrcresearchpress.com by 210.87.254.5 on 09/06/12
For personal use only.

cooling bath was removed and, after 10 min, the reaction was quenched (10% hydrochloric acid, 50 mL) and diluted with ether (≈200 mL). The aqueous phase and a first brine washing of the organic phase were combined and further extracted with ether. The combined ether phases were then washed with brine, brine – sodium bicarbonate to remove colour, and then brine again until neutral. Drying ($MgSO_4$) and evaporation of the solvent gave the keto-ester **24** (14.8 g, 94%) sufficiently pure for the next reaction. Distillation (86–88°C/4 Torr) and vpc (5 ft × ¼ in; 10% SE-30 on Chromosorb W, 160°C) gave an analytical sample; ir: 3070, 1745, 1716, 1643, 1222, 1180, 973, and 898 cm^{-1}; ^1H nmr δ: 1.11 (3H, d, J = 7 Hz, γCH_3), 1.25 (3H, t, J = 7 Hz, CH_2CH_3), 1.32 (3H, d, J = 8 Hz, αCH_3), 1.9–3.1 (3.5 H, m), 3.63 and 3.67 (1H, 2 q, J = 7 Hz, isomeric αH), 4.17 (2H, q, J = 7 Hz, OCH_2), 4.80–6.10 (3H, olefinic m); ms *m/e*: 198 (M^+), 152, 129, 97.

Keto-ester 25

A solution of dimethylformamide (70 mL) and benzene (40 mL) was dried in a Dean-Stark apparatus (17 ml removed), cooled under nitrogen, and the major part added to sodium hydride (3.66 g, 50% dispersion, 76.3 mmol, washed with pentane (2×)) and stirred in an ice/salt bath under nitrogen. Keto-ester **24** (13.7 g, 69.2 mmol) was added dropwise followed by the remainder of the solvent. After 15 min, allyl bromide (7.1 mL, 82 mmol) was added and the system was allowed to warm to RT over 15 min. After 50 min at 40°C, the reaction was quenched (10% hydrochloric acid, 40 mL), diluted with water (600 mL), and extracted with ether (3×). The combined organic fractions were washed with water until neutral, dried ($MgSO_4$), and evaporated to give keto-ester **25** (14.2 g, 86%) sufficiently pure for the next reaction. An analytical sample was prepared by vpc (5 ft. × ¼ in., 10% SE-30 on Chromosorb W, 170°C); ir: 3065, 1735, 1713, 1642, 1220, 1135, 977, and 897 cm^{-1}; ^1H nmr δ: 1.06 (3H, d, J = 7 Hz, CH_3), 1.26 (3H, t, J = 7 Hz, CH_3), 1.32 and 1.34 (3H, two s, isomeric CH_3's), 2.0–3.1 (6H, m), 4.17 (2H, q, J = 7 Hz), 4.80–6.07 (6H, olefinic m); ms *m/e*: 238 (M^+), 210, 193, 142.

Ketone 26

Keto-ester **25** (14.2 g, 59.7 mmol) in methanol (200 mL) and water (10 mL) was refluxed with sodium hydroxide (5.0 g, 125 mmol) with vigorous stirring for 3¼ h. The solvent was largely removed under reduced pressure and the residue was diluted with water and adjusted to neutral pH. Ether extraction (3×), drying ($MgSO_4$), and evaporation of the solvent followed by distillation (76–80°C/6 Torr) gave ketone **26** (7.08 g, 71.5%). An analytical sample was prepared by vpc (5 ft. × ¼ in., 10% SE-30 on Chromosorb W, 130°C); ir: 3065, 1713, 1642, 977, and 893 cm^{-1}; ^1H nmr δ: 1.04 and 1.07 (6H, two d, J = 7 Hz, isomeric CH_3), 1.73–3.02 (6H, m), 4.75–6.02 (6H, olefinic m); ^{13}C nmr δ: 16.1 and 16.2 (q, isomeric CH_3), 37.0 and 37.2 (t), 45.0 (d), 116.8, 135.9, 216.5; ms *m/e*: 166 (M^+), 97, 69.

Dibromide 27

The ketone **26** (2.39 g, 14.4 mmol) in pentane (500 mL) was placed in a water-cooled uv apparatus, cooled with ice, and purged with nitrogen for 15 min. Anhydrous hydrogen bromide was then bubbled gently into the solution with irradiation from a 450 W Hanovia mercury lamp for 15 min. The solution was again purged with nitrogen and the pentane solution was washed with 5% sodium bicarbonate containing some sodium thiosulfate (2×), then water (1×). Drying ($MgSO_4$) and evaporation gave the dibromide **27** (4.21 g, 85%) as a rapidly blackening oil which was used directly for the next step; plc (50% E/H) gave an analytical sample; ir: 1713, 1243, and 995 cm^{-1}; ^1H nmr δ: 1.08 and 1.09 (6H, two d, J = 7 Hz, isomeric CH_3), 1.4–2.1 (8H, m), 2.63 (2H, deformed quin, J = 6.5 Hz), 3.39 (4H, t, J = 6 Hz); ms *m/e*: 330, 328, 326 (M^+, 1:2:1), 249, 247 (M^+ – Br, 1:1), 179, 177 ($M^+ - C_5H_{10}Br$, 1:1).

Diacetates 28 and 29

Sodium acetate (2.70 g, 32.9 mmol) was dissolved in hexamethylphosphoramide (60 mL) and water (12 mL). To this warm solution was added the dibromide **27** (3.87 g, 11.8 mmol) and hexamethylphosphoramide (5 mL). After 21 h at 35°C the solution was diluted with water (600 mL) and ether extracted (3×). The combined ethereal phases were washed with brine (2×), dried ($MgSO_4$), and evaporated. Chromatography on silica (140 g) with increasing proportions of ether in hexane gave keto-diacetates **28** and **29** (2.27 g, 70.7%) as an inseparable mixture; plc (60% E/H) gave an analytical sample; ir: 1735, 1237, and 1017 cm^{-1}; ^1H nmr δ: 1.06 and 1.08 (6H, two d, J = 7 Hz, isomeric CH_3), 1.3–1.8 (8H, m), 2.04 (6H, s, OAc), 2.4–2.9 (2H, m), 4.04 (2H, deformed t); ^{13}C nmr δ: 16.6, 20.9, 26.5, 28.9, 29.1, 44.6, 64.2, 170.9, 216.7, 216.8; ms *m/e*: 226, 186, 166, 157. *Anal.* calcd. for $C_{15}H_{26}O_5$: C 62.91, H 9.15; found: C 62.81, H 9.35.

Spiroketals 21, 22, and 23

Diacetates **28** and **29** (3.31 g, 11.6 mmol) in methanol (90 mL), triethylamine (10 mL), and water (5 mL) were maintained at 50°C for 3 days. Evaporation of the solvent gave the diols **19** and **20** (3.06 g, 100%); ir: 3420, 1710, 1040, and 973 cm^{-1}; ^1H nmr δ: 0.96 (6H, d, J = 7 Hz), 2.30–2.85 (2H, m), 3.40 (4H, deformed t, $W/2$ = 4 Hz, CH_2O), 4.51 (2.5 H, variable s, OH); ms *m/e*: 184, 115.

Cyclization was effected in chloroform (12 mL) with consecutive additions of *p*-toluenesulfonic acid (total ≈50 mg) as the reaction was followed by nmr and vpc (5 ft × ¼ in., 5% FFAP on Chromosorb W, 105°C). The reaction occurred suddenly giving spiroketals **21**, **23**, and **22** in a ratio of 100:59:4 (R_f 3.6, 6.0, and 7.2 min respectively). The reaction was quenched with saturated sodium bicarbonate and the aqueous phase was extracted with chloroform. The combined organic phases were washed with sodium bicarbonate, dried (Na_2SO_4), and evaporated to give the product (2.13 g 115%). Chromatography on Florisil (200 g), eluting with 2% E/H, gave a partial separation of the isomeric spiroketals. From these fractions, pure material was prepared by vpc, to give (from highest R_f) the following.

Spiroketal 21: ir: 1067, 1000, 958, and 913 cm^{-1}; ^1H nmr δ: 0.86 (6H, d, J = 6 Hz), 1.3–2.0 (10H, m), 3.38–3.70 (4H, m, $W/2$ = 10 Hz); ^{13}C nmr δ: 16.2, 26.4, 27.3, 34.5, 59.9, and 99.8; ms *m/e*: 184 (M^+). *Anal.* calcd. for $C_{11}H_{20}O_2$: C 71.69, H 10.94; found: C 71.94, H 11.39.

Spiroketal 23: ir: 1062, 998, and 915 cm^{-1}; ^1H nmr δ: 0.96 (3H, d, J = 6 Hz), 1.08 (3H, d, J = 7 Hz), 1.17–2.10 (10H, m), 3.59 (4H, m, $W/2$ = 8 Hz); ^{13}C nmr δ: 16.8 (q), 17.5 (q), 20.6 (t), 24.9 (t), 26.6 (t), 29.2 (t), 35.9 (d), 36.0 (d), 59.4 (t), 60.6 (t), 100.0; ms *m/e*: 184 (M^+).

Spiroketal 22: ir: 1053, 1015, 988, 910, and 865 cm^{-1}; ^1H nmr δ: 1.01 (6H, d, J = 7 Hz), 1.13–2.42 (10H, m), 3.50–3.80 (4H, m, $W/2$ = 11 Hz); ^{13}C nmr δ: 13.6, 19.6, 25.4, 32.0, 60.7, and 99.4; ms *m/e*: 184 (M^+).

Equilibration of Spiroketal 21

To spiroketal **21** (264 mg, 1.43 mmol, >99.5% by vpc) in acetone (2 mL) was added hydrochloric acid (1 *N*, 0.50 mL) and then sufficient acetone to give a homogeneous system. The reaction was complete within 2 days by vpc. After 8 days, the reaction was quenched with sodium carbonate, diluted with ether, and concentrated under reduced pressure. Dilution with ether, drying (Na_2SO_4), and evaporation gave the product (242 mg, 91.7%) which by vpc, consisted of spiroketals **21** (96.8%), **23** (≤0.1%), and **22** (3.2%). Infrared and ^1H nmr confirmed the presence of acetal **21**. The presence of acetal **22** was confirmed by ^{13}C nmr.

Deuteration of Spiroketal 21

Spiroketal **21** (106 mg, 0.58 mmol) in d_1-methanol (0.9 mL)

Can. J. Chem. Downloaded from www.nrcresearchpress.com by 210.87.254.5 on 09/06/12
For personal use only.

and 1 *M* deuterium chloride in deuterium oxide (0.1 mL) were maintained at RT for 6 days when ^{1}H nmr showed the exchange to be 50% complete. Additional 35% deuterium chloride solution (10 μL) and d_1-methanol (0.1 mL) were added and after a further 8 days the reaction was almost complete. Complete deuteration was effected by dilution of the system with d_1-methanol (≃2 mL) and addition of further acid (20 μL, 35% solution). After 3 more days, the system was quenched with saturated sodium bicarbonate solution, diluted with ether, and the organic phase dried (Na_2SO_4). Evaporation of the solvent gave d_2-acetal (**21**) (70 mg, 66%); vpc gave an analytical sample; ir: 1090, 1052, 1035, and 995 cm^{-1}; ^{1}H nmr δ: 0.86 (6H, s, CH_3), 1.24–1.86 (8H, m), 3.44–3.76 (4H, m); ^{13}C nmr δ: 16.1, 26.4, 27.2, 59.9, anomeric carbon not observed; ms *m/e*: 186 (M^+).

Hydrolysis of Spiroketal 22

To spiroketal **22** (4.0 mg) in acetone (0.3 mL) and water (0.15 mL) was added a solution of 1 *M* hydrochloric acid (50 μL). By tlc, the isomerization was almost complete in 1 h. Work-up, as for the isomerization of spiroketal **21**, gave spiroketal **21** by vpc, tlc, ^{1}H nmr, and ir; vpc analysis gave a ratio **21**:**22** ≃ 97:3.

Hydrolysis of Spiroketal 23

Spiroketal **23** (7.9 mg) in acetone (250 μL) was treated with 1 *N* hydrochloric acid (100 μL) and the reaction was followed by vpc (≃15 min). After 18 h, the acetone was removed under reduced pressure at RT and the acid was quenched with sodium bicarbonate. Dilution with ether and adsorption of the aqueous phase with sodium sulfate gave, after evaporation, the product (11.7 mg) of composition **21** (97%), **22** (3%), **23** (≃0.09%) byvpc. Drying with EtOH–benzene azeotrope gave acetal **21** (5.5 mg, 70%) by ir, ^{1}H nmr, and tlc.

Mild Acid Hydrolysis of Spiroketal 23

To spiroketal **23** (178 mg, 0.97 mmol, composition by vpc **21** (2%), **23** (95%), **22** (3%)) in acetone (2.4 mL) and water (0.57 mL) was added 1 *M* hydrochloric acid (30 μL) and the hydrolysis was followed by vpc. After 160 min, the reaction was quenched with sodium bicarbonate and then diluted with ether. After drying (Na_2SO_4) and evaporation of the solvent, the residue was acetylated with pyridine (0.5 mL) and acetic anhydride (0.4 mL) for 2 h at room temperature. Saturated sodium bicarbonate and ether were added. The ethereal phase was washed with sodium bicarbonate (1×) and then water (2×), dried, and evaporated to give the product (0.57 g). Chromatography with ether–hexane on Florisil (30 g) gave, on elution with 2% ether–hexane (*i*) spiroketal **21** (33.6 mg, 18.9%) by ir and nmr; vpc analysis gave **21** (95%) and **23** (5%); (*ii*) a mixture of spiroketals (66.8 mg, 37.5%) consisting by vpc of **21** (67%), **23** (30%), and **22** (3%); (*iii*) a fraction of starting material (9.9 mg, 5.6%) by ir and nmr and consisting, by vpc analysis, of **21** (3%), **23** (75%), and **22** (23%).

Elution through to ether gave diacetate **29** (50 mg, 18%) as a clear oil; ir: 1735, 1234, and 1040 cm^{-1}; ^{1}H nmr δ: 1.08 (6H, d, J = 7 Hz), 1.30–1.90 (8H, m), 2.04 (6H, s), 2.37–2.90 (2H, m), 4.04 (4H, t, J = 6 Hz); ^{13}C nmr δ: 16.6, 20.9, 26.4, 29.0, 44.6, 64.3, 171.1, 217.1; ms *m/e*: 226, 166, 157.

Sodium Borohydride Reduction of Keto-acetate 29

To diacetate **29** (70 mg, 0.24 mmol) in methanol (5 mL) was added sodium borohydride (10 mg). After 95 min, the reaction was concentrated cold under reduced pressure whereupon thin layer chromatography showed incomplete reduction. Additional sodium borohydride (≃10 mg) and methanol (2 mL) were added and after 60 min the reaction was complete. The solution was again concentrated under reduced pressure, ether was added, and the organic phase was washed with saturated ammonium chloride (1×) and the brine (1×). Drying (Na_2SO_4) and evaporation gave alcohols **30** and **31** (54 mg, 77%). An analytical sample (18 mg, 26%) was obtained after plc (50% ethyl acetate – hexane); ir: 3510, 1733, 1240, and 1022 cm^{-1}; ^{1}H nmr δ: 0.92 (6H, d, J = 6 Hz), 1.30–2.87 (11H, m), 2.05 (6H, s), 3.00–3.30 (1H, m), 4.06 (4H, t, J = 6 Hz); ^{13}C nmr δ: 14.1, 16.5, 21.0, 26.2, 26.3, 27.0, 29.9, 35.1, 64.7, 64.8, 78.3, 80.6, 171.2; ms *m/e*: 159, 99.

Sodium Borohydride Reduction of Ketodiacetates 28 and 29

To diacetates **28** and **29** (90 mg, 0.31 mmol) in methanol (10 mL) was added sodium borohydride (22 mg). After 80 min, saturated ammonium chloride and ether were added. The aqueous phase was diluted with enough water to dissolve precipitated salts and extracted with ether (1×). The combined ether layers were washed with brine (1×), evaporated, and then azeotroped with benzene–ethanol to give alcohol diacetates **30**, **31**, and **32** (92 mg, 102%); plc (80 mg, 50% ethyl acetate – hexane) gave a sample (52 mg, 65%) pure by vpc (5 ft × $\frac{1}{4}$ in., Apiezon L 10% on Chromosorb W, 230°C); ir: 3500, 1733, 1240, and 1020 cm^{-1}; ^{1}H nmr δ: 0.85 and 0.91 (6H, two d, J = 6 Hz, *meso* and *dl* isomers respectively), 1.13–1.90 (11H, m), 2.04 (6H, s), 3.00– 3.30 (1H, m), 4.06 (4H, t, J = 6 Hz); ^{13}C nmr δ: 12.5, 14.1, 15.9, 16.6, 21.0, 26.2, 26.3, 26.4, 27.0, 28.8, 29.9, 30.6, 34.5, 35.1, 35.9, 64.7, 64.8, 78.2, 80.6, 171.2; ms *m/e*: 159, 99.

Spiroketal 34

To acetylene **11** (1.40 g, 9.1 mmol) in tetrahydrofuran (25 mL) at −78°C was added *n*-butyllithium (9.1 mmol of 1.6 *M* hexane solution). After 30 min, bicyclic lactone **36** (1.40 g, 9.1 mmol) in tetrahydrofuran (30 mL) was quickly added and the system was allowed to warm to RT. The reaction was quenched in water (50 mL), the organic phase was separated, and the aqueous phase was ether extracted (3×). The combined organic phases were dried (Na_2SO_4) and evaporated and the resulting residue was taken up in methanol (50 mL) and hydrogenated (40 psi over PtO_2). After filtration through silica gel, concentrated hydrochloric acid (2 drops) was added and the solution was left at RT overnight. The solvent was evaporated and the residue was taken up in ether, dried ($MgSO_4/K_2CO_3$), and again evaporated. Chromatography on silica gel gave on elution with 5% E/H, spiroketal **34** (1.18 g, 62%) as a clear oil; ir: 1164, 1150, 1132, 1020, 997, and 964 cm^{-1}; ^{1}H nmr δ: 1.32 (18H, m), 3.3–4.0 (4H, m, CH_2O); ^{13}C nmr δ: 18.6, 25.4, 26.0, 26.2, 27.7, 32.8, 35.4, 35.6, 41.8, 43.1, 60.4, 65.5, 96.0; ms *m/e*: 210 (M^+).

Deuteration (as for spiroketals **5** and **14**, but for 30 days reaction time) gave d_4 spiroketal **34**. *Exact Mass* calcd. for $C_{23}H_{28}D_4O$: 214.1871; found (ms): 214.1872.

THP-hydroxyketone 38

Compound **38** was produced, as described above for spiroketal **34**, and purified by chromatography on Florisil. Eluting with 40% E/H gave compound **38** (60–70%) as a clear oil which crystallized on standing (mp 53–55°C crystallized from hexane); ir: 3595, 3440, 1707 (weak), 1121, 1060,1048,1006 cm^{-1}; ^{1}H nmr δ: 1.58 (24H, m), 2.10 (1H, variable s, OH), 3.15–4.03 (6H, m, CH_2O), 4.56 (1H, m, OCHO).

THP-keto-acetate 39

Compound **38** (597 mg, 1.69 mmol) was treated with pyridine (2.0 mL) and acetic anhydride (2.0 mL) for 24 h at RT. Dilution with water (100 mL) and saturated sodium bicarbonate (100 mL) was followed by extraction with dichloromethane (3 × 30 mL). Washing with brine (1×), drying ($MgSO_4$), and evaporation gave THP-keto-acetate **39** (658 mg, 97.2%) as a yellow oil. Chromatography on Florisil, eluting with 20% ethyl acetate – hexane gave analytical material; ir: 1728, 1237, 1010 cm^{-1}; ^{1}H nmr δ: 1.0–1.9 (20H, m), 2.04 (3H, OAc), 2.42 (4H, m, $W/2$ = 20 Hz, CH_2COR), 3.56 (4H, m, $W/2$ = 33 Hz, CH_2O), 3.97 (2H, deformed d, J = 6 Hz, CH_2OAc), 4.56 (1H, m, OCHO); ms *m/e*: 354 (M^+), 294 (M^+ − HOAc), 270, 269, 253.

Can. J. Chem. Downloaded from www.nrcresearchpress.com by 210.87.254.5 on 09/06/12
For personal use only.

Alcohol 40 and Diacetate 41

Crystals of *p*-toluenesulfonic acid were added successively to a solution of the THP-keto-acetate **39** (467 mg, 1.32 mmol) in 10% water–methanol (25 mL) and the reaction followed by tlc. After 4 h, sodium bicarbonate was added and the solution concentrated under reduced pressure. After the addition of ether (50 mL) and removal of the aqueous phase, drying ($MgSO_4$) and evaporation gave compound **40** as a clear oil (370 mg, 104%). Pure hydroxy-acetate **40** (70% yield) could be obtained as a clear oil by chromatography on Florisil, eluting with 40% E/H; ir: 3480, 1733, 1240, and 1017 cm^{-1}; ^1H nmr δ: 1.1–1.9 (14H, m), 2.05 (3H, s, OAc), 2.45 (4H, m, $W/2 = 20$ Hz, CH_2COR), 3.63 (2H, t, $J = 6$ Hz, CH_2OH), 3.97 (2H, d, $J = 4$ Hz, CH_2OAc); ms *m/e*: 252.1685 ($M^+ - H_2O$, $C_{15}H_{24}O_3$ requires 252.1725), 210 ($M^+ -$ HOAc).

Alternatively the crude hydroxy-acetate **40** was acetylated with acetic anhydride (2.0 mL) and pyridine (2.0 mL) at RT for 17 h. Dilution with 3% sulfuric acid (150 mL), ether extraction (3×), and washing of the combined ether extracts with saturated sodium bicarbonate (1×) and brine (1×), followed by drying ($MgSO_4$) and evaporation of the solvent gave a pale oil (556 mg). Chromatography on silica gel gave, on elution with 80% E/H, keto-diacetate **41** (190 mg, 46.1% as a clear oil. A midfraction, pure by tlc and vpc (5 ft × ¼ in., Apiezon 10% on Chromosorb W, 230°C, R_t 32 min) gave ir: 1733, 1238, 1016 cm^{-1}; ^1H nmr δ: 1.0–1.8 (14H, m), 2.03 (6H, s, OAc), 2.42 (4H, m, $W/2 = 20$ Hz, CH_2COR), 3.99 (4H, m, $W/2 = 9$ Hz, CH_2OAc); ms *m/e*: 252.1724 ($M^+ -$ HOAc, $C_{15}H_{24}O_3$ requires 252.1725), 192 ($M^+ - 2$ HOAc), 158, 155, 137.

Spiroketal 35

Keto-diacetate **41** (148 mg, 0.47 mmol) in a mixture of methanol, triethylamine, and water (4:2:1; 7 mL) was warmed at 70°C for 8 days, additional solvent (3.5 mL) being added after 5 days. Removal of the solvent gave keto-diol **33** as a brown oil which crystallized on standing; mp 67–69°C; ir: 3400,1710 (weak), 1222, and 1040 cm^{-1}; ms *m/e*: 210 ($M^+ - H_2O$), 165, 155, 152, 137, 101.

This material was immediately cyclized in chloroform (2 mL) by the successive addition of small crystals of *p*-toluenesulfonic acid, the reaction being followed by tlc and vpc (5 ft × ¼ in., 3% SE-30 on Chromosorb W, 175°C). Spiroketals **34** and **35** were initially present in a ratio of 7:3 (R_t 5.0 and 5.7 min respectively) which fell to 9:1 after 5.5 h. Quenching with sodium carbonate, dilution with ether, and drying (Na_2SO_4) gave, after evaporation, a yellow oil (117 mg) which was immediately acetylated in pyridine (0.5 mL) with acetic anhydride (0.5 mL). After standing overnight at RT, the solution was diluted with ether (50 mL) and washed with saturated sodium bicarbonate (2×), brine (1×), then dried (Na_2SO_4). Evaporation gave a yellow oil (155 mg) which was chromatographed on Florisil. Elution with 5% E/H gave spiroketal **34** (27 mg, 27% from **41**) pure by vpc, tlc, nmr, and ir. Elution with ether gave keto-diacetate **41** (74 mg, 50%). Recovery of intermediate fractions gave a sample of spiroketal **35** (14 mg, 14%) containing 9% of spiroketal **34** by vpc. Preparative vpc gave an analytical sample (≃1.5 mg); ir: 1166, 1090, 1042, 1021, and 970 cm^{-1}; ^1H nmr δ: 0.8–1.9 (17 H, m), 2.10–2.43 (1H, m), 2.88–4.33 (4H, m); ms *m/e*: 210 (M^+), 155, 152, 137, 110, 101.

Isomerization of Compound 35

A sample of spiroketal **35** (≃1.5 mg, **56**:**55** = 74:26, spontaneous isomerization on sample recovery) in acetone (0.45 mL) was treated with 1 *N* hydrochloric acid (0.05 mL) at RT. Conversion to spiroketal **34** was complete within 5 min by vpc. Evaporation of the solvent gave pure spiroketal **34** by ir, nmr, tlc, and vpc.

Spiroketals 43, 44, and 46

To acetylene **16** (18.5 g, 110 mmol) in tetrahydrofuran (100 mL) at −78°C was slowly added *n*-butyllithium (100 mmol of 1.6 *M* hexane solution). After 30 min, bicyclic lactone **36** (13.9 g, 90 mmol) in tetrahydrofuran (50 mL) was quickly added and the system was allowed to warm to RT. The reaction was quenched in water (50 mL), the organic phase separated,and the aqueous phase was ether extracted (3×). The combined organic phases were dried (Na_2SO_4), evaporated, and the resulting oil was taken up in methanol (50 mL) and hydrogenated (40 psi over PtO_2). After filtration through silica gel, concentrated hydrochloric acid (2 drops) was added and the solution was left at RT overnight. The solvent was evaporated and the residue was taken up in ether, dried ($MgSO_4/K_2CO_3$), and again evaporated. Chromatography on silica gel gave, on elution with 5% E/H, (*i*) spiroketal **46**: (6.80 g, 33.5%); ir: 1383, 1229, 1092, 1087, 1048, and 992 cm^{-1}; ^1H nmr δ: 1.14 (3H, d, $J = 10.5$ Hz, CH_3), 1.19 (18H, m), 3.1–4.1 (3H,m, C*H*OR); ^{13}C nmr δ: 19.0, 21.9, 26.0, 26.2, 27.7, 32.7, 32.8, 35.1, 35.4, 41.9, 43.2, 65.2, 65.4, 96.6; ms *m/e*: 224 (M^+); (*ii*) spiroketal **44**: (2.60 g, 12.8%); ir: 1052 and 992 cm^{-1}; ^1H nmr δ: 1.12 (3H, d, $J = 10.5$ Hz, CH_3), 1.30 (18H, m), 2.8–4.5 (3H, m, CHOR); ^{13}C nmr δ: 18.4, 22.2, 25.9, 26.1, 27.7, 28.0, 32.2, 33.0, 37.2, 41.9, 44.2, 66.4, 68.3, 97.9; ms *m/e*: 224 (M^+); (*iii*) spiroketal **43**: (3.40 g, 16.7%); ir: 1068 and 1006 cm^{-1}; ^1H nmr δ: 1.21 (3H, d, $J = 10.2$ Hz, CH_3), 1.52 (18H, m); 2.8–4.3 (3H, m, CHOR); ^{13}C nmr δ: 19.3, 21.9, 26.0, 26.3, 27.7, 32.4, 32.9, 35.0, 36.0, 37.3, 41.9, 66.3, 68.6, 97.8; ms *m/e*: 224 (M^+).

Isomerization of Spiroketals 43, 44, and 46

Spiroketal **43** (224 mg, 1 mmol) in anhydrous methanol (25 mL) containing one drop of concentrated hydrochloric acid was left at RT for 20 h. The solvent was evaporated, ether was added, and the solution was dried ($MgSO_4$), filtered, and evaporated to dryness. ^1H and ^{13}C nmr analysis showed that a ≃1:1 mixture of spiroketals **43** and **44** was obtained.

The same experiment was repeated starting with spiroketal **44** and an identical result was obtained. However, spiroketal **46** was recovered unchanged when submitted to the same experimental conditions.

Deuteration of a mixture of spiroketals **43** and **44** under the conditions described previously gave the spiroketals **43** and **44** containing two deuterium atoms in ring B as shown by ^{13}C nmr analysis.

Acknowledgements

Support for this work by the National Research Council of Canada, and by the Ministère de l'Education, Québec, is gratefully acknowledged. One of us (P. Deslongchamps) is pleased to thank the John Simon Guggenheim Memorial Foundation for a Fellowship (1979–1980).

1. R. U. Lemieux and S. Koto. Tetrahedron, **30**, 1933 (1974).
2. C. Altona. Ph.D. Thesis, University of Leiden, 1964; C. Romers, C. Altona, H. R. Buys, and E. Havinga. *In* Topics in stereochemistry. Vol. 4. *Edited by* E. L. Eliel and N. L. Allinger. Wiley-Interscience, New York, NY. 1969. p. 39.
3. S. David, O. Eisentein, W. J. Here, L. Salem, and R. Hoffman. J. Am. Chem. Soc. **95**, 3806 (1973).
4. C. T. Bishop and F. P. Cooper. Can. J. Chem. **41**, 2742 (1963).
5. C. B. Anderson and D. T. Sepp. Tetrahedron, **24**, 1707 (1968).
6. J. T. Edwards, P. F. Morand, and I. Puska. Can. J. Chem. **39**, 2069 (1961).

7. R. U. LEMIEUX. Ann. N.Y. Acad. Sci. **222**, 915 (1973).
8. R. U. LEMIEUX, S. KOTO, and D. VOISIN. The *exo* anomeric effect. *In* Anomeric effect, origin and consequences. *Edited by* W. A. Szarek and D. Horton. ACS Symposium Series 87. Washington, DC. 1979. p. 17.
9. H. M. BERMAN, S. S. CHU, and G. A. JEFFREY. Science, **157**, 1576 (1967).
10. A. J. DE HOOG, H. R. BUYS, C. ALTONA, and E. HAVINGA. Tetrahedron, **25**, 3365 (1969); A. J. DE HOOG and H. R. BUYS. Tetrahedron Lett. 4175 (1969); M. GELIN, Y. BAHUREL, and G. DESCOTES. Bull. Soc. Chim. Fr. 3723 (1970).
11. G. DESCOTES, M. LISSAC, J. DELMAU, and J. DUPLAU. C.R. Acad. Sci. Ser. C, **267**, 1240 (1968).
12. N. BEAULIEU, R. A. DICKINSON, and P. DESLONGCHAMPS. Can. J. Chem. **58**, 2531 (1980).
13. G. A. JEFFREY, J. A. POPLE, and L. RADOM. Carbohydr. Res. **25**, 117 (1972).
14. H. BOOTH and J. R. EVERETT. J. Chem. Soc. Chem. Commun. 278 (1976).
15. H. J. SCHNEIDER and V. HOPPEN. Tetrahedron Lett. 579 (1974).
16. R. BAKER, R. HERBERT, P. E. HOWSE, and O. T. JONES. J. Chem. Soc. Chem. Commun. 52 (1980).
17. N. L. ALLINGER and M. A. MILLER. J. Am. Chem. Soc. **83**, 2145 (1961); H. WERNER, G. MANN, M. MÜHLSTADT, and H.-J. KÖHLER. Tetrahedron Lett. 3563 (1970).
18. E. L. ELIEL and H. HAUBENSTOCK. J. Org. Chem. **26**, 3504 (1961); G. CHIURDOGLU and W. MASSCHELEIN. Bull. Soc. Chim. Belg. **70**, 782 (1961); E. L. ELIEL and C. A. LUKACH. J. Am. Chem. Soc. **79**, 5986 (1957).
19. D. E. EVANS, C. E. SACKS, R. A. WHITNEY, and N. G. MANDEL. Tetrahedron Lett. 727 (1978).
20. T. M. CRESP, C. L. PROBERY, and F. SONDHEIMER. Tetrahedron Lett. 3955 (1978).
21. D. L. HUGHES. Tetrahedron Lett. 3959 (1978).
22. D. A. EVANS, C. E. SACKS, W. A. KLESCHICK, and T.R.TABER. J. Am. Chem. Soc. **101**, 6789 (1979).
23. J. MEINWALD and E. FRAUENGLASS. J. Am. Chem. Soc. **82**, 5235 (1960).
24. G. A. HAGGIS and L. N. OWEN. J. Chem. Soc. 389 (1953); E. ALI and L. N. OWEN. J. Chem. Soc. 2111 (1958); W. HUCKEL and W. EGERER. Ann. Chem. **645**, 162 (1961).

Can. J. Chem. Downloaded from www.nrcresearchpress.com by 210.87.254.5 on 09/06/12
For personal use only.

1,7-Dithia and 1-oxa-7-thiaspiro[5.5]undecanes. Excellent systems for the study of stereoelectronic effects (anomeric and *exo*-anomeric effects) in the monothio and the dithioacetal functions[1]

PIERRE DESLONGCHAMPS, DARYL D. ROWAN, NORMAND POTHIER, AND JOHN K. SAUNDERS

Laboratoire de Synthèse Organique, Département de Chimie, Faculté des Sciences, Université de Sherbrooke, Sherbrooke (Qué.), Canada J1K 2R1

Received September 3, 1980

PIERRE DESLONGCHAMPS, DARYL D. ROWAN, NORMAND POTHIER, and JOHN K. SAUNDERS. Can. J. Chem. **59**, 1122 (1981).

1,7-Dithiaspiro[5.5]undecane (**2**), 1-oxa-7-thiaspiro[5.5]undecane (**4**), and the tricyclic systems **3**, **5**, and **6** have been prepared by the acid cyclization of the appropriate ketone dithiol or hydroxy ketone thiol precursors.

The configuration and the conformation of the products obtained was determined by ^{13}C nmr analysis and equilibration studies. The experimental results can be rationalized by taking into account the anomeric and the *exo*-anomeric effects and the usual steric interactions.

PIERRE DESLONGCHAMPS, DARYL D. ROWAN, NORMAND POTHIER et JOHN K. SAUNDERS. Can. J. Chem. **59**, 1122 (1981).

On a préparé le dithia-1,7 spiro[5.5]undécane (**2**), le oxa-1 thia-7 spiro[5.5]undécane (**4**) et les systèmes tricycliques **3**, **5** et **6** par cyclisation en milieu acide des précurseurs dimercaptocétonique ou mercaptohydroxycétonique approprié.

La configuration et la conformation des produits obtenus ont été déterminées par la rmn du ^{13}C et par des études d'équilibration. Les résultats expérimentaux sont expliqués en tenant compte de l'effet anomère, de l'effet *exo*-anomère et des interactions stériques habituelles.

In the accompanying publications,[2] we have shown that the 1,7-dioxaspiro[5.5]undecane system exists in conformation **1***a* in preference to the other conformations **1***b* and **1***c* (Scheme 1). The relative stability of **1***a–c* was rationalized by taking into account the stereoelectronic (anomeric (3) and *exo*-anomeric (4) effects) and the classic steric effects. It can be concluded from this study that 1,7-dioxaspiro[5.5]undecane is an excellent system for the evaluation of the stereoelectronic effects in the acetal function. This work also showed that both the anomeric and the *exo*-anomeric effects correspond to a minimum value of about 1.4 kcal/mol, a value in accord with that of Descotes *et al.* (5) for the anomeric effect and which we have recently confirmed (6).

We wish to report an analogous study on the stereoelectronic effects of the monothio and the dithioacetal functions (7–9). We have studied the parent compounds, 1,7-dithiaspiro[5.5]undecane (**2**), 1-oxa-7-thiaspiro[5.5]undecane (**4**), and the three tricyclic systems **3**, **5**, and **6**.

Results and Discussion

Dithiaspiro Acetals

1,7-Dithiaspiro[5.5]undecane **2** was prepared by the method described in Scheme 2 (**7** → **8** → **2**). The ^{13}C nmr spectra of **2** at room temperature and at low temperature (≃ −130°C, $CHFCl_2$) are virtually identical and they show five peaks only.[3] This result shows that **2** is essentially a conformationally rigid system.

Compound **2** can exist theoretically in the three conformations **2***a*, **2***b*, and **2***c* (Scheme 1), which must show 5, 9, and 5 lines respectively in their ^{13}C nmr spectra. Consequently, conformer **2***b* can be eliminated on that basis and compound **2** should exist in either of the two conformations **2***a* or **2***c*.

The classic steric interactions in these three conformers can be analyzed as follows. In conformer **2***a*, the two sulfurs are axially oriented to a ring, in conformer **2***c* the two sulfurs are equatorially oriented, whereas in conformer **2***b* one sulfur is axial while the other is equatorial to a ring. If we accept that when a methylene group is axially oriented, it corresponds to two *gauche* forms of *n*-butane (2 × 0.9 = 1.8 kcal/mol),[4] and that when a sulfur is axially oriented, it corresponds to two *gauche* forms of S—CH_2—CH_2—CH_2 (2 × 0.4 = 0.8 kcal/mol (10)), then the steric effects for **2***a*, **2***b*, and **2***c* should correspond to 1.6 (4 × 0.4), 2.6 (2 × 0.4 + 2 × 0.9), and 3.6 (4 × 0.9) kcal/mol respectively. Thus, the conclusion from this study is that compound **2** should exist as a mixture of a major (**2***a*, 0 kcal/mol) and a minor (**2***b*, 1 kcal/mol) conformer. It is therefore not possible to rational-

[1]This work has been presented at the First International Symposium on Stereoelectronic Effects, University of St. Andrews, Scotland, July 1980.

[2]See refs. 1 and 2.

[3]A detailed account of the ^{13}C nmr spectral analysis is reported in the accompanying publication, see ref. 2.

[4]We make the assumption that the *gauche* form of CH_2—S—CH_2—CH_2 is equivalent to that of *n*-butane.

0008-4042/81/071122-10$01.00/0

©1981 National Research Council of Canada/Conseil national de recherches du Canada

Can. J. Chem. Downloaded from www.nrcresearchpress.com by 210.87.254.42 on 09/06/12
For personal use only.

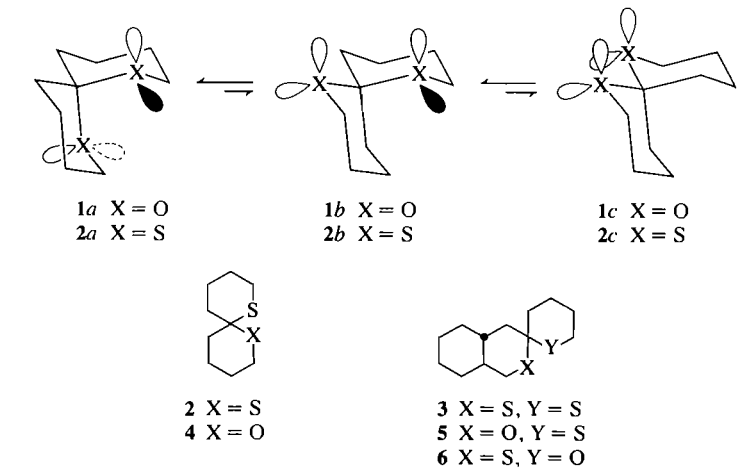

SCHEME 1

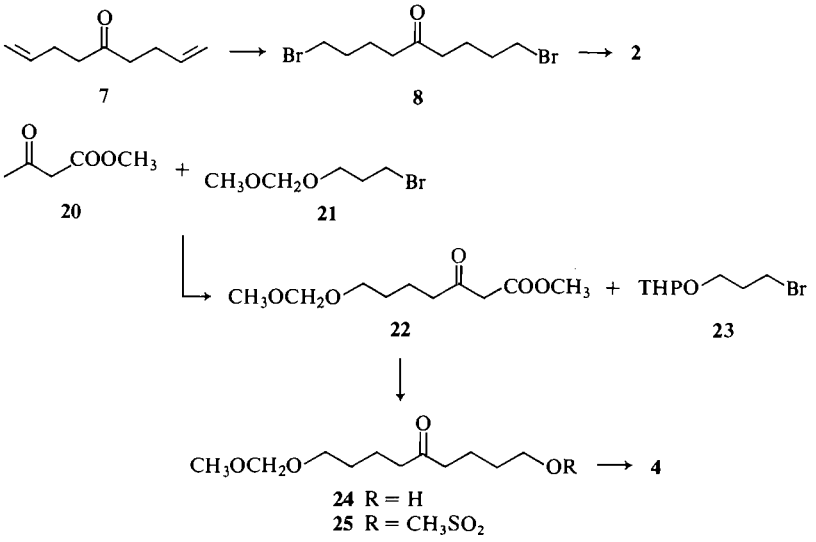

SCHEME 2

ize the experimental results on the basis of steric effects only. This indicates that stereoelectronic effects must also play a role.

Conformer **2***a* has two sulfurs each having an electron pair oriented antiperiplanar to a polar C—S bond, conformer **2***b* has only one, whereas conformer **2***c* has none. Consequently, **2***a* has two anomeric effects, **2***b* only one, and **2***c* none. If we accept that the anomeric effect is a stabilizing effect (10, 11), it must be of the order of −1.4 kcal/mol in order to arrive at a theoretical rationalization which agrees with the experimental result. Indeed with such a value, the relative energies of conformers **2***a*, **2***b*, and **2***c* become 0, 2.4, and 4.8 kcal/mol respectively (Table 1). Thus, compound **2** is a conformationally rigid system which exists in conformation **2***a* which has the least steric interactions and two anomeric effects.

The results obtained with the dithia tricyclic system **3** confirm the above conclusion. With **3**, two isomers **10** and **11** are possible from the cyclization of the ketone dithiol precursor **9** (Scheme 3) and they can exist in two conformations each, which are **10***a*–*b* and **11***a*–*b*, respectively. The detailed analysis of the relative stability of these four structures is described in Table 1. Conformer **10***a* (0 kcal/mol) is more stable than **10***b* (2.4 kcal/mol), isomer **10** should therefore exist in conformation **10***a* only. Similarly, conformer **11***a* (2.4 kcal/mol) is more stable than **11***b* (4.8 kcal/mol), isomer **11**

Can. J. Chem. Downloaded from www.nrcresearchpress.com by 210.87.254.42 on 09/06/12
For personal use only.

TABLE 1. Evaluation of steric and stereoelectronic effects*

	Effects, compound **2**			
	2*a*	**2***b*		**2***c*
	2 *ae* = −2.8	1 *ae* = −1.4		
	4 *co* = 1.6	2 *co* = 0.8		
		2 *cc* = 1.8		4 *cc* = 3.6
Total	−1.2	1.2		3.6
Relative to **2***a*	0	2.4		4.8

	Effects, compound **10**	
	10*a*	**10***b*
	2 *ae* = −2.8	1 *ae* = −1.4
	4 *co* = 1.6	2 *co* = 0.8
		2 *cc* = 1.8
Total	−1.2	1.2
Relative to **10***a*	0	2.4

	Effects, compound **11**	
	11*a*	**11***b*
	1 *ae* = −1.4	
	2 *co* = 0.8	
	2 *cc* = 1.8	4 *cc* = 3.6
Total	1.2	3.6
Relative to **10***a*	2.4	4.8

	Effects, compound **4**			
	4*a*	**4***b*	**4***c*	**4***d*
	2 *ae* = −2.8	1 *ae* = −1.4	1 *ae* = −1.4	
	2 *co* = 0.8		2 *co* = 0.8	
	2 *cs* = 0.8	2 *cs* = 0.8		
		2 *cc* = 1.8	2 *cc* = 1.8	4 *cc* = 3.6
Total	−1.2	1.2	1.2	3.6
Relative to **4***a*	0	2.4	2.4	4.8

	Effects, compound **27**	
	27*a*	**27***b*
	2 *ae* = −2.8	1 *ae* = −1.4
	2 *co* = 0.8	
	2 *cs* = 0.8	2 *cs* = 0.8
		2 *cc* = 1.8
Total	−1.2	1.2
Relative to **27***a*	0	2.4

	Effects, compound **28**	
	28*a*	**28***b*
	1 *ae* = −1.4	
	2 *co* = 0.8	
	2 *cc* = 1.8	4 *cc* = 3.6
Total	1.2	3.6
Relative to **27***a*	2.4	4.8

Can. J. Chem. Downloaded from www.nrcresearchpress.com by 210.87.254.42 on 09/06/12
For personal use only.

TABLE 1 (*concluded*)

	Effects, compound **30**	
	30*a*	**30***b*
	2 *ae* = −2.8	1 *ae* = −1.4
	2 *cc* = 0.8	2 *co* = 0.8
	2 *cs* = 0.8	
		2 *cc* = 1.8
Total	−1.2	1.2
Relative to **30***a*	0	2.4

	Effects, compound **31**	
	31*a*	**31***b*
	1 *ae* = −1.4	
	2 *cs* = 0.8	
	2 *cc* = 1.8	4 *cc* = 3.6
Total	1.2	3.6
Relative to **30***a*	2.4	4.8

*1 *ae* = one anomeric effect; 1 *co* = one *gauche* form of $OCH_2CH_2CH_2$; 1 *cs* = one *gauche* form of $S—CH_2CH_2CH_2$; 1 *cc* = one *gauche* form of *n*-butane.

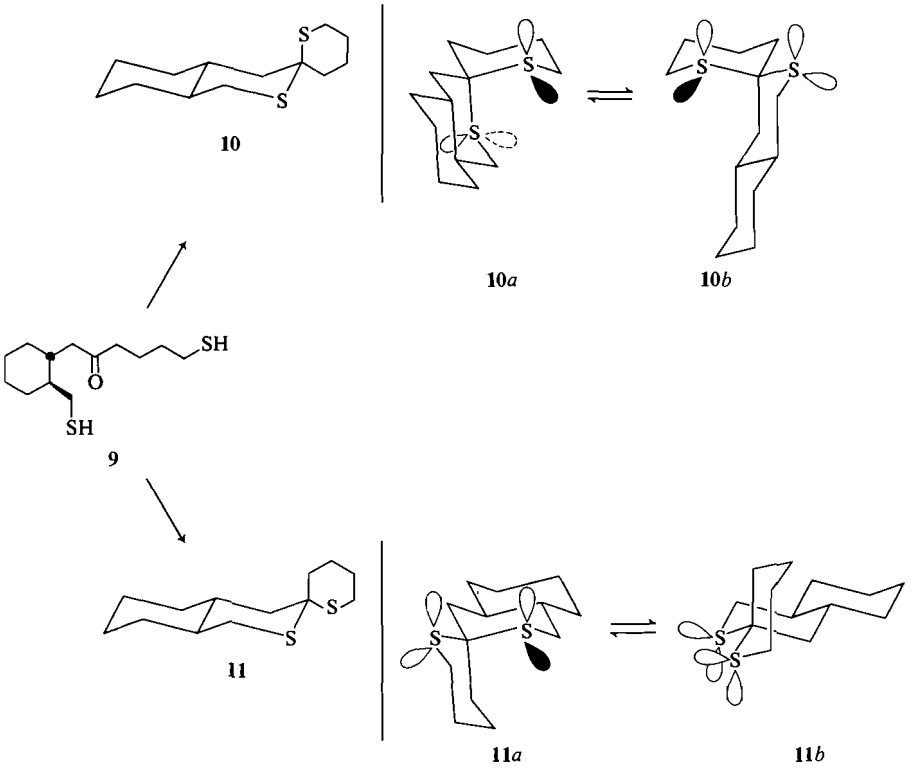

SCHEME 3

should exist in conformation **11***a* only. However, since conformer **10***a* is more stable than conformer **11***a* by 2.4 kcal/mol, and since isomers **10** and **11** can be interconverted by equilibration under acidic conditions, only isomer **10** should be observed under thermodynamically controlled conditions at low temperature.

The preparation of the diacetate derivative **19** of ketone dithiol **9** is described in Scheme 4 (**12** + **13** → **14** → **15** → **16** → **17** → **18** → **19**). Treatment of **19**

Can. J. Chem. Downloaded from www.nrcresearchpress.com by 210.87.254.42 on 09/06/12
For personal use only.

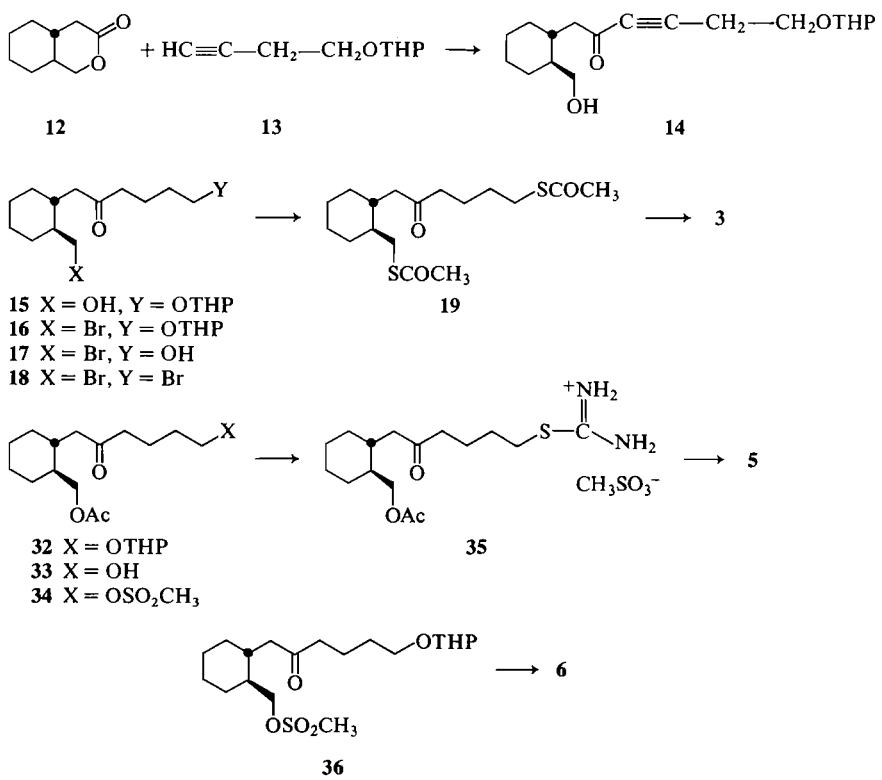

SCHEME 4

under acidic conditions (25% H_2SO_4/THF) gave a mixture of a major and a minor isomer which were separated by chromatography and identified as isomers **10** and **11**, respectively. Equilibration (concentrated HCl/benzene) of **10** gave a mixture of **10** and **11** in a 98:2 ratio. Deuteration of **10** (D_2SO_4/CH_2Cl_2) yielded a partially di- and trideuterated **10** and again the formation of a small percentage of **11** was detected. The ^{13}C nmr analysis showed that the major isomer corresponds to **10** and that it exists in conformation **10***a*.[5] The fact that a small percentage (2%) of **11** was detected at room temperature shows that, at low temperature, less than 0.1% of **11** would have been present, which confirms that, at low temperature, 1,7-dithiaspiro[5.5]undecane (**2**) is a compound which exists essentially in conformation **2***a* only.

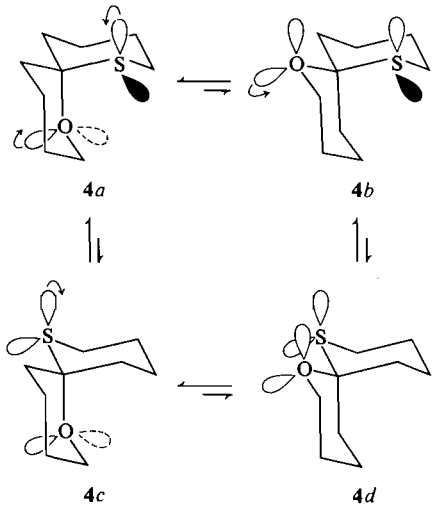

SCHEME 5

The above results show conclusively that the anomeric effect for sulfur in the dithioacetal function must be near 1.4 kcal/mol.

Monothiaspiro Acetals

1-Oxa-7-thiaspiro[5.5]undecane (**4**) can exist theoretically in four conformations (**4***a–d*, Scheme 5). The steric interactions in the four conformations **4***a–d* must be approximately 1.6, 2.6, 2.6, and 3.6 kcal/mol, respectively. Conformer **4***a* has two anomeric effects (the sulfur and the oxygen have each an electron pair oriented antiperiplanar to a polar bond), conformer **4***b* has one anomeric effect (the oxygen), conformer **4***c* has also one anomeric effect (the sulfur), and conformer **4***d* has none. If we take a value of −1.4 kcal/mol each for the

[5]Due to the small quantity obtained, the ^{13}C nmr spectra of **11** was not obtained.

Can. J. Chem. Downloaded from www.nrcresearchpress.com by 210.87.254.42 on 09/06/12
For personal use only.

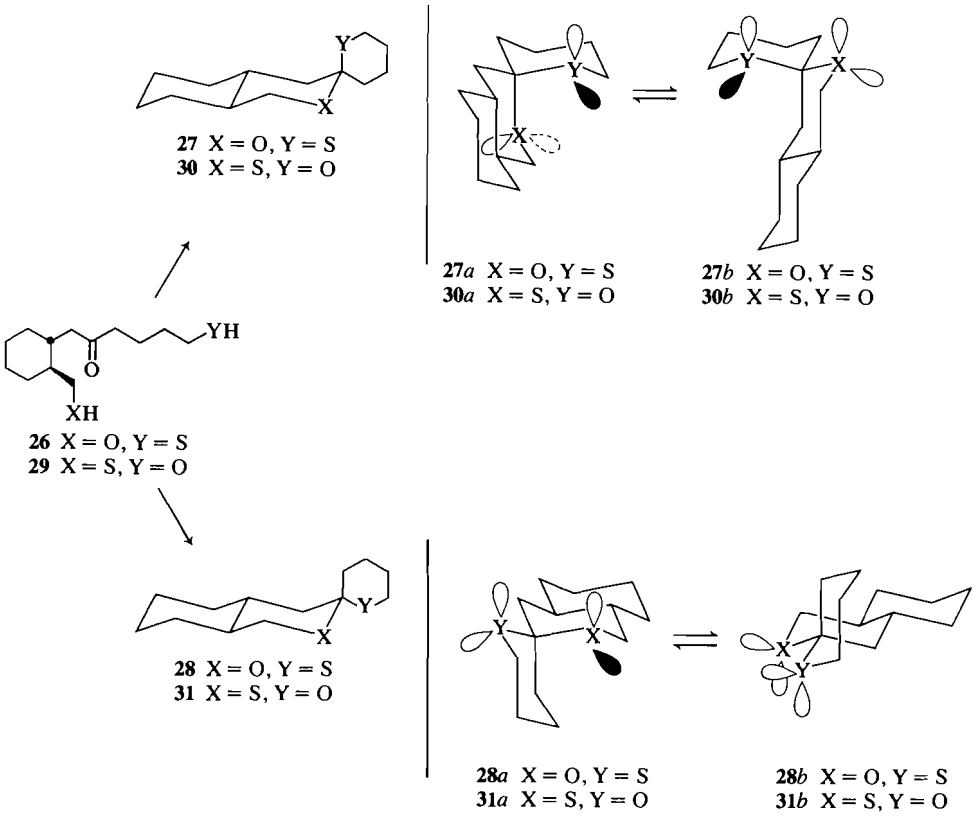

SCHEME 6

oxygen and the sulfur anomeric effect, we can predict that compound **4** will exist in conformation **4***a* only (Table 1).

1-Oxa-7-thiaspiro[5.5]undecane (**4**) was prepared by the method described in Scheme 2 (**20** + **21** → **22** + **23** → **24** → **25** → **4**) and its ^{13}C nmr spectral analysis showed that it exists in conformation **4***a* only. This conclusion was further confirmed by the study of the tricyclic spiro systems **5** and **6**.

The hydroxyketone thiol **26** (Scheme 6) can cyclize to yield the two isomers **27** and **28** which can take each two different conformations (**27***a–b* and **28***a–b*). An analysis of the steric and stereoelectronic effects leads again to the prediction that under equilibrating conditions, only isomer **27** should be formed and that it should exist in conformation **27***a* only (Table 1).

The isomeric hydroxyketone thiol **29** can also cyclize to yield two isomers (**30** and **31**) which can also take two different conformations (**30***a–b* and **31***a–b*) each. However, we can predict again that under equilibrating conditions, essentially only isomer **30** existing in conformation **30***a* should be observed (Table 1).

The preparation of the isomeric tricyclic monothio spiro systems **5** and **6** is described in Scheme 4 (**15** → **32** → **33** → **34** → **35** → **5** and **15** → **36** → **6**). An identical result was obtained in both series. With the spiro system **5**, the isomer **27** was the only product observed and ^{13}C nmr spectral analysis showed that it exists in conformation **27***a* only. Upon equilibration under acidic conditions (0.1 *N* DCl in 10% D_2O/CH_3OH, reflux), isomer **27** incorporated deuterium but the formation of isomer **28** was not observed. With the spiro system **6**, the isomer **30** was the only product observed and it was shown to exist in conformation **30***a* only. Similarly, isomer **30** does not equilibrate with isomer **31** under acidic conditions which allow deuterium incorporation.

The fact that a small percentage of isomers **28** and **31** was not observed during the deuteration experiments of isomers **27** and **30** indicates that the anomeric effect for oxygen and for sulfur must be slightly larger than 1.4 kcal/mol in the monothioacetal function.

Conclusion

These results constitute very strong evidence concerning the importance for the stereoelectronic

Can. J. Chem. Downloaded from www.nrcresearchpress.com by 210.87.254.42 on 09/06/12
For personal use only.

(anomeric and *exo*-anomeric) effects of the oxygen and the sulfur atoms in the monothio and the dithioacetal functions.

Experimental

Vapor-phase chromatographic (vpc) analysis and separations were performed on a Varian Aerograph instrument, model 2800 equipped with a thermal conductivity detector. The infrared (ir) spectra were obtained in chloroform, unless otherwise stated, on a Perkin-Elmer 257 spectrophotometer. Proton nuclear magnetic resonance (^{1}H nmr) spectra were recorded in deuterochloroform on a Bruker WP-60 instrument with TMS as an internal standard. The ^{13}C nmr spectra were recorded on a Bruker HX-90 spectrometer equipped with a Nicolet 1083 computer (8K memory for data) and operating in the Fourier transform mode. Spectra were recorded in deuterochloroform with a sweep width of 5000 Hz. Mass spectra were obtained on Hitachi-Perkin-Elmer RMU-6-A and Micromass ZAB-2F machines.

The following abbreviations are used. % E/H: % of ether in hexane; % EA/H: % of ethyl acetate in hexane; RT: room temperature; s: singlet; d: doublet; t: triplet; quin: quintet; m: multiplet; b: broad.

Ketone 7

α-Alkylation of methyl acetoacetate (11) with allyl bromide gave methyl 3-oxohept-6-enoate (84%, bp 72°C/2 Torr). α-Alkylation (12) with allyl bromide followed by decarboxylation by refluxing with aqueous sodium hydroxide gave ketone **7** (48%, bp 70–72°C/6 Torr); ir: 3075, 1715, 1640, 970, and 888 cm^{-1}; ^{1}H nmr δ: 2.34 (8H, m), 4.73–6.04 (6H, m).

Dibromide 8

Ketone **7** (1.592 g, 11.5 mmol) in pentane (500 mL) was cooled in an ice–salt bath and purged with nitrogen (≃10 min) in a photochemical apparatus. Anhydrous hydrogen bromide was bubbled in and the solution was irradiated (450 W Hanovia Hg lamp) for 15 min. After purging with nitrogen, the solution was washed with saturated sodium bicarbonate containing some sodium thiosulfate (1×), then with brine (1×), before it was dried (Na_2SO_4) and evaporated to give a black oil (3.36 g). Medium pressure chromatography on silica gel, eluting with 25% E/H gave dibromide **8** (1.97 g, 56.9%) as a clear oil; ir: 1716, 1403, 1367, 1243, and 1078 cm^{-1}; ^{1}H nmr δ: 1.76 (8H, m), 2.43 (4H, t, J = 6 Hz), and 3.38 (4H, t, J = 6 Hz); ms *m/e*: 221/219 (M^+ − Br), 165/163 (M^+ − C_4H_8Br), and 137/135 (M^+ − C_5H_8OBr).

1,7-Dithiaspiro[5.5]undecane (2)

A solution of dibromide **8** (1.239 g, 4.13 mmol) in 95% ethanol (30 mL) and thiourea (0.69 g, 9.06 mmol) was refluxed for 3 h. Solvent (10 mL) was distilled off and sodium hydroxide (10%, 10 mL) was added. After 4 h of reflux, hydrochloric acid (10%, 10 mL) was added, followed, after cooling, by ether. The mixture was left stirring overnight. The aqueous phase was diluted with brine and extracted with ether (1×). The ethereal phase was washed with brine (1×), dried (Na_2SO_4), and the solvent was evaporated. Elution with 10% E/H from a short column of silica gel gave 1,7-dithiaspiro[5.5]undecane (**2**) (685 mg, 88%) as a pale oil. Preparative vpc (R_f 9.3 min, 5% FFAP on Chromosorb W, 5 ft × ¼ in., 155°C) gave an analytical sample; ir: 1259, 1250, 1230, 978, and 924 cm^{-1}; ^{1}H nmr δ: 1.36–2.15 (12H, m), and 2.23–3.27 (4H, m); ^{13}C nmr δ: 2.16, 27.5, 42.4, C6 was not observed; ms *m/e*: 188.0694 ($C_9H_{16}S_2$ requires 188.0693), 154, and 127.

Bromoalcohol 17

The THP-hydroxyketone **15** was prepared from the bicyclic lactone **12** by the method described in ref. 1. THP-hydroxyketone **15** (846 mg, 2.71 mmol) in pyridine (5.0 mL) was cooled in an ice–salt bath and mesyl chloride (0.25 mL, 1.2 equiv.) was added dropwise. After 21 h at 0°C, tetra-*n*-butylammonium bromide (1.00 g, 3.11 mmol) was added and the mixture was warmed to 50°C with hexamethylphosphoramide (2.0 mL) for 5 h. The reaction was quenched with 5% sulfuric acid and the aqueous phase was extracted with ether (3×). The combined ether phases were washed sequentially with 5% sulfuric acid (1×), saturated sodium bicarbonate (2×), and brine (2×). Drying (Na_2SO_4) and evaporation gave bromo-THP **16** (843 mg, 87%) as an orange oil containing still some hexamethylphosphoramide; ir: 1713, 1105, 1053, 1003, and 960 cm^{-1}; ^{1}H nmr δ: 1.62 (20H, m), 2.45 (4H, m, CH_2COR), 3.51 (2H, d, J = 3 Hz, CH_2Br), and 3.67 (4H, bm, CH_2O), and 4.55 (1H, s, OCHO).

Hydrolysis of bromo-THP **16** was accomplished in methanol (10 mL) and water (1 mL) with *p*-toluenesulfonic acid. After 5 h at RT, the bulk of the solvent was removed under reduced pressure and the residue was diluted with ether. After washing with saturated sodium bicarbonate (1×) and brine (1×), the solution was dried (Na_2SO_4) and evaporated to give a yellow oil (651 mg). Chromatography on silica gel (60 g) gave on elution with 50% EA/H the bromoalcohol **17** (480 mg, 61%) as a clear oil; ir: 3445, 1706, and 1062 cm^{-1}; ^{1}H nmr δ: 0.8–2.1 (15H, m), 2.46 (4H, m), 3.51 (2H, d, J = 3 Hz, CH_2Br), and 3.62 (2H, t, J = 6 Hz, CH_2OH); ms *m/e*: 193.1592 (M^+ − Br − H_2O; $C_{13}H_{21}O$ requires 193.1593).

Dibromide 18

To a stirred solution of bromoalcohol **17** (336 mg, 1.15 mmol) in pyridine (1 mL) in an ice–salt bath was added mesyl chloride (95 μL, 1.23 mmol). After 4 h at 0°C, tetra-*n*-butylammonium bromide (540 mg, 1.68 mmol) was added and the solution was protected from light and stirred at RT for 13 h. The reaction was diluted with ether and washed sequentially with 5% sulfuric acid (2×), brine (1×), saturated sodium bicarbonate (1×), and brine (1×). Drying (Na_2SO_4) and evaporation gave dibromide **18** (401 mg, 98%) as a pale oil pure by tlc; ir: 1708 and 1285 cm^{-1}; ^{1}H nmr δ: 1.75 (14H, m), 2.46 (4H, deformed quin, J = 6 Hz), 3.52 (2H, d, J = 2.5 Hz), and 3.54 (2H, t, J = 6 Hz); ms *m/e*: no characteristic peak observed.

Dithioacetate 19

To dibromide **18** (300 mg, 8.47 mmol) in hexamethylphosphoramide (1.5 mL) was added potassium thioacetate (314 mg, 27.5 mmol) and water (0.25 mL) and the resulting red solution was stirred in the dark at RT for 10 h. Dilution with water (100 mL) and ether extraction (3×) gave, after washing with water (1×), brine (1×), and drying (Na_2SO_4), a yellow oil (366 mg). Chromatography on silica gel gave, on elution with 20% E/H, the dithioacetate **19** (299 mg, 77%) as a clear oil pure by tlc; ir: 1680 (shoulder at 1700), 1355, 1132, 1112, and 902 cm^{-1}; ^{1}H nmr δ: 2.32 (6H, s, $SCOCH_3$), and 2.22–3.25 (8H, m); ms *m/e*: 301.1309 (M^+ − CH_3CO; $C_{15}H_{25}S_2O_2$ requires 301.1304), 269 (M^+ − CH_3COS), 241, 209, and 171.

Tricyclic Spiro Dithioacetals 10 and 11

To dithioacetate **19** (266 mg, 0.77 mmol) in tetrahydrofuran (20 mL) under nitrogen was added degassed sulfuric acid (25%, 2 mL). After 24 h of reflux under nitrogen, the reaction was quenched with saturated sodium bicarbonate and the organic phase was removed and evaporated. The aqueous phase was extracted with ether (1×), and the combined organic fractions were washed with brine (1×), dried (Na_2SO_4), and evaporated

Can. J. Chem. Downloaded from www.nrcresearchpress.com by 210.87.254.42 on 09/06/12
For personal use only.

Can. J. Chem. Downloaded from www.nrcresearchpress.com by 210.87.254.42 on 09/06/12
For personal use only.

to give a pale oil (213 mg). Chromatography on Florisil gave the following, on elution with 2% E/H.

(*i*) Dithioacetal **10** (93.4 mg, 50%) as white crystals on standing, mp 43–45°C; ir (CH_2Cl_2): 1216, 1146, and 956 cm^{-1}; ^1H nmr δ: 1.72 (18H, m), and 2.20–3.06 (4H, m, CH_2S); ^{13}C nmr δ: 21.7, 26.2, 26.4, 27.1, 27.5, 32.6, 33.2, 34.0, 37.3, 42.7, 44.8, 50.4, and 55.7; ms *m/e*: 242.1164 (M^+; $C_{13}H_{22}S_2$ requires 242.1163) and 209.

(*ii*) Dithioacetals **10** and **11** (50 mg, 27%). Preparative layer chromatography (3% E/H) gave, at higher R_f, compound **10** (37 mg) and, at lower R_f, dithioacetal **11** (9.6 mg, 5%) as white crystals, mp 101–103°C; ir (CH_2Cl_2): 1235, 1142, and 961 cm^{-1}; ^1H nmr δ: 1.76 (18H, m) and 2.18–3.16 (4H, m, CH_2S); ms *m/e*: 242.1164 (M^+; $C_{13}H_{22}S_2$ requires 242.1163) and 209.

(*iii*) Elution through to 10% EA/H gave a fraction of dithioacetate **19** (22.8 mg, 8.6%).

By vpc (5 ft × ¼ in, 3% SE-30 on Chromosorb W, 220°C) compounds **10** and **11** showed R_t 6.5 and 8.0 min, respectively.

Isomerization of Dithioacetal 10

Dithioacetal **10** (8 mg) in benzene (0.5 mL) was stirred with hydrochloric acid (concentrated, one drop) for 3 days. The mixture was diluted with ether and saturated sodium bicarbonate was added. The organic phase was dried ($NaHCO_3$ and Na_2SO_4) and evaporation gave a yellow oil (6.4 mg) which was identified as dithioacetal **10** (tlc, ^1H nmr, and ir). Vapor-phase chromatography showed a mixture of **10**:**11** in a 98:2 ratio.

Deuterium Incorporation in Dithioacetal 10

Treatment of dithioacetal **10** with deuterium chloride (7% in 20% D_2O/CH_3OD, 12 h, reflux) gave dithioacetal **10** (vpc, tlc) showing $M^+ + 2$ and $M^+ + 3$ in ms; vpc indicated the presence of dithioacetal **11** (≈2%). Treatment of **10** with deuterated sulfuric acid in dichloromethane at room temperature gave also dithioacetal **10** showing $M^+ + 2$ and $M^+ + 3$ peaks in ms; vpc indicated again the presence of dithioacetal **11**.

Ketoester 22

To sodium hydride (1.43 g, 29.8 mmol, 50% dispersion) in tetrahydrofuran (25 mL) under nitrogen, stirred at 0°C, was added methyl acetoacetate (3.13 g, 27.0 mmol) dropwise. After 10 min, *n*-butyllithium (1.6 *M* in hexane, 17.0 mL, 27.2 mmol) was added to give a yellow solution. After 10 min at 0°C, the methoxymethyl ether derivative **21** of 3-bromopropanol (5.18 g, 28.2 mmol) was added to give a deep crimson solution which was allowed to warm to RT over 2.5 h. Addition to saturated ammonium chloride, and extensive ether extraction followed by washing until neutral, drying, and evaporation gave a crude product. Distillation (124–125°C/5 Torr) gave pure ketoester **22** (1.91 g, 33%); ^1H nmr δ: 1.70 (4H, m), 2.65 (2H, m), 3.34 (3H, s, CH_3OR), 3.50 (4H, m), 3.73 (3H, s, COOMe), 4.59 (2H, s, OCH_2O).

Methoxymethylbromoacetal 21

To a stirred suspension of phosphorous pentoxide (25 g) in chloroform (200 mL) and dimethoxymethane (350 mL) was added dropwise 3-bromopropanol (12 g) in chloroform (50 mL). After 5 h, the solvent was decanted and washed with saturated sodium carbonate solution. The solid residue was also dissolved in saturated sodium carbonate and extracted with chloroform (1×). The combined organic phases were further washed with saturated sodium carbonate (1×), dried (Na_2SO_4), and evaporated to give acetal **21** sufficiently pure by vpc (10% SE-30 on Chromosorb W, 5 ft × ¼ in., 100°C) for subsequent reactions. Distillation (34–35°C/4 Torr) gave pure material (4.1 g, 26%) but also extensive polymerization; ^1H nmr δ: 2.07 (2H, quin, J = 6 Hz), 3.26 (3H, s, OCH_3), 3.45 (2H, t, J = 6 Hz), 3.58 (2H, t, J = 6 Hz), 4.48 (2H, s, OCH_2O).

THP-bromide 23

To 3-bromopropanol (13.0 g, 93 mmol) in dihydropyran (9.0 g, 107 mmol) and benzene (60 mL) was added *p*-toluenesulfonic acid (10 crystals). After stirring for 12 h at 65°C, the solution was washed with saturated sodium bicarbonate (1×). The aqueous phase was extracted with ether (3×) and the combined organic phases were washed with brine (1×), dried ($MgSO_4$), and evaporated. Distillation gave **23** (14.2 g, 68.2%); bp 85–90°C/4 Torr, pure by vpc (10% SE-30 on Chromosorb W, 5 ft × ¼ in., 165°C, R_t 7.2 min); ^1H nmr δ: 1.42 (4H, m), 2.13 (2H, quin, J = 6 Hz), 3.32–4.07 (4H, m, CH_2O), 3.52 (2H, t, J = 6.6 Hz, CH_2Br), 4.59 (1H, m, OCHO).

Methoxymethyl Ether Hydroxyketone 24

To a stirred solution of sodium (220 mg, 9.57 mmol) in ethanol (30 mL) at RT under nitrogen was added dropwise the ketoester **22** (1.91 g, 8.76 mmol), and then the tetrahydropyranyl ether derivative **23** of 3-bromopropanol (2.15 g, 9.64 mmol). The resulting solution was refluxed for 12.5 h when tlc indicated a complete reaction. Sodium hydroxide (10%, 20 mL) was added and, after 3 h of reflux and standing overnight at RT, the system was saturated with sodium chloride and extracted with ether (2×). Washing with saturated ammonium chloride (1×), drying (Na_2SO_4), and evaporation gave a yellow oil (2.50 g).

Hydrolysis of the tetrahydropyranyl ether was accomplished in methanol (40 mL) and water (2 mL) with a catalytic amount of *p*-toluenesulfonic acid over 3 h at RT. Sodium bicarbonate was added and the solvent was evaporated.

The residue was diluted with ether and the aqueous phase was discarded. Further washing with saturated sodium bicarbonate (1×) and brine (1×), drying (Na_2SO_4), and evaporation gave the crude product (1.54 g) as a yellow oil. Medium pressure liquid chromatography (30% E/H to pure E) produced a number of high R_f products which were discarded. The polar fraction (≈0.5 g) was further purified on silica gel. Elution with 40% EA/H gave pure methoxymethyl ether hydroxyketone **24** (317 mg, 17%); ir: 3480, 1715, 1135, 1094, and 1020 cm^{-1}; ^1H nmr δ: 1.65 (m), 2.45 (4H, deformed t, CH_2COR), 3.45 (3H, s, CH_3O), 3.52 (4H, m, CH_2O), and 4.60 (2H, s, OCH_2—O); ms *m/e* (CI, CH_4): 219 ($M^+ + 1$), 200 ($M^+ - H_2O$), 185 ($M^+ - H_2O - CH_3$), 169, and 155; ms *m/e*: 200.1434 ($M^+ - H_2O$; $C_{11}H_{20}O_3$ requires 200.1412).

Methoxymethyl Ether Ketomesylate 25

To a stirred solution of methoxymethyl ether hydroxyketone **24** (240 mg, 1.10 mmol) in pyridine (0.44 mL) at 0°C was added dropwise mesyl chloride (0.10 mL, 1.2 equiv.). After 3.5 h, the reaction was quenched with 0.5% sulfuric acid and ether. Ether extraction (3×), followed by washing with sulfuric acid (0.5%, 1×), brine (1×), saturated sodium bicarbonate (1×), and brine (2×), drying (Na_2SO_4), and evaporation gave methoxymethyl ether ketomesylate **25** (306 mg, 94.2%) as a clear oil; ir: 1717, 1348, 1160, 1015, and 910 cm^{-1}; ^1H nmr δ: 1.64 (8H, m), 2.43 (4H, deformed t, CH_2COCH_2), 2.99 (3H, s, CH_3SO_2), 3.33 (3H, s, CH_3O), 3.49 (2H, t, CH_2O), 4.20 (2H, t, $CH_2OSO_2CH_3$), and 4.58 (2H, s, OCH_2O).

1-Oxa-7-thiaspiro[5.5]undecane (4)

To methoxymethyl ether ketomesylate **25** (306 mg, 1.03 mmol) in dry ethanol (5 mL) was added thiourea (157 mg, 2.06 mmol) and the resulting solution was refluxed under nitrogen for 4.5 h. Evaporation of the solvent and dissolution of the resulting oil in chloroform gave a white precipitate of thiourea which was filtered. Evaporation of the filtrate gave a pale viscous oil (348 mg) which was dissolved in sulfuric acid (0.5%) and washed with ether (1×). The ethereal layer was washed with sulfuric acid (0.5%) and the combined aqueous phases were made alkaline with sodium hydroxide (10%, 5 mL). Ethanol (10 mL)

Can. J. Chem. Downloaded from www.nrcresearchpress.com by 210.87.254.42 on 09/06/12
For personal use only.

was added and the mixture was refluxed for 3 h. Sulfuric acid (5%, 10 mL) was added and the solution was left at RT for 24 h. The solution was neutralized with sodium bicarbonate and was continuously extracted overnight with dichloromethane. Evaporation of the dichloromethane gave 1-oxa-7-thiaspiro[5.5]undecane (**4**) (107 mg, 57%) as a pale oil which showed one peak in vpc. Chromatography on silica gel (elution with 2% E/H) gave an analytical sample homogeneous by tlc and vpc (R_f 6.3 min, 5% FFAP on Chromosorb W, 5 ft. × ¼ in., 120°C); ir: 1269, 1095, 1078, 1068, 1042, 991, and 955 cm^{-1}; ^1H nmr δ: 1.35–1.90 (12H, m), 2.30–2.98 (2H, m, CH_2S), and 3.50–4.18 (2H, m, CH_2O); ^{13}C nmr δ: 19.2, 21.1, 25.1, 25.9, 27.2, 38.1, 41.6, 61.6, and 82.6; ms *m/e*: 172.0918 ($C_9H_{16}SO$ requires 172.0922).

Ketone Acetate Mesylate 34

Acetylation of THP-hydroxyketone **15** to give the acetate derivative **32** followed by hydrolysis to yield the hydroxyketone acetate **33** is described in ref. 1. To a stirred solution of hydroxyketone acetate **33** (212 mg, 0.79 mmol) in pyridine (0.50 mL) at 0°C was added dropwise mesyl chloride (0.08 mL, 1.3 equiv.). After 2.5 h, the reaction was poured into sulfuric acid (0.5%, 50 mL) and extracted with ether (3×). The combined ethereal layers were washed with phosphate buffer (pH 6.0, 1×) saturated sodium bicarbonate (1×), buffer (1×), and brine (1×). Drying (Na_2SO_4) and evaporation gave ketone acetate mesylate **34** (237 mg, 87%) as a clear oil; ir: 1730, 1350, 1220 (b), 1161, and 913 cm^{-1}; ^1H nmr δ: 0.83–1.93 (14H, m), 2.03 (3H, s, $OCOCH_3$), 2.44 (4H, m. $W/2$ = 14 Hz, CH_2COCH_2), 2.99 (3H, s, OSO_2CH_3), 3.94 (2H, d, J = 4 Hz, CH_2OCOCH_3), and 4.21 (2H, t, J = 6 Hz, $CH_2OSO_2CH_3$); ms *m/e*: 288 ($M^+ - CH_3CO_2H$), 252 ($M^+ - CH_3SO_3H$).

Tricyclic Monothioacetal 27

To ketone acetate mesylate **34** (232 mg, 0.67 mmol) in dry ethanol (10 mL) was added thiourea (119 mg, 1.56 mmol) and the resulting solution was refluxed for 3 h. Evaporation and dissolution of the resulting oil in chloroform gave a precipitation of thiourea which was filtered and removal of the solvent yielded the acid thiouronium salt **35** (305 mg) as a clear oil; ^1H nmr ($CDCl_3/D_2O$) δ: 2.05 (3H, s, $OCOCH_3$), 2.50 (4H, m, CH_2COCH_2), 2.77 (3H, s, $CH_3SO_2O^-$), 3.16 (2H, deformed t, CH_2SR), 3.96 (2H, b s, CH_2OCOCH_3), and 4.75 (HOD).

The thiouronium salt **35** was dissolved in sulfuric acid (0.5%, 20 mL) and extracted with ether (1×). The ethereal phase was washed with water and the combined aqueous phases were made alkaline with sodium hydroxide (10%, 5 mL). Ethanol (10 mL) was added and the mixture was refluxed for 3 h. Sulfuric acid (10%, 5 mL) was added, then ether, and the mixture was left standing at RT for 2 days. The solution was saturated with sodium chloride and extracted with ether (2×). The ethereal extracts were washed with saturated sodium bicarbonate, dried (Na_2SO_4), evaporated, and filtered through silica gel (50% E/H). Evaporation gave tricyclic monothio acetal **27** (88 mg, 58%) as a clear oil. Complete purification (162 mg) was achieved on elution from silica gel with 2% E/H which gave pure **27** as a clear oil which solidifies on cooling and melts just below RT. This compound was homogeneous by tlc and vpc (R_f 5.9 min, 3% SE-30 on Chromosorb W, 5 ft. × ¼ in., 190°C); ir: 1120, 1107, 1038, 1001, 945, and 940 cm^{-1}; ^1H nmr δ: 0.9–2.22 (18H, m), 2.28–2.98 (2H, m, CH_2S), and 3.58 (2H, m, CH_2O); ^{13}C nmr δ: 21.2, 25.4, 26.0, 26.1, 27.3, 27.6, 32.8, 36.1, 41.6, 42.5, 45.4, 66.6, and 83.4 ms *m/e*: 226.1388 ($C_{13}H_{22}SO$ requires 226.1391).

Attempted Isomerization and Deuteration of Tricyclic Monothioacetal 27

Tricyclic monothioacetal **27** (74 mg, 0.33 mmol) in methanol (1.8 mL) and hydrochloric acid (1 N, 0.2 mL) were refluxed under nitrogen for 8 h. After a further 11 h at RT, the solution was concentrated under reduced pressure and the reaction was quenched with saturated sodium bicarbonate solution. After dilution with ether, the aqueous phase was adsorbed into anhydrous sodium sulfate and the ethereal layer was removed and evaporated to give unchanged tricyclic monothioacetal **27** (vpc, tlc, ir, ^1H, and ^{13}C nmr).

Similarly, treatment of compound **27** (9.8 mg) with 0.1 N deuterium chloride in 10% deuterium oxide in monodeuterated methanol (reflux, 2.5 h and RT, 2 h) gave deuterated tricyclic monothioacetal **27** (9.4 mg, 95%); ms *m/e*: 227 ($M^+ + 1$, 9%), 228 ($M^+ + 2$, 27%), 229 ($M^+ + 3$, 39%), and 230 ($M^+ + 4$, 26%).

Tricyclic Monothioacetal 30

Mesyl chloride (0.20 mL, 2.58 mmol) was added dropwise to a solution of THP-hydroxyketone **15** (658 mg, 2.11 mmol) at 0°C. The reaction was complete after 2.5 h. Work-up consisted of filtration (washing with ether), addition of phosphate buffer (5%, pH 6, 150 mL), and extraction with ether (3×). The combined ether extracts were washed with buffer (1×), saturated sodium bicarbonate (3×), buffer (1×), and then brine (2×). Drying (Na_2SO_4) and evaporation gave crude THP-ketonemesylate **36** (752 mg, 92%) as a clear oil; ir: 1715, 1350, 1160, 1008, and 920 cm^{-1}; ^1H nmr δ: 2.36 (4H, m, CH_2COCH_2), 2.89 (3H, s, CH_3SO_2O), 3.47 (4H, b m, CH_2OR), 4.01 (2H, d, J = 3.8 Hz, $CH_2OSO_3CH_3$), and 4.46 (1H, b s, OCHO).

THP-ketonemesylate **36** (598 mg, 1.53 mmol) and thiourea (240 mg, 3.15 mmol) were refluxed in dry ethanol (15 mL) for 2.5 h. After standing at RT for 2 days, the solvent was evaporated and the resulting oil was taken up in chloroform from which crude thiourea (203 mg) precipitated. After filtration, the filtrate was concentrated (633 mg), and ether (20 mL) followed by sulfuric acid (0.5%) was added. The ether phase was washed with sulfuric acid (5%). The combined aqueous phases were washed once with ether and were then made alkaline with sodium hydroxide (10%, 5 mL). Ethanol (10 mL) was added and the solution was refluxed for 4 h. Sulfuric acid (5%, 5 mL) was added, and after standing at RT overnight, the solution was saturated with sodium chloride and extracted with ether (3×). The combined ether extracts were washed with saturated sodium bicarbonate (1×), dried (Na_2SO_4), and evaporated to give a pale oil (184 mg, 53%). Chromatography on silica gel, eluting with 2% E/H, gave crystalline tricyclic monothioacetal **30** (92 mg, 27%); mp 59.5–60.5°C (recrystallized from ethyl acetate) and homogeneous by tlc and vpc (R_f 6.1 min, 3% SE-30 on Chromosorb W, 5 ft. × ¼ in., 190°C); ir: 1058, 1018, and 954 cm^{-1}; ^1H nmr δ: 1.64 (18H, m), 2.22 (2H, m, CH_2S), and 3.48–4.34 (2H, m, CH_2O); ^{13}C nmr δ: 19.2, 26.0, 26.4, 26.7, 30.9, 33.3, 34.2, 37.0, 38.0, 44.3, 49.7, 61.6, and 83.4; ms *m/e*: 226.1383 (M^+; $C_{13}H_{22}SO$ requires 226.1391).

Attempted Isomerization and Deuteration of Tricyclic Monothioacetal 30

To tricyclic monothioacetal **30** (73 mg) dissolved in methanol (9.0 mL) was added hydrochloric acid (1 N, 1.0 mL) and the solution was refluxed for 2.5 h, then left at RT for a further 15 h; vpc and tlc showed only starting material. Saturated sodium bicarbonate was added, and the solution was diluted with ether. The aqueous phase was adsorbed into anhydrous sodium sulfate and the cloudy ethereal phase was filtered through Florisil and then evaporated to give crystalline tricyclic monothioacetal **30** (72 mg, 98%) unchanged and pure by vpc, tlc, ir, ^1H, and ^{13}C nmr.

Tricyclic monothioacetal **30** (10.8 mg) in monodeuterated methanol (1.80 mL) and deuterium oxide (0.02 mL) with deuterium chloride in deuterium oxide (1.13 M, 0.18 mL) were heated to reflux for 2.5 h. After 2 h at RT, work-up gave crystalline tricyclic monothioacetal **30** (9.4 mg, 87%), pure by vpc and tlc. Preparative thin layer chromatography gave material with ms

peaks 228 ($M^+ + 2$, 5%), 229 ($M^+ + 3$, 33%), and 230 ($M^+ + 4$, 62%).

Acknowledgements

Support for this work by the National Research Council of Canada, and by the Ministère de l'Education, Québec, is gratefully acknowledged. One of us (P. Deslongchamps) is pleased to thank the John Simon Guggenheim Memorial Foundation for a Fellowship (1979–1980).

1. P. DESLONGCHAMPS, D. D. ROWAN, N. POTHIER, and J. K. SAUNDERS. Can. J. Chem. **59**, 1105 (1981).
2. N. POTHIER, D. D. ROWAN, P. DESLONGCHAMPS, and J. K. SAUNDERS. Can. J. Chem. **59**, 1132 (1981).
3. R. U. LEMIEUX. Ann. N.Y. Acad. Sci. **222**, 915 (1973).
4. R. U. LEMIEUX, S. KOTO, and D. VOISIN. The *exo* anomeric effect. *In* Anomeric effect, origin and consequences. *Edited by* W. A. Szarek and D. Horton. ACS Symposium Series 87. Washington, DC. 1979. p. 17.
5. G. DESCOTES, M. LISSAC, J. DELMAU, and J. DUPLAU. C.R. Acad. Sci. Ser. C, **267**, 1240 (1968).
6. N. BEAULIEU, R. A. DICKINSON, and P. DESLONGCHAMPS. Can. J. Chem. **58**, 2531 (1980).
7. N. S. ZEFIROV and N. M. SHEKHTMAN. Russian Chem. Rev. **40**(4), 315 (1971), and references quoted therein.
8. F. W. NADER and E. L. ELIEL. J. Am. Chem. Soc. **92**, 3050 (1970).
9. A. S. PERLIN. Pure Appl. Chem. **50**, 1401 (1978).
10. E. L. ELIEL and B. P. THILL. Chem. Ind. London, 88 (1963); E. L. ELIEL and M. H. GIANNI. Tetrahedron Lett. 97 (1962).
11. S. N. HUCKIN and L. WEILER. J. Am. Chem. Soc. **96**, 1082 (1974).
12. C. S. MARVEL and F. D. HAGER. *In* Org. Synth. Coll. Vol. I. 2nd ed. *Edited by* H. Gilman and A. H. Blatt. John Wiley and Sons, Inc., New York, NY. 1941. p. 248.

Can. J. Chem. Downloaded from www.nrcresearchpress.com by 210.87.254.42 on 09/06/12
For personal use only.

^{13}C chemical shift data for 1,7-dioxaspiro[5.5]undecanes and related compounds

NORMAND POTHIER, DARYL D. ROWAN, PIERRE DESLONGCHAMPS, AND JOHN K. SAUNDERS
Département de chimie, Université de Sherbrooke, Sherbrooke (Qué.), Canada J1K 2R1

Received September 3, 1980

NORMAND POTHIER, DARYL D. ROWAN, PIERRE DESLONGCHAMPS, and JOHN K. SAUNDERS. Can J. Chem. **59**, 1132 (1981).

The carbon-13 chemical shift data for a series of 1,7-dioxa-, 1-oxa-7-thia-, and 1,7-dithiaspiro[5,5]undecanes and related compounds are presented. Analysis of this data led to structural and stereochemical assignments. The results show that the unsubstituted spiro bicyclic compounds exist in the conformation shown as conformation *a*. It is shown that the ^{13}C chemical shift parameters developed for cyclohexane derivatives can be applied to the sulfur but not to the oxygen heterocycles.

NORMAND POTHIER, DARYL D. ROWAN, PIERRE DESLONGCHAMPS et JOHN K. SAUNDERS. Can. J. Chem. **59**, 1132 (1981).

Les déplacements chimiques en rmn de ^{13}C de plusieurs dérivés de dioxa-1,7, oxa-1-thia-7 et dithia-1,7 spiro[5,5]undécanes sont présentés ainsi que ceux de quelques composés modèles. Les structures et la stéréochimie des composés ont été attribuées à partir de l'analyse de ces données. L'analyse conformationnelle démontre que les composés spiro-bicyclique non substitués existent dans la conformation *a*. On démontre que les paramètres de déplacement chimique de ^{13}C développés pour les dérivés du cyclohexane peuvent être appliqués aux hétérocycles sulfurés mais ils ne peuvent pas être utilisés pour les composés oxygénés.

Can. J. Chem. Downloaded from www.nrcresearchpress.com by 210.87.254.5 on 09/06/12
For personal use only.

The determination of the value of the anomeric effect using the bicyclic acetals and thioacetals described in the accompanying publications required determination of the preferred conformations and conformer populations of the various molecules. Carbon-13 chemical shifts are now accepted as one of the most valuable spectroscopic means for such determination although correlation of chemical shift with molecular geometry is generally obtained by empirical means (1–3). The idea then, for a conformationally mobile system, is to predict the chemical shift of each carbon in each conformer and then to compare these values with those obtained experimentally to ascertain the preferred conformation and in the limit, conformer populations. The empirical methods for 6-membered carbocyclic compounds in the chair conformation are reasonably well developed (3). However, the derived parameters in these systems may or may not hold true for heterocyclic compounds. For example, the effect at the β-carbon, upon introduction of a methyl group in cyclohexane, is 8.9 ppm whereas it is 5.8 or 7.3 ppm in 1,3-dioxans depending on whether the methyl group is introduced at C-4 or at C-5 (4). One is in somewhat of a quandary then, to know what value to use when the necessary parameters have not been determined for the molecule under study. In this paper we will use the parameters derived for 6-membered carbocyclic molecules (3). As will be seen, comparison of ^{13}C chemical shift values between the various compounds studied together with low temperature ^{13}C nmr led to the determination of conformational properties.

Armed with the conformational assignments, it was then of interest to examine the observed shifts to obtain more information on the effect on ^{13}C chemical shifts of introducing electronegative heterosubstituents, particularly at the β- and γ-carbons. One of the apparent anomalies in substituent effects on chemical shifts is the effect at the γ-carbon when the $C_\gamma—C_\beta$ bond is antiperiplanar to the C-substituent bond. In most examples when the α- and γ-carbons are primary or secondary, the effect is of shielding (5), whereas if either of these carbons is quaternary then deshielding is normally observed (6). The acetals and thioacetals possess heteroatoms in known, relatively rigid, orientations and should thus furnish information on substituent effects.

Results

The chemical shifts for all compounds[1] (Schemes 1 and 2) studied are given in Table 1. Spectra were assigned using the standard techniques such as single frequency off-resonance decoupled spectra, chemical shifts of model compounds, and comparison of shifts between compounds studied. For a number of compounds, the assignment of resonances to C-5 and C-11 was confirmed by deuteration since these resonances disappeared on deuteration. The presence of the spiro bicyclic function for compounds **9–25** is readily confirmed from the observation of a quaternary anomeric carbon at about 95 ppm (acetal), 80 ppm (monothioacetal), and 42 ppm (dithioacetal) respectively.

Compound **8** exists in two conformations of

[1]The chemical shifts for model compounds **3**, **6**, and **7** are taken from the Ph.D. thesis of F. Sauriol, Université de Montréal, with permission of the author and Professor St. Jacques. Their values obtained for **1** and **2** are the same as those given in Table 1.

0008-4042/81/071132-08$01.00/0
©1981 National Research Council of Canada/Conseil national de recherches du Canada

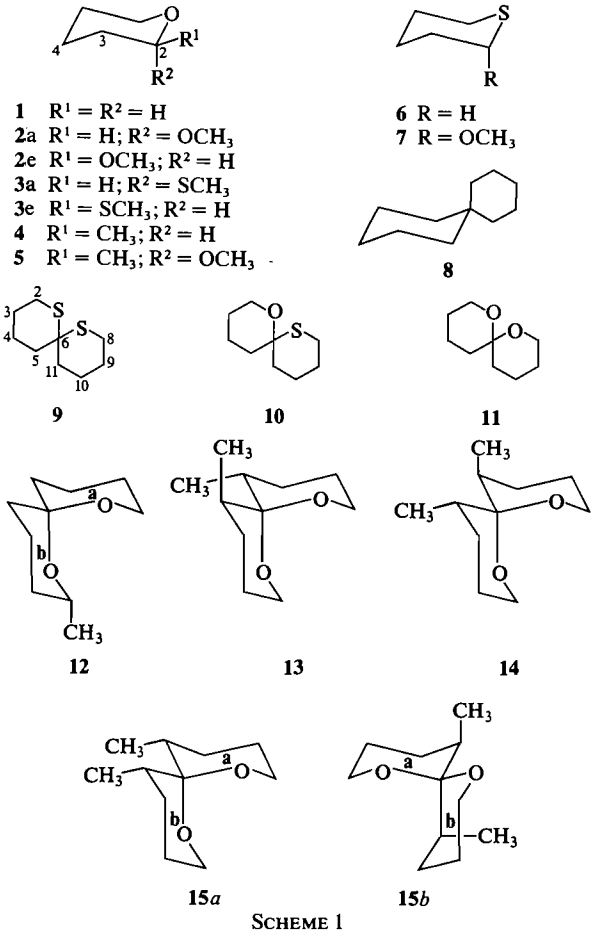

SCHEME 1

equal populations whereas there are 4 possible conformations for compounds **9–11** as illustrated in Scheme 3. The shifts for **8** and **9–11** were predicted using the chemical shifts of cyclohexane and compounds **2**, **3**, and **7**, respectively, for reference shifts and adding the increments for the various extra substituents. For example δ for C(1) of **8** is predicted to be 43 ppm which is calculated from[2] δ = reference + 3 HC + 1 CC which numerically gives 27.7 + 9 + 6.3 = 43 ppm. There are two HC interactions from C-7 and one from C-11. The CC term is for the C(11)—C(6); C(1)—C(2) *gauche* interaction. The spectra for **2**, **3**, and **7** were obtained at −130°C and the dominant, if not the exclusive, conformer of the OCH_3 group at this temperature is that in which the O—CH_3 (or S—CH_3) bond is *gauche* relative to the O(1)—C(2) (or the S(1)—C(2)) bond. This is the same orientation as in conformer *a* (Scheme 3) and thus the predicted shift for C-5 in **11***a* is 30.6 (value observed for C-3 in **2a**) + 9 (2 HC interactions from the introduction of C-11) = 39.6 ppm. By comparison the chemical shift of C-5 in conformer *d* of **11** is predicted to be 30.6 + 4.5 (1 HC from C-11) − 4.5 (the C(8)—O(7) bond is *gauche* to the C(6)—C(5) bond) = 30.6 ppm. The predicted shifts, given in Table 2, show that the only carbons which have significant conformational dependence are carbons 5 and 11. The differences in predicted shifts for the various compounds in a given conformation result from differences in the observed shifts of the reference compounds. For example, the shift induced at C-3 in the monocyclic compounds by introduction of an OCH_3 group depends on the atom at position 1 and this difference is then incorporated in the predicted shifts.

For **9**, the comparison of predicted and observed shifts infers that conformer *a* predominates. The spectrum at 160 K[3] indicates no evidence of a second conformer and is virtually identical[4] with that obtained at room temperature. We believe that our analytical method would have detected 0.5% of a second isomer if present (see Experimental). The low temperature spectrum confirms that **9** exists predominately (>95% at 25°C) as conformation *a*.

The spectrum of **10** at low temperature is essentially the same as that at room temperature. The comparison of predicted and observed shifts for C-11 suggests that either conformer *a* or *c* is predominant and that possibly a small percentage of *b* and/or *d* is also present. However, since **7** exists exclusively (or almost)[1] with the OCH_3 group in the axial orientation, conformations *c* and *d* must be neglected. Therefore **10** also exists at least predominately as conformer *a* with the shift of C-5 being more shielded than predicted.

The low temperature spectrum (160 K) of **11** shows only one symmetric conformer present since only 5 peaks are observed. Conformers *b* and *c* are equivalent and thus carbon 5 and 11 would resonate at 34.5 ppm if these were the only conformers present. This value gives the best correlation with the observed value although a significant proportion of *a* is necessary for observed and predicted values to coincide. If we take into account (*a*) that conformers *b* and *c* would give 11 peaks at low temperature whereas *a* only gives 5, (*b*) that 2-methoxy-

[2]For definitions of HC, CC, etc. see ref. 3.

[3]Assumed to be well below the coalescence temperature since separate conformers for **15** are observed at this temperature.

[4]Each carbon in **1** is more shielded at −130°C relative to 25°C by 0.4 to 0.8 ppm. Thus, any small change in chemical shift for the compounds of interest may be due to either conformational changes or changes in carbon shielding.

Can. J. Chem. Downloaded from www.nrcresearchpress.com by 210.87.254.5 on 09/06/12
For personal use only.

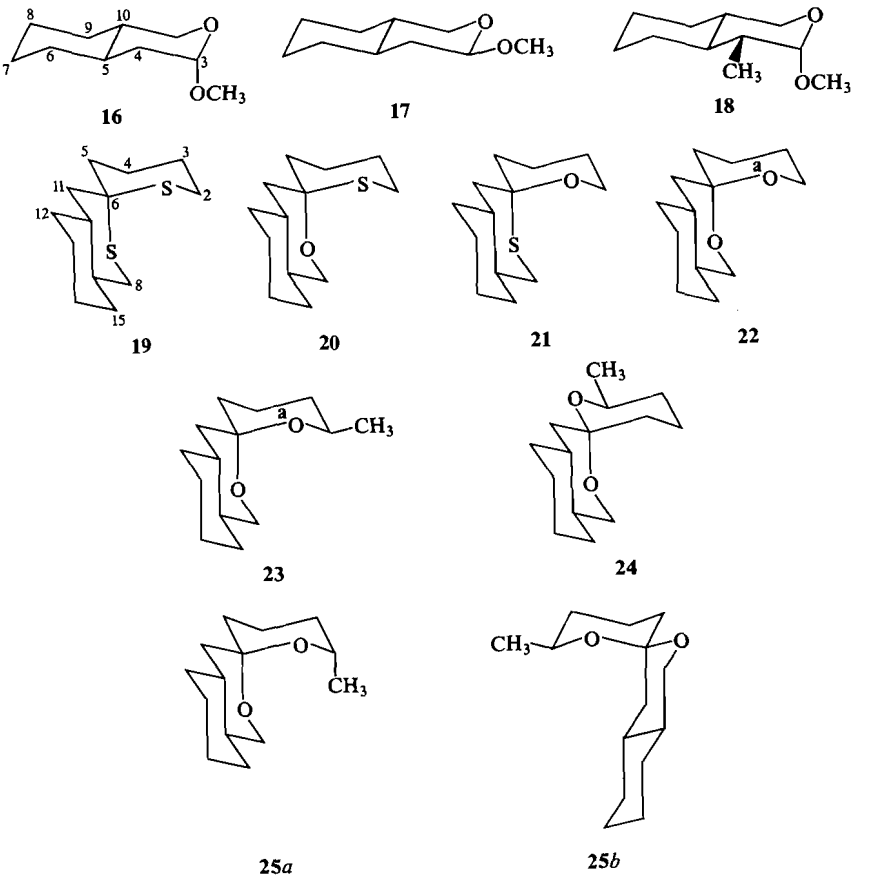

SCHEME 2

tetrahydropyran exists preferentially as **2**a (60% at 160 K), (*c*) that the observed shifts correlate better with *a* than with *d*, and (*d*) that in most oxygenated compounds, nonquaternary carbons are more shielded (5) than predicted, then it is reasonable to conclude that **11** exists predominately as conformer *a*. The X-ray data (8) discussed in the preceding paper confirm this statement. There is therefore a relatively large error in the prediction of δ(C-5) for this molecule. It should be noted at this point that the shift of C-5 in **11** is predicted by taking the observed shift for **2**a and adding the effective difference between shifts of decalin and cyclohexane, an operation which was quite successful for **8**. However, the β-effect for the introduction of a methyl group at C-4 of 1,3-dioxan is 5.8 ppm (5) and if we use this value then δ(C-5) of **11** has a predicted value of 36.0 ppm, which corresponds to that obtained experimentally.

The structure, stereochemistry, and spectra of **12** were assigned by consideration of the ^{13}C chemical shifts and SFORD spectrum. The presence of the spiro system is evident from the quaternary anomeric carbon signal at 95.5 ppm, the position of the CH_3 group follows from the methine carbon resonance at 65.2 ppm and the orientation of the methyl group follows from its chemical shift and that of C-10. The spectrum of **12** at low temperature is virtually identical with that obtained at room temperature. The chemical shifts for ring **a** of **11** and **12** are essentially the same and thus the two molecules must exist in the same conformation, and

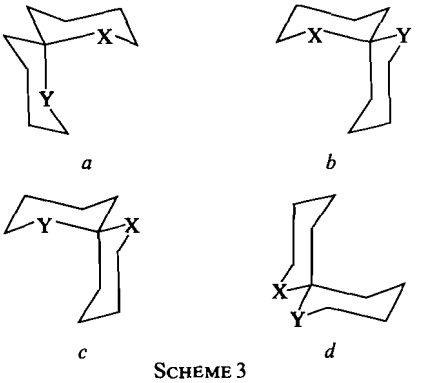

SCHEME 3

Can. J. Chem. Downloaded from www.nrcresearchpress.com by 210.87.254.5 on 09/06/12
For personal use only.

Can. J. Chem. Downloaded from www.nrcresearchpress.com by 210.87.254.5 on 09/06/12
For personal use only.

TABLE 1. ^{13}C chemical shifts[a] for compounds **1–23** relative to TMS

Compound	C-1	C-2	C-3	C-4	C-5	C-6	C-7	C-8	C-9	C-10	C-11	C-12	C-13[b]	C-14[b]	C-15	C-16
1		68.8	26.8	23.6												
1[c]		69.2	27.0	23.7												
2a[c]		98.9	30.6	18.5	26.1	60.2		55.0								
2e[c]		104.5	32.3	23.0	25.0	67.3		57.0								
3a[c]		83.7	31.1	19.8	26.5	60.2		13.5								
3e[c]		85.1	32.3	24.6	25.9	69.9		14.2								
4		74.9	34.7	24.5	26.8	69.2	22.6									
5		97.5	35.8	18.9	25.1	61.3		47.7	23.9							
6[c,d]		29.3	28.3	26.8												
7[c,d]		80.7	34.4	20.9	27.8	24.0		55.9								
8[e]	37.6	22.0	27.5			32.7										
8[e,c]	32.2	22.0	27.6	22.0	43.0	32.7										
9		26.9	27.5	21.6	42.4											
10		61.6	25.9	19.2	38.1	82.6		25.1	27.2	21.1	41.6					
11		60.3	25.4	18.6	35.8	94.9										
12		60.2	25.4	18.6	35.9	95.5		65.1	32.7	19.0	35.1	21.8				
13		60.9	27.5	28.3	35.8	100.7						16.5	16.5			
14		60.7	19.6	25.4	32.0	99.4						13.6	13.6			
15		59.4	24.9	29.3	36.0	100.9		60.6	20.6	26.6	35.9	16.8	17.5			
15a[g]		60.4	25.2	30.1	37.6	100.3		61.2	20.0	28.1	38.0	19.7	18.5			
15b[g]		63.6	19.2	25.8	31.0	100.7		62.3	25.4	26.0	26.0	12.7	15.2			
16	64.7		99.1	38.0	35.5	33.5	26.6	26.9	28.5	42.6						
17	71.0		103.9	39.3	40.5	33.5	26.5	26.6	27.9	42.6						
18	64.8		102.9	41.0	41.4	30.0	26.5	27.1	28.5	42.4						
19		27.1	27.5	21.7	42.7	55.7		34.0	44.8	37.3	50.4	33.2	26.2	26.6	32.6	
20		25.4	27.3	21.2	41.6	83.4		66.6	42.5	36.1	45.4	32.8	26.0	26.1	27.6	
21		61.6	26.0	19.5	38.0	83.4		34.2	44.3	37.0	49.7	33.3	26.4	26.7	30.9	
22		60.4	25.4	18.6	35.7	96.0		65.5	41.8	35.4	43.1	32.8	26.0	26.2	27.7	
23		65.2	32.7	19.0	35.1	96.6		65.4	41.9	35.4	43.2	32.8	26.0	26.2	27.7	21.9
24		66.4	32.2	18.4	28.0	97.9		68.3	41.9	37.2	44.2	33.0	25.9	26.1	27.7	22.2
25		68.6	32.4	19.3	37.3	97.8		66.3	41.9	35.0	36.0	32.9	26.0	26.3	27.7	21.9

[a]In $CDCl_3$ as solvent.
[b]Could be interchanged.
[c]In $CHFCl_2$ at −130°C.
[d]See footnote 1.
[e]Reference 7.
[f]Reference 7, low temperature.
[g]160 K in $CHFCl_2$.

TABLE 2. Predicted chemical shifts[a] for compounds **8–17** and **19–25**

Compound	Conformation	C-1	C-2	C-3	C-4	C-5	C-8	C-9	C-10	C-11
8		33	23	27	23	42				
9	*a*		24	28	21	43				
	b		25	27	21	43	24	28	21	34
	c		24	28	21	34	25	27	21	43
	d		25	27	21	34				
10	*a*		60	27	20	40	24	28	21	43
	b		62	27	20	40	24	28	21	34
	c		60	27	20	31	25	28	21	43
	d		62	27	20	31	25	28	21	34
11	*a*		60	26	19	40				
	b		62	25	19	39	60	26	19	31
	c		60	26	19	31	62	25	19	39
	d		62	25	19	31				
12	*a*		60	25	19	36	66	33	19	36
13	*a*		60	25	28	35				
14	*a*		60	20	25	30				
15	*a*		60	25	28	41	60	21	25	37
	b		62	20	25	32	60	21	25	28
16		69		99	39					
17		76		105	40					
19	*a*		27	27	22	42	34	42	37	50
20	*a*		25	27	21	42	71	42	34	47
21	*a*		62	26	19	38	34	42	36	50
22	*a*		60	25	19	36	69	40	34	45
23	*a*		65	33	19	35	69	40	34	45
24	*a*		66	33	19	27	66	43	36	45
25	*a*		60	31	19	36	69	43	35	45
25	*b*		68	31	19	36	69	43	35	45

[a]Reference shifts for **8**, cyclohexane; reference shifts for **9–11**, **1–3**, **6**, and **7**; reference shifts for **12–14**, compound **11**; reference shifts for **15**, compounds **13** and **14**; reference shifts for **16–17**, compound **2**; reference shifts for **19–25**, the corresponding bicyclic compound.

since introduction of a CH_3 group in ring **b** resulted in virtually no shift changes in ring **a** carbons it is evident that both **11** and **12** exist exclusively in conformation *a* even at room temperature. There is a downfield shift of C-3 by introduction of the methyl group which is not observed in **4** nor in cyclohexanes, nor in 1,3-dioxans (4).

The next compounds studied were the dimethyl bicyclic compounds **13–15**. Two of these compounds gave 6 signals whereas the third gave 11. The two former compounds must then, from symmetry arguments, have both methyl groups either axial or equatorial. For **13**, carbons 3, 4, 5, and 12 all absorb at lower field than the corresponding carbons in **14** and this must therefore be the compound with the CH_3 groups equatorial. Lowering the temperature for both compounds did not significantly alter their spectra and therefore the two exist as conformer *a*.

The third dimethyl compound gave 11 resonances including a quaternary anomeric carbon, 2 tertiary carbon, 6 secondary carbon, and 2 primary carbon resonances. Coalescence behaviour for each resonance was observed upon lowering the temperature in the following order of decreasing temperature: $35.9 > 16.8 \simeq 24.9 > 36.0 > 29.3 > 20.6 > 26.6 \simeq 59.4 > 16.8 > 60.6$. The coalescence temperatures are in a similar range as those observed for **2** and it is thus reasonable to presume that the inversion is between two chair conformations. The predicted shifts for **15***a* were obtained from **13** and **14** for rings **a** and **b**, respectively. The only carbons whose shifts should differ significantly from those in **13** and **14** are carbons 5, 11, and the methyl groups. The former have 1 less γ-*gauche* interaction than in their respective model compounds, and the methyl groups have a mutual δ-*syn*-diaxial interaction. In conformer **15***b* the shifts of carbons 2–4 and 8–10 were predicted to be the same as those in **14**. The resonance for C-5 in **15***b* should be at higher field by about 10 ppm relative to that observed in **15***a* since a γ-gauche interaction has been introduced and the methyl has changed from equatorial to axial. The difference for C-11 between the two conformations should be about 9 ppm since two γ-*gauche* interactions are present in **15***b* which are absent in **15***a*. The methyl carbon, C-13, is predicted to be shielded by 3 ppm in *b* relative to *a* since there is no δ interaction in this conformation. The CH_3 group, C-12, is axial in *b* and the change from equatorial to axial together with the lack of a δ interaction leads to a prediction

Can. J. Chem. Downloaded from www.nrcresearchpress.com by 210.87.254.5 on 09/06/12
For personal use only.

Can. J. Chem. Downloaded from www.nrcresearchpress.com by 210.87.254.5 on 09/06/12
For personal use only.

that this carbon will be shielded by approximately 8 ppm in *b* relative to *a*. The assignments given in Table 1 for **15***a* and **15***b* were made by taking into account predicted shifts, the room temperature shifts, and the coalescence behaviour. They must, however, be taken as tentative. The correlation between predicted and observed shifts is not good. The most disturbing shift is that for C-9 in **15***b* (25.4 ppm). This carbon should show very little chemical shift difference between the two conformations since it has a γ-*gauche* orientation relative to the CH_3 group in both and yet a $\Delta\delta$ value of 5.4 ppm is observed. The observed difference would in fact be best explained by placing the methyl group axial in *a* and equatorial in *b*. The conformers *c* and *d* were not considered since both have two of the very severe *syn*-diaxial interactions. The correlation between predicted and observed for the other carbons in **15***b* is acceptable. The deviation between predicted and observed for **15***a* is somewhat larger which could be indicative of a small deformation to alleviate the CH_3–CH_3 interaction. The assignments for C-5 and C-11 could be interchanged.

The assignment of *a* as the predominant conformer is based principally on the chemical shifts of C-5 and C-11. It is evident from the room temperature chemical shifts and the relative intensities at low temperature that the predominant conformer is the one in which the two methine carbons are more deshielded. It is virtually inconceivable that these carbons be more shielded in *a* than in *b* (see shifts of C-5 and C-11 in **24** and **25**). The shifts of C-2 and C-8 also infer that *a* predominates. The only doubt that persists is the shift of C-9 in *b*. Inversion of the assignments for C-3 and C-9 would infer that *b* predominates and that C-9 in *a* is more deshielded than predicted due to molecular deformation to alleviate the δ interaction. This argument does not counterbalance those for C-2, C-5, C-8, and C-11 and is therefore discarded. It should be pointed out that the difference at C-3 between **13** and **14**, 7.9 ppm, is significantly larger than that observed normally (4.5 ppm (3)). The weight of evidence indicates that the compound **15** has the structure as shown, with the conformer **15***a* being predominant by a ratio of 3:1.

The compounds **16–18** represent good models for the tricyclic compounds. The results for these compounds confirm that C-6 is deshielded relative to C-9.

For the tricyclic compounds **19–22** the predicted shifts were obtained by adding the parameters which correspond to the addition of the third ring to the spirobicyclic compounds. The correlation between predicted and observed shifts is satisfactory with the exception of C-8 in **20** and **22**. These compounds all exist in the same conformation, *a*, since the chemical shifts of ring **a** are virtually identical with those obtained for the bicyclic compounds. The structure and stereochemistry of **23** was assigned by comparison with **12**. Equilibration of **24** yields an approximate 1:1 mixture of **24** and **25** which led to the proposed structures. Confirmation of the structure for **24** was obtained from chemical shift data particularly for the methyl group (equatorial), C-5 (axial), and C-11. The spectrum of **25** at 160 K gave signals corresponding to only one conformer, **25***b*, with no trace of *a* being observed. The conformation **25***b* was assigned from the methyl carbon resonance (equatorial), the absorption of C-11 (shielded by 8.2 ppm relative to **24** and therefore axial), and C-5 (about the same as in **11**). Equilibration of **24** in deuterated medium led to an approximately 50:50 mixture of **24** and **25** with the resonances assigned to C-5 and C-11 absent in both compounds.

The conclusion that can be drawn for the chemical shift data is, with the exception of **15**, **24**, and **25**, that all spiro compounds exist almost exclusively even at room temperature in one conformation, that illustrated as *a*. At low temperature, no evidence for a second conformer was found in these compounds. Comparison of the chemical shifts of the hydrogen bearing carbons of **11** with unsubstituted ring carbons in **12** and **22** shows that the introduction of a methyl group or a third ring has not altered the chemical shift of these carbons (experimental error of ± 0.1 ppm). The conformational mobility in **12** and **22** is restricted relative to **11** yet the chemical shift is invariant. The chemical shifts of hydrogen bearing ring carbons of the methyl substituted ring of **12** and **23** are the same. Comparison of the chemical shifts of **9** with those of **19**, and **10** with either **20** or **21**, shows similar results. In light of this invariance in chemical shift upon restriction of conformational mobility, it is reasonable to conclude that the compounds **9–11** exist in one conformation.

The principal aim of developing an empirical method for predicting chemical shift is to predict chemical shifts for a large number of molecules based on a limited number of parameters. As mentioned above, a method which gives satisfactory correlation between calculated and observed shifts for six membered carbon rings in the chair conformation has been developed (3). Application of this method to compounds where sulfur replaces one of the CH_2 entities appears reasonable at least for the compounds presented herein. However, once oxy-

Can. J. Chem. Downloaded from www.nrcresearchpress.com by 210.87.254.5 on 09/06/12
For personal use only.

gen is introduced, the correlation between predicted and calculated shifts is no longer satisfactory.

Examination of the model compounds reveals a number of interesting facts. First of all the β-effect at C-3 for the introduction of an OCH_3 group is 2.8 ppm (axial) and 4.5 ppm (equatorial) for tetrahydropyran, 1.1 ppm for 2-methyltetrahydropyran, 5.4 ppm (axial) for the tetrahydrothiopyran, and 4.4 ppm (axial) and 6.3 ppm (equatorial) for 2-methoxymethylenecyclohexane (9). Thus this effect is significantly smaller for an oxygen heterocyclic compound. The β-effect for introducing a CH_3 group at C-2 varies between 7.3 ppm (**12-11**) and 7.9 ppm (**4-1**) which is somewhat smaller than that observed in cyclohexanes (9 ppm) but larger than that observed in 1,3-dioxans (5.8 ppm when substituted at C-4 (5)). Secondly, the magnitude of the γ-effect at C-6 by the introduction at C-2 of an OCH_3 (or CH_3) axial in oxygen heterocyclics is significantly larger than that observed at C-4. The latter shift is similar to that observed in cyclohexane derivatives (3).

There is a reasonably large discrepancy between predicted and observed shifts for C-5 of **11**. The difference between C-5 of **11** and C-3 of **2**a is only 5.2 ppm, which is much smaller than that using cyclohexane parameters (9 ppm) or the difference between C-3 in **4** and **1** (7.9 ppm). We assumed that the OCH_3 group in ***2a*** exists with the O—CH_3 bond *trans* with respect to the C(2)—C(3) bond, conformation A_1.[5] The other orientation possible would have the O—CH_3 bond *gauche* to this bond (conformation A_2)[5] which would lead to shielding of C-3 by the well known γ-*gauche* effect. This would at least partially explain the small β-effect at C-3 between ***2a*** and **1**. However since **11** exists in conformation *a*, the difference at C-5 between **11** and ***2a*** would be greater than predicted if ***2a*** existed in conformation A_2. The chemical shift of C-3 in 2-methyl-2-methoxytetrahydropyran is 35.8 ppm which is virtually identical to that observed for **11**. This compound will exist almost exclusively (if not exclusively) with the OCH_3 group axial since **2** exists predominately with the OCH_3 group axial and since attempts to observe the axial conformer of 2-methyltetrahydropyran proved fruitless. The shift of C-3 infers that 2-methoxy-2-methyltetrahydropyran exists with the O—CH_3 bond *gauche* with respect to the O(1)—C(2) bond, conformation A_1.

The other discrepancy between predicted and observed shifts is that for C-1 of **16–18** and C-8 of **22** and **24**. In these compounds the β-effect for the introduction of a CH_2 is about 5 ppm as compared to the normal value of 8 to 9 ppm. It is of interest to note that for **16** and **17**, C-9 is significantly shielded relative to C-6, and C-15 is significantly shielded relative to C-12 in **20** and **22**. The carbons C-9 and C-15, are γ-*trans* with respect to the oxygen and represent excellent examples of the relative shielding of this carbon when placed in this orientation relative to an electronegative substituent. However, both carbons 1 and 9 of **16** and **17** and carbons 8 and 12 of **20** and **22** are all significantly more shielded than predicted. The methyl carbons of *cis*-3,5-dimethyl tetrahydropyran are shielded by 5.9 ppm relative to that of methylcyclohexane (5), another example of the shielding effect at the γ-*trans* carbon. Carbons 2 and 4 of this compound are shielded by 5 and 18 ppm relative to **1** respectively. The effect at C-2 is similar to that discussed above whereas that at C-4 is similar to cyclohexane derivatives. The methyl carbons of **13** appear at 16.5 ppm which represents a shielding of only 1 ppm relative to those of 3,5-dimethyl tetrahydropyran. The former have two γ-*gauche* interactions which are absent in the latter and we would thus predict a difference of the order of 9 ppm, not 1 ppm. Obviously the so-called γ-*trans* shielding effect is no longer present when the α-carbon becomes quaternary. The observed shift of 16.5 ppm is comparable with that observed for the 2-methyl carbon in 1,1,2-trimethylcyclohexane. The shifts of the methyl carbons of **14** are more deshielded than predicted using cyclohexane parameters which is no doubt another example of a deshielding effect at the γ-*trans* carbon when the α-carbon is quaternary. The discussion in this paragraph infers that hydrogen–hydrogen interactions play an important role in determining carbon shieldings.

The chemical shifts for several bicyclic 1,3-dioxans have been reported (10). For compound **26** the predicted shifts for C-5, C-7, and C-11 are 42, 33, and 42 ppm, respectively. The corresponding observed shifts are 36, 30, and 41 ppm. For **27**, the predicted shifts for the same carbons are 33, 33, and 42 ppm which correspond to the observed shifts of 31, 31, and 42 ppm respectively. In both com-

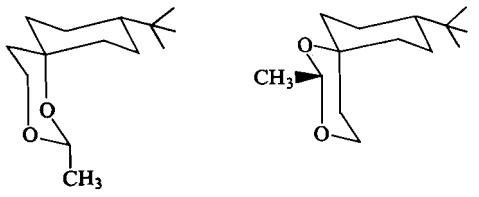

26 **27**

SCHEME 4

[5]See accompanying article.

Can. J. Chem. Downloaded from www.nrcresearchpress.com by 210.87.254.5 on 09/06/12
For personal use only.

pounds C-7 is more shielded than predicted which is most likely due to the γ-*gauche* interaction, when oxygen is present in the ring, being larger than for a CH_2 as already discussed. The correlation between observed and predicted shifts is reasonable for C-11 whereas that for C-5 is not. The chemical shifts for the carbocyclic ring are predicted satisfactorily whereas in the oxygen-containing ring, the carbon is more shielded than predicted. Compound **26** exists as conformation *a* and the chemical shift of C-5 is very close to that for C-5 in **9**.

The results from the study of these compounds demonstrate that the parameters derived from cyclohexane derivatives can be applied to sulfur but not to oxygen heterocyclics. For tetrahydropyrans, the β-effect for introduction of a methyl group equatorial at C-2 depends on the axial substituents. If the substituent is hydrogen or sulfur, the β-carbon is deshielded by 7.6 ± 0.3 ppm whereas if it is oxygen, the carbon is deshielded by 5.2 ppm. Introduction of the CH_3 at C-3 deshields C-2 by 5 ppm and C-4 by 9 ppm. It is apparent that the shielding effect at the carbon γ-*trans* to an electronegative substituent is also reflected at the α-carbon. This relative shielding effect at the γ-carbon is not present if the α-carbon is quaternary. The γ-*gauche* effect is larger if the β-atom is an oxygen rather than a carbon and this effect is even more pronounced for an oxygen than a carbon or sulfur substituent.

Experimental

The carbon-13 spectra were recorded on a Bruker HX-90 spectrometer equipped with a Nicolet 1083 computer (8K data points). Sweep widths of 5000 Hz were usually employed with TMS being used as reference. The room temperature spectra were recorded in $CDCl_3$ whereas those at low temperatures were recorded in $CHFCl_2$ with about 10% of CD_2Cl_2 added for locking purposes. The spectra of **9**, **11**, **15**, **20**, and **25** were also recorded at 160 K on a Bruker WM 250 operating at 64 MHz for carbon-13. In **9** and **11**, several peaks of very weak intensity were observed which were assigned to impurities (for example, **9** exhibited 2 of these peaks below 70 ppm which are obviously assignable to oxygen bearing carbons). These peaks varied in intensity from 0.2 to 0.5% of the intensity of the compound peaks. Since peaks were observed in the region of interest, and since these peaks could not be unequivocally assigned to impurities, the conformer purity is thus assigned to **9** and **11** as being a minimum of 99.5% at 160 K. It should be pointed out that there are very few analytical techniques capable of detecting less than 0.5% impurities.

The preparation of most of these compounds is reported in the accompanying publications. The compound **2** was obtained from the addition of methanol to dihydropyran (11). Compounds **4** and **5** were obtained from the reduction of, and the addition of methanol to, 2-methylene tetrahydropyran (12), respectively.

Acknowledgements

Financial support from the Natural Sciences and Engineering Research Council of Canada and the Ministère de l'Education du Québec is gratefully acknowledged. We are also very grateful to Bruker Canada for recording a number of spectra at 63 MHz on their WM 250, and to Professor St.-Jacques and Francoise Sauriol from the Université de Montreal for permission to use their results.

1. D. K. Dalling and D. M. Grant. J. Am. Chem. Soc. **96**, 1827 (1974).
2. J. B. Stothers. Carbon-13 nmr spectroscopy. Academic Press, New York, NY. 1972; G. C. Levy and G. L. Nelson. ^{13}C nuclear magnetic resonance for organic chemists. Wiley–Interscience, New York, NY. 1972; N. K. Wilson and J. B. Stothers. Top. Stereochem. **8**, 1 (1974).
3. H. Beierbeck, J. K. Saunders, and J. W. ApSimon. Can. J. Chem. **55**, 2813 (1977).
4. E. L. Eliel, V. S. Rao, and F. G. Riddell. J. Am. Chem. Soc. **98**, 3583 (1976).
5. E. L. Eliel, W. F. Bailey, L. D. Kopp, R. L. Willer, D. M. Grant, R. Bertrand, K. A. Christensen, D. K. Dalling, M. W. Duch, E. Wenkerl, F. M. Schell, and D. W. Cochran. J. Am. Chem. Soc. **97**, 322 (1975).
6. W. A. Ayer, L. M. Browne, S. Fung, and J. B. Stothers. Can. J. Chem. **54**, 3272 (1976).
7. D. Dalling, D. M. Grant, and E. G. Paul. J. Am. Chem. Soc. **95**, 3715 (1973).
8. D. E. Evans, C. E. Sacks, R. A. Whitney, and N. G. Mandel. Tetrahedron Lett. 727 (1978).
9. J. Lessard, P. V. M. Tan, R. Martino, and J. K. Saunders. Can. J. Chem. **55**, 1015 (1977).
10. G. F. Woods and D. N. Kramer. J. Am. Chem. Soc. **69**, 2246 (1947).
11. G. F. Woods and D. N. Kramer. J. Am. Chem. Soc. **69**, 2246 (1947).
12. R. E. Ireland and D. Habick. Tetrahedron Lett. 1389 (1980).

Separation of short fibers from bulk chrysotile asbestos fiber materials: analysis and physico-chemical characterization.[1]

CARMEL JOLICOEUR, PIERRE ROBERGE, AND JEAN-LUC FORTIER

Centre d'Application en Calorimétrie et Thermodynamique and Département de Chimie, Université de Sherbrooke, Sherbrooke (Qué.), Canada J1K 2R1

Received July 21, 1980

CARMEL JOLICOEUR, PIERRE ROBERGE, and JEAN-LUC FORTIER. Can. J. Chem. **59**, 1140 (1981).

The aqueous sedimentation behavior of commercial chrysotile asbestos fibers has been investigated and a simple method for separating short fibers (90% < 2 μm) could be devised based on selective sedimentation. Chemical, X-ray structural, and differential thermal analyses show that the short fibers have chrysotile composition and structure, with lower brucite ($Mg(OH)_2$) and iron contents than the bulk fibers. The length distribution of these short fibers exhibits a maximum at 0.3 μm and a width-at-half-height of ~0.5 μm. Surface adsorption studies yield specific areas of 20 and 28 m^2/g for N_2 and H_2O respectively. Because of their finely divided state and narrow length distribution, such fibers should be well suited for a variety of physico-chemical, chemical, and biological investigations on chrysotile fibers.

CARMEL JOLICOEUR, PIERRE ROBERGE et JEAN-LUC FORTIER. Can. J. Chem. **59**, 1140 (1981).

Une étude de la sédimentation de fibres d'amiante chrysotile en suspension aqueuse a permis la mise au point d'un procédé pour la séparation de fibres courtes (90% < 2 μm) à partir d'échantillons de fibres commerciales. L'analyse chimique, la diffraction de rayons-X et l'analyse thermique différentielle effectuées sur ces fibres courtes ont démontré qu'elles possèdent la composition et la structure du chrysotile, bien que contenant moins de brucite ($Mg(OH)_2$) et de fer que l'échantillon de départ. L'étude de l'adsorption de N_2 et H_2O par les fibres courtes a donné des surfaces spécifiques respectivement de 20 et 28 m^2/g. La distribution de longueur de ces fibres a un maximum à 0.3 μm et une largeur à demi-hauteur de ~ 0.5 μm. Il est proposé que ces fibres, vu leur état finement divisé et leur homogénéité dimensionnelle, sont bien adaptées à une variété d'études concernant les propriétés physico-chimiques, chimiques ou biologiques des fibres d'amiante chrysotile.

Introduction

The interest in the structural and surface properties of asbestos minerals has been sharply revived in recent years, because of potential health hazards resulting from human ingestion of fibrous minerals (1–4). The biological consequences of the interactions between fibrous silicates and biochemical materials (proteins, membranes, nucleic acids, etc.) remain largely unknown, but clearly the elucidation of such effects at the molecular level will require a detailed knowledge of the chemical and physico-chemical behavior of these fibrous compounds.

Among the various asbestos minerals of industrial interest, chrysotile is by far the most important. Its morphology and main structural and chemical features have been established through investigations using a variety of analytical and physical methods, for example, electron microscopy (5), infrared spectroscopy (6–8), X-ray diffraction (9–11), and surface adsorption (12–16).

Chrysotile asbestos belongs to the category of serpentine minerals (with antigorite and lizardite) having chemical composition $3MgO \cdot 2SiO_2 \cdot 2H_2O$ (17). Its basic structure consists of a sheet of silica tetrahedra which is overlayed with a sheet of magnesium hydroxide (brucite). The latter is joined to the silica layer by two out of three —Mg—O groups as illustrated in Fig. 1. Because of differences in the lattice parameters of the silica and brucite layers, the composite layer adopts a curvature (18) with the Mg—OH groups on the external surface. The growth of these curved sheets, in concentric or spiral arrangements, has lead to the naturally occurring fibrils which are found in the form of cylinders with internal and external diameters of approximately 10 nm and 25 nm respectively (17).[2] The central cavity of these cylinders has been suggested to contain amorphous minerals (12, 19) the composition of which varies depending on the origin of the chrysotile.

Attempts to perform refined studies of the physico-chemical properties of chrysotile fibers are generally difficult because of composition variations and size heterogeneity of the material. The composition variations due to substitutional elements are intrinsic to the particular material of interest and cannot be avoided. However, the situation with regards to interstitial impurities (e.g., excess brucite, amorphous minerals trapped between fibers) might be improved by using finely divided fibers, ideally monofibers (fibrils). With

[1]Part of M.Sc. Thesis of P. R., Sherbrooke 1978; work presented at A.C.F.A.S. Conference, Montreal, May 1979.

[2]Chrysotile may be found in three crystallographic varieties labelled *clino*, *ortho*, and *para*-chrysotile (9, 10); the most naturally abundant variety is *clino*-chrysotile.

0008-4042/81/071140-09$01.00/0

©1981 National Research Council of Canada/Conseil national de recherches du Canada

Can. J. Chem. Downloaded from www.nrcresearchpress.com by 210.87.254.5 on 09/06/12
For personal use only.

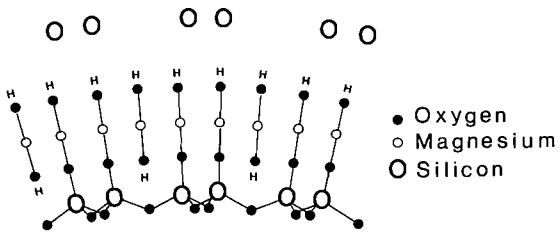

FIG. 1. Partial cross-section of a chrysotile asbestos fiber showing the composite silica–brucite layer.

such materials, the size heterogeneity should also be decreased since, in the limit, monofibers will all have comparable diameters. Finely divided fibers are also intrinsically better suited for a number of physico-chemical studies, for example, infrared absorption and surface adsorption. Investigation on fine chrysotile particles would also appear relevant to environmental and health studies, since the small fibers will be more readily airborne or transported in streams.

For one or more of the above reasons, it would thus seem highly desirable to develop methods for preparing representative samples of finely divided chrysotile fibers in a reproducible way. The present investigation was therefore undertaken with the specific aim of preparing and characterizing such samples. After various attempts with mechanical separation and size reduction procedures[3] (wet and dry), we have turned to investigate aqueous sedimentation methods. These studies have yielded a simple procedure for separating short fibers from bulk commercial samples. The separated fibers were found to have a relatively narrow length distribution and lower levels of the main interstitial impurities (brucite and iron oxides) than the starting materials. Details of the separation procedure and the results of various characterization studies including chemical and structural analysis, sedimentation rates, surface area, and differential thermal analysis are reported below. A combined thermogravimetric and infrared absorption study on the sedimented fibers will be reported in a subsequent paper (20).

Experimental

(a) Materials

The chrysotile asbestos samples used in this study were provided by Canadian Johns-Manville Ltd. through the A.M.A.Q. (Asbestos Mining Association of Quebec) laboratory. The results given in later sections were collected systematically for fibers classified as 4-T-30.[4] The water used in the various experiments was distilled and deionized on a mixed resin (Continental Deionizer). Electrolytes employed in some experiments (NaCl, $CaCl_2$) were certified reagent grade.

(b) Methods

(i) Sedimentation Rates

Two methods were adopted to measure sedimentation rates, depending on the type of fibers. With bulk 4-T-30 samples, measurements of sedimentation velocities were obtained by following the level of the solution–suspension boundary as a function of time. These measurements were carried out in Pyrex glass cylinders (diameter 7.5 cm, height 75 cm), thoroughly washed with detergents and rinsed repeatedly with deionized water. The aqueous fiber suspension was prepared at 1.00 wt%, and 50 glass beads (0.5 cm diameter) were added to assist the initial mixing. The latter was performed by inverting the stoppered cylinder 20 times in 10 min.

With short fibers the sedimentation rates were measured using a technique described, for example, by Mironov and Churaev (21). The basis of this method consists in following the weight of a horizontal glass disc, suspended from an analytical balance in the aqueous suspension. The diagram of the controlled temperature apparatus used for these measurements is illustrated in Fig. 2; the temperature was regulated to better than 0.01°C.

In the sedimentation experiments, the rates observed depended on a number of variables (standing time before experiment, stirring time, amount of material used, temperature, etc.). However, for a controlled set of experimental conditions and procedures, the half-times for sedimentation were found reproducible within 5%.

(ii) Chemical Analysis

The Mg and Fe content of samples of the 4-T-30 and of the short fibers (obtained as described in the result section, ref. 2) were determined by atomic absorption (Mg, Fe) and EDTA titration (Mg). Since prolonged acid treatment is know to leach out the metal ions of chrysotile leaving mostly amorphous silica (23, 24), the chrysotile samples were stirred vigorously in excess HCl 2.0 *M* (100 mL HCl/g chrysotile) for a period of 10 days; the resulting suspensions were centrifuged, filtered, and diluted for analysis. The Mg-EDTA titration was performed according to standard procedures using the calmagite indicator, after precipitation and removal of the iron (22).

(iii) X-ray Analysis

The diffraction pattern of sedimented short fiber samples and other materials dried at 110°C for 48 h were obtained with a Debye–Scherrer camera using the Cu, K_α line (Ni filter). The samples were confined in thin wall Pyrex capillaries having typical internal diameters of 0.5 mm. The uncertainty on the lattice parameters obtained is respectively 0.1 Å and 0.01 Å for the largest and smallest *d* spacings.

(iv) Differential Thermal Analysis (DTA)

The DTA curves of several chrysotile samples were recorded between room temperature and ~1000°C on a SETARAM thermal analyser, model Micro ATD-M4. Because of the low thermal conductivity of loose fibers, the samples (e.g. ~10 mg)

[3]There is now ample evidence that dry mechanical processes (grinding, milling) can induce profound structural modifications of the native chrysotile structure (19); such methods must therefore be avoided for the preparation of finely divided chrysotile samples.

[4]Asbestos fibers designated as 4-T-30 contain fibers with a broad distribution of lengths which may be specified from dry screening procedures. The latter show ~80% of the fibers between 1 and 4 mm with ~40% near 2 mm. Details of the procedures may be obtained from section B-2, Ro Tab Screen Analysis of Chrysotile Asbestos Test Manual (39).

Can. J. Chem. Downloaded from www.nrcresearchpress.com by 210.87.254.5 on 09/06/12
For personal use only.

Can. J. Chem. Downloaded from www.nrcresearchpress.com by 210.87.254.5 on 09/06/12
For personal use only.

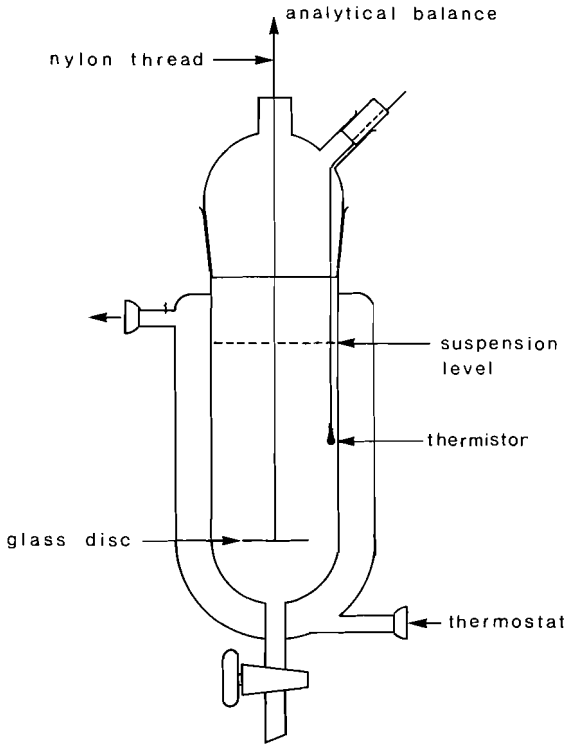

FIG. 2. Horizontal disc apparatus for the measurement of sedimentation rates.

were gently compacted in the DTA cups and the scanning rate was kept sufficiently low to avoid broadening of the transition peaks.

(v) Surface Adsorption Measurements

The specific area of chrysotile fibers was determined from nitrogen adsorption using a commercial BET apparatus (Micrometrics, Model 2200). Fibers used in these experiments and others described below were previously heated to 110°C for at least 24 h. This was sufficient to achieve constant weight and provided a reliable reference state for the various physicochemical measurements; structural modifications and dehydration of the brucite do not occur, however, until much higher temperatures.

Water adsorption measurements for short fiber samples were carried out as a function of water activity (relative humidity) using the isopiestic technique described for example by Robinson and Stokes (25) and Platford (26). The apparatus used consisted of a vacuum desiccator which housed a copper plate holding seven platinum crucibles. A solution of the isopiestic standard ($CaCl_2$ or H_2SO_4 (25)) was placed at the bottom of the desiccator and the apparatus was evacuated slowly to 2 Torr; the system was left to equilibrate, from 3 days to 1 week depending on the water partial pressure, in a constant temperature bath at 25.00 ± 0.01°C. The desiccator was then opened to a stream of dry nitrogen, the samples were quickly sealed and weighed, and the isopiestic standard solution was titrated to obtain the equilibrium water activity (25). The reproducibility in the weight of equilibrated samples (~0.5 g) for the entire operation was within ±0.0005 g.

Results and Discussion

(1) Sedimentation Studies on 4-T-30 Fibers

The sedimentation rates of 1.0 wt% aqueous suspensions of 4-T-30 fibers were investigated in electrolyte-free suspensions and in solutions of NaCl and $CaCl_2$. The time dependence of the height of the sedimentation boundary is very nearly exponential with a half-time ($t_{1/2}$) of 125 s. The latter was noted, however, to be markedly dependent on the presence of small amounts of electrolytes; for example leaching of ions from a new glass tube changed the observed rate significantly.

The measurement of sedimentation rates as a function of NaCl or $CaCl_2$ concentration yielded the results illustrated in Fig. 3. Both electrolytes retard the sedimentation of the coarse fibers with a saturation effect at ~13 m*M*. Although electrolytes have been shown to have a marked influence on the stability of chrysotile fiber suspensions (27), the behavior shown in Fig. 3 is contrary to that expected on the basis of results from ζ potential studies (28). In electrolyte-free suspensions, the ζ potential of chrysotile fibers is positive, decreasing with added salt concentration. In the absence of specific interactions as, for example with sodium silicate (28), the main influence of electrolytes should be to decrease the electrostatic repulsion between fibers (reducing the double layer thickness) and this should enhance the sedimentation rates. While the influence of various electrolytes on the sedimentation of 4-T-30 fibers was not investigated in further detail, it was noted that the sedimentation behavior with and without electrolytes differed qualitatively in an important fashion. In electrolyte-free suspensions, the supernatant liquid is a cloudy suspension of fine particles (presumably short fibers and foreign materials), whereas in the presence of sufficient electrolyte, the fine particles settled as well. From the sedimentation behavior of the fibers, it could later be concluded that the influence of electrolytes on the

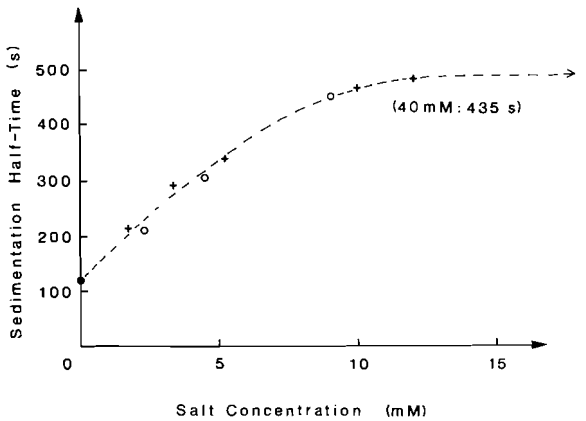

FIG. 3. Half-time for the sedimentation of aqueous suspensions of bulk 4-T-30 chrysotile fibers (1.0 wt%), as function of electrolyte concentration; +: NaCl; O: $CaCl_2$.

Can. J. Chem. Downloaded from www.nrcresearchpress.com by 210.87.254.5 on 09/06/12
For personal use only.

sedimentation rates of the coarse fibers (4-T-30) is in fact due to the properties of the short fibers; in the presence of electrolytes, the latter aggregate into a macroscopic floc and this process hinders the coarse fiber sedimentation.

(2) Method for Separation of Short Chrysotile Fibers

The experimental observations described above suggest a simple way of separating short fibers and other fine particles from bulk commercial fibers. The latter (1–2 wt%) are dispersed by gentle agitation in a column containing distilled deionized water; when sedimentation of the coarse particles is completed, the supernatant suspension is pumped out and the fine particles are precipitated by addition of low levels of electrolytes, typically NaCl 20 m*M*. If electrolyte contamination is to be avoided, the suspended material may, of course, be recovered by filtration.

The sedimentation behavior of the fine particles was examined using the suspended disc method described earlier. The influence of NaCl concentration on the sedimentation rates may be seen in Fig. 4 from the time-dependence of the disc weight in a suspension containing 0.063 wt% solids. While the disc weight is invariant in the absence of electrolyte (no sedimentation), addition of NaCl at low concentrations ($c < 2$ m*M*) leads to very slow sedimentation and an apparent weight decrease; the latter can only be understood as the result of a density gradient in the column, before a significant amount of material settles on the disc. At higher NaCl concentrations ($c > 3$ m*M*), the particles aggregate into a floc which sediments more rapidly; with an NaCl concentration of 13 m*M* (cf. the concentration required for saturation of electrolyte effects with the 4-T-30 fibers), a sedimentation half-time of ~450 s is observed, and the latter is not strongly dependent on the solid content of the suspension. This sedimentation half-time closely corresponds to that observed for the sedimentation of coarse fibers under similar conditions, an observation which is readily explained as follows: in electrolyte-free suspensions, the coarse fibers sediment with $t_{1/2} \sim 2$ min, while the fine particles remain in suspension; in the presence of electrolytes, the coarse and fine particles settle simultaneously, but the rate is now dominated by the slow ($t_{1/2} \sim 450$ s) flocculation–sedimentation process of the fine particles.

Following the method described by Michaels and Bolgers (29) in sedimentation studies of kaolin suspensions, an estimate of the average size of the floc can be obtained from the sedimentation rates. The rate determined from the positive slope of the

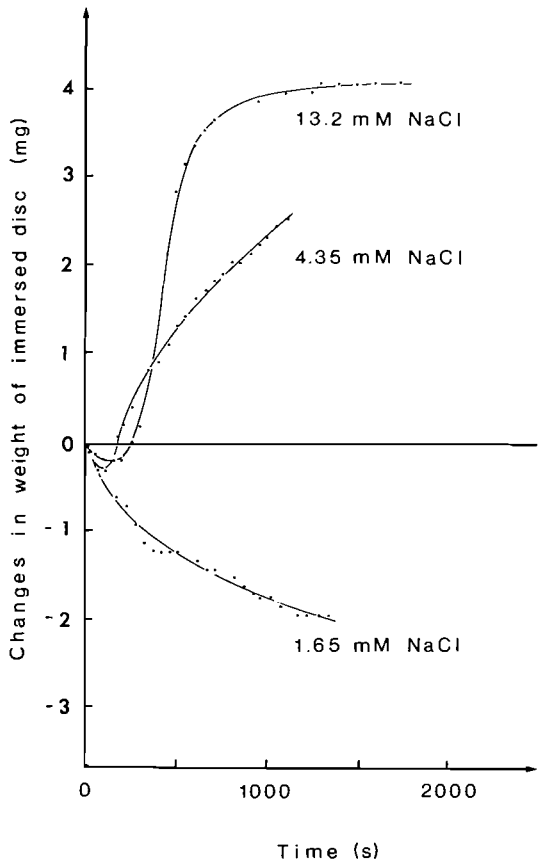

FIG. 4. Sedimentation behavior of supernatant fine particles (0.063 wt%) from the variation of immersed disc weight.

data with 13.2 m*M* NaCl (Fig. 4) leads to a floc size of 1.1 ± 0.2 mm which is compatible with the physical size of the observed aggregates.

Several experiments were carried out to determine the influence of pH on the sedimentation rate of the fine particles. In the absence of other electrolytes, addition of HCl to pH 3 does not induce significant sedimentation over a period of 2 h; sedimentation occurring at much longer times was not investigated further because of acid attack of the chrysotile fibers. On the other hand, addition of NaOH induced sedimentation, at a rate increasing with pH. The maximum sedimentation rate was found near pH 11.0 which corresponds approximately to the pH of zero-charge of chrysotile fibers for which values have been reported in the range 10.1–11.8 (30).

Finally, to determine the amount of short fibers and fine particles which could be extracted from a given bulk material, the sedimentation–separation procedure was performed repeatedly on the same sample, and this was carried out for several 60.0 g samples of 4-T-30 fibers. The total separation

Can. J. Chem. Downloaded from www.nrcresearchpress.com by 210.87.254.5 on 09/06/12
For personal use only.

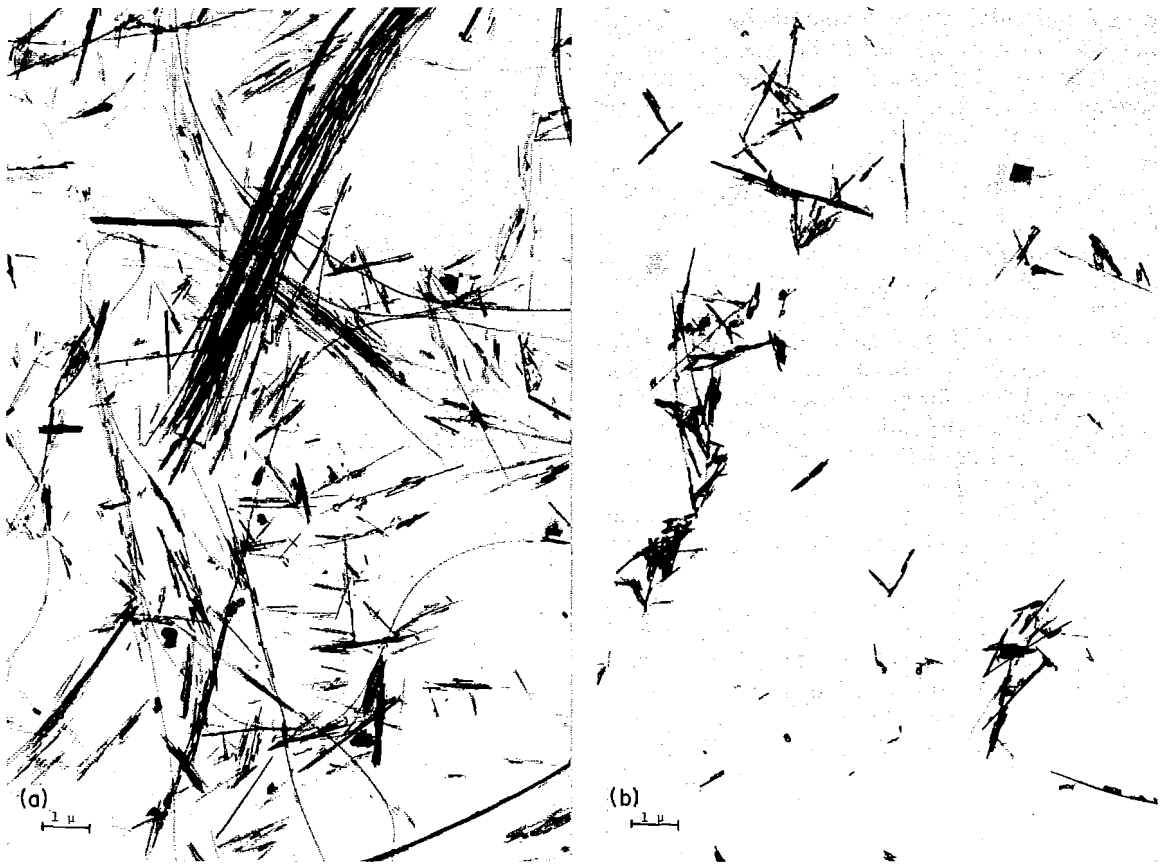

FIG. 5 (*a*) Electron micrograph of 4-T-30 chrysotile asbestos at 11 900×. (*b*) Electron micrograph of fine particles separated from the 4-T-30 chrysotile sample shown in (*a*).

yields were found as high as 10 wt% and, since the separation procedure does not involve sufficient mechanical stress to produce defibrilation, these short fibers and fine particles must be present in the starting bulk materials. The remainder of this work was concerned with the assessment of the nature and properties of these fine particles.

(3) Size Distribution Analysis

Samples obtained from consecutive extractions of fine particles on a given batch of coarse 4-T-30 fibers were examined under transmission electron microscopy and compared with the starting material. Typical electron micrographs (11 900 ×) of 4-T-30 chrysotile fibers, and of the sedimented fines are reproduced in Fig. 5 *a* and *b*, respectively. These, and a large number of other similar results, consistently showed that the fine particles are mainly short fibers rather than powdered minerals. The average diameter of these fibers could not be estimated reliably, but their length distribution was determined through fiber counting procedures using a Zeiss optical counter. The length histogram illustrated in Fig. 6 (for the 1st, 2nd, and 9th samples of consecutive extractions on a given sample) shows a sharp peak in the length distribution near 0.3 μm, more than 90% of the fibers being shorter than 2.0 μm (the peak shown at 2.5 μm is the instrument count for all fibers with lengths greater than 2.5 μm; the maximum fiber length observed was 8 μm). While these parameters are expected to vary with the type of bulk material investigated, it is interesting to note that the length distributions obtained for samples of successive separations are very similar. This shows that under the present conditions, there is no sedimentation selectivity which could allow further separation according to fiber lengths.

(4) X-ray Structural Analysis

The X-ray diffraction pattern of several chrysotile bulk and short fiber samples were obtained in thin-wall capillaries using a powder camera. The various derived lattice parameters are reported in

TABLE 1. X-ray lattice parameters obtained for 4-T-30 chrysotile fibers, sedimented short fibers, and other reference materials

d (Å)				
Original 4-T-30 sample	Short fibers 1st extraction	Cassiar[a] chrysotile	Chrysotile[b] ASTM 10-380	Brucite[c] ASTM 7-239
7.20	7.39	7.24	7.36	
				4.77
4.46	4.56	4.43	4.56	
3.63	3.65	3.63	3.66	
			2.66	
2.60		2.60	2.604	
			2.547	
2.52			2.500	
2.44	2.44	2.44	2.451	
2.36	—	—	—	2.365
			2.285	
			2.212	
2.09	2.09	2.09	2.092	
			1.972	
1.82			1.828	
1.79	—	—	—	1.794
			1.746	
				1.573
1.53	1.53	1.53	1.531	
				1.494
1.46			1.464	
1.37	—	—	—	1.373
	1.32	1.31	1.319	

[a]Natural brucite-free chrysotile.
[b]*Clino*-chrysotile (16% *ortho*-chrysotile).
[c]Most intense lines for brucite.

Table 1 with reference data for $Mg(OH)_2$ (brucite, ASTM-7-239), a brucite-free chrysotile fiber (Cassiar) and the ASTM recommended parameters for chrysotile analysis (ASTM 10-380) (31). Within the experimental error, the data for the 4-T-30 material match those of the Cassiar chrysotile and the ASTM reference data. The main chrysotile parameters are also found with the sedimented short fibers, so there can be little doubt that these fibers have chrysotile structure. Although no reliable quantitative intensity measurements could be carried out, the two most intense lines of brucite which are readily observed with the 4-T-30 sample, could not be detected in the short fiber material studied under the same conditions. This indicates a lower brucite content in the sedimented short fibers compared to the bulk initial sample; similar findings are also apparent in other analyses described below.

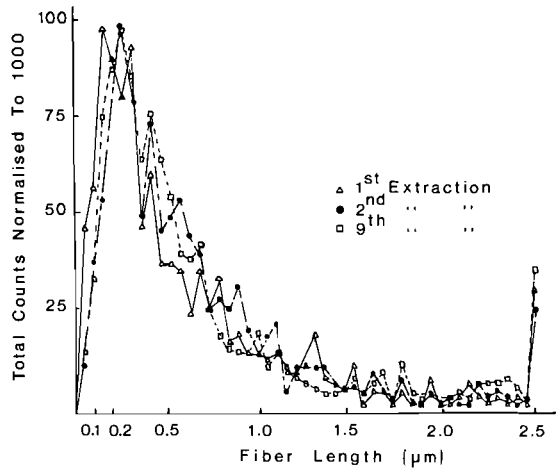

FIG. 6. Length distribution in short fibers sedimented from bulk 4-T-30 chrysotile; data obtained for 600–800 fibers and normalized to 1000.

(5) Chemical Analysis of Short Fibers

The composition of the sedimented short fibers relative to that of the bulk starting material was determined with respect to two important components: Mg and Fe. Magnesium is, of course, a key component in the chrysotile lattice, but it may also be present in excess as hydroxide (brucite) and carbonate. On the other hand, iron is one of the main substitutional and interstitial (as oxides) impurity of the chrysotile 4-T-30 material investigated. The results of Mg and Fe analysis are given in

Can. J. Chem. Downloaded from www.nrcresearchpress.com by 210.87.254.5 on 09/06/12
For personal use only.

TABLE 2. Chemical composition (wt%) of chrysotile asbestos (main components)*

Component	$3MgO \cdot 2SiO_2 \cdot 2H_2O$	Pundsack (13)	Harington (32)	Kalousek (33)	This work: Bulk sample 4-T-30	This work: Short fibers
SiO_2	43.36	42.0	39.15	41.8		
Al_2O_3		0.1	2.15	0.11		
Fe_2O_3		0.4	1.18	0.7		
					Fe: 3.4	Fe: 2.5
FeO		1.6	1.33	0.05	± 0.2	± 0.2
MgO	43.64	42.5	40.32	42.8	41.8	40.8
CaO			1.09	0.1	± 0.2	± 0.2
Na_2O			0.09	0.01		
K_2O		0.1	0.15	0.01		
H_2O	13.0	13.6	13.7	14.3		

*Similar and other composition analyses may also be found in refs. 17, 19, 34, and 35.

Table 2 along with various other chrysotile asbestos compositions reported earlier.

The elemental analysis data from different investigations illustrate typical composition variations, with Mg contents usually lower than that calculated from the chemical formula due to substitutional impurities. The same is true for the bulk and short fiber chrysotile samples studied here, and both exhibit high total Fe content. However, comparison of the results for bulk and short fibers indicate lower Mg and Fe concentrations in the latter. The significance of the lower Fe content in short fibers is difficult to assess because of the occurrence of Fe_3O_4 (magnetite) particles in the bulk material which would be partly removed in the sedimentation process. However, the lower Mg content of the short fibers confirms the lower amount of brucite in this material compared to the original 4-T-30 sample (if the difference found in entirely due to excess brucite, this means an ~2.5% difference in $Mg(OH)_2$ content).

(6) Thermal Analysis

The thermogravimetric behavior and the temperature dependence of the infrared absorption spectrum of the sedimented short fibers have been investigated in some detail and will be reported in a subsequent paper (20). The differential thermal analysis (DTA) curves provide additional evidence on the nature and composition of the sedimented short fibers as illustrated in Fig. 7. The DTA curve recorded for 4-T-30 fibers is typical of bulk chrysotile materials showing the endothermic dehydration of brucite near 400°C and dehydration of the chrysotile structure in the temperature range 600–800°C; the exothermic peak above 800°C corresponds to a rearrangement into forsterite and amorphous silica (17, 36). The DTA curve obtained with the sedimented short fibers exhibits the same features although the brucite dehydration peak is substantially lower than with 4-T-30 fibers. The ratio of the normalized brucite peak areas of short fibers and 4-T-30 fibers is ~1:10, while the ratio for the high temperature peaks is unity within experimental error.[5] The short fibers washed once with 25 vol% aqueous acetic acid exhibit no brucite peak, as expected, due to the leaching of the Mg from both the free brucite and the external brucite layer of the fibers.

The DTA curves further show that the chrysotile decomposition peak (about 780°C) is much narrower with the short fibers compared to the bulk 4-T-30 material. This may be a result of different physical properties of the samples (19), but it could also be related to differences in their decomposition mechanisms. Such effects have been observed in the thermal decomposition of loose fibers compared to fibers embedded in KBr matrices (20).

(7) Specific Area and Water Sorption Isotherm

The specific area of bulk chrysotile fibers determined from nitrogen adsorption can vary between 5–30 m^2/g, depending on the average size of the fibers (14, 16, 37, 38); specific areas up to 50 m^2/g have been obtained for mechanically dispersed fibers (14, 16) or thermally activated fibers (15). A first order calculation, taking a fiber diameter of 25 nm and a density of 2.5 g cm^{-3}, yields a specific surface area (of cylinders) of 32 m^2/g (neglecting end adsorption).

For chrysotile asbestos fibers of grade 7-R (Johns Manville),[6] Young and Healey (16) reported a nitrogen specific area of 9.7 m^2/g using a molecular

[5]The relative areas of the brucite peaks may not be taken as a measure of relative excess brucite contents until a quantitative relationship between these variables can be demonstrated.

[6]Fibers of this commercial grade are much shorter than the 4-T-30 fibers, i.e. ~75% < 0.1 mm.

Can. J. Chem. Downloaded from www.nrcresearchpress.com by 210.87.254.5 on 09/06/12
For personal use only.

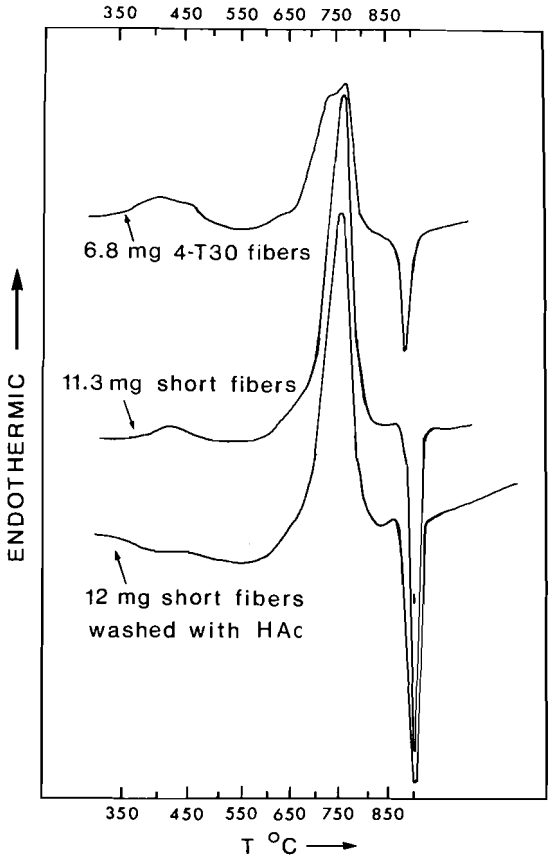

FIG. 7. Differential thermal analysis (DTA) curves for 4-T-30 fibers and short fibers before and after leaching with 25 vol% acetic acid.

adsorption area of 16.2 $(Å)^2$/molecule; data for water adsorption yielded a specific area of 17.6 m^2/g using a molecular area of 10.6 $(Å)^2$/molecule.

The specific area, determined from nitrogen adsorption, lies in the range 5–8 m^2/g for various samples of 4-T-30 fibers, and is 20 m^2/g for the sedimented short fibers. Data on water adsorption by short fibers are illustrated in Fig. 8 and compared with similar results for coarse (4-R) fibers reported by Pidgeon and Van Winsen (37). The fractional weight of sorbed water plotted against the water partial pressure yields typical BET isotherms for both types of fibers, though the short fibers exhibit substantially higher water sorption at high humidity. The origin of this difference is uncertain, but it cannot be attributed to artifacts of the isopiestic method, since Pidgeon and Van Winsen (37) had used the isopiestic and high vacuum techniques with identical results. Possibly, differences in excess brucite contents could also affect the water sorption behavior.

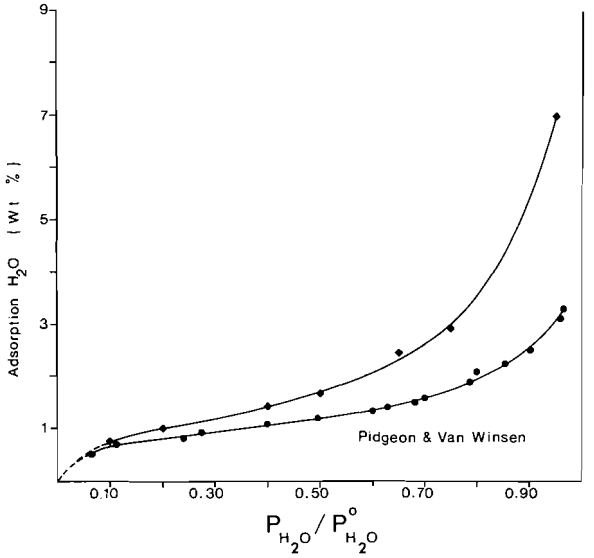

FIG. 8. Water adsorption isotherm of short fibers (25°C) compared with similar data from Pidgeon and Van Winsen (37) for coarse fibers (4-R). ◆, This work, short fibers; ●, Pidgeon and Van Winsen (37).

From the data at low water activity, monolayer coverage of the short fibers occurs at 0.8 ± 0.1 wt%; taking the H_2O molecular area as 10.6 $(Å)^2$, this yields a specific area of 28 m^2/g. Thus, from either nitrogen or water adsorption, the specific area of the sedimented short fibers appears in the upper range of values available for fibers which have not been subjected to extensive mechanical dispersion.

Conclusion

The results of the investigation described here provide a simple means for separating short chrysotile fibers from bulk commercial fibers. The selective sedimentation procedure enables rapid separation of fibers shorter than 2.0 μm, and this can be performed quantitatively by successive sedimentation–separation cycles. While the process may be of potential interest for removal of short fibers from bulk chrysotile materials, the purpose of this work was mainly to (*a*) define separation conditions, (*b*) explain the selective sedimentation behavior, and (*c*) provide some basic physico-chemical characterization of the short fibers separated in this way. Although some aspects could not be elucidated quantitatively (particularly the difficult question of excess $Mg(OH)_2$), it could be demonstrated satisfactorily that the separated short fibers are essentially native chrysotile in a form which is more homogeneous than bulk commercial fibers; in many instances, it should thus be more suitable for

Can. J. Chem. Downloaded from www.nrcresearchpress.com by 210.87.254.5 on 09/06/12
For personal use only.

further physico-chemical, biochemical, or biological investigations.

Acknowledgements

The authors gratefully acknowledge financial support of this research by the "Programme de Recherche sur l'Amiante (PRAUS)" (through Professor J. M. Lalancette) and the "Ministère de l'Education du Québec". The assistance of Marc-André Simard and Renée Hallée with some of the measurements is also acknowledged with pleasure. We also thank Mr. Marcel Cossette for providing the chrysotile samples and helpful advice, and Professor F. Kimmerle for discussion and comments on the manuscript. Finally, the assistance of Dr. R. F. Platford (Canada Center for Inland Waters) in lending the equipment for isopiestic measurements is gratefully acknowledged.

1. P. Bogovski, V. Timbrell, J. C. Gilson, and J. C. Wagner (*Editors*). Biological effects of asbestos. International Agency for Research on Cancer, Lyon. 1973.
2. J. Bignon, A. Depierre, G. Bonnaud, J. Goni, and G. Brouet. Nouv. Presse Med. **2**, 1697 (1973).
3. R. J. Fessenden and J. S. Fessenden. Adv. Drug Res. **4**, 95 (1967).
4. H. E. Whipple. Ann. N.Y. Acad. Sci. **132**, 48 (1965).
5. K. Yada. Acta Crystallogr. A**27**, 659 (1971).
6. B. D. Saksena. Trans. Faraday Soc. **57**, 242 (1961).
7. J. A. Gadsden. *In* Infrared spectra of minerals and related compounds. Butterworths, London. 1975.
8. S. Yariv and L. Heller-Kallai. Clays Miner. **23**, 145 (1972).
9. E. J. Whittaker. Acta Crystallogr. **9**, 855 (1956); **9**, 865 (1956).
10. E. J. Whittaker. Acta Crystallogr. **8**, 571 (1955).
11. J. W. Whittaker. Acta Crystallogr. **6**, 747 (1953).
12. F. L. Pundsack. J. Phys. Chem. **60**, 361 (1956); E. Martinez and J. J. Comer. Am. Miner. **49**, 153 (1964).
13. F. L. Pundsack. J. Phys. Chem. **59**, 892 (1955).
14. A. W. Nauman and W. H. Dresher. Am. Miner. **51**, 711 (1966).
15. G. H. Gorski and L. E. Stettler. Am. Indus. Hygiene Assoc. J. **34**, 345 (1974).
16. G. J. Young and F. H. Healey. J. Phys. Chem. **58**, 881 (1954).
17. A. A. Hodgson. Fibrous silicates. Lecture Series of the Royal Institute of Chemistry, No 4, p. 1–47, European Printing Co., London, 1965.
18. L. Pauling. Proc. Nat. Acad. Sci. U.S. **16**, 578 (1930).
19. E. Martinez. Can. Min. Metal. Bull. **69**, 414 (1966); A. W. Nauman and W. H. Dresher. Am. Min. **51**, 1200 (1966); A. M. Harris. Physics and chemistry of asbestos minerals. 2nd Int. Conf., Louvain 1971, paper 3:2A.
20. C. Jolicoeur and D. Duchesne. Can. J. Chem. To be published.
21. A. M. Mironov and N. V. Churaev. Coll. J. USSR, Engl. Trans. **29**, 106 (1967).
22. N. H. Furman (*Editor*). Standard methods of chemical analysis. Vol. 1. 6th ed. Van Nostrand, New York. 1962.
23. R. J. Atkinson. J. Coll. Interface Sci. **42**, 624 (1973).
24. B. Nagy and T. F. Bates. Am. Miner. **37**, 1055 (1952); A. Hargreaves and W. H. Taylor. Mineral. Mag. **27**, 204 (1946).
25. R. A. Robinson and R. H. Stokes. Electrolyte solutions. Butterworths, London. 1959.
26. R. F. Platford. Activity coefficients in electrolyte solutions. R. M. Pytkowicz (*Editor*). CRC Press, Vol. 1. 1979. p. 65.
27. A. W. Naumann and W. H. Dresher. J. Coll. Interface Sci. **27**, 133 (1968).
28. E. Martinez and G. L. Zucker. J. Phys. Chem. **64**, 927 (1960).
29. A. S. Michaels and J. C. Bolger. Ind. Eng. Chem. Fundam. **1**, 24 (1962).
30. I. Choi and R. W. Smith. J. Coll. Interface Sci. **40**, 253 (1972) and references cited therein.
31. Powder Diffraction File. American Society for Testing and Materials, Baltimore. September, 1963.
32. J. S. Harington. Ann. N.Y. Acad. Sci. **132**, 31 (1965).
33. G. L. Kalousek and L. E. Muttart. J. Mineral. Soc. Am. **42**, 1 (1957).
34. N. J. Page and R. G. Coleman. U.S. Geol. Survey Res. **575**-B, B103 (1967).
35. R. Gaze. Ann. N.Y. Acad. Sci. **132**, 23 (1965).
36. S. Chowdhury. Ph.D. Thesis. Royal School of Mines, Imperial College, London. 1972.
37. L. M. Pidgeon and A. Van Winsen. Can. J. Res. **10**, 1 (1934); **9**, 155 (1933).
38. G. H. Gorski and L. E. Stettler. Am. Indus. Hygiene Ass. J. **36**, 292 (1975).
39. Chrysotile Asbestos Test Manual. 3rd ed. 1974 (Revised 1978), Asbestos Textile Institute Inc. and Quebec Asbestos Mining Association.

Can. J. Chem. Downloaded from www.nrcresearchpress.com by 210.87.254.5 on 09/06/12
For personal use only.

Crystal structures of racemic and optically active 4,4′-dimethyl-1,1′-binaphthyl

RICHARD A. PAUPTIT AND JAMES TROTTER

Department of Chemistry, University of British Columbia, Vancouver, B.C., Canada V6T 1Y6

Received August 14, 1980

RICHARD A. PAUPTIT and JAMES TROTTER. Can. J. Chem. **59**, 1149 (1981).

The structures of the title compounds were determined to aid in understanding spontaneous resolution in binaphthyl derivatives. Crystals of the racemate, $C_{22}H_{18}$, are monoclinic, $C2/c$, $a = 13.225(8)$, $b = 10.768(4)$, $c = 11.572(7)$ Å, $\beta = 114.04(2)°$, $Z = 4$. The structure was solved by direct methods and refined to $R = 0.074$ for 886 reflections with $I \geq 3\sigma(I)$. The crystals of the optically active form are tetragonal, $P4_12_12$ or $P4_32_12$, $a = 8.3031(8)$, $c = 23.706(7)$ Å, $Z = 4$. This structure was also solved by direct methods and refined to $R = 0.060$ for 723 reflections with $I \geq 3\sigma(I)$.

RICHARD A. PAUPTIT et JAMES TROTTER. Can. J. Chem. **59**, 1149 (1981).

Les structures des composés du titre ont été déterminées pour aider la compréhension du dédoublement spontané dans les derivatives de binaphthyle. Les cristaux racémiques, $C_{22}H_{18}$, sont monocliniques, $C2/c$, $a = 13.225(8)$, $b = 10.768(4)$, $c = 11.572(7)$ Å, $\beta = 114.04(2)°$, $Z = 4$. On a déterminé la structure par les méthodes directes et l'a affinée jusqu'à une valeur de $R = 0.074$ pour 886 réflexions avec $I \geq 3\sigma(I)$. Les cristaux des antipodes optiques sont tetragonals, $P4_12_12$ ou $P4_32_12$, $a = 8.3031(8)$, $c = 23.706(7)$ Å, $Z = 4$. Cette structure a été déterminée aussi par les méthodes directes, et on l'a affinée jusqu'à une valeur de $R = 0.060$ pour 723 réflexions avec $I \geq 3\sigma(I)$.

Introduction

In contrast to 1,1′-binaphthyl (1–4), racemic 4,4′-dimethyl-1,1′-binaphthyl does not undergo spontaneous resolution upon heating from room temperature to just below the melting point (5). Optically active dimethylbinaphthyl may be obtained by seeding the racemic melt with optically active naphthidine (6). The crystal structures of both the racemic and optically active dimethylbinaphthyls were investigated in the hope of understanding these observations.

Experimental

The data for both crystals, prepared by Pincock *et al.* (6), were collected on a Datex-automated GE XRD-6 diffractometer with CuKα radiation by use of a θ–2θ scan technique. The 2θ scan was performed at 4 deg min^{-1} over a range of $(1.80 + 0.86 \tan\theta)°$ with 10 s background counts at each end of the scan.

I. Racemate

Crystal data are as follows:

$C_{22}H_{18}$, mp = 145°C fw = 282.4

Monoclinic, $C2/c$, $a = 13.225(8)$, $b = 10.768(4)$, $c = 11.572(7)$ Å, $\beta = 114.04(2)°$. $V = 1505(1)$ Å^3, $Z = 4$, $\rho_c = 1.246(1)$ g cm^{-3}.

The intensity of one check reflection was measured every 50 reflections. The first data collection showed large variations in the check reflection count (due to electronic difficulties) and although the structure was solved with this data set, another set of data was collected for the refinement. In this set the check reflection counts were used to scale the data, and 886 out of the 1497 unique reflections in the range $0 < \theta \leq 60°$ had $I/\sigma(I) \geq 3.0$, where $\sigma^2(I) = S + B + (0.06S)^2$ and S and B are the scan and background counts, respectively, and were considered observed. Lorentz and polarization corrections were applied.

The structure was solved by direct methods; the E-map revealed all 11 carbon atoms. After three isotropic and two anisotropic full-matrix least-squares refinement cycles, all but one of the hydrogens could be located on a difference map; the remaining hydrogen was placed in a calculated position. Three more refinement cycles with unit weights followed by four cycles with a polynomial weighting scheme (7) reduced R and R_w to their final values of 0.078 and 0.074, respectively. The coefficients for the polynomial weighting scheme were adjusted after every cycle and had final values $a = -0.0079$, $b = 0.08165$, $c = -0.01791$, $d = 0.001391$. The scattering factors of ref. 8 were used for the carbon atoms and those of ref. 9 for the hydrogen atoms in both structure determinations.

II. Optically Active Form

Crystal data are as follows:

$C_{22}H_{18}$, mp 158°C fw = 282.4

Tetragonal, $P4_12_12$ or $P4_32_12$, $a = 8.3031(8)$, $c = 23.706(7)$ Å, $V = 1634.3(5)$ Å^3, $Z = 4$, $\rho_c = 1.1478$ g cm^{-3}.

The intensity of a check reflection measured every 50 reflections showed very little variation and no data scaling was required. 723 out of 1117 unique reflections in the range $0 < \theta \leq 80°$ had $I/\sigma(I) \geq 3.0$.

The structure was solved by direct methods, and again the E-map revealed the positions of all 11 carbon atoms. After three isotropic and three anisotropic full-matrix least-squares refinement cycles, a difference map was calculated, but the position of only one methyl hydrogen was used and all other hydrogens were placed in calculated positions. Several more refinement cycles with use of a weighting scheme where $w = 1/\{1 + [(|F_o| - F^*)/G^*]^2\}$, $F^* = 6.0$, $G^* = 15.0$, reduced R to its final value of 0.060. Attempts at determining the absolute configuration by inclusion of the small anomalous dispersion effects were unsuccesful.

The atomic positional parameters for the two structures are presented in Table 1.[1]

Results and Discussion

Figure 1 shows the molecular drawings and numbering schemes for both molecules. The asym-

[1]Thermal parameters, mean planes, bond lengths and angles involving hydrogen atoms, and the structure factor table for both structures are available, at a nominal charge, from the Depository of Unpublished Data, CISTI, National Research Council of Canada, Ottawa, Ont., Canada K1A 0S2.

0008-4042/81/071149-04$01.00/0

©1981 National Research Council of Canada/Conseil national de recherches du Canada

Can. J. Chem. Downloaded from www.nrcresearchpress.com by 210.87.254.105 on 09/06/12
For personal use only.

Can. J. Chem. Downloaded from www.nrcresearchpress.com by 210.87.254.105 on 09/06/12
For personal use only.

TABLE 1. Fractional atomic parameters (C × 10^4, H × 10^3) with their standard deviations

	Racemate			Optically active form		
Atom	*x/a*	*y/b*	*z/c*	*x/a*	*y/b*	*z/c*
C(1)	4386(2)	2978(2)	2296(2)	951(5)	271(5)	2401(2)
C(2)	3898(2)	2039(2)	2686(2)	2489(6)	276(7)	2618(2)
C(3)	2745(2)	1996(2)	2343(2)	3641(6)	1444(9)	2431(2)
C(4)	2056(2)	2886(2)	1586(2)	3269(6)	2563(7)	2035(2)
C(5)	1834(2)	4747(2)	229(2)	1250(8)	3696(7)	1371(2)
C(6)	2277(2)	5637(3)	− 269(2)	− 243(8)	3636(9)	1130(3)
C(7)	3428(2)	5685(3)	83(2)	−1377(7)	2577(8)	1325(2)
C(8)	4112(2)	4838(2)	921(2)	−1014(6)	1493(6)	1742(2)
C(9)	3681(2)	3892(2)	1449(2)	525(5)	1450(6)	1988(2)
C(10)	2513(2)	3844(2)	1087(2)	1690(5)	2604(6)	1795(2)
C(11)	833(2)	2843(3)	1278(3)	4538(10)	3740(13)	1836(4)
H(2)	434(2)	136(2)	322(3)	271(5)	− 57(5)	291(2)
H(3)	243(2)	133(3)	270(3)	485(6)	118(5)	262(2)
H(5)	98(3)	470(3)	− 4(3)	206(7)	434(7)	121(2)
H(6)	176(2)	626(3)	− 88(3)	− 42(7)	435(7)	81(2)
H(7)	375(3)	632(3)	− 26(3)	−254(8)	259(7)	121(2)
H(8)	494(3)	492(2)	114(3)	−177(7)	86(6)	185(2)
H(111)	37(3)	266(3)	34(3)	482(8)	339(8)	139(3)
H(112)	52(2)	367(3)	144(3)	562(8)	341(8)	201(3)
H(113)	68(3)	223(3)	178(4)	408(9)	470(7)	192(3)

metric unit is one half the molecule; in each case the other half is generated by rotation about a twofold axis which bisects the C(1)—C(1′) bond. The naphthalene residues are *cis*-oriented in both molecules with a dihedral angle of 68.4° in the racemate and 80° in the optically active form.

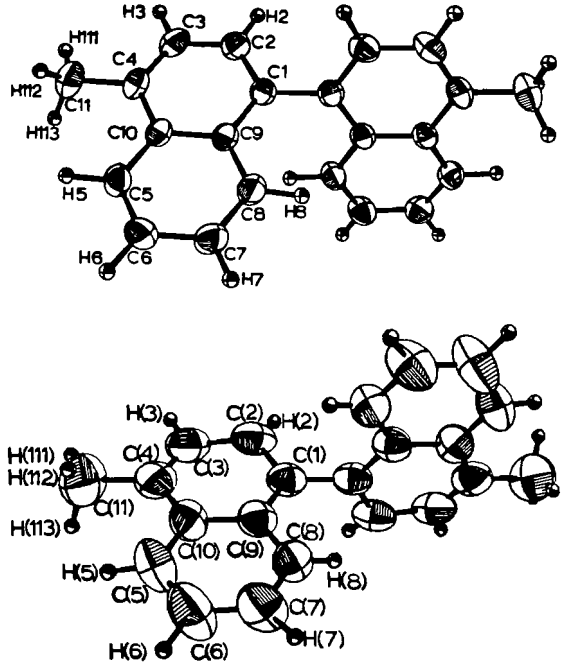

FIG. 1. Molecular views of the racemate (above) and the optically active form (below) showing 50% thermal ellipsoids.

Mean plane calculations[1] show that there is a slight bend in the asymmetric unit along the C(9)—C(10) bond: 3.1° in the racemate and 2.7° in the optically active form. For a similar distortion of 1° in 1,1′-binaphthyl the close contacts between the two halves of the molecule, e.g. C(8)...C(8′), have been suggested as possible reasons for this bending (10), but in the dimethyl compounds these contacts seem slightly too large for such an argument (e.g. C(8)...C(8′) is 3.45, 3.63, and 3.32 Å and C(9)...C(9′) is 3.34, 3.36, and 3.27 Å in the racemate, optically active form, and 1,1′-binaphthyl, respectively). At any rate, there appears to be no correlation between the proximity of these contacts and the degree of bending.

Bond lengths and angles with their standard deviations are listed in Table 2[1] and have normal values.

Packing diagrams for both compounds are shown in Fig. 2. The racemate consists of alternating layers of *R* and *S* molecules parallel to the (001) planes. Within each layer all molecules have the same orientation with respect to the crystal axes, i.e. there are only two orientations (which are enantiomorphic) with which a molecule might add to the lattice during crystallization. The optically active form packs with four orientations of molecules spiralling around a fourfold screw-axis, giving rise to quite an elongated (along *c*) unit cell. The two packing modes seem quite different.

The racemate is somewhat denser (1.25 vs. 1.15 g cm^{-3}) and hence more tightly packed and probably

Can. J. Chem. Downloaded from www.nrcresearchpress.com by 210.87.254.105 on 09/06/12
For personal use only.

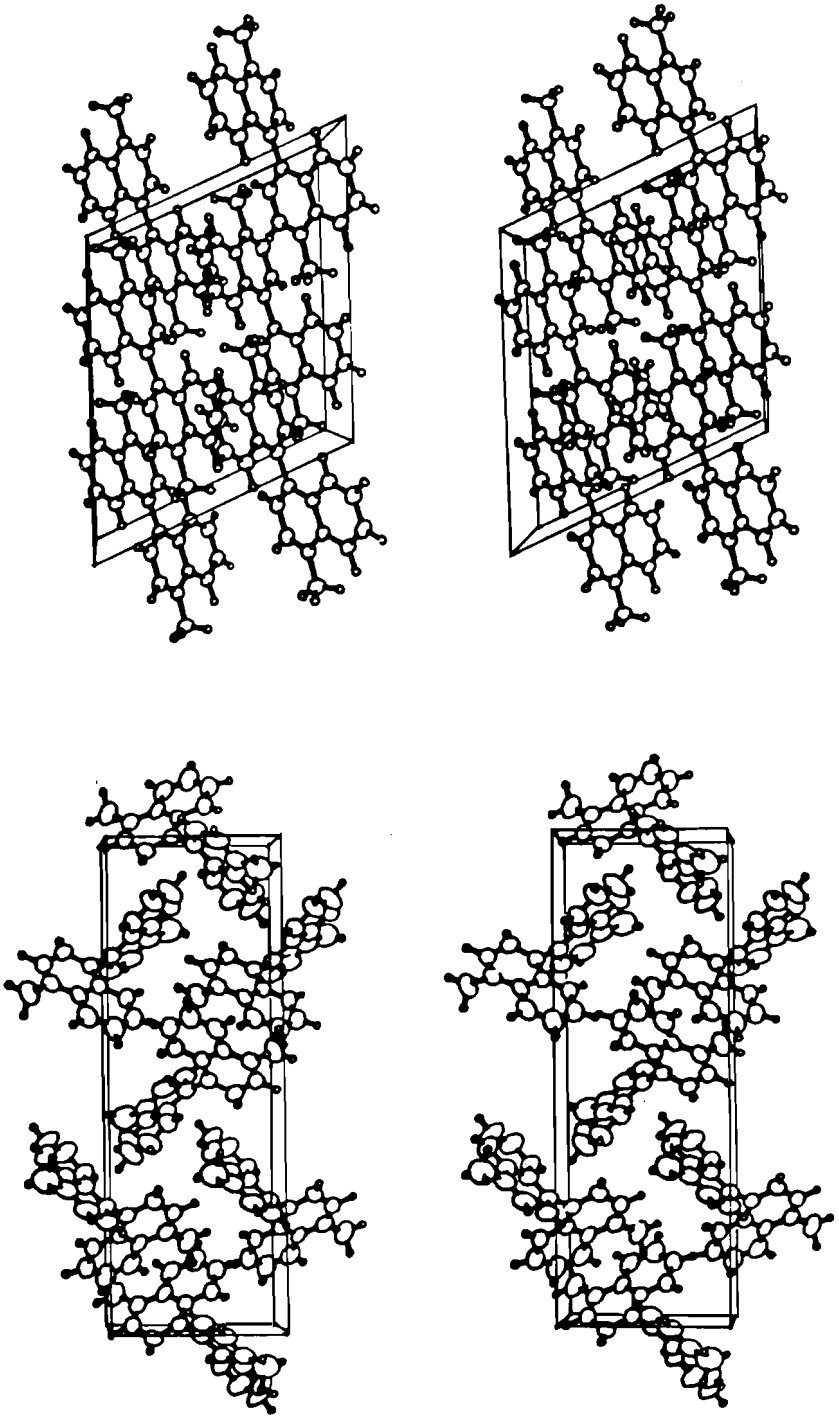

FIG. 2. Packing diagrams of the racemate (above) and the optically active form (below).

with a slightly greater lattice energy, i.e. more stable in the solid state than the optically active form. This might explain why the racemate does not undergo spontaneous resolution upon heating, but it offers no reasons for differences in behaviour between the methylated compounds and 1,1′-binaphthyl.

These results will be compared to the crystal structures of optically active naphthidine and 1,1′-binaphthyl in another paper (11).

TABLE 2. Bond lengths and angles of racemic and optically active dimethylbinaphthyl

Bond	Length (Å) Racemic	Optically active
C(1)—C(2)	1.371(3)	1.377(6)
C(1)—C(9)	1.433(3)	1.429(5)
C(1)—C(1′)	1.495(4)	1.510(8)
C(2)—C(3)	1.411(3)	1.432(8)
C(3)—C(4)	1.367(3)	1.357(7)
C(4)—C(10)	1.432(3)	1.429(6)
C(4)—C(11)	1.509(3)	1.512(8)
C(5)—C(6)	1.367(4)	1.366(8)
C(5)—C(10)	1.418(3)	1.402(7)
C(6)—C(7)	1.408(4)	1.369(8)
C(7)—C(8)	1.369(4)	1.371(7)
C(8)—C(9)	1.422(3)	1.405(6)
C(9)—C(10)	1.426(3)	1.436(6)

Bonds	Angle (deg) Racemic	Optically active
C(9)—C(1)—C(2)	118.0(2)	118.9(4)
C(1′)—C(1)—C(2)	119.5(2)	120.6(4)
C(1′)—C(1)—C(9)	122.4(2)	120.5(3)
C(1)—C(2)—C(3)	122.1(2)	120.4(5)
C(2)—C(3)—C(4)	121.3(2)	121.8(5)
C(3)—C(4)—C(11)	120.0(2)	120.0(6)
C(3)—C(4)—C(10)	118.9(2)	120.0(5)
C(10)—C(4)—C(11)	121.0(2)	120.0(6)
C(10)—C(5)—C(6)	121.2(2)	120.8(5)
C(5)—C(6)—C(7)	120.1(2)	120.5(6)
C(6)—C(7)—C(8)	120.4(2)	120.9(5)
C(7)—C(8)—C(9)	121.1(2)	121.1(5)
C(8)—C(9)—C(10)	118.3(2)	117.7(4)
C(8)—C(9)—C(1)	121.5(2)	121.6(3)
C(1)—C(9)—C(10)	120.1(2)	120.6(4)
C(9)—C(10)—C(4)	119.5(2)	118.4(4)
C(9)—C(10)—C(5)	118.9(2)	119.0(4)
C(4)—C(10)—C(5)	121.7(2)	122.6(5)

Can. J. Chem. Downloaded from www.nrcresearchpress.com by 210.87.254.105 on 09/06/12
For personal use only.

Acknowledgements

We thank the Natural Sciences and Engineering Research Council Canada and the Natural, Applied, and Health Sciences Committee, University of British Columbia, for financial support, the University of British Columbia Computing Centre for assistance, and Dr. R. E. Pincock for crystals and helpful discussion.

1. R. E. PINCOCK and K. R. WILSON. J. Chem. Ed. **50**, 455 (1973).
2. R. E. PINCOCK, R. P. BRADSHAW, and R. R. PERKINS. J. Mol. Evol. **4**, 67 (1974).
3. R. E. PINCOCK and K. R. WILSON. J. Am. Chem. Soc. **97**, 1474 (1975).
4. R. E. PINCOCK and K. R. WILSON. Can. J. Chem. **55**, 889 (1977).
5. J. SANDERS. B.Sc. Thesis, University of British Columbia, Vancouver, B.C. 1971.
6. R. E. PINCOCK, M. D. LU, and F.-N. FUNG. To be published.
7. D. W. J. CRUICKSHANK. *In* Computing methods in crystallography. *Edited by* J. S. Rollett. Pergamon Press. 1965.
8. D. T. CROMER and J. B. MANN. Acta Crystallogr. A**24**, 321 (1968).
9. R. F. STEWART, E. R. DAVIDSON, and W. T. SIMPSON. J. Chem. Phys. **42**, 3175 (1965).
10. K. A. KERR and J. M. ROBERTSON. J. Chem. Soc. B, 1146 (1969).
11. R. A. PAUPTIT and J. TROTTER. To be published.

Determination of absolute transfer free energies of hydroxyl ion from water to aqueous 2-methoxy ethanol

ABHIJIT BHATTACHARYA, ASIM K. DAS, AND KIRON K. KUNDU[1]

Physical Chemistry Laboratories, Jadavpur University, Calcutta–700 032, India

Received April 9, 1980

ABHIJIT BHATTACHARYA, ASIM K. DAS, and KIRON K. KUNDU. Can. J. Chem. **59**, 1153 (1981).

Absolute standard free energies of transfer ΔG_t^0 of OH^- from water to aqueous mixtures of 2-methoxy ethanol (ME) have been evaluated at 298.15 K by combining the apparent transfer free energies of the lyate ion that were obtained from the standard emf's of the double cell:

Hg–HgO/KOH(m), solvent/K(Hg)/KOH(m) water/HgO–Hg

and that from the autoionization constants of these mixed solvents determined by use of the cell comprising H_2– and Ag–AgCl electrodes. The required ΔG_t^0 values of K^+ and H^+ were determined earlier using the well-known tetraphenyl arsonium tetraphenyl boride (TATB) reference electrolyte method. These values and their non-Born type contributions in particular, are found to be increasingly positive in water-rich compositions, indicating that the relative stabilization of OH^- and the acidity of the mixed solvents decrease with increasing cosolvent composition. These, when compared with those in aqueous mixtures of ethylene glycol and 1,2-dimethoxy ethane, are found to lie intermediate between the latter solvent systems conforming to what is expected from the structural and electronic features of the cosolvents.

ABHIJIT BHATTACHARYA, ASIM K. DAS et KIRON K. KUNDU. Can. J. Chem. **59**, 1153 (1981).

On a évalué, à 298,15 K, les énergies standards absolues de transfert, ΔG_t^0, de l'ion OH^- à partir de l'eau jusqu'à des mélanges aqueux de méthoxy-2 éthanol (ME) en combinant les énergies libres apparentes de transfert de l'ion lyate obtenues à partir des fem standard de la double cellule:

Hg–HgO/KOH(m), solvant/K(Hg)/KOH(m) eau/HgO–Hg

et à partir des constantes d'auto-ionisation de ces solvants mixtes déterminés en utilisant une cellule formée d'électrodes H_2– et Ag–AgCl. Les valeurs nécessaires de ΔG_t^0 pour K^+ et H^+ ont été déterminées antérieurement en utilisant la méthode électrolytique de référence bien connue du tétraphényl arsonium borure de tétraphényle (TABT). On a trouvé que ces valeurs ainsi que leurs contributions de types différents de ceux prévues par Born sont de plus en plus positives dans des compositions riches en eau, indiquant ainsi que la stabilisation relative du OH^- et l'acidité des solvants mixtes décroîssent lorsque la composition du co-solvant augmente. Lorsqu'on compare ces valeurs à celles des mélanges aqueux d'éthylèneglycol et de diméthoxy-1,2 éthane, on trouve qu'elles se situent à un point intermédiaire entre celles des derniers systèmes de solvant, conformément à ce qu'on attend compte tenu des caractéristiques structurales et électroniques des co-solvants.

[Traduit par le journal]

Introduction

The knowledge of solvation behaviour of OH^- is an important prerequisite to the understanding of solvent effects on the rates of base-catalyzed reactions or equilibria involving OH^-. This is particularly true in the cases of dipolar aprotic solvents which usually cause dramatic enhancement of the rates of OH^--catalyzed reactions, H_--acidity function, and the proton transfer equilibria involving OH^- (1–6). Although all these effects are usually attributed to the well recognized "desolvation" and the accompanying enhancement of the OH^- activity caused by dipolar aprotic solvents (1–6), the thermodynamic basis of these are yet to be resolved in many cases.

It is well known that the usual source of transfer free energies ΔG_t^0, of OH^-_{app} or OH^- from water to the aquo-organic (protic as well as dipolar aprotic) solvents is the autoionization constants (K_s) of the mixed solvents (7–9) or the apparent ionization constants $(K_a)_{app}$ of water in the mixed solvents, which help determine ΔG_t^0 of $[H^+(OH^-)_{app}]$. Consider an H_2O + ROH solvent system, where ROH is a protic cosolvent. The autoionization of the aqueous mixtures of this cosolvent may be presented by the general expression [1]

$$[1] \quad SOH(s) + SOH(s) \rightleftharpoons SOH_2^+(s) + SO^-(s)$$

where SOH is a solvent molecule in the mixed solvents being either water or the cosolvent, and SOH_2^+ and SO^- are the lyonium and lyate ions, respectively, and (s) denotes that the species are in the standard state in the respective mixed solvent. In pure water the corresponding ionization process can be represented as

$$[2] \quad H_2O(w) + H_2O(w) \rightleftharpoons H_3O^+(w) + OH^-(w)$$

[1]To whom all correspondence should be addressed.

0008-4042/81/071153-07$01.00/0

©1981 National Research Council of Canada/Conseil national de recherches du Canada

Can. J. Chem. Downloaded from www.nrcresearchpress.com by 210.87.254.40 on 09/06/12
For personal use only.

Can. J. Chem. Downloaded from www.nrcresearchpress.com by 210.87.254.40 on 09/06/12
For personal use only.

where (w) denotes that the species are in the standard state in pure water. Consequently, the standard free energy change $\delta(\Delta G^0)$ accompanying the ionization of the components of the mixed solvents relative to that of water i.e. of the process [3]

[3] $H_3O^+(w) + SOH(s) + SOH(s) + OH^-(w) \rightleftharpoons H_2O(w) + SOH_2^+(s) + SO^-(s) + H_2O(w)$

which is equivalent to the sum of the free energy changes of the processes [4] and [5]:

[4] $H_3O^+(w) + SOH(s) \rightleftharpoons H_2O(w) + SOH_2^+(s)$

[5] $SOH(s) + OH^-(w) \rightleftharpoons SO^-(s) + H_2O(w)$

If we denote the free changes due to the processes [4] and [5] by $\Delta G_t^0(H^+)$ and $\Delta G_t^0(OH^-)_{app}$ respectively, it follows that

[6] $\delta(\Delta G^0) = \Delta G_t^0(H^+) + \Delta G_t^0(OH^-)_{app}$

If $\Delta G_t^0(H^+)$ is known for the system, $\Delta G_t^0(OH^-)_{app}$ could be evaluated. But $\Delta G_t^0(OH^-)_{app}$ being a composite quantity, estimation of the absolute free energies of transfer of OH^-, $\Delta G_t^0(OH^-)$ i.e. of the process [7]

[7] $OH^-(w) \rightarrow OH^-(s)$

is difficult, especially for cosolvents whose acidity is comparable to that of water. Consequently, auxiliary measurements are in order.

Another possible source of transfer free energy of OH^- in these mixed solvents is the study of emf's of suitable cells (say, cell A) containing Hg–HgO electrode – the well known OH^- reversible electrode.

[A] Hg–HgO/KOH(m), solvent/K(Hg)/KOH(m), water/HgO–Hg

The free change $\Delta G^0_{\text{cell A}}$, accompanying the overall reaction of the double cell A:

[8] $2K^+(s) + OH^-(s) + SO^-(s) + H_2O(w) = 2K^+(w) + 2OH^-(w) + SOH(s)$

as computable from the standard emf (ΔE^0) of the double cell [A] will be related as follows:

[9] $\Delta G^0_{\text{cell A}} = -2F[\Delta E^0]$

where F = Faraday. Also, from reaction [8] it follows that

[10] $\Delta G^0_{\text{cell A}} = -2\Delta G_t^0(K^+) - \Delta G_t^0(OH^-)'_{app}$

where $\Delta G_t^0(OH^-)'_{app}$ is the free energy change accompanying the process [11]

[11] $2OH^-(w) + SOH(s) \rightleftharpoons SO^-(s) + OH^-(s) + H_2O(w)$

Again, if $\Delta G_t^0(K^+)$ values are known, $\Delta G_t^0(OH^-)'_{app}$ could be evaluated. Moreover, since $\Delta G_t^0(OH^-)'_{app}$ and $\Delta G_t^0(OH^-)_{app}$ are related as follows

[12] $\Delta G_t^0(OH^-)'_{app} = \Delta G_t^0(OH^-)_{app} + \Delta G_t^0(OH^-)$

$\Delta G_t^0(OH^-)$ can be estimated, if $\Delta G_t^0(OH^-)_{app}$ is obtained from the studies of autoionization of the solvents, as indicated above. Thus it appears that the combination of the data obtainable from the studies of autoionization as well as of the cell [A], offers, for the first time, a suitable method for determining absolute transfer free energies of OH^-, $\Delta G_t^0(OH^-)$, provided ΔG_t^0 values of H^+ and K^+ are determined by use of a suitable extra-thermodynamic assumption (11, 12).

In the aqueous solutions of dipolar aprotic cosolvents, however, since SOH(s) and SO^-(s) are in fact HOH(s) and HO^-(s) respectively, it follows from eqs. [5] and [11] that

[13] $\Delta G_t^0(OH^-)_{app} = \Delta G_t^0(OH^-) - \Delta G_t^0(H_2O) = \Delta G_t^0(OH^-) + RT \ln a_w^s$

and

[14] $\Delta G_t^0(OH^-)_{app} = 2\Delta G_t^0(OH^-) - \Delta G_t^0(H_2O) = 2\Delta G_t^0(OH^-) + RT \ln a_w^s$

where a_w^s is the activity of water in the mixed solvents referred to pure water as the standard state. Thus, if a_w^s is known for the system, either autoionization constants or the ΔE^0's of the cell A would yield $\Delta G_t^0(OH^-)$. In addition to this, if $\Delta G_t^0(OH)$ is known from the combined results of both sets of measurements. eqs. [13] or [14] would provide a method for determining a_w^s in these mixed solvents.

Now, it is often observed that determination of the primary thermodynamic quantity viz. autoionization constant of water by use of suitable galvanic cells comprising either H_2 and Ag–AgCl electrodes or less preferable glass and calomel/Ag–AgCl electrodes proves difficult, especially at higher compositions of some dipolar aprotic cosolvents. Consequently, the use of cell A or the like is likely to serve as a suitable method for determining $\Delta G_t^0(OH^-)$, provided a_w^s values are known for such solvent systems.

The object of the present paper is to demonstrate the suitability of cell A or the like for evolving ΔG_t^0 values of $(OH^-)'_{app}$ in aqueous mixtures of an organic cosolvent, the nature of which lies in the borderlines of protic and dipolar aprotic characters. One such cosolvent is 2-methoxy ethanol (ME), commonly known as methyl cellosolve (MCS). Although it is basically a protic solvent, the inductive effect of methyl group is likely to facilitate intramolecular hydrogen bonding thus imparting some aprotic character to the molecule. Con-

Can. J. Chem. Downloaded from www.nrcresearchpress.com by 210.87.254.40 on 09/06/12
For personal use only.

sequently, the behaviour of cell A or the like in this solvent system, it is hoped, will be indicative of the suitability of its potential use in some aqueous dipolar aprotic solvents. Moreover, since it is a protic solvent, it is also expected that the autoionization constant of water could be easily determined by use of suitable cells referred to above. In fact, Wooley *et al.* (10*a*) have already reported the apparent ionization constant $(K_a)_{app}$ of water in this solvent system up to 65 wt% cosolvent, but by use of glass and Ag–AgCl electrodes. However, as Smits *et al.*'s (13) ΔG_t^0(HCl) values based on glass and Ag–AgCl electrodes are found to differ appreciably from those of Sadek *et al.* (14) based on H_2 and Ag–AgCl electrodes, and as similar differences are quite usual for dipolar aprotic cosolvent systems (13) we have considered it useful to determine the autoionization constant (K_s) of these solvents by use of H_2 and Ag–AgCl electrodes. Thus, in this paper we are reporting ΔG_t^0 values of $[K^+(OH^-)'_{app}]$ as well as $[H^+(OH^-)_{app}]$ in aqueous mixtures of 10, 30, 50, and 70 wt% ME as obtained by determining respectively the standard emf (ΔE^0) of the double cell A and the autoionization constants (K_s) of these mixed solvents by use of cell B

[B] H_2(g,1 atm)/KOH(m_1)KCl(m_2), solvent/AgCl–Ag

Experimental

2-Methoxy ethanol (Merck, Pure) was purified in a manner described earlier (14, 15); water used for the preparation of the mixed solvents and the electrolyte solutions was distilled thrice and made free from CO_2 and O_2 first by boiling and then by flushing pure H_2. For the studies of cell A the concentrations of the stock solutions of KOH (Merck, G.R.) were determined by standard HCl solution using phenolphthalein as indicator. Solutions of different molalities of KOH were prepared by weight dilution. As before (16), to avoid the effects of corrosion of K(Hg) the concentrations of KOH solutions used were kept above 0.02 *m*. All the manipulations and handling of the solutions were done in a chamber flushed with N_2, so as to avoid the exposure of the solutions to atmosphere as far as possible.

The methods of purification of mercury and preparation of potassium amalgam, [K(Hg)] have been described (16, 17). The amalgam reservoir and the cell design were also similar to those described earlier (17, 18).

Hg–HgO electrode consists of a j-shaped glass tube fitted with a B-19 standard joint at the upper end of the larger limb which allows placing of the electrode in the amalgam cell. The shorter limb is separated from the longer limb by a glass seal and connected electrically through a Pt-wire fused through the glass seal. The open end of the shorter limb, called the "cup" of the electrode and serving as the holder of the electrode materials, was dipped into the cell solutions. In the "cup" a small portion of triple distilled Hg was first introduced, then a paste of triturated mixture of Hg and HgO, formed by adding the respective cell solutions, was added to cover up the free surface of Hg in the "cup". Before using the HgO (red variety, Merck, G.R.) was pretreated (19) by thoroughly washing with hot water, filtering and then drying *in vacuo*. It has been observed that the asymmetry potential was reduced practically within the range of experimental uncertainty of ±0.5 mV, when a thick layer of HgO-paste was used. The electrodes were kept overnight in the respective solutions in a specially designed closed container for the attainment of equilibrium in the mixed solvents, although in aqueous solutions ageing for 2 h proved sufficient. Adequate care was taken to remove the air film often formed at the paste–solution interface, particularly in aqueous solutions. Fresh pairs of electrodes were used for each set of the cell solutions.

All studies were made at 298.15 K. Completely O_2-free atmosphere was maintained by passing pure H_2 gas through the cell solutions. The H_2 gas was presaturated with the respective solvent vapour by passing it through a train of gas saturator containing the respective cell solutions. The general experimental procedure was essentially similar to that described earlier (16, 17). Electromotive force measurements were made with the help of a Leeds and Northrup K_4-potentiometer along with a moving-coil galvanometer (Cambridge Inst. Co.) as a null point detector. Constancy of emf values within ±0.2 mV between three successive emf readings taken at 10 min intervals was taken as the criterion of equilibrium.

For the studies of cell B, the experimental set up and procedures adopted were exactly similar to those described earlier (8).

Results

Cell [A]

The observed emf's (ΔE) of cell A for different molalities (m) of KOH in each of the mixed solvents are given in Table 1. These values in each solvent mixture were used to construct an extrapolation function (17) given by eq. [15]

$$[15]\quad \Delta E' = \Delta E - 2k'[{}_sf(m) - {}_wf(m)_-] = \Delta E^0 - 2k'({}_sb - {}_wb)m$$

where

$$f(m) = -A_0B_0m^{1/2}(1 + a_0B_0m^{1/2})^{-1} - \ln(1 + 0.002\,Mm)$$

subscripts s and w indicate the mixed solvent and water respectively, $k' = RT/F$, M = molar or mean molar mass of water or of the mixed solvents respectively, a_0 is the ion-size parameter, A_0B_0 and B_0 are the familiar Debye-Hückel constants (14, 15), values of which for this solvent system were taken from a previous paper (15), and b is the empirical constant depending upon the nature of the solvent, temperature, and also the ion-size parameter used for computing $f(m)$. As in earlier studies (15, 17), since alteration of a_0 values does not impart any significant change in the extrapolated values of ΔE^0 beyond experimental error of ±0.5 mV, $a_0 = 0$ has been used. As the $\Delta E'$ function in each case was found fairly linear against mol kg^{-1} (m) of KOH solution, ΔE^0 was found by extrapolating the plots of $\Delta E'$ against m to $m = 0$. The values so obtained are presented in Table 1. The corresponding values when obtained by least squares agree within the experimental error and the

Can. J. Chem. Downloaded from www.nrcresearchpress.com by 210.87.254.40 on 09/06/12
For personal use only.

TABLE 1. Electromotive force (ΔE) in volt of cell [A] in ME + water mixtures at 298.15 K

10 wt% ME		30 wt% ME		50 wt% ME		70 wt% ME	
m/mol kg^{-1}	ΔE	m/mol kg^{-1}	ΔE	m/mol kg^{-1}	ΔE	m/mol kg^{-1}	ΔE
0.1504	0.0120	0.1323	0.0409	0.1481	0.0795	0.1500	0.1146
0.1259	0.0128	0.1155	0.0424	0.1227	0.0807	0.1228	0.1175
0.1003	0.0132	0.0856	0.0448	0.1007	0.0832	0.0996	0.1210
0.0755	0.0143	0.0644	0.0462	0.0752	0.0841	0.0762	0.1221
0.0514	0.0146	0.0524	0.0470	0.0526	0.0848	0.0528	0.1248
0.0247	0.0161	0.0216	0.0481	0.0276	0.0856	0.0246	0.1259
$\Delta E^0 = 0.0159$ V		$\Delta E^0 = 0.0472$ V		$\Delta E^0 = 0.0800$ V		$\Delta E^0 = 0.1107$ V	

average standard deviation lies well within the same limits.

Following the arguments cited earlier (see Introduction), standard free energy changes accompanying the overall reaction of cell A, $\Delta G^0_{\text{cell A}}$ were computed on mole fraction scale (20) by using eq. [16]

$$[16] \quad -\Delta G^0_{\text{cell A}} = 2\Delta G_t{}^0(\text{K}^+) + \Delta G_t{}^0(\text{OH}^-)'_{\text{app}} = 2F\Delta E^0 - 4RT \ln M_s/M_w$$

Since $\Delta G_t{}^0(\text{K}^+)$ values for this solvent system are known from a previous measurement (15) based on the most widely used tetraphenylarsonium tetraphenylboride (TATB) reference electrolyte assumption (11, 12), eq. [16] helped yield the values of $\Delta G_t{}^0(\text{OH}^-)'_{\text{app}}$. All these values are presented in Table 3.

Cell [B]

The observed emf's E (corrected to $p_{H_2} = 1$ atm) of cell B for cell solutions of different ionic strength μ in each of the solvents are presented in Table 2. These values were used to compute an extrapolation function ($_pK_s'$) defined (8) by eq. [17]

$$[17] \quad pK_s' = \frac{F[(E - E^{0,m}_{\text{AgCl-Ag}})]}{RT \log 10} + \log \frac{m_{\text{Cl}^-}}{m_{\text{OS}^-}} = pK_s{}^m - \log \frac{\gamma_{\text{Cl}^-} a_{\text{SOH}}}{\gamma_{\text{OS}^-}} = pK_s{}^m - f(\mu)$$

where the symbols have usual meanings (8) and the required $E^{0,m}_{\text{AgCl-Ag}}$ values referred to respective solvents as the standard states were taken from the paper of Sadek *et al.* (14). The standard states are so chosen that at infinite dilution in a given solvent the molal activity coefficients of the ions, and also the mole fraction of the solvent x_{SOH}, are unity. As in pure water (20*a*) and dioxane–water mixtures (20*b*) etc., since the term, $\log \gamma_{\text{Cl}^-} a_{\text{SOH}}/\gamma_{\text{OS}^-}$ is likely to be proportional to μ in dilute solutions, a plot of the function pK_s' against μ would yield pK_s value on molal scale, pK_s^m. In fact, the values of the function pK_s' for each of these solvent mixtures when plotted against μ, are found to be fairly linear. And pK_s^m values were obtained from the least-squares linear plots of pK_s' against μ. These values are given in Table 2, their standard deviations lying within ± 0.01 unit in all the cases.

Notably, these pK_s^m values are found to differ from the corresponding values $K_{a/1}$ (molal scale) of Wooley *et al.* (10*c*) by about 0.1 unit up to 65 wt% cosolvent composition. Although, the corresponding data in aqueous ethylene glycol (EG) (10*a*, 21) and glycerol (8*c*, 10*c*) agree fairly well at least up to 50 wt% cosolvents, they differ somewhat appreciably at about 70 wt% in the case of glycerol. Moreover, as mentioned earlier, since $\Delta G_t{}^0(\text{HCl})$ values obtained by glass and Ag–AgCl electrodes (13) differ appreciably from those based on H_2 and Ag–AgCl electrodes (14) in this solvent system, it leads us to wonder if the observed differences stem from the untoward behaviour of glass electrode in this cosolvent system of "semi-aprotic" character, as is usually the case in most protic – dipolar aprotic solvent systems (13).

The standard free energy changes accompanying the autoionization of the mixed solvents relative to that of water, $\delta(\Delta G^0)_{\text{cell B}}$, which stand for $\Delta G_t{}^0[\text{H}^+(\text{OH}^-)_{\text{app}}]$, have been computed on mole fraction scale by use of eq. [18]

$$[18] \quad \delta(\Delta G^0_{\text{cell B}}) = \Delta G_t{}^0[\text{H}^+(\text{OH}^-)_{\text{app}}] = 2.3026RT[p(_sK_s^m)] - p(_wK_s^m)] + 2RT \ln M_w/M_s$$

Since $\delta(\Delta G^0_{\text{cell B}})$ is the sum of $\Delta G_t{}^0(\text{H}^+)$ and $\Delta G_t{}^0(\text{OH}^-)_{\text{app}}$ (see eq. [6]), and also $\Delta G_t{}^0(\text{H}^+)$ values for this solvent system are known from a previous study (15), these $\delta(\Delta G^0_{\text{cell B}})$ values helped compute $\Delta G_t{}^0(\text{OH}^-)_{\text{app}}$ values for the system. All these values are presented in Table 3.

Combining these values of $\Delta G_t{}^0(\text{OH}^-)_{\text{app}}$ and those of $\Delta G_t{}^0(\text{OH}^-)'_{\text{app}}$ estimated from the results of cell A we have obtained $\Delta G_t{}^0(\text{OH}^-)$ values with the help of eq. [12] and listed in Table 3. The figure illustrates their variation with cosolvent composition. For the sake of comparison, the corresponding values in aqueous 1,2-dimethoxy ethane

Can. J. Chem. Downloaded from www.nrcresearchpress.com by 210.87.254.40 on 09/06/12
For personal use only.

(DME)[2] and in aqueous EG solvent systems are also shown in the figure. It should be noted that these values in DME + water system, which is an aqueous dipolar aprotic solvent system, were obtained from $\Delta G_t^0[H^+(OH^-)_{app}]$ values[2] based on autoionization constants determined by use of H_2 and Ag–AgBr electrodes and $\Delta G_t^0(H^+)$ values based on TATB method reported recently (22). And as per eq. [13] the required values of $RT \ln a_w^s$ were taken approximately equal to $RT \ln x_w^s$. Similarly, $\Delta G_t^0(OH^-)$ values for the EG–water system which is an aqueous-protic system were also obtained from literature data of $\Delta G_t^0[H^+(OH^-)_{app}]$ (8*c*) based on autoionization constants (21*a*) and $\Delta G_t^0(H^+)$ based on TATB method (21*b*). It should be particularly noted, however, that the proper correction for the ionization of EG has been made by Basu Mullick *et al.* (8*c*) following Woolley *et al.*'s method (10*c*) to make $(OH^-_{app})_{protic}$ equivalent to $(OH^-_{app})_{aprotic}$ from which $\Delta G_t^0(OH^-)$ values were obtained by adding $\Delta G_t^0(H_2O)$, i.e. $-RT \ln a_w^s$ (23) as per eq. [13]. The dotted portion in the curve for the EG–water system in Fig. 1 is to indicate the approximate nature (8*c*) of Woolley-type correction.

Discussion

It is interesting to note that while $\Delta G_t^0(OH^-)$ – composition profile (Fig. 1) in EG–water mixtures remains almost invariant, that for the other two solvent systems become increasingly positive with increased cosolvent composition in the range studied. And for any cosolvent composition $\Delta G_t^0(OH^-)$ values in the ME–water system lie in between those of the two other solvent systems, their relative order being DME > ME > EG.

As is well known, the solvation behaviour of OH^- in the mixed solvents is likely to be dictated chiefly by the combined effects of varying dielectric constant and the acidity of the solvents. So, when Born-type electrostatic effects resulting from the varying dielectric constants of the solvents (23), were computed tentatively by use of simple Born equation (24) using $r_{OH^-} = 0.156$ nm (25) and the dielectric constant values from literature (14, 20*a*, 26), and subtracted from $\Delta G_t^0(OH^-)$ values, the resulting $\Delta G_{t,ch}^0(OH^-)$ values should essentially reflect the effects of relative acidity of the mixed solvents. The observed $\Delta G_{t,ch}^0(OH^-)$ – composition profile (Fig. 1) therefore suggests that with increasing addition of the cosolvent, while the acidity of EG–water mixtures increases somewhat slowly, that of DME–water mixtures decreases quite sharply. In ME–water mixtures, as well, the

[2]J. Datta (nee Sinha) and K. K. Kundu. Unpublished results.

TABLE 2. Electromotive force (ΔE) in volt of cell [B] in ME + water mixtures at 298.15 K

10 wt% ME			30 wt% ME			50 wt% ME			70 wt% ME		
m_{NaOH} (mol kg^{-1})	m_{NaCl} (mol kg^{-1})	E	m_{NaOH} (mol kg^{-1})	m_{NaCl} (mol kg^{-1})	E	m_{NaOH} (mol kg^{-1})	m_{NaCl} (mol kg^{-1})	E	m_{NaOH} (mol kg^{-1})	m_{NaCl} (mol kg^{-1})	E
0.0442	0.0572	1.0421	0.0648	0.0366	1.0651	0.0462	0.0566	1.0481	0.0399	0.0438	1.0515
0.0388	0.0479	1.0431	0.0535	0.0294	1.0646	0.0345	0.0423	1.0461	0.0299	0.0350	1.0486
0.0329	0.0425	1.0419	0.0396	0.0218	1.0634	0.0251	0.0308	1.0460	0.0225	0.0263	1.0482
0.0357	0.0317	1.0427	0.0344	0.0189	1.0631	0.0188	0.0250	1.0456	0.0204	0.0224	1.0504
0.0176	0.0228	1.0414	0.0263	0.0145	1.0629	0.0127	0.0156	1.0454	0.0153	0.0168	1.0497
0.0122	0.0150	1.0424	0.0129	0.00709	1.0625	0.0082	0.0108	1.0452	0.0140	0.0164	1.0481
0.00598	0.00739	1.0418	0.00747	0.00411	1.0617	0.00470	0.00576	1.0446	0.00957	0.0105	1.0487
									0.00502	0.00550	1.0485
	$p(K_s^m) = 14.06$			$p(K_s^m) = 14.29$			$p(K_m^s) = 14.69$			$p(K_s^m) = 15.42$	

TABLE 3. Different free energy parameters in kJ mol^{-1} for the evaluation of absolute transfer free energies of OH^-, $\Delta G_t^0(OH^-)$, from water to ME + water mixtures at 298.15 K

wt% ME	$(\Delta G^0_{cell\,A})^a$	$\Delta G_t^0(K^+)^b$	$\Delta G_t^0(OH^-)'_{app}$	$\delta(\Delta G^0_{cell\,B})^a$	$\Delta G_t^0(H^+)^b$	$\Delta G_t^0(OH^-)_{app}$	$\Delta G_t^0(OH^-)$
10	2.28	0.6	1.1	−0.03	−0.2	0.2	1.0
30	6.54	−0.3	7.2	0.41	−2.3	2.7	4.6
50	10.68	−1.3	13.2	1.58	−4.4	6.0	7.2
70	13.80	−2.8	19.3	4.32	−5.3	9.6	9.6

[a]Estimated uncertainties in $(\Delta G^0_{cell\,A})$ and $\delta(\Delta G^0_{cell\,B})$ are ±0.05 kJ mol^{-1} while those for individual ions are ±0.3 kJ mol^{-1} (vide, ref. 15).
[b]Reference 15.

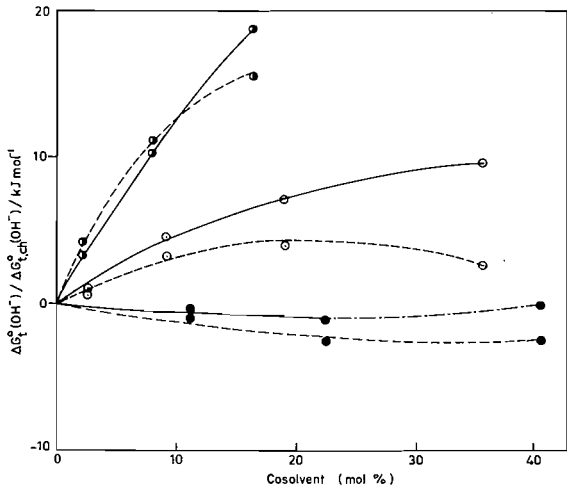

FIG. 1. Variation of $\Delta G_t^0(OH^-)$ (solid lines) and $\Delta G^0_{t,ch}(OH^-)$ (dotted lines) with cosolvent composition in ME–water mixtures (⊙), DME-water mixtures (◑), and EG–water mixtures (●).

acidity decreases, but to a much smaller extent. In fact, this is also expected from the relative acidities of the cosolvent molecules as governed by their structural features indicated below.

Simple consideration of the molecular structures of the cosolvent molecules shows that (*1*) EG is more acidic than water because the positive charge on the hydroxylic H-atom of the intramolecularly hydrogen bonded EG is enhanced by the electron withdrawing effect of the remote O-atom transferred through H-bond and (*2*) ME is less acidic than EG due to the presence of an electron releasing *O*-methyl group and also less acidic than water due to the restricted availability of the H-bonded acidic H-atom, which imparts some aprotic character to the molecule, while (*3*) DME is wholly dipolar aprotic by nature, having no acidic H-atom. Since this acidity of the cosolvents is likely to be relayed through co-operative structure of H-bonding between the cosolvent and H_2O molecules (27) in the aqueous solutions, the possible H-bonded cosolvent–water complexes should make EG–water solutions increasingly more acidic and DME–water mixtures increasingly less acidic. But the ME–water solutions should be less acidic than EG–water mixtures as well as water due to the partial aprotic character of the ME molecule but at the same time more acidic than DME–water mixtures because of its partial protic character. And this explains why the extent of stabilization of OH^- in ME–water mixtures is lying in between that in the other two cosolvent systems.

The foregoing discussions underline the importance of the absolute values of $\Delta G_t^0(OH^-)$ in obtaining information regarding solvent acidity. It will thus be useful to determine this quantity in various solvents by the method described in this work to gain better understanding of the acid–base nature of such solvents.

Acknowledgements

Thanks are due to Mr. I. N. Basu Mullick for helpful discussions and to C.S.I.R., New Delhi for financial assistance.

1. K. BOWDEN. Chem. Rev. **66**, 119 (1966).
2. C. H. ROCHESTER. Q. Rev. **20**, 511 (1966).
3. J. R. JONES. Chem. Brit. **7**, 336 (1971).
4. A. J. PARKER. Chem. Rev. **69**, 1 (1969).
5. (*a*) R. STEWART, J. P. O'DONNELL, D. J. CRAM, and B. RICKBORN. Tetrahedron, **18**, 917. (1962); (*b*) D. DOLMAN and R. STEWART. Can. J. Chem. **45**, 911 (1967).
6. K. K. KUNDU and L. AIYAR. J. Chem. Soc. Perkin Trans. II, 715 (1975).
7. (*a*) C. H. ROCHESTER. J. Chem. Soc. Dalton Trans. 5 (1972); (*b*) G. H. PARSONS and C. H. ROCHESTER. J. Chem. Soc. Faraday Trans. I, **68**, 523 (1972).
8. (*a*) A. K. DAS and K. K. KUNDU. J. Chem. Soc. Faraday Trans. I, **69**, 730 (1973). (*b*) A. K. DAS and K. K. KUNDU. J. Phys. Chem. **79**, 2604 (1975); (*c*) I. N. BASU MULLICK and K. K. KUNDU. Ind. J. Chem. **18A**, 1 (1979).
9. J. C. HALLE, R. GABORAIUD, and R. SCHAAL. Bull. Soc. Chim. Fr. 1851 (1969).
10. (*a*) E. M. WOOLLEY, D. G. HURKOT, and L. G. HEPLER. J. Phys. Chem. **74**, 3908 (1970); (*b*) E. M. WOOLLEY, J. TOMKINS, and L. G. HEPLER. J. Soln. Chem. **1**, 341 (1972); (*c*) E. M. WOOLLEY and R. E. GEORGE. J. Soln. Chem. **3**, 119 (1974).
11. O. POPOVYCH. Crit. Rev. Anal. Chem. **1**, 73 (1970).
12. B. G. COX, G. R. HEDWIG, A. J. PARKER, and D. W. WATTS. Aust. J. Chem. **27**, 477 (1974).
13. R. SMITS, D. L. MASSART, J. JULLIARD, and J. P. MOREL. Electrochim. Acta, **21**, 431 (1976).

Can. J. Chem. Downloaded from www.nrcresearchpress.com by 210.87.254.40 on 09/06/12
For personal use only.

14. H. SADEK, TH. F. TADROS, and A. A. AL-HARAKANY. Electrochim. Acta, **16**, 339 (1971).
15. A. BHATTACHARYA, A. K. DAS, and K. K. KUNDU. Ind. J. Chem. In press.
16. K. K. KUNDU, A. K. RAKSHIT, and M. N. DAS. Electrochim. Acta, **17**, 1921 (1972).
17. (*a*) K. BOSE and K. K. KUNDU. J. Soln. Chem. **8**, 175 (1979); (*b*) I. N. BASU MULLICK and K. K. KUNDU. Can. J. Chem. **58**, 79 (1980).
18. N. A. IZMAILOV and E. F. IVANOVA. Zh. Fiz. Khim. **29**, 1422 (1955).
19. D. J. G. IVES and G. J. JANE. Reference electrodes. Academic Press, New York. 1961. p. 336.
20. (*a*) H. S. HARNED and B. B. OWEN. The physical chemistry of electrolytic solutions. Reinhold, New York. 1958. (*b*) H. S. HARNED and L. D. FALLON. J. Am. Chem. Soc. **61**, 2374 (1939).
21. (*a*) S. K. BANERJEE, K. K. KUNDU, and M. N. DAS. J. Chem. Soc. A, 1166 (1967); (*b*) A. K. DAS and K. K. KUNDU. Ind. J. Chem. **16**A, 467 (1978).
22. A. BHATTACHARYA, A. K. DAS, and K. K. KUNDU. Ind. J. Chem. In press.
23. R. G. BATES. *In* Hydrogen bonded solvent systems. *Edited by* A. K. Covington and P. Jones. Taylor and Francis, London. 1968. p. 49.
24. U. SEN, K. K. KUNDU, and M. N. DAS. J. Phys. Chem. **71**, 3665 (1967).
25. D. FEAKINS. *In* Hydrogen-bonded solvent systems. *Edited by* A. K. Covington and P. Jones. Taylor and Francis, London. 1968.
26. R. N. ROY, E. E. SWENSON, G. LACROSS, JR., and C. W. KRUEGER. In Adv. Chem. Ser. No. 155. *Edited by* W. F. Furter. Am. Chem. Soc., Washington, DC. 1976. p. 220.
27. D. FEAKINS. *In* Physico-chemical processes in mixed aqueous solvents. *Edited by* F. Franks. Heinemann, London. 1967. pp. 71–91.

Can. J. Chem. Downloaded from www.nrcresearchpress.com by 210.87.254.40 on 09/06/12
For personal use only.

Conformational dynamic investigation of 1,5-benzodioxepin and its dimethyl derivative by ^1H and ^{13}C nmr

D. MENARD AND M. ST-JACQUES

Département de Chimie, Université de Montréal, Montreal (Qué.), Canada H3C 3V1

Received September 26, 1980

D. MENARD and M. ST-JACQUES. Can. J. Chem. **59**, 1160 (1981).

The conformational and dynamic properties of 1,5-dioxa-6,7-benzocycloheptene (**2**; 1,5-benzodioxepin) and its dimethyl derivative (**7**) have been investigated by dynamic ^1H and ^{13}C nmr methods. Analysis of the spectra at low temperatures (below coalescence) indicates that the most stable seven-membered ring conformations detected for solutions in CHF_2Cl are a mixture of the chair (C, 80%) and the twist-boat (TB, 20%) for **2** and a mixture of TB (64%) and C (36%) for **7**. Free energy barriers were determined for the chair inversion of **2** (6.5 kcal/mol) and **7** (7.5 kcal/mol) as well as for the twist-boat pseudorotation of **7** (6.8 kcal/mol). The conformational properties of these seven-membered heterocycles are discussed and compared to those known for 2,4-benzodioxepins.

D. MENARD et M. ST-JACQUES. Can. J. Chem. **59**, 1160 (1981).

Les propriétés conformationnelles et dynamiques du dioxa-1,5 benzocycloheptène-6,7 (**2**; benzodioxépine-1,5) et de son dérivé diméthylé (**7**) ont été étudiées par rmn dynamique des noyaux ^1H et ^{13}C. L'analyse des spectres à basse température (en-dessous de la coalescence) de ces composés en solution dans le CHF_2Cl révèle que les conformations les plus stables adoptées par le cycle à 7 chaînons sont la chaise (C, 80%) et le bateau-croisé (TB, 20%) dans le cas de 2 et un mélange de TB (64%) et C (36%) dans le cas de **7**. On a déterminé l'énergie libre d'activation de l'inversion de la chaise de **2** (6,5 kcal/mol) et de **7** (7,5 kcal/mol) de même que la barrière de pseudorotation de la forme bateau-croisé de **7** (6,8 kcal/mol). Les propriétés conformationnelles de ces hétérocycles à 7 chaînons sont discutées et comparées à celles déjà connues des benzodioxépines-2,4.

The recent observation of interesting and surprising conformational features for 1,3-dioxa-5,6-benzocycloheptene (**1**; 2,4-benzodioxepin) and its 2-substituted derivatives (**1**) as well as our continuing interest in the conformations of seven-membered ring systems led us to focus our attention on the 1,5-dioxa analogs of this family of molecules (i.e. **2** and its derivatives).

A study of the conformational characteristics of 1,5-benzodioxepins is particularly pertinent in view of the pharmaceutical activity associated with some compounds from this class of heterocyclic molecules. A number of 3-substituted aminomethyl-3-hydroxy-1,5-benzodioxepins (**3**) have been shown to possess interesting bronchial dilator activity (2) while various 3,3-disubstituted 1,5-benzodioxepin derivatives (**4**) have recently been recognized as analgesics, antiarrythmics, and sedatives (3). A precise knowledge of the conformational properties of this type of molecule therefore appears desirable in order to fully understand their biological mode of action.

At present, very few studies of the conformational properties of this class of compounds have been published. Results reported from an ultraviolet study of 1,5-benzodioxepin and its derivatives (4) have provided only partial and qualitative information on the conformations adopted by these molecules in solution. Depending on the substitution pattern, the compounds studied were often thought to exist as mixtures of conformations for

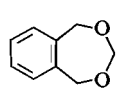

1

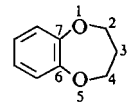

2

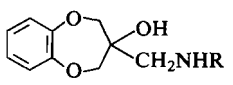

3

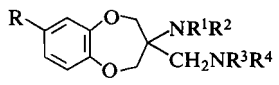

4

which no quantitative measurement could be made. Furthermore, a variable temperature ^1H nmr study of several compounds down to −80°C is reported to have failed to provide information on the conformational processes involved (4). On the other hand, X-ray diffraction data for 3,3′-spirobi[3H-2,4-dihydrobenzo[1,4]dioxepin] (**5**) showed that the seven-membered ring exists exclusively in the twist-boat conformation (5).

We therefore report the results of our study of the conformation of 1,5-benzodioxepin (**2**) and its 3,3-dimethyl derivative (**7**). Our nmr observations

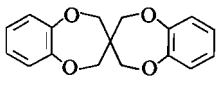

5

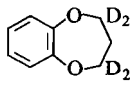

6

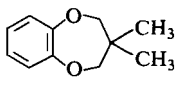

7

provide more complete insight into the conformational and dynamic features characterizing this class of heterocyclic molecules.

0008-4042/81/071160-09$01.00/0

©1981 National Research Council of Canada/Conseil national de recherches du Canada

Can. J. Chem. Downloaded from www.nrcresearchpress.com by 210.87.254.40 on 09/06/12
For personal use only.

TABLE 1. ^{1}H nmr spectral and dynamic parameters for compounds **6** and **7**

Compound	Temperature °C		δ	J_{AB} Hz	T_c °C	$\Delta G^{\ddagger}$ kcal/mol
6[a]	25	(H-3)	2.14			
	−154		1.90 (C)[b]	−15.6	≤131	6.5 (−131°C) (chair inversion)[d]
			2.39 (C)			
7[c]	25	(CH_3)	1.053			
	−140		0.741 (C)			
			1.241 (C)			
			1.009 (TB)			
	25	(H-2,4)	3.87			
	−140		3.85 (TB)	−11.9		7.46 (−140°C)[e] (chair inversion)
						7.13 (−140°C) (C → TB interconversion)
			4.01 (TB)			
			3.42 (C)	−11.7		6.84 (−140°C (TB inversion)
			3.90 (C)			

[a]At 100 MHz in CHF_2Cl containing internal Me_4Si.
[b]The letters C and TB in parentheses refer to conformations described in the text.
[c]At 250 MHz in CHF_2Cl containing internal Me_4Si and CD_2Cl_2 (about 13%) for lock.
[d]Because a transmission coefficient of 1/2 was used in the calculation of this value, the number given refers to the C ⇌ B step of the inversion pathway.
[e]These values were obtained from a computer simulation of the H-2,4 spectral change. The $\Delta G^{\ddagger}$ values correspond to k_{14}, k_{12}, and k_{23} respectively, which characterize the conformational processes given in parentheses. The estimated error is about ±0.3 kcal/mol.

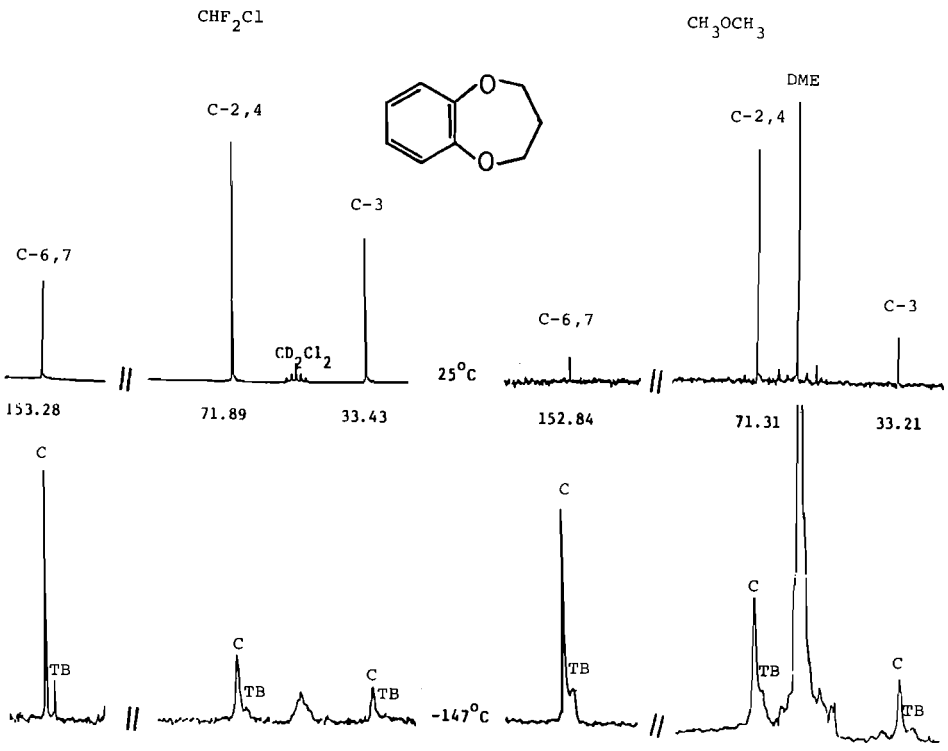

FIG. 1. The 20.15 MHz ^{13}C nmr spectra of the seven-membered ring carbons of **2** in CHF_2Cl and CH_3OCH_3 (DME identifies the CH_3 signal of the CH_3OCH_3 solvent). The symbols C and TB are defined in the text.

Results

Both compounds **2** and **7** gave dynamic proton and carbon-13 magnetic resonance (^{1}H and ^{13}C nmr) spectral changes on going to low temperatures. For spectral simplification, the variable temperature ^{1}H nmr study of **2** was performed on its 2,2,4,4-tetradeutero isomer **6**. Spectral and dynamic parameters for these compounds are listed in Tables 1 and 2.

Figure 1 illustrates the 20.15 MHz ^{13}C spectral

Can. J. Chem. Downloaded from www.nrcresearchpress.com by 210.87.254.40 on 09/06/12
For personal use only.

Can. J. Chem. Downloaded from www.nrcresearchpress.com by 210.87.254.40 on 09/06/12
For personal use only.

TABLE 2. Carbon-13 chemical shift for compounds **2** and **7** at high and low temperature[a]

Compound	Solvent	Temperature °C	C-6,7	C-8 to C-11	C-2,4	C-3	Substituents on C-3
2	CHF_2Cl	25	153.28	124.67,122.91	71.89	33.43	—
		−142	153.35 (C)[b]	125.76,124.01	73.14 (C)	33.72	—
			151.01 (TB)[b]	[c]	70.21 (TB)	[c]	
	CH_3OCH_3	25	152.84	124.01,122.48	71.31	33.21	—
		−146	153.50 (C)	124.88,123.50	74.63 (C)	34.93 (C)	—
			151.38 (TB)	121.89, [c]	72.24 (TB)	31.76 (TB)	
7	CHF_2Cl	25	152.84	124.30,122.33	81.60	37.81	22.92
		−128	153.42 (C)	125.54,120.21	81.68 (C)	38.47 (C)	21.02 (C)
			150.72 (TB)	123.72,121.45	80.43 (TB)	37.81 (TB)	22.92 (TB)
	CH_3OCH_3	25	152.40	123.72,121.96	81.02	38.10	22.48
		−142	154.17 (C)	125.27,120.27	81.02 (C)	38.67 (C)	21.09, 20.50 (C)
			151.10 (TB)	123.51,121.46	79.83 (TB)	37.68 (TB)	22.68 (TB)

[a]Solutions containing internal Me_4Si and CD_2Cl_2 (19%) for field lock purpose.
[b]The letters C and TB in parentheses refer to conformations described in the text.
[c]The chemical shifts of the less intense signals were not determined accurately at low temperature and consequently are not reported in this table.

modifications observed for **2** in CHF_2Cl. Most of the ring carbon signals have split into doublets of unequal intensities at −147°C. The more intense lines account for 80% while the less intense lines account for 20% of the total intensity. A similar spectral change was observed for this compound in dimethyl ether in which signal integration revealed 23% for the less intense lines and 77% for the major ones.

Figure 2 shows that the methylene proton singlet of the 100 MHz ^1H nmr spectrum of **6** in CHF_2Cl changes into an AB pattern below −131°C. The free energy of activation calculated from the coalescence of the AB pattern (6) is found to be 6.5 kcal/mol (at −131°C) using a transmission coefficient of one-half (*vide infra*).

The changes observed in the ^{13}C nmr spectrum of **7** as the temperature is lowered are illustrated in Fig. 3 where all ring carbons are shown to have split into doublets of unequal intensities at −128°C. For a solution of **7** in CHF_2Cl, the more intense lines account for 64% and the less intense lines account for 36% of the total intensity. A free energy of activation of 7.8 ± 0.3 kcal/mol was estimated at −113°C (the coalescence temperature) using a two site approximation (7) and a transmission coefficient of one (*vide infra*). Similar changes were observed in the ^{13}C nmr spectrum of **7** in CH_3OCH_3 with the exception that the singlet at δ 22.55 splits into three lines instead of two in CHF_2Cl at −141°C (see inset in Fig. 3). Thus, the upfield methyl line observed in CHF_2Cl constitutes an unresolved doublet and the solvent effect produced by dimethyl ether leads to better resolution of the two components of equal intensity. Integration of the signals in CH_3OCH_3 revealed 75% for the most intense lines and 25% for the minor ones.

The 250 MHz ^1H nmr spectrum of **7** in CHF_2Cl (Fig. 4) shows that the methylene singlet observed at room temperature splits into a seven line pattern below −130°C while the methyl singlet splits into a triplet below −120°C for which the center line accounts for 64% of the total intensity and the less intense lines on each side account for 18% each of the total intensity.

This figure also illustrates a series of changing spectra calculated for the methylene protons by means of the DNMR-2 computer program (8). Thus it was possible to confirm the spectral analysis reported diagrammatically under the methylene proton spectrum at −140°C (Fig. 4) where two overlapping AB patterns are identified by the solid and broken lines. The kinetic results derived from the computer spectral simulation are summarized in Table 1.

Can. J. Chem. Downloaded from www.nrcresearchpress.com by 210.87.254.40 on 09/06/12
For personal use only.

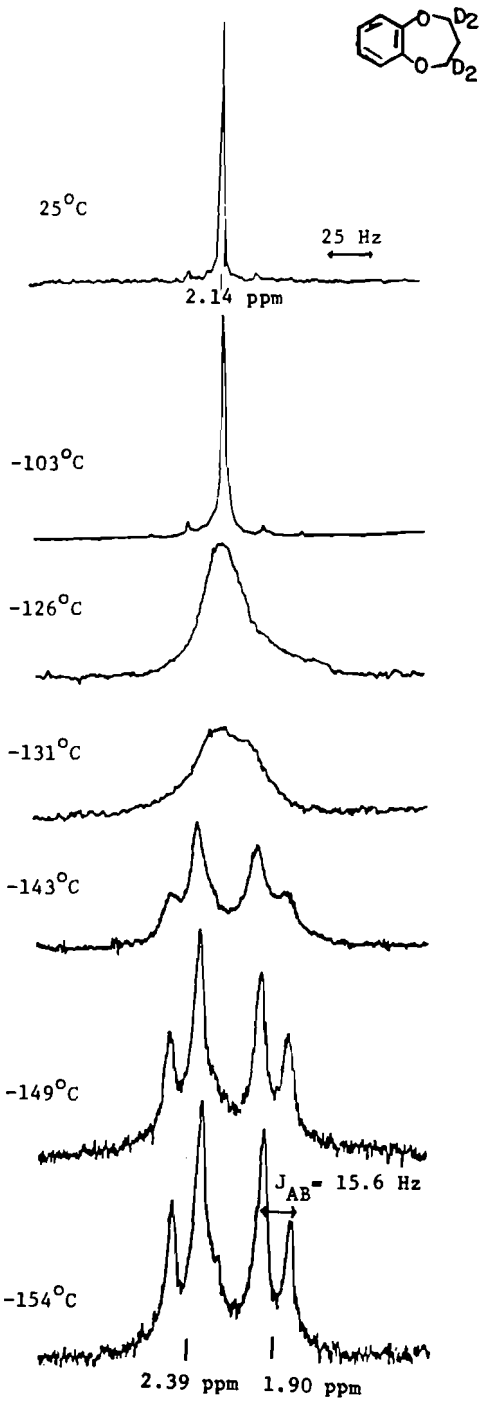

FIG. 2. The ^2H decoupled 100 MHz ^1H nmr spectra of the methylene protons of **6** in CHF_2Cl at several temperatures.

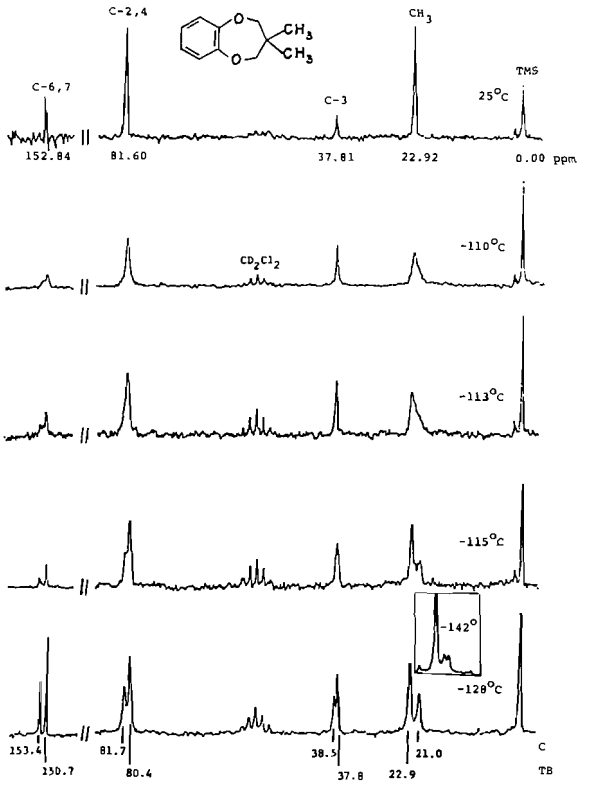

FIG. 3. The 20.15 MHz ^{13}C nmr spectra of the seven-membered ring carbons of **7** in CHF_2Cl at several temperatures. The inset shows the methyl carbon signals of **7** in dimethyl ether at −142°C.

The spectral simulation was actually carried out by means of a slightly modified version of the DNMR-2 program capable of handling four different spin systems of unequal populations instead of three in the initial version (8). The exchange model selected for the simulation is illustrated below in Scheme 1 where the numbers constitute four configurations of which 1 represents the minor conformer and 2 the major one, while 4 is the inverted form of 1 and 3 the inverted form of 2. Thus four configurations are considered whose populations in CHF_2Cl are: 1 (18%); 2 (32%); 3 (32%); 4 (18%). Each of these configurations contains two non-equivalent protons which are labelled A_1 and B_1 for 1 and 4 and A_2, B_2 for 2 and 3 and whose chemical shifts are shown in Fig. 4. Thus Scheme 1 illustrates that, for example, the transformation from 1 to 4 only exchanges the environments of A_1 and B_1. This approach therefore assumes that the methylene groups are independent of one another, as is expected from the fact that long range coupling should be small.

In addition, the following relationships were respected: $k_{12} = k_{13} = k_{43} = k_{42}$, $k_{14} = k_{41}$, $k_{23} = k_{32}$, $k_{21} = k_{34} = k_{24} = k_{31}$, and k_{21} = population ratio ([1]/[2]) k_{12}. Furthermore, the initial guess value for $k_{1,4}$ was taken as $\frac{1}{2}(k_{21})$. Best values for the rate constants at each temperature were then

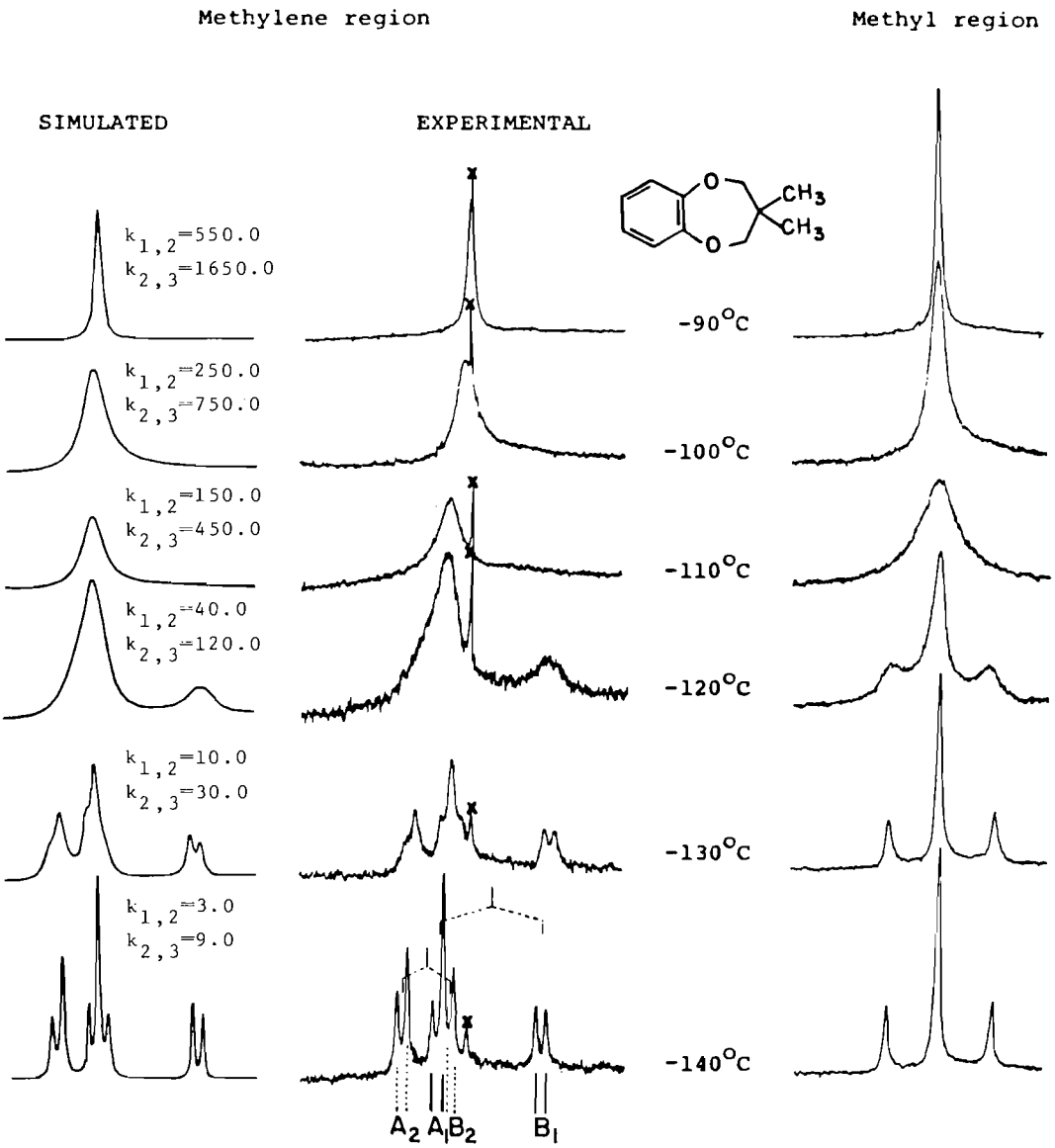

FIG. 4. The 250 MHz ^{1}H nmr spectra of the methylene and methyl protons of **7** in CHF_2Cl at several temperatures (x denotes impurity). Calculated spectra are shown on the left. The symbols A_1, B_1, A_2, B_2 identify the components of the two AB patterns observed at −140°C.

obtained by a trial and error empirical method using visual comparison as test. The values for k_{12} and k_{23} are given on Fig. 4 while that of k_{14} was found to be equal to $0.28k_{12}$.

Discussion

Conformations of the Seven-Membered Rings

The spectral modifications observed in the ^{13}C spectrum of **2** (Fig. 1) reveal the existence of a mixture of two conformers (80:20 in CHF_2Cl). Furthermore, the observation of a single AB pattern in the ^{1}H spectrum of **6** below −131°C (Fig. 2) suggests that the signals of the minor conformation are hidden under those of the major form. Examination of the symmetry properties of the three conformations possible for the seven-membered ring, namely the chair (**8***a*, C), the boat (**8***b*, B), and the twist-boat (**8***c*, TB), reveals that in both C and B, the two protons (or identical substituents) on C-3 are not chemically equivalent, whereby one proton (or substituent) occupies an axial position and the other occupies an equatorial position. On the other hand, the C_2 axis of symmetry in the twist-boat conformation makes both protons (or

Can. J. Chem. Downloaded from www.nrcresearchpress.com by 210.87.254.40 on 09/06/12
For personal use only.

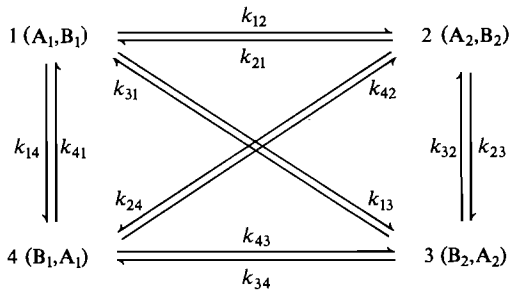

SCHEME 1

identical substituents) at the 3-position chemically equivalent. It then follows from these considerations and from the observed nonequivalence of the two H-3 in **6** that TB is ruled out as the major conformation of 1,5-benzodioxepin, whereas either the C or the B forms are compatible with this observation. Since C is generally less energetic than B (9) for unsubstituted molecules, it is expected to be the most stable conformation adopted by **2**. Later, ^{13}C chemical shift considerations will indicate that the minor conformer of **2** is TB.

The spectral modifications observed in the ^{13}C spectrum of **7** indicate that we are again in the presence of a mixture of two conformers (64:36 in CHF_2Cl or 75:25 in CH_3OCH_3). The observation of a three line pattern in the high field methyl region (Fig. 3 inset, intensity distribution 75:12.5:12.5) clearly shows that these two conformers are TB and C, whereby the most intense methyl signal is due to the two equivalent methyl carbons in the TB conformation, while the two smaller upfield signals of equal intensities are due to the nonequivalent methyl carbons in the C conformation (axial and equatorial positions). Thus, unlike the parent compound **2**, TB is the major conformation adopted by the dimethyl derivative **7** and C is the minor one.

The above conclusion is confirmed by the ^1H spectrum of **7** in CHF_2Cl (Fig. 4); the center line observed in the methyl region accounts for 64% of the total intensity and is due to the chemically equivalent methyl protons in the TB conformation, while the less intense lines on each side account for 18% each of the total intensity and are due to the methyl protons in the axial and equatorial positions of the C conformation.

8a *8b*

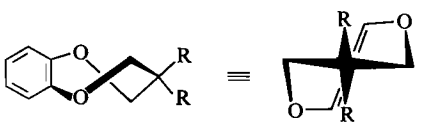

8c

Because the C-2 and C-4 methylene groups should give distinct nmr signals for the C and TB forms, it follows that the two AB patterns comprising the seven line spectrum of the methylene protons of **7** (Fig. 4 at −140°C) each belong to one conformer. Thus, the most intense AB pattern at lower field (dotted lines) corresponds to TB, while the second, less intense one, at higher field corresponds to the C form.

It has been noted that while equatorial protons generally appear at lower field than axial protons (cyclohexane : $\Delta\delta = \delta H_e - \delta H_a = 0.46$ ppm (10)), electronic polarization by a *trans* coplanar oxygen atom moves the equatorial proton of a methylene group β to an oxygen atom at higher field than the axial proton. Hence, the chemical shift difference Δδ between geminal axial and equatorial protons β to oxygen is −0.074 ppm in tetrahydropyran (11) and about −0.80 ppm in 1,3-dioxan (12). Our results seem to show that the same trend exists in seven-membered rings. A previous report (13) has shown that while Δδ for the benzylic methylene protons is −0.106 ppm in benzocycloheptene, introduction of a β oxygen atom moves the equatorial proton at 0.504 ppm upfield from the axial proton. Assuming that the same trend applies qualitatively to **2** (or **6**) we would expect the two oxygens β to the protons on C-3 to shift the equatorial proton at about 0.4 ppm upfield from the axial proton since in benzocycloheptene Δδ for the corresponding protons in 0.41 ppm (14). Results obtained from the low temperature spectrum of **6** show that the absolute value of Δδ is 0.49 ppm. The good agreement with the above prediction suggests that $\Delta\delta = -0.49$ ppm.

An important Δδ difference is observed for H-2,4 in the C and TB forms of the dimethyl derivative **7**. The Δδ value in C is 0.48 ppm while it is only 0.16 ppm in the TB form. The Δδ value for the analog H-4,6 protons of 5,5-dimethyl-1,3-dioxane, which exists as a chair, is 0.22 ppm (15). The higher field signal of the C form of **7** is therefore assigned to the axial protons on C-2,4 and the lower field signal to the equatorial protons. Lack of systems existing in the TB form, however, prevents us from further assigning the ^1H signals of this form.

The comparison of the low temperature ^{13}C spectra of **2** and **7** shows that the C-2,4, C-3, and C-6,7 signals exhibit characteristic intensities, whereby for **7** the more intense lines (those of the TB form) are upfield, while for **2** the more intense lines (those of C) are at lower field. This

Can. J. Chem. Downloaded from www.nrcresearchpress.com by 210.87.254.40 on 09/06/12
For personal use only.

Can. J. Chem. Downloaded from www.nrcresearchpress.com by 210.87.254.40 on 09/06/12
For personal use only.

observation together with the very similar chemical shifts for C-6,7 (carbons remote from the site of substitution) in both compounds identify TB as the minor conformation of **2**.

The observed differences between ^{13}C chemical shifts of the C and TB forms of **2** are 3.17 ppm for the C-3 signals, 2.93 ppm for the C-2,4 signals, and 2.34 ppm for the C-5,6 signals. Similarly differences of 0.66, 1.25, and 2.70 ppm respectively are observed for solutions of **7** in CHF_2Cl.

It is customary to analyze substituent effects on ^{13}C chemical shifts in terms of the α, β, γ, and δ shifts (16). Therefore the introduction of two methyl groups on C-3 produces an α shift of 3.74 ppm for C and 5.92 ppm for TB, while β shifts are 6.39 ppm for C and 7.59 ppm for TB. The δ shifts produced on the C-6,7 signals are very small (less than 0.6 ppm). Similarly an α shift of 3.8 ppm is observed for dimethyl substitution on the 5-position of 1,3-dioxane (which exists as a chair (17)); the β shift, being 10.0 ppm, follows the same trend although is significantly higher.

Our conformational results are in general agreement with the findings of Archer *et al.* (4) who had concluded from their uv study that **2** should exist in the chair conformation while its dimethyl derivative should exist as a mixture of C and TB conformations. Their method, however, did not allow the detection of the minor TB conformer in the case of **2** and did not provide any quantitative measurement for each conformer in the case of mixtures. Furthermore, it is not surprising that the above authors did not observe changes in the ^1H spectrum of **7** at −80°C since these occur only below −120°C.

Thus, as was the case for the 2,4-benzodioxepin family, the parent compound of the 1,5-benzodioxepin family exists predominantly in the C conformation with about 20% of the TB conformer. However, while the amount of TB for 2,4-benzodioxepin increases significantly as the polarity of the solvent is decreased, the solvent effect is small for 1,5-benzodioxepin.

The observation of an important amount of C conformer for **7** compared to the 2,4-benzodioxepin analog which exists exclusively in the TB conformation (1) can be rationalized as follows: whereas, in the case of disubstituted 2,4-benzodioxepin derivatives, the chair conformation is destabilized by nonbonding interactions between the axial methyl group and the axial benzylic protons, the fact that these protons have been replaced by the free electron pairs of the oxygen atoms in **7** leads to weaker nonbonding interactions. Thus, the chair conformation is less destabilized than in the 2,4-benzodioxepin family. A similarly attenuated nonbonding steric repulsion was observed in the case of 5-substituted 1,3-dioxanes (18, 19).

A more important solvent effect is observed for **7** than for **2**; it suggests that TB is somewhat less polar (20) than C for **7**.

Conformational Averaging Processes

The chair inversion process of benzocycloheptene (21) involves a rate-determining chair-to-boat step characterized by a free energy of activation of 10.7 kcal/mol (22). The presence of one oxygen atom in 5-oxabenzocycloheptene lowers the ΔG^* value to 9.5 kcal/mol (13), whereas the value of 8.0 kcal/mol observed for 2,4-benzodioxepin (1) indicates easier ring deformation along the inversion pathway. The even lower inversion barrier (6.5 kcal/mol) estimated from the ^1H spectral change of **6** (Fig. 2) therefore shows that chair inversion for 1,5-benzodioxepin is the most facile of these oxygenated seven-membered heterocyclic molecules.

Our inability to observe the ^1H signals of TB of **2** limited further kinetic investigation of the parent compound. Fortunately, the situation is more favorable in the case of **7** where a line shape simulation of the spectral modifications observed in the methylene region of the ^1H spectra enabled us to determine the free energies of activation of several of the conformation processes involved.

The conformational interconversion pathways applicable to **7** are shown in Scheme 2 where it is seen that the various exchange processes involve only two independent molecular transformations, namely C ⇌ B and B ⇌ TB, where the population of B is extremely small and undetermined. In other words, the C–TB interconversion involves the C ⇌ B ⇌ TB pathway while the TB inversion involves the TB ⇌ B ⇌ TB* pathway (the symbol * indicates inverted conformations), which is usually designated as a pseudorotation.

It then follows that of the various rate constants obtained from the computer spectral simulation, k_{12} corresponds to the C → TB conversion and k_{23} to the TB inversion. (i.e. 1 ≡ C; 2 ≡ TB; 3 ≡ TB*; 4 ≡ C*). The results summarized in Table 1 therefore show that at −140°C, the first process characterized by a free energy of activation of 7.13 kcal/mol is slightly more energetic than the second one (6.84 kcal/mol). A calculation of these parameters at −113°C raises the ΔG^* value for the C → TB conversion to 7.8 kcal/mol which turns out to be identical to that estimated from the ^{13}C spectrum of **7** at the coalescence temperature using the two-site approximation.

Because the B ⇌ TB step is common to both conformational processes, the higher ΔG^* value for the C → TB conversion indicates that it is the C ⇌

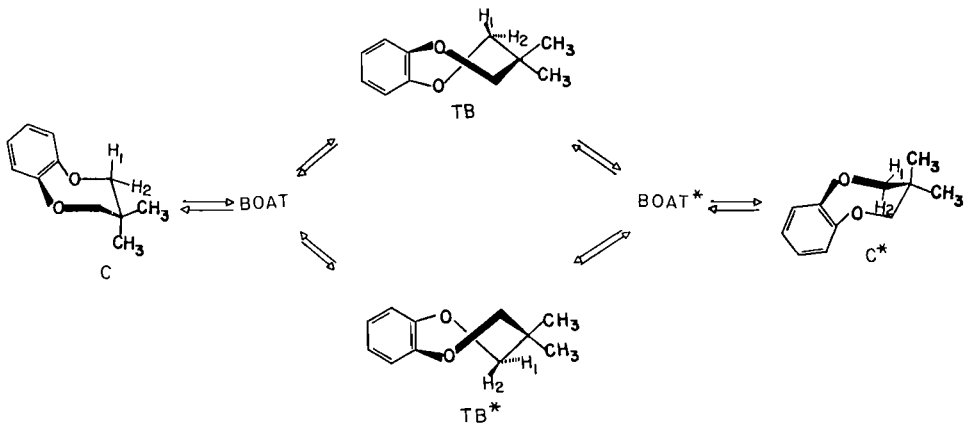

SCHEME 2

B step which is rate determining. Furthermore, the $\Delta G^{\ddagger}$ value given above for this process is about one kcal/mol higher than the corresponding value of 6.5 kcal/mol (−131°C) determined for **2** (or **6**). It is interesting to note that a similar *gem*-dimethyl substitution of benzocycloheptene also increased the chair inversion barrier by about one kcal/mol (22) (i.e. from 10.7 to 11.8 kcal/mol). This trend therefore suggests that a similar ring deformation probably takes place in the rate determining C ⇌ B step for both families of molecules, namely a flip of the benzo part of the molecule (23).

A comparison of the dynamic parameters of **7** with other seven-membered cyclic molecules is made difficult by the limited number of systems amenable to as complete an investigation as was carried out in this work. Nevertheless it is possible to compare the pseudorotation $\Delta G^{\ddagger}$ of **7** (6.8 kcal/mol) to that of 2,2-dimethyl-1,3-dioxabenzocycloheptene, for which a value of 10.0 kcal/mol was reported (1). The rather high $\Delta G^{\ddagger}$ value for the latter molecule was attributed to a *syn*-1,3 nonbonded repulsive interaction between one of the methyl groups and a benzylic hydrogen in the transition state for pseudorotation. In the case of **7**, the benzylic protons are replaced by oxygen lone pairs and consequently the methyl – lone pair interaction, being weaker (18, 19), results in a smaller pseudorotation barrier.

Experimental

Melting points are uncorrected and were determined using a Büchi melting point apparatus. The vpc analyses and separations were carried out on a Varian-aerograph model 920 instrument using helium as carrier gas.

The variable temperature ^{1}H nmr spectra of **6** at 100 MHz were obtained using a JEOL JNM-4H-100 spectrometer equipped with a temperature control unit Model JES-VT-3. Temperatures were measured accurately with a calibrated copper–constantan thermocouple placed inside a solvent containing a dummy nmr tube. A precision of ±1°C is expected. The sample was studied as a solution in chlorodifluoromethane (35 mg in 0.55 mL of solution) containing a small quantity of tetramethylsilane (TMS) in standard 5 mm tubes which had been degassed and sealed.

The variable temperature ^{1}H nmr spectra of **7** at 250 MHz were obtained in the FT mode using a Bruker WM-250 spectrometer (located at the Centre d'Etudes Nucléaires de Grenoble, France) equipped with a standard Bruker temperature control unit. Temperatures were read off the control unit and are most probably accurate to ±3°. The sample was studied as a solution in chlorodifluoromethane (11 mg in 0.55 mL of solution) containing a small quantity of TMS and about 13% of CD_2Cl_2 (for locking purposes) in a standard 5 mm tube which had been degassed and sealed. The following instrumental parameters were used: flip angle = 90°; SW = 2403 Hz; data size = 16K; AQ = 3.4 s.

The variable temperature ^{13}C nmr spectra of **2** and **7** were recorded in the FT mode with a Bruker WP-80 spectrometer operating at 20.15 MHz and equipped with the Bruker variable temperature accessory. All ^{13}C spectra were recorded with proton noise decoupling for solutions in chlorodifluoromethane or dimethyl ether (180–200 mg in 2.2 mL of solution) containing TMS and about 19% of CD_2Cl_2 (for locking purposes) in standard 10 mm tubes which had been degassed and sealed. The following instrumental parameters were used: flip angle = 35°; SW = 6000 Hz; data size = 8K; AQ = 0.679 s; pulse delay, none, except when integration of the signals was performed; a pulse repetition rate of 10 s was then used. Temperatures were measured accurately with a thermocouple as described above for the 100 MHz ^{1}H spectra.

The rate constants were estimated at the coalescence temperature using the equation $k = \pi\Delta\nu/\sqrt{2}$ for singlet to doublet splitting (in the ^{13}C spectra of **7**) (6) and the equation $k = \pi(\Delta\nu^2 + 6J^2)^{\frac{1}{2}}/\sqrt{2}$ for singlet to AB splitting (in the ^{1}H spectra of **6**) (6). The free energies values ($\Delta G^{\ddagger}$) were calculated from standard equations (24) using a transmission coefficient of one, except for the ^{1}H spectral changes of **6** for which a transmission coefficient of one half is most appropriate to describe the chair-to-boat step of the chair inversion.

Simulations were carried out using a slightly modified version of the DNMR-2 program (*vide infra*) on an CDC Cyber 173 computer. Spectra were traced by means of a Printronix plotter. Free energies of activation were calculated from a $\ln k/T$ vs. $1/T$ plot using the Eyring equation (6).

Calculations of $\Delta S^{\ddagger}$ and $\Delta H^{\ddagger}$ were not expected to be sufficiently reliable because of the uncertainty in temperature (±3°C), uncertainties in $T_2°$ arising from possible small long range coupling, as well as the fact that the conformational

Can. J. Chem. Downloaded from www.nrcresearchpress.com by 210.87.254.40 on 09/06/12
For personal use only.

Can. J. Chem. Downloaded from www.nrcresearchpress.com by 210.87.254.40 on 09/06/12
For personal use only.

populations and chemical shifts were kept constant through the whole temperature interval. As a consequence, the values of -15 ± 5 eu obtained for $\Delta S^{\neq}$ cannot be regarded as sufficiently reliable for discussion.

1,5-Benzodioxepin (2) (25)

o-Dihydroxybenzene (10.1 g, 0.092 mol), 1,3-dibromopropane (19.0 g, 0.094 mol), anhydrous potassium carbonate (12.9 g), and glycerol (0.5 g) were heated under reflux for 24 h. The mixture was cooled, diluted with water (30 mL), and made faintly alkaline with sodium hydroxide. It was then steam distilled and the distillate was extracted with chloroform. The chloroform layer was then dried ($MgSO_4$) and evaporated. There was obtained 3.45 g (24.8%) of **2** which was further purified by gas chromatography using a U.C.W. 98 column (2 m × 1 cm, T = 165°C). The product was characterized by its ^{1}H nmr spectrum which was identical with that reported (26). The ^{13}C nmr spectrum of the product (Table 2) confirmed the assigned structure.

1,3-Propanediol-1,1,3,3-d_4 *(27)*

Diethylmalonate (8.3 g, 0.052 mol) dissolved in 15 mL of anhydrous ether was added dropwise to a suspension of 29 g of $LiAlD_4$ (0.064 mol) in 100 mL of anhydrous ether. The mixture was refluxed for 6 h and then stirred magnetically at room temperature overnight. The excess of hydride was decomposed with 15 mL of a 1 *N* sodium hydroxide solution and the mixture was filtered. The yellow precipitate was washed with ether and returned to the reaction flask. Tetrahydrofuran (50 mL) was added and the mixture was brought to reflux for 30 min. The precipitate was again filtered and washed. The process of refluxing with THF was repeated twice more. The organic fractions were concentrated to give 2.56 g (1.032 mol, 61.5%) of 1,3-propanediol-1,1,3,3-d_4 which was characterized by its ^{1}H nmr spectrum; $\delta(CDCl_3)$: 1.65 (2H, s, CH_2) ppm, and was used without further purification in the next reaction.

1,3-Dibromopropane-1,1,3,3-d_4 *(27)*

Phosphorous tribromide (1.8 mL, 5.13 g, 0.019 mol) and 1,3-propanediol-1,1,3,3-d_4 (1.12 g, 0.014 mol) were mixed at 0°C and permitted to react slowly as the temperature rose. The mixture was stirred at 125°C for 3 h, then allowed to cool; 10 mL of water were added and a small amount of orange precipitate was removed by filtration. The filtrate was extracted 4 times with 20 mL of methylene chloride and the combined organic fractions were dried over magnesium sulfate; 1,3-dibromopropane-1,1,3,3-d_4 (0.84 g, 29%) was isolated and used without further purification.

1,5-Benzodioxepin-2,2,4,4-d_4 *(6)*

This compound was prepared in the same manner as **2** using 0.55 g (0.005 mol) of *o*-dihydroxybenzene and 0.84 g (0.004 mol) of 1,3-dibromopropane-1,1,3,3-d_4. The mixture was extracted with chloroform (3 × 25 mL) and the combined organic fractions were treated with charcoal, filtered, and dried over magnesium sulfate. The product was then purified by gas chromatography using a U.C.W. 98 column; 60 mg of **6** (9.5%) were obtained. The 1,5-benzodioxepin-2,2,4,4-d_4 was characterized by its retention time (which was identical to that of **2**) and by its ^{13}C nmr spectrum which was the same as **2** except for isotope effect and the lower intensity and multiplicity of the CD_2 signal.

Ditosylate of 2,2-dimethyl-1,3-propanediol

This compound was prepared by a procedure already published (28). It was characterized by its melting point, 118–121°C (lit. (28) mp 121–123°C) and its ^{1}H nmr spectrum; $\delta(CDCl_3)$:0.88 (6H, d, CH_3), 2.46 (6H, d, CH_3—Ar), 371 (4H, d, OCH_2), 7.54 (4H, AB multiplet, Ar) ppm. Yield: 86%.

3,3-Dimethyl-1,5-benzodioxepin (7)

Compound **7** was prepared by a procedure already published (4) and was characterized by its ^{1}H nmr spectrum which was identical with that reported. The ^{13}C nmr spectrum of the product (Table 2) also confirmed its structure.

Acknowledgments

We wish to acknowledge the technical assistance of Mr. R. Mayer and financial assistance from the Natural Sciences and Engineering Research Council of Canada and the Ministère de l'Education du Québec. We thank Dr. J. B. Robert from the C. E. N. Grenoble for the use of the Bruker WM-250 spectrometer.

1. A. Blanchette, F. Sauriol-Lord, and M. St-Jacques. J. Am. Chem. Soc. **100**, 4055 (1978).
2. C. S. Rooney, R. S. Stuart, B. K. Wasson, and H. W. R. Williams. Can. J. Chem. **53**, 2279 (1975).
3. T. Tahara, M. Masago, T. Fujii, and N. Anami. Jpn. Kokai Tokkyo Koho, 78 73,581; Chem. Abstr. **90**, 23131r (1979).
4. A. W. Archer, P. A. Claret, and D. F. Hayman. J. Chem. Soc. B, 1231 (1971).
5. K. Stadnicka and L. Lebioda. Acta Crystallogr. Sect. B, **35**, 2763 (1979).
6. G. Binsch. Top. Stereochem. **3**, 97 (1968).
7. D. Kost, E. H. Carlson, and M. Raban. Chem. Commun. 656 (1971).
8. G. Binsch. J. Am. Chem. Soc. **91**, 1304 (1969). A copy of the program was obtained from QCPE.
9. (*a*) N. L. Allinger and J. T. Sprague. J. Am. Chem. Soc. **94**, 5734 (1972); (*b*) G. Favini and A. Nava. Theor. Chim. Acta, **31**, 261 (1973).
10. F. A. L. Anet and A. J. R. Bourn. J. Am. Chem. Soc. **89**, 760 (1967).
11. L. Canuel and M. St-Jacques. J. Org. Chem. **41**, 1380 (1976).
12. M. Anteunis, D. Tavernier, and F. Borremans. Bull. Soc. Chim. Belg. **75**, 396 (1966).
13. L. Canuel and M. St-Jacques. Can. J. Chem. **52**, 3581 (1974).
14. M. St-Jacques and C. Vaziri. Org. Magn. Reson. **4**, 77 (1972).
15. E. Coene and M. Anteunis. Bull. Soc. Chim. Belg. **79**, 37 (1970).
16. F. W. Wehrli and T. Wirthlin. Interpretation of carbon-13 nmr spectra. Heyden, London. 1976.
17. G. M. Kellie and F. G. Riddell. J. Chem. Soc. B, 1030 (1971).
18. M. K. Kaloustian, N. Dennis, S. Mager, S. A. Evans, F. Alcudia, and E. L. Eliel. J. Am. Chem. Soc. **98**, 956 (1976).
19. E. L. Eliel. Angew. Chem. Int. Ed. Engl. **11**, 739 (1972).
20. M. K. Kaloustian. J. Chem. Educ. **51**, 777 (1974).
21. S. Kabuss, A. Lüttringhaus, H. Friebolin, H. G. Schmid, and R. Mecke. Tetrahedron Lett. 719 (1966).
22. S. Kabuss, H. G. Schmid, H. Friebolin, and W. Faisst. Org. Magn. Reson. **2**, 19 (1970).
23. M. St-Jacques and C. Vaziri. Can. J. Chem. **51**, 1192 (1973).
24. F. A. L. Anet, P. J. Degen, and J. Krane J. Am. Chem. Soc. **98**, 2059 (1976).
25. R. C. Cass, S. E. Fletcher, C. T. Mortiner, P. G. Quincey, and H. D. Springall. J. Chem. Soc. 2595 (1958).
26. A. W. Archer and P. Claret. Chem. Ind. 171 (1969).
27. J. B. Lambert. J. Am. Chem. Soc. **89**, 1836 (1967).
28. E. R. Nelson, M. Maienthal, L. A. Lane, and A. A. Benderly. J. Am. Chem. Soc. **79**, 3467 (1957).

The tetrahedral intermediate of a lactonization reaction

ROBERT A. MCCLELLAND AND MASUMA ALIBHAI

Department of Chemistry, Scarborough College, University of Toronto, West Hill, Ont., Canada M1C 1A4

Received September 29, 1980

ROBERT A. MCCLELLAND and MASUMA ALIBHAI. Can. J. Chem. **59**, 1169 (1981).

The hydrolysis of the ortho ester 1,1-diethoxy-1,3-dihydroisobenzofuran (**1**) is described. This hydrolysis proceeds with initial expulsion of an exocyclic ethoxy group, producing upon hydration of the oxocarbonium ion 1-hydroxy-1-ethoxy-1,3-dihydroisobenzofuran (**7**), the tetrahedral intermediate of the lactonization of ethyl (2-hydroxymethyl)benzoate (**6**) to phthalide (**8**). Based on the kinetic behavior of the ortho ester hydrolysis, the pH variation in the ratio of **6**:**8** initially formed from the ortho ester, and the kinetic behavior of the lactonization reaction, rate constants for the breakdown of the tetrahedral intermediate **7** have been determined, along with the equilibrium constant for its formation from the hydroxy ester **6**. The breakdown occurs in an extremely rapid hydroxide-ion-catalyzed reaction, with the rate being at the diffusion limit. Hydronium ion catalysis is also observed; this breakdown is also rapid although considerably less so than the hydroxide ion reaction. The changeover from H^+ to OH^- catalysis occurs at pH 3.5. The rate of breakdown is a minimum at this point, and corresponds to a half-life for the tetrahedral intermediate of about 0.1 s. It is concluded that this allows sufficient time for conformational changes in the tetrahedral intermediate prior to breakdown; this factor must be taken into account in stereoelectronic considerations.

ROBERT A. MCCLELLAND et MASUMA ALIBHAI. Can. J. Chem. **59**, 1169 (1981).

On décrit l'hydrolyse de l'ortho ester diéthoxy-1,1 dihydro-1,3 isobenzofuranne (**1**). Cette hydrolyse se fait avec une expulsion initiale d'un groupe éthoxy exocyclique conduisant après hydratation à l'ion oxocarbonium hydroxy-1 éthoxy-1 dihydro-1,3 isobenzofuranne (**7**), l'intermédiaire tétraédrique de la lactonisation du (hydroxyméthyl)-2 benzoate d'éthyle (**6**) en phtalide (**8**). On a déterminé la constante de vitesse de rupture de l'intermédiaire tétraédrique **7** ainsi que la constante d'équilibre conduisant à sa formation à partir de l'hydroxy ester **6** en se basant sur le comportement cinétique de l'hydrolyse de l'ortho ester, sur la variation du pH dans le rapport du produits **6**:**8** qui se forment initialement à partir de l'ortho ester et sur le comportement cinétique de la réaction de lactonisation. La rupture se produit au cours d'une réaction extrêmement rapide catalysée par l'ion hydroxyde dont la vitesse est limitée par la diffusion. On observe également la catalyse par l'ion hydronium; cette rupture est également rapide quoique considérablement plus faible que celle de la réaction catalysée par l'ion hydroxyde. Le changement de catalyseur de H^+ à OH^- se produit à un pH de 3,5. La vitesse de rupture est minimale à ce point et correspond à une demie-vie de l'intermédiaire tétraédrique d'environ 0,1 s. On en conclut que ceci accorde suffisamment de temps à des changements conformationnels de l'intermédiaire tétraédrique avant sa rupture. On doit tenir compte de ce facteur dans les considérations stéréoélectriques.

[Traduit par le journal]

Experiments have recently been reported of the direct observation of the two types of intermediates of the hydrolysis of ortho esters (1–7). These experiments obviously verify the three-stage reaction mechanism commonly accepted for this hydrolysis (8). Moreover they provide a direct measure of the kinetic behavior associated with the later two stages and, in certain cases (7), are capable of furnishing the free energy of the intermediates.

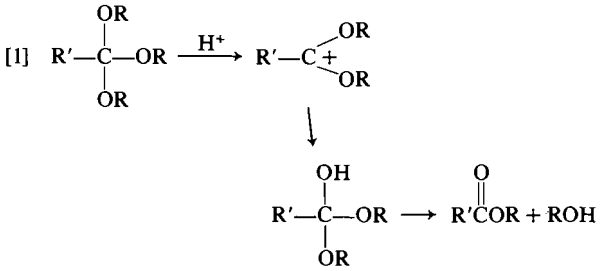

In this paper we report an analysis of the later stages in the hydrolysis of 1,1-diethoxy-1,3-dihydroisobenzofuran (**1**), an ortho ester derived from the lactone phthalide. The hydrolysis of cyclic dialkoxy ortho esters related to **1** (for example, **2**)

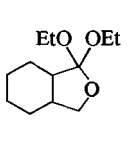

1

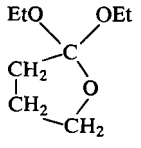

2

has been studied by Deslongchamps and coworkers (9, 10). Such investigations have played a major role in the development of the theory of stereoelectronic control of the breakdown of tetrahedral intermediates (11). The studies of Deslongchamps focused mainly on the nature of the products of the hydrolysis, and we felt it of interest to see if quantitative kinetic data could also be obtained for such a system. It can also be noted that one of the two possible hydrogen ortho ester intermediates of the hydrolysis of **1**, the one that is in fact formed (*vide infra*), is the tetrahedral intermediate of a lactonization reaction, the lactonization of ethyl 2-(hydroxymethyl)benzoate. Although lactonization reactions have seen considerable investigation in a number of cases (12–16), including the above hydroxy ester (15), no direct

0008-4042/81/071169-08$01.00/0

©1981 National Research Council of Canada/Conseil national de recherches du Canada

Can. J. Chem. Downloaded from www.nrcresearchpress.com by 210.87.254.6 on 09/06/12
For personal use only.

information regarding the tetrahedral intermediate has been reported.

Experimental

1-Ethoxy-1,3-dihydroisobenzofuran-1-ylium (3) borofluorate was prepared by the ethylation of phthalide with triethyloxonium borofluorate following a general procedure described by Deslongchamps and co-workers (10). The ^1H nmr spectrum of the salt in 100% H_2SO_4/external $(CH_3)_4Si$ had peaks at δ: 7.9–8.6 (m, 4H), 6.77 (s, 2H), 5.56 (q, J = 8 Hz, 2H), and 2.12 (t, J = 8 Hz, 3H).

1,1-Diethoxy-1,3-dihydroisobenzofuran (1) was prepared by addition of a suspension of the above salt in CH_2Cl_2 to a stirred solution at 0°C of sodium ethoxide in ethanol. Standard work-up (10) gave **1** as a clear liquid, yield 55% based on starting phthalide; bp 65°C/0.1 Torr; ^1H nmr ($CDCl_3$) δ: 7.2–7.5 (m, 4H), 5.08 (s, 2H), 3.53 (*aa'* multiplet, 4H), and 1.17 (t, 6H). *Anal.* calcd. for $C_{12}H_{16}O_3$: C 69.20, H 7.74; found: C 69.6, H 7.83.

Products of Hydrolysis

The ortho ester **1** (0.1 g) was dissolved in 500 mL of an appropriate buffer or acid and the solution allowed to stand for a period of time corresponding to 5–10 half-lives of $k_H[H^+]$ (see Results). The solution was extracted with carbon tetrachloride (100 mL), the bulk of the solvent immediately removed on a rotary evaporator, and the ^1H nmr spectrum of the residual material recorded. This spectrum contained peaks due to phthalide, δ: 7.8–8.1 (m, 1H), 7.2–7.4 (m, 3H), and 5.18 (s, 2H), and peaks due to a second material identifiable as ethyl 2-hydroxymethylbenzoate, δ: 7.8–8.1 (m, 1H), 7.3–7.4 (m, 3H), 4.70 (s*, 2H), 4.29 (q, J = 7 Hz, 2H), 3–4 variable (s*, 1H), and 1.34 (t, J = 7 Hz, 3H). (In certain samples the peaks marked with an asterisk also showed some coupling). The ratio of the two products was determined by the nmr integration of the methylene peaks at δ 5.18 and 4.70.

A solution of the ortho ester **1** dissolved in 100% H_2SO_4 exhibited an nmr spectrum identical to that of the borofluorate salt of **2** in the same acid, with additional peaks appearing from the ortho ester at δ: 4.95 (q, J = 7 Hz, 2H) and 1.87 (t, J = 7 Hz, 3H). These last two peaks are also found on dissolving ethanol in 100% H_2SO_4.

Kinetics

The procedures employed for the hydrolysis of the ortho ester (3), the detection of the oxocarbonium ion intermediate (3, 4), and the hydrolysis in H_2SO_4 solutions of the oxocarbonium ion **2** (17) have been described previously. The lactonization of ethyl 2-hydroxymethylbenzoate was followed spectroscopically at 285 nm (see Fig. 1). For measurements at pH < 4 this experiment was carried out by dissolving the ortho ester in the acid or buffer of interest, and waiting for a period of time sufficient for complete reaction of the ortho ester. For measurements at pH > 4 the ortho ester was dissolved in 0.001 M HCl, and after complete reaction of the ortho ester the solution was adjusted to the desired pH. Rate constants were determined from the slopes of plots of ln $(A_\infty - A)$ or ln $(A - A_\infty)$ versus time. Except where noted these plots were excellently linear. The error in the observed rate constants is ±2%.

Results

Kinetics of Hydrolysis of Ortho Ester 1

The hydrolysis of **1** was followed spectroscopically, from the increase in uv absorbance at 232 nm (Fig. 1). In phosphate buffers, pH 5–7, excellent first-order kinetic behavior is observed, and the

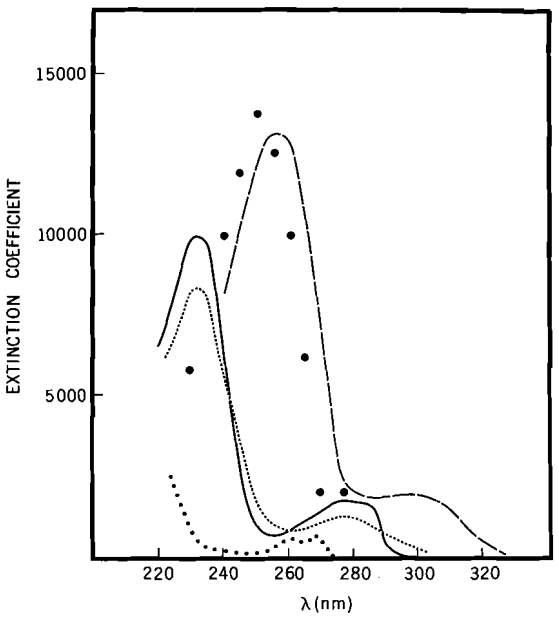

FIG. 1. Absorption spectra; (....) ortho ester **1**; (—) phthalide; (----) initial product of hydrolysis of **1** in 0.001 M HCl; (– – –) oxocarbonium **2**, spectrum taken in 90% H_2SO_4; (●) transient signal generated on hydrolysis of **1** in 0.6 M $HClO_4$; 2.4 M $NaClO_4$.

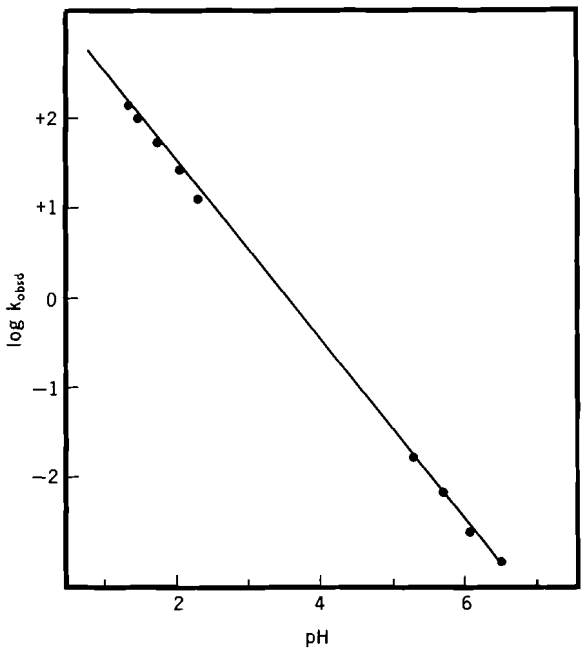

FIG. 2. Observed rate constants for the hydrolysis of **1**. The values in phosphate buffer (pH 5–7) are based on extrapolation to zero buffer concentration. The values in HCl solutions are based on the linear portion of the experimental curves. The line drawn is based on $k_H = 3.1 \times 10^3\ M^{-1}s^{-1}$.

Can. J. Chem. Downloaded from www.nrcresearchpress.com by 210.87.254.6 on 09/06/12
For personal use only.

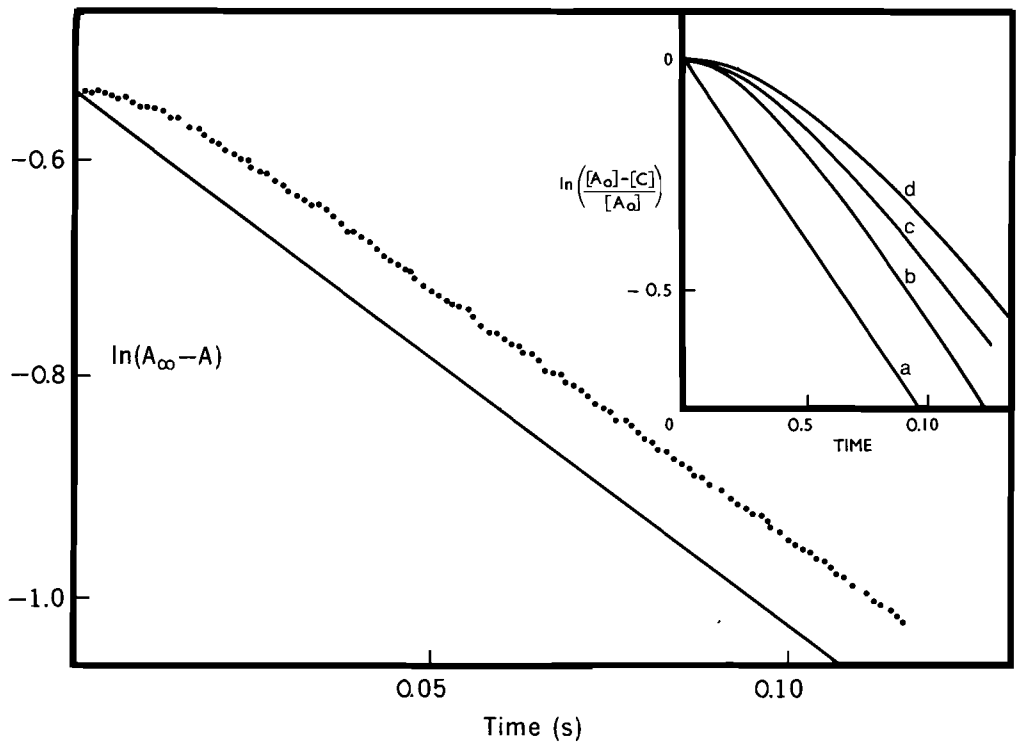

FIG. 3. First-order plot obtained for the hydrolysis of the ortho ester **1** in 0.0015 *M* HCl. The points are observed (see Experimental). The linear portion of the experimental curve ($t > 0.025$) has a least-squares slope of 4.17 s^{-1} ($2.78 \times 10^3 \times [H^+]$). The line drawn in the major figure has a slope of 4.65 s^{-1} ($3.1 \times 10^3 \times [H^+]$) and an intercept corresponding to the intercept of the experimental curve. The insert depicts the first-order plots which would be observed following the formation of the product C of two consecutive first-order reactions A → B → C, with $k_{AB} = 4.65\ s^{-1}$ and (a) $k_{BC} = \infty$ (b) $5k_{AB}$ (c) $3k_{AB}$ and (d) $2k_{AB}$.

observed first-order rate constants show the presence of both an H^+ catalyzed reaction (Fig. 2) and a general acid catalyzed reaction. The value of the second-order rate constant for H^+ catalysis is $3.1 \times 10^3\ M^{-1}s^{-1}$.

In HCl solutions, pH 1–3, the first-order kinetic plots take a form illustrated in Fig. 3. These are characterized by an initial induction period, followed by a region of reasonable linearity. The initial behavior is reproducible and is seen in all HCl solutions, although it does tend to become somewhat obscured at higher acidities where the rate becomes very large. The first-order rate constants evaluated from the linear portions of the plots are proportional to the hydronium ion concentration (Fig. 2), and give a second-order rate constant of $2.8 \times 10^3\ M^{-1}s^{-1}$. Similar behavior is also observed in dilute $HClO_4$ solutions. This observation rules out the possibility that the chloride ion in HCl is somehow responsible for the induction period.

The Oxocarbonium Ion

The cation **3** can be isolated as its borofluorate salt by treatment of phthalide with triethyloxonium borofluorate (18), and is also formed quantitatively on dissolving the ortho ester **1** in concentrated sulfuric acid. This cation has an absorption spectrum with λ_{max} near 255 nm in concentrated acid solutions (Fig. 1), where it is stable to hydrolysis. Similar spectral behavior is also observed with the related cations **4** (19) and **5** (3). The hydrolysis of **3** does occur in more dilute sulfuric acid solutions; rate constants for the hydrolysis in three acids are listed in Table 1. An approach was recently described (17) whereby such rates could be extrapolated to 0% H_2SO_4 to obtain an estimate of the rate in pure water. The average value of these estimates (Table 1) is $1.4 \times 10^2\ s^{-1}$.

Hydrolysis of the ortho ester **1** in solutions where the acid concentration is greater than 0.3 *M* reveals the presence of a transient intermediate. The uv spectrum of this transient (Fig. 1) bears a close

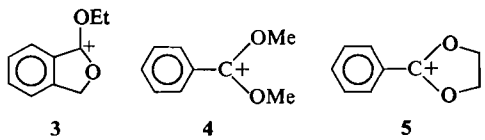

3 **4** **5**

Can. J. Chem. Downloaded from www.nrcresearchpress.com by 210.87.254.6 on 09/06/12
For personal use only.

Can. J. Chem. Downloaded from www.nrcresearchpress.com by 210.87.254.6 on 09/06/12
For personal use only.

TABLE 1. First-order rate constants (25°C) for the hydrolysis of the oxocarbonium ion **2** in H_2SO_4 solutions and estimated rate constants for its hydrolysis in water

$\%H_2SO_4$	k_{obsd}, s^{-1}	$k_{H_2O}{}^2$, s^{-1} [a]
63.9	0.0064	1.4×10^2
67.9	0.00132	1.3×10^2
72.0	0.00035	1.5×10^2

[a] $\log k_{H_2O}{}^2 = \log k_{obsd} - \log (f_R + a_{H_2O}/f_+)$. Values of the last term taken from ref. 17.

resemblance to the spectrum in concentrated acid of the authentic sample of **3**, particularly when the different solvents are taken into account (20). The first-order rate constant for the disappearance of this transient in 0.5 *M* HCl is 3×10^2 s^{-1}.

Products of Hydrolysis of Ortho Ester 1

Both phthalide and the ethyl ester of 2-hydroxymethylbenzoic acid are formed as initial products of the hydrolysis of **1**, and their relative proportion as a function of pH is provided in Fig. 4. It should be noted that these ratios do represent the products of kinetic control of the hydrolysis. The hydroxy ester does slowly convert to lactone (next section), but over the pH region of Fig. 4 this process is much slower than the hydrolysis of the ortho ester.

Lactonization of Hydroxy Ester

First-order rate constants for the conversion of the hydroxy ester to phthalide were measured. This reaction is susceptible to buffer catalysis (15), but after extrapolation to zero buffer concentration, the rate law of eq. [2] is found (Fig. 5), with k_H(lact) $= 1.4 \times 10^{-3}$ $M^{-1}s^{-1}$ and k_{OH}(lact) $= 4.4 \times 10^3$ $M^{-1}s^{-1}$.

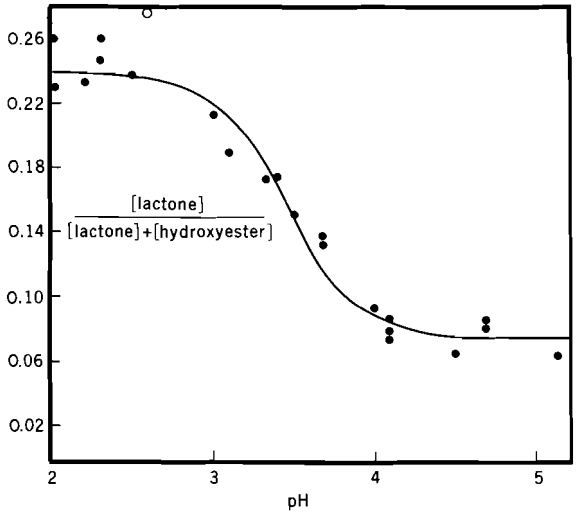

FIG. 4. Composition of the products of the hydrolysis of the ortho ester **1** as a function of pH. The curve is based on eq. [6] and values of constants listed in eqs. [7]–[9]. The point (○) represents the products obtained by addition of the borofluorate salt of the oxocarbonium ion **2**.

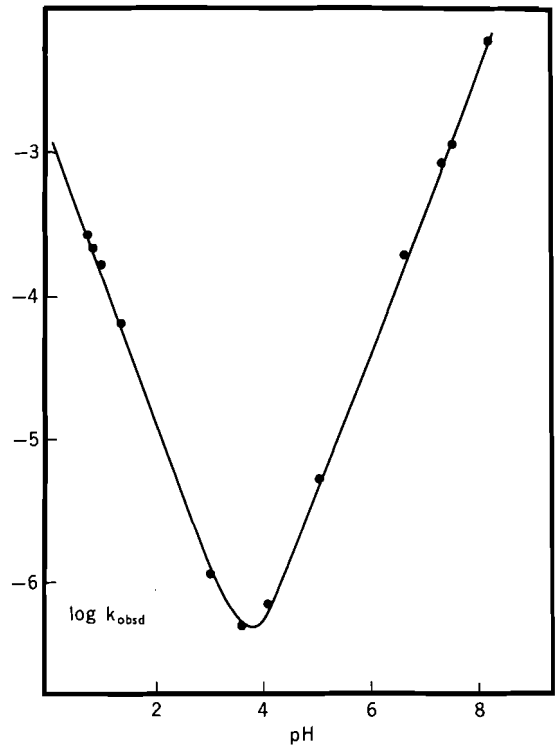

FIG. 5. First-order rate constants for the lactonization of the hydroxy ester **3**. Numbers at pH > 3 are based on extrapolation to zero buffer concentration. The curve is drawn according to eq. [2] using constants defined in the text.

[2] $k_{obsd}(lact) = k_H(lact)[H^+] + k_{OH}(lact)[OH^-]$

Fife and Benjamin (15) report $k_{OH} = 10^4$ $M^{-1}s^{-1}$ and $k_H = 3.4 \times 10^{-3}$ $M^{-1}s^{-1}$ for the same system at 30°C and ionic strength 0.5. Our rate–pH profile (Fig. 5) shows no contribution to the lactonization rate constant from a water or pH independent reaction.

Discussion

In their study of lactone derived ortho esters, Deslongchamps and co-workers presented evidence that the initial stage in the hydrolysis proceeds with loss of an exocyclic alkoxy group and not ring opening (10). The same interpretation (eq. [3]) can be made with the ortho ester **1**. This

[3] 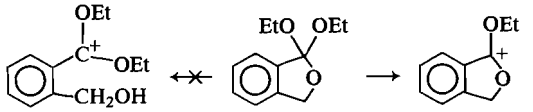

9 **1** **3**

is supported in the present case by two pieces of evidence.

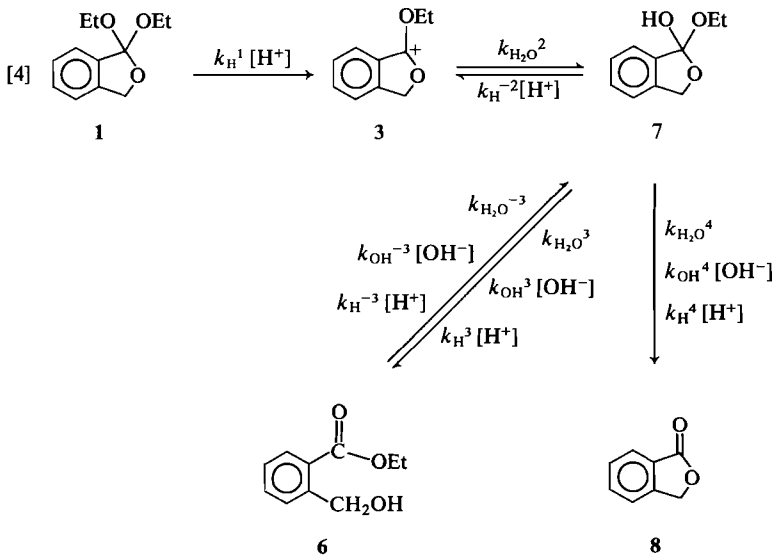

A transient uv signal attributable to an oxocarbonium ion intermediate is observed, and is more reasonably assigned to the cation **3** than to the cation **9**. The rate constant for the disappearance of this transient is close to that estimated for **3** by extrapolation of rates of an authentic sample of this cation. The cation **9** is a phenyl dialkoxy carbonium ion and, unless there is a large rate retarding effect associated with the ortho group, should be considerably more reactive (4, 17).

The products of hydrolysis of the authentic cation **3** have also been determined (Fig. 4) and are very similar to the products from the ortho ester. If the ortho ester were to be hydrolyzing to a significant extent through the cation **9**, it would have formed considerably more hydroxy ester.

The general scheme of eq. [4] can therefore be written to describe the system. The products of the ortho ester hydrolysis are both derived from the cyclic hydrogen ortho ester **7**, the same intermediate that must be involved in the subsequent lactonization of the hydroxy ester.

There can be little uncertainty in assigning the kinetic behavior observed with the ortho ester in phosphate buffers to the oxocarbonium ion-forming stage, so that we can set $k_H{}^1 = 3.1 \times 10^3\ M^{-1}s^{-1}$. This is apparent in the nature of the kinetic data which show only acid catalysis, and is confirmed by our kinetic analysis (*vide infra*). It is in fact generally true that regardless of the nature of the rate-limiting stage in acid solutions, as the acidity is decreased the oxocarbonium-ion-forming stage which requires H^+ catalysis must eventually become rate limiting.

In its oxocarbonium-ion-forming stage **1** behaves fairly similarly to a 2-phenyl-2-alkoxy-1,3-dioxolane (3, 21). Both systems exhibit general acid catalysis and react at fairly similar rates. These rates are moreover considerably greater than that associated with the acyclic trimethyl orthobenzoate. The reason for this difference has been discussed previously (21) in a comparison of the dioxolane and the acyclic ortho esters.

For the 2-aryl-2-alkoxy-1,3-dioxolanes in HCl solutions, the breakdown of the hydrogen ortho ester becomes rate-limiting for product formation (3), and the measured rate constants in HCl solutions refer to this later stage. One of the principal pieces of evidence pointing to the change between low pH and high pH is that the values of k_H obtained in HCl solutions are considerably smaller than values measured in phosphate buffers (3). This change is clearly not seen with the ortho ester **1** where, neglecting the first portion of the kinetic plots, a value of k_H is obtained in HCl solutions which is the same, within experimental uncertainty, as the value measured in phosphate buffers. Thus stage 1 must remain rate determining with **1** in acid[1] and $k_H{}^1 < k_H{}^3 + k_H{}^4$.

The curved initial regions are reminiscent of those seen with simple benzaldehyde acetals in acid solutions (22) and suggest the following analysis. The kinetic system can be described in terms of two consecutive first order reactions (eq. [5]),

[1]It can be noted that the rate constant of 3×10^2 for the decomposition of the ion **3** is actually equal to $k_{H_2O^2}(k_H{}^3 + k_H{}^4)/(k_H{}^{-2} + k_H{}^3 + k_H{}^4)$, but this must in fact be fairly close to $k_{H_2O^2}$. The argument relies on the close similarity between the reverse of the hydration stage and the oxocarbonium-ion-forming stage, such that $k_H{}^{-2}$ must be about the same as $k_H{}^1$ (3). Thus if $k_H{}^1 < k_H{}^3 + k_H{}^4$, so is $k_H{}^{-2}$.

Can. J. Chem. Downloaded from www.nrcresearchpress.com by 210.87.254.6 on 09/06/12
For personal use only.

[5] 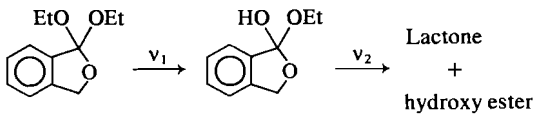

with $v1 = k_H^1[H^+] = 3.1 \times 10^3[H^+]$ and $v2 = (k_H^3 + k_H^4)[H^+]$. This neglects the hydroxide-ion-catalyzed and pH independent reactions of the hydrogen ortho ester. The step involving hydration of the oxocarbonium is also ignored, although it must become important in strongly acidic solutions. The analysis of the previous paragraph suggests that v2 is greater than v1. The insert to Fig. 3 plots theoretical curves (23) for the formation of product for several cases where the difference is not great. These curves do resemble the observed one, showing the induction period followed by the reasonably linear region whose slope is close to v1. The scatter in the experimental data makes the assignment of an exact value for v2 difficult; a number of the order of 3–6 times v1 does satisfy the observed curve reasonably well. This provides the estimate $k_H^3 + k_H^4 = (1\text{–}2) \times 10^4\ M^{-1}s^{-1}$.

It is of course possible that the initial nonlinear portion is an artifact, associated perhaps with the mixing in a stopped-flow apparatus.[2] The following analysis, however, provides support that it is real. The analysis is based on the change with pH in the ratio of products formed in the ortho ester hydrolysis, a change which is due to a variation in the partitioning of the intermediate **7**. The experimental data (Fig. 4) can be fit by eq. [6].

$$[6]\quad \frac{[\text{lactone}]}{[\text{lactone}] + [\text{hydroxy ester}]} = P = \frac{P^+[H^+]^2 + P^-(K_{app})^2}{[H^+]^2 + (K_{app})^2}$$

This equation provides a pH independent region in acid solutions (pH < 2.5 experimentally) which corresponds to breakdown of **7** by H^+ catalyzed reactions, and a pH independent region in base solutions (pH > 4.5 experimentally) which corresponds to breakdown by hydroxide ion catalyzed reactions (eqs. [7] and [8]).

$$[7]\quad P^+ = \frac{k_H^4}{k_H^3 + k_H^4} = 0.24$$

$$[8]\quad P^- = \frac{k_{OH}^4}{k_{OH}^3 + k_{OH}^4} = 0.075$$

The changeover occurs between pH 3 and 4 with an inflection point at $pH = 3.45 = pK_{app}$. The constant K_{app} is squared in eq. [6], and its value (squared) is given by eq. [9].

$$[9]\quad (K_{app})^2 = \left(\frac{k_{OH}^3 + k_{OH}^4}{k_H^3 + k_H^4}\right)K_w = 1.3 \times 10^{-7}$$

Equations [6]–[9] are derived from the general scheme of eq. [4] with the assumption being made that the decomposition of **7** occurs only by H^+ catalyzed and OH^- catalyzed reactions or, in other words, that the pH independent reactions $k_{H_2O}^3$ and $k_{H_2O}^4$ are never important. Justification for this lies in the fact that such a treatment does fit the experimental data, although admittedly the scatter in the experimental points may obscure a minor contribution from the water reactions. Corroboration can be seen in the kinetic behavior associated with the lactonization of the hydroxy ester, which must proceed by cyclization to **7**, the microscopic reverse of its breakdown. This also shows no sign of a pH independent reaction (Fig. 5).

Equations [7]–[9] can be combined with the value of $k_H^3 + k_H^4$ previously estimated to provide the absolute values of all four constants (Table 2). This operation results in very large values for k_{OH}^3 and k_{OH}^4, the former value in fact being indicative of a reaction which is proceeding at the diffusion limit (24).[3] The assignment of these rate constants relies of course on the absolute value of $k_H^3 + k_H^4$ estimated on the basis of the initially curved first-order kinetic plots observed with the ortho ester. Our argument that this region must be real is based on the consideration that if it were an artifact $k_H^3 + k_H^4$ would in fact have a larger value than $(1\text{–}2) \times 10^4\ M^{-1}s^{-1}$. The consequence of this, however, would be that k_{OH}^3 would also be required to be larger to satisfy the product data and would exceed the diffusion limit.

As seen in Table 2 large values of k_{OH} are not unexpected. The hydrogen ortho ester 2-phenyl-2-hydroxy-1,3-dioxolane also reacts with hydroxide ion at a rate near the diffusion limit, and the number in this case is actually measured when this intermediate is generated from a highly reactive precursor amide acetal (6). Rates of breakdown (and formation) of a hemiacetal analog of **7** have also been measured (27), and k_{OH} is again large, although not up to the diffusion limit.

[2]Evidence that such an artifact does not exist with our apparatus is provided by experiments carried out with trimethyl orthobenzoate, where v2 is known to be 10^4 v1 in acid solutions (5). We find excellently linear first-order traces in acid solutions, starting right from zero time.

[3]Since the hydroxide-ion-catalyzed reactions probably proceed by prior ionization (25), this could mean that a proton transfer step could be rate-limiting, an implication which we are currently investigating in other systems which also exhibit large values of k_{OH} (3, 6, 26).

Can. J. Chem. Downloaded from www.nrcresearchpress.com by 210.87.254.6 on 09/06/12
For personal use only.

TABLE 2. Rate and equilibrium constants for the formation and breakdown of hydrogen ortho esters and hemiacetals (25°C)

Constant	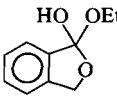 Ring opening	Loss of EtOH	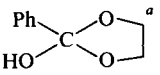 [a]	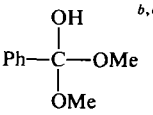 [b,c]	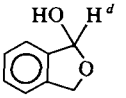 [d]
k_H^{br}, M^{-1} s^{-1}	(6–12) × 10^3	(2–4) × 10^3	3 × 10^2	2 × 10^4	4 × 10^1
$k_{H_2O}^{br}$, s^{-1}	≤2[e]	≤2[e]	1.5	0.6	0.016
k_{OH}^{br}, M^{-1} s^{-1}	(1–2) × 10^{11}	(7–14) × 10^9	6 × 10^{10}	5 × 10^8	1.4 × 10^7
K^{br}	(1–2) × 10^6		4 × 10^8	3 × 10^{11}[f]	0.15
k_H^f, M^{-1} s^{-1}	6 × 10^{-3}		8 × 10^{-7}	7 × 10^{-8}[g]	2.9 × 10^2
$k_{H_2O}^f$, s^{-1}	≤1 × 10^{-6}[e]		4 × 10^{-9}	2 × 10^{-12}[h]	0.11
k_{OH}^f, M^{-1} s^{-1}	6 × 10^4		2 × 10^2	2 × 10^{-3}[g]	9 × 10^7

[a] Reference 7.
[b] k^{br}, ref. 5.
[c] K^{br} and k^f, R. A. McClelland and G. Patel, in preparation.
[d] Reference 27.
[e] Based on the assumption that a one-third contribution of k_w to k(lact) in the pH region 3–4 would be detected.
[f] Units, M.
[g] Units M^{-2} s^{-1}.
[h] Units M^{-1} s^{-1}.

The subsequent lactonization of the initially formed hydroxy ester can be analyzed by making a stationary state assumption in the tetrahedral intermediate **7**, producing the following equations for the rate constants of eq. [2].

$$[10] \quad k_H(\text{lact}) = P^+ k_H^{-3}$$

$$[11] \quad k_{OH}(\text{lact}) = P^- k_{OH}^{-3}$$

The terms P^+ and P^- have the same meaning as in eqs. 7 and 8, providing that the partitioning of **7** is independent of its source. This was established experimentally in the case of coumarin derivatives (16) and should be true here (*vide infra*). Values of k_H^{-3} and k_{OH}^{-3} can be obtained from the observed rate constants and partitioning ratios. These can then be used in conjunction with the values of k_H^3 and k_{OH}^3 to calculate the equilibrium constant for tetrahedral intermediate formation from the hydroxy ester. The value listed in Table 2 is k_H^3/k_H^{-3}. The value of k_{OH}^3/k_{OH}^{-3} is a factor of two larger, the agreement between the two estimates pointing to the self-consistency of our analysis.

It can be noted that unlike the case with coumarinic acids (14) or esters (16) there is no dramatic change in partitioning here between high pH and low pH. To be exact, the first-order rate constants for lactonization should be expressed as in eq. [12],

$$[12] \quad k_{obsd}(\text{lact}) = (k_H^{-3}[H^+] + k_{OH}^{-3}[OH^+])\,P$$

where P is the full partitioning ratio of eq. [6]. The variation in this ratio, however, has little effect on the shape of the rate–pH profile and in particular causes no "break" of the type observed with the coumarinic acid systems (14). In fact the difference between a theoretical curve based on eq. [12] using the constants of Table 2 and the simple empirical rate law of eq. [4] is not outside experimental error.

It can also be noted according to the partitioning ratio that the rate-determining step in the lactonization must be the breakdown of the tetrahedral intermediate to lactone.[4] This has often been assumed (12, 13) for simple lactonizations, although it appears not to have been rigorously established. The same suggestion can also be made on the basis of Deslongchamp's results (9, 10).

Table 2 compares rate and equilibrium constants in several related systems. The three hydrogen ortho esters, all of which form a benzoate ester derivative, exhibit fairly similar rates of breakdown. The rates of formation are considerably slower; this is associated of course with the instability of the hydrogen ortho ester or tetrahedral intermediate relative to the ester product. As expected, these formation rate constants are significantly larger in the case of intramolecular reactions. The first and last columns offer a comparison of a hydrogen ortho ester and a closely related hemiacetal. These show a very large difference, the cyclic hemiacetal being slightly more stable than its free aldehyde form. If one assumes that the free energies of the cyclic forms are similar, the difference in equilibrium constants with these two systems corresponds to an energy difference of about 10 kcal/mol between the ring-opened hy-

[4] Although the difference in energy between the transition states for formation and breakdown is not very great.

Can. J. Chem. Downloaded from www.nrcresearchpress.com by 210.87.254.6 on 09/06/12
For personal use only.

TABLE 3. Life-time (half-life) of the tetrahedral intermediate 7 as a function of pH

pH	Half-life (s)
−1.5	2×10^{-6}
1.0	7×10^{-4}
3.5	0.1
6.0	7×10^{-4}
8.5	2×10^{-6}
11.0[a]	7×10^{-9}

[a]The calculation here is based on the assumption that 7 is not significantly ionized at pH 11.

droxy aldehyde and hydroxy ester. In the kinetic behavior the free energy difference is seen in both directions, the breakdown rates being significantly smaller for the hemiacetal, while its formation rates are larger.

We can also comment on the question of the importance of stereoelectronic control. The system of this study follows the general pattern of behavior exhibited by this type of ortho ester (10), namely a predominance of ring-opened hydroxy ester product. This result was originally explained (10) by invoking stereoelectronic arguments, although it was recognized (10, 11) that a necessary condition for these to apply was that the breakdown of the hydrogen ortho ester occur prior to any conformational change. More recent results (11*c*) have, however, indicated that this condition is not always met, particularly in the case of a hydrogen ortho ester generated in relatively neutral solutions.

The results obtained in the present study fully support this later conclusion. Table 3 lists the life-times of the tetrahedral intermediate **7** as a function of pH. This intermediate has a maximum half-life of about 0.1 s near pH 3.5; this decreases significantly in acid and base solutions. Similar life-times are obtained for the other tetrahedral intermediates of Table 2. These life-times, in the weakly acidic solutions, particularly at pH 3–4, are certainly large enough to allow the tetrahedral intermediate to undergo conformational change prior to breakdown. In fact conformational equilibrium should probably be established. In more acidic solutions and even in weakly basic solutions, the life-times do become short, and the question of conformational change prior to breakdown may arise. In strongly basic solutions the life-time is very short. It is possible in fact that the anionic form of the tetrahedral intermediate breaks down even faster than it is reprotonated.

Acknowledgements

The continued financial support of the Natural Sciences and Engineering Research Council of Canada is gratefully acknowledged. Assistance from the Research Corporation and the J. P. Bickell Foundation is also acknowledged.

1. B. CAPON, J. H. GALL, and D. M. A. GRIEVE. J. Chem. Soc. Chem. Commun. 1034 (1976); B. CAPON and D. M. A. GRIEVE. J. Chem. Soc. Perkin Trans. II, 300 (1980).
2. M. AHMAD, R. G. BERGSTROM, M. J. CASHEN, A. J. KRESGE, R. A. MCCLELLAND, and M. F. POWELL. J. Am. Chem. Soc. **99**, 4827 (1977).
3. M. AHMAD, R. G. BERGSTROM, M. J. CASHEN, Y. CHIANG, A. J. KRESGE, R. A. MCCLELLAND, and M. F. POWELL. J. Am. Chem. Soc. **101**, 2669 (1979).
4. R. A. MCCLELLAND and M. AHMAD. J. Am. Chem. Soc. **100**, 7027 (1978).
5. R. A. MCCLELLAND and R. SOMANI. J. Chem. Soc. Chem. Commun. 407 (1979).
6. R. A. MCCLELLAND and M. AHMAD. J. Org. Chem. **44**, 1855 (1979).
7. R. A. MCCLELLAND, M. AHMAD, J. BOHONEK, and S. GEDGE. Can. J. Chem. **57**, 1531 (1979).
8. E. H. CORDES and H. G. BULL. Chem. Rev. **74**, 581 (1974).
9. P. DESLONGCHAMPS, P. ATLANI, D. FREHEL, and A. MALAVAL. Can. J. Chem. **50**, 3405 (1972).
10. P. DESLONGCHAMPS, R. CHENEVERT, R. J. TAILLEFER, C. MOREAU, and J. K. SAUNDERS. Can. J. Chem. **53**, 1601 (1975).
11. P. DESLONGCHAMPS. (*a*) Tetrahedron, **31**, 2463 (1975); (*b*) Pure Appl Chem. **43**, 351 (1975); (*c*) Heterocycles, **7**, 1271 (1977).
12. D. R. STORM and D. E. KOSHLAND. J. Am. Chem. Soc. **94**, 5805 (1972); **94**, 5815 (1972).
13. S. MILSTEIN and L. COHEN. J. Am. Chem. Soc. **94**, 9158 (1972).
14. R. HERSHFIELD and G. L. SCHMIR. J. Am. Chem. Soc. **95**, 7360 (1973); **95**, 8032 (1973).
15. T. H. FIFE and B. M. BENJAMIN. J. Am. Chem. Soc. **95**, 2059 (1973).
16. R. A. MCCLELLAND, R. SOMANI, and A. J. KRESGE. Can. J. Chem. **57**, 2260 (1979).
17. R. A. MCCLELLAND and M. AHMAD. J. Am. Chem. Soc. **100**, 7031 (1978).
18. H. MEERWEIN, P. BORNER, O. FUCHS, H. J. SASSE, H. SCHRODT, and J. SPILLE. Chem. Ber. **89**, 2060 (1956).
19. R. A. MCCLELLAND and M. AHMAD. J. Am. Chem. Soc. **99**, 5356 (1977).
20. J. T. EDWARD and S. C. WONG. J. Am. Chem. Soc. **99**, 4229 (1977).
21. Y. CHIANG, A. J. KRESGE, S. SALOMAA, and C. I. YOUNG. J. Am. Chem. Soc. **99**, 4494 (1974).
22. J. L. JENSEN and P. A. LENZ. J. Am. Chem. Soc. **100**, 1291 (1978).
23. A. A. FROST and R. G. PEARSON. Kinetics and mechanism. 2nd ed. Wiley, New York. 1961. p. 167.
24. M. EIGEN. Angew. Chem. Int. Ed. Engl. **3**, 1 (1964).
25. L. H. FUNDERBURK, L. ALDWIN, and W. P. JENCKS. J. Am. Chem. Soc. **100**, 5444 (1978).
26. R. A. MCCLELLAND and S. GEDGE. J. Am. Chem. Soc. **102**, 5838 (1980).
27. J. HARRON, R. A. MCCLELLAND, C. THANKACHAN, and T. T. TIDWELL. J. Org. Chem. In press.

Can. J. Chem. Downloaded from www.nrcresearchpress.com by 210.87.254.6 on 09/06/12
For personal use only.

Mécanisme des réactions du chlorite et du dioxyde de chlore. 1. Stoechiométrie des réactions du chlorite et cinétique en présence d'*ortho*-tolidine

GUY SCHMITZ ET HENRI ROOZE

Faculté des Sciences Appliquées, Université Libre de Bruxelles, 50, avenue F. D. Roosevelt, 1050 Bruxelles, Belgique

Reçu le 9 juillet 1980

GUY SCHMITZ et HENRI ROOZE. Can. J. Chem. **59**, 1177 (1981).

La proportion de dioxyde de chlore produit par la dismutation du chlorite de sodium augmente avec la concentration du chlorite et des ions chlorures. Elle passe par un minimum lorsque la concentration de l'acide perchlorique varie de 2 *M* à 0.01 *M*. La réaction rapide entre le chlorite et l'acide hypochloreux fait partie du mécanisme de cette dismutation et sa stoechiométrie a également été étudiée. La proportion de dioxyde de chlore produit dépend du mode de mélange des réactifs et de l'acidité. Elle augmente avec la concentration du chlorite et peut dépasser la quantité prévue par:

$$HClO + 2HClO_2 \rightarrow 2ClO_2 + Cl^- + H^+ + H_2O$$

L'*ortho*-tolidine réagit très rapidement avec le chlore et avec le dioxyde de chlore mais pas avec l'acide chloreux. En milieu perchlorique (pH < 2,5) le produit de son oxydation présente une bande d'adsorption intense avec un maximum à 440 nm (ε = 59 700 M^{-1} cm^{-1}). Le chlore réagit plus vite avec l'*ortho*-tolidine qu'avec l'acide chloreux. L'étude cinétique de la dismutation de l'acide chloreux est ainsi simplifiée par l'utilisation de l'*ortho*-tolidine. En présence de chlorure ajouté initialement l'étape déterminante est $HClO_2 + Cl^- + H^+ \rightarrow 2HClO$ avec une constante cinétique

$$k = 1{,}8 \times 10^{-3}\ M^{-2}\ s^{-1}$$

Les valeurs les plus probables des enthalpies libres de formation des composés oxygénés du chlore sont déduites de la littérature.

GUY SCHMITZ and HENRI ROOZE. Can. J. Chem. **59**, 1177 (1981).

The relative amount of chlorine dioxide produced by the disproportionation of sodium chlorite increases as the concentrations of chlorite and chloride ions increase. It passes through a minimum when the concentration of perchloric acid varies from 2 *M* to 0.01 *M*. The fast reaction between chlorite and hypochlorous acid is a part of the mechanism of this disproportionation and its stoichiometry was also investigated. The relative amount of chlorine dioxide produced depends on the method of mixing the reactants and on the acidity. It increases if the concentration of chlorite increases and can exceed the amount predicted by:

$$HClO + 2HClO_2 \rightarrow 2ClO_2 + Cl^- + H^+ + H_2O$$

Ortho-tolidine reacts very rapidly with chlorine and with chlorine dioxide but not with chlorous acid. In perchloric acid solutions (pH < 2.5) the product of its oxidation has a considerable absorption with a maximum at 440 nm (ε = 59 700 M^{-1} cm^{-1}). Chlorine reacts more rapidly with *ortho*-tolidine than with chlorous acid. The kinetic investigation of the disproportionation of chlorous acid is thus simplified by the use of *ortho*-tolidine. With added chloride ions the rate determining step is $HClO_2 + Cl^- + H^+ \rightarrow 2HClO$ with a rate constant

$$k = 1.8 \times 10^{-3}\ M^{-2}\ s^{-1}$$

The most reliable values for the free enthalpy of formation of oxychlorine compounds are selected from the literature.

Introduction

Les réactions du chlorite de sodium et du dioxyde de chlore présentent un intérêt particulier dans le cadre général de l'étude du mécanisme des réactions d'oxydo-réduction des halogènes et de leurs dérivés oxygénés. Celles du type [1], avec X = Cl, Br ou I, constituent un sujet classique d'études cinétiques en solution.

$$[1] \quad XO_3^- + 5X^- + 6H^+ = 3X_2 + 3H_2O$$

Il existe neuf réactions de ce type, chacun des trois halogénates pouvant réagir avec les trois halogénures. Les lois cinétiques expérimentales sont différentes suivant les cas et ont été le sujet de nombreuses études (1–3), en particulier celles de Bray et de Skrabal. Il en résulte clairement que les réactions du type [1] font intervenir les intermédiaires HXO_2 et HXO suivant un mécanisme complexe dont certains aspects restent controversés. Un des aspects importants de celui que nous adopterons est le rôle du complexe asymétrique et probablement hydraté que nous représenterons par X_2O_2. Différentes structures de ce complexe ont été proposées par Barton et collaborateurs (4, 5). Conformément aux idées de Bray et de Skrabal, on ne peut considérer un processus du type $HXO_3 + HX \rightarrow HXO_2 + HXO$ comme une étape élémentaire impliquant un transfert d'atomes d'oxygène.[1] Un tel processus doit être décomposé en une réaction de formation du complexe X_2O_2 suivie de son hydrolyse:

$$HXO_3 + HX \rightarrow X_2O_2 + H_2O \rightarrow HXO_2 + HXO$$

[1]Intéressés par l'aspect d'oxydo-réduction des réactions étudiées nous considérons comme équivalentes celles qui ne diffèrent que par un équilibre acido–basique et ne distinguons pas toujours explicitement les molécules de leurs ions.

0008-4042/81/081177-11$01.00/0

©1981 National Research Council of Canada/Conseil national de recherches du Canada

Can. J. Chem. Downloaded from www.nrcresearchpress.com by 210.87.254.42 on 09/06/12
For personal use only.

Can. J. Chem. Downloaded from www.nrcresearchpress.com by 210.87.254.42 on 09/06/12
For personal use only.

Nous verrons que de nombreux faits expérimentaux sont alors interprétés aisément en considérant les autres réactions possibles de X_2O_2. Soulignons également les résultats de Taube et Dodgen (6) qui constituent un argument de poids pour considérer le Cl_2O_2 asymétrique comme un intermédiaire des réactions que nous étudierons.

Le cas du chlore se distingue des autres par la relative stabilité du chlorite et de l'acide hypochloreux ainsi que par la formation de dioxyde de chlore pouvant accompagner la réaction [1]. L'élaboration d'un mécanisme des réactions d'oxydo-réduction dans le système chlore peut être basée sur des faits expérimentaux d'origines plus diverses que dans le cas des autres halogènes. Nous commencerons par étudier les réactions du chlorite et la formation du ClO_2 en milieux acides. Nous envisagerons ultérieurement les réactions du ClO_2 en solutions neutres ou basiques.

Thermodynamique

Une étude critique de la littérature nous a conduit à adopter les enthalpies libres de formation reprises dans le tableau 1.

Nous avons vu antérieurement (7) pourquoi nous adoptons pour le chlorite une valeur assez différente de celle que l'on trouve généralement. Le potentiel d'oxydo-réduction de la réaction $ClO_2(aq.) + e = ClO_2^-$ a été mesuré dans des conditions diverses (8–11) et la valeur que nous avons utilisée (E_0 = 0,950 V) est probablement exacte à 0,005 V près.

Différentes méthodes de détermination de la constante d'acidité de l'acide chloreux ont donné des valeurs assez concordantes (12–15).

[2] $HClO_2 = ClO_2^- + H^+; \quad K_2 = 1{,}10 \times 10^{-2}$

La valeur de la constante d'acidité de l'acide hypochloreux déterminée par Morris (16) est quasi égale à celle adoptée antérieurement (12).

[3] $HClO = ClO^- + H^+; \quad K_3 = 3{,}0 \times 10^{-8}$

La valeur de la constante K_4 obtenue par Connick et Chia (17) par extrapolation à force ionique nulle est en accord avec les valeurs d'autres auteurs (13, 18–20) à condition de les corriger en tenant compte du coefficient d'activité de HCl.

[4] $Cl_2(aq.) + H_2O = HClO + Cl^- + H^+; \quad K_4 = 3{,}9 \times 10^{-4}$

Pour l'enthalpie libre de formation du chlorate nous avons adopté la valeur de Wagman et coll. (21). Johnson et coll. (22) ont proposé −7,95 kJ/mol. Avec les valeurs du tableau 1 on obtient pour la réaction [5] une variation d'enthalpie libre de −32 kJ/mol en bon accord avec les mesures de Olson (23).

[5] $ClO_3^- + 5Cl^- + 6H^+ = 3Cl_2(aq.) + 3H_2O; \quad K_5 = 4 \times 10^5$

TABLEAU 1. Enthalpies libres de formation à 25°C

	ΔG_f^0 (kJ/mol)	Références et valeurs utilisées pour le calcul
ClO_3^-	−3,4	(21)
$ClO_2(aq.)$	119	(7)
ClO_2^-	27,3	ΔG_f^0 (ClO_2 aq.) et E_0 (ClO_2/ClO_2^-) = 0,950 V
$HClO_2$	16,1	ΔG_f^0 (ClO_2^-) et $K_2 = 1{,}10 \times 10^{-2}$
HClO	−79,8	(12, 21) ou K_4
ClO^-	−36,9	ΔG_f^0 (HClO) et $K_3 = 3{,}0 \times 10^{-8}$
$Cl_2O(g)$	98	(21)
$Cl_2(aq.)$	6,9	(12, 21)
Cl^-	−131,9	(12, 21)

Compte tenu de la valeur de K_6 et des données de Roth (24) pour la solubilité du Cl_2O, nous ne le considérerons pas dans nos équations stoechiométriques, sa concentration étant toujours extrêmement faible. Il peut cependant intervenir comme produit intermédiaire de certaines réactions.

[6] $2HClO(aq.) = Cl_2O(g) + H_2O; \quad K_6 = 3 \times 10^{-4}$

Au point de vue thermodynamique, l'évolution d'une solution de chlorite doit conduire finalement à la formation de chlorure et d'oxygène. Expérimentalement on constate cependant qu'en l'absence d'effets photochimiques la production d'oxygène est négligeable. Nous ne considérons donc que les dismutations donnant les composés oxygénés du chlore.

A partir des valeurs du tableau 1 on peut calculer la composition d'équilibre obtenue au départ d'une solution acide de chlorite. On constate que si le pH est supérieur à 1 elle correspond à la formation de chlorate et de chlorure suivant [7] avec disparition totale du chlorite. En milieu plus acide on a également une formation non négligeable de chlore suivant [9]. Par exemple à pH = 0 et pour une concentration initiale en chlorite valant 10^{-2} M, on obtient à l'équilibre $[Cl_2]/[Cl^-] = 0{,}24$.

Les études expérimentales de la dismutation du chlorite ne conduisent généralement pas à la composition d'équilibre et l'on observe simultanément les réactions [7] et [8]. Le dioxyde de chlore formé subsiste en milieu acide pour des raisons cinétiques.

[7] $3HClO_2 = 2ClO_3^- + Cl^- + 3H^+$

[8] $5HClO_2 = 4ClO_2 + Cl^- + H^+ + 2H_2O$

[9] $5HClO_2 = 3ClO_3^- + Cl_2 + 3H^+ + H_2O$

En milieu neutre ou basique le dioxyde de chlore se dismute. On n'observe pas de production d'oxygène en solutions à l'abri de la lumière. Il a été

Can. J. Chem. Downloaded from www.nrcresearchpress.com by 210.87.254.42 on 09/06/12
For personal use only.

montré (25) que celle signalée par certains auteurs résulte en fait d'une réaction en phase gazeuse. Comme dans le cas du chlorite, on obtiendrait à l'équilibre un mélange de chlorate et de chlorure, ce qui correspond à la réaction [10], ainsi que du chlore en milieux très acides suivant [11]. La réaction [10] est extrêmement lente. Elle a été étudiée par Bray (26) en présence d'ions chlorures agissant comme catalyseur. En milieux basiques, on observe [12] au lieu de [10]. La constante d'équilibre K_{12} calculée avec les valeurs du tableau 1 vaut 9×10^{-5}, valeur beaucoup plus faible que celle calculée par Taube et Dodgen (6). La différence provient principalement de l'enthalpie libre de formation du chlorite (7). Cette réaction serait donc limitée par la réaction inverse vers pH = 2. La confirmation expérimentale directe de cette conclusion n'est cependant pas possible (6).

[10] $6ClO_2 + 3H_2O = 5ClO_3^- + Cl^- + 6H^+$

[11] $5ClO_2 + 2H_2O = 4ClO_3^- + \frac{1}{2}Cl_2 + 4H^+$

[12] $2ClO_2 + H_2O = ClO_3^- + ClO_2^- + 2H^+$

Stoechiométrie

Technique expérimentale

Le chlorite de sodium commercial à 80% est purifié par trois recristallisations successives. Ses solutions à pH naturel sont standardisées par iodométrie et peuvent être conservées plusieurs jours dans le noir. Le dioxyde de chlore est préparé par réduction du chlorate de sodium par l'acide oxalique (26). Il est dissous dans l'eau distillée et conservé dans le noir à pH naturel. Les solutions d'acide hypochloreux sont obtenues à partir de solutions de chlore où l'on précipite les ions chlorures par l'oxyde mercurique (27). Elles sont conservées dans un réfrigérateur. L'acidité des mélanges réactionnels est fixée soit avec de l'acide perchlorique, soit par un mélange tampon acide citrique–hydrogénophosphate de sodium (concentration totale = 0,1 *M*). Les produits de la qualité "pour analyses" sont utilisés sans purification supplémentaire.

Les productions de ClO_2 sont mesurées par spectrophotométrie à 360 nm. Le coéfficient d'absorption molaire obtenu expérimentalement vaut 1158 L/mol cm. En présence de grandes quantités de chlorite une petite correction doit être apportée aux mesures d'absorbances. La détermination par iodométrie en milieu acide du pouvoir oxydant des solutions étudiées permet, après déduction de la contribution du ClO_2, de calculer selon les cas le chlorite ou l'acide hypochloreux résiduel.

Dismutation du chlorite

La dismutation du chlorite en solutions acides doit être décrite par deux équations stoechiométriques, par exemple [7] et [8]. En désignant par $\Delta(HClO_2)$ la quantité de chlorite ayant réagi, on voit que les rapports stoechiométriques expérimentaux peuvent varier dans les limites suivantes.

$$0 < [ClO_2]/\Delta(HClO_2) < 0{,}80$$

$$0 < [ClO_3^-]/\Delta(HClO_2) < 0{,}66$$

De nombreux travaux (28) sont en accord avec ces relations et confirment qu'il ne faut tenir compte ni d'autres composés du chlore, ni d'une production d'oxygène. L'équation [13] souvent trouvée dans la littérature correspond à la somme de [7] et [8].

[13] $4HClO_2 = 2ClO_2 + ClO_3^- + Cl^- + 2H^+ + H_2O$

Parmi les études consacrées à l'effet des conditions expérimentales sur les rapports stoechiométriques la plus précise et la plus détaillée est celle de Kieffer et Gordon (29). Les résultats que nous avons obtenus sont en parfait accord avec cette étude. Le rapport $[ClO_2]/\Delta(HClO_2)$ augmente avec la concentration du chlorure et dépend de façon complexe de l'acidité. Entre pH = 2 et pH = 5, on trouve dans la littérature des valeurs généralement voisines de 0,5 et quasi indépendantes du pH. Hefti (30) a cependant obtenu des valeurs supérieures et augmentant avec le pH. A pH = 2,5 Kieffer et Gordon (29) ont obtenu 0,64. Ces différences résultent de l'intervention d'autres facteurs, l'un d'eux étant probablement la nature du tampon utilisé. En dessous de pH = 2 et en l'absence de chlorure ajouté initialement, ce rapport passe par un minimum aux environs de pH = 0,5 (29). Nos résultats ont confirmé cette observation. En présence de suffisamment d'ions chlorures, il augmente avec l'acidité et la stoechiométrie tend vers [8].

Un fait expérimental mérite d'être souligné car il n'apparaît pas explicitement dans la littérature. Le rapport $[ClO_2]/\Delta(HClO_2)$ diminue si l'on diminue la concentration du chlorite (cf. tableau 2). On explique ainsi la diminution de ce rapport en fonction du degré d'avancement de la réaction, observée par Kieffer et Gordon (29) à pH = 2,5. En solution 2 *M* en $HClO_4$ ce rapport augmente au cours du temps car, en milieux très acides, l'effet précédent est masqué par celui des ions chlorures produits par la réaction.

Un mécanisme permettant d'interpréter ces observations sera détaillé ultérieurement sur base des études cinétiques. Un de ses éléments importants est le rôle du complexe Cl_2O_2 proposé par Taube et Dodgen (6). Lors de la dismutation du chlorite on forme de l'acide hypochloreux qui réagit extrêmement rapidement suivant [14].

[14] $HClO + HClO_2 \rightarrow Cl_2O_2 + H_2O$

Can. J. Chem. Downloaded from www.nrcresearchpress.com by 210.87.254.42 on 09/06/12
For personal use only.

TABLEAU 2. Effet de la concentration du chlorite sur la stoechiométrie de sa dismutation à 25°C

$[HClO_4]$ (M)	$[NaClO_2]_0$ (10^{-3} M)	$\frac{[ClO_2]}{\Delta[HClO_2]}$
0,2[a]	4,08	0,40
	3,06	0,37
	2,04	0,33
0,6[b]	10,1	0,78
	6,53	0,77
	2,99	0,76
	1,79	0,72
1,0[c]	42,2	0,80
	1,05	0,76
	0,105	0,47

[a]Sans addition de chlorure, conversions = 50%.
[b]Chlorure initial = 0,08 M, conversions quasi totales.
[c]Chlorure initial = 1 M, conversions quasi totales.

Le Cl_2O_2 ainsi formé peut réagir de deux façons différentes, l'une donnant du chlorate, l'autre du dioxyde de chlore. L'étude de la stoechiométrie de la réaction entre le chlorite et l'acide hypochloreux, en vue de préciser l'effet des conditions expérimentales sur l'importance relative des réactions du Cl_2O_2, est donc le complément logique de celle de la dismutation du chlorite.

Réactions du chlorite avec le chlore et avec l'acide hypochloreux

Les vitesses des réactions du chlorite avec le chlore et avec l'acide hypochloreux sont extrêmement grandes en milieux très acides et diminuent si le pH augmente (28, 31–33). Elles semblent d'ordre un par rapport à chacun des deux réactifs. Il est généralement admis que la stoechiométrie de ces réactions peut être décrite par [15] et [16] ou leurs équivalents pour le chlore.

[15] $HClO + HClO_2 = ClO_3^- + Cl^- + 2H^+$

[16] $HClO + 2HClO_2 = 2ClO_2 + Cl^- + H^+ + H_2O$

Les études antérieures de l'importance relative de [15] et [16] ont donné des résultats discordants. Ceci peut être attribué notamment à deux aspects particuliers de ces réactions, l'effet du mode de mélange des réactifs signalé par Emmenegger et Gordon (33) et confirmé par nos expériences, et l'effet du temps écoulé entre le mélange des réactifs et les mesures. En milieu acide et en présence d'un excès de chlorite les réactions étudiées sont suivies de la dismutation du chlorite. En milieu neutre et en présence d'un excès d'hypochlorite, elles sont suivies de la réaction entre le ClO_2 et l'hypochlorite. Pour isoler la production de ClO_2 propre aux réactions chlorite–hypochlorite, il faut alors mesurer sa variation en fonction du temps et déterminer la contribution des autres réactions, ce qui est généralement possible celles-ci étant plus lentes.

Quelques exemples de nos résultats expérimentaux sont donnés par les figs 1 et 2. La variation du rapport $[ClO_2]/[HClO]_0$ en fonction de l'acidité n'est pas monotone. Dans l'acide perchlorique, il augmente si le pH varie de 0 à 2, dans le tampon citrate–phosphate, il diminue si le pH varie de 2 à 6. Ce rapport augmente avec la concentration du chlorite (fig. 1), il varie peu ou diminue si l'on augmente la quantité d'hypochlorite (fig. 2). Pour interpréter ces observations, nous admettons que le Cl_2O_2 formé suivant [14] peut réagir suivant [17] et [18], ce qui correspond respectivement aux équations stoechiométrique [15] et [16].

[17] $Cl_2O_2 + H_2O \rightarrow ClO_3^- + Cl^- + 2H^+$

[18] $Cl_2O_2 + HClO_2 \rightarrow 2ClO_2 + Cl^- + H^+$

L'augmentation du rapport $[ClO_2]/[HClO]_0$ avec la concentration du chlorite s'explique facilement, l'importance de [18] par rapport à [17] étant proportionnelle à cette concentration. Ceci explique également la diminution de ce rapport lorsque l'on augmente la quantité d'acide hypochloreux en remarquant que la concentration instantanée du chlorite dans la solution dépend de cette quantité. Pour une concentration initiale du chlorite donnée, sa concentration au cours de la réaction est plus faible si l'on introduit plus d'hypochlorite. La contribution relative de [18] est alors moins importante. Cet effet doit être d'autant plus marqué que l'excès de chlorite est plus faible. C'est effectivement ce que nous avons observé. Si au lieu de [18] on considérait la réaction $2Cl_2O_2 \rightarrow 2ClO_2 + Cl_2$,

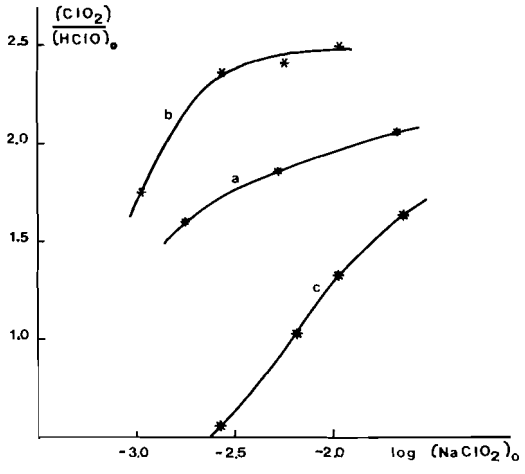

FIG. 1. Productions relatives de ClO_2 obtenues par addition de HClO à un excès de $NaClO_2$; (*a*) $[HClO_4] = 1\ M$, $[HClO]_0 = 5{,}6 \times 10^{-4}\ M$; (*b*) $[HClO_4] = 10^{-2}\ M$, $[HClO]_0 = 4{,}4 \times 10^{-4}\ M$; (*c*) tampon, pH = 6, $[HClO]_0 = 4{,}7 \times 10^{-4}\ M$.

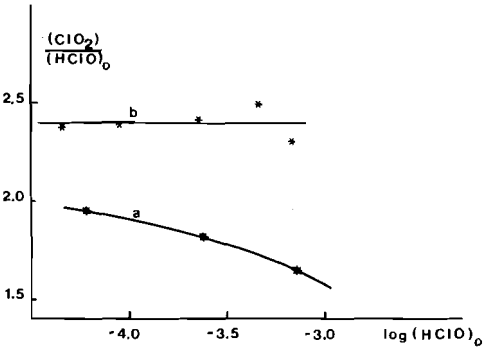

FIG. 2. Productions relatives de ClO_2 obtenues par addition de HClO à un excès de $NaClO_2$; (*a*) $[HClO_4] = 1\,M$, $[NaClO_2]_0 = 2{,}20 \times 10^{-3}\,M$; (*b*) $[HClO_4] = 10^{-2}\,M$, $[NaClO_2]_0 = 5{,}75 \times 10^{-3}\,M$.

proposée par Taube et Dodgen (6), on pourrait justifier l'effet du chlorite mais pas celui de l'hypochlorite.

Le modèle proposé explique également l'effet du mode d'addition des réactifs. On obtient moins de ClO_2 si l'on verse la solution de chlorite dans celle d'hypochlorite que si l'on suit l'ordre inverse, les autres conditions expérimentales étant identiques. En effet, si l'on verse le chlorite dans la solution d'hypochlorite où il réagit très rapidement, sa concentration instantanée reste faible, ce qui limite la contribution de [18].

Les éqs [14], [17] et [18] ne sont cependant pas suffisantes pour décrire le système. On constate que le rapport $[ClO_2]/[HClO]_0$ peut être supérieur à 2, c'est-à-dire que l'on obtient plus de dioxyde de chlore que la quantité maximale prévue par [16]. Cet excès n'est pas dû à la dismutation du chlorite en l'absence d'acide hypochloreux, réaction beaucoup plus lente que celles étudiées et généralement négligeable. De plus nos résultats en tiennent compte lorsque cela est nécessaire. Ce problème a été évoqué par Emmenegger et Gordon (33) qui ont suggéré que l'acide hypochloreux catalyse la dismutation du chlorite. Le mécanisme qui sera proposé après notre étude cinétique permettra de compléter la discussion des résultats présentés ici.

Conclusions et introduction à l'étude cinétique

La dismutation du chlorite en solutions acides donne du dioxyde de chlore et du chlorate en proportions variables. Le dioxyde de chlore, thermodynamiquement instable, apparaît pour des raisons cinétiques. Sa formation n'est cependant pas en contradiction avec les valeurs du tableau 1, la réaction [8] correspondant à une grande diminution d'enthalpie libre. Le mécanisme de la dismutation du chlorite est compliqué et sera discuté ultérieurement. Il fait intervenir un complexe asymétrique, probablement hydraté, que nous avons représenté par Cl_2O_2 et dont on peut schématiser la formation et la disparition comme suit:

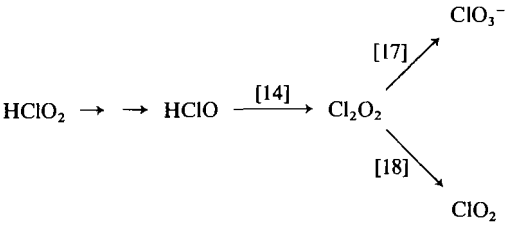

Nous avons montré que la deuxième partie de ce schéma rend compte de plusieurs faits expérimentaux relatifs à la stoechiométrie de la réaction très rapide entre le chlorite et l'acide hypochloreux. L'étude de sa première partie, la formation de l'acide hypochloreux, fait immédiatement apparaître de nombreuses complications d'origines stoechiométriques et cinétiques. En particulier, les lois admises par Gordon et coll. (28) pour les solutions $1{,}2\,M$ en acide perchlorique ne sont pas valables pour les solutions moins acides. Nous allons montrer que beaucoup de ces complications peuvent être évitées en étudiant la vitesse de dismutation du chlorite en présence d'*ortho*-tolidine (biphenyl 4,4′ diamino 3,3′ diméthyl). Il réagit très rapidement avec le chlore, l'acide hypochloreux et le dioxyde de chlore, mais pas avec le chlorite, pour donner en milieu acide une forme oxydée présentant une bande d'absorption intense dans le visible. Son coéfficient d'absorption molaire élevé constitue un des avantages de la méthode en permettant de mesurer facilement des vitesses initiales de réactions et d'élargir le domaine des mesures aux faibles concentrations en chlorite. Ses autres avantages apparaîtront au cours de l'étude cinétique.

Réaction de l'*ortho*-tolidine

Réactions avec le chlore et le dioxyde de chlore

L'*ortho*-tolidine est un réactif classique pour le dosage colorimétrique du chlore et de l'acide hypochloreux (34, 35). La coloration du produit de son oxydation dépend de l'acidité. Pour des valeurs du pH inférieures à 3, on obtient une seule espèce oxydée à laquelle Verbestel et Berger (34) ont attribué la formule $NH = C_6H_3(CH_3) = C_6H_3(CH_3) = NH$ et que nous représenterons par NHRNH. Les réactions de l'*ortho*-tolidine avec le chlore et avec l'acide hypochloreux s'écrivent ainsi sous la forme condensée [19].

[19] $NH_2RNH_2 + HClO \rightarrow NHRNH + Cl^- + H^+ + H_2O$

[19′] $NH_2RNH_2 + Cl_2 \rightarrow NHRNH + 2Cl^- + 2H^+$

Classiquement le dosage du chlore par l'*ortho*-

Can. J. Chem. Downloaded from www.nrcresearchpress.com by 210.87.254.42 on 09/06/12
For personal use only.

Can. J. Chem. Downloaded from www.nrcresearchpress.com by 210.87.254.42 on 09/06/12
For personal use only.

tolidine se fait en milieu chlorhydrique. Nous avons constaté que l'on peut également utiliser l'acide perchlorique et tous les résultats présentés ici ont été obtenus avec cet acide. Nos mesures préliminaires ont montré que plusieurs conditions relatives aux concentrations doivent être respectées. La solution d'oxydant doit être diluée; avec plus de 10^{-4} mol/L de Cl_2 on obtient des résultats par défaut. Si d'autre part la concentration de l'*ortho*-tolidine est trop grande, on observe une décroissance de l'absorbance en fonction du temps, d'autant plus rapide que le pH est élevé. Il semble qu'il y ait une réaction lente entre l'*ortho*-tolidine et sa forme oxydée. Nous avons généralement utilisé une concentration d'environ $5 \times 10^{-4}\,M$ pour laquelle cette réaction est négligeable. Il faut également que le pH soit inférieur à 2,5. La forme du spectre d'absorption est alors indépendante des concentrations avec un maximum à 440 nm. A partir de pH = 3 l'*ortho*-tolidine oxydée prend une coloration verte et il apparaît une bande d'absorption ayant son maximum à 370 nm. Dans les conditions de mesures ainsi définies, la coloration est obtenue instantanément, reste stable pendant au moins 30 min et est parfaitement reproductible. La fig. 3 montre que la loi de Beer–Lambert est satisfaite et que le coéfficient d'absorption molaire vaut $59\,700\,M^{-1}\,cm^{-1}$. Nous avons vérifié qu'il n'y a pas d'interférences des différents ions pouvant être présents lors de nos mesures cinétiques: $[ClO_3^-] \leq 0.1\,M$, $[Cl^-] \leq 1\,M$, $[Fe^{2+}] \leq 10^{-5}\,M$, $[Fe^{3+}] \leq 10^{-5}\,M$. L'effet du Fe(III) qui a parfois été signalé est uniquement d'origine spectrale (36) et n'apparaît pas aux concentrations utilisées. Il n'y a aucun effet de chlorite. L'oxydation lente de l'*ortho*-tolidine par le chlorite signalée antérieurement (35) correspond en fait au système que nous allons étudier: la dismutation du chlorite et l'oxydation de l'*ortho*-tolidine par le chlore ou le dioxyde de chlore produits.

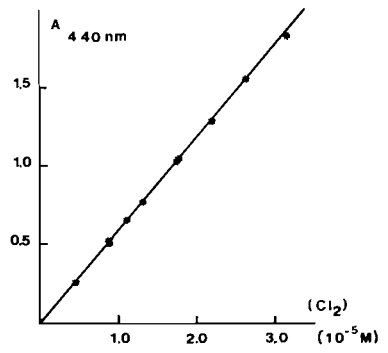

FIG. 3. Dosage du chlore par l'*ortho*-tolidine. $[HClO_4] = 0{,}1\,M$: $[NH_2RNH_2]_0 = 2{,}5 \times 10^{-4}\,M$.

L'*ortho*-tolidine est également utilisée pour le dosage du dioxyde de chlore (35). Les conclusions de nos mesures préliminaires sont identiques à celles obtenues avec le chlore. En solutions diluées dans l'acide perchlorique et pour des valeurs du pH inférieures à 2,5, on obtient le même spectre d'absorption. La coloration est obtenue instantanément, est reproductible et reste stable pendant au moins 30 min. Nos solutions de ClO_2 sont préparées par la méthode de Bray (26), préférable à la méthode standard (35), et standardisées par iodométrie. Les résultats de la fig. 4 correspondent à la réaction [20] et donnent un coéfficent d'absorption molaire de l'*ortho*-tolidine oxydée pratiquement identique à celui obtenu avec le chlore: $\varepsilon = 59\,800\,M^{-1}\,cm^{-1}$.

[20] $NH_2RNH_2 + 2ClO_2 \rightarrow NHRNH + 2HClO_2$

Pour doser le dioxyde de chlore dans des solutions contenant du chlore, on élimine ce dernier par de l'acide oxalique (35). Celui-ci ne réagit pas avec le dioxyde de chlore. Sa réaction avec le chlore apparaît lors des expériences suivantes. Dans une solution d'acide perchlorique donnant un pH final de 1,8 on a introduit $1{,}74 \times 10^{-5}$ mol/L de chlore, $2{,}5 \times 10^{-4}$ mol/L d'*ortho*-tolidine et 10^{-2} mol/L d'acide oxalique dans un ordre variant d'une expérience à l'autre. On a obtenu les absorbances suivantes.

$H_2C_2O_4 + Cl_2 + NH_2RNH_2$	$A_1 = 0$
$NH_2RNH_2 + H_2C_2O_4 + Cl_2$	$A_2 = 0{,}98$
$NH_2RNH_2 + Cl_2 + H_2C_2O_4$	$A_3 = 1{,}04$
$NH_2RNH_2 + Cl_2$	$A_4 = 1{,}04$

La comparaison de A_3 et A_4 montre que l'acide oxalique ne réduit pas l'*ortho*-tolidine oxydée. La comparaison de A_2 et A_3 montre que le chlore réagit plus vite avec l'*ortho*-tolidine qu'avec l'acide oxalique. Nous utiliserons cette propriété ultérieurement.

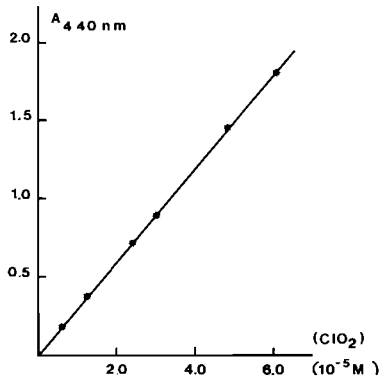

FIG. 4. Dosage du dioxyde de chlore par l'*ortho*-tolidine. $[HClO_4] = 0{,}03\,M$; $[NH_2RNH_2]_0 = 2{,}5 \times 10^{-4}\,M$.

Can. J. Chem. Downloaded from www.nrcresearchpress.com by 210.87.254.42 on 09/06/12
For personal use only.

*La réaction chlorite–chlore en présence d'*ortho-*tolidine*

La technique expérimentale est essentiellement la même que celle décrite antérieurement. Dans les conditions du tableau 3, mais en l'absence d'*ortho*-tolidine, on obtient les réactions [15] et [16], la proportion de chlorate formé étant d'autant plus importante que la concentration du chlorite est plus faible. Si par contre on ajoute du chlore ou de l'acide hypochloreux dans un mélange d'acide perchlorique, d'*ortho*-tolidine et de chlorite, on obtient uniquement la réaction [19] comme le montrent les résultats du tableau 3. Les concentrations de l'*ortho*-tolidine oxydée sont déduites des mesures d'absorbance à 440 nm corrigées pour tenir compte de la dismutation du chlorite. Si les mesures sont faites rapidement cette correction est inférieure à 5%. Les résultats sont indépendants de la concentration initiale de l'*ortho*-tolidine comprise entre 2×10^{-4} et 10^{-3} *M*.

Le rapport $[NHRNH]/[HClO]_0$ valant 1 quelle que soit la concentration du chlorite et le chlorate n'oxydant pas l'*ortho*-tolidine, il est ainsi établi que le chlore ou l'acide hypochloreux ne réagissent pratiquement pas suivant [15]. Nous admettons par conséquent que la réaction avec l'*ortho*-tolidine est encore plus rapide que celle avec le chlorite.[2] Le schéma du mécanisme de la dismutation du chlorite en est simplifié.

$$HClO_2 \rightarrow\rightarrow HClO \xrightarrow{NH_2RNH_2} NHRNH$$

La vitesse initiale de la dismutation du chlorite correspond ainsi à celle de la formation de l'*ortho*-tolidine oxydée. Par contre, en l'absence d'*ortho*-tolidine elle n'est liée à la vitesse de formation du dioxyde de chlore que par un coéfficient stoechiométrique variable. C'est un des avantages de notre méthode.

Cinétique de la dismutation du chlorite en présence de chlorure et d'*ortho*-tolidine

Technique expérimentale

Les solutions de chlorite de sodium sont préparées et standardisées comme précisé antérieurement. Elles donnent des résultats parfaitement reproductibles à condition de n'être pas trop anciennes. Les autres réactifs sont de la qualité "pour analyses" et sont utilisés sans purification supplémentaire. L'acidité est ajustée avec de l'acide perchlorique et la force ionique est fixée à 1 *M* avec du perchlorate de sodium. Toutes les mesures cinétiques sont faites à 25 ± 0,1°C. On mélange les réactifs, le chlorite étant introduit en dernier lieu, et l'on enregistre en fonction du temps l'absorbance à 440 nm mesurée par un spectrophotomètre Beckman DBGT. On obtient des droites dont la pente donne la vitesse initiale de la réaction.

$$v_0 = \frac{d}{dt}[NHRNH] = \frac{1}{59\ 700}\frac{dA}{dt}$$

Ces vitesses initiales sont obtenues très facilement, la grande sensibilité de la méthode permettant de se limiter à des taux de conversion de chlorite extrêmement faibles.

TABLEAU 3. La réaction chlorite – acide hypochloreaux en présence d'*ortho*-tolidine 2×10^{-4} à 10^{-3} *M*

$[HClO_4]$ (*M*)	$[NaClO_2]_0$ (10^{-5} *M*)	$[HClO]_0$ (10^{-5} *M*)	$\frac{[NHRNH]}{[HClO]_0}$
1	4,25	2,21	1,01
		4,42	1,00
	8,50	2,21	1,01
		4,42	0,99
	17,0	2,21	1,00
		4,42	1,00
0,1	4,25	2,21	1,01
		4,42	0,98
	8,50	2,21	1,01
		4,42	0,98
	17,0	2,21	1,02
		4,42	1,01
	34,0	2,21	1,02
		4,42	1,02

Résultats

Il n'y a aucun effet de la force ionique ni de la concentration en *ortho*-tolidine sur la valeur de v_0. Quelques résultats sont repris dans le tableau 4. Il faut éviter les temps de réaction trop longs et les mesures d'absorbances trop élevées la variation de celles-ci en fonction du temps cessant alors d'être parfaitement linéaire. Les écarts résultent probablement d'une réaction de l'*ortho*-tolidine oxydée, totalement négligeable dans les conditions de mesures que nous avons adoptées.

La fig. 5 montre que la vitesse v_0 peut être représentée par une somme de deux termes.

$$v_0 = v_I + k_{II}[Cl^-]$$

Dans la zone des concentrations en chlorure utilisées ceci est conforme aux résultats de Kieffer et Gordon (29) ainsi qu'à ceux de Hong et Rapson (37). Nous expliquerons ultérieurement les écarts

[2]On pourrait admettre également que l'on forme du Cl_2O_2 et que celui-ci réagit plus vite avec l'*ortho*-tolidine qu'il ne s'hydrolyse. Pour la suite de notre étude, cette hypothèse est strictement équivalente à celle adoptée.

Can. J. Chem. Downloaded from www.nrcresearchpress.com by 210.87.254.42 on 09/06/12
For personal use only.

TABLEAU 4. Vitesses initiales en fonction de la force ionique et de la concentration en *ortho*-tolidine. $[HClO_4] = 0{,}104\ M$, $[Cl^-] = 0{,}10\ M$

$[NaClO_2]$ $(10^{-3}\ M)$	$[NaClO_4]$ (M)	$[NH_2RNH_2]$ $(10^{-3}\ M)$	v_0 $(10^{-8}\ M\ s^{-1})$
1,07	0	0,25	4,68
	0,2	0,25	4,39
	0,5	0,25	4,52
	0,8	0,25	4,70
0,98	0	0,15	4,19
	0	0,25	4,23
	0	0,50	4,22
	0	1,00	4,23

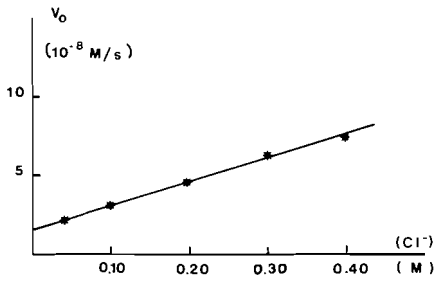

FIG. 5. Vitesses de réaction en présence d'*ortho*-tolidine $2 \times 10^{-4}\ M$. $[HClO_2] = 0{,}104\ M$; $[NaClO_2] = 5{,}02 \times 10^{-4}\ M$.

à cette relation linéaire, observés par ces auteurs pour les très faibles concentrations en ions chlorures, par un effet de ces ions sur le processus réactionnel correspondant à v_I.

Dans l'acide perchlorique $1{,}2\ M$, le terme v_I correspond à une réaction d'ordre deux par rapport au chlorite (29). En milieu moins acide la loi cinétique est beaucoup plus compliquée et sera l'objet de notre prochain article. Une étude précise de k_{II} implique d'éliminer la contribution de v_I. Pour cela, nous avons mesuré v_0 en fonction de (Cl^-) pour différentes concentrations en chlorite et en acide et déterminé k_{II} par la relation

$$k_{II} = \frac{\Delta v_0}{\Delta[Cl^-]}$$

Les résultats sont repris sur les figs 5 à 7 ainsi que dans le tableau 5.

Nous avons représenté par $[NaClO_2]$ la concentration totale du chlorite. On a donc:

$$[NaClO_2] = [HClO_2] + [ClO_2^-]$$

Pour le calcul de la concentration $[HClO_2]$ nous avons utilisé la constante d'équilibre de la réaction [2] ainsi que $\gamma_\pm = 0{,}8$ pour une force ionique fixée à $1\ M$. Le choix d'une valeur un peu différente n'aurait pas eu d'influence sur le résultat du calcul de la constante cinétique.

Le tableau 5 montre que k_{II} varie proportionnellement à la concentration de l'acide chloreux et à celle de l'acide perchlorique. Le deuxième terme de la loi donnant v_0 prend ainsi la forme.

$$v_{II} = k[HClO_2][Cl^-][H^+]$$

avec

$$k = 3{,}50 \times 10^{-3}\ M^{-2}\ s^{-1}$$

Discussion

La loi cinétique expérimentale comporte deux termes dont le second peut être interprété par le mécanisme suivant:

[21] $HClO_2 + Cl^- + H^+ \rightarrow 2HClO$

[19] $HClO + NH_2RNH_2 \rightarrow Cl^- + H^+ + NHRNH + H_2O$

L'étape [21] étant déterminante[3] la vitesse de la réaction est indépendante de la concentration de l'*ortho*-tolidine.

$$\frac{d[NHRNH]}{dt} = 2k_{21}[HClO_2][Cl^-][H^+]$$

$$k_{21} = \tfrac{1}{2}k = 1{,}75 \times 10^{-3}\ M^{-2}\ s^{-1}$$

*Comparaison avec des mesures en l'absence d'*ortho-*tolidine*

L'étude cinétique de la dismutation du chlorite en l'absence d'*ortho*-tolidine est compliquée par des problèmes stoechiométriques. Reprenons, en le complétant, le schéma considéré antérieurement.

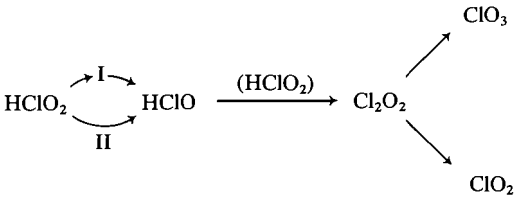

Les processus I et II correspondent aux deux termes de la loi cinétique.

Si le mécanisme de la dismutation du chlorite correspondait simplement à [21] suivi de [15], sa stoechiométrie serait donnée par [7] et sa loi cinétique par:

$$\frac{d[ClO_2]}{dt} = 0; \qquad -\frac{d[HClO_2]}{dt} = 3v_{21}$$

Si son mécanisme correspondait à [21] suivi de

[3]Pour des raisons étrangères à ce travail nous pensons que [21] n'est pas une étape élémentaire mais résulte de $HClO_2 + Cl^- + H^+ \rightarrow Cl_2O + H_2O$ suivi de $Cl_2O + H_2O \rightarrow 2HClO$. On obtient la même loi cinétique quelle que soit l'étape déterminante.

Can. J. Chem. Downloaded from www.nrcresearchpress.com by 210.87.254.42 on 09/06/12
For personal use only.

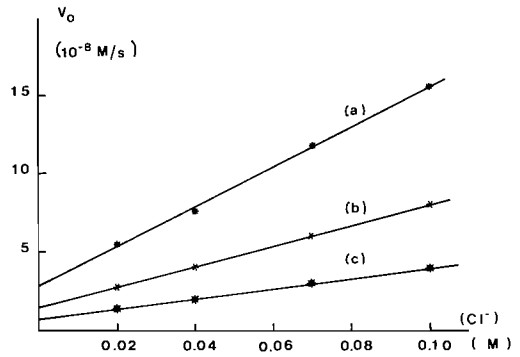

FIG. 6. Vitesses de réaction en présence l'*ortho*-tolidine 2×10^{-4} *M*. $[HClO_4] = 0{,}208$ *M*; $[NaClO_2] = 1{,}97 \times 10^{-3}$ (*a*), $9{,}86 \times 10^{-4}$ (*b*) et $4{,}93 \times 10^{-4}$ *M* (*c*).

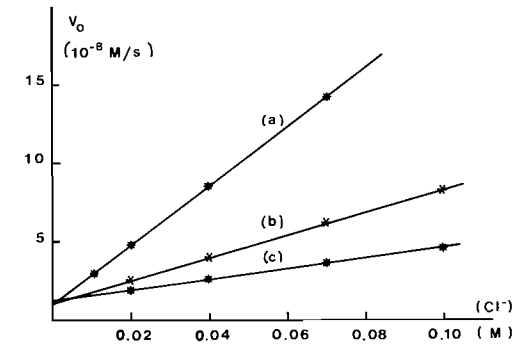

FIG. 7. Vitesses de réaction en présence d'*ortho*-tolidine 2×10^{-4} *M*. $[NaClO_2] = 1{,}07 \times 10^{-3}$ *M*; $[HClO_4] = 0{,}521$ (*a*), 0,208 (*b*) et 0,104 *M* (*c*).

TABLEAU 5. Constantes cinétiques en présence de chlorure et d'*ortho*-tolidine; 25°C; $\mu = 1$ *M*

$[HClO_4]$ (*M*)	$[NaClO_2]$ (10^{-3} *M*)	$10^6 k_{II}$ (s^{-1})	$10^3 k$ (M^{-2} s^{-1})
0,208	1,970	1,280	3,38
0,208	0,986	0,650	3,43
0,208	0,493	0,334	3,53
0,104	0,502	0,157	3,50
0,521	1,071	1,892	3,50
0,208	1,071	0,725	3,52
0,104	1,071	0,336	3,52

[16], sa stoechiométrie serait donnée par [8] et sa loi cinétique par:

$$[22] \quad \frac{d[ClO_2]}{dt} = 4v_{21}; \qquad -\frac{d[HClO_2]}{dt} = 5v_{21}$$

En général [21] est suivi de [15] et [16] simultanément. En exprimant la stationnarité de HClO ($v_{15} + v_{16} = 2v_{21}$) et en posant $v_{16} = \alpha v_{21} (0 < \alpha < 2)$, on obtient:

$$\frac{d[ClO_2]}{dt} = 2\alpha v_{21}; \qquad -\frac{d[HClO_2]}{dt} = (3 + \alpha)v_{21}$$

Pour obtenir v_{21} à partir des courbes cinétiques, il faut donc non seulement isoler la contribution du processus II, comme nous l'avons fait en présence d'*ortho*-tolidine, mais également connaître l'effet des conditions expérimentales sur α.

Dans les milieux très acides et très riches en ions chlorures le problème est plus simple. Kieffer et Gordon (29) ont montré que la stoechiométrie correspond alors quasi exclusivement à [8] ce qui implique $\alpha \simeq 2$. De plus l'importance relative du processus I est fortement réduite.

Quelques résultats expérimentaux sont repris sur la fig. 8. Ils ont été obtenus en suivant la production de dioxyde de chlore en fonction du temps par absorptiométrie à 360 nm. Pour les faibles taux de conversion du chlorite on obtient des droites dont la pente donne la vitesse initiale de la réaction. En milieux moins acides, on n'obtient plus des droites même pour les faibles taux de conversion et la mesure des vitesses initiales devient très imprécise. La raison en apparaîtra lors de notre étude du processus I.

Signalons que pour obtenir des mesures reproductibles, nous avons du recristalliser le chlorure utilisé. Cette précaution est rendue nécessaire par la présence de bromure qui, même à des concentrations extrêmement faibles, peut avoir un effet sur la vitesse de la réaction. Cet effet n'apparaît pas en présence d'*ortho*-tolidine et sera étudié ultérieurement.

La fig. 8 montre qu'en l'absence d'*ortho*-tolidine la vitesse est également donnée par une somme de deux termes dont l'un est proportionnel à la concentration en ions chlorures.

$$\frac{d[ClO_2]}{dt} = v_1' + 7{,}3 \times 10^{-3}[HClO_2][Cl^-][H^+]$$

Nous avons vu que dans ces conditions le mécanisme correspond à [21] suivi de [16] ce qui donne compte tenu de [22],

$$k_{21} = 1{,}82 \times 10^{-3}\ M^{-2}\ s^{-1}$$

La concordance avec la valeur obtenue en présence d'*ortho*-tolidine est remarquable.

La loi cinétique proposée par Kieffer et Gordon (29) correspond à celle obtenue ici lorsque la concentration en ions chlorures est suffisamment grande. Pour une solution 1,2 molaire en acide perchlorique, elle se réduit à

$$-\frac{d[HClO_2]}{dt} = 1{,}57 \times 10^{-2}[HClO_2][Cl^-]$$

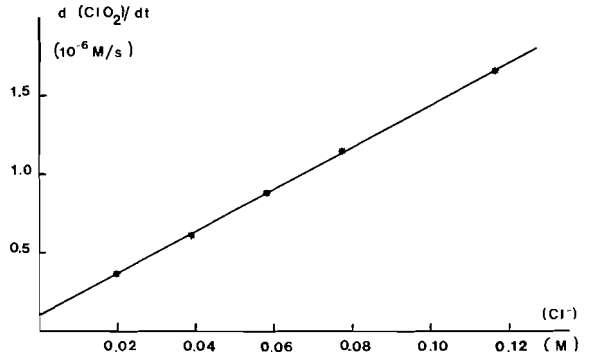

FIG. 8. Vitesses de réaction en l'absence d'*ortho*-tolidine. $[NaClO_2] = 2{,}99 \times 10^{-3}\,M$; $[HClO_4] = 0{,}624\,M$.

Ces auteurs constatent cependant que leur constante cinétique augmente avec l'acidité et admettent une variation linéaire. Leur loi devient ainsi:

$$-\frac{d[HClO_2]}{dt} = 1{,}31 \times 10^{-2}[HClO_2][Cl^-][H^+]$$

ce qui correspond, pour $\alpha \simeq 2$, à

$$k_{21} = 2{,}6 \times 10^{-3}\,M^{-2}\,s^{-1}$$

Cette valeur est compatible avec la nôtre compte tenu des différences de méthodes expérimentales, du fait qu'elle a été déduite de mesures globales de la vitesse de disparition de l'acide chloreux, sans isoler la contribution du processus II, et des complications stoechiométriques qui apparaissent en l'absence d'*ortho*-tolidine. Les résultats de Hong et Rapson (37) sont également en accord avec les nôtres moyennant des remarques similaires.

Conclusions

La loi cinétique de la dismutation du chlorite peut être représentée par une somme de deux termes dont l'un, proportionnel à la concentration des ions chlorures, peut être interprété par le mécanisme suivant:

[21] $HClO_2 + Cl^- + H^+ \rightarrow 2HClO$

[14] $HClO + HClO_2 \rightarrow Cl_2O_2 + H_2O$

[17] $Cl_2O_2 + H_2O \rightarrow ClO_3^- + Cl^- + 2H^+$

[18] $Cl_2O_2 + HClO_2 \rightarrow 2ClO_2 + Cl^- + H^+$

Ce mécanisme doit être complété pour tenir compte d'au moins deux groupes de faits expérimentaux. D'une part, nous avons vu qu'il explique l'essentiel de nos résultats relatifs à la réaction entre le chlorite et l'acide hypochloreux, mais pas leur intégralité. D'autre part, il existe un autre processus de dismutation du chlorite. En milieux 1,2 molaire en acide perchlorique ce processus est d'ordre 2 par rapport au chlorite et n'est pas influencé par le ClO_2 (29). Kieffer et Gordon ont cependant constaté que la loi qu'ils ont établie ne reste pas valable en milieux moins acides. Ce sera l'objet de notre article suivant où nous montrerons notamment que le ClO_2 peut alors inhiber la dismutation du chlorite.

L'*ortho*-tolidine simplifie grandement ces études de mécanismes en réagissant très rapidement avec l'acide hypochloreux et avec le dioxyde de chlore. En particulier il remplace les réactions [14], [17] et [18] par [19]. Grâce à la grande valeur du coéfficient d'absorption molaire de sa forme oxydée il a également l'avantage de permettre une mesure précise des vitesses initiales de réaction.

Remerciements

Les fructueuses discussions que nous avons eues avec Monsieur le Professeur C. Herbo sont à l'origine de ce travail. Nous lui adressons nos plus vifs remerciements.

1. W. C. BRAY. J. Am. Chem. Soc. **52**, 3580 (1930).
2. A. SKRABAL. Z. Elektrochem. **40**, 243 (1934).
3. (*a*) J. SIGALLA. J. Chim. Phys. **55**, 758 (1958); (*b*) Nombreuses références de cet article.
4. A. F. BARTON et G. A. WRIGHT. J. Chem. Soc. A, 1747 (1968); 2096 (1968).
5. A. F. BARTON et BOON-HIAN LOO. J. Chem. Soc. A, 3032 (1971).
6. H. TAUBE et H. DODGEN. J. Am. Chem. Soc. **71**, 3330 (1949).
7. G. SCHMITZ. J. Chim. Phys. **76**, 209 (1979).
8. G. HOLST. Sven. Papperstidn. **48**, 23 (1945).
9. T. NAITO. Kogyo Kagaku Zasshi, **65**, 749 (1962).
10. O. SCHWARZER et R. LANDSBERG. J. Electroanal. Chem. **14**, 339 (1967).
11. F. PERGOLA, R. GUIDELLI et G. RASPI. J. Am. Chem. Soc. **92**, 2645 (1970).
12. W. M. LATIMER. Oxidation potentials. Prentice Hall Inc., New York, NY. 1952.
13. M. W. LISTER. Can. J. Chem. **30**, 879 (1952).
14. G. F. DAVIDSON. J. Chem. Soc. 1649 (1954).
15. D. LEONESI et G. PIANTONI. Ann. Chim. (Rome), **55**, 668 (1965).
16. J. C. MORRIS. J. Phys. Chem. **70**, 3798 (1966).
17. R. E. CONNICK et Y. CHIA. J. Am. Chem. Soc. **81**, 1280 (1959).
18. G. ZIMMERMAN et F. C. STRONG. J. Am. Chem. Soc. **79**, 2063 (1957).
19. M. EIGEN et K. KUSTIN. J. Am. Chem. Soc. **84**, 1355 (1962).
20. K. DREYER et G. GORDON. Inorg. Chem. **11**, 1174 (1972).
21. D. D. WAGMAN et coll. Natl. Bur. Stand. U.S., Tech. Note 270-1 (1965); Tech. Note 270-3 (1968).
22. G. K. JOHNSON, P. N. SMITH, E. H. APPELMAN et W. N. HUBBARD. Inorg. Chem. **9**, 119 (1970).
23. A. R. OLSON. J. Am. Chem. Soc. **42**, 896 (1920).
24. W. A. ROTH. Z. Phys. Chem. A**191**, 248 (1942).
25. R. W. BROWN. Tappi, **35**, 75 (1952).

Can. J. Chem. Downloaded from www.nrcresearchpress.com by 210.87.254.42 on 09/06/12
For personal use only.

26. W. C. BRAY. Z. Phys. Chem. **54**, 569 (1906).
27. Inorganic Synthesis. Tome V. Therald Maeller. 1957. p. 156.
28. (*a*) G. GORDON, R. G. KIEFFER et D. H. ROSENBLATT. Prog. Inorg. Chem. **15**, 201 (1972); (*b*) cf. de nombreuses références de cet article non reprises ici.
29. R. G. KIEFFER et G. GORDON. Inorg. Chem. **7**, 235 (1968).
30. H. HEFTI. J. Text. Res. **30**, 861 (1960).
31. J. F. WHITE, M. C. TAYLOR et G. P. VINCENT. Ind. Eng. Chem. **34**, 783 (1942).
32. M. L. GRANSTROM et B. M. ISRAEL. Am. Chem. Soc., Div. Water, Air and Waste Chem., Gen. Pap. 157th. Natl. Meeting, 137 (1969).
33. F. EMMENEGGER et G. GORDON. Inorg. Chem. **6**, 633 (1967).
34. J. VERBESTEL et A. BERGER. Bull. Cent. Belge Etud. Eaux, **9**, 545 (1950).
35. Standard Methods for the Examination of Water. Am. Public Health Ass., 10th éd. New York. 1955.
36. P. URONE et E. BONDE. Anal. Chem. **32**, 1666 (1960).
37. C. C. HONG et W. H. RAPSON. Can. J. Chem. **46**, 2053 (1968).

Can. J. Chem. Downloaded from www.nrcresearchpress.com by 210.87.254.42 on 09/06/12
For personal use only.

Phosphorus-31 nuclear magnetic resonance studies of phosphido-bridged dinuclear complexes of palladium and platinum

JAMES BRADLEY BRANDON AND KEITH ROGER DIXON[1]

Department of Chemistry, University of Victoria, Victoria, B.C., Canada V8W 2Y2

Received September 15, 1980

JAMES BRADLEY BRANDON and KEITH ROGER DIXON. Can. J. Chem. **59**, 1188 (1981).

Proton decoupled ^{31}P nmr spectra are reported for a series of dinuclear metal complexes containing bridging dialkyl- or diarylphosphido groups: $[M_2Cl_2(\mu\text{-}PR'_2)_2(PR_3)_2]$, M = Pd, R′ = Ph, $R_3 = Et_3$ or HPh_2; M = Pd, R′ = Me, $R_3 = Et_3$, Ph_3, or HMe_2; M = Pt, R′ = Ph, $R_3 = Et_3$ or HPh_2; and $[M_2(\mu\text{-}PPh_2)_2(dppe)_2]Cl_2$, M = Pd, or Pt, dppe = $Ph_2P(CH_2)_2PPh_2$. Detailed analysis and computer simulation of the spectra in the AA′XX′, AA′XX′M, AA′A″A‴XX′, and AA′A″A‴XX′M spin systems leads to the following ranges and *relative* signs for coupling constants involving the bridging phosphorus atoms: $^2J(R_3P\text{—}cis\ PR'_2)$, M = Pt, −1 to +5 Hz, M = Pd, +20 to +32 Hz; $^2J(R_3P\text{—}trans\ PR'_2)$, M = Pt, +291 to +396 Hz, M = Pd, +311 to +443 Hz; $^2J(R_2P\text{—}cis\ PR_2)$, M = Pt, −162 to −208 Hz, M = Pd, −261 to −350 Hz (the assignment of negative signs to these couplings is not completely certain); $^1J(Pt\text{—}PR_2)$, *trans* to Cl, +2364 to +2635 Hz, *trans* to PR_3, +1690 to +1992 Hz. Resonances due to the bridging phosphido groups occur at very high field (−267 to −322 ppm upfield of $P(OCH_3)_3$), in strong contrast to literature reports of phosphido bridges in palladium cluster complexes where the bridged metal atoms are linked by a metal–metal bond and the bridging phosphorus occurs +57 to +82 ppm downfield of $P(OCH_3)_3$.

JAMES BRADLEY BRANDON et KEITH ROGER DIXON. Can. J. Chem. **59**, 1188 (1981).

On rapporte les spectres rmn du ^{31}P desquels on a découplé les protons d'une série de complexes métalliques binucléaires ayant en position de point des groupements dialkyle ou diaryle phosphido: $[M_2Cl_2(\mu\text{-}PR'_2)_2(PR_3)_2]$ M = Pd, R′ = Ph, $R_3 = Et_3$ ou HPh_2; M = Pd, R′ = Me, $R_3 = Et_3$, Ph_3 ou HMe_2; M = Pt, R′ = Ph, $R_3 = Et_3$ ou HPh_2; et $[M_2(\mu\text{-}PPh_2)_2(dppe)_2]Cl_2$, M = Pd ou Pt, dppe = $Ph_2P(CH_2)_2PPh_2$. Une analyse détaillée et une simulation à l'ordinateur des spectres des systèmes de spin AA′XX′, AA′XX′M, AA′A″A‴XX′ et AA′A″A‴XX′M conduisent aux intervalles et aux signes *relatifs* suivants des constantes de couplage impliquant l'atome de phosphore en position de pont: $^2J(R_3P\text{—}cis\ PR'_2)$, M = Pt, −1 à +5 Hz, M = Pd, +20 à +32 Hz; $^2J(R_3P\text{—}trans\ PR'_2)$, M = Pt, +291 à +396 Hz, M = Pd, +311 à +443 Hz; $^2J(R_2P\text{—}cis\ PR_2)$, M = Pt, −162 à −208 Hz, M = Pd, −261 à −350 Hz (l'attribution des signes négatifs à ces constantes de couplage n'est pas absolument certaine); $^1J(Pt\text{—}PR_2)$, *trans* à Cl, +2364 à +2635 Hz, *trans* à PR_3, +1690 à +1992 Hz. Les résonances dues au groupe phosphido en position de pont se produisent à très haut champ (−267 à −322 ppm à plus haut champ que $P(OCH_3)_3$) ce qui contraste fortement avec les données de la littérature au sujet des ponts phosphido dans les complexes du palladium où les atomes de métal en position de pont sont liés par une liaison métal–métal et le phosphore du pont apparaît de +57 à +82 ppm plus bas que le $P(OCH_3)_3$.

[Traduit par le journal]

Introduction

One of the objectives of our recent work has been the structural and chemical characterisation of the novel trinuclear palladium cluster cations $[Pd_3(\mu\text{-}X)(\mu\text{-}PR'_2)_2(PR_3)_3]^+$ (**1**). These clusters

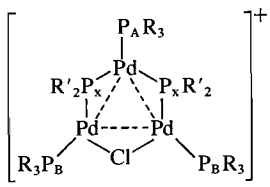

1

are unusually stable and offer opportunities for development of an extensive chemistry (1, 2). The primary technique for following their reactions is ^{31}P nuclear magnetic resonance spectroscopy (nmr) and for comparison purposes there is a need for reliable ^{31}P parameters in simple (i.e. non-metal bonded) platinum and palladium complexes containing terminal tertiary phosphines and bridging phosphido ligands. Many palladium complexes of the general type, $[Pd_2X_2(\mu\text{-}PR'_2)_2(PR_3)_2]$, were prepared in the early 1960's, initially by Issleib and Wenschuk (3) and then by the more extensive work of Hayter and co-workers (4–6). These workers utilised reactions involving elimination of HCl from secondary phosphine complexes and later Chatt and Davidson (7) extended the work to syntheses of platinum complexes using both the HCl elimination reaction and reactions of lithium diphenylphosphide with chloro-bridged complexes.

Despite the large range of known palladium and platinum species containing bridging phosphido ligands, no ^{31}P nmr data were available in the literature for these complexes. This situation prompted us to undertake a detailed ^{31}P nmr study of two groups of complexes:

[1]To whom all correspondence should be addressed.

0008-4042/81/081188-13$01.00/0

©1981 National Research Council of Canada/Conseil national de recherches du Canada

Can. J. Chem. Downloaded from www.nrcresearchpress.com by 210.87.254.42 on 09/06/12
For personal use only.

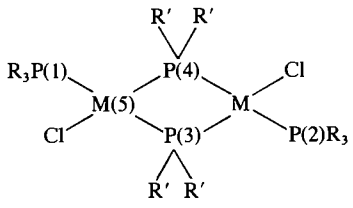

2

2: $[M_2Cl_2(\mu\text{-}PR'_2)_2(PR_3)_2]$, M = Pd, R' = Ph, $R_3 = Et_3$ or HPh_2; M = Pd, R' = Me, $R_3 = Et_3$, Ph_3, or HMe_2; M = Pt, R' = Ph, $R_3 = Et_3$ or HPh_2.

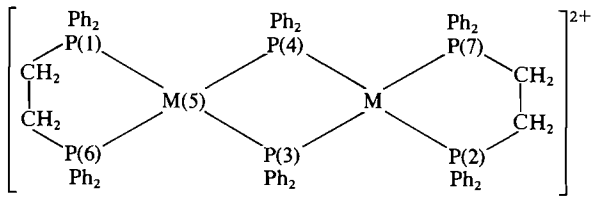

3

3: $[M_2(\mu\text{-}PPh_2)_2(dppe)_2]Cl_2$, M = Pd, or Pt, dppe = $Ph_2P(CH_2)_2PPh_2$.

The results of this ^{31}P nmr study are described in the present paper and we also note that during the preparation of our work, some parameters for the group of complexes; $[Pt_2X_2(\mu\text{-}PPh_2)_2L_2]$, X = Cl, L = PPr^n_3, PEt_3, PMe_2Ph, $AsEt_3$; X = H, L = PEt_3; X = $SiHPh_2$, L = PEt_3; have been briefly reported (8). These latter results are generally consistent with the parameters reported below except for some variations in the assigned signs of coupling constants. The brevity of the literature report (8) precludes a more detailed evaluation at the present time.

NOTE ADDED IN PROOF: We have recently learned that a more detailed report of these results is available in a Ph.D. thesis (K. J. Odell, University of Sussex, 1975).

Results

The following discussion is concerned with the proton decoupled phosphorus-31 nmr spectra of the two general types of species represented by structures **2** and **3**. The structures also show the numbering scheme (in parentheses) adopted for identification of chemical shifts and coupling constants. For the complex cations **3**, this scheme has been chosen to be consistent with that used for the neutral molecules, **2**, and to retain the same labelling for directly comparable chemical shifts and coupling constants throughout the paper. As a result the scheme for the cations is not the most logical one for these species considered independently but this should not cause any problems.

For palladium complexes, the species **2** and **3** will belong respectively to the AA'XX' and AA'A"A'"XX' spin systems as a first approximation.[2] There is a small amount of non-first order ("AB") character, as the detailed analyses given below will show, but this can be ignored in the preliminary analysis to obtain approximate parameters. For platinum complexes, a further subdivision of these spin systems is necessary since the species contain two platinum atoms and ^{195}Pt (with $I = 1/2$) is 33.8% abundant. Thus 43.8% (approximately 4/9) of the dinuclear molecules will contain no magnetically active platinum and will belong to the same spin systems as the palladium complexes; 44.8% (approximately 4/9) will contain one platinum-195 and belong to the spin systems AA'XX'M (Type **2**) and AA'A"A'"XX'M (Type **3**); and 11.4% (approximately 1/9) will contain two platinum-195 and belong to the spin systems AA'XX'MM' (Type **2**) and AA'A"A'"XX'MM' (Type **3**).[2]

Our general approach has been to analyse first spectra of Type **2** compounds of palladium in order to establish typical values for the inter-phosphorus coupling constants. We then analysed Type **2** compounds of platinum to provide platinum–phosphorus coupling constants before proceeding to the much more difficult spin systems of the Type **3** cations. As the detailed analyses will show, absorptions attributable to the approximately 1/9 of the platinum species containing two magnetically active platinum were too weak and difficult to identify for meaningful analysis. However, the only additional parameter which such an analysis could provide is ^2J(Pt,Pt) and computer simulations show that these particular spectra are not sensitive to the actual value of this coupling constant. They only depend on its approximate magnitude.

It should be noted that in all of the following discussions, identical coupling constants which are members of symmetry related sets are specified by reference to only one member of the set. For example, in Type **2** complexes a reference to $^2J(1,3)$ implies both of the identical couplings $^2J(1,3)$ and $^2J(2,4)$, or in Type **3** complexes a reference to $^2J(1,4)$ would imply the whole set $^2J(1,4)$, $^2J(4,7)$, $^2J(3,6)$, and $^2J(2,3)$.

$[Pd_2Cl_2(\mu\text{-}PPh_2)_2(PEt_3)_2]$

As noted above, the proton decoupled ^{31}P spec-

[2]In the alternative notation proposed by Haigh (35), these various spin systems would be designated $[AX]_2$, $[AX]_2M$, and $[AXM]_2$ for Type **2** species; $[[A]_2X]_2$, $[[A]_2X]_2M$, and $[[A]_2XM]_2$ for Type **3** species.

Can. J. Chem. Downloaded from www.nrcresearchpress.com by 210.87.254.42 on 09/06/12
For personal use only.

Can. J. Chem. Downloaded from www.nrcresearchpress.com by 210.87.254.42 on 09/06/12
For personal use only.

trum of this complex is, to a first approximation, an example of the AA'XX' spin system. The wave functions and transition energies for this spin system have been calculated previously in terms of four composite parameters (see ref. 9, note that this reference describes the AA'XX' spin system as A_2X_2). Using the nucleus labelling shown in structure **2** and redefining the parameters so as to be consistent with the AA'A"A'"XX' case discussed below, we obtain the following expressions for the composite parameters:[3]

$$K = \tfrac{1}{2}({}^2J(1,3) + {}^2J(1,4))$$

$$L = \tfrac{1}{2}({}^2J(1,3) - {}^2J(1,4))$$

$$P = \tfrac{1}{2}({}^4J(1,2) + {}^2J(3,4))$$

$$R = \tfrac{1}{2}({}^4J(1,2) - {}^2J(3,4))$$

The spectrum consists of identical A (terminal phosphine, downfield) and X (bridging phosphido, upfield) regions, centred on the chemical shifts δ_A and δ_X respectively, and each may be divided into two components:

(*a*) a strong doublet, separation $2K$

(*b*) two symmetrical quartets with line positions (relative to δ_A or δ_X) given by the equations:

$$+S + (S^2 + L^2)^{1/2}$$

$$-S + (S^2 + L^2)^{1/2}$$

$$+S - (S^2 + L^2)^{1/2}$$

$$-S - (S^2 + L^2)^{1/2}$$

In the first quartet $S = P$ and in the second $S = R$.

In the present example, inspection of the molecule suggests that $|{}^4J(1,2)| \ll |{}^2J(3,4)|$. Hence $|P| \simeq |R|$ and the two quartets will be almost coincident. Preliminary analysis of the A or X regions then assigns the peaks marked D in Fig. 1 to the strong doublet and the peaks marked Q to the almost coincident quartets. Closer inspection shows resolution of some of the quartet peaks and it is then possible to assign these (assuming for convenience that $P > R$ and both are positive) and to arrive at preliminary magnitudes of K, L, P, and R and hence for the coupling constants. Since only magnitudes are obtained and it is also not possible to distinguish P and R, no sign information is available except that because we find $|K| > |L|$ it follows that ${}^2J(1,3)$ and ${}^2J(1,4)$ must have the same sign. The indistinguishability of P and R also means that we cannot tell which of the two couplings ${}^4J(1,2)$ and ${}^2J(3,4)$ is which. However, couplings between phosphorus atoms in mutually *trans* positions are known to be large and positive (10, 11) and it also seems probable that the two bond coupling ${}^2J(3,4)$ will be very much larger in magnitude than the four bond coupling ${}^4J(1,2)$. With these assumptions we obtained the preliminary assignment: ${}^2J(1,3) = +407.9$ Hz, ${}^2J(1,4) = +31.2$ Hz, ${}^4J(1,2) = \pm 0.9$ Hz, and ${}^2J(3,4) = \pm 287.2$ Hz.

The actual spectrum shows significant non-first order character and so these preliminary parameters were then used as the basis for iterative computer refinements using all possible combinations of the two unknown signs. Whenever ${}^4J(1,2)$ and ${}^2J(3,4)$ were given the same sign, iteration resulted in a change of sign of ${}^4J(1,2)$ during refinement. Moreover, although the differences are subtle the plots of observed and simulated spectra shown in Fig. 1 support the assignment of ${}^2J(3,4)$ as negative. The parameters used for the plots in Fig. 1 are the result of refinement to convergence with both possible sets of signs, i.e. they are not the result of refining one set of parameters and then simply changing the signs of ${}^4J(1,2)$ and ${}^2J(3,4)$. This latter procedure is potentially very misleading

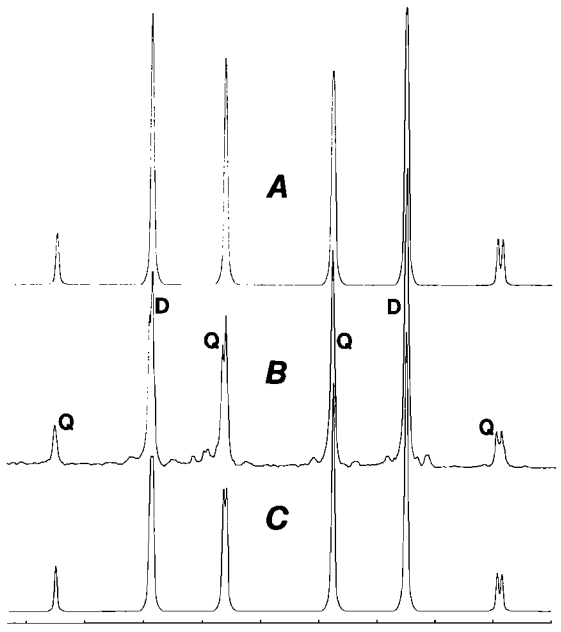

FIG. 1. Proton decoupled ^{31}P nmr spectrum of $[Pd_2Cl_2(\mu\text{-}PPh_2)_2(PEt_3)_2]$. The figure shows the terminal phosphine (lower field) region only and an identical mirror image spectrum occurs to higher field for the bridging phosphorus: (*A*) computer simulated spectrum with ${}^4J(1,2) = -2.7$, ${}^2J(1,3) = +406.7$, ${}^2J(1,4) = +29.8$, ${}^2J(3,4) = +289.0$ Hz; (*B*) observed spectrum at 24.3 MHz; (*C*) computer simulated spectrum with ${}^4J(1,2) = +2.9$, ${}^2J(1,3) = +405.9$, ${}^2J(1,4) = +31.9$, ${}^2J(3,4) = -289.5$ Hz. The significance of the doublet (D) and quartet (Q) labels is explained in the text. Each major division on the chemical shift/frequency axis represents 100 Hz.

[3]In ref. 9 the corresponding parameters are N, L, K, and M which in terms of our parameters are given by $2K$, $2L$, $2P$, and $2R$ respectively.

Can. J. Chem. Downloaded from www.nrcresearchpress.com by 210.87.254.42 on 09/06/12
For personal use only.

with complex spectra. On the basis of the plots shown in Fig. 1, the final refined parameters given in Table 1 were selected as the best fit to the observed spectrum. The signs given in Table 1 are relative to the assumption of a positive value for $^2J(1,3)$.

In the analysis of the spectrum of $[Pd_2Cl_2(\mu\text{-}PPh_2)_2(PEt_3)_2]$, and in the other cases discussed below, the preliminary assignment of the downfield resonances (δ_A in Table 1) to the terminal phosphines and the upfield (δ_X in Table 1) to the bridging phosphides, was made on the basis of known chemical shifts in terminal phosphine complexes. Thus, tabulated values (10) for a wide variety of tertiary phosphines and metals range from −66 to −166 ppm with the vast majority falling in a much smaller range, approximately −100 to −150 ppm (10). In our complexes the chemical shift assignments were confirmed by the observation in platinum compounds of two very different ^{195}Pt couplings ($^3J(2,5)$ and $^1J(1,5)$) in the low-field resonances. This unambiguously establishes these resonances as due to the terminal phosphines.

Other $[Pd_2Cl_2(\mu\text{-}PR'_2)_2(PR_3)_2]$ Spectra

These were analysed by procedures similar to that described above for $[Pd_2Cl_2(PPh_2)_2(PEt_3)_2]$ and the final refined parameters are collected in Table 1. The spectra of $[Pd_2Cl_2(\mu\text{-}PPh_2)_2(PHPh_2)_2]$ and $[Pd_2Cl_2(\mu\text{-}PMe_2)_2(PHMe_2)_2]$ showed very small magnitudes for $^4J(1,2)$ and in consequence the two quartets were not resolved from each other and it was not possible to determine the signs of $^4J(1,2)$ and $^2J(3,4)$. In Table 1 they are assumed to be similar to the other examples. Spectra of $[Pd_2Cl_2(\mu\text{-}PMe_2)_2(PEt_3)_2]$ and $[Pd_2Cl_2(\mu\text{-}PMe_2)_2(PPh_3)_2]$ showed subtle evidence that $^4J(1,2)$ is positive and $^2J(3,4)$ negative, similar to the $[Pd_2Cl_2(\mu\text{-}PPh_2)_2(PEt_3)_2]$ case discussed above.

$[Pt_2Cl_2(\mu\text{-}PPh_2)_2(PEt_3)_2]$

Observed and calculated spectra for this molecule at 24.3 MHz are shown in Fig. 2. For the purposes of analysis the spectrum must be divided into contributions from two separate species; a "centre-band" spectrum (43.8%) due to molecules having no magnetically active platinum and a "side-band" spectrum (44.8%) due to molecules containing one ^{195}Pt atom. The remaining 11.4% of the molecules (containing two magnetically active platinums) can be neglected in the preliminary analysis. The centre-band spectrum is similar to the $[Pd_2Cl_2(\mu\text{-}PPh_2)_2(PEt_3)_2]$ spectrum discussed above and was analysed in the same way using either the A (low-field, terminal) or X (high-field, bridging) to provide preliminary values for

TABLE 1. $^{31}P\{^1H\}$ nmr data for phosphido-bridged complexes

Compound	Chemical shifts[a] δ_A (terminal)	δ_X (bridge)	Coupling constants[b] $^4J(1,2)$	$^2J(1,3)$	$^2J(1,4)$	$^1J(1,5)$	$^2J(1,6)$	$^4J(1,7)$	$^3J(2,5)$	$^2J(3,4)$	$^1J(3,5)$	$^1J(4,5)$
$[Pd_2Cl_2(\mu\text{-}PPh_2)_2(PEt_3)_2]$	−125.3	−267.7	+2.9	+405.9	+31.9	—	—	—	—	−289.5	—	—
$[Pd_2Cl_2(\mu\text{-}PPh_2)_2(PHPh_2)_2]$	−142.9	−272.7	+0.2	+423.1	+20.9	—	—	—	—	−261.1	—	—
$[Pd_2Cl_2(\mu\text{-}PMe_2)_2(PHMe_2)_2]$	−194.1	−320.2	−0.4	+442.9	+24.1	—	—	—	—	−310.0	—	—
$[Pd_2Cl_2(\mu\text{-}PMe_2)_2(PEt_3)_2]$	−125.5	−321.9	+9.3	+408.4	+31.7	—	—	—	—	−344.2	—	—
$[Pd_2Cl_2(\mu\text{-}PMe_2)_2(PPh_3)_2]$	−124.1	−314.2	+12.7	+373.6	+23.5	—	—	—	—	−341.0	—	—
$[Pt_2Cl_2(\mu\text{-}PPh_2)_2(PEt_3)_2]$	−125.4	−276.0	+9.5	+374.3	+4.5	+2171.8	—	—	+31.3	−177.7	+1690.5	+2634.7
$[Pt_2Cl_2(\mu\text{-}PPh_2)_2(PHPh_2)_2]$	−142.2	−279.0	+7.6	+395.4	−1.0	+2184.0	—	—	+29.2	−162.0	+1991.1	+2364.2
$[Pd_2(\mu\text{-}PPh_2)_2(dppe)_2]Cl_2$	−92.4	−321.4	0[c]	+311.0	+28.2	—	−17.5[c]	0[c]	—	−349.4	—	—
$[Pt_2(\mu\text{-}PPh_2)_2(dppe)_2]Cl_2$	−90.5	−321.4	+7.1[c]	+291.9	0	+2112.6	0[c]	0[c]	+63.1	−207.5	+1774.7	+1774.7

[a]Recorded in dichloromethane solution. Units are parts per million from external $P(OCH_3)_3$ reference and negative shifts are upfield from the reference.
[b]Coupling constants in Hz. Labelling of coupling constants corresponds to the nucleus numbering given in structures 2 and 3. The relative sign information given in the table is that considered most probable but the Results section must be consulted for discussion of the reliability of the sign assignments.
[c]These parameters are not necessarily uniquely determined by the observed spectrum. See Results section for details.

Can. J. Chem. Downloaded from www.nrcresearchpress.com by 210.87.254.42 on 09/06/12
For personal use only.

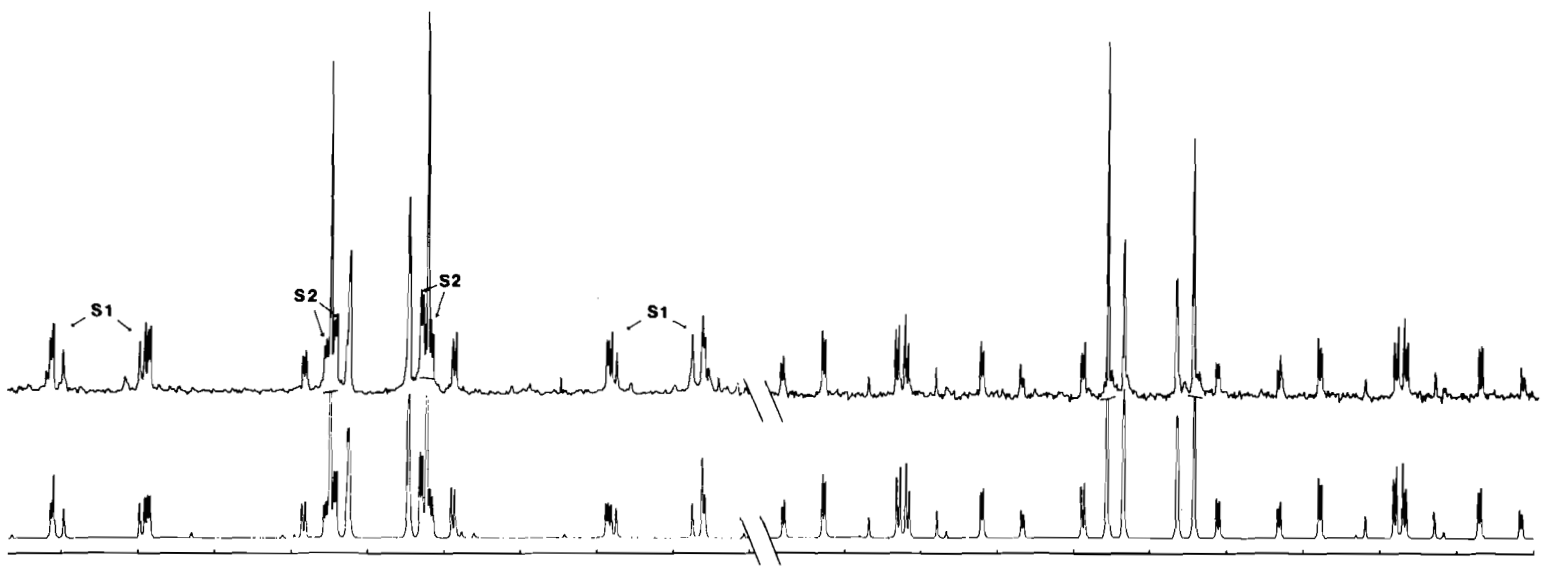

FIG. 2. Proton decoupled ^{31}P nmr spectrum of $[Pt_2Cl_2(\mu\text{-}PPh_2)_2(PEt_3)_2]$. The upper plot is the observed spectrum at 24.3 MHz and the lower plot is computer simulated using the parameters given in Table 1. The low-field (left) and high-field (right) regions are centred ca. −143 and − 273 ppm respectively and each major division on the chemical shift/frequency scale represents 300 Hz in the low-field region and 330 Hz in the high-field region. The significance of the side-band labelling (S1, etc.) is explained in the text.

Can. J. Chem. Downloaded from www.nrcresearchpress.com by 210.87.254.42 on 09/06/12
For personal use only.

the chemical shifts and phosphorus–phosphorus coupling constants. The side-band spectrum in the A region consists of two parts: (*i*) a pair of subspectra (labelled S1 in Fig. 2), associated with the spin transitions of nucleus 1 (see structue **2**) separated by the one-bond phosphorus–platinum coupling constant, $^1J(1,5)$, and (*ii*) sets of lines (labelled S2 in Fig. 2) associated with the spin transition of nucleus 2, flanking the principal lines of the centre band spectrum and having a separation of the same general magnitude (but *not* equal to) the three-bond phosphorus–platinum coupling constant, $^3J(2,5)$. It is also useful to note that $^4J(1,2)$ may be directly measured as a doublet separation of each of the principal lines of these side-band spectra. The side-band spectrum in the bridging region is more complex but consists basically of two subspectra separated by the approximate mean of the two platinum–phosphorus coupling constants, $^1J(3,5)$ and $^1J(4,5)$. Thus preliminary analysis gave direct measurement of $^1J(1,5)$, an approximate magnitude of $^3J(2,5)$ and the mean of $^1J(3,5)$ and $^1J(4,5)$.[4] Using this information together with that derived from the centre-band spectrum, the side-band spectrum was computer simulated and refined. Next the centre-band spectrum was simulated using the refined data from the side-bands and the two spectra were then combined in the correct intensity ratio to produce the plot shown in Fig. 2. The final refined parameters are collected in Table 1. As a final check on the correctness of the assignment, spectra were recorded at 101.2 MHz and the 24.3 MHz data were used, with appropriate chemical shift adjustment, to simulate the high-field results. Excellent agreement was obtained.

Careful inspection of Fig. 2 shows that only a few weak peaks are observed in addition to those accounted for in the simulated spectrum. These peaks may be attributed to the 11.4% of molecules containing two magnetically active platinums. It is clear that an analysis of these additional peaks is not necessary or indeed possible! In principle such an analysis could yield $^2J(Pt,Pt)$ but in practice the spectrum is expected to be insensitive to the precise value of this coupling.

During the refinement of the $[Pt_2Cl_2(\mu\text{-}PPh_2)_2(PEt_3)_2]$ spectra we considered that $^2J(1,3)$, $^1J(1,5)$, $^1J(3,5)$, and $^1J(4,5)$ could be assumed positive on the basis of previous sign determinations for mutually *trans* phosphorus atoms (10,11) and for one bond phosphorus–platinum couplings (12). $^2J(1,4)$ was shown by the preliminary analysis to have the same sign as $^2J(1,3)$. All possible sign combinations of $^4J(1,2)$, $^3J(2,5)$, and $^2J(3,4)$ were explored and the results showed the high-field bridging region of the spectrum to be essentially independent of the signs of these three coupling constants. The low-field terminal region was similarly non-productive as far as $^2J(3,4)$ was concerned and it appears that in this particular case this sign cannot be determined. In Table 1 it is assumed to be the same as in the palladium complexes. Changing the sign of $^4J(1,2)$ causes a reversal of the asymmetry in the outer side-bands (labelled S1 in Fig. 2) associated with spin transitions of nucleus 1 and this parameter is thus established as positive. Similarly, the inner side-bands (labelled S2 in Fig. 2), associated with spin transitions of nucleus 2, can only be satisfactorily fitted if $^3J(2,5)$ is positive.

$[Pt_2Cl_2(\mu\text{-}PPh_2)_2(PHPh_2)_2]$

Analysis of the spectrum of this complex and exploration of the possible signs of coupling constants were carried out exactly as described above for the PEt_3 analogue and the results are collected in Table 1.The only exception was that spectra at 101.2 MHz were not recorded.

$[Pd_2(\mu\text{-}PPh_2)_2(dppe)_2]Cl_2$

As noted above, the cation in this complex is a representative of the AA′A″A‴XX′ spin system (see structure **3**). This system is relatively rare in nmr literature and the analyses which have been carried out have mostly involved heteronuclear species where A and X are different magnetically active nuclei. The principal examples are P_2H_4 (13), P_2F_4 (14), $(^{13}C)_2H_4$ (15), 1,3-difluoroacetone (16), and a group of diazadiphosphetidines (17). One case which does involve a homonuclear spin system is a ^{19}F study of some hexafluorocyclopentenes (18) but these spectra are dominated and simplified by large geminal F–F couplings (i.e. couplings within the AA′A″A‴ set) and are quite different from the present example.

Theoretical approaches to the AA′A″A‴XX′ spin system have been worked out by several authors (15, 19, 20) and we have followed the work of Lynden-Bell (15) who tabulated the wave functions in C_{2v} symmetry (for P_2H_4). The $[Pd_2(\mu\text{-}PPh_2)_2(dppe)_2]^{2+}$ cation has D_{2h} symmetry but it can be shown that this has no effect on the overall analysis (15). Because certain combinations of coupling constants are repeated throughout the analysis, it is convenient to define a number of secondary parameters. Adopting the basic approach used by Lynden-Bell, and relabelling the

[4]As a starting point for the refinement an approximate magnitude for $^1J(3,5)$ was derived from the value in $[Pt_2(\mu\text{-}PPh_2)_2(dppe)_2]^{2+}$ where the assignment is unambiguous.

Can. J. Chem. Downloaded from www.nrcresearchpress.com by 210.87.254.42 on 09/06/12
For personal use only.

secondary parameters to conform to the symmetry in structure **3**, we obtain:

$$K = \tfrac{1}{2}({}^2J(1,3) + {}^2J(1,4))$$

$$L = \tfrac{1}{2}({}^2J(1,3) - {}^2J(1,4))$$

$$N = \tfrac{1}{2}({}^4J(1,2) + {}^2J(1,6))$$

$$M = \tfrac{1}{2}({}^4J(1,2) - {}^2J(1,6))$$

$$G = \tfrac{1}{2}{}^4J(1,7)$$

$$X = \tfrac{1}{2}{}^2J(3,4)$$

The indistinguishability of $^4J(1,2)$ and $^2J(1,6)$ compared to the unique nature of $^4J(1,7)$ is most easily seen by considering the effects of interchanging labels in structure **3**. Thus a change such as $2 \leftrightarrow 6$ results only in the interchange of the couplings $^4J(1,2) \leftrightarrow {}^2J(1,6)$ and the symmetry related pair $^4J(6,7) \leftrightarrow {}^2J(2,7)$. All other couplings are unchanged. However, a label change such as $2 \leftrightarrow 7$ will change not only the symmetry related pairs $^4J(1,2) \leftrightarrow {}^4J(1,7)$ and $^4J(6,7) \leftrightarrow {}^4J(2,6)$ but also the couplings to the bridging phosphorus; $^2J(2,3) \leftrightarrow {}^2J(3,7)$ and $^2J(2,4) \leftrightarrow {}^2J(4,7)$.

The lines in the A (low-field, terminal phosphine) region of the spectrum are symmetrical about δ_A,

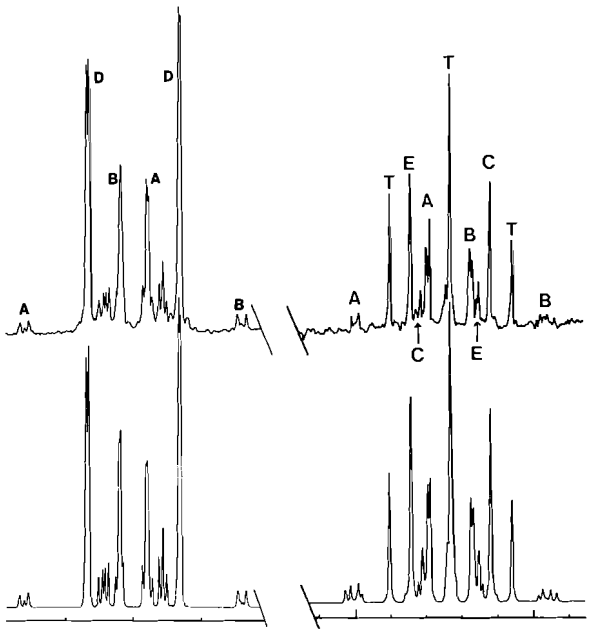

FIG. 3. Proton decoupled ^{31}P nmr spectrum of $[Pd_2(\mu\text{-}PPh_2)_2(dppe)_2]Cl_2$. The upper plot is the observed spectrum at 24.3 MHz and the lower plot is computer simulated using the parameters given in Table 1. The low-field (left) and high-field (right) regions are centred ca. −92 and −321 ppm respectively and each major division on the chemical shift/frequency axis represents 50 Hz in the low-field region and 200 Hz in the high-field region. The significance of the labelling (A, B, etc.) is explained in the text.

the chemical shift of the terminal tertiary phosphine ligands. The most prominent feature is an intense doublet with separation $2K$, and this separation also occurs in a triplet in the X (high-field, bridging) region. These features are labelled D and T respectively in Fig. 3. As in Type **2** systems described above, in the preliminary analysis we ignore complications (in this case a slight extra splitting of the doublet) caused by slight AA′A″A‴BB′ character in the basically AA′A″A‴XX′ spin system. The next most prominent feature is a set of 8 lines symmetrically disposed about $\delta_A + X$ and a corresponding mirror image set about $\delta_A - X$. The positions of these lines are given by

$$\delta_A + X + N \pm (L^2 + (X + N)^2)^{1/2}$$

$$\delta_A + X + M \pm (L^2 + (X + M)^2)^{1/2}$$

$$\delta_A + X - N \pm (L^2 + (X - N)^2)^{1/2}$$

$$\delta_A + X - M \pm (L^2 + (X - M)^2)^{1/2}$$

and

$$\delta_A - X - N \pm (L^2 + (X + N)^2)^{1/2}$$

$$\delta_A - X - M \pm (L^2 + (X + M)^2)^{1/2}$$

$$\delta_A - X + N \pm (L^2 + (X - N)^2)^{1/2}$$

$$\delta_A - X + M \pm (L^2 + (X - M)^2)^{1/2}$$

These equations contain all the terms necessary to estimate 5 of the 6 coupling constants with only the G term ($\frac{1}{2}{}^4J(1,7)$) being omitted. Thus the main interpretive problem is the assignment of these 8 lines to their corresponding algebraic expressions. The high-field bridging phosphorus region ("X" spectrum) may also be used in this assignment since in this region the two 8 line systems are repeated twice, centred on $\delta_X \pm K$ respectively (i.e. there are four 8 line systems centred on $\delta_X \pm K \pm X$ respectively). In the present case this assignment problem was solved by tabulating the A lines relative to δ_A and the X lines relative to $\delta_X + K$ and relative to $\delta_X - K$ and then searching for repeating patterns. It should be noted that exact symmetry of the repeating patterns only occurs in a true AA′A″A‴XX′ system with no AA′A″A‴BB′ character. In this tabulation it was immediately apparent that only a 4 line repeating pattern is present in the observed spectra. In the low-field region of Fig. 3, the first 4 line set is labelled A, the second B, and in the high-field region the labels A, B, C, and E are used. Reduction of the 8 line to 4 line sets is expected if $|M| \simeq |N|$, i.e. if either or both of $^4J(1,2)$ and $^2J(1,6)$ are very small. This is reasonable in the present case since the former

Can. J. Chem. Downloaded from www.nrcresearchpress.com by 210.87.254.42 on 09/06/12
For personal use only.

coupling is close to zero in the other diphenylphosphido bridged palladium complexes discussed above (see Table 1). Assuming for convenience that N and X are both positive and that N is small relative to X and L,[5] it is then possible to make an assignment of the sets of lines and to derive magnitudes for the coupling constants; $^2J(3,4)$, $^2J(1,3)$, $^2J(1,4)$, and for the parameter N.

These are approximate magnitudes because of the partial AA'A"A'"BB' character of the spectrum. Computer refinement of the spectrum was then carried out by assuming $^4J(1,2) = 0$, thereby enabling $^2J(1,6)$ to be set equal to $2N$, and also by assuming $^4J(1,7) = 0$. The refinement proceeded perfectly satisfactorily with $^4J(1,2)$ and $^4J(1,7)$ held at zero and with $^2J(1,6)$, and all other parameters, allowed to vary. The refined value of $^2J(1,6)$ is included in Table 1 with $^4J(1,2)$ set to zero but since these two parameters cannot be distinguished in this spin system (see above) and we have in any case insufficient spectral resolution to determine the parameter M, the values of $^2J(1,6)$ and $^4J(1,2)$ must be regarded as essentially undetermined, although definitely of small magnitude. Similarly $^4J(1,7)$ is undetermined although of small magnitude.

During the refinement all signs of the various coupling constants were explored. Since $|K| > |L|$ it is evident that $^2J(1,3)$ and $^2J(1,4)$ have the same sign and since couplings between mutually *trans* phosphorus atoms are known to be large and positive (10,11), it is likely that both these parameters are positive. Correct fitting of the weak lines in the central region of the A spectrum (low-field, terminal phosphines) required that a negative value of $^2J(1,6)$ be used although, as noted above, this is not a well determined parameter. Figure 3 shows the experimental spectrum together with computer simulations. The excellent fit with experiment shows the overall correctness of the analysis and, as in the Type **2** complexes described above, the detail indicates a slightly better fit when $^2J(3,4)$ is negative. As in the other cases, the evidence is suggestive only and cannot be regarded as a final proof.

$[Pt_2(\mu\text{-}PPh_2)_2(dppe)_2]Cl_2$

As in the case of $[Pt_2Cl_2(\mu\text{-}PPh_2)_2(PEt_3)_2]$ discussed above, spectra of the cation in the present complex must be divided into contributions from two separate species: (*a*) about 4/9 of the molecules contain no magnetically active platinum and give rise to a "centre-band" spectrum, (*b*) about 4/9 contains one ^{195}Pt and give rise to a "side-band" spectrum. The remaining ~1/9 of the molecules contain two ^{195}Pt and can be neglected in the preliminary analysis.

The "centre-band" spectra are similar to those described above for $[Pd_2(\mu\text{-}PPh_2)_2(dppe)_2]Cl_2$ and were analysed in basically the same way by determination of $2K$ as the separation of the large doublet in the low-field A region due to phosphorus in the dppe ligands, followed by location of the repeating 8 line patterns. In Fig. 4 the components of the centre-band spectrum are labelled in the same way as for the Pd analogue discussed above. As in the case of the palladium complex the small values of some parameters reduce the sets to 4 lines and in some cases even to two lines. These assignments yielded preliminary values for $^2J(1,3)$, $^2J(1,4)$, $^2J(3,4)$, and N, the principal difference from the palladium case being that, since $|K| \simeq |L|$, it follows that $^2J(1,4)$ is near zero. Once the centre-band spectrum is clearly identified it is easy to pick out the platinum side-bands arising from the various components and to obtain preliminary values for the coupling constants to platinum. These then permit computer simulation and refinement of the side-band spectra. Whereas, in the palladium complex it is not possible to distinguish between $^4J(1,2)$ and $^2J(1,6)$, this is possible in the side-band spectra of the platinum complex because these belong to the AA'A"A'"XX'M spin system and the principal side-band peaks due to spin transitions of nuclei 1 and 2 are doubled when $^4J(1,2) \sim 7$ and $^2J(1,6) \sim 0$ Hz but not in the reverse case. The observed spectrum shows this doubling and establishes the parameters as listed in the table. It is difficult to distinguish between the situations $^4J(1,2) \sim 7$, $^2J(1,6) \sim 0$, $^4J(1,7) \sim 0$ and $^4J(1,2) \sim 0$, $^2J(1,6) \sim 0$, $^4J(1,7) \sim 7$ Hz since both of these lead to doubling of the principal side-band peaks but examination of other spectral detail supports the former assignment.

Once refinement of the side-band spectrum was complete the refined parameters were used to simulate the centre-band spectrum and the two simulations are shown in Fig. 4. The simulated spectra of the two isotopomers were also combined in a 1:1 ratio (4/9:4/9) to produce a composite simulation (not illustrated) which showed excellent agreement with the observed spectrum. The observed spectrum in Fig. 4 contains some weak extra peaks which may be assigned to the ~1/9 of the molecules containing two magnetically active platinums. There are also 3 peaks, labelled I in Fig. 4,

[5]The assumption regarding the magnitude of N is fully justified by the likely coupling constants to be found in these molecules (see structures **2** and **3**). The assumption of positive signs is arbitrary but only interchanges line assignments without changing the final magnitudes of the derived parameters.

Can. J. Chem. Downloaded from www.nrcresearchpress.com by 210.87.254.42 on 09/06/12
For personal use only.

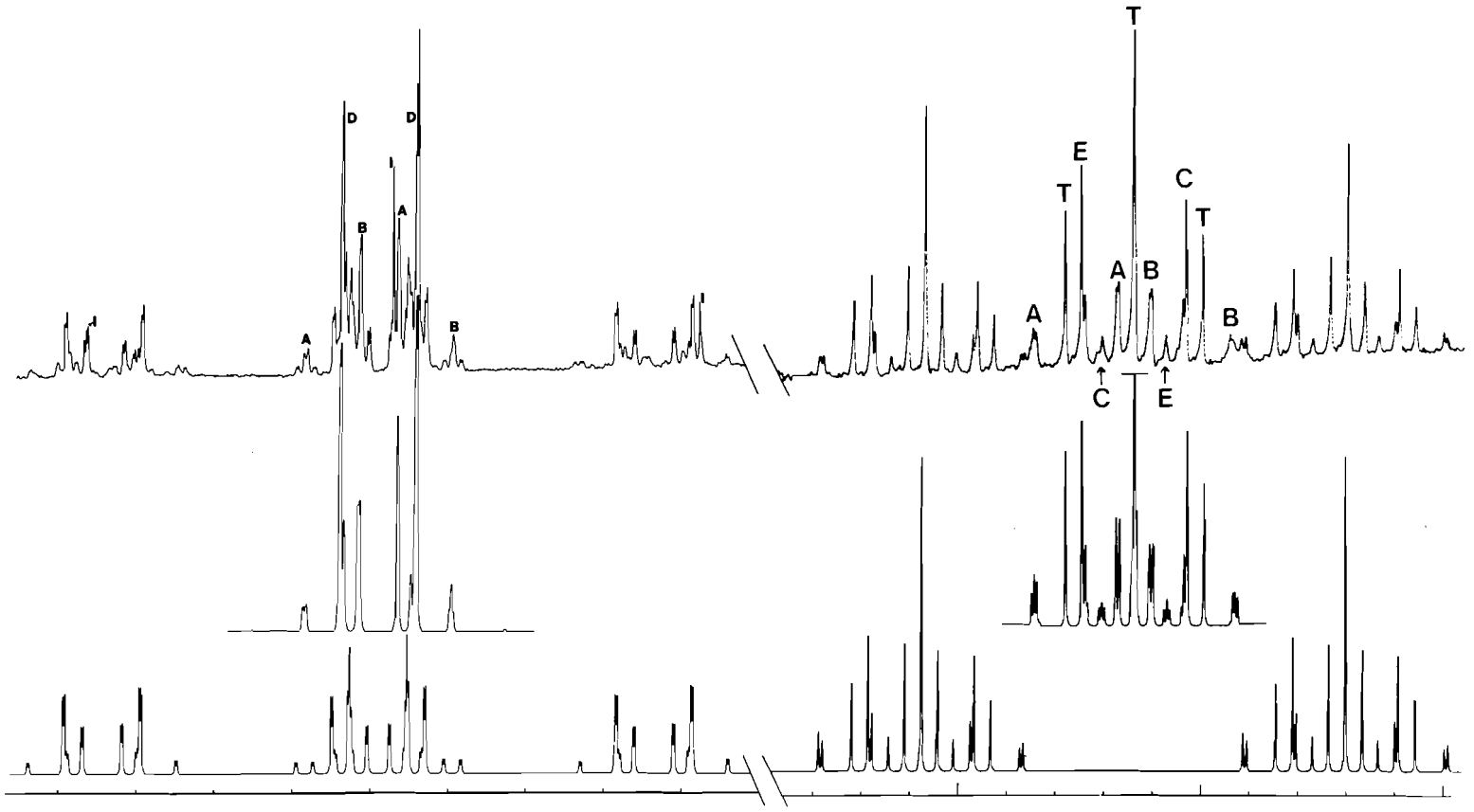

FIG. 4. Proton decoupled ^{31}P nmr spectrum of $[Pt_2(\mu\text{-}PPh_2)_2(dppe)_2]Cl_2$. The upper plot is the observed spectrum at 24.3 MHz, the centre plot is a computer simulation for molecules containing no magnetically active platinum and the bottom plot is a simulation for molecules having one ^{195}Pt atom. The simulation used the parameters given in Table 1. The low-field (left) and high-field (right) regions are centred ca. −90 and −321 ppm respectively and each major division on the chemical shift/frequency axis represents 50 Hz in the low-field region and 200 Hz in the high-field region. The significance of the labelling (A, B, etc.) is explained in the text.

Can. J. Chem. Downloaded from www.nrcresearchpress.com by 210.87.254.42 on 09/06/12
For personal use only.

which are clearly due to a simple impurity with ^{195}Pt side-bands. As in the case of $[Pt_2Cl_2(\mu\text{-}PPh_2)_2(PEt_3)_2]$ discussed above, attempted analysis of the weak "two ^{195}Pt" spectrum was not considered profitable.

Discussion

The nmr parameters for all of the complexes are collected in Table 1 using the labelling schemes shown in structures **2** and **3**. Derivation of the relative signs of the various coupling constants has already been discussed in detail in the Results section. Absolute signs for the P—P coupling constants given in Table 1 are all based on the assumption that the large coupling, $^2J(1,3)$, between mutually *trans* phosphorus atoms is positive. This has been the case in all previous examples where absolute sign has been determined (10, 11) and, although these involved phosphine or phosphite ligands rather than bridging phosphido groups, the present couplings are of very similar magnitude and it is likely that they also are positive. However, it should be noted that all of the sign information is *relative* to the assumption of a positive value for $^2J(1,3)$ and in the absence of a definitive sign determination for any phosphido system the absolute signs remain tentative assignments.

Given $^2J(1,3)$ positive, the sign of $^2J(1,4)$ is then established as positive by the relative magnitudes, $|K| > |L|$. $[Pt_2Cl_2(\mu\text{-}PPh_2)_2(PHPh_2)_2]$ is a minor exception to this statement but the negative value is of very small magnitude. The positive values for $^2J(1,4)$ are somewhat unusual in that the majority of previous sign determinations have found negative couplings between mutually *cis* phosphorus atoms (10, 11). However, none of the previous examples involved bridging phosphido and, unlike the situation with the large *trans* couplings, the small magnitudes of the *cis* couplings make sign reversals quite possible as the nature of the phosphorus groups and substituents are changed.

Continuing to discuss P—P coupling constants, the refinements suggest that the signs of the remote, $^4J(1,2)$, couplings are reliable. However, their magnitudes (especially the very small ones) are probably less accurate than those of the other couplings because these determinations depend upon resolution of the quartets which in our spectra were often almost coincident. The difficulties of distinguishing $^4J(1,2)$ from $^2J(1,6)$ in $[Pd_2(\mu\text{-}PPh_2)_2(dppe)_2]Cl_2$ and $^4J(1,2)$ from $^4J(1,7)$ in $[Pt_2(\mu\text{-}PPh_2)_2(dppe)_2]Cl_2$ have already been discussed in the Results section. A more serious problem concerns the sign of $^2J(3,4)$, the coupling between the two bridging phosphido groups. As we noted above, the majority of previous determinations for couplings between mutually *cis* phosphorus atoms have given negative signs (10, 11). However, those couplings were of relatively small magnitude and there seems to be no precedent in studies of phosphine and phosphite metal complexes for a negative coupling as large as $^2J(3,4)$. Moreover, the assignment of $^2J(3,4)$ as negative depends on some rather subtle features of the observed/simulated spectra (see figures and Results section) and it is clear that further work is needed to confirm the assignment. For the present it must be regarded as suggestive and not conclusive.

Examination of Table 1 shows that, for the exactly similar pairs of platinum and palladium complexes ($[M_2Cl_2(\mu\text{-}PPh_2)_2(PEt_3)_2]$, $[M_2Cl_2(\mu\text{-}PPh_2)_2(PHPh_2)_2]$, and $[M_2(\mu\text{-}PPh_2)_2(dppe)_2]Cl_2$), the two bond phosphorus–phosphorus coupling constants $^2J(1,3)$, $^2J(1,4)$, and $^2J(3,4)$ are always of larger magnitude in the palladium complex. The trends to be expected in J(PMP) coupling constants as M is varied down a transition triad are not well established but our observations are generally consistent with previous results. For example, in the Ni, Pd, and Pt triad the limited data available for *cis*-^2J(P—M—P) have been summarised by Carty, Johnson, and Jacobson (21). These authors show that in most cases the magnitude of *cis*-^2J(P—M—P) decreases in the sequence Ni > Pd > Pt, although the general trend is contradicted by data on $[MX_2(PMe_3)_2]$, M = Pd or Pt, X = Cl or Br. In *trans* complexes the same general trend appears to hold (i.e. decrease in magnitude of *trans*-^2J(P—M—P) down the triad) although the data are limited to platinum and palladium complexes, $[MX_2(L)_2]$, X = Cl or Br, L = PMe_3, PEt_3, or PMe_2H (10, 11). The only other well studied triad is the Cr, Mo, W group where a variety of data is available to show that *cis*-^2J(P—M—P) in *cis*-$M(CO)_4L_2$ complexes decreases in magnitude in the sequence Cr > Mo > W (10, 22). For *trans*-$M(CO)_4L_2$ complexes the data are much more limited but indicate the reverse order (10). Clearly much more data, especially with sign determinations, are needed before meaningful generalizations about these trends can be made.

One bond, platinum–phosphorus couplings are known to have positive sign (12) and this sign has been assumed for $^1J(1,5)$, $^1J(3,5)$, and $^1J(4,5)$ in Table 1. The magnitudes of $^1J(3,5)$ and $^1J(4,5)$ are consistent with the well known *trans* influence order $R_3P \gg Cl$ (23) and the relatively small values of $^1J(1,5)$, compared for example with

Can. J. Chem. Downloaded from www.nrcresearchpress.com by 210.87.254.42 on 09/06/12
For personal use only.

values for ^1J(Pt,P) of 2400 and 3520 Hz in *trans*- and *cis*-$[PtCl_2(PEt_3)_2]$ respectively (24), indicate a very high *trans* influence for the bridging diphenylphosphido group. Overall the data show the *trans* influence order

$$\mu\text{-}PPh_2 > PEt_3 > Cl$$

and this appears to represent the first determination of *trans* influence for a bridging phosphido group in platinum complexes.

Given the assumption of positive signs for the directly bonded Pt—P couplings, the detailed spectral refinements fix the indirect Pt—P coupling, ^3J(2,5) as positive. Comparatively little literature data are available for comparison with this coupling but some ^3J(Pt—P) values have been reported from ^{195}Pt spectra of a group of chloro-bridged complexes; $[Pt_2(\mu\text{-}Cl)_2(PR_3)_2]$, ^3J(Pt—P) = −21 to −27 Hz, and $[Pt_2(\mu\text{-}Cl)_2(PPr^n_3)_4][BF_4]_2$, ^3J(Pt—P) = −11 Hz (25). ^3J(Pt—P) has also been determined in $[Pt_2(\mu\text{-}Cl)_2(COEt)_2(PMe_2Ph)_2]$, *cis* isomer ±11 Hz, *trans* isomer −5.6 Hz (26) and in the sulphur bridged species $[Pt_2Cl_2(\mu\text{-}SCH_2Ph)_2(PBu^n_3)_2]$, −16 Hz, and $[Pt_2Cl_2(\mu\text{-}Cl)(\mu\text{-}SCH_2Ph)(PBu^n_3)_2]$, 0 Hz (27). The variation of ^3J(Pt—P) between zero and small negative magnitudes indicates that the coupling is sensitive to the nature of the bridging groups and other substituents on the metal. With this background our observation of positive couplings is interesting but not necessarily surprising.

As noted in the Introduction, a principal motivation for this work was to obtain nmr parameters for phosphido bridged complexes in order to assess the effect of the metal–metal bonds in our cluster complexes (see structure **1**). The most dramatic difference between the clusters and the non-metal–metal bonded systems described in the present paper is in the chemical shifts of the bridging diphenylphosphido groups. In the clusters (1, 2) these occur ca. 60–80 ppm downfield of trimethylphosphite, a sharp contrast to the ca. 270–320 ppm upfield observed in the present complexes. In their work on phosphido bridged iron carbonyl systems:

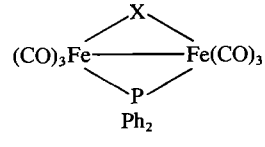

Carty and co-workers (28, 29) have shown that variation of the bridging group X causes marked shifts in the chemical shift of the PPh_2 phosphorus and have suggested that these variations are associated with changes in the Fe—P—Fe angle. The complexes give δ_P from about 0 to +60 ppm downfield of trimethylphosphite with Fe—P—Fe angles in the range 70–75° and with a tendency for δ_P to become more positive as angle increases (28, 29). In contrast, the complexes $[M_3(\mu\text{-}PPh_2)(\mu\text{-}C{\equiv}CR)(CO)_9]$, M = Ru and Os where there is no metal–metal bond between the atoms bridged by PPh_2, show M—P—M angles >90° and phosphorus chemical shifts upfield of 85% H_3PO_4 (i.e. > −140 ppm upfield from trimethylphosphite) (30). The overall effect is thus similar to the palladium case. In the clusters (structure **1**) where there is metal–metal bonding, the Pd—P—Pd angle is 81.4° (31) and the PPh_2 shift is downfield (1). For the complexes studied in the present paper the PPh_2 shifts are upfield. There is unlikely to be metal–metal bonding and comparison with the results on iron compounds leads to the expectation of large angles at the bridging phosphorus. These expectations are confirmed by very recent structure determinations (32) for $[Pt_2Cl_2(\mu\text{-}PPh_2)_2(PHPh_2)_2]$ and $[Pt_2(\mu\text{-}PPh_2)_2(dppe)_2]Cl_2$ which show Pt—PPh_2—Pt angles of 102.85(0)° and 103.9(1)° respectively and Pt....Pt separations of 358.5 and 369.9 pm. Clearly more structural information on both iron and palladium systems would be very valuable in investigating the generality of these trends.

Another important consideration is the effect of metal–metal bonds on the phosphorus–phosphorus coupling constants. Thus $J(P_A,P_B)$ in structure **1** is a 4-bond coupling if metal–metal bonding is ignored but a 3-bond coupling if it is included. $J(P_A,P_B)$ is directly comparable with the 4-bond couplings, ^4J(1,2), in Table 1 and the large difference in magnitude (~90 Hz and <10 Hz respectively) clearly shows the importance of the metal–metal bonds in the cluster.

Experimental

Phosphorus-31 nmr spectra were recorded in dichloromethane solution at 24.29 MHz on a Nicolet TT14 Fourier transform spectrometer using a Varian HA60 magnet. Protons were decoupled by broad band ("noise") irradiation at appropriate frequencies. $[P(OCH_3)_3]$ was used as external reference and C_6D_6 as external lock. Negative chemical shifts are upfield from the reference. Most spectra were recorded using 4096 real time data points in sweep widths of 6000 – 12 000 Hz and the data are thus subject to errors of the order of 1–3 Hz. Spectra of $[Pt_2Cl_2(\mu\text{-}PPh_2)_2(PEt_3)_2]$ were also recorded at 101.2 MHz using a Bruker WP250 Fourier transform spectrometer.

Simulated nmr spectra were calculated on an IBM 3031 computer and plotted on Calcomp 563 and 1039 plotters. The programmes used were a locally constructed package based on the UEAITR (33) and NMR PLOT (34) programmes from the literature.

$[Pd_2Cl_2(\mu\text{-}PPh_2)_2(PHPh_2)_2]$, $[Pd_2Cl_2(\mu\text{-}PPh_2)_2(PEt_3)_2]$, and $[Pd_2(\mu\text{-}PPh_2)_2(dppe)_2]Cl_2$ were prepared by established literature procedures (4) except that, in our hands the published

recrystallization of the PEt_3 derivative from aqueous acetone did not give satisfactory results. Our samples of this complex were purified by washing with pentane and recrystallization from acetone by addition of diethyl ether and pentane. Preparation of $[Pt_2(\mu\text{-}PPh_2)_2(dppe)_2]Cl_2$ was similar to that of the palladium analogue (4) except that the reaction mixture was heated under reflux for 30 min and the product recrystallized as pale yellow plates from methanol by addition of diethyl ether.

$[Pt_2Cl_2(\mu\text{-}PPh_2)_2(PEt_3)_2]$ has been prepared previously by reaction of $[Pt_2Cl_2(\mu\text{-}Cl)_2(PEt_3)_2]$ with $[SiMe_3(PPh_2)]$ (8). We preferred to prepare this complex by reaction of $[PtCl_2(PhCN)_2]$ with $PHPh_2$ followed by displacement of $PHPh_2$ by PEt_3.

$$2PtCl_2(PhCN)_2 + 4PHPh_2 \xrightarrow[-2PhCN]{-2HCl} Pt_2Cl_2(PPh_2)_2(PHPh_2)_2$$

$$Pt_2Cl_2(PPh_2)_2(PHPh_2)_2 + 2PEt_3 \xrightarrow{-2PHPh_2} Pt_2Cl_2(PPh_2)_2(PEt_3)_2$$

Palladium derivatives with PMe_2 bridges were prepared by similar routes based on reactions of $PHMe_2$.

$[Pt_2Cl_2(\mu\text{-}PPh_2)_2(PHPh_2)_2]$

A solution of *cis*-$[PtCl_2(PhCN)_2]$ (0.75 g, 1.6 mmol) in benzene (50 mL) was heated under reflux in a nitrogen atmosphere and $PHPh_2$ (0.56 mL, 3.2 mmol) was slowly added. After reflux for 30 min, cooling to 10°C gave $[Pt_2Cl_2(\mu\text{-}PPh_2)_2(PHPh_2)_2]$ (0.90 g, 0.75 mmol) as a white precipitate which was recrystallized from dichloromethane by addition of diethyl ether.

$[Pt_2Cl_2(\mu\text{-}PPh_2)_2(PEt_3)_2]$

PEt_3 (0.056 mL, 0.38 mmol) was added to a stirred suspension of $[Pt_2Cl_2(\mu\text{-}PPh_2)_2(PHPh_2)_2]$ (0.23 g, 0.19 mmol) in acetone (7 mL) in a nitrogen atmosphere. Stirring was continued for 30 min before the reaction mixture was evaporated under reduced pressure, washed with pentane, and the residue recrystallized from acetone by the addition of pentane to yield $[Pt_2Cl_2(\mu\text{-}PPh_2)_2(PEt_3)_2]$ (0.12 g, 0.11 mmol) as colourless crystals.

$[Pd_2Cl_2(\mu\text{-}PMe_2)_2(PHMe_2)_2]$

$[PdCl_2(PhCN)_2]$ (0.23 g, 0.59 mmol) and benzene (10 mL) were placed in a thick-walled Pyrex tube and $PHMe_2$ (0.072 g, 1.16 mmol) added *in vacuo*. The tube was sealed, shaken at ambient temperature for 4 h, cooled to −196°C and opened *in vacuo*. As the contents warmed to ambient temperature the most volatile products were removed *in vacuo* and the resulting solution was removed from the vacuum line and filtered to give $[PdCl_2(PHMe_2)_2]$ (0.17 g, 0.56 mmol) as a white solid smelling strongly of $PHMe_2$. This solid was then heated under reflux in a nitrogen atmosphere with *p*-toluidine (0.063 g, 0.59 mmol) for 20 min. The reaction mixture was evaporated under reduced pressure and extracted with dichloromethane leaving impure *p*-toluidine hydrochloride (0.089 g, ~0.6 mmol) as residue. Evaporation of the filtrate under reduced pressure gave oily yellow crystals which were partially dissolved in benzene and re-precipitated with hexane to give $[Pd_2Cl_2(\mu\text{-}PMe_2)_2(PHMe_2)_2]$ (0.12 g, 0.23 mmol).

$[Pd_2Cl_2(\mu\text{-}PMe_2)_2(PPh_3)_2]$

PPh_3 (0.6 g, 2.3 mmol) and $[Pd_2Cl_2(\mu\text{-}PMe_2)_2(PHMe_2)_2]$ (0.067 g, 0.13 mmol) were dissolved in CH_2Cl_2 (10 mL) and the mixture evaporated to dryness under reduced pressure. The solution/evaporation process was repeated 4 times to completely displace $PHMe_2$. The residues were recrystallized from dichloromethane by addition of hexane to yield $[Pd_2Cl_2(\mu\text{-}PMe_2)_2(PPh_2)_2]$ (0.10 g, 0.11 mmol) as yellow crystals.

$[Pd_2Cl_2(\mu\text{-}PMe_2)_2(PEt_3)_2]$

PEt_3 (0.15 mL, 1.0 mmol) was added to a solution of $[Pd_2Cl_2(\mu\text{-}PMe_2)_2(PHMe_2)_2]$ (0.27 g, 0.5 mmol) in dichloromethane (5 mL) under a nitrogen atmosphere. After stirring for 1 h the reaction mixture was evaporated *in vacuo* to a dark red oil. Pumping *in vacuo* was continued for several hours before the residue was dissolved in dichloromethane and the solution poured into a large volume of stirred pentane to give $[Pd_2Cl_2(\mu\text{-}PMe_2)_2(PEt_3)_2]$ (0.11 g, 0.17 mmol) as an orange powder.

1. K. R. Dixon and A. D. Rattray. Inorg. Chem. **17**, 1099 (1978).
2. S. J. Cartwright, K. R. Dixon, and A. D. Rattray. Inorg. Chem. **19**, 1120 (1980).
3. K. Issleib and E. Wenschuk. Z. Anorg. Allgem. Chem. **305**, 15 (1960).
4. R. G. Hayter. J. Am. Chem. Soc. **84**, 3046 (1962).
5. R. G. Hayter and F. S. Humiec. Inorg. Chem. **2**, 306 (1963).
6. R. G. Hayter. Inorg. Chem. **3**, 301 (1964).
7. J. Chatt and J. M. Davidson. J. Chem. Soc. 2433 (1964).
8. C. Eaborn, K. J. Odell, and A. Pidcock. J. Organomet. Chem. **170**, 105 (1979).
9. J. A. Pople, W. G. Schneider, and H. J. Bernstein. High-resolution nuclear magnetic resonance. McGraw-Hill, Toronto. 1959. pp. 138–142.
10. J. G. Verkade. Co-ord. Chem. Rev. **9**, 1 (1972); J. F. Nixon and A. Pidcock. Ann. Rev. NMR Spectrosc. **2**, 345 (1969).
11. R. J. Goodfellow and B. F. Taylor. J. Chem. Soc. Dalton, 1676 (1974).
12. W. McFarlane. J. Chem. Soc. A, 1922 (1967).
13. R. M. Lynden-Bell. Trans. Faraday Soc. **57**, 888 (1961).
14. F. A. Johnson and R. W. Rudolph. J. Chem. Phys. **47**, 5449 (1967).
15. R. M. Lynden-Bell. Mol. Phys. **6**, 601 (1963).
16. B. L. Shapiro, W. A. Thomas, J. L. McClanahan, and M. D. Johnston, Jr. J. Magn. Reson. **11**, 355 (1973).
17. R. K. Harris, M. Lewellyn, M. I. M. Wazeer, J. R. Woplin, R. E. Dunmur, M. J. C. Hewson, and R. Schmutzler. J. Chem. Soc. Dalton, 61 (1975).
18. L. Cavalli and R. K. Harris. J. Magn. Reson. **10**, 355 (1973).
19. P. Diehl. Helv. Chim. Acta, **3**, 567 (1965).
20. D. W. Aksnes. Acta Chem. Scand. A, **28**, 375 (1974).
21. A. J. Carty, D. K. Johnson, and S. E. Jacobson. J. Am. Chem. Soc. **101**, 5612 (1979) and references therein.
22. S. O. Grim, W. L. Briggs, R. C. Barth, C. A. Tolman, and J. P. Jesson. Inorg. Chem. **13**, 1095 (1974); R. B. King and J. C. Cloyd. Inorg. Chem. **14**, 1550 (1975); S. O. Grim, R. C. Barth, J. D. Mitchell, and J. D. Gaudio. Inorg. Chem. **16**, 1776 (1977).
23. T. G. Appleton, H. C. Clark, and L. E. Manzer. Co-ord. Chem. Rev. **10**, 335 (1973); F. R. Hartley. Chem. Soc. Rev. **2**, 163 (1973).
24. S. O. Grim, R. L. Keiter, and W. McFarlane. Inorg. Chem. **6**, 1133 (1967).
25. N. M. Boag, J. Browning, C. Crocker, P. L. Goggin, R. J. Goodfellow, M. Murray, and J. L. Spencer. J. Chem. Res. S(228), M(2962), (1978).
26. G. K. Anderson, R. J. Cross, L. Manojlovic-Muir, K. W. Muir, and T. Solomun. J. Organomet. Chem. **170**, 385 (1979).
27. T. Soulié, J. Y. Lallemand, and R. C. Rao. Org. Magn. Reson. **12**, 67 (1979).
28. G. N. Mott and A. J. Carty. Inorg. Chem. **18**, 2926 (1979).

Can. J. Chem. Downloaded from www.nrcresearchpress.com by 210.87.254.42 on 09/06/12
For personal use only.

29. N. J. TAYLOR, G. N. MOTT, and A. J. CARTY. Inorg. Chem. **19**, 560 (1980).
30. A. J. CARTY. Proceedings of American Chemical Society/Chemical Institute of Canada Joint Conference on "Catalytic Aspects of Metal Phosphine Complexes," Guelph, Ont., Canada. 1980.
31. G. W. BUSHNELL, K. R. DIXON, P. M. MORONEY, A. D. RATTRAY, and CH'ENG WAN. J. Chem. Soc. Chem. Commun. 709 (1977).
32. A. J. CARTY, F. HARTSTOCK, and N. J. TAYLOR. Unpublished results.
33. R. B. JOHANNSEN, J. A. FERRETI, and R. K. HARRIS. J. Magn. Reson. **3**, 84 (1970).
34. J. D. SWALEN. *In* Computer programmes for chemistry. Vol. I. *Edited by* D. F. Detar. W. A. Benjamin, New York. 1968.
35. C. W. HAIGH. J. Chem. Soc. A, 1682 (1970).

Can. J. Chem. Downloaded from www.nrcresearchpress.com by 210.87.254.42 on 09/06/12
For personal use only.

Mechanism of 2-quinizarinsulphonic acid reduction on a mercury electrode

F. CAPITAN,[1] A. GUIRAUM, AND J. L. VILCHEZ
Department of Analytical Chemistry, Faculty of Sciences, Granada, Spain
Received September 24, 1980

F. CAPITAN, A. GUIRAUM, and J. L. VILCHEZ. Can. J. Chem. **59**, 1201 (1981).

The reduction of the 1,4-dihydroxyanthraquinone-2-sulphonic acid (quinizarinsulphonic acid) at a dropping mercury electrode has been investigated. The reduction takes place in two monoelectronic steps and show $E_{1/2}$ values vs. sce $(E_{1/2})_1 = -0.380$ V and $(E_{1/2})_2 = -1.045$ V at pH 4.60. The first wave is diffusion controlled, while the second wave is kinetically controlled. The reagent captures one electron and one proton to form the semiquinonic system. The semiquinone is dimerized. The dimer captures one electron and one proton, per molecule, to form the hydroquinone. The reaction orders, together with Tafel's slopes, have been calculated.

F. CAPITAN, A. GUIRAUM et J. L. VILCHEZ. Can. J. Chem. **59**, 1201 (1981).

On a étudié la réduction de l'acide dihydro-1,4 xianthraquinone sulfonique-2 (acide quinizarinsulfonique) au niveau d'une électrode à goutte de mercure. La réduction a lieu en deux étapes monoélectroniques et a des valeurs de $E_{\frac{1}{2}}$ par rapport à sce de $(E_{\frac{1}{2}})_1 = 0{,}380$ V et $(E_{\frac{1}{2}})_2 = 1{,}045$ V à un pH de 4,60. La première onde est contrôlé par diffusion tandis que la deuxième est sous contrôle cinétique. Le réactif capte un électron et un proton en formant un système semiquinonique. La semiquinone est dimérisée. Le dimère capte un électron et un proton par molécule et donne l'hydroquinone. On a calculé l'ordre des réactions ainsi que les pentes de Tafel.

[Traduit par le journal]

Introduction

The polarographic reduction of anthraquinonic molecules has been studied by several authors (1–5). It may take place through various mechanisms (dimerization, dismutation, catalysis, etc.). The reduction product is the respective semiquinone or hydroquinone depending on the functional groups existing in the molecule, the pH of the medium and the nature of the solvent (5).

Previous to this paper the polarographic behaviour of 1,2,7-trihydroxyanthraquinone-3-methylamino-*N*,*N*-diaceticacid (anthrapurpurin complexan, reagent with anthraquinonic structure of analytical interest) has been described (4). In this paper the reduction of 1,4-dihydroxyanthraquinone-2-sulphonic acid (2-quinizarinsulphonic acid) at the DME is studied. This reagent has been previously studied with respect to some of its analytical applications; thus it has been proposed for the spectrophotometric determination of F^- (6), Zr^{4+} (7), and Th^{4+} (8), for the spectrofluorimetric determination of Al^{3+} (9) and Be^{2+} (10), and as an acid–base indicator (11).

Experimental

The *i*–*E* curves were registered either automatically or traced point by point using a 471 AMEL multipurpose unit with the damping circuit completely suppressed. The cyclic voltammetry curves were recorded on a Tectronix SSP 3 polarograph. The potentials were measured vs. sce with a Beckman Research Potentiometer, which was also used as a pH-meter.

The polarographic measurements were done using a thermostated AMEL 494 cell. A saturated calomel reference electrode was used. The working electrode was a mercury capillary with the following characteristics: rate of mercury flow $m = 1.87$ mg/s, drop time $t = 5.65$ s, open circuit, in a buffered solution at pH 4.60 and the height of the mercury column $h = 40$ cm. The cyclic voltammetry curves were carried out using an amalgamated gold electrode as a working electrode.

All the reagents used were Merck P.A. grade. As a supporting electrolyte solution, a buffered solution was used; it was composed of 0.8 *M* acetic acid and 0.8 *M* sodium acetate which were mixed in varying proportions according to the pH desired. The ionic strength was adjusted with $NaClO_4$ to 0.2 *M*. All the measurements were done in an atmosphere of nitrogen and at a temperature of 25.0 ± 0.1°C.

Results and Discussion

The 2-quinizarinsulphonic acid reduced on the DME produces two polarographic waves from aqueous solutions at concentrations smaller than 5×10^{-4} *M*. Both waves were always observed throughout the complete pH range studied (3.60–8.20). Figure 1 shows a representative polarogram at pH 4.60, $(E_{1/2})_1 = -0.380$ V, and $(E_{1/2})_2 = -1.045$ V. First of all, we investigated the dependence of the limiting current on the height of the mercury column. The results were obtained for a 5×10^{-4} *M* solution at pH 4.60. The plot of i_{lim} vs. $h^{1/2}$ (corrected for the back pressure) shows a linear dependence for the first wave. This proves that the wave height is diffusion controlled (Fig. 2). For the second wave i_{lim} is independent of the height, proving the kinetic nature of such a wave. The temperature coefficients of i_{lim} have been investigated in the range between 20 and 85°C with 10^{-4} *M* solutions at pH 4.60. The temperature coefficient is found to be $d(\log i_d)/dT = 0.0075$ for the first wave (close to the theoretical value 0.007), confirming

[1]To whom all correspondence should be addressed.

0008-4042/81/081201-04$01.00/0
©1981 National Research Council of Canada/Conseil national de recherches du Canada

Can. J. Chem. Downloaded from www.nrcresearchpress.com by 210.87.254.40 on 09/06/12
For personal use only.

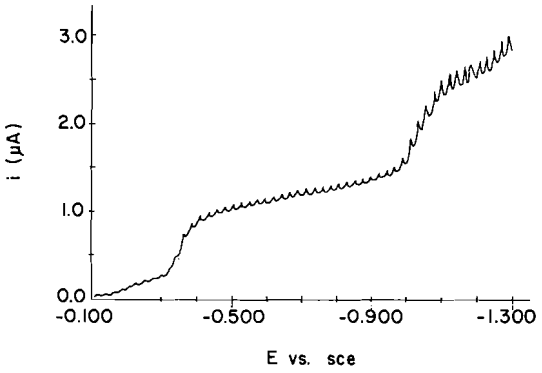

FIG. 1. Polarogram of 10^{-3} M 2-quinizarinsulphonic acid at pH 4.60 (acetate buffer).

the diffusion-controlled nature of the first wave. For the second wave $d(\log i_{lim})/dT = 0.035$, so that the kinetic nature of the wave is again confirmed. The dependence of the half-wave potential on pH was studied as well, to determine how many hydrogen ions are involved in the reduction. Polarograms were recorded for 5×10^{-4} M solutions in the pH range between 3.60 and 8.20. The dependence $E_{1/2}$ vs. pH for both waves is linear, the slopes being 57 mV and 55 mV respectively. Accordingly, the number of hydrogen ions involved in the reduction must be $p = 1$ in both cases. Likewise, the order of reaction with respect to the H^+ is 1 in both reductions. Note that the limiting currents are independent of the pH.

On the other hand, we checked whether the limiting currents are proportional to the concentration of the 2-quinizarinsulphonic acid in the bulk of the solution, in the range between 5×10^{-3} M and 10^{-4} M at pH 4.60. The value of the slope of the linear segments is: 1.6 μA L/mM and 1.2 μA L/mM for the first and the second wave respectively. Hence, the diffusion current constant is $I = i_d/m^{2/3}t^{1/6}C = 607D^{1/2}n = 0.79$, and the diffusion coefficient $D = 1.7.10^{-6}$ cm^2/s, where $n = 1$, $m = 1.87$ mg/s and $t = 5.65$ s. Such values for I and D agree with those previously published for some anthraquinones (4, 5).

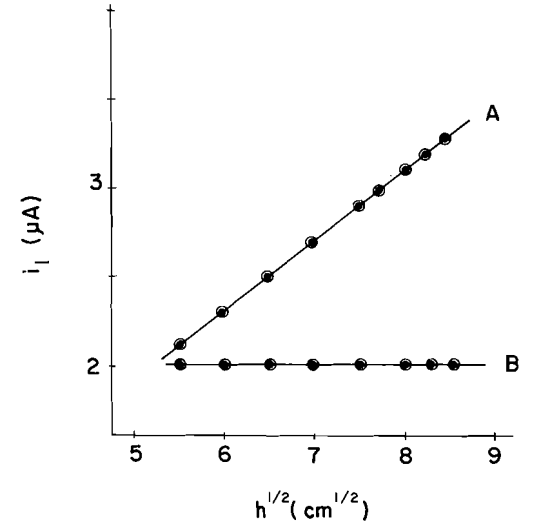

FIG. 2. Dependence of the limiting current on the height of the mercury column. A, first wave; B, second wave.

The half-wave potential $E_{1/2}$ shifts to more negative potentials with an increase in concentration. The plot $E_{1/2}$ vs.log C is linear in both waves with slopes of 13 mV and 18 mV respectively.

The transfer coefficient determined from Tafel's slope is $\alpha = 0.7$ and the orders of reaction with respect to the concentration are

$$\left(\frac{d \log i}{d \log C}\right)_E = 1$$

for the first wave and 0.53 for the second wave.

We carried out controlled-potential coulometry to determine n, i.e., the number of electrons involved in the reduction. A mercury pool was used as the cathode and a platinum wire as the auxiliary electrode; the reference electrode was a sce. The concentration of the sample before and after the electrolysis was measured polarographically to ensure that reduction reached completion. The electrolyzed samples contained 0.0348 g of solute in 100 mL of solution and a continuous stream of nitrogen was passed during the electrolysis. It appears that the reduction of 2-quinizarinsulphonic acid involves one electron in every wave.

The cyclic stationary electrode voltammetric curves for both waves at different scan rates were registered (Fig. 3). If the scan rate is medium, both systems are reversible. When the scan rate is lower both curves become irreversible. This behaviour agrees with the diagnostic criteria proposed by Wopschall and Shain (12) for reversible electrode processes followed by an irreversible chemical reaction.

Conclusions

The polarographic curves show that the reduction of the 2-quinizarinsulphonic acid proceeds by two monoelectronic steps, diffusion and kinetically controlled respectively. The reagent requires one electron and one proton in each step, to produce the semiquinone and hydroquinone consecutively.

The shape of the cyclic voltammetry curves is, in both cases, in agreement with the diagnostic criteria proposed for systems in which a single chemi-

Can. J. Chem. Downloaded from www.nrcresearchpress.com by 210.87.254.40 on 09/06/12
For personal use only.

Can. J. Chem. Downloaded from www.nrcresearchpress.com by 210.87.254.40 on 09/06/12
For personal use only.

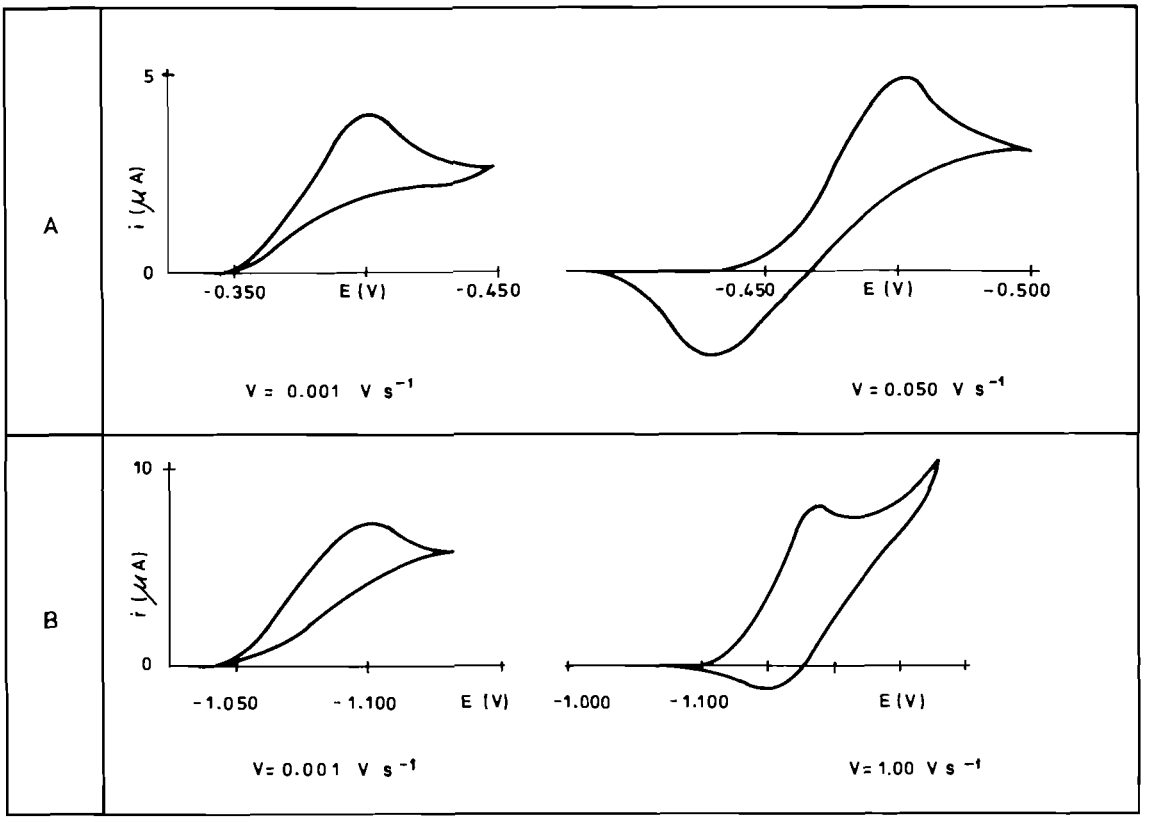

FIG. 3. Cyclic voltammetry curves of 10^{-4} *M* 2-quinizarinsulphonic acid at pH 4.60. *A*, first wave; *B*, second wave.

cal reaction follows at a reversible charge transfer (EC mechanism) (12).

On the other hand, the value $d(E_{1/2})_2/d \log C = -28$ mV agrees with the theoretical value calculated for the dimer discharge (13).

The analysis of peak voltammetry curves of the first wave lead to values $(E_p - E_{p/2}) = 36$ mV and $(E_p - E_{1/2}) = -20$ mV. This is in close agreement with the theoretical values (40.2 mV and −18 mV respectively) deduced by Shuman (14) for a discharge process followed by the hydrodimerization (15) of the reagent.

From the results and conclusions obtained, we propose for the reduction of 2-quinizarinsulphonic acid, a mechanism with the following reaction kinetic pathways:

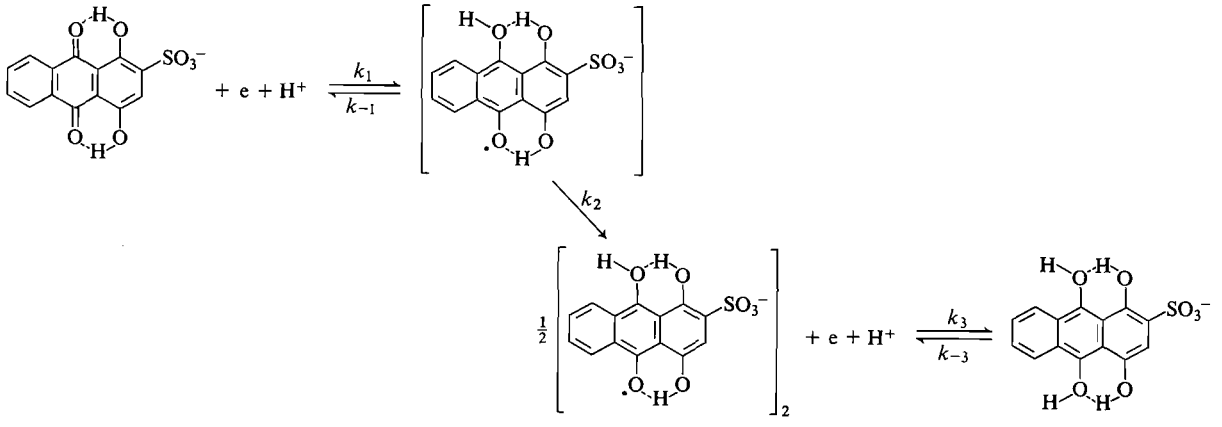

1. N. H. FURMAN and K. G. STONE. J. Chem. Soc. 3055 (1948).
2. H. BLOOM, L. H. BRIGGS, and B. CLEVERLEY. J. Chem. Soc. 178 (1959).
3. R. JONES and T. M. SPOTSWOOD. Aust. J. Chem. **15**, 942 (1962).
4. F. CAPITAN, A. GUIRAUM, and J. L. VILCHEZ. Can. J. Chem. **57**, 3243 (1979).
5. P. MASSON, J. DEVYNCK, and B. TREMILLON. J. Electroanal. Chem. **64**, 175 (1975).
6. F. CAPITAN and A. GUIRAUM. Ars Pharm. **12**, 397 (1971).
7. F. CAPITAN and A. GUIRAUM. Rev. U.I.S. Bucaramanga (Colombia) **4**, 1 (1971).
8. F. CAPITAN and A. GUIRAUM. Rev. Soc. Quim. Perú, **36**, 1 (1970).
9. F. CAPITAN, M. ROMAN, and A. GUIRAUM. An. Quim. Madrid, B**70**, 508 (1974).
10. F. CAPITAN, A. GUIRAUM, and J. L. VILCHEZ. Quim. Anal. **29**, 265 (1975).
11. F. CAPITAN and A. GUIRAUM. Quim. Ind. Madrid, **16**, 9 (1970).
12. R. H. WOPSCHALL and I. SHAIN. Anal. Chem. **39**, 13, (1967); **39**,1535 (1967).
13. V. HANUS. Chem. Zvesti, **8**, 702 (1954).
14. M. S. SHUMAN. Anal. Chem. **42**, 521 (1970).
15. C. P. ANDRIEUX and J. M. SAVEANT. Bull. Soc. Chim. Fr. 3281 (1972).

Can. J. Chem. Downloaded from www.nrcresearchpress.com by 210.87.254.40 on 09/06/12
For personal use only.

A simple ^{1}H nmr conformational study of some heterocyclic azomethines

FRANCESCO A. BOTTINO, MARIA L. LONGO, DOMENICO SCIOTTO,[1] AND MICHELE TORRE

Istituto Dipartimentale di Chimica e Chimica Industriale, Università di Catania, Viale Andrea Doria 6, 95125 Catania, Italy

Received August 6, 1980

FRANCESCO A. BOTTINO, MARIA L. LONGO, DOMENICO SCIOTTO, and MICHELE TORRE. Can. J. Chem. **59**, 1205 (1981).

The variable temperature 60 MHz ^{1}H nmr spectra of some heterocyclic azomethines exclude the presence of rotational isomerism. Chemical shift values and stereospecific long-range couplings are used to establish that *s-trans* is the existing conformation. In the case of the pyrrole derivatives a chelated *s-trans* rotamer is indicated, depending on the presence of an intramolecular hydrogen bond.

FRANCESCO A. BOTTINO, MARIA L. LONGO, DOMENICO SCIOTTO, et MICHELE TORRE. Can. J. Chem. **59**, 1205 (1981).

Le spectre rmn du proton à 60 MHz à température variable de quelques azométhines hétérocycliques excluent la présence d'une isomérie rotationnelle. On a utilisé les valeurs des déplacements chimiques et les couplages stéréospécifiques à longue distance pour prouver que la conformation *s-trans* est la seule qui existe. Dans le cas des dérivés du pyrole, on constate qu'un rotamère *s-trans* chélaté se forme en conséquence de l'existence d'une liaison hydrogène intramoléculaire.

[Traduit par le journal]

Introduction

In connection with previous studies on 2-carbonyl substituted heterocyclic systems (1) and some (*E*)-1,2-diarylethylenes (2–4), we carried out a short investigation on the conformational preferences of some heterocyclic azomethines **1**.

These molecules may populate both *s-cis* and *s-trans* rotamers.

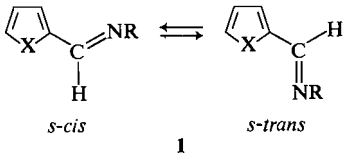

s-cis *s-trans*

1

X = N—H, N—CH_3, O; R = CH_3, *n*-C_4H_9

An electrostatic interaction between the heterocyclic heteroatom and the azomethinic nitrogen could affect the energy of the favoured *s-trans* conformation, thus allowing the existence of the *s-cis* rotamer. A similar effect was postulated to account for the conformational preferences of some diaryl ethylene derivatives (2–3) and some heterocyclic 2-carbonyl compounds (5).

Results and Discussion

In order to provide insight on the population ratio of the two planar rotational isomers we have undertaken a ^{1}H nmr variable temperature study of azomethines **1**. The ^{1}H nmr spectra of azomethines **1** show only a small line broadening or sharpening but no substantial changes of the spectral features in the range of −90°C to +100°C. The linewidth changes with the temperature were in all cases of the same order of magnitude of those observed for the TMS signal (less than 7%).

Because of the conjugation between the heterocyclic nucleus and the —C=N—R group, the rotational barrier may reasonably be considered quite similar to the one observed in the 2-carbonyl derivatives (6–8), a higher value consequently than the one required on the nmr time scale for the occurence of a process that averages the signals of the two rotational isomers. Free rotation then is excluded at lowest temperatures and the presence of only one conformational isomer is evidenced.

From ^{1}H nmr data it is possible to establish whether the *s-trans* or the *s-cis* is the existing conformation.

In the case of the molecules **1** (X = NH), ^{1}H nmr spectra ($CDCl_3$) exhibit a strong deshielding of the broad resonance of the N—H proton, which may be better evidenced by comparison with the observed value of the corresponding proton of pyrrole (see Table 1).

No significant differences are observed, in the chemical shifts of both the N—H proton and the heterocyclic protons, between the azomethines **1** (X = NH) and pyrrole-2-carboxaldehyde (see Table 1), which exists almost exclusively in the *s-trans* conformation, as supported by nmr studies (9–11) and dipole moment measurements (12). Whether an intramolecular hydrogen bond in this aldehyde is present is, however, a problem which has been investigated (9–12), but not yet unambiguously settled. In any case the ^{1}H nmr spectrum ($CDCl_3$) exhibits all the spin–spin couplings of the N—H proton with the heterocyclic ones. On the contrary no spin–spin coupling of the N—H proton

[1]Author to whom communications should be addressed.

0008-4042/81/081205-03$01.00/0

©1981 National Research Council of Canada/Conseil national de recherches du Canada

Can. J. Chem. Downloaded from www.nrcresearchpress.com by 210.87.254.6 on 09/06/12
For personal use only.

TABLE 1. Room temperature ^{1}H nmr chemical shifts (δ, ppm)[a] of azomethines **1**

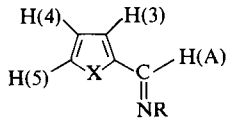

X	R	N—H	H(3)	H(4)	H(5)	H(A)
N—H	CH_3	10.42	6.42(dd)	6.17(dd)	6.80(ddd)	7.90(dq)
N—H	n-C_4H_9	10.20	6.38(dd)	6.13(dd)	6.67(ddd)	7.90(dt)
N—CH_3	CH_3	—	6.34(dd)	6.00(dd)	6.53(ddd)	7.98(dq)
N—CH_3	n-C_4H_9	—	6.27(dd)	5.98(dd)	6.47(ddd)	8.00(dt)
O	CH_3	—	6.72(dd)	6.39(dd)	7.37(m)	7.99(dq)
O	n-C_4H_9	—	6.70(dd)	6.33(dd)	7.30(m)	7.98(dt)
Pyrrole	2-Carboxaldehyde	10.50	6.97(ddd)	6.37(ddd)	7.17(m)	—
Pyrrole		7.95	6.09(m)	6.09(m)	6.60(m)	—

[a]Abbreviations: m = multiplet; dd = doublet of doublet; ddd = doublet of doublet of doublet; dq = doublet of quartet; dt = doublet of triplet.

TABLE 2. Spin–spin coupling constants (cps) of azomethines **1**[a]

X	R	$J_{H(A)-H(5)}$	$J_{H(A)-H(4)}$	$J_{H(5)-H(4)}$	$J_{H(5)-H(3)}$	$J_{H(4)-H(3)}$
NH	CH_3	0.8	0.0	2.3	1.4	3.6
NH	n-C_4H_9	0.8	0.0	2.5	1.4	3.7
NCH_3	CH_3	0.8	0.0	2.5	1.8	3.8
NCH_3	n-C_4H_9	0.8	0.0	2.6	1.8	3.9
O	CH_3	0.4	0.0	1.6	0.5	3.4
O	n-C_4H_9	0.4	0.0	1.6	0.5	3.4

[a]The J values were measured directly from the spectra run at the maximum of the scale width.

of the compounds **1** with the heterocyclic protons is evidenced in $CDCl_3$ solution.

The N—H proton chemical shift values of **1** (X = N—H) are quite insensitive to both temperature and concentration changes. Moreover ir spectra of neat **1** (X = N—H) as well as those of dilute solutions show a broad N—H stretching band in the region 3500–3000 cm^{-1}. On the basis of all these results the presence of an intramolecular hydrogen bond can be suggested in the molecules **1** (X = N—H), and the *s-trans* chelated rotamer must therefore be the populated one.

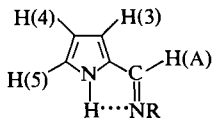

According to this hypothesis a high value of the stereospecific coupling (W_5-plan) between the a zomethinic proton H(A) and H(5) is observed (see Table 2). No spin–spin coupling occurs between H(A) and H(4), because of the *cis* coplanar disposition (dihedral angle 0°) of the two atoms. In these molecules **1** a *trans* coplanar disposition is required for the stereospecific coupling (J^5_W) to occur, as observed for aromatic (13, 9) and heterocyclic aldehydes (9, 11) and for 1,2-diarylethylenes (3, 4).

In the case of **1** (X = N—CH_3), the same value of the stereospecific spin–spin coupling between H(A) and H(5) is observed, in addition to an identical ^{1}H nmr spectral behaviour (see Tables 1 and 2). We can suggest then that the molecules **1** (X = N—CH_3) also occur exclusively in the *s-trans* conformation.

In the case of molecules **1** (X = O), from the H(A) signal of the ^{1}H nmr spectrum, a lower value of the stereospecific spin–spin coupling ($J^5_{H(A)-H(5)}$) is pointed out (see Table 2). The H(5) signal appears as an unresolved multiplet because of the presence of three small coupling constants, as typically occurs in the furan derivatives (14).

No coupling between H(A) and H(4) is observed, the H(4) signal being a clean quartet (doublet of doublet) that is the X part of an AMX system which arises from the spin–spin interaction with H(3) and H(5). The *s-trans* conformation can then be suggested also for the compounds **1** (X = O).

This behaviour is different from the corresponding 2-carbonyl-furan derivatives, where both rotamers are populated (5, 7, 9, 10, 15–19). The lower electron density on the azomethinic nitrogen of molecules **1** (X = O) with respect to the carbonyl oxygen seems to be inadequate to reduce the stability of the *s-trans* conformation because of

Can. J. Chem. Downloaded from www.nrcresearchpress.com by 210.87.254.6 on 09/06/12
For personal use only.

TABLE 3. Physical constants of azomethines **1**

X	R	Boiling point (°C/Torr) or melting point (°C)
N—H	CH_3	56–58[a]
N—H	n-C_4H_9	91–92.5/3[b]
N—CH_3	CH_3	38/0.4[c]
N—CH_3	n-C_4H_9	71/0.4[d]
O	CH_3	53/16[e]
O	n-C_4H_9	90/13[e]

[a]Reference 21.
[b]Reference 22.
[c]*Anal.* calcd. for $C_7H_{10}N_2$: C 68.82, H 8.25, N 22.93; found: C 68.94, H 8.11, N 22.98.
[d]*Anal.* calcd. for $C_{10}H_{16}N_2$: C 73.12, H 9.82, N 17.06; found: C 73.25, H 9.73, N 17.17.
[e]Reference 23.

electrostatic repulsion with intracyclic oxygen, thus allowing the existence of the alternative *s-cis* rotamer.

Experimental

The samples of the azomethines **1** were prepared by condensation of the appropriate heterocyclic aldehyde with methylamine or *n*-butylamine following the general procedure described in ref. 20. Melting points or boiling points are reported in Table 3.

The ^{1}H nmr spectra were measured in 15% solution with ca. 1% of tetramethylsilane as internal standard using $CDCl_3$ as solvent. Low temperature ^{1}H nmr spectra were obtained in a mixture of acetone-d_6 and deuterochloroform (2:1). High temperature ^{1}H nmr spectra were obtained in 5% dimethylformamide-d_7 solutions. A Varian A-60 D spectrometer with variable temperature accessories was used.

The ir spectra were recorded on a Perkin-Elmer 237 spectrophotometer. Compound **1** (X = NH, R = n-C_4H_9) was investigated as the pure liquid. For compound **1** (X = NH, R = CH_3) a KBr disk was used. Dilute solution ir spectra were obtained in CCl_4 (concentration range 0.1–5%).

Acknowledgement

The authors are grateful to the Consiglio Nazionale delle Ricerche (Rome) for financial support.

1. A. ARCORIA, S. FISICHELLA, and D. SCIOTTO. Tetrahedron Lett. 2907 (1973).
2. S. FISICHELLA, G. MINERI, G. SCARLATA, and D. SCIOTTO. Tetrahedron, **31**, 2445 (1975).
3. A. ARCORIA, F. A. BOTTINO, and D. SCIOTTO. J. Heterocycl. Chem. **14**, 1353 (1977).
4. F. A. BOTTINO, G. MINERI, and D. SCIOTTO. Tetrahedron, **34**, 1557 (1978).
5. B. ROQUES and M. L. FOURNIE-ZALUSKI. Org. Magn. Reson. **3**, 305 (1971); B. ROQUES, S. COMBRISSON, C. RICHE, and C. PASCARD-BILLY. Tetrahedron, **26**, 3555 (1970).
6. K. I. DAHLQVIST and S. FORSÈN, J. Phys. Chem. **69**, 4062 (1965).
7. L. ARLINGER, K. I. DAHLQVIST, and S. FORSÈN. Acta Chem. Scand. **24**, 662 (1970).
8. L. ARLINGER, K. I. DAHLQVIST, and S. FORSÈN. Acta Chem. Scand. **24**, 672 (1970).
9. G. J. KARABATSOS and F. M. VANE. J. Am. Chem. Soc. **85**, 3886 (1963).
10. B. P. ROQUES and S. COMBRISSON. Can. J. Chem. **51**, 573 (1973).
11. M. FARNIER and T. DRAKENBERG. Tetrahedron Lett. 429 (1973).
12. H. LUMBROSO and G. C. PAPPALARDO. J. Chim. Phys. **71**, 3 (1974); H. LUMBROSO and C. LIÉGEOIS. J. Mol. Struct. **51**, 247 (1979).
13. S. FORSÈN and B. AKEMARK. Acta Chem. Scand. **17**, 1712 (1963).
14. F. A. BOVEY. Nuclear magnetic resonance spectroscopy. Academic Press, New York and London. 1969. p. 370.
15. B. ROQUES, S. COMBRISSON, C. RICHE, and C. PASCARD-BILLY. Tetrahedron, **26**, 3555 (1970).
16. S. NAGATA, T. YAMABE, K. YOSHIKAWA, and H. KATO. Tetrahedron, **29**, 2545 (1973).
17. K. L. DAHLQVIST and S. FORSÈN. J. Phys. Chem. **69**, 1760 (1965).
18. D. J. CHADWICK and G. D. MEAKINS. Chem. Commun. 637 (1970).
19. M. L. MARTIN, J. C. ROZE, G. J. MARTIN, and P. FOURNARI. Tetrahedron Lett. **39**, 3407 (1970).
20. D. M. ROBERTSON. J. Org. Chem. **25**, 48 (1960).
21. KWAN-NAN YEH and R. H. BARKER. Inorg. Chem. **6**, 830 (1967).
22. S. VMARAWA and S. ZEN. Bull. Chem. Soc. Jpn. **36**, 1150 (1963).
23. B. L. EMLING, J. E. BEATTY, and R. J. STEVENS. J. Am. Chem. Soc. **71**, 703 (1949).

Can. J. Chem. Downloaded from www.nrcresearchpress.com by 210.87.254.6 on 09/06/12
For personal use only.

Solvolysis rates in aqueous–organic mixed solvents. IX. Solvolysis of dichloroacetate ion in water–methanol solutions

EL-HUSSIENY M. DIEFALLAH,[1] MOHAMED A. ASHY, AND AHMED O. BAGHLAF

Department of Chemistry, King Abdulaziz University, Jeddah, Saudi Arabia

Received August 19, 1980

EL-HUSSIENY M. DIEFALLAH, MOHAMED A. ASHY, and AHMED O. BAGHLAF. Can. J. Chem. **59**, 1208 (1981).

The kinetics of the alkaline solvolysis of dichloroacetate ion in water–methanol solutions have been studied in the temperature range of 50.0 to 65.0°C and the influence of solvent variation on reaction rate has been examined in terms of changes in the activation parameters. The activation parameters $\Delta H^{\ddagger}$ and $\Delta S^{\ddagger}$ for the solvolysis reaction showed a minimum at about 0.8 water mole fraction. The significance of the results was discussed in view of the electrostatic theory and the changing of solvent structure.

EL-HUSSIENY M. DIEFALLAH, MOHAMED A. ASHY et AHMED O. BAGHLAF. Can. J. Chem. **59**, 1208 (1981).

On a étudié la cinétique de la solvolyse alcaline de l'ion dichloroacétate dans des solutions de méthanol–eau dans l'intervalle de température allant de 50,0 à 65,0°C et on a examiné l'effet de la variation du solvant sur la vitesse de réaction en fonction des variations des paramètres d'activation. Les paramètres d'activation $\Delta H^{\ddagger}$ et $\Delta S^{\ddagger}$ de la réaction de solvolyse atteignent un minimum lorsque la fraction molaire de l'eau est d'environ 0,8. On discute de la signification de ce résultat par rapport à la théorie électrostatique et au changement de la structure du solvant.

[Traduit par le journal]

Introduction

Mixed solvents, in which water was frequently one component, provided a graded series of solvolytic media in which to explore the relation between rates, mechanism, and the effect of changing solvent properties (1–4). In alcohol–water binary solvent systems, an extremum in the activation parameters towards the pure water end of the composition scale has been observed (5–13). The extremum behaviour seems to reflect a common solvent behaviour (12–14) and has been related to the accompanying solvent reorganization attending the activation process in binary alcohol–water systems (13). In the present investigation, we report the results of the study of the kinetics of the alkaline solvolysis of dichloroacetate ion in water–methanol solutions. Studies of the alkaline solvolysis of mono- and trichloroacetate ions in binary alcohol–water systems were recently published (5–8). Comparisons between the mono-, di-, and trichloroacetates have shown that there are large differences in order, specific rate constant, and mechanisms of the solvolysis reactions of these ions.

Experimental

The rate of reaction was determined in the temperature range 50.0 to 65.0°C, using a titrimetric method by following the release of chloride ions according to Volhard's technique (6–8). The initial concentrations of dichloroacetic acid were in the range 0.2 to 0.5 mol/L, while the initial concentrations of the base were in the range 0.05 to 0.4 mol/L. In each reaction mixture, the concentration of the base was always less than about twice that of dichloroacetate ion in the reaction solution.

Results and Discussion

Dilute alkaline solutions of sodium dichloroacetate turn acidic on standing due to the hydrolysis of dichloroacetate ion to yield glyoxylate and hydrochloric acid (15). The rate of the reaction follows the second-order rate law:

$$[1] \quad kt = \left(\frac{1}{2A_0 - B_0}\right) \ln \frac{AB_0}{A_0B}$$

where A_0 is the initial concentration of dichloroacetate ion, B_0 is the initial concentration of base, A and B are the concentrations of dichloroacetate ion and hydroxide ion at a time t during the reaction, and k is the specific reaction rate constant. The rate constants were evaluated from the slopes of the straight lines obtained when $\ln (AB_0/A_0B)$ is plotted against t. Figure 1 shows typical plots in water–methanol solutions at 55.0°C. The mechanism of the reaction would thus involve the initial formation of the unstable chlorohydroxyacetate intermediate which, in turn, eliminates hydrochloric acid to yield glyoxylate:

$$[2] \quad CHCl_2 \cdot COO^- + OH^- \xrightarrow{-Cl^-} H{-}\underset{\displaystyle Cl}{\overset{\displaystyle OH}{\overset{|}{\underset{|}{C}}}}{-}COO^- \qquad \text{(slow)}$$

$$[3] \quad H{-}\underset{\displaystyle Cl}{\overset{\displaystyle OH}{\overset{|}{\underset{|}{C}}}}{-}COO^- \xrightarrow{-HCl} H{-}\overset{\displaystyle O}{\overset{\|}{C}}{-}COO^- \qquad \text{(fast)}$$

[1]Author to whom all communications should be addressed. Present address: Department of Chemistry, Assiut University, Assiut, Egypt.

0008-4042/81/081208-04$01.00/0

©1981 National Research Council of Canada/Conseil national de recherches du Canada

Can. J. Chem. Downloaded from www.nrcresearchpress.com by 210.87.254.5 on 09/06/12
For personal use only.

Can. J. Chem. Downloaded from www.nrcresearchpress.com by 210.87.254.5 on 09/06/12
For personal use only.

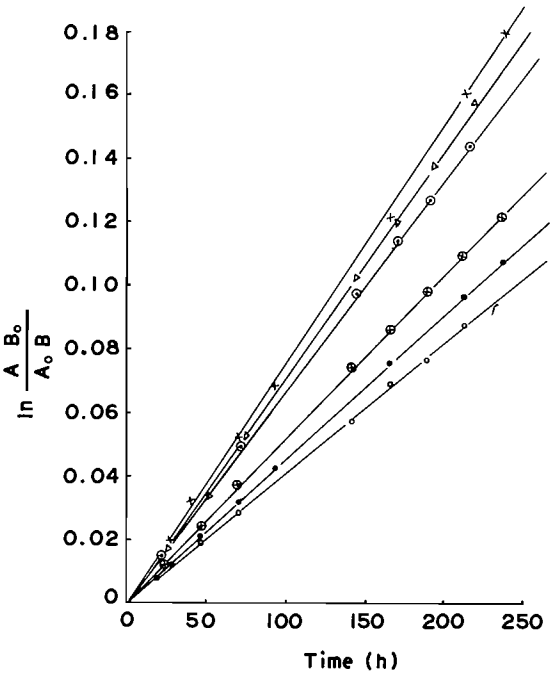

FIG. 1. Second-order plots at 55.0°C in water–methanol solutions. Water mole fraction: ●, 1.00; ⊙, 0.941; ×, 0.806; △, 0.727; ⊗, 0.542; ○, 0.308.

Table 1 lists the values of the rate constants obtained at the specified temperatures and the medium dielectric constant (D) of the various solvent mixtures investigated. The rate constants represent the average of at least three determinations and the reported errors are average errors. In each solvent mixture, D was taken from the experimental data of Akerlöf (16) or calculated from these values by interpolation between different temperatures or between different solvent mixtures. The results show that the rate of reaction first increases as the methanol content of the solution increases up to a maximum at about 0.8 water mole fraction, and then decreases. The behaviour of the solvolysis rates shows similarity to that of monochloroacetate ion in the same medium (6) but is different from those of the decarboxylation reaction of trichloroacetate ion (8). This would be due to the fact that the rate of the alkaline solvolysis in the mono- and dichloroacetates is determined by the attack of the hydroxide ion on the respective ion, whereas the rate of the alkaline decarboxylation of the trichloroacetate ion is independent of the concentration of the hydroxide ion and the rate-determining step is the breaking of the carbon–carbon bond with the concomitant release of CO_2 and the formation of trichloromethyl carbanion intermediate (7, 8). In solvent mixtures with compositions in the range 0 to 30% by weight methanol (1.0 to 0.8 water mole fraction), the results are not in the same order as that predicted by the simple electrostatic theory (17) and indicate that there is no simple correlation between the dielectric constant and the rate constant (18).

The energy of activation of the reaction was calculated from the temperature coefficient of the reaction rates by the least-squares method. The enthalpy and entropy of activations were calculated from the rate constants using absolute rate theory equations (19) and the results (calculated at 50.0°C) are tabulated in Table 2. Entropy of activation values are all negative in all solvent mixtures investigated indicating that in all of these mixtures the activated complex structure is relatively more ordered than the structure of the separated reactants. It is seen that when the concentration of methanol in the solvent mixture is increased, the enthalpy and entropy of activation first decrease to a minimum at about 0.8 water mole fraction, and then increase. The positions of the $\Delta H^{\ddagger}$ and $\Delta S^{\ddagger}$ minima appear to coincide, which is characteristic of binary solvent mixtures in which both components are hydroxylic. The depth of the $\Delta H^{\ddagger}$ minimum relative to pure water is about 4 kcal/mol and that for $\Delta S^{\ddagger}$ is 12 cal deg^{-1} mol^{-1}. These values are the same as those observed for the solvolysis of monochloroacetate ion (6) and the trichloroacetate ion (7) in the same media. The calculated values of the free energy of activation, $\Delta G^{\ddagger}$ (listed in Table 2), show that they do not change much with solvent composition. This must be due to the linear compensation between $\Delta H^{\ddagger}$ and $\Delta S^{\ddagger}$. The plot of $\Delta H^{\ddagger}$ versus $\Delta S^{\ddagger}$ gave rise to a straight line (Fig. 2), the slope of which, known as the isokinetic or isoequilibrium temperature, equals 320 K. Linear $\Delta H^{\ddagger}$–$\Delta S^{\ddagger}$ relationships were also observed for the solvolysis of monochloroacetate (5, 6) and trichloroacetate ions (7, 8) and for other systems (12, 19). This behaviour is expected if the solvents in a series perform closely similar roles in the reaction (18).

The solvolysis of dichloroacetate ion in water–methanol solutions showed that for solvent mixtures with compositions in the range 1.0 to 0.8 water mole fraction, the principal contribution toward increasing rate is from the decrease in $\Delta H^{\ddagger}$ which outweighs the decrease in rate caused by a decrease in $\Delta S^{\ddagger}$. However, at water mole fractions less than about 0.8, $\Delta S^{\ddagger}$ increases by about 15 cal deg^{-1} mol^{-1} between 0.8 and 0.3 water mole fraction, but its effect on the rate of reaction is far outweighed by the increase in $\Delta H^{\ddagger}$ (which is about

Can. J. Chem. Downloaded from www.nrcresearchpress.com by 210.87.254.5 on 09/06/12
For personal use only.

TABLE 1. Effect of temperature and solvent composition on the rate constants of the alkaline solvolysis of dichloroacetate ion in water–methanol solutions

Methanol (% by wt.)	Water mole fraction	Temperature °C	Dielectric constant	$k \times 10^7$ (L mol^{-1} s^{-1})
0	1.00	50.0	69.85	5.7 ± 0.1
		55.0	68.13	12.6 ± 0.2
		60.0	66.62	20.7 ± 0.5
		65.0	64.99	29.3 ± 0.2
10	0.941	50.0	65.66	8.2 ± 0.1
		55.0	64.14	16.8 ± 0.3
		60.0	62.77	26.0 ± 0.1
		65.0	61.14	37.2 ± 0.2
20	0.877	50.0	61.06	9.9 ± 0.3
		55.0	59.75	18.3 ± 0.3
		60.0	58.24	29.3 ± 0.2
		65.0	56.90	37.8 ± 0.3
30	0.806	50.0	56.59	11.0 ± 0.5
		55.0	55.30	19.4 ± 0.4
		60.0	53.94	30.8 ± 0.1
		65.0	52.59	40.0 ± 0.6
40	0.727	50.0	52.17	9.9 ± 0.2
		55.0	51.02	17.1 ± 0.3
		60.0	49.52	26.3 ± 0.2
		65.0	48.45	43.2 ± 0.3
50	0.640	50.0	47.82	8.8 ± 0.1
		55.0	46.71	16.9 ± 0.1
		60.0	45.28	25.4 ± 0.4
		65.0	44.26	40.8 ± 0.5
60	0.542	50.0	43.22	7.5 ± 0.5
		55.0	42.33	14.2 ± 1
		60.0	41.22	25.1 ± 0.2
		65.0	40.01	38.1 ± 0.1
80	0.308	50.0	34.62	7.2 ± 0.1
		55.0	33.82	11.8 ± 0.4
		60.0	32.74	23.3 ± 0.5
		65.0	31.94	35.9 ± 0.5

TABLE 2. Activation parameters (at 50.0°C) for the alkaline solvolysis of dichloroacetate ion in water–methanol solutions

Water mole fraction	E_a (kcal/mol)	$\Delta H^{\ddagger}$ (kcal/mol)	$-\Delta S^{\ddagger}$ (cal deg^{-1} mol^{-1})	$\Delta G^{\ddagger}$ (kcal/mol)
1.00	23.5	22.8	16.4	28.1
0.941	21.7	21.1	21.2	27.9
0.877	19.6	18.9	27.5	27.8
0.806	18.9	18.3	29.4	27.8
0.727	21.1	20.5	22.8	27.8
0.640	21.9	21.2	21.6	28.2
0.542	23.7	23.0	15.4	28.0
0.308	23.9	23.2	15.0	28.1

5 kcal mol^{-1} in the same composition range), which causes a net decrease in reaction rate for solvent mixtures with less than about 0.8 water mole fraction. Comparison of the results obtained for the solvolysis of mono-, di-, and trichloroacetates indicated that in the same solvent system the activation parameters may show similar variations irrespective of the reaction substrates, order, and mechanism. The results reflect a common solvent behaviour and emphasize the previously stated necessity of taking structural properties of the solvent into consideration.

The behaviour of the activation enthalpy and entropy towards solvent change observed here is similar to that observed for many solvolytic reactions in aqueous–organic solvent mixtures under a variety of conditions (2–6, 10). Arnett *et al.* (14) have shown that the appearance of the minimum in aqueous–organic solvent mixtures is readily explained on the basis of the behaviour of heats of

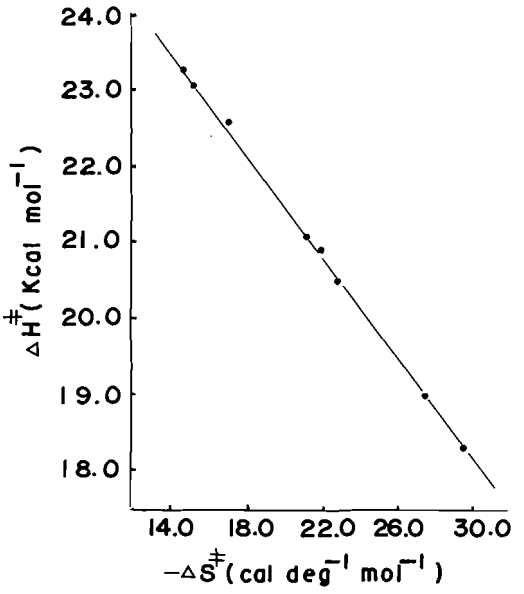

FIG. 2. A plot of $\Delta H^{\ddagger}$ versus $\Delta S^{\ddagger}$ for the alkaline solvolysis of dichloroacetate ion in a series of water–methanol solutions.

solution in aqueous alcohols. It was concluded that both heats of solution and the enthalpy of activation were related to the same kind of changes in solvent structure with changing composition. The results reported here indicate that the activation parameters $\Delta H^{\ddagger}$ and $\Delta S^{\ddagger}$ pass through a minimum at about the same composition range where other tests showed extreme behaviour, which could be attributed to a change in structural stability with composition (12–14). Hence, the behaviour of $\Delta H^{\ddagger}$ and $\Delta S^{\ddagger}$ is interpreted on the basis that the breakdown of solvent structure, as a consequence of charge separation in the activation process, parallels the sensitivity to changes in the solvent composition (13, 14).

1. R. E. ROBERTSON. Prog. Phys. Org. Chem. **4**, 213 (1967).
2. E. S. AMIS. Solvent effects on reaction rates and mechanisms. Academic Press, New York. 1966.
3. D. N. GLEW and E. A. MOELWYN-HUGHES. Proc. R. Soc. London, Ser. A, **211**, 254 (1952).
4. E. TOMMILA, M. TIILIKAINEN, and A. VOIPOI. Ann. Acad. Sci. Fenn., Ser. A1, 25 (1955).
5. EL-H. M. DIEFALLAH. Can. J. Chem. **54**, 1687 (1976).
6. A. M. AZZAM and EL-H. M. DIEFALLAH. Z. Phys. Chem. Leipzig, **91**, 44 (1974); EL-H. M. DIEFALLAH and A. M. KHALIL. Indian J. Chem. **14A**, 1012 (1976).
7. EL-H. M. DIEFALLAH and S. A. GHONAIM. J. Chem. Soc. Perkin Trans. II, 1237 (1977).
8. EL-H. M. DIEFALLAH and A. M. EL-NADI. Can. J. Chem. **56**, 2053 (1978).
9. J. B. HYNE and R. WILLS. J. Am. Chem. Soc. **85**, 3650 (1963).
10. J. B. MARTIN and R. E. ROBERTSON. J. Am. Chem. Soc. **88**, 5353 (1966).
11. H. S. GOLINKIN and J. B. HYNE. Can. J. Chem. **46**, 125 (1966).
12. R. E. ROBERTSON and S. E. SUGAMORI. J. Am. Chem. Soc. **91**, 7254 (1969).
13. R. E. ROBERTSON and S. E. SUGAMORI. Can. J. Chem. **50**, 1353 (1972).
14. E. M. ARNETT, W. G. BENTRUDE, J. J. BURKE, and P. M. DUGGLEBY. J. Am. Chem. Soc. **87**, 1541 (1965).
15. I. L. FINAR. Organic chemistry. Vol. 1. 6th ed. Longman, London. 1973. p. 239.
16. G. AKERLÖF. J. Am. Chem. Soc. **54**, 4125 (1932).
17. C. K. INGOLD. Structure and mechanism in organic chemistry. Cornell University Press, Ithaca, New York. 1953. Chapt. 7.
18. J. E. LEFFLER. J. Org. Chem. **20**, 1202 (1955).
19. A. A. FROST and R. G. PEARSON. Kinetics and mechanism. 2nd ed. John Wiley and Sons, Inc., New York. 1961. Chapt. 7.

Can. J. Chem. Downloaded from www.nrcresearchpress.com by 210.87.254.5 on 09/06/12
For personal use only.

Studies of molecular complexes of some π- and *n*-donors with iodine by the constant activity method

RAM ADHAR SING[1] AND SUBRAY N. BHAT[2]

Chemistry Department, North Eastern Hill University, Shillong - 793003, India

Received August 22, 1980

RAM ADHAR SING and SUBRAY N. BHAT. Can. J. Chem. **59**, 1212 (1981).

The iodine complexes of naphthalene, biphenyl, hexamethylbenzene, aniline, and *o*-toluidine in carbon tetrachloride were studied by using the constant activity method. The association constants and the heats of formation of the complexes were determined and the results are compared with those obtained by using conventional spectral methods. The blue-shifted iodine band maxima were determined directly.

RAM ADHAR SING et SUBRAY N. BHAT. Can. J. Chem. **59**, 1212 (1981).

On a étudié les complexes de l'iode avec le naphtalène, le biphényle, l'hexaméthylbenzène, l'aniline et la *o*-toluidine dans le tétrachlorure de carbone, en utilisant la méthode de la constante d'activité. On a déterminé les constantes d'association et les chaleurs de formation des complexes et on a comparé les résultats à ceux obtenus en utilisant les méthodes spectrales conventionnelles. On a déterminé directement les déplacements maxima vers le bleu de la liaison impliquant l'iode.

[Traduit par le journal]

Introduction

Ever since Benesi and Hildebrand (1) reported the interaction of iodine with aromatics, iodine complexes have been most extensively studied (2–6). However, it is not easy to obtain sufficiently accurate spectral measurements (particularly in the case of weak complexes) and to interpret spectral data in terms of parameters characteristic of molecular complexes of iodine. Although one can obtain a reasonably good value of $K_c\varepsilon$ from the spectral studies, the reliable separation of K_c and ε is not an easy task, particularly in the case of weakly interacting systems. So the validity of many of the published spectral and thermodynamic constants, obtained by the spectroscopic method alone has been questioned by many investigators (7–10).

Childs *et al.* (11, 12) have developed a procedure called the "spectral-solubility" or "constant activity" method which can be used to obtain the values of K_c and ε directly. In the present study, the applicability of the constant activity method in the case of iodine complexes of naphthalene, biphenyl, hexamethylbenzene (π-donors) and aniline, *o*-toluidine (*n*-donors) is investigated.

Materials and Methods

Solid tetramethylammonium pentaiodide, $TMAI_5$, was prepared as described by Chattaway and Hoyle (13). All the donors, namely, naphthalene, biphenyl, hexamethylbenzene, aniline, *o*-toluidine, and the acceptor, iodine, were purified by standard procedures (14–16). Spectral grade (BDH) carbon tetrachloride was used as such.

[1]Present address: Chemistry Department, Banaras Hindu University, Varanasi, India.

[2]To whom all correspondence should be addressed.

The procedure used to obtain the value of K_c is that developed by Childs *et al.* (11, 12). It is based on using a mixture of tetramethylammonium polyiodides to maintain a constant activity of iodine, e.g.,

[1] $(CH_3)_4NI_5(s) \rightleftarrows (CH_3)_4NI_3(s) + I_2$

Addition of a donor to this system establishes a second equilibrium (and eq. [1] is displaced to the right, to replace the iodine complexed by the donor),

[2] $D + I_2 \rightleftarrows DI_2$

and the concentration of iodine in the second equilibrium is determined directly from the increase in absorbance at the isosbestic point of iodine in the visible region. Since the extinction coefficients of the complexed and of the free (uncomplexed) iodine are equal at this wavelength (i.e. at the isosbestic point), the concentration of the complex (assuming it to be 1:1) can be calculated directly.

The equilibrium constant, K_c, for the interaction of a donor, D, with an acceptor, I_2, to form a 1:1 complex is,

[3] $K_c = C_{DI_2}/C_D C_{I_2}^t$

or

[4] $K_c = C_{DI_2}/(C_D^0 - C_{DI_2})C_{I_2}^t$

where C_{DI_2} is the equilibrium concentration of the complex (DI_2), $C_{I_2}^t$ is the equilibrium concentration of free iodine at temperature t(°C), C_D^0 is the initial donor concentration, and $(C_D^0 - C_{DI_2}) = C_D$ is the equilibrium concentration of donor. For a cell of unit path length, the increase in absorbance (assuming that the system obeys Beer's law) at the isosbestic point, ΔA_{isos}, is related to the complex concentration, C_{DI_2} as,

[5] $\Delta A_{isos} = \varepsilon_{isos} C_{DI_2}$

where ε_{isos} is the molar extinction coefficient of iodine at the isosbestic point. From eqs. [4] and [5] we get,

[6] $K_c = \Delta A_{isos}/(\varepsilon_{isos} C_D^0 - \Delta A_{isos})C_{I_2}^t$

Thus the equilibrium constant, K_c, can be calculated by knowing ΔA_{isos}, C_D^0, and $C_{I_2}^t$. In this method, a prior knowledge of the molar extinction coefficient of the complex is not needed.

The molar extinction coefficient of the charge-transfer band,

0008-4042/81/081212-06$01.00/0

©1981 National Research Council of Canada/Conseil national de recherches du Canada

Can. J. Chem. Downloaded from www.nrcresearchpress.com by 210.87.254.6 on 09/06/12
For personal use only.

Can. J. Chem. Downloaded from www.nrcresearchpress.com by 210.87.254.6 on 09/06/12
For personal use only.

ε_{CT}, or of the blue-shifted iodine band, ε_{BS}, can also be evaluated directly without a prior knowledge of K_c, if simultaneous measurements of absorbance are made at the isosbestic point, the charge-transfer band, or the blue-shifted iodine band for the same solution. It can be easily seen that

[7] $\Delta A_{CT}/\Delta A_{isos} = \varepsilon_{CT}/\varepsilon_{isos}$

and

$$\Delta A_{BS}/\Delta A_{isos} = \varepsilon_{BS}/\varepsilon_{isos}$$

For obtaining the isosbestic point as well as ε_{iso}, the spectra of pure iodine and complexed iodine in carbon tetrachloride were recorded by keeping the iodine concentration constant (~0.8 mM) and varying the donor concentrations (0.005–0.9 M). Pure $TMAI_5$ was equilibrated with carbon tetrachloride (~3 days) at constant temperature (in a thermostat) and the spectrum of iodine in the equilibrated solution was recorded. Then a series of several solutions of donors in carbon tetrachloride were similarly equilibrated with $TMAI_5$ (~150 mg) and spectra were recorded for all those solutions at constant temperature.

The spectra at 25, 30, 35, and 40°C were recorded in the uv and visible regions using a Cary-14 recording spectrophotometer fitted with thermostat jackets for temperature control of the cell. The temperature of the solutions could be controlled to within ±0.1°C.

For locating the blue-shifted iodine band of the donor–iodine complex, the spectrum of the complex was recorded with the donor and the constant activity source of iodine in the sample cell and only the constant activity source of iodine in the reference cell (17).

Results and Discussion

Heat of Dissociation of $TMAI_5$ in CCl_4

The dissociation constant, K_d for the dissociation of $TMAI_5$ into $TMAI_3$ and I_2 is given by

$$K_d = [TMAI_3][I_2]/[TMAI_5]$$

or

$$K_d = [I_2]$$

The heat of dissociation of $TMAI_5$ is obtained from Van't Hoff's plot of the absorbance of iodine at 517 nm from the $TMAI_5/TMAI_3$ equilibrium in carbon tetrachloride, and the value is 8.10 kcal/mol. This value compares well with the most recent value of Tse and Tamres (8.18 kcal/mol) (18).

Naphthalene–Iodine System

Figure 1 shows the isosbestic point of the naphthalene–iodine complex (at 497 nm). The molar extinction coefficient of iodine in carbon tetrachloride at 497 nm is 819 M^{-1} cm^{-1} (Table 1). The isosbestic point does not vary with the concentration of donor (in the experimental range of 0.11 to 0.4 M). It can be seen from Fig. 2 that as the concentration of naphthalene increases the absorbance at the isosbestic wavelength increases. It has been pointed out earlier that measurement of the increase in absorbance at the isosbestic point gives the concentration of the complex. The equilibrium

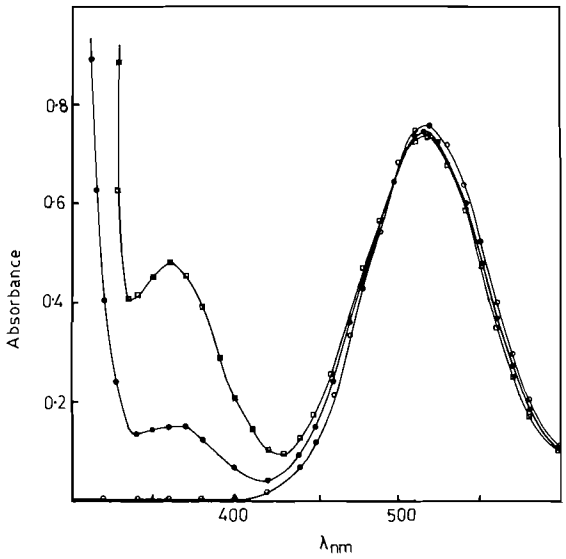

FIG. 1. Isosbestic point of the naphthalene–iodine complex in CCl_4 at 25°C; cell path = 1.00 cm; $[I_2]_0 = 8.0 \times 10^{-4}$ M; $[D]_0$ = 0.0–0.4 M.

TABLE 1. Molar extinction coefficients and isosbestic points of iodine complexes in carbon tetrachloride at 25°C (concentration of iodine = 0.8 mM, path length = 1.00 cm)

Donor	λ_{isos}* (nm)	A_{isos}	ε_{isos}† (M^{-1} cm^{-1})
Naphthalene	497	0.655	819
Biphenyl	504	0.700	875
Hexamethylbenzene	519	0.760	950
Aniline	498	0.665	837
o-Toluidine	493	0.615	766

*Error limit ± 1.
†Error limit ± 10.

constants, K_c^s (calculated by using eq. [6]) at only two temperatures and two concentrations have been listed in Table 2 for the sake of brevity. The average K_c^s and ε_{CT} at 25°C are 0.54 M^{-1} and 4850 M^{-1} cm^{-1} respectively. The value of K_c^s is slightly higher than the literature data (0.25 M^{-1}) (19); similar higher values of K_c^s have been reported by Childs *et al.* for aromatic–iodine systems (12). It has been pointed out by Christian *et al.* (11, 12) that K_c^s actually includes both the specific interaction (complex formation) and non-specific interactions between donor and iodine. If the correction term due to non-specific interactions is near zero, then the K_c^{th} value may be equal to the K_c^s value (18, 20). The enthalpy $-\Delta H^0$, (1.91 kcal/mol) calculated from a study of the temperature dependence of the absorbance of the complex using a single solution of donor with excess of $TMAI_5$ and also by the usual procedure (i.e. by knowing

Can. J. Chem. Downloaded from www.nrcresearchpress.com by 210.87.254.6 on 09/06/12
For personal use only.

TABLE 2. Formation constants and spectral data of the iodine–naphthalene complex by the constant activity method; solvent: CCl_4

	Value			
	25°C		35°C	
Parameter	(*1*)	(*2*)	(*1*)	(*2*)
C_D^0 (M)	0.09935	0.19885	0.09819	0.19643
A^0_{isos}	0.370	0.370	0.570	0.570
A_{isos}	0.390	0.410	0.595	0.625
ΔA_{isos}	0.020	0.040	0.025	0.055
C_{DI_2} ($\times 10^5$ M)	2.45	4.90	3.25	6.72
C_D (M)	0.09932	0.19880	0.09816	0.19636
K_c^s (M^{-1})	0.54	0.54	0.48	0.48
Ave K_c^s (M^{-1})*	0.54(0.25)‡		0.48	
ΔA_{CT}	0.120	0.235	0.160	0.325
ε_{CT} (M^{-1} cm^{-1})	4900	4800	4853	4840
Ave ε_{CT} (M^{-1} cm^{-1})†	4850(7250)‡		4846	
λ_{CT} (nm)	360(360)‡		360	
$-\Delta H^0$ (kcal/mol)	1.91 ± 0.1(1.80)‡			

*Error limit in K_c^s is ± 0.01.
†Error limit in ε_{CT} is ± 50.
‡Values in parentheses refer to the literature data (19).

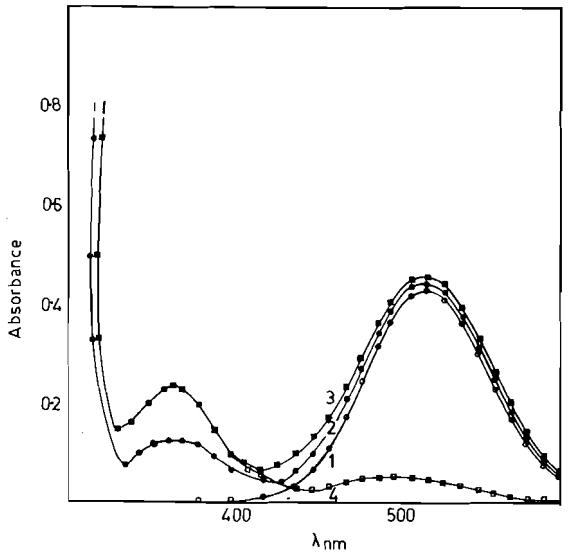

FIG. 2. Visible spectra of the naphthalene–iodine complex in CCl_4 by the constant activity method at 25°C, cell path = 1.00 cm; *1*, $[I_2]_0 = 4.53 \times 10^{-4}$, ○; *2*, $[D]_0 = 0.0994$ M, ●; *3*, $[D]_0 = 0.1989$ M, ■; *4*, Differential spectrum of *3* vs. *1*, □.

the values of K_c at different temperatures) agrees well with the literature value (1.80 kcal/mol) (21).

The concentrations of donor (range 0.05–0.2 M) used are such that we can assume that the solutions are reasonably dilute and in the low concentration region, ΔA_{CT} (the change in A_{CT} corrected for free iodine and donor) varies linearly with ΔA_{isos} and the limiting slope of the plot of ΔA_{CT} vs. ΔA_{isos} is equal to the ratio of $\varepsilon_{CT}/\varepsilon_{isos}$ (Fig. 3). The value of ε_{isos} thus calculated is 4850 M^{-1} cm^{-1} which is lower than that reported in the literature (7250 M^{-1} cm^{-1}) by the conventional spectral methods. Here it is worth mentioning that the association constant obtained by this method is higher and ε is lower but the $K\varepsilon$ product is nearly the same as that of the literature data.

The visible spectrum of the naphthalene–iodine system obtained by the constant activity method (using a differential procedure) is shown in Fig. 2. The blue shifted iodine band has a maximum at 498 ± 2 nm. An examination of the spectra at different concentrations of donor indicates that the blue-shifted iodine band position does not vary with the concentration of the donor. The molar extinction coefficient of the blue-shifted iodine band maximum, ε_{BS}, is calculated from the ratio of the change in absorbance of the blue shifted band, ΔA_{BS}, to the change in absorbance at the isosbestic point ΔA_{isos}. The molar extinction coefficient, ε_{BS}, thus obtained is 915 ± 20 M^{-1} cm^{-1}.

Biphenyl–Iodine System

The isosbestic point of the biphenyl–iodine complex is 504 nm and the molar extinction coefficient of iodine in carbon tetrachloride at 504 nm is 875 M^{-1} cm^{-1} (Table 1). The isosbestic point does not vary with the concentration (concentration range 0.1–0.9 M) of the donor. As the concentration of biphenyl in $TMAI_5$–biphenyl increases, the absorbance at the isosbestic point increases. The relevant data and the equilibrium constants for the iodine–biphenyl system are given in Table 3. The average equilibrium constant at 25°C is 0.51 M^{-1} which is slightly higher than the literature value of 0.39 M^{-1} (22) which may be due to the inclusion of

TABLE 3. Formation constants and spectral data of the iodine–biphenyl complex in CCl_4 by the constant activity method

Parameter	Value			
	25°C		35°C	
	(*1*)	(*2*)	(*1*)	(*2*)
C_D^0 (M)	0.09885	0.39609	0.09764	0.39127
A^0_{isos}	0.405	0.405	0.620	0.620
A_{isos}	0.425	0.485	0.645	0.725
ΔA_{isos}	0.020	0.080	0.025	0.105
C_{DI_2} ($\times 10^5$ M)	2.29	9.14	2.86	12.00
C_D (M)	0.09883	0.39600	0.09761	0.39115
K_c^s (M^{-1})	0.51	0.51	0.415	0.435
Ave K_c^s (M^{-1})*	0.51(0.39)‡		0.42	
ΔA_{CT}	0.060	0.240	0.075	0.310
ε_{CT} (M^{-1} cm^{-1})	2625	2625	2625	2583
Ave ε_{CT} (M^{-1} cm^{-1})†	2625(4000)‡		2604	
λ_{CT} (nm)	335			
λ_{BS} (nm)	480 ± 5			
$-\Delta H^0$ (kcal/mol)	3.45 ± 0.2			

*Error limit in K_c^s is ± 0.01.
†Error limit in ε_{CT} is ± 50.
‡Values in parentheses refer to the literature data: (*i*) ref. 22; (*ii*) ref. 23.

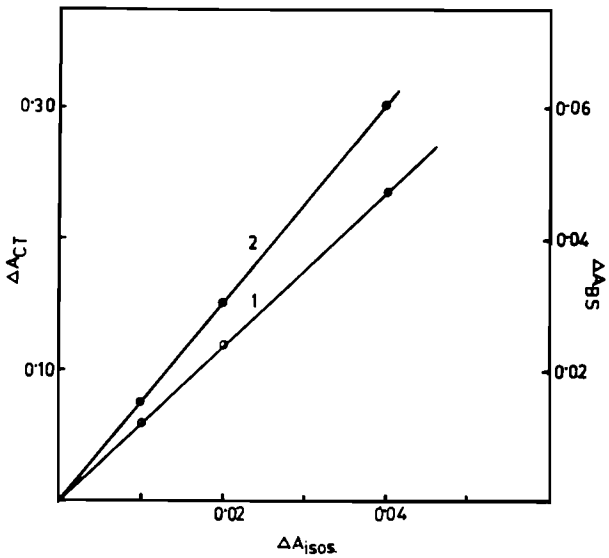

FIG. 3. Plot of ΔA_{CT} and ΔA_{BS} vs. ΔA_{isos} of the naphthalene–iodine complex at 25°C (solvent: CCl_4): *1*, ΔA_{CT} vs. ΔA_{isos}; *2*, ΔA_{BS} vs. ΔA_{isos}.

non-specific interactions in the K_c^s. The enthalpy, $-\Delta H^0$, for biphenyl–iodine is 3.45 kcal/mol.

The molar extinction coefficient of the biphenyl–iodine complex at the charge-transfer band (335 nm) calculated from the limiting slope of the plot of ΔA_{CT} vs. ΔA_{isos} is 2600 M^{-1} cm^{-1}, which is very much lower than the literature value (4000 M^{-1} cm^{-1}) (23). However, as in the case of naphthalene–iodine, the $K_c\varepsilon$ value calculated from the constant activity method is comparable to that obtained by the spectral method. It is noteworthy that Lane *et al.* (24) have rightly pointed out that, in the case of weak molecular complexes, values of ε determined using different concentration scales can differ widely.

The blue-shifted iodine band maximum (which is independent of the concentration of the donor) for the biphenyl–iodine system is at 480 ± 5 nm.

The iodine absorption band at 517 nm in CCl_4 is due to electron excitation from the antibonding π_g* molecular orbital to the antibonding σ_u* molecular orbital. Mulliken and Person (3) had pointed out that the strongly antibonding σ_u* molecular orbital must be larger in size than the outer occupied molecular orbitals in the ground state of the iodine molecule. On excitation of the iodine molecule in a complex, its swollen size introduces an exchange repulsion between it and the partner molecule. This repulsion energy, and thus the blue-shift in absorption frequency, should be greater the stronger the complex. In the present case, the shift in the visible iodine band is much more in biphenyl–iodine system compared to that in the naphthalene–iodine system and the enthalpy of the former is also higher. These results indicate that biphenyl–iodine is definitely a stronger complex than naphthalene–iodine. This observation parallels the electron-donating properties (or ionization potentials) of the donors.

Hexamethylbenzene–Iodine System

The hexamethylbenzene–iodine complex has an isosbestic point at 519 nm in CCl_4 and the molar extinction coefficient of the iodine (ε_{isos}) is 950 M^{-1} cm^{-1}. As the concentration of hexamethylbenzene (in the hexamethylbenzene–$TMAI_5$ system) in-

Can. J. Chem. Downloaded from www.nrcresearchpress.com by 210.87.254.6 on 09/06/12
For personal use only.

TABLE 4. Formation constants and spectral data of the iodine–hexamethylbenzene complex in CCl_4 by the constant activity method

Parameter	Value			
	25°C		35°C	
	(*1*)	(*2*)	(*1*)	(*2*)
C_D^0 (M)	0.05038	0.10001	0.04977	0.09879
A^0_{isos}	0.430	0.430	0.670	0.670
A_{isos}	0.475	0.520	0.725	0.780
ΔA_{isos}	0.045	0.090	0.055	0.110
C_{DI_2} ($\times 10^5$ M)	4.74	9.47	5.80	11.60
C_D (M)	0.05033	0.09992	0.04971	0.09867
K_c^s (M^{-1})	2.081	2.095	1.651	1.667
Ave K_c^s (M^{-1})*	2.088(1.35)‡		1.66	
ΔA_{CT}	0.415	0.725	0.440	0.810
ε_{CT} (M^{-1} cm^{-1})	8761	7653	7600	6995
Ave ε_{CT} (M^{-1} cm^{-1})†	8200(8200)‡		7300	
λ_{CT} (nm)	375(375)‡			
λ_{BS} (nm)	480 ± 5			
$-\Delta H^0$ (kcal/mol)	4.33 ± 0.5(3.73)‡			

*Error limit in K_c^s is ± 0.02.
†Error limit in ε_{CT} is ± 50.
‡Values in parentheses refer to literature data (27).

TABLE 5. Formation constants and spectral data of iodine–aniline and iodine–*o*-toluidine complexes by the constant activity method; solvent, CCl_4; T, 26.5°C

Parameter	Value			
	Aniline		*o*-Toluidine	
	(*1*)	(*2*)	(*1*)	(*2*)
C_D^0 (M)	0.00851	0.01338	0.00764	0.01524
A^0_{isos}	0.400	0.400	0.370	0.370
A_{isos}	0.470	0.510	0.440	0.510
ΔA_{isos}	0.070	0.110	0.070	0.140
C_{DI_2} ($\times 10^5$ M)	8.36	13.14	9.14	18.28
C_D (M)	0.00843	0.01325	0.00755	0.01506
K_c^s (M^{-1})	20.5	20.5	25.0	25.1
Ave K_c^s (M^{-1})*	20.5(12)†		25.0(11)†	

*Error limit in K_c^s is ± 0.5.
†Value in parentheses refer to literature data (26).

creases, the absorbance at the isosbestic point also increases. The equilibrium constant for the hexamethylbenzene–iodine system in CCl_4 is 2.09 M^{-1} at 25°C (lit. 1.35 M^{-1}; Table 4). However, the enthalpy is 4.33 kcal/mol which is comparable to the literature value of 3.75 kcal/mol (25).

The molar extinction coefficient of hexamethylbenzene–iodine at the charge-transfer band (375 nm) is 8200 M^{-1} cm^{-1}. This value is in very good agreement with the literature value of 8200 M^{-1} cm^{-1} (25). However, the $K_c\varepsilon$ value is higher than the literature data. In the absence of detailed information in the literature, it is not possible to comment on this.

The blue-shifted iodine band appears at 480 ± 5 nm and ε_{BS} is 1375 M^{-1} cm^{-1}. Judging from the position of the blue-shifted iodine band, it appears that hexamethylbenzene–iodine is a stronger complex than naphthalene–iodine but that its strength is comparable to that of biphenyl–iodine.

Aniline–Iodine System

The isosbestic point of the aniline–iodine system in carbon tetrachloride is located at 498 nm and ε_{isos} is 837 M^{-1} cm^{-1}. The isosbestic point neither changed with donor concentration (0.005–0.05 M) nor with time. As the concentration of aniline (in aniline–$TMAI_5$) is increased, the absorbance at the isosbestic point increases. We did not notice any change in absorbance during the experiment. This indicates that the complex is reasonably stable in CCl_4 during that time interval. The equilibrium constants K_c^s at 26.5°C is 20.5 M^{-1}, which is higher than the literature value of 12 M^{-1} (26) (Table 5). Here it may be recalled that in the literature it has been mentioned that the complex is not stable

Can. J. Chem. Downloaded from www.nrcresearchpress.com by 210.87.254.6 on 09/06/12
For personal use only.

(which may be due to some chemical reactions at high concentration of aniline). Due to this, the equilibrium constant reported may be lower compared to the present data (where the concentration of donor is low). The other possibility is that the contribution due to the non-specific interactions may be quite high, resulting in K_c^s being higher than K_c^{th}. The blue-shifted iodine band maximum is 500 ± 10 nm and the molar extinction coefficient is $\sim 830\, M^{-1}\, cm^{-1}$.

o-*Toluidine–Iodine System*

The isosbestic point of the *o*-toluidine–iodine system in carbon tetrachloride is 493 nm and ε_{isos} is $766\, M^{-1}\, cm^{-1}$. The equilibrium constant calculated by the constant activity method is $25.0\, M^{-1}$ at 26.5°C (lit. $11\, M^{-1}$) (26). This value is slightly higher than that of aniline–iodine which indicates that *o*-toluidine is a stronger complex. Here it is interesting to note that the equilibrium constant in the present case as well as in the aniline–iodine system is very much higher even though the enthalpies are nearly equal. The blue-shifted iodine band appears at 500 ± 10 nm and ε_{BS} is $\sim 770\, M^{-1}\, cm^{-1}$.

The constant activity method (sometimes known as the polyiodide-solubility method or simply solubility method) is a convenient alternative procedure for determining K_c and ε_{CT}, especially for weak molecular complexes of iodine. Secondly the blue-shifted iodine band maximum can be obtained directly. In addition to this, the heat of complexation can be determined by studying the temperature dependence of the absorbance of the complex using only a single solution of donor with excess of polyiodide.

Acknowledgement

We thank the University Grants Commission for support of this research.

1. H. A. Benesi and J. H. Hildebrand. J. Am. Chem. Soc. **71**, 2703 (1949).
2. M. Tamres. *In* Spectroscopy and structure of molecular complexes. *Edited by* J. Yarwood. Plenum Press, London. 1973.
3. R. S. Mulliken and W. B. Person. Molecular complexes. John Wiley and Sons, New York. 1969.
4. C. N. R. Rao, S. N. Bhat, and P. C. Dwiwedi. Appl. Spectrosc. Rev. **5**, 1 (1971).
5. R. Foster. Organic charge transfer complexes. Academic Press, London. 1969.
6. M. Tamres. *In* Molecular complexes. Vol. I. *Edited by* R. Foster. Elek Science, London. 1973.
7. W. B. Person. J. Am. Chem. Soc. **87**, 167 (1965).
8. P. H. Emslie, R. Foster, C. A. Fyfe, and I. Horman. Tetrahedron, **21**, 2843 (1965).
9. D. A. Deranleau. J. Am. Chem. Soc. **91**, 4044 (1969).
10. R. A. LaBudde and M. Tamres. J. Phys. Chem. **74**, 4009 (1970).
11. J. D. Childs, S. D. Christian, J. Grundnes, and S. R. Roach. Acta Chem. Scand. **25**, 1679 (1969).
12. J. D. Childs, S. D. Christian, and J. Grundnes. J. Am. Chem. Soc. **94**, 5657 (1972).
13. F. D. Chattaway and G. Hoyle. J. Chem. Soc. **123**, 654 (1923).
14. M. Brandon, M. Tamres, and S. Searles. J. Am. Chem. Soc. **82**, 2129 (1960); **82**, 2134 (1960).
15. A. I. Vogel. Text book of practical organic chemistry. ELBS, London. 1973.
16. J. A. Riddick and W. B. Bunger. Techniques of chemistry. Vol. II. Organic solvents. *Edited by* A. Weissberger. Wiley Interscience, New York, NY. 1970.
17. M. Tamres and S. N. Bhat. J. Am. Chem. Soc. **95**, 2516 (1973).
18. H. C. Tse and M. Tamres. J. Phys. Chem. **81**, 1367 (1977); **81**, 1376 (1977).
19. N. W. Blake, H. Winston, and J. A. Patterson. J. Am. Chem. Soc. **73**, 4437 (1951).
20. S. D. Christian and J. Grundnes. J. Am. Chem. Soc. **93**, 6363 (1971).
21. G. Briegleb. Elektronen–Donator–Acceptor Komplexe. Springer-Verlag, Berlin. 1962.
22. R. S. Drago and N. J. Rose. J. Am. Chem. Soc. **81**, 6141 (1959).
23. R. Bhattacharya and S. Basu. Trans. Faraday Soc. **54**, 1286 (1958).
24. E. H. Lane, S. D. Christian, and J. D. Childs. J. Am. Chem. Soc. **96**, 38 (1974).
25. L. J. Andrews and R. M. Keefer. J. Am. Chem. Soc. **74**, 4500 (1952).
26. A. K. Chandra and D. C. Mukerjee. Trans. Faraday Soc. **60**, 62 (1964).
27. R. M. Keefer and L. J. Andrews. J. Am. Chem. Soc. **74**, 4500 (1950).

Can. J. Chem. Downloaded from www.nrcresearchpress.com by 210.87.254.6 on 09/06/12
For personal use only.

Consideration on rotational isomerism in connection with its influence on some electrical properties of an interface

EDWARD DUTKIEWICZ AND STANISŁAW LAMPERSKI

Department of Electrochemistry, Institute of Chemistry, A. Mickiewicz University, ul. Grunwaldzka 6, 60-780 Poznań, Poland

Received February 25, 1980

EDWARD DUTKIEWICZ and STANISŁAW LAMPERSKI. Can. J. Chem. **59**, 1218 (1981).

The rotational isomerism contribution to some electric properties of an interface region has been considered. The mean electric dipole $\langle\mu\rangle$, the mean equilibrium constant $\langle K\rangle$ expressing the ratio of *gauche* and *trans* conformers, surface charge density σ, electric permittivity ε, differential capacity C were calculated as a function of electric field for 1,2-dichloroethane, 1-chloro-2-bromoethane, and 1,2-dibromoethane.

The results obtained suggest that in the case of adsorbed molecules exhibiting rotational isomerism, their structure and behaviour in the electrical double layer field have to be taken into account.

EDWARD DUTKIEWICZ et STANISŁAW LAMPERSKI. Can. J. Chem. **59**, 1218 (1981).

On a considéré la contribution de l'isomérie rotationnelle à quelques propriétés électriques d'une région de l'interface. On a calculé, en fonction du champ électrique, le dipôle électrique moyen $\langle\mu\rangle$ exprimant le rapport des conformères gauche et *trans*, la densité de la charge de surface σ, la permittivité électrique ε et la capacité différentielle C des dichloro-1,2, chloro-1 bromo-2 et dibromo-1,2 éthanes.

Les résultats obtenus suggèrent que dans le cas des molécules adsorbées qui montrent une isomérie rotationnelle, on doit tenir compte de leur structure et de leur comportement dans le champ électrique de l'interface.

[Traduit par le journal]

Introduction

Molecules exhibiting rotational isomerism have repeatedly been studied with interest, both experimentally and theoretically. This is, in particular, the case of the 1,2-dihalogenoderivatives of ethane, the molecule of which occurs in three stable forms, two *gauche* and one *trans*. The population ratio of *gauche* and *trans* states is referred to as the equilibrium constant of the forms and is directly dependent on the energies of the latter. This energy can be affected by many factors which, thus, modify the equilibrium constant perceptibly. Obviously, in the first place, the latter is dependent on temperature which, if raised, enhances the number of molecules in the *gauche* state (1). Also, a change in polarity of the solvent affects the equilibrium constant (2); for 1,2-dichloroethane in carbon tetrachloride it amounts to 0.9, whereas in chloroform it equals 1.0 and takes the value 1.4 for the pure liquid (3). In strongly polar solvents like acetonitryl, nitrobenzene, and nitrotoluene, it increases with increasing dilution (4, 5). An external electric field raises the equilibrium constant, as proved by the positive value of the nonlinear dielectric effect. The latter effect is characteristic for many molecular species showing rotational isomerism (5, 6). This field dependence of the electric permittivity has been considered theoretically (7, 8) with quite good results. Rotational isomerism of adsorbed molecules has been also the object of studies. Thus, for example, 1,2-dichloroethane, adsorbed on cationized zeolyte, exhibits an equilibrium constant fivefold that of the pure liquid (9). When adsorbed on a methoxylated surface, the constant decreases to 0.5 but increases even up to 2.4 on a hydroxylated surface (9). The effect can be attributed to the strong field, of the order of 10^8–10^9 V m^{-1}, existing at the phase boundary.

The above-mentioned electric field (6) and "adsorption" field effects stimulated studies of the influence of rotational isomerism in the metal/electrolyte solution interphase region (10, 11) where a strong electric field, the strength of which can be varied by applying externally a potential polarizing the electrode, exists.

On the other hand, the molecular models proposed till now in the literature (12) take into account orientational and non-orientational contributions to the electric permittivity of the surface layer of solvent. The latter contributions may be considered in terms of electric polarisation, dipole–dipole interactions, formation of associates, breaking of bonds in associates, bond formation with the metal or with the bulk, partial charge transfer, chemisorption, electrostriction, and temperature.

As can be seen, the rotational isomerism contribution connected with the increase in the number of polar molecules due to the electric field in the double layer region was not considered. Therefore, in our paper an attempt is made to estimate the role of this effect on the electric permittivity of the surface layer of solvent only. Thus the other contributions mentioned above will not be considered here.

0008-4042/81/081218-06$01.00/0

©1981 National Research Council of Canada/Conseil national de recherches du Canada

Can. J. Chem. Downloaded from www.nrcresearchpress.com by 210.87.254.105 on 09/06/12
For personal use only.

Can. J. Chem. Downloaded from www.nrcresearchpress.com by 210.87.254.105 on 09/06/12
For personal use only.

Theory

Model of the Rotational Isomer

In this paper we present a different approach to the rotational isomers of 1,2-dihalogenoderivatives of ethane than that in the method of infrared spectroscopy. The ir region vibrational modes of these molecules have a considerably greater frequency than the frequency associated with transitions among the stable isomers. In this situation the molecule analysed by means of infrared spectroscopy occurs always in one of the possible isomeric forms. Therefore, according to this method, information can be obtained about each stable form of the isomer.

The situation is otherwise in the case of dielectric methods. Here we obtain a certain "mean picture" of the molecule represented by the mean dipole moment. It is, as is well known, a fundamental quantity in the field of dielectric investigations. Therefore, it is advisable to assume a model of the rotational isomer, from which can be determined easily the mean dipole moment of the molecule. Let us assume that the molecule is at first in the state *gauche* "1" (Fig. 1) with the dipole moment μ_g. It can be assumed next that in the case of a transition to the state *trans* both halogenmethylene groups make the rotation by the same angle but in a reverse direction. The dipole moment in this state, when the halogen substituents are identical, is equal to zero. Further rotary motion of the halogenmethylene groups causes the transition of the molecule to the state *gauche* "2" in which the molecule has the dipole moment μ_g in the reverse direction.

It is obvious that the mean dipole moment calculated on the basis of the above model, for instance for 1,2-dichloroethane, amounts to zero. But the same compound will have a mean dipole moment different from zero if it is placed in an electric field F (except in the case that $F \perp \mu_g$), because, due to the interaction of the dipole moments of the *gauche* form with the electric field, one of these forms will be energetically more stable than the other.

The Electric Dipole Moment of a Molecule with Rotational Isomers

The electric moment under consideration is a function of the dihedral angle α (1), defined by the following atoms: halogen substituent – carbon – carbon – halogen substituent, as given by eq. [1]:

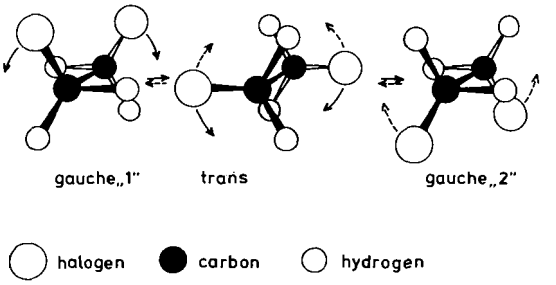

FIG. 1. Model of intramolecular rotation of 1,2-dihalogenoderivatives of ethane.

$$[1] \quad \mu(\alpha) = \pm[(\mu_1 - \mu_2)^2 + 4\mu_1\mu_2 \cos^2(\alpha/2) \sin^2\beta]^{1/2}$$

For ideal sp^3 hybridization of carbon orbitals, $\beta = 70°31'44''$. In the above equation, μ_1 and μ_2 are the dipole moments of the carbon–halogen bonds. Obviously, if the substituents are identical, $\mu_1 = \mu_2$, and we have (10):

$$[2] \quad \mu(\alpha) = 2\mu \cos(\alpha/2) \sin\beta$$

At $\alpha > \pi$, a change in sign of the dipole moment takes place. Once the function $\mu(\alpha)$ and the dependence of the potential energy on the dihedral angle $U(\alpha)$ are available, one can determine the mean dipole moment of the molecule from the Boltzmann distribution. A "6-exp" type potential can be used to describe $U(\alpha)$, applying the parametrisation proposed by Scott and Scheraga (13).

When describing the behaviour of a molecule with rotational isomers in an electric field one has still to consider the interaction energy of its dipole moment and the field F:

$$[3] \quad U(F,\Theta) = -\mu F \cos\Theta$$

F is the cavity field strength and Θ, the angle between the vectors of the dipole moment and electric field; the mean dipole moment of the isomeric molecule, called the dipole moment of the isomer, is:

$$[4] \quad \bar{\mu}(F,\Theta) = \frac{\int_0^{2\pi} \mu(\alpha) \exp\{[-U(\alpha) + \mu(\alpha)F\cos\Theta]/kT\}\, d\alpha}{\int_0^{2\pi} \exp\{[-U(\alpha) + \mu(\alpha)F\cos\Theta]/kT\}\, d\alpha}$$

$U(\alpha)$ is the potential energy per molecule.

The mean value $\langle\mu\rangle$ of the molecular dipole moment in the direction of the field allows the calculation

of the electric permittivity of an interfacial region in a strong field. Boltzmann's distribution for the mean value of the dipole moment of a rotational isomeric molecule gives:

$$[5] \quad \langle \mu(F) \rangle_{\text{rot isom}} = \frac{\int_0^\pi \bar{\mu}(F,\Theta) \exp\left[\bar{\mu}(F,\Theta) F \cos\Theta / kT\right] \cos\Theta \sin\Theta \, d\Theta}{\int_0^\pi \exp\left[\bar{\mu}(F,\Theta) F \cos\Theta / kT\right] \sin\Theta \, d\Theta}$$

Applying the definition of dipole polarizability we similarly define the dipole polarizability of the rotational isomer:

$$[6] \quad \alpha(F)_{\text{rot isom}} = \frac{\langle \mu(F) \rangle_{\text{rot isom}}}{F}$$

Influence of the Electric Field on the Equilibrium Constant

As initially stated, the field lowers the population of the *trans* state and favours the *gauche* state, thus causing an increase of the equilibrium constant K. The influence of the field is thus described by the following equation:

$$[7] \quad K(F,\Theta) = e^{-\Delta U/kT} \cos h(\mu_g F \cos\Theta / kT)$$

where μ_g is the moment of the *gauche* form and ΔU the difference in energy between the *gauche* and *trans* states.

At constant Θ, the value of K increases with increasing field strength, the sharpest change occurring if $\Theta = 0$ or π. If $\Theta = \pi/2$, K is field-independent. In the field, the molecules can assume any orientation, albeit with unequal probability. As shown above, for a given field strength K is still dependent on Θ, so that it appears useful to introduce a mean value of K defined as:

$$[8] \quad \langle K(F) \rangle = \frac{\int_0^\pi K(F,\Theta) \exp\left[\bar{\mu}(F,\Theta) F \cos\Theta / kT\right] \sin\Theta \, d\Theta}{\int_0^\pi \exp\left[\bar{\mu}(F,\Theta) F \cos\Theta / kT\right] \sin\Theta \, d\Theta}$$

Electric Permittivity

We determined the electric permittivity applying the Onsager model (14), assumed to be valid for very strong fields also. We employed for this purpose the following equation:

$$[9] \quad \varepsilon(F) = \frac{3\varepsilon(F)}{2\varepsilon(F) + 1} \frac{N g \alpha_{\text{rot isom}}(F,g)}{\varepsilon_0} + n^2$$

where g comes from Onsager's reaction field

$$[10] \quad g = \frac{[2\varepsilon(F) + 1](n^2 + 2)}{3[2\varepsilon(F) + n^2]}$$

N is the number of molecules per unit of volume, n the refractive index, and ε_0 the electric permittivity of vacuum. With the obtained permittivity and assumed distance between the condenser plates one can calculate classically the capacity per unit area of the condenser, the potential difference between its plates, and the surface charge density. We hence derive the differential capacity, defined as follows:

$$[11] \quad C_{\text{diff}} = d\sigma/dE$$

with σ being the electric charge density, and E the potential difference.

Results of Calculations

Since eqs. [4], [5], and [8] cannot be solved algebraically for strong fields, we had recourse to a numerical technique, calculating the integrals by steps of $\pi/90$ and assuming the dipole moment of C—Cl bonds to be 4.86×10^{-30} C m, C—Br, 4.6×10^{-30} C m, and H—C, 1.33×10^{-30} C m (15).

The calculated dependence of the dipole moment of the isomer (for $\Theta = 0$) as well as the mean projection in the field direction versus the field strength for 1,2-dichloroethane, 1-chloro-2-bromoethane, and 1,2-dibromoethane are presented in Fig. 2 and Fig. 3, respectively. The mean value of the equilibrium constants versus the electric field are plotted in Fig. 4. The course of the variability of the permittivity for the molecules considered as a function of the field strength is displayed in Fig. 5.

The calculated differential capacities as a function of the electrode potential (for a distance of 10 Å

Can. J. Chem. Downloaded from www.nrcresearchpress.com by 210.87.254.105 on 09/06/12
For personal use only.

Can. J. Chem. Downloaded from www.nrcresearchpress.com by 210.87.254.105 on 09/06/12
For personal use only.

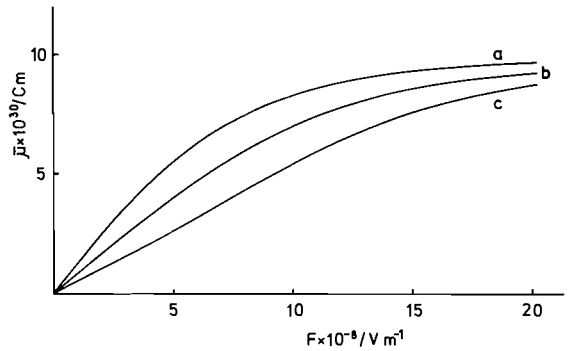

FIG. 2. Computed mean dipole moment $\bar{\mu}$ vs. electric field F curves obtained from eq. [4] for the following rotational isomers: *a*, 1,2-dichloroethane; *b*, 1-chloro-2-bromoethane; *c*, 1,2-dibromoethane.

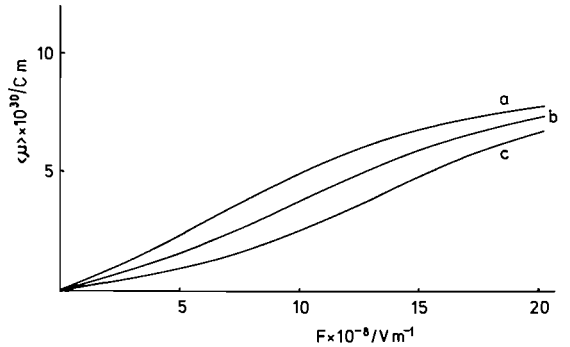

FIG. 3. Computed mean projection of dipole moment in the field direction $\langle\mu\rangle$ vs. electric field F curves obtained from eq. [5] for the following rotational isomers: *a*, 1,2-dichloroethane; *b*, 1-chloro-2-bromoethane; *c*, 1,2-dibromoethane.

between the plates of the condenser) for 1,2-dichloro-1-chloro-2-bromo-, and 1,2-dibromoethane is shown in Fig. 6. The character of these curves is due to the dependence of the electric permittivity on the electric field. Differences which occur among the curves for the investigated compounds are the result of the intramolecular hindered rotation. The hindered rotation depends on the steric effect of substituents (16).

In Table 1 there are presented some calculated values characterizing the properties of 1,2-dihalogenoderivatives of ethane in the liquid phase and they are compared with experimental data.

Discussion

In this paper the influence of a strong electric field on the behaviour of rotational isomers has been considered. Molecules can occur in a very strong electric field, when they are adsorbed, for instance, at the electrode/electrolyte solution interface. In the case of the electrode/electrolyte solution interface,

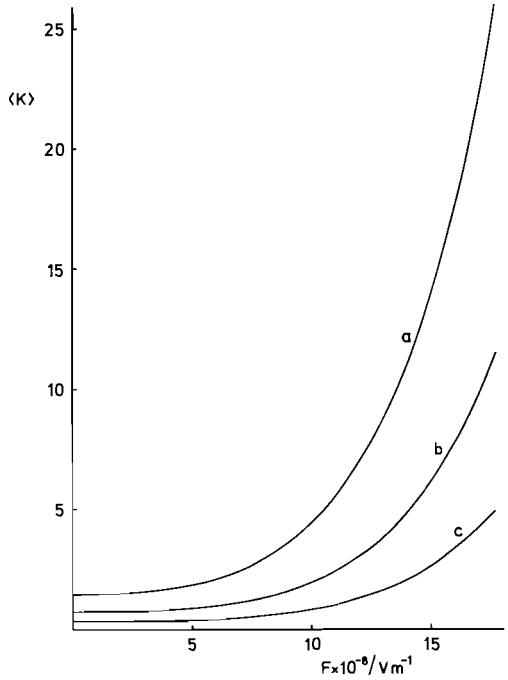

FIG. 4. Computed mean value of equilibrium constant $\langle K\rangle$ vs. electric field F curves obtained from eq. [8] for the following rotational isomers: *a*, 1,2-dichloroethane; *b*, 1-chloro-2-bromoethane; *c*, 1,2-dibromoethane.

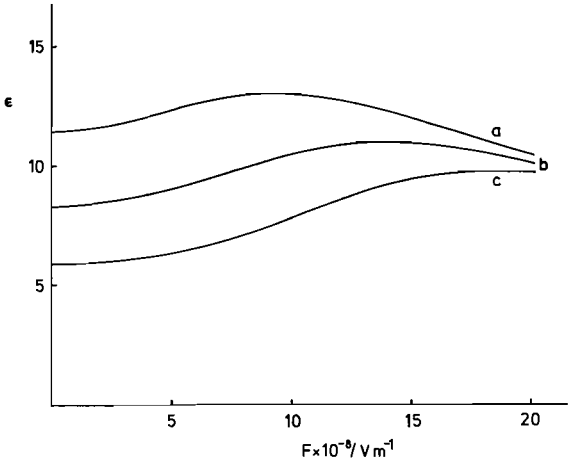

FIG. 5. Dependence of electric permittivity ε as a function of electric field F for the following rotational isomers: *a*, 1,2-dichloroethane; *b*, 1-chloro-2-bromoethane; *c*, 1,2-dibromoethane.

there exists furthermore the possibility of an increase in the intensity of the electric field at the interface with the external voltage applied to the electrode, as it has been mentioned in the Introduction.

It has been stated in the theoretical part that the change of the mean dipole moment of the rotational

Can. J. Chem. Downloaded from www.nrcresearchpress.com by 210.87.254.105 on 09/06/12
For personal use only.

TABLE 1. Comparison of some calculated and experimental physical properties of the investigated rotational isomers

Compound	Difference in energy between the *gauche* and *trans* states ΔU (k J mol^{-1})		Electric permittivity for $F = 0$ ε		Dielectric saturation coefficient $\Delta\varepsilon/E^2 \times 10^{17}$ (V^{-2} m^2)		Calculated dipole moment $\mu_g \times 10^{30}$ (C m)
	Assumed	Experimental	Calculated	Experimental	Calculated	Experimental	
1,2-Dichloroethane	0.82*	0 ± 0.56 (18)	11.43	10.85 (5)		1.8 (5)	9.84
		0 ± 0.25 (17)		10.08 (21)		1.09 (6)	
		−0.04 ± 0.4 (23)		10.58 (6)	1.35		
		0 (19)					
1-Chloro-2-bromoethane	2.59	1.96 ± 0.16 (22)	8.28	6.92 (21)			9.53
		1.38 ± 0.84 (20)					
		2.01 ± 0.29 (23)			1.02	—	
1,2-Dibromoethane	4.50	3.22 ± 0.25 (17)	5.89	4.92 (5)		1.2 (5)	9.38
		3.39 ± 0.84 (20)		4.80 (21)		0.74 (6)	
		3.81 ± 0.33 (18)		4.75 (6)	0.62		

*Taken from ref. 13.

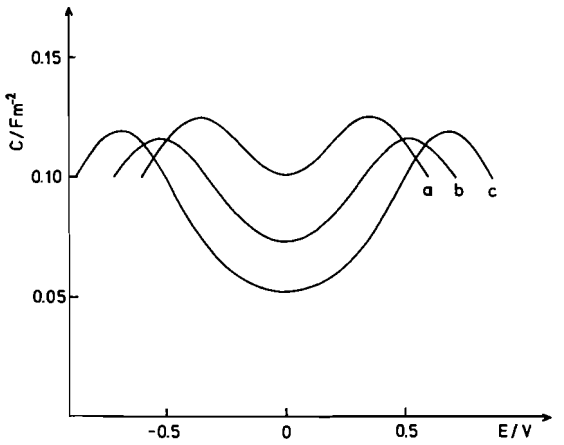

FIG. 6. Differential capacity C dependence on potential difference E for: *a*, 1,2-dichloroethane; *b*, 1-chloro-2-bromoethane; *c*, 1,2-dibromoethane.

isomer $\langle\mu\rangle$ due to the electric field F is rather complex and differs from the Langevin function (Fig. 3). The mean dipole moment versus electric field is described initially by a linear function. It follows that the polarizability of the rotational isomer is approximately constant and, therefore, that the permittivity is not subjected to great changes (Fig. 5). The value of the field intensity for such a behaviour of the molecules to be observed must be small enough. The energy corresponding to the molecule being in the *gauche* state in the electric field cannot exceed the difference in energy between the *gauche* and *trans* states. We can therefore state that the approximately linear dependence of the mean dipole moment of the rotational isomer on field is valid for field intensities smaller than 1.4×10^8 V m^{-1} for 1,2-dichloroethane, 4.5×10^8 V m^{-1}, for 1-chloro-2-bromoethane, and 8.9×10^8 V m^{-1} for 1,2-dibromoethane. It must also be stated that the mean value of the equilibrium constant $\langle K\rangle$ practically does not change (Fig. 4) in this range of electric fields. The above discussed electric fields exert a small influence on the orientation of molecules and on the transition from the *trans* to *gauche* form.

A further increase of the field intensity causes a rapid increase of the equilibrium constant $\langle K\rangle$ as well as the dipole moment $\langle\mu\rangle$. This results in an increase of the electric permittivity. This increase is due to the transition of molecules from *trans* to *gauche*.

The higher electric field intensity causes a very great increase of the equilibrium constant $\langle K\rangle$, but exerts a small influence on the value of dipole moment $\langle\mu\rangle$. The greater number of molecules is already now in the *gauche* form and the vectors of

Can. J. Chem. Downloaded from www.nrcresearchpress.com by 210.87.254.105 on 09/06/12
For personal use only.

their dipole moments are oriented parallel to the line of the electric field. As a result, the electric permittivity decreases.

The dielectric permittivity ε has been calculated on the basis of Onsager's model. From Fig. 5 one can see that the dependence of the electric permittivity of 1,2-dihalogenethane on electric field shows a maximum in a given field region before dielectric saturation is reached. A similar dependence occurs for the capacity as a function of electric potential difference (Fig. 6). These results are the main achievements of this work.

Now, the question arises whether rotational isomerism contributes to the electric permittivity of a metal/electrolyte solution interface. As was pointed out in the Introduction there is some experimental evidence for an increase in polarity of adsorbed solvent rotamers. Hence, an increase of the electric permittivity of an interface region is to be expected. Recently, Ikeda *et al.* (24) explained the change in the capacity of the inner layer in the presence of 2-methylthioethanol by means of rotation of the hydroxyl group. Adding to these facts the results presented in this paper, we suppose that a change in the electric permittivity of the metal/electrolyte solution interface in the presence of adsorbed rotamers could be partially a result of the role of rotational isomerism. Hence the differential capacity as a function of electrode potential (or surface charge) will be a more complex function as a result of various molecular and intramolecular interactions in the interface region.

The fact that molecules in adsorbed states may form a solid-like surface does not exclude the possibility of the rotation of one group within the molecule. Investigations of the dielectric properties of organic compounds have shown that, in some solid crystals, the rotation of certain groups in the molecules can also occur (25). Therefore, we assume that, in adsorbed layers, intramolecular rotation under the influence of the electric field can also take place.

Finally we would like to stress that in describing a molecular model for adsorbed solvent which consists of rotamers one has to take into account, besides the orientational and non-orientational contributions, also an intramolecular rotation contribution to the dielectric properties of the interface region.

Acknowledgements

The authors wish to thank Professor Stanisław Kielich for helpful discussion. This work was carried out within the framework of the Project MR I-11.

1. S. I. MIZUSHIMA. Structure of molecules and internal rotation. Academic Press, New York, NY. 1954.
2. M. KOKIMOTO and F. FUJIYAMA. Bull. Chem. Soc. Jpn. **48**, 3003 (1975).
3. A. V. KISELEV and V. I. LYGIN. Infrared spectra of surface compounds. Translated from Russian by N. Kaner. John Wiley and Sons, New York – Toronto. 1975.
4. D. SURMA. Ser. Fiz. Uniw. Adama Mickiewicza Poznaniu, Inst. Fiz. **28**, 41 (1978).
5. M. DUTKIEWICZ. Ser. Fiz. Uniw. Adama Mickiewicza Poznaniu, Inst. Fiz. **28**, 61 (1978).
6. A. CHEŁKOWSKI. Compte rendu du 10e Coll. Ampère, Leipzig, 80 (1961); Compte rendu du 11e Coll. Ampère, Eindhoven, 302 (1962); Compte rendu du 14e Coll. Ampère, Ljubljana, 677 (1966).
7. A. PIEKARA, S. KIELICH, and A. CHEŁKOWSKI. Arch. Sci. **12**, 59 (1959).
8. E. KLUK. Acta Phys. Pol. **20**, 845 (1961).
9. A. V. KISELEV, V. I. LYGIN, and M. F. MOSKOVSKAYA. Zh. Fiz. Khim. **40**, 2319 (1966).
10. E. DUTKIEWICZ and M. DUTKIEWICZ. J. Electroanal. Chem. **67**, 397 (1976).
11. E. DUTKIEWICZ. J. Electroanal. Chem. **90**, 211 (1978).
12. J. R. MACDONALD and C. A. BARLOW. J. Chem. Phys. **36**, 3062 (1962); R. J. WATTS-TOBIN. Philos. Mag. **6**, 133 (1961); J. O'M. BOCKRIS, M. A. V. DEVANATHAN, and K. MULLER. Proc. R. Soc. A, **274**, 55 (1963); W. R. FAWCETT. J. Phys. Chem. **82**, 1385 (1978); R. PARSONS. Electrochim. Acta, **21**, 681 (1976); B. B. DAMASKIN. J. Electroanal. Chem. **75**, 359 (1977).
13. R. A. SCOTT and H. A. SCHERAGA. J. Chem. Phys. **42**, 2209 (1965).
14. L. ONSAGER. J. Am. Chem. Soc. **58**, 1486 (1936).
15. C. P. SMYTH. Dielectric behaviour and structure. McGraw-Hill, New York, NY. 1955.
16. R. J. ABRAHAM and K. PARRY. J. Chem. Soc. B, **3**, 539 (1970).
17. YU. A. PENTIN and V. M. TATEVSKII. Dokl. Akad. Nauk S.S.S.R. **108**, 290 (1956).
18. J. HIRAISHI and T. SHINODA. Bull. Chem. Soc. Jpn. **48**, 2385 (1975).
19. J. LAMB. Z. Elektrochem. **64**, 135 (1960).
20. R. J. ABRAHAM and G. GATTI. J. Chem. Soc. B, **8**, 961 (1969).
21. H. H. LANDOLT and R. BORNSTEIN. Tables of physical constants. Lange and Springer, Berlin. 1959.
22. WEI-CHUVAN LIN. J. Chem. Phys. **50**, 1890 (1968).
23. K. TANABE. Spectrochim. Acta, Part A, **28**, 407 (1972).
24. O. IKEDA, K. KOGO, and H. TAMURA. J. Electroanal. Chem. **95**, 177 (1979).
25. C. BROT and B. LASSIER-GOVERS. Ber. Bunsenges. Phys. Chem. **80**, 31 (1976).

Préparation, réduction chimique et électrochimique d'α-nitrostyrylcétones — synthèse d'hétérocycles azotés

BERNARD MARÇOT, ALAIN RABARON ET CLAUDE VIEL
Laboratoire de Pharmacie Chimique II (ERA 317 du CNRS), Faculté de Pharmacie, 3, rue J.B. Clément 92290 Châtenay-Malabry, France

ET

CHRISTIAN BELLEC, STÉPHANE DESWARTE ET PIERRE MAITTE
Laboratoire de Chimie des Hétérocycles, Université Pierre et Marie Curie, 4 Place Jussieu, 75230 Paris Cedex 05, France

Reçu le 24 mars 1980

BERNARD MARÇOT, ALAIN RABARON, CLAUDE VIEL, CHRISTIAN BELLEC, STÉPHANE DESWARTE et PIERRE MAITTE. Can. J. Chem. **59**, 1224 (1981).

La nitration par le peroxyde d'azote des styrylcétones conduit avec de bons rendements aux cétones α-nitroéthyléniques correspondantes. Toutefois, lorsque des groupes méthoxyles sont présents sur le noyau, la nitration s'effectue sur celui-ci.

La réduction par $LiAlH_4$ des α-nitrostyrylcétones fournit les aminoalcools *érythro* et *thréo* racémiques correspondants. Après acylation puis cyclisation, on obtient une dihydroisoquinoléine ou une oxazoline-2.

La réduction électrochimique de ces nitrostyrylcétones engendre sélectivement les α-cétoximes, elles-mêmes électroréductibles en α-aminocétones. Ces dernières conduisent en milieu neutre, par condensation de deux molécules, aux dihydro-2,5 pyrazines qui s'aromatisent en pyrazines correspondantes. En milieu acide on isole un α-cétol.

Un mécanisme de réduction faisant intervenir un intermédiaire énaminol est proposé.

BERNARD MARÇOT, ALAIN RABARON, CLAUDE VIEL, CHRISTIAN BELLEC, STÉPHANE DESWARTE, and PIERRE MAITTE. Can. J. Chem. **59**, 1224 (1981).

Nitration of styryl ketones with nitrogen peroxide leads to the corresponding α-nitroethylenic ketones in good yield. However, the presence of methoxy groups involves a nitration on the aromatic nucleus.

$LiAlH_4$ reduction of α-nitrostyrylketones yields the corresponding racemic *erythro*- and *threo*-aminoalcohols; after acylation and cyclisation a dihydro-quinoline or a 2-oxazoline is obtained.

Electrochemical reduction of these nitrostyryl-ketones selectively provides the α-ketoximes, which are themselves reduced electrolytically to α-aminoketones. These latter compounds dimerise in neutral medium to dihydro-2,5-pyrazines which aromatise to the corresponding pyrazines. In acid medium an α-ketol is obtained.

A mechanism for the reduction is proposed implicating an enaminol intermediate.

[Journal translation]

Introduction

Les dérivés styréniques substitués sur le carbone β par un groupement électroattracteur sont nitrés sélectivement par le peroxyde d'azote en β-nitrostyrènes β-substitués (1–3). Ainsi s'obtiennent les α-nitrobenzylidèneacétones et les α-nitrochalcones. Nous avons pensé que la réduction de ces composés par l'hydrure de lithium et d'aluminium fournirait aisément les aminoalcools correspondants susceptibles de subir une cyclodéshydratation soit en isoquinoléines substituées en position-3, soit en oxazolines-2.

Il est particulièrement difficile de transformer en isoquinoléines les β-phényl éthylamides si le noyau aromatique est dépourvu de substituant donneur en *para* du site de cyclisation; il était donc important d'envisager la nitration de styrylcétones méthoxylées en bonne position sur le noyau.

D'autre part, et dans le cadre de nos études sur la réduction électrochimique de dérivés nitrostyréniques (4, 5) nous avons réalisé l'électroréduction de quelques β-nitrostyrylcétones.

Les résultats obtenus font l'objet du présent mémoire.

1. Nitration de styrylcétones — limites de la méthode (schémas 1 et 2)

La nitration de la benzylidène acétone (**1***a*), de la chalcone (**1***b*) et d'analogues non méthoxylés, par le peroxyde d'azote, conduit bien aux α-nitrocétones correspondantes **2** (2, 3), mais la méthode ne peut être généralisée aux styrylcétones méthoxylées sur le noyau.[1] Ainsi, pour les diméthoxy-3,4 benzylidèneacétone (**3***a*), diméthoxy-3,4 chalcone (**3***b*) et diméthoxy-3,4 chloro-4′ chalcone (**3***c*), nous constatons une nitration exclusive sur le noyau aromatique en position-6.

La structure des nitro-6 styrylcétones obtenues (**5***a*, **5***b*, **5***c*) est déterminée sans ambiguité par résonance magnétique nucléaire du proton et du

[1]Les diméthoxy-3,4 et diméthoxy-3,4 chloro 4′-chalcones décrites précédemment (2) sont par conséquent nitrées en 6 et non en α du carbonyle comme il avait été proposé.

0008-4042/81/081224-11$01.00/0
©1981 National Research Council of Canada/Conseil national de recherches du Canada

Can. J. Chem. Downloaded from www.nrcresearchpress.com by 210.87.254.6 on 09/06/12
For personal use only.

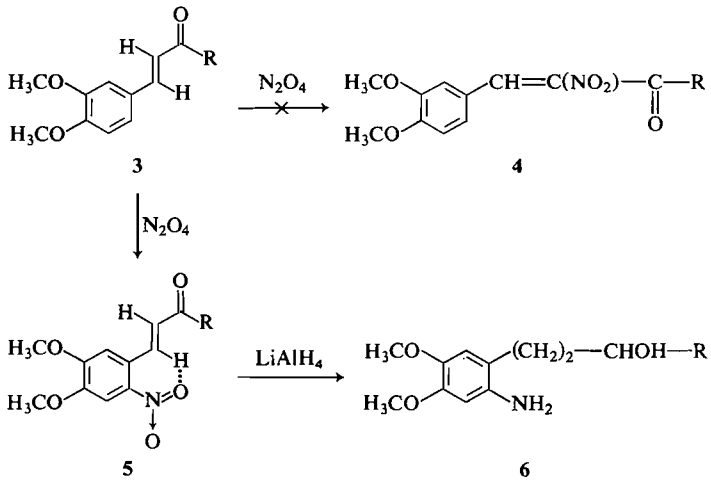

SCHÉMA 1. *a*, R = CH_3; *b*, R = C_6H_5; *c*, R = C_6H_4—*p*-Cl

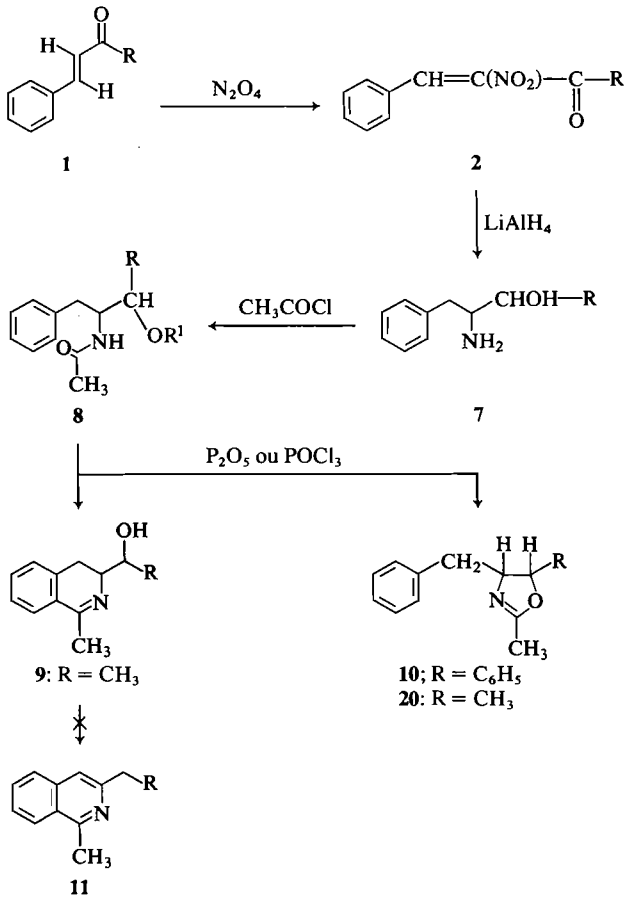

SCHÉMA 2. **1**, **2**, **7**: *a*, R = CH_3; *b*, R = C_6H_5; **8***a*: R = CH_3; R^1 = H; **8***b*: R = CH_3; R^1 = $COCH_3$; **8***c*: R = C_6H_5; R^1 = H.

Can. J. Chem. Downloaded from www.nrcresearchpress.com by 210.87.254.6 on 09/06/12
For personal use only.

Can. J. Chem. Downloaded from www.nrcresearchpress.com by 210.87.254.6 on 09/06/12
For personal use only.

^{13}C pour la nitrovératrylidèneacétone (**5***a*).[2] Les spectres protoniques de ces cétones nitrées montrent la présence de deux protons éthyléniques *trans* (J = 16 Hz) ainsi que celle de deux protons aromatiques en *para* l'un de l'autre. De même le spectre de ^{13}C de **5***a* confirme la nitrosubstitution en-6 et montre la présence d'une liaison éthylénique disubstituée. D'autre part, sur le spectre protonique de cette même cétone le déplacement à très bas champ (8,05 ppm) du signal d'un des protons éthyléniques est en faveur d'une liaison hydrogène entre ce proton et le groupe NO_2. L'effet électroattracteur de ce groupement influe également sur les protons aromatiques, le proton *ortho* sortant à champ nettement plus bas que le proton *méta* (respectivement 7,60 et 7,00 ppm). Des constatations identiques peuvent être effectuées pour les nitro-6 chalcones (**5***b* et **5***c*).

L'interprétation du spectre rmn du ^{13}C de **5***a* est effectuée par comparaison des constantes de couplage résiduel des carbones aromatiques et des hydrogènes aromatiques d'une part, des carbones éthyléniques et des hydrogènes éthyléniques d'autre part.

En ce qui concerne les carbones aromatiques, le signal à 110,2 ppm présente une constante de couplage résiduel plus faible que celle du signal à 108,2 ppm, ce qui permet d'attribuer ce dernier au carbone aromatique situé en *ortho* du groupe NO_2. De même pour les carbones éthyléniques, le signal à 131,6 ppm qui présente une constante de couplage résiduel plus grande que celui à 97,6 ppm peut être attribué au carbone éthylénique en β du carbonyle, lié à l'hydrogène chélaté avec le NO_2. Les spectres de rmn ^{13}C ont été interprétés sur la base de travaux récents relatifs aux chalcones (6), compte-tenu des incréments apportés par la nitrosubstitution en-6.

On trouve, pour les protons éthyléniques et les carbones de **1***a* et **1***b* (cf. Partie expérimentale) les déplacements chimiques attendus ce qui confirme l'existence d'une liaison hydrogène dans le cas des nitro-6 styrylcétones. On constate donc que les styrylcétones non substituées sur le noyau aromatique subissent une nitration exclusive sur la double liaison éthylénique, tandis que celles qui sont, en plus, éther de phénol sont nitrées exclusivement en position-6 sur le noyau.

Si l'on rapproche ceci du fait que des composés tels que l'anisole (7) le vératrole, l'acide vératrique et le vératraldéhyde (8) sont aisément nitrés par N_2O_4, il est logique d'admettre que l'entité réactive est l'ion NO_2^+. Dans le cas des styrylcétones, l'addition élimination doit aussi débuter par une attaque de NO_2^+ sur la double liaison éthylénique (9) puisque seul le produit de nitration dans le noyau et non sur la double liaison est obtenu dans le cas des dérivés méthoxylés. Pour ces derniers, on n'observe pas la compétition théoriquement possible entre deux sites réactionnels pour NO_2^+: noyau et double liaison. En effet, le noyau est ici activé et se nitre préférentiellement; la double liaison est ainsi appauvrie en électrons et ne peut subir l'attaque électrophile.

2. Réduction chimique des nitrostyrylcétones (schémas 1 et 2)

L'hydrure de lithium et d'aluminium transforme les α-nitrostyrylcétones (**2**) en α-aminoalcools saturés correspondants **7**; dans la série des styrylcétones diméthoxylées et nitrées dans leur noyau **5**, les aminoalcools **6** sont fragiles, et seul **6***c* issu de la diméthoxynitrochalcone chlorée a pu être cristallisé (10). Les amino-2 diphényl-1,3 propanol-1: (**7***a*) et amino-3 phényl-4 butanol-2: (**7***b*) ont été obtenus sous forme d'un mélange *érythro* et *thréo* racémiques, ainsi que le montre l'examen de leur spectre de résonance protonique: deux doublets dus au méthine du groupe —CHOH— de chaque isomère couplé au proton tertiaire adjacent (de —CH—NH_2) pour **7***b*; deux doublets dus au groupe méthyle de chaque isomère couplé au proton tertiaire adjacent (de —CHOH—) pour **7***a*.

Pour chaque aminoalcool, il a été possible de définir les proportions respectives d'isomères *érythro* et *thréo* présents dans le mélange: après transformation de ces aminoalcools en chlorhydrate, nous avons constaté dans chaque cas la cristallisation préférentielle de l'un des chlorhydrates isomères. Les constantes de couplage pour les couples de protons méthine de —CHOH—[3] (respectivement 4 Hz pour le sel de **7***a*, 4,16 Hz pour celui de **7***b*) ont été comparées aux valeurs observées pour les méthines dans l'éphédrine (4,07 Hz) et la pseudoéphédrine (8,23 Hz) (11). Elles conduisent à proposer la configuration *érythro* pour les chlorhydrates cristallisés des deux aminoalcools **7***a* et **7***b*.

A partir de chaque chlorhydrate, nous avons régénéré l'aminoalcool *érythro* pur. Ceci a permis de faire dans les spectres rmn, les attributions aux

[2]Seule cétone nitrée dans le noyau soluble à concentration suffisante pour permettre l'enregistrement du spectre de rmn ^{13}C.

[3]Après découplage du méthyle dans le cas du phénylaminobutanol.

Can. J. Chem. Downloaded from www.nrcresearchpress.com by 210.87.254.6 on 09/06/12
For personal use only.

composés *érythro* et *thréo* et de déterminer les pourcentages: compte-tenu de la précision des mesures, le rapport *érythro/thréo* pour chaque aminoalcool est de l'ordre de 50%.

3. Hétérocyclisations (schéma 2)

Vis-à-vis du chlorure d'acétyle, le comportement des aminoalcools (**7***a* et **7***b*) est différent. Alors qu'avec **7***b* seule la *N*-acylation est observée (45% en amide-alcool (**8***c*)), avec **7***a*, la double acylation des fonctions amine et alcool est prépondérante (57% en amide-ester (**8***b*); 13% en amide-alcool (**8***a*)).

Les amides **8***a*, **8***b* et **8***c* peuvent subir une cyclodéshydratation par action de l'anhydride phosphorique ou de l'oxychlorure de phosphore. Pour l'acétamido-3 acétoxy-2 phényl-4 butane (**8***b*) l'action de $POCl_3$ ou de P_2O_5 conduit à l'(α-hydroxyéthyl)-3 méthyl-1 dihydro-3,4 isoquinoléine (**9**) comme produit majeur, et seul identifiable après chromatographie du mélange réactionnel et transformation en chlorhydrate. Par contre, la cyclisation des hydroxyamides (**8***a* et **8***c*) par l'anhydride phosphorique conduit aux *cis* oxazolines-2 (**10** et **20**)[4] seuls produits identifiables après chromatographie du mélange réactionnel.

On trouve effectivement dans la littérature (13, 14) des exemples où une oxazoline-2 se forme préférentiellement à une isoquinoléine lors de la cyclisation de β-hydroxy β-phényléthylacétamides à noyau non activé; mais il est surprenant d'avoir obtenu la dihydroisoquinoléine (**9**) et non l'isoquinoléine (**11**) lors de la cyclisation de l'ester-amide (**8***b*).

Une hypothèse peut être formulée pour expliquer la formation dans un cas des oxazolines, dans l'autre celle d'une dihydroisoquinoléine. Avec les hydroxyamides (**8***a* et **8***c*), un ester phosphate peut transitoirement se former dans la réaction, et à partir de celui-ci, la formation d'une oxazoline-2 s'explique aisément. Dans le cas du bis-amide (**8***b*), la formation d'un tel intermédiaire ne pouvant avoir lieu, l'amide ester (**8***b*) subit une cyclodéshydratation isoquinoléique selon Bischler et Napieralski, suivie d'une hydrolyse de la fonction ester avec formation de la dihydroisoquinoléine (**9**).

[4]La configuration *cis* de ces composés a été attribuée à partir de la benzyl-4 méthyl-2 phényl-5 oxazoline-2 (**10**): pour ce dérivé, la valeur de la constante de couplage, 6,5 à 7 Hz, des protons CH portés par les carbones 4 et 5 a permis, par application de la règle de Karplus (12) et l'examen comparé des modèles moléculaires des oxazolines isomères, d'attribuer la configuration *cis* à l'oxazoline obtenue.

4. Réduction électrochimique des nitrostyryl-cétones

4.1. Etude polarographique

En solution hydro-organique tamponnée, la stabilité des composés **2***a* et **2***b* suivie par spectrophotométrie uv décroit par élévation du pH. Nous avons donc limité leur étude aux milieux acide et neutre.

Pour des pH inférieurs à 4–4,5, **2***a* et **2***b* présentent à l'électrode à goutte de mercure deux vagues, chacune de hauteur proche de 4 faradays. Leur potentiel de demi-vague varie linéairement avec le pH; la seconde vague est perturbée par des phénomènes d'adsorption. Au delà de pH 4,5 apparait une troisième vague dont le potentiel de demi-vague, plus négatif, reste sensiblement constant lorsque le pH croit.

Les courbes $E_{1/2} = f(\text{pH})$ pour **2***a* et **2***b* sont représentées sur la fig. 1.

4.2. Electrolyses en milieu acide (schéma 3)

4.2.1. Au niveau du palier de la première vague

Lors des *électrolyses en solution diluée* de **2***a* pH = 1,08 (50% d'acétonitrile; $c = 2 \times 10^{-3}$ *M*, $E = -0{,}5$ V) ou de **2***b*: pH = 0,75 (50% d'acétonitrile, $c = 2 \times 10^{-3}$ *M*, $E = -0{,}4$ V), on observe une décroissance de la première vague proportionnelle au nombre de coulombs consommés. A la fin de l'électrolyse, après passage de 4 électrons par molécule, subsiste une vague de hauteur 4 faradays dont le potentiel de demi-vague est identique à celui de la seconde vague de **2***a* et **2***b*.

Des électrolyses préparatives de **2***a* et **2***b*, ef-

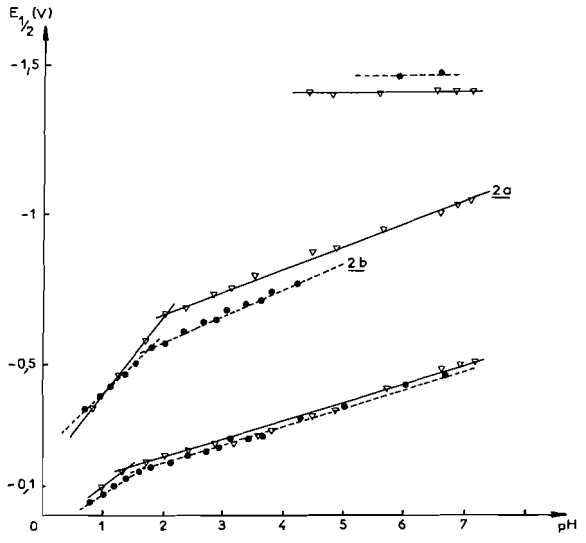

FIG. 1. Courbes $E_{1/2} = f(\text{pH})$ pour **2***a* et **2***b* en solution hydro-organique (25% de CH_3CN).

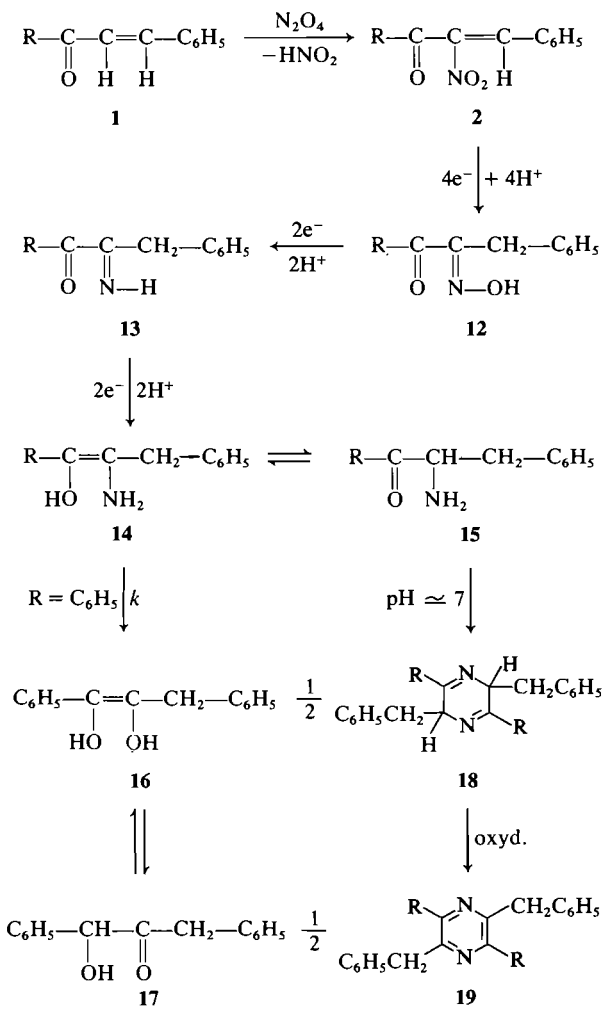

SCHÉMA 3: *a*: R = CH_3; *b*: R = C_6H_5.

fectuées dans les mêmes conditions, permettent d'isoler avec de bons rendements les α-cétoximes (**12***a* et **12***b*).

Ces résultats montrent que le premier stade de réduction de **2***a* et **2***b* correspond au schéma classique de réduction des dérivés nitrés éthyléniques en oxime selon un processus à 4 électrons. La fonction carbonyle n'est pas affectée.

Nous pouvons donc attribuer la première vague polarographique de **2***a* et **2***b*, à la réduction du motif nitré éthylénique. La hauteur (voisine de 4 faradays) et le potentiel de demi-vague à pH = 1,30: −0,15 V pour **2***a*, −0,14 V pour **2***b* sont comparables à ceux du β-nitrostyrène dans des conditions très proches (−0,16 V à pH = 1,36).

La seconde vague est attribuable à la réduction des oximes (**12***a* ou **12***b*) protonées. Le $E_{1/2}$ de cette vague (−0,55 V à pH = 1,3 pour **2***b*) est à rapprocher par exemple de celui de la phényl-1 oximino-2 propanone: −0,57 V à pH = 1 (16). De plus les échantillons authentiques de **12***a* et **12***b* obtenus par électrolyse préparative, présentent une vague cathodique de hauteur et de potentiel de demi-vague très proches de ceux de la seconde vague de **2***a* et **2***b* dans les mêmes conditions.

La troisième vague, présente au delà de pH = 4 sur le polarogramme de **2***b*, possède un $E_{1/2}$ identique à celui de la seconde vague de l'α-cétoxime (**12***b*) au même pH. Cette vague peut être attribuée à la réduction de la diphényl-1,3 propanone-1 qui résulte de l'hydrogénolyse de l'aminocétone (**15***b*) (17). Le potentiel de demi-vague: $E_{1/2}$ = −1,42 V à pH = 7,5 peut être comparé à celui de l'acétophénone: −1,4 V à pH = 7,5 (18).

4.2.2. Au niveau du palier de la seconde vague

4.2.2.1. Etude de 2a. *En solution diluée*, des électrolyses de **2***a*: pH = 1,24; (50% d'acétonitrile, E = −0,95 V; $c \simeq 2{,}5 \times 10^{-3}$ M) montrent la décroissance, proportionnelle au nombre de coulombs consommés, des deux vagues polarographiques. Après passage d'environ 8 électrons par molécule, il n'y a plus de espèce réductible en solution.

Des *électrolyses préparatives* effectuées dans des conditions très voisines permettent d'isoler le chlorhydrate de l'amino-2 phényl-1 butanone-3 (**15***a*).

Le schéma de réduction proposé est indiqué sur le schéma 3. Le premier stade de la réduction à quatre électrons de la nitrocétone éthylénique conduit à l'α-oximinocétone (**12***a*). En milieu acide il est admis que la réduction des oximes de cétones simples en amine se fait via l'imine correspondante (19). D'autre part, Armand et coll. (20) ont montré que les monoimines d'α-dicétones sont réduites en aminocétones par l'intermédiaire d'un énaminol. Au vu de ces résultats, et bien que dans le cas de **2***a*, ni l'α-cétoimine (**13**), ni l'énaminol (**14***a*) n'aient pu être décelés, le schéma de réduction proposé semble néanmoins le plus plausible. Nous verrons qu'il est justifié par les résultats exposés ultérieurement.

4.2.2.2. Etude de 2b. Au cours *d'électrolyses en solution diluée* de **2***b* à pH = 1,02 (E = −0,8 V; c = $1{,}2 \times 10^{-3}$ M; 50% d'acétonitrile), outre la décroissance des vagues 1 et 2 toujours proportionnelle au nombre de coulombs consommés, on note, au cours du temps, l'apparition d'une vague anodique de $E_{1/2}$ = −0,06 V dont la hauteur atteint son maximum aux quatre cinquièmes de l'électrolyse; en fin d'électrolyse (passage de 8 électrons par molécule), elle est encore présente mais décroit progressivement pour disparaître après environ 1 h 30 (fig. 2), la solution étant maintenue constamment sous atmosphère d'argon.

Can. J. Chem. Downloaded from www.nrcresearchpress.com by 210.87.254.6 on 09/06/12
For personal use only.

Can. J. Chem. Downloaded from www.nrcresearchpress.com by 210.87.254.6 on 09/06/12
For personal use only.

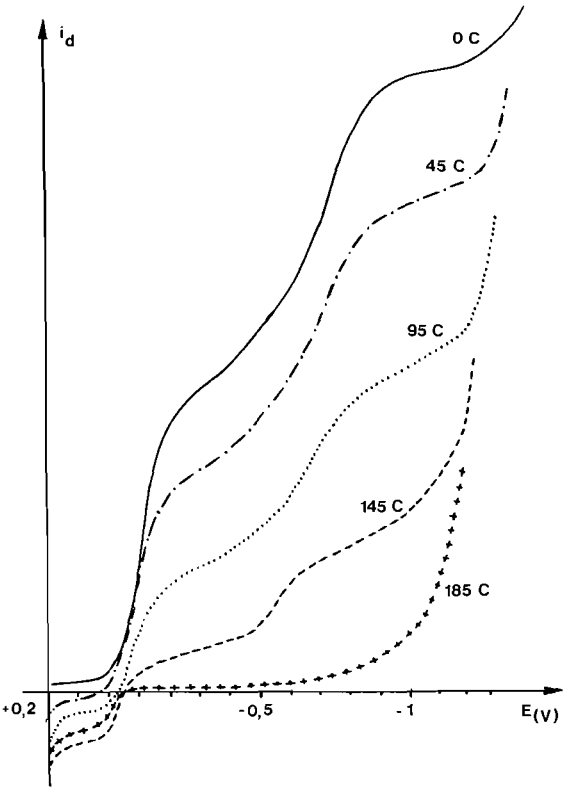

FIG. 2. Electrolyse de **2***b* en solution diluée. pH = 1,02; c = 1,2 × 10^{-3} M; CH_3CN 50%; E = −0,8 V SCE; V = 200 mL. Polarogrammes enregistrés avant (OC) pendant (45 C, 90 C, 145 C) et à la fin de l'électrolyse (185 C).

Ces résultats ne peuvent s'expliquer simplement par la réduction de **2***b* en α-cétoxime (**12***b*), puis en aminocétone (**15***b*). On devrait dans ce cas observer en fin d'électrolyse une vague cathodique due à **15***b*. La vague de l'amino-2 phényl-2 acétophénone possède en effet un $E_{1/2}$ = −0,89 V à pH = 1,2 (17).

Les faits observés montrent l'apparition d'un composé aisément oxydable évoluant lentement en solution pour conduire à une entité non réductible dans les conditions opératoires.

Des électrolyses préparatives ont été effectuées afin d'éclaircir le mécanisme de réduction. Elles permettent d'isoler avec un bon rendement l'α-cétol (**17**).

4.2.2.3. Discussion. Quatre schémas de réduction sont possibles. Les trois premiers, représentés sur le schéma 4, peuvent être éliminés:

En premier lieu, on doit rejeter l'hypothèse d'une hydrolyse de **12** en α-dicétone et la réduction de cette dernière en **17** par l'intermédiaire de l'ène-diol (**16**) (21). Nous avons en effet vérifié par ultraviolet la stabilité de l'oxime (**12***b*) dans les conditions opératoires utilisées.

Peut être exclue également la réduction de **12***b* en oxime-alcool suivie de l'hydrolyse de cette dernière en **17**. La réduction de **2***b* en **17** ne nécessiterait que 6 électrons par molécule et d'autre part, pour des composés possèdant l'enchaînement —C(=O)—C(=N)— la liaison —C=N est toujours réduite avant la fonction carbonyle (22).

Enfin, nous pouvons écarter l'hydrolyse de **13***b* en dicétone, réduite ultérieurement en **17**. En effet, on peut attendre pour cette α-cétoimine un $E_{1/2}$ proche, à pH ≃ 1,4 de 0 V. A titre de comparaison, le potentiel de demi-vague du monoanile du benzile est de −0,4 V à pH = 6 (22). Dans ces conditions, il est difficile d'envisager pour **13** une vitesse d'hydrolyse supérieure à sa vitesse de réduction à l'électrode.

Le seul schéma de réduction compatible avec les résultats expérimentaux est donc celui représenté sur le *schéma 3*.

La vague anodique observée lors des électrolyses de **2***b* à −0,8 V et qui indique la présence d'un composé aisément oxydable peut être due à l'énaminol (**14***b*) ou à l'ène-diol (**16**). Cependant, la disparition relativement lente de cette vague anodique exclut de l'attribuer à **16** l'équilibre tautomère **16** ⇌ **17** devant être beaucoup plus rapide que la réaction d'hydrolyse **14***b* → **16**.

La vague anodique est donc attribuée à **14***b*. Cet intermédiaire est par ailleurs mis en évidence par voltamétrie cyclique à balayage linéaire de tension. Pour une solution de **2***b* à pH = 1,34 (c = 10^{-3} M; 30% de méthanol, v = 0,25 V/s) on observe au balayage vers les potentiels négatifs entre 0 et −0,8 V deux pics cathodiques de potentiel de pic, E_p, proches des $E_{1/2}$ des deux vagues polarographiques de ce composé, respectivement −0,15 V et −0,56 V. Au balayage retour de −0,8 V à + 0,2 V, on note la présence d'un pic anodique de E_{pa} = −0,07 V due à l'oxydation de **14***b* (fig. 3). La décroissance de la vague anodique observée lors des électrolyses est due à l'hydrolyse de l'énaminol **14***b* en **17** via l'ène-diol **16**.

La différence de comportement observée entre **2***a* et **2***b* s'explique par les stabilités relatives des énaminols **14***a* et **14***b*. **14***a* est moins conjugué que **14***b* donc moins stable, et l'équilibre tautomère **14***a* ⇌ **15***a* est alors totalement déplacé vers la forme aminocétone **15***a*: ceci exclut une éventuelle hydrolyse de **14***a* comme nous l'observons dans le cas de **14***b*.

4.3. Electrolyses en milieu neutre (schéma 3)

Les polarogrammes enregistrés en cours d'électrolyse en solution diluée de **2***a* ou **2***b* au niveau du

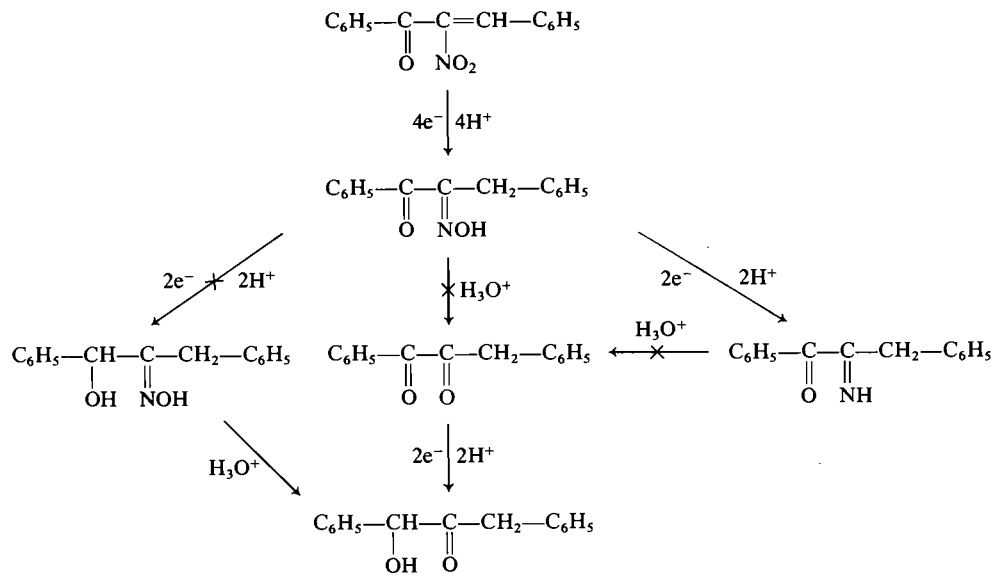

SCHÉMA 4

palier de la seconde vague et à pH ≃ 7 sont complexes. Lors des électrolyses en solution diluée, la dégradation de **2***a* et **2***b* à ce pH est négligeable. Par contre elle devient importante lors des électrolyses préparatives, beaucoup plus longues, et celles-ci ne peuvent être effectuées dans de bonnes conditions. Nous avons vérifié que la réduction primaire à quatre électrons respectivement de **2***a* et **2***b* conduisait toujours à **12***a* et **12***b* ce qui nous a permis de réaliser les électrolyses sur ces cétoximes.

Au cours d'*électrolyses en solution diluée* de **12***b* par exemple, à pH = 7,5 (50% d'acétonitrile; $c = 2 \times 10^{-3}$ *M*; $E = -1{,}05$ V), on observe une décroissance de la première vague polarographique ($E_{1/2} = -0{,}9$ V) proportionnelle au nombre de coulombs consommés tandis que la hauteur de la seconde vague ($E_{1/2} = -1{,}14$ V) attribuable à l'aminocétone **15***b* (amino-2 phényl-2 acétophénone: $E_{1/2} = -1{,}15$ V à pH = 7,4 (17)) croit avec le temps jusqu'à la demi-électrolyse. Une troisième vague de $E_{1/2}$ plus négatif apparait également. Elle peut être attribuée à la diphényl-1,3 propanone provenant de l'hydrogénolyse de la liaison C—N lors de la réduction de **15***b* (17). Ces résultats laissent penser que le produit de réduction en milieu neutre ou très faiblement basique est l'aminocétone **15***a* ou **15***b*.

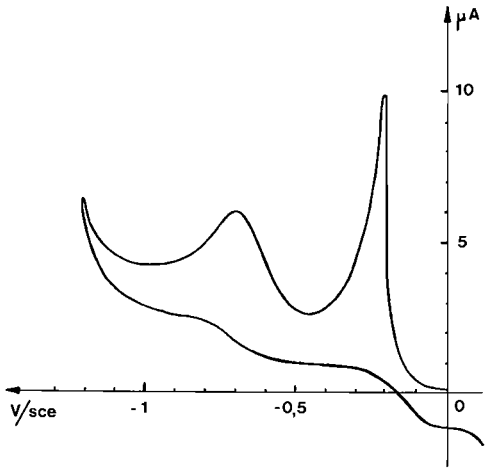

FIG. 3. Voltamogramme de **2***b* pH = 1,34; $c = 10^{-3}$ *M*; MeOH 30%; $v = 0{,}25$ V/s.

Des *électrolyses préparatives* de **12***a* et **12***b* à des pH voisins de 7: par exemple pH = 7,5–7,6 pour **12***a*; (50% d'acétonitrile, $c = 3 \times 10^{-2}$ *M*; $E = -1{,}05$ V) ou pour **12***b* pH = 7,20 (50% d'acétonitrile; $c = 2{,}8 \times 10^{-3}$ *M*; $E = -1{,}1$ V) permettent d'isoler respectivement après passage d'environ quatre électrons par molécule la dibenzyl-2,5 diméthyl-3,6 pyrazine (**19***a*) et la dibenzyl-2,5 diphényl-3,6 pyrazine (**19***b*), identifiée, par leur analyse pondérale, leurs caractéristiques physicochimiques et leur point de fusion.

Le schéma de la réduction de **2***a* et **2***b* vers pH = 7 (schéma 3) propose le passage par les α-cétoximes **12***a* et **12***b* puis les α-aminocétones **15***a* et **15***b*. Ces deux derniers composés, à ce pH, conduisent, par condensation de deux molécules (23) aux dihydropyrazines correspondantes **18***a* et **18***b*. Ces dihydropyrazines ne sont isolables qu'en prenant des précautions particulières (atmosphère inerte ...) sinon elles s'oxydent très facilement en pyrazines tétrasubstituées **19***a* et **19***b*, elles mêmes électroréductibles (24). On note par exemple pour **19***a*

Can. J. Chem. Downloaded from www.nrcresearchpress.com by 210.87.254.6 on 09/06/12
For personal use only.

Can. J. Chem. Downloaded from www.nrcresearchpress.com by 210.87.254.6 on 09/06/12
For personal use only.

une vague cathodique de hauteur proche de 2 faradays $E_{1/2}$ (V) = −0,44–0,073 pH.

Partie expérimentale

Les chromatographies en couche mince ont été réalisées sur plaques de gel de silice Riedel – De Haen. Les points de fusion sont, soit des points de fusion instantanée pris sur banc Kofler (F_K), soit des points de fusion lente pris en tubes capillaires sur appareil Buchi-Tottoli (F_T). Les microanalyses élémentaires ont été effectuées par le service central de microanalyses du CNRS. Tous les composés ont fourni des résultats analytiques correspondant à la formule à ±0,3% près.

Les spectres ultraviolets ont été enregistrés en solution éthanolique sur appareil Unicam SP 1800 (les longueurs d'onde sont exprimées en nm et les ε sont reportés entre parenthèses). Les spectres infra-rouges ont été pris en pastilles de KBr ou en solution dans $CHCl_3$ sur appareil Perkin-Elmer 177 (les nombres d'onde sont exprimés en cm^{-1}). Les spectres de rmn du proton ont été enregistrés à 60 MHz sur Varian T 60 A et les spectres de rmn ^{13}C sur Varian CFT 20 à transformées de Fourier. Dans tous les cas le tétraméthylsilane a été utilisé comme référence interne et les déplacements chimiques sont exprimés en ppm. Les abréviations s pour singulet, d pour doublet, t pour triplet, q pour quadruplet et m pour multiplet sont utilisées. Les polarogrammes sont enregistrés sur polarographe Radiometer PO_4 ou Tacussel type EPL 1B; les potentiels de demi-vague sont donnés par rapport à l'électrode à calomel saturée en chlorure de potassium. La hauteur des vagues est mesurée par rapport au β-nitrostyrène. Nous avons utilisé les tampons suivants: H_2SO_4; H_3PO_4–NaH_2PO_4; CH_3COOH–CH_3COONa; Na_2HPO_4–NaH_2PO_4. La concentration des tampons assure une force ionique comprise entre 0,1 *M* et 0,15 *M*. Les pH sont mesurés avec un pH-mètre Tacussel pH N 75 et une électrode de verre combinée verre–calomel. Les électrolyses à potentiel contrôlé sont effectuées sur cathode de mercure sous balayage d'argon ou d'azote. Le volume de la solution est généralement 200 cm^3; la solution anodique est de même composition que la solution cathodique mais sans dépolarisant. Des polarogrammes sont enregistrés en cours d'électrolyses en solution diluée en utilisant une électrode à goutte de mercure plongeant dans le compartiment cathodique et l'électrode de référence du dispositif d'électrolyse. Le potentiel est fixé par un potensiostat Tacussel ASA 4F2, la valeur exacte du potentiel est lue sur un millivoltmètre Exaprécis. Le nombre de coulombs est mesuré à l'aide d'un intégrateur Tacussel IG 31A, l'intensité du courant est lue au milliampèremètre.

Certaines abréviations ont été utilisées dans la partie expérimentale: LAH pour hydrure de lithium et d'aluminium; THF pour tétrahydrofuranne; Et_3N pour triéthylamine; N_2O_4 pour peroxyde d'azote; P_2O_5 pour pentoxyde de phosphore.

1. Action de N_2O_4 sur la benzylidène-acétone (1a) et la chalcone (1b): α-aminoalcools de réduction et composés d'hétérocyclisation

(1) cis *Benzyl-4 méthyl-2 phényl-5 oxazoline-2 (10)*
E α-nitrochalcone (2b)

Selon (2) par nitration de la chalcone par N_2O_4; 60%; F_K = 90–91°C; (2) *F* = 90–91°C. ir ($CHCl_3$): 1678 (C=O) 1640, 1600, 1583 (C=C), 1510, 1320 (NO_2); ^1H-rmn ($CDCl_3$) δ: 7,2–8,0 (m, 10, H arom.) 8,37 (s, 1, H vinylique); ^{13}C-rmn ($CDCl_3$), δ: —CH=C(NO_2)—CO—C_6H_5: 137,2; 144,6; 188,1; *i* 134,8; *o* 129,1; *m* 129,0; *p* 132,1; phényle: *i* 130,9; *o* 130,9; *m* 129,1; *p* 134,8.

Amino-2 diphényl-1,3 propanol-1 (7b)

A une suspension de 15 g (0,39 mol) de LAH dans 400 cm^3 de THF anhydre, on ajoute goutte à goutte lentement 15 g (0,06 mol) de **2***b* dissoute dans 150 cm^3 du même solvant. On chauffe 24 h à reflux. Après refroidissement du mélange réactionnel dans un bain de glace on ajoute avec précaution 100 cm^3 d'eau glacée, filtre le précipité de $Al(OH)_3$, extrait à CH_2Cl_2, sèche sur Na_2SO_4, évapore sous pression réduite et distille l'huile résiduelle: $E_{0,5}$: 135–145°C; 6,5 g (48%) d'un mélange de 55% d'aminoalcool *érythro* et de 45% de *thréo* (sur un autre essai: 57 et 43%); ir (film): 3350 et 3290 (OH et NH_2).

Chlorhydrate érythro: à la solution dans MeOH de 2 g du mélange d'aminoalcools, on ajoute HCl concentré jusqu'à pH = 1. On évapore à sec sous pression réduite puis triture le résidu avec Me_2CO anhydre. A froid précipite 0,5 g de chlorhydrate *érythro*, F_K vers 200°C avec sublimation. ^1H-rmn (DMSO d_6 + D_2O), δ: 2,73 (d, 2, $CH_2C_6H_5$); 3,5 à 4,0 (massif, 1, CH—N); 5,13 (m, 1, CHOH, *J* = 4,16 Hz); 7,37 (s, 5, arom. de CHOH—C_6H_5); 7,55 (s, 5, arom. de $CH_2C_6H_5$); ^{13}C-rmn (DMSO d_6) δ: C_6H_5—CH_2—: *i* 137,06; *o* ou *m* 128,54 ou 129,24; *p* 126,64; 32,44; —CH(NH_2)—CH(OH)—C_6H_5: 58,0; 71,22; *i* 140,76; *o* ou *m* 126,35 ou 128,31; *p* 127,52. Basifiées après évaporation du solvant et reprise par l'eau les eaux mères sont constituées encore par un mélange d'aminoalcools *érythro* et *thréo* (0,8 g) avec enrichissement important en *thréo* comme le montre la rmn; l'*aminoalcool érythro pur* est obtenu par basification d'une solution aqueuse de chlorhydrate et extraction par CH_2Cl_2; ^1H-rmn ($CDCl_3$), δ: 2,20 (s, 3, OH et NH_2, éch. D_2O); 2,70 (d, 2, CH_2); 2,8–3,3 (massif 1, CH—N); 4,55 (d, 1, CHOH, *J* = 4,16 Hz); 7,10 (m, 5, H arom.); 7,30 (s, 5, H arom.); ^{13}C-rmn ($CDCl_3$) δ: C_6H_5—CH_2—: *i* 138,9; *o*, *m*, 128,1, 128,2; *p* 127,4; 37,7; —CH(NH_2)—CH(OH)—C_6H_5: 57,9; 75,8; *i* 141,4; *o*, *m* 129,1, 126,4; *p* 126,2; *aminoalcool thréo*: la connaissance des valeurs des déplacements chimiques des carbones de l'alcool *érythro* permet dans le mélange d'aminoalcools isomères d'attribuer les valeurs des carbones non aromatiques (à l'exception des carbones *ipso*) de la base *thréo*: ^{13}C-rmn ($CDCl_3$) δ: C_6H_5—CH_2—: *i* 138,7; 39,5; —CH(NH_2)—CH(OH)—C_6H_5: 58,3; 75,7; *i* 142.5.

Acétamido-2 diphényl-1,3 propanol-1 (8c)

A 10 g (0,03 mol) d'aminoalcool **7***b* dissous dans 400 cm^3 de Et_2O anhydre, on ajoute 17,1 g (0,17 mol; 24 cm^3) de Et_3N séchée sur KOH. A cette solution refroidie par un bain de glace on ajoute lentement 7 g (0,09 mol; 6,5 cm^3) de chlorure d'acétyle. Après addition le mélange est maintenu sous agitation à température ambiante pendant 2 h. On hydrolyse par 200 cm^3 d'H_2O puis extrait la solution au toluène; la phase organique est séchée sur Na_2SO_4 puis évaporée sous pression réduite. L'huile résiduelle cristallise par addition d'un minimum de Et_2O. Après recristallisation dans MeOH: 5,30 g (45%); *F* = 150°C; ir ($CHCl_3$); 3600, 3360 (bande large, OH), 3440 (NH), 1652 (C=O), 1605 (C=C).

cis-*Benzyl-4 méthyl-2 phényl-5 oxazoline-2 (10)*

A 6 g (0,02 mol) de **8***c* dissous dans 50 cm^3 de toluène anhydre on ajoute 15 g de P_2O_5. Le mélange réactionnel est porté à reflux pendant 5 h puis refroidi par un bain de glace et traité par H_2O glacée pour décomposer l'excès de P_2O_5. La phase organique est basifiée par K_2CO_3, extraite à $CHCl_3$, lavée à H_2O jusqu'à neutralité, séchée sur Na_2SO_4 puis évaporée sous pression réduite. L'huile résiduelle est chromatographiée sur 30 fois son poids de SiO_2 G Merck. L'élution par $CHCl_3$ donne 2,5 g (45%) d'oxazoline (**10**) (R_f = 0,35, éluant CH_2Cl_2 + 20% EtOH, révélation par le réactif de Dragendorff) que l'on transforme en *chlorhydrate* par addition d'éther chlorhydrique à une solution éthérée de base; F_T = 175°C après recristallisation dans Me_2CO; uv (EtOH) 215 (496), 250 (217), 256 (271), 264 (256), 266 (210); ^1H-rmn (DMSO d_6), δ: 2,10 (s, 3, CH_3); 2,82 (m, 2, CH_2); 3,80–4,20 (massif, 1, H de CH—CH_2); 5,70 (d, 1, H de C*H*—C_6H_5, *J* = 7 Hz), 7,40 et 7,50 (2s, 10, 2 C_6H_5); ^{13}C-rmn (DMSO d_6), δ: N—CH—CH_2—C_6H_5; 55,0; 34,9; arom.: voir ci-après;

Can. J. Chem. Downloaded from www.nrcresearchpress.com by 210.87.254.6 on 09/06/12
For personal use only.

CH_3—C—O—CH—C_6H_5: 20,9; 169,4; 74,3; arom.: voir ci-après; 2 singulets arom. à 135,7 et 136,1; doublets arom.: 126,8 à 129,3.

(2)(α-Hydroxyéthyl)-3 méthyl-1 dihydro-3,4 isoquinoléine (9)
Z α-Nitrobenzylidène acétone (2a)

Selon (2) par nitration de la benzylidène-acétone par N_2O_4; 72%; F_K = 108°C (2), F = 108°C; ir ($CHCl_3$) 1690 (C=O) 1580, 1600, 1615, 1630 (C=C), 1520, 1348 (NO_2); ^{1}H-rmn ($CDCl_3$), δ: 2,47 (s, 3, CH_3), 7,47 (s large, 6, H vinylique + arom.); ^{13}C-rmn ($CDCl_3$), δ: —CH=C(NO_2)—CO—CH_3: 132,3; 147,8; 187,9; 24,9; phényle; *i* 128,7; *o* 129,7; *m* 129,3; *p* 132,2.

Amino-3 phényl-4 butanol-2 (7a)

A partir de 15 g (0,39 mol) de LAH et 15 g (0,08 mol) de **2***a* selon un mode opératoire identique à celui décrit pour **7***b* on obtient 7 g (54%) d'aminoalcool ($E_{0.5}$ = 130°C) à raison de 42% d'*érythro* et 58% de *thréo* (sur un autre essai 43 et 57%); ir ($CHCl_3$): 3300 (bande large, OH et NH_2).

Chlorhydrate érythro: 3 g du mélange d'amino alcools en solution méthanolique traités dans des conditions identiques à celles de **7***b* conduisent à froid à 0,6 g de chlorhydrate *érythro*, F_T= 162°C; ^{1}H-rmn (DMSO d_6+ D_2O), δ 1,17 (d, 3, CH_3); 2,75 à 3,37 (massif, 3, CH—N et CH_2—C_6H_5); 3,53 à 3,9 (massif, 1, CHOH; après irradiation sur le CH_3: d, J = 4 Hz); 7,33 (s, 5, H arom.); ^{13}C-rmn (DMSO d_6): δ C_6H_5—CH_2—: *i* 136,3; *o* ou *m* 130,04 ou 130,26; *p* 128,43; 36,03; —CH(NH_2)—CH(OH)—CH_3: 59,33; 67,25; 20,04. De la même façon que pour **7***b*, les eaux mères sont encore constituées par un mélange d'aminoalcools isomères (2 g) avec net enrichissement en isomère *thréo*. *L'aminoalcool* érythro *pur* est obtenu par basification d'une solution aqueuse du chlorhydrate et extraction par CH_2Cl_2; ^{1}H-rmn ($CDCl_3$), δ: 1,27 (d, 3H, CH_3); 2,17 (s, large, OH et NH_2, éch. D_2O); 2,33 à 3,03 (massif, 3, CH_2—C_6H_5 et CH—N); 3,30 à 3,85 (massif, 1, CHOH); 7,22 (s, 5, H arom.); ^{13}C-rmn ($CDCl_3$), δ: C_6H_5—CH_2—: *i* 138,84; *o* ou *m* 128,39 ou 129,06; *p* 126,18; 40,49; —CH(NH_2)—CH(OH)—CH_3: 58,33; 69,54; 20,15; *aminoalcool* thréo: la connaissance des valeurs des déplacements chimiques des carbones de la base *érythro* permet dans le mélange d'amino alcools isomères d'attribuer les valeurs des carbones non aromatiques de la base *thréo*: ^{13}C ($CDCl_3$), δ, C_6H_5—CH_2—: 38,5; —CH(NH_2)—CH(OH)—CH_3: 57,4; 65,70; 17,7.

Acétamido-3 phényl-4 butanol-2 (8a) et acétamido-3 acétoxy-2 phényl-4 butane (8b)

On ajoute goutte à goutte 20,8 g (0,26 mol, 19 cm³) de chlorure d'acétyle à une solution refroidie dans un bain de glace de 21 g (0,13 mol) de **7***a* dans 500 cm³ d'Et_2O anhydre. On ajoute alors 40 cm³ (28,8 g; 0,28 mol) de Et_3N séchée sur KOH. On poursuit l'agitation pendant 2 h à température ambiante. L'hydrolyse du mélange réactionnel par 400 cm³ d'eau puis son traitement de façon identique à celui décrit pour **8***c* conduit à 3,5 g (13%) d'acétamido-3 phényl-4 butanol-2 (**8***a*); F = 132°C; ir ($CHCl_3$): 3440 (bande large, OH et NH), 1652 et 1660 (C=O amide *érythro* et *thréo*). L'huile résiduelle après cristallisation de **8***a* est distillée sous pression réduite et donne 18 g (57%) d'acétamido-3 acétoxy-2 phényl-4 butane (**8***b*); E_5 = 165–170°C; ir ($CHCl_3$): 3280 (NH) 1730 (C=O ester), 1645–1650 (C=O amide).

En opérant la réaction d'amidification mole à mole entre le chlorure d'acétyle et l'aminoalcool (**7***a*) on obtient 20% de dérivé monoacétylé (**8***a*) et 20% de dérivé diacétylé (**8***b*).

cis Benzyl-4 diméthyl-2,5 oxazoline-2 (20)

A partir de 5 g (24 mmol) d'amide (**8***a*) dissous dans 100 cm³ de toluène anhydre et de 15 g de P_2O_5, et suivant le mode opératoire rapporté ci-dessus pour la préparation de l'oxazoline (**10**), on obtient après traitement 4 g d'une huile que l'on chromatographie sur 100 g de SiO_2 G Merck. L'élution par $CHCl_3$ + 10% EtOH donne 3,5 g (76,6%) d'oxazoline (**20**), huile qui cristallise par trituration avec de l'éther; F_T = 102°C; ^{1}H-rmn ($CDCl_3$), δ: 1,17 (d, 3, CH_3 en 5; J = 6,4 Hz); 1,92 (s, 3, CH_3 en 2); 2,85 (d élargi, 2, CH_2); 3,78 à 4,18 (m, 1, H de CH—CH_2); 5,92 à 6,15 (m, 1, H de CH—CH_3); 7,24 (s, 5, C_6H_5); ^{13}C-rmn ($CDCl_3$) δ: N—CH—CH_2—C_6H_5: 55,81; 38,05; arom.: 3 doublets: 126,27 (*p*); 128,32 et 129,11 (*o* et/ou *m*); 1 singulet à 138,20 (*i*); CH_3—C—O—CH—CH_3: 20,68; 170,60; 66,76; 23,10.

(α-Hydroxyéthyl)-3 méthyl-1 dihydro-3,4 isoquinoléine (9)

Le traitement de 7 g (0,028 mol) d'amide-ester (**8***b*) dans 60 cm³ de toluène anhydre et de 20 g de P_2O_5 de façon identique à celle décrite pour la préparation de **10** conduit après élution par $CHCl_3$ à 2,8 g (53%) d'isoquinoléine (**9**) (R_f = 0,65, éluant CH_2Cl_2 + 20% EtOH, révélation par le réactif de Dragendorff) que l'on transforme de la même façon en *chlorhydrate*; F = 150°C après recristallisation dans Me_2CO; uv (EtOH) 209 (19 100), 276 (9900); ir (KBr): 3460, 3290 (OH), 1650 (C=$\overset{+}{N}$H) 1600, 1570 (C=C); ^{1}H-rmn (DMSO d_6), δ: 1,20 (d, 3, CH_3 de CH_3—CHOH—); 2,90 (s, 3, CH_3 de CH_3—C=N^+); 3,2 (d, 2, CH_2 isoq. en 4); 3,65–4,2 (massif, 3, OH, CH isoq. en 3, CH de CH(OH)CH_3); 7,4–8,2 (m, 4, H isoq. en 5, 6, 7, 8); ^{13}C-rmn (D_2O), δ: CH(OH)—CH_3: 67,2, 18,9; CH_3—$C_{(1)}$=$N^+_{(2)}$: 20,6, 155,1: isoquinoléine: 58,7 (C_3), 25,5 (C_4), 129–131 (C_5, C_6, C_8), 138,4 (C_7), 137,7 (C_9), 125,9 (C_{10}).

II. Nitration des diméthoxy-3,4 benzylidène-acétone (3a), diméthoxy-3,4 chalcone (3b) et diméthoxy-3,4, chloro-4' chalcone (3c); alcools de réduction

Diméthoxy-3,4 nitro-6 benzylidène-acétone (5a)

On dissout 15 g (0,07 mol) de diméthoxy-3,4 benzylidène-acétone (**3***a*) (15) dans 600 cm³ de CCl_4 anhydre. Sous agitation vigoureuse on ajoute 127 g (1,38 mol) de N_2O_4 dissous dans 50 cm³ du même solvant. Après 5 mn de contact on chasse à froid et sous pression réduite l'excès de N_2O_4 et le HNO_2 formé. On ajoute 30 cm³ de MeOH à l'huile résiduelle: (**5***a*) précipite alors. Après recristallisation dans MeOH: 5,12 g (42%) de nitrocétone; F_K = 164–165°C; ir ($CHCl_3$): 1696 (C=O), 1640, 1610, 1575 (C=C), 1510, 1335 (NO_2); ^{1}H-rmn ($CDCl_3$) δ: 6,45 (d, 1, H vinylique, CH en α du CO; J = 16 Hz), 7,0 (s, 1, H arom. en *méta* du NO_2), 7,6 (s, 1, H arom. en *ortho* du NO_2), 8,05 (d, 1, H vinylique, CH en β du CO; J = 16 Hz); ^{13}C-rmn ($CDCl_3$), δ: —CH=CH—CO—CH_3: 131,6; 97,6; 187,5; 25,4; phényle: 119,8 (C_1); 110,2 (C_2); 153,8 (C_3; CH_3O); 150,5 (C_4; CH_3O); 108,2 (C_5); 139,8 (C_6; NO_2); méthoxyles: 56,6.

Diméthoxy-3,4 nitro-6 chalcone (5b)

A 10,6 g (0,02 mol) de diméthoxy-3,4 chalcone (2) dissoute dans 250 cm³ de CCl_4 anhydre, sont ajoutés 30 g (0,33 mol) de N_2O_4 dissous dans 150 cm³ du même solvant. Un abondant précipité, que l'on essore aussitôt, se forme rapidement. La chalcone nitrée est recristallisée dans MeOH: 8,67 g (77%); F_K = 184°C (2[1]) F = 182°C; ir ($CHCl_3$) 1668 (C=O), 1590, 1610, 1645 (C=C), 1508, 1338 (NO_2); ^{1}H-rmn ($CDCl_3$), δ: 4,05 (s, 6, $2CH_3O$—), 7,05–8,35 (massif, 9, 2 H vinyliques + 7 H arom.); ^{13}C-rmn.[5]

Diméthoxy-3,4 nitro-6 chloro-4' chalcone (5c)

Préparée comme la chalcone précédente à partir de 25 g (0,08 mol) de diméthoxy-3,4 chloro-4' chalcone (2) dissoute dans 400 cm³ de CCl_4 anhydre et de 45 g (0,49 mol) de N_2O_4 dans 250 cm³ du même solvant. Après recristallisation dans MeOH: 13,8 g (48%) de **5***c*; F_K = 212°C (2[1])F = 208°C; ir ($CHCl_3$): 1665 (C=O), 1645, 1608, 1590 (C=C), 1505, 1335 (NO_2); ^{1}H-rmn ($CDCl_3$), δ: 4,0 (s, 6, $2CH_3O$), 7,05 (d, 1, H vinylique, J = 17 Hz), 8,15 (d, 1, H vinylique, J = 17 Hz), 6,96–7,9 (massif, 6, H arom.); ^{13}C-rmn.[5]

[5]Composé trop peu soluble à concentration suffisante pour en effectuer le spectre de ^{13}C rmn ($CDCl_3$, DMSO d_6, $(CD_3)_2CO$).

Can. J. Chem. Downloaded from www.nrcresearchpress.com by 210.87.254.6 on 09/06/12
For personal use only.

(Amino-6 diméthoxy-3,4 phényl)-3 (chloro-4' phényl)-1 propanol-1 (6c)

Selon (10): dans la capsule d'un Soxhlet, on place 10 g (0,02 mol) de **5***c* et on introduit dans le ballon 8 g (0,21 mol) de LAH et 100 cm³ de THF anhydre. L'extraction par le solvant à reflux dure 36 h. Après refroidissement l'excès d'hydrure est détruit avec précaution par H_2O glacée et NaOH à 10%. Après essorage, on extrait l'amine avec $CHCl_3$; la phase organique est séchée sur Na_2SO_4 puis évaporée sous pression réduite. L'huile résiduelle reprise par Et_2O cristallise. Après recristallisation dans MeOH: 2 g (45%); F_K = 121–122°C; (10) F = 122°C; ir ($CHCl_3$) 3670, 3600, 3370 (bande large, OH et NH_2) 1615, 1580 (C=C); ^{1}H-rmn ($CDCl_3$), δ: 1,90 (m, 2, CH_2 de CH_2—CHOH—); 2,60 (t, 2, CH_2 de C_6H_5—CH_2—); 3,45 (s, 3, OH et NH_2, éch. D_2O); 3,80 (s, 6, $2CH_3O$); 4,55 (CH de —CHOH—); 6,25 (s, 1, CH en *ortho* de NH_2); 6,55 (s, 1, CH en *méta* de NH_2); 7,25 (s, 4, arom. de —C_6H_4—Cl).

III. Réductions électrochimiques préparatives

Phényl-1 oximino-2 butanone-3 (12a)

On prépare 250 cm³ de solution contenant 100 cm³ d'acétonitrile, 25 cm³ d'acide sulfurique N et de l'eau. On place 200 cm³ de cette solution (pH = 1,05) et 573 mg de **2***a* ($1,5 \times 10^{-2}$ *M*) dans le compartiment cathodique; la solution restante est mise dans le compartiment anodique. On fixe le potentiel à −0,4 V. Après passage de 980 C (1160 C = 4 F), i < 5 mA, l'électrolyse est arrêtée. Après évaporation de l'acétonitrile le précipité formé est lavé, séché; 487 mg (85%) puis recristallisé dans un mélange hexane–benzène 70/30 en volume. On recueille l'α-céto-oxime (**12***a*). F = 77–78°C; (25) F = 80–81°C; ^{1}H-rmn (DMSO d_6) δ: 3,35 (s, 3, CH_3); 3,93 (s, 2, CH_2); 7,3–7,4 (m, 6, arom. + N—OH).

Diphényl-1,3 oximino-2 propanone-1 (12b)

On prépare 250 cm³ de solution contenant 125 cm³ d'acétonitrile, 100 cm³ d'acide sulfurique N et de l'eau. On introduit 200 cm³ de cette solution et 910 mg de **2***b* ($1,8 \times 10^{-2}$ *M*) dans le compartiment cathodique; le reste de la solution est placé dans le compartiment anodique. Le potentiel est fixé à −0,25 V. Après passage de 1490 C (1740 C = 4 F), l'intensité résiduelle est inférieure à 5 mA et le pH de la solution est égal à 1,05. L'électrolyse est arrêtée et l'acétonitrile évaporé. Le précipité formé, lavé puis séché est l'α-céto-oxime (**12***b*): 738 mg (80%) qui est recristallisé dans un mélange hexane–benzène, 70/30 en volume, F = 122°C; (26), F = 123°C; ^{1}H-rmn (DMSO d_6), δ: 4,12 (s, 2, CH_2); 7,2–7,9 (m, 10, H arom.) 8,5 (s, éch. avec D_2O, 1, N—O*H*); uv (acétonitrile) λ_{max} = 252 nm (10 200).

Amino-2 phényl-1 butanone-3 (15a)

On prépare 250 cm³ d'une solution contenant 125 cm³ d'acétonitrile, 50 cm³ d'acide sulfurique N et de l'eau. On introduit 200 cm³ de cette solution et 1,15 g (3×10^{-2} *M*) de **2***a* dans le compartiment cathodique. Le reste est placé dans le compartiment anodique. Le potentiel est fixé à −0,95 V. Après passage de 4420 C (4630 C = 8 F) l'électrolyse est arrêtée. Le pH de la solution est alors 1,16. On évapore l'acétonitrile puis neutralise la solution par de la soude N jusqu'à pH ≃ 6. La phase aqueuse est extraite par 3 fois 30 cm³ d'éther et les phases éthérées sont séchées sur Na_2SO_4. On sature alors la solution en HCl gazeux. Le chlorhydrate de l'amino-2 phényl-1 butanone (**15***a*) précipite: F = 129–130°C; (27) F = 130°C; ^{1}H-rmn (D_2O) δ: 2,05 (s, 3, CH_3), 2,93 (d, 2, CH_2); 5,21 (t, 1, —C*H*—NH_2); 7,3–7,4 (m, 5 arom.).

Diphényl-1,3 hydroxy-1 propanone-2 (17)

On prépare 250 cm³ d'une solution contenant 125 cm³ d'acétonitrile, 50 cm³ d'acide sulfurique N et de l'eau. On place 200 cm³ de cette solution et 900 mg de **2***b* dans le compartiment cathodique; le reste de la solution est mis dans le compartiment anodique. On fixe le potentiel à −0,95 V. L'intensité résiduelle est inférieure à 10 mA après passage de 3140 C (3470 C = 8 F). L'électrolyse est arrêtée, le pH de la solution est alors 1,15. L'acétonitrile est évaporé et le précipité formé, lavé séché (702 mg: 82%) et recristallisé dans un mélange hexane–benzène 70/30 en volume conduit à l'α-cétol (**17**). F = 115°C; (28) F = 114–116°C; ^{1}H-rmn (acétone d_6): δ: 3,22 (s, 2, CH_2); 4,08 (s, éch. avec D_2O, 1, OH); 4,72 (s, 1, C*H*OH); 6,3–7 (m, 10, arom.).

Dibenzyl-2,5 diméthyl-3,6 pyrazine (19a)

On prépare 250 cm³ d'une solution contenant 100 cm³ d'acétonitrile, 50 cm³ d'acide phosphorique 0,5 *M*, 30 cm³ de soude 1 N et de l'eau. On place 200 cm³ de cette solution (pH = 7,21) et 1 g de **12***a* ($2,8 \times 10^{-2}$ *M*) dans le compartiment cathodique. La solution restante est introduite dans le compartiment anodique. On fixe le potentiel à −1,1 V. Après passage de 1920 C (2180 C = 4 F) on arrête l'électrolyse (i < 5 mA). L'acétonitrile est évaporé. Le solide obtenu est recristallisé dans un mélange méthanol–éther de pétrole 50/50. On recueille 220 mg (45%) de pyrazine (**19***a*); F = 100–102°C; (29), F = 100–101°C; uv (méthanol) λ_{max} = 282 nm. ^{1}H-rmn ($CDCl_3$), δ: 2,55 (s, 6, CH_3); 4,19 (s, 4, CH_2); 7,25 (s, 10, arom.); polarographie: vague cathodique, hauteur 2F; $E_{1/2}$(V) = 0,44–0,073 pH.

Dibenzyl-2,5 diphényl-3,6 pyrazine (19b)

On prépare 250 cm³ de solution contenant 100 cm³ d'acétonitrile, 50 cm³ d'acide phosphorique 0,5 *M*, 30 cm³ de soude N et de l'eau. On introduit 200 cm³ de cette solution (pH = 7,52) et 1,16 g de **12***b* dans le compartiment cathodique. Le reste de la solution est placé dans le compartiment anodique. Le potentiel est fixé à −1,05 V. A intervalles réguliers au cours de l'électrolyse, sont ajoutés cm³ par cm³, 5 cm³ d'acide phosphorique 0,5 *M* pour maintenir le pH à sa valeur initiale. Après passage de 1533 C (1600 C = 4 F) l'électrolyse est arrêtée, l'acétonitrile évaporé et la solution extraite par trois fois 20 cm³ d'éther. Les phases éthérées sont regroupées puis séchées sur Na_2SO_4. On obtient, après évaporation de l'éther, une gomme visqueuse orangée qui, lavée avec un minimum de chloroforme cristallise et conduit à 225 mg (40%) de pyrazine (**19***b*) qui est alors recristallisée dans l'acétonitrile; F = 151–153°C (30) F = 152°C; uv (méthanol): λ_{max} = 245 et 300 nm ^{1}H-rmn ($CDCl_3$); δ: 4,33 (s, 4, $2CH_2$); 7,23 (s, 10, arom. de C_6H_5—CH_2); 7,55 (s, 10, H arom.).

Remerciement

Nous tenons à remercier vivement Mme J. Mahuteau pour l'enregistrement des spectres de rmn.

1. J. C. Doré et C. Viel. C.R. Acad. Sci. Série C, **276**, 1641 (1973).
2. J. C. Doré et C. Viel. Eur. J. Med. Chem. **9**, 666 (1974).
3. J. C. Doré et C. Viel. Recl. Trav. Chim. Pays-Bas, **94**, 225 (1975).
4. C. Bellec, R. Colau, S. Deswarte, J. C. Doré et C. Viel. C.R. Acad. Sci. Série C, **281**, 885 (1975).
5. C. Bellec, D. Bertin, R. Colau, S. Deswarte, P. Maitte et C. Viel. J. Heterocycl. Chem. **16**, 1611 (1979); **16**, 1657 (1979).
6. E. Sol'aniová, S. Toma et S. Gronowitz. Org. Magn. Reson. **8**, 439 (1976).
7. L. Perruche. Thèse de Doctorat d'Université, Paris, 28 janvier 1921.
8. R. Colau. Résultats non publiés.
9. J. C. Doré. 2ème thèse pour l'obtention du Doctorat ès Sciences Physiques, Paris, 22 avril 1974.

10. A. ALLADÉ. Thèse de Doctorat d'Université, Paris, 28 septembre 1978.
11. M. PLAT. Il Farmaco, Ed. Prat. **25**, 143 (1970).
12. M. L. MARTIN et G. J. MARTIN. Manuel de résonance magnétique nucléaire. Azoulay, Paris. 1971. p. 75 et suiv.
13. W. KRABBE, W. EISENLOHR et H. G. SCHONE. Chem. Ber. **73**, 656 (1940).
14. W. M. WHALEY et T. R. GOVINDACHARI. Organic reactions. Vol. 6. J. Wiley, New York, NY. 1951. pp. 74–150.
15. C. F. VAN DUIN. Recl. Trav. Chim. Pays-Bas, **45**, 350 (1926).
16. J. ARMAND et J. P. GUETTE. Bull. Soc. Chim. Fr. 2894 (1969).
17. J. ARMAND et L. BOULARES. Bull. Soc. Chim. Fr. 711 (1975).
18. J. VOLKE, O. MANOUSEK et L. WASILEWSKA. J. Electroanal. Chem. **32**, 445 (1971).
19. P. SOUCHAY et S. SER. J. Chim. Phys. **49**, 172 (1952).
20. J. ARMAND, L. BOULARES, J. PINSON et P. SOUCHAY. Bull. Soc. Chim. Fr. 1918 (1971).
21. R. H. PHILP, R. L. FLURRY et R. A. DAY. J. Electrochem. Soc. **111**, 328 (1964).
22. J. ARMAND et L. BOULARES. Bull. Soc. Chim. Fr. 366 (1975).
23. W. H. CHEESEMAN et E. S. Q. WERSTIUK. Adv. Heterocycl. Chem. **14**, 115 (1972).
24. J. ARMAND, K. CHEKIR et J. PINSON. Can. J. Chem. **52**, 3971 (1974).
25. G. PONZIO. Gazz. Chim. Ital. **35**, 394 (1905).
26. T. KAMETANI et S. KANO. J. Pharm. Soc. Jpn. **72**, 1081 (1952).
27. H. DAKIN et R. WEST. J. Biol. Chem. **78**, 760 (1927).
28. W. H. HARTUNG et Y. T. CHANG. J. Am. Chem. Soc. **74**, 5927 (1952).
29. P. A. LEVENE et R. E. STEIGER. J. Biol. Chem. **79**, 101 (1928).
30. P. W. NEBER et A. UBER. Liebig's Ann. **54**, 467 (1928).

Can. J. Chem. Downloaded from www.nrcresearchpress.com by 210.87.254.6 on 09/06/12
For personal use only.

Localized excess electrons in H_2O glasses and ice[1]

GERALD J. TRUDEL,[2] HUGH A. GILLIS, NORMAN V. KLASSEN, AND GEORGE G. TEATHER
Division of Physics, National Research Council of Canada, Ottawa, Ont., Canada K1A 0R6

Received November 4, 1980

GERALD J. TRUDEL, HUGH A. GILLIS, NORMAN V. KLASSEN, and GEORGE G. TEATHER. Can. J. Chem. **59**, 1235 (1981).

The yields and decay rates of two types of localized excess electrons, absorbing in the visible (e^-_{vis}) and in the infrared (e^-_{ir}), have been compared in four pulse-irradiated H_2O glasses and their D_2O analogues, and in irradiated H_2O and D_2O ice crystals, all at 73 K. If it is assumed that extinction coefficients of e^-_{vis} and e^-_{ir} at 650 nm and 1800 nm, respectively, are independent of isotopic substitution for both glasses and ice, the G's for both types of localized electrons are lower in all the H_2O solids studied than in the corresponding D_2O solids. The largest effect of isotopic substitution was found in the lifetime of e^-_{vis} in the crystal; at 73 K the inital half-life for decay of e^-_{vis} is approximately 14 times longer in D_2O than in H_2O ice. Even at 6 K the decay of e^-_{vis} in H_2O ice is very rapid with an initial half-life of about 75 ns.

GERALD J. TRUDEL, HUGH A. GILLIS, NORMAN V. KLASSEN et GEORGE G. TEATHER. Can. J. Chem. **59**, 1235 (1981).

Opérant à 73 K, on a comparé les rendements et les vitesses de disparition de deux types d'électrons en excès localisés qui absorbent dans le visible (e^-_{vis}) et dans l'infrarouge (e^-_{ir}) et qui se forment dans quatre verres à H_2O ainsi que dans leurs analogues à D_2O irradiés par pulsation de même que dans des cristaux de glace de H_2O et de D_2O irradiés. Si on fait l'hypothèse que les coefficients d'extinction de e^-_{vis} et e^-_{ir} à 650 nm et 1800 nm respectivement sont indépendants de la substitution isotopique des deux verres et des deux glaces, les valeurs de G pour les deux types d'électrons localisés sont plus bas dans tous les H_2O solides étudiés que dans les D_2O solides correspondants. On a trouvé que l'effet de substitution isotopique est maximal dans le temps de vie e^-_{vis} dans le cristal; à 73 K, la période de demie-vie initiale de la disparition de e^-_{vis} est approximativement 14 fois plus longue dans la glace à D_2O que dans la glace à H_2O. Même à 6 K, la disparition de e^-_{vis} dans la glace à H_2O est très rapide avec une demie-vie initiale d'environ 75 ns.

[Traduit par le journal]

Introduction

In pulse radiolysis studies of some deuterated aqueous solids at low temperature, two well separated absorption bands due to excess electrons are seen (1–4). The better known of these, e^-_{vis}, has an optical absorption with a maximum around 650 nm. The more recently discovered e^-_{ir} has a maximum >2500 nm, and has been studied almost exclusively in deuterated systems because of their greater transparency in the 1200–3200 nm range; matrix absorption bands in this region in solid H_2O arising from combinations of the fundamental vibrational modes are shifted to higher wavelengths by deuterium substitution. One expects to find e^-_{ir} also in protiated systems but heretofore the possibility has remained that e^-_{ir} is peculiar to aqueous systems that are deuterated. An infrared electron band has been seen in an irradiated protiated ethylene glycol – H_2O glass (5), but there is a possibility that it is due to a presolvated electron in an alcohol environment, similar to the species which causes the infrared absorption seen in the pulse radiolysis of some pure alcohol glasses (6, 7). Hase and Kawabata (8) looked for e^-_{ir} in γ-irradiated H_2O ice at 4 K but did not find it, whereas they did find e^-_{ir} in pure D_2O ice under the same conditions. They reported that 10% by volume of H_2O in D_2O ice was sufficient to suppress the appearance of e^-_{ir}.

In this work e^-_{ir} was looked for in several protiated aqueous solids corresponding to deuterated solids in which it was found in significant yield. In all cases e^-_{ir} was found also in the protiated system. Some differences in the behaviour of e^-_{ir} and e^-_{vis} in the corresponding protiated and deuterated systems are noted.

Experimental

Most of the experimental techniques used in this work have been described earlier (1–4). The light detector for $\lambda \geq 900$ nm was a Barnes A-100 room temperature InAs photodiode. For 450 nm $\leq \lambda \leq$ 1000 nm an EG&G SHS-100 silicon photodiode was normally used, but the faster HP-4207 silicon photodiode was used in this wavelength region for measurements of e^-_{vis} in H_2O ice at 73 K.

The D_2O and DCl were used as supplied by Merck, Sharp and Dohme. All other solutes were reagent grade and were also used without further purification. Ice crystals were 5 mm thick. Glasses were irradiated in windowless cells to avoid corrections for radiation-induced absorptions in windows which can be significant for thin samples. Sample thicknesses were 1, 2, or 5 mm. Each solution was deaerated by bubbling with argon (Superpurified grade from Liquid Air Ltd.) for 15 min and was then injected into a sample holder with demountable sides. The holder was sometimes coated with a film of paraffin wax, which reduced the extent of cracking. The filled holder was immersed in liquid nitrogen to form the glass, and the polished stainless steel plates on either side were removed to leave the windowless sample. Glasses were often slightly cracked. Corresponding

[1]NRCC No. 19045.

[2]This work was carried out while G.J.T. was on leave at NRCC, Sept. 1975–May 1976. Permanent address: Chemistry Department, Concordia University, Montréal, P.Q., Canada H4B 1R6.

0008-4042/81/081235-06$01.00/0

©1981 National Research Council of Canada/Conseil national de recherches du Canada

Can. J. Chem. Downloaded from www.nrcresearchpress.com by 210.87.254.6 on 09/06/12
For personal use only.

H_2O and D_2O glasses were done on the same day to reduce as much as possible errors involved in comparing their yields.

Dosimetry was done with an oxygen saturated solution of 5×10^{-3} *M* KSCN, irradiated in a windowless holder to which two Suprasil plates were attached. Methanol was used in the irradiation Dewar to simulate liquid nitrogen. $G\varepsilon(SCN)_2^-$ at 475 nm was taken as $2.2 \times 10^4\ M^{-1}\ cm^{-1}$ $(100\ eV)^{-1}$. The dose per pulse was about 2 krad for a 10 ns pulse and 6–10 krad for a 40 ns pulse.

Results

Aqueous Glasses

The absorption spectra in four pairs of glasses as measured 100 ns after the start of a 40 ns pulse are shown in Fig. 1. The ethylene glycol glasses were made from 50% by volume of ethylene glycol-h_6 with either D_2O or H_2O. The yields of e^-_{vis} and e^-_{ir} for the D_2O glasses of ethylene glycol and 9.5 *M* LiCl were reported earlier (1) and we find approximately the same values in this work. For all four pairs both $G\varepsilon(e^-_{vis})$ and $G\varepsilon(e^-_{ir})$ at 100 ns are greater in the D_2O glasses than in those made with H_2O. The decays of e^-_{vis} and e^-_{ir} between 100 ns and about 10 μs for each glass are also shown in Fig. 1. The rates of growth or decay of e^-_{vis} are the same for the H_2O and D_2O glasses of each pair, so that the initial values of $G\varepsilon_{max}$ for e^-_{vis} are very likely higher for the D_2O glasses. The decay rates of e^-_{ir} seem to be a little faster in the H_2O glasses than in their D_2O counterparts, so that it is possible that the lower values of $G\varepsilon(e^-_{ir})$ at 100 ns in the H_2O glasses are due in part to the faster decay and not just to lower initial values. No noticeable differences in decay rates were found at different wavelengths in the e^-_{ir} band for any glass.

H_2O Ice at 73 K

Figure 2 shows the spectra found at 51 and 142 ns after irradiation of H_2O ice at 73 K with a 40 ns pulse. Absorption beyond 1000 nm could not be measured accurately at the shorter time because of the slow rise-time of the InAs detector that must be used at these wavelengths. Measurements were possible only at three wavelengths beyond 1000 nm because of the limited transparency of the sample, but these clearly indicate the high energy tail of an infrared absorption band. The visible band decays much more quickly than that in D_2O ice at the same temperature, as is seen in Fig. 3. In this figure OD_0 is the OD at mid-pulse, estimated from an extrapolation on a plot of 1/OD against time which happens to be approximately linear at short times. Estimated half-lives from mid-pulse are 25 ns for e^-_{vis} in H_2O ice, and 350 ns in D_2O ice (2). The decays of e^-_{vis} in H_2O (Fig. 3) and D_2O ice (2) give reasonably linear plots of OD against log *t*, which suggests a tunnelling mechanism of recombination. In water at room temperature ε_{700} for e^-_{aq} in D_2O is reported to be $2.02 \times 10^4\ M^{-1}\ cm^{-1}$ (9), as compared to $1.85 \times 10^4\ M^{-1}\ cm^{-1}$ in H_2O (10).[3] Here we simply assume that ε_{650} for H_2O ice at 73 K is the same ($2 \times 10^4\ M^{-1}\ cm^{-1}$) as the value used previously for D_2O ice at this temperature (2). On this basis $G(e^-_{vis})$ for H_2O ice at 73 K is approximately 0.27, as compared to 0.41 for D_2O ice (2).

The rate of decay of e^-_{ir} in H_2O ice could not be followed with much precision because the optical density at 1800 was so low (about 1.6×10^{-3} for a 40 ns pulse). However from a plot of 1/OD against time we calculate $k = 1.2 \times 10^{13}\ M^{-1}\ s^{-1}$ at 73 K by assuming (*a*) that second-order kinetics are obeyed, as they are for the e^-_{ir} in D_2O ice (2), (*b*) that the ratio $\varepsilon_{1800}/\varepsilon_{2350}$ is the same for H_2O ice as for D_2O ice, and (*c*) that $\varepsilon_{2350} = 3.8 \times 10^4\ M^{-1}\ cm^{-1}$ as for D_2O ice (2). For D_2O ice we had calculated $k = 4 \times 10^{12}\ M^{-1}\ s^{-1}$ at the same temperature (2), which is rather similar in view of the assumptions and imprecision involved. From the above assumptions about ε's for e^-_{ir}, $G(e^-_{ir})$ for H_2O ice at 73 K at mid-pulse is calculated to be 0.06, as compared to 0.11 for D_2O ice.

In order to provide further evidence that the weak infrared absorption seen in Fig. 2 is due to e^-_{ir}, the effect of accumulated dose was measured for pure H_2O ice and for samples doped with NH_4F; some results are shown in Fig. 4. The NH_4F causes a large increase in the initial yield of infrared absorption (about a factor of 8 at $7 \times 10^{-3}\ M$), and yields in the doped samples increase with accumulated dose whereas in the pure H_2O ice accumulated dose causes a small decrease in 1800 nm absorption at 100 ns. The decay rate of the absorption at 1800 nm was greatly reduced by the added NH_4F; for the conditions used to obtain the results of Fig. 4, the half-life for decay at 1800 nm from the time of maximum absorption was 170 ns in pure H_2O ice, whereas in the sample doped with $7 \times 10^{-3}\ M$ NH_4F there was about 5% decay in this time. These effects were found earlier for e^-_{ir} in D_2O ice, so there is no doubt that the infrared absorption seen in Fig. 2 is also due to e^-_{ir}.

H_2O Ice at 6 K

The spectra of irradiated H_2O ice at 6 K at 72 and 640 ns after a 40 ns pulse are shown in Fig. 5. A significant increase in infrared absorption with accumulated dose (about 25% for 10 pulses of 8 krad each) was noted; the spectra of Fig. 5 have been corrected for this effect by assuming the increase is linear with dose. Notable features of the spectra are that the ratio of infrared to visible absorption is

[3]Dr. G. Nilsson recently informed us that the value $\varepsilon_{max}(e^-_{aq})_{D_2O}/\varepsilon_{max}(e^-_{aq})_{H_2O} = 1.28$ given in Nilsson *et al.* (21) should have been 1.09 as calculated from the values given in the above text. This error is also present in our paper (22).

Can. J. Chem. Downloaded from www.nrcresearchpress.com by 210.87.254.6 on 09/06/12
For personal use only.

Can. J. Chem. Downloaded from www.nrcresearchpress.com by 210.87.254.6 on 09/06/12
For personal use only.

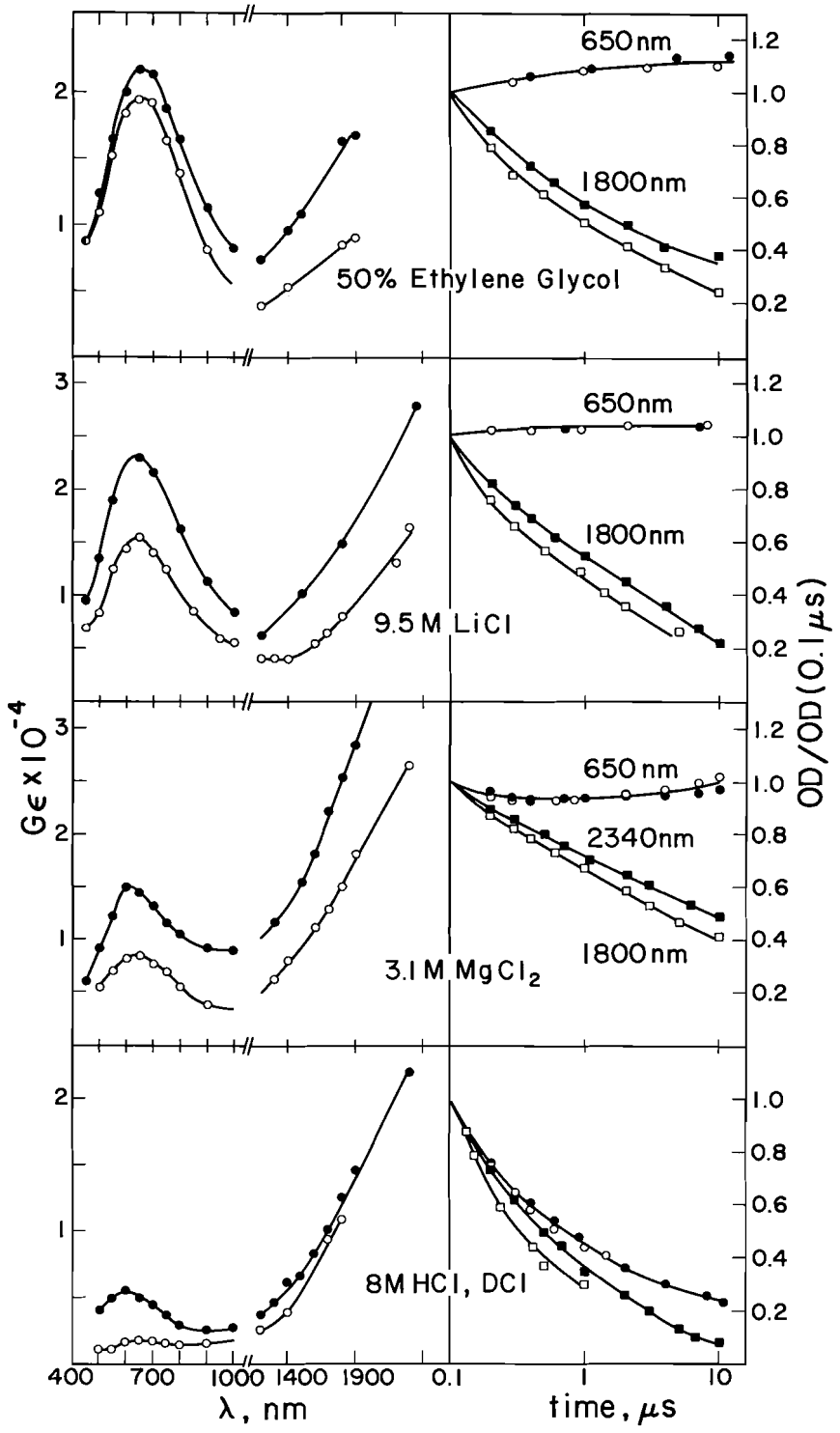

FIG. 1. Absorption spectra and decay kinetics of e^-_{vis} and e^-_{ir} in 50/50 ethylene glycol/water, 9.5 *M* LiCl/water, 3.1 *M* $MgCl_2$/water, and 8 *M* HCl/H_2O or 8 *M* DCl/D_2O glasses at 73 K. Open data points indicate H_2O glasses and filled points D_2O glasses. Absorption spectra were measured 100 ns after the start of a 40 ns pulse. The adjoining plots show representative values of the ratio of OD at a given time to the OD at 100 ns. The wavelength for each curve is indicated except for the HCl/H_2O, DCl/D_2O glasses where ○ and ● represent 650 nm, □ represents 1400 nm, and ■ represents 1900 nm. Note that a log scale is used for the time after the start of a 40 ns pulse.

Can. J. Chem. Downloaded from www.nrcresearchpress.com by 210.87.254.6 on 09/06/12
For personal use only.

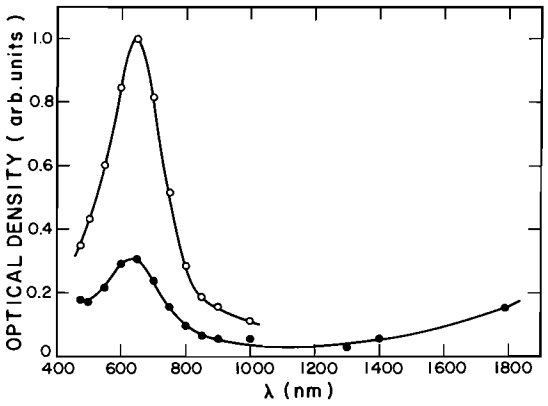

FIG. 2. Absorption spectra of irradiated crystalline H_2O ice at 73 K. ○, 51 ns after the start of a 40 ns pulse; ●, 142 ns after the start of the pulse and relative to the 51 ns spectrum.

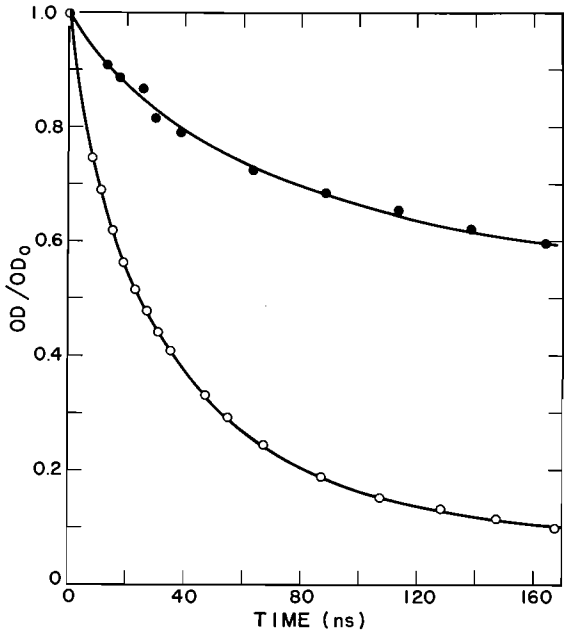

FIG. 3. Decay of absorption at 650 nm in crystalline ice at 73 K. ●, D_2O ice, pulse length 40 ns; ○, H_2O ice, pulse length 10 ns. Times are from mid-pulse.

much larger than at 73 K, the visible band decays very quickly considering the temperature ($t_{\frac{1}{2}}$ from mid-pulse ≃ 75 ns) and much more rapidly than the infrared band, and the shape of the accessible part of the infrared band is very different from the Lorentzian shape found for e^-_{ir} in D_2O ice at 73 K. The mid-pulse (pulse length of 40 ns) yields found for H_2O ice at 6 K are: for $\lambda = 650$ nm, $G\varepsilon = 5.1 \times 10^3$, very similar to the 5.3×10^3 found at 73 K; for $\lambda = 1800$ nm, $G\varepsilon = 3.3 \times 10^3$, as compared to 0.85×10^3 at 73 K. It is worth noting that our $G\varepsilon$ at 1800 nm for H_2O ice is much lower than that of 2.3×10^4

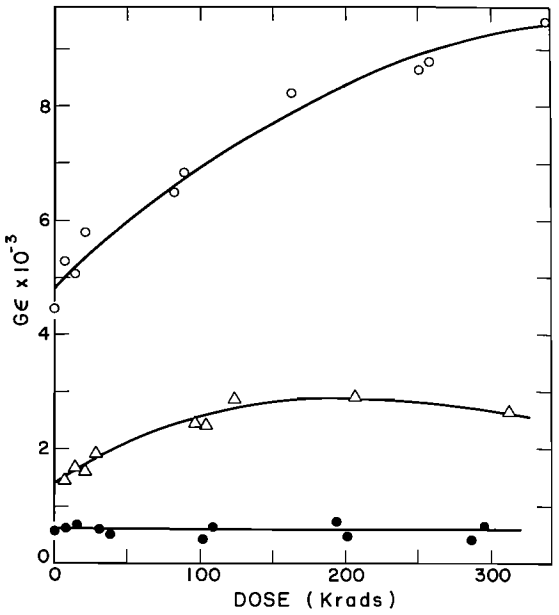

FIG. 4. Effect of accumulated dose on yields of e^-_{ir} in H_2O crystals at 73 K, measured at 1800 nm and 100 ns after the start of a 40 ns pulse. ●, no additive; △, doped with 1.1×10^{-4} *M* NH_4F; ○, doped with 7×10^{-3} *M* NH_4F. The concentrations refer to the melted crystals.

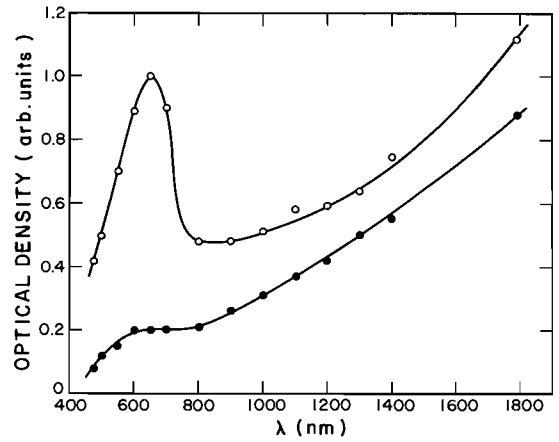

FIG. 5. Absorption spectra of irradiated crystalline H_2O ice at 6 K. ○, 72 ns after the start of a 40 ns pulse; ●, 640 ns after the start of the pulse and relative to the 72 ns spectrum.

recently published for D_2O ice at 6 K (11), but not very different from our results for D_2O ice at 6 K (23).

Discussion

Aqueous Glasses

If we assume that the values of ε_{650} and ε_{1800} are the same for D_2O glasses as for the corresponding H_2O glasses, then yields of both e^-_{vis} and e^-_{ir} are higher in all four D_2O glasses. If an effect of

Can. J. Chem. Downloaded from www.nrcresearchpress.com by 210.87.254.6 on 09/06/12
For personal use only.

deuterium substitution is to increase ε_{max} for e^-_{vis} by 9%, as it does in liquid water (9, 10), then the values of $G(e^-_{vis})$ are the same in protiated and deuterated ethylene glycol glasses, and remain higher in the D_2O glasses of the other pairs. As stated in the Results section, the lower yields ($G\varepsilon$'s) of e^-_{ir} at 100 ns in H_2O glasses could be due in part to slightly faster decay rates, rather than to smaller initial yields, but the 100 ns yields of e^-_{vis} are not subject to this reservation. In general substitution of H_2O by D_2O does not bring about the same percentage changes in yields of e^-_{vis} and e^-_{ir}. Thus in the ethylene glycol – D_2O glass values of $G\varepsilon$ of e^-_{vis} (at 650 nm) and e^-_{ir} (at 1900 nm) are larger by 12% and 87%, respectively, than the values in the corresponding H_2O glasses.

Stradowski and Hamill (12) found somewhat higher yields of e^-_{vis} in 8 *M* $NaClO_4$–D_2O glasses than in the corresponding H_2O glasses. They concluded that the initial yield of dry electrons in H_2O is slightly larger than in D_2O (13) but there is a significant isotope effect in the frequency of localization of dry electrons. They proposed that localization involves transferring to the lattice the binding energy of the dry electron as a vibrational excitation, probably through formation of H_2O^- or D_2O^-, and the cross-section for this process is smaller for D_2O. Thus localization would take place at a larger charge-pair radius in D_2O and Coulombic recombination of the localized electron, before relaxation, would be less significant than in H_2O systems. An alternative explanation they offer is that H_2O^+ and D_2O^+ have large ranges, but localization of D_2O^+ (to form D_3O^+) is slower than that of H_2O^+ so that again localization takes place at a larger charge-pair radius in D_2O (12). Evidence has been presented which indicates that both e^-_{vis} and e^-_{ir} decay geminately in LiCl and $MgCl_2$ glasses (1, 14) and the mechanism is probably tunnelling, at least for e^-_{ir} (14). The rate of decay by tunnelling is very sensitive to the distance between reactive species (15, 16). The fact that the decay rates of e^-_{ir} in corresponding H_2O and D_2O glasses are very similar (Fig. 1) argues against localization taking place at different distances from spur centers. Decays of e^-_{vis} were not followed to a large enough extent to permit any conclusion about relative localization distances for this species. (The probable reason for the rapid decay of e^-_{vis} in HCl, DCl glasses is reaction with homogeneously distributed H_3O^+ and D_3O^+.)

Our apparently higher G's of localized electrons in D_2O glasses as compared to their H_2O analogues may be due to the same mechanism that causes $G(e^-_{aq})$ to be 12% larger in liquid D_2O than in liquid H_2O (17). Various possibilities have been suggested as that mechanism. Some time ago it was suggested that the longer relaxation time and higher viscosity of D_2O as compared to H_2O would mean a greater charge-pair radius and hence a smaller amount of fast recombination (18). Anbar and Meyerstein (17) argued against this hypothesis and instead proposed the production of excited states by the reaction of subexcitation electrons, with the isotope effect arising from deuterium substituted excited states having a higher probability of undergoing non-dissociative ionization as compared with dissociative processes. More recently Singh *et al.* (19) also proposed large isotope effects in reactions of vibrationally excited states, though their proposed reactions are different from those suggested by Anbar and Meyerstein. Our results do not enable us to comment on these mechanisms for the isotope effect on yields which involve excited states.

H_2O Ice

At 73 K the yields of both e^-_{vis} and e^-_{ir} in H_2O ice, though not determined very accurately, seem to be lower than in D_2O ice. Lowering the temperature to 6 K increases considerably the yield of e^-_{ir} in H_2O ice, just as it does in D_2O ice (11, 23). The failure of Hase and Kawabata (8) to find e^-_{ir} in H_2O ice at 4 K in γ-radiolysis must have been due to its disappearance before their earliest observation time, as they suggested (8).

The biggest isotope effect we have seen in ice is in the lifetime of e^-_{vis}; at 73 K the initial half-life for decay of e^-_{vis} is approximately 14 times longer in D_2O than in H_2O ice. Lowering the temperature to 6 K increases the lifetime slightly; for e^-_{vis} in H_2O ice we find $t_{\frac{1}{2}}$'s from mid-pulse of ~25 ns at 73 K (pulse length of ~20 ns) and ~75 ns at 6 K (pulse length of ~40 ns), though these are not strictly comparable because of the difference in pulse lengths. Such a small effect of temperature strongly suggests that e^-_{vis} decays by tunnelling. Kawabata *et al.* (11) found a first observable half-life of about 5 μs after a 0.6 μs pulse for e^-_{vis} in D_2O ice at 6 K, which indicates that at this temperature also, decay is much slower than in H_2O ice.

Earlier we suggested that e^-_{vis} in D_2O ice is produced by a quasi-free electron (e^-_{qf}) dropping into a radiation-produced vacancy (□) in the same spur, with the vacancy-producing reaction being either a spur neutralization:

$$(2\,D_2O^+ + 2\,e^-_{qf}) \longrightarrow (D + OD + D_2O^+ + e^-_{qf} + \square)$$

or decomposition of an excited molecule (2). The energy of neutralization or excitation would be converted into sufficient kinetic energy of the D

plus OD fragments to expel them some distance from the lattice site. Because of conservation of momentum, the hydroxyl radical would have 1/18 of the available energy in the case of H_2O and 1/10 of the energy in D_2O ice, so that in D_2O ice the OD would be further away from the vacancy (and hence e^-_{vis}) than would OH for H_2O ice. The difference would not be large, but if it is assumed that e^-_{vis} decays by reaction with hydroxyl radical by tunnelling (2), only a small difference is required to explain the difference in lifetimes of e^-_{vis} in H_2O and D_2O ice at 73 K. If there is no inefficiency in the reaction, the distance a an electron can tunnel in time t is given by:

$$a = a_0 + 2.26\,(15 + \log t)\,B^{-1/2}$$

where a is in Å, B is the binding energy of the electron in eV, and the constant a_0 accounts for the finite radii of the electron and its reaction partner (20). We take $B = 1.2$ eV, as has been assumed for 6 M NaOH glass at 77 K (20), and $a_0 = 5$ Å. For $t =$ 25 ns and 350 ns, $a = 20.2$ Å and 22.6 Å, respectively. Thus at 73 K if half the yield of e^-_{vis} is produced within 20.2 Å and 22.6 Å of the hydroxyl radical in H_2O and D_2O ice respectively, our observed difference in half-lives is accounted for.

1. G. V. Buxton, H. A. Gillis, and N. V. Klassen. Can. J. Chem. **54**, 367 (1976).
2. G. V. Buxton, H. A. Gillis, and N. V. Klassen. Can. J. Chem. **55**, 2385 (1977).
3. H. A. Gillis, G. G. Teather, and G. V. Buxton. Can. J. Chem. **56**, 1889 (1978).
4. N. V. Klassen, G. G. Teather, and F. Keiffer. Can. J. Chem. **57**, 1488 (1979).
5. H. Hase, M. Noda, and T. Higashimura. J. Chem. Phys. **54**, 2975 (1971).
6. J. T. Richards and J. K. Thomas. J. Chem. Phys. **53**, 218 (1970).
7. N. V. Klassen, H. A. Gillis, G. G. Teather, and L. Kevan. J. Chem. Phys. **62**, 2474 (1975).
8. H. Hase and K. Kawabata. J. Chem. Phys. **65**, 64 (1976).
9. E. M. Fielden and E. J. Hart. Radiat. Res. **33**, 426 (1968).
10. E. M. Fielden and E. J. Hart. Radiat. Res. **32**, 564 (1967).
11. K. Kawabata, G. V. Buxton, and G. A. Salmon. Chem. Phys. Lett. **64**, 487 (1979).
12. C. Stradowski and W. H. Hamill. J. Phys. Chem. **80**, 1431 (1976).
13. C. Stradowski and W. H. Hamill. J. Phys. Chem. **80**, 1054 (1976).
14. H. A. Gillis and D. C. Walker. J. Chem. Phys. **65**, 4590 (1976).
15. J. R. Miller. J. Chem. Phys. **56**, 5173 (1972).
16. S. A. Rice and M. J. Pilling. Prog. Reaction Kinet. **9**, 93 (1978).
17. M. Anbar and D. Meyerstein. *In* Radiation chemistry of aqueous systems. *Edited by* G. Stein. The Weizmann Science Press of Israel. 1968. p. 130.
18. D. A. Armstrong, E. Collinson, and F. S. Dainton. Trans. Faraday Soc. **55**, 1375 (1959).
19. A. Singh, W. J. Chase, and J. W. Hunt. Discuss. Faraday Soc. **63**, 28 (1977) and following general discussion.
20. J. R. Miller. J. Phys. Chem. **79**, 1070 (1975).
21. G. Nilsson, H. Christensen, P. Pagsberg, and S. O. Nielsen. J. Phys. Chem. **76**, 1000 (1972).
22. H. A. Gillis, G. G. Teather, and C. K. Ross. J. Phys. Chem. **84**, 1248 (1980).
23. Wu Zhennan, N. V. Klassen, G. G. Teather, and H. A. Gillis. To be published.

Can. J. Chem. Downloaded from www.nrcresearchpress.com by 210.87.254.6 on 09/06/12
For personal use only.

Metal derivatives of azoles. Part VII. Gold(I) derivatives of pyrazoles

GUIDO BANDITELLI, ANNA LAURA BANDINI, AND GIOVANNI MINGHETTI
Centro CNR, Istituto di Chimica Generale dell'Università, via Venezian 21, 20133 Milano, Italy
AND
FLAVIO BONATI
Istituto Chimico dell'Università, 62032 Camerino, Italy

Received July 15, 1980

GUIDO BANDITELLI, ANNA LAURA BANDINI, GIOVANNI MINGHETTI, and FLAVIO BONATI. Can. J. Chem. **59**, 1241 (1981).

Ligand displacement by a pyrazole on Me_2SAuCl afforded L_nAuCl (n = 1 or 2, and L = 3,5-Me_2pzH, 3(5)-Me-5(3)-PhpzH; n = 1, and L = pyrazole or 3,5-Me_2-4-(p-tolylazo)pyrazole), while Ph_3PAuCl, silver fluoborate, and ligand gave both $[(Ph_3P)Au(3,5\text{-}Me_2pzH)]BF_4$ and $[(Ph_3PAu)_2(\mu\text{-}3,5\text{-}Me_2pz\text{-}N,N')]BF_4$. With iodine the last compound underwent reaction on the bridging μ-azolato ligand yielding $[(Ph_3PAu)_2(\mu\text{-}3,5\text{-}Me_2\text{-}4\text{-}Ipz\text{-}N,N')]BF_4$. The possible structures are discussed on the basis of spectral data (ir; ^1H, ^{13}C, and ^{31}P nmr).

GUIDO BANDITELLI, ANNA LAURA BANDINI, GIOVANNI MINGHETTI et FLAVIO BONATI. Can. J. Chem. **59**, 1241 (1981).

Le déplacement du ligand par un pyrazole sur Me_2SAuCl conduit aux composés L_nAuCl (n = 1 ou 2, et L = 3,5Me_2pzH, 3(5)Me-5(3)PhpzH; n = 1 et L = pyrazole ou 3,5Me_2-4-(p-tolylazo)pyrazole); d'autre façon la reaction de Ph_3PAuCl avec $AgBF_4$ et le ligand conduit soit à $[(Ph_3P)Au(3,5\text{-}Me_2pzH)]BF_4$ soit à $[(Ph_3PAu)_2(\mu\text{-}3,5\text{-}Me_2pz\text{-}N,N')]BF_4$. Par l'action de iode sur le dernier composé se produit une reaction du ligand ponté, avec formation de $[(Ph_3PAu)_2(\mu\text{-}3,5\text{-}Me_2\text{-}4\text{-}Ipz\text{-}N,N')]BF_4$. Les possibles structures sont examinés d'aprés des données spectroscopiques (i.r.; ^1H, ^{13}C et ^{31}P rmn).

Introduction

During our investigation in the field of pyrazole[1] complexes and of pyrazolates, several gold derivatives of the pyrazolato anion were obtained, including the tri-, di-, and mononuclear species **A**, **B**, and **C**, where the ligand is either bi- or monodentate (1). The first type of compound, **A**, was obtained, *inter alia*, through reaction [1]

[1] $Me_2SAuCl + pzH + KOH = (1/n)[Au(pz)]_n + KCl + H_2O + Me_2S$

A reasonable intermediate of the reaction might be a complex of the neutral pyrazole, such as $(pzH)_nAuCl$, formed by displacement of the rather volatile Me_2S ligand. In the case of gold, however, no complex of a neutral pyrazole has been reported up to now, while much work has been carried out on the related copper and silver derivatives.

Indeed, in the case of copper, the published results are abundant, and include complexes with several copper(I) and copper(II) salts (2). Other papers report the copper(II) derivatives of various anionic or neutral substituted pyrazoles, such as polypyrazolylborates (3), bis-(1-pyrazolyl)methane (4), indazole and 5-aminoindazole (5), and even the ligand $(Ph_2PCH_2)_2Pt(3,5\text{-}Me_2pz\text{-}N)_2$ (6).

Many other data are available and include: spectra (7, 8), X-ray data (9), stability constants (10), enthalpies of dissolution and of formation (11), polarographic studies (12), the thermal behaviour of $Cu(PzH)_4(SO_4)\cdot H_2O$ (13), magnetic data (14), and the extraction of the metal by pyrazoles from acid solutions (15).

Much less work is available on silver derivatives of pyrazoles (2*b*, 2*c*, 5, 16–18) which include species such as $(pzH)_2Ag^+$ (19) or $[Ag(pz)]_n$ (20); some electrochemical investigations were also published (17, 19).

In the case of gold, the only published work concerns the use of 1-phenyl-3-methyl-4-fluoroacetylpyrazol-5-one in the extraction of gold(III) from irradiated platinum (21).

In this paper we report the first gold derivatives having neutral pyrazoles as ligands and some related compounds.

Results and Discussion

The complexes reported in this paper belong to three types: (*a*) neutral complexes with one pyrazole ligand, $[(pzH)AuCl]_m$ (**I**, **II**, **III**, and **IV**); (*b*) complexes with two molecules of pyrazoles, $(pzH)_2AuCl$ (**V** and **VI**), and (*c*) ionic, bicoordinated derivatives $[(Ph_3P)Au(pzH)]BF_4$ (**VII**). In addition, two new pyrazolato complexes of the type $[(Ph_3P)Au(\mu\text{-}pz)Au(PPh_3)]^+$ (**VIII** and **IX**), where the said anion is bridging, were identified during this investigation.

The complexes of the first type were obtained

[1]1-Unsubstituted pyrazole ($C_3H_4N_2$) is indicated by PzH, while pzH represents a pyrazole on which substituents may be present (e.g.: 3,5-Me_2pzH is 3,5-dimethylpyrazole).

0008-4042/81/081241-06$01.00/0
©1981 National Research Council of Canada/Conseil national de recherches du Canada

Can. J. Chem. Downloaded from www.nrcresearchpress.com by 210.87.254.40 on 09/06/12
For personal use only.

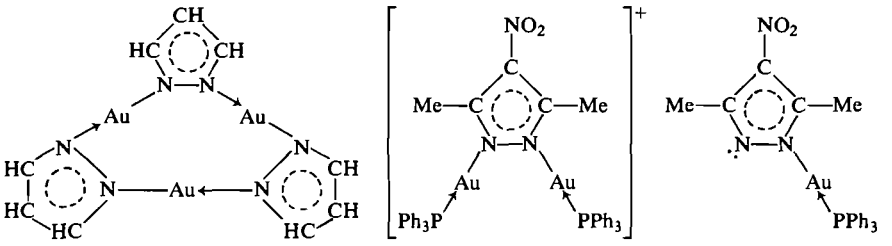

A B C

according to reaction [2]:

[2] $Me_2SAuCl + pzH = Me_2S + (1/m)[(pzH)AuCl]_m$

A few hours reflux in methylene chloride was required to displace the volatile dimethylsulphide. The reaction occurred with pyrazole, 3,5-Me_2-, 3,5-Me_2-4-(*p*-tolylazo)-, and 3(5)-Me-5(3)-PhpzH, yielding the complexes **I**, **II**, **III**, and **IV**, respectively, while when an electron-withdrawing substituent was present on the pyrazole ring, e.g. 3,5-Me_2-4-NO_2pzH (pK_{acid} 10.65 (22)), no adduct could be isolated, at least in the same conditions. In the case of 3(5)-Me-5(3)-PhpzH, the formation of the 1:1 adduct **IV** was accompanied by that of a 2:1 adduct, $(pzH)_2AuCl$, **V**. The latter, as well as the compound **VI**, could properly be obtained alone by carrying out the reaction with a ligand/Au ratio of two.

All the compounds (Table 1) are white solids (except **III**, yellow) which can be crystallized from organic solvents when freshly prepared. After standing for a few weeks, the 1:1 adducts may become insoluble, although, at least in the case of **I**, no change is observed in the infrared spectrum (4000–250 cm^{-1}). The analytical, spectroscopic, and conductivity data are reported in Tables 1–5 and at the end of the Experimental section.

The ionic compound containing two different neutral ligands, $[(Ph_3P)Au(3,5\text{-}Me_2pzH)]BF_4$, **VII**, was isolated as a by-product upon addition of the pyrazole to the CH_2Cl_2 extract obtained, after removal of AgCl, from the reaction of Ph_3PAuCl with silver fluoborate in methanol. The main product of the reaction was found to be $[(Ph_3P)Au(\mu\text{-}3,5\text{-}Me_2pz)Au(PPh_3)]BF_4$, **VIII**, i.e. a derivative of the bridging pyrazolato anion. In agreement with the behaviour of the species $[Au(\mu\text{-pz-}N,N')]_3$, **A**, previously observed (1), the sequence Au(μ-pz-*N*,*N*′)Au seems to be remarkably stable: indeed, the reaction of the complex **VIII** with iodine affords the corresponding 4-iodosubstituted derivative, **IX**, through an unusual reaction of a bridging ligand. In the phosphine containing compounds **VII** and **VIII** the coordination of the gold atoms is two: the complexes are 1:1 electrolytes in acetone solution, and both the ir spectrum in the solid state and the ^{19}F nmr spectrum (complex **VIII**) are in agreement with an uncoordinated tetrafluoborate anion (T_d). The ^1H (and ^{31}P) spectrum of the complex **VIII** shows unambiguously the presence of a symmetrically substituted exobidentate (i.e. bidentate and bridging) pyrazolato ligand.

The isolation of the compound **VIII** in the absence of any added alkali requires some comment. A scrutiny of the literature has revealed other cases where a (coordinated) pyrazole loses the 1-proton in apparently neutral conditions. Thus pyrazolato derivatives were obtained from the reaction of a diglyme solution of pyrazole complexes of copper(II) and elemental copper (2*c*), or from the reaction (23) between palladium(II) acetate and 3,5-Me_2pzH (pz′H). Furthermore, even in an acid medium, that is during attempted protonation with fluoboric acid of $Ph_3PAu(pz'')$ (pz″H = 3,5-Me_2-4-NO_2-pyrazole) a proton-free dimeric cation resulted, namely $[(Ph_3P)Au(\mu\text{-}pz'')Au(PPh_3)]^+$ (1). In the absence of contrary evidence, these reactions may be written as follows:

$$Cu(pzH)_4^{2+} + Cu = (2/n)[Cu(pz)]_n + 2pzH_2^+$$

$$2Pd(OAc)_2 + 4pz'H = [(pz'H)(AcO)Pd(\mu\text{-}pz')]_2 + 2AcOH$$

$$2Ph_3PAu(pz'') + 2H^+ = [(Ph_3P)Au(\mu\text{-}pz'')Au(PPh_3)]^+ + pz''H_2^+$$

The easy occurrence of deprotonation might be related to an increase, upon coordination, of the acidity of the N–H group. The donor bond from the nitrogen to the metal removes electron density from the ligand: the extent of the electron shift could be measured by the variation of the chemical shift in the ^{14}N nmr spectrum of the free and metal-coordinated pyrazole. Although such an experiment is out of our reach at the moment, recent data (24) on the ^{14}N nmr spectra of free and protonated pyrazole (i.e. coordination of H^+ instead of M^+) support this view.

The monomeric complexes of the type *b*, $(pzH)_2AuCl$, are an uncommon example of gold(I)

Can. J. Chem. Downloaded from www.nrcresearchpress.com by 210.87.254.40 on 09/06/12
For personal use only.

Can. J. Chem. Downloaded from www.nrcresearchpress.com by 210.87.254.40 on 09/06/12
For personal use only.

compounds stabilized by two neutral nitrogen ligands. Since they are non-electrolytes and are monomers in chloroform, they are likely to be three coordinated, at least in this solvent. Although their ir spectra (solid state) in the NH stretching region might suggest the presence of uncomplexed pyrazole, and although one of the two coordinated azoles is easily removed by donor solvents (see Experimental), the ^1H and ^{13}C nmr spectra in chloroform solution rule out a relevant amount of dissociation according to reaction [3]:

[3] $(pzH)_2AuCl = (1/m)[(pzH)AuCl]_m + pzH$

On the other hand the complexes do not display any tendency to coordinate further molecules of ligands to afford species such as $(pzH)_3AuCl$, as shown by the ^{13}C nmr spectrum of the mixture (1:1) of the compound **V** and of the ligand, where signals due to each component — and no averaged spectrum — are observed. In the ^1H and ^{13}C spectra of the complex **VI**, different signals are observed for the 3-Me and the 5-Me protons and for the C-3 and C-5 nuclei, respectively.

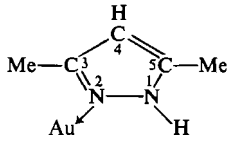

By analogy with the assignments made possible by $J(^{195}Pt\text{-}H)$ in the $[(Ph_2PCH_2)_2Pt(3,5\text{-}Me_2pzH\text{-}N)_2]^{2+}$ cation (25), in the ^1H nmr spectrum the signal at higher field is likely to be due to the 3-Me, the other one to the 5-Me group. In the case of the complex **V**, $(3,5\text{-}MePhpzH)_2AuCl$, the ^1H nmr spectrum shows two different methyl signals (partially overlapping, ca. 7:1), suggesting that both the possible coordination modes are present:

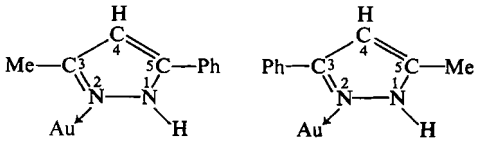

Thus, both the three coordinated species, **V** and **VI**, do not exhibit in the nmr time scale a dynamical behaviour, which, on the contrary, is observed in the case of the phosphine containing complex $[(Ph_3P)Au(3,5\text{-}Me_2pzH)]BF_4$, **VII**, as well as in pyrazole derivatives of other elements (26).

The 1:1 adducts of the type *a*, $[(pzH)AuCl]_m$, are likely to contain two coordinate gold(I), in agreement with the presence of a band at ca. 340 cm^{-1}, assigned to the terminal Au—Cl stretching vibration. However, the molecular weight determi-

TABLE 1. Analytical and other data

Compound		Decomp. range	Analyses C Found	C Calcd.	H Found	H Calcd.	N Found	N Calcd.	MW[a] Found	MW[a] Calcd.	Note
I,	(PzH)AuCl	105–106	12.3	12.0	1.36	1.33	9.2	9.3	—	300.5	[b]
II,	$(3,5\text{-}Me_2pzH)AuCl$	110–124	18.7	18.2	2.53	2.43	8.6	8.5	512	328.5	[c]
III,	$[3,5\text{-}Me_2\text{-}4\text{-}(p\text{-}MeC_6H_4N_2)pzH]AuCl$	200	32.2	32.2	3.22	3.13	12.4	12.5	892	446.5	[d]
IV,	$(3,5\text{-}MePhpzH)AuCl$	ca. 150	30.7	30.7	2.53	2.56	7.2	7.2	692	390.5	
V,	$(3,5\text{-}MePhpzH)_2AuCl$	ca. 100	44.0	43.8	3.76	3.65	10.0	10.2	509	548.5	[e]
VI,	$(3,5\text{-}Me_2pzH)_2AuCl$	From 106	27.4	28.3	3.67	3.77	12.6	13.2	404	424.5	
VII,	$[(Ph_3P)Au(3,5\text{-}Me_2pzH)]BF_4$	166–170	43.2	43.0	3.65	3.62	4.4	4.4	—	641.8	
VIII,	$[(Ph_3PAu)_2(\mu\text{-}3,5\text{-}Me_2pz)]BF_4$	ca. 220	44.8	44.7	3.38	3.18	2.4	2.5	—	1099.8	
IX,	$[(Ph_3PAu)_2(\mu\text{-}3,5\text{-}Me_2\text{-}4\text{-}Ipz)]BF_4 \cdot \frac{1}{2}Et_2O$	172	41.0	40.8	3.23	3.24	2.0	2.2	—	1264.4	[f]

[a] Molecular weight by osmometry in chloroform. See text.
[b] The compound became insoluble upon standing.
[c] Gold: found 59.5; calcd. 60.0. Chlorine: found 10.6, calcd. 10.8.
[d] Chlorine: found 7.9; calcd. 7.9.
[e] Gold: found 36.9; calcd. 36.0. Chlorine: found 7.0; calcd. 6.5.
[f] Evidence for ether is found in the nmr spectrum.

TABLE 2. Proton magnetic resonance data[a]

Compound	Solvent	Signals: Methyl groups	4-CH	NH	Aromatics	Note
II	$CDCl_3$	7.70[b], 7.65[b]	3.97	−2.12 br[c] −2.67 br[c]	—	[d]
II	CD_2Cl_2	7.68[e]	3.96	−1.99 br −2.60 br	—	—
III	$CDCl_3$	7.59[g]; 7.35[b], 7.28[b]	—	−2.4 br −3.0 br	2.78, 2.70, 2.36, 2.27	[f, h]
IV	$CDCl_3$	7.58[b], 7.51[b] [ca. 2:1]	3.48 br	−2.54[c] −3.12[c]	2.57–2.47 m, 2.34–2.18 m	—
IV	$(CD_3)_2CO$	7.59[b], 7.54[b]	3.08	[j]	2.64–2.32 m, 2.28–2.04 m	[i]
V	$CDCl_3$	7.88, 7.63 [ca. 7:1]	4.03	−4.74 br	2.73–2.44 m, 2.18–2.12 m	[k]
VI	$CDCl_3$	7.79, 7.65 [1:1]	4.36	−4.1 br[c]	—	[d]
VII	$CDCl_3$	7.60	3.89	ca. 0.6 br	2.67–2.17 m	—
VIII	$CDCl_3$	7.58	3.61	—	2.96–2.23 m	—
IX	$CDCl_3$	7.60	—	—	3.1–2.3 m	[l]

[a]τ units; room temperature. Signals are singlets unless otherwise stated; m = multiplet, br = broad.
[b]These signals overlap each other.
[c]It disappears upon deuteration.
[d]No shift of the signals upon dilution.
[e]6 Hz broad at half height.
[f]Sparingly soluble.
[g]*p*-Methyl by comparison with the spectrum of the ligand.
[h]A_2B_2 pattern for the aromatic signals.
[i]Not stable in acetone solution.
[j]Not detected.
[k]The same spectrum from +50°C to the freezing point.
[l]Et_2O: triplet at 8.80, quartet at 6.6τ, $J = 7$ Hz.

nations in chloroform solution show that the molecules do associate, independent support coming from the presence of two equally intense N—H signals in the proton nmr spectrum of **II** ($CDCl_3$ or CD_2Cl_2). The obvious possibility is that association occurs through hydrogen bond between N—H and a chlorine atom, but a simple intermolecular hydrogen bond to give extended chains is not supported by change upon dilution either in the infrared (3500–3000 cm^{-1}) or in the proton nmr spectrum. The nmr spectra of the compounds **II–IV** cannot be used in order to draw conclusions about the ways of attachment of the coordinated pyrazoles owing to the unknown nature of the intermolecular association established in solution. In the absence of additional data, such as an X-ray structure determination or Mössbauer spectra, it is not possible to state which is the structure of the complexes belonging to type *a*. It is remarkable that X-ray structural determinations of complexes of 1-unsubstituted pyrazoles have shown, in all cases (9*a*, 27), the presence of hydrogen bonding, sometimes of a rather uncommon type (28).

Experimental

General techniques and spectroscopic methods have been described previously (25). Analytical and other data are given in Table 1, ^1H and ^{13}C nmr data in Tables 2 and 3, infrared data in Table 4, and conductivity data in Table 5. All the analytical samples were pumped to constant weight (ca. 0.1 Torr, 20°C). Evaporation was always carried out under reduced pressure (water aspirator).

Freshly prepared Me_2SAuCl (29) should preferably be used because aged samples may cause catalytical decomposition with separation of a purple precipitate most likely to be colloidal gold.

While pyrazole was a commercial product, 3,5-dimethyl- (30), 3(5)-methyl-5(3)-phenyl- (31), and 3,5-dimethyl-4-(*p*-tolylazo)-pyrazole (32) were prepared according to the literature methods.

Preparation of the Compounds

(3,5-Dimethylpyrazole) chlorogold(I), II. A dichloromethane solution (50 mL) of (dimethylsulphide)chlorogold(I) (465 mg; 1.58 mmol) and 3,5-Me_2pzH (164 mg; 1.71 mmol) was refluxed for 2 h. The filtered solution was evaporated to dryness; the residue was washed with petroleum ether (50 mL; overnight; under stirring) and the solid (510 mg) was dissolved in diethyl ether (150 mL). Upon concentration to ca. 30 mL the colourless compound **II** (250 mg; 48%) was obtained. Additional compound (151 mg) was obtained upon addition of petroleum ether and concentration of the mother liquor.

The compounds **I**, **III**, and **V** were prepared analogously. The crude compound **III** was obtained by adding petroleum ether (60 mL) to the concentrated reaction mixture (15 mL) and was crystallized by concentration of its chloroform solution. The compound **I** was crystallized from CH_2Cl_2/petroleum ether. The compound **V** (or the compound **VI**) was prepared using a 2:1 ligand/Au ratio, and was isolated by precipitation with petroleum ether; if the precipitation was carried out with diethyl ether, compound **IV** was obtained. The same compound **IV** could also be obtained in the same way as **II** using a ligand/Au 1:1 ratio, but the yield was low because both **V** and unreacted Me_2SAuCl were also present.

(Triphenylphosphine)(3,5-dimethylpyrazole)gold(I) tetra-

Can. J. Chem. Downloaded from www.nrcresearchpress.com by 210.87.254.40 on 09/06/12
For personal use only.

Can. J. Chem. Downloaded from www.nrcresearchpress.com by 210.87.254.40 on 09/06/12
For personal use only.

TABLE 3. ^{13}C magnetic resonance data[a]

Compound	Signals			
	Methyl	C-4	Aryl	C-3 and C-5
V	14.3	102.1	125.8–129.9	144.8, 150.5
V + 3,5-MePhpzH	11.7, 14.3	102.0	125.8–129.3	142.8, 149.2, 144.8, 150.2
3,5-MePhpzH	11.6	102.0	125.7–132.5	143.1, 149.8
VI	11.0, 14.0	140.6	—	149.7, 142.1
3,5-Me_2pzH	12.1	103.8	—	144.0 broad

[a]δ values from internal Me_4Si, $CDCl_3$ solution, room temperature.

TABLE 4. Relevant infrared data[a]

Compound	ν(N—H)	ν(C—H)$_{pyrazole}$	1500–1600 cm^{-1}	ν(Au—Cl) region
I	3240 s	3135 m, 3104 m, 3096 m	1514 m	340 s
II[b]	3190 s, broad	3140 s, 3110 s	1575 s	340 m
III	3170 s	3121 s, 3105 sh	1596 s, 1579 s	347 s, 332 sh, 322 sh
IV	3150 vs, broad	[c]	1565	338 w
V	3300–2500	[c]	1570 m, asymm.	340 m, 330 m
VI	3600–2400	[c]	1575 s	Not observed
VII	3260	3129	1573 s	1050 s, br[d]
VIII	—	Not observed	1530 m	1050 vs, broad[d]

[a]Nujol mull.
[b]The spectrum did not change when recorded in $CHCl_3$ solution; no change also upon 1:3 dilution of the solution.
[c]Covered by the broad N—H stretching vibrations.
[d]Band due to the BF_4^- anion.

TABLE 5. Conductivity data[a]

Compound	T (°C)	Solvent	Concentration (10^{-4} M)	Conductivity (ohm^{-1} cm^2 mol^{-1})
IV[b]	19	CH_2Cl_2	15.6	0.14
V	19	CH_2Cl_2	4.1	0.31
V	19	Acetone	11.2	9.64
VI	19	CH_2Cl_2	14.1	0.33
VII	17	Acetone	1.1	125.9
VIII	19	Acetone	0.7	139.6
VIII	24	MeOH	0.77	91.4

[a]The resistance of a CH_2Cl_2 solution of the compound **II** or of an acetone solution of the compound **III** was too high to be measured.
[b]The acetone solution of the compound is not stable but, in any case, it is not conducting.

fluoroborate, **VII**, and bis[triphenylphosphinegold(I)](μ-3,5-dimethylpyrazolato-*N*,*N'*) tetrafluoroborate, **VIII**. Solid triphenylphosphinechlorogold(I) (460 mg; 0.93 mmol) was added to a methanol solution of silver fluoroborate (181 mg; 0.93 mmol). After 75 min of stirring, the filtered solution was evaporated to dryness. The oily residue was extracted with dichloromethane (80 mL) and 3,5-Me_2pzH (91 mg; 0.95 mmol) was added to the solution. After standing overnight, the solution was concentrated to ca. 20 mL and, upon addition of diethyl ether (50 mL), a precipitate formed slowly (190 mg) which was crystallized from CH_2Cl_2/Et_2O (5 + 50 mL) affording the compound **VIII** (154 mg). The first mother liquor was evaporated to dryness, and the residue was stirred under Et_2O till the oily part disappeared; the crystals (130 mg) present in the resulting solid were hand-picked under a microscope, thus affording the compound **VII**.

Compound ***IX***. To a chloroform solution (20 mL) of the compound **VIII** (73 mg; 0.066 mmol) iodine (16.8 mg; 0.066 mmol) in the same solvent (2 mL) was added. The residue after evaporation was washed with diethyl ether (2 × 50 mL), and filtered, affording **IX** (32 mg), which showed a strong ir absorption at 1050 cm^{-1}, typical of tetrahedral BF_4^- anion.

Additional nmr Data

In addition to the data reported in Tables 2 (^1H) or 3 (^{13}C), compound **VIII** showed in the ^{31}P nmr spectrum one signal at 31.55 ppm downfield from external 85% H_3PO_4, and in the ^{19}F nmr spectrum a signal at 154.8 ppm upfield from internal $CFCl_3$; both spectra were recorded in $CDCl_3$ solution at room temperature and were decoupled.

1. G. MINGHETTI, G. BANDITELLI, and F. BONATI. Inorg. Chem. **18**, 658 (1979); F. BONATI, G. MINGHETTI, and G. BANDITELLI. J. Chem. Soc. Chem. Commun. 88 (1974).
2. (*a*) K. FUKUSHIMA, A. KOBAYASHI, T. MIYAMOTO, and Y. SASAKI. Bull. Chem. Soc. Jpn. **49**, 143 (1976); (*b*) K. FUKUSHIMA, T. MIYAMOTO, and Y. SASAKI. Inorg. Chim. Acta, **15**, 105 (1975); (*c*) H. OKKERSEN, W. L. GROENEVELD, and J. REEDIJK. Recl. Trav. Chim. **92**, 945 (1973); J. REEDIJK. Recl. Trav. Chim. **88**, 1451 (1969); **89**, 605 (1970); J. REEDIJK and J. A. SMIT. Recl. Trav. Chim. **90**, 1135 (1971); D. NICHOLLS and B. A. WARBURTON. J. Inorg. Nucl. Chem. **33**, 1041 (1971); N. D. PHUNG, J.-C. TEDENAC, and M. MAURIN. J. Inorg. Nucl. Chem. **38**, 2316

(1976); M. INOUE, M. KISHITA, and M. KUBO. Inorg. Chem. **5**, 626 (1965); N. A. DAUGHERTY and J. H. SWISHER. Inorg. Chem. 7, 1651 (1968); L. I. KUZNESOVA, A. D. GARNOVSKII, O. A. OSIPOV, A. M. SLADKOV, I. R. GOLDING, and V. G. ZALETOV. Chem. Abstr. **90**, 80190h (1979).
3. A. M. ABU SALAH, M. I. BRUCE, and J. D. WALSH. Aust. J. Chem. **32**, 1209 (1979).
4. J. REEDIJK and J. VERBIEST. Transit. Met. Chem. **4**, 239 (1979); Chem. Abstr. **92**, 51142e (1980).
5. S. A. A. ZAIDI and A. S. FAROOQI. J. Inorg. Nucl. Chem. **35**, 4320 (1973); J. B. COTTON and J. R. SCHOLES. Br. Corros. J. **2**, 1 (1967).
6. A. L. BANDINI, G. BANDITELLI, G. MINGHETTI, and F. BONATI. Can. J. Chem. **57**, 3237 (1979).
7. J. REEDIJK. Recl. Trav. Chim. **90**, 117 (1971).
8. J. REEDIJK. Recl. Trav. Chim. **89**, 993 (1970).
9. (*a*) V. AGRE, I. A. KROL, V. K. TRUNOV, V. M. DZIOMKO, and O. V. IVANOV. Koord. Khim. **5**, 1406 (1979); (*b*) R. H. P. FRANCISCO, J. R. LECHAT, and Y. P. MASCARENHAS. Acta Crystallogr. B, **35**, 1468 (1979); C. BRASSY, J.-P. MORNON, J. DELETTRE', and J. LEPICARD. Acta Crystallogr. B, **30**, 2500 (1974); C. BRASSY, A. RENARD, J. DELETTRE', and J.-P. MORNON. Acta Crystallogr. B, **30**, 2246 (1974); F. VALACH, J. KOHOUT, M. DUNAJ-JURČO, M. HVASTIJOVÁ, and J. GAŽO. J. Chem. Soc., Dalton Trans. 1867 (1979).
10. B. LENARCIK and J. KULIG. Pol. J. Chem. **52**, 2089 (1978); Chem. Abstr. **90**, 93244d (1979); B. LENARCIK, K. NABIALEK, and M. GABRISZENSKI. Pol. J. Chem. **52**, 401 (1978); Chem. Abstr. **89**, 31697*z* (1978).
11. M. S. BARVINOK and L. G. LUKINA. Zh. Neorg. Khim. **23**, 2406 (1978); **22**, 2167 (1977).
12. D. R. CROW and P. K. AGGARWAL. Electrochim. Acta, **19**, 309 (1974); D. R. CROW and J. V. WESTWOOD. J. Inorg. Nucl. Chem. **30**, 179 (1968).
13. A. ANAGNOSTOPOULOS, D. NICHOLLS, and K. R. SEDDON. J. Inorg. Nucl. Chem. **36**, 2235 (1974).
14. J. C. VAN OOIJEN and J. REEDIJK. J. Chem.Soc., Dalton Trans. 1170 (1978).
15. V. M. DZIOMKO, V. N. AVILINA, and O. V. IVANOV. Tr. Vses. Nauchno-Issled. Inst. Khim. Reakiv, Osobo Chist. Khim. Veshchestv. No. 32, 34 (1970); Chem. Abstr. **76**, 158956*v* (1972).
16. R. H. P. FRANCISCO, Y. P. MASCARENHAS, and J. R. LECHAT. Acta Crystallogr. B, **35**, 117 (1979).
17. S. N. PODDAR, S. GHOSH, S. M. BATTACHARYYA, and S. R. CHAUDHURI. J. Inorg. Nucl. Chem. **39**, 739 (1977); S. N. PODDAR, S. M. BATTACHARYYA, and S. R. CHAUDHURI. Indian J. Chem. **12**, 754 (1974); Chem. Abstr. **82**, 8223*p* (1974).
18. A. M. ABU SALAH, G. S. ASHBY, M. I. BRUCE, E. A. PEDERZOLLI, and J. D. WALSH. Aust. J. Chem. **32**, 1613 (1979).
19. A. S. WHEELER and R. D. NORTON. J. Am. Chem. Soc. **50**, 2488 (1928).
20. H. REIMLINGER, A. NOELS, and J. JADOT. Chem. Ber. **103**, 1949 (1970).
21. S. M. HASANY and I. HANIF. J. Radioanal. Chem. **47**, 47 (1978); Chem. Abstr. **90**, 47821*s* (1979); S. M. HASANY, I. HANIF, and I. H. QURESHI. Int. J. Appl. Radiat. Isot. **29**, 145 (1978); Chem. Abstr. **89**, 96341 (1978).
22. C. L. HABRAKEN, P. C. M. VAN WOERKOM, H. C. DE WIND, and C. G. M. KALLENBERG. Recl. Trav. Chim. **85**, 1191 (1966).
23. J. POWELL and A. KUKSIS. Can. J. Chem. **57**, 2986 (1979).
24. I. I. SCHUSTER, C. DYLLICK-BRENZINGER, and J. D. ROBERTS. J. Org. Chem. **44**, 1765 (1979).
25. G. MINGHETTI, G. BANDITELLI, and F. BONATI. J. Chem. Soc. Dalton Trans. 1851 (1979).
26. N. F. BORKETT and M. I. BRUCE. J. Organomet. Chem. **65**, C51 (1974).
27. A. D. MIGHELL, C. W. REIMANN, and A. SANTORO. Acta Crystallogr. B, **25**, 595 (1969); J. REEDIJK, B. A. STORK-BLAISSE, and G. C. VERSCHOOR. Inorg. Chem. **10**, 2594 (1971); I. A. KROL, V. M. AGRE, V. K. TRUNOV, N. V. RANNEV, O. V. IVANOV, and V. M. DZIOMKO. Koord. Khim. **5**, 126 (1979); Chem. Abstr. **90**, 131044*y* (1979); I. A. KROL, V. M. AGRE, V. K. TRUNOV, and O. I. IVANOV. Koord. Khim. **5**, 1569 (1979); Chem. Abstr. **92**, 13921*a* (1980).
28. J. REEDIJK, J. C. JANSEN, H. VAN KONINGSVELD, and G. C. VAN KRALINGEN. Inorg. Chem. **17**, 1990 (1978).
29. F. BONATI and G. MINGHETTI. Gazz. Chim. Ital. **103**, 373 (1973).
30. R. H. WILEY, and P. E. HEXNER. Org. Synth. **31**, 43 (1951).
31. K. VON AUWERS and H. STUHLMANN. Chem. Ber. **59**, 1043 (1926).
32. C. BULOW and W. SPENGLER. Chem. Ber. **58**, 1375 (1925).

Can. J. Chem. Downloaded from www.nrcresearchpress.com by 210.87.254.40 on 09/06/12
For personal use only.

Reactions of phthalans with dienophiles. III. Formation of homoquinones by reaction of 1,1-diethoxyphthalans with quinones

LUIS CONTRERAS, DAVID B. MACLEAN, ROMOLO FAGGIANI, AND COLIN J. L. LOCK

Department of Chemistry, McMaster University, Hamilton, Ont., Canada L8S 4M1

Received August 26, 1980

LUIS CONTRERAS, DAVID B. MACLEAN, ROMOLO FAGGIANI, and COLIN J. L. LOCK. Can. J. Chem. **59**, 1247 (1981).

Treatment of 1,1-diethoxyphthalan with 1,4-benzoquinone gave the homoquinone, ethyl 2-[(1′R*,6′S*,7′S*)-2′,5′-dioxo-3′-norcaren-7′-yl]benzoate, **3**, instead of an anthracene derivative expected of a normal cycloaddition reaction. The structure of the homoquinone was deduced from an examination of its spectroscopic properties (ir, ^{1}H nmr, and ^{13}C nmr) and verified by an X-ray crystallographic study. The homoquinone, **3**, is triclinic, $P\bar{1}$, with $a = 10.601(2)$, $b = 10.434(3)$, $c = 6.491(3)$ Å, $\alpha = 105.53(3)$, $\beta = 95.21(2)$, $\gamma = 100.66(2)°$ and has two formula units per unit cell. The crystal structure was determined by direct methods and refined to $R_1 = 0.059$, $R_2 = 0.048$, based on 2378 independent reflections. The data set was obtained using a Syntex $P2_1$ diffractometer and MoKα radiation. Bond angles and distances within the molecule are normal. Homoquinones were also isolated as major products of reaction of 1,1-diethoxyphthalan and 5,6-dimethoxy-1,1-diethoxyphthalan with 1,4-benzoquinone and 1,4-naphthoquinone. A mechanism for the formation of homoquinones is offered that involves the same type of transient intermediates proposed for the reactions of 1,1-diethoxyphthalans with activated acetylenes and ethylenes.

LUIS CONTRERAS, DAVID B. MACLEAN, ROMOLO FAGGIANI et COLIN J. L. LOCK. Can. J. Chem. **59**, 1247 (1981).

La diéthoxy-1,1 phtalane réagit avec la benzoquinone-1,4 en donnant l'homoquinone, soit le [(1′*R**,6′*S**,7′*S**)dioxo-2′,5′-norcarène-3′ yl-7′]-2 benzoate d'éthyle (**3**) au lieu du dérivé de l'anthracène attendu dans une réaction normale de cycloaddition. On a déduit la structure de l'homoquinone à partir de ses spectres (ir, rmn du ^{1}H et du ^{13}C) et on l'a vérifié par diffraction de rayons-X. L'homoquinone **3** est triclinique, $P\bar{1}$, avec $a = 10{,}601(2)$, $b = 10{,}434(3)$, $c = 6{,}491(3)$Å, $\alpha = 105{,}53(3)$, $\beta = 95{,}21(2)$, $\gamma = 100{,}66(2)°$ et deux unités par maille. On a déterminé la structure du cristal par des méthodes directes et on l'a affinée jusqu'à des valeurs de $R_1 = 0{,}059$ et de $R_2 = 0{,}048$ en se basant sur 2378 réflexions indépendantes. On a obtenu l'ensemble des données en utilisant un diffractomètre de type Syntex $P2_2$ et une radiation MoKα. Les angles et les longueurs de liaison de la molécule sont normaux. L'homoquinone est également le produit principal de la réaction du diéthoxy-1,1 phtalane et des diméthoxy-5,6 diéthoxy-1,1 phtalane avec la benzoquinone-1,4 et la naphtaquinone-1,4. On propose un mécanisme de la réaction de formation de l'homoquinone qui fait intervenir des intermédiaires semblables à ceux dont l'existence a été proposée dans les cas des réactions des diéthoxy-1,1 phtalanes avec les acétylènes et éthylènes activés.

[Traduit par le journal]

In two previous papers in this series (1, 2) phthalans have been shown to react with acetylenic and ethylenic dienophiles to yield substituted naphthalenes or dihydronaphthalenes. In its reaction with activated acetylenes and ethylenes it has been proposed that 1,1-diethoxyphthalan **1** yields, on heating, an isobenzofuran as a transient intermediate which undergoes cycloaddition reactions with dienophiles (Scheme 1). In an extension of this study to carbocyclic dienophiles we treated 1,1-diethoxyphthalan with *p*-benzoquinone. Instead of the anthracene derivative expected from a cycloaddition reaction we isolated a new compound which proved to be a homoquinone derivative (3–5). The structure of this compound (**3**, $C_{16}H_{14}O_4$, formed in 30% yield) was assigned on the basis of its spectroscopic properties (ir, ^{1}H nmr, ^{13}C nmr) and confirmed by an X-ray crystallographic investigation (*vide infra*).

The ir spectrum of **3** showed two carbonyl bands, one at 1715 cm^{-1} assigned to a conjugated ester, and the second at 1685 cm^{-1}, assigned to the two carbonyl groups in the enedione system (6). The presence of an ester function was the first indication that the reaction product was not an anthracene derivative.

The ^{1}H nmr spectrum of **3** showed peaks at 1.37 δ (t, 3H) and 4.38 δ (q, 2H) corresponding to the methyl and methylene groups, respectively, of an ethoxy group in an ester function. The absorption of the methine protons, H-1′ and H-6′, was assigned to a doublet at 2.83 δ ($J = 5.4$ Hz). The methine proton at H-7′ appears as a triplet at 4.02 δ ($J = 5.4$ Hz) because of coupling to the equivalent protons, H-1′ and H-6′. The equivalence of H-1′ and H-6′ is attributed to the fact that the molecule has a symmetry plane that bisects the cyclopropane ring when the aromatic ring adopts a conformation that is at right angles to the homoquinone system. The configuration of the cyclopropane ring was assigned on the basis of the value of the coupling constant between the equivalent protons H-1′ and H-6′ and the proton of H-7′. In analogous systems, Yogev *et al.* (5) have reported values for J_{cis} in the range 9.3–10.0 Hz, and J_{trans} in the range 5.0–5.4 Hz. Clearly the coupling observed in **3** is consistent only with a *trans* relationship between the equivalent protons, H-1′ and H-6′, on the one

0008-4042/81/081247-10$01.00/0

©1981 National Research Council of Canada/Conseil national de recherches du Canada

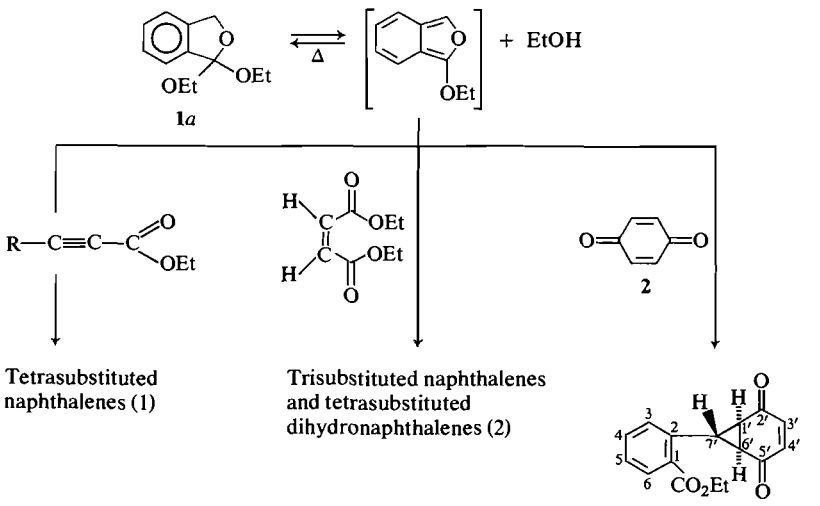

SCHEME 1

hand, and H-7′ on the other. The olefinic protons of the enedione appeared as a singlet at 6.60 δ. The aromatic protons showed two multiplets, the first centred at 7.40 δ of area 3 attributed to H-3, H-4, and H-5 and the second of area one at 8.05 δ attributed to H-6.

In the ^{13}C nmr spectrum of **3** there were four signals in the aliphatic region. The resonances at 61.5 (t) and 14.3 (q) δ, were assigned, respectively, to the methylene and methyl carbons of the ethoxy group. Two other signals at 35.8 and 36.6 δ were assigned to C-1′ and C-6′ and C-7′, respectively. The lower field signal was the more intense and assigned therefore to the two equivalent carbon atoms at C-6′ and C-7′. The signal at 138.0 δ (d) was attributed to the two ethylenic carbon atoms at C-3′ and C-4′ and that at 193.5 δ to the two carbonyl groups of the enedione. The ester carbonyl resonated at 166.4 δ. Other signals, attributed to aromatic carbon atoms appeared at 127.0 (d), 128.0 (d), 131.5 (d), 131.5 (s), 132.5 (d), and 137.3 (s) but have not been definitively assigned.

The spectroscopic data indicated strongly that **3** has the structure illustrated in Scheme 1 and this was verified through an X-ray crystallographic study described later.

The reactions of other quinones with phthalans have been investigated. Thus, when **2** was treated with **1*b*** the major product of reaction was homoquinone **4** accompanied by a small amount of its isomer **5**. Next we examined the reaction of 1,4-naphthoquinone **6** with both **1*a*** and **1*b*** and again homoquinones were formed as major products of the reaction. Two isomeric homoquinones **7** and **8** were obtained from the reaction of **1*b*** and **6** while homoquinone **9** and 2-(2′-carboethoxybenzyl)-1,4-naphthoquinone **10** were isolated from the reaction of **1*a*** with **6**. The structures of the homoquinones were deduced from a knowledge of their compositions and by comparison of their spectroscopic properties with those of **3** of established structure and relative configuration.

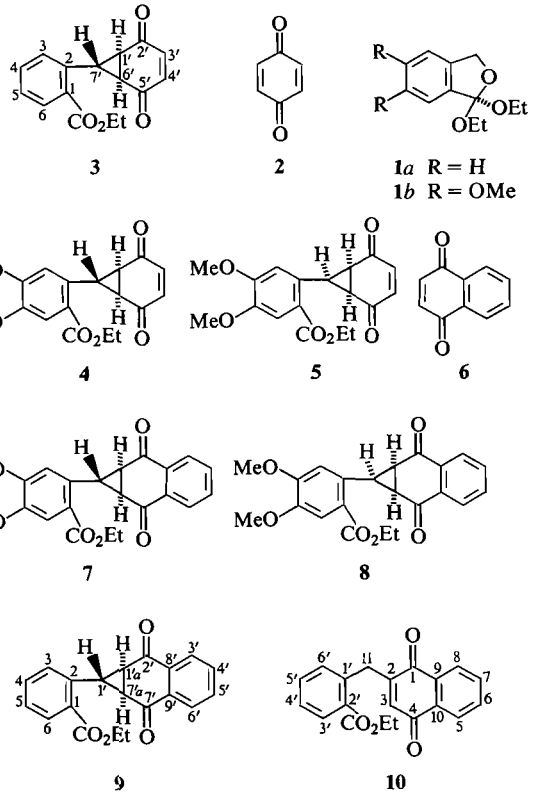

TABLE 1. ^{1}H nmr chemical shifts and coupling constants of the cyclopropyl protons of *p*-homoquinones

Compound	H-1′,6′	H-7′	H-1′a,7′a	H-1′	Coupling constant (Hz)	
3	2.83	4.02			$^3J_{1',7'}$	5.4*
4	2.77	3.97			$^3J_{1',7'}$	5.3*
5	2.87	3.55			$^3J_{1',7'}$	9.0*
7			2.96	3.83	$^3J_{1',7'a}$	5.3†
8			3.10	3.70	$^3J_{1',7'a}$	9.8†
9			3.01	3.85	$^3J_{1',7'a}$	5.3†

*$J_{1',7'} = J_{6',7'}$
†$J_{1',7'a} = J_{1'1'a}$

The infrared spectra of compounds **4**, **5**, **7**, **8**, and **9**, like the spectrum of **3**, showed two characteristic bands in the carbonyl region, the first in the range 1710–1725 cm^{-1}, attributed to the ester group, and the second in the range 1675–1685 cm^{-1}, ascribed to the two carbonyl groups of the enedione system (6). The ^{1}H nmr spectrum of **3** has already been discussed in detail and is used as a reference compound in making assignments to the new homoquinones. The resonances of the cyclopropyl protons of **3** are recorded in Table 1 along with those of other homoquinones prepared in this study. It is evident from examination of this table that compounds **4**, **7**, and **9** have the same relative configuration of protons about the cyclopropane ring and that this corresponds to the *trans* arrangement of the benzylic proton to the bridgehead protons as already established for **3**. Compounds **5** and **8** on the other hand have the *cis* arrangement. The coupling constants of similar systems have been examined previously (5, 7, 8) and are in accord with these assignments. The ^{13}C nmr spectra in the cyclopropyl region and in the carbonyl region were also examined and the resonances are recorded in Table 2. Again it is evident that there is a high degree of correspondence among the five compounds examined. Other ^{1}H and ^{13}C resonances of the compounds are listed in the Experimental and assignments made where justified. From these data it is evident that the five new compounds of this study are phenyl substituted homoquinones that carry an *ortho* carboethoxy group on the phenyl ring. Two of them, **5** and **8**, differ from the others in the stereochemistry of the cyclopropane ring. Other differences are a consequence of the starting materials employed.

TABLE 2. ^{13}C nmr chemical shifts of *p*-homoquinones*

	Compound				
Carbon	**3**	**4**	**7**	**8**	**9**
*CO*OEt	166.4	166.2	166.8		166.8
C-2′,5′	193.5	193.5			
C-2′,7′			193.3	193.0	192.2
C-1′,6′	35.8	36.0			
C-7′	36.3	36.8			
C-1′a,7′a			36.7	34.0	36.4
C-1′			36.4	34.4	36.0

*The two bridgehead carbons were differentiated from the benzylic carbon in all cases on the basis of signal intensity.

Compound **10** shows an ir absorption in the carbonyl region similar to the homoquinones but is readily differentiated from them on the basis of nmr data. The ^{1}H nmr spectrum of **10** has a number of signals which are similar to those of **9**. The methyl and methylene protons of the carboethoxy group appear at 1.28 and 4.26 δ, respectively. The aromatic region has three multiplets, the first is centered at 7.41 δ for 3H, the second at 7.73 δ for 2H, and the third centered at 8.10 δ for 3H. The major difference between **10** and **7**, **8**, and **9** is the absence of signals associated with the cyclopropane ring and the appearance of two new signals. The first is at 4.30 δ of area 2 and the other at 6.28 δ of area 1H, both of which showed a small coupling. Irradiation of the 4.30 peak produced a sharpening of the signal at 6.28. This suggests the presence of allylic coupling between the olefinic proton at 6.28 δ and the benzylic methylene protons at 4.30 δ. The presence of a methylene carbon atom was confirmed by the ^{13}C nmr spectrum of **10** which showed a signal at 34.3 ppm. This signal appeared as a triplet in the off-resonance spectrum. The aliphatic region also showed signals for the methyl and methylene carbon atoms of the ethoxy group at 14.2 and 61.0 ppm, respectively, but no other signals were present. The low field region had three signals; the first at 166.8 ppm corresponding to the carbonyl carbon atom of the ester group, and the other two at 185.0 and 185.2 ppm attributed to the nonequivalent naphthoquinone carbonyl carbon atoms. The remaining signals for the aromatic and the vinyl carbon atoms are listed in the Experimental but not assigned.

The formation of the products discussed above can be rationalized on the basis of the reactions outlined in Scheme 2 in which the reaction between

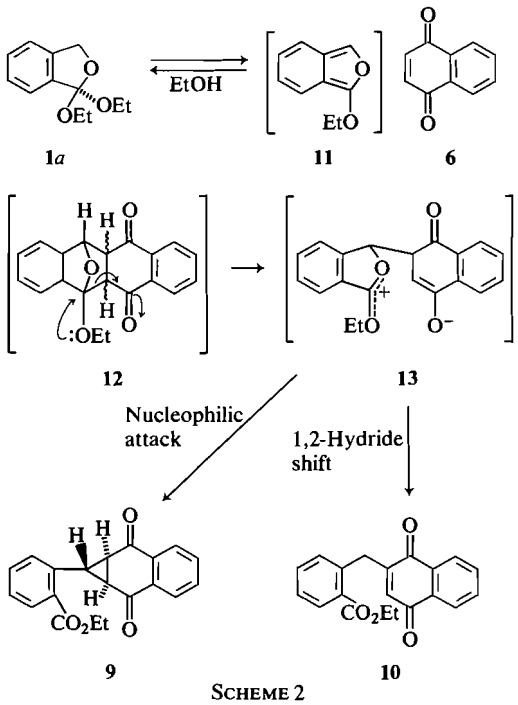

1*a* 11 6

12 13

9 10

SCHEME 2

1*a* and **6** is depicted. Intermediate **11** is considered to add to the quinone in a normal manner yielding **12**. The intermediate **12** may then undergo simultaneous C—C bond cleavage and enolization to form the zwitterion **13**. This may collapse to **10** by a 1,2 hydride shift with simultaneous C—O bond cleavage. Alternatively, this zwitterion may undergo intramolecular nucleophilic substitution by attack of the enol at the benzylic carbon atom to give *cis* ring fused *p*-homoquinone **9**. The major isomer in these reactions has the benzylic hydrogen *trans* to the bridgehead hydrogens. This would be the result expected if the adduct **12** had the *endo configuration. A cis* arrangement of all hydrogens would be the result from an *exo* adduct undergoing a similar series of reactions.

Another possible route to products beginning from **13** is outlined in Scheme 3. In this case, it is proposed that **13** is transformed to zwitterion **14***a* or **14***b*. The intermediate **14***a* may then collapse by

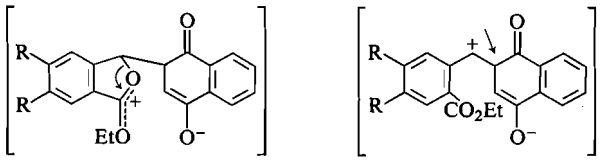

13*a* R = H
13*b* R = OMe

14*a* R = H
14*b* R = OMe

14*a* → **9** + **10**
14*b* → **7** + **8**

SCHEME 3

1,2 hydride shift and ketonization to **10** or by attack of the enolic carbon at the benzylic carbon to homoquinone **9**. In the case of **14***b*, collapse to a mixture of **7** and **8** would occur. The *trans* isomer is sterically less crowded than the *cis* isomer and would be expected to predominate. Thus, there would be no dependence of the isomer ratio on the original *endo–exo* ratio in the addition of **11** to **6**.

Similar types of C—C bond cleavage, followed by enolization as shown in Scheme 2, have been reported before. For example, it is known that compounds in the tetracycline family such as chlorotetracycline **15** (Scheme 4) undergo rearrangement to phthalide derivatives called isotetracyclines, e.g. isoaureomycin **17**, when they are treated with aqueous base under mild conditions (9). The rearrangement is initiated by nucleophilic attack of the C-6 hydroxy group on the C-11 ketone to give the hemiketal intermediate **16**. This intermediate now undergoes C—C bond cleavage and enolization to isoaureomycin **17**.

Another example comes from the work of Eugster and Bosshard (10) who have reported that the addition of furan to acetyl-1,4-benzoquinone yields an unexpected product **18**. The formation of **18** can be explained by a rearrangement of normal adduct in its enol form as shown in Scheme 5.

From the two examples given above, it is apparent that the intermediates proposed for the two reactions of Scheme 4 and 5 are related to the intermediate **12**. All the intermediates are unstable and undergo C—C bond cleavage accompanied by enolization in a retroaldol manner.

The possibility that the formation of the compounds **3**, **4**, **5**, **7**, **8**, **9**, and **10** might involve a carbene intermediate was also considered. Hamaguchi and Ibata (11) had already proposed an interrelationship between a carbene and an isobenzofuran. In this case, intermediate **19**, in equilibrium with **11**, might undergo C=C bond insertion to yield the *p*-homoquinones or C—H bond insertion, to give the compound **10**. In order to test for the presence of **19**, trapping experiments with cyclooctene and 1-phenyl-1-propyne were carried out. However, no reaction was found to occur when **1***a* and cyclooctene or **1***a* and 1-phenyl-1-propyne were heated together under a variety of conditions.

The reactions described here provide a new route to phenyl substituted homoquinones carrying an *ortho* carboethoxy group. Such compounds would be difficult to obtain by routes previously described. Because of the unusual nature of this reaction it was considered desirable to verify the structure of **3** through an X-ray study.

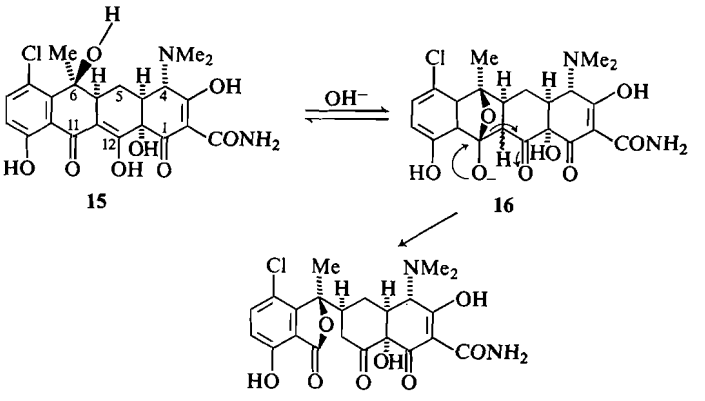

SCHEME 4

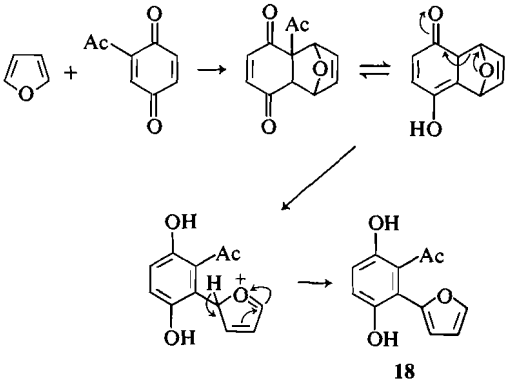

SCHEME 5

The structure of **3** derived from the X-ray study is illustrated in Fig. 1 and selected interatomic distances and angles are given in Table 3. The *trans* relationship between H(7a) and both H(1a) and H(6a) predicted from nmr spectroscopy is clearly shown. The aromatic ring is not at right angles to the homoquinone system in the crystal. Instead the angle between the aromatic ring and the C(1a)C(6a)C(7a) plane is only 53° (Table 4) and that between the aromatic ring and the C(*i*a) (*i* = 1–6) ring is 34°.

Bond lengths and angles within the ethyl benzoate portion of the molecule compare well with previous results (12–16). The C(11)O(3)O(4) plane is at a dihedral angle of 23° to the aromatic ring. This angle is quite large although values up to 18° (14, 17) have been observed previously. The twist appears to be caused by intramolecular interactions. O(3) is only 3.0 and 3.2 Å from C(1a) and C(2a), respectively, and O(4) is 2.34(5) Å from H(6), and any twist to make the CO_2 unit more nearly coplanar with the aromatic ring will decrease these distances. The short O(4)–H(6) distance may imply a weak intramolecular bonding interaction, C(6)–H(6)–O(4) is 102°. A further weak intermolecular interaction may exist as H(6a) of another molecule is only 2.5 Å from O(3) and the O(6a)–H(6a)–O(3) angle of 161° is consistent with a weak hydrogen bond. The ethyl group is almost coplanar with the CO_2 unit (7.5°) which is the usual arrangement (16).

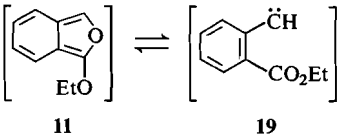

Distances and angles within the homoquinone part of the molecule also agree well with previously reported values (18, 19). The torsional distortions of the rings are very similar as well (Table 4). The quinone ring adopts a folded book conformation about the C(2a)–C(5a) axis and the dihedral angle (19.4°) is very similar to that observed in homonaphthaquinone (20.0°) (19). Similarly the angles between the cyclopropane ring and the best plane through the quinone ring are identical (83.7°, 83.8°). These angles are greater, however, than was ob-

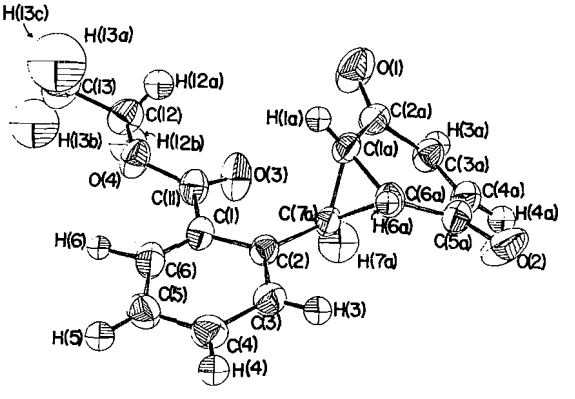

FIG. 1. The molecular structure of ethyl-2-[(1′*R**,6′*S**,7′*S**)-2′,5′-dioxo-3′-norcaren-7′yl] benzoate, $C_{16}H_{14}O_4$.

TABLE 3. Selected interatomic distances (Å) and angles (deg)

Atoms	Distance	Atoms	Distance	Atoms	Distance
C(1)–C(2)	1.402(4)	C(2)–C(3)	1.389(4)	C(3)–C(4)	1.390(4)
C(4)–C(5)	1.385(5)	C(5)–C(6)	1.375(5)	C(6)–C(1)	1.400(4)
C(2)–C(7a)	1.506(4)	C(1a)–C(2a)	1.483(4)	C(2a)–C(3a)	1.487(4)
C(3a)–C(4a)	1.328(5)	C(4a)–C(5a)	1.484(4)	C(5a)–C(6a)	1.481(4)
C(6a)–C(1a)	1.521(5)	C(1a)–C(7a)	1.503(4)	C(6a)–C(7a)	1.520(5)
C(2a)–O(1)	1.208(4)	C(5a)–O(2)	1.222(4)	C(1)–C(11)	1.497(4)
C(11)–O(3)	1.204(3)	C(11)–O(4)	1.335(4)	O(4)–C(12)	1.464(5)
C(12)–C(13)	1.493(6)	C(3)–H(3)	0.98(5)	C(4)–H(4)	1.02(4)
C(5)–H(5)	1.00(4)	C(6)–H(6)	0.98(5)	C(1a)–H(1a)	0.94(4)
C(3a)–H(3a)	0.97(4)	C(4a)–H(4a)	1.00(4)	C(6a)–H(6a)	0.98(4)
C(7a)–H(7a)	1.02(4)	C(12)–H(12a)	0.97(5)	C(12)–H(12b)	1.02(4)
C(13)–H(13a)	0.99(4)	C(13)–H(13b)	0.98(5)	C(13)–H(13c)	1.01(5)

Atoms	Angle	Atoms	Angle	Atoms	Angle
C(1)–C(2)–C(3)	118.8(3)	C(2)–C(3)–C(4)	121.4(3)	C(3)–C(4)–C(5)	119.5(3)
C(4)–C(5)–C(6)	120.0(3)	C(5)–C(6)–C(1)	121.0(3)	C(6)–C(1)–C(2)	119.4(3)
C(2)–C(3)–H(3)	119(2)	C(4)–C(3)–H(3)	120(2)	C(3)–C(4)–H(4)	120(2)
C(5)–C(4)–H(4)	120(2)	C(4)–C(5)–H(5)	119(3)	C(6)–C(5)–H(5)	121(3)
C(5)–C(6)–H(6)	124(3)	C(1)–C(6)–H(6)	115(2)	C(1)–C(2)–C(7a)	122.6(3)
C(3)–C(2)–C(7a)	118.6(3)	C(2)–C(7a)–C(1a)	121.3(2)	C(2)–C(7a)–C(6a)	119.7(2)
C(2)–C(7a)–H(7a)	114(3)	C(1a)–C(7a)–C(6a)	60.4(2)	C(1a)–C(7a)–H(7a)	115(2)
C(6a)–C(7a)–H(7a)	116(3)	C(7a)–C(1a)–C(2a)	116.4(2)	C(7a)–C(1a)–C(6a)	60.3(2)
C(7a)–C(1a)–H(1a)	118(3)	C(2a)–C(1a)–C(6a)	118.1(2)	C(2a)–C(1a)–H(1a)	115(3)
C(6a)–C(1a)–H(1a)	118(3)	C(1a)–C(2a)–C(3a)	116.7(3)	C(1a)–C(2a)–O(1)	123.2(2)
O(1)–C(2a)–C(3a)	120.1(3)	C(2a)–C(3a)–H(3a)	117(2)	C(2a)–C(3a)–C(4a)	122.6(3)
H(3a)–C(3a)–C(4a)	121(2)	C(3a)–C(4a)–H(4a)	121(2)	C(3a)–C(4a)–C(5a)	121.7(2)
H(4a)–C(4a)–C(5a)	118(2)	C(4a)–C(5a)–O(2)	120.4(3)	C(4a)–C(5a)–C(6a)	117.6(3)
O(2)–C(5a)–C(6a)	122.0(3)	C(5a)–C(6a)–C(1a)	117.8(3)	C(5a)–C(6a)–C(7a)	116.2(2)
C(5a)–C(6a)–H(6a)	114(3)	C(1a)–C(6a)–C(7a)	59.2(2)	C(1a)–C(6a)–H(6a)	121(2)
C(7a)–C(6a)–H(6a)	119(3)	C(2)–C(1)–C(11)	120.9(3)	C(6)–C(1)–C(11)	119.8(3)
C(1)–C(11)–O(3)	125.0(3)	C(1)–C(11)–O(4)	111.2(2)	O(3)–C(11)–O(4)	123.8(3)
C(11)–O(4)–C(12)	116.4(2)	O(4)–C(12)–C(13)	106.3(3)	O(4)–C(12)–H(12a)	109(3)
O(4)–C(12)–H(12b)	105(2)	C(13)–C(12)–H(12a)	110(2)	C(13)–C(12)–H(12b)	112(2)
H(12a)–C(12)–H(12b)	113(3)	C(12)–C(13)–H(13a)	113(3)	C(12)–C(13)–H(13b)	104(2)
C(12)–C(13)–H(13c)	109(2)	H(13a)–C(13)–H(13b)	105(3)	H(13a)–C(13)–H(13c)	112(3)
H(13b)–C(13)–H(13c)	113(4)				

served in the *anti* form of a homoduroquinone (75.3, 77.3°) (18). Even though the greatest difference between **3** and homonaphthaquinone is shown in the dihedral angle between the planes involving the oxygen atoms (32.7(3)° vs. 37.8(3)°) the actual distance the oxygen is out of the best plane through the quinone ring is very similar (0.500(4) 0.476(4) vs. 0.50(5) Å).

The packing of the molecules is shown in Fig. 2.

In the *c* direction the molecules are arranged such that the basic shapes (defined by the aromatic and quinone rings) are stacked like tiles on a roof. Important contacts between molecules related by the *c* translation are H(6a)....O(3) and H(12b).... phenyl ring. In the *b* direction contacts between molecules related by the *b* translation are between interleaved aromatic and quinone rings, but a further important contact at $y = \frac{1}{2}$ is between ethyl groups of molecules related by the inversion centre at $\frac{1}{2}$, $\frac{1}{2}$, $\frac{1}{2}$. In the *a* direction contacts consist of interleaved ethyl groups and quinone rings from adjacent molecules near $x = \frac{1}{2}$, and H(7a) – aromatic ring contacts near $x = 0$. All contact distances are at, or greater than, the van der Waals distances.

Experimental

Apparatus, Methods and Materials

Spectroscopic methods and procedures used in this study are the same as those described in the first paper of this series (1). The X-ray work is described below.

Collection of the X-ray Data

A parallelepiped crystal, homogeneous under the polarizing microscope, was chosen for X-ray studies and mounted roughly along [100]. Precession photographs showed the crystals were triclinic and a Delaunay test showed no hidden symmetry. Unit cell parameters were obtained from a least-squares fit of χ, ϕ, and 2θ for 15 reflections for each compound in the range $21° < 2\theta < 36°$ recorded on a Syntex $P2_1$ diffractometer using graphite-monochromated MoKα radiation (λ 0.71069 Å at 22°C). Crystal

TABLE 4. Least-squares planes and dihedral angles (errors in distances 0.004 Å and in angles 0.3°)

Plane	Distance of atoms from mean plane (Å)
1. C(*i*)(*i* = 1–6)C(7a)*	C(1) 0.005, C(2)−0.001, C(3)−0.002, C(4) 0.001, C(5) 0.002 C(6)−0.005, C(7a) 0.042.
2. C(*i*a)(*i* = 1–6)O(1)* O(2)* C(7a)*	C(1a) 0.072, C(2a)−0.147, C(3a) 0.078, C(4a) 0.069, C(5a)−0.142, C(6a) 0.069, C(7a) 1.368, O(1)−0.500 O(2)−0.476.
3. C(2a)C(1a)C(6a)C(5a)	C(2a)−0.001, C(1a) 0.002, C(6a)−0.002, C(5a) 0.001
4. C(2a)C(3a)C(4a)C(5a)	C(2a)−0.002, C(3a) 0.005, C(4a)−0.005, C(5a) 0.002
5. C(1a)C(2a)C(3a)O(1)	C(1a)−0.001, C(2a) 0.003, C(3a)−0.001, O(1)−0.001
6. C(4a)C(5a)C(6a)O(2)	C(4a) 0.000, C(5a) 0.000, C(6a) 0.000, O(2) 0.000

Plane 1	Plane 2	Dihedral angle (deg)	Equivalent angles homo-napthaquinone
C(*i*)(*i* = 1–6)	O(3)C(11)O(4)	23.2	—
C(*i*)(*i* = 1–6)	C(*i*a)C(6a)C(7a)	53.1	—
C(*i*)(*i* = 1–6)	C(*i*a)(*i* = 1–6)	33.7	—
C(1a)C(6a)C(7a)	C(*i*a)(*i* = 1–6)	83.7	83.8
C(1a)C(2a)C(5a)C(6a)	C(2a)C(3a)C(4a)C(5a)	19.4	20.0
C(1a)C(2a)C(3a)O(1)	C(4a)C(5a)C(6a)O(2)	32.7	37.8
C(12)C(13)O(4)	O(3)C(11)O(4)	7.5	—

*Atoms given no weight in calculating the best plane.
†Angles calculated from parameters in ref. 19.

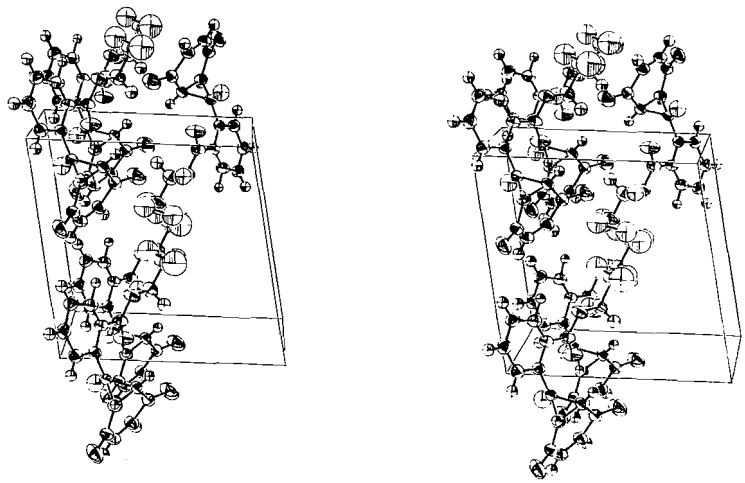

FIG. 2. The packing of the molecule within the unit cell.

data and other numbers related to data collection are:

$C_{16}H_{14}O_4$ mw = 270.12

Triclinic, $P\bar{1}$, a = 10.601(2), b = 10.434(3), c = 6.491(1) Å, α = 105.53(3), β = 95.21(2), γ = 100.66(3)°, V = 676.6(4) Å^3, Z = 2, ρ_{calc} = 1.33 g cm^{-3} at 22°C, ρ_{obs} = 1.30(1) g cm^{-3}. Crystal size, 0.20 × 0.15 × 0.25 mm, μ(MoKα) = 1.0 cm^{-1}. Max 2θ = 55° h, $\pm k$, $\pm l$. Standard reflections (esd) $\bar{3}\,2\,\bar{1}$ (1.99%), $\bar{4}\,2\,\bar{2}$ (2.76%). Number of independent reflections 2378, $I > 3\sigma(I)$, 1251, $3\sigma(I) < I < \sigma(I)$, $F_c > F_o$ 445, $3\sigma(I) < I < \sigma(I)$, $F_c < F_o$ 682, R_1 = 0.064, R_2 = 0.054 ($R_1 = \Sigma(|F_o| - |F_c|)/\Sigma|F_o|$; $R_2 = \{\Sigma w(|F_o| - |F_c|)^2/\Sigma w F_o^2\}^{1/2}$. Final shift/error: max 0.23, ave. 0.02; g(secondary extinction) 2.45 × 10^{-6}. Final residual peak: 0.33 e/Å^3, valley: −0.18 e/Å^3. Weighting scheme $\omega = (\sigma_F^2 + (0.020|F_o|)^2)^{-1}$, error in an observation of unit weight 1.238.

Densities were obtained by flotation in an aqueous zinc bromide solution. Intensity data were also recorded on the Syntex $P2_1$ diffractometer using a coupled θ(crystal)–2θ(counter) scan. The methods of selection of scan rates and initial data treatment have been described (20, 21). Corrections were made for Lorentz polarization effects but not absorption. This will make a maximum error in F of < 1.5%.

Solution of the Structure

The phase problem was solved by direct methods using 50 reflections with $|E| > 1.20$ and 12 sets of starting phases. A subsequent E map with 418 most reliable phases yielded all the

TABLE 5. Atomic positional coordinates and temperature factors (Å²)

Atom	$x(\times 10^4)$	$y(\times 10^4)$	$z(\times 10^4)$
C(1)	2123(3)	1697(3)	549(4)
C(2)	1707(3)	623(3)	1416(4)
C(3)	1032(3)	806(3)	3168(5)
C(4)	768(3)	2131(3)	4068(5)
C(5)	1186(3)	3188(3)	3209(5)
C(6)	1862(3)	2977(3)	1481(5)
C(1a)	3257(3)	−1082(3)	619(5)
C(2a)	3535(3)	−2082(3)	−1291(5)
C(3a)	2572(3)	−3401(3)	−2148(5)
C(4a)	1734(3)	−3863(3)	−974(5)
C(5a)	1687(3)	−3076(3)	1279(5)
C(6a)	2295(3)	−1602(3)	1969(4)
C(7a)	1921(3)	−791(3)	473(4)
O(1)	4491(2)	−1872(2)	−2135(4)
O(2)	1160(2)	−3638(2)	2501(4)
C(11)	2810(3)	1481(3)	−1390(4)
O(3)	2740(2)	396(2)	−2696(3)
O(4)	3513(2)	2655(2)	−1504(3)
C(12)	4235(4)	2574(4)	−3336(6)
C(13)	5074(5)	3958(4)	−2948(8)

Atom	$x(\times 10^3)$	$y(\times 10^3)$	$z(\times 10^3)$	$U(\times 10^3)$
H(3)	77(4)	13(4)	381(6)	29(7)
H(4)	29(4)	229(4)	537(6)	32(7)
H(5)	95(4)	409(4)	381(6)	31(7)
H(6)	217(4)	368(4)	79(6)	22(6)
H(1a)	396(4)	−36(4)	135(7)	25(7)
H(3a)	261(4)	−395(4)	−360(7)	35(7)
H(4a)	111(4)	−476(4)	−159(6)	33(8)
H(6a)	240(4)	−118(4)	353(7)	20(6)
H(7a)	131(4)	−134(4)	−92(7)	74(11)
H(12a)	476(4)	190(4)	−338(6)	42(10)
H(12b)	355(4)	233(4)	−467(7)	72(10)
H(13a)	562(4)	431(4)	−151(7)	150(19)
H(13b)	446(4)	455(4)	−290(7)	112(15)
H(13c)	560(4)	394(4)	−416(7)	112(12)

	Anisotropic temperature factors* $(\times 10^3)$(Å²)					
Atom	U_{11}	U_{22}	U_{33}	U_{12}	U_{13}	U_{23}
C(1)	43(2)	32(1)	37(1)	3(1)	3(1)	10(1)
C(2)	35(2)	32(1)	38(1)	4(1)	1(1)	8(1)
C(3)	44(2)	41(2)	50(2)	9(1)	14(1)	15(1)
C(4)	46(2)	49(2)	52(2)	13(1)	16(1)	9(1)
C(5)	46(2)	38(2)	56(2)	12(1)	3(1)	5(1)
C(6)	51(2)	35(2)	51(2)	6(1)	4(1)	15(1)
C(1a)	35(2)	32(1)	44(2)	−1(1)	6(1)	8(1)
C(2a)	41(2)	40(1)	52(2)	6(1)	12(1)	13(1)
C(3a)	50(2)	38(2)	47(2)	4(1)	9(2)	4(1)
C(4a)	48(2)	30(1)	55(2)	3(1)	7(1)	7(1)
C(5a)	46(2)	38(1)	54(2)	10(1)	15(1)	20(1)
C(6a)	50(2)	37(1)	36(1)	10(1)	10(1)	13(1)
C(7a)	36(1)	29(1)	37(1)	3(1)	7(1)	9(1)
O(1)	60(1)	63(1)	85(2)	−1(1)	39(1)	3(1)
O(2)	86(2)	48(1)	75(1)	12(1)	36(1)	31(1)
C(11)	56(2)	40(2)	38(2)	8(1)	4(1)	18(1)
O(3)	107(2)	40(1)	40(1)	9(1)	21(1)	9(1)
O(4)	67(1)	42(1)	50(1)	1(1)	21(1)	16(1)
C(12)	60(2)	63(2)	46(2)	9(2)	19(2)	19(1)
C(13)	92(3)	72(2)	86(3)	6(2)	52(2)	29(2)

*Anisotropic temperature factors U_{ij} were obtained from $\beta_{ij} = 2\pi^2 b_i b_j U_{ij}$ where the β_{ij}'s appear as a temperature effect for $\exp[-(\beta_{11}h^2 + \ldots + 2\beta_{12}hk + \ldots.)]$ and b_i and b_j are the reciprocal lattice vectors.

carbon and oxygen atoms. A series of full matrix least-squares refinements followed by three-dimensional difference syntheses revealed all the atoms. In subsequent refinements, the temperature factors of the carbon and oxygen atoms were made anisotropic. Tests were made to show the use of increased number of parameters was justified (22). Refinement using full matrix least squares and minimizing $\Sigma\omega(|F_o| - |F_c|)^2$ was terminated when the maximum shift/error was 0.23. Secondary extinction was applied using the method of Larson (23). Scattering factors were from Cromer and Waber (24). The final positional parameters and temperature factors are given in Table 5.[1] All calculations were carried out on a CYBER 170/730 computer.[2]

*Reaction of 1,1-Diethoxyphthalan 1*a *with 1,4-Benzoquinone 2*

Phthalan **1***a* (1.04 g, 5 mmol) and **2** (540 mg, 5.5 mmol) were heated together for 45 min at 146–148°C under an argon atmosphere. The brown oil was cooled, dissolved in methylene chloride, and filtered through alumina (neutral) to give 380 mg (29%) of colorless crystals that were recrystallized from ethanol (mp 121–122°C). The compound proved to be ethyl 2-[(1′*R**,6′*S**,7′*S**)-2′,5′-dioxo-3′-norcaren-7′-yl]benzoate, **3** and had the following spectroscopic properties. Infrared (ir) ν_{max}: 1715 and 1685 cm^{-1}; ^1H nmr δ: 1.37 (t, 3H, OCH_2CH_3, J = 7.5 Hz), 2.83 (d, 2H, H-1′ and H-6′, J = 5.4 Hz), 4.02 (t, 1H, H-7′, J = 5.4 Hz), 4.38 (q, 2H, OCH_2CH_3, J = 7.5 Hz), 6.60 (s, 2H, H-3′ and H-4′), 7.40 (m, 3H, aromatic), and 8.05 (m, 1H, aromatic). *Exact Mass* calcd. for $C_{16}H_{14}O_4$: 270.089; found (ms): 270.090. *Anal.* calcd. for $C_{16}H_{14}O_4$: C 71.09, H 5.22; found: C 70.87, H 5.28%.

*Reaction of 1*b *with 1,4-Benzoquinone 2*

Phthalan **1***b* (1.3 g, 5 mmol) and **2** (540 mg, 5.5 mmol) were heated together for 10 min at 155°C under an argon atmosphere. The dark oil was cooled, dissolved in methylene chloride, and filtered through neutral alumina to give yellow crystals that were recrystallized from benzene–pentane (800 mg, 42%) mp 191–192°C. The compound was identified as ethyl 4,5-dimethoxy-2[(1′*R**,6′*S**,7′*S**)-2′,5′-dioxo-3′-norcaren-7′-yl]benzoate, **4**, and had the following spectroscopic properties: ir ν_{max}: 1685 and 1710 cm^{-1}; ^1H nmr δ: 1.34 (t, 3H, OCH_2CH_3, J = 7.5 Hz), 2.77 (d, 2H, H-1′ and H-6′, J = 5.3 Hz), 3.97 (s, 6H, 2 × OCH_3), 4.02 (overlapping t, 1H, H-7, J = 5.3 Hz), 4.32 (q, 2H, OCH_2CH_3, J = 7.5 Hz), 6.55 (s, 2H, H-3′ and H-4′), 6.60 (s, 1H, aromatic), and 7.35 (s, 1H, aromatic); ^{13}C nmr[3] δ: (C-1) 123.2, (C-2) 131.3, (C-3) 109.8, (C-4) 152.3, (C-5) 148.3, (C-6) 114.3, (C-1′) and (C-6′) 36.0, (C-2′) and (C-5′) 193.5, (C-3′) and (C-4′) 137.9, (C-7′) 36.8, ($CO_2CH_2CH_3$) 166.2, ($CO_2CH_2CH_3$) 61.4, ($CO_2CH_2CH_3$) 14.3, (2 × OCH_3) 56.2. *Exact Mass* calcd. for $C_{18}H_{18}O_6$: 330.110; found (ms): 330.109. *Anal.* calcd. for $C_{18}H_{18}O_6$: C 65.45, H 5.45; found: C 65.14, H 5.60%.

The mother liquor was evaporated to dryness and the residue (10 mg, 0.5%) was crystallized from ether. The separated solid melted at 115–116°C. It proved to be ethyl 4,5-dimethoxy-[(1′*R**,6′*R**,7′*S**)-2′5′-dioxo-3′-norcaren-7′-yl]benzoate **5**. Infrared ν_{max}: 1680 and 1715 cm^{-1}; ^1H nmr δ: 1.41 (t, 3H, OCH_2CH_3, J = 7.5 Hz), 2.87 (d, 2H, H-1′ and H-6′, J = 9.0 Hz), 3.55 (t, 1H, H-7′, J = 9.0 Hz), 3.80 (s, 3H, OCH_3), 3.87 (s, 3H, OCH_3), 4.39 (q, 2H, OCH_2CH_3, J = 7.5 Hz), 6.18 (s, 2H, H-3′ and H-4′), 6.54 (s, 1H, aromatic), and 7.37 (s, 1H, aromatic). *Anal.* calcd. for $C_{18}H_{18}O_6$: C 65.45, H 5.45; found C 65.07, H 5.65%.

*Reaction of 1*a *with 1,4-Naphthoquinone, 6*

The phthalan (1.04 g, 5 mmol) and **6** (790 mg, 5 mmol) were heated together at 140°C for 20 min under an argon atmosphere. The resulting brown oil (1.6 g) was subjected to column chromatography (silica gel, 160 g) using methylene chloride as eluant. The first fraction (450 mg, 28%) was purified on a Lobar reversed phase chromatography column (acetonitrile–water = 70:30) and crystallized from pentane (mp 82–83°C). It proved to be 2-(2′-carboethoxybenzyl)-1,4-napthoquinone **10** and had the following spectroscopic properties. Infrared ν_{max}: 1675 and 1725 cm^{-1}; ^1H nmr δ: 1.28 (t, 3H, OCH_2CH_3, J = 6.0 Hz), 4.26 (q, 2H, OCH_2CH_3, J = 6.0 Hz), 4.30 (s, 2H, H-11), 6.28 (t, 1H, H-3), 7.41 (m, 3H, aromatic), 7.73 (m, 2H, aromatic), and 8.10 (m, 3H, aromatic); ^{13}C nmr δ: (C-1 and C-4) 185.0 and 185.2, (C-11) 34.3, ($CO_2CH_2CH_3$) 166.8, ($CO_2CH_2CH_3$) 61.0, ($CO_2CH_2CH_3$) 14.2. Other signals observed but not assigned: 126.1, 126.8, 127.4, 130.3, 131.5, 132.5, 133.7, 134.3, 134.9, 138.5. *Exact Mass* calcd. for $C_{20}H_{16}O_4$: 320.104; found (ms): 320.104. *Anal.* calcd. for $C_{20}H_{16}O_4$: C 74.97, H 5.03; found: C 75.07, H 5.20%.

The second fraction from the column was filtered through neutral alumina to remove coloured impurities and crystallized from ether to give colorless crystals that melted at 126–127°C. It was identified as ethyl 2-[(1′*R**,1′a*S**,7′a*R**)-1′a,2′,7′,7a′-tetrahydro-2′,7′-dioxo-1*H*-cyclopropa[*b*]naphthalen-1′-yl]benzoate, **9**. Infrared ν_{max}; 1685 and 1725 cm^{-1}; ^1H nmr δ: 1.28 (t, 3H, OCH_2CH_3, J = 7.0 Hz), 3.01 (d, 2H, H-1′a, and H-7′a, J = 5.3 Hz), 3.85 (t, 1H, H-1′, J = 5.3 Hz), 4.29 (q, 2H, OCH_2CH_3, J = 7.0 Hz) and 7.20–8.20 (m, 8H, aromatic); ^{13}C nmr[4] δ: (C-1′) 36.0, (C-1′a and C-7′a) 36.4, (C-2′ and C-7′) 192.2, (C-3′ and C-6′) 127.2, (C-4′ and C-5′) 134.3, (C-8′ and C-9′) 132.8, ($CO_2CH_2CH_3$) 166.8, ($CO_2CH_2CH_3$) 61.5, ($CO_2CH_2CH_3$) 14.1. Other signals observed but not assigned: 127.9, 131.4, 132.5, 137.2. *Exact Mass* calcd. for $C_{20}H_{16}O_4$: 320.104; found (ms): 320.104. *Anal.* calcd. for $C_{20}H_{16}O_4$: C 74.97, H 5.03; found: C 74.74, H 5.30%.

*Reaction of 1*b *with 1,4-Naphthoquinone 6*

Phthalan **1***b* (1.3 g, 5 mmol) and **6** (790 mg, 5 mmol) were heated together for 10 min at 150°C under an argon atmosphere. The dark oily product was filtered through neutral alumina to give a brown oil (1.4 g) that showed three spots on tlc (silica gel). Crystallization of the oil from acetone–hexane yielded 377 mg (20%) of ethyl 4,5-dimethoxy-2-[(1′*R**,1′a*S**,7′a*R**)-1′a,2′,7′,7′a-tetrahydro-2′,7′-dioxo-1*H*-cyclopropa[*b*]naphthalen-1′-yl]benzoate **7**. It melted at 151–152°C and had the following spectroscopic properties. Infrared ν_{max}: 1680 and 1710 cm^{-1}; ^1H nmr δ:

[1]The table of structure factors has been deposited and is available at a nominal charge from the Depository of Unpublished Data, CISTI, National Research Council of Canada, Ottawa, Ont., Canada K1A 0S2.

[2]Initial data treatment used the programs DATCO5, DATRDN from the XRAY 76 system (25). Most data treatment used programs from the SHELX package (26). Final data treatment used the full matrix least-squares program, CUDLS, and Fourier program, SYMFOU, written internally by J. S. Stephens and J. S. Rutherford, respectively. The least-squares plane program NRC-22 (27) was used. Diagrams were prepared using ORTEP II (28).

[3]It is known from the off-resonance spectrum that the signals at 109.8, 114.3, and 137.9 are doublets and that the signals at 123.2, 131.3, 148.3, and 152.3 are singlets. The signals at 109.8 and 114.3 are shielded by the *o*-methoxy groups and assigned to C-3 and C-6, those at 148.3 and 152.3 are deshielded by the methoxy groups and assigned to C-4 and C-5, while those at 123.2 and 131.3 are assigned to C-1 and C-2. Definitive assignments within the three pairs are not possible but those given are favoured because of observable long range coupling and known substituent effects.

[4]The assignment of signals in the quinone moiety is based on examination of the off-resonance spectrum and on comparison with the published spectrum of 1,4-naphthoquinone (29).

1.26 (t, 3H, OCH_2CH_3, J = 7.5 Hz), 2.96 (d, 2H, H-1′a and H-7′a, J = 5.3 Hz), 3.83 (t, 1H, H-1′, J = 5.3 Hz), 3.90 (s, 3H, OCH_3), 3.96 (s, 3H, OCH_3), 4.23 (q, 2H, OCH_2CH_3, J = 7.5 Hz), 6.68 (s, 1H, aromatic), 7.50 (s, 1H, aromatic), 7.75 (m, 2H, aromatic), and 8.06 (m, 2H, aromatic); ^{13}C nmr[5] δ: (C-1) 123.4, (C-2) 131.3, (C-3) 114.4, (C-4) 152.3, (C-5) 148.3, (C-6) 110.0, (C-1′) 36.4, (C-1′a and 7′a) 36.7, (C-2′ and 7′) 192.3, (C-3′ and 6′) 127.2, (C-4′ and 5′) 134.2, (C-8′ and 9′) 133.0, ($CO_2CH_2CH_3$) 166.3, ($CO_2CH_2CH_3$) 61.4, ($CO_2CH_2CH_3$) 14.3, (2 × OCH_3) 56.2. *Exact mass* calcd. for $C_{22}H_{20}O_6$: 380.125; found: 380.124. *Anal.* calcd. for $C_{22}H_{20}O_6$: C 69.53, H 5.30; found: C 69.73, H 5.54%.

The mother liquors were evaporated to dryness and the residue was subjected to column chromatography (silica gel, 100 g). Starting materials, 64 mg of 1,4-naphthoquinone and 73 mg of 5,6-dimethoxyphthalide, were eluted with methylene chloride, and products (856 mg) with methylene chloride – ether (50:50). Recrystallization of the mixture (856 mg) from acetone–hexane gave 229 mg (12%) of the compound previously described. The mother liquor from this crystallization was removed and the residue (627 mg) showed two spots on tlc (reversed phase, acetonitrile–water = 60:40). A portion of the mixture (3 × 10 mg) was subjected to Lobar reversed phase chromatography using acetonitrile–water (60:40) as eluant. The first fraction (15 mg, 50%) which was crystallized from acetone–pentane had mp 131–133°C. It proved to be ethyl 4,5-dimethoxy-2[(1′*R**,1′a*R**,7′a*S**)-1′a,2′,7′,7′a-tetrahydro-2′,7′-dioxo-1*H*-cyclopropa[*b*]naphthalene-1′-yl]benzoate, **8**, and had the following spectroscopic properties. Infrared ν_{max}: 1675 and 1710 cm^{-1}; ^{1}H nmr δ: 1.45 (t, 3H, OCH_2CH_3, J = 7.5 Hz), 3.10 (d, 2H, H-1′a and H-7′a, J = 9.8 Hz), 3.70 (overlapping t, 1H, H-1, J = 9.8 Hz), 3.70 (s, 6H, 2 × OCH_3), 4.36 (q, 2H, OCH_2CH_3, J = 7.5 Hz), 6.68 (s, 1H, aromatic), 7.08 (s, 1H, aromatic), 7.41 (m, 2H, aromatic), and 7.71 (m, 2H, aromatic); ^{13}C nmr δ: (C-3) 114.5, (C-4) 150.8, (C-5) 148.0, (C-6) 113.5, (C-1′) 34.4, (C-1′a and 7′a) 34.0, (C-2′ and 7′) 193.2, (C-3′ and C-6′) 125.8, (C-4′ and 5′) 133.7, (C-8′ and 9′) 134.0, ($CO_2CH_2CH_3$) 61.6, ($CO_2CH_2CH_3$) 14.3, (2 × OCH_3) 56.0. Signals were not observed for C-1, C-2, and the ester carbon because of low intensity of the spectrum. *Exact Mass* calcd. for $C_{22}H_{20}O_6$: 380.125; found: 380.126. *Anal.* calcd. for $C_{22}H_{20}O_6$: C 69.53, H 5.30; found: C 69.06, H 5.52%.

The second fraction (10 mg, 33%) showed spectroscopic properties similar to those of **7**.

Treatment of **1**a *with Cyclooctene or 1-Phenyl-1-propyne*

The reactions were carried out in sealed nmr tubes using $CDCl_3$ or DMSO-d_6 as solvent. In each case equivalent amounts of **3***a* and cyclooctene or 1-phenyl-1-propyne were used. The solutions were heated in an oil bath at temperatures over the range 120–190°C over a 10 h period. The tubes were examined periodically by nmr but no reaction was found to occur.

Acknowledgements

We thank the Natural Sciences and Engineering Research Council of Canada for financial support of this work and Consejo de Desarrollo Cientifico y Humanistico de la Universidad Central de Venezuela for a scholarship to L. Contreras.

[5]The signals of the aromatic carbon atoms of the benzoic ester moiety of **7** and **8** (*vide infra*) are similar to those of **4** and the assignments are made with the same reservations. The assignments in the quinone moiety are based on comparison with naphthoquinone and are very similar to those reported for **9** above.

1. L. Contreras and D. B. MacLean. Can. J. Chem. **58**, 2573 (1980).
2. L. Contreras and D. B. MacLean. Can. J. Chem. **58**, 2580 (1980).
3. W. Adam, M. Balci, and J. Rivera. Synthesis, 807 (1979).
4. (*a*) C. B. Chapleo and A. S. Dreiding. Helv. Chim. Acta, **57**, 1259 (1974); (*b*) C. B. Chapleo, C. E. Dahl, A. S. Dreiding, R. Grieb, and A. Niggli. Helv. Chim. Acta, **57**, 1876 (1974).
5. A. Yogev, J. Heller, and A. S. Dreiding. Chimia, 411 (1969).
6. K. Nakanishi. Infrared absorption spectroscopy. Holden-Day, San Francisco. 1962. p. 42.
7. H. Booth. Prog. Nucl. Magn. Reson. Spectrosc. **5**, 149 (1969).
8. T. Shono, T. Morikawa, A. Oku, and R. Oda. Tetrahedron Lett. 791 (1964).
9. D. L. J. Clive. Q. Rev. Chem. Soc. **22**, 435 (1968).
10. C. H. Eugster and P. Bosshard. Chimia, **15**, 528 (1961).
11. M. Hamaguchi and T. Ibata. Chem. Lett. 287 (1976).
12. W. R. Krigbaum and P. G. Barber. Acta Crystallogr. Sect. B, **27**, 1884 (1971).
13. J. M. Adams and S. E. Morsi. Acta Crystallogr. Sect. B, **32**, 1345 (1976).
14. R. S. Miller, I. C. Paul, and D. Y. Curtin. J. Am. Chem. Soc. **96**, 6334 (1974).
15. D. L. Hughes and J. Trotter. J. Chem. Soc. A, 2358 (1971).
16. T. S. Cameron and R. E. Cordes. Cryst. Struct. Commun. **6**, 489 (1977).
17. G. Ferguson and G. A. Sim. Acta Crystallogr. **15**, 346 (1962).
18. J. Heller, A. S. Dreiding, R. Grieb, and A. Niggli. Angew. Chem. Int. Ed. Engl. **11**, 236 (1972).
19. W. K. Grant and J. C. Speakman. Acta Crystallogr. **15**, 292 (1962).
20. R. P. Hughes, N. Krishnamachari, C. J. L. Lock, J. Powell, and G. Turner. Inorg. Chem. **16**, 314 (1977).
21. B. Lippert, C. J. L. Lock, B. Rosenberg, and M. Zvagulis. Inorg. Chem. **16**, 1525 (1977).
22. W. C. Hamilton. Acta Crystallogr. **18**, 502 (1965).
23. A. C. Larson. Acta Crystallogr. **23**, 664 (1967).
24. D. T. Cromer and J. T. Waber. International tables for X-ray crystallography. Vol. IV. *Edited by* J. A. Ibers and W. C. Hamilton. Kynoch Press, Birmingham, England. Table 2.2A. p. 72ff.
25. J. M. Stewart. The XRAY 76 system. Techn. Rep. TR-446. Computer Science Center, Univ. of Maryland, College Park, MD. 1976.
26. G. M. Sheldrick. SHELX program for crystal structure determination. Univ. of Cambridge, England. 1976.
27. M. E. Pippy and F. R. Ahmed. NRC crystallographic programs for the IBM/360 system. National Research Council of Canada, Ottawa, Ontario. 1978.
28. C. K. Johnson. ORTEP-II. Report ORNL-5138. Oak Ridge National Laboratory, Oak Ridge, TN. 1976.
29. I. A. McDonald, T. J. Simpson, and A. F. Sierakowski. Aust. J. Chem. **30**, 1727 (1977).

Excess enthalpies of aqueous solutions of biuret at 25°C. Interaction with urea

GUIDO BARONE, PASQUALE CACACE, GIUSEPPINA CASTRONUOVO, AND VITTORIO ELIA
Istituto Chimico, University of Naples, Via Mezzocannone 4, 80134 Naples, Italy

Received June 18, 1980[1]

GUIDO BARONE, PASQUALE CACACE, GIUSEPPINA CASTRONUOVO, and VITTORIO ELIA. Can. J. Chem. **59**, 1257 (1981).

The heats of dilution in water of biuret and the heats of mixing of biuret with urea have been determined by flow microcalorimetry at 25°C. The excess enthalpies obtained from the experimental data can be expressed as virial expansions of the molalities.

The value of the cross interaction coefficient h_{UB} is compared to that calculated through the empirical relation $h_{UB}^2 = (h_{UU}h_{BB})$. The agreement between the two values outlines the strict analogy in the behaviour of these two solutes. The cited combining rule, verified up to now for pairs of solutes having both h_{ii}, $h_{jj} > 0$, is here applied for the first time to a pair having h_{ii}, $h_{jj} < 0$.

GUIDO BARONE, PASQUALE CACACE, GIUSEPPINA CASTRONUOVO et VITTORIO ELIA. Can. J. Chem. **59**, 1257 (1981).

Les chaleurs de dilution dans l'eau du biurete et les chaleurs de mélange de biurete avec l'ureé ont été déterminées à 25°C par un calorimétre en flux. Les enthalpies d'excés obtenues par les données expérimentales peuvent être exprimées par une expansion du viriel en molalité. La valeur du coéfficient de l'intéraction croisée, h_{UB}, est comparée à celle évaluée par la règle empirique: $h_{UB}^2 = (h_{UU}h_{BB})$. L'accord trouvé entre les deux valeurs souligne l'analogie du comportement de ces deux solutés.

La régle combinatoriale sus-citée, verifiée jusqu'à présent seulement pour les paires de solutés ayant à la pair h_{ii} et h_{jj} positif, a été appliquée ici pour la premiére fois à une paire ayant h_{ii} et $h_{jj} < 0$.

Introduction

The study of the excess thermodynamic properties is useful to make hypotheses and to test models concerning interactions in solution. In the case of aqueous solutions of nonelectrolytes containing more than one solute, it is convenient to refer to 1 kg of solvent.

The excess enthalpy, then, is defined as:

$$[1] \quad H^E = H - H_w^{\ominus} - \sum_i m_i \bar{H}_i^0$$

where H is the enthalpy of a solution containing 1 kg of water, $H_w^{\ominus}$ is the enthalpy of 1 kg of water, and $\bar{H}_i^0$ is the standard (infinite dilution) partial molar enthalpy of each solute species. The other excess quantities, as for instance the entropy, are defined analogously.

Nonelectrolytes in water can be classified in two groups (1). The first class ($T|S^E| > |H^E|$) groups mainly hydrophobic solutes in water, while the second ($T|S^E| < |H^E|$) deals with hydrophilic solutes. The excess thermodynamic properties of predominantly hydrophobic substances of the amide or urea class have been studied extensively. On the contrary only urea, among the hydrophilic solutes of this group, has been studied in detail (2–6). Recently we studied the aqueous solutions of the predominantly hydrophilic, urea-like substances, monomethylurea (MMU) (7) and thiourea (TU) (8).

In the present paper, the heats of dilution in water of biuret (B), $NH_2CONHCONH_2$, and the heats of mixing of the same substance with aqueous solutions of urea (U) are reported. From the experimental data, the excess enthalpies, referred to 1 kg of water, are obtained. For the binary and ternary solutions they can be expressed through the following virial expansions:

$$[2] \quad H^E(m_i) = h_{ii}m_i^2 + h_{iii}m_i^3 + \ldots$$

$$[2'] \quad H^E(m_i, m_j) = h_{ii}m_i^2 + 2h_{ij}m_im_j + h_{jj}m_j^2 + h_{iii}m_i^3 + 3h_{iij}m_i^2 m_j + 3h_{ijj}m_im_j^2 + h_{jjj}m_j^3 + \ldots$$

The coefficients h_{ij}, h_{iij} characterize the interactions among pairs, triplets, etc., of molecules of the same or different species, according to the McMillan–Mayer approach (9–13). The virial expansions [2] and [2′] can be transformed to analogous expressions, as functions of the molar concentration, which are more appropriate for statistical calculations. The values of h_{BB}, h_{UU}, and h_{BU} outline the strict analogy of the molecular interactions characterizing their aqueous solutions, as a result, in our opinion, of the close similarity between the perturbations induced in water by these two solutes.

Experimental

Biuret (B) and urea (U), C. Erba (Milan) products, were crystallized twice from ethanol and dried *in vacuo* at room temperature. The solutions were prepared by weight using freshly distilled and degassed water. All the dilution and mixing experiments were performed at 25.00 ± 0.02°C. The measurements of the heats of dilution and mixing were performed by an LKB 10700-1 flow microcalorimeter equipped with a pair of gold cells, a Keithley amplifier, and two peristaltic pumps. The experimental procedure was described in preceding papers (7, 8,

[1]Revision received December 30, 1980.

0008-4042/81/081257-04$01.00/0
©1981 National Research Council of Canada/Conseil national de recherches du Canada

13). The values of ΔH^{dil} from the initial molality m_i to the final molality m_f, expressed in J kg^{-1} of water, can be obtained as follows:

$$[3]\quad \Delta H^{dil}(m_i \rightarrow m_f) = -\frac{(dQ/dt)}{P_1}$$

where dQ/dt is the heat absorbed per time unit in steady state conditions and P_1 is the total mass flow rate of water.

Mixing experiments were carried out by mixing aqueous solutions of B and U at different concentrations in different amounts. The mixing of equimolal solutions might have been employed to simplify the experimental part, but the above described procedure was preferred because of the limited solubility of B, given its relatively large heat of dilution in comparison with that of urea. The heat of mixing, ΔH^{mix}, relative to 1 kg of water in the final solution is given by:

$$[4]\quad \Delta H^{mix}[(m_B)_i, (m_U)_i \rightarrow (m_B, m_U)_f] = -\frac{dQ/dt}{P_1}$$

where m_i and m_f are the initial and final aquamolalities.

Results

The heats of dilution ΔH^{dil}, in J kg^{-1} of solvent and $\Delta\phi_L = \Delta H^{dil}/m_f$ expressed as J mol^{-1} of solute, for biuret in aqueous solutions, are reported in Table 1. Polynomial expansions of $\Delta\phi_L$ as a function of the molalities were used to interpolate the experimental data (14):

$$[5]\quad \Delta\phi_L(m_i \rightarrow m_f) = (1/m_f)\,H^E(m_f) - (1/m_i)\,H^E(m_i) = h_{BB}(m_f - m_i) + h_{BBB}(m_f^2 - m_i^2) + \ldots$$

The degree of the interpolating polynomial, obtained by a least-squares analysis, is chosen as the one for which all the coefficients exceed their own 95 percent confidence limit. According to this criterion, only h_{BB} is significant in the concentration range explored.

The heats relative to the mixing of two binary solutions of B and U, $\Delta H_{UB}{}^{mix}$, are reported in Table 2. To simplify the evaluation of the cross interaction coefficients, the auxiliary function $\Delta H^* = \Delta H_{UB}{}^{dil} - \Delta H_U{}^{dil} - \Delta H_B{}^{dil}$ is used (11, 12).

The enthalpies of dilution for the binary solutions were calculated from eq. [5], by multiplying for the appropriate m_f and using the parameters h_{ii} reported in Table 1 for B and in Table 2 for U. It is possible to correlate ΔH^* and the enthalpic coefficients through the following expression:

$$[6]\quad \Delta H^* = H^E(m_B, m_U) - H^E(m_B) - H^E(m_U) = 2\,h_{UB}m_U m_B + 3\,h_{UUB}m_U{}^2 m_B + 3\,h_{UBB}\,m_B{}^2 m_U + \ldots$$

Equation [6] can be interpolated by a least-squares method. The analysis of the relative confidence limits shows that only the pair interaction coefficient h_{UB} is significant in the concentration range studied. The limited solubility of biuret and, at the same time, its relatively large heat of dilution allowed the exploration of a range of concentration unusually low for nonelectrolytes, without loss of accuracy.

TABLE 1. Heats of dilution for aqueous solutions of biuret (B) at 25°C[a]

m_i	m_f	$\Delta H^{dil}(m_i \rightarrow m_f)$ J kg^{-1}	$\Delta\phi_L = \Delta H^{dil}/m_f$ J mol^{-1}
0.1552	0.0300	8.34	278
0.1323	0.0257	6.27	244
0.1552	0.0497	10.49	211
0.1323	0.0425	7.55	178
0.1572	0.0743	12.92	174
0.1493	0.0707	11.43	162
0.1415	0.0670	10.68	159
0.1336	0.0633	8.97	142
0.1258	0.0600	8.36	139
0.1179	0.0563	7.62	135
0.1552	0.0470	11.81	251
0.1552	0.0470	10.95	233
0.1526	0.0433	9.93	229
0.1369	0.0388	7.92	204
0.1526	0.1089	10.42	95.7
0.1369	0.0978	8.51	87.0
0.1552	0.0300	7.21	240

[a]Enthalpic pair interaction coefficient evaluated according to eq. [5]: $h_{BB} = -2120 \pm 61$ J mol^{-1} (mol kg^{-1})$^{-1}$. The error corresponds to the 95% confidence limit in the value of the coefficient.

TABLE 2. Heats of mixing for aqueous solutions of biuret (B) and urea (U) at 25°C[a]

$(m_B)_i$	$(m_B)_f$	$(m_U)_i$	$(m_U)_f$	ΔH^{mix} J kg^{-1}	$-\Delta H^*$ J kg^{-1}
0.0724	0.0410	2.0328	0.8813	257	34
0.1133	0.0509	0.9922	0.5467	30.0	54
0.1133	0.0588	0.4893	0.2353	3.4	23
0.1451	0.0906	0.4893	0.1755	3.0	25
0.1451	0.0806	0.9922	0.4413	34.9	53
0.1451	0.0818	2.0328	0.8869	208	92
0.1133	0.0286	0.9764	0.7299	26.9	34
0.1133	0.0293	1.8771	1.3912	86.7	105
0.1451	0.0598	1.8771	1.1043	147	106
0.1451	0.0576	0.9764	0.5891	25.9	57
0.1133	0.0462	1.8771	1.1124	163	84
0.1133	0.0452	0.9764	0.5873	35.6	43
0.1133	0.0445	0.4779	0.2901	4.8	20
0.1451	0.0218	2.0328	1.7277	88.9	57
0.1451	0.0209	0.9922	0.8492	13.3	30
0.1451	0.0209	0.9922	0.8492	10.9	32
0.1133	0.0201	2.0328	1.6724	100	65
0.1133	0.0185	0.9922	0.8305	19.0	28
0.1133	0.0185	0.9922	0.8305	19.3	27

[a]Enthalpic pair interaction coefficient evaluated according to eq. [6] and using $h_{UU} = -350$ (refs. 6, 12): $h_{UB} = -796 \pm 84$ J mol^{-1} (mol kg^{-1})$^{-1}$. The error corresponds to the 95% confidence limit in the value of the coefficient.

Discussion

For aqueous solutions of urea and urea-like solutes, two groups of models have been proposed. The first of them (3, 15–18) assumes the formation of reversible dimers (in some cases, polymers) of

urea. However, the close similarity between the thermodynamic excess properties of urea and thiourea (8) shows that they are not realistic. The second group of approaches focuses the attention on the perturbations induced into the solvent, more than on the direct solute–solute interactions. The first model of this group was a statistical one, developed for dilute solutions. It assumes that the main effect of urea is that of a "statistical structure breaker" (19) of water. It is supported by spectroscopic (20, 21) and nmr (22) evidence. In preceding papers (7, 8), making some hypotheses on the hydration state, we proposed an overall qualitative explanation of the thermodynamic properties of concentrated and moderately concentrated aqueous solutions of urea-like solutes. The main process in these solutions should be the coalescence of the hydration cospheres upon the concentration process. The relaxation of water from the hydration layers to the bulk state, less rich in enthalpy and in entropy, should define the signs of the excess properties.

Among the urea-like solutes, biuret is very interesting. The partial double bond character of C—N and N—C bonds makes the biuret molecule essentially planar (in the monohydrate crystals the angle between the two NH_2–CO–NH– frameworks is about 5° (23)) and partially rigid, even though it is possible to hypothesize a concerted internal rotation around the two mentioned bonds in solution. As in the case of urea, however, the excess thermodynamic properties at 25°C may be interpreted in more than one way. Even for biuret the value of h_{BB} can be due either to a relaxation of water from the cospheres coalescing during the concentration process, or to the formation of one or a pair of H-bonds. The first mechanism does not exclude completely the second one but it seems the most convincing. Friedman and Krishnan have shown, on the other hand, that if the solute–solvent interaction makes the solvent–solvent forces less attractive, the result is a net weak attraction between two solute particles (24). Anyway, the larger values of the pair interaction coefficients for biuret seem to indicate that the degrees of advancement of the involved molecular processes are more extended with respect to urea and other urea-like solutes.

The similarity of the properties of biuret and urea solutions is confirmed by the behaviour of the ternary solutions, which suggests that the same qualitative effects determine the values of all the self and cross parameters. In Table 3 the enthalpic coefficients of the pair interactions for B, U, and their mixtures are reported. Also reported is the

TABLE 3. Enthalpic pair interaction coefficients for aqueous solutions of urea (U) and biuret (B) at 25°C (units: J mol^{-1} (mol kg^{-1})$^{-1}$)

	$h_{ij(exp)}$	$h_{ij(calc)}$[a]	$h_{ij(calc)}$[b]	$h_{ij(calc)}$[c]
U–U	−350	—	−569	−280
B–B	−2120	—	−1575	−1120
B–U	−796	−861	−942	−560

[a]Calculated according to eq. [7].
[b]Calculated according to ref. 6 and to the procedure illustrated in the text.
[c]Calculated according to ref. 27 and to the procedure illustrated in the text.

value of h_{UB} predicted by the empirical rule:

$$[7] \quad h_{ij} \simeq -(h_{ii}\, h_{jj})^{1/2}$$

This is a case of the empirical rule $h_{ij}^2 = h_{ii}h_{jj}$ discussed in a preceding paper (25). This rule was first found by Franks (26) for alcohols and seems applicable to all the simple pairs of organic solutes, having both $h_{ii}, h_{jj} > 0$. The pair urea–biuret is, vice versa, a case for which both the coefficients are negative. We pointed out that the rule works better when the solutes i and j are similar and bear groups all perturbing water in the same manner. The close prediction of the value of h_{UB} (the agreement is within 8%) outlines, in our opinion, the strict analogy between the interactions determining the properties of the binary and ternary aqueous solutions of urea and biuret. Also given in Table 3 are the values of h_{ij} evaluated according to the group contribution method, following the same procedure used by Savage and Wood (6) and considering biuret as the sum of an "amide" and of a "urea group". Table 3 also contains the value for the "urea group" recalculated more recently by Wood and Hiltzik (27). Even considering biuret as the sum of two "urea groups" the disagreement was beyond the limits of uncertainty (± 220 J mol^{-1} (mol kg^{-1})$^{-1}$) found by those authors for other substances. We think that this happens because of the partial failure of the additivity principle (which is the base for the validity of the approach). For the excess enthalpy we introduced (25) a relative effectiveness coefficient $b_{i/j} = (h_{ii}/h_{jj})^{1/2}$. This coefficient accounts for the contribution of one mole of solute i in determining the value of H^E with respect to one mole of solute j. On this basis biuret seems to be 2.45 times more effective than urea in determining H^E of aqueous solutions. In our opinion, the value 2.45 found for the coefficient $b_{B/U}$ indicates, for biuret, the existence of a cooperative, intramolecular effect, which enhances its capability of undergoing interactions in these solutions, whatever the actual mechanism. At the same time, the good prediction given by eq. [7] excludes any

specific interaction in the biuret–urea solutions with respect to other urea-like solutions.

Acknowledgement

This work was carried out with the financial support of the Italian National Research Council (C.N.R.).

1. J. S. ROWLINSON. Liquids and liquid mixtures, 1st and 2nd eds. Butterworths, London. 1959, 1969.
2. F. T. GUCKER, JR. and H. B. PICKARD. J. Am. Chem. Soc. **62**, 1464 (1940).
3. R. H. STOKES. Aust. J. Chem. **20**, 2087 (1967), and references quoted therein.
4. D. HAMILTON and R. H. STOKES. J. Solution Chem. **1**, 223 (1972).
5. P. R. PHILIP, G. PERRON, and J. E. DESNOYERS. Can. J. Chem. **52**, 1709 (1974).
6. J. J. SAVAGE and R. H. WOOD. J. Solution Chem. **5**, 733 (1976).
7. G. BARONE, G. CASTRONUOVO, C. DELLA VOLPE, and V. ELIA. J. Solution Chem. **6**, 117 (1977).
8. G. BARONE, P. CACACE, G. CASTRONUOVO, and V. ELIA. Gazz. Chim. Ital. **110**, 215 (1980).
9. J. J. KOZAK, W. S. KNIGHT, and W. KAUZMANN. J. Chem. Phys. **48**, 675 (1968).
10. H. L. FRIEDMAN and C. V. KRISHNAN. J. Solution Chem. **2**, 119 (1973).
11. J. E. DESNOYERS, G. PERRON, L. AVÉDIKIAN, and J. P. MOREL. J. Solution Chem. **5**, 631 (1976).
12. F. FRANKS, M. PEDLEY, and D. S. REID. J. Chem. Soc. Faraday Trans. I, **72**, 359 (1976).
13. G. BARONE, G. CASTRONUOVO, V. CRESCENZI, V. ELIA, and E. RIZZO. J. Solution Chem. **7**, 179 (1978).
14. J. L. FORTIER, P. A. LEDUC, P. PICKER, and J. E. DESNOYERS. J. Solution Chem. **2**, 467 (1973).
15. J. A. SCHELLMAN. C.R. Lab. Carlsberg, Ser. Chim. **29**, 223 (1955).
16. G. C. KRESHECK and H. A. SCHERAGA. J. Phys. Chem. **69**, 1704 (1966).
17. R. H. STOKES. J. Phys. Chem. **69**, 4012 (1965).
18. S. J. GILL and E. L. FARQUHAR. J. Am. Chem. Soc. **90**, 3039 (1968).
19. H. S. FRANK and F. FRANKS. J. Chem. Phys. **48**, 4746 (1968).
20. G. E. WALRAFEN. J. Chem. Phys. **44**, 3726 (1966).
21. G. BARONE, E. RIZZO, and V. VITAGLIANO. J. Phys. Chem. **74**, 2230 (1970).
22. E. G. FINER, F. FRANKS, and M. J. TAIT. J. Am. Chem. Soc. **94**, 4424 (1972).
23. E. W. HUGHES, H. L. YAKEL, and H. C. FREEMAN. Acta Crystallogr. **14**, 345 (1961).
24. H. L. FRIEDMAN and C. V. KRISHNAN. *In* Water, a comprehensive treatise. Vol. 3. *Edited by* F. Franks. Plenum Press, New York, NY. 1973. Chapt. 1.
25. G. BARONE, G. CASTRONUOVO, and V. ELIA. J. Solution Chem. **9**, 607 (1980).
26. S. ABLETT, M. D. BARRATT, F. FRANKS, M. D. PEDLEY, and D. S. REID. *In* L'eau et les systèmes biologiques. *Edited by* A. Alfsen and A. J. Berteaud. Editions du CNRS Paris. 1976. p. 105.
27. R. H. WOOD and L. H. HILTZIK. J. Solution Chem. **9**, 45 (1980).

Polarisation cathodique en milieu alcalin des alliages Nb–Co

Y. UMETSU
Université Tohoku, Sendai, Japan
D. L. PIRON
Ecole Polytechnique de Montréal, Montréal (Qué.), Canada
ET
G. BÉLANGER
Institut de Recherche d'Hydro-Québec, Varennes (Qué.), Canada J0L 2P0

Reçu le 2 juillet 1980

Y. UMETSU, D. L. PIRON et G. BÉLANGER. Can. J. Chem. **59**, 1261 (1981).

L'examen microscopique des alliages de NbCo a été réalisé et a permis l'identification des différentes phases. Ces alliages furent évalués vis-à-vis leur comportement pour la réaction du dégagement de l'hydrogène (RDH) à 25°C dans une solution de 25% KOH. On observe une activité accrue par rapport au Nb ou Co pur pour les alliages entre 20 et 70% Co. Cependant cette activité pour la RDH se situe en dessous de l'activité électrocatalytique du Ni pur. Comme pour les alliages NbNi, les alliages NbCo montrent une dégradation importante de leur surface sous une polarisation cathodique prolongée (6 h) à des densités de courant variant entre 400 et 700 mA cm^{-2}. Cette dégradation se manifeste surtout pour les alliages où la teneur en Co est inférieure à 50% en poids. Pour les alliages supérieurs, la surface demeure stable vis-à-vis la RDH. La dégradation de la surface est associée à la présence de la phase δ dans l'alliage: cette phase est la solution solide de Nb.

Y. UMETSU, D. L. PIRON, and G. BÉLANGER. Can. J. Chem. **59**, 1261 (1981).

NbCo alloys were prepared and their composition characterized by optical microscopy. These alloys were evaluated for their electrochemical activity towards the hydrogen evolution reaction (HER) at 25°C in a 25% KOH solution. The alloys between 20 and 70wt% Co showed an increased activity compared to their parent metals. However the activity is below the one observed for pure Ni. As for the NbNi alloys, the NbCo undergo some surface degradation under prolonged (6 h) cathodic polarization at 400–700 mA cm^{-2}. This disintegration of the surfaces is observed for alloys below 50% in Co. Above this proportion, the alloys remain stable towards the RDH. This degradation is associated with the presence of the δ phase in the alloy: this phase is the solid solution of Nb in the alloy.

I. Introduction

Dans la quête de nouveaux matériaux pour l'électrolyse de l'eau en milieu alcalin, le niobium a été étudié par notre groupe (1–5). Le mécanisme du dégagement de l'hydrogène sur le métal pur en milieu alcalin a été démontré (1, 2) et la réaction semble obéir au mécanisme d'Heyrovsky où l'étape déterminante de la réaction est la désorption électrochimique. A la suite de ces travaux, les caractéristiques du niobium (Nb) (3, 4) et des alliages niobium–nickel (Nb–Ni) (5, 6) ont été déterminées vis-à-vis le dégagement de l'hydrogène en milieu alcalin fortement concentré (25% KOH) et à différentes températures.

Afin de continuer notre exploration des alliages du Nb et de tenter de stabiliser la surface, nous avons déterminé l'activité électrocatalytique et la stabilité des alliages Co–Nb. L'activité a été déterminée par les courbes de polarisation de différents alliages et leur stabilité par l'examen microscopique de leur surface avant et après ces polarisations.

II. Technique expérimentale

(a) Préparation des alliages

Les alliages Co–Nb furent préparés à partir de billes de cobalt de 99.9% et de poudre de niobium de même pureté. Les quantités requises furent fondues dans un four à arc sous vide utilisant une électrode de tungstène et un creuset de cuivre refroidi à l'eau. Après refroidissement et solidification, le bouton d'alliage ainsi formé a été retourné et refondu pour assurer une homogénéité complète à l'état solide de l'alliage. Ce procédé de fontes successives fut répété de 2 à 3 fois selon la composition de l'alliage. Après cette première étape les boutons furent chauffés à 1000°C sous vide pendant 24 h et pour ensuite être refroidis dans l'air. De ces spécimens, des électrodes de 5 × 5 × 3 mm furent taillées à la scie diamantée; après la taille, ces électrodes furent recuites à 1000°C sous vide (environ 10^{-6} mm Hg) pendant 10 min.

L'analyse chimique d'échantillons prélevés des boutons a montré que les alliages étaient homogènes et qu'aucune contamination soit de tungstène ou de cuivre n'avait été introduite. L'examen microscopique de la microstructure des alliages n'a pas révélé de ségrégation décelable ni l'existence de constituants non mélangés.

La surface de 5 × 5 mm fut polie sur papier de verre jusqu'à 600 et le polissage fin réalisé avec une suspension d'alumine de 0.05 μ. L'échantillon poli fut monté dans un support de Teflon et les contours isolés avec la colle époxy. Aucun polissage chimique ou électrochimique ne fut tenté pour éviter la dissolution sélective d'une des composantes de l'alliage. Avant chaque courbe de polarisation, la surface de 5 × 5 fut repolie avec la suspension de 0.05 μ d'alumine et lavée à l'eau distillée.

(b) Procédures électrochimiques

L'électrolyte utilisé a été une solution de KOH à 25% par poids. La solution a été désoxygénée avant chaque polarisation pendant 4 h par le barbotage d'hydrogène.

Un montage conventionnel à trois électrodes séparées fut utilisé: l'électrode calomel saturée fut employée comme élec-

0008-4042/81/081261-06$01.00/0
©1981 National Research Council of Canada/Conseil national de recherches du Canada

Can. J. Chem. Downloaded from www.nrcresearchpress.com by 210.87.254.42 on 09/06/12
For personal use only.

Can. J. Chem. Downloaded from www.nrcresearchpress.com by 210.87.254.42 on 09/06/12
For personal use only.

trode de référence avec un potentiostat Tacussel PRT20-2X. Une électrode auxiliaire de platine fut utilisée. La procédure potentiostatique à pseudo-équilibre fut utilisée: elle consiste essentiellement à polariser l'électrode de travail à une valeur déterminée pendant 2 min et à enregistrer le courant essentiellement constant à la fin de cet intervalle. La plage de potentiels ainsi balayée a été à partir du potentiel de repos de l'électrode dans le milieu jusqu'à −1.6 V (vs. ECS). La variation de potentiel entre chaque point a été soit 50 ou 25 mV. Les potentiels rapportés dans le texte ont été ramenés vis-à-vis l'électrode normale d'hydrogène (ENH).

Les courbes ainsi obtenues furent corrigées pour la chute ohmique entre l'électrode de travail et l'extrémité du capillaire Luggin à l'aide de la technique d'interruption de courant. L'examen microscopique des surfaces après polarisation fut réalisé pour les alliages de 30, 50 et 70% de Co par rapport à la masse.

III. Résultats

(a) Examen microscopique des alliages préparés

Le diagramme de phases du système binaire NbCo est illustré à la fig. 1 (7). Les alliages préparés furent solidifiés à partir des masses en fusion dans un creuset en cuivre refroidi à l'eau: la vitesse de solidification ne fut pas contrôlée. A la fig. 2, les photos des microstructures des alliages préparés sont présentées: les échantillons ont été attaqués par une solution HF + HNO_3 ($HF:HNO_3:H_2O$: 15:30:55 par volume) après un polissage avec une suspension de 0.05 μ d'alumine. La partie noire de la photo représente la partie riche en Co car cet élément est attaqué par la solution. Les différents échantillons furent analysés par diffraction des rayons-X, la sonde microscopique d'analyse électronique et la microscopie optique. L'alliage 1% Co et le composé intermétallique NbCo furent préparés et utilisés comme échantillons de comparaison standard pour les profils de diffraction des rayons-X. Aucune différence notable n'a été observée entre la surface des échantillons ainsi analysés et le coeur de l'alliage.

(i) Alliage 10% Co–Ni

Cet alliage est composé essentiellement de grains de phase δ (la solution solide de Nb) et une petite quantité de l'eutectique δ–γ (γ étant le composé NbCo). La seconde phase a été décelée à la frontière des grains de la phase γ. Le profil de diffraction des rayons-X laisse apparaître des fortes raies associées au Nb ou à l'alliage 1% CoNb et de faibles raies de la phase γ.

(ii) Alliage 20% Co–Nb (fig. 2a)

Cet alliage est un mélange en quantité comparable de phases δ et γ et d'une faible quantité de l'eutectique NbCo.

(iii) Alliage 30% Co–Nb (fig. 2b)

Cet alliage est constitué principalement de la phase γ et d'une faible partie de phase δ. Cette dernière phase est détectée par le spectre de diffraction des rayons-X.

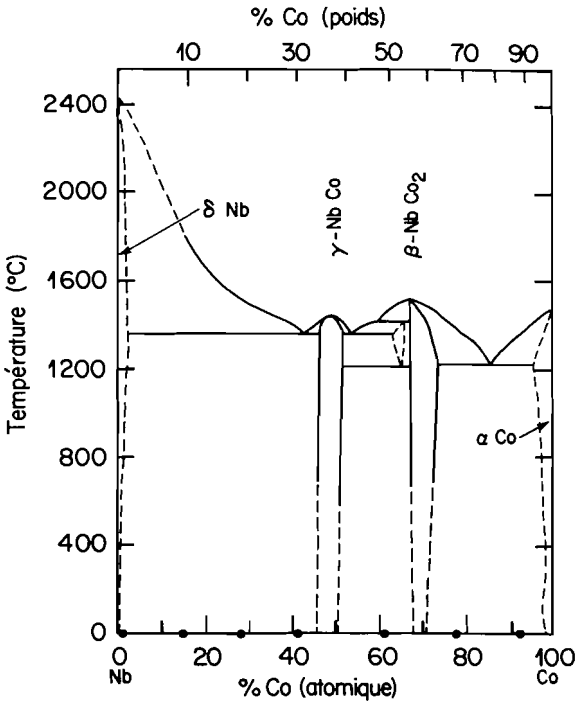

FIG. 1. Diagramme de phase du système Nb–Co d'après Shunk (7); les alliages utilisés dans cette étude sont illustrés en abscisse.

(iv) Alliage 50% Co–Nb (fig. 2c)

De longs grains de la phase γ furent observés; entre ceux-ci, la phase β ($NbCo_2$) a pu être mise en évidence. Aucune raie de la phase δ ne fut décelée.

(v) Alliage 70% Co–Nb (fig. 2d)

Cet alliage est un mélange de grains fins des phases β et α; cette dernière est la solution solide de Co.

(vi) Alliage 90% Co–Nb (fig. 2e)

Cet alliage est constitué essentiellement de la phase α; sur certains endroits de la surface on a pu observer certaine structure orientée de la phase β.

(b) Polarisation cathodique

Les courbes de polarisation du Nb, Co et certains des alliages étudiés sont illustrées à la fig. 3; en plus on inclut la courbe du Ni pour fin de comparaison. Ces courbes sont déjà corrigées pour tenir compte de la chute ohmique. Chaque courbe couvre des densités de courant s'échelonnant entre 10^{-1} à 5×10^2 mA cm^{-2}.

La courbe de polarisation du Co pur se situe entre celle de Nb et de Ni (5); le cobalt est un meilleur électrocatalyseur pour la RDH que le niobium mais moins efficace que le nickel. La fig. 3 montre que certains alliages présentent des surtensions inférieures pour la RDH que le niobium ou le cobalt pur mais sans atteindre le rendement du

Can. J. Chem. Downloaded from www.nrcresearchpress.com by 210.87.254.42 on 09/06/12
For personal use only.

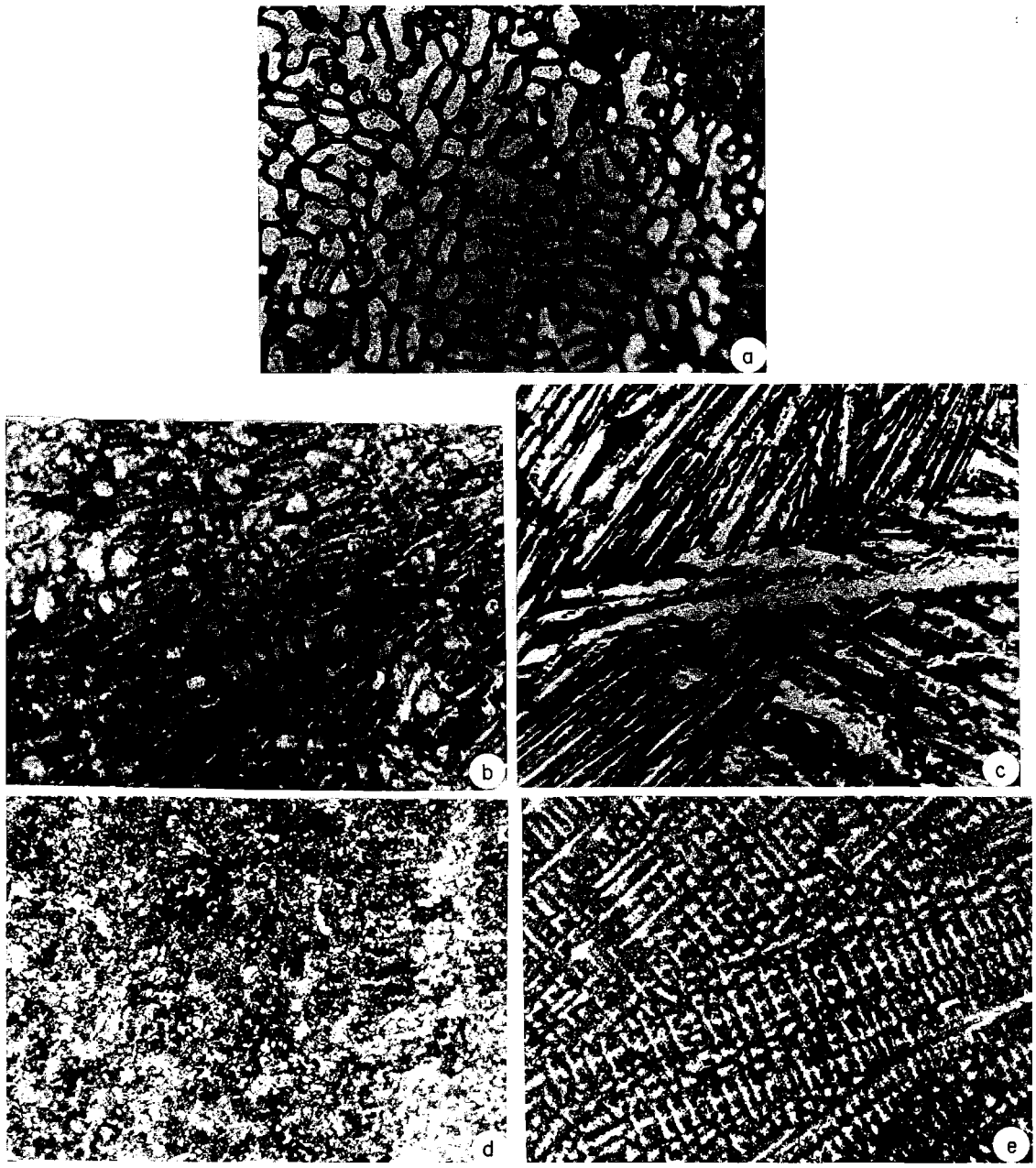

FIG. 2. Photographies microscopiques (grossissement 200 ×) des surfaces des alliages NbCo attaquées par une solution HF, HNO_3: les parties noires sont associées aux phases riches en Co. (*a*) 20% Co; (*b*) 30% Co; (*c*) 50% Co; (*d*) 70% Co; (*e*) 90% Co.

nickel. L'amélioration d'efficacité de la RDH observée précédemment (5) pour l'alliage 30% Ni–Nb ne se retrouve pas avec le cobalt.

Les pentes de Tafel furent évaluées; jusqu'à 20% de Co, les pentes demeurent inchangées à 120 mV par décade. Lorsque la proportion de cobalt augmente, cette pente s'accroît pour atteindre une valeur constante d'environ 140 mV par décade.

La surtension de la RDH pour une densité de courant de 10 mA cm^{-2} a été mesurée et tracée en fonction de la composition des alliages à la fig. 4. La surtension subit une chute importante pour l'alliage 30% Co comme cela avait été observé précédemment dans le cas des alliages Ni–Nb.

Le changement de surface apporté par la polarisation cathodique fut étudié pour les alliages de 30, 50 et 70% Co par la microscopie optique ainsi que la microscopie électronique à balayage. Chaque

Can. J. Chem. Downloaded from www.nrcresearchpress.com by 210.87.254.42 on 09/06/12
For personal use only.

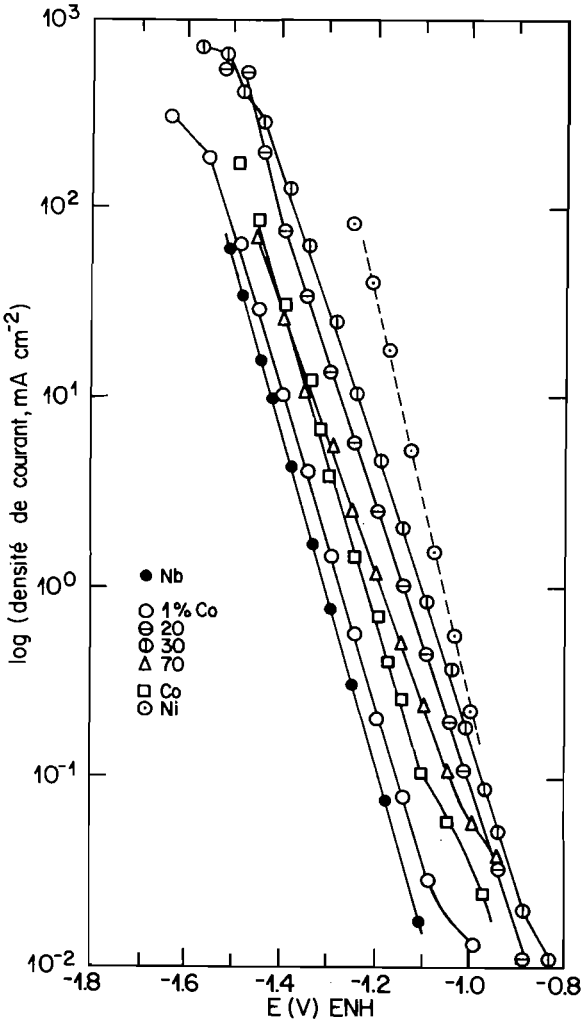

FIG. 3. Courbes de polarisation potentiostatique à l'équilibre du Nb, Ni, Co et des alliages NbCo; 25°C; sous atmosphère d'hydrogène.

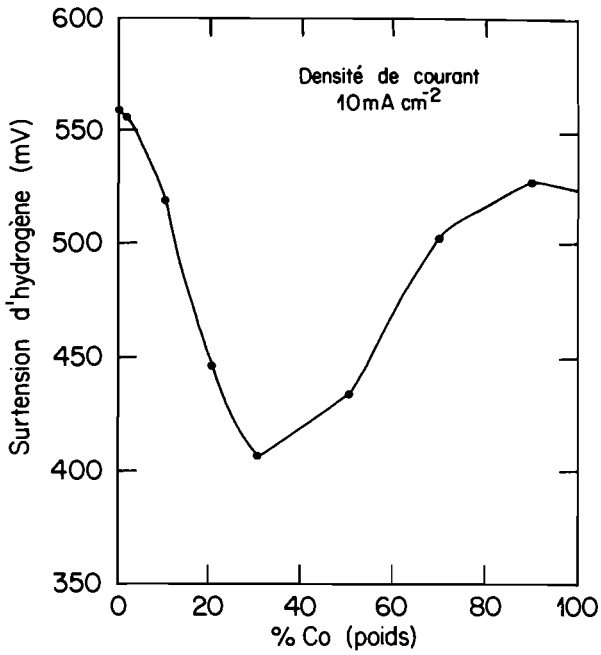

FIG. 4. Variation de la surtension de la réaction du dégagement d'hydrogène (η) en fonction de la composition de l'alliage NbCo à une densité de courant de 10 mA cm^{-2}; $\eta = E_{\text{observé}} - E_{\text{réversible}}$.

spécimen fut porté à une polarisation de -1.55 V vs. ENH pendant 6 h; les densités de courant initiales à ces tensions cathodiques variaient de 400 à 700 mA cm^{-2} selon les alliages.

A la fig. 5, nous présentons les photographies des surfaces ainsi traitées pour l'alliage 30% Co. La surface au cours de l'électrolyse est devenue uniformément noirâtre et après quelques heures, des fissures se sont révélées. A partir des photos micrographiques de la surface (figs 5*a* et *b*), on a observé un film noir sous lequel une couche brune (grise sur les photos) a été décelée. Le film de surface pouvait se détacher facilement. Les figs 5*c*, *d* et *e* sont des images de la microscopie électronique à balayage où des marches sont observées (fig. 5*c*) à la surface et le long de ces marches des fissures apparaissent et se propagent. On remarque que l'extrémité des bordures est retroussée vers l'extérieur (fig. 5*d*). Cette observation peut être associée à une expansion volumétrique importante sous la surface durant la polarisation cathodique. La forme hachurée des fragments des bordures indique la fragilité des films formés à la surface. La fig. 5*e* illustre la surface sous-jacente des films de surface à un endroit où ce film s'est décollé. Compte tenu de la nature amorphe des produits de surface, l'analyse aux rayons-X s'est avérée impuissante à identifier la composition de ces différents produits de désintégration.

Jusqu'à 30% de Co, l'addition de cet élément au niobium induit une fragilisation importante des alliages durant la polarisation cathodique. Au-delà de cette concentration, la génération et la propagation des fissures sont à toute fin pratique supprimées. Les surfaces des alliages 50 et 70% Co soumises à la polarisation cathodique décrite plus haut passent d'un fini lustré métallique à une apparence noire mate mais sans fissure. La couche de surface consiste en un produit poudreux et fin. Aux endroits où cette poudre a été balayée, on retrouve la surface métallique d'origine.

Des coupes transversales des alliages de 20% et 30% polarisés cathodiquement sont illustrées à la fig. 6. L'alliage à 20% montre une structure très

Can. J. Chem. Downloaded from www.nrcresearchpress.com by 210.87.254.42 on 09/06/12
For personal use only.

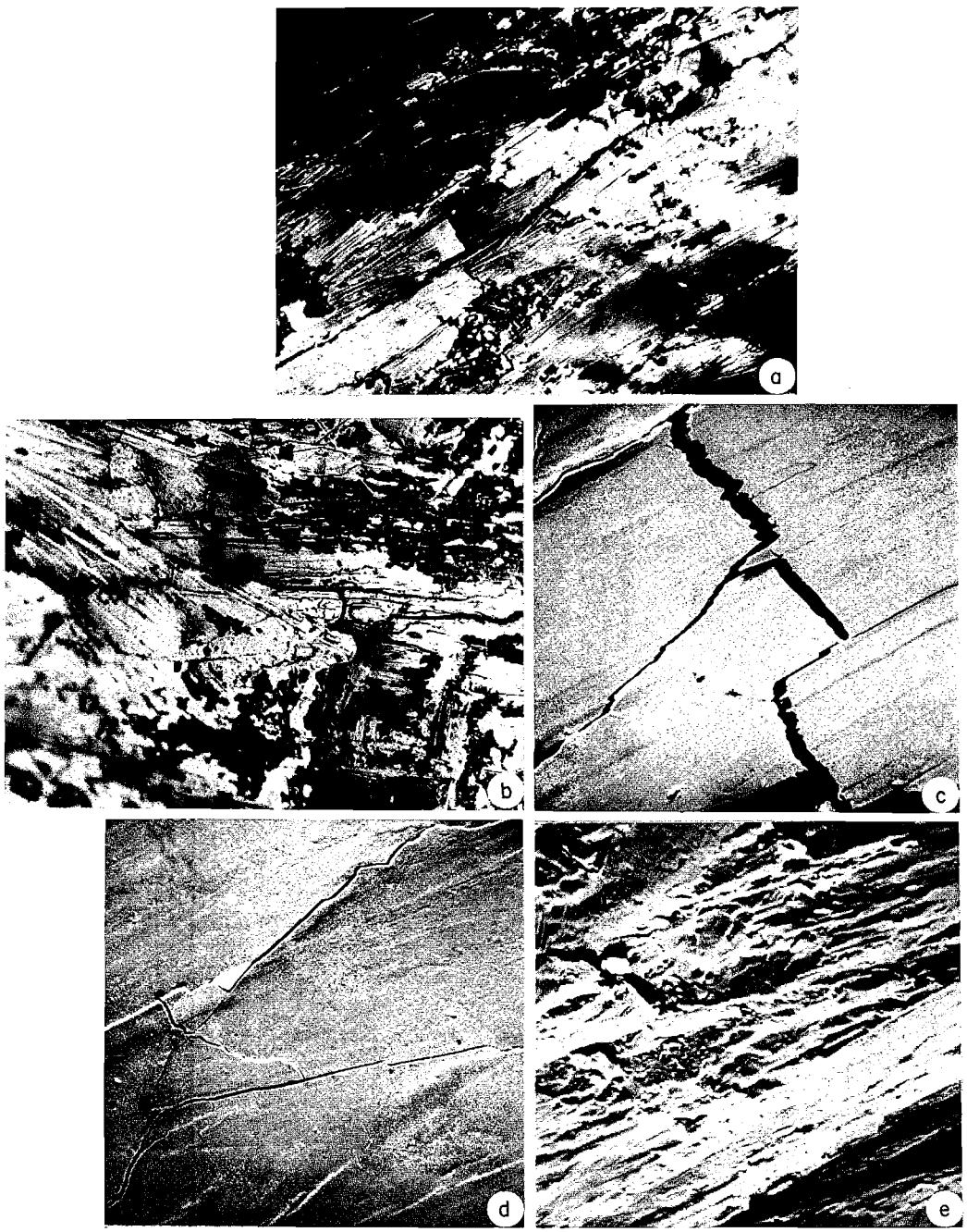

FIG. 5. Photographies microscopiques optiques (*a*, *b*) et électroniques à balayage (*c*, *d* et *e*) des surfaces de l'alliage 30% Co après une polarisation de 6 h à −1.55 V vs. ENH; (*a*) et (*b*) grossissement 200 ×; (*c*), (*d*), et (*e*) grossissement 550 ×.

modifiée par cette polarisation cathodique. Les fissures pénètrent profondément dans le métal. Pour l'alliage de 30% Co, la surface est aussi déformée par l'expansion volumétrique mais les dommages demeurent plus superficiels. Ces déformations ne furent pas observées pour les alliages de plus de 50% Co. Ces dommages ou déformations ne se manifestent pas de façon significative au cours des mesures réalisées dans l'obtention des courbes potentiostatiques illustrées à la fig. 3. Seule une polarisation prolongée (2 à 6 h) à des potentiels de −1.55 V révèlent ces dommages.

Can. J. Chem. Downloaded from www.nrcresearchpress.com by 210.87.254.42 on 09/06/12
For personal use only.

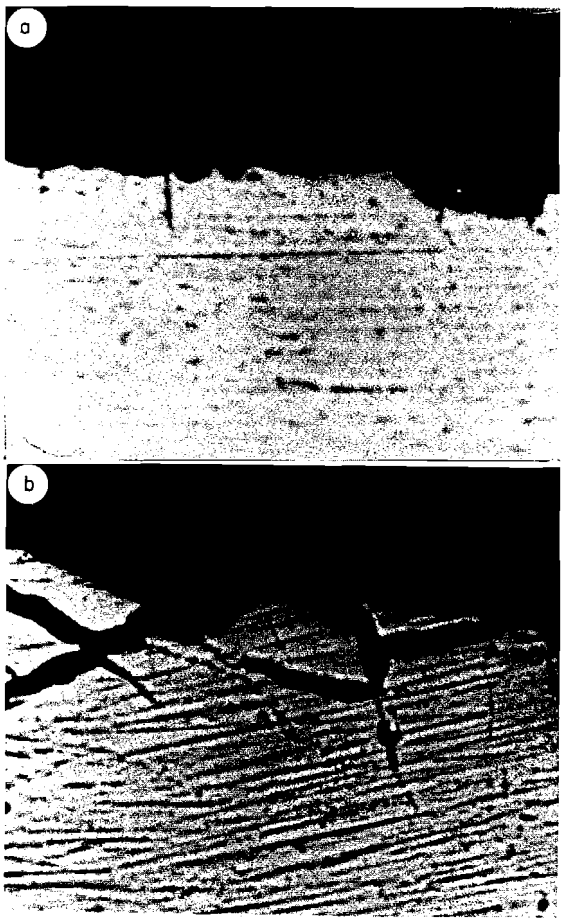

FIG. 6. Photographies microscopiques optiques (grossissement 50 ×) de coupes d'électrodes polarisées pendant 6 h à −1.55 V vs. ENH; (*a*) 20% Co; et (*b*) 30% Co.

IV. Discussion et conclusion

Comme nous l'avions observé précédemment dans le cas du nickel (5), l'alliage du cobalt et du niobium résulte en une amélioration sensible des propriétés catalytiques du nouveau matériau. En fait, pour une série d'alliages de 20 à 70% Co, le rendement dépasse celui du cobalt pur. Cependant, même le meilleur alliage ne réussit pas à surpasser le rendement du nickel pur.

Le principal problème que l'on rencontre avec les alliages du niobium est la dégradation de la surface pour les matériaux entre 20 et 30% de Co ou Ni (5, 6). Pour les alliages de plus forte teneur en Co, la stabilité s'accroît mais au détriment de l'activité électrocatalytique.

Dans le diagramme des phases à l'équilibre pour le système Co–Nb (fig. 1), il existe deux solutions solides (les phases δ et α respectivement riches en niobium et en cobalt) ainsi que deux composés intermétalliques soit le NbCo (phase γ) et le $NbCo_2$ (phase β). Le Nb et la phase δ possèdent un réseau cubique centré (c.c.) du type du tungstène, le NbCo un réseau cristallin similaire au W_6Fe_7 et enfin le $NbCo_2$ un empilement de phase de Laves (8–10). Le réseau du $NbCo_2$ passe du type $MgZn_2$ au type $MgCu_2$ lorsque la concentration de Co passe de 53 à 55.8% (poids). Les alliages utilisés dans la présente étude n'étaient pas monophasés mais bien des mélanges des phases α et β ou β et γ ou enfin γ et δ selon la composition des mélanges.

L'absence de données thermodynamiques pertinentes pour le système NbCo vis-à-vis les réactions avec l'hydrogène nous empêche de quantifier le comportement de chaque phase vis-à-vis cette molécule.

Cependant, comme la phase δ est une solution solide riche en Nb avec une faible concentration de soluté (Co), cette phase peut être associée au comportement du niobium vis-à-vis l'hydrogène. La dégradation de la surface pour les alliages où le Co est inférieur à 40% peut donc être reliée à la présence de la phase δ. Cette conclusion semble s'imposer car au-dessus de 40% où la phase δ ne se retrouve plus, la surface sous l'action de la RDH demeure relativement stable et ne présente plus de fissures. Donc en alliant le niobium avec le cobalt, la concentration de Co doit être supérieure à 40% pour obtenir une surface stable vis-à-vis la RDH.

Remerciements

L'un de nous (Y.U.) tient à remercier Hydro-Québec pour le support financier accordé pour la réalisation de cette étude.

1. D. L. PIRON et C. P. VIJAYAN. C.R. Acad. Sci. Paris C, **281**, 75 (1975).
2. C. P. VIJAYAN et D. L. PIRON. Can. J. Chem. **55**, 375 (1977).
3. M. OKUYAMA, G. BÉLANGER et D. L. PIRON. Int. J. Hydrogen Energy, **3**, 297 (1978).
4. K. SUGIMOTO, G. BÉLANGER et D. L. PIRON. J. Electrochem. Soc. **126**, 535 (1979).
5. K. SUGIMOTO, G. BÉLANGER et D. L. PIRON. Surf. Technol. **9**, 83 (1979).
6. K. SUGIMOTO, G. BÉLANGER et D. L. PIRON. Corrosion. **36**, 437 (1980).
7. F. A. SHUNK. Constitution of binary alloys. 2nd Supplement. McGraw-Hill, New York, NY. 1969. p. 180.
8. A. RAMAN. Trans. AIME, **236**, 561 (1966).
9. B. J. PIEARCY, R. JACKSON et B. B. ARGENT. J. Inst. Metals, **91**, 257 (1962–63).
10. J. K. PARGETER et W. HUME-ROTHERY. J. Less Common Met. **12**, 366 (1967).

Spectroscopic confirmation of orientational disorder of the cyanide groups in sodium cyanide dihydrate, $NaCN{\cdot}2H_2O$[1]

MICHAEL FALK

Atlantic Research Laboratory, National Research Council of Canada, 1411 Oxford Street, Halifax, N.S., Canada B3H 3Z1

Received October 1, 1980

MICHAEL FALK. Can. J. Chem. **59**, 1267 (1981).

Occurrence of orientational disorder involving the CN groups in $NaCN{\cdot}2H_2O$, suggested by van Rij and Britton on the basis of a refinement of X-ray diffraction data, has been confirmed by the doubling of CN stretching fundamentals. The ratios of doublet band areas are consistent with the energy of the orientation NC···Na being higher than that of the "normal" orientation, CN···Na by 800 ± 300 cal mol^{-1}.

MICHAEL FALK. Can. J. Chem. **59**, 1267 (1981).

En faisant appel à un affinement des données obtenues à partir d'une étude de diffraction des rayons-X, van Rij et Britton ont suggéré que l'orientation des groupes CN du $NaCN{\cdot}2H_2O$ est désordonnée. On a confirmé l'existence d'un tel désordre par l'observation d'un doublement des bandes fondamentales des vibrations de valence du groupe CN. Les rapports des aires des doublets sont en accord avec la conclusion que l'énergie de l'orientation NC···Na est plus élevée que celle de l'orientation normale, CN···Na, de 800 ± 300 cal mol^{-1}.

[Traduit par le journal]

The crystal structure of $NaCN{\cdot}2H_2O$ was first determined by Le Bihan (1), who found the cyanide groups to be oriented with their carbon atoms towards sodium, NC···Na. On the basis of subsequent refinement, using X-ray diffraction data collected at 150 K, Bats (2) found the cyanide groups to be oriented with their nitrogen atoms toward sodium, CN···Na, inverted with respect to the structure proposed by Le Bihan. A further refinement by van Rij and Britton (3), based on X-ray diffraction data collected at 295 K, led these authors to suggest that, at room temperature at least, the CN ions are partially disordered, with approximately 80% CN···Na and 20% NC···Na. Such orientational disorder should, in principle, produce a doubling of the vibrations involving the cyanide group. Upon an examination of the infrared spectrum of $NaCN{\cdot}2H_2O$ in the region of the fundamental CN stretching vibration we have, indeed, found spectroscopic confirmation of the orientational disorder postulated by van Rij and Britton.

Experimental

The dihydrate was prepared by recrystallizing sodium cyanide (BDH reagent grade) from aqueous solution at room temperature. The polycrystalline material was mulled with fluorocarbon oil and the mulls were sandwiched between calcium fluoride plates. Spectra were recorded on a Perkin Elmer model 180 spectrophotometer, fitted with a closed-cycle helium refrigerator (Displex model 202, Air Products and Chemicals Co.). Temperature readings (chromel/iron-doped-gold thermocouple) were checked against low-temperature transitions and found to be accurate to ± 1 K over most of the accessible range, 300–10 K. Spectral resolution was 2 cm^{-1}.

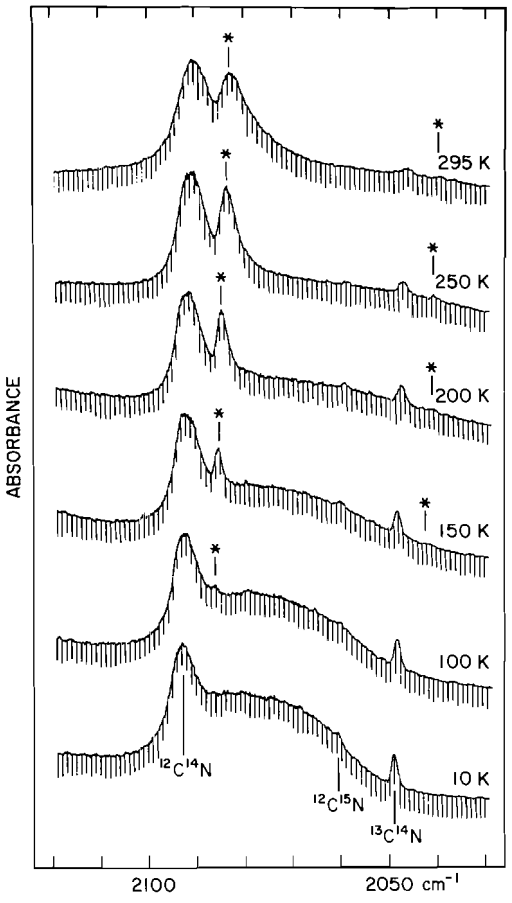

FIG. 1. The region of the CN stretching fundamental in the infrared spectrum of polycrystalline $NaCN{\cdot}2H_2O$ (fluorocarbon mull) at different temperatures. The peaks due to inverted CN groups are marked with asterisks.

[1]NRCC No. 19117.

0008-4042/81/081267-03$01.00/0

©1981 National Research Council of Canada/Conseil national de recherches du Canada

Can. J. Chem. Downloaded from www.nrcresearchpress.com by 210.87.254.42 on 09/06/12
For personal use only.

Can. J. Chem. Downloaded from www.nrcresearchpress.com by 210.87.254.42 on 09/06/12
For personal use only.

Results

In the 10 K spectrum, a broad absorption region extending from 2050 to 2100 cm^{-1} underlies the much sharper absorption peaks due to CN stretching vibrations (Fig. 1). The broad band is probably due to the combination $\nu_2 + \nu_L$ (involving the bending mode and one of the librational modes) of the water molecules in $NaCN \cdot 2H_2O$. It rapidly loses intensity with increasing temperature. At 10 K, the main CN stretching fundamental, due to the dominant isotopic species $^{12}C^{14}N$, gives rise to the band at 2092.8 cm^{-1}, while the minor isotopic species $^{13}C^{14}N$ (natural abundance 1.11%) and $^{12}C^{15}N$ (natural abundance 0.36%) give rise, respectively, to the small, sharp bands at 2060.9 and 2049.2 cm^{-1}. The calculated positions of these isotopic bands are, under a harmonic diatomic approximation, 2060.4 and 2049.1 cm^{-1}, respectively.

As the temperature increases, the $^{12}C^{14}N$ stretching band as well as its two isotopic satellites shift gradually toward lower wavenumbers (Fig. 2). At about 100 K a new absorption band becomes visible, about 7.0 cm^{-1} below the $^{12}C^{14}N$ peak, its band area rapidly increasing with temperature, until at 295 K it is about half the size of the main peak. The extra peak appears to be due to CN ions of reversed orientation.

In confirmation of this assignment, a similar doubling is observed for the $^{13}C^{14}N$ satellite band. At temperatures above 150 K a new peak emerges, 6.5 cm^{-1} below the $^{12}C^{14}N$ peak, its relative intensity increasing with temperature (Fig. 1). The barely observable $^{12}C^{15}N$ satellite band was too weak for its doubling to be seen.

Assuming that the intensity of the CN stretching fundamental is independent of orientation, the ratio of CN ions in the two orientations can be estimated from the areas of the two components of the $^{12}C^{14}N$ doublet. The results are plotted in Fig. 3, with error bars corresponding to twice the estimated standard error. Most of the experimental uncertainty arises from uncertain baseline, caused by the underlying broad absorption mentioned above. The $^{13}C^{14}N$ doublet is somewhat less affected by sloping baseline, but its very low intensity leads to even larger uncertainties in band areas.

At temperatures above 150 K the observed

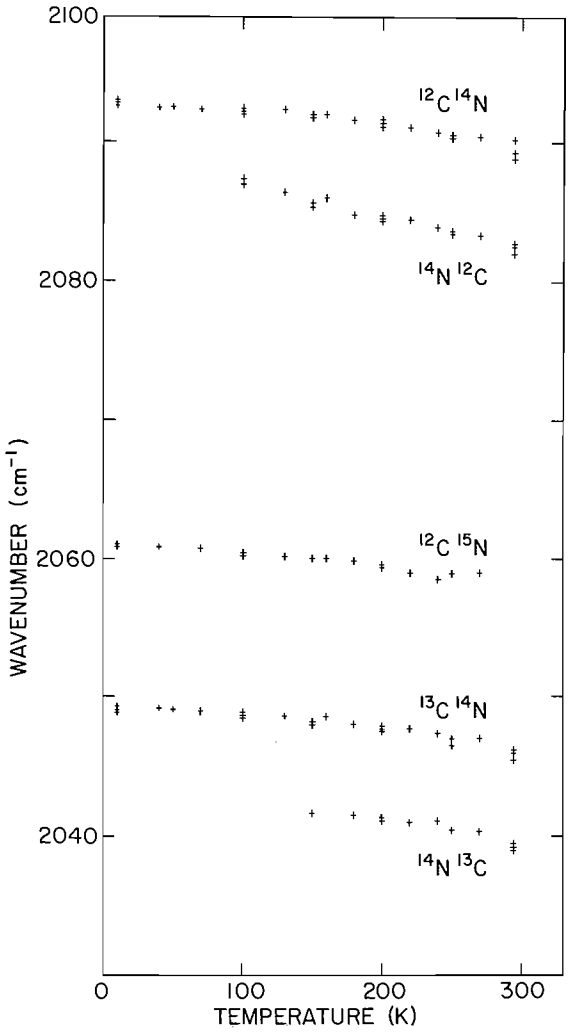

FIG. 2. Variation of peak wavenumbers of the bands in Fig. 1 with temperature.

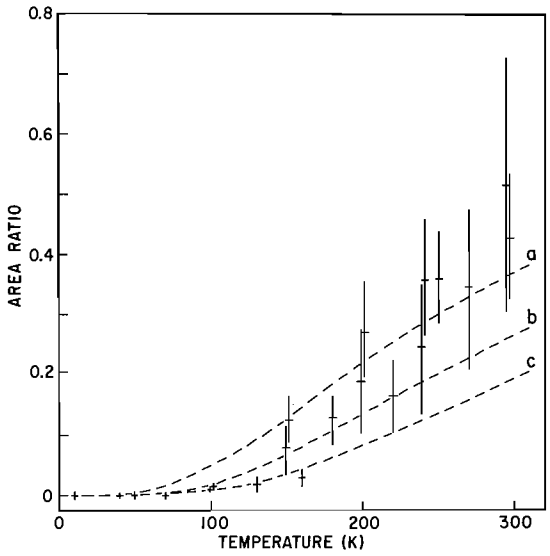

FIG. 3. Plot of the ratio of band areas of the $^{12}C^{14}N$ doublet as a function of temperature. Curves *a*, *b*, and *c* correspond to the function $\exp(-\Delta E/RT)$ where $R = 1.98$ cal deg^{-1} mol^{-1} and $\Delta E = 600$, 800, and 1000 cal mol^{-1}, respectively.

values fall within experimental error on the curve exp $(-600/RT)$, which corresponds to an order–disorder process in which there is no entropy difference between the two orientations and the energy difference is 600 cal mol^{-1}. Below 150 K the data are distinctly better fitted by exp $(-1000/RT)$, corresponding to an energy difference of 1000 cal mol^{-1}. A simple model based on CN ions with two orientations and a constant energy difference between them does not fit the data. This indicates that the disorder process is cooperative, the energy depending on the relative orientations of neighbouring CN ions, as well as on their orientation with respect to the site.[2]

[2]This type of cooperativity has been suggested by Professor Doyle Britton (personal communication).

Conclusions

The observed doubling of $^{12}C^{14}N$ and $^{13}C^{14}N$ stretching fundamentals confirms the occurrence of orientational disorder in $NaCN \cdot 2H_2O$. The ratios of the band areas are consistent with an energy difference of 800 ± 300 cal mol^{-1} between the two possible orientations. The fraction of reversed CN groups at 295 K is estimated to be 0.33 ± 0.06, greater than the estimate of 0.20 of van Rij and Britton (3). At 150 K this fraction is only 0.07 ± 0.04, which could have easily escaped detection in the study of Bats.

1. M. T. Le Bihan. Acta Crystallogr. **11**, 770 (1958).
2. J. W. Bats. Acta Crystallogr. B**33**, 466 (1977).
3. C. van Rij and D. Britton. Acta Crystallogr. B**34**, 2080 (1978).

Can. J. Chem. Downloaded from www.nrcresearchpress.com by 210.87.254.42 on 09/06/12
For personal use only.

Echange isotopique hydrogène–deutérium subi par les groupements méthyles de la triméthyl-4,5,6 pyrimidone-2

ERIC PICQUENARD ET PIERRE DIZABO

Laboratoire de Spectrochimie Moléculaire, Université Pierre et Marie Curie, 4 place Jussieu, 75230 Paris, Cedex 05, France

Reçu le 27 juin 1980

ERIC PICQUENARD et PIERRE DIZABO. Can. J. Chem. **59**, 1270 (1981).

L'échange isotopique hydrogène–deutérium des méthyles en positions 4 et 6 de la triméthyl-4,5,6 pyrimidone-2 dans D_2O à des acidités allant de pD 0,4 à 7,7 est suivie par rmn du proton. La vitesse d'échange passe par un maximum correspondant à l'équimolécularité de la pyrimidone avec son acide conjugué. Le maximum de vitesse est dû à l'arrachement par la molécule neutre d'un hydrogène du groupement méthyle de l'acide conjugué. Ce mécanisme est confirmé par l'étude de l'échange des méthyles de la tétraméthyl-1,4,5,6 pyrimidone-2.

ERIC PICQUENARD and PIERRE DIZABO. Can. J. Chem. **59**, 1270 (1981).

The rate of deuterium exchange of 4 and 6 methyl protons in 4,5,6-trimethyl-2-pyrimidone has been followed in D_2O over a range of acidity from pD 0.4 to 7.7 by means of proton magnetic resonance spectroscopy. The maximum of exchange rate represents equimolar proportions of the pyrimidone and its conjugate acid. The maximum is due to the neutral molecule acting as a base and removing a proton from one of the methyl groups of its conjugate acid. The exchange study of methyl protons in 1,4,5,6-tetramethyl-2-pyrimidone corroborates this mechanism.

Introduction

Dans des études antérieures concernant des alkyl- et aminoalkylpyrimidines (1–3), nous avons constaté, par rmn du proton, que dans les groupements alkyles en position 4 et 6, les hydrogènes portés par les carbones en α du cycle s'échangeaient en milieu acide. Nous avons proposé un mécanisme de réaction et déterminé les constantes cinétiques et isotopiques de cet échange.

Rappelons qu'en milieu acide, une double protonation est nécessaire pour déclencher le processus d'échange qui met en jeu la coupure d'une liaison C—H en α du cycle. La confrontation des résultats expérimentaux avec le traitement mathématique nous a permis de retenir un mécanisme dit séquentiel dans lequel la deuxième protonation est rapide, la coupure de la liaison C—H est lente.

Nous avons effectué une étude analogue sur des méthylpyrimidone-2. Comme pour les alkyl- et aminoalkylpyrimidines, un groupement méthyle en position 5 ne subit aucun échange isotopique, seuls les hydrogènes des méthyles en 4 et 6 s'échangent. Nous avons donc fait une étude sur la triméthyl-4,5,6 pyrimidone-2 (**1**), le méthyle en 5 servant de référence dans notre méthode expérimentale.

L'échange isotopique étudié a lieu dans l'eau lourde, soit pure, soit additionnée d'acide chlorhydrique ou de soude. A 60°C, la vitesse V de réaction varie selon l'acidité du milieu:

$$V_{\text{milieu acide}} > V_{\text{milieu basique}} > V_{\text{eau lourde pure}}$$

En milieu acide, la vitesse d'échange passe par un maximum. Dans ce mémoire, nous ne présenterons que les résultats obtenus en milieu acide. La vitesse d'échange à 60°C étant trop élevée dans ce milieu pour pouvoir, selon notre méthode expérimentale, obtenir des résultats facilement mesurables et reproductibles, nous avons effectué cette étude à 40°C.

Pour vérifier certaines hypothèses de mécanisme, nous avons été amenés à étudier l'échange isotopique hydrogène–deutérium des méthyles de la triméthyl-4,5,6 pyrimidone-2-urée (**1**-urée) et de la tétraméthyl-1,4,5,6 pyrimidone-2 (**2**).

Résultats et discussion

Triméthyl-4,5,6 pyrimidone-2

Nous avons porté sur la figure 1 le taux relatif de la réaction en fonction du temps pour différentes acidités. Le taux relatif de la réaction est défini par la relation:

$$\omega = \frac{\text{Aire du massif correspondant aux méthyles 4 et 6}}{2 \times (\text{Aire du pic correspondant au méthyle 5})}$$

Les différents mélanges sont caractérisés par le rapport ρ = [acide]/[pyrimidone], rapport des concentrations analytiques de départ, que nous avons fait varier de 0 à 2.

La vitesse de réaction passe par un maximum quand le rapport ρ est égal à 0,5, c'est à dire pour un mélange contenant deux moles de pyrimidone pour une mole d'acide.

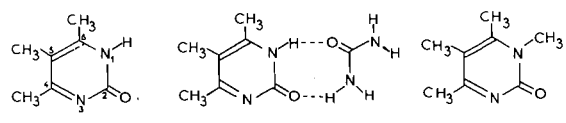

1 **1-urée** **2**

SCHÉMA 1. Composés étudiés: **1** = triméthyl-4,5,6 pyrimidone-2; **1**-urée = triméthyl-4,5,6 pyrimidone-2-urée; **2** = tétraméthyl-1,4,5,6 pyrimidone-2.

0008-4042/81/081270-07$01.00/0

©1981 National Research Council of Canada/Conseil national de recherches du Canada

Can. J. Chem. Downloaded from www.nrcresearchpress.com by 210.87.254.42 on 09/06/12
For personal use only.

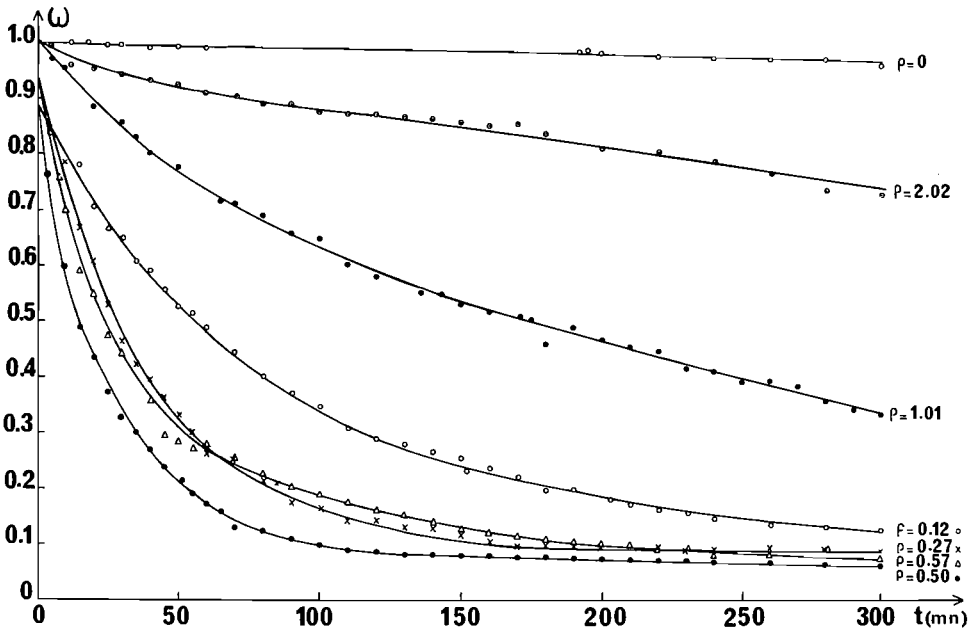

FIG. 1. Influence de la proportion d'acide présent en solution sur la vitesse d'échange de **1**.

Nous étudierons successivement la cinétique d'échange quand ρ est supérieur ou égal à 1, puis quand ρ est inférieur à 1. Nous accorderons une analyse plus détaillée à ce dernier cas.

$\rho \geq 1$: La vitesse d'échange est du même ordre de grandeur que celle des alkyl- et aminoalkylpyrimidines. De même, la réaction est du pseudo-premier ordre, toutefois, une seconde protonation ici n'est pas nécessaire pour déclencher le processus d'échange, le mécanisme de réaction est différent et le traitement mathématique établi lors des études antérieures (3) n'est pas transférable à notre cas.

Nous pouvons considérer que la réaction est principalement régie par l'attaque de l'eau sur l'acide conjugué ($\mathbf{1}D^+$) de la pyrimidone. Lorsque l'acidité augmente, la vitesse de réaction diminue, ceci est certainement dû à une baisse de l'activité de l'eau comme dans le cas de la diméthyl-1,4 pyrimidone-2 (4).

$\rho < 1$: La vitesse est plus rapide. En opérant une régression sur les valeurs expérimentales, de type $\omega = Ae^{-kt}$ et $\omega = 1/(kt + b)$ et en appliquant le test t de Student sur les déviations obtenues entre les points expérimentaux et les points calculés,[1] nous avons retenu les valeurs de k_{obs} obtenues pour une loi du pseudo-premier ordre.

La vitesse passe par un maximum pour $\rho = 0{,}5$, ce qui correspond à un pD mesuré de 4,5 (fig. 2, tableau 1). La valeur du pK_a de l'acide conjugué $\mathbf{1}H^+$ de cette pyrimidone, déterminée par rmn du carbone-13 en mesurant les déplacements chimiques des carbones en fonction du pH est de 4,4. Nous observons donc, à l'erreur expérimentale près, une vitesse maximum quand $(\mathbf{1}) = (\mathbf{1}D^+)$. Des maxima identiques ont été observés au cours d'échanges isotopiques hydrogène–deutérium pour d'autres composés (4–7). Dans tous les cas, les maxima sont expliqués par une réaction d'attaque du composé neutre sur son acide conjugué. Or lors de la synthèse de la triméthyl-4,5,6 pyrimidone-2, nous avons mis en évidence un complexe stable défini 1:1 entre la pyrimidone et l'urée (cf. partie expérimentale). La structure de ce complexe a été étudiée par spectrométrie de vibration (8). Le spectre infrarouge est compatible avec l'existence d'une double liaison hydrogène entre la pyrimidone et l'urée (**1**-urée: schéma 1). Cette constatation nous a fait envisager en premier lieu, malgré les autres résultats cités plus haut (4–7), un mécanisme où les espèces **1** et $\mathbf{1}D^+$ interviennent par formation d'un complexe intermédiaire favorisant l'échange isotopique hydrogène–deutérium:

$$1 + 1D^+ \underset{2}{\overset{1}{\rightleftharpoons}} (1D1)^+$$

[1]Apparemment, la meilleure corrélation est obtenue entre ω et le temps pour une loi du 2ième ordre, les coefficients de corrélation n'étant que peu différents de ceux obtenus pour une loi du 1er ordre pour certaines compositions initiales de mélange, c'est pourquoi nous avons dû faire une régression et utiliser le test t de Student.

Can. J. Chem. Downloaded from www.nrcresearchpress.com by 210.87.254.42 on 09/06/12
For personal use only.

Can. J. Chem. Downloaded from www.nrcresearchpress.com by 210.87.254.42 on 09/06/12
For personal use only.

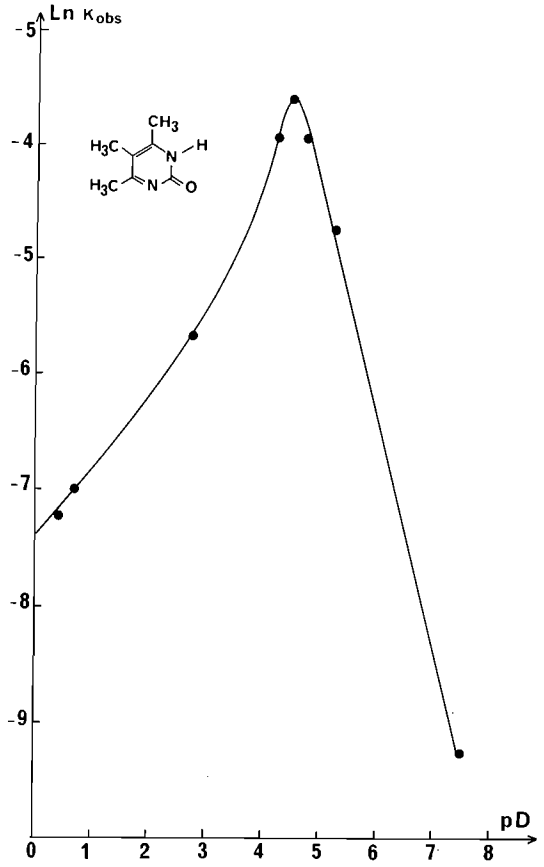

FIG. 2. Effet de l'acidité sur la vitesse d'échange de **1**.

TABLEAU 1. Constantes de vitesse observées pour l'échange de la triméthyl-4,5,6 pyrimidone-2

ρ	pD	k_{obs} mn^{-1}
2,01	0,70	$7{,}30\cdot10^{-4}$
2,00	0,40	$8{,}82\cdot10^{-4}$
1,00	2,75	$3{,}38\cdot10^{-3}$
0,57	4,25	$2{,}21\cdot10^{-2}$
0,50	4,50	$2{,}39\cdot10^{-2}$
0,27	4,80	$1{,}98\cdot10^{-2}$
$0{,}11_5$	5,25	$8{,}46\cdot10^{-3}$
0	7,70	$9{,}47\cdot10^{-5}$

Dans ce mécanisme, nous pouvons faire l'hypothèse que la pyrimidone **1** et la pyrimidone protonée $\mathbf{1D}^+$ forment un complexe identique au complexe pyrimidone–urée. Dans ce complexe, même s'il reste en faible proportion en solution, les groupements méthyles en 4 et 6 peuvent par prototropie perdre un proton, puis la recombinaison avec un deutérium du solvant conduit à l'échange. Si cette hypothèse est exacte, en milieu eau lourde le complexe **1**-urée devrait s'échanger plus rapidement que **1** seul. C'est

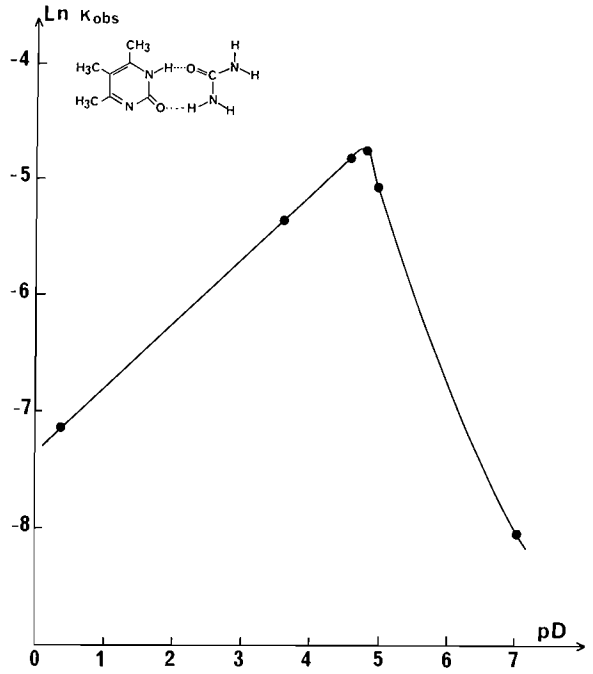

FIG. 3. Effet de l'acidité sur la vitesse d'échange du complexe **1**-urée.

pourquoi, nous avons étudié l'échange des méthyles de la triméthyl-4,5,6 pyrimidone – urée en fonction de la quantité d'acide ajoutée.

Triméthyl-4,5,6 pyrimidone-2-urée (1-urée)

Pour des raisons de solubilité, nous avons dû travailler à des concentrations plus faibles en complexe pour les solutions où ρ est inférieur à 1. Afin de mieux comparer les vitesses d'échange du complexe avec celles de la pyrimidone dans ce domaine, nous avons étudié les échanges de la pyrimidone et du complexe aux mêmes concentrations pour chaque valeur de ρ.

Nous observons que la vitesse d'échange du complexe passe par un maximum pour ρ = 0,5 (fig. 3, tableau 2). Les vitesses d'échange des deux composés **1** et **1**-urée aux mêmes concentrations pour une valeur de ρ proche de 0,5 sont les mêmes. En milieu eau lourde seule (ρ = 0), la vitesse d'échange du complexe n'est que légèrement supérieure à celle de la pyrimidone, ainsi que dans le domaine où ρ > 1.

Pour confirmer que le mécanisme proposé n'est pas vérifié, nous avons étudié l'homologue *N*-méthylé de **1** (tétraméthyl-1,4,5,6 pyrimidone-2).

Tétraméthyl-1,4,5,6 pyrimidone-2 (2)

Pour ce dernier composé, nous observons des vitesses d'échange différentes pour les groupements méthyles en position 4 et 6. Les hydrogènes du méthyle en 6 s'échangent beaucoup plus rapidement

Can. J. Chem. Downloaded from www.nrcresearchpress.com by 210.87.254.42 on 09/06/12
For personal use only.

TABLEAU 2. Constantes de vitesse observées pour l'échange du complexe pyrimidone–urée

ρ	pD	k_{obs} mn^{-1}
3,24	0,70	$7,94 \cdot 10^{-4}$
1,03	3,63	$4,75 \cdot 10^{-3}$
0,58	4,23	$8,04 \cdot 10^{-3}$
0,54	4,60	$8,64 \cdot 10^{-3}$
0,40	5,00	$6,20 \cdot 10^{-3}$*
0	7,05	$3,31 \cdot 10^{-4}$†

*Valeur estimée à partir d'un point à 223 mn.
†Valeur estimée à partir d'un point à 200 mn.

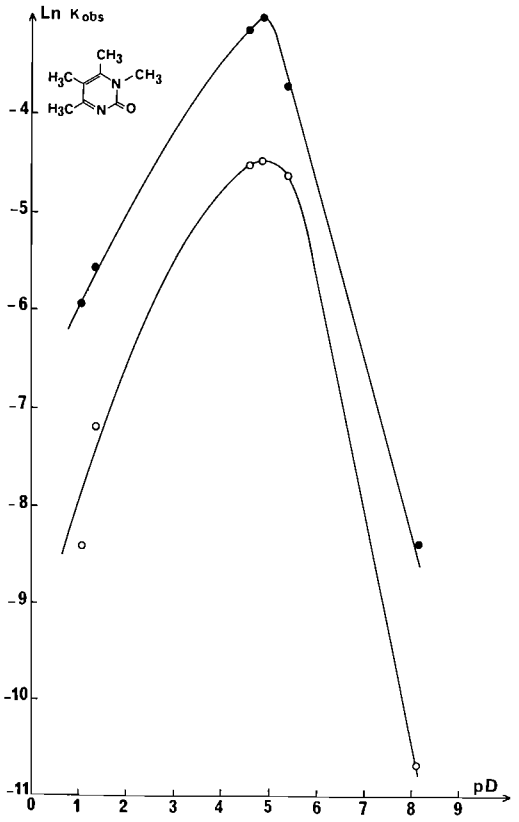

FIG. 4. Effet de l'acidité sur la vitesse d'échange de **2** (Me-6 = -●-, Me-4 = -○-).

que ceux du méthyle en 4, phénomène déjà observé par Batterham *et al.* (9) et Stewart *et al.* (10). Par rapport à l'échange des méthyles du composé **1**, l'échange du méthyle en 6 du composé **2** est plus rapide, par contre, celui du méthyle en 4 de **2** est plus lent.

Dans la région où ρ est inférieur à 1, le composé **2** présente pour l'échange des deux méthyles un maximum de vitesse pour ρ = 0,5 (fig. 4, tableau 3).

TABLEAU 3. Constantes de vitesse observées pour l'échange de la tétraméthyl-1,4,5,6 pyrimidone-2

		k_{obs} mn^{-1}	
ρ	pD	Me-4	Me-6
2,00	1,07	$2,22 \cdot 10^{-4}$	$2,66 \cdot 10^{-3}$
1,00	1,35	$7,60 \cdot 10^{-4}$	$3,79 \cdot 10^{-3}$
0,71	4,51	$1,10 \cdot 10^{-2}$	$4,29 \cdot 10^{-2}$
0,51	4,75	$1,16 \cdot 10^{-2}$	$4,90 \cdot 10^{-2}$
0,25	5,29	$9,78 \cdot 10^{-3}$	$2,41 \cdot 10^{-2}$
0	8,08	$2,30 \cdot 10^{-5}$	$2,30 \cdot 10^{-4}$

L'hypothèse du complexe intermédiaire $\mathbf{1D1}^+$ s'avère donc fausse. Même en de faibles proportions en solution, ce complexe ne contribue pas à l'échange. Le complexe **1**-urée se dissocie donc dans l'eau et l'échange se résume à l'attaque de **1** sur $\mathbf{1D}^+$.

Mise en équation du mécanisme

Examinons maintenant l'échange du composé **1** dans la région où ρ est inférieur à 1. La pyrimidone existe principalement sous forme de base libre **1** quand pD > 4,5 et sous forme d'acide conjugué $\mathbf{1D}^+$ pour pD < 4,5. L'échange est dû à l'arrachement par **1** d'un proton d'un groupement méthyle de $\mathbf{1D}^+$.

Par simplification, nous ne nous intéresserons qu'à l'échange d'un seul proton d'un groupement méthyle, les conclusions sont inchangées par cette simplification, si l'on néglige les effets isotopiques secondaires qui peuvent intervenir lors de l'arrachement d'un proton d'un groupement méthyle, qu'il soit sous forme $—CH_3$, $—CH_2D$, $—CHD_2$, ou que les azotes du cycle soient liés à des hydrogènes ou des deutériums. L'arrachement d'un proton se résume donc à l'équilibre [1]:

[1]

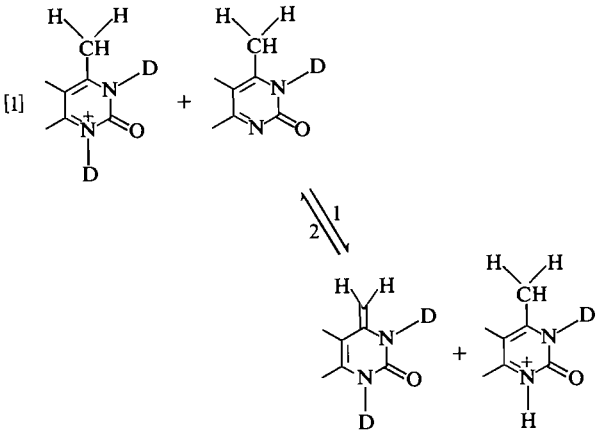

Etant donné la faible proportion d'hydrogène sous forme H_2O, H_3O^+, HDO, etc, le milieu étant à

Can. J. Chem. Downloaded from www.nrcresearchpress.com by 210.87.254.42 on 09/06/12
For personal use only.

forte teneur en deutérium, nous pouvons négliger les réactions d'équilibre acido-basique où l'hydrogène intervient. Il nous reste donc pour l'équilibre acido-basique [2]:

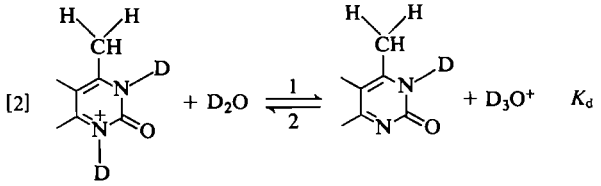

Considérons l'équilibre de recombinaison qui conduit à l'échange [3]:

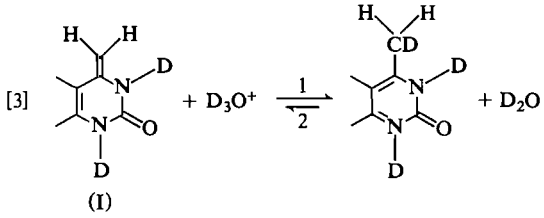

L'espèce intermédiaire I ne se recombine qu'avec D_3O^+ puisque nous négligeons H_3O^+. L'espèce I étant très réactive, l'équilibre [3] est fortement déplacé dans le sens 1.

Soit en résumé:

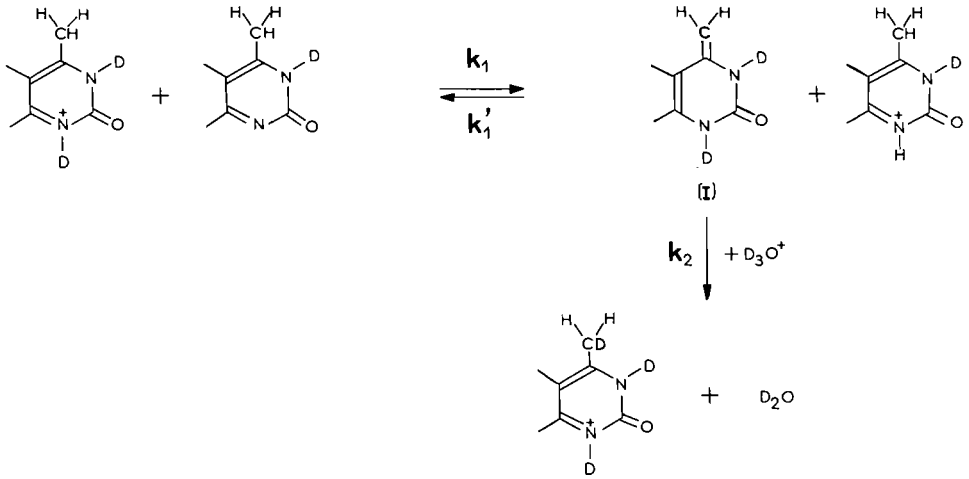

SCHÉMA 2. Mécanisme d'échange de **1** pour $0 < \rho < 1$.

Appelons $[D^+]$ la concentration en ion deutérium, [B] la concentration en pyrimidone neutre contenant l'hydrogène à échanger, [B'] la concentration en pyrimidone neutre deutériée, $[B_T]$ concentration totale en pyrimidone neutre $[B_T] = [B] + [B']$; $[BD^+]$, $[B'D^+]$ et $[B_TH^+]$ concentrations en pyrimidone protonée correspondant respectivement à B, B', B_T; X_0 concentration analytique de départ en pyrimidone et X celle correspondante aux produits non deutériés.

Si nous appliquons à l'espèce I l'hypothèse de l'état stationnaire, exprimons la vitesse de disparition des produits hydrogénés:

$$[4] \quad -\frac{dX}{dt} = k_2 \frac{k_1[BD^+][B_T][D^+]}{k_1'[B_TH^+] + k_2[D^+]}$$

Si de plus, nous considérons que la vitesse de recombinaison avec D_3O^+ est très rapide par rapport à l'établissement de l'équilibre [1] nous obtenons:

$$[5] \quad -\frac{dX}{dt} = k_1[BD^+][B_T]$$

car $k_1'[B_TH^+] \ll k_2[D^+]$. Les équilibres [2] nous donnent:

$$[6] \quad [BD^+] = X\frac{[D^+]}{[D^+] + K_d}$$

et

$$[7] \quad [B_T] = X_0\frac{K_d}{[D^+] + K_d}$$

avec $X = [B] + [BD^+]$ et $X_0 - X = [B'] + [B'D^+]$. Nous obtenons:

$$[8] \quad -\frac{dX}{dt} = k_1\frac{[D^+]K_d}{([D^+] + K_d)^2}X_0X$$

Nous mesurons le taux $\omega = X/X_0$ d'où:

Can. J. Chem. Downloaded from www.nrcresearchpress.com by 210.87.254.42 on 09/06/12
For personal use only.

$$[9] \quad -\frac{d\omega}{dt} = k_1 \frac{[D^+]K_d}{([D^+] + K_d)^2} X_0\omega$$

La réaction étant du premier ordre, nous obtenons pour

$$k_{obs} = k_1 \frac{[D^+]K_d}{([D^+] + K_d)^2} X_0$$

expression déjà établie par Stewart *et al.* lors de l'échange de la créatinine (7) où la condition k_{obs} maximum est obtenue pour $K_d = [D^+]$.

Lorsque l'on trace la courbe k_{obs} en fonction de l'expression $[D^+]K_d/([D^+] + K_d)^2$ nous obtenons une relation linéaire satisfaisante. Nous avons pris pour valeur de K_d la valeur obtenue à $\rho = 0,5$ ($pK_d = 4,5$) et de $[D^+]$ celles calculées à partir des

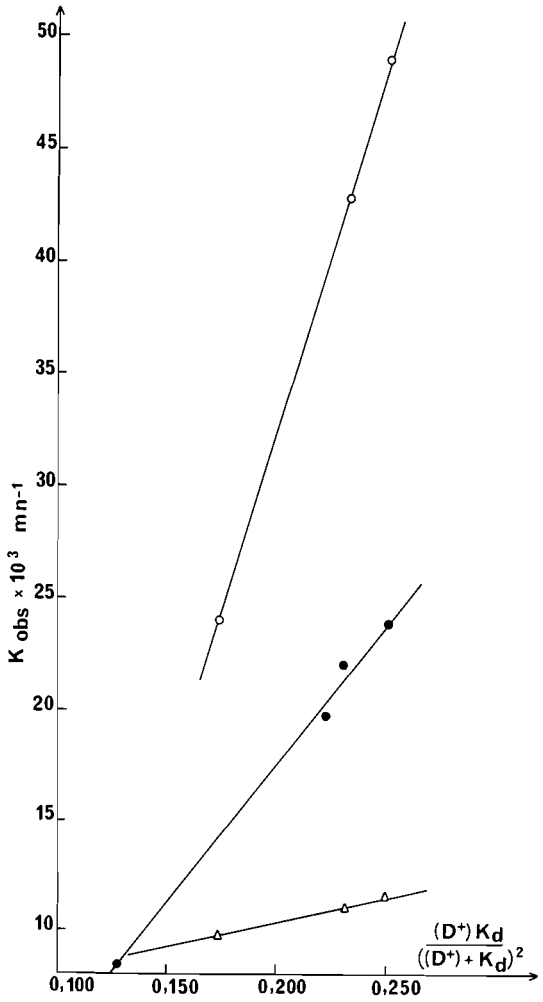

FIG. 5. Relation entre k_{obs} et $[D^+]K_d/([D^+] + K_d)^2$ pour **1**(–●–) et pour **2** (Me-6 = –○–, Me-4 = –△–).

TABLEAU 4. Constantes de vitesse k_1 obtenues à l'aide de la relation de Stewart

Composé		k_1 L mol^{-1} mn^{-1}
1		0,235
2	Me-4	0,046
	Me-6	0,649

valeurs expérimentales (fig. 5). La valeur de k_1 calculée à partir de la pente de la droite est de 0,235 mol^{-1} L mn^{-1}.

Pour le composé **2**, la comparaison des deux régressions montre que la réaction d'échange pour les méthyles en 4 et en 6 est du pseudo-premier ordre. Nous obtenons pour les deux cinétiques une relation linéaire satisfaisante (fig. 5); les valeurs de k_1 ainsi obtenues sont rassemblées dans le tableau 4.

Ces résultats nous amènent à conclure que les échanges des méthyles en position 4 et 6 sur le cycle pyrimidique des pyrimidone-2 sont dûs, dans le domaine d'acidité encadrant le pK_a de l'acide conjugué, à l'arrachement par la molécule neutre agissant comme une base, d'un proton du groupement méthyle de son acide conjugué. Ceci se traduit expérimentalement par un maximum de réactivité à l'équimolécularité de la pyrimidone avec son acide conjugué. Ce mécanisme se trouve confirmé par l'étude de l'échange des méthyles de la tétraméthyl-1,4,5,6 pyrimidone-2.

Partie expérimentale

Technique de mesure

Les réactions d'échange sont suivies par rmn du proton à l'aide d'un spectromètre Varian HA 100, équipé d'une sonde à température variable. Le deutérium ne résonnant pas dans les conditions expérimentales envisagées, nous pouvons aisément préciser de façon qualitative le site d'échange et quantitative le taux relatif de réaction. Le pic correspondant au méthyle en 5, qui ne s'échange pas, sert de référence interne à l'intégration. Nous mesurons le taux relatif de réaction ω défini dans le texte. Nous avons utilisé le signal du pic H_3O^+ ou OH^- selon le milieu, comme asservissement champ-fréquence. Dans le cas où le composé est seulement dissous dans l'eau lourde, nous avons utilisé le signal des méthyles de la pivalone, placée dans un capillaire.

Préparation des échantillons

Chaque solution est préparée par pesée en fiole jaugée, puis introduite dans un tube rmn, placé dans la sonde à 40°C. La réaction est suivie en continu en enregistrant les spectres toutes les 10 mn pendant 300 mn, jusqu'à une valeur constante, pour les réactions où $\rho < 1$, $\omega_{equilibre}$ correspondant à une deutération allant de 92 à 95% selon la composition initiale du mélange. Nous avons travaillé à concentration constante en pyrimidone (0,5 mol L^{-1}) dans l'eau lourde, provenance C.E.A. (99,84 at.% D), avec des quantités variables d'acide chlorhydrique.

Mesures d'acidités

Les mesures de pD des solutions ont été effectuées à l'aide d'un pH-mètre Orion, muni d'une électrode combinée verre–calomel. Nous avons appliqué l'équation générale pD = pH_{lu} + 0,4 (11).

Synthèse de la triméthyl-4,5,6 pyrimidone-2

Nous avons adapté pour notre composé la méthode de préparation de la diméthyl-4,6 pyrimidone-2 décrite par Kosolapoff et Roy (12). Cette méthode donne un composé blanc qui, après sublimation sous vide, a un point de fusion de 210°C; nous l'avons identifié comme étant un complexe stable pyrimidone–urée par analyse élémentaire et spectrométrie de vibration (8). *Anal.* calc.: C 48,48, H 7,07, N 28,28, O 16,26; trouvé: C 48,43, H 6,91, N 27,28, O 16,36%. Nous avons extrait la pyrimidone de la solution aqueuse du complexe en continu, avec le chloroforme, pendant 48 h. Le produit obtenu, triméthyl-4,5,6 pyrimidone-2, après recristallisation et sublimation sous vide a un point de fusion de 243°C.

A ce stade, le rendement de la réaction par rapport à la méthyl-3 pentanedione-2,4 est de 33%. *Anal.* calc.: C 60,85, H 7,29, N 20,28, O 11,58; trouvé: C 60,76, H 7,06, N 20,23, O 11,94%.

Nous avons préféré l'adaptation de la méthode de Kosolapoff à celle de Jones et Rees et celle de Brown et England qui, pour un résultat identique et un rendement équivalent, sont beaucoup plus lentes (13).

Synthèse de la tétraméthyl-1,4,5,6 pyrimidone-2

Nous avons adapté la méthode de Brown et Foster (14). Dix grammes de *N*-méthylurée (0,135 mol) sont dissous dans 60 cm^3 d'éthanol absolu. On ajoute sous agitation 14,2 g (0,125 mol) de méthyl-3 pentanedione-2,4 puis 23 cm^3 d'acide chlorhydrique concentré. La solution est laissée au repos à la température ambiante pendant 85 h. Après avoir chassé les solvants, le résidu dissous dans l'eau est neutralisé par K_2CO_3 jusqu'à pH 9 environ. Par extraction au chloroforme puis recristallisation dans l'éthanol et sublimation sous vide, nous obtenons des cristaux blancs (5 g) de tétraméthyl-1,4,5,6 pyrimidone-2; point de fusion 88–89°C. Le rendement de la réaction par rapport à la méthyl-3 pentanedione-2,4 est de 26,5%. *Anal.* calc.: C 63,13, H 7,95, N 18,41, O 10,51; trouvé: C 63,11, H 7,85, N 18,38, O 10,66%. Les cristaux obtenus sont très hygroscopiques et il est nécessaire de les conserver sous vide partiel, en présence de P_2O_5 et de les sublimer sous vide avant utilisation.

La tétraméthyl-1,4,5,6 pyrimidone-2 peut aussi être obtenue par méthylation de la pyrimidone correspondante (composé **1**) cependant cette méthode donne un produit plus difficile à purifier.

Remerciements

Nous tenons à remercier le Dr. D. Baron et Mademoiselle C. Coupry pour la détermination du pK_a de l'acide conjugué du composé **1** par rmn du carbone-13. Nous tenons également à remercier le Dr. O. S. Tee, Concordia University, Montreal, pour ses critiques constructives et ses conseils pour la mise au point de ce mémoire.

1. A. Pompon. Thèse, C.N.R.S. AO 9195, Paris, 1974.
2. A. Pompon, E. Picquenard, C. Coupry et P. Dizabo. J. Chim. Phys. **76**, 351 (1979).
3. A. Pompon. J. Chim. Phys. **72**, 505 (1975).
4. R. Stewart, S. J. Gumbley et R. Srinivasan. Can. J. Chem. **57**, 2783 (1979).
5. C. K. Ingold, C. G. Raisin et C. L. Wilson. J. Chem. Soc. 1637 (1936).
6. P. Bellingham, C. D. Johnson et A. R. Katritzky. J. Chem. Soc. B, 866 (1968).
7. R. Srinivasan et R. Stewart. Can. J. Chem. **53**, 224 (1975).
8. A. Lautie, E. Picquenard et P. Dizabo. A paraître.
9. T. J. Batterham, D. J. Brown et M. N. Paddon-Row. J. Chem. Soc. B, **3**, 171 (1967).
10. R. Stewart, S. J. Gumbley et R. Srinivasan. Tetrahedron, **35**, 1257 (1979).
11. P. K. Glasoe et F. Long. J. Phys. Chem. **64**, 188 (1960).
12. G. M. Kosolapoff et C. H. Roy. J. Org. Chem. **26**, 1895 (1961).
13. (*a*) R. L. Jones et C. W. Rees. J. Chem. Soc. C, 2251 (1969); (*b*) D. J. Brown et B. T. England. J. Chem. Soc. C, 1922 (1967).
14. D. J. Brown et R. V. Foster. J. Chem. Soc. 4911 (1965).

Can. J. Chem. Downloaded from www.nrcresearchpress.com by 210.87.254.42 on 09/06/12
For personal use only.

Theory of vibrational relaxation in mixtures of ortho- and para-hydrogen

AVYGDOR MOISE AND HUW O. PRITCHARD

Centre for Research in Experimental Space Science, York University, Downsview, Ont., Canada M3J 1P3

Received October 23, 1980

Can. J. Chem. Downloaded from www.nrcresearchpress.com by 210.87.254.40 on 09/06/12
For personal use only.

AVYGDOR MOISE and HUW O. PRITCHARD. Can. J. Chem. **59**, 1277 (1981).

A numerical study of the vibrational relaxation at 500 K of a mixture of ortho-H_2 and para-H_2 is described. The required state-to-state rate constants were calculated from the quantum results of Rabitz and co-workers, and missing pieces of data were estimated by interpolation.

It is concluded that only one relaxation time will be observed in any mixture of ortho-H_2 and para-H_2 and that (except at very high dilutions in a third inert gas) the relaxation rate constant will be close to the mean of the individual rate constants for relaxation, weighted according to the respective mole fractions of ortho-H_2 and para-H_2 present in the mixture.

We find that the relaxation process can be modelled very accurately as an electrical RC network, whose time constants can be written down quite easily as sums of the appropriate microscopic rate constants, and by using this model, it is a simple matter to explore the conditions required for a mixture of two gases to exhibit two distinct vibrational relaxation times.

AVYGDOR MOISE et HUW O. PRITCHARD. Can. J. Chem. **59**, 1277 (1981).

On décrit une étude numérique de la relaxation vibrationnelle à 500 K d'un mélange de H_2 ortho et para. On a calculé les constantes de vitesse entre états nécessaires en se basant sur les résultats quantiques de Rabitz et ses collaborateurs et on a évalué les données manquantes par interpolation.

On conclut qu'un seul temps de relaxation pourra être observé pour tous les mélanges de H_2 ortho et para et que (à l'exception des cas de très fortes dilutions dans un troisième gaz inerte), la constante de vitesse de relaxation sera voisine de la moyenne des constantes individuelles des vitesses de relaxation pondérées selon les fractions molaires respectives de H_2 ortho et para présentes dans le mélange.

Nous avons trouvé que le processus de relaxation peut être représenté d'une façon très précise par un réseau électrique RC dont on peut très facilement représenter les constantes de temps par la somme des constantes de vitesse microscopiques appropriées. L'utilisation de ce modèle permet d'explorer facilement les conditions requises pour qu'un mélange de deux gaz présente deux temps distincts de relaxation vibrationnelle.

[Traduit par le journal]

Introduction

In a recent group of papers from this laboratory, we have examined the fundamental nature of vibrational and rotational relaxation in diatomic molecules by a series of numerical experiments (1–3). To simplify matters, H_2 was considered the model molecule, and in the absence of sufficient quantum-mechanical data for individual state-to-state rate constants, such rates for the model calculations were constructed by a mixture of empiricism and guesswork. However, recent investigations, principally by Alexander (4–6) and by Rabitz and co-workers (7–9), have now reached the point where it is possible to make reasonable estimates for any state-to-state rate constant for H_2 in collision with He, among the first two or three vibrational states, and perhaps the lowest ten or twelve rotational states; most of this effort has been devoted to the even J states of H_2, i.e. para-H_2, although Alexander has also examined transitions among a few of the odd J states, i.e. ortho-H_2.

The problem we wish to address in this paper is that of the vibrational relaxation of a mixture of two diatomic gases, and the major new phenomenon to be probed here is whether the two molecules will equilibrate their vibrational energies separately or together: this problem has been addressed previously by Foster and Simpson (10) in relation to the relaxation of mixtures of N_2O and CO_2.

A feasible calculation from the point of view of consumption of computer time and computer storage space at the present time limits the number of rotation–vibration states of each molecule to an order of about ten; thus, in fact, it is only for mixtures of ortho-H_2 and para-H_2 that a full calculation of the relaxation of a mixture of two gases can be contemplated. Consequently, we describe in the following pages a calculation of the relaxation of mixtures of ortho-H_2 and para-H_2, both diluted and undiluted, using state-to-state rate constants synthesised from the tabulations of Rabitz and Zarur (7, 11). This calculation, we believe, fulfils a two-fold purpose: a reasonable description of the relaxation of ortho–para hydrogen mixtures in particular, and a realistic modelling of the relaxation of mixtures of diatomic gases in general.

State-to-state Transition Rate Constants

We begin by enumerating the kinds of processes involved in the relaxation of a mixture of ortho-H_2 with para-H_2 in the presence of a diluent M.

0008-4042/81/081277-07$01.00/0

©1981 National Research Council of Canada/Conseil national de recherches du Canada

Can. J. Chem. Downloaded from www.nrcresearchpress.com by 210.87.254.40 on 09/06/12
For personal use only.

(1) T–VR Processes

[1] $H_2^{p,o}(v, J) + M \rightleftarrows H_2^{p,o}(v', J') + M$

These are the standard atom–diatom rate processes which have been the subject of most theoretical studies in the past (4–9). We may also project out of the manifold of diatom–diatom collision processes the two sets

[1*a*] $H_2^{p,o}(v, J) + H_2^{p,o}(i) \rightleftarrows H_2^{p,o}(v', J') + H_2^{p,o}(i)$

[1*b*] $H_2^{p,o}(v, J) + H_2^{o,p}(i) \rightleftarrows H_2^{p,o}(v', J') + H_2^{o,p}(i)$

These processes are equivalent to the processes [1] in the sense that the quantum state (i) of the second H_2 on each side of the equation remains unchanged; for the present purposes, we follow our earlier model calculations (3) and make the simplification that for a given pair $(v, J) \leftrightarrow (v', J')$, all three types of process [1], [1*a*], and [1*b*] are equivalent.

(2) Self-relaxation Processes

[2] $H_2^{p,o}(v, J) + H_2^{p,o}(v', J') \rightleftarrows H_2^{p,o}(v'', J'') + H_2^{p,o}(v''', J''')$

These processes represent the exchange of vibrational and rotational excitation, with attendant dissipation because of energy mismatching, between molecules of the same species; there have been many fewer theoretical studies of these processes.

(3) Exchange Processes

[3] $H_2^{p,o}(v, J) + H_2^{o,p}(v', J') \rightleftarrows H_2^{p,o}(v'', J'') + H_2^{o,p}(v''', J''')$

Again, these processes have been the subject of a limited range of theoretical studies, but are relatively amenable to experimental study by laser fluorescence techniques. We shall see below that eq. [3] as it stands is insufficient, and that it will be necessary to subdivide [3] into two sets of processes in order to describe properly the relaxation of the mixed gases.

Our prime source of data for the construction of the required state-to-state rate constants of type [1] is an extensive tabulation (Table II) in the paper by Rabitz and Zarur (7); here, they list cross-sections for state-to-state transitions, induced by collision with He, among even states of H_2. For our purposes, we require all state-to-state rate constants among the set of levels $H_2(v, J)$ for $v, J = 0, 0; 0, 2; 0, 4; 0, 6; 0, 8; 0, 10; 1, 0; 1, 2; 1, 4;$ and $1, 6$. The cross-sections for the endothermic transitions within this group were plotted as shown in Figs. 4 and 6 of the paper of Rabitz and Zarur, and a self-consistent set of "best fit" plots was obtained using their eq. [7]. These functions of cross-section versus energy were then transformed into thermally averaged rate constants for a specific temperature T by following the development, eqs. [4.1]–[4.4] of Augustin and Rabitz (8); and finally, detailed balancing for the temperature in question was used to generate the corresponding rate constants for the reverse (exothermic) processes. For the reason that the thermal averaging procedure is extremely sensitive to small variations in the cross-section fitting procedure at low temperature, and because we cannot consider too high a temperature if we wish to truncate the energy-level system at about ten levels, we chose to perform these calculations at a single representative temperature, that of $T = 500$ K. This procedure, then, yielded a set of T–VR transition rate constants sufficient to describe the relaxation among the ten lowest states of para-H_2 at 500 K, at infinite dilution in He.

In order to extend the calculation to non-dilute mixtures of para-H_2 with He, it is necessary to know the rate constants for all the VR–VR processes of type [2] within this group of states. Here, theoretical information is much less extensive, and we used our previous parameterisation (3) of the results of Zarur and Rabitz (11), namely that for any *exothermic* VR–VR process in para-H_2 at 500 K,

[4] $$k_{ij \rightarrow kl} = 0.006Z \exp\left[-0.002\Delta\varepsilon - 2.5|\Delta J|\right]$$

where Z is the collision number for unlike particles, $\Delta J = J_i + J_j - J_k - J_l$; for processes between like reactants, reactions between $i + i'$ and $i' + i$ were each counted once.

For the analogous ortho-H_2 calculation, we require the set of state-to-state rate constants among the levels $v, J = 0, 1; 0, 3; 0, 5; 0, 7; 0, 9; 0, 11; 1, 1; 1, 3; 1,5;$ and $1, 7$. A few of these have been estimated by Alexander (4–6) for the cases where $|\Delta v| = 1$, but there are too few values from which to deduce a rule by which all the required rates may be estimated. Consequently, we examined the functions constructed from the data of Rabitz and Zarur for even J, and found that at any particular value of the total energy, rotational transfer for J, $J + 2$, and $J + 4$ states were roughly related to each other in a geometric manner. Thus, we interpolated the original tabulated data of Rabitz and Zarur (7) according to the equation

[5] $$\sigma_{v,J \rightarrow v',J'}(E) = [\sigma_{v,J-1 \rightarrow v',J'-1}(E) \times \sigma_{v,J+1 \rightarrow v',J'+1}(E)]^{1/2}$$

in order to estimate cross-sections among the odd states of H_2; thermally averaged rate constants for $T = 500$ K were then constructed as described above.

These data show one major difference from those of Alexander (c.f. Tables IX and X of ref. 4) in that

Can. J. Chem. Downloaded from www.nrcresearchpress.com by 210.87.254.40 on 09/06/12
For personal use only.

he concludes there is a larger cross-section for the transition from $v = 1, J = 1 \rightarrow v = 0, J = 1$ than for that from $v = 1, J = 0 \rightarrow v = 0, J = 0$, whereas we interpolate the data in the opposite sense. This eventually leads Alexander to the conclusion that the rate of relaxation of ortho-H_2 by He is slightly faster than that of para-H_2 (5, 6), whereas the numbers we use make it slightly slower; in fact, it appears that although ortho-H_2 is relaxed by He more quickly than is para-H_2 at low temperatures, the two rates are very nearly the same at room temperature and above (12). For our purposes, this discrepancy is of minor importance: all we require is that the relaxation times for ortho-H_2 and para-H_2 shall be different, so that we may examine meaningfully their individual behaviours in mixtures of the two gases; if we make any arbitrary adjustment to our cross-sections which makes the two relaxation rates too similar, then we will lose the ability to examine departures from the linear mixture rule, or to obtain information about the separation of relaxation times, for mixtures of gases in general.

In the absence of any theoretical data about VR–VR processes of type [2] in ortho-H_2, we again use our earlier parameterisation for the para-states, i.e. eq. [4]. Finally, for the calculations on mixtures of ortho-H_2 and para-H_2, we need to know the rate constants for the exchange processes of type [3] between the unlike species, and we also assume that these can be represented by eq. [4].

With this set of assumptions, we are now in a position to make a sequential analysis of the individual relaxation behaviours of pure ortho-H_2 and pure para-H_2, first at infinite dilution, then as a function of mole fraction in admixture with He, and finally in various mixtures of He with both ortho-H_2 and para-H_2. These calculations were performed using a slightly modified version of the numerical integration routine EPISODE, as described by Koda, McRae, and Seinfeld (13).

As in our earlier work (2, 3), the starting population for the relaxation in single species systems was taken to be a Boltzmann distribution for $T = 500$ K, but with the lowest rotational level of the $v = 1$ manifold overpopulated by a factor of 100 at the expense of the corresponding state in the $v = 0$ manifold; the reasons for using this starting distribution have been fully explained previously (2). In those cases where both H_2 species were present, we investigated starting distribution in which *either* $v = 1, J = 0$ *or* $v = 1, J = 1$ was excited, or else both were simultaneously excited: however, for reasons outlined below, the nature of the initial excitation in these systems is not important, except in highly dilute admixtures with He.

Relaxation of a Single Species at Infinite Dilution

We have made extensive investigations of single species systems involving only processes of type [1] previously (1, 2) using eigenvalue methods which, of course, are valid only at infinite dilution (3). Nevertheless, they are useful in ensuring the correct performance of the numerical integration routines, and in both the ortho-H_2 and the para-H_2 cases, we established that the two methods gave identical results to within the error criterion specified in the numerical integration routine. At this stage, we were able to confirm the exact agreement between the rate constant for energy loss calculated by integration methods and the approximate formula (5, 8)

$$[6] \qquad k_1 \equiv k_{1\rightarrow 0}(T) = \frac{\sum_J \sum_{J'} (2J + 1)[\exp(-\varepsilon_{1J}/\not{k}T)]k_{1J\rightarrow 0J'}(T)}{\sum_J (2J + 1)\exp(-\varepsilon_{1J}/\not{k}T)}$$

This is because the normal modes of relaxation for these two relaxations are very similar to those predicted previously (1) and the rotational relaxation is essentially complete (at this temperature) before the decay of the vibrational energy becomes significant.

We will find it convenient to plot the data in the form of λ, the rate constant for relaxation in the model mixture: this was always taken to comprise 3.5×10^{19} molecules $cm^{-3} \equiv [M]$, whence

$$[7] \qquad \lambda_i = k_i[M] \equiv k_i \times 3.5 \times 10^{19}\ s^{-1}$$

Relaxation of Single Species in Non-dilute Mixtures

Calculations similar to those reported previously (3) for mixtures of ortho-H_2 with He, and para-H_2 with He, for all mole-fraction ratios were performed with these new transition rate data, and the results are shown in Fig. 1. In both cases, the linear mixture rule holds quite well, but there is some downward curvature in the plots of the relaxation rate constants as the mole fraction of H_2, $x \rightarrow 0$; this curvature is of similar magnitude to that we had observed before (3), as is shown in the insets to Fig. 1 where the results for dilute mixtures are plotted on an enlarged scale.[1]

Ignoring this slight curvature, we can write that

$$[8] \qquad \lambda^{o,p}(x) \simeq \lambda_1{}^{o,p} + x\lambda_2{}^{o,p}$$

where λ_1 is given by eqs. [6] and [7], and following

[1]The values of $d\lambda/dx$ shown in Fig. 1 are much greater than that we showed previously (3). This is because, although all the processes of type [2] have the same rates as before, processes of type [1] are now a lot slower, so that $\lambda_1{}^o = 6.8 \times 10^3\ s^{-1}$ instead of $7.9 \times 10^5\ s^{-1}$; thus, type [2] processes have a relatively much larger effect on the dissipation rate in the present calculation.

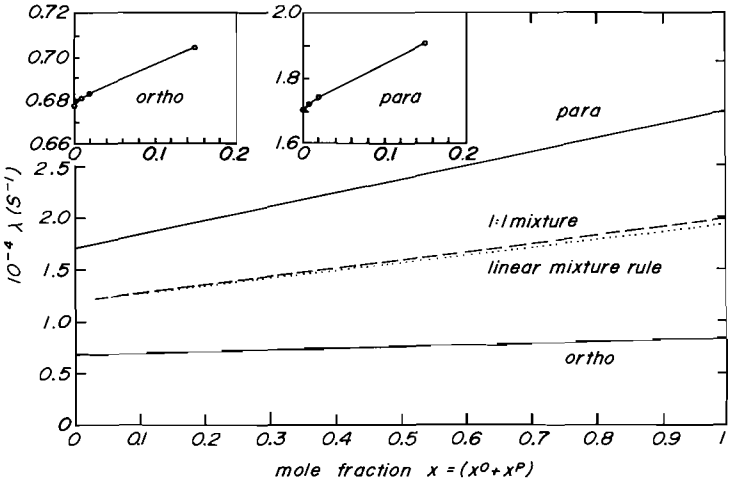

FIG. 1. Relaxation time constants λ for mixtures of H_2 and He containing a total of 3.5×10^{19} molecules cm^{-3} at 500 K. Solid lines: mixtures of He with only ortho-H_2 or only para-H_2; dashed line: 1:1 ortho-H_2:para-H_2 mixtures; dotted line: linear or mixture rule, eq. [10*b*] for the 1:1 mixture. Insets: data for ortho-H_2/He and para-H_2/He mixtures, at $x = 0, 0.01, 0.02$, and 0.15 to illustrate the magnitude of the curvature as $x \to 0$.

the reasoning by which [6] was evolved, we find that

$$[9] \qquad k_2 = \frac{\sum_J \sum_{v'} \sum_{J'} \sum_{J''} \sum_{J'''} (2J+1)(2J'+1)\{\exp[-(\varepsilon_{1J} + \varepsilon_{v'J'})/kT]\}k_{(1J+v'J')\to(0J''+v'J''')}(T)}{\left[\sum_J (2J+1)\exp(-\varepsilon_{1J}/kT)\right]\left[\sum_{v'}\sum_{J'}(2J'+1)\exp(-\varepsilon_{v'J'}/kT)\right]}$$

Equation [9] is the direct analogue of eq. [6], summing over all type [2] processes which transform a $v = 1$ state into a $v = 0$ state: thus, by using eq. [8] with $\lambda_1^{o,p}$ and $\lambda_2^{o,p}$ calculated via eqs. [6] and [9] respectively, the curves shown in Fig. 1 can be reconstructed with an accuracy of better than 0.5% for all x.

Relaxation of Mixtures of Ortho-H_2 and Para-H_2

Although we had originally intended to perform these calculations for a series of ortho-H_2 to para-H_2 mixture ratios, the simplicity of the resulting behaviour enabled us to confine our attention to equimolar mixtures of the two gases, at various dilutions in He. The results for the 1:1 ortho–para mixture at various degrees of dilution in He are shown, also in Fig. 1, as the dashed line: as long as the mole fraction x of H_2 is greater than about 1%, it can be seen that the resulting relaxation rate conforms quite closely to the form

$$[10] \qquad \lambda(x) = \lambda_1 + x\lambda_2$$

where

$$[10a] \qquad x = x^o + x^p$$

and (5)

$$[10b] \qquad \lambda_i = \frac{x^p\lambda_i^p + x^o\lambda_i^o}{x^o + x^p} \qquad i = 1, 2$$

The latter linear mixture relation is shown as the dotted line in Fig. 1; the true relaxation rate is slightly faster than the traditional average, but again the departure from the linear mixture rule is not large. Moreover, in this range of mixtures ($x > 0.01$), the vibrational energies in the ortho-H_2 and in the para-H_2 manifolds always relax together: this is because the exchange processes [3] equilibrate the excess energy between the two species so quickly that they are always virtually in equilibrium with each other.

However, in very dilute mixtures, the situation is quite different, as shown in Fig. 2. The relaxation rate constant for the mixture begins to fall below the arithmetic mean value, eq. [10], and at infinite dilution reaches the relaxation rate of the ortho-H_2/He system. Basically what is happening is that at very high dilutions, the exchange processes [3] die out, and the two manifolds tend to relax separately. However, with the rate constants we have in this calculation, this does not mean that we actually see

Can. J. Chem. Downloaded from www.nrcresearchpress.com by 210.87.254.40 on 09/06/12
For personal use only.

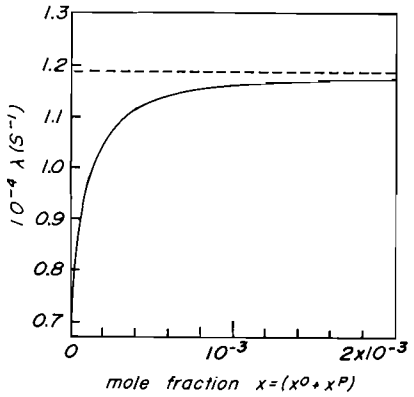

FIG. 2. Comparison of linear mixture rule, eq. [10*b*] (dashed line), with actual relaxation of a 1:1 mixture of ortho-H_2 and para-H_2 at high dilution in He (solid line). Other details as in Fig. 1.

two separate relaxation times — only that by the time either manifold reaches the stage where its energy is decaying exponentially, there is no measurable energy left in the para-H_2 manifold.

Exchange Processes

We have devoted little attention to the initial transient behaviour because there is little new information to be gleaned over and above that presented previously (2). There is however, one qualification to be made to those conclusions: we had found previously that in the simulated laser-schlieren experiment (corresponding roughly to the kinds of initial population distribution we use here), there was an initial *absorption* of energy needed to bring the $v = 1$ rotational manifold into thermal equilibrium with the initially overpopulated $v = 1$, $J = 0$ or $v = 1, J = 1$ state. In non-dilute mixtures, this does not happen: the equilibration of the $v = 1$ rotational manifold still takes place, but not by absorption from the surroundings; instead, these states are fed by $(v = 1 + v' = 0) \rightarrow (v = 0 + v' = 1)$ processes which are implicitly contained within types [2] and [3], with the result that the total energy of excitation decreases from the very beginning.

Exchange processes of this kind are very fast, and although we included them formally in defining processes [2] and [3], we have excluded them in calculating k_2 by eq. [9]. Likewise k_3 is also given by eq. [9], with the constraint that J, J'' refer to one species, J', J''' to the other. We require to project out the set of processes which lead to an exchange of vibrational energy, i.e. $(v = 1 + v' = 0) \rightarrow (v = 0 + v' = 1)$ since these lead to a rapid exchange of energy between the species, with only a small dissipative contribution (due to energy mismatch). The rate constant for such processes will be, extending the previous argument,

$$[11]\quad k_4 = \frac{\sum_J \sum_{J'} \sum_{J''} \sum_{J'''} (2J+1)(2J'+1)\{\exp[-(\varepsilon_{1J}+\varepsilon_{0J'})/kT]\}k_{(1J+0J')\rightarrow(0J''+1J''')}(T)}{\left[\sum_J (2J+1)\exp(-\varepsilon_{1J}/kT)\right]\left[\sum_{J'}(2J'+1)\exp(-\varepsilon_{0J'}/kT)\right]}$$

The numerical magnitude of k_4 is very much greater than that of k_3, because the $k(T)$ terms in the numerator are large.

As we noted above, these exchange processes are implicitly included in the type [2] self-relaxation processes, but their explicit consideration is unnecessary in order to describe the self-relaxation behaviour at long times; however, it is these particular exchange processes which are responsible for reversing the initial rise in energy observed at the beginning of the relaxation in infinitely dilute systems (2).

An Electrical Analogy

In the preceding two sections, we have defined, in terms of specific state-to-state processes, a set of relaxation rates $\lambda_1^{o,p}$, $\lambda_2^{o,p}$, $\lambda_3^{o,p}$, and λ_4, the latter being symmetrical in the species ortho-H_2 and para-H_2; we now show how it is possible to model the relaxation process (once the initial transients have died out) for any mixture of ortho-H_2, para-H_2, and He to an accuracy which for practical purposes is exact: discrepancies between the exact results found by numerical integration and those given by the following procedure never exceeded 0.5% in any of the systems we examined.

Ignoring the minor non-linearities shown in the insets in Fig. 1, we can write the rates of relaxation of the energies in the following form

$$[12]\quad \frac{dE^o}{dt} = -\left[\lambda_1^o + x^o\lambda_2^o + x^p\lambda_3^o + x^p\lambda_4\left(\frac{E^o - E^p}{E^o}\right)\right]E^o$$

$$[12a]\quad \frac{dE^p}{dt} = -\left[\lambda_1^p + x^p\lambda_2^p + x^o\lambda_3^p + x^o\lambda_4\left(\frac{E^p - E^o}{E^p}\right)\right]E^p$$

Can. J. Chem. Downloaded from www.nrcresearchpress.com by 210.87.254.40 on 09/06/12
For personal use only.

Can. J. Chem. Downloaded from www.nrcresearchpress.com by 210.87.254.40 on 09/06/12
For personal use only.

where $E^{o,p}$ are the instantaneous values of the internal energy relative to their equilibrium values. The structure of these equations arises because the processes with relaxation rates $\lambda_1^{o,p}$, $\lambda_2^{o,p}$, and $\lambda_3^{o,p}$ operate directly on the departure of the internal energy from the equilibrium value, i.e. on $E^{o,p}$, whereas the exchange process with rate constant λ_4 redistributes the energy excess between the ortho-H_2 and the para-H_2 manifolds at a rate which is proportional to the difference $E^o - E^p$ or $E^p - E^o$ depending upon the direction of the energy flow. Writing

$$[13] \quad \lambda^o = \lambda_1^o + x^o\lambda_2^o + x^p\lambda_3^o + x^p\lambda_4$$

$$[13a] \quad \lambda^p = \lambda_1^p + x^p\lambda_2^p + x^o\lambda_3^p + x^o\lambda_4$$

$$[14] \quad \lambda_\varepsilon^o = x^p\lambda_4$$

$$[14a] \quad \lambda_\varepsilon^p = x^o\lambda_4$$

These two equations may be rewritten as

$$[15] \quad dE^o/dt = -\lambda^o E^o + \lambda_\varepsilon^o E^p$$

$$[15a] \quad dE^p/dt = -\lambda^p E^p + \lambda_\varepsilon^p E^o$$

If we replace E by electric charge, these are the equations which govern the discharge of a pair of capacitances connected as shown in Fig. 3, whence it becomes clear immediately that if R_ε is very large, the two capacitances will discharge independently at rates determined by the products R_1C_1 and R_2C_2 respectively, whereas if R_ε is small, the whole system will discharge with a single relaxation time.

The exact solution to the pair of eqs. [15] and [15*a*] is given by

$$[16] \quad E^o(t) = [E^o(0) - \varepsilon^o]\exp(\lambda^+ t) + \varepsilon^o \exp(\lambda^- t)$$

$$[16a] \quad E^p(t) = [E^p(0) - \varepsilon^p]\exp(\lambda^+ t) + \varepsilon^p \exp(\lambda^- t)$$

where

$$\lambda^\pm = -\tfrac{1}{2}[\alpha \pm (\alpha^2 - 4\beta)^{1/2}]$$

$$\alpha = (\lambda^o + \lambda^p)$$

$$\beta = (\lambda^o\lambda^p - \lambda_\varepsilon^o\lambda_\varepsilon^p)$$

and

$$\varepsilon^o = \frac{\lambda^o E^p(0) - (\lambda^o + \lambda^+)E^o(0)}{\lambda^- - \lambda^+}$$

$$\varepsilon^p = \frac{\lambda^p E^o(0) - (\lambda^p + \lambda^-)E^p(0)}{\lambda^+ - \lambda^-}$$

Relaxation Together or Separately?

The values of the various relaxation rates, constructed from the state-to-state cross-sections via eqs. [6], [9], and [11], and which reproduce the relaxation behaviour calculated by numerical integration to within 0.5% when substituted into eq. [16], are as follows

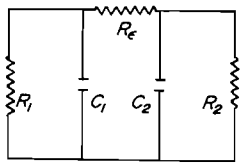

FIG. 3. Electrical circuit equivalent to the vibrational relaxation of ortho-H_2 and para-H_2 mixtures at long time, i.e. after the initial transients have ceased.

$$\lambda_1^o = 6.78 \times 10^3\ s^{-1};\quad \lambda_1^p = 1.70 \times 10^4\ s^{-1}$$
$$\lambda_2^o = 1.62 \times 10^3\ s^{-1};\quad \lambda_2^p = 1.37 \times 10^4\ s^{-1}$$
$$\lambda_3^o = 7.91 \times 10^3\ s^{-1};\quad \lambda_3^p = 8.80 \times 10^3\ s^{-1}$$
$$\lambda_4 = 9.22 \times 10^7\ s^{-1}$$

or, on a per-collision basis, with $Z = 3.68 \times 10^{-10}$ cm^3 molecule^{-1} s^{-1} taken to be the collision number for all distinguishable pairs of particles, the values of $P = \lambda/Z[M]$ are

$$P_1^o = 5.27 \times 10^{-7};\quad P_1^p = 1.32 \times 10^{-6}$$
$$P_2^o = 1.26 \times 10^{-7};\quad P_2^p = 1.06 \times 10^{-6}$$
$$P_3^o = 6.14 \times 10^{-7};\quad P_3^p = 6.83 \times 10^{-7}$$
$$P_4 = 7.16 \times 10^{-3}$$

The value of λ_1^p is very close to that calculated by Rabitz and co-workers — interpolating from Fig. 5 of ref. 9 they calculated values near 500 K in the region of 2–4 $\times 10^8$ cm^3 mol^{-1} s^{-1} compared with the value of 2.9 $\times 10^8$ cm^3 mol^{-1} s^{-1} which we find at 500 K using the same primary data. Our value of λ_1^o is somewhat smaller than λ_1^p, in contrast with Alexander's conclusion that it is slightly greater (5, 6), as we have already noted. We cannot compare our calculated values of λ_2 with experiment, although experiments do exist (14, 15), since experimentally, $d\lambda/dx = \lambda_2$ contains a contribution of the kind $[x\lambda_{1,H_2}^{o,p} + (1 - x)\lambda_{1,He}^{o,p}]$ which we have assumed to be independent of x (note that in modelling practical systems, the λ_1 components in eq. [12] would have to be expanded in this fashion). Finally, the calculated value of λ_4, which corresponds to an exchange of internal energy every 140 collisions is reasonable, c.f. a measured value of every 125 collisions for the analogous process between ^{12}CO and ^{13}CO (16).

Going back to our electrical analogy, the exchange of internal energy via λ_4 is very much faster than the decay of that energy via $\lambda_1^{o,p}$, $\lambda_2^{o,p}$, and $\lambda_3^{o,p}$ combined, and so both species relax together; obviously, we could only expect them to relax separately if $\lambda_4 < \lambda_i^{o,p}$, $i = 1, 2, 3$. However, eq. [16] shows that

Can. J. Chem. Downloaded from www.nrcresearchpress.com by 210.87.254.40 on 09/06/12
For personal use only.

if $\lambda_\varepsilon^{o,p} \ll \lambda^{o,p}$, $\lambda^{\pm}$ will be either λ^o or λ^p, in which case the two systems will relax separately: consequently, the criterion for separation of the two relaxations is not simply the intuitive one that the exchange rate constant is smaller in magnitude than the deactivation rate constants, but that the product of the mole fraction with the exchange rate constant is smaller than the deactivation rate constants. Obviously, if λ_4 is very small, the relaxations will separate, but even if λ_4 is large, it may be possible to observe a separation at high dilution in a third inert gas.

From a practical point of view, Foster and Simpson (10) studied the relaxation of N_2O and CO_2 with a view to looking for the separation of the relaxation processes. From the construction of λ_4 by eq. [11] in terms of state-to-state processes, it is clear that λ_4 will always be greater than $\lambda_{1,2,3}^{A,B}$ for any pair of molecules A and B, although as the energy mismatch becomes greater, as for example in the exchange between CO and N_2 (17), the disparity will be less marked. Then, it would seem feasible to observe a separation of relaxation times at high dilution, provided that λ_1^A and λ_1^B were not too different: if they are too different, we will find (as in our model calculation here) that all the energy has relaxed from one molecule in a non-exponential manner before the decay of the energy from the other molecule becomes exponential.

Details of the derivation of eq. [16] and an expanded set of numerical results will be made available later in thesis form (18).

1. H. O. Pritchard and N. I. Labib. Can. J. Chem. **54**, 329 (1976).
2. H. O. Pritchard. Can. J. Chem. **54**, 2372 (1976).
3. H. O. Pritchard, N. I. Labib, and A. Lakshmi. Can. J. Chem. **57**, 1115 (1979).
4. M. H. Alexander. J. Chem. Phys. **61**, 5167 (1974).
5. M. H. Alexander. Chem. Phys. **8**, 86 (1975).
6. M. H. Alexander. Chem. Phys. Lett. **38**, 417 (1976).
7. H. Rabitz and G. Zarur. J. Chem. Phys. **61**, 5076 (1974).
8. S. D. Augustin and H. Rabitz. J. Chem. Phys. **67**, 64 (1977).
9. S. D. Augustin and H. Rabitz. J. Chem. Phys. **70**, 1286 (1979).
10. M. G. Foster and C. J. S. M. Simpson. J. Chem. Soc. Faraday II, **75**, 509 (1979).
11. G. Zarur and H. Rabitz. J. Chem. Phys. **60**, 2057 (1974).
12. M. M. Audibert, R. Vilaseca, and J. Ducuing. Chem. Phys. Lett. **37**, 408 (1976).
13. M. Koda, G. J. McRae, and J. H. Seinfeld. Int. J. Chem. Kinet. **11**, 427 (1979).
14. M. M. Audibert, C. Joffrin, and J. Ducuing. Chem. Phys. Lett. **19**, 26 (1973).
15. J. E. Dove and H. Teitelbaum. Chem. Phys. **6**, 431 (1974).
16. G. L. Wolk, R. E. Weston, and G. W. Flynn. Chem. Phys. Lett. **71**, 390 (1980).
17. D. C. Allen and C. J. S. M. Simpson. Chem. Phys. **45**, 203 (1980).
18. A. Moise. Thesis, York University. To be submitted.

Boron trihalide adducts of 1,1-bis(piperidinyl)ethylene. ^{13}C and ^{11}B nmr studies of a model system for β-carbon donation in enamine adducts

J. STEPHEN HARTMAN[1] AND ERIC C. KELUSKY

Department of Chemistry, Brock University, St. Catharines, Ont., Canada L2S 3A1

Received September 9, 1980

J. STEPHEN HARTMAN and ERIC C. KELUSKY. Can. J. Chem. **59**, 1284 (1981).

1,1-Bis(piperidinyl)ethylene coordinates to the boron trihalides through the CH_2 carbon, but the covalent adducts $D.BX_3$ undergo rearrangement to give predominantly the ionic adducts $D_2BX_2^+.BX_4^-$. Striking variations in ^{11}B and ^{13}C nmr peak widths support our proposed structures. The disappearance of peaks due to excessive broadening can be misleading in the interpretation of such systems.

J. STEPHEN HARTMAN et ERIC C. KELUSKY. Can. J. Chem. **59**, 1284 (1981).

Le bis(pipéridinyl)-1,1 éthylène se coordonne aux trihalogénures de bore au moyen de l'atome de carbone du CH_2, mais les adduits covalents obtenus, $D.BX_3$, se transposent en donnant majoritairement les adduits ioniques $D_2BX_2^+.BX_4^-$. Les fortes variations observées dans les spectres de rmn du ^{13}C et du ^{11}B semblent confirmer les structures que nous proposons. La disparition des pics, due à un étalement excessif, peut conduire à une interprétation erronée de ces systèmes.

[Traduit par le journal]

Can. J. Chem. Downloaded from www.nrcresearchpress.com by 210.87.254.42 on 09/06/12
For personal use only.

Introduction

The well-known stability of the amidinium ion structure **1** (1) leads to the expectation of exclusive β-carbon protonation and complexation in 1,1-enediamines (**2**). This is well established for protonation (2). The few available studies of complexation of 1,1-enediamines to simple Lewis acids (boron trihalides (3) and Group IV tetrahalides (4)) also show that complexation is at the β-carbon site. In the boron trihalide adducts of 1,1-bis(dimethylamino)ethylene (**3**), there is restricted rotation about the central C—N bonds as a result of the amidinium-ion partial double bond character (3).

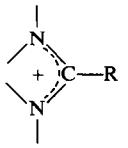

1

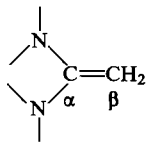

2

In our current nmr studies of enamine adducts (5), we are attempting to detect ambidentate behaviour of the enamine ligands, in which both nitrogen and the β-carbon are potential donor sites (6). Interpretation of results in the enamine adduct systems, in particular confirmation that β-carbon donation occurs, has been hampered by the scarcity of nmr data on carbon-donor boron trihalide adducts (7, 8). We now report ^{13}C and ^{11}B nmr studies of boron trihalide coordination of 1,1-bis(piperidinyl)ethylene (**4**), a 1,1-enediamine and a model compound for β-carbon donation to Lewis acids.

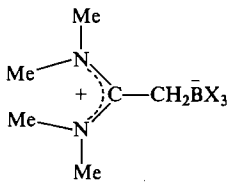

3

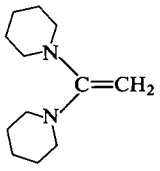

4

[1]Author to whom correspondence should be addressed.

Results and Discussion

^{13}C Spectra

^{13}C nmr parameters of **4** and its boron trihalide adducts are given in Table 1. The β-carbon of uncomplexed **4** absorbs exceptionally far to high field for an olefinic carbon, and this can be attributed to the importance of the mesomeric forms ***4b*** and ***4c***, with the buildup of appreciable negative charge on this carbon. Similar but less pronounced effects occur in enamines (5, 9). Changes in chemical shift on complex formation are consistent with the β-carbon being the donor atom. Structures ***4b*** and ***4c*** should be the only mesomeric forms contributing to the adducts, due to the localization of a lone pair at the donor position on adduct formation. The pronounced shift to high field of the β-carbon on complexation to BF_3 is consistent with the required hybridization change to sp^3. The shift back to lower field in the heavier-halogen boron trihalide adducts is consistent with the increasing Lewis acid strength of these compounds and the nearness of the BX_3 moiety. The 6 ppm chemical shift difference between the BF_3 and BCl_3 adduct β-carbon resonances is consistent with the 2.6 ppm difference between the ^{13}C resonances of $Me_3N.BF_3$ and $Me_3N.BCl_3$ (10), and the 3–7 ppm between

0008-4042/81/081284-06$01.00/0

©1981 National Research Council of Canada/Conseil national de recherches du Canada

Can. J. Chem. Downloaded from www.nrcresearchpress.com by 210.87.254.42 on 09/06/12
For personal use only.

TABLE 1. ^{13}C nmr parameters[a] of adducts of 1,1-bis(piperidinyl)ethylene

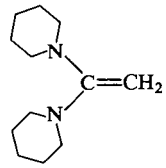

	T (K)	Chemical shifts C-α	C-β	C-2,6	C-3,5	C-4	Width at half height of the C-β peak (Hz)[b]
Free **4**	235	164.4	66.7	50.1	26.0	25.0	Sharp
	300	164.1	68.2	50.3	26.2	25.3	Sharp
4/BF_3	235	177.1, 178.2	30.6	51.9	25.7	23.4	15 ± 5
	255	177.7, 178.6	30.5	51.9	25.7	23.5	25 ± 5
	275	178.2, 178.9	[c]	51.9	25.7	23.6	[c]
4/BCl_3	235	170.6, 172.1	35.8	52.6	26.0	23.2	16 ± 5
	255	173.4	35.8	52.6	25.9	23.2	17 ± 5
	275	174.4	36.4	52.7	25.9	23.4	27 ± 5
	300	175.5	37.2	52.8	25.8	23.3	41 ± 10
4/BBr_3	255	175.2	38.8	52.6	26.0	23.1	20 ± 10
	275	175.8	38.8	52.8	26.0	23.2	20 ± 10
4/BI_3	235	175.7, 177.2	37.9	52.8	26.0	23.1	29 ± 10
	255	176.2	[c]	52.8	26.1	23.1	[c]
	300	177.9	[c]	53.1	26.1	23.1	[c]
4/H^{+}[d] (CF_3CO_2H)	255	168.7	18.1	52.7	26.2	23.4	Sharp
	275	168.8	18.1	52.7	26.1	23.2	Sharp
	300	169.1	18.0	52.8	26.0	23.2	Sharp
$(Me_2N)_2C{=}CH_2$[e]	Ambient	163.0	69.2	40.9			
$[(Me_2N)_2CCH_2PtCl]_2$[e]	Ambient	171.9	24.9	44.8			

[a]Chemical shifts are in ppm to low field of internal tetramethylsilane; 20% solutions of **4** in deuterochloroform.
[b]Spectra were transformed with 5 Hz of line broadening. Peaks described as "sharp" were not appreciably broader than the TMS peak under these conditions.
[c]Not visible.
[d]Also present in many adduct samples.
[e]Reference 25.

α-carbon resonances of BF_3 and BCl_3 adducts of ethers (11).

The α-carbon resonance shifts to low field in the adducts and in protonated **4** (Table 1). The chemical shift of 168.7 ppm for protonated **4** is consistent with values for other amidinium ions ($[(Me_2N)_2CH]^+$, 156.4 ppm (12), $[(Me_2N)(C_6H_5NH)CCl]^+$, 159 ppm (13)). However correlations of $C{=}N^+$ ^{13}C chemical shifts are generally poor, the nature of the anion having a strong influence, which can be as much as 10 ppm (12). The α-carbon shifts in the adducts (172–178 ppm, and temperature-dependent) are close to the amidinium ion range. Doubling of the adduct α-carbon resonance at low temperatures in some cases indicates additional complexity in the adduct systems, as is discussed below. The small shift to low field of the piperidinyl C-2 and C-6 carbons is consistent with adduct formation at a donor site remote from these carbons.

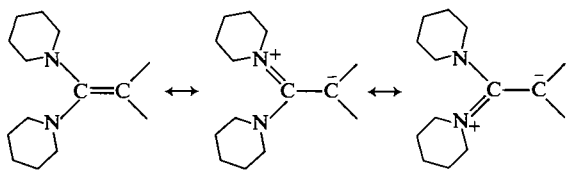

4*a* **4***b* **4***c*

Peak widths of the resonances assigned to the β-carbons are given in Table 1. The resonances are broad or even unobservable at ambient temperature, but become sharper as the temperature is lowered. This is consistent with coupling to ^{11}B which is undergoing quadrupole relaxation. Quadrupole relaxation is more effective at lower temperatures, due to slower molecular tumbling. This causes a more complete collapse of the splittings due to ^{11}B–^{13}C coupling, and of any residual peak broadening due to such coupling, at lower temperatures in the spectrum of the spin-1/2 nucleus coupled to the quadrupolar nucleus (14). Thus spectra of spin-1/2 nuclei coupled to boron are often simplified at low temperatures (7). In a

TABLE 2. ^{11}B nmr parameters of **4**/BX_3 solutions[a]

	T (K)	BX_4^-	D.BX_3	$D_2BX_2^+$	Other
4 + BI_3	253	−145.3	[b]	[b]	
	273	−146.0	[b]	[b]	
	323	−146.2	−74[c]	−38[c]	−15[c]
4 + BI_3 + $Me_4N^+I^-$	293	−146.2	[b]	[b]	
	323	−146.2	−78(320 Hz)	−36(>500 Hz[c])	−16(>500 Hz[c])
4 + BBr_3	243	−42.4	−29.1(35 Hz)	[b]	
	273	−42.9	−29.4(30 Hz)	[d]	
	323	−42.7	−29.4(15 Hz)	−28.1(280 Hz)	
4 + BCl_3	253	−11.3	[d]		
	273	−11.3	−12(~500 Hz)[e]		
	303	−11.3	−12(270 Hz)[e]		
	323	[f]	[f]		
4 + BF_3	243	−19.5	[d]		
	263	−19.6	−17.8(220 Hz)[e]		
	293	−19.7	−17.0(210 Hz)[e]		
	303	−19.6	−16.4(160 Hz)[e]		
	323	−19.5	[g]		

[a]Chemical shifts are in ppm to low field of external trimethoxyboron. (To convert to ppm to low field of boron trifluoride etherate, add 18.1 ppm.) Values in brackets are peak widths at half-height. The BX_4^- peak remains quite sharp at all temperatures.
[b]Not visible.
[c]Broad and badly overlapping peaks.
[d]Insufficient resolution.
[e]Broad resonance, likely a composite of D.BX_3 and $D_2BX_2^+$.
[f]Spectrum is complex, apparently due to decomposition.
[g]Obscured by the BF_4^- peak and by poorly-resolved fine structure which is probably due to boron–fluorine coupling.

number of cases a carbon directly bonded to boron is undetectable at ambient temperature due to excessive broadening from coupling to ^{11}B, but does give a peak at low temperatures (15). Thus our ^{13}C peak widths support our β-carbon peak assignments and the proposed adduct structure.

Splittings due to ^{11}B–^{13}C coupling can usually be seen in ^{13}C nmr spectra of tetrahedral boron compounds with C—B bonds, but these splittings are often not visible in three-coordinate boron compounds (7). This is in accord with the expectation that quadrupole relaxation of boron should be less effective in tetrahedral boron compounds due to their higher symmetry (14). The absence of such splittings in the ^{13}C spectra of the present series of adducts is thus somewhat unusual. ^{11}B chemical shifts are not consistent with three-coordinate boron. The effect of the bulky enediamine donor in slowing molecular tumbling is probably responsible for the effectiveness of ^{11}B quadrupole relaxation in these adducts, leading to ^{13}C and ^{11}B peak widths more typical of trigonal boron than of tetrahedral boron.

^{11}B Spectra

Solutions of **4** with the boron trihalides in a 1:1 molar ratio or with excess **4** give more than one ^{11}B nmr signal, and the signals have a very wide range of peak widths (Table 2 and Fig. 1). Uncomplexed boron trihalide peaks, which would absorb at low

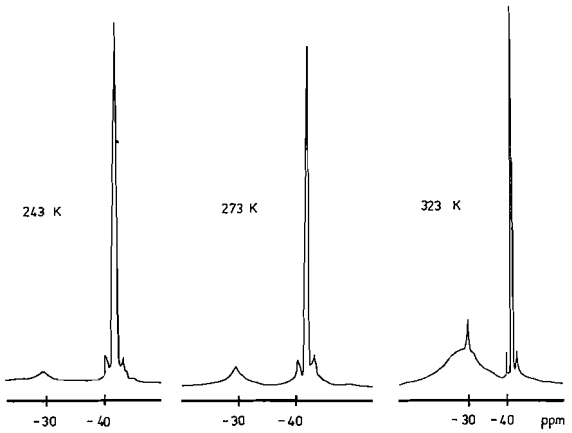

FIG. 1. ^{11}B nmr spectra of **4**.BBr_3 at various temperatures. The spectra were transformed with 5 Hz of line broadening, slightly increasing the apparent width of the BBr_4^- signal.

field, are absent, as are resonances in the RBX_2 region which is at even lower field (8). The spectra are consistent with adduct formation followed by redistribution of donor for halogen to give the ionic form of the adducts, $D_2BX_2^+.BX_4^-$.

[1] $2D.BX_3 \rightleftharpoons D_2BX_2^+ + BX_4^-$

Comparison with literature values (16–18)[2] of ^{11}B chemical shifts of adducts and related species

[2]See also Table IV of ref. 8.

Can. J. Chem. Downloaded from www.nrcresearchpress.com by 210.87.254.42 on 09/06/12
For personal use only.

TABLE 3. ^{11}B chemical shifts of model compounds[a]

X	F	Cl	Br	I	Reference
BX_4^-	−19.9	−11.6	−42.4	−146.0	16
$Me_3N.BX_3$	−15.9	−8.6	−20.9	−71.4	17
$Me_2S.BX_3$	−15.2	−11.2	−29.5	−87.0	18
BX_3	−8.6 – −6.5	28–30	20–22	−24 – −26	See ref. 8, Table 4

[a]In ppm to low field of trimethoxyboron.

(Table 3) shows that the sharpest peak in the ^{11}B spectra of the **4**/BX_3 samples corresponds to the tetrahaloborate anion BX_4^-. From the size of the peak, BX_4^- is a major species. Boron cations such as $D_2BX_2^+$ are well-known species (19, 20) but ^{11}B chemical shifts have been reported for few haloboron cations (8).

In the **4**/BBr_3 and **4**/BI_3 systems, one broad resonance has a chemical shift consistent with the values for known simple boron trihalide adducts (Table 3) and is assigned to **4**.BX_3. An additional, even broader resonance occurs at lower field, and we have assigned this to $D_2BX_2^+$. One further very broad resonance is present in the **4**.BI_3 system and might arise from a species such as D_3BI^{2+}. Precedent exists for such species, which are most easily formed when iodines, having the weakest boron–halogen bonds, are available to be displaced (19). Supporting evidence for our assignments comes from addition of tetramethylammonium iodide to solutions of **4** and BI_3. The size of the initially-small −78 ppm peak, assigned to **4**.BI_3, is greatly increased relative to both of the lower-field peaks, in accord with reactions such as [2].

[2] $D_2BI_2^+ + I^- \rightleftharpoons D.BI_3 + D$

In the ^{11}B spectrum of the **4**/BBr_3 system (Fig. 1) the resonance of intermediate chemical shift and peak width that is assigned to D.BBr_3 is small, consistent with equilibrium [1] being far to the right. The very slight chemical shift difference between the broad resonances assigned to D.BBr_3 and $D_2BBr_2^+$, together with the small range of chemical shifts of B–Br compounds when compared to analogous B–I compounds (Table 3), makes it unlikely that any further broad resonance signals, such as might arise from D_3BBr^{2+}, would be detectable. The broadest resonance could be a composite signal, rather than solely due to $D_2BBr_2^+$.

^{11}B peak areas are not consistent with $D_2BX_2^+$ and BX_4^- as the only ions in solution. The peaks assigned to cations are considerably larger than those assigned to BX_4^- ions. Halide ion is another possible counterion for $D_2BX_2^+$ (19, 20) and would not be detected in this study.

The small ^{11}B chemical shift ranges in the **4**/BCl_3 and **4**/BF_3 systems do not allow adequate resolution of peaks in addition to BX_4^-. However, there is definitely a large broad resonance underlying the BX_4^- peak in each system. It becomes less broad at higher temperatures, but resolution into separate signals has not been possible. The existence of the broad, poorly resolved resonance does indicate that reactions analogous to those in the heavier boron trihalide adduct systems are occurring.

Peak widths and their variation with temperature are the most striking feature of the ^{11}B spectra. In contrast to the ^{13}C spectra, some peaks became too broad to detect at the *lowest* temperatures, in keeping with very short lifetimes of the ^{11}B spin states due to more effective quadrupole relaxation at these temperatures (14). The variations of ^{11}B peak widths support our assignments. The tetrahaloborate ions, with full tetrahedral symmetry, give quite sharp peaks to the lowest temperatures studied, because the high electric field symmetry about boron decreases the effectiveness of quadrupole relaxation. The adducts D.BX_3, with only C_{3v} symmetry about boron and also with molecular tumbling slowed due to the attachment of a bulky donor group, undergo more effective quadrupole relaxation and hence give much broader resonances. Since the boron is in a somewhat-flexible C—CH_2—BX_3 unit, considerable local tumbling should still be possible. $D_2BX_2^+$ ions, with only C_{2v} symmetry, should give the broadest peaks. The effect should be accentuated by the much slower tumbling of the boron-containing part of the molecule due to anchoring between two very bulky donor groups. These are indeed the broadest peaks.

Boron trihalide adduct systems can be far more complex than is frequently assumed; reaction [1] is one of several possible complications (21). ^{11}B chemical shifts of the tetrahaloborates confirm reaction [1], in accord with a recent suggestion (8). Nuclear magnetic resonance studies involving only donor-molecule nuclei can be misleading in that they give no direct evidence of this reaction. ^{11}B chemical shift and peak width studies should have

Can. J. Chem. Downloaded from www.nrcresearchpress.com by 210.87.254.42 on 09/06/12
For personal use only.

Can. J. Chem. Downloaded from www.nrcresearchpress.com by 210.87.254.42 on 09/06/12
For personal use only.

similar value in other adduct systems in which such complications may occur.

Further Aspects

1,1-Enediamines have low stabilities, especially in the presence of Lewis acids, and this severely limits their usefulness as ligands. The present study has been limited by the tendency of many nmr samples to give precipitates on standing, and a few features of the spectra have not been fully explained. Thus ^{13}C spectra show that protonated **4** is present in variable amounts in our samples. Possible reactions of the initially-formed adducts include loss of an acidic β-hydrogen to give an organoboron enediamine, **5** or **6**:

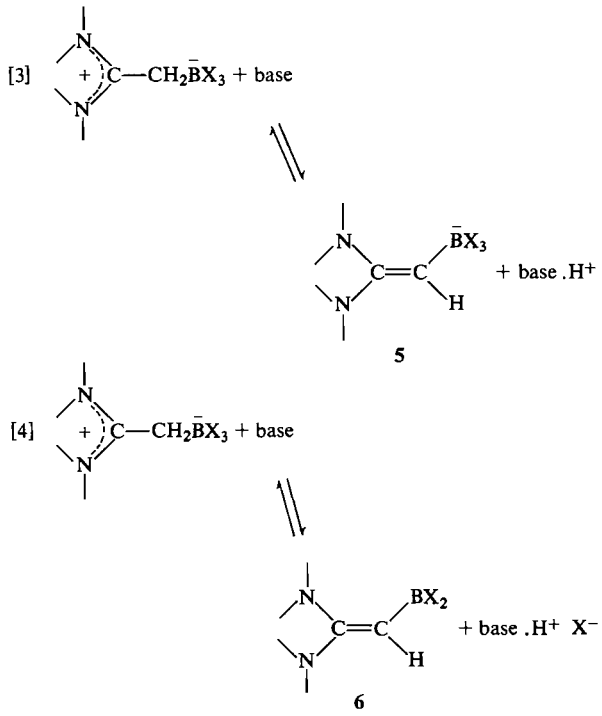

When the base in eqs. [3] and [4] is excess uncomplexed enediamine, protonated **4** would be formed. Such reactions have been reported for enediamine-group IV Lewis acid complexes by Weingarten and Wagar (4), and some evidence for similar reactions has been found for the adduct **3** (X = F) by ^{1}H and ^{19}F nmr (3). Such reactions apparently occur to a significant extent on standing in methylene chloride solution at ambient temperature for a few hours (22), consistent with the behaviour of carbon acids which often undergo relatively slow proton transfer (23). However, absence of the olefinic-carbon resonances expected for **5** or **6** argues against this reaction being the source of protonated **4**. Protonation might also arise from traces of hydrogen halide present in the boron trihalide (24) or from DCl which is often present in deuterochloroform, but this normally gives only traces of the protonated species.

Doubling of the ^{13}C α-carbon resonances in some of the adduct spectra at low temperatures could be the result of ion pairing effects, since $C{=}N^+$ shifts are quite anion-dependent (12). The absence of an equivalent doubling of the β-carbon resonances, together with the coalescence of the α-carbon resonances as the temperature is raised, excludes the possibility that the donor environments in $D.BX_3$ and $D_2BX_2^+$ give rise to the separate α-carbon resonances. The boron–carbon bonds must be long-lived to account for the broadening of the adduct β-carbon resonances at higher temperatures, and hence α-carbon resonances from $D.BX_3$ and $D_2BX_2^+$ would not coalesce. Ion pairing, on the other hand, would have the greatest effects on the α-carbon, and changes involving the counterion would be fast, consistent with the data. However, confirmation of such ion pairing effects awaits further work.

A 1,1-enediamine complex with platinum(II) has recently been reported (25). Two isomers, an η^2 (metal–olefin) complex and an η^1 (β-carbon-donor) complex analogous to our adducts, were postulated on the basis of ^{1}H and ^{13}C nmr data. ^{13}C chemical shifts for the η^1 complex are very similar to ours (Table 1) and an especially large ^{13}C–^{195}Pt coupling constant provides further evidence for the structure. The inherent interest of 1,1-enediamines as carbon-donor "ylide" ligands merits further studies of their coordination behaviour, in spite of difficulties arising from their high reactivity.

The readiness of boron trihalide adducts of 1,1-enediamines to rearrange according to eq. [1] throws light on our current studies of possible ambidentate behaviour of enamines as ligands to the boron trihalides. Initially-formed nitrogen-donor adducts of certain enamines convert to a second species, which ^{13}C nmr indicates is the β-carbon-donor adduct (5). However, ^{11}B nmr, showing only BX_4^- resonances for the second species, seemed inconsistent with the ^{13}C results. Our present study, showing that carbon-donor BX_3 adducts are especially susceptible to reaction [1], resolves the apparent inconsistency. We have apparently been unable to detect ^{11}B nmr signals of the enamine $D.BX_3$ and $D_2BX_2^+$ species due to excessive peak broadening. We will report our enamine coordination studies in a further paper.

Experimental

1,1-Bis(piperidinyl)ethylene (**4**) was synthesized by reacting

1,1,1-triethoxyethane and piperidine in the presence of toluene-4-sulfonyl chloride, according to the method of Baganz and Domaschke (26). Freshly distilled **4** is clear and colorless but it discolors on standing. The nmr samples were prepared in a nitrogen-filled glove box and made up as 20% solutions of the enediamine in deuterochloroform.

Boron tribromide and boron triiodide (Alfa Inorganics), which had been transferred and sealed into ampoules on a high-vacuum system, were opened in the glove box and added to the enediamine solutions which were cooled to −50°C. BF_3 and BCl_3 (Matheson) were added directly from the cylinder to some samples. For other samples, BF_3 and BCl_3 were purified on the high-vacuum system and condensed onto a solution of the enediamine at −196°C, and allowed to warm and react; the excess boron trihalide and the solvent were pumped off, leaving the adduct as a colorless oil.

^{13}C and ^{11}B nmr spectra were obtained on a Bruker WP-60 Fourier Transform nmr spectrometer operating at 15.08 MHz and at 19.25 MHz, respectively; 10 mm sample tubes were used. For ^{13}C spectra a 3759 Hz sweep width was used, with a 1.09 s acquisition time for 8K of data memory, using quadrature detection. A 30° pulse was used, with the Phase Alternating Pulse Sequence, and up to 5000 pulses were accumulated. The FID's were transformed with 0.5 Hz of line broadening. Off-resonance decoupled spectra were obtained to confirm peak assignments and used a proton frequency set at 250 Hz to high field of tetramethylsilane. For ^{11}B spectra various sweep widths and memory sizes were used in order to optimize spectra containing both sharp and broad resonances. Transformation of FID's with extreme line broadening (> 100 Hz) was found to be helpful in confirming the presence of very broad peaks which were difficult to detect above the noise when zero or small line broadening was applied.

Acknowledgements

We thank the Natural Sciences and Engineering Research Council of Canada for financial support of this work, and Mr. Arnold Fox and Mr. T. R. B. Jones for technical assistance.

1. W. KANTLEHNER. *In* Amidinium salts in organic chemistry. Vol. 2. *Edited by* H. Böhme. John Wiley and Sons, New York. 1979 ((Vol. 9, Part 2 of Advances in organic chemistry. Methods and results).
2. J. D. WILSON, C. F. HOBBS, and H. WEINGARTEN. J. Org. Chem. **35**, 1542 (1970).
3. J. S. HARTMAN and R. R. YETMAN. Can. J. Chem. **54**, 1130 (1976).
4. H. WEINGARTEN and J. S. WAGER. Synth. Inorg. Met.-Org. Chem. **1**, 123 (1971).
5. J. S. HARTMAN and B. D. MCGARVEY. Paper IN-28, presented at the 63rd Canadian Chemical Conference, Ottawa, Ontario, June 1980; J. S. HARTMAN, E. C. KELUSKY, and B. D. MCGARVEY. In preparation.
6. A. G. COOK (*Editor*). Enamines: synthesis, structure, and reactions. Marcel Dekker, New York. 1969.
7. B. WRACKMEYER. Prog. Nucl. Magn. Reson. Spectrosc. **12**, 227 (1979).
8. H. NÖTH and B. WRACKMEYER. NMR basic principles and progress. Vol. 14. *Edited by* P. Diehl, E. Fluck, and R. Kosfeld. Springer-Verlag, Berlin. 1978.
9. D. TOURWÉ, G. VAN BINST, S. A. G. DE GRAAF, and U. K. PANDIT. Org. Magn. Reson. **7**, 433 (1975); M. G. AHMED and P. W. HICKMOTT. J. Chem. Soc. Perkin Trans. II, 838 (1977); M. G. AHMED, P. W. HICKMOTT, and R. D. SOELISTYOWATI. J. Chem. Soc. Perkin Trans. II, 372 (1978); R. STRADI, P. TRIMARCO, and A. VIGEVANI. J. Chem. Soc. Perkin Trans. I, 1 (1978).
10. J. M. MILLER and T. R. B. JONES. Inorg. Chem. **15**, 284 (1976).
11. A. FRATIELLO, R. KUBO, D. LIU, and G. VIDULICH. J. Chem. Soc. Perkin Trans. II, 1415 (1975).
12. C. RABILLER, J. P. RENOU, and G. J. MARTIN. J. Chem. Soc. Perkin Trans. II, 536 (1977).
13. R. MERÉNYI. *In* Iminium salts in organic chemistry. Vol. 1. *Edited by* H. Böhme and H. G. Viehe. Wiley Interscience, 1976. pp. 25–105. (Vol. 9, Part 1 of Advances in organic chemistry. Methods and results).
14. M. SUZUKI and R. KUBO. Mol. Phys. **7**, 201 (1963); J. BACON, R. J. GILLESPIE, and J. W. QUAIL. Can. J. Chem. **41**, 3063 (1963); J. BACON, R. J. GILLESPIE, J. S. HARTMAN, and U. R. K. RAO. Mol. Phys. **18**, 561 (1970); R. WEISS and R. N. GRIMES. J. Am. Chem. Soc. **100**, 1401 (1978).
15. J. D. ODOM, T. F. MOORE, R. GOETZE, H. NÖTH, and B. WRACKMEYER. J. Organomet. Chem. **173**, 15 (1979); B. R. GRAGG, W. J. LAYTON, and K. NIEDENZU. J. Organomet. Chem. **132**, 29 (1977).
16. J. S. HARTMAN and G. J. SCHROBILGEN. Inorg. Chem. **11**, 940 (1972).
17. H. BINDER and E. FLUCK. Z. Anorg. Allgem. Chem. **381**, 116 (1971).
18. M. J. BULA and J. S. HARTMAN. J. Chem. Soc. Dalton Trans. 1047 (1973).
19. R. E. RYSCHKEWITSCH. *In* Boron hydride chemistry. *Edited by* E. L. Muetterties. Academic Press, New York. 1975. Chapt. 6.
20. O. P. SHITOV, S. L. IOFFE, V. A. TARTAKOVSKII, and S. S. NOVIKOV. Russ. Chem. Rev. **40**, 905 (1970).
21. G. E. RYSCHKEWITSCH and W. H. MYERS. Synth. React. Inorg. Metal-Org. Chem. **5**, 123 (1975).
22. R. R. YETMAN. M.Sc. thesis, Brock University, St. Catharines, Ont. 1975.
23. A. G. KRESGE. Acc. Chem. Res. **8**, 354 (1975).
24. J. S. HARTMAN and G. J. SCHROBILGEN. Can. J. Chem. **50**, 713 (1972).
25. P. P. PONTI, J. C. BALDWIN, and W. C. KASKA. Inorg. Chem. **18**, 873 (1979).
26. H. BAGANZ and L. DOMASCHKE. Chem. Ber. **95**, 2095 (1962).

Can. J. Chem. Downloaded from www.nrcresearchpress.com by 210.87.254.42 on 09/06/12
For personal use only.

n–π Electron donor–acceptor complexes. I. Aliphatic amines with benzonitrile

J. ANUNZIATA, J. SINGH, AND J. J. SILBER[1]

Universidad Nacional de Río Cuarto, Departamento de Química y Física, C.C. 135-5800 Río Cuarto, Córdoba, Argentina

Received September 26, 1979[2]

J. ANUNZIATA, J. SINGH, and J. J. SILBER. Can. J. Chem. **59**, 1291 (1981).

Interaction of diethyl, triethyl, *n*-butyl, di-*n*-butyl and tri-*n*-butyl amines as n-donor with benzonitrile as π-acceptor has been studied in *n*-hexane. The formation of weak electron donor–acceptor (EDA) complexes is proposed to explain the spectroscopic behavior of the mixtures. An iterative procedure was used to obtain values of stability constants (K) and extinction coefficients (ε). The fact that from the new absorption observed for these systems a value of K and a finite constant value of ε could be determined gives proof of the existence of EDA complexes. This conclusion is further supported by the temperature effect observed. Correlations of the experimental data with amine structure and other types of amine complexes were found.

J. ANUNZIATA, J. SINGH et J. J. SILBER. Can. J. Chem. **59**, 1291 (1981).

On a étudié l'interaction entre le diethyle, le triethyle, le *n*-butyle, le di-*n*-butyle et le tri-*n*-butyle amines comme donneurs n et le benzonitrile comme accepteur π dans le *n*-hexane. Pour expliquer le comportement spectroscopique des solutions de ces amines avec benzonitrile, on propose la formation de complexes faibles electron donneur–accepteur (EDA). On a employé une méthode itérative pour l'obtention de valeurs des constantes de stabilité (K) et des coefficients d'extinction (ε). En effet, á partir de la nouvelle absorption observeé dans ce systéme on a pu remarquer des valeurs de K et des valeurs limitées et constantes de ε, ce qui prouve l'existence de complexes EDA. L'effet de temperature observé renforce encore toutes ces conclusions. On a fait, des correlations parmi les éléments obtenus des expériences effectuées et la structure des amines et d'autres sortes de complexes d'amines.

Introduction

The existence of n–π type molecular complexes has been widely postulated (1). It seems characteristic of a particular n-donor to form weaker complexes with π-acceptors than with any other kind of acceptor (1*b*, 2). Thus, although the ionization potentials of aliphatic amines are mostly less than 9 eV, small enough for them to be good electron donors, their complexes with π-acceptors appear to fall in the category of weak charge-transfer complexes (3). The contribution of the charge-transfer interaction to the ground state stabilization is relatively small in these complexes, and it is appropriate to speak of them as molecular electron donor–acceptor (EDA) complexes.

The most studied π-acceptors in their interaction with aliphatic amines have been polynitroaromatic compounds (4–9). These interactions are strongly dependant on the solvent and the amine structure.

From the physicochemical properties of liquid binary systems of aliphatic amines and polar mono-substituted benzenes, the formation of EDA complexes has been inferred (10, 11), and they are considered the initially formed intermediates of nucleophilic aromatic substitution and other reactions (12–14).

The involvement of these complexes in the mechanism of general carbonyl reactions has been established (14) as well as the important biological implications of these types of interactions in protein chemistry (15).

Recently, excited charge-transfer complexes were proposed as intermediates in photochemical reactions of dicyanobenzenes and saturated amines (16–18). Furthermore intramolecular, n–π, charge-transfer interactions have been confirmed for 1-(*p*-nitrophenyl) alkanes bearing a dimethylamino group on the ω-carbon (19).

Summarizing the literature, the interaction of aliphatic amines with π-acceptors seems to follow a general pattern. In ionizing solvents, the intermediate n–π complex goes to products, making it difficult to study the complex itself; in nonpolar solvents these complexes appear to be stable but there is little information about their stabilities and thermodynamic properties. The lack of these data could be attributed to the fact that these are weak complexes and such studies, by the usual spectrophotometric methods (20), are difficult.

In order to assert most of the proposals given in the literature, a systematic study of amine complexes with π-acceptors is necessary to obtain quantitative data about stability constants and other thermodynamic properties. Also, these properties should be related to the structures of the amines and acceptors and to solvent effects.

In this work, as part of a series, the interaction of some aliphatic amines with benzonitrile as π-acceptor has been studied in the inert solvent (21)

[1]Author to whom correspondence may be addressed.
[2]Revision received May 14, 1980.

0008-4042/81/091291-06$01.00/0
©1981 National Research Council of Canada/Conseil national de recherches du Canada

Can. J. Chem. Downloaded from www.nrcresearchpress.com by 210.87.254.105 on 09/06/12
For personal use only.

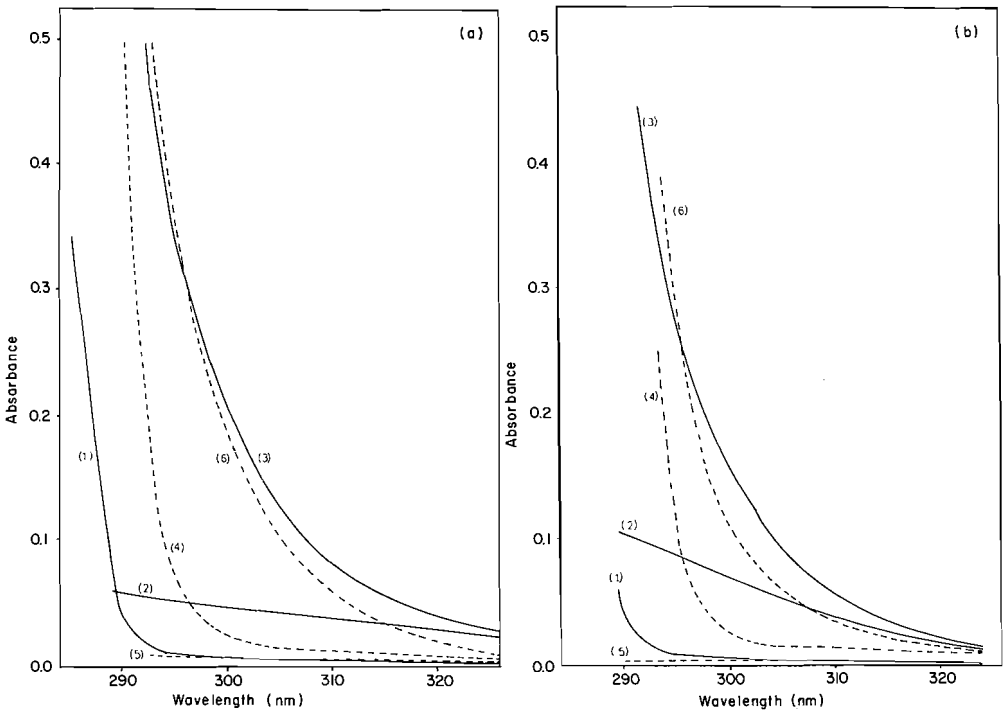

FIG. 1. Typical spectral results. (a) (—) (1) Benzonitrile 0.08 *M*, (2) triethylamine 1 *M*, (3) mixture of benzonitrile 0.08 *M* and triethylamine 1 *M*; (---) (4) benzonitrile 1 *M*, (5) triethylamine 0.08 *M*, (6) mixture of benzonitrile 1 *M* and triethylamine 0.08 *M*. (b) (—) (1) Benzonitrile 0.08 *M*, (2) di-*n*-butylamine 2 *M*, (3) mixture of benzonitrile 0.08 *M* and di-*n*-butylamine 2 *M*; (---) (4) benzonitrile 2 *M*, (5) di-*n*-butylamine 0.08 *M*, (6) mixture of benzonitrile 2 *M* and di-*n*-butylamine 0.08 *M*. Solvent: *n*-hexane. Temperature: 27 ± 0.1°C.

n-hexane. Correlations of the data with amine structure and other types of amine complexes were performed.

Experimental

n-Hexane (Carlo Erba R. P.) was purified by treatment with fuming sulfuric acid several times, washed to neutrality, dried over anhydrous $CaCl_2$, and fractionally distilled over metallic sodium. The distillate was kept over 4 Å molecular sieves (Merck). The solvent was then thoroughly degassed and distilled in a high vacuum line before use. Ultraviolet cut off point: 210 nm.

Diethylamine, triethylamine, *n*-butyl, di-*n*-butyl, and tri-*n*-butyl amines (Aldrich Chemical Co.) were purified and dried just before use by the following procedure. The amine was left over KOH pellets for several days, then refluxed, and later distilled in a dry nitrogen atmosphere over metallic sodium, collecting the middle fraction.

Benzonitrile (Fluka) was distilled over P_2O_5 under dry nitrogen atmosphere collecting the middle fraction. This distillation was repeated as many times as necessary until the residue remained colorless.

All the reagents were degassed and distilled in a high vacuum line just before use to ensure anhydrous conditions.

Spectra were measured in a thermostatted 10 mm cell in a Cary 17 spectrophotometer.

Data processing was performed in a Monroe 1860 computer and a Hewlett-Packard 9810 programable calculator.

Solutions were prepared by weighing the liquids and diluting with *n*-hexane as solvent. The complete range of concentrations used was of 0.5 to 6 *M* for benzonitrile and from 0.5 to 3.5 or 6 *M* for the amines, depending on their molecular weight. All solutions were freshly prepared prior to use.

Results

Spectral Characteristics of Solutions of Aliphatic Amine – Benzonitrile in n-*Hexane*

Typical spectral results are shown in Fig. 1. Although no new band assignable to complex formation is observed, there is an appreciable deviation from additivity of the optical density with respect to that of the amine and benzonitrile alone.

The change in the spectrum can be most likely interpreted in two ways: (*i*) a solvent shift of an absorption band of one component of the solution in the presence of the other, (*ii*) the formation of an EDA complex. For case (*i*) it is reasonable to consider that a high concentration of amine in a dilute hexane solution of benzonitrile would produce a red shift of the longer wave-length absorption of the latter, as predicted by dielectric theory (22). This is a pure electrostatic effect, which would lead to observation of an enhanced absorption in the tail of the band which has been experimentally measured, shown as full lines in Figs. 1(a) and 1(b). However, it is highly improbable that such a shift would

Can. J. Chem. Downloaded from www.nrcresearchpress.com by 210.87.254.105 on 09/06/12
For personal use only.

occur when the ratio of concentrations is reversed: i.e. excess of benzonitrile in a dilute hexane solution of amine (as is observed in Figs. 1(a) and 1(b), broken line). Furthermore it is widely recognized that solvents capable of acting as lone pair n-donors may produce anomalous shifts with respect to those expected from a purely electrostatic effect (23). The fact that amines are good n-donors, and that the deviation from additivity reaches an equivalent value with either an excess of benzonitrile or of amine suggests that the effect is caused by an alternate mechanism. The formation of EDA complexes is considered to be this mechanism. In fact, formation of EDA complexes is considered as a specific solvent effect, in addition to the electrostatic ones, and as Davis (23) has pointed out, this effect when present is likely to dominate the solvent–solute interaction.

In light of these arguments, the absorbance of the mixture (A_T) is interpreted as the sum of three components (eq. [1]).

$$[1] \quad A_T = A_A + A_D + A_{AD}$$

where A_A, A_D, and A_{AD} stand for the absorbance of the acceptor (benzonitrile), the donor (amine), and the complex at equilibrium concentration, respectively.

Assuming that Beer's Law holds for every species involved (24) and considering the formation of only a 1:1 complex, eq. [2] can be defined

$$[2] \quad A_c = A_T - (A_{Ao} + A_{Do})$$

where $A_{Ao} = \varepsilon_A$ [Ao], $A_{Do} = \varepsilon_D$ [Do], and where [Ao] and [Do] represent the initial molar concentrations of acceptor and donor; ε_A and ε_D are the molar extinction coefficients of these components.

The values of A_c calculated from A_T by eq. [2] give a measure of a deviation from additivity in the mixtures. Since no new band could be defined, A_c was obtained in the range between 295 and 305 nm where the experimental values were most accurately determined. The range of λ was restricted due to the high absorption of both donor and acceptor at shorter λ than 290 nm.

For every amine–benzonitrile system A_c values were determined by varying the concentration of either the donor or acceptor in excess with the concentration of the minor component kept constant. Some values were obtained for equal concentrations of both. Typical plots of A_c vs. concentration of the component in excess are illustrated in Fig. 2. The values of A_c obtained were independent of which component was in excess. This independence of the A_c values from the nature of the component in excess is evidence in favor of

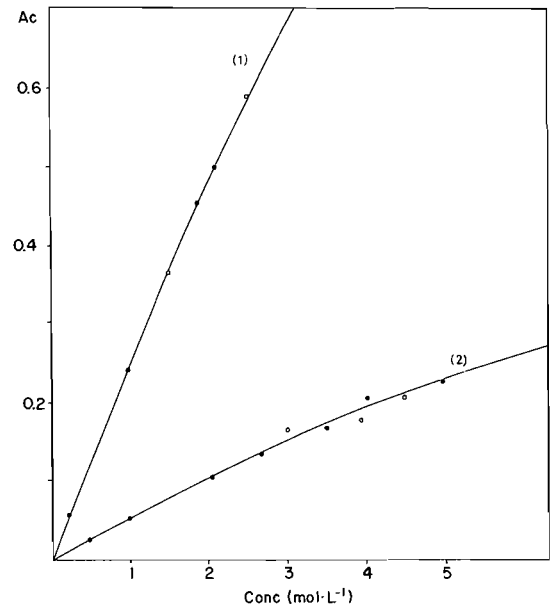

FIG. 2. Values of A_c for the systems: (1) tri-*n*-butylamine – benzonitrile, (2) di-*n*-butylamine – benzonitrile. Solvent: *n*-hexane. Temperature: 27 ± 0.1°C, λ = 300 nm. (●) Excess of amine (0.25–5 *M*); (○) excess of benzonitrile (0.25–5 *M*). Concentration of the low concentration component 0.08 *M* in all cases.

the formation of 1:1 EDA complexes. Moreover the curvature of these plots is characteristic of a particular amine, giving a qualitative picture of the equilibrium conditions. (The larger the deviation from a straight line, the greater the stability constant *K*.)

Determination of K *and* ε

By the results hitherto presented, if constancy of the ratio of activity coefficients is proposed (25), *K* can be expressed in terms of molar concentrations of benzonitrile [Ao] and amines [Do] as eq. [3];

$$[3] \quad K = [AD]/([Ao] - [AD])([Do] - [AD])$$

[AD] being the equilibrium molar concentration of the complex. If $A_{AD} = \varepsilon_{AD}$ [AD] is assumed, the following expression can be derived

$$[4] \quad \frac{[Ao]}{A_{AD}} = \frac{1}{K\varepsilon_{AD}}\frac{1}{[Do]} + \frac{[Ao]}{[Do]\varepsilon_{AD}} + \frac{1}{\varepsilon_{AD}} - \frac{[AD]}{[Do]\varepsilon_{AD}}$$

To solve eq. [4] for *K* and ε_{AD} a variety of graphical methods have been developed depending upon the system and experimental conditions (1*a*, *c*).

In the case where the absorption of the complex overlaps with the one of the donor and the acceptor, and considering

$$[5] \quad \varepsilon_c = \varepsilon_{AD} - (\varepsilon_A + \varepsilon_D)$$

Can. J. Chem. Downloaded from www.nrcresearchpress.com by 210.87.254.105 on 09/06/12
For personal use only.

TABLE 1. Experimental results for the correlations of I_p and pK_a of aliphatic amine donors in the EDA interaction with benzonitrile

Systems	Benzonitrile–amine ratio [Do]/[Ao][a]	K (L mol^{-1})[b]	ε_{AD}[b] (L mol^{-1} cm^{-1})	Correlation coefficient	I_p (amine)[c]	pK_a (amine)[d]
n-Butylamine – benzonitrile	0.015–75	0.021 ± 0.003	2	0.9860	8.71	10.60
Diethylamine–benzonitrile	0.015–75	0.062 ± 0.009	8	0.9915	8.01	10.98
Di-*n*-butylamine – benzonitrile	0.015–50	0.059 ± 0.009	12	0.9900	7.80	11.25
Triethylamine–benzonitrile	0.015–50	0.024 ± 0.003	108	0.9938	7.50	10.67
Tri-*n*-butylamine – benzonitrile	0.015–38	0.030 ± 0.005	105	0.9999	7.00	10.40

[a]The concentration of the minor component, either donor or acceptor, was kept at 0.08 *M*.
[b]Values for λ = 300 nm.
[c]Reference 37.
[d]Reference 33.

the following expression can be derived (26).

$$[6]\quad \frac{[Ao][Do]}{A_c([Ao]+[Do])} = \frac{1}{K\varepsilon_c}\frac{1}{([Ao]+[Do])} + \frac{1}{\varepsilon_c}$$

For every system studied, the values of A_c measured at different [Do] and [Ao], were plotted as in eq. [6]. A good straight line is obtained when some experimental points are neglected. From the intercept ($1/\varepsilon_c$) and the slope ($1/K\,\varepsilon_c$), the values of K and ε_c can be determined. However, the uncertainty in the determination of $1/\varepsilon_c$ is high depending upon which values of A_c are considered.

The values of the intercept change drastically if points for [Ao] = [Do] are included in the plot. Furthermore values of A_c for high values of [Ao] + [Do] seem to align better than for low donor or acceptor concentration. Therefore, calculations of K become completely unreliable. Several critical reviews about potential errors in the use of this type of graphical method for weak complexes have been published (1*c*, 20, 24, 27). Also Person (28) has shown that, for weak complexes it is very difficult experimentally to obtain concentrations of the complex which are high enough to give a good number of points sufficiently separated in the graph to allow a reliable calculation of K. In fact, this difficulty is at the root of the problems in proving the existence of weak complexes.

In order to overcome these problems, an iterative procedure was developed, where every experimental value of A_c was used independent of the initial donor or acceptor concentrations.

The method takes an approximate value of K obtained by plots of eq. [6], and then the corresponding value of [AD] is calculated by solving eq. [3] for each experimental point. Then, by using relation [7],

$$[7]\quad 1/[AD] = \varepsilon_c\, 1/A_c$$

and the usual least-squares procedure, a value of ε_c is obtained. The fit to eq. [7] obtained is measured by the correlation coefficient. An arbitrary change of K is then made and the whole process is repeated. The fit obtained is compared with the one obtained previously. The value of K is varied to obtain a better fit until there is no further improvement. In this way, the best values of both K and ε_c according to the least-squares criterion are found.

It should be noted that this method works with any ratios of [Do] to [Ao], the only restriction being that the values of A_c be sufficiently high to be measured accurately. Taking into account Person's (28) and Derenleau's (29) criteria, the best experimental points were chosen from graphs of the type shown in Fig. 2 (data corresponding to saturation fractions between 0.09 and 0.9). The same criteria (29) were used to calculate the error in the determination of K. The results obtained for measurements at λ = 300 nm are shown in Table 1.

Variation of K with λ was not appreciable; nevertheless, the range of λ that could be measured was so small that it is not possible to eliminate the possible existence of such an effect.

Since the values of ε_A and ε_D at 300 nm are very low (of the order of 10^{-2} L mol^{-1} cm^{-1}), the value of ε_c corresponds very closely to the value of ε_{AD} at this λ.

Temperature Dependance of K

The behaviour of K with temperature was studied for the system diethylamine–benzonitrile. K was determined by the described method at three temperatures; 16°C, 27°C, and 40°C ± 0.2°C. From the slope of the plot of log K vs. $1/T$ (Fig. 3) a value of -2 kcal mol^{-1} was found for the enthalpy change. This procedure assumes that ε_{AD} does not change with temperature, which is thought to be a reasonable approximation for the small range of temperature involved (30). The small negative value of ΔH encountered is consistent with the value expected for the formation of a weak EDA complex (1).

Discussion

To interpret the results from the interaction between aliphatic amines and benzonitrile, some structural properties of the molecules must be con-

Can. J. Chem. Downloaded from www.nrcresearchpress.com by 210.87.254.105 on 09/06/12
For personal use only.

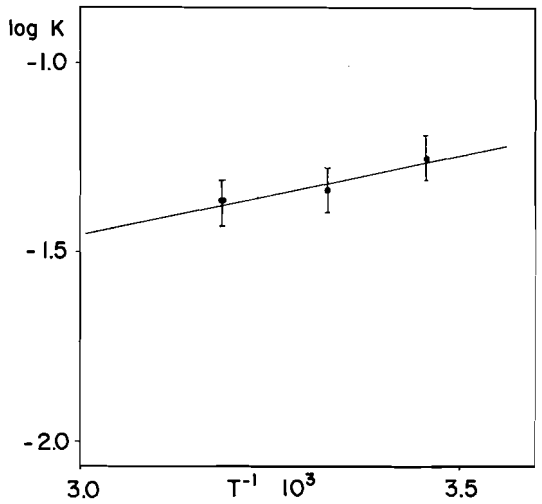

FIG. 3. Behavior of log K vs. T^{-1} for the system benzonitrile–diethylamine in n-hexane.

sidered. The presence of a cyano group in the aromatic ring, causing it to become electron deficient, makes benzonitrile a π-type of acceptor for the nonbonding electrons of a heteroatom (O, N, etc.). From these properties the formation of weak EDA complexes of benzonitrile with aliphatic amines has been proposed to explain the unusual deviation from additivity of refractive index and density of binary solutions of these compounds (10, 11). At the same time it must be recognized that, in interaction of an electron donor and acceptor to form a complex, interactions other than the charge-transfer type (such as electrostatic or dipolar) may play an important role in the ground state stabilization (22). However, the fact that from the new absorption observed in this study, a value of K and a finite constant value of ε could be determined, confirms the proposal of formation of an EDA complex between aliphatic amines and benzonitrile. Moreover, possible "contact complexes' (31) which avoid this kind of determination may be discarded as the unique cause of the spectral changes observed. These conclusions are further supported for the temperature effect observed, which is consistent with the known behaviour of weak EDA complexes.

The complexes of aliphatic amines with benzonitrile are undoubtedly very weak as judged by the small values of K. Nevertheless, the effect of the donor structure is reflected in these results. There is little correlation between the pK_a values of amines and their respective K values with benzonitrile (Table 1); this is hardly surprising, as the pK_a value is a measure of the Brönsted basicity, while the K is presumably a measure of the Lewis basicity of alkyl amines (32). It has been found that the electron donor strength of $R_3N > R_2NH > RNH_2$ predicted from the inductive effect of alkyl groups is expected to change when bulky substituent groups exert steric hindrance in the case of complex formation (33, 34). Considering that the value of the stability constant reflects the donor strength of the amine toward benzonitrile, it is possible to conclude that the same steric effects are present in these n–π complexes as in the n–v (R_3N: BMe_3) (34) and n–σ (R_3N: I_2) (35) complexes. Thus, secondary amines form stronger complexes than tertiary and primary.

The failure to observe a new maximum from the complex formed may be attributed to the fact that there is broadening of a component band, due to admixture of a component excited state with a charge transfer state (36). However, a likely possibility is that the difference in absorption of the mixture with respect to either component alone corresponds to overlap with a new band of the EDA complex. It is expected that for this type of system the new band would lie in a region of the uv spectrum which is unreachable experimentally due to the strong absorption of both donor and acceptor at the concentrations that must be used to detect such weak complexes. A maximum for such a band in aliphatic amine complexes with a stronger π-acceptor, namely 1,3,5-trinitrobenzene (6), has been found. These maxima vary with the ionization potential (I_p) of the amine in a very similar way to the variation of λ_{max} of the corresponding aliphatic amine complexes with iodine (35). In this matter, and considering that the values of ε_{AD} calculated for the amine–benzonitrile systems represent the extinction coefficient of the tail of the new absorption band at 300 nm, they would vary with the I_p of the amine, if there is a shift of λ_{max} with it. It is evident, as is shown in Table 1, that this is so. Assuming that $\varepsilon_{AD(max)}$ is not drastically different for different amines (32), the increase in ε_{AD} at 300 nm reflects the shift in λ_{max} with the order $R_3N > R_2NH > RNH_2$, as is observed for the cited n–π complexes (6).

Work is in progress to assess these conclusions from further thermodynamic data such as ΔH and ΔS measurements. Stronger π-acceptors such as nitro-substituted benzenes will be chosen in order to avoid some of the experimental difficulties found for the benzonitrile systems.

It is believed, however, that for the systems studied, the data obtained gives good evidence of complex formation which correlates with donor strength as expected and which can be used as a starting point for the elucidation of the chemical

Can. J. Chem. Downloaded from www.nrcresearchpress.com by 210.87.254.105 on 09/06/12
For personal use only.

properties of n–π complexes in reaction mechanisms.

Acknowledgements

This work has been partially supported by the Consejo Nacional de Investigaciones Científicas y Técnicas de la República Argentina.

1. (*a*) G. Briegleb. Elektronen Donator–Acceptor Komplexe. Springer-Verlag, Berlin. 1961. (*b*) W. B. Person and R. S. Mulliken. Molecular complexes: a lecture and reprint volume. Wiley, New York. 1969. (*c*) R. Foster. Organic charge transfer complexes. Academic Press, New York. 1969.
2. (*a*) W. M. Moreau and K. Weiss. J. Am. Chem. Soc. **88**, 204 (1966); (*b*) B. Nelander. Acta Chem. Scand. **20**, 2289 (1966).
3. O. B. Nagy and J. B. Nagy. Environmental effects on molecular structure and properties. D. Reidel Publishing Company, Holland. 1976. p. 179–203.
4. M. M. Labes and S. D. Ross. J. Org. Chem. **21**, 1049 (1956).
5. R. E. Miller and W. F. K. Wynne-Jones. J. Chem. Soc. 2378 (1959).
6. R. Foster and R. K. Mackie. J. Chem. Soc. 3843 (1962).
7. R. Foster and C. A. Fyfe. Rev. Pure Appl. Chem. **16**, 61 (1966), and references therein.
8. W. Liptay and N. Tamberg. Z. Electrochem. **66**, 59 (1962).
9. R. Foster and R. K. Mackie. Tetrahedron, **16**, 119 (1961).
10. M. G. Voronkov and A. Ya. Deich. Teor. Eksp. Khim. **1**, 663 (1965).
11. M. G. Voronkov, A. Ya. Deich, and E. V. Akatova. Khim. Geterotsikl. Soedin. **2**, 8 (1966).
12. (*a*) O. B. Nagy and A. Bruylants. Bull. Cl. Sci. Acad. R. Belg. **53**, 947 (1967); (*b*) **53**, 1159 (1967).
13. J. B. Nagy, A. Bruylants, and O. B. Nagy. Tetrahedron Lett. **54**, 4825 (1969).
14. (*a*) J. B. Nagy, O. B. Nagy, and A. Bruylants. Bull. Soc. Chim. Belg. **82**, 539 (1973), (*b*) O. B. Nagy, M. Muanda, and J. B. Nagy. J. Phys. Chem. **83**, 1961 (1979).
15. H. Kon and A. Szent-Gyorgyi. Proc. Natl. Acad. Sci. U.S.A. **70**, 1030 (1973).
16. M. Ohashi, K. Tsujimoto, and Y. Furukawa. Chem. Lett. 543 (1977).
17. M. Ohashi and K. Miyake. Chem. Lett. 615 (1977).
18. K. Tsujimoto, K. Miyake, and M. Ohashi. J. Chem. Soc. Chem. Commun. 386 (1976).
19. K. Mutai, K. Kobayashi, T. Kobayashi, and C. Utsunomiya. Chem. Lett. 1047 (1977).
20. E. G. Polle. Russ. Chem. Rev. **43**, 631 (1974).
21. K. M. C. Davis and M. F. Farmer. J. Chem. Soc. B, 28, (1967).
22. (*a*) E. G. McRae. J. Phys. Chem. **61**, 562 (1957); (*b*) W. Liptay. Angew. Chem. Int. Ed. Engl. **8**, 177 (1969).
23. K. M. C. Davis. Molecular association. Vol. 1. *Edited by* R. Foster. Academic Press, New York. 1975. p. 151.
24. P. H. Emslie, R. Foster, C. A. Fyfe, and I. Horman. Tetrahedron, **21**, 2843 (1965).
25. M. S. Sambhi. J. Phys. Chem. **73**, 1584 (1969).
26. S. D. Ross and M. M. Labes. J. Am. Chem. Soc. **79**, 76 (1957).
27. R. Foster. Ind. Chim. Belge, **37**, 547 (1972).
28. W. B. Person. J. Am. Chem. Soc. **87**, 167 (1965).
29. D. A. Deranleau. J. Am. Chem. Soc. **91**, 4044 (1969).
30. S. Nagakura. J. Am. Chem. Soc. **80**, 520 (1958).
31. L. E. Orgel and R. S. Mulliken. J. Am. Chem. Soc. **79**, 4839 (1957).
32. R. Foster and D. Ll. Hammick. J. Chem. Soc. 2685 (1954).
33. J. W. Smith. The chemistry of the amino group. *Edited by* S. Patai. Interscience. 1968. p. 161.
34. R. W. Taft. Steric effects in organic chemistry. *Edited by* M. S. Newman. John Wiley and Sons, New York 1956. p. 632.
35. H. Yada, J. Tanaka, and S. Nagakura. Bull. Chem. Soc. Jpn. **33**, 1660 (1960).
36. K. M. C. Davis and M. F. Farmer. J. Chem. Soc. B, 859 (1968).
37. K. Watanabe and J. R. Motte. J. Chem. Phys. **26**, 1773 (1957).

Can. J. Chem. Downloaded from www.nrcresearchpress.com by 210.87.254.105 on 09/06/12
For personal use only.

The addition of simple aromatic hydrocarbons to condensed aromatic thiophenes promoted by aluminum chloride. Part II. Naphtho[1,2-*b*]thiophene

PETER DAVID CLARK AND DAVID M. MCKINNON

Department of Chemistry, The University of Manitoba, Winnipeg, Man., Canada R3T 2N2

Received November 6, 1980

PETER DAVID CLARK and DAVID M. MCKINNON. Can. J. Chem. **59**, 1297 (1981).

The reaction of naphtho[1,2-*b*]thiophene with an aromatic hydrocarbon in the presence of aluminum chloride at 20°C gave either a 3-aryl-2,3-dihydronaphtho[1,2-*b*]thiophene by addition to the 2,3-bond or 2,3-dihydronaphtho[1,2-*b*]thiophene as a result of hydride abstraction.

Occasionally 2-aryl-2,3-dihydronaphtho[1,2-*b*]thiophenes were obtained. At higher temperatures 2-arylnaphtho[1,2-*b*]thiophenes and 2,3-dihydronaphtho[1,2-*b*]thiophene were isolated. Attempts are made to rationalize the formation of these products in terms of protonation of naphtho[1,2-*b*]thiophene by moist aluminum chloride and reaction of the resulting electrophile with an aromatic substrate.

PETER DAVID CLARK et DAVID M. MCKINNON. Can. J. Chem. **59**, 1297 (1981).

Le naphto[1,2-*b*] thiophène réagit avec un hydrocarbure aromatique en présence de chlorure d'aluminium à 20°C et conduit soit à l'aryl-3 dihydro-2,3 naphto[1,2-*b*] thiophène par une addition sur la double liaison 2,3 soit au dihydro-2,3 naphto[1,2-*b*] thiophène par suite de l'enlèvement d'un hydrure.

On obtient occasionnellement des aryl-2 dihydro-2,3 naphto[1,2-*b*] thiophènes. On a isolé, à température plus élevée, des aryl-2 naphto[1,2-*b*] thiophènes et le dihydro-2,3 naphto[1,2-*b*] thiophène. On a essayé de rationaliser la formation de ces produits en fonction d'une protonation du naphto[1,2-*b*] thiophène par le chlorure d'aluminium humide suivie de la réaction de l'électrophile ainsi obtenu avec un substrat aromatique.

[Traduit par le journal]

Introduction

Recent studies (1) have revealed that aluminum chloride promotes the addition of simple aromatic compounds to the 2,3-bond of benzo[*b*]thiophene (**1***a*) to give either 3-aryl-2,3-dihydrobenzo[*b*]thiophenes (**2***a*) or 2-arylbenzo[*b*]thiophenes (**1***b*), depending on the reaction conditions. Since the dihydro products could be dehydrogenated readily to 3-arylbenzo[*b*]thiophenes (**1***c*), a synthesis of 2- or 3-arylbenzo[*b*]thiophenes from the parent heterocycle was achieved. This work was extended to naphtho[2,1-*b*]thiophene (**3***a*) providing a general synthesis of 1- and 2-arylnaphtho[2,1-*b*]thiophenes (**3***b*, *c*) (2). For the isomeric arylnaphtho[1,2-*b*]-thiophenes (e.g., **4***b*, *c*), very few examples have been reported (3) and the general synthetic procedures for the preparation of substituted naphtho-[1,2-*b*]thiophenes are either not applicable (4) to the synthesis of arylnaphtho[1,2-*b*]thiophenes (**4***b*, *c*) or can result in mixtures (5). Consequently we have examined the addition of aromatic compounds to naphtho[1,2-*b*]thiophene (**4***a*) with aluminum chloride.

Results and Discussion

In a typical experiment naphtho[1,2-*b*]thiophene (**4***a*) was dissolved in excess of an aromatic hydrocarbon, two mol equivalents of aluminum chloride[1] were added, and the reaction mixture was

[1]The reactions proceed more slowly with one mol equivalent of aluminum chloride.

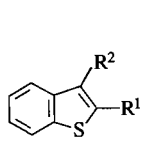

1

a $R^1 = H, R^2 = H$
b $R^1 = Ar, R^2 = H$
c $R^1 = H, R^2 = Ar$

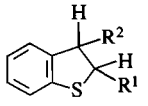

2

a $R^1 = H, R^2 = Ar$
b $R^1 = Ar, R^2 = H$

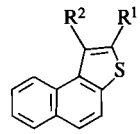

3

a $R^1 = H, R^2 = H$
b $R^1 = H, R^2 = Ar$
c $R^1 = Ar, R^2 = H$

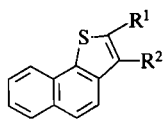

4

a $R^1 = H, R^2 = H$
b $R^1 = Ar, R^2 = H$
c $R^1 = H, R^2 = Ar$
d $R^1 = H, R^2 = C_6H_5$
e $R^1 = H, R^2 = 4\text{-}MeC_6H_4$
f $R^1 = H, R^2 = 4\text{-}EtC_6H_4$
g $R^1 = H, R^2 = 3,4\text{-}diMeC_6H_3$
h $R^1 = 4\text{-}MeC_6H_4, R^2 = H$
i $R^1 = 3,4\text{-}diMeC_6H_3, R^2 = H$
j $R^1 = 2,5\text{-}diMeC_6H_3, R^2 = H$

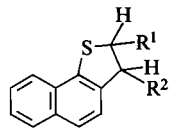

5

a $R^1 = H, R^2 = H$
b $R^1 = Ar, R^2 = H$
c $R^1 = H, R^2 = Ar$
d $R^1 = H, R^2 = C_6H_5$
e $R^1 = C_6H_5, R^2 = H$
f $R^1 = H, R^2 = 4\text{-}MeC_6H_4$
g $R^1 = H, R^2 = 4\text{-}EtC_6H_4$
h $R^1 = H, R^2 = 3,4\text{-}diMeC_6H_3$
i $R^1 = 3,4\text{-}diMeC_6H_3, R^2 = H$
j $R^1 = H, R^2 = 2,5\text{-}diMeC_6H_3$
k $R^1 = 2,5\text{-}diMeC_6H_3, R^2 = H$

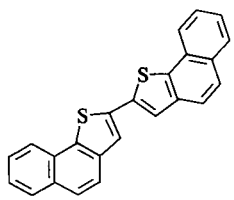

6

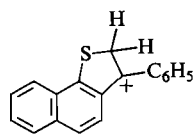

11

0008-4042/81/091297-06$01.00/0

©1981 National Research Council of Canada/Conseil national de recherches du Canada

Can. J. Chem. Downloaded from www.nrcresearchpress.com by 210.87.254.5 on 09/06/12
For personal use only.

Can. J. Chem. Downloaded from www.nrcresearchpress.com by 210.87.254.5 on 09/06/12
For personal use only.

TABLE 1. The reactions of naphtho[1,2-*b*]thiophene with aromatic hydrocarbons and aluminum chloride

			Dihydronaphtho[1,2-*b*]thiophene derivatives			Fully aromatic derivatives (%)	
Aromatic hydrocarbon	Temp (°C)	Time (h)	2-Ar (**5***b*)	3-Ar (**5***c*)	2,3-Dihydro (**5***a*)	2-Ar (**4***b*)	Dimer (**6**)
Benzene[a]	20	4		27	27		
	80	3			65	22	
Toluene	20	2		57			10
	110	4			26	47	
Ethylbenzene	0	2		73	5		18
	20	3		28	53		16
	136	2			75		
1,2-Dimethylbenzene	0	1	28	64			
	20	1	27	62			
	142					61	
1,4-Dimethylbenzene	20	1.5	38	23	15		16
	138					22	

[a]3-Phenylnaphtho[1,2-*b*]thiophene (**4***d*) (27%) was also obtained.

stirred either at 0° or 25°C or heated under reflux. An intense deep red color which always developed on addition of the aluminum chloride disappeared on addition of dilute acid during the isolation of the products. The results of these reactions are summarized in Table 1.

At 25°C naphtho[1,2-*b*]thiophene (**4***a*) reacted with simple aromatic hydrocarbons and aluminum chloride to form mainly either 3-aryl-2,3-dihydronaphtho[1,2-*b*]thiophenes (**5***c*) or 2,3-dihydronaphtho[1,2-*b*]thiophene (**5***a*). These results may be contrasted to similar reactions with benzo[*b*]thiophene (**1***a*) and with naphtho[2,1-*b*]thiophene (**3***a*) which gave the corresponding aryldihydro products almost exclusively (1, 2). The formation of 2,3-dihydronaphtho[1,2-*b*]thiophene (**5***a*) depends on the aromatic hydrocarbon being used. While toluene and 1,2-dimethylbenzene reacted to give 3-aryl-2,3-dihydronaphtho[1,2-*b*]thiophenes (**5***f*, *h*), ethylbenzene gave a mixture of the 3-aryldihydro product (**5***g*) and 2,3-dihydronaphtho[1,2-*b*]thiophene in a ratio of 2:3. Examination of probable mechanisms (Scheme 1)[2] of these reactions shows how **5***a* may arise. It is probable that protonation of naphtho[1,2-*b*]thiophene (**4***a*) by moist aluminum chloride[3] (i.e., species such as $[H^+][AlCl_4^-]$ or $[H^+][AlCl_3OH^-]$) occurs at either the 2- or 3-positions to give the carbonium ions **7** and/or **8**. It is likely that protonation at C-2 is favored since products derived from the carbonium ion **7** predominate. Also, studies (4) made on the electrophilic substitution reactions of naphtho[1,2-*b*]-thiophene indicate that attack at C-2 predominates with C-5 being the next most reactive centre.

The carbonium ion **7** may undergo two reactions, either abstraction of a hydride ion to form **5***a* or electrophilic attack on an aromatic carbon atom to form a 3-aryl-2,3-dihydronaphtho[1,2-*b*]thiophene (**5***c*). The most likely sources of hydride ions are the alkyl substituents of the aromatic hydrocarbons (8). In the reactions with toluene and 1,2-dimethylbenzene at 20°C the energy of activation for abstraction of a hydride ion seems to be unfavorable compared to reaction of the carbonium ions at an aromatic carbon atom, resulting in the production of 3-aryl-2,3-dihydro products **5***f*, *h*. However, in the reaction with ethylbenzene at 20°C, hydride abstraction by the carbonium ions becomes the dominant process and **5***a* is the major product. This

[2]Discussions of probable mechanisms for reactions with benzo[*b*]thiophene and naphtho[2,1-*b*]thiophene were given in refs. 1 and 2.

[3]Carefully dried aluminum chloride slows these reactions considerably.

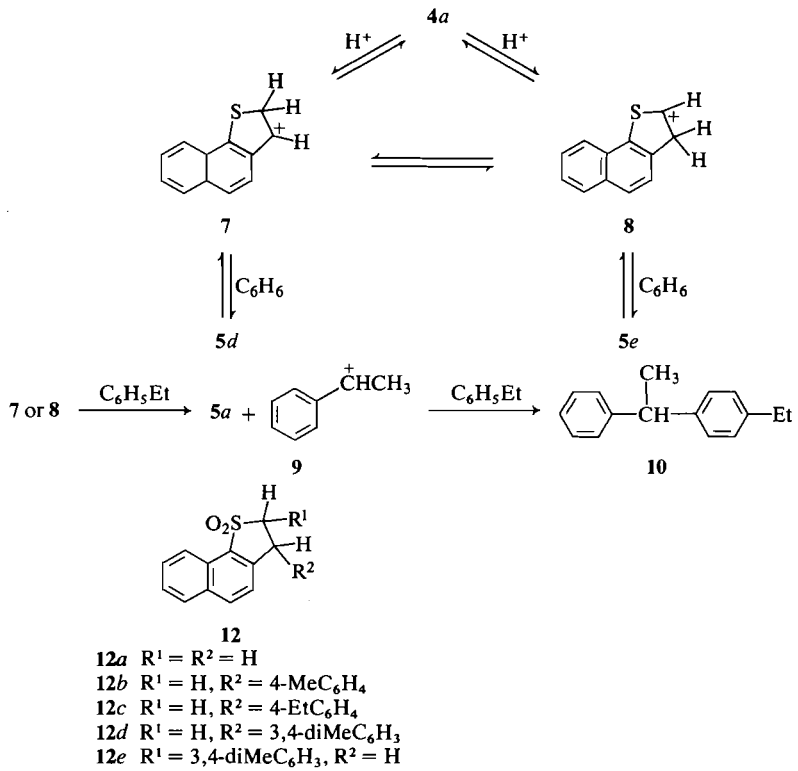

12

12a $R^1 = R^2 = H$
12b $R^1 = H$, $R^2 = 4\text{-}MeC_6H_4$
12c $R^1 = H$, $R^2 = 4\text{-}EtC_6H_4$
12d $R^1 = H$, $R^2 = 3,4\text{-}diMeC_6H_3$
12e $R^1 = 3,4\text{-}diMeC_6H_3$, $R^2 = H$

SCHEME 1. Mechanisms for the addition of aromatic hydrocarbons to naphtho[1,2-*b*]thiophene.

is reasonable, since hydride abstraction from the methylene group of ethylbenzene should be easier than abstraction from the methyl groups of toluene or 1,2-dimethylbenzene.

Interestingly, when the reaction with ethylbenzene was carried out at 0°C very little 2,3-dihydronaphtho[1,2-*b*]thiophene (**5***a*) was formed and 2,3-dihydro-3-(4-ethylphenyl)naphtho[1,2-*b*]thiophene (**5***g*) was the major product. Conversely, when the same reaction was carried out under reflux, 2,3-dihydronaphtho[1,2-*b*]thiophene (**5***a*) was the only heterocyclic product isolated. 1-Phenyl-2-(4-ethylphenyl)ethane (**10**) was also obtained. It is likely that **10** arises by attack of the α-phenethylcarbonium ion (**9**) on another molecule of ethylbenzene (Scheme 1). This reaction constitutes a more direct synthesis of both **5***a* and **10** than the syntheses already described (6, 7).

Unexpectedly, the reaction of naphtho[1,2-*b*]-thiophene with benzene gave 2,3-dihydronaphtho-[1,2-*b*]thiophene (**5***a*), along with 2,3-dihydro-3-phenylnaphtho[1,2-*b*]thiophene (**5***d*) and 3-phenylnaphtho[1,2-*b*]thiophene (**4***d*) in approximately equivalent quantities. Analysis of this mixture is described in the Experimental. Although it appears that reaction of the carbonium ion **7** with benzene is slow, after a significant quantity of **5***d* has formed, hydride abstraction from **5***d* by the carbonium ion **7** becomes significant and **5***a* results. The newly formed carbonium ion **11** loses a proton to form **4***c*.

The reactions with 1,2- and 1,4-dimethylbenzene at 25°C were unusual since only in these reactions were 2-aryl-2,3-dihydronaphtho[1,2-*b*]thiophenes (**5***i*, *k*) observed. In fact the 2-aryl product **5***k* was the major product in the reaction with 1,4-dimethylbenzene. Examination of molecular models indicates that when either 1,2- or 1,4-dimethylbenzene attacks the carbonium ion **7** there are steric interactions between the methyl groups of the benzenes and the C—H bond at C-4 of **7**. As a result products derived from the carbonium ion **8** are observed.

An interesting mechanistic feature of these reactions is that the formation of aryl-2,3-dihydronaphtho[1,2-*b*]thiophenes from the carbonium ions **7**, **8** is reversible (Scheme 1). Evidence for this was obtained as when 2,3-dihydro-3-(3′,4′-dimethylphenyl)naphtho[1,2-*b*]thiophene (**5***h*) was stirred with aluminum chloride in toluene solution 2,3-dihydro-3-(4-methylphenyl)naphtho[1,2-*b*]thiophene (**5***f*) was obtained (87% isolated yield). Similarly reactions with benzo[*b*]thiophene and naphtho-[2,1-*b*]thiophene were found to be reversible (1, 2).

Can. J. Chem. Downloaded from www.nrcresearchpress.com by 210.87.254.5 on 09/06/12
For personal use only.

TABLE 2. ^{1}H nmr data for the dihydro protons of aryl-2,3-dihydronaphtho[1,2-*b*]-thiophenes (**5**) and their *S*,*S*-dioxide derivatives (**12**)

Compound	Chemical shift (δ ppm)[a]			Coupling constants (Hz)[b]
	H_A	H_B	H_X	J_{AB}
5*a*	3.38	3.38		[c]
12*a*	3.50	3.50		[c]
5*d*	3.75	3.35	4.75	−10.8
5*f*	3.80	3.45	4.75	−10.8
12*b*	4.05	3.60	5.15	−13.2
5*g*	3.75	3.40	4.75	−11.0
12*c*	4.05	3.56	4.80	−13.4
5*h*	3.80	3.45	4.80	−11.0
5*i*	3.68	3.68	5.12	[c]
12*d*	4.06	3.58	4.80	−13.4
5*k*	3.78	3.48	5.40	−15.0
5*j*	3.85	3.40	5.10	−11.0

[a]Values are ± 0.02 ppm.
[b]Values are ± 0.2 Hz.
[c]Unobtainable from degenerate spectrum.

In many of the reactions described a small quantity of the dimer **6** was obtained (see Table 1). Its structure was confirmed by Raney-nickel hydrodesulfurization. Nevertheless when naphtho-[1,2-*b*]thiophene (**4***a*) was treated with aluminum chloride in dichloromethane the reaction proceeded very slowly. A very complex reaction mixture was obtained from which the dimer **6** could be isolated.

Because of the formation of mixtures in the reactions of naphtho[1,2-*b*]thiophene with aromatic compounds and aluminum chloride at 25°C, their usefulness as a general procedure for the synthesis of arylnaphtho[1,2-*b*]thiophenes is limited. However, when 3-aryl-2,3-dihydronaphtho-[1,2-*b*]thiophenes (**5***c*) could be isolated, it was found that dehydrogenation of these compounds with 2,3-dichloro-5,6-dicyano-1,4-benzoquinone gave 3-arylnaphtho[1,2-*b*]thiophenes (**4***c*) in excellent yield. Also reactions carried out at the boiling point of the aromatic hydrocarbon, which were expected (cf. results described in refs. 1 and 2) to give 2-arylnaphtho[1,2-*b*]thiophenes (**4***b*), in fact gave mixtures of **4***b* and 2,3-dihydronaphtho[1,2-*b*]-thiophene (**5***a*) (Table 1). Often **5***a* predominated, again limiting the method as a general synthesis of 2-arylnaphtho[1,2-*b*]thiophenes.

Product Analysis

Using ^{1}H nmr spectroscopy it was possible to differentiate between 2- and 3-aryl-2,3-dihydrobenzo[*b*]thiophenes, (**2***a*, *b*) on the basis of a difference in the value of the coupling constants (J_{AB}) for the geminal protons located at either C-2 or C-3 (1). J_{AB} values for the 3-aryl products **2***a* were always in the range -11.0 ± 0.2 Hz and, for 2-aryl products **2***b*, -15 ± 0.2 Hz. Also, while oxidation of 3-aryl products to their *S*,*S*-dioxides changed the value of J_{AB} to -13.0 ± 0.2 Hz, oxidation of the 2-aryl products did not alter the value of J_{AB}. The same technique was applied to studies on the naphtho[2,1-*b*]thiophene (**3***a*) and values of J_{AB} were almost identical for the corresponding derivatives (1, 2). In the present work, study of the ^{1}H nmr spectra of 2- and 3-aryl-2,3-dihydronaphtho-[1,2-*b*]thiophenes (**5***b*, *c*) showed analogous behaviour for the values of J_{AB} (Table 2), so enabling structural assignment. In one case (compound **5***f*) Raney-nickel hydrodesulfurization was used to confirm the structural assignment. This technique was also used to confirm the structures of 2-arylnaphtho-[1,2-*b*]thiophenes **4***b*. Full details are given in the Experimental.

Experimental

The ^{1}H nmr spectra were obtained in deuteriochloroform solution, unless stated otherwise, on a Varian model EM360 spectrometer using tetramethylsilane as an internal standard. Mass spectra were obtained on a Finnegan 1015 spectrometer. Melting points are uncorrected.

Naphtho[1,2-b]thiophene

This was prepared by the method of Clarke *et al.* (4) and had bp 125–127°C at 0.25 Torr.

Addition Reactions of Naphtho[1,2-b]thiophene at 0°C and 20°C to Form 2- and 3-Aryl-2,3-dihydronaphtho[1,2-b]-thiophenes (5b, 5c) and 2,3-Dihydronaphtho[1,2-b] thiophene (5a)

(a) General Procedure

Aluminum chloride (Fisher technical grade) (2.88 g, 0.020 mol) was added to a solution of naphtho[1,2-*b*]thiophene (2.0 g, 0.010 mol) in the appropriate aromatic hydrocarbon (100 mL). The resulting deep red mixtures were stirred for 1–4 h (see Table 1) and poured into ice-cold aqueous 20% hydrochloric acid (100 mL). The organic material was isolated by extraction with ethyl acetate. The solutions were washed with water and dried

Can. J. Chem. Downloaded from www.nrcresearchpress.com by 210.87.254.5 on 09/06/12
For personal use only.

Can. J. Chem. Downloaded from www.nrcresearchpress.com by 210.87.254.5 on 09/06/12
For personal use only.

over anhydrous magnesium sulfate. Evaporation of the solutions gave the products as oils, which either yielded crystalline material from hexane solution or were pruified further by chromatography on silica (Merck 60) and elution with hexane – ethyl acetate (20:1). Individual experiments are described below.

(b) With Toluene

The oily product was dissolved in hexane (50 mL) at 20°C and after 1 h pale yellow microcrystals of the dimer (**6**) (0.21 g, 10%), mp 257–259°C, which separated, were collected. The nmr spectrum δ: 7.0–8.2 (m, the aromatic protons). The mass spectrum: M^+ 366, calcd. 366. *Anal.* calcd. for $C_{24}H_{14}S_2$: C 78.70, H 3.85, S 17.50; found: C 78.55, H 3.90, S 17.25%.

After keeping the filtrate at −5°C for 24 h colorless plates (2.6 g, 86%), mp 76–77°C, of 2,3-dihydro-3-(4′-methylphenyl)-naphtho[1,2-*b*]thiophene (**5***f*), which were deposited, were collected. The nmr spectrum δ: 2.27 (s, Me) and 6.9–7.95 (m, the aromatic protons). The mass spectrum: M^+ 276, calcd. 276. *Anal.* calcd. for $C_{19}H_{16}S$: C 82.60, H 5.80, S 11.60; found: C 82.60, H 5.85, S 11.65%.

The structure of the dimer (**6**) was confirmed by hydrodesulfurization with Raney-nickel. A mixture of (**6**) (0.5 g) and Raney-nickel (1 g) in 95% aqueous ethanol was heated under reflux for 18 h. The reaction mixture was filtered and the filtrate was evaporated leaving an oily residue of 1,4-di-2′-naphthylbutane.[4] The nmr spectrum δ: 1.6–3.1 (m, —$(CH_2)_4$—) and 6.9–8.1 (m, the aromatic protons). The mass spectrum: M^+ 310, $C_{24}H_{22}$ requires 310. *Anal.* calcd. for $C_{24}H_{22}$: C 92.90, H 7.10; found: C 92.85, H 7.10%.

Similarly hydrodesulfurization of **5***f* gave 1-(4′-methylphenyl)-1-(2′-naphthyl)ethane as a colorless oil, bp 110–115°C at 0.6 Torr. The nmr spectrum δ: 1.65 (d, CH—*Me*), 2.15 (s, Me), 4.72 (q, *CH*—Me), and 6.9–8.1 (m, the aromatic protons). The mass spectrum: M^+, 246, $C_{19}H_{18}$ requires 246. *Anal.* calcd. for $C_{19}H_{18}$: C 92.70, H 7.32; found: C 92.90, H 7.05%.

(c) With Ethylbenzene at 0°C

Chromatography of the crude product gave an oil which was redissolved in hexane (50 mL) at 20°C. On standing at 10°C, a pale yellow microcrystalline solid (0.18 g, 9%), mp 255–259°C, corresponding to the dimer (**6**), was obtained. Cooling of the mother liquors to −5°C gave 2,3-dihydro-3-(4′-ethylphenyl)-naphtho[1,2-*b*]thiophene (**5***g*) as colorless plates (2.3 g, 73%), mp 76–77°C, which were collected. The nmr spectrum δ: 1.21 (t, Me), 2.62 (q, CH_2), and 6.8–8.0 (m, the aromatic protons). The mass spectrum: M^+ 290, calcd. 290. *Anal.* calcd. for $C_{20}H_{18}S$: C 82.75, H 6.20, S 11.05; found: C 82.55, H 6.35, S 11.05%.

(d) With Ethylbenzene at 20°C

The dimer (**6**) (0.16 g, 16%) and **5***g* (0.88 g, 28%) were isolated as described in the reaction at 0°C. Evaporation of the mother liquors gave an oil and distillation of this oil gave 2,3-dihydronaphtho[1,2-*b*]thiophene (**5***a*) (6) as a colorless oil (1.06 g, 53%), bp 110–115°C at 0.25 Torr. The nmr spectrum δ: 3.38 (s, CH_2—CH_2) and 6.8–8.2 (m, the aromatic protons). The mass spectrum: M^+ 186, calcd. for $C_{12}H_{10}S$ 186. *Anal.* calcd. for $C_{12}H_{10}S$: C 77.40, H 5.40, S 17.20; found: C 77.45, H 5.30, S 17.45%.

(e) With 1,2-Dimethylbenzene at 0°C or 20°C

The crude product was dissolved in hexane and on cooling this solution to −5°C, 2,3-dihydro-3-(3′,4′-dimethylphenyl)-naphtho[1,2-*b*]thiophene (**5***h*) was deposited as colorless prisms (1.95 g, 62%), mp 113–114°C. These were removed by filtration. The nmr spectrum δ: 2.21 (s, 2Me) and 6.9–8.0 (m, the aromatic protons). The mass spectrum: M^+ 290, calcd. 290. *Anal.* calcd. for $C_{20}H_{18}S$: C 82.75, H 6.20, S 11.05; found: C 82.80, H 6.30, S 11.10%.

[4]This compound has been reported (10) but no physical or spectroscopic data were given.

After concentration of the mother liquors and storage of this solution at −5°C for 14 days the 2-isomer (**5***i*) was collected as colorless plates, (0.88 g, 28%), mp 110–111°C. The nmr spectrum δ: 2.17 (s, 2Me) and 7.0–8.0 (m, the aromatic protons). The mass spectrum: M^+ 290, cald. 290. *Anal.* calcd. for $C_{20}H_{18}S$: C 82.75, H 6.20, S 11.05; found: C 82.60, H 6.20, S 11.05%.

(f) With 1,4-Dimethylbenzene

The crude product was dissolved in hexane (50 mL). On standing at 20°C the dimer (**6**) crystallized out as a pale yellow solid (0.31 g, 16%) which was collected. Evaporation of the mother liquors gave a clear oil (2.4 g) which could not be induced to crystallize. The ^1H nmr spectrum and the mass spectrum of the oil indicated three compounds were present: (*i*) 2,3-Dihydro-2-(2′,5′-dimethylphenyl)naphtho[1,2-*b*]thiophene (**5***k*), (*ii*) its 3-isomer (**5***j*), and (*iii*) 2,3-dihydronaphtho[1,2-*b*]thiophene (**5***a*). The nmr spectrum δ: 2.18 and 2.34 (Me's), 3.38[5] (s, due to CH_2—CH_2 of **5***a*), 3.2–4.0 (m, due to CH_2's of **5***j* and *k*), 5.10[5] (t, due to CH of **5***j*), 5.40[5,6] (t, due to CH of **5***k*), and 6.8–8.2 (m, the aromatic protons). The mixture could not be resolved by standard techniques. The mass spectrum showed peaks at 186 (due to **5***a*) and 290 (due to **5***j* and **5***k*).

(g) With Benzene

Spectroscopic studies indicated that the product was a mixture of 2,3-dihydronaphtho[1,2-*b*]thiophene (**5***a*), 2,3-dihydro-3-phenylnaphtho[1,2-*b*]thiophene (**5***d*), and 3-phenylnaphtho-[1,2-*b*]thiophene (**4***d*). Attempts to resolve this mixture were unsuccessful. The nmr spectrum δ: 3.38 (s, CH_2—CH_2 of **5***a*), 3.35–3.75 (m, CH_2 of **5***d*, 4.75 (t, CH— of **5***d*), and 7.0–8.2 (m, the aromatic protons of **5***a*, **5***d*, and **4***d*); J_{AB} for CH_2 (**5***d*) is −10.8 Hz, thus indicating a 3-aryl product. The mass spectrum: M^+, 186, 260, 262 (corresponding to **5***a*, **4***d*, and **5***d*).

Although the presence of **5***a* and **5***d* in the mixture could be determined directly by analysis of the ^1H nmr and the mass spectrum, it was not possible to determine if the remaining product was 2- or 3-phenylnaphtho[1,2-*b*]thiophene. The problem was resolved by Raney-nickel hydrodesulfurization of the reaction mixture using the procedure described earlier. The product was obtained as a clear oil and contained a mixture of 2-ethylnaphthalene and 1-(2′-naphthyl)-1-phenylethane.[7] The mixture was not resolved. The nmr spectrum, for 2-ethylnaphthalene, δ: 1.16 (t, Me), 2.57 (q, CH_2), and 7.0–8.0 (m, the aromatic protons); for 1-(2′-naphthyl)-1-phenylethane, δ: 1.72 (d, CH—Me), 4.76 (q, CH—Me), and 7.0–8.1 (m, the aromatic protons). The mass spectrum: M^+ 156, 232.

*Aryl-2,3-dihydronaphtho[1,2-*b*]thiophene-S,S-dioxides*

The aryl-2,3-dihydronaphtho[1,2-*b*]thiophenes (**5***b*, *c*) described were characterized as their *S*,*S*-dioxides (9) as an aid to structural elucidation (see Discussion). The relevant ^1H nmr data for these compounds are given in Table 2. The compounds were prepared by oxidation with hydrogen peroxide in glacial acetic acid (9) and were crystallized from ethanol. Their properties are summarized in Table 3.

[5]By integration of these signals it was determined that the mixture contained **5***k* (50%), **5***j* (30%) and **5***a* (20%).

[6]This signal was assigned to the methine proton of the 2-isomer **5***k* rather than to the methine proton of the 3-isomer **5***j* since for the isomers **5***h*, *i* the methine proton of the 2-isomer **5***i* occurred at lower field (Table 2). Also when comparing 2- and 3-aryl-2,3-dihydrobenzo[*b*]thiophenes (**2***a*, *b*), the methine signals due to the 2-aryl isomers (**2***b*) always occured to lower field (1).

[7]If the original reaction mixture had contained 2-phenylnaphtho[1,2-*b*]thiophene, 1-(2′-naphthyl)-2-phenylethane would have been formed. ^1H nmr data gave no evidence for this compound. The presence of 2-ethylnaphthalene was confirmed by comparison to an authentic sample.

TABLE 3. Aryl-2,3-dihydronaphtho[1,2-*b*]thiophene-*S*,*S*-dioxides (**12**)

Compound	Melting point °C	Yield (%)	Analysis % Calculated C	Calculated H	Calculated S	Found C	Found H	Found S
12*a*	187–188 (lit. (6) mp 186.51–188)	74	66.65	4.65	14.80	66.60	4.70	14.65
12*b*	208–209	96	74.00	5.20	10.40	73.75	5.20	10.45
12*c*	171–172	80	74.55	5.60	9.95	74.35	5.60	9.95
12*d*	236–237	78	74.55	5.60	9.95	74.50	5.55	10.00
12*e*	230–231	86	74.55	5.60	9.95	74.45	5.75	10.05

TABLE 4. 2- and 3-Arylnaphtho[1,2-*b*]thiophenes (**4***b*, *c*)

Compound	Melting point (°C)	Yield (%)	Analysis (%) Calculated C	Calculated H	Calculated S	Found C	Found H	Found S
4*e*	76–77	77	83.20	5.10	11.70	82.95	5.10	11.70
4*f*	[a]	93	83.35	5.55	11.10	83.55	5.50	10.95
4*g*	93–94	95	83.35	5.55	11.10	83.60	5.65	11.30
4*h*	129–130	[b]	83.20	5.10	11.70	82.95	5.10	11.80
4*i*	163–164	[b]	83.35	5.55	11.10	83.25	5.65	11.20
4*j*	164–165	[b]	83.35	5.55	11.10	83.45	5.60	11.08

[a]Obtained as an oil.
[b]See Table 1 for product distribution.

*The Preparation of 3-Arylnaphtho[1,2-*b*]thiophenes (**4**c)*
General Procedure

A mixture of a 3-aryl-2,3-dihydronaphtho[1,2-*b*]thiophene (**5***c*) (1 g) and 2,3-dichloro-5,6-dicyano-1,4-benzoquinone (1.25 mol equiv.) in benzene (50 mL) was heated under reflux for 2 h. The reaction mixture was cooled and filtered through a short (ca. 5 cm) alumina (tlc grade) column. The colorless filtrate was evaporated to dryness and the residue was crystallized from hexane with cooling to −5°C. The results are summarized in Table 4.

*Addition Reactions of Naphtho[1,2-*b*]thiophene Above 20°C to Form 2-Arylnaphtho[1,2-*b*]thiophenes (**4**b) and 2,3-Dihydronaphtho[1,2-*b*]thiophene (**5**a)*
General Procedure

These reactions were carried out as described for the reactions at 20°C except that each experiment was carried out at the boiling point of the aromatic hydrocarbon. All products were isolated by column chromatography on silica and elution with hexane – ethyl acetate (20:1), followed by crystallization from hexane (for products of type **4***b*) and distillation for **5***a*. The results of these experiments are presented in Table 4. The ^{1}H nmr data for the 2-arylnaphtho[1,2-*b*]thiophenes (**4***b*) are not detailed since each compound gave complex signals due to the aromatic protons and the usual resonances expected for the alkyl substituents. Likewise the infrared spectra for **4***b* are complex and uninformative[8].

[8]Full ^{1}H nmr and ir data are available on request.

Acknowledgements

We wish to thank the Natural Sciences and Engineering Research Council of Canada for support of this work, and Mr. W. Buchannon for the preparation of mass spectra.

1. P. D. CLARK, K. CLARKE, D. F. EWING, and R. M. SCROWSTON. J. Chem. Soc. Perkin Trans. I, 677 (1980).
2. P. D. CLARK and D. M. MCKINNON. Can. J. Chem. **59**, 227 (1981).
3. J. E. BANFIELD, W. DAVIES, N. GAMBLE, and S. MIDDLETON. J. Chem. Soc. 4791 (1956).
4. K. CLARKE, D. N. GREGORY, and R. M. SCROWSTON. J. Chem. Soc. Perkin Trans. I, 2956 (1973).
5. L. J. PANDYA and B. D. TILAK J. Sci. Ind. Res. India, Sect. B, **18**, 371 (1959).
6. E. CAMPAIGNE and B. HEATON. J. Org. Chem. **29**, 2372 (1964).
7. E. M. TERENT'EVA, P. I. SANIN, T. G. STEPANTSEVA, M. M. KUSAKOV, N. A. SHIMANKO, and V. I. SIDORENKO. Neftekhymiya, **1**, 141 (1961); Chem. Abstr. **57**, 9698 c (1961).
8. B. S. FRIEDMAN, F. L. MORRITZ, C. J. MORRISSEY, and R. KONCOS. J. Am. Chem. Soc. **80**, 5867 (1958).
9. B. IDDON and R. M. SCROWSTON. Adv. Heterocycl. Chem. **11**, 177 (1970).
10. R. S. DAVIDSON and T. D. WHELAN. J. Chem. Soc. Chem. Commun. 361 (1977).

Can. J. Chem. Downloaded from www.nrcresearchpress.com by 210.87.254.5 on 09/06/12
For personal use only.

Influence des groupes *tert*-butyle, triméthylsilyle et triméthylgermyle sur la stéréochimie de réactions d'addition en série cyclohexénique. IV. Réduction, par des hydrures complexes, de cyclohexanones β ou γ substituées

JEAN-CLAUDE RICHER ET MARC-ANDRÉ POIRIER

Département de Chimie, Université de Montréal, B.P. 6210, Montréal (Qué.), Canada H3C 3V1

ET

YVETTE MARONI ET GEORGES MANUEL

Laboratoire de Chimie Organique, Université Paul Sabatier, 118 Route de Narbonne, 31077 Toulouse, France

Reçu le 4 novembre 1980

Can. J. Chem. Downloaded from www.nrcresearchpress.com by 210.87.254.5 on 09/06/12
For personal use only.

JEAN-CLAUDE RICHER, MARC-ANDRÉ POIRIER, YVETTE MARONI et GEORGES MANUEL. Can. J. Chem. **59**, 1303 (1981).

On décrit la synthèse des diméthyl-5,5 *tert*-butyl-2 (**1***a*), triméthylsilyl-2 (**1***b*) et triméthylgermyl-2 (**1***c*) cyclohexanones ainsi que celle des diméthyl-2,2 *tert*-butyl-5 (**2***a*), triméthylsilyl-5 (**2***b*) et triméthylgermyl-5 (**2***c*) cyclohexanones. On examine la stéréochimie de la réaction de réduction de ces cétones par divers hydrures. Dans le cas des cétones substituées en β par un Si ou un Ge, la réduction est en compétition avec la réaction de clivage de la liaison C—M, (M = Si, Ge).

JEAN-CLAUDE RICHER, MARC-ANDRÉ POIRIER, YVETTE MARONI and GEORGES MANUEL. Can. J. Chem. **59**, 1303 (1981).

The synthesis of 5,5-dimethyl-2-*tert*-butyl- (**1***a*), -2-triméthylsilyl- (**1***b*), and -2-trimethylgermyl- (**1***c*) cyclohexanones is described as well as those of 2,2-dimethyl-5-*tert*-butyl- (**2***a*), -5-trimethylsilyl- (**2***b*), and -5-trimethylgermyl- (**2***c*) cyclohexanones. The stereochemistry of the reduction of these ketones by different hydrides is examined. This latter reaction competes with the cleavage reaction of the C—M bond in the case of β-substituted ketones (M = Si, Ge).

Introduction

Au cours de travaux antérieurs (1–3), on a mis en évidence l'influence stérique prépondérante des groupes *tert*-butyle, triméthylsilyle et triméthylgermyle sur la stéréochimie de réactions d'addition sur des cyclohexènes et lors de l'ouverture d'époxydes qui en dérivent. Dans le cadre de nos travaux sur la stéréochimie des réductions des cétones cycliques (4), nous avons donc préparé les cétones

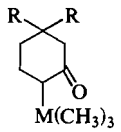

1

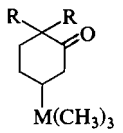

2

a R = CH_3; M = C
b R = CH_3; M = Si
c R = CH_3; M = Ge
d R = H; M = C

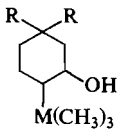

3

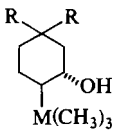

4

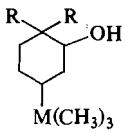

5

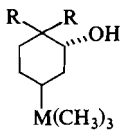

6

1 et **2** et examiné la stéréochimie de leur réduction par des hydrures complexes.

Résultats et discussion

Préparation des cétones

La cétone **1***a* a été obtenue par oxydation, par le mélange sulfochromique (5), du *tert*-butyl-2 diméthyl-5,5 cyclohexanol *trans* (**4***a*) obtenu au cours d'un travail antérieur (1), par hydroboration de l'alcène vinylique **7***a*.

Dans les mêmes conditions, l'oxydation du diméthyl-5,5 triméthylsilyl-2 cyclohexanol *cis* (**3***b*), obtenu par ouverture de l'époxyde silylé **8***b* par $LiAlH_4$ (2), conduit toutefois à la diméthyl-3,3 cyclohexanone (**9**) à la suite d'une scission de la liaison C—Si (5, 6). Cette réaction est bien connue (7, 8); la fonction carbonyle étant en β du silicium, cet arrangement représente un modèle parfait pour le clivage de la liaison C—Si (9–11). Cette réaction peut être interprétée par le schéma 1. Ce mécanisme implique la formation transitoire de la cétone β silylée (**1***b*) suivie par une attaque de l'eau sur l'atome de silicium pour conduire, avec un bon rendement, à la cétone **9**. On a pu vérifier que la cétone **1***b*, dont la préparation est décrite plus bas, conduit bien à la cétone **9** lorsqu'elle est plaçée en milieu acide.

La cétone β **1***b* a été obtenue grâce à une oxydation par un mélange oxyde de chrome – pyridine dans le chlorure de méthylène (12, 13).

0008-4042/81/091303-04$01.00/0

©1981 National Research Council of Canada/Conseil national de recherches du Canada

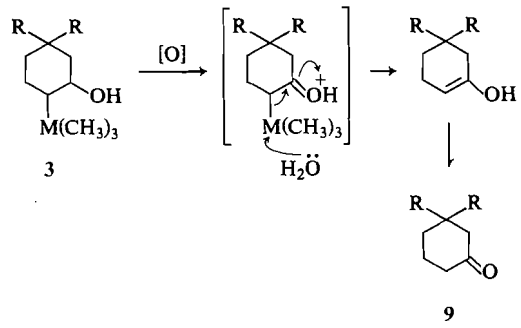

SCHÉMA 1

Cette méthode a d'ailleurs été utilisée par Hudrlik et Peterson (14, 15) pour l'obtention de cétones β silylées.

L'oxydation de l'alcool germylé **3***c* par le complexe oxyde de chrome – pyridine dans le chlorure de méthylène (12) ne nous a pas permis d'isoler la cétone **1***c* attendue. Le produit obtenu (**9**) résulte du clivage de la liaison C—Ge. On a remarqué un comportement semblable en série germylée, lors de l'époxydation de l'alcène **10***c* par l'acide *m*-chloroperbenzoïque (**3**). Il semble que les composés germylés **11***c* et **1***c* soient plus sensibles à l'effet β que leurs homologues silylés.

La synthèse de la cétone carbonée **2***a* est décrite dans un travail antérieur (1). Cette cétone **2***a* peut être obtenue soit à partir de la diméthyl-2,2 cyclohexanone (**12**) soit à partir de la *tert*-butyl-4 cyclohexanone (**13**).

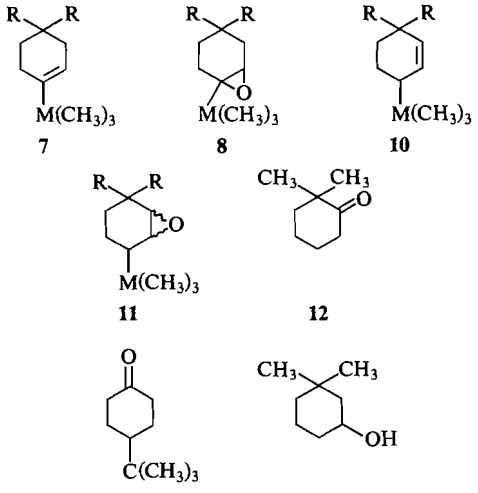

L'obtention, à l'état pur, de la cétone γ **2***b* fait appel à la propriété qu'ont les cétones β silylées de se cliver en milieu acide. L'oxydation en milieu acide du mélange d'alcools, riche en isomère γ, obtenu par réduction des époxydes silylés **11***b* (*cis*/*trans*) par $LiAlH_4$ (3), conduit à environ 88% de diméthyl-2,2 triméthylsilyl-5 cyclohexanone (**2***b*) et à de la diméthyl-3,3 cyclohexanone (**9**) résultant du clivage de la cétone β **1***b* (schéma 1) en milieu acide. La cétone γ **2***b* est ensuite obtenue à l'état pur par distillation du mélange.

TABLEAU 1. Comparaison des valeurs d'absorption du C=O (cm^{-1}) des cétones β et γ

Composés	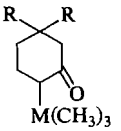	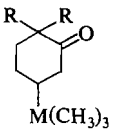
M = C; R = CH_3	1710	1710
M = Si; R = CH_3	1680	1700
M = Ge; R = CH_3	—	1700

Les études spectroscopiques sur les cétosilanes ont fait l'objet de nombreux travaux (11, 16–18). Brook et Pierce (17) ont étudié l'absorption en infrarouge du groupe carbonyle de cétones α, β et γ trialkylsilylées et ils ont fait une comparaison avec leurs homologues carbonés. Conformément aux résultats de ces auteurs, on note une augmentation de la fréquence d'absorption ν(C=O) lorsqu'on passe des β aux γ cétosilanes (tableau 1). Ces résultats sont interprétés par des interactions entre les électrons *p* de l'oxygène du carbonyle et les orbitales $3d^0$ vacantes du silicium ou germanium. La valeur de l'absorption ν(C=O) pour les γ-cétosilanes se rapproche de la position normale (soit de 1700 cm^{-1}).

La cétone germylée **2***c* est obtenue par la méthode décrite pour la série silylée. L'oxydation en milieu acide du mélange d'alcools résultant de l'hydroboration de l'alcène **10***c* (1) conduit à environ 66% de cétone γ **2***c* et à la cétone **9**. La cétone **2***c* est ensuite purifiée par distillation.

Stéréochimie de la réduction des cétones par $LiAlH_4$, $NaBH_4$ et $LiAlH(OtBu)_3$

Les études concernant la stéréochimie de la réduction de cyclohexanones différemment substituées ont fait l'objet de nombreux travaux (19–21). Les résultats concernant la réduction des cétones β (type 1) par $LiAlH_4$, $NaBH_4$, $LiAlH(OtBu)_3$ sont consignés dans le tableau 2.

Comme l'indique le tableau 2, la réduction de la cétone carbonée **1***a* par l'hydrure double de lithium et d'aluminium conduit à 98% d'alcool *cis* (**3***a*) et 2% d'isomère *trans* (**4***a*). Ces résultats suggèrent que la stéréochimie de la réduction est gouvernée par des facteurs stériques intervenant dans l'état de transition (4, 22). En effet, la comparaison de ces résultats avec ceux obtenus lors de la réduction,

Can. J. Chem. Downloaded from www.nrcresearchpress.com by 210.87.254.5 on 09/06/12
For personal use only.

TABLEAU 2. Pourcentages relatifs des différents produits obtenus par réduction des cétones β

Produit	Réducteur*	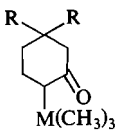 **1**	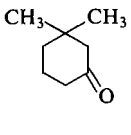 **9**	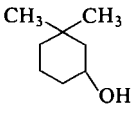 **14**	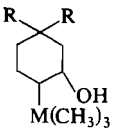 **3**	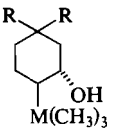 **4**
1a	$LiAlH_4$	—	—	—	98	2
1a	$NaBH_4$	100	—	—	0	0
1a	$LiAlH(OtBu)_3$	100	—	—	0	0
1b	$LiAlH_4$	—	1	17	74	8
1b	$NaBH_4$	—	42	0	48	0
1b	$LiAlH(OtBu)_3$	—	100	0	0	0

*Toutes les réductions ont été effectuées dans l'éther anhydre.

par $LiAlH_4$, de la *tert*-butyl-2 cyclohexanone (**1***d*) alors qu'on obtient un mélange 50/50 des isomères *cis* et *trans* (23), met en évidence l'importance du groupe méthyle axial supplémentaire en position 3.

Dans le cas de la réduction par $LiAlH_4$ de la cétone silylée (**1***b*), on remarque une augmentation du pourcentage en isomère *trans* (**4***b*) par rapport à la série carbonée (**1***a*–**4***a*). Cet accroissement en composé **4***b* pourrait être due à l'élongation de la liaison C—Si. La face *cis* de la cétone **1***b* deviendrait alors moins encombrée par suite de la diminution de l'interaction 1–3 diaxiale entre le réactif et l'un des méthyles du groupe triméthylsilyle et il en résulterait un accroissement d'entrée *cis* par rapport à la série carbonée.

En plus des produits normaux de réduction, on note la présence de 18% de produits **9** et **14** résultant du clivage de la liaison C—Si par un mécanisme similaire à celui représenté dans le schéma 1. Ce pourcentage de clivage est accru lors de la réduction de **1***b* par $NaBH_4$ et on note la disparition de l'isomère *trans* (**4***b*); ces résultats suggérant que le réducteur $NaBH_4$ réagit comme s'il était plus volumineux que $LiAlH_4$ s'expliquent probablement par l'insolubilité du $NaBH_4$ dans l'éther. Dans ce cas, la réaction de réduction est donc concurrencée par la réaction de clivage. Cette dernière est d'autant plus importante que le réducteur est plus volumineux. Parallèlement, en série carbonée, la réduction de la cétone **1***a* par $NaBH_4$ n'a pas lieu.

Avec un réducteur plus volumineux, tel que $LiAlH(OtBu)_3$, la réaction de clivage en série silylée est univoque et conduit uniquement à la diméthyl-3,3 cyclohexanone **9**; ce réactif ne réduit pas la cétone carbonée.

Les résultats concernant la stéréochimie de la réduction des cétones γ (**2**) par l'hydrure double de lithium et d'aluminium sont présentés dans le tableau 3.

TABLEAU 3. Pourcentages relatifs des isomères obtenus par réduction des cétones γ par $LiAlH_4$

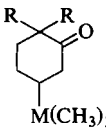	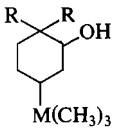	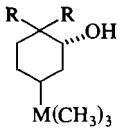
M = C; R = CH_3 (**2***a*)	85 (**5***a*)	15 (**6***a*)
M = Si; R = CH_3 (**2***b*)	85 (**5***b*)	15 (**6***b*)
M = Ge; R = CH_3 (**2***c*)	87 (**5***c*)	13 (**6***c*)

Ils mettent en évidence que les groupes *tert*-butyle, triméthylsilyle et triméthylgermyle en position 3 du groupement carbonyle à réduire n'affectent pas la stéréochimie de sa réduction.

Partie expérimentale

Les points de fusion ont été pris sur un appareil Cole-Parmer de la compagnie Instrument and Equipment.

Les spectres ir ont été pris sur un spectrophotomètre Beckman modèle IR-8 à double faisceau et, sauf indication contraire, tous les spectres ont été pris entre deux plaques de NaCl.

Les spectres de résonance magnétique nucléaire ont été déterminés sur un spectromètre modèle C-60-H de la compagnie Jeol. Le solvant choisi est le chloroforme deutéré pour la série carbonée et le tétrachlorure de carbone pour les séries silylée et germylée. Les déplacement chimiques sont exprimés en ppm et se réfèrent au tétraméthylsilane utilisé comme référence interne pour la série carbonée; le chloroforme est utilisé comme référence pour les séries silylée et germylée.

Les indices de réfraction ont été déterminés à l'aide d'un réfractomètre du type Abbe. La pureté de tous les nouveaux produits décrits dans ce travail a été déterminée par chromatographie en phase gazeuse et leur identité confirmée par spectrométrie de masse à l'aide d'un spectromètre Hitachi-Perkin-Elmer modèle RMU6-D opérant avec une énergie de faisceau d'électrons ionisants de 70 eV.

Can. J. Chem. Downloaded from www.nrcresearchpress.com by 210.87.254.5 on 09/06/12
For personal use only.

Can. J. Chem. Downloaded from www.nrcresearchpress.com by 210.87.254.5 on 09/06/12
For personal use only.

Préparation de la tert-*butyl-2 diméthyl-5,5 cyclohexanone (1a)*

Dans un ballon de 50 mL à trois tubulures, muni d'un réfrigérant et d'une ampoule à addition, on introduit 1,0 g (5,4 mmol) d'alcool **4***a* (1) en solution dans 6 mL d'éther (5). Deux millilitres d'une solution composée de 3,65 g de bichromate de sodium, de 7 mL d'eau, puis de 2,8 mL d'acide sulfurique concentré, est ajouté à 0°C par une ampoule à brome dans le ballon contenant l'alcool.

L'agitation est maintenue pendant 3 heures; le mélange réactionnel est extrait à l'éther selon la méthode habituelle. La phase organique, séchée sur du sulfate de sodium anhydre, filtrée, puis concentrée sous vide, fournit 0,93 g de cétone **1***a* (95% du rendement théorique) possédant les caractéristiques suivantes: pf: 32–33°C; pé 110°C/14 Torr; ir (pur): 1710 cm^{-1}; rmn ($CDCl_3$): 1,00 (*tert*-butyle), 0,87 et 1,05 (groupe *gem*-diméthyle) ppm.

Préparation de la diméthyl-5,5 triméthylsilyl-2 cyclohexanone (1b)

L'anhydride chromique (3,0 g; 30 mmol) est ajouté à une solution de 4,75 g de pyridine anhydre dans 20 mL de chlorure de méthylène. La solution colorée est agitée 15 min à la température de la pièce. Après cette période, une solution d'alcool **3***b* (1,0 g; 5 mmol) dans 10 mL de chlorure de méthylène est ajoutée d'un seul coup. Une suspension noire se sépare aussitôt. On laisse sous agitation pendant 2,5 heures. La solution est décantée, filtrée et la phase organique extraite à l'éther est lavée avec une solution de nitrate cuivrique, puis à l'eau. La phase éthérée est séchée sur du K_2CO_3, filtrée et concentrée sous vide. La distillation permet d'obtenir 0,8 g de cétone **1***b* (84% du rendement théorique) ayant les caractéristiques suivantes: pé 96–98°C/5 Torr; n_D^{29} 1,4615; ir: 1680, 1245 cm^{-1}; rmn (CCl_4): 0,86 et 0,79 (groupe *gem*-diméthyle), −0,07 (groupe triméthylsilyle) ppm.

Préparation de la tert-*butyl-5 diméthyl-2,2 cyclohexanone (2a)*

La synthèse de cette cétone ainsi que ses caractéristiques physiques sont décrites dans une publication antérieure (1).

Préparation de la diméthyl-2,2 triméthylsilyl-5 cyclohexanone (2b)

Cette cétone **2***b* a été préparée selon la méthode déjà décrite pour la cétone **1***a* par oxydation chromique du mélange d'alcools (1,0 g; 5 mmol) résultant de l'ouverture des époxydes *cis* et *trans* (**11***b*) par $LiAlH_4$ (3). La distillation permet d'obtenir 0,7 g de produit (85% du rendement théorique) dont les caractéristiques physiques sont les suivantes: pé 109°C/7 Torr; n_D^{21} 1,4605; ir: 1700, 1380, 1360, 1240 cm^{-1}; rmn (CCl_4): 1,09, 0,96 (groupe *gem*-diméthyle) et 0,00 ($SiMe_3$) ppm.

Préparation de la diméthyl-2,2 triméthylgermyl-5 cyclohexanone (2c)

Cette cétone **2***c* a été préparée par la méthode décrite pour la préparation de la cétone silylée **2***b* et conduit avec un rendement voisin de 80% à la cétone **2***c* et dont les caractéristiques physiques sont les suivantes: pé 110°C/5 Torr; n_D^{23} 1,4725; ir: 1700, 1380, 1360, 810 cm^{-1}; rmn (CCl_4): 1,06 et 0,96 (groupe *gem*-diméthyle), 0,06 ($GeMe_3$) ppm.

Réduction des cétones par $LiAlH_4$, $NaBH_4$, $LiAlH(OtBu)_3$

La réduction des cétones par les différents hydrures a été réalisée sur des échantillons de 5,0 mmol de cétones ajoutés à une suspension de 25,0 mmol d'hydrures dans 15 mL d'éther anhydre. Après 20 h d'agitation au reflux du solvant, l'hydrolyse par une solution de soude à 5% suivie d'une extraction à l'éther conduit au mélange d'alcool avec des rendements moyens de 95%.

Analyse des produits

Les mélanges d'alcools provenant des réactions de réduction des cétones **1** et **2** ont été analysés par chromatographie en phase gazeuse à l'aide d'un chromatographe à ionisation de flamme Research Chromatograph 700 de la compagnie F & M muni d'une colonne de 6 pi × 1/8 de po remplie de Diatoport 5750 (80–100) supportant 6% de son poids de LAC 728. Les temps de rétention (en min) des alcools dans ces conditions sont résumés dans un tableau figurant dans une publication antérieure (1).

Remerciements

Les auteurs remercient vivement le Conseil National de Recherches du Canada, le C.N.R.S. français et les autorités chargées d'administrer les accords Franco–Québécois pour l'aide financière apportée sous forme d'octroi de recherches, de bourses d'études et de frais de mission. Les auteurs tiennent à remercier le Dr. Pierre Maroni pour l'accueil chaleureux réservé à Marc-André Poirier durant son stage à Toulouse. Les auteurs tiennent aussi à exprimer leur reconnaissance aux Dr. Mazerolles et Lesbre pour leur compréhension et leurs discussions utiles.

1. C. Freppel, M. A. Poirier, J. C. Richer, Y. Maroni et G. Manuel. Can. J. Chem. **52**, 4133 (1974).
2. J. C. Richer, M. A. Poirier, Y. Maroni et G. Manuel. Can. J. Chem. **56**, 2049 (1978).
3. J. C. Richer, M. A. Poirier, Y. Maroni et G. Manuel. Can. J. Chem. **58**, 39 (1980).
4. J.-C. Richer. J. Org. Chem. **30**, 324 (1965).
5. J. Sicher et M. Tichy. Collect. Czech. Chem. Commun. **32**, 3687 (1967).
6. M. J. Carter et I. Fleming. Chem. Commun. 679 (1976).
7. P. F. Hudrlik et G. P. Withers. Tetrahedron Lett. 29 (1976).
8. K. Utimoto, M. Obayashi et H. Nozaki. J. Org. Chem. **41**, 2940 (1976).
9. W. K. Musker et G. L. Larson. J. Am. Chem. Soc. **91**, 514 (1969).
10. A. G. Brook, D. M. MacRae et A. R. Bassindale. J. Organometal. Chem. **86**, 185 (1975).
11. W. K. Musker et G. L. Larson. J. Organometal. Chem. **6**, 627 (1966).
12. G. I. Poos, G. E. Arth, R. E. Beyler et L. H. Sarett. J. Am. Chem. Soc. **75**, 422 (1953).
13. R. Ratcliffe et R. Rodehorst. J. Org. Chem. **35**, 4000 (1970).
14. P. F. Hudrlik et D. Peterson. Tetrahedron Lett. 1133 (1974).
15. P. F. Hudrlik et D. Peterson. Tetrahedron Lett. 1785 (1972).
16. I. F. Lutsenko, Yu. I. Bankov, O. V. Dudukina et E. N. Kramarova. J. Organometal. Chem. **11**, 35 (1968).
17. A. G. Brook et J. B. Pierce. Can. J. Chem. **42**, 298 (1964).
18. W. K. Musker et R. W. Ashly. J. Org. Chem. **31**, 4237 (1966).
19. G. E. Heinsohn et E. C. Ashby. J. Org. Chem. **38**, 4232 (1973).
20. H. H. Haubenstock. J. Org. Chem. **38**, 1765 (1973).
21. S. R. Landor, P. W. O'Connor, A. R. Tatchell et I. Blair. J. Chem. Soc. 473 (1973).
22. M. Chérest et H. Felkin. Tetrahedron Lett. 2205 (1968).
23. J. C. Richer et D. Eugène. Can. J. Chem. **41**, 2387 (1969).

Product distributions and isotopic selectivities in ir multiphoton dissociation of pentafluoroiodoethane[1]

E. WEINBERG,[2] M. GAUTHIER, P. A. HACKETT, AND C. WILLIS

Laser Chemistry Group, Division of Chemistry, National Research Council of Canada, Ottawa, Ont., Canada K1A 0R6

Received October 15, 1980

E. WEINBERG, M. GAUTHIER, P. A. HACKETT, and C. WILLIS. Can. J. Chem. **59**, 1307 (1981).

Infrared multiphoton dissociation of pentafluoroiodoethane leads to a complex array of reaction products. For photolysis in the ν_4 band the reaction mechanism involves C_2F_5—I bond cleavage followed by thermal dissociation of C_2F_5 radicals. For irradiation within the ν_3 band at high fluence, efficient secondary photolysis of C_2F_5 radicals is postulated. At lower fluences the dissociation is isotopically selective leading to C_4F_{10} enriched in carbon-13.

E. WEINBERG, M. GAUTHIER, P. A. HACKETT et C. WILLIS. Can. J. Chem. **59**, 1307 (1981).

Si on soumet le pentafluoroiodoéthane à une dissociation multiphotonique infrarouge il se forme une série complexe de produits de réaction. Dans le cas de la photolyse dans la bande ν_4, le mécanisme de la réaction fait intervenir un clivage de la liaison C_2F_5—I qui est suivi par une dissociation thermique des radicaux C_2F_5. Lors de l'irradiation avec une forte intensité de la bande ν_3, on croit qu'une photolyse secondaire efficace des radicaux C_2F_5 intervient. A des intensités plus faibles, la dissociation est sélective du point de vue isotopique et elle conduit à du C_4F_{10} qui est enrichi en carbone-13.

[Traduit par le journal]

Introduction

Isotopically selective infrared multiphoton dissociation of molecules is now a common experimental procedure. This is especially true for CO_2 laser induced dissociation of fluorocarbons, a consequence of particularly favourable spectral overlaps. Early work was directed at demonstrating isotopic selectivity and towards understanding the infrared multiple photon absorption and induced dissociation processes. While research in these latter areas is far from complete, other groups have pursued active research in areas where infrared multiple photon dissociation is used as a tool, e.g. synthesis of specifically isotopically enriched (labelled) compounds (1), elucidation of detailed reaction mechanisms by isotopically selective dissociation of substrates at natural isotopic abundance (2), or generation of free radicals for kinetic studies (3). It is in this vein that we have carried out the present investigation of the infrared multiple photon dissociation of pentafluoroiodoethane.

Experimental

Irradiations were carried out in a Pyrex cell (4.7 cm od × 17.5 cm long) equipped with sodium chloride windows. A Lumonics model 101 TEA-CO_2 laser, modified for closed system gas flow for use with rare isotopes of CO_2, was used for irradiations involving product analysis by gas chromatography. A second TEA-CO_2 laser (Lumonics model 103) was used for carbon-13 enrichment studies. Both lasers were equipped with high efficiency gratings (PTR Optical 135 lines/mm master ruling). Sample irradiations were performed in both parallel (2 m f.l. germanium lens) and focused beam (10 cm f.l. germanium lens) geometry with incident or exit energy monitored by a calibrated pyroelectric detector.

Pentafluoroiodoethane was obtained from PCR Inc. and purified by distillation at −131°C. Analysis by gas chromatography (9 ft Porapak S; 15 ft Chromosorb G, NAW 80–100 mesh, 3/8 in. od copper tubing, 10% silicone fluid, 90 or 120°C) (4) failed to reveal impurities, however, mass spectrometry indicated trace amounts of decafluorobutane.

Products were analysed by gas chromatography (9 ft Porapak S, 80–100 mesh, 1/4 in. od copper tubing, 100° or 140°C) or by mass spectrometry. The gc response (thermal conductivity detector) was calibrated with authentic aliquots of tetrafluoroethylene, hexafluoroethane, decafluorobutane, and pentafluoroiodoethane. No authentic sample of octafluoropropane was available to us; a response intermediate to that for the ethane and butane was assumed.

Isotopically selective dissociation was confirmed by measuring the carbon-13/carbon-12 ratio in the decafluorobutane product ($C_3F_5^+$ ion at 131, 132, 133 and $C_4F_9^+$ ion at 219, 220, 221, and 222 monitored) in the presence of substrate (reaction mixture held at −96°C) with suitable background corrections being made. A Hitachi RMU-6D mass spectrometer was used for these initial analyses.

Results and Discussion

The experimental results are summarized in Fig. 1 and in Table 1. All experiments were carried out with C_2F_5I pressure of 0.5 Torr. The distribution of products appears to be sensitive to incident fluence, irradiation geometry, and to irradiation frequency, with decafluorobutane becoming the dominant product at low fluence, in parallel beam geometry at frequencies to the red of the predominant absorption bands. Possible explanations for this are discussed below.

There is little reliable thermochemical data for fluorocarbon molecules, however, the heat of formation of C_2F_5I has recently been measured as

[1]Issued as NRCC No. 19158.

[2]NRCC Summer Student.

0008-4042/81/091307-04$01.00/0

©1981 National Research Council of Canada/Conseil national de recherches du Canada

Can. J. Chem. Downloaded from www.nrcresearchpress.com by 210.87.254.40 on 09/06/12
For personal use only.

Can. J. Chem. Downloaded from www.nrcresearchpress.com by 210.87.254.40 on 09/06/12
For personal use only.

TABLE 1. Product distributions from IRMPD of 0.5 Torr pentafluoroiodoethane at 22°C[a]

Frequency cm^{-1}	Fluence J cm^{-2}	Production rate/moles × 10^{-9} pulse^{-1}						
		CF_3I	C_2F_4	C_2F_6	C_3F_8	C_4F_{10}	C_2F_5I	A[e]
1082	1.0	[c]	[c]	[c]	[c]	0.06	nd[d]	nd
1082	[b]	2.0	3.0	1.1	1.0	0.5	−8.5	−0.20
922	1.0	2.9	4.1	[c]	5.2	32	−70	+0.04
922	0.8	1.4	0.9	[c]	1.1	15	nd	nd
922	[b]	2.2	3.0	[c]	3.4	20	−42	+0.17
920	1.05	3.5	3.0	[c]	4.6	34	nd	nd
918	0.94	4.2	3.0	[c]	4.9	32	−85	+0.15
917	0.74	2.9	1.7	[c]	2.5	24	−68	−0.22
916	0.44	[c]	0.7	[c]	1.0	20	−51	−0.19

[a]All experiments on 0.5 Torr C_2F_5I at 22°C; moles/cell = 8.5 × 10^{-6}; moles irradiated (focused geometry), 2.6 × 10^{-7}; moles irradiated (parallel geometry), 3.3 × 10^{-7}.
[b]Focused beam (estimated fluence at beam waist ≈ 100 J cm^{-2}).
[c]Below detection limit.
[d]Abbreviation nd, not determined.
[e] $A = \Sigma$(products + substrate)/-(substrate).

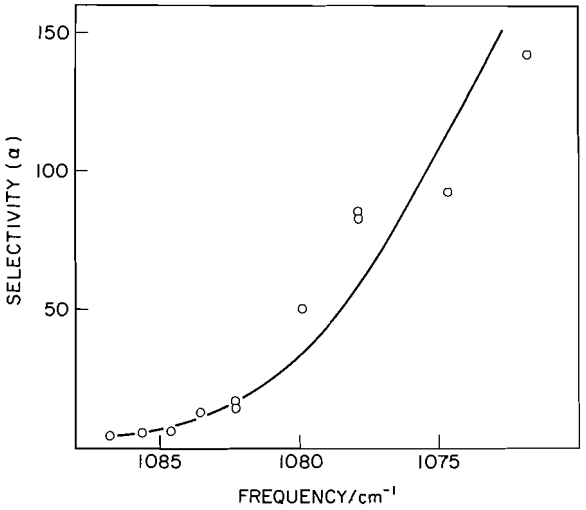

FIG. 1. Isotopic selectivities (γ) observed in the infrared multiple photon dissociation of 0.5 Torr pentafluoroiodoethane as a function of irradiation frequency. Parallel beam geometry, 1.5 J cm^{-2} fluence, temperature 22°C. γ was measured for the $C_3F_5^+$ fragment ion and is defined as γ = (carbon-13/carbon-12)

−240.0 ± 1 kcal mol^{-1} (all heats of formation and bond dissociation energies given for gas phase, 298 K) (5). This, coupled with Okafu and Whittle's recent value of $D(C_2F_5—I)$ (6), leads to a value of the heat of formation of C_2F_5 of −214.5 kcal mol^{-1} and allows the calculation of the following threshold energies:[3]

[1] $C_2F_5I \rightarrow C_2F_5 + I(^2P_{3/2})$ 51.2 kcal mol^{-1}

[2] $C_2F_5I \rightarrow CF_2 + CF_3I$ 55.7 kcal mol^{-1}

[3] $C_2F_5I \rightarrow C_2F_4 + IF$ 60.0 kcal mol^{-1}

[4] $C_2F_5 \rightarrow CF_3 + CF_2$ 58.5 kcal mol^{-1}

Of particular note is both the weakness of the $CF_3—CF_2$ bond, a result first reported by Fisher *et al.* (8), who noted the thermal decomposition of the pentafluoroethyl radical at temperatures >950°C, and the small difference in threshold energy for the molecular elimination process [3] compared to the free radical process [1]. The present value, 8.8 kcal mol^{-1}, may be contrasted to the value 21.8 kcal mol^{-1} calculated for the equivalent reactions involving CF_3I (7). This energy difference is less than the energy of three CO_2 laser photons above the first dissociation threshold. For smaller molecules the spontaneous dissociation rate rises rapidly with excess internal energy so that photon absorption is terminated at energy levels close to the first dissociation limit (9, 10). For larger molecules this rate constant is smaller and increases less rapidly so that higher levels of internal energy may be reached (11, 12). Although multiphoton absorption through the vibrational quasicontinuum depends upon the laser fluence, the degree of excess energy and hence the primary dissociative processes will depend upon laser intensity. It is certain that excess energies greater than the threshold energy of reaction [3] are achieved in the present case; what is less certain is whether one has then reached the activation energy for process [3], i.e. what is the activation energy for the addition of iodine monofluoride to tetrafluoroethylene, and also whether the rate of process [3] will compete with the rate of process [1] because of different pre-exponential (frequency) factors. These arguments apply even more stringently to the postulated difluorocarbene elimination. Thus, although our expectation is that C—I bond scission would be the dominant process, indeed it is the only process observed in multiphoton dissociation of CF_3I, we cannot reject *a priori* contributions from processes [3] and [2]. They are, however, unlikely. We are presently considering direct detection ex-

[3]Estimated energies based upon selected data from ref. 7.

Can. J. Chem. Downloaded from www.nrcresearchpress.com by 210.87.254.40 on 09/06/12
For personal use only.

periments using CF_2 $\tilde{A}(^1B_1) \rightarrow \tilde{X}(^1A_1)$ (13) and IF $\tilde{B}(^3\Pi\ 0^+) \rightarrow \tilde{X}(^1\Sigma^+)$ (14) transitions to fully elucidate the role of these intermediates in the present system.

One other observation is instructive: after infrared multiphoton irradiation with conventional gain switched TEA-CO_2 laser pulses, much vibrational energy is stored in vibrational energy levels of molecules with internal energies below the dissociation threshold (15). The collisional relaxation of this energy often leads to a high temperature thermal reaction. Thus, the purely thermal decomposition of pentafluoroiodoethane and of any perfluoroalkyl radicals (e.g. $D(C_2F_5—CF_2) \approx 49$ kcal mol^{-1}) (7) is a likely event whenever the infrared laser frequency can interact homogeneously with the ensemble of molecules, i.e. resonant excitation. When only a subset of molecules is excited, e.g. far from resonance, or when carbon-13 molecules are selectively excited, *vide infra*, we do not expect to observe this secondary thermal dissociation. Our remarks concerning the stability of the pentafluoroethyl radical are strengthened by the expectation that any excess internal energy in excited substrate will be carried away in internal excitation of the radical (16). This is because there is no exit barrier to the C—I bond cleavage and hence small probability for translational excitation (11).

Thus, an internally self consistent, but by no means unique, explanation for the results presented in the table is

$$[5]\quad C_2F_5I \xrightarrow{nh\nu} C_2F_5 + I$$

$$[6]\quad 2C_2F_5 \rightarrow C_4F_{10}$$

$$[7]\quad C_2F_5 + I \rightarrow C_2F_5I$$

$$[8]\quad I + I \rightarrow I_2$$

$$[9]\quad C_2F_5 \rightleftharpoons CF_3 + CF_2$$

$$[10]\quad C_2F_5 + CF_3 \rightarrow C_3F_8$$

$$[11]\quad CF_3 + (I, I_2, C_2F_5I) \rightarrow CF_3I + (I, C_2F_5)$$

$$[12]\quad CF_3 + CF_3 \rightarrow C_2F_6$$

$$[13]\quad C_2F_5 + CF_2 \rightleftharpoons C_3F_7 \rightarrow \text{Higher products}$$

$$[14]\quad CF_2 + CF_2 \rightarrow C_2F_4$$

A key aspect of this mechanism is the instability of the perfluoroalkyl radicals which allows $[C_2F_4] > [C_2F_6]$ as CF_3 radicals are effectively scavenged by pentafluoroethyl or iodine donors. However, another possible explanation would be the involvement of primary process [3]. We note that at suitably defined irradiation conditions the reactions [5]–[8] are sufficient to describe the production of the only product detected, namely decafluorobutane.

The sole observation outside the explanation discussed above is the product distribution due to focused beam irradiations at 1082 cm^{-1}. Although the laser interacts only with a small subset of molecules (small rate of loss of C_2F_5I), products derived from the CF_3 radical dominate those from the C_2F_5 radical. Decafluorobutane absorbs infrared radiation at this frequency (ν_{max} 1070 cm^{-1}) and hence we checked the possibility of its photolysis. Although the process

$$[15]\quad C_4F_{10} \xrightarrow{nh\nu\ (1082\,cm^{-1})} C_2F_6 + C_2F_4$$

was observed, its rate was negligible compared to the production rates reported in the table. These observations strongly support the reaction

$$[16]\quad C_2F_5 \xrightarrow{nh\nu\ (1082\,cm^{-1})} CF_3 + CF_2$$

i.e. the secondary photolysis of C_2F_5 during the 5 μs laser pulse. Similar processes have been inferred in the infrared multiphoton dissociation of CF_3Br (10), CF_3Cl (17), and C_3F_7I (18) in this same spectral region. For the trifluoromethyl compound the observation is supported by the known frequency for the ν_1 stretch of CF_3 of 1090 cm^{-1} (*7a*). Vibrational frequencies are not known for the larger radicals but both contain CF_3 groups; moreover, the carbon–carbon bond dissociation energies are certainly less than $D(CF_2—F) \approx 88$ kcal mol^{-1} (7). We conclude this discussion by noting that reaction [16] or its analogue for C_3F_7 almost certainly accounts for the product distribution observed in multiphoton dissociation of decafluorobutane.

The results of experiments investigating the isotopic selectivity of the dissociation are shown in Fig. 1. The value reported (γ) is given by:

$$\gamma = (\text{carbon-13/carbon-12})\ C_3F_5^+\ \text{ion}/0.0112$$

where 0.0112 is the carbon-13/carbon-12 ratio of the natural abundance substrate. The infrared absorption spectrum of pentafluoroiodoethane has been previously reported and a vibrational analysis has been made (19). The two strong bands within the gain profile of the CO_2 laser are ν_3 at 1114 cm^{-1}, assigned to a CF_2 stretch, and ν_4 at 922 cm^{-1} assigned to a CF_2—I stretch. This latter frequency has also been assigned to a C—C stretch (20). It is also underlain by a hot band $\nu_{13} - \nu_{10}$ at 900 cm^{-1}; for this reason we have concentrated our investigation of isotopic selectivity at frequencies to the red of the ν_3 band.

The spectral dependence of these isotopic selectivities is consistent with data obtained from dissociation of trifluoromethyl halides (21). We plan to

investigate the selective dissociation further using gc – mass spectrometry to investigate more fully the isotopic substitution of the C_4F_{10} and to observe any small amouts of C_2F_4, C_3F_8, and CF_3I in terms of carbon-13 enrichment in order to more fully define the reaction mechanisms discussed above.

In conclusion, the infrared multiphoton chemistry of C_2F_5I involves C_2F_5, CF_2, and CF_3 intermediates. At frequencies close to 9 μm the dissociation is isotopically selective and the gas phase photolysis of C_2F_5 to yield CF_2 and CF_3 seems to be a likely process. This observation suggests further pulsed laser experiments to investigate the homogeneous gas phase *photochemistry* of C_2F_5 and other free radicals.

1. J. J. RITTER. J. Am. Chem. Soc. **100**, 2441 (1978).
2. P. A. HACKETT, W. S. NIP, and C. WILLIS. J. Am. Chem. Soc. In press.
3. I. R. SLAGLE, F. YAMADA, and D. GUTMAN. Generation of polyatomic free radicals for quantitative kinetic studies using CO_2-TEA laser photolysis. Paper O-1, 14th Informal conference on photochemistry, Newport Beach, March 30–April 3, 1980.
4. D. S. ASHTON, J. M. TEDDER, and J. C. WALTON. J. Chromatogr. **90**, 315 (1974).
5. E-CHUNG WU, J. M. PICKARD, and A. S. RODGERS. J. Phys. Chem. **79**, 1079 (1975).
6. E. N. OKAFU and E. WHITTLE. Int. J. Chem. Kinetics, **8**, 287 (1975).
7. (*a*) JANAF Thermochemical Tables, Natl. Stand. Ref. Data Ser., U.S. Natl. Bur. Stand. 37. U.S. Government Printing Offices, Washington, D.C., 1971, (*b*) W. M. D. BRYANT. J. Polymer Sci. **56**, 277 (1962).
8. I. P. FISHER, J. B. HOMER, and F. P. LOSSING. J. Am. Chem. Soc. **87**, 957 (1965).
9. AA. S. SUDBO, P. A. SCHULZ, E. R. GRANT, Y. R. SHEN, and Y. T. LEE. J. Chem. Phys. **70**, 912 (1979).
10. E. WURZBERG, L. J. KOVALENKO, and P. L. HOUSTON. Chem. Phys. **35**, 317 (1978).
11. AA. S. SUDBO, P. A. SCHULZ, Y. R. SHEN, and Y. T. LEE. J. Chem. Phys. **69**, 2312 (1978).
12. P. A. HACKETT, C. WILLIS, M. DROUIN, and E. WEINBERG. J. Phys. Chem. **84**, 1873 (1980).
13. D. S. KING and J. C. STEPHENSON. Chem. Phys. Lett. **51**, 48 (1977).
14. L. STEIN, J. WANNER, and H. WALTHER. J. Chem. Phys. **72**, 1128 (1980).
15. P. A. HACKETT, M. GAUTHIER, and C. WILLIS. J. Chem. Phys. **69**, 2924 (1978).
16. J. C. STEPHENSON and D. S. KING. J. Chem. Phys. **69**, 1485 (1978).
17. A. HORWITZ, J. M. PRESES, R. E. WESTON, JR., and G. W. FLYNN. IR multiphoton chemistry of CF_3Cl. Paper A2, 14th Informal conference on photochemistry, Newport Beach, March 30–April 3, 1980.
18. M. J. ROSSI, J. R. BARKER, and D. M. GOLDEN. Kinetic and photophysical studies in collisionless IR–multiphoton dissociation of polyatomic molecules. Paper U3, 14th Informal conference on photochemistry, Newport Beach, March 30–April 3, 1980.
19. O. RISGIN and R. C. TAYLOR. Spectrochim. Acta, **15**, 1036 (1959).
20. J. R. NIELSEN, C. Y. LIANG, R. M. SMITH, and D. C. SMITH. J. Chem. Phys. **21**, 383 (1953).
21. M. DROUIN, M. GAUTHIER, R. PILON, P. A. HACKETT, and C. WILLIS. Chem. Phys. Lett. **60**, 16 (1978).

Can. J. Chem. Downloaded from www.nrcresearchpress.com by 210.87.254.40 on 09/06/12
For personal use only.

Reactions of the methylmercury(II) ion with adenine and crystal structure of (adeninato-N9)methylmercury(II) monohydrate

LEONARDO PRIZANT, MARC J. OLIVIER, ROLAND RIVEST, AND ANDRÉ L. BEAUCHAMP[1]

Département de Chimie, Université de Montréal, C.P. 6210, Succ. A, Montréal (Qué.), Canada, H3C 3V1

Received October 9, 1980

LEONARDO PRIZANT, MARC J. OLIVIER, ROLAND RIVEST, and ANDRÉ L. BEAUCHAMP. Can. J. Chem. 59, 1311 (1981).

Adenine (HAd) reacts with CH_3HgX (X = NO_3, ClO_4) in basic aqueous solution to form a compound $[CH_3HgAd]\cdot H_2O$, which crystallizes in the monoclinic space group $C2/c$, with a = 19.796, b = 7.119, c = 16.471 Å, β = 128.83°, and Z = 8. The CH_3Hg^+ group is linearly bonded to N(9) of deprotonated adenine and the molecules are held in pairs by two N(6)–H(6)···N(1) hydrogen bonds. With excess adenine, higher complexes of the formula $[(CH_3Hg)_nAd]X_{n-1}$ (where n = 2, 3) are formed, in which positions N(9) (deprotonated), N(7), and N(3) are successively filled. Compounds $[(CH_3Hg)_3(Ad\text{-}H)]X$ have been obtained at high pH by substitution of H(9) and an amino hydrogen, and with coordination of a third CH_3Hg^+ group probably to N(7). Complexation leads to significant changes in the infrared spectra and the 1750–1250 cm^{-1} regions are correlated with the substitution patterns. The structures are discussed in connection with the basicity of the donors in adenine and the basicity changes of the remaining donors when other atoms are already involved in coordination.

LEONARDO PRIZANT, MARC J. OLIVIER, ROLAND RIVEST et ANDRÉ L. BEAUCHAMP. Can. J. Chem. **59**, 1311 (1981).

L'adénine (HAd) réagit avec CH_3HgX (X = NO_3, ClO_4) en solution aqueuse basique pour former un composé $[CH_3HgAd]\cdot H_2O$, qui cristallise dans le groupe monoclinique $C2/c$ et dont les paramètres de maille sont a = 19,796, b = 7,119, c = 16,471 Å, β = 128,83° et Z = 8. Le groupe CH_3Hg^+ est lié linéairement à l'atome N(9) de l'adénine déprotonée et les molécules sont associées en paires par deux liaisons hydrogène N(6)–H(6)···N(1). En présence d'adénine en excès, il se forme des complexes supérieurs de formule $[(CH_3Hg)_nAd]X_{n-1}$ (où n = 2, 3), dans lesquels les sites N(9) (déprotoné), N(7) et N(3) sont successivement occupés. On obtient à pH élevé des composés $[(CH_3Hg)_3(Ad\text{-}H)]X$ par déplacement de H(9) et d'un atome d'hydrogène du groupe amino, et coordination d'un troisième groupe CH_3Hg^+ probablement en N(7). La complexation engendre des changements importants dans les spectres infrarouges et on relie les domaines 1750–1250 cm^{-1} de ces spectres au motif de substitution. On discute des structures de ces composés en rapport avec les basicités des atomes donneurs et les variations que subissent ces basicités lorsque certains de ces atomes donneurs sont liés au métal.

Introduction

Because of its ability to act as a unifunctional Lewis acid with minimum steric effects, the CH_3Hg^+ cation is a convenient ligating species to probe the basicities of the donor atoms in multidentate ligands such as the purine and pyrimidine molecules found in nucleic acids. Crystallographic work on complexes with 9-methlyadenine (1, 2) have confirmed the complexation sites deduced from spectroscopic work on aqueous solutions of adenosine (3–5). Under similar conditions, adenine was found to react quite differently (1, 6) and a systematic investigation of its CH_3Hg^+ complexes was undertaken in order to understand these differences.

The present paper reports on the interaction of CH_3Hg^+ with adenine (HAd) in water, as deduced from the compositions and structures of the isolated solid compounds. Complexes of various stoichiometries have been characterized and attempts have been made to relate their structures, generally known from X-ray diffraction work, with information more readily accessible, such as routine infrared spectra. The crystal structure of the neutral 1:1 complex $[CH_3HgAd]\cdot H_2O$ is also described.

Experimental

Preparation

Adenine (Aldrich) was used without further purification. CH_3HgI (Alfa) was the starting material to prepare water solutions of CH_3HgNO_3 and CH_3HgClO_4 as described elsewhere (7).

Preparations were usually run with 2 mmol (0.27 g) of ligand dissolved in 20–30 mL of hot water. A suitable volume of 1 *M* CH_3HgNO_3 or CH_3HgClO_4 solution was added to obtain the needed metal-to-ligand ratio. When necessary, 1 *M* NaOH, HNO_3, or $HClO_4$ were added in required amount or until a predetermined pH value was reached. Equilibria are normally rapid in homogeneous water solutions of CH_3Hg^+ and prolonged heating of reaction mixtures proved unnecessary. The final mixtures were allowed to stand at room temperature for 1–2 days before precipitates were collected. More soluble compounds were left uncovered for longer periods to reduce volume. The samples were usually washed with ethanol and ether. They usually decomposed when recrystallized or washed with water. The solids are colorless, generally crystalline, and stable in air, although some of them become yellowish after standing in closed bottles for several weeks.

The compounds prepared are listed below, together with the quantities of methylmercury salt, acid or base reacted with 2 mmol of ligand. All analyses were carried out by Schwarzkopf Laboratories, NY.

$[CH_3HgAd]\cdot H_2O$: CH_3HgNO_3 2 mmol, NaOH added to pH 9. *Anal.* calcd. for $C_6H_9HgN_5O$: C 19.60, H 2.47, N 19.04, Hg 54.54; found: C 19.77, H 2.35, N 18.79, Hg 54.67.

[1]Author to whom correspondence may be addressed.

0008-4042/81/091311-07$01.00/0

©1981 National Research Council of Canada/Conseil national de recherches du Canada

Can. J. Chem. Downloaded from www.nrcresearchpress.com by 210.87.254.40 on 09/06/12
For personal use only.

Can. J. Chem. Downloaded from www.nrcresearchpress.com by 210.87.254.40 on 09/06/12
For personal use only.

[(CH$_3$Hg)$_2$Ad]NO$_3$·2H$_2$O: CH_3HgNO_3 4 mmol, NaOH 2 mmol. Also obtained in smaller yield from CH_3HgNO_3 4 mmol without NaOH. *Anal.* calcd. for $C_7H_{14}Hg_2N_6O_5$: C 12.67, H 2.13, N 12.67, Hg 60.47; found: C 12.54, H 2.21, N 12.40. Hg 60.71.

[(CH$_3$Hg)$_2$Ad]ClO$_4$·H$_2$O: CH_3HgClO_4 4 mmol, NaOH 2 mmol. Also obtained in smaller yield from CH_3HgClO_4 4 mmol without NaOH. *Anal* calcd. for $C_7H_{12}ClHg_2N_5O_5$: C 12.31, H 1.77, N 10.26, Cl 5.19, Hg 58.75; found: C 12.38, H 2.08, N 10.72, Cl 4.83, Hg 58.53.

[(CH$_3$Hg)$_3$Ad](NO$_3$)$_2$: CH_3HgNO_3 6 mmol and NaOH 2 mmol, or 8 mmol without NaOH. *Anal.* calcd. for $C_8H_{13}Hg_3N_7O_6$: C 10.62, H 1.45, N 10.83, Hg 66.49; found: C 9.94, H 1.53, N 9.63, Hg 66.42.

[(CH$_3$Hg)$_3$Ad](ClO$_4$)$_2$: CH_3HgClO_4 6 mmol and NaOH 2 mmol, or 8 mmol without NaOH. *Anal.* calcd. for $C_8H_{13}Cl_2Hg_3N_5O_8$: C 9.81, H 1.34, N 7.15, Hg 61.41; found: C 9.82, H 1.38, N 7.16, Hg 60.68.

[(CH$_3$Hg)$_3$(Ad-H)]NO$_3$: CH_3HgNO_3 8 mmol, pH raised to 7 with NaOH. *Anal.* calcd. for $C_8H_{12}Hg_3N_6O_3$: C 11.41, H 1.44, N 9.98; Hg 71.47; found: C 11.39, H 1.49, N 9.83, Hg 70.67.

[(CH$_3$Hg)$_3$(Ad-H)]ClO$_4$: CH_3HgClO_4 8 mmol, pH raised to 7 with NaOH. *Anal.* calcd. for $C_8H_{12}ClHg_3N_5O_4$: C 10.93, H 1.37, N 7.96, Cl 4.03, Hg 68.43; found: C 10.81, H 1.38, N 7.82, Cl 3.77, Hg 66.90.

Crystal Data

$C_6H_9HgN_5O$ fw = 367.8

Monoclinic, space group $C2/c$, a = 19.796(6) Å; b = 7.119(3) Å, c = 16.471(4) Å, β = 128.83(2)°, V = 1808.3 Å, D_c = 2.70 g cm^{-3}, Z = 8, μ(MoKᾱ) = 169.9 cm^{-1}, λ(MoKᾱ) = 0.71068 Å (graphite monochromator), t = 23°C.

Crystallographic Measurements and Structure Resolution

The crystal selected for data collection had dimensions 0.09 × 0.14 × 0.70 mm^3. A set of precession photographs showed monoclinic Laue symmetry and indicated space group Cc or $C2/c$ (systematic absences hkl, $h + k \neq 2n$ and $h0l$, $l \neq 2n$). The crystal was mounted on an Enraf-Nonius CAD-4 diffractometer and the cell parameters were obtained from least-squares fit of the setting angles for 25 reflections centered in the counter aperture. The intensity data were collected using the ω/2θ scan technique. A fixed slit of 4 × 4 mm^2 was used and the scan range (ω) was (1.0 + 0.35 tan θ)° extended 25% on either side for backgrounds. Scan speed between 10 and 0.67 deg min^{-1} was automatically selected to make $I/\sigma(I)$ = 100, but a maximum scan time of 135 s was imposed. Prescans at 10° min^{-1} were done and all reflections having $I/\sigma(I) < 1$ were labelled "weak" and not remeasured. Three standard reflections, used as a check on instrument and crystal stability, showed only random fluctuations (esd 2.3–3.8%). Crystal orientation was checked every 100 reflections by centering three reflections. Crystal reorientation proved unnecessary.

A total of 2088 independent hkl and $\bar{h}kl$ reflections with $h + k = 2n$ were measured within a sphere $2\theta \leq 55°$. Net intensity I and esd $\sigma(I)$ were calculated as described elsewhere (8). A set of 1520 reflections with $I \geq 2.5\ \sigma(I)$ was retained for structure determination. An absorption correction was applied (Gaussian integration, grid 10 × 10 × 10, transmission coefficient 0.057–0.279). The data were finally corrected for the Lorentz and polarization effects.

The structure was solved by the heavy-atom method and refined on $|F_o|$ by full-matrix least squares. The statistical distribution of the normalized structure factors clearly favored the centric space group $C2/c$. From a Patterson map, the eight Hg atoms were positioned on a general equipoint. A Fourier map easily revealed the positions of all nonhydrogen atoms. Isotropic refinement with unit weights converged to $R = \Sigma||F_o| - |F_c||/\Sigma|F_o| = 0.123$. Refinement was continued using the block-diagonal approximation. Anisotropic temperature factors were refined for all nonhydrogen atoms. H(2), H(8), H(61), and H(62) were fixed at their calculated positions (sp^2 hybridization, C—H = 0.95 Å, N—H = 0.87 Å) with temperature factors B of 4.0 Å^2. The parameters of those hydrogens were not refined. The hydrogen atoms of the methyl group were not located. Individual weights based on counting statistics $w = 1/\sigma(F)^2$ were applied in the last least-squares cycles. Anisotropic refinement of all nonhydrogen atoms and of the scale factor converged to R = 0.051 and $R_w = [\Sigma w(|F_o| - |F_c|)^2/\Sigma w|F_o|^2]^{1/2} = 0.063$. The final difference Fourier map had a general background < ±0.7 e Å^{-3}, except for a few peaks of 1.1–2.0 e Å^{-3} within 1 Å from Hg. The refined parameters are listed in Table 1. A list of structure factors is part of the unpublished material.[2]

The form factors used were those of Cromer and Waber (9), except for hydrogen (10). Anomalous dispersion terms f' and f'' were used for Hg (11). The computer programs used are listed elsewhere (8).

Infrared Measurements

The spectra (4000–300 cm^{-1}) were recorded as Nujol mulls (CsI windows) and KBr pellets using a Beckman IR4520 spectrophotometer.

Results

Adenine is a potential pentadentate ligand. Three sites, i.e. N(1), N(3), and N(7) have available lone pairs in the undissociated ligand. Atom N(9) can become a reactive site by displacement of the weakly acidic H(9) proton (pk_a = 9.9) (12). The 6-amino group does not react as such because its lone pair participates in the ring π system, but substitution of an amino hydrogen by CH_3Hg^+ has been shown to take place under mild conditions with 9-methyladenine (1).

A number of adenine complexes containing various numbers of hydrogen and metal atoms have been structurally characterized. As the anionic form Ad^-, adenine is either monodentate through N(9) (13–16) or bridging-bidentate through N(9) and N(3) (13). The neutral form (HAd) reacts by the same donor atoms as the anion, the proton originally bonded to N(9) being displaced to N(7) (13). In the complexes with the adeninium cation H_2Ad^+, coordination usually takes place with N(3) and N(9), whereas protons are found at N(1) and N(7) (13, 17). The only exception to the latter generalization is the zwitterionic compound $[ZnCl_3(H_2Ad)]$, in which Zn is bonded to N(7), the extra proton is found at N(1), and H(9) is undissociated (18).

[2]The supplementary material includes a list of anisotropic temperature factors, a table of observed and calculated structure factors, and details of least-squares plane calculations. Complete set of data is available, at a nominal charge, from the Depository of Unpublished Data, CISTI, National Research Council of Canada, Ottawa, Ont., Canada, K1A 0S2.

Can. J. Chem. Downloaded from www.nrcresearchpress.com by 210.87.254.40 on 09/06/12
For personal use only.

TABLE 1. Refined coordinates of (adeninato-N9)-methylmercury(II) monohydrate ($\times 10^4$, H $\times 10^3$, Hg $\times 10^5$)

Atom	x	y	z
Hg(9)	44660(4)	66338(7)	53142(4)
O(1)	757(7)	1417(14)	1643(9)
N(1)	3230(7)	−428(14)	5438(9)
C(2)	3863(10)	743(20)	6117(11)
N(3)	4051(8)	2423(16)	5954(9)
C(4)	3484(9)	2950(17)	4949(10)
C(5)	2786(9)	1913(16)	4167(11)
C(6)	2656(9)	145(18)	4426(10)
N(6)	2006(8)	−1004(16)	3726(10)
N(7)	2346(7)	2888(15)	3242(9)
C(8)	2799(10)	4492(18)	3499(12)
N(9)	3513(8)	4589(14)	4543(9)
C(9)	5451(12)	8567(21)	6153(14)
H(2)*	424	32	682
H(8)*	264	546	301
H(61)*	164	−66	308
H(62)*	195	−209	392

*Parameters not refined.

Interactions of CH_3Hg^+ with Adenine

The simplest solid compound is obtained from a 1:1 solution of CH_3HgNO_3 and HAd in which pH is raised to ~9 with NaOH:

[1] $CH_3Hg^+ + HAd + OH^- \rightarrow CH_3HgAd + H_2O$

Extra CH_3Hg^+ groups are introduced into the ring without proton exchange by increasing the amount of CH_3HgX. For instance $[(CH_3Hg)_2Ad]X$ is obtained either by adding 1 equiv. of NaOH to a 2:1 mixture of CH_3HgX and HAd (eg. [2]), or by reacting a 1:1 mixture without NaOH (eq. [3]):

[2] $2CH_3Hg^+ + HAd + OH^- \rightarrow [(CH_3Hg)_2Ad]^+ + H_2O$

[3] $2CH_3Hg^+ + 2HAd \rightarrow [(CH_3Hg)_2Ad]^+ + H_2Ad^+$

In the latter case, half of adenine acts as a base to accept the liberated proton. Using one extra mole of CH_3HgX yields $[(CH_3Hg)_3Ad]X_2$. When pH is raised to ~7 in solutions containing excess CH_3HgX, complexes of composition $[(CH_3Hg)_3(Ad-H)X$ are isolated. Two hydrogen atoms, presumably H(9) and an amino proton, are displaced in that reaction:

[4] $3CH_3Hg^+ + HAd + 2OH^- \rightarrow [(CH_3Hg)_3(Ad-H)]^+ + 2H_2O$

The proton attached to N(9) in solid HAd is involved in a tautomeric equilibrium between N(9) and N(7) in water solutions (19). Hence, CH_3Hg^+ coordination to N(7) in $[CH_3HgAd]\cdot H_2O$ could not be ruled out. The X-ray work described hereafter shows, however, that mercury is bonded to the more common N(9) site (13, 15, 16). The three remaining types of compounds obtained with this system have not been reported for other metals. Coordination was found to take place with N(9) and N(7) in both $[(CH_3Hg)_2Ad]^+$ compounds (1, 20). In both salts of $[(CH_3Hg)_3Ad]^{2+}$, the third mercury atom is bonded to N(3) (6, 8). No X-ray diffraction data are available for the compounds obtained at high pH. According to the formula, two protons have been substituted, an indication that mercury bonds to N(9) and N(6). The site used by the third CH_3Hg^+ group is still uncertain, but we suggest N(7) on the basis of our present interpretation of the infrared spectra (*vide infra*).

When this work was undertaken, it was expected that low pH could reverse equilibrium [1] and lead to a series of complexes without H(9) substitution, as found in $[ZnCl_3(H_2Ad)]$ (18). Although formation of such species in solution is not ruled out, whenever pH was lowered to the point that none of the above complexes would precipitate, the solid phase isolated was adeninium nitrate or perchlorate.

Crystal Structure of $[CH_3HgAd]\cdot H_2O$

Interatomic distances and bond angles are represented in Fig. 1. The CH_3Hg group is bonded to N(9), the site formerly occupied by the displaced proton. The Hg—N (2.07(1) Å) and Hg—C (2.06(2) Å) bond lengths are similar to those found in previous studies (1, 2, 6–8). The coordination of mer-

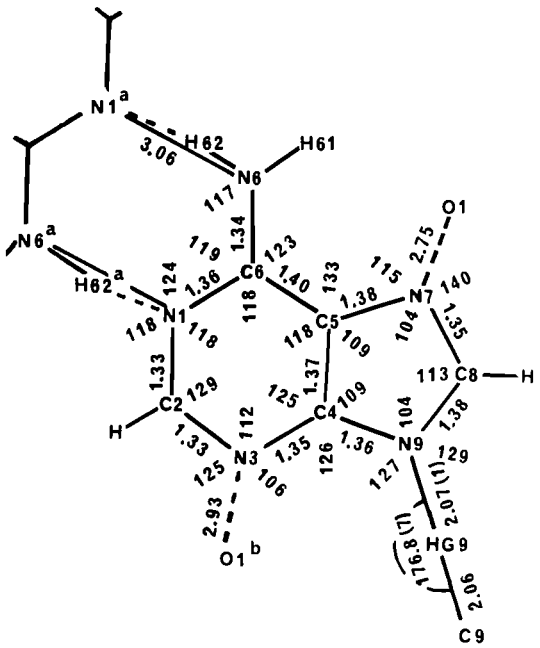

FIG. 1. Interatomic distances (Å) and bond angles (deg) in (adeninato-N9)methylmercury(II) monohydrate. Unless otherwise stated, the standard deviations on distances are 0.02 Å and on bond angles, 1°. Superscript a denotes $\frac{1}{2}-x, -\frac{1}{2}-y, 1-z$; b, $\frac{1}{2}+x, \frac{1}{2}-y, \frac{1}{2}+z$.

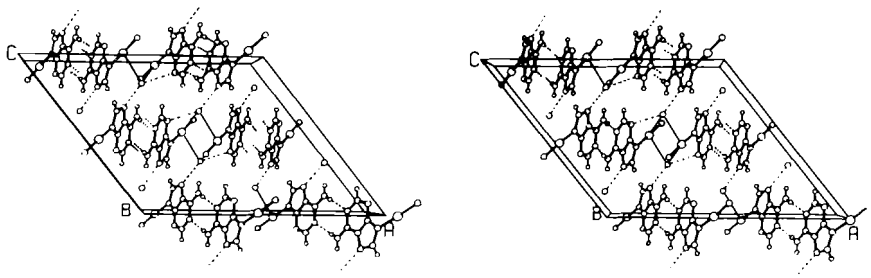

FIG. 2. Stereo view of the crystal packing. The smaller and larger spheres correspond to hydrogen and mercury atoms respectively. The hydrogen bonds are shown as dashed lines and the Hg···O contacts as thin bonds. Some of the molecules in the *ab* plane at $z = 0$ have been shifted along c to illustrate base pairing.

TABLE 2. Environments of O(1) and Hg(9) in the crystal structure*

Bond	Distance (Å)	Bond	Distance (Å)
Hg(9)—O(1)^a	3.00(1)	O(1)—N(7)	2.75(2)
Hg(9)—O(1)^b	2.97(1)	O(1)—N(3)^c	2.93(2)
		O(1)—Hg(9)^c	3.00(1)
		O(1)—Hg(9)^d	2.97(1)
Bonds	**Angle (°)**	**Bonds**	**Angle (°)**
C(9)–Hg(9)–O(1)^a	88.8(6)	N(7)–O(1)–N(3)^c	127.9(6)
C(9)–Hg(9)–O(1)^b	101.4(6)	N(7)–O(1)–Hg(9)^c	156.1(6)
N(9)–Hg(9)–O(1)^a	88.3(5)	N(7)–O(1)–Hg(9)^d	108.8(5)
N(9)–Hg(9)–O(1)^b	80.7(5)	N(3)^c–O(1)–Hg(9)^c	71.0(4)
O(1)^a–Hg(9)–O(1)^b	103.5(4)	N(3)–O(1)–Hg(9)^d	102.4(5)
		Hg(9)^c–O(1)–Hg(9)^d	76.5(3)

*Superscript a denotes $\frac{1}{2} + x, \frac{1}{2} - y, \frac{1}{2} + z$; b, $\frac{1}{2} - x, \frac{1}{2} + y, \frac{1}{2} - z$; c, $-\frac{1}{2} + x, \frac{1}{2} - y, -\frac{1}{2} + z$; d, $\frac{1}{2} - x, -\frac{1}{2} + y, \frac{1}{2} - z$.

cury is linear (N(9)–Hg(9)–C(9) = 176.8(7)°) as expected. The geometry of the ligand does not significantly differ from what has been observed for other N(9)-bonded complex (13, 15, 16) and the large standard deviations preclude any conclusions as to changes in ligand geometry (21) produced by complexation. The adenine ring, including the exocyclic N(6) atom, is planar within 1σ (0.02 Å). The CH_3Hg group is significantly out of that plane, with atom-to-plane distances of 0.177(1) Å for Hg(9) and 0.35(3) Å for C(9).

The packing diagram (Fig. 2) shows that two centrosymmetrically-related complex molecules are associated in pairs by two N(6)–H(62)···N(1′) hydrogen bonds of moderate strength: N(6)—N(1′) = 3.06(2) Å, C(6)–N(6)–N(1′) = 117(1)°, C(2′)–N(1′)–N(6) = 118(1)°, C(6′)–N(1′)–N(6) = 124(1)°.

Layers parallel to the *ab* plane at $z = 0$ and $\frac{1}{2}$ contain flat "dimers" stacked parallel with the usual separation of ~3.4 Å. The interlayer region is occupied by the water molecule O(1), which is hydrogen-bonded to N(7) in one layer, whereas it interacts with N(3) and two Hg atoms in the adjacent layer (Table 2). The N(7)···H–O(1) hydrogen bond is strong (N(7)···O(1) = 2.75(2) Å) and O(1) is close to the molecular plane, although not along the expected direction of the lone pair (the O(1)–N(7)–C angles differ by 25°, Fig. 1). The other hydrogen of O(1) interacts with N(3), but this time, the H-bond is much weaker (N(3)—O(1) = 2.93(2) Å) and O(1) is far from the molecular plane where best H-bonding is expected. The unhindered side of the water molecule bridges two mercury atoms with which it forms weak secondary bonds of 2.97(1) and 3.00(1) Å. In the resulting arrangement, each Hg atom has two such secondary bonds established as usual near the equatorial plane (assuming C(9) and N(9) as axial).

Infrared Spectroscopy

This technique has been widely used to distinguish between complexation sites in multidentate ligands. With adenine, reliable correlations between structure and spectral information are still missing. Since we had at our disposal unambiguous structural information on a series of related compounds, we carefully examined their ir spectra, hoping to detect characteristic features for each structural type. The most interesting region (1750–1250 cm^{-1}) will be discussed below.

Can. J. Chem. Downloaded from www.nrcresearchpress.com by 210.87.254.40 on 09/06/12
For personal use only.

Can. J. Chem. Downloaded from www.nrcresearchpress.com by 210.87.254.40 on 09/06/12
For personal use only.

With the exception of the weak ν C–H stretching band around 2925 cm^{-1}, the only vibration of the CH_3Hg group (22) which was clearly recognized is the Hg–C stretch showing at ~565 cm^{-1}. The band is not single when the molecule contains more than one CH_3Hg group, but the number of such groups in the compounds cannot be reliably deduced therefrom because the components are overlapping. Likewise, band position does not seem to be sensitive to the sites of attachment on the ring.

The anions present in most of our compounds produce broad and very intense bands (NO_3^-, ~1360; ClO_4^-, ~1080 cm^{-1}) (23). Except for these absorptions and other weaker anion bands, pairs of corresponding complex salts show very similar spectra and are assumed to have the same structure, a conclusion that is borne out by X-ray work for two of the three pairs of compounds (1, 6, 8, 20).

Figure 3 shows the 1750–1250 cm^{-1} portions of the ir spectra, which appear to be sensitive to the substitution pattern. This region includes mostly ring stretching vibrations, together with some in-plane deformation modes of exocyclic atoms (δ NH_2, δ NH, and δ CH). Our results for adenine are in good agreement with those reported by Lautié and Novak (24). Band assignments have been proposed by these workers for adenine and its Na salt. A normal-coordinate analysis has been carried out for the adenine ring in-plane vibrations (25).

X-ray diffraction work has been done on all the compounds in which the amino group is not substituted. Their spectra will be discussed first (Fig. 3, B, C, and D).

The scissoring motion of the 6-NH_2 group leads to a strong absorption at 1673 cm^{-1} in adenine (24). The shift to 1655 cm^{-1} observed in the complexes undoubtedly results from a change in H-bonding rather than from direct effects of complexation. The crystal structure of adenine is not known yet, but Lautié and Novak (24) have suggested a reasonable model in which each molecule is surrounded by three pairs of H-bonds (N(6)–H(62)···N(1), N(6)–H(61)···N(7), and N(9)–H(9)···N(3)) of the type found in DNA base pairing (21). Obviously, mercury binding to heterocyclic nitrogen atoms destroys most of those H-bonds. Interestingly, the N(6)–H(62)···N(1) pairing is found in all our complexes and it is the only type of base pairing observed. Even in $[CH_3HgAd]\cdot H_2O$, where N(7) is not blocked by mercury, this position is involved in H-bonding with water instead of pairing with another CH_3HgAd molecule. Consequently, the constant position of the δ NH_2 band is likely to simply reflect the similarity in H-bonding.

A set of three bands at 1604, 1570, and 1507 cm^{-1} in adenine are displaced to 1593, 1555, and 1485 cm^{-1}, respectively, in CH_3HgAd, but they return to their original positions in higher complexes. The latter vibration involves predominantly the imidazole ring (24, 25) and the shift to 1485 cm^{-1} may be characteristic of a singly N(9)-metalated ring.

The ligand band at 1449 cm^{-1} appears around 1468 cm^{-1} in all our compounds. It probably indi-

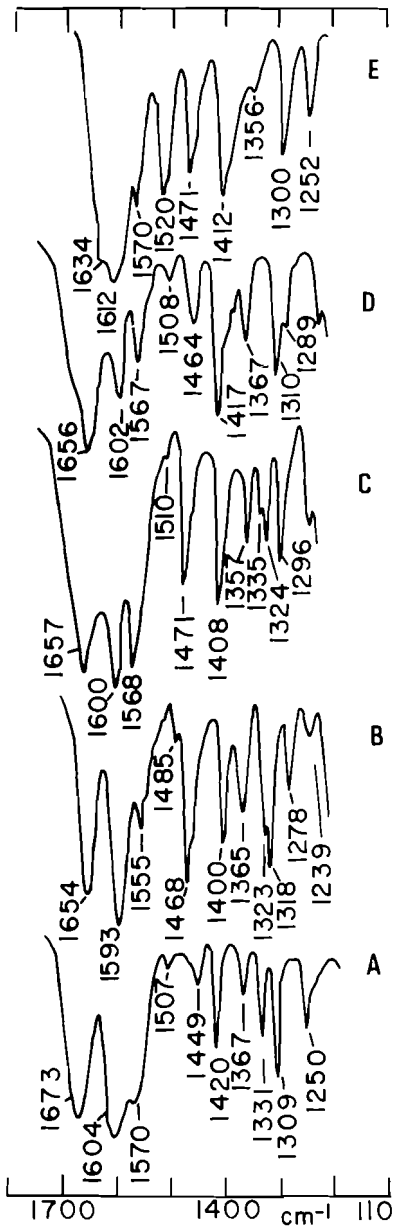

FIG. 3. The 1750–1250 cm^{-1} regions of the infrared spectra; A = adenine (HAd), B = $[CH_3HgAd]\cdot H_2O$, C = $[(CH_3Hg)_2Ad]\text{-}ClO_4\cdot H_2O$, D = $[(CH_3Hg)_3Ad](ClO_4)_2$, E = $[(CH_3Hg(Ad\text{-}H)]\text{-}ClO_4$.

Can. J. Chem. Downloaded from www.nrcresearchpress.com by 210.87.254.40 on 09/06/12
For personal use only.

cates coordination through N(9), but it is not sensitive to further reaction with N(7), or N(7) and N(3).

The position of the band around 1420 cm^{-1} in adenine is differently shifted depending on the substitution pattern.

The pair at 1331 and 1309 cm^{-1} in adenine shifts to 1323 and 1318 cm^{-1} in CH_3HgAd, to 1335 and 1324 cm^{-1} in $[(CH_3Hg)_2Ad]ClO_4$, and a single absorption at 1310 cm^{-1} is found for $[(CH_3Hg)_3Ad](ClO_4)_2$.

A band at 1250 cm^{-1} and a shoulder at 1235 cm^{-1} have been assigned to the δ NH and δ CH modes, respectively (24). The latter assignment is probably correct (25). The former vibration undoubtedly involves a large amount of ring stretching mixed with N–H bending or there may be another component (25) under the 1250 cm^{-1} peak, since the band does not disappear in the complexes, even though H(9) is no longer present. It is shifted to 1278 cm^{-1} in the 1:1 complex, it undergoes further displacement to 1296 cm^{-1} in the 2:1 complex, and probably to 1289 cm^{-1} in $[(CH_3Hg)_3Ad](ClO_4)_2$.

The structure of $[(CH_3Hg)_3(Ad\text{-}H)]X$ is not known from X-ray work. Substitution of an amino hydrogen by a CH_3Hg^+ group is consistent with the disappearance of the strong δ NH_2 band at 1673 cm^{-1} (Fig. 3, curve E). The spectrum of the nitrate shows a sharp peak at 1117 cm^{-1} (not shown). With 9-methyladenine, such a peak has been found (~1135 cm^{-1}) only in $[(CH_3Hg)_2(MAd\text{-}H)]NO_3$ (26), a compound in which mercury has displaced an amino hydrogen (1). Tobias and co-workers (5) have also reported a similar absorption at 1122 cm^{-1} in the Raman spectrum of adenosine 5′-monophosphate when reaction takes place with the amino group. Evidence for H(9) substitution comes from the band at 1471 cm^{-1}, which is common to all the N(9)-coordinated complexes above. The present complex also shows bands at 1612, 1570, and 1520 cm^{-1}, respectively. This probably rules out single occupancy of the imidazole ring, since those bands would have shifted to lower wavenumbers as in the 1:1 complex. Consequently, we suggest that the third CH_3Hg^+ group is bonded to N(7). In that case, the presence of a single band at 1300 cm^{-1} would result from perturbations in the ring caused by amino substitution. It must be stressed that the structure of $[(CH_3Hg)_3(Ad\text{-}H)]X$ is not firmly established, since this work provided unambiguous information only on three substitution patterns and the spectral changes on metal-binding elsewhere, with N(1), for example, are not easily predictable.

Discussion

This work brings out interesting aspects of CH_3Hg^+ complexation with adenine ligands. First, mercury competes favorably with the proton, since as noted by other workers (3, 5), protons are displaced by mercury at a pH much lower than that at which spontaneous dissociation would take place. For instance, an amino proton that does not dissociate in water was easily displaced in the $[(CH_3Hg)_3(Ad\text{-}H)]X$ compounds. Similarly, N(9)-mercurated compounds precipitated even at pH 2 in spite of a pk_a of 9.9 for H(9) of adenine (12). Another interesting point is the influence of substitution on the basicity of the remaining donor atoms. For example, N(9)-alkylated adenine reacts through N(1), while N(9)-mercurated adenine reacts through N(7). These peculiarities can be rationalized in terms of charge distribution.

There is no generally accepted basicity order for the donors in the adenine ring. Electrostatic potential energy calculations (27) on neutral adenine indicate that pyrimidine nitrogens N(1) and N(3) have comparable charge densities, whereas N(7) is significantly less electron-rich. This would be in agreement with the fact that adenine protonates at N(1) (12) and that N(9)-blocked adenines accept CH_3Hg^+ at the same position (2). When H(9) has been substituted by CH_3Hg^+, the theoretical considerations above have to be modified in order to explain the formation of higher complexes. Because CH_3Hg is less electron-attracting than H or CH_3, but more than nothing at all (free lone pair), the electronic distribution in CH_3HgAd should be intermediate between that of neutral adenine HAd and that of the adeninate anion Ad^-. The anion can be represented by resonance structures **1***a–d*, which are expected to contribute in the order **1***a* > **1***b* > **1***c* > **1***d*. Structures in which the charge appears on the pyrimidine ring (**1***c*, *d*) are likely to contribute less because the benzenoid structure is lost. On the other hand, N(3) is close to N(9) and is expected to receive more charge than the remote N(1) site. The net result of H(9) substitution by CH_3Hg^+ is a large basicity enhancement of N(7), a lesser effect at N(3), and probably very little effect at N(1). This work suggests that N(7) has become the best residual binding site in CH_3HgAd. Coordination to the free lone pair on N(7) will now reduce the availability of both N(1) and N(3), but probably to the same extent. Further reaction with N(3) shows either that N(3) was already more basic than N(1) in neutral adenine, or that H(9) substitution has raised its basic character above that of N(1).

In connection with the possible structures for $[(CH_3Hg)_3(Ad\text{-}H)]X$, it is interesting to speculate on the best residual binding site of an adenine ring in which H(9) and one amino hydrogen have already been substituted by CH_3Hg^+. Substitution of

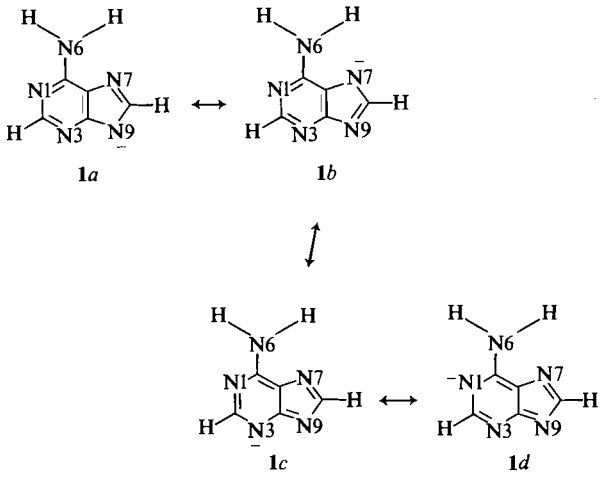

1*a* 1*b* 1*c* 1*d*

an amino hydrogen by CH_3Hg^+ should initiate a charge redistribution approaching that of the anion, for which the three predominant resonance structures are shown (**2** *a–c*). They probably contribute in the order **2***a* > **2***b* > **2***c*. Thus, initial mercuration

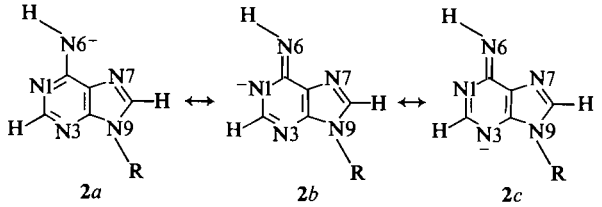

2*a* 2*b* 2*c*

on the amino group should enhance the donor basicities in the order N(1) > N(3) > N(7). On the other hand, initial mercuration at N(9) should lead to the reverse order N(7) > N(3) > N(1). Consequently, depending on the relative importance of those effects, any of the three sites would be possible. If our suggestion based on ir spectra that the compounds are N(9), N(7), N(6)-bonded is correct, it would mean that H(9) substitution directly on the imidazole ring releases more charge into the ring system than substitution on the exocyclic amino group.

1. L. PRIZANT, M. J. OLIVIER, R. RIVEST, and A. L. BEAUCHAMP. J. Am. Chem. Soc. **101**, 2765 (1979).
2. M. J. OLIVIER and A. L. BEAUCHAMP. Inorg. Chem. **19**, 1064 (1980).
3. R. B. SIMPSON. J. Am. Chem. Soc. **86**, 2059 (1964).
4. S. MANSY and R. S. TOBIAS. J. Am. Chem. Soc. **96**, 6874 (1974).
5. S. MANSY, J. P. FRICK, and R. S. TOBIAS. Biochim. Biophys. Acta, **378**, 319 (1975).
6. J. HUBERT and A. L. BEAUCHAMP. Can. J. Chem. **58**, 1439 (1980).
7. L. PRIZANT, R. RIVEST, and A. L. BEAUCHAMP. Can. J. Chem. In press.
8. J. HUBERT and A. L. BEAUCHAMP. Acta Crystallogr. Sect. B, **36**, 2613 (1980).
9. D. T. CROMER and J. T. WABER. Acta Crystallogr. **18**, 104 (1965).
10. R. F. STEWART, E. R. DAVIDSON, and W. T. SIMPSON. J. Chem. Phys. **42**, 3175 (1965).
11. D. T. CROMER. Acta Crystallogr. **18**, 17 (1965).
12. R. M. IZATT, J. J. CHRISTENSEN, and J. H. RYTTING. Chem. Rev. **71**, 439 (1971).
13. D. J. HODGSON. Prog. Inorg. Chem. **23**, 211 (1977).
14. L. G. MARZILLI. Prog. Inorg. Chem. **23**, 255 (1977).
15. W. M. BECK, J. C. CALABRESE, and N. D. KOTTMAIR. Inorg. Chem. **18**, 176 (1979).
16. H. SAKAGUCHI, H. ANZAI, K. FURUHATA, H. OGURA, Y. IITAKA, T. FUJITA, and T. SAKAGUCHI. Chem. Pharm. Bull. **26**, 2465 (1978).
17. C. GAGNON, J. HUBERT, R. RIVEST, and A. L. BEAUCHAMP. Inorg. Chem. **16**, 2469 (1977).
18. M. R. TAYLOR. Acta Crystallogr. Sect. B, **29**, 884 (1973).
19. M. DREYFUS, G. DODIN, O. BENSAUDE, and J. E. DUBOIS. J. Am. Chem. Soc. **97**, 2369 (1975).
20. A. L. BEAUCHAMP. J. Cryst. Mol. Struct. In press.
21. D. VOET and A. RICH. Prog. Nucleic Acid Res. Mol. Biol. **10**, 183 (1970).
22. J. H. S. GREEN. Spectrochim. Acta, Part A, **24**, 863 (1966).
23. K. NAKAMOTO. Infrared spectra of inorganic and coordination compounds. Interscience, New York. 1970 pp. 98 and 111.
24. A. LAUTIÉ and A. NOVAK. J. Chim. Phys. **71**, 415 (1974), and references therein.
25. M. TSUBOI, T. TAKAHASHI, and I. HARADA. Physicochemical properties of nucleic acids. Vol. 2. *Edited by* J. Duchesne. Academic Press, London. 1973. Chapt. 11.
26. L. PRIZANT, J. P. CHARLAND, R. RIVEST, and A. L. BEAUCHAMP. In preparation.
27. R. BONACCORSI, A. PULLMAN, E. SCROCCO, and J. TOMASI. Theor. Chim. Acta, **24**, 51 (1972); R. BONACCORSI, E. SCROCCO, J. TOMASI, and A. PULLMAN. Theor. Chim. Acta, **36**, 339 (1975).

Can. J. Chem. Downloaded from www.nrcresearchpress.com by 210.87.254.40 on 09/06/12
For personal use only.

Ab initio CI calculation of the band structure in the A^2B_1–X^2A_1 electronic transition of BH_2

MILJENKO PERIĆ[1] AND SIGRID D. PEYERIMHOFF

Lehrstuhl für Theoretische Chemie, Universität Bonn, Wegelerstraße 12, 5300 Bonn 1, West Germany

AND

ROBERT J. BUENKER

Lehrstuhl für Theoretische Chemie, Gesamthochschule-Universität Wuppertal, Gaußstraße 20, 5600 Wuppertal 1, West Germany

Received November 7, 1980

MILJENKO PERIĆ, SIGRID D. PEYERIMHOFF, and ROBERT J. BUENKER. Can. J. Chem. **59**, 1318 (1981).

Ab initio MRD-CI calculations have been carried out to nearly full-CI accuracy for several large AO basis sets (including *f* functions) for the potential curves of the BH_2 molecule in its X^2A_1 and A^2B_1 electronic states. A two-dimensional vibrational treatment of the bending modes in this system has been performed employing a variational method which takes account of both Renner–Teller coupling and large-amplitude motion. The resulting structural data agree to within 0.002 Å and 2° of measured bond distance and angles and the computed bending frequencies are found to be in error by less than 30 cm^{-1}; in addition predictions of the as yet unobserved stretching frequencies are also reported for both electronic states. In the best theoretical treatment the $v_2'' = 0 \rightarrow v_2' = 1$ transition energy to the linear upper state is calculated to be 4145 cm^{-1}, in excellent agreement with the corresponding value of 4190 cm^{-1} obtained by extrapolation of the three higher-energy band frequencies actually observed by Herzberg and Johns provided a renumbering of these levels (namely as $v_2' = 9$, 11, and 13) is undertaken relative to the originally preferred experimental interpretation. It is also pointed out that some of the earlier reported discrepancies between calculation and experiment regarding transition energies in this band system are actually due to a misinterpretation of the definition of the experimental fitting parameter T_{00} in previous theoretical work.

MILJENKO PERIĆ, SIGRID D. PEYERIMHOFF et ROBERT J. BUENKER. Can. J. Chem. **59**, 1318 (1981).

Utilisant plusieurs ensembles de OA avec des bases élargies (y compris les fonctions *f*), on a effectué des calculs *ab initio* MRD-CI jusqu'à une pression CI presque parfaite pour les courbes de potentiel de la molécule BH_2 dans ses états électroniques excités X^2A_1 et A^2B_1. On a effectué un traitement vibrationnel en deux dimensions des modes de déformation de ce système en utilisant une méthode de variation qui tient compte du couplage de Renner–Teller et du mouvement de grande amplitude. Les données structurales qui en résultent s'accordent à 0,002 Å et 2° avec les distances et les angles de liaison mesurés, et les fréquences calculées accusent une erreur de moins de 30 cm^{-1}. De plus on rapporte les prédictions relatives aux fréquences d'élongation qui n'ont pas encore été observées jusqu'ici, des deux états électroniques. Selon le meilleur traitement théorique, on a calculé que l'énergie de transition $v_2'' = 0 \rightarrow v_2' = 1$ vers l'état supérieur linéaire est de 4145 cm^{-1} et cette valeur est en parfait accord avec la valeur de 4190 cm^{-1} obtenue par extrapolation des trois bandes de fréquence de haute énergie observées de fait par Herzberg et Johns; cette concordance conduit à changer la numérotation de ces niveaux (soit $v_2' = 9$,11 et 13) par rapport à l'interprétation expérimentale retenue originalement. On montre également que quelques-unes des différences rapportées antérieurement entre les calculs et l'expérience relatives aux énergies de transition de ce système de bandes sont dues en fait à une mauvaise interprétation de la définition du paramètre expérimental d'accord T_{00} dans le travail théorique antérieur.

[Traduit par le journal]

I. Introduction

The triatomic radical BH_2 possesses only 7 electrons and is thus the smallest polyatomic molecule for which an electronic spectrum has yet been observed. Because of the small number of electrons the theoretical *ab initio* results should be very reliable for this species and hence very good agreement between measured and calculated data for the BH_2 structure and electronic spectrum is expected. Nevertheless up to the present when such comparison is attempted, considerable discrepancy appears to exist between the experimental and theoretical descriptions of the lowest-energy electronic transition in this spectrum.

On the experimental side an extensive study of the absorption spectrum of BH_2, observed in the flash photolysis of borine carbonyl, was undertaken by Herzberg and Johns (1). It consists of a progression of bands in the 6400–8700 Å region and is very similar to that observed for both NH_2 and CH_2. The transitions occur between the bent X^2A_1 and the upper (linear) $^2B_1$ state, whereby both states correlate with the same electronic species $^2\Pi$ in the linear nuclear arrangement (Renner–Teller effect). The progression is attributed to the bending mode, and on the basis of an extrapolation procedure, carried out under the assumption that anharmonicity effects can be neglected, it was concluded that the observed frequencies could best be fit in a polynomial series in $(v_2' + 1)$ with a constant value of $T_{00} = 4194$ cm^{-1}. No stretching frequency could be determined but on the basis of the isotope shift results between corresponding BH_2 and BD_2 bands it was concluded that one or possibly both stretch-

[1]Present address: Institut za Fizičku Hemiju, Prirodno-Matematičkog Fakulteta, Studentski Trg 12, P.O.B. 550, 11000 Beograd.

0008-4042/81/091318-10$01.00/0

©1981 National Research Council of Canada/Conseil national de recherches du Canada

Can. J. Chem. Downloaded from www.nrcresearchpress.com by 210.87.254.5 on 09/06/12
For personal use only.

Can. J. Chem. Downloaded from www.nrcresearchpress.com by 210.87.254.5 on 09/06/12
For personal use only.

ing frequencies are appreciably larger in the upper than in the X^2A_1 ground state.

Among the first *ab initio* studies of the two BH_2 states is the work of Bender and Schaefer (2), who employed a double-zeta type contracted gaussian AO basis in their natural orbital CI calculations and obtained structural data for both states which agree within 0.03 Å and 2° with the corresponding measured equilibrium quantities. Nevertheless they report a difference in the equilibrium electronic energies of the $^2A_1$ and $^2B_1$ ($^2\Pi$) species of only 2260 cm^{-1} compared to a result for this quantity given by Herzberg and Johns of 4300 cm^{-1}, and they have assumed that the resulting discrepancy arises from shortcomings in the above calculations. Staemmler and Jungen (3) have since made a very careful theoretical study of both BH_2 states in a large AO basis of 65 gaussian lobe functions contracted to 38 groups, including *d* polarization functions on boron and *p* species on hydrogen, whereby some of the original 5*p* boron exponents were reoptimized in the molecular calculation. The correlation energy is accounted for in an independent electron pair approach (IEPA) combined with the direct determination of pair natural orbitals (PNO). The calculated molecular structure constants are again in very good agreement with the experimental results (deviations of 0.006 and 0.024 Å in equilibrium bond lengths and 2.4° in X^2A_1 bond angle) in this work, but in this case the calculated energy difference (2740 cm^{-1}) between the two electronic states is only slightly greater than that obtained by Bender and Schaefer. Upon correcting for zero-point vibrational effects, Staemmler and Jungen find a value for T_{00} of 3035 cm^{-1}, and state their belief that this theoretical result is more reliable than the corresponding experimental value of 4194 cm^{-1}, suggesting that the remaining discrepancy comes about as a consequence of an incorrect numbering of the observed vibrational levels. Further theoretical work (4–6) on BH_2 has concentrated on the calculation of other molecular properties than the above transition energy or has employed a less extensive theoretical treatment, and hence has not helped to clarify this apparent discrepancy between computed and measured results.

On the basis of this literature survey it must be concluded that there is either an incorrect interpretation of the experimental results, such as an error in the assignment of the observed bands, or that the previous theoretical treatments underestimate the energy difference between the lowest vibrational levels of the two electronic states by an unexpectedly large amount. The present work attempts to clarify this situation by employing a large AO basis set in the multi-reference double-excitation CI technique (MRD-CI), which has been very successful in the study of a number of similar systems such as PH_2, H_2S^+, and NH_2, for example (7–9).

2. Technical Details of the Calculations

A. Potential Surface Treatment

The AO basis set employed in the present calculations consists of 38 contracted cartesian gaussian functions: five *s* and three *p* groups in the contraction (4,2,1,1,1/3,1,1) given by Dunning (10), in addition to a set of cartesian *d* functions with exponent $\alpha = 0.6$, located at the boron atom, and two *s* groups in the contraction (4,1) with scaling factor $\eta^2 = 2.0$ augmented by one set of *p* functions ($\alpha = 0.7$) for the hydrogen atoms; furthermore one *s* and one *p* function ($\alpha_s = 1.3$, $\alpha_p = 0.5$) located in each of the BH bonds are included. Finally for a few additional calculations at representative geometrical points a cartesian *f* function ($\alpha = 1.0$) is also employed on the boron basis set.

The calculation of the electronic energies is carried out by means of the MRD-CI method (12, 13), with configuration selection and energy extrapolation. In the present case all MO's except the highest a_1 species have been considered for variable occupation (37 total) in the construction of the configuration basis, and all electrons including those in the boron 1*s* shell are correlated. The orbital basis consists of the parent-configuration SCF MO's in each case, i.e. X^2A_1 SCF orbitals for the treatment of the X^2A_1 state and $^2B_1$ SCF MO's for the $^2B_1$ CI calculations.

The set of reference configurations employed for all nuclear conformations is listed in Table 1. All single- and double-excitation species with respect to this reference set are generated, resulting in 46 252 symmetry-adapted configuration state functions (SAF's) for the X^2A_1 and 31 988 SAF's for the $^2B_1$ state; a selection threshold of $T = 5$ μh is employed so that the actual secular problem to be solved at each nuclear conformation is in the order of 2200, while the contribution of the remaining generated configurations is accounted for by the usual extrapolation procedure (12, 13). The effect of still higher excitations is estimated by means of the perturbation formula

$$\Delta E = \left(1 - \sum_i^{\text{ref}} C_i^2\right)(E_{\text{ref}} - E_{\text{MRD-CI}})$$

so that this energy contribution, when added to the

Can. J. Chem. Downloaded from www.nrcresearchpress.com by 210.87.254.5 on 09/06/12
For personal use only.

TABLE 1. Occupation numbers for the reference configurations employed in the MRD-CI treatment for the two lowest electronic states in the BH_2 molecule

State	Occupation number							
	$1a_1$	$2a_1$	$1b_2$	$3a_1$	$1b_1$	$4a_1$	$2b_2$	$3b_2$
X^2A_1	2	2	2	1				
	2	—	2	1	2			
	2	2	—	1	—	2		
	2	—	1	—	—	2		
	2	—	2	1	—	2	—	
	2	2	—	1	—	—	—	2
	2	1	2	1	—	1	—	—
$^2B_1$	2	2	2	—	1	—		
	2	2	—	2	1	—		
	2	—	2	—	1	2		
	2	—	2	2	1	—		
	2	1	2	1	1	—		

MRD-CI value, yields a reasonable estimate (14, 15) for the full CI energy in the AO basis employed.

B. Vibrational Treatment

The vibrational treatment is carried out under the assumption that all three vibrational modes are independent of one another, i.e. the potential is represented in polynomial expansions in the vibrational coordinates including higher than second-order terms but no cross terms. Such an approach is justified since one can assume that excitation into high-lying stretching vibration levels during the electronic transition are improbable, and hence that the molecule undergoes only small-amplitude stretching vibrations, in which case it is possible to separate the bending and stretching motions from each other (16–18).

The Schrödinger equation for the symmetric and the antisymmetric vibrations is solved with the help of the variation method, involving expansion of the vibrational states in harmonic oscillator functions and employing a polynomial fit for the electronic potential, as described in more detail elsewhere (18). In the correct treatment of bending vibrations it is necessary to consider both the effect of large-amplitude vibrations as well as of the Renner–Teller vibronic interaction. A set of two-dimensional harmonic oscillator functions of the form

$$R_{v,k}(\rho) = N_{v,k} \exp(-\alpha\rho^2/2)(\alpha\rho^2)^{k/2} L^k_{(v+k)/2}(\alpha\rho)$$

is thereby employed as the functional basis ($\rho = \pi - \alpha$), just as in the related study of PH_2 (7) or NH_2 (9), and the vibronic energy levels and wavefunctions are then obtained by diagonalization of the corresponding Hamiltonian matrix.

Of the various suggestions for the kinetic energy operators allowing a treatment of the large-amplitude bending vibration (16, 17, 20), the form of Freed and Lombardi (17) as modified by Barrow *et al.* (21) is chosen for the present treatment. The operator formula 1 of ref. 21 is thereby cast in the form $T = T_0 + T'$, whereby $T_0 = \lim_{\rho\to 0} T$ (ρ denotes the bending coordinate), i.e. T_0 is the kinetic energy operator for a two-dimensional harmonic oscillator while T' has the form

$$T' = T_1'(\rho)\frac{\partial^2}{\partial\rho^2} + T_2'(\rho)\frac{\partial}{\partial\rho} + T_3'(\rho)\frac{\partial^2}{\partial\phi^2} + T_4'$$

The coefficients T_i' are expanded in a McLaurin series in ρ as described in more detail elsewhere (22), so that Hamiltonian matrix elements of the form

$$\left\langle \left| \rho^n \frac{\partial^2}{\partial\rho^2} \right| \right\rangle, \quad \left\langle \left| \rho^n \frac{\partial}{\partial\rho} \right| \right\rangle, \quad \text{and} \quad \langle|\rho^n|\rangle$$

have to be evaluated for the secular equation in the corresponding variational procedure.

If only Σ vibronic levels are of interest, there is no Renner–Teller coupling and the procedure described so far suffices. In a general treatment it is necessary to take account of the coupling between the electronic and vibrational motion which can be achieved, for example (23), by diagonalizing the total Hamiltonian in a basis consisting of products of electronic and vibrational wavefunctions obtained in the Born–Oppenheimer approximation. The coupling elements require the evaluation of the first and second derivatives of the electronic CI wavefunction with respect to the nuclear coordinate (24), which in this case is the rotation angle ϕ. An alternative procedure is the more conventional approach by Dixon (25) which has been refined (26) (and successfully applied to C_3) by taking a polynomial expansion of the Born–Oppenheimer potentials for both components of the Π electronic states under the assumption of a simple form for the electronic wavefunctions proportional to $\sin(\theta - \phi)$ and $\cos(\theta - \phi)$. Both treatments will give the same results if carried to sufficiently high order, as has been numerically demonstrated for the vibronic levels in NH_2 (19), but in the present work only the second approach (26) is actually employed.

3. Results and Discussion

A. Potential Energy Curves

The calculated potential energy curves (generally the energy corresponding to the full CI estimate) are given in Fig. 1*a*, *b* for symmetric and antisymmetric BH stretching motion respectively, and in Fig. 2 for the bending coordinate at a fixed value of the BH bond length. The total energy values of the ground state are contained in Table 2,

Can. J. Chem. Downloaded from www.nrcresearchpress.com by 210.87.254.5 on 09/06/12
For personal use only.

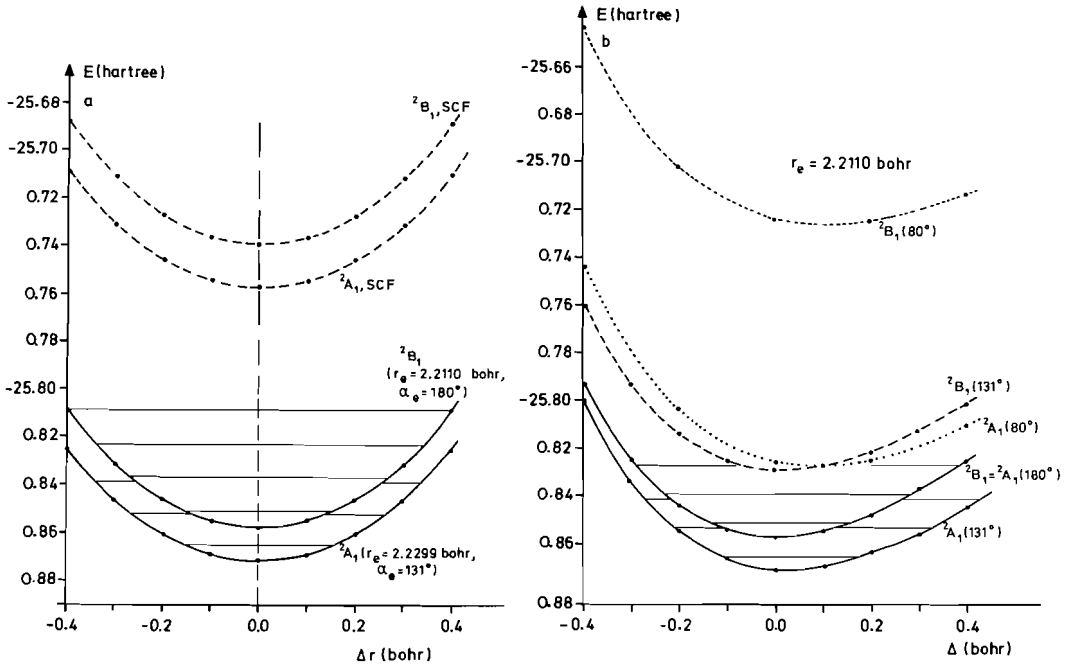

FIG. 1. Potential curves for the lowest-lying electronic states of BH_2 for the (*a*) symmetric and (*b*) antisymmetric vibrational modes obtained in the present CI treatment; corresponding SCF results are also indicated for the antisymmetric stretch motion. The values for bond lengths and angles held fixed in these calculations are given in parentheses in the figure. The lowest computed vibrational energies are also indicated in a number of instances.

TABLE 2. Total energies (in hartree) of BH_2 in its X^2A_1 ground state and relative energy T_e (in cm^{-1}) of its first excited $^2B_1$ state

	Total energy			
	Present work			
	Standard AO basis 38 groups	Additional *f* functions	Ref. 3	Ref. 2
X^2A_1 state				
SCF	−25.75679	−25.75698	−25.75251[a]	−25.70411
MRD-CI	−25.86642	−25.87068	−25.84880	−25.79078
Full CI est.	−25.87059	−25.87506	(IEPA)	(CI)
Geometry	r = 1.17 Å, α = 131°		r = 1.204 Å, α = 128.6°	r = 1.211 Å, α = 129.4°
	T_e (cm^{-1})			
	Present work			
	Standard AO basis 38 groups	Additional *f* functions	Ref. 3	Ref. 2
A^2B_1 state				
SCF	3889	3900	4020[a]	3042
MRD-CI	3050	2712	2740	2260
Full CI est.	3024	2675	(IEPA)	(CI)
Geometry	r = 1.17 Å, α = 180°		r = 1.176 Å, α = 180°	r = 1.188 Å, α = 180°

[a]The corresponding geometry is r_0 = 1.182 Å and 128.4° for X^2A_1 and 1.162 Å and 180° for $^2B_1$.

Can. J. Chem. Downloaded from www.nrcresearchpress.com by 210.87.254.5 on 09/06/12
For personal use only.

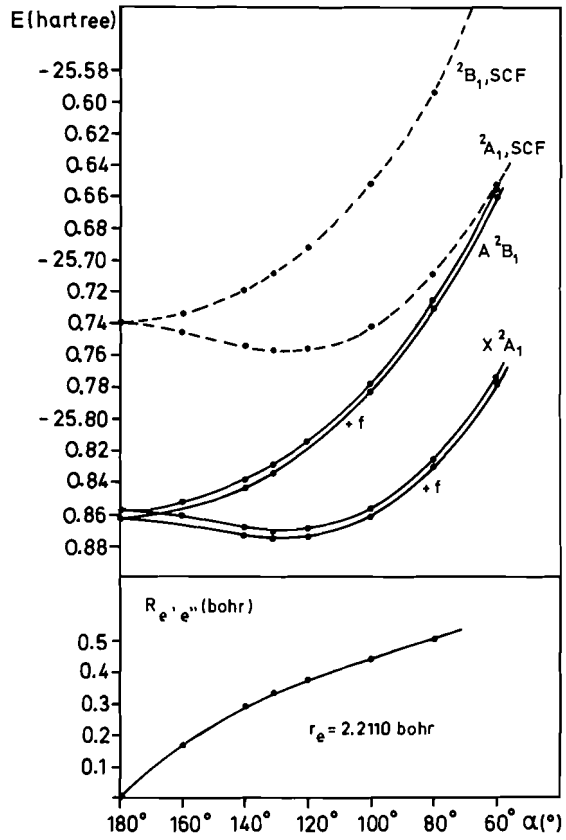

FIG. 2. Bending potential curves obtained in the SCF (dashed lines) and CI (solid lines) treatments for the A^2B_1 and X^2A_1 electronic states of BH_2; a second set of CI curves obtained for the AO basis including f functions is also indicated. In the bottom portion of the figure is given the corresponding variation in the electronic transition moment between these states.

and comparison is also made with corresponding results of previous work.

It is seen that the total energies obtained in the present work are somewhat lower than those reported previously because of the more flexible AO basis set employed. The lowering due to inclusion of f functions is only 0.00019 hartree at the SCF level but is more substantial, namely 0.00426 hartree (0.00447 hartree, full-CI estimate), at the CI level. Calculations including the f functions have only been carried out for the angular potential curve at fixed BH bond length (Fig. 2), but these results indicate that the energy lowering obtained thereby remains fairly constant for both electronic states (0.0045 hartree for $^2A_1$ and 0.0050 hartree for $^2B_1$) over a large range of internuclear angles. There is a tendency for the f functions to be somewhat more effective at very large angles, however, so that the barrier to linearity in the X^2A_1 ground state (or energy splitting between the equilibrium conformations of both states) is reduced by approximately 340 cm^{-1} as a result of this AO basis set extension. This pattern is wholly consistent with the experience for other systems such as NH_2, for example (9). It is also important to note that electron correlation is more effective in the linear geometry (Fig. 2), so that the CI potential well in the X^2A_1 state is considerably more shallow than its SCF counterpart (Table 2 and Fig. 2).

The potential energy curves for symmetric stretch (Fig. 1*a*) have been calculated for three different internuclear angles in both states to assess the dependence of the BH distance on the bending angle. The optimal values are 1.172 Å, 1.183 Å, and 1.225 Å for X^2A_1 at the angles 180°, 131°, and 80° respectively, while the $^2B_1$ counterparts for the same angles are 1.172 Å, 1.183 Å, and 1.228 Å. Hence a change of approximately 0.055 Å results in going from the equilibrium conformation to the small-angle structure.

The $^2A_1$ and $^2B_1$ curves for asymmetric distortion displayed in Fig. 1*b* run quite parallel to each other, but a definite deviation from the SCF counterparts as a result of inclusion of electron correlation is also apparent. The structural data obtained from polynomial fits to the calculated potential data are summarized in Table 3 and are seen to be in excellent agreement with the corresponding data inferred from experiment (1). A more accurate change in bond length between X^2A_1 and $^2B_1$ is also given by the present calculation, this quantity having been slightly overestimated in both previous theoretical treatments.

B. Vibrational Pattern in the X^2A_1–$^2B_1$ *Transition*

The calculated lowest vibrational levels for the two stretching modes are also indicated in Fig. 1*a*, *b*; the polynomial fit for the potential contained terms up to power 5 (symmetric) and 6 (antisymmetric mode) while a set of 15 vibrational basis functions was employed in the corresponding variational calculations in each case. The calculated frequencies are collected in Table 4 for the four common isomers of BH_2, while the corresponding Franck–Condon factors are given in Table 5*a* and *b* for the two stretching modes.

TABLE 3. Structural data for BH_2 in its two lowest electronic states obtained in the present work and comparison with corresponding results of other treatments

	Present	Ref. 3	Ref. 2	Exptl.
$X^2A_1 r_0$(Å)	1.183 (r_e)	1.204	1.211 (r_e)	1.181
α_0	129° (α_e)	128.6°	129.4° (α_e)	131°
$^2B_1 r_0$(Å)	1.172 (r_e)	1.176	1.188 (r_e)	1.17
α_0	180° (α_e)	180°	180° (α_e)	180°

TABLE 4. Calculated frequencies (in cm^{-1}) for the three normal modes of various isomers of BH_2 and comparison with previous theoretical data and experiment

	$^{10}BH_2$		$^{11}BH_2$		$^{10}BD_2$		$^{11}BD_2$	
	X^2A_1	A^2B_1	X^2A_1	A^2B_1	X^2A_1	A^2B_1	X^2A_1	A^2B_1
$\omega_1(2\varepsilon_0)$	2624	2700	2622	2700	1879	1912	1876	1912
$\omega_1(0-1)$	2588	2671	2585	2671	1860	1901	1857	1901
ω_1(ref. 3)	—	—	2487	2774	—	—	—	—
$\omega_2(\frac{1}{2}\varepsilon_0)$	—	975	—	967.5	—	744.5	—	734.5
$\omega_2(0-1)X\}^a$	1064	986	1057	978	809	751	800	742
$(\frac{1}{2}^3)A\}$								
ω_2(ref. 3)	—	—	1017	992	—	—	—	—
ω_2(ref. 1)	—	—	1030	954	—	—	—	—
$\omega_3(2\varepsilon_0)$	2858	2987	2840	2964	2157	2278	2132	2248
$\omega_3(0-1)$	2883	3014	2863	2991	2170	2293	2145	2263
ω_3(ref. 3)	—	—	2725	3054	—	—	—	—

[a]In this case the difference between the energies of the levels $v_2'' = 0$ and $v_2'' = 1$ is taken for the X^2A_1 ground state, while half of the energy difference between $v_2' = 3$ and $v_2' = 1$ of the excited A^2B_1 state is given as an alternative computation.

TABLE 5

(*a*) Calculated Franck–Condon factors for the symmetric stretching modes in the X^2A_1–A^2B_1 transition[a,b]

		$v_1' = 0$	$v_1' = 1$	$v_1' = 2$	$v_1' = 3$
$^{10}BH_2$	$v_1'' = 0$	0.9990	8.1–4	2.2–4	4.6–6
	1	8.2–4	0.9983	4.7–4	7.8–5
	2	2.0–4	5.1–4	0.9938	4.9–3
$^{11}BH_2$	$v_1'' = 0$	0.9995	2.8–4	1.8–4	3.4–6
	1	2.9–4	0.9993	3.4–5	4.1–5
	2	1.8–4	3.7–5	0.9958	3.2–3
$^{10}BD_2$	$v_1'' = 0$	0.9704	2.8–2	1.8–3	6.8–5
	1	2.9–2	0.9254	4.2–2	4.5–3
	2	3.9–5	4.8–2	0.8913	5.2–2
$^{11}BD_2$	$v_1'' = 0$	0.9771	2.1–2	1.4–3	4.0–5
	1	2.3–2	0.9419	3.2–2	3.4–3
	2	8.6–5	3.6–2	0.9183	3.9–2

[a]The reduced masses employed are μ(X) = 1.9576, μ(A) = 2.0157 for $^{10}BH_2$, μ(X) = 1.9620, μ(A) = 2.01565 for $^{11}BH_2$, μ(X) = 3.82947, μ(A) = 4.0282 for $^{10}BD_2$ and μ(X) = 3.84268 and μ(A) = 4.0282 for $^{11}BD_2$.
[b]The notation *n.m-a* stands for *n.m.* × 10^{-a}.

(*b*) Calculated Franck–Condon factors for the asymmetric stretching modes in the X^2A_1–A^2B_1 transition[a]

		$v_3' = 0$	$v_3' = 1$	$v_3' = 2$	$v_3' = 3$	$v_3' = 4$	$v_3' = 5$
$^{11}BH_2$	$v_3'' = 0$	0.9998	0	2.4–4	0	4.9–7	0
	1	0	0.9993	0	7.3–4	0	2.0–6
	2	2.4–4	0	0.9983	0	1.4–3	0
$^{11}BD_2$	$v_3'' = 0$	0.9996	0	3.6–4	0	7.6–7	0
	1	0	0.9989	0	1.1–3	0	3.5–6
	2	3.6–4	0	0.9974	0	2.2–3	0

[a]The reduced masses employed are μ(X) = 1.7503, μ(A) = 1.7037 for $^{11}BH_2$ and μ(X) = 3.09156 and μ(A) = 2.94914 for $^{11}BD_2$.

The calculated stretching frequencies are in reasonable accord with corresponding results from previous theoretical treatments (3). There are no experimental data available so far and this fact is quite understandable from the data in Table 5*a*, *b*, which show that the O—O stretching transitions are by far the most intense while excitation to $v_1' = 1$ is roughly 100 times less likely in $^{11}BD_2$ and almost 10^4 times weaker in $^{11}BH_2$.

The calculated vibrational levels are given in Fig.

Can. J. Chem. Downloaded from www.nrcresearchpress.com by 210.87.254.5 on 09/06/12
For personal use only.

Can. J. Chem. Downloaded from www.nrcresearchpress.com by 210.87.254.5 on 09/06/12
For personal use only.

3 for the rotational species $K = 0$ and $K = 1$ together with the expected intensity pattern. In this case the Franck–Condon factors $|\langle\psi_{v''}|\psi_{v'}\rangle|^2$ alone are not representative for the intensity distribution because the electronic transition moment $\boldsymbol{R}_{e'e''}$ changes drastically over the range in which the nuclear motion occurs, as seen in Fig. 2. Hence the entire integral

$$R_{e'v'e''v''} = \langle\psi_{v''}|R_{e'e''}(\rho)|\psi_{v'}\rangle$$

must be evaluated whereby for $\boldsymbol{R}_{e'e''}(\alpha)$ a polynomial fit in powers of the internuclear angle α is employed.[2] A large progression in the bending mode is apparent from these calculations, as must be expected qualitatively on the basis of the considerable difference in the internuclear angles of the X^2A_1 and $^2B_1$ electronic states.

The calculated ground state frequency of $\omega_e'' = 1057\ \text{cm}^{-1}$ is in very good accord with the measured value of $1030\ \text{cm}^{-1}$ (Table 4). The frequency of the excited state $\omega_2' = 954.65\ \text{cm}^{-1}$ has been obtained experimentally (1) via an extrapolation with the formula,

$$[1]\quad G(v_2') = \omega_2'(v_2' + 1) + x_{22}'(v_2' + 1)^2 + T_{00}$$

as will be discussed in the next section. In this connection it is important to point out that the lowest vibrational level in the two-dimensional harmonic oscillator treatment is $v_2' = 1$ in this notation, and thus the corresponding zero-point vibrational energy is not $\frac{1}{2}\omega_2'$, as in the more common one-dimensional stretching treatment, but rather $G(v_2' = 1) = 2\omega_2'$. The present calculations (Fig. 3) place $G(v_2' = 1)$ at $1935\ \text{cm}^{-1}$ and hence lead to a value for ω_2' of $967.5\ \text{cm}^{-1}$, which should be compared directly with the experimental finding of $954\ \text{cm}^{-1}$, also given in Table 4. Alternatively ω_2' can be defined as one-half of the $v_2'(1 \rightarrow 3)$ transition energy, which in the present calculations is $978\ \text{cm}^{-1}$, also in good agreement with what is inferred experimentally.

The calculated levels for states with $K > 2$ are given graphically in Fig. 4*a* and 4*b* for $^{11}BH_2$ and $^{11}BD_2$ respectively. For $^{11}BH_2$ the calculated $\Pi(K'' = 1)$, $\Delta(K'' = 2)$, $\Gamma(K'' = 3)$, and $\Phi(K'' = 4)$ levels of $v_2'' = 0$ lie higher by 34, 160, 363, and $632\ \text{cm}^{-1}$ respectively than the $K'' = 0$ energy, while the lowest levels in the excited electronic state are

[2]Since only transitions corresponding to $\Delta K = \pm 1$ are allowed the correct treatment would require the ($v_2'' = 0$, $K'' = 1$) and (v_2', $K' = 0$) functions in the evaluation of the integral for transitions to upper state levels. In the present case the radial dependance of the $K'' = 1$ and $K'' = 0$ functions is assumed to be quite similar, however, and the ground state radial function for ($v_2'' = 0$, $K'' = 0$) is employed exclusively in obtaining the intensity distributions shown in Fig. 2.

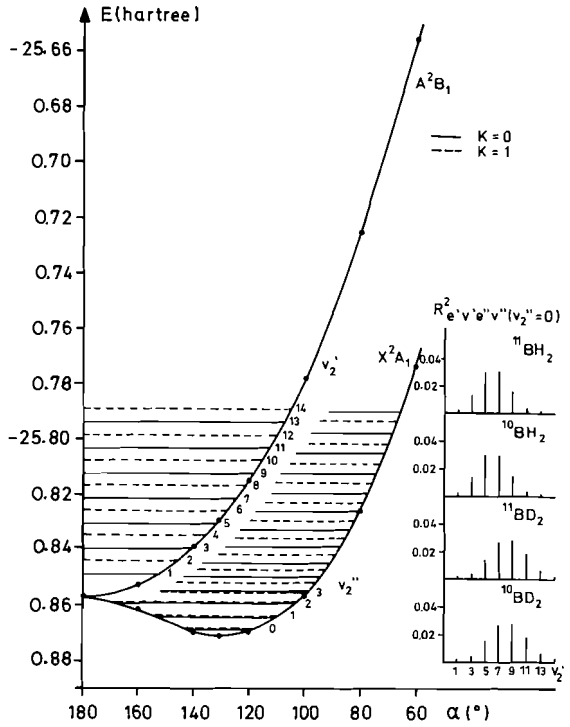

FIG. 3. Calculated bending vibrational levels and intensity distributions for the A^2B_1–X^2A_1 electronic transition of BH_2 obtained in the CI treatment without *f* functions.

above the A^2B_1 minimum by 1935 ($K' = 0$), 2894 ($K' = 1$), 3698 ($K' = 2$), 4936 ($K' = 3$), and $5701\ \text{cm}^{-1}$ ($K' = 4$).

C. *Comparison with Experiment and Revised Vibrational Assignment*

Herzberg and Johns (1) were able to fit their three measured Σ^- bands at $\bar{\nu} = 11\,767.3\ \text{cm}^{-1}$, $13\,640.6\ \text{cm}^{-1}$, and $15\,505.9\ \text{cm}^{-1}$ for $^{11}BH_2$ (Table 5 in ref. 1) in the form of eq. [1], whereby the numbering $v_2' = 7, 9, 11$ leads to $\omega_2' = 954.65\ \text{cm}^{-1}$, $x_{22} = -1.00\ \text{cm}^{-1}$, and $T_{00} = 4194.1\ \text{cm}^{-1}$. These authors prefer the above assignment even though they point out that it implies that ω_1' or ω_3', or both, are appreciably larger in the upper than in the lower state. According to Fig. 1*a*, *b* this increase in frequency is *not* to be expected, and Table 4 shows explicitly that these frequencies are not very different in the ground and excited states. In their original assignment (1) the first upper bending level ($v_2' = 1$) would then lie at $6099.4\ \text{cm}^{-1}$ above the X^2A_1 ($v_2'' = 0$) ground state energy, in considerable discrepancy (i.e. much higher) with the values calculated in the present work (Fig. 4*a*). The electronic energy difference, assuming the harmonic approximation, would then amount to

$$T_e = T_{00} + \tfrac{1}{2}\omega_2'' = 4194.1 + 515 = 4709\ \text{cm}^{-1}$$

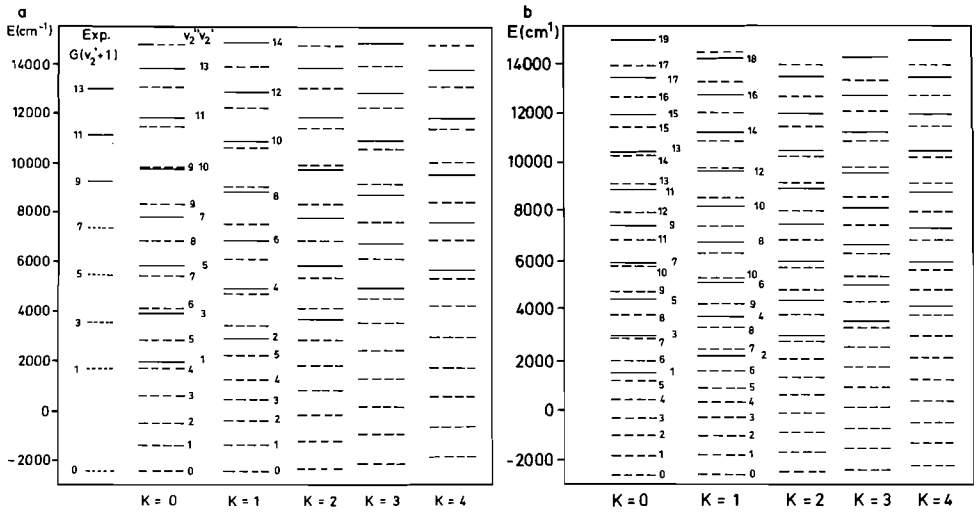

FIG. 4. Computed bending vibrational levels in the CI treatment without f functions for various values of the rotational quantum number K in the X^2A_1 ground (dashed lines, v_2'') and A^2B_1 excited (solid lines, v_2') electronic states of the (*a*) $^{11}BH_2$ and (*b*) $^{11}BD_2$ isotopes; because of the Renner–Teller coupling the distinction between ground and excited levels respectively is only clearly drawn for the $K = 0$ (Σ) levels, and hence in all other cases this designation is based on the identity of the dominant electronic component in each instance. For $^{11}BH_2$ comparison is made with the experimental results of Herzberg and Johns (1) for the Σ levels based on eq. [1] with a T_{00} value of 2285 cm^{-1} (solid lines observed, dashed lines computed from eq. [1]). The zero of energy corresponds to the location of the linear nuclear conformation of this system. Note that inclusion of f functions lowers the A^2B_1 energy results by 350 cm^{-1} relative to those of X^2A_1.

also in large disagreement with the results of all previous theoretical treatments (Table 2).[3]

If the alternative numbering for the observed lines, namely $v_2' = 9, 11, 13$ is chosen instead, i.e. an assignment which is less preferred by Herzberg and Johns (1) because it would be in apparent contradiction to their interpretation of the ^{10}B–^{11}B isotope shifts, the T_{00} value in the extrapolation formula would be 2285 cm^{-1} (1). This value, on the other hand, taken together with $\frac{1}{2}\omega_2''$ leads to $T_e = 2285 + 515 = 2800\ cm^{-1}$, again under the assumption of harmonic approximations in upper and lower states (and the same frequencies for the stretching motion), is in quite good agreement with the theoretical values for T_e given in Table 2. This fact has not been pointed out in the earlier theoretical papers (2, 3), since both sets of authors employed an incorrect definition of the T_{00} parameter in their arguments, and furthermore employed the "$\frac{1}{2}\omega$"-formula for the zero-point energy of all modes in going from T_e to the lowest possible 0–0 transition (3).

Comparison with the theoretical work thus definitely speaks in favor of the assignment $v_2' = 9, 11, 13$ for the observed bands. A direct calculation of these levels according to the Herzberg formula[4] (1) yields the levels also given in Fig. 4*a*, and the agreement between calculated and experimentally extrapolated and measured levels is excellent, especially when it is realized that the energies of the calculated levels are shifted downward by 300–400 cm^{-1} upon inclusion of f functions in the theoretical treatment (Table 2). The actual values obtained in the best theoretical treatment for the transition energies to the first three levels of the $^2B_1$ upper state agree to within 50–100 cm^{-1} with the corresponding extrapolated results obtained by fitting the experimental data according to eq. [1] when the observed bands are assigned as $v_2' = 9$, 11, and 13 (Table 6). In addition the results for higher K' values are also in good agreement with one another once this experimental interpretation is taken.

Finally, it remains to show that the results of the isotope shifts are also consistent with the revised assignment. In Fig. 5 the isotope shift for the calculated $^{10}BH_2$ and $^{11}BH_2$ lines are plotted as a function of the wavenumbers of the $^{11}BH_2$ bands. It is seen that the slope is not 0.0077 as assumed in the original work (1), i.e. by neglecting anharmonicity

[3]Note that according to eq. [1], T_{00} is the energy difference between the (0,0,0) level of the X^2A_1 state and the potential minimum ($v_2' = -1$) of A^2B_1).

[4]The new fitting with $v_2' = 9, 11, 13$ yields slightly different constants, namely $\omega_2' = 957.5\ cm^{-1}$, $x_{22} = -0.96\ cm^{-1}$, and $T_{00} = 2288\ cm^{-1}$.

Can. J. Chem. Downloaded from www.nrcresearchpress.com by 210.87.254.5 on 09/06/12
For personal use only.

TABLE 6. Comparison of the lowest calculated A^2B_1–X^2A_1 transition energies with those obtained by formula (1) from the experimental spectrum using $T_{00} = 2285\ cm^{-1}$, i.e. the alternative value for this quantity and not 4194.1 cm^{-1} as originally preferred in ref. 1

Lower state X^2A_1	($v_2'' = 0$, $K'' = 1$)	Correction for zero-point energy of ω_1 and ω_3	Correction for f-function basis augmentation	Present best calculated value	$G(v_2')$ eq. [1]
$A^2B_1(v_2' = 1, K = 0)$	4394	+101	−350	4145	4190
$A^2B_1(v_2' = 3, K = 0)$	6351	+101	−350	6102	6088
$A^2B_1(v_2' = 5, K = 0)$	8317	+101	−350	8068	7977

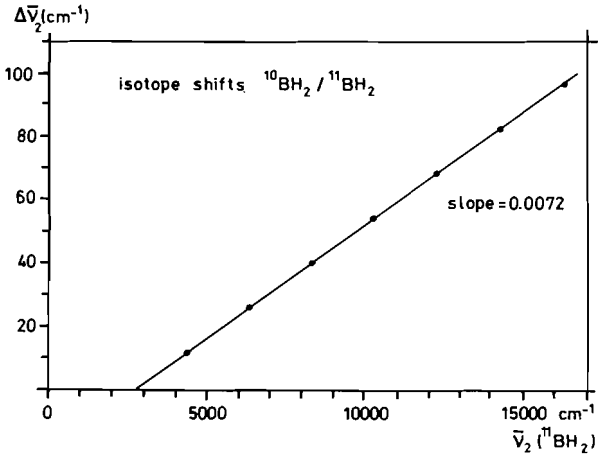

FIG. 5. Calculated $^{10}BH_2/^{11}BH_2$ isotope shifts for corresponding bending vibrational species in the A^2B_1–X^2A_1 band system plotted as a function of the $^{11}BH_2$ frequency $\bar{\nu}_2$.

effects entirely, but rather 0.0072. The latter slope can also be realistically employed to fit the measured three points, whereby a crossing of the abscissa is thereby not found around 4500 cm^{-1} as found originally, but rather below 3000 cm^{-1}, i.e. consistent with the alternative experimental choice for the value of T_{00} as 2285 cm^{-1}.[5]

In summary, then, when the above arguments are taken into account it is found that there is excellent agreement between the present calculated and the experimental structural data of BH_2 in its two lowest electronic states. The frequencies for the two stretching modes in both states have been calculated as well and are expected to constitute good predictions, awaiting experimental verification. Furthermore there is a very good correspondence in the calculated and measured energy levels in the bending progression of the A^2B_1–X^2A_1 transition and very good agreement is obtained between the lowest accessible excitation $A^2B_1(010)$–$X^2A_1(000)$ and the level extrapolated from three observed high-lying vibrational lines if they are assigned as $v_2' = 9$, 11, and 13 rather than 7, 9, and 11 as assumed originally. This reassignment, together with a correct interpretation of the T_{00} value employed in the literature as the energy difference between the lowest $v_2'' = 0$ level and the *potential minimum* of the upper state, also brings previous theoretical results in good agreement with the experimental inferences on this point, so that each of the apparent discrepancies between the experimental and theoretical description of the lowest-energy electronic transition in the BH_2 spectrum would appear to have been removed as a result of the present investigation.

[5]The intensity distribution calculated for the BH_2 isotopes (Fig. 3) indicate maxima for $v_2' = 5$ and 7, thus perhaps raising an additional argument against the $v_2' = 9$, 11, 13 assignment for the observed bands of Herzberg and Johns. It is not clear why lower energy bands were not actually seen, however, i.e. whether because of intrinsic weakness of such transitions or rather because of apparatus insensitivity in the wavelength region above 8700 Å (1), and thus in reality it is not possible to make comparison between the calculated and measured intensity distributions.

Acknowledgements

The authors wish to thank Dr. R. Marian-Runau for his assistance in carrying out some of the calculations discussed in this paper. One of us (M.P.) expresses his gratitude to the Deutsche Forschungsgemeinschaft for financial support extended during the course of this work. The services and computer time made available by the University of Bonn Computing Center (RHRZ) are also hereby gratefully acknowledged.

1. G. HERZBERG and J. W. C. JOHNS. Proc. R. Soc. A, **298**, 142 (1967).
2. C. F. BENDER and H. F. SCHAEFER III. J. Mol. Spectrom. **37**, 423 (1971).
3. V. STAEMMLER and M. JUNGEN. Chem. Phys. Lett. **16**, 187 (1972).
4. R. D. BROWN and G. R. WILLIAMS. Mol. Phys. **25**, 673 (1973).
5. G. R. WILLIAMS and W. H. HENNEKER. Mol. Phys. **27**, 1463 (1974).
6. J. D. DILL, P. R. SCHLEYER, and J. A. POPLE. J. Am. Chem. Soc. **97**, 3402 (1975).
7. M. PERIĆ, R. J. BUENKER, and S. D. PEYERIMHOFF. Can. J. Chem. **57**, 2491 (1979).
8. P. J. BRUNA, G. HIRSCH, M. PERIĆ, S. D. PEYERIMHOFF, and R. J. BUENKER. Mol. Phys. **40**, 521 (1980).

Can. J. Chem. Downloaded from www.nrcresearchpress.com by 210.87.254.5 on 09/06/12
For personal use only.

9. M. PERIĆ, R. J. BUENKER, S. D. PEYERIMHOFF, and R. MARIAN-RUNAU. To be published.
10. T. H. DUNNING JR. J. Chem. Phys. **53**, 2823 (1970).
11. S. D. PEYERIMHOFF, R. J. BUENKER, and L. C. ALLEN. J. Chem. Phys. **45**, 734 (1966).
12. R. J. BUENKER and S. D. PEYERIMHOFF. Theor. Chim. Acta, **39**, 217 (1975); **35**, 33 (1974).
13. R. J. BUENKER, S. D. PEYERIMHOFF, and W. BUTSCHER. Mol. Phys. **35**, 771 (1978).
14. P. J. BRUNA, S. D. PEYERIMHOFF, and R. J. BUENKER. Chem. Phys. Lett. **72**, 278 (1980).
15. R. J. BUENKER, S. D. PEYERIMHOFF, and P. J. BRUNA. NATO ASI Series Proceedings ASI Menton 1980.
16. J. T. HOUGEN, P. R. BUNKER, and W. C. JOHNS. J. Mol. Spectrom. **34**, 136 (1970).
17. K. F. FREED and J. R. LOMBARDI. J. Chem. Phys. **45**, 591 (1966).
18. M. PERIĆ, R. RUNAU, J. RÖMELT, S. D. PEYERIMHOFF, and R. J. BUENKER. J. Mol. Spectrom. **78**, 309 (1979).
19. Results of these laboratories, to be published.
20. W. R. THORSON and I. NAKAGAVA. J. Chem. Phys. **24**, 1119 (1956).
21. T. BARROW, R. N. DIXON, and G. DUXBURY. Mol. Phys. **27**, 1217 (1974).
22. M. PERIĆ. Mol. Phys. In press.
23. R. J. BUENKER. Gazetta Chim. Ital. **108**, 245 (1978).
24. G. HIRSCH, P. J. BRUNA, R. J. BUENKER, and S. D. PEYERIMHOFF. Chem. Phys. **45**, 335 (1980).
25. R. N. DIXON. Mol. Phys. **9**, 357 (1965).
26. M. PERIĆ and J. RADIĆ-PERIĆ. Chem. Phys. Lett. **67**, 138 (1979).

Can. J. Chem. Downloaded from www.nrcresearchpress.com by 210.87.254.5 on 09/06/12
For personal use only.

^{13}C nuclear magnetic resonance spectra of 23-hydroxy spirostane sapogenins of *Solanum hispidum*[1]

AJIT K. CHAKRAVARTY AND SATYESH C. PAKRASHI
Indian Institute of Experimental Medicine, Calcutta-700032, India
AND
JUN UZAWA
Institute of Physical and Chemical Research, Saitama, 351, Japan

Received August 13, 1980

AJIT K. CHAKRAVARTY, SATYESH C. PAKRASHI, and JUN UZAWA. Can. J. Chem. **59**, 1328 (1981).

The ^{13}C nmr spectra of some 23-hydroxy spirostane sapogenins from *Solanum hispidum* Pers., mostly as their acetates, have been studied. The effect of different orientations of the substituents at C-23 and C-25 as well as that due to change in the stereochemistry at C-22 have been discussed. The unexpected absence of the γ_g effect of the axial 23-OH on C-25 in hispigenin (**5**), a 22β*O*-spirostane derivative, presumably results from ring F deformation brought about by the steric interaction between 20-Me and 23-OH groups.

AJIT K. CHAKRAVARTY, SATYESH C. PAKRASHI et JUN UZAWA. Can. J. Chem. **59**, 1328 (1981).

On a étudié principalement sous forme d'acétates, les spectres rmn du ^{13}C de quelques sapogénines hydroxy-23 spirostanes provenant du *Solanum hispidum* Pers. On discute des effets des différentes orientations des substituants en C-23 et C-25 ainsi que de ceux provenant du changement de la stéréochimie en C-22. L'absence inattendue d'effet γ_g du OH-23 axial sur le C-25 de l'hispigénine (**5**), un dérivé 22β*O* spirostane, provient probablement de la déformation du cycle F provoquée par l'interaction stérique entre les groupes Me et OH présents respectivement en positions 20 et 23.

[Traduit par le journal]

Introduction

We have recently isolated and characterized (1, 2) five spirostane sapogenins, namely, neochlorogenin (**1**), paniculogenin (**2**), solaspigenin (**3**), neosolaspigenin (**4**), and hispigenin (**5**), from the leaves of *Solanum hispidum* Pers. Except for **1**, all the others are 23-hydroxy derivatives differing in the stereochemistry at one or more chiral centres in ring F. Furthermore, hispigenin (**5**) is the first 22β*O*-spirostane sapogenin encountered in nature.

Though the ^{13}C nmr spectra of a number of typical spirostane derivatives have been reported (3), no compound hydroxylated in ring F, except (25*S*)-5α-spirostane-25-ol, has so far been studied. It was, therefore, considered desirable to investigate the ^{13}C nmr spectra of the 23-hydroxy spirostane derivatives (**2–5**), particularly to ascertain the effect of different orientations of 23-OH and 25-Me groups as well as that due to change in stereochemistry at C-22 (as in **5**) on the chemical shifts of D, E, and F ring carbons.

Experimental

The isolation and characterization of the sapogenins and the preparation of their acetates have already been reported (1, 2). In view of the poor solubility of most of the sapogenins themselves, the spectra of the corresponding acetates, **1***a*–**5***a*, were studied.

The ^{13}C nmr spectra of the acetates were recorded in a Jeol FX-100 FT spectrometer at 25.05 MHz in $CDCl_3$ solutions at 25°C with autostacking programme. The conditions for FT measurements were as follows: spectral width, 5 KHz; data points 8K; repetition time, 0.9 or 1.2 s; flip angle, 45–60°. The spectra of paniculogenin (**2**) and hispigenin (**5**) were recorded in CD_3OD solutions in a Bruker instrument at 67.89 MHz. The chemical shifts are expressed on the δ scale from TMS as internal standard.

The methyl, methylene, and methine carbons were assigned on the basis of the multiplicities in the gated decoupled spectra. The quaternary carbon signals were identified on the basis of low-power noise-modulated decoupled spectra. Unambiguous assignment of the methyl carbon signals, particularly of 13-Me, 20-Me, and 25-Me, was done by selective proton decoupling.

Results and Discussion

The ^{13}C chemical shift data are given in Table 1. The assignments of the individual chemical shift values to specific carbons were based on the reported values for spirostane sapogenins (3), cholestanols and their acetates (4), and 3β,6α-dihydroxy cholestane (5–7).

The results showed consistent chemical shifts for the carbons of rings A, B, and C of all the acetates (**1***a*–**5***a*) as expected. Now, the chemical shifts of D, E, and F ring carbons of **1***a*, lacking the 23-substituent, were found to be in excellent agreement with the values reported (3) for a (25*S*)-spirostane, viz. sarsasapogenin. Taking **1***a* as the model, the chemical shifts for compounds **2***a*–**5***a*, however, showed significant variation with regard to D, E, and F ring carbons due to substitution at

[1]Part 62 in the series Studies on Indian Medicinal Plants. For Part 61, see S. C. Pakrashi, B. Achari, E. Ali, R. R. Sinha, and P. P. Ghosh Dastidar. Tetrahedron Lett. **21**, 2667 (1980).

0008-4042/81/091328-03$01.00/0
©1981 National Research Council of Canada/Conseil national de recherches du Canada

Can. J. Chem. Downloaded from www.nrcresearchpress.com by 210.87.254.105 on 09/06/12
For personal use only.

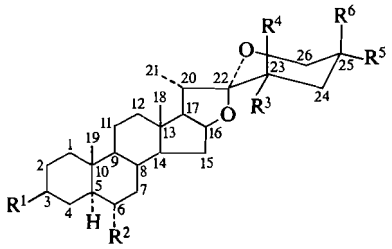

1, $R^1 = R^2 = OH$, $R^3 = R^4 = R^5 = H$, $R^6 = Me$
1*a*, $R^1 = R^2 = OAc$, $R^3 = R^4 = R^5 = H$, $R^6 = Me$
2, $R^1 = R^2 = R^3 = OH$, $R^4 = R^5 = H$, $R^6 = Me$
2*a*, $R^1 = R^2 = R^3 = OAc$, $R^4 = R^5 = H$, $R^6 = Me$
3, $R^1 = R^2 = R^4 = OH$, $R^3 = R^6 = H$, $R^5 = Me$
3*a*, $R^1 = R^2 = R^4 = OAc$, $R^3 = R^6 = H$, $R^5 = Me$
4, $R^1 = R^2 = R^4 = OH$, $R^3 = R^5 = H$, $R^6 = Me$
4*a*, $R^1 = R^2 = R^4 = OAc$, $R^3 = R^5 = H$, $R^6 = Me$

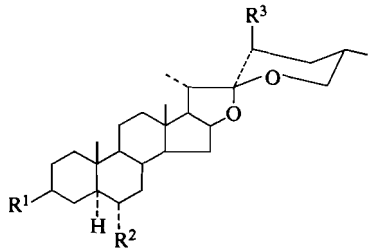

5, $R^1 = R^2 = R^3 = OH$
5*a*, $R^1 = R^2 = R^3 = OAc$

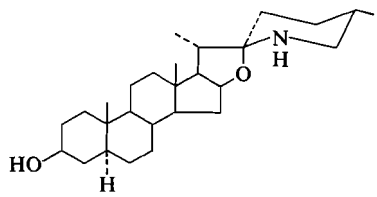

6

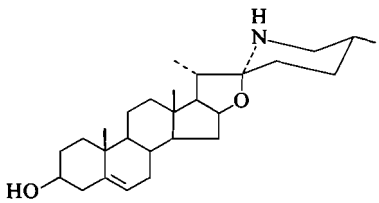

7

C-23 as well as the difference in stereochemistry at C-22, C-23, and C-25.

Thus, the equatorial 23-OAc of **2***a* exerted a γ_g effect on C-20 by 5.7 ppm. The observed deshielding of C-25 and C-27 by 3.7 and 1.2 ppm respectively in **2***a* may be ascribed to an antiperiplanar γ effect (4, 8) and the δ_2 effect (4) of equatorial 23-OAc, which also exerted an expected shielding δ_5 effect (4) on C-26 by 1 ppm. The comparatively larger deshielding (5.3 ppm) of C-25 in the alcohol **2** (spectrum measured in CD_3OD) may partly be due to the solvent effect.

On the other hand, the axial 23-OAc (as in **3***a*, **4***a*, and **5***a*) exhibited a deshielding δ_1 effect (4) on the 20-Me carbon by 1.6–1.8 ppm indicating a *skew*-pentane type interaction between the two functions. A very strong δ_1 effect (3.3 ppm) was also observed in respect of axial 25-Me carbon in **4***a* due to its *syn*-1,3-diaxial interaction with the axial 23-OAc group. The latter also caused an upfield displacement of the C-25 signal of **3***a* by 5.5 ppm due to the γ_g effect as evidenced (3) from the chemical shift (δ 30.3 ppm) of the corresponding carbon in tigogenin, a (25*R*)-23-unsubstituted spirostane sapogenin.

Contrary to expectation, however, the axial 23-OAc group of **5***a* did not apparently exert any γ_g effect on C-25. The ^{13}C nmr spectrum (Table 1) of the corresponding alcohol **5** in CD_3OD also showed similar abnormality. Although the reason for this anomaly is not very clear, a plausible explanation may be put forward as follows.

Though the ^{13}C nmr data of 23-deacetoxy-22β*O*-spirostane is not available for rationalizing the chemical shifts of D, E, and F ring carbons of **5***a*, analogy could be drawn from its 22β*N*-analogue, tomatidine (**6**). The 20-Me in the latter has been shown (9) to interact strongly with 23-methylene hydrogens since the signal of C-23 suffers an upfield shift by 7.5 ppm compared to that of the corresponding carbon of the 22α*N*-analogue, solasodine (**7**). The same type of interaction would also be expected in 23-unsubstituted 22β*O*-spirostanes. Now, introduction of an axial 23-OAc therein is likely to produce a severe *skew*-pentane type interaction with 20-Me. This interaction, however, might partially be relieved by the preferred inward bending of the 23-OAc function with concomitant outward bending of the axial 25-H, leading to such a deformation (4) of ring F as to virtually annul the γ_g effect of 23-OAc on C-25.

The assumed geometrical deformation of ring F in **5***a* received further support from the observed significant downfield shift of the signals for C-15 (1.7 ppm), C-16 (2.5 ppm), C-20 (2.0 ppm), C-22 (3.3 ppm), C-23 (0.7 ppm), C-25 (5.4 ppm), and C-26

Can. J. Chem. Downloaded from www.nrcresearchpress.com by 210.87.254.105 on 09/06/12
For personal use only.

Can. J. Chem. Downloaded from www.nrcresearchpress.com by 210.87.254.105 on 09/06/12
For personal use only.

TABLE 1. ^{13}C Chemical shifts[a]

Carbon No.	1*a*	2*a*	3*a*	4*a*	5*a*	2	5
1	36.8	36.8	36.8	36.8	36.8	38.6	38.6
2	27.1	27.1	27.1	27.1	27.1	31.7	31.7
3	73.0	72.9	73.0	73.0	72.9	72.0	72.1
4	28.4	28.4	28.4	28.4	28.3	33.0	33.0
5	48.5	48.5	48.5	48.5	48.5	52.9	53.0
6	72.0	71.9	72.0	72.0	71.9	70.0	70.1
7	37.8	37.7	37.7	37.7	37.8	42.8	42.8
8	33.7	33.8	33.8	33.8	33.6	35.2	35.2
9	53.6	53.5	53.6	53.6	53.7	55.3	55.4
10	36.6	36.6	36.6	36.6	36.6	37.4	37.5
11	20.9	20.8	20.8	20.8	20.9	22.1	22.2
12	39.8	39.6	39.3	39.3	39.9	41.3	41.3
13	40.5	41.0	40.9	40.9	41.3	42.1	42.3
14	55.9	55.9	56.0	56.0	55.2	57.3	56.7
15	31.6	31.5	31.7	31.7	33.4	32.5	34.7
16	80.6	81.1	81.2	81.4	83.7	82.6	85.4
17	61.9	61.4	63.9	63.8	63.0	63.1	64.4
18	16.4	16.0	16.1	16.1	16.2	17.0	16.5
19	13.3	13.3	13.3	13.3	13.3	13.8	13.9
20	42.1	36.4	40.3	40.6	42.3	37.0	43.4
21	14.3	13.9	16.1	15.9	16.0	14.3	16.6
22	109.6	109.2	107.0	107.6	110.3	112.6	113.5
23	27.1	65.4	72.0	71.8	72.7	64.0	70.9
24	25.7	31.5	33.8	30.6	33.6	36.0	38.6
25	25.9	29.6	24.7	25.8	30.1	31.2	31.8
26	65.1	64.1	66.5	64.7	68.5	65.0	69.5
27	16.0	17.2	16.7	19.3	16.5	17.6	17.1
Acetyl Carbonyl	170.5	170.5	170.2	170.1	169.7		
Carbonyl Carbon	170.7	170.5	170.5	170.5	170.5		
Carbon		170.8	170.8	170.7	170.7		
Acetyl Methyl	21.2	21.2	21.2	21.3	21.3		
Methyl Carbon	21.4	21.3	21.2	21.3	21.3		
Carbon		21.4	21.2	21.3	21.3		

[a]Measured in $CDCl_3$ solutions except for **2** and **5** for which CD_3OD was used as solvent.

(2.0 ppm) compared to those of the corresponding carbons in **3***a* which is enantiomeric with **5***a* at C-22.

Regarding the α-substitution effect on introduction of an acetoxyl/hydroxyl substituent at C-23, a general trend of downfield chemical shift of the carbinyl carbon in compounds with axial substituent as against the equatorial one has been observed. This may be due to a *skew*-pentane interaction existing in the axial isomer in analogy with some 10-methyl-*trans*-decalols (6) even though the two systems are not readily comparable.

Finally, besides the effects discussed above, the upfield shift of C-22, a β-carbon, and C-20, as well as a downfield displacement of C-17 signals by ca. 2 ppm compared to those for the corresponding 23-unsubstituted compounds, have been noted in 22α*O*-spirostanes with axial 23-OAc.

Acknowledgements

The authors are grateful to Bangalore NMR Facility, Bangalore, India, for the ^{13}C nmr spectra of **2** and **5**, and to Dr. M. Uramoto, Institute of Physical and Chemical Research, Saitama, Japan, for valuable discussion.

1. A. K. CHAKRAVARTY, T. K. DHAR, and S. C. PAKRASHI. Tetrahedron Lett. 3875 (1978).
2. A. K. CHAKRAVARTY, T. K. DHAR, and S. C. PAKRASHI. Phytochemistry, **19**, 1249 (1980).
3. H. EGGERT and C. DJERASSI. Tetrahedron Lett. 3635 (1975).
4. H. EGGERT, C. L. VANANTWERP, N. S. BHACCA, and C. DJERASSI. J. Org. Chem. **41**, 71 (1976).
5. C. KONNO and H. HIKINO. Tetrahedron, **32**, 325 (1976).
6. S. H. GROVER and J. B. STOTHERS. Can. J. Chem. **52**, 870 (1974).
7. J. W. BLUNT and J. B. STOTHERS. Org. Magn. Reson. **9**, 439 (1977).
8. W. A. AYER, L. M. BROWNE, and S. FUNG. Org. Magn. Reson. **11**, 73 (1978).
9. R. J. WESTON, H. E. GOTTLIEB, E. W. HAGAMAN, and E. WENKERT. Aust. J. Chem. **30**, 917 (1977).

Synthesis and complexation of the novel tridentate anionic organogallate ligands, $[Me_2Ga(N_2C_5H_7)(OCH_2CH_2SR)]^-$ (R = Et or Ph)

KENNETH S. CHONG AND ALAN STORR

Department of Chemistry, University of British Columbia, 2036 Main Mall, Vancouver, B.C., Canada V6T 1Y6

Received November 4, 1980

KENNETH S. CHONG and ALAN STORR. Can. J. Chem. **59**, 1331 (1981).

The synthesis and complexation of the novel tridentate chelating anionic organogallate ligands $[Me_2Ga(N_2C_5H_7)(OCH_2CH_2SR)]^-$ (R = Et or Ph) have been investigated. A variety of octahedral molybdenum, tungsten, and manganese carbonyl compounds have been studied in which the organogallate ligand (R = Et) is in the *fac* coordination mode. In addition tetrahedral "Cu·PPh_3" and "Ni(NO)" complexes have been characterized which display fluxional behaviour in solution. The dearth of derivatives available using the ligand where R = Ph is attributed to steric factors.

KENNETH S. CHONG et ALAN STORR. Can J. Chem. **59**, 1331 (1981).

On a étudié la synthèse et la complexation du nouveau ligand organogallate anionique chélaté de façon tridentate $[Me_2Ga(N_2C_5H_7)(OCH_2CH_2SR)]^-$ (R = Et ou Ph). On a étudié divers composés carbonylés octaédriques du molybdène, du tungstène et du manganèse dans lesquels le ligand organogallate (R = Et) est coordonné de manière *fac*. De plus, on a caractérisé les complexes tétraédriques "Cu·PPh_3" et "Ni(NO)" qui exhibent un comportement fluxionnaire en solution. On attribue à des facteurs stériques le fait qu'il existe peu de dérivés incorporant le ligand ou R = Ph.

[Traduit par le journal]

Introduction

Anionic tridentate chelating organogallate ligands incorporating "ethanolamino" and "pyrazolyl" moieties have been the subject of a number of recent publications (1, and references therein). The many novel aspects displayed by compounds containing these ligands prompted us to extend our investigations into related systems in which the "$OCH_2CH_2NR_2$" (R = H or Me) moiety is replaced by the "OCH_2CH_2SR" (R = Et or Ph) grouping. This has led to tridentate chelating ligands of the type **1**,

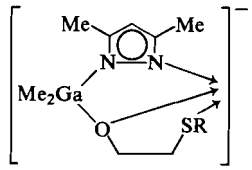

1

where R = Et or Ph, in which the three donor atoms NOS replace the NON donor atom set of the dimethylpyrazolylethanolaminogallate ligand systems (1). The new ligand where R = Et has been found to yield a wide variety of transition metal complexes but for the ligand where R = Ph the only compound fully characterized to date is the "$Mn(CO)_3$" derivative.

Experimental

Air-sensitive materials were handled in a glove box under an atmosphere of oxygen-free dry nitrogen, in a nitrogen-blanketed apparatus, or on a high-vacuum line. Tetrahydrofuran (THF) was dried by refluxing over Na/benzophenone and was used immediately following distillation. Benzene was dried by refluxing over molten potassium followed by distillation. Phenyl-2-hydroxyethyl sulphide, $HOCH_2CH_2SPh$ (2), and ethyl-2-hydroxyethyl sulphide, $HOCH_2CH_2SCH_2CH_3$, (3) were prepared by literature methods. Trimethyl gallium was prepared as described previously (4). Ni(NO)I was prepared by the method of Haymore and Feltham (5) and $Mn(CO)_5Br$ was prepared from $Mn_2(CO)_{10}$ (Strem) by a standard route (6). $(MeCN)_3M(CO)_3$ (M = Mo or W) compounds were prepared from the $M(CO)_6$ hexacarbonyls (Strem) by a literature method (7). $(C_7H_7)Mo(CO)_2I$ (6) and $(C_7H_7)W(CO)_2I$ (8) were prepared as described previously and Ph_3PCuBr was synthesized from Ph_3P and CuBr (9).

Ligand Syntheses, $Na^+[Me_2Ga(N_2C_5H_7)(OCH_2CH_2SR)]^-$ (R = Et or Ph)

Both ligands were prepared as standard THF solutions using the method established for the corresponding ligands incorporating "ethanolamino" moieties (10, 11). In the last stage of the ligand syntheses the appropriate sulphide in THF solution was added to a THF solution of $Na^+[Me_3Ga(N_2C_5H_7)]^-$ and the mixture refluxed until evolution of methane ceased (~24 h):

$$Na^+[Me_3Ga(N_2C_5H_7)]^- + HOCH_2CH_2SR \xrightarrow[\text{reflux}]{\text{THF}} Na^+[Me_2Ga(N_2C_5H_7)(OCH_2CH_2SR)]^- + MeH$$

1

Preparation of $[Me_2Ga(N_2C_5H_7)(OCH_2CH_2SEt)]$"M" Complexes

In general the transition metal complexes listed in Tables 1 and 2 were prepared by adding a slight excess of the ligand **1** (where R = Et), in 25 mL THF to the appropriate transition metal precursor compounds (~2 mmol) in 25 mL of the same solvent (see Table 1). The mixture was then stirred at room temperature for a few hours. In the preparations of the Mo and W nitrosyl derivatives, an equimolar amount of diazald was

0008-4042/81/091331-11$01.00/0

©1981 National Research Council of Canada/Conseil national de recherches du Canada

Can. J. Chem. Downloaded from www.nrcresearchpress.com by 210.87.254.40 on 09/06/12
For personal use only.

Can. J. Chem. Downloaded from www.nrcresearchpress.com by 210.87.254.40 on 09/06/12
For personal use only.

TABLE 1. Analytical, ir, and preparative data for the 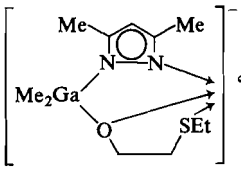 "M" complexes

"M"	Color	Yield (%)	ν_{CO} (ν_{NO}*) (cm^{-1}) Nujol	ν_{CO} (ν_{NO}*) (cm^{-1}) Cyclohexane	Calculated (%) C	Calculated (%) H	Calculated (%) N	Found (%) C	Found (%) H	Found (%) N	Transition metal precursor
$Mo(CO)_2(\eta^3\text{-}C_3H_5)$	Yellow–orange	60	1930 1834	1935 1850	39.0	5.5	5.7	38.8	5.5	5.7	$(MeCN)_3Mo(CO)_3$
$Mo(CO)_2(\eta^3\text{-}C_7H_7)$	Red–brown	50	1929 1920 1851 1834	1933 1857	44.2	5.3	5.2	44.1	5.3	5.1	$(C_7H_7)Mo(CO)_2I$
$Mo(CO)_2(NO)$	Orange	50	2015 1920 1650*	2025 1933 1668*	32.4	4.6	8.7	32.7	4.5	8.8	$(MeCN)_3Mo(CO)_3$
$W(CO)_2(\eta^3\text{-}C_7H_7)$	Red–brown	50	1923 1910 1837 1822	1927 1849	38.1	4.6	4.4	38.2	4.7	4.4	$(C_7H_7)W(CO)_2I$
$W(CO)_2(NO)$	Orange	50	1992 1897 1628*	2015 1912 1655*	27.4	3.9	7.4	27.2	3.7	7.1	$(MeCN)_3W(CO)_3$
$Mn(CO)_3$	Yellow	70	2022 1930 1900	2034 1941 1911	38.3	5.0	6.4	38.3	5.0	6.4	$Mn(CO)_5Br$
Ni(NO)	Dark blue	80	1777*	1785*	34.0	5.7	10.8	34.1	5.5	10.7	Ni(NO)I
$Cu(PPh_3)$	White	80	—	—	55.7	5.9	4.5	56.0	5.7	4.6	$Ph_3P\cdot CuBr$

Can. J. Chem. Downloaded from www.nrcresearchpress.com by 210.87.254.40 on 09/06/12
For personal use only.

TABLE 2. ^{1}H nmr data for 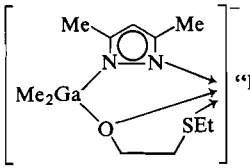 "M" complexes in C_6D_6 solution*

"M"	τ (ppm)							
	^{4}H	pz—Me	S—CH_2—*Me*	Ga—Me	O—*CH_2*—CH_2S	O—CH_2—*CH_2*S	S—*CH_2*—Me	Other
$Mo(CO)_2(\eta^3\text{-}C_3H_5)$	4.34s	7.63s, 8.03s	8.90t†	9.95s, 10.37s				H_{unique} 5.90tt (J = 10, 7 Hz)
								"allyl" H_{anti} 8.31d, 8.68d (J = 10 Hz)
								H_{syn} 6.23dd, 7.10dd (J = 7, 3 Hz)
$Mo(CO)_2(\eta^3\text{-}C_7H_7)$	4.25s	7.43s, 7.99s	9.09t†	10.00s, 10.31s	6.11dd, 6.61td	8.25td, 8.76dd	7.20m, 7.69m	C_7H_7 4.75s(br)
$Mo(CO)_2(NO)$	4.25s	7.49s, 8.00s	9.18t†	9.90s, 10.26s				Ratio of isomers 5
	4.45s	7.80s, 8.07s	9.10t†	9.78s, 10.24s				Ratio of isomers 1
$W(CO)_2(\eta^3\text{-}C_7H_7)$	4.31s	7.47s, 8.05s	9.13t†	10.03s, 10.37s	6.00dd, 6.68td	8.28td, 8.90dd	7.05m, 7.55m	C_7H_7 4.95s(br)
$W(CO)_2(NO)$	4.29s	7.48s, 8.05s	9.18t†	9.89s, 10.33s				Ratio of isomers 5
	4.50s	7.79s, 8.14s	9.12t†	9.75s, 10.29s				Ratio of isomers 1
$Mn(CO)_3$	4.24s	7.55s, 7.97s	9.19t†	9.71s, 10.29s				
Ni(NO)	3.98s	7.15s, 7.90s	9.17t†	9.86s	6.47t‡	8.42t‡	7.98q†	
$Cu(PPh_3)$	4.04s	7.68s, 7.80s	9.27t†	9.96s	6.13t‡	7.63t‡	8.07q†	Ph 2.39m, 2.97m

*$\tau_{C_6H_6}$ = 2.84 ppm; s = singlet; d = doublet; t = triplet; q = quartet; m = multiplet; tt = triplet of triplets; dd = doublet of doublets; td = triplet of doublets; br = broad.
†J = 7.5 Hz.
‡J = 5.5 Hz.

Can. J. Chem. Downloaded from www.nrcresearchpress.com by 210.87.254.40 on 09/06/12
For personal use only.

added at this point and stirring continued for a further hour. In the preparation of the "$(\eta^3$-$C_3H_5)$Mo" complex, a slight excess of allyl bromide was added in the second stage of the reaction sequence and the resulting mixture stirred for ~30 min at room temperature. In all cases, at the completion of the synthesis, the THF solvent was removed under vacuo and the resulting residue extracted with benzene. The filtered extracts were then left to evaporate slowly and yielded pure crystalline products. Elemental analysis results together with ν_{CO} and ν_{NO} stretching frequencies are listed in Table 1 for all the complexes prepared.

Preparation of $[Me_2Ga(N_2C_5H_7)(OCH_2CH_2SPh)]Mn(CO)_3$

$Mn(CO)_5Br$ (0.60 g; 2.2 mmol) in THF solution was added to 20 mL of ligand (**1**, where R = Ph) solution (2.2 mmol) and the reaction mixture stirred for 2 h. The solvent was then removed under vacuum and the solid remaining extracted with benzene. The filtered extracts yielded yellow–orange crystals of the desired product on slow evaporation of the solvent. *Anal.* calcd. for $[Me_2Ga(N_2C_5H_7)(OCH_2CH_2SPh)]Mn(CO)_3$: C 44.4, H 4.5, N 5.8; found: C 44.3, H 4.5, N 5.8. ^{1}H nmr (C_6D_6 solution): τ = 10.26s, 9.72s ($GaMe_2$); 7.93s, 7.52s (pz—Me) 4.18s (pz—H(4)). ($\tau_{C_6H_6}$ = 2.84 ppm; s = singlet; pz = pyrazolyl.) Infrared spectra: ν_{CO} (cm^{-1}) 2036, 1947, 1916 (cyclohexane); 2026, 1916 br (Nujol) (br = broad).

Spectra

Mass spectra were recorded on a Varian MAT CH4 mass spectrometer at 70 eV with a source temperature of 120–200°C. Infrared spectra were recorded on a Perkin-Elmer 457 spectrophotometer and ^{1}H nmr spectra on a Varian XL-100 spectrometer using FT techniques.

Results and Discussion

Analysis of mass spectral, ir, and ^{1}H nmr data for the complexes listed in Table 1, and also for the compound $[Me_2Ga(N_2C_5H_7)(OCH_2CH_2SPh)]Mn(CO)_3$, points to monomeric structures for the whole range of compounds studied. An octahedral structure is proposed for the molybdenum, tungsten, and manganese compounds with the tridentate gallate ligand occupying three facial positions. A schematic representation of the two manganese tricarbonyl species is shown in **2**, where R =

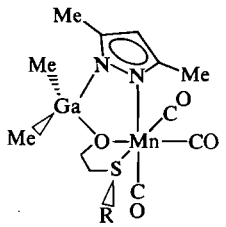

2

Et or Ph. The suggested octahedral structure of the compounds and the *fac* arrangement for the organogallate ligands has been established conclusively for the two compounds $[Me_2Ga(N_2C_5H_7)(OCH_2CH_2SEt)]Mo(CO)_2(C_7H_7)$ and $[Me_2Ga(N_2C_5H_7)(OCH_2CH_2SPh)]$ $Mn(CO)_3$ through crystal structure determinations.[1]

[1]Manuscript in preparation.

The nickel nitrosyl and triphenylphosphine copper complexes are believed to possess tetrahedral transition metal centres although if this is indeed the case then fluxional behaviour in solution must be invoked to explain their ambient temperature ^{1}H nmr spectra. The tetrahedral distribution of ligand atoms about the Ni centre in the crystalline complex $[Me_2Ga(N_2C_5H_7)(OCH_2CH_2SEt)]Ni(NO)$ has been firmly established by a crystal structure determination.[1]

Infrared Spectra

The infrared spectral data reported in Table 1 for the octahedral complexes are consistent with a *fac* tridentate gallate ligand in these molecules. In the spectrum of the manganese tricarbonyl compound three strong ν_{CO} bands are seen, an observation which discounts the possibility of a *mer* configuration for the three CO ligands since such an arrangement would lead to two weak ν_{CO} bands and one strong ν_{CO} band (12). For the molybdenum and tungsten compounds two strong ν_{CO} bands are observed in the ir spectra indicating a *cis* arrangement of the two CO ligands. This does not in itself distinguish between a *mer* or *fac* arrangement for the gallate ligand about the central metal but molecular models indicate that the *fac* mode of coordination is the sterically preferred conformation. Further, a *fac* conformation of the gallate ligand is indicated by the appearance of two strong ν_{CO} bands in the ir spectra of THF solutions of the intermediate anions $[Me_2Ga(N_2C_5H_7)(OCH_2CH_2SEt)]M(CO)_3^-$ (M = Mo or W), the lower frequency band being much broader (unresolved *e* mode) than the higher frequency band (a_1 mode). Again, a *mer* conformation of the gallate ligand in these precursor anions would give rise to two weak ν_{CO} bands and one strong ν_{CO} band in the ir spectra (12). Finally, the *fac* type of chelation has been proven in the solid state for the complex $[Me_2Ga(N_2C_5H_7)(OCH_2CH_2SEt)]Mo(CO)_2(C_7H_7)$ through a crystal structure determination.[1]

As noted previously the ν_{CO} and ν_{NO} bands for similar tungsten and molybdenum complexes are 10–20 cm^{-1} different, the lower frequency bands appearing in the spectra of the tungsten compounds (1).

Mass Spectra

With the exception of the Cu(I) compound all of the complexes prepared in this study displayed a parent ion signal in their mass spectra. No higher mass peak was observed in any of the spectra suggesting a monomeric structure for the complexes in the vapour phase. The highest *m/e* signal observed for the $[Me_2Ga(N_2C_5H_7)(OCH_2CH_2SEt]Cu{\cdot}PPh_3$ complex corresponded to the parent ion minus the

Can. J. Chem. Downloaded from www.nrcresearchpress.com by 210.87.254.40 on 09/06/12
For personal use only.

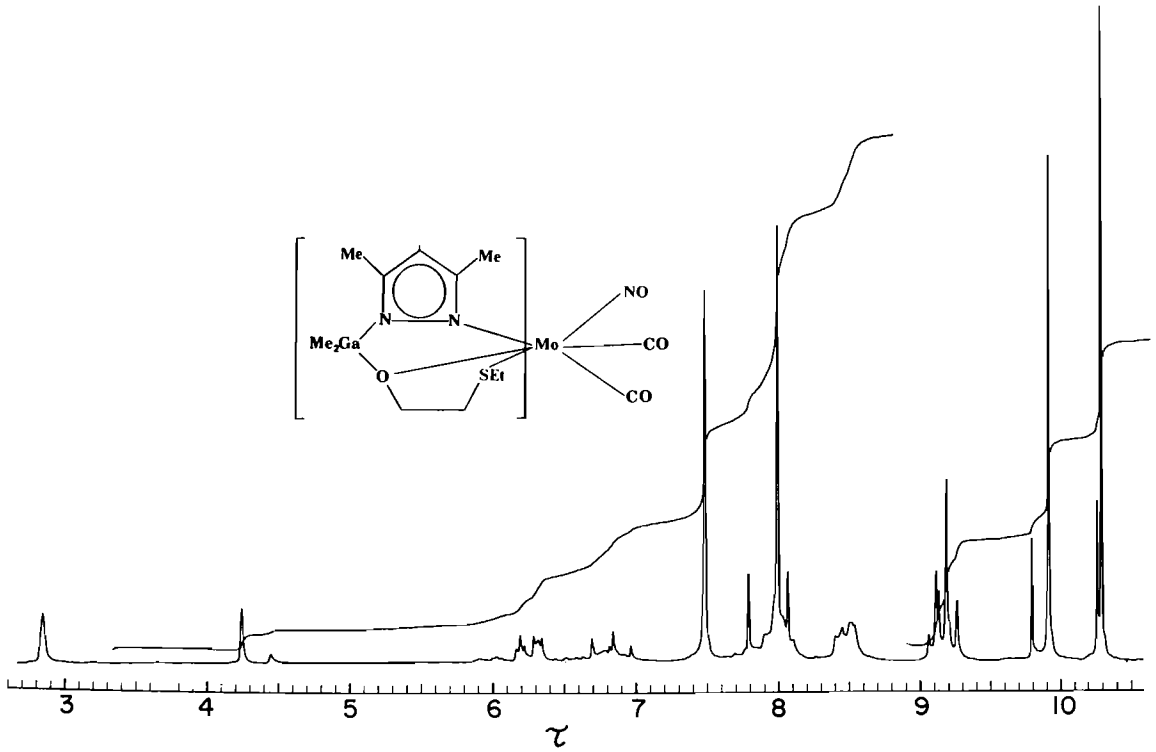

FIG. 1. Room temperature 100 MHz ^{1}H nmr spectrum of $[Me_2Ga(N_2C_5H_7)(OCH_2CH_2SEt)]Mo(CO)_2(NO)$ in C_6D_6 solution.

triphenylphosphine ligand. The appearance of signals due to other ions in all of the spectra indicated predictable fragmentation patterns for the various complexes and the intensity ratios of the individual peaks in multipeak signals agreed closely with theoretical predictions based on the percentage isotope compositions of the contributing metal atoms. The spectra of the two "$Mn(CO)_3$" derivatives were dominated by the very intense signal due to the parent ion minus the 3CO ligands, the parent ion signal being about 2% of this intensity. In all the other spectra the parent ion signal was $\geq$20% the intensity of the strongest signal in the spectrum.

^{1}H Nuclear Magnetic Resonance Spectra

Selected ^{1}H nmr data for the complexes in C_6D_6 solution are listed in Table 2. Of the five octahedral complexes where isomerism is possible only the spectra of the two nitrosyl derivatives reveal the presence of two positional isomers in solution. Thus, there are three possible positions of substitution for the incoming C_3H_5, C_7H_7, or NO groups in the decarbonylation stage of the syntheses, viz. opposite any one of the atoms of the NOS donor set. Molecular models indicate that, with a *fac* conformation for the organogallate ligand, the positions most favoured sterically for incoming substituents are those opposite the pyrazolyl nitrogen and the sulphur atoms. It is evident that the small NO group can occupy either of these positions. However, one site of substitution is distinctly preferred since the two isomers in both the Mo and W complexes occur in an approximate 5:1 ratio (see Fig. 1). The ^{1}H nmr spectra of the "C_3H_5" and "C_7H_7" compounds (see Fig. 2), on the other hand, indicate that but one positional isomer is formed in the syntheses of these complexes. Additionally, in the case of the complex $[Me_2Ga(N_2C_5H_7)(OCH_2CH_2SEt)]Mo(CO)_2(C_7H_7)$ a crystal structure determination[1] has shown the "C_7H_7" ligand to be substituted opposite to the S atom in the pseudo octahedral molecule. The asymmetric nature of the octahedral compounds is also clearly illustrated by these ^{1}H nmr spectra. In the spectrum of the η^3-C_3H_5 complex all five allyl protons give rise to separate signals. The two *anti* proton signals appear as two doublets at high field and the *unique* proton signal appears at low field as a triplet of triplets. The two *syn* proton signals occur as two doublet of doublets in an intermediate field position, the lower field *syn* proton signal being partially obscured by one of the $-CH_2-CH_2-$ proton signals. The ^{1}H nmr spectra of the "C_7H_7" compounds display a number of noteworthy features (the spectrum of the Mo complex is shown in

Can. J. Chem. Downloaded from www.nrcresearchpress.com by 210.87.254.40 on 09/06/12
For personal use only.

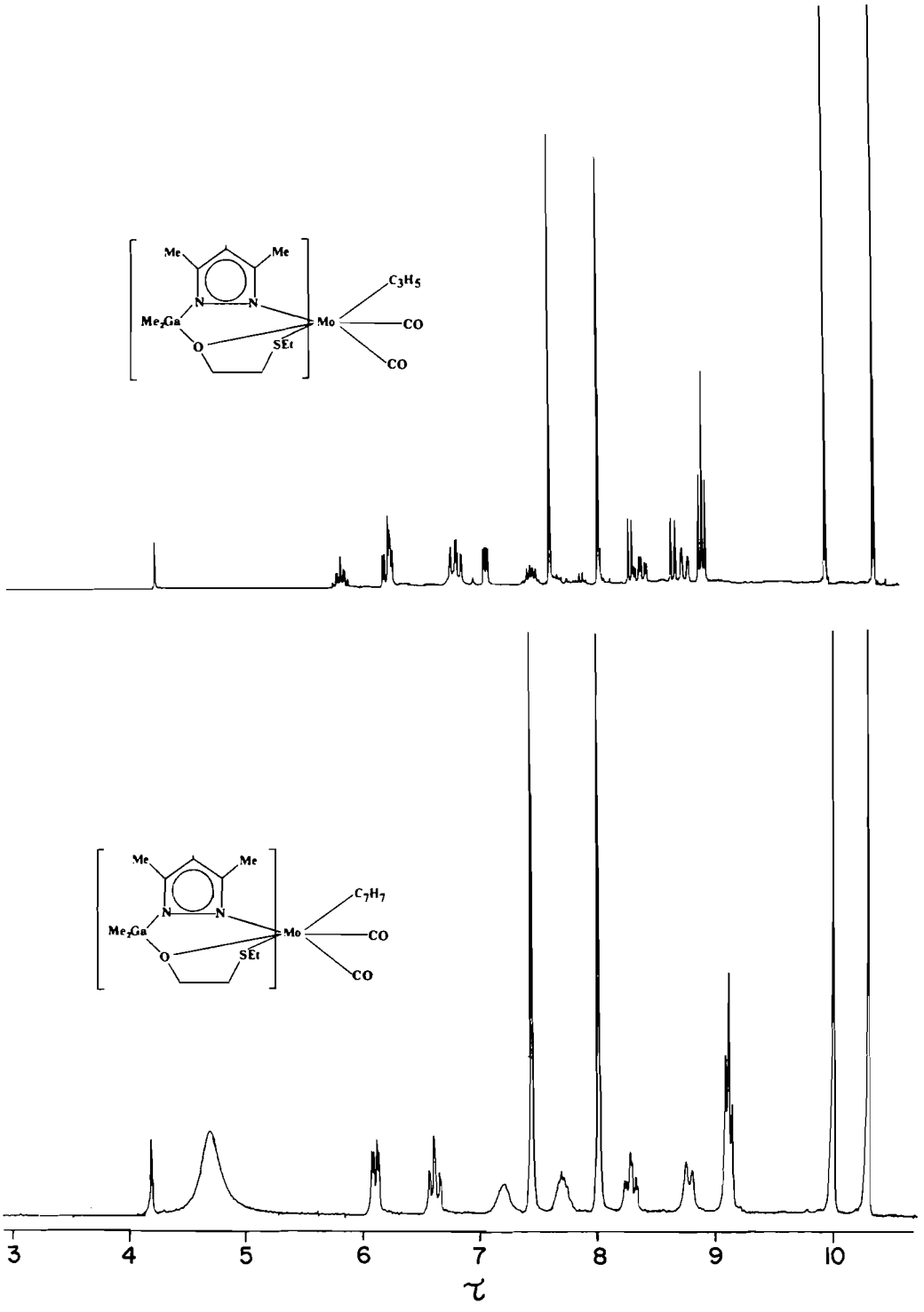

FIG. 2. Room temperature 270 MHz ^1H nmr spectra of $[Me_2Ga(N_2C_5H_7)(OCH_2CH_2SEt)]Mo(CO)_2(C_3H_5)$ (top) and $[Me_2Ga(N_2C_5H_7)(OCH_2CH_2SEt)]Mo(CO)_2(C_7H_7)$ (bottom) in C_6D_6 solution.

Can. J. Chem. Downloaded from www.nrcresearchpress.com by 210.87.254.40 on 09/06/12
For personal use only.

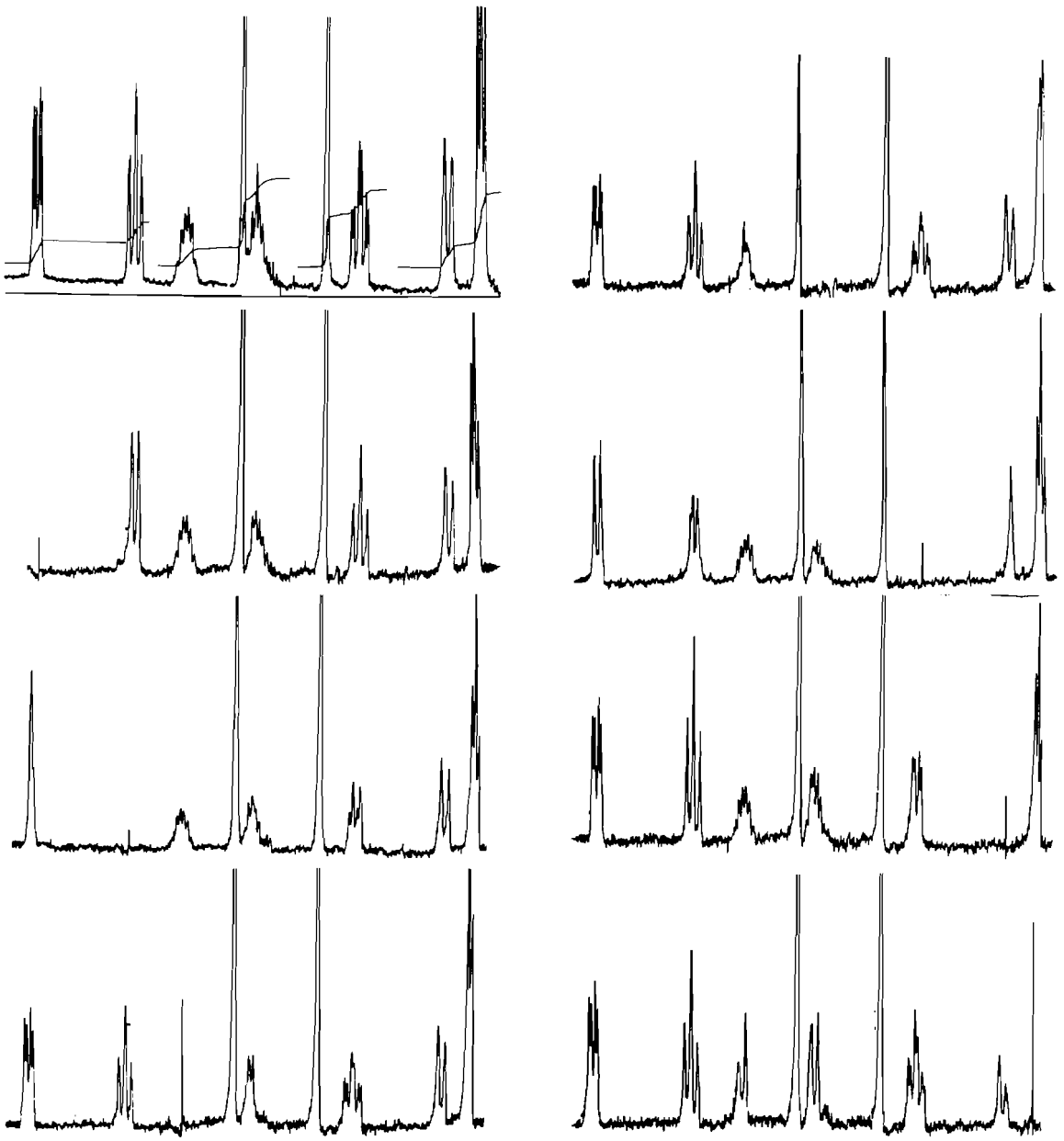

FIG. 3. Effect of double resonance experiments on the proton signals of the "$OCH_2CH_2SCH_2CH_3$" moiety in the room temperature 270 MHz spectrum of the complex $[Me_2Ga(N_2C_5H_7)(OCH_2CH_2SEt)]W(CO)_2(C_7H_7)$ in C_6D_6 solution.

Fig. 2). Firstly, the observation of one signal due to the η^3-C_7H_7 group indicates that this group is involved in a rapid fluxional process at room temperature. However, the "C_7H_7" signals are quite broad in the two spectra, especially for the W compound, and on cooling a d_6-acetone solution of this latter complex to −80°C the "C_7H_7" signal was split into a number of components. The pattern of signals observed at this lower temperature was characteristic of a rigid "η^3-C_7H_7" moiety in an asymmetric environment and was similar to the pattern reported for the C_7H_7 group in the low temperature ^1H nmr spectrum of the $[Me_2Ga(N_2C_3H_3)(OCH_2CH_2NMe_2)]W(CO)_2(C_7H_7)$ complex (1). Secondly, the six methylene protons of the

—O—CH_2—CH_2—S—CH_2—CH_3

moiety are particularly clearly distinguishable in these spectra. This distinguishability again arises from the asymmetric and rigid nature of this part

Can. J. Chem. Downloaded from www.nrcresearchpress.com by 210.87.254.40 on 09/06/12
For personal use only.

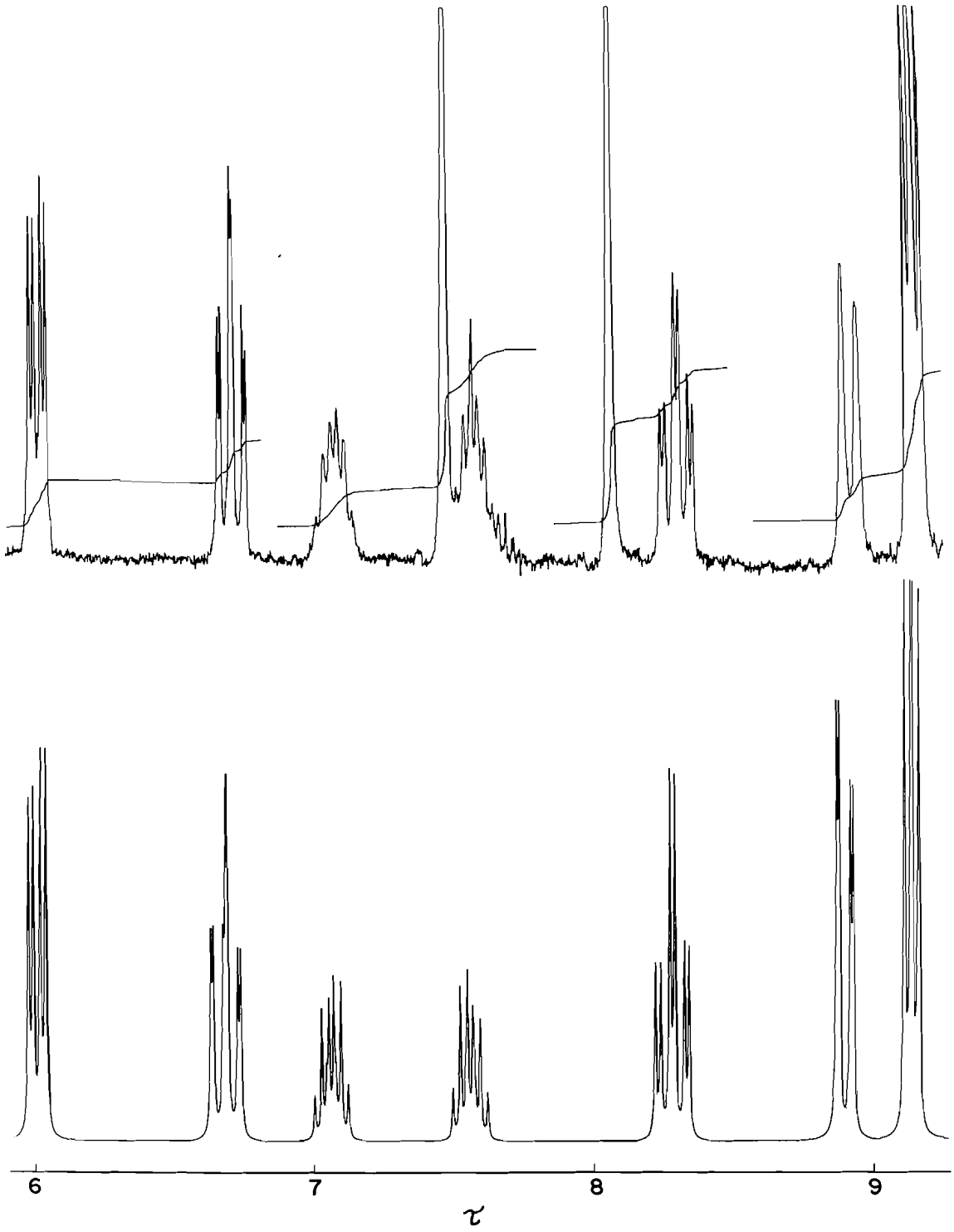

FIG. 4. Experimental room temperature 270 MHz ^1H nmr spectrum for the "$OCH_2CH_2SCH_2CH_3$" grouping in the complex $[Me_2Ga(N_2C_5H_7)(OCH_2CH_2SEt)]W(CO)_2(C_7H_7)$ in C_6D_6 (top); computer simulated spectrum (bottom).

TABLE 3. ^{1}H nmr data for the 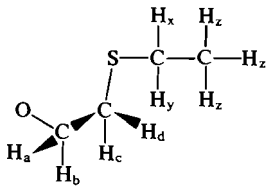 moiety† in the complex $[Me_2Ga(N_2C_5H_7)(OCH_2CH_2SEt)]W(CO)_2(C_7H_7)$

Proton*	Chemical shift (τ)‡	Coupling constants (Hz)
a	6.00	$J_{ab} = 12.0, J_{ac} = 5.0, J_{ad} = 0$
b	6.68	$J_{ba} = 12.0, J_{bc} = 14.0, J_{bd} = 2.5$
c	8.28	$J_{ca} = 5.0, J_{cb} = 14.0, J_{cd} = 14.0$
d	8.90	$J_{da} = 0, J_{db} = 2.5, J_{dc} = 14.0$
x	7.05	$J_{xy} = 12.0, J_{xz} = 7.0$
y	7.55	$J_{yx} = 12.0, J_{yz} = 7.0$
z	9.13	$J_{zx} = J_{zy} = 7.0$

*See Fig. 4.
†$H_a \ldots H_d$ *'trans'*; $H_b \ldots H_c$ *'cis'*.
‡Measured in C_6D_6 solution at toom temperature ($\tau_{C_6H_6} = 2.84$ ppm).

of the molecule. Double irradiation experiments have allowed the assignment of the S—CH_2—CH_3 methylene protons. Thus the two central multiplets (Fig. 3) both collapse to doublets when the S—CH_2—CH_3 methyl group high field triplet is irradiated. Conversely irradiation of either of these two central multiplets caused the S—CH_2—CH_3 triplet to collapse to a doublet and the other multiplet to collapse to a pseudo quartet. The remaining four multiplets can be assigned by comparison with the ^{1}H nmr spectrum of the $HOCH_2CH_2SEt$ compound. Thus the two low field multiplets can be assigned to the methylene group adjacent to the O atom and the two high field multiplets adjacent to the S—CH_2—CH_3 triplet can be assigned to the O—CH_2—CH_2—S methylene protons. The experimental ^{1}H nmr spectrum for the "$OCH_2CH_2SCH_2CH_3$" grouping is shown again in Fig. 4 together with a near-identical computer simulated spectrum based on the parameters given in Table 3.

The room temperature ^{1}H nmr spectra of both the "Ni(NO)" and "$CuPPh_3$" derivatives were very similar and both were simple first-order spectra. The spectrum of the copper complex is shown in Fig. 5. The appearance of only one signal due to the —$GaMe_2$ protons in the ^{1}H nmr spectra of both these metal complexes is compatible with a meridionally coordinated gallate ligand and a square-planar arrangement about both the Ni and Cu centres. A tetrahedral arrangement about these metal centres in solution would lead to two signals for the —$GaMe_2$ protons. However, a square-planar geometry in Cu(I) complexes is very unusual and a square-planar "Ni(NO)" complex has to date proven elusive. Further, our studies involving the analogous complexes using the ligand $[Me_2Ga(N_2C_5H_7)(OCH_2CH_2NMe_2)]^-$ have revealed fluxional behaviour for the two complexes in solution and tetrahedral structures about the metal centres in the solid state (13, 14). For the present complexes the room temperature ^{1}H nmr spectra may be explained on the basis of a rapid fluxional process which interconverts tetrahedral molecules via either a square-planar or three-coordinate intermediate (14) thus giving rise to a single averaged —$GaMe_2$ signal. Again, the tetrahedral environment about the Ni atom in the solid state has been confirmed by a crystal structure determination of the "Ni(NO)" complex.[1] In addition, low temperature ^{1}H nmr spectra of both complexes in d_6-acetone solutions display two —$GaMe_2$ proton signals, one to either side of the single room temperature signal. Thus at low temperatures in solution "static" tetrahedrally coordinated Ni and Cu centres are likely attained. Fluxional behaviour for the "Ni(NO)" and "$CuPPh_3$" complexes in solution at room temperature is also indicated by the proton signals due to the "$OCH_2CH_2SCH_2CH_3$" moiety in the ^{1}H nmr spectra. Thus these protons give rise to simple first order triplets and a quartet arrangement (see Fig. 5), much simplified from the pattern observed for these protons in the octahedral complexes (see Fig. 4).

Conclusion

It was initially puzzling that the ligand **1**, where R = Ph, was so reluctant to yield a parallel series of

Can. J. Chem. Downloaded from www.nrcresearchpress.com by 210.87.254.40 on 09/06/12
For personal use only.

Can. J. Chem. Downloaded from www.nrcresearchpress.com by 210.87.254.40 on 09/06/12
For personal use only.

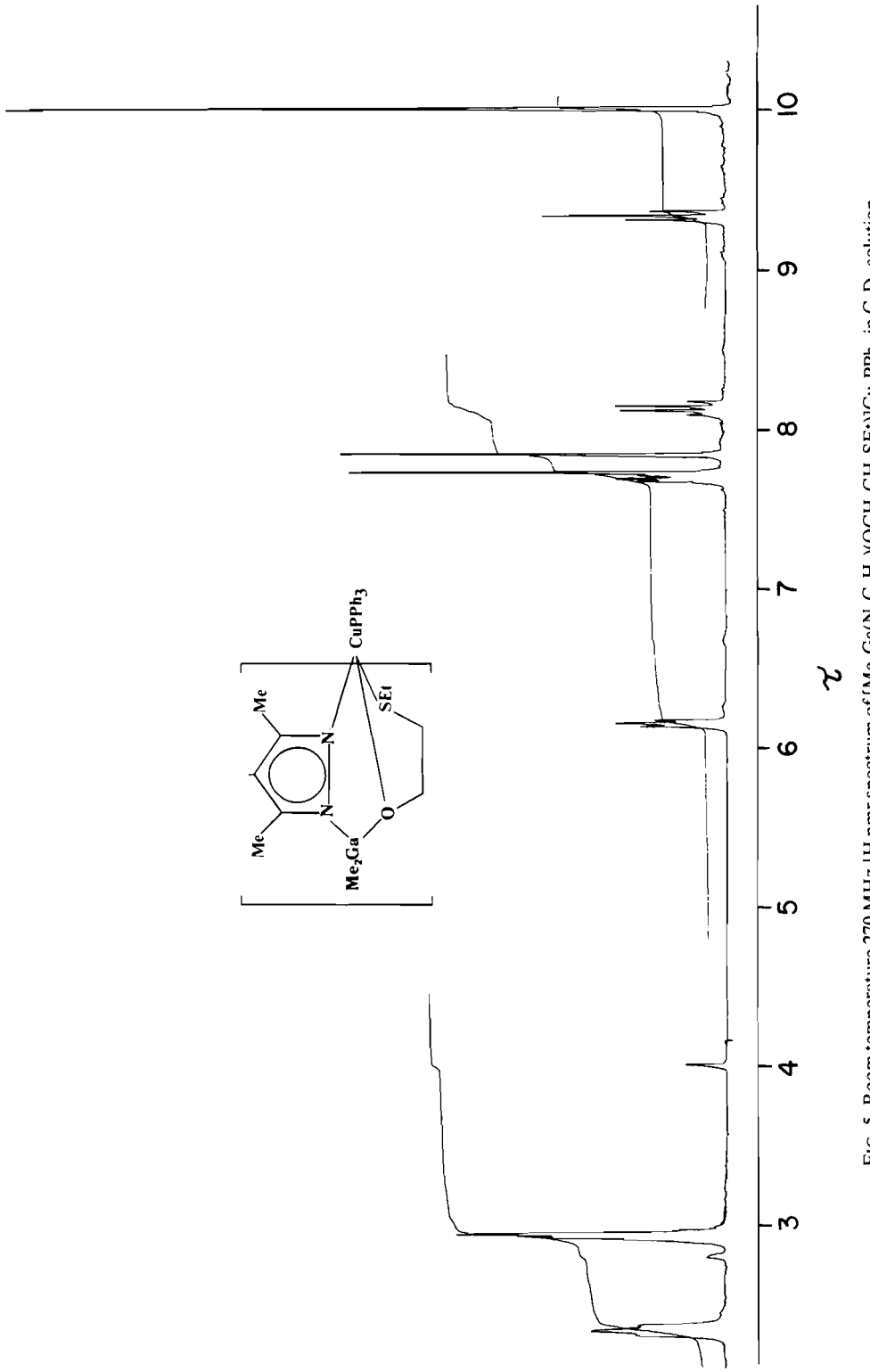

FIG. 5. Room temperature 270 MHz ^{1}H nmr spectrum of $[Me_2Ga(N_2C_5H_7)(OCH_2CH_2SEt)]Cu{\cdot}PPh_3$ in C_6D_6 solution.

compounds to the one described above for the ligand **1**, where R = Et. The only complex characterized to date is the "$Mn(CO)_3$" derivative, although evidence for a "$Mo(CO)_2(NO)$" species was obtained in one attempt to prepare this nitrosyl compound. It is conjectured that the bulky phenyl substituent on the S atom is responsible for this reluctance of the ligand **1** (R = Ph) to form complexes. The steric requirements of this ligand are discussed further in connection with the crystal structure of its "$Mn(CO)_3$" derivative.[1]

It is relevant in this regard to report that our explorations into the ligating properties of the potentially tridentate chelating ligand $[Me_2Ga(N_2C_5H_7)(OCH_2CH_2PPh_2)]^-$ have so far proven fruitless. Again the bulky "PPh_2" grouping may prohibit the tridentate chelation necessary to stabilize the various metal complexes. Our endeavours in this area of multidentate organogallate ligands are continuing with other 3-atom donor sets, and also with ligands of potentially higher denticity.

Acknowledgements

We thank the Natural Sciences and Engineering Research Council of Canada for financial support. We are grateful to Mr. P. Borda for C, H, N analyses, Mr. J. Nip for mass spectra, Ms. M. Tracey for ^1H nmr spectra, and Mr. S. Ford for experimental assistance.

1. K. S. CHONG and A. STORR. Can. J. Chem. **58**, 2278 (1980).
2. A. H. FORD-MOORE, R. A. PETERS, and R. W. WAKELIN. J. Chem. Soc. 1754 (1949).
3. N. M. VINOKUROVA and A. M. KHALETSKII. Khim.-Farm. Zh. **3**, 20 (1969); Chem. Abstr. **72**, 66307*y* (1970).
4. A. STORR and B. S. THOMAS. Can. J. Chem. **48**, 3667 (1970).
5. B. HAYMORE and R. D. FELTHAM. Inorg. Synth. **14**, 81 (1973).
6. R. B. KING. Organometallic synthesis. Vol. 1. Academic Press, New York. 1965.
7. D. P. TATE, W. R. KNIPPLE, and J. M. AUGL. Inorg. Chem. **1**, 433 (1962).
8. R. B. KING and A. FRONZAGLIA. Inorg. Chem. **5**, 1837 (1966).
9. G. COSTA, E. REISENHOFER, and L. STEFANI. J. Inorg. Nucl. Chem. **27**, 2581 (1965).
10. K. S. CHONG, S. J. RETTIG, A. STORR, and J. TROTTER. Can. J. Chem. **55**, 4166 (1977).
11. K. S. CHONG, S. J. RETTIG, A. STORR, and J. TROTTER. Can. J. Chem. **56**, 1212 (1978).
12. D. M. ADAMS. Metal–ligand and related vibrations. Edward Arnold Ltd., London. 1967. Chapt. 3.
13. K. S. CHONG, S. J. RETTIG, A. STORR, and J. TROTTER. Can. J. Chem. **57**, 3107 (1979).
14. K. S. CHONG, S. J. RETTIG, A. STORR, and J. TROTTER. Can. J. Chem. **59**, 518 (1981).

Can. J. Chem. Downloaded from www.nrcresearchpress.com by 210.87.254.40 on 09/06/12
For personal use only.

The thermal and photochemical decomposition of maleic anhydride in the gas phase[1]

R. A. BACK AND J. M. PARSONS

Division of Chemistry, National Research Council of Canada, 100 Sussex Drive, Ottawa, Canada K1A 0R6

Received October 9, 1980

R. A. BACK and J. M. PARSONS. Can. J. Chem. **59**, 1342 (1981).

The thermal decomposition of maleic anhydride has been studied in the gas phase in a static system at temperatures from 645 to 760 K and pressures from 0.7 to 20 Torr. The first-order rate constant for the homogeneous unimolecular reaction,

Maleic anhydride $\rightarrow C_2H_2 + CO + CO_2$

is described by the Arrhenius parameters $\log A\ (s^{-1}) = 14.33\ (\pm 0.3)$, and $E = 60.9\ (\pm 1)$ kcal/mol. The reaction appears to proceed through a concerted mechanism rather than a biradical one.

The photochemical decomposition, studied at wavelengths from 220 to 350 nm, yielded the same products. At 300 nm and below, the decomposition was unaffected by pressure, but at longer wavelengths collisional quenching was observed. Weak light emission was observed on excitation between 350 and 380 nm. The absorption spectrum was measured from 250 to 400 nm, and three overlapping transitions, $\pi^* \leftarrow \pi$, $\pi^* \leftarrow n_+$, and $\pi^* \leftarrow n_-$, can be distinguished. The mechanism of the photolysis is discussed and it is concluded that it probably proceeds through internal conversion to a vibrationally excited ground state.

R. A. BACK et J. M. PARSONS. Can. J. Chem. **59**, 1342 (1981).

Utilisant un système statique et opérant à des températures de 645 à 760 K et à des pressions allant de 0,7 à 20 Torr, on a étudié la décomposition thermique de l'anhydride maléique en phase gazeuse. On décrit la constante de vitesse d'ordre un de la réaction unimoléculaire homogène

Anhydride maléique $\rightarrow C_2H_2 + CO + CO_2$

par les paramètres d'Arrhénius $\log A\ (s^{-1}) = 14{,}33\ (\pm 0{,}3)$ et $E = 60{,}9\ (\pm 1)$ kcal/mol. La réaction semble se dérouler selon un mécanisme concerté de préférence à un mécanisme biradicalaire.

On obtient les mêmes produits quand on étudie la décomposition photochimique à des longueurs d'ondes allant de 220 à 350 nm. A des longueurs d'onde allant jusqu'à 300 nm, la pression n'affecte pas la décomposition mais à des longueurs d'onde plus grandes, on observe des extinctions par collision. Lorsqu'on excite entre 350 et 380 nm, on observe une faible émission de lumière. On a mesuré le spectre d'absorption à partir de 250 jusqu'à 400 nm et on peut distinguer trois transitions de recouvrement: $\pi^* \leftarrow \pi$, $\pi^* \leftarrow n_+$ et $\pi^* \leftarrow n_-$. On discute du mécanisme de la photolyse et on en conclut qu'il se fait par l'intermédiaire d'une conversion interne en un état fondamental vibrationnellement excité.

[Traduit par le journal]

Introduction

Few studies have been reported of the thermal or photochemical decomposition of the cyclic anhydrides of dicarboxylic acids in the gas phase. Krull and Arnold (1) briefly described the mercury-photosensitized decomposition of several anhydrides, while Brown and Ritchie reported qualitative results of "hot tube" pyrolysis of a number of anhydrides, both cyclic and noncyclic (2). Rice and Murphy briefly examined the pyrolysis of several cyclic anhydrides in the vapor phase in a flow system at temperatures from 750 to 900°C (3). The present paper describes a study of the thermal and photochemical decomposition of maleic anhydride (2,5-furandione) in the gas phase.

Experimental

Reaction vessels and the vacuum line for handling maleic anhydride vapor were totally enclosed in an air thermostat usually held at 100°C, well above the condensation temperature at the highest pressure employed, yet below the temperature at which thermal decomposition becomes significant. Stopcocks were greased with silicone grease, and pressure was measured by a heated quartz spiral nulled by an oil manometer outside the thermostat.

The thermal decomposition was studied in a static system using a cylindrical quartz vessel 5 cm in diameter and 7 cm long of 236 cc volume, mounted in a tube furnace controlled to ± 1°C. A similar reaction vessel packed with quartz tubing was used to test for surface effects.

The photolysis vessel was cylindrical, 5 cm in diameter and 10 cm long fitted with plane quartz windows. The light source was a 1000 W mercury–xenon arc fitted with a matching monochromator with a bandwidth that could be varied from 3.3 to 23 nm. Fluorescence was measured in a conventional quartz cell with a window at right angles to the exciting light beam and fitted with blackened Wood's horns to minimize scattered light. Emission was measured with a RCA 1P21 photomultiplier mounted behind a sharp-cutoff filter to remove most of the exciting radiation.

Product analysis was by simple low-temperature fractionation and measurement in a gas burette, followed by gas chromatography to confirm the identification and analysis. Maleic anhydride (of purity ≥99.5%) was obtained from BDH chemicals and used without further purification; it was rigorously degassed and stored as a solid in a trap cooled to about 20°C which was warmed to give the desired vapor pressure when required.

[1]NRCC No. 19258.

0008-4042/81/091342-05$01.00/0

©1981 National Research Council of Canada/Conseil national de recherches du Canada

Can. J. Chem. Downloaded from www.nrcresearchpress.com by 210.87.254.105 on 09/06/12
For personal use only.

Can. J. Chem. Downloaded from www.nrcresearchpress.com by 210.87.254.105 on 09/06/12
For personal use only.

Results and Discussion

The Thermal Decomposition

The decomposition was studied at pressures from about 0.7 to 20 Torr and temperatures from 645 to 760 K. The only products observed were CO, CO_2, and C_2H_2, formed in equimolar quantities, in agreement with the brief observations of Rice and Murphy (3) in experiments at 1093 K. There is no evidence for the formation of the propiolaldehyde or propiolic acid at 703 K suggested by Brown and Ritchie (2) even though our experiments were extended to lower temperatures and were at much lower conversions (always <5%) than theirs. No systematic search was made for products less volatile than the parent anhydride. At the higher temperatures, the change in pressure during the reaction was approximately in agreement with that expected from dissociation into the observed products. At the lowest temperatures, however, a small decrease in pressure was observed, indicating the occurrence of some condensation reactions, perhaps dimerization; this was not investigated further.

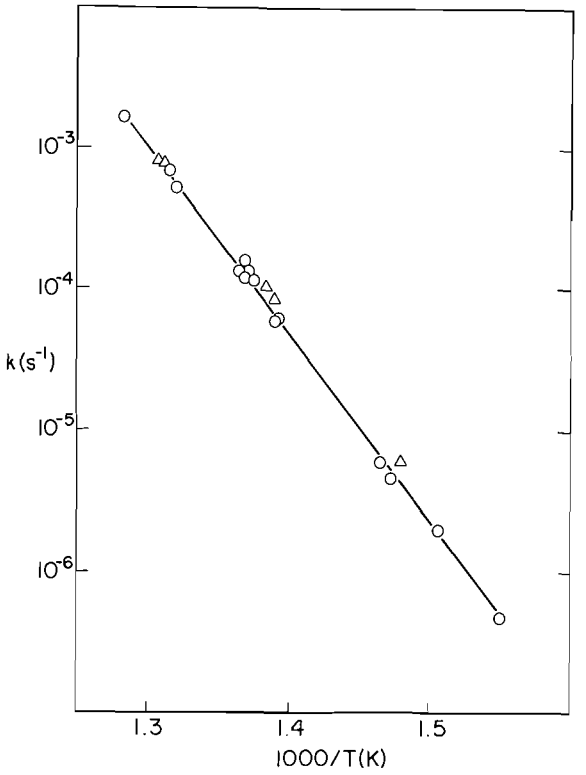

FIG. 1. Arrhenius plot for the first-order rate constant for the thermal decomposition of maleic anhydride. O = unpacked reaction vessel; Δ = packed reaction vessel, S/V increased by factor of 9.

In Fig. 1, first-order rate constants based on CO formation are shown in an Arrhenius plot; the straight line corresponds to the equation $\log k\ (s^{-1}) = 14.19 - 60.5/4.58\,T$. Experiments in the packed reaction vessel, in which the surface to volume ratio was increased by a factor of 9, showed an appreciable enhancement (Fig. 1). A small correction was made based on these data, assuming surface and homogeneous reactions to be simply additive, and surface reaction proportional to area, leading to an Arrhenius equation for the homogeneous unimolecular reaction of $\log k\ (s^{-1}) = 14.33 - 60.9/4.58T$, with uncertainties of ±0.3 in log A and ±1 in E. Between about 8 and 20 Torr, values of k were independent of pressure, and all the data in Fig. 1 were obtained in that range. At lower pressures, k decreased significantly, falling to about 60% of its high-pressure value at 0.7 Torr at 731 K. The pressure and values of k at which this occurs suggest that this is simply the normal pressure dependence of a unimolecular reaction.

The simplicity of the reaction products, the pressure dependence of k, and the values of the Arrhenius parameters indicate that the measured first-order rate constant is that for the simple homogeneous unimolecular reaction,

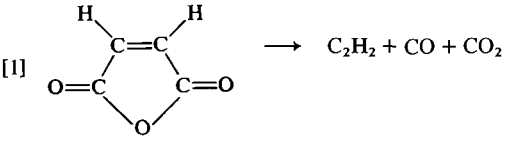

($\Delta H^0 = +34$ kcal/mol)

Biradical mechanisms are operative in the decomposition of many cyclic compounds (4). It can be estimated, however, that formation of a biradical by simple ring opening of maleic anhydride would require at least 75 kcal/mol, far above the observed activation energy. Formation of secondary biradicals or intermediates such as cyclopropenone or oxiren-2-one by molecular elimination of CO_2 or CO would also appear to be too endothermic. We conclude therefore that reaction [1] probably proceeds through a simple direct concerted mechanism. The fact that the activation energy only exceeds the endothermicity of the reaction by about 27 kcal/mol indicates a relatively loose or expanded transition state which permits CO_2 and C_2H_2 to approach their linear equilibrium configurations much more closely than is possible for maleic anhydride itself.

The Photochemical Decomposition

Products of the photolysis at all wavelengths

Can. J. Chem. Downloaded from www.nrcresearchpress.com by 210.87.254.105 on 09/06/12
For personal use only.

from 220 to 350 nm were CO, CO_2, and C_2H_2 in equimolar quantities, as in the thermal and the mercury photosensitized (1) decompositions. Relative quantum yields at 300 nm and below were independent of pressure of maleic anhydride or added CO_2. At 350 nm, quantum yields decreased with increasing pressure of maleic anhydride or of added CO_2, as shown in Stern–Volmer plots in Figs. 2 and 3; the ratio of the slopes of the two lines indicates that maleic anhydride is about 5.5 times more efficient than CO_2 in quenching the decomposition.

Weak light emission was also observed from maleic anhydride irradiated betweeen 350 and 380 nm. An excitation spectrum for this emission is shown in Fig. 4, obtained using a bandwidth of 16 nm, and normalizing the data to constant incident intensity. A spectrum of the emission excited at 366 nm was photographed on a small Hilger spectrograph with a 22 h exposure, and showed continuous emission extending from about 420 to 480 nm. The emission intensity at 366 nm was found to be a linear function of pressure, (i.e., of the light absorbed) thus indicating no collisional quenching of the emitting species.

Because of its low volatility, the absorption spectrum of maleic anhydride vapor has only been reported for wavelengths below 230 nm where the strong $\pi^*-\pi$ absorption begins; weaker absorption was observed in solution and low-temperature glasses extending to about 360 nm (5). The spectrum was therefore measured in a heated 10 cm cell at 147°C and 100 Torr pressure in a Cary spectrophotometer, and is shown in Fig. 5. Three overlapping absorption systems can be distinguished, and following McGlynn's assignments (5, 6) can be attributed to the $\pi^* \leftarrow n_-$, $\pi^* \leftarrow n_+$, and $\pi^* \leftarrow \pi$ transitions. The first two are symmetry forbidden and are quite weak with ε_{max} around 10; the dashed curves in Fig. 5 indicate only very approximately the positions of these systems. The much stronger allowed $\pi^* \leftarrow \pi$ transition was studied by Seliskar and McGlynn (5); it shows strong but diffuse vibrational bands with an origin at 213.8 nm. The tail of this absorption system, presumably an unresolved complex of hot bands, extends at least 60 to 80 nm to the red, strongly overlapping the much weaker $\pi^* \leftarrow n_+$ system and obscuring its structure. The latter shows one strong progression of diffuse vibrational bands with a spacing of about 1530 cm^{-1}, marked in Fig. 5, and a second weaker progression

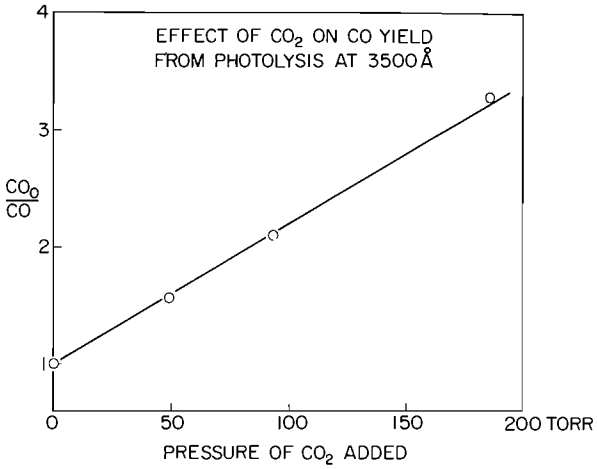

FIG. 3. Stern–Volmer plot showing the effect of CO_2 on the photolysis at 350 nm.

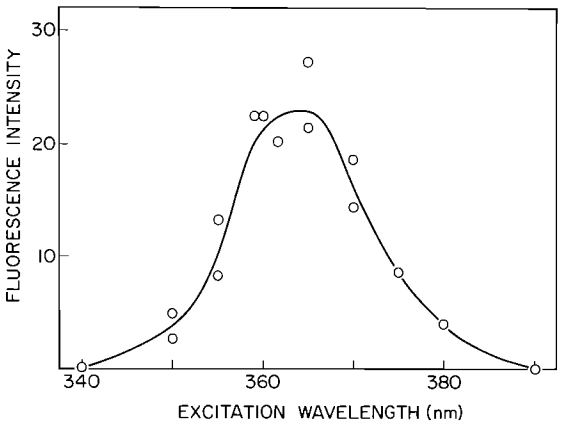

FIG. 4. Excitation spectrum for emission from maleic anhydride, normalized to constant incident intensity.

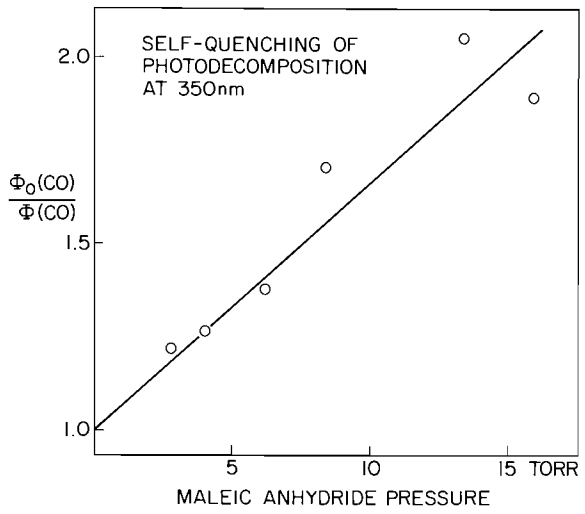

FIG. 2. Stern–Volmer plot of quantum yield of CO formation vs. pressure of maleic anhydride for the photolysis at 350 nm.

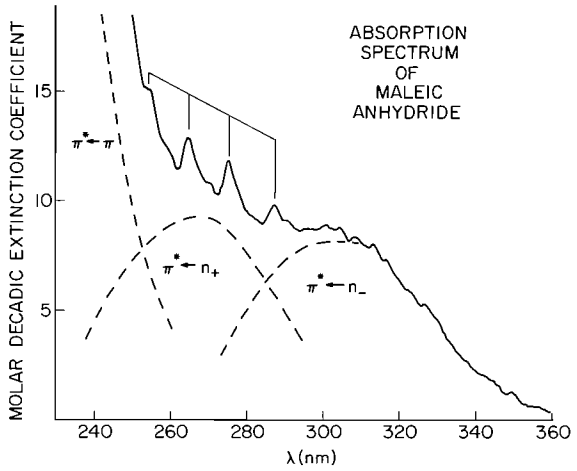

FIG. 5. Absorption spectrum of maleic anhydride vapor taken with a Cary spectrophotometer at 147°C, 100 Torr pressure, and 10 cm path length.

displaced about 700 cm^{-1} to the blue. These are presumably the same progressions observed by Seliskar and McGlynn (5) in a low-temperature glass, and probably arise from excitation of a C=O stretching vibration in the upper state. Between 290 and 320 nm a further group of diffuse vibrational bands is seen, probably belonging to the $\pi^* \leftarrow n_-$ system. Photographic spectra taken at moderately high resolution in a multi-pass 2 m cell showed that these bands are part of a complex system extending beyond 360 nm.[2] At longer wavelengths, the bands become very much sharper, showing well-resolved K-structure and rotational band contours, but spectra taken at higher resolution show that even at the longest wavelength observed (358 nm) they are ultimately diffuse, with no resolved rotational fine structure.

The Mechanism of the Photochemical Decomposition

The following generalized mechanism accounts for the observed behaviour:

[2] $MA + h\nu \rightarrow MA^*$

[3] $MA^* \rightarrow MA^{\#}$

[4] $MA^* \rightarrow h\nu' + MA$

[5] $MA^{\#} \rightarrow CO + CO_2 + C_2H_2$

[6] $MA^{\#} + X \rightarrow MA + X$

where MA = maleic anhydride and X = a collision partner. The broad diffuse bands of the $\pi^* \leftarrow \pi$ and $\pi^* \leftarrow n_+$ transitions indicate very short lifetimes for these states. The $\pi^* \leftarrow n_-$ spectrum is much sharper but at high resolution is still diffuse, and the excited state must have a lifetime no more than a few picoseconds. None of the three excited singlet states, MA*, are expected from their electronic structure to be dissociative themselves, and their short lifetime and the broadening of the spectra must be attributed to a rapid internal conversion or intersystem crossing. The corresponding triplet states are also unlikely to dissociate directly, and it seems probable that dissociation occurs from the vibrationally excited ground state ($MA^{\#}$ in the mechanism). The conversion from the initially formed singlet to the ground state might or might not proceed through a triplet state; the only experimental conclusion is that this process must be fast.

The collisional quenching of the decomposition at 350 nm is compatible with its proceeding through the vibrationally excited ground state. If no energy were lost by collision prior to internal conversion, excitation at this wavelength would yield molecules excited by about 82 kcal of vibrational energy, about 21 kcal/mol in excess of the dissociation energy measured in the thermal decomposition. Pressures of 15 Torr of maleic anhydride or 84 Torr of CO_2 were required to reduce the decomposition yield by one half (Figs. 2 and 3). This may be compared with a similar excitation of cyclobutanone by internal conversion, where a half-pressure of 600 Torr of propylene was reported for molecules with excess energy of 39 kcal/mol (7). The much lower half-pressures in the present system are a reasonable reflection of the lower excess energy.

The excitation spectrum of the emission (Fig. 4) must arise from the convolution of a decreasing extinction coefficient and an increasing quantum yield of emission with increasing wavelength. This behaviour, and the increasing diffuseness of the absorption spectrum with decreasing wavelength, suggests that only the $\pi^* \leftarrow n_-$ state is sufficiently longlived to give detectible emission, and that its lifetime decreases sharply with decreasing wavelength. Similar behaviour has been observed in many other systems, e.g., cyclobutanone (8). The observed fluorescence was very weak and while a quantum yield was not measured it must be very low. The absence of collisional quenching and the diffuseness of the absorption spectrum indicates a very short lifetime for the emitting species ($<10^{-11}$ s), while the radiative lifetime for such a weak transition must be much longer, 10^{-8} s or more, fixing the quantum yield of fluorescence at 10^{-3} or lower.

[2]We are grateful to Mr. M. Barnett of the Herzberg Institute for photographing these spectra.

Can. J. Chem. Downloaded from www.nrcresearchpress.com by 210.87.254.105 on 09/06/12
For personal use only.

Further spectroscopic and photophysical studies of the system are planned in the near future.

1. I. S. KRULL and D. R. ARNOLD. Tetrahedron Lett. **50**, 4349 (1969).
2. A. L. BROWN and P. D. RITCHIE. J. Chem. Soc. C, 2007 (1968).
3. F. O. RICE and M. T. MURPHY. J. Am. Chem. Soc. **64**, 896 (1942).
4. S. W. BENSON and H. E. O'NEAL. Kinetic data on gas phase unimolecular reactions. NSRDS-NBS 21, Washington, DC. 1970.
5. C. J. SELISKAR and S. P. MCGLYNN. J. Chem. Phys. **56**, 275 (1972).
6. D. DOUGHERTY, P. BRINT, and S. P. MCGLYNN. J. Am. Chem. Soc. **100**, 5597 (1978).
7. N. E. LEE and E. K. C. LEE. J. Chem. Phys. **50**, 2094 (1969).
8. E. K. C. LEE. Acc. Chem. Res. **10**, 319 (1977).

Can. J. Chem. Downloaded from www.nrcresearchpress.com by 210.87.254.105 on 09/06/12
For personal use only.

Synthesis of 3(2-haloethyl)aryltriazenes and study of their reactions in aqueous solution

J. WILLIAM LOWN AND RANJIT SINGH
Department of Chemistry, University of Alberta, Edmonton, Alta., Canada T6G 2G2

Received October 14, 1980

J. WILLIAM LOWN and RANJIT SINGH. Can. J. Chem. **59**, 1347 (1981).

Several 1-aryl-3-(2-haloethyl)triazenes have been synthesized and characterized spectroscopically as well as by their esterification of 3,5-dinitrobenzoic acid. Their rates of decomposition in aqueous media at pH 7 were determined polarographically employing the electrochemically active triazene moiety. In two selected cases the rates of decomposition increase markedly with lowered pH in the range 9.3 to 4.65. The products of aqueous decomposition, both volatile and involatile, were identified and quantitated by gc and gc–ms. Discrimination between alternative decomposition pathways was possible by the preparation and use of selectively deuterated triazenes. The data are consistent with initial protonation of the triazene and generation therefrom of a 2-haloethyl cation (or its kinetic equivalent) which is subject to rearrangements detected by deuterium scrambling. A second competing pathway involves cyclization of the triazene to a 1-aryl-1,2,3-triazoline intermediate which is then subject to nucleophilic opening at two sites with attendant loss of nitrogen. The effects of structural changes in the triazenes on their modes of decomposition and generation of electrophiles should assist in the interpretation of their antitumor effects.

J. WILLIAM LOWN et RANJIT SINGH. Can. J. Chem. **59**, 1347 (1981).

On a synthétisé plusieurs aryl-1 (halo-2 éthyl)-3 triazènes et on les a caractérisés par spectroscopie et en les transformant en leurs dinitro-3,5 benzoates. On a déterminé leur vitesse de décomposition en milieu aqueux à un pH = 7 en faisant appel à la polarographie et en utilisant la portion triazène électrochimiquement active. Dans deux cas sélectionnés, les vitesses de décompositions augmentent fortement lorsque le pH diminue de 9,3 à 4,65. Faisant appel à la cpg et à la cpg reliée à la sm, on a identifié les produits de décomposition volatils et non-volatils qui se forment en milieu aqueux et on a déterminé les quantités de produits formés. On peut choisir parmi les diverses voies de décomposition possibles en préparant et en utilisant des triazènes sélectivement deutérés. Les donnés sont en accord avec une protonation initiale du triazène conduisant par la suite à la formation d'un cation halo-2 éthyl (ou son équivalent cinétique) qui peut subir des transpositions qui peuvent être différenciées sur la base des produits deutérés obtenus. Une autre voie qui est en compétition avec la précédente fait intervenir la cyclisation du triazène en un intermédiaire aryl-1 triazoline-1,2,3 qui peut ensuite subir une ouverture nucléophile par attaque en deux points avec une perte concomittante d'azote. Les effets de changements structuraux dans le triazène sur leurs modes de décomposition et sur la formation d'électrophiles devraient faciliter l'interprétation de leurs effets antitumoraux.

[Traduit par le journal]

Synthetic attempts to design antagonists of 4-aminoimidazole-5-carboxamide, the ribotide of which is a precursor in purine biosynthesis, led to the development of 5(3,3-dimethyl-1-triazene)imidazole-4-carboxamide (DIC), **1***a*, which is probably the most effective agent used clinically in the treatment of melanoma (1). Among the substituted triazenes that were subsequently evaluated, 5-[3,3-bis(2-chloroethyl)-1-triazenyl]imidazole-1-carboxamide] (BIC), **1***b*, was found to be effective against brain tumors, malignant melanoma, and lymphomas (2, 3). Studies of the metabolism of DIC (5–7) and related triazenes (8) showed that oxidative *N*-demethylation gives rise to the ultimate alkylating species 5(3-methyl-1-triazene)imidazole-4-carboxamide (MIC), **1***c* (3), prior to its decomposition in water to give electrophiles which are thought to react with biological macromolecules. Mono-*N*-alkylated triazenes based on MIC, e.g. [5-[3-(2-chloroethyl)-1-triazenyl]-1*H*-imidazole-4-carboxamide], **1***d*, have exceeded MIC in activity (4). Subsequent structure–activity relationships of triazenes showed that the anticancer activity arose from the alkyltriazene portion and that the imidazole group could be replaced by an aryl ring without materially affecting activity (6, 8).

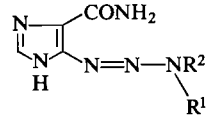

1*a* $R^1 = CH_3$, $R^2 = CH_3$
b $R^1 = CH_2CH_2Cl$, $R^2 = CH_2CH_2Cl$
c $R^1 = CH_3$, $R^2 = H$
d $R^1 = CH_2CH_2Cl$, $R^2 = H$

Studies on the chemical properties and the types of products obtained from aqueous decomposition of 2-haloethylnitrosoureas have contributed significantly to an understanding of their reactivity and mode of action (9–13). There have been few reports of a similar examination of 2-haloethyltriazenes and most studies in this field have dealt with monoalkyltriazenes (14, 15) and dialkyltriazenes (16, 17). We wish to report the synthesis, characterization, and identification of the pathways of decomposition of 2-haloethyltriazenes using specifically deuterium labelled compounds.

0008-4042/81/091347-10$01.00/0
©1981 National Research Council of Canada/Conseil national de recherches du Canada

Can. J. Chem. Downloaded from www.nrcresearchpress.com by 210.87.254.42 on 09/06/12
For personal use only.

Can. J. Chem. Downloaded from www.nrcresearchpress.com by 210.87.254.42 on 09/06/12
For personal use only.

Syntheses and Properties of Protium and Deuterium Labelled Triazenes

The aryl triazenes required in this study were prepared by coupling of the aryl diazonium cation with the 2-haloethylamine (15). The observation that the presence of an electron-withdrawing group in the phenyl ring, particularly at the *p*-position, increases the stability of the triazene and prevents formation of the pentaazadiene during the reaction of the aryldiazonium ion with the primary amine (18) was exploited in these preparations. In general it was found that a *p*-CN substituent in the phenyl ring conferred the desired stability characteristics. A special comment may be made in the case of the 2-bromoethyltriazene **8**. It was recently reported that when the *p*-nitrophenyldiazonium salt **2** was condensed with 2-bromoethylmethylamine **3** the product was that of intramolecular cyclization to the triazolinium salt (19). A similar triazolinium salt has been observed as a primary metabolite of BIC (20). No such cyclization took place in the preparation of the 2-bromoethyltriazene **8** that was obtained as a mixture of tautomers similar to the other triazenes. However, cyclization to a 1-aryl-Δ^2-1,2,3-triazoline may be significant in the aqueous decomposition of triazenes (see Discussion).

The purification of the 2-haloethyltriazenes required special care and was carried out by recrystallization at low temperatures. Purification by standard chromatographic methods was not possible owing to the rapid degradation on solid adsorbents as observed previously (21). The composition, structures, and purity of the triazenes were established by exact mass spectral measurements and by ^{1}Hmr and infrared spectroscopy. In several cases individual triazenes were characterized by their formation of ester derivatives from 3,5-dinitrobenzoic acid. The 2-haloethyltriazenes are thermally as well as chemically more labile than monoalkyl triazenes. Their instability increases in the sequence F < Cl < Br. It was also observed that the stability and reactivity are influenced by the number of methylene units intervening between the azide moiety and the halogen atom.

In common with other aryl triazenes, the 2-haloethyltriazenes were observed to exist in solution as mixtures of tautomers. Since the position of equilibrium has a direct bearing on the mechanism of decomposition, it was studied for each compound by nmr.

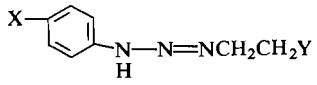

A

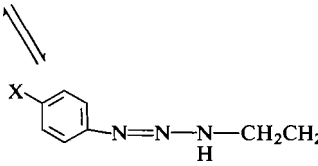

B

X = NO_2, CN, $COCH_3$, $CO_2C_2H_5$; Y = F, Cl, Br

An electron-withdrawing group X in the *para* position strongly favors tautomeric form A, whereas such a substituent in the *ortho* position gives tautomer A exclusively, results which are similar to those for other types of triazenes (22). 2-Haloethyltriazenes with an electron-withdrawing group in the *ortho* position (and therefore in tautomeric form A) are much more labile than their *para* substituted counterparts. For example triazene **14** was isolable as a stable solid whereas its *ortho* isomer decomposed as soon as it was formed. A possible explanation in accord with the proposed mechanism of decomposition is that the *ortho* triazene is fixed in tautomeric form A by hydrogen bonding:

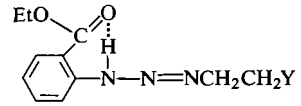

The resulting partial displacement of charge on to the aniline nitrogen should facilitate its protonation, leading to decomposition.

The presence of either tautomer in the equilibrium mixtures was detected by its characteristic bands in the infrared and ^{1}Hmr spectra. For example, the NH proton nmr signals corresponding to both tautomers are visible at −15°C. The NH proton absorbing at higher field could be assigned to

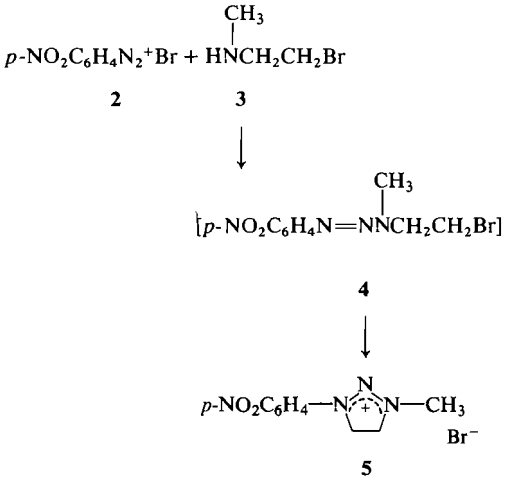

2 3 4 5

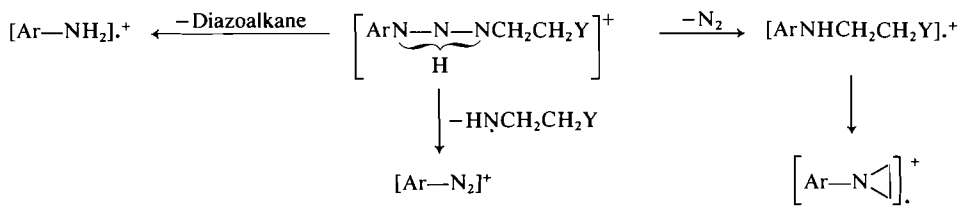

SCHEME 1

tautomer B on the basis of its coupling with the protons on the adjacent carbon at low temperature and the assigned couplings were confirmed by double resonance experiments. The mass spectra of the 2-haloethyltriazenes showed several fragmentation patterns (15) which were useful in characterizing the new compounds as shown in Scheme 1.

One new representative of the family of imidazole triazenes namely 5-[2-(2-fluoroethyl)-1-triazenyl]imidazole-4-carboxamide **28** was synthesized for a comparison of its chemical properties with those of the 2-fluoroethylaryltriazenes. Triazene **28** was light sensitive and chemically labile. It was characterized by its spectral properties and by its reaction with 3,5-dinitrobenzoic acid to form 2-fluoroethyl 3,5-dinitrobenzoate.

Certain specifically deuterated 2-haloethyltriazenes were required in order to establish the mechanistic pathways of formation of certain products. Accordingly triazenes **21** and **22** specifically deuterated on carbons C-1 and C-2, respectively, were synthesized from the corresponding deuterated amines which were in turn prepared following the procedures of Brundrett *et al.* (23).

Results

Triazenes **9**, **21**, **22**, **23**, and **28** were allowed to decompose at 37°C in phosphate buffered (0.1 *M*, pH 7.2) aqueous solution in gas-tight vials and the volatile products were analyzed by gc and identified by gc–ms (Table 1). Each product was identified by its retention time compared with a standard and by its characteristic mass spectrum (see Table 1). The involatile products were separated by chromatography and identified spectrophotometrically. 1-(*p*-Cyanophenyl)-3-(2-chloroethyl)triazene (**10**) afforded acetaldehyde (11.5% of volatiles), 1,2-dichloroethane (11.5% of volatiles), and 2-chloroethanol (77% of volatiles). In addition the following involatile products were identified: *p*-cyanoaniline (52% of involatiles), *N*-(2-chloroethyl)-*p*-cyanoaniline (30%), 1,2-di(*p*-cyanoanilino)ethane (10%), and *N*-(2-hydroxyethyl)-*p*-cyanoaniline (8%). When this triazene (**10**) was allowed to decompose in the presence of sodium bromide an additional product was 1-bromo-2-chloroethane.

Aqueous decomposition of the corresponding specifically deuterium labelled triazene 1-(*p*-cyanophenyl)-3-(2-chloro-1,1-dideuterioethyl)triazene (**21**) afforded acetaldehyde, 1,2-dichloro-1,1-dideuterioethane, a mixture of the isomeric deuterium labelled 2-chloroethanols bearing the deuterium predominantly on the carbon bearing hydroxyl (92:8), a mixture of isomeric deuterium labelled *N*-(2-chloroethyl)-*p*-cyanoanilines bearing deuteriums predominantly on carbon adjacent to chlorine (52:48), a mixture of isomeric deuterium labelled *N*-(2-hydroxyethyl)-*p*-cyanoaniline bearing deuteriums predominantly on carbon adjacent to hydroxyl (70:30), and deuterium labelled 1,2-di(*p*-cyanoanilino)ethane. Reaction of **21** in the presence of potassium bromide gave in addition labelled 1-bromo-2-chloroethane bearing deuterium mainly on the carbon bonded to bromine.

The isomeric deuterium labelled triazene 1-(*p*-cyanophenyl)-3-(2-chloro-2,2-dideuterioethyl)triazene (**22**), when allowed to decompose in pH 7 phosphate buffer, gave acetaldehyde with deuterium in the formyl group, 1,2-dichloro-1,1-dideuterioethane, a mixture of the isomeric deuterium labelled 2-chloroethanols bearing deuterium predominantly on the carbon bearing chlorine, (92:8), a mixture of isomeric deuterated *N*-(2-chloroethyl)-*p*-cyanoaniline bearing two deuteriums predominantly on carbon adjacent to nitrogen (53:47), a mixture of isomeric deuterium labelled *N*-(2-hydroxyethyl)-*p*-cyanoaniline bearing two deuteriums predominantly on carbon adjacent to nitrogen (70:30), and deuterium labelled 1,2-di(*p*-cyanoanilino)ethane. Reaction of **22** in the presence of potassium bromide gave, in addition, labelled 1-bromo-2-chloroethane bearing deuterium mainly on the carbon bonded to chlorine.

When 1-(*p*-cyanophenyl)-3-(2-chloro-2,2-dideuterioethyl)triazene **22** was allowed to react with 3,5-dinitrobenzoic acid the product was 2-chloro-2,2-dideuterioethyl 3,5-dinitrobenzoate **31** exclusively.

Aqueous decomposition of 1-(*p*-cyanophenyl)-3-

Can. J. Chem. Downloaded from www.nrcresearchpress.com by 210.87.254.42 on 09/06/12
For personal use only.

TABLE 1. Mass spectral identification of products of aqueous decomposition of protium and specifically deuterium labelled 2-haloethylaryltriazenes

Triazene	Reaction conditions	Decomposition products	*m/e* (Relative intensity, fragments)
21	Phosphate buffer	CH_3CHO	44 (42.5, M^+); 43 (21.4, CH_3CO); 29 (100, CHO)
		$ClCH_2CD_2Cl$	100 (14.2, M^+ ^{35}Cl); 102 (9.0, M^+ ^{37}Cl); 64, 66 (100, 32.3, $M^+ - HCl$); 63, 65 (31.2, 28.6, $M^+ - DCl$); 29 (79.3, C_2HD_2)
		$ClCH_2CD_2OH$	82 (2.6, M^+ ^{35}Cl); 84 (0.4, M^+ ^{37}Cl); 33
		$ClCD_2CH_2OH$	(100, CD_2OH); 31 (23.7, CH_2OH)
	Buffer + KBr	$BrCH_2CD_2Cl$	144 (5.6, M^+ ^{35}Cl); 146 (7.0, M^+ ^{37}Cl);
		$BrCD_2CH_2Cl$	65 (100, $M^+ - Br$, ^{35}Cl); 67 (31.1, $M^+ - Br$, ^{37}Cl)
22	Phosphate buffer	CH_3CDO	45 (46.2, M^+); 43 (17.6, CH_3CO); 30 (100, CDO)
		$ClCH_2CD_2Cl$	100 (7.7, M^+ ^{35}Cl); 102 (4.1, M^+ ^{37}Cl); 64, 66 (99.8, 29.6, $M^+ - HCl$); 63, 65 (25.4, 25.4, $M^+ - DCl$); 29 (100, C_2HD_2)
		$ClCH_2CD_2OH$	82 (1.4, M^+ ^{35}Cl); 84 (non visible, M^+ ^{37}Cl);
		$ClCD_2CH_2OH$	31 (100, CH_2OH); 33 (3.4, CD_2OH)
	Buffer + KBr	$BrCH_2CD_2Cl$	144 (4.4, M^+ ^{35}Cl); 146 (5.5, M^+ ^{37}Cl)
		$BrCD_2CH_2Cl$	65 (100, $M^+ - Br$, ^{35}Cl); 67 (31.4, $M^+ - Br$, ^{37}Cl)
23	Phosphate buffer	CH_3COCH_3	58 (24.9, M^+); 43 (100, $M^+ - 15$);
		$CH_3CCl{=}CH_2$	76 (43.7, M^+ ^{35}Cl); 78 (14.8, M^+ ^{37}Cl); 39 (63.8, M^+ ^{37}Cl); 41 (100, M^+ ^{35}Cl)
		$CH_3CHClCH_2Cl$	112 (4.9, M^+ ^{35}Cl); 114 (3.0, M^+ ^{37}Cl); 76, 78 (37.4, 12.7, $M^+ - HCl$); 63, 65 (100, 29.8, $M^+ - CH_2Cl$)
		$CH_3CHClCH_2OH$	65 (3.7, M^+ ^{35}Cl—CH_2OH); 67 (0.4, M^+ ^{37}Cl —CH_2OH); 58 (11.7, $M^+ - HCl$)
		CH_3COHCH_2Cl	31 (100, CH_2OH)
9 or **28**	Phosphate buffer	FCH_2CH_2F	66 (8.6, M^+); 46 (22.7, $M^+ - HF$); 33 (100, CH_2F)
		FCH_2CH_2OH	64 (12.4, M^+); 45 (15.7, $M^+ - F$); 31 (100, CH_2OH)
		$CH_3CHOHCH_2Cl$	44 (40.2, M^+); 43 (19.4, CH_3CO); 29 (100, CHO)

(2-chloropropyl)triazene at pH 7 and 37°C afforded acetone, 2-chloro-1-propanol and 1-chloro-2-propanol (3:2), 1,2-dichloropropane and 2-chloropropene, as well as *p*-cyanoaniline.

Representative examples of two 2-fluoroethyl derivatives were allowed to decompose in buffered aqueous solution and their products identified and quantitated. 5-[3-(2-Fluoroethyl)-1-triazenyl]imidazole-4-carboxamide **28** afforded 2-fluoroethanol (79% of volatiles), acetaldehyde and 1,2-difluoroethane (together constituting 21% of volatiles), 5-aminoimidazole-4-carboxamide (90% of involatiles), and 5-(2-fluoroethylamino)imidazole-4-carboxamide (~1%).

Decomposition of 1-(*p*-cyanophenyl)-3-(2-fluoroethyl)triazene **9** gave 2-fluoroethanol (76% of total volatiles), acetaldehyde and 1,2-difluoroethane (together constituting 24% of volatiles), and *p*-cyanoaniline (86%).

The kinetic half-lives of the 2-chloroethyltriazenes in buffered aqueous solution could be conveniently determined electrochemically by following the disappearance of the polarographic wave characteristic of the triazene moiety which appears in the range −0.910 to −1.038 V (Table 2). The observed half lives range from ca. 2 min to ca. 38 min. In the 1-(*p*-cyanophenyl)triazenes the sequence of stabilities depending on the halogen substituent is F > Cl > Br. For a given halogen in the 2-haloethyltriazenes the sequence of stabilities depending on the nature of the *p*-aryl substituent is CH_3CO > CH_3CH_2COO > CN. There was also observed to be a marked dependence of the decomposition half-life on the length of the alkyl chain bearing the halogen in the series of 1-(*p*-cyanophenyl)-3-(ω-chloroalkyl)triazenes such that butyl > propyl > pentyl > ethyl.

In the case of 1-(*p*-cyanophenyl)-3-(2-fluoroethyl)triazene **9** a marked pH dependence on the rate of decomposition at 26°C was observed (Table 3). The rate of decomposition increased rapidly as the pH was lowered, such that $t_{1/2}$ at pH 8, 7, and 6 was 10080 s, 7560 s, and 3180 s respectively. The rate of the more rapid decomposition of 1-(*p*-cyanophenyl)-3-(2-chloroethyl)triazene **10** at 26°C also showed a marked and progressive increase on lowering the pH in the wider range of 9.3 to 4.65.

Can. J. Chem. Downloaded from www.nrcresearchpress.com by 210.87.254.42 on 09/06/12
For personal use only.

Can. J. Chem. Downloaded from www.nrcresearchpress.com by 210.87.254.42 on 09/06/12
For personal use only.

TABLE 2. Half-life ($t_{\frac{1}{2}}$) of haloalkylaryltriazenes determined polarographically in phosphate buffered (0.1 *M*, pH 7.1) (95:5) aqueous acetonitrile at 37.5°C

	p-$YC_6H_4NHN{=}N(CH_2)_nX$				
Triazene	Y	X	n	Reduction potential (V)	$t_{\frac{1}{2}}$ (s)
9	CN	F	2	−0.925	1392
10	CN	Cl	2	−0.925	104
11	CN	Br	2	−0.942	94
12	CH_3CO	F	2	−0.925	2304
14	COOEt	F	2	−0.970	1891
15	COOEt	Cl	2	−0.980	164
23	CN	(2-Cl)	3	−0.930	1494
24	CN	Cl	3	−0.945	396
25	CN	Cl	4	−0.945	972
26	CN	Cl	5	−0.910	234
27	CH_3CO	Cl	3	−0.935	264
29[a]	CO_2Et	F	2	−0.965	1522
28[a]	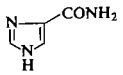	F	2	−1.038	704

[a] Determined in 95:5 aqueous DMSO.

Discussion

The types of volatile products formed from aqueous decomposition of the 2-haloethylaryltriazenes are consistent with the general Scheme 2. The observed increase in the rate of decomposition of the triazenes with lowered pH suggests a protonation step on the major tautomer first. This is followed by cleavage to produce the observed aromatic amine and the 2-chloroethyldiazonium ion or (its kinetic equivalent) the 2-chloroethyl cation. Analogy with the reactions of 2-haloethylnitrosoureas suggests hydride transfer and hydrolysis of the latter can give rise to acetaldehyde (23, 24). Alternatively, nucleophilic attack by chloride ion or water on the diazonium ion or the 2-chloroethyl cation gives rise to 1,2-dichloroethane and 2-chloroethanol, respectively. The results with the corresponding specifically deuterated 2-chloroethylaryltriazenes provided further insight into these pathways and the possible participation of the chloronium ion species.

TABLE 3. Variation of half-life ($t_{\frac{1}{2}}$) of haloalkylaryltriazenes determined polarographically as a function of solution pH at 26°C

Triazene	pH	$t_{\frac{1}{2}}$ (s)
10	4.65	161
	5.95	355
	6.0	378
	6.95	420
	8.0	516
	9.3	718
9	6.0	3175
	7.0	7549
	8.0	10080

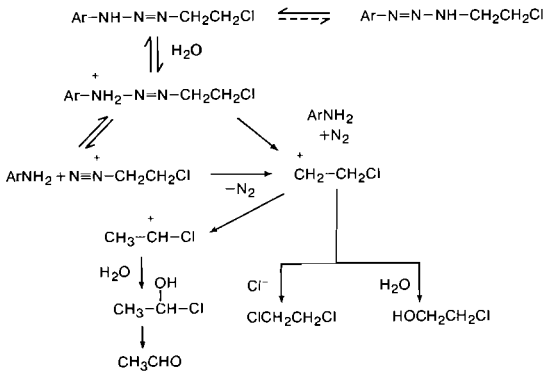

SCHEME 2

The deuterium labelled products obtained from the 2,2-dideuterio-2-chlorotriazene may be interpreted in terms of Scheme 3. The retention of the deuterium label in the formyl group of the acetaldehyde is consistent with generation of a transient 2-chloroethyl cation, a subsequent hydride shift to

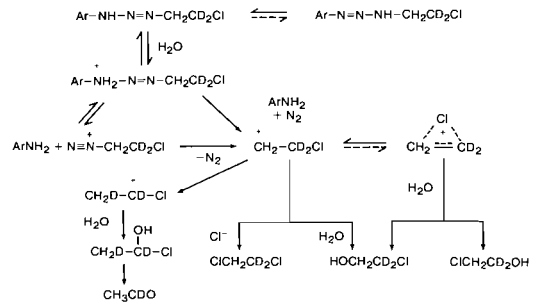

SCHEME 3

Can. J. Chem. Downloaded from www.nrcresearchpress.com by 210.87.254.42 on 09/06/12
For personal use only.

give the 1-chloroethyl cation, and hydrolysis of the latter. While either S_N2 by chloride ion attack on the conjugate acid of the triazene or S_N1 reaction via the 2-chloroethyl cation accounts for the 1,2-dichloroethane, the observed formation of a mixture of labelled 2-chloroethanols requires the intermediacy of another reactive species. The mixture of 2-chloroethanols contains predominantly (ca. 10:1) the isomer with deuterium adjacent to chlorine. As is the case with the corresponding 2-chloroethylnitrosoureas (23), the small amount (5–10%) of deuterium scrambling is consistent with a small contribution of the chloronium ion species in the overall decomposition.

Entirely complementary results are obtained in the decomposition of the 1,1-dideuterio-2-chlorotriazene. In this case, and as predicted from a pathway corresponding to Scheme 3, only unlabelled acetaldehyde is obtained. In this case, however, the two labelled 2-chloroethanols are obtained in a ratio of 10:1, containing predominantly the isomer with deuterium adjacent to hydroxyl, again in accord with a small contribution from the chloronium ion. Capture of the latter species by added bromide ion accounts for the formation of 1-bromo-2-chloroethane. Alternative decomposition pathways may be envisaged for the 2-haloethylaryltriazenes which would be indistinguishable from the main pathways outlined in Schemes 2 and 3, e.g. via the formation of a diazohydroxide.

$$ArNH{-}N{=}NCH_2CH_2Cl \xrightarrow{H_3O^+} ArNH_3^+ + HON{=}NCH_2CH_2Cl$$

The deuterium labelling experiments do, however, preclude the intermediacy of a diazoalkane since this requires the loss of one deuterium from the 2-chloroethanol and 1,2-dichloroethane isolated from the 1,1-dideuterio-2-chloroethyltriazene.

$$Ar\overset{+}{N}H_2N{=}NCH_2CH_2Cl \downarrow$$

$$ArNH_2 + N{\equiv}\overset{+}{N}CD_2CH_2Cl \not\downarrow$$

$$\bar{N}{=}\overset{+}{N}{=}CDCH_2Cl \downarrow H_2O$$

$$HOCDHCH_2Cl$$

Four involatile products were identified and quantitated from aqueous decomposition of triazene **10**. The use of specific deuterium labelling was especially informative in determining the origin of these products. While there are precedents for the direct loss of nitrogen from **10** to yield the 2-chloroethyl-*p*-cyanoaniline (15), the observation of deuterium scrambling favoring the rearrangement product (52:48) demands the intermediacy of a cyclic intermediate, but not a symmetrical one. The facts are in accord with the intermediate formation of the aryl 1,2,3-triazolinium salt (for which precedents exist, see refs. 13, 19, 25) as shown in Scheme 4. The much more marked preference for the formation of the rearrangement product with the 2-hydroxyethyl-*p*-cyanoanilines (70:30) confirms an unsymmetrical cyclic intermediate with, in this case, preferential attack by water at position 4 of the aryl 1,2,3-triazoline. Whereas the aziridine may participate as an intermediate, it alone cannot explain the observed results. Attack

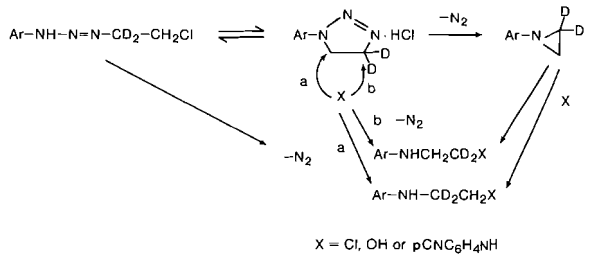

SCHEME 4

by *p*-cyanoaniline on the intermediate aryltriazenium salt (or aziridine) accounts for the formation of 1,2-*p*-cyanoanilinoethane. The results with the isomeric 1-(*p*-cyanophenyl)-3-(2-chloro-2,2-dideuterioethyl)triazene **22** are entirely consistent with Scheme 4.

The effects of a substituent α to the halogen were observed in the decomposition of 1-(*p*-cyanophenyl)-3-(2-chloropropyl)triazene. The formation of acetone is rationalized by initial formation of the diazonium ion (from protonation of the preferred tautomer) and then a formation of the 2-chloropropyl-3-cation leads to acetone by the steps indicated in Scheme 5. This requires a hydride transfer from the 2-chloropropyl cation to form the more stable 2-chloropropyl-2-cation.

In this case proton loss from the initially formed cation to give 2-chloropropene is favored by the additional methyl substituent in contrast to the 2-chloroethylaryltriazene case where no detectable quantities of vinyl chloride were produced (Schemes 2 and 3).

Nucleophilic attack by chloride ion (either S_N2 via the diazonium ion or by S_N1 reaction via the 2-chloropropyl-1-cation) accounts for 1,2-dichloropropene. Since both possible isomeric chloropropanols were identified as products, this

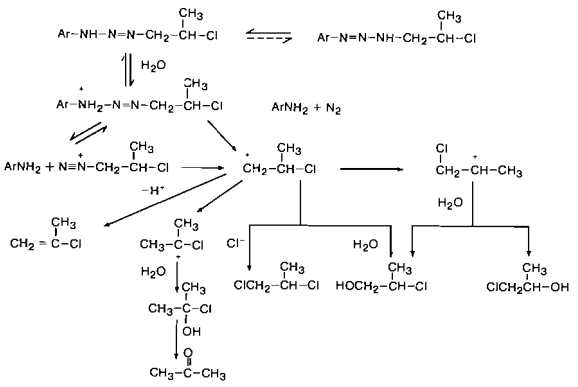

SCHEME 5

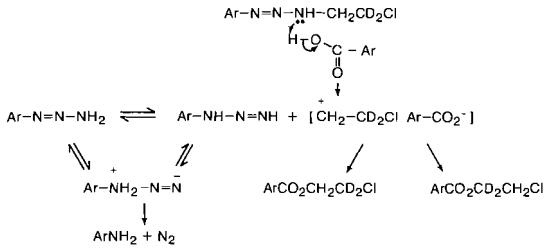

SCHEME 6

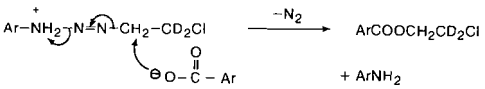

SCHEME 7

requires a rearrangement of the intermediate 2-chloro-1-propyl cation to the more stable 1-chloro-2-propyl cation. Thus in this example we employ a methyl group as a label rather than deuterium in Scheme 3. The observed ratio of 3:2 of 2-chloro-1-propanol:1-chloro-2-propanol is in accord with the expected greater contribution of this pathway compared with the approximately 10% contribution of the chloronium ion (26, 27) in Scheme 3. The fact that a greater yield of the chloropropanol product of the less stable cation is obtained suggests a substantial contribution of direct S_N2 attack on the precursor diazonium ion in Scheme 5 (such pathways have not been included in the schemes to simplify them.)

The observed order of decomposition of the homologous series of ω-haloalkyl-(*p*-cyanophenyl)-triazenes **10** > **26** > **24** > **25**, i.e. chloroethyl > chloropentyl > chloropropyl > chlorobutyl, deserves a comment. The fact that the chloroethyl homologue decomposes fastest is in accord with the intermediacy in this case only of the triazoline species. Analogous cyclization for **26**, **24**, and **25** is presumably precluded for entropic reasons. Moreover, only in the case of **10** can the chloronium ion contribute. The intervention of other pathways, involving a 1,2-hydride shift leading to a number of possible cationic intermediates in the 3, 4, and 5 carbon homologues, may account for the observed rate sequences which require detailed individual examination.

In connection with chloronium ion species, the observation of deuterium label scrambling in the decomposition of the 2-chloroethyltriazenes afforded an opportunity to investigate the mechanism of alkylation by these triazenes. Such a reaction has direct bearing on the cytotoxicity of triazenes which has been attributed in part to the alkylation of biological macromolecules. Alkylation of 3,5-dinitrobenzoic acid with 1-(*p*-cyanophenyl)-3-(2-chloro-2,2-dideuterioethyl)triazene afforded only the 2-chloro-2,2-dideuterioethyl 3,5-dinitrobenzoate, i.e. no detected label scrambling had occurred. This result is clearly at variance with one mechanism that has been suggested for this reaction (Scheme 6) (28). This mechanism requires the formation of a solvent caged ion pair which, since it permits Wagner–Meerwein rearrangement of the intermediate cation, would predict a certain degree of label scrambling as shown. A more likely pathway is by S_N2 displacement which correctly predicts the lack of label scrambling which is observed (Scheme 7). This result is then in accord with the previous conclusion of a substantial contribution from S_N2 mechanisms in the formation of products from the intermediate diazonium ions in Schemes 2, 3, and 5.

In conclusion, the above findings on the synthesis and details of the decomposition pathways of new 2-haloethylaryltriazenes may assist in the interpretation of their antitumor action. It may be noted in this connection that their observed tendency to decompose more rapidly under more acidic conditions may contribute to their selectivity of action owing to the characteristic of neoplastic tissue to exhibit somewhat lower pH than normal tissue (29, 30).

Experimental

Melting points were determined on a Fisher-Johns apparatus and are uncorrected. Infrared spectra were recorded on a Perkin-Elmer grating infrared spectrophotometer Model 421 and generally only the principal peaks are reported. Absorption spectra were measured in either distilled water or "spectrograde" solvents and were run on either a Beckman DB spectrophotometer, a Gilford 250 spectrophotometer, or a Unicam SP1700 UV spectrophotometer. Proton magnetic resonance spectra were recorded on Varian HA-100 or Bruker WH-200 instruments and were generally measured on a 10–15% (w/v) solution of the compound in the appropriate deuterated solvent. The reference compound was tetramethylsilane (TMS). Line positions are reported in ppm from the reference. Mass spectra

Can. J. Chem. Downloaded from www.nrcresearchpress.com by 210.87.254.42 on 09/06/12
For personal use only.

Can. J. Chem. Downloaded from www.nrcresearchpress.com by 210.87.254.42 on 09/06/12
For personal use only.

were determined with Associated Electrical Industries MS2, MS9, MS12, or MS50 (DS50) mass spectrometers. In general the ionization energy was 70 eV. Peak measurements were made by comparison with perfluorotributylamine at a resolving power of 1500. Kieselgel DF-5 (Camag, Switzerland) and Eastman Kodak precoated sheets were used for thin layer chromatography. Microanalyses were carried out by Mrs. D. Mahlow of this department.

General Procedure for 1(3)-Aryl-3(1)-2-haloalkyltriazenes

A solution of the aromatic amine (10 mmol) in concentrated hydrochloric acid (2.5 mL), diluted with water (12 mL) was diazotized at 0°C with sodium nitrite (0.80 g), dissolved in the minimum amount of water, and the resulting solution was stirred for 30 min or until clear. Excess acid was neutralized by addition of calcium carbonate (1.6 g). 2-Haloalkylamine hydrohalide (10 mmol) was dissolved in 5 mL water and deprotonated with potassium bicarbonate (11 mmol) (added solid) by stirring at 0°C until effervescence stopped. The diazonium salt solution was filtered cold and quickly transferred to the flask containing 2-haloalkylamine free base and then the reaction mixture was stirred for 5–10 min at 0°C. A precipitate of the triazene usually appeared immediately and was washed with cold water, air dried for 1 min, and transferred to a precooled test tube. The product was dissolved in a minimum amount of methylene chloride at room temperature whereupon an aqueous layer separated. The methylene chloride layer was carefully pipetted out and transferred to another precooled container. The triazene was precipitated out by cooling the methylene chloride solution to −30°C and adding cold petroleum ether dropwise. The precipitate was filtered, washed with cold petroleum ether, and air dried for 1–2 min.

Special precaution was exercized during the condensation of 2-bromoethylamine with the diazonium salt as well as in handling the product. The condensation was usually carried out at −10°C and the precipitate was transferred to a precooled test tube immediately after filtration in order to avoid decomposition. 2-Haloalkyltriazenes can be stored in Dry Ice for an indefinite period. The general procedure afforded the following triazenes.

1-(p-Nitrophenyl)-3-(2-fluoroethyl)triazene (6) (2.0 g, 95%), mp 98–100°C; ν_{max}: 3184, 3142, 1608, 1595, 1515, and 1340 cm^{-1}; δ (CD_2Cl_2, −20°C): 4.06 (2t, J_H = 5 Hz, J_F = 30 Hz, 2H, N—CH_2), 4.81 (2t, J_H = 5 Hz, J_F = 47 Hz, 2H, CH_2—F), 7.19–8.36 (m, 4H, aromatic), 8.5 and 9.55 (br 2s, exchangeable, 1H, NH); M^+: 212.0715 (45.90%) (calcd. for $C_8H_9FN_4O_2$: 212.0710); *m/e*: 184.0655 (M − N_2, calcd. for $C_8H_9FN_2O_2$: 184.0648), 164.0589 (2.38%) M − N_2 − HF, calcd. for $C_8H_8N_2O_2$: 164.0586), 150.0305 (68.78%) (M − NH − CH_2CH_2F, calcd. for $C_6H_4N_3O_2$: 150.0303), 138.0431 (27%) (M − N_2CHCH_2F, calcd. for $C_6H_6N_2O_2$: 138.0415), 122.0246 (100%) (calcd. for $C_6H_4NO_2$: 122.0228).

1-(p-Nitrophenyl)-3-(2-chloroethyl)triazene (7) (1.8 g, 79%) mp 64–66°C; ν_{max}: 3180, 3140, 1605, and 1595 cm^{-1}; δ ($CDCl_3$, −20°C): 3.9 (t, 2H, CH_2—Cl), 4.1 (t, 2H, N—CH_2), 7.2–8.35 (m, 4H, aromatic), 8.5 and 9.6 (1H, exchangeable, N—H); M^+: 228.0420 (2.45%) (calcd. for $C_8H_9ClN_4O_2$: 228.0414); *m/e*: 200.0361 (23.02%) (M − N_2, calcd. for $C_8H_9ClN_2O_2$: 200.0353), 164.0588 (18.12%) ((M − N_2) − HCl, calcd. for $C_8H_8N_2O_2$: 164.0586), 150.0346 (4.12%) (M − $NHCH_2CH_2Cl$, calcd. for $C_6H_4N_3O_2$: 150.0304), 138.0434 (37.79%) (M − N_2CHCH_2Cl, calcd. for $C_6H_6N_2O_2$: 138.0429).

1-(p-Nitrophenyl)-3-(2-bromoethyl)triazene (8) (1.2 g, 44%), mp 30–31°C; ν_{max} (due to rapid thermal decomposition the absorptions were too broad to be assigned to definite frequencies); δ ($CDCl_3$, −50°C): 3.8 (t, 2H, CH_2—Br), 4.25 (t, wH, N—CH_2), 7.2–8.3 (m, 4H, aromatic), 8.7 and 9.7 (br, 2s, 1H, N—H); *m/e*: 164.0599 (1.25%) ((M − N_2) − HBr, calcd. for $C_8H_8N_2O_2$: 164.0586), 138.0434 (100%).

1-(p-Cyanophenyl)-3-(2-fluoroethyl)triazene (9) (1.8 g, 93%), mp 95–96°C; ν_{max}: 3183, 3161, 2228, and 1609 cm^{-1}; δ ($CDCl_3$, −20°C): 4.08 (2t, J_H = 5 Hz, J_F = 30 Hz, 2H, N—CH_2), 4.8 (2t, J_H = 5 Hz, J_F = 47 Hz, 2H, CH_2—F), 7.2–7.75 (m. 4H, aromatic), 8.5 and 9.55 (br, 2s, exchangeable, 1H, N—H); M^+: 192.0804 (26.09%) (calcd. for $C_9H_9FN_4$: 192.0811); *m/e*: 164.0744 (1.39%) (M − N_2, calcd. for $C_9H_9FN_2$: 164.0750), 144.0683 (4.02%) ((M − N_2) − HF, calcd. for $C_9H_8N_2$: 144.0688), 130.0403 (33.87%) (M − $NHCH_2CH_2F$, calcd. for $C_7H_4N_3$: 130.0405), 118.0518 (32.11%) (M − N_2 − CH_2CH_2F, calcd. for $C_7H_6N_2$: 118.0531), 102.0342 (100%).

1-(p-Cyanophenyl)-3-(2-chloroethyl)triazene (10) (1.0 g, 48%), mp 68°C; ν_{max}: 3181, 3159, 2228, and 1608 cm^{-1}; δ (CD_2Cl_2, −45°C): 3.9 (t, 2H, CH_2—Cl). 4.1 (t, 2H, N—CH_2), 7.2–7.75 (m, 4H, aromatic), 8.55 and 9.6 (br, 2s, 1H, exchangeable, N—H); *m/e*: 182.0424 (7.23%) (M − N_2, calcd. for $C_9H_9ClN_2$: 182.0424), 144.0682 (9.74%) ((M − N_2) − HCl, calcd. for $C_9H_8N_2$: 144.0688), 132.0638 (11.06%), 131.0638 (100%), 118.0530 (62.79%).

1-(p-Cyanophenyl)-3-(2-bromoethyl)triazene (11) (yield 10–40%), mp 39°C. Compound **11** decomposed during ir scan; δ (CD_2Cl_2, −45°C): 3.7 (t, 2H, CH_2Cl), 4.9 (t, 2H, N—CH_2), 7.2–7.8 (m, 4H, aromatic), 8.7 (br, 1s, integrated for less than one proton, normally observed second broad singlet could not be traced, N—H); *m/e*: 225.9925 (20.26%) (M − N_2, calcd. for $C_9H_9N_2Br$: 225.9929), 144.0675 (9.74%) (M − N_2) − HBr, calcd. for $C_9H_8N_2$: 144.0688), 132.0638 (25.25%), 118.0531 (26.52%).

1-(p-Acetylphenyl)-3-(2-fluoroethyl)triazene (12) (0.8 g, 38%), mp 92–93°C; ν_{max}: 3192, 3161, and 1600 cm^{-1}; δ (CD_2Cl_2, − 45°C): 2.6 (s, 3H, Me), 4.08 (2t, J_H = 5 Hz, J_F = 30 Hz, 2H, N—CH_2), 4.84 (2t, J_H = 5 Hz, J_F = 47 Hz), 7.15–8.15 (m, 4H, aromatic), 8.94 and 10.0 (br, 2s, N—H); M^+: 209.0964 (35.12%) (calcd. for $C_{10}H_{12}FN_3O$: 209.0964); *m/e*: 182.0952 (41%) (M − N_2, calcd. for $C_{10}H_{13}FNO$: 182.0981), 148.0734 (16.55%), 135.0682 (44.49%), 120.0460 (87.20%) 119.0490 (100%).

1-(p-Acetylphenyl)-3-(2-chloroethyl)triazene (13) (0.6 g, 27%), mp 48–49°C; ν_{max}: 3188, 3158, and 1600 cm^{-1}; δ (CD_2Cl_2, − 45°C): 2.62 (s, 3H, Me), 3.9 (t, 2H, CH_2Cl), 4.12 (t, 2H, N—CH_2), 7.15–8.1 (m, 4H, aromatic), 8.7 and 9.75 (br, 2s, N—H); *m/e*: 197.0607 (21.67%) (M − N_2, calcd. for $C_{10}H_{12}ClNO$: 197.0607), 161.0851 (2.01%) ((M − N_2) − HCl, calcd. for $C_{10}H_{11}NO$: 161.0841), 148.0760 (77.08%), 120.0450 (100%).

1-(p-Ethoxycarbonylphenyl)-3-(2-fluoroethyl)triazene (14) (1.6 g, 56%), mp 85–87°C; ν_{max}: 3194, 3174, 1714, and 1610 cm^{-1}: δ (CD_2Cl_2, 200 MHz, − 55°C): 1.35 (t, 3H, Me), 4 (2t each accompanied by a multiplet at the base, J_H = 5 Hz, J_F = 47 Hz, 2H, N—CH_2), 4.27 (q, 2H, O—CH_2), 4.78 (2t, each accompanied by a triplet at the base, J = 5 Hz, J_F = 47 Hz, 2H, CH_2—F), 7.1–8.05 (m, 4H, aromatic), 8.6 (t, N—H, tautomer), 9.85 (br, s, N—H tautomer); M^+: 239.1077 (49.67%) (calcd. for $C_{11}H_{14}FN_3O_2$: 239.1070); *m/e*: 211.1017 (4.78%) (M − N_2, calcd. for $C_{11}H_{14}FNO_2$: 211.1008), 194.0737 (12.58%) (M − CH_2CH_3, calcd. for $C_9H_9FN_3O_2$: 194.0730), 191.0953 (6.93%) ((M − N_2 − HCl, calcd. for $C_{11}H_{13}NO_2$: 191.0947), 165.0795 (64.65%), 149.0599 (100%).

1-(p-Ethoxycarbonylphenyl)-3-(2-chloroethyl)triazene (15) (1.8 g, 70%), mp 58–60°C; ν_{max}: 3193, 3171, 1715, and 1605 cm^{-1}; δ ($CDCl_3$, − 30°C): 1.38 (t, 3H, Me), 3.84 (t, 2H, CH_2—Cl), 4.06 (t, 2H, N—CH_2), 4.34 (q, 2H, O—CH_2), 7.1–8.1 (m, 4H, aromatic), 8.55 and 9.58 (br, 2s, N—H); *m/e*: 227.0716 (21.16%) (M − N_2, calcd. for $C_{11}H_{14}ClNO_2$: 227.0713), 191.0949 (19.85%), ((M − N_2) − HCl, calcd. for $C_{11}H_{13}NO_2$: 191.0446), 165.0793 (71.29%), 120.0449 (100%).

Can. J. Chem. Downloaded from www.nrcresearchpress.com by 210.87.254.42 on 09/06/12
For personal use only.

1-(o-Nitrophenyl)-3-(2-fluoroethyl)triazene (16) (1.5 g, 70%), mp 30–31°C; ν_{max}: 3322, 1613, 1515, and 1338 cm^{-1}; δ ($CDCl_3$, −20°C): 4.08 (2t, J_H = 5 Hz, J_F = 30 Hz, 2H, N—CH_2), 4.84 (2t, J_H = 5 Hz, J_F = 47 Hz, 2H, CH_2—F), 6.94–8.34 (m, 4H, aromatic), 11.74 (s, 1H, NH); M^+: 212.0712 (67.61) (calcd. for $C_8H_9FN_4O$: 212.0710); *m/e*: 184.0650 (2.18%) (M − N_2, calcd. for $C_8H_9FN_2O_2$: 184.0648), 164.0589 (1.78%) ((M − N_2) − HF, calcd. for $C_8H_8N_2O_2$: 164.0586), 138.0430 (100%).

1(3)-(o-Nitrophenyl)3(1)-(2-chloroethyl)triazene (16a) (1.8 g, 79%), mp 55°C; ν_{max}: 3329, 1610, 1513, and 1338 cm^{-1}; δ ($CDCl_3$, −20°C): 3.92 (t, 2H, CH_2—Cl), 4.12 (t, 2H, N—CH_2), 6.94–8.34 (m, 4H, aromatic), 11.76 (s, 1H, NH); M^+: 228.0414 (21.74%) (calcd. for $C_6H_9ClN_4O_2$: 228.0414); *m/e*: 200.0353 (0.76%) (M − N_2, calcd. for $C_8H_9ClN_2O_2$: 200.0353), 164.0592 (1.02%) (calcd. for $C_8H_8N_2O_2$: 164.0586), 138.0429 (44.07%), 63.0121 (100%) (calcd. for C_2H_4Cl: 63.0001).

2-Amino-2,2-dideuterioethanol (17)

This compound was prepared by reducing glycolonitrile with lithium aluminum deuteride following the procedure of Brundrett *et al.* (23), bp 40–41°C/~0.15 Torr (lit. (23) bp 85–90°C/~10 Torr).

2-Chloro-2,2-dideuterioethylaminehydrochloride (18)

A solution of **17** (2 g, 21.6 mmol) in $CHCl_3$ (10 mL) was saturated with hydrogen chloride gas at 0°C. To the solution was added thionyl chloride (10 mL) diluted with $CHCl_3$ (10 mL) at 0°C and the solution was allowed to warm slowly to 70°C. The stirring was continued for 5 h. The solvent and the excess of the thionyl chloride were removed under vacuum. The residue was purified by recrystallization from absolute ethanol. Yield 1.5 g, 60%, mp 141–143°C (lit. (33) undeuterated, mp 143–146°C).

2-Amino-1,1-dideuterioethanol (19)

Compound **19** was prepared by reducing glycine ethyl ester with lithium aluminum deuteride following the procedure of Brundrett *et al.* (23), bp 35–38°C/~0.15 Torr (lit. (23) bp 83–88°C/~10 Torr).

1-Chloro-1,1-dideuterioethylaminehydrochloride (20)

The aminoethanol **19** was chlorinated following the procedure described for the chlorination of **17**, mp 144–146°C.

The following triazenes were also prepared by the general procedure. The diazonium salt solutions were allowed to react with the corresponding chloro-alkylamines and the products were purified by recrystallization at low temperature.

1-(p-Cyanophenyl)-3-(2-chloro-1,1-dideuterioethyl)triazene (21), mp 66–67°C; ν_{max}: 3181, 3160, 2224, and 1608 cm^{-1}; δ (CD_2Cl_2, − 10°C): 3.84 (s, 2H, CH_2—Cl), 7.2–7.75 (m, 4H, aromatic), 8.56 and 9.15 (br, 2s, exchangeable, N—H); M^+: 210.0644 (3.03%) (calcd. for $C_9H_7D_2ClN_4$: 210.0641), 182.0578 (18.69%) (M − N_2, calcd. for $C_9H_7D_2ClN_2$: 182.0580), 146.0810 (23.62%) ((M—N_2) − HCl, calcd. for $C_9H_6D_2N_2$: 146.0813), 118.0532 (100%).

1-(p-Cyanophenyl)-(3)-(2-chloro-2,2-dideuterioethyl)triazene (22), mp (67–68°C); ν_{max}: 3181, 3159, 2224, and 1608 cm^{-1}; δ (CD_2Cl_2, − 15°C): 4.03 (s, 2H, N—CH_2), 7.2–7.70 (m, 4H, aromatic), 8.5 and 9.45 (br s, exchangeable, N—H); M^+: 210.0661 (0.50%) (calcd. for $C_9H_7D_2ClN_4$: 210.0641); *m/e*: 182.0581 (63.95%) (M − N_2, calcd. for $C_9H_7D_2ClN_2$: 182.0580), 146.0811 (33.91%) ((M − N_2) − HCl, calcd. for $C_9H_6D_2N_2$: 146.0813), 133.0724 (100%).

1-(p-Cyanophenyl)-3-(2-chloropropyl)triazene (23), (1.5 g, 72%), mp 74–75°C; compound **23** decomposed during ir scan; δ (CD_2Cl_2, −20°C): 1.56 (2d, 3H, CH_3), 3.95 (2d, 2H, N—CH_2), 4.4 (m, 1H, CHCl), 7.2–7.8 (m, 4H, aromatic), 8.6 and 9.5 (br, 2s, exchangeable, N—H); M^+: 222.0672 (12.10%) (calcd. for $C_{10}H_{11}ClN_4$: 222.0672), 194.0613 (0.57%) (M − N_2, calcd. for $C_{10}H_{11}ClN_2$: 194.0611), 158.0844 (1.55%) ((M − N_2) − HCl calcd. for $C_{10}H_{10}N_2$: 158.0844), 118.0530 (30.08%), 102.0344 (100%).

1-(p-Cyanophenyl)-3-(3-chloropropyl)triazene (24), (1.5 g, 67%), mp 64–65°C; ν_{max}: 3186, 3162, 2228, and 1610 cm^{-1}; δ (CD_2Cl_2, −15°C): 2.18 (t, 2H, —CH_2—), 3.65 (t, 2H, CH_2—Cl), 6.85 (t, 2H, N—CH_2), 7.2–7.8 (m, 4H, aromatic), 8.5 and 9.5 (br, 2s, exchangeable, N—H); M^+: 222.0673 (7.79%) (calcd. for $C_{10}H_{11}ClN_4$: 222.0673), 194.0609 (3.62%) (M − N_2 calcd. for $C_{10}H_{11}ClN_2$: 194.0611), 158.0841 (7.93%) ((M − N_2) − HCl, calcd. for $C_{10}H_{10}N_2$: 158.0843), 132.0639 (2.55%), 131.0438 (1.26%), 118.0531 (100%).

1-(p-Cyanophenyl)-3-(4-chlorobutyl)triazene (25), (1.6 g 67%), mp 82°C; ν_{max}: 3186, 3163, 2220, and 1608 cm^{-1}; δ (CD_2Cl_2, −15°C): 1.85 (br, m, 4H, —CH_2CH_2—), 3.4–3.85 (br, m, 4H, N—CH_2 and CH_2—Cl), 7.2–7.8 (m, 4H, aromatic), 8.35 and 9.4 (br, 2s, exchangeable, N—H); M^+: 236.0829 (12.05%) (calcd. for $C_{11}H_{13}ClN_4$: 236.0829); *m/e*: 208.0768 (1.53%) (M − N_2, calcd. for $C_{11}H_{13}ClN_2$: 208.0768), 172.0921 (0.24%) ((M − N_2) − HCl, calcd. for $C_{11}H_{12}N_2$: 172.1010), 131.0573 (16.39%), 118.0529 (56.77%), 102.0343 (100%).

1-(p-Cyanophenyl)-3-(5-chloropentyl)triazene (26), (2.16 g, 84%), mp 66°C; ν_{max}: 3182, 3160, 2220, and 1610 cm^{-1}; δ (CD_2Cl_2, −15°C): 1.7 (br, m, 6H), 3.65 (br, sextet, N—CH_2 and CH_2—Cl), 7.2–7.8 (m, 4H, aromatic), 8.4 and 9.5 (br, 2s, exchangeable, N—H); M^+: 250 (6.12%) (calcd. for $C_{12}H_{15}ClN_4$: 250.0985); *m/e*: 222.0926 (1.33%) (M− N_2, calcd. for $C_{12}H_{15}N_2$: 222.0924), 131.0569 (12.78%), 118.0529 (100%).

1-(p-Acetylphenyl)-3-(3-chloropropyl)triazene (27), (1.2 g, 50%), mp 50–51°C; ν_{max}: 3186, 3157, 1674, and 1600 cm^{-1}; δ (CD_2Cl_2, −45°C): 2.2 (br, 2H, —CH_2—), 2.62 (s, 3H, Me), 3.67 (t, 2H, CH_2—Cl), 3.92 (t, 2H, N—CH_2), 7.15–8.1 (m, 4H, aromatic), 8.5 and 9.65 (br, 2s, N—H); M^+: 239.0825 (1.70%) (calcd. for $C_{11}H_{14}ClN_3O$: 239.0826), 211.0765 (1.09%), (M—N_2, calcd. for $C_{11}H_{14}ClNO$: 211.0766), 175.0996 (3.56%) ((M − N_2) − HCl, calcd. for $C_{11}H_{13}NO$: 175.0997), 120.0450 (83.85%).

5-[3-(2-Fluoroethyl-1-triazenyl]-imidazole-4-carboxamide (28)

Compound **28** was prepared following the procedure of Shealy *et al.* (2). 2-Fluoroethylamine free base (400 mg, 6.3 mmol) was taken in dry ethyl acetate (30 mL) and stirred under nitrogen. To the stirred solution was added thoroughly dried 5-diazoimidazole-4-carboxamide (800 mg, 4.6 mmol) in one portion. The reaction mixture was protected from light and the stirring was continued for 1 h. The resulting white solid was collected by filtration, washed with ethyl acetate, and dried *in vacuo* at room temperature, yielding 850 mg (92%) of the triazene, mp 119°C (dec); δ_{max}: 3478, 3249, 3079, 1645, 1585, 1430, and 1380 cm^{-1}; *m/e*: 138.0396 (11.75%) (M − $NHCH_2CH_2F$, calcd. for $C_4H_4N_5O$: 138.0398), 137.0341 (100%). *Anal.* calcd. for $C_6H_9N_6O$: C 36.0, H 4.5, N 42.0; found: C 35.6, H 4.5, N 41.6%.

General Procedure for the Esterification of 3,5-Dinitrobenzoic Acid by Phenyl-2-haloalkyltriazenes

The triazene (4 mmol) was suspended in ether (15 mL) at −20°C. To the stirring suspension was added dropwise 3,4-dinitrobenzoic acid (700 mg, 3.3 mmol) dissolved in ether (20 mL). After the addition was completed, the reaction mixture was allowed to warm up to room temperature and the stirring was continued for another 2 h. The reaction mixture was filtered and the solvent was evaporated leaving a syrupy residue which on tituration with chloroform deposited most of the unreacted acid. The ester was purified by chromatography on silica using benzene as eluant. When the imidazole triazene **28** was used, the reaction mixture was stirred for two days at room temperature protected from light at all times. This procedure afforded the following esters in varying yield.

2-Fluoroethyl-3,5-dinitrobenzoate (29)

From **9** and **28**, yield 60% and 30% respectively, mp 84–85°C (lit. (31) mp 86°C); ν_{max}: 1735, 1625, 1545, and 1340 cm^{-1} (in CH_2Cl_2); δ ($CDCl_3$, 200 MHz): 4.7 (m, 2H, O—CH_2), 4.99 (2m, 2H, CH_2—F), 9.18–9.3 (m, 3H). Aromatic compound **29** was identical in every respect with a sample obtained from reaction of 3,5-dinitrobenzoyl chloride with 2-fluoroethanol.

2-Chloroethyl-3,5-dinitrobenzoate (30)

From **10**, yield 40%, mp 89–90°C (lit. (32) mp 92°C); ν_{max}: 1735, 1625, 1545, and 1340 cm^{-1}; δ (CD_2Cl_2): 3.88 (t, 2H, CH_2—Cl), 4.72 (t, 2H, OCH_2), 9.14–9.28 (m, 3H, aromatic); M^+: 273.9981 (2.98%) (calcd. for $C_9H_7N_2O_6Cl$: 273.9992); *m/e*: 239.0299 (5.78%) (M − Cl, calcd. for $C_9H_7N_2O_6$: 239.0304). Compound **30** was identical with a sample obtained from reaction of 3,5-dinitrobenzoylchloride with 2-chloroethanol.

2-Chloro-2,2-dideuterioethyl-3,5-dinitrobenzoate (31)

From **22**, yield 40%, mp 89°C; ν_{max}: 1735, 1625, 1535, and 1340 cm^{-1}; δ ($CDCl_3$): 4.6 (s, 2H, O—CH_2), 9.1–9.3 (m, 3H, aromatic); M^+: 276.0117 (8.53%) (calcd. for $C_9H_5D_2ClN_2O_6$: 276.0117). *Anal.* calcd. for $C_9H_5D_2ClN_2O_6$: C 39.05, N 10.12; found: C 39.18, N 9.83%.

2-Bromoethyl-3,5-dinitrobenzoate (32)

From **11**, yield 10%, mp 82°C (lit. (33) mp 85–86°C); ν_{max}: 1740, 1625, 1540, and 1340 cm^{-1}; δ ($CDCl_3$): 3.70 (t, 2H, CH_2—Br), 4.66 (t, 2H, O—CH_2), 9.1–9.3 (m, 3H, aromatic). Compound **32** was identical with a sample obtained from reaction of 3,5-dinitrobenzoylchloride with 2-bromoethanol.

Acknowledgements

We would like to thank Mr. Jacques Gibeau and Miss Susan Ranson for the electrochemical determinations. This investigation was supported by grant 1R01-CA21488-01 awarded by the National Cancer Institute, DHEW (U.S.A.) to J.W.L. and by a grant from the Alberta Provincial Cancer Hospitals Board.

1. S. K. Carter and M. A. Friedman. Eur. J. Cancer, **8**, 85 (1972).
2. Y. F. Shealy and C. A. Krauth. Nature, **210**, 208 (1966).
3. G. Hoffman, I. Kline, M. Gang, D. D. Tyrer, J. M. Venditti, and A. Goldin. Cancer Chemother. Rep. Part 1, **52**, 715 (1968).
4. Y. F. Shealy, C. A. O'Dell, and C. A. Krauth. J. Pharm. Sci. **64**, 177 (1969).
5. J. L. Skibba, G. Ramirez, D. D. Beal, R. O. Johnson, and G. T. Bryan. Proc. Am. Assoc. Cancer Res. **10**, 83 (1969).
6. J. L. Skibba and G. T. Bryan. Toxicol. Appl. Pharmacol. **18**, 707 (1971).
7. R. Preussman, A. von Hodenberg, and H. Hengy. Biochem. Pharmacol. **18**, 1 (1969).
8. Y. F. Shealy. J. Pharm. Sci. **59**, 1533 (1970).
9. T. P. Johnston, G. S. McCaleb, P. S. Opliger, and J. A. Montgomery. J. Med. Chem. **9**, 892 (1966).
10. J. A. Montgomery, T. P. Johnston, and Y. F. Shealy. *In* Medicinal chemistry. Part II. 4th ed. *Edited by* A. Burger. Wiley–Interscience, New York. 1979. pp. 629–633.
11. G. D. Wheeler. *In* Cancer chemotherapy. *Edited by* A. C. Sartorelli. American Chemical Society, Washington, DC. 1976. pp. 87–119.
12. T. A. Connors. Top. Curr. Chem. **52**, 160 (1974).
13. J. A. Montgomery. Cancer Treat. Rep. **60**, 651 (1976).
14. K. Vaughan and M. F. G. Stevens. Q. Rev. 377 (1977).
15. T. P. Ahern, H. Fong, and K. Vaughan. Can. J. Chem. **55**, 170 (1977).
16. G. J. Katheway, C. Hansch, K. H. Kim, S. R. Milstein, G. L. Schmidt, R. N. Smith, and F. R. Quinn. J. Med. Chem. **21**, 563 (1978).
17. A. J. Lin and T. L. Loo. J. Med. Chem. **21**, 268 (1978).
18. T. P. Ahern and K. Vaughan. Chem. Commun. 701 (1973).
19. H. Hansen, S. Hunig, and K. Kishi. Chem. Ber. **112**, 445 (1979).
20. J. A. Montgomery. Cancer Treat. Rep. **60**, 125 (1976).
21. R. J. LeBlanc and K. Vaughan. Can. J. Chem. **50**, 2544 (1972).
22. K. Vaughan. J. Chem. Soc. Perkin Trans. II, 17 (1977).
23. R. B. Brundrett, J. W. Cowens, M. Colvin, and I. Jardin. J. Med. Chem. **19**, 958 (1976).
24. D. B. Ludlum, B. S. Kramer, J. Want, and C. Fenselau. Biochemistry, **14**, 5480 (1975).
25. H. W. Heine and D. A. Tomalia. J. Am. Chem. Soc. **84**, 993 (1962).
26. W. J. Hehre and P. C. Hiberty. J. Am. Chem. Soc. **96**, 2665 (1974).
27. G. A. Olah, D. A. Beal, and P. W. Westerman. J. Am. Chem. Soc. **95**, 3387 (1973).
28. N. S. Isaacs and E. Rannala. J. Chem. Soc. Perkin Trans. II, 899 (1974); 902 (1974).
29. T. A. Connors, B. C. V. Mitchley, V. M. Rosenoer, and W. C. J. Ross. Biochem. Pharmacol. **13**, 395 (1964).
30. W. C. J. Ross. Biochem. Pharmacol. **8**, 235 (1961).
31. B. C. Saunders, G. J. Tracey, and I. G. E. Wilding. J. Chem. Soc. 773 (1949).
32. L. W. Jones and G. R. Burns. J. Am. Chem. Soc. **47**, 2966 (1925).
33. O. Theodorebenfy, J. R. Stanmyer, Jr., B. Millimgan, and E. W. Westhead, Jr. J. Org. Chem. **20**, Part 2, 1777 (1955).

Can. J. Chem. Downloaded from www.nrcresearchpress.com by 210.87.254.42 on 09/06/12
For personal use only.

Solvent induced frequency shifts of the C—H stretching bands of *n*-octane. A Fourier transform infrared study[1]

D. G. CAMERON, S. C. HSI,[2] J. UMEMURA,[3] AND H. H. MANTSCH

Division of Chemistry, National Research Council of Canada, Ottawa, Ont., Canada K1A 0R6

Received December 10, 1980

D. G. CAMERON, S. C. HSI, J. UMEMURA, and H. H. MANTSCH. Can. J. Chem. **59**, 1357 (1981).

Using a Fourier transform spectrometer the frequencies and bandwidths of the infrared active C—H stretching modes of *n*-octane were determined in a variety of solvents with refractive indices from 1.63 (carbon disulfide) to 1.28 (*n*-perfluorooctane), and dielectric constants from 37.5 (acetonitrile) to 1.8 (*n*-perfluorooctane). The frequency shifts were correlated with the refractive indices and dielectric constants of the solvents, and fitted with the equation of David and Hallam (Spectrochim. Acta, Part A, **23**, 593 (1967)). Generally, solution results in shifts to frequencies lower than those observed in the gas phase. However, solution in *n*-perfluorooctane resulted in a shift to a higher frequency, behavior in accord with the above equation but not previously observed.

D. G. CAMERON, S. C. HSI, J. UMEMURA et H. H. MANTSCH. Can. J. Chem. **59**, 1357 (1981).

Utilisant un spectromètre à transformation de Fourier et opérant dans des solvants dont l'indice de réfraction varie de 1,63 (sulfure de carbone) à 1,28 (*n*-perfluorooctane) et la constante diélectrique varie de 37,5 (acétonitrile) à 1,8 (*n*-perfluorooctane), on a déterminé les fréquences et les largeurs des bandes de vibration du C—H, du *n*-octane actives dans l'infrarouge. On a établi une corrélation entre les déplacements des fréquences et les indices de réfraction et les constantes diélectriques des solvant et on les a ajustés avec l'équation de David et Hallam (Spectrochimica Acta, Part A, **23**, 593 (1967)). Généralement la mise en solution provoque des déplacements de fréquence qui sont plus faibles que ceux observés en phase gazeuse. Cependant la mise en solution dans le *n*-perfluorooctane provoque un déplacement vers les hautes fréquences; ce comportement, en accord avec l'équation mentionnée ci-dessus, n'avait pas encore été observé jusqu'à maintenant.

[Traduit par le journal]

Introduction

In a recent study (1) of micelle formation in aqueous solutions of sodium *n*-alkanoates the C—H stretching bands of the acyl chains were observed at frequencies substantially higher than those reported in the literature. These high frequencies were found at low concentrations at which the alkanoates are present in the monomeric form, and we tentatively attributed the shifts to solvent induced effects.

Solvent induced frequency shifts have been extensively studied since the initial applications of Onsager's theory (2–4). However, the studies have generally been restricted to localized vibrations of small molecules in order to approximate a diatomic oscillator (5–7). We were unable to locate a report on solvent effects on the C—H stretching bands of acyl chains. Consequently, we have investigated the solvent induced frequency shifts of *n*-octane using a Fourier transform infrared spectrometer, and report the results herein.

Experimental

Materials were of spectroscopic or analytical reagent grade and their purities were checked by gas–liquid chromatography prior to their use.

The gas phase spectrum was recorded in a 100 cm pathlength cell at a pressure of 10 Torr. For solution spectra, demountable 25 μm pathlength calcium fluoride cells were used. The spectrum of pure *n*-octane was recorded in a 2.5 μm calcium fluoride cell. As the peak absorbances in the solutions used in the study (1% by volume) were about 0.01, frequency errors due to anomalous dispersion effects were negligible (8). Slight frequency errors can be expected in the case of pure *n*-octane. However, as the bands are quite broad (20–30 cm^{-1} half bandwidth) the effect is expected to be small. This was confirmed by plotting frequency versus concentration over the concentration range 1% v/v to 100% v/v. Linear plots were obtained with both CS_2 and CCl_4 as solvents, whereas nonlinearities would be expected if there were appreciable anomalous dispersion effects.

Spectra were recorded at 25°C on a Digilab FTS-11 Fourier transform infrared spectrometer equipped with a 15 μm low frequency cutoff high sensitivity mercury cadmium telluride detector (Infrared Associates, New Brunswick, NJ). Typically, 400 interferograms recorded with an optical velocity of 1.2 cm s^{-1} and maximum optical retardation of 0.25 cm were co-added, apodized with a triangular function, and Fourier transformed with 4 levels of zero filling resulting in a spectral resolution of 4 cm^{-1}.

Frequencies were determined by computing the center of area of the topmost segment of a band employing data points within ±1 cm^{-1} of the frequency of the maximum encoded data point. As the frequency scale of this instrument is reproducible to within ≤ ±0.005 cm^{-1} this technique yields frequencies accurate and reproducible to better than ±0.1 cm^{-1} (9). Bandwidths were determined by subtracting a baseline interpolated between 2990 and 2820 cm^{-1} from the spectrum and computing the width at nine-tenths height of the resultant band.

Refractive indices were determined at 25°C at the sodium

[1]NRCC Publication No. 19040.

[2]On leave from the Institute of Applied Chemistry, Changchun, China.

[3]NRCC Postdoctoral Fellow 1978–1980. Permanent address: Institute for Chemical Research, Kyoto University, Uji, Kyoto-fu, 611 Japan.

0008-4042/81/091357-04$01.00/0

©1981 National Research Council of Canada/Conseil national de recherches du Canada

Can. J. Chem. Downloaded from www.nrcresearchpress.com by 210.87.254.5 on 09/06/12
For personal use only.

Can. J. Chem. Downloaded from www.nrcresearchpress.com by 210.87.254.5 on 09/06/12
For personal use only.

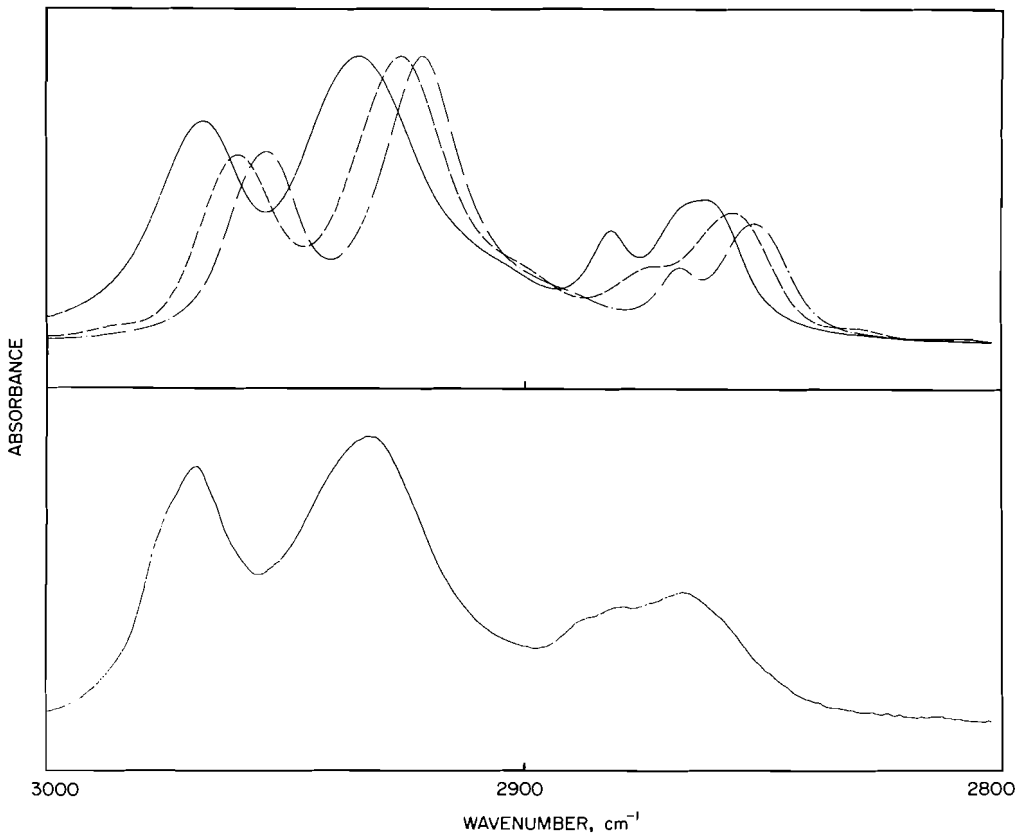

FIG. 1. C—H stretching region of the infrared spectrum of *n*-octane. Top: pure liquid (---); 1% v/v solution in carbon disulfide (——·——); 1% v/v solution in *n*-perfluorooctane (—). Bottom: vapour phase, 40 Torr in 1 m cell.

wavelength using an Abbé refractometer and agreed with literature values. The refractive index of perfluoromethylcyclohexane was determined by linear extrapolation of a plot of refractive index versus concentration of a series of solutions of perfluoromethylcyclohexane in hexafluorobenzene. Experimental values were linear over the range 1% v/v to 70% v/v. Dielectric constants were taken from the literature (10).

Results and Discussion

Figure 1 shows the C—H stretching region of the infrared spectrum of *n*-octane as a gas, liquid, and 1% v/v solutions in carbon disulfide and *n*-perfluorooctane. Four fundamentals are present in each spectrum. They result from the asymmetric and symmetric methyl and methylene stretching modes although in the vapour phase spectrum the symmetric bands can not be distinguished due to overlap of the bands and the superposition of rotational structure.

The changes on going from the gas to the liquid phases are typical of those observed on condensation. The rotational structure is lost and all bands shift to lower frequency. Solution in carbon disulfide, which has the highest refractive index ($n_D = 1.632$) of the solvents employed in this study, results in further shifts to lower frequency and some reduction of the bandwidth. Solution in *n*-perfluorooctane ($n_D = 1.282$) results in shifts to frequencies close to those of the gas phase, and broadening of the bands.

These spectra and spectral changes represent the largest variations observed in the study. The detailed results observed with these and the other solvents are discussed below.

Frequency Shifts

Table 1 lists the frequencies of the asymmetric C—H stretching bands in the infrared spectra of gaseous and liquid *n*-octane, and 1% v/v solutions of *n*-octane in a variety of solvents. Also listed are the refractive indices and the dielectric constants of the solvents.

Attempts were made to relate the frequency shift on solution to the refractive indices and dielectric constants of the solvents. Of the various equations used (3, 5, 11) only that of David and Hallam (11) resulted in a satisfactory fit of the data. The equation has the form

$$[1] \quad \Delta\nu = C_1 + C_2(n^2 - 1)/(n^2 + 2) + C_3(\varepsilon - 1)/(\varepsilon + 2)$$

TABLE 1. Solvent induced frequency shifts (in cm^{-1}) of the asymmetric C—H stretching bands of *n*-octane

	Asymmetric CH_3 stretch		Antisymmetric CH_2 stretch			
	ν	Δν	ν	Δν	n_D	ε
Vapour	2969.2		2932.6			
Liquid	2959.0	10.2	2925.0	7.6	1.397	1.904
1% v/v in:						
Carbon disulfide	2953.9	15.3	2921.3	11.3	1.632	2.663
Tetrachloroethylene	2958.7	10.5	2926.8	5.8	1.505	2.365
Carbon tetrachloride	2959.4	9.8	2927.3	5.3	1.460	2.234
Chloroform-*d*	2959.2	10.0	2927.5	5.1	1.445	4.813[b]
Hexafluorobenzene	2964.1	5.1	2932.6	0.0	1.377	2.029
Acetone-d_6	2961.2	8.0	2929.0	3.6	1.356	21.4[b]
Acetonitrile	2962.5	6.7	[a]		1.344	37.5
n-Perfluorooctane	2967.3	1.9	2934.8	−2.2	1.282	1.79
Perfluoromethylcyclohexane	2966.3	2.9	2932.4	0.4	1.278	1.85

[a]Not determined because of overlap with the CH_3 stretching band of acetonitrile.
[b]Values are those of perhydro compounds.

TABLE 2. Differences (in cm^{-1}) between calculated and observed frequency shifts, and bandwidths at nine-tenths peak height of the C—H stretching bands of *n*-octane

	Asymmetric CH_3 stretch		Antisymmetric CH_2 stretch	
	$\nu_{obs} - \nu_{calc}$	$\Delta\nu_{0.9}$	$\nu_{obs} - \nu_{calc}$	$\Delta\nu_{0.9}$
Carbon disulfide	−0.1	7.2	−0.9	6.8
Tetrachloroethylene	+0.4	7.5	+0.6	8.4
Carbon tetrachloride	−0.6	7.2	−0.4	7.9
Chloroform-*d*	−0.3	7.5	+0.3	8.5
Hexafluorobenzene	+1.0	9.0	+2.0	10.3
Acetone-d_6	−0.5	7.3	−0.1	9.4
Acetonitrile	+0.6	6.5	—	—
n-Perfluorooctane	+0.3	7.9	+0.7	10.9
Perfluoromethylcyclohexane	−0.8	8.9	−2.1	12.9

where Δν is the difference in frequency between the gas and solution phase spectra, and C_1, C_2 and C_3 are constants. Using the data in Table 1, the coefficients of the equations for the asymmetric methyl and methylene stretching bands obtained by least-squares solution are:

CH_3 asymmetric stretch

$$C_1 = -10.7, C_2 = 68.8, C_3 = 3.62$$

CH_2 antisymmetric stretch

$$C_1 = -13.4, C_2 = 63.1, C_3 = 3.64$$

In these equations the refractive index term dominates and the effects of the dipolar interactions are an order of magnitude smaller. Nonetheless the latter term is critical; even in the case of low dielectric constant solvents, neglect of the term results in a less satisfactory fit of the data.

The degree to which the data are fitted is shown in Table 2, which lists the differences between the observed (ν_{obs}) and calculated (ν_{calc}) frequency shifts. The maximum differences for the methyl and methylene bands are 1.0 and 2.1 cm^{-1}, respectively. The fit of the methyl frequencies is slightly better than that of the methylene frequencies. The most probable cause is that the methyl band of *n*-octane is not affected by differences in conformational distribution in the various solvents, while the methylene band is (12).

We also note that in *n*-perfluorooctane solution the methylene stretching band is at a higher frequency than in the gas phase. That this can occur when $\varepsilon - 1$ is small, C_1 is negative, and $|C_1| > C_2(n^2 - 1)/(n^2 + 2)$, is apparent from eq. [1]; furthermore, Buckingham (7) has suggested the possibility of a blue frequency shift from his theoretical treatment. However, as far as we can ascertain, a shift to higher frequency of the C—H stretching band has not been previously reported. The situation in another example of such a shift, the nitroxyl chloride stretching band (13), is quite different from the present case, in that the band shifts to higher frequencies as the polarity or the dielectric constant of the solvent increases.

Can. J. Chem. Downloaded from www.nrcresearchpress.com by 210.87.254.5 on 09/06/12
For personal use only.

Bandwidths

Table 2 also lists the widths at nine-tenths height of the asymmetric CH_3 and CH_2 stretching bands of *n*-octane in 1% v/v solutions. There is no simple correlation between refractive index and bandwidth. However, it is evident that in the fluorinated solvents the bandwidths are substantially greater. As this effect is observed in both the aromatic and aliphatic fluorocarbon solvents, it appears to be associated with the presence of fluorine. Broadening is indicative of either increased rotational relaxation or increased vibrational relaxation, and these are generally incompatible with each other. Fluorocarbons are known to have very low surface tensions which are another expression of the low intermolecular forces present (14). Therefore, the solute–solvent interaction is expected to be substantially smaller in the fluorocarbon solvents than in others, resulting in greater motional freedom of the solute molecule and hence rapid rotational relaxation in fluorocarbons, thus suppressing the vibrational relaxation.

Summary

The frequencies of the C—H stretching bands of acyl chains have been shown to be sensitive to solvent–solute interactions and behave as predicted by the David and Hallam equation. A shift to higher frequency has been demonstrated on going from the gas phase to an *n*-perfluorooctane solution. In addition, fluorinated solvents produce a substantial broadening of the C—H stretching bands compared to the other solvents studied.

In general, although the frequency shifts are not large, their precise determination is well within the capability of modern infrared instrumentation. Acyl chains are found in a wide variety of systems, such as polymers, fatty acids, surfactants, and lipids. As vibrational spectroscopic techniques are increasingly used to monitor the acyl chain properties in such systems, it is apparent that as more complex systems are more precisely studied, solvent induced shifts must be carefully considered in the interpretation of the data.

1. J. UMEMURA, D. G. CAMERON, and H. H. MANTSCH. J. Phys. Chem. **84**, 2272 (1980).
2. L. ONSAGER. J. Am. Chem. Soc. **58**, 1468 (1936).
3. J. G. KIRKWOOD. J. Chem. Phys. **4**, 592 (1936).
4. E. BAUER and M. MAGAT. J. Phys. Radium, **9**, 319 (1938).
5. A. D. BUCKINGHAM. Proc. R. Soc. London, Ser. A, **248**, 169 (1958).
6. A. D. BUCKINGHAM. Proc. R. Soc. London, Ser. A, **255**, 32 (1960).
7. A. D. BUCKINGHAM. Trans. Faraday Soc. **56**, 753 (1960).
8. T. FUJIYAMA, J. HERRIN, and B. L. CRAWFORD. Appl. Spectrosc. **24**, 9 (1969).
9. J. KAUPPINEN, T. KÄRKKÄINEN, and E. KYRÖ. J. Mol. Spectrosc. **71**, 15 (1967).
10. R. C. WEAST (*Editor*). Handbook of chemistry and physics. 53rd ed. The Chemical Rubber Co., Cleveland, OH. 1972.
11. J. G. DAVID and H. E. HALLAM. Spectrochim. Acta, Part A, **23**, 593 (1967).
12. R. G. SNYDER. J. Chem. Phys. **47**, 1316 (1967).
13. L. J. BELLAMY. The infrared spectra of complex molecules. 2nd ed. Methuen, London. 1958. p. 382.
14. T. J. BRICE. *In* Fluorine chemistry. Vol. I. *Edited by* J. H. Simons. Academic Press, New York. 1950. p. 438.

Can. J. Chem. Downloaded from www.nrcresearchpress.com by 210.87.254.5 on 09/06/12
For personal use only.

Effect of short-chained sodium alkylsulfate micelles on the kinetics of metal complex formation

PAUL D. I. FLETCHER[1] AND VINCENT C. REINSBOROUGH

Department of Chemistry, Mount Allison University, Sackville, N.B., Canada E0A 3C0

Received November 10, 1980

PAUL D. I. FLETCHER and VINCENT C. REINSBOROUGH. Can. J. Chem. **59**, 1361 (1981).

The kinetics of the reaction between Ni_{aq}^{2+} and the bidentate ligand pyridine-2-azo-*p*-dimethylaniline (PADA) have been investigated in micellar solutions of sodium decyl-, octyl-, and hexylsulfates using the stopped-flow technique. The rate of enhancement decreased with decreasing alkyl-chain length and from the Berezin or Robinson model could be quantitatively related to the independently measured binding constants of Ni^{2+} ion and PADA to the micelle surface. The dramatic effect of micelles upon the reaction rates in different directions of the Ni^{2+}/PADA and the Ni^{2+}/ murexide reactions served as sensitive indicators of the cmc even at the very limit of micelle formation which relatively concentrated sodium hexylsulfate solutions represent.

PAUL D. I. FLETCHER et VINCENT C. REINSBOROUGH. Can. J. Chem. **59**, 1361 (1981).

En utilisant la technique de flux stoppé, on a étudié la cinétique de la réaction entre le Ni_{aq}^{2+} et le ligand bidentate, pyridine azo-2 *p*-diméthylaniline (PADA), dans des solutions micellaires de décylsulfate, d'octylsulfate et d'hexylsulfate de sodium. Le taux d'augmentation de la vitesse diminue avec la longueur de la chaîne alkylée et, à partir du modèle de Berezin ou de Robinson, on peut le relier quantitativement aux constantes de liaison entre l'ion Ni^{2+} et la PADA à la surface de la micelle que l'on peut mesurer indépendamment. L'effet dramatique des micelles sur les vitesses de réaction dans les différentes directions des réactions de Ni^{2+}/PADA et du Ni^{2+}/murexide servent d'indicateurs sensibles de cmc même à la limite de la formation de la micelle ce qui est le cas pour des solutions relativement concentrées d'hexylsulfate de sodium.

[Traduit par le journal]

Introduction

The mechanism whereby sodium dodecylsulfate (SLS) micelles increase the rate of complex formation between Ni_{aq}^{2+} and neutral bidentate ligands such as pyridine-2-azo-*p*-dimethylaniline (PADA) has been adequately characterized (1–4). The kinetic model successfully predicts the effect of changes of pH, of ligand, and of reactant concentrations. The reaction occurs in the surface region of the micelle and the rate increase depends upon the independently measured extent of binding of ligand to the micelle.

In SLS micellar solutions at concentrations greater than twice the critical micelle concentration (cmc), both the nickel ion and PADA are strongly adsorbed into the surface region of the micelle so that any effects of partitioning of the reactants at low ionic strength into the bulk water upon the apparent rate are negligible. With ligands less hydrophobic than PADA, where an appreciable amount of the ligand is in the bulk water, the rate enhancement of the SLS micelles upon the Ni^{2+}–ligand complex formation is less dramatic (2). The kinetic model successfully accounts for the observed kinetic constant by allowing for this distribution of ligand between the micellar surface region and the bulk water.

The effect of significant partitioning of the other reactant, Ni^{2+}, into the bulk water from the micellar surface upon the enhancement of the rate of these reactions has not hitherto been reported. White[2] had noted in a preliminary study that decreasing the length of the carbon chain in the members of the sodium alkylsulfate series had led to a decrease in the rate enhancing effect of the micelles for this particular reaction.

In the case of both reactants partitioning significantly between the micelle surface and the bulk water, the more complex kinetic expression can still be readily interpreted. It was for this reason that the reaction between Ni_{aq}^{2+} and the ligand PADA was studied kinetically in sodium decylsulfate (SDS) solutions, in sodium octylsulfate (SOS) solutions, and in sodium hexylsulfate (SHS) solutions. We wished also to gain more information on the micellization phenomenon as it occurs with short-chained surfactants with which little work has been done.

Experimental

The stopped-flow instrumentation and technique did not differ significantly from that described previously (2, 5); the deadtime was less than two milliseconds. The nickel ion concentrations were varied from 5×10^{-4} to 1.5×10^{-3} mol dm^{-3} while the PADA concentration, to maintain pseudo-first order conditions, was kept constant at 5×10^{-6} mol dm^{-3}. The pH of

[1]Visiting Research Fellow from the University of Kent at Canterbury, England.

[2]N. C. White, University of Kent, U.K. Unpublished results.

0008-4042/81/091361-07$01.00/0

©1981 National Research Council of Canada/Conseil national de recherches du Canada

all solutions was manually adjusted with a glass electrode to 8.2 ± 0.2 to prevent protonation of the ligand and hydrolysis of the nickel ion (1) on the micelle surface. Analysis of the experimental transients was performed from Polaroid photographs of the storage oscilloscope traces. When the micellar reaction rate was much faster than the bulk solution rate, exponential traces were obtained. In SHS solutions especially, where the rates were within an order of magnitude of each other, the initial region of the observed trace was used to obtain the observed kinetic constant (k_{obs}) for the micellar reaction.

The solubilities of PADA in the various micellar solutions were measured at 25°C by means of a Cary 219 spectrophotometer. The electrical conductivities of SOS solutions were measured using a dip-cell and a RC-18A Beckman conductivity bridge. The sharp break in the plot of the conductivity vs. concentration was interpreted as the cmc. The presence of 5×10^{-4} mol dm^{-3} Ni_{aq}^{2+} did not alter the cmc in SOS solutions within experimental error. This was presumably due to the large excess of Na_{aq}^{+} ions (approx. 0.2 mol dm^{-3}) largely present as surfactant counter ions. In contrast, for very pure SLS, the cmc is $\sim 8 \times 10^{-3}$ mol dm^{-3} and is strongly dependent on the concentration of added electrolyte.

PADA was supplied by Sigma Chemicals, SDS by Schwarz-Mann, and SOS and SHS by Eastman Kodak. All of the reagents were of the highest purity except SHS (practical grade), where it was felt that purifying the surfactant would not improve the results. Only an approximate value of k_{obs} could be obtained with SHS because, as mentioned above, coupling of the fast and slow reactions could not be eliminated.

Results and Discussion

The overall reaction between Ni_{aq}^{2+} and PADA may be represented as

$$Ni_{aq}^{2+} + PADA \underset{k_{-1}}{\overset{k_1}{\rightleftharpoons}} NiPADA^{2+}$$

for which the kinetic equation is

$$[1] \quad k_{obs} = k_1 [Ni^{2+}]_T + k_{-1}$$

where k_{obs} is the observed first-order rate constant for metal-complex formation and $[Ni^{2+}]_T$ is the total nickel ion concentration in mol dm^{-3} (2). Equation [1] is valid when $[Ni^{2+}]_T \gg [PADA]$.

When the reaction occurs in the micelle surface region as well as in the bulk water, the reaction scheme is enlarged as follows (2):

$$\begin{array}{ccc} Ni_w^{2+} + PADA_w & \underset{k_{-1}^{w}}{\overset{k_1^{w}}{\rightleftharpoons}} & NiPADA_w^{2+} \\ \Big\downarrow\Big\uparrow K_{Ni} \quad \Big\downarrow\Big\uparrow K_{PADA} & & \Big\downarrow\Big\uparrow K_c \\ Ni_M^{2+} + PADA_M & \underset{k_{-1}^{M}}{\overset{k_1^{M}}{\rightleftharpoons}} & NiPADA_M^{2+} \end{array}$$

The subscript or superscript M denotes the micellar surface region and w, the bulk water. K_{Ni}, K_{PADA}, and K_c are the equilibrium constants for the distribution between the bulk water and micellar surface regions for Ni^{2+} ion, PADA ligand, and metal–ligand complex, respectively. The equilibrium constants are defined for the general case as

$$K_A = [A_M]/C[A_W]$$

where C is (C_T − cmc) with C_T being the total surfactant concentration. C is a measure of the concentration of the micellar surfactant and is proportional to the micellar surface area.

The metal–ligand complex should be the most strongly adsorbed species of the three into the micellar surface region since both hydrophobic and coulombic interactions are operative. Thus, it is reasonable to neglect the K_c contribution to the overall rate of reaction.

When this pathway is neglected, the kinetic expressions, which result from a treatment analogous to that of Berezin (6), for the apparent forward rate constant for a pseudo-first order reaction in the micellar surface region, become

$$[2a] \quad {}^{M}k_1^{app} = k_1{}^{M}/[CV\{1 + (CK_{Ni})^{-1}\} \times \{1 + (CK_{PADA})^{-1}\}]$$

and

$$[2b] \quad {}^{w}k_1^{app} = k_1{}^{w}/[(1 + CK_{Ni}) \times (1 + CK_{PADA})(1 - CV - C_T\bar{V}]$$

where V is the reaction volume per mole of micellar surfactant and $\bar{V}$ is the partial molar volume of surfactant.

The surface and bulk water reactions can couple together to produce a composite overall rate under certain partitioning conditions. Since the kinetic trace was analyzed only for the faster pseudo-first order rate constant, eq. [2*a*] only need be considered, i.e.

$$[3] \quad k_1{}^{app} = k_1{}^{M}/CV\{1 + (CK_{Ni})^{-1}\} \times \{1 + (CK_{PADA})^{-1}\}$$

It must be noted that eqs. [2] and [3] are valid only when the partitioning equilibria are established rapidly relative to the reaction rate.

If the alternative analysis of Robinson and coworkers (1, 2) is followed, then a similar expression is obtained with the same assumptions:

$$[4] \quad k_1{}^{app} = k_1{}^{M}/CAN\{1 + (CK_{Ni})^{-1}\} \times \{1 + CK_{PADA})^{-1}\}$$

where A is the effective surface area per head group at the micelle surface and N is Avogadro's Number. The two $k_1{}^{M}$ values cannot be compared since they are dimensionally different, reflecting the different conceptual approaches of the two models. Berezin defines the surface reaction as occurring within a certain volume V which probably amounts

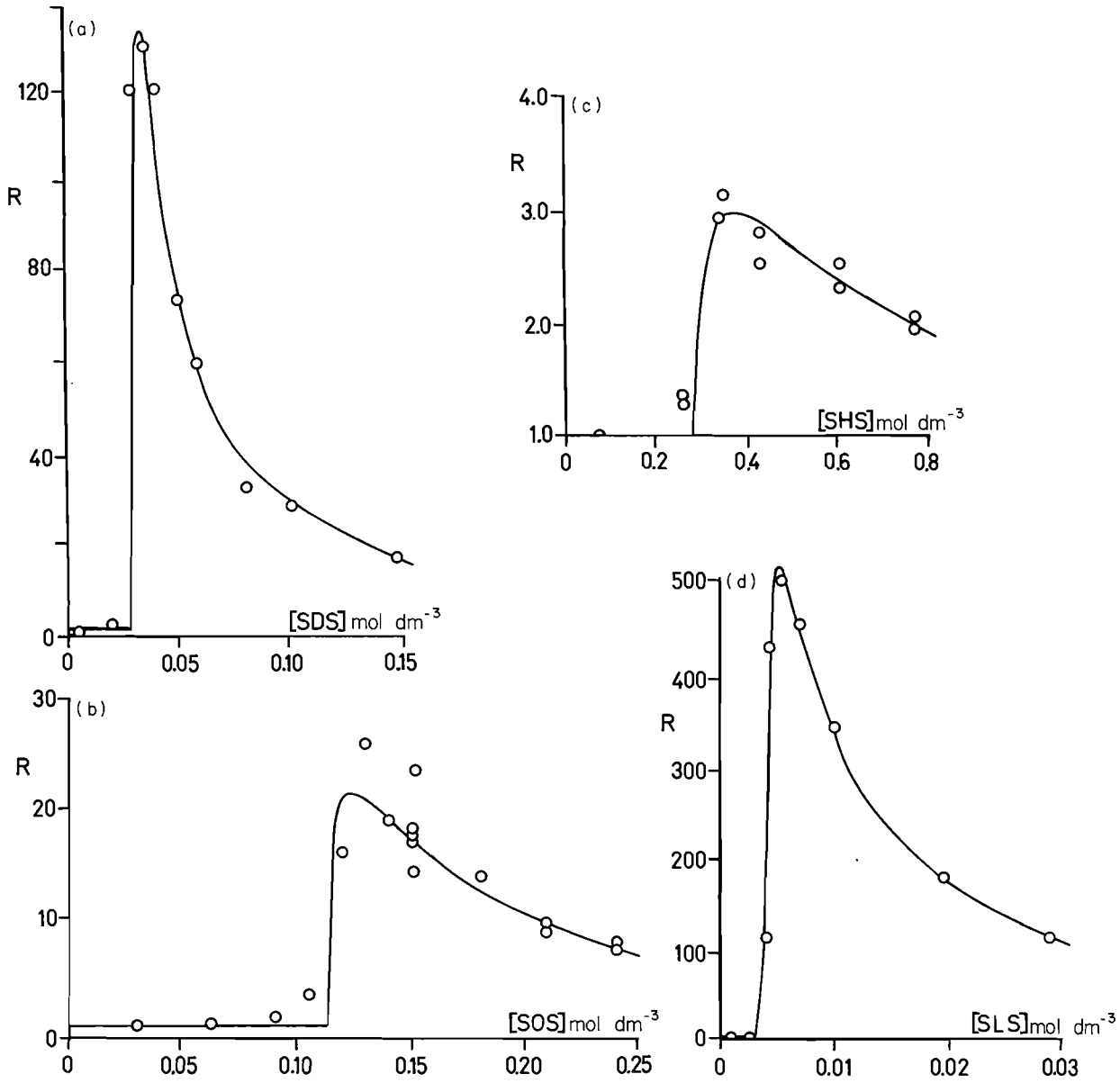

FIG. 1. Dependence of k_1^{app}/k_1^0 or R upon surfactant concentration at 25°C for (a) SDS, (b) SOS (c) SHS, and (d) SLS solutions. The open circles are data points while the curves have been fitted according to eq. [3].

to the combined volumes of the Stern layer and the shell of deepest penetration of the reactants. Berezin estimated V to be 3/4 of the total volume for the SLS micelle and approximated V by the molar volume of the surfactant (6). As yet, V cannot be independently measured and remains an adjustable parameter. Robinson and co-workers (1, 2) view the reaction as occurring on the outer skin of the micelle thus reducing the reaction volume to a reaction area defined by the effective cross-sectional area of the polar group of the surfactant.

The relationship between k_{obs} and k_1^{app} is given by the equation

$$[5] \quad k_{obs} = k_1^{app}[Ni^{2+}]_T + k_{-1}^M$$

Values of k_{-1}^M were obtained as the intercepts of the linear plots of k_{obs} against $[Ni^{2+}]_T/C\{1 + (CK_{Ni})^{-1}\}\{1 + (CK_{PADA})^{-1}\}$. Since k_{-1}^M was normally much less than $k_1^{app}[Ni^{2+}]_T$, values of k_1^{app} were not strongly dependent on the relatively inaccurate values obtained for k_{-1}^M. The ratio $R(= k_1^{app}/k_1^w)$, where k_1^w is the forward rate constant

for the metal–ligand complex formation in water at 25°C ($k_1^w = 1.2 \pm 0.1 \times 10^3$ dm^3 mol^{-1} s^{-1} (1)), gives a direct measure of the forward rate enhancement and these ratios for the SDS, SOS, and SHS systems are shown in Figs. 1(a), (b), and (c), respectively. Corresponding data from the literature for SLS (3) are given in Fig. 1(d). The curves are all similar and the four zones of Holzwarth *et al.* (3) are clearly delineated. On approaching the cmc region from the dilute concentration side in very short-chained surfactant solutions, the slight increase in the rate of reaction that occurs can be explained simply as a concentrative effect as the volume fraction of the solution due to surfactant monomer becomes appreciable. This increase cannot be interpreted as evidence for micellar precursors.

The maximum rate enhancement occurs in the region of the cmc for each surfactant with the maximum ratios being estimated as 520 for SLS, 130 for SDS, 22 for SOS, and 2.9 for SHS solutions. In Fig. 2, where these values are plotted against the number of carbon atoms in the alkyl chain of the surfactant, an extrapolation suggests that shorter members of the series will have no rate enhancing effect.

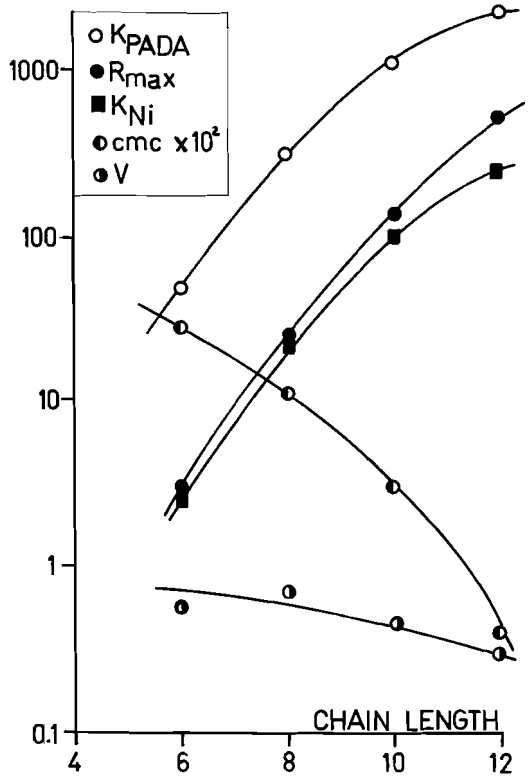

FIG. 2. Variation of various micellar parameters with chain length for the sodium alkylsulfates.

This dramatic decrease in rate enhancing activity with decrease in chain length of the surfactant could mean that either one or both of the reactants

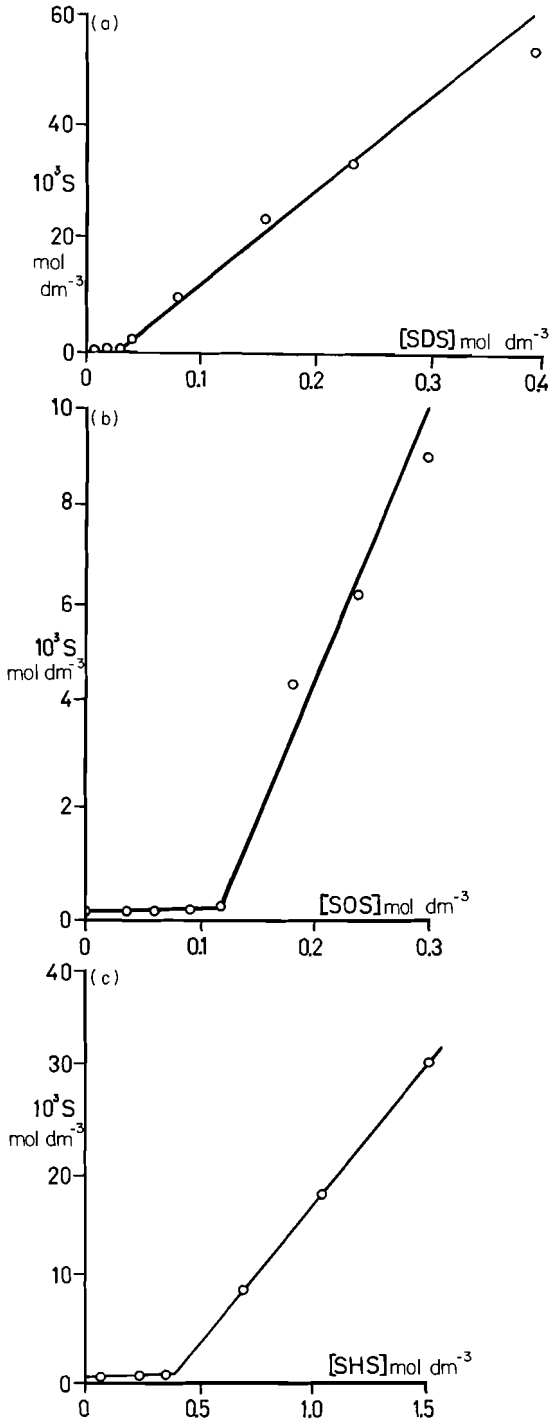

FIG. 3. Solubility (S) of PADA in (a) SDS, (b) SOS, and (c) SHS solutions at 25°C.

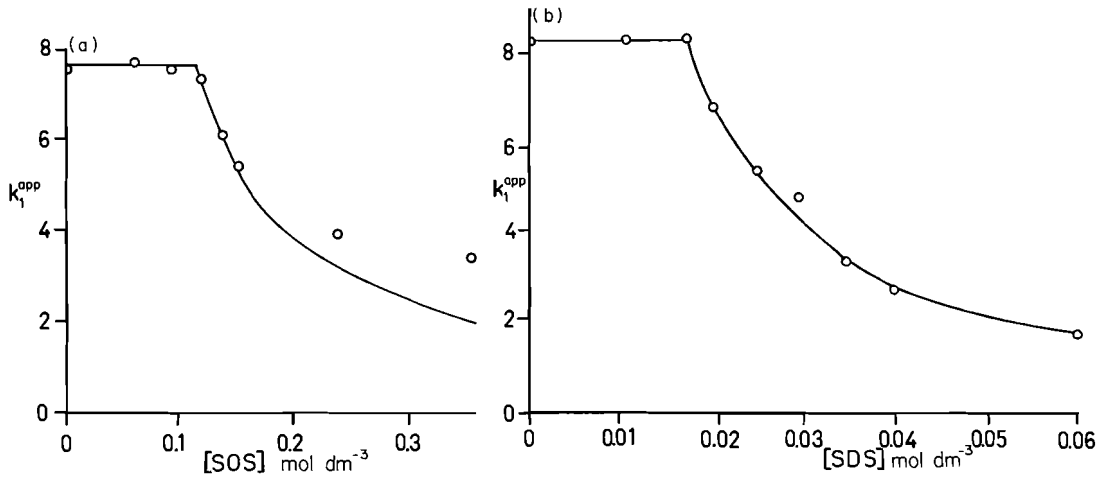

FIG. 4. Apparent forward rate constants (k_1^{app} in 10^3 dm^3 mol^{-1} s^{-1}), for the Ni^{2+}/murexide reaction in (a) SDS and (b) SOS solutions at 25°C. The open circles are data points while the solid line represents the best fitted curve. In the case of SOS, the first few data points beyond the cmc have been more heavily weighted.

are less available for reaction on the micelle surface, i.e. in terms of eq. [3] or [4], K_{Ni} or K_{PADA} or both are much lower in value than for SLS micelles. Both these quantities can be independently measured. Alternatively, the factor k_1^M/V could be changing.

The distribution constant for the PADA ligand between bulk water and the micelle surface, K_{PADA}, was obtained from solubility measurements. Figures 3(a), (b), and (c) show the variation of the solubility of PADA with surfactant concentration for SDS, SOS, and SHS solutions at 25°C. Again there is a clear indication of the cmc from the two linear portions of the curves, even for SHS solutions. K_{PADA} was calculated as $[PADA]_M/[PADA]_w C$ with $[PADA]_w$ being equated to the solubility of PADA at the cmc since, below the cmc, a slight increase in solubility was noted. The values of K_{PADA} at 25.0°C determined by this method were 50 dm^3 mol^{-1} for SHS, 300 dm^3 mol^{-1} for SOS, and 1050 dm^3 mol^{-1} for SDS (2800 dm^3 mol^{-1} for SLS (2)) (see Fig. 2). The degree of binding of the PADA ligand to the micelle decreases as the chain length is decreased reflecting weaker hydrophobic interaction.

K_{Ni} was determined using the murexide complexation technique (7, 8) for SDS and SOS solutions. The negatively-charged murexide ion avoids the anionic micelles so that, when Ni^{2+} ion is also present in solution, any complex formation between Ni^{2+} and murexide will occur only in the bulk water. The rate constant for $NiMu^+$ complex formation is conveniently obtained by the stopped-flow technique using optical detection. Thus, the ratio of the amount of Ni^{2+} ion in the bulk water ("free" Ni^{2+}) to the amount of Ni^{2+} ion in the surface region ("bound" Ni^{2+}) is readily determined from the decrease in observed rate constant with increasing surfactant concentration. The data were corrected for ionic strength according to the Davies equation (7) and plotted as values of apparent rate constants k_1^{app} for complex formation. The Davies equation is not satisfactory above approximately 0.2 mol dm^{-3} so that no attempt was made to measure K_{Ni} in SHS solutions by this method. A value of k_1^w of 2.1 s^{-1} was used in the calculation of k_1^{app} since this was the appropriate value for the experimentally used pH of 4.0 (7). The best fitted curves to the corrected data points for SDS and SOS solutions are shown in Figs. 4(a) and (b). In the SOS situation, the first few points above the cmc were more heavily weighted. The K_{Ni} values thus determined were 90 dm^3 mol^{-1} for SDS and 12 dm^3 mol^{-1} for SOS. The literature value for K_{Ni} for SLS solutions by this method is 650 dm^3 mol^{-1} when data from ref. 12 of that paper is recalculated according to its modified eq. [7], i.e., ${}^wk_1^{app} = k_1^w/(1 + K_{Ni}C)$.

At first glance, it is surprising that Ni^{2+} ions are so weakly bound, especially to the anionic SOS micelles. At 0.2 mol dm^{-3} above the cmc, about half the Ni^{2+} ions are bound, whereas with SLS micellar solutions they are almost totally bound. However, the much greater Na^+ counter ion concentration in micellar SOS solutions must nullify the charge density advantage that the Ni^{2+} ion would have in dilute micellar SLS solutions. Hence, the decrease of K_{Ni} with decreasing chain length is due to the ionic strength changes caused by the increasing cmc values. The much weaker binding

TABLE 1. Rate enhancement parameters

Surfactant	Experimental[a] K_{PADA} dm^3 mol^{-1}	Experimental[a] K_{Ni} dm^3 mol^{-1}	Best-fit K_{Ni} dm^3 mol^{-1}	Best-fit V dm^3 mol^{-1}
SLS	2800	650	250	0.29
SDS	1050	90	100	0.45
SOS	300	12	25	0.70
SHS	50	—	2.5	0.55

[a]The experimental values of K_{PADA} were used in obtaining the fitted K_{Ni} and V values.

of the Ni^{2+} ion to the micelle as compared with the PADA ligand binding to the micelle largely accounts for the reduced rate enhancement with short-chained surfactants.

The curves of the forward rate enhancement ratio R against surfactant concentration were computer fitted. Figures 1(a), (b), (c), and (d) show the experimental data together with the "best-fit" solid curve. The curves were fitted using the experimental values of K_{PADA} and the values of K_{Ni} and k_1^M/V were adjusted until a best fit was obtained. The values of K_{Ni} determined experimentally using the Ni^{2+}/murexide indicator system do not necessarily correspond to the Ni^{2+}/PADA reaction and hence were adjusted independently. This point is discussed in more detail below. It was further assumed that $k_1^M = k_1^w$ and hence the two adjustable parameters were reduced to K_{Ni} and V. This assumption is reasonable in that the activation enthalpy of this reaction is unchanged in SLS micellar solutions (1). The values of the "best fit" parameters are shown graphically in Fig. 2 and listed for purposes of comparison with the experimental values of K_{Ni} in Table 1. Considering that the kinetics can be confidently calculated only within a factor of 2 over almost 3 orders of magnitude, the agreement between the parameters is remarkably good.

The small apparent divergence between "best-fit" and experimental values of K_{Ni} can be rationalized in this manner. The "best-fit" values apply to partitioning of the nickel ion between the bulk water and the surfactant surface region defined by CV. The experimental values apply to partitioning between the bulk water pseudophase as "seen" by the murexide ion and a surface region "not seen" be the murexide ion which can be defined by CV'. The value of V' could be different from V leading to different values of K_{Ni}.

The increase of the parameter V with decreasing chain length may reflect an increase in the effective surface area of sulfate head groups, indicating in turn a looser packed micelle structure with decreasing chain length. Since only the ratio k_1^M/V can be determined, an alternative explanation is that k_1^M decreases with decreasing chain length. Combinations of these two factors must also be possible.

Another conclusion from this study is that C_8 and even C_6 surfactant solutions show well defined cmc's which agree well between the different methods used. The cmc values for SOS at 25°C as determined by four methods were 0.117 mol dm^{-3} (PADA solubility), 0.114 mol dm^{-3} (Ni–murexide), 0.11 to 0.12 mol dm^{-3} (onset of micellar rate enhancement), and 0.115 mol dm^{-3} (electrical conductivity). These agree well with cmc values of 0.118 and 0.115 mol dm^{-3} from two different ultrasonic absorption studies (9, 10). The nickel murexide experiment was particularly impressive (Fig. 4(b)) as the abrupt fall-off of the forward rate signalled the sudden emergence of micelles to which some Ni^{2+} ion had been adsorbed. The two estimates for the cmc of SHS solutions were 0.40 mol dm^{-3} from PADA solubility measurements and 0.28–0.32 mol dm^{-3} from the onset of micellar rate enhancement (0.43 mol dm^{-3} at 40°C from ultrasonic absorption data (9)). Even with this presumably last micelle former of the sodium alkylsulfate series, the appearance of these solution aggregates is dramatic, especially from the sudden increase in the rate enhancement factor, and occurs over a narrow concentration range.

In conclusion, the kinetic behaviour of these systems can be very well characterized from a simple model that is successful even with the extreme case of micellization that sodium hexylsulfate solutions represent (perhaps less than 10 monomers per aggregate). The indicator methods provide simple, sensitive, and flexible probes of micellar solution structure.

Acknowledgements

We thank the Natural Sciences and Engineering Research Council of Canada for financial support and Mount Allison University for providing a Visiting Research Fellowship (to P.F.). The support

and helpful comments of Dr. Brian Robinson in this project are much appreciated.

1. A. D. JAMES and B. H. ROBINSON. J. Chem. Soc. Faraday Trans. I, **74**, 10 (1978).
2. V. C. REINSBOROUGH and B. H. ROBINSON. J. Chem. Soc. Faraday Trans. I, **75**, 2395 (1979).
3. J. HOLZWARTH, W. KNOCHE, and B. H. ROBINSON. Ber. Bunsenges. Phys. Chem. **82**, 1001 (1978).
4. V. C. REINSBOROUGH and B. H. ROBINSON. Techniques and applications of fast reactions in solution. *Edited by* W. J. Gettins and E. Wyn-Jones. D. Reidel Press, Dordrecht, Holland. 1979. p. 275.
5. B. H. ROBINSON, N. C. WHITE, and C. MATEO. Adv. Mol. Relaxation Processes, **7**, 321 (1975).
6. K. MARTINEK, A. K. YATSIMIRSKI, A. V. LEVASHOV, and I. V. BEREZIN. Micellization, solubilization and microemulsions. Vol. 2. *Edited by* K. L. Mittal. Plenum Press, New York. 1977. p. 489.
7. M. FISCHER, W. KNOCHE, B. H. ROBINSON, and J. WEDDERBURN. J. Chem. Soc. Faraday Trans. I, **75**, 119 (1979).
8. M. FISCHER, W. KNOCHE, P. D. I. FLETCHER, B. H. ROBINSON, and N. C. WHITE. Colloid Polym. Sci. **258**, 733 (1980).
9. D. A. W. ADAIR, V. C. REINSBOROUGH, N. PLAVAC, and J. P. VALLEAU. Can. J. Chem. **52**, 429 (1974).
10. J. GETTINS, P. L. JOBLING, M. F. WALSH, and E. WYN-JONES. J. Chem. Soc. Faraday Trans. II, **76**, 794 (1980).

The relative rates of bromination of cyclohexane and cyclopentane with molecular bromine. Comparison of the reactions in solution and in vapor phase

DENNIS D. TANNER,[1] TOMOKI C-S. RUO, HIDEKI TAKIGUCHI,[2] AND ANDRE GUILLAUME[3]

Department of Chemistry, University of Alberta, Edmonton, Alta., Canada T6G 2G2

Received September 25, 1980

DENNIS D. TANNER, TOMOKO C-S. RUO, HIDEKI TAKIGUCHI, and ANDRE GUILLAUME. Can. J. Chem. **59**, 1368 (1981).

The relative rates of transfer of the cyclopentyl radical with molecular bromine and hydrogen bromide (k_2'/k_{-1}') and with hydrogen tribromide and hydrogen bromide (k_3'/k_{-1}') have been determined. The relative transfer rates are compared with the analogous values previously reported for the reactions of cyclohexyl radicals (k_2/k_{-1} and k_3/k_{-1}). Utilizing the values of k_2'/k_{-1}' and k_2/k_{-1} the competitive vapor phase rates of bromine atom abstraction of hydrogen from the two substrates could be obtained. An expression using a combination of the five sets of relative rate constants was used to determine the effect of competitive cage reversal which occurs in the solution phase bromination of the two substrate radicals with caged hydrogen bromide. For two structurally similar radicals, cage reversal (internal return) was found to affect the relative rates of bromination by 30%, while the relative transfer rates, although differing each by a factor of two, fortuitously nearly cancel each other's effect.

The effect of both internal and external reversal reactions on the relative rates of bromination of structurally dissimilar substrates, halogenated alkanes and their parent hydrocarbons, is discussed.

DENNIS D. TANNER, TOMOKO C-S. RUO, HIDEKI TAKIGUCHI et ANDRE GUILLAUME. Can. J. Chem. **59**, 1368 (1981).

On a déterminé les vitesses relatives de transfert du radical cyclopentyle avec le brome moléculaire et le bromure d'hydrogène (k_2'/k_{-1}') et avec le tribromure d'hydrogène et le bromure d'hydrogène (k_3'/k_{-1}'). On a comparé les vitesses relatives de transfert aux valeurs analogues rapportées précédemment pour les réactions des radicaux cyclohexyles (k_2/k_{-1}) et (k_3/k_{-1}). En utilisant les valeurs de k_2'/k_{-1}' et k_2/k_{-1}, on peut obtenir les vitesses compétitives en phase gazeuse de l'enlèvement d'un atome d'hydrogène par l'atome de brome à partir des deux substrats. On a utilisé une expression faisant intervenir une combinaison des 5 ensembles des constantes relatives de vitesse pour déterminer l'effet de l'inversion compétitive de cage qui a lieu au cours de la bromation en solution des deux radicaux avec du bromure d'hydrogène encagé. On a trouvé que, pour deux radicaux ayant des structures identiques, l'inversion de cage (renversement interne) modifie de 30% les vitesses relatives de bromation; par ailleurs, dans le cas des vitesses relatives de transfert qui diffèrent l'une de l'autre par un facteur de deux, elles annulent par hasard leurs effets respectifs.

On discute de l'effet des réactions d'inversion interne et externe sur les vitesses relatives de bromation des substrats ayant des structures différentes soit les alcanes et leurs dérivés halogénés.

[Traduit par le journal]

Introduction

Recently the kinetics of the solution phase free radical bromination of alkanes has been shown to be complicated by transfer of the radicals formed with hydrogen bromide in the solvent cage (internal return) and transfer of the radicals external to the solvent cage with both hydrogen bromide and hydrogen tribromide (external return) (1–3), see Scheme 1.

From studies of the relative rates of bromination of alkanes and substituted alkanes it has become apparent that the above mentioned reversal reactions seriously affect the magnitude of the values of the relative rates obtained for competitive bromination reactions (4).[4] Studies on the bromination of several model compounds, cyclohexane (1), 1-chlorobutane (5), and 1-bromobutane (6) in the vapor phase, where neither the cage reaction nor the transfer reaction with hydrogen tribromide are important, gave values of k_2/k_{-1} of 2.81, 12.3, and 28.2, respectively. Transfer reactions with unsubstituted alkyl radicals with the polar species hydrogen bromide appear to show less polar deactivation than do their substituted analogs (4). Competitive rates of bromination between substituted and unsubstituted alkanes will be the more seriously affected by

$$\mathrm{Br_2} \xrightarrow{h\nu} 2\,\mathrm{Br^\cdot}$$

$$\mathrm{Br^\cdot + RH} \underset{k_{-1}}{\overset{k_1}{\rightleftharpoons}} (\mathrm{R^\cdot + HBr})^{\mathrm{cage}}$$

$$(\mathrm{R^\cdot + HBr})^{\mathrm{cage}} \xrightarrow{k_d} \mathrm{R^\cdot + HBr}$$

$$\mathrm{R^\cdot + HBr} \xrightarrow{k_{-1}} \mathrm{RH + Br^\cdot}$$

$$\mathrm{R^\cdot + Br_2} \xrightarrow{k_2} \mathrm{RBr + Br^\cdot}$$

$$\mathrm{R^\cdot + HBr_3} \xrightarrow{k_3} \mathrm{RH + Br_3^\cdot}$$

$$\mathrm{HBr + Br_2} \underset{}{\overset{K}{\rightleftharpoons}} \mathrm{HBr_3}$$

SCHEME 1

[1]Author to whom correspondence may be addressed.

[2]Postdoctoral Fellow, University of Alberta, 1974–1975.

[3]Postdoctoral Fellow, University of Alberta, 1976–1977.

[4]Under the usual bromination condition of excess substrate to bromine, the concentration of bromine varies from $C^0 \rightarrow 0$ while hydrogen bromide concentration varies from $0 \rightarrow C^0$. Examples of the effect of reversal on substrate pairs are discussed in ref. 4.

0008-4042/81/091368-07$01.00/0

©1981 National Research Council of Canada/Conseil national de recherches du Canada

Can. J. Chem. Downloaded from www.nrcresearchpress.com by 210.87.254.40 on 09/06/12
For personal use only.

Can. J. Chem. Downloaded from www.nrcresearchpress.com by 210.87.254.40 on 09/06/12
For personal use only.

reversal. The substituted, deactivated radicals will reverse less frequently, to reform starting material, than the unsubstituted radicals. The kinetic results of this process lead to the erroneous conclusion that the substituted reactant undergoes a relatively greater amount of reaction during the competitive brominations. The values for the relative rates of bromination in solution of pairs of unsubstituted alkanes can be strongly affected by reversal. These effects, however, may be fortuitously diminished or cancelled out by competitive sets of reversible reactions. One such set of competitive reversal reactions has been reported in the study of the relative rates of bromination of cyclohexane and cyclopentane (7). Under conditions favoring reversible abstraction, the relative rate obtained at 60°C, $k_{C_5H_{10}}/k_{C_6H_{12}}$, was determined to be 6.8 (C_5H_{10}:C_6H_{12}:Br_2, 10:10:1) whereas under conditions favoring no reversal, $k_{C_5H_{10}}/k_{C_6H_{12}} = 8.0$ (C_5H_{10}:C_6H_{12}:Br_2, 1:1:100). Since under the condition favoring reversibility the kinetics of the bromination of cyclohexane itself has been shown to be greatly influenced by hydrogen bromide reversal (1), the similarity between the two competitive reactions reported for cyclohexane vs. cyclopentane could be interpreted as being due to the concomitant cancellation of the effects of reversibility for the two substrates.

Kinetic data is now available for the bromination reactions of cyclohexane in the vapor phase and in solution (1). If similar data for the bromination of cyclopentane were also available, a method could be designed to combine these results and obtain the solution phase relative rates of abstraction for these two cycloalkanes. The objective of this study is to devise such a method and test the bromination scheme (Scheme 1) proposed for the competitive solution phase bromination of these two unsubstituted alkanes.

Discussion and Results

The rate of bromination of cyclohexane (RH) in solution, as depicted in Scheme 1, can be derived using the steady state assumption for the caged radical – hydrogen bromide pair and the cyclohexyl radicals free of the solvent cage, eq. [1].[5]

$$[1] \quad \frac{-d[RH]}{dt} = \frac{k_1[RH][Br\cdot]k_2[Br_2]k_d}{(k_d + k_{-1}[HBr]^c)(k_2[Br_2] + k_3[HBr_3] + k_{-1}[HBr])}$$

A similar derivation for the bromination of cyclopentane, R′H, can be obtained. Dividing these two equations gives eq. [2], the relative rates of bromination of cyclohexane vs. cyclopentane.

$$[2] \quad \frac{d[RH]/dt}{d[R'H]/dt} \cdot \frac{[R'H]}{[RH]} = \frac{k_1}{k_1'} \frac{k_2}{k_{-1}} \frac{k_{-1}'}{k_2'} \frac{k_d}{k_d'} \frac{k_d' + k_{-1}'[HBr]^c}{k_d + k_{-1}[HBr]^c} \frac{\left(\frac{k_2'}{k_{-1}'}\right)\left(\frac{[Br_2]}{[HBr]}\right) + \left(\frac{k_3'}{k_{-1}'}\right)\left(\frac{[HBr_3]}{[HBr]}\right) + 1}{\left(\frac{k_2}{k_{-1}}\right)\left(\frac{[Br_2]}{[HBr]}\right) + \left(\frac{k_3}{k_{-1}}\right)\left(\frac{[HBr_3]}{[HBr]}\right) + 1}$$

The relative rates of disappearance of the two substrates in solution can be evaluated when the reactions are carried out using high concentrations of hydrogen bromide and molecular bromine, when the concentrations of these reactants remain essentially constant, if the relative transfer rates k_2/k_{-1} and k_3/k_{-1} and the cage contribution k_d ($k_d + k_{-1}[HBr]^c$) are known for both substrates, and if the equilibrium concentration of hydrogen tribromide is known.

The relative transfer rate constants for the bromination of cyclohexane (23°C), k_2/k_{-1}, k_3/k_{-1}, and the equilibrium constant, K, for the formation of hydrogen tribromide have previously been determined (k_2/k_{-1}, 2.81; k_3/k_{-1}, 21.8; K, 2.8) (1, 3). Similar determinations of the relative transfer rate constants for cyclopentane were carried out by determining the relative rates of transfer of perdeuteriocyclopentyl radicals after their formation in the presence of an excess of hydrogen bromide and molecular bromine, see Table 1.

$$C_5D_{10} + Br^\cdot \longrightarrow C_5D_9^\cdot + DBr$$

$$C_5D_9^\cdot + HBr \xrightarrow{k_{-1}'} C_5D_9H + Br^\cdot$$

$$C_5D_9^\cdot + Br_2 \xrightarrow{k_2'} C_5D_9Br + Br^\cdot$$

[5]Caged species are treated as bimolecular and the same rate constant, k_{-1}, is used for reaction within the solvent cage and outside the solvent cage. For a more detailed explanation of this treatment, first proposed by Flory for initiator efficiency, see ref. 12.

Can. J. Chem. Downloaded from www.nrcresearchpress.com by 210.87.254.40 on 09/06/12
For personal use only.

TABLE 1. Photobromination of perdeuteriocyclopentane with excess bromine and hydrogen bromide (23°C)

Reaction	Concentration[a] (mol/L) × 10^5								Material balance %,[b]	% Reaction	k_2'/k_1'[c]	k_3'/k_{-1}'
	$[C_5D_{10}]^0$	$[C_5D_9H]^0$	$[Br_2]^0$	$[HBr]^0$	$[C_5D_{10}]^f$	$[C_5D_9H]^f$	$[C_5D_9Br]$	$[C_5D_8Br_2]$				
1[d]	23.50	1.33	38.69	280.6	15.99	5.82	1.81	0.44	96.9	9.1	3.73	
2[d]	27.57	1.55	38.56	146.9	19.41	4.78	2.90	0.67	95.4	12.3	4.41	
3[d]	24.51	1.38	38.73	151.1	20.67	2.37	0.99	0.07	93.1	4.1	4.28	
4[d]	16.06	0.92	38.14	38.2	12.13	1.56	2.18	0.63	97.2	16.6	4.58	
											ave. 4.26 ± 0.26	
5[e]	1959	111	1715	4145	1701	279	73.6	17.5	99.0	6.22	1.3	47.4
6[e]	2881	174	2109	7570	2415	539	82	19	102	5.51	1.0	56.0
7[e]	1311	79	3247	3713	893	324	102	71	81	9.30	0.85	50.4
8[e]	1920	115	3671	4015	1657	265	94	19	108	3.30	0.83	44.1
												ave. 49.5 ± 0.38

[a]Superscripts 0 refers to initial concentrations and f to final concentrations.
[b]Material balances are based on hydrocarbon and bromination products accounted for.
[c]Calculated using eq. [3]; the values for the average concentration of Br_2 and HBr during the reactions were used. This correction is only significant when the conversion is greater than 10% (reactions 2 and 4). The value of $[C_5D_9Br]$ in eq. [3] was taken as the sum of $[C_5D_9Br]$ and $[C_5D_8Br_2]$.
[d]Gas phase 12 L reaction bulb.
[e]Freon 113 solution.

The relative rates of formation of the two products are given by eq. [3].

$$[3] \quad \{d[C_5D_9Br]/dt\}/\{d[C_5D_9H]/dt\} = k_2'[Br_2]/k_{-1}'[HBr]$$

The ratio of rate constants, $(k_2'/k_{-1}')^{vp}$, in the vapor phase was determined by carrying out the reaction of perdeuteriocyclopentane with excess bromine and added hydrogen bromide to low conversion and the products were analyzed by glpc and mass spectrometry in the same manner as was reported for cyclohexane (1). The values obtained are reported in Table 1, reactions 1–4. The ratio of transfer rate constants in solution (Freon 113), k_3'/k_{-1}', was calculated from the data (Table 1, reactions 5–8) obtained from the photobromination of perdeuteriocyclopentane with excess bromine and added hydrogen bromide using the integrated form of eq. [4], derived from the reactions listed in Scheme 1 (see ref. 1).

$$[4] \quad (d[C_5D_9Br]/dt)/(d[C_5D_9H]/dt) = \frac{k_2'([Br_2]^0 - [HBr_3])}{k_{-1}'([HBr]^0 - [HBr_3]) + k_3'[HBr_2]}$$

Equation [4] could be integrated, eq. [5], when the reactions were carried out to low conversion where the concentrations of bromine and hydrogen bromide were essentially unchanged.[6]

$$[5] \quad \frac{[C_5D_9Br]^f}{[C_5D_9H]^f}\left(\frac{k_{-1}'}{k_2'}\right)^{vp} = \frac{[Br_2]^0 - [HBr_3]}{[HBr]^0 - [HBr_3] + (k_3'/k_{-1}')[HBr_3]}$$

The equilibrium concentration of hydrogen tribromide was calculated using the previously determined equilibrium constant (3), $K = 2.8 \pm 0.3$, at 23°C.

The relative rate constants for abstraction of hydrogen from cyclopentane and cyclohexane could be determined in the vapor phase by carrying out the competitive bromination of the two substrates using high concentrations of bromine and hydrogen bromide (see Table 2, reactions 9–10). Since in the vapor phase the reactions of the radicals formed are exclusive of the cage and do not include the reaction of the radicals with hydrogen tribromide, the relative rate constants for abstraction, k_1'/k_1, can be calculated from the integrated form of eq. [2], eq. [6].[7]

$$[6] \quad \frac{\log \frac{(R'H)^0}{(R'H)^f}}{\log \frac{(RH)^0}{(RH)^f}} = \frac{k_1'}{k_1}\frac{k_2'}{k_{-1}'}\frac{k_{-1}}{k_2}\frac{1 + k_2/k_{-1}[Br_2]/[HBr]}{1 + k_2'/k_{-1}'[Br_2]/[HBr]}$$

Likewise the value k_1'/k_1 could be obtained by an analysis of the products formed during the competitive vapor phase bromination of the two substrates (low conversion) using excess bromine and hydrogen bromide, eq. [7] (see Table 2, reactions 11–13), or using high concentrations of excess bromine with no added hydrogen bromide (see Table 2, reactions 14–15), eq. [8].

$$[7] \quad \frac{[R'Br]}{[RBr]} \approx \frac{[R'H]}{[RH]}\frac{k_1'}{k_1}\frac{k_2'}{k_{-1}'}\frac{k_{-1}}{k_2}\frac{1 + k_2/k_{-1}[Br_2]/[HBr]}{1 + k_2'/k_{-1}'[Br_2]/[HBr]}$$

$$[8] \quad \frac{[RH]}{[R'H]}\frac{[R'Br]}{[RBr]} = \frac{k_1'}{k_1}$$

The agreement between the determination of the relative rates of abstraction, k_1'/k_1 (9.66 ± 0.26), by the three methods used lends support to the validity of the mechanistic scheme (Scheme 1) and substantiates the values obtained for the relative transfer rate constants.

The cage contribution, the kinetic result of competitive cage reversal (k_{-1}) and diffusion (k_d) of two different hydrogen bromide – radical pairs, (C), was calculated (eq. [9]) using all of the relative rate constants and the data obtained for the relative rates of product formation obtained from the competitive, low conversion, solution phase brominations of cyclopentane and cyclohexane in the presence of excess bromine and added hydrogen bromide.

[6]The validity of using the values of relative rate constants obtained in the vapor phase for the calculation of relative rates for a solution phase reaction has previously been substantiated, see refs. 1–3.

[7]It has previously been established that the relative rates of transfer obtained for deuterated radicals could be considered as equivalent to the same relative rate constants obtained for the protiated species, see refs. 1, 3, 5, 6.

Can. J. Chem. Downloaded from www.nrcresearchpress.com by 210.87.254.40 on 09/06/12
For personal use only.

TABLE 2. Competitive vapor phase brominations of cyclohexane and cyclopentane (22°C)

	Concentration[a] (mol/L) × 10^5								
Reaction[b]	$[C_5H_{10}]^0$	$[C_6H_{12}]^0$	$[Br_2]^0$	$[HBr]^0$	$[C_5H_{10}]^f$	$[C_6H_{12}]^f$	$[C_5H_9Br]^c$	$[C_6H_{11}Br]^c$	k_1'/k_1
9	0.410	0.422	105.8	55.6	0.0307	0.327	—	—	9.62[d]
10	0.410	0.422	56.5	76.1	0.0779	0.362	—	—	9.64[d]
11	1.33	6.43	43.9	29.8	—	—	0.0451	0.0202	10.08[e]
12	1.30	7.14	14.6	74.9	—	—	0.0111	0.00502	9.49[e]
13	1.71	7.10	56.5	163.9	—	—	0.0625	0.0227	9.46[e]
14	1.67	6.06	45.1	0.0	—	—	0.0622	0.0222	10.17[f]
15	1.19	6.54	46.8	0.0	—	—	0.0430	0.0258	9.16[f]
									ave. 9.66 ± 0.26

[a]Superscript 0 refers to initial concentrations and f to final concentrations.
[b]Reactions 11 and 15 were carried out in a 12 L glass vessel. All of the remaining reactions were carried out in a 22 L reaction vessel.
[c]The values listed for $[C_5H_9Br]$ and $[C_6H_{11}Br]$ are the sum of $[C_5H_9Br]$ + $[C_5H_8Br_2]$ and $[C_6H_{11}Br]$ + $[C_6H_{10}Br_2]$.
[d]Calculated using eq. [10].
[e]Calculated using eq. [7].
[f]Calculated using eq. [8].

$$[9]\quad \frac{[C_5H_9Br]\,[C_6H_{12}]^0}{[C_6H_{11}Br]\,[C_5H_{10}]^0} = \frac{k_1'}{k_1}\frac{k_2'}{k_{-1}'}\frac{k_{-1}}{k_2}\,C\,\frac{\left(\frac{k_2}{k_{-1}}\right)\left(\frac{[Br_2]}{[HBr]}\right) + \left(\frac{k_3}{k_{-1}}\right)\left(\frac{[HBr_3]}{[HBr]}\right) + 1}{\left(\frac{k_2'}{k_{-1}'}\right)\left(\frac{[Br_2]}{[HBr]}\right) + \left(\frac{k_3'}{k_{-1}'}\right)\left(\frac{[HBr_3]}{[HBr]}\right) + 1}$$

$$C = \left(\frac{k_d'}{k_d}\right)\left(\frac{k_d + k_{-1}[HBr]^c}{k_d' + k_{-1}'[HBr]^c}\right)$$

The data obtained from these reactions (reactions 16–18) as well as a summary of the rate constants used for the calculation of C are listed in Table 3.

The magnitude of the cage contribution, $C = 1.43 \pm 0.02$, demonstrates that even in the case of structurally similar substrates such as cyclohexane and cyclopentane, differential cage reversal can affect the apparent relative rates of abstraction by as much as 30%. A further analysis of the cage contribution is not justified, however, since although the function is mathematically correct its physical significance is unclear. In the previous observations of differential cage reversal (2, 3) the cage contribution was simplified by assuming that k_d/k_d' was equal to unity. The approximation was justified on the basis of the assumption that the relative rates of diffusion of a perdeuteriocyclohexyl radical and a cyclohexyl radical were the same or that the same simplification could be made for the isomeric radicals formed during the bromination of 1-chlorobutane. The relative rates of diffusion of the cyclohexyl and cyclopentyl radicals are not necessarily expected to be as similar (8) and therefore this approximation was not made.

The observation, that the relative rates of bromination of two substrates in the absence of external return (high concentrations of bromine and low conversion of substrates) were not the same as the values obtained in their vapor phase brominations carried out under the same reaction conditions, has been attributed to competitive internal return reactions of the geminate radical – hydrogen bromide pairs (2, 3). It was demonstrated (2, 3) that in solvent liquid bromine the radicals, both external and internal to the solvent cage, could be effectively scavenged by molecular bromine and that both the vapor phase bromination of a substrate (carried out in absence of external return) and the reactions run in neat bromine give the same relative rates of bromination. This scheme could be further tested in the study of the competitive bromination of cyclopentane and cyclohexane.

When the competitive bromination was carried out in solvent liquid bromine (14–18 M) and the reaction mixture was analyzed for the relative disappearance of the two substrates, the relative rate of abstraction of hydrogen (per molecule), k_1'/k_1, was found to be 9.20 ± 0.28 (see Table 4), well within the experimental limits found for the vapor phase reactions, 9.66 ± 0.26 (see Table 4, reactions 19–22). These values are in excellent agreement with the value, 8.0, previously reported by Traynham and Lee (7) for the bromination of the two substrates at 60°C using high concentrations of molecular bromine.

Conclusions

The relative rates of bromination of hydrocarbon substrates in solution, whether they be deactivated

Can. J. Chem. Downloaded from www.nrcresearchpress.com by 210.87.254.40 on 09/06/12
For personal use only.

TABLE 3. Concentrations and relative rate constants used to calculate C for the bromination of cyclohexane and cyclopentane in solvent Freon 113 (23°C)

Reaction	Concentration mol/L × 10^3 $[C_5H_{10}]^0$	$[C_6H_{12}]^0$	$[Br_2]^0$	$[HBr]^0$	$[C_5H_9Br]/[C_6H_{11}Br]$	C^a
16	22.4	35.9	41.1	111.2	7.48	1.44
17	9.04	50.6	165	95.1	1.93	1.40
18	7.12	39.5	516	91.5	2.07	1.44
						ave. 1.43±0.02
	$k_2/k_{-1} = 2.81^b$				$k_2'/k_{-1}' = 4.26$	
	$k_3/k_{-1} = 21.8^b$				$k_3'/k_{-1}' = 49.5$	
			$K^{23°} = 2.8^c$			
			$k_1'/k_1 = 9.66$			

[a]Calculated using eq. [9].
[b]Taken from ref. 1.
[c]Taken from ref. 3.

TABLE 4. The competitive bromination of cyclopentane and cyclohexane at very high concentrations of molecular bromine (23°C)

Reaction	Concentration[a] mol/L × 10^2 $[C_5H_{10}]^0$	$[C_6H_{12}]^0$	$[Br_2]^0$	Area ratio, glpc[a] $(C_5H_{10}/Freon)^0$	$(C_5H_{10}/Freon)^f$	$(C_6H_{12}/Freon)^0$	$(C_6H_{12}/Freon)^f$	$k_1'/k_1{}^b$
19	6.08	6.04	18.0	0.665	0.124	0.742	0.615	8.99
20	6.08	6.04	18.0	0.665	0.152	0.742	0.631	9.13
21	6.08	6.04	18.0	0.660	0.235	0.741	0.660	8.92
22	83.6	59.4	14.1	0.879	0.272	0.693	0.615	9.77
								ave. 9.20±0.28

[a]Superscript 0 refers to initial values and f to final values.
[b]The values reported were calculated using eq. [10].

by electronegative substituents or be hydrocarbon pairs of a similar structure, are affected by both internal and external reversal. In the case of the substrates cyclohexane and cyclopentane these reversal reactions fortuitously nearly cancel each other.

Competitive brominations carried out to obtain information on structure reactivity relationships between chlorinated or brominated substrates and their parent unsubstituted hydrocarbons will lead to serious errors in mechanistic interpretation (9) unless these effects are considered (4).

Although detailed evidence for internal and external reversal has been obtained in the case of bromination reactions only, these processes should similarly affect the interpretation of structure reactivity relationships in other substitution processes which have comparable energetics.

Experimental

Materials

Perdeuteriocyclopentane (Merck, Sharp and Dohme, Canada) was used without further purification. Gas–liquid partition chromatography (glpc) (10 ft × 1/4 in. 10% SE-30 on Chromosorb P AW) showed it to be >99.9% pure, and mass spectral analysis (AEJ MS 50, 12 eV) showed it to contain 99.47 at.% D.

Cyclopentane (Philips 66, research grade) and cyclohexane (Aldrich Chemical) were heated to reflux over P_2O_5 and fractionally distilled using an 18 in. Vigreux column; the middle fractions were collected; glpc analysis (10% SE-30) showed them to be >99.9% pure.

Freon 112 (PCR) and Freon 113 (Matheson of Canada Ltd.) were fractionally distilled (18 ft Vigreux column) from P_2O_5; the middle fractions were collected.

Bromine (Fisher Scientific) was washed twice with concentrated sulfuric acid, decanted, and fractionally distilled (18 ft Vigreux column) from P_2O_5. The middle fraction was collected.

Analysis

The glpc area ratios were determined using either a HP digital integrator or a HP disk integrator. Concentrations determined by glpc analysis were calculated using standard calibration curves obtained from plots of area ratios vs. mole ratios of known mixtures.

The protium in perdeuteriocyclopentane was determined as previously described (1) using an AEI MS 9 mass spectrometer (12 eV) and the percentage ^1H was calculated by the method of Biemann (10).[8]

Vapor Phase Bromination of Perdeuteriocyclopentane

Perdeuteriocyclopentane (about 0.2 g) was accurately weighed into a Pyrex break seal, and this was degassed by the freeze–thaw method three times and finally sealed. Bromine (about 0.7 g) was similarly weighed, degassed, and sealed in a separate break seal. Hydrogen bromide was degassed and distilled in a vacuum line, measured manometrically, and distilled into a break seal. The three break seals were attached to the reaction vessel (12 L), and the system was evacuated. The

[8]For details of the analytical procedure see ref. 1.

Can. J. Chem. Downloaded from www.nrcresearchpress.com by 210.87.254.40 on 09/06/12
For personal use only.

Can. J. Chem. Downloaded from www.nrcresearchpress.com by 210.87.254.40 on 09/06/12
For personal use only.

break seals were broken in the absence of light (in the order C_5D_{10}, HBr, Br_2, with 20 min intervals between each break seal), the mixture of the three substrates was allowed to equilibrate (30 min, 23°C), and then the vessel was irradiated (one 100 W incandescent lamp). The contents of the bulb were condensed into a tube attached to the reaction vessel in the absence of light. The tube was cooled (−198°C), opened, and a CCl_4 solution of an internal standard (chlorobenzene) was added, and the excess bromine and hydrogen bromide was destroyed with cold (0°C) sodium bisulfite. The organic phase was washed with a solution of sodium bicarbonate (0°C) and then with water, and dried (anhydrous $MgSO_4$). The mixture was analyzed by glpc (10 ft × 0.25 in. 10% Carbowax 20 M on Chromosorb P AW, glass column) for remaining starting material and products and the unbrominated deuterated cyclopentane was collected and submitted for mass spectral analysis. As controls, known mixtures of the three substrates and their products were placed in the reaction vessel, in the absence of light, and isolated and reanalyzed in the same manner. The control experiments gave material balances within the experimental errors quoted. The concentrations and results of the analyses of the reaction mixtures are listed in Table 1, reactions 1–4.

Bromination of Perdeuteriocyclopentane in Freon 113

A Freon 113 solution of bromine and hydrogen bromide was allowed to equilibrate at 23°C. An aliquot of the solution was titrated iodometrically for both bromine and hydrogen bromide (11). A Freon 113 solution of perdeuteriocyclopentane was added and the mixture was irradiated (2 × 200 W incandescent lamps) after equilibration at 23°C. Several aliquots of the mixture were again analyzed for both bromine and hydrogen bromide, after adequate irradiation. The mixture, in the absence of light, was freed from the excess bromine and hydrogen bromide by washing with a cold (0°C) solution of $NaHSO_3$. The organic phase was washed with aqueous sodium bicarbonate, then water, and dried over anhydrous Na_2SO_4. The mixture was then analyzed by glpc (10 ft × 0.25 in. 10% SE 30 and Chromosorb P AW, glass column) for starting material and products. The deuterated cyclopentane was collected by preparative glpc (10% SE 30) and subjected to mass spectral analysis (reaction 5, Table 1) or concentrated by preparative glpc and subjected to glpc–ms (10% SE 30, AEI-MS12 mass spectrometer) analysis directly (reactions 6–8, Table 2). The concentrations and results used are listed in Table 1, reactions 5–8. Control experiments on known mixtures of reactants and products gave analytical results within the experimental values quoted.

Competitive Bromination of Cyclohexane and Cyclopentane in the Vapor Phase

The reactions were carried out with mixtures of cyclohexane and cyclopentane as substrates in the manner described previously for the gas phase brominations of perdeuteriocyclopentane, except that Freon 112 was used as an internal standard and a 24 ft × 0.25 in. 7% SE 30 on Chromosorb P AW, glass column was used to analyze the mixture. The results are listed in Table 2, reactions 9–10.

When the reaction mixture was analyzed for the disappearance of reactants (Table 2, reactions 9–10), the reaction mixture was condensed in the isolated compartment of a break seal attached to the reaction vessel. The break seal contained one mL of toluene and 10 mL of an aqueous solution containing excess Na_2SO_3. The collecting tube was sealed and after the break seal was opened and the materials mixed, the tube was opened and the organic phase was subjected to analysis by glc (7% SE 30 on Chromosorb P AW, glass column). The concentrations and results, calculated using eqs. [6] and [10], are listed in Table 2, reactions 9–10.

$$[10]\quad \frac{\log \dfrac{[C_5H_{10}]^0/[\text{Freon 112}]^0}{[C_5H_{10}]^f/[\text{Freon 112}]^f}}{\log \dfrac{[C_6H_{12}]^0/[\text{Freon 112}]^0}{[C_6H_{12}]^f/[\text{Freon 112}]^f}} = \frac{\log [C_5H_{10}]^0/[C_5H_{10}]^f}{\log [C_6H_{12}]^0/[C_6H_{12}]^f}$$

When the reaction was analyzed for the appearance of products (reactions 11–15, Table 2), the same method was used as that described for the product analysis used in the bromination of perdeuteriocyclopentane.

Competitive Brominations of Cyclohexane and Cyclopentane in Freon 113

The reactions were carried out and analyzed in the manner described for the bromination of perdeuteriocyclohexane in Freon 113 (1) except that the reaction mixture was concentrated by distillation using a 24 in. Teflon spinning band column, and the concentrated mixture was analyzed by glpc (24 ft × 0.25 in. 7% SE 30 on Chromosorb P AW glass column). Control experiments showed the analytical method to be accurate. The concentrations and results are listed in Table 3.

Competitive Brominations of Cyclohexane and Cyclopentane in Liquid Bromine

Aliquots of a pre-analyzed mixture of cyclohexane, cyclopentane, and Freon 112, as an internal standard, were placed in reaction tubes containing molecular bromine, degassed, and sealed in the absence of light. The mixtures were allowed to equilibrate at 23°C and were then irradiated with 4 × 200 W incandescent lamps. The tubes were cooled, opened, and an aliquot of toluene and an aqueous solution of $NaHSO_3$ were added. The organic layer was washed with a cold aqueous solution of Na_2CO_3, then water, dried over anhydrous Na_2SO_4, and analyzed by glpc (24 ft, 7% SE 30). The concentrations and results, calculated using eq. [11], are listed in Table 4, reactions 19–22.

$$[11]\quad \frac{\log \dfrac{[C_5H_{10}]^0/[\text{Freon 112}]^0}{[C_5H_{10}]^f/[\text{Freon 112}]^f}}{\log \dfrac{[C_6H_{12}]^0/[\text{Freon 112}]^0}{[C_6H_{12}]^f/[\text{Freon 112}]^f}} = k_1'/k_1$$

Acknowledgments

The authors wish to thank the National Research Council of Canada and the University of Alberta for their generous support of this work.

1. D. D. TANNER, T. PAĆE, and T. OCHIAI. J. Am. Chem. Soc. **97**, 4303 (1975).
2. D. D. TANNER, T. OCHIAI, and T. PAĆE. J. Am. Chem. Soc. **97**, 6163 (1975).
3. D. D. TANNER, T. OCHIAI, J. ROWE, T. PAĆE, H. TAKIGUCHI, and P. W. SAMAL. Can. J. Chem. **55**, 3536 (1977).
4. D. D. TANNER, J. E. ROWE, T. PAĆE, and Y. KOSUGI. J. Am. Chem. Soc. **95**, 4705 (1973).
5. D. D. TANNER, T. PAĆE, and T. OCHIAI. Can. J. Chem. **53**, 2202 (1975).
6. D. D. TANNER, Y. KOSUGI, R. ARHART, N. WADA, T. PAĆE, and T. RUO. J. Am. Chem. Soc. **98**, 6275 (1976).
7. J. G. TRAYNHAM and Y. S. LEE. J. Am. Chem. Soc. **96**, 3590 (1974).
8. R. D. BURKHART and R. J. WONG. J. Am. Chem. Soc. **95**, 7203 (1973).
9. P. S. SKELL and K. J. SHEA. J. Am. Chem. Soc. **94**, 6550 (1972).
10. K. BIEMANN. Mass spectrometry, applications to organic chemistry. McGraw-Hill, New York, NY. 1962.
11. G. H. CADY. Inorg. Synth. **5**, 156 (1975).
12. C. WALLING. Free radicals in solution. Wiley, New York, NY. 1957. p. 76.

Le potentiel chimique d'excès dans des systèmes binaires: acides dicarboxyliques – acides monocarboxyliques ou esters. L'énergie libre d'interéchange entre groupes aliphatiques et carboxyliques

GIANFRANCESCO BERCHIESI, GIANCARLO GIOIA-LOBBIA, GIOVANNI VITALI ET MARIA A. BERCHIESI

Istituto Chimico dell'Università, Via S. Agostino 1, 62032 Camerino, Italie

Reçu le 6 octobre 1980

GIANFRANCESCO BERCHIESI, GIANCARLO GIOIA-LOBBIA, GIOVANNI VITALI et MARIA A. BERCHIESI. Can. J. Chem. **59**, 1375 (1981).

Les auteurs rapportent des donnés experimentales concernant les températures d'équilibre solide–liquide et liquide–liquide de systèmes binaires entre acides aliphatiques dicarboxyliques et l'hexadecanoate d'éthyle. Le potentiel chimique d'excès est deduit à partir de la courbe de crystallization soit pour ces systèmes soit pour des systèmes étudiés précédemment et publiés seulement sous forme graphique. Cette quantité thermodynamique est comparée avec la valeur correspondante calculée selon la théorie d'interaction des groupes.

GIANFRANCESCO BERCHIESI, GIANCARLO GIOIA-LOBBIA, GIOVANNI VITALI, and MARIA A. BERCHIESI. Can. J. Chem. **59**, 1375 (1981).

We report experimental data concerning the solid–liquid and liquid–liquid equilibrium temperatures for some binary systems composed of ethyl hexadecanoate and some bicarboxylic aliphatic acids. The crystallization curves of these systems and of others, previously published only in a graphical form, are used in order to obtain the excess chemical potential of the bicarboxylic acid along its crystallization curve. This thermodynamic quantity is compared with that calculated from the theory of group interaction, by means of the areas of the contact surfaces and of three interchange energy parameters.

Introduction

Les propriétés thermodynamiques des mélanges de composés organiques peuvent être traitées théoriquement selon la théorie d'interaction des groupes developpée par Kehiahian (1). Depuis quelques années nous avons étudié (2–8)[1] les mélanges binaires entre acides dicarboxyliques (composé **1**) et acides monocarboxyliques ou esters (composé **2**) par la méthode cryoscopique, qui permet de calculer le potentiel chimique d'excès (9–12). Dans cette note les valeurs expérimentales des équilibres de phase dans les systèmes binaires $CH_3(CH_2)_{14}-COOC_2H_5-COOH(CH_2)_nCOOH$ ($2 \leq n \leq 7$) sont données. Les composés ont été choisis pour étudier l'interaction entre groupes carboxyliques et aliphatiques, à cause de l'importance de ces groupes dans le domain industriel et biologique. L'interpretation du potentiel chimique d'excès dans les systèmes étudiés jusqu'à présent est essayée sur la base de la théorie proposée récemment par Kehiahian (1).

Méthode expérimentale

La méthode expérimentale employée est décrite en detail dans une note précédente (13): le mélange fondu, contenu dans une éprouvette en Pyrex, est placé dans un four thermoréglé au moyen d'une thermocouple Chromel Alumel jointe à un système CAT Leeds & Northrup. La température du four est reglée quelques dégrés au dessous de la température de fusion et une resistence auxiliaire, enroulée autour de l'éprouvette, permet de fondre le mélange partiellement crystallisé et de régler la vitesse de refroidissement à une valeur approximative de 0,25 K/min. La température du mélange est mesurée par une seconde thermocouple (Chromel Alumel) placée dans la cavité interne de la canne en verre du vibrobrouilleur et jointe à un potentiomètre Leeds & Northrup K-3. La thermocouple de mesure est étalonnée par comparaison avec un thermomètre à résistance de platine (avec garantie NBS). Les mélanges étudiés sont thermiquement stables pendant 3 ou 4 h à la température du composé plus haut-fondant. Pour un temps plus long les mesures de température de crystallisation d'une même composition ne sont plus reproductibles entre ±0,1 K et, en plus, le mélange brunit. Chaque mésure est répétée deux ou trois fois et l'accord est toujours meilleur que 0,1 K. A plus hautes températures (p.e. dans les courbes d'équilibre L–L), les mélanges sont moins stables et ont été employés pour une période plus courte. Des produits Fluka ou Ega ont été employés (purété 99%), après une recristallisation d'alcool.

Théorie et calculs

Les courbes cryoscopiques sont employées dans les études thermodynamiques et cette méthode est largement décrite en littérature (14) et a été employée dans des études précédentes (10–12). La courbe T/x peut être représentée mathematiquement par une des équations suivantes (9, 10, 14):

$$[1] \quad T = (H_{f1} + \Sigma H_{t1} + \mu_{E1})/(S_{f1} + \Sigma S_{t1} - R \ln x_1)$$

$$[2] \quad T = (H_{f1} + \Sigma H_{t1} + \bar{H}_1)/(S_{f1} + \Sigma S_{t1} + \bar{S}_1)$$

qui peuvent être déduites de l'équation $\mu_{1s} =$

[1] A cause d'une erreur de presse dans le tableau 1 de ref. 3 x_2 est écrit au lieu de x_1 et dans le tableau 3 de ref. 7 le terme A_3 du système binaire acide adipique + diphenyl ether a été écrit 956,0 au lieu de −956,0.

0008-4042/81/091375-06$01.00/0

©1981 National Research Council of Canada/Conseil national de recherches du Canada

Can. J. Chem. Downloaded from www.nrcresearchpress.com by 210.87.254.40 on 09/06/12
For personal use only.

Can. J. Chem. Downloaded from www.nrcresearchpress.com by 210.87.254.40 on 09/06/12
For personal use only.

TABLEAU 1. Volumes et aires de surfaces selon Bondi des molécules des composés étudiés. Exprimés en unité V_{CH_4} ou A_{CH_4} (*: CH_2, CH_3; **: COOH(**1**); ***: COOH(**2**); ****: COO)

Substance	r_i	q_i	α_i*	α_i**	α_i***	α_i****
b	3,98	3,51	0,3980	0,6012		
c	4,57	3,97	0,4690	0,5316		
d	5,17	4,44	0,5242	0,4753		
e	5,77	4,90	0,5700	0,4307		
f	6,36	5,37	0,6068	0,3930		
g	6,96	5,83	0,6388	0,3620		
h	9,66	7,84	0,8651		0,1346	
i	10,26	8,30	0,8733		0,1271	
l	10,85	8,77	0,8796		0,1203	
m	11,45	9,23	0,8862		0,1143	
n	10,86	8,74	0,9132			0,0868
o	11,46	9,20	0,9176			0,0824
p	12,06	9,67	0,9214			0,0785
q	12,65	10,13	0,9256			0,0749
r	12,65	10,13	0,9256			0,0749

μ_{1L} à condition que les crystaux en équilibre avec le mélange liquide soient une phase pure. Dans cette note nous employons l'éq. [1] qui permet d'obtenir μ_{E1}, quand H_{f1} et H_{t1} seulement sont connus. μ_{E1} est exprimé par un polynôme $\sum_1^n A_i x_2^i$ et la limite est n choisie de façon à avoir une valeur de rms comparable à l'erreur expérimentale. Dans la statistique employée la fonction de partition configurationnelle est calculée sur un modèle de liquide quasi-réticulaire, en employant l'approximation quasi-chimique et l'hypothèse que les molécules sont en contact sur toute leur surface. Le potentiel chimique d'excès deduit est donné par la formule suivante:

$$[3]\quad \mu_{E1}/RT = \mu_{E1}^*/RT + zq_1 \Sigma_s \alpha_{s1} \ln (X_s\alpha_{s1}/X_{s1}\alpha_s)$$

où le terme combinatoire est exprimé dans la forme de Guggenheim:

$$[4]\quad \mu_{E1}^*/RT = \ln \varphi_1/x_1 + (zq_1/2) \ln \xi_1/\varphi_1$$

et X_s, égale à $\sqrt{2A_{ss}/A}$ est obtenu à l'aide d'un système d'équations de Barker (1):

$$[5]\quad X_s(X_s + \Sigma_t X_t \eta_{st}) = \alpha_s$$

où η_{st} est en relation avec l'énergie libre d'interéchange g_{st}

$$[6]\quad \eta_{st} = \exp(-g_{st}/zRT)$$

Les volumes et l'aire des surfaces des molécules sont obtenus selon la méthode de Bondi (15) et sont donnés au tableau 1.

Analyse des erreurs expérimentales

μ_{E1} calculé selon la méthode cryoscopique le long de la courbe de cristallisation est affecté par l'influence de ces causes d'erreur: (*1*) l'erreur expérimentale en T; (*2*) l'erreur expérimentale en H_f et S_f; (*3*) le fait que, si la capacité calorifique partielle des composés dans le mélange n'est pas connue, en général H_f et S_f sont considérés constants le long de la courbe de cristallisation. L'expression pour ces causes d'erreurs peut être obtenue à partir de l'éq. [1].

L'erreur relative au point *1* est: $\delta\mu_{E1} = (S_f - R \ln x_1)\delta T$, qui peut être estimé en employant la valeur S_f relative à l'acide hexanedioique publiée précédemment (16). Dans l'intervalle de concentration $0{,}9 > x_1 > 0{,}1\mu_{E1}$ change entre 2,0 et 2,4 cal/mol.

L'erreur relative au point *2* est: $\delta\mu_{E1} = T\delta S_f - \delta H_f$; dans l'intervalle de concentration entre le composé **1** pur et le mélange eutectique $\delta\mu_{E1}$ change entre 0 et 23 cal/mol (calcul effectué sur l'acide hexanedioique).

Le point *3* donne une erreur:

$$[7]\quad \delta\mu_{E1} = T\int_{T_f}^{T} (\Delta\bar{c}_p/T)\,dT - \int_{T_f}^{T} \Delta\bar{c}_p\,dT \simeq T\Delta\bar{c}_p \ln (T/T_f) + \Delta\bar{c}_p(T_f - T)$$

A cause du fait que $\bar{c}_p$ n'est pas connu pour l'acide hexanedioique ou pour les autres acides employés, une évaluation approximative peut être effectuée en employant une valeur $\Delta\bar{c}_p = 10$ cal/K mol, valable pour d'autres substances aliphatiques (17–19). $\delta\mu_{E1}$ change entre 0,0 et 195 cal/mol dans l'intervalle de concentration entre le composé **1** pur et le mélange eutectique. Pour cette raison une incertitude de 10 ou 15% est attendue pour les valeurs de μ_{E1}.

Résultats et discussion

Les températures expérimentales d'équilibre L–L et L–S sont données au tableau 2 avec les

Can. J. Chem. Downloaded from www.nrcresearchpress.com by 210.87.254.40 on 09/06/12
For personal use only.

TABLEAU 2

(*a*) Températures d'équilibre liquide–solide et liquide–liquide pour les systèmes binaires: o–a; o–b; o–c

o–a			o–b			o–c		
x_2*	T_{sl} (K)	T_{ll} (K)	x_2*	T_{sl} (K)	T_{ll} (K)	x_2*	T_{sl} (K)	T_{ll} (K)
0,0	457,0		0,0	371,0		0,0	425,5	
0,0031	456,4		0,0063	370,8		0,0023	425,3	
0,0094	456,7	465,8	0,0152	370,7	403,7	0,0080	424,5	
0,0115	456,5	483,2	0,0195	370,7	437,7	0,0277	423,7	
0,0160	456,1	492,6	0,0215	370,3	460,2	0,0381	423,4	446,0
—	—	—	0,0232	369,9	475,7	0,0461	423,6	465,3
0,7466	457,6	484,7	—	—	—	0,0550	423,3	483,5
0,7677	456,6	476,7	0,8029	370,9	457,0	—	—	—
0,8082	457,1	458,4	0,8369	370,8	419,1	0,6777	423,2	454,6
0,8335	456,8		0,8538	370,1	390,7	0,6970	423,9	443,7
0,9263	445,2		0,8738	369,7		0,7125	423,7	436,2
0,9671	433,1		0,8965	367,5		0,7597	423,2	
0,9874	401,0		0,9097	365,0		0,8066	421,6	
1,0	294.2		0,9505	347,3		0,8614	417,4	
			0,9760	331,3		0,9011	414,9	
x_{2m}' = 0,008			1,0	294,2		0,9344	406,7	
x_{2m} = 0,814						0,9586	398,1	
T_m = 456,8 K			x_{2m}' = 0,014			0,9879	360,1	
			x_{2m} = 0,860			1,0	294,2	
			T_m = 370,5 K					
						x_{2m}' = 0,030		
						x_{2m} = 0,734		
						T_m = 423,5 K		

*1 représente le composé acide dicarboxylique, 2 l'autre composé.

(*b*) Températures d'équilibre liquide–solide pour les systèmes binaires: o–d; o–f; o–e

o–d		o–f		o–e			
x_2*	T_{sl} (K)	x_2*	T_{sl} (K)	x_2*	T_{sl} (K)	x_2	T_{sl} (K)
0,0	377,5	0,0	380,0	0,0	415,5	0,7598	402,4
0,0469	375,9	0,0162	379,5	0,0162	414,7	0,8030	400,4
0,0995	375,0	0,0674	378,2	0,0446	413,6	0,8724	396,2
0,1565	374,7	0,0984	378,0	0,0859	411,9	0,9215	391,2
0,2398	373,7	0,1487	377,6	0,1363	410,6	0,9521	384,2
0,3465	373,2	0,2292	376,6	0,1940	409,4	0,9707	376,3
0,4218	372,9	0,2610	375,8	0,2553	408,6	0,9871	362,9
0,5218	372,6	0,3379	375,3	0,3067	408,1	0,9904	352,7
0,6603	372,0	0,4096	374,5	0,3555	407,7	1,0	294,2
0,7765	369,7	0,4859	373,6	0,4330	407,4		
0,8716	364,8	0,5660	372,8	0,5181	406,5		
0,9132	360,4	0,6720	372,4	0,5735	405,9		
0,9704	345,5	0,7236	371,1	0,6274	404,9		
0,9881	327,4	0,7877	369,3	0,6705	404,0		
1,0	294,2	0,8321	368,1	0,7041	403,4		
		0,8710	366,8				
		0,9287	361,1				
		0,9682	351,6				
		0,9859	332,6				
		1,0	294,2				

*1 représente le composé acide dicarboxylique, 2 l'autre composé.

coordonnées des points invariants. La courbe de cristallisation du composé **1** est étendue jusqu'à des valeurs très faibles de x_1 et, comme observé souvent précédemment (3–8), il n'a pas été possible de mettre en évidence le point eutectique. Ce fait peut être attribué à la grande différence de point de fusion des deux composés (20). Les systèmes binaires avec les acides butanedioique, pentanedioique et hexanedioique présentent la region d'immiscibilité à l'état liquide, qui n'a pas été étudiée complètement à cause des raisons de stabilité thermique. Les autres systèmes binaires présentent

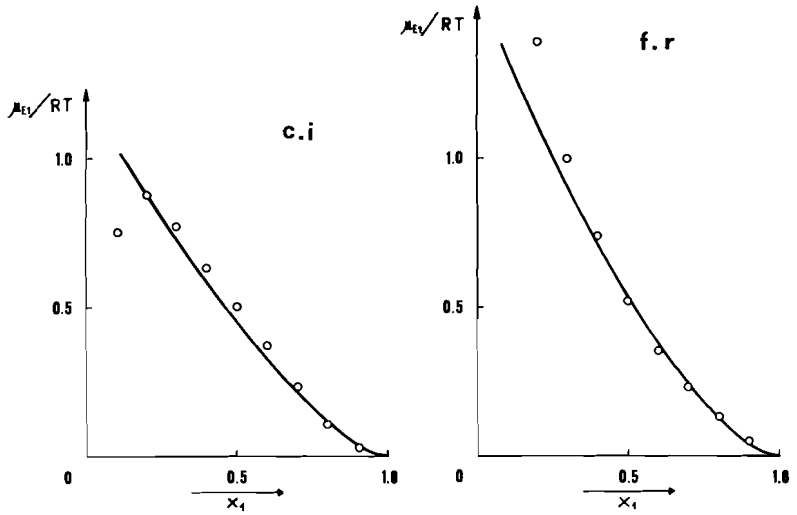

FIG. 1. Comparaison entre le potentiel chimique d'excès expérimental (points) et théorique (ligne) pour les systèmes suivants: b–i; b–h; d–m; g–m; f–m; e–m; c–m; c–i; c–l; c–h; d–p; f–p; f–q; f–n; f–r; e–r; f–o; d–o; e–n; e–p; e–q; d–n; dans cette note les systèmes c–i et f–r sont publiés, les autres figures sont placées dans le dépôt.[2]

une courbe de cristallisation T/x en forme de S, comme dans les systèmes avec "region d'immiscibilité submergée" (20).

Dans les systèmes étudiés jusqu'à présent (2–8) et dans ceux rapportés dans cette note il est assez probable que les équilibres L–S soient entre phase liquide et phase solide pure: en effet dans une note précédente (2) nous avons mis en évidence le fait que la constante cryoscopique $\Delta T/m$ s'approche à la valeur thermodynamique $RT_f^2M_1/1000H_f$ pour des solutions diluées de 2 en 1. Même les acides nonanedioique, octanedioique et heptanedioique présentent un comportement cryoscopique regulier avec l'hexadecanoate d'éthyle; en effet les mesures effectuées jusqu'à une concentration 1,2 m du composé **2** donnent les valeurs $\Delta T/m$ suivantes, extrapolées à $m = 0$: 6,0, 8,3, 6,0 K/molalité qui sont en accord avec les valeurs thermodynamiques (16): 6,9, 8,6, 6,9 K/molalité.

Ce fait, comme aussi le nombre remarquable de systèmes qui présentent la region d'immiscibilité dans cette famille de systèmes binaires supporte l'hypothèse que la déviation positive des courbes T/x est due au potentiel chimique d'excès plutôt que à une solubilité partielle du composé **2** dans le composé **1** solide.

Après ces considérations et au moyen des données calorimétriques publiées précedemment (16), μ_{E1} a été calculé pour les mélanges étudiés et exprimé en polynômes $\sum_1^n A_i x_2^i$, dont les coefficients concernant les systèmes en hexadécanoate d'éthyle et en nonadécanoate de methyle ont été donnés au tableau 3 avec les valeurs rms.[2] Les valeurs des coefficients des autres systèmes étudiés ont été données dans une note précédente (5). Les valeurs g_{st} d'énergie libre d'interéchange ont été déterminées sur les systèmes b–h et f–q et elles sont: 6480 J/mol, pour le contact (CH_3, CH_2)–COOH(**1**); 4800 J/mol pour le contact (CH_3, CH_2)–COOH(**2**); 400 J/mol pour le contact COOH(**1**)–COOH(**2**); 4400 J/mol pour le contact (CH_3, CH_2)–COO; 3600 J/mol pour le contact COOH(**1**)–COO; z étant 4 dans cette note. Les valeurs de μ_{E1} expérimentales et calculées sont comparées en fig. 1, montrant un accord satisfaisant. Les groupes carboxyliques COOH(**1**) et COOH(**2**) ne semblent pas équivalents. Précédemment nous avons mis en évidence du point de vue expérimentale (2) que l'interaction COOH(**2**)–COOH(**2**) prévaut sur l'interaction COOH(**1**)–COOH(**2**) quand la concentration du composé **2** augmente. La présence de deux groupes identiques dans une molécule semble changer les propriétés du groupe, comme rapporté en littérature pour les diols (21). Les valeurs g_{st} élevées et la valeur z faible peuvent expliquer les déviations positives de l'idéalité comme dues à une déviation du mélange casuel.

Etant $X_sX_t\eta_{st}$ la surface de contact entre les surfaces s et t dans le système, le produit $g_{st}X_sX_t\eta_{st}/A$

[2]On peut obtenir les données mises en dépôt, à un prix nominal, en s'adressant au Dépôt de données non publiées, ICIST, Conseil national de recherches du Canada, Ottawa (Ont.), Canada K1A 0S2.

Can. J. Chem. Downloaded from www.nrcresearchpress.com by 210.87.254.40 on 09/06/12
For personal use only.

Can. J. Chem. Downloaded from www.nrcresearchpress.com by 210.87.254.40 on 09/06/12
For personal use only.

peut être considéré égal à l'énergie libre d'interéchange totale dans le mélange. La fonction $F = \Sigma g_{st} X_s X_t \eta_{st}$ étendue à tous les contacts montre un maximum (fig. 2) dans la zone riche en composé **1**, probablement comme conséquence de la constitution géométriques et cimique des composés. En fig. 2 on peut aussi remarquer que F augmente avec la longueur de la chaîne aliphatique du composé **2**; du point de vue expérimentale on a remarqué une tendance plus forte à la separation en deux phases liquides au fur et à mesure que la chaîne du composé **2** augmente.

La composition des deux phases liquides en équilibre à une température T sont en relation, dans l'intervalle de température étudié, selon la formule suivante, tel que remarqué précédemment (8)

$$[8] \quad \ln x_2/x_2' = a - b(T - T_m)$$

où $x_2 > x_2'$ et T_m est la température monotectique. D'une façon empirique on peut montrer que a et b dependent des groupes présents dans les composés. En effet les paramètres

$$[9] \quad \delta = (n_{COOH}/n_C)_{dicarb} - (n_{COO(H)}/n_C)_{ester,\ (monocarb)}$$

et b sont en relation linéaire (fig. 3); tandis que le paramètre a dépend de la température monotectique selon la relation $a/\gamma T_m \simeq 0{,}0011\ K^{-1}$ ($\sigma = 0{,}0003$). γ est définie: $\gamma = (n_{COOH}/n_C)_{dicarb}/(n_{COO(H)}/n_C)_{ester(mon)}$. La valeur 0,0011 K^{-1} est la moyenne sur 25 systèmes (8) et a varie entre 1,58 et 4,78, γ entre 5,70 et 10,00, T_m entre 369,2 et 455,2 K.

Ces considérations empiriques montrent que la region d'immiscibilité peut être traitée par une théorie des groupes et qu'il est nécessaire de developper une convenable statistique pour les systèmes binaires de composés polaires et associés. L'utilité pratique de la fig. 3 à été expliqué précédemment (8).

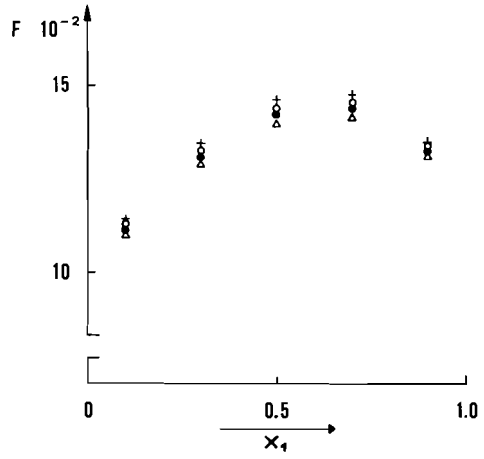

FIG. 2. Comportement de la fonction F contre x_1 dans les systèmes: c–i ●; c–l ○; c–h △; c–m +. F est exprimé en J/mol.

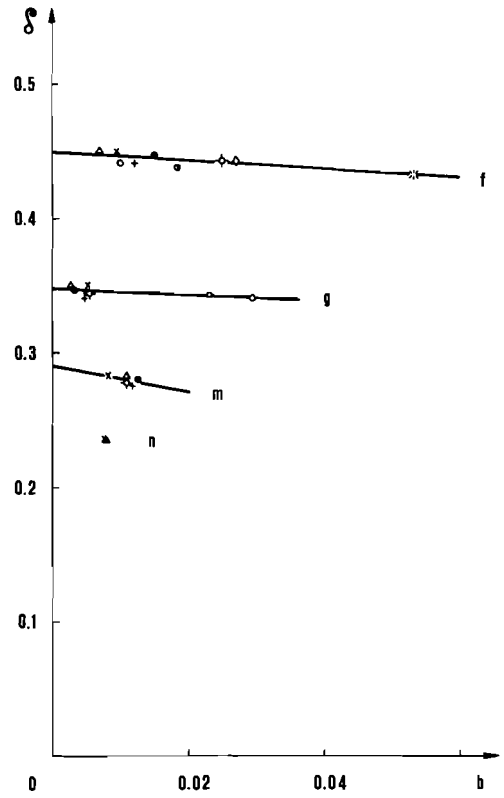

FIG. 3. Comportement δ/b (K^{-1}) dans les systèmes binaires entre: *a* et (à partir de gauche) q, r, l, o, n, p, i, u, h; *b* et (à partir de gauche) q, p, n, o, r, m, l; *c* et (à partir de gauche) r, q, o, n, p; *d* et (à partir de gauche) r, q.

Remerciements

Nous remercions le Dr. Ing. A. Polzonetti, directeur du Centro di Calcolo dell'Università di Camerino, pour nous avoir mis à disposition le programme pour la resolution des systèmes d'équations de Barker et nous remercions aussi le CNR (Rome) pour l'aide financière.

1. H. V. KEHIAHIAN, J. P. E. GROLIER et G. C. BENSON. J. Chim. Phys. **75**, 1031 (1978).
2. G. BERCHIESI, A. CINGOLANI et D. LEONESI. J. Therm. Anal. **6**, 91 (1974).
3. G. GIOIA LOBBIA, G. BERCHIESI et M. A. BERCHIESI. J. Therm. Anal. **10**, 133 (1976).
4. G. GIOIA LOBBIA, G. BERCHIESI et M. A. BERCHIESI. J. Ther. Anal. **12**, 449 (1977).
5. G. GIOIA LOBBIA, G. BERCHIESI, M. A. BERCHIESI et G. VITALI. Ann. Chim. (Rome), **67**, 407 (1977).

6. G.GIOIA LOBBIA, G. BERCHIESI et M. A. BERCHIESI. Gazz. Chim. **107**, 43 (1977).
7. G. GIOIA LOBBIA, A. CINGOLANI et G. BERCHIESI. Ann. Chim. (Rome), **67**, 535 (1977).
8. G. GIOIA LOBBIA, G. BERCHIESI, M. A. BERCHIESI et G. VITALI. J. Therm. Anal. **16**, 41 (1979).
9. C. SINISTRI et P. FRANZOSINI. Ric. Sci. Sez. A, Ser. 2, **3**, 419 (1963).
10. G. BERCHIESI et M. LAFFITTE. J. Chim. Phys. **6**, 877 (1971).
11. G. BERCHIESI, A. CINGOLANI, D. LEONESI et G. PIANTONI. Can. J. Chem. **50**, 1972 (1972).
12. A. CINGOLANI, G. BERCHIESI et P. FRANZOSINI. Gazz. Chim. **101**, 981 (1971).
13. M. BRAGHETTI, D.LEONESI et P. FRANZOSINI. Ric. Sci. **38**, 116 (1968).
14. G. PETIT. La cryométrie à haute température et ses applications. Masson & Cie, Paris. 1965. p. 10 suivantes.
15. A. BONDI. J. Phys. Chem. **68**, 441 (1964).
16. A. CINGOLANI et G. BERCHIESI. J. Therm. Anal. **6**, 87 (1974).
17. G. S. PARKS et K. K. KELLEY. J. Am. Chem. Soc. **47**, 2089 (1925).
18. K. S. PITZER. J. Am. Chem. Soc. **62**, 331 (1940).
19. G. S. PARKS et D. W. LIGHT. J. Am. Chem. Soc. **56**, 1511 (1934).
20. J. E. RICCI. The phase rule and heterogeneous equilibrium. Dover Inc., New York, NY. 1966. pp. 88, 175.
21. E. JIMENEZ, M. I. PAZ. ANDRADE et C. CASANOVA. J. Chim. Phys. **76**, 46 (1979).

Appendix

Tableau des symboles

A	aire de la surface totale des molécules du système
α_s	fraction de surface de type s dans le système
α_{si}	fraction de surface de type s dans une molécule de type i
ΔT	dépression cryoscopique
δ	différence entre le caractère polaire des composés dans le mélange
$\Delta\bar{c}_p$	différence de capacité calorifique du composé impliqué dans la fusion, dans la phase liquide et dans la phase solide
φ_i	fraction de volume des molécules de type i
γ	rapport entre le caractère polaire des composés
H_{f1}, H_{t1}	enthalpie de fusion et de transition du composé **1**
$\bar{H}_1$	enthalpie molaire partielle du composé **1**
M_1	poids moléculaire du composé **1**
μ_{1S}, μ_{1L}	potentiel chimique du composé **1** dans les phases solides et liquides en équilibre respectivement
μ_{E1}	potentiel chimique d'excès du composé **1**
m	molalité
n_C, n_{COOH}, n_{COO}	nombre d'atomes de carbon, de groupes COOH et de groupes COO dans une molécule respectivement
g_{st}	énergie libre d'interéchange
q_i	surface de la molécule i en unité de surface de CH_4
r_i	volumes des molécules i en unité de volume de CH_4
rms	$\sqrt{S/N}$; $S = \Sigma(\mu_{E1} - \mu_{E1}\ \text{calc})^2$; N = nombre de points expérimentaux
S_{f1}, S_{t1}	entropie de fusion et de transition, respectivement, du composé **1**
$\bar{S}_1$	entropie molaire partielle du composé **1**
T_f	température de fusion
T_m	température monotectique
T_{sl}, T_{ll}	température d'équilibre solide–liquide et liquide–liquide respectivement
ξ_i	rapport de surface du composé i
z	nombre de coordination (= 4 dans cette note)
$x_{2m'}$, x_{2m}	composition des deux phases en équilibre à T_m, determinée graphiquement

Symboles des composés

a	Acide butanedioique
b	acide pentanedioique
c	acide hexanedioique
d	acide heptanedioique
e	acide octanedioique
f	acide nonanedioique
g	acide décanedioique
h	acide pentadécanoique
i	acide hexadécanoique
l	acide heptadécanoique
m	acide octadécanoique
n	hexadécanoate de methyle
o	hexadécanoate d'ethyle
p	octadécanoate de methyle
q	octadécanoate d'ethyle
r	nonadécanoate de methyle
u	octadécan-1ole

Can. J. Chem. Downloaded from www.nrcresearchpress.com by 210.87.254.40 on 09/06/12
For personal use only.

Charge distributions and chemical effects. XXIV. On the role of vibrational energies in determining molecular stabilities

SÁNDOR FLISZÁR AND J.-L. CANTARA
Department of Chemistry, University of Montreal, Montreal, P.Q., Canada H3C 3V1
Received September 10, 1980

Can. J. Chem. Downloaded from www.nrcresearchpress.com by 178.218.224.3 on 09/06/12
For personal use only.

SÁNDOR FLISZÁR and J.-L. CANTARA. Can. J. Chem. **59**, 1381 (1981).

A simple equation has been derived for calculating accurate ZPE + $H_T - H_0$ (zero-point and heat content) energies of saturated hydrocarbons from their enthalpies of formation and carbon-13 nuclear magnetic resonance spectra. Applications to conformational analysis indicate a near invariance of vibrational energies with respect to chair–boat conformational changes of the cyclohexane ring, the loss in molecular stability arising then from a weakening of the chemical binding due to a reorganization of the electronic charges. The origin of the destabilizing effect of butane *gauche* interactions is found, in the cyclohexane series, in a weakening of the chemical binding (~1.85 kcal/mol) which is partially compensated by a lowering (~0.85 kcal/mol) vibrational energy, thus offering an explanation for the loss in molecular stability of ~1.00 kcal/mol for one *gauche* interaction without invoking Coulomb-type repulsions between non-bonded atoms. Calculated enthalpies of formation are presentd for a number of cycloalkanes.

SÁNDOR FLISZÁR et J.-L. CANTARA. Can. J. Chem. **59**, 1381 (1981).

On a déduit une équation simple pour calculer avec précision les énergies ZPE + $H_T - H_0$ (point zéro et contenu de chaleur) des hydrocarbures saturés à partir de leurs enthalpies de formation et de leurs spectres rmn du ^{13}C. Les applications à l'analyse conformationnelle indiquent une quasi invariance des énergies vibrationnelles par rapport aux changements de conformation chaise-bateau du cycle cyclohexane, la perte de la stabilité moléculaire provient alors de l'affaiblissement des liaisons chimiques provoquées par une réorganisation des charges électroniques. En série cyclohexanique l'origine de l'effet déstabilisant des interactions butane gauche réside dans un affaiblissement des liaisons chimiques (~1,85 kcal/mol) qui est partiellement compensé par un abaissement (~0,85 kcal/mol) de l'énergie vibrationnelle, apportant ainsi une explication de la perte de stabilité moléculaire de ~1,00 kcal/mol pour une interaction gauche sans invoquer des répulsions de type Coulombien entre les atomes non liés. On présente des enthalpies de formation calculées pour un certain nombre de cycloalcanes.
[Traduit par le journal]

The atomization

$$\text{Molecule} \rightarrow n_1A_1 + n_2A_2 + \ldots$$

of a molecule into its constituent n_1 atoms A_1, n_2 atoms A_2, ... provides a direct insight into fundamental aspects of molecular energies. The relevant thermodynamic information is usually expressed in terms of enthalpy of formation, ΔH_f, or enthalpy of atomization, ΔH_a, of the molecule under consideration, i.e.

$$[1] \quad \Delta H_a = \Sigma n_i \Delta H_f(A_i) - \Delta H_f$$

where the $\Delta H_f(A_i)$'s are the enthalpies of formation of the gaseous atoms A_i. A number of schemes viewing the molecule as an assembly of chemical bonds or groups and the " molecular energy" as a sum of appropriately defined contributions has been proposed for calculating ΔH_a (1). In the study of isolated molecules, however, we refer more conveniently (2) to the *energy* of atomization ΔE_a, i.e.

$$[2] \quad \Delta E_a = \Delta H_a - (\Sigma n_i - 1)RT$$

Both ΔE_a and ΔH_a are considered at some temperature, say 25°C, i.e. under working conditions which are of real practical interest. This situation may be compared with that referring to molecules in their hypothetical vibrationless state at 0 K, whose atomization energy is ΔE_a^*. The relation between ΔE_a and ΔE_a^* is described by eq. [3]

$$[3] \quad \Delta E_a = \Delta E_a^* - \Sigma F(\nu_i,T) + 3(\Sigma n_i - 2)RT/2$$

which states that the energy of atomization at, say, 25°C is that of the hypothetical vibrationless molecule at 0 K *less* the sum $\Sigma F(\nu_i,T)$ (over $3\Sigma n_i - 6$ degrees of freedom) of vibrational energy corresponding to the fundamental frequencies ν_i, which is already present in the molecule at 25°C. The term $3(\Sigma n_i - 2)RT/2$ accounts for the formation of Σn_i atoms with translational energy and the disappearance of one nonlinear molecule with 3 translational and 3 rotational $RT/2$ contributions. It follows from eqs. [1]–[3] that

$$[4] \quad \Delta E_a^* = \Sigma n_i[\Delta H_f^0(A_i) - 5RT/2] + \Sigma F(\nu_i,T) + 4RT - \Delta H_f^0$$

where all enthalpies are now referred to standard conditions (gas, $T = 298.16$ K). The vibrational energy may be separated into a zero-point energy term (ZPE) and a thermal energy term (E_{vibr}). It is, therefore,

$$\Sigma F(\nu_i, T) + 4RT = \text{ZPE} + E_{vibr} + 4RT$$

0008-4042/81/091381-07$01.00/0
©1981 National Research Council of Canada/Conseil national de recherches du Canada

Can. J. Chem. Downloaded from www.nrcresearchpress.com by 178.218.224.3 on 09/06/12
For personal use only.

On the other hand, $E_{vibr} + 4RT$ is the increase in enthalpy $(H_T - H_0)$ of nonlinear molecules due to their warming up from $T = 0$ to $T = T$. Consequently, eq. [4] can now be written as follows.

$$[5] \quad \Delta E_a^* = \Sigma n_i[\Delta H_f^0(A_i) - 5RT/2] + \text{ZPE} + (H_T - H_0) - \Delta H_f^0$$

This analysis of the energy components illustrates that there is a long way to go from the knowledge of the behavior of hypothetical motionless molecules to the understanding of their actual behavior at some temperature T. Postponing the questions about the derivation of accurate ΔE_a^*'s, it appears that the real problem is one of estimating the vibrational contributions in a simple manner. The object of this paper is to report some information about vibrational energies of saturated hydrocarbons, thus opening a way towards the construction of a simple empirical scheme for their evaluation. Saturated hydrocarbons $C_nH_{2n+2-2m}$ containing m (≥ 0) six-membered rings are selected because it is presently the only class of compounds for which we possess sufficient experimental information, namely both thermochemical and spectroscopic data.

Outline of calculations

For the $C_nH_{2n+2-2m}$ hydrocarbons under study, it is possible to calculate accurate ΔE_a^* energies from carbon-13 nuclear magnetic resonance shifts δ (ppm from ethane) by means of eq. [6] (3)

$$[6] \quad \Delta E_a^* = (1 - m)\Delta E_a^*(C_2H_6) + (n - 2 + 2m) \times [\Delta E_a^*(C_2H_6) - \Delta E_a^*(CH_4)] + \lambda_1 \Sigma N_{CC}\delta + \lambda_2[(n - 2 + 2m)\delta(CH_4) + \Sigma\delta]$$

in which $\Delta E_a^*(C_2H_6)$ and $\Delta E_a^*(CH_4)$ are, respectively, the appropriate values for ethane and methane. N_{CC} is the number of CC bonds formed by the C atom whose shift is δ. The parameters λ_1 and λ_2, which are derived from theory (3), are constants for this class of compounds. Equation [6] enables a simple and remarkably accurate calculation of the ΔE_a^*'s, considerably outperforming in rapidity and precision their quantum chemical evaluation. Indeed, eq. [6] was shown to agree with experimental ΔE_a^* values (eq. [5]) within experimental uncertainty, the average deviation being ~0.23 kcal/mol (3, 4). On the physical side, eq. [6] contains the information that, for vibrationless molecules, the prime factors governing molecular stabilities are found in the behavior of the charge dependent energy contributions associated with the chemical bonds indicating, namely, that 1 millielectron (= 10^{-3} e) of electronic charge added to hydrogen stabilizes a CH bond by 0.632 kcal/mol, whereas 1 me added to carbon has a stabilizing effect of 0.247 on a CH bond and of 0.488 kcal/mol on a CC bond (3).

At this stage we have two expressions for ΔE_a^*, i.e. eqs. [5] and [6]. Inserting the experimental values (3–5) (kcal/mol at $T = 298.16$ K) $\Delta H_f^0(C) = 170.89$, $\Delta H_f^0(H) = 52.09$, $\Delta E_a^*(C_2H_6) = 710.54$, $\Delta E_a^*(CH_4) = 419.27$, $\lambda_1 = 0.03244$, $\lambda_2 = 0.05728$, and $\delta(CH_4) = -8$ ppm, the following new energy formula is obtained from eqs. [5] and [6] (in kcal/mol at 298.16 K)

$$[7] \quad \text{ZPE} + H_T - H_0 = 27.692(1 - m) + 20.184n + 0.03244\Sigma N_{CC}\delta + 0.05728\Sigma\delta + \Delta H_f^0$$

which enables a rapid calculation of ZPE + H_T − H_0 energies from standard enthalpies of formation and C-13 nmr spectra. Of course, eq. [7] is as accurate as eq. [6] which has been tested earlier (3). The possibility of deriving ZPE + H_T − H_0 energies in a simple manner by means of eq. [7] offers now a new way of recognizing possible structure-related regularities from an examination of numerous cases. The results are as follows.

Results

Non-cyclic Alkanes

To begin with, we apply eq. [7] to all the non-cyclic alkanes (through C_9) which are either linear or contain only CH_3 branching but no quaternary C atoms. The idea is to avoid any case involving an *a priori* visible steric hindrance of internal rotations. The results obtained in this way are well reproduced by the simple new additivity scheme, eq. [8].

$$[8] \quad \text{ZPE} + H_T - H_0 = 11.479 + 18.213n_1 + 17.870n_2$$

where n_1 = number of CH_2 groups forming the linear chain and n_2 = number of CH_3 branchings.

Indeed, Table 1 indicates, firstly, that the ZPE + H_T − H_0 energies derived from eq. [7] are in excellent agreement with their experimental counterparts and, secondly, that these results are well reproduced by eq. [8], which gives the ZPE + H_T − H_0 values with a standard error of 0.176 kcal/mol (average deviation = 0.125 kcal/mol) and a multiple correlation coefficient of 0.99997. The change in ZPE + H_T − H_0 associated with methyl substitutions giving quaternary carbon atoms, however, can only be estimated as a rough average (17.55 kcal/mol) suggested by the experimental incre-

Can. J. Chem. Downloaded from www.nrcresearchpress.com by 178.218.224.3 on 09/06/12
For personal use only.

TABLE 1. ZPE + $H_T - H_0$ energies of selected paraffins containing no quaternary carbon atoms

Molecule	ZPE + $H_T - H_0$, kcal/mol		
	Exptl.[a]	Eq. [7][b]	Eq. [8]
C_1	29.5	29.53	29.69
C_2	48.02	48.02	47.91
C_3	65.94	66.20	66.12
C_4	84.38	84.37	84.33
2-MeC_3	83.89	84.32	83.99
C_5	102.83	102.59	102.54
2-MeC_4	102.14	101.96	102.20
C_6	120.99	120.78	120.76
2-MeC_5		120.66	120.41
3-MeC_5		120.56	120.41
2,3-Me_2C_4	119.65	119.90	120.07
C_7	139.29	138.93	138.97
2-MeC_6		138.65	138.63
2,3-Me_2C_5		138.05	138.28
2,4-Me_2C_5		138.25	138.28
C_8		157.16	157.18
2,3-Me_2C_6		156.87	156.50
2,4-Me_2C_6		156.52	156.50
2,3,4-Me_3C_5		156.23	156.15
C_9		175.35	175.40
4-MeC_8		175.03	175.05
2,3,5-Me_3C_6		174.26	174.37

[a]Zero-point energies were calculated in the harmonic oscillator approximation (ZPE = $N_{Av}\Sigma h\nu/2$) using the frequencies taken from ref. 6. The $H_T - H_0$ values are from ref. 7.
[b]The experimental ^{13}C and ΔH_f^0 data used in eq. [7] are indicated in Table 2.

ments in going from 2-MeC_3 to 2,2-Me_2C_3 (17.41), from 2-MeC_4 to 2,2-Me_2C_4 (17.37), from 2,3-Me_2C_4 to 2,2,3-Me_3C_4 (17.66), and from 2,2,3-Me_3C_4 to 2,2,3,3-Me_4C_4 (17.77), and should, therefore, be used with due care. The practical aspects of eq. [8] are clear: together with the ΔE_a*'s derived from carbon-13 nmr spectra (eq. [6]) they give access to accurate enthalpies of formation (eq. [5], Table 2).

Of course, the construction of an additivity scheme involving vibrational energies is, in itself, not free from conceptual difficulties and is considered here only on an empirical basis. It is also true, however, that the problems raised in this manner are no more acute than those hidden in additivity schemes involving directly ΔH_a or ΔE_a, because any such scheme implicitly distributes vibrational energies by treating them *de facto* as if they were additive. This point can be shown as follows. Let us temporarily assume that one single value (e.g., 18.213 kcal/mol) describes the increment in ZPE + $H_T - H_0$ for one added CH_2 group, regardless of the point of methyl substitution, i.e.,

$$\text{ZPE} + H_T - H_0 = 11.479 + 18.213n$$
$$= 47.905 + 18.213(n - 2)$$

where 47.905 is the value for ethane. Then, using eqs. [1], [5], and [6], we obtain the following expressions

$$[9] \quad \Delta H_a = \Delta H_a(2) + (n - 2)\,[\Delta H_a(2) - \Delta H_a(1)] + \lambda_1 \Sigma N_{CC}\delta + \lambda_2[(n - 2)\delta(1) + \Sigma\delta]$$

$$[10] \quad \Delta H_f^0 = \Delta H_f^0(2) + (n - 2)\,[\Delta H_f^0(2) - \Delta H_f^0(1)] - \lambda_1 \Sigma N_{CC}\delta - \lambda_2[(n - 2)\delta(1) + \Sigma\delta]$$

in which the indices 1 and 2 refer to methane and ethane, respectively. These equations describe in fact a bond-enthalpy additivity scheme, $\Delta H_a = \Sigma\Delta H_a$(bond) with individual bond contributions depending on the charges of the bond-forming atoms, implying exact additivity not only of non-bonded interactions, but also of the vibrational energy contributions. Now we know that the latter do depend on structural features. It so happens that the terms $\Sigma N_{CC}\delta$ and $\Sigma\delta$ are also structure-dependent. Equations [9] and [10] give generally satisfactory results (Table 2) because a readjustment of the parameters λ_1 and λ_2 compensates for the error introduced in assuming exact additivity of the vibrational energy terms. Hence, the success of eqs. [9] and [10] is in part due to fortunate compensations and should not be interpreted as a proof for postulated intrinsic qualities of bond-enthalpy additivity schemes. Of course, *marked* departures from "quasi-additivity" of the interactions between non-bonded atoms occurring in situations of extreme steric crowding represent a source of errors which should not be overlooked (14).

Cycloalkanes

We can now turn to the study of cyclic hydrocarbons and examine to what extent the additivity scheme describing ZPE + $H_T - H_0$ energies in acyclic compounds (eq. [8]) is applicable to cyclic structures. To begin with, we select molecules which are free from steric effects, such as butane *gauche* or *skew* pentane interactions.

Firstly, we note that a CH_2 group contributes 18.213 kcal/mol if no tertiary C atom is formed and 17.870 kcal/mol when branching occurs to give a tertiary C atom. We construct tentatively the ZPE + $H_T - H_0$ energies of cycloalkanes by counting 18.213 kcal/mol for each C atom of the molecule (rule 1) and subtract 18.213 − 17.870 = 0.343 kcal/mol for each tertiary C atom that is formed (rule 2). A number of H atoms is removed in the formation of polycyclic compounds, e.g., 2H atoms in *trans* decalin. The 11.479 kcal/mol term of eq. [8] represents roughly the contribution of two H atoms. Accordingly, we approximate the decrease in ZPE + $H_T - H_0$ due to the loss of one H atom by subtracting 11.479/2 = 5.740 kcal/mol per H atom that is removed (rule 3). These rules express clearly

TABLE 2. Comparison of ΔH_f^0's calculated from eqs. [7] and [8] or eq. [10], with experimental results[a]

Molecule	$\Sigma N_{CC}\delta$	$\Sigma\delta$	$-\Delta H_f^0$, kcal/mol		
			Exptl.	Eqs. [7], [8]	Eq. [10]
C_1	0	−8.0	17.89	17.73	18.15
C_2	0	0	20.04	20.15	20.08
C_3	39.8	29.6	25.02	25.11	24.97
C_4	91.0	52.8	30.03	30.07	30.03
2-MeC_3	113.4	74.8	32.07	32.40	32.22
C_5	139.6	77.6	35.00	35.05	35.05
2-MeC_4	161.6	87.7	36.92	36.68	36.59
2,2-Me_2C_3	190.4	124.4	40.27		39.85
C_6	188.0	102.0	39.96	39.98	40.05
2-MeC_5	211.8	116.1	41.66	41.91	41.88
3-MeC_5	212.5	102.9	41.02	41.17	41.21
2,3-Me_2C_4	223.8	110.6	42.49	42.32	42.13
C_7	235.4	125.7	44.89	44.85	44.97
2-MeC_6	257.5	138.2	46.60	46.62	46.64
3-MeC_6	255.5	126.7	45.96	45.90	45.93
2,3-Me_2C_5	267.2	123.2	46.65	46.42	46.27
2,4-Me_2C_5	274.6	151.3	48.30	48.27	48.11
2,2-Me_2C_5	288.4	159.7	49.29		49.18
2,2,3-Me_3C_4	290.1	145.7	48.96		48.51
C_8	284.2	150.0	49.82	49.80	49.98
2-MeC_7	306.5	162.8	51.50	51.59	51.67
3-MeC_7	307.4	153.0	50.82	51.06	51.19
4-MeC_7	303.4	153.6	50.69	50.96	51.04
2,3-Me_2C_6	315.8	150.0	51.13	51.50	51.41
2,4-Me_2C_6	321.1	163.8	52.44	52.46	52.39
2,5-Me_2C_6	327.8	174.6	53.21	53.30	53.27
3,4-Me_2C_6	314.2	139.0	50.91	50.82	50.75
2,3,4-Me_3C_5	324.3	148.7	51.97	52.05	51.72
2,2-Me_2C_6	331.7	180.8	53.71		53.77
3,3-Me_2C_6	319.1	159.0	52.61		52.04
2,2,3-Me_3C_5	344.8	164.8	52.61		53.51
2,3,3-Me_3C_5	319.0	145.7	51.73		51.32
2,2,3,3-Me_3C_4	353.8	178.0	53.99		54.63
C_9	332.0	174.1	54.54	54.69	54.93
4-MeC_8	350.7	177.3	56.19	55.83	55.95
2,3,5-Me_3C_6	378.0	185.4	57.97	57.86	57.62

[a]The ^{13}C data were taken from ref. 8 (C_1, C_2), ref. 9 (C_3–C_6), and ref. 10 (C_7–C_9). Except as noted below, the experimental ΔH_f^0 values are from ref. 7. The values for C_2, C_3, C_4, and 2-MeC_3 are taken from ref. 11, and that of 2,2-Me_2C_3 from ref. 12. The value for 2,3-Me_2C_6 and for the C_9 alkanes are taken from ref. 13. The present selection of experimental ΔH_f^0 values is not intended to represent a critical collection of "best values". Slightly different results are reported in ref. 13*a* for C_2 (−20.24), C_3 (−24.82), and C_4 (−30.15 kcal/mol), all other values being those given in this table. Similarly, one finds (13*b*), in kcal/mol, −35.07 for C_5, −36.55 (2-MeC_4) and −40.09 (2,2-Me_2C_3). Experimental uncertainties of this magnitude do not affect the general conclusions drawn in the present work. The parameters of eq. [10] are $\lambda_1 = 0.04531$ and $\lambda_2 = 0.05338$.

the fact that so far cyclic compounds are considered on the same basis as the acyclic ones, following strictly the description given by eq. [8]. Considering now that eq. [8] describes non-cyclic compounds in which internal rotations are as free as possible and, moreover, that internal rotations are hindered in cyclic compounds, we subtract tentatively $\frac{1}{2}RT = 0.296$ kcal (at 298.16 K) for each C—C bond in the cycle (rule 4). The results are presented in Table 3.

The comparison of the ZPE + $H_T - H_0$ energies derived from eq. [7] with their experimental counterparts clearly confirms the validity of eq. [7] for this class of compounds. The remarkable agreement between ZPE + $H_T - H_0$ energies constructed from the admittedly crude rules 1–4 and their "experimental" counterparts deduced from eq. [7] suggests that these cycloalkanes behave in essence like acylic alkanes inasmuch as vibrational energies are concerned, provided that the suppression of internal rotations is adequately taken into account. The fact that the $RT/2$ correction appears to be adequate further suggests that in acyclic hydrocarbons the contributions from internal rotations seem to be fairly close to $RT/2$, within experimental accuracy, even in relatively long chains.

Can. J. Chem. Downloaded from www.nrcresearchpress.com by 178.218.224.3 on 09/06/12
For personal use only.

TABLE 3. ZPE + $H_T - H_0$ energies of selected cycloalkanes

Molecule	ZPE + $H_T - H_0$, kcal/mol		
	Exptl.[a]	Eq. [7][b]	Rules 1–4
Cyclohexane	107.54	107.58	107.50
Methylcyclohexane	125.73	125.37	125.37
Ethylcyclohexane		144.17	143.59
n-Butylcyclohexane		180.30	180.01
cis-1,3-Dimethylcyclohexane		143.46	143.24
trans-1,4-Dimethylcyclohexane		143.46	143.24
1-*cis*-3-*cis*-5-Trimethylcyclohexane		161.54	161.11
trans-Decalin	166.90	166.96	166.71
trans-syn-trans-Perhydroanthracene		225.64	225.90
trans-anti-trans-Perhydroanthracene		225.96	225.90
Adamantane	153.54	153.64	154.25
Bicyclo[2.2.2]octane	130.83	131.17	130.87

[a]The value for bicyclo[2.2.2]octane is given in ref. 15. The other results are given in ref. 4 and were deduced from the spectroscopic data of ref. 6 and the $H_T - H_0$ values reported in ref. 7.
[b]The experimental ^{13}C and ΔH_f^0 data used in eq. [7] are indicated in Table 4.

Now, of course, there is no reason to assume that the individual energy contributions in cycloalkanes are necessarily *exactly* the same as in noncyclic paraffins. To begin with, the comparison of ZPE + $H_T - H_0$ energies derived by means of eq. [7] for isomer pairs differing by the number of butane *gauche* interactions (e.g., *cis*- vs. *trans*-decalin) indicates a lowering of the ZPE + $H_T - H_0$ energy by 0.853 kcal/mol for one *gauche* interaction. A multiple regression analysis carried out using ZPE + $H_T - H_0$ energies derived for sixteen cycloalkanes containing no quaternary C atoms indicated, firstly, a contribution of 18.249 kcal/mol for each carbon atom and, secondly, a decrease of 0.322 kcal/mol for each tertiary C atom of the molecule. Moreover, the removal of one H atom in the formation of polycyclic structures reduces the ZPE + $H_T - H_0$ energy by 5.925 kcal/mol. Finally, this energy is further lowered by 0.296 ($= \frac{1}{2}RT$) kcal/mol for each CC bond of the cycle(s). These results are expressed by eq. [11], where n_C and $n_C + m - 1$ are, respectively, the numbers of C atoms and CC bonds in the cycle(s) and $2(m - 1)$ is the number of H atoms removed in the formation of polycyclic compounds.[1] The number of butane *gauche* interactions is n_g.

$$[11]\quad \text{ZPE} + H_T - H_0 = 11.850(1 - m) + 18.249n - 0.322n_{\text{tert}} - (n_C + m - 1)RT/2 - 0.853n_g$$

This approximation yields accurate estimates of ZPE + $H_T - H_0$ energies and involves only the knowledge of the molecular structures. Indeed, enthalpies of formation calculated from eq. [7] (or eqs. [5] and [6]) using the results given by eq. [11] and the appropriate ^{13}C nmr data are accurate within 0.168 kcal/mol (average deviation) when compared with their experimental counterparts. The results are given in Table 4.

This verification by means of experimental ΔH_f^0 values includes two compounds (**9** and **34**) which were not considered in the parameterization of eq. [11] because of the quaternary C atoms contained in their structures. Here, quaternary C atoms were tentatively treated like tertiary carbons. While the present results clearly support the validity of this approximation, additional verifications would be desirable. The enthalpy differences between **9**, **10**, and **11** calculated in this fashion can nevertheless be regarded as being reasonably reliable, as well as the difference of 1.41 kcal/mol between the *trans*- and *cis*-9-methyldecalins. For the latter compounds, the experimental ΔH_f^0 difference in the liquid phase is 1.39 ± 0.64 kcal/mol (24).

It is noteworthy that the change from chair to boat cyclohexane has no effect (or only a very minor one) on ZPE + $H_T - H_0$. This is clearly indicated by the results obtained for *trans-anti-trans*-perhydroanthracene (**26**) and bicyclo[2.2.2]-octane (**32**) and is further supported by the ZPE + $H_T - H_0$ energy determined for **32** by Boyd *et al.* (15), 130.83 kcal/mol, which is precisely the value derived from eq. [11].

As regards the perhydroanthracenes, our calculated ΔH_f^0 values can be compared with the results derived from Allinger's equilibration experiments in the liquid phase (25). Of course, liquid and gas phase results are not identical. *cis*-Decalin, for example, is less stable than its *trans* isomer by

[1]Not too much importance should be attached to the precise values of these parameters as they are subject to slight changes depending upon whether or not one or another compound is left out of the regression analysis. Inclusion of a constant term in the correlation yields an insignificant improvement (~0.02 kcal/mol in average deviation) and cannot be justified within the precision of this type of analysis.

Can. J. Chem. Downloaded from www.nrcresearchpress.com by 178.218.224.3 on 09/06/12
For personal use only.

TABLE 4. Calculated ΔE_a^*, ZPE + $H_T - H_0$ and ΔH_f^0 (298.16 K, gas) energies (kcal/mol) of cycloalkanes[a]

Molecule	$\Sigma N_{CC}\delta$	$\Sigma\delta$	ΔE_a^*	ZPE + $H_T - H_0$	$-\Delta H_f^0$ Calcd.	$-\Delta H_f^0$ Exptl.
1, Cyclohexane	261.6	130.8	1760.86	107.72	29.36	29.50
2, Methylcyclohexane	349.8	169.7	2056.77	125.65	36.71	36.99
3, Ethylcyclohexane	402.1	186.8	2350.26	143.89	41.33	41.05
4, *n*-Butylcyclohexane	492.1	234.3	2937.52	180.39	50.83	50.92
5, *cis*-1,3-Dimethylcyclohexane	437.0	208.5	2352.63	143.57	44.02	44.13
6, *trans*-1,3-Dimethylcyclohexane	373.9	180.4	2348.97	141.87	42.06	42.20
7, *trans*-1,4-Dimethylcyclohexane	436.8	208.5	2352.62	143.57	44.01	44.12
8, *cis*-1,4-Dimethylcyclohexane	378.7	179.3	2349.07	141.87	42.16	42.22
9, 1,1-Dimethylcyclohexane	391.4	194.5	2350.35	142.19	43.12	43.26
10, 1,1,3-Trimethylcyclohexane	483.6	237.7	2646.63	160.12	50.84	
11, 1,1,4-Trimethylcyclohexane	474.8	231.1	2645.97	160.12	50.18	
12, 1-*cis*-3-*cis*-5-Trimethylcyclohexane	527.3	248.9	2648.69	161.50	51.52	51.48
13, 1-*cis*-3-*trans*-5-Trimethylcyclohexane	462.6	223.1	2645.11	159.79	49.65	49.37
14, *trans*-Decalin	630.8	277.1	2815.56	166.74	43.74	43.52
15, *cis*-Decalin	527.0	232.5	2809.64	164.18	40.38	40.43
16, *trans-anti*-1-Methyldecalin	717.9	308.2	3110.98	183.81	51.46	
17, *cis-syn*-1-Methyldecalin	606.0	259.4	3104.56	181.25	47.60	
18, *trans-syn*-2-Methyldecalin	712.6	313.7	3111.13	184.67	50.75	
19, *cis-syn*-2-Methyldecalin	620.2	273.8	3105.84	182.11	48.02	
20, *trans*-9-Methyldecalin	637.6	274.7	3106.46	181.58	49.17	
21, *cis*-9-Methyldecalin	590.7	261.6	3104.19	180.72	47.76	
22, *trans-syn*-2-*syn*-7-Dimethyldecalin	797.1	351.8	3406.87	202.59	57.94	
23, *trans-anti*-1-*syn*-8-Dimethyldecalin	709.1	301.3	3401.12	199.18	55.60	
24, *trans-anti*-1-*syn*-3-Dimethyldecalin	794.4	342.8	3406.26	201.74	58.18	
25, *trans-syn-trans*-Perhydroanthracene	997.4	422.9	3870.15	225.76	58.01	58.13
26, *trans-anti-trans*-Perhydroanthracene	900.5	389.2	3865.08	225.76	52.94	52.74
27, *cis-trans*-Perhydroanthracene	890.1	379.2	3864.17	223.20	54.59	
28, *cis-anti-cis*-Perhydroanthracene	779.6	333.8	3857.98	220.64	50.96	
29, *trans-anti-trans*-Perhydrophenanthrene	977.9	408.5	3868.66	224.91	57.37	
30, *trans-anti-cis*-Perhydrophenanthrene	872.0	366.4	3862.85	222.35	54.12	
31, *trans-syn-cis*-Perhydrophenanthrene	879.0	368.9	3863.22	222.35	54.49	
32, Bicyclo[2.2.2]octane	363.7	163.1	2218.74	130.83	24.09	23.75
33, Adamantane	662.3	285.4	2688.15	153.95	30.34	30.65
34, Spiro[5.5]undecane	552.2	249.4	3102.24	181.60	44.93	44.81

[a]The carbon-13 nmr are extracted from ref. 16 (**1**, **2**, **5**–**13**), ref. 17 (**3**, **4**), ref. 18 (**14**–**24**, **34**), ref. 19 (**25**–**31**), ref. 20 (**32**), and ref. 21 (**33**). The experimental enthalpies of formation are taken from ref. 1*a* (**1**–**8**, **14**, **15**, **25**, **26**), ref. 7 (**9**), ref. 22 (**12**, **13** from equilibration experiments), ref. 15 (**32**, **33**), and ref. 23 (**34**).

2.69 kcal/mol in the liquid and by 3.36 kcal/mol in the gas phase (26). Relative to **25**, the compounds **27**, **26**, and **28** are less stable, in that order, by 2.76, 4.15, and 5.58 kcal/mol in the liquid phase and by 3.42, 5.07, and 7.05 kcal/mol, as calculated for the gas phase.

In Table 4 we have only considered molecules for which the structural dependence of the ZPE + $H_T - H_0$ energies has been substantiated by an adequate body of experimental data, thus leaving out structural features (e.g., *skew* pentane, or interactions between methyl substituents in a 1,2 position) for which no, or too little, experimental information is presently available. Because of this selection, our predicted ΔH_f^0 values should represent reasonably good estimates.

Conclusions

The energetic factors governing molecular stabilities are conveniently classified into, firstly, a part which relates to molecules in their hypothetical vibrationless state at 0 K and, secondly, a contribution arising from vibrational energies.

In the part not involving vibrational energies, the prime factors are found in the behavior of the charge dependent bonded contributions, whereas interaction energies between non-bonded atoms are little affected by structural features and do not account for the bulk of the energy differences between isomers or conformers (14). The atomization energy ΔE_a^*, covering both bonded and non-bonded interactions, is a measure of the molecular energy component referring to vibrationless molecules.

Combining the description given for ΔE_a^* in terms of an additivity scheme explicitly involving atomic charges with the thermochemical definition of ΔE_a^*, we obtain a new formula for ZPE + $H_T - H_0$ energies, which can now be calculated accurately in a very simple way from ^{13}C nmr data and the appropriate enthalpies of formation. The examination of numerous ZPE + $H_T - H_0$ energies

Can. J. Chem. Downloaded from www.nrcresearchpress.com by 178.218.224.3 on 09/06/12
For personal use only.

Can. J. Chem. Downloaded from www.nrcresearchpress.com by 178.218.224.3 on 09/06/12
For personal use only.

derived in this fashion has led to simple empirical formulas for their evaluation from structural features. Noteworthy aspects are (*i*) the decrease in ZPE + $H_T - H_0$ energy by $\sim RT/2$ for each hindered internal rotation in cycloalkanes, (*ii*) its invariance with respect to the change from the chair to the boat conformation of the cyclohexane ring, and (*iii*) the decrease in vibrational energy by ~0.85 kcal/mol for one *gauche* interaction involving H atoms of the cycle.

The thermochemical stabilities are a blend of both ΔE_a* and vibrational energy components. Isomer pairs differing by the number of *gauche* interactions (e.g., *trans*- vs. *cis*-decalin) usually reveal a decrease of ~1.85 kcal/mol in ΔE_a* energy for one *gauche* interaction, i.e., a weakening of the chemical bonds. Because of the concurrent decrease in vibrational energy by ~0.85 kcal/mol, which is a stabilizing effect, the total destabilization due to one *gauche* interaction is ~1.0 kcal/mol. This analysis of the *gauche* effect clearly shows that it has nothing to do with Coulomb-type repulsions between non-bonded atoms. In comparisons between isomers, the order of stability indicated by the ΔE_a* energies is in most cases also reflected in the ΔH_f^0's. An interesting exception is the *cis-trans*-perhydroanthracene[2] which is 0.91 kcal/mol less stable in ΔE_a* energy than its *trans-anti-trans* isomer but more stable in terms of ΔH_f^0 by 1.65 kcal/mol because of its low content in vibrational energy. This point is confirmed by Allinger's equilibration experiments (25).

While this last example further stresses the important role of the vibrational contributions in determining molecular stabilities, it is clear that the present analysis is incomplete as it would not account for a number of possible structural features. In turn, the possibility of deriving ZPE + $H_T - H_0$ energies in a simple manner by means of eq. [7] offers a new way of recognizing the occurrence of other possible regularities from an examination of numerous cases.

Acknowledgement

The financial aid given by the National Research Council of Canada is gratefully acknowledged.

[2]We express our gratitude to Dr. D. K. Dalling for his co-operation in helping us to duplicate and confirm the ^{13}C nmr spectrum (19) of this compound.

1. (*a*) J. D. Cox and G. Pilcher. Thermochemistry of organic and organometallic compounds. Academic Press, New York, NY. 1970; (*b*) W. C. Herndon. Progress in physical organic chemistry. Vol. 9. *Edited by* A. Streitwieser, Jr., and R. W. Taft. Wiley-Interscience, New York, NY. 1972.
2. B. Nelander and S. Sunner. J. Chem. Phys. **44**, 2476 (1966).
3. S. Fliszár. J. Am. Chem. Soc. **102**, 6946 (1980).
4. H. Henry, G. Kean, and S. Fliszár. J. Am. Chem. Soc. **99**, 5889 (1977).
5. D. R. Stull and G. C. Sinke. Adv. Chem. Ser. No. 18 (1956).
6. R. G. Snyder and J. H. Schachtschneider. Spectrochim. Acta, **21**, 169 (1965).
7. F. D. Rossini. Selected values of physical and thermodynamic properties of hydrocarbons and related compounds. Carnegie Press, Pittsburgh, PA. 1952.
8. H. Spiesecke and W. G. Schneider. J. Chem. Phys. **35**, 722 (1961).
9. D. M. Grant and E. G. Paul. J. Am. Chem. Soc. **86**, 2984 (1964).
10. L. P. Lindeman and J. Q. Adams. Anal. Chem. **43**, 1245 (1971).
11. D. A. Pittam and G. Pilcher. J. Chem. Soc. Faraday Trans. I, **68**, 2221 (1972).
12. G. Pilcher and J. D. M. Chadwick. Trans. Faraday Soc. **63**, 2357 (1967).
13. (*a*) G. R. Somayajulu and B. J. Zwolinski. J. Chem. Soc. Faraday Trans. II, **68**, 1971 (1972); **70**, 967 (1974); (*b*) W. D. Good. J. Chem. Thermodyn. **2**, 237 (1970).
14. S. Fliszár and M. T. Béraldin. Can. J. Chem. **57**, 1772 (1979).
15. R. H. Boyd, S. N. Sanwal, S. Chary-Tehany, and D. M. McNally. J. Phys. Chem. **75**, 1264 (1971).
16. D. K. Dalling and D. M. Grant. J. Am. Chem. Soc. **89**, 6612 (1967).
17. J. B. Stothers. Carbon-13 nmr spectroscopy. Academic Press, New York. NY. 1972.
18. D. K. Dalling, D. M. Grant, and E. G. Paul. J. Am. Chem. Soc. **95**, 3718 (1973).
19. D. K. Dalling and D. M. Grant. J. Am. Chem. Soc. **96**, 1827 (1974).
20. G. E. Maciel and H. C. Dorn. J. Am. Chem. Soc. **93**, 1268 (1971).
21. G. E. Maciel, H. C. Dorn, R. L. Green, W. A. Kleschick, M. R. Peterson, and G. H. Wahl. J. Org. Magn. Reson. **6**, 178 (1974).
22. C. J. Egan and W. C. Buss. J. Phys. Chem. **63**, 1837 (1959).
23. D. J. Subach and E. Zwolinski. J. Chem. Eng. Data, **20**, 232 (1975).
24. W. G. Dauben, O. Rohr, A. Labbauf, and F. D. Rossini. J. Phys. Chem. **64**, 283 (1960).
25. N. L. Allinger and M. T. Wuesthoff. J. Org. Chem. **36**, 2051 (1971).
26. G. F. Davies and E. C. Gilbert. J. Am. Chem. Soc. **63**, 1585 (1971). D. M. Speros and F. D. Rossini. J. Phys. Chem. **64**, 1723 (1960); T. Miyazawa and K. S. Pitzer. J. Am. Chem. Soc. **80**, 60 (1958).

Aggregation of a symmetrical metalloporphyrin. Concentration and temperature dependence of the absorption and magnetic circular dichroism spectra of dilute zinc octamethyltetrabenzporphyrin solutions

KENNETH J. REIMER[1]

Departments of Chemistry, Royal Roads Military College, FMO Victoria, B.C., Canada V0S 1B0 and University of Victoria, Victoria, B.C, Canada V8W 2Y2

MONICA M. REIMER

Department of Chemistry, University of Victoria, Victoria, B.C., Canada V8W 2Y2

AND

MARTIN J. STILLMAN[1]

Department of Chemistry, University of Western Ontario, London, Ont., Canada N6A 5B7

Received November 7, 1980

KENNETH J. REIMER, MONICA M. REIMER, and MARTIN J. STILLMAN. Can. J. Chem. **59**, 1388 (1981).

Absorption and magnetic circular dichroism (mcd) spectra of toluene solutions of zinc octamethyltetrabenzporphyrin, Zn(OMBP), exhibit marked concentration and temperature dependence. Monomeric Zn(OMBP), **1**, characterized by a 429 nm Soret band, dominates at low concentrations (10^{-7} *M*, 300 K) and higher temperatures (10^{-5} *M*, 320 K) in toluene solution. Decreasing temperatures (320 to 235 K for a 10^{-5} *M* solution) and increasing concentrations (10^{-7} *M* to 10^{-4} *M*, 300 K) result in 8–10 nm red shifts in this band. These spectral changes are attributed to the concurrent formation of a species **2** with a low extinction coefficient and another compound, **3**, with λ_{max} at 439 nm. At the highest concentrations (10^{-3} *M*) and lowest temperatures (225–190 K) used, a dramatic blue shift (439 to 422 nm) due to a fourth species (**4**) is observed. All the spectral changes observed are completely reversible. In addition, and consistent with self-association, species **2**, **3**, and **4** are formed at higher temperatures as the concentration is increased. Possible aggregate structures are proposed and evidence is presented for a novel Zn—N (pyrrole) intermolecular bond.

KENNETH J. REIMER, MONICA M. REIMER et MARTIN J. STILLMAN. Can. J. Chem. **59**, 1388 (1981).

Les spectres d'adsorption et de dichroïsme circulaire magnétique (dcm) de solutions d'octaméthyltétrabenzporphyrine de zinc, Zn(OMBP), dans le toluène varient d'une façon importante avec la concentration et la température. Le monomère Zn(OMBP), **1**, caractérisé par une bande de Soret à 429 nm, domine aux faibles concentrations (10^{-7} *M*, 300 K) et aux températures élevées (10^{-5} *M*, 320 K) en solution dans le toluène. Si on diminue la température (de 320 à 235 K, pour des solutions 10^{-5} *M*) et si on augmente la concentration (de 10^{-7} à 10^{-4} *M* à 300 K) il se produit des déplacements de 8 à 10 nm de cette bande vers le rouge. On attribue ces changements spectraux à la formation simultanée d'une espèce, **2**, avec un faible coefficient d'extinction et d'un autre composé, **3**, caractérisé par un λ_{max} à 439 nm. Si on utilise des concentrations plus élevées (10^{-3} *M*) et des températures plus basses (225–190 K), on observe un déplacement dramatique vers le bleu (439 à 422 nm) provoqué par une quatrième espèce (**4**). Tous les changements observés dans les spectres sont réversibles. De plus et en accord avec l'auto-association, les espèces **2**, **3** et **4** se forment à des températures plus élevées quand on augmente la concentration. On propose des structures associées possibles et on présente des données relatives à une nouvelle liaison intermoléculaire Zn—N (pyrrole).

[Traduit par le journal]

Introduction

Self-association of metalloporphyrins (1) and related compounds (2) has been known for some time. Because of their biological significance, and potential catalytic importance (3), current interest has focussed on the structures and intermolecular bonding of such aggregates (4). Dimers have been characterized in aqueous media and organic solvents at concentrations of 10^{-2}–10^{-3} *M* by nmr and epr spectroscopy (1, 4), and observed at 10^{-6} *M* by optical methods (5), but higher aggregates, particularly at low concentration ($< 10^{-4}$ *M*) are essentially unknown (1, 4).

This paper describes the facile self-association of zinc octamethyltetrabenzporphyrin (Fig. 1). Although benzporphyrins are known to have unique optical (6) and redox characteristics (7) there have been no reports of concentration dependent phenomena (for a preliminary report see ref. 8). Particularly unusual in the present instance is the formation of several aggregate species in dilute solutions. These observations can be attributed to

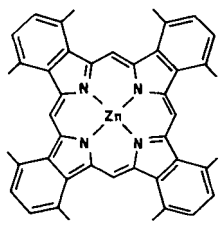

FIG. 1. Zinc octamethyltetrabenzporphyrin.

[1]Address correspondence to these authors; K.J.R. at the University of Victoria.

0008-4042/81/091388-07$01.00/0

©1981 National Research Council of Canada/Conseil national de recherches du Canada

Can. J. Chem. Downloaded from www.nrcresearchpress.com by 210.87.254.40 on 09/06/12
For personal use only.

Can. J. Chem. Downloaded from www.nrcresearchpress.com by 210.87.254.40 on 09/06/12
For personal use only.

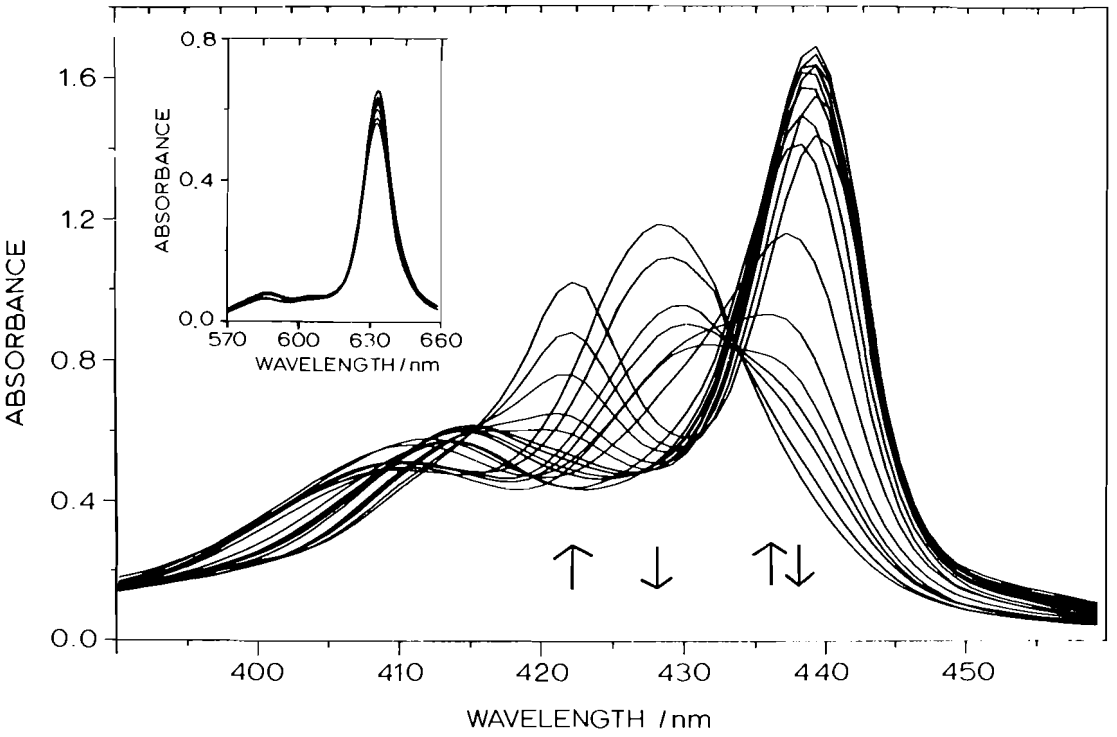

FIG. 2. Temperature dependence of the absorption spectrum of a 10^{-5} *M* toluene solution of Zn(OMBP). The major portion shows the Soret region for spectra recorded between 320 and 190 K. The arrows indicate the spectral changes that occur upon cooling the solution from 320 K. The intensity in the 439 nm region first increases and then decreases at the lowest temperatures. The inset shows the *Q* band region at all temperatures.

the special donor properties of the $OMBP^{2-}$ ligand described herein.

Experimental

A sample of Zn(OMBP), prepared by a modification (9) of the original procedure, was generously supplied by J. R. Sams and T. B. Tsin. Solutions freshly prepared without exclusion of air using Fisher "spectroscopy grade" toluene gave identical results to anaerobic control experiments employing toluene distilled from calcium hydride.

A Cary 14 spectrometer was used to record all of the absorption data. Each trace was simultaneously digitized using equipment designed and constructed at the U.W.O. The spectra presented here are computer plots of these original data. An Oxford Instruments exchange gas cryostat, CF204, coupled to a digital temperature controller, DTC2, was used to maintain the temperature of each sample within ±0.1 K. The absolute temperature is correct to ±1 K. Magnetic circular dichroism (mcd) spectra were recorded with a Jasco J5 spectrometer modified to Sproul SS20 specifications, and using an Oxford Instruments SM2 superconducting magnet operating at 5.5 T. The mcd data were digitized as above. The spectrometer was calibrated by measuring the negative band of aqueous $CoSO_4$, which gave a value of $[\theta]_M = -61.0$ deg cm^2 dmol^{-1} T^{-1}.

Results

Temperature Dependence

Figure 2 is a composite of all of the spectra obtained from a 10^{-5} *M* Zn(OMBP) toluene solution from 320–190 K. In contrast to the relative invariance of the 630 nm band (inset), the Soret spectral region displays extremely complex behavior. Several distinctive features may be discerned within this data set and for greater clarity representative spectra are plotted in Figs. 3–5.

Figure 3 shows that the 429 nm absorption which dominates the spectrum at 320 K undergoes a red shift with decreasing temperature, 320–295 K; cooling below 295 K results in a further red shift at the expense of the 429 nm absorption. In the range 255–235 K, subsequent to the complete disappearance of the 429 nm band, an isosbestically related series of spectra (Fig. 4) is defined by an increase in intensity at 439 nm due to a further red shift from a very weak absorption. A new isosbestic set of spectra (Fig. 5) results from the loss of the 439 nm species and the formation of a new blue-shifted band at 422 nm. This band continues to grow to 190 K (near the fp of toluene). All spectral features are reproducible at different Zn(OMBP) concentrations and are completely reversible with temperature.

Can. J. Chem. Downloaded from www.nrcresearchpress.com by 210.87.254.40 on 09/06/12
For personal use only.

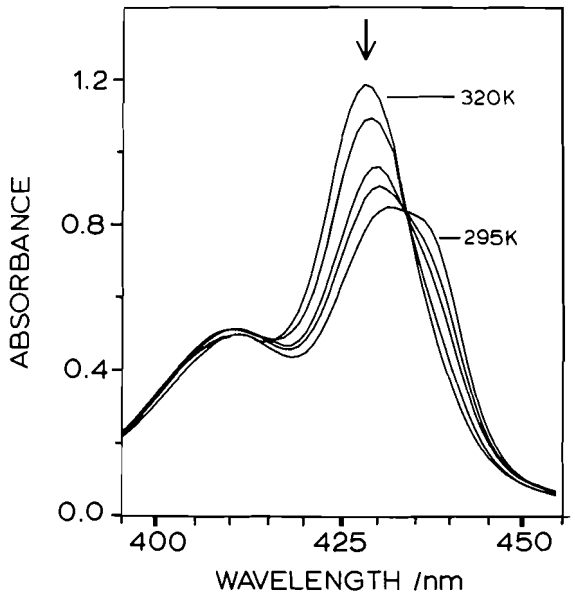

FIG. 3. High temperature spectral set, 320–295 K, using selected data taken from Fig. 2.

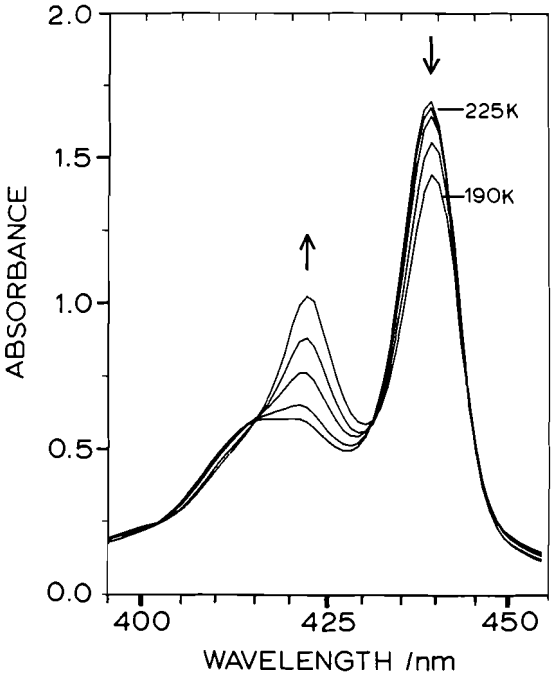

FIG. 5. Low temperature set, 225–190 K.

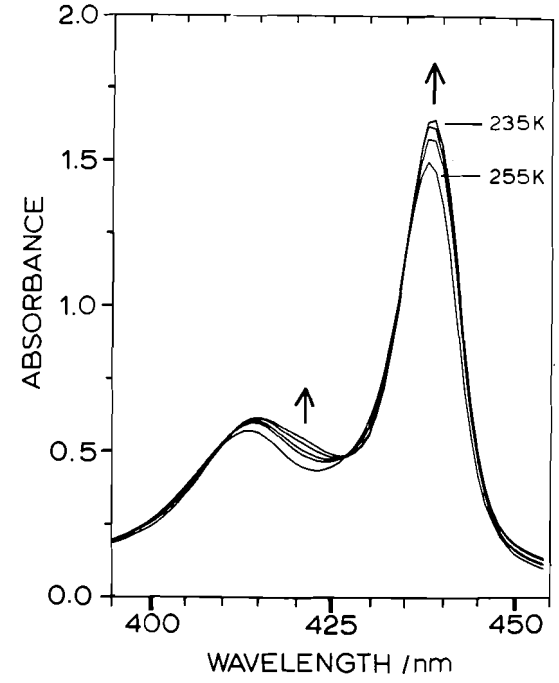

FIG. 4. Mid temperature data set, 255–235 K.

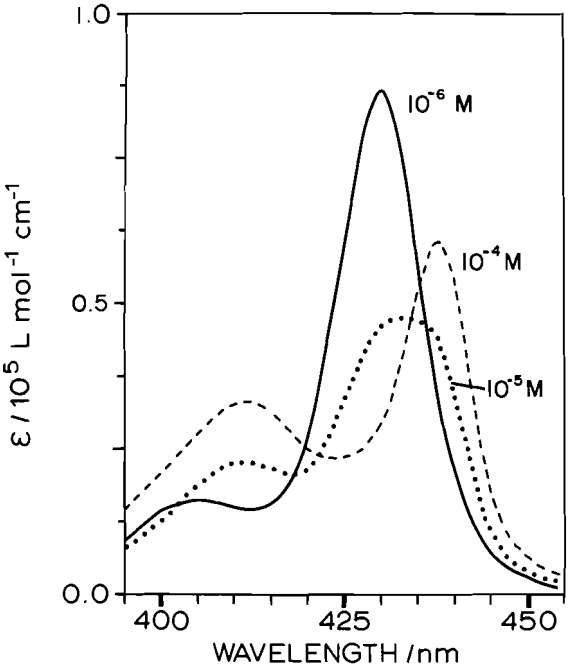

FIG. 6. Concentration dependence of the absorption spectrum of Zn(OMBP). Extinction coefficient calculated on the basis of the total monomeric porphyrin concentration.

Concentration Dependence

Unlike the temperature dependence data, isosbestic points were not seen in the related room temperature concentration dependence results despite considerable experimental effort. Representative data from one experiment are summarized in Fig. 6, for a range of concentrations from 10^{-6} (a similar band is observed for 10^{-7} *M* solutions) to 10^{-4} *M*. Red shifts accompany increasing concentration as does an increase in the intensity of the 439 nm band. There is only a slight increase in

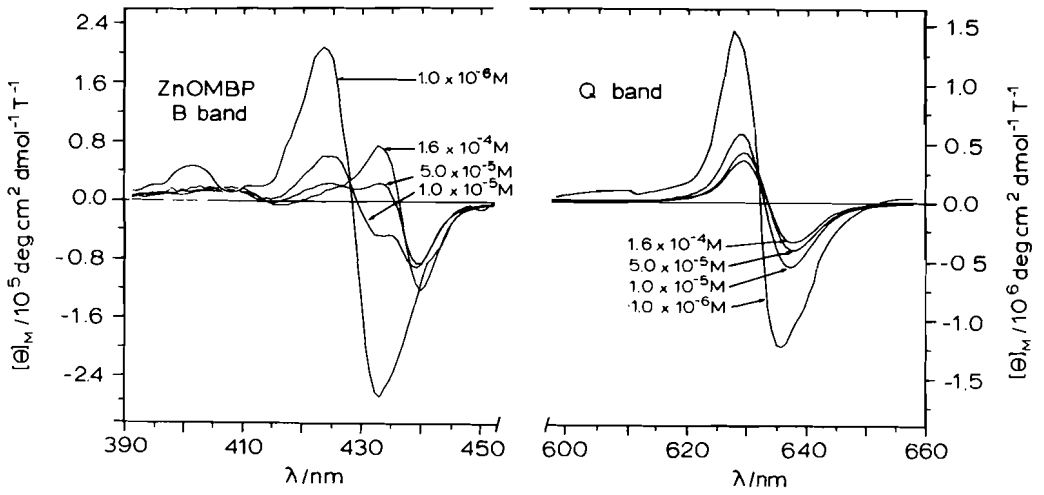

FIG. 7. Concentration dependence of the mcd spectra of Zn(OMBP). Ordinate values were calculated on the basis of the total monomeric porphyrin concentration.

absorbance at 422 nm at the highest concentrations ($\sim 10^{-3}\,M$) suggesting that this might be the next species to develop as it is found at the lowest temperatures used.

It is notable that the extinction coefficient of the 439 nm band, calculated on a monomer basis, is far less than that of the initial monomer, contrasting the considerable increase in absorbance observed for the 439 nm band at low temperatures.

Magnetic Circular Dichroism Concentration Dependence

Figure 7 shows a series of mcd spectra recorded for Zn(OMBP) solutions ranging in concentration from 1×10^{-6} to $1.6 \times 10^{-4}\,M$, a range similar to that in Fig. 6. The ordinate units were calculated using the nominal monomer porphyrin concentration with no account taken for aggregation.

Following the absorption spectrum, the mcd of the most concentrated solution shows a Soret band that is weaker and has a slightly smaller half-width than the spectrum of the most dilute solution. Although an initial analysis of the mcd data in Fig. 7 suggests that a two-species system may be present, the lack of isosbestic points in each of several concentration experiments requires a more complicated system. Two species must be formed with increasing concentration but one (with a 439 nm maximum) dominates at the highest concentration.

It is also apparent that the mcd intensity of the other species is very low, as no clear spectral features can be identified, apart from the lack of isosbestic points. The visible region Q band envelope similarly loses intensity as the solution concentration increases, the band centre being slightly red-shifted at the highest concentration.

Figure 8 shows the absorption and mcd spectra of the most concentrated solution used ($1.6 \times 10^{-4}\,M$). From the sequence of the absorption data in Fig. 6 it can be seen that the dominant species is an aggregate. Surprisingly the spectra in Fig. 8 have all the characteristics of a monomeric species (10). The Q_{00} region is clearly resolved, especially in the mcd spectrum where individual components of the Q_{vib} envelope can be discerned, and the band half-widths are almost the same as the most dilute solution ($10^{-6}\,M$), see the insert in Fig. 2.

In the Soret region, we observe a well resolved positive A term under the 439 nm band, clearly identifying the degeneracy of the second $\pi \rightarrow \pi^*$ transition, followed, to higher energy, by a weak shoulder at about 424 nm. It is rather easier to see the shoulder in the mcd spectrum, and it is likely that this band is the B_{01} transition normally buried in a broader Soret band envelope. In spectra where the B_{00} band is very sharp, for example ZnTPP, a weak and fairly well resolved shoulder is seen to higher energy. For ZnTPP, CuOEP, and CoOEP, the mcd shows (10*c*) a weak positive band at this wavelength, quite similar to the overlapping positive mcd signal at 425 nm in the ZnOMBP spectrum.

The prominent resolved band at 411 nm is associated with a weak mcd signal that appears to be a positive A term centred on the absorption band centre. Although it is common for Q band envelopes to exhibit a series of well resolved vibrational components, often extending some 2000–3000 cm^{-1} from Q_{00}, and of significant intensity in both absorption and mcd spectra, it would be unusual for the B_{01} bands to be as intense and well separated from the B_{00} transition as would be the

Can. J. Chem. Downloaded from www.nrcresearchpress.com by 210.87.254.40 on 09/06/12
For personal use only.

Can. J. Chem. Downloaded from www.nrcresearchpress.com by 210.87.254.40 on 09/06/12
For personal use only.

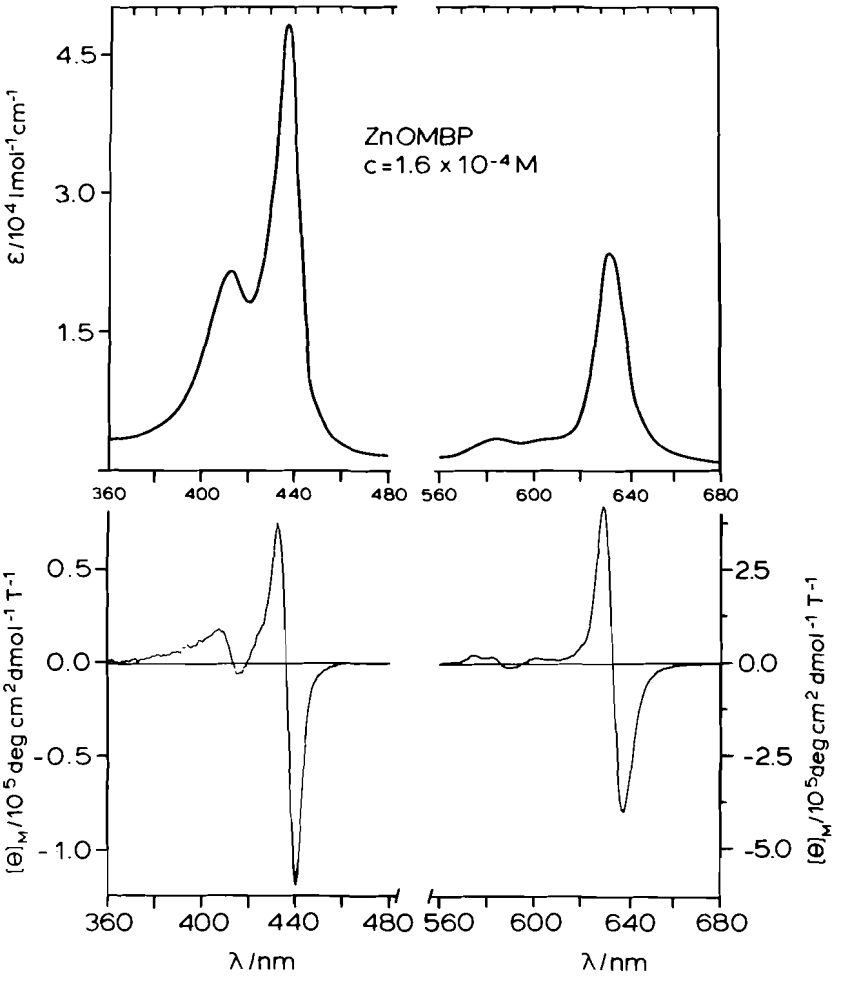

FIG. 8. Absorption and mcd spectra of a concentrated (1.6×10^{-4} *M*) toluene solution.

case if the 411 nm band was a vibronic band. It is more reasonable to suggest that this is the *N* band of the porphyrin, i.e., the third $\pi \rightarrow \pi^*$ transition (10, 11). A similar band is also clearly visible in the spectra of many zinc porphyrins (10*a*, *c*) and phthalocyanines (12).

Discussion

Aggregation phenomena reported to date are not nearly as complicated as those exhibited by Zn(OMBP) in toluene. Typically, the observed spectral changes are isosbestically related and have been interpreted in terms of a monomer $\rightleftharpoons$ dimer equilibrium (1, 4, 5). The data presented in this paper show unambiguously that more than one species is formed with Zn(OMBP). Of even greater significance, it is clear that the type of association found at intermediate concentrations ($\sim 10^{-5}$ to 10^{-6} *M*), close to room temperature (295 K, 10^{-5} *M*), and which is characterized by red shifts of the Soret band, is completely different from the association observed at the lowest temperatures (<225 K for 10^{-5} *M*) where a 17 nm (439 to 422 nm) blue shift is seen.

Species **1**, with a 429 nm Soret band, is undoubtedly monomeric as it is observed for all low concentration solutions (10^{-7} *M*) and at the highest temperatures (320 K) used. This is additionally verified by an analysis of separate ligand binding data (13). We assume that the toluene solvates the porphyrin under these conditions, however, it is not clear whether the interaction is through the metal or the porphyrin π system.[2] As the solution temperature is lowered, or as the concentration of the porphyrin is increased, the Soret band shifts some 8–10 nm to higher wavelength.

[2]Both types of interaction have been observed in the solid state (14). No spectral changes are observed when hexamethylbenzene is added to dilute dichloromethane solutions of Zn(OMBP).

Can. J. Chem. Downloaded from www.nrcresearchpress.com by 210.87.254.40 on 09/06/12
For personal use only.

It is tempting to interpret the 320–295 K spectral changes shown in Fig. 3 in terms of a simple equilibrium between the monomer and a single compound characterized by this red-shifted Soret band. However, a closer examination of the composite temperature dependence spectra (Fig. 2), and the 410 nm region in particular, indicates that the apparent isosbestic point at 435 nm is fortuitous. It is lost at temperatures below 295 K and no isosbestic point is ever found in the concentration dependent spectra (including the mcd data). These concentration data argue strongly against successive compound formation (with overlapping equilibria) but are consistent with the simultaneous formation of two species, **2** and **3**, at concentrations $< 10^{-5} M$. Similarly, both species are probably present at most temperatures between 320 and 255 K. As the spectral changes are dominated by the 439 nm absorption due to **3**, species **2** must have a low extinction coefficient and is also mcd inactive. It is therefore difficult to assign a peak position to this compound, but it must lie in the range 435–439 nm. This is verified by the 255–235 K spectral set (Fig. 4) which is indicative of a **2** to **3** transformation. In the concentration data, the low intensity of the 439 nm band relative to 429 nm at $10^{-4} M$ (Fig. 6) suggests that this band is still a composite of absorptions due to both species **2** and **3**. Finally, at the lowest temperature studied, a fourth species, **4**, (λ_{max} at 422 nm) replaces compound **3** (Fig. 5). The combination of temperature and concentration data, and the reversibility of all spectra, can only be explained by the formation of aggregated species.

Three main modes of aggregation have been described (15) for dimers reported in the literature: (*i*) an electrostatic metal $d\pi$ – porphyrin π interaction (4), (*ii*) a donor–acceptor complex involving a porphyrin π–π interaction (16), and (*iii*) a peripheral substituent-to-metal coordination of the type found in chlorophyll dimers (2). The extent of aggregation through modes (*i*) and (*ii*) is enhanced by asymmetric substitution (particularly with electron-withdrawing groups) of the porphyrin ring; indeed it appears that an asymmetric electronic distortion may be a necessary condition for dimer formation through (*i*) or (*ii*) (4, 16). The complicated aggregation observed for Zn(OMBP) is unusual because $OMBP^{2-}$ is a symmetric porphyrin.

Structural assignments in the present case are complicated by the relatively few optical studies available, as aggregation is usually only significant at concentrations more accessible by nmr and epr measurements (1, 4). The only related example of a symmetrical porphyrin is zinc octaethylporphyrin, Zn(OEP), which undergoes discrete dimer formation accompanied by a blue shift (5).

Red shifts in zinc porphyrin Soret bands are associated with axial ligand coordination to the zinc, the extent of the red shift being directly related to the nature of the donor atom (17). Zinc must therefore play an important role in species **2** and **3**. The coincidence of the spectrum of **3** recorded (13) for monomeric Zn(OMBP) in the presence of pyridine or any neutral nitrogen donor ($\lambda_{max} = 439$ nm) provides compelling support for a geometrical arrangement of **3** that involves the coordination of zinc to one of the ring nitrogens on an adjacent porphyrin. The structure depicted in Fig. 9 is consistent with the above data and the (maximum) five-coordinate stoichiometry observed for all (13, 17) zinc porphyrin complexes including Zn(OMBP).

An alternative explanation involving coordination of adventitious water can be dismissed on the following grounds. First, spectra of toluene solutions of Zn(OMBP) prepared under rigorously anhydrous conditions are identical to those obtained using water-saturated toluene. (Similarly weak binding of water to Zn(TPP) has been reported (17).) Secondly, O-donor ligands such as dimethylacetamide induce small (~3 nm) red shifts and intense ($\varepsilon \sim 10^5 M^{-1}cm^{-1}$) Soret bands, behavior which is inconsistent with the spectroscopic properties of both **2** and **3**. Finally, the concentration of adventitious water should be constant, yet the same red shifts are observed with increasing concentration of Zn(OMBP) as are noted with decreasing temperature. Thus, the concentration dependence experiments demonstrate unequivocally the involvement of a donor group other than water.

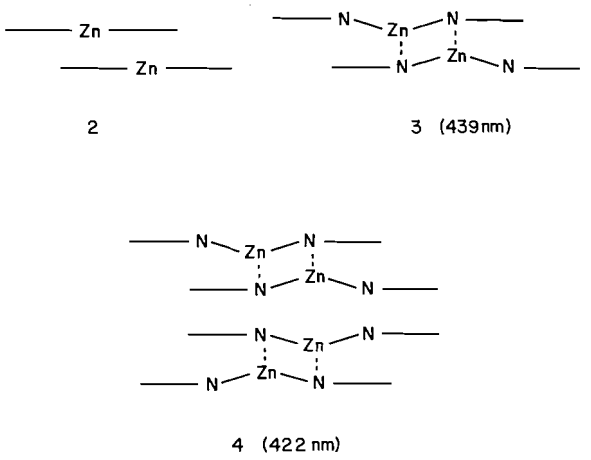

FIG. 9. Proposed aggregate structures for species **2**, **3**, and **4**.

Can. J. Chem. Downloaded from www.nrcresearchpress.com by 210.87.254.40 on 09/06/12
For personal use only.

Further support for a Zn—N coordinative interaction comes from related experiments with CH_2Cl_2 solutions. Only slight red shifts (<2 nm) and increasing absorbance are observed with increasing concentration of Zn(OMBP); identical effects are again noted on pyridine addition to solutions of the monomer. Although the extent of Zn(OMBP) aggregation is less in CH_2Cl_2, it is notable that it occurs at all (1) in this polar solvent.

While the above data support a model for **3** that involves a zinc—N (pyrrole) intermolecular bond, we find little direct evidence for the geometrical arrangement of **2**. However, it is not inconsistent that mode (*i*) may obtain a weak electrostatic interaction between the zinc and the porphyrin π orbitals (Fig. 9).

Finally, at the lowest temperatures (<225 K) a new species, **4**, (λ_{max} = 422 nm) forms at the expense of **3**. Similar large blue shifts (ca. 20 nm) have been observed for cofacial porphyrins (18) and with the dimerization of Zn(OEP) (5). These two examples suggest that the blue shift arises from $\pi-\pi$ interactions of the porphyrins rather than metal specific interactions (especially as the same shifts occur for metal-free cofacial porphyrins (18)). In the present case polymerization of the **3** dimers through $\pi-\pi$ interactions provides a reasonable model (Fig. 9). Thus units of **3** begin to associate through a weaker interaction to form dimers or higher aggregates.

Conclusion

The spectra of toluene solutions of Zn(OMBP) indicate that at least three aggregates form at high concentrations or low temperatures. The unusual behavior of the Soret band in exhibiting both red and blue shifts is only consistent with a scheme that involves axial coordination to the central metal for the red-shifted species. This result follows the general trend of an extremely electron deficient central metal in M(OMBP) species. The equilibrium constant for Zn(OMBP) + py $\rightleftharpoons$ Zn(OMBP)py is the largest yet reported (13) (log K = 5.63 compared with 3.76 for the analogous reaction with zinc tetraphenylporphyrin (17)) and similar trends are found for ligand binding to Co(OMBP) and Mn(OMBP).[3] The blue shifted species is an aggregate comprised of more typical, weaker $\pi-\pi$ association.

Acknowledgements

We thank the Natural Sciences and Engineering Research Council of Canada for financial support (to K.J.R. and M.J.S.) and the Academic Development Fund at the University of Western Ontario for an equipment grant (to M.J.S.). M.J.S. is a member of the Centre for Interdisciplinary Studies in Chemical Physics, University of Western Ontario. K.J.R. also acknowledges the assistance of the Chemistry Department, University of Guelph, where this work was initiated.

[3]Enhanced ligand binding and the formation of novel six-coordinate Co(OMBP)L_2 (19) and Mn(OMBP)L_2 (20) have been noted.

1. W. I. WHITE. *In* The porphyrins. Vol. V. *Edited by* D. Dolphin. Academic Press, New York. 1978. Chapt. 7.
2. J. J. KATZ, L. L. SHIPMAN, T. M. COTTON, and T. R. JANSON. *In* The porphyrins. Vol. V. *Edited by* D. Dolphin. Academic Press, New York. 1978. Chapt. 9.
3. A. D. ADLER, V. VÁRADI, and N. WILSON. Ann. N.Y. Acad. Sci. **244**, 685 (1975).
4. (*a*) K. M. SMITH. Acc. Chem. Res. **12**, 374 (1979); (*b*) R. J. ABRAHAM, S. C. M. FELL, H. PEARSON, and K. M. SMITH. Tetrahedron, **35**, 1759 (1979).
5. K. A. ZACHARIASSE and D. G. WHITTEN. Chem. Phys. Lett. **22**, 527 (1973).
6. L. EDWARDS, M. GOUTERMAN, and C. B. ROSE. J. Am. Chem. Soc. **98**, 7638 (1976).
7. (*a*) A. VOGLER, H. KUNKELY, and B. RETHWISCH. Inorg. Chim. Acta, **46**, 101 (1980); (*b*) T. E. PHILLIPS, R. P. SCARINGE, B. M. HOFFMAN, and J. A. IBERS. J. Am. Chem. Soc. **102**, 3435 (1980).
8. K. J. REIMER, M. REIMER, and M. J. STILLMAN. Paper IN-41. 63rd CIC Conference, Ottawa, Ont. June 8–11, 1980.
9. J. R. SAMS, T. B. TSIN, and D. DOLPHIN. Inorg. Synth. **20**, 155 (1980).
10. (*a*) R. GALE, A. J. MCCAFFERY, and M. D. ROWE. J. Chem. Soc. Dalton Trans. 596 (1972); (*b*) G. BARTH, R. E. LINDER, E. BNNENBERG, C. DJERASSI, L. SEAMANS, and A. MOSCOWITZ. J. Chem. Soc. Perkin Trans. II, 1706 (1974); (*c*) W. R. BROWETT and M. J. STILLMAN. Inorg. Chim. Acta, **49**, 1 (1981).
11. L. EDWARDS, D. DOLPHIN, and M. GOUTERMAN. J. Mol. Spectrosc. **35**, 90 (1970).
12. (*a*) M. J. STILLMAN and A. J. THOMSON. J. Chem. Soc. Faraday Trans. II, **70**, 890 (1974); (*b*) K. A. MARTIN. M.Sc. thesis, University of Western Ontario, London, Ont., 1979.
13. K. J. REIMER, M. REIMER, and C. SPIDLE-SPRAGUE. Paper IN-45. 62nd CIC Conference, Vancouver, B.C. June 3–6, 1979.
14. (*a*) W. R. SCHEIDT, M. E. KASTNER, and K. HUTANO. Inorg. Chem. **17**, 706 (1978); (*b*) W. R. SCHEIDT and C. A. REED. Inorg. Chem. **17**, 710 (1978).
15. H. SCHEER and J. J. KATZ. *In* Porphyrins and metalloporphyrins. *Edited by* K. M. Smith. Elsevier, Amsterdam. 1975. p. 494.
16. D. B. VISCIO and G. N. LAMAR. J. Am. Chem. Soc. **100**, 8092 (1978).
17. M. NAPPA and J. S. VALENTINE. J. Am. Chem. Soc. **100**, 5075 (1978).
18. C. K. CHANG. Adv. Chem. Ser. **173**, 162 (1979).
19. B. R. JAMES, D. W. SMITH, and K. J. REIMER. Paper IN-44. 62nd CIC Conference, Vancouver, B.C. June 3–6, 1979.
20. K. J. REIMER, H. R. HARMER, and C. SIBLEY. Paper IN-67. 63rd CIC Conference, Ottawa,Ont. June 8–11, 1980.

Lewis acid promoted reactions of ethyl cyanoformate. Reaction with 2,5-dimethylfuran[1]

ARCHIBALD W. MCCULLOCH, A. GAVIN MCINNES, AND DONALD G. SMITH

Atlantic Research Laboratory, National Research Council of Canada, Halifax, N.S., Canada B3H 3Z1

Received September 8, 1980

ARCHIBALD W. MCCULLOCH, A. GAVIN MCINNES, and DONALD G. SMITH. Can. J. Chem. **59**, 1395 (1981).

Aluminum chloride promoted reaction of 2,5-dimethylfuran with ethyl cyanoformate affords, depending on the experimental conditions, *cis* and *trans* ethyl 5-cyano-2,5-dimethyl-2,5-dihydrofuran-2-carboxylates, **3** and **4**, ethyl 2,5-dimethylfuran-3-carboxylate **5**, 4,8-dicyano-1,2,4,8-tetramethyl-3,9-dioxatricyclo-[5.2.1.$0^{2,6}$]decane **6**, and ethyl 3-(2,5-dimethyl-3-furyl)-5-cyano-2,5-dimethyltetrahydrofuran-2-carboxylate **7**. Structures were elucidated from spectral evidence and chemical transformations.

ARCHIBALD W. MCCULLOCH, A. GAVIN MCINNES et DONALD G. SMITH. Can. J. Chem. **59**, 1395 (1981).

Le chlorure d'aluminium initie la réaction du diméthyl-2,5 furanne avec le cyanoformate d'éthyle et conduit, selon des conditions expérimentales, aux cyano-5 diméthyl-2,5 dihydro-2,5 furanne carboxylates-2 d'éthyle *cis* et *trans*, **3** et **4**; au diméthyl-2,5 furanne carboxylate-3 d'éthyle, **5**; au dicyano-4,8 tétraméthyl-1,2,4,8 dioxa-3,9 tricyclo[5.2.1.$0^{2,6}$] décane, **6**, et au (diméthyl-2,5 furyl-3)-3 cyano-5 diméthyl-2,5 tétrahydrofurannecarboxylate-2 d'éthyle **7**. On a déterminé les structures des produits obtenus à partir de données spectroscopiques et de transformations chimiques.

[Traduit par le journal]

Introduction

We have recently studied the $AlCl_3$-promoted reaction of 2,5-dimethylfuran **1** with ethyl cyanoformate **2**. This study was prompted in part by the reported isolation of azanorbornadiene adducts **18** from highly dienophilic sulfonyl cyanides (1), and also by our own experience with the influence of Lewis acids on certain Diels–Alder reactions of acetylenic dienophiles (e.g. ref. 2). Although no Diels–Alder addition was observed between **1** and **2**, a number of interesting heterocyclic products were obtained; these are described in the present communication.

Results and Discussion

The reaction of **1** with **2** in the presence of $AlCl_3$ in CH_2Cl_2 yielded a mixture of products, amongst which we have identified the *cis*- and *trans*-2-carbethoxy-5-cyano-2,5-dimethyl-2,5-dihydrofurans **3** and **4**, the 3-carbethoxyfuran **5**, the tricyclic derivative **6**, and the 2:1 adduct **7**. No Diels–Alder adduct **19** was detected.

Under all reaction conditions used, polymerization of **1** was a major factor, resulting in low yields of **3–7**. When the reaction was carried out at 10–15°C for 60 s only, the major products were **3** (11%) and **4** (5%), while reaction at 25°C for 1 h

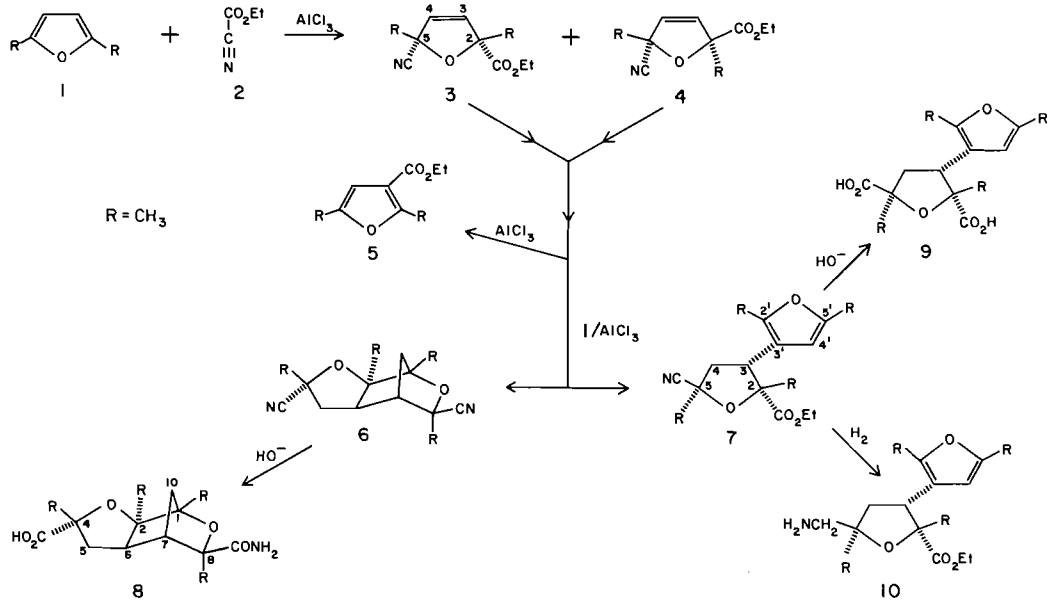

[1]Issued as NRCC No. 19148.

0008-4042/81/091395-08$01.00/0

©1981 National Research Council of Canada/Conseil national de recherches du Canada

Can. J. Chem. Downloaded from www.nrcresearchpress.com by 210.87.254.42 on 09/06/12
For personal use only.

Can. J. Chem. Downloaded from www.nrcresearchpress.com by 210.87.254.42 on 09/06/12
For personal use only.

TABLE 1. ^{1}H nmr data ($CDCl_3$)[a]

No.	C—CH_3(s)	Ester CH_3(t)	Ester CH_2(q)	=CH	—CH— and —CH_2—	—CH_2—N	NH; OH
	At C-2, C-5			H-3, H-4			
3	1.58, 1.74	1.32	4.25	ABq centered at 6.06, $\Delta\nu_{3,4} = 8.3$; $J_{3,4} = 5.8$ Hz			
4	1.63, 1.74	1.28	4.22	ABq centered at 6.03, $\Delta\nu_{3,4} = 11.0$; $J_{3,4} = 5.8$ Hz			
					H-3, H-4	—CH_2—N	
11	1.49, 1.67	1.34	4.25		1.70–2.90(m, 4H)		
12	1.59, 1.71	1.27	4.20		1.80–2.70(m, 4H)		
13	1.27, 1.46	1.28	4.19		1.40–2.55(m, 4H)	2.65(m, 2H)	
14	1.29, 1.45	1.27	4.15		1.40–2.50(m, 4H)	2.62(m, 2H)	
16[c]	1.60			6.04(s)			9.99(bs)
17[c]	1.57			6.05(s)			10.48(bs)
	At C-2, C-5 / At C-2^1, C-5^1			H-4^1			
7	1.57, 1.85 / 2.19, 2.26	1.11	3.99	5.65(bs)	3.55[b](t, 1H, 9.8 Hz); 2.53[b](bd, 2H, 9.8 Hz)		
10	1.47, 1.57 / 2.17, 2.21	1.13	4.01	5.73(bs)	3.35(bm, 1H); 1.90–2.50(m, 2H)	2.72(bs, 2H)	
9	1.53, 1.68 / 2.17, 2.25			5.90(bs)	3.41(q, 1H); 2.54(m, 2H)		5.75(b)
	At C-1, C-5				H-6, H-7		
15	1.42, 1.50				1.65–2.45(m, 4H)	ABq centered at 3.26[e]; $\Delta\nu_{AB}$ = 21.0; J_{AB} = 11.2 Hz	7.05(b)
	At C-1, C-2, C-4, C-8				H-5, H-6, H-7, H-10		
6	1.33, 1.49, 1.60, 1.66				1.50–3.10(m, 6H)		
8[d]	1.20(6H), 1.23, 1.36				1.25–3.20(m, 6H)		7.00(b)

[a]b = broad, s = singlet, d = doublet, t = triplet, q = quartet, m = multiplet.
[b]The 100 MHz spectrum of 7 in benzene-d_6 showed an ABX system for these three hydrogens: AB centered at 2.28, X part centered at 3.46, $J_{AB} = 12.7$, $J_{AX} = 13.1$, $J_{BX} = 6.5$, $\Delta\nu_{AB} = 23.7$ Hz.
[c]In acetone-d_6.
[d]In DMSO-d_6.
[e]The high-field proton was coupled (2.9 Hz) to the NH.

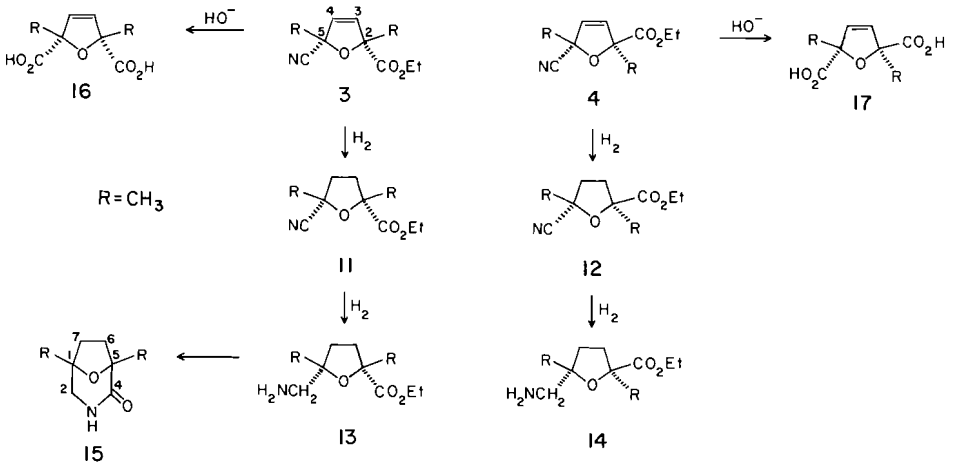

favored **5** (11%) and **7** (8%). Independent experiments established that at 25°C both **3** and **4** react (*a*) with $AlCl_3$ to give **5**, and (*b*) with **1** and $AlCl_3$ to give **6** and **7**.

Structures

The structures of all products were elucidated chiefly on the basis of their spectral properties (see Experimental and Tables 1 and 2). Mass measurement of the molecular ions of **3** and **4** established that each possessed the molecular formula $C_{10}H_{13}NO_3$, indicating 1:1 adducts formed by reaction of **1** and **2**. Mass spectral fragmentation of each isomer involved facile cleavage of a $—CO_2C_2H_5$ moiety. The ^1H nmr spectrum (Table 1) in each case showed an AB quartet for two olefinic hydrogens with a coupling (J_{AB} = 5.8 Hz) consistent with a 2,5-dihydrofuran system (3), two nonequivalent *C*-methyl singlets, and signals corresponding to the protons of a carbethoxyl substituent. The ^{13}C nmr spectra (Table 2) showed corresponding signals for the carbons of two olefinic methine, two nonequivalent methyl, and one carbethoxyl group. Signals near 82 and 92 ppm for the two quaternary carbons bonded to methyl groups were consistent with deshielding by oxygen. The remaining resonance was identified as a nitrile carbon by its characteristic chemical shift (ca. 119 ppm). (This was supported by weak ir absorption at ca. 2230 cm^{-1}.) The combined evidence is compatible only with the dihydrofuran structures **3** and **4**. The quaternary carbon resonances (C-2 and C-5) of each compound could be clearly differentiated on the basis of the known shielding effects of attached nitrile and carbethoxyl substituents (4). The methyl and olefinic carbons could be similarly assigned.

Catalytic reduction of **3** and **4** gave the corresponding tetrahydrofurans **11** and **12**. The ^1H nmr spectrum of each of the latter showed four ring methylene, but no olefinic, hydrogens. Their high-resolution ^{13}C nmr spectra confirmed that the two olefinic carbons of **3** and **4** had in each case been replaced by two methylene carbons, while characteristic resonances (and also ir absorptions) for cyano groups established that the nitrile functions of **3** and **4** were retained in **11** and **12**.

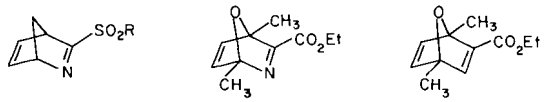

18 **19** **20**

The cyano groups of **11** and **12** could be reduced on exhaustive hydrogenation. The products, amino-esters **13** and **14**, were unstable, and attempts to isolate pure samples were unsuccessful. In each instance ^1H and ^{13}C nmr spectra of the freshly-prepared material were consistent with the amino-ester structure. The most important features of the ^{13}C spectra were the absence of the CN resonance and the presence of new signals near 59 ppm which could be assigned to methylene carbons deshielded by an attached nitrogen.

The products of exhaustive hydrogenation of **3** also included the lactam **15**, establishing that the cyano and carbethoxyl groups in **3** have a *cis* orientation. No lactam was formed after reduction of **4**, which must therefore have the corresponding *trans* stereochemistry. Mass measurement of **15** established the molecular formula $C_8H_{13}NO_2$. The combined ^1H and ^{13}C nmr evidence confirmed that the ethyl group of the carbethoxyl function of **3** had been lost and that new methylene (δ_C 54.2, carbon deshielded by the attached N) and —NH—(δ_H 7.05) groups had been formed. Characteristic carbonyl and NH absorptions for a cyclic amide were observed in the ir.

Finally, saponification of **3** and **4** afforded the corresponding *cis* and *trans* diacids **16** and **17**, which for symmetry reasons gave signals for pairs

Can. J. Chem. Downloaded from www.nrcresearchpress.com by 210.87.254.42 on 09/06/12
For personal use only.

Can. J. Chem. Downloaded from www.nrcresearchpress.com by 210.87.254.42 on 09/06/12
For personal use only.

TABLE 2. ^{13}C nmr data ($CDCl_3$)

δ_C (ppm) multiplicity[a,b] $^nJ_{CH}$(Hz)

No.	CH_3				C=O	C≡N	C—O (m)		Other C			
	At C-2		At C-5				C-2	C-5	C-3		C-4	
3	27.54q ^1J 130.8		24.46q ^1J 129.48		170.66m	118.60m	91.83	81.86	133.81dqu ^1J 176.3, $^2J = {}^3J$ = 3.7		129.48dqu ^1J 178.5, $^2J = {}^3J$ = 3.7	
4	26.77q ^1J 131.1		23.91q ^1J 130.1		171.06m	119.43m	92.21	81.97	133.88dqu ^1J 176.3, $^2J = {}^3J$ = 3.8		129.17dqu ^1J 178.0, $^2J = {}^3J$ = 3.8	
11	26.91qm ^1J 130.0		25.02qm ^1J 128.9		173.49m	121.08m	85.84	76.53	38.44tm ^1J 136.5		35.61tm ^1J 136.1	
12	25.71qd ^1J 130.4, ^3J 4.0		24.46qd ^1J 129.0, ^3J 4.0		173.42m	121.70m	85.97	77.08	39.17tm ^1J 136.3		37.34tm ^1J 134.4	
												CH_2—N
13		26.13q, 26.23q ^1J 128.3 ^1J 128.3			175.38m		83.86, 85.90			36.67tm, 34.73tm ^1J 133.7 ^1J 132.8		59.18tm ^1J 132.5
14		25.35q, 25.53q ^1J 128.1 ^1J 128.1			175.53m		83.85, 85.89			36.91tm, 34.37tm ^1J (133) ^1J (132)		59.32tm ^1J (132)
												C-4[1]
7	23.45qd ^1J 128.8, ^3J 5.2		25.42qdd ^1J 130.5, ^3J 2.5 ^3J 1.9		172.14dq ^3J 6.5 ^3J 3.4	122.06tq ^3J 6.7 ^3J 4.5	88.67	76.12	47.30dq ^1J 130.0, ^3J 4.1		44.13tq ^1J 135.0, ^3J 4.1	104.79dm ^1J 170.5
	At C-2[1]		At C-5[1]						C-2[1]		C-3[1]	C-5[1]
	11.79q ^1J 128.8		13.26qd ^1J 128.0, ^3J 0.7						147.62ddq ^3J 6.7, ^3J 4.9, ^3J 6.7		113.53m	149.90dq ^2J 8.5, ^2J 7.2
10	11.79q ^1J 127.8		13.31q ^1J 128.0		173.59m		84.84,	87.49	146.85m		115.75m	149.24qu ^2J = 8.0
	At C-2		At C-5						C-3	C-4	C-4[1]	CH_2—N
		23.89qm, 24.66qm ^1J (128) ^1J (128)							47.06dm ^1J 127.2	41.46btm ^1J (128)	105.27dm ^1J 170.4	60.93 ^1J (134)
15	At C-1		At C-5				C-1	C-5	C-6	C-7	CH_2—N	
	19.47q ^1J 127.6		24.04q ^1J 126.6		174.68bs		78.44,	82.71	39.34tm ^1J 134.9	35.66tm ^1J 133.8	54.21tm ^1J 137.5	
		At C-1, C-2, C-4, C-8					C-1, C-2	C-4, C-8	C-6, C-7		C-5, C-10	
6	13.43q ^1J 127.2	16.32qd ^1J 127.0 ^3J 3.4	21.24q ^1J 129.9	26.11qd ^1J 130.1 ^3J 5.1		121.80m, 122.43m	88.95 93.30	75.14 76.08	45.83dm ^1J 140.0	50.24dm ^1J 150.6	39.07tm, 46.28t ^1J 136.2 ^1J 133.8	
8[c]	13.82q ^1J 126.8	16.91qm ^1J 126.2	19.28q ^1J 127.6	24.70qm ^1J 128.7	176.42m, 177.57bs		87.20, 83.22,	91.08 83.53	45.87dm, ^1J 134.4	46.76dm ^1J (145)	36.47tm, 41.54tm ^1J (135) ^1J (133)	

[a]b = broad, s = singlet, d = doublet, t = triplet, q = quartet, qu = quintet, m = multiplet. Multiplicities and coupling constants were derived from first-order analysis of high-resolution spectra. Those in parentheses could only be estimated because of signals being partially obscured by solvent resonances or by signal overlap, or being extremely broad.

[b]Resonances for the methyl and methylene carbons of the carbethoxyl groups were observed in the ranges 13.81–14.21 (qt, ^2J 126.9–127.5, ^1J 2.3–2.5 Hz) and 60.55–61.76 (tq, ^1J 147.5–148.2, ^2J 4.0–4.4 Hz) ppm respectively.

[c]In DMSO-d_6.

Can. J. Chem. Downloaded from www.nrcresearchpress.com by 210.87.254.42 on 09/06/12
For personal use only.

of chemically equivalent methyl groups and olefinic hydrogens (Table 1).

Identification of the 3-carbethoxyfuran **5** posed no problem since we had previously isolated this compound as a product of Diels–Alder retrogression of the oxanorbornadiene **20** (5).

The mass, ir, ^{1}H nmr, and ^{13}C nmr spectra of compound **6** suggested a product comprised of two 2-cyano-2,5-dimethyltetrahydrofuran moieties linked together. Structure **6** was established through X-ray analysis of its crystalline derivative **8** (6).

In the case of **7**, mass measurement established the molecular formula $C_{16}H_{21}NO_4$, suggesting a 2:1 product of **1** with **2**. The ir spectrum confirmed the presence of ester (1720 cm^{-1}) and nitrile (2235 cm^{-1}) groups. The ^{1}H nmr spectrum showed two broadened *C*-methyl signals at 2.19 and 2.26 ppm, both coupled to a single hydrogen at 5.65 ppm. In addition, the ^{13}C nmr spectrum showed resonances for two *C*-methyl carbons at 11.79 and 13.26 ppm, a single ring CH at 104.79 ppm, and three quaternary ring carbons at 113.53, 147.62, and 149.90 ppm. These combined data indicated the presence of a 3-substituted 2,5-dimethylfuryl ring system (cf. ref. 7 and also ref. 4, p. 253). Furthermore, ^{13}C signals for two quaternary carbons linked to oxygen (76.12 and 88.67 ppm), and a nitrile (122.06 ppm), and ^{1}H and ^{13}C resonances for a carbethoxyl, a —CH_2CH—, and two chemically nonequivalent methyl groups, indicated that the second ring of **7** is a β-substituted 2-carbethoxy-5-cyano-2,5-dimethyltetrahydrofuryl moiety. The two rings can be linked together at either β-position of the tetrahydrofuran ring. The ester-substituted (88.67 ppm) and cyano-substituted (76.12 ppm) ring carbons of **7** can be readily distinguished on the basis of substituent effects (4). The fact that the carbon bearing the carbethoxyl in **7** is deshielded (by about 3 ppm) compared to the corresponding carbon in **11** and **12**, while the nitrile substituted carbon is virtually unaffected, indicates that the furyl substituent in **7** is located on the carbon (C-3) adjacent to the ester-bearing carbon. This was confirmed by selective decoupling experiments. Irradiation of the methine hydrogen (H-3) had a significant effect on the carbonyl carbon resonance (causing the doublet of quartets to collapse to a broad quartet), but negligible effect on the nitrile resonance. Similarly, irradiation of the methylene ring hydrogens (H-4) caused a significant change in the nitrile carbon resonance (causing the triplet of quartets to collapse to a quartet), but had little effect on the carbonyl signal.

The relative stereochemistry of **7** was deduced on the basis of (*a*) nuclear Overhauser enhancement (13%) of the ^{1}H nmr signal for H-3 upon irradiation of the adjacent methyl hydrogens, establishing their *cis* relationship, and (*b*) failure to form either an anhydride from diacid **9** (obtained by saponification) or a lactam from the amino-ester **10** (obtained by catalytic reduction), showing that the ester and nitrile functions of **7** must be *trans*.

Mechanisms

Electrophilic attack of the cyanoformate – $AlCl_3$ complex at position 2 of the 2,5-dimethylfuran ring (to give **21**) followed by intramolecular attack at position 5 by cyanide results in formation of the favored isomer **3**. Elimination of cyanide (from **21**) to give **22** and its reinsertion may result in either **3** or **4** (Scheme 1).

Intermediate **22** is also likely in the formation of **5**. Thus, migration of the carbethoxyl group of **22** accounts for the observed formation of **5** from

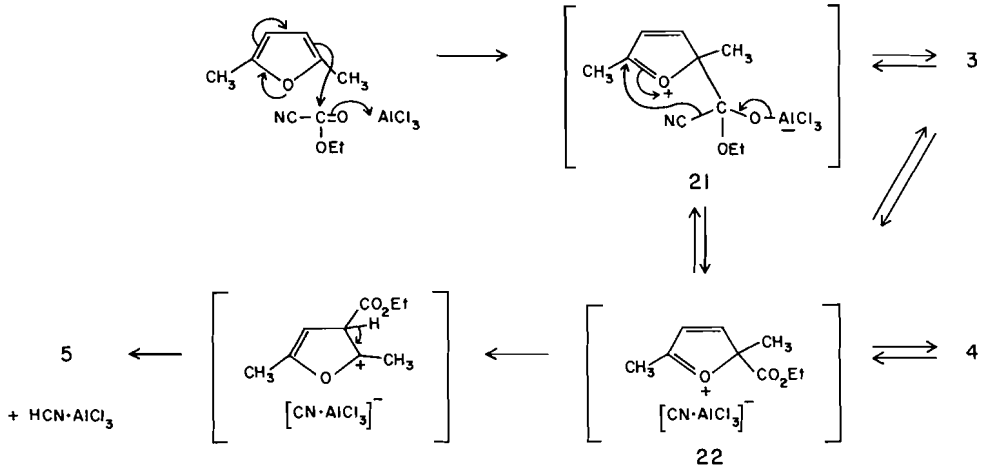

SCHEME 1

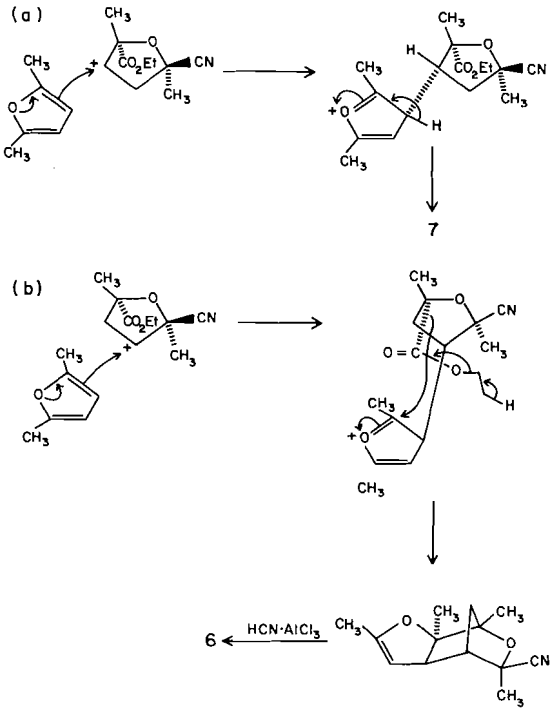

SCHEME 2

either **3** or **4** (Scheme 1); analogous ester migrations are well documented (8).

Any explanation of the formation of **6** and **7**, which are co-products of **5** in the $AlCl_3$-promoted reaction of **3** or **4** in the presence of **1**, must explain the observed stereochemistry of each product. Additional experiments showed that **6** was not formed through $AlCl_3$-promoted reactions of (*a*) **1** with HCN, (*b*) **7** with HCN, or (*c*) **7** with **2**. Pathways involving **4** as a common intermediate, and initiated in each case by protonation of the double bond (presumably by $H^+AlCl_3CN^-$ formed during production of **5**), are outlined in Schemes 2a and 2b.

The second step in each pathway is nucleophilic attack by **1**. Examination of molecular models indicates that there is less steric hindrance to approach of **1** on the face of the molecule substituted by the carbethoxyl group. (Presumably such approach can indeed only occur when the two methyl groups are *trans*, and hence is confined to **4**).

Protonation at C-4, attack by **1** at C-3, and elimination of a proton leads directly to compound **7** (Scheme 2a). Protonation at C-3 and attack by **1** at C-4, followed by a decarboxylative ring-closure affords a tricyclic derivative; addition of HCN to the latter gives **6** (Scheme 2b).

Experimental

The ^1H nmr spectra were obtained on a Varian A-60A spectrometer using $CDCl_3$ as solvent (unless otherwise stated) and tetramethylsilane as internal standard. Nuclear Overhauser enhancement measurements were made on a degassed solution of **7** in dimethyl sulfoxide-d_6, using a Varian HA-100D spectrometer. Carbon-13 nmr spectra were recorded in $CDCl_3$ on a Varian XL-100-15 or Varian FT-80 spectrometer. The operating conditions, including those used in the selective decoupling experiments on **7**, were similar to those detailed previously (9). High-resolution mass spectra were recorded using a Dupont-CEC 21-110B instrument with electrical detection being used for mass measurements. Infrared spectra were measured with Perkin-Elmer 180, 521, or 237 spectrometers. Column chromatographic separations were carried out on Mallinckrodt silicic acid (100 mesh) and preparative thin-layer chromatography (plc) on 2.0 mm Merck silica gel F-254 precoated plates. In all cases $CHCl_3$ was used for elution.

Reaction of 2,5-Dimethylfuran 1 with Ethyl Cyanoformate 2

No reaction occurred when a mixture of equimolar amounts of **1** and **2** was refluxed for 48 h.

$AlCl_3$-Promoted Reaction

(*a*) To a stirred suspension of $AlCl_3$ (6.65 g, 0.05 mol) in CH_2Cl_2 (175 mL) was added a solution of **2** (4.95 g, 0.05 mol) in CH_2Cl_2 (50 mL). To the resultant yellow-green solution was then added a solution of **1** (4.80 g, 0.05 mol) in CH_2Cl_2 (25 mL). There was an exothermic reaction, the mixture turned red, and some gummy material precipitated. Stirring was continued for 1 h at room temperature, during which the mixture became dark red and further tarry material was deposited. The mixture was poured into ice-water and the tarry residue in the reaction flask dissolved in a CH_2Cl_2/H_2O mixture. The combined organic and aqueous solutions were separated (after shaking vigorously) and the aqueous layer extracted twice with CH_2Cl_2. The combined CH_2Cl_2 solutions were then dried (Na_2SO_4) and evaporated to give a red-brown oil (7.85 g) which was chromatographed. In order of their elution from the column the following were obtained.

(*i*) *Ethyl 2,5-dimethylfuran-3-carboxylate* **5** as a yellow oil (723 mg, 8.6%). Repeated chromatography gave a pale yellow oil, n_D^{23} = 1.4690, whose spectral properties were identical with those of an authentic sample (5). (*ii*) A yellow oil (242 mg) composed of **5** and **7** in a molar ratio of 5:2. (*iii*) A semi-solid fraction (965 mg), crystallization of which from a small amount of ethyl acetate/petroleum ether gave cream colored prisms (420 mg). Preparative thin-layer chromatography afforded a solid fraction and final crystallization from petroleum ether gave pure **7** as colorless prisms (193 mg), mp 74–75°C; ν_{max} ($CHCl_3$):2235(w), 1720 cm^{-1}; λ_{max} (EtOH):217 nm (ε 7400). Molecular ion (55%) at *m/e* 291.1462 ($C_{16}H_{21}NO_4$ requires 291.14706), base peak at *m/e* 151, strong ions at *m/e* 218 (73%), 175 (80%), and 160 (37%). (iv) Oily material (585 mg), containing some **7**. (*v*) A yellow-brown oil (633 mg). Repeated column chromatography gave a solid fraction; crystallization from ethyl acetate/petroleum ether gave **6** as colorless prisms (102 mg, 1%), mp 117.5–118.5°C; ν_{max} ($CHCl_3$):2234 cm^{-1}, no absorption in carbonyl region. Molecular ion (2%) at *m/e* 246.1371 ($C_{14}H_{18}N_2O_2$ requires 246.13683); base peak at *m/e* 188.0946 ($C_{11}H_{12}N_2O$ requires 188.09496); strong ion (50%) at *m/e* 123.0684 (C_7H_9NO requires 123.06841). Estimated total yields (from ^1H nmr): **5** (11%), **6** (3%), and **7** (8%).

(*b*) To a mixture of $AlCl_3$ (13.30 g, 0.10 mol) and **2** (9.90 g, 0.10 mol) in CH_2Cl_2 (450 mL), cooled to 10–15°C, was added with stirring a similarly cooled solution of **1** (9.60 g, 0.10 mol) in CH_2Cl_2 (50 mL). The mixture was stirred for 60 s only, and was

Can. J. Chem. Downloaded from www.nrcresearchpress.com by 210.87.254.42 on 09/06/12
For personal use only.

Can. J. Chem. Downloaded from www.nrcresearchpress.com by 210.87.254.42 on 09/06/12
For personal use only.

then worked up as in (*a*) above to give a red oil. The crude product was distilled under vacuum. The initial distillate contained mainly unreacted **2**. The intermediate fractions (5.44 g) were combined. High-boiling fractions contained mainly polymeric material and were discarded. The intermediate distillate was then chromatographed. In order of their elution, the following were obtained.

(*i*) A fraction (564 mg), containing approximately equal amounts of **4** and **7**. (*ii*) Pure trans *ethyl 5-cyano-2,5-dimethyl-2,5-dihydrofuran-2-carboxylate* **4** as a pale yellow oil (104 mg), $n_D^{24} = 1.4391$; ν_{max} (liq. film):2230 (w), 1750 (sh), 1735 cm^{-1}. Molecular ion (<1%) at *m/e* 195.0899 ($C_{10}H_{13}NO_3$ requires 195.08954); base peak at *m/e* 122.0603 (C_7H_8NO requires 122.06059). (*iii*) A fraction (1.056 g) containing equal amounts of **3** and **4**. (*iv*) A fraction (702 mg) containing **3**, contaminated by ca. 5% **4**. (*v*) Pure cis *ethyl 5-cyano-2,5-dimethyl-2,5-dihydrofuran-2-carboxylate* **3** as a pale yellow oil (522 mg), $n_D^{23} = 1.4448$; ν_{max} (liq. film):2230 cm^{-1} (w), 1750 (sh), 1732 cm^{-1}. Molecular ion (<1%) at *m/e* 195.0895 ($C_{10}H_{13}NO_3$ requires 195.08954); base peak at *m/e* 122.0606 (C_7H_8NO requires 122.06059). (*vi*) A final fraction (607 mg) consisting chiefly of **3**, together with ca. 20% **6**. Estimated total yields (from ^1H nmr): **3** (11%), **4** (5%), **6** (1%), and **7** (1%).

Reaction of 3 or 4 with $AlCl_3$

A 1:1 mixture (105 mg, 0.00054 mol) of **3** and **4** in CH_2Cl_2 (2 mL) was added to a stirred suspension of $AlCl_3$ (157 mg, 0.00118 mol) in CH_2Cl_2 (3 mL). The mixture was stirred at room temperature for 1 h, then worked up in the usual way to give a yellow oil (96 mg); ^1H nmr analysis indicated almost quantitative conversion to **5**; plc afforded pure **5** (46 mg, 51%). (Low recovery is due to volatility of **5**.)

A similar result was achieved with pure **3** or **4**.

Reaction of 3 (or 4) with 1 and $AlCl_3$

A mixture of **3** (155 mg, 0.0008 mol) and **1** (96 mg, 0.001 mol) in CH_2Cl_2 (3 mL) was added to a stirred, cooled suspension of $AlCl_3$ (215 mg, 0.0016 mol) in CH_2Cl_2 (2 mL). The mixture was stirred at 25°C for 1 h and then worked up as above to give a brown oil; plc of this product afforded **5** (45 mg, 34%), **7** (34 mg, 15%), and slightly impure **6** (20 mg, estimated 7%).

Similar reaction of **4** (52 mg, 0.00027 mol), **1** (41 mg, 0.00043 mol), and $AlCl_3$ (76 mg, 0.00057 mol) in CH_2Cl_2 (5 mL) gave **5** (15 mg, 34%), **7** (17 mg, 22%), and slightly impure **6** (7 mg, estimated 7%).

A comparable product was obtained from a corresponding reaction of **3** (390 mg, 0.002 mol), **1** (192 mg, 0.002 mol), $AlCl_3$ (532 mg, 0.004 mol), and HCN (generated from 500 mg NaCN) in CH_2Cl_2 (12 mL).

Attempted Reaction of 1 with HCN and $AlCl_3$

A solution of **1** (200 mg) in CH_2Cl_2 (3 mL) was added to a stirred suspension of $AlCl_3$ (266 mg) in CH_2Cl_2 (3 mL). The resultant solution was treated with HCN (liberated from 300 mg NaCN). After stirring in a stoppered flask for 1 h at 25°C, the usual work-up gave a yellow oil (194 mg); ^1H nmr indicated no **6**.

Attempted Conversion of 7 to 6

An almost quantitative recovery of **7** was made after 1 h treatment of a 0.2 *m* solution of this compound in CH_2Cl_2 at 25°C (stoppered flask) with (*a*) up to three molar equivalents of $AlCl_3$, (*b*) a mixture of $AlCl_3$ (two molar equivalents) and HCN (generated from 250 mg NaCN), or (*c*) $AlCl_3$ (two molar equivalents) and **2** (one molar equivalent). In no case could **6** be detected in the product.

cis-*Ethyl 5-Cyano-2,5-dimethyltetrahydrofuran-2-carboxylate 11*

A solution of **3** (278 mg) in 100% EtOH (35 mL) was hydrogenated over 5% Pd/C (35 mg). The reduction was stopped after uptake of one mole of H_2 (10 min). Filtration and evaporation gave a product, plc of which afforded **11** as a mobile pale yellow oil (185 mg, 66%), $n_D^{26} = 1.4381$; ν_{max} (liq. film):2235 (w), 1732 cm^{-1}. Molecular ion not detected; base peak at *m/e* 124.0759 ($C_7H_{10}NO$ requires 124.07624, corresponding to loss of $CO_2C_2H_5$ from $C_{10}H_{15}NO_3$).

cis-*Ethyl 5-Aminomethyl-2,5-dimethyltetrahydrofuran-2-carboxylate 13 and 3-Aza-1,5-dimethyl-8-oxabicyclo-[3.2.1] octan-4-one 15*

A solution of **11** (413 mg) in 100% EtOH (40 mL) was hydrogenated over 5% Pd/C (60 mg). After uptake ceased (2 h) filtration and evaporation gave a product which partially crystallized on standing overnight. Trituration with petroleum ether gave **15** as a colorless crystalline solid (114 mg, 35%). Crystallization from ethyl acetate/petroleum ether gave colorless prisms, mp 131–133°C; ν_{max} (KBr):3450, 3320, 3200, 1675 cm^{-1}. Molecular ion (100%) at *m/e* 155.0946 ($C_8H_{13}NO_2$ requires 155.09463); other ions at *m/e* 126 (19%), 112 (20%), 98 (69%), and 97 (75%).

The petrol-soluble portion of the product was a colorless oil. All attempts to obtain a completely pure sample were unsuccessful, although ^1H and ^{13}C nmr data were obtained, consistent with this fraction being predominantly **13**.

trans-Ethyl 5-Cyano-2,5-dimethyltetrahydrofuran-2-carboxylate 12

A solution of **4** (156 mg) in 100% EtOH (20 mL) was hydrogenated over 5% Pd/C (16 mg). The reaction was stopped after one mole of H_2 had been taken up (3 h); plc of the crude product afforded **12** as a pale yellow oil (92 mg, 59%), $n_D^{25} = 1.4438$; ν_{max} (liq. film):2230 (w), 1732 cm^{-1}. Molecular ion not detected; base peak at *m/e* 124.0769 ($C_7H_{10}NO$ requires 124.07624, corresponding to loss of $CO_2C_2H_5$ from $C_{10}H_{15}NO_3$).

trans-*Ethyl 5-Aminomethyl-2,5-dimethyltetrahydrofuran-2-carboxylate 14*

A solution of **12** (172 mg) in 100% EtOH (25 mL) was hydrogenated over 5% Pd/C (80 mg). When uptake of H_2 ceased the reaction was worked up in the usual way to give a colorless oil (166 mg). All attempts to obtain pure **14** were unsuccessful, although consistent ^1H and ^{13}C nmr data were obtained on the freshly prepared material.

Ethyl 5-Aminomethyl-2,5-dimethyl-3-(2,5-dimethyl-3-furyl)-tetrahydrofuran-2-carboxylate 10

Compound **7** (235 mg) in 100% EtOH (25 mL) was hydrogenated over 5% Pd/C (100 mg) for 24 h at room temperature. The usual work-up gave **10** as a viscous yellow oil (217 mg). The nature of the product was established by characteristic ^1H and ^{13}C nmr signals, although attempts to obtain a pure sample by chromatography or crystallization were unsuccessful.

cis-*2,5-Dimethyl-2,5-dihydrofuran-2,5-dicarboxylic Acid 16*

A solution of **3** (364 mg) in 95% EtOH (3 mL) and 30% NaOH (10 mL) was refluxed for 3 h. The dark red-brown mixture was cooled and diluted with water (10 mL). The aqueous solution was filtered, extracted with ether, and then acidified with 50% H_2SO_4. The acid solution was thoroughly extracted with ether. After drying (Na_2SO_4), evaporation of solvent from the extract afforded **16** as a colorless crystalline residue (302 mg, 87%). Crystallization from water gave cream-colored prisms, mp 178–179°C; ν_{max} (KBr):3500–2500 (br. env.), 1700 (b) cm^{-1}. Molecular ion not detected; base peak at *m/e* 141.0551 ($C_7H_9O_3$ requires 141.05517, corresponding to loss of CO_2H from $C_8H_{10}O_5$).

trans-*2,5-Dimethyl-2,5-dihydrofuran-2,5-dicarboxylic Acid 17*

A solution of **4** (197 mg) in 95% EtOH (2 mL) and 30% NaOH

(6 mL) was refluxed for 3 h. The red-brown solution was then worked up as for **16** above to give a solid residue. Crystallization from ethyl acetate/petroleum ether gave **17** as colorless prisms (110 mg, 60%), mp 148–149°C; ν_{max} (KBr):3500–2500 (br. env.), 1700 (b) cm^{-1}. Molecular ion not detected; base peak at m/e 141.0549 ($C_7H_9O_3$ requires 141.05517, corresponding to loss of CO_2H from $C_8H_{10}O_5$).

4-Carboxy-1,2,4,8-tetramethyl-3,9-dioxatricyclo[5.2.1.0^{2,6}] decane-8-carboxamide 8

A solution of **6** (120 mg) in 95% EtOH (2 mL) and 30% NaOH (10 mL) was refluxed for 3 h. Work-up as for **16** above gave a solid residue (132 mg). Crystallization from ethyl acetate gave **8** as colorless prisms, mp 240–242°C; ν_{max} (KBr):3600–2800 (br. env., with bands superposed at 3460 and 3220 cm^{-1}), 1723, 1642 cm^{-1}. Molecular ion (8%) at *m/e* 283.1412 ($C_{14}H_{21}NO_5$ requires 283.14197); base peak at *m/e* 239.1278 ($C_{13}H_{19}O_4$ requires 239.12834).

3-(2,5-Dimethylfuryl)-2,5-dimethyltetrahydrofuran-2,5-dicarboxylic Acid 9

A solution of crude **7** (450 mg) in 95% EtOH (3 mL) and 30% NaOH (20 mL) was refluxed for 3 h. The dark brown solution was worked up as for **16** above to give a brown solid (400 mg). Crystallization from ethyl acetate gave pure **9** (163 mg), mp (dec.) 230–232°C; ν_{max} (KBr):3600–2300 (br. env.), 1712 (b) cm^{-1}. Molecular ion (66%) at *m/e* 282.1108 ($C_{14}H_{18}O_6$ requires *m/e* 282.11034); base peak at *m/e* 149.0966 ($C_{10}H_{13}O$ requires 149.09664).

Reaction of 9 with Acetyl Chloride

A solution of **9** (90 mg) in acetyl chloride (10 mL) was refluxed for 24 h. Evaporation gave a dark brown residue. Attempts to isolate an anhydride from this product by recrystallization or chromatography resulted only in recovery of **9**.

Acknowledgments

We gratefully acknowledge the excellent technical assistance of Mrs. M. G. Flack, and the useful contributions made to this work by J. Walker (N.R.C.C. summer student, 1973) and D. Appleton (technical assistant 1976–1977). Our thanks go also to D. J. Embree for all mass measurements and to P. F. Seto for ir spectra.

1. J. C. Jagt and A. M. Van Leusen. J. Org. Chem. **39**, 564 (1974).
2. A. W. McCulloch, D. G. Smith, and A. G. McInnes. Can. J. Chem. **52**, 1013 (1974).
3. T. J. Batterham. NMR spectra of simple heterocycles. John Wiley and Sons, Inc. New York. 1973. p. 378.
4. J. B. Stothers. Carbon-13 nmr spectroscopy. Academic Press, New York. 1972.
5. A. W. McCulloch and A. G. McInnes. Can. J. Chem. **53**, 1496 (1975).
6. A. W. Hanson. Acta Crystallogr. Sect. B, **33**, 889 (1977).
7. T. F. Page, T. Alger, and D. M. Grant. J. Am. Chem. Soc. **87**, 5333 (1965).
8. R. M. Acheson. Acc. Chem. Res. **4**, 177 (1971).
9. R. A. F. Matheson, A. W. McCulloch, A. G. McInnes, and D. G. Smith. Can. J. Chem. **57**, 2743 (1979).

Can. J. Chem. Downloaded from www.nrcresearchpress.com by 210.87.254.42 on 09/06/12
For personal use only.

Can. J. Chem. Downloaded from www.nrcresearchpress.com by 210.87.254.6 on 09/06/12
For personal use only.

COMMUNICATION

On cardioactive steroids. IV.[1] A new synthesis of cardenolides

RINALDO MARINI-BETTOLO, PETR FLECKER, THOMAS Y. R. TSAI, AND KAREL WIESNER

Natural Products Research Centre, University of New Brunswick, Bag Service #45222, Fredericton, New Brunswick, Canada E3B 6E2

Received January 19, 1981

This paper is dedicated to Prof. Raymond U. Lemieux on the occasion of his 60th birthday

RINALDO MARINI-BETTOLO, PETR FLECKER, THOMAS Y. R. TSAI, and KAREL WIESNER. Can. J. Chem. **59**, 1403 (1981).
A new and efficient synthesis of Digitalis cardenolides via methoxyfuryl intermediates is described.

RINALDO MARINI-BETTOLO, PETR FLECKER, THOMAS Y. R. TSAI, et KAREL WIESNER. Can. J. Chem. **59**, 1403 (1981).
Une nouvelle synthèse efficace des cardenolides de Digitalis à partir des intermediaires methoxyfuryle est décrit.
[Traduit par le journal]

Some time ago we reported a short and efficient synthesis of digitoxigenine via the furyl intermediate **I**. This material was converted by oxidation and reduction to the 15β-hydroxy cardenolide **II** and hence in three simple steps to digitoxigenine (2).

We now wish to disclose an even more effective (second generation (4)) variant of this method which dispenses with the oxidation and reduction.

We describe first the preparation of the new organometallic reagent 2-methoxy-4-furyl lithium **1**.[2]

The dibromo carboxylic ester **2** (5) was heated to 120°C in a pressure bottle with methanolic sodium methoxide for 30 min. The methoxy derivative **3** (mp 93–95°C) was obtained in a yield of 58% besides starting material.[3] (Infrared ($CHCl_3$): 1720 ($-CO.OCH_3$) cm^{-1}; ^{1}Hmr ($CDCl_3$): τ = 4.45 (s, 1H, aromatic H), 6.03 (s, 3H, $-OCH_3$), 6.10 (s, 3H, $-CO.OCH_3$).) Saponification of the ester **3** to the carboxylic acid **4** (mp 185°C (dec.)) and decarboxylation of this material at 185°C gave 2-methoxy-4-bromofuran **5** in a yield of 50%. For purification compound **5** was simply distilled without fractionation (100°C bath temperature, 14 Torr). (^{1}Hmr ($CDCl_3$): τ = 3.12 (d, J = 1 Hz, 1H, C5H), 4.69 (d, J = 1 Hz, 1H, C3H), 6.18 (s, 3H, $-OCH_3$).)

The methoxy bromofuran **5** was converted to the lithium derivative **1** by stirring with *n*-butyllithium (2.3 mol) in ether at −78°C for 1 h. The steroid ketone **III** (2)[4] (0.3 mol) was added in benzene solution and stirring was continued for 1 h. The crude compound **6** was obtained practically pure in a quantitative yield. On purification by chromatography on silica gel about 20% of the material was hydrolyzed to the corresponding lactone, which is useless for the continuation of the synthesis. (^{1}Hmr ($CDCl_3$): τ = 3.3 (d, J = 1 Hz, 1H, α-furyl H), 4.75 (d, J = 1 Hz, 1H, β-furyl H), 6.18 (s, 3H, $-OCH_3$), 8.94, 8.97 (2s, 3H each 2-CH_3).)

To avoid losses of compound **6** due to its facile hydrolysis on purification, the crude material **6** was acetylated with acetic anhydride and pyridine and a catalytic amount of *p*-dimethylaminopyridine for 48 h at room temperature. The crude acetyl derivative was refluxed in aqueous acetone in the presence of calcium carbonate for 48 h. On purification by chromatography, the allylic rearrangement product **7** was again partially hydrolyzed to the lactone **8**. The pure compound **7** remained oily. (^{1}Hmr ($CDCl_3$): τ = 3.00 (broad s, 1H, α-furyl H), 4.67 (broad s, 1H, β-furyl H), 6.15 (s, 3H, $-OCH_3$), 4.12 (d, J = 4 Hz, 1H, C16H).)

The hydrolysis of compound **7** to the lactone **8**

[1]References 1, 2, and 3 are considered the first three communications of this series.

[2]The method is actually not shorter in absolute terms. It is, however, shorter and more efficient with respect to the far more expensive steroid starting material **III**. Experiments to prepare the reagent **1** by a much simpler method are in progress.

[3]All compounds gave molecular ions in mass spectrometry and ir and ^{1}Hmr spectra compatible with the structures assigned to them. All crystalline compounds gave satisfactory C/H analyses.

[4]The preparation of **III** has now been made fully stereospecific by substituting reduction of the C3 ketone with "Selectride" for hydrogenation at the appropriate stage of the synthesis (cf. 2).

0008-4042/81/091403-02$01.00/0
©1981 National Research Council of Canada/Conseil national de recherches du Canada

FOR ERRATA SEE
v.59#22 19...81...p.3135

ERRATA

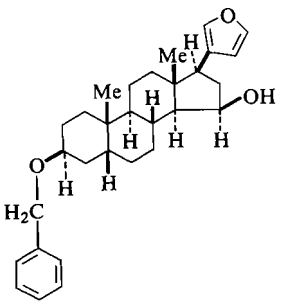

I

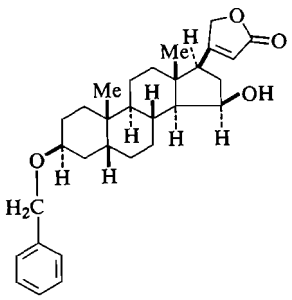

II

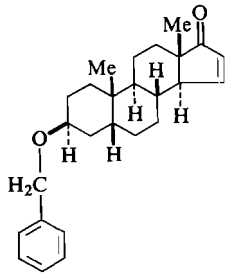

III

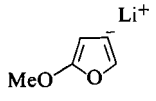

1

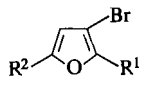

2 $R^1 = CO_2CH_3$, $R^2 = Br$
3 $R^1 = CO_2CH_3$, $R^2 = OCH_3$
4 $R^1 = CO_2H$, $R^2 = OCH_3$
5 $R^1 = H$, R^2OCH_3

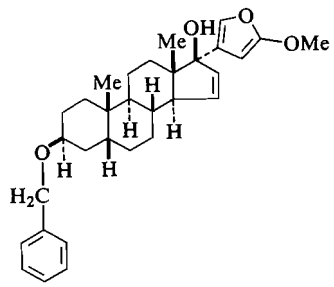

6

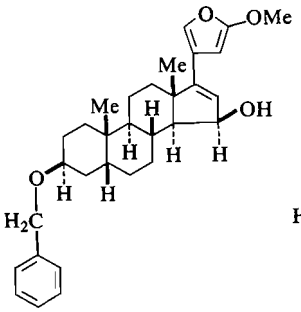

7

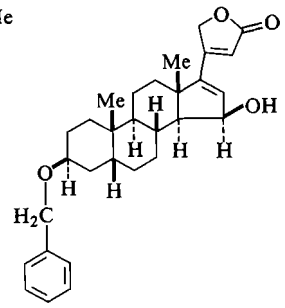

8

was accomplished quantitatively by stirring with dilute hydrochloric acid in aqueous THF for 5 h at room temperature. Compound 8 was recrystallized from ether and melted at 129–131°C. (Infrared ($CHCl_3$): 3600, 3475 (OH), 1790, 1750 (lactone) cm^{-1}; uv λ_{max}(EtOH): 268 nm (ε = 13 170); ^{1}Hmr ($CDCl_3$): τ = 3.75 (d, J = 4 Hz, 1H, C16H), 3.84 (s, 1H, C22H), 5.06 (broad s, 2H, C21H), 5.35 (m, 1H, C15H).)

The lactone **8** was obtained in a yield of 75% from the starting steroid **III** if the entire operation was performed without purification of the intermediates **6** and **7**. Hydrogenation of compound **8** with $Pd/CaCO_3$ in ethanol gave quantitatively the already described intermediate **II** (2). We have originally described this material as oily, but it crystallized after several months in the refrigerator and was recrystallized from ethanol (mp 147–148°C). Identity was established by mixture mp and spectral and chromatographic data.

Acknowledgements

We wish to thank the Natural Sciences and Engineering Research Council of Canada and the Canadian Heart Foundation for support of this work. K.W. and R.M.B. thank the Canada Council for an Izaak Walton Killam Memorial Scholarship and the Italian Research Council for a leave of absence, respectively.

1. J. M. Ferland, Y. Lefebvre, R. Deghenghi, and K. Wiesner. Tetrahedron Lett. 3617 (1966).
2. T. Y. R. Tsai, A. Minta, and K. Wiesner. Heterocycles, **12**, 1397 (1979).
3. R. Marini-Bettolo, Connie S. J. Tsai, T. Y. R. Tsai, and K. Wiesner. Heterocycles, **15**, 305 (1981).
4. K. Wiesner. Centenary Lecture. Chem. Soc. Rev. **6**, 413 (1977).
5. D. J. Chadwick, J. Chambers, G. D. Meakins, and R. L. Snowden. J. Chem. Soc. Perkin Trans. I, 1770 (1973).

Can. J. Chem. Downloaded from www.nrcresearchpress.com by 210.87.254.6 on 09/06/12
For personal use only.

Removal of allergens from natural oils by selective binding to polymer supports. II.[1] Application of aminated resins to isoalantolactone and costus oil

ANNIE CHEMINAT AND CLAUDE BENEZRA[2]

Laboratoire de Dermato-Chimie, Université Louis Pasteur, Clinique Dermatologique, C.H.R. de Strasbourg, 67091 Strasbourg, France

AND

M. JEAN FARRALL AND JEAN M. J. FRÉCHET[2]

Department of Chemistry, University of Ottawa, Ottawa, Ont., Canada K1N 9B4

Received January 29, 1981

ANNIE CHEMINAT, CLAUDE BENEZRA, M. JEAN FARRALL, and JEAN M. J. FRÉCHET. Can. J. Chem. **59**, 1405 (1981).

A number of crosslinked polymers containing primary or secondary amine functional groups were prepared by chemical modification of styrene–divinylbenzene or styrene–acrylonitrile–divinylbenzene resins. The polymers were tested in the binding of α-methylene-γ-butyrolactone allergens via Michael addition of their nucleophilic ends with the conjugated system of the lactones. Best results were obtained using 1% crosslinked poly(aminoethylstyrene) in ethanol; polymers with higher crosslinking or other functional groups were somewhat less reactive. This technique for the removal of α,β-unsaturated lactones from solution was applied successfully to the selective removal of the allergenic components of costus oil, a natural oil of plant origin used in the cosmetics industry. After purification of the costus extracts, the allergens which were retained by the polymer could be cleaved by permethylation followed by base treatment, and characterized. The polymer-treated natural oil had lost its allergenic properties while the polymer-retained materials were found to be powerful allergens.

ANNIE CHEMINAT, CLAUDE BENEZRA, M. JEAN FARRALL et JEAN M. J. FRÉCHET. Can. J. Chem. **59**, 1405 (1981).

On a préparé des polymères réticulés contenant des amines primaire ou secondaire comme groupes fonctionnels en modifiant chimiquement des résines de styrène–divinylbenzène ou de styrène–acrylonitrile–divinylbenzène. On a vérifié les possibilités que pourront avoir ces polymères à se lier à l'allergène α-méthylène γ-butyrolactone par le biais d'une addition de Michael de leurs extrémités nucléophiles sur le système conjuguée des lactones. On obtient les meilleurs résultats en utilisant le poly(aminoéthylstyrène) réticulé à 1% dans l'éthanol; les polymères plus fortement réticulés ou porteurs d'autres groupes fonctionnels sont un peu moins réactifs. On a appliqué avec succès cette technique de fixation des lactones-α,β non saturées pour enlever sélectivement des composés allergènes de l'huile de costus, une huile végétale naturelle utilisée dans l'industrie des cosmétiques. Après la purification des extraits de costus, les allergènes qui se sont fixés sur le polymère peuvent être clivés par une perméthylation suivie d'un traitement basique, et être ensuite caractérisés. L'huile naturelle ainsi traitée perd ses propriétés allergènes alors que les produits retenus par le polymère sont des allergènes puissants.

[Traduit par le journal]

Introduction

Synthetic functional polymers have been used in a number of very varied applications in organic chemistry (1). For example, polymers have been used as regenerable reagents (2) or supports (3) in organic synthesis or chiral column packings for the resolution of racemates (4). Another potentially important application of polymers is derived from their ability to "fish out" selectively one type of functionality from a complex mixture (5). Thus we have recently experimented with the use of poly(*p*-2-aminoethyl styrene) in the removal of an α-methylene-γ-butyrolactone from solution (6). This reaction was the test of a system for the removal of certain allergy-causing compounds from natural oils.

Many plants, especially those of the very common Compositae family, contain sesquiterpene α-methylene-γ-butyrolactones (7). These substances are extremely reactive and their biological activity has been reviewed recently (8). Among their numerous properties, they are capable of inducing allergic contact dermatitis. Since numerous plant extracts are used in cosmetology, perfumery, or pharmacy, it is desirable to devise a method for the selective removal of these undesirable allergy-causing compounds from the complex mixtures which make up these extracts. Two main benefits would accrue from the development of a specific removal procedure: first the mixtures would become anallergic; second the compounds which have been removed could be isolated, characterized, and tested, thus providing a better insight into the complex mechanism of allergenic reactions.

Results and Discussion

Studies of the mechanism of action (8) of α-methylene-γ-butyrolactone allergens have suggested that Michael additions of thiol or amine

[1]For part I see ref. 6. Presented in part at the 180th Meeting of the American Chemical Society, Las Vegas, NV, August, 1980.

[2]Author to whom correspondence may be addressed.

0008-4042/81/101405-10$01.00/0

©1981 National Research Council of Canada/Conseil national de recherches du Canada

Can. J. Chem. Downloaded from www.nrcresearchpress.com by 210.87.254.5 on 09/06/12
For personal use only.

Can. J. Chem. Downloaded from www.nrcresearchpress.com by 210.87.254.5 on 09/06/12
For personal use only.

nucleophiles to the unsaturated lactones are involved. Our method for the removal of these lactones is patterned after this supposed *in vivo* reaction and makes use of an insoluble but very reactive nucleophilic polymer which can bind the conjugated lactones by a Michael addition and thus is able to remove them from solution (Fig. 1).

We have described recently the preparation of several polymeric nucleophiles (6, 9, 10) by chemical modification of styrene–divinylbenzene copolymers. Among these, the resins containing amine or thiol groups have the greatest potential in the role of polymeric nucleophiles for the binding of α-methylene-γ-butyrolactones.

Our first tests were centered on the use of aminated polymers for the extraction from solution of a single sesquiterpene lactone, isoalantolactone, which is isolated from a plant of the Compositae family: *Inula helenium L.* Our results have then been extended to the much more demanding problem of extracting selectively several α-methylene-γ-butyrolactones from a complex plant extract, costus oil, which is obtained from the dried roots of another member of the Compositae family, *Saussurea Lappa C.*

Synthesis of the Polymers

Copolymers of styrene and divinylbenzene were chosen as substrates because their properties are well known and their chemical modification is readily carried out. For example, polymers containing thiol or phenol groups on a 1% crosslinked polystyrene matrix can be prepared easily by bromination of the aromatic rings, followed by lithiation and reaction with elemental sulfur or oxygen (9). We have observed that this reaction sequence results in the introduction of some additional crosslinks in the polymer beads. However, this increase in the degree of crosslinking does not affect noticeably the performance of the polymers. Another route to similar polymers involved the copolymerization of *m*-mercapto- (11) or *o*-hydroxystyrene (12) with divinylbenzene.

In an attempt to ascertain whether small differences in polymer structure had an influence on the binding of unsaturated lactones, a series of resins containing amine functional groups was prepared. Variations in structure included the degree of functionalization, the extent and type of crosslinking (micro or macroporous), the nature of the amine (primary or secondary), and the length of the spacer arm between the polymer backbone and the amino group.

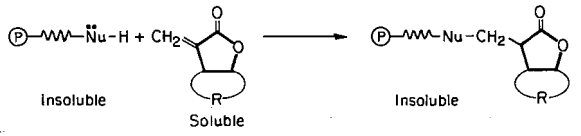

FIG. 1. Insolubilization of α-methylene-γ-butyrolactones by Michael addition with a nucleophilic polymer.

A first type of polymer in which the amino group is linked through a short 1–3 carbon chain to some of the aromatic rings of polystyrene was prepared from partially chloromethylated or partially lithiated polystyrene. Poly(aminomethylstyrene) is obtained (13) by reaction of the chloromethylated polymer with potassium phthalimide followed by treatment with hydrazine hydrate. Poly(aminoethylstyrene) is prepared by cyanation (6, 14) of poly(chloromethylstyrene) followed by reduction of the polymeric nitrile with lithium aluminium hydride – aluminium chloride. We have prepared poly(aminopropylstyrene) **5** via two different routes (Scheme 1). One involves the reaction

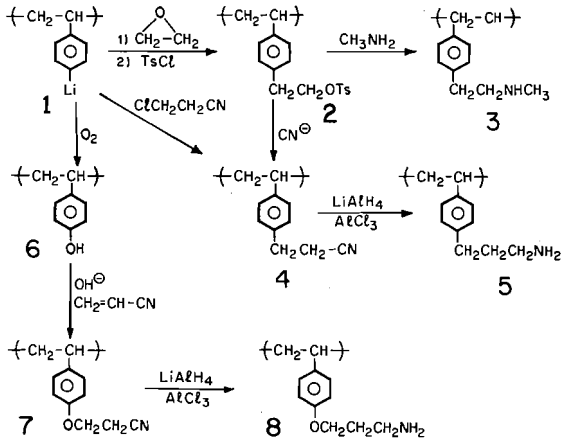

SCHEME I

of the lithiated polymer **1** with 3-chloropropionitrile to yield **4** which can then be reduced to **5**; the second route is somewhat longer but also gives the nitrile **4** in good functional yield. The lithiated polymer **1** is quenched with ethylene oxide, then tosylated to afford **2**, which can either be treated with cyanide to produce a polymer with propionitrile pendant groups **4** or with methylamine to give a polymer with secondary amine functionalities **3**. The polymers prepared through the intermediate tosylate **2** had capacities of up to 2.5 mequiv./g.

Another preparation by chemical modification makes use of the cyanoethylation of the hydroxylated polymer **6** with acrylonitrile in the presence of base. This simple reaction affords a nitrile polymer **7** which can be reduced to the corresponding primary amine **8**.

A different approach to the synthesis of a

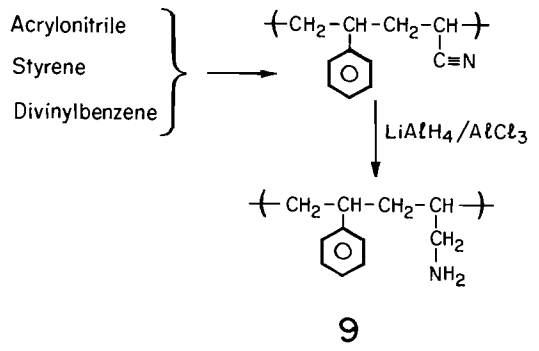

SCHEME 2

polymer containing amino groups (Scheme 2) involves the preparation of a terpolymer containing styrene, acrylonitrile, and divinylbenzene and its subsequent reduction to **9**. Although the final composition of the terpolymer can be varied by changing the polymerization conditions, monomer feed ratio, etc., we have concentrated on the preparation of polymers with a capacity of approximately 3 mequiv. of functional group per gram to maintain the desirable physical characteristics (porous bead formation, mechanical stability, etc.) of the more classical styrene–divinylbenzene copolymers.

Use of Aminated Polystyrenes for the Removal of Isoalantolactone From Solution

The ability of aminated polymers to bind allergenic lactones by Michael addition to their α,β-unsaturated system was first tested in the insolubilization of isoalantolactone **10** using poly(aminoethylstyrene) (Scheme 3). The reaction was carried out simply by stirring a solution containing a known concentration of **10** in the presence of polymer **11** while monitoring the soluble phase by gas chromatography. Comparison of the chromatograms with those obtained for calibrated solutions afforded a fairly accurate measurement of the uptake of lactone by polymer **11**. This was confirmed by gravimetric measurements both on the soluble phase after evaporation of the solvent and on the solid phase after washing and drying.

In order to optimize the reaction conditions we have studied the influence of the nature of the solvent, lactone concentration, lactone-to-polymer

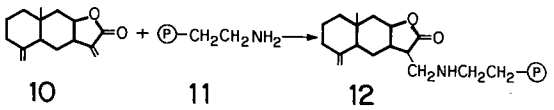

SCHEME 3

ratio, and nature of the polymer on the binding of **10**.

Influence of Solvent

Reactions involving insoluble functional polymers are usually extremely solvent sensitive (1, 3). In particular, when microporous resins are used, it is desirable to use good swelling solvents such as halogenated hydrocarbons, cyclic ethers, or aromatic solvents, to ensure that most of the reactive sites located within the polymer beads are fully exposed to the reagents in solution. Macroporous resins having a more rigid and very porous structure are usually much less affected by the nature of the reaction solvent; however, their reactivity is often less than that of swollen microporous polymers. Another important point to be considered in choosing a solvent for the reaction of polymer **11** with isoalantolactone is that Michael additions are usually best carried out in polar solvents such as alcohols. Thus it appears that it might be difficult to reconcile the solvent requirements of both the Michael addition and the microporous polymer, although a careful survey of the literature shows that in some cases good results can be obtained even in nonswelling solvents. For example, Leznoff and Wong (15) succeeded in the preparation of chalcones in quantitative yields using a microporous polymer support with ethanol as solvent.

Table 1 summarizes the results we obtained using an excess of polymer **11** with a capacity of 3.1 mequiv. of amino groups per gram. Best results were obtained in ethanol with essentially complete removal of isoalantolactone from solution in approximately seven hours. Mixtures of ethanol with dichloromethane or dioxane were almost as efficient while nonpolar solvents gave poor results. A kinetic study of the reaction carried out under similar conditions but in homogeneous phase with primary amines (*n*-butylamine and phenethylamine) in ethanol, showed that the reaction rates were comparable whether the amine was in solution or polymer-bound. Binding of the lactone to the polymer was confirmed both by the gain in weight of the polymer **12**, which indicated attachment of all the lactone originally present in the solution, and by the infrared spectrum of **12**, which included a broad peak at 1770 cm^{-1} and a weaker one at 1640 cm^{-1}, consistent with the presence of a γ-lactone and a disubstituted double bond on **12**.

Influence of Concentration

As can be seen in Table 2, a large excess of amino reactive sites on the polymer results in complete removal of the lactone from solution, while at constant resin sites to lactone ratio (exp. 9 and 12). best

Can. J. Chem. Downloaded from www.nrcresearchpress.com by 210.87.254.5 on 09/06/12
For personal use only.

TABLE 1. Influence of solvent on the loading of isoalantolactone onto resin **11**

Experiment No.	Solvent	% Loading[a] 1 h	3 h	5 h	7 h	24 h
1	Dioxane	37	38	39	41	50
2	Acetone	2	4	5	6	10
3	Benzene	3	5	7	8	14
4	Chloroform	4	10	14	16	25
5	Ethanol	52	77	91	96	99
6	Ethanol–dichloromethane 3:2	34	50	60	67	90
7	Ethanol–dioxane 1:1	28	43	53	61	85

[a]% Of isoalantolactone removed from solution in the reaction of a 0.026 *M* solution of **10** with a suspension containing 0.31 equiv./L of $\text{P}\sim\text{NH}_2$ functional groups at room temperature for the time indicated.

TABLE 2. Influence of the relative concentrations on the loading of isoalantolactone **10** onto resin **11**

Experiment No.	[Lactone **10**] mol/L	[Resin sites][a] equiv./L	$\frac{\text{[Resin sites]}}{\text{[Lactone 10]}}$	% Bound[b]
8	0.001	0.236	236	100
9	0.021	0.236	11	100
10	0.042	0.236	5.6	98
11	0.004	0.118	30	95
12	0.011	0.118	11	73

[a]Calculated for a polymer having a capacity of 2.4 mequiv./g.
[b]After 24 h stirring at room temperature.

results are obtained with a higher concentration of lactone. It should be noted, however, that even with a low resin sites to lactone ratio, most of the lactone can be removed from solution provided sufficient reaction time is allowed. Table 1 shows clearly that the rate of addition decreases as binding increases, a result which can be explained easily by the decrease in concentration of the reactive species and by increasing hindrance about the remaining sites of the polymer. A saturation test using a large excess of isoalantolactone showed that for resins with capacities of 3–4 mequiv./g up to 80% of the amine sites of the polymer were available for binding of the lactone.

Although all of the experiments described in Tables 1 and 2 were performed using a stirred suspension of the aminoethyl resin in a solvent, removal techniques involving the use of columns packed with resin **11** were also tested. Complete retention of the isoalantolactone on the column could be achieved by changing such variables as the size of the column, concentration, and rate of elution, or by passing the eluate several times over the column.

Influence of Polymer Structure

Table 3 summarizes the results which were obtained with nucleophilic polymers containing amine functional groups. Although best results were obtained using 1% crosslinked aminoethyl polystyrene **11**, most of the polymers which were tested performed satisfactorily. Neither the length of the spacer between the aromatic ring of the styrene units and the amino group, nor the primary or secondary nature of the nucleophile seemed to have a drastic effect on coupling provided the contact time was long enough (Fig. 2). Surprisingly perhaps, since ethanol is not a good swelling solvent for microporous polymers, the 1% crosslinked swellable resin performed better than the macroporous one. This seems to confirm the general trend to higher reactivity of microporous polymers. Also, better results were obtained with the less crosslinked resins and therefore microporous 1% crosslinked **11**, having shown the best performance, was used in almost all of the experiments described below. However, it is worthwhile noting that polymer **9**, obtained by reduction of crosslinked styrene–acrylonitrile beads, is the cheapest and most easily prepared aminated resin and may be the reagent of choice in larger scale applications.

Cleavage of Isoalantolactone From Polymer 12

Cleavage of the polymer-bound isoalantolactone was carried out by permethylation with methyl iodide followed by base treatment to regenerate the conjugated exocyclic double bond (Scheme 4). Unfortunately, with polymer **12** the yield of this reaction was usually only 40–50% and two or three

Can. J. Chem. Downloaded from www.nrcresearchpress.com by 210.87.254.5 on 09/06/12
For personal use only.

TABLE 3. Influence of polymer structure

Experiment[a] No.	Polymer	Crosslinking[b] (%)	$-NH_2$ mequiv./g	% **10** bound 12 h	% **10** bound 24 h
13	Ⓟ$-CH_2NH_2$	1	3.7	80	90
14	Ⓟ$-(CH_2)_2NH_2$ **11**	1	2.0	98	100
15	Ⓟ$-(CH_2)_2NH_2$ **11**	1	3.2	100	100
16	Ⓟ$-(CH_2)_3NH_2$ **5**	1	2.4	80	86
17	Ⓟ$-(CH_2)_2NHCH_3$ **3**	1	2.0	72	95
18	Ⓟ$-O(CH_2)_3NH_2$ **8**	1	1.2	70	80
19	Ⓟ$-(CH_2)_2NH_2$ **11**	2	2.0	80	85
20	Ⓟ$-(CH_2)_2NH_2$ **11**	4M	2.6	72	90
21	**9**	2	2.7	88	95

[a]Reactions performed using a 0.043 *M* solution of **10** in ethanol with a five-fold excess of polymer.
[b]Crosslinked microporous SX-1 beads from Bio-Rad; 2% crosslinked microporous beads from Eastmann # 11180; 4 M refers to macroporous Amberlite XE-305 beads with 4% divinylbenzene from Rohm and Haas.

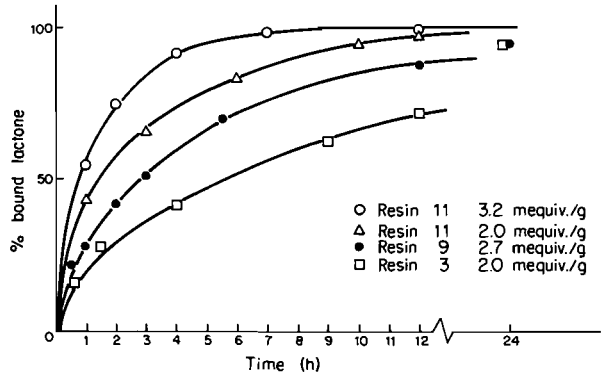

FIG. 2. Influence of the nature and loading of the polymer on lactone binding. The measurements were made on 0.5 g polymer with 0.05 g isoalantolactone in 5 mL ethanol at room temperature.

successive sequential permethylation–bicarbonate treatments were required to liberate up to 80% of the bound lactone. Attempts were made to improve the reaction by increasing the permethylation time or by using other methylating agents such as methylfluorosulfonate or Meerwein's reagent but these were unsuccessful. The only improvement which could be made was the addition of ether during the bicarbonate cleavage step. This served to remove the isoalantolactone from the reaction medium as it was formed and prevented its involvement in side reactions. The recovered isoalantolactone was identical (ir, nmr, gc, tlc) to an authentic sample.

Somewhat better results were obtained in the cleavage of isoalantolactone bound to the secondary amine polymer **3** with a 65% yield in a single treatment. This may be due to a more efficient permethylation step.

An obvious drawback of polymer **11** and indeed of all the aminated polymers we have tested to date is that they cannot be regenerated in simple fashion. The permethylation step causes the deactivation of all the amine sites of the polymer, whether they are involved in the binding of lactone or not. Although a fully regenerable polymer would be highly desirable, it should be emphasized that the unique advantages inherent to the use of insoluble nucleophiles are amply sufficient to justify their use.

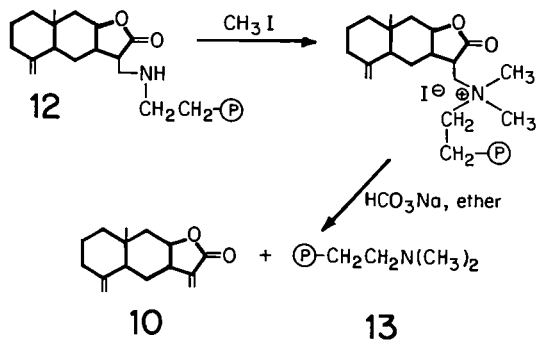

SCHEME 4

Application to Other Unsaturated Lactones

To ensure that the results obtained for isoalantolactone would be applicable to similar compounds, the binding of two other α,β-unsaturated lactones, alantolactone **14** and dehydrocostuslactone **15**, was attempted using polymer **11**. Figure 3 shows that the three lactones react with the polymer at approximately the same rate. Cleavage of the lactones from the polymer by permethylation–bicarbonate treatment gave results identical to those reported above.

Can. J. Chem. Downloaded from www.nrcresearchpress.com by 210.87.254.5 on 09/06/12
For personal use only.

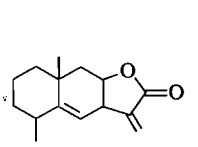

14

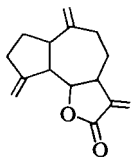

15

Application of Poly(aminoethylstyrene) to the Treatment of Costus Oil

Costus oil is a natural oil which is extracted from the roots of *Saussurea Lappa C.* (Costus), a plant of the Compositae family growing in the western Himalayas. This oil, which has a very characteristic and persistent odor, has been used extensively in perfumery. Unfortunately, costus oil contains some α-methylene-γ-butyrolactones which can cause allergic contact dermatitis (16); to prevent potential undesirable reactions to products containing plant extracts such as costus oil, it is useful to effect the selective removal of the α-methylene-γ-butyrolactones from the natural oils.

Costus extracts are available in two forms, costus essential oil, a light yellow viscous liquid which is obtained by steam distillation of the dried roots of *Saussurea Lappa C,* and costus oil, which is obtained by solvent extraction of costus roots. Both of these extracts contain at least two α-methylene-γ-butyrolactones: costunolide **16** and dehydrocostuslactone, DHC **15**.

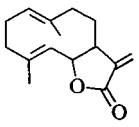

16

Both extracts were treated with poly(aminoethylstyrene) **11** suspended in a minimum amount of ethanol (Table 4). Binding of the lactones onto the polymer was followed by gas–liquid chromatography. As can be seen in Table 4, significant amounts of material were retained by the polymer: 13% of the essential oil and 40% of the oil. Examination of the chromatograms before (Fig. 4a) and after (Fig. 4b) polymer treatment of the essential oil show that most of the components of the oil remain untouched. One main component, identified as dehydrocostuslactone, is essentially completely removed by the polymer (peak 16, Fig. 4a). Two other minor components (peaks 11 and 15, Fig. 4a) were also removed. These were later identified as α- and β-cyclocostunolide, **17** and **18**. Similarly, the chromatograms of costus oil before and after treatment with polymer **11** show that two major components are removed by reaction with the

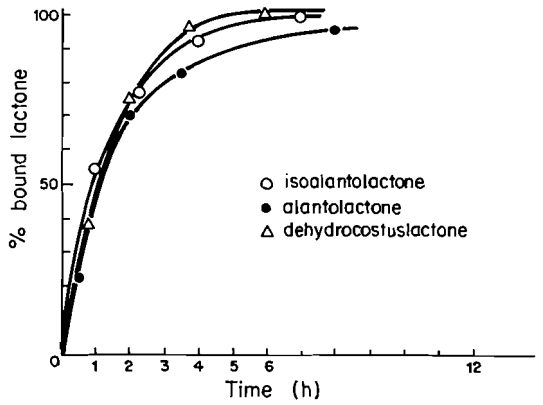

FIG. 3. Influence of lactone structure on coupling. The measurements were made on 0.5 g polymer (3.2 mequiv./g) with 0.05 g lactone in 5 mL ethanol at room temperature.

polymer: dehydrocostuslactone **15** and a product tentatively identified as costunolide **16**.[3]

The polymer-bound products were cleaved from their supports using the procedure which was developed with isoalantolactone. Analysis of the cleaved products was carried out by gc–ms and also by nmr spectrometry of the various components after separation by preparative thin layer chromatography. In the case of the polymer-retained products recovered after treatment of costus essential oil, the chromatogram (Fig. 5a) shows several products, including 80% of dehydrocostuslactone **15** (peak 4, Fig. 5a) and some small amounts of α-cyclocostunolide (peak 2, Fig. 5a) and β-cyclocostunolide (peak 3, Fig. 5a). Another 10% of the mixture are unidentified products.[4] In the case of the products liberated from the polymer after treatment of costus oil, the chromatogram shows four different peaks (Fig. 5b). The major peak (4, 65% of total) corresponds to dehydrocostuslactone, with sizeable peaks for α-cyclocostunolide (2, 14%) and β-cyclocostunolide (3, 21%). A very small peak (1) has tentatively been assigned to arbusculin-B **19**. Table 5 summarizes the composition of the lactone mixtures cleaved from the polymer.

It is noteworthy that no costunolide is found among the products which are cleaved from the polymer although costus oil is known to contain costunolide. In contrast, α- and β-cyclocostunolide

[3]The product decomposes thermally on the glc column. However, analysis of the product cleaved from the polymer after reaction suggests that it is indeed costunolide.

[4]One of these, peak 1 with $M^+ = 230$ has a mass spectrum consistent with that of an unsaturated lactone. A smaller peak with $M^+ = 232$ could not be analyzed satisfactorily.

Can. J. Chem. Downloaded from www.nrcresearchpress.com by 210.87.254.5 on 09/06/12
For personal use only.

TABLE 4. Treatment[a] of costus extract with polymer **11**

Costus extract	Weight of extract (g)	Weight of polymer[b] (g)	Amount retained by **11** (g)	Extract retained (%)	Amount of DHC **15** (g)
Essential oil	2	1	0.270	13	0.220
Oil	1.19	1.47	0.486	40	0.300

[a]Stirring of the amounts indicated in 2.5 mL of ethanol for 3 days at room temperature.
[b]Capacity of the polymer: 3.2 mequiv./g.

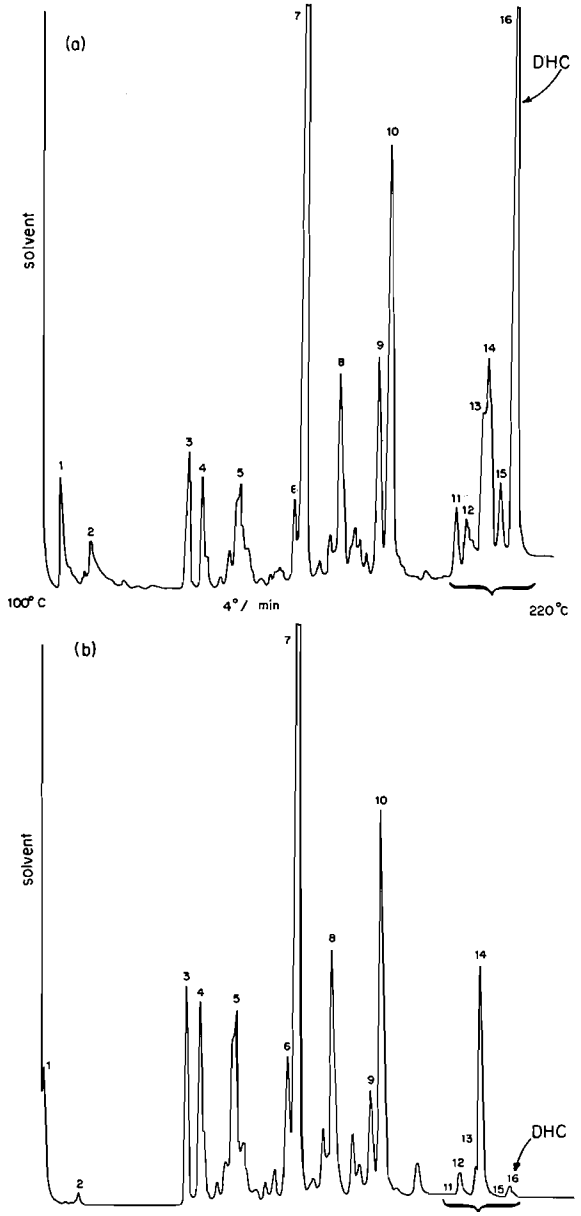

FIG. 4. (a) Chromatogram of crude costus essential oil. (b) Chromatogram of costus essential oil after treatment with polymer **11**.

and arbusculin-B have never been reported in costus oil, yet they have been identified as important components of the cleavage mixture. Since it is well known (17) that costunolide can cyclize readily in acidic medium (Scheme 5) to yield both cyclocostunolides and arbusculin-B, it is likely that our treatment of costus oil has resulted in the cyclization of costunolide, probably during the cleavage step. To verify this hypothesis pure costunolide was bound to the poly(aminoethylstyrene) in the usual fashion and the cleavage reaction was carried out with gc–ms analysis of the cleaved material. As expected, α- and β-costunolide, as well as arbusculin-B were found in the cleaved material. The composition of the mixtures recovered from the polymers after cleavage is given in Table 5.

Allergy-Testing of the Polymer-Purified Costus Extracts

This testing, which was carried out on laboratory

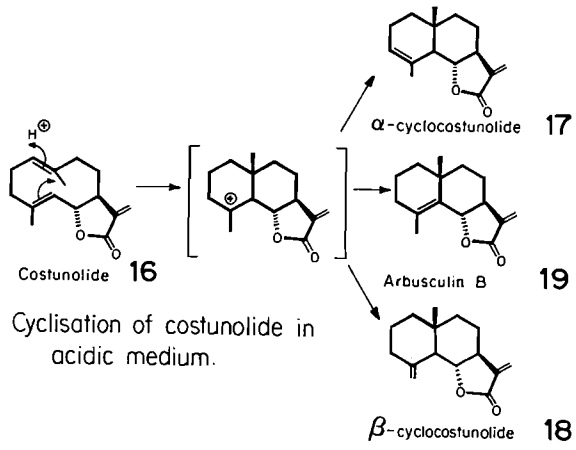

SCHEME 5

TABLE 5. Composition of the mixtures cleaved from the polymers

	Recovered lactones (%)				
Extracted from	**15**	**19**	**17**	**18**	Unknown
Costus essential oil	80	—	8	2	10
Costus oil	64	2	14	20	—

Can. J. Chem. Downloaded from www.nrcresearchpress.com by 210.87.254.5 on 09/06/12
For personal use only.

Can. J. Chem. Downloaded from www.nrcresearchpress.com by 210.87.254.5 on 09/06/12
For personal use only.

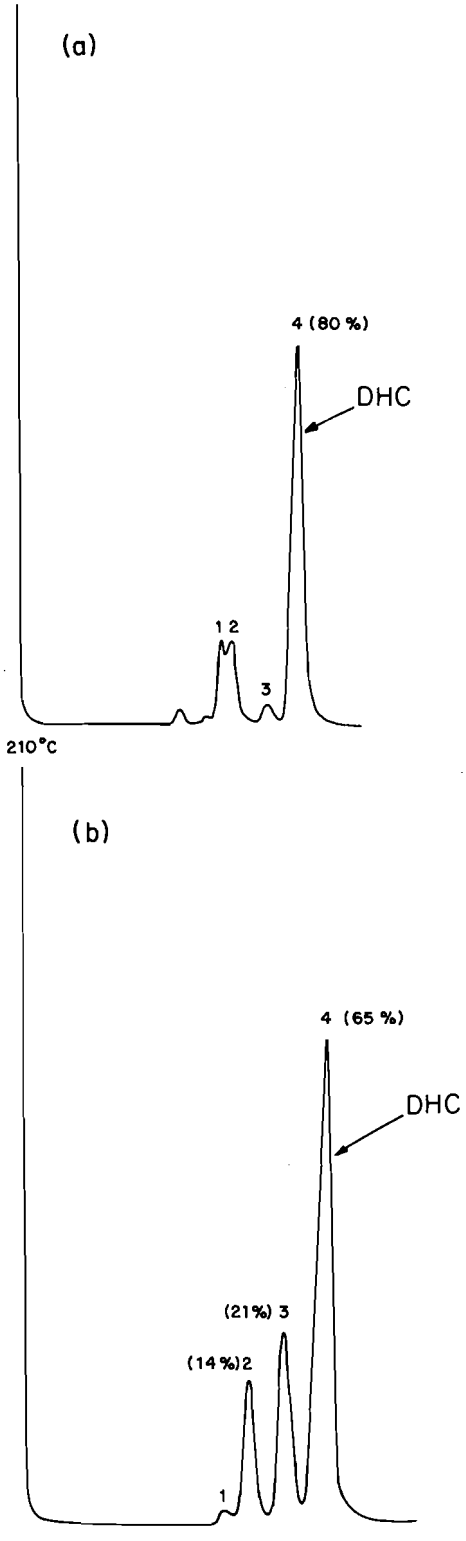

FIG. 5. (a) Chromatogram of the polymer-retained products from costus essential oil after cleavage. (b) Chromatogram of the polymer-retained products from costus oil after cleavage.

animals sensitized to crude costus extracts with appropriate control experiments, confirmed that the polymer-treated extracts were anallergic. In contrast, the mixtures recovered by cleavage of the polymer-retained materials were shown to contain powerful allergens. The complete results of this animal testing are being reported elsewhere.[5]

Conclusion

These results confirm clearly the great potential of polymers containing amino groups for the removal of α,β-unsaturated lactones from complex mixtures. Complete selectivity of the polymers cannot be claimed since the α,β-unsaturated aldehydes and ketones which are reported (18) to be present in small amounts in costus essential oil might also have been retained by the polymer. These compounds are present in such small amounts that they are likely to escape detection by our method. However, since one of the aims of this project is to remove all potential allergens from natural extracts, their removal would in fact be a benefit. We are currently studying the selectivity of poly(aminoethylstyrene) with test mixtures of various α,β-unsaturated compounds. We are also testing the reactivity of polymers containing thiol groups since much of the biological activity of α-methylene lactones seems to derive from their affinity for the thiol side-groups of sulfhydryl enzymes. Our preliminary work has indicated that almost instantaneous binding is achieved when thiolate reactive ends are present on the polymer.

Several improvements to our procedure are also under investigation. These include the development of a better and more quantitative cleavage procedure which would be free of side reactions such as the cyclization of costunolide and the preparation of fully regenerable polymers which could be used repeatedly in the removal of allergy-causing substances.

Experimental

Infrared spectra were recorded on a Pye-Unicam SP 1100 spectrophotometer using KBr pellets or NaCl discs. The nmr spectra were obtained on a 250 MHz spectrometer in $CDCl_3$ using approximately 1 mg samples. The gc–ms results were obtained on a LKB 900 S with LKB 2130 interface, and a PDP 11/10 Digital Equipment computer using a 25 m SE-30 capillary column with temperature programming 110–280°C, 3°/min. The gc chromatograms were obtained on a Girdel 300 gas chromatograph with FID on a 2 m, 1/8 in. column of 10% OV 17 on Chromosorb. Analytical thin-layer chromatography was carried out on silica gel without binder with three successive migrations using 1:1 ether–hexane. The polymers used were Bio-Beads SX-1 or SX-2 from Bio-Rad Laboratories, or Amber-

[5]A. Cheminat, J. L. Stampf, C. Benezra, M. J. Farrall, and J. M. J. Fréchet, unpublished data.

Can. J. Chem. Downloaded from www.nrcresearchpress.com by 210.87.254.5 on 09/06/12
For personal use only.

lite XE-305 from Rohm and Haas. Elemental analyses were performed by MHW Laboratories (Phoenix, AZ) or at the University of Ottawa. Isoalantolactone was isolated from Helenin (Sigma Chemical Co.). Costus oil and costus essential oil were obtained through Roure and Bertrand (Grasse, France). All other chemicals were obtained from commercial sources and used without further purification except when otherwise stated.

Preparation of Ⓟ $-CH_2CH_2NH_2$ *11*

Bio-Beads SX-1 (103 g) were chloromethylated using 260 mL of chloromethyl ethyl ether and 20 mL of $SnCl_4$ in 600 mL $CHCl_3$ as previously described (9, 14, 19) to give 130 g of polymer containing 4.1 mequiv./g of Cl. This polymer (100 g) was then transformed into the nitrile by treatment with 70 g of sodium cyanide in 1 L DMF at 60°C (6, 14) to give 98 g of Ⓟ $-CH_2CN$ which was reduced as follows. To a cooled and stirred solution of 18 g of $LiAlH_4$ in 1 L of dry THF were added slowly 60 g of anhydrous $AlCl_3$ followed by 97 g of the nitrile polymer. After refluxing overnight, the reaction was stopped by addition of excess dilute HCl which dissolved all of the aluminium salts. After filtration the polymer was washed with H_2O (3×), THF/2 *N* NaOH (3:1), H_2O (3×), THF, acetone, CH_2Cl_2, and CH_3OH, and dried to give polymer **11**. The infrared spectrum showed no remaining nitrile absorption at 2200 cm^{-1} and had a large NH_2 band centered at 3450 cm^{-1}. Elemental analysis showed that the polymer contained 4.42% N, indicating a capacity of 3.2 mequiv./g or a degree of functionalization of 0.38.

This procedure was also used to prepare poly(aminoethylstyrene) using Eastman 2% crosslinked polystyrene and macroporous Amberlite XE-305.

Preparation of Ⓟ $-CH_2CH_2OTs$ *2*

Ⓟ –Li **1** was prepared as described in the literature (20) from 15 g of brominated polystyrene (3 mequiv./g) and 75 mL *n*-BuLi (1.1 *N*) in 200 mL of dry benzene. After three hours of reaction at 65°C, the polymer was filtered, washed 2× with benzene, then 150 mL anhydrous THF, and 14 mL of ethylene oxide were added and allowed to react 15 h at room temperature. The polymer was filtered, washed, and dried as previously described (20), to give 13 g of Ⓟ $-CH_2CH_2OH$. The ir spectrum showed a large OH absorption at 3400 cm^{-1}. Ⓟ $-CH_2CH_2OH$ (7 g) was then treated with 8 g of tosyl chloride in 75 mL of pyridine at 4°C for 5 days followed by washing with water, THF, and ether, and drying to give 9.7 g of Ⓟ $-CH_2CH_2OTs$ **2**. The ir spectrum of **2**, showed large bands at 1160 and 1350 cm^{-1}.

Preparation of Ⓟ $-CH_2CH_2NHCH_3$ *3*

Polymer **2** prepared above (2.45 g) was suspended in 30 mL THF and 30 mL methylamine and the suspension was refluxed 6 h, then left at room temperature 18 h. After filtration and washing with H_2O, 1 *N* NaOH, H_2O, THF, acetone, CH_2Cl_2, CH_3OH, and ether, the polymer was dried (1.85 g). The infrared spectrum of **3** still showed very small bands at 1160 and 1350 cm^{-1}. Analysis, found: N 2.85%; 2.0 mequiv./g.

Preparation of Ⓟ $-CH_2CH_2CN$ *4*

Method A: Ⓟ –Li **1** prepared from 10 g of Ⓟ –Br (3.0 mequiv./g) and 35 mL of *n*-BuLi (2 *N*) as described previously was treated with 11 mL of 3-chloropropionitrile in 150 mL THF at room temperature for 18 h. The polymer was filtered, washed with H_2O (3×), THF/2 *N* HCl (3:1), H_2O (3×) THF, acetone, CH_2Cl_2, and CH_3OH, and dried to give 10 g of polymer **4**. The ir spectrum showed a CN absorption at 2240 cm^{-1}. Analysis, found: N 4.38%; 3.1 mequiv./g.

Method B: Ⓟ $-CH_2CH_2OTs$ **2** (3.0 g) suspended in 60 mL of DMF was reacted with 1 g of NaCN at 60°C for 5 h, then 18 h at room temperature. The polymer was then filtered, washed with DMF, H_2O (3×), THF/H_2O (3:1), THF, acetone, CH_2Cl_2, and CH_3OH, and dried to give 2.33 g of polymer **4**. The ir spectrum showed a CN peak at 2240 cm^{-1} and no residual tosylate absorptions. Analysis, found: N 3.43%; 2.45 mequiv./g.

Preparation of Ⓟ $-CH_2CH_2CH_2NH_2$ *5*

Ⓟ $-CH_2CH_2CN$ **4** (9.8 g, 3.1 mequiv./g) was treated with 4 g of $LiAlH_4$ and 13.4 g of $AlCl_3$ in 150 mL anhydrous THF as described above for Ⓟ $-CH_2CH_2NH_2$ **11**. After washing and drying, 10.0 g of polymer **5** was obtained. The ir spectrum showed the disappearance of the CN absorption and appearance of a $-NH_2$ band at 3400 cm^{-1}.

Preparation of Ⓟ *–OH 6*

Ⓟ –OH was prepared as described in the literature (9) from 15 g of SX-1 resin, 37 mL of *n*-BuLi (2.6 *N*), 15 mL of tetramethylethylenediamine, and O_2. After washing and drying, 15.5 g of polymer **6** were obtained. Analysis, found: O 2.52%; 1.6 mequiv./g.

Preparation of Ⓟ $-OCH_2CH_2CN$ *7*

Ⓟ –OH **6** (10 g, 1.6 mequiv./g) was suspended in 70 mL of acrylonitrile and 2 mL of 5% aqueous NaOH. After 18 h of reflux, the polymer was filtered, washed with THF, THF/2*N* HCl (3:1), CH_3CN (2×), H_2O (3×), THF, acetone, CH_2Cl_2, and CH_3OH, and dried to give 10.5 g of polymer **7**. The infrared spectrum showed a CN absorption at 2260 cm^{-1}. Analysis, found: N 1.86%; 1.33 mequiv./g.

Preparation of Ⓟ $-OCH_2CH_2CH_2NH_2$ *8*

Ⓟ $-OCH_2CH_2CN$ **7** (9.0 g, 1.33 mequiv./g) was reduced with 2 g of $LiAlH_4$ and 7 g of $AlCl_3$ in 250 mL of dry THF as described above. After washing and drying, 9.0 g of polymer **8** was obtained. The ir spectrum showed complete disappearance of the CN band. Analysis, found: N 1.70%; 1.21 mequiv./g.

Preparation of Ⓟ $-CH_2NH_2$

Ⓟ $-CH_2NH_2$ was prepared as described by Sparrow (13) from 50 g of Ⓟ $-CH_2Cl$ (4.28 mequiv./g) by reaction with 50 g of potassium phthalimide in 400 mL DMF followed by 17 g of hydrazine hydrate in 300 mL ethanol. After washing and drying, 50 g of polymer were obtained, containing 3.73 mequiv./g of N.

Preparation of an Acrylonitrile–Styrene–Divinylbenzene Terpolymer and Reduction to 9

To a solution of 1 g of sodium oleate in 400 mL deoxygenated water was added 13 g of acrylonitrile, 37 g of styrene, and 2 g of divinylbenzene (50%) followed by 0.2 g of benzoyl peroxide. The reaction mixture was stirred vigorously at 60°C for 12 h. The product was filtered, washed with H_2O, CH_3OH, and ether and dried to yield 37 g of fine white polymer beads. The ir spectrum showed a strong CN band at 2240 cm^{-1}. Analysis, found: N 4.23%; 3.0 mequiv./g.

The polymer (10 g, 3.0 mequiv./g) was then treated with 2.5 g of $LiAlH_4$ and 9.0 of $AlCl_3$ in 350 mL of anhydrous THF as described above. After washing and drying 9.0 g of polymer **9** were obtained. The ir spectrum contained a NH_2 band at 3480 cm^{-1} and no residual CN absorption. Analysis, found: N 3.8%; 2.7 mequiv./g.

General Procedure for the Binding of Isoalantolactone on an Aminated Polymer

All the preliminary tests for the study of the influence of solvent on the binding of isoalantolactone were carried out using 0.5 g of polymer **11** in 5 mL of a solution containing 0.030 g of isoalantolactone in the solvent tested. Tests to determine the influence of the nature of the polymer were carried out in similar fashion but with 5 mL of a solution containing 0.050 g of isoalantolactone in ethanol. The polymer suspensions were stirred at room temperature and the liquid phase was monitored by

gas chromatography on 10% OV 17 at 220°C. Final uptake of isoalantolactone by the polymer was confirmed by gravimetry both on the soluble phase and the polymer phase. In some cases the reaction was also monitored by uv spectrophotometry. An infrared spectrum of the polymer after reaction showed a strong band at 1770 cm^{-1} with no remaining absorption at 1660 cm^{-1}.

Determination of the Capacity of Polymer 11: Saturation Test

To a solution of 0.1091 g isoalantolactone in 4 mL ethanol was added 0.1137 g of polymer **11** (3.2 mequiv./g). The mixture was stirred at room temperature for 7 days. After thorough washing and Soxhlet extraction, the polymer weighed 0.1840 g while the combined liquid phases after evaporation yielded only 0.0380 g of isoalantolactone. This saturation test indicated that 83% of the sites of the polymer reacted with isoalantolactone. Duplicate tests gave results ranging from 74 to 84%.

General Procedure for the Cleavage of the Polymer-Retained Products from Their Support

A suspension of 1 g of a polymer containing bound lactones in 5 mL DMF (or ethanol) was treated with a large excess (1–2 mL) of CH_3I. The mixture was stirred in the dark at room temperature for 2 days. After filtration the polymer was washed repeatedly and dried *in vacuo*. The permethylated polymer was then suspended in 5 mL dioxane and 10 mL of a 10% aqueous $NaHCO_3$ solution were added. After addition of 20 mL ether, the polymer remained in the aqueous phase. The mixture was then stirred vigorously for 3–10 h while appearance of the lactone in the ether phase was monitored by gas chromatography. Once no further progress of the reaction was observed, the ether phase was separated from the aqueous phase, washed with dilute aqueous HCl, with aqueous $NaHSO_3$, and finally with water. After extraction of the aqueous wash water, the combined ether phases were dried and evaporated to yield a light yellow oily material which was characterized.

Purification of Costus Extracts

To a suspension of 1.470 g of **11** (1% crosslinked, 3.2 mequiv./g) in 2.5 mL ethanol was added 1.190 g costus oil (Roure and Bertrand). The mixture was stirred in the dark at room temperature and the disappearance of dehydrocostuslactone from the liquid phase was followed by gas chromatography. Once the reaction appeared to be complete (1–3 days), the polymer was filtered, washed with ethanol, then extracted in a Soxhlet for 24 h with CH_2Cl_2. The combined soluble phases were evaporated *in vacuo* to yield the purified costus oil (0.70 g). After drying *in vacuo* the polymer weighed 1.956 g indicating that 0.486 g (40%) of the original extract had been retained by the polymer.

A similar experiment carried out on 2 g of costus essential oil with 1 g of **11** in 2.5 mL ethanol resulted in the retention of 0.270 g (13.5%) of material by the polymer. The bound products were cleaved from their support as described above.

Acknowledgements

The authors thank N.A.T.O. for grant no. 1678. Additional support of this work through a Natural Sciences and Engineering Research Council of Canada operating grant (to J.M.J.F.) and a postdoctoral fellowship (to M.J.F.) is also acknowledged. Finally, thanks are due to I.N.S.E.R.M. for financial support (contrat libre 77-1-097-3) and to Dr. P. Teisseire from Roure and Bertrand for the generous gift of costus oil and costus essential oil.

1. P. Hodge and D. C. Sherrington (*Editors*). Polymer-supported reactions in organic synthesis. J. Wiley and Sons Limited, London. 1980; N. K. Mathur, C. K. Narang, and R. E. Williams. Polymers as aids in organic chemistry. Academic Press, New York. 1980.
2. J. M. J. Fréchet, G. Darling, and M. J. Farrall. Polym. Prepr. **21**, 270 (1980); **21**, 272 (1980).
3. J. M. J. Fréchet. Synthesis and applications of organic polymers as supports and protecting groups. Tetrahedron Rep. No. 103. **37**, 663 (1981).
4. R. Audebert. J. Liq. Chromatogr. **2**, 1063 (1979); G. Wulff, W. Vesper, R. Grobe Einsler, and A. Sahan. Makromol. Chem. **178**, 2799 (1977).
5. I. T. Harrison and S. Harrison. J. Am. Chem. Soc. **89**, 5723 (1967); E. Seymour and J. M. J. Fréchet. Tetrahedron Lett. 3669 (1976); C. C. Leznoff and P. I. Svirskaya. Angew. Chem.Int. Ed. Engl. **17**, 947 (1978).
6. A. Cheminat, C. Benezra, M. J. Farrall, and J. M. J. Fréchet. Tetrahedron Lett. 617 (1980).
7. J. C. Mitchell, G. Dupuis, and T. A. Geisman. Br. J. Dermatol. **87**, 235 (1972); J. C. Mitchell and G. Dupuis. Br. J. Dermatol. **84**, 139 (1971).
8. E. Fujita and Y. Nagao. Bioorg. Chem. **6**, 287, (1977); S. M. Kupchan, D. C. Fessler, M. A. Eakin, and T. J. Giacobbe. Science, **168**, 376 (1970); S. M. Kupchan, M. A. Eakin, and A. M. Thomas. J. Med. Chem. **14**, 1147 (1971); J. C. Mitchell and W. L. Epstein. Arch. Dermatol. **110**, 871 (1974); G. Schlewer, J. L. Stampf, and C. Benezra. J. Med. Chem. **23**, 1031 (1980); G. Dupuis, C. Benezra, G. Schlewer and J. L. Stampf. Mol. Immunol. 1980. In press; J. P. Corbet and C. Benezra. Can. J. Chem. **57**, 213 (1979).
9. J. M. J. Fréchet, M. de Smet, and M. J. Farrall. Polymer, **20**, 675 (1979).
10. J. M. J. Fréchet, M. de Smet, and M. J. Farrall. Tetrahedron Lett. 137 (1979).
11. O. Nuyken, M. Hofinger, and R. Kerber. Polymer Bull. **2**, 21 (1980).
12. M. Kato. J. Polymer Sci. Part A-1, **7**, 2405 (1969).
13. J. T. Sparrow. J. Org. Chem. **41**, 1350 (1976).
14. J. M. J. Fréchet, M. de Smet, and M. J. Farrall. J. Org. Chem. **44**, 1774 (1979).
15. C. C. Leznoff and J. Y. Wong. Can. J. Chem. **51**, 3756 (1973).
16. J. C. Mitchell and W. L. Epstein. Arch. Dermatol. **110**, 871, (1974); W. L. Epstein, G. W. Reynolds, and E. Rodriguez. Arch. Dermatol. **116**, 59 (1980).
17. T. C. Jain and J. E. McCloskey. Tetrahedron, **31**, 2211 (1975).
18. B. Maurer and A. Grieder. Helv. Chim. Acta, **60**, 2177 (1977).
19. K. W. Pepper, H. M. Paisley, and M. A. Young. J. Chem. Soc. 4097 (1953).
20. M. J. Farrall and J. M. J. Fréchet. J. Org. Chem. **41**, 3877 (1976).

Can. J. Chem. Downloaded from www.nrcresearchpress.com by 210.87.254.5 on 09/06/12
For personal use only.

γ- and δ-epoxy sulfones. Formation of different ring-sized products upon reaction with CH_3MgI or $LiN[CH(CH_3)_2]_2$

JOHN M. DECESARE, BERNARD CORBEL,[1] AND TONY DURST
Department of Chemistry, University of Ottawa, Ottawa, Ont., Canada K1N 9B4

AND

JOHN F. BLOUNT
Chemical Research Department, Hoffmann-LaRoche Inc., Nutley, NJ 07110, U.S.A.

Received July 30, 1980

JOHN M. DECESARE, BERNARD CORBEL, TONY DURST, and JOHN F. BLOUNT. Can. J. Chem. **59**, 1415 (1981).

γ-Epoxy sulfones in which the epoxide function is terminal yield cyclopropylmethanol derivatives on reaction with methyllithium or lithium diisopropylamide. In contrast, treatment of these epoxides with two equivalents of CH_3MgI gives only *cis*-3-phenylsulfonylcyclobutanols. The *cis*-relationship between the OH and sulfonyl groups was proven in one instance by an X-ray structure determination. Internal γ-epoxy sulfones yield cyclopropylmethanols with all bases studied. All δ-epoxy sulfones studied furnished *cis*-3-phenylsulfonylcyclopentanols upon reaction with the Grignard reagent. These same epoxides gave either cyclopentanols or noncyclic products upon reaction with LDA; no cyclobutane ring containing products were obtained contrary to the expectations based on Stork's results with the corresponding epoxy nitriles (ref. 2). The mechanism of the Grignard-mediated reaction involves epoxide opening by iodide ion, α-sulfonyl Grignard formation, and, finally, cyclization. When LDA or CH_3Li is used the products are formed by an intramolecular S_N2 opening of the epoxide by an α-lithio sulfone.

JOHN M. DECESARE, BERNARD CORBEL, TONY DURST et JOHN F. BLOUNT. Can. J. Chem. **59**, 1415 (1981).

Les γ-époxysulfones ayant la fonction époxyde en position terminale réagissent avec le méthyllithium ou le diisopropylamidure de lithium en donnant des dérivés du cyclopropylméthanol. Par contre, ces mêmes époxydes réagissent avec deux équivalents de CH_3MgI en donnant uniquement des phénylsulfonyl-3 cyclobutanols *cis*. Dans un cas, on a établi la relation *cis* entre les groupes OH et sulfonyle par une détermination de structure par diffraction de rayons-X. Sous l'influence de toutes les bases utilisés les γ-époxy sulfones internes conduisent aux cyclopropylméthanols. Toutes les δ-époxy sulfones étudiées fournissent les phénylsulfonyl-3 cyclopentanols *cis* après réaction avec le réactif de Grignard. Ces mêmes époxydes réagissent avec le DAL en donnant des cyclopentanols ou des produits non cycliques; on n'a pas obtenu de produit contenant un cycle cyclobutane, contrairement à ce qui etait attendu selon les résultats de Stork relatifs aux époxy nitriles correspondants (ref. 2). Le mécanisme de la réaction induite par le réactif de Grignard fait intervenir une ouverture de l'époxyde par l'ion iodure, la formation d'un réactif de Grignard avec le groupement α-sulfonyle et finalement une cyclisation. Avec le DAL ou le CH_3Li, la formation des produits implique une ouverture intramoléculaire du type S_N2 de l'époxyde par une α-lithio-sulfone.

[Traduit par le journal]

Introduction

Examples of intramolecular attack by a carbanion on an epoxide as a method of ring formation have been known for some time (1). However, the general synthetic potential of this type of reaction was not appreciated or systematically investigated until 1974 when Stork and co-workers (2) studied the base-induced cyclization of a series of epoxy nitriles. These workers generalized that the epoxy nitriles **1** always cyclized to yield preferentially the smaller ring when both ends of the epoxide were equally substituted (path **a** rather than **b** in structure **1**). The regioselectivity was due to a more ready attainment of the necessary co-planar arrangement of the attacking group, epoxide carbon, and oxide leaving group, thus resulting in the smaller of the two ring sizes. (See structures **2** and **3** for 4- vs. 5-membered ring formation.)

The preference for cyclobutyl vs. cyclopentyl ring formation was later reinvestigated by Lallemand and Onanga (3) who noted that the epoxide stereochemistry also played a role in the regioselectivity of the epoxide opening. *cis*-δ-Epoxy nitriles bearing equal degrees of substitution on the epoxide ring continued to give cyclobutanes, selectively, whereas similarly substituted *trans*

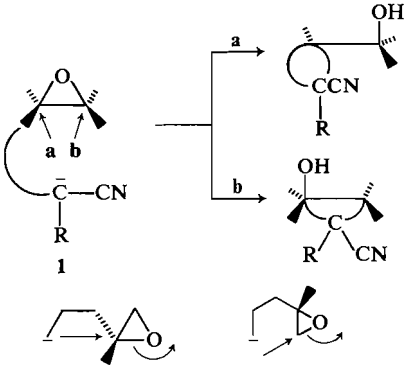

[1]Scientific exchange visitor, N.R.C.C.–France, 1975–1976.

0008-4042/81/101415-10$01.00/0

©1981 National Research Council of Canada/Conseil national de recherches du Canada

Can. J. Chem. Downloaded from www.nrcresearchpress.com by 210.87.254.5 on 09/06/12
For personal use only.

Can. J. Chem. Downloaded from www.nrcresearchpress.com by 210.87.254.5 on 09/06/12
For personal use only.

TABLE 1. Reactions of epoxy sulfones with bases

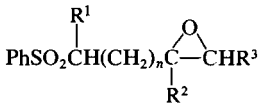

Entry	n	R^1	R^2	R^3	Base	Product: Ring size	Product: Yield, %
1	1	H	H	H	LDA	3	85
2	1	H	H	H	CH_3Li	3	81
3	1	H	H	H	CH_3MgI	4	96, 46[a]
4	1	Ph	H	H	LDA	3	95
5	1	Ph	H	H	CH_3MgI	4	98, 60[a]
6	1	C_4H_9	H	H	CH_3MgI	4	92
7	1	C_7H_{15}	H	H	CH_3MgI	4	95
8	1	CH_2Ph	H	H	CH_3MgI	4	89
9	1	H	CH_3	H	LDA	3	36
10	1	H	CH_3	H	CH_3MgI	4	51
11	1	H	H	CH_3	LDA	3	71
12	1	H	H	CH_3	CH_3MgI	3	30
13	1	H	H	Ph	LDA	3	98
14	1	H	H	Ph	CH_3Li	3	90
15	1	H	H	Ph	CH_3MgI	3	70
16	2	H	H	H	LDA	—	—
17	2	H	H	H	CH_3MgI	5	75, 35[a]
18	2	Ph	H	H	CH_3MgI	5	75[a]
19	2	H	H	CH_3	LDA	—	—
20	2	H	H	CH_3	CH_3MgI	5	50
21	2	H	H	Ph	LDA	5	75
22	2	H	H	Ph	CH_3MgI	5	67

[a]Yield obtained via a "one-pot" reaction

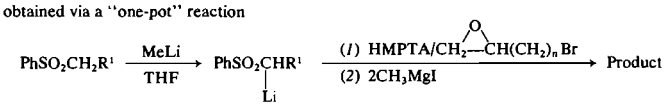

epoxides yielded mixtures of 4- and 5-membered ring products. Cyclopropanes were formed from γ-epoxy nitriles irrespective of the epoxide substitution pattern (2).

We have recently reported in preliminary form that a variety of γ-epoxy sulfones **4***a* and γ-epoxy nitriles **4***b* can be converted into either cyclopropyl methanols **5** or cyclobutanols **6** upon treatment with lithium diisopropylamide (LDA) and CH_3MgI respectively (4). The ability to generate at will two different ring sizes from the same starting material greatly increases the value of these epoxy sulfones and nitriles as synthetic intermediates.

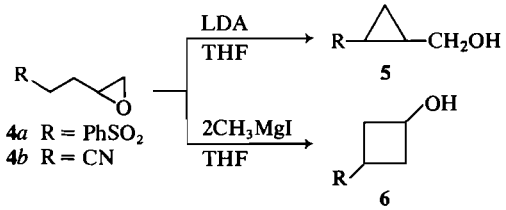

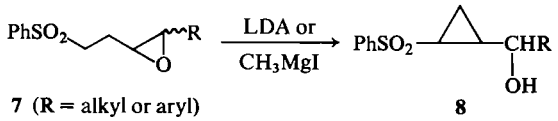

7 (R = alkyl or aryl) 8

Discussion and Results

In our previous publications (4, 5) we reported the reactions of a number of γ- and δ-epoxy sulfones with both LDA (or CH_3Li) and CH_3MgI (Table 1). Also included in Table 1 are the cyclization results of several new nonterminal epoxides. In general, the terminal epoxides in the γ-epoxy sulfone and γ-epoxy nitrile series yield cyclopropyl derivatives when treated with LDA and cyclobutanols upon reaction with CH_3MgI. Gaoni (6) had earlier reported several examples of the reaction of γ-epoxy sulfones with *n*-butyllithium, each yielding cyclopropane derivatives. In contrast to these results, internal γ-epoxy sulfones such as **7** gave only cyclopropyl derivatives with either LDA or CH_3MgI as the cyclizing reagents.

In the δ-epoxy sulfone series, the three examples investigated, **9***a–c*, gave only 3-phenylsulfonyl cyclopentanols **10***a–c* when reacted with CH_3MgI. Unfortunately, the reaction of these epoxy sulfones with LDA failed to give the expected cyclobutylmethanols (2). The parent γ-epoxy sulfone **9***a* and the methyl derivative **9***b* gave few or no monomeric products while the styrene oxide **9***c* afforded, upon reaction with LDA, the same cyclopentanol as was

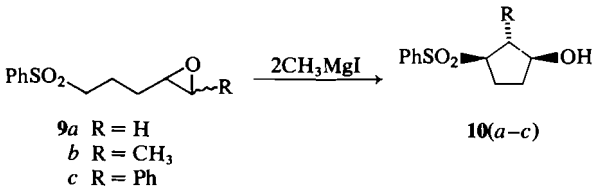

9*a* R = H
b R = CH_3
c R = Ph

10(*a–c*)

obtained with CH_3MgI. The response of the various epoxides to CH_3MgI can be explained in terms of the mechanism shown in Scheme 1.

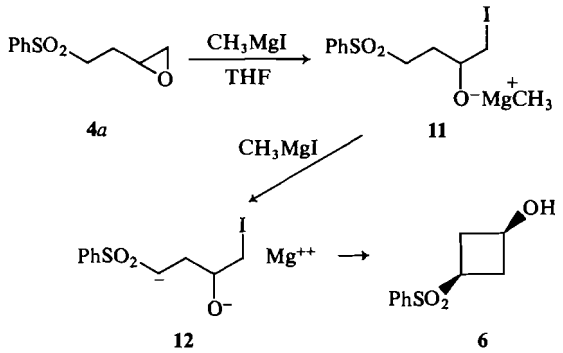

4*a* **11** **12** **6**

SCHEME 1. Mechanism of conversion of γ-epoxy sulfones to cyclobutanols.

Some evidence for this mechanism has been described in our initial publication (4). This involved isolation of the iodohydrin **13** derived from **11** when the reaction mixture was hydrolyzed before warming to above −20°C. The epoxide **4** was also opened to a bromohydrin corresponding to **13** upon reaction with $MgBr_2$. Both these bromo- and iodohydrins were converted to **6** upon exposure to two or more equivalents of CH_3MgI or CH_3MgBr (4).

The opening of the epoxide ring in **4***a* was shown to be faster than abstraction of a hydrogen α to the sulfonyl group. Hydrolysis of the reaction mixture at low temperature with D_2O (see above) furnished **13** bearing 30% D α to the sulfonyl group (nmr). If α-sulfonyl Grignard formation had been complete prior to the epoxide opening monodeuterated **13** should have resulted. The isolation of **13** containing some deuterium suggests that the cyclization of the dimagnesium derivative **12** is not instantaneous, thus allowing some buildup of **12**, hydrolysis of which with D_2O would give mono-deuterated iodohydrin.

We have now shown that the cyclization **4***a* to **6***a* requires two equivalents of Grignard reagent. Thus reaction of **4***a* with 1 equivalent of CH_3MgI at −70°C followed by warming to room temperature for as long as 52 h gave only the iodohydrin derived from **13**, no cyclobutanol **6***a* could be detected by ^1H nmr. In contrast, when two equivalents of CH_3MgI were utilized, **6***a* was formed in approximately 95% yield after 26 h. It appears that the methylmagnesium alkoxide **11** is not sufficiently basic to cause abstraction of a hydrogen α to the sulfone group; thus a second equivalent of CH_3MgI is required.

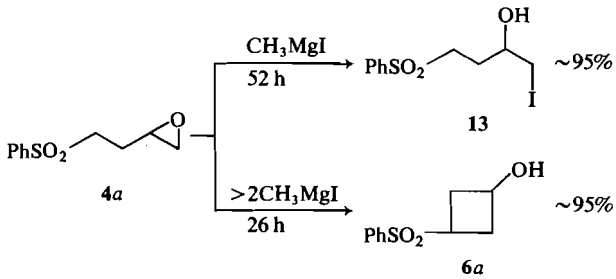

4*a* **13** **6***a*

In contrast to the conversion of **4** to **6**, compounds such as **14**, in which the epoxide function is internal, furnished only cyclopropylmethanols, **15**, irrespective of the base employed. The formation of only cyclopropane derivatives from all γ-epoxy sulfones and CH_3Li or LDA has been explained in terms of stereoelectronic requirements (see above); the CH_3MgI mediated reaction may best be rationalized as follows. In contrast to **4**, the opening of the epoxides in **14** by iodide is not expected to be regioselective and both the iodoalkoxides **16** and **17** should be formed, deprotonation of which would yield **18** and **19**, respectively. Cyclization of **18** to **15** should be rapid relative to the conversion of **19** to **20** since cyclopropanes are formed up to 10^6 times more rapidly than cyclobutanes in this type of cyclization (*exo*-tetrahedral) (7). If the conversion of **19** to **20** is indeed slow, reepoxidation to **21** and subsequent rapid intramolecular epoxide opening, thereby again yielding the cyclopropane **15**, may become the dominant route.

As mentioned above, the δ-epoxy sulfones afforded 3-phenylsulfonylcyclopentanols upon treatment with excess CH_3MgI. This was expected since the relative rates of cyclization of the α-sulfonyl derivatives of the two possible iodoalkoxides **22** and **22***a* should greatly favour **22** and hence the cyclopentanol product **10**. A pathway similar to the type discussed above for the reactions of **14** could also come into play and thus help form **10** rather than **23** from **22***a*.

Reaction of **9***c* (R = Ph, 85% *trans*-epoxide) with LDA afforded in 75% yield the cyclopentanol **10***c* (R = Ph), identical in all respects with that obtained using CH_3MgI as base. This result is reminiscent of those of Lallemand and Onanga (3) who showed that *trans*-δ-epoxy nitriles gave mainly cyclopentanol rather than cyclobutylmethanol derivatives.

Based on the stereochemistry of the in-

Can. J. Chem. Downloaded from www.nrcresearchpress.com by 210.87.254.5 on 09/06/12
For personal use only.

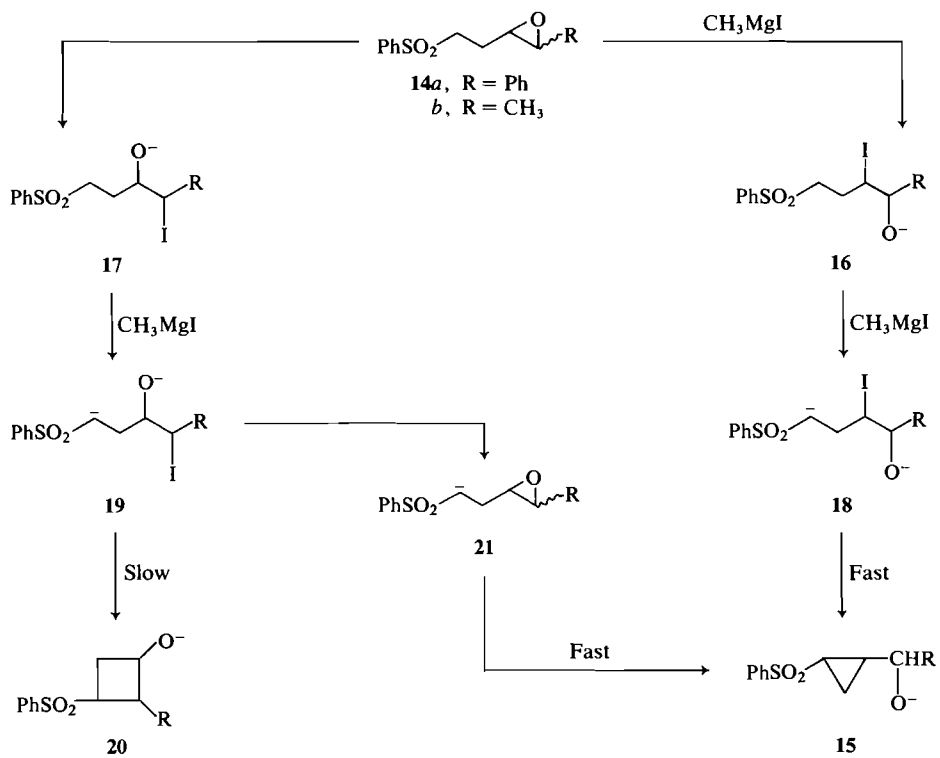

SCHEME 2. Possible mechanism of the reaction of 1,2 disubstituted γ-epoxy sulfones with CH_3MgI.

tramolecular epoxide opening by the α-lithiosulfone, the epoxide stereochemistry in the starting material, and the 75% yield of a single isomeric product, we have assigned the stereochemistry of **10***c* as shown below. The relative configuration of the $PhSO_2$ and OH as *cis* is based on an X-ray structure determination in the 3-phenylsulfonylcyclobutanol series (see below). The product **10***c*, mp 105–106°C, was oxidized with CrO_3 to 3-phenylsulfonylcyclopentanone (ir 1750 cm^{-1}), which on further treatment with triethylamine afforded a 2-phenylcyclopent-2-enone (8).

The formation of **10***c* in 67% yield from **9***c* with CH_3MgI probably results from an iodide-catalyzed epimerization at the benzylic carbon of the intermediate iodoalkoxide **24**, since a simple S_N2 opening of the epoxide by iodide (formation of **24***a*) followed by intramolecular cyclization would give **10***c* having the OH and phenyl groups *cis* to each other. Cyclization of the intermediate **24***b* leading to **10***c* should be much faster than that of **24***a* lead-

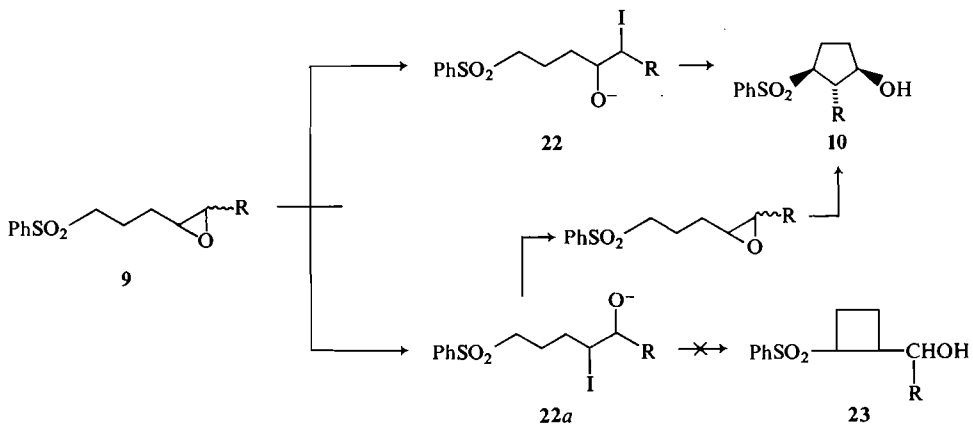

Can. J. Chem. Downloaded from www.nrcresearchpress.com by 210.87.254.5 on 09/06/12
For personal use only.

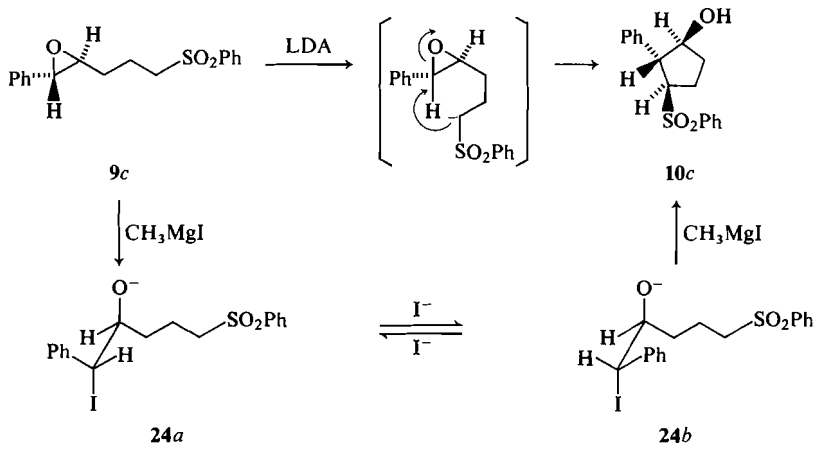

SCHEME 3

ing to the isomer of **10***c* in which all substituents are *cis* (Scheme 3).

In the cyclization of γ- and δ-epoxysulfones of the type **27** to **28** only one isomeric product was obtained. This was ascertained by comparing the nmr spectra of both the crude and purified reaction products with that of diastereomeric mixtures prepared by C-alkylation of the dianion of 3-phenylsulfonylcyclobutanol (5). The mixtures obtained showed two distinct areas of absorption for C*H*—OH at δ = 4.0–4.3 and 4.3–4.6. The cyclization products showed only the absorption at the higher field and thus it seems likely that all cyclization products belong to the same stereochemical series. The stereochemistry of one of the cyclization products was unambiguously shown to have the OH and $PhSO_2$ groups *cis* to each other by an X-ray structure determination (Fig. 1). This *cis* relationship is proposed to result from chelation of the magnesium(II) in the intermediate **29** by both the alkoxide and sulfonyl groups thus holding these two groups *cis* to each other. Admittedly, the basicity of a typical sulfone is not very high (9). It would, however, be expected to increase due to the adjacent Grignard function. Marquet[2] and coworkers have noted a decrease of approximately 60 cm^{-1} in both the symmetric and asymmetric S—O stretching frequencies in going from sulfones to α-lithio sulfones. This change indicates that the S—O bond in the α-lithio sulfones, and hence in the α-sulfonyl Grignards, is becoming somewhat like that in sulfoxides in which the oxygen acts as a strong Lewis base.

Highly stereoselective cyclizations were also observed for appropriately substituted δ-epoxy sulfones; presumably in these compounds the OH and the phenylsulfonyl group are also *cis* to each other.

If the formation of the parent compound **6***a* from **4***a* was carried out for a minimum amount of time, the isomer having its C*H*—OH absorption at higher field was obtained. Prolonged reaction times caused isomerization, presumably via an O,C dianion.

We attempted to investigate the importance of

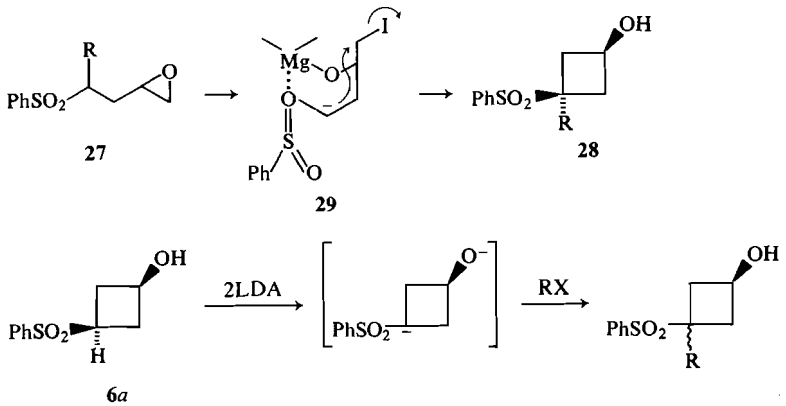

[2]A. Marquet, private communication.

Can. J. Chem. Downloaded from www.nrcresearchpress.com by 210.87.254.5 on 09/06/12
For personal use only.

Can. J. Chem. Downloaded from www.nrcresearchpress.com by 210.87.254.5 on 09/06/12
For personal use only.

the proposed chelation in controlling the stereochemistry of the cyclization. To this end the tetrahydropyranyl ethers **30** were prepared. Reaction of these with up to 3 equivalents of CH_3MgI under the usual conditions for up to 7 days failed to give any reaction other than halogen exchange. Inadvertent quenching of the CH_3MgI was ruled out as a possible cause for the lack of reactivity since quenching of one reaction trial with benzophenone resulted in an 85% yield of 1,1-diphenylethanol. The lack of reactivity of **30** is not obvious, especially since the iodo sulfone **31** furnished cyclobutyl phenyl sulfone **32** in 90% isolated yield upon reaction with 2 equivalents of CH_3MgI for 24 h. One is left with the suggestion that failure to observe cyclization in **30** is due to adverse steric effects.

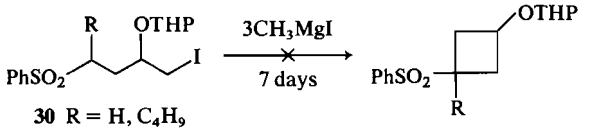

30 R = H, C_4H_9

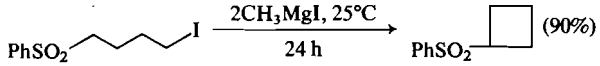

31 **32**

(Reaction of one equiv. of CH_3MgI with **31** produced **32** in 60% yield after 24 h; 20% of **31** was also recovered).

X-ray Structure Determination of 3-Phenyl-3-phenylsulfonylcyclobutanol (33) (Fig. 1)

The cyclobutanol **33** was prepared in 60% yield via a one-pot reaction according to

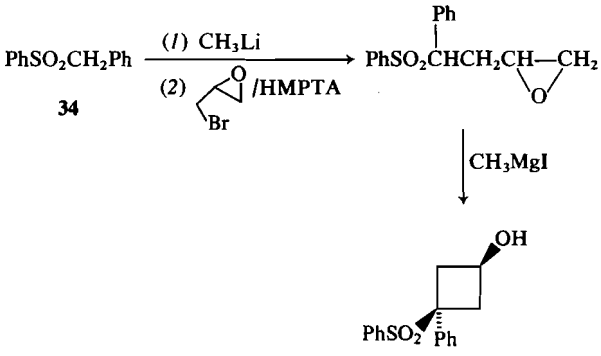

34 **33**

Replacement of epibromohydrin by 4-bromo-1,2-epoxybutane in the above reaction furnished the 5-membered ring homologue, 3-phenyl-3-phenylsulfonylcyclopentanol (75%). The parent 3-phenylsulfonylcyclobutanol and -cyclopentanol were similarly obtained in 46 and 35% yield respectively by alkylation of the lithio salt of methyl phenyl sulfone with the appropriate bromo epoxide followed by CH_3MgI treatment.

Suitable crystals of **33**, mp 132°C, were grown from methanol. The crystal data are:

$C_{16}H_{16}O_3S$ fw 288.36

Monoclinic, space group $P2_1/n$, a = 18.399(2), b = 10.607(2), c = 15.384(3) Å, β = 107.24(1)° and d_{calcd} = 1.335 g cm^{-3} for Z = 8. The intensity data were measured on a Hilger-Watts diffractometer (Ni filtered CuKα radiation, θ–2θ scans, pulse height discrimination). A crystal fragment measuring approximately 0.15 × 0.5 × 0.6 mm was used for data collection; the data were corrected for absorption (μ = 19.9 cm^{-1}). A total of 3727 reflections were measured for $\theta < 57°$, of which 3322 were considered to be observed ($I > 2.5\sigma(I)$). The structure was solved by a multiple solution procedure (10). The final refinement was carried out by block-diagonal least squares in which the matrix was partitioned into two blocks. In the final refinement anisotropic thermal parameters were used for the heavier atoms and isotropic temperature factors were used for the hydrogen atoms. The hydrogen atoms were included in the structure factor calculations but their parameters were not refined. The final discrepancy indices are R = 0.057 and wR = 0.075 for the 3322 observed reflections. The final difference map has no peaks greater than ±0.3 Å^{-3}.

The conformations of the two independent molecules of **33** into the unit cell are essentially the same except for a rotation of about 15° around the S—C(3) bond. The dihedral angles between the plane C(1)–C(2)–C(3) and the plane C(1)–C(4)–C(3) are 32.8 and 32.2° in the unprimed and primed molecules, and the dihedral angles between the planes C(2)–C(3)–C(4) and C(2)–C(1)–C(4) are 33.2 and 32.8° (Fig. 1).

Conclusions

Treatment of a variety of γ- and δ-epoxy sulfones with different bases (CH_3Li, LDA, or CH_3MgI) results in products whose ring size depends on both the structure of the epoxide and the base used. The results are summarized in Table 2.

Experimental

General Comments (See also ref. 5)

The synthesis of the epoxy sulfones involved in entries 1–18 (Table 1) and the preparation of 3-phenylsulfonylcyclobutanols (entries 3, 5–8, 10) and 3-phenylsulfonylcyclopentanol (entry 17) have been described. The reactions of the various epoxy sulfones with different bases are described below and are referenced with respect to their entry number in Table 1.

Reaction of Epoxy Sulfones with LDA or CH_3Li. General Procedure

To a solution of LDA in THF at −78°C was added via syringe the epoxy sulfone as a concentrated THF solution. The reaction mixture was then allowed to warm to room temperature and

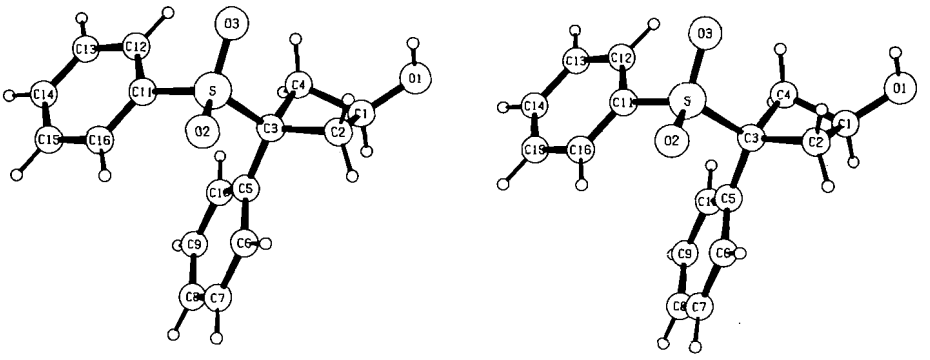

FIG. 1. X-ray structure of 3-phenyl-3-phenylsulfonylcyclobutanol.

TABLE 2. Products obtained in γ- and δ-epoxy sulfone "cyclizations"

Epoxy sulfone structure	Base	Product
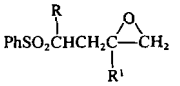	CH_3Li or LDA	Cyclopropylmethanols
	$2CH_3MgI$	Cyclobutanols
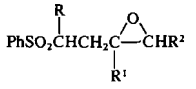	LDA or CH_3Li or $2CH_3MgI$	Cyclopropylmethanols
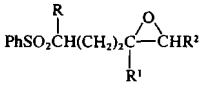	LDA	Cyclopentanols or noncyclic products
	$2CH_3MgI$	Cyclopentanols

[a] R, R^1, R^2 = alkyl or aryl.

stored for the indicated times. Work-up was accomplished by quenching with a saturated ammonium chloride solution, extracting with CH_2Cl_2, drying the organic extracts with anhydrous $MgSO_4$, and evaporating the solvent. The products were purified by silica gel chromatography. The yields in Table 1 refer to purified materials. When CH_3Li was used as base, it was added to the epoxy sulfone dissolved in THF at −78°C and the reaction was allowed to proceed as above.

Reactions of 4-Phenylsulfonyl-1,2-epoxybutane

(a) With LDA (Entry 1)

Epoxide (2.12 g, 10 mmol) was added to 30 mL of dry THF containing 10 mmol of LDA at −78°C. The reaction mixture was allowed to warm to room temperature over a 15 min period. Work-up followed by chromatography (ethyl acetate – hexane) yielded 1.8 g, 85%, of 2-hydroxymethyl-1-phenylsulfonylcyclopropane as a clear oil; nmr (after D_2O):1.1–1.5 (m, 1H), 1.5–2.2 (m, 2H), 3.0–3.5 (m, 2H), 3.6–4.1 (m, 1H), 7.5–8.2 (m, 5H).

(b) With CH_3Li (Entry 2)

Epoxy sulfone (0.244 g, 1.15 mmol), dissolved in 30 mL of THF at −78°C was reacted with 0.9 mL of 1.3 *M* CH_3Li in ether. The reaction mixture was stirred for 15 min at −78°C, warmed to 25°C, and quenched with saturated NH_4Cl solution. Work-up and chromatography gave 198 mg (81%) of 2-hydroxymethyl-1-phenylsulfonylcyclopropane as a mixture of *cis–trans* isomers; nmr (after D_2O): 0.7–1.5 (m, 2H), 1.6–2.6 (m, 2H), 3.0–4.0 (m, 2H), 7.4–8.1 (m, 5H). *Anal.* calcd. for $C_{10}H_{12}O_3S$: C 56.60, H 5.66; found: C 56.92, H 5.63.

Reactions of 4-Phenyl-4-phenylsulfonyl-1,2-epoxybutane

(a) With LDA (Entry 4)

Epoxy sulfone (0.23 g, 0.8 mmol), dissolved in 2 mL of THF, was added to 20 mL of THF containing 0.9 mmol of LDA. The reaction mixture was kept at low temperature for 15 min, warmed to 25°C, and then worked up. Chromatography on silica gel with 1:2 ethyl acetate – hexane gave 104 mg (48%) and 91 mg (43%) respectively of the less and more polar isomers of 2-hydroxymethyl-1-phenyl-1-phenylsulfonylcyclopropane. More polar isomer (mp 92–93°C), nmr: 1.1–1.3 (m, 1H), 1.7–2.1 (m, 2H including O*H*), 2.3–2.8 (m, 1H), 3.43 (d, J = 6 Hz, 2H), 7.1–7.7 (m, 10H). *Anal.* calcd. for $C_{16}H_{16}O_3S$: C 66.64, H 5.60; found: C 66.51, H 5.70. Less polar isomer (mp 84–86°C), nmr: 1–2.1 (m, 3H), 3.0 (O*H*), 4.33 (d, J = 6 Hz, 2H), 7.1–7.7 (m, 10H). *Anal.* found: C 66.62, H 5.65.

The more polar isomer is tentatively assigned the structure in which the phenyl and CH_2OH groups are *trans*, since the chemical shift of the CH_2OH group is considerably shielded, 3.43 vs 4.33, when CH_2OH and $PhSO_2$ are *cis* (less polar isomer).

5-Phenylsulfonyl-2,3-epoxypentane

(a) Reaction with LDA (Entry 11)

Epoxy sulfone (39.5 mg, 1.76 mmol) was added to 25 mL of THF containing 1.9 mequiv. of LDA at −78°C. The reaction mixture was stirred at low temperature for 1 h, then warmed to room temperature and quenched with saturated NH_4Cl. The organic product was purified on chromatography to yield 223 mg of isomeric product as a clear oil; nmr (after D_2O exchange): CH_3 (2 doublets at 1.05 and 1.03, J = 6 Hz), 1.0–2.0 (m, 3H), 2.2–2.6 (m, 1H), 3.3–3.7 (m, 1H), 7.5–8.1 (m, 5H). *Anal.* calcd. for $C_{11}H_{14}O_3S$: C 58.38, H 6.23; found: C 58.12, H 6.14.

(b) Reaction with CH_3MgI (Entry 12)

Epoxy sulfone (353 mg, 1.56 mmol) was reacted in the usual manner with 1.72 mmol of CH_3MgI. Work-up gave several products including 30% of 1-hydroxyethyl-2-phenylsulfonylcyclopropane, having a different isomer mixture than in (*a*) above. The other products were not identified.

Reactions of 1-Phenyl-4-phenylsulfonyl-1,2-epoxybutane

(a) With LDA (Entry 13)

Epoxy sulfone (284 mg, 0.99 mmol) was added to 20 mL of THF at −78°C containing 1.05 mmol of LDA. The reaction mixture was kept at −78°C for 20 min, then warmed to room temperature. Work-up gave 280 mg (98%) of a single alcohol, 1-hydroxyphenyl-2-phenylsulfonylcyclopropane, as a white solid, mp 126°C (ether–hexane); nmr: 1.1–1.7 (m, 2H), 1.8–2.2 (m, 1H), 2.3–2.9 (m, 2H, including O*H*), 4.43 (d, J = 5 Hz, 1H),

Can. J. Chem. Downloaded from www.nrcresearchpress.com by 210.87.254.5 on 09/06/12
For personal use only.

Can. J. Chem. Downloaded from www.nrcresearchpress.com by 210.87.254.5 on 09/06/12
For personal use only.

7.1–7.9 (m, 10H). *Anal.* calcd. for $C_{16}H_{16}O_3S$: C 66.64, H 5.60; found: C 66.81, H 5.75.

(b) With CH_3Li (Entry 14)

Reaction of 107 mg of epoxy sulfone in 20 mL THF at −78°C with 1.1 equiv. of CH_3Li furnished, in 90% yield, the same product as described in (*a*) above.

(c) With CH_3MgI (Entry 15)

To 203 mg of epoxy sulfone in THF (20 mL) at −78°C was added 2 equiv. of CH_3MgI. The reaction mixture was allowed to warm to room temperature and stirred overnight. Work-up, followed by chromatography on silica gel, furnished 142 mg (70%) of the alcohol described in (*a*) above.

"One-pot" Reactions

(a) Preparation of 3-Phenyl-3-phenylsulfonylcyclopentanol (Entry 18)

Benzyl phenyl sulfone (786 mg, 3.3 mmol) was dissolved in 25 mL of THF containing 1 mL of HMPTA. The solution was cooled to −70°C, reacted with 3.6 mmol of CH_3Li for 5 min, followed by 543 mg (3.6 mmol) of 4-bromo-1,2-epoxybutane. The reaction mixture was warmed to room temperature and kept until the starting sulfone had disappeared as evidenced by tlc. The reaction mixture was then cooled again to −70°C, reacted with 6.9 mmol of CH_3MgI, warmed to room temperature, and kept for 48 h. Work-up followed by chromatography (1:2 ethyl acetate – hexane) gave 750 mg of viscous oil identified as the title compound; ir: 3500 (broad), 1300(s) and 1130(s) cm^{-1}; nmr: 2.0–3.4 (m, 6H), 3.4–3.8 (O*H*), 4.2–4.6 (m, 1H), 7.0–7.6 (m, 10H). *Anal.* calcd. for $C_{17}H_{18}O_3S$: C 67.55, H 5.96; found: C 67.33, H 6.10.

(b) 3-Phenylsulfonylcyclopentanol (Entry 17)

Using the above procedure, methyl phenyl sulfone (4.9 g, 31.5 mmol) was converted to its carbanion with 35 mmol of CH_3Li, treated with 4.72 g (32 mmol) of 4-bromo-1,2-epoxybutane, and then 65 mmol of CH_3MgI. The yield of 3-phenylsulfonylcyclopentanol (**5**) was 2.5 g (35%).

*(c) 3-Phenyl-3-phenylsulfonylcyclobutanol (**33**) (Entry 5)*

To the α-lithio derivative derived from 3.5 g (15 mmol) of benzyl phenyl sulfone was added 2.4 mL (excess) of epibromohydrin followed, as in (*a*) above, by 35 mmol of CH_3MgI. Work-up followed by chromatography provided 2.6 g (60%) of the title cyclobutanol as white granules, mp 132°C (CH_2Cl_2–CCl_4); ir: 3500 (broad), 1305(s), 1150(s) cm^{-1}; nmr: 2.9–3.3 (m, 5H; 4H after D_2O treatment), 4.18 (J = 6 Hz, 1H), and 6.8–7.7 (m, 10H). *Anal.* calcd. for $C_{16}H_{16}O_3S$: C 66.64, H 5.60; found: C 66.58, H 5.64.

(d) 3-Phenylsulfonylcyclobutanol (5) (Entry 3)

This compound (**5**) was obtained in 46% isolated yield from 711 mg (4.6 mmol) of methyl phenyl sulfone, 4.7 mmol of CH_3Li, 1.0 mL of epibromohydrin, and 10 mmol of CH_3MgI using the procedure outlined in (*a*) above.

Syntheses of New Epoxy Sulfones

Epoxy Sulfone 9c (R = Ph)

To a solution of 32.3 g (0.29 mol) of thiophenol dissolved in 200 mL of methanol containing 16.8 g (0.3 mol) of KOH was added dropwise 42.3 g (0.28 mol) of 1-acetoxy-4-chlorobutane. The mixture was stirred overnight and then saponified by addition of a further 26 g of KOH. After the saponification was complete the mixture was diluted with 200 mL of H_2O, extracted with 2 × 100 mL of CH_2Cl_2, and worked up further in the usual manner. The yield of 4-phenylthiobutan-1-ol was 84%.

The above alcohol (5.0 g, 27.5 mmol) dissolved in 5 mL of CH_2Cl_2 was added over 15 min to a mixture of 226 mmol pyridinium chlorochromate (12 g, 56 mmol) and sodium carbonate (24 g), suspended in 25 mL of dry CH_2Cl_2. After stirring for an additional 10 min the granular precipitate was filtered and washed with 50 mL of CH_2Cl_2. The crude organic product was purified by column chromatography on 100 g of silica gel using hexane as eluent. The yield of 4-phenylthiobutanal (clear oil) was 70%; ir: 1710 cm^{-1}; nmr: 1.3–1.9 (m, 2H), 2.1–2.6 (m, 2H), 2.83 (t, J = 7 Hz, 2H), 6.8–7.2 (m, 5H), 10.0 (s, 1H).

4-Phenylthiobutanal (7.5 g, 41.6 mmol) was dissolved in 30 mL of CH_2Cl_2 containing 8.5 g (46 mmol) of benzyldimethylsulfonium chloride and 300 mg of benzyltriethylammonium chloride. To this mixture, well stirred and cooled in an ice-bath, was added dropwise 40 mL of a 50% NaOH solution. After 1 h of reaction time the mixture was diluted with 50 mL each of H_2O and CH_2Cl_2. Further work-up afforded, after silica gel chromatography (ethyl acetate – hexane, 1:20), 8.0 g of 1-phenyl-5-phenylthio-1,2-epoxypentane as a clear oil; nmr: 1.4–2.0 (m, 4H), 2.5–3.0 (m, 3H), 3.40 (d, J = 2 Hz), and 3.83 (d, J = 4 Hz, combined 1H), 6.7–7.1 (m, 10H).

The above epoxide was refluxed overnight with 2 equiv. of MCPBA in CH_2Cl_2. Work-up followed by chromatography (1:2 ethyl acetate – hexane) afforded the epoxy sulfone **9***c* (R = Ph) in 87% yield. Infrared: 1310(s), 1150(s) cm^{-1}; nmr: 1.5–2.1 (m, 4H), 2.8–3.4 (m, 3H), 3.56 (d, J = 2 Hz), and 4.04 (d, J = 4 Hz, combined 1H), 7.1–8.0 (m, 10H); ms: M^+ = 302 (0.01%); other key fragments at m/e = 105(100), 91(74), 77(62).

Epoxy Sulfone 9b (R = CH_3)

To 75 mL of dry THF containing 33 mmol of ethylidenetriphenylphosphorane was added at room temperature 4.0 g (22 mmol) of 4-phenylthiobutanal (see above). The light orange reaction mixture was stirred for an additional 5 min and then worked up. The yield of 6-phenylthiohex-2-ene was 90% after purification on silica gel chromatography using hexane as eluent; nmr: 1.0–2.3 (m, 7H), 2.80 (t, J = 6 Hz, 2H), 4.7–5.4 (m, 2H), 6.7–7.1 (m, 5H). This olefin-sulfide was refluxed overnight in CH_2Cl_2 with 3 equiv. of MCPBA to furnish, after chromatography (1:2 ethyl acetate – hexane), 4.2 g (85%) of epoxy sulfone **9***b* (R = CH_3) as a light yellowish oil; ir: 1310(s), 1150(s) cm^{-1}; nmr: 1.18 (d, J = 5 Hz) and 1.30 (d, J = 5 Hz, total 3H), 1.0–2.1 (m, 4H), 2.3–3.4 (m, 4H), 7.4–8.0 (m, 5H).

Reaction of Epoxy Sulfone 9c with CH_3MgI (Entry 22)

Epoxy sulfone **9***c*, 2.0 g (6.6 mmol) dissolved in 50 mL of THF at −78°C was treated with 16.5 mmol of CH_3MgI. The resultant white suspension was allowed to warm to room temperature and stirred for an additional 24 h. Work-up followed by chromatography on 100 g of silica gel (2:8 ethyl acetate – hexane) furnished 1.35 g, 67%, of **10***c*, white crystals, mp 105–106°C (methylene chloride – hexane). Infrared: 3500 (broad), 1310(s), 1145(s) cm^{-1}; nmr: 1.7–2.6 (m, 5H; 4H, following D_2O treatment), 3.2–3.4 (m, 1H), 3.5–3.8 (m, 1H), 3.9–4.2 (m, 1H), and 6.8–7.8 (m, 10H). *Anal.* calcd. for $C_{17}H_{18}O_3S$: C 67.55, H 5.96, S 10.60; found: C 67.47, H 6.08, S 10.99.

Reaction of 22a with LDA (Entry 21)

Reaction of **9***c* (1.41 g, 4.7 mmol) with 5.1 mmol of LDA in 50 mL of THF at −78 to 25°C (1 day), gave 1.10 g (75%) of **10***c*.

Oxidation of 10c

Alcohol **10***c* (660 mg, 2.2 mmol) was dissolved in 10 mL of "Spectrograde" acetone and reacted with 2.5 mmol of Jones' reagent for 30 min. Excess oxidizing agent was destroyed by addition of 10% $Na_2S_2O_3$ solution. Chromatography, followed by recrystallization, yielded 260 mg (75%) of 2-phenylcyclopent-2-enone, mp 67–68°C (lit. (8) mp. 71°C).

Can. J. Chem. Downloaded from www.nrcresearchpress.com by 210.87.254.5 on 09/06/12
For personal use only.

2-Methyl-3-phenylsulfonylcyclopentanol (Entry 20)

Epoxy sulfone **9*b***, (1.0 g, 4.2 mmol) was dissolved in 50 mL of THF at −78°C and reacted with 10 mmol of CH_3MgI (in ether solution). The resultant white suspension was allowed to warm to ambient temperature and then quenched with saturated NH_4Cl solution. Further work-up and chromatography of the crude product yielded 0.5 g (50%) of the title compound; nmr: 1.02 (d, J = 6 Hz, 3H), 1.6–2.5 (m, 5H), 2.5–2.9 (O*H*), 3.0–3.3 (m, 1H), 3.6–3.9 (m, 1H), 7.4–7.9 (m, 5H). *Anal.* calcd. for $C_{12}H_{16}O_3S$: C 60.00, H 6.66; found: C 59.93, H 6.83.

2-Methyl-3-phenylsulfonylcyclopentanone

Cyclopentanol **10*b*** (110 mg, 0.45 mmol) was oxidized with 0.50 mmol of Jones' reagent in 10 mL of "Spectrograde" acetone for 5 min. The reaction mixture was treated with 5 mL of 10% $Na_2S_2O_3$ solution and then worked up to yield 88 mg of the title compound, mp 82–83°C. Infrared: 1750, 1310, 1150 cm^{-1}; nmr: 1.13 (d, J = 6 Hz, 3H), 2.0–2.8 (m, 5H), 3.3–3.5 (m, 1H), 7.5–8.0 (m, 5H). *Anal.* calcd. for $C_{12}H_{14}O_3S$: C 60.50, H 5.88, S 13.44; found: C 60.50, H 6.01, S 13.22.

Reaction of Epoxy Sulfone 9b *with LDA (Entry 19)*

Epoxy sulfone **9*b*** (600 mg, 2.5 mmol) was added to 75 mL of THF at −78°C containing 3.0 mmol of LDA. The solution was allowed to warm to room temperature and stirred for 24 h. Work-up followed by chromatography gave 450 mg of a slightly yellow oil whose nmr showed peaks at 1.0–1.2 (m, 6H), 1.5–2.5 (m, 11H), 2.7–3.2 (m, 3H; 2H after D_2O treatment), 3.6–3.9 (m, 2H), 7.5–8.1 (m, 10H); the infrared showed bands at 3400 (OH), 1155, and 1320 (SO_2) cm^{-1}. The material was not further characterized.

Mechanistic Studies

Iodohydrin 13

Epoxy sulfone **4*a*** (4.0 g, 18.8 mmol) was added to 20 mmol of CH_3MgI dissolved in 100 mL of dry THF at −78°C. The reaction mixture was allowed to warm to room temperature and then quenched with 20 mL of saturated ammonium chloride solution. Usual work-up provided, after recrystallization from CH_2Cl_2–hexanes, 5.4 g (85%) of iodohydrin **13**, mp 88–89°C. Infrared: 3480 (broad), 1310(s), 1150(s) cm^{-1}; nmr: 1.6–2.3 (m, 2H), 2.6 (O*H*), 3.2–3.4 (m, 2H), 3.5–3.9 (m, 1H), 7.4–8.0 (m, 5H). *Anal.* calcd. for $C_{10}H_{13}IO_2S$: C 37.09, H 4.04, S 9.89; found: C 36.51, H 4.03, S 9.58.

Reaction of Epoxy Sulfone 4a *With One or Two Equivalents of CH_3MgI*

To two flasks, each containing 500 mg (2.4 mmol) of epoxy sulfone **4*a*** dissolved in 25 mL of THF at −78°C, were added 2.4 and 6.0 mmol, respectively, of CH_3MgI solution which had been standardized just prior to use. The reaction mixtures were warmed to room temperature and stirred for up to 52 h and the progress of the reactions was monitored by tlc. In the case where a 1:1 epoxide to CH_3MgI ratio was employed, work-up gave a 95% yield of the iodohydrin **13**, whereas formation of **6*a*** (~95%) was observed in the second reaction. Gas evolution, presumed to be methane, was observed from each mixture on addition of saturated NH_4Cl solution.

Tetrahydropyranyl Derivative 30

To a solution of 5.11 g of iodohydrin **13** in 50 mL of CH_2Cl_2 was added 2.52 g of dihydropyran and 200 mg of TsOH. The reaction mixture was stirred for 30 h, diluted with 50 mL of H_2O, worked up, and chromatographed on silica gel. Elution furnished 5.0 g (78%) of THP derivative as a yellowish oil. Infrared: no OH; nmr: 0.8–2.7 (m, 8H), 2.9–4.2 (m, 7H), 4.3–4.9 (m, 1H), 7.0–7.9 (m, 5H).

To 50 mL of freshly distilled THF was added 1.33 g (3.13 mmol) of the above THP. The solution was cooled to −78°C and reacted with 6.3 mmol of CH_3MgI. A white precipitate formed immediately. The reaction mixture was stirred for 24 h and then worked up. Nuclear magnetic resonance and tlc analysis of the reaction mixture indicated the presence of only **30**. When the crude product was exposed to 5% methanolic HCl for several hours the iodohydrin **13** was obtained in 80% yield.

The above reaction was repeated with 3 and 4 equivalents of Grignard reagent per equivalent of **30** and for reaction times varying from 1–4 days. No **6*a*** was ever detected by nmr or tlc. Finally, at the end of one of the above runs, an equivalent of benzophenone was introduced prior to work-up. The product, besides recovered **30** (90%), was 1,1-diphenyl ethanol (85%).

Cyclobutyl Phenyl Sulfone 32

An ethanol solution (100 mL) containing 20 g of 1,4-dibromobutane and 16 g of $PhSO_2Na$ was refluxed for 24 h, diluted with 200 mL of H_2O, and extracted twice with 100 mL of CH_2Cl_2. The crude organic-soluble product was chromatographed on silica gel (1:3 ethyl acetate – hexane) to furnish 4.6 g (18%) of 1-bromo-4-phenylsulfonylbutane, mp 58–59°C (CH_2Cl_2–hexanes); nmr: 1.7–2.1 (m, 4H), 3.12 (t, J = 6 Hz, 2H), 3.36 (t, J = 6 Hz, 2H), 7.4–7.9 (m, 5H); M^+ calcd: 276. 278; found (ms): 276. 278.

The above bromo sulfone (3.0 g) was dissolved in 30 mL of acetone containing 1.8 g of NaI. The solution was stirred for 12 h at room temperature, diluted with 100 mL of H_2O, and further worked up. The crude product was recrystallized from CH_2Cl_2–hexanes to give 83% of **31** as colorless needles, mp 74–75°C; nmr: 1.7–2.1 (m, 4H), 3.0–3.3 (m, 4H), 7.5–8.0 (m, 5H). *Anal.* calcd. for $C_{10}H_{13}IO_2S$: C 37.04, H 4.03, I 39.17; found; C 36.78, H 4.21, I 38.81.

The above iodo sulfone (1.34 g, 4.1 mmol) dissolved in 25 mL of THF at −78°C was reacted with 10 mmol of CH_3MgI. The solution was warmed to room temperature, stirred for 24 h, and worked up. Chromatography of the crude product on 40 g of silica gel using 1:9 ethyl acetate – hexane afforded 700 mg (90%) of cyclobutyl phenyl sulfone as a viscous slightly yellowish oil; nmr: 1.8–2.6 (m, 6H), 3.56 (quintet, J = 8 Hz, 1H), 7.4–7.9 (m, 5H); ^{13}C nmr: 16.8(t), 22.8(t), 56.9(d), in addition to the aromatic carbons.

1-Iodo-4-phenylsulfonylbutane, **31**, was reacted as above with about 1.2 equiv. of CH_3MgI. Nuclear magnetic resonance inspection of the crude reaction product indicated approximately 45% of **32**, 45% of recovered **31**, and 5–10% of 1-phenyl sulfonyl pentane.

Acknowledgement

The authors would like to thank the Natural Sciences and Engineering Research Council of Canada for continued financial support.

1. (*a*) R. R. Sauers, R. A. Parent, and S. B. Bamle. J. Am. Chem. Soc. **88**, 2257 (1966); (*b*) Y. Gaoni. Isr. J. Chem. 63 (1971); Tetrahedron, **28**, 5525 (1972); **28**, 5533 (1972); (*c*) G. Hodgson, D. F. MacSweeney, and T. Money. Tetrahedron Lett. 3683 (1972); (*d*) J. Babler and A. Tortorella. J. Org. Chem. **41**, 885 (1976); (*e*) C. R. Johnson, J. E. Kaiser, and J. C. Sharp. J. Org. Chem. **38**, 3091 (1973); (*f*) R. J. Schultz, W. H. Staas, and L. A. Spurlock. J. Org. Chem. **38**, 3091 (1973); (*g*) L. A. Spurlock and R. G. Fayter, Jr. J. Am. Chem. Soc. **94**, 2707 (1972); (*h*) N. R. Williams. Adv. Carbohydr. Chem. **25**, 109 (1970), and references therein.

2. (*a*) G. STORK, L. D. CAMA, and R. D. COULSON. J. Am. Chem. Soc. **96**, 5268 (1974); (*b*) G. STORK and J. F. COHEN. J. Am. Chem. Soc. **96**, 5270 (1974).
3. J. Y. LALLEMAND and M. ONANGA. Tetrahedron Lett. 585 (1975).
4. B. CORBEL and T. DURST. J. Org. Chem. **41**, 3448 (1976).
5. J. M. DECESARE, N. CORBEL, and T. DURST. Can. J. Chem. **56**, 505 (1978).
6. Y. GAONI. Tetrahedron Lett. 503 (1976).
7. A. C. KNIPE and J. C. M. STIRLING. J. Chem. Soc. B, 67 (1968).
8. Y. AMIEL, A. LOFFLER, and D. GINSBERG. J. Am. Chem. Soc. **76**, 3625 (1973).
9. (*a*) J. N. GARDNER, S. KAISER, A. KUBINER, and H. LUCAS. Can. J. Chem. **51**, 1419 (1973); (*b*) G. A. OLAH, A. T. KU, and J. A. OLAH. J. Org. Chem. **35**, 3904 (1970); (*c*) T. DURST. *In* Comprehensive organic chemistry. Vol. III. *Edited by* D. H. R. Barton and W. D. Ollis. Pergamon Press, Oxford. 1979. p. 171.
10. G. GERMAIN, P. MAIN, and M. M. WOOLFSON. Acta Crystallogr. Sect. A, **27**, 368 (1971).

Can. J. Chem. Downloaded from www.nrcresearchpress.com by 210.87.254.5 on 09/06/12
For personal use only.

Investigation of a Ziegler–Natta catalyst system derived from a mixture of lithium tetraalkylaluminate, aluminum chloride, and titanium tetrachloride and its usefulness in polymerizations involving styrene

ANU MISHRA

Uniroyal Research Laboratories, Guelph, Ont., Canada N1E 5L7

Received September 29, 1980

This paper is dedicated to Professor W. E. Harris on the occasion of his retirement from the University of Alberta

ANU MISHRA. Can. J. Chem. **59**, 1425 (1981).

Vinyl ethers, 1-olefins, and styrene were homo- and copolymerized by the use of catalyst derived from a mixture of lithium tetraalkylaluminate ($LiAlR_4$), aluminum chloride ($AlCl_3$), and titanium tetrachloride ($TiCl_4$), in order to determine the nature of the active components present.

It is postulated that the active catalyst in the stereospecific polymerization of vinyl ethers is ether-coordinated $TiCl_3 \cdot LiCl$, while in the polymerization of 1-olefins and styrene, it is the alkylated derivatives of $TiCl_3 \cdot LiCl$.

For homo- and copolymerization of styrene, AlR_3 seems to be the preferred alkylating agent. About 3 to 4 equivalents of AlR_3 are needed for complete alkylation of $TiCl_3 \cdot LiCl$, probably due to heterogeneity of the system.

Highly isotactic polystyrene and copolymers of styrene with 1-olefins can be prepared in good yields by the use of this catalyst.

ANU MISHRA. Can. J. Chem. **59**, 1425 (1981).

Dans le but de déterminer la nature des composants actifs présents, on a utilisé un catalyseur provenant d'un mélange de tétraalkylaluminate de lithium ($LiAlR_4$), de chlorure d'aluminium ($AlCl_3$) et de tétrachlorure de titane ($TiCl_4$) pour polymériser et copolymériser des éthers vinyliques, des oléfines-1 et le styrène.

On pense que le catalyseur actif lors de la polymérisation stéréospécifique des éthers vinyliques est le $TiCl_3 \cdot LiCl$ coordonné à l'éther alors que les dérivés alkylés du $TiCl_3 \cdot LiCl$ seraient les catalyseurs actifs pour la polymérisation des oléfines-1 et du styrène.

Il semble que la AlR_3 soit l'agent alkylant privilégié lors de la polymérisation et de la copolymérisation du styrène. Il faut environ 3 à 4 équivalents de AlR_3 pour alkyler complètement le $TiCl_3 \cdot LiCl$; ce phénomène est probablement dû à l'hétérogénéité du système.

L'utilisation de ce catalyseur permet de préparer, avec d'excellents rendements, du polystyrène et des copolymères du styrène avec les oléfines-1 qui sont fortement isotactiques.

[Traduit par le journal]

Introduction

In our study of polymer electrets (1), we wanted to evaluate the copolymers of styrene and 1-olefins for their electret behaviour. Since such copolymers are not commercially available, we decided to prepare them by the use of Ziegler–Natta type catalysts (2). Ziegler–Natta catalysts are susceptible to oxygen, moisture, and other electron-rich compounds. The catalyst components, generally aluminum alkyls and halides of lower valent titanium and vanadium are pyrophoric and thus difficult to handle. However, a simple system comprised of a lithium tetraalkylaluminate and titanium tetrachloride as described by Campbell and Haven (3) seemed easier to handle.

Although Campbell and Haven discovered this catalyst system over twenty years ago, not much work has since been carried out to elucidate the nature and efficiency of this system. We believe that we have determined the nature of the active catalyst present by following its action on vinyl ethers, 1-olefins, and styrene. As a result, we have been able to modify this catalyst to prepare isotactic polystyrene and copolymers of styrene with various 1-olefins in reasonably good yields.

Experimental

All temperatures are in degrees Celsius.

Reagents

Monomers

Commercial vinyl ethers from GAF Corporation were washed several times with distilled water, dried over potassium hydroxide pellets, and finally distilled under reduced pressure over calcium hydride.

Commercial styrene from Fiberglass, Canada, was washed several times with 1% sodium hydroxide solution and distilled water, then dried over anhydrous magnesium sulfate and fractionally distilled under reduced pressure just before use. The 1-olefins used were high purity commercial materials obtained from Aldrich or Gulf Chemicals.

Solvents

Normal hexane was of spectroscopic grade, from Caledon Laboratory, Georgetown, Ontario. Toluene was purified by treatment with concentrated sulfuric acid, followed by aqueous sodium hydroxide solution and distilled water, dried over anhydrous magnesium sulfate, and distilled over metallic sodium, under nitrogen.

Catalyst Components

Titanium tetrachloride, lithium aluminum hydride, and anhydrous aluminum chloride were purchased from Anachemia, and *n*-butyl lithium from Alpha Inorganics.

Catalyst Preparation

The catalysts were all prepared in a clean three-necked round bottom flask which was oven-dried (140°) overnight and flushed with nitrogen while cooling. The flask was equipped with a

0008-4042/81/101425-08$01.00/0

©1981 National Research Council of Canada/Conseil national de recherches du Canada

Can. J. Chem. Downloaded from www.nrcresearchpress.com by 210.87.254.42 on 09/06/12
For personal use only.

Can. J. Chem. Downloaded from www.nrcresearchpress.com by 210.87.254.42 on 09/06/12
For personal use only.

thermometer, condenser, and a nitrogen inlet tube. Stirring, which took place during the preparation, was achieved by a magnetic stirrer and Teflon-coated magnetic stirring bar.

Vinyl Ethers

The catalyst for the polymerization of vinyl ethers was prepared by mixing lithium aluminum hydride (500 mg, 13.1 millimol) and 1-hexadecene (20 mL, 70.1 millimol) under a nitrogen atmosphere in the three-necked round bottom flask described above. The reaction mixture was heated at 160° with stirring for four hours. The temperature was lowered to 120°, a given amount of anhydrous aluminum chloride added, and stirring continued at that temperature for one hour. Then, heat was turned off and the reaction mixture was allowed to cool, after 50 mL toluene or *n*-hexane had been added. When the temperature was about 50°, a given amount of titanium tetrachloride was injected into the mixture through a hypodermic syringe. The black suspension of catalyst particles thus formed in the reaction mixture was aged for 30 min while it slowly cooled down to room temperature. At this point, the catalyst was ready for use.

To obtain a catalyst without using aluminum derivatives, a mixture of *n*-butyl lithium (5 mL of 4.25 *m* in *n*-hexane, 21.3 millimol) and toluene (50 mL) was stirred for 5 min at room temperature in a dry three-necked flask, kept under nitrogen. Titanium tetrachloride (1.2 mL, 12 millimol) was added through a syringe and the mixture exothermed to 45°. After ageing for 30 min, the catalyst was ready for use.

Styrene and 1-Olefins

The catalyst used in the polymerization and copolymerization of styrene and 1-olefins was prepared in a manner similar to that used in the vinyl ether polymerization.

Polymerization

The polymerizations took place in the same three-necked flask in which the catalysts were prepared. A flow of nitrogen was maintained during the polymerization reaction as was also rapid stirring with a magnetic stirrer.

Vinyl Ethers

The flask containing the catalyst (prepared from 7 millimol of $LiAlH_4$) was placed in a water bath at 25°. A vinyl ether (50 mL) was added dropwise so that the temperature of the reaction mixture was maintained between 25 and 35°. After the addition, the polymerization was allowed to continue overnight for a period of about 17 h.

A mixture of methanol (100 mL) and concentrated hydrochloric acid (5 mL) was added to the polymerization mixture to decompose the catalyst and precipitate the polymer. The supernatant liquid which was quite dark was decanted. The precipitated polymer was washed several times with additional methanol until it was decolourized. The polymers were isolated and dried in a vacuum oven at 60° for 10 h.

Styrene and 1-Olefins

After the catalyst (prepared from 26 millimol of $LiAlH_4$) had aged, a vinyl monomer (200 mL) was added to the flask at room temperature and the polymerization continued overnight.

The polymerization reaction was stopped by adding a mixture of isopropanol (150 mL) and hydrochloric acid (5 mL). After a few hours, the contents of the flask were transferred to a beaker and additional isopropanol added until the polymer completely precipitated. The polymer was washed several times with isopropanol until most of the dark colour of the catalyst had disappeared. The polymer was filtered under suction, washed further with isopropanol, and dried in a vacuum oven at 60° for 10 h.

Determination of Stereospecificity

Percentage isotacticity of a polyvinyl ether was determined by measuring the percent of that material insoluble in boiling acetone (5). For polystyrene, percentage of isotacticity was similarly determined by using boiling methyl ethyl ketone. Infrared spectra of these materials were used as further checks of isotacticity content. Infrared spectra were also used to determine the composition of copolymers of styrene and 1-olefins.

Results and Discussion

Lithium Alkylaluminates as Reducing Agents

Lithium aluminum hydride is a widely used reducing agent for organic synthesis (4), usually in ether as solvent. However, in Ziegler–Natta polymerizations, electron-rich compounds such as ethers cannot be used as solvents because they coordinate with the transition metals and render them ineffective as catalysts.

Alkylation of lithium aluminum hydride makes the derivatives soluble in hydrocarbon solvents so that they can be used as reducing agents for the transition metal halides. Thus, with $LiAlR_xH_y$ where R = alkyl group, $x + y = 4$ and $x = 1$ to 4, reduction of titanium tetrachloride occurs readily in hexane and toluene, as evidenced by the production of dark coloured lower valent compounds. In contrast, no reaction occurs when titanium tetrachloride is added to a suspension of lithium aluminum hydride in toluene even at 80°, although in diethyl ether these compounds react vigorously at room temperature.

Campbell and Haven (3) have shown that the catalyst prepared from lithium tetraalkylaluminate and titanium tetrachloride is not very active for styrene polymerization. Actually, for steric reasons, styrene is not very reactive towards Ziegler–Natta catalysts in general. Therefore, one can judge the relative reactivities of Ziegler–Natta catalysts belonging to a particular group by the amount of polystyrene obtained when styrene is polymerized by these catalysts under exactly the same conditions. Table 1 shows the results of varying R and x in $LiAlR_xH_y$, $(x + y = 4)$ on the amount of polystyrene obtained employing the catalyst prepared by the action of $LiAlR_xH_y$ on $TiCl_4$.

Varying R from ethyl to 1-hexadecyl increases the yield of polystyrene. Actually, when R = ethyl, over-reduction of $TiCl_4$ is indicated by production of metallic mirrors on the side of the reaction flask. Longer chain-length in R makes the final product a mild reducing agent. There was no effect due to variation in x from 2 to 4 (R = 1-hexadecyl) showing that this is not as important. However, when $x = 0$, exothermic cationic polymerization due to unreduced $TiCl_4$ took place, indicating again that $LiAlH_4$ is insoluble in toluene and does not react with $TiCl_4$ in this solvent.

For further work, $LiAlR_4$, where R = 1-hexadecyl, was adopted as the reducing agent be-

TABLE 1. Effect of varying R and x on polymerization of styrene by $LiAlR_xH_y$ ($x + y = 4$)*

R ($x = 3$)	Yield of polystyrene (%)	x (R = 1-hexadecyl) from stoichiometry	Yield of polystyrene (%)
Ethyl	0	0 ($LiAlH_4$)	Cationic polymerization
1-Octyl	5	2 ($LiAlR_2H_2$)	20
1-Decyl	15	3 ($LiAlR_3H$)	20
1-Hexadecyl	20	4 ($LiAlR_4$)	20

*Polymerization condition: toluene, 50 mL; $LiAlR_xH_y$, 27 mmol; $TiCl_4$, 13 mmol; styrene, 200 mL. Room temperature, 16 h.

cause of its mild reducing nature. Since this compound does not contain any hydride ion, production of hydrogen gas during the isolation of the polymer product would not occur.

The Nature of the Reduced Titanium Species

The nature of the reduced titanium species can be deduced from the study of polymerization of isobutyl vinyl ether and decyl vinyl ether with these catalysts. It has been reported by Joh *et al.* (5) that substantially different kinds of polymers are obtained from vinyl ethers due to difference in the structure of VCl_3 and $TiCl_3$ catalysts employed.

In Table 2, the nature of polyvinyl ethers prepared by us with various titanium catalysts is shown.

From Tables 2 and ref. 5, it is clear that when the VCl_3 and $TiCl_3$ used are free of other metallic salts, because they are prepared by reduction with hydrogen or by thermal decomposition, they give rise to mostly atactic polyvinyl ethers (5). In sharp contrast, however, when VCl_3 and $TiCl_3$ are produced by reaction with *n* BuLi, Al, or $LiAlR_4$ (R = 1-hexadecyl), they are in association with LiCl and $AlCl_3$ (5*c*) and these catalysts are isospecific.

According to Joh *et al.* (5*c*), the isospecific catalysts produced by reduction of VCl_4 and $TiCl_4$ with *n* BuLi may be $VCl_3 \cdot LiCl$ and $TiCl_3 \cdot LiCl$ (eq. [1])

[1] $VCl_4 + n\ BuLi = VCl_3 \cdot LiCl + n\ BuCl$

$TiCl_4 + n\ BuLi = TiCl_3 \cdot LiCl + n\ BuCl$

In Table 2, it can be seen that the polyvinyl ethers produced are about 50 to 70% isotactic. Therefore, the action of $TiCl_3$, produced from $TiCl_4$ by $LiAlR_4$, should be very similar to that produced by *n*-BuLi and the following equation may be valid (eq. [2]):

[2] $LiAlR_4 + TiCl_4 = TiCl_3 \cdot LiCl + AlR_3 + \frac{1}{2}R{-}R$

The above equation also explains why an equimolar mixture of $LiAlR_4$ and $TiCl_4$ is a good polymerization catalyst for 1-olefins, because 1 equivalent of AlR_3 is produced in this reaction and this alkylates $TiCl_3 \cdot LiCl$ to produce an active Ziegler–Natta catalyst.

TABLE 2. Polymerization of vinyl ethers by titanium halide catalysts*

Vinyl ether	Catalyst	Conversion (%)	Isotacticity (% insoluble in boiling acetone)
Decyl	$TiCl_3$[a]	76	68
Decyl	$TiCl_3$[b]	90	56
Decyl	$TiCl_3$[c]	100	64
Decyl	$TiCl_3$[d]	100	66
Isobutyl	$TiCl_3$[b]	90	50

*Polymerization conditions: toluene, 50 mL; monomer, 50 mL; catalyst, 10 mmol; 30°C, 17 h. (*a*) $TiCl_4$/*n*-BuLi = 1/2; (*b*) $TiCl_4/LiAlR_4$ = 1/1; (*c*) $TiCl_4/LiAlR_4/AlCl_3$ = 1/1.75/.25; (*d*) $TiCl_4/LiAlR_4/AlCl_3$ = 1.0/4.75/1.25 R = 1-hexadecyl.

Alkyl Lithium, Lithium Alkylaluminate, and Aluminum Alkyls as Organic Bases and Reducing Agents

It is known (4*b*) that aluminum alkyls react with alkyl lithium compounds to produce lithium alkyl aluminates (eq. [3]).

[3] $LiR + AlR_3 = LiAlR_4$

Because lithium alkyls are strong bases, they can initiate anionic polymerization of vinyl monomers such as styrene (6). Neither AlR_3 nor $LiAlR_4$ alone can polymerize styrene. We have found that in toluene at 80° for 20 h no polymer was obtained from styrene by the action of $LiAlR_4$ (R = 1-hexadecyl). This shows that, in toluene, $LiAlR_4$ does not dissociate appreciably into LiR and AlR_3.

These three classes of organometallic compounds (RLi, $LiAlR_4$, and AlR_3, R = alkyl) behave quite characteristically towards titanium tetrachloride. It is known (7) that the reduction of $TiCl_4$ with *n*-butyllithium is complicated by complex formation. Complete reduction is not achieved and the extent of reduction depends on the order of reagent addition, Li/Ti ratio, and concentration of the reagents. Maximum reduction to about 55% Ti^{3+} occurs at a Li/Ti ratio of 2.0. At Li/Ti <1.5,

Can. J. Chem. Downloaded from www.nrcresearchpress.com by 210.87.254.42 on 09/06/12
For personal use only.

Can. J. Chem. Downloaded from www.nrcresearchpress.com by 210.87.254.42 on 09/06/12
For personal use only.

sufficient free $TiCl_4$ is present in the system to initiate cationic polymerization of *N*-vinyl carbazole. At Li/Ti >4, almost all the titanium is in the tetravalent state but complexed with *n*-BuLi, so it no longer retains its Lewis acidity. This is another example of the highly basic nature of *n*-BuLi that prefers salt formation with acidic $TiCl_4$ rather than effecting its reduction.

The reduction of $TiCl_4$ with alkyl aluminum compounds such as triethyl aluminum (Et_3Al) has been described in a simplified form as a succession of alkyl–chlorine group exchanges, followed by a reductive dealkylation of unstable alkyltitanium halide (eq. [4]):

[4] $TiCl_4 + Et_3Al = EtTiCl_3 + Et_2AlCl$
$TiCl_4 + Et_2AlCl = EtTiCl_3 + EtAlCl_2$ etc.
$EtTiCl_3 \rightarrow TiCl_3 + Et$
or $2EtTiCl_3 \rightarrow 2TiCl_3 + Et—Et$

Beerman and Bestian (8) have shown a strong solvent effect on the mechanism of decomposition of CH_3TiCl_3. In hydrocarbon solvents, no evidence for the intermediate formation of free radicals could be found whereas, in diethyl ether, methyl radicals were the primary decomposition products. It seems that aluminum alkyls preferably alkylate titanium trichloride rather than reduce it to Ti^{2+} or lower valent species. Therefore, most active and stereoselective catalysts are prepared from $TiCl_3$ and aluminum alkyls (2).

The reduction of $TiCl_4$ by $LiAlR_4$ can similarly occur (eq. [5]).

[5] $2LiAlR_4 + 2TiCl_4 \rightarrow 2RTiCl_3 \cdot LiCl + 2AlR_3$
$2RTiCl_3 \cdot LiCl \rightarrow 2TiCl_3 \cdot LiCl + R—R$

On the basis of the above discussion, we can readily explain the observation made by Ludlum *et al.* (9) in the polymerization of ethylene by catalysts derived from titanium tetrachloride through the reductive action of *n*-hexyl lithium, lithium tetra-1-heptylaluminate, and triisobutyl aluminum or triethyl aluminum. This is illustrated in Fig. 1. The maximum yield of polyethylene is apparently produced by a catalyst formed by reaction of the stoichiometric amount of the reducing agent required to reduce titanium tetrachloride to its trivalent state followed by alkylation. Thus in the case of *n*-hexyl lithium, the ratio of $C_6H_{13}Li$:$TiCl_4$ is 2:1 and in the case of lithium tetra-1-heptylaluminate, $LiAl(C_7H_{15})_4$:$TiCl_4$ is 1:1. In the case of aluminum alkyls, reduction and subsequent alkylation require a ratio of alkylaluminum:$TiCl_4 \gg 1$.

It can be easily seen that *n*-hexyl lithium does not produce a very active catalyst but lithium tetra-1-heptylaluminate does. In this example, actions of

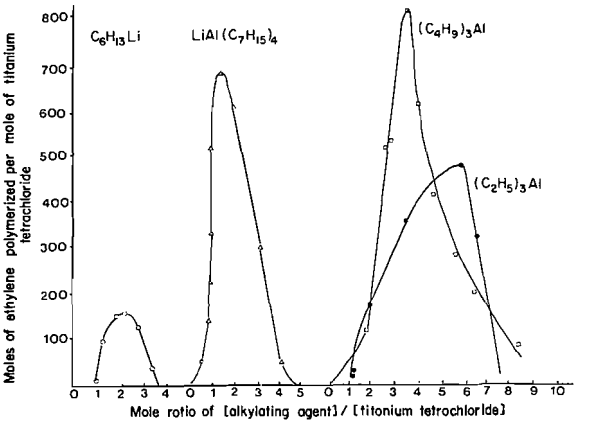

FIG. 1. Catalytic activity versus catalyst composition at 100°C (9), for ethylene polymerization.

$LiAlR_4$ and aluminum alkyls appear to be very similar.

The Nature of the Active Catalyst in the $LiAlR_4$ (R = Alkyl) and $TiCl_4$ System

From the above results, it seems that when equimolar amounts of $LiAlR_4$ and $TiCl_4$ are mixed together, an active catalyst is produced, according to the following scheme (Fig. 2).

With the above catalyst, copolymerization between vinyl ether and 1-olefin or styrene cannot be accomplished. It seems that vinyl ethers coordinate initially with the catalyst and this can polymerize only vinyl ethers but not styrene or 1-olefins. It is known (5) that styrene can be polymerized by $VCl_3 \cdot LiCl$ but not by VCl_3LiCl,THF where THF = tetrahydrofuran. Production of atactic polystyrene and isotactic poly(1-olefin) by this catalyst is interesting. It shows that 1 mole of AlR_3 produced cannot completely alkylate the $TiCl_3 \cdot LiCl$ and because 1-olefins are very reactive, they can be polymerized easily by the alkylated $TiCl_3 \cdot LiCl$ species present. Styrene, however, is polymerized preferentially by $TiCl_3 \cdot LiCl$ to an atactic polymer. It should not be cationic by nature because the rate of polymerization is very low at room temperature, resulting in low yields. It is characteristic of Ziegler–Natta catalysts to be sensitive to steric factors.

A Truly Isotactic Specific Ziegler–Natta Catalyst in $LiAlR_4/AlCl_3/TiCl_4$ System

It is known (4) that anhydrous $AlCl_3$ reacts with $LiAlR_4$ (eq. [6]):

[6] $3LiAlR_4 + AlCl_3 = 3LiCl + 4AlR_3$

It is clear from Table 3 that activity of $TiCl_3$ depends on its relative concentration with respect to the alkylating agent AlR_3. However, at a ratio of AlR_3:$TiCl_3 \simeq 3:1$, saturation is achieved in the rate

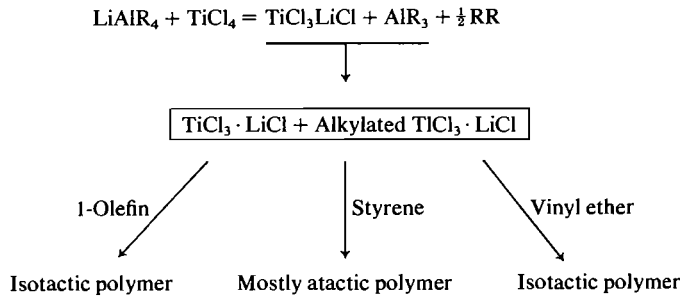

FIG. 2. Probable catalyst composition in 1 : 1 molar mixture of $LiAlR_4$ and $TiCl_4$.

TABLE 3. Catalyst composition versus polymer yield and isotacticity in styrene polymerization by $TiCl_3LiCl + x\ AlR_3$ (R = 1-hexadecyl)*

x	$[TiCl_3]$ mol	Polystyrene g	Polystyrene g/mol $TiCl_3$	Isotacticity (%)	Isotactic polystyrene g/mol $TiCl_3$
1	0.025	11	440	30	132
2	0.015	36	2400	100	2400
3	0.011	34	3100	100	3100
4	0.009	32	3400	80	2720

*Polymerization conditions: $LiAlR_4$, 26.5 mmol; toluene, 50 mL; styrene, 200 mL; anhydrous $AlCl_3$ added, 0 (x = 1), 450 mg (x = 2), 600 mg (x = 3), and 700 mg (x = 4); time, 16 h at room temperature.

TABLE 4. Effect of reaction conditions on styrene polymerization by $TiCl_3 \cdot LiCl + 3\ AlR_3$ (R = 1-hexadecyl, $TiCl_3 \cdot LiCl$ = 11 mmol)

Time (t) (h)	Temperature (°C)	Styrene (mL)	Toluene (mL)	Volume fraction of styrene (V)	$V \times t$ (h)	Polymer yield (g)	Isotacticity (%)
16	22	200	50	0.80	12.8	34	100
16	22	100	50	0.67	10.7	30	100
16	22	50	300	0.14	2.3	6	90
64	22	50	300	0.14	9.0	21	90
64	22	150	300	0.33	21.2	40	90
64	22	125	50	0.71	45.5	49	85
16	60	200	50	—	—	29	40

of polymerization, yield, and isospecificity in styrene polymerization. At this particular catalyst concentration, the amount of polystyrene obtained depends on styrene concentration (Table 4 and Fig. 3).

A few interesting observations can be made from Table 4. Higher temperature, e.g. 60°C, dramatically decreases the isotacticity of the polymer without much change in yield. This indicates that the catalyst is sensitive to temperature to lose much of its isospecific character. At room temperature (22°C) the catalyst is highly isospecific and, in dilute solution and at lower conversions, the amount of polystyrene obtained is proportional to the product $V \times t$ (Table 4) as it can be seen from Fig. 3. This shows that the polymerization of styrene is of first order in styrene at lower conversions and the order tends to be zero at higher values of $V \times t$.

Proof of Copolymerization between Styrene and 1-Olefins

To prove that styrene is copolymerizing with 1-olefins in the presence of $TiCl_3 \cdot LiCl + 3AlR_3$ catalyst, we chose 1-hexene as the olefin, because it is known (2) that poly(styrene-co-1-hexene) is soluble in *n*-hexane and polystyrene is not. Table 5 shows the analysis of the copolymers obtained from these monomers by the action of the above catalyst. The portion of the copolymer mixture insoluble in *n*-hexane was found to be polystyrene by infrared analysis. Thus, from Table 5, it is clear that copolymerization between styrene and 1-hexene occurs to a very significant degree.

Generally, styrene polymerizes at a yield of 25–30% and 1-hexene at 95–100% yield under the polymerization conditions given in Tables 4 and 5. Under the same conditions, the copolymer yield is

Can. J. Chem. Downloaded from www.nrcresearchpress.com by 210.87.254.42 on 09/06/12
For personal use only.

Can. J. Chem. Downloaded from www.nrcresearchpress.com by 210.87.254.42 on 09/06/12
For personal use only.

TABLE 5. Analysis of styrene/1-hexene copolymers*

Catalyst	Mol% styrene in feed	% Copolymer soluble in *n*-hexane (by weight)	Mol% styrene in copolymer†
$TiCl_3 \cdot LiCl$	50	88	7
$+ 3\ AlR_3$	67	80	14
(R = 1-hexadecyl)	75	75	20

*Polymerization condition: catalyst concentration, 11 mmol; total monomer, 100 mL; *n*-hexane, 50 mL; 16 h at room temperature.
†Analyzed by nmr spectroscopy.

TABLE 6. Copolymerization of styrene and 1-hexene (2:1 molar) by $LiAlR_4/AlCl_3/TiCl_4$ (R = 1-hexadecyl) catalyst system*

Initial $LiAlR_4$ (mol × 10^{-4})	$AlCl_3$ added (mol × 10^{-4})	$TiCl_3$ added (mol × 10^{-4})	Excess $LiAlR_4$ after reaction with $AlCl_3$ and $TiCl_4$ (mol × 10^{-4})	Molar ratio: aluminum/titanium	Copolymer yield	
					g	g/mol $TiCl_3$
264	0	135	129	1.9:1.0	26	1930
264	22.5	150	47	1.9:1.0	33	2200
264	45.0	160	0	1.9:1.0	32	2000
264	67.5	170	0	2.0:1.0	36	2120
264	89.0	180	0	2.0:1.0	17	950
264	0	97	167	2.7:1.0	14	1440
264	22.5	105	92	2.8:1.0	22	2090
264	45.0	113	16	2.7:1.0	27	2390
264	67.5	121	0	2.7:1.0	32	2640
264	89.0	131	0	2.7:1.0	23	1760
264	112.5	138	0	2.7:1.0	17	1230
264	0	73	191	3.6:1.0	0	0
264	22.5	79	117	3.7:1.0	8	1010
264	67.5	91	0	3.6:1.0	27	2970
264	134.5	110	0	3.5:1.0	12	1100

*Polymerization condition: total monomer, 100 mL; *n*-hexane, 50 mL; 16 h at room temperature.

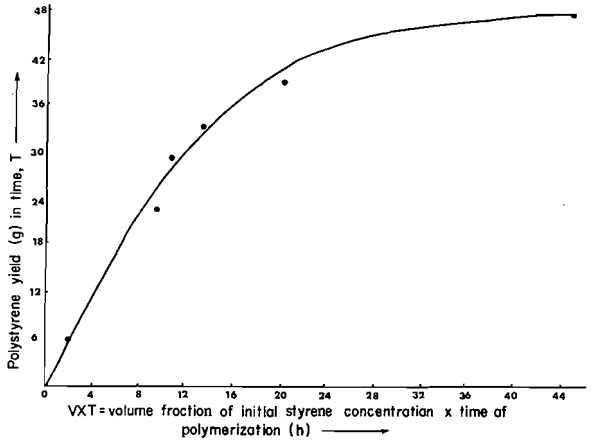

FIG. 3. Dependence of polystyrene yield on styrene concentration.

also 25–30% and the unreacted monomers, even 1-hexene, could be recovered. This shows that the catalyst preferentially coordinates with styrene and although 1-hexene polymerizes faster than styrene in the copolymerization reaction, the overall reaction rate is controlled by styrene.

Effect of Varying the Catalyst Composition on the Copolymerization Behaviour of Styrene and 1-Hexene

Table 6 shows that when a mixture of styrene and 1-hexene (2:1 molar) is copolymerized in the presence of a catalyst system, derived from a fixed amount of $LiAlR_4$ (R = 1-hexadecyl) but varying amounts of $AlCl_3$ and $TiCl_4$, a pattern develops that enables us to determine the right catalyst composition for optimum yield.

The nature and amount of the various catalyst components may be explained by the following reactions (eq. [7]):

[7] $3LiAlR_4 + AlCl_3 = LiCl + 4AlR_3$
$LiAlR_4 + TiCl_4 \equiv TiCl_3 \cdot LiCl + AlR_3 + \frac{1}{2}RR$
$AlR_3 + TiCl_4 \equiv TiCl_3 + AlR_2Cl + \frac{1}{2}RR$

Addition of $AlCl_3$ converts $LiAlR_4$ into AlR_3. Thus for complete conversion of $LiAlR_4$ to AlR_3 in Table 6, only 88 × 10^{-4} moles of $AlCl_3$ is necessary. Figure 4 shows that the maximum activity of the catalyst occurs well before addition of 88 × 10^{-4} moles of $AlCl_3$, indicating that for the production of

TABLE 7. Copolymerization of styrene and 1-olefins having branched sidechains*

Comonomers	Feed styrene (mol fraction)	Copolymer styrene (mol fraction)	Yield of the copolymer
3-Methyl-1-butene	0.75	0.77	19
	0.50	0.75	15
	0.25	0.64	24
4-Methyl-1-pentene	0.75	0.58	31
	0.50	0.46	41
	0.25	0.32	70

*Polymerization conditions: total monomers, 100 mL; *n*-hexane, 50 mL; $TiCl_3 + 3AlR_3$, 11 mmol; 16 h at room temperature.

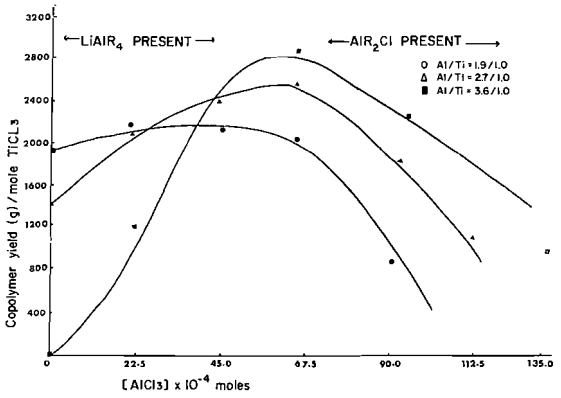

FIG. 4. Effect of varying catalyst compositions on copolymer yield for styrene/1-hexene (2:1 molar) system.

active $TiCl_3$, $LiAlR_4$ is a much better reagent than AlR_3 when R = 1-hexadecyl.

In all three cases (Table 6, Fig. 4), at the point of maximum activity, the concentration of $LiAlR_4$ equals that of $TiCl_4$. Presence of excess of $LiAlR_4$ is deleterious. Presence of not enough $LiAlR_4$ results in the reduction of $TiCl_4$ by AlR_3 producing AlR_2Cl and this is also deleterious. In all three cases, presence of excess $LiAlR_4$ is more harmful than the presence of excess AlR_2Cl. At the point of maximum polymerization activity, the catalyst corresponds to $TiCl_3 \cdot LiCl + xAlR_3$ with no $LiAlR_4$ and AlR_2Cl present. This shows that copolymerization of styrene proceeds best in the presence of catalysts prepared by the alkylation of $TiCl_3$ by simple aluminum alkyls.

Copolymerization of Styrene and 1-Olefins with Branched Side Chains

1-Olefins with normal side chains polymerize faster than styrene, resulting in lower incorporation of styrene into their copolymers. The lower reactivity of styrene is attributed to steric hindrance presented by the phenyl group. In the copolymerization of styrene and 1-hexene it has been established that the catalyst coordinates preferentially with styrene. Therefore, the copolymerization rate reflects the rate of styrene polymerization, although the greater reactivity of 1-hexene is reflected in the final copolymer structure.

1-Olefins with branched side chains such as 3-methyl-1-butene, and 4-methyl-1-pentene possess steric features similar to styrene. Therefore we thought that it would be interesting to determine the copolymer structures and copolymerization rates when styrene and branched chain 1-olefins are copolymerized. Table 7 shows the results.

It is clear from Table 7 that (*a*) the rate of copolymerization of styrene and 3-methyl-1-butene is lower than the homopolymerization rate of styrene, and (*b*) that of styrene and 4-methyl-1-pentene is slightly higher. This indicates that with the 1-olefins having branched side chains the copolymerization rate depends on the steric nature of the side chains.

Table 7 shows the copolymer composition in relation to the feed composition of poly(styrene-co-4-methyl-1-pentene). The copolymer composition was determined by infrared spectral analysis following the relationship established by Kissin *et al.* (10) and given below (eq. [8]):

$$[8] \quad \frac{D1388}{D1603} = 1.68\left(\frac{1}{C\ \text{styrene}} - 1\right) + 0.25$$

where D1388 and D1603 are the absorbance in the infrared spectrum of the copolymers at 1388 cm^{-1} (methyl group) and 1603 cm^{-1} (benzene ring) respectively.

It is expected that the above relationship should be applicable in the infrared analysis of poly(styrene-co-3-methyl-1-butene). The results obtained for this copolymer are based on that assumption.

Data from Table 7 show that the copolymerization rates and copolymer compositions involving branched 1-olefins and styrene can be very susceptible to the steric structure of the side chain of the 1-olefins. Thus, it is really interesting to note that more styrene than 1-olefin can be incorporated into the copolymer structure in poly(styrene-co-3-methyl-1-butene), a situation completely opposite to that in poly(styrene-co-1-hexene).

Can. J. Chem. Downloaded from www.nrcresearchpress.com by 210.87.254.42 on 09/06/12
For personal use only.

1. A. MISHRA. U.S. Patent 4,086,499. Apr. 25, 1978.
2. (*a*) I. H. ANDERSON, G. M. BURNETT, and P. J. T. TAIT. J. Polym. Sci. **56**, 391 (1962); (*b*) I. H. ANDERSON, G. M. BURNETT, and W. C. GEDDES. Eur. Polym. J. **3**, 161 (1967); (*c*) I. H. ANDERSON, G. M. BURNETT, and W. C. GEDDES. Eur. Polym. J. **3**, 171 (1967); (*d*) B. BAKER and P. J. T. TAIT. Polymer, **8**, 225 (1967).
3. (*a*) T. W. CAMPBELL and A. C. HAVEN JR. J. Appl. Polym. Sci. **1**, 73 (1959); (*b*) T. W. CAMPBELL. J. Appl. Polym. Sci. **5**, 184 (1961).
4. (*a*) N. G. GAYLORD. Reduction with complex metal hydrides. Interscience, New York 1956; (*b*) E. C. ASHBY. Adv. Inorg. Chem. Radiochem. **8**, 283 (1966).
5. (*a*) Y. JOH, H. YUKI, and S. MURAHASHI. J. Polym. Sci. Polym. Chem. Ed. **8**, 2775 (1970); (*b*) J. Polym. Sci. Polym. Chem. Ed. **8**, 3311 (1970); (*c*) Y. JOH, K HARADA, H. YUKI, and S. MURAHASHI. J. Polym. Sci. Polym. Chem. Ed. **9**, 1089 (1971).
6. (*a*) M. SZWARC. Carbanion, living polymers and electron-transfer process. Interscience, New York. 1968; (*b*) R. W. LENZ. Organic chemistry of synthetic high polymers. Interscience, New York. 1968. Chapt. 13.
7. (*a*) H. N. FRIEDLANDER and K. OITA. Ind. Eng. Chem. **49**, 1885 (1957); (*b*) J. HELLER, D. O. TIESZEN, and D. E. PARKINSON. J. Polym. Sci. Part A, **1**, 125 (1963).
8. C. BEERMAN and H. BESTIAN. Angew. Chem. **71**, 618 (1959).
9. D. B. LUDLUM, A. W. ANDERSON, and C. E. ASHBY. J. Am. Chem. Soc. **80**, 1380 (1958).
10. Y. V. KISSIN, Y. Y. GOLDFARB, B. A. KREUTSEL, and H. EYLIEN. Eur. Polym. J. **8**, 487 (1972).

Can. J. Chem. Downloaded from www.nrcresearchpress.com by 210.87.254.42 on 09/06/12
For personal use only.

A novel approach to the synthesis of a variety of aminodeoxy-α-D-glycopyranosides

RAYMOND U. LEMIEUX, FAWZY F. Z. GEORGES,[1] AND ZYGFRYD SMIATACZ[2]

Department of Chemistry, University of Alberta, Edmonton, Alta., Canada T6G 2G2

Received October 14, 1980

This paper is dedicated to Professor W. E. Harris on the occasion of his retirement from the University of Alberta

RAYMOND U. LEMIEUX, FAWZY F. Z. GEORGES, and ZYGFRYD SMIATACZ. Can. J. Chem. **59**, 1433 (1981).

Conditions for the replacement of the 3-acetoxy group of ethyl 3,4,6-tri-*O*-acetyl-2-deoxy-2-oximino-α-D-*arabino*-hexopyranoside (**1**) by nucleophiles including azide, phthalimide, hydride, and thiophenoxide are reported. The reaction was discovered through the formation of dimeric and trimeric derivatives of deacetylated **1** in the course of its alkaline hydrolysis. The possible use of the replacement reaction to achieve precursors for the formation of 3-deoxy-, 3-amino-3-deoxy-, 2-amino-2,3-dideoxy-, 2,3-diamino-2,3-dideoxy-, and 2-amino-2,3,4-trideoxy-α-glycopyranosides is demonstrated.

RAYMOND U. LEMIEUX, FAWZY F. Z. GEORGES et ZYGFRYD SMIATACZ. Can. J. Chem. **59**, 1433 (1981).

On rapporte les conditions qui permettent de remplacer le groupe acétoxy en position 3 du tri-*O*-acétyl-3,4,6 déoxy-2-oximino-2-α-D-arabino hexopyrannoside d'éthyle (**1**) par des nucléophiles comprenant: l'azoture, la phtalimide, l'hydrure et le thiophénolate. On a découvert cette réaction par le biais de la formation de dérivés dimères et trimères du composé **1** désacétylé au cours de son hydrolyse alcaline. On démontre l'utilisation possible de cette réaction de déplacement pour obtenir les précurseurs nécessaires à la formation de déoxy-3, amino-3-déoxy-3, amino-2-didéoxy-2,3, diamino-2,3 didéoxy-2,3 et amino-2-tridéoxy-2,3,4-α-glycopyrannosides.

[Traduit par le journal]

A wide variety of aminocyclitol-type antibiotics (1) possess the 3-amino-3-deoxy-α-D-glucopyranosyl group. Others, such as kasugamycin, sisomycin, tobramycin, and the lividomycin antibiotics contain a 2-amino-2,3-dideoxyglycosyl group. The 2,3-diamino-2,3-dideoxyglycosyl group occurs in the antibiotic seldomycin factor 5 (2). Furthermore, a 2-amino-2,3,4-trideoxyglycosyl derivative is present in the gentamicin C antibiotics (3). All these structural units represent either glycopyranosides or glycopyranosaminides modified at the 3-position. It is evident, therefore, that a general synthetic methodology for the replacement of the 3-hydroxyl group of glycopyranosides or glycopyranosaminides either by a hydrogen atom or an amino group is of substantial interest to this important field of inquiry. Since all of these glycosyl groups occur as α-anomers, it would be of special interest if the methodology produced the groups in this configuration. That these requirements can, in principle, be met by way of suitably 3-*O*-substituted 2-deoxy-2-oximino-α-glycopyranosides (4) was the subject of a preliminary communication (5). In the following discussion of the results, the various transformations which were observed starting with such a glycoside (**1**) are first to be outlined. The evidence for the structural assignments is then presented.

Discussion of Results

The reaction of the nitrosyl chloride adducts of acetylated glycals with alcohols in *N*,*N*-dimethylformamide (DMF) was shown (6) to provide acetylated 2-deoxy-2-oximino-α-glycopyranosides in high yield. Furthermore, the further processing of these oximinoglycosides under acidic and neutral conditions provided access to both α-glycosides (7) and 2-amino-2-deoxy-α-glycosides (8). However, a number of observations made at that time showed the acetylated oximinoglycosides to be alkali labile and this lability was tacitly attributed to the reversal of the glycosylation reaction. That the situation was more complex became apparent in the course of an attempt to de-*O*-acetylate ethyl 3,4,6-tri-*O*-acetyl-2-deoxy-2-oximino-α-D-glucopyranoside (**1**) using triethylamine in aqueous methanol. In addition to the formation of the expected product (**2**), the dimeric (**3**) and trimeric (**4**) forms of **2** were also formed. Indeed, **3** was the major product of the reaction (49% isolated yield). The products **2**, **3**, and **4** were formed in nearly the following ratios, 4:6:1, respectively. Once the nature of the products **3** and **4** was established, it was apparent that the 3-substituent of a 2-oximino-α-glycoside can compete with the aglycon as leaving group in the alkaline degradation to form nitrosoalkene (**5**). In the event that elimination of the 3-substituent (route 1) is more rapid than elimination of the aglycon (route 2), the route for the formation of compounds **3** and **4** is evident. Once formed, compound **2** was highly stable under the conditions

[1]University of Alberta postdoctoral fellow, 1977–1979.

[2]Visiting Research Associate, 1976–1977. Present address: Institute of Chemistry, University of Gdansk, Poland.

0008-4042/81/101433-06$01.00/0

©1981 National Research Council of Canada/Conseil national de recherches du Canada

Can. J. Chem. Downloaded from www.nrcresearchpress.com by 210.87.254.40 on 09/06/12
For personal use only.

Can. J. Chem. Downloaded from www.nrcresearchpress.com by 210.87.254.40 on 09/06/12
For personal use only.

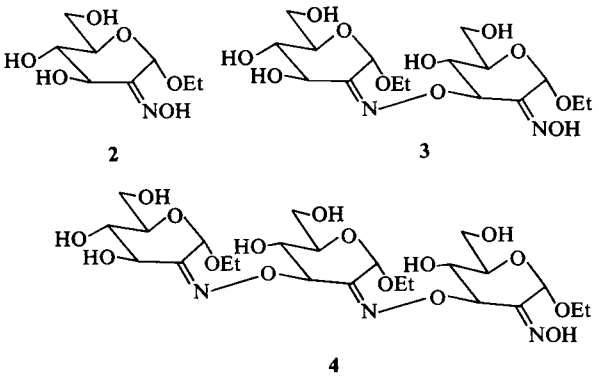

2 3 4

which led to the formation of **3** and **4** from **1** in keeping with the fact that the acetate ion is a much better leaving group than the hydroxyl ion.

The above described results suggested a novel route for the preparation of glycosides modified at the 3-position. In order to test this possibility, **1** was treated with sodium azide in commercial DMF at room temperature. Indeed, a slow transformation occurred which led to the formation of a nearly equimolar mixture of the azides **6** and **7**. The *Z*-configuration of the oximino groups was assigned on the basis of the ^{1}H nmr chemical shifts of H-1 (6.02 and 5.90 ppm) as compared to that for H-1 (6.00 ppm) of **1** (9). The reaction was much more rapid at 65°C. Under these conditions, the *E*-isomer **8** was formed (10% yield). As expected (9), the change in the configuration of the oximino group of **7** to form **8** resulted in a deshielding of H-3 by 0.9 ppm and shielding of H-1 by 0.75 ppm.

An attempt to convert **1** into the azides **6**, **7**, and **8** using specially dried DMF failed. However, the reaction observed using commercial DMF readily occurred on adding water (1%) to the reaction mixture prepared using dry DMF. The effect of the water appears to be related to the energy required to separate the sodium and azide ions, since the reaction occurred at a useful rate on adding 18-Crown 6 (10) to the reaction mixture prepared in the pure DMF. Furthermore, the remarkable sensitivity to solvent of the reaction involving replacement of the 3-acetoxy group of **1** was observed in deacetylation reactions. As noted above, treatment of **1** with triethylamine in aqueous methanol led to the formation of compounds **3** and **4**. However, only **2** was formed in appreciable amount when dry methanol was used as solvent. This is not likely due to too rapid deacetylation since **3** was formed when sodium methoxide was used as the base in dry methanol. These matters are noteworthy since they show the elimination of the acetoxy group to be dependent on the presence in the medium of an efficient proton acceptor (B^-). Compounds **6**, **7**, and **8** were formed on reaction of **1** with sodium azide at elevated temperatures in aqueous dioxane and it therefore appears that a wide range of solvents may be used. Treatment of either **6** or **7** with sodium azide in wet DMF converted the compound to the near 1:1 equilibrium mixture. When, instead of the ethyl glycoside **1**, the corresponding *tert*-butyl glycoside was used, the azides corresponding to replacement of the 3-acetoxy group were formed. However, attempts to replace the 3-acetoxy groups of the 4,5-di-*O*-(3,4,6-tri-*O*-acetyl-2-deoxy-2-oximino-α-D-*arabino*-hexopyranosyl) derivative of *N*,*N*′-dicarbobenzoxy-2,5-dideoxystreptamine led to cleavage of the glycosyl bonds (route 2 as shown for compound **1**). It appears, therefore, that applications of the reaction for the formation of complex aminoglycosides may require a leaving group at the position α to the oximino group which is superior to the acetate ion. It was not possible to further investigate this matter.

In order to achieve greater stereochemical con-

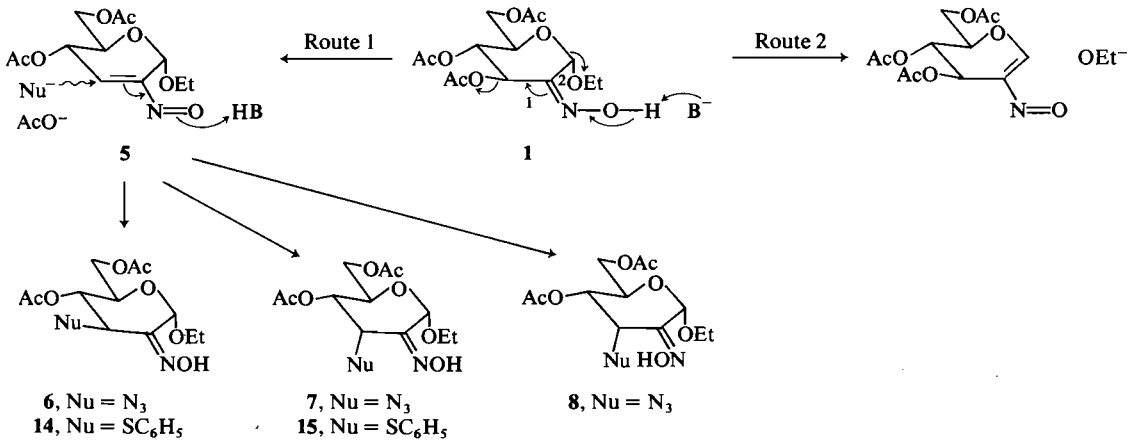

5 1

6, Nu = N_3
14, Nu = SC_6H_5

7, Nu = N_3
15, Nu = SC_6H_5

8, Nu = N_3

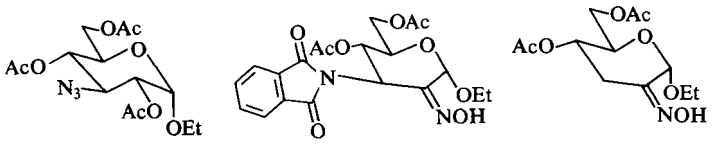

9 10 11

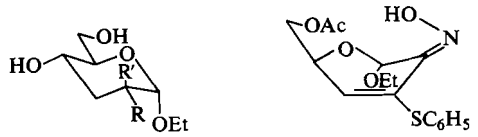

12, R = NHAc, R′ = H
13, R = OH, R′ = H

16

trol of the replacement than that provided by sodium azide, the use of potassium phthalimide as nucleophilic reagent was examined. Under the conditions used, the acetylated form of the dimeric product (**3**) was the main product. However, a 25% yield of the desired *arabino*-phthalimido compound **10** was obtained as the only phthalimide product of the reaction. Reaction conditions which may be more favorable to the formation of **10** were not investigated.

It could be anticipated that the proposed nitrosoalkene intermediate would be reduced by borohydride and, if so, the reaction would provide a new access to either 3-deoxyglycosides or 2,3-dideoxy-2-aminoglycosides. Indeed, the 3-deoxyoxime **11** was obtained in 70% yield on reaction of **1** with sodium borohydride in DMF.

When sodium thiophenoxide was used as the nucleophilic reagent, the reaction with **1** in acetonitrile was nearly complete in 1.5 h at 75°C and the main product of the reaction was the α,β-unsaturated oxime **16**. The expected products of substitution, namely, **14** and **15**, were also present in the reaction mixture. It is apparent that H-3 of these latter compounds is sufficiently acidic to render facile the elimination of the 4-acetoxy group to form **16**. In the course of the deoximation of **14** using an acidic solution of acetaldehyde, followed by borohydride reduction and acetylation, the 4-acetoxy group was lost since reductive desulfurization of the olefinic product produced ethyl 2,6-di-*O*-acetyl-3,4-dideoxy-α-D-*erythro*-hexopyranoside (**23**).

The structure of compounds **3** and **4** were evident from the ^{1}H nmr spectral data. Deoximation of **3** with acetaldehyde, then borohydride reduction, followed by acetylation of the product to form **17** and **18** confirmed these conclusions.

The structure of **6**, which could be assigned on the basis of the ^{1}H nmr spectrum, was confirmed by deoximation followed by borohydride reduction and acetylation to form the azide **9** which was converted to ethyl 3-acetamido-2,4,6-tri-*O*-acetyl-3-deoxy-α-D-glucopyranoside (**19**). Similarly, **7** was converted to ethyl 3-acetamido-2,4,6-tri-*O*-acetyl-3-deoxy-α-D-allopyranoside (**20**). The phthalimide **10** was unequivocally characterized by its ^{1}H nmr spectrum.

The azido groups in compounds **6** and **7** could be preferentially hydrogenated to amine groups. *N*-Acetylation then provided the products **21** and **22**. It is fully expected that borane reduction (8) of compounds **6** and **7** will produce 2,3-diamino-2,3-dideoxyglycosides but this matter was not investigated.

Borane reduction of **11** and acetylation of the product gave ethyl 2-acetamido-4,6-di-*O*-acetyl-2,3-

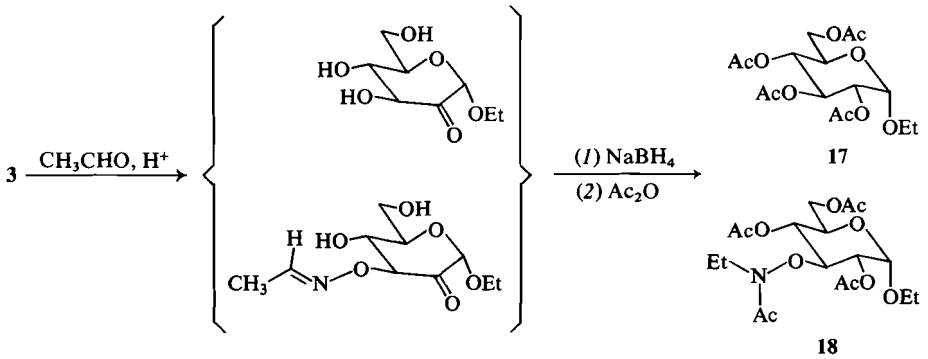

17

18

Can. J. Chem. Downloaded from www.nrcresearchpress.com by 210.87.254.40 on 09/06/12
For personal use only.

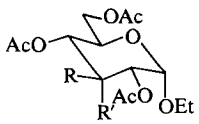

19, R = NHAc, R′ = H
20, R = H, R′ = NHAc

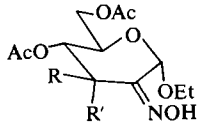

21, R = NHAc, R′ = H
22, R = H, R′ = NHAc

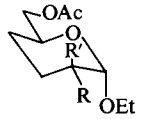

23, R = OAc, R′ = H
24, R = NHAc, R′ = H
25, R = H, R′ = NHAc

dideoxy-α-D-*ribo*-hexopyranoside, the *O*-acetylated form of **12**, in 80% yield. Deoximation of **11** followed by borohydride reduction provided ethyl 3-deoxy-α-D-*ribo*-hexopyranoside (**13**) in 85% yield.

Reductive desulfurization of **14** and acetylation of the product provided ethyl 2-acetamido-6-*O*-acetyl-2,3,4-trideoxy-α-D-*erythro*-hexopyranoside (**24**) in 77% yield along with the D-*threo*-isomer (**25**) in 15% yield. The same products were obtained on the similar treatment of compounds **15** and **16**.

The foregoing transformations are considered to demonstrate the potential value of the elimination of groups neighboring to an oximino group for the preparation of a wide range of deoxy and aminodeoxysugars of special interest to the general area of aminoglycoside antibiotics.

Experimental

Thin-layer chromatography was performed on Merck silica gel plates type 60 F_{254}, layer thickness 0.25 mm. Spots were made visible by heating the plates sprayed with 5% sulfuric acid in methanol. Unless otherwise indicated, the following systems were used as chromatographic solvents: carbon tetrachloride – acetone mixtures A, 1:1; B, 3:1; and C, 5:1; D, carbon tetrachloride – ether 4:3; E, benzene – ethyl acetate 10:1; F, 3% methanol in chloroform; G, ethyl acetate – petroleum ether 1:2.

Unless specified otherwise, the ^{1}H nmr data refer to 100 MHz spectra obtained with $CDCl_3$ as solvent (lock signal, tetramethylsilane). External TMS was used when D_2O was the solvent. The ^{13}C nmr data refer to 22.6 MHz spectra recorded on a Bruker HFX-90 spectrometer. The optical rotations were measured at room temperature (21–23°C).

The column chromatograms employed silicic acid (Merck 7736, type 60 for thin-layer chromatography) using 20 g per gram of reaction product with the specified developing solvents.

*Products **2**, **3**, and **4**. Deacetylation of Ethyl 3,4,6-Tri-O-acetyl-2-deoxy-2-oximino-α-D-*arabino*-hexopyranoside (**1**)*

With Triethylamine in Aqueous Methanol

Compound **1** (2.09 g, 6 mmol) was dissolved in 80 mL of methanol–water (1:1) containing 4.2 mL of triethylamine. On standing at 4°C for 6 h, tlc (solvent B) showed the presence of three products in the approximate ratio 1:1.5:0.1. Solvent removal left a crystalline mass which was subjected to column chromatography (solvent A).

The first fraction (0.40 g, 30% yield) was characterized (^{1}H nmr, mass spectrum) to be ethyl 2-deoxy-2-oximino-α-D-*arabino*-hexopyranoside (**2**), mp 136°C; $[\alpha]_D$ 94° (ethanol). *Anal.* calcd. for $C_8H_{15}NO_6$: C 43.43, H 6.78, N 6.33; found: C 43.34, H 6.72, N 5.46.

The second fraction (0.62 g, 49% yield) crystallized from acetone, mp 146–150°C; $[\alpha]_D$ +138° (ethanol), was characterized (^{1}H nmr, mass spectrum) as the dimer **3**. The ^{1}H nmr spectrum (D_2O) showed singlets for H-1 and H-1′ at 6.14 and 6.18 ppm. The ^{13}C nmr showed nine lines for ring atoms with the signals for C-1, C-5, and C-6 superimposed. *Anal.* calcd. for $C_{16}H_{28}N_2O_{11} \cdot 2H_2O$: C 41.73, H 6.13, N 6.09; found: C 41.15, H 5.95, N 5.77.

The third fraction (0.10 g, 8% yield) was assigned the structure **4** on the basis of its nmr spectra and was not further investigated.

The oxime **2** (221 mg, 1 mmol) was dissolved in water (5 mL), 1 *N* hydrochloric acid (1 mL), and acetaldehyde (3 mmol). After 3.5 h at room temperature, the stirred solution was cooled to 0°C and treated with sodium borohydride (189 mg, 5 mmol) in small portions. After 30 min, the solution was kept at room temperature for 2 h. After neutralization with acetic acid, the solvent was removed and the residue was acetylated with acetic anhydride in pyridine. An 80% yield of ethyl 2,3,4,6-tetra-*O*-acetyl-α-D-glucopyranoside (**17**) was obtained.

The dioxime **3** was treated as described above. The product was chromatographed (solvent C) to yield two fractions. One product was identical to **17**. The other product, obtained in low yield, gave nmr spectra in accord with expectations for structure **18**. As expected, de-*O*-acetylation provided a product possessing (^{1}H nmr) an *O*-ethyl, an *N*-ethyl, and an acetyl group. Spin decoupling required the substituent to be at the 3-position.

*Ethyl 4,6-Di-O-acetyl-3-azido-2,3-dideoxy-2-Z-oximino-α-D-arabino-pyranoside (**6**) and the Z- and E-ribo-Isomers (**7** and **8**)*

(a) In Dimethylformamide at Room Temperature

The glycoside **1** (1.04 g, 3 mmol) and sodium azide (780 mg, 12 mmol) were stirred together in DMF (50 mL, Fisher Reagent Grade) for 30 h at room temperature. Complete conversion of **1** into two new products was revealed by tlc (solvent E, 3 developments). The mixture was treated with anhydrous ether and the inorganic salts were removed by filtration. The filtrate was diluted with dichloromethane (250 mL) and washed with water (4 × 50 mL), dried over magnesium sulfate, and taken to dryness. Column chromatography of the residue by use of solvent E provided ethyl 4,6-di-*O*-acetyl-3-azido-2,3-dideoxy-2-*Z*-oximino-α-D-*arabino*-hexopyranoside (**6**) in 40% yield (400 mg), mp 88–90°C (recrystallized from ethyl acetate – hexane); $[\alpha]_D$ 55° (*c* 1, in chloroform); ir_{max}: 2100 (N_3) cm^{-1}; ^{1}H nmr data: 6.02 (s, 1H, H-1), 5.06 (t, 1H, $J_{4,5}$ = 10 Hz, H-4), 4.43 (d, 1H, $J_{3,4}$ = 10 Hz, H-3). *Anal.* calcd. for $C_{12}H_{18}N_4O_7$ (330.2): C 43.63, H 5.45, N 16.96; found: C 43.83, H 5.58, N 17.10.

Further developments of the column gave ethyl 4,6-di-*O*-acetyl-3-azido-2,3-dideoxy-2-*Z*-oximino-α-D-*ribo*-hexopyranoside (**7**) (400 mg, 40%), mp 73–75°C; $[\alpha]_D$ 123° (*c* 1, in chloroform); ir_{max}: 2105 (N_3) cm^{-1}; ^{1}H nmr data: 5.90 (s, 1H, H-1), 4.94 (q, 1H, $J_{4,5}$ = 9 Hz, H-4), 4.75 (d, 1H, $J_{3,4}$ = 4 Hz, H-3). *Anal.* calcd. for $C_{12}H_{18}N_4O_7$ (330.2): C 43.63, H 5.45, N 16.96; found: C 43.39, H 5.54, N 16.93.

(b) In Dimethylformamide at 65°C

A mixture of glycoside **1** (796 mg, 2.3 mmol) and sodium azide (1.52 g, 23.4 mmol) in the commercial DMF (25 mL) was heated at 65°C for 3 h. Thin-layer chromatography (solvent E) then indicated complete conversion of **1** into two major products that were accompanied by a small proportion of a third product. The mixture was brought to room temperature and processed as described in (*a*). Column chromatography (solvent E) of this

Can. J. Chem. Downloaded from www.nrcresearchpress.com by 210.87.254.40 on 09/06/12
For personal use only.

Can. J. Chem. Downloaded from www.nrcresearchpress.com by 210.87.254.40 on 09/06/12
For personal use only.

mixture furnished **6** (240 mg, 32%), **7** (230 mg, 30.6%), and its *E*-isomer **8** as an oil (75 mg, 10%); $[\alpha]_D$ 57° (*c* 1, in chloroform); ir_{max}: 2100 (N_3) cm^{-1}; ^1H nmr data: 5.15 (s, 1H, H-1), 5.64 (d, 1H, $J_{3,4}$ = 3 Hz, H-3), 4.87 (q, 1H, $J_{4,5}$ = 9 Hz, H-4).

(c) In Dry Dimethylformamide

An attempt to repeat the preparation reported in (*b*) above using DMF distilled from phosphorus pentoxide failed to indicate an appreciable extent of reaction after 12 h at 65°C. However, on making the solution 1% in water, the rates of reaction and products formed were comparable to those mentioned in (*b*) above.

(d) In Dry Dimethylformamide and Using 18-Crown 6 (10)

Under the conditions reported in (*c*) above using dry DMF but adding equivalent amounts of the sodium azide and the crown ether, the reaction at 65°C was complete in 2 h to give the same mixture of **6**, **7**, and **8** obtained in (*b*) above. The reaction took 18 h at room temperature.

(e) In Aqueous Dioxane

To a solution of the oxime **1** (3.0 g, 8.6 mmol) in dioxane (30 mL) was added a saturated aqueous solution (4 mL) of sodium azide (1.7 g, 25.9 mmol), and the stirred mixture was heated under reflux for 8 h. Solvent removal *in vacuo* left a residue which was extracted into ethyl acetate and filtered through Celite. Evaporation of the solvent and column chromatographic separation of the resulting syrup as above, gave **6**, **7**, and **8** in 40, 45, and 10% yield, respectively.

*Ethyl 3-Acetamido-2,4,6-tri-*O*-acetyl-3-deoxy-α-D-gluco-pyranoside (**19**)*

Compound **6** (300 mg, 0.9 mmol) was deoximated and the uloside directly reduced with borohydride as was described above for the conversion of **2** to **17**. The crude product was stirred in methanol (10 mL) and a hydrogen atmosphere in the presence of 5% palladium on charcoal (300 mg) for 24 h at room temperature. The product of acetylation with acetic anhydride in pyridine was recrystallized from ethyl acetate – heptane (212 mg, 63% yield), mp 132–134°C; $[\alpha]_D$ 94° (*c* 1, in chloroform); ^1H nmr: 6.03 (d, broad, exchangeable with D_2O, *J* = 9 Hz, N—H), 4.95 (d, 1H, $J_{1,2}$ = 3 Hz, H-1), 2.08 (s, 6H, 2 × OAc), 2.05 (s, 3H, OAc), 1.90 (s, 3H, NAc). *Anal.* calcd. for $C_{16}H_{25}NO_9$ (375.3): C 51.19, H 6.7, N 3.73; found: C 50.79, H 6.61, N 3.51.

De-*O*-acetylation of **19** with triethylamine in methanol gave the ethyl 3-acetamido-3-deoxy-α-D-glucopyranoside in 85% yield, mp 194–195°C (recrystallized from ethanol – ethyl acetate – Skellysolve B); $[\alpha]_D$ 126° (*c* 1, in ethanol); ^1H nmr (D_2O): 5.20 (d, 1H, $J_{1,2}$ = 3 Hz, H-1), 4.36 (t, 1H, $J_{2,3}$ = $J_{3,4}$ = 10 Hz, H-3), 2.32 (s, 3H, NAc). *Anal.* calcd. for $C_{10}H_{19}NO_6$ (249.2): C 48.18, H 7.68, N 5.61; found: C 48.12, H 7.89, N 5.59.

*Ethyl 3-Acetamido-2,4,6-tri-*O*-acetyl-3-deoxy-α-D-allo-pyranoside (**20**)*

In the same manner as described for the preparation of **19**, the azide **7** was converted in 61% yield to the title compound, mp 120–121°C; $[\alpha]_D$ 85° (*c* 0.7, in chloroform); ^1H nmr: 6.89 (d, broad, exchangeable with D_2O, *J* = 7.4 Hz, N—H), 2.08 (s, 3H, OAc), 2.03 (s, 3H, OAc), 2.00 (s, 3H, NAc). *Anal.* calcd. for $C_{16}H_{25}NO_9$ (375.3): C 51.19, H 6.71, N 3.73; found: C 51.11, H 6.75, N 3.54.

*Ethyl 4,6-Di-*O*-acetyl-2,3-dideoxy-2-Z-oximino-3-phthalimido-α-D-*arabino*-hexopyranoside (**10**)*

A solution of **1** (1.74 g, 5 mmol) and potassium phthalimide (1.5 g) in DMF was stirred for 10 h at room temperature. Solvent removal and extraction of the residue with benzene provided a product which was chromatographed on a column of silicic acid and eluted with diethyl ether – heptane (1:1). The first fraction was unreacted compound **1** (200 mg). The second fraction was the title compound (**10**) (550 mg, 25%) which was recrystallized from chloroform – petroleum ether, mp 157–158°C; $[\alpha]_D$ 71° (*c* 1, in chloroform); ^1H nmr: 7.68 (m, 4H, Ar), 6.00 (s, 1H, H-1), 5.74 (t, 1H, $J_{3,4}$ = $J_{4,5}$ = 10 Hz, H-4), 5.22 (d, 1H, $J_{3,4}$ = 10 Hz, H-3). *Anal.* calcd. for $C_{20}H_{22}N_2O_9$ (434.4): C 55.29, H 5.10; found: C 55.43, H 5.19.

The third fraction proved to be the acetylated form of **3**, ethyl 4,6-di-*O*-acetyl-2-deoxy-3-*O*-(ethyl 3,4,6-tri-*O*-acetyl-2-deoxy-2-iminyl-α-D-*arabino*-hexopyranoside)-2-oximino-α-D-*arabino*-hexopyranoside which crystallized from ethyl acetate – petroleum ether. Yield, 635 mg (20%), mp 178–179°C; $[\alpha]_D$ 44.6° (*c* 0.15, in chloroform); ^1H nmr data: 6.03 (s, 1H, H-1′), 5.90 (s, 1H, H-1), 5.72 (d, 1H, $J_{3,4}$ = 10 Hz, H-3′). *Anal.* calcd. for $C_{26}H_{38}N_2O_{16}$ (634.6): C 49.20, H 6.03; found: C 49.40, H 5.78.

*Mixture of Ethyl 4,6-Di-*O*-acetyl-2,3-dideoxy-2-Z-oximino-α-D-*erythro*-hexopyranoside (**11**) and its* E*-Isomer*

The *Z*-oxime **1** (2.0 g, 5.7 mmol) was dissolved in dry DMF (20 mL) and treated with sodium borohydride (1.06 g, 28.0 mmol) in portions over a period of 30 min. After stirring for 16 h at room temperature, excess borohydride was destroyed by the addition of methanol with cooling. The solvent was then removed *in vacuo* and several portions of methanol were successively evaporated from the remaining residue which was finally purified through a column of silicic acid by means of solvent G. The syrupy product thus obtained (1.13 g, 70%) was found to be a mixture of the isomeric *Z*- and *E*-oximes, in the ratio of 1:2, by the appearance, in the ^1H nmr spectrum, of singlets at 5.87 and 5.03 corresponding to the anomeric protons of these isomers, respectively.

*Ethyl 2-Acetamido-2,3-dideoxy-α-D-*ribo*-hexopyranoside (**12**)*

A 1 *M* solution of borane–tetrahydrofuran complex (20 mL) was added under nitrogen to a stirred solution of the above mixture of oximes (**11**) (0.6 g, 2.07 mmol) in tetrahydrofuran (1 mL), cooled to −5°C. The solution was then kept at room temperature for 24 h. The excess borane was reacted with methanol and solvent removal left a residue which was dissolved in methanol and treated with Dowex 1-X8 resin (hydroxide form). Acetic anhydride (0.45 mL) was added to the filtered solution and the mixture was stirred at room temperature for 1 h. Excess commercial sodium methoxide was then added cautiously until the solution became basic (~pH 9). Stirring was continued for an additional hour prior to treatment with Amberlite IR-120 (H^+) ion exchange resin. Solvent removal left a syrupy residue which was washed several times with ether. Crystallization from ethyl acetate furnished pure **12** (385 mg, 80%), mp 186–188°C; $[\alpha]_D$ 140° (*c* 0.25, in methanol) (lit. (11) mp 185–187°C; $[\alpha]_D$ 149° (*c* 1.05, in methanol). The ^1H nmr data (in D_2O): 5.02 (d, 1H, $J_{1,2}$ = 3.8 Hz, H-1), 3.85 (complex m, 7H), 2.07 (multiplet including a sharp singlet at 2.20, 5H, H-3a, H-3e, and NAc); ^{13}C nmr: 174.2 (C=O), 9.58 (C-1), 73.2 (C-5), 64.8 (C-4, or OCH_2), 64.3 (OCH_2 or C-4), 61.3 (C-6), 48.3 (C-2), 32.4 (C-3), 22.4 ($AcCH_3$), 14.7 (CH_3) ppm.

*Ethyl 3-Deoxy-α-D-*ribo*-hexopyranoside (**13**)*

The mixture of **11** and its *E*-isomer (0.5 g, 1.7 mmol) was deoximated and the uloside reduced with borohydride as described for the preparation of **17**. For purposes of purification, the crude product was acetylated with acetic anhydride and pyridine in the usual way and, after isolation, was deacetylated with sodium methoxide in methanol. Treatment of the solution with Amberlite IR-120 (H^+) resin, filtration, and solvent removal left a residue which was washed with cold chloroform and recrystallized from chloroform – petroleum ether. Yield, 283 mg (85%), mp 92–93°C; $[\alpha]_D$ 144.8° (*c* 1.75, in methanol); ^1H nmr (in D_2O): 4.84 (d, 1H, $J_{1,2}$ = 3 Hz, H-1), 3.88 (m, 7H), 2.34 (m, 1H, H-3e), 1.91 (m, 1H, H-3a). *Anal.* calcd. for $C_8H_{16}O_5$ (192.2): C 49.98, H 8.39; found: C 49.71, H 8.23.

Can. J. Chem. Downloaded from www.nrcresearchpress.com by 210.87.254.40 on 09/06/12
For personal use only.

*Products **14**, **15** and **16**. Reaction of Ethyl 3,4,6-Tri-O-acetyl-2-deoxy-2-oximino-α-D-*arabino*-hexopyranoside (**1**) with Sodium Thiophenoxide*

Compound **1** (1.44 g, 4 mmol) was added to a suspension of sodium thiophenoxide (1.9 g, 14.4 mmol) in acetonitrile (75 mL) and the mixture was stirred at 75°C for 1.5 h. Filtration and removal of the solvent left a solid which was taken up in chloroform, washed with water, dried, and taken to dryness. The yellow solid, which tlc (solvent E) indicated to be a mixture of three products together with some unreacted starting material, was applied to a column of silicic acid and the chromatogram developed with solvent E. The following compounds were obtained in order of elution.

Ethyl 4,6-di-*O*-acetyl-2,3-dideoxy-2-oximino-3-*S*-phenyl-3-thio-α-D-*ribo*-hexopyranoside (**15**), (90 mg, 5.5%), mp 96–97°C; $[\alpha]_D$ 164° (*c* 1.5, in chloroform). The ^{1}H nmr data: 7.36 (m, 5H, Ar), 5.90 (s, 1H, H-1), 5.06 (q, 1H, $J_{3,4}$ = 4.25 Hz, $J_{4,5}$ = 10 Hz, H-4), 4.70 (d, 1H, $J_{3,4}$ = 4.25 Hz, H-3). *Anal.* calcd. for $C_{18}H_{23}NO_7S$ (397.4): C 54.39, H 5.83; found: C 54.71, H 5.84.

Ethyl 6-*O*-acetyl-2,3,6-trideoxy-2-oximino-3-*S*-phenyl-3-thio-α-D-*glycero*-hex-3-enopyranoside (**16**) as an oil (485 mg, 35%); $[\alpha]_D$ 84° (*c* 1, in chloroform). The ^{1}H nmr data: 7.39 (m, 5H, Ar), 6.00 (s, 1H, H-1), 5.62 (d, 1H, $J_{4,5}$ = 2 Hz, H-4), 4.67 (sextet, 1H, $J_{4,5}$ = 2 Hz, $J_{5,6}$ = $J_{5,6'}$ = 4.5 Hz, H-5), 4.11 (d, 2H, $J_{5,6}$ = $J_{5,6'}$ = 4.5 Hz, H-6 and 6'). *Anal.* calcd. for $C_{16}H_{20}NO_5S$ (338.3): C 56.78, H 5.95, S 9.47; found: C 56.05, H 5.74, S 9.52.

Ethyl 4,6-di-*O*-acetyl-2,3-dideoxy-2-*Z*-oximino-3-*S*-phenyl-α-D-*arabino*-hexopyranoside (**14**) (410 mg, 24.9%) as a syrup which solidified on standing, mp 80–85°C; $[\alpha]_D$ 64° (*c* 1, in chloroform). The ^{1}H nmr data: 7.34 (m, 5H, Ar), 6.00 (s, 1H, H-1), 5.18 (t, 1H, $J_{3,4}$ = $J_{4,5}$ = 9 Hz, H-4), 4.30 (d, 1H, $J_{3,4}$ = 9 Hz, H-3). *Anal.* calcd. for $C_{18}H_{23}NO_7S$ (397.4): S 8.06; found: S 7.69.

Unreacted starting material (120 mg, 8.3% recovery).

*Compounds **24** and **25**. Reaction of **14** with Raney Nickel*

The glycoside **14** (300 mg, 0.75 mmol) was treated in methanol (10 mL) with Raney Nickel in the presence of hydrazine hydrate (1 mL) under reflux for 5 h. The catalyst was then removed by filtration and washed with methanol. The combined filtrates gave, upon evaporation, 160 mg of white solid, which was acetylated with acetic anhydride in pyridine. An oil (120 mg) was obtained which was found by tlc (solvent B, 5 developments) to consist of two products. Column chromatography with solvent F yielded ethyl 2-acetamido-6-*O*-acetyl-2,3,4-trideoxy-α-D-*erythro*-hexopyranoside (**24**) (150 mg, 77%), mp 58–61°C; $[\alpha]_D$ 121° (*c* 1, in chloroform); ^{1}H nmr data: 4.72 (d, 1H, $J_{1,2}$ = 3.5 Hz, H-1), 1.65 (m, 4H, H-3a, H-3e, H-4a, and H-4e). *Anal.* calcd. for $C_{12}H_{21}NO_5$ (259.2): C 55.59, H 8.15; found: C 55.53, H 7.94.

Further elution of the column afforded ethyl 2-acetamido-6-*O*-acetyl-2,3,4-trideoxy-α-D-*threo*-hexopyranoside (**25**) as an oil (30 mg, 15.4%); $[\alpha]_D$ 79° (*c* 0.5, in chloroform); ^{1}H nmr: 4.62 (s, 1H, H-1), 1.59 (m, 4H, H-3a, H-3e, H-4a, and H-4e). *Anal.* calcd. for $C_{12}H_{21}NO_5$ (259.2): C 55.59, H 8.15; found: C 55.15, H 7.89.

Compounds **24** and **25** were also obtained when the unsaturated glycoside **16** was treated in the same manner.

Acknowledgements

The authors wish to acknowledge the support of the University of Alberta and the National Research Council of Canada (Grant A-172 to R. U. Lemieux). The nmr spectra and analyses were provided by the spectroscopy and microanalytical laboratories of this Department.

1. S. UMEZAWA. Adv. Carbohydr. Chem. **30**, 111 (1974).
2. J. B. MCALPINE, A. C. SINCLAIR, R. S. EGAN, R. L. DEVAULT, R. S. STANASZEK, M. CIROVIC, S. L. MUELLER, P. C. GOODLEY, R. J. MAURITZ, N. E. WIDEBURG, L. A. MITSCHER, K. SHIRAHATA, H. MATSUSHIMA, S. SATO, and T. IIDA. J. Antibiot. **30**, 39 (1977).
3. D. J. COOPER, M. D. YUDIS, H. M. MARIGLIANO, and T. TRAUBEL. J. Chem. Soc. C, 2876 (1971).
4. R. U. LEMIEUX, T. L. NAGABHUSHAN, K. J. CLEMETSON, and L. C. N. TUCKER. Can. J. Chem. **51**, 53 (1973).
5. R. U. LEMIEUX, F. F. Z. GEORGES, and Z. SMIATACZ. Heterocycles, **13**, 169 (1979).
6. R. U. LEMIEUX, Y. ITO, K. JAMES, and T. L. NAGABHUSHAN. Can. J. Chem. **51**, 7 (1973).
7. R. U. LEMIEUX, K. JAMES, and T. L. NAGABHUSHAN. Can. J. Chem. **51**, 42 (1973).
8. R. U. LEMIEUX, K. JAMES, and T. L. NAGABHUSHAN. Can. J. Chem. **51**, 48 (1973).
9. R. U. LEMIEUX, R. A. EARL, K. JAMES, and T. L. NAGABHUSHAN. Can. J. Chem. **51**, 19 (1973).
10. G. W. GOKAL and H. D. DURST. Aldrichimica Acta, **9**, 3 (1976).
11. E. JEGOU, J. CLEOPHAX, J. LEBOUL, and S. D. GERO. Carbohydr. Res. **45**, 323 (1975).

Products from interaction of aromatic nitrocompounds with argon metastables inside a gas chromatograph[1]

WALTER A. AUE, VELUPPILLAI PARAMASIGAMANI,[2] AND JAE H. KIM

Chemistry Department, Dalhousie University, Halifax, N.S., Canada B3H 4J3

Received August 12, 1980

This paper is dedicated to Professor W. E. Harris on the occasion of his retirement from the University of Alberta

WALTER A. AUE, VELUPPILLAI PARAMASIGAMANI, and JAE H. KIM. Can. J. Chem. **59**, 1439 (1981).

The neutral products resulting from the degradation of aromatic nitrocompounds, following interaction with argon metastables (presumably by Penning ionization), have been studied inside a gas chromatographic system. The simplest but typical example, nitrobenzene, yields benzene and phenol. Product ratios sometimes resemble results of mass spectrometry more than they do data obtained by pyrolysis. The ease of elimination of substituents from monohalogenated nitrobenzenes follows the order I > NO_2 > Br > Cl. Ratios of the products resulting from loss of NO (rearrangement) versus loss of NO_2 have been measured for a variety of compounds. The leaving NO_2 group can be replaced by I if the system is doped with iodine vapour. Reduction of the nitro group and ring closures are observed with some of the more complex substrates, similar to results known from discharge chemistry.

WALTER A. AUE, VELUPPILLAI PARAMASIGAMANI et JAE H. KIM. Can. J. Chem. **59**, 1439 (1981).

On a étudié dans un système de chromatographie en phase gazeuse, les produits neutres de dégradation des composés nitrés aromatiques résultant d'une interaction avec des métastables de l'argon (probablement par une ionisation de Penning). L'échantillon à la fois le plus simple et le plus représentatif, le nitrobenzène, conduit au benzène et au phénol. Les rapports des produits ressemblent quelquefois d'avantage aux résultats de la spectrométrie de masse qu'aux données obtenues par pyrolyse. La facilité d'élimination des substituants à partir des nitrobenzènes monohalogénés varie selon l'ordre suivant: I > NO_2 > Br > Cl. On a mesuré, pour un certain nombre de composés, les rapports entre les quantités de produits provenant de la perte de NO (transposition) et ceux dus à la perte de NO_2. Le groupe labile NO_2 peut être remplacé par I si on ajoute de la vapeur d'iode au système. Dans le cas de substrats plus complexes, on observe la réduction du groupe nitro et des annellations; ces résultats ressemblent à ceux observés dans la chimie de la décharge.

[Traduit par le journal]

Introduction

Aromatic nitro compounds are used widely as explosives, propellants, biocides, and intermediates for chemical synthesis. As a consequence, they are often found dispersed at trace levels in the environment. In this form they pose a formidable challenge to the analyst.

Not the least of the analyst's problems is the need for confirmation. Popular methods involve chemical derivatization and, more often, degradation methods that monitor ions such as mass spectrometry.

In contrast, methods that monitor *neutral* products of gas-phase degradations are far less common. To wit: gas chromatography – mass spectrometry (gc–ms) is the most esteemed of all confirmation methods, while gas phase pyrolysis of gc peaks (1) is rarely encountered in the literature. There are good reasons for this, for instance the great advantage of knowing accurate fragment masses, the much larger ms literature, and the difference between ionic and radical degradation processes.

Beyond this relatively narrow analytical context, the gas-phase reactions of aromatic nitro compounds, ionic or radical, have been the subject of numerous studies in organic and physical chemistry. This study, although undertaken with future analytical goals in mind, reports likewise on the characteristic behaviour of nitro compounds in a particular type of gas-phase degradation. It starts with ionization but ends with the determination of neutral products.

In past years we had performed various ionic and radical degradation processes right inside a two-dimensional gas chromatograph. This was done to produce and separate neutral products that would be indicative of the original analyte.

Some of the chosen fragmentation techniques, e.g. electron capture (2) or photolysis (3), worked to our satisfaction. However, these could be used only for compounds that suitably capture electrons or absorb radiation, and then only within relatively limiting concentration ranges.

A third approach, which could be used on a much more varied selection of compounds, involved Penning ionization. The term denotes ionization by electronically excited neutrals, particularly by noble gas atoms in long-lived states.

$$Ar^* + M \rightarrow Ar + M^+ + e^-$$

[1]Presented at the 62nd conference of the Chemical Institute of Canada in Vancouver, B.C., June 1979.

[2]Current address: B19 Environmental Health Centre, Health and Welfare Canada, Tunney's Pasture, Ottawa, Ont., Canada K1A 0L2.

0008-4042/81/101439-10$01.00/0

©1981 National Research Council of Canada/Conseil national de recherches du Canada

Can. J. Chem. Downloaded from www.nrcresearchpress.com by 210.87.254.105 on 09/06/12
For personal use only.

Can. J. Chem. Downloaded from www.nrcresearchpress.com by 210.87.254.105 on 09/06/12
For personal use only.

This is the basis of the well-known gc "argon detector" (4, 5), which monitors ionization of organic solute molecules by argon metastables.

We have shown that the use of an argon plasma is feasible for *in situ* degradation of gas chromatographic peaks (6). Argon was chosen for similar reasons as apply to the argon detector. It is inexpensive enough to be used as a gc carrier gas and it can be easily purified. Its metastable states ($^3P_2$ and $^3P_0$, 11.54 and 11.72 eV, lifetime at atmospheric pressure 0.2×10^{-6} s; also argon molecules, about 10.1 eV, lifetime 3.4×10^{-6} s, as cited in ref. 5) are suitably long-lived. Their energy is high enough to ionize most organic compounds, yet low enough to avoid excessive degradation. (It should be noted, however, that Penning ionization is only one of a number of processes, both ionic and radical, that can initiate degradation in an argon plasma.)

In our experiments, argon (or other noble gases) could be used, while nitrogen could not. The latter carrier degraded the analyte but did not yield significant fragmentation products. In fact, small amounts of nitrogen in argon inhibited formation of gc-separable products. This was taken as indication that the products do indeed arise from initial Penning ionization. There are prominent metastable states of N_2 much below the ionization potential of organic compounds, and N_2 reacts efficiently with Ar*. The glow originating from the latter reaction is often used as a test for the presence of argon metastables.

Degradation techniques that start with the molecular cation should show similarities to processes postulated for EI-ms, CI-ms, API-ms and plasma chromatography, although, of course, the latter systems recognize only ionic products while the gas chromatographic approach is restricted to volatile, neutral species. Also, there should be similarities to the discharge chemistry of larger organic molecules (7). It must be realized, however, that syntheses in discharges are assumed to involve mainly *radical* processes, although ionic intermediates have been postulated for certain cases and there is a general lack of mechanistic information in this area.

Regardless of the nature of the intermediates, however, the fact that products have to be neutral and relatively stable to be recognized in either technique makes for some similarity. After all, there is only a limited number of stable structures that one can reasonably expect to emerge from a given substrate. Furthermore, even the fragmentation of positive ions generates various neutral species. These would not be directly "seen" in a mass spectrometer, but they, or their fragments, can form compounds separable by gc. Especially important in this context are larger radicals that can emerge as stable compounds via hydrogen abstraction from a suitable substrate.

It needs to be emphasized here that the pressure in our system is the highest of all degradation methods mentioned so far, ranging typically between two and three atmospheres. This has obvious consequences for the probability of ion–molecule reactions vs. unimolecular degradations.

The literature of the various ionic degradation methods for nitro compounds is an interesting one. A part of it relating to explosives has recently been reviewed (8). The nitro group can leave in either anionic, radical, or cationic form. The second prominent fragmentation pathway is the loss of NO (9).

There is little, if any, evidence for such losses in plasma chromatography (10, 11). The ions observed by this technique are usually MH^+ or M^-. The loss of NO_2 is thought to occur only at higher energy. Halogenated nitroaromatics lose Cl, Br, or I, but not NO_2 (12). In an API source, *o*- and *p*-chloronitrobenzene exchange the halide against oxygen (from O_2 traces), but the *meta* isomer forms the molecular anion (13).

The neutral products from pentachloro- and tetrachloronitrobenzene in an electron capture detector, however, do show loss of NO_2: pentachloro- and tetrachlorobenzene are the primary products and there is no evidence for products that retained the nitro group (14). Generally, though, nitro compounds are assumed to engage in associative, halogen compounds in dissociative, electron capture. The lifetimes of a great number of relevant negative ions have been determined (15).

Considerable work has been done with free radicals from the pyrolysis of nitro compounds. Parallel to electron impact mass spectrometry, the primary losses are those of NO and NO_2 (16). In this review as well as in a later paper (17), attention is drawn to the fact that widely disparate degradation methods, presumably based on totally different principles and/or processes, can lead to surprisingly similar results.

Thus it is also with the results obtained in this study. The neutral products of gas chromatographic peaks subjected to Penning ionization conditions showed general similarities to mass spectroscopy on the one, to discharge chemistry on the other hand.

It must be mentioned that Penning ionization mass spectra have been described (ref. 18 and literature cited therein). Unfortunately, the number of

Can. J. Chem. Downloaded from www.nrcresearchpress.com by 210.87.254.105 on 09/06/12
For personal use only.

such spectra is very small. When comparisons with mass spectra are made in this paper, they refer therefore to electron-impact ms.

Experimental

The instrument used for this study has been recently described (6). Its essential capability is that a gc peak of interest can be separated from other sample components on a first gc column and routed to a flow-through reactor. Reactors with parallel plate and pin-cup geometries employ ^{63}Ni-coated gold foils, and are operated in constant-current mode (typically 20 to 200 μA) or, less often, in constant-voltage mode (typically 2000–4000 V). The approximate argon flow through the reactor is 50 mL/min, its temperature 250°C. (These settings are not overly critical.) The degradation products plus residual analyte flow on to a second gc column where they are separated.

In this study, FID detection and highly purified argon carrier gas were used throughout. On occasion, the fragmentation took place in the presence of small amounts of dopants such as hydrogen and iodine. Hydrogen was added directly to the effluent from the first column. Iodine was introduced at the same junction by a low flow of argon that had passed over I_2 crystals at room temperature ($vp_{I_2} \approx 0.3$ Torr; or $\approx 10^{-5}$ g I_2 per min).

Model compounds were injected, degraded at various voltage or current settings, and the nature and relative yield of major degradation products determined. Frequent "blanks" (with the power supply turned off) had to be run to ensure that the observed products did not arise from extraneous reactions (i.e. solute degradation in the chromatographic system).

Identification of products was done only by retention, sometimes on two different columns, and co-chromatography with authentic standards. It must be stressed that, as a consequence, the results are subject to the well-known limitations of gas chromatography in this respect. However, the simplicity of product patterns and their obvious relationship to the parent compound leave little doubt about the general correctness of structural assignments.

Mass spectra were obtained on a CEC 21-104 instrument, operated with a source temperature of 150°C and an anode current of 10^{-4} A. Its approximate resolution was 600, thus certain important doublets were unresolved.

Results and Discussion

Besides the uncertainties peculiar to qualitative analysis by gc, a few very general and fairly obvious points need to be kept in mind whenever the output of the system, a series of gas chromatographic peaks, is subjected to speculation concerning their origin. Such speculation is likely to arise, mainly because this particular degradation methodology may well transcend its original analytical mission. The following points will therefore be discussed in some detail.

First, analyte reactions with argon metastables at a pressure of two to three atmospheres can be considered a relatively "soft" degradation method. The energy of the metastables is not far above the ionization potentials of most organic compounds, and dissipation of excess energy is relatively easy. The high pressure favors two and three-body processes and the establishment of equilibria.

Second, degradation of solute molecules may be initiated by processes other than Penning ionization.

While the system has been devised with Penning ionization in mind, and while evidence gathered so far does not deny the assumption that this mode prevails, the fact is that relatively complex organic molecules are used as substrates and that the chromatogram can describe only the final result of a possibly quite complex sequence of reactions. Different types of analytes may differ in regard to breakdown mechanism and, at best, only very thorough, detailed, and comprehensive studies could establish with some degree of certainty their mechanistic classification. This is a predicament shared with, among other established approaches, discharge synthesis. And the fact that ours is a technique yet in its infant stage certainly aggravates the problem.

What processes, beside Penning ionization by the argon $^3P_2$ and $^3P_0$ species, could initiate compound degradation? There is the obvious possibility that higher excited states may become involved, and the fact that the plasma can be pushed to degrade even methane (whose ionization potential is higher than the energy available from the metastables) certainly attests to that. There are the possibilities of associative (Hornbeck–Molnar) ionization

$$Ar^* + M \rightarrow ArM^+ + e^-$$

dissociative ionization

$$Ar^* + MX \rightarrow Ar + M^+ + X^- \text{ (or } X + e^-)$$

and ionizations with various types of rearrangements. Generally, however, Penning ionization yielding the molecular cation is perceived as a main, but not the exclusive, ionic reaction channel on the basis of experiments with relatively simple molecules (19). One would assume that the complex organic molecules of this study are even more likely to react in this manner.

Ionization of analyte molecules can also occur by charge transfer from Ar^+ (ionization potential of argon 15.76 eV), from Hornbeck–Molnar species such as Ar_2^+ or ArM^+, or from various other ions of lower energy that are present when a peak passes through the reactor. After all, the current is usually around 1×10^{-4} A or 1×10^{-9} F/s (compared with a typical 10 s peak of 10^{-4} g or 10^{-7} mole/s). To be noted in this context, though, are calculations by Collinson *et al.* (5) showing that, for a particular argon detector geometry, the number of metastables generated is ca. 55 times as large as the number of positive ions. (If this applies also to our system, the number of metastables would be

Can. J. Chem. Downloaded from www.nrcresearchpress.com by 210.87.254.105 on 09/06/12
For personal use only.

roughly of the same order of magnitude as the number of solute molecules.)

Another possibility of cation (or possibly ion-pair) formation is electron impact. Collisions with electrons also excite the neutral molecules and lead to radical fragmentation, i.e. processes that are considered responsible for most of discharge chemistry. The preferred status of noble gases, however, militates against a major role for this process in our system.

Radicals are sure to be present, though. For one, the fragmentation of a radical cation usually produces an even-electron ion and a radical. While radicals (and their further products) are not "seen" in ms, they can proceed to form stable compounds recognizable by gc.

Another possibility about which little is known, but which cannot be easily discounted with compounds carrying nitro or halogen substituents, is negative ion formation. In EI-ms systems, anion abundance is highly dependent on pressure. The fact that, in our system, the random substitution typical of, say, the chlorine radical has not been observed, may indicate the presence of the alternative chloride anion.

Aside from electron impact and the fragmentation pathways of a molecular ion, excitation of analyte molecules and subsequent radical fragmentation can also occur by energy transfer from the same argon metastables that are responsible for Penning ionization. There is ample spectroscopic evidence for this process happening with a variety of simple molecules; in fact, excitation by argon metastables is an excellent way of obtaining certain interesting emission spectra (20). The question to what extent, and on what substrates, such processes compete with Penning ionization will, it is hoped, become somewhat clearer in the future as more product patterns become available.

Finally, there is the rather disturbing but ever-present possibility of wall reactions (21) without or with catalytic effects (e.g. on the Ni-63 foil). One would also expect the "cleanliness" of the reactor to be of importance in this context. Whether or not wall reactions do play a significant role in our system, however, is unclear at present.

Third, a variety of processes can or must occur before fragmentation products appear as chromatographic peaks on the recorder chart. Given that ions and radicals exist in the reactor, these species have to form stable compounds that can pass through a gc column. It should be noted that, in our system, 100% yields (of products plus residual analyte) would be quite rare, although values above 50% are not uncommon. (In fact, this is remarkably good for degradation processes of all sorts running at ~3 atm pressure. The present reactor cell has been in operation for over three years and has yet to be cleaned.) Still, low yields indicate the possibility that certain processes will go unnoticed because the species involved do not lead to peaks in the final chromatogram.

To produce peaks, ions have to neutralize, and little is known about the direct neutralization process (cation/anion or cation/electron). If such neutralization were to liberate energy anywhere close to the typical ionization energies, one would expect extensive fragmentation to result. If they are not neutralized in the gas phase, some ions should reach the electrodes, provided their lifetime in this particular environment allows them to do so. (Under typical conditions, it should take an ion about 10^{-4} s to traverse the reactor.) What happens then at the electrode is, again, a matter of speculation.

Ions can also transfer charge to become, often after hydrogen abstraction from a suitable substrate, stable compounds. This process could perhaps be considered the "softest" type of neutralization, and much more is known about it from chemical ionization mass spectrometry.

Fourth, the *same* product can be formed by different pathways. For instance, the formation of benzene from nitrobenzene, just counting mass spectrometric evidence, could start from a positive, neutral, or negative C_6H_5 species.

Fifth, the formation of stable compounds from ions or radicals often requires the presence of another reactant (e.g. a hydrogen donor for the phenoxy precursor of phenol). Also, degradation products can react with each other (for instance forming biphenyl from a substituted benzene).

Sixth, the yield of a product from a particular precursor reflects not only the rate of formation but also the rate of further degradation of that product. Elementary as that appears, it is easily overlooked in front of a pretty chromatogram presenting a number of "final" products.

Seventh, the geometry of the argon reactor, the flow patterns and field gradients in it, and the power level at which it is run, can all influence relative product yields. This is not too surprising and can be compared, perhaps, to the difference in mass spectra related to pressure and temperature, not to speak of the cleanliness of either degradation enclosure. As one point out of many, the lifetime of argon metastables (in argon at atmospheric pressure) allows them to diffuse about 10^{-4} cm from a position close to the anode (5). Obviously, solute molecules entering the cell in that spot are likely to

TABLE 1. Product patterns of nitrobenzene[a]

Product	Pyrolyzer (16)	Argon reactor[b]	Mass spectrometer 13 eV	Mass spectrometer 30 eV	Mass spectrometer Ions
Benzene	1.0	1.0	1.0	1.0	$C_6H_5^+$
Phenol	5.4	0.63	0.55	0.20	$C_6H_5O^+ + NO^+$
Aniline	0.28	Hidden; small if present			
Benzonitrile	1.0	0.06			
Biphenyl	4.0	Hidden; small if present			
Dibenzofuran	3.0	Not detected			
	Various biphenyl and higher structures in considerable amounts				

[a]Normalized to benzene.
[b]FID peak areas in temperature-programmed run.

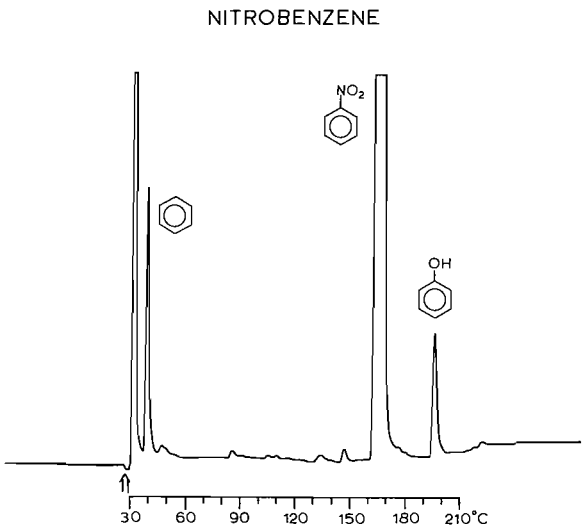

FIG. 1. Degradation pattern of nitrobenzene in an argon plasma reactor. Separation of degradation products by column 2, as seen by FID-2. Column 2: 5% Carbowax 20M on Chromosorb W, 45/60 mesh, in 200 × 0.4 cm id borosilicate tube; temperature-programmed as indicated; Ar ca. 50 mL/min.

encounter a different reaction milieu than if they had entered, say, around the cathode. Product ratios can therefore vary.

To end the fairly obvious points on an experimental note, any quantitative comparison of product ratios from the argon reactor, such as in Tables 3 or 4, implies that these were obtained under conditions as similar as possible.

In Fig. 1, the degradation of nitrobenzene leads, as expected, to benzene and phenol, but very few other peaks are evident. One can compare this result (subject, as always, to the various caveats mentioned above) to results from pyrolysis (16) and from mass spectrometry (Table 1). When comparing mass spectrometric data in particular, one has to be aware of the rather tenuous connection between neutral molecules presumed to have arisen from initial Penning ionization, and the apparent cations (and, by inference, neutrals, radicals, and their possible fragments) from the mass spectrum that could have served as their precursors. Furthermore, the argon metastables are about 11.6 eV above ground state; therefore the ms has to be run pretty well at the lowest possible energy setting (in our case a nominal 13 eV). To indicate the direction in which electron energy influences relative ion intensity, a scan at 30 eV is included.

Table 1 suggests (based, however, on only one ratio) that the argon reactor results are closest to those of 13 eV electron-impact ms, as one would have expected for Penning ionization. In contrast, they seem to have little in common with the pyrolysis pattern. It should be realized, though, that the abundance of dimerization products is obviously concentration-dependent, hence less useful for comparison of product ratios. The significance of comparing the argon reactor data with mass spectrometry and pyrolysis lies, of course, in the fact that the former method starts with ionization, the latter with radical bond fission. By analogy, the assumption of Penning ionization as the decisive mechanism in the argon reactor is buttressed by such results.

The difference between the argon reactor and the pyrolyzer (16) is also evident in the degradation of 2-nitroethylbenzene (Table 2). While there are, of course, some common compounds, the main pyrolysis product, aniline, was not even detected in the argon reactor effluent. Conversely, the prominent argon plasma products *o*-ethylphenol and phenol seem not to have been formed in the pyrolyzer.

Table 2 also contains mass spectrometric infor-

Can. J. Chem. Downloaded from www.nrcresearchpress.com by 210.87.254.105 on 09/06/12
For personal use only.

TABLE 2. Product patterns of 2-nitroethylbenzene

Product	Pyrolyzer (16)	Argon reactor	Mass spectrometer 13 eV[a]	Mass spectrometer 30 eV[a]	Ions	m/e
Indole	68	32				
O-ethylphenol		44	3.4 + 2.7 = 6.1	1.6 + 9.7 = 11.3	$(M - NO)^+$ + NO^+	121 30
Phenol		27	4.4	28.6	$(M - C_2H_5 - NO)^+$	92[b]
O-nitrotoluene		20				
Styrene	24	100				
Ethylbenzene		48	11.5	13.1	$(M - NO_2)^+$	105
Aniline	100	Not detected				
O-toluidine	11	Not detected				

[a]Base peak (100) is $(M - OH)^+$.
[b]Corrected for C-13 contribution from presumed tropylium ion at 91.

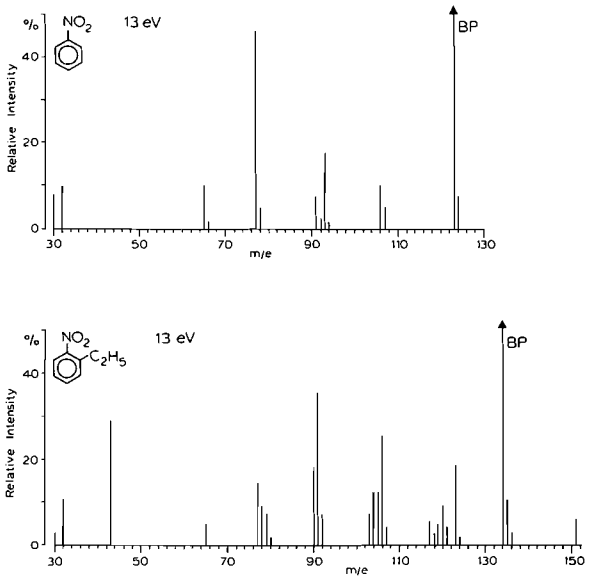

FIG. 2. Electron impact mass spectra at 13 eV of nitrobenzene and *o*-ethylnitrobenzene. BP = base peak.

mation, but the greater complexity of the test compounds makes meaningful comparisons close to impossible. For instance, the base peak, $(M - OH)^+$, has no directly equivalent neutral product, although one could consider it a precursor of indole. Obviously, Table 2 lists only selected ions. For further comparison, the 13 eV electron impact mass spectrum of *o*-nitroethylbenzene is reproduced in Fig. 2, together with that of nitrobenzene itself.

Sometimes it may be more fruitful to compare defined product ratios, rather than whole product patterns. For instance, one would expect the competition between rearrangement and elimination of the nitro group to provide such a comparison. That is, the ratio R—OH/R—H (arising from degradation of $R—NO_2$) should, first, decrease with increasing energy and, second, depend on the nature of the aromatic system and its substituents.

TABLE 3. R—OH/R—H ratios of products from $R—NO_2$

R	Argon reactor[a] R—OH/R—H	Mass spectrometer $\left(\frac{(M-NO)^+ + NO^+}{(M-NO_2)^+ + NO_2^+}\right)$ 13 eV	30 eV
Phenyl	0.6	0.6	0.2
2-Biphenyl	0.5(0.6[b])	3.6	1.4
3-Biphenyl	0.4	0.5	0.1
4-Biphenyl	0.4	0.08	0.03
o-Tolyl	1.0	0.2	0.1
m-Tolyl	0.9	0.1	0.1
p-Tolyl	1.0	0.5	0.2
1-Naphthyl	1.2	2.4	2.5
2-Naphthyl	0.7	0.07	0.06
2-Ethylphenyl	0.9	0.5	0.9

[a]FID peak area ratios from temperature-programmed runs.
[b]Includes dibenzofuran.

To check out the first expectation one would have to use metastables of different energy. Some preliminary experiments in this direction have been done, but the results appear rather contradictory at present. They will be the subject of a separate study.

The second expectation was easier to pursue. Table 3 shows ratios from various aromatic nitro compounds. Certain trends are obvious, as can be seen, for instance, from a comparison of the three nitrobiphenyls to the three nitrotoluenes. In-

Can. J. Chem. Downloaded from www.nrcresearchpress.com by 210.87.254.105 on 09/06/12
For personal use only.

TABLE 4. Product ratios from monohalonitrobenzenes

Compound (X in X-ϕ-NO_2)	Argon reactor[a] ϕ-X / ϕ-NO_2	Mass spectrometer[b] ϕ-X^+ / $HX^+ + X^+$ 13 eV	30 eV	Argon reactor[a] X-ϕ-OH / ϕ-X	Mass spectrometer[b] X-ϕ-$O^+ + NO^+$ / ϕ-X^+ 13 eV	30 eV
o-Cl	5.0	4.9	7.1	1.1	1.5	0.57
m-Cl	7.8	4.6	6.9	0.50	0.42	0.18
p-Cl	6.1	3.8	9.4	0.71	1.9	0.53
o-Br	1.3	7.5	9.7	0.46	1.7	0.76
m-Br	1.9	10.3	9.0	0.43	0.92	0.42
p-Br	0.96(?)	9.6	13.8	0.55	2.0	0.54
o-I	0.27	5.2	9.1	0.24	1.0	0.59
m-I	0.41	1.6	1.0	0.27	0.35	0.31
p-I	0.24	5.2	11.0	0.60	1.1	0.50

[a]FID peak area ratios from temperature-programmed runs.
[b]Both isotopes considered for Cl and Br.

teresting is also the clear difference between the 1 and 2 positions on the naphthalene ring.

Mass spectrometric ratios have been included in Table 3. There is no clear-cut correlation, although some trends do correspond. This is not too surprising. Besides experimental variation, one could expect considerable differences between the behavior of, say, the tropylium ion in the low-pressure, essentially unipolar environment of the mass spectrometer and the high-pressure, bipolar argon reactor cell. Furthermore, some of the mass spectral data remain ambiguous in the absence of high-resolution measurements. For instance, our instrument cannot distinguish between the masses of NO and H_2CO and doublets are likely in some cases. In the tables we have, of necessity, ignored the problem, but it would have to be addressed if more than "trends" were at stake.

Peaks resulting from the elimination of either NO or NO_2 appeared prominent, and it was therefore interesting to compare them with peaks resulting from the loss of other substituents. Subject to the limited information content of peak amplitude and position as discussed above, a semi-quantitative answer can be given to the "ease of removal" of the NO_2 group vs. one of three halogens from various monohalonitrobenzene substrates. Figure 3 presents an example and Table 4 lists, aside from other data, the product peak height ratios of $\phi X/\phi NO_2$; i.e. an approximate measure of the extent to which NO_2 is removed in comparison to a particular halogen. Clearly, NO_2 leaving is more likely than Cl or Br but less likely than I; on average by factors of 6.3, 1.4, and 0.3 in this experimental series. It should be noted that these values can vary somewhat with current or voltage settings; however, the general sequence Cl < Br < NO_2 < I was always observed.

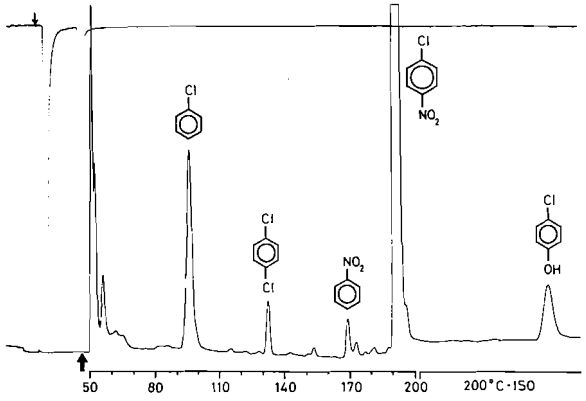

FIG. 3. Degradation pattern of *p*-chloronitrobenzene. Top chromatogram (inverted): Separation of title compound from solvent in column 1, as seen by FID-1, for introduction to plasma reactor. Column 1: 5% Carbowax 20M on Chromosorb W, 45/60 mesh, in 90 × 0.4 cm id borosilicate tube; isothermal at 190°C; Ar ca. 35 mL/min. Bottom chromatogram: Separation of degradation products by column 2, as seen by FID-2. Column 2: 5% Carbowax 20M on Chromosorb W, 45/60 mesh, in 200 × 0.4 cm id borosilicate tube; temperature-programmed as indicated; Ar ca. 50 mL/min.

Scanning through the argon-reactor numbers in Table 4 makes it obvious that, on a relative basis, halogen elimination from the *ortho* and *para* positions appears to be preferred to removal from *meta* ("appears" because the departure of halogen is only one of several processes necessary to bring about the finally observed result). The peculiar role of the *meta* position is, of course, well known from studies of aromatic substitution patterns in organic chemistry.

We have to admit to the temptation of drawing, in analogy, mesomeric structures of preferred transition states. However, this would be unmitigated speculation. At this early stage, we do not even know the forms assumed by the various leaving and

Can. J. Chem. Downloaded from www.nrcresearchpress.com by 210.87.254.105 on 09/06/12
For personal use only.

Can. J. Chem. Downloaded from www.nrcresearchpress.com by 210.87.254.105 on 09/06/12
For personal use only.

entering species. They may be cationic, radical, or anionic in free or associated states, not to mention their relative concentration if one species occurs in more than one form. The best one could do for now would be to use analogies from API, CI, or EI mass spectrometry or from plasma chromatography. None of these methods, however, uses energy transfer from noble gas metastables.

Valuable as comparisons of congeneric series are, there is always the complication of possible changes in mechanism. The argon reactor results vary relatively smoothly from chlorine to iodine, and predictions based on the carbon–halogen bond strength would have been qualitatively fulfilled. The trends are clearly evident from the data of Table 4.

Not so with the appended mass spectrometric data. Trends occur, but they are not as clearly expressed. "Mechanisms" change, as seen for instance by the varying relative contributions of HX^+ and X^+ to the removal of halogen. Even though our first quantitative results (on chloronitrobenzenes) promised good correlation between data from the argon reactor and the mass spectrometer, the scans involving bromine and iodine analogues did not follow suit.

Clearly, the matter is more complex than thought at first. What would be needed for a clean experimental approach is a mass spectrometer with a high-pressure Penning ionization source. This instrument does not exist at present, but would certainly be interesting, likely difficult, and probably most worthwhile to build. However, it might fit better into a lab that is not primarily chromatographic and analytical in nature as ours happens to be.

Chromatographically motivated, we have in the past used iodine doping in a two-dimensional gc system (22). Here, as in many other investigations from different fields, the addition of iodine leads to new products. In this study of nitro compounds, iodine was used with the intention of trapping reactive intermediates. An experiment of this sort is shown in Fig. 4. When NO_2 leaves, iodine and hydrogen compete for the vacant position. Whether this represents the usual radical-scavenging effect of the ground-state iodine molecule, or whether particularly reactive states of iodine are involved, is uncertain. Interesting is, in any case, the fact that NO_2 can be exchanged in this direct manner against I. In comparing Figs. 1 and 4, the formation of phenol (as could be expected from a reaction whose essential step is presumably an intramolecular rearrangement) appears undisturbed, while the abundance of products resulting

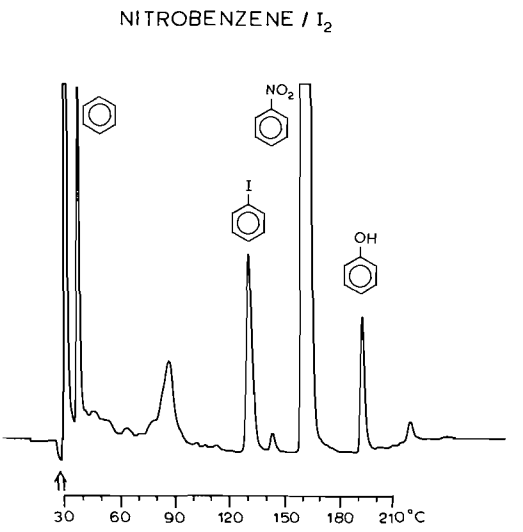

FIG. 4. Degradation pattern of nitrobenzene in iodine-doped argon; ca. 15 mL/min of argon, saturated with iodine at ambient temperature, were added to column 1 effluent prior to entering the reactor. Other conditions as in Fig. 1.

from elimination of NO_2 seems enhanced. However, no further study was made of this aspect.

One can further attempt to scavenge the intermediates from chloro- or bromonitrobenzene by iodine doping. Figure 5 demonstrates this for the former compound. The $\phi X/\phi NO_2$ ratios are not exactly duplicated by the corresponding $I\phi X/I\phi NO_2$ ratios. However, the same tendency is clearly evident, as can be seen from a comparison of Figs. 1 and 4 (X = H), and 3 and 5 (X = Cl).

Halogen can replace the nitro group not only when the former is present, as in the case of iodine, as a dopant. The halogen leaving a molecule of, say, chloronitrobenzene, is available for another

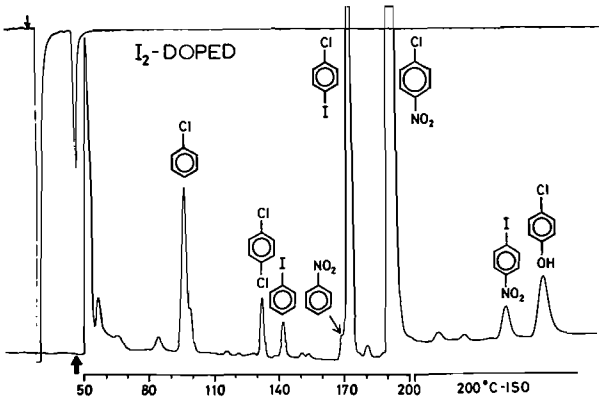

FIG. 5. Degradation pattern of *p*-chloronitrobenzene in iodine-doped argon; ca. 15 mL/min argon, saturated with iodine at ambient temperature, were added to column 1 effluent prior to entering the reactor. Other conditions as in Fig. 3.

Can. J. Chem. Downloaded from www.nrcresearchpress.com by 210.87.254.105 on 09/06/12
For personal use only.

molecule that loses the nitro group, thus leading to the formation of dichlorobenzene (Figs. 3 and 5). Such products, whose structures are alien to that of the original analyte, are usually formed in relatively small amounts. Isomeric configuration, however, is preserved. For nitro compounds as well as for other compounds so far tested, a, say, *para* structure will generally not yield significant amounts of *ortho, meta*, or higher substituted products.

The nature and position of various substituents also appears to influence the relative amount of phenol formed. Tables 3 and 4 contain R—OH/R—H ratios for a variety of compounds. There are definite trends in these numbers, although the experimental evidence is too scarce and too imprecise to allow these to be formulated as rules. It appears that the formation of phenol is usually favored from the *ortho* and *para* positions. The mass spectrometric data of Table 4 correlate herein.

Returning to data of a more synthetic nature, a number of interesting cyclizations were noted. These often parallelled reactions of discharge chemistry, the "*ortho* effect" of mass spectrometry, etc. Correspondence of this sort is not too unusual. Although surprising in view of mechanistic model pathways clearly delineated one against the other, there exists a large amount of similarity among the results of various degradation methods designed to probe different properties of matter with different forms of energy (23). It may be that the stability of products, in this method perhaps more than in others, determines the experimental outcome. For instance, 2-nitrobiphenyl yielded, among others, the following products in regular and H_2-doped systems.

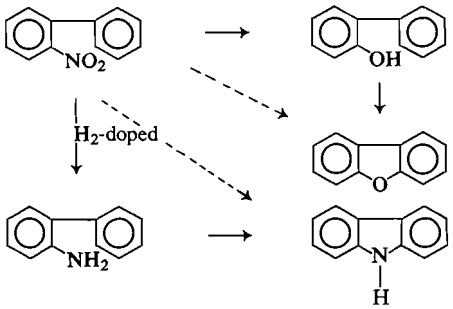

All of the above reactions are also found in discharge chemistry (24), except that, there, the presence of H_2 is not due to its deliberate introduction as a dopant.

2-Amino- and 2-hydroxybiphenyl, when degraded by themselves, do indeed yield carbazole and dibenzofuran, respectively. Whether the former neutral compounds are the main intermediates in the reaction of 2-nitrobiphenyl to the tricyclic structures, or whether they arise from common, higher-energy species has not been established.

Obviously, *meta* and *para* structures do not cyclize. Similarly, only the *ortho* isomer of nitroanisole leads to (among many other products) a second ring.

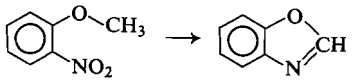

It must be noted that the formation of benzoxazole from *o*-nitroanisole was predicted for a pyrolysis system (16).

Further structures could undoubtedly be obtained from suitable precursors. In general, compounds formed in the argon reactor are of potential interest to a variety of areas. Three applications that come to mind most easily are that the products promise analytical methodology for solute identification or confirmation, that they may provide mechanistic inferences about other degradation methods such as mass spectrometry, and that they could offer synthetic routes to compounds difficult to obtain by conventional means. In each case, problems involving isomeric structure are particularly suitable ones to study with this system, owing to its chromatographic separation capabilities.

Acknowledgements

This research was supported by NSERC grant A-9604, a contribution from Dalhousie's Research Development Fund, and a Killam Fellowship for one of us (V.P.). The valuable advice of D. Jamieson is gratefully acknowledged.

1. D. A. Leathard and B. C. Shurlock. Identification techniques in gas chromatography. Wiley Interscience, New York. 1970. pp. 123–130.
2. W. A. Aue and S. Kapila. Anal. Chem. **50**, 536 (1978).
3. R. Aigner-Held and W. A. Aue. J. Chromatogr. **189**, 127 (1980).
4. J. E. Lovelock. Anal. Chem. **33**, 162 (1961).
5. A. J. L. Collinson, J. R. Bennett, and D. W. Hill. Brit. J. Appl. Phys. **16**, 631 (1965).
6. W. A. Aue, V. Paramasigamani, and S. Kapila. Mikrochim. Acta, 193 (1978).
7. H. Suhr. Pure Appl. Chem. **39**, 395 (1974).
8. J. Yinon. Analysis of explosives. CRC Critical Reviews in Analytical Chemistry. December, 1977. p. 1.
9. J. H. Beynon, M. Bertrand, and R. G. Cooks. J. Am. Chem. Soc. **95**, 1739 (1973).
10. F. W. Karasek and D. M. Kane. J. Chromatogr. **93**, 129 (1974).
11. G. E. Spangler and P. A. Lawless. Anal. Chem. **50**, 884 (1978).
12. F. W. Karasek and D. M. Kane. Anal. Chem. **46**, 780 (1974).

13. I. DZIDIC, D. I. CARROLL, R. N. STILLWELL, and E. C. HORNING. Anal. Chem. **47**, 1308 (1975).
14. S. KAPILA and W. A. AUE. J. Chromatogr. **148**, 343 (1978).
15. L. G. CHRISTOPHOROU, M. W. GRANT, and D. L. MCCORKLE. Adv. Chem. Phys. **36**, 413 (1977).
16. E. K. FIELDS and S. MEYERSON. Adv. Free-Radical Chem. **5**, 101 (1975).
17. S. MEYERSON. 175th Am. Chem. Soc. Meeting, Anaheim, CA. April, 1978. Abstract PETR-43.
18. E. G. JONES and A. G. HARRISON. Int. J. Mass Spectrom. Ion Phys. **5**, 137 (1970).
19. A. FONTIJN. Prog. React. Kinet. **6**, 75 (1971).
20. D. H. STEDMAN and D. W. SETSER. Prog. React. Kinet. **6**, 193 (1971).
21. B. D. BLAUSTEIN and Y. C. FU. *In* Techniques of chemistry. Vol. I. Part IIb. *Edited by* A. Weissberger and B. W. Rossiter. Wiley–Interscience, New York. 1971. p. 184.
22. V. PARAMASIGAMANI and W. A. AUE. Anal. Chem. **52**, 373 (1980).
23. R. C. DOUGHERTY. Top. Curr. Chem. **45**, 93 (1974).
24. H. SUHR. Top. Curr. Chem. **36**, 39 (1973).

Can. J. Chem. Downloaded from www.nrcresearchpress.com by 210.87.254.105 on 09/06/12
For personal use only.

A nuclear Overhauser effect difference study and a two-dimensional *J* proton magnetic resonance study of (6*S*)-prostaglandin I_1 [1]

GEORGE KOTOVYCH,[2] GERDY H. M. AARTS, AND TOM T. NAKASHIMA
Department of Chemistry, University of Alberta, Edmonton, Alta., Canada T6G 2G2

Received August 22, 1980

This paper is dedicated to Professor W. E. Harris on the occasion of his retirement from the University of Alberta

GEORGE KOTOVYCH, GERDY H. M. AARTS, and TOM T. NAKASHIMA. Can. J. Chem. **59**, 1449 (1981).

High-field nuclear Overhauser effect difference measurements allowed the assignment of the proton resonances for (6*S*)-prostaglandin I_1 in phosphate buffer solutions. The two-dimensional *J* proton magnetic resonance experiments complemented these studies, as they also allowed the structure of several multiplets to be obtained when these multiplets are hidden by nearby resonances in a normal spectrum. The chemical shifts and coupling constants are compared with the data obtained previously for (6*R*)-prostaglandin I_1.

GEORGE KOTOVYCH, GERDY H. M. AARTS et TOM T. NAKASHIMA. Can. J. Chem. **59**, 1449 (1981).

Les mesures de différence d'effet nucléaire Overhauser à haut champ permettent d'identifier les résonances des protons de la (6*S*)-prostaglandine I_1 dans des solutions tampon de phosphate. Des expériences de résonance magnétique du proton *J* en deux dimensions constituent un complément à cas études en ce sens qu'elles permettent également d'obtenir la structure de plusieurs multiplets lorsque ces derniers sont masqués par les résonances voisines dans un spectre normal. On a comparé les déplacements chimiques et les constantes de couplage aux données obtenues antérieurement avec la (6*R*)-prostaglandine I_1.

[Traduit par le journal]

Introduction

Prostacyclin (PGI_2) is extremely important in the cardiovascular system as a potent vasodilator and inhibitor of platelet aggregation (1–3, and references therein), as well as a potent inhibitor of gastric acid secretion (4).

Because of the PGI_2 instability and its extreme biological importance, a variety of stable analogs have been prepared, among them 5,6-dihydroprostacyclin, or prostaglandin I_1 (PGI_1) (5–10; see also Johnson *et al.*, ref. 2, pp. 17–29). The two epimers at C6 are designated (6*R*)-PGI_1 and (6*S*)-PGI_1 (11) (Figs. 1 and 2). The PGI_2 structure contains a double bond between C5 and C6, the hydrogen atom at C5 has the 5*Z* configuration, but the rest of the molecule is identical to PGI_1.

The biological activity of the 5,6-dihydro PGI_2 compounds has been studied (9, 12–17; see also Johnson *et al.*, ref. 2, pp. 17–29; and Whittle and Boughton-Smith, ref. 2, pp. 159–171). The results of one study (12) indicate that the orientation of the α chain may play a key role in explaining the potency of these compounds with respect to PGI_2. This suggests specificity in the platelet receptor which may prove useful for pharmacological manipulation (12). Compound (6*S*)-PGI_1 was always more active than (6*R*)-PGI_1 when the activity of both epimers was compared (13).

Nuclear Overhauser effect (nOe) difference measurements have proved to be invaluable in the nmr studies of PGI_2 (18) and (6*R*)-PGI_1 (19). In the present study, these measurements, together with two-dimensional *J* nmr studies and inversion-recovery experiments, are applied to obtain the chemical shifts and coupling constants for (6*S*)-PGI_1 (Figs. 1 and 2), also referred to as *exo* or 6β-PGI_1. These data are compared with those for (6*R*)-PGI_1 (19). In this way, we hope to correlate the structure and activity of these compounds in solution.

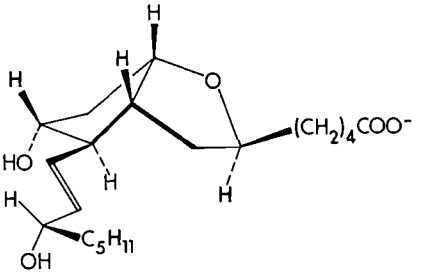

FIG. 1. The structure of (6*S*)-PGI_1.

Materials and Methods

Compound (6*S*)-PGI_1 was a gift from Dr. R. A. Johnson of the Upjohn Co., Kalamazoo, MI. The present measurements were carried out in phosphate buffer (0.2 *M*) in D_2O. The sample preparation was discussed in ref. 19. All of the data were collected in the Fourier transform mode using the Bruker WH-400/DS nmr spectrometer and the Aspect 2000 Data System utilizing 16 or 32K of data memory. All of the experiments were carried out at ambient temperature (298 K). The deuterium

[1]This paper is No. 7 in a series of high-field nmr studies on prostaglandins and vitamins. Paper No. 6 is ref. 19.

[2]Formerly G. Kotowycz.

0008-4042/81/101449-06$01.00/0

©1981 National Research Council of Canada/Conseil national de recherches du Canada

Can. J. Chem. Downloaded from www.nrcresearchpress.com by 210.87.254.5 on 09/06/12
For personal use only.

Can. J. Chem. Downloaded from www.nrcresearchpress.com by 210.87.254.5 on 09/06/12
For personal use only.

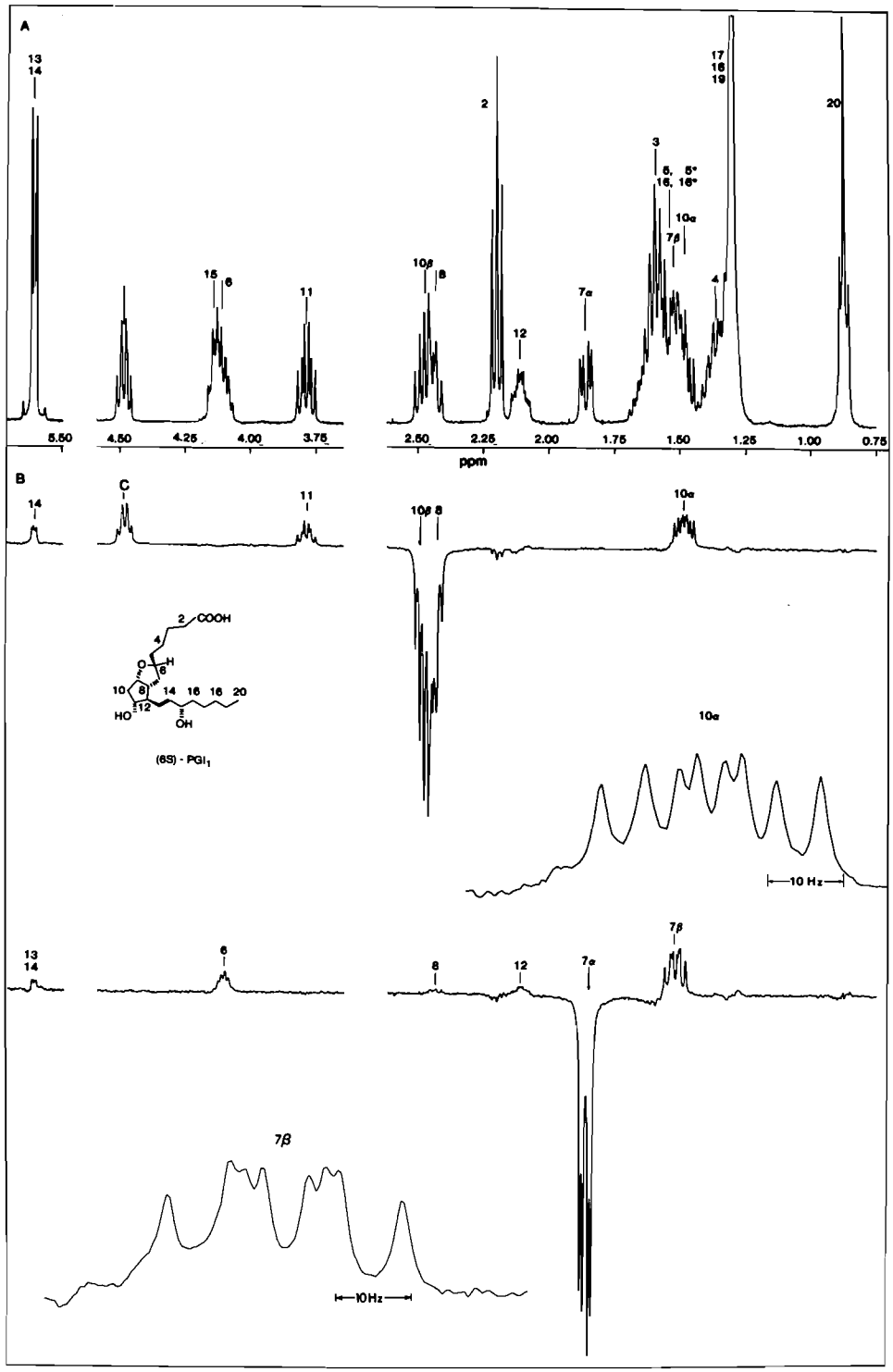

FIG. 2. Results of the nOe difference experiments performed on (6*S*)-PGI_1 in phosphate buffer in D_2O. The normal spectrum is seen in (A). In (B), H-10β and H-8 are saturated with the irradiation frequency centred on H-10β. In (C) H-7α is saturated. The expanded H-10α and H-7β multiplets are shown in (B) and (C).

Can. J. Chem. Downloaded from www.nrcresearchpress.com by 210.87.254.5 on 09/06/12
For personal use only.

resonance of the solvent was used for the lock signal. The chemical shifts and coupling constants were calculated to first order at 400 MHz and are reported with an accuracy of about ±0.010 ppm and ±0.20 Hz, respectively. For maximum accuracy, spectra were expanded to a width of 1 or 2 Hz/cm. The inversion-recovery experiments were carried out using the 180°–τ–90° two-pulse sequence.

The nOe difference experiments (18–23) involve the measurement of the intensity change of a proton resonance upon saturating another proton. A strong nOe indicates that the two protons are in close proximity. The experimental procedure for this technique has been described elsewhere (19).

The two-dimensional *J* nmr spectra (24–26) allow the possibility of restricting one nuclear parameter to one frequency dimension (the chemical shift) and the other parameter (coupling constant) to the other dimension. The structure of a multiplet can thus be obtained, even though in a normal spectrum it may overlap nearby multiplets. The present 2D *J* nmr spectra were obtained using the software provided by Bruker. The standard Hahn spin echo pulse sequence (90°–τ–180°–τ–Acq-RD-) was used with the 90° pulse equal to 10.7 μs and the 180° pulse equal to 21.4 μs. The relaxation delay (RD) was 10 s, and 48 scans per τ value were accumulated. The resolution was 0.610 Hz/point along both the *J* and δ axes corresponding to a spectral width of 39 Hz along the *J* axis (128 points) and 2500 Hz along the δ axis (8192 points). A Gaussian weighting function was applied to the data.

Results

The proton resonances were assigned on the basis of double resonance and nOe difference experiments. From inversion recovery measurements, the H-6 and H-15 multiplets and the H-8 and H-10β multiplets were resolved. The H-7β and H-10α multiplets were resolved from the many overlapping peaks in the region of 1.45 to 1.70 ppm by means of the 2D *J* nmr and the nOe difference experiments. The resonances for H-2, H-13, H-14, H-17 to H-19, and H-20 were assigned on the basis of their characteristic chemical shifts.

The results of the nOe experiments are as follows. When the H-13 and H-14 multiplet is saturated, enhancements are observed by H-15, H-11, H-8, and H-12. Saturation of the H-6 and H-15 protons, with the irradiation frequency centred on H-6, results in nOe's for H-13 and H-14, H-12, H-7α, and H-17 to H-19. Two broad multiplets also appear at ~1.55 ppm and these were assigned to H-5 and H-16, and H-5* and H-16*, respectively, as these protons are adjacent to H-6 and H-15. These assignments were confirmed by carrying out the nOe difference experiments on a (6*S*)-PGI_1 sample in $CDCl_3$ solution where the H-6 and the H-15 multiplets are resolved. The enhancements observed by H-12, H-7α, and H-5,5* are due to saturation of H-6. Saturation of H-11 results in enhancements for H-13 and H-14, H-9, H-10β, and H-8, as well as H-12. This confirms the assignment of H-10β.

Further nOe experiments are shown in Fig. 2. In Fig. 2B, H-10β as well as H-8 are saturated. The irradiation frequency is centred on H-10β. As expected, enhancements are observed by H-13 and H-14, H-9, H-11, and H-10α. This allows the assignment of the chemical shift and determination of the coupling constants for H-10α. The expanded H-10α multiplet is seen in the figure. The assignment of H-10β to low field of H-10α is in agreement with the torsion angle dependency of chemical shifts for five-membered prostanoid precursors (27). Finally, saturation of H-7α (Fig. 2C) results in nOe's for H-13 and H-14, H-6, H-12, H-7β, as well as a very small nOe for H-8. The large nOe experienced by H-6 confirms the assignment for H-7α. The detailed, expanded H-7β multiplet is also shown in Fig. 2C. The enhancement to H-12 cannot be quantitated since it is perturbed by the irradiating field, but a large nOe is also expected. Additional nOe experiments include irradiation of H-2, confirming the chemical shift for H-3. Irradiation of H-9 results in enhancements for H-11, H-8, and H-10β. Nuclear Overhauser effects across the ring, from H-7α to H-8 as seen in Fig. 2C, from H-11 to H-12, and from H-12 to H-11 (upon saturating H-12), were observed in the present nOe studies.

Since the H-7β and H-10α multiplets are buried under many other resonances, the chemical shifts and multiplicity of these multiplets were confirmed using 2D *J* nmr techniques. The results of these experiments are shown in Fig. 3. In this figure, the stacked plot of the partial two-dimensional *J* spectra is seen together with the projection of the tilted 2D *J* spectra to give the totally decoupled spectrum. The multiplicity for H-7β and H-10α, obtained by displaying the cross section of the 2D *J* spectra, is identical to that obtained by the nOe difference technique. These spectra are shown in Figs. 2B and 2C.

Other proton assignments were made on the basis of the homonuclear decoupling experiments. Decoupling of H-13 and H-14 results in a triplet for H-15, which appears to low field of the overlapping H-6 multiplet (Fig. 2A). As well, the H-12 multiplet is assigned, and it simplifies to a triplet with the removal of second order virtual coupling (28, 29). This indicates that $J(8–12)$ and $J(11–12)$ are equal to 10.0 Hz. Decoupling of H-12 results in a doublet of doublets for H-11, corresponding to $J(10\alpha–11)$ and $J(10\beta–11)$. When H-10β is decoupled, a triplet is observed for H-11 corresponding to $J(10\alpha–11)$ and $J(11–12)$. Decoupling of H-8 sharpens the H-7α resonances, indicating that $J(7\alpha–8) \cong 0.5$ Hz. Finally, the chemical shift for H-4 is determined by

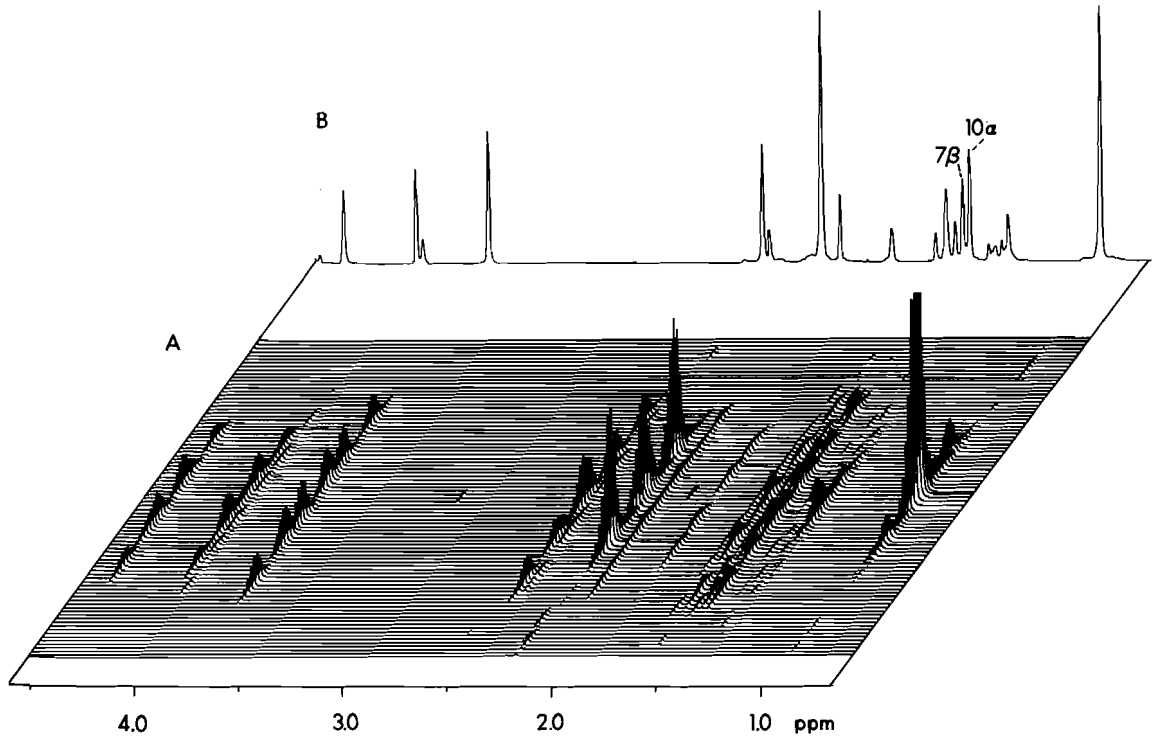

FIG. 3. (A). The stacked plot of the partial 2D *J* spectra. (B). Projection of the 2D *J* spectra to give the totally decoupled spectrum. The cross sections of the 2D *J* spectra for protons H-7β and H-10α are identical to those obtained using the nOe difference technique, shown in Figs. 2B and 2C.

integration, since the multiplet between 1.2 and 1.45 ppm corresponds to eight protons, including six for H-17 to H-19.

The results of the above experiments are tabulated in Table 1 and the proton magnetic resonance spectrum, including all assignments, is shown in Fig. 2A.

Discussion

The nOe difference experiments have been applied previously to the study of prostaglandins including PGI_2 (18), (6*R*)-PGI_1 (19), and prostaglandin E_2 (23). Very small effects can be measured, since a control spectrum without an nOe is subtracted from the spectrum with an nOe. In the present study, the nOe measurements proved invaluable in the assignment of the proton resonances, in the determination of chemical shifts, and in the evaluation of the coupling constants. The 2D *J* nmr experiments allowed the structure of several multiplets to be obtained, even though in a normal spectrum these multiplets are buried by many other multiplets. The data are in excellent agreement with the nOe difference results.

The proton chemical shifts and coupling constants are presented in Table 1. All data are calculated to first order. A comparison of these data with those obtained for (6*R*)-PGI_1 in phosphate buffer in D_2O at 25°C, pH 7.0 (19) can be made. The pH's are uncorrected meter readings. The largest observed changes in the chemical shifts are for H-7α and H-7β. For (6*S*)-PGI_1 these shifts are 1.86 and 1.52 ppm, respectively, whereas for (6*R*)-PGI_1 these shifts are 1.36 and 2.23 ppm, respectively. Obviously, changing the configuration of the chain at C-6 from the β-position in (6*S*)-PGI_1 to the α-position in (6*R*)-PGI_1 shifts H-7β from 1.52 ppm to 2.23 ppm. At the same time, H-7α shifts from 1.86 ppm to 1.36 ppm. Hence the H-7 proton that is *cis* to the C-6 substituent is always more shielded, due to the anisotropy of the C-5—C-6 bond. On the other hand, the next-nearest neighbors in the ring, namely H-8, H-9, H-10α, and H-12 are deshielded by the side chain. For (6*S*)-PGI_1 these shifts are 2.44, 4.49, 1.48, and 2.11 ppm, respectively, whereas for (6*R*)-PGI_1 these shifts are 2.38, 4.25, 1.61, and 2.20 ppm, respectively. These long-range effects are much smaller and difficult to explain.

In comparing the coupling constants, the largest difference is observed for $J(7\alpha\text{–}8)$. For (6*S*)-PGI_1 it is 0.5 Hz, whereas for (6*R*)-PGI_1 it is 5.0 Hz. Hence

Can. J. Chem. Downloaded from www.nrcresearchpress.com by 210.87.254.5 on 09/06/12
For personal use only.

Can. J. Chem. Downloaded from www.nrcresearchpress.com by 210.87.254.5 on 09/06/12
For personal use only.

TABLE 1. Proton chemical shifts and coupling constants for (6*S*)-PGI$_1$ (0.02 *M*) in phosphate buffer (0.2 *M*) in D_2O (pH 7.0)[a]

Proton	Chemical shift (ppm)	Coupling constants (Hz)
2	2.20	$J(2–3) = 7.5$
3	1.59[b,c]	$J(2–3) = J(3–4) = 7.5$[b,c]
4	~1.36[c]	
5, 5*	1.58[b], 1.49[b]	
6α	4.11[c]	$J(5–6\alpha)$ } = 6.3[c] $J(5^*–6\alpha)$ }
7α	1.86	$J(6\alpha–7\alpha) = 4.6$ $J(7\alpha–7\beta) = 12.4$ $J(7\alpha–8) = 0.5$[d]
7β	1.52[b]	$J(6\alpha–7\beta) = 10.4$[b,c] $J(7\alpha–7\beta) = 12.4$[b,e] $J(7\beta–8) = 8.1$[b,e]
8	2.44[c]	$J(8–12) = 10.0$[d]
9	4.49	$J(9–10\beta) = 7.6$ $J(8–9) = 7.6$ $J(9–10\alpha) = 6.0$
10α	1.48[b]	$J(9–10\alpha) = 5.9$[b,e] $J(10\alpha–10\beta) = 12.9$[b,e] $J(10\alpha–11) = 10.5$[b,e]
10β	2.48[c]	$J(9–10\beta) = 7.6$ $J(10\alpha–10\beta) = 12.9$ $J(10\beta–11) = 6.8$
11	3.79	$J(10\alpha–11) = 10.2$ $J(10\beta–11) = 6.8$ $J(11–12) = 10.0$[d]
12	2.11	$J(8–12) = 10.0$[d]
13	5.61	
14	5.61	
15	4.14[c]	$J(14–15) = 6.6$[e], $J(15–16) = J(15–16^*) = 6.6$[d,e]
16, 16*	1.58[b], 1.49[b]	
17, 18, 19	1.30	
20	0.87	$J(19–20) = 6.8$

[a]The chemical shifts, with respect to TSP-d_4, and the coupling constants are calculated to first order.
[b]Value obtained from nOe difference spectra.
[c]Value obtained from inversion recovery spectra.
[d]Value obtained from decoupled spectra.
[e]Value obtained from 2D *J* nmr experiment.

in (6*S*)-PGI$_1$, the H-7α to H-8 dihedral angle is about 90°. In (6*R*)-PGI$_1$, the large value for this coupling constant indicates that the dihedral angle is larger. For both molecules this indicates that the chain at C-6 adopts the pseudo-equatorial conformation. The other coupling constants between the ring protons are consistent with this view.

In summary, the nOe difference experiments are extremely valuable in assigning the proton multiplets for (6*S*)-PGI$_1$ in phosphate buffer solutions. The 2D *J* nmr measurements complemented these studies, as they also allowed the structure of several multiplets to be obtained when these multiplets are hidden by nearby resonances in a normal spectrum.

Acknowledgements

The authors are grateful to Dr. R. A. Johnson of the Upjohn Company in Kalamazoo, MI, for providing the sample of (6*S*)-PGI$_1$, the Natural Sciences and Engineering Research Council of Canada for a grant towards the purchase of the Bruker WH-400 nmr spectrometer, and the Natural Sciences and Engineering Research Council, the Alberta Heart Foundation and the University of Alberta for generous financial assistance.

1. J. M. ARMSTRONG, G. J. DUSTING, S. MONCADA, and J. R. VANE. Circ. Res. **43**, I 112 (1978).
2. S. MONCADA and J. R. VANE. *In* Prostacyclin. *Edited by* J. R. Vane and S. Bergstrom. Raven Press, New York, NY. 1979. pp. 5–16.
3. S. MONCADA and J. R. VANE. *In* Advances in prostaglandin and thromboxane research. Vol. 6. *Edited by* B. Samuelsson, P. W. Ramwell, and R. Paoletti. Raven Press, New York, NY. 1980. pp. 43–60.
4. B. J. R. WHITTLE, N. K. BOUGHTON-SMITH, S. MONCADA, and J. R. VANE. Prostaglandins, **15**, 955 (1978).
5. E. J. COREY, G. E. KECK, and I. SZÉKELY. J. Am. Chem. Soc. **99**, 2006 (1977).
6. R. A. JOHNSON, F. H. LINCOLN, J. L. THOMPSON, E. G. NIDY, S. A. MIZSAK, and U. AXEN. J. Am. Chem. Soc. **99**, 4182 (1977).
7. N. A. NELSON. J. Am. Chem. Soc. **99**, 7362 (1977).
8. R. A. JOHNSON, F. H. LINCOLN, E. G. NIDY, W. P. SCHNEIDER, J. L. THOMPSON, and U. AXEN. J. Am. Chem. Soc. **100**, 7690 (1978).
9. G. TOGNA, C. GANDOLFI, A. ANDREONI, A. FUMAGALLI, C. PASSAROTTI, F. FAUSTINI, and C. PATRONO. Pharmacol. Res. Commun. **9**, 909 (1977).
10. E. J. COREY, H. L. PEARCE, I. SZÉKELY, and M. ISHIGURO. Tetrahedron Lett. 1023 (1978).
11. R. A. JOHNSON, D. R. MORTON, and N. A. NELSON. Prostaglandins, **15**, 737 (1978).
12. B. H. CRANE, T. L. MAISH, Y. T. MADDOX, E. J. COREY, I. SZÉKELY, and P. W. RAMWELL. J. Pharmacol. Exp. Ther. **206**, 132 (1978).
13. B. J. R. WHITTLE, N. K. BOUGHTON-SMITH, S. MONCADA, and J. R. VANE. J. Pharm. Pharmacol. **30**, 597 (1978).
14. S. BUNTING, S. MONCADA, P. REED, J. A. SALMON, and J. R. VANE. Prostaglandins, **15**, 565 (1978).
15. K. SCHRÖR. Naunyn-Schmiedeberg's Arch. Pharmakol. **306**, 213 (1979).
16. G. L. KAUFFMAN, JR., B. J. R. WHITTLE, D. AURES, J. R. VANE, and M. I. GROSSMAN. Gastroenterology, **77**, 1301 (1979).
17. B. J. R. WHITTLE, S. MONCADA, F. WHITING, and J. R. VANE. Prostaglandins, **19**, 605 (1980).
18. G. KOTOVYCH, G. H. M. AARTS, T. T. NAKASHIMA, and G. BIGAM. Can. J. Chem. **58**, 974 (1980).
19. G. KOTOVYCH and G. H. M. AARTS. Can. J. Chem. **58**, 2649 (1980).

20. R. RICHARZ and K. WÜTHRICH. J. Magn. Reson. **30**, 147 (1978).
21. G. E. CHAPMAN, B. D. ABERCROMBIE, P. D. CARY, and E. M. BRADBURY. J. Magn. Reson. **31**, 459 (1978).
22. G. KOTOVYCH, G. H. M. AARTS, and K. BOCK. Can. J. Chem. **58**, 1206 (1980).
23. G. KOTOVYCH, G. H. M. AARTS, and G. BIGAM. Can. J. Chem. **58**, 1577 (1980).
24. W. P. AUE, J. KARHAN, and R. R. ERNST. J. Chem. Phys. **64**, 4226 (1976).
25. G. BODENHAUSEN, R. FREEMAN, R. NIEDERMEYER, and D. L. TURNER. J. Magn. Reson. **26**, 133 (1977).
26. R. FREEMAN and G. A. MORRIS. Bull. Magn. Reson. **1**, 5 (1979).
27. M. ANTEUNIS and D. DANNEELS. Org. Magn. Reson. **7**, 345 (1975).
28. F. A. L. ANET. Can. J. Chem. **39**, 2262 (1961).
29. J. I. MUSHER and E. J. COREY. Tetrahedron, **18**, 791 (1962).

Can. J. Chem. Downloaded from www.nrcresearchpress.com by 210.87.254.5 on 09/06/12
For personal use only.

Synthesis and properties of silicon, germanium, and tin derivatives of cyclopentadienyltricarbonylrhenium

D. F. DONG, J. K. HOYANO, AND W. A. G. GRAHAM

Department of Chemistry, University of Alberta, Edmonton, Alta., Canada T6G 2G2

Received August 20, 1980

This paper is dedicated to Professor Walter E. Harris on the occasion of his retirement from the University of Alberta

D. F. DONG, J. K. HOYANO, and W. A. G. GRAHAM. Can. J. Chem. **59**, 1455 (1981).

The preparation and properties of a series of rhenium compounds of the general formula $(\eta\text{-}C_5H_5)Re(CO)_2XY$ in which X or Y or both is a silyl, germyl, or stannyl ligand are reported. The silyl hydrides *cis*-$(\eta\text{-}C_5H_5)Re(CO)_2(SiR_3)H$ (R = Ph, CH_2Ph) and *cis*-$(\eta\text{-}C_5H_5)Re(CO)_2(SiPh_2H)H$ were obtained by ultraviolet irradiation of $(\eta\text{-}C_5H_5)Re(CO)_3$ and the appropriate silane. The hydrides *trans*-$(\eta\text{-}C_5H_5)Re(CO)_2XH$ (X = $SiPh_3$, $GeCl_3$, $GeBr_3$, $SnCl_3$) were obtained by protonation of the corresponding anions. These new anions $[(\eta\text{-}C_5H_5)Re(CO)_2X]^-$ also reacted with other electrophiles to yield compounds of the type *trans*-$(\eta\text{-}C_5H_5)$-$Re(CO)_2XY$ (Y = Me, halogen, SnR_3). The reaction of $(\eta\text{-}C_5H_5)Re(CO)_3$ with Cl_3GeH or Ph_3SnH yielded only the compounds *trans*-$(\eta\text{-}C_5H_5)Re(CO)_2(GeCl_3)_2$ and *trans*-$(\eta\text{-}C_5H_5)Re(CO)_2(SnPh_3)_2$ respectively. Infrared and ^1H nmr spectra are reported for all compounds, and v(Re–H) values for the hydrides have been obtained from Raman spectra.

D. F. DONG, J. K. HOYANO et W. A. G. GRAHAM. Can. J. Chem. **59**, 1455 (1981).

On rapporte la synthèse et les propriétés d'une série de composés du rhénium de formule générale $(\eta\text{-}C_5H_5)Re(CO)_2XY$ dans lesquels X ou Y ou les deux à la fois représentent un ligand silyle, germyle ou stannyle. On a obtenu les hydrures silylés $(\eta\text{-}C_5H_5)Re(CO)_2(SiR_3)H$ *cis* (R = Ph, CH_2Ph) et $(\eta\text{-}C_5H_5)Re(CO)_2(SiPh_2H)H$ *cis*, par irradiation ultraviolette du $(\eta\text{-}C_5H_5)Re$-$(CO)_3$ et du silane approprié. Par protonation des anions correspondants, on obtient les hydrures $(\eta\text{-}C_5H_5)Re(CO)_2XH$(X-$SiPh_3$, $GeCl_3$, $GeBr_3$, $SnCl_3$). Ces nouveaux anions $[(\eta\text{-}C_5H_5)Re(CO)_2X]^-$ réagissent également avec d'autres agents électrophiles et conduisent aux composés du type $(\eta\text{-}C_5H_5)Re(CO)_2XY$ *trans* (Y = Me, halogène, SnR_3). La réaction de $(\eta\text{-}C_5H_5)Re(CO)_3$ avec Cl_3GeH ou Ph_3SnH conduit uniquement aux composés $(\eta\text{-}C_5H_5)Re(CO)_2(GeCl_3)_2$ *trans* et $(\eta\text{-}C_5H_5)Re(CO)_2(SnPh_3)_2$ *trans*. On rapporte les spectres infrarouges et RMN du ^1H de tous les composés ainsi que les valeurs v(Re—H) de ces hydrures obtenus à partir des spectres Raman.

[Traduit par le journal]

Can. J. Chem. Downloaded from www.nrcresearchpress.com by 210.87.254.105 on 09/06/12
For personal use only.

Introduction

Earlier work from this laboratory (1–4) has shown that reactions of silanes with transition metal carbonyls provide a useful synthetic route to compounds having silicon – transition-metal bonds. In particular, the photochemical reaction shown below in general terms has afforded numerous silyl transitional-metal – hydrides which exhibit interesting structural, spectroscopic, and kinetic features (4–7). We now describe the synthesis and properties of a series of rhenium compounds of the type $(\eta\text{-}C_5H_5)Re(CO)_2XY$. These are *formally* the products of oxidative addition reactions on $(\eta\text{-}C_5H_5)Re(CO)_3$ by various silicon, germanium, and tin species. However, most of them are not accessible by such a direct route, so alternative pathways have been developed.

At present, very few dicarbonyl-η-cyclopentadienylrhenium(III) derivatives are known. The first to be reported was $(\eta\text{-}C_5H_5)Re(CO)_2Br_2$ (8), followed by several of its derivatives such as $(\eta\text{-}C_5H_5)Re(CO)_2(Br)CH_3$, $(\eta\text{-}C_5H_5)Re(CO)_2$-$(CH_3)_2$, and $(\eta\text{-}C_5H_5)Re(CO)_2(Br)H$ (9). The alkylrhenium hydride $(\eta\text{-}C_5H_5)Re(CO)_2(CH_2Ph)H$ was reported in 1978 (10). The present work on silicon, germanium, and tin derivatives was undertaken to extend our knowledge of this potentially large but currently underdeveloped class of compounds.

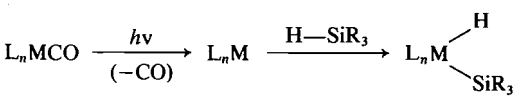

Results and Discussion

Preparation of Hydrides

The silyl hydrides were obtained by ultraviolet irradiation of the appropriate silane with $(\eta\text{-}C_5H_5)Re(CO)_3$ in hydrocarbon solvent:

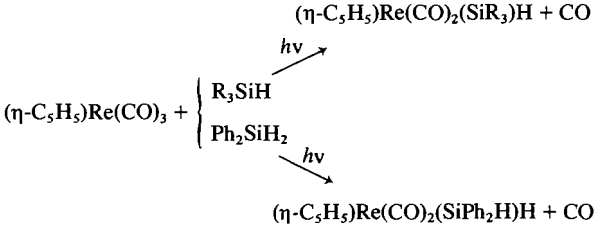

where R = Ph, CH_2Ph. This reaction is completely analogous to our previously reported photochemical reactions of silanes with metal carbonyls, and a likely mechanism of formation has been discussed

0008-4042/81/101455-08$01.00/0

©1981 National Research Council of Canada/Conseil national de recherches du Canada

TABLE 1. Colors, melting points, and analytical data for the hydrides and the anions

Compound	Color	Melting point (°C)	Calcd. (%)			Found (%)		
			C	H	X[a]	C	H	X
cis-(η-C_5H_5)Re(CO)$_2$($SiPh_3$)H	White	151–153	52.9	3.73	—	52.5	3.75	—
cis-(η-C_5H_5)Re(CO)$_2$($SiPh_2H$)H	White	103–105	46.4	3.49	—	46.5	3.77	—
(η-C_5H_5)Re(CO)$_2$($Si(CH_2Ph)_3$)H	Pale-yellow	130 dec.	55.1	4.46	—	55.1	4.51	—
trans-(η-C_5H_5)Re(CO)$_2$($SiPh_3$)H	White	123–125	52.9	3.73	—	52.6	3.91	—
trans-(η-C_5H_5)Re(CO)$_2$($GeCl_3$)H	White	110–115	17.3	1.24	21.8	17.1	1.22	22.2
trans-(η-C_5H_5)Re(CO)$_2$($GeBr_3$)H	Pale-brown	139–145	13.6	0.97	38.6	13.6	1.15	39.8
trans-(η-C_5H_5)Re(CO)$_2$($SnCl_3$)H	Pale-yellow	125 dec.	15.8	1.13	19.8	15.9	1.30	20.9
[Et_4N][(η-C_5H_5)Re(CO)$_2$($SiPh_3$)]	Pale-yellow	140 dec.	56.9	4.03	—	56.0	4.94	—
[Et_4N][(η-C_5H_5)Re(CO)$_2$($GeCl_3$)]	Yellow	144–146	29.2	4.09	17.3	29.3	4.35	17.1
[Et_4N][(η-C_5H_5)Re(CO)$_2$($GeBr_3$)]	Yellow	100 dec.	24.0	3.36	32.0	23.8	3.60	32.2
[Et_4N][(η-C_5H_5)Re(CO)$_2$($SnCl_3$)]	Pale-yellow	124–125	27.2	3.80	16.1	27.1	3.90	15.8

[a]X = halogen.

(4, 6). Compared to the corresponding manganese derivatives (4, 7, 11), those of rhenium are much more stable. Purifications require column chromatography on silica gel followed by recrystallization. The complex (η-C_5H_5)Re(CO)$_2$($SiPh_3$)H obtained in the above manner is the *cis* (or lateral) isomer (see spectroscopic section below for discussion of the stereochemical assignments). The corresponding *trans* (or diagonal) isomer was obtained by deprotonation of this *cis* hydride followed by reprotonation with phosphoric acid at 0°C:

cis-(η-C_5H_5)Re(CO)$_2$($SiPh_3$)H + KOH
→ (EtOH)
[(η-C_5H_5)Re(CO)$_2$($SiPh_3$)]$^-$
→ (H^+(0°C))
trans-(η-C_5H_5)Re(CO)$_2$($SiPh_3$)H

Deprotonation of silyl hydrides has been effected with amines such as Et_3N (12), but the low acidity of the above rhenium hydride requires the stronger base ethanolic KOH. The anion [(η-C_5H_5)Re(CO)$_2$($SiPh_3$)]$^-$ has been isolated as the moderately air-stable tetraethylammonium salt; other reactions of this anion are described below.

Reactions of germanes of the type R_3GeH with (η-C_5H_5)Re(CO)$_3$ do not yield any isolable amounts of the expected germyl hydrides of rhenium. In some cases, complexes such as (η-C_5H_5)Re(CO)$_2$($GeCl_3$)$_2$ were obtained, and these are discussed in the next section. Similarly, tin hydrides did not produce the anticipated hydride products. However, as an alternative route, the new anions [(η-C_5H_5)Re(CO)$_2$(EX_3)]$^-$ were prepared, and subsequent protonation gave the *trans* hydrides:

[Et_4N][EX_3] + (η-C_5H_5)Re(CO)$_3$
→ (THF, *hν*)
[Et_4N][(η-C_5H_5)Re(CO)$_2$(EX_3)]
→ (H^+)
trans(η-C_5H_5)Re(CO)$_2$(EX_3)H

(E = Ge, X = Cl, Br; E = Sn, X = Cl). The corresponding anions of manganese have been previously reported by Ruff (13), and the preparations here were carried out in a similar manner (see Experimental).

The physical properties and analytical data for the hydrides and anions described are listed in Table 1. All the complexes are moderately air-stable in the solid state.

The rhenium hydrides undergo a reductive elimination reaction with PPh_3 in the same way as the manganese analogs (7):

(η-C_5H_5)Re(CO)$_2$($SiPh_3$)H + PPh_3
↓
(η-C_5H_5)Re(CO)$_2$(PPh_3) + $HSiPh_3$

However, the reaction is much slower than for the corresponding manganese complex, presumably owing to differences in the M—H and M—Si bond strengths.

Preparation of other Group IV Metal Derivatives

Besides protonation, the anions described above were found to undergo a number of other reactions. The triphenylsilyl derivative reacts with electrophiles in a way similar to the more familiar carbonylate anions such as $Re(CO)_5^-$ and $Mn(CO)_5^-$, and to the more closely related anions such as

Can. J. Chem. Downloaded from www.nrcresearchpress.com by 210.87.254.105 on 09/06/12
For personal use only.

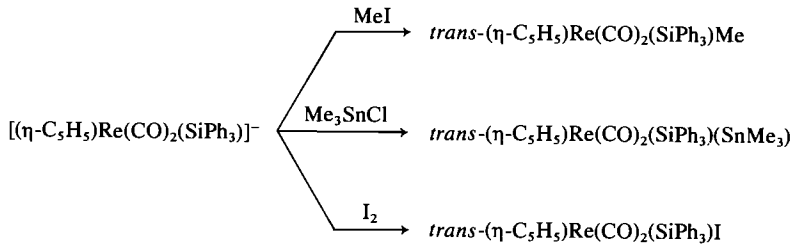

$[Ru(CO)_4SiMe_3]^-$ (14) and $[(\eta\text{-}C_5H_5)Mn(CO)_2SiCl_3]^-$ (12). The following equations summarize the reactions, which indicate that the anion is a moderately strong nucleophile.

The germanium- and tin-containing anions are trihalogeno species, and it is not surprising that their nucleophilicity is lower than that of the triphenylsilyl analogs, as their reactions suggest. In particular, the $[(\eta\text{-}C_5H_5)Re(CO)_2(EX_3)]^-$ anions *did not react* with MeI, EtI, Me_3SnCl, $MeGeCl_3$, or acetyl chloride. The methyl compounds were obtained when stronger alkylating agents were used:

$[(\eta\text{-}C_5H_5)Re(CO)_2(EX_3)]^- \xrightarrow{Me_3OPF_6 \text{ or } MeOSO_2F} trans\text{-}(\eta\text{-}C_5H_5)Re(CO)_2(EX_3)Me$

(E = Ge, X = Cl, Br; E = Sn, X = Cl). We note that the nucleophilicity of $[(\eta\text{-}C_5H_5)Mn(CO)_2(SiCl_3)]^-$ (12) appears to be greater than that of the trihalogeno-germanium and -tin rhenium anions.

While the trihalogenogermanium anions react normally with iodine, the tin–rhenium bond is cleaved in the reaction. Covalent bonds of tin of transition metals often undergo cleavage of this type (15).

$[(\eta\text{-}C_5H_5)Re(CO)_2(GeX_3)]^- \xrightarrow{I_2} trans\text{-}(\eta\text{-}C_5H_5)Re(CO)_2(GeX_3)I$

$[(\eta\text{-}C_5H_5)Re(CO)_2(SnCl_3)]^- \xrightarrow{I_2} trans\text{-}(\eta\text{-}C_5H_5)Re(CO)_2I_2$

As mentioned above, reactions of the germanium and tin hydrides did not yield the corresponding rhenium hydrides. Instead, germanium and tin complexes of rhenium were obtained as shown in the equations below:

$(\eta\text{-}C_5H_5)Re(CO)_3 + Cl_3GeH \xrightarrow{20°C} trans\text{-}(\eta\text{-}C_5H_5)Re(CO)_2(GeCl_3)_2$

$(\eta\text{-}C_5H_5)Re(CO)_3 + Ph_3SnH \xrightarrow{h\nu} trans\text{-}(\eta\text{-}C_5H_5)Re(CO)_2(SnPh_3)_2$

It would be reasonable to suppose that in both of these reactions, the first step is the formation of an intermediate rhenium hydride. For the trichlorogermane reaction, there is good evidence for this. An infrared spectrum taken immediately after mixing showed bands of both *trans*-$(\eta\text{-}C_5H_5)Re(CO)_2(GeCl_3)H$ and *trans*-$(\eta\text{-}C_5H_5)Re(CO)_2(GeCl_3)_2$; the latter species was dominant, and the only one remaining after an hour. A separate experiment showed that the following reaction proceeds easily under similar conditions:

trans-$(\eta\text{-}C_5H_5)Re(CO)_2(GeCl_3)H + Cl_3GeH \xrightarrow[\text{hexane}]{20°C} trans\text{-}(\eta\text{-}C_5H_5)Re(CO)_2(GeCl_3)_2$

This step of the reaction must occur more rapidly than the first since even with a slight excess of $(\eta\text{-}C_5H_5)Re(CO)_3$, $(\eta\text{-}C_5H_5)Re(CO)_2(GeCl_3)_2$ is the major product observed immediately after mixing.

The first step of the reaction for Ph_3SnH clearly involves oxidative addition to the photochemically generated 16-electron $(\eta\text{-}C_5H_5)Re(CO)_2$ fragment. It is remarkable, however, that reaction of Cl_3GeH with the rather inert $(\eta\text{-}C_5H_5)Re(CO)_3$ proceeds *in the dark* at room temperature within minutes if excess Cl_3GeH is used. We think this unusual reaction can be understood on the assumption that Cl_3GeH is sufficiently acidic to protonate the rhenium atom to some extent forming $[(\eta\text{-}C_5H_5)Re(H)(CO)_3]^+$. A carbonyl group in this cation would then be displaced by the Cl_3Ge^-. Precedent for labilization of carbonyls by protonation is found, for example, in the catalysis of exchange between carbon monoxide and iron pentacarbonyl by trifluoroacetic acid (16).

The physical properties and analytical data for the complexes described in this section are shown in Table 2. The following section describes the structures and spectroscopic properties of the prepared complexes.

Spectroscopic Properties and Structures

Except for the anionic species, all complexes prepared in this study are of the general form $(\eta\text{-}$

Can. J. Chem. Downloaded from www.nrcresearchpress.com by 210.87.254.105 on 09/06/12
For personal use only.

TABLE 2. Colors, melting points, and analytical data for group IV – metal derivatives of $(\eta\text{-}C_5H_5)Re(CO)_3$

Compound	Color	Melting point (°C)	Calcd. (%)			Found (%)		
			C	H	X[a]	C	H	X
trans-$(\eta\text{-}C_5H_5)Re(CO)_2(SiPh_3)Me$	White	185–187	53.68	3.98	—	54.57	3.75	—
trans-$(\eta\text{-}C_5H_5)Re(CO)_2(SiPh_3)(SnMe_3)$	White	158–160	46.04	4.01	—	46.10	4.20	—
trans-$(\eta\text{-}C_5H_5)Re(CO)_2(SiPh_3)I$	Yellow	150–152	43.29	2.91	—	43.60	3.05	—
trans-$(\eta\text{-}C_5H_5)Re(CO)_2(GeCl_3)_2$	White	90 dec.	12.6	0.76	32.0	12.7	0.99	30.4
trans-$(\eta\text{-}C_5H_5)Re(CO)_2(SnPh_3)_2$	Pale-brown	240–250	51.3	3.50	—	50.2	3.47	—
trans-$(\eta\text{-}C_5H_5)Re(CO)_2(GeCl_3)Cl$	Yellow	140–144	16.1	0.97	27.2	16.4	0.93	27.0
trans-$(\eta\text{-}C_5H_5)Re(CO)_2(GeCl_3)Br$	Orange	148–155	14.9	0.89	32.9[b]	15.3	1.04	31.2
trans-$(\eta\text{-}C_5H_5)Re(CO)_2(GeCl_3)I$	Orange	136–139	13.7	0.82	17.4[c]	13.9	0.91	17.3
trans-$(\eta\text{-}C_5H_5)Re(CO)_2(GeCl_3)Me$	Pale-brown	163–168	19.2	1.61	21.2	19.7	1.68	21.4
trans-$(\eta\text{-}C_5H_5)Re(CO)_2I_2$	Red-brown	120 dec.	15.0	0.90	45.2	14.6	1.19	44.6

[a]X = Cl, Br, or I.
[b]Total halogen content.
[c]For Cl: calcd. for I 20.7: found 20.4.

TABLE 3. Infrared carbonyl stretching frequencies of group IV – metal derivatives of $(\eta\text{-}C_5H_5)Re(CO)_3$

Compound	Stretching frequencies (cm^{-1})[a]	
cis-$(\eta\text{-}C_5H_5)Re(CO)_2(SiPh_3)H$	1999(s)	1932(ms)
cis-$(\eta\text{-}C_5H_5)Re(CO)_2(SiPh_2H)H$	2001(s)	1934(s)
$(\eta\text{-}C_5H_5)Re(CO)_2(Si(CH_2Ph)_3)H$	*cis*: 1995(s)	1920(s)
	trans: 1998(m)	1931(s)
trans-$(\eta\text{-}C_5H_5)Re(CO)_2(SiPh_3)H$	2004(m)	1940(s)
trans-$(\eta\text{-}C_5H_5)Re(CO)_2(GeCl_3)H$	2043(m)	1981(s)[b]
trans-$(\eta\text{-}C_5H_5)Re(CO)_2(GeBr_3)H$	2041(m)	1980(s)[b]
trans-$(\eta\text{-}C_5H_5)Re(CO)_2(SnCl_3)H$	2040(m)	1981(s)[b]
trans-$(\eta\text{-}C_5H_5)Re(CO)_2(SiPh_3)Me$	1995(m)	1932(s)
trans-$(\eta\text{-}C_5H_5)Re(CO)_2(SiPh_3)(SnMe_3)$	1957(m)	1898(s)
trans-$(\eta\text{-}C_5H_5)Re(CO)_2(SiPh_3)I$	2016(m)	1958(s)
trans-$(\eta\text{-}C_5H_5)Re(CO)_2(GeCl_3)_2$	2052(m)	2004(s)
trans-$(\eta\text{-}C_5H_5)Re(CO)_2(SnPh_3)_2$	1954(m)	1897(s)[b]
trans-$(\eta\text{-}C_5H_5)Re(CO)_2(GeCl_3)Cl$	2066(m)	2011(s)
trans-$(\eta\text{-}C_5H_5)Re(CO)_2(GeCl_3)Br$	2063(m)	2010(s)
trans-$(\eta\text{-}C_5H_5)Re(CO)_2(GeCl_3)I$	2053(m)	2003(s)
trans-$(\eta\text{-}C_5H_5)Re(CO)_2(GeCl_3)Me$	2034(m)	1971(s)[b]
trans-$(\eta\text{-}C_5H_5)Re(CO)_2I_2$	2048(m)	1987(s)[b]
$[Et_4N][(\eta\text{-}C_5H_5)Re(CO)_2(SiPh_3)]$	1862(ms)	1782(s)[b]
$[Et_4N][(\eta\text{-}C_5H_5)Re(CO)_2(GeCl_3)]$	1923(s)	1852(s)[b]
$[Et_4N][(\eta\text{-}C_5H_5)Re(CO)_2(SnCl_3)]$	1923(s)	1856(s)[b]

[a]In cyclohexane solution unless otherwise noted; w = weak, m = medium, s = strong.
[b]Dichloromethane solution.

$C_5H_5)Re(CO)_2XY$ where the ligands X and Y may be different or the same. For this formulation two stereoisomers are possible, the *cis* and *trans*, as shown below; recently the terms lateral and diagonal have been suggested as being more precise because the "*trans*" angles are not 180° (17).

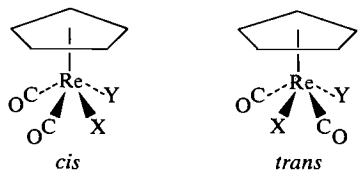

cis *trans*

The assignments of *cis* or *trans* configuration for the complexes reported here are based mainly on the relative intensities of the two carbonyl stretching bands in the infrared spectrum, and this method of assignment is now fairly well established as being correct (16, 17). Basically, the *cis* arrangement is assigned to complexes with a more intense higher energy (symmetric) stretching band, while the *trans* arrangement is assigned to complexes with a more intense lower energy (asymmetric) stretching band. For the compounds reported here, Table 3 shows the ir carbonyl stretching bands and the stereochemical assignments.

For $(\eta\text{-}C_5H_5)Re(CO)_2(SiPh_3)H$, both *cis* and *trans* isomers were obtained in pure form as described above, while the compound $(\eta\text{-}C_5H_5)Re(CO)_2[Si(CH_2Ph)_3]H$ appears to exist as a

Can. J. Chem. Downloaded from www.nrcresearchpress.com by 210.87.254.105 on 09/06/12
For personal use only.

TABLE 4. Proton nmr data

Compound	Proton chemical shifts (δ)[a]	
	η-C_5H_5	M–H
cis-(η-C_5H_5)Re(CO)$_2$($SiPh_3$)H	5.17	−9.10
cis-(η-C_5H_5)Re(CO)$_2$($SiPh_2$H)H[c]	5.12	−9.70 (doublet[c])
(η-C_5H_5)Re(CO)$_2$($Si(CH_2Ph)_3$)H	4.69	−10.59, −10.63
trans-(η-C_5H_5)Re(CO)$_2$($SiPh_3$)H	5.06	−10.30
trans-(η-C_5H_5)Re(CO)$_2$($GeCl_3$)H[b]	5.58	−9.39
trans-(η-C_5H_5)Re(CO)$_2$($GeBr_3$)H	5.54	−9.18
trans-(η-C_5H_5)Re(CO)$_2$($SnCl_3$)H	5.63	−9.29
trans-(η-C_5H_5)Re(CO)$_2$($SiPh_3$)Me	4.90	—
trans-(η-C_5H_5)Re(CO)$_2$($SiPh_3$)($SnMe_3$)	4.91	—
trans-(η-C_5H_5)Re(CO)$_2$($GeCl_3$)Me[d]	5.54	—
[Et_4N][(η-C_5H_5)Re(CO)$_2$($SiPh_3$)][b]	4.75	—

[a]In $CDCl_3$ solution unless otherwise noted.
[b]Dichloromethane solution.
[c]For Si—H, δ = 5.97 (doublet, J = 2.7 Hz).
[d]Methyl singlet at δ 1.15.

mixture of *cis* and *trans* forms, at least in solution. The other hydrides (the Ge and Sn species) were obtained only in the *trans* form. The other derivatives, which contain two bulkier ligands, were found only in the *trans* form, and this would be the more stable form on steric grounds. As Table 3 shows, infrared bands appear at higher frequencies for the *trans* form in those cases where both stereochemistries have been observed, and this is consistent with what is observed for *cis*- and *trans*-(η-C_5H_5)Re(CO)$_2$$Br_2$ (17). Although stable in the solid state, *trans*-(η-C_5H_5)Re(CO)$_2$($SiPh_3$)H readily converts to the *cis* form in solution (10 h at 70°C, or at room temperature in the presence of Et_3N); this is opposite to (η-C_5H_5)Re(CO)$_2$$Br_2$, where the *cis* isomer is converted to the *trans* upon heating in solution.

Table 4 summarizes the proton nmr data. All the compounds exhibit a sharp singlet for the cyclopentadienyl protons in the expected region. The hydride complexes show characteristic high field resonances due to transition metal bonded hydrogen, and there is little variation in the chemical shifts among the complexes. The cyclopentadienyl resonance in *trans*-(η-C_5H_5)Re(CO)$_2$($SiPh_3$)H lies 0.09 ppm to higher field than in the *cis*-isomer. For (η-C_5H_5)Re(CO)$_2$$Br_2$ (17), the *trans* resonance lies 0.40 ppm to higher field than *cis*. However, this is not generally true even for the small number of cases where both isomers are known; in the tribenzylsilyl hydride (Table 4) it would appear that in the *cis–trans* mixture, the cyclopentadienyl resonances are accidentally degenerate.

All the neutral compounds listed in Table 3 exhibited the expected isotope patterns for the molecular ions in the mass spectra, while the fragmentation patterns were consistent with the proposed formulations. Some of the spectra showed features of special interest. All complexes showed ions due to the successive loss of one and two carbonyl groups from the parent ion. The spectrum of *cis*-(η-C_5H_5)Re(CO)$_2$($SiPh_3$)H showed a medium intensity peak due to Ph_3Si^+ and only a weak peak due to Ph_3SiH^+, whereas the corresponding manganese compound exhibited Ph_3SiH^+ as the strongest peak in the spectrum. This property is reflected in the facile displacement of Ph_3SiH in the manganese compound (7). The mass spectra of *trans*-(η-C_5H_5)Re(CO)$_2$(EX_3)H (E = Ge, Sn) showed strong peaks due to the loss of HX from the molecular ions.

An interesting structural feature of a hydride complex like *cis*-(η-C_5H_5)Re(CO)$_2$($SiPh_3$)H is the possibility of an attractive interaction between the hydrogen and silicon, as found in the X-ray structure determinations of analogous manganese compounds (7, 18, 19). The infrared, Raman, and other spectroscopic properties have been discussed, and at present there is no clear cut diagnostic spectroscopic indicator of this interaction. The transition-metal hydride stretching modes have been observed at normal terminal M–H frequencies, although they may be very weak or absent in the infrared spectra. Recently it has been suggested that broadening of the hydrogen mode in the Raman spectrum may be an indication of the Si–H interaction (20). Also, rather than an inherently attractive interaction, steric factors have been suggested as forcing the close approach of silicon to hydrogen in related compounds (21).

Some of the cyclopentadienylrhenium(III) hydrides reported here were investigated with regard to this possible Si–H interaction. All the hydrides described here, including the *trans* isomers, showed no detectable bands in the infrared spectra which could be assigned to the rhenium–hydrogen

Can. J. Chem. Downloaded from www.nrcresearchpress.com by 210.87.254.105 on 09/06/12
For personal use only.

Can. J. Chem. Downloaded from www.nrcresearchpress.com by 210.87.254.105 on 09/06/12
For personal use only.

TABLE 5. Raman spectral data for the hydrides[a]

Compound	ν(Re–H) or (Re–D) (cm^{-1})
cis-(η-C_5H_5)Re(CO)$_2$($SiPh_3$)H	2013
cis-(η-C_5H_5)Re(CO)$_2$($SiPh_3$)D	1440
trans-(η-C_5H_5)Re(CO)$_2$($GeCl_3$)H	1987
trans-(η-C_5H_5)Re(CO)$_2$($GeCl_3$)D	1426
trans-(η-C_5H_5)Re(CO)$_2$($GeBr_3$)H	1981
trans-(η-C_5H_5)Re(CO)$_2$($GeBr_3$)D	1421
trans-(η-C_5H_5)Re(CO)$_2$($SnCl_3$)H	1990

[a]Solid-state spectra.

stretching mode. However, ν(Re–H) bands were observed in the Raman spectra, and these bands shifted to appropriate energies for the deuterides (see Table 5). A bridging interaction in the *trans* isomer is highly unlikely, so the mere absence of an ir band for ν(Re–H) appears not to be diagnostic either way. As stated above, the nmr and mass spectra showed no major differences among the various hydrides.

Single-crystal X-ray structures have now been determined for *cis*-(η-C_5H_5)Re(CO)$_2$($SiPh_3$)H **1** (22), *trans*-(η-C_5H_5)Re(CO)$_2$($GeCl_3$)H **2** (23), and [Et_4N][(η-C_5H_5)Re(CO)$_2$($GeCl_3$)] **3** (23), and some interesting features have emerged. The assigned stereochemistries have been confirmed as evidenced by the OC—Re—CO angles of 84° and 103° for the silyl- and germyl-hydride complexes, respectively. Also, the structure of the deprotonated germanium anion **3** has a corresponding angle of

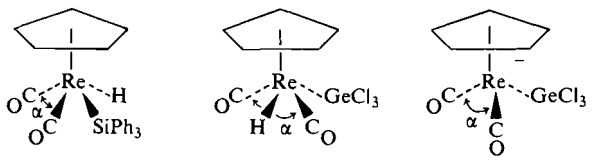

1 (α = 84°) **2** (α = 103°) **3** (α = 89°)

89°, suggesting the proton has been removed from the position *trans* to the germanium atom. The hydrogens were not located in these X-ray determinations, although for *cis*-(η-C_5H_5)Re(CO)$_2$($SiPh_3$)H it is estimated (22) that the hydrogen-to-silicon distance is 2.2 Å, relatively short but longer than in the manganese analogue (18). It appears that a neutron diffraction study may be required to resolve the issue.

Experimental

Materials and General Methods

A nitrogen atmosphere was maintained during all reactions and during work-up procedures by the use of Schlenk apparatus. Irradiations were carried out in quartz vessels and using a Hanovia utility lamp (Model 30620, 140 W) or the more powerful Hanovia lamp (No. L699A, 450 W) in conjunction with a water-jacketed sample compartment. The (η-C_5H_5)Re(CO)$_3$ was prepared by a slight modification of a published procedure (24). The silicon, germanium, and tin compounds were purchased from commercial suppliers or prepared according to published procedures. All reagents and solvents were purified or dried according to standard methods.

Melting points were obtained using a microscope with a Kofler hot stage. Microanalyses were performed in the microanalytical laboratory of this department. Infrared spectra were obtained using a Perkin-Elmer 337 spectrometer with scale expansion and calibration as previously described (1). Raman spectra were obtained on a Spex Laser Raman spectrometer (Ramalog) using argon on krypton lasers. Varian A-60, 56-60A, or HA-100 instruments were used to record nmr spectra. Mass spectra were obtained on Associated Electrical Industries MS-9 or MS-12 spectrometers.

Preparation of cis-(η-C_5H_5)Re(CO)$_2$($SiPh_3$)H

A solution of (η-C_5H_5)Re(CO)$_3$ (2.3 g or 6.9 mmol) and triphenylsilane (5.0 g, 19 mmol) in 200 mL of cyclohexane was irradiated with the 450 W source for 7 h. The reaction mixture was then suction filtered through a 100 g silicic acid column (compounds adsorbed on column). Elution with 300 mL *n*-hexane removed all of the unreacted triphenylsilane. Then the column was eluted with two 100 mL portions of 30% dichloromethane – *n*-hexane; the first fraction contained (η-C_5H_5)Re(CO)$_3$ (1.0 g), and the second fraction contained the product and a small amount of (η-C_5H_5)Re(CO)$_3$. Sublimation of the second fraction at 60°C removed the tricarbonyl; crystallization of the unsublimed solid from dichloromethane–hexane afforded white crystals of *cis*-(η-C_5H_5)Re(CO)$_2$($SiPh_3$)H (0.55 g, 15%).

The complexes *cis*-(η-C_5H_5)Re(CO)$_2$($SiPh_2$H)H and (η-C_5H_5)Re(CO)$_2$($Si(CH_2Ph)_3$)H were prepared in the same way, with yields of the pure products being 10% and 36% respectively. The yields in these reactions appear to be low, but the unreacted starting materials can be recovered and recycled to yield more product.

Preparation of [Et_4N][(η-C_5H_5)Re(CO)$_2$($SiPh_3$)]

Solid *cis*-(η-C_5H_5)Re(CO)$_2$($SiPh_3$)H (0.40 g, 0.70 mmol) was magnetically stirred with 5 mL of 1.0 *M* ethanolic KOH; the hydride solid slowly dissolved and a clear yellow solution formed after 1.5 h of stirring. Addition of Et_4NBr (0.95 mmol in 3 mL ethanol) gave an immediate pale-yellow precipitate. The mixture was centrifuged and the ethanol was decanted. The remaining solid was dried *in vacuo*; crystallization from dichloromethane–hexane yielded pale-yellow prisms of the product (0.35 g, 72%).

Preparation of trans-(η-C_5H_5)Re(CO)$_2$($SiPh_3$)H

A solution of [Et_4N][(η-C_5H_5)Re(CO)$_2$($SiPh_3$)] (0.10 g, 0.14 mmol) in 20 mL of dichloromethane was vigorously stirred with 0.5 mL of phosphoric acid at 0°C for 30 min. After allowing the mixture to settle, the dichloromethane layer was decanted and evaporated at reduced pressure (0°C). The white solid was recrystallized from hexane–dichloromethane to yield crystals of the pure *trans* product (0.06 g, 75%).

Preparation of trans-(η-C_5H_5)Re(CO)$_2$($SiPh_3$)Me

A solution of methyl iodide (0.1 mL) and [Et_4N][(η-C_5H_5)Re(CO)$_2$($SiPh_3$)] (0.05 g, 0.07 mmol) in 15 mL of dichloromethane was stirred at 20°C for 30 min. After removal of solvent and excess methyl iodide at reduced pressure, recrystallization from hexane–dichloromethane afforded white crystals of the product (0.03 g, 55%).

Preparation of trans-(η-C_5H_5)Re(CO)$_2$($SiPh_3$)($SnMe_3$)

A solution of $ClSnMe_3$ (0.04 g, 0.2 mmol) and [Et_4N][(η-C_5H_5)Re(CO)$_2$($SiPh_3$)] (0.1 g, 0.14 mmol) in 25 mL of dichloro-

Can. J. Chem. Downloaded from www.nrcresearchpress.com by 210.87.254.105 on 09/06/12
For personal use only.

methane was stirred for 30 min. Removal of solvent at reduced pressure and crystallization from hexane–chloroform afforded white crystals of the products (0.09 g, 70%).

Preparation of trans-$(\eta\text{-}C_5H_5)Re(CO)_2(SiPh_3)I$

A solution of I_2 (0.05 g) and $[Et_4N][(\eta\text{-}C_5H_5)Re(CO)_2(SiPh_3)]$ (0.05 g, 0.07 mmol) in 10 mL of dichloromethane was stirred for 1 h. Removal of solvent at reduced pressure and crystallization from hexane–chloroform afforded yellow crystals of the product (0.35 g, 65%).

Preparation of $[Et_4N][(\eta\text{-}C_5H_5)Re(CO)_2GeCl_3]$

A solution of $(\eta\text{-}C_5H_5)Re(CO)_3$ (2.45 g, 7.35 mmol) and $[Et_4N][GeCl_3]$ (5.55 g, 18.0 mmol) in 300 mL of THF was irradiated at reflux temperature with the 140 W source for 26 h. After irradiation, the solution was reduced in volume to about 20 mL on a rotary evaporator and 75 mL of methanol was then added. Cooling to −20°C afforded 2.04 g yellow crystals, after filtering, washing with cold methanol, and drying *in vacuo*. Reducing the volume of the mother liquor to about 30 mL afforded a second crop of 0.44 g (total yield 55%).

The complexes $[Et_4N][(\eta\text{-}C_5H_5)Re(CO)_2(GeBr_3)]$ and $[Et_4N][(\eta\text{-}C_5H_5)Re(CO)_2(SnCl_3)]$ were prepared in a similar fashion, and the yields were 33% and 73% respectively.

Preparation of trans-$(\eta\text{-}C_5H_5)Re(CO)_2(GeBr_3)H$

To a rapidly stirred solution of $[Et_4N][(\eta\text{-}C_5H_5)Re(CO)_2(GeBr_3)]$ (1.1 g, 1.5 mmol) in 10 mL of dichloromethane was added dropwise 3 mL of phosphoric acid. Stirring was continued for 2.5 h, after which the bottom of the tube was cooled to −78°C. As soon as the acid had solidified and the suspended solids had settled to the bottom, the dichloromethane solution was syringed into another Schlenk tube. Cooling of this solution by slow immersion into a −78°C bath initiated crystallization; addition of small amounts of heptane to the cold solution completed crystallization and afforded pale-brown crystals of *trans*-$(\eta\text{-}C_5H_5)Re(CO)_2(GeBr_3)H$ (0.49 g, 53%).

The other hydrides *trans*-$(\eta\text{-}C_5H_5)Re(CO)_2(GeCl_3)H$ and *trans*-$(\eta\text{-}C_5H_5)Re(CO)_2(SnCl_3)H$ and their corresponding deuterides were prepared by the same method, and the yields were in the 30–60% range.

Preparation of trans-$(\eta\text{-}C_5H_5)Re(CO)_2(GeCl_3)Cl$

Chlorine gas was bubbled rapidly for 2 min through a solution of $[Et_4N][(\eta\text{-}C_5H_5)Re(CO)_2GeCl_3]$ (0.20 g, 0.32 mmol) in 20 mL of dichloromethane. Removal of solvent on a rotary evaporator and vacuum sublimation at 80°C yielded 0.035 g (21%) of microcrystalline product.

Preparation of trans-$(\eta\text{-}C_5H_5)Re(CO)_2(GeCl_3)Br$

A solution of $[Et_4N][(\eta\text{-}C_5H_5)Re(CO)_2GeCl_3]$ (0.30 g, 0.49 mmol) and bromine (0.030 mL, 0.55 mmol) in 10 mL of dichloromethane was stirred for 10 min. Crystallization was effected by adding cold diethylether (10 mL), and then cold petroleum ether. Subsequent cooling to −20°C gave 0.21 g (75%) of orange *trans*-$(\eta\text{-}C_5H_5)Re(CO)_2(GeCl_3)Br$.

The complex *trans*-$(\eta\text{-}C_5H_5)Re(CO)_2(GeCl_3)I$ was prepared by the same method in 98% yield.

Preparation of trans-$(\eta\text{-}C_5H_5)Re(CO)_2I_2$

A solution of $[Et_4N][(\eta\text{-}C_5H_5)Re(CO)_2SnCl_3]$ (0.66 g, 1.0 mmol) and iodine (0.25 g, 1.0 mmol) in 15 mL of dichloromethane was stirred for 1 h. Addition of 10 mL of petroleum ether, removal of a small amount of solvent at reduced pressure, and cooling to −20°C yielded red–brown crystals of *trans*-$(\eta\text{-}C_5H_5)Re(CO)_2I_2$ (0.17 g, 30%).

Preparation of trans-$(\eta\text{-}C_5H_5)Re(CO)_2(GeCl_3)Me$

A mixture of $[Et_4N][(\eta\text{-}C_5H_5)Re(CO)_2(GeCl_3)]$ (0.72 g, 1.2 mmol) and $MeOSO_2F$ (0.30 g, 2.6 mmol) in 10 mL of toluene was rapidly stirred for 8 h. The fine white precipitate was filtered off and heptane was added to the filtrate until turbidity occurred. Cooling slowly to −78°C afforded pale-brown crystals of the product (0.41 g, 58%).

Preparation of trans-$(\eta\text{-}C_5H_5)Re(CO)_2(GeCl_3)_2$

A solution of $(\eta\text{-}C_5H_5)Re(CO)_3$ (0.335 g, 1.00 mmol) and Cl_3GeH (1.84 g, 10.0 mmol) in 10 mL of hexane was stirred for 1 h. Excess Cl_3GeH was destroyed by reaction with 20 mL of methanol, and then solvents were removed *in vacuo*. Extraction of the residue with 100 mL of hot heptane and cooling the extract to −20°C afforded white crystals of product (0.20 g, 30%).

Preparation of trans-$(\eta\text{-}C_5H_5)Re(CO)_2(SnPh_3)_2$

A solution of $(\eta\text{-}C_5H_5)Re(CO)_3$ (1.0 g, 3.0 mmol) and $HSnPh_3$ (2.1 g, 6.0 mmol) in 200 mL of petroleum ether was irradiated with the 450 W source for 23 h. The solution and solid residues washed out with dichloromethane were combined and the mixture was reduced to dryness on a rotary evaporator. Unreacted $(\eta\text{-}C_5H_5)Re(CO)_3$ was sublimed off, and the residue was adsorbed onto a 100 g silicic acid column in a small amount of 1:1 petroleum ether – dichloromethane. Elution by suction filtration with 300 mL of petroleum ether and 100 mL of a 1:1 mixture of petroleum ether – dichloromethane removed most of the remaining $(\eta\text{-}C_5H_5)Re(CO)_3$. Further elution with 200 mL acetone led to a solution containing the product and a small amount of $(\eta\text{-}C_5H_5)Re(CO)_3$, which was sublimed off after removal of the solvent. Recrystallization of the residue from dichloromethane–heptane gave pale-brown crystals of *trans*-$(\eta\text{-}C_5H_5)Re(CO)_2(SnPh_3)_2$ (50 mg, 1.7%).

Acknowledgments

We thank the Natural Sciences and Engineering Research Council of Canada for financial support and for a Postgraduate Scholarship to D.F.D. The University of Alberta also provided support and a Dissertation Fellowship to D.F.D.

1. W. Jetz, P. B. Simons, J. A. J. Thompson, and W. A. G. Graham. Inorg. Chem. **5**, 2217 (1966).
2. W. Jetz and W. A. G. Graham. J. Am. Chem. Soc. **89**, 2773 (1967).
3. L. Vancea and W. A. G. Graham. Inorg. Chem. **13**, 511 (1974).
4. W. Jetz and W. A. G. Graham. Inorg. Chem. **10**, 4 (1971).
5. J. K. Hoyano, M. Elder, and W. A. G. Graham. J. Am. Chem. Soc. **91**, 4568 (1969).
6. J. K. Hoyano and W. A. G. Graham. Inorg. Chem. **11**, 1265 (1972).
7. A. J. Hart-Davis and W. A. G. Graham. J. Am. Chem. Soc. **93**, 4388 (1971).
8. A. N. Nesmeyanov, N. E. Kolobova, Y. V. Makarov, and K. N. Animisov. Isv. Akad. Nauk SSSR, Ser. Khim. (Engl. Trans.), 1687 (1969).
9. A. N. Nesmeyanov, N. E. Kolobova, Y. V. Makarov, and K. N. Animisov. Zh. Obshch. Khim. (Engl. Trans.), 2179 (1974).
10. E. O. Fischer and A. Frank. Chem. Ber. **111**, 3740 (1978).
11. J. K. Hoyano. Ph.D. Thesis, University of Alberta, Alberta, 1971.
12. W. Jetz and W. A. G. Graham. Inorg. Chem. **10**, 1647 (1971).
13. J. K. Ruff. Inorg. Chem. **10**, 409 (1971).
14. S. A. R. Knox and F. G. A. Stone. J. Chem. Soc. (A), 2559 (1969).

15. M. J. ASH, A. BROOKES, S. A. R. KNOX, and F. G. A. STONE. J. Chem. Soc. A, 458 (1971); M. R. BOOTH, D. J. CARDIN, N. A. D. CAREY, H. C. CLARK, and B. R. SREENATHAW. J. Organomet. Chem. **21**, 171 (1970); R. E. BICHLER, H. C. CLARK, B. K. HUNTER, and A. T. RAKE. J. Organomet. Chem. **69**, 367 (1974).
16. K. NOACK and M. RUCH. J. Organomet. Chem. **17**, 309 (1969).
17. R. B. KING and R. H. REIMANN. Inorg. Chem. **15**, 179 (1976); R. B. KING, R. H. REIMANN, and D. J. DARENSBOURG. J. Organomet. Chem. **93**, C23 (1975).
18. W. L. HUTCHEON. Ph.D. Thesis, University of Alberta, Alberta, 1971; Chem. Eng. News, **48**, 75 (1970).
19. K. A. SIMPSON. Ph.D. Thesis, University of Alberta, Alberta, 1973.
20. M. A. ANDREWS, S. W. KIRTLEY, and H. D. KAESZ. *In* Transition metal hydrides. *Edited by* R. Bau. American Chemical Society, Washington, DC. 1978. pp. 215–231.
21. M. COWIE and M. J. BENNETT. Inorg. Chem. **16**, 2321 (1977); **16**, 2325 (1977).
22. R. A. SMITH and M. J. BENNETT. Acta Crystallogr. **B33**, 1113 (1977).
23. L. L. Y. CHAN and W. A. G. GRAHAM. Unpublished results.
24. M. L. H. GREEN and G. WILKINSON. J. Chem. Soc. 4314 (1958).

Can. J. Chem. Downloaded from www.nrcresearchpress.com by 210.87.254.105 on 09/06/12
For personal use only.

The structure of benzoylphenyldiazomethane

MARTIN COWIE[1] AND MICHELE D. GAUTHIER

Chemistry Department, The University of Alberta, Edmonton, Alta., Canada T6G 2G2

Received September 5, 1980

This paper is dedicated to Professor W. E. Harris on the occasion of his retirement from the University of Alberta

MARTIN COWIE and MICHELE D. GAUTHIER. Can. J. Chem. **59**, 1463 (1981).

The structure of benzoylphenyldiazomethane has been established by an X-ray structure determination. The packing of the molecules within the unit cell is related to the complex esr spectral results. Apart from the observed N—N distance of 1.132(5) Å the structural parameters in the molecule suggest conjugation between the diazo and carbonyl functions. The N—N distance is probably anomalously short owing to thermal vibration of the diazo moiety. Benzoylphenyldiazomethane crystallizes in the space group $P2_12_12_1$ with $a = 5.600(1)$, $b = 13.347(2)$, $c = 15.018(3)$, and $Z = 4$. Based on 888 unique observed reflections the structure has been refined to $R = 0.052$ and $R_w = 0.070$.

MARTIN COWIE et MICHELE D. GAUTHIER. Can. J. Chem. **59**, 1463 (1981).

On a déterminé la structure du benzoylphényldiazométhane par diffraction de rayons-X. L'entassement des molécules dans la maille explique la complexité des spectres de rpe. A l'exception de la distance de 1,132(5) Å observée pour la liaison N—N, les paramètres structuraux de la molécule suggèrent une conjugaison entre les fonctions diazo et carbonyle. Il est probable que la distance N—N est anormalement courte à cause de la vibration thermique de la portion diazo. Le benzophényldiazométhane cristallise dans le groupe d'espace $P2_12_12_1$ avec $a = 5,600(1)$, $b = 13,347(2)$, $c = 15,018(3)$ et $Z = 4$. En se basant uniquement sur 888 réflexions observées, on a affiné la structure jusqu'à des valeurs de $R = 0,052$ et de $R_w = 0,070$.

[Traduit par le journal]

Introduction

The esr spectrum of benzoylphenyldiazomethane, commonly known as azibenzil, has been reported by Trozzolo (1) and by Murai, Torres, and Strausz (2). The latter group noted that photolysis of a microcrystalline sample of $PhCOCN_2Ph$ at 77 K resulted in a complex esr spectrum, consisting of a strong and a weak triplet signal and a quintet signal. The strong triplet was assigned to the *trans* conformer of the benzoylphenylmethylene radical, which is formed through loss of N_2 from the starting diazoketone molecule, also assumed to have the *trans* geometry in the solid state. The weak triplet was assigned to the presence of small amounts of the *cis* conformer of this radical, and the novel quintet state was attributed to a triplet–triplet radical pair formed by the pairwise interaction of two triplet state benzoylphenylmethylene radicals. For such a radical pair to form, two radicals must be in close proximity in the crystal, which could result if, in a crystal of the parent diazoketone species, two molecules were oriented such that there were close interactions between the diazo functions. A determination of the structure of benzoylphenyldiazomethane was therefore undertaken to determine the intermolecular interactions within the crystal in order to gain a further understanding of the esr spectrum and to confirm the proposed trans geometry of the molecule.

Semiempirical CNDO/2 calculations (3) on benzoylphenyldiazomethane indicate that two geometries are preferred, having the carbonyl and diazo groups either *cis* or *trans* across the single bond, and having an essentially planar molecular framework. Other conformations resulting from rotations about the C—C bond were not favored. However, the measured electric dipole moments (4) are compatible with either two *cis–trans* conformers in equilibrium or with only a single skewed conformer.

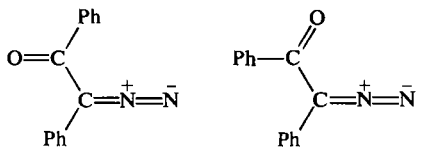

trans *cis*

In addition, few diazoalkane molecules have been structurally characterized (5–10). Therefore the structure of $PhCOCN_2Ph$ is important as a basis for comparison with other diazoalkane molecules to help establish structural and chemical trends within these molecules.

[1]Besides local programs the following were used in the solution and refinement of the structure: AGNOST, the Northwestern University absorption program which includes Coppens-Leiserowitz-Rabinowvich logic for Gaussian integration; FORDAP, the Fourier summation program by A. Zalkin; MULTAN, for the automatic solution of Crystal Structures using the weighted tangent formula, by G. Germain, P. Main, and M. M. Woolfson; ORFFE, for calculating bond lengths, angles, and associated standard deviations by W. Busing and H. A. Levy; ORTEP, plotting program by C. K. Johnson; SFLS-5, structure factor and least-squares refinement by C. J. Prewitt.

0008-4042/81/101463-07$01.00/0

©1981 National Research Council of Canada/Conseil national de recherches du Canada

Can. J. Chem. Downloaded from www.nrcresearchpress.com by 210.87.254.42 on 09/06/12
For personal use only.

Can. J. Chem. Downloaded from www.nrcresearchpress.com by 210.87.254.42 on 09/06/12
For personal use only.

TABLE 1. Summary of data and intensity collection for benzoylphenyldiazomethane

Formula	$C_{14}H_{10}N_2O$
Formula weight	222.25
Cell parameters	
a	5.600(1) Å
b	13.347(2) Å
c	15.018(3) Å
V	1122.5 Å^3
Z	4
Density	1.315 g cm^{-3} (calcd.) 1.30(1) g cm^{-3} (exptl., flotation)
Space group	$D_2^4 - P2_12_12_1$
Crystal dimensions	0.384 × 0.216 × 0.129 mm^3
Crystal volume	0.0107 mm^3
Crystal shape	Orthorhombic prism with faces $0\bar{1}1$, 011, $0\bar{1}2$, $01\bar{2}$, 100, $\bar{1}00$
Temperature	20°C
Radiation	CuKα_1 (λ = 1.540562 Å); Ni filter
μ	6.447 cm^{-1}
Transmission factors	0.854–0.924
Receiving aperture	4 mm × 4 mm; 30 cm from the crystal
Takeoff angle	5.50°
Scan speed	2° in 2θ/min
Scan range	1.0° below Kα_1 to 1.0° above Kα_2
Background counting time	20 s
2θ limits	3.0°–123°
2θ limits for centered reflections	50.0° ≤ 2θ ≤ 70.0°
Final number of parameters	94
Unique data collected	1068
Unique data used ($F_0^2 \geq 3\sigma(F_0^2)$)	888
Error in observation of unit weight	1.948 electrons
R	0.052
R_w	0.070

Experimental

Orange needles of benzoylphenyldiazomethane recrystallized from ether were kindly supplied by Dr. M. Torres and Professor O. P. Strausz (University of Alberta). A suitable crystal fragment, cut from one of the needles, was mounted in the air on a glass fibre. Preliminary film data showed Laue symmetry mmm with systematic absences ($h00$, $h = 2n + 1$; $0k0$, $k = 2n + 1$; $00l$, $l = 2n + 1$) consistent with the space group $P2_12_12_1$. The cell parameters along with the pertinent crystal data and intensity collection details are listed in Table 1.

Data were collected by the θ–2θ scan method on a Picker four-circle automated diffractometer, equipped with a scintillation counter and pulse height analyzer tuned to accept 90% of the CuKα peak. Background counts were measured at both ends of the scan range with both crystal and counter stationary. Standard deviations in the intensities were calculated using a p factor of 0.05 (11). The intensities of three standard reflections were measured every 100 reflections. No significant decrease in these intensities was noted.

Structure Solution and Refinement

The structure was solved by direct methods using the program MULTAN (12). The solution was based on 300 reflections having $|E| > 1.03$ and 2000 phase relationships. The E-map corresponding to the solution with the best combined figure of merit yielded the positions of all non-hydrogen atoms. All hydrogen atoms were found in a subsequent electron density difference map phased on the heavier atom framework. Full matrix least-squares techniques were used, with atomic scattering factors from Cromer and Waber (13) for all atoms except hydrogen, for which the values from Stewart, Davidson, and Simpson (14) were used. Anomalous dispersion terms for O, N, and C (15) were included in F_c. All non-hydrogen atoms were refined as individual atoms, with the phenyl carbon atoms having isotropic thermal parameters, and the rest having anisotropic thermal parameters. The hydrogen atoms were included as fixed contributions in their idealized positions, with thermal parameters of 1 Å^2 greater than the equivalent isotropic B for the corresponding carbon atom. Absorption corrections were applied to the data using Gaussian integration.[1] In the final electron density difference map, the top 20 residuals ranged from 0.31 to 0.14 e/Å^3, and were in the vicinities of the two phenyl rings. In earlier difference Fourier maps, a typical hydrogen atom had an electron density of about 0.27 e/Å^3.

A stereoview of the unit cell is shown in Fig. 1. Figure 2 showing a perspective view of the molecule indicates the numbering scheme used within the molecule (hydrogen atoms have the same number as their attached carbon atoms). The final positional and thermal parameters for the non-hydrogen atoms are listed in Table 2. Selected interatomic distances are listed in Table 3, while bond angles and torsion angles are presented in Table 4. A listing of the observed and calculated structure amplitudes, the table of idealized hydrogen positions and thermal parameters, and the table of least-squares planes are available.[2]

Description of Structure and Discussion

Within the unit cell of benzoylphenyldiazomethane there are four discrete molecules. Figure 1

[2]This material (5 pages) is available, at a nominal charge from the Depository of Unpublished Data, CISTI, National Research Council of Canada, Ottawa, Ont., Canada K1A 0S2.

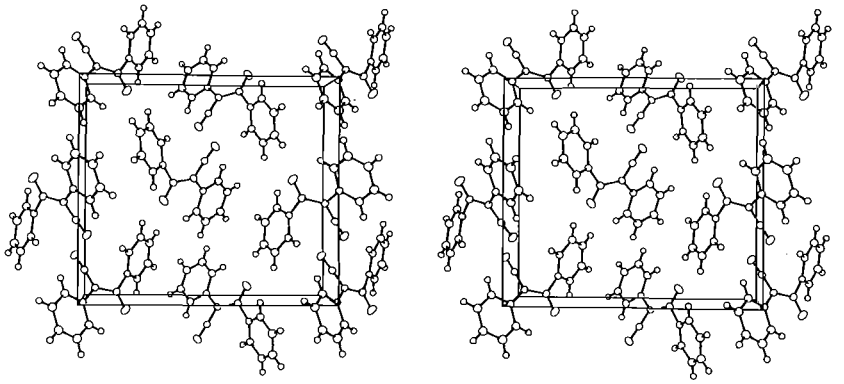

FIG. 1. A stereoview of the unit cell of benzoylphenyldiazomethane. The x-axis goes into the page, the y-axis runs from top to bottom, and the z-axis is from right to left. 20% thermal ellipsoids are drawn, except for hydrogen atoms which are drawn artificially small. Extra molecules are shown as an aid in visualizing the packing.

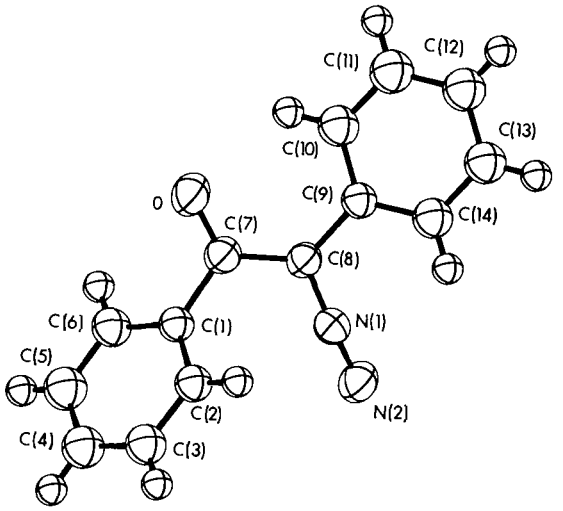

FIG. 2. A perspective view of benzoylphenyldiazomethane showing the numbering scheme. 50% thermal ellipsoids are drawn.

indicates that these molecules can be grouped in pairs along the crystallographic screw axis in the x-direction. In this arrangement the molecules have their diazomethylene groups directed towards each other but inclined somewhat along a such that zig-zag arrays of diazomethylene groups, parallel to the a axis, result. These diazomethylene groups therefore come into rather close contact; the N(2)—N(2)′ distance along the zig-zag chain is 3.238(4) Å.[3] Although it is difficult to establish a normal van der Waals contact for such an interaction, this contact can be related to the radius of an aromatic ring (1.85 Å) (16). It is not unreasonable to assume that the π system of the diazomethylene function is similar to that of an aromatic ring, and thus we estimate that a normal van der Waals contact between two diazo functions is approximately 3.70 Å. As such, the N(2)—N(2)′ distance in the present structure indicates a significant interaction between the two diazomethylene groups.

In the esr study by Strausz and co-workers (2), photolysis of a microcrystalline sample of the title complex at 77 K resulted in the production of the benzoylphenylmethylene radical. Since the elimination of N_2 at this temperature in the solid state is not expected to change the geometry of the molecule, the cell packing diagram shown in Fig. 1 should be representative of the orientation of the radicals immediately after photolysis and should prove useful in interpreting the esr results. Initially, the esr spectrum showed a strong triplet signal (assigned to the *trans* configuration of the benzoylphenylmethylene radical), a weak triplet signal (assigned to the *cis* configuration of this group), and a quintet signal. The quintet signal was thought to arise from the pairwise interaction of two neighboring triplet radicals (2). Within the unit cell of benzoylphenyldiazomethane, there are two close contacts between neighboring carbene carbon atoms which could give rise to this interaction. The first is along the zig-zig chain, where the C(8)—C(8)′ separation is 6.133(6) Å, and the second occurs between molecules separated by one unit cell translation in a, in which the C(8)—C(8)′ distance is 5.600(1) Å. Both possibilities are consistent with the separation expected between radical pairs producing the quintet signal, as indicated by the small zero field splitting parameter, D(0.0943 cm^{-1}) (2), which is a function of the separation of unpaired electrons in the radicals.

Upon warming the sample from 77 K to 90 K, the quintet esr signal decays to a new triplet signal which was postulated to result from the formation of a diradical through spin inversion and a single,

[3]Primed atoms are related to unprimed atoms by the symmetry transformations shown in Table 3.

Can. J. Chem. Downloaded from www.nrcresearchpress.com by 210.87.254.42 on 09/06/12
For personal use only.

Can. J. Chem. Downloaded from www.nrcresearchpress.com by 210.87.254.42 on 09/06/12
For personal use only.

TABLE 2. Positional and thermal parameters for the non-hydrogen atoms of [$PhCOCN_2Ph$]

Atom	x^a	y	z	$U_{11}{}^b$	U_{22}	U_{33}	U_{12}	U_{13}	U_{23}
O	0.4284(7)	0.5492(2)	0.6751(2)	8.3(2)	4.5(2)	6.7(2)	−1.4(2)	1.8(2)	−1.5(2)
N(1)	0.4459(7)	0.3660(2)	0.5106(2)	5.3(2)	4.4(2)	4.6(2)	−0.4(2)	0.4(2)	0.2(2)
N(2)	0.3784(8)	0.3006(3)	0.4698(2)	7.2(3)	5.4(2)	5.8(2)	−1.3(2)	0.6(2)	−1.3(2)
C(7)	0.4020(8)	0.4677(3)	0.6379(3)	4.7(2)	3.6(2)	5.2(2)	−0.0(2)	0.0(2)	−0.1(2)
C(8)	0.5264(8)	0.4448(3)	0.5551(3)	4.9(3)	3.6(2)	4.4(2)	−0.2(2)	0.2(2)	−0.2(2)
C(1)	0.2441(7)	0.3908(3)	0.6795(2)	3.23(7)[c]					
C(2)	0.3138(8)	0.2906(3)	0.6874(3)	3.62(8)					
C(3)	0.1689(9)	0.2233(3)	0.7328(3)	4.34(9)					
C(4)	−0.0428(10)	0.2540(3)	0.7685(3)	4.7(1)					
C(5)	−0.1111(9)	0.3538(4)	0.7616(3)	4.9(1)					
C(6)	0.0326(9)	0.4215(3)	0.7183(3)	3.98(9)					
C(9)	0.7247(7)	0.5008(3)	0.5126(3)	3.32(7)					
C(10)	0.7799(9)	0.5975(3)	0.5381(3)	4.34(9)					
C(11)	0.972(1)	0.6463(3)	0.4985(3)	5.0(1)					
C(12)	1.102(1)	0.6020(3)	0.4323(3)	4.8(1)					
C(13)	1.0465(9)	0.5068(3)	0.4059(3)	4.55(9)					
C(14)	0.8588(9)	0.4563(3)	0.4463(3)	4.19(9)					

[a]Estimated standard deviations in the least significant figure(s) are given in parentheses in this and all subsequent tables.
[b]The form of the thermal ellipsoid is: $\exp[-2\pi^2(a^{*2}U_{11}h^2 + b^{*2}U_{22}k^2 + c^{*2}U_{33}l^2 + 2a^*b^*U_{12}hk + 2a^*c^*U_{13}hl + 2b^*c^*U_{23}kl)]$. The quantities given in the table are the thermal coefficients × 10^2.
[c]Isotropic B(Å^2).

TABLE 3. Selected interatomic distances (Å) for $PhCOCN_2Ph$

(*a*) Bonded contacts

Bond	Distance	Bond	Distance
N(1)—N(2)	1.132(5)	C(4)—C(5)	1.391(7)
N(1)—C(8)	1.325(5)	C(5)—C(6)	1.373(6)
C(7)—O	1.231(4)	C(6)—C(1)	1.382(6)
C(1)—C(7)	1.491(5)	C(9)—C(10)	1.381(6)
C(7)—C(8)	1.458(6)	C(10)—C(11)	1.390(7)
C(8)—C(9)	1.484(6)	C(11)—C(12)	1.367(7)
C(1)—C(2)	1.398(5)	C(12)—C(13)	1.367(6)
C(2)—C(3)	1.390(6)	C(13)—C(14)	1.389(7)
C(3)—C(4)	1.364(7)	C(14)—C(9)	1.381(6)

(*b*) Non-bonded contacts

Atoms	Distance	Atoms	Distance
O–H(10)	2.29	N(1)–C(14)	2.781(6)
N(1)–H(14)	2.47	N(2)–N(2)[a,c]	3.238(4)
N(1)–H(2)	2.62	N(2)–N(1)[a]	3.301(5)
C(7)–H(6)	2.62	C(13)–N(1)[d]	3.319(6)
C(7)–H(2)	2.70	C(13)–N(2)[d]	3.458(6)
C(8)–H(14)	2.63	O–C(6)	2.870(5)
C(8)–H(10)	2.67	O–C(10)	2.920(6)
C(3)–H(14)[a]	2.98	O–C(8)[e]	5.541(6)
C(12)–H(5)[b]	2.93	O–C(8)[f]	6.251(5)
C(13)–H(5)[b]	2.88	C(8)–C(8)[a,c]	6.133(6)
H(14)–C(2)[c]	2.97	C(8)–C(8)[d,e]	5.600(1)
H(14)–C(3)[c]	2.98		

[a]Atom is located at the position $-\frac{1}{2} + x, \frac{1}{2} - y, 1 - z$.
[b]Atom is located at the position $\frac{1}{2} - x, 1 - y, -\frac{1}{2} + z$.
[c]Atom is located at the position $\frac{1}{2} + x, \frac{1}{2} - y, 1 - z$.
[d]Atom is located at the position $1 + x, y, z$.
[e]Atom is located at the position $-1 + x, y, z$.
[f]Atom is located at the position $\frac{1}{2} - x, 1 - y, \frac{1}{2} + z$.

covalent bond formation (2). Based on an inspection of the packing of the molecules, two mechanisms seem possible for formation of the new triplet signal. The first could result from a covalent bond formation between the carbene carbon of one diradical and a carbonyl group of another leading to a species as shown in **a**.

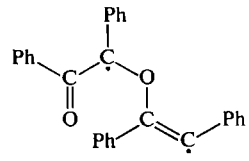

a

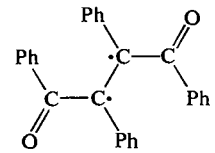

b

This bond formation would require some reorientation of the radicals in the crystal (see Fig. 1) and it is uncertain whether at 90 K the required reorientation is possible. From a structural point of view, possibly the more obvious mechanism would involve covalent bond formation between two adjacent carbene carbon atoms, which are related by the crystallographic screw axis, resulting in the diradical shown in **b**. As can be seen in Fig. 1 very little molecular reorientation is required in this case. However, it seems that based on the small zero-field splitting parameters obtained from the esr spectrum (D = 0.0189 cm^{-1} and E = 0.0008 cm^{-1}), the required separation of the unpaired electrons is too great to accommodate diradical **b** but seems consistent with the diradical **a** formed from C—O bond formation (2, 17). Based on the present crystallographic study both mechanisms seem feasible. The closest contacts of type **a** occur between molecules separated by one cell translation along the a axis, where the O—C(8)′ distance is 5.541(6) Å. The next closest such interaction is 6.251(5) Å (see Table 3). The two closest in-

Can. J. Chem. Downloaded from www.nrcresearchpress.com by 210.87.254.42 on 09/06/12
For personal use only.

teratomic distances between carbene carbon atoms (C(8)–C(8)′) are 5.600(1) and 6.133(6) Å (*vide supra*).

Within the molecule, the carbonyl and diazo groups are *trans* to each other across the C—C single bond, as expected from the esr results (2). This geometry and the *cis* conformation are the two which are favored owing to π-delocalization within the molecule, as has been suggested by theoretical calculations (3). The preference of one of these two conformations over the other is dependent on both electronic and steric factors. For optimum delocalization of the π electrons, the whole molecular fragment should be planar (18). This planarity is opposed by steric interactions, the greatest of which occurs between the two phenyl groups in the *cis* configuration. Thus, the two phenyl rings cannot both be coplanar with the carbonyl and diazo groups, and delocalization through the phenyl rings is lost in this conformation. However, the *cis* conformation is stabilized by an electrostatic attraction between the carbonyl and diazo functions, as shown below, which is not possible in a *trans* geometry.

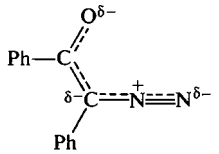

The *trans* conformation is favoured by steric considerations since this allows the bulky phenyl groups to avoid each other. Which of the two preferred conformations is favored will depend on which of the above stabilizing or destabilizing forces predominate. In the present compound, the observed *trans* geometry implies that the steric repulsion between the two phenyl groups predominates. It is also possible that the observed *trans* conformer may be favored in the present structure by packing considerations.

In the present structure the molecule is not totally planar but is skewed somewhat. For example, the O—C(7)—C(8)—N(1) torsion angle is −165.3(4)° and the torsion angle between phenyl ring 2 and the diazomethylene group (C(10)—C(9)—C(8)—N(1)) is 161.9(4)°. These two values suggest that some conjugation may be possible between the carbonyl and diazomethylene groups and between the diazomethylene group and the adjacent phenyl ring since the skewing from planarity is only 14.7(4)° and 18.1(4)°, respectively. On the other hand the C(1)—C(6) phenyl ring is twisted considerably from the adjacent carbonyl group (torsion angle C(2)—C(1)—C(7)—O = −133.9(4)°), allowing very little electron delocalization between this phenyl and the carbonyl group. This twisting probably results from steric interactions between the phenyl ring and the diazo and carbonyl groups, with the phenyl rings skewing to avoid contacts with these groups.

The C—C distances within ring 1 (C(1)—C(6), average 1.383(13) Å)[4] and ring 2 (C(9)—C(14), average 1.379(10) Å) are somewhat shorter than the values found in benzene and its derivatives (19). This apparent bond shortening probably results from thermal vibrations of the rings, with the shortest C—C distances occurring at the C(4) and C(12) ends of the rings, where the thermal motion is the greatest. The C(1)—C(7) and C(8)—C(9) distances (1.491(5) and 1.484(6) Å) agree well with the predicted value for a single bond between sp^2 hybridized carbon atoms (16), indicating that there is little actual delocalization between either of the phenyl rings and the carbonyldiazomethylene backbone. The C(7)—C(8) bond length (1.458(6) Å), on the other hand, is intermediate between a single and a double bond (18*a*) and suggests significant conjugation between the carbonyl and diazomethylene functions. A similar pattern of C—C bond lengths was observed in dibenzoyldiazomethane (20) where the C—C_{Ph} bond lengths (1.486(2) and 1.485(3) Å) indicated little conjugation and the C—C distances between carbonyl and diazomethylene carbon atoms (1.472(3) and 1.476(3) Å) showed some delocalization between these groups. The carbonyl distance (C(7)—O) in the present compound, at 1.231(4) Å, is normal for a C=O double bond (21) but is somewhat longer than the analogous distance of 1.222(2) Å observed in the related compound, dibenzoyldiazomethane. However, we expect that these observed C—O distances are somewhat shorter than the true values owing to thermal vibrations involving the carbonyl groups (22).

The diazomethylene fragment of the present structure is virtually linear (177.5(4)°) as expected and the C(8)—N(1) bond length of 1.325(5) Å is intermediate between a single and a double bond (23). This latter value is comparable with the analogous distance of 1.338(2) Å in dibenzoyldiazomethane (20) and can be compared with the values predicted for C=N double and C—N single bonds (1.29 and 1.47 Å, respectively) based on covalent radii (18*b*). The N(1)—N(2) bond length,

[4]For average quantities, the estimated standard deviation is the larger of an individual standard deviation or the standard deviation of a single observation as calculated from the mean.

TABLE 4. Selected angles (deg) for $PhCOCN_2Ph$

(*a*) Bond angles

Bonds	Angle	Bonds	Angle
N(2)—N(1)—C(8)	177.5(4)	C(1)—C(2)—C(3)	119.9(4)
N(1)—C(8)—C(7)	115.8(4)	C(2)—C(3)—C(4)	120.4(4)
N(1)—C(8)—C(9)	116.0(4)	C(3)—C(4)—C(5)	119.9(5)
O—C(7)—C(8)	121.0(4)	C(4)—C(5)—C(6)	120.3(5)
O—C(7)—C(1)	119.3(4)	C(5)—C(6)—C(1)	120.5(4)
C(1)—C(7)—C(8)	119.7(3)	C(6)—C(1)—C(2)	119.1(4)
C(7)—C(8)—C(9)	128.2(3)	C(9)—C(10)—C(11)	119.5(4)
C(7)—C(1)—C(2)	121.9(4)	C(10)—C(11)—C(12)	121.4(4)
C(7)—C(1)—C(6)	118.7(3)	C(11)—C(12)—C(13)	119.4(5)
C(8)—C(9)—C(10)	121.3(4)	C(12)—C(13)—C(14)	119.8(5)
C(8)—C(9)—C(14)	120.0(4)	C(13)—C(14)—C(9)	121.2(4)
		C(14)—C(9)—C(10)	118.7(4)

(*b*) Torsion angles

Bonds	Angle
C(1)—C(7)—C(8)—N(1)	16.0(6)
C(1)—C(7)—C(8)—C(9)	−166.8(4)
O—C(7)—C(8)—C(9)	11.9(7)
O—C(7)—C(8)—N(1)	−165.3(4)
C(10)—C(9)—C(8)—N(1)	161.9(4)
C(2)—C(1)—C(7)—O	−133.9(4)

at 1.132(5) Å, is significantly longer than the analogous distances reported for other diazoalkane structures (5–10) and is longer than that observed (20) in dibenzoyldiazomethane (1.113(2) Å). As a comparison, typical N—N triple and double bond distances are 1.10 Å (24) and 1.24 Å (25), respectively. This observed N(1)—N(2) distance, like those previously reported, is unexpectedly short considering that the C(8)—N(1) bond length corresponds to a bond order of 1.5. Again however, as with the C(7)—O bond length, we suggest that this shortening is apparent, resulting from thermal vibration of the diazomethylene moiety. Ideally diffraction data should be collected at low temperature to minimize these effects.

The present structural parameters for benzoylphenyldiazomethane indicate that there is a significant amount of conjugation between the carbonyl and diazomethylene groups. However there seems to be very little, if any, conjugation between the phenyl rings and the carbonyl or diazomethylene groups. For ring 1 which is skewed significantly from the carbonyl–diazomethylene plane this is not surprising, however, for ring 2 which is twisted only 14.8° from this plane, this is rather surprising. Finally, taken as a whole, the structural parameters indicate more delocalization in the benzoylphenyldiazomethane compound than is observed in the similar species, dibenzoyldiazomethane (20).

Acknowledgements

We thank the University of Alberta and the Natural Sciences and Engineering Research Council of Canada for financial support and Dr. M. Torres and Professor O. P. Strausz for supplying the crystals and for helpful discussions.

1. A. M. TROZZOLO. Acc. Chem. Res. **1**, 329 (1968).
2. H. MURAI, M. TORRES, and O. P. STRAUSZ. J. Am. Chem. Soc. **102**, 5104 (1980).
3. S. SORRISO and A. STØGARD. J. Chem. Soc. Perkin **II**, 538 (1976).
4. S. SORRISO and A. FOFFANI. J. Chem. Soc. Perkin II, 1497 (1973).
5. T. H. TULIP, P. W. R. CORFIELD, and J. A. IBERS. Acta Crystallogr. B, **34**, 1549 (1978).
6. H. HOPE and K. T. BLACK. Acta Crystallogr. B, **28**, 3632 (1972).
7. G. B. ANSELL. J. Chem. Soc. B, 729 (1969).
8. C. T. PRESLEY and R. L. SASS. Acta Crystallogr. B, **26**, 1195 (1970).
9. D. J. ABRAHAM, T. G. COCHRAN, and R. D. ROSENSTEIN. J. Am. Chem. Soc. **93**, 6279 (1971).
10. A. P. COX, L. F. THOMAS, and J. SHERIDAN. Nature (London) **181**, 1000 (1958).
11. R. J. DOEDENS and J. A. IBERS. Inorg. Chem. **6**, 204 (1967).
12. G. GERMAIN, P. MAIN, and M. M. WOOLFSON. Acta Crystallogr. A, **27**, 368 (1971).
13. D. T. CROMER and J. T. WABER. International tables for X-ray crystallography. 3rd ed. The Kynoch Press, Birmingham, England. Vol. IV. 1974. Table 2.2 A.
14. R. F. STEWART, E. R. DAVIDSON, and W. T. SIMPSON. J. Chem. Phys. **42**, 3175 (1965).

Can. J. Chem. Downloaded from www.nrcresearchpress.com by 210.87.254.42 on 09/06/12
For personal use only.

15. D. T. CROMER and D. J. LIBERMAN. J. Chem. Phys. **53**, 3175 (1970).
16. F. A. COTTON and G. WILKINSON. Advanced inorganic chemistry. 3rd ed. Wiley, New York. 1972. pp. 117–120.
17. H. MURAI, M. TORRES, and O. P. STRAUSZ. To be published.
18. L. PAULING. The nature of the chemical bond. 3rd ed. Cornell University Press, Ithaca, New York. 1960. (*a*) Chapt. 8.7; (*b*) Table 7.5.
19. K. TAMAGAWA, T. IIJIMA, and M. KIMURA. J. Mol. Struct. **30**, 243 (1976).
20. M. COWIE and M. D. GAUTHIER. Acta Crystallogr. In press.
21. International tables for X-ray crystallography. 2nd ed. The Kynoch Press, Birmingham, England. Vol. III. 1968, Tables 4.2.2 to 4.2.5.
22. D. W. J. CRUICKSHANK. Acta Crystallogr. **9**, 757 (1956).
23. R. J. KURLAND and E. B. WHITE, JR. J. Chem. Phys. **27**, 585 (1957).
24. C. ROMMING and T. TJORNHAM. Acta Chem. Scand. **22**, 2934 (1968); C. ROMMING. Acta Chem. Scand. **17**, 1444 (1963); P. G. WILKINSON. Astrophys. J. **126**, 1 (1957).
25. C. J. BROWN. Acta Crystallogr. **21**, 146 (1966); C. J. BROWN. Acta Crystallogr. **21**, 153 (1966); A. TROMBETTI. Can. J. Phys. **46**, 1005 (1968).

Can. J. Chem. Downloaded from www.nrcresearchpress.com by 210.87.254.42 on 09/06/12
For personal use only.

Epithermal neutron activation analysis with a SLOWPOKE nuclear reactor

DONALD CRAIG STUART[1] AND DOUGLAS EARL RYAN

Trace Analysis Research Centre, Chemistry Department, Dalhousie University, Halifax, N.S., Canada B3H 4J1

Received June 18, 1980

This paper is dedicated to Professor W. E. Harris on the occasion of his retirement from the University of Alberta

DONALD CRAIG STUART and DOUGLAS EARL RYAN. Can. J. Chem. **59**, 1470 (1981).

Epithermal neutron activation analysis is examined using a SLOWPOKE nuclear reactor. Data are given for 69 elements using cadmium and boron shielding. Cadmium ratios calculated from literature values of resonance integrals are compared with experimental values. All elements except cadmium are shielded more effectively by boron. Advantage factors for a selection of elements under cadmium, natural boron, and enriched boron shields are given. Boron shields are of particular practical value for rapid instrumental analysis.

DONALD CRAIG STUART et DOUGLAS EARL RYAN. Can. J. Chem. **59**, 1470 (1981).

On examine l'analyse par l'activation épithermique des neutrons en utilisant un réacteur nucléaire du type SLOWPOKE. On rapporte des données relatives à 69 éléments en utilisant un écran au cadmium et au bore. On compare les valeurs expérimentales des taux de cadmium à celles calculées à partir des valeurs rapportées dans la littérature pour des intégrales de résonance. A l'exception du cadmium tous les éléments sont mieux protégés par le bore. On rapporte les facteurs qui favorisent la sélection des éléments sous des écrans de cadmium, de bore naturel et de bore enrichi. Les écrans de bore sont d'une valeur pratique particulière pour une analyse instrumentale rapide.

[Traduit par le journal]

Introduction

A number of researchers (1–13) have demonstrated the usefulness of irradiating samples surrounded by a thermal neutron shield. The activation of many elements can be greatly reduced in this way, whereas the activation of a number of other elements is only reduced by a small amount, since the activation of these is largely due to higher energy neutrons which are not absorbed appreciably by the shield. The usefulness of this epithermal neutron activation analysis (ENAA) technique in a given situation thus depends upon whether or not any significant advantage over interfering elements can be obtained for the elements that are to be determined.

For the most part, cadmium has been utilized as a shield material. This method of ENAA has been applied to silicate rocks with particular success (3–7, 12, 13). Other applications include aerosols (9), coal and fly ash (11), and biological materials (8, 10).

A recent compilation of resonance integrals by Gryntakis and Kim (14) is very extensive and shows how calculations may be carried out by the Westcott method (15) or by a simplified "normal" method (16, 17) to estimate the relative effects of cadmium shielding. Unfortunately, as the authors point out (14), values frequently vary an order of magnitude or more, depending on the technique used.

In attempting to apply ENAA to chemical analysis, it would be more valuable to have a consistent set of results produced under practical analytical conditions, such as the data of Brunfelt and Steinnes (3) for some twenty elements with half-lives greater than two days.

Van Der Linden and co-workers have compiled a list of resonance integrals (18) following the practical method of Hogdahl (19), using a cylindrical cadmium box with a wall thickness of 1 mm as the shield. These values were derived from data in three irradiation sites where the thermal-to-epithermal flux ratios were estimated to be 23.8:1, 18.3:1, and 144:1. Another compilation by Van Der Linden *et al.* gives values for fifteen very short-lived isotopes in a site with a ratio of 14.7:1 (20).

Other neutron filter materials besides cadmium may be used. The possibility of using boron is discussed by Rossitto *et al.* (21). Hanna and Al-Shahristani (22) and Randa (23) have compared some combinations of shield materials for a few elements, and arsenic, gallium, and bromine have been determined in some standard reference materials (24, 25).

The use of boron as a shield material may offer several distinct advantages over cadmium. Boron may be advantageous in utilizing very short-lived isotopes for rapid analysis, since the shield itself is not strongly activated so that post-irradiation handling is simplified. Boron absorbs neutrons with

[1]Present address: The Radiochemical Company, Atomic Energy of Canada Ltd., P.O. Box 6300, Ottawa, Ont., Canada K2A 3W3.

0008-4042/81/101470-06$01.00/0

©1981 National Research Council of Canada/Conseil national de recherches du Canada

Can. J. Chem. Downloaded from www.nrcresearchpress.com by 210.87.254.40 on 09/06/12
For personal use only.

Can. J. Chem. Downloaded from www.nrcresearchpress.com by 210.87.254.40 on 09/06/12
For personal use only.

higher energy than does cadmium, so that it should form a more effective shield for many elements. Also, varying the boron thickness will vary the effective neutron cutoff energy of the shield over quite a wide range (21). This may allow some discrimination among elements, depending upon the energy of epithermal neutron resonance absorptions.

This paper presents results of an examination of ENAA utilizing a SLOWPOKE nuclear reactor (26). Data obtained under consistent experimental conditions are given for 69 elements using cadmium and boron shielding, so that results may be directly compared in a practical way. The advantages of utilizing a boron shield for ENAA are emphasized.

Experimental and Results

Irradiation and Counting

A "standard" set of conditions consisting of a 10 min irradiation (at a neutron flux of 1×10^{12} n cm^{-2} s^{-1}), a 1 min decay, and a 10 min accumulation of the γ-ray spectrum from the sample has been previously described, with data given for the peak areas obtained for 78 elements (26). These conditions have again been used in this work to establish the effectiveness of the shielding by cadmium and by boron, so that results are directly comparable, with the exception that in the present study the neutron flux employed was 5×10^{11} n cm^{-2} s^{-1}, exactly one-half that used in ref. 26.

The γ-ray spectrometer used consisted of a 60 cm^3 Canberra high-resolution Ge(Li) detector, 1.88 keV FWHM at the 1.33 MeV ^{60}Co peak, peak-to-Compton ratio 35:1, and a 9.5% (of NaI) efficiency, in conjunction with a Tracor Northern TN 11 pulse-height analyzer.

Thermal Neutron Shields

Cadmium shields were fashioned from 1 mm thick sheets in a cylindrical shape with top and bottom discs to completely enclose the sample.

Table 1 gives the experimentally determined cadmium ratios for 69 elements, where the cadmium ratio is the peak area obtained for the unshielded sample divided by the peak area obtained when the sample was irradiated under the cadmium shield. The actual peak areas obtained for 1 μg of unshielded material, and the γ-ray energies, are given in Table 3 of ref. 26.

Following the simple practical method of Hogdahl (19), the cadmium ratio, R_{Cd}, is given by the formula,

$$R_{Cd} = \frac{A}{A_{Cd}} = \frac{\sigma_{th}\phi_{th} + I_0\phi_{epi}}{I_0\phi_{epi}} = \frac{\sigma_{th}\phi_{th}}{I_0\phi_{epi}} + 1$$

where A and A_{Cd} are the sample activities from irradiation without and with cadmium cover, σ_{th} = thermal neutron cross section, ϕ_{th} = thermal neutron flux, I_0 = the resonance integral (includes $1/v$ contribution), ϕ_{epi} = epithermal neutron flux.

The SLOWPOKE reactor cadmium ratio for gold for an inner site is 2.1. Using the above equation and the I_0/σ_{th} ratio for gold of 15.7, the thermal-to-epithermal flux ratio is estimated to be 17.3:1. From this, the cadmium ratios expected may be calculated from literature values of resonance integrals, for comparison purposes with the experimental values. Calculated values using data from refs. 18 and 20 are included in Table 1. For the most part, agreement is very good. Titanium and mercury show particularly large discrepancies. For titanium, the expected cadmium ratio calculated from the resonance integral determined by Ryves (27) is 27, more in line with the present work.

Boron shields were formed using a mixture of boron carbide powder and paraffin wax. The mixture was heated to about 70°C (paraffin melting point = 56°C) and cast into cylindrical forms. A central hole was made in the form as it solidified by using a heated metal rod of appropriate diameter, which was centred in a guide tube through which it moved to a fixed depth into the form. This resulted in a cylindrical shield with a central cavity, closed at one end. Samples were sealed in plastic and placed in the cavity, and then a top placed over the open end to totally enclose the samples. The open end of the form was made concave to accommodate a convex-shaped top, in order to avoid neutron leaks but to allow rapid assembly and dis-assembly of the capsules.

These shields may be re-used many times. The wall thickness was 4 mm and corresponded to an approximate neutron energy cutoff of 10 eV (21). It should be noted that while this method of construction is very simple and convenient, this type of shield is only suitable for a low temperature reactor such as SLOWPOKE, because if the paraffin melts (with considerable expansion), the integrity of the shield will be lost.

Table 2 gives data for the experimentally obtained boron ratios, under conditions directly comparable with those for the data in Table 1. All elements save cadmium are shielded more effectively by the boron shield. Isotopes having resonance absorption at low neutron energy are particularly well shielded by boron. These include Dy, Eu, Au, In, Ir, Rh, Sc, and Tm. At the same time, there are many isotopes which exhibit a small boron ratio suggesting that those elements could be advantage-

TABLE 1. Cadmium ratios

Element	Isotope measured	Cadmium ratio	Calculated value	Element	Isotope measured	Cadmium ratio	Calculated value
Aluminum	^{28}Al	37	17	Neodymium	^{151}Nd	1.8	2.1
Antimony	^{122}Sb	1.2	1.8	Nickel	^{65}Ni	31	35
Argon	^{41}Ar	27	—	Niobium	^{94m}Nb	3.1	3.4
Arsenic	^{76}As	1.9	2.8				
				Osmium	^{193}Os	7	9
Barium	^{139}Ba	24	21	Oxygen	^{19}O	4.2	4.0
Bromine	^{80}Br	2.0	1.9				
				Palladium	^{109m}Pd	4.1	2.5
Cadmium	^{111m}Cd	2.3	1.9	Platinum	^{199}Pt	3.0	2.3
Calcium	^{49}Ca	41	22	Potassium	^{42}K	23	20
Cerium	^{143}Ce	7	17	Praeseodymium	^{142}Pr	7	11
Cesium	^{134m}Cs	2.3	2.6				
Chlorine	^{38}Cl	43.5	36	Rhenium	^{188m}Re	5.5	4.9
Chromium	^{51}Cr	30	36	Rhodium	^{104m}Rh	3.9	1.3
Cobalt	^{60m}Co	9.0	10	Rubidium	^{86m}Rb	1.4	1.9
Copper	^{66}Cu	18	15	Ruthenium	^{105}Ru	2.2	2.3
	^{64}Cu	15	14				
				Samarium	^{155}Sm	3.9	5.1
Dysprosium	^{165m}Dy	99	68	Scandium	^{46m}Sc	76	33
				Selenium	^{77m}Se	27	—
Erbium	^{171}Er	4.3	5.1		^{79m}Se	2.4	—
Europium	^{152m}Eu	26	20	Silver	^{108}Ag	5.2	5.4
					^{110}Ag	2.7	2.4
Fluorine	^{20}F	8	5	Sodium	^{24}Na	28	27
				Strontium	^{87m}Sr	4.5	4.0
Gadolinium	^{161}Gd	8.9	4.6	Sulphur	^{37}S	39	16
Gallium	^{72}Ga	3.0	7.4				
Germanium	^{75m}Ge	8	8	Tantalum	^{182m}Ta	1.6	1.6
Gold	^{198}Au	2.1	(2.1)[a]	Tellurium	^{131}Te	9.4	11.2
				Terbium	^{160}Tb	1.8	2.1
Hafnium	^{179m}Hf	1.9	1.9	Thorium	^{233}Th	2.9	2.8
Holmium	^{166}Ho	2.6	2.7	Thulium	^{170}Tm	1.7	2.3
				Tin	^{125m}Sn	1.4	1.3
Indium	^{116m}In	2.4	2.3	Titanium	^{51}Ti	26	1.6
Iodine	^{128}I	1.3	1.7	Tungsten	^{187}W	2.3	2.5
Iridium	^{194}Ir	2.8	2.4				
Iron	^{59}Fe	26	13	Uranium	^{239}U	1.1	1.2
Lanthanum	^{140}La	19	15	Vanadium	^{52}V	30	30
Lead	^{204m}Pb	1.0	—				
Lutetium	^{176m}Lu	3.9	1.6	Ytterbium	^{177}Yb	7.3	8.2
				Yttrium	^{89m}Y	1.1	—
Magnesium	^{27}Mg	32	18		^{90}Y	3.7	—
Manganese	^{56}Mn	16	18				
Mercury	^{197}Hg	4.7	33	Zinc	^{69m}Zn	4.6	6.6
	^{199m}Hg	1.5	1.2	Zirconium	^{97}Zr	1.0	—
Molybdenum	^{101}Tc	1.6	1.8				

[a]Values calculated from resonance integral data given in refs. 18 and 20, using a cadmium ratio for gold of 2.1.

ously determined in a matrix containing elements with high boron ratios (e.g. Al, Cl, Na). The use of thicker boron shields to give a higher effective neutron energy cutoff has also been investigated. This has been done by maintaining the same shield geometry, but replacing the boron carbide with boron powder which is 92.94% enriched in ^{10}B. The estimated effective neutron energy cutoff of these shields is approximately 150 eV. Table 3 gives data for a selection of elements and demonstrates that in all cases greater shielding has been obtained.

The data in Tables 1–3 have been presented in a format which allows a decision to be quickly formed as to whether or not one of these shields can be employed to advantage for any specific sample being analyzed. In general, a given sample type will exhibit several isotopes which dominate the γ-ray spectrum (e.g. Al, Cl, Mn, Na, Sc). These will often cause serious interference in determining other isotopes of interest, particularly ones which give minor peaks in the spectrum. It is noteworthy that the elements that typically cause interference can be

Can. J. Chem. Downloaded from www.nrcresearchpress.com by 210.87.254.40 on 09/06/12
For personal use only.

TABLE 2. Boron ratios for a neutron cutoff energy of ~10 eV

Element	Isotope measured	Boron ratio	Element	Isotope measured	Boron ratio
Aluminum	^{28}Al	79	Neodymium	^{151}Nd	2.4
Antimony	^{122}Sb	3.6	Nickel	^{65}Ni	100
Argon	^{41}Ar	50	Niobium	^{94m}Nb	3.8
Arsenic	^{76}As	3.3			
			Osmium	^{193}Os	18
Barium	^{139}Ba	44	Oxygen	^{19}O	4.8
Bromine	^{80}Br	3.9			
			Palladium	^{109m}Pd	7.3
Cadmium	^{111m}Cd	1.9	Platinum	^{199}Pt	4.8
Calcium	^{49}Ca	180	Potassium	^{42}K	41
Cerium	^{143}Ce	30	Praeseodymium	^{142}Pr	16
Cesium	^{134m}Cs	7.5			
Chlorine	^{38}Cl	147	Rhenium	^{188m}Re	13
Chromium	^{51}Cr	120	Rhodium	^{104m}Rh	57
Cobalt	^{60m}Co	13	Rubidium	^{86m}Rb	1.7
Copper	^{66}Cu	31	Ruthenium	^{105}Ru	2.7
	^{64}Cu	23			
			Samarium	^{155}Sm	7.2
Dysprosium	^{165m}Dy	720	Scandium	^{46m}Sc	460
			Selenium	^{77m}Se	60
Erbium	^{171}Er	6.9		^{79m}Se	3.2
Europium	^{152m}Eu	260	Silver	^{108}Ag	11
				^{110}Ag	12
Fluorine	^{20}F	11	Sodium	^{24}Na	64
			Strontium	^{87m}Sr	5.5
Gadolinium	^{161}Gd	12	Sulphur	^{37}S	>150
Gallium	^{72}Ga	4.4			
Germanium	^{75m}Ge	11	Tantalum	^{182m}Ta	5.6
Gold	^{198}Au	9.5	Tellurium	^{131}Te	12
			Terbium	^{160}Tb	3.8
Hafnium	^{179m}Hf	7	Thorium	^{233}Th	4.9
Holmium	^{166}Ho	7.8	Thulium	^{170}Tm	7.3
			Tin	^{125m}Sn	2.4
Indium	^{116m}In	32	Titanium	^{51}Ti	71
Iodine	^{128}I	2.6	Tungsten	^{187}W	2.7
Iridium	^{194}Ir	17			
Iron	^{59}Fe	40	Uranium	^{239}U	2.9
Lanthanum	^{140}La	34	Vanadium	^{52}V	95
Lead	^{204m}Pb	1			
Lutetium	^{176m}Lu	4.7	Ytterbium	^{177}Yb	10
			Yttrium	^{89m}Y	1.1
Magnesium	^{27}Mg	101		^{90}Y	5.0
Manganese	^{56}Mn	30			
Mercury	^{197}Hg	8.4	Zinc	^{69m}Zn	6.4
	^{199m}Hg	1.8	Zirconium	^{97}Zr	1.3
Molybdenum	^{101}Tc	1.9			

highly shielded. ^{24}Na is often taken as an example to estimate the advantage factor obtainable using the ENAA technique. The advantage factor (1) is calculated as the shield ratio for sodium divided by the shield ratio for the isotope of interest (e.g. in the case of gold under a cadmium shield, the advantage factor for gold over sodium is 28/2.1 = 13). The advantage factor represents the degree to which the particular interference will be reduced by using the shield.

Table 4 gives advantage factors over sodium for a selection of elements under the three shields (data from Tables 1–3). For elements with very low energy resonances (Au, Hf, In, Ir, Rh) cadmium gives the best advantage factor. For a number of others (Ba, Cd, Mo, Rb, Ru, Sr, Zn) a thick boron shield is best. This is especially true for fast-neutron induced reactions such as for ^{204}Pb(n,n')^{204m}Pb or ^{29}Si(n,p)^{29}Al, or ^{19}F(n,p)^{19}O. However, for many elements (As, Br, Co, Ga, I, La, Pd, Pt, Sm, Th, Sn, W, Zr) the advantage factor is optimised by the "intermediate" cutoff energy afforded by the natural boron shield.

Thus it is indeed possible to optimise the shield-

Can. J. Chem. Downloaded from www.nrcresearchpress.com by 210.87.254.40 on 09/06/12
For personal use only.

Can. J. Chem. Downloaded from www.nrcresearchpress.com by 210.87.254.40 on 09/06/12
For personal use only.

TABLE 3. Boron ratios for a neutron cutoff energy of ~150 eV

Element	Isotope measured	Boron ratio	Element	Isotope measured	Boron ratio
Aluminum	^{28}Al	125	Manganese	^{56}Mn	70
Antimony	^{122}Sb	17	Mercury	^{197}Hg	19
Arsenic	^{76}As	9.3		^{199m}Hg	2.2
			Molybdenum	^{101}Tc	3.0
Barium	^{139}Ba	70			
Bromine	^{80}Br	9.2	Palladium	^{109m}Pd	34
			Platinum	^{199}Pt	14
Cadmium	^{111m}Cd	2.6	Potassium	^{42}K	62
Cesium	^{134m}Cs	36			
Chlorine	^{38}Cl	360	Rubidium	^{86m}Rb	2.5
Chromium	^{51}Cr	230	Ruthenium	^{105}Ru	4.3
Cobalt	^{60m}Co	28			
Copper	^{66}Cu	59	Samarium	^{155}Sm	21
	^{64}Cu	48	Sodium	^{24}Na	130
			Strontium	^{87m}Sr	8.4
Gallium	^{72}Ga	12			
Gold	^{198}Au	90	Thorium	^{233}Th	12
			Tin	^{125m}Sn	9.6
Hafnium	^{179m}Hf	96	Titanium	^{51}Ti	109
			Tungsten	^{187}W	34
Indium	^{116m}In	250			
Iodine	^{128}I	10	Uranium	^{239}U	11
Iridium	^{194}Ir	89			
			Vanadium	^{52}V	190
Lanthanum	^{140}La	130			
			Zinc	^{69m}Zn	9.8
			Zirconium	^{97}Zr	2.9

TABLE 4. Advantage factors for selected elements relative to ^{24}Na[a]

	Advantage factors calculated from Tables 1–3		
Element	Cadmium	Boron	Boron-10
Arsenic	14	19	14
Barium	1.1	1.5	1.9
Bromine	13	16	14
Cadmium	12	34	50
Cobalt	3.0	4.9	4.6
Gallium	9.3	15	11
Gold	13	6.7	1.4
Hafnium	14	9.1	1.4
Indium	11	2.0	0.5
Iodine	21	25	13
Iridium	9.6	3.8	1.5
Lanthanum	1.4	1.9	1.0
Lead	27	64	130
Molybdenum	17	34	43
Palladium	6.6	8.8	3.8
Platinum	9.0	13	9.3
Rhodium	6.9	1.1	—
Rubidium	19	38	52
Ruthenium	12	24	30
Samarium	6.9	8.1	6.2
Strontium	6.2	12	15
Thorium	9.3	13	11
Tin	19	27	14
Tungsten	12	24	3.8
Zinc	6.1	10	13
Zirconium	27	49	45

[a]Isotope measured as listed in Table 3.

ing conditions to discriminate among the elements present in a sample, in order to give the largest advantage to elements of particular interest.

We have found the use of boron shields to be of particular practical advantage for rapid instrumental analysis in a number of instances, including the analysis for the trace element content of a natural salt matrix, analysis for the fluorine content of soil, analysis for the silicon content of geological material, and as part of an instrumental NAA scheme for the essentially complete determination of the major, minor, and trace components of rock, sediment, and soil samples (to be published).

Acknowledgement

This work was supported by a grant from the Natural Sciences and Engineering Research Council of Canada.

1. D. BRUNE and K. JIRLOW. Nukleonik, **6**, 242 (1964).
2. D. BRUNE. Anal. Chim. Acta, **46**, 17 (1969).
3. A. O. BRUNFELT and E. STEINNES. Anal. Chim. Acta, **48**, 13 (1969).
4. E. STEINNES. Z. Anal. Chem. **247**, 23 (1969).
5. E. STEINNES and D. BRUNE. Talanta, **16**, 1326 (1969).
6. E. STEINNES. *In* Activation analysis in geochemistry and cosmochemistry. *Edited by* A. O. Brunfelt and E. Steinnes. Universtets-forlaget, Oslo. 1971. p. 113.
7. H. G. MEYER. J. Radioanal. Chem. **7**, 67 (1971).

8. N. V. BAGDAVADZE and L. M. MOSULISHVILI. J. Radioanal. Chem. **24**, 65 (1975).
9. M. JANSSENS, B. DESMET, R. DAMS, and J. HOSTE. J. Radioanal. Chem. **26**, 305 (1975).
10. H. AL-SHAHRISTANI and K. ABBASS. J. Radioanal. Chem. **27**, 105 (1975).
11. E. STEINNES and J. J. ROWE. Anal. Chim. Acta, **87**, 451 (1976).
12. J. J. ROWE and E. STEINNES. J. Radioanal. Chem. **37**, 849 (1977).
13. P. A. BAEDECKER, J. J. ROWE, and E. STEINNES. J. Radioanal. Chem. **40**, 115 (1977).
14. E. M. GRYNTAKIS and J. I. KIM. Part 1: J. Radioanal. Chem. **29**, 175 (1976); Part 2: J. Radioanal. Chem. **42**, 181 (1978).
15. C. H. WESTCOTT, W. H. WALKER, and T. K. ALEXANDER. 2nd Int. Conf. Peaceful Uses of Atomic Energy, IAEA, Geneva, **16**, 70 (1958).
16. R. W. STOUGHTON and J. HALPERIN. Nucl. Sci. Eng. **6**, 100 (1959).
17. J. I. KIM and F. ADAMS. Radiochim. Acta, **9**, 61 (1968).
18. R. VAN DER LINDEN, F. DE CORTE, P. VAN DEN WINKEL, and J. HOSTE. J. Radioanal. Chem. **11**, 133 (1972); R. VAN DER LINDEN, F. DE CORTE, and J. HOSTE. J. Radioanal. Chem. **20**, 695 (1974).
19. O. T. HOGDAHL. Radiochemical methods of analysis. IAEA, Geneva. 1965.
20. R. VAN DER LINDEN, F. DE CORTE, and J. HOSTE. J. Radioanal. Chem. **23**, 113 (1974).
21. F. ROSSITTO, M. TERRANI, and S. TERRANI. Nucl. Instrum. Methods, **103**, 77 (1972).
22. A. G. HANNA and H. AL-SHAHRISTANI. J. Radioanal. Chem. **37**, 581 (1977).
23. Z. RANDA. Radiochem. Radioanal. Lett. **24**, 157 (1976).
24. L. E. WANGEN and E. S. GLADNEY. Anal. Chim. Acta, **96**, 271 (1978).
25. E. S. GLADNEY and D. R. PERRIN. Anal. Chem. **51**, 2015 (1979).
26. D. E. RYAN, D. C. STUART, and A. CHATTOPADHYAY. Anal. Chim. Acta, **100**, 87 (1978).
27. T. B. RYVES. J. Nucl. Energy, **24**, 35 (1974).

Can. J. Chem. Downloaded from www.nrcresearchpress.com by 210.87.254.40 on 09/06/12
For personal use only.

The determination of copper, cadmium, and lead in sea water by anodic stripping voltammetry with a thin film mercury electrode

D. G. GREEN, L. W. GREEN,[1] J. A. PAGE,[2] J. S. POLAND, AND G. VAN LOON

Department of Chemistry, Queen's University, Kingston, Ont., Canada K7L 3N6

Received July 15, 1980

This paper is dedicated to Professor W. E. Harris on the occasion of his retirement from the University of Alberta

D. G. GREEN, L. W. GREEN, J. A. PAGE, J. S. POLAND, and G. VAN LOON. Can. J. Chem. **59**, 1476 (1981).

The application of anodic stripping voltammetry to the determination of Cu, Pb, and Cd in acidified sea water samples has been examined. The analyses were carried out using a thin film mercury electrode prepared *in situ* by the method of Florence. The electrode was rotated in the collection step but held stationary in the stripping step. The stripping involved a linear DC potential ramp and background compensation was employed. Resolution of the stripping peaks required "curve fitting" of the baseline.

In the acidified sea water electrolyte it was found that the Pb and Cd stripped to Pb(II) and Cd(II) while the Cu stripped to Cu(I). A good correlation was found between the stripping signals and predictions based on the Levich equation for deposition at a rotating disk electrode and the De Vries and Van Dalen equation for stripping from a thin film electrode. The effect of sample acidity was examined and it was concluded that in unpolluted, filtered sea water the total metal was free for analysis at pH 2. Calibration was by the method of standard addition and intercalibration studies showed that the results agreed well with those obtained by other methods.

D. G. GREEN, L. W. GREEN, J. A. PAGE, J. S. POLAND et G. VAN LOON. Can. J. Chem. **59**, 1476 (1981).

On a étudié la possibilité d'appliquer la technique de redissolution anodique au dosage du Cu, du Pb et du Cd dans des échantillons d'eau de mer acidifiée. Les analyses ont été faites en utilisant une électrode à film mince de mercure préparée *in situ* par la méthode de Florence. On fait tourner l'électrode lors du dépôt des cations mais on la maintient fixe lors de l'étape de redissolution. La redissolution est effectuée avec un balayage linéaire du potentiel en utilisant une compensation du courant résiduel. La résolution des pics de redissolution requiert un ajustement de la ligne de base.

On a trouvé que dans l'eau de mer acidifiée, la Pb et le Cd se redissolvent sous forme de Pb(II) et de Cd(II) tandis que le Cu se redissout sous forme de Cu(I). On observe une bonne corrélation entre les pics de redissolution et les prévisions faites à partir de l'équation de Levich pour le dépôt sur une électrode à disque tournant et l'équation de De Vries et Van Dalen pour la redissolution à partir d'une électrode à film mince. On a étudié l'effet de l'acidité de l'échantillon et on en conclut que, dans le cas de l'eau de mer non polluée et filtrée, la quantité totale de métal est sous forme libre lors des analyses à un pH de 2. La calibration a été faite par la méthode des additions standard et des études d'intercalibration ont montré que les résultats sont en bon accord avec ceux obtenus par d'autres méthodes.

[Traduit par le journal]

Introduction

The determination of trace metals in seawater (SW) is receiving increasing attention because of the interest in the spatial and temporal variation of the elements and their role in the biochemical and geochemical cycles of the oceans. However, despite considerable past efforts reliable data are still difficult to obtain and there are presently active programs concerned with the development and evaluation of appropriate analytical methods (1). The analyses are difficult because almost all of the elements of interest in unpolluted sea water are in the sub μg L^{-1} concentration range; in addition there are major questions concerning the speciation or form of the trace element and even uncertainties regarding the sampling and storage procedures used. The questions cannot be resolved until the accuracy and precision of the analytical techniques have been satisfactorily established.

Riley (2) has reviewed the analytical methods currently used in the analysis of sea water; of the various instrumental techniques anodic stripping voltammetry (ASV) appears particularly advantageous for the determination of trace Cu, Zn, Cd, and Pb. The technique is sensitive and requires only simple instrumentation; it is also unique in that it can directly probe the sea water matrix after a minimal pretreatment of the sample. The "concentration step" prerequisite to the application of most instrumental methods in trace analysis becomes a simple deposition that does not require the addition of reagents or other sample manipulation; anodic stripping of the deposited metal in the "analytical step" yields the current signal used for quantitative evaluation. Both steps are carried out using a single working electrode under programmed potential control. The technique is somewhat restricted and works best with those elements that can be deposited and collected as amalgams at a mercury electrode; even here the metal must strip from the amalgam at potentials that do not result in oxidation of the mercury itself.

[1]Present address: Atomic Energy of Canada Limited Research Laboratories, Chalk River, Ont., Canada K0J 1J0.

[2]To whom all correspondence should be addressed.

0008-4042/81/101476-11$01.00/0

©1981 National Research Council of Canada/Conseil national de recherches du Canada

Can. J. Chem. Downloaded from www.nrcresearchpress.com by 210.87.254.40 on 09/06/12
For personal use only.

Can. J. Chem. Downloaded from www.nrcresearchpress.com by 210.87.254.40 on 09/06/12
For personal use only.

However, there are variants involving direct deposition on other substrates and these permit the determination of additional elements; this and other aspects have been considered in detail in the monograph by Vdyra *et al.* (3), while Nurnberg (4) has discussed the potentialities of the method as regards sea water analysis.

An important feature of ASV analysis is that only the metal that is in a "labile" form for deposition ultimately yields an analytical stripping signal. It is recognized that a trace metal can be present in a variety of forms in sea water and whether a particular species is ASV "labile" or "inert" is mainly dependent upon the kinetics of dissociation of the complex as well as the electrode potential and electrode parameters in the deposition stage (5). ASV analysis is usually carried out with calibration by the method of standard additions and while this approach might be expected to give a value for the total metal concentration in the sample this would occur only if the added standard correctly proportioned itself amongst all the forms of the metal in the sample. The slope of the resultant standard addition plot would depend upon the proportion of added standard in the ASV labile form while the intercept on the concentration axis would give the true value for the total metal.

At another extreme, standard addition ASV analysis would be expected to give values for the true labile metal concentration if the added standard proportioned itself (only) amongst the ASV labile species in the sample. The slope of the standard addition plot would then be constant and independent of the proportions of labile and inert metal species.

In the case of a sea water sample the form and distribution of the metal in the sample is unknown as is the partition of an added standard amongst the various forms. The interpretation of a set of standard addition ASV results may then be complex. It is known that the absolute value of an ASV signal generally increases with acidification of a sea water sample, suggesting a conversion of inert to labile metal, but the distribution of an added standard can still be uncertain.

The "total" metal in a sample can be unambiguously ascertained if the sea water is treated in such a way as to convert all of a metal to ASV labile forms. In most procedures for the ASV analysis of sea water the sample is filtered through a conventional 0.45 μm filter and then acidified to pH ~2; it is assumed that on standing in the weakly acid solution the metals are quantitatively converted to labile forms for the analysis. Other more intensive treatments including ultraviolet irradiation and nitric acid digestion have been used to ensure complete conversion (6) but these involve sample handling and reagent addition and are liable to produce significant contamination at the trace level. In many cases the need for such robust treatment is questionable and at least one paper (7) implies that it is unnecessary in the case of unpolluted sea water samples.

The actual "speciation" of the trace metal in sea water is of interest since the form determines the properties of the metal. Davison (8) has reviewed the use of electroanalytical techniques to actually define the metal species present in natural waters; a variety of ASV experiments were summarized including titration with either metal or ligand to determine the complexing capacity and properties of the sample, model experiments to determine the behaviour of metal species added to the sample, and direct probing of real samples. In the latter experiments the ASV response is usually determined as a function of acidity; any increase in analytical signal with acidity is interpreted in terms of displacement of active metal from inert complex species. Other than model studies, this approach has been exploited only to a limited extent with sea water because of the low concentrations of the metals and the difficulties in analysis of the trace level.

In the present study the determination of Cu, Cd, and Pb in sea water by ASV was examined. There have been a number of recent papers concerned with the determination of these elements (sometimes with an accompanying Zn determination) and the variants include differential pulse ASV at a hanging mercury drop electrode (9) and direct ASV (10), potentiometric stripping (11), and differential pulse ASV (12) at a thin film mercury electrode (TFME). In the present study a thin film mercury electrode was used; the electrode was rotated in the collection step but stripping was carried out from a stationary electrode using a linear potential ramp. The method was chosen over other variants because it had the requisite sensitivity and importantly because the deposition and stripping parameters are well defined and it is possible to correlate the stripping signal and unknown concentration without calibration. Unlike some of the other studies the simultaneous determination of Zn was not examined since the element, if deposited, can interfere in the ASV determination of Cu, Cd, and Pb by the formation of intermetallic compounds (3, 13). This effect can be severe in the relatively concentrated amalgams formed at thin

Can. J. Chem. Downloaded from www.nrcresearchpress.com by 210.87.254.40 on 09/06/12
For personal use only.

film electrodes but the difficulty can be avoided if the analyses are carried out without deposition of Zn in the collection step.

The reported determinations of Zn in sea water have been by differential pulse ASV at a mercury drop electrode with the sample normally buffered in the pH 4–5 range. One method has been reported with the sample acidified to pH 1 in the presence of additional added chloride (9), but such an acid level produces a severe depression of the Zn differential pulse stripping peak. In the present work some attempts were made to determine Zn by the differential pulse technique using a mercury drop electrode with samples buffered to pH 4.5, but the results with the various sea water samples appeared high and a measure of Zn contamination was suspected.

Experimental

An EG and G Princeton Applied Research Model 174A Polarographic Analyzer was used for the ASV measurements. The instrument has an I/E converter with a maximum sensitivity corresponding to a full scale output of 10 V for a 20 nA electrolysis current. The 174A unit was linked to a programmable timer[3] that provided bias voltages and switching for automation of the ASV cycle.

The actual Faradaic stripping peaks were found to be superimposed on a relatively large background process and could not be recorded without a partial compensation of this part of the signal. This was achieved using an instrumentation amplifier to subtract a linear ramp from the stripping signal. The ramp was derived from the *X* axis drive of the 174A instrument; this output tracks the ramp signal fed to the summing amplifier in the stripping process. The signal fed to the instrumentation amplifier was generated using the *X* output as the input to an operational amplifier with calibrated variable gain. The compensated stripping signals were recorded on a Hewlett Packard Model 7005 X-Y recorder; a 10× normal expansion of the stripping peaks was achieved by recording the current at a *Y* axis sensitivity of 0.1 V/in. While other methods of background compensation including storage and subtraction of a blank scan (14) and dual electrodes operating in a subtractive mode (15) have been suggested, they were not employed in this study. The latter technique was investigated but found impractical because of the difficulty in matching the background characteristics of the dual electrodes while the former requires complex digital circuitry. A block diagram of the apparatus is given in Fig. 1*A*, while a diagram of a quartz ASV cell with a rotatable TFME is shown in Fig. 1*B*.

The cells were made either from quartz glass or machined from polytetrafluoroethylene (PTFE) rod. These materials were chosen to minimize contamination problems. The sample compartment of each cell had a diameter of ~1.6 cm and a 5–10 cm^3 sample capacity. The auxiliary electrode was a Pt wire while the reference was either a Ag/AgCl/SW electrode (−0.010 V vs. SCE) prepared from Ag wire or a $Hg/Hg_2Cl_2/SW$ electrode (+0.045 V vs. SCE). The latter electrode was formed from a slug of Hg packed in a small diameter passage through a PTFE insert in the cell wall. Contact with the Hg was made using a clean

[3]The timer was based on a National Semiconductor MM57161N SIT processor chip. Circuit diagrams are available from the authors.

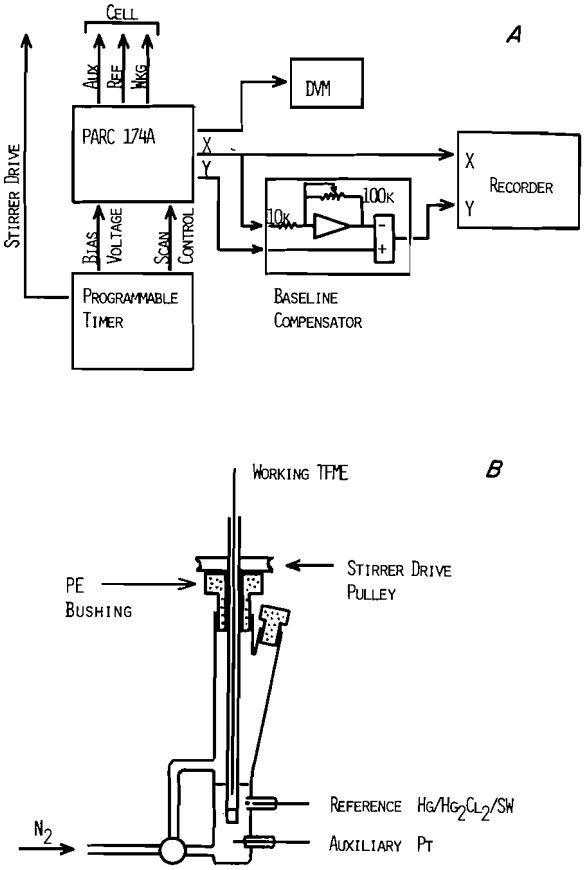

FIG. 1. *A*, block diagram of apparatus; *B*, quartz ASV cell with rotated TFME. IA is Analog Devices 603K, OA is Analog Devices 43K.

amalgamated Pt wire press fitted into the passage. After electrolytic conditioning of the Hg to produce a surface layer of Hg_2Cl_2, the reference was well poised with a potential independent of the presence of any Hg(II) added to the acidified SW samples. The use of this electrode eliminated the standard saturated calomel reference probe as a source of contamination in the trace analysis experiments. The ASV analyses were carried out with the electrolyte at room temperature (25 ± 2°C); O_2 was rigorously removed and excluded from the electrolyte by an initial deaeration and subsequent blanketing with N_2 gas. The N_2 gas used was purified by passage over hot BASF Cu catalyst to remove trace O_2, then thoroughly scrubbed by passage through H_2O before use.

The TFME was prepared according to Florence (16) by *in situ* electrodeposition after the addition of Hg(II) to the sample. The substrate consisted of a disk of GC-20 glassy carbon supplied by the Tokai Electrode Manufacturing Company. The material was in the form of 3 mm *d* × 4 mm *l* rod mounted and sealed in a glass tube with epoxy cement. The exposed face was polished, initially with 6 μm diamond dust and finally to a mirror finish with 0.05 μm alumina. The electrode had a surface area of 0.066 cm^2 and was rotated at precisely 1800 rpm (N = 30 Hz) in the deposition and conditioning stages of the ASV cycle; electrical contact was made through a stationary Pt wire inserted into Hg contained in the electrode tube. The electrode was mounted in the cell through a polyethylene (PE) bearing with PE bushings bored to allow free true rotation of the electrode. In any series of

Can. J. Chem. Downloaded from www.nrcresearchpress.com by 210.87.254.40 on 09/06/12
For personal use only.

analyses there was a continual deposition and thickening of the film and the Hg was removed from the substrate after each set of analyses using a clean nylon brush. Between analyses the electrode was stored in distilled water. Good electrodes had a life span of up to 4 months with failure evident in the form of increased background currents in the stripping process. The failure was usually attributed to deterioration of the epoxy seal rather than to change in the substrate surface.

In some studies of the SW with pH as a variable the addition of Hg(II) to the sample was undesired and "preformed" films, prepared in a separate experiment by electrodeposition from an acid Hg(II) electrolyte, were used in the ASV experiments. Such films were difficult to handle and gave more irreproducible results than the *in situ* formed films.

The sample vessels, glassware, cells, and electrodes used were conditioned before use by long soaking in aqueous 3 *M* nitric acid followed by thorough rinsing with distilled water. Stringent precautions were taken to exclude contamination and the sample handling, transfer operations, and cell experiments were carried out in a laminar flow clean hood. The approximately sized SW samples were transferred directly from the sample vessel to the cell with the sample volume determined after the analysis. On occasion a number of attempts with successive emptying and refilling of the cell with fresh sample were required before low and consistent analytical results could be obtained. If pH was a variable, the adjustments were made by the addition of calculated amounts of reagent to the sample or cell electrolyte; glass electrodes were found to be a source of metal contamination and measurements were made only after the sample was removed from the cell or alternatively the pH was tracked in a separate parallel experiment. Standard solutions were prepared determinately from pure metals dissolved in excess nitric acid; the stock solutions were diluted using a 0.1 *M* HNO_3 electrolyte as required. The reagents used were BDH "Aristar" quality and the HNO_3 and HCl acids were redistilled in quartz apparatus before use. The distilled water was obtained from a well aged and conditioned three stage borosilicate glass still.

ASV Analysis

A standard procedure with optimized parameters was developed for the SW analyses; potentials are quoted relative to the $Hg/Hg_2Cl_2/SW$ reference electrode.

The cell was rinsed and filled with sample adjusted to pH 2 and 25 μL of a 10 m*M* Hg(II) solution was added for each 5 mL of sample. This gave a Hg(II) concentration of 50 μ*M* (10 ppm) for the *in situ* film deposition. After deaeration for 15 min under open circuit conditions, a preliminary deposition of Hg was made at −1.00 V with the electrode rotated; deposition was continued for 30 min to produce a film thickness of ~100 nm as estimated from the deposition current (~5 μA). The electrode was then scanned to −0.10 V and conditioned at that potential, with rotation, for 40 s. This stripped the metals which had codeposited with the Hg film back into the electrolyte in preparation for the subsequent series of analyses involving the sample and calibration.

The analysis for the metals was then carried out using a deposition potential of −1.00 V with electrode rotation and a collection period (τ) typically of 300 s. At the end of this period the potential was maintained for a further 30 s without electrode rotation to establish quiescent conditions for the stripping stage.

The deposited metals were then stripped from the Hg film by scanning from −1.00 V to −0.10 V with $dE/dt = 0.050$ V s^{-1} and a predetermined level of background compensation. The Cd, Pb, and Cu stripping peaks appeared near −0.75, −0.56, and −0.35 V respectively. On reaching −0.10 V the scan was terminated and the Hg film conditioned at that potential for a minimum period of 40 s before continuing with replicate analysis. Calibration was by the method of standard additions and the microaliquots of standard solution were added at this stage. Potentiostatic control of the electrode potential was maintained throughout. In an analysis the increments of the three metals were made simultaneously and the total of the standard additions was chosen to give an ~2× increase of each stripping peak.

For each single analysis the unknown and three standard additions were run; in general each instrumental measurement in this set was repeated three times. During the series of analyses there was a continued growth of Hg film thickness from the *in situ* deposition but the non-dependence of the stripping signal on the film thickness can be demonstrated provided a film of minimum thickness has been predeposited. The calibration line and the best single estimate of unknown concentration (z) and standard error (s_z) were determined from the set of data by linear regression (17, 18). When replicate analyses were carried out the individual concentration values were pooled to give a mean concentration ($\Sigma z/n$), an estimated standard deviation (s), and the standard error ($s/\sqrt{n}$). The errors associated with the individual calibration lines were also combined to give a pooled standard error ($(s_z)_p$); this pooled error is a measure of imprecision in the instrumental procedure (19). The data given in this paper (Tables 2 and 5) show the standard error of the concentration values is in general only marginally greater than the pooled standard error of the individual calibration lines; this indicates that handling of the sample for replicate analyses is only a marginally greater source of error than the measurement itself. When comparisons were possible with the work of other investigators (Table 2), the imprecision of the ASV results was found comparable to that obtained in analyses involving atomic absorption measurements.

The metal concentrations in uncontaminated SW are at the sub μg L^{-1} level and the linearity of the response over the concentration ranges typically investigated is demonstrated by the correlation coefficients in Table 1. A time dependency of the ASV signals after a standard addition was not detected with acidified SW samples. In separate experiments the calibrations were extended to ~10 μg L^{-1} of each metal; there was no evidence of curvature and the slopes of the calibration lines remained consistent with those obtained over the working ranges of concentration.

Figure 2 shows stripping curves as obtained in the analysis of a typical SW sample; the diagram shows both an uncompensated curve and a curve as recorded with an appropriate degree of linear compensation. The compensation level has been adjusted to give an output with a small positive slope over the mid range of the stripping ramp and this results in rapidly changing base line values at the beginning and end of the potential range. These changes occur at potentials corresponding to the cessation of H^+ discharge and the onset of Hg oxidation respectively. In Fig. 3, a "blank" curve obtained using a SW sample and an analysis cycle with zero deposition time ($\tau = 0$) is compared with an analytical curve obtained on the same sample ($\tau = 300$ s). A shift in the baseline between the blank and the analytical curve is evident in the region of the Cu stripping peak even though the compensation level and output offset were unchanged between recordings.

The stripping peaks for the three metals were resolved from the background by "curve fitting"; the background curve was approximated graphically using the blank curve to estimate the position of the baseline under the individual stripping peaks. While "tangent fitting" of the baseline was considered this would have produced peak values for Cu significantly less than the true value while blank subtraction would have produced peak values greater than the true value. Table 1 gives the responses for the

Can. J. Chem. Downloaded from www.nrcresearchpress.com by 210.87.254.40 on 09/06/12
For personal use only.

TABLE 1. TFME–ASV analysis of SW

Parameter	Value		
	Cu	Pb	Cd
$E_{1/2}$/(V vs. SCE)[a]	>0, −0.20	−0.48	−0.68
D_0/(cm^2 s^{-1})[a]	0.62×10^{-5}	0.83×10^{-5}	0.66×10^{-5}
i_l/C_0*[b]			
A/(mol l^{-1})	0.0797	0.0960	0.0830
E_p/(V vs. Hg/Hg_2Cl_2/SW)	−0.35	−0.56	−0.75
$b_{1/2}$/V	0.080	0.038	0.039
i_p/C_0*			
A/(mol L^{-1})[b]	6.98	33.7	29.1
μA/(μg L^{-1})[b]	0.110	0.163	0.258
$i_p/\Delta C$*			
A/(mol L^{-1})[c]	3.5–6.7	28.4 (1.2)	21.0 (2.0)
μA/(μg L^{-1})[c]	0.055–0.106	0.137 (0.006)	0.186 (0.018)
r[d]	0.9967	0.9983	0.9988

[a]Polarography of spiked SW.
[b]Calculated according to eqs. [1]–[4].
[c]Range of slope or mean slope and standard deviation.
[d]Typical correlation coefficient for slope.

TABLE 2. Comparative results on a coastal SW sample

Parameter	Value		
	Cu	Cd	Pb
TFME–ASV[a,c]	1.14 *3* (0.14)	0.120 *5* (0.016)	0.29 *5* (0.07)
$(s_z)_p$[d]	0.090	0.0084	0.019
Atomic absorption[b,c]	1.20 *5* (0.09)	0.098 *5* (0.010)	0.39 *5* (0.07)

[a]Analyses at pH 1.6.
[b]Atomic absorption results by solvent extraction/heated graphite atomizer as reported in ref. 30.
[c]Mean concentrations (μg L^{-1}), number of replicates, and standard deviation.
[d]Pooled standard error from individual calibration lines.

three metals in the SW electrolyte in terms of the slope of the standard addition calibration plots obtained with the given set of experimental and kinetic parameters. The comparison in the response of the three metals is probably best made in terms of molar concentrations but weight/volume relations are typically used in trace analysis and both conventions are expressed.

ASV Response

The equations that relate the kinetic parameters to both the deposition current at the rotated TFME or "disk" electrode and the anodic current peak in the subsequent stripping step are well defined (for definition of symbols, see Table 3) and it is possible to predict the ASV response for a given concentration of analyte.

For the deposition of the metal under conditions of limiting mass transfer, the current can be related to the apparent diffusion layer thickness:

$$[1]\quad M^{n+} + ne \xrightarrow{\text{TFME}} M(Hg)$$
$$i_l = (nFA)D_0(C_0^*/\delta)$$

In the special case of a rotated disk electrode, the limiting current can be calculated according to Levich (20) and is given by:

$$[2]\quad i_l = 0.62(nFA)D_0^{2/3}\omega^{1/2}\gamma^{-1/6}C_0^*$$

If the reduction of the metal ion is unaffected by the coreduction of other species and if there is no significant depletion of the active species in the collection period, the amount of metal deposited is proportional to the deposition time and

$$[3]\quad n_r = (i_l\tau)/(nF)$$

In the subsequent oxidation, the peak anodic stripping current from the TFME can be estimated according to De Vries and Van Dalen (21) and is given by:

$$M(Hg) - n'e \xrightarrow{\text{TFME}} M^{n'+}$$
$$[4]\quad i_p = 0.30(n'FA)\sigma l C_r = 0.30(n'F)\sigma n_r;\quad \sigma = (n'F/RT)v$$

The relation as derived applies only to homogeneous amalgam films sufficiently thin that diffusion of reduced metal to the film surface is not a limiting feature of the oxidation. De Vries and Van Dalen estimate the relation is valid within 2% if their defined kinetic parameter is sufficiently small ($H < 0.144$, $H = l^2\sigma/D_r$) and in the present case it can be shown that this holds for any film thickness less than 10^{-3} cm. These authors also estimated the half-width of the stripping peak and the effect of the kinetic parameters on the stripping peak potential:

$$[5]\quad n'b_{1/2} = 0.0755V\quad (H < 0.45)$$

$$[6]\quad n'(E_p - E_{1/2}) = 0.0014V + 0.02958V \log H$$

These equations permit correlation of the concentration of metal ion in a sample to the peak stripping current and Table 1 includes the predicted responses (i_p/C^*) for the three metals in the SW electrolyte. The values are based on the standard electrode and kinetic parameters as defined in the procedure, values of the diffusion coefficients determined from polarography, and the known kinematic viscosity of the SW electrolyte. In the case of Cu the response value is based on an (assumed) 1-electron

Can. J. Chem. Downloaded from www.nrcresearchpress.com by 210.87.254.40 on 09/06/12
For personal use only.

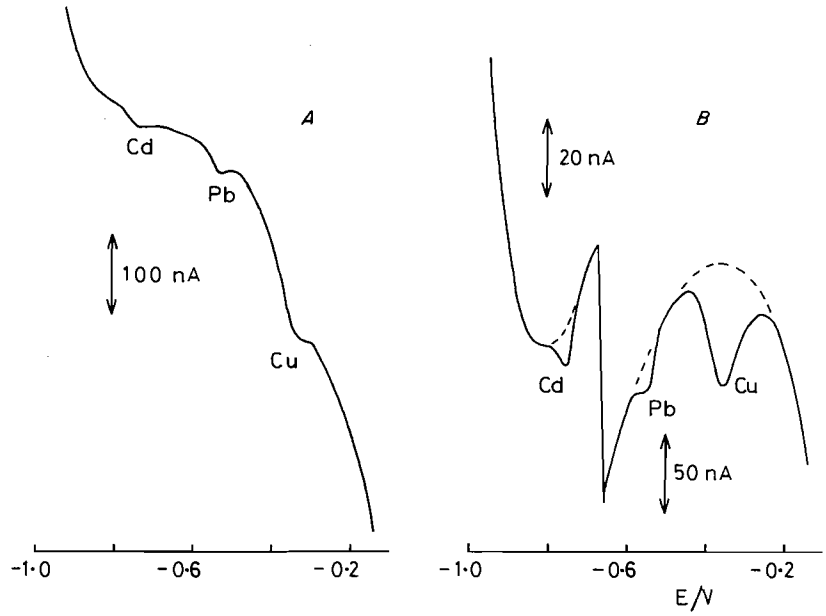

FIG. 2. ASV stripping peaks: SW sample at pH 2, TFME, Hg/Hg_2Cl_2/SW reference; *A*, uncompensated signal; *B*, compensated signal.

stripping process giving a response factor that would be 1/4 × that for Cd and Pb, other than for differences in the diffusion coefficients of the metal species. The predicted responses can be compared to the slopes of the experimental standard calibration addition plots.

In the cases of Cd and Pb the stripping peaks were well defined and readily resolved from the background. The height and half-width of the peaks were in keeping with 2-electron processes and the slopes of the experimental calibration plots were reproducible and showed little variation from sample to sample. The agreement with the predicted value was best with Pb; in the case of Cd the calibration slope was somewhat low. The result with Cd is probably best rationalized by assuming that there is a slow step in the deposition of the metal and the limiting current is less than that predicted by eq. [2]. This would not be unexpected at the potential used for the deposition.

In the case of Cu, the resolved stripping peak had a half-width consistent with a 1-electron stripping process giving a stable Cu(I) species. However, it appeared that the deposition and stripping processes were much more dependent on the state of the electrode than in the cases of Pb and Cd. The slopes of the Cu calibration plots were somewhat variable but always significantly less than the value calculated for the possible 2-electron stripping process; the experimental values approached but never exceeded that for a 1-electron stripping process. It was found that the calibration line slopes could vary from run to run when replicates of a given sample were analyzed though the calibration slopes for Cd and Pb remained constant. Despite such variation in slope good standard addition calibration plots and consistent values of Cu concentration were obtained in replicate analyses.

The resolution from the background and measurement of the Cu peak was dependent upon "curve fitting". When blank subtraction as shown in Fig. 3 ($A - B$) was used to resolve the Cu peak it was apparent that the (resolved) 1-electron oxidation peak was accompanied by a second process giving a broad background peak. The nature of this second process was not established though it did not appear to be a Faradaic process associated with a further oxidation of the Cu(I) product. It was found that the background peak grew only to a limit with increasing time at the deposition potential and the limiting value was independent of the magnitude of the resolved Cu stripping peak. Some experiments were carried out in which the SW

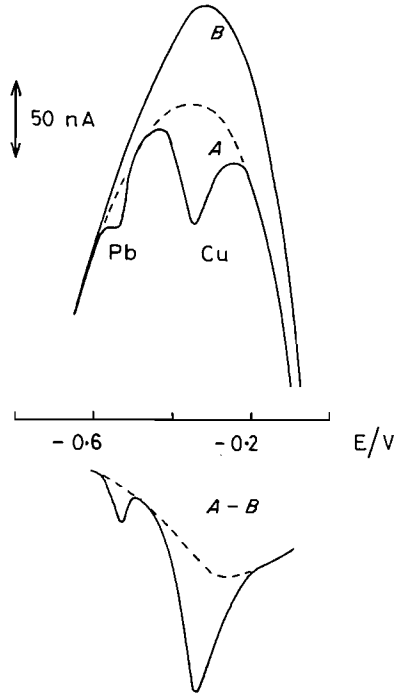

FIG. 3. ASV stripping peaks: SW sample at pH 2, TFME, Hg/Hg_2Cl_2/SW reference; *A*, sample (τ = 300 s); *B*, blank (τ = 0 s); ($A - B$), difference of sample and blank signal.

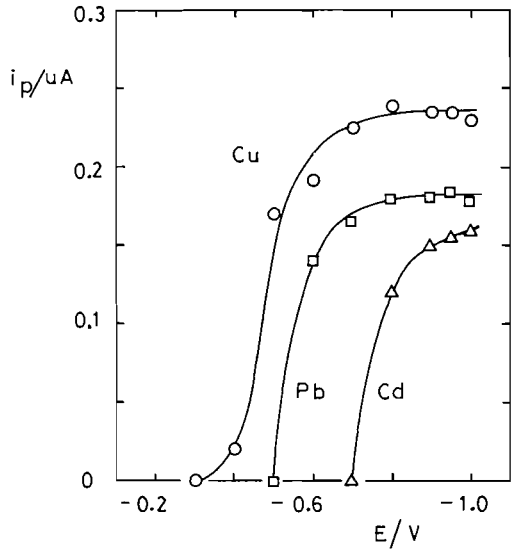

FIG. 4. ASV stripping signals as function of deposition potential: spiked SW sample at pH 2, TFME, $Hg/Hg_2Cl_2/SW$ reference.

samples were exposed to ultraviolet irradiation or digested to destroy organic material. This treatment was found to eliminate a component from the background although the resolved Cu stripping peak was unchanged. The component removed was positive to the Cu stripping peak potential and shaded into the Hg oxidation process; the background under the stripping peak itself was unchanged.

Other electrochemistry is in keeping with the assumed 1-electron Faradaic stripping process for Cu in the SW electrolyte. The polarography of Cu(II) spiked SW samples at pH 2 shows a two step reduction; $E_{1/2}$ for the reduction of the Cu(II) to Cu(I) is more positive than the potential for oxidation of the Hg of the electrode itself, while $E_{1/2}$ for the second stage of the Cu(II) reduction occurs at −0.20 V vs. SCE. Triangular wave voltammetry using a Hg drop electrode and a scan rate of 0.050 V s^{-1} shows composite behaviour with a cathodic peak on the forward scan corresponding to the reduction of Cu(I) to Cu at −0.25 V vs. SCE, and an anodic peak corresponding to the formation of Cu(I) at −0.17 V on the reverse scan; the peaks for the initial reduction and reoxidation to Cu(II) occur at potentials more positive than those for the oxidation of the Hg electrode. While the Cu stripping process in SW has not been previously so characterized other workers have observed related behaviour; Zirino and Kounaves (22) noted the apparent reduction of Cu(II) to Cu(I) in the stripping polarography of SW at a Hg drop electrode, while Pinchin and Newham (23) observed a "mixed" ASV stripping of Cu to Cu(I) and Cu(II) at a TFME in a buffered pH 5–0.2 *M* chloride electrolyte. In the latter case, the apparent *n* values were non-integral and the two stripping reactions could not be resolved.

In the cases of Cd and Pb, the slopes of the experimental calibration plots were quite reproducible and in close keeping with prediction, but with Cu there was considerably more variability. While all the analytical results reported in this paper were based on calibration by the method of standard additions, absolute analysis based solely on measurements on the sample and the calculated i_p/C^* values appears possible. The statistical evaluation of the results of such analysis will be presented in a subsequent paper.

Optimization of ASV Parameters

The procedure for the ASV analyses employed the following standard set of parameters:

SW: pH 1.5–2.0; 50 μ *M* added Hg(II); ~0.005 L sample
TFME: $A = 0.066\ cm^2$, $l > 100$ nm, $N = 30$ Hz
E_d: −1.00 V vs. $Hg/Hg_2Cl_2/SW$, $\tau = 300$ s
ASV: $dE/dt = 0.050\ V\ s^{-1}$, stationary TFME

A series of experiments was carried out to study the effect of variation of some of these parameters; in each case the value of one parameter was varied while the others were maintained, if possible, at their standard values.

(1) Deposition Potential (E_d)

A spiked SW sample was analyzed with E_d varied in steps from −0.5 to −1.0 V. The plot of i_p vs. E_d shown in Fig. 3 then gives the collection efficiency of each element at a given deposition potential. For each element there is a characteristic rising curve and a range of potentials over which a limiting deposition rate is indicated. In the case of Cd the rising part of the curve is less steep than in the case of Cu and Pb and the potentials corresponding to the limiting deposition plateau are relatively cathodic to the polarographic $E_{1/2}$ given in Table 1. This indicates a measure of kinetic control in the electron transfer step and while the limiting plateau for the Cd deposition was barely defined at −1.0 V, more negative potentials were not employed since these would favour Zn codeposition and H^+ reduction from the SW electrolyte. The choice of E_d for the ASV analyses may then be responsible for the less than expected slopes reported for the Cd calibration lines in Table 1. The potentials corresponding to the limiting deposition plateau of Cu are also relatively cathodic to the $E_{1/2}$ for the polarographic Cu(I) → Cu(Hg) step but this may result from the limited solubility of Cu in the Hg substrate. The Pb deposition appeared to proceed smoothly without hindrance.

(2) Film Thickness (l)

This variable was studied in a series of repetitive experiments beginning without predeposition of a Hg film. When unspiked SW or low level spiked samples were subjected to analysis the stripping peaks grew to a limiting value over the initial 2–3 analysis cycles, then remained constant through the 20 cycles investigated in the experiments. It was assumed that the initial low values of the stripping peaks resulted either from incomplete coverage of the substrate with Hg so that only a fraction of the electrode area was operative in the collection step, or perhaps to saturation of the Hg film with the metals deposited in an analysis cycle. This would also be expected to reduce the collection efficiency of the electrode and both effects would decrease as the amount of Hg present on the substrate increased from cycle to cycle. The deposition current resulting from the 50 μ*M* Hg(II) added to the SW was ~5 μA and this corresponds to a film growth of ~17 nm in each 300 s deposition period provided the film is uniform and depletion of the added Hg(II) is not significant. Complete deposition of the Hg(II) from a 0.005 L sample would correspond to a maximum film thickness of ~550 nm.

The standard procedure is based on a 30 min predeposition of the Hg, corresponding to a film thickness of ~100 nm. It was assumed that this gave a uniform film with complete coverage of the substrate and the Hg was in excess of that required to amalgamate the amounts of Cu, Pb, and Cd deposited in an analysis. Of the three metals, Cu has a limited solubility (0.01 atom% (24, 25)) and would be most likely to give saturated films. In the absence of predeposition, the solubility data indicate that film saturation would be expected only if Cu(II) > 0.3 μg L^{-1}, provided that the Hg and Cu deposit together in a similar fashion and the added Hg(II) is present at the 50 μ*M* level. However, if a 100 nm film is predeposited, calculations based on eq. [1] and the appropriate kinetic factors indicate that amalgam saturation would occur in a 300 s deposition only if Cu(II) > 3.0 μg L^{-1}.

Can. J. Chem. Downloaded from www.nrcresearchpress.com by 210.87.254.40 on 09/06/12
For personal use only.

TABLE 3. Definitions and units of symbols

Symbol	Definition	Unit
A	Surface area of electrode	
$b_{1/2}$	Stripping peak width at half maximum	V
C_0*	Bulk concentration of reducible M^{n+}	mol L^{-1}
C_r	Concentration of reduced M in amalgam	mol L^{-1}
D_0	Diffusion coefficient of reducible ion $\sim 7 \times 10^{-6}$ cm^2 s^{-1} for M_{aq}^{2+} in SW	
D_r	Diffusion coefficient of metal in amalgam $\sim 2 \times 10^{-5}$ cm^2 s^{-1} for M in Hg (3)	
E_p	Stripping peak potential	V
$E_{1/2}$	Polarographic half-wave potential	V
F	Faraday	96 485 C mol^{-1}
H	Kinetic parameter ($= l^2\sigma/D_r$) (21)	
i_l	Limiting current in deposition step	A
i_p	Peak stripping current	A
l	Thin layer film thickness	cm
n_r	Amount of metal collected for stripping	mol
δ	Diffusion layer thickness	cm
γ	Kinematic viscosity of electrolyte $\sim 9.4 \times 10^{-3}$ cm^2 s^{-1} for SW at 298 K (33)	
v	Potential scan rate in stripping step (dE/dt)	V s^{-1}
σ	$n(F/RT)v = n(38.92\ V^{-1})v$ at 298 K	s^{-1}
ω	Angular rotation velocity of electrode $= 2\pi N$ where N is frequency of rotation	s^{-1}
τ	Deposition time with electrode rotation	s

If the Cu collected should exceed the solubility limits then a multi phase deposit with a complex stripping behaviour might be expected. However, Stojek *et al.* (26) found that even with a calculated 160× excess of total over amalgamated Cu the ASV peak was "somewhat asymmetric, thinner and displaced" but still close to the form and shape predicted for the homogeneous amalgam. Pinchin and Newham (23) also studied the stripping of Cu from a TFME and found that while film saturation produces an anodic shift in peak potential the stripping peak height remains proportional to the amount of Cu present. Figure 5 shows the results obtained in this study with a heavily spiked SW sample; the concentration of Cu(II) was estimated from the peak stripping currents as $\sim 5\ \mu g\ L^{-1}$, a value sufficiently high that film saturation is conceivable in the initial stages of the experiment. The experiment was carried out without film predeposition and through the initial cycles the Cu stripping peak was sharp and narrow with a shape characteristic of the stripping of a solid deposit. As the number of cycles and the amount of Hg on the substrate increased, the peak height decreased but both the peak width and peak area grew until limiting values characteristic of amalgam stripping were obtained. With Cu(II) at 5 $\mu g\ L^{-1}$, it can be estimated that a 300 s deposition would saturate a ~ 167 nm film and some 10 ASV cycles would be required to produce this film thickness. The behaviour shown in Fig. 5 is near prediction in this respect although the initial behaviour of the Cu can also be explained by incomplete coverage of the electrode with Hg and deposition and stripping of Cu directly from the substrate. With Pb and Cd the stripping peaks grew to a limiting value through the initial 1–5 cycles with the shapes of the peaks always characteristic of amalgam stripping. It would appear that predeposition of a 100 nm Hg film is sufficient for ASV analyses at the higher levels of Cu, Pb, and Cd.

(3) pH

The dependency of the ASV experiment on the pH of the electrolyte was investigated using fresh but unacidified SW samples that had been filtered through a 3 μm polycarbonate filter (Nucleopore™). The cell was initially filled with sample of pH ~ 8 and ASV measurements, using preformed TFME electrodes, were made as a function of pH. The results showing the ASV response are shown in Fig. 6.

At the natural pH of the SW sample there was little response in the case of Cu and Pb although Cd gave a well defined stripping peak. The ASV peaks increased with acidity with limiting peak heights appearing near pH 4. The increases are likely a combination of changing electrode response and displacement of metal from inert forms by the increased proton activity. It was assumed that at pH 2 all the metals are in a form labile to ASV deposition; this assumption is supported by the near theoretical slopes of the standard addition calibration plots, the lack of a time dependency to the ASV signal after a standard addition increment, and the lack of any significant increase in the ASV signals after ultraviolet irradiation of the SW samples.

(4) Rotation Rate ($\omega = 2\pi N$)

The Levich relation as given in eq. [2] predicts that the amount of a metal collected in the deposition step at the rotated TFME is proportional to $\omega^{1/2}$. Since the parameters in the stripping step are independent of those in the collection step one would predict that the sensitivity of the method would increase with $\omega^{1/2}$ and the electrode rotation rate should be as large as possible. Experiments were carried out using spiked SW samples with N varied from 10 to 60 Hz; for each metal i_p was found to vary linearly with $\omega^{1/2}$ over the range of rotation rates studied. However, considerations concerned with bearing wear at the rotating electrode dictated a practical upper value for the rotation rate and the analyses were carried out with $N = 30$ Hz.

(5) Scan Rate (dE/dt, v)

Equation [4] predicts that the stripping current peak is directly proportional to the rate of potential scan but background processes associated with charging of the double layer at the electrode surface would be expected to increase at the same rate (27) so that a gain in the signal-to-noise ratio would not be expected.

Experiments were carried out using spiked SW samples with dE/dt in the stripping step varied from 0.005 to 0.1 V s^{-1}. The highest scan rate investigated was just within the ability of the

Can. J. Chem. Downloaded from www.nrcresearchpress.com by 210.87.254.40 on 09/06/12
For personal use only.

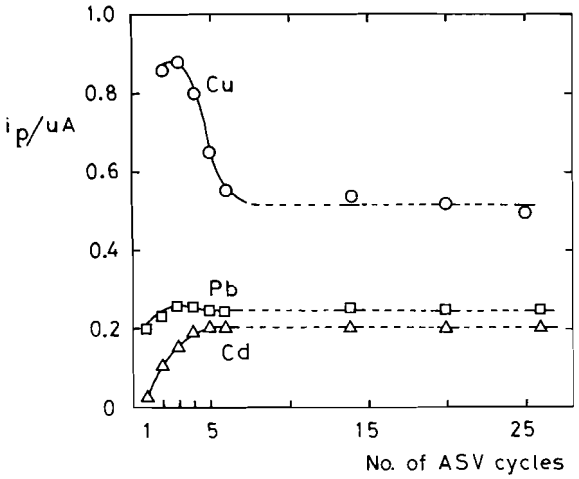

FIG. 5. ASV stripping signals as function of Hg film growth: spiked SW sample at pH 2, TFME, Hg/Hg_2Cl_2/SW reference, no Hg film predeposition.

recorder to accurately track the stripping peaks. Over the range investigated the peak heights were proportional to scan rate but there was little change in the apparent signal-to-noise ratio. However, the peak potentials and background currents were a function of scan rate and it was found that the Cd peak was best resolved from the initial rapid change in background at fast scan rates while the Cu peak was best resolved from the final rapid change in background at slow scan rates. A compromise scan rate was selected and the stripping analyses were carried out with $dE/dt = 0.05\ V\ s^{-1}$.

(6) Deposition Time (τ)

Equation [3] predicts that the amount of a metal deposited and the sensitivity of the method should increase directly with deposition time. Experiments with spiked SW showed a direct correlation between the observed stripping peak currents and deposition time provided that the time at the deposition potential with rotation was sufficiently large ($\tau > 100$ s) that the additional metal deposited in the 30 s period without rotation is not significant. A deposition with $\tau = 300$ s was selected for the analyses and the calibration data are based on this value. Longer deposition times will increase the sensitivity of the method at the expense of analysis time.

Results and Discussion

(1) Blank Analysis

It is not possible to obtain or directly synthesize a "blank" SW, that is a sample containing insignificant background concentrations of the analyte elements. Nevertheless it is useful to measure blank values on other appropriate samples as a measure of the extent of contamination during the course of an ASV analysis.

A blank NaCl solution with ionic strength equivalent to that of SW was prepared (0.55 mol L^{-1} NaCl). The solution had a pH of 7.5 and it was stripped of trace metals by a single pass through a 1 cm × 15 cm column of Chelex 100 (100–200 mesh, Na form, flow rate ~1 mL min^{-1}) (28). The eluent was acidified to pH 2 with HCl and then analyzed for Cu, Cd, and Pb. Detectable ASV peaks were observed for each element with peak signals marginally greater than the limit of detection but less than 1 nA corresponding to < 11 ng L^{-1} Cu, < 6 ng L^{-1} Cd, and < 7 ng L^{-1} Pb (as determined from the experimental calibration slopes in Table 1). Such blank signals with stripping peaks of less than 1 nA were consistently obtained using the sample handling and cell pretreatment procedures developed in this study. Comparison of the blank with the results given for typical SW samples in Tables 2, 4, and 5 show the values to be of the order of 10% of the SW values. The question remains as to whether such blank values should be deducted from the SW sample values. Correction should be made if the NaCl blanks represent contamination from sample handling or reagent addition during the procedure but no correction is required if these values are in fact only the base line levels of the metals remaining after the Chelex 100 exchange.

Other experiments were carried out to assess possible sources of contamination. In one set of experiments, the concentration of Hg(II) added to the NaCl blank for the *in situ* film formation was increased stepwise to 150 μM and in another set, the blank solutions were allowed to stand in the ASV cell for periods of up to 12 h before analysis. Detectable changes in the ASV signals were not observed, indicating that the metals found in the blank were not related to the added Hg(II) and there was no significant net release of metal from the cell. There is the possibility that low blank values are in part due to the adsorption of metals on the cell walls. However, the increased signals resulting from 20 ng L^{-1} additions of metal to the NaCl blank showed no time dependency and the slope of the resultant standard addition plots were comparable to those given in Table 1 for real SW samples (mean values: Cu 5.1; Pb 28.4; Cd 22.9 A/(mol L^{-1})). It was concluded that a blank correction was not required in the SW analyses.

(2) Intercalibration Studies

Although low blanks are a prerequisite for trace analysis, they are not a test of accuracy. The conventional means of testing accuracy of an analytical method is to analyze standard reference materials of the same matrix as the sample. However, there are no standard reference seawater samples (29) and thus an alternate test of accuracy must be employed.

Two intercalibration studies were undertaken for this purpose. The first involved a coastal sea water sample obtained from the Atlantic Regional Laboratory of the National Research Council of Canada

Can. J. Chem. Downloaded from www.nrcresearchpress.com by 210.87.254.40 on 09/06/12
For personal use only.

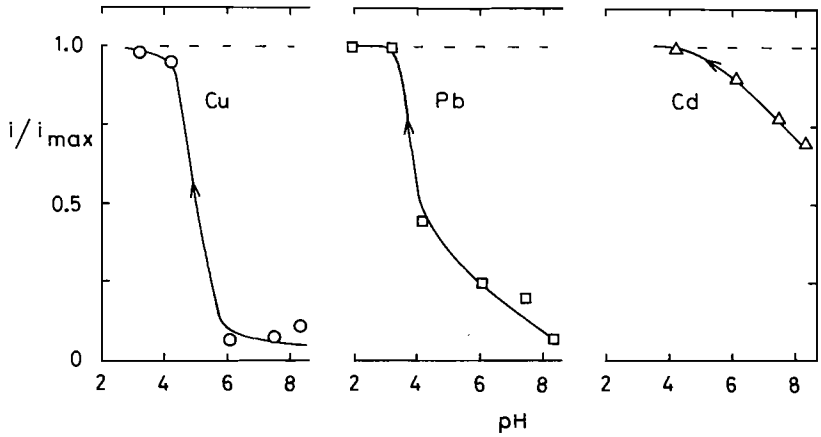

FIG. 6. ASV stripping signals as function of sample pH: filtered SW sample, TFME, Hg/Hg_2Cl_2/SW reference. $(i_p)_{max}$: Cu = 32 nA; Pb = 15 nA; Cd = 8 nA.

TABLE 4. Intercalibration results for trace metals in SW

Sample	Value[a] Cu	Cd	Pb	
Spike	1.95 *2* (0.13)	0.220 *2* (0.004)	0.43 *3* (0.08)	ASV
	1.84 (0.37)	0.207 (0.076)	0.39 (0.09)	ICES
Dummy	0.63 *4* (0.22)	0.070 *4* (0.020)	0.42 *4* (0.09)	ASV
	0.29 (0.27)	0.063 (0.020)	0.27 (0.07)	ICES
R1	0.17 *4* (0.04)	0.035 *4* (0.010)	0.47 *4* (0.02)	ASV
R2	0.25 *4* (0.14)	0.047 *4* (0.009)	0.51 *4* (0.03)	ASV
R3[b]	2.82 *4* (0.75)	0.058 *3* (0.003)	0.68 *3* (0.05)	ASV
R1, R_2[c]	0.21 (0.11)	0.041 (0.011)	0.49 (0.03)	ASV
	0.33 (0.20)	0.059 (0.020)	0.45 (0.08)	ICES

[a]Mean concentration (μg L^{-1}), number of replicates, and standard deviation, ASV, analyses as reported in this work; ICES, high precision results from intercalibration study as reported in ref. 31.
[b]Replicate R3 (only) was provided as a portion of original sample in a second PE container. Cu contamination suspected.
[c]Mean of replicates R2 and R3.

TABLE 5. Trace metal concentrations in Sandy Cove SW samples

	Cu	Cd	Pb
3 μm filter, acidified (pH 1.8)[a]			
[b]	0.18 *6* (0.09)	0.042 *10* (0.013)	0.095 *10* (0.015)
$(s_z)_p$[c]	0.015	0.0016	0.0041
0.45 μm filter, non-acidified (pH 8)[a]			
[b]	0.20 *4* (0.04)	0.035 *4* (0.008)	0.074 *3* (0.02)
$(s_z)_p$[c]	0.035	0.0077	0.0040

[a]Mean concentrations (μg L^{-1}), number of replicates, and standard deviation.
[b]ASV–TFME analyses at pH 2.
[c]Pooled standard error from individual calibration lines.

in Halifax, Nova Scotia. The sample had been filtered through a 0.45 μm filter, acidified to pH 1.6 and stored in a PE bottle. The sample was also analyzed by the Analytical Section Laboratories of the National Research Council in Ottawa, Ontario using graphite furnace atomic absorption spectrometry after a preconcentration of the trace metals (30). The comparative results are given in Table 2 and the agreement is good. The atomic absorption procedure involved solvent extraction of samples adjusted to pH 4 (and digested at 80°C) while the ASV procedure was a direct probing of the SW as supplied at pH 1.6. The agreement in the results would reasonably indicate that all of a metal in the SW is labile to the two procedures or alternatively the proportion of inert metal is unaffected by the alteration of electrolyte conditions.

A second intercalibration study involved samples taken as part of the 1978 fourth round intercalibration study organized by International Council for the Exploration of the Sea (ICES). The samples were obtained as the residual water supplied to an original participant and the analytical data have been presented as part of the ICES report (31). The results are summarized in Table 4 and the values obtained are in good agreement with the high preci-

Can. J. Chem. Downloaded from www.nrcresearchpress.com by 210.87.254.40 on 09/06/12
For personal use only.

sion values selected from the results of the other participants in the study. Again it would appear that the three metals are completely labile to the ASV procedure.

(3) Sandy Cove Water

In order to integrate the ASV procedures described into a total system of analysis a sampling excursion was undertaken to Sandy Cove, Nova Scotia. Water from this site has been analyzed in other studies (30, 32) and it is considered to be representative of relatively unpolluted but near shore SW. The samples were collected on June 7, 1979 at a distance of 0.8 km from shore (44° 28′ N, 63° 34′ W) and at a depth of 20 m. The SW had a salinity of 30.9‰, a pH of 8.06, and a temperature of 9.5°C.

The samples were collected using a water sampler designed as part of this work and constructed entirely of high purity polymethylmethacrylate and PE plastics. The sampler is described elsewhere (18) and has been shown capable of retrieving uncontaminated sub-surface samples. Of the samples taken one was filtered through a 0.45 μm cellulose acetate filter (Millipore™) and stored without acidification and another was filtered through a 3 μm polycarbonate filter (Nucleopore™) then acidified to pH 1.8 with HCl. The samples were stored in preconditioned PE bottles and subsequently analyzed. The analyses were carried out by the standard ASV procedure with the sample stored at the natural pH and brought to pH 2 with HCl prior to analysis.

The results are given in Table 5 and the values for Cd and Cu are near those for the 1978 ICES acidified samples. The ICES samples were similar in that they were taken from the Scotian Shelf but at a depth of 180 m and 100 km offshore. The Pb values are much less than the ICES replicates, supporting a suggestion that Pb contamination occurred during sampling and handling for that intercalibration study. The results are thought to represent typical values for the total trace Cu, Cd, and Pb in the samples and there seems to be no significant differences between the two samples despite the differences in filtration and storage with and without acidification.

Acknowledgements

We are grateful to the Natural Sciences and Engineering Research Council of Canada and to the Committee on Marine Analytical Chemistry of the National Research Council and the Advisory Research Committee of Queen's University for financial assistance. A scholarship from the Aluminum Company of Canada in support of the Ph.D. studies of L. W. Green is also gratefully acknowledged.

1. Anal. Chem. **52**, 749A (1980).
2. J. P. Riley. *In* Chemical oceanography. Vol. 3. 2nd ed. *Edited by* J. P. Riley and G. Skirrow. Academic Press, New York. 1975. Chapt. 19.
3. F. Vydra, K. Štulík, and E. Juláková. Electrochemical stripping analysis. Halsted Press, John Wiley and Sons, Inc., New York. 1976.
4. H. W. Nürnberg. Electrochim. Acta, **22**, 935 (1977).
5. D. R. Turner and M. Whitfield. J. Electroanal. Chem. **103**, 43 (1979); **103**, 61 (1979).
6. T. M. Florence and G. E. Batley. Talanta, **24**, 151 (1977).
7. L. Sipos, J. Golimovski, P. Valenta, and H. W. Nürnberg. Fresenius Z. Anal. Chem. **298**, 1 (1979).
8. W. Davison. J. Electroanal. Chem. **87**, 395 (1978).
9. G. Gillain, G. Duyckaerts, and A. Disteche. Anal. Chim. Acta, **106**, 23 (1979).
10. T. M. Florence. J. Electroanal. Chem. **35**, 237 (1972).
11. D. Jagner and K. Årén. Anal. Chim. Acta, **107**, 23 (1979).
12. P. Valenta, L. Mart, and H. Rützel. J. Electroanal. Chem. **82**, 327 (1977).
13. M. S. Shuman and G. P. Woodward. Anal. Chem. **48**, 1979 (1976).
14. S. D. Brown and B. R. Kowalski. Anal. Chim. Acta, **107**, 13 (1979).
15. J. Wang and M. Ariel. J. Electroanal. Chem. **85**, 289 (1977).
16. T. M. Florence. J. Electroanal. Chem. **27**, 273 (1970).
17. L. W. Green. Ph.D. Thesis, Queen's University, Kingston, Ont. 1979.
18. I. L. Larsen, N. A. Hartmann, and J. J. Wagner. Anal. Chem. **45**, 1511 (1973).
19. A. L. Wilson. Talanta, **17**, 31 (1970).
20. V. G. Levich. Physiochemical hydrodynamics. Prentice-Hall Inc., New Jersey. 1962.
21. W. T. De Vries and E. Van Dalen. J. Electroanal. Chem. **14**, 315 (1967).
22. A. Zirino and S. P. Kounaves. Anal. Chim. Acta, **113**, 79 (1980).
23. M. J. Pinchin and J. Newham. Anal. Chim. Acta, **90**, 91 (1977).
24. M. Hansen. Constitution of binary alloys. 2nd ed. McGraw-Hill Book Company, New York. 1958.
25. E. A. Zakharova, G. A. Kataev, L. A. Ignat'eva, and V. E. Morozova. Tr. Tomsk. Gos. Univ. **249**, 103 (1973); Chem. Abstr. **82**, 104858 (1975).
26. Z. Stojek, B. Stępnik, and Z. Kublik. J. Electroanal. Chem. **74**, 277 (1976).
27. P. Delahay. New instrumental methods in electrochemistry. Interscience Publishers, John Wiley and Sons, Inc., New York. 1965.
28. T. M. Florence and G. E. Batley. Talanta, **23**, 179 (1976).
29. M. Stoeppler, P. Valenta, and H. W. Nürnberg. Fresenius Z. Anal. Chem. **297**, 22 (1979).
30. R. E. Sturgeon, S. S. Berman, A. Desaulniers, and D. S. Russell. Talanta, **27**, 85 (1980).
31. J. M. Bewers, J. Dalziel, P. A. Yeats, and J. L. Barron. International Council for the Exploration of the Sea, Report of the ICES Fourth Round Intercalibration for Trace Metals in Seawater, CM 1979/E:37.
32. R. E. Sturgeon, S. S. Berman, J. A. H. Desaulniers, A. Mykytiuk, J. W. McLaren, and D. S. Russell. Anal. Chem. **52**, 1585 (1980).
33. F. J. Millero. The sea. Vol. 5. *Edited by* E. D. Goldberg. Wiley-Interscience, John Wiley and Sons, Inc., New York. 1974. Chapt. 1.

Can. J. Chem. Downloaded from www.nrcresearchpress.com by 210.87.254.40 on 09/06/12
For personal use only.

A simple method to characterize feed-coals for liquefaction

SUJIT K. CHAKRABARTTY

Coal Research Department, Alberta Research Council, 11315-87th Avenue, Edmonton, Alta., Canada T6G 2C2

Received July 15, 1980

This paper is dedicated to Professor W. E. Harris on the occasion of his retirement from the University of Alberta

SUJIT K. CHAKRABARTTY. Can. J. Chem. **59**, 1487 (1981).

The analytical techniques for identification of coal-properties relevant to liquefaction processes are not well-developed. A simple method is described to satisfy this need.

SUJIT K. CHAKRABARTTY. Can. J. Chem. **59**, 1487 (1981).

Les techniques analytiques d'identification des propriétés du charbon correspondant aux procédés de liquéfaction ne sont pas bien développées. On décrit une méthode simple qui vient combler cette lacune.

[Traduit par le journal]

Can. J. Chem. Downloaded from www.nrcresearchpress.com by 210.87.254.6 on 09/06/12
For personal use only.

Introduction

The problem of declining supplies of petroleum and natural gas has encouraged the industrial nations of the world to expand R and D work for better utilization of coal reserves which make up to 47% of the energy content of the recoverable resources of the planet's fossil fuels. Two conversion techniques for producing transportable fuels from coal, namely, solvent refining and liquefaction, are now being considered as advanced technology for the eighties. The essential aspects of these conversion processes are broadly described (1) as a thermal fragmentation of macromolecular units in the presence of a hydrogen-donor solvent at the temperature range 375–425°C, associated with the scrambling of hydrogen atoms in the reactants to produce pyridine-soluble solids, and the progressive hydrogenation of the fragmented products to yield finally a transportable fuel or synthetic crude oils.

The rates of the fragmentation reactions are very fast and depend on the nature of coals. The microcomponents, as identified by the microscopic examination of coal particles as "vitrinite" and "exinites", are the most reactive materials which undergo rapid fragmentations. The other components, known as "semifusinite" and "fusinite", produce insignificant amounts of liquid products but may act as nuclei for coke-formation which might be deleterious to ultimate conversion.

Presently, the selection of coals for these processes is conducted on the basis of very expensive and time-consuming autoclave tests in high-pressure laboratory facilities. In this report, a simplified analytical version of the autoclave test procedure is presented. The method is based on the chemistry of coal–solvent interactions and identifies the yield of products generated by the very fast kinetic paths only.

Experimental

The sample coal with solvent is flash-heated in a reactor tube for a specified time and subsequently quenched by immersing the tube in cold water. The reactor tube, shown in Fig. 1, is made from pressure-rated 316 type stainless steel tubing, closed at one end, and fitted with swagelock fittings, thermocouple, and pressure gauge. A metal bath, electrically heated up to 500°C, is used as heat source. A typical experimental procedure is described below.

A sample of anhydrous subbituminous coal from Alberta, (−10 +30 Tyler particle sizes, 5 g) was placed in the reactor along with the solvent, tetrahydronaphthalene (73 mol). The vessel was purged with hydrogen until all air was removed. A nominal gauge pressure of 10 psi was maintained after closing the shut-off valve to isolate the pressure gauge. (The pressure gauge has to be isolated from the reactor vessel during reaction to avoid condensation of solvent vapors and products in the cooler chamber of the gauge.) The vessel was dipped into the hot metal bath maintained at 400°C. The temperature of the reactants reached the bath temperature in 3 min. A series of experi-

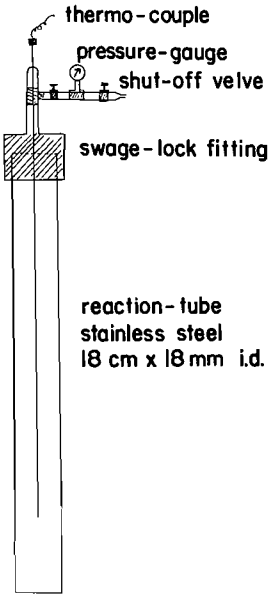

FIG. 1. The reactor tube.

0008-4042/81/101487-03$01.00/0

©1981 National Research Council of Canada/Conseil national de recherches du Canada

TABLE 1. Data of flash-solvolysis of Forestburg coal in tetralin (expressed as mmol per 5 g dry coal)

Product-yield	Residence time in min								
	5	10	15	20	30	30†	40	40*	60
Hydrogen	0.681	0.279	0.771	0.458	0.202	1.125	1.720	1.727	0.638
Hydrogen sulfide	0.025	0.129	0.095	0.184	0.220	0.050	0.089	0.154	0.038
Carbon oxides	7.460	8.168	9.619	9.563	10.791	10.226	10.577	10.279	10.077
Hydrocarbon C_1–C_4	0.511	0.828	1.267	1.656	2.120	1.837	2.512	2.414	3.044
Total gas, cm^3, STP	194	210	263	266	299	298	326	333	309
Conversion %, dry coal	11.0	17.0	24.0	30.0	31.0	28.0	38.0	37.0	39.0
Conversion to liquid %, dry coal	7.0	12.0	12.0	15.0	18.0	13.0	18.0	19.0	26.0
Solvent dehydrogenation: 73 mmol of tetralin changes to									
Tetralin	67	64.7	61.6	61.7	59.2	59.8	57.2	57.2	56.2
Naphthalene	6	8.1	11.4	11.5	13.8	13.2	15.8	15.7	16.8
Hydrogen transferred to coal, mmol/5 g	11.3	16.4	23.5	22.5	27.8	25.2	33.3	33.1	34.2

*Duplicate run to establish the repeatability of the experiment.
†Duplicate run with finer particle size.

ments was undertaken under this condition varying the length of the reaction times and the particle sizes of the coal. At the end of the specified times, the vessel was taken out of the metal bath and cooled by water spraying. After the contents of the vessel attained room temperature, pressure was recorded to calculate the gas yield. An increase of 74 psig pressure was noted in a 60 min run with this specific coal.

The system was connected to the gas-sampling port of a Carle's analytical gas chromatography apparatus to analyze the gas composition. After venting out the gases inside a fume hood, the contents of the reaction tube were poured onto 200 mL of *n*-pentane solvent. After thorough mixing and transferring all the products from the tube, the solids were separated by filtration, and the pentane-soluble materials were subjected to gc–ms analysis. The pentane-insoluble solid was extracted with chloroform at room temperature until the extract was colorless. The total conversion of coal to gas and extractable matters (bitumen) was calculated based on the residue left after chloroform extraction.

Results and Discussion

The following results are described as an example to demonstrate the usefulness of the proposed method in terms of simplicity, reproducibility, and efficiency to meet the necessary objectives, viz. screening of coal for liquefaction-processes.

When coal is heated in a slurrying vehicle, it is "liquefied" at 400–500°C. Though the reaction-mechanism involving conversion of coal to oil is very complex, it appears that the interaction of coal with solvent at the initial stage of the reactions plays the vital role to determine the sequential conversion of coal substances – first to a pyridine-soluble solid and thereafter to benzene-soluble liquid hydrocarbons and light oils (2). Thus the isolation and identification of the products of coal–solvent interactions to yield pyridine-soluble matter may provide information regarding the suitability of the sample-coal for liquefaction. The experimental results, given in Table 1, show the effects of residence time on the sequential reactions and ultimate conversion-yields. The gc–ms analysis of the pentane-soluble products indicated that light oils (C_8–C_{12} hydrocarbons) started to form after 30 min along with decahydronaphthalene, methyltetrahydronaphthalene, methylnaphthalene, and indene. The gas yield reached the maxima at this point and was stabilized afterward with minor fluctuation in C_1–C_4 hydrocarbon yields. Increasing the residence time beyond 30 min showed gradual improvement of liquid conversion values. From this observation, it was surmised that the reaction up to 30 min was predominately due to coal–solvent interaction. The gradual decrease of tetrahydronaphthalene in the reaction mixture associated with gradual increase of dehydrogenated and methylated solvent with reaction time possibly indicated that these products were derived from solvent, and not from coal. At the initial stages, tetrahydronaphthalene and naphthalene contributed to more than 99% of the total extract on pentane-free basis.

Tetrahydronaphthalene, by itself, was found to be stable under these temperature and pressure conditions. In the presence of coal, tetrahydronaphthalene is dehydrogenated very rapidly. In the absence of solvent (Table 2), liquid conversion yield was negligible, though the yield and composition of the gaseous products remained similar to earlier results. Repeating the experiment with nitrogen instead of hydrogen as gaseous atmosphere, did not show any significant differences in the

Can. J. Chem. Downloaded from www.nrcresearchpress.com by 210.87.254.6 on 09/06/12
For personal use only.

TABLE 2. Flash-solvolysis of Forestburg coal: effect of solvent and gaseous atmosphere

	Conversion total	% dry liquid	Gaseous products, mmol/5 g dry coal				Gas volume cm^3 STP/5 g dry coal
			H_2	CO_x	HC	H_2S	
Coal/dry/N_2/30 min	14	0.1	0.087	8.104	1.098	0.012	208
Coal/tetralin/N_2/30 min	33	16.0	0.675	10.783	2.262	0.152	310
Coal/tetralin/H_2/30 min	31	18.0	0.202	10.791	2.120	0.220	299
Tetralin/H_2/400°C/60 min	Nil	100% recovery of the starting material					

results, indicating that molecular hydrogen present in the gas-phase did not participate in the initial stages of coal-liquefaction. The solvolysis reaction with the test coal was conducted earlier (3) in a standard 300 cm^3 autoclave with tetrahydronaphthalene as solvent. The rate of heating was approximately 4.5°C per min, and the reaction time of 60 min was measured from the moment the autoclave had reached 400°C. The conversion as defined on the basis of benzene-insoluble matters was 26.8% dry basis (30% as dry, ash-free basis). The value is lower than the conversion obtained in tube-reactor for the 30 min run (Table 2). Due to long heat-up and cooling time in an autoclave run, the reactions cannot be quenched at the initial stage of coal–solvent interaction and are difficult to define. The quenching of the reactions before the light oils started to form would identify the yield of products generated by the very fast kinetic path only.

From this discussion it can be concluded that the reactivity of coal towards tetrahydronaphthalene can be determined by the described procedure and the results used to characterize the feed coal for liquefaction processes. Since the different micro-components react differently, it would be necessary to separate them as several gravity-cut by flotation technique, and establishing their reactivities separately. The reactivity of the as-mined coal (composite sample), along with the reactivities of micro-components, would be a valuable parameter. The test method would also provide data for yield and composition of gaseous products, and minimum hydrogen requirement that has to be fed in the reactor using solvent as a carrier. The spectroscopic characterization of the extractable matters would provide information helpful in down-stream processing of the primary liquefaction products.

1. N. BERKOWITZ. An introduction to coal technology. Academic Press, New York. 1979. Chapts. 7, 13, 14 and references therein.
2. R. C. NEAVEL. Fuel, **55**, 237 (1976).
3. S. E. MOSCHOPEDIS. Fuel, **59**, 67 (1980).

Can. J. Chem. Downloaded from www.nrcresearchpress.com by 210.87.254.6 on 09/06/12
For personal use only.

The extraction of alkali metal picrates by polyurethane foam using crown ether

ANJUM S. KHAN, W. G. BALDWIN, AND A. CHOW
Department of Chemistry, University of Manitoba, Winnipeg, Man., Canada R3T 2N2

Received July 30, 1980

This paper is dedicated to Professor W. E. Harris on the occasion of his retirement from the University of Alberta

ANJUM S. KHAN, W. G. BALDWIN, and A. CHOW. Can. J. Chem. **59**, 1490 (1981).

The distribution of alkali metal picrates between water and polyurethane foam was studied in the presence of dicyclohexyl 18-crown-6 (DCHC-6). The extraction constants and dissociation constants for the ion pair (MCrA) in polyurethane foam were determined. The extraction constant sequence of the alkali metal ions with DCHC-6 is $K^+ > Rb^+ > Cs^+ > Na^+$ and mainly depends on the stability of the alkali metal – crown ether complex.

ANJUM S. KHAN, W. G. BALDWIN et A. CHOW. Can. J. Chem. **59**, 1490 (1981).

On a étudié la distribution des picrates de métaux alcalins entre l'eau et la mousse de polyuréthane en présence de l'éther dicyclohexyl-18 couronne-6 (DCHC-6). On a déterminé les constantes d'extraction et de dissociation de la paire d'ions (MCrA) dans la mousse de polyuréthane. La constante d'interaction des ions de métaux alcalins avec le DCHC-6 varie dans l'ordre suivant: $K^+ > Rb^+ > Cs^+ > Na^+$ et dépend principalement de la stabilité du complexe métal alcalin éther couronne.

[Traduit par le journal]

Can. J. Chem. Downloaded from www.nrcresearchpress.com by 210.87.254.40 on 09/06/12
For personal use only.

During the last few years, the high distribution coefficients obtained (1) and the ease of handling of the system have aroused considerable interest in using polyurethane foam for the extraction and separation of inorganic and organic species from aqueous solutions (2, 3). Recently the extraction of platinum metals from organic media by polyurethane foam has also been reported (4). Polyurethane foam has been used for the extraction of Fe(III) (5), Ga(III) (6), Sn(IV) (7), Sb(III) and Sb(IV) (8) from acidic chloride systems. The extraction of thiocyanate complexes of Ru, Pd, Rh, Os, and Pt has also been reported with distribution coefficients as high as 10^5 (9). Even higher values were reported for the Co/SCN system (1).

Crown ethers, first prepared by Pedersen (10), form stable complexes with a number of metal ions, particularly the alkali metal ions. In a typical cation – crown ether complex, the cation is located in the center of the main ring in the plane or almost in the plane, of the oxygen atoms (10). The complexation is said to result mainly from electrostatic ion–dipole attraction between the metal ion and the oxygen atoms surrounding it (11). The stability and the stoichiometry of the complexes depend mainly on the ratio of the ionic size of the cation to the cavity size of the crown ether (12). If the ionic diameter of the cation is such that it just fits into the cavity of the crown ether, a stable complex is formed. However, if the cation is too small to closely fit into the cavity of the ring, either incomplete complexation or the formation of 2:1 and 3:2 (M:L) complexes may result. Similarly a metal ion of relatively large size may form 1:2 or 2:3 complexes (13). The charge of the cation, the nature of anion and the solvent can also influence the stability of the complexes (12). The ionic diameters of alkali metals and cavity sizes of some crown ethers are listed in Table 1. From these data it is seen that 18-crown-6 is optimum in size for K^+ and 15-crown-5 for Na^+.

Although some solvent extraction studies of alkali metal cations in the presence of crown ethers have appeared in the literature (14), there is no reported use of polyurethane foam for the extraction of alkali metal – crown ether complexes. The present study was undertaken to explore the use of polyurethane foam for the extraction of alkali metal cations with crown ethers and to determine the extraction constants for the alkali metal – crown ether/picrate ion system between polyurethane foam and water.

Dicyclohexyl 18-crown-6 (DCHC-6) was chosen for the present study because this cyclic polyether has been thoroughly investigated and forms stable complexes with alkali metals. Since a large anion is easily extracted into a low dielectric constant media, the picrate anion was used as the counter anion. The effect of other anions on the extraction has also been investigated.

TABLE 1. Ionic radii of alkali metals and cavity radii of crown ethers (Å)

Cation	Pauling ionic radius (19)	Crown ether	Cavity radius (16)
Li^+	0.6	14-Crown-4	0.6 –0.75
Na^+	0.95	15-Crown-5	0.85–0.11
K^+	1.33	18-Crown-6	1.3 –1.6
Rb^+	1.48		
Cs^+	1.69		

0008-4042/81/101490-07$01.00/0
©1981 National Research Council of Canada/Conseil national de recherches du Canada

Can. J. Chem. Downloaded from www.nrcresearchpress.com by 210.87.254.40 on 09/06/12
For personal use only.

Experimental

Apparatus

The absorption and pH measurements were made on a model 306 Perkin Elmer atomic spectrometer and a Fisher Accumet model 520 digital pH meter respectively.

Reagents

Dicyclohexyl 18-crown-6 (DCHC-6) was obtained from Aldrich Chemical Co. and was used without further purification. No attempt was made to separate the two isomers, therefore the results are valid only for the isomeric mixture. KCl, NaCl, LiCl, RbCl, and CsCl were of reagent grade. 8-Anilino-1-napthalene sulphonic acid as the magnesium salt (ANS) was obtained from Eastman Kodak Co. A 0.05 *M* solution of picric acid was prepared from BDH reagent grade picric acid hydrate and was standardized potentiometrically with sodium hydroxide. A sheet of commercial polyurethane foam (polyether type) was used. The water used was doubly distilled and deionized.

Procedure

Small cubes of approximately 0.2 g each were cut from the polyurethane foam sheet. These foam cubes were soaked in 0.5 *M* HNO_3 for 12 h, washed with double distilled water, extracted with acetone in a Soxhlet apparatus for 6 h and finally, air dried.

The sample solution and foam were placed in one of the glass cells shown in Fig. 1. The foam was squeezed by means of the plunger at 15 min intervals for 6 h at room temperature. The amount of metal extracted was determined by measuring the concentration before and after extraction with the foam, using atomic absorption or flame emission.

The distribution coefficient for metal ion is given by the ratio of the concentration of the metal on the foam to the concentration of the metal left in solution at equilibrium and is equal to:

$$[1] \quad D = \frac{\text{amount of metal on foam}}{\text{weight of foam}} \times \frac{\text{volume of solution}}{\text{amount of metal left in solution}}$$

Defined in this way, D has the units of volume per weight, i.e., of mL g^{-1} or of L kg^{-1}.

Trial experiments showed little or no extraction of the metal ions if either the crown ether or picric acid was absent from the alkali metal solution.

The Distribution Coefficient of Crown Ether and Picric Acid

The distribution ratio between foam and water for DCHC-6 was determined as follows. A 50 mL aliquot of crown ether solution was first equilibrated with polyurethane foam as in the metal extraction procedure. After 6 h, 25 mL of solution was transferred to a separatory funnel and a large excess of KOH and picrate solution added. This was then extracted with an equal volume of methylene chloride. A second 25 mL aliquot of crown ether solution, not previously equilibrated with foam, had a large excess of KOH and picric acid solution added, and the resulting solution extracted with an equal volume of methylene chloride. Under these conditions crown ether is extracted together with an equivalent quantity of picrate ion (14*b*). Thus the spectrophotometric analysis of picrate in the two methylene chloride extracts allowed us to calculate the concentration of crown ether before and after foam extraction. The amount of crown ether extracted by foam was thus easily determined. The distribution ratio of crown ether was determined in this way for a number of initial crown ether concentrations between 0.001 and 0.01 mol L^{-1}. The average distribution coefficient (K_{1ex}) was found to be 15 ± 3 L kg^{-1} (the standard deviation of 10 measurements is given).

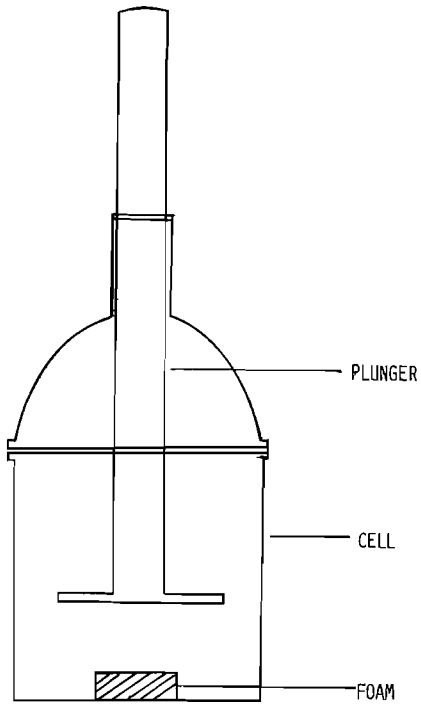

FIG. 1. Cell used in squeezing.

The distribution ratio for picrate ion between water and polyurethane foam was determined by studying the extraction of picric acid in the absence of both alkali metal ions and crown ether. The picric acid extraction was studied using solutions with an initial picric acid concentration of 4×10^{-3} mol L^{-1} in the aqueous phase, and over a pH range of 2.0 to 8. The picrate ion concentration was determined spectrophotometrically. The distribution ratios thus obtained were found to be constant over the pH range 2.5 to 8. The average value, together with the standard deviation was found to be 35 ± 5 L kg^{-1}.

Results and Discussion

The overall extraction equilibrium between an aqueous phase containing a metal ion (M^+), picrate ion (A^-), a crown ether (Cr), and the polyurethane foam may be represented by the following equation:

$$[2] \quad M^+(aq) + Cr(aq) + A^-(aq) \rightleftharpoons MCrA(f)$$

$$[3] \quad K_{ex} = [MCrA(f)]/[M^+(aq)][Cr(aq)][A^-(aq)]$$

where MCrA represents the ion pair between the metal – crown ether cation MCr^+ and picrate anion A^-. The labels "aq" and "f" denote the aqueous and foam phases respectively. The overall equilibrium is thought to consist of the following equilibria:

(*a*) The distribution of free crown ether between foam

Can. J. Chem. Downloaded from www.nrcresearchpress.com by 210.87.254.40 on 09/06/12
For personal use only.

and aqueous phases

[4] $Cr(aq) \underset{}{\overset{K_{1ex}}{\rightleftharpoons}} Cr(f)$

[5] $K_{1ex} = [Cr(f)]/[Cr(aq)]$

(*b*) The distribution of picric acid between the two phases:

[6] $HA(aq) \overset{K_{2ex}}{\rightleftharpoons} HA(f)$

[7] $K_{2ex} = [HA(f)]/[HA(aq)]$

(*c*) The dissociation of picric acid in both phases:

(i)

[8] $HA(aq) \overset{K_{3d}}{\rightleftharpoons} H^+(aq) + A^-(aq)$

[9] $K_{3d} = [H^+(aq)][A^-(aq)]/[HA(aq)]$

(ii)

[10] $HA(f) \overset{K_{3d}^*}{\rightleftharpoons} H^+(f) + A^-(f)$

[11] $K_{3d}^* = [H^+(f)][A^-(f)]/[HA(f)]$

(*d*) The reaction of the metal ion with the crown ether:

[12] $M^+(aq) + Cr(aq) \overset{K_4}{\rightleftharpoons} MCr^+(aq)$

[13] $K_4 = [MCr^+(aq)]/[M^+(aq)][Cr(aq)]$

(*e*) The association of complexed cation with the picrate anion

[14] $MCr^+(aq) + A^-(aq) \overset{K_5}{\rightleftharpoons} MCrA(aq)$

[15] $K_5 = [MCrA(aq)]/[MCr^+(aq)][A^-(aq)]$

(*f*) The distribution of the ion pair between the two phases:

[16] $MCrA(aq) \overset{K_{5ex}}{\rightleftharpoons} MCrA(f)$

[17] $K_{5ex} = [MCrA(f)]/[MCrA(aq)]$

(*g*) The dissociation of the ion pair in the foam:

[18] $MCrA(f) \overset{K_{5d}^*}{\rightleftharpoons} MCr^+(f) + A^-(f)$

[19] $K_{5d}^* = [MCr^+(f)][A^-(f)]/[MCrA(f)]$

(*h*) The dissociation of the metal ion – crown ether complex in the foam:

[20] $MCr^+(f) \overset{K_{4d}^*}{\rightleftharpoons} M^+(f) + Cr(f)$

[21] $K_{4d}^* = [M^+(f)][Cr(f)]/[MCr^+(f)]$

The distribution of picric acid in the absence of both metal ion and crown ether was studied at different pH values and was found to be constant over the pH range from 2.5 to 8. The distribution ratio, D', of picrate in the absence of metal ion is equal to:

[22] $$D' = \frac{\text{total picrate per unit weight foam}}{\text{total picrate per unit volume of solution}} = ([HA(f)] + [A^-(f)])/([HA(aq)] + [A^-(aq)])$$

Substituting for the values of [HA(f)] and [HA(aq)] using eqs. [9] and [11],

[23] $$D' = \left\{\frac{[H^+(f)][A^-(f)]}{K_{3d}^*} + [A^-(f)]\right\} \Big/ \left\{\frac{[H^+(aq)][A^-(aq)]}{K_{3d}} + [A^-(aq)]\right\}$$

[24] $$= \frac{[A^-(f)]}{[A^-(aq)]} \frac{K_{3d}([H^+(f)] + K_{3d}^*)}{K_{3d}^*([H^+(aq)] + K_{3d})}$$

The value of K_{3d} has been determined (15) as 0.51 mol L^{-1}. Thus, at pH values higher than 2, $([H^+(aq)] + K_{3d})$ is approximately equal to K_{3d} and the expression for D' reduces to

[25] $$D' = \frac{[A^-(f)]}{[A^-(aq)]} \frac{K_{3d}([H^+(f)] + K_{3d}^*)}{K_{3d}^* K_{3d}}$$

Since the distribution ratio for picric acid was constant over the pH range from 2.5 to 8, it seems reasonable to assume that $([H^+(f)] + K_{3d}^*)$ is approximately equal to K_{3d}^* over the pH range studied. Thus

[26] $D' = [A^-(f)]/[A^-(aq)]$

over the pH range 2.5 to 8.

The distribution of crown ether was also studied in the absence of both picrate and of metal ion. The distribution ratio

[5] $K_{1ex} = [Cr(f)]/[(Cr(aq)]$

Can. J. Chem. Downloaded from www.nrcresearchpress.com by 210.87.254.40 on 09/06/12
For personal use only.

was determined for various initial concentrations of crown ether (0.001 to 0.01 mol L^{-1}) and was found to be constant with a value of 15 ± 3 L kg^{-1}.

The distribution ratio of the metal ion is defined as

$$[1] \quad D = \frac{\text{total metal on foam per unit weight of foam}}{\text{total metal in solution per unit volume of solution}}$$

Thus, using the equilibria in [4] through [21]

$$[27] \quad D = \frac{[M^+(f)] + [MCr^+(f)] + [MCrA(f)]}{[M^+(aq)] + [MCr^+(aq)] + [MCrA(aq)]}$$

Substituting from eqs. [13], [15], [17], [19], and [21] gives

$$[28] \quad D = \frac{K_{4d}{}^*K_{5d}{}^*K_{5ex}K_5K_4mca/c_fa_f + K_{5d}{}^*K_{5ex}K_5K_4mca/a_f + K_{5ex}K_5K_4mca}{m + K_4mc + K_5K_4mca}$$

where $m = [M^+(aq)]$, $c = [Cr(aq)]$, $a = [A^-(aq)]$, $c_f = [Cr(f)]$, $a_f = [A^-(f)]$. Substituting for c_f and a_f using eqs. [5] and [26] respectively

$$[29] \quad D = \frac{K_{4d}{}^*K_{5d}{}^*K_{5ex}K_5K_4/K_{1ex}D' + K_{5d}{}^*K_{5ex}K_5K_4c/D' + K_{5ex}K_5K_4ca}{1 + K_4c + K_5K_4ca}$$

Since for all the experiments the total metal ion is always less than 1/10th of the total crown ether, it seems reasonable to approximate

$$vCr_T = vc + wc_f$$

where Cr_T is the initial concentration of crown ether in the aqueous phase, v is the volume of solution, and w is the weight of foam used. Thus,

$$[30] \quad vCr_T = vc + wK_{1ex}c$$

$$[31] \quad c = Cr_T/(1 + K_{1ex}w/v)$$

Similarly,

$$[32] \quad a = A_T/(1 + D'w/v)$$

Substituting these values of c and a into eq. [29] gives:

$$[33] \quad D = \frac{\frac{K_{4d}{}^*K_{5d}{}^*K_{5ex}K_5K_4}{K_{1ex}D'} + \frac{K_{5d}{}^*K_{5ex}K_5K_4Cr_T}{D'(1 + K_{1ex}w/v)} + K_{5ex}K_5K_4Cr_TA_T/(1 + K_{1ex}w/v)(1 + D'w/v)}{1 + K_4Cr_T/(1 + K_{1ex}w/v) + K_5K_4Cr_TA_T/(1 + K_{1ex}w/v)(1 + D'w/v)}$$

Both K_{1ex} and D' have been determined above. The stability constants of alkali metal ion – DCHC-6 complexes, K_4 in the above equation, have been reported in the literature (12, 16) and are listed in Table 2.

The ion pair association constants, K_5, have not been determined. They may be estimated using the following equation derived by Fuoss (17) for ions in contact

$$[34] \quad K = 2.524 \times 10^{-3}\mathring{a}^3e^b$$

$$[35] \quad b = Z^2/aDkT$$

where Z is the electron charge, a is the center-to-center distance of the ions in a pair, D is the dielectric constant of the medium, and k is Boltzmann's constant. Using the Pauling ionic radii given in Table 1 and a value of 2.23 Å for the radius of the picrate ion (18), values for the ion pair association constants, K_5, were estimated. The values are given in Table 2. Substituting the appropriate values of K_4, K_5, Cr_T, and A_T, it can be seen that the denominator in eq. [33] can be approximated by

$$1 + K_4Cr_T/(1 + K_{1ex}w/v)$$

Thus, after rearranging it can be seen that plots of $D(1 + K_4Cr_T/(1 + K_{1ex}w/v))$ against both A_T and

TABLE 2. "Best" combinations of equilibrium constants, K, for alkali metal ion – crown ether – picrate ion extraction into polyurethane foam

Cation	K_4‡ / L mol^{-1}	K_5† / L mol^{-1}	K_5K_{5ex} / L^2 mol^{-1} kg^{-1}	K_{4d}* / mol kg^{-1}	K_{5d}* / mol kg^{-1}	K_{ex} / L^3 mol^{-2} kg^{-1}
Na^+	16	0.77	2.5×10^4	2×10^{-3}	0.06	4.0×10^5
K^+	104	0.85	9.2×10^4	5×10^{-5}	0.12	9.6×10^6
Rb^+	34	0.88	1.3×10^5	0.03	0.05	4.4×10^6
Cs^+	17	0.94	5.2×10^4	0.05	0.11	8.8×10^5

†Estimated by Fuoss equation (17).
‡Reference 12.

Cr_T will be straight lines, the slopes and intercepts of which allow us to estimate K_{4d}*, K_{5d}*, and K_5K_{5ex}.

The extraction behaviour of the cations Na^+, K^+, Rb^+, and Cs^+ (lithium showed no extraction under the conditions of the experiments) into polyurethane foam from aqueous solution containing DCHC-6 and picric acid was studied as a function of the total initial picric acid concentration, A_T. The concentration of the picric acid was varied from 0.5×10^{-3} to 15×10^{-3} mol L^{-1} for each cation (1×10^{-4} mol L^{-1}) with the crown ether concentration kept constant at 4×10^{-3} mol L^{-1}. The results are shown in Fig. 2 where it is clear that the extraction of metal ion increases with an increase in the picric acid concentration.

The effect of crown ether concentration on extraction of K^+, Rb^+, Cs^+, and Na^+ was studied at constant initial picric acid concentration and constant metal ion concentration. The results shown in Fig. 3 indicate that the extraction increases with an increase in crown ether concentration. The extraction behaviour of the cations shown in Figs. 2 and 3 is consistent with the ion pair extraction of cation – crown ether and picrate complexes as predicted from eq. [33].

Figure 4 shows the plot of D vs. initial crown ether concentration for three different concentrations of K^+

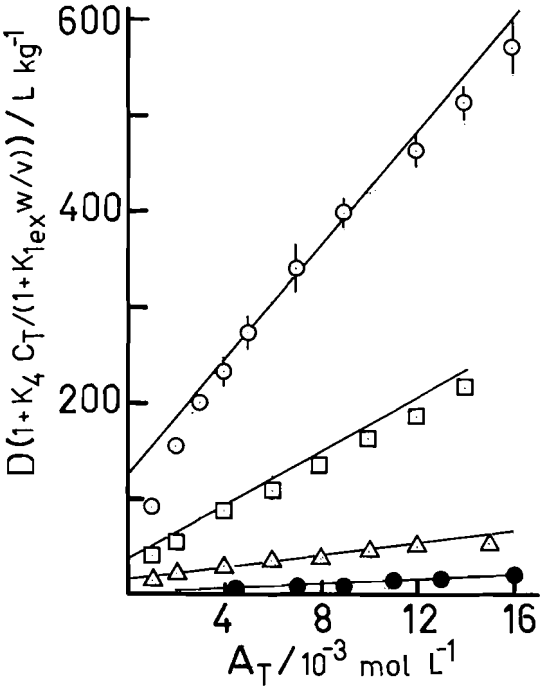

FIG. 2. The effect of varying the initial concentration of picric acid, A_T, on the distribution ratio, D, for the distribution of various alkali metal cations between polyurethane foam and aqueous solution. Total metal ion concentration 1×10^{-4} mol L^{-1}; total crown ether concentration 4×10^{-3} mol L^{-1}; weight of foam 0.2 g; volume of solution 40 mL: K^+ (○), Rb^+ (□), Cs^+ (△), and Na^+ (●).

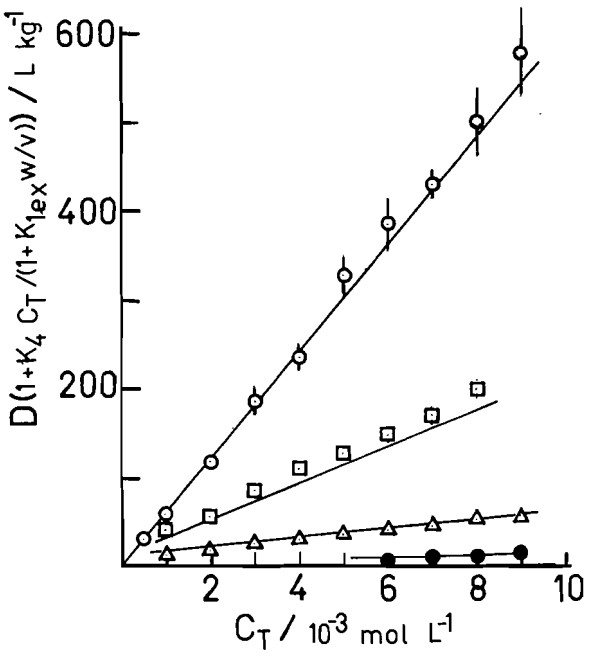

FIG. 3. The effect of varying the initial concentration of crown ether, C_T, on the distribution ratio, D, for the distribution of various alkali metal cations between polyurethane foam and aqueous solution. Initial metal ion concentration 1×10^{-4} mol L^{-1}; initial picric acid concentration 4×10^{-3} mol L^{-1}; weight of foam 0.2 g; volume of solution 40 mL: K^+ (○), Rb^+ (□), Cs^+ (△) and Na^+ (●).

Can. J. Chem. Downloaded from www.nrcresearchpress.com by 210.87.254.40 on 09/06/12
For personal use only.

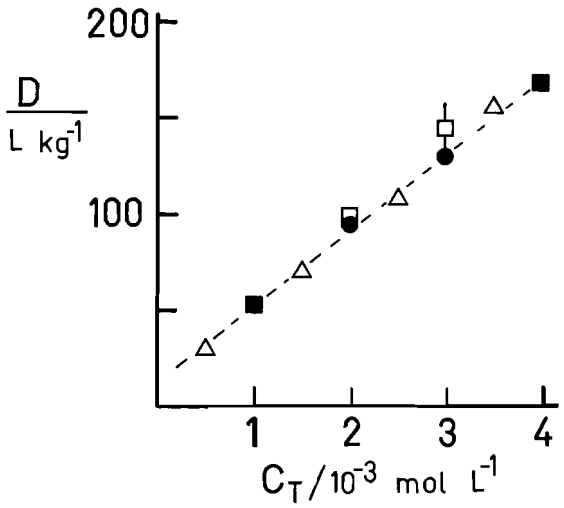

FIG. 4. Distribution coefficient as a function of initial concentration of DCHC-6 at different total concentrations of K^+: $K^+ = 0.25 \times 10^{-4}$ *M* (●), 0.5×10^{-4} *M* (□), 1×10^{-4} *M* (△), [picric acid] = 4×10^{-3} *M*. Weight of foam 0.2 g.

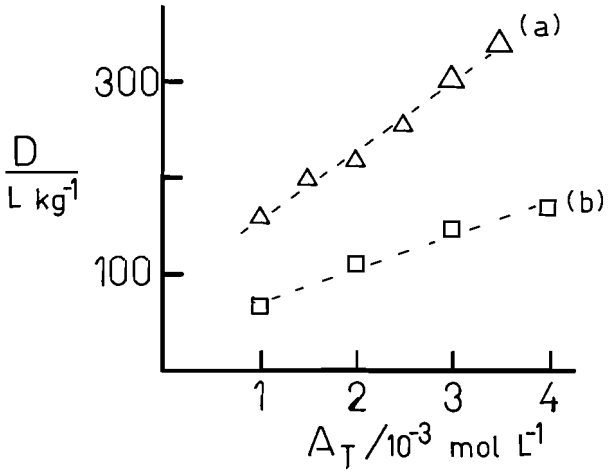

FIG. 5. Distribution coefficient as a function of initial concentration of anions, ANS (△), picric acid (□), $[K^+]$ 1×10^{-4} *M*, [DCHC-6] 4×10^{-3} *M*. Weight of foam 0.2 g.

with picric acid concentration constant at 4×10^{-3} *M*. The results shown in Fig. 4 indicate that the extraction is independent of metal ion concentration under these conditions (i.e. $[M^+]_T < [A_T]$ and $[Cr_T]$). This behaviour is predicted from eq. [33]. In Fig. 5, curves *a* and *b* show the plot of *D* vs. the initial concentration of picric acid and ANS respectively at constant initial concentration of K^+ and DCHC-6. It is expected that the bulky anions are more hydrophobic and therefore ought to enhance the extraction into foam. This is clearly shown in Fig. 5 for K^+, where the *D* values are higher for ANS than for picric acid. Under similar conditions no extraction was observed with 2,6- and 2,4-dinitrophenols. These findings demonstrate that the efficiency of ion pair extraction depends, in addition to the other factors mentioned, on the nature of the counter ion.

The effect of pH on the extraction of K^+ was studied at constant picric acid and crown ether concentrations. The pH values were adjusted by the addition of hydrochloric acid or tetraethyl ammonium hydroxide (10% solution in H_2O). The extraction increases rapidly with the increase in pH, reaching a maximum at pH ~ 2.5 and remaining constant up to pH 8. From this result, it is obvious that the *D* values are independent of hydrogen ion concentration above pH 2.5, which is in agreement with our approximations.

Values for the constants K_5K_{5ex}, K_{4d}*, and K_{5d}* were calculated according to eq. [33] from the values of the slopes and intercepts obtained from Figs. 2 and 3. A best fit was made to the data. The preferred or "best" values for the constants are given in Table 2. The solid lines in Figs. 2 and 3 were calculated using these best fit values.

Similar results have been reported for the solvent extraction of ion pairs of Na^+, K^+, and Ca^{2+} complexes of DCHC-6 with picrate and other anions (14*d*). Solvent extraction data are commonly reported as overall extraction coefficients, K_{ex}, defined analogously to eq. [3]. From eqs. [17], [15], and [13], it can be shown that

$$K_{ex} = K_5K_{5ex}K_4$$

Values of K_{ex} have been calculated, and are given in Table 2. It is seen from these K_{ex} values that the extraction increases in the order $Na^+ < Cs^+ < Rb^+ < K^+$. This is consistent with the results obtained by previous workers (14) for solvent extraction studies and is due to the fact that the stability of the cation – crown ether complex depends mainly on the ratio of the ionic size of the cation to the cavity size of the crown ether (12). From Table 1, one might have predicted that K^+ just barely fits into the DCHC-6 ring. The cations larger (Rb^+ and Cs^+) or smaller (Na^+ and Li^+) than the optimum size form less stable complexes because in the former case the cation is too large to fit into the cavity, while in the latter case, the ring is too large and thus the cation cannot be simultaneously close to all the oxygens. Thus a weaker complexation of Li^+, Na^+, Rb^+, and Cs^+ with DCHC-6 results in the poor extraction of these cations compared to K^+, which forms the most stable complex with DCHC-6 (Table 2).

The similarity of our results to those for solvent extractions (14) tends to suggest that extraction of alkali metals in the presence of crown ether and

Can. J. Chem. Downloaded from www.nrcresearchpress.com by 210.87.254.40 on 09/06/12
For personal use only.

picric acid by polyurethane foam from an aqueous system can be considered as the ion pair extraction of MCrA by an organic solvent of moderate dielectric constant.

Acknowledgment

This work was supported by the Natural Sciences and Engineering Research Council of Canada.

1. R. F. HAMON and A. CHOW. Abstracts of 60th CIC Conference held at Montreal, P.Q., Canada. 1977.
2. G. J. MOODY and J. D. R. THOMAS. The Analyst, **104**, 1 (1979).
3. T. BRAUN and A. B. FARAG. Anal. Chim. Acta, **99**, 1 (1978).
4. R. A. MOORE and A. CHOW. Talanta, **27**, 315 (1980).
5. J. J. OREN, K. M. GOUGH, and H. D. GESSER. Can. J. Chem. **57**, 2032 (1979).
6. H. D. GESSER and G. A. HORSFALL. J. Chim. Phys. **74**, 1072 (1977).
7. V. S. K. LO and A. CHOW. Anal. Chim. Acta, **106**, 161 (1979).
8. V. S. K. LO and A. CHOW. Talanta, in press.
9. S. J. AL-BAZI and A. CHOW. Abstracts of 62nd CIC Conference held at Vancouver, B.C., Canada. 1979.
10. C. J. PEDERSEN. J. Am. Chem. Soc. **89**, 7017 (1967).
11. C. J. PEDERSEN. J. Am. Chem. Soc. **89**, 2495 (1967).
12. R. M. IZATT, D. J. EATOUGH, and J. J. CHRISTENSEN. Struct. Bonding, **16**, 161 (1973).
13. (*a*) D. BRIGHT and M. R. TRUTER. Nature, London, **225**, 176 (1970); (*b*) D. BRIGHT and M. R. TRUTER. J. Chem. Soc. B, 1544 (1970); (*c*) M. A. BUSH and M. R. TRUTER. Chem. Commun. 1439 (1970).
14. (*a*) C. J. PEDERSEN. Fed. Proc. Fed. Am. Soc. Expt. Biol. **27**, 1305 (1968); (*b*) H. K. FRENSDORFF. J. Am. Chem. Soc. **93**, 4684 (1971); (*c*) A. SADAKANE, T. IWACHIDO, and K. TOEI. Bull. Chem. Soc. Jpn. **48**, 60 (1975); (*d*) M. JAWAID and FOLKE INGMAN. Talanta, **25**, 91 (1978).
15. G. KORTUM, M. VOGEL, and K. ANDRESSON. (*Editors*). Dissociation constants of organic acids in aqueous solutions. Butterworth, London, 1961.
16. H. K. FRENSDORFF. J. Am. Chem. Soc. **93**, 600 (1971).
17. R. M. FUOSS. J. Am. Chem. Soc. **80**, 5059 (1958).
18. T. C. WADDINGTON. Adv. Inorg. Chem. Radiochem. **1**, 180 (1959).
19. L. PAULING. The nature of the chemical bond. 3rd ed. Cornell Univ. Press. 1960.

Can. J. Chem. Downloaded from www.nrcresearchpress.com by 210.87.254.40 on 09/06/12
For personal use only.

Solvent extraction of anionic surfactants. The stearic acid – metal triethylenetetramine chelate ion-pair

DAVID JEFFRIES AND JAMES FRESCO

Otto Maass Chemistry Building, McGill University, Montreal, P.Q., Canada H3A 2K6

Received August 5, 1980

This paper is dedicated to Professor W. E. Harris on the occasion of his retirement from the University of Alberta

DAVID JEFFRIES and JAMES FRESCO. Can. J. Chem. **59**, 1497 (1981).

The solvent extraction behaviour of nickel(II) and copper(II) chelates of triethylenetetramine with stearic acid in a cyclohexane–isobutanol mixed solvent has been investigated. The results indicate that carboxylic acid selectivity by charged chelate extraction is based on partition constant differences rather than ion-pair formation constants. A computational technique for determination of partition and dimerization constants of high molecular weight carboxylic acids has been tested.

DAVID JEFFRIES et JAMES FRESCO. Can. J. Chem. **59**, 1497 (1981).

On a étudié le comportement, lors d'extraction par des solvants, des chélates de Ni(II) et du Cu(II) de la triéthylènetétramine avec l'acide stéarique dans un solvant mixte cyclohexane–isobutanol. Les résultats indiquent que la sélectivité de l'acide carboxylique par rapport à l'extraction du chélate chargé, est relié à des différences de constante de partage plutôt qu'aux constantes de formation de paire d'ions. On a vérifié une technique de calcul des constantes de partage et de dimérisation des acides carboxyliques de poids moléculaire élevé.

[Traduit par le journal]

Introduction

The determination of low-level concentrations of surfactants is achieved by solvent extraction and colorimetric analysis of a suitable chromophore-containing component of the extracted ion-pair (1). In this manner alkyl sulphates and alkane sulphonates in polluted waters and environmental samples have been measured employing substituted 1,10-phenanthroline and 2,2′-bipyridine chelates of iron(II) (2–4). In addition to organic sulphates and sulphonates, long chain carboxylate surfactants have been determined in mineral flotation liquors by means of the copper(II) chelate of triethylenetetramine (5).

The success of this analysis after modifying the detection system to include an atomic absorption spectrometer (6) provoked the present investigation. The analysis of stearic acid using copper(II) trien and nickel(II) trien was chosen for detailed study to expose significant features of this extraction system and as a consequence advance surfactant analysis.

Experimental

Chemicals

Triethylenetetramine (trien) supplied by Fisher Scientific Co. was purified by preparation of the dihydrate of the sulphate salt (7). The purity of the product was determined as 99.9% by potentiometric titration with standard sodium hydroxide.

Copper-61 and -64 were coproduced by proton bombardment of a 99.99% pure copper foil target positioned in the McGill University Foster Radiation Laboratory Synchrocyclotron. After dissolution of the foil, traces of Co, Ni, and Zn were separated by anion exchange chromatography (8). The radiochemical purity of the copper from each irradiation was checked by analysis of the two-component decay curves obtained.

Nickel-56 and -57 were obtained by proton bombardment of 99.9% pure nickel powder enclosed in an aluminum capillary. The irradiation facility and radiochemical purification procedure were similar to those used for ^{61}Cu and ^{64}Cu. γ-Ray spectra obtained for each nickel irradiation after ion exchange separation did not show peaks for nuclides other than those expected for nickel.

All other chemicals and solvents were either reagent or spectral grade and were used without further purification.

Solutions

Isobutanol/cyclohexane mixed solvent used as the organic phase was prepared by mixing 200 mL isobutanol and 800 mL cyclohexane.

Stearic acid stock solutions were prepared by dissolution of weighed portions of stearic acid in the mixed solvent. For the extraction studies further dilutions were performed as required.

Trien solutions were prepared by dissolution of 7.56 g of triethylenetetrammonium sulphate in 50 mL 1.6 *M* sodium hydroxide. A 90% reduction in volume was achieved under vacuum in a rotary evaporator and the resultant slurry of concentrated trien and solid Na_2SO_4 was filtered. After dilution of the filtrate to 100 mL this 2% trien solution possessed pH 11.8.

Metal(II) trien solutions were prepared by dilution of a fraction of the metal-containing effluent from the ion-exchange column with 2% trien solution. The concentration of these intermediate metal ion solutions was determined colorimetrically. Aqueous phases were prepared by mixing aliquots of the standardized metal trien solutions with sufficient small volumes of HCl and dilution to volume with 2% trien solution. The pH after extraction ranged from 10 to 12.

Procedure

The extractions were conducted at ambient temperature, 24 ± 1°C, and the aqueous phase ionic strength ranged between 0.010 and 0.015 *M*. Aliquots of 4 mL of the metal(II) trien solutions and stearic acid in 20% isobutanol/80% cyclohexane mixed sol-

0008-4042/81/101497-04$01.00/0

©1981 National Research Council of Canada/Conseil national de recherches du Canada

Can. J. Chem. Downloaded from www.nrcresearchpress.com by 210.87.254.40 on 09/06/12
For personal use only.

Can. J. Chem. Downloaded from www.nrcresearchpress.com by 210.87.254.40 on 09/06/12
For personal use only.

vent were transferred to 10 mL centrifuge tubes. After capping, the tubes were shaken for 10 min and then centrifuged to separate the phases. Equilibration was checked by examining the phases after shorter and longer periods of agitation. The less dense organic phase was sampled first and the aqueous phase was sampled by applying positive pressure to a pipet as it was lowered through the residual organic phase.

The aliquots of each phase were delivered to separate 150 mm × 10 mm test tubes and capped. The metal ion activities were measured in a γ-well counter and the pH values of the equilibrated aqueous phases were recorded. The aqueous phase volume increase and organic phase volume decrease both by a factor of 5% were considered in the calculations.

Calculations

Resolution of mixed nuclide activities: since the half-life of ^{61}Cu was significant relative to the duration of the counting measurements, the observed activities were resolved and extrapolated to an initial time before distribution ratios were calculated. The observed counting rate for a sample containing mixed activities can be expressed by eq. [1] (10):

$$[1] \quad Y_j = \sum_{i=1}^{n} x_i \exp(-\lambda_i t_j) \frac{1 - \exp[-\lambda_i(\Delta t)_j]}{\lambda_i(\Delta t)_j}$$

where Y_j is the activity observed in the jth measurement, λ_i is the decay constant of the ith species, x_i is the contribution to the initial activity from the ith species at time t_0, t_j is the time relative to t_0 at the beginning of the jth measurement, and Δt_j is the duration of the jth measurement.

This equation was solved for the coefficients x_i by a weighted least-squares method using data obtained for a reference sample monitored during the counting of the separated phases. The weighting of data was achieved by dividing eq. [1] by the standard deviation of Y_j. Values for the initial activities of ^{61}Cu and ^{64}Cu were calculated by a FORTRAN subroutine in the data reduction program *vide infra*.

The activity of each sample was corrected to an arbitrarily selected time, t_0, using eq. [2].

$$[2] \quad Z_0 = \frac{G/\Delta t_G - B/\Delta t_B}{\sum_{i=1}^{n} f_i \exp(-\lambda_i t) \frac{1 - \exp(-\lambda_i \Delta t_G)}{\lambda_i \Delta t_G}}$$

where Z_0 is total activity corrected to time t_0, G is the gross count at time t, B is the background count, Δt_G and Δt_B are the durations of these counts, f_i the fraction of Z_0 due to the ith species is determined from the values of x_i.

Accordingly, the extraction data were corrected for decay before distribution ratios were calculated. The average of the sums of the corrected aqueous and organic phase activities for each extraction was within one sd of the activity of the resolution standard.

The magnitude of the Nitrien^{2+} and Cutrien^{2+} formation constants (9), excess trien employed, and range of pH values of the aqueous phases studied precluded existence of significant metal species other than the chelate. Plots of the logarithm of the metal ion distribution ratio, D, for the Mtrien^{2+} – stearic acid system versus pH or log stearate ion concentration first increased according to a slope of two and then changed continuously toward slope zero. The span of log D values was from less than −2 to 0.8 for copper and 1.2 for nickel while log stearate ion concentrations ranged from less than −4.5 to −2.5. On this basis the extractable species was assigned as the chelate distearate, MtrienA$_2$, and the observed values for the distribution ratio was represented as

$$D = \overline{[\text{MtrienA}_2]}/([\text{MtrienA}_2] + [\text{MtrienA}^+] + [\text{Mtrien}^{2+}])$$

Inversion and introduction of equilibrium constants give

$$1/D = 1/K_{D_C} + 1/K_{D_C}K_2[A^-] + 1/K_{D_C}K_1K_2[A^-]^2$$

which is a binomial equation with respect to $[A^-]^{-1}$ where K_{D_C} is the partition constant for the distearate species and K_1 and K_2 are the stepwise formation constants of the same species. The equation is solvable for the coefficients $1/K_{D_C}$, $1/K_{D_C}K_2$, and $1/K_{D_C}K_1K_2$ after values for $[A^-]$ are established.

Since the total stearic acid concentration, $[HA]_T$, was much greater than the total metal concentration, the free stearate ion concentration is obtained by solving the quadratic equation

$$2K_P H^2 K_{D_R}{}^2[A^-]^2/K_a{}^2 + (H + K_a + HK_{D_R})[A^-]/K_a - [HA]_T = 0$$

where H is the hydrogen ion concentration and K_P, K_{D_R}, and K_a are the dimerization constant, partition constant, and dissociation constant of stearic acid. A value for K_a of 1.29×10^{-5} typical for fatty acids above C_8 was assumed. The values K_{D_R} and K_P were too large to be determined directly by a two-phase titration or the analytical procedure on which this study is based. These constants were evaluated simultaneously with those for K_{D_C}, K_1, and K_2 according to the following method.

Trial values for K_{D_R} and K_P were varied independently in an iterative computer program. For each pair of values, the weighted least-squares solution of eq. [1] was carried out by von Holdt's matrix method (10). The values of all five constants were taken to be those values for which χ^2 was a minimum. A three-dimensional plot of χ^2 vs. log K_{D_R} and log K_P showed one marked minimum for both metals studied and the corresponding coordinates were assigned to log K_{D_R} and log K_P.

Can. J. Chem. Downloaded from www.nrcresearchpress.com by 210.87.254.40 on 09/06/12
For personal use only.

Results and Discussion

Enhanced extraction of uncharged chelates through neutral adduct formation has been extensively studied and summarized (11). Although the extraction of charged chelates and metal carboxylates (12) has considerable practical importance, detailed information on the formation of extractable species of the former type is meagre. In this work the distribution ratio of the charged substrate has been employed to indirectly establish properties of the free ligand heretofore ignored or determined independently.

The computer solution for the partition coefficients and stepwise formation constants of metal trien distearates was tested by using the published data for the extraction of thorium(IV) with acetylacetone (13) as well as results obtained for the iron(III) and vanadium(V) chelates of β-isopropyltropolone using the program OMNITAB (14). Agreement was excellent for all constants. Unsuccessful attempts to determine the partition and dimerization constants of stearic acid by two-phase titrations and extractions using either Gregory's method (5) or radiotracer copper trien as a stearate ion monitor indicated that log K_{D_R} for stearic acid would be greater than 5, if dimerization was negligible.

The results of the extraction studies of copper(II) and nickel(II) trien distearates appear in Table 1. Dimerization and partition constants have been reported for acetic, propionic, and butyric acids in the CCl_4/H_2O system (15). However, the precision of the extraction data for valeric acid would not permit the calculation of the corresponding constants.

Dimerization constants of C_2 to C_6 carboxylic acids have been shown to be independent of chain length (16) by solvent extraction. This study also showed that for the same series of acids the value of log K_{D_R} increases by 0.56–0.60 for every methylene group added. The values of K_{D_R} and K_P for propionic acid in cyclohexane (16) are −2.54 and 3.71, respectively. Accordingly, log K_{D_R} for stearic acid should have a value between 5.6–6.2.

The predictions for stearic acid in the cyclohexane/water system may be compared to the values in Table 1 where the organic solvent was 80% cyclohexane – 20% isobutanol. The agreement between the dimerization constants obtained by the copper and nickel extractions is considerably better than that obtained for the partition constant of stearic acid, the value of which may be considered $(1.0 \pm 0.3) \times 10^6$. The presence of isobutanol would be expected to depress the dimerization constant and enhance the partition constant. This trend was only apparent in the case of the dimerization constant.

The composition of the phases extracted was similar to that described by Gregory (5) except ethanolamine was excluded from the present study. Since carboxylic acids of chain lengths less than C_{14} were not extracted by Cutrien^{2+}, the results of this study suggest the basis of the carboxylic acid selectivity is the magnitude of K_{D_C} values rather than differences in adduct formation constants.

It is of further interest to examine the basis for the nonextractability of Cutrien distearate into cyclohexane in the absence of isobutanol reported earlier (5). If stearate ions had occupied the axial positions of the metal ion in the extractable species, a significant difference between copper and nickel adduct formation constants would have been almost certainly observed. Since this was not the case, the axial positions were probably occupied by isobutanol and the extraction of "solvent-separated" ion pairs occurred. The larger partition constant of Nitrien distearate could reflect tighter bonding of the adduct and consequent increase in shielding of the metal ion.

TABLE 1. Equilibrium constants of nickel(II) and copper(II) triethylenetetramine distearate for the H_2O/cyclohexane–isobutanol solvent pair

Parameter	Value			
	NitrienA$_2$		CutrienA$_2$	
log K_{D_R}	6.2		5.6	
log K_P	3.2		3.4	
log K_{D_C}	1.49	$\binom{+0.10}{-0.13}$	0.87	$\binom{+0.05}{-0.06}$
log K_1		*	2.99	$\binom{+0.23}{-0.51}$
log K_2		*	2.9	$\binom{+0.3}{-1.3}$
log K_1K_2	6.10	$\binom{+0.11}{-0.15}$	6.02	$\binom{+0.08}{-0.09}$

*log K_1 and log K_2 values for nickel were unresolvable.

Acknowledgment

We are grateful to the National Research Council of Canada for financial support of this work.

1. J. T. Cross (*Editor*). Anionic surfactants – chemical analysis. Marcel Decker, Inc., New York, NY. 1977.
2. J. Courtot-Coupez and A. LeBihan. Anal. Lett. **2**, 211 (1969).
3. C. G. Taylor and J. Waters. Anal. Chim. Acta, **69**, 363 (1974).
4. C. G. Taylor, J. Waters, and P. V. Williams. Anal. Chim. Acta, **69**, 373 (1974).
5. G. R. Gregory. Analyst, **91**, 257 (1966).
6. R. H. Yoon. Ph.D. Thesis, McGill University, Montreal, P.Q. 1977.

7. C. N. REILLEY and A. VAVOULIS. Anal. Chem. **31**, 243 (1959).
8. K. A. KRAUS and G. E. MOORE. J. Am. Chem. Soc. **75**, 1460 (1953).
9. L. G. SILLEN and A. E. MARTELL. Stability constants of metal-ion complexes. The Chemical Society, London, U.K. 1964.
10. P. C. STEVENSON. Processing of counting data. NAS-NS 3109, Natl. Bur. Stand. U.S. Dept. of Commerce, Springfield, VA. 1966. pp. 61–63.
11. T. SEKINE and Y. HASEGAWA. Solvent extraction chemistry. Marcel Decker, Inc., New York, NY. 1977.
12. F. MILLER. Talanta, **21**, 685 (1974).
13. J. RYDBERG. Acta Chem. Scand. **4**, 1603 (1950); **15**, 1723 (1961).
14. O. MENIS, B. E. MCCLELLAN, and D. S. BRIGHT. Anal. Chem. **43**, 431 (1971).
15. T. SEKINE *et al.* Bull. Chem. Soc. Jpn. **40**, 27 (1967).
16. I. KOJIMA, M. YOSHIDA, and M. TANAKA. J. Inorg. Nucl. Chem. **32**, 987 (1970).

Can. J. Chem. Downloaded from www.nrcresearchpress.com by 210.87.254.40 on 09/06/12
For personal use only.

Basicity of *N*-substituted anilines and pyridine in dimethylsulfoxide

ROBERT L. BENOIT, MOYRA J. MACKINNON, AND LÉON BERGERON[1]

Département de Chimie, Université de Montéal, C.P. 6210, Succ. A, Montréal (Qué.), Canada H3C 3V1

Received August 8, 1980

This paper is dedicated to Professor W. E. Harris on the occasion of his retirement from the University of Alberta

ROBERT L. BENOIT, MOYRA J. MACKINNON, and LÉON BERGERON. Can. J. Chem. **59**, 1501 (1981).

The ionization constants of the conjugated acids BH^+ of aniline, *N*-methyl- and *N*,*N*-dimethylaniline, and pyridine have been determined potentiometrically in Me_2SO. The heats of neutralization of the amines B and their heats of solution have been obtained by calorimetry. The p*K*'s and enthalpies of ionization of these BH^+ ions and alkylammonium ions are linearly related. Comparisons with gas phase data show that the abnormal basicity order of the amines B in Me_2SO is mainly due to the decreasing exothermicity of the heat of solution of the BH^+ ions with the number of N—H protons available for H-bonding to Me_2SO. The large increase in basicity difference between equally substituted aromatic and alkylamines, when passing from the gas phase to Me_2SO, is linked to the larger heat of vaporization of the aromatic amines.

ROBERT L. BENOIT, MOYRA J. MACKINNON et LÉON BERGERON. Can. J. Chem. **59**, 1501 (1981).

Les constantes d'ionisation des acides conjugués BH^+ de l'aniline, de la *N*-méthyl et la *N*,*N*-diméthylaniline, et de la pyridine on été déterminées par potentiométrie dans le Me_2SO. Les chaleurs de neutralisation des amines B et leurs chaleurs de solution ont été obtenues par calorimétrie. On a trouvé une relation linéaire entre les p*K* et les enthalpies d'ionisation de ces ions BH^+ et d'autres ions alkylammonium. Des comparaisons avec des données en phase gazeuse montrent que l'ordre anormal de basicité des amines B dans le Me_2SO est principalement dû à l'exothermicité décroissante de la chaleur de solution des ions BH^+ celle-ci étant fonction du nombre de protons N—H pouvant former des liaisons hydrogène avec le Me_2SO. L'augmentation importante de la différence de basicité entre les amines aromatiques et les alkylamines également substituées, lorsque l'on passe de la phase gazeuse au Me_2SO, provient de la plus grande chaleur de vaporisation des amines aromatiques.

While the acid–base properties of compounds belonging to related series often follow a rational sequence in the gas phase, the sequence can be complex when the compounds are present as solutes. The modifications in the basicity of alkylamines B according to the nature and number of alkyl substituents is a case in point (1, 2). For example, in the gas phase the basicity order is

$$Me_3N > Me_2NH > n\text{-}PrNH_2 > EtNH_2 > MeNH_2 > NH_3$$

while in the solvent dimethylsulfoxide (Me_2SO) the order becomes

$$MeNH_2 \sim EtNH_2 > n\text{-}PrNH_2 > NH_3 \sim Me_2NH \gg Me_3N$$

thus NH_3 is more basic than Me_3N by 2.0 p*K* units. Then in water, the sequence changes to

$$Me_2NH \sim EtNH_2 \sim MeNH_2 \sim n\text{-}PrNH_2 > Me_3N > NH_3$$

so that NH_3 is now a weaker base than Me_3N with a 0.6 p*K* difference. Comparison of amines protonation data in solvents and in the gas-phase provides a full understanding of the solvent effect and reveals some interesting variations in the solvation of both B and BH^+. We have recently reported such a comparison (2) and we present here the results of our work on the solution and protonation of four aromatic amines in Me_2SO, aniline (ϕNH_2), *N*-methyl- ($\phi NHMe$) and *N*,*N*-dimethylaniline (ϕNMe_2), and pyridine (Py). Potentiometric and calorimetric determinations were carried out to provide the necessary data in Me_2SO and some supplementary data in water and CCl_4.

Experimental

Materials

Me_2SO (BDH) was reagent grade. It was dried (water content less than 0.02%) and stored over 4A molecular sieves. Aniline (Anachemia), *N*,*N*-dimethylaniline (Fisher Scientific), and pyridine (BDH, 99.5% purity) were reagent grade and used without further purification. *N*-Methylaniline (Eastman Kodak practical grade) was distilled under reduced pressure and the middle fraction used. Trifluoromethanesulfonic acid (3M Chemical) was used as received, as were tetraethylammonium iodide (Baker reagent grade) after drying 12 h at 50°C and tetraethylammonium perchlorate (Eastman reagent) after similar drying.

Potentiometric Determinations

Potentiometric titrations of Me_2SO solutions of the amines (2×10^{-3} to 1×10^{-2} *M*) with standardized solutions of HCF_3SO_3 in Me_2SO were carried out in a glove box under a stream of dry nitrogen. The solution in the cell was maintained at 25.0°C by means of a jacket through which temperature-controlled water circulated. The electrodes used were a glass electrode (Radiometer G202B) which was calibrated twice with standard HCF_3SO_3 to give a 62.4 ± 0.3 mV slope (intercept: 85.76 ± 0.10 mV, $r = 0.9999$) in a ΔE vs. log [HA] plot, and an I^-/I_3^- reference electrode consisting of a platinum wire in a Me_2SO solution 10^{-2} *M* in I_2 and 2×10^{-2} *M* in Et_4NI (2). The junction consisted of a 0.10 *M* Et_4NClO_4 solution in Me_2SO. An essentially constant ionic strength was maintained in the amine solutions by making them initially 0.1 *M* in Et_4NI. The potentiometer used was a Tacussel Model Aries 10 000–15 562. Titration of the anilines and pyridine, which are weak bases, did not show a

[1]Present address: Alcools de Commerce, Varennes, P.Q., Canada.

0008-4042/81/101501-04$01.00/0

©1981 National Research Council of Canada/Conseil national de recherches du Canada

sharp end-point so their concentration was pre-determined by weight.

Calorimetry

The heats of solution and of neutralization of the liquid amines were measured at 25.0°C with a LKB Model 8725-2 isoperibol calorimeter as previously described (3), the amount of amine dissolved or reacted being known from the weight of the glass ampoules. An excess of 0.1 *M* HCF_3SO_3 in Me_2SO and 0.1 *N* HCl in water were used in the neutralization experiments. For each amine 3–6 separate determinations were made at different concentrations.

Results

Potentiometry

The values of the ionization constants *K* of the ammonium ions BH^+ were obtained from the potentiometric titration curves for each amine B. Analyses were made of each plot giving ΔE against $\log R$ where

$$R = \frac{C_B - (C_{HA} - [H^+])}{C_{HA} - [H^+]}$$

C_B representing the intial amine concentration, and C_{HA} the concentration of added HCF_3SO_3. The average slopes of the plots for $-0.2 < \log R < +0.5$ were respectively 64.2 ± 1.5 mV (ϕNH_2), 63.0 ± 1.0 mV (ϕNHMe), 62.9 ± 1.1 mV (ϕNMe_2), and 63.6 ± 1.4 mV (Py). These values are in satisfactory agreement with 62.4 mV, the calibration slope obtained with HCF_3SO_3, a strong acid in Me_2SO (4). From the values of the half-neutralization potentials, ΔE for $\log R = 0$, the p*K* values listed in Table 1 were calculated and averaged ($\Delta pK \leq 0.02$). Our values for aniline and pyridine are in good agreement with data from previous investigators who used different electrode systems and calibration techniques (1, 5).

Calorimetry

Table 2 presents our values of the heat of solution, ΔH_s^0(B), of the liquid amines in Me_2SO and also of aniline in water. The final concentrations of the amines ranged from 0.03 to 0.3 *M* and since the average deviation of the 3–6 values of the molar heats of solution was less than 2%, the average value was assumed to be equal to ΔH_s^0(B). The solubilities of ϕNHMe and ϕNMe_2 in water are low so that their ΔH_s^0 values for this solvent could not be determined. Literature values of the heat of vaporization ΔH_v^0 of aniline and pyridine (6) are also given in Table 2. Since no values of ΔH_v^0 for ϕNHMe and ϕNMe_2 were available, two methods were used for their estimation. First, the heats of solution of ϕNH_2, ϕNHMe, and ϕNMe_2 were determined in CCl_4 at 25°C and extrapolated to zero concentration since there is a slight concentration effect between 0.02 and 0.06 *M*. The values are listed in Table 2. Then, it was assumed that the heat of vaporization of the three amines from dilute CCl_4 would be equal. This led to the following two ΔH_v^0 values: 52.7 kJ mol^{-1} (ϕNHMe) and 47.7 (ϕNMe_2). In the second method, ΔH_v^0 was estimated from the extrapolated linear relations between ΔH_v^0 and t_{eb} given by Wadsö (7) for aliphatic amines, since we found that the values for ϕNH_2 also obeyed this relation. The ΔH_v^0 values thus obtained were: 56.5 kJ mol^{-1} (ϕNHMe) and 52.7 (ϕNMe_2). The values reported in Table 2 are averages from both methods. Table 3 gives values of $\Delta H_{n,s}^0$ the heat of neutralization of the liquid amines by HCF_3SO_3 in Me_2SO for the reaction

$$B(l) + H^+(s) = BH^+(s)$$

These $\Delta H_{n,s}^0$ values are averages of 4 determinations, the average deviation being less than 3%. The $\Delta H_{n,s}^0$ values for the aqueous neutralization of ϕNHMe and ϕNMe_2, respectively −24.7 ± 2.1 kJ mol^{-1} and −31.4 ± 5.0 kJ mol^{-1} have uncomfortably large margins of error caused by the slow rate of reaction of these poorly soluble amines. The calculated heat of protonation of the amines $\Delta H_{p,s}^0$ for reaction

$$B(s) + H^+(s) = BH^+(s)$$

were obtained by combining ΔH_s^0(B) values from Table 2 and the previous $\Delta H_{n,s}^0$ values. These $\Delta H_{p,s}^0$ values are presented in Table 4.

TABLE 1. Ionization constants *K* of BH^+ ions at 25°C

	p*K*			
B	ϕNH_2	ϕNHMe	ϕNMe_2	Py
Me_2SO	3.72	2.76	2.51	3.45
Water	4.60[a]	4.85[a]	5.16[a]	5.17[b]

[a]Reference 8.
[b]Reference 15.

TABLE 2. Heats of solution ΔH_s^0 and heats of vaporization ΔH_v^0 of the amines B (in kJ mol^{-1} at 25°C)

	B	ϕNH_2	ϕNHMe	ϕNMe_2	Py
ΔH_s^0	Me_2SO	−9.36	−3.43	3.51	1.17
	Water	1.84			−9.70[a]
	CCl_4	9.2	5.8	1.05	
ΔH_v^0		55.6[b]	54.3	50.2	40.1[b]

[a]Reference 15.
[b]Reference 6.

TABLE 3. Heats of solution ΔH_n^0 of the amines B in 0.1 *M* HCF_3SO_3 in Me_2SO (in kJ mol^{-1} at 25°C)

B	ΔH_n^0
ϕNH_2	−40.1
ϕNHMe	−27.0
ϕNMe_2	−20.3
Py	−26.5

TABLE 4. Heats of protonation of the amines B (in kJ mol^{-1} at 25°C)

	B	ϕNH_2	$\phi NHMe$	ϕNMe_2	Py
$\Delta H^0_{p,s}$	Me_2SO	−30.8	−23.5	−23.8	−27.7
	Water	−30.1[a]			−20.3[a,b]
$\Delta H^0_{p,g}$	Gas phase	−872.8[c]	−894.5[d]	−920.0[c]	−911.7[c]

[a] Reference 16.
[b] Reference 15.
[c] Reference 12.
[d] Estimated from ref. 13.

Discussion

Considering first the ionization constants K of the conjugate acids BH^+ of aniline, N-methyl, and N,N-dimethylaniline, the data in Table 1 indicate that the addition of an N-methyl substituent lowers the anilines basicity in Me_2SO according to

$$\phi NH_2 > \phi NHMe > \phi NMe_2$$

The effect is similar to that found for the methylamines (2) where

$$MeNH_2 > Me_2NH > Me_3N$$

On the other hand the trend of the pK values in water for the three anilinium ions (8) is opposite, and this time in agreement with the expected methyl base-strengthening effect. It is then clear why the pK differences of these BH^+ ions in Me_2SO and water, $pK_s - pK_w$, increase with the number of Me substituents: −0.9 (ϕNH_3^+), −2.0 (ϕNH_2Me^+), −2.6 ($\phi NHMe_2^+$) (Table 1). Values for the pK of a large series of substituted alkylammonium ions BH^+ in Me_2SO and water (1, 2, 5) also exhibit similar trends, although the $pK_s - pK_w$ differences are less negative and change sign: +1.2 (NH_4^+), +0.4 (RNH_3^+), −0.6 ($R_2NH_2^+$), and −1.5 (R_3NH^+), the R_3NH^+ difference being close to that for PyH^+, −1.7.

The data in Tables 1 and 4 for the pK of the conjugate acids BH^+ and the enthalpy of protonation of the amines B in Me_2SO both follow the same basicity sequence

$$\phi NH_2 > Py > \phi NHMe \gtrsim \phi NMe_2$$

The implied correlation between free energy ($\Delta G^0_{i,s} = 5.68\,pK$) and enthalpy of ionization ($\Delta H^0_{i,s} = -\Delta H^0_{p,s}$) of BH^+ ions indicates an ionization entropy contribution $\Delta S^0_{i,s}$ either approximately constant or linearly related to $\Delta H^0_{i,s}$. First, we calculated $\Delta S^0_{i,s}$ and found indeed that the values varied by less than 8.3 J K^{-1} mol^{-1}. However, when we included data for alkylammonium ions (2) and plotted the pK values against $\Delta H^0_{i,s}$ (Fig. 1), we obtained a good straight line,

$$\Delta H^0_{i,s} = 6.855pK + 4.907 (r = 0.997)$$
$$\text{for } 2.5 < pK < 11.0$$

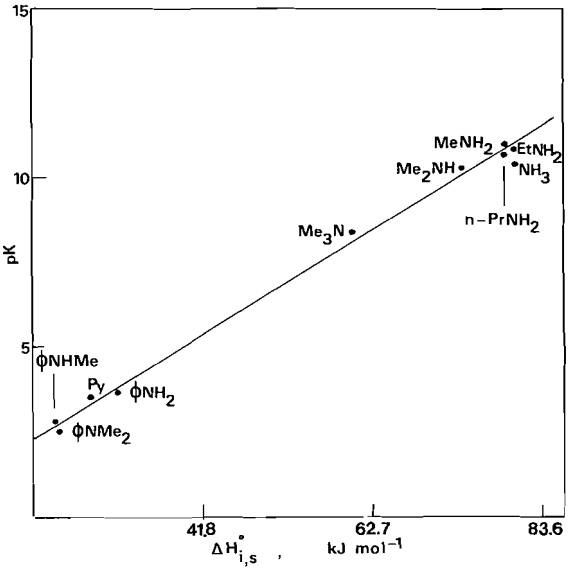

FIG. 1. Constants and enthalpies of ionization of conjugate acids of substituted amines in dimethylsulfoxide.

This is evidence of a clear enthalpy–entropy type relationship (9) since both $\Delta H^0_{i,s}$ and $pK(\Delta G^0_{i,s})$ are independently determined. We have recently found a similar relationship for HCl and 8 carboxylic acids ($2.0 < pK < 11.5$) in Me_2SO (10):

$$\Delta H^0_{i,s} = 5.43pK - 15.9 (r = 0.983)$$

while Arnett *et al.* (11) obtained

$$\Delta H^0_{i,s} = 5.64pK + 2.5 (r = 0.97)$$

for 12 weaker acids ($10 < pK < 30$) but an average slope of 7.06 for the correlation line for the deprotonation of neutral anilines and diphenylamines. Not only the slopes of the lines then depend on the class of acids but they also vary with the dipolar aprotic solvent used (10).

The basicity sequence obtained in Me_2SO

$$\phi NH_2 > Py > \phi NHMe \gtrsim \phi NMe_2$$

is at odds with the intrinsic gas phase order

$$\phi NH_2 < \phi NHMe < Py < \phi NMe_2$$

deduced from the amines proton affinity ($PA = -\Delta H^0_{p,g}$) (12, 13) listed in Table 4. This quasi-reversal of the basicity order in Me_2SO can be analyzed by using a thermodynamic cycle to relate the protonation processes in both media. The following equation is then deduced to connect both enthalpies of protonation:

$$[1]\quad \Delta H^0_{p,s} = \Delta H^0_{p,g} - \Delta H^0_s(B)_g + \Delta H^0_s(BH^+)_g - \Delta H^0_s(H^+)_g$$

with

$$\Delta H^0_s(B)_g = -\Delta H^0_v(B) + \Delta H^0_s(B)$$

TABLE 5. Heats of solution of gaseous amines B and BH^+ ions in Me_2SO (in kJ mol^{-1} at 25°C)

B	$\Delta H_s^0(B)_g$	$\Delta H_s^0(BH^+)_g$
ϕNH_2	−64.8	−377.0
$MeNH_2$[a]	−26.8	−376.6
$\phi NHMe$	−57.7	−340.7
Me_2NH[a]	−25.1	−341.9
ϕNMe_2	−46.8	−304.3
Py	−38.9	−308.9
Me_3N[a]	−19.6	−305.6

[a]Reference 2.

where $\Delta H_s^0(X)_g$ is the enthalpy of solution of gaseous X. The corresponding free energy equation could not be used here because the low volatility of the anilines made the determination of $\Delta G_s^0(B)_g$ impracticable. We calculated $\Delta H_s^0(BH^+)_g$ from eq. [1], data in Tables 4, 2 and $\Delta H_s^0(H^+)_g = -1154.1$ kJ mol^{-1} (2). The values of $\Delta H_s^0(BH^+)_g$, as well as those of $\Delta H_s^0(B)_g$ obtained from data in Table 2, are listed in Table 5. These data show conclusively that the increasing exothermicity of the gas-phase protonation in the order $\phi NH_2 < \phi NHMe < \phi NMe_2$ is reversed in Me_2SO essentially because the heat of solution of BH^+ ions becomes much less exothermic according to $\phi NH_3^+ > \phi NH_2Me^+ > \phi NHMe_2^+$. The changes in $\Delta H_s^0(B)_g$ have a small opposite effect. When comparing ϕNMe_2 and Py, the basicity reversal in Me_2SO is due to changes in both $\Delta H_s^0(BH^+)_g$ and $\Delta H_s^0(B)_g$, the latter being now more important.

We can now compare the values of $\Delta H_s^0(BH^+)_g$ for the anilinium and pyridinium ions with values for the methylammonium ions $MeNH_3^+$, $Me_2NH_2^+$, and Me_3NH^+ (2) listed in Table 5. We see that the heat of solution in Me_2SO is nearly the same for each pair of primary and secondary ammonium ions and for the three tertiary ammonium ions. This corroborates previous findings (2, 14) that the exothermic heat of solution of substituted ammonium ions $R_{4-n}NH_n^+$ decreases with the number n of N—H protons which can H-bond to the solvent, the size of the substituent R being of lesser importance. There is an interesting consequence of the closeness of the heats of solution of equally substituted ammonium ions in both methylamine and aniline series. In the gas phase, the anilines are only slightly less basic than the corresponding methylamines: for example, the proton affinity of ϕNH_2 is only 10.9 kJ mol^{-1} less than that of $MeNH_2$ (i.e. 1.8 units on the pK scale). In contrast, in Me_2SO the corresponding heats of protonation differ by 48.1 kJ mol^{-1} (i.e. 8.4 units on the pK scale), the pK's being 3.7 and 10.9 respectively (Fig. 1), so that ϕNH_2 is now a much weaker base than $MeNH_2$. Since the heat of solution of ϕNH_3^+ und $MeNH_3^+$ are nearly identical (Table 5), the 37.7 kJ mol^{-1} increase in basicity difference between ϕNH_2 and $MeNH_2$ from the gas phase to Me_2SO must come from a large difference in the heat of solution of gaseous ϕNH_2 and $MeNH_2$, and this is indeed shown by the $\Delta H_s^0(B)$ values in Table 5, −64.8 and −26.8 kJ mol^{-1} respectively. The same comparisons could be made between $\phi NHMe$ and Me_2NH on the one hand, and ϕNMe_2, Py, and NMe_3 on the other hand. We can then conclude that the much weaker basicity of the anilines and pyridine in Me_2SO when compared with that of the alkylamines comes from a much larger heat of solution of the gaseous aromatic amines. Moreover since the heats of solution of the liquid alkylamines in Me_2SO are low (2), as are also those of the aromatic amines (the most exothermic one if for ϕNH_2 probably because of H-bonding) (Table 2), we can further advance that the large increase in basicity difference between the aromatic and alkylamines, when passing from the gas phase to Me_2SO, is essentially due to the larger heat of vaporization of the aromatic amines (i.e. 55.6 kJ mol^{-1} for ϕNH_2 against 24.3 kJ mol^{-1} for $MeNH_2$).

Acknowledgement

We acknowledge support by the Natural Sciences and Engineering Research Council of Canada.

1. I. M. KOLTHOFF, M. K. CHANTOONI, JR., and S. BHOWMIK. J. Am. Chem. Soc. **90**, 23 (1968).
2. A. MUCCI, R. DOMAIN, and R. L. BENOIT. Can. J. Chem. **58**, 953 (1980).
3. R. L. BENOIT, M. RINFRET, and R. DOMAIN. Inorg. Chem. **11**, 2603 (1972).
4. R. L. BENOIT and C. BUISSON. Electrochim. Acta, **18**, 105 (1973).
5. J. COURTOT-COUPEZ and M. LE DÉMEZET. Bull. Soc. Chim. Fr. 1033 (1969).
6. J. D. COX and G. PILCHER. *In* Thermochemistry of organic and organometallic compounds. Academic Press, New York, NY. 1970.
7. I. WADSÖ. Acta Chem. Scand. **23**, 2061 (1969).
8. N. F. HALL and M. R. SPRINKLE. J. Am. Chem. Soc. **54**, 3469 (1932).
9. O. EXNER. Collect. Czech. Chem. Commun. **38**, 799 (1973).
10. A. RAKSHIT. Unpublished work.
11. E. M. ARNETT, T. C. MORIARITY, L. E. SMALL, J. P. RUDOLPH, and R. P. QUICK. J. Am. Chem. Soc. **95**, 1492 (1973).
12. P. KEBARLE. Ann. Rev. Phys. Chem. **28**, 445 (1977).
13. Y. K. LAU, P. P. S. SALUJA, P. KEBARLE, and R. W. J. ALDER. J. Am. Chem. Soc. **100**, 7328 (1978).
14. R. W. TAFT, M. TAAGEPERA, K. D. SUMMERHAYS, and J. MITSKY. J. Am. Chem. Soc. **95**, 3811 (1973).
15. L. SACCONI, P. PAOLETTI, and M. CIAMPOLINI. J. Am. Chem. Soc. **82**, 3828 (1960).
16. J. J. CHRISTENSEN, R. M. IZATT, D. P. WRATHALL, and L. D. HANSEN. J. Chem. Soc. A, 1212 (1969).

Nuclear magnetic resonance studies of the solution chemistry of metal complexes. XVII. Formation constants for the complexation of methylmercury by sulfhydryl-containing amino acids and related molecules

R. Stephen Reid and Dallas L. Rabenstein[1]

Department of Chemistry, University of Alberta, Edmonton, Alta., Canada T6G 2G2

Received August 26, 1980

This paper is dedicated to Professor W. E. Harris on the occasion of his retirement from the University of Alberta

R. Stephen Reid and Dallas L. Rabenstein. Can. J. Chem. **59**, 1505 (1981).

Complexation of methylmercury, $CH_3Hg(II)$, by mercaptoacetic acid, mercaptoethanol, mercaptosuccinic acid, cysteine, penicillamine, homocysteine, and *N*-acetylpenicillamine has been studied by ^1H nuclear magnetic resonance spectroscopy. The equilibrium constant for displacement of mercaptoacetic acid from its $CH_3Hg(II)$ complex by each of the other thiols was measured over a wide range of pH. From the displacement constants and a literature value for the formation constant of the mercaptoethanol complex of $CH_3Hg(II)$, formation constants were calculated for thiol complexes with the other ligands, including microscopic formation constants for cysteine and penicillamine complexes in which the amino groups are protonated and deprotonated. Detailed information on the acid–base chemistry of the free amino and carboxylic acid groups in the complexes is also reported. The formation constants increase as the Brønsted basicity of the deprotonated sulfhydryl group increases according to the relation $\log K_f = pK + 6.86$. The conditional formation constants of the $CH_3Hg(II)$ complexes are strongly pH dependent due to competitive reactions involving hydrogen and hydroxide ions at low and high pH. The results at physiological pH are discussed with reference to the effectiveness of mercaptosuccinic acid, *N*-acetylpenicillamine, and penicillamine as antidotes for methylmercury poisoning.

R. Stephen Reid et Dallas L. Rabenstein. Can. J. Chem. **59**, 1505 (1981).

Utilisant la spectroscopie de rmn du ^1H, on a étudié la complexation du méthylmercure, $CH_3Hg(II)$, par l'acide mercaptoacétique, le mercaptoéthanol, l'acide mercaptosuccinique, la cystéine, la pénicillamine, l'homocystéine et la *N*-acétylpénicillamine. Dans un large intervalle de pH, on a mesuré la constante d'équilibre de la réaction de déplacement de l'acide mercaptoacétique de son complexe avec le $CH_3Hg(II)$ par chacun des autres thiols. En utilisant les constantes de déplacement et les données de la littérature relatives à la constante de formation du complexe de $CH_3Hg(II)$ avec le mercaptoéthanol, on a calculé les constantes de formation des complexes de thiol avec d'autres ligands en incluant les constantes de formation microscopiques des complexes de la cystéine et de la pénicillamine dans lesquels les groupes amino sont protonés et déprotonés. On rapporte également une information détaillée de la chimie acide–base des groupes carboxyliques libres de ces complexes. Les constantes de formation augmentent avec la basicité de Brønsted du groupe sulfhydryle déprotonée selon l'équation: $\log K_f = pK + 6{,}86$. Les constantes de formation conditionnelle des complexes de $CH_3Hg(II)$ dépendent fortement du pH à cause des réactions compétitives qui font intervenir les ions hydrogènes et hydroxyles aux pH faible et élevé. On discute des résultats au pH physiologique dans le but d'évaluer l'efficacité de l'acide mercaptosuccinique, de la *N*-acétylpénicilline et de la pénicillamine comme antidotes lors d'empoisonnement par le méthylmercure.

[Traduit par le journal]

Introduction

Mercury ions bind strongly to sulfur donor groups. For example, methylmercury(II) ($CH_3Hg(II)$) binds preferentially to the sulfhydryl group of amino acids and small peptides from $pH < 1$ to >13 (1, 2). Since the toxicity of mercury results from the formation of such complexes, a good understanding of their solution chemistry is desirable. Surprisingly, however, detailed stability data are sparse, due possibly to the difficulty in measuring such large stability constants. Schwarzenbach and Schellenberg (3) measured the formation constant of the $CH_3Hg(II)$–mercaptoethanol complex potentiometrically, using competition with iodide to lower the equilibrium constant into a measurable range. Simpson (4) estimated formation constants for the $CH_3Hg(II)$ complexes of cysteine and glutathione by means of halide competition and toluene extraction.

This paper reports formation constants for the $CH_3Hg(II)$ complexes of several thiol and amino acids of biological and pharmaceutical interest. The formation constants have been measured by allowing two thiols, RSH and R′SH, to compete for $CH_3Hg(II)$.

$$RSHgCH_3 + R'S^- \overset{K_d}{\rightleftharpoons} RS^- + R'SHgCH_3$$

K_d has been determined from ^1H nmr chemical shift data. Since two thiols are competing for the $CH_3Hg(II)$, K_d is relatively small and the equilibrium position can be measured precisely. Mercaptoacetic acid (MAA), which displays only a single ^1H resonance in aqueous solution, is used as one of the thiols throughout in competition experiments with mercaptoethanol (ME), penicillamine (PSH), *N*-

[1]To whom all correspondence should be addressed.

0008-4042/81/101505-10$01.00/0

©1981 National Research Council of Canada/Conseil national de recherches du Canada

Can. J. Chem. Downloaded from www.nrcresearchpress.com by 210.87.254.42 on 09/06/12
For personal use only.

Can. J. Chem. Downloaded from www.nrcresearchpress.com by 210.87.254.42 on 09/06/12
For personal use only.

acetylpenicillamine (NPSH), cysteine (CYS), homocysteine (HCYS), and mercaptosuccinic acid (MSA). The formation constant for the mercaptoacetic acid complex is obtained from the K_d for the competition experiment with mercaptoethanol and the formation constant for the mercaptoethanol complex (3). Formation constants for the other complexes are then obtained from competition experiments with the other thiols. Various other parameters, including acid dissociation constants for $CH_3Hg(II)$-complexed species, are obtained simultaneously. The characterization of the solution chemistry of the complex is then complete, and the apparent thiol affinity for $CH_3Hg(II)$ can be predicted at any pH.

Experimental

Chemicals

Mercaptoethanol, mercaptoacetic acid (Eastman Kodak Co.), cysteine, penicillamine, 2-mercaptosuccinic acid (Aldrich Chem. Co.), *N*-acetylpenicillamine (Sigma Chem. Co.), and homocysteine (Nutritional Biochemicals Corp.) were used as received. The determination of purity and preparation of solutions is described below.

Methylmercury(II) iodide (Alfa Division, Ventron Corp.) was converted to a solution of methylmercury(II) hydroxide by reaction with silver oxide. In a typical preparation, 0.100 mol of Ag_2O was reacted with 0.022 mol of CH_3HgI in 50 mL of water. Since Ag_2O is sparingly soluble in water, the more water-insoluble CH_3HgI was used in slight excess to ensure no silver contamination of the product solution. After stirring for 10 h, the solution was vacuum filtered through paper and then through a 0.2 μm Nalgene millipore filter (Nalge Sybron Corp.), and diluted to volume in a 100 mL volumetric flask. The solution was standardized with respect to $CH_3Hg(II)$ by titration with chloride (1). The conversion of CH_3HgI to CH_3HgOH was quantitative with respect to the equivalents of silver ion added. Because of the toxicity of $CH_3Hg(II)$, this concentrated stock solution was opened only in the fumehood, and handled with gloves.

Iodoacetamide (Aldrich Chem. Co., Sigma Chem. Co.) was used as received. All other chemicals were reagent grade and were used without further purification. Water used in making solutions was doubly distilled and deionized by passage through a Barnstead D8902 Ultrapure mixed bed ion-exchange resin.

pH Measurements

All pH measurements were made at 25 ± 1°C with an Orion Model 701 digital pH meter, equipped with either a standard glass electrode – porous ceramic junction reference electrode pair, or a microcombination electrode. Fisher certified buffers of nominal pH values 4.00, 7.00, and 10.00 were used for three-point calibration of the pH meter. The exact pH of each of these buffers was established, and periodically checked, by comparison with freshly prepared N.B.S. pH standard solutions (5).

^1H Nuclear Magnetic Resonance Measurements

^1H nmr spectra were obtained on a Varian A60D spectrometer at a probe temperature of 25 ± 1°C. Spectra were recorded at a sweep rate of 0.1 Hz s^{-1}. Chemical shifts were measured relative to either the central resonance of the triplet for the tetramethylammonium ion or the singlet for 1,4-dioxane. A small amount of the reference compound was added to solutions before pH adjustments. Chemical shifts are reported relative to the methyl resonance of sodium 2,2-dimethyl-2-silapentane-5-sulphonic acid (DSS). Positive shifts correspond to resonances of protons less shielded than the methyl protons of DSS.

Solution Preparation

(i) Thiol solutions. Procedures used for preparation of thiol solutions were designed to minimize oxidation of the sulfhydryl group. Na_2H_2EDTA was added to freshly deionized water to a concentration of 2×10^{-5} *M*. The solution was purged with argon, and then thiol was added in an amount to give a concentration of ~0.3 *M*. When necessary, the final pH was adjusted to <7 by the addition of nitric acid. With the exception of *N*-acetylpenicillamine, the thiols are all readily soluble at the 0.3 *M* level. To attain this concentration with *N*-acetylpenicillamine, the pH was repeatedly increased to ~6 following the addition of small amounts of *N*-acetylpenicillamine. After filling the air space with argon, the flasks were stoppered and stored at 4°C. Under these conditions, the thiols appeared to show little oxidation with time, as determined by the iodoacetamide procedure described below (6). Homocysteine, the least stable, showed only slight oxidation after 2 days. At the other extreme, mercaptoacetic acid showed no measurable loss of thiol content over a period of 4 months.

The thiol content of the stock solutions was determined by reaction of the thiol with iodoacetamide, followed by reaction of the protons displaced from the thiol group with strong base (6). For the concentration of protons displaced and titrated to equal the concentration of sulfhydryl group, the initial and final pH must be the same, and also low enough to ensure that the thiol is quantitatively in the RSH form. However, to obtain precise endpoints, the pH should also be in a region where buffering does not occur. To illustrate, details will be given here for standardization of mercaptoacetic acid solutions. Since the p*K*'s of the carboxyl and sulfhydryl groups of MAA are 3.50 and 10.08, the above conditions are satisfied at pH 7. So that reaction would occur in a reasonable time, the pH was raised to approximately 9 midway through the reaction. pH adjustments were followed and endpoints located by color matching using mixtures of phenolphthalein and bromothymol blue. This mixture of indicators is yellow at low pH, through green at pH 7 to blue, and then purple above pH 9. The mixture of indicators was added to water, the solution purged with argon for 5 min, and an aliquot of the MAA stock solution added. The solution was brought to pH 7. Iodoacetamide (0.2 g in 5 mL of water) was added to the flask, followed by a measured amount of standardized base to raise the pH to 9. As reaction proceeded and the pH decreased, more base was added to maintain the pH at 9. When reaction was complete (generally after 2 min), the solution was titrated back to pH 7 with standardized acid. Three or four replicate titrations were normally done, with a precision of 5 ppt or better.

This procedure gave satisfactory results for mercaptoacetic acid and mercaptosuccinic acid. For ligands with a sulfhydryl p*K* below 10, a similar procedure employing an initial and final pH of 5 and a methyl red/phenolphthalein indicator system was used. For all standardizations, a blank titration was performed.

(ii) Solutions for pK measurements. In cases where no literature p*K* values were available, or where those available were considered questionable, they were determined by ^1H nmr. Solutions were 0.05–0.10 *M* in the compound of interest, and the ionic strength was brought to 0.3 *M* by adding KNO_3. Typically, 10 to 30 mL of solution were prepared under argon, and the pH was adjusted to the highest value desired with KOH. Solution (0.3 mL) was then trans-

TABLE 1. Acid dissociation constants for the thiol ligands[a,b,c]

Ligand	Acid group	Acid dissociation constant	pK	Reference
Mercaptoacetic acid	CO_2H	K_1	3.50±0.01	[d]
	SH	K_2	10.08±0.02	[d]
Mercaptoethanol	SH	K_1	9.62	15
N-Acetylpenicillamine	CO_2H	K_1	3.33	16
	SH	K_2	10.19	16
Penicillamine	CO_2H	K_1	1.94	14
	NH_3^++SH	K_2[e]	7.93	14
	NH_3^++SH	K_3[e]	10.39	14
	SH	k_{12}[f]	8.05	14
	NH_3^+	k_{13}[f]	8.61	14
	NH_3^+	k_{123}[f]	10.29	14
	SH	k_{132}[f]	9.70	14
Cysteine	CO_2H	K_1	1.93	17
	NH_3^++SH	K_2[e]	8.22	18
	NH_3^++SH	K_3[e]	10.25	18
	SH	k_{12}[f]	8.38	18
	NH_3^+	k_{13}[f]	8.73	18
	NH_3^+	k_{123}[f]	10.09	18
	SH	k_{132}[f]	9.74	18
Homocysteine	CO_2H	K_1	2.27±0.02	[d]
	NH_3^++SH	K_2[e]	8.66	19
	NH_3^++SH	K_3[e]	10.55	19
Mercaptosuccinic acid	CO_2H	K_1	3.13	20
	CO_2H	K_2	4.63	20
	SH	K_3	10.26	20

[a]25°C and 0.3 *M* ionic strength.
[b]Literature values were recalculated to an ionic strength of 0.3 *M* using the Davies equation (7).
[c]Mixed constants: a_{H^+} and concentration of acid and its conjugate base.
[d]This work.
[e]Composite macroscopic constants due to simultaneous dissociation of the NH_3^+ and SH groups over the same pH region. See Fig. 4.
[f]Microscopic constants as defined in Fig. 4.

ferred to an nmr tube, and the tube was flushed with argon before being capped. Nitric acid was then added to adjust the pH, and the next sample removed. Following each adjustment of pH, the approximate ionic strength was calculated, and KNO_3 or distilled water added as necessary to restore the ionic strength to 0.3 *M*.

(iii) Solutions for formation constant measurements. The main requirement in preparing solutions for the formation constant determinations was that the relative amounts of MAA, $CH_3Hg(II)$, and competing thiol be known. Usually the mole ratio was 1:1:1. The procedure followed was to first prepare a MAA–$CH_3Hg(II)$ solution having an exact 1:1 stoichiometry, and then to add the desired amount of competing thiol stock solution. The 1:1 stoichiometry for the MAA–$CH_3Hg(II)$ solution was achieved with an nmr titration procedure. Sufficient MAA stock solution to make the final solution 0.07 *M* in MAA was transferred to a beaker. An amount of $CH_3Hg(II)$ stock solution corresponding to 99% of the MAA was then added, the volume adjusted with water, and the pH increased to ~12 with base. A 0.3 mL sample was transferred to an nmr tube. The additional amount of $CH_3Hg(II)$ solution necessary to give a 1:1 stoichiometry was calculated from the chemical shift of the MAA singlet resonance, which is the weighted average of that for the free and the complexed MAA due to rapid ligand exchange. The competing thiol ligand was then added and samples for ^1H nmr measurements were withdrawn as the pH was lowered with nitric acid. To maintain a reasonably constant ionic strength, the necessary amount of KNO_3 was added to give an initial ionic strength of 0.40 *M*. The nitric acid solution used for pH adjustment was 0.3 *M* in KNO_3. Calculations indicate that the ionic strength remained between 0.4 and 0.25 *M*. Activity coefficients, as estimated by the Davies equation (7), vary only slightly in this ionic strength range.

Results

Determination of Acid Dissociation Constants

Reliable literature values were available for the acid dissociation constants of most of the ligands. Ionic strength corrections to the present conditions were made using the Davies equation (7). The values so obtained are listed in Table 1.

Because of the lack of agreement among literature values for MAA (8–11) and the central nature of MAA to this work, its acid dissociation constants were redetermined. The equilibria and associated constants are:

[1] $HSCH_2CO_2H \rightleftarrows HSCH_2CO_2^- + H_3O^+$

Can. J. Chem. Downloaded from www.nrcresearchpress.com by 210.87.254.42 on 09/06/12
For personal use only.

Can. J. Chem. Downloaded from www.nrcresearchpress.com by 210.87.254.42 on 09/06/12
For personal use only.

$$[2] \quad K_1 = \frac{[HSCH_2CO_2^-]a_{H_3O^+}}{[HSCH_2CO_2H]}$$

$$[3] \quad HSCH_2CO_2^- \rightleftarrows {}^-SCH_2CO_2^- + H_3O^+$$

$$[4] \quad K_2 = \frac{[{}^-SCH_2CO_2^-]a_{H_3O^+}}{[HSCH_2CO_2^-]}$$

K_1 and K_2 are mixed concentration–activity constants, as are all the other constants listed in Table 1. Proton exchange involving the various MAA species is rapid on the nmr time scale. The chemical shift of the exchange-averaged resonance is the weighted average of the chemical shifts of the various species:

$$[5] \quad \delta_{obs} = P_1\delta_1 + P_2\delta_2 + P_3\delta_3$$

where δ_{obs} is the observed chemical shift, δ_1, δ_2, and δ_3 the chemical shifts, and P_1, P_2, P_3 the fractional concentrations of $HSCH_2CO_2H$, $HSCH_2CO_2^-$, and ${}^-SCH_2CO_2^-$ respectively. P_1, P_2, and P_3 can be expressed in terms of K_1 and K_2, which leads to:

$$[6] \quad \delta_{obs} = (a_{H^+}{}^2\delta_1 + a_{H^+}K_1\delta_2 + K_1K_2\delta_3)/D$$

where $D = a_{H^+}{}^2 + a_{H^+}K_1 + K_1K_2$. δ_1, δ_2, and δ_3 were determined by inspection from Fig. 1*A*. K_1 and K_2 were obtained by fitting chemical shift vs. pH data for MAA to eq. [6] using the nonlinear least-squares curve fitting program KINET (12). Satisfactory correlations were observed in this and all cases discussed. The results for MAA are listed in Table 1. For comparison, literature values are: $pK_1 = 3.40$ and $pK_2 = 10.07$ (8); $pK_1 = 3.53$ (9); $pK_1 = 3.27$, $pK_2 = 10.05$ (10); and $pK_1 = 3.53$ and $pK_2 = 10.40$ (11).

The acid dissociation constant for the carboxylic acid group of homocysteine (K_1 in Table 1) was measured since no literature value was available. The method used was similar to that for MAA, except that the system was treated as a monoprotic acid since dissociation of the carboxylic acid group is essentially complete before dissociation of the sulfhydryl and ammonium groups begins. The resonance pattern for the methine proton on the α carbon was used.

Acid dissociation constants were also determined for the carboxylic and ammonium groups of the sulfhydryl-complexed ligands. To distinguish them from acid dissociation constants for the free ligands, they are primed, e.g. K_1'. In most cases, these constants were obtained from the formation constant studies, as described below. The exceptions are the acid dissociation constants for the carboxylic groups of CH_3Hg(II)-complexed MAA and *N*-acetylpenicillamine, which were determined directly from the exchange-averaged chemical shifts of ligand resonances. For the MAA complex, the resonance

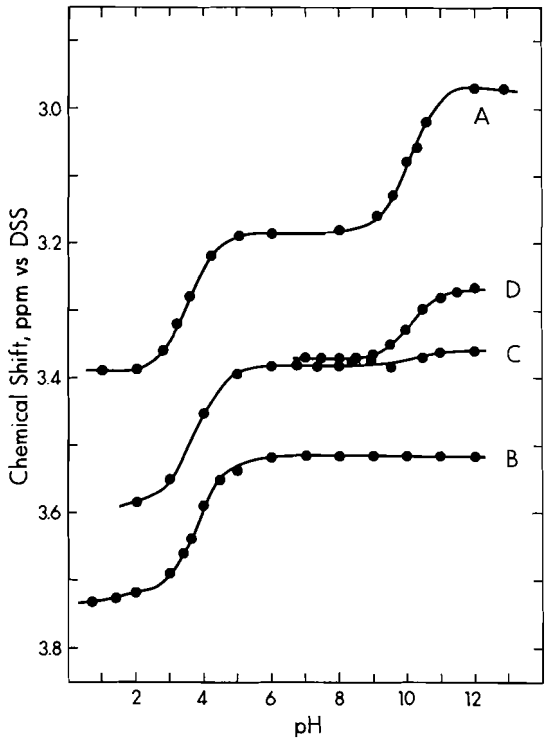

FIG. 1. pH dependence of the chemical shift of mercaptoacetic acid (MAA) in solutions containing (*A*) 0.10 *M* MAA, (*B*) 0.10 *M* MAA and 0.10 *M* CH_3Hg(II), (*C*) 0.10 *M* MAA, 0.10 *M* CH_3Hg(II), and 0.10 *M* mercaptoethanol, and (*D*) 0.10 *M* MAA, 0.10 *M* CH_3Hg(II), and 0.10 *M* *N*-acetylpenicillamine. 0.25–0.4 *M* ionic strength and 25°C. The solid curves are theoretical curves calculated from formation constants determined in this work. Approximately one-half the experimental points are shown.

for the methylene protons of MAA was used; for the *N*-acetylpenicillamine complex, the chemical shift separation between the resonances for the nonequivalent methyl groups of *N*-acetylpenicillamine was used. Results are reported in Table 2.

Determination of Formation Constants

Formation constants for the CH_3Hg(II)–thiol complexes were determined from the exchange-averaged chemical shift measured over a wide range of pH values, of the MAA resonance in solutions containing MAA, CH_3Hg(II), and the various thiols. For example, chemical shift data are shown in Fig. 1 for the methylene protons of MAA in (*A*) a solution containing only free MAA, (*B*) a solution containing the CH_3Hg(II)–MAA complex, and (*C*) a solution containing MAA, CH_3Hg(II), and mercaptoethanol in a 1:1:1 ratio. Throughout the entire pH range, curve *C* lies between curves *A* and *B*, indicating displacement of some of the complexed MAA by ME and fast exchange of the MAA between its free and complexed forms. Also, the position of

Can. J. Chem. Downloaded from www.nrcresearchpress.com by 210.87.254.42 on 09/06/12
For personal use only.

TABLE 2. Acid dissociation constants for methylmercury(II)-complexed thiols[a]

Complex	Acid group	Acid dissociation constant	pK'
$CH_3HgSCH_2CO_2H$	CO_2H	K_1'	3.80±0.01
$CH_3CONHCH(CH_3)(SHgCH_3)CO_2H$	CO_2H	K_1'	3.10±0.07
$^+H_3NCH(CH_3)(SHgCH_3)CO_2H$	CO_2H	K_1'	2.33±0.05
	NH_3^+	K_2'	8.14±0.01
$^+H_3NCH(CH_2SHgCH_3)CO_2H$	CO_2H	K_1'	2.44±0.08
	NH_3^+	K_2'	8.80±0.02
$^+H_3NCH(CH_2CH_2SHgCH_3)CO_2H$	CO_2H	K_1'	2.26±0.06
	NH_3^+	K_2'	9.12±0.02
$HO_2CCH(SHgCH_3)CH_2CO_2H$	CO_2H	K_1'	3.53±0.03
	CO_2H	K_2'	4.85±0.02

[a]25°C and 0.3 *M* ionic strength.

curve *C* relative to curves *A* and *B* is pH-dependent, indicating that the relative affinities of MAA and ME for $CH_3Hg(II)$ are pH-dependent.

The calculation procedure will be illustrated for the general case with the competing thiol RSH. At high pH, the ligand exchange reaction is

$$[7] \quad RS^- + CH_3HgSCH_2CO_2^- \rightleftarrows RSHgCH_3 + {}^-SCH_2CO_2^-$$

for which we define a displacement constant

$$[8] \quad K_d = \frac{[RSHgCH_3][{}^-SCH_2CO_2^-]}{[RS^-][CH_3HgSCH_2CO_2^-]} = \frac{K_{f,RSH}}{K_{f,MAA}}$$

where

$$[9] \quad K_{f,RSH} = \frac{[CH_3HgSR]}{[CH_3Hg^+][RS^-]}$$

$$[10] \quad K_{f,MAA} = \frac{[CH_3HgSCH_2CO_2^-]}{[CH_3Hg^+][{}^-SCH_2CO_2^-]}$$

K_d does not depend upon $[CH_3Hg^+]$, and thus the changes in speciation of $CH_3Hg(II)$ in solution with pH (13) need not be considered. For systems having a MAA:$CH_3Hg(II)$:RSH mole ratio of 1:1:1, substitution of eqs. [9], [10], and the acid dissociation constant expressions for the various acidic groups into eq. [8], yields the equation

$$[11] \quad K_d = \left(\frac{P_f}{1 - P_f}\right)^2 \frac{\alpha_1\alpha_3}{\alpha_2\alpha_4}$$

where P_f is the fraction of MAA present in the free, uncomplexed form, α_1 is the fraction of this MAA in the fully deprotonated form ($= K_1K_2/(a_{H^+}{}^2 + a_{H^+}K_1 + K_1K_2)$), α_2 is the fraction of $CH_3Hg(II)$-complexed MAA present in the $CH_3HgSCH_2CO_2^-$ form ($= K_1'/(a_{H^+} + K_1')$), α_3 is the fraction of the complexed RSH in the fully deprotonated form, and α_4 is the fraction of the free RSH in the fully deprotonated form. Equations for α_3 and α_4 for the various competing thiols are given below.

P_f was determined over a range of pH values from the exchange-averaged chemical shift of the MAA methylene resonance, whose observed chemical shift, δ_{obs}, is given by

$$[12] \quad \delta_{obs} = \delta_f P_f + (1 - P_f)\delta_c$$

δ_f and δ_c are the chemical shifts of the free and complexed forms. Rearrangement of eq. [12] gives

$$[13] \quad P_f = \frac{\delta_{obs} - \delta_c}{\delta_f - \delta_c}$$

P_f was calculated at each sample pH using δ_{obs} and calculated values for δ_f and δ_c. In these calculations, K_1, K_2, and K_1' for MAA and the $CH_3Hg(II)$–MAA complex were set equal to the values determined above. K_d and any unknown acid dissociation constants for the $CH_3Hg(II)$-complexed form of the competing thiol were then calculated by fitting the P_f vs. pH data to eq. [11] using the non-linear least-squares curve fitting program KINET (12). $K_{f,RSH}$ was calculated from K_d using the relation $K_{f,RSH} = K_{f,MAA}K_d$.

$K_{f,MAA}$ was calculated from K_d for the MAA–$CH_3Hg(II)$–mercaptoethanol system, using the value reported by Schwarzenbach and Schellenberg for $K_{f,mercaptoethanol}$ (3). For the mercaptoethanol system, $\alpha_3 = 1$ and $\alpha_4 = K_1/(a_{H^+} + K_1)$ where K_1 is the acid dissociation constant for mercaptoethanol. K_d is calculated to be 0.16 ± 0.01 from the data in Fig. 1*C*. The formation constant calculated for the MAA complex is listed in Table 3. The quality of the fit can be judged by the agreement between the experimental points of Fig. 1*C* and the smooth curve,

Can. J. Chem. Downloaded from www.nrcresearchpress.com by 210.87.254.42 on 09/06/12
For personal use only.

TABLE 3. Formation constants for methylmercury(II)–thiol complexes[a]

Ligand	log K_f
$^-SCH_2CH_2OH$	16.12[b]
$^-SCH_2CO_2^-$	16.92
$CH_3CONHCH(CH_2SCH_3)CO_2^-$	16.76
$H_2NCH(CH_2SC(CH_3)_2)CO_2^-$	16.94
$^+H_3NCH(CH_2SC(CH_3)_2)CO_2^-$	14.79
$H_2NCH(CH_2SH)CO_2^-$	16.67
$^+H_3NCH(CH_2SH)CO_2^-$	15.38
$H_2NCH(CH_2CH_2SH)CO_2^-$	16.45
$^-O_2CCH(CH_2SH)CH_2CO_2^-$	17.31

[a]25°C and 0.3 *M* ionic strength.
[b]Reference 3.

which was calculated using the derived formation constant.

Chemical shift vs. pH data for the competition experiment with *N*-acetylpenicillamine are shown in Fig. 1*D*. Samples were prepared over the pH region 12 to 1.5. However, as the pH was lowered from 12, the MAA resonance became very broad due to relatively slow exchange of MAA between its free and complexed forms in this region. Below pH 7, no signal was observed. Since the amide group of *N*-acetylpenicillamine is nonbasic, the molecule has only two ionizable groups. Its acid–base scheme is therefore identical to that of MAA, differing only in the values of the dissociation constants. However, since at pH 7 the carboxylic acid group is fully deprotonated in the free and bound forms, the data above pH 7 can be fitted to the same scheme as used for the mercaptoethanol system. Non-linear least-squares calculations yielded $K_d = 0.70 \pm 0.02$, from which the formation constant listed in Table 3 for the *N*-acetylpenicillamine complex was calculated.

Chemical shift vs. pH data for the penicillamine system are shown in Fig. 2*C*. Penicillamine is a triprotic acid, whose acid–base chemistry is further complicated by the dissociation of the sulfhydryl and ammonium groups over approximately the same pH range (14). A full description of its acid–base chemistry at the molecular level requires the use of microconstants (Fig. 3); however the definition of K_d in eq. [7] is in terms of fully-deprotonated species, which can be calculated using the macroscopic acid dissociation constants K_1, K_2, and K_3 for PSH. Thus α_3 in eq. [11] is $K_1K_2K_3/(a_{H^+}{}^3 + K_1a_{H^+}{}^2 + K_1K_2a_{H^+} + K_1K_2K_3)$. The $CH_3Hg(II)$ complex of

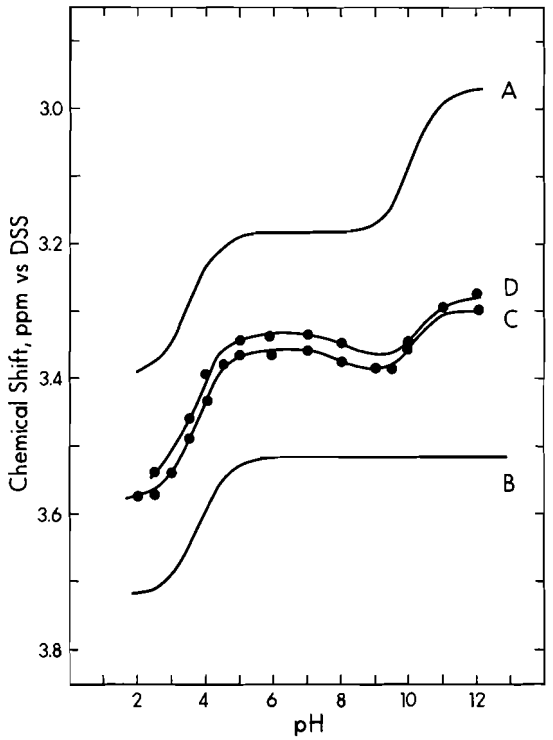

FIG. 2. pH dependence of the chemical shift of MAA in solutions containing (*A*) 0.10 *M* MAA, (*B*) 0.10 *M* MAA and 0.10 *M* $CH_3Hg(II)$, (*C*) 0.10 *M* MAA, 0.10 *M* $CH_3Hg(II)$, and 0.10 *M* penicillamine, and (*D*) 0.10 *M* MAA, 0.10 *M* $CH_3Hg(II)$, and 0.10 *M* cysteine. 0.25–0.4 *M* ionic strength and 25°C. Approximately one-half the experimental points are shown.

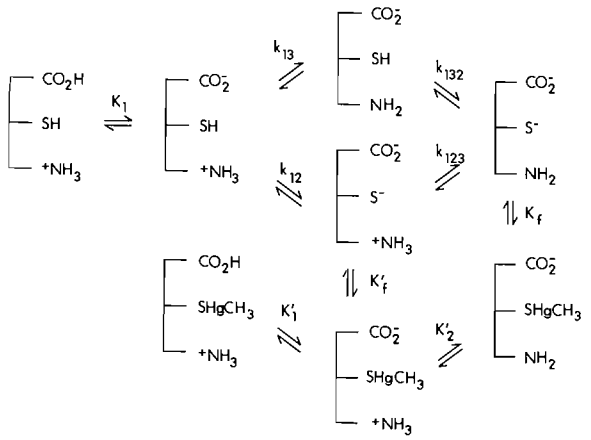

FIG. 3. Microscopic acid–base and complexation equilibria for cysteine and penicillamine in solutions containing $CH_3Hg(II)$.

PSH has two acidic groups. Assigning K_1' and K_2' respectively to the carboxylic acid and ammonium groups $\alpha_4 = K_1'K_2'/(a_{H^+}{}^2 + K_1'a_{H^+} + K_1'K_2')$. K_d, K_1', and K_2' were obtained by fitting the data in Fig. 2*C* to eq. [11]. The value obtained for $K_d = 1.06 \pm 0.02$; those obtained for K_1' and K_2' are listed in Table 2. The formation constant calculated for the $CH_3Hg(II)$ complex with the fully deprotonated form of PSH is listed in Table 3. Using this value for K_f, the value for K_2' in Table 2 and the value in Table 1 for the microscopic acid dissociation constant k_{123}, the microscopic formation constant listed in Table 3 for the complexation of $CH_3Hg(II)$ by the amino protonated form of penicillamine (K_f') was calculated with the relation $K_f' = k_{123}K_f/K_2'$.

Data for the cysteine, homocysteine, and mercaptosuccinic acid systems are presented in Figs. 2*D*, 4*C*, and 4*D*, respectively. The acid–base chemistry of the free forms of each of these ligands and their $CH_3Hg(II)$ complexes can be described by the same macroscopic dissociation schemes as for PSH and its $CH_3Hg(II)$ complex. Thus α_3 and α_4 are defined as for the PSH system. Fitting of the data in Figs. 2*D*, 4*C*, and 4*D* yielded $K_d = 0.57 \pm 0.01$, 0.34 ± 0.005, and 2.50 ± 0.06 for the cysteine, homocysteine, and mercaptosuccinic acid systems and the values listed in Table 2 for K_1' and K_2'. The values calculated for K_f for each of the complexes with the fully deprotonated ligands are given in Table 3.

The microscopic formation constant K_f' listed in Table 3 for complexation of $CH_3Hg(II)$ by the amino-protonated form of cysteine was calculated as described above for the penicillamine complex. K_f' could not be calculated for the analogous homocysteine complex because microscopic acid dissociation constants are not available for homocysteine.

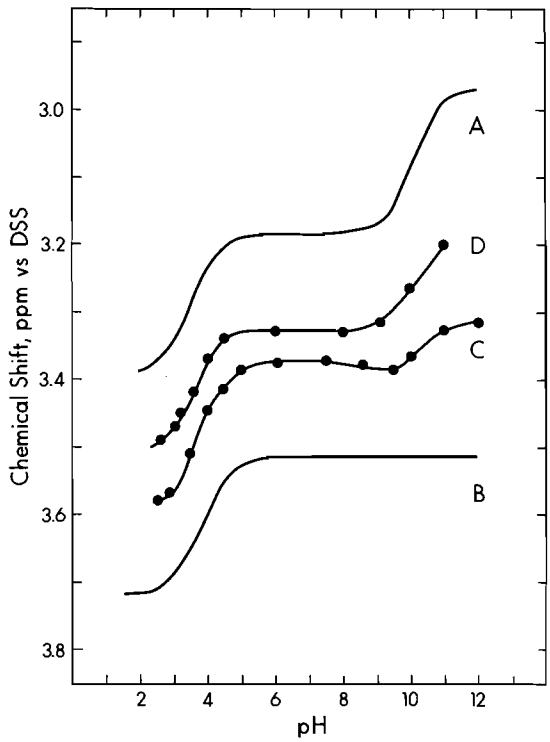

FIG. 4. pH dependence of the chemical shift of MAA in solutions containing (*A*) 0.1 *M* MAA, (*B*) 0.10 *M* MAA and 0.10 *M* $CH_3Hg(II)$, (*C*) 0.10 *M* MAA, 0.10 *M* $CH_3Hg(II)$, and 0.10 *M* homocysteine, and (*D*) 0.10 *M* MAA, 0.10 *M* $CH_3Hg(II)$, and 0.10 *M* mercaptosuccinic acid. 0.25–0.4 *M* ionic strength at 25°C. Approximately one-half the experimental points are shown.

Discussion

The thiol ligands studied contain various combinations of carboxylate, amino, and sulfhydryl groups, all of which can complex $CH_3Hg(II)$. Most of these ligands can form chelate complexes; however, the mercury in $CH_3Hg(II)$ has a strong tendency towards linear two-coordination (2). The complexation of $CH_3Hg(II)$ by these ligands is therefore considered to involve binding to a single donor group. Since previous experiments have shown that the sulfhydryl group binds $CH_3Hg(II)$ most strongly over the pH range <1 to >13 (1, 2) and since the competition experiments were performed with a thiol to $CH_3Hg(II)$ stoichiometry of 2:1, we can assume that only sulfhydryl complexes are formed. Crystallographic studies have shown the $CH_3Hg(II)$ in $CH_3Hg(II)$–cysteine and $CH_3Hg(II)$–penicillamine complexes of 1:1 stoichiometry to be bonded to the deprotonated sulfhydryl group (21, 22).

The acid dissociation constants for the ammonium and carboxylic acid groups of the $CH_3Hg(II)$-complexed ligands (Table 2) show no trend due to

Can. J. Chem. Downloaded from www.nrcresearchpress.com by 210.87.254.42 on 09/06/12
For personal use only.

Can. J. Chem. Downloaded from www.nrcresearchpress.com by 210.87.254.42 on 09/06/12
For personal use only.

$CH_3Hg(II)$ complexation. For example, complexation of the sulfhydryl groups of mercaptoacetic acid, penicillamine, cysteine, and mercaptosuccinic acid causes a decrease in the acidity of the carboxylic acid group, whereas complexation of the sulfhydryl groups of *N*-acetylpenicillamine and homocysteine causes, respectively, an increase and no change in the acidity of their carboxylic acid groups. The acid dissociation constants for the ammonium groups of the sulfhydryl complexed forms of both cysteine and penicillamine are closer to k_{13} than to k_{123} in the microscheme shown in Fig. 4. This was also found for the analogous trimethyllead(IV) ($(CH_3)_3Pb(IV)$) complexes of these ligands (15). It appears that, when complexed to the sulfhydryl group, both $CH_3Hg(II)$ and $(CH_3)_3Pb(IV)$ closely mimic a similarly bonded hydrogen ion, in terms of their effect on the acid strength of neighboring ammonium groups.

Although the $CH_3Hg(II)$ is bonded to the deprotonated sulfhydryl group in each of the complexes, formation constants listed in Table 3 cover a range of values. The plot of log K_f vs. pK of the thiol group in Fig. 5 clearly shows the Brønsted basicity of the deprotonated sulfhydryl group to be a major factor in determining the magnitude of the formation constant. From the results in Fig. 5, which also include formation constants for $CH_3Hg(II)$ complexes of fully deprotonated glutathione (h) and amino-protonated glutathione (i), the relation between formation constant and acid dissociation constant is found to be log K_f = pK + 6.86. A similar dependence has been reported for carboxylic acid complexes of $CH_3Hg(II)$ (23).

It is worth comparing the formation constant determined in this work for the cysteine complex with that reported by Simpson (4). The latter is one of few values in the literature for complexation of $CH_3Hg(II)$ by a biological thiol ligand and consequently has been used in many discussions of the chemistry of $CH_3Hg(II)$ in biological systems. The constant reported by Simpson is an "association constant", which was calculated in terms of the macroscopic acid–base chemistry of cysteine rather than the microscheme shown in Fig. 4. Thus this constant actually reflects a composite of complexation, sulfhydryl acid–base, and amino acid–base behavior. Recalculation of Simpson's association constant using more recent pK values for cysteine (18) yields a value of 15.3. The "association constant" calculated from the formation constant determined in this work is 15.2. Similar agreement is observed for the glutathione–$CH_3Hg(II)$ complex association constants (25).

Such good agreement is not obtained with the results of Hojo *et al.* for the $CH_3Hg(II)$ complexes of penicillamine and cysteine (26). CH_3HgCl was used as the source of $CH_3Hg(II)$ in that study, but no mention was made of correcting for the competitive complexation of $CH_3Hg(II)$ by chloride ion or for $CH_3Hg(II)$ speciation (13).

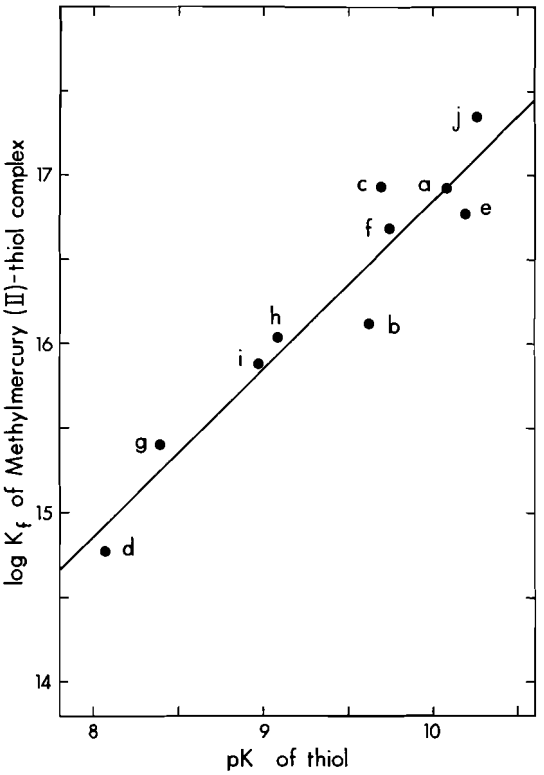

FIG. 5. Correlation between log K_f of the $CH_3Hg(II)$–thiol complexes and the pK of the thiol groups. The letters a–j refer to the complexes of MAA, ME, PSH (amino deprotonated), PSH (amino protonated), NPSH, CYS (amino deprotonated), CYS (amino protonated), glutathione (amino deprotonated), glutathione (amino protonated), and MSA, respectively.

The formation constants listed in Table 3 show the affinity for $CH_3Hg(II)$ to decrease in the order

mercaptosuccinic acid > penicillamine > mercaptoacetic acid > *N*-acetylpenicillamine > cysteine > homocysteine > mercaptoethanol

However, because of competing reactions, this order of stability is rather misleading with respect to effective binding strength. For ligands such as penicillamine and cysteine, the situation is further complicated by the dependence of the pK of the thiol group on the protonation states of acidic groups in the ligand. For example, the formation constant of the penicillamine complex decreases from log K_f = 16.94 to 14.79 upon protonation of the amino group, while that for the cysteine complex decreases from 16.67 to 15.38.

Can. J. Chem. Downloaded from www.nrcresearchpress.com by 210.87.254.42 on 09/06/12
For personal use only.

These effects can be most easily visualized with conditional formation constants, K_{fc}, which are defined as pH-dependent equilibrium constants for the reaction

$$CH_3Hg_{free} + L_{free} \rightleftarrows CH_3HgL_{total}$$

where CH_3Hg_{free} and L_{free} include all the free forms of $CH_3Hg(II)$ and ligand and CH_3HgL_{total} includes all the complexed forms of the ligand.

The logarithm of K_{fc} is plotted vs. pH in Fig. 6. In all cases, the conditional formation constant is orders of magnitude smaller than the formation constant listed in Table 3 due to competing reactions. Also, the conditional formation constants are pH dependent, reaching a maximum in each case around neutral pH, and decreasing at higher and lower pH values due to competing reactions involving hydroxide ion and hydrogen ion, respectively. The various curves in Fig. 6 show that the exact pH dependence of K_{fc} for the different complexes is strongly dependent on the acid–base chemistry of the sulfhydryl group, with the striking result that the order of relative affinity for $CH_3Hg(II)$ undergoes some major changes with change in pH. Thus, at pH 10, K_{fc} for the mercaptosuccinic acid complex is largest while at pH 4 it is smallest. At pH 10, K_{fc} for the cysteine complex is second smallest while at pH 4 it is largest.

Of particular interest with respect to the chemistry

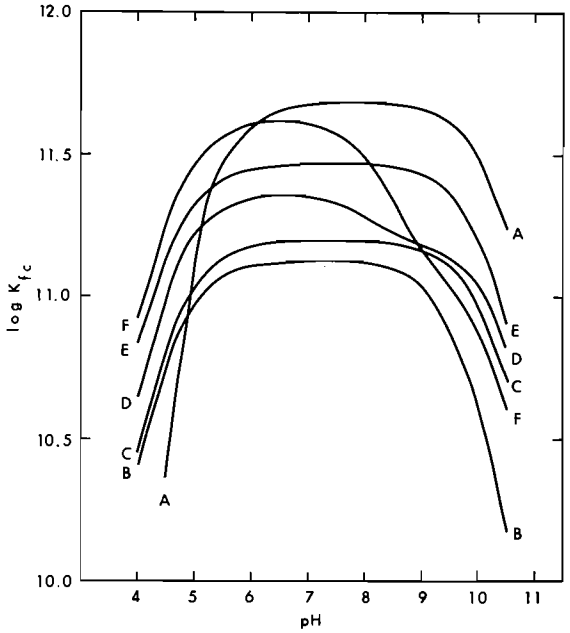

FIG. 6. pH dependence of the conditional formation constants for the $CH_3Hg(II)$–thiol complexes of (*A*) MSA, (*B*) ME, (*C*) NPSH, (*D*) PSH, (*E*) MAA, and (*F*) CYS.

TABLE 4. Conditional formation constants for the methylmercury(II)–thiol complexes at pH 7.4

Ligand	log $K_{f,conditional}$
Mercaptoethanol	11.13
Mercaptoacetic acid	11.47
N-Acetylpenicillamine	11.20
Penicillamine	11.33
Cysteine	11.57
Homocysteine	11.15
Mercaptosuccinic acid	11.68

of methylmercury toxicology are the relative binding affinities at pH 7.4 (24). From the conditional formation constants listed in Table 4, the order of decreasing ligand affinity for $CH_3Hg(II)$ at pH 7.4 is

mercaptosuccinic acid > cysteine > mercaptoacetic acid > penicillamine > *N*-acetylpenicillamine > homocysteine > mercaptoethanol

The logarithm of K_{fc} for the $CH_3Hg(II)$ complex of glutathione is 11.48 at pH 7.4 (25), which places glutathione with mercaptoacetic acid in the above sequence. Of these ligands, mercaptosuccinic acid, penicillamine, and *N*-acetylpenicillamine have been found to increase the rate of elimination of $CH_3Hg(II)$ in animal studies of antidotes for methylmercury poisoning (27–30). Considering that K_{fc} for the glutathione complex is larger than those for the penicillamine and *N*-acetylpenicillamine complexes at pH 7.4 and that glutathione is quite abundant in most cellular systems it is perhaps surprising that penicillamine and *N*-acetylpenicillamine are effective antidotes. For example, glutathione is present at a level of about 2 m*M* in human red blood cells (31, 32). The order of effectiveness as antidotes for methylmercury poisoning in animal studies is (30)

mercaptosuccinic acid > *N*-acetylpenicillamine > penicillamine

It appears that factors in addition to relative binding strengths are important, such as the ease with which the thiol ligand can penetrate cellular membranes and convert the nondiffusible intracellular $CH_3Hg(II)$ into a freely diffusible complex (27).

Acknowledgements

This research was supported by the Natural Sciences and Engineering Research Council through its Strategic Grants Program and by the University of Alberta. Financial support of R.S.R. by an I. W. Killam Fellowship is gratefully acknowledged.

1. D. L. RABENSTEIN and M. T. FAIRHURST. J. Am. Chem. Soc. **97**, 2086 (1975).
2. D. L. RABENSTEIN. Acc. Chem. Res. **11**, 100 (1978).

3. G. SCHWARZENBACH and M. SCHELLENBERG. Helv. Chim. Acta, **48**, 28 (1967).
4. R. B. SIMPSON. J. Am. Chem. Soc. **83**, 4711 (1961).
5. R. G. BATES. Determination of pH. 2nd ed. Wiley-Interscience, New York, NY. 1973.
6. R. BENESCH and R. E. BENESCH. Biochim. Biophys. Acta, **23**, 643 (1957).
7. C. W. DAVIES. J. Chem. Soc. 2093 (1938).
8. W. LUND and E. JAKOBSEN. Acta Chem. Scand. **19**, 1783 (1965).
9. E. LARSSON. Z. Anorg. Chem. **172**, 375 (1928).
10. D. L. LEUSSING. J. Am. Chem. Soc. **80**, 4180 (1958).
11. O. S. MUSAILOV, B. A. DUNAI, and N. P. KOMAR. J. Anal. Chem. USSR, **23**, 123 (1968).
12. J. L. DYE and V. A. NICELY. J. Chem. Educ. **48**, 443 (1971).
13. D. L. RABENSTEIN, C. A. EVANS, M. C. TOURANGEAU, and M. T. FAIRHURST. Anal. Chem. **47**, 338 (1975).
14. E. W. WILSON and R. B. MARTIN. Arch. Biochim. Biophys. **142**, 445 (1971).
15. S. J. BACKS and D. L. RABENSTEIN. Inorg. Chem. In press.
16. D. A. DOORNBOS. Pharm. Weekbl. **102**, 269 (1967).
17. J. H. RITSMA and E. JELLINEK. Recueil, **91**, 923 (1972).
18. E. COATES, C. MARSDEN, and B. RIGG. Trans. Faraday Soc. **65**, 863 (1969).
19. K. WALLENFELS and C. STREFFER. Biochem. Z. **346**, 119 (1966).
20. L. J. PORTER and D. D. PERRIN. Aust. J. Chem. **22**, 267 (1969).
21. N. J. TAYLOR, Y. S. WONG, P. C. CHIEH, and A. J. CARTY. J. Chem. Soc. Dalton, 438 (1975).
22. Y. S. WONG, P. C. CHIEH, and A. J. CARTY. J. Chem. Soc. Chem. Commun. 741 (1973).
23. S. LIBICH and D. L. RABENSTEIN. Anal. Chem. **45**, 118 (1973).
24. D. L. RABENSTEIN. J. Chem. Educ. **55**, 292 (1978).
25. R. S. REID and D. L. RABENSTEIN. Unpublished results.
26. Y. HOJO, Y. SUGIURA, and H. TANAKA. J. Inorg. Nucl. Chem. **38**, 641 (1976).
27. J. AASETH. Acta Pharmacol. Toxicol. **39**, 289 (1976).
28. J. AASETH, A. WANNAG, and T. NORSETH. Acta Pharmacol. Toxicol. **39**, 302 (1976).
29. T. SUZUKI, S. SHISHIDO, and N. ISHIHARA. Br. J. Ind. Med. **33**, 88 (1976).
30. J. AASETH and E. A. FRIEDHEIM. Acta Pharmacol. Toxicol. **42**, 248 (1978).
31. E. BEUTLER, O. DURON, and B. M. KELLY. J. Lab. Clin. Med. **61**, 882 (1963).
32. D. L. RABENSTEIN and R. SAETRE. Clin. Chem. **24**, 1140 (1978).

Can. J. Chem. Downloaded from www.nrcresearchpress.com by 210.87.254.42 on 09/06/12
For personal use only.

Electroreduction of uranyl ion in aqueous calcium nitrate solutions

NAROTTAM P. BANSAL[1] AND JAMES A. PLAMBECK

Department of Chemistry, University of Alberta, Edmonton, Alta., Canada T6G 2G2

Received August 26, 1980

This paper is dedicated to Professor W. E. Harris on the occasion of his retirement from the University of Alberta

NAROTTAM P. BANSAL and JAMES A. PLAMBECK. Can. J. Chem. **59**, 1515 (1981).

The electroreduction of uranyl ions in buffered and unbuffered 0.5 *M* calcium nitrate has been studied using polarography, cyclic voltammetry, chronopotentiometry, and chronoamperometry. The results are compared with those in molten calcium nitrate tetrahydrate.

NAROTTAM P. BANSAL et JAMES A. PLAMBECK. Can. J. Chem. **59**, 1515 (1981).

Faisant appel à la polarographie, la voltamétrie cyclique, la chronopotentiométrie et la chronoampérométrie, on a étudié la réduction électrolytique des ions uranyles dans des solutions 0,5 *M* de nitrate de calcium tamponnées et non tamponnées. On a comparé les résultats à ceux obtenus dans du nitrate de calcium tétrahydrate fondu.

[Traduit par le journal]

Introduction

In electrochemical studies both in aqueous solvents and in melts, little attention appears to have been paid to the application of the same techniques to systems of some electrochemical complexity in an aqueous solution and also in a fused-salt melt as comparable as possible to the aqueous solution. We have previously studied (1) the reduction of uranyl ion in fused calcium nitrate tetrahydrate. The present paper compares aqueous results with those obtained in the hydrated melt.

The reduction of U(VI) has been extensively studied in aqueous media by different electrochemical methods (2–14).[2] Most of these studies have been carried out in acidic ($HClO_4$, HCl, H_2SO_4, HNO_3) media (2–11). In sufficiently acidic solution, the reduction mechanism (12) is that uranyl is reduced in a one-electron step and that the resulting U(V) species disproportionates, regenerating U(VI). The disproportionation rate has been found to be first order in H^+ concentration according to the following scheme:

(E) $UO_2^{2+} + e^- \rightleftarrows UO_2^+$

(C) $UO_2^+ + H^+ \rightleftarrows UO_2H^{2+}$

(D) $UO_2^+ + UO_2H^{2+} \rightleftarrows UO_2^{2+} + UO_2H^+$

(E) $UO_2H^{2+} + e^- \rightleftarrows UO_2H^+$

followed by other reactions to yield stable forms of U(IV). These steps following the initial reduction of U(VI) to U(V) are all strongly pH-dependent. Reaction of the electrochemically produced U(V) or U(IV) with components of the solution (nitrate ion) is also possible.

In less acidic solutions the situation is simplified because the disproportionation of U(V) does not take place (13), but studies in weakly acid to neutral aqueous media (13, 14) are few.

The studies were carried out in unbuffered aqueous 0.5 *M* $Ca(NO_3)_2$ and aqueous 0.5 *M* $Ca(NO_3)_2$ buffered at pH 3.65 or 4.65 with acetate. The latter was used to help elucidate processes in the unbuffered solution, since electroreduction of uranyl requires protons and the solution in the immediate vicinity of the electrode is more basic than the bulk electrolyte in unbuffered solution. These solutions at 25°C are compared with molten calcium nitrate tetrahydrate at 55°C. The temperature difference is unavoidable because comparison with aqueous work at 25°C is necessary. The ratio of H_2O to Ca^{2+} changes from about 110:1 (aqueous) to 4:1 (melt), with concomitant changes in structure and viscosity.

Experimental

The electrochemical cell was a Princeton Applied Research (P.A.R.) Model 9300-9301 polarographic cell employed in a three electrode configuration. The working electrode was either a P.A.R. Model 9323 hanging mercury drop electrode (HMDE) or a P.A.R. Model 172A dropping mercury electrode (DME). These electrodes were set up using triply distilled mercury (Englehard). For the HMDE, a fresh mercury drop of constant known area (0.0176 or 0.0349 cm^2) was taken for each observation. The auxiliary electrode was a large platinum flag. A saturated calomel reference electrode (sce), Corning 47600 with fibre junction, was used. All values of potential in this work are with reference to this sce.

The polarographic behavior was studied using a P.A.R. Model 174A polarographic analyzer. The chronopotentiometric potential–time curves and the chronoamperometric current–time curves were obtained with a P.A.R. Model 173 potentiostat/galvanostat. The cyclic voltammetry was performed with the Model 173 coupled to a P.A.R. Model 175 universal programmer. The polarograms, current–time curves, some of the potential–time traces, and the cyclic voltammograms at slow

[1]On leave of absence from Department of Chemistry, Ramjas College, University of Delhi, Delhi-110007, India.

[2]For earlier work see the references cited therein.

0008-4042/81/101515-06$01.00/0

©1981 National Research Council of Canada/Conseil national de recherches du Canada

Can. J. Chem. Downloaded from www.nrcresearchpress.com by 210.87.254.6 on 09/06/12
For personal use only.

Can. J. Chem. Downloaded from www.nrcresearchpress.com by 210.87.254.6 on 09/06/12
For personal use only.

scan rates (< 1 V/s) were recorded with an $x-y$ and $x-t$ recorder (Houston Instrument Type 2000). The cyclic voltammograms at higher scan rates and the chronopotentiograms were photographed from the screen of a Tektronix Model 535A oscilloscope. The polarographic currents were corrected for the residual current of the base electrolyte, which was 0.5 M $Ca(NO_3)_2$ throughout; at this concentration, no additional supporting electrolyte is necessary. The pH of the unbuffered aqueous solutions were measured and found to be 3.65 ± 0.05 depending on the batch of $Ca(NO_3)_2 \cdot 4H_2O$ employed. Buffered solutions were buffered at 3.65 ± 0.02 or 4.65 ± 0.02 with acetate.

Before electrolysis, all solutions were purged with purified pre-saturated wet nitrogen for at least 15 min and blanketed with it during the run. Analytical reagent grade uranyl nitrate and calcium nitrate tetrahydrate (BDH AnalaR), acetic acid, and sodium acetate were used without further purification. The experiments were all carried out at 25°C.

Results

Polarograms of aqueous uranyl solutions (Fig. 1) show two reduction waves. In all solutions the first wave is a reversible one-electron reduction of uranyl to U(V), as it is in the melt, as shown by Heyrovsky–Ilkovic plots. The values of the half-wave potential are: unbuffered aqueous, −0.180 ± 0.005 V; pH 3.65 buffer, −0.254 ± 0.05 V; pH 4.65 buffer, −0.323 ± 0.005 V; melt (silver reference), −0.475 ± 0.005 V (1). The plateau height is directly proportional to uranyl concentration.

The second wave near −1.0 V in unbuffered solutions is absent in both of the buffered solutions; it is an artifact of the local basicity produced by use of hydrogen ions near the electrode of the unbuffered solution in the electroreduction of uranyl. In the region of −1.0 V the shape of the current–time curves for individual drops is anomalous, though both positive and negative of this region it appears normal (Fig. 2).

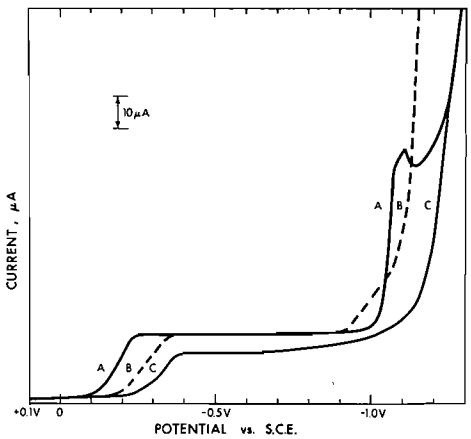

FIG. 1. Polarograms of reduction of uranyl ion in aqueous solution. Curve A, unbuffered, pH 3.65; curve B, acetate buffer, pH 3.65; curve C, acetate buffer, pH 4.65. 0.5 M $Ca(NO_3)_2$, maximum current, controlled drop time 2 s, uranyl concentration 1.00 mmol/L (A, B), 0.70 mmol/L (C).

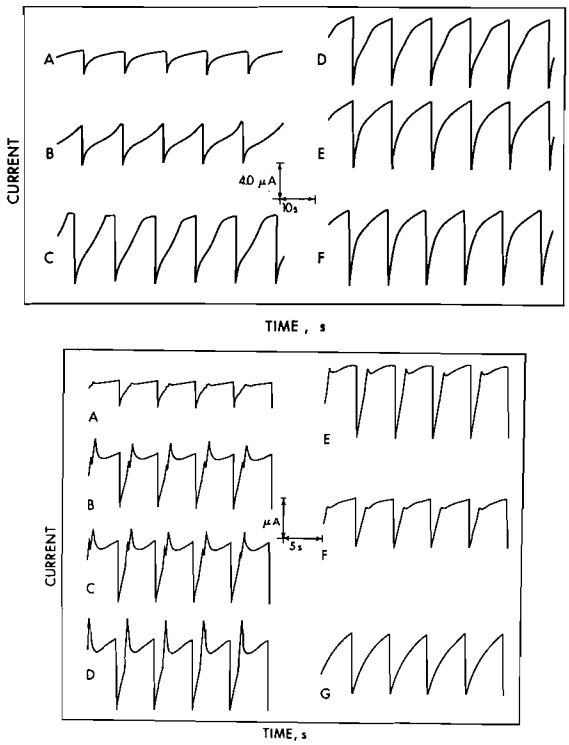

FIG. 2. Variation of instantaneous current during drop life. Upper data, unbuffered solution, 1.006 mmol/L uranyl, current scale 4 μA/unit; curve A, −0.90 V; B, −0.95 V; C, −0.98 V; D, −1.00 V; E, −1.02 V; F, −1.10 V. Lower data, solution buffered at pH 4.65, 1.016 mmol/L uranyl; curve A, −0.20 V, 4 μA/unit; B, −0.40 V, 10 μA/unit; C, −0.60 V, 10 μA/unit; D, −0.80 V, 10 μA/unit; E, −1.00 V, 10 μA/unit; F, −1.10 V, 20 μA/unit; G, −1.15 V, 50 μA/unit. Data in buffered solution of pH 3.65 is intermediate between these.

In unbuffered solution (Fig. 3) the chronopotentiometric curves show one sharp transition with quarter-time potential $E_{\tau/4}$ of −0.175 ± 0.010 V. The Sand plot of $\tau^{1/2}$ against the reciprocal of the current density for this process was a straight line passing through the origin. The Karaoglanoff plot of E vs. log $(\tau^{1/2} - t^{1/2})/t^{1/2}$ was a straight line of slope 0.061 V which is in reasonable agreement with the theoretical value of 0.059 V for a reversible, single-electron, reduction process at 25°C where the product of the electrode reaction is soluble. For a reversible process (15), the polarographic half-wave potential, $E_{1/2}$, is equal to $E_{\tau/4}$ whereas for the reoxidation process after the current reversal, it should correspond to the potential at time $0.222\tau'$. For the first transition both $E_{\tau/4}$ and the potential at $0.222\tau'$ were found to be the same as $E_{1/2}$ regardless of the time at which the current was reversed.

Chronopotentiometry with current reversal was carried out at various points in the $E-t$ curve, i.e.

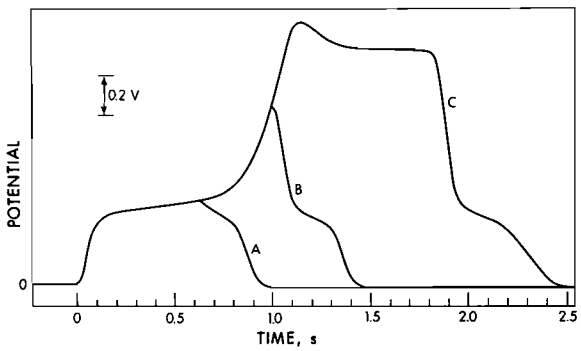

FIG. 3. Chronopotentiograms obtained on reduction of UO_2^{2+} in unbuffered solution. Curve *A*, current reversed on first plateau; *B*, current reversed on rising portion following first plateau; *C*, current reversed on second plateau at time 1.81 s. Concentration of UO_2^{2+}, 1.006 mmol/L; current density 0.285 mA/cm² both forward and reverse.

towards the end of the first transition, at the rising portion after the first transition and after the appearance of the peak where the second process commences (Fig. 3*A*, *B*, *C*). When the direction of the electrolysis current was reversed even at some time after the peak, the electrode potential immediately dropped to a value corresponding to the first reduction process. The value of the *first* forward to reverse transition times, τ_f/τ_r, was found to be approximately three in all cases and independent of the length of time beyond τ_f. These observations show that the product of the second reduction reaction cannot be reoxidized at more negative potential than the product of the first process and that the product of the first process is being regenerated, perhaps catalytically, during the second reduction reaction. These results are similar to those obtained in the melt (1).

Cyclic voltammetry was employed in all three solutions using voltage scan rates v between 0.02 and 100 V/s. In all solutions, the first process was the reversible one-electron U(VI)/U(V) system, for which the peak current is proportional to $v^{1/2}$ and the cathodic/anodic peak ratio is unity. If the potential scan was restricted, only this process was observed (Fig. 4); the value of ΔE_p corresponds to a reversible one-electron process. If the scan range extended to or beyond −1.0 V a large cathodic peak was obtained and the anodic wave was distorted in buffered or unbuffered solutions.

The curves obtained using potential-step chronoamperometry in unbuffered solution are presented in Fig. 5. The shape of the *I–t* curves was normal for applied potentials corresponding to the first reduction step, up to −0.92 V. The curves show maxima for applied potentials in the range −0.94 to −1.12 V corresponding to the second electrode process, but are of normal shape at more negative potentials. After the initial capacitive current decay, the current increases and then slowly decreases after reaching a maximum. The position and intensity of the maxima depend upon the potential step; the height of the maximum increases and it appears after shorter times as the potential is stepped to more negative values. No maxima in the *I–t* curves are observed at applied potentials more negative than −1.12 V. At such negative potentials, it may be that the maxima appear at such a short time interval that it is not possible to detect them on the pen recorded transients and only the usual diffusion controlled curves, in which *I* is proportional to $t^{-1/2}$, are observed. The *I–t* curves for buffered solutions are similar but with more regular progression.

It is easier to interpret the chronoamperometric curves by integration rather than directly because the separation of the different processes can then be achieved. The integrated area (16) from $t = 0$ to $t = 16$ s is plotted in Fig. 6. This length of time was necessary in order to include the peak of *D*, Fig. 5, but even such a long time does not permit inclusion of the peak of *C* so that the point at −0.94 V on Fig. 6 is anomalously low. The contribution of double-layer charging on this time scale is negligible but the coulombs due to the first reduction of UO_2^{2+} are not. Since, however, the process is reversible this charge can be calculated by integration of the Cottrell equation as $Q = 2nFC(Dt/\pi)^{1/2}$. Using the experimental values of 16 s, 1.006 mmol/L, 1 electron/ion, and appropriate values of the fundamental constants, *Q* is an insensitive function only of the diffusion coefficient of uranyl ion. The diffusion coefficient obtained in this and other work is 7.7 × 10^{-6} cm²/s, which yields 1.22 mC/cm² for charge due to the UO_2^{2+} reduction to UO_2^{+}. This value, plotted as a solid horizontal line in Fig. 6, is in excellent agreement with the coulombs observed for the first wave. For the second wave even a value of three times this, plotted as a broken line in Fig. 6, cannot describe the coulometry of this process which then cannot be $UO_2^{2+} \rightarrow$ U(III). Indeed, it

TABLE 1. Diffusion coefficients of uranyl ion in aqueous media at 25°C

$D \times 10^6$ (cm² s⁻¹)	Medium/technique	Reference
7.1	1 *M* $HClO_4$; transfer function curves	8
5.30 ± 0.08	1 *M* K_2SO_4, pH 2; cyclic voltammetry	5
6.8	ClO_4^-, pH 0.83; mean of UO_2^{2+}, UO_2^{+}	12
5.7 ± 0.4	0.5 *M* $Ca(NO_3)_2$; cyclic voltammetry	This work
8.0 ± 0.4	0.5 *M* $Ca(NO_3)_2$; chronoamperometry	This work
9.3 ± 0.4	0.5 *M* $Ca(NO_3)_2$; chronopotentiometry	This work

Can. J. Chem. Downloaded from www.nrcresearchpress.com by 210.87.254.6 on 09/06/12
For personal use only.

Can. J. Chem. Downloaded from www.nrcresearchpress.com by 210.87.254.6 on 09/06/12
For personal use only.

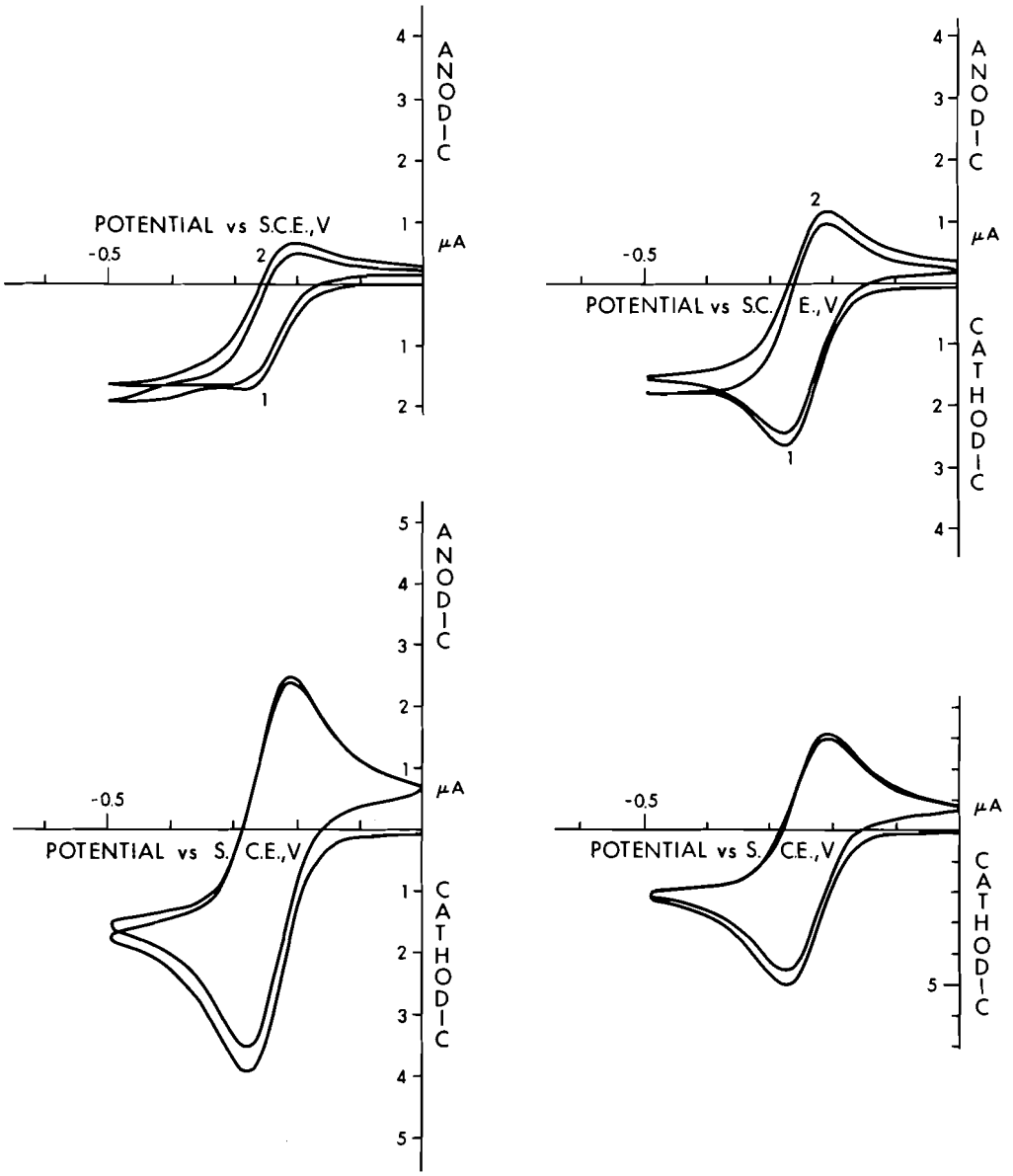

FIG. 4. Cyclic voltammetry of uranyl reduction. Solution buffered at pH 3.65. Initial cathodic direction, 2 cycles, uranyl concentration 1.016 mmol/L. Clockwise from upper left: 20 mV/s, 50 mV/s, 200 mV/s, 100 mV/s.

cannot be limited by diffusion of UO_2^{2+} at all and thus must correspond to the catalytic reduction of nitrate, whose concentration is sufficiently great that the observed coulombs can be passed without exceeding the limit imposed by mass transport.

Discussion

The experimental results described above are consistent with a coherent interpretation in which the first step of the reduction is the one-electron reversible reduction of UO_2^{2+} to UO_2^{+}. The absence of complications in this process can be observed from the Heyrovsky–Ilkovic polarographic plot, the variation of current during drop life, the current-reversal chronopotentiometry, and the chrono-amperometric and cyclic voltammetric studies.

This uranyl reduction is simpler than that in neutral 0.1 *M* aqueous KCl, in which Harris and Kolthoff (14) observed two polarographic waves. The diffusion current constant for the first wave decreased when the concentration of uranyl ions present in the solution was decreased. They attrib-

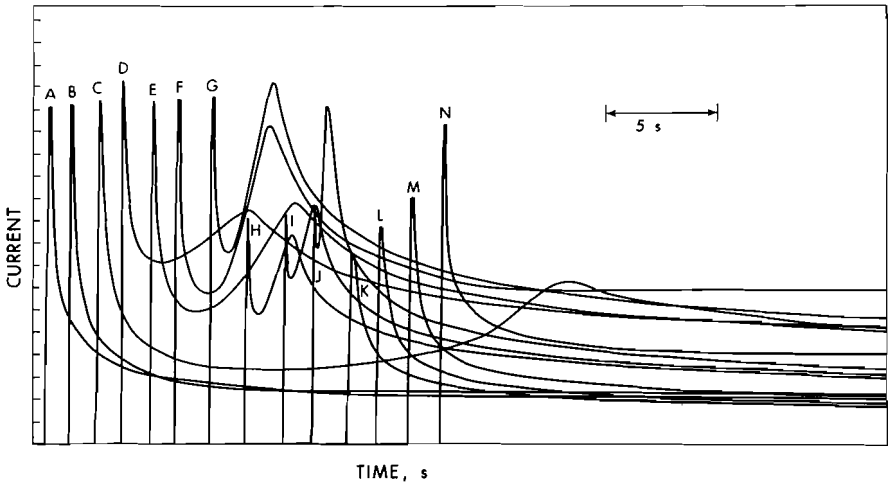

FIG. 5. Chronoamperometric curves of uranyl ion reduction in unbuffered 0.5 *M* $Ca(NO_3)_2$. Concentration of UO_2^{2+}, 1.006 mmol/L. Potential steps applied (from 0.0 V): *A*, −0.90 V; *B*, −0.92 V; *C*, −0.94 V; *D*, −0.96 V; *E*, −0.98 V; *F*, −1.00 V; *G*, −1.02 V; *H*, −1.04 V; *I*, −1.06 V; *J*, −1.08 V; *K*, −1.10 V; *L*, −1.12 V; *M*, −1.14 V; *N*, −1.20 V. Curve *K*, as *J*, possesses peak distinguishable from initial rise while curves *L*, *M*, and *N* do not. Current scales: curves *A*–*G*, 0.5 μA/division, curves *H*–*J*, 1.0 μA/div; curves *K*–*N*, 2.5 μA/div. Curves arbitrarily displaced on time axis. Area of HMDE, 0.0176 cm². Curves in buffered solutions similar but progression is more regular.

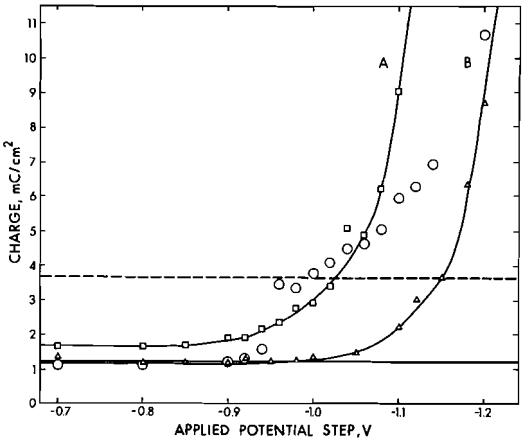

FIG. 6. Chronoamperometric charge. Curves integrated to 16.0 s; concentration of UO_2^{2+}, 1.006 mmol/L; electrode area 0.0176 cm². Circles correspond to experimental points in unbuffered solution. Curve *A* is obtained in buffered solution of pH 3.65 and *B* in buffered solution of pH 4.65. For explanation of horizontal lines see text.

uted this to the hydrolysis of the uranyl ion, the first wave resulting from the one-electron reduction of UO_2^{2+} alone; the hydrolyzed species UO_2OH^+ is not reduced at the potential of the first wave. The degree of hydrolysis of UO_2^{2+} increases, and its relative concentration decreases, with decreasing concentration resulting in the decrease of the diffusion current constant. In the present study the polarographic diffusion current constant and the factor $I_p v^{-1/2}/C^\circ$ in cyclic voltammetry are independent of the bulk uranyl concentration, indicating the absence of the hydrolysis of UO_2^{2+} in 0.5 *M* $Ca(NO_3)_2$.

Collat and Lingane (17) have shown that U(VI) or U(V) is reduced at a potential of −1.1 V vs. sce in aqueous KCl at pH 2–3. In the absence of uranium, nitrate ion is not reduced at this potential; the reduction of nitrate occurs at potentials about 0.2 V more negative than the half-wave potential (−1.58 V) for the hydrogen ion wave. But during the uranium-catalyzed reduction of nitrate the nitrate ion is reduced by a lower oxidation state of uranium at the electrode surface, this uranium being reoxidized to U(V) which is rapidly re-reduced to produce a catalytic cycle. The reduction of nitrate removes hydrogen ions. The catalytic reaction at this pH is not complicated by insolubility of UO_2, which precipitates in more basic solutions (14) and in the melt (1), or by the more complex behavior observed in highly acidic solutions (2–10).

The aqueous mechanism is similar to that in the melt, though precipitation of $UO_{2(s)}$ does not occur. The results are consistent with the UO_2^{2+}/UO_2^+ reversible reduction followed by onset of catalytic nitrate reductions at −1.0 V. The variation in drop shape with onset of the catalytic reduction (Fig. 2) is consistent with initial diffusion-controlled reduction of U(V) followed by catalysis of nitrate reduction leading to eventual diffusion control by nitrate at much higher current. The changeover appears more clearly in the buffered solution because reduction of both UO_2^+ and NO_3^- consumes hydrogen ions; the pH in the immediate vicinity of the

Can. J. Chem. Downloaded from www.nrcresearchpress.com by 210.87.254.6 on 09/06/12
For personal use only.

electrode in unbuffered solution is increased more than in the buffered solutions. The greater pH increase also appears in Figs. 1 and 6; the unbuffered curve shifts, as the catalytic reaction becomes greater, toward the curve obtained at a buffered pH higher than that of the unbuffered bulk solution.

Acknowledgement

The authors are grateful to the National Research Council of Canada for support of this research through an Operating Grant (to J.A.P.).

1. N. P. BANSAL and J. A. PLAMBECK. Electrochim. Acta, **23**, 1053 (1978).
2. M. R. DHANESHWAR and R. G. DHANESHWAR. Proc. Seminar Electrochem., 14th, 207, 1973 (published 1974); Central Electrochem. Research Inst., Karaikudi, India.
3. M. MASTRAGOSTINO and J. M. SAVEANT. Electrochim. Acta, **13**, 751 (1968).
4. L. NADJO and J. M. SAVEANT. Electrochim. Acta, **16**, 887 (1971).
5. S. CASADIO and L. LORENZINI. Anal. Lett. **6**, 809 (1973).
6. S. CASADIO and F. ORLANDINI. Electrochim. Acta, **17**, 441 (1972).
7. S. W. FELDBERG and C. AUERBACH. Anal. Chem. **36**, 505 (1964).
8. D. T. PENCE and G. L. BOOMAN. Anal. Chem. **38**, 112 (1966).
9. B. KASTENING. Collect. Czech. Chem. Commun. **30**, 4033 (1965).
10. A. I. STABROVSKII. Zh. Neorg. Khim. **13**, 406 (1968).
11. D. M. H. KERN and E. F. ORLEMANN. J. Am. Chem. Soc. **71**, 2102 (1949).
12. R. T. IWAMOTO. J. Phys. Chem. **63**, 303 (1959).
13. E. F. ORLEMANN and D. M. H. KERN. J. Am. Chem. Soc. **75**, 3058 (1953).
14. W. E. HARRIS and I. M. KOLTHOFF. J. Am. Chem. Soc. **69**, 446 (1947).
15. P. DELAHAY. New instrumental methods in electrochemistry. Interscience, New York. 1954.
16. N. P. BANSAL and J. A. PLAMBECK. J. Electrochem. Soc. **124**, 1036 (1977).
17. J. W. COLLAT and J. J. LINGANE. J. Am. Chem. Soc. **76**, 4214 (1954).

Can. J. Chem. Downloaded from www.nrcresearchpress.com by 210.87.254.6 on 09/06/12
For personal use only.

Infrared and thermogravimetric studies of the thermal degradation of chrysotile asbestos fibers: evidence for matrix effects

CARMEL JOLICOEUR AND DANIEL DUCHESNE

Centre d'Application en Calorimétrie et Thermodynamique (C.A.C.T.U.S.), Département de chimie, Université de Sherbrooke, Sherbrooke (Qué.), Canada J1K 2R1

Received August 26, 1980

This paper is dedicated to Professor W. E. Harris on the occasion of his retirement from the University of Alberta

CARMEL JOLICOEUR and DANIEL DUCHESNE. Can. J. Chem. **59**, 1521 (1981).

Thermal decomposition of short chrysotile asbestos fibers under static heating has been studied by infrared spectroscopy and thermogravimetry. The spectral changes were monitored at room temperature for fibers heated (*a*) in the free state or (*b*) in KBr matrix. In either case dehydration occurs sharply near 550°C. However, subsequent transformations of the chrysotile anhydride were found to be markedly different for (*a*) and (*b*), suggesting important matrix effects. This provides an explanation for earlier observations in which the thermal decomposition scheme appeared dependent of the size of the chrysotile fibers.

CARMEL JOLICOEUR et DANIEL DUCHESNE. Can. J. Chem. **59**, 1521 (1981).

La décomposition thermique de fibres courtes d'amiante chrysotile en chauffage statique a été étudiée par spectroscopie infrarouge et par analyse thermogravimétrique. Les spectres infrarouges ont été enregistrés à la température ambiante avec les fibres incorporées dans des fenêtres de KBr. L'influence de la température de chauffe sur les spectres a été étudiée pour (*a*) des fibres libres et (*b*) des fibres déjà incorporées dans le KBr. En chauffage statique, la déshydratation du chrysotile se produit de façon abrupte près de 550°C et la réaction semble peu dépendante de l'état physique des fibres lors du traitement thermique. Les réactions subséquentes de l'anhydride diffèrent, toutefois, selon l'état des fibres, suggérant l'existence d'effets de matrice. De tels effets permettent d'expliquer les observations antérieures concernant l'influence de la grosseur des fibres sur leur mécanisme de décomposition thermique.

Introduction

The thermal stability of fibrous magnesium silicates is of obvious relevance to many high-temperature uses of asbestos fibers or composite materials containing such fibers. Consequently, the surface and structural transformations resulting from heat treatment of these fibrous minerals have been the subject of numerous physico-chemical investigations using various techniques namely, X-ray diffraction, infrared spectroscopy, electron microscopy, differential thermal analysis, and thermogravimetric analysis. Summaries of the conclusions from much of the previous work may be found, for example, in reviews by Hodgson (2), Harington *et al.* (3), Martinez (4), and Brett and MacKenzie (5).

In the case of chrysotile asbestos,[1] which is the most abundant and most widely investigated, the various steps involved in the thermal degradation (dehydration, dehydroxylation, structural transformations) have been characterized within reasonable limits, and mechanisms for dehydroxylation and structural rearrangements have been proposed by Ball and Taylor (6) and Brindley and Hayami (7–9). From the data available, it is noteworthy, however, that the dehydroxylation temperature and that for the breakdown of the chrysotile structure, are markedly dependent on the physical properties (size, specific area) of the fibers. While such effects are expected and frequently observed in dynamic heating experiments (e.g. DTA, TGA (10–13)), static heating investigations have also shown significant variations in thermal decomposition behavior. For instance, Naumann and Dresher (11) reported variations in the dehydroxylation and recrystallization temperatures which were related to the surface area of the chrysotile fibers (essentially brucite-free, Cassiar chrysotile). Also in static heating experiments, Murphy and Ross (14) showed that a chrysotile material having a high brucite content (~10%) retained the chrysotile silicate structure at temperatures higher than brucite-free samples. Both of these observations point out the possibility of matrix effects, whether these are related to the "ease of water removal" and "degree of cementation" of the monofibers (11) or to "solid–solid interactions" between chrysotile fibers and interstitial brucite (14).

To unravel the intrinsic decomposition behavior of chrysotile fibers and the influence of confining matrices, it appeared desirable to carry out further quantitative investigations of the surface and structural modifications, first, of finely divided fibers (ideally monofibers) and, second, of the same fibers

[1]The morphology and chemical structure of chrysotile fibers have been described in a preceding paper (1) and we refer to the latter for details; only those aspects essential to the present discussion will be recalled here.

0008-4042/81/101521-06$01.00/0

©1981 National Research Council of Canada/Conseil national de recherches du Canada

Can. J. Chem. Downloaded from www.nrcresearchpress.com by 210.87.254.40 on 09/06/12
For personal use only.

incorporated in various solid matrices. The present work was undertaken with this aim, using short fibers obtained by an aqueous sedimentation method described in a previous paper (1). The infrared absorption and thermogravimetric results presented below have been used to characterize the thermal dehydroxylation and structural changes of these fibers in the "free" state and incorporated in KBr matrices.

Experimental

(a) Materials

The chrysotile fibers used throughout this work were extracted by a selective aqueous sedimentation technique (1) from bulk 4-T-30 commercial fibers (Johns Manville, Quebec). The chemical and structural characterization of these fibers was described in detail elsewhere (1) and may be summarized as follows. The fibers have the chrysotile composition and structure, with a low brucite content (~1%) as determined from X-ray and DTA analyses. The average length of these fibers is of the order of 0.5 μm; their length distribution peaks at ~0.3 μm and the distribution width-at-half-height is 0.5 μm. The surface area of the fibers is 20 m^2/g from N_2 adsorption and 28 m^2/g from H_2O adsorption. Taking a specific area of 25 m^2/g and a bulk density of 2.5 g cm^{-3}, the average cylinder diameter of the fiber is readily calculated as 64 nm which is approximately three times larger than that of monofibers, ca. 25 nm (15). For all experiments, the fibers were previously heated to 110°C for 24 h to ensure removal of physisorbed water.

The KBr was BDH reagent grade, used after heating for 24 h at 120°C.

(b) Methods

The KBr discs used for all infrared measurements (13 mm diameter, ~0.5 mm thick) were prepared from 200 mg of finely ground KBr and various amounts ranging between 1 and 3 mg of dry (110°C, 24 h) chrysotile fibers. In part of this work, a fixed amount of potassium thiocyanate was added as internal standard (16) for quantitative absorbance measurements. The powder mixture was transferred into an evacuable die (Beckman model K-13) and slowly compressed at 10 000 psi, producing pellets having 50–80% transmittance. The disc was dried at 120°C overnight and the ir spectra recorded immediately after. In cases where heating led to a significant loss of transparency due to microfractures, the discs were recompressed as described above.

The infrared spectra were recorded at room temperature in the range 300–4000 cm^{-1} using a double beam Perkin-Elmer spectrometer model 621 under scanning rates between 0.5 and 3 cm s^{-1}. The frequency calibration was checked against absorption bands of a polystyrene film; the accuracy of the frequencies reported here varies between 3 and 20 cm^{-1}, and the uncertainty is mainly due to the width of the absorption lines, especially in the Si—O region. Frequency measurements on the relatively narrow O—H stretching bands in five independent samples showed a standard deviation inferior to 1 cm^{-1}.

(c) Heat Treatment

As mentioned earlier, the chrysotile samples were heat-treated following two distinct procedures. In the first method, loose chrysotile fibers were heated to a given temperature for 3–4 h (8); after cooling in a desiccator over P_2O_5, the sample was weighed and, part of it was pressed in a KBr disc for spectral studies. The remaining loose fiber sample was then heated to the next higher temperature for 3–4 h and the procedure repeated at several temperatures between 110 and 900°C.

In the second method, five KBr–chrysotile discs were prepared from the same fiber stock sample, and these were heat-treated under conditions given above for the loose fiber samples. Since KBr melts at 730°C, the maximum achievable temperature in these experiments was 700°C.

Thermogravimetric analyses of loose chrysotile fibers were also carried out under a scanning rate of 5°C/min, using a SETARAM thermal analyser Model 1133.

Results and Discussions

A partial cross section of a chrysotile fiber is illustrated in Fig. 1, showing the concentric layer structure of the chrysotile fiber. Each layer is formed by the superimposition of a plane of silica tetrahedra and arrays of MgO and MgOH groups. As is readily seen, one out of every four Mg—OH groups is pointing inwards to the chain of silicates, while the remaining three are oriented towards the external surface.

The main events in the thermal decomposition pattern of chrysotile ($3\,MgO \cdot 2SiO_2 \cdot 2H_2O$) containing some adsorbed water (xH_2O) and varying amounts of brucite ($yMg(OH)_2$) are given in Fig. 2, as generally observed in dynamic heating studies, DTA or TGA. Between room temperature and ~250°C, a chrysotile sample looses 1–2 wt.% due to sorbed water (monolayer coverage was earlier shown as 0.8 wt.% (1)). Near 400°C, the excess brucite present is dehydrated, and at significantly higher temperatures (≃600°C), dehydroxylation of

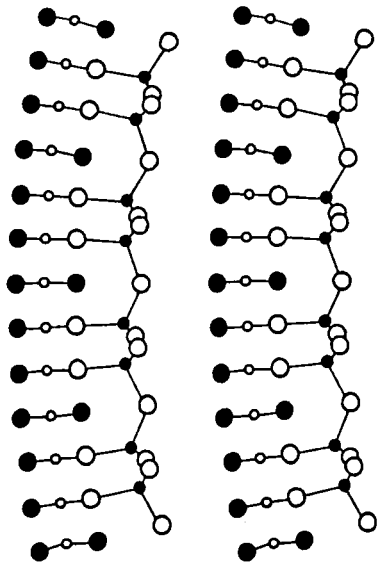

FIG. 1. Schematic representation of the concentric layer structure of chrysotile. Each layer consists of a plane of silica tetrahedra which are interlinked by three apices; this plane is overlayed with a sheet of Mg—OH groups (redrawn from Martinez (4)). A chrysotile monofiber will contain some 10–20 such combined layers in concentric or spiral arrangements. Symbols: ●, —OH; ○, oxygen; ○, Mg; ●, Si.

Can. J. Chem. Downloaded from www.nrcresearchpress.com by 210.87.254.40 on 09/06/12
For personal use only.

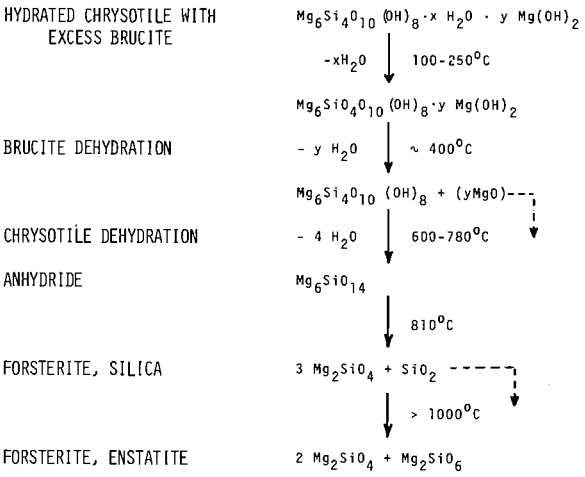

FIG. 2. Overall thermal reaction scheme of chrysotile fibers under dynamic heating conditions (DTA, TGA).

the Mg—OH groups in the chrysotile lattice occurs with a weight loss of ≃13% (theoretical: 13.0%). The amorphous (or partially amorphous) anhyride product of this reaction recrystallizes exothermically into forsterite and amorphous silica at ≃810°C; further heating to temperatures above 1000°C yields some enstatite.

The reaction mechanisms proposed by Ball and Taylor (6) and Brindley and Hayami (8) for these various events are illustrated in the comparison diagram given by the latter authors (Fig. 3). Both mechanisms invoke a concept of "donor–acceptor regions", although they differ in the stoichiometries of these regions and in the transfer of ions or atoms (H, Mg, Si) between them. The two mechanisms account for chrysotile lattice dehydration (≃600°C) on the basis of proton migration from the acceptor to the donor region; water is formed in the latter by reaction with hydroxyl groups, and expelled leaving either pores (6) or silica (8), depending on the extent of the inverse Si migration. It does not appear that any distinction was required for the two different types of OH groups in the chrysotile lattice (one internal vs. three external), in spite of the different environments of these groups. There seems, however, no specific evidence that both types of hydroxyl groups are removed simultaneously, and this question will be considered further below.

Another significant difference in the mechanisms proposed by Ball and Taylor (6) and Brindley and Hayami (8) concerns the structure of the dehydration products. In the former, an anhydride is formed which is converted to forsterite at higher temperatures following further ion migration (Si, Mg); in the Brindley–Hayami mechanism, disordered forsterite is formed immediately, and crystallizes at higher temperatures (≃800°C). This difference in reaction pathways could also result from matrix effects as shown below.

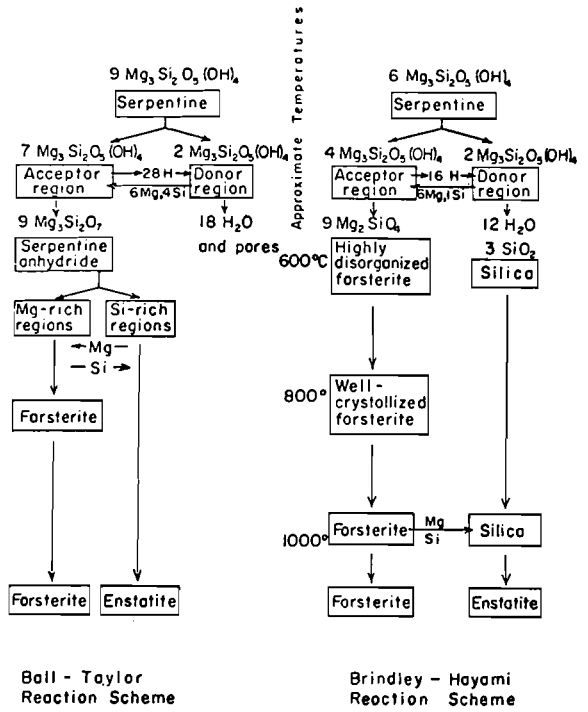

FIG. 3. Comparison of the reaction pathways proposed by Ball and Taylor (6) and Brindley and Hayami (8) for the thermal degradation of chrysotile structure (reproduced from ref. 8 with permission).

(a) Thermogravimetric Results for Dehydration

The fractional weight loss observed upon heating samples of loose chrysotile fibers is illustrated in Fig. 4 as function of temperature for dynamic and stepwise heating. The TGA curve obtained under continuous scanning (5°C/min) is comparable to those reported by other authors (2, 4, 5, 17, 18) and not markedly dependent on the sample size between 50–600 mg. The curve exhibits three distinct portions corresponding to removal of residual water up to ≃200°C, brucite dehydration at ≃400°C, and chrysotile dehydration between 600 and 800°C. By comparison, the data from stepwise heating show that chrysotile dehydration is essentially complete at 650°C. The results at lower temperatures $T < 550$°C are in good agreement with those of Chowdhury (19) who showed that the brucite and chrysotile dehydration occurs distinctly.

The difference between the mid-point temperatures for dehydration of the chrysotile under dynamic and static heating illustrates the slow kinetics of the diffusion-controlled process (9).

Can. J. Chem. Downloaded from www.nrcresearchpress.com by 210.87.254.40 on 09/06/12
For personal use only.

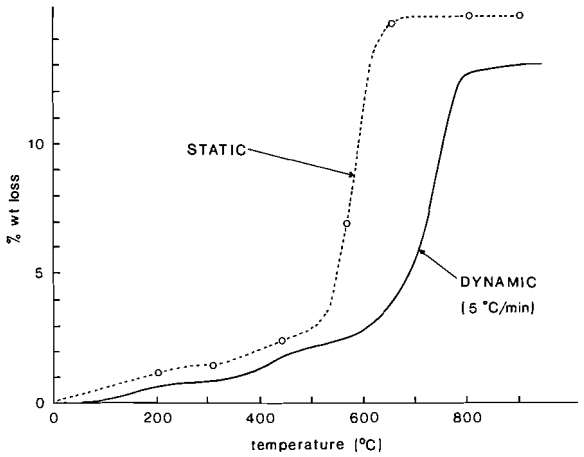

FIG. 4. Fractional weight loss of chrysotile fibers as function of temperature in dynamic heating (5°C/min) and stepwise heat treatments (3–4 h at constant temperature).

(b) Infrared Spectra in the OH Stretching Region

The infrared absorption spectrum of short chrysotile fibers in the hydroxyl stretching region is illustrated in Fig. 5 as a function of heat treatment temperature. The spectra shown are those obtained with fibers heated in their KBr matrix, but these are identical to spectra recorded with fibers heated before incorporation in KBr discs, except for changes in the broad band at ~3450 cm^{-1}. Such differences could not be established reliably, however, since water adsorbed in, or on, the KBr discs during manipulations also shows absorption in this region.

The OH stretching spectrum exhibits three fairly well resolved components, the frequencies of which are given in Table 1, along with data for brucite and other reference materials. The values reported here are consistent with data from various other sources for chrysotile (20–26), brucite (20, 27), and other minerals (20, 26–29). The sharp doublet (ca. 3687 cm^{-1}) is of particular interest in relation to the lattice OH groups. Because brucite exhibits only a single sharp OH absorption (27), and since the short fibers are randomly oriented in the KBr matrix, the OH doublet is readily assigned to Mg—OH groups in different environments.

The peak absorbance of the two bands was determined after graphical deconvolution assuming symmetry of the 3687 cm^{-1} component. Overlap of the doublet band with the broad low frequency band (3450 cm^{-1}) was also accounted for by subtraction of the high frequency tail of the 3450 cm^{-1} band. A plot of A_{3687} vs. A_{3644} for data obtained in the temperature range 120–555°C yielded a slope of 2.96 with a standard deviation of 0.05. This confirms the assignment of the OH doublet to the

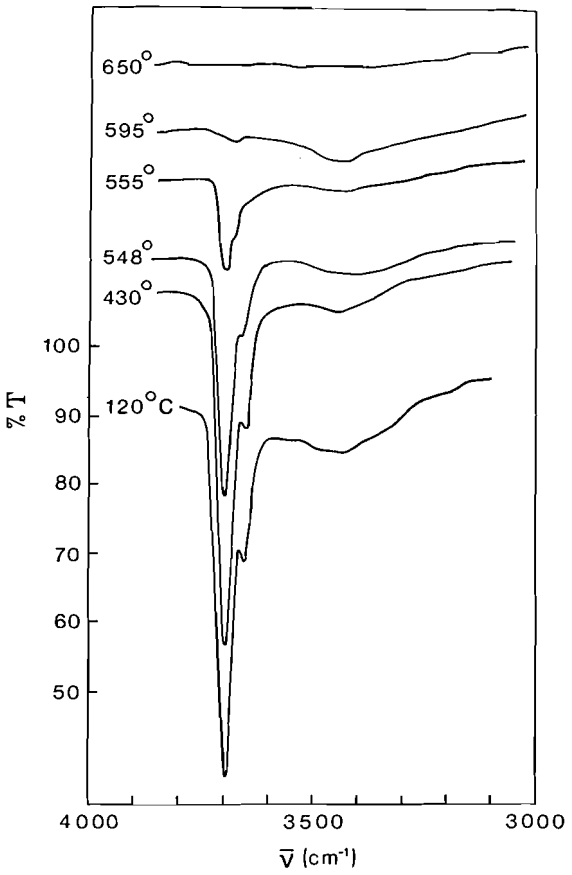

FIG. 5. Infrared spectra of the OH stretching region for short chrysotile fibers in KBr discs as function of heat treatment temperatures.

external and internal Mg—OH groups present in a 3:1 molar ratio, and further shows that dehydration of chrysotile under static heating occurs by simultaneous removal of these OH groups.

A correlation of the ir and thermogravimetric data is illustrated in Fig. 6, where the temperature dependence A_{3687} is shown for three different samples of chrysotile fibers heat-treated in KBr discs.[2] The thermogravimetric results obtained under stepwise heating clearly demonstrate related behaviors, as expected.

(c) Infrared Results in the Si—O Region

The infrared absorption of minerals in the Si—O region has been extensively investigated, for example, by Saskena (31) and Chen (25) and the

[2]The results of experiments where the loose fibers are heated and subsequently incorporated in KBr are not significantly different from those in Fig. 6. For such experiments, however, the absorbances had to be measured relative to that of an internal standard (KCNS) and the overall uncertainty was found larger.

Can. J. Chem. Downloaded from www.nrcresearchpress.com by 210.87.254.40 on 09/06/12
For personal use only.

TABLE 1. Frequencies of selected ir absorption bands of chrysotile and related materials

Material	ν_{OH} (stretching)/cm^{-1}[a]			ν_{Si-O}/cm^{-1}			
Short chrysotile fibers	3687 (3)	3644 (3)	3450 (20)	1075 (5)	1022 (5)	950 (5)	
Brucite ($Mg(OH)_2$)[b]	3694		3420 (sorbed water)				
Amorphous silica[c]				1042	998(s)	798	
Forsterite[d]					984	885 (weak bands at 954 and 837)	
Enstatite[e]				1070(s)	1020	980	942(s)

[a]Spectra recorded with 0.5–1 wt.% samples in KBr discs at scanning rates of 0.5–3 cm^{-1}/s; (s) indicates strong absorption; numbers show estimated wavelength uncertainties.
[b]Finely powdered $Mg(OH)_2$.
[c]Reference 25.
[d]Reference 30.
[e]Reference 20.

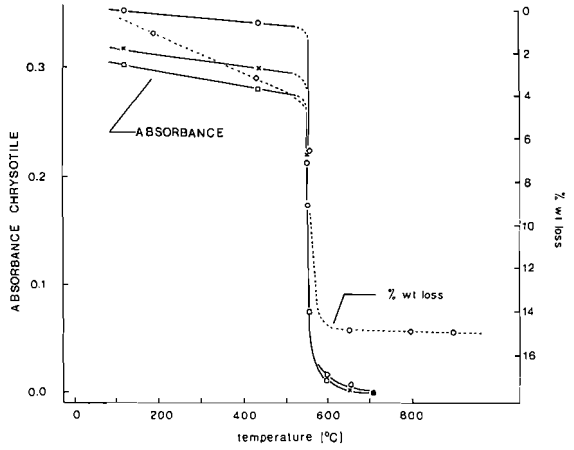

FIG. 6. Influence of heat treatment temperature on the peak absorbance at 3687 cm^{-1} compared to weight loss.

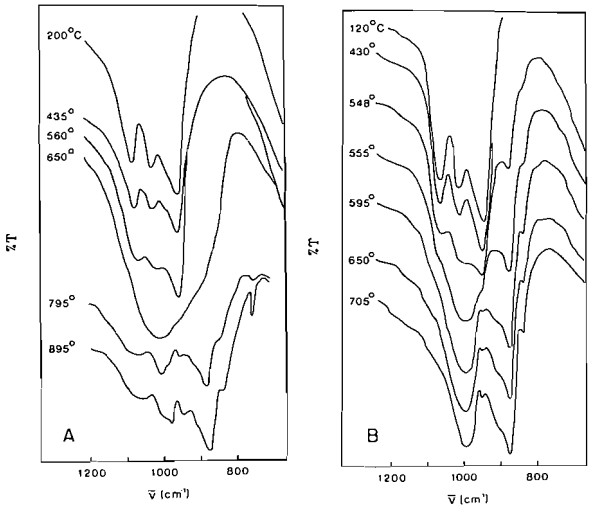

FIG. 7. Influence of heat treatment temperature on the infrared absorption of chrysotile fibers (KBr pellets) in the Si—O stretching region: *A*, fibers heated stepwise before incorporating in KBr discs; *B*, fibers heated stepwise in KBr pellets.

results generally indicate absorption bands sufficiently characteristic to identify a particular mineral, or group of minerals. Of special interest in chrysotile studies is the ν_3 mode of SiO_4 tetrahedra which is degenerated in the isolated tetrahedron, but not in chain silicate minerals. Because of the lower symmetry in the chrysotile lattice, the degeneracy is lifted and the ν_3 mode of SiO_4 appears as a triplet (ca. 1085, 1017, and 962 cm^{-1} (31)) characteristic of chain silicate structures. The frequencies observed in the present work are reported in Table 1 with similar data for amorphous silica and forsterite.

The influence of the heat treatment temperature on the infrared absorption of chrysotile fibers in the Si—O stretching region is illustrated in Fig. 7. The spectra shown in Fig. 7*A* correspond to fibers heated stepwise and later pressed into KBr discs. The triplet structure of the ν_3 mode, initially well resolved, coalesces in samples heat-treated above 600°C; at 650°C, the absorption is a broad structureless band, typical of amorphous materials. In samples heated at still higher temperatures (795°C), the bands of forsterite (984 cm^{-1} and 885 cm^{-1}) become clearly resolved. Changes observed following heat treatment to 900°C (e.g. increase in intensity at ~940 cm^{-1}) may be attributed to the appearance of enstatite (4). Except for the occurrence of enstatite at temperatures lower than 1000°C, these observations are in full agreement with the reaction scheme of Ball and Taylor (6), forsterite appearing only after complete dehydration of the chrysotile into an amorphous anhydride.

The temperature dependence of the Si—O spectral features of chrysotile fibers heat-treated in KBr

Can. J. Chem. Downloaded from www.nrcresearchpress.com by 210.87.254.40 on 09/06/12
For personal use only.

discs (Fig. 7*B*) shows marked departure from the behavior described above. For temperatures lower than ~450°C, the ν_3 triplet lineshape is fairly independent of the fiber history, i.e., whether they are heated before pressing into a KBr matrix or heated within the matrix. However, heating at 550°C results in sharp loss of the triplet structure (between 545 and 555°C), while the 885 cm^{-1} band of forsterite becomes clearly evident. The appearance of the latter band before the complete disappearance of the chrysotile triplet is compatible with the mechanism of Brindley and Hayami (8) who proposed the formation of forsterite immediately after dehydration at 600°C based on X-ray diffraction results

The observations described here are strikingly analogous to those reported by Nauman and Dresher (11) in their X-ray diffraction studies of the thermal decomposition of chrysotile fibers of different sizes. Under static heating, coarse chrysotile fibers (specfic area 12 m^2/g) convert to forsterite between 550 and 600°C. However, when the same material is defibrilated in a ball mill to a specific area of 40 m^2/g, static heating in the range 550–600°C leads to an amorphous phase which converts to forsterite only at higher temperatures, ca. 650–700°C. The similar effects found here with chrysotile fibers in a completely different matrix suggest a general basis for explanation of matrix effects involving mostly physical factors such as pressure or stress on the fibers. Whether more specific interactions (electrostatic, chemical reactions) also play a significant part remains to be determined from studies involving different types of matrices. This would clearly seem a worthy investigation, considering the many applications where chrysotile fibers are used as reinforcing agents in high-temperature materials.

Acknowledgements

The authors gratefully acknowledge financial support of this work by the Ministère de l'Education du Québec, the Natural Sciences and Engineering Research Council of Canada, and the Programme de recherche sur l'Amiante through Professor Jean-Marc Lalancette. The assistance of Dr. Jean-Luc Fortier and M. Pierre Roberge with several experimental aspects of this work is also kindly acknowledged.

1. C. Jolicoeur, P. Roberge, and J.-L. Fortier. Can. J. Chem. **59**, 1140 (1981).
2. A. A. Hodgson. R. Ins. Chem. Lect. Ser. No. 4, 1 (1965).
3. J. S. Harington, A. C. Allison, and D. V. Badami. Adv. Pharm. Chem. **12**, 292 (1975).
4. E. Martinez. Can. Min. Metall. Bull. **69**, 414 (1966).
5. N. H. Brett, K. J. D. MacKenzie, and J. H. Sharp. Q. Rev. **24**, 185 (1970).
6. M. C. Ball and H. F. W. Taylor. Mineral. Mag. **33**, 467 (1963); **32**, 754 (1961).
7. G. W. Brindley and R. Hayami. Clays Clay Miner. **12**, 35 (1964).
8. G. W. Brindley and R. Hayami. Mineral. Mag. **35**, 189 (1965).
9. G. W. Brindley, B. N. Narahari Achar, and J. H. Sharp. Am. Mineral. **52**, 1697 (1967).
10. T. Otouma, S. Take, and S. Udagawa. J. Jpn. Ass. Miner. Pet. Econ. Geol. **69**, 364 (1974).
11. A. W. Nauman and W. H. Dresher. Am. Mineral. **51**, 1200 (1966).
12. A. M. Harris. *In* The physics and chemistry of asbestos minerals. Abst. 3:2A, Inst. Nat. Sci. Louvain, Belgium. 1971.
13. J. B. Donnet and P. J. Cosme. Silic. Ind. **38**, 133 (1973).
14. W. J. Murphy and R. A. Ross. Clays Clay Miner. **25**, 78 (1977).
15. K. Yada. Acta Crystallogr. A**27**, 659 (1971).
16. S. E. Wiberley. Anal. Chem. **29**, 210 (1957).
17. G. L. Kalousek and L. E. Muttart. Am. Mineral. **42**, 1 (1957).
18. W. D. Johns. Bull. Am. Ceram. Soc. **44**, 682 (1965).
19. S. Chowdhury. Ph.D. Thesis, Imperial College, London. 1972.
20. J. A. Gadsen. Infrared spectra of minerals and related compounds. Butterworths, London. 1975.
21. S. Yariv and L. Heller-Kallai. Clays Clay Miner. **23**, 145 (1975).
22. G. W. Brindley and J. Zussman. Am. Mineral. **44**, 185 (1957).
23. H. W. van der Marel and J. H. L. Zwiers. Silic. Ind. **24**, 359 (1959).
24. J. D. Russell, V. C. Farmer, and B. Velde. Miner. Mag. **37**, 869 (1970).
25. J.-Y. T. Chen. J. Ass. Off. Anal. Chem. **60**, 206 (1977).
26. J.-P. Mouchalin, J.-M. Gagne, J.-L. Parpal, and L. Bertrand. Appl. Phys. Lett. **35**, 360 (1979).
27. H. A. Benesi. J. Chem. Phys. **30**, 852 (1959).
28. B. D. Saksena. Trans. Faraday Soc. **60**, 1714 (1964).
29. J. M. Serratosa and W. F. Bradley. J. Phys. Chem. **62**, 1164 (1958).
30. D. A. Duke and J. D. Stephens. Am. Mineral, **49**, 1388 (1964).
31. B. D. Saksena. Trans. Faraday Soc. **57**, 242 (1961).

Can. J. Chem. Downloaded from www.nrcresearchpress.com by 210.87.254.40 on 09/06/12
For personal use only.

A rapid method for the determination of bitumen, water, and solids in oil sands

D. Lorne Ball,[1] E. D. Cooke, Jean M. Cooley,[2] M. Coreen Hamilton,[3] and Robert Schutte

Research Department, Syncrude Canada Ltd., P.O. Box 5790, Edmonton, Alta., Canada T6C 4G3

Received September 8, 1980

This paper is dedicated to Professor W. E. Harris on the occasion of his retirement from the University of Alberta

D. Lorne Ball, E. D. Cooke, Jean M. Cooley, M. Coreen Hamilton, and Robert Schutte. Can. J. Chem. **59**, 1527 (1981).

A simple and rapid method has been developed to measure the bitumen, water, and solids content of Athabasca oil sand samples in order to efficiently serve both plant operations and research needs. A solvent blend of 74% toluene and 26% isopropyl alcohol extracts both the bitumen and the water from the solids producing a homogeneous liquid phase. The bitumen is determined gravimetrically on an aliquot of this solution. A Karl Fischer titration is used to measure the water concentration. Solids are measured gravimetrically or can be reported by difference. Mass balances between 99.05 and 100.25% are achieved routinely.

D. Lorne Ball, E. D. Cooke, Jean M. Cooley, M. Coreen Hamilton et Robert Schutte. Can. J. Chem. **59**, 1527 (1981).

Dans le but d'aider tant les opérations industrielles que la recherche, on a mis au point une méthode simple et rapide pour mesurer le bitume, l'eau et les solides contenus dans des échantillons de sable bitumineux de l'Athabasca. Grâce à un mélange de solvant formé de 74% de toluène et de 26% d'alcool isopropylique on peut extraire le bitume et l'eau des solides et former une phase liquide homogène. Grâce à la gravimétrie, on peut déterminer le contenu en bitume d'un échantillon de cette solution. On utilise le titrage de Karl Fischer pour mesurer la teneur en eau. On mesure les solides par gravimétrie ou par différence. On effectue de façon courante des bilans qui valent entre 99,05 et 100,25%.

[Traduit par le journal]

Introduction

The extensive Athabasca oil sands are assuming an increasing role in supplying Canada's liquid hydrocarbon needs. One commercial plant, Suncor Inc., has operated since 1967. It extracts bitumen from the oil sands and subsequently upgrades it to synthetic crude oil. Syncrude Canada Ltd., which is designed to produce 109 000 barrels of synthetic crude per day, began production in 1978. Fundamental to the successful utilization of this oil sand resource and to the economic operation of the extraction plant is a reliable analytical method for the assessment of bitumen in reserves and plant feed. Because economics require that only feed of 6% bitumen or greater enters the process and because different grades of oil sand require changes in process conditions for efficient operation, the analytical method must also be rapid and efficient.

Oil sand is a variable mixture of organics (bitumen), water, and solids. The bitumen content varies between 0 and 16% by weight, the water content between 0 and 8% by weight, and the solids make up the remainder of the sample. Methods for measuring the bitumen as well as the water and solids in oil sand samples have been used for many years. A well established procedure is the modified Dean–Stark method (1). In that method the bitumen is extracted with hot toluene, and, as with the solids, is determined gravimetrically. The water is collected in the Dean–Stark trap and determined volumetrically. The method yields highly reliable results as exemplified in a 1973 study by the Canadian Petroleum Association Tar Sands Council (2). A serious disadvantage of the method, however, is the extraction time of at least 8 h and an elapsed time of 24 h. For feedback to plant operators and often for research purposes such a long turnaround time cannot be tolerated. Therefore, a need existed for a faster method for analysis of oil sand.

Specifically, the criteria for a new method of bitumen, water, and solids analysis in oil sand are: an analysis time of less than 1 h per sample, the technique must be simple, the reagents must be safe, all three components must be able to be determined from a single sample, higher operator productivity than with the current method, and the maintenance of accuracy and precision of the method in current use.

Because oil sand is highly variable, the parameters by which it can be assayed are limited. Bitumen itself is a complex mixture of a large number of organic molecules and is therefore difficult to be measured quantitatively. Spectroscopic techniques have been investigated, but as Patel reported (3), measuring bitumen from its response at 530 nm is valid only if the standards and samples are obtained from within the same imme-

[1]Present address: East Kootenay Community College, P.O. Box 8500, Cranbrook, B.C., Canada V1C 4J6.

[2]To whom all correspondence should be addressed.

[3]Present address: Oil Sands Research Department, Alberta Research Council, 11315 - 87 Avenue, Edmonton, Alta., Canada T6G 2C2.

0008-4042/81/101527-04$01.00/0

©1981 National Research Council of Canada/Conseil national de recherches du Canada

Can. J. Chem. Downloaded from www.nrcresearchpress.com by 210.87.254.40 on 09/06/12
For personal use only.

diate area of the deposit which is not practical in the commercial laboratory. Furthermore, Syncrude's experience has shown that spectrophotometric response for bitumen obtained from different depths of the same core hole can vary as much as 30%. Severe response variations in the infrared and ultraviolet regions were similarly encountered, and these techniques were necessarily discarded. The use of gravimetric/ashing and pyrolysis techniques was also eliminated because of the random presence of finely divided coal. As a consequence, mass was identified as the only reliable parameter by which bitumen could be determined. The choice of this parameter demanded an initial separation of the bitumen from the solids.

Although water is present in the oil sands in a complex manner, its determination was considered to be relatively straightforward and possible by a variety of techniques, e.g., Karl Fischer titration or gas chromatography.

The determination of solids was complicated by the extreme variation in solids composition, ranging in all combinations from sand to silt to clay. Thus, it required a determination by mass.

Experimental

Analytical Procedure

The extraction solvent, 74% toluene (conforming to ASTM D841-50 for nitration grade), 26% isopropyl alcohol (ACS reagent grade) blend (vol.%) is prepared by mixing the appropriate volumes of each solvent in a large closed container. Type 4A molecular sieves are added to dry the solvent. Unless the weather is unusually humid, the solvent should dry within 24 h. The density of this blend is 0.8440 kg/L at 20°C and this value is used as a check on its composition. The solvent density, which should be kept in the range 0.8435 to 0.8445 kg/L, is measured daily and recorded. The solvent blend is also analyzed daily by Karl Fischer titration to ensure that it is dry.

Six standard water solutions, in the range of 0.2–2.0 g water per 100 mL solution, are prepared by weighing distilled water (to the nearest 0.0001 g) into a volumetric flask and diluting it to volume with the toluene/isopropyl alcohol solvent blend. The solutions are mixed, transferred to 125 mL serum bottles and sealed. These solutions keep for several months if the glassware used for their preparation and storage has been treated with a silylating agent, dimethyldichlorosilane, to prevent adsorption of the water from the solutions.

A Photovolt Aquatest II Automatic Karl Fischer Titrator is calibrated daily using the standard water solutions. A 200 μL Hamilton push button syringe is adjusted to deliver a volume of 100 μL. The syringe is then rinsed three times with the most dilute water standard, a minute is allowed for the syringe to return to its equilibrium volume, the syringe filled, and the aliquot injected into the titration cell of the instrument. The value of the aliquot titre is recorded and two more aliquots of the same standard solution are titrated. In the same manner, three aliquots of each of the five remaining standard water solutions are titrated.

An oil sand sample (between 20 and 50 g) is transferred to a preweighed 500 mL Nalgene bottle (linear polyethylene) and its weight is recorded. Approximately 250 mL of the solvent blend is then added. The bottle is tightly capped, and reweighed to determine the exact quantity of solvent added. The Nalgene bottle is then placed on a reciprocating shaker (40 mm stroke, 5 cycles/s) and the oil sand/solvent mixture shaken for at least 10 min. When the bottle is removed from the shaker, it is allowed to stand upright for 3 min to settle the coarse solids. Aliquots of the resultant extract solution are analyzed for bitumen and water content.

Fifteen cm diameter glass fiber filters are dried in a 110°C oven for 1 h, cooled, and then weighed to the nearest 0.0001 g. For the bitumen analysis approximately 10 mL of the extract solution is filtered to remove fine solids. A 0.45 μm 25 mm Millipore Millex filter assembly is attached to a Luer-lok syringe and the filtrate is collected in a small Erlenmeyer flask which is then stoppered. A calibrated 5 mL transfer pipet is rinsed with the filtered extract solution and then used to distribute an aliquot of the extract to a weighed glass fiber filter. This is hung for 15 min to evaporate the water and the solvent and then reweighed to measure the bitumen present.

If the water determination is not done immediately after the Nalgene bottle is removed from the shaker, the bottle is shaken by hand and then a 100 μL aliquot is analyzed by Karl Fischer titration following the procedure used for the water standard.

After the aliquots of sample extract solution have been removed for bitumen and water analyses, the remaining extract is filtered to separate the solids. A 350 mL fine pore glass frit filtering funnel is filled with a 30 mm layer of Celite 499 filter aid and then weighed to the nearest 0.01 g. The funnel is placed on a filtering flask, the filter aid is wetted with solvent blend, and the vacuum turned on. The sample extract solution and solids are poured into the filtering funnel. The inside of the Nalgene bottle is washed with solvent blend and the washings are also poured into the funnel. The solids in the funnel are washed with several portions of solvent blend until the effluent appears colourless. The clean solids are finally washed with acetone to aid in drying. The funnel and solids are dried in the oven at 110°C, allowed to cool and then reweighed.

Calculations

The Karl Fischer titrator calibration data are subjected to a linear regression analysis to obtain the slope and the intercept of the median Karl Fischer titrator reading versus water standard concentration.

The volume of the extract solution is calculated using correction factors to account for non-ideal solution mixing. Volume of extract solution = solvent volume + 1.02 (grams of bitumen in sample) + 0.98 (grams of water in the sample). By solving simultaneous equations the percent bitumen and water can be computed. If the solids were measured the percent solids and mass balance check are then calculated.

Results and Discussion

Solvent Composition

Bitumen is defined as the toluene extractable portion of an oil sand sample (4). After extensive experimentation a solvent blend of 74 vol.% toluene and 26 vol.% isopropyl alcohol proved to have the optimum extraction capability for both the bitumen and water in the amounts likely to be found in oil sand. It is a relatively non-toxic blend and readily available. Simple mixing of an oil sand sample with a quantity of this solvent blend will effect extraction within 10 min.

Can. J. Chem. Downloaded from www.nrcresearchpress.com by 210.87.254.40 on 09/06/12
For personal use only.

TABLE 1. Solvent evaporation time study on filter paper containing solvent or sample extract solution

Aliquot pipetted	Weight on filter* (g) After 9 min	After 11 min	After 13 min	After 15 min	After 18 min	After 20 min	After 25 min	After 45 min
2.5 mL solvent	0.0007	0.0001	0.0000	0.0000	0.0000	0.0000	0.0000	0.0000
2.5 mL sample extract	0.0481	0.0470	0.0470	0.0468	0.0466	0.0464	0.0462	0.0460
5.0 mL solvent	0.0016	0.0008	0.0003	0.0000	0.0000	0.0000	0.0000	0.0000
5.0 mL sample extract	—	0.0955	0.0945	0.0938	0.0937	0.0937	0.0934	0.0926

*Each number is the average of six determinations.

Bitumen Measurement

A fast gravimetric determination requires rapid evaporation of the solvent and water from the extract solution. A 15 cm glass fiber filter adequately absorbs 5 mL of a sample extract solution and, when hung on a clip to dry, exposes a very large area to the atmosphere, permitting the solvent to evaporate quickly. The pipet used to transfer the aliquot must be calibrated with a solution that approximates the sample extract solution, and the evaporation time of the solvent from the filter must be carefully controlled. Data are shown in Table 1 for the weight of glass fiber filters as a function of time for filters on which aliquots of pure solvent blend or sample extract solutions have been pipetted. These data indicate that incorrect evaporation times will result in an error in the bitumen analysis. Too short an evaporation time will give a high result while too long an evaporation time will give a low bitumen result, presumably due to loss of volatile bitumen components. These data also show that there is more leeway in the evaporation time for a 5 mL aliquot (15–20 min) than for a 2.5 mL aliquot (11–13 min), suggesting that the 5.0 mL aliquot measurement will be less operator sensitive and more suitable for routine laboratory use. Determinations on a 5.0 mL aliquot are also more precise than those on a 2.5 mL aliquot. For example, ten 2.5 mL determinations on a typical oil sand extract solution give an average of 0.0418 g bitumen with a standard deviation of 0.0004 g. Ten 5.0 mL measurements on the same solution give an average bitumen value of 0.0836 g and a standard deviation of 0.0002 g. Extrapolating this uncertainty from the 5 mL aliquot to the bulk extract solution (approximately 250 mL total volume) gives an uncertainty of 0.010 g. For a 30 g sample containing 10% bitumen this means an uncertainty of 0.033% (absolute) or 0.33% (relative) in the bitumen determination.

Water Measurement

The Karl Fischer method of water determination was chosen because it is a fast and reliable way to obtain water measurements of high accuracy and precision. The Aquatest II Karl Fischer Titrator is a constant current coulometer which needs minimal maintenance and calibration. However, the instrument is calibrated daily to compensate for fluctuations in the current and to eliminate the need to measure the volume of sample delivered by the syringe. It titrates 10^{-5} g of water per second so only small volumes of sample are analyzed to allow the titration to be completed quickly. The Hamilton push button syringe delivers the sample with excellent repeatability. Calibration data are given in Table 2 for solutions of solvent blend containing various amounts of water. The calibration data indicate that there is a linear relationship between the instrument response and the water concentration over the entire range of water solubility in the solvent blend.

Solids Measurement

Even samples containing large proportions of fine material filter easily with no detectable loss of fines when a filter aid, such as Celite 499, is used to separate the sample solids from the extract solution.

Calculations

To determine the percent bitumen and water in the sample the total volume of the extract solution

TABLE 2. Calibration data for the Aquatest II Automatic Karl Fischer Titrator*

Concentration of standard (g H_2O/100 mL)	Titrator readings	Median reading
0.2571	330, 314, 314	314
0.5004	606, 599, 612	606
0.8255	982, 986, 987	986
1.2041	1436, 1433, 1437	1436
1.6091	1927, 1922, 1930	1927
2.0078	2391, 2413, 2405	2405

*Linear regression analyis results: slope = 1193.7748, intercept = 4.8443, $r^2 = 0.99997$.

Can. J. Chem. Downloaded from www.nrcresearchpress.com by 210.87.254.40 on 09/06/12
For personal use only.

TABLE 3. Comparison of the modified Dean–Stark and Syncrude bitumen, water, solids analyses on subsamples of a medium grade oil sand

Method	No. of samples analyzed	% Bitumen (average ± std. dev.)	% Water (average ± std. dev.)	% Solids (average ± std. dev.)
Modified Dean–Stark	12	11.14 ± 0.21	4.48 ± 0.16	84.38 ± 0.25
This method	12	11.00 ± 0.26	4.49 ± 0.15	84.50 ± 0.22

must be determined. The volume of extract solution is calculated from the amount of solvent blend used to extract the sample and the weights of bitumen and water extracted into the solvent. Volume correction factors for the dissolution of bitumen (1.02 mL/g) and water (0.98 mL/g) have been determined.

Accuracy and Precision

In the absence of primary standards or standard reference materials the accuracy of this method cannot be determined. The absence of determinate errors was shown by comparing the results of analysis by this method to the results by the modified Dean–Stark procedure for subsamples of the same bulk oil sand sample. Results by the two methods compare favourably. Data are shown in Table 3 for the bitumen/water/solids analysis by the two methods for subsamples of a medium grade oil sand sample. The precision of the analyses of all three components is comparable to the precision obtained from the modified Dean–Stark analyses, and is well within the 5% relative standard deviation limit expected by the Canadian Petroleum Association Tar Sands Council (2).

The method has been used routinely in Syncrude Canada Ltd.'s laboratories for several years. All types and compositions of oil sands were amenable to analysis by this method. Less than 5% of a set of 3000 core oil sand analyses had to be repeated because of analyses falling outside the 99.05 to 100.25% mass balance limits which Syncrude requires for both methods.

Conclusions

A new method was developed which allows the accurate analysis of an oil sand sample within a 40 min turnaround time. The bitumen and water in the sample are extracted from the oil sand by shaking the sample with a known quantity of dry solvent. The solvent blend, 74% toluene, 26% isopropyl alcohol (vol.%), dissolves both the bitumen and the water and results in a homogeneous liquid phase plus the solids. An aliquot of this extract is filtered and evaporated to remove the solvent and water, and the bitumen is determined gravimetrically. Another aliquot of the extract is analyzed for water content by an automatic Karl Fischer titrator. Before the percentages of bitumen and water are calculated the volume of solvent blend used is corrected to take into account dissolved bitumen and water. Solids are routinely filtered, dried, and weighed so that a mass balance check is obtained on the analysis. The elapsed time for the analysis of a single sample (solids by difference) is 40 min and the total elapsed time for a set of 10 samples (solids by difference) is 2 h. The determination of the solids content of a set of 10 samples requires an additional 40 min.

This method is a fast, safe, and reliable method for determining the bitumen, water, and solids content of oil sand samples. Analytical results can be obtained in a significantly shorter time than with the conventional method, and with equal accuracy and precision.

Acknowledgements

The authors wish to thank Syncrude Canada Ltd. for permission to publish this work and R. E. Hoyle, C. G. Paton, L. Darichuk, and K. Nastiuk of the Syncrude Research Department for their considerable assistance in this study.

1. R. G. DRAPER, A. YATES, and H. McD. CHANTLER. Canada Department of Mines and Technical Surveys, Mines Branch, Rep. FRL-211, Fuels Division. December, 1955.
2. Round Robin Study of Analytical Procedures of Various Laboratories on Assay Analysis of Athabasca Tar Sands. Canadian Petroleum Association Tar Sands Council, J. R. Eade, Shell Canada Ltd., Chairman, November, 1974.
3. M. S. PATEL. Anal. Chem. **46**, 794 (1974).
4. C. W. BOWMAN. Proc. Seventh World Petroleum Congress, **3**, 583 (1967).

Can. J. Chem. Downloaded from www.nrcresearchpress.com by 210.87.254.40 on 09/06/12
For personal use only.

Streaming current detector for reversed-phase liquid chromatography

SHIGERU TERABE, KIYOSHI YAMAMOTO, AND TEIICHI ANDO

Department of Industrial Chemistry, Faculty of Engineering, Kyoto University, Sakyo-ku, Kyoto, 606 Japan

Received September 8, 1980

This paper is dedicated to Professor W. E. Harris on the occasion of his retirement from the University of Alberta

SHIGERU TERABE, KIYOSHI YAMAMOTO, and TEIICHI ANDO. Can. J. Chem. **59**, 1531 (1981).

Fundamental characteristics of the electrokinetic detector for high performance liquid chromatography, whose operating principle is based on the measurement of the streaming current between both ends of a bundle of glass capillaries, were studied under reversed-phase chromatographic conditions. The detector is specifically sensitive to ionizable compounds like carboxylic acids and amines, but is also universally responsive to nonionic compounds. The detection limit for the former compounds was about 10^{-8} g and for the latter about 10^{-4} g. The lowest amount actually measured was 5.8×10^{-9} g. The universal detectability makes this type of detector unsuitable for gradient elution. The observed streaming current was in the range of 10^{-7} to 10^{-8} A and was highly dependent on the flow rate of the mobile phase. Characteristics of the detectors equipped with some packed beds prepared from porous materials instead of glass capillaries were also investigated.

SHIGERU TERABE, KIYOSHI YAMAMOTO et TEIICHI ANDO. Can. J. Chem. **59**, 1531 (1981).

En utilisant la chromatographie en phase inversée, on a étudié les caractéristiques fondamentales d'un détecteur électrocinétique pour un chromatographie en phase liquide à haute performance, dont le principe d'opération repose sur la mesure du courant gazeux aux extrémités d'un groupe de tubes capillaires en verre. Le détecteur est sensible spécifiquement aux composés susceptibles de s'ioniser tels les acides carboxyliques et les amines, mais d'une façon générale il est également sensible aux composés non ioniques. La limite de détection des premiers composés est d'environ 10^{-8} g et dans le cas des derniers la limite est d'environ 10^{-4} g. La plus faible quantité mesurée actuellement est de $5{,}8 \times 10^{-9}$ g. La détection universelle rend ce type de détecteur impropre à l'utilisation de gradients d'élution. Le courant observé varie de 10^{-7} à 10^{-8} A et il dépend fortement de la vitesse d'écoulement de la phase mobile. On a également étudié les caractéristiques de détecteurs équipés de lits entassés à partir de matériels poreux au lieu de tubes de verre.

[Traduit par le journal]

Introduction

Among various detecting devices for high performance liquid chromatography (HPLC), uv photometers and refractometers are now mainly used although their performance characteristics are not always satisfactory. New detectors having higher sensitivity or higher specificity than the currently available detectors are desirable for many purposes.

A new type of detector, whose operating principle is based on the measurement of electrokinetic phenomenon, has been developed by Czechoslovak chemists (1, 2). They have investigated the generation of the streaming current in low-conductivity liquids both by theory and by experiment. This paper describes the results of our studies which were made in order to explore the performance characteristics of such a detector under reversed-phase chromatographic conditions.

When a liquid is forced to flow through a capillary or a packed bed, an electrical potential is produced between its ends. This potential is called the streaming potential, and is given by (3)

$$E = (\varepsilon\zeta/4\pi\eta\kappa)P$$

where ε, κ, and η are the permittivity, specific conductivity, and viscosity of the liquid, respectively, ζ is the ζ-potential, and P is the pressure drop of the liquid transported through a capillary or a packed bed.

The parameters appearing in the above equation, ε, ζ, η, and κ, are all dependent on the composition of the liquid. When the composition of the mobile phase is kept constant, i.e., under isocratic conditions, the variation of the composition with a solute is very slight and the permittivity and viscosity of the eluent and the pressure drop can be assumed to remain practically unchanged.

This implies that the detection of a solute in the eluent by measurement of the streaming current, if possible, should be based on the change in the ζ-potential and conductivity of the eluent, and leads to the expectation that such a detector should be specifically sensitive to ionic compounds because both the ζ-potential and the conductivity are highly dependent on the concentration of ionic species in the liquid. The ζ-potential is also dependent on the material of which a capillary or a packed bed is made.

In this study, two kinds of streaming current detector cells, i.e., a bundle of glass capillaries and a polytetrafluoroethylene (PTFE) tube packed with various porous materials (porous beds) were prepared and their fundamental characteristics as a

0008-4042/81/101531-07$01.00/0

©1981 National Research Council of Canada/Conseil national de recherches du Canada

Can. J. Chem. Downloaded from www.nrcresearchpress.com by 210.87.254.40 on 09/06/12
For personal use only.

Can. J. Chem. Downloaded from www.nrcresearchpress.com by 210.87.254.40 on 09/06/12
For personal use only.

detector, such as the dependence of baseline current on the kind, composition, and flow rate of the mobile phase, the dynamic range of the response, and the detection limits for various compounds, were investigated under reversed-phase chromatographic conditions adopted most widely in modern HPLC.

Experimental

Schematic diagram of the streaming current detector is shown in Fig. 1. The eluent from a separation column was transported to the detector cell through PTFE tubing of 0.25 mm id and 1.5 mm od. The entrance end of the cell was grounded and the electrical current from the exit end to the ground was measured with a Takeda Riken TR-8651 electrometer, used as an electronic ammeter. The direction of the current was designated positive when it flowed from the exit end to the ground. The input resistance of the electrometer was chosen so that it did not exceed 1% of the resistance of the liquid in the detector cell. It was usually in the range of 10^4–10^6 Ω. In some cases, the current was measured with different input resistances in order to confirm the correct choice of the input resistance.

Figure 2 shows scanning electronmicrographs of a cross section of the bundle of glass capillaries used in this study as detector cell. The bundle was made by drawing a glass tube of 3.4 mm id and 5 mm od packed with glass capillaries of 0.1 mm id and 0.15 mm od. The glass capillary cell used was 1.5 mm od, 2 cm in length, and contained about 300 capillaries of 15–20 μm in diameter. Packed beds used for detector cells are listed in Table 1.

Three combinations of a pump and an injector were used: a Waters 6000A pump and a Waters U6K injector, a Jasco Tri Rotar and a Jasco VL-611, and a Jasco A700 and a Rheodyne 7120. When 6000A or Tri Rotar was employed, not only the pulse damper belonging to each pump but also an air damper of a stainless tube of 8 mm id and 50 cm in length were used to reduce pulsating flows generated by the reciprocating pump. In some cases, a variable-wavelength photometric detector, a Cecil CE212 or a Jasco Uvidec-100-II, was connected with the streaming current detector in series in order to evaluate the detector. Two sizes of chromatographic columns, 4.6 mm id × 20 cm and 4.6 mm id × 10 cm, were used and they were packed with Nucleosil $7C_{18}$, average particle size 7.5 μm (Macherey-Nagel & Co., Düren, G.F.R.) by the modified viscosity method recommended by the manufacturer. A column of 20 cm in length was used unless otherwise mentioned.

Methanol and acetonitrile were of HPLC-quality; acetone and tetrahydrofuran (THF) were of reagent grade. The carboxylic acids, amines, and other chemicals used as injection samples were of reagent grade and used without further purification. All the solvents and chemicals were purchased from Nakarai Chemicals Ltd. (Kyoto, Japan) or Wako Pure Chemical Industries Ltd. (Osaka, Japan). Water was purified by means of an ion-exchange column followed by single distillation in glassware.

Results and Discussion

Baseline Current

Dependence of the streaming current (baseline current) on the flow rate of the mobile phase was first examined with a glass capillary detector cell. As shown in Fig. 3, the current was directly proportional to the flow rate for all solvents tested: e.g., an increase of the flow rate of water by 0.1 mL/min caused an increase of the current by about 1.8×10^{-8} A. On the other hand, the change of the baseline current by an eluted sample is usually less than 10^{-8} A as will be shown later. This means that the fluctuation of the flow rate of the mobile phase should be kept as small as possible to assure high sensitivity in detection.

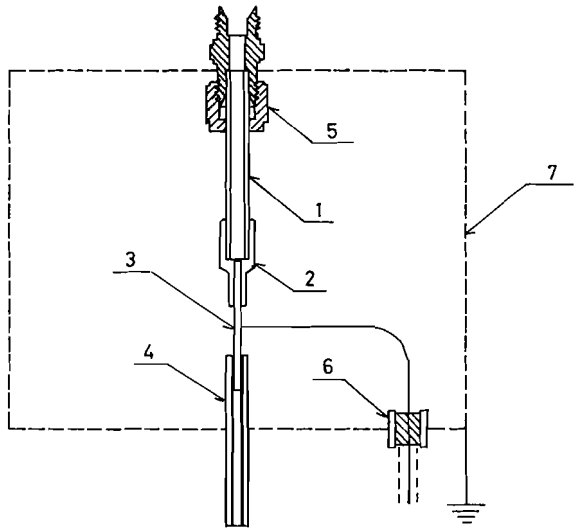

FIG. 1. Schematic diagram of the streaming current detector. *1* = Detector cell (bundle of glass capillaries or packed bed); *2* = shrinkable PTFE tubing; *3* = platinum tubing (0.25 mm id × 10 mm); *4* = PTFE tubing for draining off the mobile phase or for connecting to another detector; *5* = Swagelok union (1/16 in.); *6* = connector to electrometer; *7* = shielding box of aluminum (7 cm × 7 cm × 5 cm).

The same type of dependency was observed when the packed beds listed in Table 1 were used instead of the glass capillaries. Table 2 shows the baseline currents observed for four kinds of solvents at the flow rate of 1.0 mL/min with glass capillary and porous bed cells. The direction of the current was positive in all cases.

In Fig. 4 is shown the dependence of the baseline current on the composition of aqueous organic solvents used as mobile phase. Examples shown in Fig. 4 were obtained when the bundle of glass capillaries was used as detector cell at the flow rate of 1.0 mL/min. Dependence of the current on the compositions was also examined for the porous bed cells by using mixtures of methanol and water. No linear relationship was observed between the current and the composition of the mobile phase except for the methanol–water system in glass capillaries.

The substantial variation of the streaming current with the composition of the mobile phase makes the streaming current detector unsuitable for the gradient elution technique.

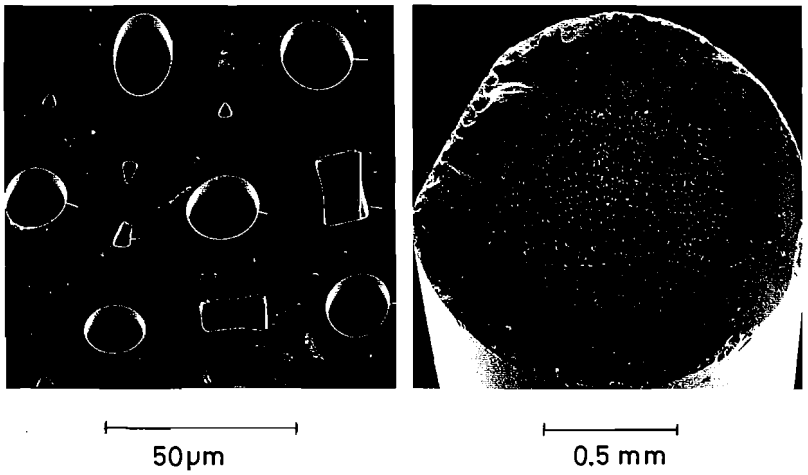

FIG. 2. Scanning electronmicrographs of a cross section of a bundle of glass capillaries.

TABLE 1. Packed beds in PTFE tubing used for the streaming current detector

Packed bed	Packing material	Size
Alumina	Woelm, neutral, 70 μm	0.5 mm id × 7 mm
Silica gel	Du Pont, Zipax, 25–37 μm	0.5 mm id × 7 mm
Silica gel	M.-Nagel, Polygosil, 10 μm	0.8 mm id × 5 mm
ODS	Du Pont, Permaphase, 25–37 μm	0.5 mm id × 7 mm
Titania	Alfa, crashed in a mortar	0.8 mm id × 10 mm

Linear Dynamic Range

As a response characteristic of the streaming current detector, the relationship between the quantity of the sample injected and the peak area was investigated. Since the change of the baseline current caused by the solute in the eluent was small relative to the baseline current, it was necessary to operate the electrometer at a higher sensitivity than for measuring the baseline current. It was performed by shifting the baseline current to near zero by means of the current compensator belonging to the electrometer.

Calibration curves for nonanoic acid, 3,4-xylidine, and *p*-nitrophenol, obtained with the glass capillary cell, are shown in Fig. 5. All the calibration curves obtained were straight in the range of two orders of sample quantity, regardless of the

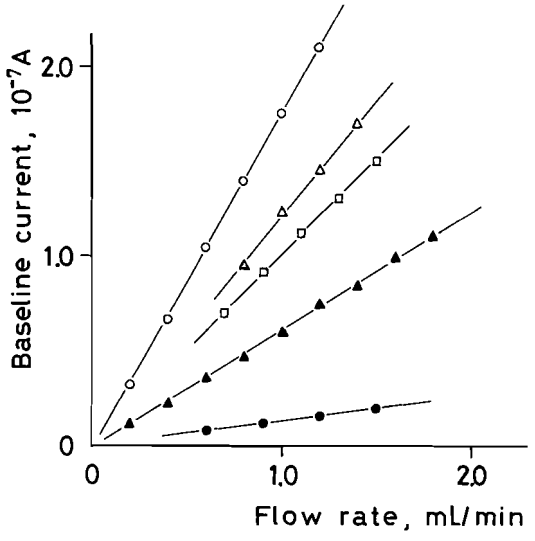

FIG. 3. Dependence of baseline current on the flow rate of mobile phase. Detector cell, bundle of glass capillaries; mobile phase, water (○), methanol (▲), acetonitrile (△), acetone (□), and THF (●).

TABLE 2. Baseline current (10^{-7} A) at the flow rate of the mobile phase of 1.0 mL/min

	Mobile phase			
Detector cell	Water	Methanol	Acetone	Acetonitrile
Bundle of glass capillaries	1.7	0.61	1.0	1.2
Packed bed				
Alumina	0.17	0.084	0.11	0.15
Silica gel (Zipax)	0.60	0.49	0.24	0.48
ODS	1.3	0.58	0.65	0.32
Silica gel (Polygosil)	0.92	0.90	0.13	0.19
Titania	0.093	0.072	0.37	0.23

Can. J. Chem. Downloaded from www.nrcresearchpress.com by 210.87.254.40 on 09/06/12
For personal use only.

Can. J. Chem. Downloaded from www.nrcresearchpress.com by 210.87.254.40 on 09/06/12
For personal use only.

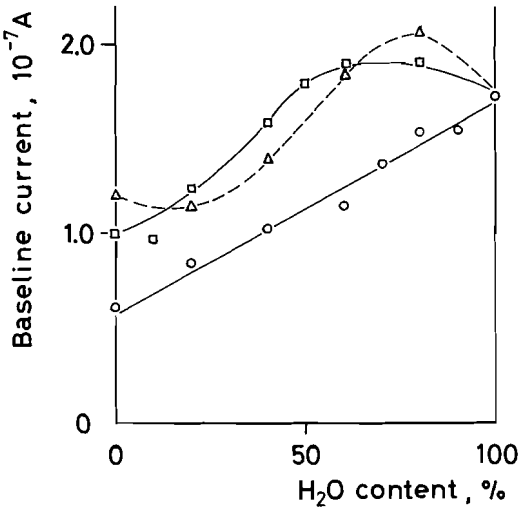

FIG. 4. Dependence of baseline current on the composition of mobile phase. Detector cell, bundle of glass capillaries; flow rate, 1.0 mL/min; mobile phase, methanol–water (○), acetone–water (□), and acetonitrile–water (△).

mobile phase or the flow rate. When the sample quantity exceeded a certain limit, the curve altered to a convex one, as indicated in Fig. 5 for nonanoic acid.

It was also noticed that the peak heights were nearly proportional to the sample quantity in the linear region of the calibration curve but not in the non-linear region: an increase of the sample quantity caused little or no increase of the peak height but a substantial increase of the peak width instead in the non-linear region.

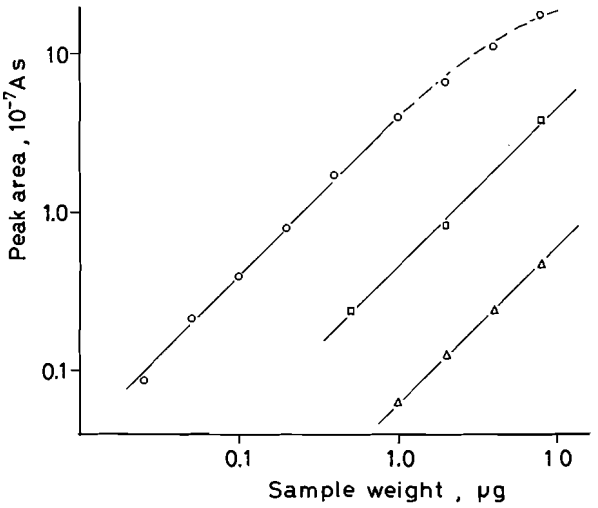

FIG. 5. Dependence of detector response on the amount of sample injected. Detector cell, bundle of glass capillaries; sample, nonanoic acid (○), 3,4-xylidine (□), and *p*-nitrophenol (△); see Table 3 concerning other conditions.

To learn the reason for this abnormal peak shape, a variable-wavelength uv photometer was connected in series with the streaming current detector and the linear dynamic ranges of the two detectors were compared by use of compounds absorbing uv light such as toluic acids. Peak heights with the uv detector were proportional to the sample quantity even in the non-linear region of the calibration curve obtained with the streaming current detector. These results evidently show that abnormal peak shapes observed at the non-linear region are not due to overloading on the separation column but to the intrinsic nature of the streaming current detector.

The linear dynamic range of the porous bed detector cells was also found to be about two orders of the quantity of the carboxylic acids investigated. No substantial differences in the linear dynamic ranges were recognized among the porous bed detector cells tested.

Noises

Two chromatograms of a mixture of three isomeric toluic acids were simultaneously recorded, as shown in Fig. 6, with the glass-capillary type streaming current detector and a uv detector connected in series. The uv detector was operated at 264 nm, where the three toluic acids had nearly the same molar absorptivity.

The marked deviation of the baseline at the injection point in the chromatogram with the streaming current detector can be attributed to the instantaneous pressure drop caused by the large volume (about 2 mL) of the sample loading loop of a Waters U6K injector, which was at atmospheric pressure before injection.

The chromatogram shown in Fig. 7 is another example of the detection with the streaming current detector; the titania bed was used as detector cell and six fatty acids having an even number of carbon atoms from C_{12} to C_{22} as samples. Periodic fluctuation observed in the baselines in Figs. 6 and 7 were associated with the pulsating flow by the reciprocating pumps employed, although the frequencies were different because of the difference in pumping mechanism of the two pumps.

This pulsating flow, which could not completely be eliminated even by the use of an air damper in addition to the pulse damper belonging to each pump, was the dominant factor responsible for the detector noises.

Relationship between Sensitivity and Streaming Current

The baseline current increased linearly with the flow rate of the mobile phase as mentioned above.

Can. J. Chem. Downloaded from www.nrcresearchpress.com by 210.87.254.40 on 09/06/12
For personal use only.

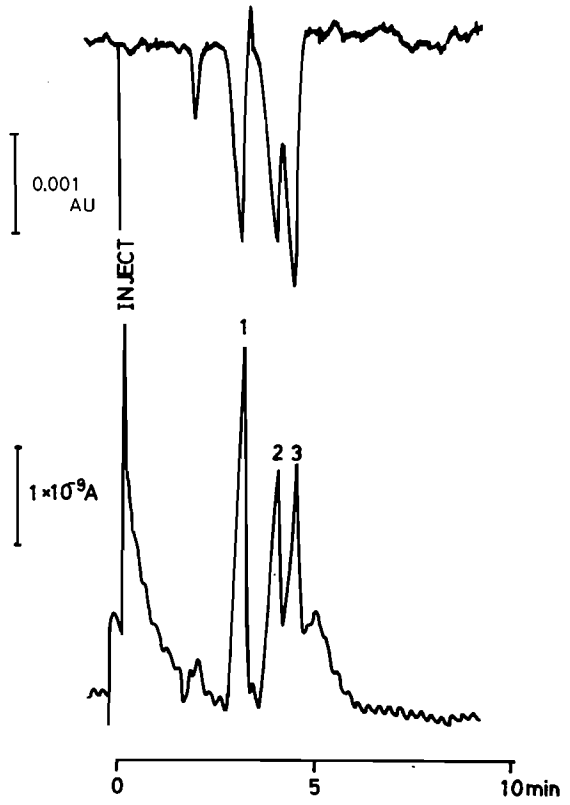

FIG. 6. Chromatogram of toluic acids obtained with the streaming current and a uv detector. Detector, a Cecil CE212 variable-wavelength uv photometer at 264 nm (upper trace) and the streaming current detector equipped with a bundle of glass capillaries (lower trace); pump, a Waters 6000A; injector, a Waters U6K; mobile phase, methanol–water (40:60); flow rate, 0.7 mL/min; sample, mixture of equal amounts (0.17 μg each) of *o*-(*1*), *m*-(*2*), and *p*-toluic acid (*3*).

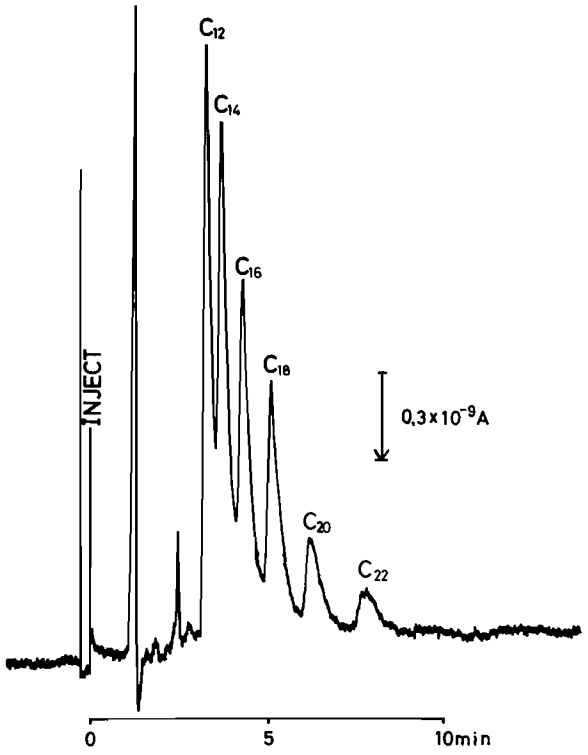

FIG. 7. Chromatogram of fatty acids of C_{12}–C_{22} obtained with the streaming current detector. Detector cell, packed bed with titania; pump, a Jasco Tri Rotar; injector, a Jasco VL-611; mobile phase, methanol; flow rate, 1.0 mL/min; sample, 1 μg each.

An example of the dependence of the detector sensitivity on the flow rate is given in Fig. 8. Peak heights were practically proportional to the flow rate, but peak areas were virtually independent of the flow rate because peak widths ordinarily decreased with an increase of the flow rate. This is a characteristic of the streaming current detector distinctly different from other detectors widely used in modern HPLC such as uv photometer, refractometer, and fluorimeter, where peak heights are independent of, but peak areas are dependent on, the flow rate.

The detection limits of this detector for various kinds of compounds will be given later. The relationship between the detection limit and the flow rate was examined under the following conditions: palmitic acid as sample, methanol as mobile phase, and the glass capillaries as detector cell. It was found that the detection limit was inversely proportional to the flow rate, i.e, the larger the baseline current, the smaller the detection limit. The same relationship was observed when the porous beds were used instead of the glass capillaries.

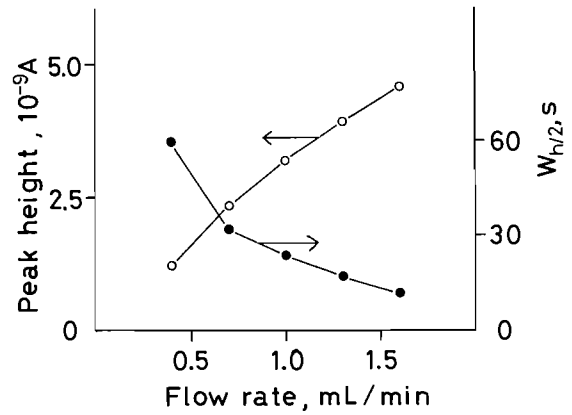

FIG. 8. Dependence of peak height and peak width at half-height on the flow rate of mobile phase. Detector cell, bundle of glass capillaries; mobile phase, methanol; sample, palmitic acid 0.3 μg.

The baseline current was seriously affected by the addition of a small amount of a salt. For exam-

Can. J. Chem. Downloaded from www.nrcresearchpress.com by 210.87.254.40 on 09/06/12
For personal use only.

TABLE 3. Detection limits of various compounds by the streaming current detector with a bundle of glass capillaries[a]

Sample	Mobile phase[b]	Flow rate (mL/min)	Direction of peak[c]	Detection limit (g)
Heptanoic acid	Methanol 50%	0.6	−	7.2×10^{-9}
Nonanoic acid	Methanol 70%	0.7	−	8.7×10^{-9}
Palmitic acid	Methanol 90%	1.0	−	2.0×10^{-8}
o-Toluic acid	Methanol 40%	0.7	−	6.0×10^{-9}
p-*t*-Butylbenzoic acid	Methanol 50%	0.7	−	8.7×10^{-9}
m-Nitrophenol	Methanol 60%	0.8	−	8.0×10^{-6}
p-Nitrophenol	Methanol 60%	0.8	−	5.0×10^{-7}
2,4-Dinitrophenol	Methanol 40%	1.0	−	6.9×10^{-9}
Picric acid	Methanol 40%	1.0	−	5.8×10^{-9}
Phenol	Methanol 80%	1.0	+	2.5×10^{-4}
N-*s*-Butylaniline	Methanol 80%	1.0	+	1.7×10^{-7}
N,*N*-Dimethylaniline	Methanol 80%	1.0	+	2.5×10^{-7}
N-Ethylaniline	Methanol 80%	1.0	+	1.9×10^{-7}
3,4-Xylidine	Methanol 80%	1.0	+	4.4×10^{-8}
p-Chloroaniline	Methanol 70%	1.0	+	1.0×10^{-6}
Pyridine	Methanol 80%	1.0	+	5.0×10^{-7}
2-*t*-Butylpyridine	Methanol 80%	1.0	+	3.0×10^{-7}
2,4,6-Trimethylpyridine[d]	Methanol 10% + AcOH 0.6 m*M*	1.0	+	1.0×10^{-6}
Benzylamine[d]	Methanol 10% + AcOH 0.4 m*M*	1.0	+	5.3×10^{-8}
Octylamine[d]	Methanol 10% + AcOH 0.6 m*M*	1.0	+	1.0×10^{-6}
Acetylacetone	Methanol 40%	1.0	+	1.0×10^{-4}
Toluene	Methanol 80%	1.0	−	5.0×10^{-4}

[a]Column, Nucleosil $7C_{18}$ 4.6 mm id × 20 cm unless otherwise mentioned.
[b]Mixture of methanol and water; content other than water is given.
[c]Minus sign means the direction of decreasing current, see text.
[d]Column, Nucleosil $7C_{18}$ 4.6 mm id × 10 cm.

ple, when sodium nitrate (1 m*M*) was added to the water as mobile phase, the baseline current was reduced to one-fifth and concurrently the sensitivity to one-tenth of the values obtained with pure water.

These results clearly show that the streaming current detector must be used at a baseline current as large as possible to secure high sensitivity in detection.

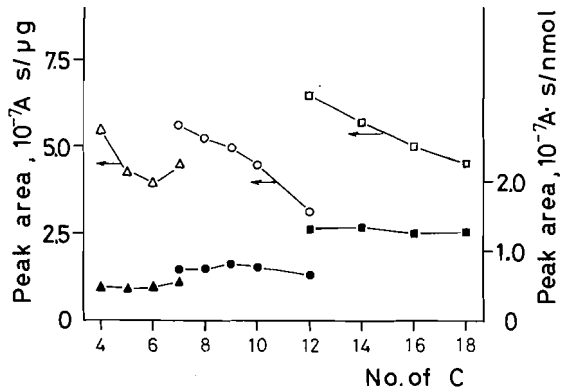

FIG. 9. Dependence of sensitivities (peak area per μg and per μmol) on the number of carbon atoms of fatty acids. Detector cell, bundle of glass capillaries; mobile phase and flow rate, methanol–water (50:50) and 0.6 mL/min (△,▲), methanol–water (70:30) and 0.7 mL/min (○,●), and methanol–water (90:10) and 1.0 mL/min (□,■).

Detection Limits for Various Compounds

Figure 9 shows the relationship between the peak area expressed per weight or per mole and the number of carbon atoms of fatty acids having C_4–C_{18} straight chains. The peak area per mole was practically constant irrespective of the number of carbon atoms, if the mobile phase was unchanged. Very probably, the constancy of the peak area per mole for fatty acids is closely related to their similarity in pK_a values (4).

The detection limit, expressed as the quantity of an injected sample which gave a peak height equal to twice the peak-to-peak noise level, was evaluated for various kinds of compounds. Values of detection limits obtained with the glass capillaries as detector cell are summarized in Table 3. The direction of peak is also indicated in the table. As a rule, acidic compounds caused a decrease of the baseline current, i.e., they gave negative peaks; on the contrary, basic compounds generally gave rise to positive peaks.

As shown in Fig. 6, the streaming current detector and a variable-wavelength uv photometer gave

TABLE 4. Detection limits of palmitic and *o*-toluic acids by the streaming current detector with a packed bed cell

Detector cell	Palmitic acid[a]		*o*-Toluic acid[b]	
	Direction of peak	Detection limit (g)	Direction of peak	Detection limit (g)
Bundle of glass capillaries	−	1.0×10^{-8}	−	6.0×10^{-9}
Packed bed				
Alumina	−	1.2×10^{-8}	−	1.1×10^{-8}
Silica gel (Zipax)	−	2.0×10^{-7}	−	1.0×10^{-8}
ODS	−	1.1×10^{-7}	−	6.2×10^{-9}
Silica gel (Polygosil)	+	2.5×10^{-7}	+	5.0×10^{-8}[c]
Titania	−	8.9×10^{-8}	−	2.5×10^{-8}

[a]Mobile phase, methanol; flow rate, 1.5 mL/min.
[b]Mobile phase, methanol–water (40:60); flow rate, 1.0 mL/min unless otherwise mentioned.
[c]Flow rate, 0.8 mL/min.

nearly equal sensitivities for aromatic carboxylic acids. The relationship between the detection limits for acidic compounds and their pK_a values (4) can be summarized as follows: the detection limits for the compounds whose pK_a values are less than 5, such as fatty acids, picric acid, toluic acid, etc., are nearly identical, whereas that for *p*-nitrophenol (pK_a 7.1) is two-orders higher and that for *m*-nitrophenol (pK_a 8.4) three-orders higher than those for the acids cited above.

The same type of pK_a effect is also found in Fig. 6, a chromatogram of a mixture of equal amounts of three isomeric toluic acids. The peak of *o*-toluic acid (pK_a 3.9) is definitely higher than those of *m*- (pK_a 4.3) and *p*-isomer (pK_a 4.4).

The detection limit for toluene is much larger than for acids, as shown in Table 3. This low sensitivity for toluene may be interpreted as follows. It is reasonable to assume that ionic dissociation of toluene in the neutral mobile phase (aq. methanol) can be neglected. If 1 mg of toluene, which is twice the detection limit, is injected, the concentration of toluene in the eluent from the separation column is expected to be more than 0.1%. The change of this order in the composition of the eluent must affect its ζ-potential, permittivity, and viscosity rather than its specific conductivity. Under such circumstances the detector can act only non-selectively and with low sensitivity. This characteristic seems to render an advantage to the detector for use in the preparative liquid chromatography.

In contrast, the ζ-potential and the conductivity are dominant factors determining the sensitivity for ionic compounds and, therefore, in such cases it can be expected that the larger the pK_a of the sample, the larger the detection limit.

Table 4 lists the detection limits of the detector equipped with porous beds for palmitic acids and *o*-toluic acids. The directions of the peak were all negative except for a silica gel (Polygosil) bed. There was no significant difference among the porous beds in any other performance characteristic including detection limits.

In conclusion, the bundle of glass capillaries is superior to the porous beds as detector cell with respects to baseline stability, reproducibility, and sensitivity, whereas the porous beds are preferred in ease of preparation and handling. Since the volume of the cell is very small, the detector has an advantage that it can be connected with another detector without any peak broadening. The streaming current detector is expected to be useful especially in specific and sensitive detection of ionic species such as carboxylic acids, amines, inorganic ions, etc.

Acknowledgements

The authors gratefully acknowledge the assistance of Mr. T. Kadono of Shionogi Research Laboratory for preparation of the bundle of glass capillaries. One of the authors (S.T.) wishes to express his gratitude to Professor R. S. Juvet, Jr. for giving him the opportunity to start this study, and to Professor W. E. Harris for generous encouragement. The authors also thank the Asahi Glass Foundation for Industrial Technology for financial assistance.

1. K. ŠLAIS and M. KREJČÍ. J. Chromatogr. **148**, 99 (1978).
2. M. KREJČÍ, K. ŠLAIS, and K. TESAŘÍK. J. Chromatogr. **149**, 645 (1978).
3. D. N. SHAW. Introduction to colloid and surface chemistry. 2nd ed. Butterworths, London. 1973.
4. G. KORTÜM, W. VOGEL, and K. ANDRUSSOV (*Editors*). Dissociation constants of organic acids in aqueous solution. Butterworths, London. 1961.

Can. J. Chem. Downloaded from www.nrcresearchpress.com by 210.87.254.40 on 09/06/12
For personal use only.

Simulation of electrochemical processes by orthogonal collocation. Spherical electrode geometry

B. STANLEY PONS

Department of Chemistry, University of Alberta, Edmonton, Alta., Canada T6G 2G2

Received September 16, 1980

This paper is dedicated to Professor W. E. Harris on the occasion of his retirement from the University of Alberta

B. STANLEY PONS. Can. J. Chem. **59**, 1538 (1981).

Discretization formulas for the digital simulation of the diffusional processes associated with a variety of electrochemical processes at a spherical electrode are given. The formulas are based on orthogonal collocation techniques. Several mechanisms are represented, and the technique is demonstrated for chronoamperometry, chronopotentiometry, and cyclic voltammetry.

B. STANLEY PONS. Can. J. Chem. **59**, 1538 (1981).

On donne des formules uniques pour la simulation numérique des processus diffusionnels associées à différentes réactions électrochimiques au niveau d'une électrode sphérique. Les formules sont établies à partir des techniques de collocation orthogonale. On représente plusieurs mécanismes, et on démontre l'application de cette technique à la chronoampérométrie, à la chronopotentiométrie et à la voltamétrie cyclique.

[Traduit par le journal]

Can. J. Chem. Downloaded from www.nrcresearchpress.com by 210.87.254.42 on 09/06/12
For personal use only.

Orthogonal collocation techniques for the simulation of second order partial differential equations have been demonstrated for a variety of problems in electrochemistry (1–7), chemical engineering (8–11), differential scanning calorimetry (12), and other fields (13). The advantages over other methods have been described, but noteworthy is generally increased accuracy for decreased computational effort (1–7).

In electrochemical diffusion problems, the algorithms needed to compute concentration profiles, chronopotentiograms, chronoamperometric responses, spectrophotometric responses of individual species, cyclic voltammograms, and chronocoulometric responses, all to planar electrode configurations, have been given. This paper deals with some of the same experiments applied to a common configuration, the static spherical electrode (Fig. 1).

The programs for solving the equations described herein have been given (7). Basically, the orthogonal collocation technique is implemented by the following steps. (*1*) Make the Ficks laws equations suitably dimensionless. (*2*) Discretize the resulting equations at the roots (zeros) of an orthogonal polynomial of suitable symmetry. The resulting set of equations now consists of first order ordinary differential equations. (*3*) Integrate the set of simultaneous differential equations to obtain the set of concentration profiles with respect to distance from the electrode surface and with time. (*4*) Use these concentrations in the suitably discretized equations to obtain the desired electrochemical parameter (current, absorbance, etc.).

Chronoamperometry

We will only consider diffusion on the solution side of the electrode–solution interface. For a chronoamperometric experiment on the simple charge transfer mechanism at a spherical electrode

$$[1] \quad A \overset{ne^-}{\rightleftharpoons} B$$

we have the following imposed conditions:

$$[A]_{R,0} = [A]_{\infty,T} = [A^0]$$

$$[2] \quad [A]_{r_0,T} = [B]_{\infty,T} = [B]_{R,0} = 0$$

$$\left(\frac{\delta[A]}{\delta R}\right)_{R=r_0} = -\left(\frac{\delta[B]}{\delta R}\right)_{R=r_0}$$

where R is the distance parameter (radial) from the center of the spherical electrode and r_0 = the radius of the electrode. Since interpolation methods using orthogonal polynomials are simpler to use in a [0,1] interval, we will define M as some distance in the R direction such that no diffusion effects are experienced there during the time frame of the experiment. The differential equation for the A species is:

0008-4042/81/101538-10$01.00/0

©1981 National Research Council of Canada/Conseil national de recherches du Canada

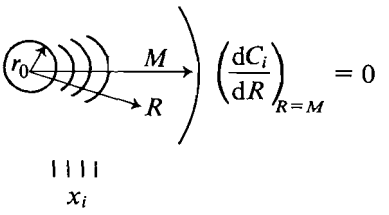

FIG. 1. Spherical electrode geometry.

$$[3] \quad \frac{\delta[A]}{\delta T} = \frac{D_A \delta^2[A]}{\delta R^2} + \frac{2D_A}{R}\frac{\delta[A]}{\delta R}$$

For dimensionless variables, we choose

$$[4] \quad c_A = \frac{[A]}{[A^0]}; \qquad t = \frac{DT}{(M - r_0)^2}; \qquad r = \frac{R - r_0}{M - r_0}$$

We note then that

$$[5] \quad dT = \frac{(M - r_0)^2}{D_A} dt; \qquad \text{and} \qquad dR = (M - r_0)\, dr$$

Substitution of the new variables [4] into [3] gives

$$[6] \quad \frac{D_A[A^0]\delta c_A}{(M - r_0)^2 \delta t} = \frac{D_A[A^0]\delta^2 c_A}{(M - r_0)^2 \delta r^2} + \left(\frac{2D_A}{(M - r_0)r + r_0}\right)\frac{[A^0]\delta c_A}{(M - r_0)\delta r}$$

which, after simplification, leads to

$$[7] \quad \frac{\delta c_A}{\delta t} = \frac{\delta^2 c_A}{\delta r^2} + \frac{2}{r + \beta}\frac{\delta c_A}{\delta r}$$

where

$$\beta = \frac{r_0}{M - r_0}$$

The general spatial derivatives in terms of their polynomial interpolation coefficients (1) are given by

$$[8a] \quad \left(\frac{dQ}{dX}\right)_{X=X_i} = \sum_{j=1}^{N+2} A_{i,j} Q(X_j, t)$$

$$[8b] \quad \left(\frac{d^2Q}{dX^2}\right)_{X=X_i} = \sum_{j=1}^{N+2} B_{i,j} Q(X_j, t)$$

where N is the order of the approximation polynomial chosen, the X_i represents the roots of that polynomial collocation points, and A_{ij} and B_{ij} are given by (10)

$$[9] \quad [A_{ij}] = \begin{bmatrix} dX_1^0/dX & dX_1^1/dX & \cdots & dX_1^{N+2}/dX \\ dX_2^0/dX & & & \\ dX_{N+2}^0/dX & & \cdots & dX_{N+2}^{N+2}/dX \end{bmatrix} \begin{bmatrix} \\ S \\ \\ \end{bmatrix}^{-1}$$

and

$$[10] \quad [B_{ij}] = \begin{bmatrix} d^2X_1^0/dX^2 & d^2X_1^1/dX^2 & \cdots & d^2X_1^{N+2}/dX \\ d^2X_2^0/dX^2 & & & \\ d^2X_{N+2}^0/dX^2 & & \cdots & d^2X_{N+2}^{N+2}/dX \end{bmatrix} \begin{bmatrix} \\ S \\ \\ \end{bmatrix}^{-1}$$

The matrix $[S]$ is given by

Can. J. Chem. Downloaded from www.nrcresearchpress.com by 210.87.254.42 on 09/06/12
For personal use only.

$$[11] \quad [S] = \begin{bmatrix} X_0{}^0 X_0{}^1 \ldots X_0{}^{N+2} \\ X_1{}^0 \quad \ldots \\ X_{N+2}{}^0 \quad \ldots X_{N+2}{}^{N+2} \end{bmatrix}$$

The algorithms for finding the roots of any orthogonal polynomial and the corresponding $[A_{ij}]$ and $[B_{ij}]$ matrices have been given previously (9). The $N + 2$ terms arise because $X = 0$ and $X = 1$ are included as roots to the orthogonal polynomial. The concentration profile will be evaluated at the collocation point, i.e. at concentric spheres surrounding the spherical electrode. Each sphere has radius $r = X_1, X_2, X_3$, etc., i.e. at the collocation points.

Equation [7] is thus written in terms of [8*a*] and [8*b*] at the discrete points X_i:

$$[12] \quad \left.\frac{dc_A}{dt}\right|_{r_i=X_i} = \sum_{j=1}^{N+2} B_{ij}c_A(r_j, t) + \frac{2}{r_i + \beta}\sum_{j=1}^{N+2} A_{ij}c_A(r_j, t)$$

Thus we have $N + 2$ simultaneous first order differential equations to solve for the $N + 2$ $c_A(r_j,t)$ unknowns. Any one of several methods may be used for solving this system of equations (1, 4, 9).

Inserting the boundary conditions [2] further defines the electrochemical method used, and reduces the number of equations from $N + 2$ to N. This is done by first expanding eq. [12] partially, exposing the boundary points at $r_1 = X_1 = 0$ and $r_{N+2} = X_{N+2} = 1$:

$$[13] \quad \left.\frac{dc_A}{dt}\right|_{r_i=X_i} = B_{i,1}c_A(0, t) + B_{i,N+2}c_A(1, t) + \sum_{j=2}^{N+1} B_{ij}c_A(r_j, t) + \frac{2}{r_i + \beta}\left[A_{i,1}c_A(0, t) + A_{i,N+2}c_A(1, t) + \sum_{j=2}^{N+1} A_{ij}c_A(r_j, t)\right]$$

We have from the original boundary conditions [2] that $c_A(0,t) = 0$ and $c_A(1,t) = 1$, so [13] becomes

$$[14] \quad \left.\frac{dc_A}{dt}\right|_{r_i=X_i} = B_{i,N+2} + \sum_{j=2}^{N+1} B_{ij}c_A(r_j, t) + \frac{2}{r_i + \beta}\left[A_{i,N+2} + \sum_{j=2}^{N+1} A_{ij}c_A(r_j, t)\right]$$

So we have one equation to solve at each of the N interior collocation points X_i, $i = 2, \ldots, N + 1$ for the N unknown $c_A(r_j,t)$.

The concentration profile for the B species is derived similarly, and leads to identically the same result as eq. [12]:

$$[15] \quad \left.\frac{dc_B}{dt}\right|_{r_i=X_i} = \sum_{j=1}^{N+2} B_{ij}c_B(r_j, t) + \frac{2}{r_i + \beta}\sum_{j=1}^{N+2} A_{ij}c_B(r_j, t)$$

Partial expansion leads again to eq. [13] with $c_B(r_j,t)$ substituted for the $c_A(r_j,t)$. However, even though it is true that one boundary condition, $c_B(i,t) = 1$ may be immediately substituted, the other boundary condition $c_B(0,t)$ is not known explicitly. This problem is easily resolved in collocation methods. We note the flux relation

$$[16] \quad D_A\left.\frac{dc_A}{dr}\right|_{r_1=X_1=0} = -D_B\left.\frac{dc_A}{dr}\right|_{r_1=X_1=0}$$

We will let $D_A = D_B$ here for convenience even though it presents no problem in setting up the equations if we do not (1, 4). The flux relation is replaced by eq. [8*a*] on each side:

$$[17] \quad \sum_{j=1}^{N+2} A_{1,j}c_A(r_j, t) = -\sum_{j=1}^{N+2} A_{1,j}c_B(r_j, t)$$

Partially expanding so that known conditions may be inserted, we have

$$[18] \quad A_{1,1}c_A(0, t) + A_{1,N+2}c_A(1, t) + \sum_{j=2}^{N+2} A_{1,j}c_A(r_j, t) = -\left[A_{1,1}c_B(r_j, t) + A_{1,N+2}c_B(1, t) + \sum_{j=2}^{N+1} A_{1,j}c_B(r_j, t)\right]$$

Can. J. Chem. Downloaded from www.nrcresearchpress.com by 210.87.254.42 on 09/06/12
For personal use only.

Can. J. Chem. Downloaded from www.nrcresearchpress.com by 210.87.254.42 on 09/06/12
For personal use only.

Inserting known quantities, we deduce

$$[19]\quad A_{1,N+2} + \sum_{j=1}^{N+1} A_{1,j}c_A(r_j, t) = -\left[A_{1,1}c_B(0, t) + \sum_{j=2}^{N+1} A_{1,j}c_B(r_j, t)\right]$$

Solving for our unknown boundary condition,

$$[20]\quad c_B(0, t) = U + \sum_{j=2}^{N+1} C_{1,j}(c_A(r_j, t) + c_B(r_j, t))$$

where

$$U = -\frac{A_{1,N+2}}{A_{1,1}}; \qquad \text{and} \qquad C_{1,j} = -\frac{A_{1,j}}{A_{1,1}}$$

We can now substitute this explicit value for $c_B(0,t)$ in eq. [15], along with $c_B(1,t) = 0$ to obtain the equation necessary to represent the concentration profiles for B:

$$[21]\quad \left.\frac{dc_B}{dt}\right|_{r_i=X_i} = V_i + \sum_{j=2}^{N+1} D_{ij}c_A(r_j, t) + \sum_{j=2}^{N+1} E_{ij}c_B(r_j, t)$$

where

$$V_i = B_{i,1}U + \frac{2A_{i,1}U}{r_i + \beta}$$

$$D_{ij} = C_{1,j}\left[B_{i,1} + \frac{2A_{i,1}}{r_i + \beta}\right]$$

$$E_{ij} = B_{ij} + C_{1,j}\left[B_{i,1} + \frac{2A_{i,1}}{r_i + \beta}\right] + \frac{2A_{ij}}{r_i + \beta}$$

Again we have N equations in the N unknown $c_B(r_j,t)$ to solve simultaneously.

Table 1 compares results obtained for the current obtained by eq. [33] and the analytic solution for this case, which is

$$[22]\quad i = \frac{nFAD_A^{1/2}[A^0]}{\pi^{1/2}T^{1/2}} + \frac{nFAD_A[A^0]}{r_0}$$

We use, by example, $D_A = 1 \times 10^{-5}$ cm^2 s^{-1}, $[A^0] = 10^{-6}$ mol cm^{-3}, A $= \pi r_0^2$, $r_0 = 0.1$ cm, and $n = 1$. β for the example was 10^4.

For the mechanism

$$A \rightleftharpoons B \xrightarrow{k} C$$

the profile for the A species is the same as eq. [14]. The B species has a different profile due to loss of material through the chemical reaction, i.e.

$$[23]\quad \frac{\delta[B]}{\delta t} = D_B\frac{\delta^2[B]}{\delta R^2} + \frac{2D_B}{R}\frac{\delta[B]}{\delta R} - k[B]$$

After discretization to the collocation points and insertion of the dimensionless variables [4], we have

$$[24]\quad \left.\frac{dc_B}{dt}\right|_{r_i=X_i} = \sum_{j=1}^{N+2} B_{i,j}c_B(r_j, t) + \frac{2}{r_i + \beta}\sum_{j=1}^{N+2} A_{i,j}c_B(r_j, t) - \alpha c_B(r_i, t)$$

where

$$\alpha = \frac{k(M - r_0)^2}{D_B}$$

Continuing precisely as for the simple electron transfer case, except with the addition of this last chemical kinetic term, we find that

TABLE 1. Comparison of exact and simulated currents for the simple change transfer chronoamperometric experiment. ($N = 6$ collocation points), see text for parameters

Time (s)	i_{exact} (mA)	$i_{simulated}$ (mA)
1×10^{-5}	1.7104	1.7104
1×10^{-4}	0.5411	0.5412
1×10^{-3}	0.1713	0.1712
1×10^{-2}	0.0054	0.0054
1×10^{-1}	0.0017	0.0017
1×10^{0}	0.0001	0.0001

$$[25] \quad \left.\frac{dc_B}{dt}\right|_{r_i=X_i} = V_i + \sum_{j=2}^{N+1} D_{ij}c_A(r_j, t) + \sum_{j=2}^{N+1} E_{ij}c_B(r_j, t) - \alpha c_B(r_j, t)$$

For the catalytic mechanism

$$[26] \quad A \rightleftharpoons B \xrightarrow{k} C + A$$

both the A and B profiles are modified by the presence of the chemical reaction. The differential equations are

$$[27] \quad \frac{\delta[A]}{\delta t} = D_A\frac{\delta^2[A]}{\delta R^2} + \frac{2D_A}{R}\frac{\delta[A]}{\delta R} + k[B]$$

$$\frac{\delta[B]}{\delta t} = D_B\frac{\delta^2[B]}{\delta R^2} + \frac{2D_A}{R}\frac{\delta[B]}{\delta R} - k[B]$$

The boundary conditions are exactly as the previous cases, so that discretization is the same. We find that

$$[28] \quad \left.\frac{dc_A}{dt}\right|_{r_i=X_i} = B_{i,N+2} + \sum_{j=2}^{N+1} B_{ij}c_A(r_j, t) + \frac{2}{r_i + \beta}\left[A_{i,N+2} + \sum_{j=2}^{N+1} A_{ij}c_A(r_j, t)\right] + \alpha c_B(r_j, t)$$

$$[29] \quad \left.\frac{dc_B}{dt}\right|_{r_i=X_i} = V_i + \sum_{j=2}^{N+1} D_{ij}c_A(r_j, t) + \sum_{j=2}^{N+1} E_{ij}c_B(r_j, t) - \alpha c_B(r_j, t)$$

again letting $D_A = D_B$.

To calculate the current at any time for the mechanisms listed above under the chronoamperometric experiment, we note the following:

$$[30] \quad i = nFAD_A\left(\frac{d[A]}{dR}\right)_{R=0}$$

where A is the electrode surface area and F is the Faraday constant. The flux term is converted to dimensionless terms by insertion of the newly defined variables (4).

$$[31] \quad i = \frac{nFAD[A^0]}{M - r_0}\left(\frac{dc_A}{dr}\right)_{r_1=X_1=0}$$

The flux term may then be discretized to

$$[32] \quad i = \frac{nFAD[A^0]}{M - r_0}\left[A_{1,1}c_A(0, t) + A_{1,N+2}c_A(1, t) + \sum_{j=2}^{N+1} A_{1,j}c_A(r_j, t)\right]$$

or

$$[33] \quad i = \frac{nFAD[A^0]}{M - r_0}\left[A_{1,N+2} + \sum_{j=2}^{N+1} A_{1,j}c_A(r_j, t)\right]$$

after insertion of the known values of $c_A(0,t)$ and $c_A(1,t)$.

So the current i may be calculated at any time $T = (M - r_0)^2t/D$ by insertion of the calculated concentrations from eqs. [14] or [28] into eq. [33]. If there are additional electroactive species in the mechanism,

Can. J. Chem. Downloaded from www.nrcresearchpress.com by 210.87.254.42 on 09/06/12
For personal use only.

Can. J. Chem. Downloaded from www.nrcresearchpress.com by 210.87.254.42 on 09/06/12
For personal use only.

their contribution is simply added into eq. [33], since generally,

$$[34] \quad i = \frac{nFAD[A^0]}{M - r_0} \sum_{n=1}^{m} \left(\frac{dc_n}{dr}\right)_{r=X_1=0}$$

where m is the total number of electroactive species.

The charge or spectroelectrochemical absorbance can be calculated by use of Gaussian quadrature weights (4, 9, 10) for the integration of the current in time or the concentration profiles in time.

Cyclic Voltammetric Response

Several modifications have to be made to the method of Speiser and Rieker (6) to develop the cyclic voltammetric responses for the spherical electrode. We define new dimensionless time and distance variables

$$[35] \quad t = \frac{DTa}{(M - r_0)^2} \quad \text{and} \quad r = \frac{(R - r_0)a^{1/2}}{M - r_0}$$

where

$$a = nFv/R'T'$$

with v = the potential sweep rate in V s^{-1}, R' the gas constant, and T' the temperature. Thus,

$$dT = (M - r_0)^2 dt/aD$$

and

$$[36] \quad dR = (M - r_0)dr/a^{1/2}$$

For the simple electron transfer reaction [1], the differential equation [6] becomes

$$[37] \quad \frac{aD[A^0]\delta c_A}{(M - r_0)^2 \delta t} = \frac{aD[A^0]\delta^2 c_A}{(M - r_0)^2 \delta r^2} + \frac{2D[A^0]}{((M - r_0)r + r_0)(M - r_0)} \frac{\delta c_A}{\delta r}$$

which simplifies to

$$[38] \quad \frac{\delta c_A}{\delta t} = \frac{\delta^2 c_A}{\delta r^2} + \frac{2a^{1/2}}{r + \beta} \frac{\delta c_A}{\delta r}$$

The derivation now proceeds as described by Speiser and Rieker (6).

The cyclic voltammetric boundary conditions are

$$[39] \quad \begin{aligned} &[A]_{R,0} = [A]_{\infty,t} = [A^0] \\ &[B]_{R,0} = [B]_{\infty,t} = 0 \\ &(\delta[A]/\delta R)_{R=0} = -(\delta[A]/\delta R)_{R=0} \\ &[A]_{0,T}/[B]_{0,T} = \exp[nF/R'T'(E^{\ominus}_{A/B} - E)] = \theta_{A/B} S_\lambda(t) \end{aligned}$$

Inserting the potential sweep rate [14] v, we have

$$\theta_{A/B} = \exp[nF/R'T'(E^{\ominus}_{A/B} - E_{START})]$$

$$[40] \quad S_\lambda(T) = \begin{cases} \exp(-nFvT/R'T') = \exp(-aT) & \text{for } T \le T_\lambda \\ \exp(at - 2aT_\lambda) & \text{for } T_\lambda \le T \le 2T \end{cases}$$

where T is the time when the forward potential sweep is reversed.

We convert eqs. [39] to dimensionless form normalized to t and M:

$$[41] \quad \begin{aligned} &c_A(r, 0) = c_A(1, t) = 1 \\ &c_B(r, 0) = c_B(1, t) = 0 \\ &\left(\frac{\delta c_A}{\delta r}\right)_{r=0} = \left(\frac{-\delta c_B}{\delta r}\right)_{r=0} \\ &\frac{c_A(0, t)}{c_B(0, t)} = \theta_{A/B} S_\lambda(t) \end{aligned}$$

Can. J. Chem. Downloaded from www.nrcresearchpress.com by 210.87.254.42 on 09/06/12
For personal use only.

Discretizing using eqs. [8*a*] and [8*b*] on [38], we have

$$[42]\quad \left.\frac{dc_A}{dt}\right|_{r_i=X_i} = \sum_{j=1}^{N+2} B_{ij}c_A(r_j, t) + \frac{2a^{1/2}}{r_i + \beta}\sum_{j=1}^{N+2} A_{ij}c_A(r_j, t)$$

or after partial expansion

$$[43]\quad \left.\frac{dc_A}{dt}\right|_{r_i=X_i} = B_{i,1}c_A(0, t) + B_{i,N+2}c_A(1, t) + \sum_{j=2}^{N+1} B_{ij}c_A(r_j, t) + \frac{2a^{1/2}}{r_i + \beta}\left[A_{i,1}c_A(0, t) + A_{i,N+2}c_A(1, t) + \sum_{j=2}^{N+1} A_{ij}c_A(r_j, t)\right]$$

Inserting the explicit boundary conditions, we have

$$[44]\quad \left.\frac{dc_A}{dt}\right|_{r_i=X_i} = B_{i,1}c_A(0, t) + B_{i,N+2} + \sum_{j=2}^{N+1} B_{ij}c_A(r_j, t) + \frac{2a^{1/2}}{r_i + \beta}\left[A_{i,1}c_A(0, t) + A_{i,N+2} + \sum_{j=2}^{N+1} A_{ij}c_A(r_j, t)\right]$$

Identical treatment for the B species yields

$$[45]\quad \left.\frac{dc_B}{dt}\right|_{r_i=X_i} = B_{i,1}c_B(0, t) + \sum_{j=2}^{N+1} B_{ij}c_B(r_j, t) + \frac{2a^{1/2}}{r_i + \beta}\left[A_{i,1}c_B(0, t) + \sum_{j=2}^{N+1} A_{ij}c_B(r_j, t)\right]$$

We discretize the flux relation in [41] to get an equation relating $c_A(0,t)$ and $c_B(0,t)$, presently implicit boundary conditions.

$$[46]\quad \sum_{j=1}^{N+2} A_{k,j}c_A(r_j, t) = -\sum_{j=1}^{N+2} A_{i,j}c_B(r_j, t)$$

Speiser and Rieker (6) showed that after expansion of eq. [46], one may then substitute in eq. [44] and arrive at the following result giving the time (potential) dependence of $c_A(0,t)$ and $c_B(0,t)$:

$$[47]\quad \begin{aligned} c_A(0, t) &= -\frac{\theta_{A/B}S_\lambda(t)}{A_{1,1}[1 + \theta_{A/B}S_\lambda(t)]}A_{1,N+2} + \sum_{j=2}^{N+1} A_{1,j}(c_A(r_j, t) + c_B(r_j, t)) \\ c_B(0, t) &= -\frac{1}{A_{1,1}[1 + \theta_{A/B}S_\lambda(t)]}A_{1,N+2} + \sum_{j=2}^{N+1} A_{1,j}(c_A(r_j, t) + c_B(r_j, t)) \end{aligned}$$

Inserting these time-dependent boundary conditions into the discretized eqs. [44] and [45] yield the $2N$ simultaneous first order differential equations necessary to solve for the concentration profiles in time:

$$[48]\quad \begin{aligned} \left.\frac{dc_A}{dt}\right|_{r_i=X_i} &= W_i + \sum_{j=2}^{N+1} F_{ij}c_A(r_j, t) + \sum_{j=2}^{N+1} G_{ij}c_B(r_j, t) \\ \left.\frac{dc_B}{dt}\right|_{r_i=X_i} &= X_i + \sum_{j=2}^{N+1} H_{ij}c_A(r_j, t) + \sum_{j=2}^{N+1} I_{ij}c_B(r_j, t) \end{aligned}$$

with

$$W_i = \frac{\theta_{A/B}S_\lambda(t)}{A_{1,1}[1 + \theta_{A/B}S_\lambda(t)]}\left[B_{i,1}A_{1,N+2} + \frac{2a^{1/2}}{r_i + \beta}A_{i,1}A_{1,N+2}\right] + B_{i,N+2} + \frac{2a^{1/2}}{r_i + \beta}A_{i,N+2}$$

$$F_{ij} = B_{ij} + \frac{2a^{1/2}}{r_i + \beta}A_{ij} - \frac{2a^{1/2}A_{i,1}A_{1,j}\theta_{A/B}S_\lambda(t)}{(r_i + \beta)A_{1,1}[1 + \theta_{A/B}S_\lambda(t)]} - \frac{B_{i,1}A_{1,j}\theta_{A/B}S_\lambda(t)}{A_{1,1}[1 - \theta_{A/B}S_\lambda(t)]}$$

$$G_{ij} = \frac{\theta_{A/B}S_\lambda(t)}{A_{1,1}[1 + \theta_{A/B}S_\lambda(t)]}\left[B_{i,1}A_{1,j} + \frac{2a^{1/2}A_{i,1}A_{1,j}}{(r_i + \beta)}\right]$$

$$W_i = -\frac{1}{A_{1,1}[1 + \theta_{A/B}S_\lambda(t)]}\left[B_{i,1}A_{1,N+2} + \frac{2a^{1/2}}{r_i + \beta}A_{i,1}A_{1,N+2}\right]$$

$$H_{ij} = -\frac{1}{A_{1,1}[1 + \theta_{A/B}S_\lambda(t)]}\left[B_{i,1}A_{1,j} - \frac{2a^{1/2}A_{i,1}A_{1,j}}{r_i + \beta}\right]$$

$$I_{ij} = B_{ij} + \frac{2a^{1/2}}{r_i + \beta}A_{ij} - \frac{2a^{1/2}A_{j,1}A_{1,j}}{(r_i + \beta)A_{1,1}[1 + \theta_{A/B}S_\lambda(t)]} - \frac{B_{i,1}A_{1,j}}{A_{1,1}[1 + \theta_{A/B}S_\lambda(t)]}$$

The $2N$ equations [48] are solved simultaneously as before to get $c_A(r_j,t)$ and $c_B(r_j,t)$. The current response is represented similar to the chronoamperometric case:

$$[49] \quad i = nFAD_A\left(\frac{\delta[A]}{\delta R}\right)_{R=0}$$

or in the dimensionless space

$$[50] \quad i = \frac{nFAD_A[A^0]a^{1/2}}{(M - r_0)}\left(\frac{dc_A}{dr}\right)_{r_1 = X_1 = 0}$$

Discretizing the flux and inserting the boundary conditions leads to [6]

$$[51] \quad \left.\frac{dc_A}{dr}\right|_{r_1 = X_1} = \frac{1}{1 + \theta_{A/B}S_\lambda(t)}\left[A_{1,N+2} + \sum_{j=2}^{N+1} A_{1,j}c_A(r_j, t) - \theta_{A/B}S_\lambda(t)\sum_{j=2}^{N+1} A_{1,j}c_B(r_j, t)\right]$$

So that

$$[52] \quad i = \frac{nFAD_A[A^0]a^{1/2}}{(M - r_0)}\left[\frac{1}{1 + \theta_{A/B}S_\lambda(t)}\left[A_{1,N+2} + \sum_{j=2}^{N+1} A_{1,j}c_A(r_j, t) - \theta_{A/B}S_\lambda(t)\sum_{j=2}^{N+1} A_{1,j}c_B(r_j, t)\right]\right]$$

The concentrations $c_A(r_i,t)$ and $c_B(r_i,t)$ found at each time $T = (M - r_0)^2t/aD$ are used in eq. [52] to determine the current as a function of time and hence potential by the relation

$$[53] \quad E = \begin{cases} E_{START} + \dfrac{(M - r_0)^2tR'T'}{nFD} & t \leq t \\ E_{START} + 2vt_\lambda - \dfrac{(M - r_0)^2tR'T'}{nFD} & t \leq t \leq 2t \end{cases}$$

where t is the dimensionless potential sweep reversal time

$$t_\lambda = \frac{aDT_\lambda}{(M - r_0)^2}$$

Chronopotentiometry

The chronopotentiometric case for planar electrodes was described in a previous paper. For a chronopotentiometric response to the simple reversible charge transfer reaction, we must consider the following conditions:

$$[54] \quad \begin{aligned} &[A]_{r,0} = [A]_{\infty,T} = [A^0] \\ &[B]_{r,0} = [B]_{\infty,T} = 0 \\ &E + E^{\ominus}_{A/B} - \frac{R'T'}{nF}\ln[B]_{r_0} \end{aligned}$$

$$[55] \quad \left(\frac{\delta[A]}{\delta R}\right)_{r_0} = -\left(\frac{\delta[B]}{\delta R}\right)_{r_0}$$

$$i = nFAD_A\left(\frac{\delta[A]}{\delta R}\right)_{R=r_0} = \text{constant}$$

The new dimensionless parameters are

$$[56] \quad t = T/\tau; \qquad r = \frac{R - r_0}{M - r_0}$$

Can. J. Chem. Downloaded from www.nrcresearchpress.com by 210.87.254.42 on 09/06/12
For personal use only.

where τ is the transition time of the experiment. Insertion of these values into the differential equation [3] and simplification yields

$$[57]\quad \frac{\delta c_A}{\delta t} = \alpha \frac{\delta^2 c_A}{\delta r} + \frac{2\alpha}{r + \beta} \frac{\delta c_A}{\delta r}$$

where

$$\alpha = D\tau/(M - r_0)^2$$

The conditions [54] and [55] in dimensionless form become

$$[58]\quad \begin{aligned} c_A(r,0) &= c_A(1,t) = 1 \\ c_B(r,0) &= c_B(1,t) = 0 \\ \left(\frac{\delta c_A}{\delta r}\right)_{r_0} &= -\left(\frac{\delta c_B}{\delta r}\right)_{r_0} \end{aligned}$$

$$[59]\quad i = \frac{nFAD[A^0]}{(M - r_0)} \left(\frac{dc_A}{dr}\right)_{r_0} = \frac{nFAD^{1/2}[A^0]\alpha^{1/2}}{\tau^{1/2}} \left(\frac{dc_A}{dr}\right)_{r_0}$$

The flux relation at the electrode is given from [8*a*]

$$[60]\quad \begin{aligned} \left(\frac{dc_A}{dr}\right)_{r_0} &= \sum_{j=1}^{N+2} A_{1,j} c_A(r_j, t) \\ \left(\frac{dc_B}{dr}\right)_{r_0} &= \sum_{j=1}^{N+2} A_{1,j} c_B(r_j, t) \end{aligned}$$

Upon entering the known boundary conditions and expanding, and then substituting these into [59] we have

$$[61]\quad \begin{aligned} c_A(0, t) &= Q - \sum_{j=2}^{N+1} a_j c_A(r_j, t) \\ c_B(0, t) &= R - \sum_{j=2}^{N+1} a_j c_B(r_j, t) \end{aligned}$$

with

$$Q = \frac{1}{A_{1,1}} \left[\frac{i\tau^{1/2}}{nFA[A^0]D^{1/2}\alpha^{1/2}} - A_{1,N+2}\right]$$

$$R = \frac{1}{A_{1,1}} \left[\frac{i\tau^{1/2}}{nFA[A^0]D^{1/2}\alpha^{1/2}}\right]$$

$$a_j = \frac{A_{1,j}}{A_{1,1}}$$

The discretized equations for A and B are thus

$$[62]\quad \begin{aligned} \left.\frac{dc_A}{dt}\right|_{r_i = X_i} &= \sum_{j=1}^{N+2} B_{ij} c_A(r_j, t) + \frac{2\alpha}{r_i + \beta} \sum_{j=1}^{N+2} A_{ij} c_A(r_j, t) \\ \left.\frac{dc_B}{dt}\right|_{r_i = X_i} &= \sum_{j=1}^{N+2} B_{ij} c_B(r_j, t) + \frac{2\alpha}{r_i + \beta} \sum_{j=1}^{N+2} A_{ij} c_B(r_j, t) \end{aligned}$$

The known boundary conditions from eqs. [58] and [61] are entered, and we have

$$[63]\quad \begin{aligned} \left.\frac{dc_A}{dt}\right|_{r_i = X_i} &= \alpha Q_i' + \alpha \sum_{j=2}^{N+1} b_{ij} c_A(r_j, t) \\ \left.\frac{dc_B}{dt}\right|_{r_i = X_i} &= \alpha R_i' + \alpha \sum_{j=2}^{N+1} b_{ij} c_B(r_j, t) \end{aligned}$$

Can. J. Chem. Downloaded from www.nrcresearchpress.com by 210.87.254.42 on 09/06/12
For personal use only.

where

$$Q_i' = B_{i,1}Q + B_{i,N+2} + \frac{2\alpha}{r_i + \beta}(A_{i,1}Q + A_{i,N+2})$$

$$R_i' = B_{i,1}R + \frac{2A_{i,1}R}{r_i + \beta}$$

$$b_{ij} = -B_{i,1}a_j + B_{ij} = \frac{2}{r_i + \beta}(A_{i,1}a_j - A_{ij})$$

The usual display of the response is given by

$$[64] \quad E = E^{\circ}_{A/B} - \frac{R'T'}{nF} \ln \left(\frac{c_B(0, t)}{c_A(0, t)}\right)$$

where the two concentration terms in parentheses are found from eq. [61]. The concentration terms in [61] are found by integration of the simultaneous equation [63] by the methods described (1, 4, 5, 9) previously.

1. L. F. WHITING and P. W. CARR. J. Electroanal. Chem. **81**, 1 (1977).
2. A. BEWICK, J. MELLOR, and B. S. PONS. Electrochim. Acta, **23**, 77 (1978).
3. A. BEWICK, J. MELLOR, and B. S. PONS. Electrochim. Acta, **25**, 931 (1980).
4. B. S. PONS and P. P. SCHMIDT. Electrochim. Acta, **25**, 987 (1980).
5. B. S. PONS. Electrochim. Acta. In press.
6. B. SPEISER and A. RIEKER. J. Electroanal. Chem. **102**, 1 (1979).
7. B. SPEISER. J. Electroanal. Chem. **110**, 69 (1980).
8. J. VILLADSEN. Selected approximation methods for chemical engineering problems. Reproset, Copenhagen. 1970.
9. J. VILLADSEN and M. L. MICHELSEN. Solution of differential equation models by polynomial approximation. Prentice Hall, Englewood Cliffs, NJ. 1978.
10. J. VILLADSEN and W. E. STEWART. Chem. Eng. Sci. **22**, 1483 (1967).
11. J. VILLADSEN and J. P. SORENSON. Chem. Eng. Sci. **24**, 1337 (1969).
12. L. F. WHITING and P. W. CARR. Anal. Chem. **50**, 1997 (1978).
13. B. A. FINLAYSON. *In* Mathematics in science and engineering. Vol. 87. *Edited by* Richard Bellman. Academic Press, New York, NY. 1972.

Can. J. Chem. Downloaded from www.nrcresearchpress.com by 210.87.254.42 on 09/06/12
For personal use only.

Ionic strength effect on extraction of potassium complexed with crown ether 18-crown-6. Preliminary communication

IZAAK MAURITS KOLTHOFF

Department of Chemistry, University of Minnesota, 207 Pleasant Street SE, Minneapolis, MN 55455, U.S.A.

Received October 15, 1980

This paper is dedicated to Professor W. E. Harris on the occasion of his retirement from the University of Alberta

IZAAK MAURITS KOLTHOFF. Can. J. Chem. **59**, 1548 (1981).

As part of a broad study of the factors which affect extraction of salts of cations, complexed with an uncharged ligand, L, a critical study has been made of the extraction into dichloromethane of K^+ complexed with 18-crown ether-6 in the form of picrate (LKPi). In using extraction analysis for the determination of very small concentrations of K^+ in the presence of other salts activities of $(K^+)_w$ and $(Pi^-)_w$ in the aqueous phase must be written in the expression for K^{ext}(LKPi). The salting out effect on $P(L) = [L]_o/[L]_w$ can greatly affect the concentration of potassium ions left in the aqueous phase. Selectivity of K^+/Na^+ in extractions with 18-crown-6 has been determined.

The extraction method is very suitable for the determination of traces of potassium in salts of sodium, magnesium, and calcium after calibration with, e.g., potassium chloride in potassium-free salts and also, after proper calibration, in routine analysis of liquids which contain little K^+ and a large excess of Na^+ (e.g. sea water, blood serum).

IZAAK MAURITS KOLTHOFF. Can. J. Chem. **59**, 1548 (1981).

Dans le cadre d'une étude complète des facteurs influençant l'extraction des sels des cations, complexés à un ligand non chargé, L, on a réalisé une étude critique de l'extraction à l'aide de dichlorométhane de K^+, existant sous formes picrates (LKPi), complexés par de l'éther 18-couronne-6. Lors de l'utilisation de l'analyse par extraction dans le but de déterminer des concentrations très faibles d'ions K^+ en présence d'autres sels, on doit décrire les activités $(K^+)_w$ et $(Pi^-)_w$ en phase aqueuse par l'expression K^{ext}(LKPi). L'effet de relargage sur $P(L) = [L]_o/[L]_w$ peut affecter d'une façon importante la concentration résiduelle en ions potassium de la phase aqueuse. On a déterminé la sélectivité K^+/Na^+ lors d'extractions à l'éther 18-couronne-6.

La méthode d'extraction est très appropriée à la détermination de traces de potassium dans des sels de sodium, de magnésium et de calcium après calibration avec, par exemple, du chlorure de potassium dans des sels libres de potassium et également, après une calibration convenable, à l'analyse de routine de liquides qui contiennent peu de K^+ et un grand excès de Na^+ (par exemple l'eau de mer, le sérum sanguin).

[Traduit par le journal]

Introduction

In recent years a large number of papers, many of them from Japanese laboratories, have been published dealing with extraction constants of salts composed of alkali or alkaline earth ions complexed with a crown ether and a lipophilic anion (usually picrate). Eisenman *et al.* (1) represented the extraction equilibrium as

$$[1] \quad M^+_w + A^-_w + L_o \rightleftharpoons (LMA)_o$$

in which the subscripts w and o denote the aqueous and organic phases, while L denotes the ligand. The equilibrium constant of reaction [1] was designated by them as the extraction constant K^{ext}.

$$[2] \quad K^{ext} = [LMA]_o/(a_{M^+})_w(a_{A^-})_w[L]_o = [LMA]_o/y_{M^+}[M^+]_w y_{A^-}[A^-]_w[L]_o$$

Eisenman, as well as Frensdorff (2), who with Pedersen (3) was the first to apply crown ethers in extractions, used such low ionic concentrations (potassium and sodium) that the activity coefficients y_{M^+} and y_{A^-} in eq. [2] could be taken equal to unity. This is also the situation in more recent publications in which "extraction constants"

$$K^{ext}_{conc} = [LMA]_o/[M^+]_w[A^-]_w[L]_o$$

have been reported where concentrations have been used instead of activities. As a result of the slight dissociation of electrolytes in the low dielectric constant organic phase, even at high ionic strengths in the aqueous phase, the activity of L in the organic phase can be taken equal to its concentration. The effect of ionic strength on the distribution of L

$$[3] \quad P(L) = [L]_o/[L]_w$$

can be large on $[M^+]_w$ at extraction equilibrium. The extraction method has been applied at appreciable ionic strengths, e.g. for determination of K^+ in blood serum (4) and in sea water (5) when K^{ext}_{conc} differs considerably from K^{ext} in eq. [2].

At present we are engaged in a detailed study of various factors which affect extraction constants of potassium and sodium, including selectivity of K^+/Na^+ with various crown ethers, extraction of

0008-4042/81/101548-04$01.00/0

©1981 National Research Council of Canada/Conseil national de recherches du Canada

Can. J. Chem. Downloaded from www.nrcresearchpress.com by 210.87.254.5 on 09/06/12
For personal use only.

Can. J. Chem. Downloaded from www.nrcresearchpress.com by 210.87.254.5 on 09/06/12
For personal use only.

homoconjugated ($LMA \cdot (HA)_n$) and heteroconjugated ($LMA \cdot (HX)_n$) salts, effect of organic polar additives to the aqueous phase, and effect of temperature.

In the present note we report mainly the effect of ionic strength on the extraction constant of potassium, using 18-crown-6 as the ligand, L, and picrate (Pi^-) as the anion. Examples of the use of extraction analysis for determination of traces of potassium in lithium and sodium salts are also presented. Dichloromethane has served as an extractant.

Experimental

The ligand, 18-crown-6, was a Parish Co., Provo, Utah, product. Its purity was estimated by the following extraction procedure: aqueous solutions of the sample, which were 3.5×10^{-4} to 1.2×10^{-3} *M* in L, 5×10^{-3} *M* in potassium picrate, and 2.5×10^{-2} *M* in potassium hydroxide, were extracted with an equal volume of dichloromethane. The extraction of the residual aqueous phase was repeated. It appeared that no more LKPi was extracted after the second extraction, as the absorbance became practically equal to zero. The concentration of LKPi in the organic phase was determined spectrophotometrically at 370 nm. The molar extinction coefficient, ε, was determined using known amounts of potassium picrate in dichloromethane saturated with water and containing $1.4–2.7 \times 10^{-3}$ *M* 18-crown-6. The value of ε was $1.7_9 \times 10^4$ cm^{-1} M^{-1} at 25°C. By the above method the sample of 18-crown-6 used in the present work was 97% pure.

Lithium chloride (Mallinckrodt), sodium chloride (Fisher), potassium hydroxide (Matheson, Coleman & Bell) were analytical reagent grade, while lithium hydroxide was from Ventron Corp. Sodium and potassium picrates were prepared by neutralizing Baker Co. picric acid with the hydroxides in water, while lithium picrate (dihydrate), calcium and magnesium picrates were prepared by neutralization of picric acid with the corresponding carbonate (General Chemical or Mallinckrodt). Lithium carbonate was recrystallized from hot water; the picrates were recrystallized from water. All salts were dried *in vacuo* at 100°C. Dichloromethane (MCB Omnisolv) was found to contain 0.3 ppm residue upon evaporation and 0.004% water. The solubility of water in CH_2Cl_2 given in the literature (6) is 1.30% by weight (0.153 *M*) and that of CH_2Cl_2 in water 1.98% (0.145 *M*).

Extraction Procedure

Lithium picrate was usually added to the aqueous phase in a concentration of 2×10^{-3} *M* or less. In order to avoid presence of picric acid, all mixtures were made 5×10^{-5} *M* in lithium hydroxide. In all experiments equal volumes of the aqueous and organic phases were used. No volume change was observed upon attainment of extraction equilibrium. The quantity $[\sum LMPi]_0$ was determined spectrophotometrically at 370 nm. From the value thus found and the estimated dissociation constant $K^d(LMPi)$, the concentration of undissociated $(LMPi)_0$ was found. Under all conditions $[LK^+]_w$ was negligibly small.

Results

The partition coefficient *P*(L) at zero ionic strength (eq. [3]) between water and dichloromethane of 18-crown-6 was found equal to 4.50 at 25°C. This value is much larger than those reported in benzene at 25°C, 0.0634 (7) and 0.0572 (8). In Table 1 are reported values of K^{ext} (eq. [2]) and of $K^d(LMPi)$ in the organic phase of potassium and sodium, both as picrates. For comparison are added literature values of K^{ext}_{conc} of two substituted 18-crown-6 ligands and of K^{ext}_{conc} between water and benzene with 18-crown-6.

Effect of Ionic Strength on $K^{ext}(LKPi)$

The effect of ionic strength was determined by adding lithium chloride (labelled to contain 0.01% K^+; by extraction analysis we found 0.024%, v.i.). Values of *P*(L) were determined at various concentrations of lithium chloride and are reported in Table 2. These values of *P*(L) were used to calculate K^{ext}. Values of $K^{ext}(LKPi)$ were calculated using eq. [2] in which the activity coefficients, *y*, of $[K^+]_w$ and $[Pi^-]_w$ were computed from the partially extended Debye–Hückel relation

$$-\log y = 0.5115\sqrt{\pi}/(1 + 0.329a\sqrt{\pi})$$

taking $a = 3.0$ for K^+ and 7.0 for Pi^-. In this way values of $y_{K^+}y_{Pi^-}$ were found to be 0.70, 0.59, and 0.53 at lithium chloride concentrations of 0.04, 0.12, and 0.20 *M*, respectively (Table 2). In Table 2 K^{ext} is a true constant within experimental error, up to an ionic strength of 0.12. At higher ionic strengths deviations from constancy must be attributed to uncertainties in calculated values of $y_{K^+}y_{Pi^-}$. Clearly, the ionic strength and salting out effects must be considered in quantitative analysis by extraction of electrolytes complexed with an uncharged ligand. The smaller values of K^{ext}_{conc}, reported by Smid *et al.* (9), than that reported in the present study (Table 1) may be attributed to the fact that these authors determined K^{ext}_{conc} at an ionic strength of 0.01 (or greater).

Effect of Temperature

A few extractions of K^+ have been carried out at 20°C and 15°C as well as at 25°C. Using a total potassium concentration of 4×10^{-4} *M* and of 18-crown-6 of 4×10^{-3} *M*, the percentages of K^+ extracted were 46.5 at 25°C, 42.0 at 20°C, and 40.5 at 15°C. More work is planned in order to find the effects over a larger range of temperature on *P*(L), K^{ext}, and stability constants of LK^+ in water and dissociation constant of LKPi in dichloromethane.

Determination of K^+ *in Salts of* Na^+, Li^+, Ca^{2+}, *and* Mg^{2+}

Sodium has a value of log K^{ext} of 3.3_4 as compared to 6.2_1 of K^+ (Table 1). This corresponds to a selectivity of K^+/Na^+ of 750 when extracted with 18-crown-6 as picrate. In the determination by ex-

TABLE 1. log K^{ext}(LMPi) and K^{d}(LMPi) of K^+ and Na^+ at 25°C

Crown ether	Ion	CH_2Cl_2 as extractand		Benzene as extractand log K^{ext}
		log K^{ext}	$K^{d}(LMPi)_0$	
18-cr-6	K^+	6.21 (5.5)[c]	3×10^{-5} (1×10^{-5})[c]	6.00[a]
	Na^+	3.34 (3.1)[c]	9×10^{-5} (3×10^{-5})[c]	3.31[a]
Dicyclohexyl-18-cr-6 (mixed isomers)	K^+	6.32[b]	3.7×10^{-5}[b]	
	Na^+	4.18[b]	1×10^{-4}[b]	
VB-18-cr-6[d]	K^+	5.48[c]	1×10^{-5}[c]	
	Na^+	3.08[c]	3×10^{-5}[c]	

[a]Reference 8.
[b]Reference 2.
[c]Reference 10.
[d]VB-18-cr-6 = 4′-vinylmonobenzo-18-cr-6.

TABLE 2. Effect of ionic strength (LiCl) on K^{ext}_{conc} and K^{ext} at 25°C; total concentrations: $c_L = 2.5 \times 10^{-3}$, $c_{K^+} = 4 \times 10^{-4}$, $c_{Pi} = 2 \times 10^{-3}$

LiCl M	P(L)	$[LKPi]_0$ $M \times 10^4$	$[K^+]_w$ $M \times 10^5$	%K^+ extracted	log K^{ext}_{conc}	log K^{ext} (eq. [2])
0	4.5	2.5_6	5.4	86	6.2_0	6.2_1
0.04	5.1	2.4_0	7.2	81	6.0_4	6.1_9
0.12	5.8	2.2_7	8.7	78	5.9_2	6.1_5
0.20	6.4	2.2_1	10.5	73	5.7_9	(6.0_6)
0.40	7.4	—	—	—	—	—

traction of small amounts of K^+ in sodium salts the effect of sodium upon the extraction of K^+ can be calculated, but this calculation becomes quite involved as the ionic strength effect on both K^{ext}(LKPi) and K^{ext}(LNaPi) must be taken into account.

It is much simpler to determine empirically the effect of sodium on the percentage of K^+ extracted by adding known amounts of K^+ to solutions of a pure sodium salt. For example, in solutions which were 4×10^{-4} M in K^+, 2×10^{-3} M in picrate, 2.7×10^{-3} M in 18-crown-6, and 0, 0.008, and 0.02 M in pure sodium chloride the amounts of picrate extracted, expressed in % of K^+_{total}, were 46.5, 46.0, and 46.8, respectively. Under the above conditions the ionic strength effect of the large excess of sodium is compensated by $[LNaPi]_0$ extracted (expressed as K^+). It is easy to find conditions to carry out the determination of less than 0.2% of K^+ in sodium salts by extraction analysis.

The extractibility of Li^+ and of Mg^{2+} as picrate with 18-crown-6 is very small. We determined the K^+ content of a Mallinckrodt C.P. lithium chloride product in the following way: a solution was prepared which was 0.2 M in LiCl, 0.002 M in LiPi, and 0.0025 M in 18-crown-6. The picrate found in the first extract corresponded to an apparent concentration of 8.5×10^{-5} M K^+ in the aqueous phase. After the first extraction the concentrations of L and LiPi in the aqeuous phase were adjusted to their original values. After the second, third, fourth, and fifth extractions the concentration of $\sum[LMPi]_0$ corresponded to 6.2×10^{-5}, 5.2×10^{-5}, 5.0×10^{-5}, and 5.0×10^{-5} M in the aqueous phase. Thus, the concentration of lithium, extracted as picrate from 0.2 M LiCl solution was 5×10^{-5} M, and the potassium content of the 0.2 M LiCl solution was 4.7×10^{-5} M. Thus, under the above conditions all the potassium was in the organic phase after three extractions. The lithium chloride appeared to contain 0.02_4 mol or wt% K (it was labelled to contain 0.01% K).

From 2.5×10^{-3} M solutions the amount of Mg^{2+} extracted was 0.6 of that of lithium, while that of calcium was 30 times greater than that of lithium. Thus K^+ can be determined simply in magnesium salts in the same way as was done in lithium chloride. The determination of K^+ in calcium salts can be done in the same way as described for sodium salts.

Discussion

From the results in Table 1 it is seen that the selectivity K^+/Na^+ expressed as log $K^{ext}(K^+)$ − log $K^{ext}(Na^+)$ using dichloromethane as extractand is 2.9 with L = 18-crown-6, 2.1 with L = dicyclohexyl-18-crown-6 (mixed isomers) (2), and 2.4 with 4′-vinylmonobenzo-18-crown-6 (9). In unpublished work we find with dibenzo-18-crown-6 a selectivity of 2.3. With 18-crown-6, but in benzene as extract-

Can. J. Chem. Downloaded from www.nrcresearchpress.com by 210.87.254.5 on 09/06/12
For personal use only.

and, the selectivity is reported to be 2.7 (ref. 8, Table 1).

Quite generally, for analytical purposes, solvents like benzene, toluene, chloroform are preferred over the polar solvent dichloromethane as ionic dissociation of $(LMPi)_0$ in the organic phase is negligibly small and need not be considered when use is made of eq. [2].

It is of interest to add that in dichloromethane, $K^q(LMPi)_0$ of sodium has been reported with three crown ethers (Table 1) to be three times as large as that of potassium. Whether this indicates that an equilibrium between solvent separated and contact ion pairs of LNaPi is more favorable towards the former than that of LKPi needs further study.

Extraction analysis for determination of traces of potassium in lithium, sodium, and calcium salts is very suitable, particularly when calibration is made using potassium-free salts. It is also suitable for routine analysis for potassium in liquids which contain large but only slightly variable excesses of sodium, like sea water and blood serum.

Acknowledgements

Acknowledgement is made to the donors of the Petroleum Research Fund, administered by the American Chemical Society, for support of this research.

Acknowledgement is also made to Dr. Sadayuki Himeno, who carried out the experimental work described in this paper, and to Dr. M. K. Chantooni, Jr. for his supervision of the experimental work and his comments on the manuscript.

1. G. Eisenman, S. M. Ciani, and G. Czabo. Fed. Proc. **27**, 1289 (1968).
2. H. K. Frensdorff. J. Am. Chem. Soc. **93**, 4684 (1971).
3. C. J. Pedersen. J. Am. Chem. Soc. **89**, 7017 (1967).
4. H. Sumiyoshi and K. Nakahara. Talanta, **24**, 763 (1977).
5. H. Nakamura, M. Takagi, and K. Ueno. Talanta, **26**, 921 (1979).
6. J. A. Riddick and W. Bunger (*Editors*). Techniques of chemistry. Vol. II. Organic solvents. 3rd ed. Wiley-Interscience, New York. 1970.
7. Y. Takeda and H. Kato. Bull. Chem. Soc. Jpn. **52**, 1027 (1979).
8. T. Iwachido, A. Sadakane, and K. Toei. Bull. Chem. Soc. Jpn. **51**, 629 (1978).
9. S. Kopolow, T. E. Hogen-Esch, and J. Smid. Macromolecules, **4**, 359 (1973).
10. S. Kopolow, T. E. Hogen-Esch, and J. Smid. Macromolecules, **6**, 133 (1973).

Can. J. Chem. Downloaded from www.nrcresearchpress.com by 210.87.254.5 on 09/06/12
For personal use only.

Rational orbitals for two-electron ^1S states

F. W. BIRSS AND W. DEN HERTOG

Department of Chemistry, University of Alberta, Edmonton, Alta, Canada T6G 2G2

Received August 28, 1980

This paper is dedicated to Professor W. E. Harris on the occasion of his retirement from the University of Alberta

F. W. BIRSS and W. DEN HERTOG. Can. J. Chem. **59**, 1552 (1981).

The concept of rational orbitals is introduced, based upon finding that pair of orbitals which yield the single configuration function which maximally overlaps with a configuration interaction wave function. They are simply obtained from the natural orbitals by an elementary orthogonal transformation and are more appropriate than natural orbitals to analysis of functions for open-shell states. The CI wave functions of a number of ^1S states of helium are analyzed and the nature of the rational orbitals investigated.

F. W. BIRSS et W. DEN HERTOG. Can. J. Chem. **59**, 1552 (1981).

On propose le concept d'orbitales rationnelles, en se basant sur la découverte de la paire d'orbitales qui conduit à la fonction de configuration unique qui assure un recouvrement maximal avec une fonction d'onde d'interaction de configuration. On les obtient simplement à partir des orbitales naturelles par une transformation orthogonale élémentaire et elles sont plus appropriées que les orbitales naturelles pour l'analyse des fonctions des états où la couche électronique est incomplète. On a analysé les fonction d'onde IC d'une série d'états ^1S de l'helium on a étudié la nature des orbitales rationnelles.

[Traduit par le journal]

I. Natural Orbitals for ^1S States

The concept of natural orbitals was first developed by Löwdin (1) in the context of density matrix theory. For states of two-electron systems they provide a particularly efficient expression of a configuration interaction wave function (2). Consider such a function:

$$[1] \quad \Phi = \sum_{(kl)} C_{(kl)}[\chi_k\chi_l]$$

The summation is taken over independent pairs of orthonormal one-electron basis functions χ_k, χ_l. $[\chi_k\chi_l]$ indicates a symmetry adapted, antisymmetrized, and normalized single configuration function constructed from such a pair. The natural orbital expansion of the same function is

$$[2] \quad \Phi = \sum_k C_k{}^N[\chi_k{}^N\chi_k{}^N]$$

which represents a significant reduction in the number of terms required for expression of the function.

Natural orbitals for the ^1S two-electron case can be discovered as the answer to the question: what is the single determinant, $[\chi_1{}^N\chi_1{}^N]$ which maximally overlaps with the original CI wave function? We thus seek to maximize

$$[3] \quad S = \langle[\chi_1{}^N\chi_1{}^N]\|\Phi\rangle$$

subject to the normalization constraint

$$[4] \quad \langle\chi_1{}^N|\chi_1{}^N\rangle = 1$$

The natural orbitals are expanded in the basis of functions used to construct the CI function,

$$[5] \quad \chi_i{}^N = \sum_j \chi_j N_{ji}$$

Substituting for Φ and $\chi_1{}^N$ in [3] and [4] we obtain (assuming all orbitals to be real and orthonormal),

$$[6] \quad S = \sum_{(kl)} C_{(kl)}(1 + \delta_{kl})^{1/2} N_{k1} N_{l1}$$

$$[7] \quad \langle\chi_1{}^N|\chi_1{}^N\rangle = \sum_k N_{k1}{}^2 = 1$$

The condition for maximum overlap is obtained by applying the Lagrange method of undetermined multipliers. It is

$$[8] \quad \sum_l C_{(kl)}(1 + \delta_{kl})^{1/2} N_{l1} = \lambda_1 N_{k1}$$

with $-\lambda_1$ the multiplier used upon the constraint [7]. Defining the elements of the matrix **D** as

$$[9] \quad D_{kl} = D_{lk} = C_{(kl)}(1 + \delta_{kl})^{1/2}$$

and N_1 as the vector with components N_{i1}, [8] may be written as the matrix equation

$$[10] \quad \mathbf{D}N_1 = N_1\lambda_1$$

The matrix **D** is the "fundamental" matrix defined by Löwdin (1), with eigenvectors the coefficients of the basis χ in the expansion of the natural orbitals and eigenvalues the coefficients, $C_k{}^N$, in the expansion of the CI function in the basis of configurations constructed from natural orbitals.

II. Rational Orbitals for ^1S States

For approximate closed shell state functions, the determinant associated with the dominant $C_k{}^N$

0008-4042/81/101552-05$01.00/0

©1981 National Research Council of Canada/Conseil national de recherches du Canada

Can. J. Chem. Downloaded from www.nrcresearchpress.com by 210.87.254.105 on 09/06/12
For personal use only.

Can. J. Chem. Downloaded from www.nrcresearchpress.com by 210.87.254.105 on 09/06/12
For personal use only.

should be a reasonable approximation to the Hartree–Fock function if an adequate basis set of functions has been used in constructing the CI function (3). For excited states the best one-term approximation would be of the form $[\chi_k\chi_l]$ with $k \neq l$. Thus the usual natural orbital expansion in determinants involving double occupied orbitals is inappropriate for truncation to a single term. We define rational orbitals in this situation by requiring maximal overlap of a single term of the form $[\chi_1{}^R\chi_2{}^R]$ with a CI wave function ascribable to a state for which the orbital description would be two singly occupied orbitals. In terms used in Section I, we can obtain the matrix **R** defined by

$$[11] \quad \boldsymbol{\chi}^R = \boldsymbol{\chi}\mathbf{R}$$

by requiring **R** to be that matrix which effects the transformation

$$[12] \quad \mathbf{D}^R = \mathbf{R}^\dagger\mathbf{D}\mathbf{R}$$

such that the (1,2) and (2,1) elements of $\mathbf{D}^R$ have maximum magnitude.

Consider the natural orbital transformation

$$[13] \quad \boldsymbol{\lambda} = \mathbf{N}^\dagger\mathbf{D}\mathbf{N}$$

and the subsequent transformation which modifies only the (1,1), (2,2), (1,2), and (2,1) elements:

$$[14] \quad \mathbf{D}^R = \mathbf{Q}^\dagger\boldsymbol{\lambda}\mathbf{Q} = \mathbf{Q}^\dagger\mathbf{N}^\dagger\mathbf{D}\mathbf{N}\mathbf{Q} = \mathbf{R}^\dagger\mathbf{D}\mathbf{R}$$

We now prove the implied statement of [14]: it is this transformation which maximizes the magnitude of the (1,2) and (2,1) elements of $\mathbf{D}^R$, presuming the λ_i to be ordered in decreasing magnitude. Consider the elementary orthogonal matrix $\mathbf{Q}^{(ij)}$ which differs form the unit matrix only by having

$$[15] \quad \begin{aligned} Q_{ii}^{(ij)} &= Q_{jj}^{(ij)} = \cos\theta \\ Q_{ji}^{(ij)} &= -Q_{ij}^{(ij)} = \sin\theta \end{aligned}$$

The effect of the transformation by $\mathbf{Q}^{(12)}$ upon the ordered diagonal matrix $\boldsymbol{\lambda}$ is to yield

$$[16] \quad D_{12}{}^R = D_{21}{}^R = (\lambda_2 - \lambda_1)\sin\theta\cos\theta$$

which maximizes the magnitude $D_{12}{}^R$ and $D_{21}{}^R$ when $\theta = \pi/4$ (or, equivalently, $3\pi/4$, $5\pi/4$, etc.). Then

$$[17] \quad \begin{aligned} D_{11}{}^R &= D_{22}{}^R = \tfrac{1}{2}(\lambda_1 + \lambda_2) \\ D_{12}{}^R &= D_{21}{}^R = \tfrac{1}{2}(\lambda_2 - \lambda_1) \end{aligned}$$

A further transformation with $\mathbf{Q}^{(ij)}$ in an attempt to increase the magnitude of $D_{12}{}^R$ and $D_{21}{}^R$ must have either i or j equal to 1 or 2 in order to affect the values of the elements. Since $D_{11}{}^R$ and $D_{22}{}^R$ are equal, either i or j equal to either 1 or 2 leads to an equivalent result. Consider the transformation using $\mathbf{Q}^{(1j)}$ with $j \neq 1$ or 2. Then

$$[18] \quad D_{12}{}^{R\prime} = D_{12}{}^R\cos\theta + D_{j2}{}^R\sin\theta$$

But, since $D_{j2}{}^R$ is zero except for $j = 1$ and 2, this is simply $D_{12}{}^R\cos\theta$. Since $\theta = n\pi$ is the only choice which leaves $D_{12}{}^R$ maximal in magnitude, $\mathbf{Q}^{(1j)}$ is a trivial multiple of the unit matrix.

Thus the process of obtaining the rational orbital transformation matrix **R** is first to perform the diagonalization of the fundamental matrix which yields **N** and $\boldsymbol{\lambda}$ and then to selectively "disdiagonalize" $\boldsymbol{\lambda}$ by the elementary orthogonal transformation $\mathbf{Q}^{(ij)}$ with $\theta = \pi/4$; i and j are chosen to select those λ_i and λ_j which yield the largest possible magnitude of the symmetric pair of off-diagonal elements in $\mathbf{D}^R$. Then **R** is $\mathbf{N}\mathbf{Q}^{(ij)}$.

III. Configuration Interaction Functions for Helium

In the two series of calculations reported here the original configuration functions were prepared from Slater type orbitals with symmetry adaptation and antisymmetrization after inclusion of spin.

In the first series of calculations the selected Slater type orbitals were the eight s functions with $1 \leq n \leq 8$, the six p functions with $2 \leq n \leq 7$, the four d functions with $3 \leq n \leq 6$ and the two f functions with $4 \leq n \leq 5$. Since the intent of this series was to obtain energies and wave functions of high precision, all seventy possible configurations of ^1S type were ultimately used. The orbital exponents were varied independently for each of the five lowest states in order to achieve minimum energy for the state in question. Thus, from the point of view of the calculations, there was no relation between the orbital exponents and CI coefficients, $C_{(kl)}$, obtained for any two states. The minimization with respect to orbital exponents was carried out in stages. First the energy was minimized using the 36 configurations constructed from the s functions, varying their orbital exponents. The 21 configurations constructed from the six p functions were then added and exponent variation for the p functions carried out. The s functions were not further varied. The d and f functions were in turn similarly treated.

Since the original configuration functions were constructed from Slater orbitals, they were not orthonormal. Some difficulty was experienced with loss in numerical precision in the orthogonalization carried out as a preliminary to solution of the eigenvalue problem. A test of the quality of the unit matrix which should be generated by transforming the metric matrix with the orthogonalization matrix

Can. J. Chem. Downloaded from www.nrcresearchpress.com by 210.87.254.105 on 09/06/12
For personal use only.

TABLE 1. First series calculations for helium: energies (hartree)

	State				
	$1s^2$	$1s2s$	$1s3s$	$1s4s$	$1s5s$
This work	−2.90322	−2.14593	−2.06126	−2.03358	−2.02117
Exact[a]	−2.90372	−2.14597	−2.06127	−2.03359	−2.02118
Hartree–Fock[b]	−2.86168	−2.14344	−2.06045	−2.03324	−2.02099
Rational orbital	−2.86165	−2.14141	−2.05999	−2.03306	−2.02090
Δs	−0.01726	−0.00028	−0.00008	−0.00003	−0.00002
Δp	−0.02157	−0.00016	−0.00004	−0.00002	−0.00001
Δd	−0.00124	−0.00001	—	—	—
Δf	−0.00060	—	—	—	—

[a]Reference 4.
[b]$1s^2$, ref. 5; $1s2s$ to $1s4s$, ref. 6.

was performed. It was found that selection of the orbital exponents from sets of relatively low and high magnitudes obviated precision difficulties without jeopardizing the quality of the energies obtained.

The intent of the second series was to obtain reasonably good results for a broad range of more highly excited states using a common basis of configurations. The Slater type s functions consisted of three $1s$, two $2s$ and one function each with $3 \leq n \leq 25$. The orbital exponents of two of the $1s$ and one of the $2s$ functions were obtained by minimization of the ground state energy obtained in the basis of the six configurations constructed using these three functions. The orbital exponent of the third $1s$ function was fixed at 2.0. The orbital exponents of the second $2s$ and functions of higher n were determined by the formula

$$[19] \quad \zeta_n = a + b/n + c/n^2$$

The coefficients, a, b, and c, were determined by collective minimization of the fifth through the second highest eigenvalues; i.e., if alteration of a coefficient resulted in the sum of the changes of those eigenvalues being negative, that alteration was considered acceptable.

The configurations were constructed as described above but not all those possible were used. The six configurations involved in the selection of the orbital exponents of the two $1s$ and one $2s$ functions were included plus those involving the $1s$ function with orbital exponent 2.0 with itself and with each of the remaining functions. There were thus $N + 6$ configurations constructed from s functions, with N the n of the highest order s function used. The configurations involving p, d, and f functions were those determined for the fifth state in the first series of calculations, carried over unchanged.

IV. The First Series

The energies obtained for the five lowest ^1S states of helium[1] are gathered in Table 1. The headings $1s^2$, $1s2s$, etc., are used here and elsewhere as state labels according to the dominant orbital description. The exact energies are the results of Pekeris and co-workers (4).

Although the criterion for obtaining the dominant term is that it shall maximally overlap with the total CI function, it should be a reasonable approximation to the Hartree–Fock function obtained on the basis of minimum energy for a single configuration. The comparison between the Hartree–Fock and rational orbital single-term energies is included in Table 1. It is clear that, for the excited states, as correlation plays a less important role in contributing to the description of the state, the two wave functions approach each other more closely. What is particularly remarkable is the goodness of the approximation to Hartree–Fock in the closed-shell case. To a certain extent this is consistent with the relative behaviour of the ground and excited states upon inclusion of terms which take correlation into account. For the excited states, the quantity Δs of Table 1, which gives the energy lowering upon inclusion of s configurations beyond the rational orbital level, is greater than $\Delta p + \Delta d + \Delta f$, which gives the energy lowering upon subsequent inclusions of angular correlation. The opposite is the case for the ground state.

In Table 2 are given the configuration occupation numbers for the states considered in the first series. These numbers are the squares of the coefficients, C_{ij}^R and C_k^N, in the rational-natural orbital expansion:

$$[20] \quad \Phi = C_{12}^R[\chi_1^R\chi_2^R] + C_{11}^R[\chi_1^R\chi_1^R] + C_{22}^R[\chi_2^R\chi_2^R] + \sum_{k\geq 3} C_k^N[\chi_k^N\chi_k^N]$$

The $1s$ state is expanded only in natural orbitals

[1]The orbital exponents and expansion coefficients are available from F.W.B. upon request.

TABLE 2. First series calculations for helium: configuration occupation numbers

Orbitals	State				
	$1s^2$	$1s2s$	$1s3s$	$1s4s$	$1s5s$
s_1s_2	—	0.993352	0.998347	0.999347	0.999674
s_1^2	0.991952	0.003000	0.000733	0.000288	0.000143
s_2^2	0.003797	0.003000	0.000733	0.000288	0.000143
All s	0.995817	0.999530	0.999875	0.999950	0.999975
All p	0.003976	0.000450	0.000119	0.000048	0.000024
All d	0.000182	0.000019	0.000006	0.000003	0.000001
All f	0.000023	0.000003	0.000001	—	—

TABLE 3. Second series calculations for helium

State	Energies (hartree)			Configuration occupation numbers	
	This work	Pekeris	Hydrogenic	s_1s_2	s_1^2 and s_2^2
5	−2.02110	−2.02118	−2.02000	0.999675	0.000142
6	−2.01452	−2.01456	−2.01389	0.999815	0.000082
7	−2.01060	−2.01063	−2.01020	0.999886	0.000050
8	−2.00808	−2.00809	−2.00781	0.999925	0.000033
9	−2.00636	−2.00637	−2.00617	0.999947	0.000023
10	−2.00514	−2.00514	−2.00500	0.999961	0.000017
11	−2.00424	−2.00424	−2.00413	0.999971	0.000013
12	−2.00355	−2.00355	−2.00347	0.999978	0.000010
13	−2.00302	−2.00302	−2.00296	0.999983	0.000008
14	−2.00260	−2.00260	−2.00255	0.999986	0.000006
15	−2.00226	−2.00226	−2.00222	0.999989	0.000005
16	−2.00199	—	−2.00195	0.999991	0.000004
17	−2.00176	—	−2.00173	0.999992	0.000004
18	*−2.00155*	—	−2.00154	0.999987	0.000006
19	−1.99957	—	−2.00139	—	—
20	−1.94675	—	−2.00125	—	—

which are the rational orbitals for a doubly occupied state in the orbital description.

In all cases the occupation numbers indicated that addition of further functions of the symmetries already used would have a minor effect upon the energy. Further major improvement should be sought in functions of higher l quantum number, a conclusion parallel to that of Weiss (7) in similar work on the helium ground state.

As the degree of excitation increases, the importance of correlation decreases sharply so that the accuracy of functions, such as these, based upon the same number and type of configurations, increases correspondingly. It is this feature, coupled with the technique of adapting the basis functions to a particular state, which holds promise for the use of the CI method for excited states of larger atoms and molecules.

Consistent with the decreasing importance of correlation, the weight of the dominant term approaches unity more closely as more highly excited states are considered. This number is also the square of the overlap between the single term and the total CI function. This same trend is displayed by the stepwise energy quantities, Δs, Δp, Δd, and Δf given in Table 1. The single-term function takes into account a greater portion of the total energy and the convergence is more rapid as more highly excited states are considered.

V. The Second Series

The energy results for this series[1] are given in Table 3 for $N = 20$, i.e., for configurations constructed with s Slater functions of this maximum principle quantum number. The italicized value indicates the end of the range of eigenvalues included in the process of collective minimization for obtaining the values

$$a = 1.3 \times 10^{-4}, b = 1.1113, c = 9.2 \times 10^{-4}$$

of [19]. The results of Pekeris and co-workers (4) are given for comparison. The hydrogenic energies are based upon the idealized situation of a $1s$ orbital of He^+, with no perturbation by the outer electron, and a ns orbital of H, with perfect shielding by the inner electron.

Can. J. Chem. Downloaded from www.nrcresearchpress.com by 210.87.254.105 on 09/06/12
For personal use only.

The configuration occupation numbers for the dominant s configurations are given in the latter columns of Table 3. The trends already evident in the lower states are continued here, with both angular and radial correlation playing a less important role as greater excitation is encountered. It is evident that the $1s18s$ function is of poorer quality than the others since the trend toward unity of the s_1s_2 configuration occupancy is abruptly interrupted at this point. It was this observation that led us to choose only up to the $N - 2$ state for collective minimization: without seriously sacrificing the quality of the upper bounds for a large number of lower states, one cannot achieve reasonable approximations to the upper bounds of the highest three states. This feature was also found in the calculations with $N = 15$ and 25, which were performed as a check upon the convergence of the results reported here.

VI. Conclusion

The modification of the natural orbital analysis to obtain rational orbitals for excited states of two-electron species has been useful in exposing some aspects of the structure of such states. As the need arises, the technique can be extended to open shell states of many-electron systems.

The particular results for the helium atom have not contained any surprises but the analysis does provide a firm numerical basis for the discussion of excited states in terms of the relative importance of various aspects of the model: the Hartree–Fock level, radial correlation and angular correlation.

Acknowledgments

This work was supported by the Natural Sciences and Engineering Research Council of Canada with the award of a PIER fellowship and a grant-in-aid of research. The use of the facilities of the Computing Services of the University of Alberta and the assistance of Mr. Peter Senn in helping with the calculations are gratefully acknowleged.

1. P.-O.LÖWDIN. Phys. Rev. **97**, 1474 (1955).
2. H. SHULL and P.-O. LÖWDIN. J. Chem. Phys. **23**, 1565 (1955); **30**, 617 (1959).
3. G. V. NAZAROFF and J. O. HIRSCHFELDER. J. Chem. Phys. **39**, 715 (1963).
4. C. L. PEKERIS. Phys. Rev. **127**, 509 (1962); Y. ACCAD, C. L. PEKERIS, and B. SCHIFF. Phys. Rev. A, **4**, 516 (1971).
5. C. C. J. ROOTHAAN, L. M. SACKS, and A. W. WEISS. Rev. Modern Phys. **32**, 186 (1960).
6. E. R. DAVIDSON. J. Chem. Phys. **41**, 656 (1964); J. Chem. Phys. **42**, 4199 (1965).
7. A. W. WEISS. Phys. Rev. **122**, 1826 (1961).

Can. J. Chem. Downloaded from www.nrcresearchpress.com by 210.87.254.105 on 09/06/12
For personal use only.

Synthesis of *N*-acyl-1,3-oxathiol-2-imines

MARSHALL KULKA
Research Laboratories, Uniroyal Limited, Guelph, Ont., Canada N1H 6N3
Received November 27, 1980

MARSHALL KULKA. Can. J. Chem. **59**, 1557 (1981).

A facile synthesis of *N*-acyl-1,3-oxathiol-2-imines, **7**, is reported. It comprises the reaction of *O*-alkyl acylcarbamothioates, **4**, with 2-chloroketones in the presence of alcoholic sodium alkoxide. The resulting *O*-alkyl-*S*-substituted-*N*-acylcarbonimidothiates, **6**, undergo cyclization with elimination of alcohol, spontaneously, or upon heating in boiling toluene to form **7**.

MARSHALL KULKA. Can. J. Chem. **59**, 1557 (1981).

On rapporte une synthèse facile des *N*-acyl oxathiol-1,3 imines-2 (**7**). Cette synthèse fait intervenir la réaction des *O*-alkyl acylcarbamothioates (**4**) avec les chloro-2 cétones en présence d'un alcoolate de sodium. Les *O*-alkyl *N*-acylcarbonimidothiates portant un substituant sur le soufre (**6**) obtenus se cyclisent avec élimination d'alcool soit spontanément, soit par chauffage dans le toluène bouillant et conduisent aux dérivés (**7**).

[Traduit par le journal]

Prior to 1966 few simple 1,3-oxathioles were known (1). Since that time there has been some activity in this field but not to any great extent. Kuhlmann and Dittmer (2) found that by treating 2-thiocyanato-2-phenylacetophenone with excess sodium hydride, 2,4,5-triphenyl-1,3-oxathiole was formed in 55% yield. Kempe *et al.* (3) demonstrated that dehydrobromination of 1-(2-oxo-2-phenylethyl)-2,5-dihydrothiophenium bromide, followed by heating, resulted in a 55% yield of 2-benzoyl-5-phenyl-1,3-oxathiole. Ried and Kaiser (4) reacted 3-phenyl-2-propynethioamides ($C_6H_5C{\equiv}CCSNHR$) with 2-bromoketones in the presence of triethylamine and obtained 2-phenylethynyl-5-substituted-1,3-oxathiol-2 amines. Russian workers (5) report that 2,4,5-trimethyl-1,3-oxathiole was formed in 30% yield when acetylene and sodium sulfide were heated. A number of *N*-phenyl- and *N*-butyl-1,3-oxathiol-2 imines (6) have been prepared by the reaction of *N*-phenyl- and *N*-butyl-carbonochlorimidothioic acid chlorides (C_6H_5- and C_4H_9—N=C(SCl)(Cl) with ketones.

This paper reports a facile synthesis of *N*-acyl-1,3-oxathiol-2-imines, **7**, from *O*-alkyl acylcarbamothioates, **4**, and 2-chloroketones, **5**. The *O*-methyl acylcarbamothioates, **4**, were readily obtained through the reaction of acid chlorides, **1**, with ammonium thiocyanate, **2**, and addition of methanol to the resulting acyl isothiocyanates, **3**, (7, 8). Phenylmethyl chloride and 2-chloroketones, **5**, reacted with *O*-methyl acylcarbamothioates, **4**, at room temperature in the presence of methanolic sodium methoxide to yield the corresponding *O*-methyl-*S*-substituted-*N*-acylcarbonimidothioates. The products, **6**, of the reaction of 2-chloroketones, **5**, with **4** were found to be quite unstable. They liberated methanol and underwent cyclization at room temperature or upon heating in toluene to form the *N*-acyl-1,3-oxathiol-2-imines (**7**). Thus when *O*-methyl benzoylcarbamothioate (**4**, R = phenyl) was treated with ethyl 2-chloroacetoacetate (**5**, R′ = CH_3. R″ = $COOC_2H_5$) in methanol solution in the presence of sodium methoxide at room temperature, ethyl 2-benzoylimino-5-methyl-1,3-oxathiole-4-carboxylate (**7**, R = phenyl, R′ = CH_3, R″ = $COOC_2H_5$) precipitated in 87% yield and no intermediate **6** could be isolated. *O*-Methyl (2-furanyl)carbonylcarbamothioate (**4**, R = 2-furanyl) reacted similarly with ethyl 2-chloroacetoacetate to produce the corresponding 1,3-oxathiole directly, and no intermediate.

On the other hand, when *O*-methyl benzoylcarbamothioate (**4**, R = phenyl) was treated with 2-oxo-2-phenylethyl chloride (**5**, R′ = phenyl, R″ = H) under the same conditions, the intermediate *O*-methyl *S*-(2-oxo-2-phenylethyl)-*N*-benzoylcarbonimidothioate (**6**, R = R′ = phenyl, R″ = H) precipitated in 85% yield. To cyclize this intermediate to **7** (R = R′ = phenyl, R″ = H) it was necessary to heat it under reflux in toluene. In most of the other preparations the reactions of **4** with **5** yielded mixtures of the intermediate **6** and the 1,3-oxathiole **7** and it was necessary to heat the isolated **6** or the mixture in toluene in order to produce the maximum yield of **7**. Structural assignments were based on nmr and ir spectra and elemental analysis.

The 2-chloroketones that successfully reacted with **4** to give the corresponding *N*-acyl-1,3-oxathiol-2-imines were ethyl 2-chloroacetoacetate, 3-chloro-2,4-pentanedione, 2-chloro-*N*,*N*-dimethylacetoacetamide, ethyl 2-chlorobenzoylacetate,

0008-4042/81/111557-03$01.00/0
©1981 National Research Council of Canada/Conseil national de recherches du Canada

Can. J. Chem. Downloaded from www.nrcresearchpress.com by 210.87.254.105 on 09/06/12
For personal use only.

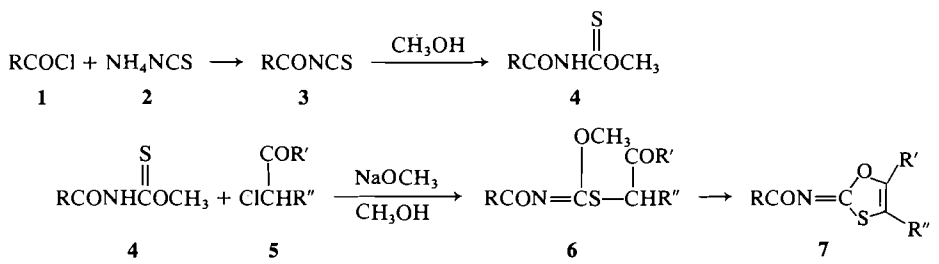

2-oxo-2-phenylethyl chloride, 2-chloro-3-butanone, 2-chloro-1-(4-methylphenyl)propanone, 2-chloro-1-(2,4-dimethylphenyl) propanone, and 2-chlorocyclohexanone. 1-Chloro-2-propanone and 2-chloroacetoacetanilide failed in this synthesis.

Experimental

Infrared spectra were obtained on Perkin-Elmer 237B or 521 grating ir spectrometers. The nmr spectra were recorded using an R-20 Hitachi Perkin-Elmer spectrometer and are expressed in ppm (δ values) relative to tetramethylsilane as standard. Melting points were determined on a Gallenkamp melting point apparatus and are uncorrected. Analyses were performed on a Perkin-Elmer 240 elemental analyzer. Ultraviolet spectra were obtained on a Varian model G34 spectrophotometer.

O-*Methyl (5,6-Dihydro-2-methyl-1,4-oxathiin-3-yl)carbonyl carbamothioate (4, R = 5,6-dihydro-2-methyl-1,4-oxathiin-3-yl)*

5,6-Dihydro-2-methyl-1,4-oxathiin-3-carbonyl isothiocyanate (3, R = 5,6-dihydro-2-methyl-1,4-oxathiin-3-yl) prepared (8) from 5,6-dihydro-2-methyl-1,4-oxathiin-3-carboxylic acid (40 g) and ammonium thiocyanate was treated with methanol (100 mL) and then allowed to stand at room temperature overnight. The excess methanol was distilled off *in vacuo*, the residue dissolved in toluene (500 mL), and the solution washed with water. Concentration of the toluene solution *in vacuo* and allowing the concentrate to cool yielded 35 g (60%) of light-yellow crystals melting at 86–88°C. Two crystalline modifications could be obtained, one melting at 89–91°C when recrystallized from aqueous methanol and the other melting at 98–100°C when recrystallized from methanol alone. Solutions of these in chloroform gave identical ir and nmr spectra; ir (KBr): 3350, 1675, and 1580 cm^{-1}; nmr ($CDCl_3$): 9.38(1H, s, NH), 4.42(2H, m, OCH_2), 4.12(3H, s, OCH_3), 2.96(2H, m, SCH_2), 2.25(3H, s, CH_3). *Anal.* calcd. for $C_8H_{11}NO_3S_2$: C 41.20, H 4.76, N 6.01; found: C 41.34, H 4.66, N 6.19.

O-*Ethyl (2-Furanyl)carbonylcarbamothioate*

This was prepared in 57% yield as above from 2-(furanyl)-carbonyl isothiocyanate and absolute ethanol, mp 67–69°C; nmr ($CDCl_3$): 9.40(1H, s, NH), 7.60(1H, m, aromatic), 7.30(1H, m, aromatic), 6.60(1H, m, aromatic), 4.55(2H, q, CH_2), 1.42(3H, t, CH_3). *Anal.* calcd. for $C_8H_9NO_3S$: C 48.24, H 4.56, N 7.03; found: C 48.52, H 4.68, N 7.04.

O-*Methyl 3-Methylbenzoylcarbamothioate*

This was prepared in 80% yield as above from 3-methylbenzoyl isothiocyanate and methanol, mp 75–77°C; nmr ($CDCl_3$): 9.40 (1H, s, NH), 7.60(2H, m, aromatic), 7.35(2H, m, aromatic), 4.15(3H, s, OCH_3), 2.40(3H, s, CH_3). *Anal.* calcd. for $C_{10}H_{11}NO_2S$: C 57.41, H 5.30, N 6.70; found: C 57.61, H 5.24, N 6.68.

O-*Methyl*-S-*phenylmethyl*-N-*(5,6-dihydro-2-methyl-1,4-oxathiin-3-yl)carbonyl Carbonimidothioate*

To a solution of sodium (1.1 g) in methanol (75 mL) cooled to 15°C was added *O*-methyl (5,6-dihydro-2-methyl-1,4-oxathiin-3-yl)carbonylcarbamothioate **4** (10 g) and phenylmethyl chloride (6.2 g). The resulting solution was allowed to stand at room temperature for 5 h. The precipitated sodium chloride was filtered and the filtrate concentrated to about half the original volume and allowed to crystallize. The white prisms melted at 87–89°C after recrystallization from methanol. The yield was 10 g (60%); nmr ($CDCl_3$): 7.28 (5H, s, aromatic), 4.25 (2H, m, OCH_2), 4.14 (2H, s, CH_2), 3.98 (3H, s, OCH_3), 2.86 (2H, m, SCH_2), 2.37 (3H, s, CH_3). *Anal.* calcd. for $C_{15}H_{17}NO_3S_2$: C 55.72, H 5.30, N 4.33; found: C 55.69, H 5.35, N 4.20.

Other O-*alkyl*-S-*substituted*-N-*acylcarbonimidothioates* ($RCON{=}C(O\text{-alk})SCH_2Ar$) prepared, for which yields, analyses and nmr spectra are available from the Depository of Unpublished Data,[1] are: R = C_6H_5, Alk = CH_3, Ar = C_6H_5, mp 80–82°C; R = C_6H_5, Alk = CH_3, Ar = 4-OCH_3-3-BrC_6H_3, mp 96–98°C; R = 3-$CH_3C_6H_4$, Alk = CH_3, Ar = 4-ClC_6H_4, mp 81–82°C; R = 5,6-dihydro-2-methyl-1,4-oxathiin-3-yl, Alk = CH_3, Ar = 4-ClC_6H_4, mp 102–104°C; R = 2-furanyl, Alk = C_2H_5, Ar = 4-ClC_6H_4, mp 103–104°C.

N-*Benzoyl-5-phenyl-1,3-oxathiol-2-imine (7, R = R′ = phenyl, R″ = H)*

To a solution of sodium (1.85 g) in methanol (100 mL) was added *O*-methyl benzoylcarbamothioate (7) (**4**, R = phenyl) (15.6 g). To the resulting solution was added a solution of 2-oxo-2-phenylethyl chloride (**5**, R′ = phenyl, R″ = H) (12.3 g) in methanol (50 mL) and the reaction mixture was allowed to stand 3 h. The precipitated O-*methyl*-S-*(2-oxo-2-phenylethyl)*-N-*benzoylcarbonimidothioate (6, R = R′ = phenyl, R″ = H)* containing sodium chloride was filtered off, washed with water and with aqueous methanol, and dried, yielding 21.4 g (85%) of white crystals melting at 97–99°C. Recrystallization from methanol did not change the melting point; nmr ($CDCl_3$): 8.20 (2H, m, aromatic), 8.00 (2H, m, aromatic), 7.55 (6H, m, aromatic), 4.42 (2H, s, CH_2), 4.02 (3H, s, CH_3). *Anal.* calcd. for $C_{17}H_{15}NO_3S$: C 65.17, H 4.82, N 4.47; found: C 65.05, H 4.67, N 4.51.

The intermediate *O*-methyl-*S*-(2-oxo-2-phenylethyl)-*N*-benzoylcarbonimidothioate (**6**, R = R′ = phenyl, R″ = H) (11.3 g) was dissolved in toluene (50 mL) and the solution heated under reflux for 1 h. The resulting solution was concentrated and allowed to cool, when white crystals, mp 164–165°C, were obtained. The yield of *N*-benzoyl-5-phenyl-1,3-oxathiol-2-imine (**7**, R = R′ = phenyl, R″ = H) was 10 g (85%). Ultraviolet (CH_3OH) λ_{max}: 334.5 nm (ε 21 285); nmr ($CDCl_3$): 8.32 (2H, m, aromatic), 7.70 (2H, m, aromatic), 7.40 (6H, m, aromatic), 6.80 (1H, s, CH). *Anal.* calcd. for $C_{16}H_{11}NO_2S$: C 68.32, H 3.94, N 4.98; found: C 68.15, H 4.18, N 4.90.

[1]This information may be obtained at a nominal charge from the Depository of Unpublished Data, CISTI, National Research Council of Canada, Ottawa, Ont., Canada, K1A 0S2.

Can. J. Chem. Downloaded from www.nrcresearchpress.com by 210.87.254.105 on 09/06/12
For personal use only.

Ethyl 2-(5,6-Dihydro-2-methyl-1,4-oxathiin-3-yl)-carbonyl-imino-5-methyl-1,3-oxathiole-4-carboxylate (7, R = 5,6-Dihydro-2-methyl-1,4-oxathiin-3-yl, R′ = CH_3, R″ = $COOC_2H_5$)

To a solution of sodium (1.1 g) in methanol (40 mL) was added *O*-methyl (5,6-dihydro-2-methyl-1,4-oxathiin-3-yl)carbonyl-carbamothioate (**4**, R = 5,6-dihydro-2-methyl-1,4-oxathiin-3-yl) (10 g). To the resulting solution was added ethyl 2-chloroacetoacetate (8.0 g). The reaction mixture was allowed to stand for 5 h, then the precipitate was filtered, washed with methanol and with water, and dried. The 1,3-oxathiole (4.0 g) melted at 159–160°C after recrystallization from methanol. The filtrate from the reaction mixture was taken to "dryness" *in vacuo* and the residue was dissolved in ether and extracted with ice-cold dilute aqueous sodium hydroxide. The alkaline extract was acidified with cold dilute hydrochloric acid and extracted with ether. The ether extract was washed with water and the ether distilled, leaving a residue of the crude intermediate, **6** (R = 5,6-dihydro-2-methyl-1,4-oxathiin-3-yl, R′ = CH_3, R″ = $COOC_2H_5$). This was dissolved in toluene (25 mL), the solution heated under reflux for 45 min and then allowed to stand overnight. The precipitate was filtered, washed with toluene and with methanol, and dried, yielding 5.9 g more of the above 1,3-oxathiole, mp 159–160°C. The total yield was 9.9 g (70%). Ultraviolet (CH_3OH) λ_{max}: 304 nm (ε 11 432); nmr ($CDCl_3$): 4.38 (2H, m, OCH_2), 4.30 (2H, m, CH_2), 3.00 (2H, s, SCH_2), 2.62 (3H, s, CH_3), 2.46 (3H, s, CH_3), 1.35 (3H, t, CH_3). *Anal.* calcd. for $C_{13}H_{15}NO_5S_2$: C 47.42, H 4.59, N 4.25; found: C 47.42, H 4.67, N 4.35.

Other N-*Acyl-1,3-oxathiol-2-imines*

Other *N*-acyl-1,3-oxathiol-2-imines prepared, for which yields, analyses, and uv and nmr spectra are available from the Depository of Unpublished Data[1] are 7 where R = C_6H_5, R′ = CH_3, R″ = $CO_2C_2H_5$, mp 167–169°C; R = C_6H_5, R′ = CH_3, R″ = $COCH_3$, mp 196–197°C; R = C_6H_5, R′ = CH_3, R″ = $CON(CH_3)_2$, mp 106–107°C; R = C_6H_5, R′ = R″ = CH_3, mp 162–164°C; R = R′ = C_6H_5, R″ = $CO_2C_2H_5$, mp 160–161°C; R = 3-$CH_3C_6H_4$, R′ = CH_3, R″ = $CO_2C_2H_5$, mp 132–134°C; R = 3-$CH_3C_6H_4$, R′ = CH_3, R″ = $CON(CH_3)_2$, mp 101–103°C; R = C_6H_5, R′ = 4-$CH_3C_6H_4$, R″ = CH_3, mp 149–150°C; R = C_6H_5, R′ = 2,4-di$CH_3C_6H_3$, R″ = CH_3, mp 105–106°C; R = 5,6-dihydro-2-methyl-1,4-oxathiin-3-yl, R′ = C_6H_5, R″ = H, mp 178–180°C; R = 5,6-dihydro-2-methyl-1,4-oxathiin-3-yl, R′ and R″ together = -$CH_2CH_2CH_2CH_2$-, mp 143–145°C; R = 5,6-dihydro-2-methyl-1,4-oxathiin-3-yl, R′ = C_6H_5, R″ = $CO_2C_2H_5$, mp 158–160°C; R = 2-furanyl, R′ = CH_3, R″ = $CO_2C_2H_5$, mp 126–127°C; R = 2-furanyl, R′ = CH_3, R″ = $COCH_3$, mp 179–180°C; R = 2-furanyl, R′ = R″ = CH_3, mp 143–145°C; R = 2-furanyl, R′ = CH_3, R″ = $CON(CH_3)_2$, mp 163–165°C; R = 2-furanyl, R′ = C_6H_5, R″ = $CO_2C_2H_5$, mp 163–165°C; R = C_2H_5O, R′ = CH_3, R″ = $CO_2C_2H_5$, mp 64–65°C; R = cyclohexyl, R′ = CH_3, R″ = $CO_2C_2H_5$, mp 55–56°C.

Acknowledgements

Grateful acknowledgement is made to W. R. Boos, M. J. Ross, Mary-Ann Fitzsimmons, and Helen van Veggel for the analyses and the nmr, uv, and ir spectra.

1. D. S. Breslow and H. Skolnik. Heterocyclic compounds, multisulfur and sulfur and oxygen five- and six-membered heterocycles. Part one. *Edited by* A. Weissburger. Interscience Publishers Inc., New York, NY. 1966. p. 203.
2. G. E. Kuhlmann and D. C. Dittmer. J. Org. Chem. **34**, 2006 (1969).
3. U. J. Kempe, T. Kempe, and T. Norin. J. Chem. Soc. Perkin Trans.I, 1547 (1978).
4. W. Ried and L. Kaiser. Ann. Chem. 958 (1975); Chem. Abstr. **83**, 114304w (1975).
5. B. A. Trofimov, S. V. Amosova, V. V. Kryuchkov, G. A. Kalabin, U. K. Voronov, M. V. Sigolov, L. I. Azerova, and O. A. Tarasova. Tezisy Dokl. Nauchn. Sess. Khim. Tekhnol. Org. Soedin Sery Sernistykh Neftei, **13**, 121 (1974); Chem. Abstr. **85**, 159952p (1976).
6. G. Ottman, G. D. Vickers, and H. Hooks, Jr. J. Heterocycl. Chem. **4**, 527 (1967).
7. A. R. Katritzky, B. Wallis, R. T. C. Brownlee, and R. D. Topson. Tetrahedon, **21**, 1681 (1965).
8. M. Kulka. Can. J. Chem. **58**, 2044 (1980).

Can. J. Chem. Downloaded from www.nrcresearchpress.com by 210.87.254.105 on 09/06/12
For personal use only.

Medium effects in protonation equilibrium studies. Accurate acidity constants using the excess acidity method[1]

ROBIN A. COX AND KEITH YATES

Department of Chemistry, University of Toronto, 80 St. George St., Toronto, Ont., Canada M5S 1A1

Received November 20, 1980

ROBIN A. COX and KEITH YATES. Can. J. Chem. **59**, 1560 (1981).

Ultraviolet spectra of *N-tert*-butylbenzamide taken in 0–92% sulfuric acid solutions clearly show that two processes, having roughly equal effects on the spectra, take place over this acidity range. One is protonation of the molecule, and the other is either tautomerization from N- to O-protonated forms, or a pronounced medium effect on the latter. Attempted separation of these two processes using characteristic vector analysis fails. However, separation is possible using an analysis based on the excess acidity (*X*-function) method. This shows that the second process is a medium effect. The analysis permits accurate calculation of pK_{BH^+} and m^* values in the presence of medium effects on the acid form, the base form, or both.

ROBIN A. COX et KEITH YATES. Can. J. Chem. **59**, 1560 (1981).

Les spectres ultraviolets de la *N-tert*-butylbenzamide dans des solutions d'acide sulfurique à des concentrations allant de 0 à 92% révèlent clairement que, sur cet intervalle d'acidité, deux processus se superposent et qu'ils ont chacun à peu près le même effet sur le spectre. L'un deux est la protonation de la molécule tandis que l'autre correspond soit à une tautomérisation de la forme N-protonée en forme O-protonée, soit à un effet du milieu assez prononcé sur la dernière forme. Il est impossible de différencier ces deux processus en utilisant une analyse vectorelle caractéristique. Cependant il est possible d'obtenir une différenciation en utilisant une analyse basée sur la méthode d'excès d'acidité (fonction de *X*). Ceci révèle que le deuxième procédé est un effet du milieu, L'analyse a permis de calculer d'une façon précise les valeurs du pK_{BH^+} et de m^* en présence des effets du milieu sur la forme acide, sur la forme basique ou sur les deux à la fois.

[Traduit par le journal]

Introduction

The site of protonation is of central importance to the study of amide protonation equilibria (1) and hydrolysis mechanisms (2). Much evidence now exists in favour of oxygen protonation; for instance McClelland and Reynolds' decisive ^{13}C nmr study showed oxygen protonation of *N,N*-dimethylformamide at all acidities (3), and recently Benedetti *et al.* presented an X-ray structure of *N,N*-dimethylacetamide hydrochloride (4), in which a difference-Fourier synthesis clearly shows the molecule to be oxygen-protonated in the solid state. However, the latter workers (4) leave open the possibility of a tautomeric equilibrium between N- and O-protonated forms in solution, as has been suggested by Liler (5). Also, a recent theoretical study (6), which favours oxygen protonation in the gas phase, finds that increasing "pyramidization" of the NH_2 group, which might occur in solution, increases the nitrogen and decreases the oxygen basicity.

In view of this we decided to apply the method of characteristic vector analysis (CVA) (7, 8) to uv spectra of amides taken over the whole sulfuric acid concentration range. In this case CVA separates the data into orthogonal vectors according to eq. [1], where D is optical density at

$$[1] \quad D_\lambda = \bar{D}_\lambda + c_1 v_{1\lambda} + c_2 v_{2\lambda} + \ldots$$

eq. [1], where D is optical density at wavelength λ, $\bar{D}$ is the average D at that wavelength over the acidity range, v's are vectors, independent of acidity, and c's are weighting coefficients, independent of wavelength. The protonation information is supposedly contained in c_1 when the method is used to separate protonation from medium effects (8–10). For a separation into different vectors to occur the effects involved must be orthogonal, i.e. independent of one another (7). This should apply, at least formally, to subsequent protonation and tautomerism (eq. [2]), insofar as

[2] 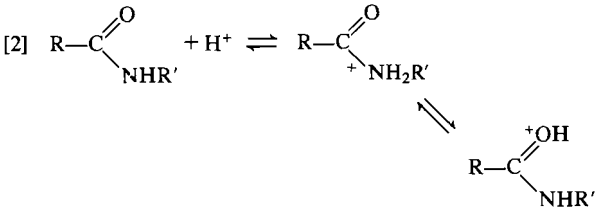

the first equilibrium involves a proton, and so would be acidity-dependent, whereas the second does not.

This approach, the problems found with it, and the excess acidity (11) analysis of medium effects on protonation equilibrium measurements which

[1]Presented in part at the 62nd Chemical Conference of the Chemical Institute of Canada, Vancouver, B.C., June, 1979, No. OR-107.

0008-4042/81/111560-08$01.00/0

©1981 National Research Council of Canada/Conseil national de recherches du Canada

Can. J. Chem. Downloaded from www.nrcresearchpress.com by 210.87.254.42 on 09/06/12
For personal use only.

Can. J. Chem. Downloaded from www.nrcresearchpress.com by 210.87.254.42 on 09/06/12
For personal use only.

was developed as a result, form the subject of this paper, with *N-tert*-butylbenzamide being used as an example. Other examples will be found in the following paper (12), which uses this method for dissecting medium effects from protonation equilibria in the protonation of many different amides and lactams.

Experimental

The CVA program was written from Simonds' (7) algorithm and is essentially the same as that used by Edward and Wong (8).[2] The *X*-function analysis program was an adaptation of the general-purpose curve-fitting program CURFIT due to Bevington (13), quite similar to that used before for calculating *X*-functions for HCl and HBr (14), and for fitting kinetic equations (15). Details may be obtained from the authors; most computer centres offer similar curve-fitting routines. The uv spectra of *N-tert*-butylbenzamide were already available (12, 16) (Fig. 1). Ten absorbance measurements, at 5 nm intervals over the wavelength range 212.5–257.5 nm, were taken from each of 26 spectra covering the acidity range from water to 92% H_2SO_4. These data were arranged into a 26 row by 10 column matrix and used for both CVA and the excess acidity analysis without further modification.[2]

Characteristic Vector Analysis

The uv spectra of *N-tert*-butylbenzamide at different acidities are illustrated in Fig. 1. At low acidities a peak is present at about 225 nm, which shifts to some 237 nm at intermediate acidities and continues shifting to the 245–250 nm region in strongly acidic solutions. Clearly more than one process is occurring; presumably protonation, and either tautomerization as in eq. [2] or a pronounced medium effect, are taking place. It is also apparent that each of the two spectral processes contributes approximately equally to the total spectral variation.

This is contradicted by the CVA results, however. The analysis found two statistically significant vectors, the first accounting for 92.4% of the observed variation and the second 5.0%, the remaining 2.6% of the variation being random. The spectra reconstituted using the vectors and coefficients obtained were in good agreement with the originals, the root-mean-square residual error being ±0.010 absorbance units. The coefficients of the two vectors are plotted as a function of $-H_0$ (17), for illustrative purposes, in Fig. 2. Now simple

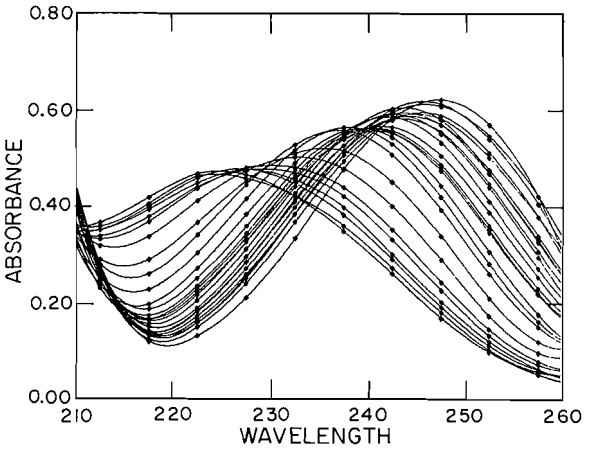

FIG. 1. Ultraviolet spectra of *N-tert*-butylbenzamide at different acidities. Points are the data points used in the CVA and the excess acidity analysis. The acidity ranges from water to 92% sulfuric acid at approximately 3.7% intervals, increasing from top to bottom at the left of the figure and from bottom to top at the right.

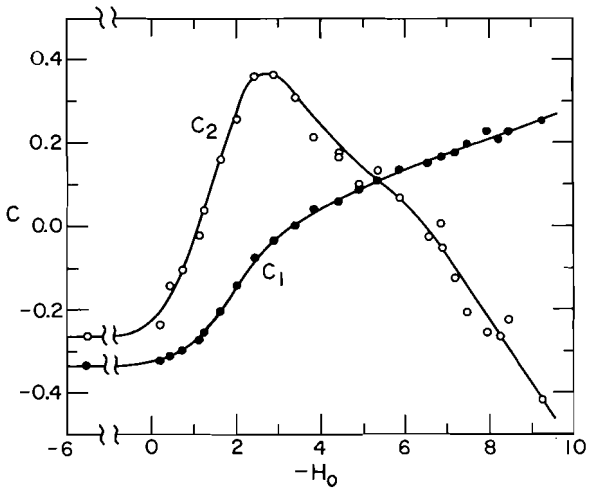

FIG. 2. Coefficients of the first and second characteristic vectors resulting from CVA of the spectra in Fig. 1, plotted as a function of $-H_0$.

protonation would give a sigmoid titration curve, changing from a constant c_B to a constant c_{BH^+}, when plotted in this way. It is evident that c_1 behaves like this initially, but does not reach a stable final value, continuing to vary slowly, and roughly linearly, with $-H_0$. This behaviour is very similar to that observed in some cases by Reeves (9), in his study of phenylazobenzenes and phenylazonaphthols in sulfuric acid. The only reasonable conclusion is that both protonation and the second effect are contained in c_1, which accounts for most

[2]The CVA program, together with the data matrix used, the derived vectors and coefficients, the reconstituted data matrix provided by the program, and the residuals, are on deposit and may be obtained, at a nominal charge, from the Depository of Unpublished Data, CISTI, National Research Council of Canada, Ottawa, Ont., Canada K1A 0S2. The *X*-function analysis program is given as a supplement to the following paper (12).

Can. J. Chem. Downloaded from www.nrcresearchpress.com by 210.87.254.42 on 09/06/12
For personal use only.

of the variation; c_2 has no obvious physical or chemical counterpart (8).

Ultraviolet spectra as a function of acidity were obtained for many of the amides studied in the following paper (12), in addition to *N-tert*-butylbenzamide. Application of CVA resulted in very similar behaviour for all of them, with one vector accounting for almost all of the observed variation; in some cases this was the only statistically significant vector obtained. It should be emphasized that *N-tert*-butylbenzamide is quite typical; in fact when CVA is used in this way this behaviour is very common (8–10).

In hindsight this is what would be expected. CVA as used (7–10) is in fact *principle component* analysis (18), i.e., first the maximum possible variation is assigned to the first *eigen*vector, then the maximum amount of the remainder is assigned to the second, and so on. This unique eigenvector orientation is based solely on mathematical, not chemical, properties, and the eigenvectors which result may be linear combinations of chemical properties rather than the properties themselves (18). This seems to be the case here. Coordinate rotation is generally required to obtain the true chemical properties; some criteria for this have been given (18). A suitable linear combination of the vectors obtained may well give the proper sigmoid acidity dependence for the coefficients,[3] but the CVA method (7) as used here and elsewhere (8–10) evidently does not. It is true that spectra reconstituted according to eq. [1] using only $\bar{D}$ and v_1 show excellent isosbestic points, as spectra should when only one process is taking place, exemplified in papers by Edward and Wong (8), Reeves (9), and Zalewski (10). However, an isosbestic point necessarily results whenever v_1 is zero (see eq. [1]), which happens at least once in all cases (8–10), so this behaviour is forced upon the system.

Therefore we had to abandon unmodified CVA as a method for separating these different spectral processes. However, Fig. 2 is useful insofar as it shows that the second process is more likely to be a medium effect than a tautomerization. A process such as eq. [2] would likely produce two superimposed sigmoid curves, reaching a constant value at high acidity, rather than the continuous increase with $-H_0$ that is found for c_1. Also the observed nonseparation makes tautomerization seem less likely. Accordingly we determined to see whether the new excess acidity method, which has had considerable success in measuring pK_{BH^+} values (11, 14) and in the study of organic reaction mechanisms in these nonideal strong acid systems (15, 19), could be used for the determination of pK_{BH^+} values from spectral measurements in the presence of medium effects.

[3]Of course when only one statistically significant vector results none of this is possible.

Excess Acidity Analysis

The chemical process of interest is a base B being protonated to an acid A (as abbreviated here for convenience, usually written HA or BH^+), the dissociation constant of A being K_a (or K_{BH^+}), as in eq. [3]. According to the excess acidity method (11, 14), in terms of molarity C and molar activity coefficient f the pK_a is given by eq. [4]. The basic assumption of this treatment is eq. [5], where B* is a standard reference base (11, 14); eqs. [4] and [5] are well-tested and have been shown to be valid (11, 20).

$$[3]\quad B + H^+ \underset{}{\overset{K_a}{\rightleftharpoons}} A \qquad I = C_A/C_B$$

$$[4]\quad \log I - \log C_{H^+} = pK_a + m^*X$$

$$[5]\quad \log (f_B f_{H^+}/f_A) = m^* \log (f_{B^*} f_{H^+}/f_{A^*}) = m^*X$$

Since K_a as defined is solvent-independent, that is, the states of hydration of B, A, and H^+ are not specified, a series of equations like eq. [3], with the same K_a, can be written for different states of hydration (say 1 and 2) of A and B, as in eq. [6].

$$[6]\quad \begin{aligned} B_1 + H^+ &\overset{K_a}{\rightleftharpoons} A_1 \qquad I_1 = C_{A_1}/C_{B_1} \\ B_1 + H^+ &\overset{K_a}{\rightleftharpoons} A_2 \qquad I_2 = C_{A_2}/C_{B_1} \\ B_2 + H^+ &\overset{K_a}{\rightleftharpoons} A_1 \qquad I_3 = C_{A_1}/C_{B_2} \\ &\vdots \qquad\qquad \vdots \end{aligned}$$

Now by definition $a_{A_1} = a_{A_2} = \ldots = a_A$ and $a_{B_1} = a_{B_2} = \ldots = a_B$; as the medium is changed, the activities of the different hydrates remain equal, but the concentrations do not. If state 1 is more hydrated than state 2, its activity coefficient will increase and its concentration decrease as the medium becomes more acidic and more dehydrating, and vice versa. If the states have different physical properties (uv spectrum, nmr chemical shift) this will cause a medium effect as the acidity is varied.

Excess acidity equations are easily derived for eq. [6] as in eq. [7]. By considering the equilibria between states 1 and 2, eq. [8], the ratios I_A and I_B can be obtained by subtracting the appropriate X-function equations in eq. [7], giving eq. [9] for the base B and eq. [10] for the acid A. If the states 1 and 2 have different properties, then Δm_B^* and $\Delta m_A^* \neq 0$

Can. J. Chem. Downloaded from www.nrcresearchpress.com by 210.87.254.42 on 09/06/12
For personal use only.

and a real medium shift will be apparent.

$$\begin{aligned} \log I_1 &= pK_a + \log C_{H^+} + m_1{}^*X \\ \log I_2 &= pK_a + \log C_{H^+} + m_2{}^*X \\ \log I_3 &= pK_a + \log C_{H^+} + m_3{}^*X \\ &\vdots \end{aligned} \quad [7]$$

$$B_1 \underset{}{\overset{K=1}{\rightleftharpoons}} B_2 \quad I_B = C_{B_2}/C_{B_1} = I_1/I_3 \quad [8]$$

$$A_1 \underset{}{\overset{K=1}{\rightleftharpoons}} A_2 \quad I_A = C_{A_2}/C_{A_1} = I_2/I_1 \quad [8]$$

$$\log I_B = \log I_1 - \log I_3 = (m_1{}^* - m_3{}^*)X = \Delta m^*{}_B X \quad [9]$$

$$\log I_A = \log I_2 - \log I_1 = (m_2{}^* - m_1{}^*)X = \Delta m^*{}_A X \quad [10]$$

Now one protonation equation, say that for $\log I_1$ in eq. [7], and the two medium effect equations [9] and [10], suffice to describe the variation of (say) optical density with the changing medium:

$$\begin{aligned} C_T &= C_{B_1} + C_{B_2} + C_{A_1} + C_{A_2} \\ &= C_{B_1}(1 + I_B + I_1 + I_1 I_A) \end{aligned}$$

$$\begin{aligned} D &= \varepsilon_{B_1} l C_{B_1} + \varepsilon_{B_2} l C_{B_2} + \varepsilon_{A_1} l C_{A_1} + \varepsilon_{A_2} l C_{A_2} \\ &= \frac{C_T(\varepsilon_{B_1} l + \varepsilon_{B_2} l I_B + \varepsilon_{A_1} l I_1 + \varepsilon_{A_2} l I_1 I_A)}{1 + I_B + I_1(1 + I_A)} \end{aligned}$$

$$D = \frac{D_{B_1} + D_{B_2} I_B + D_{A_1} I_1 + D_{A_2} I_1 I_A}{1 + I_B + I_1(1 + I_A)} \quad [11]$$

(since $\varepsilon_{B_1} l C_T = D_{B_1}$, etc.). In the aqueous reference state $X = 0$ (11) and $I_A = I_B = 1$ (also $\log I_1 = pK_a - pH$), and eq. [11] reduces to

$$D = \frac{(D_{B_1} + D_{B_2})/2 + I_1(D_{A_1} + D_{A_2})/2}{1 + I_1}$$

Thus in water we can write $D_{Baq} = (D_{B_1} + D_{B_2})/2$ and $D_{Aaq} = (D_{A_1} + D_{A_2})/2$. D_{B_1}, D_{A_2} etc. are hypothetical limits, never attained in practice because it is not possible to observe B_1 in the *absence* of B_2, etc. (It may be convenient to regard state 1 as being solvated by all the water molecules present and state 2 as being unsolvated.) So now we may make the more practical definition above, based on the aqueous reference state, and define a medium shift δ:

$$D_{B_2} = D_{Baq} + \delta D_B \qquad D_{A_2} = D_{Aaq} + \delta D_A$$

With these substitutions eq. [11] becomes:

$$D = \frac{D_{Baq} + \delta D_B\left(\frac{I_B - 1}{1 + I_B}\right) + D_{Aaq}\left(\frac{I_1(1 + I_A)}{1 + I_B}\right) + \delta D_A\left(\frac{I_1(I_A - 1)}{1 + I_B}\right)}{1 + \frac{I_1(1 + I_A)}{1 + I_B}}$$

From the definitions of I_1, I_A, and I_B it is apparent that

$$I_1(1 + I_A)/(1 + I_B) = (C_{A_1} + C_{A_2})/(C_{B_1} + C_{B_2}) = C_A/C_B = I$$

and that

$$I_1(I_A - 1)/(1 + I_B) = I(I_A - 1)/(1 + I_A)$$

For simplicity we define

$$\begin{aligned} (I_A - 1)/(1 + I_A) &= I'_A \\ (I_B - 1)/(1 + I_B) &= I'_B \end{aligned}$$

With these substitutions we obtain

$$D = \frac{D_{Baq} + \delta D_B I'_B + I(D_{Aaq} + \delta D_A I'_A)}{1 + I} \quad [12]$$

Equation [12] is a general equation with eight unknowns (D_{Baq}, D_{Aaq}, δD_B, δD_A, pK_a, m^*, $\Delta m_B{}^*$ and $\Delta m^*{}_A$). Thus large amounts of good data over the entire acidity range will be required if eq. [12] is to be used directly; however, it can be simplified.

Case 0

No medium effect; $\delta D_B = \delta D_A = 0$. Equation [12] becomes

$$D = (D_B + I D_A)/(1 + I) \quad [13]$$

with

$$\log I = pK_a + \log C_{H^+} + m^*X$$

(In water, $I_B = I_A = 1$ and $I'_B = I'_A = 0$, so the same equation applies, only with $\log I = pK_a - pH$.)

Case 1

Compounds which protonate in weak acid, medium effects on the base form not observable, $\delta D_B = 0$; eq. [12] becomes

$$D = (D_B + I(D_{Aaq} + \delta D_A I'_A))/(1 + I) \quad [14]$$

with

$$I'_A = (I_A - 1)/(1 + I_A) \quad \text{and} \quad \log I_A = \Delta m^*{}_A X$$

Case 2

Compounds protonating in strong acid, medium

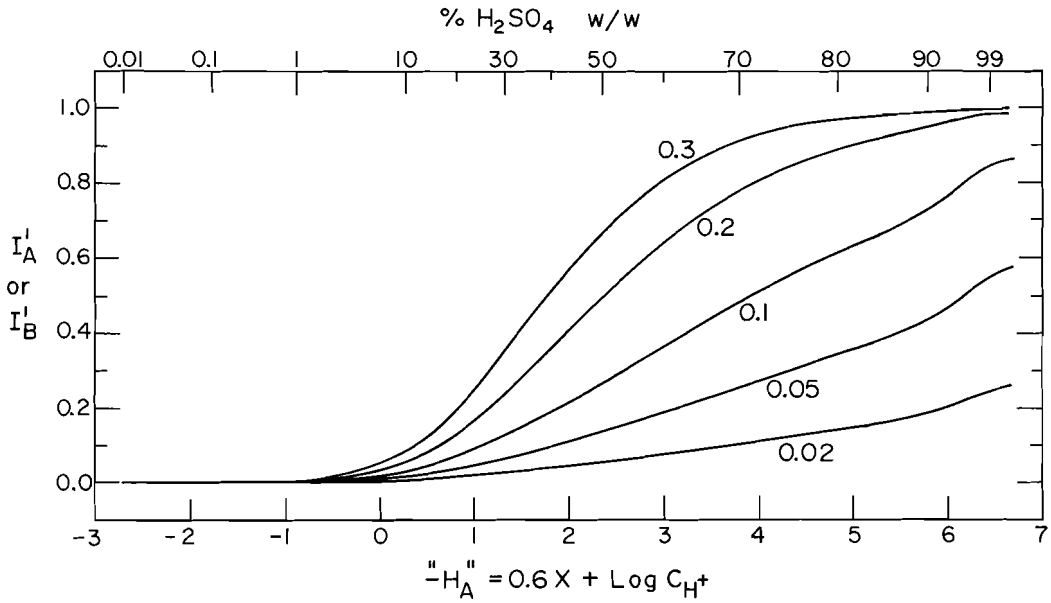

FIG. 3. I'_A or I'_B for various values of Δm^*, plotted against an acidity function for average amides. For comparison purposes a percent H_2SO_4 scale is included at the top of the figure.

effects on the acid form not observable, $\delta D_A = 0$; eq. [12] becomes

[15] $$D = (D_{Baq} + \delta D_B I'_B + I D_A)/(1 + I)$$

with

$$I'_B = (I_B - 1)/(1 + I_B) \quad \text{and} \quad \log I_B = \Delta m^*_B X$$

These equations make intuitive sense. When medium effects are absent, eq. [13] with constant D_A and D_B values applies; if medium effects are present, either D_A or D_B or both become variable functions of acidity, e.g. $D_A = D_{Aaq} + \delta D_A I'_A$, exactly as would be expected. I_B and I_A have limiting values of unity, since X cannot be negative (11); both must be ≥ 1 since the states of hydration of B and BH^+ must decrease with increasing acidity, i.e. $B_1 \rightarrow B_2$ and $A_1 \rightarrow A_2$. Thus Δm^*_B and Δm^*_A must be positive. I'_A and I'_B have limiting values of zero, in the aqueous standard state, and unity, when I_A and I_B are very large.

The behaviour of I' as a function of changing acidity (in terms of an acidity function for average amides (11), "$-H_A$" = $0.6X + \log C_{H^+}$) is illustrated for various values of Δm^* in Fig. 3. For $\Delta m^* \leq 0.1$, I' is practically linear with acidity functions over the 20–95% H_2SO_4 range, in agreement with experience (9, 21, 22); for instance Katritzky *et al.* (21) found that the medium effect on protonated amides was accounted for by assuming that ε_{BH^+} ($\equiv D_A$ here) was linear in $-H_0$, and Yates and McClelland (22) found that the same assumption applied to the unprotonated form (D_B) in ester protonation studies. This agreement is gratifying; it must be pointed out that it is not "built into" the excess acidity method, as the only assumption used in obtaining eq. [12] is that of eq. [5] above. Our experience has been that $\Delta m^* \simeq 0.1$ in most cases (12); occasionally $\Delta m^* > 0.1$, however, and plots of D_A or D_B against acidity functions are curved. An example is given in a following paper (12). If the data are insufficient to permit calculation of six coefficients using eq. [14] or eq. [15], fixing Δm^* at 0.1 (or 0.05) and calculating pK_a, m^*, D_{Baq}, D_{Aaq}, and δD is usually satisfactory (12). Often D_{Baq} is accurately known too. In extreme cases m^* can also be fixed at a likely value (11), but this is far less satisfactory. Equations [12]–[15] are best solved using a computer curve-fitting routine (see Experimental); only the familiar (11, 23) eq. [13] can be conveniently linearized (using fixed D_A and D_B values). Values of $\log C_{H^+}$ and X for use with these equations are available (11, 14).

Results and Discussion

Amides protonate in relatively dilute sulfuric acid (1, 16), so only medium effects on the acid form should be visible, Case 1 above. Accordingly eq. [14] was used, with the data already available from the characteristic vector analysis. These data consist of optical density measurements at 10 separate wavelengths, in 26 different sulfuric acid solutions, so the equation solved was actually ten separate eq. [14]'s, each one with different D_B,

Can. J. Chem. Downloaded from www.nrcresearchpress.com by 210.87.254.42 on 09/06/12
For personal use only.

Can. J. Chem. Downloaded from www.nrcresearchpress.com by 210.87.254.42 on 09/06/12
For personal use only.

D_{Aaq}, and δD_A values, but with the same pK_a, m^*, and Δm^*_A applying to all of them. Techniques for fitting a series of equations of this type were already available (14). One advantage to this is that 260 data points are used to calculate $3 \times 10 + 3 = 33$ coefficients, which is 7.9 points per coefficient, as compared to only 4.3 points per coefficient if 26 points are used to calculate 6 coefficients at a single wavelength, so the precision is higher. Another advantage is that the resulting D_B, D_{Aaq}, and δD_A values can be used to construct theoretical uv spectra for comparison with experiment.

For *N-tert*-butylbenzamide, $pK_a = -1.34 \pm 0.05$, $m^* = 0.68 \pm 0.05$, and $\Delta m^*_A = 0.107 \pm 0.007$ (12). The computer-drawn spectra constructed using these and the calculated D_B, D_{Aaq}, and δD_A values are given in Fig. 4. As can be seen the comparison between Figs. 1 and 4 is very good; the root-mean-square deviation between theory and experiment on the data points is marginally better than that given by the CVA, ± 0.009 optical density units, mainly due to the minor substrate concentration fluctuations to be expected from the experimental method used (12, 16). The appearance that the spectra would have in the absence of medium effects can also be determined, by assuming that D_A remains constant at D_{Aaq} and using eq. [13]; this is presented in Fig. 5. This shows that in water the protonated form has a λ_{max} of 237 nm, compared to 225 nm for the free amide. Similarly the medium effect on the protonated form can be examined in isolation, using $D_A = D_{Aaq} + \delta D_A I'_A$, and is given in Fig. 6. The λ_{max} of the acid form is seen to shift from 237 nm in water to 247 nm in 92% sulfuric acid. The second process is clearly revealed to be a medium effect by the regular shift pattern and the

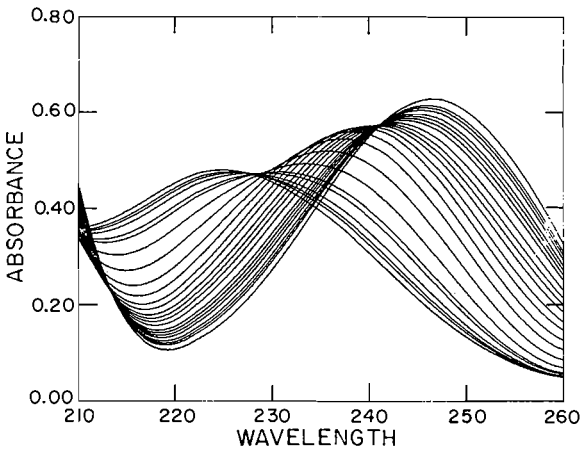

FIG. 4. Reconstructed uv spectra of *N-tert*-butylbenzamide at different acidities, resulting from the excess acidity analysis of the data in Fig. 1 via eq. [14]. See Fig. 1.

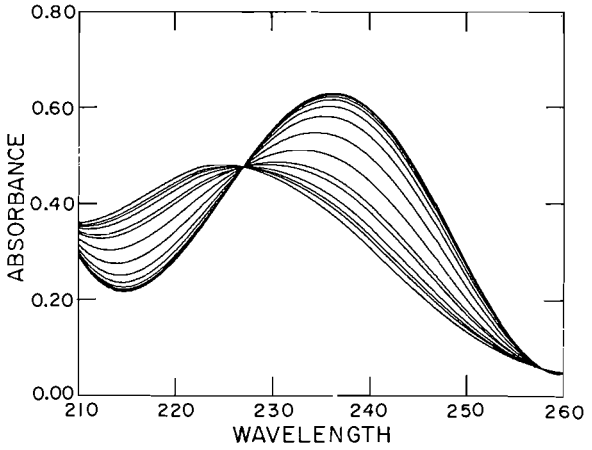

FIG. 5. Protonation; how the uv spectra of *N-tert*-butylbenzamide at different acidities would appear in the absence of a medium effect. See text and Fig. 1.

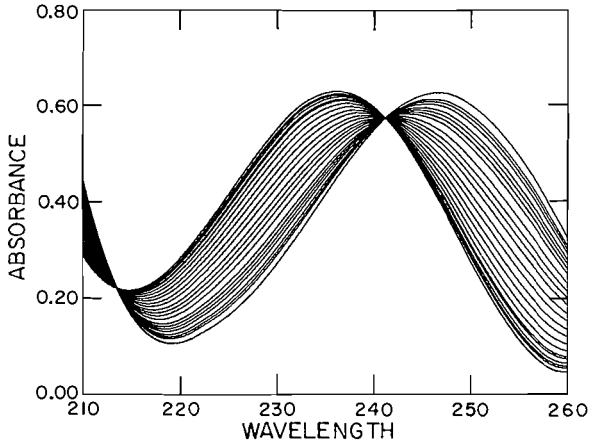

FIG. 6. The medium effect; how the uv spectra of protonated *N-tert*-butylbenzamide at different acidities would appear in the absence of spectral changes due to protonation. See text and Fig. 1.

closely similar peak shapes. Protonation is essentially complete at the 13th spectral scan (60% H_2SO_4); subsequent spectra only show the medium effect.

Returning to the CVA results and Fig. 2, eq. [14] should apply to c_1 also, if c_1 contains both medium effect and protonation information. Accordingly eq. [14] was written in terms of c (dropping the subscript 1 for clarity) and recast as eq. [16], in

$$[16] \quad (c(1 + I) - c_B)/I = c_{Aaq} + \delta c_A I'_A$$

order to determine c_{Aaq} and δc_A. The values of pK_a, m^*, and Δm^*_A given above were used to calculate I and I'_A, and c_B was taken to be the value in water, -0.335; the resulting plot was accurately linear (correlation coefficient 0.998 over 24 points),

Can. J. Chem. Downloaded from www.nrcresearchpress.com by 210.87.254.42 on 09/06/12
For personal use only.

showing that the analysis does indeed apply to c_1 also. An intercept, $c_{Aaq} = -0.118 \pm 0.003$, and a slope, $\delta c_A = 0.486 \pm 0.007$, were obtained; these were used to calculate a theoretical curve, and to dissect c_1 into two parts, as before, and the result is compared with the experimental points in Fig. 7. Here c_1 is plotted against the proper substrate acidity function (11) for *N-tert*-butylbenzamide, $-H_S = \log C_{H^+} + m^*X$, rather than $-H_0$; the values of c_{Aaq}, c_B, and δc_A are also indicated. As can be seen, agreement with the experimental c_1 values is excellent; the sigmoid protonation curve is seen to account for slightly less than half of the total variation. The true pK_a occurs half-way along such titration curves, as shown; it differs considerably from the value that would be chosen if the entire c_1 curve was taken as being due to protonation. The fact that this dissection of c_1 into two parts works so well reinforces the conclusion reached earlier, that CVA as used *does not* separate medium effects from protonation equilibria.

The possibility that the second process is a tautomerization, and not a medium effect, can now be discounted. Without going into detail, it is not difficult to derive X-function equations like eq. [14] based on this possibility, only now I' involves a ΔpK_a for protonation at the two sites, as well as a Δm^*, which would be the difference in m^* between protonation at N and O atoms, 0.4 or more (11). In order to obtain the good agreement with eq. [14] found in this work Δm^* would have to be 0.1, as found, and ΔpK_a would have to be zero. Thus tautomerism seems highly improbable on this basis. The uv spectra of benzamide given by Liler (5), which she takes as evidence of tautomerism, are in fact very similar to the *N-tert*-butylbenzamide spectra in this paper; undoubtedly they represent a medium effect in that case also. Very large medium shifts are found for other carbonyl compounds in strong acids, e.g. acetone (24), and it is unreasonable not to expect them for amides too; dilute and concentrated H_2SO_4 are, after all, very different media (25). The only evidence of Benedetti *et al.* for tautomerism is that a solution of dimethylacetamide hydrochloride in water does not have the same uv spectrum as does a solution in HCl (4). Presumably the aqueous solution would not have a pH lower than about one, as the only source of acid is the dimethylacetamide hydrochloride itself, at low uv spectral concentrations. This is insufficient to support full protonation of dimethylacetamide (diethylacetamide has a pK_{BH^+} of -0.33 (12)), and the observed spectrum will be that of a combination of free and protonated amides, not a combination of N- and O-protonated amides as stated (4).

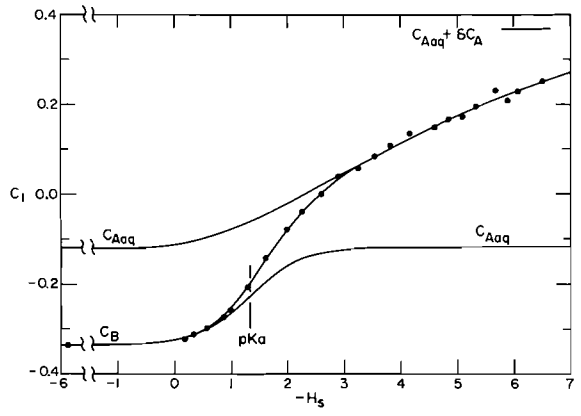

FIG. 7. The first characteristic vector coefficients from Fig. 2 compared with the theoretical curve from eq. [14], as a function of $-H_S$, the substrate acidity function for *N-tert*-butylbenzamide. Also shown is the dissection into the protonation titration curve and the medium effect curve (see text).

Summarizing: characteristic vector analysis as used does *not* separate medium effects from protonation equilibria, and its use for this purpose requires modification; medium effects are of major importance in the protonation of amides, as shown here and in a following paper (12); the excess acidity method enables accurate pK_{BH^+} determinations in the presence of large medium effects via eqs. [12]–[15]; and oxygen protonation is the only observable protonation process for amides at any acidity.

Acknowledgements

Financial support of this research is by the Natural Sciences and Engineering Research Council of Canada. Helpful comments by a referee are also appreciated.

1. K. YATES, J. B. STEVENS, and A. R. KATRITZKY. Can. J. Chem. **42**, 1957 (1964); K. YATES and J. B. STEVENS. Can. J. Chem. **43**, 529 (1965).
2. C. R. SMITH and K. YATES. J. Am. Chem. Soc. **93**, 6578 (1971).
3. R. A. MCCLELLAND and W. F. REYNOLDS. J. Chem. Soc. Chem. Commun. 824 (1974).
4. E. BENEDETTI, B. DI BLASIO, and P. BAINE. J. Chem. Soc. Perkin Trans. II, 500 (1980).
5. M. LILER. J. Chem. Soc. Perkin Trans. II, 71 (1974).
6. J. CATALÁN and M. YÁÑEZ. Tetrahedron, **36**, 665 (1980).
7. J. L. SIMONDS. J. Opt. Soc. Am. **53**, 968 (1963).
8. J. T. EDWARD and S. C. WONG. J. Am. Chem. Soc. **99**, 4229 (1977).
9. R. L. REEVES. J. Am. Chem. Soc. **88**, 2240 (1966).
10. R. I. ZALEWSKI. J. Chem. Soc. Perkin Trans. II, 1637 (1979).
11. R. A. COX and K. YATES. J. Am. Chem. Soc. **100**, 3861 (1978).
12. R. A. COX, L. M. DRUET, A. E. KLAUSNER, T. A. MODRO, P. WAN, and K. YATES. Can. J. Chem. **59**, 1568 (1981).
13. P. R. BEVINGTON. Data reduction and error analysis for the

physical sciences. McGraw-Hill, New York. 1969. pp. 232–242.
14. R. A. Cox and K. Yates. Can. J. Chem. In press.
15. R. A. Cox, M. F. Goldman, and K. Yates. Can. J. Chem. **57**, 2960 (1979).
16. T. A. Modro, K. Yates, and F. Beaufays. Can. J. Chem. **55**, 3050 (1977).
17. C. D. Johnson, A. R. Katritzky, and S. A. Shapiro. J. Am. Chem. Soc. **91**, 6654 (1969).
18. R. W. Rozett and E. M. Petersen. Anal. Chem. **47**, 1301 (1975).
19. R. A. Cox and K. Yates. Can. J. Chem. **57**, 2944 (1979); R. A. Cox, C. R. Smith, and K. Yates. Can. J. Chem. **57**, 2952 (1979).
20. R. Passerini, N. C. Marziano, and P. Traverso. Gazz. Chim. Ital. **105**, 901 (1975); N. C. Marziano, P. G. Traverso, and R. C. Passerini. J. Chem. Soc. Perkin Trans. II, 306 (1977).
21. A. R. Katritzky, A. J. Waring, and K. Yates. Tetrahedron, **19**, 465 (1963).
22. K. Yates and R. A. McClelland. J. Am. Chem. Soc. **89**, 2686 (1967).
23. C. H. Rochester. Acidity functions. Academic Press, London. 1970. Chapt. 1.
24. H. J. Campbell and J. T. Edward. Can. J. Chem. **38**, 2109 (1960).
25. R. A. Cox. J. Am. Chem. Soc. **96**, 1059 (1974).

Can. J. Chem. Downloaded from www.nrcresearchpress.com by 210.87.254.42 on 09/06/12
For personal use only.

Protonation acidity constants for some benzamides, acetamides, and lactams

ROBIN A. COX, LINDA M. DRUET, ADI E. KLAUSNER, TOMASZ A. MODRO, PETER WAN, AND KEITH YATES

Department of Chemistry, University of Toronto, 80 St. George St., Toronto, Ont., Canada M5S 1A1

Received November 20, 1980

ROBIN A. COX, LINDA M. DRUET, ADI E. KLAUSNER, TOMASZ A. MODRO, PETER WAN, and KEITH YATES. Can. J. Chem. **59**, 1568 (1981).

Protonation acidity constants for 27 benzamides, acetamides, and lactams have been determined. Ultraviolet, and ^{13}C and ^{1}H nmr, spectroscopic methods were used; almost all the spectra were found to be subject to medium effects, some quite severe, as the sulfuric acid concentration was increased. Despite this, the excess acidity (X-function) method gave accurate pK_{BH^+} and m^* values. In all cases protonation, followed by a medium shift in the spectrum of the protonated form, was the only process taking place; protonation was essentially complete in 60% H_2SO_4. The results for the different bases are interpreted in terms of the resonance, inductive, and steric effects in operation in the acid and base forms.

ROBIN A. COX, LINDA M. DRUET, ADI E. KLAUSNER, TOMASZ A. MODRO, PETER WAN et KEITH YATES. Can. J. Chem. **59**, 1568 (1981).

On a déterminé les constantes d'acidité de la protonation de 27 benzamides, acétamides et lactames. A cette fin on a utilisé la rmn du ^{1}H et du ^{13}C ainsi que la spectroscopie ultraviolette; lorsque la concentration en acide sulfurique augmente, presque tous les spectres subissent des effets de milieu qui sont quelquefois très importants. En dépit de cette influence, la méthode d'excès d'acidité (fonction X) donne des valeurs précises de pK_{BH^+} et de m^*. Dans tous les cas, la protonation, suivie d'un déplacement moyen dans le spectre de la forme protonée, est le seul processus qui a lieu; la protonation est tout à fait complète dans du H_2SO_4 à 60%. On interprète les résultats des différentes bases en fonction de la résonance ainsi que des effets inductifs et stériques présents dans les formes acide et basique.

[Traduit par le journal]

Introduction

A knowledge of the acidity constants of weakly basic substrates is of central importance to the study of the mechanisms of reactions which take place in acidic media (1), one example of which is the hydrolysis reaction of amides (2, 3) and lactams (4) in moderately concentrated aqueous sulfuric acid. Acidity constants are obtained from an analysis of the variation of some physical property of the substrate with changing acid concentration. The three properties most commonly used are the uv–visible spectrum (1), and the ^{1}H and ^{13}C nmr spectra (5, 6); the change observed with increasing acidity is from a spectrum characteristic of the free base to that of the protonated base. For carbonyl compounds the situation is more complex, however, since the spectra of one or both forms are usually subject to substantial medium effects (6–8). In view of this we recently developed a method for obtaining accurate acidity constants in spite of possible medium effects, based on the excess medium acidity X, which is a measure of the deviation of the acid system from ideality with increasing acid concentration (9).

The variation of ionization ratio, $I = C_{BH^+}/C_B$, with medium acidity is given for the protonation process of eq. [1] by eq. [2] according to the excess acidity (X-function) method (10); C_{H^+} is the proton concentration and X the excess acidity, values of which as a function of weight percent composition are available for the aqueous sulfuric acid system (10), and other common acid media (10, 11). The acidity constant pK_{BH^+} is as defined in eq. [1], and

$$[1]\quad B + H^+ \overset{K_{BH^+}}{\rightleftharpoons} BH^+$$

$$[2]\quad \log I = pK_{BH^+} + \log C_{H^+} + m^*X$$

inclusion of the slope parameter m^*, which expresses the sensitivity of the substrate to the changing acidity, obviates the necessity for considering differing acidity function behaviour among different substrates (10). When medium effects are present, a second ionization ratio is introduced, defined as in eq. [3]; I'_A when the medium effect is on the acid form BH^+, and I'_B for the base form B (9). Here the

$$[3]\quad I'_A = (I_A - 1)/(1 + I_A);\ \log I_A = \Delta m^*_A X$$

slope parameter Δm^*_A reflects the differing sensitivities to the medium of BH^+ in strongly hydrated (aqueous media) and weakly hydrated (strong acid media) forms (9). Amides protonate in relatively weak acid (2, 3), and so come under Case 1 in the accompanying paper (9), i.e. medium effects on the base form are assumed to be negligible, $\Delta m^*_B = 0$. The equation that describes the variation of optical density (or nmr chemical shift) D with changing acidity in this case is eq. [4] (9), where D_B and D_{BH^+aq} are the optical densities of the pure B and

0008-4042/81/111568-06$01.00/0

©1981 National Research Council of Canada/Conseil national de recherches du Canada

Can. J. Chem. Downloaded from www.nrcresearchpress.com by 210.87.254.105 on 09/06/12
For personal use only.

BH^+ forms in water, and δD_{BH^+} is a medium shift term, i.e. $D_{BH^+} = D_{BH^+aq} + \delta D_{BH^+} I'_A$. If medium effects are absent the simpler form of eq. [4] with $\delta D_{BH^+} = 0$ can be used.

$$[4] \quad D = \frac{D_B + I(D_{BH^+aq} + \delta D_{BH^+} I_A')}{1 + I}$$

As a result of continuing kinetic studies in this area (2–4) we needed accurate pK_{BH^+} values for a number of lactams, acetamides, and benzamides, **1–27**. For practical reasons (e.g. the acetamides and lactams do not have useful uv spectra), and in order to test the general applicability of eq. [4], uv, ^1H and ^{13}C spectroscopy were all used in this work.

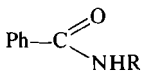

1 R = H
2 R = CH_3
3 R = CH_2CH_3
4 R = $CH(CH_3)_2$
5 R = $CH_2CH(CH_3)_2$
6 R = $CH(CH_3)CH_2CH_3$
7 R = $C(CH_3)_3$
8 R = CH_2Ph
9 R = $CH(CH_3)Ph$

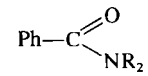

10 R = CH_3
11 R = CH_2CH_3
12 R = $CH(CH_3)_2$
13 $R_2 = (CH_2)_5$

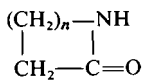

14 $n = 1$
15 $n = 2$
16 $n = 3$
17 $n = 4$
18 $n = 5$
19 $n = 6$

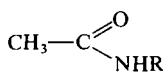

21 R = H
22 R = CH_2CH_3
23 R = $C(CH_3)_3$
24 R = CH_2Ph
25 R = $CH_2C_6H_4OCH_3$-*p*
26 R = $CH_2C_6H_4Cl$-*p*

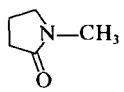

20

$CH_3CON(CH_2CH_3)_2$

27

Experimental

Most of the amides and lactams were available commercially or had been previously prepared (2–4). *N*-benzyl- and α-methyl-*N*-benzylbenzamide were prepared according to Beckmann (12); benzoyl piperidine was obtained using Pasto and Johnson's procedure (13) and purified by column chromatography over alumina. Literature preparations were also available for *N-tert*-butyl- (14), *N*-benzyl- (15), *N-p*-methoxybenzyl- (15), and *N-p*-chlorobenzylacetamide (16). All synthesized compounds had appropriate spectral properties and melting points in agreement with literature values. Sulfuric acid solutions were diluted from the commercial acid and analyzed by measuring their densities at 25°C, using available tabulated composition/density data (17) and a DMA 02C digital precision density meter from Anton Paar.

Unicam SP 1800 or Cary 14 spectrophotometers and matched 1 cm cuvettes were used for the uv measurements, with the cell holders thermostatted at 25°C. Stock substrate solutions in methanol were prepared, of sufficient concentration that adding several microlitres to 3 mL of the test acid by syringe gave optical densities between 0.5 and 0.8, in general. Ultraviolet spectra in the 200–280 nm range were measured for each substrate in at least 20 acids covering the water – 90% H_2SO_4 region, in most cases, using as reference the same acid/methanol mixture, which was subsequently analyzed for concentration if the methanol content was greater than 0.2%. Optical density values at several different wavelengths for each acid were analyzed by computer as described before (9).[1]

A Varian CFT-20 instrument was used for the ^{13}C nmr spectroscopy studies; measurements were relative to a dioxane insert reference, at the probe temperature of 33 ± 2°C. At least 25 different acid strengths between zero and 90% were used; the substrate concentration was 0.5 *M*. For the pK_{BH^+} analysis differences in chemical shift between two carbons in the molecule were employed; 2–4 data columns could be obtained per substrate, which were analyzed in the same way as the uv data (9). Shift differences changed sufficiently with acidity to allow accurate analysis in all cases; for the 9-membered lactam **19**, however, the changes were quite small. Proton nmr measurements were obtained and analyzed in a similar fashion, using Varian T-60 and EM-360 instruments. In this case the number of data columns for analysis was occasionally reduced due to substrate peaks being swamped by solvent peaks at some acidities. For β-propiolactam **14**, very little difference between protonated and unprotonated spectra was apparent, and only approximate results could be obtained.[1]

Results

The benzamides **1–13** were all studied by uv spectroscopy. Data were already available for **1**, **2**, and **10** (18); the available spectra for **3**, **4**, **7**, and **11** (3) were supplemented by measurements at additional acidities. Optical density readings at several different wavelengths were read from spectra taken at each of 20–30 different acid concentrations. Using these data, eqs. [2]–[4] were solved using a computer curve-fitting program (9, 19).[1] For each base, values of D_B, D_{BH^+aq}, and δD_{BH^+} at each of the wavelengths used, as well as pK_{BH^+}, m^*, and Δm^*_A, were obtained, as already described for *N-tert*-butylbenzamide (9). The latter values for all of the compounds studied are given in Table 1, together with the number of data columns analyzed, the total number of data points, the root-mean-square error σ_y and the percent sulfuric acid concentration at which each compound is half-protonated. Occasionally the data did not permit calculation of Δm^*_A; in these cases it was given a fixed value, 0.2, 0.1, or 0.05 (9), and the one which resulted in the lowest σ_y used. In any case pK_{BH^+} and m^* did not vary by more than ±0.02 regardless of Δm^*_A. Those cases in which no

[1]The computer program used, and all of the experimental optical density and chemical shift data for **1–27**, are on deposit and may be obtained, at a nominal charge, from the Depository of Unpublished Data, CISTI, National Research Council of Canada, Ottawa, Ont., Canada K1A 0S2.

Can. J. Chem. Downloaded from www.nrcresearchpress.com by 210.87.254.105 on 09/06/12
For personal use only.

TABLE 1. Acidity constants for the amides **1–27**

Compound	Method[a]	pK_{BH^+}[b]	m^*[b]	Δm^*_A[b,c]	No.[d]	$\pm\sigma_y$[e]	%[f]
1, Benzamide	uv, 3	−1.54±0.02	0.54±0.02	0.1	66 (1)	0.017	36.54
2, Benzamide, *N*-Me	uv, 3	−1.46±0.01	0.53±0.01	0.1	60 (2)	0.005	35.16
3, Benzamide, *N*-Et	uv, 11	−1.52±0.08	0.57±0.08	0.165±0.046	132 (5)	0.019	35.31
4, Benzamide, *N*-*i*-Pr	uv, 11	−1.54±0.06	0.60±0.08	0.1	154 (11)	0.012	34.74
5, Benzamide, *N*-*i*-Bu	uv, 14	−1.50±0.03	0.52±0.03	0.1	308 (19)	0.011	36.28
6, Benzamide, *N*-*s*-Bu	uv, 14	−1.55±0.03	0.68±0.03	0.061±0.013	308 (15)	0.008	33.21
7, Benzamide, *N*-*t*-Bu	uv, 10	−1.34±0.05	0.68±0.05	0.107±0.007	260 (7)	0.009	29.29
8, Benzamide, *N*-benzyl	uv, 12	−1.83±0.07	0.67±0.05	0.135±0.008	276 (10)	0.010	38.50
9, Benzamide, α-Me-*N*-benzyl	uv, 13	−1.58±0.05	0.49±0.04	0.113±0.011	299 (12)	0.008	38.78
10, Benzamide, *N*,*N*-Me_2	uv, 3	−1.00±0.02	0.58±0.03	0.1	66 (2)	0.009	24.22
11, Benzamide, *N*,*N*-Et_2	uv, 10	−1.14±0.06	0.64±0.08	0.094±0.012	260 (9)	0.007	26.13
12, Benzamide, *N*,*N*-*i*-Pr_2	uv, 13	−0.55±0.03	0.60±0.08	0.124±0.009	286 (15)	0.005	15.12
13, Benzoyl piperidine	uv, 13	−0.97±0.03	0.45±0.04	0.060±0.023	286 (14)	0.008	25.91
14, β-Propiolactam	^{1}H, 2	−0.96±0.09[g]	0.21±0.22[g]	0	26	0.92	32.37[g]
15, 2-Pyrrolidone	^{13}C, 2	−0.65±0.01	0.68±0.04	0.178±0.007	54 (1)	0.02	16.33
16, δ-Valerolactam	^{13}C, 2	−0.18±0.02	0.80±0.07	0.085±0.009	54	0.02	8.31
17, ε-Caprolactam	^{13}C, 2	−0.46±0.01	0.54±0.02	0.095±0.006	54 (2)	0.02	13.74
18, 2-Azacyclooctanone	^{13}C, 2	−0.38±0.01	0.59±0.05	0.101±0.011	58 (2)	0.01	12.01
19, 2-Azacyclononanone	^{13}C, 4	−0.18±0.03	0.63±0.18[g]	0.1	100 (7)	0.05	8.79
20, *N*-Me-2-pyrrolidone	^{13}C, 3	−0.75±0.01	0.68±0.03	0.139±0.007	81 (2)	0.02	18.09
21, Acetamide	^{13}C, 3	−0.73±0.02	0.55±0.04	0.075±0.025	84 (2)	0.05	19.05
22, Acetamide, *N*-Et	^{13}C, 2	−0.49±0.01	0.43±0.03	0.05	50 (2)	0.03	15.07
23, Acetamide, *N*-*t*-Bu	^{1}H, 1	−0.41±0.02	0.81±0.06	0.1	118 (6)	0.49	11.49
24, Acetamide, *N*-benzyl	^{1}H, 1	−1.08±0.08	0.86±0.17	0.1	152 (11)	1.37	22.12
25, Acetamide, *N*-*p*-OMe-benzyl	^{1}H, 1	−0.94±0.04	0.69±0.05	0	103 (2)	1.11	21.55
26, Acetamide, *N*-*p*-Cl-benzyl	^{1}H, 1	−1.23±0.05	0.6[h]	0	52 (2)	1.68	28.73
27, Acetamide, *N*,*N*-Et_2	^{13}C, 4	−0.33±0.02	0.84±0.05	0.068±0.014	108 (6)	0.05	10.32

[a]Experimental method, and number of data columns used in the mathematical analysis.
[b]Obtained using eq. [4].
[c]Values without errors indicate a fixed Δm^*_A. A zero means that medium effects were absent.
[d]Total data points. The number rejected by the program as not forming part of the data set, to 95% confidence, are in parentheses. Rejected data points are not used in obtaining pK_{BH^+} and other coefficients.
[e]Optical density units for uv; chemical shift differences in ppm for ^{13}C and Hz for ^{1}H nmr.
[f]Percent sulfuric acid in which the base is half-protonated.
[g]Approximate; see Experimental.
[h]Fixed value.

medium effect was apparent are indicated in the Table by $\Delta m^*_A = 0$.

Using the calculated D_B, D_{BH^+aq}, and δD_{BH^+} values at several different wavelengths, the Table 1 data, and eqs. [2]–[4], it is possible to construct theoretical uv spectra in several different ways. Some of the possibilities are illustrated for *N*-*tert*-butylbenzamide in an accompanying paper (9); the behaviour of all the benzamides was very similar to this. For all compounds spectra for pure B and pure BH^+ in water were derived, as were spectra for BH^+ in 80% H_2SO_4, enabling λ_{max} to be obtained under standard conditions. The resulting spectra were very similar for all of the monoalkylbenzamides, with which benzamide itself is included. For Baq, BH^+aq, and BH^+(80% H_2SO_4), respectively, λ_{max} (ε) was 227 ± 1 (10 500 ± 300), 238 ± 1 (13 200 ± 200), and 246 ± 1 (12 700 ± 300) nm, averaging over **1–9**. The only exception was *N*-*tert*-butylbenzamide, **9**, with almost the same λ_{max} values but slightly reduced extinction coefficients at 9700, 12 700, and 12 000 (not included in the averages). Again for the dialkylbenzamides the spectra were similar; only a trailing end absorption was visible for Baq, but BH^+aq and BH^+(80% H_2SO_4) had λ_{max} (ε) of 230 ± 4 (8 700 ± 200) and 238 ± 2 (8900 ± 200) nm, averaging over **10–13**. Here the exception was *N*,*N*-diisopropylbenzamide, **12**, with considerably reduced extinction coefficients of 5 500 and 5 800. In general the dialkylbenzamide peaks were broader than the monoalkylbenzamide ones.

The lactams **15–20** and the acetamides **21**, **22**, and **27** were studied by ^{13}C nmr spectroscopy. Carbon chemical shifts δ at 20–30 different acidities were recorded, and differences in δ between pairs of carbon atoms were used as data, 2–4 data columns showing reasonable changes with acidity being recorded.[1] For instance, for the lactam **16** ($\delta_\alpha - \delta_\beta$) and ($\delta_\delta - \delta_\gamma$) both gave noticeable changes, as illustrated in Fig. 1. Differences in δ were used in order to avoid bulk susceptibility corrections, and in the hope that medium effects would be minimized (6). This hope was not realized, however, as Fig. 1 clearly shows. Rather than a simple sigmoid curve between B and BH^+, a considerable

Can. J. Chem. Downloaded from www.nrcresearchpress.com by 210.87.254.105 on 09/06/12
For personal use only.

Can. J. Chem. Downloaded from www.nrcresearchpress.com by 210.87.254.105 on 09/06/12
For personal use only.

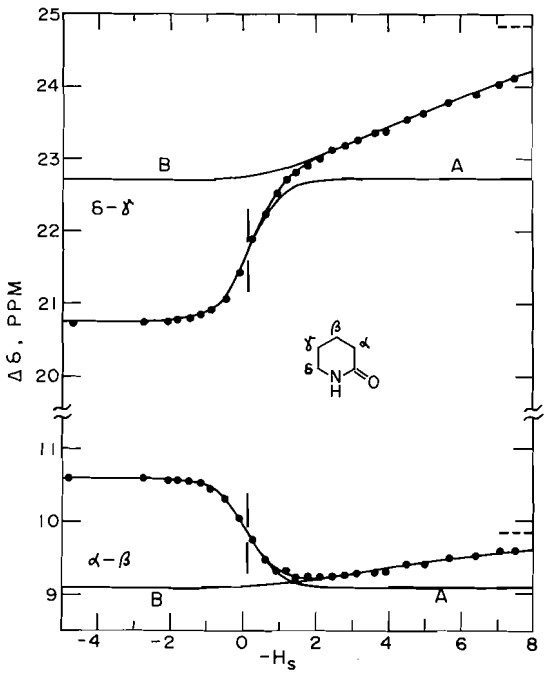

FIG. 1. ^{13}C chemical shift differences $\Delta\delta$ for δ-valerolactam as a function of its substrate acidity function $-H_S$. Points are experimental, curves theoretical for (A) protonation alone, (B) medium effect on the protonated form BH^+ alone, (through points) both protonation and medium effect. Upper, $\delta_\delta - \delta_\gamma$; lower, $\delta_\alpha - \delta_\beta$. The pK_{BH^+} is indicated by the vertical lines, and the theoretical $\Delta\delta$ for unsolvated BH^+ by the dashed lines at the right.

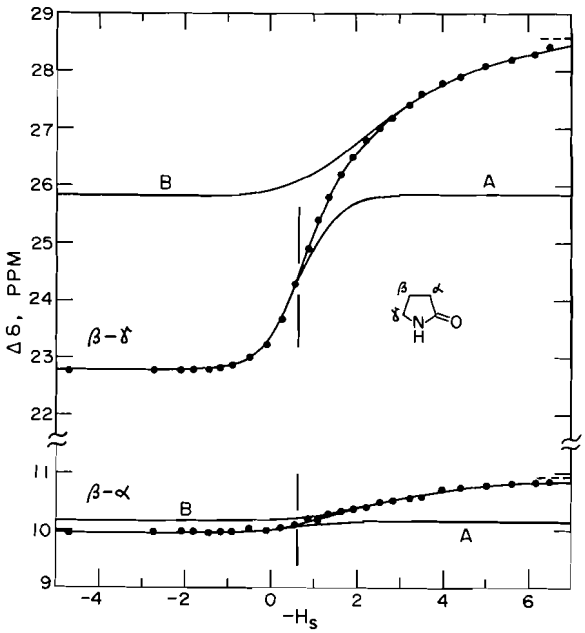

FIG. 2. ^{13}C chemical shift differences for 2-pyrrolidone as a function of $-H_S$. Upper, $\delta_\beta - \delta_\gamma$, lower, $\delta_\beta - \delta_\alpha$; see Fig. 1.

medium effect on the BH^+ form is apparent. Both large and small medium effects were observed, either augmenting the change due to protonation (upper part of Fig. 1) or opposing it (lower part). In some cases the medium effect caused larger changes in the spectrum than protonation itself, as illustrated for the lactam **15** in Fig. 2. As can be seen, without a method for allowing for the medium effect it would be difficult or impossible to assign an accurate pK_{BH^+} for this compound.

Because of the evident medium effects, the data were treated in exactly the same way as the uv data, using eqs. [2]–[4]. The results are in Table 1; the data are fitted to ±0.03 ppm on average, this representing excellent agreement between theory and experiment. In addition to pK_{BH^+}, m^*, and Δm^*_A, values of $\Delta\delta_B$, $\Delta\delta_{BH^+aq}$, and $\delta\Delta\delta_{BH^+}$ were obtained; e.g. for **16** these were 10.58 ± 0.01, 9.09 ± 0.01, and 0.76 ± 0.07, and 20.74 ± 0.01, 22.70 ± 0.02, and 2.11 ± 0.14 ppm, respectively, for the two shift differences in Fig. 1. Using these with eqs. [2]–[4] as before, theoretical curves can be constructed for comparison with experiment, as can curves to illustrate protonation in the absence of a medium effect, and the medium effect alone (9). These are all illustrated in Figs. 1 and 2, showing the large contribution from the medium effect.

Proton nmr was used for the acetamides **23–26**, and the β-lactam **14**. The procedure was the same as for the ^{13}C measurements, and the results are in Table 1.[1] Again chemical shift differences plotted as a function of acidity sometimes showed appreciable medium effects, as illustrated for **23**, *N-tert*-butylacetamide, in Fig. 3.[2] Here only one data column was available for the excess acidity analysis, the difference in δ between the CH_3 and $C(CH_3)_3$ protons, and replicate measurements were made to compensate for this. The precision, ±0.5–1.5 Hz, was not as high as it was for the ^{13}C measurements, but the method had compensating advantages, in that the medium effects were in general not as severe, and that measurements were faster. This was an important consideration for the easily hydrolysable compound **14** (4), which did not survive long enough in the more concentrated acids to allow time for the accumulation of adequate ^{13}C signals. Even so, the pK_{BH^+} and m^* values for **14** in Table 1 are only approximate, since the spectral change on protonation was very small.

[2]In Fig. 3, as in Figs. 1 and 2, $\Delta\delta$ is plotted as a function of the substrate acidity function $-H_S = \log C_{H^+} + m^*X$ (**10**); e.g. use of m^* for **23** means that $-H_S$ is specifically applicable to **23**. For comparison purposes a percent H_2SO_4 concentration scale is included at the top of Fig. 3.

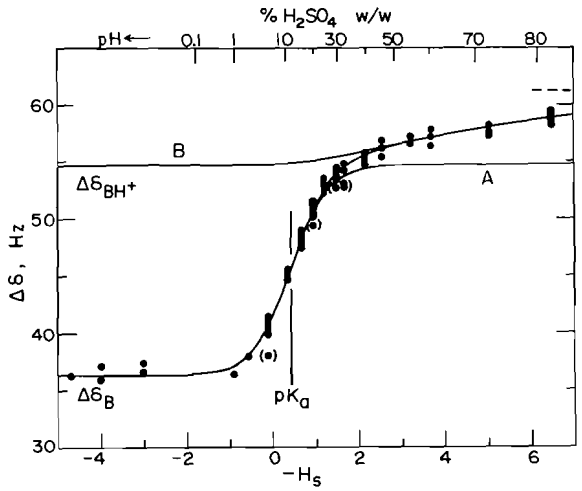

FIG. 3. Proton chemical shift differences for *N-tert*-butylacetamide as a function of $-H_S$; see Fig. 1. For convenience a percent sulfuric acid concentration scale is included at the top of the figure.

Discussion

For *N-tert*-butylbenzamide we have previously shown that the fact that the protonation data were so well fitted by eq. [4] was only consistent with protonation on oxygen, in the presence of a medium effect on the protonated form, and that the evidence was not consistent with a tautomerization from nitrogen- to oxygen-protonated isomers (9). The compounds studied in this work further support this conclusion; the experimental data are fitted by eq. [4] to high precision. In general, protonation of all the amides in this study was complete by about 60% H_2SO_4, further changes in the spectra with increasing acidity being entirely due to the medium effect.

Many of the trends in the pK_{BH^+} values in Table 1 run counter to intuition, and several factors must be taken into account when comparing them. For instance, it is apparent from Table 1 that acetamide is more basic than benzamide by 0.81 pK units. Part of this must be due to the higher electronegativity of the sp^2 carbons in benzamide, causing electron withdrawal and making protonation more difficult, but this should be counteracted by the resonance stabilization of positive charge into the ring possible in benzamide, making it a stronger base and the protonated form a weaker acid. However, this is an effect on the enthalpy, and pK (i.e. free energy) also contains an entropy contribution. Substituting phenyl for methyl is worth +3 to +8 entropy units in acid ionizations in water (somewhat less in the gas phase (20)), e.g. methylammonium ion, ΔS = −4.7 eu (21), anilinium ion, ΔS = +3.7 eu (22); acetic acid, −22.1 (21), benzoic acid, −19.0 (21). The 1–3 kcal/mol available from this at 25°C may be enough to overcome the resonance effect. Benzoic acid, for instance, is stronger than acetic acid, pK 4.213 vs. 4.756 (21), despite resonance stabilization of the acid form.

Steric effects should be apparent for those compounds with substituents bulky enough to interfere with the coplanarity of the molecule. Here, for the benzamides, we have independent evidence, from their uv spectra. All of the monoalkylbenzamides have the same spectrum except for *N-tert*-butylbenzamide, **7**, which has slightly reduced extinction coefficients. Application of the equation $\cos^2\theta = \varepsilon/\varepsilon_0$ (23) reveals that it is twisted with respect to benzamide by some 14°. Similarly the dialkylbenzamides are twisted with respect to the monoalkyl ones by 34°, with *N*,*N*-diisopropylbenzamide **12** twisted an additional 37°; this is supported by the 8 nm shift to high energy for the dialkyl compounds, indicative of reduced conjugation. The degree of twist is the same for the free base and protonated forms; addition of a proton has no effect on the coplanarity. Examination of Table 1 reveals that, with the exception of the *N*-benzyl compounds **8** and **9**, increased twisting changes the pK from benzamide-like to acetamide-like; the dialkylbenzamides are about 0.5 pK units more basic than the monoalkyl ones, and **7** and **12** have increased basicities within their series. This shows that whatever the nature of the effect which causes benzamide to be less basic than acetamide, the degree of coplanarity in the molecule is important to it.

Alkyl groups attached to nitrogen should have an acid-weakening effect; in the gas phase increasing methyl substitution in the series $HCONH_2$, $HCONHCH_3$, and $HCON(CH_3)_2$ stabilizes the protonated form by about 4 pK units per methyl group (24). This can be seen in the acetamides **21–23** and **27** in Table 1; for instance going from zero to one to two *N*-ethyl groups increases the pK from −0.7 to −0.5 to −0.3. However, this effect is not apparent in the benzamides, where benzamide and the monoalkylbenzamides all have pK's of −1.5; the increase to −1.0 in the dialkyl compounds is partly due to the steric effect discussed above. Something is counteracting the expected acid-weakening effect, and the most likely possibility appears to be steric inhibition of solvation. Protonated benzamide can partially delocalize its positive charge into the solvating water molecules; this will be more difficult when NH_2 becomes NHR, almost regardless of the size of R, and will be more difficult in any case with a phenyl group pres-

Can. J. Chem. Downloaded from www.nrcresearchpress.com by 210.87.254.105 on 09/06/12
For personal use only.

Can. J. Chem. Downloaded from www.nrcresearchpress.com by 210.87.254.105 on 09/06/12
For personal use only.

ent, rather than a methyl. Thus there is more charge requiring internal stabilization in the *N*-alkylbenzamides, and presumably this is fortuitously exactly neutralized by the inductive effect of the alkyl group in going from benzamide to a monoalkylbenzamide.

This factor, steric inhibition of solvation countering the inductive effect, may also account for the reduced basicity of the *N*-benzyl compounds **8–9** and **24–26**. Entropy effects, discussed above, may also be important. The same situation may apply to **15** and **20**, where *N*-methylation of 2-pyrrolidone has a slight acid-strengthening effect, counter to intuition. The situation may clarify when more amide (particularly benzamide) gas-phase basicity measurements are available for comparison. The trends apparent in the p*K*'s of the lactams **14–19** have been discussed elsewhere (4); in general they are acetamide-like in their behaviour.

The m^* values in Table 1 offer no real clues to the behaviour of these compounds. By analogy with Bunnett–Olsen ϕ values (25), $m^* > 1$ should indicate a larger than usual change in solvation by water molecules in going from $B + H^+$ to BH^+ (perhaps due to low solvation of BH^+ (25), as in carbonium ions (11)), and $m^* < 1$ should indicate the opposite. The average of the values in Table 1 is 0.63 ± 0.12 (excluding the fixed value for **26** and the less certain one for **14**), typical of amides (10). Three compounds, **9**, **13**, and **22**, have anomalously low values and another four, **16**, **23**, **24**, and **27**, have high ones. It is apparent that the lactams and acetamides show more variation in m^* than the benzamides; this is reasonable, since the latter can better delocalize charge internally by resonance and induction, resulting in less interaction with the solvent and less influence of structure upon m^*. Further work in this area, including temperature studies with determination of ΔS, may help to clarify the situation.

The medium effect coefficient Δm^*_A should reflect the differing sensitivity to the medium of BH^+ in highly solvated and unsolvated forms (9). However, much more information will have to be collected before significance can be attached to this quantity. For those cases in which Δm^*_A could be calculated, the average from Table 1 is 0.107 ± 0.036. For $\Delta m^*_A < 0.1$, the medium effect upon the spectrum of BH^+ is almost linear with acidity functions, in agreement with experience (8), as can be seen in Figs. 1 and 3. For Δm^*_A values considerably in excess of 0.1, curvature becomes noticeable, however, as is apparent for 2-pyrrolidone in Fig. 2. In general, it appears that, although all three experimental methods used here are susceptible to medium effects, they are less troublesome for proton nmr, and worst for ^{13}C spectroscopy.

Acknowledgements

We thank Elizabeth A. Stubley for measurements on **8** and **9**. Financial support of this research is by the Natural Sciences and Engineering Research Council of Canada.

1. M. Liler. Reaction mechanisms in sulphuric acid. Academic Press, London. 1971; C. H. Rochester. Acidity functions. Academic Press, London. 1970.
2. C. R. Smith and K. Yates. J. Am. Chem. Soc. **93**, 6578 (1971).
3. T. A. Modro, K. Yates, and F. Beaufays. Can. J. Chem. **55**, 3050 (1977).
4. P. Wan, T. A. Modro, and K. Yates. Can. J. Chem. **58**, 2423 (1980).
5. D. G. Lee and M. H. Sadar. J. Am. Chem. Soc. **96**, 2862 (1974).
6. R. A. McClelland and W. F. Reynolds. Can. J. Chem. **54**, 718 (1976).
7. H. J. Campbell and J. T. Edward. Can. J. Chem. **38**, 2109 (1960).
8. A. R. Katritzky, A. J. Waring, and K. Yates. Tetrahedron, **19**, 465 (1963); K. Yates and R. A. McClelland. J. Am. Chem. Soc. **89**, 2686 (1967).
9. R. A. Cox and K. Yates. Can. J. Chem. **59**, 1560 (1981).
10. R. A. Cox and K. Yates. J. Am. Chem. Soc. **100**, 3861 (1978).
11. R. A. Cox and K. Yates. Can. J. Chem. In press.
12. E. Beckmann. Chem. Ber. **23**, 3331 (1890).
13. D. J. Pasto and C. R. Johnson. Laboratory text for organic chemistry. Prentice-Hall, Inc., Englewood Cliffs, N.J. 1979. p. 454.
14. H. Fernholz and H. J. Schmidt. Angew. Chem. Int. Ed. Engl. **8**, 521 (1969).
15. C. L. Parris and R. M. Christenson. J. Org. Chem. **25**, 331 (1960).
16. R. L. Shriner, R. C. Fuson, and D. Y. Curtin. The systematic identification of organic compounds. 5th. ed. Wiley, New York. 1964. pp. 259–260.
17. International Critical Tables. Vol. 3. McGraw-Hill, New York. 1930. p. 56.
18. C. R. Smith. Ph.D. Thesis, University of Toronto. 1971.
19. P. R. Bevington. Data reduction and error analysis for the physical sciences. McGraw-Hill, New York. 1969. pp. 232–242.
20. J. E. Bartmess, J. A. Scott, and R. T. McIver, Jr. J. Am. Chem. Soc. **101**, 6046 (1979).
21. J. E. Leffler and E. Grunwald. Rates and equilibria of organic reactions. Wiley, New York. 1963. pp. 371–373.
22. P. D. Bolton and F. M. Hall. Aust. J. Chem. **20**, 1797 (1967).
23. R. A. Cox and E. Buncel. Can. J. Chem. **51**, 3143 (1973).
24. R. S. Brown and A. Tse. J. Am. Chem. Soc. **102**, 5222 (1980).
25. J. F. Bunnett and F. P. Olsen. Can. J. Chem. **44**, 1899 (1966).

Enzymes in organic syntheses. 19.[1] Evaluation of the stereoselectivities of horse liver alcohol dehydrogenase; catalyzed oxidoreductions of hydroxy- and ketothiolanes, -thianes, and -thiepanes

J. Bryan Jones and Harold M. Schwartz

Department of Chemistry, University of Toronto, Toronto, Ont., Canada M5S 1A1

Received December 5, 1980

J. Bryan Jones and Harold M. Schwartz. Can. J. Chem. **59**, 1574 (1981).

The specificity of horse liver alcohol dehydrogenase (HLADH) with respect to unsubstituted five-, six-, and seven-membered ring 3- and 4-thiaketone and -thiaalcohol substrates has been examined. The enzyme is found to have a broad tolerance of the structural variations within this series. HLADH also exhibits encouraging (up to 46%) enantiotopic and enantiomeric specificity in preparative-scale reduction and oxidation reactions of the heterocyclic ketones and alcohols respectively.

J. Bryan Jones et Harold M. Schwartz. Can. J. Chem. **59**, 1574 (1981).

On étudie la spécificité de la déshydrogénase d'alcool provenant du foie de cheval par rapport à des substrats thiacétones et thialalcools en positions 3 ou 4 de cycles à 5, 6 et 7 chaînons ne portant pas de substituants. On a trouvé que l'enzyme présente une grande tolérance vis-à-vis des variations structurales à l'intérieur de cette série. Cette déshydrogénase présente également une spécificité énantiotope et énantiomère encourageante (jusqu'à 46%) lors de réactions préparatives de réduction et d'oxydation respectivement de cétones et d'alcools hétérocycliques.

[Traduit par le journal]

The broad range of asymmetric synthetic opportunities provided by exploitation of the ability of horse liver alcohol dehydrogenase (HLADH)[2] to effect stereospecific oxidations and reductions of a broad structural range of alcohol and ketone substrates has been extensively documented (2, 3). Up till now, the substrates evaluated have been almost exclusively carbocyclic in nature, and with very few exceptions (2*c*, 3–5), heterocyclic compounds have received little attention as potential substrates. Accordingly, in view of the considerable asymmetric synthetic value of chiral heterocyclic synthons, we have initiated a general survey of the structural- and stereospecificity of HLADH towards substrates containing heteroatoms.

Sulfur was the heteroatom chosen for our initial studies. Its selection was dictated by several considerations. The enzyme was known to be tolerant of the sulfide functional group (2*c*, 4, 5) and the facilities of oxidoreductions of cyclic thiaketones and -alcohols were expected to parallel those of their well documented carbocyclic analogues. Also, it was anticipated that the carbocyclic substrate-derived active site model for predicting substrate stereospecificity would be equally applicable to thia-compounds since the longer C—S bond lengths and smaller C—S—C bond angles (6) do not alter the basic geometries of the rings sufficiently to invalidate the diamond lattice coordinate analyses normally applied (2*a*). Furthermore, subsequent application of the methodology of sulfur chemistry to enzyme-derived chiral thia-products of predictable absolute configurations opens up exciting asymmetric synthon possibilities. The additional benefit of providing access to otherwise difficult-to-prepare acyclic alcohols of predetermined chiralities via desulfurization of enzymically produced chiral cyclic thia-alcohols and ketones has been noted previously (2*c*).

In this paper we report on the specificity of HLADH-catalyzed oxidations and reductions of the hydroxy- and ketothiolanes, -thianes, and -thiepanes **1–10**.

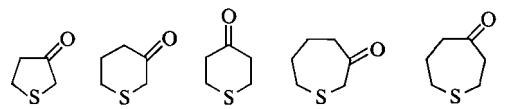

1 **2** **3** **4** **5**

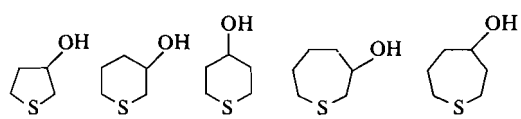

(±)-**6** (±)-**7** **8** (±)-**9** (±)-**10**

Results

The potential substrates **1–10** were all prepared in good yields by literature procedures or by straightforward modification of published routes.

[1]For Part 18, see ref. 1.

[2]Abbreviations used: HLADH, horse liver alcohol dehydrogenases; NAD^+ and NADH, oxidized and reduced forms respectively of nicotinamide adenine dinucleotide; V_{rel}, relative velocity; V_{max}, maximum velocity; K_m(app), apparent Michaelis constant; FMN, flavin mononucleotide (riboflavin phosphate); $Eu(fod)_3$, Tris(6,6,7,7,8,8,8-heptafluoro-2,2-dimethyl-3,5-octanedionato)europium (III); MTPA, (+)-α-methoxy-α-trifluoro phenyl acetate; ee, enantiomeric excess.

0008-4042/81/111574-06$01.00/0

©1981 National Research Council of Canada/Conseil national de recherches du Canada

Can. J. Chem. Downloaded from www.nrcresearchpress.com by 210.87.254.42 on 09/06/12
For personal use only.

Can. J. Chem. Downloaded from www.nrcresearchpress.com by 210.87.254.42 on 09/06/12
For personal use only.

The relative rates of HLADH-catalyzed reductions of the ketones **1–5** and of their five-, six-, and seven-membered ring carbocyclic analogues are recorded in Table 1, together with the steady-state kinetic constants for each substrate. The corresponding data for HLADH-catalyzed oxidations of **6–10** and of cyclopentanol, cyclohexanol, and cycloheptanol are given in Table 2. With the exception of 4-thiepanone (**5**), all thia-compounds of Tables 1 and 2 were sufficiently good substrates for preparative-scale reactions to be undertaken with confidence.

The preparative-scale HLADH-catalyzed oxidoreductions of **1**, **2**, **4**, **6**, **7**, **9**, **10** were carried out on ~1 g of substrate. Ketone **3** and alcohol **8** were omitted because both substrates and products are achiral. The results for enzyme-mediated reductions of **1**, **2**, and **4** are summarized in Table 3 and for oxidation of (±)-**6** – (±)-**10** in Table 4.

The stereochemical course of HLADH-catalyzed oxidation of (±)-3-thianol (**7**) was seen to be anomalous, since the thianol recovered from both it and the corresponding reduction of 3-thianone had the same, 3*S*, configuration. Accordingly, the oxidation reaction was repeated in the presence of semicarbazide to trap the ketone as it was formed. (3*R*)-Thianol was then obtained, as shown in Scheme 1.

The enantiomeric excesses (ee) of the chiral alcohols were determined by preparing their MTPA esters (7) and monitoring the 220 MHz ^{1}H nmr absorptions of the diastereotopic methoxyl protons in the presence of Eu(fod)$_3$. The $\Delta\Delta\delta$ values observed for the racemic MTPA esters are recorded in Table 5. The ee values determined by this procedure are given in Tables 3 and 4.

The absolute configurations of the chiral thia-alcohols **6**, **7**, **9**, and **10** obtained enzymically were assigned by their desulfurization with lithium in diethylamine (8) to optically active 2-butanol, 2-pentanol, 2-hexanol, and 3-hexanol respectively. These were converted directly to their hydrogen phthalate esters (9), the absolute configurations of which were known (10–13). The absolute configuration assignments are recorded in Tables 3 and 4.

TABLE 1. Kinetic data for HLADH-catalyzed reductions of **1–5**[a]

Substrate	V_{rel}[b]	K_m (app)[c] (m*M*)	V_{max}[c] (s^{-1})	V_{max}/K_m (app) ($\times 10^{-3}\ M^{-1}\ s^{-1}$)
		2.83	0.15	0.05
1	0.10	3.07	1.02	0.33
	1.00	7.69	28.1	3.65
2	2.18	4.15	32.5	7.01
3	1.24	12.39	50.6	4.08
		1.33	0.12	0.09
4	0.20	8.00	4.97	0.62
5	0.01	0.46	0.04	0.09

[a]Determined in 0.1 *M* phosphate buffer, pH 7 at 25°C with [NADH] 1.75×10^{-4} *M*.
[b][Ketone] = 10^{-3} *M*. Rates relative to cyclohexanone = 1.0.
[c][Ketone] 10^{-3}–10^{-4} *M*.

TABLE 2. Kinetic data for HLADH-catalyzed oxidations of (±)-**6**–(±)-**10**[a]

Substrate	V_{rel}[b]	K_m (app)[c] (m*M*)	V_{max}[c] (s^{-1})	V_{max}/K_m (app) ($\times 10^{-3}\ M^{-1}\ s^{-1}$)
		0.08	0.56	6.77
(±)-**6**	0.03	0.70	0.10	0.14
	1.00	0.54	4.06	7.53
(±)-**7**	0.43	3.59	2.30	0.64
8	0.45	2.88	1.88	0.65
		0.18	3.21	18.0
(±)-**9**	0.75	0.65	2.28	3.51
(±)-**10**	0.49	2.73	2.72	1.00

[a]Determined in 0.1 *M* glycine–NaOH buffer, pH 9 at 25°C with [NAD^+] 5×10^{-4} *M*.
[b][Alcohol] 5×10^{-3} *M*. Rates relative to cyclohexanol = 1.0.
[c][Alcohol] 10^{-3}–10^{-5} *M*.

TABLE 3. Preparative-scale HLADH-catalyzed reductions of **1**,**2**, and **4**[a]

Substrate	%Reduction	Reaction time	Products [yield][b](ee)
	64	4 days	
1			(−)-**6**[41%] (33%)
	54	3 h	
2			(−)-**7**[35%] (28%)
	35	10 days	
4			(+)-**9**[26%] (10%)

[a]Phosphate buffer, pH 7, room temperature (20°C), EtOH as coupled substrate for NADH recycling.
[b]Yields reported are of isolated, purified, materials.

Can. J. Chem. Downloaded from www.nrcresearchpress.com by 210.87.254.42 on 09/06/12
For personal use only.

TABLE 4. Preparative-scale HLADH-catalyzed oxidations of **6**, **7**, **8**, and **10**[a]

Substrate	% Oxidation	Reaction time	Products [yield][b](ee)
(±)-**6**	16	7 days	+ **1** [7%] (+)-**6** [46%] (9%)
(±)-**7**	28	2.5 days	+ **2** [17%] (−)-**7** [36%] (8%)
(±)-**9**	51	1.3 h	+ **4**[c] (−)-**9** [25%] (34%)
(±)-**10**	52	5 h	+ **5**[c] (−)-**10** [29%] (25%)

[a]Glycine–NaOH buffer, pH 9, room temperature (20°C), FMN-recycling of NAD^+.
[b]Yields reported are of isolated, purified, materials.
[c]Removed with Girard T reagent.

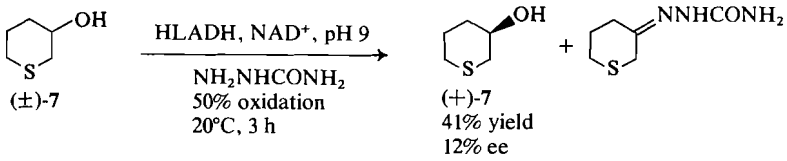

SCHEME 1

Discussion

In general, we have found that any substrate which undergoes HLADH-catalyzed reduction or oxidation at a rate > 1–2% of that of the reference substrates cyclohexanone or cyclohexanol respectively will be a satisfactory candidate for preparative-scale reactions. From the relative velocity data of Tables 1 and 2, it is seen that with the exception of 4-thiepanone (**5**), each of the thia-compounds evaluated is a good candidate for preparative-scale reactions. However, the relative oxidation rate of (±)-3-thiolanol (**6**) is only 3% of that of cyclohexanol, thus placing it at the lower limit of preparative viability.

TABLE 5. Enantiomeric shift differences for the methoxyl protons of the racemic MTPA esters of (±)-**6**, **-7**, **-9**, and **-10**[a]

MTPA ester of	$Eu(fod)_3$ (equiv.)	ΔΔδ (ppm)
(±)-**6**[b]	0.15	0.30
(±)-**7**[c]	0.36	0.15
(±)-**9**[c]	0.25	0.07
(±)-**10**[c]	0.28	0.18

[a]Determined at 220 MHz.
[b]In C^2HCl_3.
[c]In CCl_4.

The steady-state kinetic descriptors K_m(app) and V_{max} were obtained using Lineweaver–Burk plots. No deviations from linearity were observed in any of the ketone plots (Table 1) but cyclopentanol, cyclohexanol, cycloheptanol, and (±)-3-thiepanol (**9**) showed substrate activation at high substrate concentration in the presence of saturating coenzyme levels.

For HLADH-catalyzed oxidoreductions, the mechanism is often a highly ordered one with enzyme–coenzyme (E–CoE) association preceding the binding of substrate (S). The hydride transfer step takes place following the formation of the E–CoE–S ternary complex. For many simple carbonyl and alcohol substrates the final step of the mechanism, dissociation of the enzyme-reacted coenzyme complex, is rate-determining (2*a*, *d*, 14). However, for all of the carbonyl substrates of Table 1, the V_{max} values are slower than that observed when $E.NAD^+$ dissociation is rate limiting (2*a*, *d*, 14). Thus hydride transfer is at least partially rate-limiting to varying degrees for each of

Can. J. Chem. Downloaded from www.nrcresearchpress.com by 210.87.254.42 on 09/06/12
For personal use only.

the thiaketones **1**–**5**. The situation is quite different for oxidation (Table 2), E.NADH dissociation is rate-determining for cyclohexanol oxidation (2*a*, 14), and is also largely so for the thiaalcohols **7**–**10**, whose V_{max}'s are of a similar magnitude. Only for the five-membered ring alcohols are the V_{max} values significantly lower. This indicates that the hydride-transfer step is sufficiently slower for these substrates to become kinetically dominant.

V_{max}/K_m(app) ratios (or their equivalents) can serve as useful indicators of overall substrate reactivity when coenzyme release is rate-limiting (2*d*, 15). It is of interest to note that even for the thia-compounds of Tables 1 and 2, which do not all meet the rate-determining E–CoE dissociation condition, the V_{max}/K_m (app) variations tend to parallel those of the V_{rel} values.

The ring-size effects are similar for both carbocyclic- and thia-substrate series. In the reduction mode the reactivity order is clearly six- > seven- > five-membered ring ketone. For the corresponding alcohols, the variations are much less marked, but the five-membered ring alcohols remain the poorest substrates.

Although the substrate activities of analogous carbocyclic and thia-compounds are similar, the introduction of sulfur is seen to have a dramatic activating effect on the ketone reduction rates, particularly for the 3-thiaketones **1**, **2**, and **4** (Table 1). The reasons for these activating effects cannot be identified from the current data.[3] In contrast, the replacement of methylene by sulfur in the cyclic alcohol substrates was found to be uniformly deleterious (Table 2).

All preparative-scale HLADH-catalyzed reactions were carried out using ethanol as the coupled-substrate for NADH-recycling (16) and FMN for NAD^+-recycling (2*e*). Since the enantiomeric excesses attained were not high enough to be of great asymmetric synthesis value, no attempt was made to optimize the reaction conditions. The enantiomeric excesses were conveniently determined by nmr analysis of the Mosher esters (7). Desulfurizations of the thiaalcohols **6**, **7**, **9**, and **10** were first attempted using Raney nickel under the conditions previously found satisfactory (2*c*). However, these experiments met with little success and lithium-diethylamine was used instead. The results with the latter reagent paralleled the literature reports, with only one C—S bond cleaved at −78°C (17) and complete desulfurization being achieved at 0°C (8).

[3]There is ample evidence in the literature of the importance of electronic factors in sulfur–carbonyl interactions. Details are provided in the Ph.D. thesis of H.M.S., University of Toronto, 1979, and are available on request.

Initially, the fact that the alcohol (−)-**7** produced by reduction of 3-thianone (**2**) and recovered from oxidation of (±)-3-thianol (**7**) had the same (3*S*)-configuration was puzzling. Subsequently, this anomaly was found to be the result of (±)-3-thianol (**7**) being a slowly oxidized substrate while 3-thianone (**2**) was reduced with great facility. Accordingly, the 3-thianone being produced by HLADH-catalyzed oxidation of (±)-**7** was undergoing reduction back to (−)-**7** under the Table 4 reaction conditions. When the initial thiaketone product **2** was trapped with semicarbazide (4) to prevent this reverse reaction, the expected (3*R*)-alcohol (+)-**7** accumulated (Scheme 1).

The ee levels recorded in Tables 3 and 4 are of moderate magnitude only and are not of immediate chiral synthon value. Nevertheless, when it is considered that HLADH has been able to make these significant degrees of enantiotopic and enantiomeric distinctions on the basis of such a minor structural difference as the position of the sulfur atom in the ring, the enantiomeric excesses achieved are truly remarkable. It is clear that the enzyme has a broad structural tolerance of cyclic sulfur-containing substrates and that much higher (up to 100% (2*c*)) ee levels can be attained with larger and more dissymmetric molecules as substrates. These studies are now in hand.

Experimental

Melting points were determined on a Fisher-Johns apparatus and are uncorrected. Spectra were obtained on the following instruments: ir, Perkin-Elmer 237; nmr (TMS internal standard), Varian T60 and HR220; ms, Bell and Howell 21-490. Optical rotations were measured on a Perkin-Elmer 141 polarimeter and glc analyses were performed on a Hewlett-Packard 5710A instrument using 3% QF1 or OV101 on Chromosorb 6 columns. All substrates used were glc-pure. NAD^+ was purchased from Kyowa Hakko Kogyo Co., New York, and NADH from Sigma. HLADH was a gift from Hoffmann La-Roche Inc. (18). The activity of the enzyme was determined (19) prior to each use and the amounts of HLADH quoted refer to milligrams of active enzyme. (±)-3-Thianol (**7**) was purchased from Aldrich.

Preparation of Substrates

All substrates were prepared by literature methods, or unexceptional modifications thereof, as follows.

3-Thiolanone (**1**), bp 68–70°C/12 Torr (lit. (20) bp 74.5°C/15 Torr), by the procedure of Woodward and Eastman (20).

3-Thianone (**2**), bp 42–44°C/0.25 Torr (lit. (21) bp 55–60°C/0.1 Torr), via the method of Young and Heitz (21).

4-Thianone (**3**), mp 61–63°C after recrystallization from pentane (lit. (22) mp 58–62°C), by the procedure of Barkenbus *et al.* (23).

3-Thiepanone (**4**), bp 80°C/1.5 Torr (lit. (24) bp 55°C/0.55 Torr, by the route of Leonard and Figueras (24).

4-Thiepanone (**5**), bp 80°C/0.5 Torr (lit. (25) bp 72–75°C/1.5 Torr), using the route reported by Overberger and Katchman (25).

Can. J. Chem. Downloaded from www.nrcresearchpress.com by 210.87.254.42 on 09/06/12
For personal use only.

(±)-3-Thiolanol (**6**), bp 40–42°C/0.3 Torr (lit. (26) bp 53°C/0.25 Torr), by the method of Wilson and Albert (26).

(±)-4-Thianol (**8**), mp 49–50°C after recrystallization from pentane (lit. (27) mp 48–49°C), with the procedure as for (±)-**6** above.

(±)-3-Thiepanol (**9**), bp 80°C/5 Torr and *(±)-4-thiepanol* (**10**), bp 75°C/2 Torr (lit. (25) bp 75–77°C/1 Torr), by the method of Borsdorf *et al.* (28).

Relative Rate and Kinetic Studies of HLADH-catalyzed Reductions of 1–5 and Oxidations of 6–10

These were performed by the assay methods described previously (2*c*, *d*). The results obtained (correlation coefficients 0.95–0.99) are recorded in Tables 1 and 2.

Preparative-scale HLADH-catalyzed Oxidoreductions

Reductions of 1, 2, and 4

The following general procedure was employed. The thiaketone (~1 g) was dissolved in 0.1 *M* potassium phosphate buffer, pH 7, (500 mL) at 20°C. NAD^+ (~1 g) and ethanol (~2 g) were added and the reaction was initiated with HLADH (30–40 mg). The extent of reaction was monitored periodically by glc. After an appropriate conversion level, the mixture was continuously extracted with chloroform for 1 day. The dried ($MgSO_4$) chloroform extract was evaporated and the residual oil (~quantitative recovery) was separated into its components by thick layer chromatography on silica gel (230–400 mesh) with $CHCl_3$/CCl_4 (4:1) development followed by Kugelrohr distillation. The overall data are summarized in Tables 3 and 4. The individual reactions gave the following results.

Reduction of 3-thiolanone (**1**, 990 mg, 9.7 mmol) with enzyme (37 mg), NAD^+ (1.0 g, 1.4 mmol), and ethanol (2 g, 43 mmol) for 4 days gave unchanged **1** (329 mg) and (−)-(3*S*)-thiolanol (**6**, 411 mg, 33% ee), bp 44–48°C/0.3 Torr; $[\alpha]_D^{25}$ −4.31° (*c* 1.1, $CHCl_3$); ir (film): 3356 cm^{-1}; ^1H nmr (C^2HCl_3) δ: 1.5–2.4 (2H, m), 2.6–3.2 (4H, m), and 3.6 (1H, s) ppm.

Oxidations of (±)-6, -7, -9, and -10

In the general procedure used, the thiaalcohol (~1 g), NAD^+ (~1 g), and FMN (~10 g) were dissolved in 0.1 *M* glycine – NaOH buffer, pH 9, (500 mL) at 20°C. The enzyme (15–40 mg) was then added and the pH readjusted to 9 with 10 *M* aqueous NaOH. The course of the reaction was monitored by glc and when an acceptable conversion level had been reached, the solution was continuously extracted with chloroform for 1 day. The extract was filtered through a plug of silica (2 g), dried ($MgSO_4$), and evaporated to give an oil which was separated into its components by thick layer chromatography on silica gel 60 (230–400 mesh) with $CHCl_3$/CCl_4 (4:1) development. Final purification was effected by Kugelrohr distillation.

Oxidation of (±)-3-thiolanol (**6**, 980 mg, 9.4 mmol) with enzyme (38 mg), NAD^+ (1.0 g, 1.4 mmol), and FMN (10.0 g, 20.9 mmol) for 4 days, followed by further addition of enzyme (8 mg) and 3 more days reaction time gave 3-thiolanone (**1**, 67 mg) and (+)-(3*R*)-thiolanol (**6**, 453 mg, 9% ee), bp 40°C/0.3 Torr; $[\alpha]_D^{25°}$ +1.44° (*c* 1.04, $CHCl_3$); ir and nmr spectra identical with those detailed above.

Oxidation of (±)-3-thianol (**7**, 1.1 g, 9.32 mmol) with HLADH (37 mg), NAD^+ (1.0 g, 1.3 mmol), and FMN (10.0 g, 20.0 mmol) for 2.5 days gave 3-thianone (**2**, 183 mg) and (−)-(3*S*)-thianol (**7**, 390 mg, 8% ee), bp 40°C/0.25 Torr, $[\alpha]_D^{25°}$ −3.89° (*c* 1.0, $CHCl_3$); ir and nmr spectra identical with those detailed above.

Oxidation of (±)-4-thiepanol (**10**, 802 mg, 6.08 mmol) with enzyme (25 mg), NAD^+ (1.0 g, 1.4 mmol), and FMN (10.0 g, 20.9 mmol) for 5 h gave 4-thiepanone (**5**, 52% by glc, removed by treatment with Girard T reagent) and (−)-(4*S*)-thiepanol (**10**, 235 mg, 25% ee), bp 76°C/2 Torr; $[\alpha]_D^{25°}$ −2.69° (*c* 1.0, $CHCl_3$); ir and nmr spectra identical with those detailed above.

Enantiomeric Excess Determinations

The optically active and, for calibration purposes, the racemic alcohols **6**, **7**, **9**, and **10** were converted to their MTPA esters in quantitative yields by the standard literature procedure (7) using freshly prepared (+)-(2*R*)-2-methoxy-2-trifluoromethylphenylacetyl chloride, $[\alpha]_D^{25°}$ +128.2° (*c* 0.93, CCl_4) (lit. (7) $[\alpha]_D^{25°}$ 129° (*c* 5.17, CCl_4)). The enantiomeric excesses of the HLADH-derived MTPA esters were determined by 220 MHz ^1H nmr examination of the methoxyl protons in the presence of $Eu(fod)_3$, using the corresponding racemic alcohol MTPA esters for reference. The ΔΔδ values for each pair of diastereotopic methoxyl groups are shown in Table 5.

Absolute Configuration Determinations

The absolute configurations of the optically active alcohols (−)-**6**, (−)-**7**, (−)-**9**, and (−)-**10** (Tables 3 and 4) were established by desulfurization. The procedure for (−)-**6** is representative.

To a stirred solution of (−)-3-thiolanol (**6**, 270 mg, 2.6 mmol, $[\alpha]_D^{25°}$ −4.37° (*c* 2.01, $CHCl_3$)) in anhydrous ethylamine (5 mL) at 0°C was added lithium (1 g, 144 mmol) in small chunks. The mixture was stirred for 10 h at 0°C and was then added slowly to an ether (100 mL) – ice (20 g) mixture at −78°C. The ether layer was then separated, dried ($MgSO_4$), and evaporated to give an oil (97 mg, 1.31 mol). This was converted directly into its hydrogen phthalate ester with resublimed phthalic anhydride (271 mg, 1.83 mmol) in dry pyridine (5 mL). The mixture was refluxed for 3 h, stirred overnight at 20°C, and then poured onto ice (5 g). Concentrated hydrochloric acid (1.75 mL) was added and the aqueous mixture extracted with chloroform (3 × 50 mL). The chloroform extract was dried ($MgSO_4$) and evaporated to give the (−)-hydrogen phthalate ester of (2*R*)-butanol (253 mg), mp (±) 58–58.5°C after recrystallization from hexane (lit. (10) mp 56–57°C); $[\alpha]_D^{25}$ −4.35° (*c* 0.09, $CHCl_3$) (lit. (10) (+)-2*S*-enantiomer, $[\alpha]_D^{25}$ +33.54° ($CHCl_3$)); ir (film): 3700–2200, 1735, and 1700 cm^{-1}; ^1H nmr (C^2HCl_3) δ: 0.8–1.2 (3H, t, *J* = 6 Hz), 1.2–1.9 (5H, overlapping q, *J* = 6 Hz and d, *J* = 6 Hz), 5.2 (1H, sextet, *J* = 6 Hz), 7.4–8.1 (4H, m), and 11.9 (1H, s) ppm.

The alcohols (−)-7, (−)-**9**, and (−)-**10** were treated similarly.

Desulfurization of (−)-3-thianol (**7**, 192 mg, 1.63 mmol, $[\alpha]_D^{25}$ −17; 2° (*c* 1.0, $CHCl_3$)) yielded the (−)-hydrogen phthalate ester of (2*R*)-pentanol (149 mg), mp(±) 63.5–64.5°C, after recrystallization from hexane (lit. (10) mp 60–61°C); $[\alpha]_D^{25}$ −12.01° (*c* 0.33, $CHCl_3$) (lit. (10) (+)-(2*S*) enantiomer $[\alpha]_D^{25}$ +36.94° ($CHCl_3$)); ir (film): 3600–2200, 1735, and 1700 cm^{-1}; ^1H nmr (C^2HCl_3): 0.8–2.0 (10H, m overlapping and at δ 1.3, *J* = 6 Hz), 5.3 (1H, sextet, *J* = 6 Hz), 7.4–8.0 (4H, m), and 11.1 (1H, s) ppm.

Desulfurization of (−)-3-thiepanol (**9**, 151 mg, 1.15 mmol, $[\alpha]_D^{25}$ −9.38° (*c* 1.06, $CHCl_3$)) produced the (−)-hydrogen phthalate ester of (2*R*)-hexanol (159 mg), mp (±) 48–48.5°C after recrystallization from hexane (lit. (10) mp 48°C), $[\alpha]_D^{25}$ −12.33° (*c* 1.59, $CHCl_3$) (lit. (10) (+)-(2*S*)-enantiomer $[\alpha]_D^{25}$ +43.39° ($CHCl_3$)); ir (film): 3600–2200, 1735, and 1700 cm^{-1}; ^1H nmr (C^2HCl_3) δ: 0.8–2.0 (12H, m overlapping d at δ 1.3, *J* = 6 Hz), 5.3 (1H, sextet, *J* = 6 Hz), 7.4–8.0 (4H, m), and 10.8 (1H, s) ppm.

Desulfurization of (−)-4-thiepanol (**10**, 150 mg, 1.14 mmol, $[\alpha]_D^{25}$ −2.69° (*c* 1.3, $CHCl_3$)) afforded the (−)-hydrogen phthalate ester of (3*R*)-hexanol (218 mg), mp (±) 75.5–77°C after recrystallization from hexane (lit. (10) mp 76–77°C), $[\alpha]_D^{25}$ −3.03° (*c* 2.18, $CHCl_3$) (lit. (10) (+)-(3*S*)-enantiomer $[\alpha]_D^{25}$ +9.31 ($CHCl_3$)); ir (film): 3600–2200, 1735, and 1700 cm^{-1}; ^1H nmr (C^2HCl_3) δ: 0.8–1.2 (6H, m), 1.2–2.0 (6H, m), 5.1 (1H, quintet, *J* = 6 Hz), 7.4–8.0 (4H, s), and 11.1 (1H, s) ppm.

Acknowledgements

This work was supported by the Natural Sci-

ences and Engineering Research Council of Canada. We are also indebted to Hoffmann-La Roche, Inc. Nutley, NJ for a generous gift of enzyme.

1. D. H. PLIURA and J. B. JONES. Can. J. Chem. **58**, 2633 (1980).
2. (*a*) J. B. JONES and J. F. BECK. Tech. Chem. (N.Y.), **10**, 107 (1976); (*b*) I. J. JAKOVAC, G. NG, K. P. LOK, and J. B. JONES. Chem. Commun. 515 (1980), and references therein; (*c*) J. DAVIES and J. B. JONES. J. Am. Chem. Soc. **101**, 5405 (1979); (*d*) A. J. IRWIN, K. P. LOK. K. W-C. HUANG, and J. B. JONES. J. Chem. Soc. Perkin Trans. I, 1636 (1978); (*e*) J. B. JONES and K. E. TAYLOR. Can J. Chem. **54**, 2969 (1976).
3. (*a*) J. J. VAN LUPPEN, J. A. LEPOIVRE, T. A. VAN OSSELAER, G. L. LEMIERE and F. C. ALDERWEIRELDT. Bull. Soc. Chim. Belg. **88**, 829 (1979).
4. J. A. HINSON and R. A. NEAL. J. Biol. Chem. **247**, 7106 (1972); Biochim. Biophys. Acta, **384**, 1 (1975).
5. R. W. FRIES, D. P. BOHLKEN, and B. V. PLAPP. J. Med. Chem. **22**, 356 (1979).
6. W. TAGAKI. *In* Organic chemistry of sulfur. *Edited by* S.Oae. Plenum, New York. 1977. p. 231.
7. J. A. DALE, D. L. DULL, and H. S. MOSHER. J. Org. Chem. **34**, 2543 (1969).
8. K. KONDO, A. NEGISHI, K. MATSUI, D. TUNEMOTO, and S. MASAMUNE. J. Chem. Soc. Chem. Commun. 1311 (1972).
9. A. W. INGERSOLL. Org. React. **2**, 400 (1944).
10. R. H. PICKARD and J. KENYON. J. Chem. Soc. **99**, 45 (1911); **103**, 1942 (1913).
11. P. A. LEVENE and A. ROTHEN. J. Org. Chem. **1**, 76 (1936).
12. R. WIBERG. J. Am. Chem. Soc. **74**, 3891 (1952).
13. R. S. AIRS, M. P. BALFE, and J. KENYON. J. Chem. Soc. 18 (1942).
14. K. DALZIEL. *In* The enzymes. Vol. 11. 3rd ed. *Edited by* P. D. Boyer. Academic, New York. 1975. p. 1.
15. C. S. TSAI. Can. J. Biochem. **46**, 381 (1968).
16. B. ZAGALAK, P. A. FREY, G. L. KARABATSOS, and R. H. ABELES. J. Biol. Chem. **241**, 3028 (1966).
17. E. E. VAN TAMELEN, P. MCCURRY, and U. HUBER. Proc. Natl. Acad. Sci. U.S.A. **68**, 1294 (1971).
18. S. K. ROY and A. H. NISHIKAWA. Biotechnol. Bioeng. **21**, 775 (1979).
19. K. DALZIEL. Acta Chem. Scand. **11**, 397 (1957).
20. R. B. WOODWARD and R. H. EASTMAN. J. Am. Chem. Soc. **68**, 2229 (1946).
21. T. E. YOUNG and J. L. HEITZ. J. Org. Chem. **38**, 1562 (1973).
22. E. A. FEHNEL and M. CARMACK. J. Am. Chem. Soc. **70**, 1813 (1948).
23. C. BARKENBUS, V. C. MIDKIFF, and R. M. NEWMAN. J. Org. Chem. **16**, 232 (1951).
24. N. J. LEONARD and J. FIGUERAS. J. Am. Chem. Soc. **74**, 917 (1952).
25. C. G. OVERBERGER and A. KATCHMAN. J. Am. Chem. Soc. **78**, 1965 (1956).
26. G. E. WILSON, JR. and R. ALBERT. J. Org. Chem. **38**, 2156 (1973).
27. E. ADLEROVA and M. PROTIVA. Collect. Czech. Chem. Commun. **24**, 1268 (1959).
28. R. BORSDORF, H. KASPER, and A. D. REPP. Angew. Chem. Int. Ed. Engl. **6**, 872 (1967).

Can. J. Chem. Downloaded from www.nrcresearchpress.com by 210.87.254.42 on 09/06/12
For personal use only.

Comportement anodique des alliages Nb–Co en milieu alcalin

Y. UMETSU
Université Tohoku, Sandai, Japon
J. P. BAILLON ET D. L. PIRON
Ecole Polytechnique, Montréal (Qué.), Canada
ET
G. BÉLANGER
Institut de recherche d'Hydro-Québec, Varennes (Qué.), Canada J0L 2P0

Reçu le 30 octobre 1980

Y. UMETSU, J. P. BAILLON, D. L. PIRON et G. BÉLANGER. Can. J. Chem. **59**, 1580 (1981).

Les alliages Nb–Co sont stables à la corrosion à circuit ouvert en présence d'oxygène dans une solution de 25% KOH en autant que le pourcentage en poids de Co excède 50%. En deça de cette valeur des coupons soumis à ces conditions se sont désagrégés après 30 jours. Lorsque les alliages sont soumis à une polarisation anodique, on observe la dissolution active suivie d'une passivation et en présence de cobalt, la réaction du dégagement d'oxygène se manifeste. L'analyse par spectroscopie électronique Auger (SEA) du niobium pur et des alliages 30 et 90% de Co montre que le film d'oxyde croît de façon irrégulière selon la nature de la surface. Ainsi pour une polarisation anodique identique (0,845V vs. ENH pendant 6 heures) le film d'oxyde passe de $4{,}13 \times 10^{-2}$ µm pour le Nb pur à 0,10 µm pour l'alliage à 30% de Co et redevient aussi mince que 8×10^{-4} µm pour l'alliage à 90% de Co. Le profil de concentration révélé par SEA indique une dissolution préférentielle du Nb comparativement au Co dans le film d'oxyde.

Y. UMETSU, J. P. BAILLON, D. L. PIRON, and G. BÉLANGER. Can. J. Chem. **59**, 1580 (1981).

Niobium–cobalt alloys are stable to corrosion in an open circuit in the presence of oxygen in 25% KOH solution as long as the weight percentage of cobalt exceeds 50%. Below this value, samples submitted to these conditions disintegrate after 30 days. When these alloys are submitted to anodic polarization an active dissolution is noted followed by passivation and in the presence of cobalt production of oxygen occurs. Electronic Auger Spectroscopic (EAS) analysis of pure niobium and its alloys with 30% and 90% cobalt indicates that the oxide film grows in an irregular manner according to the nature of the surface. Thus, for an identical anodic polarization (0.845 V vs. ENH for 6 hours) the oxide film changes from 4.13×10^{-2} µm for pure Nb to 0.10 µm for the 30% Co–Nb alloy and becomes as thin as 8×10^{-4} µm for the 90% Co–Nb alloy. The concentration profile as shown by EAS indicates a preferential dissolution of Nb over Co in the oxide film.

[Journal translation]

Introduction

Dans le cadre des travaux de notre groupe sur la réaction du dégagement de l'hydrogène (RDH), une série de mesures furent réalisées illustrant certains avantages électrocatalytiques du niobium (1–3) et ses alliages avec le Ni (4, 5). En effet, lors d'une polarisation cathodique, le niobium acquiert une activité catalytique comparable au nickel pour la RDH (2, 3). En alliant le niobium au nickel, cette activité se manifeste pour l'alliage 30% Ni (4); cependant la surface de ce matériau se désintègre sous la formation d'hydrure. Une activité accrue par rapport au Nb se retrouve en alliant celui-ci au Co mais dans une moindre mesure que l'alliage Ni–Nb (6). Pour compléter notre évaluation des alliages Ni–Nb, nous avons étudié le comportement de ceux-ci à l'état de repos dans une solution aérée de KOH de même que sous l'effet d'une polarisation anodique (5); les alliages à basse teneur de Ni sont rapidement corrodés à l'état de repos. Par contre, le niobium pur soutient une croissance d'un oxyde lors d'une polarisation anodique (5, 7, 8).

Dans cette présente étude, nous avons étendu nos travaux pour évaluer le comportement anodique des alliages Co–Nb en milieu alcalin; les observations électrochimiques ont été complétées par l'évaluation par spectroscopie Auger de la composition chimique de la surface après une polarisation anodique prolongée.

Partie expérimentale

La préparation des alliages et leur montage en électrodes de 5 × 5 × 3 mm ont été décrits précédemment (6). L'électrolyte utilisé a été une solution de 25% (en poids) de KOH dans l'eau distillée. Les solutions furent désaérées pendant 4 h sous argon avant le début des polarisations.

La technique de polarisation potentiostatique à l'équilibre fut utilisée dans le cours des mesures électrochimiques (2, 3); le saut de potentiel a été de 50 mV et le courant noté après 2 min sous une polarisation constante. La gamme de potentiels explorés a été à partir du potentiel de repos jusqu'au dégagement de l'oxygène. Les essais électrochimiques furent réalisés en utilisant une électrode calomel saturée comme référence mais les potentiels rapportés dans ce travail furent ramenés à l'électrode normale de l'hydrogène (−245 mV vs. ECS).

Les essais de corrosion furent réalisés en immergeant les échantillons dans une solution de 25% KOH saturée d'air de 100 mL pendant 30 jours.

0008-4042/81/111580-05$01.00/0
©1981 National Research Council of Canada/Conseil national de recherches du Canada

Can. J. Chem. Downloaded from www.nrcresearchpress.com by 210.87.254.42 on 09/06/12
For personal use only.

Can. J. Chem. Downloaded from www.nrcresearchpress.com by 210.87.254.42 on 09/06/12
For personal use only.

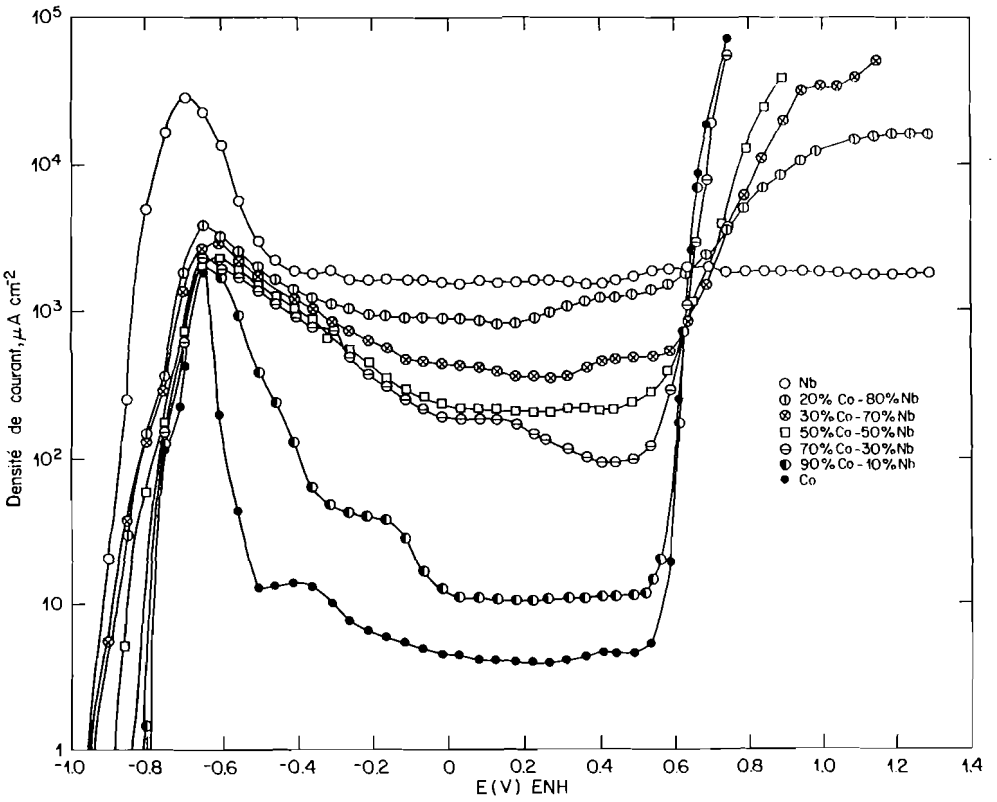

FIG. 1. Courbe potentiostatique à l'équilibre du comportement anodique du Nb et des alliages Nb–Co: 25% KOH (par poids); 25°C.

Les profils de concentration du Nb, Co et de l'oxygène dans les films d'oxyde furent déterminés pour le Nb et des alliages typiques soit 30 et 90% Co. Pour ces expériences, les échantillons furent polarisés dans la solution de KOH à 845 mV vs. ENH pendant 6 h. Après ce traitement anodique, l'électrode fut lavée abondamment à l'eau distillée et asséchée dans un desiccateur. Les analyses des films d'oxyde par spectroscopie électronique Auger (SEA) ont été réalisées dans un système de la compagnie Varian. Les conditions expérimentales étaient les suivantes: (*a*) faisceau d'électrons primaires: énergie, 3 keV; courant, 15 μA; diamètre du faisceau ≃ 5 μm; modulation, 2 V crête à crête; (*b*) décapage ionique: ions d'argon de 1 keV; densité de courant ≃ 85 μA cm^{-2}; pression ≃ 5×10^{-5} Torr. Sous ces conditions, la vitesse de décapage est approximativement de l'ordre de 5×10^{-5} μm (0.5 Å) par seconde pour les couches d'oxyde de niobium.

Résultats et discussion

(a) Essais de corrosion

Après 30 jours d'immersion dans une solution aérée de 25% KOH les alliages 10, 20 et 30% Co sont sérieusement attaqués et on y note la formation de grains ou de poudres. Pour les alliages de 50% Co et plus, seul celui contenant 90% Co montre une certaine attaque du milieu.

L'alliage 10% Co a subi une attaque le long des limites des grains et s'est fissuré en de petites unités séparées. Les alliages de 20 et 30% Co se sont désintégrés en fine poudre. En conclusion, seuls les alliages de 50% et plus montrent une stabilité à la corrosion en milieu alcalin en présence d'oxygène; ces mêmes échantillons en solution désaérée ne présentent pas de corrosion notable.

(b) Polarisation anodique

Les courbes de polarisation anodique sont illustrées à la fig. 1. A l'encontre des alliages Ni–Nb, les alliages de Co montrent une région de dissolution active à des potentiels de −800 mV vs. ENH. Le niobium pur illustre le comportement typique d'un métal "valve" où suite à une dissolution, un oxyde de surface croît jusqu'à de grandes épaisseurs (7, 8).

La présence de cobalt ne modifie pas le potentiel de courant maximum bien que le potentiel de repos subisse en déplacement anodique.

Les alliages à forte teneur de Co montrent une passivation importante; le courant anodique chute de façon abrupte à des potentiels plus anodiques que −600 mV. Ce phénomène est très marqué pour le Co pur ainsi que pour l'alliage 90% Co.

Can. J. Chem. Downloaded from www.nrcresearchpress.com by 210.87.254.42 on 09/06/12
For personal use only.

Pour les alliages, on observe un dégagement d'oxygène à des potentiels de 600 mV ou plus. Pour les alliages de 20 à 50% Co, un film à la surface de l'électrode se manifeste suite à une polarisation prolongée. Pour les alliages de 70% et plus, l'effet du niobium est pratiquement absent et les courbes de polarisation de la réaction du dégagement d'oxygène se confondent avec celles observées pour le cobalt pur.

A la fig. 2 on a rapporté la densité de courant à un potentiel de 445 mV (dans la région de passivation). On remarque une chute importante de ce courant suite à l'augmentation de la teneur en Co des alliages; la densité de courant tombe à 3 $\mu A\,cm^{-2}$ pour le Co pur comparativement à 1,5 $mA\,cm^{-2}$ pour le Nb pur.

(c) Profils de concentrations dans les films anodiques

La réaction du dégagement d'oxygène (RDO) se déroule sur un film d'oxyde et les caractéristiques de celui-ci déterminent à la fois le mécanisme de la réaction et aussi les propriétés anodiques du métal. Pour le niobium pur, le film d'oxyde forme une barrière au dégagement d'oxygène (7, 8) et la croissance de cet oxyde confère au métal des propriétés diélectriques particulières; un tel comportement se retrouve pour l'aluminium et le tantale entre autres (7, 8). La formation de films d'oxydes conducteurs électroniques permet à la RDO de se produire et c'est le cas des métaux précieux (Pt, Au) ou d'autres métaux catalytiques Ni et Co.

Récemment Romand *et al.* (9) ont rapporté l'analyse par spectroscopie Auger des films anodiques d'oxyde sur le Nb et certains de ses alliages à l'exclusion des alliages CoNb. En plus de la complexité du film d'oxyde, on doit noter que la composition chimique des alliages du système NbCo présente certains traits particuliers. Comme l'ont rapporté Shunk (10) et Dwight (11), on note la présence de deux composés intermétalliques soit le NbCo et le $NbCo_2$ ainsi que des phases de Laves. Les alliages étudiés dans ce travail comportaient deux phases (6).

Le spectre électronique Auger (SEA) pour le film anodique du Nb pur pour différents temps de décapage ionique est illustré à la fig. 3. Le changement de l'amplitude crête à crête des signaux du Nb et de l'oxygène indique la présence d'un profil de concentration de ces éléments dans le film. La fig. 4 illustre ce profil en traçant l'amplitude du signal en fonction du temps de décapage ionique. On remar-

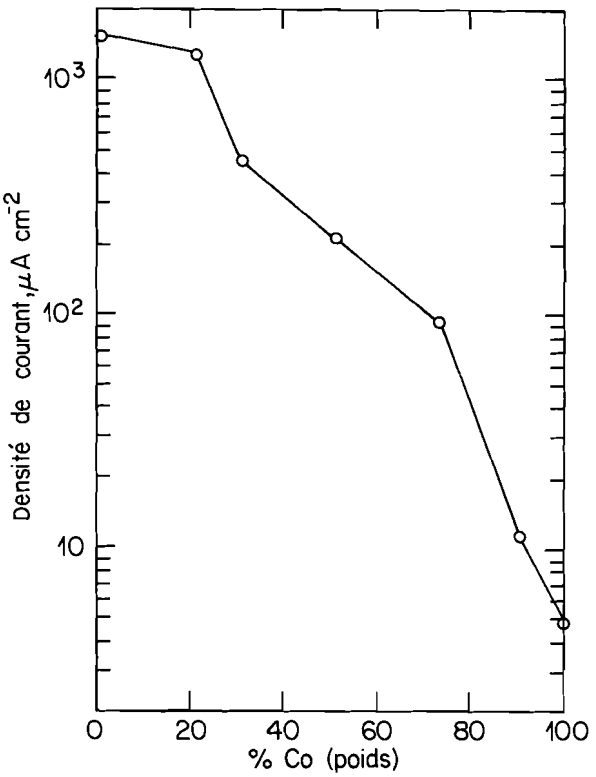

FIG. 2. Densité de courant à 445 mV en fonction de la composition de l'alliage Nb–Co; 25% KOH à 25°C.

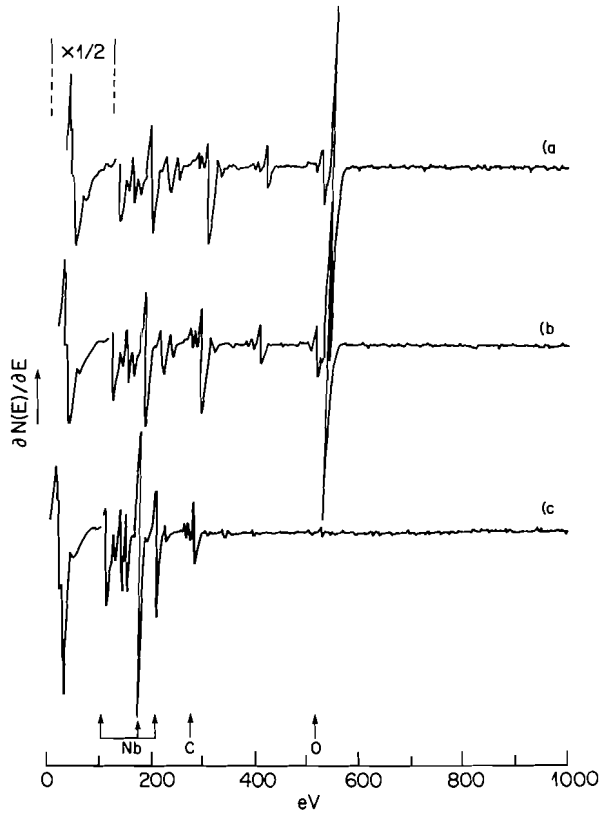

FIG. 3. Spectre électronique Auger du niobium anodisé pour différents temps de décapage ionique de la surface: (a) 20 s; (b) 40 s; (c) 1100 s.

Can. J. Chem. Downloaded from www.nrcresearchpress.com by 210.87.254.42 on 09/06/12
For personal use only.

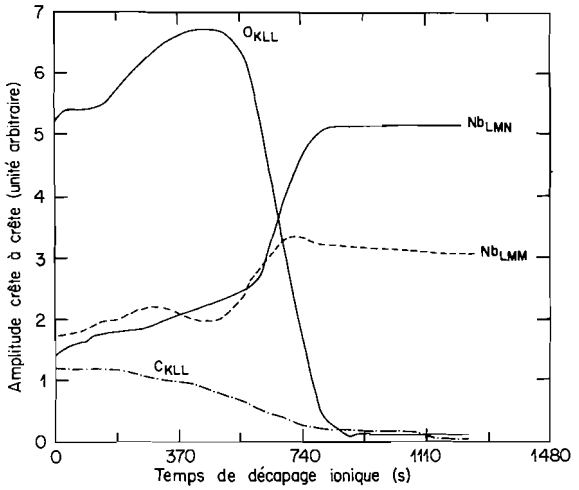

FIG. 4. Profil des amplitudes crête à crête des pics Auger en fonction du temps de décapage ionique pour la surface anodisée du niobium.

que que le signal associé à l'oxygène tombe pratiquement à zéro après environ 825 s; à ce même moment, le signal associé au Nb demeure constant indiquant la fin du film d'oxyde ce qui représente $4{,}13 \times 10^{-2}$ µm d'épaisseur. La présence du carbone est associée au contact de l'échantillon avec l'air ambiant tel que suggère par Lumsden et Staehle (12).

On remarque que la concentration d'oxygène augmente légèrement sous la couche superficielle de l'oxyde mais que cette concentration tombe rapidement à zéro lorsque le métal est atteint. Les deux signaux du Nb (Nb_{LMN} et Nb_{LMM}) ont essentiellement un comportement identique.

A la fig. 5, le SEA pour l'alliage 30% Co polarisé anodiquement est présenté; on remarque que les pics du Nb, de l'oxygène et du Co sont bien séparés l'un de l'autre et les amplitudes crête à crête représentent bien les concentrations respectives de ces éléments. La fig. 6 illustre donc les profils de concentration en fonction du temps de décapage de la surface. Il est à noter que le temps nécessaire pour atteindre le métal est plus long que celui nécessaire pour se débarrasser de l'oxyde de niobium. Cette observation nous donne à penser que l'épaisseur du film d'oxyde est plus importante pour l'alliage 30% Co–Nb que pour le Nb pur et ceci pour une période de polarisation identique. En utilisant la même vitesse de décapage on arrive à une épaisseur de l'ordre de 0,10 µm. On peut remarquer qu'à l'interface métal–oxyde, le film est plus riche en oxygène qu'à la surface; cette augmentation de l'oxygène est couplée à une diminution correspondante du Co et Nb. La concentration du Co dans le film d'oxyde est très voisine de celle dans le coeur de l'alliage mais ce n'est pas le cas

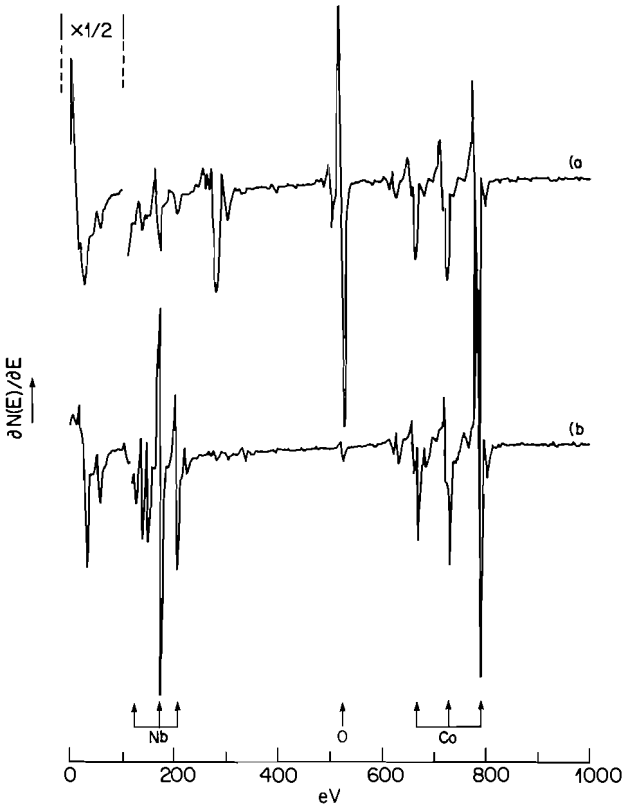

FIG. 5. Spectre électronique Auger de l'alliage Nb–Co (30%) anodisé pour deux temps de décapage ionique de la surface: (a) 20 s; (b) 3500 s.

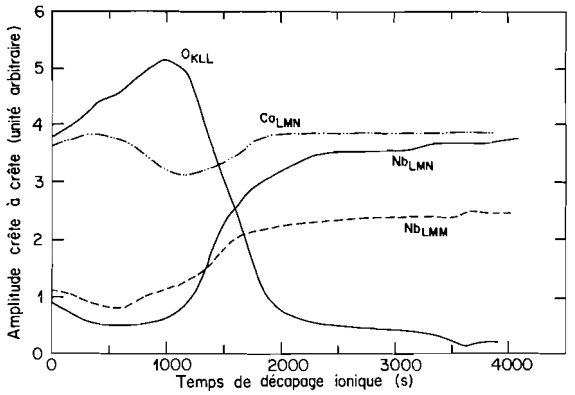

FIG. 6. Profil des amplitudes crête à crête des pics Auger en fonction du temps de décapage ionique de la surface anodisée de l'alliage Nb–Co (30%).

pour le Nb. La polarisation anodique semble donc favoriser une dissolution active du Nb mais une croissance de l'oxyde de Co.

Les résultats du SEA de l'alliage de 90% Co sont illustrés aux figs. 7 et 8. Pour cet alliage, le film d'oxyde est très mince ($\simeq 8 \times 10^{-4}$ µm); en plus, le niobium s'est complètement dissous à la surface et par l'analyse des résultats illustrés à la fig. 8, on

peut conclure que la surface est essentiellement composée d'un film d'oxyde de Co.

Compte tenu de la sensibilité analytique voisine de la transition Nb_{LMN} et du Co_{LMN}, nous pouvons conclure par l'examen de la fig. 6 que le faisceau électronique s'est concentré sur un point où la composition de l'alliage était essentiellement le composé NbCo. Les analyses microscopiques réalisées précédemment (6) ont montré que cet alliage était composé de deux phases: la phase γ (le NbCo) en majeure partie et la phase δ qui est essentiellement une solution solide de Nb. En plus, la fig. 6 illustre une diminution sensible de la concentration du Nb dans le film d'oxyde.

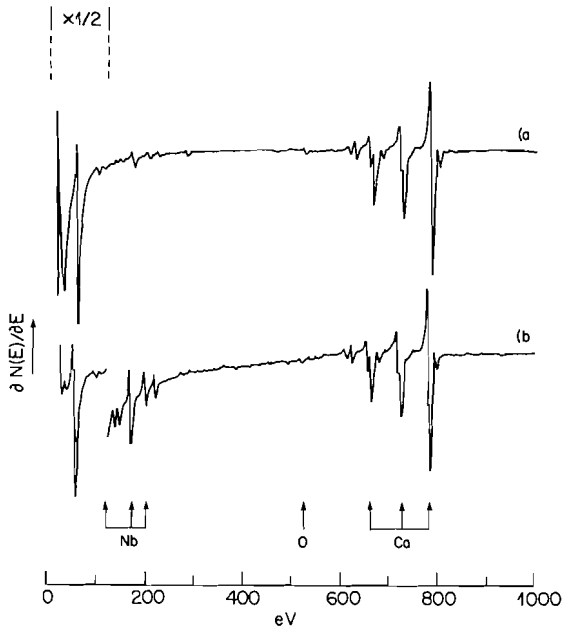

FIG. 7. Spectre électronique Auger de l'alliage Nb–Co (90%) anodisé pour deux temps de décapage ionique de la surface: (a) 40 s; (b) 200 s.

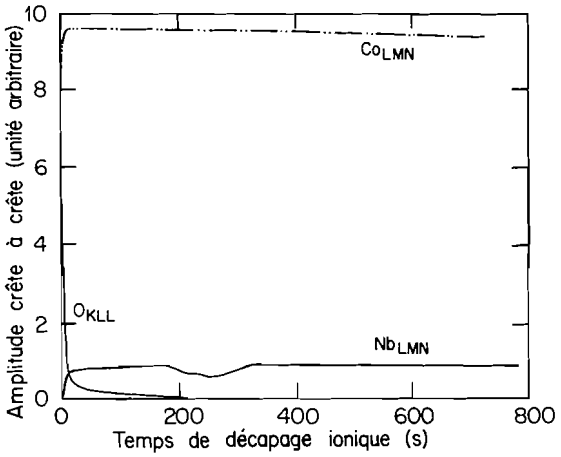

FIG. 8. Profil des amplitudes crête à crête des pics Auger en fonction du temps de décapage ionique de la surface anodisée de l'alliage Nb–Co (90%).

Conclusion

Dans cette étude, le comportement sous polarisation anodique des alliages Nb–Co fut déterminé; cette évaluation électrochimique fut complétée par une étude par spectroscopie électronique Auger des profils de concentration de surface de certains alliages typiques. Les résultats peuvent se regrouper ainsi.

(*a*) Les alliages de Co–Nb ayant une teneur en Co inférieure à 50% sont fortement corrodés par une solution aérée de 25% KOH. En absence d'oxygène tous les alliages sont stables à circuit ouvert.

(*b*) L'alliage du Nb par le Co ne déplace pas le potentiel de passivation mais ce procédé réduit la densité de courant dans l'état de passivation.

(*c*) Sous potentiel anodique, la surface du niobium pur se couvre d'un film d'oxyde bleuâtre qui augmente en épaisseur en fonction du potentiel anodique de polarisation. Même à des tensions anodiques importantes, aucune évolution d'oxygène ne fut observée.

(*d*) La présence de cobalt permet à la réaction du dégagement d'oxygène de se manifester: pour les alliages de 70% Co et plus, la RDO se confond avec celle observée sur le Co pur.

(*e*) Pour les alliages, le niobium se dissout sous polarisation anodique et la concentration de cet élément dans le film d'oxyde est plus faible que dans le coeur de l'alliage. Le cobalt demeure pratiquement stable pour les alliages étudiés (30% et 90%) à la fois au travers le film comme dans l'alliage métallique lui-même.

1. C. P. VIJAYAN et D. L. PIRON. Can. J. Chem. **55**, 375 (1977).
2. Y. OKUYAMA, G. BÉLANGER et D. L. PIRON. Int. J. Hydrogen Energy, **3**, 297 (1978).
3. K. SUGIMOTO, G. BÉLANGER et D. L. PIRON. J. Electrochem. Soc. **126**, 535 (1979).
4. K. SUGIMOTO, G. BÉLANGER et D. L. PIRON. Surf. Technol. **9**, 83 (1979).
5. K. SUGIMOTO, G. BÉLANGER et D. L. PIRON. Corrosion, **36**, 437 (1980).
6. Y. UMETSU, D. L. PIRON et G. BÉLANGER. Can. J. Chem. Sous presse.
7. D. A. VERMILYEA. *Dans* Advances in electrochemistry and electrochemical engineering. Vol. 3. Interscience, New York. 1963.
8. L. YOUNG. Anodic oxide films. Academic Press, New York. 1961.
9. M. ROMAND, J. S. SOLOMON et W. L. BAUN. Mater. Res. Bull. **11**, 517 (1976).
10. F. A. SHUNK. *Dans* Constitution of binary alloys. 2nd Supplement. McGraw-Hill, New York. 1969. p. 180.
11. A. E. DWIGHT. AIME Metallurgical Society Conf. Vol. 10. Interscience Inc., New York. 1961.
12. J. B. LUMSDEN et R. W. STAEHLE. Scripta Metallurgica, **16**, 1703 (1972).

Can. J. Chem. Downloaded from www.nrcresearchpress.com by 210.87.254.42 on 09/06/12
For personal use only.

An ^{129}I Mössbauer study of organotin iodides

C. H. W. JONES AND M. DOMBSKY
Department of Chemistry, Simon Fraser University, Burnaby, B.C., Canada V5A 1S6
Received September 9, 1980

C. H. W. JONES and M. DOMBSKY. Can. J. Chem. **59**, 1585 (1981).

Iodine-129 Mössbauer data for SnI_4, $MeSnI_3$, Me_2SnI_2, Me_3SnI, $Me_3SnI_2^-$, $Me_3SnI.py$, and $Me_2SnI_2.2py$ are reported. The data are compared with available nqr data for the corresponding chlorides and bromides. The Mössbauer data are interpreted as evidence that $MeSnI_3$, Me_2SnI_2, and Me_3SnI are distorted from tetrahedral geometry in the solid state. The applicability of the additive model in interpreting ^{119}Sn quadrupole splittings in these compounds is commented on.

C. H. W. JONES et M. DOMBSKY. Can. J. Chem. **59**, 1585 (1981).

On rapporte des données de Mössbauer relatives à l'iode-129 présent dans les composés suivants: SnI_4, $MeSnI_3$, Me_2SnI_2, Me_3SnI, $Me_3SnI_2^-$, $Me_3SnI.py$ et $Me_2SnI_2.2py$. On a comparé ces données à celles de rqn disponibles pour les chlorures et bromures correspondants. Les données de Mössbauer indiquent qu'à l'état solide les composés $MeSnI_3$, Me_2SnI_2 et Me_3SnI sont déformés par rapport à la géométrie tétraédrique. On discute de l'utilisation du modèle additif dans l'interprétation des dédoublements quadrupolaires du ^{119}Sn dans ces composés.

[Traduit par le journal]

Can. J. Chem. Downloaded from www.nrcresearchpress.com by 210.87.254.6 on 09/06/12
For personal use only.

Introduction

There have been a large number of studies in the past relating to the nature of the bonding in, and the structure of, the organotin halides, $R_{4-n}SnX_n$ (R = alkyl or aryl; X = Cl, Br, or I; n = 1, 2, or 3). In particular, a number of crystal structures have been reported (1–4), while ir (5), ^{119}Sn Mössbauer (see ref. 6 and references therein) and halogen nqr (7–9) spectroscopy have all been used to probe the bonding and structure in the solid state. These compounds have also been studied in solution by proton nmr (10, 11) while electron diffraction techniques have provided information on the molecular geometry in the gas phase (12).

Marks *et al.* (13) have recently studied the ^{129}I Mössbauer spectra of Me_3SnI and $MeSnI_3$ in frozen solutions in methylcyclohexane. They interpreted the ^{119}Sn and ^{129}I Mössbauer data, together with the proton nmr data of the solutions, in terms of the valence shell orbital populations on the tin and iodine. In their interpretation they assumed that the coordination about the tin is close to tetrahedral in both the solid state and in solution. This assumption appears to be at variance with the findings drawn from other studies, where it has generally been concluded that the methyltin halides are distorted from regular tetrahedral geometry in the solid state.

In the present study the ^{129}I Mössbauer spectra of SnI_4, $MeSnI_3$, Me_2SnI_2, Me_3SnI, Ph_3SnI, $Me_3SnI.py$, $[Bu_4N^+][Me_3SnI_2^-]$, and $Me_2SnI_2.2py$ have been measured at 4.2 K. The Mössbauer data are interpreted in the light of the previous ir, nqr and crystal structure studies in terms of the coordination about the tin.

Results

The ^{129}I Mössbauer parameters are reported in Table 1 and sample spectra are given in Fig. 1. The ^{119}Sn Mössbauer spectra of these compounds were also recorded to help in their identification and these results are reported in Table 2.

The ^{129}I parameters obtained in the present work for solid $MeSnI_3$ (Table 1) are in excellent agreement with those reported for the frozen solution experiment in ref. 13, suggesting that the iodine environment is similar in the two cases. The isomer shifts, coupling constants, and asymmetry parameters for Me_3SnI as a solid and in frozen solution do not show as good an agreement, although the values are similar. It may be noted that in the ^{129}I frozen solution spectrum of Me_3SnI reported in ref. 13, the absorption at $-6\,mm\,s^{-1}$ was exceptionally broad and showed evidence of structure, while a pronounced shoulder at $+4\,mm\,s^{-1}$ was clearly not part of the major component of the spectrum. However, the key point is that the iodine atoms again appear to be in similar environments in both the solid and the frozen solution.

The iodine coupling constant for Me_2SnI_2 (Table 1) lies between that of $MeSnI_3$ and Me_3SnI. Bryuchova *et al.* (23) have reported the ^{127}I nqr spectrum of Et_2SnI_2 at 77 K and observed resonances equivalent to $e^2qQ(127) = -971\,MHz$ ($\eta = 0.122$) in comparison with $-1035\,MHz$ ($\eta = 0$) for Me_2SnI_2 found here.

0008-4042/81/111585-07$01.00/0
©1981 National Research Council of Canada/Conseil national de recherches du Canada

Can. J. Chem. Downloaded from www.nrcresearchpress.com by 210.87.254.6 on 09/06/12
For personal use only.

TABLE 1. ^{129}I Mössbauer data

	δ* mm s^{-1}	e^2qQ† MHz		$\Gamma_{Exp.}$ mm s^{-1}	χ^2/N‡	Reference§
		^{129}I	^{127}I			
SnI_4	0.38	-971 ± 9	-1387	1.07	262/238	
	0.43	-956				14
$MeSnI_3$	0.27	-864 ± 6	-1234	0.79	292/238	
	0.26	-876				13
Me_2SnI_2	0.03	-725 ± 2	-1035	0.92	286/235	
Me_3SnI	-0.21	-584 ± 6 ($\eta = 0.18$)	-834	0.75	212/233	
	-0.15	-518				13
Ph_3SnI	-0.01	-715 ± 3	-1021	0.76	214/235	
$[Bu_4N][Me_3SnI_2]$	-0.18	-298 ± 9	-425	1.00	277/240	
$Me_3SnI.py$	-0.30	-326 ± 5	-466	0.89	240/238	
$Me_2SnI_2.2py$	-0.12	-357 ± 3	-510	0.86	228/234	
I_2	0.84	-1490 ± 9 ($\eta = 0.17$)	-2129	1.10	258/238	
	0.83	-1510 ($\eta = 0.17$)				15
NaI	-0.48	0		1.17	211/250	
	-0.46	0				16

*δ with respect to ZnTe, source and absorbers at 4.2 K.
†Ground state coupling constants for ^{129}I and ^{127}I, $\eta = 0$, except where noted.
‡χ^2/N chi^2 divided by the number of degrees of freedom.
§References: this work except where noted.

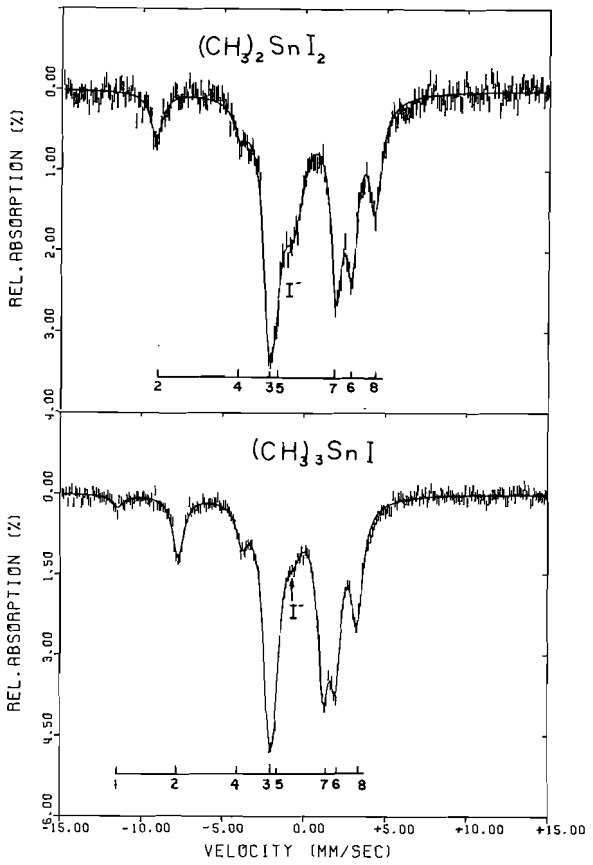

FIG. 1. ^{129}I Mössbauer spectra recorded at 4.2 K against a $Zn^{129m}Te$ source.

TABLE 2. ^{119}Sn Mössbauer data

	δ* ($\pm$0.03 mm s^{-1})	Δ ($\pm$0.03 mm s^{-1})	Reference†
SnI_4	1.48	0	
	1.55	0	14
$MeSnI_3$	1.51	1.68	
	1.58	1.68	13
Me_2SnI_2	1.52	2.76	
Me_3SnI	1.42	3.05	
	1.48	3.05	17
Ph_3SnI	1.34	2.27	
	1.41	2.05	18
$[Bu_4N][Me_3SnI_2]$	1.42	3.31	
$[Et_4N][Me_3SnBr_2]$	1.43	3.45	19
$Me_3SnI.py$	1.36	3.35	
$Me_3SnBr.py$	1.30	3.18	20
$Me_2SnI_2.2py$	1.44	3.79	
$Me_2SnBr_2.2py$	1.67	3.90	21

*δ with respect to SnO_2 source and absorber at 77 K.
†References: this work except where noted. In the referenced works the source was at room temperature and the absorbers at ca. 77 K.

The compound Ph_3SnI yielded a coupling constant e^2qQ (127) of -1020 MHz which is much larger than that of Me_3SnI. A previous ^{127}I nqr study of Ph_3SnI (22) yielded only one resonance which, assuming that this corresponds to the 1/2–3/2 transition, gives a $|e^2qQ\ (127)| = 1028$ MHz.

The X-ray crystal structure of $Me_3SnCl.py$ has shown this compound to be trigonal bipyramidal with the chlorine and pyridine ligands in axial positions (22). The vibrational spectra (4) of $[Bu_4N][Me_3SnI_2]$ and $Me_3SnI.py$ are consistent with the tin being in a similar environment. The ^{119}Sn

TABLE 3. The halogen reduced coupling constants of the organotin halides

	Reduced coupling constants*		
	Cl	Br	I
SnX_4	0.427–0.439(a)	0.504–0.514(a)	0.603–0.608(a) 0.60(4.2 K)(b)
$MeSnX_3$	0.38(c)	0.427, 0.457 (c)	0.54(4.2 K)(b)
	0.354, 0.398 (d)	0.429, 0.461 (d)	
Me_2SnX_2	0.282(c)	0.339, 0.343 (c)	0.45(4.2 K)(b)
	0.282(d)	0.342, 0.346 (d)	
	0.276, $\eta = 0.36$(e)		
Me_3SnX	0.208(c) 0.272(80 K)(e)	0.218(c) 0.291(d)	0.36(4.2 K)(b)
$Me_3SnX.py$		0.195, 0.194, 0.185 (d)	0.20(4.2 K)(b)
$Me_2SnX_2.2py$		0.204(d)	0.22(4.2 K)(b)
$PhSnX_3$	0.367–0.388(e)		
Ph_2SnX_2	0.318–0.341(e)		
Ph_3SnX	0.305–0.310(303 K)(e) 0.250(e)	0.362–0.368(e)	0.447(e) 0.45(4.2 K)(b)

*Measured at 77 K except where noted. References are: (a) ref. 23, (b) this work, (c) ref. 8, (d) ref. 7, (e) ref. 6.

quadrupole splittings (Table 2) are also consistent with this assignment. These compounds yielded ^{129}I coupling constants much smaller than that of Me_3SnI. In the compound $Me_2SnI_2.2py$ the tin is octahedrally coordinated and the methyl groups are *trans* and the iodine ligands *cis*. (5) This compound has an ^{129}I coupling constant comparable with that of $[Bu_4N][Me_3SnI_2]$ and $Me_3SnI.py$.

Discussion

As noted above, the present Mössbauer data appear to be in reasonable agreement with the previous ^{129}I solution work and the limited amount of ^{127}I nqr data available. The data of Table 1 clearly show that there is a decrease in the iodine coupling constant, and hence an increase in the Sn—I bond ionicity, in the order $SnI_4 < MeSnI_3 < Me_2SnI_2 < Me_3SnI < MeSnI_2.2py < Me_3SnI.py \sim Me_3SnI_2^-$ while the Sn—I bond in Ph_3SnI is more covalent than that in Me_3SnI.

The present data are compared in Table 3 and Fig. 2 with the previously published ^{35}Cl and ^{81}Br nqr data for the corresponding chlorides and bromides. The data are compared in terms of reduced coupling constants,[1] defined (6) as the experimentally observed coupling constant divided by the appropriate atomic coupling constants (^{35}Cl 109.746 MHz, ^{81}Br 643.032 MHz, ^{127}I 2292.712 MHz, ^{129}I 1607.0 MHz). It can be seen from Fig. 2 that the trends in halogen reduced coupling constants for

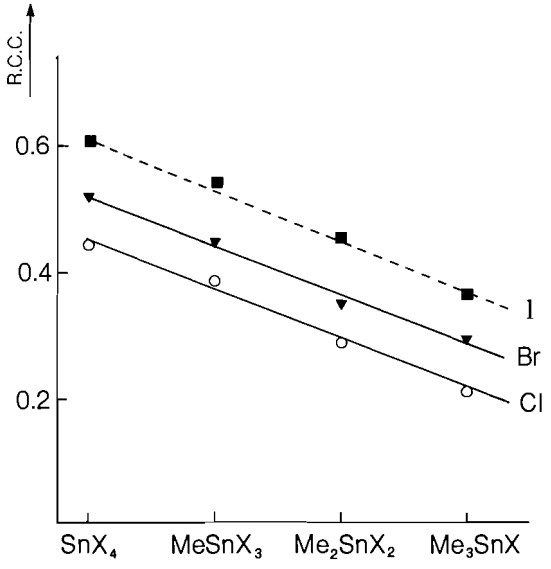

FIG. 2. The halogen reduced coupling constants of the organotin halides.

[1]The reduced coupling constant is also called the *p*-orbital imbalance, U_p.

Can. J. Chem. Downloaded from www.nrcresearchpress.com by 210.87.254.6 on 09/06/12
For personal use only.

Can. J. Chem. Downloaded from www.nrcresearchpress.com by 210.87.254.6 on 09/06/12
For personal use only.

the organotin iodides parallel those for the chlorides and bromides throughout the series $Me_{4-n}SnX_n$ (n = 1 to 3). It may be noted in Table 3 that there are discrepancies in the literature values for the ^{35}Cl and ^{81}Br coupling constants for Me_3SnCl and Me_3SnBr. From the trends of Fig. 2 it would appear that the values of 0.208 and 0.291 are the more consistent for the reduced coupling constants for Me_3SnCl and Me_3SnBr, respectively.

From Table 3 it is also apparent that the small reduced coupling constants for $Me_3SnI.py$ and $Me_2SnI_2.2py$ are reasonably consistent with the small ^{81}Br values observed for the corresponding bromine compounds. Similarly, the fact that Ph_3SnI yields a significantly larger coupling constant than Me_3SnI is consistent with the observation that for the phenyltin chlorides $Ph_{4-n}SnCl_n$, the ^{35}Cl coupling constants are greater, for any given value of n, than for the corresponding methyl compounds.

While ^{35}Cl and ^{81}Br nqr measurements on polycrystalline samples yield only the magnitude of the coupling constant, ^{129}I Mössbauer spectroscopy also allows the determination of the sign of the coupling constant, the magnitude of the asymmetry parameter, and the sign and magnitude of the isomer shift. For SnI_4, $MeSnI_3$, Me_2SnI_2, and Me_3SnI e^2qQ is negative in sign and the asymmetry parameter was zero except for Me_3SnI where η = 0.18.

The Mössbauer isomer shift can be used to crudely estimate the number of p-electrons, h_p, removed from the iodine in bonding, assuming that the s-electrons are not bonding; i.e., $h_s = 0$. This can be done employing the empirical equation (13)

$$\delta = 1.5\,h_p - 0.54$$

Moreover, the coupling constant yields the p-orbital imbalance in the usual way (13):

$$U_p = e^2qQ/e^2q_0Q$$

For a nonbridging Sn—I bond, h_p should just be equal to U_p. The values of h_p and U_p are given in Table 4. There is reasonable agreement between h_p and U_p for SnI_4, $MeSnI_3$, and Me_2SnI_2 assuming h_s = 0. (In ref. 13 an error was made in calculating h_s for $MeSnI_3$ and rather than a value of 0.07 a value of 0.004 should have been obtained.) However, for Me_3SnI where $\eta \neq 0$, h_p and U_p, as calculated on this overly simplistic model, are not in good agreement.

The significance of these observations is that for $MeSnI_3$ and Me_2SnI_2 the iodine Mössbauer data suggest that the Sn—I bond is axially symmetrical, that the bonding to iodine occurs through an iodine 5p orbital, and that there is no evidence for significant intermolecular interactions in either compound. For Me_3SnI the presence of a small asymmetry parameter, together with the fact that $h_p < U_p$, may be interpreted as evidence for an intermolecular interaction in which the Sn—I...Sn linkage is not linear, although such an interaction would not appear to be very strong. The participation of a small amount of iodine 5s character in bonding could lead to a nonlinear bridging interaction and this would also result in the apparently low value of h_p.

TABLE 4. The p-hole and p-orbital imbalances calculated from δ and e^2qQ, respectively

	h_p	U_p
SnI_4	0.61	0.60
$MeSnI_3$	0.54	0.54
Me_2SnI_2	0.38	0.45
Me_3SnI	0.22	0.36 (η = 0.18)

The X-ray crystal structures of Me_2SnCl_2, Me_3SnCl, Ph_2SnCl_2, Ph_3SnCl, and Et_2SnX_2 (X = Cl, Br, or I) have all been reported (Table 5) and the dihalides all exhibit a significant distortion from tetrahedral geometry, the environment about the tin being distorted octahedral with two distant bridging halogen contacts. The weight of the evidence suggests (24) that in the dichlorides and dibromides these distant contacts represent weak intermolecular bonds while in Et_2SnI_2, these contacts are greater than the sum of the van der Waal's radii. The compounds Me_3SnCl and Ph_3SnCl also show distortion from regular tetrahedral geometry, although the distortion is much greater in the former than the latter. In Me_3SnCl the Me_3Sn group approaches a planar geometry (4) and a relatively short Sn---Cl bridging contact completes a ψ-tbp environment about the tin.

Evidence from ir spectra also suggests that in the trimethyltin halides the Me_3Sn-moiety is nearly planar, consistent with a ψ-tbp environment about the tin with the halogens bridging. The Sn—X stretching frequencies also give some evidence for association in the Me_2SnX_2 compounds.

The marked similarity in the behaviour of the halogen reduced coupling constants illustrated in Fig. 2, together with the structures of Me_2SnCl_2, Et_2SnI_2, and Me_2SnCl_2 noted above, suggest that in the methyltin iodides in the solid state there is increasing distortion from tetrahedral geometry in the series $SnI_4 < MeSnI_3 < Me_2SnI_2 < Me_3SnI$. As the number of methyl groups attached to the tin increases the Sn—I bond becomes more ionic and the iodine coupling constant decreases.

The compounds $[Bu_4N][Me_3SnI_2]$ and $Me_3SnI.py$

Can. J. Chem. Downloaded from www.nrcresearchpress.com by 210.87.254.6 on 09/06/12
For personal use only.

TABLE 5. X-ray crystal structure data

Bond lengths (Å)	Ph_2SnCl_2(2)	Me_2SnCl_2(3)	Et_2SnCl_2(24)	Et_2SnBr_2(24)	Et_2SnI_2(24)	Ph_3SnCl(1)	Me_3SnCl(4)
Sn—C	2.114	2.21	2.132	2.167	2.178	2.122	2.14
Sn—X	2.346	2.40	2.385	2.505	2.719	2.316	2.434
Sn—X	3.77	3.54	3.483	3.777	4.284		3.259
Bond angles							
X–Sn–X	99.8	93	96	98.5	104		
C–Sn–C	125.5	123.5	134	135.9	130	112.9	117.2
C–Sn–X	107	109	106.3	97.5	105.6	106	98.5

are important in this context since they provide the coupling constant for iodine bound to tin in a tbp environment, the methyl groups occupying equatorial positions. It can be seen that in Me_3SnI the iodine coupling constant is intermediate between that of SnI_4, on the one hand, and $Me_3SnI_2^-$ or Me_3SnI.py on the other. Again, this would be consistent with distortion from tetrahedral towards tbp geometry in Me_3SnI.

There is no evidence for intermolecular bridging in the ^{129}I Mössbauer data for $MeSnI_3$ or Me_2SnI_2 and this is consistent with the known structure of Et_2SnI_2 referred to above. For Me_3SnI the ^{129}I data is consistent with the presence of a nonlinear Sn—I---Sn intermolecular interaction analogous to that observed in Me_3SnCl.

It has been recognized for some considerable time that the ^{119}Sn quadrupole splittings in the organotin halides do not accord to a simple point charge or additive model (see ref. 25 and references therein), and this was itself interpreted as evidence for divergence from tetrahedral geometry in these compounds. It is interesting to note that the halogen nqr and ^{129}I Mössbauer data are consistent with the ^{119}Sn quadrupole splittings. Thus, in Table 6 the ^{119}Sn quadrupole splittings for some methyl and phenyl chlorides and iodides are compared along with the reduced halogen coupling constants. For $MeSnCl_3$ and $PhSnCl_3$ the ^{119}Sn Δ values are very similar, as expected on a point-charge model, and the Sn—Cl bonds are very similar as reflected in the halogen coupling constants. On the other hand, Me_3SnCl and Ph_3SnCl yield very different ^{119}Sn Δ values. For these compounds the Sn—Cl bonds are significantly different as reflected in the chlorine coupling constants and in the crystal structures of these compounds. Thus the Sn—Cl bond length in Ph_3SnCl is 2.316 Å and that in Me_3SnCl 2.434 Å. Similarly, for Me_3SnI and Ph_3SnI the ^{119}Sn quadrupole splittings are significantly different and the iodine coupling constants point to a considerable difference in the Sn—I bonds.

Thus for both the chlorides and the iodides the methyl compounds appear to show a greater divergence from tetrahedral geometry as the number of methyl groups on the tin increases than is the case for the phenyl compounds. This is reflected both in the ^{119}Sn quadrupole splittings and in the halogen coupling constants. The phenyl group would appear to be more electronegative than the methyl group in these compounds.

TABLE 6. The ^{119}Sn Mössbauer parameters and the halogen reduced coupling constants (RCC) for a number of methyl and phenyltin chlorides and iodides

	^{119}Sn* δ (mm s^{-1})	^{119}Sn* Δ (mm s^{-1})	Reference	Average halogen† RCC
$MeSnCl_3$	1.32	2.07	21	0.38
$PhSnCl_3$	1.22	1.84	19	0.37
Me_3SnCl	1.43	3.41	17	0.21
Ph_3SnCl	1.31	2.56	19	0.31
Me_3SnI	1.42	3.05	This	0.36
Ph_3SnI	1.34	2.27	work	0.45

*δ is given with respect to $BaSnO_3$ at 77 K.
†Taken from Table 2.

Another point concerns the application of the additive model to the ^{119}Sn quadrupole splittings of molecules of different geometry. It can be shown (26) that the relative [L] values for ligands bonded to tin in complexes of given geometry are given by

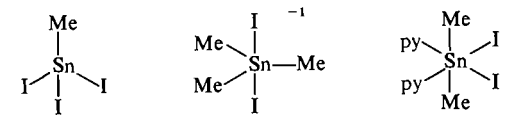

$$-\frac{3}{10}\langle r\rangle_p^{-3}\sigma_{tet.} \qquad -\frac{1}{5}\langle r\rangle_p^{-3}\sigma_{tbp}^{ax.} \qquad -\frac{1}{5}\langle r\rangle_p^{-3}\sigma_{oct.}$$

where the terms 3/10, 1/5, and 1/5 reflect the relative p character of sp^3, pd, and sp^3d^2 hybrids on the tin atom, respectively, and the σ terms are the populations of those tin hybrid orbitals. From the iodine coupling constants of $MeSnI_3$, $Me_3SnI_2^-$, and Me_2SnI_2.py it can be seen that the $\sigma_{tet.} = 0.54$, $\sigma_{tbp}^{ax.} = 0.20$, and $\sigma_{oct.} = 0.22$. Not surprisingly, the σ values are very different for an sp^3 hybrid orbital

Can. J. Chem. Downloaded from www.nrcresearchpress.com by 210.87.254.6 on 09/06/12
For personal use only.

on tin bonded to iodine and for a *pd* hybrid orbital, since the latter gives rise to a much longer bond in which much of the electron density resides on the iodine. Thus in addition to taking account of the different hybrid orbitals used, the wide variations in σ should also be taken into account when attempting to apply the additive model to tin compounds of different geometry.

Finally, it may also be noted that the iodine coupling constant in Me_3SnI is roughly twice that in $Me_3SnI_2^-$ while the ^{119}Sn quadrupole splittings of the two are very similar. In Me_3SnI the Sn—I bond will have considerable tin *5p* orbital character. In $Me_3SnI_2^-$ the I–Sn–I linkage may be viewed as involving a single tin *5p* orbital in a *3c–2e* bond or alternatively as involving *pd* hybrids on the tin.

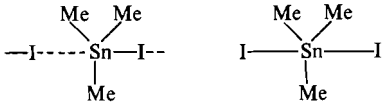

In terms of a simple additive model, it would be anticipated that the former would give rise to an iodine coupling constant roughly twice that of the latter and this is indeed observed. Thus the point-charge model appears to retain its validity and Me_3SnI is more appropriately compared with $Me_3SnI_2^-$ than with $MeSnI_3$.

Experimental

The ^{129}I was obtained as $Na^{129}I$ in Na_2SO_3 solution from Oak Ridge National Laboratory and was converted into pure dry solid, $Na^{129}I$ by oxidation to I_2, extraction into CCl_4, reduction back to I^- with thiosulphate, precipitation as PbI_2, treatment with aqueous Na_2CO_3 to produce NaI in solution, and finally, evaporation and drying on heating.

Tin tetraiodide, $MeSn^{129}I_3$, $Me_2Sn^{129}I_2$, and $Ph_3Sn^{129}I$ were prepared by stirring a small excess of $Na^{129}I$ solid with the corresponding chloride compounds, either in dry chloroform or dry ethanol, for several hours. The preparations were carried out under dry nitrogen and the resulting solutions were finally evaporated in a stream of nitrogen in the Teflon holders in which Mössbauer measurements were to be subsequently made.

The compound $Me_3Sn^{129}I$ was made by addition of dry elemental $^{129}I_2$ to Me_6Sn_2 in stoichiometric quantity. This reaction was again carried out under nitrogen in the Teflon holder in which the Mössbauer spectrum was to be recorded.

The pyridine adducts $Me_3Sn^{129}I.py$ and $Me_2Sn^{129}I_2.2py$ were prepared by the addition of an excess of dry pyridine to the parent methyltin iodide and removal of the excess of pyridine in a stream of dry nitrogen. The compound $[Bu_4N]Me_3Sn^{129}I_2$ was prepared by adding $Bu_4N^{127}I$ to $Me_3Sn^{129}I$ in dry methanol and subsequently evaporating off the solvent in a stream of dry nitrogen.

Each of the above preparations was initially carried out using $Na^{127}I$ and $^{127}I_2$ both on a larger scale and also on the scale to be used in the ^{129}I preparations. The compounds were characterized, where appropriate, by nmr in solution, by C, H, and N analysis in the cases of the pyridine adducts and the tetrabutyl ammonium salt, and by ^{119}Sn Mössbauer spectroscopy. The $J(^{119}Sn—C—^1H)$ frequencies in Hz were found to be $MeSnI_3$ 76(73), Me_2SnI_2 64(62.5), Me_3SnI 59(58.5), and $Me_3SnI.py$ 65(64), where the values in brackets are those reported in the literature (10, 11). The spectra of the first three compounds were recorded in $CDCl_3$ and that of the last compound in pyridine, using a Varian 56A/60 spectrometer. The ^{129}I Mössbauer spectra were recorded using a 100 mg $Zn^{129m}Te$ source, prepared by heating zinc and elemental tellurium, labelled with ^{129m}Te, *in vacuo*. The ^{129m}Te was obtained as $^{129m}TeO_3^{2-}$ in aqueous solution from New England Nuclear and this was reduced to elemental tellurium with SO_2 in 6 *M* HCl. The source had an initial activity of 2 mCi. Each absorber contained 10–15 mg cm^{-2} of ^{129}I and was mounted in a Teflon holder with screw cap. Spectra were recorded with the source and absorbers immersed in liquid helium in a Harwell Instruments MHC 200 cryostat. The source was driven in constant acceleration using a Harwell Instruments 200 series transducer, function generator, and attenuator. The spectrometer was routinely calibrated using a $^{57}Co/Pd$ (New England Nuclear) source and iron foil and α-Fe_2O_3 absorbers at room temperature. The ^{129}I parameters in Table 1 for SnI_4, I_2, and NaI also provide a calibration of the spectrometer.

The ^{119}Sn Mössbauer spectra were recorded, using a $Ba^{119m}SnO_3$ source supplied by New England Nuclear, with the source and absorbers at 77 K.

The Mössbauer spectra were computer fitted to independent Lorentzians and in the analysis of the ^{129}I data the approach outlined by Pasternak (27) was followed, although the revised value (28) of $Q^*/Q = 1.238$ for ^{129}I was used.

Acknowledgement

The authors wish to thank the Natural Sciences and Engineering Research Council of Canada for a grant in support of this work.

1. N. G. Bokii, G. N. Zakharova, and Yu. T. Struchkov. Zh. Strukt. Khim. **11**, 895 (1970).
2. P. T. Greene and R. F. Bryan. J. Chem. Soc. A, 2549 (1971).
3. A. G. Davies, H. J. Milledge, D. C. Puxley, and P. J. Smith. J. Chem. Soc. A, 2862 (1970).
4. M. Bilayet Hossain, J. L. Lefferts, K. C. Malloy, D. Van Der Helm, and J. J. Zuckerman. Inorg. Chim. Acta, **36**, L409 (1979).
5. V. S. Petrosyan, N. S. Yashina, and O. A. Reutov. Adv. Organomet. Chem. **14**, 63 (1976).
6. N. W. G. Debye and M. Linzer. J. Chem. Phys. **61**, 4770 (1974).
7. V. S. Petrosyan, N. S. Yashina, and O. A. Reutov. J. Organomet. Chem. **52**, 321 (1973).
8. D. F. Van de Vondel, H. Willemen, and G. P. Van der Kelen. J. Organomet. Chem. **63**, 205 (1973).
9. P. J. Green and J. D. Graybeal. J. Am. Chem. Soc. **89**, 4305 (1967).
10. E. V. Van den Berghe and G. P. Van der Kelen. J. Organomet. Chem. **6**, 515 (1966).
11. E. V. Van den Berghe and G. P. Van der Kelen. J. Organomet. Chem. **11**, 479 (1968).
12. B. Beagley, K. McAloon, and J. M. Freeman. Acta Crystallogr. Sect. B, **30**, 444 (1974).
13. A. P. Marks, R. S. Drago, R. H. Herber, and M. J. Potasek. Inorg. Chem. **15**, 259 (1976).
14. S. Bukshpan and R. H. Herber. J. Chem. Phys. **46**, 3375 (1967).
15. M. Pasternak and T. Sonnino. J. Chem. Phys. **48**, 1997 (1968).

16. D. W. HAFEMEISTER, G. DE PASQUALI, and H. DE WAARD. Phys. Rev. **135**, B1089 (1964).
17. M. CORDEY-HAYES, R. D. PEACOCK, and M. NUCELIC. J. Inorg. Chem. **29**, 1177 (1967).
18. V. V. KHARPOV, V. I. GOLDANSKII, A. K. PROKOFIEV, and R. G. KOSTYANOVSKII. J. Gen. Chem. U.S.S.R. **37**, 1 (1967).
19. R. V. PARISH and R. H. PLATT. Inorg. Chim Acta, **4**, 65 (1970).
20. J. NASIELSKI, N. SPRECHER, J. DEVOOGHT, and S. LEJEUNE. J. Organomet. Chem. **8**, 97 (1967).
21. V. S. PETROSYAN, N. S. YASHINA, S. G. SACHAROV, O. A. REUTOV, V. YA ROCHEV, and V. I. GOLDANSKII. J. Organomet. Chem. **52**, 333 (1973).
22. R. HULME. J. Chem. Soc. 1525 (1963).
23. E. V. BRYUCHOVA, G. K. SEMIN, V. I. GOLDANSKII, and V. V. KHRAPOV. Chem. Commun. 491 (1968).
24. N. W. ALCOCK and J. F. SAWYER. J. Chem. Soc. Dalton Trans. 1090 (1977).
25. R. V. PARISH. Prog. Inorg. Chem. **15**, 101 (1972).
26. G. M. BANCROFT and R. H. PLATT. Adv. Inorg. Chem. Radiochem. **15**, 82 (1972).
27. M. PASTERNAK. Symp. Faraday Soc. **1**, 119 (1967).
28. H. DE WAARD. *In* Mössbauer effect data index. *Edited by* J. G. Stevens and V. E. Stevens. Plenum, New York. 1973. p. 447.

Can. J. Chem. Downloaded from www.nrcresearchpress.com by 210.87.254.6 on 09/06/12
For personal use only.

Stability and reactivity of the benzyl and tropylium cations in the gas phase

D. K. SEN SHARMA AND P. KEBARLE

Chemistry Department, University of Alberta, Edmonton, Alta., Canada T6G 2G2

Received November 4, 1980

D. K. SEN SHARMA and P. KEBARLE. Can. J. Chem. **59**, 1592 (1981).

A measurement of equilibrium [4]: $t\text{-}C_4H_9^+ + BzCl = t\text{-}C_4H_9Cl + C_7H_7^+$ led to equilibrium constants K_4 which are in fair agreement with earlier work by Abboud *et al.* However, the present temperature dependence predicts a ΔS_4^0 which is sufficiently different from that by Abboud *et al.* to put in question the indentification of $C_7H_7^+$ as Bz^+ on the basis of the measured ΔS_4^0 value. Therefore experiments were made to confirm that $C_7H_7^+$ produced in [4] is Bz^+ and not the tropylium cation. A $C_7H_7^+$ cation was produced by hydride abstraction from 1,3,5-cycloheptatriene. The behaviour of that $C_7H_7^+$ ion was entirely different from $C_7H_7^+$ produced by chloride abstraction from BzCl or hydride abstraction from toluene. While the benzyl derived $C_7H_7^+$ engaged in a number of reactions like hydride abstraction, chloride abstraction, addition, condensation, etc., the $C_7H_7^+$ from the heptatriene remained completely unreactive. On this basis the $C_7H_7^+$ ions were identified as Bz^+ and tropylium$^+$, respectively. Rate constants for several reactions of Bz^+ were determined. It is concluded that a rearrangement from benzyl to tropylium cations and vice versa does not occur at least up to 300°C. The ions also retain their identity if they are produced with considerable internal excitation energy.

D. K. SEN SHARMA et P. KEBARLE. Can. J. Chem. **59**, 1592 (1981).

Une mesure de l'équilibre [4]: $t\text{-}C_4H_9^+ + BzCl = t\text{-}C_4H_9Cl + C_7H_7^+$ a permis de déterminer la valeur de la constante d'équilibre K_4 qui est en bon accord avec les travaux antérieurs de Abboud *et al.* Cependant l'influence de la température suggère que le ΔS^0_4 est assez différent de celui de Abboud et ses collaborateurs pour remettre en question l'identification de $C_7H_7^+$ en tant que Bz^+, en se basant sur la valeur mesurée de ΔS^0_4. En conséquence, on a effectué des expériences afin de confirmer que le $C_7H_7^+$ produit dans l'équilibre [4] est bien le Bz^+ et non le cation tropylium. On a produit un cation $C_7H_7^+$ par enlèvement d'un hydrure du cycloheptatriène-1,3,5. Le comportement de cation $C_7H_7^+$ est complètement différent de celui obtenu par enlèvement de chlorure du BzCl ou par enlèvement d'un hydrure du toluène. Le $C_7H_7^+$ provenant du chlorure de benzyle peut donner des réactions comme l'enlèvement d'un hydrure, l'enlèvement d'un chlorure, l'addition, la condensation, etc., alors que le $C_7H_7^+$ provenant de l'heptatriène est complètement inactif. A partir de ces faits, on a identifié les deux ions $C_7H_7^+$ comme étant respectivement le Bz^+ et le tropylium. On a déterminé les constantes de vitesse de plusieurs réactions du Bz^+. On en conclut qu'il ne se produit pas de transposition entre le cation benzyle et le cation tropylium, du moins jusqu'à 300°C. Les ions retiennent leur identité également s'ils sont produits avec une grande énergie d'excitation interne.

[Traduit par le journal]

Introduction

A number of studies dealing with the benzyl and tropylium cations in the gas phase have been published. Interest in the identity and properties of the two ions was first aroused by Meyerson and co-workers (1) who in 1957 suggested that the $C_7H_7^+$ ions, formed by electron impact from toluene and other alkyl derivatives of benzene, do not have the expected benzyl structure but are tropylium cations. The evidence of Meyerson was largely based on a comparison of the mass spectra of various deuterated ethyl benzenes and toluenes. The formation of tropylium from toluene may proceed by two routes. The excited $C_7H_8^+$ ion of toluene structure may rearrange to $C_7H_8^+$ with the cycloheptatriene structure. This is followed by dissociation to the tropylium cation, (see route [a,b], eq. [1]). In the second alternative the toluene ion dissociates to the benzyl cation which then rearranges to tropylium (see route [c,d] eq. [1]). Meyerson pointed out that his results favored the route [a,b].

[1] $C_7H_8^+$ (toluene$^+$) $\xrightarrow{a}$ $C_7H_8^+$ (*c*-heptatriene)

$\downarrow c$ $\qquad\qquad$ $\downarrow b$

$C_7H_7^+$ (benzyl$^+$) + H $\xrightarrow{d}$ $C_7H_7^+$ (tropylium$^+$) + H

McLafferty and co-workers (2) studied the collisional activation spectra of $C_7H_7^+$ ions produced by electron impact from various parent compounds. Analysis of the rather complex results led these authors to conclude that the $C_7H_7^+$ ions obtained from electron impact on substituted toluenes are composed of as many as five isomers, benzyl, tropylium, and the *o*, *m*, and *p*-tolyl cations. McLafferty and Winkler also concluded that, probably, the tropylium ions obtained from toluene are due to a rearrangement to the C_7 ring structure prior to dissociation, i.e. they are produced by route [a,b], eq. [1].

The reactivity of the $C_7H_7^+$ ions produced by electron impact with toluene was studied in high pressure mass spectrometers by Giardini-Guidoni and Zocchi (3) and by Wexler and Clow (4), who found that most of the ions react with toluene to give two products as shown in eqs. [2] and [3]. A

[2] $C_7H_7^+ + C_6H_5CH_3 = C_{14}H_{15}^+$

[3] $C_7H_7^+ + C_6H_5CH_3 = C_8H_9^+ + C_6H_6$

0008-4042/81/111592-10$01.00/0

©1981 National Research Council of Canada/Conseil national de recherches du Canada

Can. J. Chem. Downloaded from www.nrcresearchpress.com by 210.87.254.42 on 09/06/12
For personal use only.

Can. J. Chem. Downloaded from www.nrcresearchpress.com by 210.87.254.42 on 09/06/12
For personal use only.

small fraction of the $C_7H_7^+$ ions were found to be unreactive. More recently Dunbar and co-workers (5) using an ICR spectrometer also observed that the $C_7H_7^+$ ions obtained by electron impact from toluene divide into a larger fraction of reactive ions and a smaller fraction which is unreactive towards toluene. These authors suggested that the unreactive $C_7H_7^+$ ions are tropylium cations while the reactive ions are mostly benzyl. Dunbar also concluded that the tropylium ions are probably made from the cyclic $C_7H_8^+$ ion, i.e. via route [a,b].

In spite of the conclusions by Meyerson and coworkers (1), McLafferty and Winkler (2) and Dunbar and coworkers (5) that tropylium is formed by route [a,b], i.e. not by a rearrangement of the benzyl cation, there has been concern amongst gas phase chemists that the benzyl rearrangement might be occurring. For example, Lossing (6) considered the isomerization [d] as a possible complication in measurements of the ionization potential of the benzyl radical. More recently Abboud *et al.* (7) felt it pertinent to provide evidence for the stable existence of the benzyl cation in the gas phase. The major experimental feature in this work was a measurement of the temperature dependence of the equilibrium [4]

$$[4]\quad C_6H_5CH_2Cl + (CH_3)_3C^+ \underset{r}{\overset{f}{\rightleftharpoons}} C_7H_7^+ + (CH_3)_3CCl$$

observed in an ICR mass spectrometer. The equilibrium constant K_4 was measured at two temperatures, 303 and 408 K. This allowed the determination of ΔH^0_4 and ΔS^0_4. One expects (7) a $\Delta S_4 \approx 0$ for $C_7H_7^+$ being benzyl. On the other hand, the high symmetry of the tropylium cation would lead (7) to a $\Delta S^0_4 \approx -4$ eu. The experimental ΔS^0_4 was -0.5 eu which is evidence that the $C_7H_7^+$ produced by chloride abstraction from benzyl chloride is the benzyl cation and that the benzyl cation does not rearrange to tropylium.

Recently, in this laboratory, we initiated studies of chloride and hydride transfer equilibria involving various carbonium ions. These studies are planned to provide ladders of chloride and hydride affinities and thus result in useful new thermochemical data on carbocations. One series of ions that we were interested in was *o*, *m*, and *p*-substituted benzyl cations. A preliminary report of this work has been presented (8). In connection with this work it was of some importance to convince ourselves that the cations obtained from chloride abstraction from benzyl chlorides were actually benzyl and not tropylium. It was also necessary to obtain a connection of our ladder of free energy changes to some standard ion whose heat of formation is presumed to be well known. Since t-$C_4H_9^+$ is a much used standard, we decided to remeasure the chloride transfer equilibrium [4] and extend the determinations of Abboud *et al.* over a wider temperature range. To our surprise we could not confirm the $\Delta S^0_4 \approx 0$ obtained by Abboud *et al.* (7). In fact the preliminary ΔS^0_4 obtained by us agreed with that expected for $C_7H_7^+$ being tropylium. Since we expected that the $C_7H_7^+$ occurring in [4] is in fact benzyl we saw ourselves challenged to investigate the situation more closely. The present work consists of three parts: (*a*) the measurement of the equilibrium [4] over an extended temperature range and a kinetic study of [4] and the side reactions involved, (*b*) studies of the reactivity of $C_7H_7^+$ produced from chloride and hydride abstraction from benzyl chloride and toluene, and (*c*) studies of the reactivity and the behaviour of $C_7H_7^+$ obtained by hydride abstraction from 1,3,5-cycloheptatriene.

Experimental

The measurements were made with a pulsed electron beam high pressure ion source mass spectrometer which has been described previously (9).

Most of the rate constants quoted in Results and Discussion were obtained by the following technique. Consider the reaction $A^+ + B = C^+ +$ neutrals. A^+ may be an ion present at time $t = 0$ or a reaction product which appears at a later time. Since the neutral reactants are in vast excess over the ions all ionic reactions are pseudo first order. The reaction frequency equals $\nu = k[B]$. Integration of: $d[C^+]/dt = \nu[A^+]$ leads to:

$$[C^+]_t - [C^+]_{t_o} = \nu \int_{t_o}^{t} [A^+]dt$$

Plots of $[C^+]_t$ versus the integral obtained by graphical integration of the concentration–time dependence of A^+ lead to straight lines with slope ν. Since [B] is known k can be evaluated.

Results and Discussion

(*a*) *The Chloride Transfer Equilibrium of Benzyl and* tert-*Butylchloride and Side Reactions*

The chloride transfer equilibrium [4] was measured over the temperature range 300 K–640 K. A van't Hoff plot of the equilibrium constants K_4 is shown in Fig. 1. The results of Abboud *et al.* (7) and a more recent determination by Lias and coworkers (10) at room temperature are also included in Fig. 1. Inspection of Fig. 1 shows that at room temperature there is relatively good agreement between the present determinations of K_4 and those of Abboud *et al.* (7) and Lias and coworkers (10). However, the present results agree less well with Abboud's single measurement at 408 K, where Abboud's K_4 is higher by a factor of 1.6. The van't

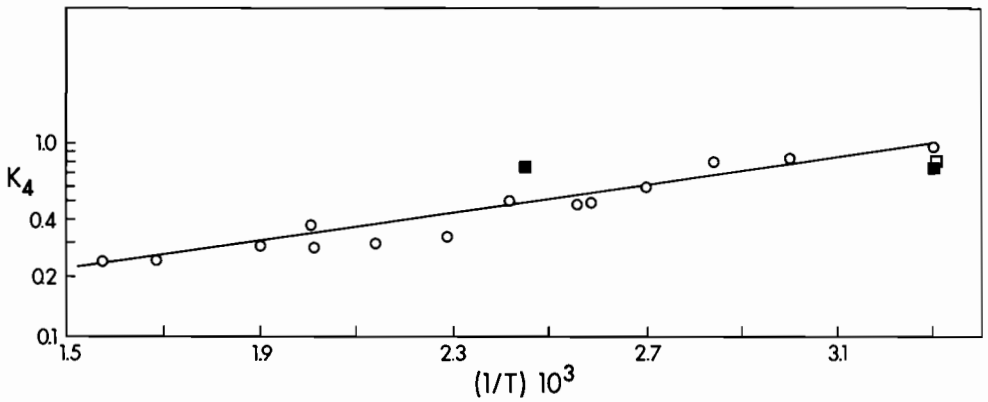

FIG. 1. van't Hoff plot for equilibrium [4]: t-$C_4H_9^+ + BzCl = t$-$C_4H_9Cl + C_7H_7^+$. ○ Present work, ■ Abboud *et al.* (7), □ Jackson *et al.* (10). Although present results are close to those of Abboud *et al.*, the temperature dependence predicted is somewhat different. Present results predict $\Delta S_4 \approx -4$ eu, while Abboud *et al.*'s data lead to $\Delta S_4 = -0.5$ eu. Present results, if correct, invalidate Abboud *et al.*'s entropy argument identifying $C_7H_7^+$ as Bz^+.

Hoff plot based on the present results shown in Fig. 1 leads to $\Delta H^0_4 = -0.8 \pm 0.3$ kcal/mol, $\Delta S^0_4 = -4.1 \pm 0.6$ cal/degree, and $\Delta G^0(300) = 0.0$ kcal/mol $\pm$ 0.3 kcal/mol while Abboud's data based on the two-point determination are $\Delta H^0_4 = 0.03$ kcal/mol, $\Delta S^0_4 = -0.05$ cal/degree, and $\Delta G^0_4(300) = +0.2$ kcal/mol. Thus the enthalpies agree within 0.8 kcal/mol and the entropies within 4 cal/degree. This is not a serious disagreement; however the present data, if correct, invalidate the entropy argument used by Abboud *et al.* (7) to show that the $C_7H_7^+$ ion is the benzyl cation. In fact the present entropy difference fits the predicted entropy change (7) for $C_7H_7^+$ being tropylium. We shall present evidence later showing that the $C_7H_7^+$ ion is in fact benzyl. Accepting this result one has two choices. Either the ΔS^0_4 predicted on the basis of symmetry numbers alone (7) is incorrect or the decrease of K_4 with temperature, observed in the present work (Fig. 1), is not a valid result. In an attempt to resolve this difficulty a detailed examination of the reaction system in which the equilibrium [4] occurred was made.

The ion concentration – time dependence observed in a typical run at room temperature is shown in Fig. 2. Ionization by electron impact and fast ion molecule reactions in pure methane lead to CH_5^+ and $C_2H_5^+$ which are roughly in 1:1 ratio. In the presence of benzyl chloride and *tert*-butyl chloride, these ions produce almost exclusively $C_7H_7^+$ and $C_4H_9^+$. The ethyl cation can produce these ions by chloride abstraction from the parent compounds. CH_5^+ must be protonating the chlorides which then decompose to HCl and the corresponding carbocation, t-$C_4H_9^+$ and $C_7H_7^+$, respectively. Since, for the concentrations used in Fig. 2, all the above reactions are fast, $C_4H_9^+$ and

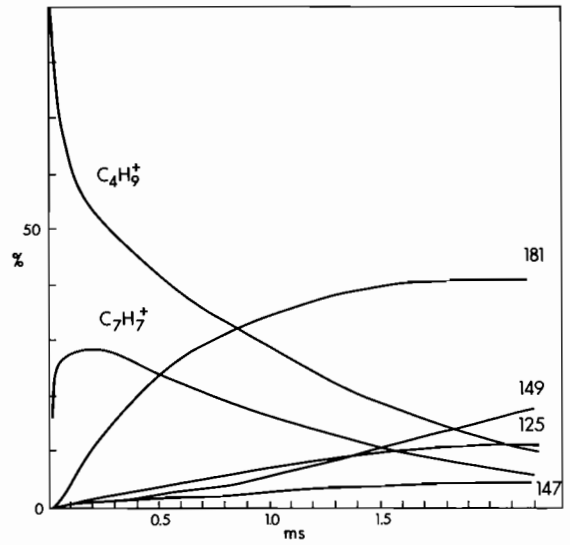

FIG. 2. Concentration time dependence for a run used for measurement of equilibrium [4]. 30°C (4 Torr CH_4, 0.2 mTorr t-BuCl, 0.1 mTorr BzCl). Equilibrium [4] between $C_4H_9^+$ and $C_7H_7^+$ leads to a constant concentration ratio for these ions after some 0.3 ms. Ion $m = 181$ is formed by the condensation reaction [5] involving $C_7H_7^+$ and BzCl, while ion $m = 125$ is formed by hydride abstraction, [7] and [8], from $BzCl^{35}$. The Cl^{37} isotope leads to $m = 127$. The intensity of this ion was added to $m = 125$ shown in the figure.

$C_7H_7^+$ appear as the initial ions. After a short ($\sim$200 μs) kinetic stage, $C_4H_9^+$ and $C_7H_7^+$ reach equilibrium, i.e. their concentration ratio becomes constant. However, the concentrations of both ions decrease with time due to a number of relatively slow reactions. Three ions of molecular mass $m = 181$, 147, and 125 were observed to be major reaction products under a variety of conditions. The production of these ions can be explained by reactions [5]–[8].

Can. J. Chem. Downloaded from www.nrcresearchpress.com by 210.87.254.42 on 09/06/12
For personal use only.

Can. J. Chem. Downloaded from www.nrcresearchpress.com by 210.87.254.42 on 09/06/12
For personal use only.

[5] $Bz^+ + BzCl =$ 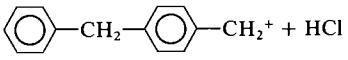 $+ HCl$

$m = 181$

[6] $t\text{-}C_4H_9^+ + BzCl =$ 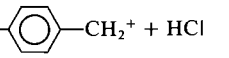 $+ HCl$

$m = 147$

[7] $Bz^+ + BzCl = BzH +$ 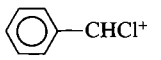

$m = 125$

[8] $t\text{-}C_4H_9^+ + BzCl = \text{iso-}C_4H_{10} +$ 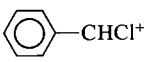

Reactions [5] and [6] are analogous. One might assume that this type of reaction proceeds in two steps, alkylation of the benzene ring by the electrophilic attack of the carbocation, as shown in structure **1**, and migration of the proton followed by loss of HCl as shown in **2**. The $C_7H_7^+$ ion participating in [5]and [7] is shown in the equations as Bz^+. It will be shown later that tropylium$^+$ does not add to BzCl and does not hydride abstract from benzyl chloride. Reactions [7] and [8] are hydride abstractions. The new benzyl cation created is chlorosubstituted in the α position. Electron pair donation from the chlorine atom makes this ion more stable than benzyl, therefore reactions [7] and [8] are exothermic (8).

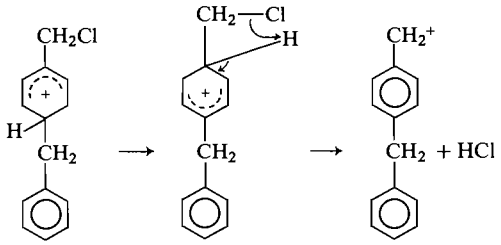

1 **2** **3**

Results from a run at the considerably higher temperature 218°C are shown in Fig. 3. Again, after a short time (~250 μs) the ratio $C_4H_9^+/C_7H_7^+$ becomes stationary. Evidently reaction [5], which was the major side reaction at 30°C, is very much slower at higher temperature. The ion $m = 181$ is now only a minor product. The corresponding *tert*-butyl reaction [6], leading to $m = 147$, and the hydride transfer reactions [7] and [8], leading to $m = 125$, are still observed. The major long reaction time product is an ion of mass 107. This mass corresponds to protonated xylene. The origin of this product is unclear.

Taking into consideration that the $C_4H_9^+$ and $C_7H_7^+$ do not only participate in the chloride transfer equilibrium [4] but also engage in side reactions like [5]–[7] one may ask whether these side reactions could be affecting the equilibrium measurements. For the evaluation of the equilibrium constant K_4 in Fig. 1 we have used the stationary ratio $[C_7H_7^+]/[C_4H_9^+]$ observed at longer reaction times. However, that ratio will be the equilibrium ratio only if the rates of the side reactions are relatively slow compared with the equilibrium rates.

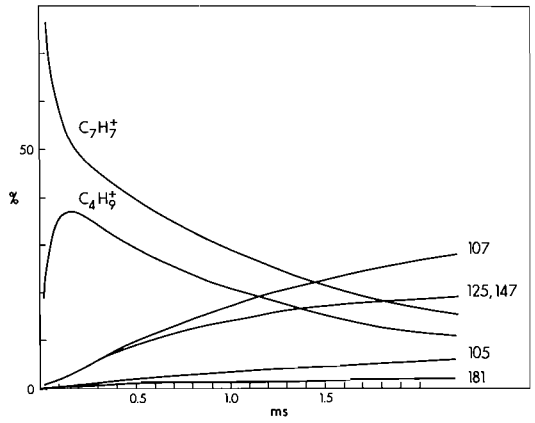

FIG. 3. Equilibrium [4] and side reactions: 218°C, (4 Torr CH_4 2.5 mTorr BzCl, 0.5 mTorr *t*-BuCl).

In order to examine the effect of the side reactions on the equilibrium, we fitted the concentrations observed in Fig. 3 by computer calculated concentrations for a reaction system consisting of the forward [4_f] and reverse [4_r] of the equilibrium

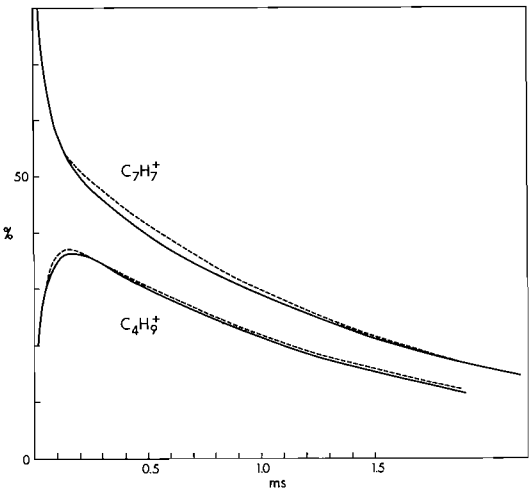

FIG. 4. Computer fit of equilibrium [4].—Experimental results from Fig. 3. ------ Computer fit of reaction system. Computer fit provides values for forward and reverse rate constants k_{4f} and k_{4r}. From these equilibrium constant $K_4 = k_{4f}/k_{4r}$ is evaluated. This result is essentially identical to K_4 obtained from stationary ratio of $C_7H_7^+$ and $C_4H_9^+$ at long reaction times. This means that side reactions are too slow to affect equilibrium measurement.

TABLE 1. Summary of rate and equilibrium constants determinations[a]

	Reaction	Constants
[4]	$BzCl + t\text{-}C_4H_9^+ = Bz^+ + t\text{-}C_4H_9Cl$	$\Delta G^0(300) = 0.0$ kcal/mol (0.2)[b] $\Delta H^0 = -0.8 \pm 0.3$ kcal/mol (0.03)[b] $\Delta S^0_4 = -4.1 \pm 0.6$ cal/deg (−0.5)[b] k_4(forward) = 1.4×10^{-9}(303 K); 2.8×10^{-10} (491 K) k_4(reverse) = 1.3×10^{-9}(303 K); 9.7×10^{-10} (451 K)
[5]	$Bz^+ + BzCl = C_6H_5CH_2{\cdot}C_6H_5CH_2^+ + HCl$	$k_5 = 5 \times 10^{-10}$ (303 K) $k_5 = 7 \times 10^{-11}$ (346 K)
[7]	$Bz^+ + BzCl = C_6H_5CH_3 + C_6H_5CHCl^+$	$k_7 = 3 \times 10^{-11}$ (346 K) $k_7 = 3 \times 10^{-12}$ (523 K) $k_7 = 1.1 \times 10^4 T^{-5.733}$ (340–550 K)
[13]	$Bz^+ + C_6H_5CH_3 = Bz{\cdot}C_6H_5CH_3^+$	$k_{13} = 2 \times 10^{-9}$ (303 K) or 1.6×10^{-26} molecules^{-2} cm^6 s^{-1} (303 K)
[13] + [14]	$Bz^+ + C_6H_5CH_3 = BzC_6H_5CH_3^+ + MeC_6H_4CH_2^+ + C_6H_6$	$k_{13} + k_{14} = 1 \times 10^{-9}$ (430 K) $k_{13} + k_{14} = 6 \times 10^{-10}$ (452 K)
[14]	$BzC_6H_5CH_3^+ = MeC_6H_4CH_2^+ + C_6H_6$	k_{14}[c] $= 5.9 \times 10^{18} \exp(-32.5\text{ kcal/mol}/RT)$ s^{-1}
[16]	$t\text{-}C_4H_9^+ +$ 1,3,5-cycloheptatriene $= C_4H_9{\cdot}C_7H_8^+$	k_{16}[d] $= 2.5 \times 10^{-10}$ (423 K)
[17]	$t\text{-}C_4H_9^+ +$ 1,3,5-*c*-heptatriene $=$ iso-$C_4H_8 + C_7H_9^+$	$k_{16} = 1.7 \times 10^{-10}$ (473 K) $k_{17} = 1.1 \times 10^{-10}$ (423 K)
[18]	$t\text{-}C_4H_9^+ +$ 1,3,5-*c*-heptatriene $=$ iso-$C_4H_{10} + C_7H_7^+$(tropylium)	$k_{18} = 1.1 \times 10^{-10}$ (423 K) $k_{18} \approx 1.0 \times 10^{-10}$ (473 K)
[19]	$C_7H_9^+ +$ 1,3,5-*c*-heptatriene $= C_7H_{10} + C_7H_7^+$(tropylium)	$k_{19} \approx 2.5 \times 10^{-11}$ (452 K)
[20]	$t\text{-}C_4H_9^+ + C_6H_5CH_3 =$ iso-$C_4H_{10} + Bz^+$	$\Delta H_{20} = 3.8$ kcal/mol[e]
[21]	$t\text{-}C_4H_9^+ +$ 1,3,5-*c*-heptatriene $=$ iso-C_4H_{10} + tropylium$^+$	$\Delta G^0_{21} < -13.4$ kcal/mol[f] (452 K) $\Delta H^0_{21} \approx -37.1$ kcal/mol[g]
[21]	$Bz^+ +$ 1,3,5-*c*-heptatriene $=$ tropylium$^+ + C_6H_5CH_3$	$\Delta H_{22} \approx -40.9$ kcal/mol[g]

[a]Units for all second order rate constants are cm^3 molecules^{-1} s^{-1}.
[b]Abboud *et al.* (7).
[c]Thermal decomposition [14] was assumed to be first order. However, reaction requires thermal activation and might be second order. To obtain second order rate constant divide by methane concentration, 9×10^{16} (molecules·cm^{-3}).
[d]Reaction assumed to be second order. However, since association occurs, reaction may be third order. To obtain third order rate constant divide by methane concentration, 9×10^{16} (molecules·cm^{-3}).
[e]From ΔH_4 and $\Delta H_f(t\text{-BuCl}) = -43.7$ kcal/mol, $\Delta H_f(BzCl) = 4.5$ kcal/mol.
[f]From lower limit of equilibrium constant K_{21}, present work.
[g]From estimate of Jackson *et al.* (10) $\Delta H_f(Bz^+) - \Delta H_f(\text{tropylium}^+) = 9$ kcal/mol.

and a fictitious reaction [9]. Since the origin of the

[9] $Bz^+ + BzCl$ or $BuCl \rightarrow$ Products (m = 107, 125, 147 etc.)

long reaction times products m = 107, 125, 147, etc. could not be assigned unambiguously to Bz^+ or t-but$^+$, we assume in reaction [9] that they are all due to Bz^+. The computer fit of the concentrations is shown in Fig. 4. From the rate constants k_{4f} and k_{4r} obtained from the computer fit one evaluates a $K_4 = 0.29$. The K_4 obtained by taking the constant ratio $[C_7H_7^+]/[C_4H_9^+]$ observed at long reaction times is $K_4 = 0.27$. The two equilibrium constants are essentially identical. Reaction [9] induces a (maximum) lowering of the $[C_7H_7^+]/[C_4H_9^+]$ stationary ratio at long reaction times. The fact that the equilibrium constants K_4 are nearly identical means that the side reactions are too slow to affect the equilibrium concentrations. The rate constants k_{4f} and k_{4r} obtained from the computer fit are given in Table 1. A similar treatment of the low temperature results in Fig. 2 showed that, there again, the ratio of $[C_7H_7^+]/[C_4H_9^+]$ read off from the figure at long reaction times leads to a K_4 which is nearly identical to a K_4 calculated from k_{4f}/k_{4r}. From the above considerations we conclude that the side reactions cannot be affecting the equilibrium measurements shown in the van't Hoff plot Fig. 1.

Thermal decomposition of the BzCl in the ion source could be a source of error. Such decomposition will lower the actual concentration of BzCl present at higher temperatures and lead to an apparent decrease of K_4. It is not easy to detect directly the occurrence of thermal decomposition with the apparatus used; however thermal decomposition is unlikely for the following reasons. Assuming that K_4 is independent of temperature, the van't Hoff plot in Fig. 1 becomes equivalent to an Arrhenius plot for the thermal decomposition. The resulting activation energy is only ~1 kcal/mol, a value much too small even for a surface catalyzed thermal decomposition of benzyl chloride on the metal surface of the ion source.

Can. J. Chem. Downloaded from www.nrcresearchpress.com by 210.87.254.42 on 09/06/12
For personal use only.

Can. J. Chem. Downloaded from www.nrcresearchpress.com by 210.87.254.42 on 09/06/12
For personal use only.

Thermal decomposition was also shown not to occur by the following experiment. The flow rate of gas through the ion source was slowed down at constant ion source pressure. Decrease of the flow rate increases the residence time of benzyl chloride in the ion source. In the presence of thermal decomposition this would lead to a decrease of the benzyl chloride concentration and an apparent decrease of K_4. Such a decrease was not observed.

We come to the conclusion that our result, $\Delta S^0_4 = -4$ cal/mol may be the true value. It may also be an erroneous result due to causes that we don't understand at present.

(b) Reactions of the Benzyl Cation with Benzyl Chlorides and Toluene

Reactions [5] and [7] involving $C_7H_7^+$ produced by chloride abstraction from benzyl chloride were considered in section (a). A more extensive study of these reactions was undertaken in runs where only BzCl and the major gas methane were present. The results from a run at the intermediate temperature of 73°C are shown in Fig. 5. The condensation product $m = 181$ formed by reaction [5] is now the major product. The next most abundant ion is $C_6H_5CHCl^+$ $m = 125$, formed by the hydride abstraction [8]. The hydrocarbon ions $C_8H_9^+$ $m = 105$, $C_8H_{11}^+$ $m = 107$, $C_{13}H_{12}^+$ $m = 155$, and $C_{15}H_{17}^+$ $m = 197$ were observed in this and other runs at low and intermediate temperatures. Their origin is not understood.

A run at the considerably higher temperature 250°C is shown in Fig. 6.

The $[C_7H_7^+]$ decrease, observed at this temperature, is slower, even though the benzyl chloride reactant is present at 30 times higher concentration. This means that the rate of the overall reaction [10] decreases greatly with temperature.

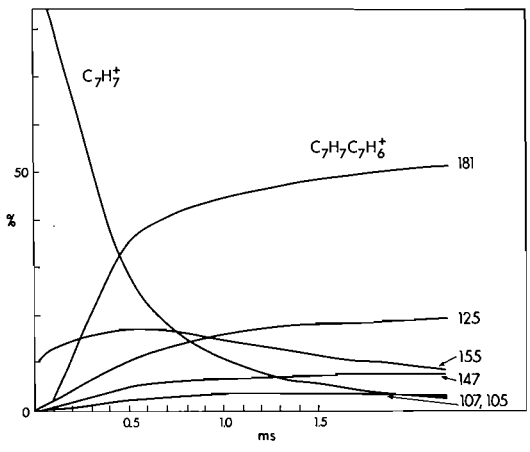

FIG. 5. Reactions of Bz^+ ($C_7H_7^+$) with BzCl: 73°C, (4 Torr CH_4, 0.5 mTorr BzCl). The two main reactions are the condensation [5] leading to $m = 181$ and the hydride abstraction [7] leading to $m = 125$, $C_6H_5CHCl^+$.

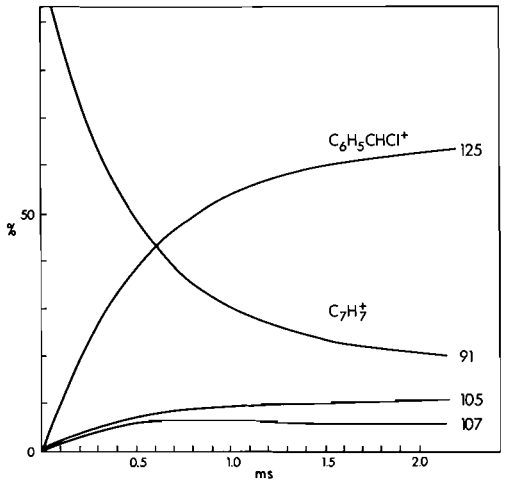

FIG. 6. Reactions of Bz^+ with BzCl at higher temperature: 250°C (4 Torr CH_4, 15 mTorr BzCl). Condensation [5] leading to $m = 181$ is very slow at this temperature, main reaction now is hydride abstraction [7] leading to $m = 125$.

[10] $Bz^+ + BzCl =$ products (other than $BzCl + Bz^+$)

The major product now is $C_6H_5CHCl^+$, $m = 125$, produced by the hydride abstraction [7]. The condensation product **3**, $m = 181$ from reaction [5] was barely visible at this temperature. A large decrease of the rate of [5] with temperature was observed also in the preceding section, Figs. 2 and 3.

The temperature dependence of the rate constants k_7 and k_{10} was determined in a series of runs, like those in Figs. 5 and 6, made in the temperature range 73 to 250°C. These results are shown in Fig. 7. The hydride abstraction [7] has a negative temperature dependence, $k_7 = 3.2 \times 10^{-11}$ at 73°C decreases to 3×10^{-12} (cm^3 $molecules^{-1}$ s^{-1}) at 250°C. Salomon and co-workers (11–13) have observed negative temperature dependence for several hydride transfer reactions involving alkyl cations. The rate constant k_{10} has a much larger negative temperature dependence than k_7 (see Fig. 7). This reflects the very large negative temperature dependence of the condensation [5]. At low temperatures $k_{10} \approx k_5$, while at high temperatures $k_{10} \approx k_7$. The very large negative temperature dependence for the condensation [5] is expected. Reactions involving a complex rearrangement of the reaction intermediate (see structures **1**, **2**, **3**) require a long lived intermediate (a tight reaction complex). At high temperature the lifetime of the complex is shorter and simpler reactions like back dissociation to $Bz^+ + BzCl$ and hydride transfer [7] will dominate.

Can. J. Chem. Downloaded from www.nrcresearchpress.com by 210.87.254.42 on 09/06/12
For personal use only.

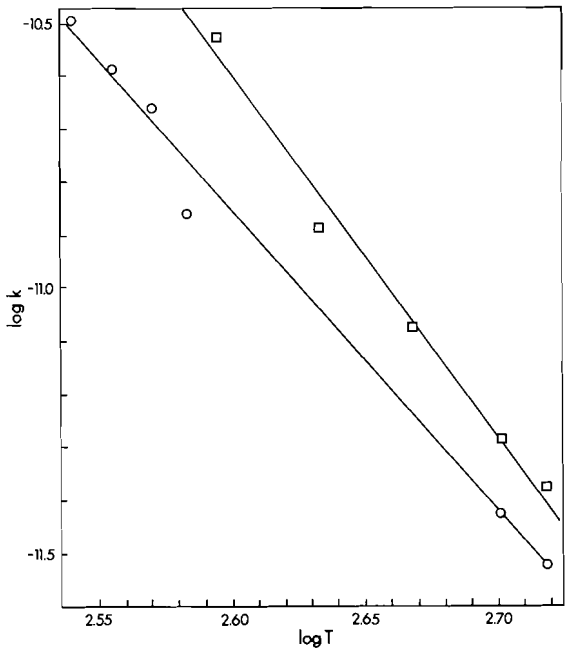

FIG. 7. Plots of log k versus log T for rate constants of reactions [7] and [10]; ○ k_7, □ k_{10}.

Meot-Ner *et al.* [12, 13] found that hydride abstraction can increase up to the Langevin collision rate as the temperature is lowered. Evidently this cannot be the case for the systems studied here, where symmetric chloride transfer and the condensation [5] are fast reactions that dominate over the hydride transfer [7] at low temperature.

A number of chloride transfer equilibria involving $C_7H_7^+$ produced by chloride abstraction from BzCl were observed and measured (X = *o*, *m*, *p*-F, o, *m*, *p*-Cl, *o*, *m*, *p*-Me). The thermodynamic data obtained from these measurements will be described elsewhere (8). The point of interest in connection with the present discussion is that ions produced by chloride abstraction from substituted benzyl chlorides like *p*-Me, which led to more stable cations, were able to shift the equilibrium [11] completely to the right i.e. to the almost complete disappearance of the $C_7H_7^+$ ion. In contrast to this, as will be shown in the next section, $C_7H_7^+$ produced by hydride abstraction from 1,3,5-cycloheptatriene did not abstract chloride from any of the substituted benzyl chlorides, i.e. had a lower chloride affinity than any of the substituted benzyl ions.

[11] $C_6H_5CH_2^+ + XC_6H_4CH_2Cl = C_6H_5CH_2Cl + XC_6H_4CH_2^+$

Reactions of the benzyl cation with toluene observed at two temperatures are shown in Figs. 8 and 9. The reaction mixture of 4 Torr CH_4 and 10 mTorr isobutane produces, after a few micro-

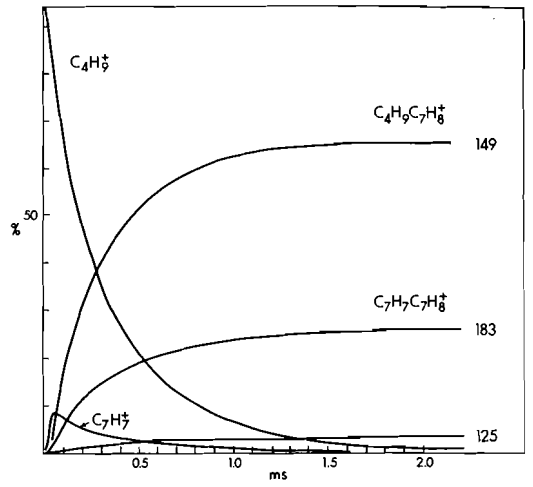

FIG. 8. Reactions of the benzyl cation with toluene. 31°C, (4 Torr CH_4, 10 mTorr isobutane, 0.1 mTorr BzCl, 0.1 mTorr toluene). $Bz^+(C_7H_7^+)$, produced via chloride abstraction by $C_4H_9^+$ from BzCl, forms adduct m = 183 with toluene. Adduct is thermally stable at this temperature.

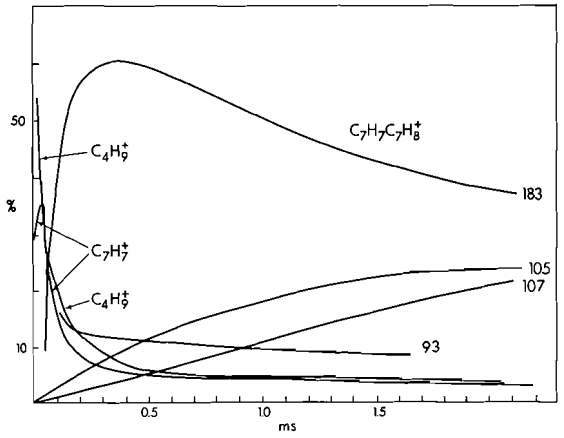

FIG. 9. Reactions of the benzyl cation with toluene. 168°C (4 Torr CH_4, 10 mTorr isobutane, 1 mTorr BzCl, 1 mTorr toluene). The adduct formed from Bz^+ and toluene, m = 183, is thermally unstable at this temperature and decomposes to m = 105, $CH_3C_6H_4CH_2^+$.

seconds, $C_4H_9^+$ as the only ion. In the presence of small amounts of toluene and benzyl chloride, (each at 0.1 mTorr, see Fig. 8), $C_4H_9^+$ produces $C_7H_7^+$. Most of the $C_7H_7^+$ is due to the fast chloride abstraction from BzCl; a smaller amount should result from the slow hydride abstraction from toluene. A side reaction is the addition of $C_4H_9^+$ to toluene, i.e. reaction [12]. The addition of Bz^+ to

[12] $C_4H_9^+ + \text{toluene} =$ 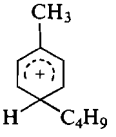 (m = 149)

Can. J. Chem. Downloaded from www.nrcresearchpress.com by 210.87.254.42 on 09/06/12
For personal use only.

[13] Bz^+ + toluene = 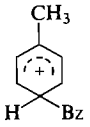 (m = 183)

[14] 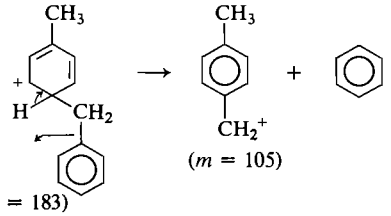
(m = 183) (m = 105)

toluene is also observed. The rate constant for the addition reaction k_{13} obtained from data in Fig. 8 is given in Table 1.

The concentration changes in Fig. 9 show what happens at higher temperature. Since all reactions are slower, 10 times higher concentrations of toluene and BzCl were used. The higher yield of the addition product of Bz^+ to toluene (m = 183) can be explained by the virtual absence of the addition product of Bu^+ to toluene (m = 149). The Bu^+ addition product must be unstable at this temperature, i.e. it back-dissociates to Bu^+ and toluene. Thus, at this higher temperature more Bu^+ is available to produce more Bz^+ by [1]. It is interesting to note that at the higher temperature, the adduct of Bz^+ and toluene (m = 183) also dissociates, but slowly, to give an ion m = 105, (see Fig. 9). The mechanism for this reaction, [14], was suggested by Dunbar and co-workers (5). Reactions [13] and [14] are the same as [2] and [3] observed by earlier workers (3–5, 10). Dunbar and co-workers observed, with their ICR mass spectrometer, only the ion m = 105 and not the adduct precursor m = 183. At the very low total pressures used in the ICR instrument ($p \approx 10^{-5}$ Torr) collisional stabilization of the excited adduct m = 183 is slow, therefore, even at room temperature, the adduct undergoes back dissociation or dissociation to the xylyl cation, m = 105.

From several runs like those in Figs. 8 and 9, performed in the temperature range 30–180°C, the temperature dependence of k_{14} could be determined. In the evaluation of k_{14} it was assumed that the xylyl cation m = 105 reacts further to give m = 107. This reaction is indicated in Fig. 9 (and more clearly in other runs which are not shown) by the different shapes of the concentration curves of m = 105 and 107 at short and long reaction times. An Arrhenius plot of k_{14} gave a good straight line which defined k_{14} as shown in eq. [15].

[15] $k_{14} = A \exp -E_{14}/RT$

E_{14} = 32.5 kcal/mol, $A_{14} = 5.9 \times 10^{18}$ s^{-1}

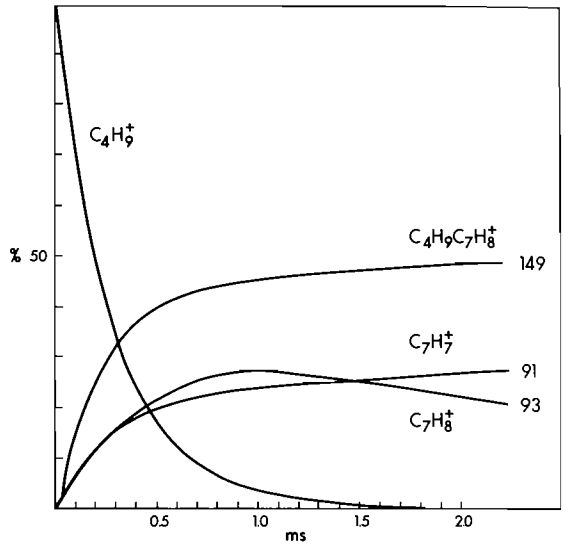

FIG. 10. Production and reactivity of the tropylium cation. 179°C (4 Torr isobutane, 0.4 mTorr 1,3,5-cycloheptatriene) $C_7H_7^+$ ion produced via hydride abstraction by t-$C_4H_9^+$ from the heptatriene, cannot be Bz^+ since Bz^+ cannot exist in 4 Torr isobutane. The $C_7H_7^+$ present has a very low hydride affinity and can be only the tropylium cation.

We have assumed k_{14} is first order. We worked at constant total pressure of 4 Torr. Probably [14] is second order due to third body requirement for activation at low pressures.

(c) Reactions of the Tropylium Cation

Tropylium was produced from 1,3,5-cycloheptatriene. Concentration changes with time of one such experiment are shown in Fig. 10. The final ion in pure isobutane is t-Bu^+. In the presence of small quantities of the heptatriene, t-Bu^+ engages in three reactions: addition, protonation, and hydride abstraction. Reactions [16] and [17] are alkylation

[16] t-$C_4H_9^+$(57) + c-heptatriene (92) = $C_4H_9 \cdot C_7H_8^+$(149)

[17] t-$C_4H_9^+$(57) + c-heptatriene (92) = $C_7H_9^+$(93) + iso-C_4H_8

[18] t-$C_4H_9^+$(57) + c-heptatriene (92) = $C_7H_7^+$(91) + iso-C_4H_{10}

[19] $C_7H_9^+$ + c-heptatriene = $C_7H_7^+$(91) + C_7H_{10}

and protonation at a double bond of the heptatriene. The resulting structure is probably **4**, where X

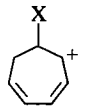

4

is t-Bu or H respectively. The rate constant k_{16} was measured in the temperature range 423–473 K. It was found to have a small negative temperature dependence, see Table 1. The rate constant for the protonation and hydride abstraction reactions [17]

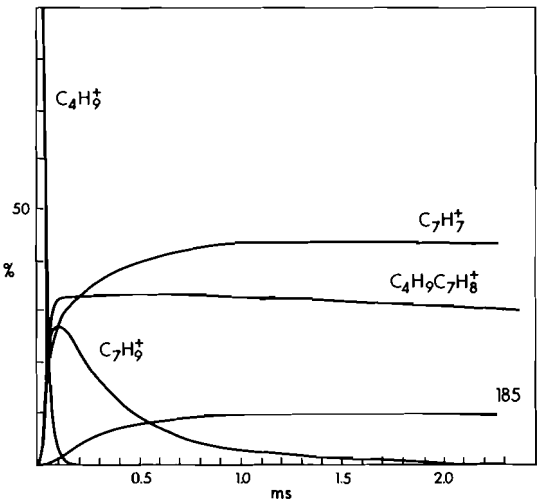

FIG. 11. Production and reactivity of the tropylium cation, 179°C (4 Torr isobutane, 5 mTorr 1,3,5-cycloheptatriene). The higher concentration of heptatriene used in this run makes reaction [19] more clearly visible. Protonated cycloheptatriene, $m = 93$, hydride abstracts from cycloheptatriene to yield tropylium $m = 91$. Almost 100% tropylium can be obtained with same concentrations of neutrals at higher reaction temperatures.

and [18] were found to be very similar, see Fig. 10. At 179°C, $k_{17} \approx k_{18} = 10^{-10}$ cm^3 molecules^{-1} s^{-1}. The rate for hydride transfer reactions is generally lower than the Langevin collision rate. On the other hand, protonation, when exothermic, generally proceeds at near collision rate. The relatively low value of the protonation rate constant k_{17} suggests that this reaction is slightly endothermic, i.e. PA(*c*-heptatriene) < PA(isobutene). 1,3-Pentadiene has a proton affinity which is some 5 kcal/mol higher than that of isobutene (14). One would expect the proton affinity of the straight chain 1,3,5-heptatriene to be even higher. However, 1,3,5-cycloheptatriene is a highly strained molecule. Molecular models show that protonation to structure **4** does not cause significant removal of strain. The ion remains twisted and π conjugation is highly hindered. This indicates a low proton affinity and makes PA(*c*, 1,3,5-cycloheptatriene) < PA(isobutene), rather likely.

The protonated *c*-heptatriene reacts with *c*-heptatriene to give more $C_7H_7^+$ (tropylium), see eq. [19]. This reaction is clearly indicated in Fig. 11, which gives results for a run at the same temperature as Fig. 10 but at 20 times higher concentration of heptatriene. The hydride abstraction [19] is considerably slower than the hydride abstraction by *t*-Bu$^+$ [18]. Thus, at 179°C, $k_{18} \approx 10^{-10}$ cm^3 molecules^{-1} s^{-1}, while $k_{19} \approx 2.5 \times 10^{-11}$ cm^3 molecules^{-1} s^{-1}. The operation of reactions [18] and [19] results in high yields of $C_7H_7^+$ (tropylium) as is evident from Fig. 11. Even higher yields are obtained at higher temperatures because of the negative temperature dependence of the addition reaction [16] and an observed thermal decomposition of the addition product $C_4H_9 \cdot C_7H_8^+$.

The fact that $C_7H_7^+$ produced from *c*-heptatriene can exist in pure isobutane at 4 Torr pressure is a direct proof that this species is very different from the $C_7H_7^+$(benzyl$^+$) obtained from benzyl chloride or toluene. The enthalpy change $\Delta H_4 = -0.8$ kcal/mol obtained in section (a) taken together with the heats of formation: ΔH_f(*t*-BuCl) = −43.7, ΔH_f(BzCl) = 4.5 and ΔH_f(iso-C_4H_{10}) = −32.4, ΔH_f(toluene) = 11.99 (all in kcal/mol) (15) leads to $\Delta H_{20} = 3.8$ kcal/mol. This result shows that benzyl could not have been observed under the conditions of the experiments in Figs. 10 and 11. The presence of isobutane at vast excess (4 Torr) would have converted all Bz$^+$ to *t*-Bu$^+$ by the reverse of [20].

[20] t-$C_4H_9^+ + C_6H_5CH_3 =$ iso-$C_4H_{10} + C_7H_7^+$(benzyl)

[21] t-$C_4H_9^+ +$ 1,3,5-*c*-heptatriene = iso-$C_4H_{10} + C_7H_7^+$(tropylium)

[22] $C_7H_7^+$(benzyl) + 1,3,5-*c*-heptatriene = $C_6H_5CH_3 + C_7H_7^+$(tropylium)

The $C_7H_7^+$ observed in these runs is a species which is much more stable than Bz$^+$, i.e. it must be tropylium. The concentrations observed in Fig. 10 permit one to set an upper limit to $\Delta G^0_{21} \approx \Delta H^0_{21}$. Taking $C_7H_7^+ = 28\%$ and $C_4H_9^+ = 0.1\%$ one obtains $\Delta G^0_{21} < -13.4$ kcal/mol. Lias and coworkers (10) have estimated that the heat of formation of tropylium$^+$ is 9 kcal/mol lower than that of benzyl$^+$. Using this value, ΔH_f(1,3,5-cycloheptatriene) = 43.9 kcal/mol and $\Delta H_{20} = 3.8$ kcal/mol, one evaluates $\Delta H_{21} = -37.1$ kcal/mol. The $\Delta G^0_{21} < -13.4$ kcal/ mol from the present experiments is consistent with the thermochemical ΔH_{21}, but it is obvious that a reactant with much lower hydride affinity than *t*-butyl$^+$ will be required if one is to achieve a hydride transfer equilibrium with tropylium.

The enthalpy change $\Delta H_{22} = -40.9$ kcal/mol calculated with the Lias (10) estimate for ΔH_f tropylium$^+$ predicts a hydride affinity of tropylium some 41 kcal/mol lower than that of benzyl. This vast difference is due to 9 kcal/mol difference in the heats of formation of benzyl$^+$ and tropylium$^+$ and 32 kcal/mol difference in the heats of formation of the heptatriene and toluene. The very low hydride affinity of the tropylium cation is thus not so much a result of the greater stability of tropylium$^+$ versus Bz$^+$, but the much lower stability of the very strained cycloheptatriene as compared to that of toluene.

Can. J. Chem. Downloaded from www.nrcresearchpress.com by 210.87.254.42 on 09/06/12
For personal use only.

Can. J. Chem. Downloaded from www.nrcresearchpress.com by 210.87.254.42 on 09/06/12
For personal use only.

Several experiments were made in which the reactivity of the $C_7H_7^+$(tropylium) produced by hydride abstraction from cycloheptatriene was tested. These experiments showed that the tropylium ion is completely unreactive, i.e. does not engage in any of the reactions observed with Bz^+. Thus the chloride transfer equilibria [4] in the presence of heptatriene shifted completely to $C_7H_7^+$ as final cation. The $C_7H_7^+$ was tropylium produced by hydride abstraction. Substituted benzyl cations like p-CH_3-benzyl, which are more stable than unsubstituted Bz^+, were also found to completely disappear in the presence of the heptatriene and produce the tropylium cation. The tropylium cation was found not to hydride abstract from various substituted benzyl chlorides, i.e. did not engage in reactions analogous to [7]. The tropylium cation did not add to benzyl chloride or toluene, i.e. it did not undergo reactions analogous to [5] and [13] + [14]. Addition of water vapor to benzyl produced ions of mass corresponding to protonated benzyl alcohol and higher hydrates $Bz(OH_2)_n^+$. No such hydrates were observed with tropylium under the same conditions.

The experiments in the present and preceding section show that the benzyl and tropylium cations preserve their distinctive characteristics at temperatures up to 300°C. There are no rearrangements from benzyl to tropylium and vice versa. Even extremely exothermic reactions like the chloride abstraction by ethyl from benzyl chloride (exothermicity ~83 kcal/mol) in which a considerable fraction of the exothermicity may be expected to be present as excitation energy in the newly created Bz^+, do not cause the conversion from benzyl to tropylium. Similarly the highly exothermic hydride abstraction by t-Bu^+ from cycloheptatriene (exothermicity ~42 kcal/mol) produces only tropylium.

The present findings support earlier conclusions in the literature. Tropylium must be created by electron impact on toluene, it cannot have resulted from a rearrangement of benzyl$^+$ to tropylium$^+$ (1, 2, 5). The unreactive $C_7H_7^+$ ion created by electron impact from toluene must be tropylium$^+$, (5, 10). It is the benzyl cation produced by electron impact from toluene that engages in the reactions [12] and [13] with toluene, (5, 10).

It is interesting to note that no rearrangements of tropylium$^+$ to Bz^+ and vice versa seem to have been reported in the voluminous organic literature (16) dealing with the reactions of the benzyl and tropylium cations in condensed media. The present work shows that there is also no rearrangement in the gas phase. One qualification may be added. In the present work only electronic ground state benzyl and tropylium cations were involved. Therefore, the present results do not preclude rearrangements of benzyl$^+$ to tropylium$^+$ and vice versa for electronically excited species or ground state species with extremely large internal excitation, i.e. excitation sufficient to lead to fragmentation of these ions.

1. P. N. Rylander, S. Meyerson, and H. M. Grubb. J. Am. Chem. Soc. **79**, 842 (1957); S. Meyerson and P. N. Rylander. J. Chem. Phys. **27**, 901 (1957).
2. J. Winkler and F. W. McLafferty. J. Am. Chem. Soc. **95**, 7533 (1973); F. W. McLafferty and J. Winkler. J. Am. Chem. Soc. **96**, 5182 (1974).
3. A. Giardini-Guidoni and Z. Zocchi. Trans. Faraday Soc. **64**, 2342 (1968).
4. S. Wexler and R. P. Clow. J. Am. Chem. Soc. **90**, 3940 (1968).
5. J. Shen, R. C. Dunbar, and G. A. Olah. J. Am. Chem. Soc. **96**, 6227 (1974); E. W. Fu, P. P. Dymerski, and R. C. Dunbar. J. Am. Chem. Soc. **98**, 337 (1976).
6. F. P. Lossing. Can. J. Chem. **49**, 361 (1971).
7. J. L. M. Abboud, W. J. Hehre, and R. W. Taft. J. Am. Chem. Soc. **98**, 6072 (1976).
8. D. K. Sen Sharma and P. Kebarle. 28th Ann. Conference on Mass Spectrometry, New York, 1980. To be published.
9. A. J. Cunningham, J. D. Payzant, and P. Kebarle. J. Am. Chem. Soc. **94**, 7627 (1972).
10. J. A. Jackson, S. G. Lias, and P. Ausloos. J. Am. Chem. Soc. **99**, 7521 (1977).
11. J. J. Solomon, M. Meot-Ner, and F. H. Field. J. Am. Chem. Soc. **96**, 3727 (1974).
12. M. Meot-Ner and F. H. Field. J. Chem. Phys. **64**, 277 (1976).
13. M. Mautner. *In* Gas phase ion chemistry. *Edited by* M. T. Bowers. Academic Press, New York. 1979.
14. D. H. Aue and M. T. Bowers. *In* Gas phase ion chemistry. Vol. 2. *Edited by* M. T. Bowers. Academic Press, New York. 1979. p. 32.
15. J. D. Cox and G. Pilcher. Thermochemistry of organic and organometallic compounds. Academic Press, New York, NY. 1970.
16. K. M. Harmon. *In* Carbonium ions. Vol. IV. *Edited by* G. A. Olah and P. v. R. Schleyer. Wiley Interscience, New York. 1973.

A study of aqueous sodium cholate by ^2H nmr

WILLIAM B. SMITH AND GARETH D. BARNARD
Texas Christian University, Fort Worth, TX 76129, U.S.A.
Received November 17, 1980

WILLIAM B. SMITH and GARETH D. BARNARD. Can. J. Chem. **59**, 1602 (1981).

Solutions of aqueous sodium 7-^2H-cholate have been studied as a function of cholate concentration by ^2H nmr. Relaxation times and solution viscosities have been used to show that cholate is monomeric in solution at 0.1 *M*. Increasing concentration leads to tetramer formation which is complete at 0.1 *M*. The tetramer solutions are stable up to 55°C. Solutions of cholate in aqueous pyridine also form tetramers in the same fashion. Evidence was found, however, for a weak hydrogen bonding interaction between the two.

WILLIAM B. SMITH et GARETH D. BARNARD. Can. J. Chem. **59**, 1602 (1981).

Des solutions aqueuses du sel sodique de l'acide cholique-7-^2H ont été étudiés par rmn du ^2H en fonction de la concentration en cholate. Des mesures de temps de relaxation et de viscosité démontrent que le sel est monomère en solution centimolaire. Un accroissement de la concentration entraîne la formation d'un tetramère et celle-ci s'avère complète à une concentration de 0.1 *M*. Ces solutions de tetramère sont stables jusqu'à 55°C. En solution aqueuse de pyridine, il se forme également des tetramères. Nous observons cependant une faible interaction cholate–pyridine par liaison hydrogène.

Because of their complex biological function the solution properties of the bile acids and their salts continue as a subject of considerable interest (1–5). Recently, it was demonstrated that chloroform solutions of noninteractive steroids such as cholesteryl chloride and cholesteryl acetate are well behaved in the sense that their ^{13}C spin lattice relaxation time (T_1's) follow the viscosity relation of the simple Stokes–Einstein–Debye approach (4). In contrast, the methyl esters of a series of bile acids showed a more complex behavior attributable to hydrogen bond formation between the molecules. Furthermore, this interaction varied with the number of available hydroxyl groups and their steric environments in a rational fashion.

It has been known for years that sodium cholate and sodium deoxycholate form micelles in aqueous media. Small *et al.* (1, 2) have combined data from light scattering, ultracentrifugation, and proton nmr to provide a model in which sodium cholate forms a dimeric primary micelle at the critical micelle concentration (cmc). These dimers were postulated to have their hydrophobic β-sides inward and their hydroxyl-bearing α-sides outward in the polar medium. Such a model is, of course, quite different from that required to explain the behavior of the bile acid esters referred to above.

Recently, Oakenfull and Fisher (5) reported on the conductivity of aqueous sodium cholate and deoxycholate. They noted for both cases a sharp break in the curve of equivalent conductance versus the square root of the concentration about the cmc (ca. 0.01 *M* bile salt). They conclude that premicellar aggregation is occurring. At the cmc higher aggregates (tetramers) are formed. While a hydrophobic interaction between dimers might be possible, they propose that these higher aggregates are formed by polyfunctional hydrogen bonding since there is a negative volume of micelle formation at the cmc.

Because of these two divergent models which have been used to describe the aggregation of bile salts in aqueous media, we felt it worthwhile to extend our previous nmr relaxation measurements to these systems. Because both the proton and ^{13}C nmr spectra of solutions of sodium cholate are poorly resolved and suffer from low signal to noise ratios, ^2H nmr was used on singly labeled sodium cholate. The use of deuterium for such studies offers the advantage that the relaxation times are determined solely by the quadrupolar mechanism. Previously, Fung and Peden (3) had determined ^2H relaxation times for solutions of specifically deuterated sodium deoxycholate over the range of 0.12–0.17 *M*. They concluded that within this range the deoxycholate is a tetramer.

As an adjunct to the above study, we have also carried out studies in dilute solutions of aqueous pyridine. Earlier, Liebfritz and Roberts (6) had shown by ^{13}C nmr that methylnaphthalene undergoes some sort of restrictive interaction when solubilized within a sodium deoxycholate micelle. Pyridine is capable of both hydrophilic and hydrophobic interactions with the bile salt micelle. Furthermore, the molecular motions of perdeuteropyridine have been previously studied (7).

Experimental

Cholic acid (mp 195–196°C) and perdeuteropyridine were from Steraloids and Aldrich respectively. Sodium cholate was

0008-4042/81/111602-05$01.00/0
©1981 National Research Council of Canada/Conseil national de recherches du Canada

Can. J. Chem. Downloaded from www.nrcresearchpress.com by 210.87.254.105 on 09/06/12
For personal use only.

Can. J. Chem. Downloaded from www.nrcresearchpress.com by 210.87.254.105 on 09/06/12
For personal use only.

from ICN Pharmaceuticals. Since the ^{13}C nmr spectra of the steroids indicated no impurities, they were used directly.

Cholic acid was partially oxidized to the 7-ketoacid by the method of Hoehn and Linsk (8). The crude reaction product was then reduced as the potassium salt with sodium deuteroborohydride (Ventron). The crude 7-^2H-acid was recovered and crystallized from methanol, mp 194–195°C, mixture melting point with starting acid was undepressed. The borohydride reduction of the 7-ketocholanic acid to the 7-α-hydroxyacid is known to proceed in 75% yield with no isolable amount of the 7-β-hydroxyacid (9). The ^{13}C nmr of the reaction product was that of pure cholic acid except that the intensity of the C-7 line at 68 ppm was greatly reduced. Sodium cholate was prepared by careful titration with standard sodium hydroxide and evaporation to dryness.

Viscosities were measured in a standard Ostwald viscometer at the appropriate temperature with flow times in excess of 100 s so that no correction for kinetic energy was required.

All nmr measurements were made at 9.19 MHz on a JEOL FX-60 instrument using 8K transforms. Pyridine relaxation times (T_1's) were determined by the standard inversion-recovery technique with a pulse repetition time in excess of $5 \times T_1$. The 90° pulse on this instrument was 400 μs. The standard auto-T_1 program was used. The T_1's for neat perdeuteropyridine at 23°C were 0.72, 0.79, and 0.74 s respectively for the α-, β-, and γ-positions. These are in good agreement with the values of 1.14, 1.17, and 1.20 s determined at 30°C by Kintzinger and Lehn (7). The ^{13}C T_1 values for neat pyridine were determined three times giving an average value of 17.1 ± 0.7 s for the combined data of the three carbon types (10). The ^{13}C and ^2H relaxation times can be compared by the equation

$$[1] \quad \frac{T_1(^{13}C)}{T_1(^2H)} = \frac{3\pi^2\chi_D^2 r^6}{2N\hbar^2\gamma_C^2\gamma_H^2}$$

where χ_D is the nuclear quadrupole coupling constant, r is the C—H bond length, N is the number of hydrogens attached to the carbon, and γ_C and γ_H are the magnetogyric ratios for ^{13}C and ^1H respectively (11). The value of χ_D for pyridine of Kintzinger and Lehn (193 KHz) was used (7). The average C—H bond length for pyridine is 1.08 Å (12). On this basis, the calculated ^2H-T_1 value for neat pyridine is 0.70 s in good agreement with the experimental values.

The FX-60 does not have sufficiently short pulse interval times to allow determination of the short T_1 values found for aqueous sodium cholate (below 0.01 s for the most part). Consequently, the width of the ^2H-line at half height was used to get a T_2 value. A correction for magnetic field inhomogeneity was made where appropriate using the natural line width of perdeuteroacetone which was routinely found to be 1.5 Hz. The assumption was made that for the small aggregates found here the motional narrowing condition was fulfilled, i.e. $T_2 = T_1$. While this method of determining T_1's is less desirable than the standard pulse method, line widths here were 50–200 Hz and reproducible to ±10%, i.e., about the same as the inversion-recovery method. Furthermore, the above was checked as follows. Four inversion-recovery ^{13}C determinations were carried out on a 0.2 M solution of sodium cholate at 30°C giving a value of 0.063 ± 0.01 s for the monoprotonated carbons. The appropriate ^2H value was then calculated from the equation above. The C—H bond length of the C-7 hydrogen was taken as 1.05 Å from the value of the hydroxyl-bearing carbons in myo-inositol (13). The values of χ_D used were 165 KHz (CH_3OH) and 170 KHz (cyclohexane) (14). This range leads to calculated values of 4.0 to 4.2 ms in excellent agreement with the line width determined ^2H-T_2 for a comparable solution of sodium 7-^2H-cholate of 4.0 ms.

Results and Discussion

Small (1) has surveyed the various literature values for the critical micelle concentration (cmc) of aqueous sodium cholate. It would be best to say that the value falls in the range of 0.01 to 0.02 M since different experimental techniques have provided different values. Equilibrium ultracentrifugation data were interpreted as indicating a dimer as the first formed micelle (1*a*). As the concentration increases dimer formation persists until at some unspecified point "secondary" micelle formation sets in with the formation of tetramers and higher aggregates. Ekwall *et al.* (15) proposed the association process to be divided into three concentration regions for each bile salt, i.e., monomer, primary micelle, and secondary micelles. The previously mentioned structure for the cholate dimer derives primarily from observation of line width changes in the proton nmr of cholate solutions (2). It was reported that the methyl absorptions widen with increasing concentration as does the methylene envelope. Unfortunately, no consideration was given to viscosity effects on these spectra or to the variety of inter- and intramolecular phenomena which can influence proton relaxation times.

In contrast, deuterium relaxation times are determined primarily by nuclear quadrupole interactions (16). When combined with the Stokes–Einstein approximation and Debye theory (17) the relaxation time may be written as:

$$[2] \quad \frac{1}{T_1} = \frac{3(\pi^2)(\chi_D^2)\tilde{V}_m}{2RT}\eta$$

where $\tilde{V}_m$ is the apparent molar volume of interest and η is the viscosity in poise. Strictly speaking, eq. [2] applies only to a spherical molecule, and η is a rotational microviscosity. However, it has been established that these approximations are valid for noninteracting steroids (4), and that ^2H nmr can be used to demonstrate that the deoxycholate ion is a monomer in methanol but a tetramer in water (3). The use of an experimental translational viscosity for η seems warranted on the basis that steroid tumbling must always move a substantial number of solvent molecules out of the way. It is likely that more linear hydrogen bonded complexes do not follow the form of [2].

The ^2H-T_2's for sodium 7-^2H-cholate in water and in dilute pyridine solutions are given in Table 1. Viscosities for the solutions in water and in 0.14 M pyridine are shown in a semi-log plot in Fig. 1. The viscosity data for the 0.07 M and 0.28 M pyridine systems were indistinguishable from those plotted.

Low molecular weight aggregates should fall in

Can. J. Chem. Downloaded from www.nrcresearchpress.com by 210.87.254.105 on 09/06/12
For personal use only.

the region of motional narrowing, i.e. $1/T_1 = 1/T_2$ and eq. [2] above should apply for T_2. The justification for this assumption applied to solutions of sodium cholate is given in the Experimental. In Fig. 2, plots are given of $1/T_2$ vs. viscosity for aqueous sodium cholate at 23°C and 55°C and for sodium cholate in dilute pyridine solutions at 23°C. These plots are characteristic of all the data in Table 1. In each case, the plot is linear over the range of 0.01 to 0.10 *M* cholate. The value of T_2 decreases rapidly over the range, while viscosity increases only slightly. Beyond a viscosity of ca. 1.0 (approximately 0.1 *M*) the plot shows a change of slope as though some aspect of structure of the system had been subject to a discontinuity in the 0.10 to 0.12 *M* region of cholate concentration. Above this point the plot appears to be more curvilinear. Unfortunately, the conductivity data of Oakenfull and Fischer (5) did not extend to this concentration.

Application of eq. [2] to the data for 0.01 *M* cholate at 23°C gives an experimental molar volume of 464 mL. A density determination of 0.1 *M* sodium cholate gives an apparent molar volume of 363 mL in good agreement with the published value (5). Small (1) has published the value of 325 mL for the "anhydrous" molar volume. Thus, one concludes that at 0.01 *M* sodium cholate at 23°C the bile salt is essentially a mixture of monomers and dimers in approximately equal amounts. Due to limits of instrument sensitivity it is impracticable to make determinations below 0.01 *M* sodium cholate so we can not confirm the break observed in the conductivity curve in this region.

In Fig. 2*a* at 0.11 *M*, the calculated molar volume is 1.3×10^3 mL corresponding to an aggregation number of 4 using Small's molar volume. It appears that the discontinuity occurs at that concentration where tetramer formation is complete. The linear behavior of the $1/T_2$ vs. viscosity plot from 0.01 to 0.10 *M* cholate rationally results from the fact that over this region there is very little change in the viscosity. Consequently, the experimental value of $1/T_2$ can be shown to be a linear function of the corresponding terms for the monomer, dimer, and

TABLE 1. ^{2}H-Relaxation times for sodium 7-^{2}H-cholate in water and in dilute pyridine solutions at 23°C[a]

	[Pyridine]				
[Sodium cholate]	None	None[c]	0.07	0.14	0.28
0.010	12.3	—	12.6	12.3	12.6
0.025	8.7	—	8.8	6.9	5.9
0.050	4.7	14.7	4.9	7.4	5.2
0.075	—	9.8	4.9	4.3	3.7
0.10	3.7	8.3	3.3	4.0	3.7
0.20	2.9	—	2.6	3.9	3.2
0.30	2.3	4.9	2.5	2.8	2.7
0.40	1.5[b]	4.6	2.2	2.9	2.0
0.50	—	—	1.4	1.9	1.4
0.60	1.2	2.9	1.2	1.3	1.3

[a] T_2's in ms.
[b] Determined for 0.45 *M* cholate.
[c] Taken at 55°C.

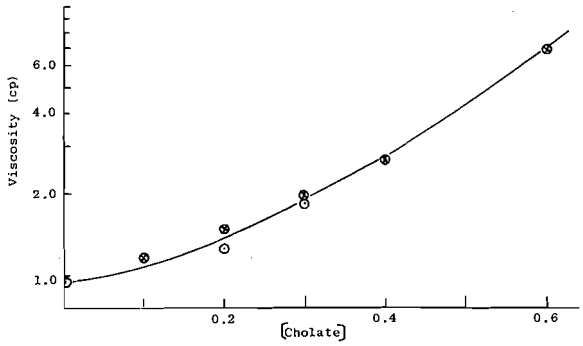

FIG. 1. The viscosity of sodium cholate solutions in water (dots) and in 0.14 *M* pyridine (×).

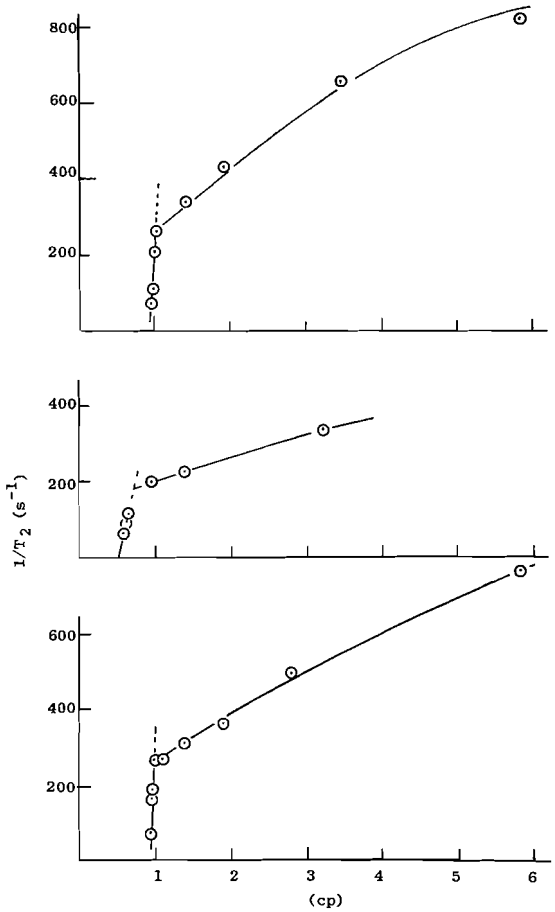

FIG. 2. Plots of $1/T_2$ versus solution viscosity for various sodium cholate solutions; upper at 23°C in water; middle at 55°C in water; and lower in 0.28 *M* pyridine at 23°C.

Can. J. Chem. Downloaded from www.nrcresearchpress.com by 210.87.254.105 on 09/06/12
For personal use only.

tetramer. Beyond 0.11 *M* cholate the viscosity changes rapidly, and the linear relationship breaks down.

Small *et al.* (2) found the line widths of the proton nmr spectra of sodium cholate solutions to be decreased on raising the temperature. This was interpreted as implying a dissociative process which became complete above 70°C. Unfortunately, these data are hard to interpret. No viscosity measurements were made, and so decreasing line widths could be due entirely to viscosity effects. Furthermore, the methylene envelope is a forest of lines caused by the many different proton chemical shifts and the strong spin–spin couplings between many of these nuclei. Conclusions based on the width of the methylene envelope are fraught with difficulty.

The ^{2}H-T_2 for a 0.10 *M* sodium 7-^{2}H-cholate solution was determined at several temperatures up to 55°C. The viscosities of these solutions were also determined. The data are given in Fig. 3 in the form of semi-log plots of $1/T_2$ and of η respectively against $1/T$. Over this range of temperatures linear behavior is observed as expected for a simple first order process. There is a slight divergence of slopes as can be seen. However, the calculated molar volume of the cholate micelle at 55°C is 93% of that at 23°C, so dissociation has not yet become very significant at that temperature.

Finally, it had been our expectation that the presence of pyridine would alter the pattern of cholate micelle formation. The data in Table 1 and in Figs. 1 and 2 do not support that expectation. In Fig. 4 are plotted the $1/T_1$ vs. viscosity data for the α-^{2}H of perdeuteropyridine (0.14 *M*) with increasing concentrations of cholate. The interpretation of the ^{2}H-T_1's for pyridine are made complex by the fact that the molecule possesses a significant rotation in the molecular plane negating the application

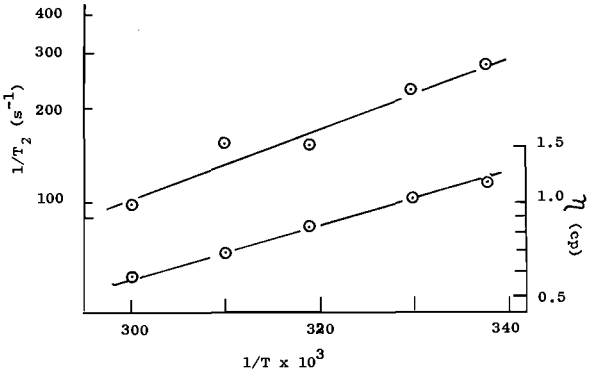

FIG. 3. The relation of $1/T_2$ (upper) and of log viscosity respectively to the reciprocal of the Kelvin temperature for 0.10 *M* sodium cholate.

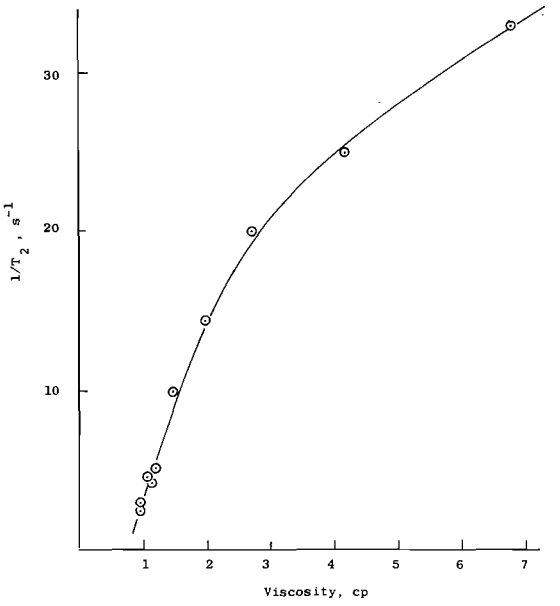

FIG. 4. The change in $1/T_2$ for perdeuteropyridine (0.14 *M*) at 23°C in varying concentrations of sodium cholate.

of eq. [2] (7). However, if the pyridine were to be rigidly bound to the micelle both would have the same correlation time for rotation. Such is not the case here.

Yet there is a bit of evidence for a cholate–pyridine interaction. In keeping with the absence of a preferred rotational axis, the ^{2}H-T_1's for neat pyridine are the same at all positions. In aqueous 0.14 *M* pyridine the ratio of $T_{1\alpha}/T_{1\gamma}$ is 1.35. The introduction of hydrogen bonding to water produces a preferred rotation axis about the C_γ—N axis. Upon addition of 0.01 *M* cholate this ratio increases to 1.46, and with 0.025 *M* cholate is found to be 1.50. Beyond this point the γ-^{2}H resonance becomes too broad to measure and merges with the β-^{2}H line. These results suggest that some hydrogen bonding of the pyridine to the cholate occurs, but reasonably this might be on the outer surface of the micelle.

Acknowledgements

We wish to express here our appreciation to the Robert A. Welch Foundation and to the Texas Christian University Research Foundation for support of this work.

1. (*a*) D. M. SMALL. Adv. Chem. Ser. **84**, 31 (1968); (*b*) D. M. SMALL. The bile acids. Vol. 1. *Edited by* P. Nair. Plenum Press, New York. 1972. p. 249.
2. D. M. SMALL, S. A. PENKETT, and D. CHAPMAN. Biochem. Biophys. Acta, 176 (1969); 178 (1969).
3. B. M. FUNG and M. C. PEDEN. Biochem. Biophys. Acta, 273 (1976); 437 (1976).

4. (*a*) W. B. SMITH. J. Phys. Chem. **82**, 234 (1978); (*b*) Annual reports of nmr spectroscopy. Vol. 8. *Edited by* G. A. Webb. Academic Press, London. 1979. p. 199.
5. D. G. OAKENFULL and L. R. FISCHER. J. Phys. Chem. **81**, 1838 (1977).
6. D. LIEBFRITZ and J. D. ROBERTS. J. Am. Chem. Soc. **95**, 4996 (1973).
7. J. P. KINTZINGER and J. M. LEHN. Mol. Phys. **22**, 273 (1971).
8. W. M. HOEHN and J. LINSK. J. Am. Chem. Soc. **67**, 312 (1945).
9. E. H. MOSBACH, W. MEYER, and F. E. KENDALL. J. Am. Chem. Soc. **76**, 5799 (1954).
10. G. C. LEVY, J. D. CARGIOLI, and F. A. ANET. J. Am. Chem. Soc. **95**, 1527 (1973).
11. H. SAITO, H. H. MANTSCH, and I. C. P. SMITH. J. Am. Chem. Soc. **95**, 8453 (1973).
12. B. BAK, H. HANSEN-NYGAARD, and J. RASTRUP-ANDERSON. J. Mol. Spectrosc. **2**, 361 (1958).
13. I. N. RABINOWITZ and J. KRAUT. J. Acta Crystallogr. **17**, 159 (1964).
14. J. C. ROWELL, W. D. PHILLIPS, L. R. MELBY, and M. PANAR. J. Chem. Phys. **43**, 3442 (1965).
15. P. EKWALL, K. FONTELL, and A. STEN. Proceedings of the second international congress of surface activity. Butterworths, Washington, DC. 1957. p. 357.
16. A. ABRAGAM. The principles of nuclear magnetism. Oxford Press, London. 1961.
17. N. BLOEMBERGAN, E. M. PURCELL, and R. V. POUND. Phys. Rev. **73**, 679 (1948).

Can. J. Chem. Downloaded from www.nrcresearchpress.com by 210.87.254.105 on 09/06/12
For personal use only.

Quantum yield of solution photolysis of bicyclo[3.1.0]hexan-3-one and derivatives[1]

KARL R. KOPECKY AND RODRIGO RICO GOMEZ[2]
Department of Chemistry, University of Alberta, Edmonton, Alta., Canada T6G 2G2
Received November 21, 1980

KARL R. KOPECKY and RODRIGO RICO GOMEZ. Can. J. Chem. **59**, 1607 (1981).

The quantum yields for photolysis of 0.25 *M* solutions of bicyclo[3.1.0]hexan-3-one, 1,5-dimethylbicyclo[3.1.0]hexan-3-one, and tricyclo[4.3.1.0]decan-8-one in pentane or cyclohexane with 313 nm light are 0.44, 0.52, and 0.32, respectively.

KARL R. KOPECKY et RODRIGO RICO GOMEZ. Can. J. Chem. **59**, 1607 (1981).

Les rendements quantiques de la photolyse à 313 nm de la bicyclo[3.1.0]hexanone-3, de la diméthyl-1,5 bicyclo[3.1.0]hexanone-3 et de la tricyclo[4.3.1.0]décanone-8 en solution à 0,25 *M* dans le pentane ou le cyclohexane sont respectivement de 0,44, 0,55 et 0,32.

[Traduit par le journal]

Introduction

The yield of excited cyclopentanone formed from 3,3:4,4-dibutano-1,2-dioxetane, **1**, as measured by the amount of 4-pentenal formed, eq. [1],

[1] 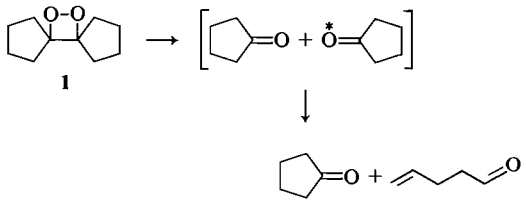

1

is subject to considerable uncertainty because the ratio of cyclopentanone to 4-pentenal is quite large (1). This is because of a small yield of excited cyclopentanone and a moderate quantum yield for photolysis of cyclopentanone to 4-pentenal, Φ = 0.27 (1), so that a small error in the absolute yield of 4-pentenal results in a large error in the calculated yield of excited cyclopentanone. Use of a 1,2-dioxetane which would produce a ketone that photolyzed with a much higher quantum yield might provide more accurate results.

It was felt that bicyclo[3.1.0]hexan-3-one, **2**, might undergo photodecomposition in solution with a higher quantum yield than does cyclopentanone. In the gas phase both cyclopentanone (2) and **2** (3) are destroyed with high quantum efficiencies, Φ = 0.69 and 0.77, respectively, independent of pressure. However, the product distribution from cyclopentanone is affected considerably by pressure while that from **2** is not. A change from the gas phase to solution should affect the photolysis of cyclopentanone more than that of **2**.

[1]This research was supported by the Natural Sciences and Engineering Research Council of Canada.

[2]Present address: Departamento de Quimica Organica, Facultad de Ciencias, Universidad de Malaga, Malaga, Spain.

The solution photolysis of **2** and of several derivatives has been studied (4) but the quantum yields have not been determined. In the present work the quantum yields for photolysis in solution of **2** and of its 1,5-butano and 1,5-dimethyl derivatives, **3** and **4**, respectively, have been determined.

Results

The ketones **2** (3) and **3** (4*a*) were prepared as described and **4** was prepared from 3,4-dimethyl-2-cyclopentenone (6) by the sequence shown in Scheme 1.

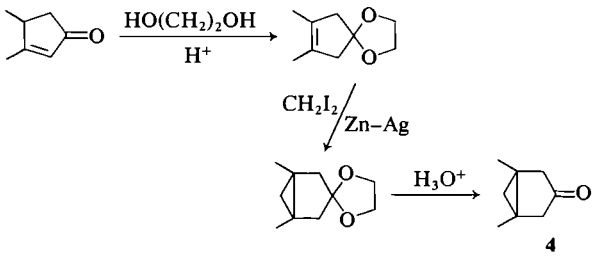

SCHEME 1

Degassed solutions containing about 0.25 *M* ketone were irradiated with 313 nm light from a medium pressure mercury arc. From each ketone only the one product indicated, eqs. [2], [3], and

[2] 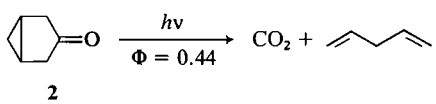

2

[3] 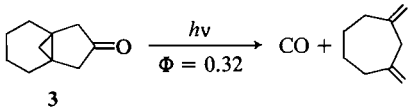

3

[4] 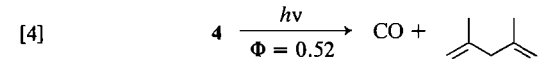

0008-4042/81/111607-03$01.00/0
©1981 National Research Council of Canada/Conseil national de recherches du Canada

Can. J. Chem. Downloaded from www.nrcresearchpress.com by 210.87.254.40 on 09/06/12
For personal use only.

Can. J. Chem. Downloaded from www.nrcresearchpress.com by 210.87.254.40 on 09/06/12
For personal use only.

[4], could be detected by gc, in agreement with the report that the photolysis of **3** in solution produced 1,3-dimethylenecycloheptane in 100% yield (4*a*). Cyclopentanone, 0.26 *M* in pentane, was irradiated in parallel with the other ketones to about 5% conversion and served as the actinometer. The quantum yield of 4-pentenal formation was taken as 0.27 (1). Quantum yields for formation of the dienes from the other ketones are given in the equations.

Discussion

In the gas phase, photolysis of **2** produces 1,4-pentadiene, vinylcyclopropane, and 1,3-butadiene in about a 7:1:0.2 ratio (3). The latter two products were not found in solution. Similarly, ethylene and cyclobutane, which are major products of the photolysis of cyclopentanone in the gas phase (2) are formed only in trace amounts in solution (5). As well, the quantum yield for photolysis of these two ketones is smaller in solution. The excess vibrational energy of the intermediates is quenched much more quickly in solution than in the gas phase.

The quantum yields for solution photolysis of **2**, **3**, and **4** vary from a value nearly double that of cyclopentanone to one only slightly greater. The results may be rationalized if the assumption is made that the amount of α-cleavage (7), Scheme 2, is nearly the same for **2**, **3**, and **4**. The quantum yield for α-cleavage is not known but is likely greater than that for diene formation. The only information on this point is that there is epimerization of the isomeric thujones during photolysis (4*b*). Cyclization of the diradical **6** would give back starting ketone **2** and opening of the cyclopropane ring would produce the secondary diradical **7**. The latter process would be retarded by the butano bridge of the corresponding diradical from **3** and favored by the relief of strain between the two methyl groups of the corresponding diradical from **4**. The trend in quantum yields is consistent with the predicted effects of the substituents. There would be little or no effect of substituents if the initial diradical **6** lost CO to give the diradical **8** more rapidly than ring opening to **7** occurred. Intramolecular hydrogen atom transfer to give **9** does not take place at all on solution photolysis of **2**, although the corresponding process occurs with moderate efficiency on photolysis of cyclopentanone.

Although the quantum yields for photolysis of **2**, **3**, and **4** are greater than that for cyclopentanone, the improvement is not large enough to make these ketones significantly better than cyclopentanone for measurement of excited state yields from 1,2-dioxetanes.

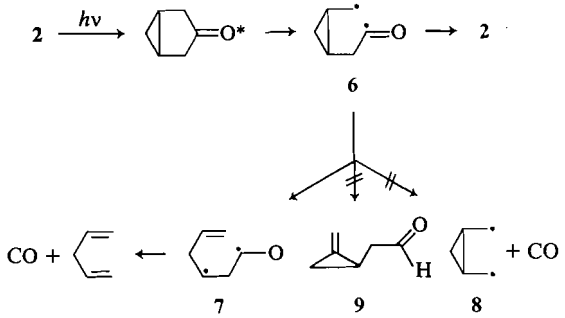

SCHEME 2

Experimental

Boiling points are uncorrected. Nuclear magnetic resonances were recorded on Varian A56-60A and Bruker WH200 spectrometers in carbon tetrachloride with tetramethylsilane as internal standard. Gas chromatographic analyses were carried out on an Aerograph A-90-P3 gas chromatograph using a 5 ft × ¼ in. column of FFAP on 60/80 Chromosorb W at 70°C to analyze reaction mixtures from photolysis of cyclopentanone and of **3**, and a 10 ft × ¼ in. column of 23% dimethylsulfolane on 60/80 Chromosorb P at 48°C to analyze reaction mixtures from photolysis of **2** and **4**. Solutions were dried with magnesium sulfate. Microanalyses were performed by Mrs. Darlene Mahlow and staff.

Compounds **2** (3),[3] **3**(4*a*), 1,4-pentadiene (8),[3] and 4-pentenal (9) were prepared according to literature directions; 1,3-dimethylenecycloheptane was prepared by photolysis (4*a*) of **3**; 2,4-dimethyl-1,4-pentadiene was obtained from K and K Chemicals. Reagent grade cyclopentanone was distilled just prior to use.

3,4-Dimethyl-3-cyclopentenespiro-(2',5'-dioxacyclopentane)

A mixture of 3,4-dimethyl-2-cyclopentenone (6) (7.5 g), 1,2-ethanediol (100 g), benzene (200 mL), and toluenesulfonic acid (0.15 g) was heated under reflux for 30 h in a round-bottomed flask fitted with a Soxhlet thimble which contained calcium carbide (10). The reaction mixture was cooled and some sodium hydroxide pellets and aqueous sodium bicarbonate were added. The organic layer was shaken twice with water, dried, and the solvent removed to leave a dark brown oil which was distilled at 15 Torr through a short-path still to give 4 g of a colorless oil, bp 108–140°C, which was shown to consist of a mixture of acetal and starting ketone. The mixture was separated by flash chromatography (11) through a 5 × 15 cm column of silica gel, Merck No. 9385, using 85:15 ether–pentane as eluent. The product was purified by bulb-to-bulb distillation at 710 Torr, 180°C pot temperature to give 1.9 g (20%) of a colorless oil; ^{1}H nmr τ: 8.34 (t, J = 1 Hz, 6H), 7.48 (q, J = 1 Hz, 4H), 6.06 (s, 4H). *Anal.* calcd. for $C_9H_{14}O_2$: C 70.09, H 9.15; found: C 70.23, H 9.12.

3,4-Dimethylbicyclo[3.1.0^{3,4}]hexanespiro(2',5'-dioxacyclopentane)

The above olefinic acetal, 1.18 g, was converted to the cyclopropyl derivative with 8.4 g diiodomethane using the zinc–silver couple method (12) to give 1.89 g (95%) of a colorless oil which had a moderate carbonyl absorption in the infrared spectrum. This product was purified by flash chromatography (10) on a 5 × 30 cm column of silica gel using 75:25 ether–pentane as eluent to give 1.5 g product which was isolated by bulb-to-bulb distillation at 15 Torr and 80°C (pot); ^{1}H nmr τ: 6.18

[3]We thank Mr. A. Miller for these preparations.

(d, J = 3 Hz, 2H), 6.22 (d, J = 3 Hz, 2H), 8.04 (s, 4H), 8.88 (s, 6H), 9.11 (m, 1H), 9.98 (m, 1H). *Anal.* calcd. for $C_{10}H_{16}O_2$: C 71.42, H 9.52; found: C 70.79, H 9.76.

1,5-Dimethylbicyclo[3.1.0]hexan-3-one **4**

A stirred mixture of 3 g silica gel (28–200 mesh) in 5 mL dichloromethane was treated with 0.4 mL of 10% aqueous oxalic acid (13), then 0.8 g of the above acetal was added and the resulting mixture was stirred for 20 h, after which hydrolysis was complete. The mixture was filtered, solvent removed from the filtrate, and the residual oil was distilled from bulb to bulb at 710 Torr and 180°C (pot) to give 0.5 g product. The ^{1}H nmr τ: 7.65 (m, 4H), 8.75 (s, 6H), 9.58 (H_{6exo}, m, 1H), 9.73 (H_{6endo}, d, J = 5 Hz, 1H). *Anal.* calcd. for $C_8H_{12}O$: C 77.37, H 9.66; found: C 76.62, H 9.66.

Quantum Yields

Degassed pentane solutions 0.25 M in **3** and **4** and degassed cyclohexane solutions 0.25 M in **2** were irradiated in parallel with degassed pentane solutions 0.26 M in cyclopentanone, which served as the actinometer, at 22°C on a merry-go-round apparatus (14) with a 200 W medium pressure Hanovia lamp and a potassium chromate filter to isolate the 313 nm line. Pyrex tubes were used and the irradiations were carried out to no more than 4% decomposition of cyclopentanone. The amounts of photolysis products were determined by gc using solutions of known concentrations of these materials to make calibration charts. The quantum yield of 4-pentenal was taken to be 0.27 (1).

1. K. R. Kopecky and J. A. Lopez Sastre. Can. J. Chem. **58**, 2089 (1980).
2. (*a*) R. Srinivasan. J. Am. Chem. Soc. **83**, 4344 (1961); (*b*) J. Am. Chem. Soc. **83**, 4348 (1961).
3. L. D. Hess and J. N. Pitts, Jr. J. Am. Chem. Soc. **89**, 1973 (1967).
4. (*a*) E. J. Starr and R. H. Eastman. J. Org. Chem. **31**, 1393 (1966); (*b*) G. D. Lyon. Ph.D. Thesis, University of Oregon (1975).
5. P. Dunion and D. N. Trumbore. J. Am. Chem. Soc. **87**, 4211 (1965).
6. J. M. Conia and M. L. Leriverend. Bull. Soc. Chim. Fr. 2981 (1970).
7. F. E. Blacet and A. Miller. J. Am. Chem. Soc. **79**, 4327 (1957); (*b*) B. Rickborn, R. L. Alumbaugh, and G. O. Pritchard. Chem. Ind. London, 1951 (1964); (*c*) R. L. Alumbaugh and G. O. Pritchard. J. Phys. Chem. **69**, 3225 (1965); (*d*) H. M. Frey. Chem. Ind. London, 947 (1966); (*e*) C. C. Badcock, M. J. Perona, G. O. Pritchard, and B. Rickborn. J. Am. Chem. Soc. **91**, 543 (1969).
8. R. E. Benson and B. C. McKusick. *In* Org. Synth. Coll. Vol. 4. *Edited by* N. Rabjohn. John Wiley and Sons, Inc., New York. 1963. p. 746.
9. L. K. Montgomery and J. W. Matt. J. Am. Chem. Soc. **89**, 6556 (1967).
10. E. J. Corey and H. Uda. J. Am. Chem. Soc. **85**, 1788 (1965).
11. W. C. Still, M. Kahn, and A. Mitra. J. Org. Chem. **43**, 2923 (1978).
12. J. M. Denis, C. Girard, and J. M. Conia. Synthesis, 549 (1972).
13. F. Huet, A. Lechevallier, M. Pellet, and J. M. Conia. Synthesis, 63 (1978).
14. S. Murov. Handbook of Photochemistry. Marcell Dekker, New York. 1973. pp. 132–128.

Can. J. Chem. Downloaded from www.nrcresearchpress.com by 210.87.254.40 on 09/06/12
For personal use only.

Nickel(III)–tris(di-imine) complexes: a series of strong one-electron oxidants

J. C. BRODOVITCH, R. I. HAINES, AND A. MCAULEY[1]

Department of Chemistry, University of Victoria, P.O. Box 1700, Victoria, B.C., Canada V8W 2Y2

Received November 14, 1980

J. C. BRODOVITCH, R. I. HAINES, and A. MCAULEY. Can. J. Chem. **59**, 1610 (1981).

The complexes $[Ni(III)(LL)_3](ClO_4)_3$ (LL = phen, bipy, and substituted derivatives) have been isolated as products of the electrolysis in acetonitrile of the corresponding nickel(II) species. Electron spin resonance measurements for all nickel(III) species in frozen anhydrous CH_3CN and in frozen 4.0 *M* $HClO_4$ solutions (77 K) show a single near symmetric line shape ($g \approx 2.10$) with fine structures appearing only in the presence of mixed solvent systems. In a CH_3CN/5% H_2O glass (77 K) quintets in the $g_{||}$ and $g_{\perp}$ regions are observed ($g_{||} \approx 2.03$, $A_{||} \approx 22$ G; $g_{\perp} \approx 2.135$, $A_{\perp} \approx 16$ G) consistent with Jahn–Teller distortion expected for a low-spin d^7 system. Ultraviolet–visible spectra are also reported. Electrode potentials for the $Ni(LL)_3^{3+/2+}$ couples in CH_3CN (0.1 *M* $NaClO_4$) lie in the range 1.51 V ($Ni(4,4'\text{-}Me_2bipy)_3^{3+}$) to 1.82 V ($Ni(5\text{-}NO_2\text{-}phen)_3^{3+}$) and the powerful oxidizing nature of these species has been confirmed in reaction with both organic and inorganic substrates.

J. C. BRODOVITCH, R. I. HAINES et A. MCAULEY. Can. J. Chem. **59**, 1610 (1981).

On a isolé les complexes de $[Ni(III)(LL)_3]$ $(ClO)_4)_3$ (LL = phen, bipy et des dérivés substitués) comme produits de l'électrolyse des espèces correspondantes du nickel(II) dans l'acétonitrile. Les spectres de rpe de toutes ces espèces du nickel(III) dans du CH_3CN anhydre solide et dans des solutions solides de $HClO_4$ 4,0 *M* (77 K) se présentent tous sous la forme d'une raie unique presque symétrique ($g \approx 2{,}10$) sur laquelle se superpose une structure fine uniquement en présence de systèmes de solvants mixtes. Dans du CH_3CN/5% H_2O (77 K), on observe des quintuplets dans les régions $g_{||}$ et $g_{\perp}$ ($g_{||} \approx 2{,}03$, $A_{||} \approx 22\,G$; $g_{\perp} \approx 2{,}135$ $A_{\perp} \sim 16\,G$) qui sont en accord avec la distorsion de Jahn–Teller attendue pour un système de faible spin d^7. On rapporte également les spectres uv–visible. Les potentiels d'électrode du couple $Ni(LL)_3^{3+/2+}$ dans le CH_3CN (0,1 *M* $NaClO_4$) varient de 1,51 V pour ($Ni(Me_2bipy\text{-}4,4')_3^{3+}$) à 1,82 V pour ($Ni(NO_2\text{-}phen\text{-}5)_3^{3+}$) et la réaction de ces produits avec des substrats organiques et inorganiques confirme la nature fortement oxydante de ces espèces.

[Traduit par le journal]

There has been considerable recent interest in the characterization and reactions of nickel(III) complexes. In many instances (1–4), tetraazamacrocyclic ligands have been used to stabilize this higher oxidation state of the metal and although considerable stability is shown in acetonitrile (5), only when the macrocycle is saturated are these species stable with respect to intramolecular reduction in aqueous media (2, 4, 6–8). A feature of many of these studies has been the interpretation of esr spectra (1, 9) where, owing to the localization of the unpaired electron in the d_z^2 orbital of these low spin d^7 complexes, differing g values are observed for the $g_{||}$ and $g_{\perp}$ parameters. In this paper we wish to report the results of studies on nickel(III)–di-imine complexes which in some cases, although relatively easily prepared in acetonitrile, exhibit very powerful oxidizing capabilities. The complex ion $Ni(bipy)_3^{3+}$ has been prepared electrolytically in strongly acidic aqueous media (10, 11) and results of oxidations of H_2O_2 (10), Br^- (10), and N_3^- (11) have been published. The complexes were not, however, isolated as solids. In the present study, the results of esr, uv–visible, and cyclic voltammetric investigations on these systems are presented.

[1]Author to whom correspondence may be addressed.

Experimental

Reagent grade acetonitrile was refluxed for 24 h over calcium hydride and copper(II) chloride, then distilled onto molecular sieves prior to use. Tetraethylammonium perchlorate (G. F. Smith) and silver nitrate (Englehardt) were used as received.

Nickel(II) complexes were prepared as their perchlorate salts by addition of 3.5 equivalents of ligand to 1 equivalent of nickel(II) perchlorate in methanol. The precipitated products were washed copiously with methanol and ether and dried *in vacuo*. Abbreviations used in this paper are: phen = 1,10-phenanthroline; bipy = 2,2'-bipyridyl; (5-Me phen), (4,4'-Me_2-phen), (5-Cl-phen), and (5-NO_2-phen) refer to the substituents in the ring positions noted. The corresponding nickel(III) complex perchlorates were prepared by electrolysis of an acetonitrile solution of the nickel(II) precursor (ca. 0.1 g/50 mL) containing 0.1 *M* tetraethylammonium perchlorate as supporting electrolyte. The procedure was carried out in the dark at 5°C overnight at a constant potential of 15 V using Pt wire electrodes. Products were isolated by slow evaporation of solvent at 5°C. The dark-green crystalline solids were filtered, washed with a little cold acetonitrile, and dried *in vacuo*. All products were found to be quite stable in the solid state in the dark, except the chloro and nitro substituted ligand complexes which reverted to the nickel(II) state generally within 24 h. In some instances dilute solutions of the nickel(III) complexes were prepared in acetonitrile containing 0.1 *M* $NaClO_4$. Electron spin resonance spectra derived from this source showed no differences from those prepared similarly from solid samples.

Electrode potentials and cyclic voltammograms were measured using a Princeton Applied Research polarographic analyser model 174. Studies were made using 10^{-4} *M* solutions of the nickel(II) complex in CH_3CN containing 0.1 *M* $NaClO_4$. The three-compartment cell was constructed with two medium

0008-4042/81/111610-05$01.00/0

©1981 National Research Council of Canada/Conseil national de recherches du Canada

Can. J. Chem. Downloaded from www.nrcresearchpress.com by 210.87.254.42 on 09/06/12
For personal use only.

TABLE 1. Electron spin resonance parameters for $Ni(LL)_3^{3+}$ complexes, $T = 77$ K

LL	$g_{\|}$ (± 0.001)	$A_{\|}$ (G)[a]	$g_{\perp}$ (± 0.001)	$A_{\perp}$ (G)[b]	g_{iso}[c]
bipy	2.027	22.2	2.137	15	2.102[d]
4,4'-diMebipy	2.026	23.0	2.133	15	2.098
phen	2.027	23.2	2.136	16	2.106
5-Me-phen	2.027	22.5	2.137	18	2.107
5-Cl-phen	2.027	22.0	2.137	17	2.107
5-NO_2-phen	2.030	22.3	2.135	16	2.107

[a](±0.3 G)
[b](±1 G)
[c]Unresolved spectra, measured in anhydrous CH_3CN.
[d]A value of 2.095 ± 0.002 is observed in $HClO_4/H_2O$, $T = 77$ K (ref. 11).

porosity glass scinters separating the anode and cathode assemblies. The centre section was filled with a solution of 0.1 *M* $NaClO_4$ in acetonitrile. In this way any diffusion was reduced to a minimum. The working electrode was a Pt sphere, with a Pt-wire counter electrode. An agar bridge (containing $NaClO_4$) led to an aqueous solution (0.1 *M* $NaClO_4$) into which the reference electrode (calomel/saturated NaCl) was introduced. A constant stream of dry N_2 gas was passed through the reacting solution. All solutions were prepared in the cell in a dry box prior to measurements being made.

Electron spin resonance spectra of the series of nickel(III) complexes were measured in frozen acetonitrile solutions at 77 K, using a Varian E6 spectrometer; *g* values were determined from spectra using a scan range of 400 G and DPPH ($g = 2.0037$) was used as an internal reference standard. As observed previously (12), better resolution of esr spectra may be obtained with frozen samples of mixed solvent solutions. Results presented include those obtained from binary mixtures of 4 *M* $HClO_4$/5–10% CH_3CN or acetone, or CH_3CN/5–10% H_2O or acetone.

Ultraviolet–visible spectra were measured using either a Cary 17 or Beckman DU8 spectrometer. Extinction coefficients were determined using solutions prepared from solid samples or by electrolytic oxidation of a solution of the corresponding nickel(II) complex. Nickel(III) concentrations were derived by potentiometric titration with either hydroquinone (CH_3CN medium) or ferrous ammonium sulphate (4.0 *M* $HClO_4$).

Results and Discussion

The unequivocal existence of nickel(III) complexes rather than nickel(II)–radical systems has been confirmed in many instances using esr data (1, 4, 9, 11). For a low spin d^7 tetragonally distorted octahedral ion values of $g_{\|} \sim 2.00$ and $g_{\perp} \sim 2.2$ are consistent with the axially symmetric systems (13). Also, the unpaired electron has been shown to occupy principally the d_z^2 orbital as evidenced by the observed superhyperfine splitting of the $g_{\|}$ feature, owing to interaction of the electron with the axially bound ligands (e.g. in $Ni(cyclam)Cl_2^+$, the septet observed centred at $g_{\|} \sim 2.027$ is attributed to this effect) (4, 14). Table 1 shows the data for the nickel(III) di-imine complexes and in Fig. 1 the spectrum of the $Ni(bipy)_3^{3+}$ complex ion is presented, being typical of all such data for these complexes. If the electron were delocalized into

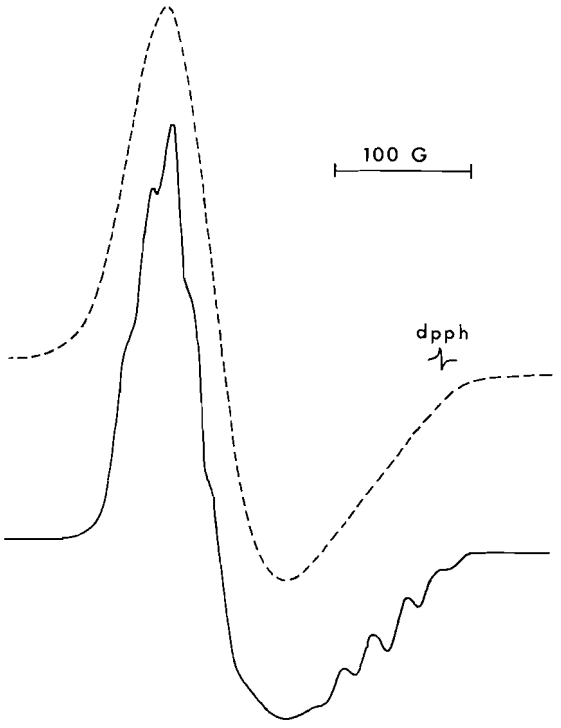

FIG. 1. Electron spin resonance spectra of frozen solutions at 77 K; $Ni(bipy)_3(ClO_4)_3$ --- in CH_3CN (0.1 *M* $NaClO_4$), — binary mixture CH_3CN/5% H_2O.

the bipyridyl ligand systems in what may be written formally as a (Ni(II)–LL$^{\cdot}$) radical complex ion, a *g* value very close to 2.00 would be expected (15, 16) for the (principally *C* centred) paramagnetic species. Frozen solutions at 77 K using only one solvent system (either CH_3CN or 2–4 *M* $HClO_4$) yielded only a near symmetric isotropic signal ($g_{iso} \approx 2.10$). This is in agreement with the previous observation of Wells and co-workers (11) using frozen aqueous perchloric acid solutions where partial oxidation to nickel(III) had occurred ($g = 2.095 \pm 0.002$). In the latter study, the possibility of weak features at higher fields indicating *g* aniso-

Can. J. Chem. Downloaded from www.nrcresearchpress.com by 210.87.254.42 on 09/06/12
For personal use only.

Can. J. Chem. Downloaded from www.nrcresearchpress.com by 210.87.254.42 on 09/06/12
For personal use only.

tropy could not be discerned owing to interference from the resonance of the unoxidized Ni(II) present in excess. Greater resolution of the spectra was obtained in all cases using mixed solvent systems (Fig. 1). Quintets in the $g_{\|}$ and $g_{\perp}$ regions are observed with $g_{\|} \approx 2.027$, $A_{\|} \approx 22$ G, $g_{\perp} \approx 2.137$, and $A_{\perp} \approx 15$ G. This is consistent with the assignment of the metal centre as Ni(III) and with a local symmetry of D_{4h} around the nickel as would be expected for a Jahn–Teller distorted low spin d^7 species. Interaction with the two axial nitrogen atoms gives rise to the observed quintets. The use of mixed solvents (H_2O/5–20% propane-diol) has been shown to provide a greatly enhanced spectral resolution in the study of cobalt(II)–corrin complexes (12). In frozen aqueous solutions, variations in the packing of the solute and solvent molecules occur and inhomogeneities in solute concentrations are to be expected. This effect may give rise to a variable microcrystalline environment for each paramagnetic centre and so lead to variation in spin Hamiltonian parameters and broadening of spectral lines. Local high concentrations of paramagnetic species have an adverse influence on spin–relaxation processes. In a glassy solid (solvent/H_2O mixtures), however, a vitreous rather than a polycrystalline medium is obtained on rapid freezing. A more uniform distribution of solute molecules is expected under these conditions, reducing the line broadening by spin–spin relaxation. It is of interest, in comparing the hyperfine coupling constants derived in the present systems with those for other macrocyclic nickel(III) complex ions, that $A_{\|}$ values of similar magnitude (25 ± 3 G) are observed whereas the $A_{\perp}$ coupling (≈ 15 G) in the tris di-imine complexes is greater than that for the saturated tetra-aza 14-membered ring systems (4). (< 5 G).

Electrochemical measurements on Ni(II)/Ni(III) systems have commonly employed acetonitrile as solvent (5), since it permits a wide range of potentials to be covered without decomposition and because the nickel(III) complexes are generally stable for long periods in the anhydrous medium. Results of electrolytic studies are presented in Table 2 where some measurements on the oxidation of iron(II)–di-imine complexes have been included. Whereas the iron(II)/(III) data show reasonable reversibility with peak separations of 60–70 mV, the values for the nickel(III) complexes are higher (Fig. 2). This quasi-reversibility has been shown to be a feature of several studies on nickel(III) systems (9). The most marked feature of these data is the very strongly oxidizing nature of the nickel(III) complexes. In some instances (e.g. the 5-chloro and 5-nitro species) the oxidation peaks were close to the limit possible for study without oxidation of the solvent. Comparison with the iron(III) species shows the nickel complexes to be much more powerful oxidants. This has been observed previously in aqueous media by Wells and co-workers (11). An attempt may be made to estimate the redox potentials of the nickel(III) complexes in aqueous media. Data for three iron(III) complexes, presented in Table 2, include the E^0 values in 1.0 M $HClO_4$ (17). In all cases the $Fe(LL)_3^{3+}$ cations are known to be fairly strongly oxidizing (18) and react via an outer sphere electron transfer mechanism. For the three systems shown, $\Delta E'$ (the differences between the potentials in 1.0

TABLE 2. Electrochemical data on $Ni(LL)_3^{2+/3+}$ complexes (in CH_3CN, I = 0.1 M ($NaClO_4$), T = 25°C)

Complex	E (V)[a]	ΔmV[b]	Scan rate (Vs^{-1})	E^0 (V)[c]
$Fe(phen)_3^{2+}$	0.937	74	0.1	1.06
$Fe(5\text{-Me phen})_3^{2+}$	0.911	77	0.05	1.02
$Fe(bipy)_3^{2+}$	0.918	63	0.05	1.035
$Ni(phen)_3^{2+}$	1.641	104	0.05	(1.73)
$Ni(bipy)_3^{2+}$	1.625	107	0.05	(1.71)
$Ni(4,4'\text{-Me}_2\text{ bipy})_3$	1.507	(208)	0.02	(1.59)
$Ni(5\text{-Cl phen})_3^{2+}$	1.747	98	0.01	(1.83)
$Ni(5\text{-NO}_2\text{ phen})_3^{2+}$	1.820	(170)	0.02	(1.90)
$Ni(5\text{-Me phen})_3^{2+}$	1.609	150	0.01	(1.69)

[a] Determined by cyclic voltammetry at the scan speed shown, $[Ni(II)]_t \sim 4 \times 10^{-4} M$.
[b] Peak to peak separation indicating reaction reversibility.
[c] In 1.0 M $HClO_4$ (ref. 16). Values in parentheses are estimates derived in comparison with $Fe(LL)_3^{2+/3+}$ couples.

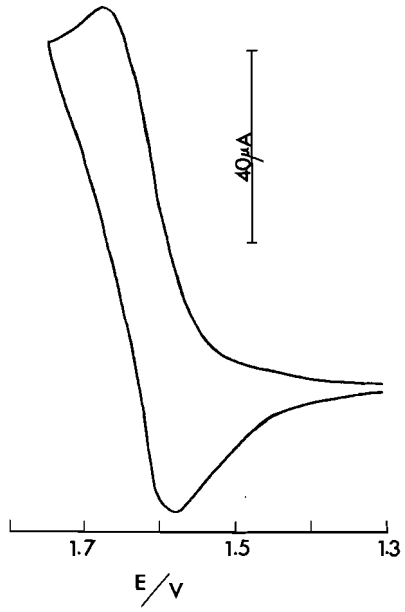

FIG. 2. Platinum sphere cyclic voltammetry of Ni(II)-$(bipy)_3(ClO_4)_2$ in CH_3CN (0.1 M $NaClO_4$), recorded at 20 mV/s using S.C.E./NaCl (satd) reference.

Can. J. Chem. Downloaded from www.nrcresearchpress.com by 210.87.254.42 on 09/06/12
For personal use only.

M $HClO_4$ and CH_3CN (0.1 M $NaClO_4$)) measured with the present reference system are 85 mV, 71 mV, and 85 mV respectively for $Fe(phen)_3^{3+}$, $Fe(5\text{-Me-phen})_3^{3+}$, and $Fe(bipy)_3^{3+}$. Estimates for the $Ni(LL)_3^{3+}$ ions in 1.0 M aqueous acidic media have been made (Table 2) by adding 85 mV to the potential for these species in CH_3CN. The redox potentials are all in excess of 1.59 V and the complexes are among the strongest one-electron oxidants available both in aqueous and nonaqueous media. The value for $Ni(phen)_3^{3+}$ (1.73 V) is almost identical (1.70 V) to that of Ce(IV) in $HClO_4$ (19) and only slightly lower than that (1.84 V) for $Co(III)_{aq}$ (20) in the same medium. The very high values (>1.8 V) for the 5-chloro and 5-nitro complexes may be the reason for the observation that even in the solid state the complexes decomposed readily. The preparation in CH_3CN requires rigorous exclusion of moisture since the potentials are in excess of that necessary to oxidize water.

In general, tervalent nickel complexes have been reported characteristically as dark green (1, 5), unless axially coordinated non-ammine ligands are present (14). Intense absorptions in the range 200–300 nm are also observed for these species (5) and have been assigned to metal–ligand charge transfer. This description may also be applied to the Ni(III) $(LL)_3^{3+}$ complex ions. For example, the $Ni(bipy)_3^{3+}$ ion shows maxima at wavelengths ($\varepsilon >$ 10^4 $M^{-1}cm^{-1}$) at 225 nm, 267 nm, and 292 nm in CH_3CN, associated with the ligand system. In the range λ = 300–450 nm, in both CH_3CN and 4.0 M $HClO_4$, increased absorbance of the Ni(III) complexes over the Ni(II) species was observed. In Fig. 3 the characteristic absorbance of nickel(III) ($Ni(bipy)_3^{3+}$ in CH_3CN is presented with evidence for the weak transition at ~620 nm (ε = 275 ± 25 $M^{-1}cm^{-1}$). The corresponding spectrum of $Ni(bipy)_3^{3+}$ in 4.0 M $HClO_4$ agrees with that of Wells and co-workers (11) in 2 M acid. The measured extinction coefficient at 350 nm, 5300 ± 300 $M^{-1}cm^{-1}$ may be compared with an interpolated value of ~6000 $M^{-1}cm^{-1}$ (ref. 11). A similar value at 350 nm (ε = 6020 ± 300 $M^{-1}cm^{-1}$) is observed in acetonitrile. For $Ni(III)(phen)_3^{3+}$ the high wavelength transition (λ = 620 nm) has been confirmed in 5.0 M $HClO_4$.

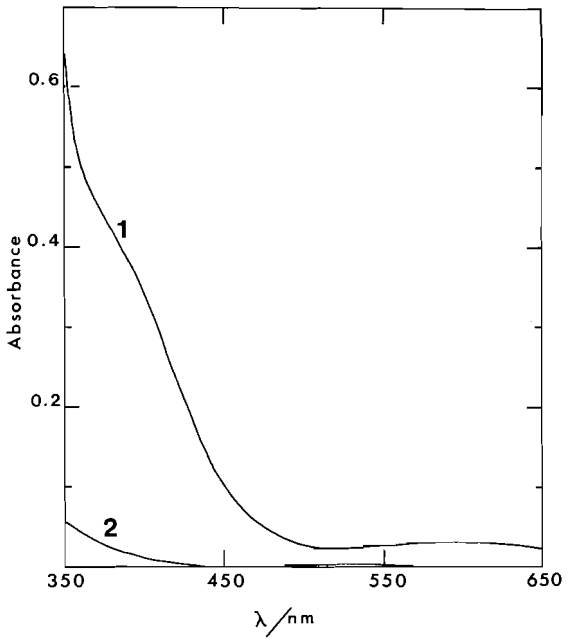

FIG. 3. Ultraviolet–visible spectra of $Ni(bipy)_3^{2+/3+}$ complexes in CH_3CN; (1) 1.2 × 10^{-4} M $Ni(bipy)_3^{3+}$ containing 1 × 10^{-4} M $Ni(bipy)_3^{2+}$, (2) solution (1) reduced to $Ni(II)(bipy)_3^{2+}$.

Previous kinetic measurements were made at 350 nm where interference from Ni(II) is negligible. Solutions of Ni(III) (prepared from the solid form) were reacted against various concentrations of either hydroquinone (H_2Q) or iodide. Spectrophotometric titrations confirmed the reaction stoichiometries:

$$2Ni(LL)_3^{3+} + H_2Q \rightarrow 2Ni(LL)_3^{2-} + Q + 2H^+$$

and

$$2Ni(LL)_3^{3+} + 3I^- \rightarrow 2Ni(LL)_3^{2+} + I_3^-$$

Concentrations of nickel(III) solutions prepared electrolytically were confirmed using such reactions and spectra and extinction coefficients (to ±6%) derived using solutions diluted from these stocks. The increased stability of solutions of these complexes in anhydrous CH_3CN was confirmed by the very small changes in absorbance (<1–2%) over two–three week periods when stored in the dark at 0°C compared with the aqueous media where reduction occurred over a matter of hours.

The outer-sphere nature of the redox reactions of $Ni(bipy)_3^{3+}$ has been demonstrated in aqueous perchloric acid solutions (10, 11), in reactions with H_2O_2, HN_3, and Br^-. Preliminary results of studies with metal ion reductants confirm these observations. The oxidation of $Ni^{II}(cyclam)^{2+}$ (~10^{-4} M) by $Ni(bipy)_3^{3+}$ in 1.5 M $HClO_4$ is too fast for measurement in the stopped-flow system (ΔE^0 ~ 0.75 V), whereas the reaction with Ce^{3+} under the same conditions (ΔE^0 < 0.1 V) is much slower ($t_{\frac{1}{2}}$ ~ 200 s). In the reaction of $Fe(phen)_3^{2+}$ with $Ni(bipy)_3^{3+}$ in 1.0 M H_2SO_4, ($\Delta E^0 \approx$ 0.6 V) the second order rate constant is ~10^5 $M^{-1}s^{-1}$. These redox processes are at present being studied.

In nonaqueous media, a parallel chemistry with a

similar reaction mechanism may be investigated. In these media, oxidation of Cu(I), Tl(I), hydroquinone, and I^- are all observed. Also, the powerful oxidizing nature of the species is confirmed in the transient formation of the radical cation from the polynuclear aromatic perylene (21). Further work on these systems is in progress.

Acknowledgements

We thank Drs. T. Oswald and J. M. Winfield for helpful discussions. Financial support from NATO (Research Grants) and from the Natural Sciences and Engineering Research Council of Canada and the University of Victoria is gratefully acknowledged.

1. E. S. Gore and D. H. Busch. Inorg. Chem. **12**, 1 (1973).
2. E. Zeigerson, G. Ginsburg, N. Schwartz, Z. Luz, and D. Meyerstein. J. Chem. Soc. Chem. Commun. 241 (1979).
3. L. Fabrizzi. J. Chem. Soc. Chem. Commun. 1063 (1979).
4. R. I. Haines and A. McAuley. Inorg. Chem. **19**, 719 (1980).
5. D. C. Olsen and J. Vasilevskis. Inorg. Chem. **8**, 1611 (1969).
6. K. D. Whitburn and G. S. Laurence. J. Chem. Soc. Dalton Trans. 139 (1979).
7. P. Maruthamuthu, L. K. Patterson, and G. Ferraudi. Inorg. Chem. **17**, 3157 (1978).
8. M. Jaacobi, D. Meyerstein, and J. Lilie. Inorg. Chem. **18**, 429 (1979).
9. F. P. Bossu and D. W. Margerum. J. Am. Chem. Soc. **98**, 4003 (1976).
10. C. F. Wells and D. Fox. J. Chem. Soc. Dalton Trans. 1498 (1977); 1502 (1977).
11. J. K. Brown, D. Fox, M. P. Hayward, and C. F. Wells. J. Chem. Soc. Dalton Trans. 735 (1979).
12. S. Cockle, H. A. O. Hill, S. Risdale, and R. J. P. Williams. J. Chem. Soc. Dalton Trans. 297 (1972).
13. A. G. Lappin, C. K. Murray, and D. W. Margerum. Inorg. Chem. **17**, 1630 (1978).
14. A. Desideri, J. B. Raynor, and C. K. Poon. J. Chem. Soc. Dalton Trans. 2051 (1977).
15. A. L. Balch, F. Rohrscheid, and R. H. Holm. J. Am. Chem. Soc. **87**, 2301 (1965).
16. E. I. Steifel, J. H. Waters, E. Billig, and H. B. Gray. J. Am. Chem. Soc. **87**, 3016 (1965).
17. E. Pelizzetti, E. Mentasti, and E. Pramauro. Inorg. Chem. **15**, 2898 (1976).
18. C. O. Adedinsewo and A. Adegite. Inorg. Chem. **18**, 3597 (1979).
19. D. Benson. Mechanisms of oxidation by metal ions. Elsevier, New York. 1976. p. 10.
20. G. Davies and B. Warnqvist. Coord. Chem. Rev. **5**, 349 (1970).
21. P. R. West, A. McAuley, and T. Oswald. To be published.

Can. J. Chem. Downloaded from www.nrcresearchpress.com by 210.87.254.42 on 09/06/12
For personal use only.

An experimental study of the reactivity of the hydroxide anion in the gas phase at room temperature, and its perturbation by hydration

SCOTT D. TANNER, GERVASE I. MACKAY, AND DIETHARD K. BOHME

Department of Chemistry and Centre for Research in Experimental Space Science, York University, Downsview, Ont., Canada M3J 1P3

Received August 11, 1980

SCOTT D. TANNER, GERVASE I. MACKAY, and DIETHARD K. BOHME. Can. J. Chem. **59**, 1615 (1981).

Flowing afterglow measurements are reported which provide rate constants and product identifications at 298 ± 2 K for the gas-phase reactions of OH^- with CH_3OH, C_2H_5OH, CH_3OCH_3, CH_2O, CH_3CHO, CH_3COCH_3, CH_2CO, HCOOH, $HCOOCH_3$, $CH_2{=}C{=}CH_2$, $CH_3{-}C{\equiv}CH$, and $C_6H_5CH_3$. The main channels observed were proton transfer and solvation of the OH^-. Hydration with one molecule of H_2O was observed either to reduce the rate slightly and lead to products which are the hydrated analogues of the "nude" reaction, or to stop the reaction completely, $k \leq 10^{-12}$ cm^3 molecule^{-1} s^{-1}. The reaction of $OH^-{\cdot}H_2O$ with $CH_3{-}C{\equiv}CH$ showed an uncertain intermediate behaviour.

SCOTT D. TANNER, GERVASE I. MACKAY et DIETHARD K. BOHME. Can. J. Chem. **59**, 1615 (1981).

On rapporte des mesures avec la technique de la lueur d'écoulement qui permettent d'obtenir les constantes de vitesse et d'identifier les produits des réactions en phase gazeuse à 298 ± 2 K de l'ion OH^- avec CH_3OH, C_2H_5OH, CH_3OCH_3, CH_2O, CH_3CHO, CH_3COCH_3, CH_2CO, HCOOH, CH_3COOH, $CH_2{=}C{=}CH_2$, $CH_3{-}C{\equiv}CH$ et $C_6H_5CH_3$. Les principales voies observées sont celles du transfert du proton et de la solvatation du OH^-. On a observé que l'hydratation par une molécule d'eau provoque soit l'arrêt complet de la réaction, $k \leq 10^{-12}$ cm^3 molécule^{-1} s^{-1}, soit une légère réduction de la vitesse avec la formation de produits qui sont les analogues hydratés de la réaction "nue". La réaction entre $OH^-{\cdot}H_2O$ et $CH_3{-}C{\equiv}CH$ présente un comportement incertain de l'intermédiaire.

[Traduit par le journal]

Introduction

The hydroxide anion is a relatively strong base in the gas phase where it can be readily generated in a variety of ways. Consequently it is often implicated in the chemical evolution of negative ions in electronegative plasmas such as hydrocarbon flames (1) and planetary ionospheres (2). One important practical consequence of the reactivity and ease of production of OH^- has been its use in negative chemical ionization mass spectrometry (3). While certain qualitative aspects of the gas-phase reactivity of OH^- have been well documented in the literature, only a few quantitative studies have been reported so far. Here we present an extensive flowing afterglow study of the kinetics and mechanisms of reactions of OH^- with a variety of oxygen-containing hydrocarbons, allene, propyne, and toluene. The results complement our earlier flowing afterglow studies of reactions of OH^- with olefins (4, 5), acetylene (6), simple cyanides (7), nitromethane (8), silane (9), and halogenated methanes (10), and therefore serve to extend our understanding of the intrinsic reactivity patterns of this ion. As such they also provide a benchmark for the reactivity of OH^- in solution where its basicity is much depressed as a result of solvation. An attempt is also made in this study to begin to explore the influence of hydration on the intrinsic reactivity of this ion.

Experimental

The measurements were carried out in a conventional flowing plasma mass spectrometer (flowing afterglow) system which has been described previously (11). The OH^- and $OH^-{\cdot}H_2O$ ions were established by introducing water vapor past the electron gun in either a flowing helium or hydrogen plasma. In certain instances, to avoid the presence of water vapor, OH^- was produced by the reaction of O^- with CH_4 with O_2 serving as the source gas for O^-.

The reactant neutrals were added into the reaction region either in their pure form or diluted with helium. The determination of their flows required separate viscosity measurements as has been described (12). The sources of most of the neutral reactants and their purities have also been given previously (13). The allene, propyne, and toluene were of normal research grade. Rate constants were determined in the usual manner from measurements of the $m/e = 17$ and $m/e = 35$ signals as a function of added reactant. The contribution due to $^{35}Cl^-$ was subtracted to arrive at the true $OH^-{\cdot}H_2O$ signal. The magnitude of $^{35}Cl^-$ was derived from the 37 isotope which was monitored concomitantly with product ions. The operating conditions in these experiments encompassed total gas pressures, P, in the range 0.20 to 0.53 Torr, average gas velocities, $\bar{v}$, from 7.3 to 8.0 × 10^3 cm s^{-1}, effective reaction lengths, L, between 45 and 125 cm, and a gas temperature, T, of 298 ± 2 K.

Results and Discussion

The results of the measurements are summarized in Tables 1 and 2. The sources of uncertainty associated with the determination of the rate constants have been described previously (11). Initial measurements of the charge transfer reaction:

[1] $OH^- + NO_2 \rightarrow NO_2^- + OH$

0008-4042/81/111615-07$01.00/0

©1981 National Research Council of Canada/Conseil national de recherches du Canada

Can. J. Chem. Downloaded from www.nrcresearchpress.com by 210.87.254.6 on 09/06/12
For personal use only.

Can. J. Chem. Downloaded from www.nrcresearchpress.com by 210.87.254.6 on 09/06/12
For personal use only.

TABLE 1. Rate constants measured in this study for reactions of the bare hydroxide ion at 298 ± 2 K

Reaction	k^a
$OH^- + NO_2 \rightarrow NO_2^- + OH$	1.1 ± 0.4
$OH^- + CH_3OH \rightarrow CH_3O^- + H_2O$	2.2 ± 0.6
$OH^- + C_2H_5OH \rightarrow C_2H_5O^- + H_2O$	2.7 ± 0.8
$OH^- + CH_3OCH_3 \rightarrow$ products	$\lesssim$ 0.001
$OH^- + CH_2O + He \rightarrow HOCH_2O^- + He$	$(2 \pm 1) \times 10^{-26}$ [b]
$OH^- + CH_3CHO \rightarrow {}^-CH_2CHO + H_2O$	3.1 ± 0.8
$OH^- + CH_3COCH_3 \rightarrow CH_3COCH_2^- + H_2O$	3.7 ± 0.9
$OH^- + CH_2CO \rightarrow {}^-CHCO + H_2O$	2.2 ± 0.5
$OH^- + HCOOH \rightarrow HCO_2^- + H_2O$	2.2 ± 0.7
$\rightarrow OH^-\cdot H_2O + CO$	
$OH^- + HCOOCH_3 \rightarrow HCO_2^- + CH_3OH$	1.9 ± 0.5
$\rightarrow CH_3O^-\cdot H_2O + CO$	
$OH^- + CH_2{=}C{=}CH_2 \rightarrow CH_2{=}C{=}CH^- + H_2O$	1.7 ± 0.4
$OH^- + CH_3{-}C{\equiv}CH \rightarrow {}^-CH_2{-}C{\equiv}CH + H_2O$	1.7 ± 0.3
$\rightarrow CH_3{-}C{\equiv}C^- + H_2O$	
$OH^- + C_6H_5CH_5 \rightarrow C_6H_5CH_2^- + H_2O$	2.6 ± 0.6
$OH^- + C_6H_5CH_2D \rightarrow C_6H_5CHD^- + H_2O$	2.8 ± 0.7
$\rightarrow C_6H_5CH_2^- + HOD$	

[a] The measured rate constant along with the estimated uncertainty in units of 10^{-9} cm^3 molecule^{-1} s^{-1}.
[b] Termolecular rate constant measured at a total pressure of 0.26 Torr.

TABLE 2. Rate constants measured in this study for reactions of the singly-hydrated hydroxide ion at 298 ± 2 K

Reaction	k^a
$OH^-\cdot H_2O + C_2H_5OH \rightarrow C_2H_5O^-\cdot H_2O + H_2O$	2.1 ± 0.5
$OH^-\cdot H_2O + CH_3CHO \rightarrow {}^-CH_2CHO\cdot H_2O + H_2O$	3 ± 1
$OH^-\cdot H_2O + CH_3COCH_3 \rightarrow CH_3COCH_2^-\cdot H_2O + H_2O$	3 ± 1
$OH^-\cdot H_2O + HCOOCH_3 \rightarrow CH_3O^-\cdot 2H_2O + CO$	1.6 ± 0.5
$\rightarrow (HCO_2^-\cdot H_2O + CH_3OH)$	
$OH^-\cdot H_2O + CH_2{=}C{=}CH_2 \rightarrow$ products	$\lesssim$ 0.001
$OH^-\cdot H_2O + CH_3{-}C{\equiv}CH \rightarrow C_2H_3O^- + CH_3OH$	0.058 ± 0.023
$OH^-\cdot H_2O + C_6H_5CH_3 \rightarrow$ products	$\lesssim$ 0.001

[a] The measured rate constant along with the estimated uncertainty in units of 10^{-9} cm^3 molecule^{-1} s^{-1}.

provided a rate constant of $(1.1 \pm 0.4) \times 10^{-9}$ cm^3 molecule^{-1} s^{-1} in exact agreement with the accepted value (14). The following section provides a more detailed account of the observed hydroxide ion chemistry.

CH_3OH, C_2H_5OH, CH_3OCH_3

The reaction with CH_3OH was investigated over a wide range in total gas pressure (0.307 to 0.52 Torr) and effective reaction length (59, 85, and 120 cm). Also the flow of H_2O was varied over a large range from 7.8×10^{16} to 9.3×10^{19} molecules^{-1} s^{-1} in an attempt to drive reaction [2] to equilibrium:

[2] $OH^- + CH_3OH \rightleftharpoons CH_3O^- + H_2O$

Proton transfer was the only observed reaction channel and k_2 was determined to be $(2.2 \pm 0.6) \times 10^{-9}$ cm^3 molecule^{-1} s^{-1}. Significant amounts of reverse reaction, as manifested by curvature in the decay of OH^-, became apparent only at the highest additions of H_2O ($>10^{19}$ molecules s^{-1}) and the long reaction lengths ($L > 85$ cm). However, under these relatively extreme conditions, a variety of competing and secondary reactions came into play as both the OH^- and CH_3O^- were observed to cluster with H_2O (up to $OH^-\cdot 3H_2O$) and CH_3OH (up to $CH_3O^-\cdot CH_3OH$), respectively. Also, the observation of mixed cluster ions of the type $CH_3O^-\cdot nH_2O$ ($n = 1$ to 3) and $CH_3O^-\cdot H_2O\cdot CH_3OH$ was indicative of some interconversion between cluster ions. These complicating reactions apparently prevented the establishment of equilibrium for the unsolvated reaction [2]. The ratio of the rate constants, k_2/k_{-2}, determined from our usual fitting procedure (11) was strongly dependent on the H_2O concentration as were the mass discrimination plots which exhibited strong curvature. Also, the ratio plots were observed to be curved for all additions of CH_3OH. Such a behaviour is expected for a reaction with a large equilibrium constant proceeding in the presence of secondary reactions. Indeed, available thermochemical information indicates a very large value for K_2 of $(2.2 \pm 0.4) \times 10^7$

Can. J. Chem. Downloaded from www.nrcresearchpress.com by 210.87.254.6 on 09/06/12
For personal use only.

(15). Equilibrium did appear to be established between several of the cluster ions as we have recently reported in a study which followed the transition in the relative acidity of water and methanol, viz. the magnitude of K_2, from the completely unsolvated behaviour in the gas phase to that in solution.

The proton-transfer reaction of OH^- with ethanol was also observed to proceed rapidly at room temperature.

[3] $OH^- + C_2H_5OH \rightarrow C_2H_5O^- + H_2O$

with $k_3 = (2.7 \pm 0.8) \times 10^{-9}$ cm^3 molecule^{-1} s^{-1}. Equilibrium could again not be achieved under the available operating conditions. Solvation with one molecule of water reduced the reactivity of the hydroxide ion only slightly. The rate constant for the hydrated proton transfer [4] was

[4] $OH^-\cdot H_2O + C_2H_5OH \rightarrow C_2H_5O^-\cdot H_2O + H_2O$

measured to be $(2.1 \pm 0.5) \times 10^{-9}$ cm^3 molecule^{-1} s^{-1}. The hydrated product ion was readily observed. Formation of "nude" $C_2H_5O^-$ is endothermic since the 25 kcal mol^{-1} of hydration energy for OH^- (16) exceeds the 10 kcal mol^{-1} of exothermicity for reaction [4] (17).

Dimethyl ether failed to react with OH^-, $k < 10^{-12}$ cm^3 molecule^{-1} s^{-1}. The failure to observe proton transfer in this case is a manifestation of the low gas-phase acidity of dimethyl ether.

CH_2O, CH_3CHO, CH_3COCH_3

Formaldehyde was observed to react quite rapidly with OH^-, but not by proton transfer; an ion with mass 47 was produced instead. Apparently an association reaction was taking place but with an unexpectedly large rate. At the total pressure of the measurements (0.56 Torr) the observed OH^- decay was equivalent to a three-body rate constant of $(2 \pm 1) \times 10^{-26}$ cm^6 molecule^{-2} s^{-1}. This value is much larger than those expected for association reactions involving a similar number of atoms in which a "loose" adduct is formed through electrostatic interaction or proton bonding. Therefore it has been taken as a manifestation of the formation of a "tight" adduct through chemical bonding to a tetrahedrally coordinated carbon atom (18):

[5] $OH^- + C{=}O \rightarrow [HO{-}C{-}O^-]^* \xrightarrow{He} H_2C(O^-)(OH)$

Formation of the conjugate base of methyl peroxide, $CH_3O_2^-$, would require extensive chemical redisposition and so is not expected to occur efficiently. We have observed a similar addition of hydride and methoxide to formaldehyde (18).

Acetaldehyde and acetone were both observed to react rapidly with OH^- by proton transfer (see Table 1). Deuterium-labeling experiments have established previously that acetaldehyde loses the proton from the methyl position (19). Figure 1 shows a representative result obtained with acetaldehyde. Solvation with a single water molecule was seen to leave the reactivity of OH^- essentially unchanged. Since the singly-hydrated product ions were observed, we may write:

[6] $OH^-\cdot H_2O + CH_3CHO \rightarrow {}^-CH_2CHO\cdot H_2O + H_2O$

[7] $OH^-\cdot H_2O + CH_3COCH_3 \rightarrow CH_3COCH_2^-\cdot H_2O + H_2O$

Both of these reactions were measured to proceed with a rate constant of $(3 \pm 1) \times 10^{-9}$ cm^3 molecule^{-1} s^{-1}.

CH_2CO

Ketene was observed to react rapidly with the hydroxide ion with $k = (2.2 \pm 0.5) \times 10^{-9}$ cm^3 molecule^{-1} s^{-1} to form a mass 41 ion for which the following resonance structure may be written

[8] $H{-}\bar{C}{=}C{=}O \leftrightarrow H{-}C{\equiv}C{-}O^-$

Figure 2 shows the formation of a secondary product ion with mass 39. The HC_2O^- apparently was being consumed further by reaction with ketene to produce $C_3H_3^-$ for which the following

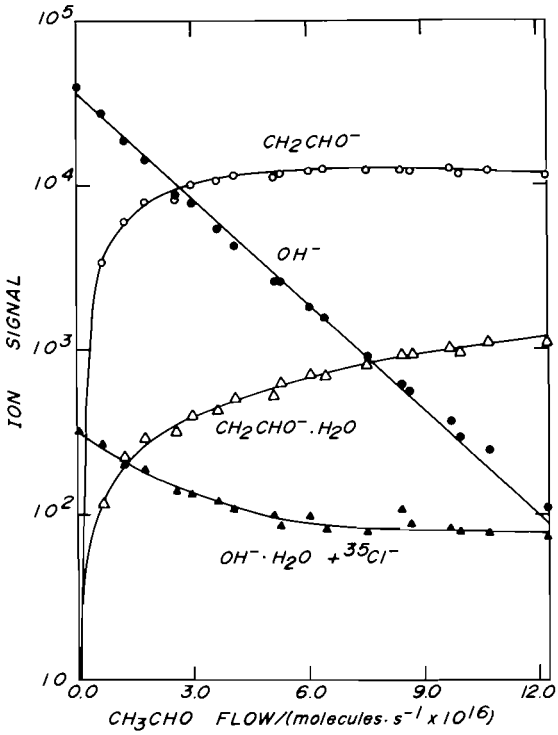

FIG. 1. The observed variation in the dominant ion signals recorded upon the addition of acetaldehyde into a flowing H_2/H_2O plasma; $T = 298$ K, $P = 0.312$ Torr, $\bar{v} = 7.8 \times 10^3$ cm s^{-1}, and $L = 84$ cm.

Can. J. Chem. Downloaded from www.nrcresearchpress.com by 210.87.254.6 on 09/06/12
For personal use only.

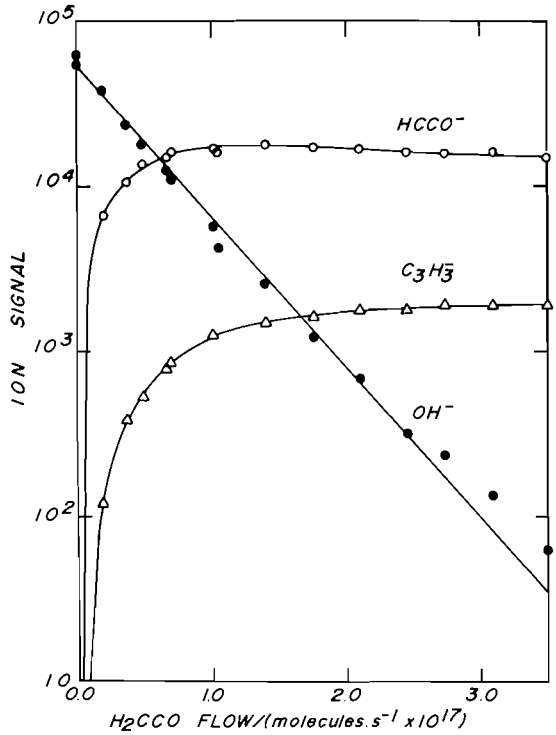

FIG. 2. The observed variation in the dominant ion signals recorded upon the addition of ketene into a flowing H_2/H_2O plasma; T = 298 K, P = 0.301 Torr, $\bar{v}$ = 7.9 × 10^3 cm s^{-1}, and L = 59 cm.

resonance structures may be written:

[9] $H—\bar{C}=C=CH_2 \leftrightarrow H—C\equiv C—\bar{C}H_2$

The mechanism of this latter reaction presumably involves the formation of a four-centered intermediate which fragments to eliminate CO_2:

[10] 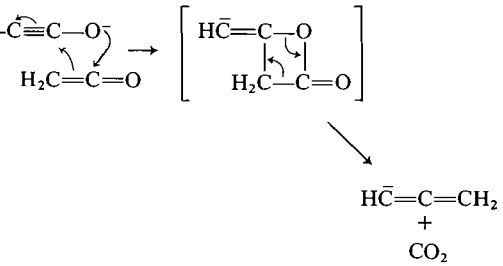

The $C_3H_3^-$ in turn appeared to react further with ketene to regenerate the HC_2O^- by proton transfer,

[11] $C_3H_3^- + H_2C_2O \rightarrow HC_2O^- + C_3H_4$

This reaction, together with the previous reaction which produces $C_3H_3^-$, represents an ion-catalyzed reaction scheme for the conversion of ketene into CO_2 and C_3H_4,

[12] $H_2C_2O + H_2C_2O \rightarrow CO_2 + C_3H_4$

The overall exothermicity of reaction [12] is 18.9 kcal mol^{-1} for the formation of allene. An analysis of the steady-state ion abundance ratio for $HC_2O^-/C_3H_3^-$ indicated a value for the ratio of rate constants k_{11}/k_{10} approximately = 10.

HCOOH

The analysis of the formic acid data also indicated a high rate, k = (2.2 ± 0.7) × 10^{-9} cm^3 $molecule^{-1}$ s^{-1}, but with only 0.75 ± 0.05 of the reactive collisions leading to the proton-transfer product, HCO_2^-. The remaining 0.25 ± 0.05 of the collisions gave rise directly (in a bimolecular fashion) to singly-hydrated OH^-,

[13*a*] $OH^- + HCOOH \rightarrow HCO_2^- + H_2O$

[13*b*] $\rightarrow OH^-\cdot H_2O + CO$

For the experimental results shown in Fig. 3, the reactant OH^- was produced by the reaction of O^- with CH_4 to eliminate all but impurity H_2O and so to minimize the direct association of OH^- with H_2O. The initial signal at mass 35 was entirely accounted for under these conditions by the chlorine isotope, $^{35}Cl^-$. The change in this signal with

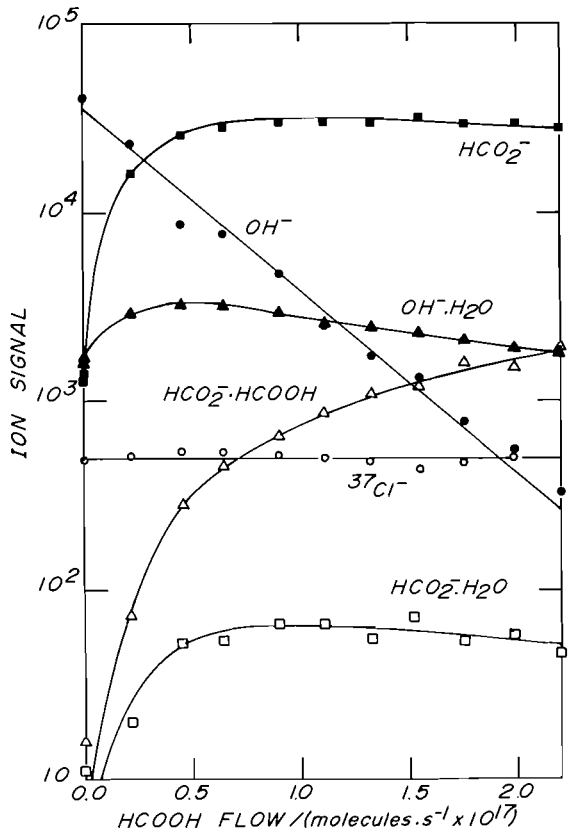

FIG. 3. The observed variation in the dominant ion signals recorded upon the addition of formic acid into a flowing $He/O_2/CH_4$ plasma; T = 301 K, P = 0.450 Torr, $\bar{v}$ = 8.4 × 10^3 cm s^{-1}, and L = 47 cm.

Can. J. Chem. Downloaded from www.nrcresearchpress.com by 210.87.254.6 on 09/06/12
For personal use only.

addition of formic acid could then be attributed entirely to the bimolecular formation of $OH^-\cdot H_2O$ and its subsequent reaction. The channel leading to the formation of the cluster ion is rendered exothermic by the hydration energy of OH^-, 25 kcal mol^{-1} (16), without which it would be endothermic by 6 kcal mol^{-1} (16). Its mechanism may involve a nearly concerted loss of CO and capture of the water molecule by the OH^-:

[14] $OH^- + HCOOH \longrightarrow$ 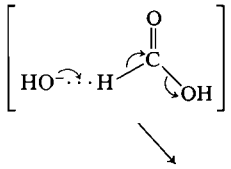

$H_2O\cdot OH^- + CO$

The products of the reaction of the cluster ion were not established with certainty. They may include the following:

[15*a*] $OH^-\cdot H_2O + HCOOH \rightarrow HCO_2^- + 2H_2O$

[15*b*] $\rightarrow HCO_2^-\cdot H_2O + H_2O$

[15*c*] $\rightarrow OH^-\cdot 2H_2O + CO$

Channel [15*a*] was masked by the production of HCO_2^- from "nude" OH^-. Channel [15*c*] is the analogue of channel [13*b*]. The $OH^-\cdot 2H_2O$ was observed above the background only in those experiments in which the initial OH^- was produced from H_2O and higher signals of $OH^-\cdot H_2O$ were present initially. Channel [15*b*] was observed only in depressed amounts due to a secondary "solvent switching" reaction with HCOOH:

[16] $HCO_2^-\cdot H_2O + HCOOH \rightarrow HCO_2^-\cdot HCOOH + H_2O$

The reactivity of the nude hydroxide ion is reminiscent of the behaviour reported previously by Isolani and Riveros (20) in their ICR study of analogous reactions of negative ions with esters of formic acid. In the next section we report a study of the reaction of OH^- with the first member of this homologous series, methyl formate.

$HCOOCH_3$

Two main products were observed in the ICR studies of the reaction on OH^- with methyl formate at water pressures of 5×10^{-5} Torr (21):

[17*a*] $OH^- + HCOOCH_3 \rightarrow HCO_2^- + CH_3OH$

[17*b*] $\rightarrow CH_3O^-\cdot H_2O + CO$

The rate constant k_{17} and branching ratio [17*a*]/[17*b*] were reported to be 1.5×10^{-9} cm^3 $molecule^{-1}$ s^{-1} and 0.80, respectively. The results of the flowing afterglow measurements for this reaction are virtually identical: $k_{17} = 1.9 \times 10^{-9}$ cm^3 $molecule^{-1}$ s^{-1} and [17*a*]/[17*b*] = 1.0 ± 0.2 for the measurements carried out with and without added water vapour. The $CH_3O^-\cdot H_2O$ product rapidly reacted further, $k > 9 \times 10^{-10}$ cm^3 $molecule^{-1}$ s^{-1}, apparently to produce an ion at $m/e = 63$, presumably $CH_3O^-\cdot CH_3OH$, which is known to be formed from the "nude" CH_3O^- (22). The mechanism of reaction [17] has been reviewed by Nibbering (23).

The singly-hydrated OH^- appeared to react in a fashion analogous to the bare ion. The reaction was rapid, $k = (1.6 \pm 0.5) \times 10^{-9}$ cm^3 $molecule^{-1}$ s^{-1}, and ions were observed to be produced which correspond to the singly-hydrated counterparts of the products of reaction [17]:

[18*a*] $OH^-\cdot H_2O + HCOOCH_3 \rightarrow CH_3O^-\cdot 2H_2O + CO$

[18*b*] $\rightarrow HCO_2^-\cdot H_2O + CH_3OH$

The assignment of the latter product ion was ambiguous since it has the same mass as the $CH_3O^-\cdot CH_3OH$ believed to be produced by $CH_3O^-\cdot H_2O$. In contrast, the second hydrate, $OH^-\cdot 2H_2O$, reacted in a much slower fashion, $k < 3 \times 10^{-10}$ cm^3 $molecule^{-1}$ s^{-1}.

C_3H_4

Both allene and propyne were observed to lose a proton to OH^-. The rate constant measured for the reaction with allene

[19] $OH^- + CH_2{=}C{=}CH_2 \rightarrow CH_2{=}C{=}CH^- + H_2O$

was $(1.7 \pm 0.4) \times 10^{-9}$ cm^3 $molecule^{-1}$ s^{-1}, which exceeds an earlier value of $(7.5 \pm 2.3) \times 10^{-10}$ cm^3 $molecule^{-1}$ s^{-1} (4). The reaction with propyne

[20*a*] $OH^- + CH_3{-}C{\equiv}CH \rightarrow {}^-CH_2{-}C{\equiv}CH + H_2O$

[20*b*] $\rightarrow CH_3{-}C{\equiv}C^- + H_2O$

was observed to be equally rapid with $k = (1.7 \pm 0.3) \times 10^{-9}$ cm^3 $molecule^{-1}$ s^{-1}. Previous deuterium-labelling experiments (19) have shown that ≥ 60% of the deprotonation of propyne initially produces $^-CH_2{-}C{\equiv}CH$ which may relax to the more stable allenyl anion, $CH_2{=}C{=}CH^-$ (24). The allenyl anion is computed to be less stable than $CH_3{-}C{\equiv}C^-$ but the profile for this interconversion shows a high energy barrier (25). We have probed the relative reactivity of the $C_3H_3^-$ ions produced from allene and propyne in a separate study (25). The observed relative reactivity with methyl formate suggested that only 10 ± 5% of the deprotonation of propyne in fact occurs at the C≡CH position. Nonempirical molecular orbital calculations predict that the acetylenic proton is slightly more acidic than the proton at the methyl position (26). Such an order of acidity would imply that the deprotonation observed experimentally is controlled kinetically rather than thermodynamic-

Can. J. Chem. Downloaded from www.nrcresearchpress.com by 210.87.254.6 on 09/06/12
For personal use only.

ally. Indeed, on the basis of the electrostatic interaction during a collision of OH^- with polar propyne, deprotonation by OH^- can be expected to proceed preferentially at the positive methyl end of propyne.

Hydration of OH^- stops the reaction with allene, $k \leq 10^{-12}$ cm^3 molecule^{-1} s^{-1}. Apparently the exothermicity of the bare reaction, together with the hydration energy of the $C_3H_3^-$, is insufficient to compensate for the 25 kcal mol^{-1} of hydration energy of OH^-. The reaction of $OH^-\cdot H_2O$ with propyne showed the more surprising result given in Fig. 4. A slow decay is observed with addition of propyne which corresponds to a rate constant of $(5.8 \pm 2.3) \times 10^{-11}$ cm^3 molecule^{-1} s^{-1}. An ion with $m/e = 43$ rises concomitantly, in part due to the association of C_2H^- with H_2O. A number of options are allowed by stoichiometry, for example:

$$[21a]\quad OH^-\cdot H_2O + CH_3CCH \rightarrow C_3H_7^- + O_2$$

$$[21b]\quad \rightarrow C_2H^-\cdot H_2O + CH_3OH$$

$$[21c]\quad \rightarrow {}^-CH_2CHO + CH_3OH$$

Channel [21*a*] is unattractive on both energetic and mechanistic grounds. Channel [21*b*] corresponds to a hydrated nucleophilic displacement reaction which is probably endothermic because of the endothermicity of the bare reaction and the high hydration energy of OH^-. However, separate experiments have shown that C_2H^- hydrates with a three-body association rate constant similar in magnitude to that for the hydration of OH^-. This result suggests that the two hydration energies may be similar, at least to the extent that these rate constants correlate with the stability of the associated species (18). The slow reaction observed would be consistent with a hydrated nucleophilic displacement reaction endothermic by 2 kcal mol^{-1}. Channel [21*c*] is exothermic but would require an unlikely reaction mechanism. A fourth option might involve the formation of an enol type ion such as $HOCHCH^-$ which is isomeric with the $C_2H^-\cdot H_2O$ cluster ion and ${}^-CH_2CHO$, the conjugate base of acetaldehyde. The enol anion might result from a 1,3 nucleophilic attack in the following manner:

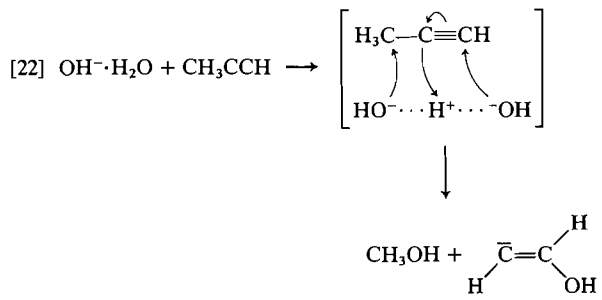

The stability of this ion is likely to fall in between the lower stability of $C_2H^-\cdot H_2O$ and the higher stability of ${}^-CH_2CHO$. Consequently its formation may well be exothermic.

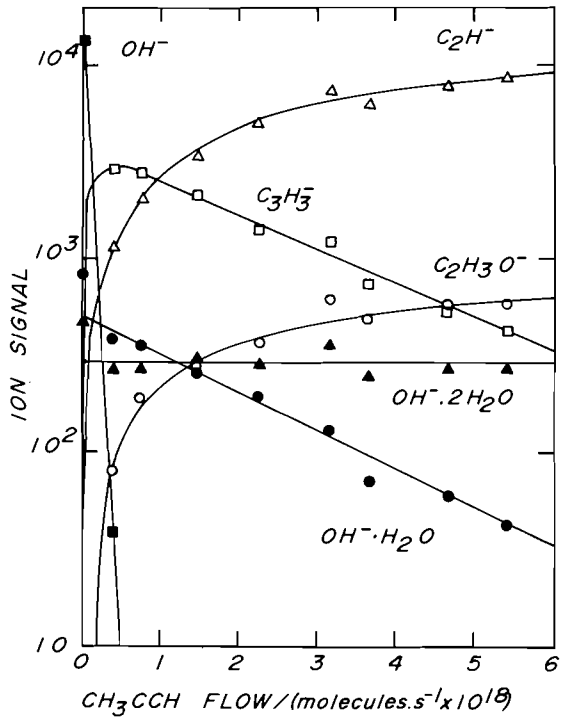

FIG. 4. The observed variation in the dominant ion signals recorded upon the addition of propyne into a flowing H_2/H_2O plasma; $T = 296$ K, $P = 0.354$ Torr, $\bar{v} = 7.6 \times 10^3$ cm s^{-1}, and $L = 46$ cm.

$C_6H_5CH_3$, $C_6H_5CH_2D$

The proton transfer from toluene to the bare hydroxide ion was also observed to be rapid, $k = (2.6 \pm 0.6) \times 10^{-9}$ cm^3 molecule^{-1} s^{-1}. Deuteration at one of the methyl positions failed to reveal an isotope effect; the new rate constant was measured to be $(2.8 \pm 0.7) \times 10^{-9}$ cm^3 molecule^{-1} s^{-1}. Furthermore, in those experiments in which OH^- was produced from O^- and CH_4 in the absence of added water vapour in helium buffer, the branching ratio [23*a*]/[23*b*] was observed to be 0.5 ± 0.1:

$$[23a]\quad OH^- + C_6H_5CH_2D \rightarrow C_6H_5CH_2^- + HOD$$

$$[23b]\quad \rightarrow C_6H_5CHD^- + HOH$$

The implication of this result is that the proton transfer proceeds in a direct fashion rather than through a long-lived complex for which complete scrambling would produce a branching ratio of 1.0 rather than 0.5. In those experiments in which OH^- was derived from water vapour the observed product ion ratio $[C_6H_5CH_2^-]/[C_6H_5CHD^-]$ was a

Can. J. Chem. Downloaded from www.nrcresearchpress.com by 210.87.254.6 on 09/06/12
For personal use only.

function of the added water vapour, becoming as large as 11 at the highest additions. This was interpreted to reflect a rapid H/D exchange between H_2O and $C_6H_5CHD^-$. Stewart *et al.* have previously reported that $C_6H_5CH_2^-$ will exchange two hydrogen atoms in the presence of D_2O (19).

Several unsuccessful attempts were made with additions of water vapour as large as 4.2×10^{19} molecules s^{-1} at a reaction length of 125 cm to drive to equilibrium the reaction

[24] $OH^- + C_6H_5CH_3 \rightarrow C_6H_5CH_2^- + H_2O$

We can report only a limit to the equilibrium constant of $K \geq 3 \times 10^5$.

Summary

The bare hydroxide ion has been observed to react rapidly, $k > 10^{-9}$ cm^3 molecule^{-1} s^{-1}, by proton transfer, with a variety of oxygen and carbon acids stronger than H_2O in the gas phase. With formic acid and methyl formate the proton transfer competes with the formation of a solvated hydroxide ion.

Hydration of the bare ion with one molecule of water was observed to result in either a slightly or a considerably reduced reactivity depending on the nature of the acid and the exothermicity of the bare reaction. The reactivity remains high when the hydration energy of the conjugate base produced is comparable to that of OH^-, or the exothermicity of the "nude" reaction is correspondingly high. The products are then also analogous to those observed for the "nude" reaction. Such was the case with the observed reactions of OH^- with C_2H_5OH, CH_3CHO, HCOOH, and $HCOOCH_3$. For the reactions with allene, propyne, and toluene, proton transfer was closed to the hydrated OH^- in the gas phase. Apparently the hydration energy of the carbanions produced in these cases is not sufficient to compensate for the high hydration energy of OH^- so that the acidity of the conjugate acids relative to that of H_2O has been reversed. The reaction with propyne showed an uncertain intermediate behaviour. The reduced reactivity in this case may be associated with a change in mechanism with solvation from proton transfer to hydrated displacement.

Acknowledgement

We thank the Natural Sciences and Engineering Research Council of Canada for financial support.

1. D. K. Bohme. *In* Kinetics of ion–molecule reactions. *Edited by* P. Ausloos. Plenum Press, New York, NY. 1979. p. 323.
2. F. C. Fehsenfeld and E. E. Ferguson. J. Chem. Phys. **61**, 3181 (1974).
3. A. L. C. Smit and F. H. Field. J. Am. Chem. Soc. **99**, 6471 (1977).
4. D. K. Bohme and L. B. Young. J. Am. Chem. Soc. **92**, 3301 (1970).
5. G. I. Mackay, M. H. Lien, A. C. Hopkinson, and D. K. Bohme. Can. J. Chem. **56**, 131 (1978).
6. D. K. Bohme, G. I. Mackay, H. I. Schiff, and R. S. Hemsworth. J. Chem. Phys. **61**, 2175 (1974).
7. G. I. Mackay, L. D. Betowski, J. D. Payzant, H. I. Schiff, and D. K. Bohme. J. Phys. Chem. **80**, 2919 (1976).
8. G. I. Mackay and D. K. Bohme. Int. J. Mass Spectrom. Ion Phys. **26**, 327 (1978).
9. J. D. Payzant, K. Tanaka, L. D. Betowski, and D. K. Bohme. J. Am. Chem. Soc. **98**, 894 (1976).
10. K. Tanaka, G. I. Mackay, J. D. Payzant, and D. K. Bohme. Can. J. Chem. **54**, 1643 (1976).
11. D. K. Bohme, R. S. Hemsworth, H. W. Rundle, and H. I. Schiff. J. Chem. Phys. **58**, 3504 (1973).
12. G. I. Mackay, R. S. Hemsworth, and D. K. Bohme. Can. J. Chem. **54**, 1624 (1976).
13. G. I. Mackay, S. D. Tanner, A. C. Hopkinson, and D. K. Bohme. Can. J. Chem. **57**, 1518 (1979).
14. D. L. Albritton. At. Data Nucl. Data Tables, **22**, 1 (1978).
15. G. I. Mackay and D. K. Bohme. J. Am. Chem. Soc. **100**, 327 (1978).
16. P. Kebarle. Ann. Rev. Phys. Chem. **28**, 445 (1977).
17. J. E. Bartmess, J. A. Scott, and R. T. McIver. J. Am. Chem. Soc. **101**, 6046 (1979).
18. D. K. Bohme, G. I. Mackay, and S. D. Tanner. J. Am. Chem. Soc. **102**, 407 (1980).
19. J. H. Stewart, R. H. Shapiro, C. H. DePuy, and V. M. Bierbaum. J. Am. Chem. Soc. **99**, 7650 (1977).
20. P. C. Isolani and J. M. Riveros. Chem. Phys. Lett. **33**, 362 (1975).
21. J. F. G. Faigle, P. C. Isolani, and J. M. Riveros. J. Am. Chem. Soc. **98**, 2049 (1976).
22. J. M. Riveros. Adv. Mass Spectrom. **6**, 277 (1974).
23. N. M. M. Nibbering. *In* Kinetics of ion–molecule reactions. *Edited by* P. Ausloos. Plenum Press, New York, NY. 1979. p. 165.
24. A. C. Hopkinson. Prog. Theor. Org. Chem. **2**, 194 (1977).
25. G. I. Mackay and D. K. Bohme. Org. Mass Spectrom. **15**, 593 (1980).
26. A. C. Hopkinson, M. H. Lien, K. Yates, P. G. Mezey, and I. G. Csizmadia. J. Chem. Phys. **67**, 517 (1977).

Crystallographic studies and physico-chemical properties of π-electron compounds. Part I. Crystal and molecular structure of 6-*N*,*N*-diacetylaminochrysene (DAAC)

TADEUSZ WIĘCKOWSKI AND TADEUSZ M. KRYGOWSKI

Department of Chemistry, University of Warsaw, 02093 Warsaw, ul. Pasteura 1, Poland

Received August 1, 1980

TADEUSZ WIĘCKOWSKI and TADEUSZ M. KRYGOWSKI. Can. J. Chem. **59**, 1622 (1981).

The molecules of 6-*N*,*N*-diacetylaminochrysene, $C_{22}H_{17}NO_2$, crystallize in orthorhombic space group *Pbca* with $a = 15.120(1)$ Å, $b = 7.8706(9)$ Å, and $c = 28.504(2)$ Å, $Z = 8$, $V = 3392.3(6)$ Å^3, $D_x = 1.28$ g cm^{-1}. The structure was essentially solved by direct phase determination with assistance of Fourier and difference Fourier maps and finally was refined to $R = 0.050$ for 2320 reflections. The DAA-group is almost perpendicular to the plane of chrysene moiety. The simple harmonic oscillator model for calculating the stabilization energy of π-electron systems by means of negative value of energy deformation necessary to transform the real molecule (or its fragments) to its Kekulé structure is presented. It shows high delocalization of π-electrons in both independent π-electron systems of DAAC molecule: the DAA-group and the chrysene moiety.

TADEUSZ WIĘCKOWSKI et TADEUSZ M. KRYGOWSKI. Can. J. Chem. **59**, 1622 (1981).

Les molécules de *N*,*N*-diacétylamino-6 chrysène, $C_{22}H_{17}NO_2$, cristallisent dans le groupe d'espace orthorhombique *Pbca* avec $a = 15,120(1)$ Å, $b = 7,8706(9)$ Å et $c = 28,504(2)$ Å, $Z = 8$, $V = 3392,3(6)$ Å^3, $D_x = 1,28$ g cm^{-1}. On a résolu la structure essentiellement par la détermination directe de la phase en s'appuyant sur des diagrammes et des différences de diagrammes de Fourier et on l'a affinée jusqu'à une valeur de $R = 0,050$ pour 2320 réflexions. Le groupe DAA est presque perpendiculaire au plan de la portion chrysène. On présente le modèle d'oscillation harmonique simple pour le calcul de l'énergie de stabilisation du système d'électrons π au moyen de la valeur négative de l'énergie de déformation nécessaire pour transformer la molécule réelle (ou son fragment) en sa structure de Kékulé. Il révèle une forte délocalisation des électrons π dans les deux systèmes indépendants d'électrons π de la molécule DAAC: le groupe DAA et le noyau chrysène.

[Traduit par le journal]

Crystal and molecular structure of benzenoid hydrocarbons and some of their derivatives has long been studied by means of various diffraction techniques (1–4). Chrysene (5) and its derivatives (6–8) have often been studied for their possible carcinogenic properties. 6-*N*,*N*-Diacetylaminochrysene DAAC is supposed to be also carcinogenic (9) and additionally in its molecule one may find two interesting features: (*i*) interference between two π-electron systems, i.e. chrysene moiety and *N*,*N*-diacetylamine-group (DAA), and (*ii*) a considerable overcrowding of hydrogen atoms in the chrysene moiety as well as of some fragments in the DAA-group. The above mentioned problems are discussed in this paper on the basis of full X-ray diffraction studies of DAAC-crystals.

Experimental

Preparation and Crystallization

A solution of 6-aminochrysene in acetic anhydride was refluxed for 2 h, cooled somewhat, and diluted to cloudiness with water. 6-*N*,*N*-Diacetylaminochrysene was separated in the shape of glistening tan needles. A sample for analysis, recrystallized twice from benzene – petroleum ether mixtures, using decolorizing carbon, formed large colorless prisms, mp 222.5–223.5°C. *Anal.* calcd. for $C_{22}H_{17}NO_2$: C 80.71, H 5.24, N 4.28; found: C 80.80, H 5.18, N 4.26%.

Optical Properties

The refraction coefficients were measured by applying the immersion method by Berek's (Leitz) microrefractometer in Na-light at 20°C. The coefficients $n\alpha_D$ and $n\beta_D$ were determined in the mixture of 1-bromonapththalene and petroleum and were equal to 1.609 ± 0.001 and 1.658 ± 0.001, respectively. The coefficient $n\gamma_D$ was determined in methylene iodide with addition of small amounts of sulphur and phosphorus and was equal to 1.867 ± 0.001. The microrefractometer was adjusted by use of Jolley's refractometer and testing plates. The angle between optical axes, $2V_\gamma$, was measured applying the conoscope method in the Waldmann's sphere in which the crystal was mounted, and the sphere filled up with a fluid of refractive index $n\beta_D$. The $2V_\gamma$ quantity was calculated applying the measured refractive indices $n\alpha_D$, $n\beta_D$, and $n\gamma_D$ and the value obtained was 56°46′ whereas the measured quantity was 56±1°. The dihedral of the acute angle is directed to γ and hence the optical sign of the crystal is positive. The plane of optical axes is parallel to (100).

Crystallographic Measurements

Preliminary cell dimensions and the space group were determined from oscillation and Weissenberg photographs indicating that the crystal belongs to the orthorhombic system. For data collection a prismatic crystal, 0.31 × 0.31 × 0.35 mm, was mounted on a Syntex $P2_1$ four-circle computer-controlled diffractometer. X-Ray diffraction data were measured with graphite-monochromated CuKα radiation. Least-squares fitting of 2θ, ω, and χ for 15 intense reflections centred on a diffractometer gave accurate cell constants. Crystal data (at 20°C) are:

$C_{22}H_{17}NO_2$ fw = 327.37

Orthorhombic, $a = 15.120(1)$, $b = 7.8706(9)$, $c = 28.504(2)$ Å, $V = 3392.3(6)$ Å^3, $\rho_m = 1.28$ (flotation in aqueous KI), $Z = 8$, $\rho_c = 1.28$ g cm^{-3}, $F(000) = 1376$, $\mu(CuK\alpha) = 6.6$ cm^{-1}, $\lambda(CuK\alpha) = 1.54178$ Å, mp: 222.5–223.5°C. Absent reflections $0kl$, $k \neq 2n$; $h0l$, $l \neq 2n$; $hk0$, $h \neq 2n$. Space group *Pbca*. A variable-speed (2.01 to 29.30° min^{-1}) θ–2θ scan technique was used in measuring 2320 independent reflections to a maximum 2θ of 115.0°. 1606 reflections from the data set had $I > 1.960\sigma(I)$ and were used in

0008-4042/81/111622-08$01.00/0

©1981 National Research Council of Canada/Conseil national de recherches du Canada

Can. J. Chem. Downloaded from www.nrcresearchpress.com by 210.87.254.5 on 09/06/12
For personal use only.

Can. J. Chem. Downloaded from www.nrcresearchpress.com by 210.87.254.5 on 09/06/12
For personal use only.

the analysis. Structure factors and normalized structure factors were derived from the intensities by application of the Lorentz-polarization corrections. The absorption and extinction corrections were negligible because of the low value of μ. The reflections were adjusted to an absolute scale by Wilson statistics; a Wilson plot (10) gave an overall isotropic temperature factor of 3.04 Å^2.

Structure Solution and Refinement

The structure was essentially solved by direct phase determination with the MULTAN system using 235 E's $\geq$ 1.58 for which 3768 Σ_2 relationships were generated. 16 phase sets were derived using one special and two general multisolution phases, and an E map with the highest combined figure of merit CFOM (2.990) obtained with the unit weight of ABSFOM (1.169) and RESID (21.75) gave initial coordinates for 24 out of 25 non-hydrogen atoms of the asymmetric unit. The missing C atom was easily located on Fourier and difference Fourier maps. Full-matrix least-squares refinement of all non-hydrogen atoms positional and isotropic thermal parameters converged at R = 0.133. The vibrational model was then changed to an anisotropic one and a similar least-squares refinement was attempted; R reduced to 0.101. The positional parameters of all the H atoms were found from two successive difference Fourier syntheses. The isotropic thermal factor for each H atom was fixed at 1.0 Å^2 greater than that for the C to which it is bounded. These H atoms contributions were included in the structure factor calculations but their positions and temperature factors were not refined. Three subsequent cycles of refinement gave agreement indices $R = \Sigma||F_o| - |F_c||/\Sigma|F_o| = 0.050$ and $R_w = [\Sigma w(F_o - F_c)^2/\Sigma wF_o^2]^{1/2} = 0.046$. The quantity minimized in the least-squares calculations was $\Sigma w(|F_o| - |F_c|)^2$. The weighting scheme was based on counting statistics; $w = 1/\sigma^2(F_o)$. The final fractional coordinates and thermal parameter from the last cycle of the least-squares refinement for non-hydrogen and hydrogen atoms, respectively, are given in Tables 1, 2, and 3.[1]

All calculations were performed on a Nova minicomputer with the Syntex XTL programs for structure determination (11).

Results

The atom labelling scheme and the anisotropic thermal ellipsoids of the DAAC are shown in Fig. 1. Bond lengths and angles are listed in Tables 4*a* and 4*b*[1] whereas in Fig. 2 there are presented distances between non-bonded H-atoms, bond lengths, and displacements of atoms from the best plane for atoms: C5, C6, C7, C8, C9, C14, C15, C16, C17, C18. Table 5 gives the best planes for fixed sets of atoms and displacements of atoms from them, whereas Table 6 presents angles between the above mentioned planes. Table 7 presents the torsion angles for the DAA-fragment. Figures 3 and 4 present projections of the elementary cell contents on planes *ab* and *ac*, respectively.

TABLE 1. Fractional coordinates ($\times 10^5$) for non-hydrogen atoms. Estimated standard deviations from the final full-matrix least-squares cycle are given in parentheses

	x	*y*	*z*
C1	20745/21/	3079/43/	9285/13/
C2	20110/24/	4880/47/	4498/14/
C3	13568/25/	−3671/48/	2006/12/
C4	7765/21/	−13976/47/	4299/12/
C5	8299/20/	−16194/41/	9218/12/
C6	2297/20/	−26873/42/	11758/12/
C7	2799/21/	−28801/40/	16437/12/
C8	9442/20/	−20365/40/	19177/12/
C9	9939/20/	−22367/39/	24205/12/
C10	4071/24/	−32293/47/	26832/12/
C11	4986/27/	−34333/51/	31560/13/
C12	11897/28/	−26454/51/	33933/13/
C13	17614/25/	−16481/48/	31590/13/
C14	16830/23/	−14161/45/	26665/12/
C15	22982/25/	−4098/51/	24174/14/
C16	22391/23/	−1913/51/	19552/13/
C17	15570/21/	−9980/41/	16836/12/
C18	14946/20/	−7591/40/	11783/12/
C19	−12642/22/	−26191/48/	8714/12/
C20	−3107/24/	−51510/47/	7085/13/
C21	−20440/23/	−33665/48/	6381/13/
C22	5738/27/	−59234/48/	8055/16/
N	−4728/16/	−35609/33/	9180/08/
O1	−12866/16/	−11957/33/	10305/09/
O2	−8488/17/	−58382/34/	4635/09/

Discussion

There are a few problems which seem to be more general and deserve a greater interest. The electronic properties of the *N*,*N*-diacetylamine group (DAA) need comment since as a result of the high delocalization of π-electrons in the group no tendency of conjugation between DAA group and chrysene moiety occurs. In order to tackle the problem of π-electron delocalization in DAA-group the HOSE (13) model is extended in this paper into the system with such bonds as CN and CCH_3. Another problem worth mentioning and deeper discussion here is the presence of very short and very long CC-bonds as well as the overcrowding of protons leading to non-planarity of the chrysene moiety.

(i) Extension of the Harmonic Oscillator Model of Calculating Stabilization Energy from Bond Lengths and Electronic Properties of the DAA-group

When the bonds of a real molecule are deformed to the lengths such as in the Kekulé structure of the molecule the deformation energy, E_{def}, may be calculated by means of applying a simple harmonic

[1]The structure factor table and Tables 2 (thermal parameters for non-H atoms), 3 (fractional coordinates and isotropic temperature factors for H-atoms), 4*b* (bond lengths and valency angles involving H-atoms), 5 (equations of the best planes and distances of individual atoms from them), 6 (angles between normals to planes), 7 (torsion angles) are available, at a nominal charge, from the Depository of Unpublished Data, CISTI, National Research Council of Canada, Ottawa, Ont., Canada K1A 0S2.

Can. J. Chem. Downloaded from www.nrcresearchpress.com by 210.87.254.5 on 09/06/12
For personal use only.

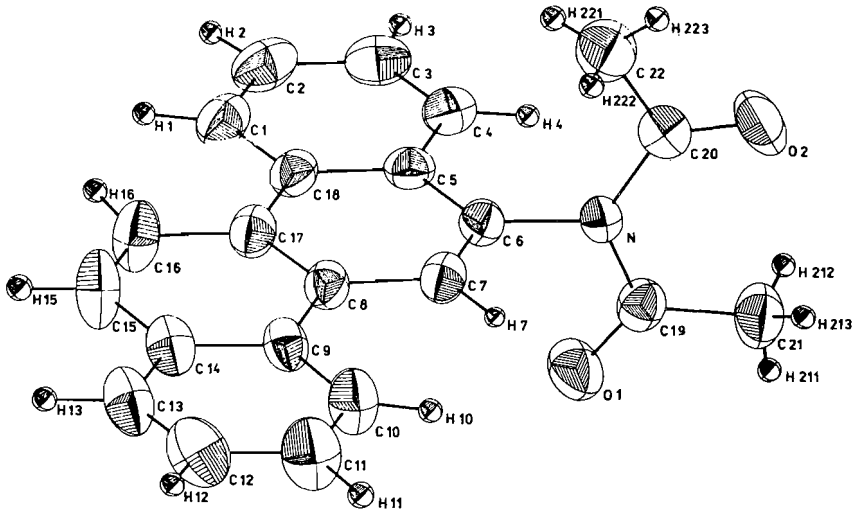

FIG. 1. Thermal ellipsoid plot (ORTEP, Johnson (12)) showing vibration ellipsoids at the 50% probability level.

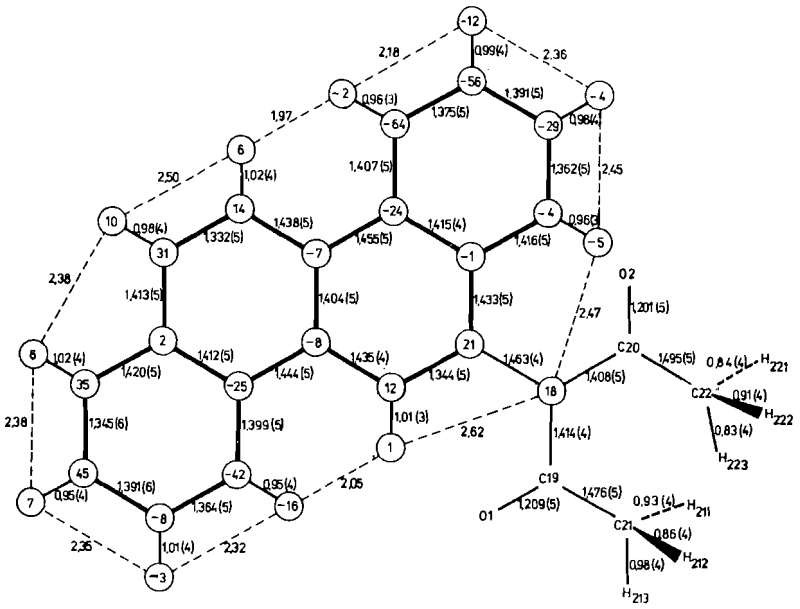

FIG. 2. Displacements of atoms from the best plane C5 through C9, C14 through C18 in circles. For non-hydrogen atoms × 10^3 Å, for hydrogen atoms × 10^2 Å. Bond lengths (Å) along bonds whereas distances (Å) between non-bonded hydrogen atoms are given along dotted lines.

oscillator model in the following way (13):

$$[1]\quad E_{\text{def}} = -\frac{1}{2}\left[\sum_{r=1}^{n_1}(R_r - R_r^0)^2 k_r' + \sum_{r=1}^{n_2}(R_r - R_r^0)^2 k_r''\right]$$

where R_r are the bond lengths in the real molecule, n_1 and n_2 are numbers of single and double bonds in the Kekulé structure, respectively. In the process of deformation the n_1 longest CC-bonds are lengthened and the n_2 shortest CC-bonds are shortened to the bond lengths R_r^0 for C—C and C=C, respectively. The R_r^0-values for C—C and C=C are adopted such as those in acyclic polyenes. In our case we have taken bond lengths for butadiene–1,3 (14). In the case of bonds other than CC the properly chosen reference bonds have to be used. These data for CC, CO, and CN bonds are collected in Table 8 together with appropriate force constants k for each of the single and double bonds. k' and k'' in eq. [1] are the force constants for bonds which are lengthened and shortened, respectively. Assuming reverse proportionality k_r against R_r as

Can. J. Chem. Downloaded from www.nrcresearchpress.com by 210.87.254.5 on 09/06/12
For personal use only.

TABLE 4*a*. Bond lengths (Å) and valency angles (deg) for the DAAC molecule with estimated standard deviations in parentheses
(*a*) Non-H atoms

Bond	Length (Å)	Bond	Length (Å)
C1 —C2	1.375/5/	C16—C17	1.438/5/
C2 —C3	1.391/5/	C17—C18	1.455/5/
C3 —C4	1.362/5/	C18—C1	1.407/5/
C4 —C5	1.416/5/	C5 —C18	1.415/4/
C5 —C6	1.433/5/	C8 —C17	1.404/5/
C6 —C7	1.344/5/	C9 —C14	1.412/5/
C7 —C8	1.435/4/	C6 —N	1.463/4/
C8 —C9	1.444/5/	N —C19	1.414/4/
C9 —C10	1.399/5/	C19—O1	1.209/5/
C10—C11	1.364/5/	C19—C21	1.476/5/
C11—C12	1.391/6/	N —C20	1.408/5/
C12—C13	1.345/6/	C20—O2	1.201/5/
C13—C14	1.420/5/	C20—C22	1.495/5/
C14—C15	1.413/5/		
C15—C16	1.332/5/		

Bonds	Angle (deg)	Bonds	Angle (deg)
C2 —C1 —C18	121.3/3/	C9 —C14—C13	119.6/3/
C3 —C2 —C1	120.4/3/	C9 —C14—C15	119.5/3/
C2 —C3 —C4	120.1/3/	C13—C14—C15	120.9/3/
C3 —C4 —C5	120.8/3/	C14—C15—C16	121.7/3/
C4 —C5 —C6	122.4/3/	C15—C16—C17	121.6/3/
C4 —C5 —C18	119.6/3/	C16—C17—C8	118.3/3/
C6 —C5 —C18	118.0/3/	C16—C17—C18	121.5/3/
C5 —C6 —C7	122.1/3/	C18—C17—C8	120.2/3/
C5 —C6 —N	118.8/3/	C1 —C18—C17	122.5/3/
C7 —C6 —N	119.1/3/	C5 —C18—C17	119.7/3/
C6 —C7 —C8	121.8/3/	C17—C18—C1	122.5/3/
C7 —C8 —C9	121.8/3/	C6 —N —C19	114.5/3/
C7 —C8 —C17	118.2/3/	C6 —N —C20	120.3/3/
C9 —C8 —C17	120.1/3/	C19—N —C20	125.0/3/
C8 —C9 —C10	124.0/3/	N —C19—O1	118.3/3/
C8 —C9 —C14	118.8/3/	N —C19—C21	120.6/3/
C10—C9 —C14	117.2/3/	O1 —C19—C21	121.1/3/
C9 —C10—C11	122.0/3/	N —C20—O2	121.9/3/
C10—C11—C12	120.3/4/	N —C20—C22	116.0/3/
C11—C12—C13	120.1/4/	O2 —C20—C22	122.0/3/
C12—C13—C14	120.8/3/		

given below:

[2] $k_r = a + bR_r$

and applying the data of Table 8 the sets of constants[2] were obtained: for CC-bond $a = 44.39$ and $b = -26.02$, for CN bond $a = 43.18$ and $b = -25.73$, and for CO bond $a = 52.35$ and $b = -32.88$. These constants permit the estimation of force constants k_r for a bond with a given bond length R_r.

Resonance energy (RE), is usually defined as an excess of energy over the additive sum of energy of a reference molecule calculated for the molecule with "purely" single and double bonds (for hydrocarbons these are C=C and C—C as in acylic polyenes), cf. refs. 21, 22. In the model proposed in this paper, the RE is approximated by the negative value of E_{def} calculated by use of the harmonic oscillator, and hence called stabilization energy, abbreviated HOSE (harmonic oscillator stabilization energy). It is the energy which must be applied to deform the real molecule to its Kekulé structure. Due to this energy the real molecule is more stable than its Kekulé structure. Combining eqs. [1] and [2] we may write the formula for HOSE in a convenient way for calculating:

[3] $$\text{HOSE} = C\left[\sum_{r=1}^{n_1}(a + bR_r')(R_r' - R_r^0)^2 + \sum_{r=1}^{n_2}(a + bR_r'')(R_r'' - R_r^0)^2\right]$$

where $C = 301.15$ is a constant converting HOSE's into kJ whereas the bond lengths are in Å, R_r' and R_r'' are the bond lengths for bonds shortened and lengthened in the process of deformation respectively.[3] There are n_1 bonds of the first kind, i.e. the number of single bonds in the Kekulé structure; n_2 is the number of double bonds (R'') in the Kekulé structure, a and b in [3] are constants as estimated by eq. [2] chosen dependent on the bond in question, and summations in [3] have to run over all the bonds of interest. It is important to know that [3] may be applied to fragments of π-electron systems as it has been done for the DAA-group. The HOSE-value for it, calculated from experimental bond lengths (Table 4*a*), results in 19.0 kJ,

TABLE 8. Bond lengths and appropriate force constants applied to get eq. [2]

Bond	Bond length (Å)	Stretching force constant (15) (dyn cm^{-1} × 10^5)
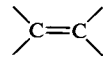	1.337[a]	9.6
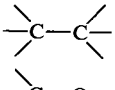	1.533[b]	4.5
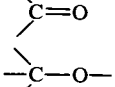	1.208[c]	12.6
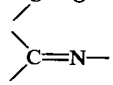	1.428[d]	5.4
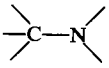	1.270[e]	10.5
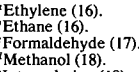	1.474[f]	5.25

[a]Ethylene (16).
[b]Ethane (16).
[c]Formaldehyde (17).
[d]Methanol (18).
[e]Interpolation (19).
[f]Methylamine (20).

[2]Dimensions of constants a and b are: 10^{-5} dyn cm^{-1} and 10^3 dyn cm^{-2}, respectively.

[3]kJ read kJ/mol throughout the paper.

Can. J. Chem. Downloaded from www.nrcresearchpress.com by 210.87.254.5 on 09/06/12
For personal use only.

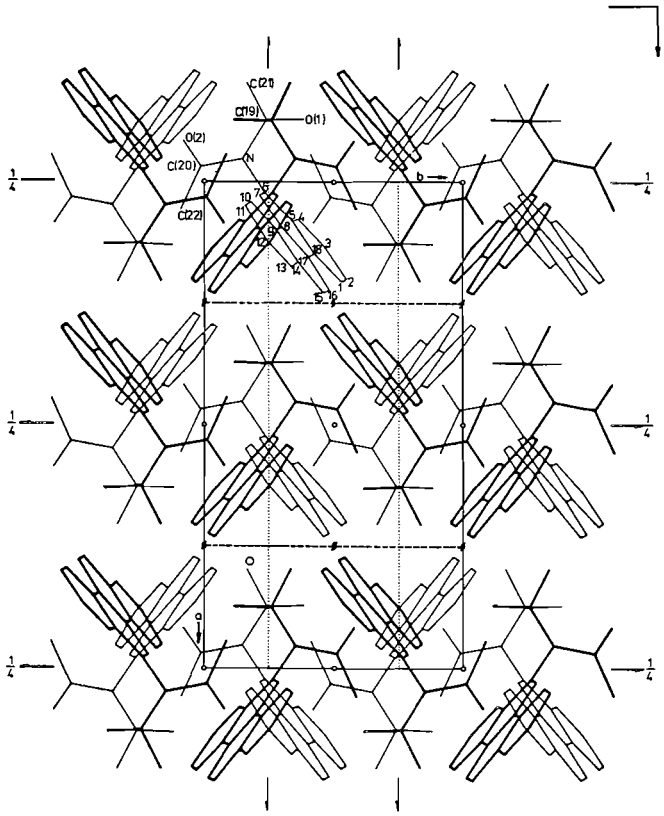

FIG. 3. View of the crystal structure down *c*.

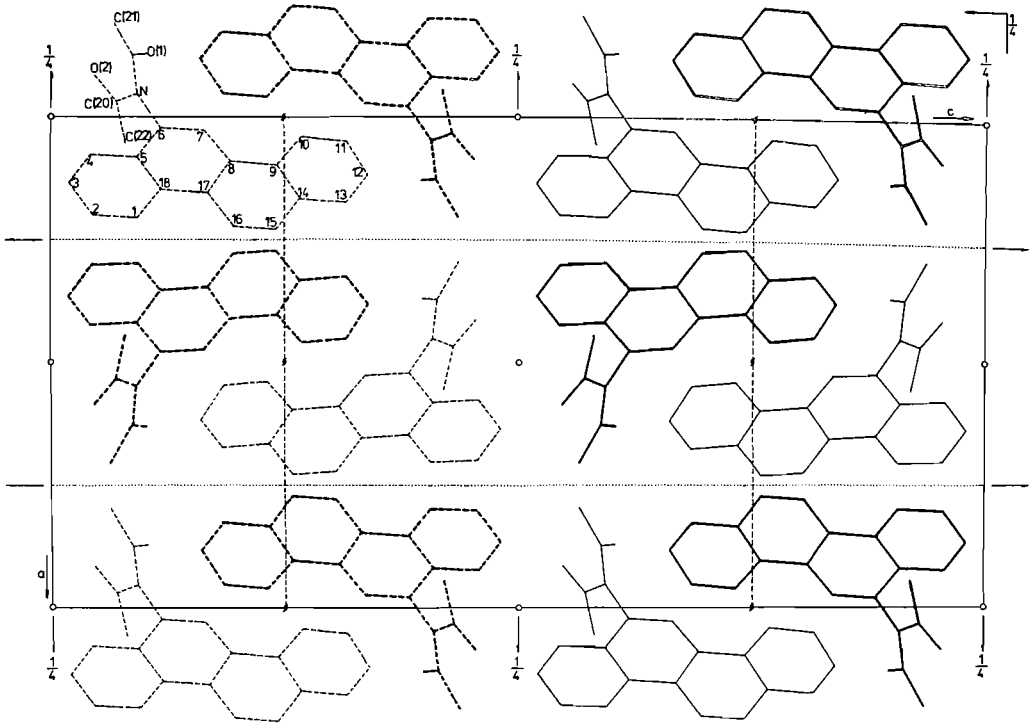

FIG. 4. View of the crystal structure down *b*.

Can. J. Chem. Downloaded from www.nrcresearchpress.com by 210.87.254.5 on 09/06/12
For personal use only.

i.e. 2.7 kJ per one bond. If the CN-bond linking the DAA-group with the chrysene moiety is excluded from the calculation, the HOSE/bond value for DAA becomes still higher resulting in 3.1 kJ, the value which is not far from the HOSE/bond for the rings in chrysene. In Table 9 there are collected HOSE as well as HOSE/bond-values for some more familiar systems for the scale of comparison with the data for DAAC. From these data one derives that the substituted ring is somewhat destabilized in comparison with other rings in chrysene moiety. The same tendency is observed in the case of substituted benzenes for which the HOSE-values are lower than for their parent system, i.e. benzene itself.

In calculation of HOSE for DAA we have chosen R^0 for $\diagdown\!\!=\!\!\diagup C—CH_3$ equal to 1.510 Å, i.e. that estimated by electron diffraction studies for *trans*-butene-2 (16).

The results of the HOSE-model are in line with an independent description of DAA by means of inductive and resonance substituent constants. For the DAA-group these constants are (23) $\sigma_R = -0.04$ and $\sigma_I = 0.37$. Due to the opposite electron the properties of the N-atom in the amine group, $\sigma_R = -0.48$ and $\sigma_I = 0.12$, and in the acetyl groups, $\sigma_R = -0.16$ and $\sigma_I = 0.28$, a rather strong delocalization of π-electrons within the frame of the DAA-group may be expected. Hence its conjugation with the chrysene moiety may be low and it is chiefly an inductive effect of DAA that seems to operate. Thus it is not a surprise that the plane of the DAA-group is almost perpendicular to the plane of chrysene: the angle between them is 91.06°. As a result of the inductive effect of DAA on chrysene the valence angle at C_6 is 122.1° and remarkably higher than that observed for amine derivatives of benzene where $\alpha = 118.4°$ (24). It is quite comparable with the α value for nitro- or cyano-derivatives of benzene for which $\alpha = 122.1$ and 121.8° (24), respectively. The relationship between valence angle at the substituted carbon and the nature of the substituent may be discussed (25) in terms of Walsh's (26) rule. It implies an increase of the value of the endocyclic angle, at the substituted carbon with an increase of electronegativity of the substituent. Hence, the electronegativity of the DAA-group may be assumed to be close to that of CN- or NO_2-groups. This finding is also supported by the values of σ_I for these two groups which are 0.65 and 0.67, respectively in comparison with 0.37 for DAA.

Analyzing the bond lengths in the DAA-group the π-electron delocalization within the group is argued by: (*i*) the shortening of NC_{20} and NC_{19} bonds, which are 1.408 and 1.414 Å, respectively, in comparison with NC_6 bond length 1.463 Å which by no means is influenced by the mesomeric effect, (*ii*) $C_{19}C_{21}$ and $C_{20}C_{22}$ bond lengths are 1.476 Å and 1.495 Å, respectively, and they are distinctly shorter than $C—CH_3$ bond lengths in xylene (1.510 Å (27)) where the mesomeric effect seems to be much lower.

TABLE 9. HOSE-values for DAAC and its fragments. For comparison there are added HOSE's for several π-electron compounds

Compound	Hose (kJ)	HOSE/bond (kJ)
DAAC 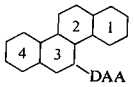	150.2	5.4
Chrysene moiety	131.2	6.2
Rings: 1	46.8	7.8
2	42.1	7.0
3	36.4	6.1
4	46.9	7.8
DAA-group	19.0	2.7
DAA-group without CN linkage	18.8	3.1
Benzene (13)	79.9	13.3
Anthracene (13)	103.5	6.5
Pyrene (13)	132.8	7.0
Chrysene (13)	164.4	7.8
p-N,N-Dimethylnitroaniline (13)	58.3	9.7
p-Nitrobenzoic acid (13)	77.2	12.9

(ii) Too Short and too Long CC-bonds and the Problems of Overcrowding

In the DAAC molecule there are both very short CC-bonds, 1.332 Å or 1.344 Å, and very long ones, 1.455 or 1.444 Å. Since the X-ray diffraction measurement for a CC bond in ethene yields 1.337 Å (28) the values reported here are not very striking. The short CC bond lengths measured by X-ray diffraction are shortened as a result of non-sphericity of electron clouds around C-atoms involved in the C=C bond by some 0.02 Å. It seems to be a rule that the shortened CC-bonds are those of HC=CH type and shorter than 1.375 Å. For this kind of bond the difference between X-ray and neutron (N) – or electron (E) – diffraction bond lengths $\overline{R}(X) - \overline{R}(N \text{ or } E) = 0.019$ Å. This difference between mean values of $\overline{R}(X)$ and $\overline{R}(N \text{ or } E)$ was calculated applying the data concerning the following molecules: phenanthrene (29), naphthalene (30), anthracene (30), pyrene (31), and triphenylene (32). It seems to be another rule, at least for angular benzenoid hydrocarbons, that most often very short bonds are located opposite very long bonds: in the DAAC molecule such pairs may be distinguished, i.e. C_6C_7 and $C_{17}C_{18}$ as well as $C_{15}C_{16}$ and C_8C_9 as it is well shown in Fig. 2. Following the ideas of Coulson and Haigh

Can. J. Chem. Downloaded from www.nrcresearchpress.com by 210.87.254.5 on 09/06/12
For personal use only.

(33) the lengthening of $C_{17}C_{18}$ and C_8C_9 bonds is caused by the overcrowding of hydrogens H_{16} and H_1 as well as H_7 and H_{10}, which are as close as 1.97 Å and 2.05 Å, respectively. It is much less than the sum of the van der Waals radii of hydrogen, i.e. 2.12 Å for the closest H···H distance between non-bonded hydrogens. Another consequence of the overcrowding is a considerable nonplanarity of the chrysene moiety, as presented in Fig. 2, where displacement of the atoms from the best plane C_5 through C_9 and C_{14} through C_{18} are given in Å × 10^3 for non-hydrogen atoms and in Å × 10^2 for hydrogen atoms. It is immediately apparent that the chrysene moiety of DAAC is twisted in such a way that the fragments containing $C_1H_1C_2H_2$- and $C_{10}H_{10}C_{11}$-H_{11}-atoms are bent out off the plane of the figure, whereas fragments containing $C_{15}H_{15}C_{16}H_{16}$ and C_7H_7 and C_6 and the CN-bond are twisted in an opposite direction. As a result of the overcrowding the saddle-type shape of the chrysene moiety is observed. Quantitatively it is seen from the angles between the normals to the planes of the successive rings. In Table 6 one may readily find these quantities: they are 0.66°, 2.28°, and 2.76°, the latter value being the angle of overall bending of the chrysene moiety. This property of the chrysene moiety is clearly expressed by a high value of a standard deviation of carbon atom displacements from plane 2, SD = 0.026, whereas this quantity is much lower for particular rings, being in the range from 0.004 (plane 4) to 0.008 (plane 6). According to Coulson and Haigh (33) the overcrowding of H···H in a chrysene molecule may result in the lengthening of C_8C_9- and $C_{17}C_{18}$-bonds by some 0.02 Å, whereas C_5C_6-, C_7C_8-, $C_{14}C_{15}$-, and $C_{16}C_{17}$-bonds are lengthened by some 0.01 Å. The same kind of interactions is expected to occur in a DAAC-molecule. It is supported by a decrease of HOSE-values for rings 2 and 3, 42.0 and 36.4 kJ, respectively. In comparison with HOSE ≃ 47 for rings 1 and 4 where no particular overcrowding effect is present. Another consequence of overcrowding is perpendicularity of the DAA-group and chrysene moiety. If the DAA-group was coplanar with the chrysene moiety, the H_4-atom would have to be surrounded by three H-atoms of the methyl group (C_{22}), with the closest distance between H_4 and C_{22} equal to about 0.3 Å. This is certainly the main reason of non-coplanarity of these two π-electron systems, which is additionally supported by their own mesomeric effects causing a very low tendency for any mesomeric interactions to occur between DAA and the chrysene moiety. However, a slight deviation from exact perpendicularity is observed, the torsion angles $C_7C_6NC_{20}$ and $C_5C_6NC_{20}$ being −94.97° and 86.52°, respectively. This asymmetry of the torsion angles may be explained in terms of very different bond lengths 1.344 and 1.433 Å for C_6C_7- and C_5C_6-bonds, respectively. The plane of DAA is inclined towards the longer C_5C_6-bond because of the larger space in this direction. The overcrowding is also a reason of equal interatomic distances H_{212} and O_2 as well as O_2 and H_{223}, which are 2.40 Å, whereas the sum of van der Waals radii for H and O is 2.64 Å (34).

(iii) Comparison with Other Studies of Chrysene or its Derivatives

It should be mentioned that there are some differences and similarities between our results and those referring to other studies of similar structures. As a rule, precision of refinement is not high enough to draw too far reaching conclusions but it seems likely that certain characteristic features are common.

(*i*) Very short CC-bonds are usually in the same places in molecules, ranging from 1.365 Å for chrysene (5) through 1.353 Å for the chrysene 7,7,8,8-tetracyanoquinodimethane CT-complex (6) ending up with 1.370 Å for the fluoranilchrysene CT-complex (7). In the case of DAAC this bond is as short as 1.332 Å.

(*ii*) Very long CC-bonds are usually also in the same region of the molecules as a result of overcrowding. In the above mentioned CT-complex (6) the longest CC-bonds in the chrysene moiety are in the same places as in DAAC and are equal to 1.461 Å in comparison with 1.455 Å for 1.444 Å in DAAC. The CT-interactions, as we can see, do not influence the lengthening significantly. In a slightly different molecule, dibenzo (q,p) chrysene (8) the longest CC-bonds are also present in the same region being in the range of 1.444–1.467 Å. In this case, however, the overcrowding should be expected to be stronger due to q and p benzene rings added to the chrysene moiety.

As it is easily seen from Fig. 3 the stacking in the DAAC-crystal is different from that in chrysene (5) or the chrysene–TCNQ complex (6).

Acknowledgements

The authors wish to thank Professor Z. Kosturkiewicz for her kind interest in this work and Dr. M. Jaskólski (both from A. Mickiewicz University in Poznań) for his kind assistance during the collecting of the data as well as for numerous discussions.

The work was sponsored by the Chemical Sciences Committee of the Polish Academy of Sciences.

1. G. FERGUSON and J. M. ROBERTSON. Adv. Phys. Org. Chem. **1**, 203 (1963).
2. A. ALMENINGEN, O. BASTIANSEN, and F. DYVIK. Acta Crystallogr. **14**, 1056 (1961).
3. A. C. HAZELL, F. K. LARSEN, and M. S. LEHMANN. Acta Crystallogr. B, **28**, 2977 (1972).
4. J. TROTTER. Crystal-structure studies of aromatic hydrocarbons. The Royal Institute of Chemistry, Lecture Series 1962. No. 2.
5. D. M. BURNS and J. IBALL. Proc. R. Soc. A, **257**, 491 (1960).
6. P. J. MUNNOCH and J. D. WRIGHT. J. Chem. Soc. Perkin II, 1397 (1974).
7. P. J. MUNNOCH and J. D. WRIGHT. J. Chem. Soc. Perkin II, 1071 (1975).
8. F. H. HERBSTEIN. Acta Crystallogr. B, **35**, 1611 (1979).
9. P. SHUBIK and J. L. HARTWELL. Survey of compounds which have been tested for carcinogenic activity, Supplement 2. U.S. Government Printing Office, Washington, DC. 1969.
10. A. J. C. WILSON. Nature, **150**, 151 (1942).
11. Synthex XTL Operation Manual (1973). Cupertino: Syntex Analytical Intruments.
12. C. K. JOHNSON. ORTEP, Report ORNL-3794. Oak Ridge National Laboratory, Tennessee. 1965.
13. T. M. KRYGOWSKI and T. WIĘCKOWSKI. Croat. Chim. Acta, in press.
14. D. R. LIDE, JR. Tetrahedron, **17**, 125 (1962).
15. G. HERZBERG. Molecular spectra and molecular structure. Vol. II. 12th printing. D. van Nostrand, New York, NY. 1966.
16. K. KUCHITSU. MTP International review of science, physical chem., Ser. 1, Molecular structure and properties. *Edited by* G. Allen. Butterworth and Co. Ltd. 1972.
17. K. TAGAKI and T. OKA. J. Phys. Soc. Jpn. **18**, 1174 (1963).
18. K. KIMMA and M. KUBO. J. Chem. Phys. **30**, 151 (1959).
19. G. HÄFELINGER. Chem. Ber. **103**, 2902 (1970).
20. T. NIKISHAWA. J. Phys. Soc. Jpn. **12**, 668 (1957).
21. M. J. S. DEWAR and C. DE LLANO. J. Am. Chem. Soc. **91**, 789 (1969).
22. A. B. HESS, JR. and L. J. SCHAAD. J. Am. Chem. Soc. **93**, 305 (1971).
23. O. EXNER. *In* Correlation analysis in chemistry recent advances. *Edited by* N. B. Chapman and J. Shorter. Plenum Press, New York, NY. 1978. Chapt. 10.
24. A. DOMENICANO, P. MAZZEO, and A. VACIAGO. Tetrahedron Lett. 1032 (1976).
25. A. DOMENICANO, A. VACIAGO, and C. A. COULSON. Acta Crystallogr. B, **31**, 221 (1975).
26. A. WALSH. Discuss. Faraday Soc. **2**, 18 (1947).
27. A. DOMENICANO, G. SCHULTZ, M. KOLONITS, and I. HARGITTAI. J. Mol. Struct. **53**, 197 (1979).
28. J. H. VAN NES and A. VOS. Acta Crystallogr. B, **34**, 1947 (1978).
29. M. I. KAY, Y. OKAYA, and D. E. COX. Acta Crystallogr. B, **27**, 26 (1971).
30. A. ALMENINGEN, O. BASTIANSEN, and F. DYVIK. Acta Crystallogr. **14**, 1056 (1961).
31. A. C. HAZELL, F. K. LARSEN, and M. S. LEHMANN. Acta Crystallogr. B, **28**, 2977 (1972).
32. G. FERRARIS, D. W. JONES, and J. YERKESS. Z. Kristallogr. **138**, 113 (1973).
33. C. A. COULSON and C. W. HAIGH. Tetrahedron, **19**, 527 (1963).
34. C. A. COULSON. Ind. Chim. Belge, **2**, 149 (1963).

Can. J. Chem. Downloaded from www.nrcresearchpress.com by 210.87.254.5 on 09/06/12
For personal use only.

Orthophosphoric acid: calculation of concentration quotients for the first ionization equilbrium at 25.0°C[1]

DONALD S. GAMBLE

Chemistry and Biology Research Institute, Agriculture Canada, Ottawa, Ont., Canada K1A 0C6

Received November 19, 1980

DONALD S. GAMBLE. Can. J. Chem. **59**, 1630 (1981).

Equilibrium concentration quotients, K_1, have been calculated for the first ionization step of orthophosphoric acid at 25.0°C. Literature information for γ_{HCl} in mixed orthophosphate–chloride solutions has made it possible to use the published electrochemical data of Bates and Nims for this purpose. K_1 is found to be a function of two independent variables for orthophosphate concentrations from 9×10^{-2} *m* down to at least 1.0×10^{-2} *m*. K_1 is described in terms of total orthophosphate concentration C_T and the degree of ionization, α_1. Linear multiple regression analysis was used to produce the empirical equation $K_1 = K_1^* + A_0 C_T^{1/2} - \beta\alpha_1 C_T^{1/2}$, in which K_1^* is an experimental constant not identified with the thermodynamic equilibrium constant, $\mathcal{K}_1$.

DONALD S. GAMBLE. Can. J. Chem. **59**, 1630 (1981).

On a calculé les quotients K_1 de concentration à l'équilibre pour la première ionisation de l'acide orthophosphorique à 25°C. Les données de la littérature relatives à γ_{HCl} dans des solutions mixtes de orthophosphate et de chlorure ont rendu possible l'utilisation des données électrochimiques rapportées par Bates et Nims dans ce but. On a trouvé que K_1 est une fonction de deux variables indépendantes pour des concentrations d'orthophosphate allant de 9×10^{-2} *m* jusqu'à au moins 1×10^{-2} *m*. On décrit K_1 en fonction de la concentration totale C_T en orthophosphate et du degré d'ionisation α_1. On a utilisé l'analyse par regression multiple linéaire pour obtenir l'équation empirique $K_1 = K_1^* + A_0 C_T^{1/2}\ \beta\alpha_1 C_T^{1/2}$ dans laquelle K_1^* est une constante expérimentale qui n'est pas reliée à la constante d'équilibre thermodynamique $\mathcal{K}_1$.

[Traduit par le journal]

Introduction

Equilibrium data for the first step of orthophosphoric acid ionization are required for various practical purposes. One of these is the investigation of aluminum orthophosphate complexes in soil solutions (1). Also included are instrument calibrations for the measurement of H^+ concentrations (1), and conventional pH measurements (2). The first two of these applications require that concentrations rather than activities be calculated with the use of equilibrium data from the literature. The available activity coefficient data are based, however, on the assumption that aqueous orthophosphoric acid solutions contain only such monomers as H_3PO_4, $H_2PO_4^-$, and H^+ (3, 4). Published experimental evidence indicates that this is not the case (5–10). Fortunately, an alternative procedure exists for the calculation of equilibrium concentrations. Instead of the thermodynamic equilibrium constant being used with activity coefficients, a more direct procedure is the use of the corresponding concentration quotient. This requires that the concentration quotient be a known function of solution composition.

The objective of this work was therefore to determine the concentration quotient K_1 for the first ionization step, as a function of solution composition at 25.0°C. It is intended that an empirical description be produced for use in accurate practical calculations. Experimental data and observations published by Bates (11), Nims (12), and Elmore *et al.* (6) have been used for this purpose. Bates and Nims used their electrochemical data only for evaluating the extrapolation functions with which they determined the thermodynamic constant, $\mathcal{K}_1$. Their extrapolation functions were derived solely from Debye–Hückel equations, since orthophosphate dimers were not yet suspected. Bates quite properly pointed out that thermodynamically rigorous values of $\gamma_H\gamma_{Cl}$ were then unavailable for orthophosphate–chloride mixed systems. Rigorous calculations of K_1 were therefore impossible. Elmore *et al.* (6) have since published an important experimental observation which removes this difficulty. They found that for orthophosphate–chloride solutions with total concentration less than 1 *m*, $\gamma_H\gamma_{Cl}$ has the same values as for HCl solutions at the same ionic strengths. The high concentration theoretical results of Pitzer and Silvester (13) show no disagreement with this experimental observation by Elmore *et al.* The theoretical parameters of Pitzer and Silvester were evaluated empirically for pure electrolytes having concentrations up to 6 *m*. With allowance for extrapolation and other assumptions, no disagreement can be shown for the mixed electrolyte at ionic strengths below 9×10^{-2} *m*. Rigorous calculations of K_1 from the electrochem-

[1]C.B.R.I. Contribution No. 1219.

0008-4042/81/111630-06$01.00/0

©1981 National Research Council of Canada/Conseil national de recherches du Canada

Can. J. Chem. Downloaded from www.nrcresearchpress.com by 210.87.254.42 on 09/06/12
For personal use only.

Can. J. Chem. Downloaded from www.nrcresearchpress.com by 210.87.254.42 on 09/06/12
For personal use only.

ical data of Bates (11) and Nims (12) have therefore become possible.

It was found necessary to do the chemical calculations and the computing in a sequence of four steps: (*1*) the calculation of K_1 from the hydrogen electrode measurements of Bates and Nims; (*2*) the identification and separation of independent variables; (*3*) development of an analytical equation that describes K_1 in terms of the independent variables; (*4*) obtaining optimum statistical use of the data, by fitting them to the analytical equation by multiple regression analysis.

1. Calculation of the Concentration Quotient, K_1, *for the First Ionization Step*

Using hydrogen and Ag–AgCl electrodes in cells without liquid junction, Bates (11) made measurements on samples prepared with ranges of KH_2PO_4 to HCl mole ratios, and ranges of total concentrations. He tabulated experimental values of

$$[1] \quad \log (m_H\gamma_H\gamma_{Cl}) = -\left[\frac{(E - E^0)F}{2.3026RT} + \log m_{HCl}\right]$$

together with values of m_{HCl} and the mole ratio

$$[2] \quad \alpha = C_T/m_{HCl}$$

m is the molality of the indicated reagent or chemical species, and C_T is the molality of total orthophosphate. Other symbols have the usual electrochemical meanings.

The first part of the present calculation used the following working equations, which are well known relationships employed by Bates:

$$[3] \quad \mu = c_1 + m_H$$

$$[4] \quad \mu_0 \approx c_1 + (m_H\gamma_H\gamma_{Cl})$$

$$[5] \quad \gamma_{HCl} \equiv \sqrt{\gamma_H\gamma_{Cl}} = f(\mu)$$

$$[6] \quad \log m_H = -\left[\frac{(E - E^0)F}{2.3026RT} + \log m_{HCl}\right] - 2 \log \gamma_{HCl}$$

μ is the ionic strength and μ_0 is its zero order approximation, c_1 is the molality of total orthophosphate singly ionized, E is the experimental cell potential, and E^0 is the standard cell potential of the Ag–AgCl reference electrode. The relationship in eq. [5] was obtained from the data of Harned and Owen (3). μ, γ_{HCl}, and m_H were calculated together in a simple iterative procedure until m_H values had converged to within four or five significant figures. This typically required three or four iterations. The concentration quotient and the degree of ionization were next calculated according to eqs. [7] and [8],

$$[7] \quad K_1 = c_1 m_H/c_p$$

$$[8] \quad \alpha_1 = c_1/C_T$$

in which c_p is the molality of total unionized orthophosphoric acid.

Nims (12) had previously done the same kind of electrochemical experiment, with the published results tabulated as values of E, E^0, and m_{HCl}. After the calculation of log $(m_H\gamma_H\gamma_{Cl})$ according to eq. [1], the calculations were the same as those using Bates' data.

The calculation results are listed in Table 1 for subsequent use.

2. The Identification and Separation of Independent Variables

The composition variables of fundamental chemical interest include total orthophosphate concentration, degree of ionization, and ionic strength. H^+ concentration is of practical and operational interest, primarily because it provides the experimental means for adjusting one or more of the other variables.

A plot of the K_1 data in Table 1 against any one of the composition variables produces a family of curves rather than a single curve. Figure 1 gives an example. This confirms the report by Elmore *et al.* (6) that K_1 is a function of at least two independent variables. The results of Elmore *et al.* were reported for somewhat higher concentrations. With the three composition variables C_T, α_1, and μ, and one constraint imposed by the ionization equilibrium, the net result is two independent variables. Because of their direct practical importance, C_T and α_1 are chosen for totally specifying the chemical composition of the system. That is, at the constant temperature,

$$[9] \quad K_1 = f_1(C_T,\alpha_1)$$

The analytical form of this function must be determined, so that the data of Table 1 may be fitted in a multiple regression analysis. To achieve separation of the independent variables for this purpose, the data were fitted to empirical polynomials by the method of least squares, and interpolated. This was done in two steps:

(*a*) For each of the eight experiments of Table 1 taken in turn, K_1 and α_1 were separately fitted as functions of C_T, and interpolated at the same round values of C_T. This produced data for a family of K_1 vs. α_1 curves, for which C_T is the parameter.

(*b*) Each of these K_1 vs. $\alpha_1$curves was fitted, and all of them were interpolated at the same round

Can. J. Chem. Downloaded from www.nrcresearchpress.com by 210.87.254.42 on 09/06/12
For personal use only.

TABLE 1. First ionization step* of orthophosphoric acid at 25.0°C data from Bates (11) and Nims (12); concentration quotient, $K_1 = c_1 m_H / c_p$

Experiment No.	Sample No.	K_1	C_T (molal)	α_1	m_H (molal)	μ
Bates 1	1	12.0730×10^{-3}	8.765×10^{-2}	0.40057	1.80663×10^{-2}	1.05716×10^{-1}
	2	11.0138×10^{-3}	4.705×10^{-2}	0.46431	1.27017×10^{-2}	5.97486×10^{-2}
	3	10.0182×10^{-3}	2.870×10^{-2}	0.51855	9.30140×10^{-3}	3.7997×10^{-2}
	4	9.7741×10^{-3}	2.427×10^{-2}	0.53895	8.36134×10^{-3}	3.26294×10^{-2}
	5	9.0240×10^{-3}	1.057×10^{-2}	0.65145	4.83029×10^{-3}	1.54001×10^{-2}
Bates 2	6	11.9889×10^{-3}	8.642×10^{-2}	0.41065	1.72062×10^{-2}	1.03661×10^{-1}
	7	11.4831×10^{-3}	6.759×10^{-2}	0.43353	1.50043×10^{-3}	8.25906×10^{-2}
	8	11.0392×10^{-3}	5.386×10^{-2}	0.45603	1.31679×10^{-3}	6.69347×10^{-2}
	9	10.1578×10^{-3}	3.196×10^{-2}	0.51312	9.63833×10^{-3}	4.15960×10^{-2}
	10	9.4344×10^{-3}	1.549×10^{-2}	0.60659	6.11882×10^{-3}	2.15998×10^{-2}
	11	9.0137×10^{-3}	1.105×10^{-2}	0.68067	4.84673×10^{-3}	1.58927×10^{-2}
Bates 3	12	11.9636×10^{-3}	9.439×10^{-2}	0.49008	1.24482×10^{-2}	1.06838×10^{-1}
	13	11.0649×10^{-3}	5.590×10^{-2}	0.53219	9.72640×10^{-3}	6.56240×10^{-2}
	14	10.7588×10^{-3}	4.646×10^{-2}	0.54868	8.84971×10^{-3}	5.53076×10^{-2}
	15	10.5298×10^{-3}	4.230×10^{-2}	0.55655	8.39001×10^{-3}	5.06900×10^{-2}
	16	9.5141×10^{-3}	1.957×10^{-2}	0.63619	5.44080×10^{-3}	2.50118×10^{-2}
Bates 4	17	11.2148×10^{-3}	7.075×10^{-2}	0.63373	6.48164×10^{-3}	7.72316×10^{-2}
	18	11.0469×10^{-3}	6.118×10^{-2}	0.64256	6.14504×10^{-3}	6.73266×10^{-2}
	19	10.4107×10^{-3}	4.076×10^{-2}	0.66868	5.15835×10^{-3}	4.58296×10^{-2}
	20	9.4632×10^{-3}	1.976×10^{-2}	0.72437	3.60132×10^{-3}	2.33648×10^{-2}
Bates 5	21	11.1770×10^{-3}	9.540×10^{-2}	0.85345	1.91925×10^{-3}	9.73197×10^{-2}
	22	10.9829×10^{-3}	8.354×10^{-2}	0.85554	1.85455×10^{-3}	8.53946×10^{-2}
	23	10.6146×10^{-3}	5.932×10^{-2}	0.86198	1.69955×10^{-3}	6.10196×10^{-2}
	24	10.6958×10^{-3}	5.927×10^{-2}	0.86218	1.70973×10^{-3}	6.09793×10^{-2}
Nims 1	1	10.5958×10^{-3}	4.628×10^{-2}	0.64379	5.86264×10^{-3}	5.21412×10^{-2}
	2	10.1963×10^{-3}	3.780×10^{-2}	0.65756	5.30988×10^{-3}	4.31086×10^{-2}
	3	9.9640×10^{-3}	3.177×10^{-2}	0.67092	4.88719×10^{-3}	3.66549×10^{-2}
	4	9.5745×10^{-3}	2.172×10^{-2}	0.70316	4.04195×10^{-3}	2.57630×10^{-2}
	5	9.1559×10^{-3}	1.434×10^{-2}	0.74067	3.20574×10^{-3}	1.75437×10^{-2}
	6	8.8651×10^{-3}	9.597×10^{-3}	0.77908	2.51383×10^{-3}	1.21103×10^{-2}
Nims 2	7	11.4173×10^{-3}	9.243×10^{-2}	0.72452	4.34118×10^{-3}	9.67712×10^{-2}
	8	10.4134×10^{-3}	6.462×10^{-2}	0.73551	3.74465×10^{-3}	6.83647×10^{-2}
	9	10.7134×10^{-3}	5.525×10^{-2}	0.73876	3.68235×10^{-3}	5.89315×10^{-2}
	10	9.7127×10^{-3}	2.723×10^{-2}	0.77883	2.75824×10^{-3}	2.99880×10^{-2}
	11	9.3968×10^{-3}	1.782×10^{-3}	0.80519	2.27347×10^{-3}	2.00885×10^{-2}
	12	8.9093×10^{-3}	9.009×10^{-3}	0.85087	1.56150×10^{-3}	1.05705×10^{-2}
Nims 3	13	11.2643×10^{-3}	7.981×10^{-2}	0.72796	4.20948×10^{-3}	8.40195×10^{-2}
	14	11.0305×10^{-3}	7.073×10^{-2}	0.73223	4.03372×10^{-3}	7.47637×10^{-2}
	15	10.4268×10^{-3}	4.500×10^{-2}	0.75174	3.44338×10^{-3}	4.84434×10^{-2}
	16	10.0507×10^{-3}	3.537×10^{-2}	0.76333	3.11611×10^{-3}	3.84861×10^{-2}
	17	9.0984×10^{-3}	1.360×10^{-2}	0.82104	1.98315×10^{-3}	1.55832×10^{-2}
	18	8.9102×10^{-3}	1.048×01^{-2}	0.83871	1.71351×10^{-3}	1.21945×10^{-2}

*The required error analyses have been produced by the subsequent computing and are given with the rest of the computing results in Tables 2 and 3. The rounding off to significant figures has been done after the computing, in order to avoid truncation errors.

values of α_1. This in turn provided a family of K_1 vs. C_T curves, for which α_1 is the parameter.

3. *The Analytical Form of the Function* $K_1 = f(C_T, \alpha_1)$

Examination of the K_1 vs. C_T family of curves from step (*b*) of the data processing has yielded three important observations:

(*a*) At constant α_1, K_1 is found by least-squares fit to be a linear function of $C_T^{1/2}$. Figure 2 shows the resulting family of straight lines,

$$[10] \quad K_1 = K_1^* + AC_T^{1/2}$$

(*b*) K_1^* is independent of α_1, so that the whole family of straight lines has a common intercept. K_1^* is a totally empirical constant, and because of long extrapolations one cannot assume a priori that it may be identified with the thermodynamic constant, $\mathcal{K}$.

(*c*) Figure 3 shows that for $\alpha_1 > 0.55$, A is a decreasing linear function of α_1,

$$[11] \quad A = A_0 - \beta\alpha_1$$

The available data do not permit conclusions to be drawn for $\alpha_1 < 0.55$, but from the appearance of

Can. J. Chem. Downloaded from www.nrcresearchpress.com by 210.87.254.42 on 09/06/12
For personal use only.

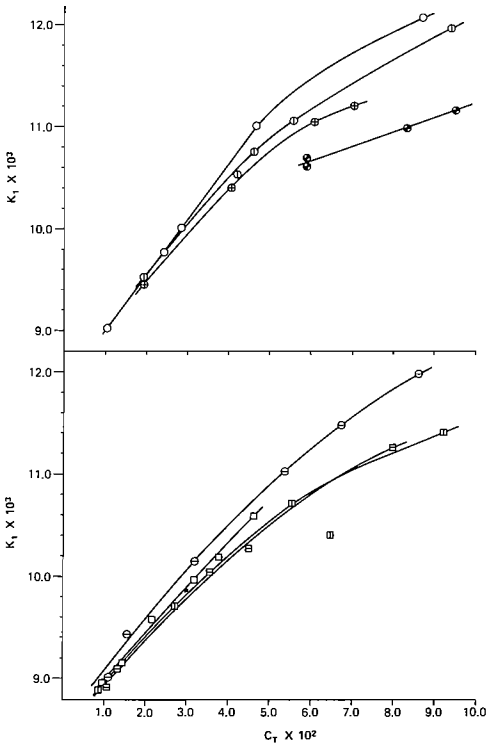

FIG. 1. $K_1 = c_1 m_H / c_p$ at 25.0°C. Bates' experiments: ○, $0.40 < \alpha_1 < 0.65$; ⊖, $0.41 < \alpha_1 < 0.68$; ◑, $0.49 < \alpha_1 < 0.64$; ⊕, $0.63 < \alpha_1 < 0.72$; ◕, $0.85 < \alpha_1 < 0.86$. Nims' experiments: □, $0.64 < \alpha_1 < 0.78$; ⊟, $0.72 < \alpha_1 < 0.85$; ◫, $0.73 < \alpha_1 < 0.84$.

Fig. 3 it is postulated that in this region,

[12] $A = A_0, \neq A(\alpha_1)$

Substituting for A this gives:

[13] $\alpha_1 > 0.55, K_1 = K_1^* + A_0 C_T^{1/2} - \beta\alpha_1 C_T^{1/2}$

$\alpha_1 < 0.55, K_1 = K_1^* + A_0 C_T^{1/2}$

The K_1 vs. α_1 family of curves obtained from step (*a*) of the data processing has the following characteristics:

(*a*) At constant C_T, a least-squares fit produces the decreasing linear function seen in Fig. 4,

[14] $K_1 = C_0 + C_1\alpha_1$

(*b*) C_0 is an increasing linear function of $C_T^{1/2}$,

[15] $C_0 = 7.40 \times 10^{-3} + 18.67 \times 10^{-3} C_T^{1/2}$

$\sigma = \pm 0.69\%$

But $C_0 \equiv K_1(C_T, 0)$ is the $\alpha_1 = 0$ limiting case of the family of curves in Fig. 2. K_1 therefore depends strongly on total orthophosphate concentration even in the limit of zero ionic strength.

(*c*) The computing results show that the experimental and calculation errors in C_1 are too large to permit their quantitative interpretation. Semiquantitatively it is found however, that

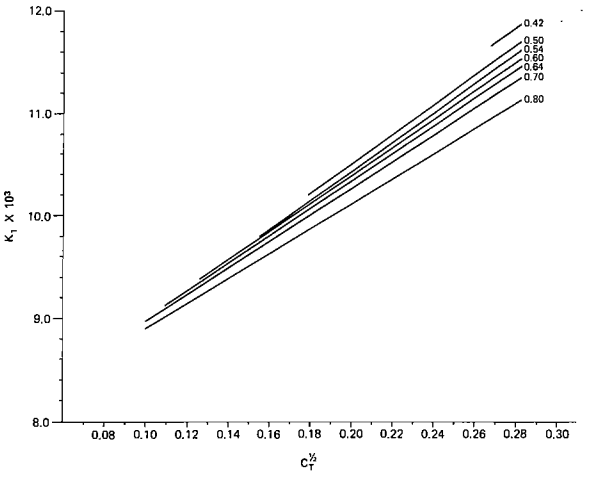

FIG. 2. $K_1 = K_1^* + Ac_T^{1/2}$, 25.0°C. Values of α_1 as the parameter are indicated for the curves. $\sigma = \pm 0.20\%$ to 0.46%. A $\equiv (\partial K_1/\partial C_T^{1/2})_{\alpha_1} = f(\alpha_1)$. For all of the curves, $K_1^* = 7.69 \times 10^{-3} \pm 0.69\%$.

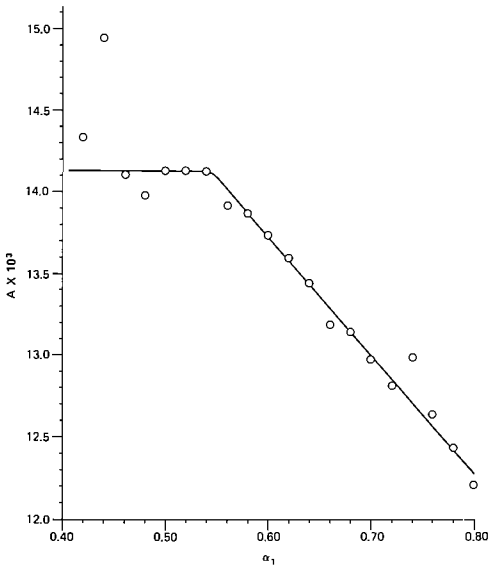

FIG. 3. $A \equiv (\partial K_1/\partial C_T^{1/2})_{\alpha_1} = f(\alpha_1)$, 25.0°C, ○, interpolated data points.

[16] $C_1 \equiv \left(\frac{\partial K_1}{\partial C_T^{1/2}}\right)_{\alpha_1} = f(C_T)$

The reason for the large error in C_1 is that K_1 is a much less sensitive function of α_1 than it is of C_T.

It is concluded from these results that eq. [13] is the function required for multiple regression analysis.

4. Linear Multiple Regression Analysis of $K_1 = K_1(C_T^{1/2}, \alpha_1)$

Data from Table 1 were fitted to eq. [13] for the case in which $\alpha_1 > 0.55$. The linear multiple

TABLE 2. Multiple regression analysis of $K_1 = f_1(C_T, \alpha_1)$ at 25.0°C;$\alpha_1 \geq 0.55$, stepwise addition of terms in the computed order of importance: step *1*: $K_1 = K_1^* + A_0 C_T^{1/2}$ step *2*: $K_1 = K_1^* + A_0 C_T^{1/2} - \beta\alpha_1 C_T^{1/2}$

Step No.	Error in K_1 ±‰σ	Reduction in total sum of squares %	Multiple correlation coefficient	K_1^* Value	K_1^* Standard error ±%	A_0 Value	A_0 Standard error ±%	β Value	β Standard error ±%
1	1.36	96.8	0.984	7.70×10^{-3}	1.11	12.6×10^{-3}	3.58		
2	1.06	98.1	0.990	7.72×10^{-3}	0.87	16.8×10^{-3}	6.29	5.9×10^{-3}	24.1

TABLE 3. Linear least-squares fit of $K_1 = f_1(C_T^{1/2})$ at 25.0°C, $\alpha_1 < 0.55$, $K_1 = K_1^* + A_0 C_T^{1/2}$

Error in K_1 ±‰σ	K_1^* Value	K_1^* Standard error ±%	A_0 Value	A_0 Standard error ±%
0.87	7.2×10^{-3}	0.48	16.5×10^{-3}	3.0

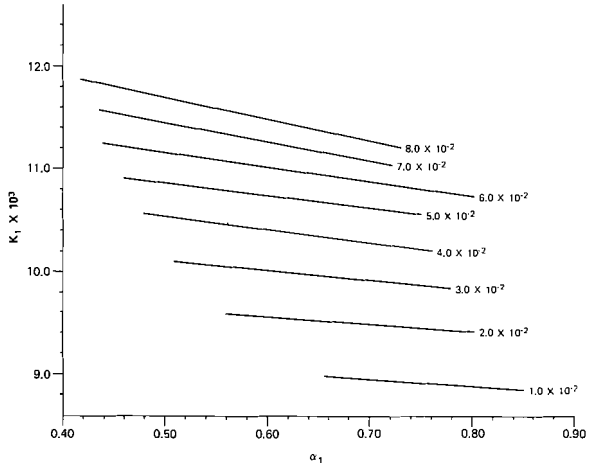

FIG. 4. $K_1 = C_0 + C_1\alpha$, 25.0°C. Values of C_T as the parameter are indicated for the curves. $\sigma = \pm 0.3\%$ to 0.7%. $C_1 \equiv (\partial K_1/\partial\alpha_1)_{C_T} = -f_1(C_T)$. $C_0 = 7.40 \times 10^{-3} + 18.67 \times 10^{-3} C_T^{1/2}$; $a = \pm 0.69\%$.

regression was carried out with a Fortran V program "SOO4C Regression" provided by the Engineering and Statistical Research Institute, Research Branch, Agriculture Canada. The linear regression required the transformation of variables according to eq. [17].

$$[17] \quad \begin{aligned} Y_4 &= C_T^{1/2} \\ Y_5 &= \alpha_1 C_T^{1/2} \end{aligned}$$

The transformed variables were added to the function consecutively in the computed order of importance. Table 2 gives the regression analysis results.

For the simpler case in which $\alpha_1 < 0.55$, K_1 vs. $C_1^{1/2}$ was fitted to a straight line by the ordinary linear least-squares procedure. The results are tabulated in Table 3 for comparison with the multiple regression output in Table 2.

Discussion

Preston and Adams (14) investigated orthophosphoric acid by laser Raman spectroscopy, over wide ranges of concentrations and pressures. Although their data had considerable scatter, they were able to observe that up to 0.1 *m* total orthophosphate, $K_1/\mathcal{K}_1$ attained values greater than 2. In addition to the limitations of the spectroscopic method, variable α_1 may have contributed to the experimental scatter. Qualitatively however, their results agree with those of Table 1. Elmore *et al.* (6) found K_1 to be a function of two independent variables for the relatively large concentrations 0.1 *m* to 10 *m*. This is now found to be true down to at least 0.01 *m* total orthophosphate, and for $\alpha_1 > 0.55$. At 1×10^{-3} *m* total orthophosphate, however, moderate changes in α_1 will have only slight effects on K_1.

The computed order of importance found in Table 2 for the terms in eq. [13] proves that $C_T^{1/2}$ is a more important independent variable than is α_1. A comparison of Tables 2 and 3 also shows that for the same value of A_0 to be obtained in the two cases of $\alpha_1 < 0.55$ and $\alpha_1 > 0.55$, the extra term $\beta\alpha_1 C_T^{1/2}$ must be added for the higher range of α_1 values. This is consistent both with the observation that α_1 is an important variable when $\alpha_1 > 0.55$, and with the postulate that K_1 becomes independent of α_1 below $\alpha_1 = 0.55$.

It is now clear why Bates' extrapolation to log $\mathcal{K}_1$ in his Fig. 2 exist as a family of curves. His use of the extended Debye–Hückel equation in his extrapolation formula for the calculation of log $\mathcal{K}_1$ introduced one independent variable, ionic

Can. J. Chem. Downloaded from www.nrcresearchpress.com by 210.87.254.42 on 09/06/12
For personal use only.

Can. J. Chem. Downloaded from www.nrcresearchpress.com by 210.87.254.42 on 09/06/12
For personal use only.

strength, but left the second independent variable unaccounted for. The result is a family of curves having a common intercept, in just the same way that the present Fig. 2 does. His procedure required however, the arbitrary adjustment of the Debye–Hückel ion size parameter, in order to obtain the common intercept for the family of curves. Recognition that K_1 is a function of two independent variables, for example $K_1 = f_1(C_T^{1/2}, \alpha_1)$, avoids this difficulty. Some of the observations by Pitzer and Silvester (13) lead to the same conclusion. Nims followed a very similar extrapolation procedure for the calculation of log $\mathcal{K}_1$, and his set of plotted curves is comparable. By using the limiting Debye–Hückel equation, Nims avoided the problem of the arbitrarily adjusted ion size parameter.

There are three indications that the behaviour of K_1 is not properly accounted for by the Debye–Hückel ion cloud model, as originally assumed first by Nims and later by Bates.

(*a*) K_1 is not just a function of ionic strength as required by the Debye–Hückel theory, but instead is a function of two independent variables.

(*b*) K_1 is a decreasing function of α_1, and therefore the apparent activity coefficient quotient is an *increasing* function of α_1,

$$[18] \quad \left(\frac{\gamma_\pm^2}{\gamma_p}\right)_{app} = \frac{\mathcal{K}_1}{K_1} = f_{app}(\alpha_1)$$

If α_1 simply reflected the ionic strength μ, then this result would be contrary to the predictions of the Debye–Hückel theory.

(*c*) According to the empirical result in eq. [15], K_1 increases substantially as $C_T^{1/2}$ increases, even when the ionic charge approaches zero.

It is concluded from these observations that the behaviour of K_1 is caused by something more than simply ionic charge. Several authors have presented evidence for the existence of orthophosphate dimers. The observed dependence of K_1 on $C_T^{1/2}$ is consistent with the existence of dimers, assuming some reaction such as that of eq. [19]:

$$[19] \quad H_3PO_4 \overset{K_{dim}}{\rightleftharpoons} \tfrac{1}{2}[H_2PO_4^-]_2 + H^+$$

Any equilibrium model postulated for the interpretation of the properties of K_1 must account for three points:

(*a*) It must be shown how the effects of the dimer concentration may be related to the observed behaviour of total orthophosphate concentration;

(*b*) It is necessary to account for a second independent variable;

(*c*) The dependence of K_1 on α_1 instead of $(\alpha_1 C_T)^{1/2}$ requires that some phenomenon other than ordinary ionic strength be invoked.

A preliminary examination reveals that a model meeting such requirements will have a more complicated mathematical description. This would make any calculations employing it more speculative, and it would also tend to magnify the experimental errors. The need for practical calculations and the importance of providing chemical insight have requirements that are to some extent mutually exclusive. The empirical description offered here is intended to serve the first objective. An equilibrium model should be separately postulated, for the purpose of interpretation. Its development, verification, and demonstration constitute a substantial problem outside the scope of the present report.

It follows from these results that the Debye–Hückel theory alone is not directly applicable to extrapolation functions for the calculation of $\mathcal{K}_1$. A family of K_1 vs. μ curves having an appropriate parameter may give the correct numerical value of $\mathcal{K}_1$ however, simply because μ reflects total orthophosphate concentration when α_1 does not vary too widely.

It is of some interest to note that in Table 2, K_1^* is greater than the $\mathcal{K}_1$ values of 7.11×10^{-3} and 7.52×10^{-3} calculated by Bates and Nims, while its value in Table 3 is moderately close to Bates' value. These eqs. [13] are strictly empirical, however, and the interpretation of constants such as β, A_0, and K_1^* should be deferred until a chemical equilibrium model is available for the first ionization step.

1. D. S. GAMBLE. Can. J. Chem. **58**, 2150 (1980).
2. R. G. BATES. Determination of pH, theory and practice. 2nd ed. John Wiley and Sons, New York. 1973.
3. H. S. HARNED and B. B. OWEN. The physical chemistry of electrolyte solutions. 3rd ed. Am. Chem. Soc. Monograph Series. Reinhold Publishing Corporation New York. 1958.
4. R. A. ROBINSON and R. H. STOKES. Electrolyte solutions. 2nd ed. Butterworths, London. 1959.
5. M. SELVARATNAM and M. SPIRO. Trans. Faraday Soc. **61**, 360 (1965).
6. K. L. ELMORE, J. D. HATFIELD, R. L. DUNN, and A. D. JONES. J. Phys. Chem. **69**, 3520 (1965).
7. C. W. CHILDS. J. Phys. Chem. **73**, 2956 (1969).
8. A. A. IVAKIN and E. M. VORONOVA. Russ. J. Inorg. Chem. **18**, 465 (1973).
9. R. H. WOOD and R. F. PLATFORD. J. Solution Chem. **4**, 977 (1975).
10. W. A. ADAMS, C. M. PRESTON, and H. A. M. CHEW. J. Chem. Phys. **70**, 2074 (1979).
11. R. G. BATES. J. Res. Natl. Bur. Stand. **47**, 127 (1951).
12. L. F. NIMS. J. Am. Chem. Soc. **56**, 1110 (1934).
13. K. S. PITZER and L. F. SILVESTER. J. Solution Chem. **5**, 269 (1976).
14. C. M. PRESTON and W. A. ADAMS. Can. J. Spectrosc. **22**, 125 (1977).

Rearrangement studies with ^{14}C. XLV. The decomposition of *cis*- and *trans*-1,2-dianisyl-2-phenyl[2-^{14}C]vinylphenyltriazenes in acetic acid

CHOI CHUCK LEE AND CRAIG A. OBAFEMI

Department of Chemistry and Chemical Engineering, University of Saskatchewan, Saskatoon, Sask., Canada S7N 0W0

Received November 19, 1980

CHOI CHUCK LEE and CRAIG A. OBAFEMI. Can. J. Chem. **59**, 1636 (1981).

The decomposition of *cis*- or *trans*-1,2-dianisyl-2-phenyl[2-^{14}C]vinylphenyltriazene (*cis*- or *trans*-**1**-NNNHPh-2-^{14}C) in HOAc gave a 1:1 mixture of *cis* and *trans* products which showed about 3% scrambling of the label from C-2 to C-1 due to 1,2-phenyl shifts in the 1,2-dianisyl-2-phenylvinyl cation. The presence of the more nucleophilic acetate ion from the addition of different amounts of NaOAc was found to decrease or even completely suppress the extent of isotopic scrambling. Comparisons with earlier data such as those obtained from the decomposition of trianisyl[2-^{14}C]vinylphenyltriazene (**2**-NNNHPh-2-^{14}C) led to a calculated $k_{r(An)}/k_{r(Ph)}$ of about 25 for the relative anisyl to phenyl migration ratio. A k_{OAc}/k_{HOAc} ratio of about 1.5×10^3 for the product forming capture reactions in the 1,2-dianisyl-2-phenylvinyl cation from the decomposition of **1**-NNNHPh-2-^{14}C was also obtained.

CHOI CHUCK LEE et CRAIG A. OBAFEMI. Can. J. Chem. **59**, 1636 (1981).

La décomposition des dianisyl-1,2 phényl-2[^{14}C-2] vinylphényltriazènes *cis* ou *trans* (NNNHPh-**1** ^{14}C-2 *cis* ou *trans*) dans du AcOH donne un mélange 1:1 de produits *cis* et *trans* dont le marquage est échangé d'environ 3% entre C-2 et C-1 par suite des déplacements 1,2 du phényle du cation dianisyl-1,2 phényl-2 vinyle. On a trouvé que la présence d'un ion acétate plus nucléophile, provenant de l'addition de différentes quantités de AcONa, diminue ou même supprime complètement le degré d'échange isotopique. Une comparaison avec des données antérieures, comme celles obtenues à partir de la décomposition du trianisyl[^{14}C-2]vinylphényltriazène (NNNHPh-**2** ^{14}C-2), a conduit à une valeur calculée de $k_{r(An)}/k_{r(Ph)}$ d'environ 25 pour le rapport de migration de l'anisyle vers le phényle. On a également obtenu un rapport k_{AcO}/k_{AcOH} d'environ $1,5 \times 10^3$ pour le produit engendrant les réactions de capture dans le cation dianisyl-1,2 phényl-2 vinyle à partir de la décomposition du NNNHPh-**1** ^{14}C-2.
[Traduit par le journal]

The isomeric *cis*- and *trans*-1,2-dianisyl-2-phenylvinyl bromides and chlorides (*cis*- and *trans*-**1**-Br and **1**-Cl) were prepared and their stereochemistry determined in 1969 by Rappoport and Apeloig (1). Solvolytic studies in various solvents, with or without added nucleophiles, gave a 1:1 mixture of the *cis* and *trans* products and it was concluded that S_N1 reactions took place via the dissociated 1,2-dianisyl-2-phenylvinyl cation. Further work with *cis*- and *trans*-**1**-Br, *cis*-**1**-Cl, and the methanesulfonates *cis*- and *trans*-**1**-OMs, including kinetic studies and *cis–trans* isomerization in the recovered reactant, were reported in 1975 (2, 3). The results were interpreted by a mechanism involving formation of an ion-pair, which gave internal return with isomerization, or further ionization to dissociated ions, which could either give external ion return or solvolysis product. In 1976, Lee and Oka (4) reported that the reaction of either *cis*- or *trans*-1,2-dianisyl-2-phenyl[2-^{13}C]vinyl bromide (*cis*- or *trans*-**1**-Br-2-^{13}C) with HOAc–AgOAc gave a 1:1 mixture of *cis*- and *trans*-**1**-OAc-2-^{13}C with no isotopic scrambling, indicating no detectable degenerate rearrangement from 1,2-phenyl shifts in the 1,2-dianisyl-2-phenylvinyl cation under the conditions employed. A similar lack of scrambling was reported by Rappoport and co-workers (5) for the solvolysis in HOAc–NaOAc of a 5:1 mixture of *cis*- and *trans*-1-anisyl-2-*p*-[$^2H_3$]methoxyphenyl-2-phenylvinyl bromides (*cis*- and *trans*-**1**-Br-2-methoxy-d_3), but some scrambling was observed in the solvolysis of this D-labeled substrate in aqueous ethanol or in 2,2,2-trifluoroethanol. In the present work, a study was made on the possible degenerate rearrangement from 1,2-phenyl shifts in the 1,2-dianisyl-2-phenylvinyl cation generated from the decomposition in HOAc of 1,2-dianisyl-2-phenyl[2-^{14}C]vinylphenyltriazene (**1**-NNNHPh-2-^{14}C). Since the extents of degenerate rearrangement arising from 1,2-anisyl shifts in the trianisylvinyl cation generated from the decomposition of trianisyl[2-^{14}C]vinylphenyltriazene (**2**-NNNHPh-2-^{14}C) have already been reported (6), isotopic scrambling data from the present work with **1**-NNNHPh-2-^{14}C may be compared with those from **2**-NNNHPh-2-^{14}C to provide information such as the relative anisyl to phenyl migration ratio in vinyltriazene decompositions.

Using $[^{14}C]CO_2$ instead of $[^{13}C]CO_2$ as the source of label, *cis*- and *trans*-**1**-Br-2-^{14}C were synthesized in the same way as reported for the synthesis of *cis*- and *trans*-**1**-Br-2-^{13}C (4). The pure *cis*- or *trans*-**1**-Br-2-^{14}C, separated by fractional crystallization (4), was converted to the corresponding Grignard reagent and then treated with

0008-4042/81/111636-05$01.00/0
©1981 National Research Council of Canada/Conseil national de recherches du Canada

Can. J. Chem. Downloaded from www.nrcresearchpress.com by 210.87.254.5 on 09/06/12
For personal use only.

Can. J. Chem. Downloaded from www.nrcresearchpress.com by 210.87.254.5 on 09/06/12
For personal use only.

phenyl azide to give the triazene, *cis*- or *trans*-**1**-NNNHPh-2-^{14}C (6). Decomposition of either *cis*- or *trans*-**1**-NNNHPh-2-^{14}C was carried out in HOAc or HOAc containing various amounts of NaOAc and the product obtained was a 1:1 mixture of the *cis*- and *trans*-acetates, *cis*- and *trans*-**1**-OAc-1,2-^{14}C, scrambling of the ^{14}C-label from C-2 to C-1 being observed in some of the experiments. Degradation of the product was effected by $LiAlH_4$ reduction to an *erythro* and *threo* mixture of 1,2-dianisyl-2-phenyl[1,2-^{14}C]ethanol (**3**-1,2-^{14}C) (4), followed by $KMNO_4$ oxidation to give anisyl phenyl [^{14}C]ketone (**4**-^{14}C) (7). The difference in specific activities between **3**-1,2-^{14}C and **4**-^{14}C gave the extent of scrambling of the ^{14}C-label from C-2 to C-1 in the original reaction product. The results are summarized in Table 1. An alternative degradation was carried out on the first set of experiments (Table 1) and this involved the separation of the *cis* and *trans* product mixture, with the aid of added carrier, to give the pure *trans*-**1**-OAc-1,2-^{14}C, followed by ozonolysis to **4**-^{14}C (8). Essentially the same extent of scrambling was obtained, thus confirming the validity of the degradation method used on the mixture of *cis*- and *trans*-**1**-OAc-1,2-^{14}C.

The acid catalyzed decomposition of triazenes presumably proceeds via the diazonium ion which gives rise to the dissociated triarylvinyl cation (6, 9). The isotopic scramblings observed in the present system would arise from 1,2-phenyl shifts in the 1,2-dianisyl-2-phenylvinyl cation as depicted in Scheme 1. The formation of a 1:1 mixture of *cis* and *trans* products from either *cis* or *trans* reactant and the suppression of or decrease in the extent of scrambling (Table 1) by the presence of the more nucleophilic acetate ion in the reaction medium (8–10) are observations that would also support the formation of the dissociated cation as reaction intermediate.

From Table 1, it is seen that the largest extent of scrambling observed in the present work was only about 3%, which was found in the decomposition of *cis*- or *trans*-**1**-NNNHPh-2-^{14}C in HOAc with no added NaOAc. This relatively low degree of degenerate rearrangement could be attributable to a low migratory aptitude for the phenyl group and a relatively high stability of an α-anisyl substituted triarylvinyl cation. In discussing the relative amounts of scrambling arising from 1,2-phenyl shifts in the triphenylvinyl, 2-phenyl-1,2-ditolylvinyl, and 1,2-dianisyl-2-phenylvinyl cations generated from reactions of the corresponding bromides with HOAc–AgOAc (11), it was pointed out

TABLE 1. Data from the decomposition of *cis*- or *trans*-1,2-dianisyl-2-phenyl[2-^{14}C]vinylphenyltriazene in HOAc with or without the presence of added NaOAc

Expt.	Triazene	Reaction medium	Specific activities (10^{-6} × dpm/mmol)				Scrambling from C-2 to C-1 (%)	
			An(Ph)CHCH(OH)An		AnCOPh			
			Run 1	Run 2	Run 1	Run 2	Run 1	Run 2
1	*cis*, 144 m*M*	HOAc	6.17	6.58	5.98	6.38	3.1[a]	3.0[a]
2	*cis*, 144 m*M*	HOAc, 720 m*M* NaOAc	6.38	6.20	6.38	6.20	0	0
3	*cis*, 144 m*M*	HOAc, 1440 m*M* NaOAc	6.32	6.27	6.32	6.27	0	0
4	*trans*, 144 m*M*	HOAc	5.99	6.35	5.81	6.15	3.0	3.1
5	*trans*, 144 m*M*	HOAc, 720 m*M* NaOAc	6.21	6.33	6.21	6.33	0	0
6	*cis*, 15 m*M*	HOAc	1.62	1.68	1.57	1.63	3.1	3.0
7	*cis*, 15 m*M*	HOAc, 45 m*M* NaOAc	2.113	2.593	2.100	2.575	0.6	0.7
8	*cis*, 15 m*M*	HOAc, 75 m*M* NaOAc	1.692	1.589	1.684	1.584	0.5	0.3

[a]Essentially the same results were obtained using an alternative degradation involving ozonolysis of the purified *trans*-1,2-dianisyl-2-phenyl[1,2-^{14}C]vinyl acetate product.

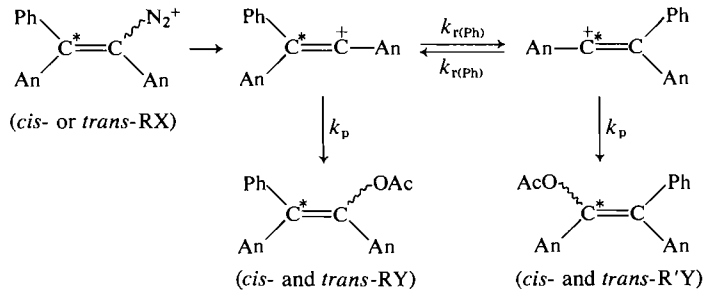

SCHEME 1

that if one were to consider a bridged ion as a model of the transition state for the 1,2-aryl shift, in going from a linear triarylvinyl cation such as **5** to a bridged transition state such as **6**, the higher stability of an α-anisyl substituted vinyl cation would lead to a higher activation energy and hence a lower extent of scrambling. Such an effect likely also contributed to the observed relatively low extents of scrambling in the present study.

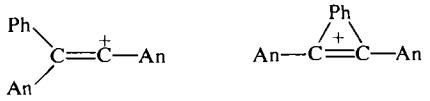

5 6

In the decomposition of trianisyl[2-^{14}C]-vinylphenyltriazene (**2**-NNNHPh-2-^{14}C) (6), the scrambling arising from 1,2-anisyl shifts in the trianisylvinyl cation was found to be 37.8 and 38.4% in duplicate runs. Obviously, a higher migratory aptitude for the anisyl group relative to that of the phenyl group would play an important role in giving rise to the greater extent of scrambling than the 3.0–3.1% observed in the present study with **1**-NNNHPh-2-^{14}C. Relative migratory aptitudes for aryl groups in triarylvinyl cations have been evaluated using isotopic scrambling data (11–13). Thus for a scrambling mechanism as depicted in Scheme 1, it has been shown that eq. [1] would apply (11–13),

$$[1] \quad [RY]/[R'Y] = 1 + (k_p/k_{r(Ph)})$$

It is seen from eq. [1] that the extent of scrambling, related to [RY]/[R'Y], would be independent of the initial concentration of the substrate RX, and this is in agreement with the finding that the same 3.0–3.1% scrambling was obtained whether the initial concentration of **1**-NNNHPh-2-^{14}C was 144 m*M* or 15 m*M* (Table 1).

Using eq. [1] and a mean scrambling value of 3.05% for the decomposition of **1**-NNNHPh-2-^{14}C in HOAc, $k_p/k_{r(Ph)}$ can be calculated as given in eq. [2].

$$[2] \quad k_p/k_{r(Ph)} = (96.95/3.05) - 1 = 30.8$$

For the similar decomposition of **2**-NNNHPh-2-^{14}C in HOAc, a statistical factor of 2 should be applied to the 1,2-anisyl shift in the trianisylvinyl cation and eq. [1] is modified to give eq. [3] (13), from which $k_p'/k_{r(An)}$ can be obtained for the mean scrambling of 38.1% as given in eq. [4]. By dividing [2] by [4], one would obtain $k_p k_{r(An)}/k_p' k_{r(Ph)}$. If one were to assume that in the triazene decomposition in HOAc, k_p and k_p' for the product formation from the 1,2-dianisyl-2-phenylvinyl and trianisylvinyl cations are about equal, then $k_{r(An)}/k_{r(Ph)}$ would be 30.8/1.25 = 25.

$$[3] \quad [RY]/[R'Y] = 1 + (k_p'/2k_{r(An)})$$

$$[4] \quad k_p'/k_{r(An)} = 2[(61.9/38.1) - 1] = 1.25$$

It is of interest to note that a similar calculation using scrambling data from reactions with HOAc–AgOAc for triphenyl[2-^{14}C]vinyl and *trans*-2-anisyl-1-phenyl-2-[$^2H_5$]phenylvinyl bromides gave a $k_{r(An)}/k_{r(Ph)}$ ratio of 162 (13), which is considerably different from the presently obtained value of 25. This difference, however, is not unexpected since the calculations were based on data from two types of reactions (decomposition of triazene and reaction of bromide with HOAc–AgOAc) involving different triarylvinyl cations. In a recent book on vinyl cations, it was pointed out that in saturated cationic systems, the anisyl to phenyl migratory ratios have been found to be about 6 to 500 for solvolysis and related reactions and much lower (1.2 to 2.0) for deamination reactions (14). For vinyl cationic systems, various values for the anisyl to phenyl migration ratio have also been obtained and it was concluded that the $k_{r(An)}/k_{r(Ph)}$ ratios of ≥ 11 to ≥ 67 for these vinyl cations are much higher than unity, thus showing similar behavior to the saturated carbocations (14). The present results would also fit into this general conclusion.

As indicated earlier, the effect of added NaOAc in decreasing or even suppressing the extent of scrambling has been regarded as evidence for the formation of dissociated triarylvinyl cations in a

Can. J. Chem. Downloaded from www.nrcresearchpress.com by 210.87.254.5 on 09/06/12
For personal use only.

Can. J. Chem. Downloaded from www.nrcresearchpress.com by 210.87.254.5 on 09/06/12
For personal use only.

mechanism as shown in Scheme 1 since, in the presence of the more nucleophilic OAc^- ion, the scrambling process would compete less effectively with product formation (8–10). From the actually observed decrease in scrambling, calculations can be made to give the selectivity of the cation in its product forming capture reactions with OAc^- and with HOAc, k_{OAc}/k_{HOAc}. In the decomposition of 2-NNNHPh-2-^{14}C in HOAc, the presence of 1.7 equiv. (240 m*M*) of NaOAc was found to decrease the mean scrambling from 38.1% to 16.8% (6). These data led to a calculated k_{OAc}/k_{HOAc} of 3.9×10^2 (10). In the present work, the decomposition of 1-NNNHPh-2-^{14}C in HOAc with no added NaOAc gave 3.0–3.1% scrambling, while the presence of 45 and 74 m*M* NaOAc, respectively, decreased the scrambling to about 0.6 and 0.4% (Expts. 7 and 8). Since these scrambling values are very small, calculated k_p/k_r using variations of eq. [1] are subjected to large deviations with small changes in the observed scrambling. Nevertheless, utilizing the data from Expts. 6, 7, and 8, and employing the same method used in the treatment of the data from 2-NNNHPh-2-^{14}C (10), k_{OAc}/k_{HOAc} values of the order of 1.5×10^3 were obtained for the decomposition of 1-NNNHPh-2-^{14}C, but this value is considerably different from the k_{OAc}/k_{HOAc} of 3.9×10^2 found for the decomposition of 2-NNNHPh-2-^{14}C (10).

Some difference in the k_{OAc}/k_{HOAc} values for 1-NNNHPh-2-^{14}C and 2-NNNHPh-2-^{14}C is to be expected since two different cations (the trianisylvinyl and 1,2-dianisyl-2-phenylvinyl cations) and widely different concentrations of added OAc^- are involved in the reactions with 1-NNNHPh-2-^{14}C and 2-NNNHPh-2-^{14}C. Even for the same reaction involving the same cation as in the solvolysis of trianisyl[2-^{14}C]vinyl bromide (2-Br-2-^{14}C) in 70% HOAc – 30% H_2O with the presence of varying amounts of added NaOAc (10), the calculated $k_{OAc}/k_{SOH'}$, $k_{SOH'}$ being defined as $[HOAc]k_{HOAc} + [H_2O]k_{H_2O} + [OAc^-]k_{OAc}$, was found to vary with changing amounts of added NaOAc. It was pointed out (10) that a major factor that contributed to these variations could be due to the use of concentrations rather than activities in the calculations, and corrections for such effects would be greater the higher the concentration of the added NaOAc. In the present work, the k_{OAc}/k_{HOAc} ratio was obtained from Expts. 7 and 8 involving the use of 45 and 75 m*M* of added NaOAc. In the calculation of k_{OAc}/k_{HOAc} based on data from the decomposition of 2-NNNHPh-2-^{14}C, a much higher acetate concentration of 240 m*M* was utilized and its wider deviation from the true acetate activity would lead to a lower calculated k_{OAc}/k_{HOAc}, as was obtained.

Experimental

cis- *or* trans-*1,2-Dianisyl-2-phenyl[2-^{14}C]vinylphenyltriazene (*cis- *or* trans-**1**-*NNNHPh-2-^{14}C)*

The pure *cis*- or *trans*-1,2-dianisyl-2-phenyl[2-^{14}C]vinyl bromide (*cis*- or *trans*-**1**-Br-2-^{14}C), prepared as previously described for the analogous ^{13}C-labeled compound (4), was converted to the corresponding Grignard reagent and then treated with phenyl azide to give the desired triazene (6). A typical preparation is described below.

To a mixture of 0.75 g (30 mmol) of Mg in 60 mL of anhydrous ether in a 3-neck flask and under N_2 a small amount of bromoethane was added to initiate the Grignard reaction. A solution of 10.0 g (25 mmol) of *cis*-**1**-Br-2-^{14}C in 30 mL of anhydrous ether was added dropwise with stirring, and then the mixture was heated under reflux for 2 days. The resulting Grignard solution was cooled in an ice bath and a solution of 3.0 g (25 mmol) of freshly prepared phenyl azide (15) in 25 mL of anhydrous ether was slowly added. The mixture was stirred at room temperature for 3 h before being treated with a solution of 10% NH_4OH – 10% NH_4Cl. The ether layer was separated and the aqueous layer was extracted with more ether. After drying over $MgSO_4$ and removal of the ether, the resulting yellow oil partially solidified upon refrigeration. The material was stirred with a 1:10 mixture of $CHCl_3$–hexane, leaving some undissolved crystalline material which proved to be *cis*-1,2-dianisyl-2-phenylethylene, showing the same mp and ^{1}H nmr spectrum as previously reported for this olefin (1). The $CHCl_3$–hexane solution was evaporated off at room temperature under reduced pressure. The residual oil was purified by passage through an alumina column using 90% petroleum ether – 10% ether as eluant (6). More *cis*-1,2-dianisyl-2-phenylethylene was removed as a first fraction, and the desired product, *cis*-**1**-NNNHPh-2-^{14}C, was recovered as a second component. After recrystallization from hexane containing a small amount of $CHCl_3$, 3.3 g (30%) of *cis*-**1**-NNNHPh-2-^{14}C was obtained, mp 110–112°C (dec.); ^{1}H nmr δ($CDCl_3$): 3.69, 3.73 (two CH_3O, two singlets), 6.63–7.43 (aromatic, m). *Anal.* calcd. for $C_{28}H_{25}N_3O_2$: C 77.22, H 5.79, N 9.65; found: C 77.18, H 5.48, N 9.80.

The *trans*-isomer, *trans*-**1**-NNNHPh-2-^{14}C, prepared in the same way from *trans*-**1**-Br-2-^{14}C, melted at 125–126°C (dec.); ^{1}H nmr δ($CDCl_3$): 3.70, 3.79 (two CH_3O, two singlets), 6.67–7.61 (aromatic, m). *Anal.* calcd. for $C_{28}H_{25}N_3O_2$: C 77.22, H 5.79, N 9.65; found: C 77.51, H 5.45, N 9.71. Both *cis*- and *trans*-**1**-NNNHPh-2-^{14}C were stored in the dark since they appeared to decompose slowly in the presence of light.

Decomposition of cis- *or* trans-*1-NNNHPh-2-^{14}C*

The conditions used in the various experiments are summarized in Table 1. A typical experiment (Expt. 2) is described below.

A mixture of 500 mg (1.15 mmol) of *cis*-**1**-NNNHPh-2-^{14}C and 472 mg (5.76 mmol) of NaOAc in 8.0 mL of glacial HOAc was stirred at room temperature for 10 min, evolution of N_2 being observed in the first couple of min. Most of the solvent was then removed at room temperature under reduced pressure. The residual oil was redissolved in ether and washed with a saturated $NaHCO_3$ solution and then with H_2O. After drying over $MgSO_4$, removal of the ether gave 360 mg (84%) of product mixture, the nmr spectrum of which showed it to be a 1:1 mixture of *cis*- and *trans*-**1**-OAc-1,2-^{14}C (4) (1:1 ratio of the two AcO absorptions at δ($CDCl_3$) 1.95, 2.00 ppm).

Degradation Procedures

The 1:1 mixture of *cis* and *trans* acetate products was treated twice (7) with $LiAlH_4$ to give a mixture of *erythro*- and *threo*-1,2-dianisyl-2-phenyl[1,2-^{14}C]ethanol (**3**-1,2-^{14}C) as previously described (4). Oxidation of the **3**-1,2-^{14}C from each

experiment with alkaline $KMNO_4$ (7) gave the anisyl phenyl [^{14}C]ketone (**4**-^{14}C) which melted alone or in admixture with an authentic sample at 61–63°C.

In Expt. 1, about one-half of the *cis* and *trans* acetate product was mixed with about 700 mg of *trans*-**1**-OAc as carrier, the latter being prepared and purified by fractional crystallization as described by Rappoport and Apeloig (1). Repeated crystallizations from CH_3OH gave the pure *trans*-**1**-OAc-1,2-^{14}C, mp 140–142°C (lit. (1), mp 140–141°C). Ozonolysis of this sample of *trans*-**1**-OAc-1,2-^{14}C using the same procedure as previously employed in the ozonolysis of trianisylethylene (8) gave **4**-^{14}C and the extent of scrambling.

Acknowledgment

The financial assistance given by the Natural Sciences and Engineering Research Council of Canada is gratefully acknowledged.

1. Z. Rappoport and Y. Apeloig. J. Am. Chem. Soc. **91**, 6734 (1969).
2. Z. Rappoport and Y. Apeloig. J. Am. Chem. Soc. **97**, 821 (1975).
3. Z. Rappoport and Y. Apeloig. J. Am. Chem. Soc. **97**, 836 (1975).
4. C. C. Lee and M. Oka. Can. J. Chem. **54**, 604 (1976).
5. Y. Houminer, E. Noy, and Z. Rappoport. J. Am. Chem. Soc. **98**, 5632 (1976).
6. C. C. Lee and E. C. F. Ko. Can. J. Chem. **54**, 3041 (1976).
7. C. C. Lee, A. J. Cessna, B. A. Davis, and M. Oka. Can. J. Chem. **52**, 2679 (1974).
8. C. C. Lee, U. Weber, and C. A. Obafemi. Can. J. Chem. **57**, 1384 (1979).
9. W. M. Jones and F. W. Miller. J. Am. Chem. Soc. **89**, 1960 (1967).
10. C. C. Lee, E. C. F. Ko, and Z. Rappoport. Can. J. Chem. **58**, 2369 (1980).
11. C. C. Lee, A. J. Paine, and E. C. F. Ko. J. Am. Chem. Soc. **99**, 7267 (1977).
12. Z. Rappoport, E. Noy, and Y. Houminer. J. Am. Chem. Soc. **98**, 2238 (1976).
13. C. C. Lee, E. C. F. Ko, and Z. Rappoport. Can. J. Chem. **58**, 884 (1980).
14. P. J. Stang, Z. Rappoport, M. Hanack, and L. R. Subramanian. Vinyl cations. Academic Press, New York, NY. 1979. pp. 404–406.
15. R. O. Lindsay and C. F. H. Allen. Organic syntheses. Coll. Vol. III. John Wiley and Sons, New York. 1955. p. 710.

Can. J. Chem. Downloaded from www.nrcresearchpress.com by 210.87.254.5 on 09/06/12
For personal use only.

Bridged-ring steroids. II. The synthesis of bridged steroids with a bicyclo[2.2.1]heptane ring A system[1]

PETER YATES AND FRANÇOISE M. WINNIK[2]

Lash Miller Chemical Laboratories, University of Toronto, Toronto, Ont., Canada M5S 1A1

Received December 4, 1980

PETER YATES and FRANÇOISE M. WINNIK. Can. J. Chem. **59**, 1641 (1981).

Bridged steroids with a bicyclo[2.2.1]heptane ring A system are formed on thermolysis of 5-vinyl 3-keto steroids. 5-Vinyl-5α-cholestan-3-one (**26**) on being heated at 350°C in decalin gave 2α,5-(*syn*-methylmethano)-5α-cholestan-3-one (**27**). Similar treatment of 17β-hydroxy-5-vinyl-5β-estran-3-one (**21**) gave 17β-hydroxy-2β,5-(*syn*-methylmethano)-5β-estran-3-one (**30**), which was also obtained by reduction of 2β,5-(*syn*-methylmethano)-5β-estrane-3,17-dione (**31**) with sodium borohydride on alumina. Compound **31** was formed as the major product on thermolysis of 5-vinyl-5β-estrane-3,17-dione (**24**) at 350°C, together with 5-(*trans*-propenyl)-*A*-nor-5β-estrane-3,17-dione (**32**). Compounds **27**, **30**, and **31** are considered to arise via intramolecular ene reactions of the Δ^2-enols of compounds **26**, **21**, and **24**, respectively. Compound **32** is postulated to be formed via an analogous reaction of the Δ^3-enol of **24**, followed by thermolysis of the resulting 3′-methyl-4β,5-dihydrocyclopropa[4, 5]-5β-estrane-3,17-dione (**36**). Photolysis of **30** in methanol results in α-cleavage of the C2—C3 bond and the formation of a ketene-derived ester and two enal-derived oxetanes.

PETER YATES et FRANÇOISE M. WINNIK. Can. J. Chem. **59**, 1641 (1981).

La thermolyse des vinyl-5 céto-3 stéroïdes conduit à la formation de stéroïdes pontés portant au niveau du cycle A un bicyclo[2.2.1] heptane. Si on chauffe la vinyl-5 5α-cholestanone-3 (**26**) dans de la décaline à 350°C, on obtient la (méthylméthano *syn*)-2α,5 5α-cholestanone-3 (**27**). L'hydroxy-17β vinyl-5 5β-estranone-3 (**21**), traitée de la même façon, fournit l'hydroxy-17β (méthylméthano *syn*)-2β,5 5β-estranone-3 (**30**) que l'on obtient également par réduction de la (méthylméthano *syn*)-2β,5 5β-estranedione-3,17 (**31**) par le borohydrure de sodium sur l'alumine. Le composé **31** se forme comme le produit principal de la thermolyse de la vinyl-5 5β-estranedione-3,17 (**24**) à 350°C à côté de la (propènyl-*trans*)-5 A-nor 5β-estranedione-3,17 (**32**). On considère que les composés **27**, **30** et **31** proviennent respectivement de réactions *ène* intramoléculaires des Δ^2 énols des composés **26**, **21** et **24**. On pense que le composé **32** se forme par l'intermédiaire d'une réaction analogue du Δ^3 énol de **24** suivie de la thermolyse de la méthyl-3′ dihydro-4β,5 cyclopropa[4,5] 5β-estranedione-3,17 (**36**). La photolyse du composé **30** dans le méthanol provoque un clivage α de la liaison C2—C3 et la formation d'un ester provenant d'un cétène et de deux oxétanes provenant d'un énal.

[Traduit par le journal]

Bridged steroids are of interest both because of their potential biological activity and because they can serve as substrates for the study of the effects of the constraints imposed on bridged bicyclic systems by the steroid skeleton in the course of the reactions of such systems.

We and others have previously investigated the synthesis of steroids incorporating a bicyclo-[2.2.2]octane (2, and references therein quoted) or bicyclo[3.2.1]octane system (3). Here we are concerned with the incorporation of a bicyclo-[2.2.1]heptane system. Solo *et al.* have made extensive investigations of bridged ring D steroids of this type, which they synthesized by Diels–Alder addition of dienophiles to steroid 14,16-dienes (4, and earlier papers in this series). However, the only previous work to our knowledge that led to the incorporation of a bicyclo[2.2.1]heptane system into a steroid ring other than ring D is that of Nazer (5), who obtained compounds **1***a* and **1***b* by treatment of **2***a* and **2***b*, respectively, with lithium aluminum hydride. We report now on the synthesis of ring-A bicyclo[2.2.1]-steroids.[3]

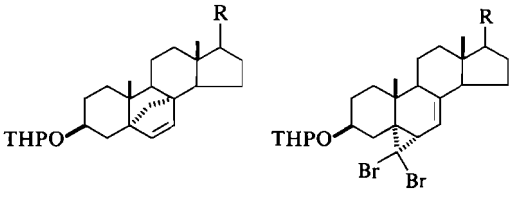

1 **2**

a, R = $CH(CH_3)CH{=}CHCH(CH_3)CH(CH_3)_2$
b, R = $CH(CH_3)CH_2CH_2CH(CH_3)CH(CH_3)_2$

Three types of ring-A bicyclo[2.2.1]-steroid can be envisaged with a one-carbon bridge between C1 and C4 (**3**), C2 and C5 (**4**), or C3 and C10 (**5**) (the last being possible only in the 19-nor series). Our initial approach was to a system of type **3**. It was thought possible that this could be obtained by a Diels–Alder reaction of the known des-A-cholestane derivative **6** with cyclopentadiene. However, neither this nor the α,β-unsaturated nitrile **7** could be induced to undergo cycloaddition to cyclopentadiene. It

[1]For Part I, see ref. 1; for a preliminary account of part of this work, see ref. 2.

[2]Née Françoise M. Walliser.

[3]We use the term bicyclo[2.2.1]-steroid to denote a steroid incorporating a bicyclo[2.2.1]heptane system in one of its rings.

0008-4042/81/111641-10$01.00/0

©1981 National Research Council of Canada/Conseil national de recherches du Canada

Can. J. Chem. Downloaded from www.nrcresearchpress.com by 210.87.254.42 on 09/06/12
For personal use only.

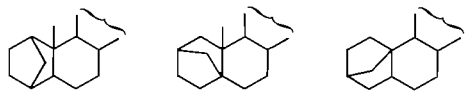

3 4 5

had been planned to isomerize **7** to **8** in order to obtain a system of type **3** via the Diels–Alder route. However, the failure of **7** to undergo cycloaddition led us to abandon this approach.

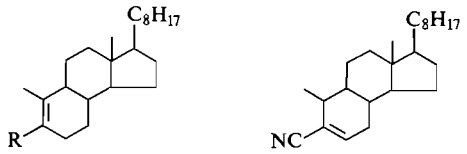

6, R = OAc
8, R = CN

7

We then turned our attention to the synthesis of bridged compounds of type 4. We chose target molecules with a carbonyl function at C3 both because this is a common feature of conventional steroids and because one of our eventual aims was to study the photochemistry of bicyclo[2.2.1]-steroidal ketones. Such targets suggested two types of approach: carbon–carbon bond formation either by nucleophilic displacement of a leaving group X in the enolate ion **9** to give **10** or by an intramolecular ene reaction of the enol **11** to give **12**.

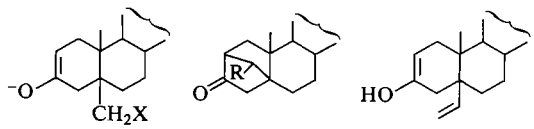

9 **10**, R = H; **12**, R = CH_3 11

The former approach is not without intrinsic interest since in terms of Baldwin's rules (6) it is a favored *exo*-5 process and a disfavored *endo*-5 process at the same time. In terms of precedent it may be compared with the closure of **13** to the sativene precursor **14** (7). However, this approach showed little promise in the case of **15** because of our failure to generate the Δ^2 rather than the Δ^3

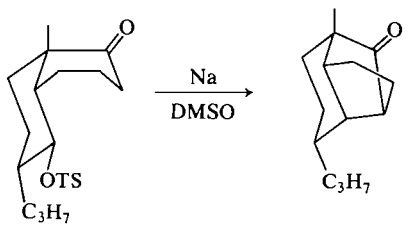

13 14

enolate ion and the ready closure of the latter ion to the cyclopropane **16**.

The approach via an intramolecular ene reaction of a compound of type **11** has ample precedent in the case of simpler systems in the extensive work of Conia and LePerchec (8). It has the advantage

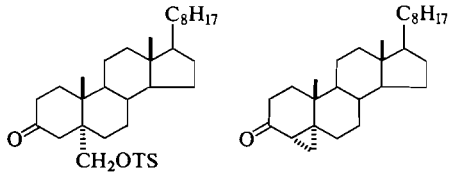

15 16

over the route via compounds of type **15** that closure to cyclopropyl ketones via the Δ^3 enol is reversible while closure to the bicyclo[2.2.1]-heptane system via the Δ^2 enol is not (9). Interestingly the closure of **11** to **12** is again an ambiguous type of reaction in terms of Baldwin's rules.

The most direct route to the 5-vinyl 3-keto steroids related to **11** that were required for this approach appeared to be the conjugate addition of lithium divinylcuprate to the corresponding Δ^4-3-keto steroids. It is known that both lithium dimethylcuprate and diethylcuprate add to cholest-4-en-3-one (**17**) to give exclusively the 5β-methyl derivative **18** (10) and 5β-ethyl derivative **19** (11), respectively. In spite of the reported greater reactivity of lithium divinylcuprate relative to lithium dimethylcuprate (12) we were unable to effect vinylation either in the presence of dimethyl sulfide (13) or tri-*n*-butylphosphine (14). This failure may be related to the lower thermostability of lithium divinylcuprate (15).

However, success was achieved in the vinylation by this method of a Δ^4-3-keto steroid lacking a C19

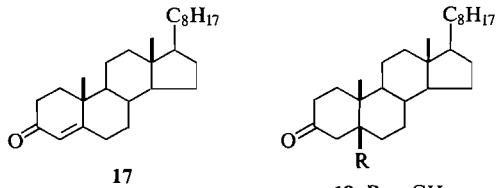

17

18, R = CH_3
19, R = C_2H_5

methyl group. Treatment of 19-nortestosterone (**20**) with lithium divinylcuprate – tri-*n*-butylphosphine complex gave a product that is assigned structure **21**. Its gross structure follows from its ir (2.80 (w), 5.86, 6.08 (w), 10.1 (w), 10.90 (w) μm), uv (272–282 nm (ε 21)), and ^{1}H nmr spectra (δ 0.80 (s, 3H), 3.5–3.8 (m, 1H), 4.8–6.0 (m, 3H)). The 5β-vinyl configuration is assigned on the basis of analogy with the 5β configuration of the addition products **18** and **19**; the stereochemistry of the formation of these has been interpreted in terms of

Can. J. Chem. Downloaded from www.nrcresearchpress.com by 210.87.254.42 on 09/06/12
For personal use only.

Can. J. Chem. Downloaded from www.nrcresearchpress.com by 210.87.254.42 on 09/06/12
For personal use only.

hindrance of α attack by the axial 7α and 9α hydrogens (16) and it is to be expected that the absence of a C19 methyl group in **20** would yet further favor β over α attack. Furthermore, the reaction of the closely related enone **22** with vinylmagnesium bromide catalyzed by cupric acetate has been shown to give the 5β product **23** (17). Oxidation of **21** with chromium trioxide gave the dione **24**, as shown by its ir spectrum (5.75, 5.84, 6.09 (w), 10.10 (w), 10.90 (w) μm).

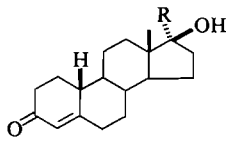

20, R = H
22, R = CH_3

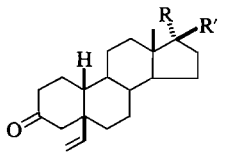

21, R = H, R′ = OH
23, R = CH_3, R′ = OH
24, R, R′ = O

Since it was desired to examine bridge formation in both the 5β and 5α series, the preparation of a 5α-vinyl 3-keto steroid was also undertaken. Because of the high β stereoselectivity of the addition reactions discussed above, it was necessary to take a more pedestrian approach to the 5α-vinyl compound. Cholest-4-en-3-one (**17**) was converted in several steps to the aldehyde **25** (18),[4] which in turn was converted by a Wittig reaction followed by trans-ketalization to the 5α-vinyl 3-keto steroid **26**.

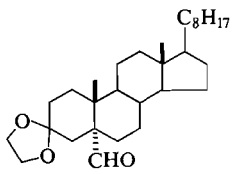

25

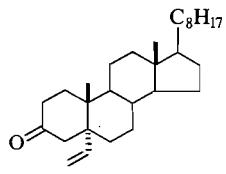

26

Heating of a 3% solution of **26** in decalin in a sealed tube at 350°C for 14 h gave a product in 41% yield that is assigned the desired structure **27**. Its ir spectrum showed a carbonyl-stretching band at 5.74 μm, characteristic of a bicyclo[2.2.1]heptan-2-one. A maximum at 280 nm (ε 50) in its uv spectrum and a signal at δ 218.5 in its ^{13}C nmr spectrum are also in accord with the presence of this system.[5] As expected, its ^1H nmr showed no signals downfield of δ 2.70. Recording of this spectrum at 80 MHz in conjunction with lanthanide-induced shift experiments utilizing increasing amounts of $Eu(fod)_3$ established the *syn*-stereochemistry of the methyl group at C1′ (the latter carbon is assigned the α configuration on the basis of the configuration at C5 in **26**).[6] These experiments permitted the assignment of signals in the δ 1.9–2.7 region as follows (cf. **28***a*): δ 1.92 (d, J = 17 Hz, H_C), 2.08 (dd, J = 17, 3.5 Hz, H_D), 2.33 (br d, J = 5 Hz, H_A), 2.61 (v br q, J = 8 Hz, H_B). The splitting pattern of the H_D signals shows that in addition to geminal coupling with H_C (J = 17 Hz) it is coupled with another proton (J = 3.5 Hz); this is only possible in the *syn* isomer **27** (**28***a*), where long range coupling with the H_B proton will occur as a result of the "W" arrangement of these protons; in the *anti* isomer **28***b* no such coupling is to be anticipated (19). The H_B signal appears as a very broad quartet (J = 8 Hz); the primary coupling is with the C1′ methyl protons and the broadness is attributable to further, unresolved coupling with

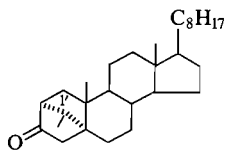

27

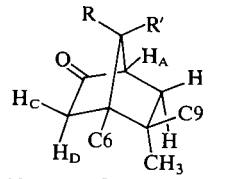

28*a*, R = CH_3, R′ = H_B
28*b*, R = H_B, R′ = CH_3

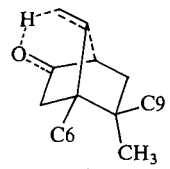

29

H_A and H_D. The configuration assigned to C1′ in **27** on this basis is that anticipated in terms of the transition state for the ene reaction of the enol of **26** (cf. **29**).

Thermolysis of the 19-nortestosterone derivative **21** is complicated by the presence of the thermally unstable 17β hydroxyl group. Under the optimum conditions for the isomerization of **26** to **27**, **21** gave a complex mixture, including aromatic compounds, as indicated by the ^1H nmr spectrum of the crude product. A pure product could be isolated in 11% yield whose spectra showed it to be **30** (the *syn* configuration at C1′ is assigned by analogy with **27**). In this case the signal of the C1′ methyl group at δ 0.87 (d, J = 8 Hz) could readily be identified in the ^1H nmr spectrum of the product; in the case of **27**, the corresponding signal was obscured by the side chain signals. Attempts to improve the yield of the ene reaction by protection of the hydroxyl group of **21** as the acetate or

[4]This aldehyde was also an intermediate in the preparation of **15** (see Experimental).

[5]The ^{13}C nmr spectra of **27** and related compounds will be discussed in full elsewhere.

[6]The terms *syn* and *anti* refer to the relationship of the bridge methyl group to the C3 carbonyl group.

Can. J. Chem. Downloaded from www.nrcresearchpress.com by 210.87.254.42 on 09/06/12
For personal use only.

tert-butyldimethylsilyl ether were unsuccessful. However, thermolysis of the corresponding dione **24** proceeded much more smoothly to give a 41% yield of a product assigned structure **31** on the basis of its spectroscopic properties (as in the case of **30**, the signal of the C1′ methyl group is readily discernible in the ^{1}H nmr spectrum of the product at δ 0.88 (d, J = 8 Hz)) and the fact that it is selectively reduced by sodium borohydride adsorbed on alumina (20) to **30** and is formed on chromic acid oxidation of the latter. Compound **31** was also formed in significant amount (~10%) on thermolysis of **21** when the decalin solution was not carefully freed of oxygen, presumably resulting from oxidation of the C17 hydroxyl group by decalin hydroperoxide formed by oxidation of decalin at 350°C.

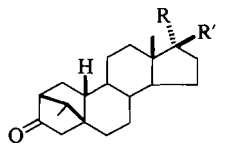

30, R = H, R′ = OH
31, R, R′ = O

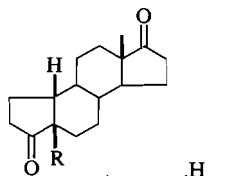

32, R =

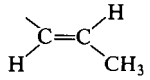

33, R = $CH_2CH_2CH_3$

A second product was isolated in 7% yield from the thermolysate of **24**. This product is isomeric with **31** and is assigned structure **32** based on the following considerations. It has two five-membered ring ketonic groups as revealed by a strong carbonyl-stretching band in its ir spectrum at 5.74 μm and signals at δ 218.5 and 220.8 in its ^{13}C nmr spectrum.[5] The presence of a *trans*-1-propenyl group is vouchsafed by a two-proton multiplet at δ 5.20–5.42 and a three-proton broad doublet (J = 5 Hz) at δ 1.61 in its ^{1}H nmr spectrum, and a band at 10.35 μm in its ir spectrum. The *trans* stereochemistry is also indicated by the occurrence of the vinyl methyl signal at δ 18.2 in its ^{13}C nmr spectrum.[5] The intensity of the $n \rightarrow \pi^*$ band at 296 nm (ε 200) in its uv spectrum suggests that there is homoconjugative interaction between the ethylenic bond and one of the carbonyl groups and thus that it is a β,γ unsaturated ketone (21). Hydrogenation gave a dihydro compound that is assigned structure **33**. The mass spectrum of this product has a weak molecular ion at *m/e* 302 (4%) and a base peak at *m/e* 260 that results from loss of a fragment C_3H_6, as shown by accurate mass measurement. This loss can readily be interpreted in terms of a McLafferty rearrangement:

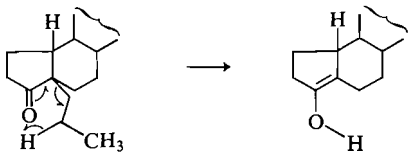

m/e 302 → *m/e* 260 + CH_2=$CHCH_3$

The occurrence of this rearrangement confirms that the *n*-propyl group in **33**, and thus the *trans*-propenyl group in **32**, is in the α relationship to one of the carbonyl groups.

The configuration of **32** at C5 is assigned on the basis of the sign of the Cotton effect shown by the C3 carbonyl group. In order to determine this it was necessary to remove the C17 carbonyl group, and this was accomplished by selective reduction to **34** with sodium borohydride adsorbed on alumina (20). The mass spectrum of the product showed it to be a dihydro compound and the fact that the C17 rather than the C3 carbonyl group is reduced is evidenced by a shift of the C18 methyl signal from δ 0.90 in the ^{1}H nmr spectrum of **32** to δ 0.80 in that of **34** (22) and by the retention of enhanced $n \rightarrow \pi^*$

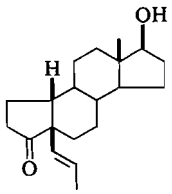

34

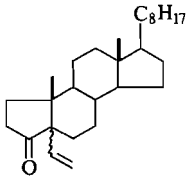

35*a*, 5α
35*b*, 5β

absorption in the uv spectrum of **34** (296 nm (ε 185)). The 17β configuration is assigned to **34** by analogy with the reduction of **31** to **30** by this reagent. It has been found for ketones **35***a* and **35***b* that the CD may be considered as a special case of the ketone octant rule where the double bond has the effect of increasing the magnitude of the chiroptical effect (11). Application of similar considerations to the closely related case of **34**, which exhibits a positive Cotton effect, leads to the assignment of the *cis* stereochemistry of the ring A/B junction as depicted. The amplitude of the chiroptical effect is smaller than that reported for **35***b* and this may be attributed in part to the additional methyl substituent on the double bond, which is located in a negative octant.

The formation of **32** in addition to **31** in the thermolysis of **24** may be interpreted as involving the intermediacy of the cyclopropyl ketone **36**,

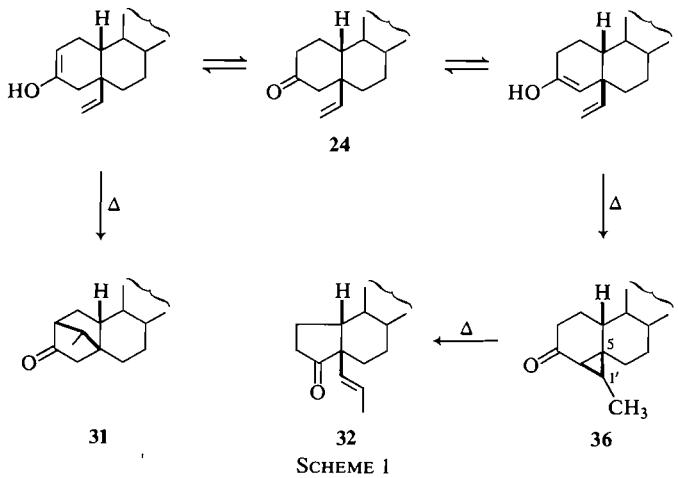

SCHEME 1

formed by an ene reaction of the Δ^3 enol of **24** (Scheme 1). This ketone can revert to **24**, but can also undergo a cyclopropyl–allylic rearrangement to give **32**. Such a rearrangement could occur by cleavage of the C5—C1′ bond and migration of the carbonyl group in either a concerted (cf. **37***a*) or stepwise fashion (cf. **37***b*). A precedent for such a rearrangement is found in the thermal rearrangement of **38** to **39** (23), which on the basis of kinetic evidence has been proposed to involve a concerted $_{\sigma}2_s + {}_{\sigma}2_a$ process analogous to that shown in **37***a*. In

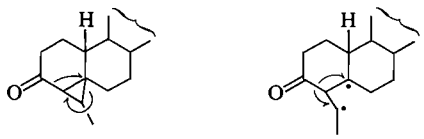

37*a* **37***b*

the present case the observation of the formation of only the A/B-*cis* isomer provides some grounds for favoring the concerted mechanism. The *trans* configuration of the olefinic bond in the final product may have no mechanistic significance, since thermal isomerization of this bond could occur after its formation.

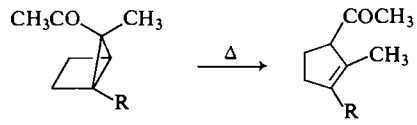

38 **39**

We conclude by referring briefly to the results of a preliminary study of the photochemistry of **30** in methanol. Three products were formed in a ~2:3:4 ratio as shown by vpc analysis. One product was separated by column chromatography and identified by its spectra as the ester **40**. The other two products, which could not be separated from each other by column chromatography are assigned structures **41** and **42**. The three products are considered to arise by the routes shown in Scheme 2, which are analogous to processes previously observed in the photochemistry of bicyclo[2.2.1]-heptan-2-ones (24, 25). Three features are noteworthy in comparison with the photochemistry of the simpler 7-*syn* substituted bicyclo[2.2.1]heptan-2-ones, camphor (**46**) (26) and apocamphor (**47**) (24, 25). First, the postulated enal intermediate **44** could not be detected among the products, while in the cases of **46** and **47** the enals of type **48** are the major isolated products and oxetane formation is only observed upon prolonged irradiation. Second, no products could be detected that arise from closure of the diradical **43** to a cyclic oxacarbene, whereas products derived from oxacarbene **49** are formed in the cases of **46** and **47**. Third, ketene **45** is implicated as an intermediate although ketene-derived products are not observed in the cases of **46** and **47**. We attribute these special features to the geometrical restrictions imposed by the steroidal framework in **43** and **44**. In the former case we suggest that these favor hydrogen transfer to give **45** over cyclization to an oxacarbene; a similar proposal has been made previously (25) to account for the formation of the ketene-derived product **50** on photolysis of carvonecamphor (**51**) in methanol (27). In the latter case we suggest that these favour exciplex formation between the $n \rightarrow \pi^*$ singlet state of the carbonyl group and the olefinic bond (28), thus facilitating oxetane formation. It may finally be noted that the formation of enal **44** from **43** rather than enal **52**, which would give rise to oxetanes distinguishable from **41** and **42**, confirms the earlier *syn* assignment of the methyl group at

Can. J. Chem. Downloaded from www.nrcresearchpress.com by 210.87.254.42 on 09/06/12
For personal use only.

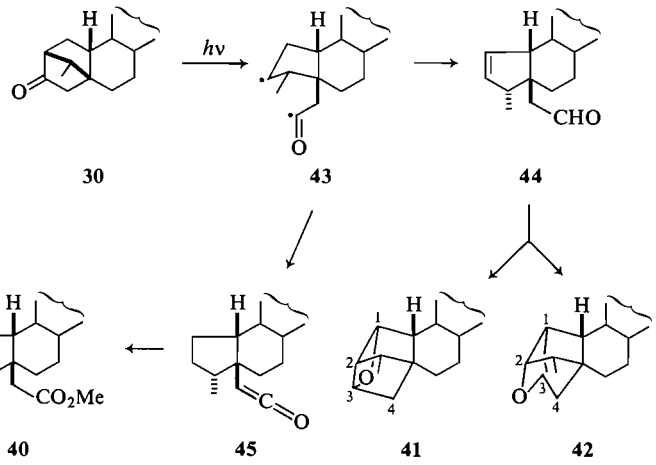

30 43 44 40 45 41 42

SCHEME 2

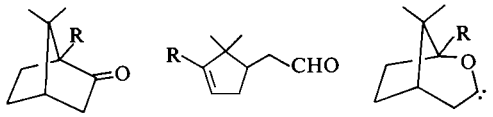

46, R = CH_3 **48** **49**
47, R = H

C1′, since the *anti*-stereoisomer would be expected to give **52** rather than **44** (24, 25).

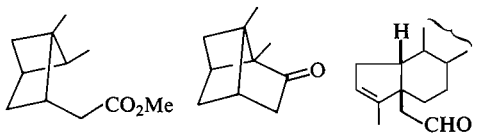

50 **51** **52**

Experimental

Melting points were determined on a Fisher-Johns apparatus and are uncorrected.The ir and nmr spectra were taken in $CHCl_3$ and $CDCl_3$ solutions, respectively. The relative abundance (%) of low resolution mass spectral peaks is given in parentheses after their *m/e* values. Vapor phase chromatographic (vpc) analyses were carried out on a Varian 2700 gas chromatograph, equipped with a flame ionization detector. The temperature of the in-column injector and detector were set at 325°C and 340°C, respectively; oven temperatures ranging from 240°C to 280°C were used. The flow rate of the carrier gas (nitrogen) was adjusted at 40 mL/min. A 6 ft. glass column (od 1/8 in., id 2 mm) packed with 3% OV-17 on Chromosorb W-HP, 80/100 was utilized. The relative intensities and retention times were determined with a Varian chromatography Data System 111C. Analytical thin-layer chromatography (tlc) was carried out on 70 × 20 × 0.25 mm silica gel Q6-F plates from Quantum Industries. After elution, they were sprayed with a solution of ethanol/concentrated sulfuric acid 3:1 v/v containing a small amount of vanillin, and developed at 150°C for a few seconds. Preparative tlc was carried out on 20 × 20 cm plates coated with a 1-mm or 2-mm silica gel layer and activated at 150°C for 30 min prior to use. Column chromatography was performed on silica gel (Grace Davison, grade 923, 100/200) or neutral alumina (Woelm, activity I, 70/290, pH 7.5).

In a standard work-up the organic solution was washed twice with 5% aqueous sodium bicarbonate solution, twice with distilled water, and twice with brine. It was dried over anhydrous magnesium sulfate and concentrated *in vacuo* on a rotary evaporator under water aspirator pressure. All diethyl ether and pentane used for extraction was distilled prior to use.

*10α-des-*A*-Cholestan-5-one and 10β-des-*A*-Cholestan-5-one*

A solution of 5-oxo-*A*-nor-3,5-secocholestan-3-oic acid (29) (1.69 g, 4.2 mmol) in methanol (25 mL) was titrated with 0.2 *N* methanolic sodium hydroxide (22.3 mL). At the end-point a drop of very dilute aqueous hydrochloric acid was added. Evaporation of the solvent afforded the sodium salt of the acid (1.54 g, 86%). An intimate mixture of the salt (0.80 g, 1.85 mmol) and sodium phenylacetate (3.0 g, 19.0 mmol) was heated at 295°C in a 40:7:53 w/w/w $NaNO_2/NaNO_3/KNO_3$ bath under reduced pressure (0.05 Torr) for 3 h (30). The cooled reaction mixture was dissolved in diethyl ether. The usual work-up and chromatography on silica gel with benzene gave 10α-des-*A*-cholestan-5-one (0.50 g, 81%), which was recrystallized from methanol; mp 58–60°C (lit. (30) mp 62–63°C); λ_{max}: 5.85 μm; $^{H}\delta$: 0.70–2.60 (m), 0.76 (s, 3H), 1.01 (d, J = 6 Hz, 3H); *m/e*: 332 (100) (M^+). Further elution gave 10β-des-*A*-cholestan-5-one (80 mg, 13%), which was crystallized from methanol; mp 71–72°C; λ_{max}: 5.86 μm; $^{H}\delta$: 0.70–2.60 (m), 0.76 (s, 3H), 1.10 (d, J = 7 Hz, 3H); *m/e*: 332 (100) (M^+). *Anal.* calcd. for $C_{23}H_{40}O$: C 83.07, H 12.12, Mol. Wt. 332.3079; found: C 82.81, H 12.15, Mol. Wt. (ms) 332.3077.

*Epimerization of 10β-des-*A*-Cholestan-5-one*

A 3 *M* solution of sodium ethoxide in dry ethanol (5 drops) was added to a solution of 10β-des-*A*-cholestan-5-one (10 mg, 0.03 mmol) in dry ethanol (2 mL). After 90 min the 1:6 equilibrium mixture of this with 10α-des-*A*-cholestan-5-one was obtained, as determined by tlc with benzene as eluent.

*des-*A*-Cholest-5(10)-en-5-yl Acetate (6)*

A solution of 10α-des-*A*-cholestan-5-one (170 mg, 0.51 mmol) in carbon tetrachloride (3 mL) was treated with freshly distilled acetic anhydride (0.80 mL) and 70% aqueous perchloric acid (1 drop) and kept at room temperature for 24 h. The dark brown solution was diluted with diethyl ether (30 mL) and worked up in the usual manner to give a mixture of des-*A*-cholest-5(10)-

Can. J. Chem. Downloaded from www.nrcresearchpress.com by 210.87.254.42 on 09/06/12
For personal use only.

Can. J. Chem. Downloaded from www.nrcresearchpress.com by 210.87.254.42 on 09/06/12
For personal use only.

en-5-yl acetate (**6**) and 10α-des-*A*-cholest-5-en-5-yl acetate in an approximately 7:3 ratio (30). Chromatography with benzene on a 2-mm silica gel preparative plate afforded pure **6** (95 mg, 50%), which was crystallized from methanol/acetone; mp 72–74°C (lit. (30) mp 73–74°C); λ_{max}: 5.74, 6.15 (w) μm; $^H\delta$: 0.7–2.2 (m), 0.70 (s, 3H), 1.45 (br s, 3H), 2.10 (s, 3H).

*Reaction of des-*A*-Cholest-5(10)-en-5-yl Acetate (6) with Cyclopentadiene*

(*i*) Dicyclopentadiene (30 mg, 0.23 mmol) and **6** (270 mg, 0.45 mmol) were heated in a sealed tube at 180°C for 12 h. Purification of the reaction mixture by column chromatography on silica gel eluted with pentane followed by pentane/benzene (4:1 v/v) afforded 10α-des-*A*-cholestan-5-one (90 mg) and unconsumed **6** (10 mg).

(*ii*) A solution of **6** (140 mg, 0.38 mmol) and cyclopentadiene (50 mg, 0.76 mmol) in freshly distilled acetic anhydride (4 mL) was heated in a sealed tube at 180°C for 17 h. Evaporation of the solvent and chromatography on a 2-mm silica gel preparative plate eluted with benzene yielded unconsumed starting material (85 mg).

(*iii*) Aluminum trichloride (15 mg, 0.12 mmol) was added to a solution of **6** (45 mg, 0.12 mmol) and cyclopentadiene (15 mg, 0.25 mmol) in dry dichloromethane (15 mL). The reaction mixture was stirred at room temperature under nitrogen for 15 h. Slow addition of water followed by the usual work-up afforded an oil (41 mg), which was a complex mixture, as indicated by tlc analysis.

*des-*A*-Cholest-5-en-5-carbonitrile (7)*

Potassium cyanide (3.0 g, 0.046 mol) was added to a solution of 10α-des-*A*-cholestan-5-one (0.55 g, 1.6 mmol) in absolute ethanol (25 mL). Glacial acetic acid (3.2 mL) was added dropwise to the mixture kept at 0°C. At the end of the addition the reaction mixture was stirred at 0°C for 1 h and at room temperature for 2 h. Addition of water, extraction with ether, and the usual work-up afforded 5ξ-cyano-10α-des-*A*-cholestan-5ξ-ol (500 mg, 87%) as a white powder; λ_{max}: 2.90 (w), 4.48 (w) μm; $^H\delta$: 0.60–2.30 (m), 0.69 (s, 3H), 1.05 (d, J = 7 Hz, 3H), 3.55 (br s, 1H).

A solution of 5ξ-cyano-10α-des-*A*-cholestan-5ξ-ol (220 mg, 0.63 mol) and phosphorus oxychloride (0.2 mL) in pyridine (3 mL) was heated at reflux under nitrogen for 18 h. The reaction mixture was poured into ice-water acidified with concentrated hydrochloric acid (1 mL). Extraction with diethyl ether followed by the usual work-up and chromatography with benzene on a 2-mm silica gel preparative plate afforded **7**; λ_{max}: 4.50 (w), 6.08 (w) μm; $^H\delta$: 0.70–2.30 (m), 0.70 (s, 3H), 1.20 (d, J = 7 Hz, 3H), 6.45–6.75 (m, 1H).

Reaction of 7 with Cyclopentadiene

A mixture of **7** (130 mg, 0.38 mmol) and cyclopentadiene (25 mg, 0.40 mmol) was heated in a sealed tube at 170°C for 14.5 h. After evaporation of the solvent and of the remaining cyclopentadiene, **7** was recovered together with polymeric compounds, as shown by tlc analysis and ir and ^{1}H nmr spectroscopy. A similar result was obtained when the reaction was carried out for 4 days at 180°C with a tenfold excess of cyclopentadiene.

5-Cyano-5α-cholestan-3-one and 5-Cyano-5β-cholestan-3-one

(*i*) *Potassium Cyanide in Methanol*

5-Cyano-5α-cholestan-3-one was obtained in 10% yield by reaction of potassium cyanide and cholest-4-en-3-one (**17**) in aqueous methanol, as described by Nagata *et al.* (31); mp 182–184°C (lit. (31) mp 182–184°C); λ_{max}: 4.52 (w), 5.83 μm; $^H\delta$: 0.65–2.30 (m), 0.66 (s, 3H), 1.11 (s, 3H), 2.32–2.45 (m, 2H); *m/e*: 411 (50) (M^+).

(*ii*) *Calcium Cyanide in* N*-Methylpyrrolidone*

Calcium cyanide (90%, 0.50 g, 5.2 mmol)[7] was added to a solution of cholest-4-en-3-one (**17**) (0.50 g, 1.3 mmol) in dry *N*-methylpyrrolidone (50 mL) (32). The suspension was stirred at room temperature for 6 days. The gray suspension was poured into water and the mixture was extracted with ethyl acetate. The usual work-up followed by column chromatography on silica gel with hexane/ethyl acetate (85:15 v/v) as eluent afforded 5-cyano-5α-cholestan-3-one (135 mg, 25%), mp 181–183°C, and 5-cyano-5β-cholestan-3-one (255 mg) contaminated by a small amount of **17** as indicated by ir and ^{1}H nmr spectroscopy; λ_{max}: 4.52 (w), 5.83 μm; $^H\delta$: 0.70 (s 3H), 1.28 (s, 3H).

5-Cyano-5α-cholestan-3-one Ethylene Acetal

A solution of 5-cyano-5α-cholestan-3-one (1.70 g, 40 mmol), ethylene glycol (1.37 g, 22 mol), and *p*-toluenesulfonic acid (76 mg, 0.80 mmol) in dry toluene (150 mL) was heated at reflux in a Dean-Stark apparatus for 21 h (18). The usual work-up afforded 5-cyano-5α-cholestan-3-one ethylene acetal (1.54 g, 85%); λ_{max}: 4.55 (w) μm; $^H\delta$: 0.65–2.10 (m), 0.66 (s, 3H), 0.95 (s, 3H), 3.70–4.30 (m, 4H); *m/e*: 455 (75) (M^+).

3,3-Ethylenedioxy-5α-cholestane-5-carbaldehyde (25)[8]

To a solution of 5-cyano-5α-cholestan-3-one ethylene acetal (1.20 g, 3.74 mmol) in hexane (freshly distilled from $LiAlH_4$; 110 mL) kept at 0°C under nitrogen diisobutylaluminum hydride (1 *M* in hexane; 10 mL, 10 mmol) was added over a period of 1 h.[9] The mixture was stirred for 1 h at 0°C and for 18 h at room temperature and then added to saturated aqueous sodium sulfate (1 mL). No immediate reaction occurred, but after 10 min the temperature of the solution increased (29°C) and a white gel formed; after 1 h the temperature had decreased and the white solid formed was separated by filtration. The usual work-up of the filtrate afforded 5-iminomethyl-5α-cholestan-3-one ethylene acetal (1.26 g, 74%); λ_{max}: 3.10 (w), 6.11 (w) μm; $^H\delta$: 0.65–2.10 (m), 0.66 (s, 3H), 1.10 (s, 3H), 3.70–3.85 (m, 5H), 8.46 (br s, 1H); *m/e*: 457 (100) (M^+).

A solution of the iminomethyl compound (140 mg, 0.31 mmol) and dilute aqueous acetic acid (10%, 4 mL) in THF (15 mL) was kept at room temperature for 1 h and then neutralized with aqueous 5% $NaHCO_3$. Extraction with diethyl ether and the usual work-up afforded **25** (114 mg, 81%), which crystallized from diethyl ether; mp 113–114°C (lit. (18) mp 110–112°C); λ_{max}: 5.86 μm; $^H\delta$: 0.6–2.1 (m), 0.66 (s, 3H), 1.03 (s, 3H), 3.5–4.0 (m, 4H), 9.9 (s, 1H); *m/e*: 458 (1) (M^+).

5-Tosyloxymethyl-5α-cholestan-3-one (15)

Compound **25** was reduced with lithium aluminum hydride (35) to yield 5-hydroxymethyl-5α-cholestan-3-one ethylene acetal (91 mg, 82%),[8] which was recrystallized from acetone: mp 170–171°C (lit. (35) mp 175–177°C); λ_{max}: 2.95 (w) μm; $^H\delta$:

[7]Identical results were obtained with calcium cyanide that was purified before use by formation of the ammonia complex $[Ca(CN)_2 \cdot 2NH_3]$ (33).

[8]This experiment was conducted under rigorously anhydrous conditions under a positive pressure of argon or nitrogen.

[9]Cf. ref. 34 for a related reduction with diisobutylaluminum hydride, where, however, the iminomethyl compound was not isolated; cf. also the reduction of 5-cyano-5α-cholestan-3-one ethylene acetal with lithium triethoxyaluminum hydride to give the iminomethyl compound (18).

Can. J. Chem. Downloaded from www.nrcresearchpress.com by 210.87.254.42 on 09/06/12
For personal use only.

0.60–2.20 (m), 0.63 (s, 3H), 1.03 (s, 3H), 2.20–2.60 (br m, 1H, absent after D_2O treatment), 3.30–4.10 (br m, 4H); *m/e*: 460 (35) (M^+).

The 5-hydroxymethyl acetal was converted to the corresponding tosylate, 5-tosyloxymethyl-5α-cholestan-3-one ethylene acetal (65 mg, 47%) (36); λ_{max}: 6.24 (w), 8.50 μm; $^H\delta$: 0.60–2.0 (m), 0.61 (s, 3H), 1.00 (s, 3H), 2.43 (br s, 3H), 3.70–3.80 (m, 4H), 4.33 and 4.60 (AB system, J = 10 Hz, 2H), 7.26 and 7.76 (AB system, J = 8 Hz, 4H).

A solution of the tosyloxymethyl acetal (23 mg, 0.03 mmol) and *p*-toluenesulfonic acid hydrate (1 mg, 0.005 mmol) in acetone (5 mL) was heated at reflux for 1 h. The acetone was evaporated and the residue was extracted with chloroform. Work-up in the usual manner afforded a mixture of 5-tosyloxymethyl-5α-cholestan-3-one (**15**) and 4α,5-dihydro-3′*H*-cyclopropa[4,5]-5α-cholestan-3-one (**16**) as a white solid (17 mg). Fractional crystallization from ether afforded **15** (10 mg, 58%); mp 129–131°C (lit. (36) mp 116–117°C); λ_{max}: 5.85, 6.24 (w), 8.48 μm; $^H\delta$: 0.65–2.10 (m), 0.66 (s, 3H), 1.18 (s, 3H), 2.15–2.24 (m, 2H), 2.45 (br s, 3H), 4.33 and 4.60 (AB system, J = 10 Hz, 2H), 7.26 and 7.76 (AB system, J = 8 Hz, 4H); *m/e*: 398 (100) (M^+ − 172).

3′,4β-Dihydrocyclopropa[4,5]-5α-cholestan-3-one (16)

A solution of **15** (15 mg, 0.028 mmol) and *p*-toluenesulfonic acid (1 mg, 0.005 mmol) in acetone (4 mL) was heated at reflux for 5 h. The acetone was evaporated and the residue was extracted with chloroform. Work-up in the usual manner afforded **16** (10 mg, 90%), which was crystallized from diethyl ether/methanol; mp 135–137°C (lit. (36) mp 134–137°C); λ_{max}: 5.94 μm; λ_{max} (hexane) (ε): 272 (48) nm; $^H\delta$: 0.50–2.50 (m), 0.70 (s, 3H), 1.08 (s, 3H); *m/e*: 398 (100) (M^+).

Attempted Cyclization of 15 via its Δ^2 Enolate[8]

(*i*) To a solution of diisopropylamine (9.8 μL, 0.70 mmol) in THF (5 mL) cooled to −78°C, methyllithium in diethyl ether (1.67 *M*, 31 μL, 0.05 mmol) was added, and the resulting solution was stirred at −78°C for 1 h. A solution of **15** (31 mg, 0.050 mmol) in THF (5 mL) was added over a period of 10 min, and the reaction mixture was stirred at −78°C for 1 h, then at room temperature for 1 h. The excess base was decomposed by addition of water, and the reaction mixture was diluted with diethyl ether. Work-up in the usual manner afforded a crystalline material (27 mg), identified by ir and ^{1}H nmr spectroscopy as starting material.

(*ii*) The reaction was carried out under the same conditions as in (*i*) except that the reaction mixture was boiled under reflux for 4 h after it had warmed up to room temperature. After work-up, a solid product was obtained; λ_{max}: 5.80 (w), 5.94 μm; this was shown by tlc analysis to be a mixture of at least two products, one of which was identified as **16**; no spectroscopic evidence for the formation of a bicyclo[2.2.1]heptan-2-one system was obtained.

(*iii*) A solution of **15** (34 mg, 0.060 mmol) in 1,2-dimethoxyethane (2 mL) was added at −78°C over a period of 15 min to a solution of lithium diisopropylamide (0.080 mmol) in 1,2-dimethoxyethane, prepared at −78°C. The reaction mixture was stirred at −78°C for 1 h, then at room temperature for 16 h. After the usual work-up, a white solid was obtained, which by tlc analysis appeared to be a mixture of three compounds, including **16**; no spectroscopic evidence for the formation of a bicyclo-[2.2.1]heptan-2-one system was obtained.

17-β-Hydroxy-5-vinyl-5β-estran-3-one (21)[8]

A solution of vinyllithium in THF (1.56 *M*, titrated before use (37); 10.39 mL, 16.2 mmol) was added slowly under argon to a cooled (−78°C), stirred, solution of tetrakis[iodotri-(*n*-butylphosphine)copper(I)] (3.19 g, 8.14 mmol) (38) in THF (220 mL). The first-formed dark suspension became a clear yellow-orange solution when the addition of vinyllithium was complete. A solution of 17β-hydroxyestr-4-en-3-one (19-nortestosterone; **20**) (446 mg, 1.63 mmol) in THF (25 mL) was added slowly to the lithiumdivinyl cuprate solution kept at −78°C. After completion of the addition, the reaction mixture was stirred at −78°C for 2 h, allowed to warm up slowly to 0°C, and maintained at 0°C for 2 h; the initially clear solution became black after a few minutes at 0°C. The reaction mixture was poured into a saturated aqueous ammonium chloride solution and stirred overnight. The mixture was extracted with diethyl ether, and the combined extracts were washed with dilute aqueous ammonia, water, and brine, and dried over anhydrous magnesium sulfate. Evaporation of the solvent afforded an oil (420 mg, 85%),which crystallized from diethyl ether to give **21**, mp 171–172°C; λ_{max}: 2.80 (w), 5.86, 6.08 (w), 10.10 (w), 10.90 (w) μm; λ_{max} (CH_3OH) (ε): 272–282 (21) nm; $^H\delta$: 0.78–3.0 (m), 0.80 (s, 3H), 3.50–3.80 (m, 1H), 4.80–5.96 (m); *m/e*: 302 (60) (M^+). *Anal.* calcd. for $C_{20}H_{30}O_2$: C 79.42, H 10.00; found: C 79.43, H 9.92.

5-Vinyl-5β-estrane-3,17-dione (24)[8]

Chromium trioxide (dried *in vacuo* over P_2O_5; 0.60 g, 6.10 mmol) was added to a stirred solution of pyridine (distilled from barium oxide; 948 mg, 965 μL, 12 mmol) in dry dichloromethane (30 mL) under nitrogen at room temperature. The deep red solution was stirred at room temperature for 15 min and then a solution of **21** (300 mg, 1.00 mmol) in dichloromethane (5 mL) was added all at once. The orange-brown suspension was stirred for 20 min and filtered. The filtrate was diluted with diethyl ether (30 mL), washed with aqueous 5% sodium hydroxide and aqueous 10% hydrochloric acid, and subjected to the usual work-up. Compound **24** was obtained as a white solid (244 mg, 81%) and recrystallized from diethyl ether; mp 138–139°C; λ_{max}: 5.75, 5.84, 6.09 (w), 10.10 (w), 10.90 (w) μm; λ_{max} (CH_3OH) (ε): 285–291 (56) nm; $^H\delta$: 0.90–2.90 (m), 0.91 (s, 3H), 4.80–5.96 (m, 3H); *m/e*: 300 (100) (M^+). *Anal.* calcd. for $C_{20}H_{28}O_2$: C 79.96, H 9.39; found: C 79.90, H 9.29.

5-Vinyl-5α-cholestan-3-one (26)

5-Vinyl-5α-cholestan-3-one ethylene acetal was prepared from compound **25** by treatment with methylenetriphenylphosphorane (39); λ_{max}: 6.13 (w), 10.31 (w), 11.0 (w) μm; $^H\delta$: 0.65–2.0 (m), 0.65 (s, 3H), 1.05 (s, 3H), 3.80–3.92 (m, 4H), 4.73–5.22 (AB portion of ABX system), 6.30 (X portion of ABX system, $J_{AX} + J_{BX}$ = 27 Hz, 1H).

A solution of the 5-vinyl acetal (172 mg, 0.48 mmol) and *p*-toluenesulfonic acid (10 mg, 0.05 mmol) in acetone (20 mL) was heated at reflux for 1 h. After cooling, the solvent was evaporated, and the residue was dissolved in chloroform. The usual work-up afforded **26** (152 mg, 97%), which was recrystallized from diethyl ether/methanol (1:1 v/v); mp 141–143°C (lit. (39) mp 144–145°C); λ_{max}: 5.84, 6.12 (w), 10.28, 10.84 μm; $^H\delta$: 0.65–2.40 (m), 0.66 (s, 3H), 1.16 (s, 3H), 4.81–5.26 (AB portion of ABX system), 6.35 (X portion of ABX system, $J_{AX} + J_{BX}$ = 27 Hz, 1H); *m/e*: 412 (100) (M^+).

*2α,5-(*syn*-Methylmethano)-5α-cholestan-3-one (27)*

A solution of 5-vinyl-5α-cholestan-3-one (**26**) (85 mg, 0.21 mmol) in decalin (3 mL) was heated at 350°C for 14 h.[10] Evaporation of the decalin and chromatography on silica gel with elution with chloroform afforded **27** (35 mg, 41%) and unconsumed **26** (16 mg). Compound **27** was crystallized from methanol; mp 87–88°C; λ_{max}: 5.74 μm; λ_{max} (CH_3OH) (ε): 280 (50) nm; $^H\delta$: 0.65–2.38 (m), 0.66 (s, 3H), 0.93 (s, 3H), 2.38–2.70

[10]For details of the thermolytic conditions, see the thermolysis of compound **24** described below.

Can. J. Chem. Downloaded from www.nrcresearchpress.com by 210.87.254.42 on 09/06/12
For personal use only.

(br q, J = 6 Hz, 1H); *m/e*: 412 (50) (M^+). *Mol. Wt.* calcd. for $C_{29}H_{48}O$: 412.3705; found (ms): 412.3720.

*17β-Hydroxy-2β,5-(*syn-*methylmethano)-5β-estran-3-one (30)*

(i) Thermolysis of 17β-Hydroxy-5-vinyl-5β-estran-3-one (21)

Compound **21** (500 mg, 1.66 mmol) was thermolyzed in decalin (15 mL).[10] A complex mixture was obtained, as indicated by tlc and vpc analysis. After evaporation of the decalin and chromatography on silica gel with ethyl acetate/hexane (1:4 v/v), a small amount of compound **30** (54 mg, 11%) was isolated. This was crystallized from methanol; mp 205–206°C; λ_{max}: 2.80 (w), 2.90 (w), 5.75 μm; λ_{max} (CH_3OH) (ε): 271–284 (36) nm; $^H\delta$: 0.75–2.42 (m), 0.76 (s, 3H), 0.87 (d, J = 8 Hz, 3H), 3.55–3.76 (m, 1H); *m/e*: 302 (100) (M^+). *Mol. Wt.* calcd. for $C_{20}H_{30}O_2$: 302.2246; found (ms): 302.2248.

*(ii) Reduction of 2β,5-(*syn-*Methylmethano)-5β-estrane-3,17-dione (31)*

A solution of **31** (120 mg, 0.40 mmol) (*vide infra*) in diethyl ether (25 mL) was added all at once to a vigorously stirred suspension of $NaBH_4/Al_2O_3$[11] (1.20 g, 12.7 mmol $NaBH_4$) in diethyl ether. After 5.5 h tlc analysis indicated that all the starting material had reacted to give one major product together with a minor product of higher polarity. Filtration, evaporation of the solvent, and chromatography on a 2-mm silica gel preparative plate with hexane/ethyl acetate (7:3 v/v) afforded **30** (73 mg, 60%), which crystallized from methanol; mp 205–206°C; the ir, ^1H nmr, and mass spectra of the reduction product were identical to those of the product obtained as in (*i*).

*Thermolysis of 24. Formation of 2β,5-(*syn-*Methylmethano)-5β-estrane-3,17-dione (31) and 5-(*trans-*Propenyl)-*A-*nor-5β-estrane-3,17-dione (32)*

A solution of **24** (0.800 g, 2.67 mmol) in decalin (distilled under reduced pressure from $LiAlH_4$ and kept in the dark over molecular sieves; 12 mL) was transferred into three pyrolysis tubes, previously rinsed with an alkaline solution, then with distilled water, and dried at 120°C for 3 h. These tubes were connected to a vacuum line and after two freeze–thaw cycles were sealed under vacuum. The ampoules were placed inside a 1-L stainless steel Parr bomb containing decalin (120 mL) and heated at 350°C for 14 h.[12] At the end of this period the tubes were cooled to room temperature, opened, and the decalin was evaporated to give a pale yellow oil. Chromatography on a silica gel column with elution with hexane/ethyl acetate (9:1 v/v and 4:1 v/v) afforded three fractions: unconsumed **24** (147 mg), **31** (326 mg, 41%), and **32** (57 mg, 7%). Compound **31** was recrystallized from methanol; mp 191–192°C; λ_{max}: 5.74 μm; λ_{max} (CH_3OH) (ε): 269–276 (110) nm; $^H\delta$: 0.80–2.90 (m), 0.88 (d, J = 8 Hz, 3H), 0.90 (s, 3H); *m/e*: 300 (100) (M^+). *Anal.* calcd. for $C_{20}H_{28}O_2$: C 79.96, H 9.39, *Mol. Wt.* 300.2089; found: C 79.54, H 9.36, *Mol. Wt.* (ms) 300.2094.

Compound **32** was crystallized from diethyl ether; mp 195–196°C; λ_{max}: 5.74, 10.35 (w) μm; λ_{max} (methanol) (ε): 295–297 (200) nm; $^H\delta$:0.85–2.90 (m), 0.90 (s, 3H), 1.61 (br d, J = 5 Hz, 3H), 5.20–5.42 (m, 2H). *Mol. Wt.* calcd. for $C_{20}H_{28}O_2$: 300.2089; found (ms): 300.2091.

Compound **31** was also obtained by oxidation of **30** with Jones reagent under the conditions used for the oxidation of **21** to **24**.

[11]Prepared by addition of a slurry of $NaBH_4$ (1.0 g) in distilled water (1.0 mL) to neutral alumina (10 g); the mixture was stirred for 6 h until it was homogeneous and dried overnight *in vacuo* (20).

[12]Alternatively, the tubes were inserted into an electrically heated, cylindrical glass-oven and heated at 350°C.

*5-(*n-*Propyl)-*A-*nor-5β-estrane-3,17-dione (33)*

A solution of **32** (20 mg, 0.067 mmol) in ethyl acetate (5 mL) was added to a stirred suspension of activated Adams catalyst (3 mg) in ethyl acetate (3 mL) under atmospheric pressure of hydrogen. After 1 h one equivalent of hydrogen (1.6 mL) had been taken up. The catalyst was removed by filtration and the ethyl acetate was evaporated to give **33** as a white amorphous solid; λ_{max}: 5.76 μm; $^H\delta$: 0.85–2.80 (m), 0.90 (s); *m/e*: 302 (4) (M^+), 260 (100) (M^+-42). *Mol. Wt.* calcd. for $C_{20}H_{30}O_2$: 302.2246; found (ms): 302.2245; calcd. for $C_{17}H_{24}O_2$: 260.1776; found (ms): 260.1795.

*17β-Hydroxy-5-(*trans-*propenyl)-*A-*nor-5β-estran-3-one (34)*

A solution of **32** (20 mg, 0.067 mmol) in diethyl ether (2 mL) was added all at once to a stirred suspension of $NaBH_4/Al_2O_3$[11] (500 mg; 5.28 mmol $NaBH_4$) in diethyl ether (5 mL). After 1 h all the starting material had been converted into a single product, as indicated by tlc and vpc analysis. Filtration and evaporation of the solvent from the filtrate gave **34** (17 mg, 85%) as a white amorphous solid; λ_{max}: 2.90 (w), 5.75, 10.44 (w) μm; λ_{max} (ε): 296 (185) nm; $^H\delta$: 0.70–2.20 (m), 0.80 (s, 3H), 1.61 (d, J = 5 Hz, 3H), 3.45–3.90 (m, 1H), 5.20–5.40 (m, 2H); *m/e*: 302 (100) (M^+); CD (*c* 1.24, MeOH) 22°C: $[\theta]_{340}$ 0, $[\theta]_{297}$ +1200, $[\theta]_{240}$ 0. *Mol. Wt.* calcd. for $C_{20}H_{30}O_2$: 302.2246; found (ms): 302.2242.

*Irradiation of 17β-Hydroxy-2β,5-(*syn-*methylmethano)-5β-estran-3-one (30)*

A solution of **30** (100 mg, 0.33 mmol) in methanol (boiled under reflux over magnesium and then distilled; 20 mL) was irradiated in Pyrex under nitrogen with a Hanovia 450-W medium-pressure mercury arc lamp for 12 h to give a mixture of three components in the approximate ratio 2:3:4, as determined by vpc analysis. The usual work-up and chromatography on a 2-mm silica gel preparative plate afforded two major fractions. The slower moving fraction (10 mg) was shown by vpc analysis to be a single product, compound **40**; λ_{max}: 2.80 (w), 5.78 μm; $^H\delta$: 0.55–2.22 (m), 0.75 (s, 3H), 0.91 (br d, J = 6 Hz, 3H), 3.61 (s, 3H), 3.4–3.6 (br m); *m/e*: 334 (9) (M^+), 260 (100) (M^+-74). *Mol. Wt.* calcd. for $C_{21}H_{34}O_3$: 334.2508; found (ms) 334.2500; calcd. for $C_{18}H_{28}O$: 260.2140; found: 260.2135.

The second fraction was a mixture of **41** and **42**; λ_{max}: 2.80 (w), 10.5 (m), 11.0 (m) μm; $^H\delta$: 3.5–3.8 (m), 4.5–4.7 (m). Gas chromatographic – mass spectral analysis showed that one component has *m/e* 320 (M^+) and 260 ($M^+ - C_2H_2O$; base peak) and the other *m/e* 302 (M^+) and 258 ($M^+ - C_2H_4O$; base peak).

Acknowledgement

We thank the Natural Sciences and Engineering Research Council of Canada for support of this work.

1. P. YATES and F. M. WALLISER. Can. J. Chem. **54**, 3508 (1976).
2. F. M. WALLISER and P. YATES. Chem. Commun. 1025 (1979).
3. W. NAGATA, M. NARISADA, and T. WAKABAYASHI. Chem. Pharm. Bull. **16**, 875 (1968).
4. A. J. SOLO, S. ENG, and B. SINGH. J. Pharm. Sci. **62**, 1474 (1973).
5. M. Z. NAZER. J. Org. Chem. **30**, 1737 (1965).
6. J. E. BALDWIN and L. I. KRUSE. Chem. Commun. 233 (1977); J. E. BALDWIN. Chem. Commun. 734 (1976).
7. J. E. MCMURRY. J. Am. Chem. Soc. **90**, 6821 (1968).
8. J. M. CONIA and P. LEPERCHEC. Synthesis, 1 (1975).
9. G. L. LANGE and J. M. CONIA. Nouv. J. Chem. **1**, 189 (1977); J. M. CONIA and G. L. LANGE. J. Org. Chem. **43**, 564 (1978).

10. R. E. IRELAND and G. PFISTER. Tetrahedron Lett. 2145 (1969); D. C. MUCHMORE. Org. Synth. **52**, 109 (1972).
11. T. AKIYAMA, D. PEDDER, J. V. SILVERTON, J. I. SEEMAN, and H. ZIFFER. J. Org. Chem. **40**, 3675 (1975).
12. H. O. HOUSE, C. Y. CHU, J. M. WILKINS, and M. J. UMEN. J. Org. Chem. **40**, 1460 (1975); G. H. POSNER, C. E. WHITTEN, J. J. STERLING, and D. J. BRUNELLE. Tetrahedron Lett. 2591 (1974).
13. R. D. CLARK and C. H. HEATHCOCK. J. Org. Chem. **41**, 1396 (1976).
14. J. HOOZ and R. B. LAYTON. Can. J. Chem. **48**, 1626 (1970).
15. H. O. HOUSE and J. M. WILKINS. J. Org. Chem. **43**, 2443 (1978); H. O. HOUSE. Acc. Chem. Res. **9**, 59 (1976).
16. J. A. MARSHALL, W. I. FANTA, and H. ROEBKE. J. Org. Chem. **31**, 1016 (1966).
17. H. MORI and R. OH-UCHI. Chem. Pharm. Bull. **23**, 559 (1975).
18. W. NAGATA, S. HIRAI, H. ITAZAKI, and K. TAKEDA. Justus Liebigs Ann. Chem. **641**, 196 (1961)
19. M. BARFIELD and B. CHAKRABARTI. Chem. Rev. **69**, 757 (1969).
20. E. SANTANIELLO, F. PONTI, and A. MANZOCCHI. Synthesis, 891 (1978).
21. M. FISCHER and B. ZEEH. Chem. Ber. **101**, 2360 (1968).
22. W. ARNOLD, W. MEISTER, and G. ENGLERT. Helv. Chim. Acta, **57**, 1559 (1974).
23. J. P. GROSCLAUDE, H. U. GONZENBACH, J. C. PERLBERGER, and K. SCHAFFNER. Helv. Chim. Acta, **59**, 2919 (1976); M. J. JORGENSON and A. F. THACHER. Chem. Commun. 1030 1969).
24. P. YATES. Pure Appl. Chem. **16**, 93 (1968); P. YATES and R. O. LOUTFY. Acc. Chem. Res. **8**, 209 (1975).
25. P. YATES. J. Photochem. **5**, 91 (1976); J. C. L. TAM and P. YATES. Chem. Commun. 739 (1975).
26. W. C. AGOSTA and D. K. HERRON. J. Am. Chem. Soc. **90**, 7025 (1968).
27. J. MEINWALD and R. A. SCHNEIDER. J. Am. Chem. Soc. **87**, 5218 (1965); T. GIBSON and W. F. ERMAN. J. Org. Chem. **31**, 3028 (1969); J. MEINWALD, R. A. SCHNEIDER, and A. F. THOMAS. J. Am. Chem. Soc. **89**, 70 (1967).
28. R. R. SAUERS, A. D. ROUSSEAU, and B. BYRNE. J. Am. Chem. Soc. **97**, 4947 (1975).
29. J. T. EDWARDS, D. HOLDER, W. H. LUNN, and I. PUSKAS. Can. J. Chem. **39**, 599 (1961).
30. M. P. HARTSHORN and E. R. H. JONES. J. Chem. Soc. 1312 (1962).
31. W. NAGATA, S. HIRAI, H. ITAZAKI, and K. TAKEDA. J. Org. Chem. **26**, 2413 (1967).
32. H. B. HENBEST and W. R. JACKSON. J. Chem. Soc. C, 2465 (1967).
33. H. H. FRANCK and C. FREITAG. Angew. Chem. **39**, 1430 (1926); L. J. CHRISTMANN and A. G. HOUPT. U.S. Patent No. 2,386,434 (1945); Chem. Abstr. **40**, 684 (1946).
34. J. A. MARSHALL, N. H. ANDERSON, and J. W. SCHLICHER. J. Org. Chem. **35**, 858 (1970).
35. S. HIRAI. Chem. Pharm. Bull. **9**, 854 (1961).
36. W. NAGATA and M. NARISADA. Chem. Pharm. Bull. **16**, 867 (1968).
37. W. G. KOFRON and L. M. BACLAWSKI. J. Org. Chem. **41**, 1879 (1976).
38. G. B. KAUFFMAN and L. A. TETER. Inorg. Synth. **7**, 9 (1963).
39. W. NAGATA, M. NARISADA, T. SUGASAWA, and T. WAKABAYASHI. Chem. Pharm. Bull. **16**, 885 (1968).

Can. J. Chem. Downloaded from www.nrcresearchpress.com by 210.87.254.42 on 09/06/12
For personal use only.

Microbial hydroxylation of steroids. 7. Hydroxylation of *B*-nortestosterone and related compounds by *Rhizopus arrhizus* ATCC 11145, and ^{13}C nuclear magnetic resonance spectra of some *B*-norsteroids

HERBERT L. HOLLAND

Department of Chemistry, Brock University, St. Catharines, Ont., Canada L2S 3A1

Received December 29, 1980

HERBERT L. HOLLAND. Can. J. Chem. **59**, 1651 (1981).

The incubation of *B*-norandrost-4-ene-3-ones and *B*-nor-3β-hydroxyandrost-5-enes with *Rhizopus arrhizus* ATCC 11145 has been described. The products are consistent with a mechanism of oxidation at C-6 in which the stereochemistry of substitution at C-6 is controlled by stereoelectronic interactions in the substrate, and is not dictated by enzymic constraint during the reaction. The carbon-13 nuclear magnetic resonance spectra of several *B*-nor-Δ^4 and Δ^5 steroids have been presented.

HERBERT L. HOLLAND. Can. J. Chem. **59**, 1651 (1981).

On décrit l'incubation des *B*-norandrostène-4 ones-3 et des *B*-norhydroxy-3β androstènes-5 avec le *Rhizopus arrhizus* ATCC 11145. Les produits sont en accord avec un mécanisme d'oxydation au niveau du carbone en position 6 dans lequel la stéréochimie de la substitution en C-6 est contrôlée par des interactions stéréoélectroniques dans le substrat et elle n'est nullement due à une contrainte enzymatique au cours de la réaction. On présente les spectres de résonance magnétique nucléaire du C-13 de plusieurs *B*-nor-Δ^4 et Δ^5 stéroides.

[Traduit par le journal]

Introduction

The mechanism of the hydroxylation of androst-4-ene-3,17-dione (**1***a*) at C-6β by the fungus *Rhizopus arrhizus* ATCC 11145 has been studied in some detail (1–6). The reaction proceeds by enzymic enolization of the Δ^4-3-ketone, followed by stereoelectronically controlled axial addition of electrophilic oxygen to the resulting enol, giving rise to **1***b* stereospecifically. A feature of this mechanism is that the stereochemistry of substitution at C-6 of the product is determined largely by conventional stereoelectronic interactions during the oxidation process, rather than being dictated by constraints placed upon the reactants by their interaction with the enzyme.

In this paper, the incubations with *R. arrhizus* of the Δ^4-3-keto-*B*-norsteroids **2***a* and **3***a*, and of the Δ^5-*B*-norsteroids **4***a* and **4***b* are described, which support the mechanistic interpretation outlined above. In addition, the ^{13}C nuclear magnetic resonance spectra of several *B*-norsteroids are presented.

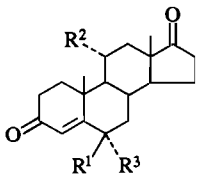

1

a $R^1 = R^2 = R^3 = H$
b $R^1 = OH, R^2 = R^3 = H$
c $R^1 = R^3 = H, R^2 = OH$
d $R^1 = R^2 = H, R^3 = OH$

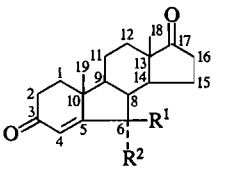

2

a $R^1 = R^2 = H$
b $R^1 = OH, R^2 = H$
c $R^1 = H, R^2 = OH$

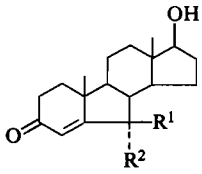

3

a $R^1 = R^2 = H$
b $R^1 = OH, R^2 = H$
c $R^1 = H, R^2 = OH$

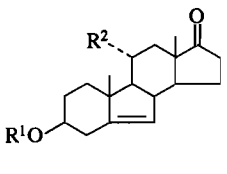

4

a $R^1 = R^2 = H$
b $R^1 = Ac, R^2 = H$
c $R^1 = H, R^2 = OH$

Results and Discussion

B-norandrost-4-ene-3,17-dione (**2***a*) was metabolized by *R. arrhizus* to give three products in low yield. The difficulty of separation of these products precluded their large scale preparation, but by repeated chromatography pure samples were obtained and identified as *B*-nortestosterone (**3***a*), and the 6α- and 6β- hydroxy-*B*-norandrost-4-ene-3,17-diones, (**2***c*) and (**2***b*) respectively. The identification of **3***a* was trivial, and **2***c* has been reported previously as the product of microbial transformation of **2***a* by *Absidia orchidis* (7, 8). Confirmation of the structures of **2***b* and **2***c* rested largely on comparisons of their ^1H nmr spectral data (Table 1) with those of **1***b* and **1***c*, and, more significantly, with those of **3***b* and **3***c*. The ^1H nmr spectra of the latter two compounds, the only products of the incubation of *B*-nortestosterone (**3***a*) with *R. arrhizus*, were analysed by spin decoupling experiments.[1] In each case the C-4 hydrogen, which

[1]These experiments were performed at 250 MHz by Dr. C. Rogers of Bruker Spectrospin (Canada) Ltd.

0008-4042/81/111651-05$01.00/0

©1981 National Research Council of Canada/Conseil national de recherches du Canada

Can. J. Chem. Downloaded from www.nrcresearchpress.com by 210.87.254.40 on 09/06/12
For personal use only.

TABLE 1. Principal ^1H nmr signals of **1***a–c* and the *B*-norsteroids **2–7***

Compound	δ ppm					
	C-3H	C-4H	C-6H	C-11H	C-18H	C-19H
1*a*	—	5.74 (s, $W_{\frac{1}{2}}$ 3 Hz)	—	—	0.93	1.22
1*b*	—	5.84 (s, $W_{\frac{1}{2}}$ 1.8 Hz)	4.40 (t, *J* 7 Hz)	—	0.95	1.41
1*c*	—	5.77 (s, $W_{\frac{1}{2}}$ 3 Hz)	—	3.6–4.3 (m)	0.94	1.36
1*d*	—	6.20 (d, *J* 2 Hz)	4.37 (dd, *J* 5, 11 Hz)	—	0.92	1.21
2*a*	—	5.83 (t, *J* 1.5 Hz)	—	—	0.95	1.12
2*b*	—	6.00 (d, *J* 2 Hz)	4.40 (dd, *J* 2, 8 Hz)	—	0.95	1.24
2*c*	—	6.07 (d, *J* 2 Hz)	4.76 (dd, *J* 2, 7 Hz)	—	0.95	1.11
3*a*	—	5.78 (t, *J* 1.5 Hz)	—	—	0.82	1.08
3*b*	—	5.95 (d, *J* 2 Hz)	4.24 (dd, *J* 2, 8 Hz)	—	0.82	1.20
3*c*	—	6.02 (d, *J* 2 Hz)	4.60 (dd, *J* 2, 7 Hz)	—	0.81	1.10
4*a*	3.25–3.65	—	5.44 (br s)	—	0.93	0.93
4*b*	4.35–4.80	—	5.46 (d, *J* 2 Hz)	—	0.94	0.94
4*c*	3.30–3.70	—	5.41 (br s)	—	0.94	1.06
5	3.65–4.20	—	3.38 (s)	—	0.94	0.88
6*a*†	3.30–3.70	—	5.30 (d, *J* 2 Hz)	—	0.75	0.88
6*b*	4.50–4.90	—	5.46 (d, *J* 2 Hz)	—	0.83	0.92
7*a*	4.35–4.80	—	5.45 (d, *J* 2 Hz)	—	0.67	0.93

*Solvent $CDCl_3$ unless otherwise stated.
†Solvent $CDCl_3$/DMSO-d_6, 1:1.

appears in the undecoupled spectrum as a doublet, collapsed to a singlet upon irradiation at the resonance position of the hydrogen geminal to hydroxyl, thus confirming the location of the latter functional group at C-6. The chemical shifts observed for the C-19 methyl hydrogens, diagnostic of the stereochemistry of substitution at C-6 (9), are also consistent with the structures presented, as are their ^{13}C nmr data (*vide infra*).

R. arrhizus has been reported to hydroxylate 17α-methyl-*B*-nortestosterone at C-6α, C-6β, and C-11α, but without quantification or discussion of the results (10). Hydroxylation of **2***a* or **3***a* at C-11α was not observed in the present study but hydroxylation at C-6 of both substrates occurred, to give α and β isomers in approximately equal amounts in each instance. Control experiments in which **3***b* and **3***c* were used as substrate demonstrated that epimerization at C-6 does not occur under the conditions of the incubation or work-up, the C-6 alcohols being recovered unchanged in each case. The concurrent formation of both α and β alcohols at C-6 from **2***a* and **3***a* is consistent with the mechanism outlined in the Introduction: the conformation of the 5-membered B ring of *B*-norsteroids is such that both α and β positions at C-6 are stereochemically equivalent with respect to the plane of the O—C-3—C-4—C-5 enone system. This is reflected in the observed multiplicity of the C-4 hydrogen signal in the ^1H nmr spectra of **2***a* and **3***a*, appearing as a symmetrical triplet (J = 1.5 Hz) (Table 1) due to the influence of both hydrogens at C-6. Interaction of developing electron density at C-6 from a $\Delta^{3,5}$ enol of **2***a* or **3***a* with an electrophilic oxidizing species will therefore occur equally favourably on both α and β faces of the molecule. This assumes that the transition state for the reaction is product-like, an assumption which is consistent with available data on such processes (2, 11, 12).

The reaction of a $\Delta^{3,5}$ enol acetate or enol ether with *m*-chloroperoxybenzoic acid has been used successfully as a model system to study the stereoelectronic control of product formation during electrophilic oxidation at C-6 in the normal steroid series (3) and related bicyclic enones (1, 3). In an attempt to use this reaction in the *B*-nor series, the preparation of compounds **8***a* and **8***b* was undertaken, using standard procedures for the preparation of $\Delta^{3,5}$ enol ethers (13) and acetates (14) from Δ^4-3-ketosteroids. Although tlc analysis indicated that product formation had occurred, all attempts at isolation resulted in reversion to the Δ^4-3-ketone. An alternative procedure, successful in converting a bicyclo [4.3.0] nonenone to its enol acetate **10**, (15), was used with *B*-nortestosterone (**3***a*) as starting material in an effort to produce the enol diacetate **9**; once again, although **9** was apparently formed in the reaction, it reverted to *B*-nortestosterone acetate on attempts at isolation. Compound **10** is reportedly unstable (15), and the extra steric strain in ring B of the steroid caused by the presence of rings C and D can account for an increased reactivity of **8***a*, **8***b*, and **9** with respect to **10**. It has therefore not been possible to pursue the model oxidations of **8***a*, **8***b*, or **9**.

Can. J. Chem. Downloaded from www.nrcresearchpress.com by 210.87.254.40 on 09/06/12
For personal use only.

TABLE 2. ^{13}C Chemical shifts of Δ^5-*B*-norsteroids **4–7**

	δ ppm						
Carbon	**4***a*	**4***b*	**4***c*	**5**	**6***a*†	**6***b*	**7**
1	37.1	36.9	38.6	30.9*	37.3	37.0*	37.0
2	32.0	27.9	32.0	31.2*	31.9	28.1**	28.0
3	71.4	73.5	70.8	69.7	71.2	73.7	73.7
4	36.6	32.8	36.6*	34.6	37.3	32.8	32.8
5	150.4	149.1	150.8	69.4	150.0	148.4	148.3
6	123.4	124.3	122.0	59.2	124.8	125.5	125.8
8	45.8	45.8	42.1	42.3	46.4	45.9	46.0
9	62.6	62.6	67.6	46.3	62.9	62.5	62.3
10	44.7	44.8	45.4	38.9	45.0	44.9***	44.8
11	20.2	20.1	68.6	19.7	20.8	20.5	21.0
12	32.0	31.9	43.4	31.7	37.3	37.1*	39.3
13	49.4	49.4	50.9	49.3	46.4	44.6***	46.0
14	49.8	49.7	49.3	48.8	49.7	49.1	54.8
15	22.4	22.5	21.9	22.4	23.9	23.9	24.5
16	35.8	35.8	36.4*	35.7	30.7	27.8**	23.4
17	220.4	220.1	218.7	219.7	81.3	82.4	63.2
18	14.1	14.2	14.7	14.0	11.5	12.4	13.7
19	15.1	15.0	15.2	15.6	15.1	15.0	15.0
20							209.6
21							31.5
Other		21.4				21.2	21.4
						21.4	
		170.5				170.5	170.5
						171.1	

*Chemical shifts with asterisks may be interchanged.
†Solvent $CDCl_3$/DMSO-d_6, 1:1.

The lack of enzyme control of oxidation at C-6 is observed more strikingly in the oxidation of the Δ^5-*B*-norsteroids **4***a* and **4***b* by *R. arrhizus*. Both gave identical products, the ester function of **4***b* being hydrolyzed in conjunction with oxidative metabolism. The product of hydroxylation at C-11α, **4***c*, was identified by spectral analysis (see tables) and by comparison of physical data with those published (7, 8). The 5,6α epoxide **5** was identified by ^1H and ^{13}C nmr spectral data (Tables 1 and 2). This compound has also previously been reported as the result of the transformation of **4***a* by *Rhizopus nigricans* (7, 8).

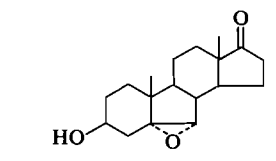

5

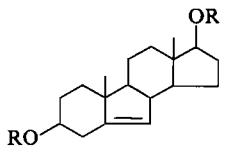

6
a R = H
b R= Ac

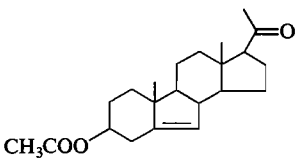

7

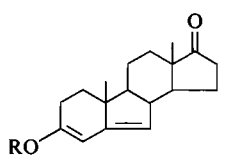

8
a R = Ac
b R = Et

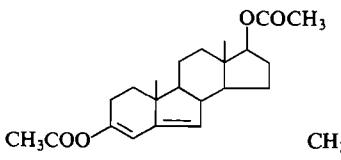

9

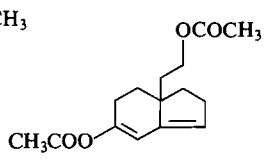

10

The stereospecific formation of the 5,6α epoxide by a micro-organism which produces the C-6β alcohol from Δ^4-3-keto substrates of the normal steroid series once again emphasizes that the stereochemistry of oxidation in this region of the molecule is controlled by the configuration and conformation of the substrate and is largely independent of the enzyme; peracid oxidation of the 5,6-double bond in *B*-norsteroids proceeds stereoselectively from the α side (16).

Product characterization in this study relied heavily upon the interpretation of carbon-13 nuclear magnetic resonance data, presented in Tables 2 and 3. The chemical shifts of the unsubstituted Δ^4-3-keto-*B*-norsteroids **2***a* and **3***a* and of the Δ^5-*B*-norsteroids **4***a*, **4***b*, **6***a*, **6***b*, and **7** were readily assigned by comparison with published data for analogous *B*-norcholestenes (Rings A and B) (17) and androstane derivatives (Rings C and D) (18). Compound **4***c* shows chemical shifts in accord with

Can. J. Chem. Downloaded from www.nrcresearchpress.com by 210.87.254.40 on 09/06/12
For personal use only.

Can. J. Chem. Downloaded from www.nrcresearchpress.com by 210.87.254.40 on 09/06/12
For personal use only.

TABLE 3. ^{13}C Chemical shifts of Δ^4-3-keto-*B*-norsteroids **2** and **3**

	δ ppm			
Carbon	**2***a*	**3***a*	**3***b*	**3***c*
1	35.3*	35.4	35.5	36.0
2	33.5	33.7	33.8	33.7
3	199.1	199.5	200.4	200.2
4	123.0	122.6	124.1	124.1
5	177.4	178.7	177.8	179.6
6	33.5	34.3	76.6	71.8
8	38.2	38.5	47.5	44.1*
9	58.5	58.5	53.3	53.7
10	43.8	43.9	42.4	43.2
11	20.1	20.5	20.3	20.3
12	31.3	36.5	36.1	36.0
13	49.2	44.8	44.7	44.7
14	51.1	50.9	49.6	44.7*
15	22.6	23.9	23.8	23.4
16	35.7*	30.6	30.8	30.6
17	219.5	81.2	81.2	81.2
18	14.3	11.5	11.4	11.4
19	17.5	17.5	18.6	17.8

*Chemical shifts with asterisks may be interchanged.

those anticipated for C-11α hydroxyl substitution (in normal steroids) (18), while **5** shows shifts, particularly those of C-1 and C-9, which confirm the α stereochemistry of the epoxide (19). The 6-hydroxy-*B*-norsteroids **2***b* and **2***c* were not obtained in sufficient quantity for acceptable ^{13}C spectra to be easily obtained, but chemical shift assignments for the analogous *B*-nortestosterone derivatives **3***b* and **3***c* are presented in Table 3.

The observed shifts at C-6, C-8, C-14, and C-19, with respect to those of the corresponding carbons of **3***a*, are characteristic of the stereochemistry of substitution at C-6 and are entirely consistent with the structures proposed.

Experimental

Apparatus, Materials, and Methods

The apparatus and techniques used were as previously described (3, 19). Analytical samples were purified and final separation of **3***b* and **3***c* performed by chromatography using a Perkin-Elmer series 3A HPLC. Incubations with *R. arrhizus* were performed as described earlier (1).

Preparation of Substrates

The following compounds were prepared by published procedures: *B*-norandrost-4-ene-3,17-dione (**2***a*) (20, 21), 3β-acetoxy-*B*-norandrost-5-ene-17-one (**4***b*) (20), *B*-norandrost-5-ene-3β-ol-17-one (**4***a*) (20), *B*-norandrost-5-ene-3β,17β-diol (**6***a*) (20), 3β,17β-diacetoxy-*B*-norandrost-5-ene (**6***b*) (20), 3β-acetoxy-*B*-norpregn-5-ene-20-one (**7**) (20). All compounds had analytical (mp) and spectral (ir) properties consistent with those reported previously (20, 21). The ^1H nmr and ^{13}C nmr data are presented in the tables.

B-*Norandrost-4-ene-17β-ol-3-one* (B-*nortestosterone*), (**3***a*)

This was prepared by the procedure used by Eder for the preparation of testosterone from androst-4-ene-3,17-dione (22). A solution of *B*-norandrost-4-ene-3,17-dione (**2***a*) (7 g) in toluene (400 mL) was flushed with N_2 and heated until 200 mL of solvent had been distilled out. The solution was then cooled to 0°C, and a solution of di-isobutyl aluminum hydride in toluene (35 mL, 25%) added by syringe over a period of 10 min. The solution was stirred at 0°C for 1 h, and then acetone (14 mL) was added, followed by 2-propanol (14 mL). The resulting mixture was allowed to stand at room temperature for 3 h, and then poured onto *N* H_2SO_4 (200 mL). The product was then extracted into ether, (4 × 200 mL), and the extract washed (saturated $NaHCO_3$, water, and brine), dried (Na_2SO_4), and evaporated. The residue (6.1 g) on crystallization from ethyl acetate afforded *B*-nortestosterone (**3***a*), (5.8 g, 83%), mp 163–165°C (lit. (21) mp 163–164°C).

Incubations with R. arrhizus *ATCC 11145*

B-*Norandrost-4-ene-3,17-dione* (2a)

Incubation of **2***a* (1 g) by the standard procedure (1) gave extracts from the medium (0.9 g) and mycelium (1.3 g). The latter contained endogenous fungal material, plus **2***a* as the only readily detectable steroid. The former extract was chromatographed on silica gel using benzene–ether gradient elution and afforded **2***a* (0.7 g) and a mixture of **3***a*, **2***b*, and **2***c* (total 0.18 g), which was separated by repeated preparative layer chromatography (Merck Silica gel 60 F_{254}, 3% methanolic chloroform) to give, in order of decreasing R_f, *B*-nortestosterone (**3***a*) (35 mg), identified by mp, tlc, and spectral comparison with an authentic sample prepared as above; 6α-hydroxy-*B*-norandrost-4-ene-3,17-dione (**2***c*) (8 mg after crystallization from ethyl acetate – hexane), mp 205–210°C (lit. (7, 8) mp 210–213°C); ir ν_{max}: 1670, 1750, 3450 cm^{-1}; *ms m/e* (%): 288 (100), 273 (35), 270 (20), 260 (15), 255 (15), 244 (40), 242 (25), 232 (60); ^1H nmr, see tables; and 6β-hydroxy-*B*-norandrost-4-ene-3,17-dione (**2***b*) (6 mg after crystallization from ethyl acetate – hexane), mp 195–198°C; ir ν_{max}: 1670, 1750, 3450 cm^{-1}; ms, M^+ calcd. for $C_{18}H_{24}O_3$: 288.172; found: 288.169; *m/e* (%): 288 (100), 273 (45), 270 (20), 260 (30), 255 (25), 244 (35), 242 (20), 232 (40); ^1H nmr, see tables.

B-*Nortestosterone* (3a)

Incubation of **3***a* (2 g) gave extracts from the mycelium (1.8 g) and medium (1.6 g). The former contained **3***a* as the only readily detectable steroid. The latter extract was chromatographed on silica gel using benzene–ether – 2% methanolic ether as eluting solvents, and gave **3***a* (0.66 g), identified by comparison with a sample of authentic material, and a mixture of **3***b* and **3***c* (total 0.81 g, ca. 1:1) separated by high pressure liquid chromatography on a column of silica gel (Whatman Partisil 20, 800 × 7.8 mm) using chloroform – ethyl acetate (40:60) as eluting solvent. Crystallization from ethyl acetate – hexane gave 6β-hydroxy-*B*-nortestosterone (**3***b*), mp 172–174°C; ir ν_{max}: 1660, 3450 cm^{-1}; ms, M^+ calcd. for $C_{18}H_{26}O_3$: 290.188; found: 290.181; *m/e* (%): 290 (100), 288 (20), 275 (50), 272 (46), 257 (57), 246 (16), 234 (70), 215 (80), 213 (70); R_f, benzene – ethyl acetate 30:70, 4 elutions, 0.5; chloroform – ethyl acetate 30:70, 4 elutions, 0.63; nmr, see tables; and 6α-hydroxy-*B*-nortestosterone (**3***c*), mp 191–193°C; ir ν_{max}: 1660, 3450 cm^{-1}; ms, M^+ calcd. for $C_{18}H_{26}O_3$: 290.188; found: 290.184; *m/e* (%): 290 (28), 288 (6), 275 (12), 272 (20), 257 (32), 246 (30), 234 (100), 215 (40), 213 (42); R_f benzene – ethyl acetate 30:70, 4 elutions, 0.42; chloroform – ethyl acetate 30:70, 4 elutions, 0.56; nmr, see tables.

3β-*Hydroxy*-B-*norandrost-5-ene-17-one* (*4a*)

Incubation of **4***a* (2.4 g) gave extracts from the medium (1.8 g) and mycelium (0.8 g). The latter contained starting material as the only readily detectable steroid (tlc) and was not examined further. The extract from the incubation medium was chromatographed on silica gel (gradient elution from benzene through ether to 5% methanolic ether) and gave **4***a* (0.57 g), identified by

Can. J. Chem. Downloaded from www.nrcresearchpress.com by 210.87.254.40 on 09/06/12
For personal use only.

comparison with authentic material, 5,6α-epoxy-3β-hydroxy-*B*-nor-5α-androstan-17-one (**5**) (0.45 g from ethyl acetate – hexane), mp 193–196°C (lit. (8) mp 195–198°C); ms *m/e* (%): 290 (100), 275 (35), 272 (66), 257 (52), 244 (46), 217 (63), 215 (95); nmr, see tables; and 3β,11α-dihydroxy-*B*-norandrost-5-ene-17-one (**4***c*) (0.49 g from ethyl acetate – hexane), mp 135–138°C (softening at 115°C) (lit. (8) mp 114–120°C (from ethyl acetate)), ms *m/e* (%): 290 (100), 275 (24), 272 (24), 257 (25), 246 (36), 231 (18), 228 (27), 215 (30), 213 (32); nmr, see tables.

3β-*Acetoxy*-B-*norandrost-5-ene-17-one* (**4***b*)

Incubation of **4***b* (1 g), and work-up as described above for the incubation of **4***a*, gave **4***b* (trace), **4***a* (trace), **4***c* (0.25 g), and **5** (0.09 g). Compounds **4***c* and **5** produced in this way were identical with samples produced by incubation of **4***a* with *R. arrhizus*.

Attempted Preparations of 3-Acetoxy- and 3-Ethoxy-B-*norandrosta-3,5-diene-17-one* (**8**a *and* **8**b), *and 3,17*β*-Diacetoxy*-B-*norandrosta-3,5-diene* (**9**)

3-Acetoxy-B-*norandrosta-3,5-diene-17-one* (**8**a)

Perchloric acid (8 μL, 70%) was added to a solution of *B*-norandrost-4-ene-3,17-dione (**2***a*) (0.1 g) in dry ethyl acetate (20 mL) and freshly distilled acetic anhydride (2 mL). The reaction was allowed to stand at room temperature, and was monitored by tlc analysis. After a period of 2 h, when reaction was judged to be virtually complete, the mixture was poured onto 2*M* sodium bicarbonate and the product extracted into ethyl acetate. The extract was washed with water, dried (Na_2SO_4), and evaporated to yield an oil which by ^{1}H nmr analysis was found to consist of a mixture of **2***a* (ca. 80%) and the desired product (**8***a*) (ca. 20%). All attempts at separation of this mixture by chromatography on silica gel or alumina resulted only in the recovery of **2***a*.

3-Ethoxy-B-*norandrosta-3,5-diene-17-one* (**8**b)

B-Norandrost-4-ene-3,17-dione (**2***a*) (1.5 g) was dissolved in acetone cyanohydrin (3 mL) by gentle warming, and then aqueous ammonia (sg. 0.880, 4 drops) added to the solution. The resulting mixture was allowed to stand at room temperature for 3 h, and then filtered to yield 17ξ-cyano-17ξ-hydroxy-*B*-norandrost-4-ene-17-one (1.35 g), which was washed with ether and dried *in vacuo* to give a sample of mp 163–165°C; ir ν_{max}: 1660, 2220, 3350 cm^{-1}; ^{1}H nmr δ: 0.95 (3H, s, C-18H), 1.10 (3H, s, C-19H), 5.86 (1H, br s, C-4H); ms *m/e* (%): 299 (1), 284 (2), 272 (54), 257 (14), 274 (29), 230 (100). *Anal.* calcd. for $C_{19}H_{25}NO_2$: C 76.21, H 8.41, N 4.69%; found: C 75.98, H 8.39, N 4.59%.

The above cyanohydrin (1.1 g) was dissolved in benzene (20 mL), and then 10 mL of solvent was removed by distillation. When the solution had cooled to 65°C, freshly distilled ethyl orthoformate (2.0 mL), absolute ethanol (0.9 mL), and ethanolic HCl (80 μL of a solution of 15 mL concentrated HCl in 65 mL ethanol) were added. The resulting mixture was maintained at 65°C for 2½ h, after which time tlc analysis indicated that formation of **8***b*-cyanohydrin was essentially complete. The mixture was then neutralized by the addition of pyridine (14 μL) and evaporated *in vacuo* to yield a pale yellow solid (1.31 g), which was subsequently redissolved in 95% ethanol (20 mL) containing pyridine (2 drops). This solution was heated (steam bath) for 20 min, and then diluted with hot water and allowed to crystallize to yield 1.0 g of a solid, which by ^{1}H nmr analysis was found to consist of a mixture of **2***a* (ca. 60%) and **8***b* (ca. 40%). Attempted separation as described above gave only **2***a*.

*3*β*,17*β*-Diacetoxy*-B-*norandrosta-3,5-diene* (**9**)

Preparation of **9** was attempted using the method of Peet and Cargill (15) on *B*-nortestosterone (0.515 g). The only isolable product was *B*-nortestosterone acetate (0.47 g).

Acknowledgements

Financial support was provided by the Natural Sciences and Engineering Research Council of Canada. Thanks are due to Bruker Spectrospin (Canada) Ltd. for ^{1}H nmr spectra of compounds **3***b* and **3***c*.

1. H. L. Holland and B. J. Auret. Can. J. Chem. **53**, 2041 (1975).
2. H. L. Holland and B. J. Auret. Tetrahedron Lett. 3787 (1975).
3. H. L. Holland and P. R. P. Diakow. Can. J. Chem. **56**, 694 (1978).
4. H. L. Holland and P. R. P. Diakow. Can. J. Chem. **57**, 436 (1979).
5. H. L. Holland and P. R. P. Diakow. Can. J. Chem. **57**, 1585 (1979).
6. H. L. Holland and G. J. Taylor. Can. J. Chem. **58**, 2326 (1980).
7. Z. Prochazka, J. Fajkos, J. Joska, and F. Sorm. Collect. Czech. Chem. Commun. **26**, 2068 (1961).
8. J. Joska, Z. Prochazka, J. Fajkos, and F. Sorm. Collect. Czech. Chem. Commun. **38**, 1398 (1973).
9. J. E. Bridgeman, P. C. Cherry, A. S. Clegg, J. M. Evans, Sir Ewart R. H. Jones, A. Kasal, V. Kumar, G. D. Meakins, Y. Morisawa, E. E. Richards, and P. D. Woodgate. J. Chem. Soc. C, 250 (1970).
10. L. R. Fare, K. G. Holden, and J. R. Valenta. U.S. Patent 3,293,300 (20 Dec. 1966). Chem. Abstr. **66**, 64376x (1967).
11. S. K. Malhotra and H. J. Ringold. J. Am. Chem. Soc. **86**, 1997 (1964).
12. G. Subramanyam, S. K. Malhotra, and H. J. Ringold. J. Am. Chem. Soc. **88**, 1332 (1966).
13. A. Ercoli and P. de Ruggieri. J. Am. Chem. Soc. **75**, 650 (1953).
14. B. E. Edwards and P. Narashima. J. Org. Chem. **31**, 324 (1966).
15. N. P. Peet and R. L. Cargill. J. Org. Chem. **38**, 1215 (1973).
16. J. Joska, J. Fajkos, and F. Sorm. Collect. Czech. Chem. Commun. **28**, 82 (1963).
17. V. Dave and J. B. Stothers. Can. J. Chem. **57**, 1550 (1979).
18. J. W. Blunt and J. B. Stothers. Org. Magn. Reson. **9**, 439 (1977).
19. H. L. Holland, P. R. P. Diakow, and G. J. Taylor. Can. J. Chem. **56**, 3121 (1978).
20. L. Knof. Ann. Chem. **657**, 171 (1962).
21. J. Joska, J. Fajkos, and F. Sorm. Collect. Czech. Chem. Commun. **25**, 1086 (1960).
22. U. Eder. Chem. Ber. **109**, 2954 (1976).

Orientations of the hydroxyl and isopropyl groups in the *cis* and *trans* conformers of 2-isopropylphenol and 2-isopropyl-6-methylphenol

TED SCHAEFER, BRENDA M. ADDISON, RUDY SEBASTIAN, AND TIMOTHY A. WILDMAN

Department of Chemistry, University of Manitoba, Winnipeg, Man., Canada R3T 2N2

Received November 28, 1980

TED SCHAEFER, BRENDA M. ADDISON, RUDY SEBASTIAN, and TIMOTHY A. WILDMAN. Can. J. Chem. **59**, 1656 (1981).

Measurement of the long-range spin–spin coupling constants between methine or hydroxyl protons and the ring protons in 2-isopropylphenol shows that the *trans* conformer is favored by 2.5 ± 0.3 kJ/mol for a 2 mol% solution in CCl_4 at 305 K. In this conformer the methine C—H bond of the isopropyl group points towards the hydroxyl group. In the *cis* conformer, the C—H bond points away from the hydroxyl group. In 2-isopropyl-6-methylphenol the conformation in which the O—H bond lies *trans* to the isopropyl group is preferred by 1.2 ± 0.3 kJ/mol in free energy at 305 K in CCl_4 solution. This result agrees with an additive superposition of the conformational preferences of the hydroxyl groups in the monosubstituted phenol derivatives. Molecular orbital calculations do not agree with the existence of a *cis* conformer.

TED SCHAEFER, BRENDA M. ADDISON, RUDY SEBASTIAN et TIMOTHY A. WILDMAN. Can. J. Chem. **59**, 1656 (1981).

La mesure des constantes de couplage à longue distance entre les protons méthinique ou hydroxyle et les protons du cycle de l'isopropyl-2 phénol montre que le conformère *trans* est favorisé par 2,5 ± 0,3 kJ/mol pour une solution à 2 mol% dans le CCl_4 à 305 K. Dans ce conformère, la liaison C—H du méthine de l'isopropyle est orientée vers le groupe hydroxyle. Dans le conformère *cis*, la liaison C—H est orientée en *trans* par rapport à l'hydroxyle. Dans l'isopropyl-2 méthyl-6 phénol, la conformation privilégiée est celle où la liaison O—H se situe en position *trans* par rapport au groupe isopropyle; du point de vue de l'énergie libre, cette conformation est favorisée par 1,2 ± 0,3 kJ/mol à 305 K en solution dans le CCl_4. Ce résultat est en accord avec une superposition additive des préférences conformationnelles des groupes hydroxyles dans les dérivés monosubstitués du phénol. Les calculs d'orbitales moléculaires ne sont pas en accord avec l'existence d'un conformère *cis*.

[Traduit par le journal]

Introduction

If intermolecular proton exchange can be retarded sufficiently (1–8), then the measurement of the stereospecific long-range proton–proton coupling constants over five bonds, ${}^5J_m{}^{H,OH}$, provides a direct measure of the *cis–trans* equilibrium in phenol derivatives. This measurement may be the only direct method for some phenols, e.g., 2-methylphenol (2), for which hydroxyl stretching bands cannot be resolved into two components (9) and for which low-frequency Raman and infrared vibrations cannot be assigned unambiguously (10, 11).

The hydroxyl stretching band in 2-isopropylphenol is also unresolvable (9), and is shifted by only 2 cm^{-1} from the phenol value. The twofold barrier to internal rotation of the isopropyl group in isopropylbenzene is 8.4 ± 0.8 kJ/mol. The preferred conformation has the methine C—H bond in the plane of the aromatic framework (12). Again, phenol prefers a planar conformation to the extent of 14.6 kJ/mol (13, 14). At ambient temperatures, the equilibrium **1***a*/**1***b* appears as an hypothesis; the barriers to rotation about the C—O and exocyclic C—C bonds being rather larger than kT. Intuitively, **1***a* should be *much* less stable than **1***b*, as is suggested by molecular orbital calculations, and consistent with the infrared data. The present experiments show otherwise. Note that correlated orientations of the sidechains are implied by **1***a* and **1***b*.

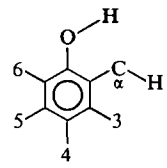

1*a cis*

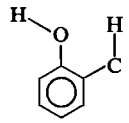

1*b trans*

Experimental

A solution containing 1.9$_5$ mol% of 2-isopropylphenol (Ethyl Corporation) and 4.0 mol% of tetramethylsilane (TMS) in CCl_4 was transferred to a 5 mm od nmr sample tube, was degassed by five freeze–thaw–pump cycles, and was then flame-sealed. Intermolecular hydroxyl proton exchange was retarded as described previously (7). The ^1H nmr spectrum was recorded on an HA100 spectrometer in the frequency sweep mode at a probe temperature of 305 K. Calibrations involved the reading of sweep and lock oscillator frequencies for markers placed at ca. 5 Hz intervals. Fivefold repetition of this procedure and interpolation sequences yielded peak frequencies whose standard deviations were typically ≤ 0.02 Hz.

A 6.0 mol% solution in CCl_4 of 2-isopropyl-6-methylphenol, prepared from the aniline derivative (Ethyl Corporation) via diazotization, was degassed and flame sealed into a 5 mm od nmr sample tube. Its ^1H nmr spectrum was recorded at 100 MHz and a probe temperature of 205 K. Decoupling of methyl protons yielded a spectrum in which fine structure in the hydroxyl proton band could be resolved. The peaks due to H-3 were broadened by small couplings to the isopropyl substituent. The ring proton region was not calibrated precisely.

Calculations at the STO 3G level of *ab initio* molecular orbital

0008-4042/81/111656-04$01.00/0

©1981 National Research Council of Canada/Conseil national de recherches du Canada

Can. J. Chem. Downloaded from www.nrcresearchpress.com by 210.87.254.40 on 09/06/12
For personal use only.

Can. J. Chem. Downloaded from www.nrcresearchpress.com by 210.87.254.40 on 09/06/12
For personal use only.

theory (15), as well as at the INDO level of semiempirical MO theory (16), were performed on an Amdahl 470/V7 system.

Results and Discussion

Spectral Analysis

The spectral parameters for **1** in Table 1 were obtained via the computer program LAME (17, 18). There were no substantial correlations between the parameters. However, the peaks due to H-3 were broadened by small couplings to the methyl protons. Decoupling procedures did not lead to linewidths for H-3 acceptable in a precise analysis, perhaps because one of the CH_3 peaks occurred near 120 Hz from the lock frequency. The H-3 peaks were therefore not assigned in the iterations, nor were those of the methine proton. Nevertheless 110 of the 128 calculated transitions of the other four protons were assigned and led to a calculated spectrum in good agreement with experiment. Figure 1 displays the calculated and observed spectra for the hydroxyl proton. The distortion of the experimental spectrum *may* arise from unresolved interactions with the isopropyl protons. Such distortions do not occur for 4-chloro-2-methylphenol (2).

The ring proton spectrum of 2-isopropyl-6-methylphenol corresponds to a loosely coupled ABC spin system, complicated by long-range couplings to the hydroxyl proton, to the protons of the methyl substituent, to the methine proton of the isopropyl group, and, for H-3, by additional small couplings with the six methyl protons of the isopropyl substituent. Precise spectral parameters for the ring protons were not obtainable. Approximate δ values are 6.83, 6.67, and 6.92 ppm for H-5, H-4, and H-3, respectively.

TABLE 1. ^{1}H nmr spectral parameters for a 2 mol% solution of 2-isopropylphenol in CCl_4 at 305 K

Parameter	Value	Parameter	Value
ν_{OH}[a]	438.684(3)[b]	$^5J_o^{CH,OH}$	0.0
ν_{CH}	318.4	$^5J_m^{H_3,OH}$	0.509(6)
ν_{CH_3}	123.6	$^5J_m^{H_5,OH}$	0.189(5)
ν_3	709.7	$^6J_p^{H,OH}$	0.0
ν_4	678.330(4)	$^4J_o^{H,OH}$	−1.66(5)
ν_5	693.186(5)	$^4J_o^{H_3,CH}$	−0.7
ν_6	657.195(4)	$^5J_m^{H_4,CH}$	0.450(7)
$^3J^{H,CH_3}$	6.9	$^5J_m^{H_6,CH}$	0.178(7)
$^3J_{34}$	7.684(7)	$^6J_p^{H,CH}$	−0.252(8)
$^3J_{45}$	7.402(5)	Rms error	0.016
$^3J_{56}$	7.975(6)	Largest deviation	0.038
$^4J_{35}$	1.671(8)	Peaks observed	74
$^4J_{46}$	1.224(5)	Transitions assigned	110
$^5J_{36}$	0.330(8)	Transitions calculated	128[c]

[a] In Hz at 100.001 MHz (centreband) to low field of TMS.
[b] Numbers in parentheses are standard deviations in the last significant figure.
[c] Excluding 32 for H-3 and 32 for the methine proton (see text).

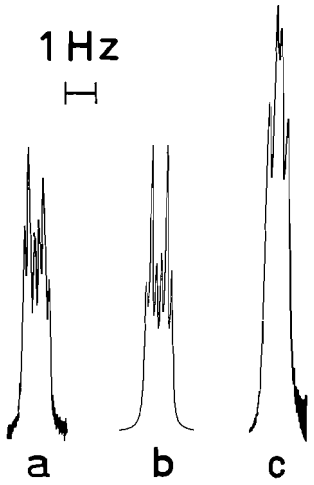

FIG. 1. In (a) is shown the ^{1}H nmr spectrum at 100 MHz of the hydroxyl proton of a 1.9_5 mol% solution of 2-isopropylphenol in CCl_4. δ_{OH} is 4.387 ppm at 305 K. The calculated spectrum in (b) used the parameters in Table 1 and a linewidth at half height of 0.10 Hz. Some of the distortion and broadening (compare Fig. 1 in ref. 2) may arise from unresolved couplings to the methine and/or methyl protons. No coupling to H-4 was indicated by decoupling experiments. In (c) is displayed the hydroxyl proton resonance of 2-isopropyl-6-methylphenol. The methyl protons are being decoupled, the probe temperature is 305 K, δ_{OH} is 4.381 ppm, and some residual coupling to isopropyl protons may be present. $^5J_m^{H_3,OH}$ is 0.38 ± 0.02 Hz and $^5J_m^{H_5,OH}$ is 0.24 ± 0.02 Hz. Corrections for overlapping Lorentzian lines would give 0.42 nd 0.26 Hz.

The hydroxyl proton is coupled to the 6-methyl protons (very likely by a proximate interaction) by an amount sufficient to obscure its interactions with the ring protons. Irradiation at δ_{CH_3}= 2.182 ppm yielded the hydroxyl proton spectrum at δ = 4.381 ppm shown in Fig. 1c (a 3.6 mol% solution had δ_{OH} as 4.365 ppm). It is clear that the couplings to H-3 and H-5 are unequal.

Under these conditions, the ring proton spectrum allowed the extraction of $^5J_m^{H_4,CH}$ as 0.375 ± 0.02 Hz and also showed that the smaller $^5J_m^{H,OH}$ involves H-5. The ring proton chemical shift assignment, based initially on the broadened lines from H-3, was confirmed by irradiation of the hydroxyl proton band. The ensuing spectrum showed that $^6J_p^{H,CH}$ is (−)0.24 ± 0.02 Hz, $^6J_p^{H,CH_3}$ is (−)0.6 Hz, and $^4J_o^{H,CH_3}$ is (−)0.7 Hz. Consequently, no doubt exists about the assignment of the H-3 and H-5 multiplets. The methine proton of the isopropyl group resonates at 3.140 ppm.

The cis–trans *Equilibrium*

The sum of the two $^5J_m^{H,OH}$ values is 0.69_8 Hz, as compared to 0.69_5 Hz for a 2.5 mol% solution of 2-methylphenol (2). It is therefore assumed that ^5J_m

depends only on the conformational equilibria, the latter being different for the two compounds. If $^5J_m^{H_3,OH}$ in **1***a* and $^5J_m^{H_5,OH}$ in **1***b* are negligibly small (see refs. 3 and 4 for more extensive discussions of this point), it follows that the free energy difference between **1***a* and **1***b* is $-RT \ln K = -RT \ln 0.509/0.189 = -2510 \pm 290$ J/mol. The quoted error assumes that the standard deviations in Table 1 are to be multiplied by 3 (99% confidence limits). In 2-methylphenol in CCl_4 solution at the same temperature (305 K), the *trans* form is favored by 1590 ± 170 J/mol in free energy.

No coupling between the *para* proton, H-4, and the hydroxyl proton could be detected, strongly indicating (3, 8) that conformers in which the O—H bond lies out of the benzene plane can be ignored in this discussion.

The Conformations of the Isopropyl Group

$^5J_m^{H,CH}$ is stereospecific in benzene derivatives containing sidechains such as CHO (19–21), $CHCl_2$ (22), $CHBr_2$ (23), and CHI_2 (24). All the evidence points to a vanishing magnitude of couplings analogous to $^5J_m^{H_4,CH}$ in **1***a* and $^5J_m^{H_6,CH}$ in **1***b*. Furthermore, substituents on the ring cause only minor changes in the magnitude of $^5J_m^{H,CH}$. In particular, in *p*-nitroisopropylbenzene (25) $^5J_m^{H,CH}$ is 0.30 ± 0.02 Hz, i.e. the coupling analogous to $^5J_m^{H_6,CH}$ in **1***a* or $^5J_m^{H_4,CH}$ in **1***b* would be 0.60 ± 0.04 Hz. In *p*-fluoroisopropylbenzene, $^5J_m^{H,CH}$ is 0.31 ± 0.02 Hz (26). The sum of the two $^5J_m^{H,CH}$ values in 2-isopropylphenol is 0.62_8 ± 0.04 Hz (error equal to three times the sum of the standard deviations).

Accordingly, if the orientation of the isopropyl group is correlated with that of the hydroxyl group as indicated by **1***a* and **1***b*, the free energy difference favoring **1***a* can also be written as $-RT \ln 0.450/0.178 = -2340 \pm 420$ J/mol. The quoted error again assumes that the standard deviations in the individual $^5J_m^{H,CH}$ values are to be tripled. It appears that **1***a* and **1***b* are good approximations to the preferred orientations of the sidechains. The structures are discussed further below.

cis–trans *Equilibrium in 2-Isopropyl-6-methylphenol*

Decoupling of the methyl protons yielded the spectrum of the hydroxyl proton in Fig. 1c. Some residual breadth of the lines suggests that the splittings should be corrected for overlap of Lorentzian peaks (see figure caption). The free energy difference favoring the conformer in which the hydroxyl group lies *trans* to the isopropyl group is 1200 ± 290 J/mol (1170 ± 330 J/mol if the uncorrected couplings are used). The additive preference derived from the monosubstituted phenols is (−1590 ± 170) + (2510 ± 290) or 920 ± 460 J/mol.

$^5J_m^{H_4,CH}$ is $0.37_5 \pm 0.02$ Hz. If methyl substitution does not cause a significant perturbation of this parameter, one may write the free energy difference favoring the *trans* conformer as $-RT \ln (0.628 - 0.375)/0.375 = 990 \pm 335$ J/mol. Again, the isopropyl group apparently points towards the hydroxyl group when the latter lies *trans* to the isopropyl substituent.

The Methine and Hydroxyl Proton Shifts

At 308 K, δ_{OH} of phenol at infinite dilution in CCl_4 is 4.26 ppm (27). The first important association process very likely (27–30) involves trimerization. The assumption that *only* trimerization occurs yields a δ_{OH} of 7.89 ppm for the trimer (27), an association shift of 3.63 ppm. The first important association in 2-methylphenol apparently is also trimerization (2). If this is true for 2-isopropylphenol, the δ_{OH} of 4.39 ppm for the 2 mol% solution in CCl_4 at 305 K (Table 1) suggests that, at this concentration, more than 90% exists as monomer. This suggestion contains the additional assumption that δ_{OH} in the 2-isopropylphenol is not appreciably different from δ_{OH} in phenol. For 2-isopropyl-6-methylphenol, δ_{OH} is 4.38 ppm at 305 K for a 6 mol% solution in CCl_4 and is 4.36_5 ppm for a 3.6 mol% solution. These numbers are also consistent with a small degree of self-association.

In the crystal, the isopropyl group of 2-isopropyl-5-methylphenol is turned (31) so that the two methyl groups are as far as possible from the oxygen atom (compare structure **1***b*). By way of contrast, in dilute solution 2-isopropylphenol exhibits also a *cis* conformer, **1***a*.

There is evidence from Schroeder–Lippincott potential functions (32) for very weak C—H···O hydrogen bonds, perhaps as much as 1.2 kJ/mol in energy for a geometry such as in **1***b*. The chemical shift, δ_{CH}, in **1***b* may be obtained as follows. A 2 mol% solution of isopropylbenzene in CCl_4 had δ_{CH} as 2.86_4 ppm, whereas δ_{CH} is 3.18_4 ppm for the 2 mol% solution of 2-isopropylphenol. Assuming that δ_{CH} in **1***a* is the same as in isopropylbenzene and knowing that the fraction of **1***b* is 0.72, one has δ_{CH} as 3.30_8 ppm in **1***b*. Then the shift due to the C—H···O interaction is 0.43 ppm to low-field, i.e. a deshielding interaction. This number is *consistent* with a weak hydrogen-bonding (attractive) interaction in **1***b*. The early surmise (33), that the methine C—H bond prefers to lie *cis* to the hydroxyl group, is correct for the form **1***b*.

In 2-isopropyl-6-methylphenol δ_{CH} is 3.14_0 ppm. Since the fraction of the conformer analogous to **1***b*

Can. J. Chem. Downloaded from www.nrcresearchpress.com by 210.87.254.40 on 09/06/12
For personal use only.

Can. J. Chem. Downloaded from www.nrcresearchpress.com by 210.87.254.40 on 09/06/12
For personal use only.

is 0.61 (see above), the predicted δ_{CH} is 3.13_5 ppm. This number assumes that δ_{CH} in the conformer analogous to **1***a* is the same as in isopropylbenzene. Therefore the observed δ_{CH} suggests that the isopropyl group in the two conformers of 2-isopropyl-6-methylphenol orients in the same way as in the analogous conformers **1***a* and **1***b* (note that the methyl substituent is *meta* to the isopropyl group and is therefore not expected to alter significantly the electron density at the methine proton).

Molecular Orbital Calculations

STO 3G calculations involving optimization of external bond angles and of C—O and O—H bond lengths gave **1***b* as the stable conformer (−417.471739 au in energy), but found **1***a* at least 50 kJ/mol less stable than **1***b*; dipole moments of **1***a* and **1***b* were 1.59 and 0.99 D, respectively. On the other hand, a conformer, **1***c*, in which the O—H and the methine C—H bonds were *trans*, was calculated as only 1.8 kJ/mol above **1***b* in energy and had a dipole moment of 1.17 D. Such a distribution of conformers **1***b* and **1***c* (67 and 33% at 305 K) would reproduce the observed $^5J_m^{H,CH}$ numbers in Table 1. However, the available evidence (1–8) would then suggest that $^5J_m^{H_5,OH}$ be zero or at least much smaller than the observed value of 0.19 Hz. Furthermore, the conformer distribution of 2-isopropyl-6-methylphenol then cannot be derived on an additive basis, as it can for other hydrocarbon groupings (1). Solvent effects (34) are not large enough to stabilize the more polar **1***a* by the required 32 kJ/mol.

Accordingly, the STO 3G predictions are rejected. INDO MO computations on the STO-3G geometries gave **1***c* as at least 8.9 kJ/mol more stable than **1***a* or **1***b* and are therefore also inadequate.

Acknowledgements

We are grateful to the Ethyl Corporation for gifts of 2-isopropylphenol and 2-methyl-6-isopropylaniline. This research was supported by the Natural Sciences and Engineering Research Council of Canada.

1. T. SCHAEFER, R. SEBASTIAN, and T. A. WILDMAN. Can. J. Chem. **57**, 3005 (1979).
2. T. SCHAEFER and K. CHUM. Can. J. Chem. **56**, 1788 (1978).
3. T. SCHAEFER and T. A. WILDMAN. Can. J. Chem. **57**, 450 (1979).
4. J. B. ROWBOTHAM and T. SCHAEFER. Can. J. Chem. **52**, 3037 (1974).
5. J. B. ROWBOTHAM, M. SMITH, and T. SCHAEFER. Can. J. Chem. **53**, 986 (1975).
6. T. SCHAEFER and J. B. ROWBOTHAM. Can. J. Chem. **54**, 2243 (1976).
7. T. SCHAEFER, J. B. ROWBOTHAM, and K. CHUM. Can. J. Chem. **54**, 3666 (1976).
8. T. SCHAEFER, T. A. WILDMAN, and S. R. SALMAN. J. Am. Chem. Soc. **102**, 107 (1980).
9. K. U. INGOLD and D. R. TAYLOR. Can. J. Chem. **39**, 471 (1961).
10. A. S. MANOCHA, G. L. CARLSON, and W. G. FATELEY. J. Phys. Chem. **77**, 2094 (1973).
11. G. L. CARLSON and W. F. FATELEY. J. Phys. Chem. **77**, 1157 (1975).
12. T. SCHAEFER, W. J. E. PARR, and W. DANCHURA. J. Magn. Reson. **25**, 167 (1977).
13. H. D. BIST, J. C. D. BRAND, and D. R. WILLIAMS. J. Mol. Spectrosc. **24**, 402 (1967).
14. E. MATHIER, D. WELTI, A. BAUDER, and Hs. H. GÜNTHARD. J. Mol. Spectrosc. **37**, 63 (1971).
15. W. J. HEHRE, W. A. LATHAN, R. DITCHFIELD, M. D. NEWTON, and J. A. POPLE. QCPE, **11**, 236 (1979).
16. P. A. DOBOSH. QCPE, **11**, 141 (1979).
17. C. W. HAIGH and J. M. WILLIAMS. J. Mol. Spectrosc. **32**, 398 (1969).
18. S. CASTELLANO and A. A. BOTHNER-BY. J. Chem. Phys. **41**, 3863 (1964).
19. G. J. KARABATSOS and F. M. VANE. J. Am. Chem. Soc. **85**, 3886 (1963).
20. D. G. KOWALEWSKI and S. CASTELLANO. Mol. Phys. **16**, 567 (1969).
21. R. WASYLISHEN and T. SCHAEFER. Can. J. Chem. **49**, 3216 (1971).
22. J. PEELING, T. SCHAEFER, and C. M. WONG. Can. J. Chem. **48**, 2839 (1970).
23. J. PEELING, L. ERNST, and T. SCHAEFER. Can. J. Chem. **52**, 849 (1974).
24. J. PEELING, J. B. ROWBOTHAM, L. ERNST, and T. SCHAEFER. Can. J. Chem. **52**, 2414 (1974).
25. D. W. BEISTEL and H. E. CHEN. J. Chem. Phys. **59**, 4642 (1973).
26. T. SCHAEFER, W. DANCHURA, W. NIEMCZURA, and J. PEELING. Can. J. Chem. **56**, 2442 (1978).
27. A. J. DALE and T. GRAMSTAD. Spectrochim. Acta, Part A, **28**, 639 (1972).
28. E. E. TUCKER, S. D. CHRISTIAN, and LUNG-NAN LIU. J. Phys. Chem. **78**, 1443 (1974).
29. E. E. TUCKER and E. LIPPERT. *In* Recent advances in hydrogen bonding. *Edited by* P. Schuster, G. Zundel, and C. Sandorfy. North-Holland Publishing Co., Amsterdam. 1976. Chapt. 17.
30. B. U. PETELENZ and H. F. SHURVELL. Can. J. Chem. **58**, 353 (1980).
31. A. THOZET and M. PERRIN. Acta Crystallogr. Sect. B, **36**, 1444 (1980).
32. J. N. SPENCER, G. J. CASEY, J. BUCKFELDER, and H. D. SCHREIBER. J. Phys. Chem. **78**, 1415 (1974).
33. B. G. SOMERS and H. S. GUTOWSKY. J. Am. Chem. Soc. **85**, 3065 (1963).
34. R. J. ABRAHAM and E. BRETSCHNIEDER. *In* Internal rotation in molecules. *Edited by* W. J. Orville-Thomas. J. Wiley, New York. 1974. Chapt. 13.

Cyclic neutron activation analysis of biological and metallurgical samples

A. CHATT,[1] K. N. DESILVA, J. HOLZBECHER, D. C. STUART, R. E. TOUT, AND D. E. RYAN
Trace Analysis Research Centre, Department of Chemistry, Dalhousie University, Halifax, N.S., Canada B3H 4J1
Received August 7, 1980[2]

A. CHATT, K. N. DESILVA, J. HOLZBECHER, D. C. STUART, R. E. TOUT, and D. E. RYAN. Can. J. Chem. **59**, 1660 (1981).

A rapid pneumatic transfer cyclic system for use with the SLOWPOKE reactor has been designed which allows detection of nuclides with half-lives as short as 0.8 s. Reliable reproducibility is achieved with a 1 s transfer period from reactor to detector. Both accuracy and relative standard deviation are significantly improved with some matrices as the number of cycles is increased but the gains in detection limits increase with the square root of the number of cycles. Cyclic instrumental neutron activation analysis has been successfully applied to the determination of Ag, F, Hf, Pb, Rb, Sc, and Se in a variety of biological and metallurgical matrices. The detection limits ranged from 0.01 to 2.2 ppm for all elements studied except Pb.

A. CHATT, K. N. DESILVA, J. HOLZBECHER, D. C. STUART, R. E. TOUT, and D. E. RYAN. Can. J. Chem. **59**, 1660 (1981).

On propose un système cyclique de transfert pneumatique rapide, pouvant être utilisé de concert avec le réacteur SLOWPOKE, qui permet de détecter les noyaux dont les demi-vies pourraient aller jusqu'à 0,8 s. On obtient une reproductibilité parfaite avec une période de transfert de 1s du réacteur au détecteur. On améliore de façon importante la précision ainsi que la déviation normale relative à l'aide de quelques matrices lorsque le nombre de cycles augmente; toutefois les gains sur les limites de détection augmentent selon la racine carré du nombre de cycles. On applique avec succès l'analyse intrumentale cyclique de l'activation du neutron à la détermination de Ag, F, Hf, Pb, Sc et Se dans différentes matrices biologiques et métallurgiques. Pour tous les éléments étudiés, à l'exception du Pb, les limites de détection se situent entre 0,01 et 2,2 ppm.

[Traduit par le journal]

Instrumental neutron activation analysis (INAA) involving conventional irradiation, decay, and counting periods has been widely applied for multielement determination in biological and metallurgical samples. Short (<30 s) irradiation, decay, and counting times have been used in recent years for measuring the levels of a few selected elements (1–3). At least 38 stable elements, however, produce short- (and long-) lived nuclides under thermal neutron bombardment. Many of these short-lived nuclides can be used for sensitive determinations of a number of trace elements in a variety of sample matrices (4).

To detect the γ-rays emitted by short-lived (half-life <65 s) nuclides, it is necessary to develop methods based on the principles of cyclic activation analysis. In cyclic INAA (CINAA), a sample is irradiated for a short time, is rapidly transferred to a detector for counting, and the entire process is repeated for a number of cycles. The CINAA technique was suggested in 1960 (5) and the theory of CINAA has been recently described in detail (6). The concentrations of trace elements in biological and environmental materials have been determined during the past few years using this technique (7–13).

A pseudo-cyclic INAA method, which involved manual transfer of samples, was initially developed for use with the Dalhousie University SLOWPOKE-2 Reactor (DUSR) facility; it was successfully applied to multielement determinations in biological samples (14, 15). A rapid automated transfer cyclic system has been subsequently designed and installed. The design and timing parameters of this system are described here. CINAA methods for the determination of several elements in biological and metallurgical samples are reported in this paper. Precision, accuracy, and detection limits are also discussed.

Experimental

Irradiations

All samples and standards were irradiated in the pneumatic site #1 of the DUSR facility. The composition, homogeneity, and reproducibility of the DUSR neutron flux were determined and reported in a previous publication (16). The excellent stability and reproducibility of the DUSR neutron flux are particularly advantageous for CINAA methods where samples and comparator standards have to be irradiated separately in an identical flux.

Counting System

Neutron irradiated samples were counted using a 35-cm^3 PGT Ge(Li) detector with a full width at half maximum of 2.4 keV at the 1332-keV photopeak of ^{60}Co, peak-to-Compton ratio of 30:1, and an efficiency of 7.1%. The detector was coupled to a TN-1700 model 4096-Channel pulse height analyzer.

Cyclic System

A rapid automated transfer cyclic system was designed in collaboration with Atomic Energy of Canada Limited, Commercial Products. The system consists of two main components: a recycle irradiation controller and a switching unit. The recycle irradiation controller contains an irradiation timer, a delay timer, a counting timer, and a recycle counter. The

[1]To whom all correspondence should be addressed.
[2]Revision received February 25, 1981.

0008-4042/81/111660-05$01.00/0
©1981 National Research Council of Canada/Conseil national de recherches du Canada

Can. J. Chem. Downloaded from www.nrcresearchpress.com by 210.87.254.105 on 09/06/12
For personal use only.

Can. J. Chem. Downloaded from www.nrcresearchpress.com by 210.87.254.105 on 09/06/12
For personal use only.

switching unit contains two 2-way diverters and a solenoid valve. A schematic diagram of this system is shown in Fig. 1.

The cyclic system was operated according to the following sequence. A carefully sealed polyethylene capsule containing the sample to be irradiated was manually placed in the breech. The recycle option of the transfer system was switched on for automatic recycling of the sample between the reactor core and the Ge(Li) detector. The irradiation, delay, and counting timers were then set to desired time intervals. The required number of cycles was selected on the recycle counter. The polyethylene capsule was inserted into the reactor from the breech by pushing a button. The capsule photodetector unit located in the irradiation tube at the top of the reactor signalled the passage of the capsule; this signal, in turn, started the irradiation timer. At the end of the set irradiation time, the capsule was ejected to the detector. The counting system and the counting timer were activated when the delay timer reached zero from a preset time. The capsule was reinserted into the reactor when the counting time expired. The capsule was recycled (i.e., re-irradiated and re-counted) for the preselected number of cycles, and then was ejected to the capsule receiver through the diverter and the Y-section of the switching unit.

The various factors which could influence the transit time of a capsule between reactor and detector were studied. These factors included weight of a capsule, shape of the top and bottom portions of a capsule, and air pressure in the pneumatic tube. The variation of air pressure between 30 and 60 p.s.i. appeared to make little difference on the transit time of a capsule of a given weight. Capsules weighing between 4 and 6 g were generally used at an air pressure of about 40 p.s.i. in developing the CINAA methods. The time taken to transfer a capsule from the reactor core to the detector surface under the above operating conditions was approximately 600 ms at best. In order to achieve reliable reproducibility, a delay time of 1 s was normally sufficient.

Sealing of Irradiation Capsules

The irradiation capsules used were polyethylene vials (5.5 cm length, 1.6 cm outer diameter, and 7 cm^3 capacity) fitted with polyethylene snap caps and were supplied by the Durham Aircraft Corporation, New York. The snap cap was always heat-sealed to the vial prior to irradiation. The general method of sealing (consisting of fitting the cap on the vial, trimming the sides of the cap, and heat-sealing the edges) although ideal for conventional one-shot irradiation, could not be used in cyclic irradiations. Rough edges at the top of the vial lengthened transfer time and vial caps came off after a few recycle periods ($n < 5$). A sealing technique that permits a large number of cycles with minimum transfer time consists of inserting an inverted snap cap (edges trimmed) of an irradiation vial into the vial and heat sealing the edges of the vial and cap together. The sealed vials could be transferred within 600 ms from reactor to detector, and could be used for a large number ($n > 100$) of recycling periods.

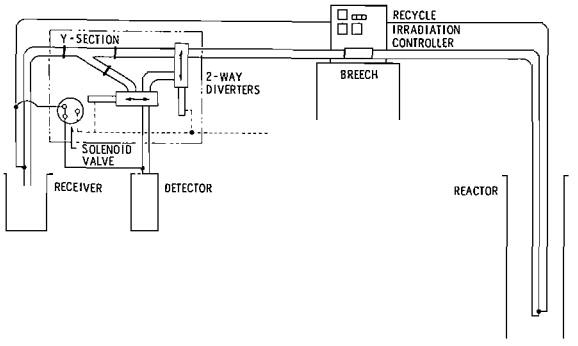

FIG. 1. A schematic diagram of the DUSR cyclic system.

Standards and Samples

Monoelement comparator standards were prepared by depositing microlitre portions of "atomic absorption standard solutions (Alfa-Ventron Corporation)" on either Nucleopore polycarbonate membrane or prewashed (with HNO_3 and H_2O) Whatman #1 filters. The spotted filters were evaporated to dryness at low heat under an infrared lamp and then sealed in a precleaned polyethylene envelope. Ultrapure lead wires were used as comparator standards for lead.

Two standard reference materials (SRM) were analyzed to evaluate the precision and accuracy (22, 23) of the CINAA method. These included Orchard Leaves (NBS SRM-1571) and Bovine Liver (NBS SRM-1577) supplied by the U.S. National Bureau of Standards (NBS).

Other analyzed samples were: Fish Flour obtained from the International Council for the Exploration of the Sea (ICES), cod liver collected from fish caught off the coast of Prince Edward Island, Canada (1); hair obtained from a population group previously studied (17); "Analyzed Brass" from Thorn Smith; "Specpure" zirconium salts from Johnson-Matthey Co.; and ultrapure zirconium wires supplied by Alfa-Ventron Corporation.

All samples were contained in precleaned polyethylene envelopes which were then heat-sealed. Each envelope was placed in a separate 1.5 cm^3 polyethylene vial which was then inserted into the irradiation vial. A second vial was used as a spacer to keep the bottom vial in place and to prevent any impulses on the sealed cap. The irradiation vial was then sealed according to the procedure described in a preceding section.

Results and Discussion

Seven short-lived neutron activation products which decay by the emission of γ-rays have been investigated in the present work; their nuclear data are given in Table 1. Photopeaks used are free from interference under the experimental conditions described. The isotopic abundances of the targets are generally high except for ^{76}Se. The cross sections are also fairly large (i.e. $\geq$0.10b) except those of ^{19}F and ^{206}Pb. The combination of high isotopic abundance and cross section indicates that most of the nuclides listed in Table 1 will be produced in high yields. Since the half-lives of these nuclides vary over two orders of magnitude, different timing parameters (i.e. irradiation, decay and counting times) had to be developed for their sensitive measurements. The composition of sample matrix also needed to be considered for selecting appropriate timing parameters.

For the determinations of Ag, F, Rb, Sc, and Se in biological materials (namely, cod liver and otolith, Fish Flour, Bovine Liver, and Orchard Leaves), the timing parameters selected were: irradiation time (t_i) = 10 s, decay time (t_d) = 2 s,

TABLE 1. Nuclear data for elements determined by CINAA[a]

Element	Target isotope	Isotopic abundance %	Cross section,[b]	Product nuclide	Half-life, s	γ-Ray energy used, keV	Intensity of γ-ray, %
Ag	^{109}Ag	48.17	89	^{110}Ag	24.4	658	4.52
F	^{19}F	100	0.0098	^{20}F	11.0	1633	100
Hf	^{178}Hf	27.1	52	^{179m1}Hf	18.7	214	95.2
Pb	^{206}Pb	24.1	0.03	^{207m}Pb	0.81	570	97.9
Rb	^{85}Rb	72.17	0.10	^{86m}Rb	62.4	556	98.2
Sc	^{45}Sc	100	11	^{46m}Sc	18.7	142	62.1
Se	^{76}Se	9.0	21	^{77m}Se	17.4	162	52.5

[a]Reference 26.

counting time (t_c) = 10 s, and number of cycles (n) = 12. The Se content of scalp hair was measured using t_i = 60 s, t_d = 1 s, t_c = 60 s, and n = 10. Macroquantities of Pb were determined with t_i = 3 s, t_d = 1 s, t_c = 3 s, and n = 10. Concentrations of Hf in "specpure" zirconium salts and wires were measured using t_i = 60 s, t_d = 1.5 s, t_c = 60 s, and n = 10. Results are shown in Table 2.

The fluorine content of ICES Fish Flour was determined through its only thermal neutron activation product, ^{20}F. The same nuclide could also be produced by two interfering reactions: ^{23}Na(n,α)^{20}F and ^{20}Ne(n,p)^{20}F. Appropriate corrections were made considering the sodium content of biological materials and neon content of the empty space in irradiation capsules; contributions from the interfering reactions were experimentally determined.

The concentrations of Ag, Rb, Sc, and Se could also be determined using long-lived nuclides of these elements. However, the use of short-lived nuclides not only reduces total experimental time but also improves the precision of measurements. No competing reactions interfered in the determinations of these nuclides under the experimental conditions and sample matrices used.

The determination of Hf in Zr is an example of a system particularly amenable to CINAA. Measurement of trace amounts of Hf in the presence of a large excess of Zr (or vice versa) is ordinarily very difficult because of the extreme similarities in chemical properties of these two elements and their ions. In samples analyzed by CINAA, however, the matrix element (Zr) does not become activated to any significant degree under the experimental conditions used (t_i = 60 s, t_d = 1.5 s, t_c = 60 s, and n = 10) while ^{179m1}Hf is formed in sufficient amounts so that microgram quantities of Hf in ultrapure Zr standard wires can be determined. The hafnium content of spectrographically analyzed (specpure) Zr salts was determined by CINAA. The Hf level of the zirconium sulfate was too high to be analyzed directly; a sample was therefore dissolved in dilute sulfuric acid and microlitre portions were deposited onto filter papers for analysis. The sample was found to contain 0.741 ± 0.009% by CINAA compared to the spectrographic estimation of 0.7%. The hafnium content of "specpure" ZrO_2 was directly determined by CINAA at a reduced flux of 5×10^9 n cm^{-2} s^{-1}. The activity due to ^{179m1}Hf was high in comparison to other Zr–Hf samples analyzed, but its concentration could be estimated (1.67%).

TABLE 2. Typical elemental content of biological and metallurgical samples determined by CINAA

Element	Sample material	Content, ppm
Ag	Cod liver	0.65 ± 0.05
F	Fish Flour	62 ± 8
Hf	Zirconium standard wire	195 ± 2
	"Specpure" zirconium sulfate	0.741 ± 0.009[a]
	Zirconium dioxide	1.67 ± 0.01[a]
Pb	Brass #16	19 ± 2.4[a]
Rb	Cod liver	0.50 ± 0.04
Sc	Cod otolith	0.48 ± 0.05
Se	Cod liver	0.67 ± 0.04
	Hair	0.42 ± 0.03

[a]Content expressed in %.

The determination of Pb through ^{207m}Pb by CINAA using the present cyclic system is not very sensitive. An attempt was made, however, to measure macroquantities of Pb in an alloy because of the advantages (over classical techniques) of speed and ease of analysis of solid samples. Brass was analyzed for Pb using the timing parameters described earlier at a flux of 5×10^{10} n cm^{-2} s^{-1}; this 10-fold reduction in normal flux was necessary to reduce matrix activity. To minimize errors due to shielding, a brass sample with a certified Pb content was used as a comparator standard. The Pb levels determined by CINAA could be in error by as much as 15% relative because of coincidence losses as indicated by high dead times. Methods are presently being developed to correct for such losses.

Although CINAA was generally used for single

Can. J. Chem. Downloaded from www.nrcresearchpress.com by 210.87.254.105 on 09/06/12
For personal use only.

TABLE 3. Optimum timing parameters for a number of short-lived nuclides

Nuclide	Half-life, s	Optimum value of t_i and t_c (90% S_{max} range)		
		Orchard Leaves	Bovine Liver	Coal
^{77m}Se	17.4	19(5–32)	13(5–32)	19(5–32)
^{179m_1}Hf	18.7	19(5–32)	19(5–34)	19(6–32)
^{110}Ag	24.4	19(6–42)	19(6–42)	22(6–42)

element measurement, it can be applied to simultaneous multielement determinations (18–20). Using a computer program for optimizing timing parameters (21), the maximum value of the significance of a photopeak (S_{max}) and the range of 90% S_{max} have been calculated for a number of nuclides; the results are presented in Table 3. It is evident from the table that a value of $t_i = t_c = 11$ s will produce values of $S \geq 90\%\ S_{max}$ for nuclides with half-lives ranging between 5.3 and 49 s in all three matrices. This means that only one CINAA experiment need to be performed for the simultaneous detection of several short-lived nuclides with varying half-lives.

Precision of measurement generally improves in CINAA with an increasing number of cycles (n). The precision of determining Sc in the Orchard Leaves by CINAA is shown in Fig. 2. The improvement in precision was almost four-fold. The relative standard deviation decreased from 34% in the first cycle to 9% in the twelfth cycle. A relative standard deviation of 10% was achieved at $n = 8$; an increase in the number of cycles from 9 to 12 decreased the relative standard deviation by only

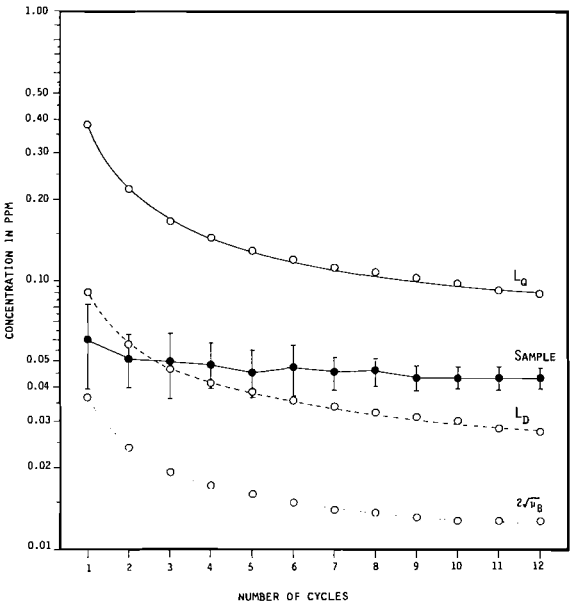

FIG. 2. Determination of Sc in Orchard leaves by CINAA.

TABLE 4. Concentrations of elements in NBS standard reference materials determined by CINAA

Sample material	Element	Concentration, ppm	
		This work[a]	Literature
Bovine Liver (NBS SRM-1577)	Rb	17.6 ± 1.2	18.3 ± 1.0[b]
Orchard Leaves (NBS SRM-1571)	Sc	0.043 ± 0.004	0.054 ± 0.004[c]
Bovine Liver (NBS SRM-1577)	Se	1.03 ± 0.06	1.1 ± 0.1[b]

[a]Average of 3 determinations.
[b]NBS certified values, ref. 23.
[c]Reference 25.

TABLE 5. Detection limits of elements by CINAA

Sample material	Element	Detection limit, ppm
Cod liver	Ag	0.017
Fish flour	F	2.2
Zirconium (wire) standard	Hf	0.93
Brass	Pb	3.6[a]
Bovine liver	Rb	2.0
Orchard leaves	Sc	0.012
Bovine liver	Se	0.31
Hair	Se	0.10

[a]Expressed in %.

1%. Accuracy of measurement was evaluated by analyzing two well-characterized SRM provided by the NBS. The averages of 3 determinations for each element are shown in Table 4. The agreement with certified values (23) is generally good, wherever such comparison is feasible.

Limits of detection, defined by $2\sqrt{\mu_B}$, where μ_B is the number of background counts under the photopeak, were calculated for each of the elements analyzed. The limits are shown in Table 5. Except for Pb, the limits are generally low and of the order that is required of a trace analytical technique. Both qualitative detection limit (L_D) and quantitative determination limit (L_Q), as defined by Currie (24), were also calculated; the results for Sc in Orchard Leaves are shown in Fig. 2.

It is also evident from Fig. 2. that although detection limits decrease with increasing number of cycles, the rate of decrease slows down consider-

Can. J. Chem. Downloaded from www.nrcresearchpress.com by 210.87.254.105 on 09/06/12
For personal use only.

ably after 7 or 8 cycles. The detection limit of an element is highly dependent on the composition of a given sample matrix. For example, the detection limit of Se in Bovine Liver (high background activity due to ^{24}Na, ^{38}Cl, and ^{28}Al) is approximately 3 times poorer than that in hair (very little background activity).

The pneumatic transfer cyclic system used in this work needs to be modified for detecting nuclides with half-lives less than 800 ms. Due to complexity of diverters used in the present system (Fig. 1), the capsule transit time occasionally reached values greater than 1 s. Extensive dead time corrections are necessary to determine trace element concentrations with high accuracy. With the availability of low energy photon detectors and improved cyclic systems, a number of very short-lived (half-life < 0.80 s) nuclides can be used for multielement determinations.

Acknowledgment

This work was supported by grants from the Natural Sciences and Engineering Research Council of Canada.

1. A. CHATTOPADHYAY, K. M. ELLIS, and K. N. DESILVA. Proc. Intern. Symp. on Nuclear Activation Techniques in the Life Sciences 1978, IAEA, Vienna, 667 (1979).
2. N. I. WARD and D. E. RYAN. Anal. Chim. Acta, **105**, 185 (1979).
3. R. DAMS, J. BILLIET, and J. HOSTE. Intern. J. Environ. Anal. Chem. **4**, 141 (1975).
4. R. E. TOUT and A. CHATT. Anal. Chim. Acta, **118**, 341 (1980).
5. O. U. ANDERS. Anal. Chem. **32**, 1368 (1960).
6. N. M. SPYROU and S. A. KERR. J. Radioanal. Chem. **48**, 169 (1979).
7. A. EGAN and N. M. SPYROU. Anal. Chem. **48**, 1959 (1976).
8. A. EGAN and N. M. SPYROU. J. Radioanal. Chem. **37**, 775 (1979).
9. A. EGAN, S. A. KERR, and M. J. MINSKI. Radiochem. Radioanal. Lett. **28**, 369 (1977).
10. S. A. KERR and N. M. SPYROU. J. Radioanal. Chem. **44**, 159 (1978).
11. F. GRASS and R. NIESNES. Nucl. Instrum. Methods, **151**, 589 (1978).
12. F. GRASS. Atomkernenergie, **25**, 243 (1975).
13. F. GRASS and G. P. WESTPHAL. Nucl. Instrum. Methods, **140**, 97 (1977).
14. A. CHATTOPADHYAY and K. N. DESILVA. Trans. Am. Nucl. Soc. **32**, 185 (1979).
15. K. N. DESILVA and A. CHATT. Anal. Chim. Acta, To be published.
16. D. E. RYAN, D. C. STUART, and A. CHATTOPADHYAY. Anal. Chim. Acta, **100**, 87 (1978).
17. D. E. RYAN, J. HOLZBECHER, and D. C. STUART. Clin. Chem. **24**, 1996 (1978).
18. A. CHATT, K. N. DESILVA, and R. E. TOUT. Trans. Can. Nucl. Soc. **1**, 80 (1980).
19. A. CHATT and K. N. DESILVA. Proc. 4th Intern. Conf. on Nuclear Methods in Environment and Energy Research, Univ. of Missouri, Columbia, U.S.A. In press.
20. A. CHATT, K. N. DESILVA, and R. E. TOUT. J. Radioanal. Chem. In press.
21. R. E. TOUT and A. CHATT. Anal. Chim. Acta, In press.
22. National Bureau of Standards, Certificate of Analysis, Standard Reference Material 1571, Orchard Leaves, Washington, D.C. (1976).
23. National Bureau of Standards, Certificate of Analysis, Standard Reference Material 1577, Bovine Liver, Washington, D.C. (1977).
24. L. A. CURRIE. Anal. Chem. **40**, 586 (1968).
25. H. A. VAN DER SLOOT, G. D. WALS, C. A. WEERS, and H. A. DAS. Anal. Chem. **52**, 112 (1980).
26. C. M. LEDERER and V. S. SHIRLEY (*Editors*). Table of isotopes. 7th. ed. Wiley-Interscience, Toronto. 1978.

Can. J. Chem. Downloaded from www.nrcresearchpress.com by 210.87.254.105 on 09/06/12
For personal use only.

Crystal and molecular structure of [dimethyl(3,5-dimethyl-1-pyrazolyl)(ethanolamino)gallato ($N(2),O,N(3)$)](η^3-cycloheptatrienyl)dicarbonylmolybdenum

KENNETH S. CHONG, STEVEN J. RETTIG, ALAN STORR, AND JAMES TROTTER

Department of Chemistry, University of British Columbia, 2036 Main Mall, Vancouver, B.C. V6T 1Y6

Received December 3, 1980

KENNETH S. CHONG, STEVEN J. RETTIG, ALAN STORR, and JAMES TROTTER. Can. J. Chem. **59**, 1665 (1981).

Crystals of [dimethyl(3,5-dimethyl-1-pyrazolyl)(ethanolamino)gallato($N(2),O,N(3)$)](η^3-cycloheptatrienyl)dicarbonylmolybdenum are monoclinic, $a = 10.511(1)$, $b = 8.335(1)$, $c = 24.138(3)$ Å, $\beta = 102.22(1)°$, $Z = 4$, space group $P2_1/c$. The structure was solved by Patterson and Fourier syntheses and was refined by full-matrix least-squares procedures to $R = 0.028$ and $R_w = 0.046$ for 3708 reflections with $I \geq 3\sigma(I)$. The crystal structure consists of discrete molecules linked by N—H...O hydrogen bonds (N...O = 2.929(5) Å). The Mo atom is in a distorted octahedral environment with the η^3-C_7H_7 ligand occupying one coordination site, trans to the amino nitrogen, as a π-donating ligand. Important bond distances (corrected for libration) are: Mo—O, 2.245(2), Mo—N(amino), 2.249(3), Mo—N(pyrazolyl), 2.270(3), Mo—C(O), 1.950(4) and 1.947(4), Mo—C(C_7H_7), 2.176(4), 2.364(4), and 2.380(4), Ga—O, 1.919(3), Ga—N, 1.984(3), and Ga—C, 1.982(5) and 1.983(5) Å. An unusual type of disorder is present in which a second image of the molecule, approximately mirrored by the plane $y = 1/4$, is in evidence at low occupancy.

KENNETH S. CHONG, STEVEN J. RETTIG, ALAN STORR et JAMES TROTTER. Can. J. Chem. **59**, 1665 (1981).

Les cristaux de [diméthyl(diméthyl-3,5 pyrazolyl-1) (éthanolamino) gallato ($N(2),O,N(3)$)] (η^3-cycloheptatriényl) dicarbonylmolybdène sont monocliniques avec $a = 10,511(1)$, $b = 8,335(1)$, $c = 24,138(3)$ Å, $\beta = 102,22(1)°$, $Z = 4$, groupe d'espace $P2_1/c$. On a résolu la structure à l'aide des synthèses de Fourier et de Patterson et on les a affinées par la méthode des moindres carrés (matrice entière) jusqu'à des valeurs de $R = 0,028$ et de $R_w = 0,046$ pour 3708 réflexions avec $I \geq 3\sigma(I)$. Du point de vue structural, le cristal est constitué de molécules discrètes liées par des liaisons hydrogènes N—H...O (N...O) 2,929(5) Å. L'atome de Mo est dans un environnement tétraédrique déformé avec le ligand η^3-C_7H_7 occupant un des sites de coordination en position *trans* par rapport à l'azote du groupement amino comme un ligand donneur π. Les distantes importantes de liaison (corrigées pour la libration) sont: Mo—O, 2,245(2), Mo—N(amino), 2,249(3), Mo—N(pyrazolyl), 2,270(3), Mo—C(O), 1,950(4) et 1,947(4), Mo—C(C_7H_7), 2,176(4), 2,364(4) et 2,380(4), Ga—O, 1,919(3), Ga—N, 1,984(3) et Ga—C, 1,982(5) et 1,983(5) Å. On trouve un type inhabituel de désordre dans lequel on rencontre une deuxième image de la molécule qui est approximativement réfléchie par le plan $y = 1/4$, et qui ne correspond qu'à un faible taux d'occupation.

[Traduit par le journal]

Introduction

The synthesis and coordinating properties of the anionic ligands **1** have been discussed in a number of previous publications (1–9). Recently a series of $LM(CO)_2(C_7H_7)$ (where L = **1** and M = Mo or W) derivatives was described (10). The present paper describes the crystal structure analysis of the complex $[Me_2Ga(N_2C_5H_7)OCH_2CH_2NH_2]Mo(CO)_2(\eta^3\text{-}C_7H_7)$, **2**. The structure confirms our earlier predictions (10) regarding the *fac* tridentate chelating nature of the organogallate ligand and the presence of an η^3-C_7H_7 grouping. Steric factors which influence the position of substitution of the C_7H_7 group in the pseudo-octahedral complex are discussed.

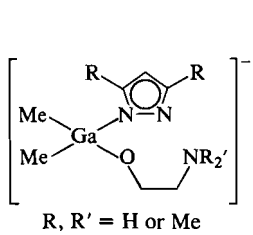

R, R' = H or Me

1

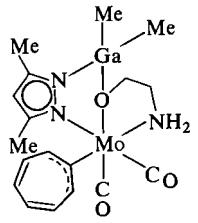

2

Experimental

The preparation of the title complex has been described in a previous publication (10). Crystals suitable for X-ray analysis were obtained by recrystallization from benzene. A crystal ca. 0.18 × 0.40 × 0.14 mm in size was mounted in a general orientation. Unit-cell parameters were refined by least-squares on 2 sin θ/λ values for 25 reflections measured on a diffractometer with Mo K_α radiation ($\lambda = 0.71073$ Å). Crystal data at 22°C are:

$C_{18}H_{26}GaMoN_3O_3$ f.w. = 498.09

Monoclinic, $a = 10.511(1)$, $b = 8.335(1)$, $c = 24.138(3)$ Å, $\beta = 102.22(1)°$, $V = 2066.6(4)$ Å^3, $Z = 4$, $\rho_c = 1.601$ g cm^{-3}, $F(000) = 1008$, μ(Mo K_α) = 19.8 cm^{-1}. Absent reflections: $h0l$, $l \neq 2n$ and $0k0$, $k \neq 2n$ uniquely indicate the space group $P2_1/c$ (C_{2h}^5, No. 14).

Intensities were measured with graphite-monochromatized Mo K_α radiation on an Enraf-Nonius CAD4-F diffractometer. An ω–θ scan at 1.26–10.06° min^{-1} over a range of (0.65 + 0.35 tan θ) degrees in ω (extended by 25% on both sides for background measurement) was employed. Data were measured to $2\theta = 55°$. The intensities of 3 check reflections, measured every 3600 s throughout the data collection, remained constant to within ±2%. After data reduction, an absorption correction was applied using the Gaussian integration method (11, 12). Transmission factors ranged from 0.692 to 0.793 for 224

0008-4042/81/111665-06$01.00/0

©1981 National Research Council of Canada/Conseil national de recherches du Canada

Can. J. Chem. Downloaded from www.nrcresearchpress.com by 210.87.254.40 on 09/06/12
For personal use only.

Can. J. Chem. Downloaded from www.nrcresearchpress.com by 210.87.254.40 on 09/06/12
For personal use only.

sampling points. Of the 4740 independent reflections measured, 3708(78%) had intensities greater than $3\sigma(I)$ above background where $\sigma^2(I) = S + 2B + (0.04(S - B))^2$ with S = scan count and B = background count.

The positions of the Mo and Ga atoms were determined from the Patterson function and those of the remaining non-hydrogen atoms from a subsequent Fourier synthesis. After full-matrix least-squares refinement with anisotropic thermal parameters to $R = 0.083$ a difference map showed one large peak related to the Mo atom by reflection in the plane $y = 1/4$ and second peak similarly related to the Ga atom. Careful inspection of the difference map showed that an image of the original molecule, approximately mirrored by the plane $y = 1/4$, was present at a relatively low occupancy. Before continuing the refinement additional photographs were taken using several different crystals including that used for data collection. Even after long exposures, no evidence of twinning nor of a supercell was discovered. The original choice of space group and cell parameters was confirmed and the structure assumed to possess this unusual type of disorder.

Occupancy factors were estimated from the relative peak heights of the two partial Mo atoms on a Fourier map and were later adjusted to give nearly equal equivalent isotropic thermal parameters for the Mo atoms. These values were determined to be 0.895 and 0.105 and were not subsequently varied. Eventually the non-hydrogen atoms of the low-occupancy molecule as well as the hydrogen atoms associated with the predominant structure were located by Fourier synthesis. A three-dimensional model indicated that several atoms were too close for individual refinement. These atoms were included in the refinement as fixed atoms, their coordinates being taken from the Fourier maps. Thermal parameters for fixed low-occupancy O and C atoms were fixed at values near those observed for the high-occupancy counterparts. Fixed hydrogen atoms were assigned U values related to the equivalent isotropic U of the atom to which they are bonded ($U_H = k \cdot U_C$, where $k = 1.25$ for Me—H and 1.10 for other types). The scattering factors of ref. 13 were used for non-hydrogen atoms and those of ref. 14 for hydrogen atoms. Anomalous scattering factors from ref. 15 were used for the Mo and Ga atoms. The weighting scheme, $w = 1/\sigma^2(F)$ where $\sigma^2(F)$ is derived from the previously defined $\sigma^2(I)$ gave uniform average values of $w(|F_o| - |F_c|)^2$ over ranges of $|F_o|$ and was employed in the final stages of refinement. Convergence was reached at $R = 0.028$ and $R_w = 0.046$ for 3708 reflections with $I \geq 3\sigma(I)$. For all 4740 reflections $R = 0.047$ and $R_w = 0.046$. The function minimized was $\Sigma w(|F_o| - |F_c|)^2$, $R = \Sigma||F_o| - |F_c||/\Sigma|F_o|$ and $R_w = (\Sigma w(|F_o| - |F_c|)^2/\Sigma w|F_o|^2)^{1/2}$.

On the final cycle of refinement the mean and maximum parameter shifts corrsponded to 0.13 and 2.4σ respectively. The mean error in an observation of unit weight was 1.572. A final difference map showed no unusual features. The final positional and thermal parameters appear in Tables 1 and 2[1] respectively. Measured and calculated structure factors have been placed in the Depository of Unpublished Data.[1]

The ellipsoids of thermal motion for the non-hydrogen atoms are shown in Fig. 1. The thermal motion has been analysed in terms of the rigid-body modes of translation, libration, and screw motion (16) using the compuer program MGTLS. The rms standard error in the temperature factors σU_{ij} (derived from the least-squares analysis) is 0.0025 Å^2. Analysis of all 26 non-hydrogen atoms of the high-occupancy molecule gave rms $\Delta U_{ij} = 0.0065$ Å^2 and physically reasonable rigid-body parameters. The appropriate bond distances have been corrected for libration (17), using shape parameters q^2 of 0.08 for all atoms involved. Corrected bond lengths appear along with the uncorrected values in Table 3. The esd's of the corrected bond lengths are assumed to be the same as those obtained from the least-squares for the uncorrected values. Corrected bond angles are not different from the uncorrected values in Table 4 by more than 1σ. Intra-annular torsion angles defining the ring conformations are listed in Table 5. Derived results presented in Tables 3–5 refer to the predominant molecule, those for the low-occupancy structure being far less accurate. The low-occupancy Ga–Me_2 moiety is not well resolved and represents the only region of the low-occupancy model which differs significantly from that of the predominant structure, most likely a result of the overlap.

[1]The structure factor table and Table 2 (thermal parameters) are available, at a nominal charge, from the Depository of Unpublished Data, CISTI, National Research Council of Canada, Ottawa, Ont., Canada K1A 0S2.

Results and Discussion

The crystal structure of **2** consists of discrete molecules, each linked to two others along the crystallographic b axis by weak symmetric bifurcated N—H...O hydrogen bonds involving one of the carbonyl oxygen atoms (N(3)—H(N3a)/H(N3b)...O(1) ($1 - x$, $1/2 + y$, $1/2 - z$), O...N = 2.929(5), O...H = 2.42(4) and 2.43(5) Å, O...H—N = 122(4) and 120(4), C—O...H = 161(1) and 159(1)°). All other intermolecular distances correspond to normal van der Waals contacts.

The ligand **1** displays *fac* coordination as in **3** (2), resulting in a distorted pseudo-octahedral coordination geometry about the Mo atom with an η^3-C_7H_7 ligand occupying one coordination site as a π-donating ligand. Unlike **3**, in which the η^3-2-methylallyl ligand is situated *trans* to the pyrazolyl nitrogen, the allylic portion of the η^3-C_7H_7 ligand is located *trans* to the amino nitrogen. Steric effects are most likely responsible for this difference. If the cycloheptatrienyl ligand were *trans* to the pyrazolyl nitrogen close contacts with the amino group would occur. In the observed orientation two of the C_7H_7 protons are near the pyrazolyl nitrogen and may even be weakly interacting with the pyrazolyl π-system (N(1)...H(11) = 2.59(4) and N(1)...H(5) = 2.65(5) Å). This stereochemical difference between **2** and **3** leads to significant differences between the coordination spheres of these two closely related molecules.

The orientation of the allylic portion of the η^3-C_7H_7 ligand is normal, the central carbon atom

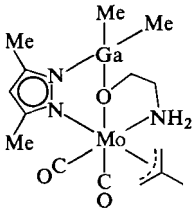

3

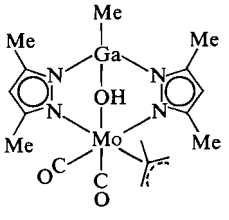

4

Can. J. Chem. Downloaded from www.nrcresearchpress.com by 210.87.254.40 on 09/06/12
For personal use only.

TABLE 1. Final positional parameters (fractional × 10^4, Mo and Ga × 10^5, H and primed O, N, and C × 10^3*) with estimated standard deviations in parentheses

Atom	x	y	z
Mo	60847(3)	33452(4)	15588(1)
Ga	92417(7)	26812(11)	12775(3)
Mo′	6077(3)	1627(4)	1558(1)
O(1)	4234(3)	783(5)	1888(2)
O(2)	3758(3)	5324(5)	1814(1)
O(3)	7906(2)	1890(3)	1636(1)
N(1)	7528(3)	5310(3)	1486(1)
N(2)	8635(3)	4926(4)	1282(1)
N(3)	7076(4)	3562(5)	2476(1)
C(1)	4955(4)	1683(5)	1755(2)
C(2)	4643(4)	4619(5)	1706(2)
C(3)	8963(6)	1845(7)	494(2)
C(4)	10984(4)	2430(7)	1781(2)
C(5)	5805(4)	3217(6)	643(2)
C(6)	5477(5)	1680(6)	756(2)
C(7)	4198(7)	943(8)	590(3)
C(8)	3024(6)	1625(9)	408(3)
C(9)	2747(7)	3272(14)	393(4)
C(10)	3567(5)	4540(8)	530(2)
C(11)	5000(5)	4552(7)	697(2)
C(12)	7447(4)	6911(5)	1490(2)
C(13)	8462(8)	7571(8)	1300(4)
C(14)	9185(4)	6278(5)	1159(2)
C(15)	8336(4)	1393(5)	2220(2)
C(16)	8392(4)	2850(7)	2591(2)
C(17)	6379(6)	7768(6)	1684(3)
C(18)	10373(5)	6277(8)	916(2)
Ga′	9238(10)	2237(10)	1266(4)
H(N3a)	717(4)	450(5)	257(2)
H(N3b)	653(5)	345(6)	267(2)
H(3a)	935(6)	202(7)	23(3)
H(3b)	858(8)	44(12)	50(4)
H(3c)	906	308	42
H(4a)	1101(5)	146(6)	210(2)
H(4b)	1149(9)	287(11)	155(4)
H(4c)	1097	291	217
H(5)	649(5)	358(6)	58(2)
H(6)	613(4)	88(6)	78(2)
H(7)	428(6)	− 34(8)	55(3)
H(8)	228(5)	85(6)	34(2)
H(9)	187(6)	341(7)	28(3)
H(10)	320(7)	586(10)	46(3)
H(11)	542(4)	530(5)	71(2)
H(13)	866	874	126
H(15a)	764(4)	64(5)	235(1)
H(15b)	907(4)	109(5)	232(2)
H(16a)	905	362	251
H(16b)	861(4)	265(6)	293(2)
H(17a)	649(7)	877(10)	175(3)
H(17b)	560(4)	758(5)	144(2)
H(17c)	646	745	210
H(18a)	1021(5)	564(7)	54(2)
H(18b)	1116(6)	586(8)	122(3)
H(18c)	1071(6)	725(8)	84(2)
O(1′)	416(4)	422(6)	187(2)
O(2′)	375(3)	−37(5)	185(1)
O(3′)	789	311	162
N(1′)	752(3)	−35(4)	150(1)
N(2′)	862(3)	6(4)	127(1)
N(3′)	705(3)	136(4)	249(1)
C(1′)	491(4)	323(5)	173(2)
C(2′)	463(4)	41(5)	174(2)
C(3′)	906	308	42
C(4′)	1059	246	157
C(5′)	574	181	54
C(6′)	554	337	52
C(7′)	440(6)	419(6)	61(2)
C(8′)	306(8)	358(11)	34(4)
C(9′)	277	204	43
C(10′)	372(6)	68(7)	55(2)
C(11′)	508(5)	23(6)	70(2)
C(12′)	743(7)	−206(9)	152(3)
C(13′)	861(6)	−267(7)	119(2)
C(14′)	920	−126	116
C(15′)	833	361	222
C(16′)	842(5)	186(7)	260(3)
C(17′)	637	−277	169
C(18′)	1023(6)	−156(7)	87(3)

*Primed atoms have occupancy 0.105, all others are 0.895.

being directed away from the carbonyl groups and closest to the Mo atom as in the related complexes **4** (18), **5** (19), $[H_2B(N_2C_5H_7)_2]Mo(CO)_2(\eta^3\text{-}C_7H_7)$ **6** (20), and $[PhB(N_2C_3H_3)_3]Mo(CO)_2$(allyl) (21) where allyl = η^3-C_7H_7, **7**, or η^3-C_3H_5, **8**. This is in contrast to the "reverse" orientation of the η^3-C_4H_7 ligand in **3** where the Mo—C bond to the central carbon atom is the longest of the three. In the η^3-C_7H_7 complexes **2**, **6**, and **7** the central Mo—C(allyl) bond is about 0.19 Å shorter than the "outer" Mo—C bonds. This difference is larger than that generally observed for η^3-C_3H_5 or η^3-C_4H_7 complexes and is the result of steric effects. The distance from the Mo atom to the centre of mass of the three coordinated allylic carbon atoms (*D′*) in **2** is 2.051 Å, shorter than the values found for the closely related structures of **3–8** which range from 2.067 Å in **4** to 2.103 Å in **3**. A structural *trans* effect is probably responsible since the allylic ligands in **3–8** are *trans* to a pyrazolyl nitrogen while that in **2** is *trans* to an amino nitrogen atom. All of these Mo—*D′* distances are in the usual range of 2.02–2.10 Å observed for d^4-M(allyl)L_5 complexes (22).

The Mo—O distance of 2.245(2) Å is significantly shorter than the values of 2.269(2) and 2.272(4)

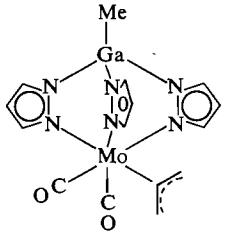

5

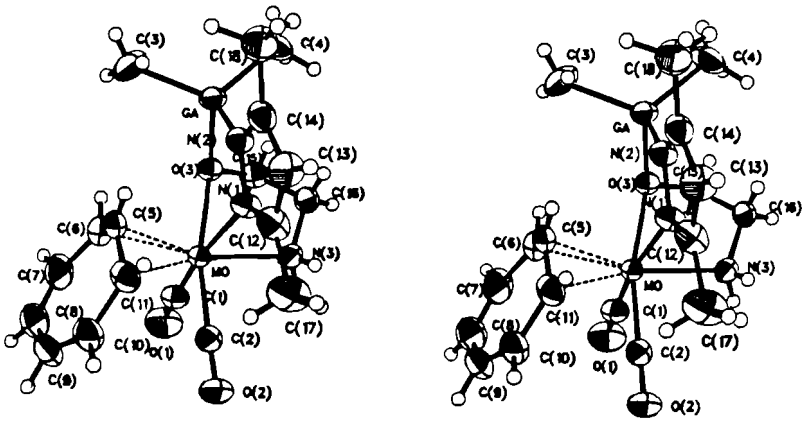

FIG. 1. Stereo view of the [dimethyl(3,5-dimethyl-1-pyrazolyl)(ethanolamino) gallato (*N(2),O, N(3)*](η³-cycloheptatrienyl) dicarbonylmolybdenum molecule. 50% thermal ellipsoids are shown for the non-hydrogen atoms.

TABLE 3. Bond lengths (Å) with estimated standard deviations in parentheses

	Length			Length	
Bond	Uncorr.	Corr.	Bond	Uncorr.	Corr.
Mo —O(3)	2.241(2)	2.245	N(1) —C(12)	1.338(5)	1.339
Mo —N(1)	2.264(3)	2.270	N(2) —C(14)	1.329(5)	1.330
Mo —N(3)	2.246(3)	2.249	N(3) —C(16)	1.476(5)	1.478
Mo —C(1)	1.947(4)	1.950	C(5) —C(6)	1.369(7)	1.372
Mo —C(2)	1.943(4)	1.947	C(5) —C(11)	1.420(7)	1.423
Mo —C(5)	2.170(4)	2.176	C(6) —C(7)	1.455(8)	1.456
Mo —C(6)	2.359(4)	2.364	C(7) —C(8)	1.345(10)	1.347
Mo —C(11)	2.374(4)	2.380	C(8) —C(9)	1.403(12)	1.405
Ga —O(3)	1.916(3)	1.919	C(9) —C(10)	1.359(12)	1.361
Ga —N(2)	1.977(3)	1.984	C(10)—C(11)	1.474(7)	1.475
Ga —C(3)	1.979(5)	1.982	C(12)—C(13)	1.363(9)	1.364
Ga —C(4)	1.983(5)	1.983	C(12)—C(17)	1.487(7)	1.489
O(1)—C(1)	1.158(5)	1.162	C(13)—C(14)	1.402(8)	1.403
O(2)—C(2)	1.176(5)	1.179	C(14)—C(18)	1.489(6)	1.489
O(3)—C(15)	1.446(5)	1.447	C(15)—C(16)	1.503(7)	1.505
N(1)—N(2)	1.393(4)	1.395			

Å observed for **3** and **4** respectively. As noted previously (2, 18–21) the Mo—N bonds *trans* to the allylic ligand are significantly shortened relative to those *trans* to CO. The Mo—N(amino) bond in **2**, *trans* to the η^3-C_7H_7 ligand, at 2.249(3) Å, is significantly shorter than the corresponding bond of 2.285(2) Å *trans* to CO in **3**. The Mo—N(pyrazolyl) distance of 2.270(3) Å is shorter than the corresponding distances (*trans* to CO) of 2.283(4)–2.328(3) Å in the pyrazolyl gallate complexes **4** and **5**, but is longer than the values of 2.222(5)–2.260(3) Å in the pyrazolyl borate structures **6–8**. The Mo—N(pyrazolyl) distances which are *trans* to the allylic ligands in **3–8** are shorter, ranging from 2.173(5) Å in **6** to 2.242(4) Å in **4**. The longer Mo—N(pyrazolyl) bond in **2** relative to that in **3** is compensated by a significant shortening of the Ga—N distance, from 2.006(2) Å in **3** to 1.984(3) Å in **2**.

The two Mo—C(O) distances in **2** (1.950(4) and 1.947(4) Å) are equal within experimental error, in sharp contrast to the markedly different values in **3** (1.961(2) Å *trans* to amino N and 1.902(3) Å *trans* to (O)). The two C—O distances, however, differ by 2.4σ and the O(2)—C(2) distance of 1.179(5) Å is one of the longest observed in this type of compound (2). The ν_{CO} values for **2** in cyclohexane solution of 1932 and 1855 cm^{-1} (10) are reasonably consistent with the solid state C—O distances (2) although involvement of carbonyl oxygen atoms in hydrogen-bonding (in **2** and **3**) as well as crystal packing forces tend to reduce the probability of

Can. J. Chem. Downloaded from www.nrcresearchpress.com by 210.87.254.40 on 09/06/12
For personal use only.

Can. J. Chem. Downloaded from www.nrcresearchpress.com by 210.87.254.40 on 09/06/12
For personal use only.

TABLE 4. Bond angles (deg) with estimated standard deviations in parentheses, non-hydrogen atoms

Bonds	Angle (deg)	Bonds	Angle (deg)
O(3)—Mo—N(1)	79.8(1)	Mo —O(3) —Ga	118.1(1)
O(3)—Mo—N(3)	75.6(1)	Mo —O(3) —C(15)	108.8(2)
O(3)—Mo—C(1)	98.5(1)	Ga —O(3) —C(15)	115.5(2)
O(3)—Mo—C(2)	165.0(1)	Mo —N(1) —N(2)	119.0(2)
O(3)—Mo—C(5)	89.3(1)	Mo —N(1) —C(12)	132.6(3)
O(3)—Mo—C(6)	80.1(1)	N(2) —N(1) —C(12)	106.9(3)
O(3)—Mo—C(11)	123.1(1)	Ga —N(2) —N(1)	120.9(2)
N(1)—Mo—N(3)	80.8(1)	Ga —N(2) —C(14)	130.2(3)
N(1)—Mo—C(1)	170.6(1)	N(1) —N(2) —C(14)	108.6(3)
N(1)—Mo—C(2)	100.4(1)	Mo —N(3) —C(16)	111.9(3)
N(1)—Mo—C(5)	84.6(1)	Mo —C(1) —O(1)	175.0(4)
N(1)—Mo—C(6)	115.5(1)	Mo —C(2) —O(2)	176.4(4)
N(1)—Mo—C(11)	80.3(2)	Mo —C(5) —C(6)	80.1(3)
N(3)—Mo—C(1)	89.8(2)	Mo —C(5) —C(11)	79.8(2)
N(3)—Mo—C(2)	89.6(1)	C(6) —C(5) —C(11)	122.3(4)
N(3)—Mo—C(5)	160.5(2)	Mo —C(6) —C(5)	65.0(2)
N(3)—Mo—C(6)	147.7(2)	Mo —C(6) —C(7)	123.3(4)
N(3)—Mo—C(11)	150.1(2)	C(5) —C(6) —C(7)	126.7(5)
C(1)—Mo—C(2)	78.8(2)	C(6) —C(7) —C(8)	129.9(6)
C(1)—Mo—C(5)	104.8(2)	C(7) —C(8) —C(9)	126.4(6)
C(1)—Mo—C(6)	73.1(2)	C(8) —C(9) —C(10)	129.6(6)
C(1)—Mo—C(11)	108.1(2)	C(9) —C(10) —C(11)	129.1(7)
C(2)—Mo—C(5)	105.7(2)	Mo —C(11) —C(5)	64.1(3)
C(2)—Mo—C(6)	112.7(2)	Mo —C(11) —C(10)	123.5(4)
C(2)—Mo—C(11)	71.4(2)	C(5) —C(11) —C(10)	124.3(6)
C(5)—Mo—C(6)	34.9(2)	N(1) —C(12) —C(13)	110.1(5)
C(5)—Mo—C(11)	36.1(2)	N(1) —C(12) —C(17)	122.3(4)
C(6)—Mo—C(11)	62.2(2)	C(13)—C(12) —C(17)	127.5(5)
O(3)—Ga —N(2)	93.2(1)	C(12)—C(13) —C(14)	106.0(5)
O(3)—Ga —C(3)	109.7(2)	N(2) —C(14) —C(13)	108.3(4)
O(3)—Ga —C(4)	110.9(2)	N(2) —C(14) —C(18)	121.9(4)
N(2)—Ga —C(3)	110.9(2)	C(13)—C(14) —C(18)	129.8(5)
N(2)—Ga —C(4)	110.7(2)	O(3) —C(15) —C(16)	108.3(3)
C(3)—Ga —C(4)	118.7(2)	N(3) —C(16) —C(15)	107.3(4)

TABLE 5. Intra-annular torsion angles (deg) chelate and C_7H_7 rings

Bond	Obs.	Bond	Obs.
Mo —N(1)	26.3(2)	C(5) —C(6)	42.9(5)
N(1) —N(2)	−18.7(2)	C(6) —C(7)	−16.0(7)
N(2) —Ga	−2.8(2)	C(7) —C(8)	−7.4(9)
Ga —O(3)	23.4(1)	C(8) —C(9)	3.1(9)
O(3) —Mo	−27.8(1)	C(9) —C(10)	4.7(10)
		C(10)—C(11)	12.1(7)
Mo —O(3)	23.4(2)	C(11)—C(5)	−39.4(5)
O(3) —C(15)	−51.2(3)		
C(15)—C(16)	58.2(4)		
C(16)—N(3)	−36.3(3)		
N(3) —Mo	7.7(2)		

good correlation between solution ν_{CO} values and solid state C—O distances.

The remaining bond lengths and angles in the molecule are as expected. The pyrazolyl ring is slightly, but significantly, non-planar ($\chi^2 = 13.7$ for N_2C_3) with the metal atoms considerably displaced from the mean plane of the pyrazolyl ring (Mo by 0.4425(3) and Ga by −0.1903(8) Å). The cycloheptatrienyl ring has six atoms roughly coplanar with C(5), the central coordinated atom, displaced from the plane defined by the other atoms (see torsion angles in Table 5). The η^3-C_7H_7 ligand was found to be fluxional in solution (10), a result also noted for the complexes **6** and **7** (20, 21).

Acknowledgments

We thank the Natural Sciences and Engineering Research Council of Canada for financial support and the University of British Columbia Computing Centre for assistance.

1. K. S. CHONG and A. STORR. Can. J. Chem. **57**, 167 (1979).
2. K. S. CHONG, S. J. RETTIG, A. STORR, and J. TROTTER. Can. J. Chem. **57**, 1335 (1979).
3. K. S. CHONG, A. STORR, S. J. RETTIG, and J. TROTTER. Can. J. Chem. **55**, 4166 (1977).

4. K. S. CHONG, S. J. RETTIG, A. STORR, and J. TROTTER. Can. J. Chem. **56**, 1212 (1978).
5. K. S. CHONG, S. J. RETTIG, A. STORR, and J. TROTTER. Can. J. Chem. **57**, 3107 (1979).
6. K. S. CHONG, S. J. RETTIG, A. STORR, and J. TROTTER. Can. J. Chem. **57**, 3113 (1979).
7. K. S. CHONG, S. J. RETTIG, A. STORR, and J. TROTTER. Can. J. Chem. **58**, 1091 (1980).
8. K. S. CHONG, S. J. RETTIG, A. STORR, and J. TROTTER. Can. J. Chem. **58**, 1080 (1980).
9. K. S. CHONG, S. J. RETTIG, A. STORR and J. TROTTER. Can. J. Chem. **59**, 518 (1981).
10. K. S. CHONG and A. STORR. Can. J. Chem. **58**, 2278 (1980).
11. P. COPPENS, L. LEISEROWITZ, and D. RABINOVICH. Acta Crystallogr. **18**, 1035 (1965).
12. W. R. BUSING and H. A. LEVY. Acta Crystallogr. **22**, 457 (1967).
13. D. T. CROMER AND J. B. MANN. Acta Crystallogr. Sect. A, **24**, 321 (1968).
14. R. F. STEWART, E. R. DAVIDSON, and W. T. SIMPSON. J. Chem. Phys. **42**, 3175 (1965).
15. D. T. CROMER and D. LIBERMAN. J. Chem. Phys. **53**, 1891 (1970).
16. V. SCHOMAKER and K. N. TRUEBLOOD. Acta Crystallogr. Sect. B, **24**, 63 (1969).
17. D. W. J. CRUICKSHANK. Acta Crystallogr. **9**, 747 (1956); **9**, 754 (1956); **14**, 896 (1961).
18. K. R. BREAKELL, S. J. RETTIG, A. STORR, and J. TROTTER. Can. J. Chem. **57**, 139 (1979).
19. K. R. BREAKELL, S. J. RETTIG, D. L. SINGBEIL, A. STORR and J. TROTTER. Can. J. Chem. **56**, 2099 (1978).
20. F. A. COTTON, M. JEREMIC and A. SHAVER. Inorg. Chim. Acta **6**, 543 (1972).
21. F. A. COTTON, C. A. MURILLO and R. B. STULTS. Inorg. Chim. Acta, **22**, 75 (1977).
22. J. A. KADUK, A. T. POULOS, and J. A. IBERS. J. Organomet. Chem. **127**, 245 (1977).

Can. J. Chem. Downloaded from www.nrcresearchpress.com by 210.87.254.40 on 09/06/12
For personal use only.

Methyl group inequivalence and rotational barrier heights from ^{1}H nmr lineshapes: dimethylsulphoxide and trimethylsulphoxonium iodide[1]

J. A. RIPMEESTER

Division of Chemistry, National Research Council of Canada, Ottawa, Ont., Canada K1A 0R9

Received December 16, 1980

J. A. RIPMEESTER. Can. J. Chem. **59**, 1671 (1981).

The ^{1}H nmr lineshapes obtained for a solid solution of DMSO-d_3 in DMSO-d_6 and for $CH_3(CD_3)_2SO^+I^-$ indicated the presence of inequivalent methyl groups in each solid. The effect of methyl group tunnelling on the lineshapes at low temperatures was used to derive barrier heights of 4.15 and 5.0 kcal/mol of a DMSO and 3.70 and 3.85 kcal/mol for $CH_3(CD_3)_2SO^+I^-$. Using ^{1}H nmr lineshapes, including temperature dependent effects, may well be one of the more sensitive techniques to detect inequivalent methyl groups.

J. A. RIPMEESTER. Can. J. Chem. **59**, 1671 (1981).

La forme des lignes obtenues en rmn du ^{1}H pour des solutions solides de DMSO-d_3 dans du DMSO-d_6 et pour le $CH_3(CD_3)_2SO^+I^-$ indique qu'il existe dans chaque solide des groupes méthyles qui ne sont pas équivalents. On a utilisé l'effet tunnel du groupe méthyle sur la forme des lignes à basse température pour déduire les hauteurs des barrières qui sont de 4,15 et 5,0 kcal/mol pour le DMSO et de 3,7 et 3,85 kcal/mol pour le $CH_3(CD_3)_2SO^+I^-$. L'utilisation de la forme des lignes en incluant l'effet de la température, peut bien être une des techniques les plus sensibles pour détecter des groupes méthyles non équivalents.

[Traduit par le journal]

Introduction

In most molecules containing more than one methyl group bonded to a single centre, the methyl groups are equivalent in the gas or liquid phases. On freezing, crystal packing forces may well render such chemically equivalent methyl groups crystallographically inequivalent. Unless detailed crystal structures are available, information on methyl group inequivalence in a solid must be obtained by spectroscopic techniques. Crystal field effects may cause factor group splittings in vibrational spectroscopy or detectable differences in nuclear shielding in nmr spectroscopy. If there are significant differences in methyl group barrier heights, low frequency vibrational spectroscopy or inelastic neutron scattering may be used to detect torsional bands, or ^{1}H nmr may be used to measure distinct methyl group rotation activation energies.

In this contribution the use of CW nmr lineshapes to detect methyl group inequivalence will be illustrated. Solid systems studied include dimethylsulphoxide and trimethylsulphoxonium iodide.

Experimental

Dimethylsulphoxide-d_6 was obtained from Merck, Sharp and Dohme Ltd.; methyl iodide was reagent grade material.

Trimethylsulphoxonium-d_6 iodide ($CH_3(CD_3)_2SO^+I^-$) was prepared by heating dimethylsulphoxide-d_6 and methyliodide (1) together in a sealed tube for a week. The resulting crystalline material was purified by recrystallization from water acidified with HCl to suppress H–D exchange. A solution of DMSO-d_3 in DMSO-d_6 was prepared by heating the $CH_3(CD_3)_2SO^+I^-$ to 190°C under vacuum and fractionating the decomposition products in a series of cold traps (1). In order to suppress exchange, the solution was frozen and stored as a solid.

The nmr samples were prepared by sealing in Pyrex tubes small quantities of the appropriate materials. A low pressure of helium gas was included to ensure good thermal contact of the samples with the tube walls. The ^{1}H nmr lineshapes were recorded at ~56 MHz using a low level marginal oscillator. Low temperatures were achieved using the crystal and control systems described earlier (2).

Results and Discussion

Dimethyl Sulphoxide

In order to illustrate that methyl group inequivalence often is not observed, although expected, the relevant data on solid DMSO will be reviewed.

Two X-ray structure determinations, one for DMSO-d_6 at −60°C (3), the other for DMSO at 5°C (4), agree that the methyl groups are crystallographically inequivalent. For normal DMSO, the two S—C bond lengths were found to be significantly different, 1.766 and 1.827 Å (4). For the deuterated solid, however, both bond lengths were found to be 1.801 Å (3). A wide-line ^{1}H nmr study (5) as a function of temperature showed that above ~120 K, both methyl groups rotate at a rate faster than several tens of kHz. Solid state nmr studies did not show evidence of inequivalence in nuclear shielding for either ^{1}H or ^{13}C nuclei (6, 7). In a study (8) of the low frequency vibrational spectrum, a single band was assigned to methyl torsion. Two bands were assigned to methyl torsion in an inelastic

[1]NRCC No. 19225.

0008-4042/81/111671-04$01.00/0

©1981 National Research Council of Canada/Conseil national de recherches du Canada

Can. J. Chem. Downloaded from www.nrcresearchpress.com by 210.87.254.105 on 09/06/12
For personal use only.

Can. J. Chem. Downloaded from www.nrcresearchpress.com by 210.87.254.105 on 09/06/12
For personal use only.

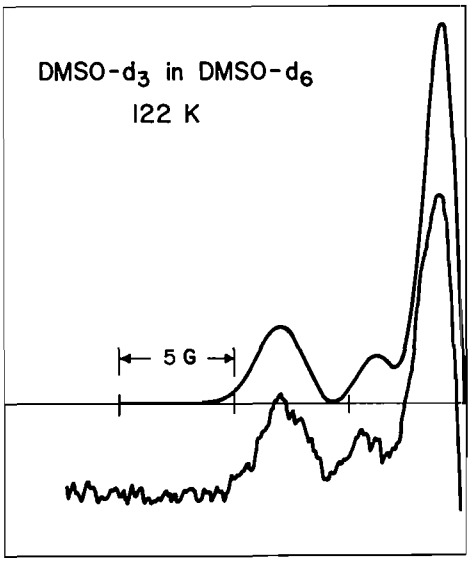

FIG. 1. Experimental (bottom) and calculated ^{1}H nmr lineshapes at 122 K for a solid solution of DMSO-d_3 in DMSO-d_6.

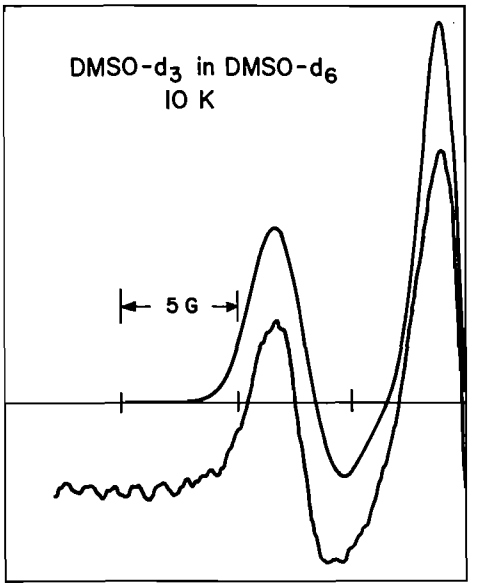

FIG. 2. Experimental (bottom) and calculated ^{1}H nmr lineshapes at 10 K for a solid solution of DMSO-d_3 in DMSO-d_6.

neutron scattering study (9), although the assignment may be somewhat in doubt (8). Two minima in the ^{1}H relaxation time vs. temperature plot were interpreted in terms of dynamically inequivalent methyl groups in a pulsed nmr study (10). Activation energies for methyl group reorientation were found to be 3.0 and 3.8 kcal/mol. This brief summary illustrates that only the X-ray technique and nuclear relaxation, and perhaps inelastic neutron scattering, showed there to be inequivalent methyl groups.

In view of the large difference in methyl group rotational activation energies found from nuclear relaxation measurements, there should be a limited temperature region where half the methyl groups are rotating, and half stationary, on an nmr timescale. Examination of the ^{1}H lineshapes shown in ref. 5 shows that the intermethyl nuclear dipolar coupling obscures fine structure in the temperature region of interest.

In order to reduce the effect of intermethyl group broadening, a sample of DMSO-d_3 in DMSO-d_6 was prepared and the ^{1}H lineshape studied between 100 and 150 K. Between ~120 and 130 K distinct contributions from static and rotating methyl groups are observable. The lineshape observed at 122 K is shown in Fig. 1; the feature ~8 G from the centre is contributed by static methyl groups, the feature ~4 G from the centre mainly by rotating methyl groups. The upper lineshape in Fig. 1 was calculated using the equations given by Andrew and Bersohn (11) assuming there to be equal numbers of static and rotating methyl groups.

Under certain assumptions, the ^{1}H nmr lineshape for a methyl group in its torsional ground state, because of a perturbation of the dipolar energy levels due to tunnelling, can give information on the methyl group barrier heights (12, 13). The lineshape for a 50% DMSO-d_3/DMSO-d_6 solid solution recorded at 10 K is shown in Fig. 2. Distinguishable features for the two distinct methyl groups are not evident.

The lineshape was simulated using the formalism of Apaydin and Clough (14), again assuming there to be two methyl groups each with its distinct tunnelling frequency. The parameters used in the simulation procedure are J, μd, and β. Here $3J/\hbar$ is the tunnelling frequency, $\mu = \gamma\hbar/2$, $d = (3/2)\mu/R^3$, γ is the proton gyromagnetic ratio, R is the interproton distance, and β the Gaussian broadening parameter to account for intermethyl group broadening. Using a value of a $\mu d/\hbar = 7.82$ kHz, the lineshape can be simulated reasonably well using $J/\mu d$ ratios of 0.1 and 0.8. For the geometry assumed, this leads to tunnelling frequencies of 12.3 and 18.8 kHz. The relation derived by Hecht and Dennison (15) may then be used to derive methyl group barrier heights of 4.15 and 5.0 kcal/mol.

It should be noted that the Hecht and Dennison relation (15), although aproximate, agrees within a

Can. J. Chem. Downloaded from www.nrcresearchpress.com by 210.87.254.105 on 09/06/12
For personal use only.

few percent with explicit calculations of the dependence of tunnelling splitting on barrier heights based on a solution of the Matthieu equation for a threefold sinusoidal potential. Uncertainties in the barrier heights obtained are more likely to occur because of approximations such as the assumption of a threefold sinusoidal shape for the barrier, or uncertainties in the moment of inertia of the methyl group.

The activation energies for methyl group rotation derived from the spin–lattice relaxation methods (10), 3.0 and 3.8 kcal/mol, are much lower than the barrier heights derived. Some of the difference may be accounted for by the zero point energy, although significant errors may also occur because of the method used to derive activation energies. Limiting slopes of the log T_1 vs. inverse temperature plots were used, rather than fitting or simulation procedures in order to resolve the double T_1 minimum.

By considering the crystal structure (4), the barrier heights may be assigned to specific methyl groups. Since methyl group I has three short intermolecular C—O distances indicative of hydrogen bond formation, as opposed to methyl group II which has only one such distance, this group can be assigned the higher barrier height.

It is relevant to point out that SCF-MO calculations (19) have indicated that thio-organic molecules in general, and DMSO in particular, can easily distort in the presence of even weak intermolecular interactions.

Trimethylsulphoxonium Iodide

Relatively little is known about the structure of the trimethylsulphoxonium ion. In solution, it has C_{3v} symmetry (16), whereas in the solid the symmetry is generally lower. In the perchlorate salt (17), two of the methyl groups in the ion are related by a mirror plane, in the tetrafluoroborate (18) salt the ion has no symmetry elements although in neither salt are distortions from C_{3v} symmetry severe.

A single band in the far infrared spectrum (16) of the iodide was assigned to methyl torsion and the corresponding methyl group rotational barrier was calculated to be 3.4 kcal/mol.

The ^{1}H nmr lineshape of the partially deuterated salt $CH_3(CD_3)_2SO^+I^-$ recorded at 2.4 K is shown in Fig. 3. In simulating the lineshape (Fig. 3), emphasis was placed on fitting the position and amplitude of tunnelling sidebands. The best fit was achieved by assuming there to be two methyl groups with a $J/\mu d$ ratio of 2.5, and one with $J/\mu d$ of 1.6; the

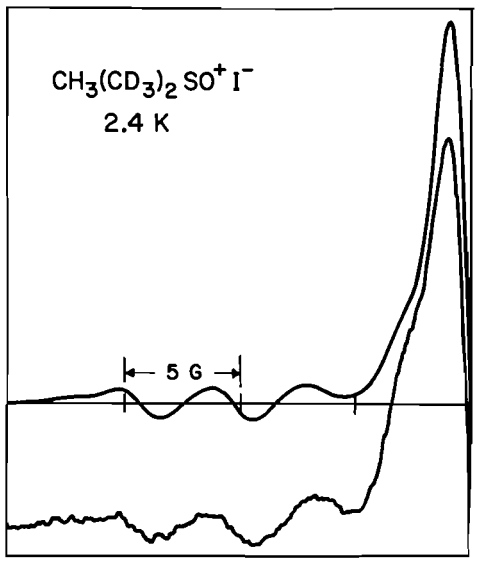

FIG. 3. Experimental (bottom) and calculated ^{1}H nmr lineshapes at 2.4 K for solid $CH_3(CD_3)_2SO^+I^-$.

Gaussian broadening parameter β was taken to be 0.9. Assuming $\mu d/\hbar$ to be 7.82 kHz, this leads to tunnelling frequencies of 58.7 and 37.5 kHz, and application of the Hecht and Dennison relation (15) yields barrier heights of 3.70 and 3.85 kcal/mol.

In molecular solids, crystal forces which render methyl groups inequivalent are usually much weaker than the bonding forces within the molecule. The use of barrier heights and/or motional properties of methyl groups to detect methyl group inequivalence should be quite sensitive as these properties usually depend on the crystal forces as well. The success of the technique depends on resolution of dipolar fine structure either with or without the effect of tunnelling perturbations so that magnetic dilution is often necessary. Under favourable conditions it should be possible to resolve methyl groups with barrier height differences greater than ~5–10% provided at least one of the barriers is greater than 3.5 kcal/mol.

1. R. KUHN and H. TRISCHMANN. Ann. Chem. **611**, 117 (1958).
2. S. K. GARG, B. MORRIS, and D. W. DAVIDSON. J. Chem. Soc. Faraday Trans. II, **68**, 481 (1972).
3. M. A. VISWAMITRA and K. K. KANNAN. Nature, **209**, 1016 (1966).
4. R. THOMAS, C. B. SHOEMAKER, and K. ERIKS. Acta Crystallogr. **21**, 12 (1966).
5. J. DUFOURQ, J. M. CHEZEAU, and B. LEMANCEAU. C.R. Acad. Sci. Paris, **265**, 761 (1967).
6. A. PINES, S. VEGA, and M. MEHRING. Phys. Rev. B, **18**, 112 (1978).

7. A. PINES, M. G. GIBBY, and J. S. WAUGH. Chem. Phys. Lett. **15**, 373 (1972).
8. J. R. DURIG, C. M. PLAYER, and J. BRAGIN. J. Chem. Phys. **52**, 4224 (1979).
9. G. U. SAFFORD, P. C. SCHAFFER, P. S. LEUNG, G. F. DOEBBLER, G. W. BRADY, and E. F. X. LYDEN. J. Chem. Phys. **50**, 2140 (1969).
10. Z. PAJAK, K. JURGA, and S. JURGA. Acta Phys. Pol. A, **45**, 837 (1974).
11. E. R. ANDREW and R. BERSOHN. J. Chem. Phys. **18**, 159 (1950).
12. C. MOTTLEY, T. COBB, and C. S. JOHNSON. J. Chem. Phys. **55**, 5823 (1971).
13. J. A. RIPMEESTER, S. K. GARG, and D. W. DAVIDSON. J. Chem. Phys. **67**, 2275 (1977).
14. F. APAYDIN and S. CLOUGH. J. Phys. C, **1**, 932 (1968).
15. K. T. HECHT and D. M. DENNISON. J. Chem. Phys. **26**, 31 (1957).
16. J. A. CREIGHTON, J. H. GREEN, D. J. HARRISON, and S. M. WALLER. Spectrochim. Acta, Part A, **23**, 2973 (1967).
17. C. L. COULTER, P. K. GANTZEL, and J. D. MCCULLOUGH. Acta Crystallogr. **16**, 676 (1963).
18. I. C. ZIMMERMAN, M. BARLOW, and J. D. MCCULLOUGH. Acta Crystallogr. **16**, 883 (1963).
19. P. G. MEZEY and A. KAPUR. Can. J. Chem. **58**, 559 (1980).

Can. J. Chem. Downloaded from www.nrcresearchpress.com by 210.87.254.105 on 09/06/12
For personal use only.

Acid-catalyzed rearrangement of cyclobutanones. VI.[1] Syntheses of chrysenes and steroid-like substances

EDWARD LEE-RUFF, ALAN C. HOPKINSON, AND LE H. DAO
Department of Chemistry, York University, Downsview, Ont., Canada M3J 2R3

Received December 2, 1980

EDWARD LEE-RUFF, ALAN C. HOPKINSON, and LE H. DAO. Can. J. Chem. **59**, 1675 (1981).

Cyclobutanones derived from 1-naphthylketenes and 1,3-cycloalkadienes were prepared. These undergo acid rearrangements under a variety of conditions to give tetracyclic ketones. The tetracyclic ketones were converted to chrysene and substituted cyclopentenophenanthrenes. A mechanistic scheme is proposed for the rearrangement process.

EDWARD LEE-RUFF, ALAN C. HOPKINSON et LE H. DAO. Can. J. Chem. **59**, 1675 (1981).

On a préparé des cyclobutanones à partir de naphtyl-1 cétènes et de cycloalcadiènes-1,3. Ces cétones se transposent en milieux acides variés en donnant des cétones tétracycliques. On a pu transformer ces cétones tétracycliques en chrysène et en cyclopentenophénanthrènes substitués. On propose un mécanisme pour la transposition.

[Traduit par le journal]

Can. J. Chem. Downloaded from www.nrcresearchpress.com by 210.87.254.42 on 09/06/12
For personal use only.

Cyclobutanones have recently attracted considerable interest as synthetic intermediates (2). Their stereoselective formation (3) and their often spontaneous ring-opening reactions (4) resulting from ring strain permit the preparation of stereoselectively functionalized olefins and ring systems found in natural products. We have been interested in the acid-catalyzed ring-opening processes of cyclobutanones both from a theoretical standpoint in view of the well-studied cyclobutyl–cyclopropyl–carbinyl – allylcarbinyl cation interconversions (5) as well as developing novel approaches to ring annelations and syntheses of polycyclic systems. Our recent findings that α-arylcyclobutanones (i.e. **1**) substituted by a β-positive charge-stabilizing group rearrange under

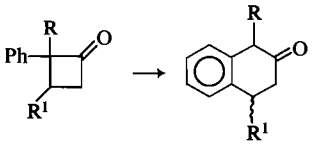

1 **2**

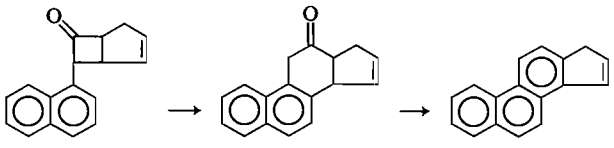

3a *4a* *7a*

acid catalysis to β-tetralones (i.e. **2**) led us to develop a synthesis of tetracyclic steroid analogues (1). In a preliminary communication (1*c*) we reported that the α-naphthylcyclobutanone **3***a* could be converted to the steroid-like derivative **4***a* and aromatized to cyclopenteno[*a*]phenanthrene (**7***a*). We would like to report here the full details of this conversion as well as extensions of this reaction to include the preparation of *D*-homosteroid and chrysene derivatives. Compounds such as **7** as well as substituted chrysenes are of current interest in environmental pollution and have been implicated in the initiation of cancer (6).

Results and Discussion

The cyclobutanone derivatives **3** *a–c* were prepared by the *in situ* generation of 1-naphthylketenes (from dehydrochlorination of 1-naphthylacetyl chloride) in the presence of 3- to 5-fold

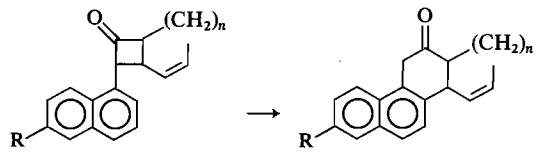

3*a* R = H *n* = 1 **4***a* R = H *n* = 1
b R = H *n* = 2 *b* R = H *n* = 2
c R = OCH_3 *n* = 1 *c* R = OCH_3 *n* = 1

excess of 1,3-cyclopentadiene or 1,3-cyclohexadiene. The yields of the cyclobutanones vary from 40–65% depending upon temperature and concentration effects. Aldoketenes are known to spontaneously dimerize (7) and specific experimental conditions have to be met to maximize the yield of competing olefin cycloadditions. All of these derivatives are heat sensitive and revert to naphthylketene dimer and 1,3-cycloalkadienes at higher temperatures. The structures are assigned

[1]For Part V see ref. 1*a*.

0008-4042/81/111675-05$01.00/0
©1981 National Research Council of Canada/Conseil national de recherches du Canada

Can. J. Chem. Downloaded from www.nrcresearchpress.com by 210.87.254.42 on 09/06/12
For personal use only.

based on spectral and analytical data and by analogy with other ketene 1,3-diene cycloaddition products (8). The regiospecificity of cycloadditions of ketenes is well established (9, 10); however, the stereochemistry of the naphthyl group with respect to the ring junction has not been unequivocally defined, although there is evidence that when two ketene substituents differ in steric bulk the larger one tends to occupy the more hindered *endo* position in the product (11, 12). In all three derivatives it appears that one major stereoisomer is formed.

The acid-catalyzed rearrangements were accomplished using a variety of conditions including methanesulfonic acid (ethereal solution of ketone added to acid at ambient temperature), refluxing trifluoroacetic acid in chloroform solutions, refluxing toluenesulfonic acid in benzene solutions, polyphosphoric acid heated to 100°C, and stannic chloride in benzene. Yields of the rearranged products ranged from 20% to 80%. Optimum yields were obtained using methanesulfonic acid. The structures of ketones **4** *a–c* were assigned based on their

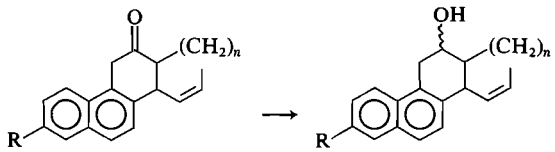

4*a* R = H *n* = 1
b R = H *n* = 2
c R = OCH_3 *n* = 1

5*a* R = H *n* = 1
b R = H *n* = 2
c R = OCH_3 *n* = 1

spectral and analytical data as well as their conversions to the alcohols **5** *a–c* with lithium aluminum hydride and subsequent dehydration and dehydrogenation with 2,3-dichloro-5,6-dicyano-1,4-benzoquinone (DDQ) to the known chrysene (**6**) and cyclopentenophenanthrene (**7***a*) (from **5***a* and *b*, respectively[2]). The aromatized products **6** and **7***a* were found to be identical in all respects with authentic samples. In the case of ketone **4***c*, the above sequence of conversions resulted in its conversion to cyclopentenophenanthrene **7***b*. This derivative was hydrogenated to the known cyclopentanophenanthrene which was obtained independently from Wolff–Kischner reduction and dehydrogenation of equilenin methyl ether. The stereochemistry of the C/D ring junction was assigned to **4** *a–c*, the *cis* configuration based on the nmr coupling constants for the bridgehead protons (J = 4–7 Hz). *trans* Diaxial hydrogen coupling constants are of the order of 12–15 Hz (16).

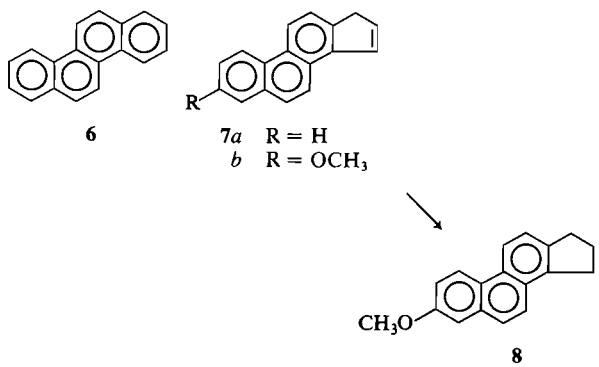

6

7*a* R = H
b R = OCH_3

8

It is noteworthy and contrary to expectation that cyclobutanone **3***c* demonstrates a marked inertness in its tendency towards rearrangement. Using trifluoroacetic acid in refluxing benzene, **3***c* gave the half reacted trifluoroacetate **11** and attempts to

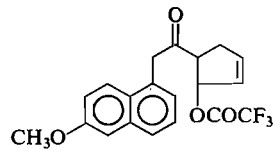

11

cyclize **11** to the tetracyclic ketone **4***c* failed under a variety of conditions. The rearrangement could only be accomplished using stannic chloride in benzene.

These rearrangements can be rationalized according to Scheme 1. Ring opening of protonated cyclobutanone **3** results in formation of ions **9** and/or **10** (classical structure) or a nonclassical ion which is represented by canonical forms **9** and **10**. The subsequent ring annelation could proceed from ion **9** by the known electrophilic substitution pathway for aromatic systems or proceed via ion **10** via cyclopropane ring opening and nucleophilic annelation on aromatic carbon. The observation that no cyclization occurs at the more electron-rich *peri* position of the naphthalene ring, the decreased reactivity of the 6-methoxyl derivative **3***c*, as well as the absence of products derived from ring annelation of the other allylic site in the delocalized ion **9**, suggest that it is not the immediate precursor to the rearrangement product. On the other hand, **10** could conceivably provide two regioisomeric products resulting from the two different modes of

[2]Higher yields of the aromatized products **6** and **7** could be obtained by dehydration of the alcohols **5***a* and *b* with P_2O_5 followed by dehydrogenation with DDQ.

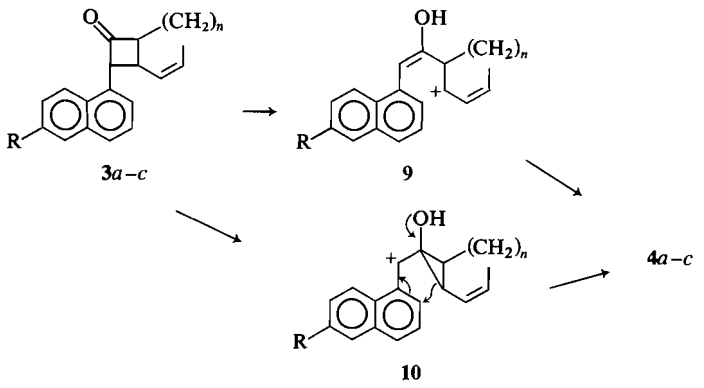

SCHEME I

cyclopropane ring opening processes. Analysis of the reaction product **7***a* derived from **3***a* indicated regiospecific formation of **4***a* during the acid rearrangement, barring any equilibration between **7***a* and its regioisomer 15*H*-cyclopentenophenanthrene during the dehydration/dehydrogenation process.

In view of current interest in specific site alkylated polynuclear hydrocarbons and functionalized steroids we investigated the alkylations of ketones **4** *a–c* by Grignard and alkyl lithium reagents. Mainly starting material and aldol type dimers were observed with both of these reagents. This would suggest that the benzylic hydrogens at C-11 (steroid numbering system) are quite acidic and susceptible to being abstracted by these very strong bases. Attempted electrophilic alkylations at C-11 by way of the enolate using alkyl halides did not provide any transformed material. The alkylation of the carbonyl function was, however, successfully accomplished by nucleophilic addition to the starting cyclobutanones **3** *a–b* and subsequent acid rearrangements of the corresponding cyclobutanols. These observations will be reported in a subsequent paper. The acid-catalyzed rearrangements of α-naphthyl bicyclic cyclobutanones provide a novel entry in the synthesis of steroids, *D*-homosteroids, cyclopentenophenanthrenes, and chrysenes. Work is in progress to specifically alkylate derivatives **4** *a–c* in order to obtain analogues of physiologically active oestrogens.

Experimental

Melting points were determined on a Reichert melting point apparatus and were uncorrected. The ir spectra were recorded on a Unicam SP1000 instrument. The nmr spectra were recorded on a Varian EM-360 spectrometer using $CDCl_3$ solutions and TMS as internal standard. Mass spectra were recorded on a V.G. Micromass 16F spectrometer. Microanalyses were performed by Guelph Chemical Laboratories Ltd. Naphthylacetic acid and 1,3-cyclohexadiene were obtained from Aldrich chemicals and not further purified. 1,3-Cyclopentadiene was obtained by pyrolysis of its dimer (Aldrich chemicals). 6-Methoxy-1-naphthylacetic acid was prepared using a modified literature preparation (14).

Preparation of 1-Naphthylacetyl Chlorides

The acid chlorides were prepared by stirring neat carboxylic acid with 5 mole equivalents of thionyl chloride for 3–24 h at room temperature. The excess thionyl chloride was evaporated and the residual acid chlorides (1-naphthylacetyl chloride and 6-methoxy-1-naphthylacetyl chloride) were used without further purification; ir: 1810 cm^{-1} (C=O of acid chloride).

Preparation of Cyclobutanones **3** a–c

A solution of 10 mmol of acid chloride was dissolved in 50 mL of dry benzene. To this solution was added 50 mmol of 1,3-cyclopentadiene or 1,3-cyclohexadiene and the solution heated to reflux for **3***a* and **3***b* but only to 50°C for **3***c*. Triethylamine (11 mmol) was added over a period of 15 min. After complete addition the reaction mixture was stirred for 30 min at room temperature. It was then poured over 50 mL of ice-water and 50 mL of ether was added. The organic layer was washed with water, 2 × 20 mL of 2 *N* HCl solution, 3 × 30 mL of saturated $NaHCO_3$ solution, and further washed with water. The ether extract was dried over anhydrous $MgSO_4$ and evaporated. In the case of **3***a* and **3***b*, the oily residue was crystallized in boiling hexane. In the case of **3***c* the residue was chromatographed on silica gel using $CH_2Cl_2/CHCl_3$ gradient eluents. Isolated yields for **3** *a–c* are 55, 60, and 30% respectively.

Cyclobutanone **3**a: mp: 114–115°C; ir: 1770, 1600, 1510 cm^{-1}; nmr δ: 2.70 (2H, m), 4.10 (2H, m), 5.40 (2H, m), 5.38 (1H, m), 7.25–8.00 (7H, m); ms (70 ev): 234 (M^+), 168 (naphthylketene, 100%). *Anal.* calcd. for $C_{17}H_{14}O$: C 87.18, H 5.98; found: C 86.60, H 5.85%.

Cyclobutanone **3**b: mp: 126–127°C; ir: 1770 (C=O), 1590, 780 cm^{-1}; nmr δ: 0.9–2.2 (4H, complex multiplet), 3.7 (2H, broad singlet), 4.9–5.3 (2H, m), 5.4–5.8 (1H, m), 7.3–8.0 (7H, m). *Anal.* calcd. for $C_{18}H_{16}O$: C 87.10, H 6.45; found: C 87.26, H 6.59%.

Cyclobutanone **3**c: mp: 86°C; ir (KBr): 1780, 1725, 1632, 1600, 1520, 1480, 1430 cm^{-1}; nmr δ: 2.70 (2H, m), 3.54 (1H, m), 3.90 (3H, s), 4.30 (1H, m), 5.20 (1H, m), 5.70 (2H, m), 7.10–8.00 (6H, m); ms (70 ev); 264 (M^+), 198 ($M^+ - C_5H_6$). *Anal.* calcd. for $C_{18}H_{16}O_2$: C 81.82, H 6.06; found: C 82.24, H 5.92%.

Can. J. Chem. Downloaded from www.nrcresearchpress.com by 210.87.254.42 on 09/06/12
For personal use only.

Can. J. Chem. Downloaded from www.nrcresearchpress.com by 210.87.254.42 on 09/06/12
For personal use only.

Acid-Catalyzed Rearrangements of Cyclobutanones **3** a–c

The following general methods were used for the acid-catalyzed rearrangements.

Method A

A solution of polyphosphoric acid was prepared by heating a 1:1 mixture of P_2O_5 and orthophosphoric acid for 12 h. To 5 mL of polyphosphoric acid heated to 100°C was added 500 mg of cyclobutanone derivative and the mixture stirred vigorously for 5 min. To this mixture was added ice-water and 75 mL of ether. The ether extract was washed with saturated aqueous sodium bicarbonate solution and then with water. The ether extract was then dried over $MgSO_4$ and evaporated. The residue was directly crystallized from ether or chromatographed on a silica gel column.

Method B

To 50 mL of chloroform was added 10 mmol of cyclobutanone and 10 mmol of trifluoroacetic acid. The mixture was refluxed for 4–10 h. This mixture was diluted with 30 mL of benzene and washed with aqueous saturated sodium bicarbonate solution, water, and subsequently dried over $MgSO_4$. After evaporation the residue was chromatographed on a silica gel column and the products eluted with benzene.

Method C

To 10 mL of neat methanesulphonic acid stirred at 0°C was added 2 mmol of cyclobutanone dissolved in 20 mL of ether. The solution in all cases developed a deep colour (brown to purple). After stirring at room temperature for one hour the mixture was poured over crushed ice in water and extracted with 3 × 50 mL of ether. The ether extract was washed with saturated $NaHCO_3$ solution, water, and dried with anhydrous $MgSO_4$. After evaporation the residue was crystallized from ether or ether–ethanol mixtures.

Method D

To a 10^{-2} *M* benzene solution of cyclobutanone was added 50 mg of toluenesulphonic acid. The solution was heated to reflux for 1–4 h. After cooling, the solution was diluted with ether, washed with aqueous $NaHCO_3$ solution, water, and dried with $MgSO_4$. After evaporation the residue was chromatographed on a silica gel column and eluted with benzene.

Method E

To a solution containing 5 mmol of cyclobutanone in 50 mL of benzene was added 1.30 g (5 mmol) of stannic chloride. The reaction mixture was stirred at room temperature. After usual work-up (see above) the residue was chromatographed on a silica gel column and eluted with benzene.

Ketone **4**a Percentage yields from method A: 40%; B: 70%; C: 85%; D: 30%;mp: 84–85°C; ir (Nujol): 1715 cm^{-1} (C=O); nmr δ: 2.90 (2H, m), 3.30 (1H, m, J = 4Hz, 7 Hz), 3.95 (2H, s), 4.52 (1H, br d), 5.88 (2H, m, J = 7 Hz), 7.25–8.05 (6H, m); ms (70 ev): 234 (M^+). *Anal.* calcd. for $C_{17}H_{14}O$: C 87.18, H 5.98; found: C 87.43, H 6.03%.

Ketone **4**b Percentage yields from method A: 70%; B: 35%; C: 85%; D: 30%; mp: 132–133°C; ir (KBr): 1710 cm^{-1}; nmr δ: 1.6–2.7 (4H, m), 2.90 (1H, d of d, J = 2Hz, 7 Hz), 4.0 (3H, s superimposed on m, J = 7 Hz), 5.70 (2H, s) 7.3–8.0 (6H, m); ms (70 ev): 248 (M^+). *Anal.* calcd. for $C_{18}H_{16}O$: C 87.10, H 6.45; found: C 86.78, H 6.57%.

Ketone **4**c Percentage yields from method E: 20%; mp: 103–104°C; ir (KBr): 1720 cm^{-1} (C=O), 1632, 1610, 1520, 1480, 1445; nmr δ: 2.80 (2H, m), 3.70 (1H, m), 3.90 (5H, s), 4.10 (1H, m), 5.80 (2H, m), 7.2–7.8 (5H, m); ms (70 ev): 264 (M^+). *Anal.* calcd. for $C_{18}H_{16}O_2$: C 81.82, H 6.06; found: C 82.17, H 5.85.

Trifluoroacetic Acid Reaction of Cyclobutanone **3**c

A solution of 1.32 g of **3***c* (5 mmol) and 0.57 g (5 mmol) of trifluoroacetic acid in 20 mL of dry chloroform was heated to reflux for 10 h. The cooled mixture was diluted with 20 mL of benzene, washed with water, $NaHCO_3$ and water, and dried over $MgSO_4$. After evaporation the yellow oil crystallized from hexane to give yellow-green crystals of **11**; mp: 64°C; ir (Nujol): 1790, 1740, 1632, 1610, 1510, 1440 cm^{-1}; nmr δ: 2.80 (2H, m), 3.80 (2H, s), 3.90 (3H, s), 4.00 (1H, m), 4.88 (1H, m), 5.80 (2H, m), 7.10–7.80 (6H, m); ms (70 ev): 378 (M^+), 266, 264, 250, 238, 222, 211.

General Method for Reduction of Ketones **4** a–c *to Alcohols* **5** a–c

0.1 *M* Ethereal solutions of ketones **4** *a–c* were added to a dispersion of 3 equiv. of $LiAlH_4$ in anhydrous ether. The mixtures were stirred for 3 h at room temperature. A solution containing 10% NH_4Cl in water (2 mL) was used to quench the excess $LiAlH_4$. The precipitate was filtered off and the filtrate was washed neutral with water, dried over $MgSO_4$, and evaporated. The crude residue was used for the subsequent transformation.

Alcohol **5**a: ir: 3400, 1600, 1518 cm^{-1}; nmr δ: 2.5–2.8 (2H, m), 3.20 (1H, m), 3.80 (2H, t, J = 7 Hz), 4.20 (2H, m), 5.80 (2H, m), 7.10–8.00 (6H, m); ms (70 ev): 236 (M^+), 218.

Alcohol **5**b: ir: 3600, 3460–3200, 1580, 1385, 890 cm^{-1}; nmr δ: 1.7–2.3 (6H, m), 2.90 (1H, t, J = 6 Hz), 3.45 (1H, br, t, J = 8 Hz), 4.50 (1H, t, J = 8 Hz), 5.0 (1H, br t, J = 6 Hz), 5.80 (2H, quintet), 7.2–8.2 (6H, m); ms (70 ev): 250 (M^+), 232.

Alcohol **5**c: mp: 108°C; ir: 3400 cm^{-1}; nmr δ: 3.70 (2H, m), 3.90 (3H, s), 7.10–8.00 (7H, m); ms (70 ev): 246 (M^+), 205.

Dehydrogenation of Alcohols **5** a–c *with DDQ*

To a 50 mL solution (0.1 *M*) of alcohols **5** *a–c* in benzene was added 2.3 g (11 mmol) of DDQ. The solution was heated to reflux for 3 h. The solution was concentrated to 15 mL and chromatographed on a silica gel column and eluted with hexane–benzene mixtures.

Hydrocarbon **7**a: Yield 60% (crystallized from hexane); mp: 169–170°C (lit. (14) mp 164–165°C); ir (Nujol): 1600, 1490, 1420; nmr δ: 3.68 (2H, d of t), 6.71 (2H, m), 7.30–8.10 (6H, m), 8.50–8.80 (2H, m); ms (70 ev): 216 (M^+); uv and ir identical with authentic sample (15).

Chrysene: Yield 55%; ir, nmr, uv identical with a commercial sample.

Ether **7**b: Yield 60%; mp 108–109°C; nmr δ: 3.70 (2H, m), 3.90 (3H, s), 7.10–8.00 (7H, m); ms (70 ev): 246 (M^+), 205, 171, 161, 141, 129, 115.

Hydrogenation of Ether **7**b

A solution of 0.126 g of **7***b* and 0.1 g of Pd on charcoal in ethyl acetate was stirred under H_2 in a closed system containing a gas burette. Reaction was complete after one equivalent of H_2 was absorbed. The solution was filtered and evaporated to give an oily residue which crystallized from hot 95% ethanol to give 0.084 g of **8**; mp: 135–137°C (lit. (13) mp 136–137°C); ms (70 ev): 248 (M^+). A sample was prepared by a literature method (13) from equilenin and found identical (tlc and ms) to the sample prepared above.

Acknowledgements

We would like to thank the Natural Sciences and Engineering Research Council of Canada for financial support and Miss Susan Strach for technical assistance. We are grateful to Ayerst (Montreal) Labs for providing a sample of equilenin.

1. (*a*) P. DUPERROUZEL and E. LEE-RUFF. Can. J. Chem. **58**, 51 (1980); (*b*) L. H. DAO, A. C. HOPKINSON, and E. LEE-RUFF. Tetrahedron Lett. 1413 (1978); (*c*) V. P. ABEGG, A. C. HOPKINSON, and E. LEE-RUFF. Can. J. Chem. **56**, 99 (1978).
2. B. M. TROST. Acc. Chem. Res. **7**, 85 (1974).
3. W. T. BRADY and R. M. LLOYD. J. Org. Chem. **44**, 2560 (1979).
4. R. F. NEWTON, D. P. REYNOLDS, N. M. CROSSLAND, D. R. KELLY, and S. M. ROBERTS. J. Chem. Soc. Chem. Commun. 683 (1979).
5. H. C. BROWN. The nonclassical ion problem. Plenum Press, New York. 1977. Chapt. 5.
6. J. A. ALLEN and M. M. COOMBS. Nature, **287**, 244 (1980).
7. H. ULRICH. Cycloaddition reactions of heterocumulenes. Academic Press, New York. 1967. Chapt. II.
8. R. W. HOLDER, H. S. FREIMAN, and M. F. STEFANCHIK. J. Org. Chem. **41**, 3303 (1976).
9. P. OTTO and R. HUISGEN. Chem. Ber. **102**, 3985 (1969).
10. R. W. HOLDER. J. Chem. Educ. **53**, 81 (1976).
11. M. REY, S. ROBERTS, A. DIEFFENBACHER, and A. S. DREIDING. Helv. Chim. Acta, **53**, 417 (1970).
12. W. T. BRADY and R. ROE, JR. J. Am. Chem. Soc. **93**, 1662 (1971).
13. A. COHEN, J. W. COOK, C. L. HEWETT, and A. GIRARD. J. Chem. Soc. 653 (1934).
14. A. L. GREEN and D. H. HEY. J. Chem. Soc. 4306 (1954).
15. M. M. COOMBS. J. Chem. Soc. C, 963 (1966).
16. M. KARPLUS. J. Am. Chem. Soc. **85**, 2870 (1963)

Can. J. Chem. Downloaded from www.nrcresearchpress.com by 210.87.254.42 on 09/06/12
For personal use only.

The structure of chicanine, a new lignan from *Schisandra sp.*

JIA-SEN LIU,[1] MEI-FEN HUANG, AND YAO-LIANG GAO
Shanghai Institute of Materia Medica, Chinese Academy of Sciences, 319 Yueyang Road, Shanghai (200031), China
AND
JOHN A. FINDLAY
Chemistry Department, University of New Brunswick, Bag Service #45222, Fredericton, N.B., Canada E3B 6E2

Received December 18, 1980

JIA-SEN LIU, MEI-FEN HUANG, YAO-LIANG GAO, and JOHN A. FINDLAY. Can. J. Chem. **59**, 1680 (1981).

A new lignan, chicanine, isolated from the fruit of *Schisandra sp.*, is shown to possess structure **1**, 2*S*-(3-methoxy-4-hydroxyphenyl)-3*R*,4*S*-dimethyl-5*S*-(3,4-methylenedioxyphenyl)tetrahydrofuran, from spectra analysis and chemical conversions. The tetrahydrofuran ring exists in a "twist envelope" conformation.

JIA-SEN LIU, MEI-FEN HUANG, YAO-LIANG GAO et JOHN A. FINDLAY. Can. J. Chem. **59**, 1680 (1981).

A partir d'une analyse spectrale et de transformations chimiques, on montre qu'un nouveau lignan, la chicanine, que l'on a isolé du fruit de *Schisandra sp.*, possède la structure **1**, (méthoxy-3 hydroxy-4 phényl)-2*S*, diméthyl-3*R*,4*S* (méthylènedioxy-3,4 phényl)-5*S* tétrahydrofuranne. Le cycle tétrahydrofuranne existe selon une conformation "enveloppe croisée".
[Traduit par le journal]

Can. J. Chem. Downloaded from www.nrcresearchpress.com by 210.87.254.42 on 09/06/12
For personal use only.

It was reported (1–3) that several dibenzocyclooctadiene lignan compounds, schisantherin A, B, C, D, and schisanhenrin, which were isolated from the fruits of *Schisandra sphenanthera* Rehd et Wils and *S. henryi* Clarke, had been used in clinical studies to lower abnormally high serum glutamic-pyruvic transaminase (SGPT) levels of patients suffering from chronic virus hepatitis. In the process of searching for new active principles, an unknown lignan compound named chicanine was isolated from the fruits of *Schisandra sp.* which had been collected in the district of Xiangfan, Hubei province of China. In pharmacological tests of mice with abnormally high SGPT levels induced by carbon tetrachloride, chicanine was shown to be ineffective but it was evident that chicanine is a tetrahydrofuran type lignan and not a dibenzocyclooctadiene type, the usual constituent of this genus. Furthermore, chicanine is the first tetrahydrofuran lignan to be isolated from this genus. This paper reports the elucidation of the structure **1** for chicanine by means of spectral analysis and chemical conversions.

Chicanine, $C_{20}H_{22}O_5$ (M^+ 342.1459), mp 122–124°C, $[\alpha]_D^{31}$ +118.8° (*c* 4.568, $CHCl_3$), affords the same ultraviolet spectrum (uv) and mass spectrum (ms) as those of austrobailignan-7, **5** (4), but the compounds differ in other respects (see Table 1). Also, their proton magnetic resonance (^1H nmr) spectra indicate significant differences in signals for H-2, H-3, and H-4 (see Table 2). It was evident that chicanine is a diastereomer of austrobailignan-7.

The relative stereochemistry of chicanine was elucidated by decoupling experiments and by measuring intramolecular nuclear Overhauser effects (nOe) on dinitrochicanine ethyl ether **6**. On irradiation at H-3 (δ 3.04) of compound **6**, the signals for H-2 (δ 5.95) and CH_3-3 (δ 0.64) were decoupled simultaneously and a 10.5% nOe enhancement of H-2 was introduced, indicating the *cis* configuration between H-3 and H-2. On respective irradiation at CH_3-4 (δ 1.00) and CH_3-3 (δ 0.64), 12.5% and 10% nOe enhancements of H-5 (δ 5.72) were observed, and when H-4 (δ 2.50) was irradiated, both signals of CH_3-4 and H-5 were decoupled. This indicates *cis* relationships also for CH_3-3, CH_3-4, and H-5. In addition, by a series of reactions, *vide infra*, chicanine **1** was converted into *meso*-dihydroguaiaretic acid dimethyl ether **12**, which can only be explained if a *cis* relationship exists between CH_3-3 and CH_3-4. Thus, all the facts mentioned above lead to the conclusion that H-5, CH_3-4, CH_3-3, and Ar-2 are *cis*, and thus the aromatic moieties Ar-2 and Ar-5 are *trans*.

The positions of the aromatic substituents at C-2 and C-5 can also be established independently by the results of other nOe experiments on dinitrochicanine ethyl ether **6**. When the ethoxyl methylene (δ 4.13) and the methoxyl (δ 3.93) were irradiated, the signals of H-5′ (δ 7.48) and H-2′(δ 7.12) showed 25% and 12.5% nOe enhance-

[1]Present address: Chemistry Department, University of New Brunswick, Bag Service #45222, Fredericton, N.B., Canada E3B 6E2.

0008-4042/81/111680-05$01.00/0
©1981 National Research Council of Canada/Conseil national de recherches du Canada

Can. J. Chem. Downloaded from www.nrcresearchpress.com by 210.87.254.42 on 09/06/12
For personal use only.

TABLE 1. Physical properties of chicanine and austrobailignan-7

Compound	Melting point (°C)	Melting point of acetates (°C)	Melting point of methyl ethers (°C)	$[\alpha]_D^a$	$[\alpha]_D$ of acetates	$[\alpha]_D$ of methyl ethers
Chicanine **1**	122–124	95–97	135–136	+118.8°	+131.1°	+125.2°
Austrobailignan-7 **5** (4)	oil (bp 130°C/ 0.02 Torr)	81–82	93–94	+12°	+23°	+33°

[a] $[\alpha]_D$ measured in $CHCl_3$.

TABLE 2. Comparison of ^1H nmr parameters of chicanine and austrobailignan-7[a]

Compounds	CH_3-3	CH_3-4	H-3, H-4	OCH_3	H-5	H-2	OH	$-OCH_2O-$	Ar-H
Chicanine **1**	0.54 d, 7	0.94 d, 7	2.10–2.50 m	3.80 s	4.48 d, 8.5	5.24 d, 4.0	5.20 br	5.80 s	6.60–6.80 m
Austrobailignan-7 **5** (4)	0.63 d, 6.6	1.02 d, 6.1	1.45–2.40 m	3.82 s	4.33 d, 8.8	5.07 d, 8.2	5.68 br	5.92 s	6.50–7.10 m

[a] In $CDCl_3$. Chemical shifts in ppm relative to internal TMS. Coupling constants, J, in Hz.

ment, respectively. Also, the signals of H-2′ and H-2″ (δ 7.28) showed 21% and 7% nOe enhancement, respectively, when H-2 (δ 5.95) and H-5 (δ 5.72) were irradiated. These results showed that the 3-methoxy-4-hydroxyphenyl group must be attached to C-2 and the 3,4-methylenedioxyphenyl group to C-5.

In order to elucidate the absolute stereochemistry, the following chemical conversions were carried out. First, chicanine **1** was hydrogenated in the presence of palladium oxide, giving a mixture of **7** and **8**, which on demethylation in acetic acid/sulfuric acid and phloroglucinol afforded desoxydemethylenechicanine **9** and demethyldihydroguaiaretic acid **10**. These were separated and methylated with dimethyl sulfate. The known isoguaiacin dimethyl ether **11** (*5a*) and *meso*-dihydroguaiaretic acid dimethyl ether **12** (*5a*, 6) were obtained from **9** and **10**, respectively. Next, treatment of chicanine methyl ether **3** with 2% perchloric acid in acetic acid gave anhydrochicanine **13**, which was hydrogenated in the presence of platinum oxide, affording (+)galcatin **14**, the enantiomer of the known (−)galcatin (7–10), isolated from *Himantandra baccata* Bail.

Since the absolute configuration of isoguaiacin dimethyl ether **11** has been previously established as 3*R*,2*R* (*5a*), it follows that the absolute configuration of chicanine **1** is 3*R*,4*S* and 2*S*,5*S* since C-3 and C-4 are unchanged in the above-mentioned transformations. Confirmation of this assignment is provided by the transformation of chicanine into (+)galcatin **14**, enantiomer of (−)galcatin (7–10), of known absolute configuration.

Consistent with coupling constant data, ($J_{2,3} \cong$ 4.0 Hz and $J_{4,5} \cong$ 8.5 Hz) from the ^1H nmr spectrum of chicanine, the dihedral angles between H-2 and H-3 and between H-4 and H-5 should be about 40° and 150°, respectively. This suggests that the tetrahydrofuran ring possesses the "twist envelope" conformation, readily explained by the mutual steric repulsion of the *cis* substituents CH_3-3, CH_3-4, and Ar-2. Thus, the structure of chicanine should be written as **1**, namely, 2*S*-(3-methoxy-4-hydroxyphenyl)-3*R*,4*S*-dimethyl-5*S*-(3,4-methylenedioxyphenyl)tetrahydrofuran.

Experimental

Melting points were determined on a Kofler hot stage apparatus and are uncorrected. Infrared spectra were obtained with a Unicam SP-100 or Perkin-Elmer 727B spectrophotometer and uv spectra with a Unicam SP-1800 instrument. Jeol PS-100 and Varian T-60 spectrometers were employed for recording ^1H nmr spectra and the former for measuring nOe in 4% $CDCl_3$ solution. Varian MAT-711 or AEI MS 50 were used for

Can. J. Chem. Downloaded from www.nrcresearchpress.com by 210.87.254.42 on 09/06/12
For personal use only.

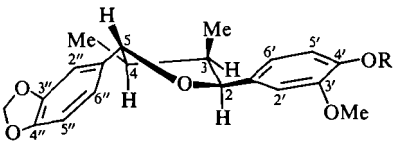

1 R = H
2 R = Ac
3 R = Me
4 R = Et

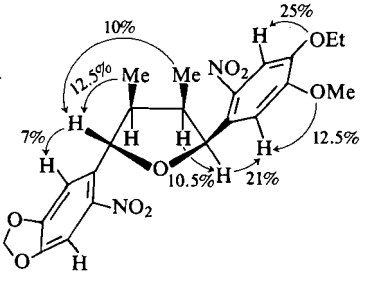

6

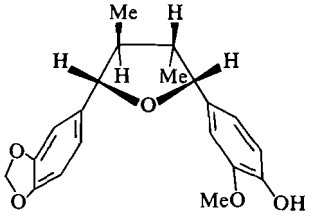

5

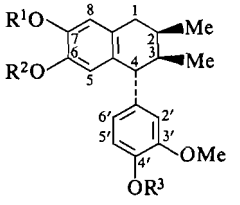

7 R^1, R^2 = —CH_2—, R^3 = H
9 R^1 = R^2 = R^3 = H
11 R^1 = R^2 = R^3 = Me

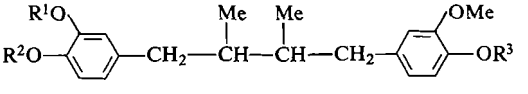

8 R^1, R^2 = —CH_2—, R^3 = H
10 R^1 = R^2 = R^3 = H
12 R^1 = R^2 = R^3 = Me

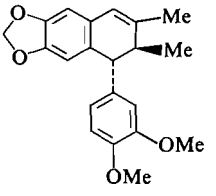

13

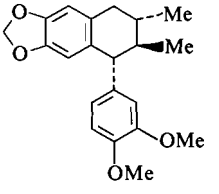

14

recording high resolution mass spectra. The ord curves were obtained on a Jasco ORD/UV-5 spectrometer at 26°C.

Chicanine 1

The crude benzene extracts of the fruit of *Schisandra sp.*, gathered in the district of Xiangfan, Hubei province, China, were chromatographed on a silica gel column eluting with benzene, then benzene/ethyl acetate (10:1). The late benzene fractions and the fractions of benzene/ethyl acetate (10:1) gave chicanine which was recrystallized from chloroform/hexane giving prisms, mp 122–124°C (yield ~ 0.2%); $[\alpha]_D^{31}$ +118.8° (*c* 4.568, $CHCl_3$); uv (MeOH) λ_{max} nm (log ε): 233 (4.10), 284 (3.87); ir (KBr) ν_{max}: 3495, 3075, 3045, 2970, 2945, 2880, 2850, 1855, 1610, 1520, 1495, 1445, 1380, 1370, 1295, 1275, 1260, 1250, 1230, 1200, 1175, 1165, 1140, 1125, 1115, 1100, 1070, 1040, 1000, 980, 950, 935, 895, 870, 865, 820, 810, 735, 725, 715 cm^{-1}; ord (MeOH): $[\phi]_{296}$ = +5521 pk, $[\phi]_{245}$ = +19000 pk, $a \times 10^{-2}$ = −135; ^1H nmr (CCl_4) δ_{TMS}: 0.54, 0.94 (d, each 3H, J = 7, CH_3-3, CH_3-4, respectively), 2.10–2.50 (m, 2H, H-3, H-4), 3.80 (s, 3H, OCH_3), 4.48 (d, 1H, J = 8.5, H-5), 5.24 (d, 1H, J = 4.0, H-2), 5.20 (br, 1H, exchangeable with D_2O, OH), 5.80 (s, 2H, —OCH_2O—), 6.60–6.80 (m, 6H, Ar-H × 6); ms *m/e*: 342.1459 (26.74%, $C_{20}H_{22}O_5$, ca. 342.1467, M^+), 218.0925 (4.01%, $C_{13}H_{14}O_3$, M − ϕ (OCH_3) (OH) − H), 192.1145 (100%, $C_{12}H_{16}O_2$, M − (CH_2O_2)ϕCHO), 190.0988 (39.42%, $C_{12}H_{14}O_2$, M − (CH_3O) (OH)ϕCHO), 180.0789 (8.72%, $C_{10}H_{12}O_3$, (CH_3O)(OH)ϕCH—CHCH$_3$ ⌝$^+$), 177.0918 (37.09%, $C_{11}H_{13}O_2$, M − (CH_2O_2)ϕCHO − CH_3), 175.0768 (12.63%, $C_{11}H_{11}O_2$, M −

Can. J. Chem. Downloaded from www.nrcresearchpress.com by 210.87.254.42 on 09/06/12
For personal use only.

(CH_3O) $(OH)\phi CHO - CH_3$), 164.0848 (29.19%, $C_{10}H_{12}O_2$, $(CH_2O_2)\phi CH{=}CHCH_3]^+$), 137.0550 (7.62%, $C_8H_9O_2$, (CH_3O) $(OH)\phi CH_2]^+$), 135.0400 (5.42%, $C_8H_7O_2$, $(CH_2O_2)\phi CH_2]^+$).

Chicanine Acetate 2

Chicanine **1** was acetylated in acetic anhydride/pyridine at room temperature for 3 days, affording its acetate in quantitative yield which crystallized as plates from methanol, mp 95–97°C; $[\alpha]_D^{18}$ +133.1° (*c* 0.969, $CHCl_3$); uv (MeOH) λ_{max} nm (log ε): 222 (sh, 4.01), 278 (sh, 3.70), 282 (3.74), 288 (sh, 3.59); ir (nujol) ν_{max}: 1760 (>C=O) cm^{-1}. No hydroxyl. ^1H nmr (CCl_4) δ_{TMS}: 0.56, 1.01 (d, each 3H, J = 7, CH_3-3, CH_3-4), 2.16 (s, 3H, CH_3CO), 2.32 (m, 2H, H-3, H-4), 3.74 (s, 3H, OCH_3), 4.55 (d, 1H, J = 8.5, H-5), 5.26 (d, 1H, J = 4.0, H-2), 5.82 (s, 2H, —OCH_2O—), 6.60–6.90 (m, 6H, Ar-H × 6); ms *m/e*: 384 (M^+), 341 (M − Ac), 234 (M − $(CH_2O_2)\phi CHO$).

Chicanine Methyl Ether 3

Chicanine **1** was methylated in the usual manner with dimethyl sulphate and potassium carbonate in acetone, affording its methyl ether (~70%) which crystallized as plates from acetone/methanol, mp 135–136°C, $[\alpha]_D^{18}$ +125.2° (*c* 1.31, $CHCl_3$); uv (MeOH) λ_{max} nm (log ε): 233 (4.12), 284 (3.86). ir (KBr) ν_{max}: no OH absorption; ^1H nmr (CCl_4) δ_{TMS}: 0.54, 0.94 (d, each 3H, J = 7, CH_3-3, CH_3-4), 2.28 (m, 2H, H-3, H-4), 3.70, 3.72 (s, each 3H, OCH_3 × 2), 4.46 (d, 1H, J = 8.5, H-5), 5.22 (d, 1H, J = 4.0, H-2), 5.80 (s, 2H, —OCH_2O—), 6.60–6.80 (m, 6H, Ar-H × 6). ms *m/e*: 356 (M^+), 192, 178, 175.

Chicanine Ethyl Ether 4

Chicanine (100 mg) in dichloromethane was refluxed for 40 h with bromoethane (0.3 mL) in the presence of potassium carbonate (300 mg) and a trace of 18-crown-6. The reaction mixture was chromatographed on a silica gel column eluting with hexane/ether (3:1). The early fractions gave chicanine ethyl ether **4** (70%) which crystallized as plates from ether/hexane, mp 80–81°C; ^1H nmr (CCl_4) δ_{TMS}: 0.54, 0.94 (d, each 3H, J = 7, CH_3-3, CH_3-4), 1.34 (t, 3H, J = 7, CH_3CH_2O—), 2.30 (m, 2H, H-3, H-4), 3.74 (s, 3H, OCH_3), 3.92 (q, 2H, J = 7, OCH_2CH_3), 4.46 (d, 1H, J = 8.5, H-5), 5.24 (d, 1H, J = 4.0, H-2), 5.80 (s, 2H, —OCH_2O—), 6.60–6.80 (m, 6H, Ar-H × 6); ms *m/e*: 370.1730 (26.90%, $C_{22}H_{26}O_5$, ca. 370.1780, M^+), 220.1465 (96.78%, $C_{14}H_{20}O_2$, M − $(CH_2O_2)\phi CHO$), 218.0925 (5.62%, $C_{13}H_{14}O_3$, M − $\phi(OCH_3)$ (OCH_2CH_3) − H), 208.1124 (11.64%, $C_{12}H_{16}O_3$, (CH_3O) $(CH_3CH_2O)\phi CH$—$CHCH_3$]$^+$), 205.1256 (31.49%,

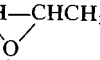

$C_{13}H_{17}O_2$, M − $(CH_2O_2)\phi CHO$ − CH_3), 192.1168 (100%, $C_{12}H_{16}O_2$, (CH_3O) $(CH_3CH_2O)\phi CH{=}CHCH_3]^+$), 190.1026 (61.93%, $C_{12}H_{14}O_2$, M − (CH_3CH_2O) $(CH_3O)\phi CHO$), 175.0750 (41.51%, $C_{11}H_{11}O_2$, M − (CH_3CH_2O) $(CH_3O)\phi CHO$ − CH_3), 164.0830 (11.00%, $C_{10}H_{12}O_2$, $(CH_2O_2)\phi CH{=}CHCH_3]^+$), 135,0390 (9.66%, $C_8H_7O_2$, $(CH_2O_2)\phi CH_2]^+$).

Dinitrochicanine Ethyl Ether 6

Nitric acid (0.5 mL, d 1.42) in acetic acid/acetic anhydride (0.5 mL, 1:1) cooled to −5 to −10°C was added to chicanine ethyl ether (200 mg) in acetic acid/acetic anhydride (2.5 mL, 1:1) at −5 to −10°C. The mixture was kept for 15 min at that temperature, then poured into ice water. The solid product was chromatographed on silica gel column with ether/hexane (1:2). The early and late fractions contained impurities. The middle fractions yielded dinitrochicanine ethyl ether (105 mg) which crystallized as yellow plates, mp 144–146°C from chloroform/hexane; ^1H nmr ($CDCl_3$), δ_{TMS}: 0.64, 1.00 (d, each 3H, J = 7, CH_3-3, CH_3-4), 1.44 (t, 3H, J = 7, OCH_2CH_3), 2.50 (m, 1H, H-4), 3.04 (m, 1H, H-3), 3.93 (s, 3H, OCH_3), 4.13 (q, 2H, J = 7, —OCH_2CH_3), 5.72 (d, 1H, J = 9.5, H-5), 5.95 (d, 1H, J = 5.5, H-2), 6.08 (s, 2H, OCH_2O), 7.12, 7.28, 7.48, 7.55 (s, each 1H, H-2′, H-2″, H-5′, H-5″); ms *m/e*: 460 (M^+), 264 (M − ϕ(OC-H_3)$(OCH_2CH_3)(NO_2)$), 250 (M − $(CH_2O_2)\phi(CHO)(NO_2)$ − CH_3), 234 (M − $\phi(OCH_3)(OCH_2CH_3)(CHO)(NO_2)$ − H).

Desoxydemethylenechicanine 9 and Demethyldihydroguaiaretic Acid 10

Chicanine (1 g) in ethanol (20 mL) was hydrogenated in the presence of palladium oxide (230 mg) at 60–70°C for 2 h. The reaction mixture was chromatographed on silica gel column with ether/hexane (1:3). The early fractions gave a mixture of **7** and **8** (0.7 g) (ratio 4:1) as shown by ^1H nmr (3.63 (d, 0.80H, J = 7), 3.80 (s, 2.40H), 5.83 (s, 1.60H), and 6.37 (s, 0.80H) for respective H-4, OCH_3, —OCH_2O— and H-5 of **7**; 3.80 (s, 0.60H) and 5.90 (s, 0.40H) for respective OCH_3 and —OCH_2O— of **8**) and ms data (*m/e* 326, M^+ of **7**; 328, M^+ of **8**). The mixture of **7** and **8** (0.69 g) in acetic acid (30 mL) was heated with phloroglucinol (1 g) and 50% sulfuric acid (20 mL) under nitrogen on a steam bath for 2 h, then diluted with water (50 mL) and extracted with ether. The extract was chromatographed on a silica gel column using ether/hexane (2:1). The phenolic fractions (detected by $FeCl_3$) were rechromatographed on a silica gel column and eluted with the same solvent. The early fractions yielded desoxydemethylenechicanine **9** (110 mg) which crystallized as needles from methanol, mp 153–155°C; $[\alpha]_D^{26}$ −40.7° (*c* 0.08116, MeOH). The late fractions afforded demethyldihydroguaiaretic acid **10** (30 mg), a pale yellow solid. Infrared values for **9** ($CHCl_3$) ν_{max}: 3610, 3560, 3300 (br). The ord (MeOH) of **9**: $[\phi]_{300}$ = +5223 pk, $[\phi]_{284}$ = −18959 tr, $a \times 10^{-2}$ = +242, $[\phi]_{242}$ = −8899 tr; ^1H nmr ($CDCl_3$) of **9** δ_{TMS}: 0.90 (d, 6H, J = 7, CH_3-2, CH_3-3), 1.80–2.30 (m, 2H, H-2, H-3), 2.55 (d, 1H, J = 7, H-1a), 2.78 (d, 1H, J = 5, H-1e), 3.60 (d, 1H, J = 7, H-4), 3.84 (s, 3H, OCH_3), 6.35 (s, 1H, H-5), 6.40–6.90 (m, 4H, H-2′, H-5′, H-6′, H-8), 6.38 (br, 3H, exchangeable with D_2O, OH × 3); ms of **9** *m/e*: 314.1520 (100%, $C_{19}H_{22}O_4$, ca. 314.1518, M^+), 258.0880 (20.48%, $C_{15}H_{14}O_4$, M − C_4H_8), 257.0814 (35.62%, $C_{15}H_{13}O_4$, M − C_4H_9), 241.0863 (33.34%, $C_{15}H_{13}O_3$, M − C_4H_8 − OH), 227.0706 (61.08%, $C_{14}H_{11}O_3$, M − C_4H_8—OCH_3), 226.0628 (19.06%, $C_{14}H_{10}O_3$, M − C_4H_9 − OCH_3), 197.0603 (12.23%, $C_{13}H_9O_2$, M − C_5H_9 − OCH_3 − OH), 190.0987 (22.68%, $C_{12}H_{14}O_2$, M − ϕ(OH)(OCH_3) − H), 175.0759 (21.10%, $C_{11}H_{11}O_2$), 137.0603 (9.49%, $C_8H_9O_2$, $(CH_3O)(OH)\phi CH_2^+$). Infrared values for **10** ($CHCl_3$) ν_{max}: 3600, 3550, 3300 (br); ^1H nmr ($CDCl_3$) of **10** δ_{TMS}: 0.85 (d, 6H, J = 6.5, >$CHCH_3$ × 2), 1.50–2.00 (m, 2H, >CH— × 2), 2.06–2.90 (m, 4H, Ar-CH_2- × 2), 3.85 (s, 3H, OCH_3), 5.30 (br, 3H, exchangeable with D_2O, OH × 3), 6.50–6.90 (m, 6H, Ar-H × 6); ms of **10** *m/e*: 316 (M^+), 137 $(CH_3O)(OH)\phi CH_2^+$).

Isoguaiacin Dimethyl Ether 11

The desoxydemethylenechicanine in acetone was methylated in the usual manner with dimethyl sulphate in the presence of potassium carbonate, affording isoguaiacin dimethyl ether **11** (~95%) (*5a*) which crystallized as needles from methanol, mp 100–101°C; $[\alpha]_D^{26}$ −46° (*c* 0.1054, $CHCl_3$). The ir spectrum in $CHCl_3$ was identical with that of its enantiomer, isogalbulin (*5b*); ord (MeOH): $[\phi]_{295}$ = +4052 pk, $[\phi]_{282}$ = −16883 tr, $a \times 10^{-2}$ = +209, $[\phi]_{242}$ = −21273 tr; ^1H nmr ($CDCl_3$) δ_{TMS}: 0.90 (d, 6H, J = 7, CH_3-2, CH_3-3), 1.70–2.30 (m, 2H, H-2, H-3), 2.57 (d, 1H, J = 7, H-1a), 2.77 (d, 1H, J = 5, H-1e), 3.70, 3.83 (s, each 3H, OCH_3 × 2), 3.90 (s, 6H, OCH_3 × 2), 3.75 (d, 1H, J = 7, covered, H-4), 6.37 (s, 1H, H-5), 6.40–6.90 (m, 4H, H-2′, H-5′, H-6′, H-8); ms *m/e*: 356.1990 (100%, $C_{22}H_{28}O_4$, ca. 356.1987, M^+), 299.1271 (10.42%, $C_{18}H_{19}O_4$, M − C_4H_9), 285.1129 (6.77%, $C_{17}H_{17}O_4$, M − C_5H_{11}), 269.1170 (78.31%, $C_{17}H_{17}O_3$, M − C_4H_8 − OCH_3), 238.0993 (6.42%, $C_{16}H_{14}O_2$, M − C_4H_8 −

Can. J. Chem. Downloaded from www.nrcresearchpress.com by 210.87.254.42 on 09/06/12
For personal use only.

$(OCH_3)_2$), 218.1304 (7.45%, $C_{14}H_{18}O_2$, M − $\phi(OCH_3)_2$ − H), 187.1124 (3.18%, $C_{13}H_{15}O$, M − $\phi(OCH_3)_2$ − H − OCH_3), 165.0914 (3.19%, $C_{10}H_{13}O_2$), 151.0750 (8.41%, $C_9H_{11}O_2$, $(CH_3O)_2\phi CH_2^+$), 150.0678 (7.65%, $(CH_3O)_2\phi CH^{+\cdot}$).

meso-*Dihydroguaiaretic Acid Dimethyl Ether 12*

Compound **12** was obtained by methylation of compound **10** with dimethyl sulfate by the above-mentioned method and crystallized as colorless needles from ether/hexane, mp 99–101°C; $[\alpha]_D^{26}$ 0° (*c* 0.2018, EtOH); ^{1}H nmr ($CDCl_3$) δ_{TMS}: 0.85 (d, 6H, *J* = 6, $>CHCH_3$ × 2), 1.77 (m, 2H, >CH— × 2), 2.10–2.95 (m, 4H, $ArCH_2$ × 2), 3.87 (s, 12H, OCH_3 × 4), 6.60–6.80 (m, 6H, Ar-H × 6); ms *m/e*: 358.2137 (38.93%, $C_{22}H_{30}O_4$, ca. 358.2144, M^+), 179.1069 (4.52%, $C_{11}H_{15}O_2$, $ArCH_2CHCH_3$), 151.0754 (100%, $C_9H_{11}O_2$, $ArCH_2^+$). All the data agreed with that in literature (*5a*, 6).

Anhydrochicanine Methyl Ether 13

Chicanine methyl ether **4** (100 mg) was dissolved in acetic acid (5 mL) containing 2% perchloric acid and kept at room temperature for 1.5 h. Then the reaction mixture was poured into a solution of sodium hydroxide (15 mL). The solid products were chromatographed on a silica gel column eluting with hexane/ether (5:1). Anhydrochicanine methyl ether (80 mg) was obtained from the early fractions and crystallized as needles from methanol, mp 70–72°C; $[\alpha]_D^{26}$ −108.05° (*c* 0.17158, MeOH); ord (MeOH): $[\phi]_{308}$ = −16991 tr, $[\phi]_{254}$ = +74857 pk, $a \times 10^{-2}$ = −918; ^{1}H nmr ($CDCl_3$) δ_{TMS}: 1.09 (d, 3H, *J* = 7.5, CH_3-3), 1.80 (d, 3H, *J* = 1.5, CH_3-2), 2.40 (q, d, 1H, *J* = 7.5, *J* = 3.5, H-3), 3.66 (d, 1H, *J* = 3.5, H-4), 3.83, 3.86 (s, each 3H, OCH_3 × 2), 5.86 (s, 2H, —OCH_2O—), 6.12 (q, 1H, *J* = 1.5, H-1), 6.41–6.70 (m, 5H, Ar-H × 5); ms *m/e*: 338.1518 (100%, $C_{21}H_{22}O_4$, ca. 338.1518, M^+), 323,1288 (44.76%, $C_{20}H_{19}O_4$, M − CH_3), 307.1322 (12.12%, $C_{20}H_{19}O_3$, M − OCH_3), 292.1089 (10.51%, $C_{19}H_{16}O_3$, M − CH_3 − OCH_3), 200.0832 (23.45%, $C_{13}H_{12}O_2$, M − $\phi(OCH_3)_2$), 151.0744 (16.95%, $C_9H_{11}O_2$, $(CH_3O)_2\phi CH_2^+$).

(+) *Galcatin 14*

Anhydrochicanine methyl ether **13** (100 mg) in ethanol (10 mL) was hydrogenated in the presence of platinum oxide (30 mg). Thin-layer chromatography showed two products, the major product having higher R_f. After chromatography on a silica gel column using hexane/ether (5:1) as eluant, the main product, (+)galcatin **14**, was obtained (90 mg) and crystallized as prisms from methanol, mp 111–113°C. This compound showed identity in all respects with data reported for (−)galcatin (7–10) except for the sign of optical rotation: $[\alpha]_D^{26}$ +9.8° (*c* 0.10206, $CHCl_3$); ord (MeOH): $[\phi]_{304}$ = +10327 pk, $[\phi]_{285}$ = −24319 tr, $a \times 10^{-2}$ = +346, $[\phi]_{264}$ = +1999 pk, $[\phi]_{252}$ = 0 tr; ^{1}H nmr ($CDCl_3$) δ_{TMS}: 0.86, 1.06 (d, each 3H, *J* = 6, CH_3-2, CH_3-3), 1.57 (m, 2H, H-2, H-3), 2.67 (d, 2H, *J* = 5.8, H-1), 3.40 (d, 1H, *J* = 9.5, H-4), 3.85, 3.90 (s, each 3H, OCH_3 × 2), 5.85 (s, 2H, —OCH_2O—), 6.20 (s, 1H, H-5), 6.50–6.80 (m, 4H, Ar-H × 4); ms *m/e*: 340.1671 (100%, $C_{21}H_{24}O_4$, ca. 340.1674, M^+), 283.0972 (15.21%, $C_{17}H_{15}O_4$, M − C_4H_9), 269.0816 (5.06%, $C_{16}H_{13}O_4$, M − C_5H_{11}), 253.0857 (94.81%, $C_{16}H_{13}O_3$, M − C_4H_8 − OCH_3), 238.0632 (5.70%, $C_{15}H_{10}O_3$, M − C_5H_{11} − OCH_3), 222.0680 (5.08%, $C_{15}H_{10}O_2$, M − C_4H_8 − $(OCH_3)_2$), 202.0987 (12.67%, $C_{13}H_{14}O_2$, M − $\phi(OCH_3)_2$ − H), 187.0760 (9.97%, $C_{12}H_{11}O_2$, M − $\phi(OCH_3)_2$ − H − CH_3).

Acknowledgements

We thank Dr. Thomas Y. R. Tsai for helpful discussions and Professor Karel Wiesner for his interest. We are grateful to the Department of Analytical Chemistry and the Mass Spectrometry Lab, Shanghai Institute of Materia Medica, Chinese Academy of Sciences, China, for recording ir, uv, some mass spectra, and some $[\alpha]_D$ measurements, and also to the Mass Spectrometry Lab and Spectral Services Lab, University of Alberta, Canada, for providing some mass spectra and some $[\alpha]_D$ and ord measurements

1. C-S. Liu (J-S. Liu), S-D. Fang, M-F. Huang, Y-L. Kao (Y-L. Gao), and J-S. Hsu. Sci. Sin. **21**, 483 (1978).
2. J-S. Liu, M-F. Huang, and Y-L. Gao. Acta Chim. Sin. **38**, 361 (1980).
3. (*a*) Shanghai Institute of Materia Medica & Third People's Hospital of Shanghai, 2nd Med. College. Acta Biochim. Biophys. **8**, 333 (1976); (*b*) Shanghai Institute of Traditional Chinese Medicine & Shanghai Hongqiao Hospital. Chunghua Neike Zhazi, **1**, 184 (1976).
4. S. T. Murphy, E. Ritchie, and W. C. Taylor. Aust. J. Chem. **28**, 81 (1975).
5. (*a*) F. E. King and J. G. Wilson. J. Chem. Soc. 4011 (1964); (*b*) A. W. Schrecker and J. L. Hartwell. J. Am. Chem. Soc. **77**, 432 (1955).
6. Y. Ikeya, H. Taguchi, I. Yosioka, and H. Kobayashi. Chem. Pharm. Bull. **27**, 1583 (1979).
7. G. K. Hughes and E. Ritchie. Aust. J. Chem. **7**, 104 (1954).
8. A. Pelter. J. Chem. Soc. C, 74 (1968).
9. R. Wallace, A. L. Porte, and R. Hodges. J. Chem. Soc. 1445 (1963).
10. S. M. Adjangba and D. Billet. Bull. Soc. Chim. Fr. 1970 (1962).

Can. J. Chem. Downloaded from www.nrcresearchpress.com by 210.87.254.42 on 09/06/12
For personal use only.

COMMUNICATION

Annelation of β-keto thiolesters and synthetic application

HSING-JANG LIU, LI-KANG HO, AND HOI KIONG LAI
Department of Chemistry, University of Alberta, Edmonton, Alta., Canada T6G 2G2
Received March 5, 1981

HSING-JANG LIU, LI-KANG HO, and HOI KIONG LAI. Can. J. Chem. **59**, 1685 (1981).

The use of β-keto thiolesters in the construction of fused (e.g. **8**) and bridged (e.g. **12**) ring systems possessing a functionalized substituent at the angular position is described. Some synthetic applications of the annelation procedure are demonstrated including: selective reduction of the thiol ester group; the concomitant removal of ketone carbonyl and reduction of thiolester to the alcohol level via thioketal intermediate; and direct conversion of the ketone carbonyl to a *gem*-dimethyl group using lithium dimethylcuprate.

HSING-JANG LIU, LI-KANG HO et HOI KIONG LAI. Can. J. Chem. **59**, 1685 (1981).

On décrit l'utilisation de β-cétothiolesters dans l'édification des systèmes cycliques condensés (par exemple **8**) et des systèmes cycliques ayant un pont (par exemple **12**) possédant des substituants fonctionnels en position angulaire. On démontre quelques applications synthétiques de la méthode d'annellation incluant: la réduction sélective du groupe thiolester; l'élimination concomitante du carbonyle de la cétone et la réduction du thiolester en alcool via un intermédiaire thiocétal; et la transformation directe du groupe carbonyle de la cétone en *gem*-diméthyle par le diméthylcuprate de lithium.

[Traduit par le journal]

Robinson annelation[1] and the closely related reaction leading to bridged polycyclic systems[2] are important synthetic processes. We wish to describe the first examples of annelation reactions using a β-keto thiolester moiety[3] which facilitates the formation of polycyclic compounds possessing a functionalized substituent at the angular position.

In the presence of a tertiary amine, β-keto thiolesters were found to undergo Michael reaction readily with conjugated enones. Several amines were examined including triethylamine, 1,5-diazabicyclo[4.3.0]non-5-ene, 1,8-diazabicyclo[5.4.0]undec-7-ene, and 1,4-diazabicyclo[2.2.2]octane (DABCO). Of these, DABCO was shown to be most effective, giving consistently high yields of the products under mild conditions. In a typical experiment, DABCO (497 mg, 4.43 mmol) and methyl vinyl ketone (311 mg, 4.43 mmol) were added to a solution of 2-ethylthiocarbonylcyclohexanone (690 mg, 3.7 mmol) in 1,2-dimethoxyethane (15 mL). After stirring at room temperature under a nitrogen atmosphere for 24 h, the reaction mixture was acidified with 1 *N* aqueous hydrochloric acid and extracted with ether. The usual work-up of the organic solution, followed by column chromatography of the crude product on silica gel eluting with ether–benzene (3:7), gave adduct **1** (944 mg; 100% yield). The generality of this procedure is illustrated by the additional examples listed in Table 1 which also includes a case involving an α,β-unsaturated aldehyde.

The Michael adducts were readily cyclized to the octalone system under the influence of *p*-toluenesulfonic acid using a well-documented procedure (1). Treatment of diketone **1** with a small amount (1/6 of **1** by weight) of *p*-toluenesulfonic acid in refluxing benzene (Dean–Stark trap) for 10 h gave rise to a 98% yield of enone **8**. Similarly, reaction of diketone **2** gave enone **9** in quantitative yield. The cyclization of the two five-membered ring compounds **4** and **5** was shown to be equally facile and the resulting enones **10** and **11** were obtained in a yield of ca. 90% each.

The second possible mode of aldol condensation leading to a bridged system could be effected using sulfuric acid (2). For instance, when diketone **2** (150 mg) was exposed to cold (2–4°C) concentrated H_2SO_4 (0.2 mL) in benzene (1 mL) for 1 h, enone **12** was formed in 95% yield. Other examples gave similar results (e.g. **1** → **13** (93%), **4** → **14** (53%), **6** → **15** (100%), and **7** → **16** (81%)). The cyclization of keto aldehyde **3** was not as successful. In the best case the yield of the desired enone **17** was 20%.

This method provides a viable alternative to the

[1]For a review, see ref. 1.
[2]See ref. 2 for a review.
[3]β-Keto thiolesters are readily accessible via Dieckmann condensation of dithioesters (3) or α-methylthiocarbonylation of ketones (4).

0008-4042/81/111685-04$01.00/0
©1981 National Research Council of Canada/Conseil national de recherches du Canada

TABLE 1. Michael addition of β-keto thiolesters to conjugated enones.

β-Keto thiolester	Enone	Time (h)	Product	Yield (%)
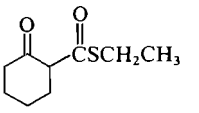	CH_2=CHCOCH$_3$	24	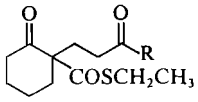	
			1 R = CH_3	100
	CH_2=CHCOCH$_2$CH$_3$	16	**2** R = CH_2CH_3	88
	CH_2=CHCHO	11	**3** R = H	88
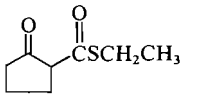	CH_2=CHCOCH$_3$	2.5	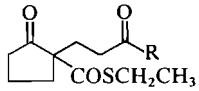	
			4 R = CH_3	100
	CH_2=CHCOCH$_2$CH$_3$	6	**5** R = CH_2CH_3	98
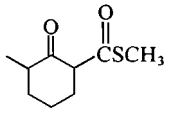	CH_2=CHCOCH$_3$	48	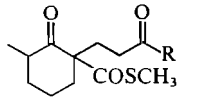	
			6 R = CH_3 (Two isomers)	97
	CH_2=CHCOCH$_2$CH$_3$	48	**7** R = CH_2CH_3 (Two isomers)	100

commonly used β-keto ester approach (1, 2) to the construction of bridged and fused ring systems with concomitant introduction of a reactive functionalized substituent at the angular position. The thiol ester group may be transformed to a number of other important functionalities, often under mild and specific conditions (5), thus providing greater flexibility in the annelation reaction. A feature which is of obvious synthetic utility is the direct reduction of the thiolester to the alcohol using Raney nickel without need of protection of the ketone carbonyl. This worked particularly well in the case of the bridged compounds. Thus, treatment of enone **13** with ca. ten-fold (by weight) excess of W-2 Ra-Ni in benzene for 0.5 h resulted in the formation of alcohol **18** in 88% yield. Comparable yields were also obtained for alcohols **19**, **20**, and **21** from enones **12**, **15**, and **16** respectively. In the fused system, however, this selective reduction process was found to be less satisfactory due to the competing elimination of the thiol ester group.[4] Even under carefully controlled conditions using deactivated (refluxing acetone; 20 min) Ra-Ni, this side reaction could not be completely suppressed and the reduction of enone **8** gave only a modest yield (45%) of the corresponding alcohol **22**.

Another area of synthetic utility is illustrated in the following examples, which show that the removal of the ketone carbonyl of the annelation product and the reduction of the angular substituent to the alcohol level can be simultaneously effected via a thioketal derivative. Treatment of enone **9** with 1,2-ethanedithiol in methylene chloride in the presence of a catalytic amount of boron trifluoride etherate gave the corresponding thioketal **23** (89% yield), which was subjected to reduction with Ra-Ni in benzene at room temperature for 1.5 h to give a 75% yield of alcohol **24**. Similarly, thioketalization of **10** followed by reduction afforded alcohol **25** in an overall yield of 88%.

We also examined the reaction of enone **8** with lithium dimethylcuprate. The reaction was expected to give diketone **26** as a result of a conjugate addition of the reagent to the enone moiety (7) with simultaneous conversion of the thiol ester substituent into a methyl ketone (5*h*). Towards this end, enone **8** was treated with lithium dimethylcuprate (4 mol equiv.) in ether at −40°C for 2 h. Contrary to expectation, an acidic product, mp 88–88.5°C, was formed in 78% yield, to which structure **27** was readily assigned on the basis of the spectroscopic

[4]For examples of reductive elimination of the thiol ester group of β-keto thiolesters with Ra-Ni, see refs. 3 and 6.

Can. J. Chem. Downloaded from www.nrcresearchpress.com by 210.87.254.42 on 09/06/12
For personal use only.

Can. J. Chem. Downloaded from www.nrcresearchpress.com by 210.87.254.42 on 09/06/12
For personal use only.

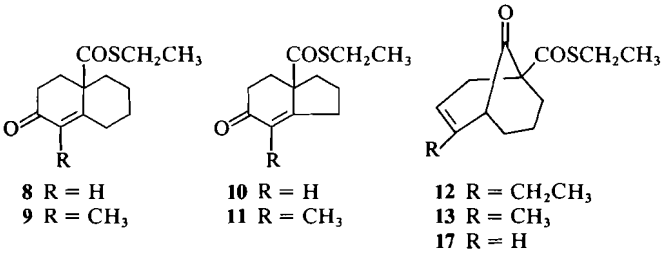

8 R = H
9 R = CH_3

10 R = H
11 R = CH_3

12 R = CH_2CH_3
13 R = CH_3
17 R = H

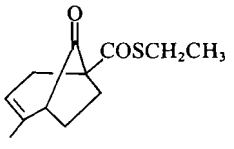

14

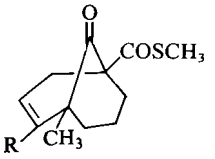

15 R = CH_3
16 R = CH_2CH_3

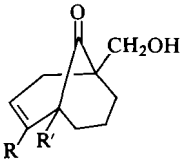

18 R = CH_3; R′ = H
19 R = CH_2CH_3; R′ = H
20 R = CH_3; R′ = CH_3
21 R = CH_2CH_3; R′ = CH_3

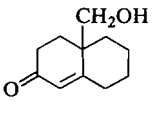

22

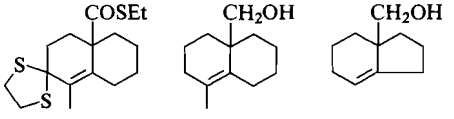

23 **24** **25**

data.[5] The structural assignment was further confirmed by esterification (CH_3I–K_2CO_3–acetone) to give **28**, which was identical with an authentic sample prepared from 3,3-dimethylcyclohexanone by an unambiguous route.

The direct conversion of a ketone carbonyl into a *gem*-dimethyl group by the action of lithium dimethylcuprate is, to our knowledge, unprecedented. This transformation appears to be general for compounds structurally related to enone **8**. Consistent results were obtained for enones **9** and **10** which gave directly and in comparable yields acids **29** (mp 105–106°C) and **30** (mp 92.5–93.5°C), respectively, upon treatment with $(CH_3)_2$-LiCu at −40°C.

It is worth noting that the formation of **27** from **8** is in sharp contrast to the result obtained for the *O*-ester analog **31**, which on similar treatment with

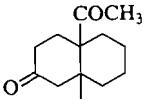

26

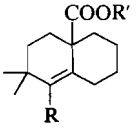

27 R = R′ = H
28 R = H; R′ = CH_3
29 R = CH_3; R′ = H

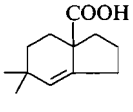

30

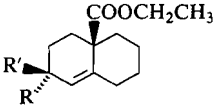

31 R, R′ = O
32 R = OH; R′ = CH_3
33 R = CH_3; R′ = OH

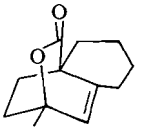

34

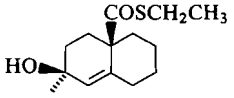

35

lithium dimethylcuprate gave rise to a 3:1 mixture of two epimeric alcohols **32** and **33**. Mechanistic-

[5]Mass spectrum M^+ 208.1463 (calcd. for $C_{13}H_{20}O_2$: 208.1463); ir ($CHCl_3$) 2400–3700 and 1700 cm^{-1} (acid); nmr (CCl_4) δ: 12.18 (s, 1H, —COOH), 5.19 (s, 1H, =CH—), 0.97 (s, 3H, —CH_3), and 0.91 (s, 3H, —CH_3).

ally, the unusual replacement of a ketone carbonyl with a *gem*-dimethyl may be rationalized by invoking a lactone intermediate such as **34**. In agreement with this postulation are the following observations. Treatment of enone **8** with methyllithium in ether at −78°C for 1 h resulted in the formation of a single alcohol **35**[6] (88% yield), which was readily cyclized to lactone **34** using sodium hydride in 1,2-dimethoxyethane at room temperature.[7] When lactone **34** was treated with lithium dimethylcuprate (3 mol equiv.) in ether at −40°C for 2 h, acid **27** was isolated in 85% yield.

In conjunction with the easy accessibility of the required precursors, the unique and efficient transformation —CO— → —$C(CH_3)_2$— described above should have broad synthetic application, particularly in the area of pentacyclic triterpenoids, many of which have D/E ring systems similar to that of **27** (8).

We are currently examining the coupling reaction of allyl pivalates and organocopper reagents. Preliminary results are encouraging.

[6]It is noteworthy that on treatment with methyllithium the *O*-ester analog **31** gave quantitatively a mixture of alcohols **32** and **33** in 1:3.5 ratio as compared with the 3:1 ratio obtained using $(CH_3)_2LiCu$ (*vide supra*).

[7]Our initial attempts to prepare lactone **34** from alcohol **33** were unsuccessful. Whereas no cyclization occurred even after prolonged treatment with sodium hydride in 1,2-dimethoxyethane at room temperature, at reflux temperature alcohol **33** gave exclusively 3-methylbicyclo[4.4.0]deca-1(6),2-diene, apparently as a result of lactone formation followed by a retro-Diels–Alder reaction.

Acknowledgments

We are grateful to the Natural Sciences and Engineering Research Council of Canada and the University of Alberta for financial support.

1. M. E. JUNG. Tetrahedron, **32**, 3 (1976).
2. J. A. PETERS. Synthesis, 321 (1979).
3. H. J. LIU and H. K. LAI. Tetrahedron Lett. 1193 (1979).
4. H. J. LIU, S. K. ATTAH-POKU, and H. K. LAI. Synth. Commun. **9**, 883 (1979).
5. (*a*) V. PRELOG, J. NORYMBERSKI, and O. JEGER. Helv. Chim. Acta, **29**, 360 (1946); (*b*) M. L. WOLFROM and J. V. KARABI NOS. J. Am. Chem. Soc. **68**, 742 (1946); (*c*) H. J. BESTMANN and B. ARNASON. Chem. Ber. **95**, 1513 (1962); (*d*) J. ŠAVRDA and D. H. VEYRAT. Tetrahedron Lett. 6253 (1968); (*e*) T. KUMAMOTO and T. MUKAIYAMA. Bull. Chem. Soc. Jpn. **41**, 2111 (1968); (*f*) K. LLOYD and G. T. YOUNG. J. Chem. Soc. C, 2890 (1971); (*g*) T. MUKAIYAMA, M. ARAKI, and H. TAKEI. J. Am. Chem. Soc. **95**, 4763 (1973); (*h*) R. J. ANDERSON, C. A. HENRICK, and L. D. ROSENBLUM. J. Am. Chem. Soc. **96**, 3654 (1974); (*i*) S. MASAMUNE, Y. HAYASE, W. SCHILLING, W. K. CHAN, and G. S. BATES. J. Am. Chem. Soc. **99**, 6756 (1977); (*j*) E. J. COREY and S. BHATTACHARYYA. Tetrahedron Lett. 3919 (1977); (*k*) Y. NAGAO, K. KAWABATA, and E. FUJITA. Chem. Commun. 330 (1978); (*l*) I. ERNEST, J. GOSTELI, C. W. GREENGRASS, W. HOLICK, D. E. JACKMAN, H. R. PFAENDLER, and R. B. WOODWARD. J. Am. Chem. Soc. **100**, 8214 (1978); (*m*) Y. KOBUKE and J. C. YOSHIDA. Tetrahedron Lett. 367 (1978); (*n*) M. J. S. LOBO and H. J. CHAVES DAS NEVES. Tetrahedron Lett. 2171 (1978); and references cited therein.
6. H. J. LIU, H. K. LAI, and S. K. ATTAH-POKU. Tetrahedron Lett. 4121 (1979).
7. G. POSNER. *In* Organic reactions. Vol. 19. J. Wiley and Sons, Inc., New York, NY. 1972. Chapt. 1.
8. T. K. DEVON and A. I. SCOTT. Handbook of naturally occurring compounds. Vol. II. Terpenes. Academic Press, New York, NY. 1972.

Can. J. Chem. Downloaded from www.nrcresearchpress.com by 210.87.254.42 on 09/06/12
For personal use only.

An investigation of the ^1H nmr isotropic shifts for some methyl-substituted bipyridine complexes with Ni(II) and Co(II)

T. L. JOSEPH HUANG AND DOUGLAS G. BREWER[1]

Department of Chemistry, University of New Brunswick, P.O. Box 4400, Fredericton, N.B., Canada E3B 5A3

Received November 13, 1980

T. L. JOSEPH HUANG and DOUGLAS G. BREWER. Can. J. Chem. **59**, 1689 (1981).

In order to extend existing ideas on isotropic spin transfer mechanisms in bipyridine–metal complexes, a series of unsymmetrical methyl-substituted bipyridine ligands, and their nickel(II) and cobalt(II) complexes, have been prepared, and their ^1H nmr isotropic shifts measured experimentally. Simulating different electron spin density transfer mechanisms, from direct σ-electron density transfer to indirect π-mechanisms involving spin polarization or hyperconjugation, various INDO calculations have been performed on model cations and anions of the free ligand, producing good agreement with the experimental results.

T. L. JOSEPH HUANG et DOUGLAS G. BREWER. Can. J. Chem. **59**, 1689 (1981).

Dans le but d'étendre les concepts existants relatifs aux mécanismes de transfert isotrope de spin dans les complexes bipyridine–métal on a préparé une série de ligands bipyridines non symétriques portant des substituants méthyles ainsi que leurs complexes de Ni(II) et de Co(II) et on a mesuré expérimentalement leurs déplacements isotropes en rmn du ^1H. Simulant divers mécanismes de transfert de densité de spin électronique, allant du transfert direct de la densité d'électron σ jusqu'à des mécanismes π indirects impliquant la polarisation du spin ou l'hyperconjugaison, on a réalisé divers calculs INDO sur des modèles de cations et d'anions du ligand libre et l'on a obtenu un bon accord avec les résultats expérimentaux.

[Traduit par le journal]

Introduction

The isotropic chemical shifts in the ^1H nmr spectra of nickel(II) complexes of pyridines and some methyl-substituted pyridines have previously been studied in solution (1–8). In a perfectly octahedral crystal field, the ground term ^3F of Ni(II) is split into two ^3T excited states and one $^3A_{2g}$ ground level; this $^3A_{2g}$ level corresponds to an isotropic magnetic susceptibility. In a slightly distorted octahedral field, since the energy separation between the ground state and the excited state is large (9, 10) ($\gg 800\ cm^{-1}$), spin–orbit coupling may be insignificant. For this reason, the contribution to the chemical shifts of protons from dipolar interactions is usually neglected and the isotropic shifts are attributed solely to Fermi contact hyperfine interaction. In such cases, electron spin densities on nuclei of the ligand in Ni(II) pyridine-type complexes result primarily from charge transfer between metal and ligand via a σ-mechanism, as described by Happe and Ward (1).

Work has also been done previously on some Co(II) complexes with pyridine-type ligands (11–14). Using ligand field theory, Abragam and Pryce (15) have shown that the Co(II) ground term ^4F is split by an octahedral field producing a $^4T_{1g}$ ground state. Because there is strong spin–orbit coupling, this $^4T_{1g}$ state is further split into six doubly degenerate levels (Kramer's doublets) (16, 17) with the energy difference between two consecutive levels being less than $\sim 200\ cm^{-1}$. At room temperature, the electrons are distributed over all of these levels, with the population in each level being related to the Boltzmann distribution factor. Therefore the experimentally determined magnetic susceptibility for a cobalt complex will only correspond closely to the calculated spin-only value when the sample is cooled to liquid helium temperature. At other temperatures, the second-order Zeeman mixing terms make an important contribution to the magnetic susceptibility (18).

Wicholas and Drago (19) have assumed that the mechanism for the electron spin transfer and distribution in a Co(II) complex is similar to that in the corresponding Ni(II) complex. If this were true, the correlation of the isotropic shift in a Ni(II) compound to the difference between the isotropic shift and the dipolar shift, on an equivalent proton of the corresponding Co(II) compound, should be unity. Many studies have shown that this is not the case. To accurately calculate the dipolar and contact shifts in Co(II) complexes is somewhat difficult, since one needs to know the molecular structure and the magnetic moments along the principal axes (20, 21). Horrocks (22) used Krishnan's critical torque (flip angle) method (23) to measure the magnetic susceptibilities along the principal axes of a single crystal of Co(2,2′-bipyridine)$_3$·Br_2·$6H_2O$. Using this information, the second-order Zeeman terms can then be included in the magnetic mo-

[1]Author to whom correspondence may be addressed.

0008-4042/81/121689-12$01.00/0

©1981 National Research Council of Canada/Conseil national de recherches du Canada

Can. J. Chem. Downloaded from www.nrcresearchpress.com by 210.87.254.105 on 09/06/12
For personal use only.

Can. J. Chem. Downloaded from www.nrcresearchpress.com by 210.87.254.105 on 09/06/12
For personal use only.

ments at that temperature, and the dipolar and contact shift terms are determinable. The contact shifts of the Co(II) complexes determined in this way will therefore represent a mixture of contributions from first and second order Zeeman terms. If data on the temperature variation of these observed shifts had been available (this was not possible with the instrumentation available in this laboratory) then a more exact analysis according to McGarvey (17, 24) might have been attempted. Moreover, several "pure" spin-orbitals are in reality mixed in each Kramer's doublet state function, and therefore the hyperfine coupling constant of a particular nucleus in the complexed ligand would no longer be directly proportional to the electron density at that nucleus because of spin–orbital coupling. Thus eq. [3], used later in this paper, is not strictly valid; however, within the accuracy of the simplified calculations used in this investigation, and in the absence of isotropic shift temperature data, further refinement was deemed unnecessary.

La Mar and Van Hecke (25) claimed that it is impossible for a π-spin transfer mechanism to account for the isotropic shifts in octahedral Ni(II) complexes because there is no unpaired electron in the t_{2g}-orbitals. However, a π-spin transfer mechanism was reported to predominate in the ^1H nmr isotropic shifts of some octahedral Schiff base Ni(II) complexes (26–29). The charge transfer from metal to ligand via a π-mechanism in the divalent tris(2,2′-bipyridine) metal complexes of the first transition metals was also confirmed by Torii and co-workers (30), by Felix *et al.* (31), and by Nakamoto and co-workers (32). The isotropic proton chemical shifts of 2,2′-bipyridine and its symmetrical methyl-substituted Ni(II) complexes have been investigated by Wicholas and Drago (33). However, the calculated electron spin densities for the protons of bipyridine via the EHT (Extended Huckel Theory) method, neglecting the contribution from the π-back-donation mechanism, gave poor agreement with the experimental values.

In unsymmetrical methyl-substituted 2,2′-bipyridine Ni(II) complexes, the isotropic shifts show multiple resonance peaks for a particular proton, similar to that of the Co(II) and Cr(II) complexes. La Mar and Van Hecke (34, 35) indicated that there are two isomers (*cis* and *trans*) formed, and the multiple peaks are due to the unpaired d^{π}-electron(s) being unequally delocalized in the three ligands. In this work, both σ- and π-spin transfer mechanisms were considered operable in both Ni(II) and Co(II) complexes, and the theoretical estimation of the spin densities at the ligand nuclei was carried out via the INDO (intermediate neglect of differential overlap) method. The valence orbitals of the metal fragment were excluded in this simplified treatment, although calculations including the valence orbitals of the metal ion are technically feasible (36–38).

Experimental

A. *Preparation of Ligands*

2,2′-Bipyridine was purchased from Aldrich Chemical Co. Inc.; 4,4′- and 5,5′-dimethyl-2,2′-bipyridine were prepared by the procedures of Case (39) and Sasse and Whittle (40). The unsymmetrical methyl-substituted 2,2′-bipyridines were synthesized via the schemes designed by Krohnke (41), as follows.

(*1*) *4,5-Dimethyl-2,2′-bipyridine*: 1-(2-acetyl-pyridine)-pyridinium iodide and a stoichiometric amount of 2-methyl-2-butenal with excess ammonium acetate in methanol as solvent were stirred on a water bath (35–40°C) for 4–5 h. The methanol was evaporated and the residue was extracted with ethyl ether. The pure compound was recrystallized from light petroleum ether.

(*2*) *4-Methyl-2,2′-bipyridine*: the preparation was similar to the procedure (*1*) above, except 2-butenal was used in place of 2-methyl-2-butenal and the temperature was controlled at 60–65°C. The mixture of products was extracted with ethyl ether and then with hexane, and separated on a basic alumina column, eluting with hexane/acetone (9:1) mixture. The pure compound was recrystallized from 8% ethanol.

(*3*) *5-Methyl-2,2′-bipyridine*, *6-methyl-2,2′-bipyridine*, *4,6-dimethyl-2,2′-bipyridine*, *and 5,6-dimethyl-2,2′-bipyridine* were prepared in the same manner, using 2-methylpropenal, methyl vinyl ketone, 3-penten-2-one, and 3-methyl-3-buten-2-one, respectively, reacting with stoichiometric amounts of 1-(2-acetyl-pyridine)-pyridinium iodide in excess ammonium acetate in formamide, and heating in a water bath at 60–70°C for 6–8 h. The purification involved the same method as for 4-methyl-2,2′-bipyridine.

The starting material 1-(2-acetyl-pyridine)-*pyridinium* iodide was prepared according to the procedure of Krohnke and Gross (42). The elemental microanalysis and/or the molecular weight from high resolution mass spectroscopy for these compounds are tabulated in Table 1.

For the sake of brevity, the 2,2′-bipyridine is abbreviated to "bipy", and the substituents are identified according to the numbering scheme in Fig. 1. Also, a mono-methyl substituent is simplified as "me", and dimethyl substituents as "dm".

B. *Preparation of Ni(II) Complexes*

The tris ligand 2,2′-bipyridine, 4,4′-dm-bipy, and 5,5′-dm-bipy Ni(II) chloride complexes were prepared according to the procedure of Wicholas and Drago (33). Tris-ligand 4-me-bipy and 4,5-dm-bipy Ni(II) chloride complexes were prepared according to the procedure for $Ni(5,5'\text{-dm-bipy})_3Cl_2$.

The bis-ligand 4,6-dm-bipy, 5,6-dm-bipy, 5-me-bipy, and 6-me-bipy Ni(II) chloride complexes were prepared according to the following procedure. An excess amount of ligand was added to a solution of $NiCl_2 \cdot 6H_2O$ in a minimum amount of absolute ethanol and stirred for a few minutes. The solution immediately changed to a reddish-purple color. Ethyl ether was added dropwise until a slight turbidity was noticed. The green crystals were filtered, washed with ether, and dried in vacuum over P_5O_5.

The elemental analyses of these unsymmetric methyl-substituted bipyridine Ni(II) complexes are given in Table 2.

C. *Preparation of Co(II) Complexes*

$Co(2,2'\text{-bipyridine})_3(PF_6)_2$ was prepared by dissolving a stoi-

TABLE 1. Elemental analyses and molecular weights of unsymmetrical methyl-substituted 2,2′-bipyridines

Compound	Molecular weight	Found (%)†			Calculated (%)		
		C	H	N	C	H	N
4,5-dm-bipy	184	78.27	6.63	15.30	78.22	6.58	15.21
4,6-dm-bipy	184.0999*	Not available					
5,6-dm-bipy	184	78.33	6.54	15.25	78.22	6.58	15.21
4-me-bipy	170	77.65	5.89	16.40	77.61	5.93	16.46
5-me-bipy	170.0840*	Not available					
6-me-bipy	170.0847*	Not available					

*The molecular weights of these oily compounds were taken from mass spectra of high resolution mass spectroscopy (University of Alberta).
†Elemental analyses were performed by Franz Pascher Microanalytical Laboratory (Germany).

TABLE 2. Elemental analyses of bipyridine Ni(II) complexes

Compound	Found (%)*				Calculated (%)				Color
	Ni	C	H	N	Ni	C	H	N	
$Ni(4\text{-me-bipy})_3Cl_2 \cdot 3\ 1/2\ H_2O$†	8.26	56.38	4.77	11.92	8.35	56.35	5.31	11.95	Red
$Ni(5\text{-me-bipy})_2Cl_2 \cdot 1/2\ H_2O$†	11.42	55.35	4.85	11.37	12.27	55.16	4.39	11.70	Green
$Ni(6\text{-me-bipy})_2Cl_2 \cdot 1\ 1/2\ H_2O$†	12.13	52.85	4.60	11.52	11.81	53.15	4.67	11.27	Green
$Ni(4,5\text{-dm-bipy})_3Cl_2 \cdot 1\ 1/2\ H_2O$†	7.32	59.70	5.83	11.34	8.17	60.18	5.63	11.70	Red
$Ni(4,6\text{-dm-bipy})_2Cl_2 \cdot H_2O$†	10.86	56.65	5.17	10.82	11.37	55.84	5.09	10.86	Green
$Ni(5,6\text{-dm-bipy})_2Cl_2$	11.18	57.84	5.15	11.02	11.79	57.86	4.87	11.25	Green

*Elemental analyses were performed by Analytical Laboratory, Elbach (Germany).
†The water of crystallization was verified by the broad band at 3400 cm^{-1} using a Perkin-Elmer 467 infrared spectrometer.

chiometric amount of $CoCl_2 \cdot 6H_2O$ in absolute ethanol, and then adding an excess of 2,2′-bipyridine, which was previously dissolved in ethanol. The mixture was stirred and refluxed for one-half hour. After the solution had cooled to room temperature, a large amount of water was added to dilute the solution and an excess amount of NH_4PF_6 in water was added. The precipitate formed immediately. After filtering and washing, first with water, then with ethanol, the complex was dried under vacuum over P_2O_5, and then was recrystallized from acetone/methanol mixture. In this preparation all the solvents were completely degassed before using and the whole procedure was performed in a glove bag under nitrogen. All other methyl-substituted 2,2′-bipyridine Co(II) di(hexafluorophosphorate) complexes were prepared in a similar manner to that of $Co(2,2'\text{-bipyridine})_3(PF_6)_2$.

The $Co(2,2'\text{-bipyridine})_3Br_2 \cdot 2H_2O$ complex was prepared by mixing a stoichiometric amount of $CoBr_2 \cdot 6H_2O$ with an excess of 2,2′-bipyridine in absolute ethanol, and then refluxing for one-half hour. After allowing the solution to cool to room temperature, ethyl ether was added dropwise until the solution turned cloudy. The precipitate was filtered, washed with ether, and dried under vacuum over P_2O_5. The same precautions must be taken as in the previous preparation. Elemental analyses of all complexes as performed by Analytical Laboratory, Elbach (Germany) are given in Table 3.

D. *Spectral Measurements*

The ^1H nmr spectra of unsymmetrical methyl-substituted 2,2′-bipyridines in 0.1 *M* CCl_4 solution were taken on a Varian T-60 nmr spectrometer, with TMS as internal standard at a temperature of 35 ± 1°C. The proton chemical shifts of the metal complexes were measured at ca. 35°C with a Varian 4300B high resolution nmr spectrometer with 56.4 MHz radio frequency oscillator. A side band technique using a model 225C universal counter–timer (Computer Measurement Company) was employed to measure the proton resonance peaks, against an internal reference TMS in CD_3OD solution. The Co(II) complexes with hexafluorophosphorate as the anion were dissolved in acetone-d_6 and those with bromine as the anion were dissolved in methanol-d_4. TMS was used as reference.

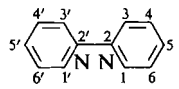

FIG. 1

E. *Measurement of Magnetic Susceptibility*

A single-temperature Gouy Balance SG1 (Newport Instruments) using a Newport 1.5 in. electromagnet (type C) was employed. The sample tube was calibrated using $[Ni(en)_3]S_2O_3$.

F. *Theoretical Calculations*

INDO open-shell calculations were performed on an IBM 370-158 computer system, using the CNINDO program obtained through the quantum chemistry program exchange (43). Bond angles and bond lengths for 2,2′-bipyridine were estimated using the structural parameters for $[Cu(bipy)_2I]I$ (44).

Experimental Results

Assignment of ^1H nmr Spectra of Free Ligand

The ^1H nmr spectra of unsymmetrical methyl-substituted 2,2′-bipyridines are similar to those for the symmetrical methyl derivatives, and by inspection and comparison, these peaks can be assigned uniquely. All proton chemical shifts for 2,2′-bipyridine and its methyl derivatives are listed in Table 4.

Assignment of ^1H nmr Spectra of Ni(II) Complexes

The ^1H nmr isotropic chemical shifts of nickel(II)

Can. J. Chem. Downloaded from www.nrcresearchpress.com by 210.87.254.105 on 09/06/12
For personal use only.

TABLE 3. Elemental analyses of Co(II) complexes*

Compound	Found (%)			Calculated (%)		
	C	H	N	C	H	N
$Co(bipy)_3Br_2 \cdot 2H_2O$	49.96	3.87	11.53	49.81	3.90	11.62
$Co(bipy)_3(PF_6)_2$	44.13	3.10	10.36	44.08	2.97	10.28
$Co(4,4'\text{-dm-bipy})_3(PF_6)_2$	47.92	4.16	9.37	47.95	4.03	9.32
$Co(5,5'\text{-dm-bipy})_3(PF_6)_2$	48.05	4.16	9.31	47.95	4.03	9.32
$Co(4,5\text{-dm-bipy})_3(PF_6)_2$	47.71	4.00	9.37	47.95	4.03	9.32
$Co(4\text{-me-bipy})_3(PF_6)_2$	45.86	3.48	9.69	46.11	3.53	9.78
$Co(5\text{-me-bipy})_3(PF_6)_2$	46.00	3.58	9.90	46.11	3.53	9.78

*Elemental analyses were performed by Analytical Laboratory, Elbach (Germany).

TABLE 4. The proton chemical shifts of 2,2'-bipyridine and its methyl substituted* derivatives

Proton position	bipy†	4,4'-dm† -bipy	5,5'-dm† -bipy	3,3'-dm† -bipy	4,5-dm -bipy	4,6-dm -bipy	5,6-dm -bipy	4-me -bipy	5-me -bipy	6-me -bipy
6'-	−515	−505	−502	−503	−510	−514	−512	−520	−519	−514
6-	−515	−505	−502	−503	−507	(−149)‡	(−151)	−512	−510	(−153)
3'-	−508	−497	−497	(−130)	−496	−508	−506	−506	−504	−510
3-	−508	−497	−497	(−130)	−492	−487	−489	−496	−498	−499
5'-	−429	−420	(−139)	−426	−425	−426	−426	−433	−432	−424
5-	−429	−420	(−139)	−426	(−133)	−407	(−136)	−424	(−138)	−416
4'-	−460	(−146)	−448	−451	−458	−456	−459	−466	−464	−457
4-	−460	(−146)	−448	−451	(−138)	(−136)	−443	(−144)	−452	−446

*Chemical shifts in Hz, referenced against TMS, were taken on a Varian T-60 nmr spectrometer.
†Data from ref. 53.
‡Numbers in parentheses are chemical shifts of methyl protons.

bipyridine and its symmetrical methyl-substituted complexes were assigned on the basis of line widths and the results of methyl substitution on the aromatic rings by Wicholas and Drago (33). The assignments for the tris(4,5-dm-bipy) and tris(4-me-bipy) nickel(II) complexes prepared in this study are listed in Table 5. In general, the ^1H nmr spectra have similar features to those of the simple pyridine complex. The 6,6'-proton resonance is too broad to be observed and the 4,4'-proton peak has a small half-width. The other two protons have similar half-widths and give resonances at ca. −45 ppm and ca. −60 ppm with intensity 1:1 for 4-me-bipy and 0.5:1 for 4,5-dm-bipy complexes, respectively. Since methyl substitution causes very little change in the position of the aromatic ring proton peaks compared to their positions in the unsubstituted bipyridine Ni(II) complex, the upper field resonance at ca. −45 ppm is assigned to the 5,5'-protons and the lower field one at ca. −60 ppm to the 3,3'-protons.

In complexes having a 6-methyl substituted ligand, the 3,3'- and 5,5'-protons multiple resonance peaks are spread over the region from ca. −45 to −60 ppm. Obviously, this is evidence of *cis* and *trans* isomers of the tris-ligand Ni(II) complexes, as in the case of unsymmetrical methyl-substituted 1,10-phenanthroline Cr(II), Fe(III), and Co(II) complexes (25). When the ligand/Ni(II) ratio is increased from 1:1 to 3:1, the ^1H nmr spectra show proton chemical shifts which can be interpreted in terms of the ligand changing from a uni-chelate to a bis-chelate, and then to a tris-chelate. For a ratio less than 1:1, the major species is the uni-chelated ligand. One can unambiguously assign each peak to its corresponding proton position from the resonance peak shape (45) and the ^1H nmr chemical shifts of each ligand in these complexes are listed in Table 5.

Assignment of ^1H nmr Spectra of Co(II) Complexes

For the tris unsymmetrical methyl-substituted 2,2'-bipyridine Co(II) complexes, the ^1H nmr spectra show four resonance peaks with equal intensities for each particular proton. Obviously, two stereoisomers exist for these complexes, and the concentrations of the two isomers are established statistically resulting in a ratio of *cis*/*trans* = 1:3. The methyl substituent in the bipyridine Co(II) complexes has no effect on the magnetic properties of the unsubstituted tris complex and the chemical shifts are consistent for each particular proton. This allows each peak to be assigned unambig-

Can. J. Chem. Downloaded from www.nrcresearchpress.com by 210.87.254.105 on 09/06/12
For personal use only.

Can. J. Chem. Downloaded from www.nrcresearchpress.com by 210.87.254.105 on 09/06/12
For personal use only.

uously, as tabulated in Table 6. The magnetic properties of these Co(II) complexes are also not affected by a variation in the anion group, as has been confirmed by a study of the chemical shifts in Co(2,2′-bipyridine)$_3$X$_2$ with X = Cl^-, Br^-, ClO_4^-, and PF_6^-. The *cis* form of the Co(II) complexes belongs to a monoclinic system with approximate D_3 symmetry, similar to that of tris-(2,2′-bipyridyl) Ni(II) sulphate hydrate and trisacetylacetonato Co(II) (46, 47).

Discussion and Results

The ^{1}H nmr chemical shifts of a paramagnetic metal complex can be written as:

$$[1] \quad \Delta\nu_{obsd} = \Delta\nu_{con} + \Delta\nu_{dip} + \Delta\nu_{dia}$$

where $\Delta\nu_{obsd}$ is the observed proton chemical shift of a paramagnetic complex from a reference (TMS) peak; $\Delta\nu_{con}$ and $\Delta\nu_{dip}$ are the shifts contributed from contact and dipolar interactions, respectively; $\Delta\nu_{dia}$ is the proton chemical shift of either an analogous diamagnetic complex or the free ligand.

For the Co(II) complexes with a cylindrically symmetric susceptibility tensor, the contact and dipolar shifts have been expressed in a simple form by Jesson (48, 49):

$$[2] \quad \left(\frac{\Delta\nu_{dip}}{\nu_0}\right) = \frac{-1}{3r^3}(3\cos^2\theta - 1)(\chi_{\parallel} - \chi_{\perp})$$

and

$$[3] \quad \left(\frac{\Delta\nu_{con}}{\nu_0}\right) = -\frac{A_N}{6\hbar\gamma_N\beta}\left(\frac{\chi_{\parallel}g_{s\parallel}}{g_{\parallel}} + \frac{2\chi_{\perp}g_{s\perp}}{g_{\perp}}\right)$$

where A_N is the Fermi hyperfine coupling constant of the proton N, and can be expressed as

$$[4] \quad A_N = \frac{16\pi}{3}\hbar\gamma_N\beta\sum_i \delta(r_i)$$

For a complex possessing an essentially spin-only magnetic moment, the contact shift can be shown to exhibit Curie behaviour.

$$[5] \quad \left(\frac{\Delta\nu_{con}}{\nu_0}\right) = -A_N\frac{g\beta S(S+1)}{\gamma_N\hbar\cdot 3kT}$$

A. *The Fermi Contact Shifts of Ni(II) Complexes*

In the study of a series of solutions of varying ligand/Ni(II) ratio, the ^{1}H nmr resonance for a particular proton has a shift range which is not affected by the number of bipyridines coordinated with the metal ion. The isotropic shifts of these unsymmetrical methyl-substituted bipyridines were determined by subtracting the diamagnetic ligand shifts from the uni-chelated Ni(II) complexes ligand shifts, and are listed in Table 9. These Ni(II) complexes have a $^3A_{2g}$ ground state which is isotropic, and then the dipolar contribution can usually be neglected. In this situation, the isotropic shift arises solely from the Fermi contact interaction, which is proportional to the hyperfine coupling constant resulting from electron spin delocalization on the proton, as shown in eq. [5].

B. *The Fermi Contact Shifts of Co(II) Complexes*

As indicated previously, the octahedrally axial Co(II) complexes have a $^4T_{1g}$ ground state, and thus magnetic anisotropy is expected. The isotropic shifts are interpreted in terms of Fermi contact and dipolar hyperfine interactions.

(*i*) *Dipolar Shifts*

To calculate the dipolar shifts of the protons in these Co(II) complexes, one has to determine the magnetic susceptibilities along the principal axes of the complexes. Horrocks (22) studied the single crystal Co(2,2′-bipyridine)$_3$Br$_2$·6H$_2$O and found the molar magnetic susceptibilities are $\chi_{\parallel}^M = 7500 \times 10^{-6}$ and $\chi_{\perp}^M = 12250 \times 10^{-6}$ cgsu/mol at 40°C. For the methyl-substituted 2,2′-bipyridine Co(II) complexes, these principal magnetic susceptibilities are unavailable. In this work, the average magnetic susceptibility of some tris-ligand complexes was measured by the Gouy method. The main contribution to the magnetic susceptibility of the complex is due to the paramagnetic metal ion, χ_{corr}^M, and is nearly constant (within ± 3%) for all tris-ligand complexes. It is therefore assumed that the methyl-substituents in these complexes only slightly affect the magnetic properties along the principal axes and that any such effect can be neglected. The ratio of $\chi_{\parallel}^M$ and $\chi_{\perp}^M$ was chosen as 0.61, i.e. ($7500 \times 10^{-6}/12250 \times 10^{-6}$), for these Co(II) complexes. The values of $\chi_{\parallel}^M$ and $\chi_{\perp}^M$ were estimated from the solution of the following two equations and are tabulated in Table 7.

$$[6] \quad \chi^M = 1/3(2\chi_{\perp}^M + \chi_{\parallel}^M)$$

$$[7] \quad \chi_{\parallel}^M/\chi_{\perp}^M = 0.61$$

For calculation of the geometric factor $(3\cos^2\theta - 1)/r^3$ as shown in eq. [1], the geometric parameters of bipyridine Co(II) complex are taken from the data of X-ray structure of [Cu(2,2′-bipyridine)$_2$I]I compound (44); the bond length of Co—N was chosen as 2.00 Å with a bond angle for N—Co—N as 82°. For the *trans* isomer of the methyl-substituted bipyridine Co(II) complexes, there is no symmetry axis. The angle θ is taken from the corresponding value for the *cis* form, since the isotropic shifts have been averaged over all isomers (*vide infra*). The calculated geometric factors of

TABLE 5. The proton chemical shifts of bipyridine ligands in Ni(II) complexes when ligand/nickel = 3/1, 2/1, and 1/1*

Ligand	Nucleus	Tris-ligand	Bis-ligand	Mono-ligand
bipy	6,6'-	−144.3		
	3,3'-	−65.1		
	5,5'-	−48.6		
	4,4'-	−15.1		
4,4'-dm-bipy	6,6'-	—		
	3,3'-	−64.1		
	5,5'-	−48.1		
	4,4'-	(+8.1)†		
5,5'-dm-bipy	6,6'-	—		
	3,3'-	−64.4		
	5,5'-	(−8.7)		
	4,4'-	−13.9		
4,5-dm-bipy	6'-	—		
	6-	—		
	3'-	−61.5	−63.0	−59.7 §, −57.9
	3-			
	5'-	−45.8	−48.1	−43.4
	5-	(−8.6)	(−8.6)	(−9.7)
	4'-	−14.6	−15.1	−14.5
	4-	(+8.0)	(+8.7)	(+7.6)
4,6-dm-bipy	6'-	—	—	—
	6-	(+9.6)	(+7.7)	(+6.8)
	3'-	−63.0[3]‡ §, −59.6[1]	−56.3[1]	−56.3
	3-	−55.1[1], −52.7[2]		−46.9
	5'-	−51.3[2], −50.0[3]	−49.8[1]	−45.3
	5-	−46.9[3], −43.1[1]	−43.8[2]	−46.9
	4'-	−16.2	−15.9	−15.9
	4-	(+5.5)[3], (+3.8)[1]	(+4.9)	(+5.4)
5,6-dm-bipy	6'-	—	—	—
	6-	(+7.0)	(+7.8)	(+5.4)
	3'-	−60.7[2], −56.6[2]		−56.4
	3-	−52.9[3], −49.6[2]	−65.5[1], −60.5[1]	−50.1
	5'-	−45.0[2], −41.5[1]	−49.7[1]	−45.6
	5-	(−6.9)	(−6.6)	(−8.5)
	4'-	−15.7[3]	−18.1	−15.9
	4-	−11.0[1]	−11.6	−11.3
4-me-bipy	6'-			
	6-	—	—	—
	3'-	−57.3	−60.5	−54.0
	3-			−52.5
	5'-	−42.4	−44.9	−41.1
	5-			−39.5
	4'-	−13.4	−15.0	−13.7
	4-	(+7.4)	(+7.6)	(+6.6)
5-me-bipy	6'-	−172.9	—	−159.9
	6-			

Can. J. Chem. Downloaded from www.nrcresearchpress.com by 210.87.254.105 on 09/06/12
For personal use only.

TABLE 5 (*Concluded*)

Ligand	Nucleus	Tris-ligand	Bis-ligand	Mono-ligand
	3'-			−60.7
	3-	−65.3	−57.4	−58.3
	5'-	−48.3	−43.1	−43.7
	5-	(−8.5)	(−7.3)	(−9.3)
	4'-			−14.7
	4-	−14.8	−12.7	−14.0
6-me-bipy	6'-	—	—	—
	6-	(+9.0)	(+8.6)	(+8.1)
	3'-	−61.7[3] −57.7[1]	−54.4[1]	−56.2
	3-	−54.7[1] −51.7[3]	−48.9[1]	−48.2
	5'-	−49.7[3] −47.2[3]	−47.0[1]	−46.1
	5-	−44.4[1] −43.0[1]	−45.6[1]	−48.2
	4'-	−15.7[1] −13.2[3]	−14.4	−15.7
	4-	−11.8[4]	−11.7	−13.0

*Chemical shifts in ppm at 35°C in CD_3OD solution, referenced against TMS.
†Numbers in parentheses are chemical shifts of methyl protons.
‡Numbers in brackets are overlapping peaks.
§Shifts for designated protons are indistinguishable from each other, with respect to assignments.

TABLE 6. The ^1H nmr isotropic chemical shifts of Co(II) bipyridine complexes*

Compound	6,6'-H	3,3'-H	5,5'-H	4,4'-H	4-CH_3	5-CH_3	6-CH_3
$Co(bipy)_3Br_2 \cdot 2H_2O$	−85.3	−80.6	−44.9	−14.1			
$Co(bipy)_3(PF_6)_2$	−86.3	−81.0	−44.9	−14.2			
$Co(4,4'\text{-dm-bipy})_3(PF_6)_2$	−88.3	−78.3	−43.3		−0.59		
$Co(5,5'\text{-dm-bipy})_3(PF_6)_2$	−86.8	−82.6		−13.5		−1.88	
$Co(4,5\text{-dm-bipy})_3(PF_6)_2$	−101.5[1]†	−85.3[1]	−44.6[2]	−14.8[1]	−4.71[1]	−3.72[1]	
	−93.2[2]	−83.4[1]	−40.2[2]	−13.6[1]	−3.47[1]	−2.48[2]	
		−81.8[1]					
	−82.6[2]	−80.8[1]		−11.9[1]	−1.49[1]	−2.08[1]	
	−76.1[2]	−79.4[2]		−10.9[1]	−0.74[1]		
	−57.1[1]	−77.1[1]					
		−75.1[1]					
$Co(4\text{-me-bipy})_3(PF_6)_2$	−101.1[1]	−83.6	−47.9	−15.3	−3.89		
	−93.5[2]	−82.7	−45.4	−14.3	−2.70		
	−86.6[2]	−81.9	−43.3	−12.4	−1.78		
	−80.6[1]	−81.0	−40.9	−11.4	−0.64		
	−73.4[2]	−80.0					
		−78.9					
		−78.1					
		−77.2					
$Co(5\text{-me-bipy})_3(PF_6)_2$	−87.5	−82.6	−44.6	−14.0		−1.98	
	−84.1	−80.4		−13.5		−3.27	

*Chemical shifts in ppm at 35°C in solution, referenced against TMS.
†Numbers in brackets are overlapping peaks.

Can. J. Chem. Downloaded from www.nrcresearchpress.com by 210.87.254.105 on 09/06/12
For personal use only.

Can. J. Chem. Downloaded from www.nrcresearchpress.com by 210.87.254.105 on 09/06/12
For personal use only.

TABLE 7. The magnetic susceptibilities of Co(II) complexes*

Compound	χ_g†	χ^M	$\chi_{corr}{}^M$‡	$\chi_{\|\|}{}^M$	$\chi_\perp{}^M$
$Co(bipy)_3Br_2 \cdot 2H_2O$	13.02	9418	9778	6600	10830
$Co(bipy)_3(PF_6)_2$	11.77	9619	9992	6740	11060
$Co(4,4'\text{-dm-bipy})_3(PF_6)_2$	10.23	9223	9667	6470	10600
$Co(5,5'\text{-dm-bipy})_3(PF_6)_2$	10.00	9017	9461	6320	10360
$Co(4,5\text{-dm-bipy})_3(PF_6)_2$	10.46	9594	10038	6730	11030
$Co(5\text{-me-bipy})_3(PF_6)_2$	10.81	9292	9778	6520	10680
$Co(4\text{-me-bipy})_3(PF_6)_2$	10.29	8840	9249	6200	10160

*Unit in VVK (1 VVK = 1×10^{-6} cgsu).
†Magnetic susceptibilities are measured at 20 ± 1°C.
‡$\chi_{corr}{}^M = \chi^M - \chi_{dia}$; $\chi_{corr}{}^M$ is attributed to paramagnetic metal ion, and χ_{dia}; is the diamagnetic contributions for ligand and anion. Data taken from ref. 54.

TABLE 8. Hyperfine chemical shifts of protons in Co(II) complexes*

Proton	$\Delta\nu_{obsd}$**	$\Delta\nu_{dia}$†	$\Delta\nu_{iso}$‡	$\Delta\nu_{dip}$¶	$\Delta\nu_{con}$§
$Co(bipy)_3Br_2 \cdot 2H_2O$					
6,6′-H	−85.3	−8.6	−76.7	72.6	−149.3
3,3′-H	−80.6	−8.5	−72.1	−17.1	−55.0
5,5′-H	−44.9	−7.2	−37.8	8.1	−45.9
4,4′-H	−14.1	−7.7	−6.4	−3.2	−3.2
$Co(bipy)_3(PF_6)_2$					
6,6′-H	−86.3	−8.6	−77.7	74.1	−151.8
3,3′-H	−81.0	−8.5	−72.5	−17.5	−55.0
5,5′-H	−44.9	−7.2	−37.8	8.2	−46.0
4,4′-H	−14.2	−7.7	−6.5	−3.3	−3.2
$Co(4,4'\text{-dm-bipy})_3(PF_6)_2$					
6,6′-H	−88.3	−8.4	−79.9	70.9	−150.8
3,3′-H	−78.3	−8.3	−70.0	−16.7	−53.3
5,5′-H	−43.3	−7.0	−36.3	7.9	−44.2
4,4′-CH_3	−0.59	−2.43	+1.84	−2.17	+4.01
$Co(5,5'\text{-dm-bipy})_3(PF_6)_2$					
6,6′-H	−86.8	−8.4	−78.4	69.3	−147.7
3,3′-H	−82.6	−8.3	−74.3	−16.3	−58.0
4,4′-H	−13.5	−7.5	−6.0	−3.0	−3.0
5,5′-CH_3	−1.88	−2.32	+0.44	7.58	−7.14
$Co(4,5\text{-dm-bipy})_3(PF_6)_2$					
6,6′-H	−82.8	−8.5	−74.3	73.8	−148.1
3,3′-H	−80.3	−8.2	−72.1	−17.4	−54.7
5′-H	−42.3	−7.1	−35.3	8.2	−43.5
4′-H	−12.8	−7.6	−5.2	−3.2	−2.0
4-CH_3	−2.60	−2.30	−0.30	−2.26	+1.96
5-CH_3	−2.69	−2.22	−0.47	8.07	−8.54
$Co(5\text{-me-bipy})_3(PF_6)_2$					
6,6′-H	−85.8	−8.6	−77.2	71.4	−148.6
3,3′-H	−81.5	−8.4	−73.1	−16.8	−56.3
5′-H	−44.6	−7.2	−37.4	7.9	−45.3
4,4′-H	−13.8	−7.6	−6.2	−3.1	−3.1
5-CH_3	−2.30	−2.30	0.00	7.81	−7.81
$Co(4\text{-me-bipy})_3(PF_6)_2$					
6,6′-H	−86.1	−8.6	−77.5	+68.0	−145.5
3,3′-H	−80.4	−8.4	−72.0	−16.0	−56.0
5,5′-H	−44.4	−7.1	−37.3	+7.5	−44.8
4′-H	−13.4	−7.8	−5.6	−3.0	−2.6
4-CH_3	−2.25	−2.40	+0.15	−2.08	2.23

TABLE 8 (*Concluded*)

Proton	$\Delta\nu_{obsd}$**	$\Delta\nu_{dia}$†	$\Delta\nu_{iso}$‡	$\Delta\nu_{dip}$¶	$\Delta\nu_{con}$§
Co(4,6-dm-bipy)(bipy)$_2$(PF$_6$)$_2$§§					
6′-H	−86	−8.6	−77	70	−147
3,3′-H	−80	−8.3	−72	−17	−55
5,5′-H	−42	−6.9	−35	7.8	−43
4′-H	−14	−7.6	−6.4	−3.1	−3.3
4-CH$_3$	−2.0	−2.3	−0.3	−2.2	1.9
6-CH$_3$	90	−2.5	93	54	39
Co(5,6-dm-bipy)(bipy)$_2$(PF$_6$)$_2$§§					
6′-H	−86	−8.5	−78	70	−147
3,3′-H	−80	−8.3	−72	−17	−55
5′-H	−45	−7.1	−38	7.8	−46
4,4′-H	−14	−7.5	−6.5	−3.1	−3.4
5-CH$_3$	−3.0	−2.3	−0.7	7.7	−8.4
6-CH$_3$	90	−2.5	93	54	39
Co(6-me-bipy)(bipy)$_2$(PF$_6$)$_2$§§					
6′-H	−88	−8.6	−79	70	−149
3,3′-H	−83	−8.4	−75	−17	−58
5,5′-H	−42	−7.0	−35	7.8	−43
4,4′-H	−14	−7.5	−6.5	−3.1	−3.4
6-CH$_3$	90	−2.6	93	54	39

*The unit in ppm.
**Data ($\Delta\nu_{obsd}$) from ^{1}H nmr isotropic chemical shifts of Co(II) complexes.
†Data ($\Delta\nu_{dia}$) from free ligand.
‡$\Delta\nu_{iso} = \Delta\nu_{obsd} - \Delta\nu_{dip}$.
¶Data ($\Delta\nu_{dip}$) from dipolar shifts calculation.
§Fermi contact shifts $\Delta\nu_{con}$, $\Delta\nu_{con} = \Delta\nu_{iso} - \Delta\nu_{dip}$.
§§Shifts are the average of all corresponding protons on bipyridine ring. $\chi_{||}^M$ and $\chi_{\perp}^M$ are taken from the average value of tris-methyl-substituted bipyridine Co(PF$_6$)$_2$ complexes.

these protons are given by the following values (in Å^{-3} unit):

6,6′-H	5,5′-H	4,4′-H	3,3′-H	4-CH$_3$	5-CH$_3$	6-CH$_3$
0.03099	0.00344	−0.00136	−0.00730	−0.00095	0.00339	0.02363

Basically, these values agree well with those of Horrocks (22), except for that of the 4,4′-H. This high discrepancy (18%) can be rationalized by considering the two pyridyl rings in bipyridine as being slightly bent towards the metal ion. The calculated dipolar shifts using eq. [1] are given in Table 8. When the 6-proton on the bipyridine is substituted by a methyl group, dipolar shift calculations predict an isotropic shift for the methyl protons of some +70 ppm. An attempt to verify this directly failed, since the compounds Co(6-me-bipy)$_3$(PF$_6$)$_2$ and Co(4,6-dm-bipy)$_3$(PF$_6$)$_2$ could not be prepared, apparently due to strong steric hindrance by the 6-methyl groups. However, the tris-mixed complexes Co(6-me-bipy)(bipy)$_2$(PF$_6$)$_2$, Co(4,6-dm-bipy)(bipy)$_2$(PF$_6$)$_2$, and Co(5,6-dm-bipy)-(bipy)$_2$(PF$_6$)$_2$ have been prepared and their ^{1}H nmr spectra studied. In the calculation of the dipolar shifts of these compounds the magnetic susceptibilities ($\chi_{||}^M$ = 6500, $\chi_{\perp}^M$ = 10600 VVK) are taken from the average values of all Co(II) dihexafluorophosphate complexes. The isotropic shift of the protons indicated in Table 8 is the average of the values for all corresponding protons on the mixed ligand set.

(*ii*) *Fermi Contact Shifts*

The isotropic shifts were determined by subtracting the diamagnetic ligand shifts from the average values of equivalent protons of ligand shifts in *cis* and *trans* stereoisomers of tris-chelated Co(II) complexes, in a way similar to the determination of the isotropic shifts in Ni(II) complexes. The contact shifts of protons were determined by the difference between the isotropic shifts and the dipolar shifts, Table 8. Since the unpaired electrons fluctuate between the multiple levels (six Kramer's doublets), and with the mixing of several "pure" spin orbitals in each Kramer's doublet state function, a quantitative study of the unpaired electron

Can. J. Chem. Downloaded from www.nrcresearchpress.com by 210.87.254.105 on 09/06/12
For personal use only.

TABLE 9. Comparison of relative contact shifts of bipyridine ligand in Ni(II) and Co(II) complexes with calculated relative hyperfine coupling constants of free ligand model compounds

Ligand	Proton position	A^{σ}	A^{π}	$A^{\sigma} + A^{\pi}$	Calculated (relative A_H) Free ligands	Experimental* (relative A_H) Ni(II) complexes	Co(II) complexes
bipy	6,6'-H	16.57	−2.15	14.42	2.82	2.44(−136.4)	2.76(−151.8)
	3,3'-H	5.82	−0.70	5.12	1.00	1.00(−55.9)	1.00(−55.0)
	5,5'-H	6.60	0.92	7.52	1.47	0.73(−40.7)	0.84(−46.0)
	4,4'-H	8.79	−8.74	0.05	0.01	0.12(−6.4)	0.06(−3.2)
4,4'-dm-bipy	6,6'-H	16.69	−0.82	15.87	3.05	—	2.83(−150.8)
	3,3'-H	6.27	−1.07	5.20	1.00	1.00(−55.0)	1.00(−53.3)
	5,5'-H	7.25	−0.18	7.07	1.36	0.73(−40.4)	0.83(−44.2)
	4,4'-CH_3	−1.34	—	−1.34	−0.26	−0.20(+10.8)	−0.08(+4.01)
5,5'-dm-bipy	6,6'-H	14.56	−0.36	14.20	2.98	3.17(−175.5)	2.55(−147.7)
	3,3'-H	5.21	−0.45	4.76	1.00	1.00(−55.3)	1.00(−58.0)
	4,4'-H	9.87	−9.29	0.58	0.12	0.10(−5.4)	0.05(−3.0)
	5,5'-CH_3	1.92	—	1.92	0.40	0.11(−6.3)	0.12(−7.1)
4,5-dm-bipy†	6,6'-H	15.58	−0.58	15.00	3.07	—	2.71(−148.1)
	3,3'-H	5.73	−0.84	4.89	1.00	1.00(−50.0)	1.00(−54.7)
	5'-H	6.63	0.11	6.74	1.38	0.72(−35.9)	0.80(−43.5)
	4'-H	8.75	−8.47	0.28	0.06	0.13(−6.4)	0.04(−2.0)
	4-CH_3	−1.38	—	−1.38	−0.28	−0.20(+10.0)	−0.04(+1.96)
	5-CH_3	1.93	—	1.93	0.39	0.15(−7.3)	0.16(−8.54)
4,6-dm-bipy†	6'-H	16.23	−0.34	15.89	3.13	—	2.67(−147)
	3,3'-H	6.31	−1.24	5.07	1.00	1.00(−43.3)	1.00(−55)
	5,5'-H	6.41	0.63	7.04	1.39	0.91(−39.2)	0.78(−43)
	4'-H	8.81	−8.14	0.67	0.13	0.18(−7.8)	0.06(−3.3)
	4-CH_3	−1.17	—	−1.17	−0.23	−0.18(+7.8)	−0.03(+1.9)
	6-CH_3	−0.83	—	−0.83	−0.16	−0.22(+9.4)	−0.71(+39)
5,6-dm-bipy†	6'-H	16.28	−1.02	15.26	3.20	—	2.67(−147)
	3,3'-H	5.74	−0.97	4.77	1.00	1.00(−44.9)	1.00(−55)
	5'-H	6.64	0.12	6.76	1.42	0.86(−38.5)	0.84(−46)
	4,4'-H	9.46	−8.21	1.25	0.26	0.12(−5.6)	0.06(−3.4)
	5-CH_3	1.84	—	1.84	0.39	0.13(−6.0)	0.15(−8.4)
	6-CH_3	−1.07	—	−1.07	−0.22	−0.15(+6.6)	−0.71(+39)
4-me-bipy†	6,6'-H	16.63	−1.29	15.34	3.00	—	2.60(−145.5)
	3,3'-H	6.05	−0.93	5.12	1.00	1.00(−44.3)	1.00(+56.0)
	5,5'-H	6.92	0.26	7.18	1.40	0.74(−32.7)	0.80(−44.8)
	4'-H	8.78	−8.51	0.27	0.05	0.12(−5.5)	0.05(−2.6)
	4-CH_3	−1.34	—	−1.34	−0.26	−0.20(+9.0)	−0.04(+2.23)
5-me-bipy†	6,6'-H	15.56	−1.24	14.32	2.90	2.98(−150.8)	2.64(−148.6)
	3,3'-H	5.51	−0.57	4.94	1.00	1.00(−50.6)	1.00(−56.3)
	5'-H	6.63	+0.90	7.53	1.53	0.71(−36.1)	0.80(−45.3)
	4,4'-H	9.34	−9.02	0.32	0.06	0.12(−6.2)	0.06(−3.1)
	5-CH_3	1.96	—	1.96	0.40	0.13(−6.8)	0.14(−7.81)
6-me-bipy†	6'-H	16.38	−0.86	15.52	3.12	—	2.57(−149)
	3,3'-H	6.07	−1.10	4.97	1.00	1.00(−43.8)	1.00(−58)
	5,5'-H	6.09	1.18	7.27	1.46	0.92(−40.2)	0.74(−43)
	4,4'-H	8.96	−7.78	1.18	0.24	0.14(−6.3)	0.06(−3.4)
	6-CH_3	−0.99	—	−0.99	−0.20	−0.25(+10.8)	−0.67(+39)

*Numbers in parentheses are contact shifts ($\Delta\nu_{con}$) in ppm.
†Values for unsymmetrical ligands are taken from the average of the equivalent protons.

spin densities at the protons is impossible without data on the temperature dependence of the observed shifts. Therefore at a particular temperature, the contact shift of the proton in a Co(II) complex is taken to be approximately proportional to the hyperfine coupling constant, which is related to the unpaired electron spin density at the proton as shown in eq. [3].

C. *Electron Spin Transfer Mechanisms in Ni(II) and Co(II) Complexes*

When one considers the dynamics of bond for-

Can. J. Chem. Downloaded from www.nrcresearchpress.com by 210.87.254.105 on 09/06/12
For personal use only.

Can. J. Chem. Downloaded from www.nrcresearchpress.com by 210.87.254.105 on 09/06/12
For personal use only.

mation in these complexes, the lone pair electrons on the ligand are first donated to the metal ion forming a σ-bond. To reduce the build-up of high electron density on the central metal ion, some electron density will be back-donated from the d^{π}-orbitals of the metal to a π*-bonding orbital of the ligand (50). The σ-mechanism results in cationic character being attributed to the ligand, while the π-mechanism imparts anionic character to the ligand. These σ-donations and π-back-donations have been well documented by measurement of infrared stretching bands (30) and by electronic absorptions (32).

In this work, the INDO method has been used to calculate the electron spin density at each nucleus in both σ- and π-orbitals of the ligand, for a model free ligand cation (representing unpaired electron density on the σ-orbitals of the ligand) and a model free ligand anion (representing unpaired electron density on the π*-bonding orbital of the ligand). The valence *d*-orbitals of Ni(II) or Co(II) were excluded in this simplified treatment. The electron spin density of the protons on the aromatic ring and that of the protons on the methyl substituent have been considered separately.

(*i*) *Aromatic Protons on the Bipyridine Ring*

For a σ-spin transfer mechanism, the free ligand cation is used to simulate the ligand with α-spin in its σ-orbitals, and the calculated hyperfine coupling constants (A_H^{σ}) arise from electron spin density on the 1*s*-orbital on the protons.

To calculate any "induced" electron spin density on a proton (28), the free ligand anion is used to simulate the ligand with α-spin in its π*-orbital, and the hyperfine coupling constant (A_H^{π}) is obtained from McConnell's relation $A_H^{\pi} = Q_{CH}\rho_C^{\pi}$ (51), where all notations are standard (44). Q_{CH} has a value of 22.5 gauss.

The resultant calculated hyperfine coupling constant of the proton, A_H, is a combination of A_H^{σ} and A_H^{π}, of the general form $A_H = C_{\sigma}A_H^{\sigma} \pm C_{\pi}A_H^{\pi}$. In several trial fits with the experimental data, it was determined that the coefficients C_{σ} and C_{π} were very nearly equal, and therefore in this calculation were both assigned a value of unity. Note that if α-spin is used for the calculation for both the cation and the anion models, the hyperfine coupling constant is the sum of these two factors, i.e. $A_H = A_H^{\sigma} + A_H^{\pi}$. If β-spin is used for the anion model, only the difference of A_H^{σ} and A_H^{π} fits the experimental results, that is, $-A_H^{\pi}$ (β-spin) is equal to A_H^{π} (α-spin). Thus one can infer that the unpaired electron densities in the σ- and π*-bonding orbitals of the ligand have the same spin (α-spin). The values of the calculated A_H are listed in Table 9.

In comparing the calculated and experimental results, it can be seen that there is qualitative agreement in both Ni(II) and Co(II) complexes; the proton peaks for the 6,6′-positions are shifted to very low field and the protons in the 4,4′-positions show a very slight shift. While the calculated A_H for the 5,5′- and 3,3′-protons and the measured contact shifts are in reasonable agreement, the positions are reversed. This may result from neglecting the interactions between the two pyridyl rings of the 2,2′-bipyridine in the complexes.

(*ii*) *Protons on the Methyl Substituent(s)*

The calculated hyperfine coupling constant of the methyl proton A_{CH_3} is considered to have arisen primarily from a σ-mechanism, and any "induced" electron spin density arising from a hyperconjugative π-back donation mechanism has been neglected. This is consistent with the scheme described by La Mar (52) for paramagnetic complexes where the hybrid σ-orbitals of the methyl group already possess some unpaired spin density before any π-back donation occurs, and because of electron repulsions, is probably not significant. The values of A_{CH_3} are calculated from the cation model with α-spin on the ligand and are listed in Table 4. Comparison of the calculated A_{CH_3} with the experimental contact shift of the methyl protons shows that the sign of the 6- and 4(4′)-methyl protons are all negative, having an upfield shift with respect to TMS, and the sign of the 5(5′)-methyl protons is positive, having a downfield shift. The magnitude of the calculated values of A_{CH_3} is in reasonable agreement with the experimental results, with those for the 6- and 4(4′)-positions being noticeably better than those for the 5(5′)-positions.

Acknowledgements

The authors wish to gratefully acknowledge the financial support of U.N.B. through the Department of Chemistry, Dr. F. Grein (Chemistry Department) for his assistance with theoretical aspects, and Dr. R. Kaiser (Physics Department) for the use of his nmr facilities.

1. J. A. Happe and R. L. Ward. J. Chem. Phys. **39**, 1211 (1963).
2. R. E. Cramer and R. S. Drago. J. Am. Chem. Soc. **92**, 66 (1970).
3. D. Forster. Inorg. Chem. Acta, **5**, 465 (1971).
4. W. D. Horrocks, Jr. and D. L. Johnston. Inorg. Chem. **10**, 1837 (1971).
5. M. S. Sun, F. Grein, and D. G. Brewer. Can. J. Chem. **50**, 2626 (1972).
6. M. S. Sun. Ph.D. Thesis, University of New Brunswick, 1974.
7. M. J. Scarlett, A. T. Casey, and R. A. Craig. Aust. J. Chem. **23**, 1333 (1970).

8. M. J. SCARLETT, A. T. CASEY, and R. A. CRAIG. Aust. J. Chem. **24**, 31 (1971).
9. L. SACCONI. Transition metal chemistry. Vol. 4. *Edited by* R. L. Carlin. Marcel Dekker, New York. 1968. p. 199.
10. R. D. HANCOCK and G. J. MCDOUGALL. J. Chem. Soc. Dalton Trans. 67 (1977).
11. R. W. KLUIBER and W. D. HORROCKS, JR. Inorg. Chem. **6**, 166 (1967).
12. D. DODDRELL and J. D. ROBERTS. J. Am. Chem. Soc. **92**, 6839 (1970).
13. I. MORISHIMA, T. YONEZAWA, and K. GOTO. J. Am. Chem. Soc. **92**, 6651 (1970).
14. D. FORSTER. Inorg. Chem. **12**, 4 (1973).
15. A. ABRAGAM and M. H. L. PRYCE. Proc. R. Soc. London Ser. A. **206**, 173 (1951).
16. J. P. JESSON. J. Chem. Phys. **45**, 1049 (1966).
17. B. R. MCGARVEY. J. Chem. Phys. **53**, 86 (1970).
18. A. REUVENI, V. MALATESTA, and B. R. MCGARVEY. Can. J. Chem. **55**, 70 (1977).
19. M. L. WICHOLAS and R. S. DRAGO. J. Am. Chem. Soc. **90**, 2196 (1968).
20. G. P. FULTON and G. N. LA MAR. J. Am. Chem. Soc. **98**, 2124 (1976).
21. C. SRIVANAVIT and D. G. BROWN. J. Am. Chem. Soc. **98**, 4447 (1976); **100**, 5777 (1978).
22. W. D. HORROCKS, JR. Inorg. Chem. 690 (1970).
23. W. D. HORROCKS, JR. Coord. Chem. Rev. **6**, 147 (1971).
24. R. J. KURLAND and B. R. MCGARVEY. J. Magn. Reson. **2**, 286 (1970).
25. G. N. LA MAR and G. R. VAN HECKE. Inorg. Chem. **9**, 1546 (1970).
26. W. D. HORROCKS, JR., R. C. TAYLOR, and G. N. LA MAR. J. Am. Chem. Soc. **86**, 3031 (1964).
27. J. D. THWAITES and L. SACCONI. Inorg. Chem. **5**, 1029 (1966).
28. A. CHAKRAVORTY, J. P. FENNESSEY, and R. H. HOLM. Inorg. Chem. **4**, 26 (1965).
29. G. N. LA MAR. Mol. Phys. **12**, 427 (1967).
30. I. FUJITA, T. YAZAKI, Y. TORII, and H. KOBAYASHI. Bull. Chem. Soc. Jpn. **45**, 2156 (1972).
31. F. FELIX, J. FERGUSON, H. U. GUDEL, and A. LUDI. J. Am. Chem. Soc. **102**, 4096 (1980); **102**, 4102 (1980).
32. Y. SAITO, J. TAKEMOTO, B. HUTCHINSON, and K. NAKAMOTO. Inorg. Chem. **11**, 2003 (1972).
33. M. WICHOLAS and R. S. DRAGO. J. Am. Chem. Soc. **90**, 6946 (1968).
34. G. N. LA MAR and G. R. VAN HECKE. J. Am. Chem. Soc. **92**, 3021 (1970).
35. G. N. LA MAR and G. R. VAN HECKE. J. Magn. Reson. **4**, 384 (1971).
36. T. MAITANI, M. CHIKUMA, and H. TANAKA. J. Inorg. Nucl. Chem. **41**, 1115 (1979); **41**, 1121 (1979).
37. C. SRIVANAVIT and D. G. BROWN. Inorg. Chem. **14**, 2950 (1975).
38. O. A. GANSOW, P. A. LOEFFLER, R. E. DAVIS, R. E. LENKINSKI, and M. R. WILLCOTT. J. Am. Chem. Soc. **98**, 4250 (1976).
39. F. H. CASE. J. Am. Chem. Soc. **68**, 2574 (1964).
40. W. H. F. SASSE and C. P. WHITTLE. J. Chem. Soc. 1347 (1961).
41. F. KROHNKE. Synthesis, 1 (1976).
42. F. KROHNKE and K. F. GROSS. Chem. Ber. **92**, 24 (1959).
43. P. A. DOBOSH and N. S. OSTLUND. QCPE. **10**, 141 (1969).
44. G. A. BARCLAY, B. F. HOSKINS, and C. H. L. KENNARD. J. Chem. Soc. 5691 (1963).
45. A. CARRINGTON and A. D. MCLACHLAN. Introduction to magnetic resonance. Harper and Row, New York. 1967.
46. A. WADA, N. SAKABE, and J. TANAKA. Acta Crystallogr. Sect. B, **32**, 1121 (1976).
47. G. J. KRUGER and E. C. REYNHARDT. Acta Crystallogr. Sect. B, **30**, 822 (1974).
48. J. P. JESSON. J. Chem. Phys. **47**, 579 (1967).
49. J. P. JESSON. NMR of paramagnetic molecules, principles and applications. *Edited by* G. N. La Mar, W. D. Horrocks, Jr., and R. H. Holm. Academic Press, New York. 1973. Chapt. 1.
50. A. B. P. LEVER. J. Chem. Educ. **51**, 612 (1974).
51. H. M. MCCONNELL. J. Chem. Phys. **24**, 632 (1956); **24**, 764 (1956).
52. G. N. LA MAR. NMR of paramagnetic molecules, principles and applications. *Edited by* G. N. La Mar, W. D. Horrocks, Jr., and R. H. Holm. Academic Press, New York. 1973. Chapt. 3.
53. T. J. BATTERHAM. NMR spectra of simple heterocycles. Wiley-Interscience, New York. 1972. p. 28.
54. W. L. JOLLY. The synthesis and characterization of inorganic compounds. Prentice-Hall, NJ. 1970.

Can. J. Chem. Downloaded from www.nrcresearchpress.com by 210.87.254.105 on 09/06/12
For personal use only.

Etude d'interactions moléculaires en solution par analyse de la relaxation quadripolaire du deutérium. II.[1] Associations de l'albumine sérique de bœuf en solution aqueuse

YVES VAN HAVERBEKE, ANDRÉ MAQUESTIAU, ROBERT MULLER ET LUCE VANDER ELST[2]
Département de chimie organique, Université de l'Etat, 7000 Mons, Belgique

Reçu le 19 novembre 1980

YVES VAN HAVERBEKE, ANDRÉ MAQUESTIAU, ROBERT MULLER et LUCE VANDER ELST. Can. J. Chem. **59**, 1701 (1981).

Les associations de plusieurs substances organiques avec de l'albumine sérique de bœuf (BSA) ont été analysées soit par l'étude directe de leur affinité pour la macromolécule, soit par le biais de leur compétition vis à vis d'un équilibre de référence. Cette dernière méthode évite l'enrichissement isotopique de la drogue à tester.

L'examen de l'influence du pH sur l'association de la pyridine-d_5 et de l'albumine sérique permet de préciser la nature de l'interaction. Plusieurs aspects des procédures de mesures sont discutés.

YVES VAN HAVERBEKE, ANDRÉ MAQUESTIAU, ROBERT MULLER, and LUCE VANDER ELST. Can. J. Chem. **59**, 1701 (1981).

Deuterium longitudinal relaxation time is used for assessing the interaction between bovine serum albumin (BSA) and some drugs. The study of unenriched compounds by means of a reference equilibrium is successfully applied.

The deuterium relaxation rate of pyridine versus the pH profile allows a better understanding of the nature of the interactions. Some experimental aspects are discussed.

Introduction

Parmi l'éventail des méthodes d'investigation de la dynamique moléculaire, la relaxation nucléaire occupe une position privilégiée. Cependant, tandis que l'intérêt revêtu par le phénomène apparaît clairement, le choix du noyau et des procédures expérimentales appropriés à l'examen d'un système donné relève souvent du cas d'espèce. Les noyaux quadripolaires dont la relaxation est généralement dominée par un seul mécanisme se prêtent particulièrement bien à l'approche des mobilités et des associations moléculaires. Ainsi, Baldeschwieler et coll. (1–3), ont-ils étudié les structures et associations de quelques protéines par examen de la relaxation transversale du ^{35}Cl dans des systèmes marqués par des groupes chloromercuriques.

Le noyau de deutérium qui possède une constante de couplage quadripolaire relativement faible peut être examiné au sein d'un lien covalent. Les divers avantages que présente l'étude de la relaxation de ce noyau dans le cadre de la dynamique moléculaire ont été démontrés par plusieurs auteurs (4–12).

Dans le présent travail, nous examinons les interactions entre petites molécules organiques et l'albumine sérique de bœuf (BSA) par extension des procédures appliquées au cours d'une étude antérieure (12). Notre choix s'est porté sur cette macromolécule en raison de l'important rôle de vecteur qu'elle assure vis à vis de très nombreuses substances chimiques.

[1]Pour la première partie, voir réf. 12.

[2]Titulaire d'un mandat d'aspirant au F.N.R.S.

Partie expérimentale

1. *Appareillage*

Les spectres de rmn du ^2H sont relevés à 9,2 MHz à la température de 30 ° ± 1°C, sur un appareil Bruker WP-60 équipé d'un calculateur Nicolet-BNC-12 (8K données, 4K programme).

Les solutions sont contenues soit dans des tubes de 8 mm concentriques à des tubes de 10 mm renfermant de l'hexafluorobenzène utilisé pour la stabilisation champ-fréquence (lock ^{19}F), soit dans des tubes de 10 mm, la stabilisation champ-fréquence est alors assurée par un lock ^2H externe.

Tous les signaux de précession libre sont enregistrés sur 1K mémoire et la transformé de Fourier est effectuée sur 4K (zero filling).

Les séquences d'impulsions utilisées sont les séquences d'inversion–récupération (IRFT et FIRFT) décrites par Freeman et Hill (13), et Canet *et al.* (14); la durée de l'impulsion nécessaire à l'inversion de la magnétisation est égale à 21 μs. Les valeurs de T_1 sont calculées par régression linéaire sur la droite de $\ln (M_\infty - M_\tau)$ en fonction de τ et sont reproductibles à ±5%.

Le pH des solutions est mesuré avant et après chaque série de mesures au moyen d'un appareil Metrohm type E 353 B équipé d'une électrode Orion (91-15).

2. *Produits*

La pyridine-d_5, le 1,4-dioxanne-d_8 et l'acétonitrile-d_3 sont des produits commerciaux (Merck). Le sulfacétamide est synthétisé suivant la méthode de Bretschneider et Klotzer (15) par acylation du sulfanilamide (16). Le *N*-acétyl-d_3-benzènesulfonamide est obtenu par addition de chlorure d'acétyle-d_3 sur le benzènesulfonamide (17).

Deux lots d'albumine sérique sont utilisés; ils proviennent des firmes Cabiochem Behring (cat no. 12659, pureté électrophorétique >95%) et Boehringer-Mannheim (cat no. 238031, électrophorétiquement pure Mol. Wt.: 68 000) et seront dénommés respectivement lot I et lot II dans la suite du texte.

3. *Préparation des échantillons*

Le tampon utilisé est le tris(hydroxyméthyl) aminométhane. Une série de mesures effectuées sur des solutions tamponnées au dihydrogénophosphate de potassium a montré que la nature du tampon ne jouait aucun rôle. Le pH des solutions est compris

0008-4042/81/121701-04$01.00/0

©1981 National Research Council of Canada/Conseil national de recherches du Canada

Can. J. Chem. Downloaded from www.nrcresearchpress.com by 210.87.254.5 on 09/06/12
For personal use only.

entre 7,4 et 8,2. Les échantillons sont préparés par mélange de solutions stock de macromolécule et de drogues; leur volume total est égal à 1 mL. Pour les mesures à pH variable, le pH est ajusté par addition de solutions de NaOH et HCl.

Résultats expérimentaux et discussion

La vitesse de relaxation longitudinale observée pour un noyau de deutérium situé au sein d'un substrat S de petite taille interagissant, de manière réversible et rapide, avec une macromolécule A dont la concentration est très inférieure à celle du substrat vaut (18, 19):

$$[1] \quad \frac{1}{T_1^{obs}} = \frac{a^0}{K_D + s^0}\frac{1}{T_1^c} + \frac{1}{T_1^1}$$

avec $a°$: concentration totale en macromolécule; $s°$: concentration totale en substrat; K_D: constante de dissociation de l'équilibre $A + S \rightleftharpoons AS$; T_1^c: T_1 du noyau au sein de la molécule complexée; T_1^1: T_1 du noyau au sein de la molécule libre et $T_1^c \ll T_1^1$; T_1^{obs}: T_1 observé.

A $s°$ constante, la vitesse de relaxation observée varie linéairement en fonction de la concentration totale en macromolécule. Grâce à un minimum de deux séries de mesures à concentrations totales en drogue différentes, il est donc possible de déterminer K_D et T_1^c par la pente des droites expérimentales (méthode à $s°$ constante).

Par transformation de l'éq. [1], on obtient la relation [2]:

$$[2] \quad \left(\frac{1}{T_1^{obs}} - \frac{1}{T_1^1}\right)^{-1} = \frac{K_D}{a^0}T_1^c + \frac{s^0}{a^0}T_1^c$$

A $a°$ constante et moyennant une détermination préalable de la vitesse de relaxation de la drogue en l'absence de protéine, la pente de la droite de $(1/T_1^{obs} - 1/T_1^1)^{-1}$ en fonction de $s°$ fournit le temps de relaxation du complexe tandis que l'ordonnée à l'origine permet de calculer la constante de dissociation (méthode à $a°$ constante).

Les résultats obtenus pour l'équilibre pyridine-d_5/BSA (lot I) sont très voisins quelle que soit la méthode employée (tableau 1 et figs. 1 et 2). La valeur du T_1^c déterminée expérimentalement concorde bien avec celle que l'on estime grossièrement par la relation de Stokes–Einstein sur base du rapport des masses des entités libres et complexées.

Pour le *N*-acétyl-d_3-benzènesulfonamide, la différence sensible entre les T_1^c calculés par le rapport des masses et observés est due à la rotation indépendante du groupe méthyle sur lequel porte la mesure. L'erreur commise au niveau des temps de corrélation se répercute sur la valeur de K_D.

La méthode de détermination des T_1^c et K_D à $a°$ constante s'étant avérée plus rapide et précise, son utilisation a été généralisée pour la suite de l'étude des équilibres simples.

Trois séries de mesures effectuées sur un échantillon différent de BSA (lot II) témoignent de façon reproductible d'une interaction plus faible avec la pyridine-d_5. Cette différence de comportement doit être mise en rapport avec le degré de pureté des deux lots d'albumine.

Les interactions du 1,4-dioxanne-d_8 et de l'acétonitrile-d_3 sont, quant à elles, nettement plus faibles que celles enregistrées pour la pyridine-d_5.

Equilibres compétitifs

Dans un travail précédent (12), nous avons montré qu'il est possible de caractériser l'interaction d'un compétiteur quelconque (C) avec une entité déterminée (A) en mesurant simplement la perturbation que ce compétiteur provoque sur un équilibre de référence (A + S).

Un traitement analogue à celui utilisé pour les équilibres simples permet d'obtenir une relation linéaire entre l'inverse de l'accroissement de la vitesse de relaxation du substrat et la concentration en compétiteur lorsque les quantités $a°$ et $s°$ sont maintenues constantes (éq. [3]).

$$[3] \quad \left(\frac{1}{T_1^{obs}} - \frac{1}{T_1^1}\right)^{-1} = \frac{K_{D_1} + s^0}{a^0}T_1^c + \frac{c^0}{a^0}\frac{K_{D_1}}{K_{D_2}}T_1^c$$

K_{D_1}: constante de dissociation de l'équilibre de référence; K_{D_2}: constante de dissociation de l'équilibre de compétition; $c°$: concentration totale en compétiteur.

Si l'on a déterminé indépendamment l'un des deux paramètres de l'équilibre de référence (T_1^c ou K_{D_1}), la pente et l'ordonnée à l'origine du graphique de $(1/T_1^{obs} - 1/T_1^1)^{-1}$ en fonction de la quantité de compétiteur ajoutée permettent le calcul de l'autre paramètre (K_{D_1} ou T_1^c) et celui de la constante de dissociation de l'équilibre compétitif.

Pour tous les systèmes étudiés, on observe une augmentation du temps de relaxation longitudinal du substrat (S), la pyridine-d_5, lors de l'addition de *N*-acétyl-d_3-benzènesulfonamide, de sulfacétamide, de 1,4-dioxanne-d_8 ou d'acétonitrile-d_3. Ceci témoigne de l'existence d'une interaction compétitive des deux ligands pour la macromolécule. On peut également envisager que l'association avec le compétiteur modifie la structure de la protéine d'une manière néfaste à la liaison avec le substrat.

Tant pour l'équilibre de référence relatif à l'association pyridine-d_5/albumine que pour les inter-

Can. J. Chem. Downloaded from www.nrcresearchpress.com by 210.87.254.5 on 09/06/12
For personal use only.

TABLEAU 1. T_1^c et K_D pour les équilibres simples

	Méthode à $s°$ constante		Méthode à $a°$ constante	
	T_1^c (s)	K_D (mol L^{-1})	T_1^c (s)	K_D (mol L^{-1})
Pyridine-d_5/BSA (lot I)	$5{,}2\ 10^{-4}$ $(7{,}4\ 10^{-4})^j$	$(5{,}0 \pm 3{,}2)10^{-2a}$	$(4{,}3 \pm 0{,}5)10^{-4}$ $(7{,}4\ 10^{-4})^j$	$(6{,}8 \pm 1{,}4)10^{-2b}$
N-acétyl-d_3-benzènesulfonamide/BSA (lot I)	$4{,}2\ 10^{-4}$ $(26{,}3\ 10^{-4})^j$	$(11{,}3 \pm 10{,}2)10^{-2c}$	$(11{,}4 \pm 1{,}0)10^{-4}$ $(26{,}3\ 10^{-4})^j$	$(1{,}7 \pm 0{,}6)10^{-2d}$
Pyridine-d_5/BSA (lot II)			$(1{,}2 \pm 0{,}4)10^{-4}$ $(1{,}2 \pm 0{,}3)10^{-4}$ $(1{,}4 \pm 0{,}4)10^{-4}$ $(7{,}4\ 10^{-4})^j$	$(17{,}9 \pm 7{,}6)10^{-2e}$ $(18{,}8 \pm 6{,}0)10^{-2f}$ $(14{,}4 \pm 5{,}2)10^{-2g}$
1,4-dioxanne-d_8/BSA (lot II)			$(6{,}4 \pm 2{,}4)10^{-4}$ $(9{,}4\ 10^{-4})^j$	$(34{,}7 \pm 17{,}6)10^{-2h}$
Acétonitrile-d_3/BSA (lot II)			$(26{,}1 \pm 28{,}0)10^{-4}$ $(37{,}4\ 10^{-4})^j$	$(53{,}9 \pm 67{,}0)10^{-2i}$

[a] Voir Fig. 1.
[b] Voir Fig. 2.
[c] $s_1° = 2{,}78\ 10^{-2}$ mol L^{-1} et $a° (0 \rightarrow 9{,}30)10^{-4}$ mol L^{-1}; $s_2° = 6{,}50\ 10^{-2}$ mol L^{-1} et $a° = (0 \rightarrow 10{,}30)10^{-4}$ mol L^{-1}.
[d] $a° = 9{,}01\ 10^{-4}$ mol L^{-1} et $s° = (2{,}88 \rightarrow 10{,}00)10^{-2}$ mol L^{-1}.
[e] $a° = 3{,}90\ 10^{-4}$ mol L^{-1} et $s° = (3{,}10 \rightarrow 12{,}50)10^{-2}$ mol L^{-1}.
[f] $a° = 4{,}05\ 10^{-4}$ mol L^{-1} et $s° = (2{,}50 \rightarrow 18{,}75)10^{-2}$ mol L^{-1}.
[g] $a° = 4{,}43\ 10^{-4}$ mol L^{-1} et $s° = (2{,}50 \rightarrow 12{,}50)10^{-2}$ mol L^{-1}.
[h] $a° = 5{,}26\ 10^{-4}$ mol L^{-1} et $s° = (2{,}50 \rightarrow 15{,}00)\ 10^{-2}$ mol L^{-1}.
[i] $a° = 6{,}52\ 10^{-4}$ mol L^{-1} et $s° = (3{,}80 \rightarrow 19{,}00)10^{-2}$ mol L^{-1}.
[j] Valeurs de T_1^c déterminées par le rapport des masses.

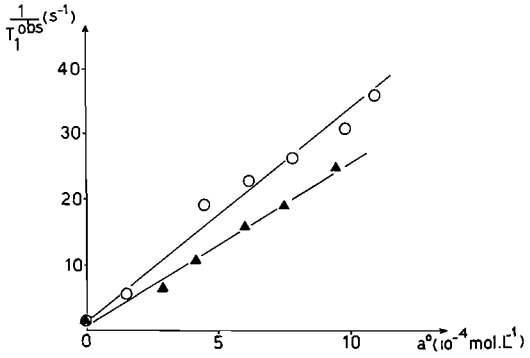

FIG. 1. Variation de $1/T_1^{obs}$ en fonction de $a°$ à $s°$ constante pour le système pyridine-d_5/BSA (lot I); ○: $s° = 1{,}25\ 10^{-2}$ mol L^{-1}; ▲: $s° = 2{,}50\ 10^{-2}$ mol L^{-1}.

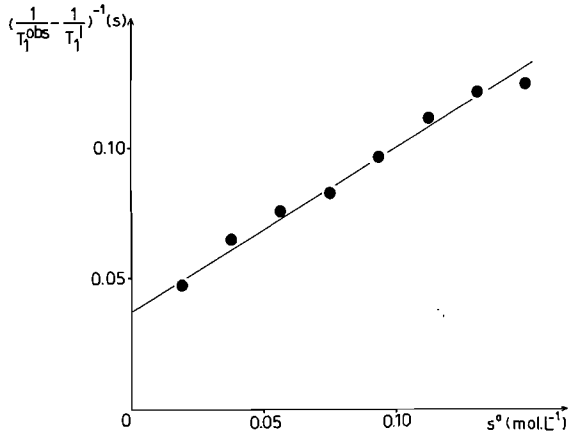

FIG. 2. Variation de $(1/T_1^{obs} - 1/T_1^l)^{-1}$ en fonction de $s°$ à $a°$ constante pour le système pyridine-d_5/BSA (lot I); ●: $a° = 7{,}12\ 10^{-4}$ mol L^{-1}.

actions compétitives, les valeurs de K_D obtenues ici concordent très bien avec celles qui ont été déterminées plus haut (tableaux 1 et 2). Vis à vis de cet équilibre de référence, le *N*-acétyl-d_3-benzènesulfonamide, le 1,4-dioxanne-d_8 et l'acétonitrile-d_3 sont des compétiteurs "faibles" contrairement au sulfacétamide.

Influence du pH

La figure 3 représente la variation de la vitesse de relaxation d'une solution pyridine-d_5/BSA en fonction du pH. La courbe présente vers pH 5,25, un point d'inflexion correspondant au pK_a de la pyridine. Le temps de relaxation à pH 2 est égal à celui de la pyridine-d_5 en solution aqueuse de même acidité; on peut donc admettre que l'ion pyridinium n'interagit pratiquement pas avec l'albumine.

La vitesse de relaxation est maximale dans une zone de pH s'étendant de 7 à 9. Ceci reflète une meilleure fixation à la protéine et non un phénomène d'agrégation des macromolécules puisque le palier se situe dans une zone de pH nettement supérieure au pH isoélectrique de la protéine (pI ≃ 4.7).

Enfin, la diminution importante de la vitesse de relaxation observée pour les pH supérieurs à 9, correspond à la déprotonation des groupements $NH_3^{(+)}$ et OH des acides aminés à chaîne latérale basique (lysine, histidine, arginine, tyrosine) qui

Can. J. Chem. Downloaded from www.nrcresearchpress.com by 210.87.254.5 on 09/06/12
For personal use only.

TABLEAU 2. T_1^c et constantes de dissociation des équilibres compétitifs

Compétiteur	T_1^c (s)[a]	K_{D_1} (mol L^{-1})	K_{D_2} (mol L^{-1})
N-acétyl-d_3-benzènesulfonamide[b,d]	$(4,3 \pm 0,5)10^{-4}$	$(6,0 \pm 1,4)10^{-2}$	$(9,0 \pm 4,9)10^{-2}$
Sulfacétamide[c,e]	$(1,2 \pm 0,3)10^{-4}$	$(17,9 \pm 8,9)10^{-2}$	$(14,9 \pm 11,7)10^{-2}$
1,4-dioxanne-d_8[c,f]	$(1,2 \pm 0,3)10^{-4}$	$(17,1 \pm 8,1)10^{-2}$	$(21,7 \pm 32,2)10^{-2}$
Acétonitrile-d_3[c,g]	$(1,2 \pm 0,3)10^{-4}$	$(17,3 \pm 6,8)10^{-2}$	$(115,9 \pm 192,0)10^{-2}$

[a] T_1^c déterminé par la méthode à $a°$ constante employée pour les équilibres simples.
[b] BSA: lot I.
[c] BSA: lot II.
[d] $a° = 4,24\ 10^{-4}$ mol L^{-1}, $s° = 2,50\ 10^{-2}$ mol L^{-1}, $c° = (0,00 \rightarrow 14,00)10^{-2}$ mol L^{-1}.
[e] $a° = 4,43\ 10^{-4}$ mol L^{-1}, $s° = 12,50\ 10^{-2}$ mol L^{-1}, $c° = (0,00 \rightarrow 13,00)10^{-2}$ mol L^{-1}.
[f] $a° = 5,26\ 10^{-4}$ mol L^{-1}, $s° = 12,50\ 10^{-2}$ mol L^{-1}, $c° = (0,00 \rightarrow 12,00)10^{-2}$ mol L^{-1}.
[g] $a° = 6,52\ 10^{-4}$ mol L^{-1}, $s° = 10,00\ 10^{-2}$ mol L^{-1}, $c° = (0,00 \rightarrow 36,00)10^{-2}$ mol L^{-1}.

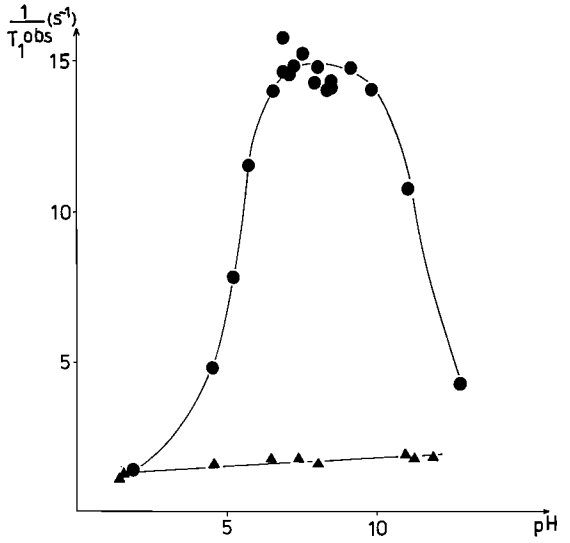

FIG. 3. Variation de $1/T_1^{obs}$ du système pyridine-d_5/BSA (lot II) en fonction du pH; ●: pyridine-d_5/BSA, $a° = 4,40\ 10^{-4}$ mol L^{-1}, $s° = 10,00\ 10^{-2}$ mol L^{-1}; ▲: pyridine-d_5 (deutérium en γ) $s° = 5,00\ 10^{-2}$ mol L^{-1}.

représentent 28% de la composition totale de l'albumine sérique de bœuf (20).

Conclusions

L'analyse de la relaxation nucléaire du deutérium peut être considérée, à plusieurs titres, comme une excellente méthode d'approche de la dynamique moléculaire. Le présent travail démontre l'efficacité de la démarche dans le cadre d'une application à l'étude d'associations en phase aqueuse.

Il est important de remarquer que l'affinité d'un substrat quelconque pour une macromolécule peut être rapidement appréciée, notamment par le biais de sa compétition avec un équilibre de référence. Cette procédure qui rend superflu le marquage isotopique du substrat peut s'avérer particulièrement rentable pour des études systématiques portant sur des séries de composés.

Il convient enfin de souligner que les valeurs observées dépendent étroitement du degré de pureté du matériel biologique utilisé.

1. T. R. STENGLE et J. D. BALDESCHWIELER. Proc. Natl. Acad. Sci. U.S.A. **55**, 1020 (1966).
2. P. HAUGLAND, L. STRYER, T. R. STENGLE et J. D. BALDESCHWIELER. Biochemistry, **6**, 498 (1967).
3. T. R. STENGLE et J. D. BALDESCHWIELER. J. Am. Chem. Soc. **89**, 3045 (1967).
4. H. H. MANTSCH, H. SAITO et I. C. P. SMITH. Prog. Nucl. Magn. Reson. Spectrosc. **11**, 211 (1977).
5. M. A. BERNSTEIN, L. D. HALL et W. E. HULL. J. Am. Chem. Soc. **101**, 2744 (1979).
6. CH. BREVARD, J. P. KINTZINGER et J. M. LEHN. Tetrahedron, **28**, 2429 (1972).
7. D. E. WOESSNER, B. S. SNOWDEN JR., et E. STROM. Mol. Phys. **14**, 265 (1968).
8. T. T. BOPP. J. Chem. Phys. **47**, 3621 (1967).
9. J. A. GLASEL, V. J. HRUBY, J. F. MCKELVY et A. F. SPATOLA. J. Mol. Biol. **79**, 555 (1973).
10. W. EGAN. J. Am. Chem. Soc. **98**, 4091 (1976).
11. K. J. NEUROHR, N. LACELLE, H. H. MANTSCH et I. C. P. SMITH. Biophys. J. **32**, 931 (1980).
12. Y. VAN HAVERBEKE, A. MAQUESTIAU, R. N. MULLER et L. VANDER ELST. Spectrochim. Acta, Part A, **36**, 627 (1980), et références incluses.
13. R. FREEMAN et H. D. W. HILL. J. Chem. Phys. **53**, 4103 (1971).
14. D. CANET, G. C. LEVY et I. R. PEAT. J. Magn. Reson. **18**, 199 (1975).
15. H. BRETSCHNEIDER et W. KLOTZER. Chem. Abstr. **50**, 15542 (1956).
16. R. M. ROBERTS, J. C. GILBERT, L. B. RODEWALD et A. S. WINGROVE. An introduction to modern experimental organic chemistry. Holt, Rinehart and Winston Inc., New York. 1969.
17. T. DEWING, W. H. GRAY, B. C. PLATT et D. STEPHENSON. J. Chem. Soc. 239 (1942).
18. O. JARDETZKY et N. G. WADE-JARDETZKY. Mol. Pharmacol. **1**, 214 (1965).
19. M. SARRAZIN, J. C. SARI, M. BOURDEAUX-PONTIER et C. BRIAND. Mol. Pharmacol. **15**, 71 (1979).
20. T. W. PUTNAM. *Dans* The proteins. Vol. III. *Edité par* H. Neurath. Academic Press, New York. 1965. Chapt. 14.

Can. J. Chem. Downloaded from www.nrcresearchpress.com by 210.87.254.5 on 09/06/12
For personal use only.

Ion exchange properties of trialkylammonium salts

MICHEL GÉRIN AND JAMES FRESCO[1]
Department of Chemistry, McGill University, Montreal, P.Q., Canada, H3A 2K6
Received February 25, 1981[2]

MICHEL GÉRIN and JAMES FRESCO. Can. J. Chem. **59**, 1705 (1981).

Two phase acid–base titrations of amines from tributyl to tridodecyl and their salts have been performed for the nitrobenzene–water system. Hydrolysis constants were determined and from these anion-exchange constants were calculated. For these series of salts values of hydrolysis and anion-exchange constants were independent of the amine and strongly influenced by the nature of the anions.

MICHEL GÉRIN et JAMES FRESCO. Can. J. Chem. **59**, 1705 (1981).

Dans un système biphase nitrobenzène–eau on a effectué des titrages acide–base d'amines et de leurs sels allant de tributyl à tridodecyl. On a déterminé les constantes d'hydrolyse et on en a déduit les constantes d'échange anionique. Pour ces séries de sels les constantes d'hydrolyse et d'échange anionique sont indépendantes de l'amine et fortement dépendantes de la nature de l'anion.

Introduction

To date studies of phase transfer catalysts have been focussed most usually on crown ethers and quaternary ammonium salts. Recently tridodecylammonium bisulphate has been used as a phase transfer reagent in inorganic synthesis for the first time (1). That differences in phase transfer properties exist between tetraalkylammonium ions and comparable trialkylammonium ions is suggested by the stability of their simple salts. Formation constants of salts of the latter ion are at least 100 times greater than the former, when the alkyl is butyl (2).

Values of partition constants have been reported (3) for a series of low to medium molecular weight tertiary alkylammonium salts of the type R_3NHX. These values were combined with dissociation constants, K_d, established in nitrobenzene (2) to provide partition coefficients, K_p, for the nitrobenzene–water system. Partition constants were not obtainable beyond alkyl chain lengths of five or six. In addition, conductivity measurements of the most concentrated nitrobenzene solutions of the salts indicated the possibility of triple-ion aggregation.

It is possible (4–7) to compare properties of higher molecular weight tertiary ammonium salts on the basis of two-phase equilibria of the type

$$\overline{R_3NHX} \rightleftarrows \overline{R_3N} + H^+ + X^-$$

The corresponding hydrolysis constant, K, representing the inverse of the formation constant of the salt from the organic dissolved amine and aqueous acid, has been evaluated by several methods (8). The two-phase emf titration technique (9, 10) and subsequent slope analysis of a log–log plot of the data (11) provide a rapid description of the nature of solute aggregation. This approach has been applied here to higher molecular weight salts from tributylammonium perchlorate to the tridodecylamine halides.

Experimental

Aqueous Solutions

After drying potassium halides at 120°C, stock molar aqueous solutions of KCl, KBr, KI, $NaClO_4$, HCl, HBr, HI, and $HClO_4$ were prepared. The molarity of the sodium perchlorate stock solution was determined by titration of the acid equivalent displaced on a cation exchange resin (12). A standardized decimolar NaOH solution was used to determine the normalities of the aqueous acids. The NaOH solution was prepared from a carbonate-free 50% solution. The carbonate was removed from a stock KOH solution (ca. 1.5 *M*) by addition of small quantities of concentrated $BaCl_2$ solutions until no more precipitate formed. After filtration through glass fibres, alkali solutions were stored in polyethylene bottles and protected from atmospheric carbon dioxide during delivery. Primary standard potassium hydrogen phthalate was used for standardization.

All other solutions were prepared by dilution of the stock solutions and when necessary their normalities were checked by standard methods. Water used to prepare solutions was distilled, deionized, and boiled shortly before use, and saturated with nitrobenzene at room temperature.

Organic Solutions

Organic trialkylammonium salt solutions of sixteen different salts were prepared. These were the chlorides, bromides, iodides, and perchlorates of tridodecylammonium, TLA, to tributylammonium, TBA, with the exceptions of TBAHCl, TBAHBr, TBAHI, and tripentylammonium chloride, TPTAHCl. The preparation of trialkylammonium salts and the purification of trialkylamines and nitrobenzene have been described (3). Solutions were prepared by either direct dissolution of the salt or solvent extraction from the organic amine solution. These were identical to procedures previously described (2). The decimolar solutions were standardized by potentiometric titration with ethanolic KOH. Centimolar and millimolar solutions were prepared by dilution.

Organic decimolar trialkylamine solutions were prepared by

[1]Author to whom correspondence may be addressed.

[2]Manuscript originally received March 27, 1980 but was misplaced due to clerical error.

0008-4042/81/121705-06$01.00/0
©1981 National Research Council of Canada/Conseil national de recherches du Canada

Can. J. Chem. Downloaded from www.nrcresearchpress.com by 210.87.254.5 on 09/06/12
For personal use only.

Can. J. Chem. Downloaded from www.nrcresearchpress.com by 210.87.254.5 on 09/06/12
For personal use only.

direct dissolution of the purified amines. Pipettes were not used to deliver volumes of these solutions since these were found to deliver unevenly. Known quantities were thus transferred gravimetrically. The decimolar solutions were standardized by titration with $HClO_4$ in acetic acid. The procedure used was the same as the one described for amines (3).

Potential Measurements

The electrodes used were a Beckman double shielded 39000 glass electrode and a Fisher calomel electrode #13-639-51. The originally saturated calomel electrode was modified to a 1 *M* KCl calomel electrode.

The calomel electrode was separated from the solution in which a potential measurement was to be done by a salt bridge of 1 *M* KCl provided by a Remote Reference Junction (Fisher #13-639-55). The reference electrode was placed ca. one foot above the solution, dipping three cm in a 125 mL separatory funnel connected by the stem to the remote reference through Tygon tubing. The funnel, tubing, and remote reference were filled with 1 *M* KCl solution. The hydrostatic head gave improved stability to the flow of electrolyte in the porous ceramic plug serving as liquid junction between the salt bridge and the solution. Stable potentials could be read with a reproducibility of ± 0.2 mV shortly after inserting the solutions.

The potential of the electrode pair was measured using a Fisher Accumet pH meter Model 320 with expanded scale. The expanded mV scale only was used and calibrated using a precision potentiometer (Leeds and Northrup Volt Potentiometer #8687). Overlap of the different scales was adjusted. The meter was found not to be perfectly linear in the low mV range.

Experimental Procedure

The two-phase emf titrations were carried out in a 100-mL jacketed beaker maintained at 25.0°C by circulation of thermostated water. A 50 mL volume of aqueous constant ionic strength (0.1 *M* KCl, KBr, KI, or $NaClO_4$) solution was pipetted into the beaker which was later covered with a lid to maintain a nitrogen blanket. The solution was agitated for 30 min in order to degas. The organic phase was then introduced, usually by means of a 10 mL pipette. Decimolar amine solutions were transferred directly from their flasks and the volume calculated by weight difference. The electrodes were introduced through holes in the lid. The titrant was added from a burette, the tip of which was inserted in another hole in the lid.

For each salt six titrations were performed covering approximately three decades of total organic salt concentrations from 10^{-1} to 10^{-4} *M*. Three titrations were performed by titrating the amine in nitrobenzene with aqueous acidic titrant and have been referred to as direct titrations elsewhere. Three titrations involved titrating the ammonium salt in nitrobenzene with base and were described as reverse titrations. The three titrations covered an organic amine or salt concentration which was successively decimolar, centimolar, and millimolar. For each titration five points were usually recorded, i.e. at 10%, 20%, 40%, 60%, and 80% of equivalence.

After addition of titrant the two phases were mixed by means of a magnetic bar immersed in the lower organic phase. Equilibrium was attained when the potential reached a stable value. The speed of rotation of the stirrer had no significant influence on the equilibrium potential reading. It had, however, an influence on the equilibration time. A high enough rotation speed was adopted so that equilibrium could be reached in less than one hour for each point. The two phases never formed a stable emulsion and separated quickly into two transparent phases when stirring was stopped.

For the various 0.1 *M* aqueous salt solutions the potential of the glass – reference electrode pair was found to conform to the equation, $E = E_A^0 + 59.16 \log [H^+]$. The constant E_A^0 was determined before and after every titration by measuring the potential of an appropriate standard acid solution. Values for the ion product of water in each aqueous salt medium were established according to Liberti and Light (13).

Calculations

Values of the total concentration of ammonium salt (ion-paired, dissociated, or aggregated) in the organic phase, $[\overline{R_3NHX}]_T$, and $[\overline{R_3N}][H^+][X^-]$ are related through the concentration quotient, Q', expressed in logarithms as $\log [\overline{R_3NHX}]_T = \log [\overline{R_3N}][H^+][X^-] - \log Q'$. In the region where the salt exists essentially as an ion-pair a plot of the first term versus the second term of the preceding equation will be a straight line of slope one. A straight line of slope ½ is obtained for the case of a completely dissociated salt. Where the salt exists as a dimer in the organic phase, the slope of the plot would be two.

Proceeding from low concentrations the shape of a log–log plot reflects changing solute conditions from, for example, dissociated ions to ion-pairs to dimers etc. Values for the concentration quotient, Q', are determined from two phase titration data. After replacing $\overline{R_3NHX}_T$ by $\overline{R_3NHX}$ a corrected quotient, Q, is obtained. The relationship between Q and K is $K = Q\,\gamma_\pm^2$ where $\gamma_\pm$ is the mean activity coefficient of HX.

For each point in a two-phase emf titration the quantities $[\overline{R_3NHX}]_T$, $[\overline{R_3N}]$, $[H^+]$, and $[X^-]$ can be determined from the potential measurement and the initial concentrations: the total concentration of amine, c_B^0 (or ammonium salt, c_A^0) in the organic phase of volume V_{org} and the alkali metal salt concentration c of MX in the aqueous phase of volume V_{aq}^0. A known volume V_{add} of titrant of known composition is added and the concentration of H^+ ions in the aqueous phase is determined by the potentiometric measurement. The number of mequiv. of acid (or base) introduced by the titrant was denoted as n_{H^+} (or n_{OH^-}) and $V_{aq} = V_{aq}^0 + V_{add}$.

The following expressions can be deduced for direct titrations:

$$[1]\quad \overline{[R_3N]} = c_B^0 - \frac{n_{H^+}}{V_{org}} + \frac{V_{aq}}{V_{org}}\{[H^+] - [OH^-]\}$$

$$[2]\quad \overline{[R_3NHX]}_T = \frac{n_{H^+}}{V_{org}} - \frac{V_{aq}}{V_{org}}\{[H^+] - [OH^-]\}$$

$$[3]\quad [X^-] = c + [H^+] - [OH^-]$$

In the reverse titration of the organic ammonium salt by aqueous alkali, eqs. [1] and [2] are changed to:

$$[4]\quad \overline{[R_3N]} = \frac{n_{OH^-}}{V_{org}} + \frac{V_{aq}}{V_{org}}\{[H^+] - [OH^-]\}$$

$$[5]\quad \overline{[R_3NHX]}_T = c_A^0 - \frac{n_{OH^-}}{V_{org}} - \frac{V_{aq}}{V_{org}}\{[H^+] - [OH^-]\}$$

In the cases described above the ammonium salt is considered absent from the aqueous phase. However, for some medium and low molecular weight species a significant fraction of the ammonium salt might migrate to the aqueous phase.

Constants, K_p, representative of the equilibrium $\overline{R_3NHX} \rightleftarrows R_3NH^+ + X^-$ have been reported previously (3). The partition ratio $[R_3NH^+]/[\overline{R_3NHX}]_T$ of salt between nitrobenzene and the aqueous phase can be equated to $K_p/\gamma_\pm^2\, c$ and the percentage loss of organic salt to the aqueous phase to $100\, K_p V_{aq}/\gamma_\pm^2 V_{org}\, c$, i.e. ca. $8000\, K_p$. If an error of 1% (corresponding to the potentiometric error of 0.2 to 0.3 mV) is incurred, the maximum value of K_p, acceptable before appreciable loss of organic salt to the aqueous phase occurs, is seen to be: $K_p = 1/8000 = 1.25 \times$

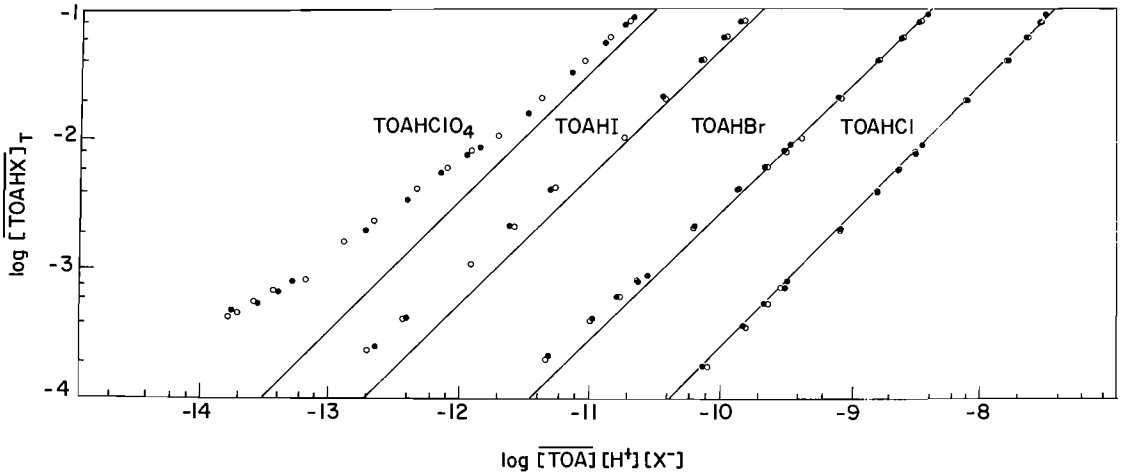

FIG. 1. Log–log plots of two phase titration measurements for trioctylamine salts, TOAHX, where X denotes ClO_4, I, Br, and Cl. Solid and open circles represent values obtained by direct and reverse titrations respectively.

10^{-4}. On this basis the following thirteen salts were considered to be negligibly extracted into the aqueous phase: TLAHCl, TOAHCl, TLAHBr, TOAHBr, THAHBr, TLAHI, TOAHI, THAHI, TPTAHI, $TLAHClO_4$, $TOAHClO_4$, $THAHClO_4$, and $TPTAHClO_4$ where TLAH denotes trilaurylammonium, TOAH trioctylammonium, THAH trihexylammonium, TPTAH tripentylammonium, TBAH tributylammonium, and TPRAH tripropylammonium.

For the other salts of low molecular weight in each series, eqs. [2], [3], and [5] do not apply. Appropriate expressions were derived for these by including K_p. The range of applicability was, however, limited to the less water partitioned salts; THAHCl,TPTAHBr, and $TBAHClO_4$.

In the preceding considerations the assumption was made that the free amine dissolved in the organic phase did not migrate significantly to the aqueous phase. This was verified for tripropylamine. The constant corresponding to the equilibrium $\overline{R_3N} \rightleftarrows R_3N$ was measured to be ca. 10^{-3}. Constants for higher molecular weight amines were considered to be even smaller and the concentration of free amine in the aqueous phase to be in all cases negligible.

The partition of MX between the aqueous medium and the nitrobenzene phase was disregarded since conductivity measurements performed on nitrobenzene phases equilibrated with 0.1 *M* aqueous solutions of $NaClO_4$, KI, KBr, or KCl showed the concentration of ionized inorganic salt in nitrobenzene was negligible in all cases.

Results

Log–log plots for the trioctylammonium salts which appear in Fig. 1 are typical of the results obtained from two phase emf titrations of all the amine salts studied.

In the low concentration decade, 10^{-3} to 10^{-4} *M* in total ammonium salt, drift and oscillations were frequently observed. Drifty values were not recorded and oscillating values were averaged. In the case of the iodide salt solutions systematic drifts towards lower *E* values were observed in the three concentration decades for solutions with *E* values above certain thresholds. This seems to indicate the onset of a decomposition reaction and renders uncertain the values recorded even for the more stable points. It was found that in this system all values would eventually drift in the low concentration ranges (10^{-2} to 10^{-4} *M* total ammonium salt). No attempt was made to clarify the reaction responsible for these drifts. One possibility is oxidation of iodide.

Chloride System

The plots for all R_3NHCl salts were linear with a slope of one. On this basis the solute should exist in the form of an ion-pair over the concentration range studied. No significant dissociation was evident. Values of *Q*, the concentration quotient, were essentially constant from the trihexyl to the tridodecylammonium salt.

Bromide System

Plots for R_3NHBr appeared linear with a slope of one over the 10^{-1} *M* concentration decade. Deviations which appeared in the 10^{-2} *M* decade increased in the 10^{-3} *M* decade. The solute may be considered as ion-paired at higher concentrations and to undergo progressive dissociation in the lower concentration ranges. Values of *Q* determined from the first decade were constant from the tripentyl to the tridodecylammonium salt.

Iodide System

Behaviour similar to that of the bromide system was observed for R_3NHI. However, deviations from a slope one in the lower concentration decades were larger than in the bromide plots, indicating greater dissociation. Values of *Q* determined over the first decade were constant from tripentyl to tridodecyl salts.

Can. J. Chem. Downloaded from www.nrcresearchpress.com by 210.87.254.5 on 09/06/12
For personal use only.

Can. J. Chem. Downloaded from www.nrcresearchpress.com by 210.87.254.5 on 09/06/12
For personal use only.

Perchlorate System

All plots showed similar behaviour. The slope decreased regularly from high to low concentrations of R_3NHClO_4 corresponding to a value close to one to a value close to one-half. Thus ion-pairs seemed to be predominant at high concentration and dissociated ions at low concentrations. The relative positions of the plots at high concentration seemed to indicate that Q values are similar from tributyl to tridodecylammonium perchlorates.

Examination of the region of highest amine salt concentrations on all log–log plots showed that in no system did the experimental curve have a slope significantly larger than one. This indicated no appreciable formation of species of higher molecular weight than the ion-pair occurred in the range of concentration studied.

Since the systems can be represented by two equilibria corresponding to the constants K and K_d, a graphical procedure was devised to obtain preliminary values for the constants. A family of curves was calculated to represent the theoretical log–log plots of a number of systems for a general Q value with varying K_d values. The straight line of slope one represents the system without dissociation; systems with varying K_d values (from 10^{-5} to 7×10^{-3}) increasingly deviate from the straight line. The deviation is small for $K_d = 10^{-5}$ and detectable only at the lowest concentrations. A change in Q value does not change this pattern but shifts the set of curves horizontally on the log–log plot. The set of curves was calculated by an iteration method.

The experimental log–log plots were compared to the standard curves by superimposition. The K_d values obtained for the amine chlorides were $<10^{-5}$, bromides $\sim 5 \times 10^{-5}$, iodides $\sim 2 \times 10^{-4}$, and perchlorates $\sim 3 \times 10^{-3}$. The corresponding Q values were chlorides 3.5×10^{-7}, bromides 3.5×10^{-8}, iodides 2.0×10^{-9}, and perchlorates 3.0×10^{-10}. The relative error for Q ranged between 5–10%.

Final values for Q were calculated directly from the data by an iteration method where each $[\overline{R_3NHX}]_T$ value yielded a value of $[\overline{R_3NHX}]$ for a given K_d value and Q was calculated for each point as $[R_3N][H^+][X^-]/[\overline{R_3NHX}]$. If the correct value of K_d has been selected, Q, should be a constant over the whole concentration range and the plot of $[\overline{R_3NHX}]$ vs. $[\overline{R_3N}][H^+][X^-]$ should be a straight line of slope one.

A series of K_d values were tested starting with the graphically determined K_d value. The value that minimized the spread on Q values was selected together with the corresponding Q value. In Fig. 1 straight lines of slope one were drawn on this basis.

The Chloride Series

These salts gave log–log plots which were linear and of slope one and computation of Q or K by iteration was unnecessary. Values of Q' calculated directly for each data point were averaged over the entire concentration range giving the following results: THAHCl, $Q = (3.6 \pm 0.2) \times 10^{-7}$; TOAHCl, $Q = (3.3 \pm 0.2) \times 10^{-7}$; TLAHCl, $Q = (3.4 \pm 0.2) \times 10^{-7}$.

The Bromide Series

Values of K_d over the range 10^{-5} to 10^{-4} were used to minimize the standard deviation of Q. The corresponding Q values are TPTAHBr, $Q = (4.2 \pm 0.2) \times 10^{-8}$, $K_d = (5 \pm 3) \times 10^{-5}$; THAHBr, $Q = (3.7 \pm 0.2) \times 10^{-8}$, $K_d = (5 \pm 3) \times 10^{-5}$; TOAHBr, $Q = (3.7 \pm 0.2) \times 10^{-8}$, $K_d = (7 \pm 3) \times 10^{-5}$; TLAHBr, $Q = (3.6 \pm 0.3) \times 10^{-8}$, $K_d = (5 \pm 4) \times 10^{-5}$.

The Iodide Series

Since relatively few stable data points were found in this system and all of these in the upper concentration decade, a direct computation of K_d and Q was not attempted but rather the results from the graphical method were believed to give a reasonable value for Q. These were TPTAHI 2.0×10^{-9}, THAHI 1.9×10^{-9}, TOAHI 1.8×10^{-9} and TLAHI 2.0×10^{-9}. In the case of iodides the accuracy of the graphical method was close to ± 5%. To this a standard deviation of 10% was added giving a range of ± 15% around the preceding values.

The Perchlorate Series

Values for K_d ranging between 10^{-3} and 4.5×10^{-3} were tested and the corresponding values of Q obtained were $TBAHClO_4$, $Q = (3.0 \pm 0.3) \times 10^{-10}$, $K_d = (2.0 \pm 0.5) \times 10^{-5}$; $TPTAHClO_4$, $Q = (2.7 \pm 0.2) \times 10^{-10}$, $K_d = (2.0 \pm 0.5) \times 10^{-5}$; $THAHClO_4$, $Q = (2.5 \pm 0.3) \times 10^{-10}$, $K_d = (2.0 \pm 0.5) \times 10^{-5}$; $TOAHClO_4$, $Q = (2.7 \pm 0.3) \times 10^{-10}$, $K_d = (2.0 \pm 0.5) \times 10^{-5}$, $TLAHClO_4$, $Q = (3.0 \pm 0.4) \times 10^{-10}$, $K_d = (2.5 \pm 1.0) \times 10^{-5}$.

In all cases attainment of equilibrium in the two-phase emf titrations was verified by comparing data points on the log–log plots obtained by direct and reverse titrations (see Fig. 1). In general, titrations of organic amine by acid and of organic ammonium salt by base in the same concentration decade gave data points that agreed within 5% or less. The difference arose in large part from potentiometric errors (0.2/0.3 mV or 1% in concentration on each potential reading).

Final K *Values and Ion Exchange Constants,* K_{12}

The thermodynamic constant K was obtained

TABLE 1. Hydrolysis constants, $-\log K$, of trialkylammonium salts at 25.0°C

Salt	Cl^-	Br^-	I^-	ClO_4^-
$TBAH^+$				9.71 ± 0.05
$TPTAH^+$		7.58 ± 0.02	8.90 ± 0.06	9.77 ± 0.03
$THAH^+$	6.65 ± 0.03	7.64 ± 0.02	8.90 ± 0.06	9.76 ± 0.05
$TOAH^+$	6.69 ± 0.03	7.64 ± 0.02	8.95 ± 0.06	9.74 ± 0.05
$TLAH^+$	6.67 ± 0.03	7.65 ± 0.03	8.90 ± 0.06	9.69 ± 0.06

from Q values, by applying the extended form of the Debye–Hückel law. A value of 0.79 for $\sqrt{\gamma_{H^+}\gamma_{X^-}}$ was obtained in all cases.

In Table 1 the log K values are presented.

The constants K can be combined for each series of salts to give ion exchange equilibrium constants. The equilibria

$$\overline{R_3NHX_1} \rightleftarrows \overline{R_3N} + H^+ + X_1^-$$

and

$$\overline{R_3NHX_2} \rightleftarrows \overline{R_3N} + H^+ + X_2^-$$

with constants K_1 and K_2, are combined to yield the following equilibrium

$$\overline{R_3NHX_1} + X_2^- \rightleftarrows \overline{R_3NHX_2} + X_1^-$$

This equilibrium describes the exchange of anion X_1 from the ion-paired salt in nitrobenzene R_3NHX_1 for anion X_2 in the aqueous solution.

The constant for the ion-exchange equilibrium is K_{12} with:

$$K_{12} = \frac{\overline{[R_3NHX_2]}[X_1^-]}{\overline{[R_3NHX_1]}[X_2^-]} = \frac{K_1}{K_2}$$

Similarly for the salts of low to middle molecular weight for which no value of K was obtainable, K_p values (3) can be combined to obtain the ion exchange constants:

$$K_{12} = K_{p1}/K_{p2}$$

In Table 2 the ion exchange constants for the couples Cl^-/Br^-, Br^-/I^-, I^-/ClO_4^- are listed for each trialkylammonium series.

For THAH Cl^-/Br^-, Br^-/I^- and TPTAH Br^-/I^-, I^-/ClO_4^- log K_{12} values obtained from partition constants were also available and except for possibly THAH Cl^-/Br^- there was no significant difference between the two values.

TABLE 2. Ion exchange constants, log K_{12}, of trialkylammonium salts at 25.0°C

Salt	Cl^-/Br^-	Br^-/I^-	I^-/ClO_4^-
$TPRAH^+$	1.01 ± 0.01*	1.26 ± 0.03*	0.92 ± 0.04*
$TBAH^+$	0.98 ± 0.01*	1.35 ± 0.03*	0.82 ± 0.03*
$TPTAH^+$	1.01 ± 0.03*	1.32 ± 0.08	0.87 ± 0.09
$THAH^+$	0.99 ± 0.05	1.26 ± 0.08	0.86 ± 0.11
$TOAH^+$	0.95 ± 0.05	1.26 ± 0.08	0.84 ± 0.11
$TLAH^+$	0.98 ± 0.06	1.25 ± 0.09	0.79 ± 0.12

*Obtained from K_p values.

Discussion

Dissociation constants obtained by two-phase emf titration are comparable to values previously obtained by conductometry (2). The pK_d values by conductometry (chlorides ~ 5.0, bromides ~ 4.5, iodides ~ 3.4, perchlorates ~ 2.4) are in fair agreement with values from two-phase emf titrations (chlorides < 5, bromides ~ 4.3, iodides ~ 3.7, perchlorates ~ 2.7). Since the errors associated with the constants obtained by potentiometry were large, subtle differences that might arise from chain length differences, for example, were not observed.

Conductometric studies (3) did not entirely exclude the possibility of limited triple ion formation at the most concentrated extreme of the chloride and bromide systems. The analysis of two-phase titration data does not support the possibility of significant aggregation other than simple ion pairs beyond the conductometric concentration maximum.

Several hydrolysis constants, $-\log K$, presented in Table 1 have been reported previously by other workers: TOAHCl, 6.75 (4) vs. 6.69 ± 0.03; TLAHCl, 6.78 (6) vs. 6.67 ± 0.03; TLAHBr, 7.70 (6) vs. 7.65 ± 0.03; TLAHI, 9.00 (6) vs. 8.90 ± 0.06. The agreement is satisfactory if the errors of the early measurements were comparable to the recent values. Müller and Diamond (6) gave a value of $pK = 7.45$ for $TLAHClO_4$ corresponding to the following equilibrium

$$\overline{R_3NH^+} + \overline{ClO_4^-} \rightleftarrows \overline{R_3N} + H^+ + ClO_4^-$$

A corresponding value from this work would be 7.0 ± 0.1 (calculated as $pK - pK_d$). The Müller and Diamond treatment, however, was approximate since association of separated ions to ion-pairs was ignored.

From an examination of K values obtained in this work for a variety of salts two major elements appear, the constancy of K with increasing carbon chain length for the same anion and the marked influence of the nature of the anion.

Can. J. Chem. Downloaded from www.nrcresearchpress.com by 210.87.254.5 on 09/06/12
For personal use only.

No significant trend was evident in the K values for any series of salts proceeding up the series from tributyl or tripentylamine to tridodecylamine (Table 1). If the acid–base reaction in the organic solvent

$$\overline{R_3NHX} \rightleftarrows \overline{R_3N} + \overline{HX}$$

is considered, the corresponding equilibrium constant K_a is related to K as $K_a = KK_{HX}$ where K_{HX} represents the partition equilibrium constant of HX corresponding to the partition reaction:

$$H^+ + X^- \rightleftarrows \overline{HX}$$

For a given anion, K_{HX} is a constant and since K does not vary with alkyl chain length, $\overline{K_a}$ is a constant too. This suggests that the basicity of trialkylamines in nitrobenzene does not change with increasing chain length from tributylamine.

The inductive effect should increase the basicity of trialkylamines as alkyl chain length is increased (14). This effect has been observed in water proceeding from trimethyl to tributylamine (15). Trémillon (16), by a spectrophotometric method, found that the base strength of amines in various solvents was not significantly influenced by the chain length from tributyl to trioctylamine. Grinstead (7) reported a similar affinity of THA and TOA for HCl in toluene.

The influence of the nature of the anion on the values of the hydrolysis constant is large. Hydrolysis assumes increasing importance in the order $ClO_4^- < I^- < Br^- < Cl^-$. There is approximately an order of magnitude difference in the hydrolysis constant when going from ClO_4^- to I^-, from I^- to Br^-, and from Br^- to I^-. Anion exchange constants (Table 2) also reflect these differences. As is the case with basicity of the amine, ion exchange does not seem to be influenced significantly by alkyl chain length for the series C_3–C_{12} reported here.

The order of anion exchange can be attributed to the nature of the aqueous and organic phases. In the organic phase, cation–anion interaction through electrostatic interaction and hydrogen bonding should favor the extraction of Cl^- vs. Br^-, Br^- vs. I^-, and I^- vs. ClO_4^- (3). However, this interaction is believed to be less important than interactions in the aqueous phase. Hydration is more favorable in the case of a smaller more basic anion. Furthermore, anions of larger diameter are also energetically more favored in the organic phase than small anions because of the water structure breaking factor.

Acknowledgement

Financial support by the National Research Council of Canada is gratefully acknowledged.

1. A. K. Shukla and W. Preetz. Angew. Chem. Int. Ed. Engl. **18**, 151 (1979).
2. M. Gérin and J. Fresco. Anal. Chim. Acta, **97**, 155 (1978).
3. M. Gérin and J. Fresco. Anal. Chim. Acta, **97**, 165 (1978).
4. A. D. Nelson, J. L. Fasching, and R. L. McDonald. J. Inorg. Nucl. Chem. **27**, 439 (1965).
5. J. J. Bucher and R. M. Diamond. J. Phys. Chem. **69**, 1565 (1965).
6. W. Müller and R. M. Diamond. J. Phys. Chem. **70**, 3469 (1966).
7. J. Bizot and B. Trémillon. Bull. Soc. Chim. Fr. 122 (1959); L. Newman and P. Klotz. J. Phys. Chem. **65**, 796 (1961); G. Duyckaerts, J. Fuger, and W. Müller. Euratom Report EUR-426 (1963); A. S. Wilson and N. A. Wogman. J. Phys. Chem. **66**, 1552 (1962); W. E. Keder and A. S. Wilson. Nucl. Sci. Eng. **17**, 287 (1963); R. R. Grinstead. Solvent extraction chemistry. *Edited by* D. Dyrssen, J. O. Liljenzin, and J. Rydberg. North-Holland, Amsterdam. 1967. p. 426; J. M. P. J. Verstegen and J. A. A. Ketelaar. Trans. Faraday Soc. **57**, 1527 (1961); K. A. Allen. J. Phys. Chem. **60**, 239 (1956).
8. A. S. Kertes. Critical evaluation of some equilibrium constants involving alkylammonium extractants. Pergamon, Oxford. 1977.
9. E. Högfeldt. Ion exchange. Vol. 1. *Edited by* J. A. Marinsky. Marcel Dekker, New York. 1966. Chapt. 4.
10. E. Högfeldt and F. Fredlund. Trans. R. Inst. Technol. Stockholm, N226 (1964).
11. R. M. Diamond. Solvent extraction chemistry. *Edited by* D. Dyrssen, J. O. Liljenzen, and J. Rydberg. North-Holland, Amsterdam. 1967. p. 349.
12. O. Samuelson. Ion exchange separations in analytical chemistry. Wiley, New York. 1963. p. 241.
13. A. Liberti and T. S. Light. J. Chem. Educ. **39**, 236 (1962).
14. J. Clark and D. D. Perrin. Q. Rev. **18**, 295 (1964).
15. H. K. Hall. J. Am. Chem. Soc. **79**, 5441 (1957).
16. B. Trémillon. Bull. Soc. Chim. Fr. 1053 (1964).

Can. J. Chem. Downloaded from www.nrcresearchpress.com by 210.87.254.5 on 09/06/12
For personal use only.

Structure and electrochemical behaviour of 2-nitrosoquinoxaline

JOSEPH ARMAND, YVETTE ARMAND, AND LINE BOULARES

Laboratoire de Physicochimie des Solutions, L.A. CNRS 161, Université Pierre et Marie Curie, Bâtiment F, 8, Rue Cuvier, 75230 Paris Cedex 05, France

MICHÈLE PHILOCHE-LEVISALLES

Laboratoire de Chimie Systématique, Université Pierre et Marie Curie, Bâtiment F, 8, Rue Cuvier, 75230 Paris Cedex 05, France

AND

JEAN PINSON

Laboratoire d'Electrochimie, Université Paris 7, 2, Place Jussieu, 75221 Paris Cedex 05, France

Received November 7, 1980

JOSEPH ARMAND, YVETTE ARMAND, LINE BOULARES, MICHÈLE PHILOCHE-LEVISALLES, and JEAN PINSON. Can. J. Chem. **59**, 1711 (1981).

It is shown by X-ray crystallography that 2-nitrosoquinoxaline crystallizes as a dimer, the structure of which is established. In solution the monomeric form predominates and the dimerisation equilibrium constant is measured. The electrochemical reduction of 2-nitrosoquinoxaline in acidic medium leads to the oxime of quinoxaline (1*H*)-2-one (**3**) through the intermediate hydroxylamine. **3** is electrochemically reoxidized directly to 2-nitrosoquinoxaline.

JOSEPH ARMAND, YVETTE ARMAND, LINE BOULARES, MICHÈLE PHILOCHE-LEVISALLES et JEAN PINSON. Can. J. Chem. **59**, 1711 (1981).

Les données cristallographiques obtenues par diffraction des rayons X montrent que la nitroso-2 quinoxaline cristallise sous forme de dimère dont la structure est établie. En solution le monomère prédomine et la constante d'équilibre est mesurée. La réduction électrochimique de la nitroso-2 quinoxaline en milieu acide conduit à l'oxime de la quinoxaline (1*H*)-one-2 (**3**) par l'intermédiaire de l'hydroxylamine correspondante. **3** est réoxydée par électrochimie directement en nitroso-2 quinoxaline.

There has been considerable recent interest in the structure of monomeric and dimeric nitroso-compounds, both in the solid state and in solution, as well as in the monomer dimer equilibrium (**1**).

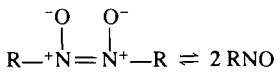

[A]

In the aromatic series, nitrosobenzenes have been mostly investigated. In the solid state, nitrosobenzene itself exists as a dimer (2), while its derivatives bearing an electron-donating group crystallize as monomers (3). In solution, the constant of equilibrium [A] depends on the electron-donating or -withdrawing ability of the substituents but also on their steric bulkiness. Correlations have been established between the redox potentials of monomers and the uv absorption frequencies (4, 5) on one side and the equilibrium constants k_A (6) on the other side.

As 2-nitrosoquinoxaline is one of the few nitroso heterocyclic derivatives we became interested in its structure both in the solid state and in solution. As in the case of *p*-aminonitrosobenzene (3) and of 9-nitrosojulolidine (7) a resonance form (*b*) resembling an oxime ion can be written which may contribute significantly to the structure of the monomer:

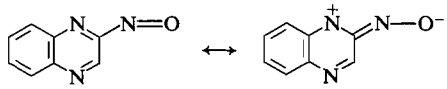

(*a*) (*b*)

In relation with the structure in solution we investigated the electrochemical behaviour as several possible schemes were possible: reduction of the quinoxaline ring, of the nitroso group, or of the azodioxide group.

(1) Structure in the Solid State

Atomic positions are given in Table 1. Tables of observed and calculated structure factor amplitudes and of temperature factors are available from the Depository of Unpublished Data.[1] Table 2 lists the bond lengths and Table 3 the bond angles. Figure 1 is an ORTEP (9) diagram of the crystal structure and the crystal packing is shown in Fig. 2.

The results of the X-ray analysis show that 2-nitrosoquinoxaline exists in the solid state in the *cis*-azodiquinoxaline dioxide structure **1**. While the results obtained with the crystals of pentafluoro-nitrosobenzene (10) show that it is possible for monomeric and dimeric aromatic nitroso com-

[1]Complete set of data is available, at a nominal charge, from the Depository of Unpublished Data, CISTI, National Research Council of Canada, Ottawa, Ont., Canada K1A 0S2.

0008-4042/81/121711-06$01.00/0

©1981 National Research Council of Canada/Conseil national de recherches du Canada

Can. J. Chem. Downloaded from www.nrcresearchpress.com by 210.87.254.40 on 09/06/12
For personal use only.

Can. J. Chem. Downloaded from www.nrcresearchpress.com by 210.87.254.40 on 09/06/12
For personal use only.

TABLE 1. Position of parameters (esd's) for *cis*-azodiquinoxaline dioxide*

Atom	*x*	*y*	*z*
O(1)	5007(3)	16(2)	3768(2)
O(2)	7786(3)	664(2)	4839(2)
N(1)	4963(4)	837(2)	4006(2)
N(2)	3816(4)	2113(2)	3083(2)
N(3)	47(4)	1666(2)	3471(2)
N(4)	6362(4)	1181(2)	4586(2)
N(5)	4578(4)	2417(2)	5153(2)
N(6)	8016(4)	3439(2)	5576(2)
C(1)	3395(4)	1432(2)	3608(2)
C(2)	1536(5)	1174(2)	3809(2)
C(3)	394(4)	2414(2)	2925(2)
C(4)	−1157(5)	2983(3)	2573(3)
C(5)	− 840(6)	3734(3)	2023(3)
C(6)	1015(5)	3936(3)	1793(3)
C(7)	2540(5)	3396(2)	−2128(2)
C(8)	2267(4)	2631(2)	2716(2)
C(9)	6245(5)	2114(2)	4979(2)
C(10)	7987(5)	2610(3)	5187(3)
C(11)	6300(5)	3799(3)	5771(2)
C(12)	6226(6)	4692(3)	6188(3)
C(13)	4533(6)	5064(3)	6374(3)
C(14)	2820(6)	4561(3)	−6143(3)
C(15)	2826(5)	3693(3)	−5749(3)
C(16)	4572(4)	3294(2)	5552(3)
H(2)	1304(54)	679(29)	4276(26)
H(4)	−2398(59)	2820(29)	2787(27)
H(5)	−1862(60)	4100(30)	1760(28)
H(6)	1231(57)	4399(30)	1330(28)
H(7)	3830(57)	3525(28)	−1946(26)
H(10)	9179(56)	2327(30)	5014(26)
H(12)	7312(63)	5004(33)	6324(30)
H(13)	4458(62)	5671(33)	6690(29)
H(14)	1739(62)	4814(32)	6272(29)
H(15)	1729(60)	3333(30)	−5633(28)

*× 10^4

TABLE 2. Bond lengths (Å) (esd's) in *cis*-azodiquinoxaline dioxide

Bond	Length
O(1) —N(1)	1.259(6)
N(1) —C(1)	1.461(7)
C(1) —C(2)	1.419(8)
C(2) —N(3)	1.312(7)
N(3) —C(3)	1.368(7)
C(3) —C(4)	1.411(8)
C(4) —C(5)	1.370(9)
C(5) —C(6)	1.411(9)
C(6) —C(7)	1.366(9)
C(7) —C(8)	1.415(8)
C(8) —C(3)	1.419(7)
C(8) —N(2)	1.376(7)
N(2) —C(1)	1.291(7)
N(1) —N(4)	1.328(6)
N(4) —O(2)	1.264(6)
N(4) —C(9)	1.449(7)
C(9) —C(10)	1.416(8)
C(10)—N(6)	1.306(8)
N(6) —C(11)	1.368(8)
C(11)—C(12)	1.409(9)
C(12)—C(13)	1.356(10)
C(13)—C(14)	1.410(10)
C(14)—C(15)	1.359(10)
C(15)—C(16)	1.410(9)
C(16)—C(11)	1.418(8)
C(16)—N(5)	1.374(7)
N(5) —C(9)	1.299(7)
C(2) —H(2)	1.009(67)
C(4) —H(4)	0.987(70)
C(5) —H(5)	0.936(72)
C(6) —H(6)	0.971(71)
C(7) —H(7)	0.990(68)
C(10)—H(10)	0.986(69)
C(12)—H(12)	0.886(77)
C(13)—H(13)	0.982(77)
C(14)—H(14)	0.879(76)
C(15)—H(15)	0.925(72)

pounds to coexist in the crystalline state, in the case of the crystals 2-nitrosoquinoxaline there is no evidence for the existence of any species other than **1**.

The dimer of 2-nitrosoquinoxaline has a *cis* configuration as the dimer of nitrosobenzene (2). In both cases the central azodioxide group is not planar, and an important twist is observed along the N—N bond, coupled with some displacement of the nitrogen atoms from the plane defined by its three bonded neighbours. For the *cis*-azobenzene dioxide, the C(phenyl)—N—N—C(phenyl) and O—N—N—O torsion angles are 18.0 and 3.0° respectively while the out-of-plane distortions at N(1) and N(2) are 0.048 Å and 0.049 Å. In the case of **1**, the corresponding torsion angles are 11° 05′ and 5° 04′ while the out-of-plane distortions are 0.015 Å and 0.025 Å. The N—O, N—N, and C_1—N_1 bond lengths in **1** and *cis*-azobenzene dioxide are quite similar within experimental errors.

The existence of 2-nitrosoquinoxaline under a dimeric structure in the solid state points to a very low weight of resonance structure (*b*).

(2) Structure in Solution

A solution of 2-nitrosoquinoxaline shows a uv maximum at λ_{max} = 800 nm corresponding to the n → π* transition of the nitroso group which is classically observed between 630 and 830 nm.

The molar extinction coefficient ε_0 of the monomer **2** has been determined by linear extrapolation (Ostwald law) of the usual (11) ε vs. $\varepsilon^2 c_0$ plots (where c_0 is the concentration of total nitroso compounds all figured as monomer) to zero concentration: ε_0 = 30 L mol^{-1} cm^{-1}. The constant K_A of equilibrium [A] was then determined to be 3×10^{-2} mol L^{-1} at 20°C, this value corresponding to 32% of monomers in a $c_0 = 0.1\ M$ solution. As in the case of nitrosobenzene (6) the nature of the solvent plays a minor role; the percentage of monomer in $CHCl_3$ for a $c_0 = 0.1\ M$ solution is 29%. The value of the equilibrium constant K_A was also determined in a 50–50 water–dimethylformamide mixture at pH 1.7, the solvent in which the electrochemical in-

Can. J. Chem. Downloaded from www.nrcresearchpress.com by 210.87.254.40 on 09/06/12
For personal use only.

TABLE 3. Bond angles (esd's) in *cis*-azodiquinoxaline dioxide

Bonds	Angle
O(1) —N(1) —C(1)	118.7(0.9)
N(1) —C(1) —C(2)	116.1(1.0)
C(1) —C(2) —N(3)	120.0(1.1)
C(2) —N(3) —C(3)	116.8(1.0)
N(3) —C(3) —C(8)	121.6(1.1)
N(3) —C(3) —C(4)	118.8(1.1)
C(8) —C(3) —C(4)	119.6(1.1)
C(3) —C(4) —C(5)	119.6(1.2)
C(4) —C(5) —C(6)	120.9(1.3)
C(5) —C(6) —C(7)	120.6(1.3)
C(6) —C(7) —C(8)	119.9(1.2)
C(7) —C(8) —C(3)	119.3(1.1)
C(7) —C(8) —N(2)	119.8(1.0)
C(8) —N(2) —C(1)	114.4(0.9)
N(2) —C(1) —N(1)	117.5(1.0)
N(2) —C(1) —C(2)	126.4(1.2)
C(3) —C(8) —N(2)	120.8(1.0)
O(1) —N(1) —N(4)	119.6(0.9)
O(2) —N(4) —N(1)	119.3(0.9)
O(2) —N(4) —C(9)	119.0(0.9)
N(4) —C(9) —N(5)	118.1(1.0)
N(4) —C(9) —C(10)	117.0(1.0)
C(9) —C(10) —N(6)	120.9(1.2)
C(10)—N(6) —C(11)	117.1(1.1)
N(6) —C(11)—C(16)	121.1(1.2)
N(6) —C(11)—C(12)	120.1(1.2)
C(16)—C(11)—C(12)	118.9(1.2)
C(11)—C(12)—C(13)	120.7(1.5)
C(12)—C(13)—C(14)	120.0(1.5)
C(13)—C(14)—C(15)	121.2(1.5)
C(14)—C(15)—C(16)	119.6(1.3)
C(15)—C(16)—C(11)	119.6(1.2)
C(15)—C(16)—N(5)	119.6(1.1)
C(11)—C(16)—N(5)	120.9(1.1)
C(16)—N(5) —C(9)	115.3(1.0)
N(5) —C(9) —C(10)	124.8(1.2)

vestigation was carried out. The value obtained, $K = 1.28 \times 10^{-2}$ mol L^{-1} at 20°C leads, for a value of $c_0 = 10^{-3}$ M, to 6% of the dimer, i.e. to a value of $c_2 = 0.6 \times 10^{-4}$ M.

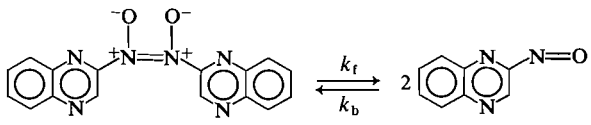

$$K_A = k_f/k_b$$

The rate constant of the forward dimer → monomer rate constant was measured by the stopped-flow technique and was found to be $k_f = 7.8\ s^{-1}$, which leads to $k_b = 6.1 \times 10^2\ M^{-1}\ s$.

The above value of K_A obtained for 2-nitrosoquinoxaline is much lower than that obtained for nitrosobenzene, in this last case, the percentage of monomer is higher than 99% for $c_0 = 0.1\ M$ (11). The value of K_A for 2-nitrosoquinoxaline is of the same order of magnitude as that of 2,4,6-trimethylnitrosobenzene (6). For this latter compound the lower value of K_A has been assigned to a steric inhibition of resonance in the monomer (6) or in the dimer (12). In our case it is difficult to rationalize the origin of the decreased value of K_A from the different influences of the phenyl and quinoxalyl rings.

(3) Electrochemical Reduction

In an hydroorganic medium, 2-nitrosoquinoxaline is unstable above pH 4. In a 50/50 water–dimethylformamide solution at pH 1.7, the polarogram shows two waves, the first one is a 2 F wave the half-wave potential of which cannot be measured at the dropping mercury electrode ($E_{1/2} > 0.2$ V), the second one is a 4 F wave with an $E_{1/2} = -0.48$ V. This second wave is that of the oxime of quinoxaline (1*H*)-2-one (**3**) which evidences the same cathodic wave. Besides a preparative electrolysis of 2-nitrosoquinoxaline at the level of the first wave gives **3**.

The voltammogram recorded at 200 mV s^{-1} on a vitreous carbon electrode shows, besides the peak of **3** at −0.48 V, two cathodic peaks I*c*, II*c*, and two anodic peaks III*a* and IV*a* (Fig. 3). The same voltammogram is obtained starting from the oxime of quinoxaline (1*H*)-2-one **3** and scanning +1.0 V → 0 V → +1.0 V. Peak I*c*, $E_p = +0.28$ V, corresponds to the transfer of two electrons. On a rotating vitreous carbon disc electrode, the height of the wave corresponding to peak I*c* varies linearly with the square root of the rotation speed, $\omega^{1/2}$, indicating that this plateau of the wave is diffusion-controlled. Upon increasing the scan rate peak I*c* shifts to more negative potentials.

Peak II*c* is a small peak which appears at +0.15 V, its height which is rather irreproducible from one experiment to the other never reaches more than 20% of that of I*c*. Upon scanning repetitively between +0.1 V and 0 V its height decreases less than 10% of its initial height. Upon increasing the scan rate peak II*c* becomes symmetrical and spiky. Thus peak II*c* appears as an adsorption peak. Peak III*a* ($E_p = +0.33$ V at 200 mV s^{-1}) is not related to peak II*c*; indeed when the cathodic scan is reversed before peak II*c*, peak III*a* still appears on the voltammogram. The height of peak III*a* increases with the sweep rate: while it is not observed at a scan rate of 0.025 V s^{-1} it reaches about one third of the height of peak I*c* at 20 V s^{-1}. Besides, this peak is not observed in a solution of **3** when scanning from 0 to +1 V.

Peak IV*a* corresponds to the oxidation of **3** into **2**. Indeed, in a solution of **3** under the same conditions as above the first anodic scan (0 → +1.0 V) shows an anodic peak identical to peak IV*a* and on

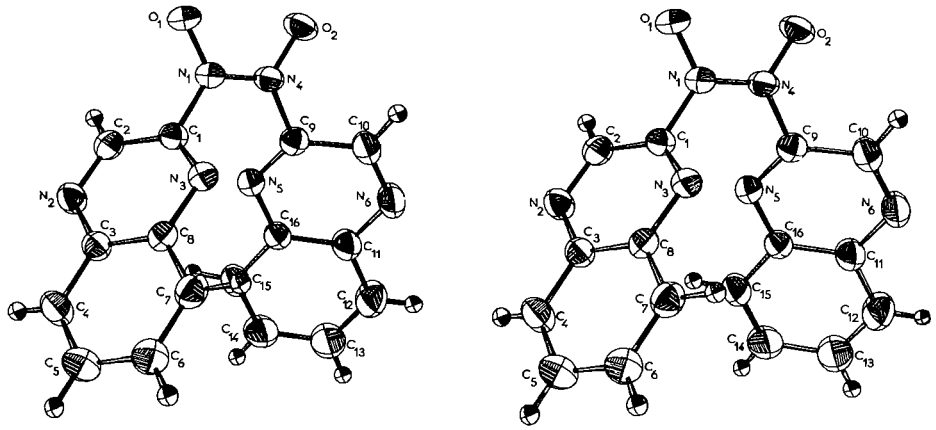

FIG. 1. Stereoscopic view of the solid state structure of *cis*-azodiquinoxaline dioxide.

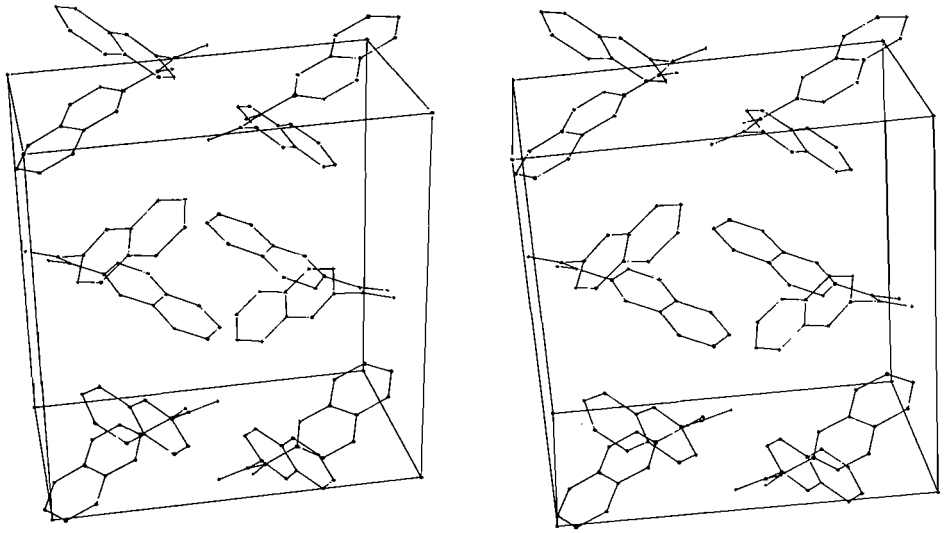

FIG. 2. Crystal packing of *cis*-azodiquinoxaline dioxide.

the reverse cathodic scan peaks Ic and IIc are observed. The height of peak IV*a* is equal to that of peak Ic at 0.025 V s^{-1} and decreases with the sweep rate, at 20 V s^{-1} it is reduced to one third of that of Ic and is nearly equal to that of II*a*.

Discussion

Our results show that while 2-nitrosoquinoxaline is entirely in a dimeric form in the solid state, the monomer predominates in the solution. Let us first consider the problem of the dimer, i.e., does one of the peaks observed on the voltammogram correspond to the dimer? The only azodioxide which has been investigated by electrochemistry is the 4,5,9,10- tetraza-4,5-pyrene di-*N*-oxide (14). Mugnier and Laviron have shown, by voltammetry, that the first 2 F reduction peak corresponds to the cleavage of an oxygen atom, while the second 4 F peak corresponds to the reduction of the azoxy derivative into the corresponding hydrazo compound. The potential difference between the two peaks is about 0.2 V. Thus if peak IIc was that of the dimer **1**, one should observe the peak of the azoxyquinoxaline at about −0.05 V. No peak is observed in this region of the voltammogram, in the same way the polarogram shows only a clean plateau between +0.1 V and −0.4 V. Besides the height of peak IIc does not increase significantly with the concentration between $c_0 = 5 \times 10^{-4}$ and 2×10^{-3} *M*. This leads to the conclusion that peak IIc does not belong to the dimer and that monomer **2** is the only species which is reduced at the electrode, equilibrium [A] is drawn to the right by reduction of **2**.

Can. J. Chem. Downloaded from www.nrcresearchpress.com by 210.87.254.40 on 09/06/12
For personal use only.

Can. J. Chem. Downloaded from www.nrcresearchpress.com by 210.87.254.40 on 09/06/12
For personal use only.

Two mechanisms can be taken into account for the reduction of 2-nitrosoquinoxaline (*i*) a reduction into 2-hydroxylaminoquinoxaline **4** followed by its rearrangement into **3**:

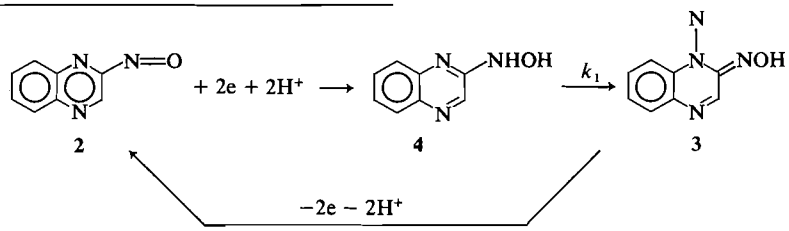

(*ii*) a direct electrochemically irreversible reduction of **2** into **3**

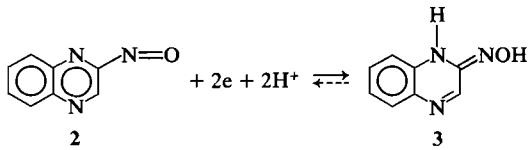

The appearance of peak II*a* on the voltammogram of **2** clearly indicates that the first mechanism is operative. This peak must correspond to the intermediate hydroxylamine **4**. The difference $E_p(Ic) - E_p(IIIa) = 50$ mV which is close to that of the reversible system nitrosobenzene–phenylhydroxylamine also observed on vitreous carbon (13). It is not observed on the first anodic scan of a solution of **3** but it appears on the reverse anodic scan of a solution of **2** and its height increases with the sweep rate. Peak IV*a* corresponds to the direct reoxidation of **3** into **2**. The **2/3** couple thus appears as an electrochemically irreversible but chemically reversible couple.

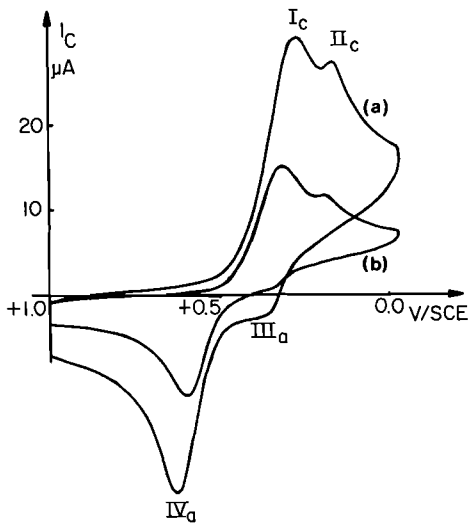

FIG. 3. Cyclic voltammogram of 2-nitrosoquinoxaline–water –dimethylformamide 50/50, pH 1.7, $c_0 = 10^{-3}$ *M*, on a vitreous carbon electrode. Scan rate (*a*), 0.2 V s^{-1}; (*b*), 0.025 V s^{-1}.

Experimental

The 2-nitrosoquinoxaline as well as the oxime of quinoxaline (1*H*)-2-one have been prepared according to ref. 15. The monocrystal used in the crystallographic study was obtained by slow evaporation of a methanolic solution.

Crystallographic Study

Crystal data are as follows:

$C_{16}H_{10}N_6O_2$ f.w. = 318.29

Monoclinic, $a = 7.019$ (2), $b = 14.143$ (3), $c = 14.788$ (3) Å, $\beta = 96.12$ (1)°, $V = 1459.62$ Å^3, $Z = 4$, $\rho_c = 1.44$ g cm^{-3}, $\rho_0 = 1.48$ (2) g cm^{-3} (20°C, MoK$_\alpha\lambda = 0.707$ Å, $\mu = 1.0$ cm^{-1}). Preliminary X-ray photographs showed the following systematic absences: $h0l, l = 2n + 1$; $0k0, k = 2n + 1$. The space group is the $P2_1/c$. A crystal (0.60 × 0.15 × 0.35 mm) was mounted with the *a* axis parellel to the ϕ axis of a Philips automated diffractometer equipped with a graphite monochromator. The intensities of all reflection having 2θ less than 50° were measured using the variable ω–2θ scan technique. During the course of the data collection three standard reflections were measured every 54 reflections. A total of 2572 independent reflections were measured 1665 of which had $I > 4\sigma(I)$. The data were reduced to $|F_o|$ by the routine procedure. Lorentz and polarization but not absorption or extinction corrections were applied. The scattering factors for neutral atoms were taken from ref. 16. The structure was determined by direct methods (MULTAN) (17) and refined by large block least-squares $(\Sigma\omega|F_o| - |F_c|)^2 = \min$ with $\omega = 1/\sigma^2$. The refinement with anisotropic thermal parameters on the non-hydrogen atoms converged with $R = 0.068$. At this stage, a difference Fourier map revealing the position of all the hydrogens was calculated; refinement of their positional parameters was carried out using the thermal parameters of the corresponding heavy atoms at the end of isotope refinement. The refinement including all atoms and all observed reflections converged with $R = 0.040$ and $R_w = 0.046$.

Electrochemical techniques have been previously described (18). All the potentials are referred to the aqueous saturated calomel electrode. A vitreous carbon electrode (3 mm diameter) was used, it was polished with 1 μ diamond paste before each experiment. The uv spectra have been recorded on Beckmam model 25 apparatus.

The rate constant of the dimer → monomer reaction has been determined with a Durrum stopped-flow spectrophotometer D 150, the cell compartment of which was maintained at 20 ± 0.5°C. Equal volumes of a pH 1.7 solution of **1** ($c_0 = 3 \times 10^{-3}$ *M*) containing 50% of dimethylformamide and of the same solution without **1** were mixed and the optical density vs. time curve recorded at $\lambda = 800$ nm.

Preparative Electrolysis

It was performed on mercury in a cell previously described (8), the cathodic compartment contained 100 mL of an aqueous

solution containing 500 mg of **1** (which were only partly dissolved), 50 mL of methanol, and 10 mL of H_2SO_4; the anodic compartment contained the same solution without depolarizer. The potential was set at −0.2 V. After consumption of 600 C (2F/mol = 607 C) the current decreased to less than 3 mA and the cell was disconnected. The cathodic solution was filtered, neutralized to pH 7 with sodium carbonate, the methanol was evaporated *in vacuo* at room temperature. The solid which precipitated was filtered, washed with water, and dried to give 320 mg (yield 64%) of **3** mp = 200°C (dec.) (lit. (15) mp = 198–200°C (dec.)). This compound was identified by comparison (ir, nmr) with an authentic sample (15).

1. J. H. BOYER. The chemistry of the nitro and nitroso groups. Interscience Publishers, New York. 1969. p. 253.
2. D. A. DIETRICH, I. C. PAUL, and D. Y. CURTIN. J. Am. Chem. Soc. **96**, 6372 (1974).
3. H. J. TALBERG. Acta Chem. Scand. A, **31**, 743 (1977) and references therein.
4. W. KEMULA and T. M. KRYGOWSKI. *In* Encyclopedia of electrochemistry of the elements. Vol. XIII. *Edited by* A. J. Bard and H. Lund. Marcel Dekker, New York. 1979. p. 131.
5. L. HOLLECK and R. SCHINDLER. Z. Electrochem. **60**, 1142 (1956).
6. R. H. HOLMES. J. Org. Chem. **29**, 3076 (1964).
7. R. DUNLOP, R. D. U. HARDY, H. H. MILLS, R. K. MACKENZIE, D. D. MACNICOL, and D. A. R. WILLIAMS. J. Chem. Res. (S) 152 (1979), (M) 1848 (1979).
8. J. ARMAND, K. CHEKIR, and J. PINSON. Can. J. Chem. **56**, 1804 (1978).
9. C. K. JOHNSON. ORTEP, Report ORNL-3794, Oak Ridge National Laboratory, Oak Ridge, TN. 1965.
10. C.K. PROUT, A. CODA, R. A. FORDER, and B. KAMENAR. Cryst. Struct. Commun. **3**, 39 (1974).
11. V. KEUSSLER and W. LUTTKE. Z. Electrochem. **63**, 614 (1959).
12. W. LUTTKE. Z. Electrochem. **61**, 982 (1957).
13. L. CHUANG, I. FRIED, and P. J. ELVING. Anal. Chem. **36**, 2426 (1964).
14. Y. MUGNIER and E. LAVIRON. Bull. Soc. Chim. Fr. 1486 (1976).
15. K. HARSANYI, C. GONCZJ, and D. KARBONITZ. Annelen, 190 (1973).
16. International Tables for X ray crystallography. Vol. IV. The Kynoch Press, Birmingham, England. 1974.
17. G. GERMAIN, P. MAIN, and M. M. WOOLFSON. Act. Crystallogr. A. **27**, 268 (1971).

Can. J. Chem. Downloaded from www.nrcresearchpress.com by 210.87.254.40 on 09/06/12
For personal use only.

A novel type rearrangement in cyclic β-dicarbonyl compounds in strong acid media[1]

KIMITOSHI SAITO AND HIDETAKA YUKI
School of Pharmaceutical Science, Toho University, Miyama 2-2-1, Funabashi, Chiba 274, Japan
TOSHIYUKI OHYAMA AND RYOHEI NAKANE
The Institute of Physical and Chemical Research, Wako, Saitama 351, Japan
AND
KATSUYUKI NAGUMO AND TADASHI SATO
Department of Applied Chemistry, Waseda University, Ookubo, Shinjuku-ku, Tokyo 160, Japan
Received June 18, 1980

KIMITOSHI SAITO, HIDETAKA YUKI, TOSHIYUKI OHYAMA, RYOHEI NAKANE, KATSUYUKI NAGUMO, and TADASHI SATO. Can. J. Chem. **59**, 1717 (1981).

5,5-Dimethylcyclohexane-1,3-dione and its derivatives were shown to isomerize to give 5,6-dihydropyran-4-ones on irradiation in FSO_3H or 98% H_2SO_4. The 2,2-dimethyl derivative, lacking hydrogen on C2, failed to give any products under the same conditions. A similar type of isomerization was also observed with thiolane-2,4-dione and its derivatives, while no photoisomerization was observed with their nitrogen or oxygen analogs. A possible reaction mechanism is proposed.

KIMITOSHI SAITO, HIDETAKA YUKI, TOSHIYUKI OHYAMA, RYOHEI NAKANE, KATSUYUKI NAGUMO et TADASHI SATO. Can. J. Chem. **59**, 1717 (1981).

En milieu acide à 98% H_2SO_4 ou à FSO_3H, nous avons obtenu la dihydro-5,6 pyrane-4, par isomérisation sous l'action de l'irradiation, de la diméthyl-5,5 cyclohexenedione-1,3 et de ses dérivés. Par contre, le dérivé 2,2-diméthylé, sans hydrogène en C2, n'est pas isomérisé dans les mêmes conditions expérimentales. Le même type de photoisomérisation a été obtenu avec la thiolanedione-2,4 sauf avec ses composés oxygénés et azotés. Nous proposons ici un des méchanismes possibles de réaction.

The photochemistry of ketones in strong acid media has been characterized by a unique reaction pattern induced by controlled excitation due to the protonation on the carbonyl group. The reaction has been extensively investigated particularly in cyclic dienone systems, and isomerization to bicyclo systems or ring contraction has been identified as the typical reaction pattern (2–7).

Previously, we reported that the photoreaction of ketones in methanol in the presence of $TiCl_4$ or UO_2Cl_2 proceeds through C—C bond formation, and proposed a scheme involving the coordination of the ketone and methanol to the metal ion as an essential step for the reaction to proceed (8–10). In connection with this reaction, we thought it of interest to compare the catalytic effect of Lewis acids with that of protonic acids. Childs and Hor (11) investigated the effects of boron trihalides and protonic acid on the photobehavior of eucarvone, and observed a similarity in their catalytic effects for the major reaction paths.

We have studied the effect of protonic acids on the photoreaction of a variety of carbonyl compounds, and found a novel reaction pattern with cyclic β-dicarbonyl compounds upon irradiation in strong acid media.

[1]Preliminary report, see ref. 1.

Results and Discussion

Irradiation of 5,5-dimethylcyclohexane-1,3-dione, **1***a*, in FSO_3H or 98% H_2SO_4 with quartz-filtered light from a high pressure mercury lamp for 24 h, and subsequent work-up with water gave 2,6,6-trimethyl-5,6-dihydro-4*H*-pyran-4-one, **2***a*, as sole product in 19% yield. The acid solution became darkened toward the end of the irradiation, and the longer irradiation times did not increase the yield. Olah *et al.* (12) reported that carbonyl compounds such as **1***a* and **2***a* exist in a protonated form, **1***aH* and **2***aH*, respectively. We confirmed this result from the nmr spectra of **1***a* and **2***a* in FSO_3H as shown in Table 1. Although the isolated yield of **2***a* was low, the ^1H nmr analysis of the acid solution after the irradiation revealed that no other signals were noticeable except those of **2***aH* and the starting material, **1***aH*. Although the 2-methyl derivative, **1***b*, afforded **2***b* in 18% yield, the 2,2-dimethyl derivative, **1***c*, lacking hydrogen on C2, failed to give any products under the same conditions. The structures of **2***a* and **2***b* were identified by comparing the spectroscopic data with the reported values (13).

It has been reported that the photo-induced ring contraction of protonated cyclic dienones proceeds through the initial electrocyclic opening of the ring, while the ring contraction of protonated cyclo-

0008-4042/81/121717-05$01.00/0
©1981 National Research Council of Canada/Conseil national de recherches du Canada

Can. J. Chem. Downloaded from www.nrcresearchpress.com by 210.87.254.5 on 09/06/12
For personal use only.

TABLE 1. ^{1}H nmr spectral data of protonated and unprotonated ketones[a]

Compound	Solvents	Chemical shift (ppm)[b] C1	C2	C3	C4	C5	C6
1*a*	$CDCl_3$[c]	6.58 (OH)	5.46 (H)		2.22 (H)	1.04 (GM)[d]	2.22 (H)
	FSO_3H		6.16 (H)		2.75 (H)	1.22 (GM)	2.75 (H)
2*a*	CCl_4		1.92 (Me)	5.13 (H)		2.28 (H)	1.40 (GM)
	FSO_3H		2.75 (Me)	6.45 (H)		3.29 (H)	1.95 (GM)
1*b*	$CDCl_3$[c]	5.38 (OH)	1.00 (Me)		2.09 (H)	1.02 (GM)	2.09 (H)
	FSO_3H		1.82 (Me)		2.64 (H)	1.09 (GM)	2.64 (H)
5*c*	DMSO[f,i]		5.21 (H)		2.3–2.6 (H)[e]	3.0–3.3 (H)[e]	2.3–2.6 (H)[e]
	FSO_3H[g]		6.28 (H)		3.06 (H)[h]	3.3–3.8 (H)[e]	3.06 (H)[h]
7*aS*	DMSO[i]			5.37 (H)	9.02 (OH)	4.00 (H)	
	FSO_3H			5.87 (H)		4.08 (H)	
8*a*	CCl_4				5.15 (H)[j]	2.11 (Me)[k]	
	FSO_3H				6.29 (H)	1.91 (Me)	
7*bS*	CCl_4[l]		16.7 (OH)	2.54 (AM)[m]		3.86 (Me)	
	FSO_3H			2.60 (AM)		4.31 (Me)	
8*b*	CCl_4				2.50 (AM)	2.32 (Me)	
	FSO_3H				2.92 (AM)	3.02 (Me)	

[a] All spectra were obtained at 34°C.
[b] External TMS was used as reference (sealed capillary tube).
[c] Only the data of enol form are shown.
[d] *gem*-Dimethyl.
[e] Multiplet.
[f] Phenyl signal was observed at 7.44(s).
[g] Phenyl signal was observed at 7.37(s).
[h] Broad signal.
[i] Completely exists in enol form.
[j] Quintet, J = 1.2 Hz.
[k] Doublet, J = 1.2 Hz.
[l] Only the data of major components of two tautomeric enol mixtures (30) are shown.
[m] Acetyl methyl.

hexenones proceeds through the initial 1,2-shift (14). Since the concerted 1,3-shift of C5 from C4 to oxygen is unlikely due to the structural requirement, we envisaged the isomerization **1** → **2** as a stepwise reaction involving ring-opening and recyclization. The ring-opening could proceed through either electrocyclic opening of the cyclohexadienone system, **3**, which could possibly exist as a minor equilibrium component even in strong acid media (Scheme 1), or simple 1,2-bond fission of the protonated species (Scheme 2, see later).

In order to distinguish between the two plausible paths, we carried out the irradiation in deuterated sulfuric acid. When **1***a* was irradiated in D_2SO_4 and then worked up with H_2O, a deuterated **2***a* was obtained. The ^{1}H nmr and mass spectroscopic analyses of this product indicated that 100% of one proton on the C2-methyl group and 84% of the C3-proton had been exchanged with deuterium. On the other hand, the irradiation of **1***a* in H_2SO_4 and subsequent work-up with D_2O gave **2***a*, in which a major portion (62%) of the C3-proton had been exchanged with deuterium. This result indicates that the C3-proton of **2***a* is exchangeable with solvent proton with great ease, and we concluded that the primary product of the reaction in D_2SO_4 is a dideuterated compound, **4**, from which 16% of C3-D was expelled by proton during the work-up procedure. In spite of the deuteration at the C3 and C2-methyl groups, no indication of deuteration at C5 was observed at all, and the possibility of intervening in the electrocyclic opening as shown in Scheme 1 was thus eliminated.

The presence of *gem*-dimethyl substituents at C5 in the starting material is necessary for the present reaction to proceed, and compounds **5***a–c* were recovered unchanged under the same irradiation conditions. These findings induced us to propose the following scheme for the present isomerization (Scheme 2). As mentioned above, the starting material **1***a* exists in a protonated form **1***aH* under the present reaction conditions. This was also suggested from the comparison of the ultraviolet spectra in organic solvents and acidic media (Table 2). This cationic species undergoes a C4–C5 bond fission upon irradiation to give a cation, **6***aH*, followed by cyclization at carbon and oxygen atoms to give **2***aH*. Upon work-up, it affords the observed

Can. J. Chem. Downloaded from www.nrcresearchpress.com by 210.87.254.5 on 09/06/12
For personal use only.

Can. J. Chem. Downloaded from www.nrcresearchpress.com by 210.87.254.5 on 09/06/12
For personal use only.

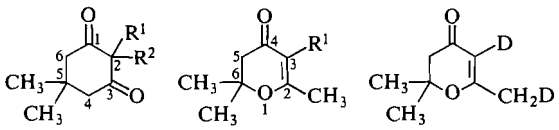

1 **2** **4**

a $R^1 = R^2 = H$
b $R^1 = CH_3$, $R^2 = H$
c $R^1 = R^2 = CH_3$

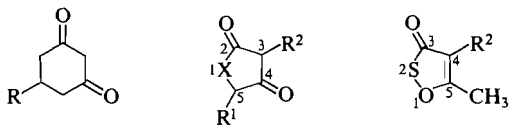

5 **7** **8**

a R = H
b $R = CH_3$
c R = Ph

a $R^1 = R^2 = H$
b $R^1 = H$, $R^2 = COCH_3$
S X = S
N X = NH
O X = O

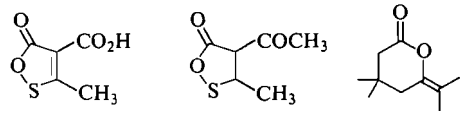

9 **10** **11**

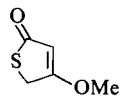

12

product **2***a*. Presumably, the stabilization of the positive charge in **6***aH* by the *gem*-dimethyl groups would play an important role in the success of the reaction.

In view of Scheme 2, it is hard to rationalize the unreactivity of the phenyl derivative **5***c*. In our previous communication, we ascribed the inertness to protonation on the phenyl ring. However, we observe now that such a speculation is erroneous in view of the ^1H nmr data as shown in Table 1. Probably a different type of excited state might be responsible, although no experimental work has been carried out on this problem.

The same type of rearrangement was also observed in sulfur-containing cyclic β-diketones. Irradiation of thiolane-2,4-dione, **7***aS*, in FSO_3H and subsequent work-up with water afforded 5-methyl-3-oxo-3*H*-1,2-oxathiole, **8***a*, in 76% yield. Similarly, the 3-acetyl derivative, **7***bS*, afforded **8***b* in 49% yield. Although the ultraviolet spectra of

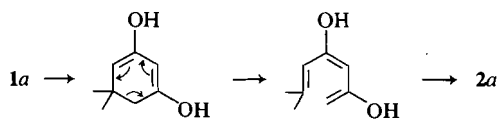

3

SCHEME 1

7*aS* and **7***bS* in 98% H_2SO_4 showed three absorption maxima in the range of 220–340 nm (Table 2), the yields of **8***a* and **8***b* were almost independent of whether the light was filtered by quartz or Pyrex. Presumably, the absorption at the longer wavelength might be responsible for the reaction. The ^1H nmr analysis indicated that no other products except the starting materials are present in the acid solution after the irradiation.

There seems to be no precedent for the 3-oxo-3*H*-1,2-oxathiole ring system, and the structure of the product, **8***b*, was determined by its elemental analysis and ^1H and ^{13}C nmr spectra. Since the spectroscopic analyses alone do not eliminate another possible structure **10** for the product, we attempted its synthesis. However, every effort to convert the known compound **9** (15) into **10** failed, and we could not elaborate any other way but to compare the spectroscopic data of **8***b* with those of **9**.

Hall and Wemple (16) have reported that the ^{13}C nmr signals of the carbonyl carbon and the carbon α to the carbonyl function in thiol esters are shifted downfield relative to those of the corresponding carboxylic acid derivatives. The comparison of ^{13}C nmr data of **8***b* and **9** revealed that the chemical shift of the ring carbonyl carbon appears at higher field in **9** relative to **8***b*, while the chemical shifts of the carbon β to the ring carbonyl function

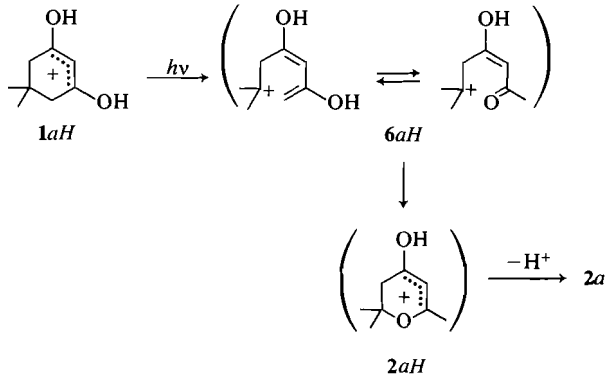

1*aH* **6***aH* **2***aH*

SCHEME 2

and the methyl carbon on the ring appear at lower field in **9** relative to **8***b*. The ^1H nmr shift of the methyl group in **9** (δ 2.92) also appears at lower field as compared with that in **8***b* (δ 2.50). All these trends could be explained more satisfactorily by assuming the different orientation of the S—O moiety in the ring system, rather than by assuming a different substituent effect between carboxylic and acetyl groups. Although there remains some ambiguity in the structure **8***b* in view of the lack of

Can. J. Chem. Downloaded from www.nrcresearchpress.com by 210.87.254.5 on 09/06/12
For personal use only.

TABLE 2. Ultraviolet absorption data of starting ketones

Compounds	Solvents	λ_{max} (log ε)		
1*a*	EtOH	257 (4.19)		
	98% H_2SO_4	276 (4.21)		
1*b*	EtOH	264 (2.59)		
	98% H_2SO_4	293 (3.37)		
1*c*	EtOH	248 (2.56)		
	98% H_2SO_4	277 (2.99)		
7*aS*	EtOH	231 (4.22)	257 (3.72)	345 (3.04)
	98% H_2SO_4	228 (3.73)	296 (3.62)	340 (2.62)
7*bS*	EtOH	216 (3.86)	240 (3.86)[a]	273 (3.93)
	98% H_2SO_4	218 (3.97)	255 (3.98)	292 (3.92)

[a]Shoulder band.

independent synthesis, we believe structure **8***b* is the most probable among other alternatives.

Although the isolated product from 7*aS* was too unstable to permit elemental analysis, the spectroscopic data were consistent with the structure **8***a* (see Experimental).

In contrast with the facile rearrangement in sulfur analogs, both the nitrogen analog, 7*bN*, and oxygen analog, 7*bO*, were stable when irradiated in FSO_3H, and most of the starting materials were recovered.

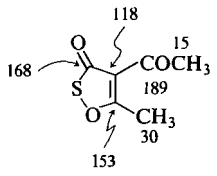

8*b*

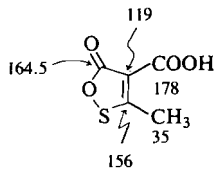

9

The ^1H nmr spectra of 7*aS* and 7*bS* in FSO_3H (Table 1) are indicative of the formation of the corresponding hydroxyl cations, 7*SH*, under these conditions. By analogy with the case of the carbocyclic β-dicarbonyl system, we envisaged the photoisomerization as involving S—C5 bond fission and subsequent recyclization with S—O bond formation (Scheme 3). Again, the stabilization of the open-chain cationic species would be responsible for the isomerization. It is known that a sulfenium cation is more stable than the univalent oxygen or nitrogen cations (17), and this trend reflects the facile rearrangement of sulfur compounds only.

As a reference, the photoreaction of these cyclic

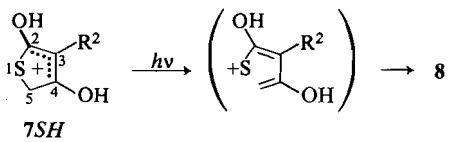

7*SH*

SCHEME 3

β-diketones under unprotonated conditions was investigated. It is reported (18) that the irradiation of **1***c* in benzene gives δ-lactone, **11**, by the C1—C2 bond cleavage and subsequent recyclization. This reaction proceeds irrespective of the presence or absence of the methyl group(s) on C5. In the present study, we confirmed that cyclic β-diketones having no methyl group on C2, such as **1***a*, were photochemically inert when irradiated in methanol. Thiolane-2,4-dione, 7*S*, and its oxygen or nitrogen analogs, 7*bO* or 7*bN*, were also intact under neutral conditions in methanol except in the case of 7*aS* in which 4-methoxy-2-oxo-2,5-dihydrothiophene, **12**, was obtained as the main product accompanied by a 22% yield of methyl acetoacetate (19).

Experimental

General

The mass spectra were obtained with a Hitachi RMS-4 spectrometer, the ir spectra with a Hitachi 215 spectrometer, the ^1H nmr spectra with a JEOL PS-100 spectrometer (with Me_4Si as the internal standard), and ^{13}C nmr spectra with a JEOL FX-10 spectrometer operated at 25.1 MHz.

Materials

The starting materials **1***a* and **5***a* were commercial samples, and **1***b*(20), **1***c*(20), **5***b*(21), **5***c*(22), 7*aS*(23), 7*bS*(24), 7*bN*(25), 7*bO*(26), and **9**(27) were prepared according to the procedures described in the literature cited. FSO_3H was prepared from 60% fuming sulfuric acid and H_2KF (28) and distilled twice under N_2 before use. D_2SO_4 was prepared by anhydrous sulfuric acid and D_2O (29).

General Procedure for the Photolysis in FSO_3H or 98% H_2SO_4

Starting ketone was dissolved in FSO_3H or 98% H_2SO_4, and the solution (0.1–0.3 *M*) was irradiated in Pyrex or quartz test tubes by means of a high pressure mercury lamp (Ushio UM 452 (450 W)) for 24 h. After the irradiation, the solution was poured onto crushed ice, and then extracted with chloroform. The chloroform solution, after washing with 10% aqueous sodium carbonate solution, was dried over sodium sulfate and evaporated *in vacuo*. The residue was treated as indicated below.

Photolysis of **1**a *or* **1**b

The viscous residue obtained by the general procedure was purified by vacuum distillation. Compound **2***a* or **2***b* was isolated

as a single product; **2***a*, bp 87°C/18 Torr (lit.12) bp 63°C/1 Torr); **2***b*, bp 110°C/18 Torr (lit.(12) bp 62°C/1 Torr). The structures of **2***a* and **2***b* were identified by comparing spectroscopic data with the reported values (12).

Photolysis of **1**a *in* D_2SO_4

A solution of **1***a* in 60% deuteriosulfuric acid was irradiated for 6 h. The viscous residue obtained by the general procedure, after work-up with H_2O, gave dideuterated compound, **4**; ^{1}H nmr (CCl_4) δ: 1.4(s, 6H), 1.92 (t, 2H, one proton of C2-methyl was deuterated), 2.3 (s, 2H), and no C3-proton was detected; mass/intensity ratio of *m/e* 140(M^+): 141 (M^+ + 1): 142 (M^+ + 2) was calculated to be 1:4.5:24.

A solution of **1***a* in 98% H_2SO_4 was irradiated for 6 h. After the irradiation, the solution was poured onto crushed ice mixed with D_2O, and then extracted with chloroform. The chloroform solution was dried over sodium sulfate and then evaporated *in vacuo*. The residue was analysed by ^{1}H nmr spectroscopy; ^{1}H nmr (CCl_4) δ: 1.4(s, 6H), 1.92(s, 3H), 2.3(s, 2H), and 5.1(s, 0.387H; H–D exchange ratio is calculated to be 61.3%).

Photolysis of **7**aS *or* **7**bS

The viscous residue obtained from **7***bS* by the general procedure gave white crystals of **8***b* upon sublimation at 55–65°C (bath)/18 Torr. In the same way, the crude solid of **8***a* was obtained from **7***aS*. Since **8***a* was unstable, the analysis was carried out on a sample without purification. For **8***a*, ir (CCl_4) ν: 1745–1710 cm^{-1}; the ^{1}H nmr spectral data are shown in Table 1; mass spectrum *m/e*: 116 (M^+), 88, and 43. For **8***b*, mp 66°C; ir(CCl_4) ν: 1745, 1650, and 1610 cm^{-1}; the ^{1}H nmr spectral data are shown in Table 1, and the ^{13}C nmr spectral data are given in the text. Mass spectrum *m/e*: 158 (M^+), 114, 87, and 43. *Anal.* calcd. for $C_4H_6O_3S$: C 45.58, H 3.83; found: C 44.82, H 3.70.

1. T. Sato, K. Nagumo, K. Saito, T. Ohyama, and R. Nakane. Chem. Lett. 1203 (1979).
2. D. G. Cornell and N. Filipescu. J. Org. Chem. **42**, 3331 (1977).
3. J. W. Pavlik and R. J. Pasterius. J. Am. Chem. Soc. **96**, 6107 (1977).
4. J. W. Pavlik, D. R. Bolin, K. C. Bradford, and W. G. Anderson. J. Am. Chem. Soc. **99**, 2816 (1977).
5. R. Noyori, Y. Ohyama, and M. Kato. J. Am. Chem. Soc. **97**, 928 (1975).
6. R. F. Childs and C. V. Rogerson. J. Am. Chem. Soc. **100**, 649 (1978).
7. K. E. Hine and R. F. Childs. J. Am. Chem. Soc. **95**, 6116 (1973).
8. T. Sato, S. Yamaguchi, and M. Kaneho. Tetrahedron Lett. 1863 (1979).
9. T. Sato, G. Izumi, and T. Imamura. J. Chem. Soc. Perkin Trans. I. 788 (1976).
10. T. Sato, K. Tamura, K. Maruyama, S. Ogawa, and T. Imamura. Chem. Lett. 295 (1976).
11. R. F. Childs and Y. C. Hor. Can. J. Chem. **55**, 3501 (1977).
12. G. A. Olah, J. L. Grant, and P. W. Westerman. J. Org. Chem. **40**, 2102 (1975); G. A. Olah and M. Calin. J. Am. Chem. Soc. **90**, 4672 (1968).
13. S. Gellin and R. Gellin. Bull. Soc. Chim. Fr. 288 (1968); 4901 (1969).
14. R. F. Childs, K. E. Hine, and E. A. Hung. Can. J. Chem. **57**, 1442 (1979).
15. C.-E. Hargberg, O. Bohaman, and C. Endahl. Tetrahedron Lett. 3689 (1972).
16. C. M. Hall and J. Wemple. J. Org. Chem. **42**, 2118 (1977).
17. E. Block. *In* Reaction of organosulfur compounds. Academic Press, New York. 1978. p. 128; M. Z. Krimer, V. A. Smit, and A. A. Shamshrin. Dokl. Akad. Nauk SSSR, **208**, 867 (1973).
18. H. Nozaki, Z. Yamaguchi, T. Okada, and M. Kawanishi. Tetrahedron, **23**, 3993 (1976).
19. K. Saito and T. Sato. Bull. Chem. Soc. Jpn. **52**, 3601 (1979).
20. T. G. Halsall and D. B. Thomas. J. Chem. Soc. 2431 (1956).
21. R. J. Friary, S. J. M. Gilligan, R. P. Szajewski, K. J. Falci, and R. W. Frank. J. Org. Chem. **38**, 3940 (1973).
22. K. W. Rosemund, H. Herzberg, and H. Schutt. Chem. Ber. **87**, 1258 (1954).
23. D. M. O'Mant. J. Chem. Soc. C, 1501 (1968).
24. E. Benery. Chem. Ber. **45**, 2103 (1901).
25. S. A. Harris. J. Med. Chem. **8**, 478 (1954).
26. R. N. Lacey. J. Chem. Soc. 832 (1954).
27. S. Allenmark and O. Bohman. Acta Chem. Scand. **22**, 1404 (1968).
28. J. Meyer and G. Schramm. Z. Anorg. Chem. **206**, 24 (1945).
29. A. Murray and D. L. Williamsons. *In* Organic synthesis with isotopes. Part 2. Interscience. 1958. p. 1311.
30. T. Yamaguchi, K. Saito, T. Tsujimoto, and H. Yuki. J. Heterocyclic Chem. **13**, 533 (1976).

Can. J. Chem. Downloaded from www.nrcresearchpress.com by 210.87.254.5 on 09/06/12
For personal use only.

Metal-catalyzed organic photoreactions. $TiCl_4$-catalyzed photoreaction of 2-acetyl-1,3-dicarbonyl compounds in methanol

KIMITOSHI SAITO AND HIDETAKA YUKI

School of Pharmaceutical Science, Toho University, Miyama 2-2-1, Funabashi, Chiba 274, Japan

AND

TOMOYUKI SHIMADA AND TADASHI SATO

Department of Applied Chemistry, Waseda University, Ookubo, Shinjuku-ku, Tokyo 160, Japan

Received January 23, 1981

KIMITOSHI SAITO, HIDETAKA YUKI, TOMOYUKI SHIMADA, and TADASHI SATO. Can. J. Chem. **59**, 1722 (1981).

When five- and six-membered cyclic β-dicarbonyl compounds having an acetyl group on the 2-position were irradiated in methanol in the presence of $TiCl_4$, a coupling reaction between the acetyl carbonyl atom and the α-carbon atom of the methanol took place, giving γ-ketoaldehydes or dihydrofurans as the main product.

KIMITOSHI SAITO, HIDETAKA YUKI, TOMOYUKI SHIMADA et TADASHI SATO. Can. J. Chem. **59**, 1722 (1981).

Lors de l'irradiation de composés β-dicarbonylés cycliques formés de 5 ou 6 chaînons et portant un groupement acétyle en position 2 dans le méthanol et en présence de $TiCl_4$, il y a formation principalement des γ-cétoaldéhydes ou des dihydrofurannes par suite d'une réaction de couplage du carbonyle du groupement acétyle et l'atome de carbone en α du méthanol.

[Traduit par le journal]

Can. J. Chem. Downloaded from www.nrcresearchpress.com by 210.87.254.5 on 09/06/12
For personal use only.

Previously we reported that a cyclic β-dicarbonyl compound, **1**, when irradiated in methanol in the presence of $TiCl_4$, underwent a novel type of reaction with the formation of a C—C bond between the substrate and the alcohol, and produced

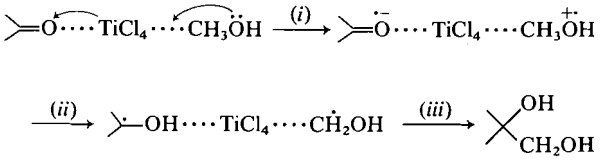

SCHEME 1

an acetal, **2** (1). The photoreaction has been pictured as involving (*i*) a photo- and metal-assisted electron transfer from alcohol to carbonyl compound, (*ii*) the succeeding proton transfer, and (*iii*) the cross-coupling of the two species to give a 1,2-diol (Scheme 1). The whole process is believed to proceed within the coordination sphere of the titanium (2). The intermediate 1,2-diols, which are in some cases isolable, further decomposed to aldehydes by dehydration, and then to the final products.

In our preceding paper (3), we described a novel effect of protonic acids on the photoreaction of five- and six-membered cyclic β-dicarbonyl compounds having an acetyl group on the 2-position. We next carried out the $TiCl_4$-catalyzed photoreaction on these compounds in order to see whether there is a similarity in the effects of $TiCl_4$ and protonic acids, and which of the three carbonyl groups is susceptible to the photoreaction under these conditions.

Results and Discussion

When a methanol solution of **3***aS* was irradiated in the presence of $TiCl_4$ for 4 h, a γ-ketoaldehyde, **5***aS*, and its acetal, **4***aS*, were obtained in 18% and 29% yields, respectively, along with a cyclization product, **6***a* (9%). Similarly, the 2-methyl deriva-

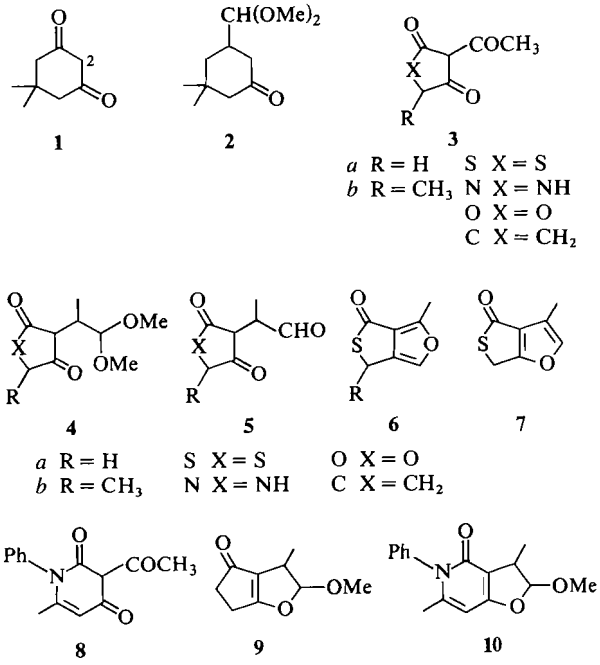

1 **2** **3**

a R = H S X = S
b R = CH_3 N X = NH
O X = O
C X = CH_2

4 **5** **6** **7**

a R = H S X = S O X = O
b R = CH_3 N X = NH C X = CH_2

8 **9** **10**

0008-4042/81/121722-02$01.00/0

©1981 National Research Council of Canada/Conseil national de recherches du Canada

Can. J. Chem. Downloaded from www.nrcresearchpress.com by 210.87.254.5 on 09/06/12
For personal use only.

tive, **3***bS*, gave **4***bS* (25%), **5***bS* (17%), and **6***b* (9%) under the same irradiation conditions. Acetals **4***aO* and **4***aN* were also obtained as the main products from the photolyses of **3***aO* and **3***aN*. The ^{1}H nmr signal of the furan proton of **6***a* at δ 7.17 splits into a triplet (J = 1.25 Hz) due to the coupling with methylene protons, and the alternative structure **7** was thus eliminated. Evidently, **4** and **5** are products from hydroxymethylation at the acetyl carbonyl group, while **6** is a product from hydroxymethylation at the ring carbonyl group. The $TiCl_4$-catalyzed reaction on **3***aC* and **8** resulted in hydroxymethylation exclusively on the acetyl carbonyl group, and **9** and **10** were isolated as major products, respectively.

In conclusion, it was found that there was no similarity in the reaction patterns of $TiCl_4$- and proton-catalyzed photoreactions, and the acetyl carbonyl group is more reactive towards the $TiCl_4$-catalyzed reactions as compared with the carbonyl group in the ring system.

Experimental

General

The mass spectra were obtained with a Hitachi RMS-4 spectrometer, the ir spectra with a Hitachi 215 spectrometer, and the ^{1}H nmr spectra with a JEOL PS-100 spectrometer (with Me_4Si as the internal standard).

Materials

The starting materials **3***aS* (4), **3***bS* (4), **3***aN* (5), **3***aO* (6), **3***aC* (7), and **8** (8) were prepared according to the procedures described in the literature cited.

General Procedures for the Photolysis in Methanol in the Presence of $TiCl_4$

Unless otherwise noted, a solution (0.02–0.03 *M*) of the starting material containing an equivalent amount of $TiCl_4$ was irradiated in a Pyrex test tube by means of a high pressure mercury lamp (Ushio UM 452 (450 W)) for 4 h. After the irradiation, the solution was concentrated *in vacuo*, and the crude residue was placed on a short Florisil column and then eluted with chloroform. The solvent was removed *in vacuo* from the eluate, and the residue was treated as indicated below.

Photolysis of **3**aS *or* **3**bS

The viscous residue obtained from **3***aS* by the general procedure was purified by preparative tlc (silica gel, 10% methanol in chloroform). Compounds **4***aS* and **5***aS* were isolated, along with **6***a*; **4***aS*, ir (CCl_4) ν: 2980, 1780, 1690, 1640, 1220, and 1020 cm^{-1}; ^{1}H nmr (CCl_4) δ: 1.05 (d, J = 7.5 Hz, 3H), 2.02 (m, 1H), 3.26 (s, 1H), 3.38 (s, 3H), 3.55 (s, 3H), 3.70 (s, 2H), and 4.38 (d, J = 3.3 Hz, 1H). Compound **5***aS*, ir ($CHCl_3$) ν: 2970, 1760, 1720, 1620, and 1420 cm^{-1}; ^{1}H nmr ($CDCl_3$) δ: 1.31 (d, J = 7 Hz, 3H), 2.04 (m, 1H), 3.32 (s, 1H), 3.94 (s, 2H), and 8.56 (s, 1H). Compound **6***a*, mp 99°C; ir ($CHCl_3$) ν: 1730, 1700, 1620, 1570, and 860 cm^{-1}; ^{1}H nmr ($CDCl_3$) δ: 2.46 (s, 3H), 4.15 (d, J = 1.25 Hz, 2H), and 7.17 (t, J = 1.25 Hz, 1H); mass spectrum *m/e*: 154 (m$^+$), 126, 125, 112, 111, 97, 83, 65, and 43. *Anal.* calcd. for $C_7H_6O_2S$: C 54.53; H 3.92; found: C 54.09, H 4.02.

Similarly, **3***bS* afforded a viscous residue by the general procedure. The formation and yield of **4***bS*, **5***bS*, and **6***b* were determined by means of their ^{1}H nmr spectra (tetrachloroethane was used as the internal standard) without further purification; ^{1}H nmr ($CDCl_3$) δ: 3.34 (s, OMe of **4***bS*), 3.91 (s, OMe of **4***bS*), 7.04 (s, furan proton of **6***b*), 8.47 (s, CHO of **5***bS*), and others.

Photolysis of **3**aN *or* **3**aO

When the viscous residue obtained from **3***aN* or **3***aO* by the general procedure was chromatographed on a Florisil column (chloroform), **4***aN* or **4***aO* was obtained as a main product; **4***aN*, ^{1}H nmr ($CDCl_3$) δ: 1.10 (d, J = 7 Hz, 3H), 3.55 (s, 3H), 3.96 (s, 2H), 4.22 (d, J = 3 Hz, 1H), and others. Compound **4***aO*, ^{1}H nmr ($CDCl_3$) δ: 1.07 (d, J = 7 Hz, 3H), 3.45 (s, 3H), 3.64 (s, 3H), 4.54 (s, 2H), and others.

Photolysis of **3**aC

When the viscous residue obtained from **3***aC* by the general procedure was chromatographed by preparative tlc (silica gel, 5% methanol in chloroform), **4***aC* and **9** were isolated; **4***aC*, ir (CCl_4) ν: 1695, 1640, 1465, 1270, and 1080 cm^{-1}; ^{1}H nmr (CCl_4) δ: 1.05 (d, J = 7 Hz, 3H), 2.3–3.0 (m, 5H), 3.20 (s, 3H), 3.32 (s, 3H), 3.92 (s, 3H), and 4.75 (d, J = 10 Hz, 1H). Compound **9**, ir ($CHCl_3$) ν: 1712 cm^{-1}; ^{1}H nmr ($CDCl_3$) δ: 1.06 (d, J = 7.5 Hz, 3H), 2.27–2.64 (m, 4H), 3.45 (s, 3H), and others.

Photolysis of **8**

When the solid obtained from **8** by the general procedure was washed with carbon tetrachloride, **10** was obtained as a single product; ir ($CHCl_3$) ν: 1640, 1600, 1570, 1490, and 1400 cm^{-1}; ^{1}H nmr ($CDCl_3$) δ: 1.48 (s, 3H), 1.85 (s, 3H), 3.83 (ABq, J = 12 Hz, 2H), 5.93 (s, 1H), and 7.1–7.7 (m, 5H).

1. T. Sato, S. Yoshiie, T. Imamura, K. Hasegawa, M. Miyahara, and O. Ito. Bull. Chem. Soc. Jpn. **50**, 2714 (1977).
2. T. Sato, H. Kaneko, and S. Yamaguchi. J. Org. Chem. **45**, 3778 (1980).
3. K. Saito, H. Yuki, T. Ohyama, R. Nakane, K. Nagumo, and T. Sato. Can. J. Chem. **59**, 1717 (1981).
4. E. Benerry. Chem. Ber. **45**, 2103 (1901).
5. S. A. Harris. J. Med. Chem. **8**, 478 (1964).
6. R. N. Lacey. J. Chem. Soc. 832 (1954).
7. F. Merenyi and M. Nilsson. Acta Chem. Scand. **18**, 1368 (1964).
8. H. Yuki, T. Tsujimoto, T. Sawada, K. Takiura, and T. Yamaguchi. J. Pharm. Soc. Jpn. **96**, 536 (1976).

Membrane transport systems. I. Synthesis and characterization of carriers for a proton driven alkali metal cation pump

LAUREL A. FREDERICK, THOMAS M. FYLES,[1] NARINE P. GURPRASAD, AND DENNIS M. WHITFIELD

Department of Chemistry, University of Victoria, Victoria, B.C., Canada V8W 2Y2

Received December 12, 1980

LAUREL A. FREDERICK, THOMAS M. FYLES, NARINE P. GURPRASAD, and DENNIS M. WHITFIELD. Can. J. Chem. **59**, 1724 (1981).

The synthesis of a series of macrocyclic polyethers (crown ethers) of interest as carriers for the countertransport of metal ions and protons across artificial membranes is described. Thallium mediated cyclization of oligoethyleneglycol diiodides with (+)−*N*,*N*,*N*′,*N*′-tetramethyltartaramide gave 15-crown-5 and 18-crown-6 diamides which were converted, via the diacids and anhydrides, to crown ether monoamides bearing long chain alkyl groups (octyl, tetradecyl, and octadecyl). The alkali metal salts and complexes of these carriers are soluble in nonpolar solvents and alkali metal ions are extracted from aqueous solutions into chloroform solutions of the carriers. Acidity constants and stability constants for complex formation in methanol/water (90:10 v/v) solutions have been determined using a combination of ion selective electrode and pH-metric techniques. Deprotonation of the ligand carboxylic acid group results not only in more stable complexes but also more selective complexation. Implications for membrane transport are discussed.

LAUREL A. FREDERICK, THOMAS M. FYLES, NARINE P. GURPRASAD et DENNIS M. WHITFIELD. Can. J. Chem. **59**, 1724 (1981).

On décrit la synthèse de polyéthers macrocycliques (éthers couronnes) qui sont intéressants en tant que phases mobiles pour le transport en sens contraire des ions métalliques et des protons à travers les membranes artificielles. La cyclisation des diiodures d'oligoéthylèneglycols avec la (+)−*N*,*N*,*N*′*N*′tétraméthyltartramide initiée par le thalium donne les diamides 15-couronne-5 et 18-couronne-6 que l'on transforme par l'intermédiaire des diacides et des anhydrides monoamides d'éthers couronnes portant une longue chaîne alkylée (octyle, tétradécyle et octadécyle). Les sels des métaux alcalins et les complexes de ces supports sont solubles dans les solvants non polaires et on extrait les ions des métaux alcalins des solutions aqueuses à l'aide des solutions des phases mobiles dans le chloroforme. On a déterminé les constantes d'acidité et de stabilité de la formation des complexes dans des solutions de méthanol/eau (90:10 v/v) en utilisant une combinaison d'électrode ionique sélective et les techniques de mesure de pH. La déprotonation du groupe acide carboxylique du ligand conduit non seulement à des complexes plus stables mais aussi à une complexation plus sélective. On discute des implications pour le transport à travers les membranes.

[Traduit par le journal]

The coupled flow of different substances across membranes is an essential feature of biological systems (1). The realization of artificial model systems which mimic the transport behaviour of natural membranes should allow detailed mechanistic analyses of single components of complex natural systems and in addition should lead to applications in analytical chemistry and separation science. Simple model systems are known. Naturally occurring ionophore antibiotics (2) and synthetic macrocyclic compounds such as the crown ethers (3) and cryptands (4) have been shown to carry metal ions across hydrophobic liquid membranes. Transport occurs by carrier mediated facilitated diffusion (5) in the direction of the concentration gradient of the transported ion.

Of particular interest from the point of view of eventual applications is the ability of biological membranes to exploit ion or proton gradients to "pump" a solute of interest from a region of low concentration to a region of higher concentration. Again, several artificial systems which model this type of behaviour have been reported. All involve a mobile carrier in the membrane phase which forms a complex with the solute of interest. The complex crosses the membrane by diffusion and the solute is released to the receiving phase. The ion whose gradient drives the process either diffuses with the complex (co-transport) or diffuses with the carrier on its return to the intake side of the membrane (countertransport) (6). For example, picrate anion can be accumulated against its concentration gradient by the co-transport of potassium ion using crown ethers as carriers (7). Similarly, crown ethers act as carriers for the countertransport of thallium and sodium ions, the gradient in sodium pumping the thallium (8). These and other similar schemes (9) are hampered by very slow transport rates, low efficiencies, and low selectivities, hence are suited neither as models for biological membranes nor as the basis for potentially useful separation schemes.

Schemes exploiting proton gradients appear to be more generally promising. In these cases the carrier is a weak acid and cations are pumped from basic to acidic solution by the countertransport of protons. Phosphatidylethanolamine (10) and stearic acid (11) have been reported to act as

[1]Author to whom correspondence should be addressed.

0008-4042/81/121724-10$01.00/0

©1981 National Research Council of Canada/Conseil national de recherches du Canada

Can. J. Chem. Downloaded from www.nrcresearchpress.com by 210.87.254.40 on 09/06/12
For personal use only.

Can. J. Chem. Downloaded from www.nrcresearchpress.com by 210.87.254.40 on 09/06/12
For personal use only.

carriers for the countertransport of potassium ions and protons. These carriers are, however, unselective and the transport rates were low. A more efficient system uses the ionophore antibiotic, monensin (2), as the carrier (12). The antibiotic, as the carboxylate, forms a stable and selective complex with sodium ion in which the carrier molecule is wrapped around the cation in a fashion similar to many other types of alkali metal ion inclusion complexes (13). Transport rates with this carrier are much higher than those reported for other model systems and, in addition, the carrier selectively transports sodium ion as the sodium complex is more stable than complexes of the other alkali metal ions. This monensin-based transport system thus bears at least qualitative resemblance to some naturally occurring transport systems (1).

Our interest in this area was stimulated by the possibilities for the design and synthesis of other carriers which, like monensin, could mediate the countertransport of protons and alkali metal ions, but unlike the natural product would be susceptible to extensive structural modifications. These modifications could influence factors such as liposolubility, overall shape, and size, and would thus influence the *rate* of transport or could influence the ability of the carrier to complex metal ions and hence would influence the *selectivity* of transport. A systematic investigation of the relationship between structure and function would thus be possible.

We chose initially to examine carriers based upon a macrocyclic polyether (crown ether) framework. Compounds of this type form inclusion complexes with metal ions; a large number of these compounds have been prepared (14) and many of the structural factors which influence complex structure, stability, and selectivity have been investigated (15). In addition lipophilic crown ethers have been shown to extract metal ions into nonpolar solvents (16) and, as described above, to act as carriers for the collapse of ion gradients across artificial and natural membranes. Crown ethers thus appeared to be a suitable starting point for consideration.

In order to mimic monensin, the proposed carrier must be a carboxylic acid, must contain donor sites for ion complexation (the crown ether), and must bear enough hydrophobic groups to render the carrier and its salt complexes soluble in a nonpolar membrane phase. In addition, the carboxylate group should be located so as to provide additional stabilization for a metal ion held in the crown ether. Several types of crown ethers (17) and "noncyclic" crown ethers (18) bearing pendant carboxylic acid groups have been described. In basic solution, the carboxylate can act as the counter-ion for a complexed metal ion (electrostatic stabilization) and, if suitably positioned, can act as an addition binding site (coordinative stabilization). The X-ray crystal structures of monensin (19) and related antibiotics of the nigericin group (2) reveal both types of behaviour. If optimally positioned, a coordinating carboxylate or other convergent binding site could result in substantially more stable and selective complexes than would be possible using the crown ether monocycle alone. This effect has been clearly demonstrated by Cram and co-workers (20). However, the additional conformational demands of such a complex imply a more elaborate molecular architecture than would be required if electrostatic stabilization alone were considered. The only structural requirement in this case is that the distance between the carboxylate group and the coordinated metal ion be as minimal as possible. In order to achieve some stabilization without the expenditure of considerable synthetic effort, we chose initially to examine carriers bearing carboxylic acid groups directly attached to the crown ether periphery. Compounds of this type have been prepared (21, 22) and the expected stabilization has been clearly revealed (23). The effect is apparently electrostatic in nature but coordination of the metal ion by the carboxylate cannot be excluded.

A large number of potential candidate carriers have structures consistent with all the design requirements cited above. One of the synthetically simplest types, of which compounds **1***a–c* and **2***a–d* are examples, was chosen for initial investigation. This paper describes the synthesis and characterization of carriers **1***a–c* and **2***a–d*. An adjoining paper describes the transport behaviour of an artificial membrane system containing **1***a–c* and **2***a–c* as carriers for the coupled countertransport of protons and alkali metal ions (24). A preliminary account of part of this work has appeared (25).

Results and Discussion

Synthesis

The syntheses of **1***a–c* and **2***a–d* were accomplished from (+)-tartaric acid. Although chiral crown ethers have been shown to exhibit chiral recognition in the complexation and transport of chiral ammonium salts (26), this feature is not at issue in this case since the substrates, metal ions, are achiral. Rather, in order to limit the number of stereoisomers, we chose to begin with a precursor

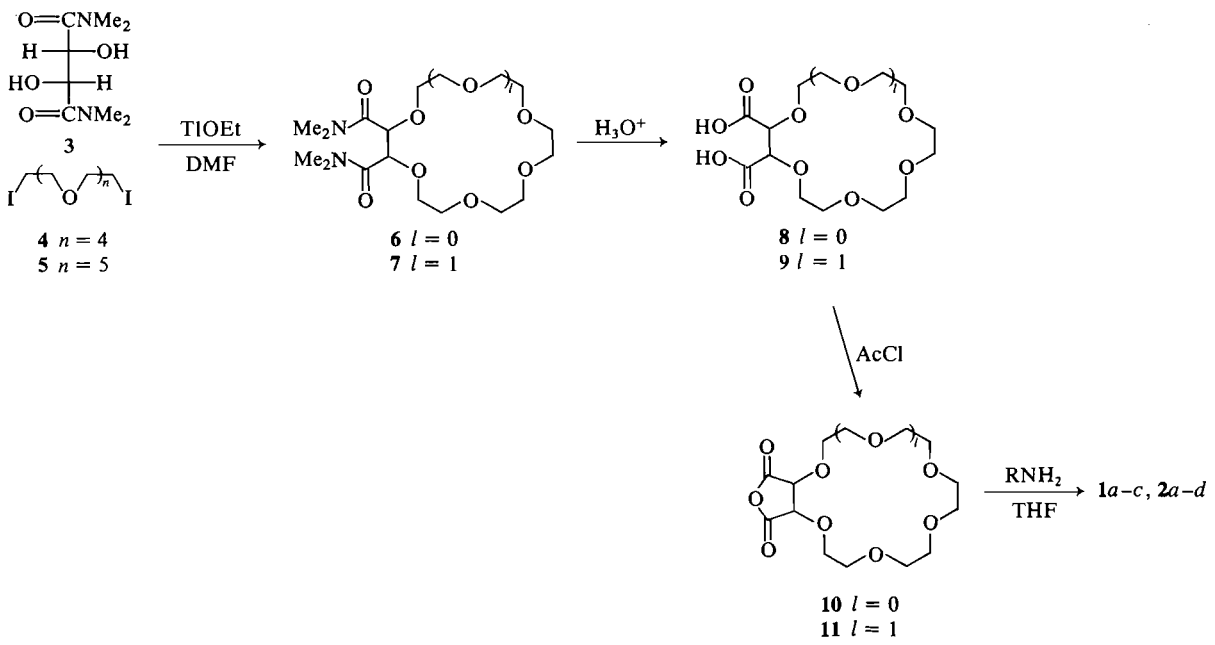

FIG. 1

of known configuration and to employ methods which would permit this configuration to be retained in the final product. Thus of the four potential isomers we have prepared only the 2*R*,3*R* isomers from 2*R*,3*R*-(+)-tartaric acid.

The synthetic scheme is outlined in Fig. 1. The bis-dimethylamide **3** (27) and the oligoethyleneglycol diiodides **4** and **5** (28) were prepared by literature methods. Alkylation of thallium(I) alkoxides is a useful modification of the Williamson ether synthesis which is compatible with readily racemized chiral centers and has been used to prepare ethers of tartaric acid (29) and crown ethers containing 2 or 3 tartarate-derived moieties (21, 22) without loss of configuration. Thus treatment of **3** in DMF with two equivalents of thallium ethoxide led to an immediate precipitation of the dithallium salt of **3**. On addition of **4** the precipitate slowly turned to the orange color of thallium iodide. Removal of TlI by filtration and evaporation of the solvent gave a yellow oil from which the 15-crown-5 diamide **6** could be isolated by chromatography.[2] In a similar fashion **3** and **5** gave the 18-crown-6 derivative **7**. Yields in both cases were ca. 40%.

Acidic hydrolysis of **6** or **7** gave the diacids **8** and **9** respectively[2] which on reflux with a vast excess of acetyl chloride were smoothly dehydrated to the crown ether anhydrides **10** and **11**. The carriers **1***a–c* and **2***a–d* were prepared from **10** or **11** by treatment with 2.2 equivalents of octylamine, tetradecylamine, octadecylamine, or butylamine in dry THF. The product initially isolated by evaporation of the solvent is the corresponding alkylammonium salt of **1***a–c* or **2***a–d*. In the case of **2***d*, butylammonium was removed by extraction with aqueous acid. In the other cases, ion exchange was necessary as the alkylammonium halides are water insoluble. However, even after several treatments with strongly acidic ion exchange resins, significant amounts of the alkylammonium salts remained, which may be in part due to the complexation of the ammonium group by the crown ether. The carriers **1***a–c* and **2***a–c* could be freed of the last traces of ammonium salt by gel permeation chromatography, in which the salt or complex having the higher molecular weight and larger size was eluted first, or by reverse phase chromatography in which the more polar salt was eluted first.

Properties

With the exception of **2***d* which was prepared primarily for thermodynamic studies, the carriers are all clear viscous oils or low melting waxy solids. They are soluble in all organic solvents but are virtually insoluble in water. Attempts to determine coefficients for the distribution of the carriers between chloroform and various aqueous solutions (acidic, basic, with or without metal ions) met with

[2]Another independent synthesis of **6** and **8** by the same methods has recently been reported (37).

Can. J. Chem. Downloaded from www.nrcresearchpress.com by 210.87.254.40 on 09/06/12
For personal use only.

Can. J. Chem. Downloaded from www.nrcresearchpress.com by 210.87.254.40 on 09/06/12
For personal use only.

only limited success. Basic or metal ion containing solutions inevitably gave emulsions which separated to three phases after long times. Deprotonation with or without metal ion binding produces an amphiphilic molecule, hence emulsion formation is not surprising. In cases where emulsions did not form (acidic solution, no metal ions) the distribution coefficients ($D = [X]_{org}/[X]_{aq,org} = CDCl_3$) were large; log D ca. 3.8 for **2***a*, log D ca. 3.0 for **1***a* as estimated by nmr (15). The corresponding values for **1***b*,*c* and **2***b*,*c* are larger but the method was insufficiently sensitive for the accurate determination of the small amounts of the carriers in the aqueous phase.

Qualitatively, all the potential extraction equilibria favour forms in which the carrier or its complexes remain in the organic phase. The potassium, sodium, and rubidium salts of the carriers can be prepared by gently stirring a chloroform solution of the carrier with aqueous solutions of the metal hydroxide. The carriers will dissolve solid alkali metal salts into chloroform solution. None of the carriers can be extracted into homogeneous aqueous solution, either by bases or by alkali metal ion solutions. It is thus probable that during the transport experiments, little, if any of the carrier would be lost from the membrane phase.

Acidity and Stability Constants

In order to define suitable conditions for transport experiments and to rationalize observed transport selectivities (24) we have determined the acidity constants of the carriers and the concentration stability constants for complex formation with alkali metal cations (30). Consider the following set of equilibria involving a ligand (the carrier) in its protonated (LH) and deprotonated forms (L) and a metal ion (M).[3]

[1] $LH \rightleftharpoons L + H$ $\qquad K_a = [L][H]/[LH]$

[2] $LH + M \rightleftharpoons LHM$ $\qquad K_1 = [LHM]/[LH][M]$

[3] $L + M \rightleftharpoons LM$ $\qquad K_2 = [LM]/[L][M]$

Equation [1] defines the normal acidity constant for LH, eq. [2] defines the concentration stability constant K_1 for formation of the 1:1 complex LHM from LH and M, and eq. [3] defines a stability constant K_2 for a 1:1 complex between L and M. Additional equilibria involving other complex stoichiometries are possible. Of interest is the apparent acidity constant for the complex LHM, defined by eq. [4].

[4] $LHM \rightleftharpoons LM + H$ $\qquad K_{a'} = [LM][H]/[LHM]$

Equations [1]–[4] overdefine the set of 1:1 complexes between L, H, and M, and it is straightforward to show that:

[5] $K_{a'} = (K_2/K_1)K_a$

or

[6] $pK_a - pK_{a'} = \log K_2 - \log K_1$

Independent determinations of K_a, $K_{a'}$, K_1, and K_2 will allow the data to be internally tested using [6]. Should the relationship [6] be found to hold, other equilibria involving other complexes must therefore be unimportant under the conditions of the experiment and the equilibria [1]–[3] may be assumed to adequately model the solution behaviour of L, H, and M.

The acidity constants $K_{a'}$ were determined from the pH metric titration curves obtained on addition of tetramethylammonium hydroxide to a methanol/water (90:10 v/v) solution of the free acid. The data were analysed as previously described (31) using a modified version of the program SCOGS (32). The stability constants for complex formation with sodium, potassium, and rubidium ions were determined using glass electrodes sensitive to these ions. Commercially available potassium electrodes are sufficiently sensitive to rubidium to allow the direct determination of rubidium ion (in the absence of interfering potassium ion). The method has been previously described (30) and our modifications are outlined in the Experimental. Solutions were buffered to ensure that to a good approximation only LH or L was present. The stability constant determined in acidic solution is thus K_1 and the stability constant determined in basic solution is K_2.

A knowledge of K_1 and K_2 permits an estimation of the minimum metal ion concentration at which effectively all the ligand, whether protonated or not, will be present as a metal ion complex. Determination of an acidity constant under these conditions will give the apparent acidity constant of the complex LHM, i.e. $K_{a'}$. The results of these determinations are reported in Table 1 for the case of **2***d*, together with the value of $pK_{a'}$ calculated using eq. [6]. The agreement between the measured and calculated values of $pK_{a'}$ is good and well within the limits of the experimental errors. This confirms that the eqs. [1]–[3] adequately model the solution behaviour of L, H, and M.

With this assurance we can turn to a more efficient method of determining K_1 and K_2 directly from pH metric titration data albeit with the loss of

[3]Charges are omitted throughout for clarity. In all cases LH and LM are neutral, L is negatively charged, and M and H are unipositively charged.

Can. J. Chem. Downloaded from www.nrcresearchpress.com by 210.87.254.40 on 09/06/12
For personal use only.

the internal cross checks of the ion selective electrode determinations. Consider a generalized cumulative association constant defined as

$$[7] \quad \beta_{lmh} = [L_l M_m H_h]/[L]^l[M]^m[H]^h$$

where l, m, and h are integers including zero which denote the number of ligands, metal ions, and protons respectively, bound in a given species. Thus β_{110} is the formation constant for a species containing one ligand, one metal ion, and no protons, i.e. K_2 as defined by eq. [3]. It can be similarly shown that $\beta_{101} = 1/K_a$ and $\beta_{111} = K_1/K_a$ ($\log \beta_{101} = -pK_a$ and $\log \beta_{111} = \log K_1 + pK_a$). In a fashion analogous to that previously described with respect to the complexation of anions by polyguanidinium salts (31), computer analysis of the pH-metric titration curves obtained at various ratios of L/M gave a set of β_{lmh} which described the system, from which values of K_1 and K_2 were calculated.

The results for the various different types of analyses for alkali metal ions and the carriers prepared are given in Table 2. It appeared unnecessary and redundant to determine all the stability constants for all pairs of ligand and metal ions as the effect of varying the alkyl side chain on complex formation was expected to be small. Thus **1***a* and **2***d* were chosen as "typical" representative 15-crown-5 and 18-crown-6 derivatives and a complete set of constants was determined for these two ligands. Spot checks of the above assumption proved it to be substantially correct; **1***a*/K^+ the same as **1***c*/K^+ and **2***d*/Na^+ the same as **2***a*/Na^+.

Insofar as acidity constants are concerned, all carriers were found to have $pK_a = 5.95 \pm 0.10$. As such they are somewhat stronger acids than acetic (pK_a 7.15 in methanol/water (90:10 v/v) under our conditions). It is not clear what the pK_a would be in pure water. In general, simple carboxylic acids are ca. 1–2 pK_a units weaker acids in methanol/water solution (31) than in water itself. A pK_a in water of about 4 is not inconsistent with the transport results reported in the accompanying paper which suggest an apparent pK_a at the water/chloroform interface greater than 3.3 (24).

TABLE 1. Acidity constants and stability constants for the complexation of sodium, potassium, and rubidium ions by **2***d*[a,b]

	Na^+	K^+	Rb^+
$\log K_1$[c]	3.3	4.5	4.0
$\log K_2$[c]	4.4	5.8	5.0
$pK_{a'}$ measured[c]	4.82	4.63	5.01
$pK_{a'}$ calculated[d]	4.91	4.71	5.01

[a]In methanol/water (9:1 v/v) at 25 ± 0.1°C. For concentrations, conditions, and other experimental detail see Experimental.
[b]pK_a **2***d* = 6.01.
[c]pK_a ± 0.10, log K ± 0.2; for a discussion of accuracy and precision see Experimental.
[d]Using eq. [6].

The stability constants follow the expected trends. The 18-crown-6 derivatives show peak selectivity (30) for potassium; the 15-crown-5 derivatives show complex stability decreasing along the series Na^+, K^+, Rb^+. The increase in complex stability between the acidic and basic forms of the ligand is also expected. Work with related systems (22, 23) has shown that carboxylate groups stabilize ammonium and metal ion complexes by electrostatic interactions. The effect can be very large, up to a factor of 5000 for ammonium complexation in water solution induced by the presence of four carboxylate groups. The factors of 5–25 fold stabilization observed in our case are perhaps smaller than might have been expected but the different solvents involved may partly explain the smaller effect. Since methanol/water mixtures are less polar than pure water, complexation of any type is to be favoured, hence the importance of other interactions must be diminished.

It is interesting to note, especially with reference to the complexes of **2***d*, that the electrostatic stabilization afforded the ion by the carboxylate group is most pronounced for the ion which is most strongly complexed. Thus K^+, selectively complexed by **2***d*, is a factor of 20 times more strongly complexed in basic solution than in acidic solution compared to factors of 10 and 12 times for Rb^+ and Na^+ respectively. Looked at from another point of view, the basic forms of the ligands are more selective than are the acidic forms; the K^+/Na^+ selectivity of **2***d* in acidic solution is ca. 16 while in basic solution it is ca. 25. These results suggest additional structural recognition of the ion by the ligand, possibly with the carboxylate acting as an additional binding site.

These thermodynamic results hold a number of implications for the transport of alkali metal ions using carriers **1***a–c* and **2***a–c*. It has been noted in other systems that transport rate is a complex function of many parameters including the stability of the complex formed (33, 34). The optimal value of the equilibrium constant for complexation is about 10^5–10^6 ($6 \gtrsim \log K \gtrsim 5$) in methanol (34); complexes less stable than this are not efficiently extracted, while complexes more stable than this are too efficiently held in the membrane. Our values suggest that of the ions and carriers considered, potassium will be selectively transported by 18-crown-6 derivatives while overall rates will be lower with 15-crown-5 derivatives but selective for sodium. The potassium ion complex of **2***d* has a log K_2 value within the optimal range. The thermody-

TABLE 2. Stability constants for the complexation of sodium, potassium, and rubidium ions by the carriers[a]

Carrier	Stability constant[b]	Na^+		K^+		Rb^+	
		ISE[c]	pH[d]	ISE[c]	pH[d]	ISE[c]	pH[d]
1*a*	log K_1	2.7	2.7	2.2	2.1	[e]	1.8
	log K_2	3.4	3.4	3.0	2.9	2.6	2.7
2*d*	log K_1	3.3	3.1	4.5	4.2	4.0	3.8
	log K_2	4.4	4.2	5.8	5.5	5.0	4.8
1*c*	log K_1	—	—	—	2.1	—	—
	log K_2	—	—	—	2.9	—	—
2*a*	log K_1	—	3.1	—	—	—	—
	log K_2	—	4.2	—	—	—	—
2*b*	log K_1	—	—	4.4	—	—	—

[a]In methanol/water (9:1 v/v) at 25 ± 0.1°C. For concentrations, conditions, and other experimental detail see Experimental.
[b]log K ± 0.2, K_1 and K_2 defined in text.
[c]Determined using ion selective electrode techniques (30).
[d]Determined using pH-metric techniques (31).
[e]Complex stability too low to be accurately determined log $K \cong 1.7$.

namic results also suggest that extraction and transport of ions from a basic solution will be a more selective process for a given carrier than extraction and transport of the same ions from an acidic solution. The transport scheme envisaged involves the pumping of ions from basic to acidic solution; pumping is likely therefore to be more selective than any "leakage" from the acidic to the basic side which might occur. In a system of this type, the membrane selectivity might then be enhanced by *allowing* the membrane to leak, for example by providing a liposoluble anion in the acidic phase (3, 33).

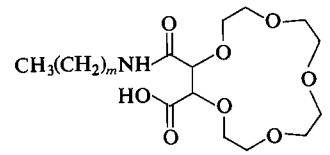

1*a* $m = 7$
1*b* $m = 13$
1*c* $m = 17$

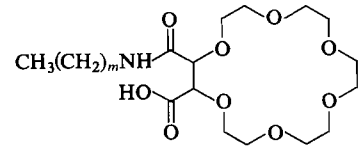

2*a* $m = 7$
2*b* $m = 13$
2*c* $m = 17$
2*d* $m = 3$

Experimental

General Details

Melting points were taken using a Koefler hotstage microscope and are uncorrected. The ir spectra were recorded using a Perkin Elmer 283 spectrometer in $CHCl_3$ as solvent unless otherwise stated. The proton nmr spectra were recorded using a Perkin Elmer R12B (60 MHz) or R32 (90 MHz) spectrometer using $CDCl_3$ as solvent containing tetramethylsilane (TMS) as internal standard. The carbon nmr spectra were recorded using a Nicolet TT14 spectrometer (15.1 MHz) in $CDCl_3$ containing TMS unless otherwise specified. The mass spectra were recorded using a Finnegan 3300 GC-MS using methane chemical ionization. Specific rotations were calculated from optical rotation values obtained using a Perkin Elmer 141 polarimeter and a 1 dm cell in $CHCl_3$ as solvent unless otherwise stated. Elemental analyses were performed by Canadian Microanalytical Services, Vancouver, B.C.

Precursors

(*a*) *R,R*-(+)-*N,N,N',N'*-Tetramethyltartaramide (**3**) was prepared from (+)-tartaric acid by dimethylammonolysis of the diester (27); $[\alpha]_D^{20}$ +43.2° (*c* 3.0, ethanol) (lit. (19) +42.7° (*c* 3.6, ethanol)).

(*b*) 1,11-Diiodo-3,6,9-trioxaundecane (**4**) was prepared from tetraethylene glycol via the dichloride (28); bp 95°C/0.5 Torr (lit. (28) "about 95°C/0.4 Torr"). The dichloride in acetone was allowed to reflux overnight with a fivefold excess of NaI and the solution was concentrated to a thick sludge which was taken up in water, extracted with CH_2Cl_2, the organic layer dried over Na_2SO_4 and evaporated to yield a thick yellow oil. The crude diiodide was used directly without further purification; ^1H nmr δ: 3.70 (4H) and 3.30 (4H) (A_2B_2, J_{AB} 7 Hz, OCH_2CH_2I), 3.60 (10H, brs, all other protons).

(*c*) 1,14-Diiodo-3,6,9,12-tetraoxatetradecane (**5**) was prepared by a sequence similar to that described for (**4**). Triethylene glycol was converted to the dichloride (bp 65°C/1 Torr). The dichloride was heated in ethylene glycol containing 2.2 equivalents of sodium to give pentaethylene glycol (28) (bp 155–160°C/1 Torr) which gave the dichloride (bp 120°C/1 Torr) and finally the diiodide **5**; ^1H nmr δ: 3.70 (4H) and 3.30 (4H) (A_2B_2 J_{AB} 7 Hz, OCH_2CH_2I), 3.60 (12H, brs, all other protons).

2R,3R-(+)-N,N,N',N',-Tetramethyl-2,3-dicarboxamido-1,4,7,10,13-pentaoxacyclopentadecane (7) (37)

A 2 L 3-neck flask fitted with an argon inlet and bubbler, condenser, and mechanical stirrer was charged with 1600 mL of dry dimethylformamide (DMF) and 20.5 g (0.100 mol) of **3**. The solution was heated to 90°C under a stream of argon and 14.5 mL

Can. J. Chem. Downloaded from www.nrcresearchpress.com by 210.87.254.40 on 09/06/12
For personal use only.

Can. J. Chem. Downloaded from www.nrcresearchpress.com by 210.87.254.40 on 09/06/12
For personal use only.

(14.0 mequiv./mL, 0.200 equiv.) of thallium ethoxide (35) was added via a syringe which resulted in immediate formation of a white precipitate, presumably the dithallium salt of **3** (21, 22). To this slurry was added a total of 42.5 g (0.21 equiv.) of diiodide **4** in 20 mL of DMF via syringe over a period of 10 min. The resultant mixture was stirred at 90°C and gradually turned orange as thallium iodide was formed. After 4 h the mixture was cooled to room temperature, 100 mL of water was added, and the precipitate was removed by filtration. The bulk of the solvent was removed on a rotary evaporator and the crude product containing DMF and traces of thallium iodide was passed through a short column (10 cm) of alumina followed by a washing with 250 mL of chloroform. The combined filtrates were evaporated and pumped at high vacuum overnight. The crude product was taken up in chloroform, absorbed on 50 g of Celite, and pumped at high vacuum for a second night. In this fashion the bulk of the DMF was removed. The subsequent chromatographic separation is strongly dependent upon the proportion of DMF remaining at this stage. The crude product on Celite was added to the top of a column of alumina (activity II, 5 × 80 cm) and eluted with a gradient of methanol in chloroform (0 → 4% v/v, 4 L total volume). Depending on the amount of DMF the product was eluted at about 2% methanol in chloroform. Fractions were monitored by tlc (10% methanol in chloroform, alumina, R_f **6** ~ 0.7) and by nmr. Product containing fractions were combined and rechromatographed on the same size of alumina column using the same solvent gradient to give 14.8 g of a clear, colorless oil. This material is sufficiently pure to carry on to further reactions.[4] Gel permeation chromatography (Sephadex LH20, 2.5 × 90 cm, 3.0 mL/min, 5.0 mL fractions, $CHCl_3/CH_3OH$ 2:1 (v/v) as eluent) of a 0.50 g sample of this oil gave a small faster moving fraction (35 mg) enriched in the cyclic dimer, a 30-crown-10 derivative (37) and a well separated slower moving major fraction (465 mg) of **6** as a clear colorless oil; ir cm^{-1}: 2880, 2920 (CH), 1650 (C=O), 1120 (C—O); $[\alpha]_D^{20}$ +74.7 (*c* 5.8); ^1H nmr δ: 4.78 (2H, s, OCHC=O), 3.65 (16H, brs, CH_2O), 3.15 and 2.90 (6H, s, CH_3N); ^{13}C nmr δ: 169.5 (C=O), 76.5 (CH), 70.6–68.8 (CH_2O), 37.3 and 35.6 (CH_3N); ms *m/e*: 363 (M + 1, 95), 290 (M − DMF + 1, 15), 245 (characteristic of a 15-crown-5 bearing a carbonyl, i.e. 15-crown-5 $C{\equiv}O^+$, 100). *Anal.* calcd. for $C_{16}H_{30}N_2O_7$: C 53.02, H 8.34, N 7.73; found: C 52.81, H 8.31, N 7.59.

2R,3R-(+)-N,N,N′,N′-Tetramethyl-2,3-carboxamido-1,4,7,10,13,16-hexaoxacyclooctadecane (7)

By a method analogous to that described for **6**, 20.5 g of **3**, 14.5 mL of thallium ethoxide, and 46.5 g of **5** gave 16.1 g of **7** (40%) as a clear colorless oil. A small sample was crystallized from hexane/ether but the bulk of the sample was used as an oil; mp 69.5–70°C; ir cm^{-1}: 1660 (C=O), 1120 (C—O); $[\alpha]_D^{20}$ +51.5° (*c* 2.6); ^1H nmr δ: 4.80 (2H, s, OCHC=O), 3.65 (20H, brs, CH_2—O), 3.15 and 2.88 (6H, s, CH_3N); ^{13}C nmr δ: 169.5 (C=O), 76.6 (CH—O), 70.6–68.9 (CH_2O), 37.3 and 35.6 (CH_3N); ms *m/e*: 407 (M + 1, 100), 289 (characteristic of 18-crown-6 + carbonyl, i.e. 18-crown-6 $C{\equiv}O^+$, 20). *Anal.* calcd. for $C_{18}H_{34}N_2O_8$: C 53.19, H 8.43, N 6.89; found: C 52.96, H 8.39, N 6.71.

2R,3R-(+)-2,3-Dicarboxyl-1,4,7,10,13-pentaoxacyclopentadecane (8) (37)

A mixture of 13.0 g of **6**, 25 mL of concentrated hydrochloric acid, and 100 mL of water was stirred at reflux overnight. The resultant solution was cooled, concentrated to about 50 mL total volume, placed in a heavy liquid continuous extractor, and extracted for 4 days with purified (alcohol-free) dichloromethane. The extract was dried over Na_2SO_4 and evaporated to give a viscous oil which contained a small amount of water. Complete drying of this oil by azeotropic distillation or by pumping at high vacuum was not successful. The hydrate could be crystallized from wet acetone/ether (overall yield 65%); mp ca 60°C; ir (KBr) cm^{-1}: 3600–2400 (OH), 1750 (C=O), 1120 (C—O); $[\alpha]_D^{20}$ +14.5 (*c* 0.7); ^1H nmr (D_2O, external TMS) δ: 4.40 (2H, s, $CHCO_2H$), 3.65 (16H, brs, CH_2O); ^{13}C nmr (D_2O, external TMS) δ: 174 (CO_2H), 80.7 ($CHCO_2H$), 72–71.2 (CH_2O); ms *m/e*: 309 (hydrate − H_2O + 1, 100), 245 (15-crown-5 $C{\equiv}O^+$, 25). *Anal.* calcd. for $C_{12}H_{20}O_{10}$ (8·H_2O): C 44.17, H 6.79; found: C 43.81, H 6.89.

2R,3R-(+)-2,3-Dicarboxyl-1,4,7,10,13,16-hexaoxacyclooctadecane (9)

By a method analogous to that described for **8**, **7** gave **9** in 75% yield; mp 108°C (acetone/ether); ir (KBr) cm^{-1}: 3500–2500 (OH), 1745 (C=O), 1100 (C—O); $[\alpha]_D^{25}$ +34.7 (*c* 1.5, H_2O); ^1H nmr (D_2O, external TMS) δ: 4.48 (2H, s, $CHCO_2H$), 3.70 (20H, brs, CH_2O); ^{13}C nmr (D_2O, external TMS) δ: 174.5 (CO_2H), 80.5 ($CHCO_2H$), 70.0 (CH_2O); ms *m/e*: 353 (M + 1, 100), 289 (18-crown-6 $\overset{+}{C}{\equiv}O$, 20). *Anal.* calcd. for $C_{14}H_{24}O_{10}$: C 47.72, H 6.87; found: C 47.81, H 6.86.

General Method for the Preparation of Crown Ether Monoamides

The diacid (**8** or **9**) was dissolved in acetyl chloride (~15 mL/g diacid) and stirred at reflux overnight. The solution was cooled and evaporated four times with 20 mL of benzene and pumped at high vacuum for 2 h. The crude anhydrides **10** or **11** were not further purified; for **10**, ir cm^{-1}: 1880, 1805 (5 membered cyclic anhydride); ^1H nmr δ: 4.84 (2H, s, —CHCO), 4.0 (2H, m), 3.70 (14H, brs); for **11**, ir cm^{-1}: 1880, 1805 (5 membered cyclic anhydride); ^1H nmr δ: 4.91 (2H, s, CHC=O), 4.0 (2H, m), 3.72 (16H, brs), 3.65 (2H, m).

The crude anhydride (**10** or **11**) was taken up in 10 mL/g freshly dried THF and treated with 2.2 equivalents of a primary alkyl amine. The mixture was stirred at reflux for 2 h, cooled, and evaporated to dryness. The crude alkylammonium crown ether amidocarboxylate was dissolved in isopropanol/chloroform (1:3 v/v) and passed slowly through a bed of strongly acidic cation exchange resin in the same solvent. The resin was washed exhaustively and the combined washings were evaporated to oils. Purification was achieved in two ways: (*1*) by gel permeation chromatography on Sephadex LH20 (2.5 × 90 cm column, 3.0 mL/min gravity flow, 5.0 mL fractions) using chloroform/methanol (4:3 v/v) as eluent, in which case the heavier impurity was eluted first, or (*2*) by reverse phase chromatography on RP-8 (Merck Lobar prepacked column, pressurized with 150 Torr of argon, 3.0 mL/min, 5.0 mL fractions) using 0–15% chloroform in methanol as eluent, in which case the desired product was eluted after the impurities. Fractions were monitored by tlc (reverse phase Merck RP2 on glass, 25% methanol in chloroform, R_f ~ 0.7–0.8 for **1***a–c*, **2***a–c*) and by ^1H nmr. In the acidity constant determination, alkylammonium contamination could be detected below 1.0

[4]Purification of the oil is not required as the cyclic dimer is mostly removed at the diacid (tetracid) stage and finally eliminated during final gel permeation chromatography of **1***a–c*. A recent synthesis of **6** by an analogous route (37) reports **6** as a solid mp 65°C. Solid samples of **6** may be obtained from our oily fraction on lengthy standing to give physical properties identical with those reported (37) except the ^1Hmr spectra show additional very broad signals at 10.5–9.5 (about 3H). Elemental analyses suggest these solids are hydrates. *Anal.* calcd. for $C_{16}H_{33}O_{8.5}N_2$(**6**,1.5H_2O): C 49.34, H 8.54, N 7.19; found: C 49.44, H 8.48, N 7.51. The solids go to oils on drying in vacuum and give correct elemental analyses for the anhydrous material.

Can. J. Chem. Downloaded from www.nrcresearchpress.com by 210.87.254.40 on 09/06/12
For personal use only.

wt.%. All samples were better than this level of purity. In this fashion were prepared the following.

2R,3R-(+)-N-Octyl-2-carboxamido-3-carboxyl-1,4,7,10,13-pentaoxacyclopentadecane (1a)

Purified by gel permeation, as a clear colorless oil in 70% yield from **8**; ir (neat) cm^{-1}: 3340 (NH), 3600–2400 (OH), 1745 (CO_2H), 1670, 1635, 1540 (amide), 1120 (C—O); $[\alpha]_D^{20}$ +16.4 (*c* 5.4); ^1H nmr δ: 8.4 (1H, br, CO_2H), 7.4 (1H, brt, NH), 4.48 and 4.35 (2H, dd, AB, J_{AB} 3 Hz, O—CH—CH—O), 3.60 (16H, brs, CH_2O), 3.30 (2H, m, CH_2N), 1.30 (12H, brs, —CH_2—), 0.90 (3H, brt, CH_3); ^{13}C nmr δ: 172.0, 169.2 (CO_2H, CONH), 80.3, 79.4 (CH—CH), 70.6–69.4 (CH_2O), 39.5 (CH_2N), 31.8 (—CH_2—), 29.3, 26.9, 22.6, 14.1 (alkyl chain end); ms *m/e*: 420 (M + 1, 100), 245 (15-crown-5 C≡O^+, 25). *Anal.* calcd. for $C_{20}H_{37}NO_8$: C 57.26, H 8.89, N 3.34; found: C 57.60, H 8.97, N 3.39.

2R,3R-(+)-N-Tetradecyl-2-carboxamido-3-carboxyl-1,4,7,10,13-pentaoxacyclopentadecane (1b)

Purified by gel permeation, as a waxy solid in 60% yield from **8**; ir cm^{-1}: 3320 (NH), 3600–2400 (OH), 1740 (CO_2H), 1670, 1635, 1530 (amide), 1120 (C—O); $[\alpha]_D^{20}$ +16.8 (*c* 5.0); ^1H nmr δ: 7.4 (1H, brt, NH), 6.5 (1H, brs, CO_2H + trace H_2O), 4.48 and 4.35 (2H, dd, AB, J_{AB} 2.5 Hz, OCH—CHO), 3.65 (16H, brs, CH_2O), 3.30 (2H, m, CH_2N), 1.30 (24H, brs, —CH_2—), 0.9 (3H, brt, CH_3); ^{13}C nmr δ: 172.2, 168.9 (CO_2H, CONH), 80.5, 79.5 (CH—CH), 70.7, 70.3, 69.8, 69.4 (CH_2O), 39.5 (CH_2N), 31.9 (—CH_2—), 29.6, 26.9, 22.7, 14.1 (alkyl chain end); ms *m/e*: 504 (M + 1, 100), 245 (15-crown-5 C≡O^+, 60). *Anal.* calcd. for $C_{24}H_{49}NO_8$: C 62.00, H 9.80, N 2.78; found: C 61.83, H 9.72, N 2.64.

2R,3R-(+)-N-Octadecyl-2-carboxamido-3-carboxyl-1,4,7,10,13-pentaoxacyclopentadecane (1c)

Purified by reverse phase chromatography, as a waxy solid, recrystallized from pentane in 78% yield from **8**, mp 57°C; ir cm^{-1}: 3340 (NH), 3600–2500 (OH), 1745 (CO_2H), 1670, 1635, 1550 (amide), 1120 (C—O); $[\alpha]_D^{20}$ +16.8 (*c* 4.8); ^1H nmr δ: 8.6 (1H, brs, CO_2H), 7.4 (1H, brt, NH), 4.45 and 4.35 (2H, dd, AB J_{AB} 2.5 Hz, CH—CH), 3.65 (16H, brs, CH_2O), 3.30 (2H, m, CH_2N), 1.30 (32H, brs, —CH_2—), 0.90 (3H, brt, CH_3); ^{13}C nmr δ: 172.3, 168.8 (CO_2H, CONH), 80.6, 79.5 (CH—CH), 70.6–69.4 (CH_2O), 39.5 (CH_2N), 31.9 (—CH_2—), 29.7, 26.9, 22.7 and 14.1 (alkyl chain end); ms *m/e*: 542 (M − H_2O + 1, 100), 245 (15-crown-5 C≡O^+, 70), no M + 1. *Anal.* calcd. for $C_{30}H_{57}NO_8$: C 64.37, H 10.26, N 2.50; found: C 64.37, H 10.48, N 2.60.

2R,3R-(+)-N-Octyl-2-carboxamido-3-carboxyl-1,4,7,10,13,16-hexaoxacyclooctadecane (2a)

Purified by gel permeation, as a wax in 80% yield from **9**; ir cm^{-1}: 3360 (NH), 3600–2400 (OH), 1750 (CO_2H), 1670, 1635, 1540 (amide), 1110 (C—O); $[\alpha]_D^{20}$ +28.7 (*c* 7.3); ^1H nmr δ: 8.5 (1H, brs, CO_2H), 7.40 (1H, brt, NH), 4.42 and 4.34 (2H, dd, AB J_{AB} 2.0 Hz, CH—CH), 3.64 (20H, brs, CH_2O), 3.30 (2H, m, CH_2N), 1.30 (12H, brs, —CH_2—), 0.9 (3H, t, CH_3); ^{13}C nmr δ: 171.8, 169.5 (CO_2H, CONH), 81.0, 80.0 (CH—CH), 70.1 (CH_2O), 39.4 (CH_2N), 31.8 (—CH_2—), 29.3, 27.0, 22.6 and 14.1 (alkyl chain end); ms *m/e*: 464 (M + 1, 60), 446 (M − H_2O + 1, 100), 289 (18-crown-6 C≡O^+, 51). *Anal.* calcd. for $C_{22}H_{41}NO_9$: C 57.00, H 8.91, N 3.02; found: C 57.04, H 9.04, N 3.09.

2R,3R-(+)-N-Tetradecyl-2-carboxamido-3-carboxyl-1,4,7,10,13,16-hexaoxacyclooctadecane (2b)

Purified by reverse phase chromatography, as a clear oil in 61% yield from **9**; ir cm^{-1}: 3350 (NH), 3600–2400 (OH), 1740 (CO_2H), 1670, 1630, 1530 (amide), 1110 (C—O); $[\alpha]_D^{20}$ +28.4 (*c* 6.6); ^1H nmr δ: 7.8 (1H, br, CO_2H), 7.3 (1H, brt, NH), 4.42 and 4.32 (2H, dd, AB J_{AB} 3 Hz, —CH—CH—), 3.64 (20H, brs, CH_2O—), 3.30 (2H, m, CH_2N—), 1.30 (24H, brs, —CH_2—), 0.9 (3H, brt, CH_3); ^{13}C nmr δ: 171.5, 169.1 (CO_2H, CONH), 80.9, 80.4 (CH—CH), 69.9 (CH_2O), 39.4 (CH_2N), 31.9 (—CH_2—), 29.6, 26.9, 22.7 and 14.1 (alkyl chain end); ms *m/e*: 548 (M + 1, 100), 289 (18-crown-6 C≡O^+, 31). *Anal.* calcd. for $C_{28}H_{53}NO_9$: C 61.40, H 9.75, N 2.55; found: C 61.53, H 9.91, N 2.59.

2R,3R-(+)-N-Octadecyl-2-carboxamido-3-carboxyl-1,4,7,10,13,16-hexaoxacyclooctadecane (2c)

Purified by reverse phase chromatography, followed by gel permeation, as a wax in 58% yield from **9**; ir cm^{-1}: 3360 (NH), 3600–2500 (OH), 1740 (CO_2H), 1670, 1635, 1540 (amide), 1110 (C—O); $[\alpha]_D^{20}$ +29.0 (*c* 9.75); ^1H nmr δ: 8.5 (1H, br, CO_2H), 7.30 (1H, brt, NH), 4.42 and 4.38 (2H, dd, AB J_{AB} 2.5 Hz, —CH—CH—), 3.65 (20H, brs, CH_2—O—), 3.30 (2H, m, CH_2N), 1.30 (32H, brs, —CH_2—), 0.9 (3H, brt, CH_3); ^{13}C nmr δ: 172.3, 169.6 (CO_2H, CONH), 81.2, 80.3 (CH—CH), 70.3 (CH_2O), 39.4 (CH_2N), 31.9 (—CH_2—), 29.7, 27.0, 22.7 and 14.1 (alkyl chain end); ms *m/e*: 604 (M + 1, 100), 586 (M − H_2O + 1, 65), 289 (18-crown-6 C≡O^+, 12). *Anal.* calcd. for $C_{32}H_{61}NO_9$: C 63.65, H 10.18, N 2.32; found: C 63.48, H 10.28, N 2.38.

2R,3R-(+)-N-Butyl-2-carboxamido-3-carboxyl-1,4,7,10,13,16-hexaoxacyclooctadecane (2d)

The crude product was isolated as described above, taken into chloroform and stirred (gently) with three portions of aqueous HCl for 1 h each portion. The product obtained on evaporation of the solvent was ammonium free and was crystallized from ether/pentane to give **2d** in 90% yield from **9**; mp 93°C; ir cm^{-1}: 3420, 3350 (NH), 3600–2500 (CO_2H), 1755 (CO_2H), 1670, 1530 (amide), 1120 (C—O); $[\alpha]_D^{20}$ +45.5 (*c* 8.1); ^1H nmr δ: 10.0 (1H, br, CO_2H), 7.40 (1H, brt, NH), 4.46 and 4.35 (2H, dd, AB J_{AB} 3.0 Hz, —CH—CH—), 3.64 (20H, brs, CH_2O—), 3.30 (2H, m, CH_2N), 1.7–1.3 (4H, m, CH_2CH_2), 0.95 (3H, t, *J* 6 Hz, CH_3); ^{13}C nmr δ: 171.7, 169.0 (CO_2H, CONH), 81.2, 80.6 (CH—CH—), 71.4, 70.3 (CH_2—O), 39.0 (CH_2N), 31.6, 20.0 and 13.8 (alkyl chain); ms *m/e*: 408 (M + 1, 100), 436 (M + 29, 18), 390 (M − H_2O, 40), 289 (18-crown-6 C≡O^+, 20). *Anal.* calcd. for $C_{18}H_{30}NO_9$: C 53.06, H 8.16, N 3.43; found: C 53.47, H 8.50, N 3.43.

Determination of Acidity and Stability Constants

Apparatus and Materials

Titrant was delivered from a Radiometer Autoburet ABU11 in aliquots of 10.0 μL to a 5.0 mL cell jacketed to permit thermostating (25 ± 0.1°C for all determinations). Electrodes used: pH electrode, Fisher glass electrode; reference electrode, Ag/AgCl linked to the cell by a porous plug salt bridge containing 1.0*M* tetramethylammonium chloride in methanol/water (M/W) (90:10 v/v); sodium selective glass electrode, Phillips type G15Na; potassium selective glass electrode, Phillips type G15K or AH Thomas type 4202 Q10. The electrodes were conditioned in M/W for several days before use. Cell potential was read using a Fisher Accumet 610 pH/mV meter. All salts were analytical grade or better, water was purified using a Barnsted Nanopure water purifier, and methanol was HPLC grade.

Methods

Methanol/water solutions were prepared from 1 part water made to 10 parts with methanol.

(*1*) *Standardization of pH** Three buffers, interpolated from the data of deLigny *et al.* (36) for solutions 90:10 v/v M/W (87.68 wt.% methanol) were used as primary standards; pH* 3.59, 0.01*m* oxalic acid/0.01*m* ammonium hydrogen oxalate from 0.7639 g of oxalic acid dihydrate plus 0.2870 g of diammonium oxalate monohydrate dissolved in 50.0 mL of water and made to 500.0 mL with methanol; pH* 6.55, 0.01*m* succinic

Can. J. Chem. Downloaded from www.nrcresearchpress.com by 210.87.254.40 on 09/06/12
For personal use only.

acid/0.01 *m* lithium hydrogen succinate from 0.9540 g of succinic acid plus 0.1695 g of lithium hydroxide monohydrate dissolved in 50.0 mL of water and made to 500.0 mL with methanol; pH* 9.80, $7.4 \times 10^{-3} m$ hexylamine/$1.095 \times 10^{-3} m$ hexylammonium chloride from 0.1517 g of freshly distilled hexylamine plus 0.861 mL of 1.0 *M* HCl plus 9.14 mL of water made to 100.0 mL with methanol. Cell potentials for the three buffers were used to give a linear regression line from which pH* could be calculated. Before every set of determinations, a standard solution of ethylene diammonium dihydrochloride was titrated with tetramethylammonium hydroxide. The pK_a values calculated from this titration were compared with previous determinations. Day to day and long term variations were always less than ± 0.1 pK_a unit.

(*2*) *pH Metric Determinations* Duplicate M/W solutions, $2.5 \times 10^{-3} M$ in ligand containing tetramethylammonium chloride (0.1 *M*) to maintain ionic strength, were titrated with $5.0 \times 10^{-2} M$ tetramethylammonium hydroxide in M/W. The titration data were analysed as previously described (31). In cases where metal ions were present, some tetramethylammonium chloride was omitted so that the total ionic strength remained at 0.1 *M*. Acidity constants are precise to $pK_a \pm 0.10$ and stability constants from pH metric determinations are precise to $\log K \pm 0.2$ as assessed from the accuracy and reproducibility of the measurements.

(*3*) *Ion Selective Electrode Determinations* Electrodes were conditioned in buffered M/W solutions $10^{-2} M$ in MCl for several days before use. Selectivity is sufficiently poor for the potassium electrodes that they could be used as rubidium selective electrodes following a few days of conditioning in rubidium salt solutions. Buffers: acidic solution, $1.0 \times 10^{-3} M$ HCl, pH* 3.01; basic solution, tris-hydroxymethylaminomethane (Tris)/Tris·HCl, $2.5 \times 10^{-2} M$ in Tris, from pH 8.60 Tris buffer in water, [Tris] = $2.5 \times 10^{-1} M$ (24) diluted tenfold with methanol, pH* 9.30. Methanol/water solutions containing 0.1 *M* tetramethylammonium chloride in the appropriate buffer were titrated with $2.5 \times 10^{-2} M$ metal chlorides in M/W. Potential as a function of $\log [M]_{total}$ was plotted and the process was repeated until a stable series of straight lines was obtained. Duplicate M/W solutions of ligand, $5 \times 10^{-4} M$ to $2.5 \times 10^{-3} M$ (depending on *K* (30)) containing 0.1 *M* tetramethylammonium chloride in the buffer were titrated under conditions identical with the calibration. The standard curve was checked between each solution. Curves of potential as a function of $\log [M^+]_{total}$ were plotted. For all ligands clear end points at 1 equivalent of added metal ion were observed, indicating 1:1 complex formation. For the formation of a 1:1 complex the concentration stability constant, *K*, can be calculated using:

$$K = ([M]_{tot} - [M]_{free})/[M]_{free}([L]_{tot} - [M]_{tot} + [M]_{free})$$

where $[M]_{tot}$ and $[L]_{tot}$ are the total metal ion and ligand concentrations and $[M]_{free}$ is the free metal ion concentration sensed by the electrode (30). A value of *K* was calculated for each titration point between 0.2 and 0.8 equivalents of added metal ion and the results were averaged. Further experimental considerations are to be found in ref. 30. Stability constants determined by this method are precise to $\log K \pm 0.2$ in the range $2 < \log K < 5$ (outside this range $\log K \pm 0.3$) as assessed from the accuracy and reproducibility of the measurements.

Acknowledgements

We would like to acknowledge the continued financial support of the University of Victoria and the Natural Sciences and Engineering Research Council of Canada. We thank Mr. Helmi Rafla for technical assistance in part of this work.

1. P. MITCHELL. *In* Membranes and ion transport. Vol. I. *Edited by* E. E. Bittar. Wiley, London. 1970; D. E. GREEN and S. REIBEL. Proc. Natl. Acad. Sci. U.S.A. **71**, 4850 (1974); **72**, 253 (1975); V. P. SKULACHEV. Biomembranes, **28**, 371 (1972).
2. YU. A. OVCHINNIKOV, V. T. IVANOV, and A. M. SHKROB. Membrane active complexones. Elsevier, Amsterdam. 1974.
3. C. F. REUSCH and E. L. CUSSLER. A. I. Ch. E. Journal, **19**, 736 (1973); K. H. WONG, K. YAGI, and J. SMID. J. Membr. Biol. **18**, 379 (1974); Y. KOBUKE, K. HANJI, K. HORIGUCHI, M. ASADA, Y. NAKAYAMA, and J. FURUKAWA. J. Am. Chem. Soc. **98**, 7414 (1976); J. D. LAMB, J. J. CHRISTENSEN, S. R. IZATT, K. BEDKE, M. S. ASTIN, and R. M. IZATT. J. Am. Chem. Soc. **102**, 3399 (1980), and references cited therein.
4. M. KIRCH and J. M. LEHN. Angew. Chem. Int. Ed. Engl. **14**, 555 (1975).
5. K. SOLLNER. *In* Diffusion processes. *Edited by* J. N. Sherwood, A. V. Chadwick, W. H. Muir, and F. L. Swinton. Gordon and Breach, London. 1971.
6. E. L. CUSSLER. A. I. Ch. E. Journal, **17**, 1300 (1971); F. CARACCIOLO, E. L. CUSSLER, and D. F. EVANS. A. I. Ch. E. Journal, **21**, 160 (1975); W. E. MORF, S. ARVANITIS, and W. SIMON. Chimia, **33**, 452 (1979).
7. M. SUGIURA and T. SHINBO. Bull. Chem. Soc. Jpn. **52**, 684 (1979).
8. M. SUGIURA, T. SHINBO, and N. TAKIZAWA. Nippon Kagaku Kaishi, 1427 (1979); Chem. Abstr. **91**, 217228u (1979).
9. M. SUGIURA and T. SHINBO. Bull. Chem. Soc. Jpn. **52**, 2209 (1979).
10. H. L. ROSANO, J. H. SCHULMAN, and J. B. WIESBUCH. Ann. N. Y. Acad. Sci. **92**, 457 (1961).
11. J. H. MOORE and A. S. SCHECHTER. Nature, **222**, 476 (1969).
12. E. M. CHOY, D. F. EVANS, and E. L. CUSSLER. J. Am. Chem. Soc. **96**, 7085 (1974).
13. M. R. TRUTER. Struct. Bonding (Berlin), **16**, 71 (1973).
14. J. S. BRADSHAW and P. E. STOTT. Tetrahedron, **36**, 461 (1980).
15. J. M. LEHN. Struct. Bonding (Berlin), **16**, 1 (1973); D. J. CRAM and J. M. CRAM. Acc. Chem. Res. **11**, 8 (1978); Synthetic multidentate macrocyclic compounds. *Edited by* R. M. Izatt and J. J. Christensen. Academic Press, New York. 1978.
16. C. J. PEDERSEN and H. K. FRENSDORFF. Angew. Chem. Int. Ed. Engl. **11**, 16 (1972); Y. TAKEDA. Bull. Chem. Soc. Jpn. **52**, 2501 (1979), and references cited therein; K. KIMURA, T. MAEDA, and T. SHONO. Talanta, **26**, 945 (1979); M. J. REYES, A. G. MADDOCK, G. DUPLATNE, and J. J. SCHIEFFER. J. Inorg. Nucl. Chem. **41**, 1365 (1979).
17. R. UNGARO, B. EL HAJ, and J. SMID. J. Am Chem. Soc. **98**, 5198 (1976); I. TABUSHI, Y. KOBUKE, K. ANDO, M. KISHIMOTO, and E. OHARA. J. Am. Chem. Soc. **102**, 5947 (1980).
18. W. WIERENGA, B. R. EVANS, and J. A. WOLTERSOM. J. Am. Chem. Soc. **101**, 1334 (1979).
19. A. AGTARAP, J. W. CHAMBERLIN, M. PINKERTON, and L. STEINRAUF. J. Am. Chem. Soc. **89**, 5737 (1967).
20. D. J. CRAM, R. C. HELGESON, K. KOJA, E. P. KYBA, K. MADAN, L. R. SOUSA, M. G. SIEGEL, P. MOREAU, G. W. GOKEL, J. M. TIMKO, and G. D. Y. SOGAH. J. Org. Chem. **43**, 2758 (1978); R. C. HELGESON, G. R. WEISMAN, J. L. TONER, T. L. TARNOWSKI, Y. CHAO, J. M. MAYER, and D. J. CRAM. J. Am. Chem. Soc. **101**, 4928 (1979).
21. J. M. GIRODEAU, J. M. LEHN, and J. P. SAUVAGE. Angew. Chem. Int. Ed. Engl. **14**, 764 (1975).

22. J. P. BEHR, J. M. LEHN, and P. VIERLING. J. Chem. Soc. Chem. Commun. 621 (1976); J. M. LEHN, P. VIERLING, and R. C. HAYWARD. J. Chem. Soc. Chem. Commun. 296 (1979).
23. J. M. LEHN. Pure Appl. Chem. **50**, 871 (1978).
24. T. M. FYLES, V. A. MALIK-DIEMER, and D. M. WHITFIELD. Can. J. Chem. **59**, 0000 (1981).
25. L. A. FREDERICK, T. M. FYLES, V. A. MALIK-DIEMER, and D. M. WHITFIELD. J. Chem. Soc. Chem. Commun. 1211 (1980).
26. M. NEWCOMB, J. L. TONER, R. C. HELGESON, and D. J. CRAM. J. Am. Chem. Soc. **101**, 4941 (1979).
27. D. SEEBACH and H. A. OEI. Angew. Chem. Int. Ed. Engl. **14**, 634 (1975).
28. C. J. PEDERSEN. J. Am. Chem. Soc. **89**, 7017 (1967).
29. H. O. KALINOWSKI, D. SEEBACH, and G. CRASS. Angew. Chem. Int. Ed. Engl. **14**, 762 (1975).
30. J. M. LEHN and J. P. SAUVAGE. J. Am. Chem. Soc. **97**, 6700 (1975).
31. B. DIETRICH, D. L. FYLES, T. M. FYLES, and J. M. LEHN. Helv. Chim. Acta, **62**, 2763 (1979).
32. I. G. SAYCE. Talanta, **15**, 1397 (1968); **18**, 653 (1971).
33. J. M. LEHN. Pure Appl. Chem. **51**, 979 (1979).
34. J. D. LAMB, J. J. CHRISTENSEN, J. L. OSCARSON, B. L. NIELSEN, B. W. ASSAY, and R. M. IZATT. J. Am. Chem. Soc. **102**, 6820 (1980).
35. L. F. DAHL, G. L. DAVIS, D. L. WAMPLER, and R. WEST. J. Inorg. Nucl. Chem. **24**, 357 (1962).
36. C. L. DELIGNY, P. F. M. LUYKX, M. REHBACH, and A. A. WIENEKE. Recl. Trav. Chim. Pays-Bas, **79**, 699 (1960), and references cited therein.
37. J. P. BEHR, J. M. GIRODEAU, R. C. HAYWARD, J. M. LEHN, and J. P. SAUVAGE. Helv. Chim. Acta, **63**, 2096 (1980).

Can. J. Chem. Downloaded from www.nrcresearchpress.com by 210.87.254.40 on 09/06/12
For personal use only.

Membrane transport systems. II. Transport of alkali metal ions against their concentration gradients

THOMAS M. FYLES,[1] VIRGINIA A. MALIK-DIEMER, AND DENNIS M. WHITFIELD

Department of Chemistry, University of Victoria, Victoria, B.C., Canada V8W 2Y2

Received December 12, 1980

THOMAS M. FYLES, VIRGINIA A. MALIK-DIEMER, and DENNIS M. WHITFIELD. Can. J. Chem. **59**, 1734 (1981).

An artificial membrane system based on a series of macrocyclic polyether carriers (crown ethers) is described. Under the influence of a proton gradient the carriers move alkali metal ions from basic to acidic solution through a chloroform membrane phase. Transport occurs against the concentration gradient of the transported ion as a result of a coupled counterflow of protons. Different transport behaviors are observed depending upon the metal ion concentration. At high metal ion concentration the amount transported is a linear function of time; at lower metal ion concentration the amount transported is a complex function of time which may be described as the result of a pair of consecutive first order processes. Effects of metal ion, carrier, and proton concentration on transport rate are considered. The rate increases with increasing metal ion or carrier concentration but is essentially independent of the pH of either aqueous phase. Increased lipophilicity of the carrier also results in a rate increase. Carriers derived from 18-crown-6 transport potassium selectively and all ions more rapidly than 15-crown-5 derivatives which are, however, selective for sodium. The overall efficiency of the system is discussed in terms of competing "leak" reactions, either of cations from the basic phase or of anions from the acidic phase.

THOMAS M. FYLES, VIRGINIA A. MALIK-DIEMER et DENNIS M. WHITFIELD. Can. J. Chem. **59**, 1734 (1981).

On décrit un système de membrane artificielle basée sur une série de polyéthers macrocycliques (éthers couronnes) en tant que phases mobiles. Sous l'influence d'un gradient de proton, les phases mobiles déplacent les ions des métaux alcalins d'une solution basique vers une solution acide à travers la phase chloroforme de la membrane. Le transport se fait à l'opposé du gradient de concentration des ions transportés; ceci est dû à un contre-courant simultané de protons. On observe différents comportements lors du transport en fonction de la concentration de l'ion métallique. Pour une concentration élevée de l'ion métallique, la quantité transportée est une fonction linéaire du temps; pour une plus faible concentration de l'ion métallique, la quantité transportée est une fonction complexe du temps qui peut être décrite comme le résultat de deux processus consécutifs de premier ordre. On considère les effets de l'ion métallique, de la phase mobile et de la concentration du proton sur la vitesse de transport. La vitesse augmente avec la concentration de l'ion métallique ou de la phase mobile mais elle est essentiellement indépendante du pH d'une phase aqueuse quelconque. L'augmentation de la lipophilicité de la phase mobile augmente également la vitesse. Les phases mobiles dérivées des éthers 18-couronne-6 transportent sélectivement le potassium et tous les ions plus rapidement que celles dérivant des éthers 15-couronne-5 qui sont cependant sélectives vis-à-vis du sodium. On discute de l'efficacité globale du système en fonction de réactions compétitives impliquant des fuites soit de cations à partir de la phase basique soit d'anions à partir de la phase acide.

[Traduit par le journal]

The ability of macrocyclic polyethers (crown ethers) to selectively dissolve or extract metal ions into nonpolar solvents has been exploited in a wide range of applications from fundamental studies of ion solvation to phase transfer catalysis (1). However, one of the potentially most useful areas of application, that of the transport of ions through membranes, remains relatively unexplored. Of particular interest is the possibility that an ion of interest could be "pumped" against its concentration gradient by a coupled counterflow of ions (2), electrons (3), or protons (4). Potential applications include the separation and concentration of specific chemical species, the decontamination of wastes or biological fluids, or the direct analysis of a particular substrate in a mixture (5). Such applications will depend on a complete analysis of the mechanisms of transport and the effects of structural modifications of the carrier on transport rate, efficiency, and selectivity.

We have recently described the synthesis and characterization of a series of crown ether derivatives **1***a–c* and **2***a–c* (6) which in principle could act, like the ionophore antibiotic monensin (7), as carriers for the coupled counterflow of cations and protons across bulk liquid membranes. This simple system is susceptible to extensive structural modification, hence many of the features mentioned above may be examined in a much more detailed fashion than is possible either with natural biological transport systems (8) or with natural ionophores in artificial membranes (7, 9).

We envisage the transport to occur by the schematic mechanism outlined in Fig. 1. The carrier, by virtue of its lipophilic nature, remains dissolved in the hydrophobic membrane phase. At the left interface the carrier, a carboxylic acid, gives up a proton to the basic aqueous phase. To maintain electroneutrality in the membrane a metal ion is extracted to form the salt of the carrier which is also a crown ether – cation inclusion complex (1). The complex diffuses down its concentration grad-

[1]Author to whom correspondence should be addressed.

0008-4042/81/121734-11$01.00/0

©1981 National Research Council of Canada/Conseil national de recherches du Canada

Can. J. Chem. Downloaded from www.nrcresearchpress.com by 210.87.254.5 on 09/06/12
For personal use only.

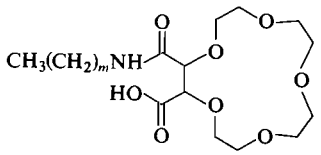

1*a* $m = 7$
1*b* $m = 13$
1*c* $m = 17$

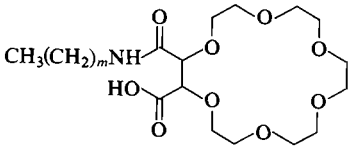

2*a* $m = 7$
2*b* $m = 13$
2*c* $m = 17$

ient to the right acidic interface, whereupon it becomes protonated. Again, in order to maintain electroneutrality, the metal ion must be lost to the aqueous phase (or a counter ion must be extracted, see later discussion). The free carrier diffuses down its own concentration gradient to the left interface to recommence the cycle. The net result is the transport of a metal ion from left to right at the expense of a proton transported from right to left. If the metal ion concentration is greater on the right (acidic) side than on the left side, the metal ion is pumped against its own concentration gradient. The necessary energy is provided by the flux of protons in the opposite sense, from acidic to basic solution.

That the carriers 1*a–c* and 2*a–c* do in fact pump alkali metal ions from basic to acidic solution was the subject of a preliminary communication (10). The present article seeks to outline the phenomenon in detail and to address the questions of mechanism, efficiency, and selectivity using this model system.

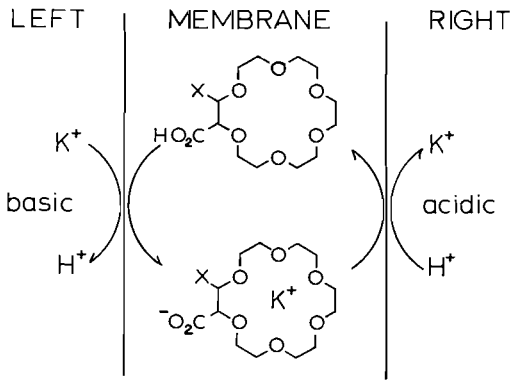

FIG. 1. A schematic mechanism for the carrier mediated countertransport of a metal ion and a proton.

Experimental

Apparatus

Transport experiments were performed in a U-shaped apparatus similar to those previously described (11), constructed of 15 mm id Pyrex tubing bent to a 20 mm radius bend. Two cell volumes were used (25 and 100 mL total volume). The bends in both cases were identical but one cell had flared arms to provide a larger volume. The "membrane," chloroform (12 mL), was placed in the base of the U and filled the cell into the vertical portions of the arms. The interface was thus of constant and reproducible area (1.54 cm^2). The two aqueous solutions were added simultaneously to the arms of the U and floated on the chloroform. All phases were efficiently stirred at 450 Hz. Dyes placed in any compartment were completely distributed throughout the compartment after ten seconds of stirring. The interfaces were only slightly perturbed by the constant stirring. The entire cell was jacketed and thermostated at 25 ± 0.1°C.

Materials

The synthesis and purification of the carriers 1*a–c* and 2*a–c* has been described (6). Other carriers are commercially available, monensin (Cal Biochem), dicyclohexano 18-crown-6 (Aldrich, a mixture of isomers), and were used as received. Alkali metal salts were of analytical grade or better, materials for buffer solutions were reagent or analytical grade and were analysed for alkali metal content before use. Water was purified using a Barnsted Nanopure water purifier, chloroform was distilled and stored under water to give a constant source of water saturated chloroform. Stock acidic buffer solutions were prepared from 0.5 mol of phosphoric acid in 0.750 L of water. A base (tetramethylammonium hydroxide pentahydrate, tetraethylammonium hydroxide 20% in water or triethanolamine) was added to give a target value of pH (1.25, 2.0, 3.0) and the solution was made to 1 L with water. Stock basic buffers were prepared similarly from 0.5 mol of tris(hydroxymethyl)aminomethane (Tris) or glycine in 0.750 L of water made to a target pH (8.50, 10.50) with concentrated hydrochloric acid or tetramethylammonium hydroxide pentahydrate, respectively, and then made to 1 L with water. Solutions for transport experiments were made up, from 0.1 *M* stock solutions of the alkali metal chlorides and the stock buffers, to result in a twofold dilution of the buffer.

Analytical Methods

The U cell was charged with chloroform and the two aqueous solutions then equilibrated for ca. 1 h. A stock solution of carrier (usually 1.0 mL) was injected to make the membrane phase to 12.0 mL total volume. The time of injection was taken as time = 0. Samples were withdrawn by microliter syringe from the aqueous solutions at various times. Sample size depended upon the metal ion concentration and the analysis required (typically 10–25 μL for metal ion concentration alone or 1.1 mL for proton concentration plus metal ion concentration). Metal ion samples (Na^+, K^+, Rb^+) were diluted with 1.0 mL of water and analysed by atomic emission spectrometry using a Varian 475 atomic absorption spectrometer. Values were typically in the range 0.5–5 ppm for which the method was reproducible to ±0.05 ppm between duplicates. Cesium ion concentrations were determined by pulse polarography. Proton transport rates were determined by acid/base titration of a 1.0 ml sample in 4.0 mL of 0.1 *M* KCl solution. Titration curves of pH vs. volume were plotted and end points were determined graphically. Kinetic data were analysed as described in the text. The reported transport rates are accurate to ±15% as assessed from the precision and reproducibility of the methods used and the long term repeatability of the experiments using different stock solutions and samples of carriers.

Can. J. Chem. Downloaded from www.nrcresearchpress.com by 210.87.254.5 on 09/06/12
For personal use only.

Can. J. Chem. Downloaded from www.nrcresearchpress.com by 210.87.254.5 on 09/06/12
For personal use only.

Results and Discussion

Cation–Proton Countertransport: the Phenomenon

The membrane transport of alkali metal cations by carriers **1***a–c* and **2***a–c* was studied using a U-shaped apparatus. The "membrane," chloroform, was placed in the base of the U and aqueous solutions were added to the arms of the U and floated on the chloroform. The aqueous solutions were initially of equal metal ion concentration but were buffered to impose a proton gradient across the membrane. The carrier was added to the membrane and aliquots of the aqueous solutions were withdrawn at various time intervals thereafter and analysed for metal ion and proton concentration. The counter transport of protons and alkali metal cations can be readily demonstrated with reference to Fig. 2 for the case of potassium and **2***b*. On the basic side of the membrane (the lower dashed line), the potassium ion concentration *decreases* with time while on the acidic side (the upper solid line) it *increases*. At the same time the proton concentration on the basic side of the membrane *increases* while on the acidic side it *decreases*. Qualitatively the change in potassium concentration roughly parallels the change in proton concentration for each side of the membrane although the two sides are different. The form of the curves is complex and is further complicated by the fact that part of the "transport" is due to the removal of samples for analysis. Thus some of the decrease in potassium concentration on the basic side is simply due to sampling while on the acidic side the increase is not as large as it would have been in the absence of sampling. The effect is not small; about 30% of the initial volume was consumed in samples.

Nonetheless, the cation–proton stoichiometry of countertransport may be demonstrated using this example since sampling of equal volumes occurred at equal times for both sides of the cell and perturbed the potassium and proton concentrations of a given compartment by an equal amount. "Transport" due to sampling is thus a constant factor and may be eliminated by plotting the change in proton concentration to a given time as a function of the change in potassium ion concentration to the same time (Fig. 3). The solid line is the linear regression line for all the data points and has a slope of 0.98 (residual 0.995) clearly indicating that the exchange of a single proton for a single potassium ion has occurred as is required by the schematic mechanism of Fig. 1. Furthermore, since the line has essentially the theoretical slope, the *efficiency* of the transport must be high. Little or no "leakage" of potassium from acidic to basic solution can have occurred (see later discussion).

Kinetic Analysis of Transport Data

Having outlined the basic features of the coupled countertransport of cations and protons we turned to a more precise method for the determination of transport rates using a smaller cell (10 mL aqueous phases) and a much smaller sample size (10–25 μL). Perturbations due to sampling are thus small, even with respect to uncontrollable

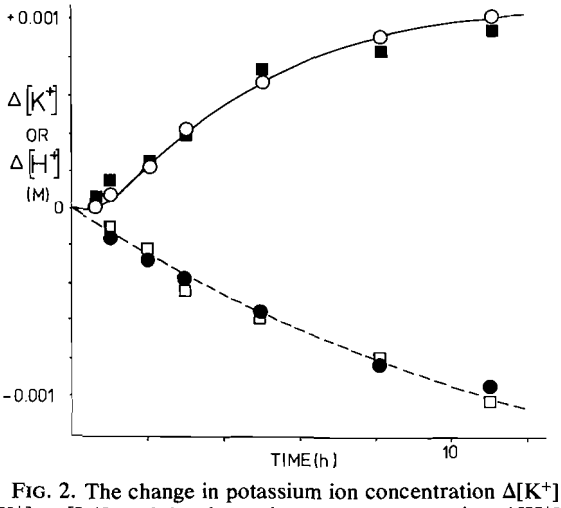

FIG. 2. The change in potassium ion concentration $\Delta[K^+] = [K^+]_t - [K^+]_0$ and the change in proton concentration, $\Delta[H^+] = [H^+]_0 - [H^+]_t$, as functions of time for the carrier **2***b*. The cell initially consisted of: 5×10^{-3} *M* KCl in 5×10^{-3} *M* Tris/Tris-HCl buffer (pH 8.69) || **2***b* 5.0×10^{-4} *M* in $CHCl_3$ || 5×10^{-3} *M* KCl in 1×10^{-2} *M* HCl (pH 2.15), ○, ●, Δ [K⁺]; □, ■ Δ [H⁺]; dashed line, basic side; solid line, acidic side.

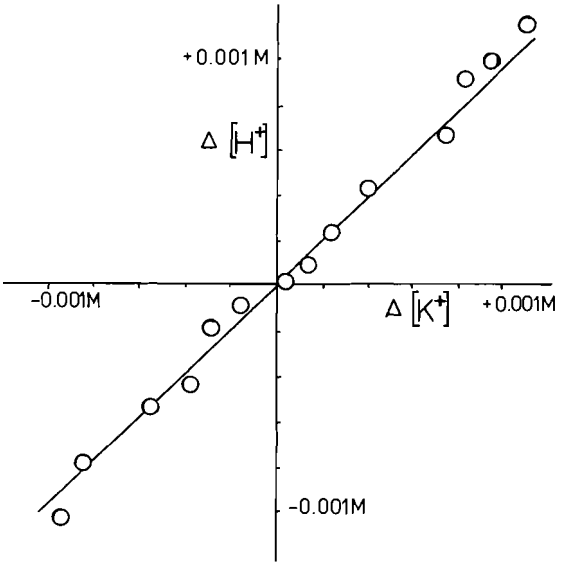

FIG. 3. The change in proton concentration, $\Delta [H^+] = [H^+]_0 - [H^+]_t$ as a function of the change in potassium ion concentration, $\Delta [K^+] = [K^+]_t - [K^+]_0$. Data taken from the experiment of Fig. 2.

Can. J. Chem. Downloaded from www.nrcresearchpress.com by 210.87.254.5 on 09/06/12
For personal use only.

variations in volume due to evaporation (ca. 0.2 mL/day). Detailed proton transport rates in these cases are unknown but are assumed to follow a pattern similar to those of Fig. 2. Checks of the final pH values of the aqueous phases allowed a calculation of the approximate number of moles of protons absorbed or liberated by the buffers. Values consistent with the number of moles of cation transport were obtained in all cases.

Two types of transport are observed depending upon the relative amounts of carrier and of metal ion. When the metal ion is present in a large excess, the amount of metal ion transported is a linear function of time (Fig. 4) referred to hereafter as type A behavior. The transport is apparent zero order in metal ion and the amount of metal ion at any time is given by

$$[1] \quad M_t^+ = M_0^+ \pm k_0 t$$

where M_t^+, M_0^+ are the amounts of metal ion in the phase of interest at a time t or initially, + refers to the acidic side and − refers to the basic side, and k_0 is the apparent zero order rate constant in units of moles per unit time (typically μmol h^{-1}). The rate constant k_0 must be dependent upon carrier concentration and proton concentration but these are imposed as constants for a given experiment. In type A cases there is commonly a brief induction period for the acidic side while the membrane achieves a steady state. The rates of uptake and of release are typically the same within experimental error but this is not uniformly observed.

The second type of transport (type B behavior), illustrated in Fig. 5, is more complex and occurs

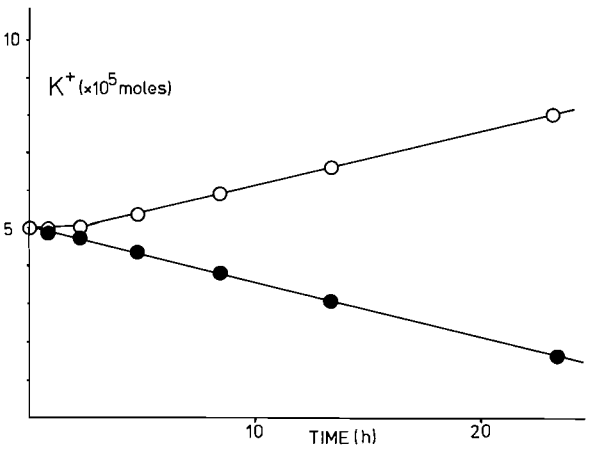

FIG. 4. The number of moles of potassium ion transported as a function of time by the carrier **2***b* showing typical type A behavior. The cell initially consisted of: 5 × 10^{-3} *M* KCl in tetramethylammonium glycinate buffer (pH 10.54) || 5.5 × 10^{-4} *M* **2***b* in $CHCl_3$ || 5 × 10^{-3} *M* KCl in tetramethylammonium dihydrogenphosphate buffer (pH 2.30). Data of the experiment of entry 14, Table 1; ●, basic side; ○, acidic side.

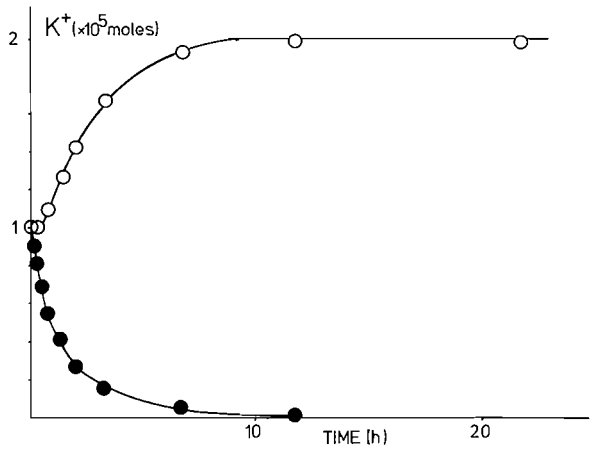

FIG. 5. The number of moles of potassium transported as a function of time by the carrier **2***b* showing typical type B behavior. The cell initially consisted of: 1 × 10^{-3} *M* KCl in Tris/Tris HCl buffer (pH 8.56) || 1.14 × 10^{-3} *M* **2***b* in $CHCl_3$ || 1 × 10^{-3} *M* KCl in tetramethylammonium dihydrogenphosphate buffer (pH 3.35). Data of the experiment of entry 13, Table 1; ●, basic side; ○, acidic side.

when the amounts of metal ion and of carrier are comparable. The kinetic behavior can be described by assuming a pair of consecutive first order processes.

$$[2] \quad \mathbf{A} \xrightarrow{k_1} \mathbf{B} \xrightarrow{k_2} \mathbf{C}$$

A in this case is the metal ion in the basic aqueous solution, **B** is presumably the carrier/metal ion complex in the membrane, and **C** is the metal ion in the acidic aqueous solution. Both **A** and **C** are observable as a function of time; **B** can be calculated from a knowledge of **A** and **C** and the total amount of metal ion initially present. The rate constant, k_1, is the rate at which a metal ion is taken into the membrane at the basic interface in exchange for a proton and k_2 is the rate of the reverse reaction occurring at the acidic interface.

Values for both k_1 and k_2 can be determined by standard methods (12). The decrease in metal ion concentration in the basic solution is a simple first order case from which k_1 is readily determined. The ratio of the rate constants $\kappa = k_2/k_1$ can be estimated graphically (12) to give an initial estimate for k_2 from the known value of k_1. The value of k_2 was further refined by an iterative procedure[2] to

[2]Since the value of t is known to a few seconds in several hours, the time at each experimental point was treated as an exact value. Using the values of k_1 and k_2, the potassium ion concentration in the acidic phase was calculated for each experimental time. The squares of the differences between experimental and calculated potassium concentrations were summed for the entire curve and this parameter was minimized by varying the value of k_2.

Can. J. Chem. Downloaded from www.nrcresearchpress.com by 210.87.254.5 on 09/06/12
For personal use only.

give a value which best reproduced the experimental curve of metal ion concentration in the acidic phase as a function of time. The solid lines of Fig. 5 are typical of curves calculated using this "best fit" pair of rate constants.

Data from type A experiments are in the form of moles of metal ion transported per unit time whereas data from type B experiments are in the form of time^{-1}. In order to compare the two cases we consider the **maximum rate of release** of the metal ion to the acidic phase. This is just k_0 for the acidic side of type A experiments. In type B experiments, the rate will be maximal when the concentration of **B**, the carrier complex, is at a maximum. It can be shown (12) that the **time**, t_{max}, at which **B** is a maximum is given by

$$[3] \quad t_{max} = \ln \kappa / k_1(\kappa - 1)$$

where $\kappa = k_2/k_1$.

The value of t_{max} can be calculated from k_1 and k_2 and gives the time at which the rate of formation of **C**, that is the rate that metal is released to the acidic phase, is at a maximum. From the integrated rate equation (12),

$$[4] \quad \left(\frac{dC}{dt}\right)_{max} = \frac{k_2 k_1 A_0}{k_2 - k_1} \times [\exp(-k_1 t_{max}) - \exp(-k_2 t_{max})]$$

where A_0 is the initial concentration of **A** and k_1, k_2, and t_{max} are defined above. All the parameters to the right of eq. [4] are known, thus the maximum rate of release of the metal ion to the acidic phase can be calculated.

This analysis permits comparisons between the two types of behavior but obscures the fact that these are only **apparent** rates of transport. As can be seen from the explicit derivation above, the maximum release rate contains terms in the initial concentration of metal ion on the basic side of the membrane, the rate of uptake, and the rate of release. In addition, each of the latter must have some dependence upon carrier and proton concentration. Nonetheless, the composite value is useful in examining the system as a whole and for comparing the effect of a change on the total behavior of the system.

The results obtained with carriers **1***a*–*c* and **2***a*–*c* for a variety of metal ions, concentrations and proton gradients are given in Table 1. Also included are results obtained with other carriers: monensin, stearic acid, and dicyclohexano 18-crown-6. Before going on to a detailed examination of the data, it would be useful to examine the type of information which is wholly or partly obscured by the analysis used. Firstly, the maximum release rate of the metal ion is clearly a composite value as shown by the data of entries 5 and 6. The overall behavior of these two systems is very similar and this is reflected by the similar maximum release rates. However, for **2***b* the uptake of potassium is rate limiting, while for **2***c* the release is rate limiting. The simple conclusion that **2***b* and **2***c* will always behave in a similar fashion is not borne out by the data. Presumably in other cases, e.g., entries 20 and 21 or 25 and 26, these competing effects cancel one another to different extents to result in different overall transport rates. A different sort of effect can be seen in the data of entries 5 and 12 and 13. Clearly in this case uptake rate controls the overall behavior of the system even though the release rates vary somewhat as well. This latter fact is lost in the maximum release rate calculation.

The extent to which these problems are to be found among the type A cases is not clear. Certainly after a miminum period of time the system will achieve a steady state. Subsequent to this time the release and uptake rates cannot be totally independent. The difference between the apparent zero order rates of uptake and of release might thus be considerably attenuated from the values for the individual isolated reactions. Even with these reservations, the data of Table 1 clearly reveal specific concentration and structural effects on the rate, selectivity, and efficiency of transport.

Influence of Concentration on Transport

Using our experimental cell, the antibiotic monensin pumps sodium ion against a concentration gradient at the rate of 1.03 μmol h^{-1} (entry 28). From the data of Choy *et al.* (7), a rate of ca. 1220 μmol h^{-1} for the transport of sodium across a thin octanol membrane of the same area as our cell by an amount of monensin 400 times greater than in our cell can be calculated. The form of the concentration dependence is not known either in their system or in ours. Assuming the rate increases as a direct linear function of the carrier concentration gives an estimate of about 3 μmol h^{-1} for monensin at the same concentration as in our experiment, in reasonable agreement with our value. Any differences can be attributed to the assumptions required and to the different liquid phases involved. Comparison of monensin/Na^+ with **2***a*–*c*/K^+ (entries 8, 10, and 11) reveals that, at the same concentration level in the same experimental cell, the model system performs as well as or better than the natural product. Admittedly, this is a comparison of best cases; carriers **2***a*–*c* are relatively ineffective carriers of Na^+, monensin is a relatively ineffective carrier of K^+ (7). Comparisons between **1***a*–*c* or

TABLE 1. Experimental parameters and carrier mediated transport rates of metal ions through a chloroform membrane[a]

Entry	Metal ion[b]	Carrier	Carrier concentration ($\times 10^3$ M)	Experimental conditions[c]	Intake rate[d]	Release rate[e]	Maximum release rate[f]
1	K^+	1*a*	1.40	I	0.06	0.05	[g]
2	K^+	1*b*	1.40	I	0.06	0.05	[g]
3	K^+	1*c*	1.35	I	0.08	0.06	[g]
4	K^+	2*a*	1.67	I	0.29	0.49	1.36
5	K^+	2*b*	1.37	I	0.46	1.14	2.48
6	K^+	2*c*	1.48	I	0.71	0.66	2.53
7	K^+	2*b*	0.55	I	0.23	0.31	0.95
8	K^+	2*b*	0.55	II	1.59	1.60	[g]
9	K^+	2*b*	0.55	III	2.12	1.86	[g]
10	K^+	2*a*	0.65	II	0.89	0.76	[g]
11	K^+	2*c*	0.67	II	1.92	1.69	[g]
12	K^+	2*b*	1.14	IV	0.44	0.95	2.26
13	K^+	2*b*	1.14	V	0.49	1.19	2.35
14	K^+	2*b*	0.55	VI	1.34	1.53	[g]
15	K^+	2*b*	0.55	VII	1.60	1.68	[g]
16	Na^+	1*a*	0.48	II	0.08	0.09	[g]
17	Na^+	1*b*	0.43	II	0.32	0.27	[g]
18	Na^+	1*c*	0.44	II	0.27	0.23	[g]
19	Na^+	2*a*	0.65	II	0.13	0.17	[g]
20	Na^+	2*b*	0.50	II	0.36	0.43	[g]
21	Na^+	2*c*	0.67	II	0.60	0.52	[g]
22	Rb^+	1*b*	0.43	II	0.04	0.04	[g]
23	Rb^+	1*c*	0.44	II	0.03	0.03	[g]
24	Rb^+	2*a*	0.65	II	0.28	0.24	[g]
25	Rb^+	2*b*	0.50	II	0.37	0.34	[g]
26	Rb^+	2*c*	0.67	II	0.83	0.62	[g]
27	Cs^+	2*b*	0.50	II	0.20	0.20	[g]
28	Na^+	[h]	0.42	II	1.12	1.03	[g]
29	K^+	[i]	0.50	II	0.05	0.02	[g]
30	K^+	[j]	[j]	II	0.06	0.02	[g]
31	K^+[k]	2*b*	0.50	II	0.72	0.98	[g]
32	K^+[l]	2*b*	0.50	II	1.03	1.17	[g]

[a] Determined at 25 ± 0.1°C. Values accurate to ± 15%.
[b] Metal ion salts as chlorides unless otherwise indicated.[k, l]
[c] Initial conditions of the cell: I, 1×10^{-3} M MCl, basic pH = 8.56, acidic pH = 2.30; II, 5×10^{-3} M MCl, pH 8.6/2.3; III, 1×10^{-2} M MCl, pH 8.6/2.3; IV, 1×10^{-3} M MCl, pH 8.6/1.4; V, 1×10^{-3} M MCl, pH 8.6/3.3; VI, 5×10^{-3} M MCl, pH 10.5/2.3; VII, 5×10^{-3} M MCl, pH 11.8/2.3. Carriers were initially as the free acids unless otherwise noted.[h]
[d] Rate at which the metal ion is extracted from the basic aqueous phase in μmol h^{-1} except for type B cases, entries 4–7 and 12–13, where the first order rate constant k_1 is in s^{-1}.
[e] Rate at which the metal ion is released to the acidic aqueous phase in μmol h^{-1} except for type B cases, entries 4–7 and 12–13, where the first order rate constant k_2 is in s^{-1}.
[f] The maximum rate at which the metal ion is released to the acidic aqueous phase in μmol h^{-1} calculated using eq. [4].
[g] For type A cases the maximum rate is equal to the zero order release rate.
[h] Monensin, initially as the sodium salt.
[i] Stearic acid.
[j] Stearic acid, 5.0×10^{-4} M and dicyclohexano 18-crown-6, 5.0×10^{-4} M.
[k] PF_6^- salt used.
[l] ClO_4^- salt used.

2*a*–*c* and other "carriers," e.g., stearic acid (entry 29), are even more favorable.

In principle, the carrier of the ion and the carrier of the proton need not be in the same molecule. Coupling between the substrate and pumping fluxes would be electrostatic, the carboxylate of the acid providing a liposoluble counter ion for the extracted metal ion. This is the basis of a redox driven cation pump (3) and various anion pumps (13). As the data of entry 30 show, however, this approach was not very successful in our system. The separated carriers were a factor of 80 times less efficient than 2*b*–*c*. The extraction rate is somewhat larger than with stearic acid alone but the net transport is the same with or without crown ether. Quite apart from other considerations, separate carriers must be entropically disfavored and would likely require an organized aggregation at the interface in order to achieve ion extraction and proton release by an efficient low-energy pathway.

Examination of Table 1 reveals a variety of general effects which have been noted in other

Can. J. Chem. Downloaded from www.nrcresearchpress.com by 210.87.254.5 on 09/06/12
For personal use only.

Can. J. Chem. Downloaded from www.nrcresearchpress.com by 210.87.254.5 on 09/06/12
For personal use only.

systems (14) or might be predicted from simple considerations. The rate of transport increases with increasing carrier concentration (e.g., entries 5 and 7) and with increasing metal ion concentration (e.g., entries 7–9). It is not straightforward to obtain data suitable for the determination of the kinetic order in carrier or in metal ion, as the observed transport behavior is strongly dependent upon the relative concentrations of carrier and of metal ion. The fivefold concentration increase in potassium ion between the experiments of entries 7 and 8 was sufficient to change the system from type B to type A behavior.

The dependence of transport rate on proton gradient was investigated in the experiments of entries 5, 12, and 13 and 8, 14, and 15. As is evident for 5, 12, and 13, the extraction step is rate limiting, hence it is not surprising that there is no change in rate due to changes in the acidic phase. It is not clear, however, why there should be virtually no rate changes produced by changes in the pH of the basic solution. The analysis of Cussler (15) predicts a dependence of 1/rate on $1/[M^+]\ [OH^-]$ for the basic side of the membrane and this relationship was found to hold for the carriers cholanic acid and monensin (7). The data of entries 8, 14, and 15 vary the hydroxide ion concentration by three orders of magnitude; the rate remains essentially unchanged (within the experimental error). The analysis referred to above explicitly assumed that all chemical reactions (i.e., proton release, metal ion extraction), are fast with respect to diffusion. It is not unreasonable to suppose that this criterion is not met in our well-stirred system and that the rate of extraction or release controls the transport. This conclusion is supported by the observation that extraction is not always rate limiting (entry 6, possibly 11 and 26). In order for the acidic side to play any role at all, some diffusional processes must have already occurred. This is not to imply that the pH plays no role whatsoever in determining rate; as the pH approaches the pK_a of the carrier, some effect due to diminished concentrations of the protonated or deprotonated carrier should be observable. The cases examined are remote from this value and are sufficient to check for an effect similar to that predicted by Cussler (15) but do not adequately examine the more complex questions associated with smaller proton gradients.

Structural Influences on Transport

Since diffusional restraints in our system appear to be unimportant, it is not surprising to note that increasing the length of the alkyl chain, which must decrease the ability of the carrier to diffuse freely, does not result in a rate decrease. On the contrary, in most cases the maximum release rates increase along the series octyl < tetradecyl < octadecyl (entries 4–6, 14, 10 and 15, 24–26, etc.). This is reasonable; in most cases intake is rate limiting and this rate should increase with increasing lipophilicity. The data of entries 4–6 reflect this trend but show in addition that the release rates pass through a maximum at the tetradecyl derivative. The thermodynamic data (6) show that the metal ion complexes of **2***a–c* are of comparable stability, hence both these trends must reflect changes in the lipophilicity of the carrier. The issue is further clouded by the observation that, although separated spatially, the intake and release reactions are formally the forward and reverse directions of the proton–cation exchange equilibrium [5]

$$[5] \quad M^+ (aq) + HCrn (org) \rightleftharpoons MCrn (org) + H^+ (aq)$$

where HCrn and MCrn are the carrier and metal ion complex respectively.

If the reaction occurs by a common pathway at both interfaces, microscopic reversibility will require that factors which accelerate the forward reaction will retard the reverse reaction. This is incompatible with the rate maximum at the acidic interface which is absent at the basic interface (entries 4–6). Special or extenuating circumstances at the acidic interface of the experiment of entry 4 such as the loss of **2***a* into the aqueous phase are not supported by other data. The potassium concentrations of these entries show the expected evolution with time and the values of k_1 and k_2 accurately reproduce the experimental curves. The distribution data (6) suggest that less than 0.2% of the **2***a* initially present would be lost to achieve equilibrium with the aqueous phase.

It is therefore evident that although eq. [5] formally represents the process, the uptake and release reactions must occur by different sequences of events and the relative rates within the sequence must change according to the lipophilicity of the carrier. Although speculation is possible, a more detailed discussion will be retained for a more comprehensive kinetic analysis of the isolated reactions.

Turning from comparisons within a structurally related series to comparisons between series, the data show that in general the 18-crown-6 derivatives (**2**) transport all ions more effectively than do the 15-crown-5 derivatives (**1**). This is presumably related to the stability of the complexes formed. The stability constants for complex formation have been determined in methanol/water solution (M/W

Can. J. Chem. Downloaded from www.nrcresearchpress.com by 210.87.254.5 on 09/06/12
For personal use only.

90:10 v/v) (6). Typically, 18-crown-6 carboxylates complex K^+ (log K = 5.8) more strongly than Na^+ (log K = 4.4) or Rb^+ (log K = 5.0) as well as more strongly than 15-crown-5 carboxylates (Na^+, log K = 3.4; K^+, log K = 3.0; Rb^+, log K = 2.7). The relationship between complex stability determined in homogeneous solution (usually methanol) and transport rate has been investigated in other systems (16) and is found to pass through a maximum about log K (methanol) ≈5–6. Complexes less stable than this do not extract the ion sufficiently well; complexes more stable than this fail to release the ion (14–16). All the values for **1***a–c* and **2***a–c* lie to the low side of the optimal value, hence one would expect to observe only an increase in rate with an increase in log K. The 18-crown-6 derivatives would thus be expected to transport ions more effectively than the 15-crown-5 derivatives on this basis alone.

An additional effect may also be important. As discussed above, an increase in lipophilicity results in an increase in metal ion extraction rate. Comparing the coefficients for the distribution of **1***a* and **2***a* between chloroform and aqueous acid (6) shows that **1***a* is less lipophilic than **2***a* even though both bear octyl side chains. The 15-crown-5 head group must thus be less lipophilic than the 18-crown-6 head group. Although there is no other quantitative data to support this view, there is a large body of qualitative evidence. Among other observations, the synthetic precursors in the 15-crown-5 series are uniformly more difficult to extract from water and to dry than are the 18-crown-6 counterparts.

The two effects (complex stability and lipophilicity) act in the same sense and allow one to predict that for a given side chain, the rate of intake should decrease along the series K^+/**2** > Rb^+/**2** > Na^+/**2** > Na^+/**1** > K^+/**1** > Rb^+/**1**. This is clearly found for both the octyl and octadecyl series. The tetradecyl case is less clear cut as the rates for Rb^+/**2**, Na^+/**2**, and Na^+/**1** are the same within the experimental error. In general, therefore, it is clear that the uptake rates are dominated by these two factors; an increase in complex stability or in ligand lipophilicity results in an increased rate of extraction.

This being the case, one might expect that membrane selectivity might be simply explained in terms of the selectivity of complexation determined from stability constants. In general, this is found to be the case; the 18-crown-6 derivatives complex K^+ selectively and transport K^+ most effectively. Unfortunately, the magnitude of the two effects is not the same. Whereas the carboxylates of the 18-crown-6 derivatives exhibit a K^+/Na^+ selectivity (thermodynamic selectivity) of about 20 (6) this results in a transport K^+/Na^+ selectivity of only 4 (entries 8 and 20 or 11 and 21, etc.). Other thermodynamic selectivities are similarly diminished to modest transport selectivities with the exception of the Na^+/K^+ selectivity of **1***a* which remains roughly the same (but small). This attenuation can be noted in other systems; monensin shows a thermodynamic Na^+/K^+ selectivity of 7 (9) in methanol which translates to a transport selectivity of 3 (7); the cryptand [2.2.C_8] (14, 17) exhibits a thermodynamic K^+/Na^+ selectivity of 22 (18) but a transport selectivity of only 2.8 (14, 19). In all these cases the membrane retains some selectivity and the overall behavior is closely controlled by the magnitude of the constant of stability. It therefore seems reasonable to suppose that the transport selectivity truly reflects the thermodynamic selectivity of the carrier in the **medium where complexation occurs**. Both complex stability and selectivity are strongly medium dependent and in general both values tend to increase as the solvent polarity decreases (18). For example, the K^+/Na^+ selectivity of the cryptand [2.2.C_8] increases from 22 to 50 as the solvent is changed from M/W (95:5 v/v) to pure methanol (18). The change from water to M/W is more dramatic: a tenfold increase in the K^+/Na^+ selectivity of the cryptand [2.2.2] is reported (18).

The selectivities of **1***a–c* and **2***a–c* were determined in M/W (90:10 v/v) (6). The ligands are insoluble in water, hence the values in this solvent are unobtainable, but may safely be assumed to be less than the values determined. A K^+/Na^+ selectivity of 3 has been reported for dicyclohexano 18-crown-6 (isomer A) in water (20). The transport selectivities observed in our system are consistent with a thermodynamic selectivity of about this magnitude and suggest therefore that the complexation step occurs in a predominantly aqueous environment.

Other Aspects

There are a variety of other aspects of the membrane system which serve to outline the general phenomenon. Electrostatic effects have been widely investigated in both a biological and chemical context (9) and are due to the potential created by the concentration gradient across the membrane. In our system (e.g., the cell of entry 8), the potential was ca. 260 mV and fell to 205 mV after all the potassium had been removed from the basic phase. The cell potential may be eliminated using a voltage clamp (21) (an applied potential which opposes the membrane potential). Transport with a membrane potential of 0 mV occurred at the same rate as with the full membrane potential. This is a

Can. J. Chem. Downloaded from www.nrcresearchpress.com by 210.87.254.5 on 09/06/12
For personal use only.

case of an "electrically silent antiport" transport mechanism (8) as is observed in both biological (9) or chemical (7) systems and is consistent with the mechanism outlined above (Fig. 1). The species within the membrane must therefore migrate as undissociated molecules or as tight ion pairs.

Turning to the question of **efficiency**, it is of interest to enquire why the system functions in such a highly efficient fashion (Figs. 2 and 3). Efficiency in this system refers to the ratio of protons to metal ions transported; the value 1 indicates an efficient system, larger values indicate that more protons must be expended to pump the same amounts of metal ions. The question arises since one might expect the carrier to act, not only to create a concentration gradient, but also to collapse the gradient so created. This question may be analysed in terms of a competition at the acidic interface between the pumping reaction [6] and a "leak" reaction [7].

[6] $MCrn\ (org) + H^+\ (aq) \rightleftharpoons HCrn\ (org) + M^+\ (aq)$

[7] $MCrn\ (org) + H^+\ (aq) + X^-\ (aq) \rightleftharpoons MHCrn^+X^-\ (org)$

In the pumping reaction [6], protonation of the carrier results in metal ion release. The "leak" reaction [7] occurs by extraction of an anion X^- to form a protonated carrier ion pair complex which can diffuse to the basic interface. This results in proton transfer with no net metal ion transfer. Membrane efficiency might be determined by the relative rates of the two forward reactions or by the relative positions of the two equilibria. For whatever reason, reaction [6] clearly dominates in our system.

The efficiency may be partly explained in terms of the relative stabilities of the two complexes. The thermodynamic data (6) show that the complexes of the protonated carriers are an order of magnitude less stable than the complexes of the deprotonated carriers, presumably as a result of lost electrostatic stabilization (22). As demonstrated above, the weaker complex would be expected to be transported less quickly, hence the reaction [7] would be expected to result in lower transport rates than the uptake rates for the same carrier at the basic interface. However, this effect is probably not large enough to explain the efficiency obtained. The thermodynamic data demonstrate that the K^+/18-crown-6 complex in acidic solution is about as stable as the Na^+/18-crown-6 complex in basic solution (6). Taking the Na^+ transport rates as a model for the rate of transport of K^+ by a protonated carrier, the difference in stability constant is seen to amount to at most a fivefold difference in rate. This is insufficient to account for the observed efficiency.

It is more likely that the efficiency is related to the anion dependence of the leak. In order for [7] to occur, an anion must be extracted from aqueous solution. This process strongly depends upon the solvation of the anion in both phases and may be referred to in qualititative terms as the "liposolubility" of the anion (14). The "anion effect" has been noted several times in membrane systems involving the transport of cations with an associated anion and can be very large (over eight orders of magnitude difference between the liposoluble anion picrate and the hydrophilic anion fluoride) (23). The effect roughly correlates with the free energy of hydration of the anion (23). The standard experiment has chloride (5×10^{-3} *M*), hydrogen phosphate (HPO_4^{2-}, $\sim 1 \times 10^{-3}$ *M*), and dihydrogenphosphate ($H_2PO_4^{2-}$, ~ 0.1 *M*) as extractible anions. Insofar as [7] is concerned, neither the Cl^- nor the HPO_4^{-2} present a suitable choice for X^-; both are highly solvated, are not liposoluble anions (23, 24), and are present at low concentration. The role of the $H_2PO_4^-$ is less clear; it may (23) or may not (3) be a liposoluble anion and it is present in large excess. In our system it is clear that $H_2PO_4^-$ is not a liposoluble anion as is shown by the following observations: (*i*) varying the $H_2PO_4^-$ concentration over a factor of 100 resulted in no change in rate of transport (entries 5, 12, and 13); (*ii*) the metal ion transport rate did not change when phosphate buffers were replaced by aqueous HCl; and, (*iii*) a standard cell, maintained for three days after the transport of 1.5×10^{-4} moles of K^+ had occurred, showed only 1.25 ppm of phosphorus (as phosphate) on the basic side of the membrane. This latter result indicates that an $H_2PO_4^-$ dependent leak is negligible to the level of 0.01% of the K^+ transported.

The membrane can be induced to "leak" by the use of KPF_6 or $KClO_4$ as the salts for the transport experiment (entries 31 and 32). Both perchlorate and hexafluorophosphate are much more liposoluble than chloride, hence the importance of [7] would be expected to be enhanced. This is borne out by the data; the system still pumps K^+ but at a reduced rate. The KPF_6 results suggest that on average, one protonated carrier/metal ion complex in three extracts an anion instead of releasing a metal ion to the aqueous solution. These results corroborate the discussion of the liposolubility of $H_2PO_4^-$. Relatively minor amounts of liposoluble anions observably disrupt the system; it follows that $H_2PO_4^-$ is not liposoluble or the transport would be unobservable.

Can. J. Chem. Downloaded from www.nrcresearchpress.com by 210.87.254.5 on 09/06/12
For personal use only.

Having examined anion dependent leaks, it is important to examine cation leaks as well in order to verify that such leaks could occur but did not in the standard experiment. The leak may be envisaged again, in terms of a competition between the pumping reaction and the leak at either the basic or acidic interfaces.

[8] $CrnH\ (org) + M^+\ (aq) + OH^-\ (aq) \rightleftharpoons CrnM\ (org) + H_2O$

[9] $CrnH\ (org) + C^+\ (aq) + OH^-\ (aq) \rightleftharpoons CrnC\ (org) + H_2O$

[10] $CrnM\ (org) + H^+\ (aq) \rightleftharpoons CrnH\ (org) + M^+\ (aq)$

[11] $CrnM\ (org) + C^+\ (aq) \rightleftharpoons CrnC\ (org) + M^+\ (aq)$

At the basic interface ([8]/[9]), the competition is between the ion of interest M^+ and an interfering cation C^+. At the acidic interface ([10]/[11]), the competition is between a proton and an interfering cation C^+. Both leak reactions generate the complex CrnC in the membrane, will result in a scrambling of C^+ between the two aqueous phases, and will degrade efficiency by disrupting the apparent M^+/H^+ stoichiometry. The available cations in the standard experiment are, on the basic side, tris(hydroxymethyl)ammoniomethane ($TrisH^+$) and on the acidic side, tetramethylammonium. The roles of both these cations as potential cation leaks were shown to be negligible by varying buffer concentration (no effect on rate) and by varying the cation. On the basic side, tetramethylammonium glycinate gave the same metal ion transport rates as the $TrisH^+$ buffers (entries 8 and 14) and on the acidic side tetramethylammonium, tetraethylammonium, and triethanolammonium dihydrogenphosphate buffers all gave the same transport rates for potassium. These results are somewhat surprising considering that the tetramethylammonium salts of the carriers are extremely soluble in chloroform and are easily prepared from aqueous tetramethylammonium hydroxide and the carriers in chloroform. However, the stability constants for complex formation were all determined in the presence of a vast excess of tetramethylammonium. A log K of 5.8 for the 18-crown-6 derivatives with K^+ thus means that the K^+ complex is at least six orders of magnitude more stable than a tetramethylammonium "complex."

Nonetheless, the membrane can be induced to leak tetramethylammonium by using $5 \times 10^{-3}\ M$ KCl in $0.1\ M$ tetramethylammonium chloride and $0.01\ M$ tetramethylammonium hydroxide as the basic aqueous phase. A plot similar to that of Fig. 3 in this case showed a line of slope 5, that is five times as many protons were transported as potassium ions. This is an extreme case; the other experiments in which the basic solution contained tetramethylammonium had at least a tenfold lower concentration of the interfering cation. At this level the leak is undetectable.

To summarize the question of efficiency, it appears likely the efficient functioning of the system depends upon the absence of interfering counterions. Among the cations available on the basic side, only the desired metal ion is sufficiently extractible to be drawn into the membrane. On the acidic side, protonation and metal ion release are preferred over the extraction of an anion since the choice of anions is so poor. The net result is that the system does what it was designed to do: pumps metal ions from basic to acidic solution.

Acknowledgements

We thank the Natural Sciences and Engineering Research Council of Canada and the University of Victoria for financial support of this project. Ms. Laurel A. Frederick was instrumental in developing the general procedures for the analyses on which this study is based.

1. R. M. IZATT and J. J. CHRISTENSEN (*Editors*). Synthetic multidentate macrocyclic compounds. Academic Press, New York. 1978; G. A. MELSON (*Editor*) Coordination chemistry of macrocyclic compounds. Plenum, New York. 1979.
2. M. SUGIURA and T. SHINBO. Bull. Chem. Soc. Jpn. **52**, 2209 (1979), and references cited therein.
3. J. J. GRIMALDI and J. M. LEHN. J. Am. Chem. Soc. **101**, 1333 (1979), and references cited therein.
4. W. E. MORF, S. ARVANITIS, and W. SIMON. Chimia, **33**, 452 (1979).
5. R. A. SCHWIND, T. J. GILLIGAN, and E. L. CUSSLER. *In* Synthetic multidentate macrocyclic compounds. *Edited by* R. M. Izatt and J. J. Christensen. Academic Press, New York. 1978.
6. L. A. FREDERICK, T. M. FYLES, N. P. GURPRASAD, and D. M. WHITFIELD. Can. J. Chem. **59**, 1724 (1981).
7. E. M. CHOY, D. F. EVANS, and E. L. CUSSLER. J. Am. Chem. Soc. **96**, 7085 (1974).
8. E. RACKER. Acc. Chem. Res. **12**, 338 (1979).
9. YU. A. OVCHINNIKOV, V. T. IVANOV, and A. M. SHKROB. Membrane active complexones. Elsevier, Amsterdam. 1974.
10. L. A. FREDERICK, T. M. FYLES, V. A. MALIK-DIEMER, and D. M. WHITFIELD. J. Chem. Soc. Chem. Commun. 1211 (1980).
11. M. NEWCOMB, J. L. TONER, R. C. HELGESON, and D. J. CRAM. J. Am. Chem. Soc. **101**, 4941 (1979).
12. A. A. FROST and R. G. PEARSON. Kinetics and mechanism. Wiley, New York. 1961. pp. 166–169.
13. M. SUGIURA and T. SHINBO. Bull. Chem. Soc. Jpn. **52**, 684 (1979); T. Shinbo, K. Kurihara, Y. Kobatake, and N. Kamo. Nature, **270**, 277 (1977).
14. J. M. LEHN. Pure Appl. Chem. **51**, 979 (1979).
15. E. L. CUSSLER. A. I. Ch. E. Journal, **17**, 1300 (1971).
16. J. D. LAMB, J. J. CHRISTENSEN, J. L. OSCARSON, B. L. NIELSEN, B. W. ASAY, and R. M. IZATT. J. Am. Chem. Soc. **102**, 6820 (1980).

17. B. DIETRICH, J. M. LEHN, and J. P. SAUVAGE. J. Chem. Soc. Chem. Commun. 15 (1973).
18. J. M. LEHN and J. P. SAUVAGE. J. Am. Chem. Soc. **97**, 6700 (1975).
19. M. KIRCH and J. M. LEHN. Angew. Chem. Int. Ed. Engl. **14**, 555 (1975).
20. C. J. PEDERSEN and H. K. FRENSDORFF. Angew. Chem. Int. Ed. Engl. **11**, 16 (1972).
21. J. W. MOORE. *In* Biophysics and physiology of excitable membranes. *Edited by* W. J. Adelman Jr. Van Nostrand Reinhold, New York. 1971.
22. J. P. BEHR, J. M. LEHN, and P. VIERLING. J. Chem. Soc. Chem, Commun. 621 (1976); M. M. LEHN, P. VIERLING, and R. C. HAYWARD. J. Chem. Soc.Chem. Commun. 296 (1979).
23. J. D. LAMB, J. J. CHRISTENSEN, S. R. IZATT, K. BEDKE, M. S. ASTIN, and R. M. IZATT. J. Am. Chem. Soc. **102**, 3399 (1980).
24. J. J. CHRISTENSEN, J. D. LAMB, S. R. IZATT, S. E. STARR, G. C. WEED, M. S. ASTIN, B. D. STITT, and R. M. IZATT. J. Am. Chem. Soc. **100**, 3219 (1978).

Can. J. Chem. Downloaded from www.nrcresearchpress.com by 210.87.254.5 on 09/06/12
For personal use only.

Erratum: 1,7-Dioxaspiro[5.5]undecanes. An excellent system for the study of stereoelectronic effects (anomeric and *exo*-anomeric effects) in acetals

PIERRE DESLONGCHAMPS, DARYL D. ROWAN, NORMAND POTHIER, GILLES SAUVÉ, AND JOHN K. SAUNDERS

Laboratoire de Synthèse Organique, Département de Chimie, Faculté des Sciences, Université de Sherbrooke, Sherbrooke (Qué.), Canada J1K 2R1

(Ref.: Can. J. Chem. **59**, 1105 (1981))
Received April 13, 1981

Our apologies are extended to author Gilles Sauvé for misspelling his name in this article.

Erratum: The role of the molecular environment for the primary photoprocesses of phenol in solution

J. ZECHNER, G. KÖHLER, G. GRABNER, AND N. GETOFF

Institut für Theoretische Chemie und Strahlenchemie der Universität Wien und Ludwig Boltzmann Institut für Strahlenchemie, Währingerstraße 38, A-1090 Vienna, Austria

(Ref.: Can. J. Chem. **58**, 2006 (1980))
Received April 23, 1981

In Table 1 α_e in water should read 0.018 and $Q_F(S_1)$ in cyclohexane 0.08.
In Fig. 2 the scale is to be divided by a factor of 10 for Q_e and for Q_H.
In Fig. 3 the scale is to be divided by a factor of 10 for α_e and by a factor of 3 for $\alpha_{(e+H)}$.

Configuration and conformation of alkoxyalkyl and hydroxyalkyl trifluoromethyl nitroxides. Anomeric effects and nitroxide conformations[1]

C. CHATGILIALOGLU[2] AND K. U. INGOLD

Division of Chemistry, National Research Council of Canada, Ottawa, Ont., Canada K1A 0R6

Received June 17, 1980

This paper is dedicated to Dr. F. P. Lossing of the National Research Council of Canada on the occasion of his 65th birthday

C. CHATGILIALOGLU and K. U. INGOLD. Can. J. Chem. **59**, 1745 (1981).

The epr spectral parameters for some $F_3CN(\dot{O})C(R_1R_2)OR$ radicals have been measured over a range of temperatures. These radicals are probably non-planar at nitrogen. Their OR groups are in the eclipsed position with respect to the N $2p_z$ orbital, a conformational preference which is attributed to a combination of steric factors and the anomeric effect. For $F_3CN(\dot{O})CH_2OR$ the *H* hyperfine splittings (hfs) are of unusually small magnitude. It is pointed out that all other known $R_3N(\dot{O})CHR_2OR$ also have anomalously low *H* hfs. It is suggested that this is due to the anomeric effect which not only promotes the eclipsed conformation but also causes the OR group to bend towards the semioccupied orbital, thereby moving *H* and R_2 towards the nodal plane of this orbital.

C. CHATGILIALOGLU et K. U. INGOLD. Can. J. Chem. **59**, 1745 (1981).

Opérant à différentes températures et faisant appel à la rpe, on a mesuré les paramètres spectraux de quelques radicaux $F_3CN(\dot{O})C(R_1R_2)OR$. Ces radicaux ne sont probablement pas plans au niveau de l'azote. Leurs groupes OR sont dans une position décalée par rapport à l'orbitale $2p_z$ de l'azote; on attribue cette préférence conformationnelle à une combinaison de facteurs stériques et de l'effet anomérique. Dans le cas du $F_3CN(\dot{O})CH_2OR$ les découplages hyperfins du H (fhs) ont une valeur qui est anormalement faible. On signale le fait que tous les autres radicaux $R_3N(\dot{O})CHR_2OR$ connus ont également des valeurs anormales de *H* hfs. On suggère que cela est dû à l'effet anomérique qui non seulement favorise la conformation décalée mais provoque également une déformation du groupe OR vers l'orbitale semi-occupée, déplaçant ainsi *H* et R_2 ver le plan nodal de cette orbitale.

[Traduit par le journal]

Introduction

The configurations and conformations of free radicals[3] can frequently be determined from the absolute magnitudes and/or the temperature coefficients of the hyperfine splittings (hfs) of various nuclei in the electron paramagnetic resonance (epr) spectra of the radicals (1).[4] During the course of an investigation into the mechanism by which radicals having the general structure **1** are formed

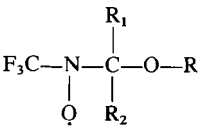

1

"spontaneously" when trifluoronitrosomethane is mixed with ethers or alcohols (3), we became intrigued by the fact that the N and F hfs for some **1** exhibited large temperature coefficients which were of *opposite* sign to those reported by Scheidler and Bolton (4) for bistrifluoromethyl nitroxide, $(CF_3)_2N\dot{O}$ (see also ref. 5). This prompted the present more detailed epr spectroscopic study of certain alkoxyalkyl and hydroxyalkyl trifluoromethyl nitroxides.[5] This leads us to conclude that in their configuration **1** are probably non-planar (at nitrogen) and that the conformations of **1** and of other alkoxyalkyl and hydroxyalkyl nitroxides are, in part, determined by anomeric effects (for leading references see ref. 6).

Experimental

Radicals were generated by mixing CF_3NO and the ether or alcohol in $CFCl_3$ and in CF_2Cl_2 with the usual freeze–thaw degassing. Spectra were recorded on a Varian E-104 EPR spectrometer. The epr parameters were measured by Griller and Preston's (7) very accurate procedure which utilizes an nmr field marker and a microwave frequency counter. A least-squares treatment is then used to obtain the best fit for all the measured lines. No sample was heated above room temperature because of the danger of bursting the epr tubes from the internal pressure.

Results

The $CF_3N(\dot{O})CR_1R_2OR$ radicals studied and their epr parameters at various temperatures are summarized in Table 1. The N and F hfs for four of these radicals ($R_1 = R_2 = H$ and CH_3, $R = H$ and CH_3) have been plotted against temperature in

[1]NRCC No. 18706.

[2]NRCC Research Associate 1979–1980.

[3]Following Kochi's suggestion (1) configuration is used herein to describe the geometry at the radical center (nitrogen) and conformation is used to describe the geometry of the whole radical, particularly as it relates to the orientation of the RO group with respect to the remainder of the radical.

[4]For a review of temperature dependent hfs see ref. 2.

[5]The atoms in **1** are identified as follows: $F_\gamma C_\beta N_\alpha(\dot{O})C_\beta(R_1R_2)_\gamma O_\gamma R_\delta$.

0008-4042/81/121745-08$01.00/0

©1981 National Research Council of Canada/Conseil national de recherches du Canada

Can. J. Chem. Downloaded from www.nrcresearchpress.com by 210.87.254.105 on 09/06/12
For personal use only.

Can. J. Chem. Downloaded from www.nrcresearchpress.com by 210.87.254.105 on 09/06/12
For personal use only.

Figs. 1 and 2, respectively, together with the epr data of Scheidler and Bolton (4) for $(CF_3)_2N\dot{O}$.

Discussion

Configuration

As can be seen from Figs. 1 and 2 $\partial a^N/\partial T$ is positive and $\partial a^F/\partial T$ is negative for bis-trifluoromethyl nitroxide. Scheidler and Bolton (4) suggested that the sign of these temperature coefficients, together with the small value of the N hfs relative to that for $[(CH_3)_3C]_2N\dot{O}$, resulted from conjugation of the fluorine *p* orbitals with the nitrogen $2p_z$ orbital. As they pointed out (4), the direct transfer of electron spin to the fluorine atoms must be significant because Rogers and Whiffen's study (8) of the single crystal epr spectra of the $HOOC—CH_2—\dot{C}F—COOH$ radical has shown that most of the spin density in the two β-fluorines lies in *p*-orbitals perpendicular to the C—F bond. This implies that there is a direct across-space interaction with the semi-occupied orbital. When the central atom is nitrogen this effect may be more pronounced because C—N bonds are shorter than C—C bonds.[6] Scheidler and Bolton therefore predicted that there should be a partial hindering of rotation about the C—N bonds. However, Morokuma (10) later concluded, on the basis of INDO calculations, that the average spin density of the fluorines in the two most stable planar conformers were the same, thus ruling out hindered rotation as a cause of the F hfs temperature coefficient. More detailed INDO calculations by Underwood and Vogel (ref. 11*a*, for related calculations on $H_2NO^{\cdot}$ see ref. 11*b*) showed that the structure of minimum energy was non-planar at nitrogen with a low barrier to inversion. Furthermore, the temperature dependence of the N hfs for $(CF_3)_2N\dot{O}$ could best be accounted for as being due to an increase in the out-of-plane vibration amplitude with increase in temperature, the energy required to produce such deformation being quite small (11*a*). The increase in the N hfs as the temperature rises is due to the fact that the amount of *s* character in the semi-occupied orbital will increase as the radical becomes, on average, less planar. Underwood *et al.* (11*c*) have also concluded that spin is transmitted to the fluorines by hyperconjugation rather than via the fluorine *p* orbitals. Since there is disagreement regarding the relative importance of the two mechanisms of spin transmission to fluorine the origin of the temperature dependence of the F hfs in $(CF_3)_2N\dot{O}$ remains uncertain.

There can, however, be no doubt that $(CF_3)_2N\dot{O}$ is non-planar. This has been shown by electron diffraction; the angle between the NO bond and the CNC plane being $22 \pm 3°$ (12). Furthermore, we (13) have shown by ^{17}O labelling that the unusually small N hfs of $(CF_3)_2N\dot{O}$ is due to a high spin density on oxygen (compared to dialkyl nitroxides) and not to spin transfer to the fluorine atoms.

The theory of the symmetric double minimum

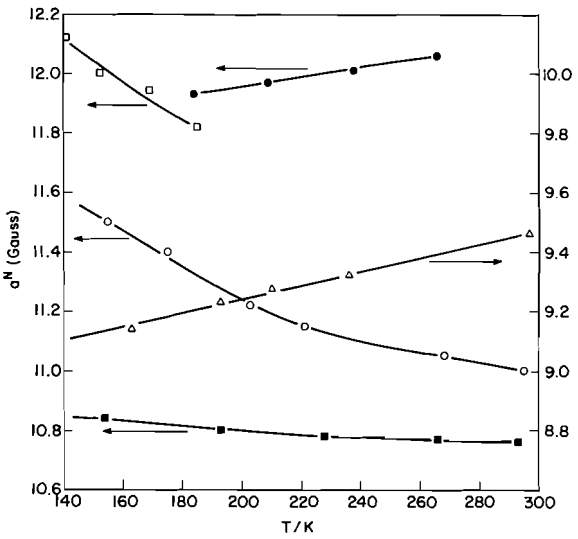

FIG. 1. N hfs as a function of temperature for $(CF_3)_2N\dot{O}$ (△, ref. 4), $CF_3N(\dot{O})CH_2OH$ (■), $CF_3N(\dot{O})C(CH_3)_2OH$ (●), $CF_3N(\dot{O})CH_2OCH_3$ (□), and $CF_3N(\dot{O})C(CH_3)_2OCH(CH_3)_2$ (○).

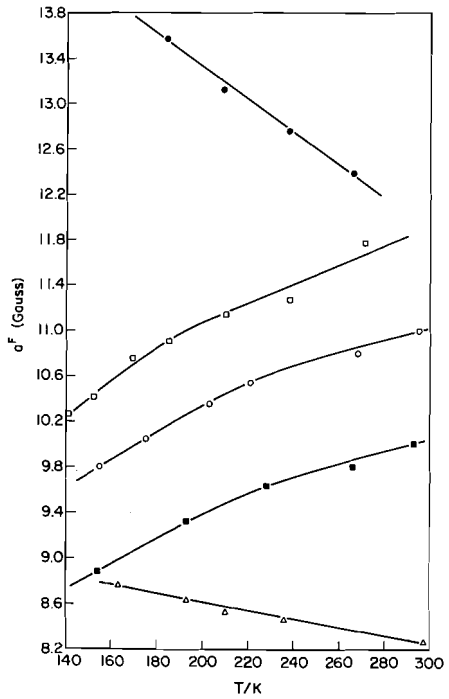

FIG. 2. F hfs as a function of temperature. Symbols are the same as in Fig. 1.

[6]Suggested by an anonymous referee.

TABLE 1. Electron paramagnetic resonance parameters for $CF_3N(\dot{O})C(R_1R_2)OR$ radicals in $CFCl_3$[a]

Radical (g)	T/K	a^N	a^F	$a^H(R_1R_2)$	$a^H(R)$	ΔH_{pp}[b]
$CF_3N(\dot{O})CH_2OH$	293	10.76	10.00	3.67(2H)	[c]	0.50
(2.0068)	266	10.77	9.79	3.42(2H)	[c]	0.41
	248	10.78	9.63	3.12(2H)	0.20(1H)	0.20
	213	10.80	9.32	2.84(2H)	0.28(1H)	0.15
	174	10.84	8.88	2.54(2H)[d]	0.30(1H)	0.15
$CF_3N(\dot{O})CH(CH_3)OH$	260	11.22	10.49	2.75(1H)	[c]	0.45
(2.0067)	216	11.24	10.36	2.74(1H)	[c]	0.58
	178	11.25	9.83	2.69(1H)	0.32(1H)	0.63
	150	11.27	9.35	2.67(1H)	[c]	0.75
$CF_3N(\dot{O})CD(CD_3)OD$	297	11.17	10.65	0.42(1D)		0.30
(2.0067)	266	11.17	10.55	0.42(1D)		0.23
	233	11.18	10.33	0.40(1D)		0.18
	204	11.19	10.00	0.39(1D)		0.14
	162	11.24	9.31	0.39(1D)		0.20
$CF_3N(\dot{O})CH(CH_2CH_3)OH$	293	[c]	10.96	2.22(1H)		0.50
(2.0067)	263	[c]	10.88	2.09(1H)		0.50
	218	10.94[f]	10.74	1.88(1H)		0.53
	188	10.96[f]	10.44	1.76(1H)		0.60
	167	11.00[f]	10.20	1.66(1H)		0.70
$CF_3N(\dot{O})C(CH_3)_2OH$	266	12.06	12.38			0.38
(2.0064)	238	12.01	12.76			0.40
	209	11.97	13.12			0.43
	184	11.93	13.57			0.50
$CF_3N(\dot{O})CH_2OCH_3$	271	[c]	11.77	3.08(1H);[c]	[c]	1.38
(2.0067)	237	[c]	11.27	3.09(1H);[c]	[c]	1.36
	210	[c]	11.14	3.09(1H); 1.07(1H)	[c]	0.30
	185	11.82	10.90	3.17(1H); 1.11(1H)	0.30(3H)	0.15
	169	11.94	10.75	3.25(1H); 1.12(1H)	0.30(3H)	0.15
	152	12.00	10.41	3.32(1H); 1.14(1H)	0.30(3H)	0.15
	141	12.12	10.26	3.47(1H); 1.17(1H)	0.30(3H)	0.15
$CF_3N(\dot{O})CH_2OC(CH_3)_3$	293	10.49	9.40	3.85(2H)		0.43
(2.0067)	248	10.42	9.24	3.76(2H)[d]		0.36
	216	10.37	9.14	3.70(2H)		0.30
	175	10.30	8.97	3.67(2H)[g]		0.30
	153	10.22	8.88[h]	3.65(2H)		0.30
$CF_3N(\dot{O})CH(CH_3)OCH_2CH_3$	298	[c]	10.68	1.65(1H)		0.81
(2.0068)	265	[c]	10.11	1.48(1H)		0.70
	229[i]	[c]	9.96	1.24(1H)		0.61
$CF_3N(\dot{O})C(CH_3)_2OCH(CH_3)_2$	295	11.00	11.00	[c]	3.50(1H)	1.40
(2.0067)	268	11.05	10.80	[c]	3.55(1H)	1.10
	221	11.15	10.54	0.40(6H)	3.75(1H)	0.25
	203	11.22	10.35	0.40(6H)	3.83(1H)	0.25
	175	11.40	10.05	0.40(6H)	3.97(1H)	0.25
	155	11.50	9.80	0.40(6H)	4.10(1H)	0.30

[a]Hyperfine splittings are given in G. The error is generally ± 0.04 G. In every case examined the epr parameters were, within experimental error, identical in CF_2Cl_2.
[b]Peak-to-peak line width in G.
[c]Not resolved.
[d]Centre line of 1:2:1 triplet starting to broaden.
[e]Resolved via second derivative spectrum.
[f]Tentative value.
[g]Center line of 1:2:1 triplet barely detectable.
[h]Center lines of the 1:3:3:1 quartet starting to broaden.
[i]At lower temperatures the interpretation of the spectrum became ambiguous. Other radicals may have been present.

Can. J. Chem. Downloaded from www.nrcresearchpress.com by 210.87.254.105 on 09/06/12
For personal use only.

Can. J. Chem. Downloaded from www.nrcresearchpress.com by 210.87.254.105 on 09/06/12
For personal use only.

potential energy function for out-of-plane bending as it relates to epr hfs parameters is now firmly established (14–17). For a radical, $A_\gamma B_\beta \dot{C}_\alpha D$, dissolved in an ideal (i.e., non-interacting) solvent:

(*i*) A *negative* tempertature coefficient for C_α implies a double minimum potential function (i.e., non-planarity at C_α) with at least three vibrational levels lying below the top of the barrier to inversion. Furthermore, it implies that the measurements were made at relatively low temperatures.[7]

(*ii*) A *positive* temperature coefficient for C_α may be observed under three different sets of conditions: (*1*) $AB\dot{C}D$ prefers a planar configuration (single potential minimum) but out-of-plane vibration is substantial (i.e., is thermally excited). (*2*) $AB\dot{C}D$ prefers a non-planar configuration but there are fewer than three vibrational levels below the top of the barrier. (*3*) $AB\dot{C}D$ prefers a non-planar configuration and has more than three vibrational levels below the top of the barrier but the measurements have been made at high temperatures.[7]

(*iii*) Provided the *conformation* of the radical is temperature independent (i.e., provided hindered rotation is unimportant) the temperature coefficients for A_γ and C_α will generally[8] be of opposite sign whether the out-of-plane motion is governed by a single (7) or a double (14, 17) minimum potential function.

Since $(CF_3)_2N\dot{O}$ is *non-planar* (12) it follows that the observation that its N and F hfs are temperature dependent[9] with positive and negative coefficients, respectively, means only that there is relatively little resistance to further out-of-plane deformation at nitrogen.

There are only a few other reports of trifluoromethyl nitroxides for which the N and F hfs have been shown to be temperature dependent (19–21). For $CF_3N(\dot{O})C(CH_3)_3$ (19), and for $CF_3N(\dot{O})CH[C(O)CH_3]_2$ and $CF_3N(\dot{O})COCH_3$ (20), the temperature dependencies of the N and F hfs are positive and negative, respectively, i.e., they are of the same sign as those for $(CF_3)_2N\dot{O}$. These three radicals may, therefore, be *either planar or non-planar*. The only *firm* conclusion that can be drawn from the experimental observations is that they all undergo extensive out-of-plane bending motion in the temperature range in which they were examined.

The results with most of the $CF_3N(\dot{O})C(R_1R_2)OR$ radicals, **1**, we have examined stand in sharp contrast to this earlier work in that the temperature coefficients for the N hfs are *negative* (or zero within the limits of our experimental accuracy) and for the F hfs are *positive* (see Table 1 and Figs. 1 and 2). It would appear, therefore, that most radicals of this type are probably non-planar, undergo extensive out-of-plane vibration, and have more than three vibrational levels below the top of the inversion barrier. Unfortunately, our experimental procedure confined us to ambient temperatures and below. We were therefore unable to observe even one example of a change in the sign of the temperature coefficients of the N and F hfs at high temperatures, which is predicted both on theoretical grounds (14–17) and by analogy with the observed behavior of *tert*-butyl (17). The preferred conformation of **1** has the C—O bond and the time averaged axis of the semi-occupied orbital eclipsed (*vide infra*) and so inversion at nitrogen can be represented by the non-equivalent structures, **2** and **3**.

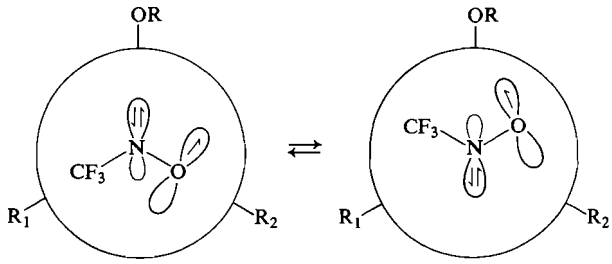

2 **3**

It must be added that the negative temperature coefficient for the N hfs can be explained *without* invoking a non-planar radical configuration. In a polar, or polarizable, solvent the interaction between the N—O dipole of the radical and neighbouring solvent molecules will become more important as the temperature decreases (22). That is, canonical structure **4***b* will become favored relative to **4***a* at lower temperatures and this means that the N hfs will increase with a decrease in temperature.[10] The experimental data do not, therefore, allow a decision to be made as to whether **1** are planar or non-planar. However, the latter seems the more probable in view of the known non-planarity of $(CF_3)_2N\dot{O}$ (12) and many (23), though perhaps not all (24), dialkyl nitroxides.

[7]Low and high temperature are defined in terms of the barrier height (15).

[8]Exceptions are known. For example, in $(CH_3)_3\dot{C}$, the out-of-plane motion of which is probably governed by a double minimum potential function, the maximum in a^H and the minimum in a^{13C_α} do not occur at the same temperature in all solvents (17).

[9]$|\partial a^N/\partial T| < |\partial a^F/\partial T|$ because N is "less sensitive" than F to *s* spin density. The calculated (18) hfs for an electron in an N 2*s* orbital (i.e., A_0^N) is 646 G and in a F 2*s* orbital it is 18 866 G.

[10]That is, the change in hfs with temperature may be due to the change in volume of the solvent; there being no intrinsic change with temperature at constant volume (22). However, changes in N hfs with temperature from this cause are fairly small (22).

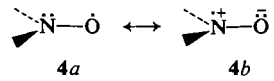

4a 4b

There are two **1** for which the temperature coefficients of the hfs differ from those generally observed. The first, $CF_3N(\dot{O})C(CH_3)_2OH$, has coefficients for N and F with the *same* sign as $(CF_3)_2N\dot{O}$ (see Figs. 1 and 2). Provided this radical is non-planar it would appear to have a lower barrier to out-of-plane motion than most other **1**. The second $CF_3N(\dot{O})CH_2OC(CH_3)_3$ has a positive temperature coefficient for both the N and F hfs. The same unusual behavior has been previously observed for the $CF_3N(\dot{O})C(CH_3)_2C(O)CH_3$ radical (21), and we suggest it arises either because of hindered rotations in these two radicals (which is certainly the case for $CF_3N(\dot{O})CH_2OC(CH_3)_3$, see footnote *h* to Table 1) or because of a greater than "normal" difference in energy between 2 and 3 (which would imply that out-of-plane motion will be easier in one direction than in the other).

To summarize, $(CF_3)_2N\dot{O}$ is unquestionably non-planar (12) and it has $\partial a^N/\partial T > 0 > \partial a^F/\partial T$. However, these temperature coefficients *do not require* that the radical be non-planar. In contrast, most $CF_3N(\dot{O})C(R_1R_2)OR$ radicals have $\partial a^N/\partial T < 0 < \partial a^F/\partial T$. *Unless* these temperature coefficients are due to solvent effects (22) these radicals must be non-planar *and* have a barrier to inversion which is higher than 3 vibrational levels. It seems likely that other radicals of this particular type *and* other radicals having the general structure[11] $CF_3N(\dot{O})CRR_1R_2$ (19–21) are non-planar. That is, theoretical calculations not withstanding, we think it probable that *all* $CF_3N(\dot{O})CRR_1R_2$ radicals are non-planar at nitrogen.

Conformation

The magnitude of the hfs of the hydrogen(s) directly attached to C_β provides a simple method for determining the approximate conformation of the $ROCHR_2$ group with respect to the $CF_3N(\dot{O})$ moiety. For a radical with a planar configuration the magnitude of a^H is related to the dihedral angle (θ) between the C_β—*H* bond and the axis of the semi-occupied orbital (see **5**) by the equation:

$$[1] \quad a^H = A + B\cos^2\theta$$

In this equation A and B are constants and A is generally taken to be zero (1, 2). For any new family of radicals B is assumed to be twice a^H for the methyl group because this group is not subject to hindered rotation and therefore the average value of θ is 45°. In the present instance the required radical, i.e., methyl trifluoromethyl nitroxide, was unknown. We therefore prepared it by photolysis of acetyl peroxide or methyl iodide and CF_3NO in $CFCl_3$.

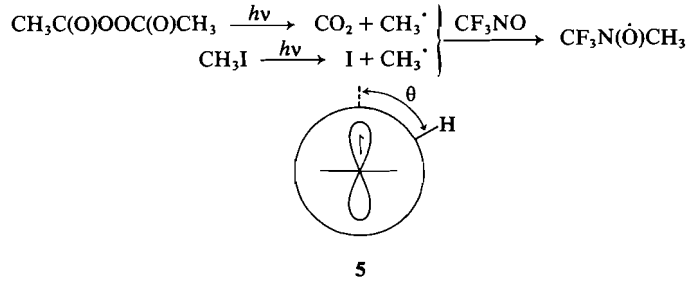

5

The epr parameters for $CF_3N(\dot{O})CH_3$ are given in Table 2. The hfs show small but interesting temperature dependencies in that the F hfs increases and the H hfs decreases with an increase in temperature. We prefer not to speculate on whether this is due to different mechanisms of spin transmission to H and F or to the different dynamic properties of the CH_3 and CF_3 groups. The H hfs is ca. 10.6 G (the necessary distinction between the H and F hfs having been achieved by preparing $CF_3N(\dot{O})CD_3$), and therefore $B \approx 21.2$ G for alkyl trifluoromethyl nitroxides.

Although this value of B can be used to obtain "exact" values of θ for many of the radicals listed in Table 1, there is a problem with the $CF_3N(\dot{O})CH_2OR$ radicals. For these radicals θ will have its *maximum* value when the RO group is in the eclipsed position (see structures **2** and **3**). This maximum is 60°, which would lead to a predicted *minimum* a^H value of $B/4 = 5.3$ G. However, all three $CF_3N(\dot{O})CH_2OR$ radicals have a^H values which are less than 4 G (see Table 1).

Unexpectedly small a^H values have been re-

[11]Represented in this way to exclude radicals such as $CF_3N(\dot{O})C_6H_5$ which are more likely to be planar. For a variable temperature epr study of some aryl fluoroalkyl nitroxides see ref. 25.

Can. J. Chem. Downloaded from www.nrcresearchpress.com by 210.87.254.105 on 09/06/12
For personal use only.

Can. J. Chem. Downloaded from www.nrcresearchpress.com by 210.87.254.105 on 09/06/12
For personal use only.

TABLE 2. Electron paramagnetic resonance parameters for $CF_3N(\dot{O})CH_3$ in $CFCl_3$[a]

T/K	a^N	a^F	a^H	ΔH_{pp}[b]
270	11.78	11.23	10.51	0.62
233	11.87	11.20	10.57	0.30
201	11.91	11.12	10.65	0.24
163	11.95	10.94	10.88	0.30

[a] g = 2.0066. Hyperfine splittings are given in G with an estimated error of ± 0.04 G.
[b] Peak-to-peak line width in G.

ported on several occasions. The 2-chloroethyl radical, $ClCH_2CH_2^{\bullet}$, provides a well known case in point (1). For this radical a^H = 10.2 G while the estimated value (based on a^H = 26.87 G in $CH_3CH_2^{\bullet}$) for θ = 60° is 13.4 G (1). Many other examples of the same phenomenon are known (1). They are usually interpreted in terms of the eclipsed conformation *plus* an attractive interaction between the heteroatom, or heteroatom-centered group, X, and the semi-occupied orbital which causes X to move towards the radical center (1, 26). As a consequence the hydrogens of the CH_2X group are displaced towards the nodal plane and their interaction with the unpaired electron decreases (1, 26), see **6**. It has also been suggested

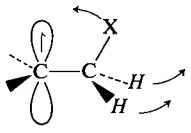

6

that the electron-attracting X will reduce a^H simply by reducing the electron releasing power of the C_β—H bonds (27).

Either of the above explanations might account for the small H hfs of $CF_3N(\dot{O})CH_2OR$ radicals. There is, in addition, the possibility that with non-planar radicals the A term in eq. [1] is not so small that it can be neglected.

While there may be some doubt about the reason for their small a^H values, there can be no doubt that $CF_3N(\dot{O})CH_2OR$ radicals preferentially adopt a conformation with the RO group in the eclipsed position, i.e., **2** and **3**. The same would seem to be true for $CF_3N(\dot{O})CH(R_2)OR$ radicals and is presumably true for $CF_3N(\dot{O})C(R_1R_2)OR$ radicals. This conformational preference contrasts with that of 2-alkoxyethyl and 2-hydroxyethyl radicals which prefer the staggered conformation, **7** (1, 2).

We attribute the preference of **1** for the eclipsed conformation to a combination of steric factors and the anomeric effect (6). Steric factors must be significant since even $CF_3N(\dot{O})CH_2CH_3$ would appear, from its a^H value of 7.5 G at 300 K (28), to have

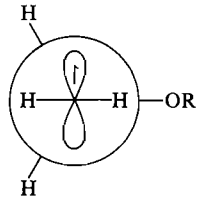

7

the methyl group close to the eclipsed position. The anomeric effect, which results from delocalization of a heteroatom lone pair into the region of an adjacent polar bond, produces an increase in the stability of conformations in which the lone pair is in the same plane as the polar bond (6). In **1** the interaction between the N lone pair (or, more correctly, the NO 3 electron system) and the antibonding σ_{CO}^* orbital will favor RO being in the eclipsed position. Furthermore, this interaction is attractive and thus provides a simple explanation for the small magnitudes of H hfs in $CF_3N(\dot{O})CH_2OR$ radicals (*vide supra*, cf. 6) and in other alkoxyalkyl and hydroxyalkyl nitroxides (*vide infra*).

A second anticipated manifestation of the anomeric effect would be between the *p*-type lone pair on the oxygen of the RO group and the polar C_β—$N(O)CF_3$ bond. This interaction will favor conformations in which the R—O bond is approximately perpendicular to the N—C_β—O plane, i.e., **8** and **9**. This will lead to restricted rotation about the C_β—O bond. However, in many **1** conformations **8** and **9** may not be attained because of overriding steric interactions (e.g., those between R and R_2 in **8** and possibly those between R and CF_3 in **9**).

At low temperatures the methylene hydrogens in $CF_3N(\dot{O})CH_2OR$ radicals become non-equivalent. For R = CH_3 this inequivalence manifests itself as two distinct H hfs at 210 K and below, while for R = H and R = $C(CH_3)_3$ inequivalence manifests itself as a broadening of the central line of the 1:2:1 triplet which becomes noticeable at 174 K and 248 K, respectively. Assuming that inversion at N has only a low barrier (*vide supra*), the non-equivalence of the hydrogens implies that rotation about both the C_β—O bond (**10** ⇄ **11**) and C_β—N bond (**11** ⇄ **12**) can be frozen-out.

Finally, attention is drawn to the unusually large H hfs of $CF_3N(\dot{O})C(CH_3)_2OCH(CH_3)_2$ (ca. 4 G, see

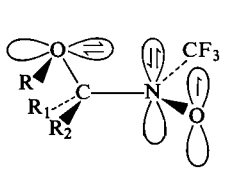

8 $R_1 = R_2$

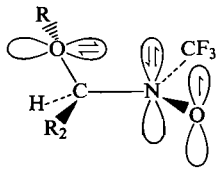

9 R_2 = alkyl

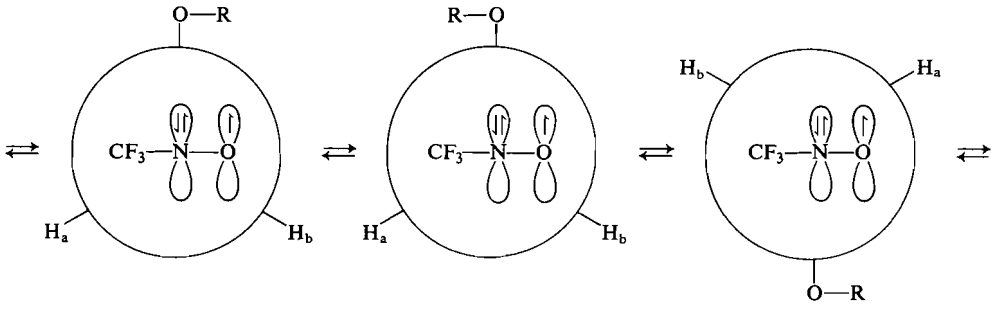

10 11 12

Table 1). It is clear that this radical is quite firmly locked in a conformation which allows a long-range H hfs. This might be a W, **13**, an anti-W, or a U, **14**, conformation (29). It would seem that in this radical steric factors override the anomeric effect, which favors conformation **8**.

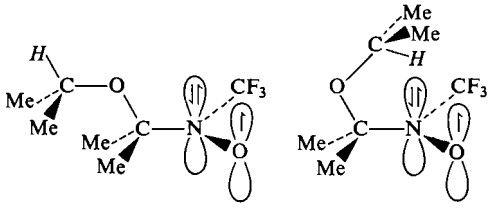

13 14

Other Alkoxyalkyl and Hydroxyalkyl Nitroxides

As far as we can tell all alkoxyalkyl and hydroxyalkyl nitroxides, i.e., all $R_3N(\dot{O})CHR_2OR$ radicals which have been reported have anomalously low *H* hfs (30). For example, $(CH_3)_3CN(\dot{O})CH_3$ has $a^H = 11.3$ G, which yields a "minimum" a^H for $(CH_3)_3CN(\dot{O})CH_2X$ radicals of 5.5 G (i.e. for $\theta = 60°$), yet for $(CH_3)_3CN(\dot{O})CH_2OH$ a^H has a value of 4.8 G in methanol at 298 K (31), 4.1 G (32*a*) or 4.0 G (32*b*) at 195 K and 4.5 G (32*c*) or 4.0 G (32*d*) at 228 K. As a second example, spin-trapping of HO· and RO· radicals by 5,5-dimethyl-1-pyrroline-1-oxide has yielded nitroxides, **15**,

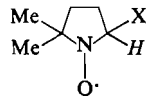

15

X	a^H (G)	Reference
H	18.9	34
CH_3	20.5	33
HO	15.3	35
MeO	7.6	33
EtO	7.0	33
Me_3CO	7.9	33

which also exhibit unexpectedly small *H* hfs (33–37).

No self-consistent explanation of the above results has been advanced.[12] However, they can be simply explained as a consequence of the anomeric effect which favors conformation **17** for

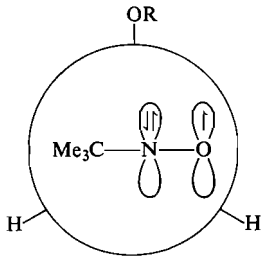

17

$(CH_3)_3CN(\dot{O})CH_2OR$ radicals and **18** for **15** having X = HO and RO. Distortions of 5-membered rings from planarity are known in related structures (9) which can also be attributed to anomeric effects.

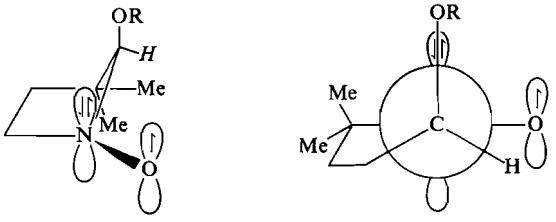

18

1. J. K. KOCHI. Adv. Free Radical Chem. **5**, 189 (1975).
2. P. D. SULLIVAN and E. M. MENGER. Adv. Magn. Reson. **9**, 1 (1977).
3. C. CHATGILIALOGLU and K. U. INGOLD. To be published.
4. P. J. SCHEIDLER and J. R. BOLTON. J. Am. Chem. Soc. **88**, 371 (1966).
5. W. R. KNOLLE and J. R. BOLTON. J. Am. Chem. Soc. **91**, 5411 (1969); **93**, 3337 (1971).
6. (*a*) R. U. LEMIEUX. Pure Appl. Chem. **25**, 527 (1971); (*b*) N.

[12]A proposal by Janzen *et al.* (34) that the nitroxyl function becomes more and more non-planar as the electronegativity of X increases would, as these authors point out, lead to an increase in a^N which is contrary to their observations. A polar or inductive effect from X was suggested as an offsetting factor (34).

Can. J. Chem. Downloaded from www.nrcresearchpress.com by 210.87.254.105 on 09/06/12
For personal use only.

Can. J. Chem. Downloaded from www.nrcresearchpress.com by 210.87.254.105 on 09/06/12
For personal use only.

S. ZEFIROV and N. M. SHEKHTMAN. Russ. Chem. Rev. **40**, 315 (1971); (*c*) S. DAVID, O. EISENSTEIN, W. J. HEHRE, L. SALEM, and R. HOFFMANN. J. Am. Chem. Soc. **95**, 3806 (1973); (*d*) R. U. LEMIEUX, K. B. HENDRIKS, R. V. STICK, and K. JAMES. J. Am. Chem. Soc. **97**, 4056 (1975); (*e*) L. B. HARDING and W. A. GODDARD III. Tetrahedron Lett. 747 (1978); (*f*) W. A. SZAREK and D. HORTON (*Editors*). Anomeric effect. Origin and consequences. Am. Chem. Soc. Symp. Ser. No. 87, 1979; (*g*) S. WOLFE, M.-H. WHANGBO, and D. J. MITCHELL. Carbohydr. Res. **69**, 1 (1979).

7. D. GRILLER and K. F. PRESTON. J. Am. Chem. Soc. **101**, 1975 (1979).
8. M. T. ROGERS and D. M. WHIFFEN. J. Chem. Phys. **40**, 2662 (1964).
9. (*a*) K. MÜLLER and A. ESCHENMOSER. Helv. Chim. Acta, **52**, 1823 (1969); (*b*) M. DOBLER, J. D. DUNITZ, and D. M. HAWLEY. Helv. Chim. Acta, **52**, 1831 (1969); (*c*) V. MALATESTA and K. U. INGOLD. J. Am. Chem. Soc. In press.
10. K. MOROKUMA. J. Am. Chem. Soc. **91**, 5412 (1969).
11. (*a*) G. R. UNDERWOOD and V. L. VOGEL. Mol. Phys. **19**, 621 (1970); (*b*) Y. ELLINGER, R. SUBRA, A. RASSAT, J. DOUADY, and G. BERTHIER. J. Am. Chem. Soc. **97**, 476 (1975); (*c*) G. R. UNDERWOOD, V. L. VOGEL, and I. KREFTING. J. Am. Chem. Soc. **92**, 5019 (1970).
12. C. GLIDEWELL, D. W. H. RANKIN, A. G. ROBIETTE, G. M. SHELDRICK, and S. M. WILLIAMSON. J. Chem. Soc. A, 478 (1971).
13. C. CHATGILIALOGLU, V. MALATESTA, and K. U. INGOLD. J. Phys. Chem. To be published.
14. J. B. LISLE, L. F. WILLIAMS, and D. E. WOOD. J. Am. Chem. Soc. **98**, 227 (1976).
15. P. J. KRUSIC and P. MEAKIN. J. Am. Chem. Soc. **98**, 228 (1976).
16. G. BRUNTON, K. U. INGOLD, B. P. ROBERTS, A. L. J. BECKWITH, and P. J. KRUSIC. J. Am. Chem. Soc. **99**, 3177 (1977).
17. D. GRILLER, K. U. INGOLD, P. J. KRUSIC, and H. FISCHER. J. Am. Chem. Soc. **100**, 6750 (1978).
18. J. R. MORTON and K. F. PRESTON. J. Magn. Reson. **30**, 577 (1978).
19. K. J. KLABUNDE. J. Am. Chem. Soc. **92**, 2427 (1970).
20. B. L. BOOTH, D. J. EDGE, R. N. HASZELDINE, and R. G. G. HOLMES. J. Chem. Soc. Perkin Trans. 2, 7 (1977).
21. Y. KATSUMURA, K. ISHIGURE, and Y. TABTA. J. Phys. Chem. **83**, 3152 (1979).
22. D. GRILLER. J. Am. Chem. Soc. **100**, 5240 (1978).
23. (*a*) J. LAJZÉROWICZ-BONNETEAU. Acta Crystallogr. Sect. B, **24**, 196 (1968); (*b*) D. M. HAWLEY, G. FERGUSON, and J. M. ROBERTSON. J. Chem. Soc. B, 1255 (1968); (*c*) A. CAPIOMONT, B. CHION, and J. LAJZÉROWICZ-BONNETEAU. Acta Crystallogr. Sect. B, **27**, 322 (1971); (*d*) A. CAPIOMONT. Acta Crystallogr. Sect. B, **28**, 2298 (1972); (*e*) A. CAPIOMONT. Acta Crystallogr. Sect. B, **29**, 1720 (1973); (*f*) A. CAPIOMONT and J. LAJZÉROWICZ-BONNETEAU. Acta Crystallogr. Sect. B, **30**, 2160 (1974).
24. (*a*) B. CHION, A. CAPIOMONT, and J. LAJZÉROWICZ. Acta Crystallogr. Sect. B, **28**, 618 (1972); (*b*) J. W. TURLEY and F. P. BOER. Acta Crystallogr. Sect. B, **28**, 1641 (1972); (*c*) J. C. A. BOEYENS and G. J. KRUGER. Acta Crystallogr. Sect. B, **26**, 668 (1970); (*d*) B. CHION and M. THOMAS. Acta Crystallogr. Sect. B, **31**, 472 (1975); (*e*) B. CHION and J. LAJZÉROWICZ. Acta Crystallogr. Sect. B, **31**, 1430 (1975).
25. S. A. FAIRHURST and L. H. SUTCLIFFE. J. Chem. Soc. Faraday Trans. 1, 1521 (1979).
26. (*a*) P. J. KRUSIC and J. K. KOCHI. J. Am. Chem. Soc. **93**, 846 (1971); (*b*) D. J. EDGE and J. K. KOCHI. J. Am. Chem. Soc. **94**, 6485 (1972); (*c*) A. J. BOWLES, A. HUDSON, and R. A. JACKSON. Chem. Phys. Lett. **5**, 552 (1970); (*d*) T. KAWAMURA, D. J. EDGE, and J. K. KOCHI. J. Am. Chem. Soc. **94**, 1752 (1972); (*e*) M. C. R. SYMONS. Chem. Phys. Lett. **19**, 61 (1973); (*f*) J. COOPER, A. HUDSON, and R. A. JACKSON. Tetrahedron Lett. 831 (1973); (*g*) K. S. CHEN, I. H. ELSON, and J. K. KOCHI. J. Am. Chem. Soc. **95**, 5341 (1973); (*h*) I. BIDDLES and A. HUDSON. Chem. Phys. Lett. **18**, 45 (1973); (*i*) D. GRILLER and K. U. INGOLD. J. Am. Chem. Soc. **96**, 6715 (1974); (*j*) S. A. FIELDHOUSE, A. R. LYONS, H. C. STARKIE, and M. C. R. SYMONS. J. Chem. Soc. Dalton Trans. 1966 (1974); (*k*) M. C. R. SYMONS. Tetrahedron Lett. 793 (1975); (*l*) J. C. SCAIANO and K. U. INGOLD. J. Phys. Chem. **80**, 275 (1976).
27. (*a*) J. A. BRIVATI, K. D. J. ROOT, M. C. R. SYMONS, and D. J. A. TINLING. J. Chem. Soc. A, 1942 (1969); (*b*) A. R. LYONS and M. C. R. SYMONS. J. Chem. Soc. Faraday Trans. 2, **68**, 622 (1972).
28. V. A. GINSBURG, A. N. MEDVEDEV, S. S. DUBOV, and M. F. LEBEDEVA. Zh. Obshch. Khim. **37**, 601 (1967).
29. F. W. KING. Chem. Rev. **76**, 157 (1976).
30. A. R. FORRESTER. *In* Landolt-Börnstein, New Series. Vol. 9. Part cl. *Edited by* H. Fischer and K.-H. Hellwege. 1979. Chapt. 6. pp. 192–1066.
31. M. J. PERKINS, P. WARD, and A. HORSFIELD. J. Chem. Soc. B, 395 (1970).
32. (*a*) J. A. WARGON and F. WILLIAMS. J. Am. Chem. Soc. **94**, 7917 (1972); (*b*) F. P. SARGENT and E. M. GARDY. Can. J. Chem. **52**, 3645 (1974); (*c*) F. P. SARGENT, E. M. GARDY, and H. R. FALLE. Chem. Phys. Lett. **24**, 120 (1974); (*d*) F. P. SARGENT and E. M. GARDY. J. Phys. Chem. **80**, 854 (1976).
33. E. G. JANZEN and J. I.-P. LIU. J. Magn. Reson. **9**, 510 (1973).
34. E. G. JANZEN, C. A. EVANS, and J. I.-P. LIU. J. Magn. Reson. **9**, 513 (1973).
35. J. R. HARBOUR, V. CHOW, and J. R. BOLTON. Can. J. Chem. **52**, 3549 (1974).
36. F. P. SARGENT and E. M. GARDY. Can. J. Chem. **54**, 275 (1976).
37. C. A. EVANS. Aldrichim. Acta, **12**, 23 (1979).

Charge exchange mass spectra of some C_5H_{10} isomers

YIP HOI LI, JAN A. HERMAN,[1] AND ALEX. G. HARRISON

Department of Chemistry, University of Toronto, Toronto, Ont., Canada M5S 1A1

Received October 13, 1980

This paper is dedicated to Dr. F. P. Lossing of the National Research Council of Canada on the occasion of his 65th birthday

YIP HOI LI, JAN A. HERMAN, and ALEX. G. HARRISON. Can. J. Chem. **59**, 1753 (1981).

Reagent gas systems are described for use in a single-source chemical ionization mass spectrometer which permit charge exchange mass spectra to be obtained using $CS_2^{+\cdot}$ (~ 10.2 eV), $COS^{+\cdot}$ (11.2 eV), $Xe^{+\cdot}$ (~ 12.5 eV), $CO^{+\cdot}$ (14.0 eV), $N_2^{+\cdot}$ (15.3 eV), and $Ar^{+\cdot}$ (15.8 eV) (recombination energies in brackets) as the major reactant ions. Using these reagent gas systems the charge exchange mass spectra of cyclopentane, 1-pentene, 3-methyl-1-butene, 2-methyl-1-butene, 2-pentene, and 2-methyl-2-butene have been obtained. It is shown that these spectra can be used to construct breakdown graphs which adequately depict the relative energy dependences of the fragmentation pathways and rationalize the 70 eV electron impact mass spectra.

YIP HOI LI, JAN A. HERMAN et ALEX. G. HARRISON. Can. J. Chem. **59**, 1753 (1981).

Des spectres de masse de transfert de charge ont été obtenus avec un spectromètre de masse muni d'une source simple à chimiionisation en utilisant des milieux réactionnels comportant comme ion réactif principal l'une des espèces suivantes: $CS_2^{+\cdot}$ (~ 10.2 eV), $COS^{+\cdot}$ (11.2 eV), $Xe^{+\cdot}$ (~ 12.5 eV), $CO^{+\cdot}$ (14.0 eV), $N_2^{+\cdot}$ (15.3 eV) et $Ar^{+\cdot}$ (15.8 eV) (énergie de recombinaison données entre parenthèses). Cette étude a porté sur les cyclopentane, pentène-1, méthyl-3 butène-1, méthyl-2 butène-1, pentène-2 et méthyl-2 butène-2. Ces spectres de transfert de charge peuvent ensuite servie à construire des diagrammes de seuil d'apparition permettant de décrire les dépendances énergétiques relatives des voies de fragmentation et de rendre compte des spectres de masse par impact électronique à 70 eV.

When a gaseous sample of a polyatomic molecule, M, of ionization energy, IE, is bombarded with a beam of electrons of energy, E, the molecular ions produced possess internal energies ranging from 0 to E − IE, with a distribution which is unknown but depends on the electron energy E and the identity of the molecule M. The mass spectrum observed results from a series of competing and consecutive unimolecular fragmentation reactions, starting from $M^{+\cdot}$, each with rate coefficients dependent on the internal energy, summed over the unknown internal energy distribution (1). In effect, the primary kinetic data, i.e., the reaction channels and the relative rates of competing channels, are obscured by the summation procedure. Although qualitative kinetic information can be obtained by varying the energy of the impacting electrons, quantitative data, in the form of a breakdown graph, can be obtained only by determining the normalized second derivatives of the ion signals as a function of the ionizing electron energy (2).

The breakdown graph, i.e., the fractional ion intensities as a function of the internal energy of $M^{+\cdot}$, provides detailed information on the fragmentation channels of $M^{+\cdot}$ and on the competition between these channels as a function of internal energy. It has long been recognized (3, 4) that breakdown graphs can be obtained directly by charge exchange ionization (reaction [1]),

$$[1] \quad R^{+\cdot} + M \rightarrow M^{+\cdot} + R$$

where the internal energy of $M^{+\cdot}$ is determined by the difference between the recombination energy (RE) of the reactant ion $R^{+\cdot}$ and the ionization energy (IE) of the molecule M. The internal energy of $M^{+\cdot}$ can be varied in a controlled manner by suitable choice of reagent ions $R^{+\cdot}$. Most charge transfer experiments to date have been performed using tandem mass spectrometers (3, 4) and, for the most part, have studied in detail relatively simple molecules with the aim of comparing experimental breakdown graphs with those calculated from theory (4, 5), although several recent publications (6–8) have been concerned with the question of distinguishing among isomeric molecules from their charge exchange mass spectra.

With the advent of high pressure chemical ionization mass spectrometry, a number of groups have used charge exchange ionization either separately, or in conjunction with proton transfer ionization in analytical applications (9–14). However, with the exception of two reports by Einolf and Munson (15, 16), there have been no attempts to develop charge exchange reagent ion systems covering a range of recombination energies suitable for the derivation of breakdown graphs from single-source experiments. Such data for complex molecules should provide considerable information on fragmentation mechanisms and the energy dependence of the reactions occurring. The present work reports the development of charge exchange reagent ion sys-

[1]Visiting Professor 1979–1980, Permanent address: Département de Chimie, Université Laval (Qué.), Canada G1K 7P4.

0008-4042/81/121753-07$01.00/0

©1981 National Research Council of Canada/Conseil national de recherches du Canada

Can. J. Chem. Downloaded from www.nrcresearchpress.com by 210.87.254.105 on 09/06/12
For personal use only.

Can. J. Chem. Downloaded from www.nrcresearchpress.com by 210.87.254.105 on 09/06/12
For personal use only.

tems covering recombination energies from ~10 eV to ~16 eV and the application of the systems developed to the determination of the charge exchange mass spectra of six C_5H_{10} isomers. Some years ago Turk and Shapiro (17) reported breakdown graphs for a number of simple ketones obtained from single-source experiments using the method of Cermak and Herman (18). This method suffers from a number of experimental problems and it appeared that the approach of high pressure mass spectrometry might prove to be simpler and more useful.

We have chosen to study the C_5H_{10} isomers in part because they have been extensively studied by electron impact. In particular, the energetics of formation of the molecular ion and the $C_4H_7^+$ fragment ion have been clearly established by Lossing (19); this allows us to evaluate the recombination energies achieved in the present high pressure systems. The 70 eV mass spectra of the C_5 olefins are quite similar (20, 21), the most striking difference being the enhanced loss of C_2H_4 from the molecular ion of 1-pentene. Similarly, the mass spectrum of cyclopentane shows a dominant loss of C_2H_4 from the molecular ions (20, 21). The major low energy fragmentation reactions, which are observed as metastable peaks, correspond to loss of CH_3 and to loss of C_2H_4 from the molecular ion; the ratio of metastable peak intensities is independent of molecular structure (22) making distinction among the isomers impossible on this basis. In addition, the collisional activation mass spectra of the C_5H_{10} isomers are very similar (23), making isomer identification by this method extremely difficult. Thus, the study also provides a test of the utility of charge exchange mass spectrometry in distinguishing among isomers.

Charge Exchange Reagent Ions

$CS_2^{+\cdot}$

Electron impact ionization of a mixture of 10–20% CS_2 in N_2 at ~0.2 Torr total pressure gave $CS_2^{+\cdot}$ as the major reactant (>80%) with minor yields of $S_2^{+\cdot}$ (<10%), $(CS_2)_2^{+\cdot}$ (<10%), and a very small amount of CS_3^+. The use of CS_2/N_2 mixtures to produce $CS_2^{+\cdot}$ as a low energy charge exchange reagent has been reported previously (24, 25).

The photoelectron spectrum of CS_2 shows (26) the lowest energy ionic state as a doublet and yields ionization energies of 10.06 and 10.12 eV, with very little vibrational structure apparent. The $\tilde{A}^2\pi_\mu$ state of $CS_2^{+\cdot}$ with an energy of 12.69 eV could be formed by charge exchange from $N_2^{+\cdot}$. This state has a lifetime of ~4 μs (27) and could play a role in subsequent charge exchange reactions. Lindholm (3, 4) reports the recombination energy of $CS_2^{+\cdot}$ to be ~9.5 or 10 eV. The recombination energy of $(CS_2)_2^{+\cdot}$ should be lower than that of $CS_2^{+\cdot}$ while the recombination energy of $S_2^{+\cdot}$ should be equal to or less than the ionization energy of 9.4 eV (28).

$COS^{+\cdot}$

Attempts to prepare $COS^{+\cdot}$ by electron impact ionization of COS/N_2 mixtures resulted in $S_2^{+\cdot}$ as the major product ion. Presumably charge exchange of $N_2^{+\cdot}$ with COS resulted largely in formation of $S^{+\cdot}$ (AE = 13.6 eV (28)) which reacts with COS by reaction [2], as previously reported (29).

[2] $S^{+\cdot} + COS \rightarrow S_2^{+\cdot} + CO$

By contrast electron impact ionization of a 10% COS – 90% CO mixture at 0.1–0.2 Torr pressure yielded $COS^{+\cdot}$ (~76%) with $S_2^{+\cdot}$ (~14%), $CS_2^{+\cdot}$ (~4%), and $(COS)_2^{+\cdot}$ (~4%) as the major ions; the $(COS)_2^{+\cdot}/COS^{+\cdot}$ intensity ratio increased with increasing pressure as expected. Kebarle *et al.* (29) have reported the ion–molecule reaction

[3] $COS^{+\cdot} + COS \rightarrow S_2^{+\cdot} + 2CO$

This reaction probably accounts for the major part of the $S_2^{+\cdot}$ observed.

The photoelectron spectrum of COS shows (26) the lowest energy band as a doublet (ionization energies of 11.18 and 11.23 eV) with weak vibrational structure. Bands at higher energies give ionization energies of 15.5 eV, 16.0 eV, and 18.0 eV. The $\tilde{A}^2\pi$ state (15.5 eV) has an upper lifetime for decay by fluorescence of 30 ns, the major decay channel being predissociation to S^+ (^4S) (27). The role of the higher states in charge exchange is not known. Lindholm (3, 4) reports a recombination energy of 11.2 eV for $COS^{+\cdot}$. The major impurity of $S_2^{+\cdot}$, with a recombination energy ≤9.4 eV could effect ionization of molecules with IE's below this value, but in the present system would not lead to fragment ion formation.

$Xe^{+\cdot}$

Electron impact ionization of Xe at source pressures of ~0.1 Torr yielded only Xe^+ ions. The recombination energy of $Xe^{+\cdot}$ is 12.13 eV for the $^2P^0_{3/2}$ state and 13.44 eV for the $^2P^0_{1/2}$ state (3, 4). In construction of the breakdown graphs in the following, a mean recombination energy of 12.5 eV has been used; this assumes the 66:33 statistical weights of the two states. Electron impact on Xe could produce the long-lived $^3P_2$ and $^3P_0$ states of Xe which could react by Penning ionization (30);

Can. J. Chem. Downloaded from www.nrcresearchpress.com by 210.87.254.105 on 09/06/12
For personal use only.

the energies of these states are 8.31 eV and 9.44 eV, respectively (31), with the result that only molecular ion formation should occur and only for C_5H_{10} isomers of low ionization energy.

$CO^{+\cdot}$

Electron impact ionization of CO at source pressures of 0.1–0.2 Torr yielded $CO^{+\cdot}$ with only a minor yield of $(CO)_2^{+\cdot}$. The photoelectron spectrum of CO yields (32) ionization energies of 14.01, 16.54, and 19.67 eV. The lifetime of the latter (*B*) state has been reported as 54 ns (33). Lindholm (3, 4) reports a recombination energy of 14.0 eV for $CO^{+\cdot}$.

$N_2^{+\cdot}$

Electron impact ionization of N_2 at 0.1–0.2 Torr produced $N_2^{+\cdot}$ with only minor amounts of $(N_2)_2^{+\cdot}$. The photoelectron spectrum of N_2 shows (32) ionization energies of 15.58, 16.69, and 18.26 eV; the latter state has a lifetime of ~60 ns (33). Lindholm (3, 4) reports a recombination energy of 15.3 eV for $N_2^{+\cdot}$. Penning ionization by long-lived neutral states of N_2 has been reported (34–36) and attributed (34) to two states capable of releasing energy in the range 11.4–11.6 eV and 10.2–11.4 eV. Single-source experiments (37) indicate that the ion currents produced by Penning ionization are less than 5% of the ion currents resulting from charge exchange using N_2; it does not appear that this mode of ionization will seriously affect the present results.

$Ar^{+\cdot}$

The $Ar^{+\cdot}$ reactant ion was produced by electron impact ionization of argon at 0.1–0.2 Torr source pressure. The recombination energies of $Ar^{+\cdot}$ are 15.76 eV ($^2P^0_{3/2}$) and 15.94 eV ($^2P^0_{1/2}$) (3, 4). Penning ionization by the long-lived $^3P_2$ and $^3P_0$ states of Ar (11.54 and 11.72 eV respectively) may occur; earlier work (37, 38) indicates that Penning ionization normally is less than 5% of that resulting from charge exchange involving $Ar^{+\cdot}$.

Charge Exchange Mass Spectra

The complete charge exchange mass spectra of cyclopentane, 1-pentane, 3-methyl-1-butene, 2-methyl-1-butene, 2-pentene, and 2-methyl-2-butene, obtained with the reagent gas systems described above, are recorded in tables in the Depository of Unpublished Data.[2] The essential data are summarized in the form of breakdown graphs

[2]Complete set of data may be obtained, at a nominal charge, from the Depository of Unpublished Data, CISTI, National Research Council of Canada, Ottawa, Ont., Canada K1A 0S2.

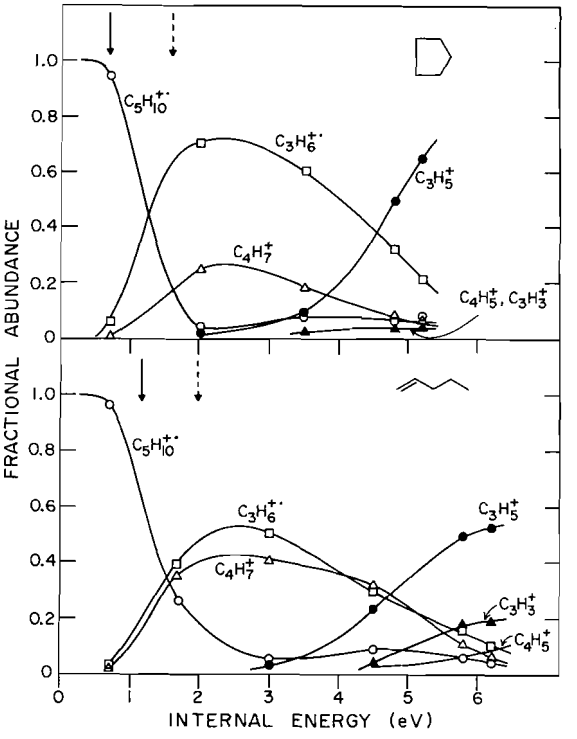

FIG. 1. Breakdown graphs for cyclopentane and 1-pentene: —, critical energy for formation of $C_3H_6^{+\cdot}$ and $C_4H_7^+$; --- critical energy for formation of $C_3H_5^+$. Data points in order of increasing energy from $CS_2^{+\cdot}$, $COS^{+\cdot}$, $Xe^{+\cdot}$, $CO^{+\cdot}$, N_2^+, and $Ar^{+\cdot}$ charge exchange (cyclopentane graphs begin with $COS^{+\cdot}$ charge exchange).

for the six isomers shown in Figs. 1 to 3. These graphs have been constructed by plotting the fractional ion intensities as a function of the internal energy of the $M^{+\cdot}$ ion, taken as RE − IE, using the IE values given in Table 1. The recombination energies used were those given in the above discussion except for $CS_2^{+\cdot}$ where an effective value of ~10.2 eV is indicated by more extensive but unpublished work in this laboratory. The charge exchange mass spectra showed (usually) low intensity $C_5H_9^+$ ion signals. These ions may arise by H^- abstraction reactions rather than by dissociative charge exchange; consequently, they have not been included in deriving the breakdown graphs. In the ionization of cyclopentane with the CS_2/N_2 reagent system $C_5H_9^+$ was the major product ion with only a minor (~4%) yield of $C_5H_{10}^{+\cdot}$. The ionization energy of cyclopentane (10.49 eV) is above the recombination energy of ground state $CS_2^{+\cdot}$; the low intensity $C_5H_{10}^{+\cdot}$ ion signal may result from reaction of the $\tilde{A}\,^2\pi_\mu$ state of $CS_2^{+\cdot}$, present in low abundance, or from reaction of vibrationally excited $CS_2^{+\cdot}$ ions. The $C_5H_9^+$ product presumably

Can. J. Chem. Downloaded from www.nrcresearchpress.com by 210.87.254.105 on 09/06/12
For personal use only.

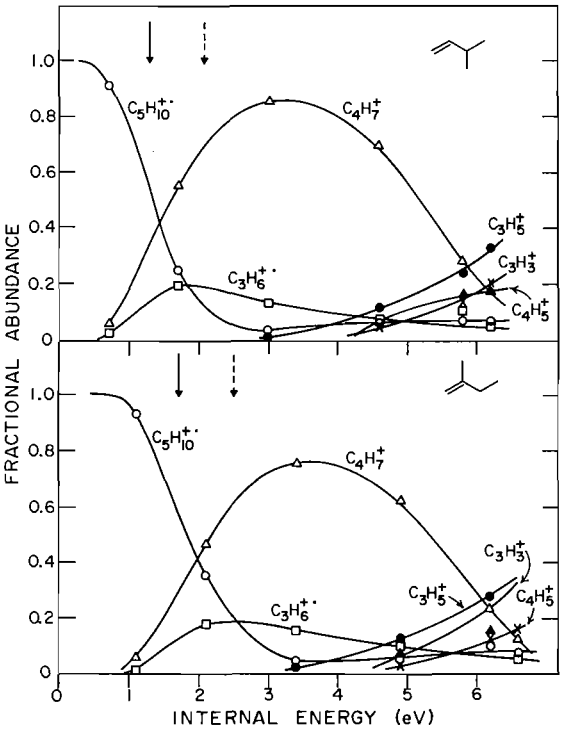

FIG. 2. Breakdown graphs for 3-methyl-1-butene and 2-methyl-1-butene, see caption for Fig. 1.

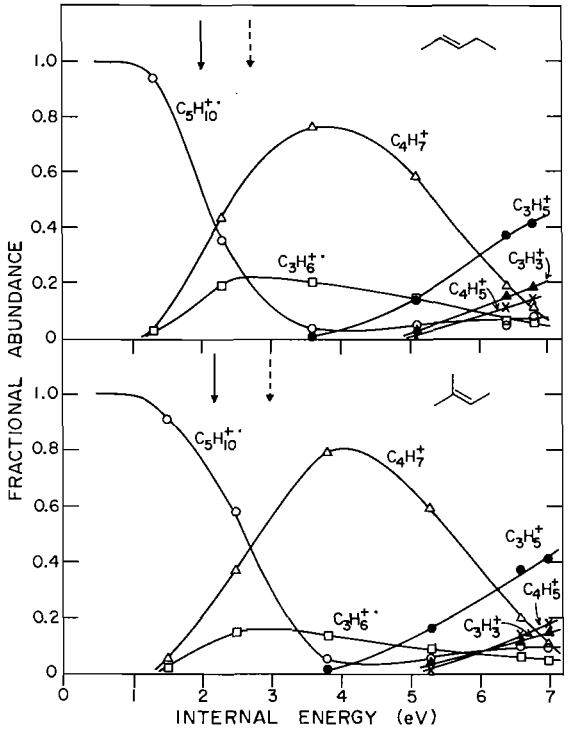

FIG. 3. Breakdown graphs for 2-pentene and 2-methyl-2-butene, see caption for Fig. 1.

arises by H^- abstraction although the reactant ion is unknown. It should be noted that the total additive ion signal was considerably lower in the CS_2/N_2–cyclopentane system than in any of the other systems studied. The lowest energy data for the cyclopentane breakdown graph are derived from the $COS^{+\cdot}$ charge exchange spectrum.

The discussion which follows is based on the energetics data for the major ions summarized in Table 1 and the fragmentation scheme, Scheme 1.

For each isomer the calculated appearance energy for formation of $C_3H_6^{+\cdot}$ is identical, within experimental error, with the measured appearance energy for $C_4H_7^+$. These appearance energies, translated into critical energies for fragmentation, are shown as the single solid arrows on the breakdown graphs. Also shown by dashed arrows are the critical energies for formation of $C_3H_5^+$ by the process indicated in Scheme 1.

With the exception of cyclopentane the ionization energies of the C_5H_{10} isomers are below $RE(CS_2^{+\cdot})$ and charge exchange to give $C_5H_{10}^{+\cdot}$ is the dominant reaction channel; however, in all cases low yields of $C_3H_6^{+\cdot}$ and/or $C_4H_7^+$ are observed despite the fact that the critical energies for formation of these fragments are 0.2 to 0.7 eV higher than the energy transferred by ground state $CS_2^{+\cdot}$. A minor participation of a higher energy species, possibly the $\tilde{A}^2\pi_\mu$ state of $CS_2^{+\cdot}$ is indicated.

The $COS^{+\cdot}$ ion has a recombination energy of 11.2 eV. This is above the IE of cyclopentane but almost coincident with the appearance energies of $C_3H_6^{+\cdot}$ and $C_4H_7^+$; charge exchange leads predominantly to formation of $C_5H_{10}^{+\cdot}$ with only minor fragmentation to form $C_3H_6^{+\cdot}$. For the isomeric acyclic olefins $RE(COS^{+\cdot})$ is above the appearance energies of $C_3H_6^{+\cdot}$ or $C_4H_7^+$ and extensive, structure dependent, fragmentation of the molecular ion is observed. The charge exchange mass spectra using $Xe^{+\cdot}$, $CO^{+\cdot}$, $N_2^{+\cdot}$, and $Ar^{+\cdot}$ as reagent ions all show low yields of molecular ions which are most readily interpreted in terms of a minor contribution from a species of low recombination energy; as discussed above, Penning ionization is a possibility for the rare gases and N_2. Another, less likely, explanation is deactivation of the $M^{+\cdot}$ ions by collision with the gas bath mole-

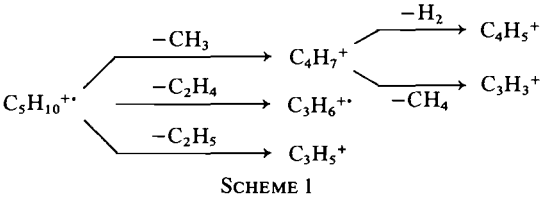

SCHEME 1

TABLE 1. Energetics of C_5H_{10} systems[a]

Molecule	IE(M)[b]	AE($C_4H_7^+$)[b]	AE($C_3H_6^{+\cdot}$)[c]	AE($C_3H_5^+$)[c]
c-C_5H_{10}	10.49	11.14	11.29	12.09
	9.48	10.64	10.71	11.52
	9.52	10.74	10.76	11.56
	9.12	10.85	10.83	11.64
	8.92	10.68	10.81	11.61
	8.70	10.84	10.93	11.73

[a]All data in eV.
[b]From ref. 19.
[c]Calculated from thermochemical data of ref. 28.

cules. At the source pressures used the bimolecular collision rate is $\sim 10^7\ s^{-1}$. It would be expected that most molecular ions, particularly those of higher internal energies, would fragment before undergoing a collision; hence collisional deactivation should play only a minor role.

Although the data points for the breakdown graphs are rather widely separated they have been connected by smooth curves; consequently fine structure will not be seen but only the major trends will be. This procedure also has the result that significant fragmentation of the molecular ion is indicated below the critical energy for fragmentation of the acyclic isomers. The graphs could have been drawn with the onset of fragmentation coinciding with the critical onset energies; this would not have altered the major features. The breakdown graphs summed over the appropriate internal energy distribution produced by electron impact should yield the electron impact mass spectra. Approximate internal energy distribution functions can be obtained from photoelectron spectra (39). The He I photoelectron spectra of the C_5 olefins (see that for 2-pentene in Fig. 4) show a highly structured band at threshold with a broad band having an onset ~ 2 eV above threshold which peaks between 3 and 4 eV and drops off sharply at higher energies. Comparison of this distribution with the breakdown graphs shows that ionization to the states below 1 eV will lead predominantly to molecular ion formation while ionization to the states above 2 eV will lead to the $C_4H_7^+$ and/or $C_3H_6^{+\cdot}$ fragment ion depending on the isomer. The major peaks in the 70 eV electron impact mass spectra (40) of the C_5H_{10} isomers are indicated in Table 2. Clearly the electron impact mass spectra are in accord with the breakdown graphs and the approximate energy distribution function suggested by the photoelectron spectra. The relatively low yield of $C_3H_5^+$ is to be expected in light of the small yield of molecular ions with internal energies >6 eV where this fragment dominates the breakdown graph. The onset of formation of $C_3H_5^+$ in the breakdown graphs is considerably higher than the calculated critical energy, most likely a reflection of a kinetic shift (2, 41).

Although the present study of C_5H_{10} isomers was designed primarily to assess the properties of the

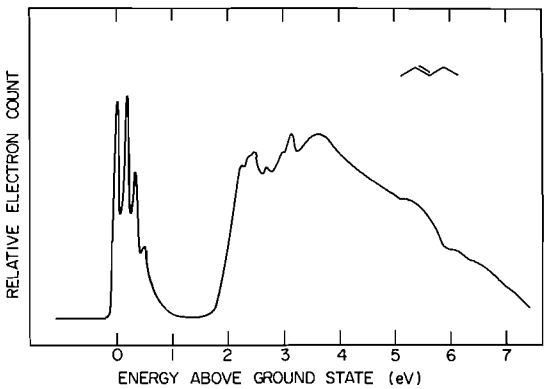

FIG. 4. He I photoelectron spectrum of 2-pentene. Abscissa scale as energy above ground state $C_5H_{10}^{+\cdot}$.

TABLE 2. Partial EI mass spectra of C_5H_{10} isomers

Compound	$C_5H_{10}^{+\cdot}$	$C_4H_7^+$	$C_3H_6^{+\cdot}$	$C_3H_5^+$
Cyclopentane	30	29	100	29
1-Pentene	32	58	100	45
3-Methyl-1-butene	26	100	28	21
2-Methyl-1-butene	26	100	27	21
2-Pentene	34	100	46	29
2-Methyl-2-butene	35	100	31	36

Can. J. Chem. Downloaded from www.nrcresearchpress.com by 210.87.254.105 on 09/06/12
For personal use only.

TABLE 3. $COS^{+\cdot}$ charge exchange mass spectra (% of base peak)

Ion	*c*-C_5H_{10}					
$C_5H_{10}^{+\cdot}$	100	73	46	75	84	100
$C_5H_9^+$	21	58	33	29	35	15
$C_4H_7^+$	1	94	100	100	100	77
$C_3H_6^{+\cdot}$	7	100	36	39	44	29

charge exchange reagent systems developed rather than to solve significant problems of ion chemistry, some comment on the fragmentation of the different isomers appears desirable. Despite the fact that the critical energies for formation of $C_4H_7^+$ and $C_3H_6^{+\cdot}$ are identical, $C_4H_7^+$ is the dominant ion in the breakdown graphs for 2-pentene and the methylbutenes while $C_3H_6^{+\cdot}$ is the dominant ion in the breakdown graph of cyclopentane and is more important than $C_4H_7^+$ for 1-pentene. This differing behaviour is not reflected in the metastable ion intensity ratios which are similar for all isomers (22). The metastable ion intensity ratios reflect primarily the relative critical decomposition or fragmentation energies. By contrast, the relative intensities observed at higher internal energies in the breakdown graphs are influenced not only by the relative critical fragmentation energies but also by the energy independent terms (or so-called frequency factors) in the $k(E)$ expressions for the fragmentation reactions. It is clear that, for the $C_5H_{10}^{+\cdot}$ ions derived from cyclopentane and 1-pentene, the fragmentation reactions leading to $C_3H_6^{+\cdot}$ must have a more favourable frequency factor than the reactions leading to $C_4H_7^+$, while the converse is true for the other isomers. It follows that over the major part of the internal energy range studied the $C_5H_{10}^{+\cdot}$ ions derived from cyclopentane and 1-pentene are not isomerizing to a common structure (or mixture of structures) accessible to the remaining $C_5H_{10}^{+\cdot}$ molecular ions, although such an isomerization is indicated (22) for long-lived ions fragmenting in drift regions (metastable ions). It is interesting to note that the $C_5H_{10}^{+\cdot}$ ions derived from the cyclopentane and 1-pentene structures can yield $C_3H_6^{+\cdot}$ by relatively simple pathways, reactions [5] and [6],

[5] 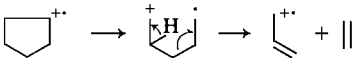

[6] 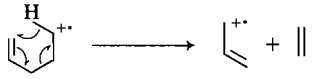

which should have relatively favourable frequency factors. Deuterium labelling studies (42) of the electron impact induced fragmentation of cyclopentane and 1-pentene cannot be explained solely on the basis of these reactions; however, the EI studies represent a summation of reactions of molecular ions covering a wide range of internal energies and, hence, lifetimes and more than one fragmentation route could be involved. Charge exchange studies of labelled compounds should provide useful information on the energy, and lifetime, dependence of these routes. In principle, it should be possible to quantitate these arguments through calculation of the breakdown graphs by suitable application of absolute rate theory (5). However, such calculation requires a knowledge of the vibrational frequencies not only of the molecular ion but also of the transition states leading to $C_4H_7^+$ and $C_3H_6^{+\cdot}$. In view of our rudimentary knowledge of the transition state structures, let alone vibrational frequencies, calculations do not appear fruitful at the present time.

Finally, we note that the $COS^{+\cdot}$ charge exchange mass spectra of the C_5H_{10} isomers (Table 3) show large differences in the relative intensities of the $C_5H_{10}^{+\cdot}$, $C_4H_7^+$, and $C_3H_6^{+\cdot}$ ions. Clearly, with the exception of 2-methyl-1-butene and 2-pentene, the isomeric molecules can be identified by the charge exchange mass spectra obtained with reactant ions of recombination energies of ~11.2 eV. The differences are more pronounced than those observed in the 70 eV mass spectra, while both the metastable ion spectra (22) and the collisional activation spectra (23) are incapable of distinguishing among the isomers.

Experimental

The charge exchange mass spectra were obtained using a Du Pont 21-490 mass spectrometer equipped with a high pressure source. The ionizing electron energy was 70 eV with the repellers held at cage potential. The ion source temperature was ~100°C, with the C_5H_{10} samples being introduced from a heated inlet system at ~100°C.

Reagent gas mixtures were prepared by pressure–volume measurements. All reagent gases and liquids and C_5H_{10} isomers were commercially available samples of high purity.

Can. J. Chem. Downloaded from www.nrcresearchpress.com by 210.87.254.105 on 09/06/12
For personal use only.

Acknowledgements

The authors are indebted to the Natural Sciences and Engineering Research Council of Canada for financial support. J.A.H. gratefully acknowledges the leave of absence provided by Université Laval while A.G.H. is indebted to Dr. S. Leach for helpful discussions.

1. H. M. Rosenstock, M. B. Wallenstein, A. L. Wahrhaftig, and H. Eyring, Proc. Natl. Acad. Sci. U.S. **38**, 667 (1952).
2. W. A. Chupka. J. Chem. Phys. **30**, 191 (1959).
3. E. Lindholm. *In* Ion molecule reactions in the gas phase. *Edited by* P. Ausloos. Am. Chem. Soc., Washington. 1966. p. 1.
4. E. Lindholm. *In* Ion–molecule reactions. Vol. 2. *Edited by* J. L. Franklin. Plenum Press, New York. 1972. Chapt. 10.
5. M. Vestal. *In* Fundamental processes in radiation chemistry. *Edited by* P. Ausloos. J. Wiley and Sons, New York. 1968. Chapt. 2.
6. J. Sunner and I. Szabo. Int. J. Mass Spectrom. Ion Phys. **25**, 241 (1977).
7. J. Sunner and I. Szabo. Int. J. Mass Spectrom. Ion Phys. **25**, 263 (1977).
8. J. Jalonen, J. M. Tedder, and P. H. Vidaud. J. Chem. Soc. Faraday Trans. In press.
9. D. F. Hunt and J. F. Ryan. Anal. Chem. **44**, 1306 (1972).
10. B. L. Jelus, B. Munson, and C. Fenselau. Biomed. Mass Spectrom. **1**, 96 (1974).
11. M. L. Lee and R. A. Hites. J. Am. Chem. Soc. **99**, 2008 (1977).
12. B. Munson. Anal. Chem. **49**, 772A (1977).
13. S. C. Subba Rao and C. Fenselau. Anal. Chem. **50**, 511 (1978).
14. J. Sunner and I. Szabo. Adv. Mass Spectrom. 7, 1383 (1978).
15. N. Einolf and B. Munson. Org. Mass Spectrom. **5**, 397 (1971).
16. N. Einolf and B. Munson. Org. Mass Spectrom. **7**, 155 (1973).
17. J. Turk and R. H. Shapiro. Org. Mass Spectrom. **5**, 1373 (1971).
18. V. Cermak and Z. Herman. Nucleonics, **19**, 106 (1961).
19. F. P. Lossing. Can. J. Chem. **50**, 3973 (1972).
20. J. H. Beynon, R. A. Saunders, and A. E. Williams. The mass spectra of organic molecules. Elsevier, Amsterdam. 1968. p. 65.
21. E. Stenhagen, S. Abrahamsson, and F. W. McLafferty. Registry of mass spectral data. Wiley–Interscience, New York. 1974. pp. 21, 41.
22. R. D. Bowen and D. H. Williams. Org. Mass Spectrom. **12**, 453 (1977).
23. T. Nishishita and F. W. McLafferty. Org. Mass Spectrom. **12**, 75 (1977).
24. M. Meot-Ner and F. H. Field. Chem. Phys. Lett. **44**, 484 (1976).
25. M. Meot-Ner, P. Hamlet, E. P. Hunter, and F. H. Field. J. Am. Chem. Soc. **100**, 5466 (1978).
26. C. R. Brundle and D. W. Turner. Int. J. Mass Spectrom. Ion Phys. **2**, 195 (1965).
27. J. H. D. Eland, M. Devoret, and S. Leach. Chem. Phys. Lett. **43**, 97 (1976).
28. H. M. Rosenstock, K. Draxl, B. W. Steiner, and J. T. Herron. J. Phys. Chem. Ref. Data Vol. 6, Suppl. 1, 1977.
29. I. Dzidic, A. Good, and P. Kebarle. Can. J. Chem. **48**, 664 (1970).
30. F. M. Penning. Z Physik. **46**, 225 (1975); **57**, 723 (1929).
31. V. Cermak and Z. Herman. Coll. Czech. Chem. Commun. **30**, 169 (1965).
32. H. Hotop and A. Niehaus. Int. J. Mass Spectrom. Ion Phys. **5**, 415 (1970).
33. A. J. Smith, F. H. Read, and R. E. Imhoff. J. Phys. B**8**, 2869 (1975).
34. V. Cermak. J. Chem. Phys. **44**, 3318 (1966).
35. W. T. Huntress, Jr. and J. L. Beauchamp. Int. J. Mass Spectrom. Ion Phys. **3**, 149 (1969).
36. E. G. Jones and A. G. Harrison. Int. J. Mass Spectrom. Ion Phys. **5**, 137 (1970).
37. E. G. Jones. Ph.D. Thesis, University of Toronto. 1969.
38. E. G. Jones and A. G. Harrison. Int. J. Mass Spectrom. Ion Phys. **6**, 77 (1971).
39. G. G. Meisels, C. T. Chen, B. G. Giessner, and R. H. Emmel. J. Chem. Phys. **56**, 793 (1972).
40. A. Cornu and R. Massot. Compilation of mass spectral data. Heyden and Son Ltd., London. 1966.
41. B. J. Millard and D. F. Shaw. J. Chem. (B), 664 (1966).
42. A. G. Harrison. *In* Topics in organic mass spectrometry. *Edited by* A. L. Burlingame. J. Wiley and Sons, New York. 1970. Chapt. 3.

Can. J. Chem. Downloaded from www.nrcresearchpress.com by 210.87.254.105 on 09/06/12
For personal use only.

Hydrocarbon ions in fuel-rich, CH_4–C_2H_2–O_2 flames as a probe for the initiation of soot: an experimental approach

SCOTT D. TANNER,[1] JOHN M. GOODINGS, AND DIETHARD K. BOHME
York University, Department of Chemistry, 4700 Keele Street, Downsview, Ont., Canada M3J 1P3

Received October 22, 1980

This paper was presented at a Special Symposium "The Structure and Thermochemistry of Gaseous Ions", held in honour of Dr. F. P. Lossing of the National Research Council of Canada, during the Second Canadian Conference on the Gas Phase Chemistry of Ions, Trent University, June 5–8, 1980, and is dedicated to him on the occasion of his 65th birthday

SCOTT D. TANNER, JOHN M. GOODINGS and DIETHARD K. BOHME. Can. J. Chem. **59**, 1760 (1981).

The natural hydrocarbon ions $C_nH_x^{\pm}$ ($n \geq 2$, $x \geq 0$) present in premixed, fuel-rich, nearly sooting, CH_4–C_2H_2–O_2 flames at atmospheric pressure were studied as a probe of the early chemical stages of soot formation. Ion concentration profiles were measured mass-spectrometrically along the flame axis through the reaction zone into the burnt gas downstream. Total ionization profiles were examined for their dependence on both temperature and equivalence ratio, ϕ. Families of individual $C_nH_x^-$ negative ion profiles exhibit concentration peaks in three distinct regions; predominantly oxygenated ions occur upstream, giving way to moderately unsaturated hydrocarbon ions near the end of the reaction zone, leading to highly unsaturated carbonaceous ions further downstream. The concentrations of the downstream ions alternate with the parity of n, the even-n species being larger. Series of $C_nH_x^+$ positive ion profiles, for a given n, show profile peak positions which move steadily downstream with decreasing x, indicative of progressive dehydrogenation. The positive ion chemistry of these series is essentially independent of n. As ϕ is increased at constant temperature towards the sooting point, the concentrations of $C_nH_x^{\pm}$ ions increase while those of the oxygenated ions decrease; the positive ions show a relative enhancement of species having high values of n.

SCOTT D. TANNER, JOHN M. GOODINGS et DIETHARD K. BOHME. Can. J. Chem. **59**, 1760 (1981).

Dans le but d'évaluer la nature des réactions impliquées dans les stades préliminaires de la formation de la suie, on a étudié les ions des hydrocarbures naturels, $C_nH_x^{\pm}$ ($n \geq 2$, $x \geq 0$), présents à la pression atmosphériques dans des flammes de CH_4–C_2H_2–O_2, riches en combustible, prémélangés et pratiquement au point de former de la suie. On a mesuré les profils des concentrations des ions par spectrométrie de masse en fonction de l'axe de la flamme traversant la zone de réaction et procédant vers la section des gaz brûlés. On a examiné les profils d'ionisation totale tant au point de vue de l'influence de la température que du point de vue du rapport d'équivalence, ϕ. Les familles individuelles d'ions négatifs $C_nH_x^-$ présentent des pics de concentrations dans trois régions distinctes; près de la zone de réaction, on retrouve principalement des ions oxygénés et si on procède vers la zone des gaz brulés on retrouve d'abord des ions d'hydrocarbures modérément insaturés puis des ions carbonés fortement insaturés. Les concentrations des ions dans la zone des gaz brulés alternent avec la parité de n; les concentrations des espèces où n est pair sont plus élevées. Les séries de profils des ions positifs $C_nH_x^+$, pour une valeur donnée de n, indiquent que le profil des positions du pic se déplace d'une façon régulière vers la zone des gaz brulés lorsque n diminue; ceci indique une déshydrogénation progressive. La chimie des ions positifs de ces séries est pratiquement indépendante de n. Lorsqu'augmente ϕ, à température constante, vers le point de formation de suie, les concentrations des ions $C_nH_x^{\pm}$ augmentent alors que celles des ions oxygénés diminuent et les concentrations des ions positifs sont relativement plus élevés lorsque les valeurs de n sont élevées.

[Traduit par le journal]

Introduction

Flame chemists are divided on the mechanism of soot formation in hydrocarbon combustion. There are proponents of both an ion-based synthesis of carbon and a neutral chemistry scheme. Most of the research which has been done on soot has been directed at its phenomenology in the burnt gas (1). This is too late in the flame to gain information about the initial chemistry of soot formation. One technique with which it is possible to study the reaction zone of a flame involves the measurement of ion concentrations and their axial profiles with a flame-ion mass spectrometer. An understanding of the relevant ion–molecule reactions then allows the flame-ion data to be interpreted to give insight into both the ionic and the neutral chemical evolution of the flame.

Detailed studies of the ionic composition of flames have very recently been reported for fuel-rich methane combustion by Goodings *et al.* (2, 3) and for fuel-rich and sooting acetylene and ethylene flames by Tse *et al.* (4) and Delfau *et al.* (5). In each of these works particular attention was drawn to the observation of high-mass carbonaceous ions in the burnt gas just downstream of the luminous flame front. Goodings *et al.* (2, 3) measured concentration profiles for all detectable ions of both polarities for $m/e < 100$ amu. The chemistry of their formation, interconversion, and loss was discussed. The observation of carbonaceous positive ions for $m/e < 200$ amu in the reaction zone of a

[1]Present address: Sciex Inc., 55 Glencameron Rd., #202, Thornhill, Ont., Canada L3T 1P2.

0008-4042/81/121760-11$01.00/0

©1981 National Research Council of Canada/Conseil national de recherches du Canada

Can. J. Chem. Downloaded from www.nrcresearchpress.com by 210.87.254.5 on 09/06/12
For personal use only.

Can. J. Chem. Downloaded from www.nrcresearchpress.com by 210.87.254.5 on 09/06/12
For personal use only.

fuel-rich acetylene flame was taken by Tse *et al.* (4) to indicate early pyrolysis of the fuel. The novel application of a 360° magnetic mass analyzer by Delfau *et al.* (5) permitted the observation of positive ions up to $m/e \simeq 7000$ amu downstream in sooting flames.

The present work was undertaken in order to provide some insight into the mechanisms of formation of these carbonaceous ions in the belief that they constitute a source of information about the early chemical stage of soot formation. The evolution of the flame-ion distribution was monitored through the reaction zones of a fuel-rich methane–oxygen flame and a nearly-sooting flame with acetylene added to the methane fuel. The excellent spatial resolution provided by the flame-ion mass spectrometer employed for these studies permitted the ion distribution of these flames to be mapped in detail. Additional measurements were made to record the response of this distribution when sooting conditions are approached.

The experimental results of this investigation and a preliminary discussion are presented in this paper. A considerable range of observations is organized in summary form at the end of the paper. The detailed interpretation of these data will be discussed in a later publication.

Experimental

The ion concentration data were obtained with a flame-ion mass spectrometer which has been described previously (2). A fuel-rich premixed, laminar flame was stabilized vertically on a simple, cylindrical, quartz burner at atmospheric pressure. The flame was conical with a base diameter of about 4 mm and a height of about 6 mm with a rounded tip. It was surrounded by a flowing argon shield to exclude atmospheric air. Compressed methane and oxygen of CP grade (>99% CH_4, >99.6% O_2) and acetylene of Purified grade (>99.6% C_2H_2 dissolved in acetone) were used directly from the cylinders without further purification.

Two flames were studied in detail in this work. One of these was a pure methane–oxygen flame having an equivalence ratio $\phi = 2.15$ (alternatively, a carbon/oxygen ratio C/O = 0.538). Ionic data for this flame have been reported previously (2, 3). A more fuel-rich methane flame with added acetylene having the same burnt-gas temperature as measured with a pneumatic probe (6) was also studied. The equivalence ratio for such a mixed-fuel flame of unburnt composition CH_4:C_2H_2:$O_2 = a:b:c$ is given by $\phi = (4a + 5b)/2c$ (C/O = $(a + 2b)/2c$). A more fuel-rich flame is cooler than another one nearer to stoichiometric composition, whereas C_2H_2–O_2 mixtures burn at higher temperatures than do CH_4–O_2 mixtures. Therefore, by properly choosing the CH_4–C_2H_2 fuel mixture, a fuel-rich flame may be burned having the same temperature as a less fuel-rich pure CH_4–O_2 flame. It was found that a flame having $\phi = 2.47$ (C/O = 0.696) and containing 17.7% C_2H_2 in the fuel had a temperature in the burnt gas at a distance $z = 3$ mm downstream of the reaction zone which was the same as that measured at the same point for the methane–oxygen flame with $\phi = 2.15$. The flames were of the same shape and size so that the distance scales upstream of, and within, the reaction zones were comparable. A faint yellow luminescence from soot particles was observed for the more fuel-rich flame.

The burner itself was mounted on a motor-driven carriage, and the flame axis was carefully aligned with respect to the mass spectrometer sampling orifice. A voltage proportional to the calibrated displacement of the burner carriage was fed to the *X*-axis of an *XY* recorder such that 0.1 mm along the flame axis corresponded to either 1.00 cm or 0.75 cm on the recorder. In a typical experiment, the quadrupole mass filter was tuned to a specific m/e and the output from an electrometer connected to a Faraday cage was coupled to the *Y*-axis of the *XY* recorder. In this manner, the concentration profile of the ion species corresponding to the specified m/e was recorded as a function of distance axially through the tip of the flame. Total ionization profiles were obtained in the same fashion by removing the dc voltage from the mass filter. The pressure in the second vacuum chamber of the mass spectrometer was monitored with an ionization gauge and displayed on a second *XY* recorder. The pressure profile derived in this manner showed a minimum corresponding to the downstream edge of the reaction zone. This minimum was adopted as a reproducible origin ($z = 0$ mm) *in the flame* for the distance scale of the ion profiles.

In the experiments reported previously from this laboratory, the flame ions were sampled through a pinhole 0.1 mm in diameter in a platinum–iridium disc welded into a water-cooled stainless-steel mounting. The flat disc against which the flame burned was approximately 2.0 mm in diameter. For the present experiments, this sampling nozzle was replaced with a thin-walled chromium cone which had a sharp-edged orifice of diameter 0.10 mm at its apex and a total tip diameter of approximately 0.28 mm. This sampling cone was made in a manner similar to that suggested by Burdett and Hayhurst (7). The change in orifice design considerably decreased the thickness of the thermal/momentum boundary layer which covers the sampling plate as discussed in the work of Hayhurst and co-workers (8, 9). It is known that the gas sample may be chemically perturbed during passage through the boundary layer. One reaction which proceeds in this region is the three-body hydration of H_3O^+ (9). In the present study, the ratio $R = [H_3O^+ \cdot H_2O]/[H_3O^+]$ was observed to decrease from a value of $R = 0.34$ obtained with the "old" Pt/Ir sampling disc to $R = 0.09$ with the Cr nozzle. This may be taken as evidence of a considerable decrease in the thickness of the boundary layer. An additional advantage of using the sharp-tipped Cr nozzle over the blunt Pt/Ir disc is an increased spatial resolution. This may be understood by making reference to the flow streamline calculations of Hayhurst *et al.* (8) for a conical nozzle similar to that employed in the present study. The tip of this Cr nozzle is blunt over a radius which is less than the stagnation radius. The Pt/Ir disc, on the other hand, is considerably more blunt causing a thicker momentum boundary layer; this, in turn, causes an increase in the stagnation radius. As a result, some of the ions included in the sample drawn through the Pt/Ir nozzle are taken from a region further from the flame axis than are included in the sample passing through the Cr nozzle. When sampling upstream in a conical flame, gas originating at a point further from the flame axis can derive from a region in the flame downstream of the sampling point, thereby decreasing the spatial resolution.

Differences between the ion profiles presented here and those reported earlier for the same $\phi = 2.15$ flame (2, 3) may be ascribed to these changes in sampling conditions. In fact, the maximum total positive ion signal detected with the two different sampling nozzles was the same within experimental error, although the maximum negative ion signal decreased by a

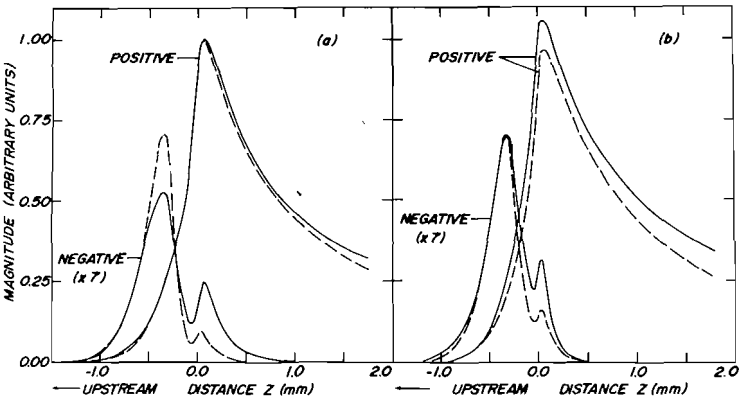

FIG. 1. Total positive and negative ionization profiles: (*a*) for two flames having similar adiabatic flame temperatures, T_{ad} but different equivalence ratios, ϕ. Dashed curves: $\phi = 2.15$ (C/O = 0.538), no C_2H_2, $T_{ad} = 2455$ K. Solid curves: $\phi = 2.47$ (C/O = 0.696), 17.7% C_2H_2, $T_{ad} = 2443$ K. % C_2H_2 refers to the percentage in the fuel; (*b*) for two CH_4–C_2H_2–O_2 flames having similar ϕ's but different values of T_{ad}. Dashed curves: $\phi = 2.22$ (C/O = 0.560), 1.1% C_2H_2, $T_{ad} = 2401$ K. Solid curves: $\phi = 2.23$ (C/O = 0.587), 7.1% C_2H_2, $T_{ad} = 2488$ K.

factor of 3.5 when the Cr nozzle was used (c.f. Fig. 1(*a*) here with Fig. 1(*b*) of ref. 3). This latter decrease is expected because the boundary layer cooling is reduced when sampling with the new nozzle. Consequently, negative ion equilibria shift in the endothermic direction causing electron detachment from negative ions; the free electron concentration is enhanced at the expense of the negative ion concentration. It should be clearly understood, however, that all of the data considered hereafter, including those for the $\phi = 2.15$ flame, were obtained using the new Cr sampling nozzle.

A quadrupole mass filter discriminates to some extent against the transmission of larger *m/e* ions. The effect is more pronounced when the resolving power of the filter is increased. For most of the experiments reported here, a relatively high resolving power was employed in order to distinguish between neighbouring ions of high *m/e*. For this reason, care was taken to assure that the resolving power was maintained constant for all the experiments involving relative magnitudes. In this way, the mass discrimination profile was maintained constant, and trends in the relative magnitudes of ion signals at the same mass numbers in different flames are still valid. In a few instances, the resolving power was lowered either to gain an appreciation for the extent of the mass discrimination or to increase the sensitivity for the larger *m/e* ions.

In order to achieve a consistent set of ion signals, a reference ion profile was recorded frequently during the experiments. The magnitude of each profile was normalized to the maximum signal measured for the total ionization profile of the same polarity. These normalized ion signal magnitudes (all < 1.0) are referred to as *relative magnitudes*, although those for positive ions have been multiplied by 10^4 and those for negative ions by 10^3 to eliminate cumbersome negative powers of ten. Magnitude ratios for individual ion profiles for different flames may be obtained by using the ratio of the peak magnitudes of the total ionization profiles as a multiplier applied to the relative magnitudes. The relevant peak magnitudes are given in Fig. 1.

Results and Preliminary Discussion

Total Ionization Profiles

Total ionization profiles for the two flames which were studied in detail in this work are given in Fig. 1(*a*). The phenomenology of the profiles for the flame having $\phi = 2.15$ (C/O = 0.538) has been discussed previously (3); the improved spatial resolution is apparent in the negative ionization profile whose minimum between the two peaks earlier had been hidden when sampling with the Pt/Ir nozzle. The profiles may be contrasted with those given in Fig. 1(*b*) for two flames which have similar equivalence ratios but distinctly different adiabatic flame temperatures.

Several observations can be made from these results. The first is that the peak magnitude of the total positive ionization curve increases with increasing flame temperature. Such a trend is consistent with an increase in the rate of chemi-ionization with temperature.

Secondly, the magnitude of the upstream peak of the negative ionization profile seems to depend mainly on the equivalence ratio of the unburnt gas. Several reasons for this dependence may be envisaged. The decrease with increasing ϕ (or C/O ratio) may result from a decreased rate of attachment of electrons as would result, for example, from a decrease in the concentration of O_2. Alternatively, the rate of loss of negative ions may be enhanced by an increase in the non-equilibrium concentration of radicals, especially H, which participate in ion–radical associative detachment reactions.

Finally, the magnitude of the downstream maximum of the total negative ionization profile is seen to increase considerably with an increase in both ϕ (or C/O ratio) and the flame temperature. This behaviour is consistent with an increase in the rate of electron attachment to hydrocarbon neutrals, for example polyacetylenes or their radicals, whose

Can. J. Chem. Downloaded from www.nrcresearchpress.com by 210.87.254.5 on 09/06/12
For personal use only.

Can. J. Chem. Downloaded from www.nrcresearchpress.com by 210.87.254.5 on 09/06/12
For personal use only.

concentrations increase rapidly with both equivalence ratio and temperature.

Downstream Ion Spectra

A more detailed view of the ionic composition of the flame is provided by measurements of the ion mass spectra. Figure 2 presents the spectra measured at a distance $z = 0.05 \pm 0.02$ mm downstream of the reaction zone of the flame with $\phi = 2.47$. At this point in the flame the total positive and negative ionization profiles maximize. It should be noted that the sampling position is referenced to an origin within the flame itself. Such a procedure is necessary given the high spatial resolution of this method. Our experience has shown that the observed mass spectra can be extremely sensitive to small changes in the sampling position within, and downstream of, the reaction zone.

Negative Ions: It is significant that the dominant negative ions in this fuel-rich flame are the highly unsaturated hydrocarbons $C_nH_x^-$ with $n \geq 2$ and $x \leq 5$. Operation of the mass filter at low resolving power permitted the detection of groups of ions spaced by roughly 12 amu having values of n up to and including 10. These are shown in Fig. 2(*a*) which, for the most part, gives the mass numbers of the maximum signals for the various ion groups. The individual ions which compose these broad groups were resolved at high resolving power, as shown in Fig. 2(*b*). It was noticed that the ions corresponding to C_2H^- and C_4H^- have significantly higher concentrations than do the ions with odd values of n. In fact, this alternation of intensity with the parity of n was observed all the way up to $n \sim 10$ in the experiments with low resolving power, and is consistent with the earlier observations reported by Green (10). This alternation attests to the importance of polyacetylenes or their radicals at this point in the flame. Nearly all of the hydrocarbon ions are more abundant in the more fuel-rich flame.

Positive Ions: The groups of $C_nH_x^+$ ions observed in the positive ion spectrum shown in Fig. 2(*c*) are remarkable for their similarity to one another in structure. The lower-x, more unsaturated components of each family seem to be strongly preferred; the largest signal in each family occurs for $x = 3$. Since the spectra for the different families are similar, it would seem that the chemistry of the $C_nH_x^+$ ions is essentially independent of n. The fall-off in the magnitudes of the $C_nH_x^+$ ion groups with increasing n may reflect to some extent an increase in mass discrimination of the quadrupole mass filter with increasing mass number at the high resolving power used to obtain these data. Consequently, this overall trend in the magnitudes of the $C_nH_x^+$ ion signals with n is not included in the summary of results given at the end of the paper. A comparison with the spectrum obtained at the same position in the more fuel-lean ($\phi = 2.15$, no C_2H_2) flame (not shown) revealed several other noteworthy features (11). Ions corresponding to $n \leq 2$ and oxygenated species have higher concentrations in the flame with $\phi = 2.15$, whereas ions corresponding to $n > 2$ seem to be more abundant in the more fuel-rich flame. The degree of this enhancement increases with increasing n. Furthermore, within a group of given n, there is a relative enhancement of ions with small x.

Reaction Zone

A view of the evolution of the ionic composition requires measurements of the axial concentration profiles for the individual ion species. In this section we present profiles measured with the intent to characterize their early behaviour upstream in the reaction zone.

Positive Ions: Figure 3 shows normalized profiles measured for the $C_4H_x^+$ family of ions from 49 to 57 amu. There is a clearly-resolved progression downstream from high to low mass ions. This behaviour is exemplary of that observed for the other $C_nH_x^+$ families.

More than 70 individual positive ion concentration profiles were measured for each flame studied. This vast amount of detailed information is unwieldy to manipulate. The data for the flame with $\phi = 2.47$ are presented in Fig. 4 in such a manner as to provide a simplified overview. The mass of each ion is plotted against the position (distance coordinate, z) at which the corresponding profile was observed to maximize. We have called such a plot a profile–peak–position or 3P plot. It provides an appreciation for the spatial relationships of the various ion concentration maxima at a glance. Similar data for the $\phi = 2.15$ flame are available (11). Of course, the details of the shapes of the profiles are necessarily lost in such a treatment. In addition to the profile peaks noted in Fig. 4, several profiles displayed broad peaks with maxima well downstream, given in Table 1. These involve the protonation of major combustion products in the burnt gas (H_2O, CO, CO_2 and their isotopic derivatives; a small amount of nitrogen is present from air entrainment, which leads to NH_3).

In the interpretation of this 3P plot it should be remembered that the precise locations and magnitudes of the profile maxima are intimately related to

Can. J. Chem. Downloaded from www.nrcresearchpress.com by 210.87.254.5 on 09/06/12
For personal use only.

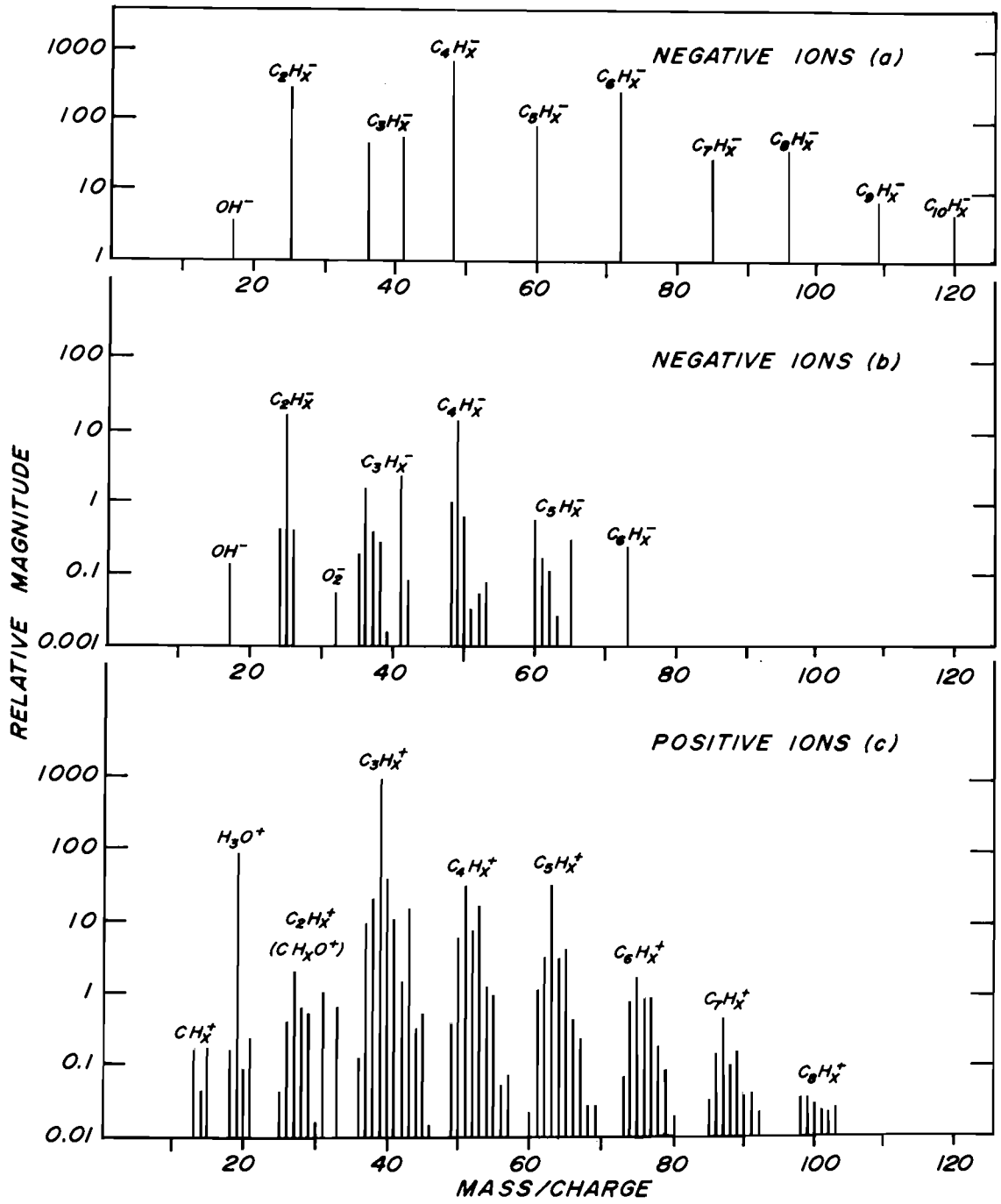

FIG. 2. Ion mass spectra recorded at a distance $z = 0.04 \pm 0.02$ mm downstream of the reaction zone of a CH_4–C_2H_2–O_2 flame (ϕ = 2.47, 17.7% C_2H_2). (*a*) Negative ions, low resolving power. (*b*) Negative ions, high resolving power. (*c*) Positive ions, high resolving power.

the rates of the formation and loss processes of the ions concerned. A large relative magnitude in the peak concentration of an ion may indicate either a relatively lower reactivity of the ion or a more prolific source.

Figure 4 shows eight distinct series of concentration maxima. The members of each series shift monotonically downstream with decreasing amu. Each series originates well upstream near the beginning of the reaction zone with its highest amu

TABLE 1. Peak positions of positive ion concentration profiles which showed broad maxima downstream of $z = 0.4$ mm

amu	Assignment	Peak position[a]	Relative magnitude
18	H_2O^+ (NH_4^+)	>3.3	>3.1
19	H_3O^+	2.68±0.08	384
20	H_2DO^+	2.60±0.10	0.31
21	$H_3{}^{18}O^+$	2.70±0.08	0.82
29	CHO^+	2.59±0.09	0.80
37	$H_3O^+ \cdot H_2O$	2.93±0.09	20.5
45	CHO_2^+	0.72±0.08	0.70
46	$^{13}CHO_2^+$, CDO_2^+, $CH^{17}O^{16}O^+$	0.68±0.09	0.02

[a]Measured in mm with respect to the origin ($z = 0$) at the end of the reaction zone.

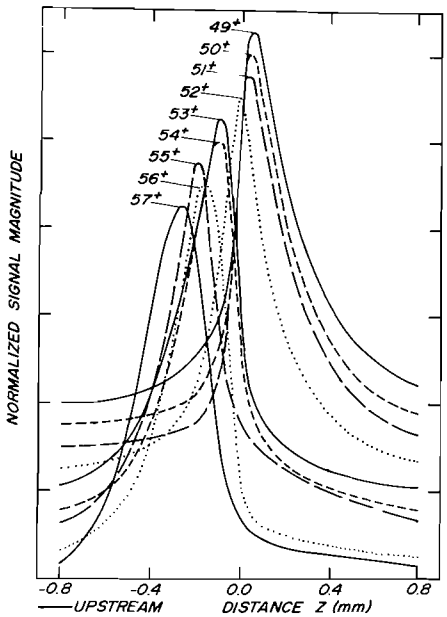

FIG. 3. Positive ion profiles observed for the ions from 49 to 57 amu. The magnitudes of the profiles have been normalized, and the zero baseline has been displaced vertically by a 1/4 scale interval per amu. These data were obtained for the flame with $\phi = 2.22$, 1.1% C_2H_2, $T_{ad} = 2401$ K.

members, and ends downstream at about $z = 0.1$ mm where its lowest amu members are gathered. The series are separated from each other by approximately 12 amu.

The relative magnitudes of the peak concentrations alternate quite regularly within each series, with those for ions of odd amu being appreciably larger than those for even amu ions. Over the limited mass range of any one of the eight series, mass discrimination effects are not significant. On the other hand, mass discrimination may play a significant role in the apparent decay in the relative magnitudes observed for the eight series, particularly beyond about 60 amu, at the high resolving power employed for these measurements. Therefore, this latter trend is not included in the summary of results given at the end of the paper. The actual concentrations of the higher mass ions may be quite considerable and comparable to the concentrations of the lower mass ions.

With the exception of a number of ions which may constitute sub-series of empirical formulae $C_nH_xO^+$ corresponding, for example, to protonated alcohols and aldehydes, the majority of the detected ions appear to be of the type $C_nH_x^+$ with n taking the values 1 through 8 and x taking values in the range 0 to $(2n + 3)$. Each value of n denotes a separate series for which the peak positions of the individual members are determined by the value of x. The spatial evolution of each series reflects a stepwise dehydrogenation leading to the highly unsaturated carbonaceous products at the end of the reaction zone. Presumably the higher-n homologues of these series ($n > 8$) are also present, but these were beyond the range of detection.

Negative Ions: The negative ion 3P plot for the flame with $\phi = 2.47$ is given in Fig. 5. It shows rather less structure than that for the positive ions and provides less insight into the assignment of the corresponding ion identities. Nearly all of the negative ion profiles show a maximum well upstream near the beginning of the reaction zone. All of these subsequently show a rather abrupt decrease with many recovering to a secondary maximum just downstream of the reaction zone. Some of these profiles show one additional maximum in the "valley" of the total ionization profile.

The larger of the upstream negative ion peaks are likely to be associated with oxygenated ions such as CHO_2^- and $C_2H_5O^-$ (45 amu), O_2^- (32 amu), $CHCO^-$ (41 amu), CO_3^- (60 amu), HCO_3^- (61 amu), and CH_2CHO^- (43 amu). One exception is the ion at 25 amu corresponding to C_2H^-.

The major downstream ions are readily identified as very highly unsaturated hydrocarbons. The most abundant of these are the acetylenic species

Can. J. Chem. Downloaded from www.nrcresearchpress.com by 210.87.254.5 on 09/06/12
For personal use only.

Can. J. Chem. Downloaded from www.nrcresearchpress.com by 210.87.254.5 on 09/06/12
For personal use only.

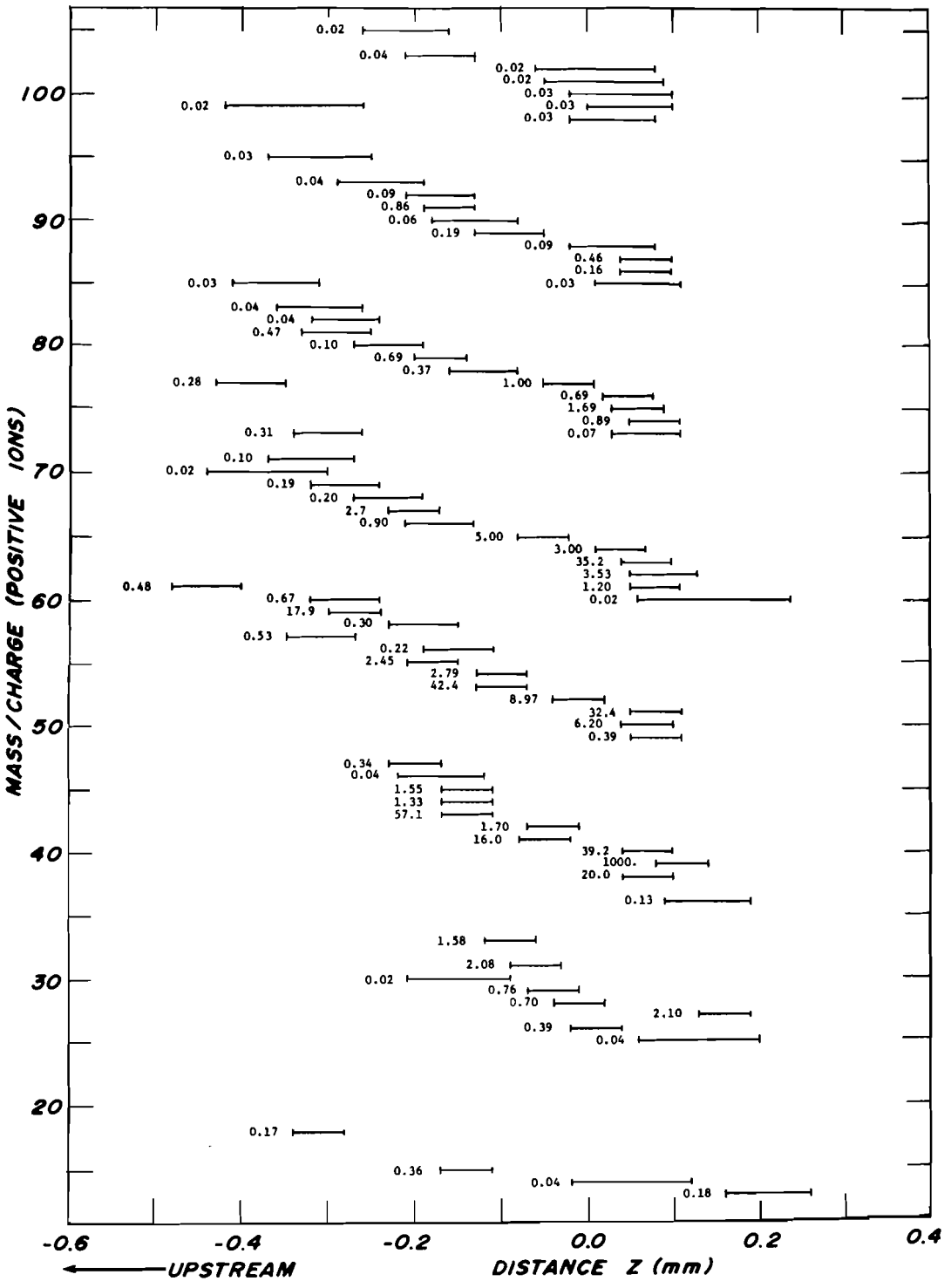

FIG. 4. The positive ion profile–peak–position (3P) plot for the flame with $\phi = 2.47$, 17.7% C_2H_2, $T_{ad} = 2443$ K. The number beside each bar is the relative magnitude of the profile maximum. The lengths of the bars represent the estimated uncertainties in the positions of the profiles which may arise from either the shapes or the magnitudes of the profiles.

Can. J. Chem. Downloaded from www.nrcresearchpress.com by 210.87.254.5 on 09/06/12
For personal use only.

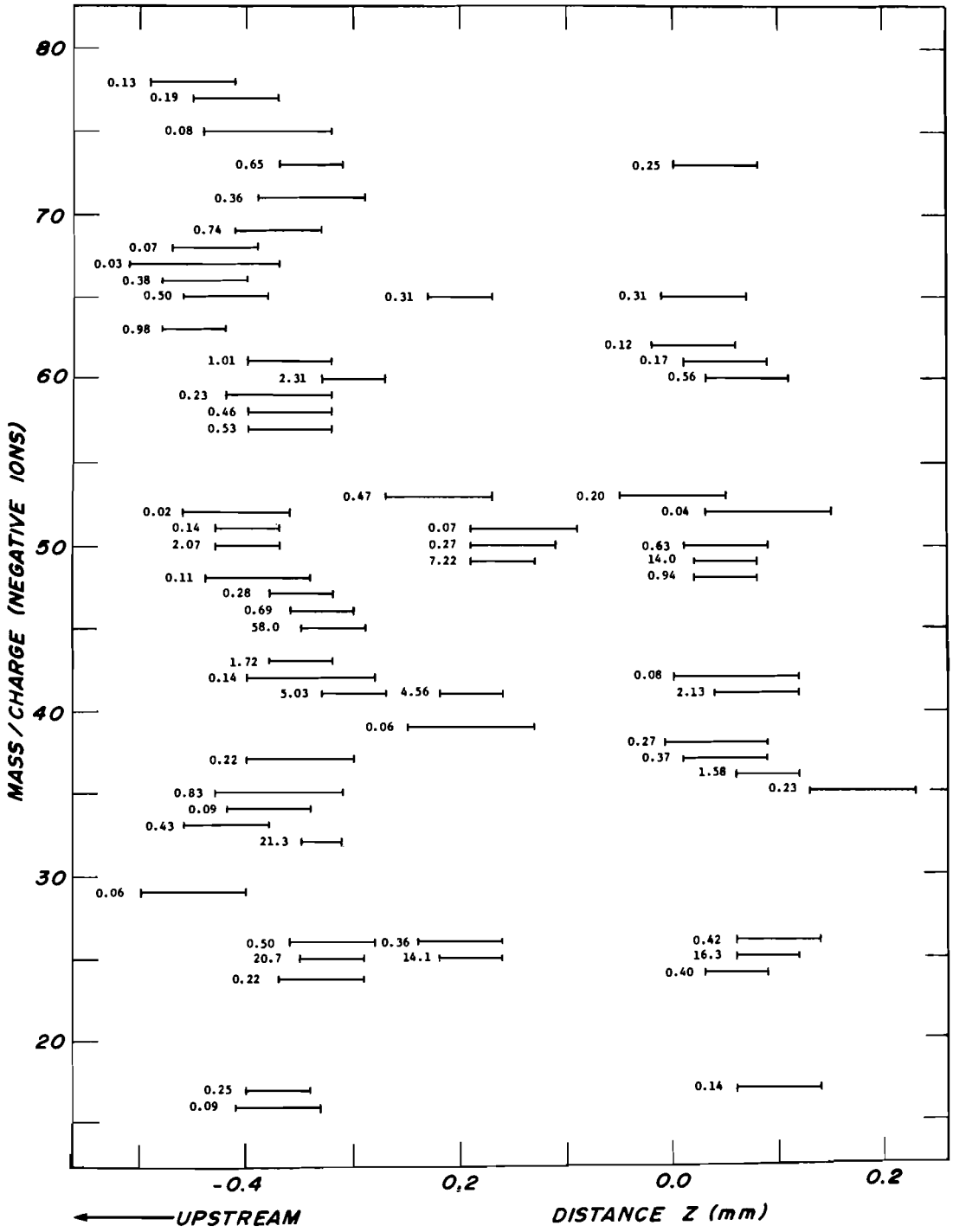

FIG. 5. The negative ion profile–peak–position (3P) plot for the flame with $\phi = 2.47$, 17.7% C_2H_2, $T_{ad} = 2443$ K. The number beside each bar is the relative magnitude of the profile maximum. The lengths of the bars represent the estimated uncertainties in the position of the profiles which may arise from either the shapes or the magnitudes of the profiles.

Can. J. Chem. Downloaded from www.nrcresearchpress.com by 210.87.254.5 on 09/06/12
For personal use only.

C_2H^- (25 amu) and C_4H^- (49 amu) with some C_6H^- (73 amu). The downstream odd-number carbon ion signals appear largest for $x = 0$ and 5; i.e., for C_3^- (36 amu), $C_3H_5^-$ (41 amu), and C_5^- (60 amu), $C_5H_5^-$ (65 amu).

The species C_2H^- and C_4H^- also show strong peaks in the intermediate valley region (as do their ^{13}C isotopic counterparts at 26 and 50 amu). The ion at 41 amu, which has been assigned as $CHCO^-$ upstream and as $C_3H_5^-$ downstream, also shows a major peak in this region. The remaining ions in the valley show much smaller maxima; interpreted as $C_nH_x^-$, these ions may represent moderately unsaturated intermediates in the overall dehydrogenation which appears to proceed through the reaction zone.

Variations with Fuel Composition

A comparison of the 3P plots for the flame having $\phi = 2.47$ (Figs. 4 and 5) with those for the flame having $\phi = 2.15$ (not shown) exhibited some interesting variations in both peak positions and magnitudes, albeit the gross features were quite insensitive to the change in equivalence ratio (11). As regards changes in peak positions, it was noticed that the upstream ion peak positions shifted downstream while the downstream ion peak positions shifted upstream with the change to the more fuel-lean flame. These features may reflect a real change in the width of the reaction zone resulting from changes in the reaction rates and burning velocity, and a change in the flame geometry. For the most part, however, these changes were only of the order of 0.05 mm. In general the peak magnitudes changed by not more than a factor of 5, although for a few ions changes as large as a factor of 20 were observed.

Of course, for a full appreciation of changes due to a change in fuel composition, there is no substitute for the profiles themselves. For example, the 3P plots do not contain information about the actual shapes of the peaks which reflect rates of formation and loss. Most of the observed peaks are skewed: the upstream peaks upstream and the downstream peaks downstream.

Some of the differences in shapes as well as peak magnitudes and positions observed with the change in fuel composition are illustrated in Figs. 6, 7, and 8 for several positive and negative ion profiles. It can be readily seen that the shapes in fact do not change dramatically over the range of conditions adopted in this study. This attests to the usefulness of the 3P-plot treatment introduced earlier.

As a general observation, the peak magnitudes of ions upstream decrease whereas the downstream peak magnitudes increase. This is illustrated for positive ions in Fig. 6. The increase downstream in the ions at mass 49 amu (C_4H^+) and 61 amu (C_5H^+) would appear to be associated with the increase in the acetylene concentration. The reason for the decrease in the upstream profile at 61 amu is less clear. A likely cause is proton transfer from protonated acetic acid to acetone present as an impurity in the added acetylene. The dramatic decrease in the intermediate CH_3^+ peak at 15 amu no doubt is due to its rapid reaction with C_2H_2 yielding $C_3H_3^+$ (12). A corresponding result is recorded for negative ions in Fig. 7. Here the downstream profiles at 25 and 60 amu (C_2H^- and C_5^-) increase with the addition of acetylene to the fuel. Of the upstream ions, C_2H^- increases at the expense of OH^- (and O^-, not shown) which is known to react with acetylene (13). The decrease in the upstream portion of the profile at 60 amu (CO_3^-) is likely a result of the depletion of its source ion, O^-.

As regards the individual ion profiles, only a few showed shifts in peak positions which were significantly larger than the small shifts of ± 0.05 mm discussed earlier. Notable amongst these are the profiles for H_3O^+, its hydrate $H_3O^+ \cdot H_2O$ and HCO^+. The last of these is shown in Fig. 8, where its peak is seen to shift by 1.79 ± 0.18 mm. The sharp peak upstream which does not show a shift may be identified as $C_2H_5^+$. The late downstream rise of HCO^+ may be related to the unusual persistence of $C_3H_3^+$. These two ions are believed to be coupled through the reaction (14)

$$C_3H_3^+ + O \rightleftharpoons HCO^+ + C_2H_2$$

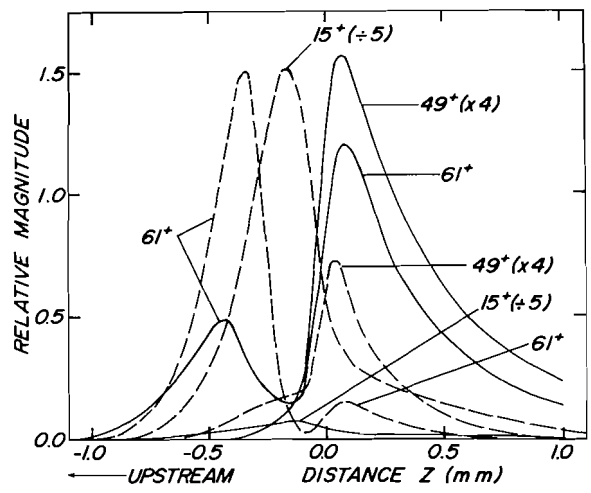

FIG. 6. A comparison of selected positive ion profiles which show significant changes in peak magnitudes measured for the flames having $\phi = 2.47$ (solid curves) and $\phi = 2.15$ (dashed curves).

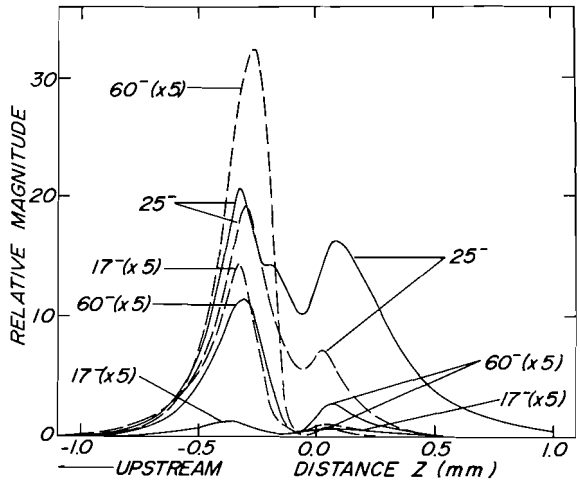

FIG. 7. A comparison of selected negative ion profiles which show significant changes in peak magnitudes measured for the flames having $\phi = 2.47$ (solid curves) and $\phi = 2.15$ (dashed curves). It should be noted that the peak magnitudes have been normalized to the maximum signal measured for the total negative ionization profile (see Fig. 1(*a*)).

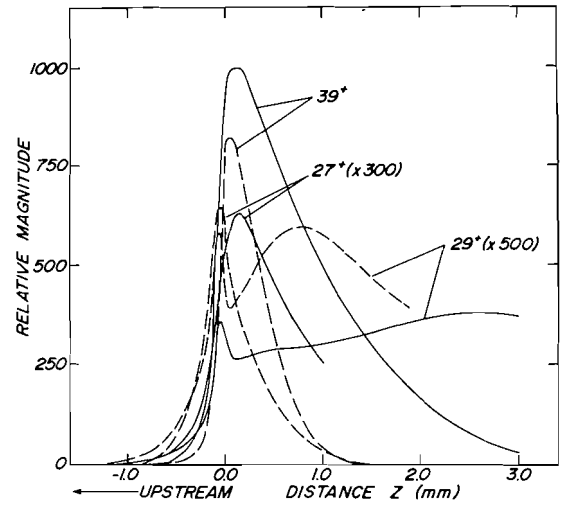

FIG. 8. A comparison of selected positive ion profiles which show significant changes in peak positions measured for the flames having $\phi = 2.47$ (solid curves) and $\phi = 2.15$ (dashed curves).

whose reverse rate will be enhanced by the added acetylene. Finally, the $C_2H_3^+$ profile at 27 amu shows the transition from a symmetric profile typical of intermediate ions to a more skewed profile characteristic of the more persistent ions downstream of the reaction zone. The small concomitant shift reflects the continued protonation of acetylene.

Summary

A large amount of experimental data has been presented in this report employing improved methods for the measurement of the flame-ion concentration profiles with high spatial resolution and novel approaches for their analysis. The following list summarizes many of the observations made in this study.

1. The spatial resolution of ion profile data is increased by the use of a conical sampling nozzle compared with a nozzle of more blunt geometry, for the same-sized orifice.

2. The peak magnitude of the total positive ionization curve increases with an increase in temperature; chemi-ionization has a positive temperature dependence (T-dependence).

3. The total negative ion profile is double-peaked. For fuel-rich flames, the magnitude of the upstream peak decreases with increasing equivalence ratio (negative ϕ-dependence) and has little T-dependence. The magnitude of the downstream peak shows both positive ϕ- and T-dependence.

4. The negative ion profile peaks for $C_nH_x^-$ ions appear in three distinct regions. (*i*) Oxygenated anions are found upstream; C_2H^- is an exception. (*ii*) Very highly unsaturated hydrocarbon ions are observed downstream peaking just beyond the reaction zone. Their concentrations alternate with the parity of n, the even-n species being larger. This implicates acetylene or its polymers in the anionic chemistry. For even n, the most abundant carbonaceous species are the acetylenic anions C_2H^-, C_4H^-, C_6H^-, ... with $x = 1$. For n odd, the most abundant tend to be those with $x = 0$ and 5. (*iii*) Moderately unsaturated hydrocarbon ions seem to be present in the intermediate region.

5. The positive ion peaks are observed to form a number of series through the flame reaction zone. (*i*) Each series is defined by the value of n, and the profile peak positions evolve downstream through the flame front with decreasing values of x, amounting to progressive dehydrogenation. (*ii*) The peak magnitudes tend to be larger for small values of x; the largest signal in each series is obtained for $x = 3$. Within each series, there is a fairly regular alternation in magnitude with x; the larger peaks are associated with odd values of x. (*iii*) The positive ion chemistry of these series seems to be essentially independent of the value of n.

6. As ϕ of a fuel-rich flame is increased at constant temperature towards the sooting point by the addition of acetylene, a number of changes occur. (*i*) The concentrations of the unsaturated positive and negative hydrocarbon ions within and

Can. J. Chem. Downloaded from www.nrcresearchpress.com by 210.87.254.5 on 09/06/12
For personal use only.

downstream of the reaction zone increase; the upstream (oxygenated) ions decrease. (*ii*) The profile peaks due to hydrocarbon ions spread out somewhat both upstream and downstream; possibly the thickness of the reaction zone is increased. (*iii*) The shapes of these profiles do not change greatly, except that they become more skewed in the downstream direction; a key factor to be considered is chemical reactions involving acetylene. (*iv*) The concentrations of positive ions having high n-values are enhanced relative to those of low n; the degree of this enhancement appears to increase with increasing n. Also, within a series of given n, there is a relative enhancement of ions with small x.

Acknowledgements

One of us (S.D.T.) is grateful for the award of an Ontario Graduate Scholarship. Support of this work by the Natural Sciences and Engineering Research Council of Canada under Grant Numbers A1604 (J.M.G.) and A6258 (D.K.B.) is acknowledged.

1. J. LAHAYE and G. PRADO. Chem. Phys. Carbon, **14**, 167 (1978).
2. J. M. GOODINGS, D. K. BOHME, and C.-W. NG. Combust. Flame, **36**, 27 (1979).
3. J. M. GOODINGS, D. K. BOHME, and C.-W. NG. Combust. Flame, **36**, 45 (1979).
4. R. S. TSE, P. MICHAUD, and J.-L. DELFAU. Nature, **272**, 153 (1978).
5. J.-L. DELFAU, P. MICHAUD, and A. BARASSIN. Combust. Sci. Technol. **20**, 165 (1979).
6. C.-W. NG. M.Sc. Thesis. York University, Downsview, Ont., Canada M3J 1P3. 1977.
7. N. A. BURDETT and A. N. HAYHURST. Proc. R. Soc. London A, **355**, 377 (1977).
8. A. N. HAYHURST, D. B. KITTELSON, and N. R. TELFORD. Combust. Flame, **28**, 123 (1977).
9. A. N. HAYHURST and D. B. KITTELSON. Combust. Flame, **28**, 137 (1977).
10. J. A. GREEN. 26th AGARD Propulsion and Energetics Panel, Pisa, Italy, AGARD Conference Proceedings No. 8. Vol. I. *Edited by* H. D. Wilsted. 1965. p. 191.
11. S. D. TANNER. Ph.D. Thesis, York University, Downsview, Ont., Canada M3J 1P3. 1980.
12. W. T. HUNTRESS, JR. Astrophys. J. Suppl. Ser. **33**, 495 (1977).
13. D. K. BOHME, G. I. MACKAY, H. I. SCHIFF, and R. S. HEMSWORTH. J. Chem. Phys. **61**, 2175 (1974).
14. J. M. GOODINGS, D. K. BOHME, and T. M. SUGDEN. Sixteenth Symposium (International) on Combustion, The Combustion Institute, Pittsburgh, PA. 1977. p. 891.

Can. J. Chem. Downloaded from www.nrcresearchpress.com by 210.87.254.5 on 09/06/12
For personal use only.

A room-temperature study of the kinetics and energetics for the protonation of ethane

G. I. MACKAY, H. I. SCHIFF, AND D. K. BOHME

Department of Chemistry and Centre for Research in Experimental Space Science, York University, Downsview, Ont., Canada M3J 1P3

Received November 3, 1980

This paper was presented at a Special Symposium "The Structure and Thermochemistry of Gaseous Ions", held in honour of Dr. F. P. Lossing, of the National Research Council of Canada, during the Second Canadian Conference on the Gas Phase Chemistry of Ions, Trent University, June 5–8, 1980, and is dedicated to him on the occasion of his 65th birthday

G. I. MACKAY, H. I. SCHIFF, and D. K. BOHME. Can. J. Chem. **59**, 1771 (1981).

The flowing afterglow and selected-ion flow tube (SIFT) techniques have been applied in room-temperature measurements of the kinetics for proton-transfer reactions of ethane with HeH^+, H_3^+, N_2H^+, CH_5^+, N_2OH^+, and HCO^+. The fragmentation of $C_2H_7^+$ was followed over a range in excess energy of 100 kcal mol^{-1}. Equilibrium constants were measured at low excess energies for the proton-transfer reactions with HCO^+ and N_2OH^+. The latter provided values for the proton affinity of ethane and $\Delta H_f^0(C_2H_7^+)$ and, indirectly, values for the proton affinity of ethylene and $\Delta H_f^0(C_2H_5^+)$. Additional measurements of the kinetics of the reactions of C_2H_6 with H^+ itself, O^+, OH^+, and H_2O^+ provided insight into the competition between proton-transfer and other reaction channels and the fragmentation associated with the $C_2H_6^+$ ion.

G. I. MACKAY, H. I. SCHIFF et D. K. BOHME. Can. J. Chem. **59**, 1771 (1981).

Opérant à la température ambiante, on a utilisé les techniques de la lueur d'écoulement et de tube à écoulement d'ions sélectionnés (TEIS) pour mesurer la cinétique des réactions de transfert de proton de l'éthane avec HeH^+, H_3^+, N_2H^+, CH_5^+, N_2OH^+ et HCO^+. On a contrôlé la fragmentation de $C_2H_7^+$ sur une large étendue d'énergie en excès de 100 kcal mol^{-1}. On a mesuré les constantes d'équilibre en utilisant de faibles énergies en excès pour les réactions de transfert du proton avec HCO^+ et N_2OH^+. Ces dernières permettent de déterminer les valeurs de l'affinité de l'éthane pour le proton et le $\Delta H_f^0(C_2H_7^+)$ et, indirectement, les valeurs de l'affinité de l'éthylène pour le proton ainsi que la $\Delta H_f^0(C_2H_5^+)$. Des mesures additionnelles des cinétiques des réactions du $C_2H_6^+$ avec H^+ lui-même, O^+, OH^+ et H_2O^+ fournissent de nouvelles connaissances quant à la compétition entre le transfert de proton et d'autres voies de réaction et de la fragmentation associée avec l'ion $C_2H_6^+$.

[Traduit par le journal]

Introduction

The low stability of $C_2H_7^+$ against dissociation into $C_2H_5^+$ and H_2 has presented a special challenge to the determination of the tendency for ethane to gain a proton. Here we report a systematic investigation of the kinetics and energetics for the protonation of ethane by reactions of the type:

$$[1] \quad AH^+ + C_2H_6 \rightarrow [C_2H_7^+]^* + A \xrightarrow{} C_2H_5^+ + H_2$$

We adopted the approach which we have recently applied to studies of the dissociative protonation of other molecules such as nitromethane (1), formic and acetic acid (2), and several formate and acetate esters (3). The method involves the preparation of a variety of acids, AH^+, by prereaction in a Flowing Afterglow or Selected Ion Flow Tube apparatus, which are then invoked systematically in proton-transfer reactions of type [1]. The concomitant variation in excess energy allowed the nature and extent of the fragmentation of $C_2H_7^+$ to be monitored in a controlled fashion as a function of the degree of its chemical activation by AH^+. Furthermore, several relatively mild acids were identified for which the fragmentation was minimal. Their reactions with ethane permitted the involvement of $C_2H_7^+$ in an equilibrium state and consequently the determination of the relative proton affinity of ethane from equilibrium constant measurements (4). An extension of these studies to radical cations and H^+ itself introduced still other competing channels together with the fragmentation associated with the $C_2H_6^+$ ion.

Experimental

The experiments were carried out using both the Flowing Afterglow, FA, and Selected Ion Flow Tube, SIFT, techniques for which details of construction and methods of operation have been described elsewhere (4, 5). The equilibrium measurements were made with the conventional flowing afterglow using H_2 as the carrier gas. N_2OH^+ and HCO^+ ions were produced from H_3^+ according to the following rapid reactions:

$$[2] \quad H_3^+ + N_2O \rightarrow N_2OH^+ + H_2$$

$$[3] \quad H_3^+ + CO \rightarrow HCO^+ + H_2$$

The H_3^+ itself was established as usual by the rapid reaction of H_2 with H_2^+ produced by electron impact on the carrier gas in the region of the electron gun. The ethane was added sufficiently downstream of the ion production region to ensure that reactions [2] and [3] had gone to completion and that the N_2OH^+ and HCO^+ ions had thermalized to the ambient temperature of 298 ± 2 K.

Except for the reaction of ethane with CH_5^+ which was

0008-4042/81/121771-08$01.00/0

©1981 National Research Council of Canada/Conseil national de recherches du Canada

Can. J. Chem. Downloaded from www.nrcresearchpress.com by 210.87.254.6 on 09/06/12
For personal use only.

followed in a H_2 carrier in the flowing afterglow mode, the kinetic measurements were carried out with the apparatus in the SIFT configuration. Helium was employed as the carrier gas in the reaction region while both H_2 and He were used in the source region at total pressures of ca. 0.5 Torr. CH_5^+ was produced in the manner of reactions [2] and [3]. H_3^+, HCO^+, and N_2H^+ were produced in the SIFT source as in the FA mode. The OH_x^+ ions were produced from water vapour introduced into a SIFT source containing a weak He plasma.

The purities of the gases have been given previously (6) except that for ethane which was 99.9% (Matheson Research Grade).

Results

The data analysis associated with the determination of rate constants and equilibrium constants has been described in detail elsewhere together with the various sources of error (4, 5).

H^+, HeH^+, H_3^+

With the SIFT quadrupole tuned to H_3^+ both H^+ and HeH^+ were observed to be produced in the reaction tube containing helium buffer at pressures in the range 0.357 to 0.50 Torr. The translational energy acquired by the H_3^+ apparently was sufficient to cause some collisional dissociation:

[4*a*] $H_3^+ + He \rightarrow H^+ + H_2 + He$

and to overcome the endothermicity of the proton-transfer reaction:

[4*b*] $H_3^+ + He \rightarrow HeH^+ + H_2$

Figure 1 shows the response of these ions to the addition of ethane into the reaction region sufficiently downstream to allow for their thermalization. All three are rapidly replaced by the ions $C_2H_3^+$, $C_2H_4^+$, and $C_2H_5^+$ in a distribution with respect to the three individual reactant ions which is not readily discernable from the data. The $C_2H_3^+$ is known to react further with ethane to produce $C_2H_5^+$ (7). There was no evidence for the formation of $C_2H_7^+$ (< 1%).

$C_2H_5^+$ is the only one of the three observed product ions which may be formed exothermically by the reaction of ethane with thermalized H_3^+, so that we may write:

[5] $H_3^+ + C_2H_6 \rightarrow C_2H_5^+ + 2H_2$

The formation of both $C_2H_3^+$ and $C_2H_5^+$ is exothermic for the reaction with HeH^+:

[6] $HeH^+ + C_2H_6 \rightarrow C_2H_5^+ + H_2 + He$
$\rightarrow C_2H_3^+ + 2H_2 + He$

Because of the small initial signal of HeH^+ only a small fraction of the observed $C_2H_3^+$ can be attributed to reaction [6]. The $C_2H_4^+$ and most of the $C_2H_3^+$ must, by elimination, come from the free protons:

[7] $H^+ + C_2H_6 \rightarrow C_2H_4^+ + H_2 + H$
$\rightarrow C_2H_3^+ + 2H_2$

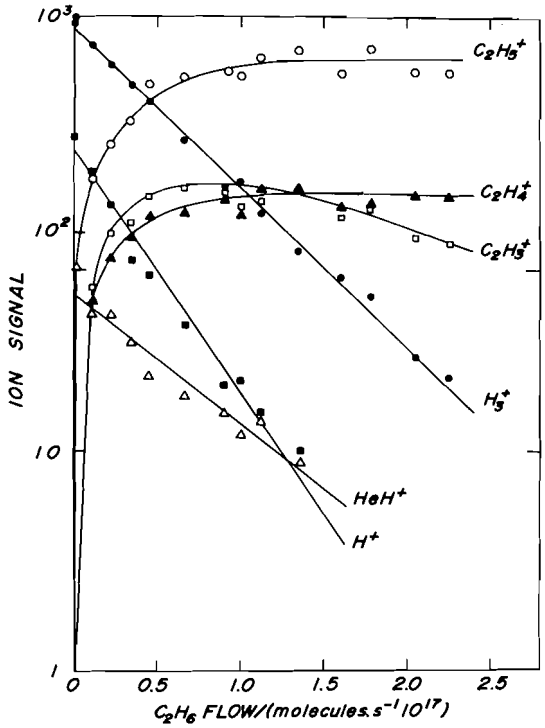

FIG. 1. The variation in ion signals detected upon the addition of C_2H_6 into the reaction region with the SIFT quadrupole tuned to H_3^+ and He Buffer gas in the flow tube. $T = 297$ K, $L = 46$ cm, $P = 0.366$ Torr, and $\bar{v} = 8.5 \times 10^3$ cm s^{-1}.

N_2H^+, CH_5^+

The reaction of N_2H^+ with ethane was investigated in the SIFT mode with H_2 as carrier gas. Figure 2 shows a representative observation of changes in ion signals. The decay of the N_2H^+ is masked in this case by the rise in $C_2H_5^+$ at $m/e = 29$ as is evident from the concomitant rise in the $m/e = 30$ isotope of $C_2H_5^+$. A fit to the rise in the $m/e = 31$ signal provided a rate constant of 1.3×10^{-9} cm^3 molecule^{-1} s^{-1} with an uncertainty of 35%. 87% of the reactive collisions apparently lead to $C_2H_5^+$:

[8] $N_2H^+ + C_2H_6 \rightarrow C_2H_5^+ + H_2 + N_2$
$\rightarrow C_2H_7^+ + N_2$

The association reaction:

[9] $C_2H_5^+ + H_2 \rightarrow C_2H_7^+$

which may ensue in the H_2 buffer is too slow to alter significantly the $C_2H_5^+/C_2H_7^+$ branching ratio under our operating conditions. Experiments in which $C_2H_5^+$ was injected into H_2 buffer at typical

Can. J. Chem. Downloaded from www.nrcresearchpress.com by 210.87.254.6 on 09/06/12
For personal use only.

Can. J. Chem. Downloaded from www.nrcresearchpress.com by 210.87.254.6 on 09/06/12
For personal use only.

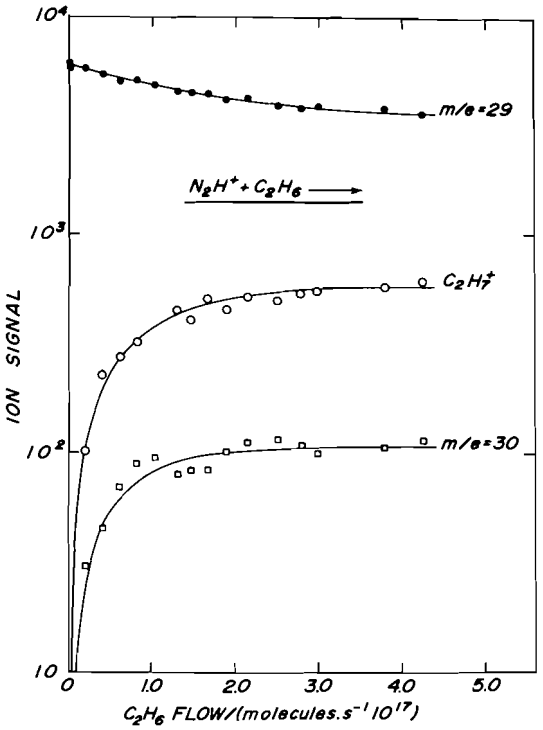

FIG. 2. The variation in ion signals recorded upon the addition of C_2H_6 into the reaction region with the SIFT quadrupole tuned to N_2H^+ and H_2 buffer gas in the flow tube. T = 300 K, L = 46 cm, P = 0.347 Torr, and $\bar{v}$ = 7.6 × 10^3 cm s^{-1}.

operating pressures failed to reveal any formation of $C_2H_7^+$. This observation is consistent with the results obtained by Hiraoka and Kebarle (8) who observed reaction [9] to be second order overall at H_2 pressures down to 2.4 Torr and to have a rate constant of only about 1 × 10^{-14} cm^3 molecule^{-1} s^{-1} at 298 K.

The protonation of ethane by CH_5^+ was investigated in a H_2 buffered flowing afterglow at total pressures from 0.420 to 0.51 Torr. The decays of CH_5^+ were observed to be linear and indicated rapid reaction with k = 1.5 × 10^{-9} cm^3 molecule^{-1} s^{-1} and an estimated uncertainty of ± 25%. Both $C_2H_7^+$ and $C_2H_5^+$ were observed as product ions in the ratio of 5.5 ± 1.0 to 1 under these operating conditions:

[10] $CH_5^+ + C_2H_6 \rightarrow C_2H_7^+ + CH_4$
$\rightarrow C_2H_5^+ + H_2 + CH_4$

The linearity of the observed CH_5^+ decays persisted for at least three orders of magnitude over a range of methane flows from 4.27 × 10^{17} up to 1.9 × 10^{19} molecules s^{-1} which is indicative of a slow reverse reaction and a high equilibrium constant.

N_2OH^+

Rapid protonation of ethane was also observed to occur in H_2 buffer in which N_2OH^+ was initially a dominant ion. Other exothermic channels which lead to the formation of a m/e = 31 ion are conceivable but these involve considerable bond redisposition and could be ruled out on the basis of the observed m/e = 32 ion which had the correct isotopic abundance for $C_2H_7^+$. Some formation of an ion at m/e = 29($C_2H_5^+$) was again apparent but in much smaller relative amounts, about 5%:

[11] $N_2OH^+ + C_2H_6 \rightarrow C_2H_7^+ + N_2O$
$\rightarrow C_2H_5^+ + H_2 + N_2O$

Sufficient curvature was introduced into the N_2OH^+ decays at flows of N_2O from 5.25 × 10^{17} to 1.87 × 10^{19} molecules s^{-1} to allow for the analysis of the kinetics for the reverse reaction and the establishment of equilibrium for the reaction:

[11a] $N_2OH^+ + C_2H_6 = C_2H_7^+ + N_2O$

as demonstrated in Fig. 3 and Fig. 4, respectively. The total pressure was in the range from 0.300 to 0.424 Torr.

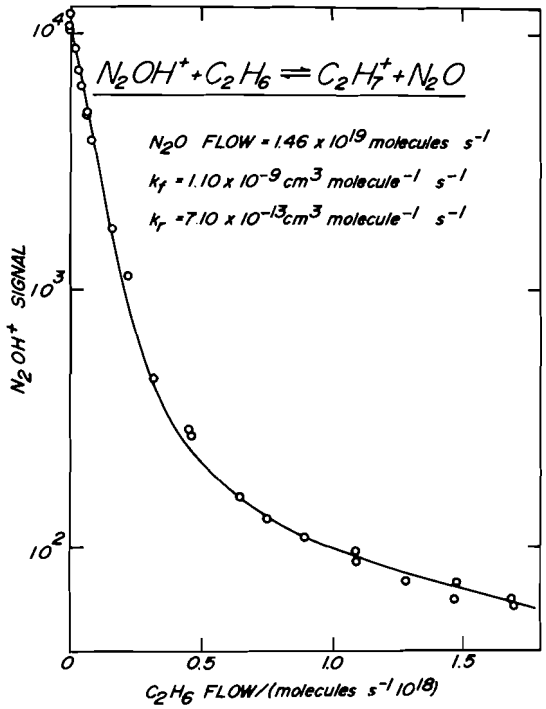

FIG. 3. The variation of the N_2OH^+ signal observed as a function of the flow of ethane at a fixed flow of N_2O in the flowing afterglow mode. T = 296 K, L = 85 cm, P = 0.405 Torr, and $\bar{v}$ = 8.3 × 10^3 cm s^{-1}. The open circles are experimental and the curve is calculated using the values indicated for k_f, k_r, and the flow of N_2O.

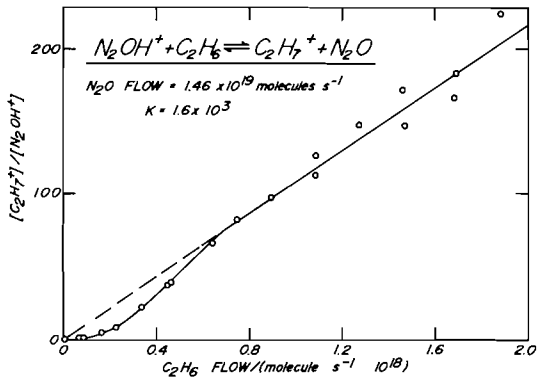

FIG. 4. The observed variation in the ion concentration ratio $[C_2H_7^+]/[N_2OH^+]$ (corrected for mass discrimination) as a function of ethane addition showing the approach to and attainment of equilibrium at a fixed flow of N_2O in the flowing afterglow. The best straight line through the open circles at high ethane flows yields the indicated value for the equilibrium constant.

Thirteen runs provided a value for the forward rate constant of $(1.1 \pm 0.2) \times 10^{-9}$ cm^3 molecule^{-1} s^{-1}. In nine of these runs the curvature in the decays of N_2OH^+ provided a reverse rate constant of $(6.9 \pm 2.1) \times 10^{-13}$ cm^3 molecule^{-1} s^{-1} and a ratio of rate constants of $(1.5 \pm 0.45) \times 10^3$. The measured ratio of equilibrium concentrations provided a value for K of $(1.5 \pm 0.3) \times 10^3$ which is identical to the rate constant ratio.

HCO^+

The proton-transfer reaction of HCO^+ with ethane was expected to have a small equilibrium constant on the basis of the N_2OH^+ results and the known proton affinities of N_2O and CO (9). Indeed, strong curvature was observed in the decays of HCO^+ at all flows of CO which ranged from 1.53×10^{18} to 9.9×10^{19} molecules s^{-1} and at total pressures from 0.331 to 0.420 Torr. Equilibrium appeared to be established in the flowing afterglow already at small additions of ethane. The curvature in the HCO^+ decay was fitted to provide a ratio of rate constants of 10.8 ± 3.2. Because of the early establishment of equilibrium the fitting procedure could not yield unique values for the individual rate constants. The analysis of the equilibrium ratio plots yielded a value for K of 11.9 ± 4.0 which combines with the measured ratio of rate constants to provide a true value for the thermodynamic equilibrium constant of 11.3 ± 2.4. This value is in excellent accord with the ratio of equilibrium constants $(1.5 \pm 0.3) \times 10^3/(1.4 \pm 0.2) \times 10^2 = 11 \pm 4$ derived from the equilibrium constant measurements for reactions [11*a*] and [12] (10):

[12] $N_2OH^+ + CO = HCO^+ + N_2O$

The SIFT measurements performed with H_2 buffer gas at pressures between 0.283 and 0.451 Torr and in the absence of CO in the reaction region, provided a rate constant for the protonation of ethane by HCO^+ of $(1.2 \pm 0.2) \times 10^{-10}$ cm^3 molecule^{-1} s^{-1}. There was no evidence for any formation of $C_2H_5^+$.

OH_x^+

The reactions of O^+, OH^+, and H_2O^+ with ethane were investigated in the SIFT mode in helium buffer gas at pressures in the range 0.298 to 0.359 Torr. All three ions reacted rapidly with the added ethane and at least two product ions were apparent in each case. With O^+ the apparent reaction was the following:

[13] $O^+ + C_2H_6 \rightarrow C_2H_4^+ + (H_2O)$
$\rightarrow C_2H_5^+ + (OH)$

The observed branching ratio $C_2H_4^+/C_2H_5^+$ was 7/3. The proton affinity of O is close to that of N_2 (9) so that the proton transfer from OH^+ to ethane is quite exothermic. But so are many other reaction channels in this instance. Indeed, the product spectrum observed in this case was quite elaborate:

[14*a*] $OH^+ + C_2H_6 \rightarrow C_2H_4^+ + (H_2 + OH)$

[14*b*] $\rightarrow C_2H_5^+ + (H_2 + O)$

[14*c*] $\rightarrow H_3O^+ + C_2H_4$

[14*d*] $\rightarrow C_2H_6^+ + OH$

[14*e*] $\rightarrow C_2H_7^+ + O$

The observed branching ratio was a:b:c:d:e = 65:20:10:3:2. Proton transfer appears to be completely swamped by other reaction channels in the case of H_2O^+ for which it is still exothermic but now only slightly so. The observed product spectrum was the following:

[15*a*] $H_2O^+ + C_2H_6 \rightarrow H_3O^+ + C_2H_5$

[15*b*] $\rightarrow C_2H_4^+ + H_2 + H_2O$

[15*c*] $\rightarrow C_2H_6^+ + H_2O$

[15*d*] $\rightarrow C_2H_5^+ + H + H_2O$

Evidently H-atom transfer predominates almost exclusively as the branching ratio a:b:c:d was estimated to be 83:12:4:1.

Discussion

The measurements reported in this study yield both rate and equilibrium data for the protonation of ethane. The latter provides the basis for a determination of the proton affinity of ethane as

Can. J. Chem. Downloaded from www.nrcresearchpress.com by 210.87.254.6 on 09/06/12
For personal use only.

Can. J. Chem. Downloaded from www.nrcresearchpress.com by 210.87.254.6 on 09/06/12
For personal use only.

will be discussed in a later section. The former provides insight into the efficiency of protonation, the stability of the resulting $C_2H_7^+$ against further dissociation, and the degree to which proton transfer competes with other reaction channels when these become viable options, as is the case with radical ions.

Kinetics of Protonation

Table 1 summarizes the rate constants determined in this study along with the observed product ion distributions. Except for the reaction of HCO^+ which proceeds at only about 10% efficiency, all of the reactions in Table 1 proceed within 25% of the collision rate calculated from the Langevin (11) or Average-Quadrupole-Orientation, AQO, theories (12, 13).

The free protons were observed to react most rapidly. Their reaction proceeded at 80% of the AQO rate. The observed $C_2H_4^+$ and $C_2H_3^+$ product ions may be envisaged to arise from what is formally a dissociative hydride ion transfer:

$$[16]\quad H^+ + C_2H_6 \rightarrow [C_2H_7^+]^* \rightarrow \begin{cases} [C_2H_5^+]^* + H_2 \\ \rightarrow C_2H_4^+ + H \\ \rightarrow C_2H_3^+ + H_2 \end{cases}$$

and/or by dissociative charge transfer:

$$[17]\quad H^+ + C_2H_6 \rightarrow [C_2H_6^+]^* + H \begin{cases} \rightarrow C_2H_5^+ + H \\ \rightarrow C_2H_4^+ + H_2 \end{cases}$$

However, the formation of $C_2H_3^+$ by dissociative charge transfer may be ruled out since it is endothermic.

It is interesting to compare the reaction with protons to that with O^+ ions since H and O atoms have essentially identical ionization potentials. The reaction with O^+ seems more efficient with the measured rate constant being 25% larger than the calculated collision rate constant. $C_2H_4^+$ is a major product but $C_2H_3^+$ is not observed even though the overall exothermicities of the H^+ and O^+ reactions are very similar. $C_2H_5^+$ appears as a product ion instead. The higher stability of $C_2H_5^+$ in this case may arise from a larger amount of the excess energy appearing in the neutral OH in the analogue of reaction [16].

An inspection of the product distributions in Table 1 for the reactions of the even-electron acids $AH^+ = HeH^+$, H_3^+, N_2H^+, CH_5^+, N_2OH^+, and HCO^+, reveals the trend expected on the basis of the dissociative proton-transfer mechanism expressed in eq. [1]. The most energetic product ions $C_2H_3^+$ and $C_2H_5^+$ are associated with the strongest acid HeH^+ for which the excess energy is largest, while the least energetic product ion $C_2H_7^+$ is associated predominantly with the weakest acid in this series, HCO^+, for which the excess energy is smallest.

TABLE 1. Summary of rate constants and product distributions for reactions with ethane measured in this study at 298 ± 2 K

Reactant ion	Product ions	Product distribution	Rate constant[a]
H^+	$C_2H_4^+$ $C_2H_3^+$ $(C_2H_5^+)$		3.9 ± 0.8
O^+	$C_2H_4^+$ $C_2H_5^+$	0.7 0.3	1.9 ± 0.4
OH^+	$C_2H_4^+$ $C_2H_5^+$ H_3O^+ $C_2H_6^+$ $C_2H_7^+$	0.65 0.20 0.10 0.03 0.02	1.6 ± 0.3
H_2O^+	H_3O^+ $C_2H_4^+$ $C_2H_6^+$ $C_2H_5^+$	0.83 0.12 0.04 0.01	1.6 ± 0.3
HeH^+	$C_2H_5^+$ $C_2H_3^+$		2.1 ± 0.4
H_3^+	$C_2H_5^+$	1.00	2.4 ± 0.5
N_2H^+	$C_2H_5^+$ $C_2H_7^+$	0.87 0.13	1.3 ± 0.5
CH_5^+	$C_2H_7^+$ $C_2H_5^+$	0.85 0.15	1.5 ± 0.3
N_2OH^+	$C_2H_7^+$ $(C_2H_5^+)$	0.95 0.05	1.1 ± 0.2
HCO^+	$C_2H_7^+$	1.00	0.12 ± 0.02

[a]Rate constant for the total loss of the reactant ion along with the estimated accuracy in units of 10^{-9} cm^3 molecule^{-1} s^{-1}.

The trend in the product distribution with reaction exothermicity observed in this study for the protonation of C_2H_6 is shown in the form of a bargraph in Fig. 5. Clearly the fraction of $C_2H_7^+$ ions which have sufficient energy to decompose, and do so under the experimental conditions, increases dramatically when the reaction exothermicity exceeds the 13.0 kcal mol^{-1} required for the dissociation as is indicated in the potential energy diagram shown in the insert in Fig. 5. The observed efficiency of dissociative proton transfer will depend on the total energy initially deposited in the $C_2H_7^+$ product, the dependence of the rate constant of the fragmentation on this internal energy, and the degree to which the internal energy is moderated by collisions with the buffer gas molecules. Since the time between collisions with the buffer gas molecules is ca. 1 μs, fragmentations

TABLE 2. Product distributions observed for various degrees of excitation of ions in reactions with ethane

Reaction	Product ions[a]	Product distribution: Tandem-ICR[b] Excited	Tandem-ICR[b] Relaxed	FA[c]
$N_2H^+ + C_2D_6/C_2H_6$	$C_2D_6H^+$	0.00	0.09	0.13
	$C_2D_5^+ + C_2D_4H^+$	1.00	0.91	0.87
$CD_5^+/CH_5^+ + C_2H_6$	$C_2H_6D^+$	0.26	0.58	0.85
	$C_2H_5^+ + C_2H_4D^+$	0.74	0.42	0.15
$N_2OD^+/N_2OH^+ + C_2H_6$	$C_2H_6D^+$		0.89	0.95
	$C_2H_5^+$, $C_2H_4D^+$		0.11	0.05
$DCO^+/HCO^+ + C_2D_6/C_2H_6$	$C_2D_7^+$		0.84	1.00
	$C_2D_5^+$		0.16	0.00

[a]Only the deuterated product ions observed in the tandem-ICR experiments are indicated. The FA experiments were carried out only with undeuterated reactants.

[b]Reactions proceeded at average ion translational energies of 0.1 eV and typical pressures of 10^{-6} Torr. The average number of ion–neutral collisions of an ion prior to reaction was varied between 0 and 10 collisions by increasing the pressure in the ion source.

[c]Product distributions measured in the flowing afterglow or SIFT mode at 298 ± 2 K.

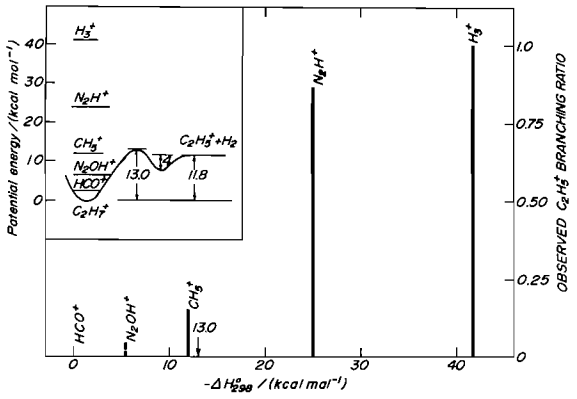

FIG. 5. The observed trend in the extent of dissociative proton transfer to C_2H_6 with reaction exothermicity. The exothermicities have been calculated from the proton affinities determined previously in this laboratory (9) and that of C_2H_6 derived in the text. The potential energy diagram is based on rate and equilibrium measurements for the association of $C_2H_5^+$ and H_2 as a function of temperature carried out by Hiraoka and Kebarle (8).

which require more time than this may be discriminated against and so obscure the initial product distribution in that they may appear as stabilized $C_2H_7^+$ product ions.

It is interesting to compare, as is done in Table 2, the product distributions observed at the relatively high pressures of the FA/SIFT experiments with those obtained previously at the much lower pressures, viz. 10^{-6} Torr, of tandem-ICR experiments (14). In the latter experiments the product distributions were found to be quite sensitive to the excitation of the reactant ion AH^+, shifting towards decreased dissociation of the $C_2H_7^+$ with an increase in the average number of ion–neutral collisions experienced by AH^+ prior to reaction. The product distributions obtained in the FA/SIFT experiments, in which the reactant ions experience a sufficient number of ion–neutral collisions to be thermalized to the buffer gas temperature, are consistent with the trend established at the low pressures in that they show a still further shift towards $C_2H_7^+$ formation. The further shift is expected since there still is a spread in internal energies of several tenths of an eV associated with the "relaxed" AH^+ ions in the tandem-ICR experiments. For example, for the proton-transfer reaction with HCO^+ for which the flowing afterglow measurements show no dissociation, and indeed the dissociation is clearly endothermic, the tandem-ICR experiments show that 16% of the reaction produces $C_2H_5^+$. Dissociative proton-transfer is also endothermic for N_2OH^+ but in this case the energetics are somewhat unique in that several other exothermic routes are possible for the observed formation of the ion at $m/e = 29$:

$$[18a]\quad N_2OH^+ + C_2H_6 \rightarrow C_2H_5^+ + H_2O + N_2$$

$$[18b]\quad \rightarrow N_2H^+ + C_2H_5OH/(C_2H_4 + H_2O)$$

Channels [18*a*] and [18*b*] are exothermic by 69 and 36/(26) kcal mol^{-1}, respectively. Channel [18*a*] seems more probable on mechanistic grounds since it can be viewed to proceed by hydride transfer to N_2OH^+ followed by the dissociation of the resulting neutral species into stable N_2 and H_2O.

Proton Affinity of Ethane

The results of the pertinent equilibrium constant

Can. J. Chem. Downloaded from www.nrcresearchpress.com by 210.87.254.6 on 09/06/12
For personal use only.

Can. J. Chem. Downloaded from www.nrcresearchpress.com by 210.87.254.6 on 09/06/12
For personal use only.

measurements are shown in Table 3. They provide a best estimate of the true value of the equilibrium constant for the protonation of ethane by HCO^+ of 11.2 ± 2.1:

[19] $HCO^+ + C_2H_6 = C_2H_7^+ + CO$

This result is very useful for the determination of the proton affinity of ethane since the proton affinity of CO is well established. The equilibrium constant corresponds to a standard free energy change at 298 K for reaction [19] of -1.43 ± 0.11 kcal mol^{-1}. A standard entropy change of $+2.3 \pm 2.2$ cal mol^{-1} K^{-1} may be estimated from the absolute entropies for HCO^+, $C_2H_7^+$, and CO, of 48.04 ± 0.2 (15), 54.9 (16), 58 ± 3, and 47.21 (17) cal mol^{-1} K^{-1}. The entropy of $C_2H_7^+$ was estimated from a comparison with the entropies of the isoelectronic species CH_3NH_2 and CH_3OH and ethane itself (16). The standard free energy and entropy changes can be combined to provide a value for the standard enthalpy change of -0.74 ± 0.77 kcal mol^{-1}, or a difference in the proton affinities of C_2H_6 and CO, $\Delta PA(C_2H_6, CO) = 0.7 \pm 0.8$ kcal mol^{-1}. With a value for PA(CO) of 141.4 ± 0.4 kcal mol^{-1} as in ref. 9, the value for $PA(C_2H_6)$ becomes 142.1 ± 1.2 kcal mol^{-1}. This result is consistent with the limiting values $136 < PA(C_2H_6) < 159$ kcal mol^{-1} which we obtained previously from bracketing measurements (18), but it exceeds the value of 127.0 ± 1.0 kcal mol^{-1} obtained on the basis of mass-spectrometer ion-source measurements (19) of the proton-transfer reaction:

[20] $CH_5^+ + C_2H_6 = C_2H_7^+ + CH_4$

This discrepancy has been discussed previously (18). *Ab initio* molecular orbital calculations (20) of the geometry and energy of $C_2H_7^+$ have led to a theoretical value for $PA(C_2H_6) = 140.1$ kcal mol^{-1} (not corrected for zero point vibrations) which compares very favourably with our experimental value. Accepted heats of formation for ethane and the proton (16, 17) lead to a heat of formation for $C_2H_7^+$ of 204.8 ± 1.3 kcal mol^{-1}.

TABLE 3. Summary of equilibrium constants measured at 298 ± 2 K for proton-transfer reactions of the type $XH^+ + Y \rightleftharpoons YH^+ + X$. The preferred direction of proton transfer is towards the top of the table

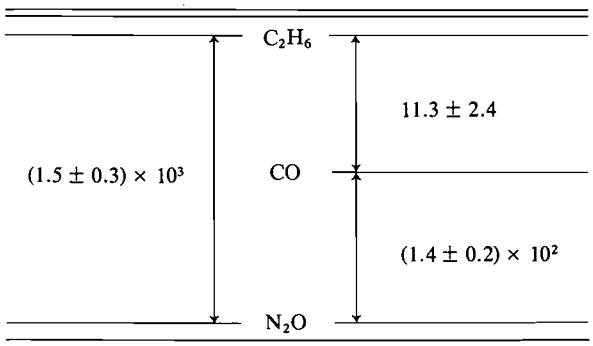

Proton Affinity of Ethylene

Having established a value for the proton affinity of ethane, we may take advantage of previous measurements of the equilibrium constant for the association reaction [9] to derive a value for the proton affinity of ethylene. Equilibrium [9] has been investigated by Hiraoka and Kebarle (8) between 358 and 473 K in a high-pressure ion-source mass spectrometer. The corresponding van't Hoff plot provided a value for the standard enthalpy change for reaction [9] of -11.8 ± 0.4 kcal mol^{-1}. $PA(C_2H_4)$ is related to this enthalpy change and $PA(C_2H_6)$ by the equation:

[21] $PA(C_2H_4) = PA(C_2H_6) + \Delta H_f^0(C_2H_4) - \Delta H_f^0(C_2H_6) - \Delta H_9^0$

The accepted values for the heats of formation of ethylene and ethane (16) lead to a value for $PA(C_2H_4) = 163.0 \pm 1.7$ kcal mol^{-1}. Also the heat of formation of $C_2H_7^+$ determined above leads to a heat of formation for $C_2H_5^+$ of 216.6 ± 1.7 kcal mol^{-1}.

The heat of formation of $C_2H_5^+$ has recently received renewed attention. Previous values have been based exclusively on non-equilibrium studies of the appearance of this ion by dissociative ionization and by the ionization of the ethyl radical and have led to a higher value of 220.5 kcal mol^{-1} (21) (here the electron is treated as a conventional element (17)). The shortcomings of these two methods have been described recently by Baer in connection with a report of results obtained by him in a photoionization and photoion-photoelectron coincidence (PIPECO) study of the appearance of $C_2H_5^+$ from C_2H_5I (22). The onset of $C_2H_5^+$ in the I atom loss process:

[22] $h\nu + C_2H_5I \rightarrow C_2H_5^+ + I + e$

was measured in delayed coincidence with zero energy electrons. The kinetic energy release was also measured and found to be zero at the dissociation onset. Baer has derived from these observations a room-temperature heat of formation for $C_2H_5^+$ of 216.8 ± 1.0 kcal mol^{-1} (or 215.3 ± 1.0 kcal mol^{-1} with the stationary electron convention (21)) which is in excellent agreement with the value obtained in our study.

Acknowledgement

We thank the Natural Sciences and Engineering Research Council of Canada for financial support.

1. G. I. MACKAY and D. K. BOHME. Int. J. Mass Spectrom. Ion Phys. **26**, 327 (1978).
2. G. I. MACKAY, A. C. HOPKINSON, and D. K. BOHME. J. Am. Chem. Soc. **100**, 7460 (1978).
3. A. C. HOPKINSON, G. I. MACKAY, and D. K. BOHME. Can. J. Chem. **57**, 2996 (1979).
4. D. K. BOHME, R. S. HEMSWORTH, H. W. RUNDLE, and H. I. SCHIFF. J. Chem. Phys. **58**, 3504 (1973).
5. G. I. MACKAY, G. D. VLACHOS, D. K. BOHME, and H. I. SCHIFF. Int. J. Mass Spectrom. Ion Phys. **36**, 259 (1980).
6. G. I. MACKAY, L. D. BETOWSKI, J. D. PAYZANT, H. I. SCHIFF, and D. K. BOHME. J. Phys. Chem. **80**, 2919 (1976).
7. L. W. SIECK and S. G. LIAS. J. Phys. Chem. Ref. Data, **5**, 1123 (1976).
8. K. HIRAOKA and P. KEBARLE. J. Am. Chem. Soc. **98**, 6119 (1976).
9. D. K. BOHME, G. I. MACKAY, and H. I. SCHIFF. J. Chem. Phys. **73**, 4976 (1980).
10. R. S. HEMSWORTH, H. W. RUNDLE, D. K. BOHME, H. I. SCHIFF, D. B. DUNKIN, and F. C. FEHSENFELD. J. Chem. Phys. **59**, 61 (1973).
11. G. GIOUMOUSIS and D. P. STEVENSON. J. Chem. Phys. **29**, 294 (1958).
12. T. SU and M. T. BOWERS. Int. J. Mass Spectrom. Ion Phys. **17**, 309 (1975).
13. T. SU and M. T. BOWERS. Int. J. Mass Spectrom. Ion Phys. **21**, 417 (1976).
14. R. D. SMITH and J. H. FUTRELL. Int. J. Mass Spectrom. Ion Phys. **20**, 347 (1976).
15. P. J. BRUNA. Ap. L. **16**, 107 (1975).
16. D. D. WAGMAN, W. H. EVANS, V. B. PARKER, I. HALOW, S. M. BAILY, and R. H. SCHUMM. Natl. Bur. Stand. Tech. Note 207–3 (1968).
17. JANAF Thermochemical Tables, 2nd ed., Natl. Bur. Stand. Ref. Data Ser. 37 (1971).
18. D. K. BOHME, P. FENNELLY, R. S. HEMSWORTH, and H. I. SCHIFF. J. Am. Chem. Soc. **95**, 7512 (1973).
19. S. L. CHONG and J. L. FRANKLIN. J. Am. Chem. Soc. **94**, 6347 (1972).
20. W. A. LATHAN, W. J. HEHRE, and J. A. POPLE. J. Am. Chem. Soc. **93**, 808 (1971).
21. H. M. ROSENSTOCK, K. DRAXL, B. W. STEINER, and J. T. HERRON. J. Phys. Chem. Ref. Data Suppl. **1**, 6 (1977).
22. T. BAER. J. Am. Chem. Soc. **102**, 2482 (1980).

Can. J. Chem. Downloaded from www.nrcresearchpress.com by 210.87.254.6 on 09/06/12
For personal use only.

Relative methylmercury cation affinities in the gas phase determined by high pressure mass spectrometry

JOHN A. STONE AND DENA E. SPLINTER
Chemistry Department, Queen's University, Kingston, Ont., Canada K7L 3N6

Received November 5, 1980

This paper is dedicated to Dr. F. P. Lossing of the National Research Council of Canada on the occasion of his 65th birthday

JOHN A. STONE and DENA E. SPLINTER. Can. J. Chem. **59**, 1779 (1981).

A pulsed electron beam, high pressure mass spectrometer has been used to determine equilibrium constants for the exchange of CH_3Hg^+ between bases; $CH_3Hg{\cdot}B_1^+ + B_2 \rightleftharpoons CH_3Hg{\cdot}B_2^+ + B_1$. A series of aromatic, hydrocarbon bases has been studied at 417 K and several nitrogen bases have been studied at 580 K. There is a good linear correlation between differences in CH_3Hg^+ affinity (ΔG^0) and H^+ affinity for bases in each series. The single sulfur base examined ($(C_3H_7)_2S$) shows anomalously high relative affinity for CH_3Hg^+ compared with H^+ while two oxygen bases (CH_3COOCH_3 and $C_6H_5NO_2$) show lesser relative affinity. These results are in qualitative agreement with the hard–soft acid base theory. ΔH^0 and ΔS^0 values have been obtained from Arrhenius plots. For a pair of aromatic bases (toluene–ethylbenzene) ΔH^0 is of the same magnitude as that for H^+ and ΔS^0 may be calculated using partition functions for translation and external rotation. For toluene/methylacetate the difference in binding energy is much greater for H^+ than for CH_3Hg^+ and a similar calculation of ΔS^0 gives a result not consistent with the experimental value.

JOHN A. STONE et DENA E. SPLINTER. Can. J. Chem. **59**, 1779 (1981).

On a utilisé un spectromètre de masse à haute pression et à faisceau pulsé d'électrons pour déterminer les constantes d'équilibre de l'échange de CH_3Hg^+ entre des bases: $CH_3Hg{\cdot}B_1^+ + B_2 \rightleftharpoons CH_3Hg{\cdot}B_2^+ + B_1$. On a étudié à 417 K une série d'hydrocarbures aromatiques agissant comme bases et à 580 K plusieurs bases azotées. Dans chacune des séries, on a noté une bonne corrélation linéaire entre les différences d'affinités (ΔG^0) des bases pour CH_3Hg^+ et H^+. La seule base sulfurée étudiée ($(C_3H_7)_2S$) présente une affinité anormalement élevée pour CH_3Hg^+ par rapport à son affinité pour le H^+; toutefois les deux bases oxygénées (CH_3COOCH_3 et $C_6H_5NO_2$) montrent une affinité relative beaucoup plus faible. Ces résultats sont en accord quaiitatif avec la théorie des acides et des bases durs et mous. On a obtenu les valeurs de ΔH^0 et de ΔS^0 à partir des courbes d'Arrhénius. Pour une paire de bases aromatiques (toluène–éthylbenzène), le ΔH^0 est du même ordre de grandeur que celui de H^+; on peut calculer le ΔS^0 en utilisant les fonctions de partition pour la translation et la rotation externe. Dans le cas du toluène/acétate de méthyle, la différence du point de vue de l'énergie de liaison est beaucoup plus grande pour H^+ que pour CH_3Hg^+ et un calcul analogue de ΔS^0 conduit à des résultats qui ne concordent pas avec la valeur expérimentale.

[Traduit par le journal]

Introduction

The gas phase basicities of a very large number of molecules have now been reported and both qualitative and quantitative interpretations of the values have been given. The majority of these values have been obtained with respect to the proton as acid but the present concept of acidity encompasses many other cations and as has been emphasized, a basicity scale is dependent on the particular acid employed in obtaining it (1). Basicities with respect to a small but growing number of singly charged gas phase metallic ions are now being reported (2).

One of the concepts that has found some favour in qualitative explanations of chemical reactivity in solution is that of hard and soft acids and bases (3). This idea correlates with the covalent (soft) and ionic (hard) contributions to acid base interactions and although its severe limitations have been noted (4) it is still popular. The proton is classified as a hard acid, as are the alkali metal ions, while soft acids are represented by ions such as Ag^+, Hg^{2+}, and CH_3Hg^+ (5). The metal ions which have received the most study in the gas phase are those of the alkali metals which are readily obtained from thermionic sources. Kebarle (6) has summarized the results obtained. Gas phase metal ions from other groups of the periodic table are less easy to produce in a controlled manner and hence have received much less attention. Castleman and coworkers (7) studied the singly charged alkaline earth ions and found, for example, significantly stronger binding to H_2O than for the alkali ions. This he associated with an increasing covalent character to the binding. In order to obtain a greater understanding of the behaviour of acids and bases in the gas phase it is now necessary to extend the range of acid types.

We reported earlier (8) that CH_3Hg^+, obtained by chemical ionization of $(CH_3)_2Hg$ in a high pressure ion source, forms complexes with both π- and n-donor bases. We also reported an ordering of

0008-4042/81/121779-08$01.00/0
©1981 National Research Council of Canada/Conseil national de recherches du Canada

Can. J. Chem. Downloaded from www.nrcresearchpress.com by 210.87.254.42 on 09/06/12
For personal use only.

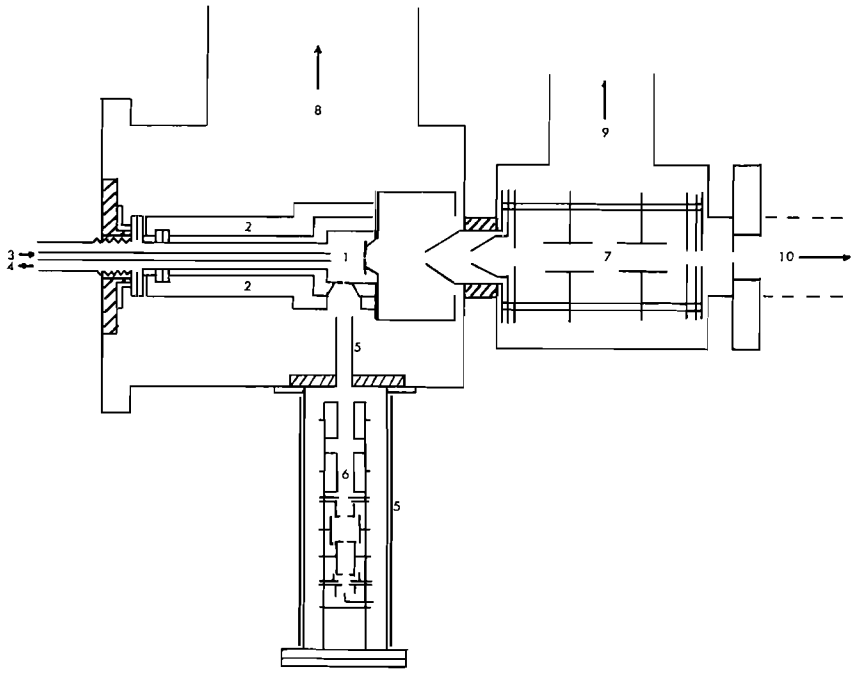

FIG. 1. Schematic diagram of ion source, ion lens and electron gun assemblies. *1*, ion source; *2*, copper heating sheath; *3*, gas flow in; *4*, gas flow out; *5*, mu metal magnetic shielding; *6*, electron gun; *7*, ion lens; *8*, to 4 in. diffusion pump; *9*, to 2 in. diffusion pump; *10*, to magnetic analyzer.

basicities with respect to CH_3Hg^+ for a range of molecules at ambient temperature. This work has now been extended to obtain absolute values for the differences in gas phase basicities (ΔG^0) for a variety of bases with this cation.

Experimental

The high pressure mass spectrometer is patterned after the one described by Kebarle (9). The basic instrument is a Hitachi RMU-6E from which the original ion source and ion multiplier housings have been removed. Figure 1 illustrates the new ion source, ion focusing lens, and electron gun and their housing. The original small diffusion pump now pumps only the flight tube and detector. The flight tube is separated from the lens housing by a fixed source slit of dimensions 10 × 0.5 mm. The lens housing is pumped by an Edwards 2 in. diffusion pump while the ion source housing is pumped by an Edwards 4 in. diffusion pump. All diffusion pumps are backed by the same Edwards 660 L min^{-1} rotary pump. When the ion source pressure is 1 Torr, the pressures in the flight tube, ion lens housing, and ion source housing are roughly 10^{-6}, 2×10^{-5}, and 2×10^{-4} Torr, respectively.

All seals in the stainless steel ion source have gold gaskets. The electron entrance and ion exit slits are fabricated by spot welding razor blades over holes drilled through the thin ends of stainless steel flanges. They have dimensions 1.5 × 0.025 mm^2. Four cartridge heaters embedded in a copper block surrounding the ion source allow operation up to 600 K, as measured with a copper–constantan thermocouple. The electron gun is mounted well away from the ion source and the focussed 2000 V, 2μA electron beam reaching the source has a negligible heating effect.

In dc operation the ionizing electron beam of $3–10 \times 10^{-8}$ μA gives good, intense spectra. This beam strength can be measured at an electron collector inside the ion source when no gas is present. In actual operation the source is used in the field-free mode with no ion repeller and with the electron collector shorted to the chamber. In the pulsed mode the electron beam is gated on for 50 μs every 10 ms by removing a 90 V bias on the first electrode of the electron gun. Ions escaping through the ion exit slit are accelerated through 1900 V, subjected to mass analysis and detected by a Galileo 4800 continuous dynode ion multiplier which is operated at 1200–1400 V in the analogue mode and at 2200 V for ion counting which is used in the pulsed mode. In the latter mode the individual multiplier pulses are amplified by a factor of 200 with an Ortec 9302 amplifier–discriminator the output pulses of which go to a Nicolet 1170 signal averager. In most runs the dwell time per channel is 35 μs and data are collected in 150 channels after the start of the electron pulse. Accumulation of data from many individual pulses is required to obtain ion residence time curves. The number required varies from 2×10^3 to 16×10^3 depending on the signal strength.

Results and Discussion

We have previously described the behaviour of dimethylmercury in the chemical ionization source with CH_4 as the reagent gas (8). We will first present a brief account of this behaviour together with details of subsequent experiments which further clarify our knowledge.

Low concentrations of $(CH_3)_2Hg$ in CH_4 form $(CH_3)_3Hg_2^+$ as the major product at all temperatures from 300 to 600 K. $(CH_3)_3Hg_2^+$ may be regarded as the CH_3Hg^+ adduct of $(CH_3)_2Hg$ just as $(CH_3)_2Hg{\cdot}H^+$ is the proton adduct. The latter ion

Can. J. Chem. Downloaded from www.nrcresearchpress.com by 210.87.254.42 on 09/06/12
For personal use only.

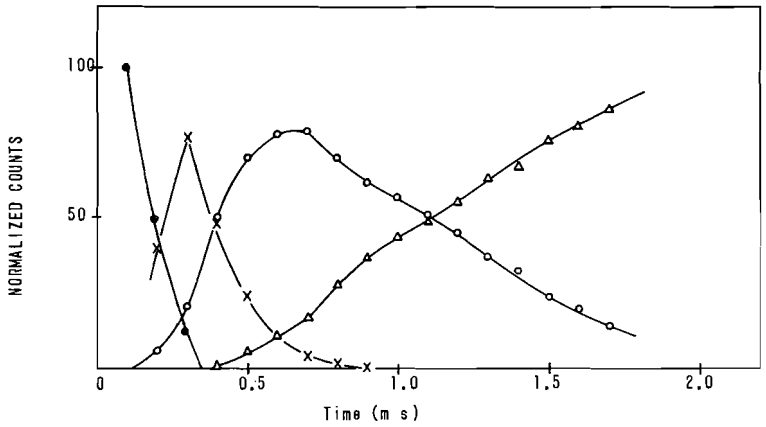

FIG. 2. Normalized ion intensities as functions of residence time in the ion source for 4×10^{-4} Torr $(CH_3)_2Hg$ in 1 Torr CH_4 at 340 K. ●, CH_5^+; ×, H_3O^+; ○, CH_3Hg^+; △, $(CH_3)_3Hg_2^+$.

is observed, together with CH_3Hg^+, at 300 K and both are presumed to be precursors of $(CH_3)_3Hg_2^+$ although this could not be verified because of the extremely low ion currents. At temperatures above 400 K, $(CH_3)_2Hg{\cdot}H^+$ is not observed and presumably dissociates to $CH_3Hg^+ + CH_4$. Reactions [1]–[4] summarize the presumed ambient temperature chemistry.

$$[1] \quad CH_5^+ + (CH_3)_2Hg \rightarrow CH_4 + (CH_3)_2Hg{\cdot}H^{+*}$$

$$[2a] \quad (CH_3)_2Hg{\cdot}H^{+*} \rightarrow CH_3Hg^+ + CH_4$$

$$[2b] \quad \xrightarrow{M} (CH_3)_2Hg{\cdot}H^+$$

$$[3] \quad CH_3Hg^+ + (CH_3)_2Hg \xrightarrow{M} (CH_3)_3Hg_2^+$$

$$[4] \quad (CH_3)_2Hg{\cdot}H^+ + (CH_3)_2Hg \rightarrow (CH_3)_3Hg_2^+ + CH_4$$

Above 400 K the yield of CH_3Hg^+ relative to that of $(CH_3)_3Hg_2^+$ increases but is always very small. Figure 2 shows the normalized, time resolved ion intensities for a system containing a very low concentration of $(CH_3)_2Hg$ in CH_4 in the absence of SF_6. No precautions were taken to dry any of the reagents and the intermediate H_3O^+ ion signifies the presence of a considerable amount of water. Under normal operating conditions the signal due to H_3O^+ is insignificant since all bases used, including $(CH_3)_2Hg$, have much higher proton affinities than H_2O. The sequence of ions determined by the results in Fig. 1 is,

$$CH_4^+ \xrightarrow{a} CH_5^+ \xrightarrow{b} H_3O^+ \xrightarrow{c} CH_3Hg^+ \xrightarrow{d} (CH_3)_3Hg^{2+}$$

There is no equilibrium observed in step *d* which prevents the direct determination of thermodynamic data for the association reaction forming $(CH_3)_3Hg_2^+$ (reaction [3]).

When a base B is added to the $CH_4/(CH_3)_2Hg/SF_6$ system, three new products appear. There is competition between B and $(CH_3)_2Hg$ for reaction with CH_5^+ and H_3O^+ and since $(CH_3)_2Hg$ has a proton affinity between those of benzene and toluene (10), any base with a proton affinity greater than that of benzene shows a BH^+ peak with intensity directly dependent on the molar ratio of B and $(CH_3)_2Hg$. The other two products CH_3M^+ and CH_3Hg. M^+ arise from the reaction of the base with CH_3Hg^+ and $(CH_3)_3Hg_2^+$. The relative yields are pressure dependent, that of CH_3HgM^+ increasing with increasing total pressure as seen in Fig. 3 for M = *m*-xylene. Obviously collisional deactivation of an initially formed excited complex is occurring.

$$[5] \quad CH_3Hg^+ + C_6H_4(CH_3)_2 \rightarrow CH_3Hg{\cdot}C_6H_4(CH_3)_2^{+*}$$

$$[6a] \quad CH_3Hg{\cdot}C_6H_4(CH_3)_2^{+*} \xrightarrow{M} CH_3Hg{\cdot}C_6H_4(CH_3)_2^+$$

$$[6b] \quad \rightarrow CH_3{\cdot}C_6H_4(CH_3)_2^+ + Hg$$

The half-life of the excited complex may be estimated from Fig. 3. Assuming that stabilization

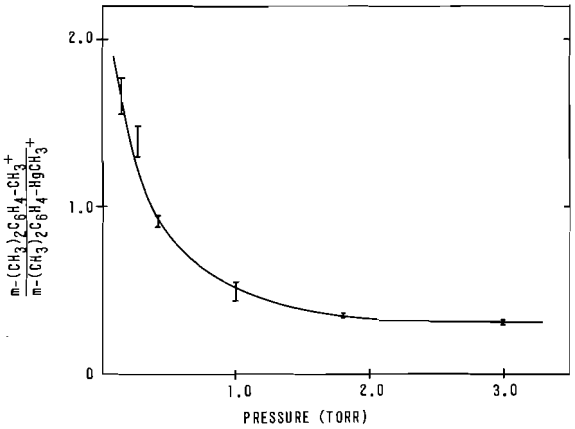

FIG. 3. The ratio of the *m*-xylene·CH_3^+ and *m*-xylene·$HgCH_3^+$ yields as a function of ion source pressure. Sample composition (mole fractions) *m*-xylene, 4×10^{-3}; $(CH_3)_2Hg$, 8×10^{-3}; SF_6, 2×10^{-3}; methane, 0.99 (588 K).

Can. J. Chem. Downloaded from www.nrcresearchpress.com by 210.87.254.42 on 09/06/12
For personal use only.

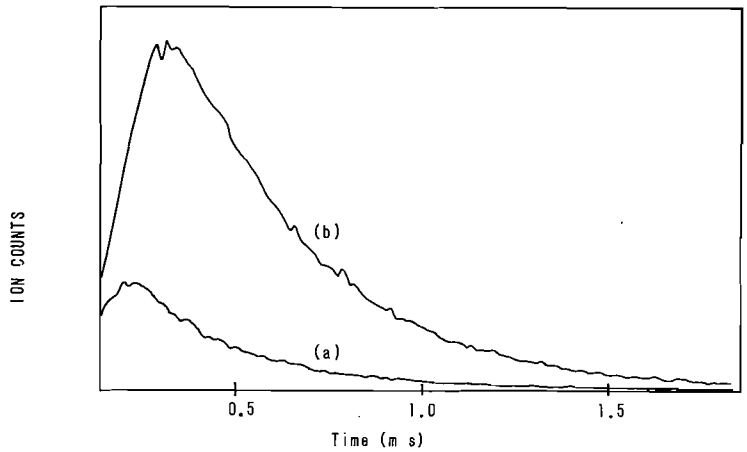

FIG. 4. Ion counts as functions of ion residence times in the ion source for (*a*) (*o*-xylene·$HgCH_3$)$^+$ and (*b*) (mesitylene·$HgCH_3$)$^+$, 2.1×10^{-3} Torr *o*-xylene, 1.8×10^{-3} Torr mesitylene, 8×10^{-3} Torr $(CH_3)_2Hg$, 1.4 Torr methane (577 K).

occurs at every collision with a neutral molecule and since 50% stabilization occurs at a pressure of ~0.25 Torr (8×10^{15} molecules cm^{-3}) and taking the collision rate to be 10^{-9} cm^3 $molecule^{-1}$ s^{-1}, the pseudo first order rate constant for [6*a*] is $\sim 10^{-9} \times 8 \times 10^{15}$ s^{-1}, i.e. $t_{1/2} \geq 1 \times 10^{-7}$ s. It is possible that $CH_3Hg \cdot M^{+*}$ formed in reaction [5] is a π complex which is a precursor of the more stable $CH_3Hg \cdot M^+$ and $CH_3 \cdot M^+$ σ complexes.

$(CH_3)_3Hg_2^+$ also reacts with bases, the reaction being the transfer of CH_3Hg^+ from the weak base $(CH_3)_2Hg$. Again, both CH_3^+ and CH_3Hg^+ addition products are observed.

[7*a*] $CH_3Hg \cdot (CH_3)_2Hg^+ + C_6H_4(CH_3)_2 \rightarrow CH_3 \cdot C_6H_4(CH_3)_2^+ + Hg + (CH_3)_2Hg$

[7*b*] $\rightarrow CH_3Hg \cdot C_6H_4(CH_3)_2^+ + (CH_3)_2Hg$

All the bases studied yield a CH_3^+ adduct. For aromatic bases these will be initially the ipso-protonated form of a higher aromatic, for example benzene forms protonated toluene. When a mixture of two bases is studied then the relative yields of the methyl adducts change as functions of ion residence time due to the setting up of proton transfer equilibria. These CH_3^+ addition products were not mentioned in our earlier communication since they were ascribed to the presence of impurities. They were not investigated further but might be usefully employed in low pressure icr studies to obtain additional information on ipso-protonation.

Figure 4 shows the intensities of the CH_3Hg^+ adducts of *o*-xylene and mesitylene as functions of time from the start of the electron pulse. The constancy of the ratio of the two ion intensities after ~0.5 ms^{-1} is shown when the normalized ion intensities are considered (Fig. 5). This time invariance of the ratio at long residence times indicates the attainment of the equilibrium

[8] $CH_3Hg \cdot C_6H_4(CH_3)_2^+ + C_6H_3(CH_3)_3 \rightarrow C_6H_4(CH_3)_2 + CH_3Hg \cdot C_6H_3(CH_3)_3^+$

The equilibrium constant is obtained from this constant ratio and the known molar ratio of the bases

$$K = \frac{[C_6H_4(CH_3)_2]}{[C_6H_3(CH_3)_3]} \cdot \frac{i_{CH_3Hg \cdot C_6H_3(CH_3)_3^+}}{i_{CH_3Hg \cdot C_6H_4(CH_3)_2^+}} = \exp \frac{-\Delta G^0}{RT}$$

The usual criteria for confirmation of the attainment of equilibrium are found to apply, i.e. K is independent of total pressure (0.5–3.5 Torr) and independent of the molar ratio of the two bases over more than a 10-fold range.

Reaction [8] may be considered the difference of two reactions

[9] $CH_3Hg^+ + C_6H_3(CH_3)_3 \rightarrow CH_3Hg \cdot C_6H_3(CH_3)_3^+$

[10] $CH_3Hg^+ + C_6H_4(CH_3)_2 \rightarrow CH_3Hg \cdot C_6H_4(CH_3)_2^+$

$$\Delta G^0 = -RT \ln K = \Delta G_9^0 - \Delta G_{10}^0$$

ΔG_9^0 and ΔG_{10}^0 will be defined as the gas phase methylmercury cation basicities (MMCB) of mesitylene and *o*-xylene respectively. Only differences in these values are measurable by this technique, neither the absolute values for MMCB nor the binding energies of CH_3Hg^+ to the bases (ΔH^0) being at present obtainable either experimentally or theoretically. Table 1 gives the differences in MMCA values for a series of bases, mainly aromatic, at 425 K, the values being checked for consistency by the usual ladder technique. Similarly Table 2 gives the differences in MMCB values for

Can. J. Chem. Downloaded from www.nrcresearchpress.com by 210.87.254.42 on 09/06/12
For personal use only.

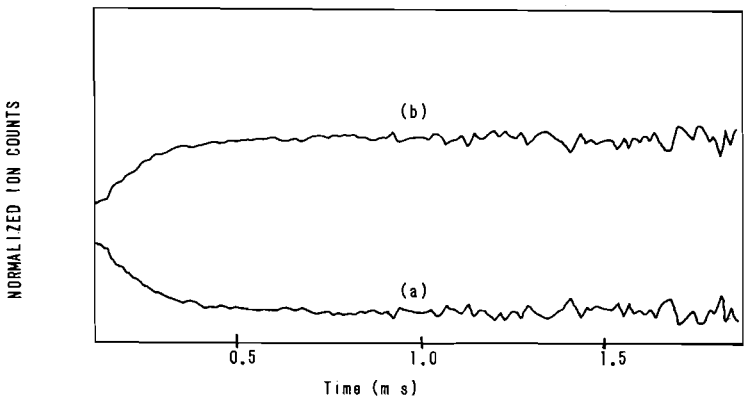

FIG. 5. The normalized yields of $(o\text{-xylene}\cdot HgCH_3)^+$ (*a*) and $(\text{mesitylene}\cdot HgCH_3)^+$ (*b*) from the data in Fig. 4.

TABLE 1. Free energy differences (kcal mol^{-1}) for the attachment of CH_3Hg^+ to aromatic and ester bases, the direction of increasing basicity is upwards (425 K)

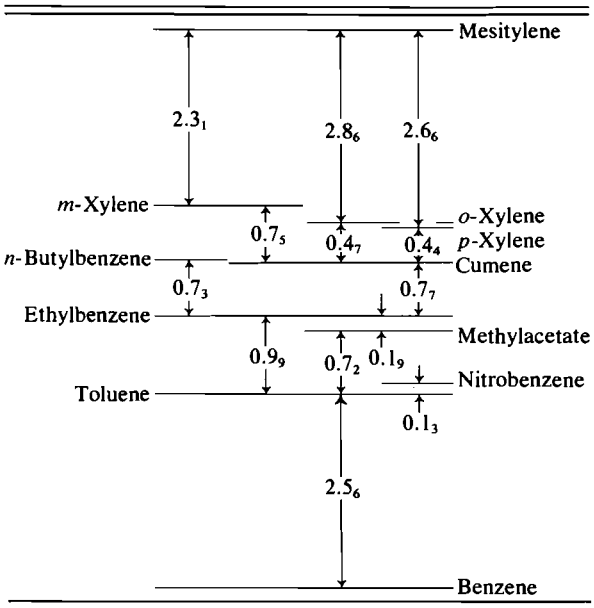

several nitrogen and one sulfur base at 580 K. This higher temperature was required to overcome problems associated with solvation. We have so far not obtained a linking up of the two series, but 2-chloropyridine is more basic than mesitylene at the same temperature.

The effect of molecular structure on gas phase basicity with respect to the proton has been presented and discussed in detail (11, 12) and it is of interest to seek comparisons with MMCB values (Figs. 6 and 7). The correspondence between the two scales of basicity is striking. In both cases basicity increases with increasing alkyl chain length in both π-donor (benzene<toluene<ethylbenzene<*n*-butylbenzene) and n-donor bases $((C_2H_5)_3N < (C_3H_7)_3N)$, and with increasing methyl or ethyl substitution (benzene<toluene<xylene <mesitylene), $((C_2H_5)_2NH<(C_2H_5)_3N)$. Even the finer nuances of basicity in the xylenes is the same (*p*<*o*<*m*). These correlations surely prove that the aromatic binding sites of the adducts are the same in both the H^+ and CH_3Hg^+ complexes. H^+ addition leads to the formation of an arenium ion and the same must hold true for CH_3Hg^+ addition. Such σ bonded adducts have been postulated on the evidence of nmr spectroscopy in strongly acidic solutions of dialkylmercury compounds (13, 14).

The slope of the line drawn through the points for the lower aromatic bases in Fig. 6 is 0.7 which implies that the changes in absolute basicity with change in substituent is almost the same for

TABLE 2. Free energy differences (kcal mol^{-1}) for the attachment of CH_3Hg^+ to N and S bases, the direction of increasing basicity is upwards (580 K)

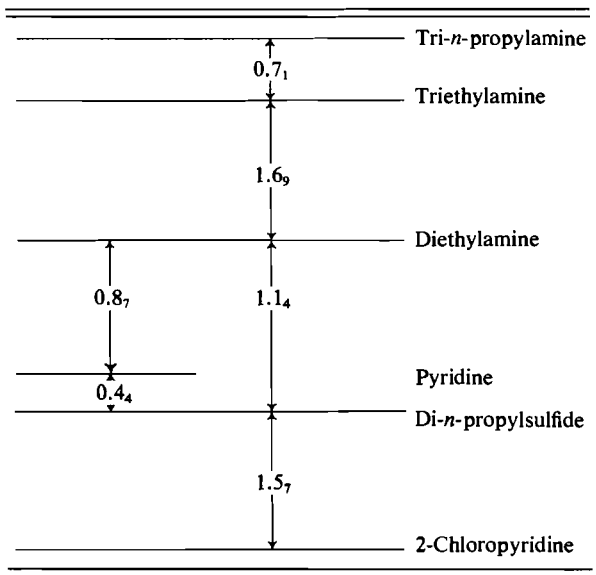

Can. J. Chem. Downloaded from www.nrcresearchpress.com by 210.87.254.42 on 09/06/12
For personal use only.

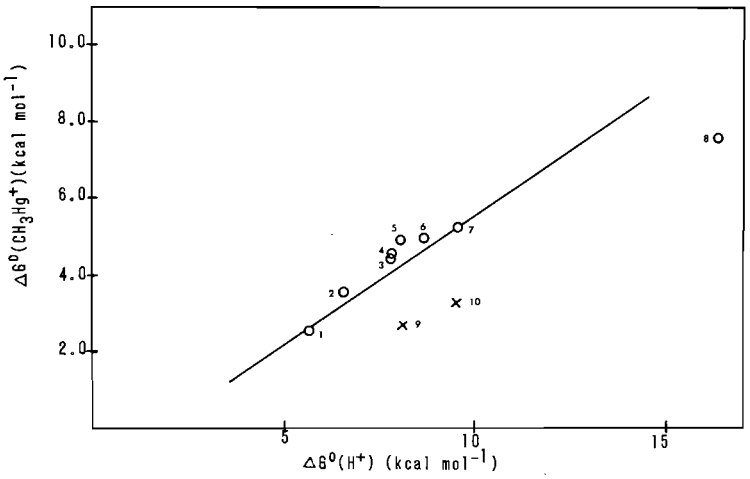

FIG. 6. Gas phase basicities (relative to that of benzene) with respect to the acids H^+ and CH_3Hg^+. *1*, toluene; *2*, ethylbenzene; *3*, cumene; *4*, *n*-butylbenzene; *5*, *p*-xylene; *6*, *o*-xylene; *7*, *m*-xylene; *8*, mesitylene; *9*, methylacetate; *10*, nitrobenzene (417 K).

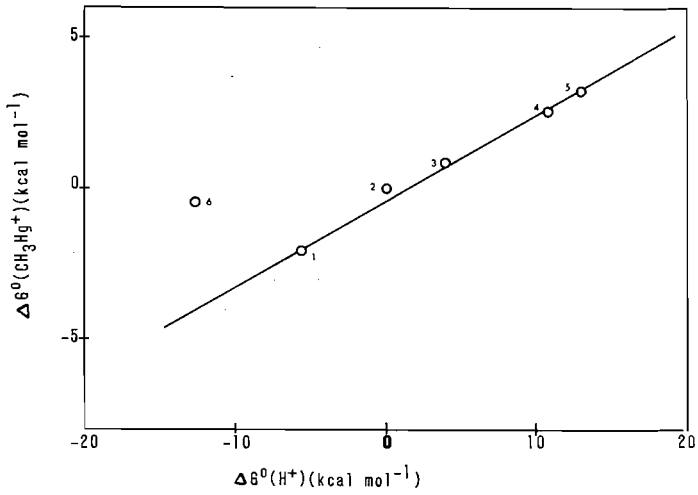

FIG. 7. Gas phase basicities (relative to that of pyridine) with respect to the acids H^+ and CH_3Hg^+. *1*, 2-chloropyridine; *2*, pyridine; *3*, diethylamine; *4*, triethylamine; *5*, tri-*n*-propylamine; *6*, di-*n*-propylsulfide (580 K).

CH_3Hg^+ as for H^+. This is in spite of the fact that the strengths of the bonds formed are vastly different. (An upper limit of 24 kcal mol^{-1} has been estimated for $D(CH_3Hg^+—C_6H_6)$ (8) while $D(H^+—C_6H_6)$ is 186 kcal mol^{-1} (10).) Both nitrobenzene and methylacetate protonate on oxygen and presumably this is also the basic site for CH_3Hg^+. Compared with the π-donor bases, a relatively weaker interaction with CH_3Hg^+ is indicated.

The slope of the line in Fig. 7 is 0.3 showing a lesser discrimination for nitrogen compounds by CH_3Hg^+ relative to H^+ than for the aromatics. However, $(C_3H_7)_2S$ is well off the line, signifying a much stronger relative interaction with CH_3Hg^+ than for the nitrogen bases. This is in contrast to the much weakened basicity (enthalpy of binding) of $(CH_3)_2S$ compared with $(CH_3)_2O$ or $(CH_3)_3N$ for Li^+ relative to that for H^+ (15). An increased covalent character relative to both H^+ and Li^+ of the binding of the larger CH_3Hg^+ to the more polarizable second row element is indicated. In a qualitative sense this is in keeping with the idea of the hard–soft acid base interaction.

Basicity is defined in terms of a change in free energy but in this ΔG^0 term entropy changes may be dominant. Of more immediate interest is the relative change in binding energy. For proton

Can. J. Chem. Downloaded from www.nrcresearchpress.com by 210.87.254.42 on 09/06/12
For personal use only.

TABLE 3. Thermochemical data derived from temperature studies of the equilibrium $AX^+ + B \rightleftharpoons A + BX^+$

A	B	X	$-\Delta H^\circ$ (kcal mol^{-1})	$-\Delta S^\circ$ (cal K^{-1} mol^{-1})
Toluene	Ethylbenzene	CH_3Hg^+	1.2_6	0.6_9
Toluene	Ethylbenzene	H^{+a}	0.9	0
Toluene	Methylacetate	CH_3Hg^+	1.9_4	3.0
Toluene	Methylacetate	H^{+a}	6.7	0

[a]Data from ref. 11 in which ΔH^0 values are obtained from isothermal (300 K) ΔG^0 values using calculated ΔS^0 values which are based on changes in rotational symmetry.

transfer equilibria most enthalpy changes have been obtained from free energy differences using the approximation that the entropy change is calculable from changes in external rotation symmetry numbers (16). The moment of inertia of a molecule changes little upon protonation but there will be drastic changes when CH_3Hg^+ is added and simple symmetry calculations will not be sufficient for determining ΔS^0. In addition, vibrational modes involving Hg will be of very low frequency and may also be of significance in the ΔS^0 term. Theoretical calculations of entropy changes are not immediately possible and experimental values of ΔH^0 must be obtained from plots of log K vs. $1/T$ (6). Two such plots are shown in Fig. 8 and the derived thermodynamic data are shown in Table 3 where they are compared with data for the corresponding proton transfer equilibria.

The difference in energy for binding CH_3Hg^+ to toluene and ethylbenzene is comparable to that for the proton. ΔS^0 is small for the reaction since the ions are very similar in geometry. It is therefore expected that only rotational and translational partition functions need be considered in calculating entropy changes. Therefore for the equilibrium

$$CH_3HgT^+ + E \rightleftarrows T + CH_3Hg{\cdot}E^+$$

where T = toluene and E = ethylbenzene

$$\Delta S^0 = \Delta S^0_{trans} + \Delta S^0_{rot}$$

$$= \frac{3}{2} R \ln \left[\frac{M_{CH_3Hg\cdot E} + M_T}{M_{CH_3Hg\cdot T} + M_E}\right] + \frac{3}{2} R \ln \left[\frac{I_{CH_3Hg\cdot E} + I_T}{I_{CH_3Hg\cdot T} + I_E} \frac{\sigma_{CH_3Hg\cdot T} + \sigma_E}{\sigma_{CH_3Hg\cdot E} + \sigma_T}\right]$$

where M is the molar mass, I the moment of inertia about the centre of mass, σ the rotational symmetry number, and T and E are toluene and ethylbenzene respectively (17). The moments of inertia were calculated for structures in which CH_3Hg was bonded to an sp^3 hybridized carbon in the para position of the aromatic ring with unchanged C—C distances. ΔS^0 (calcd) = -0.8 cal mol^{-1} K^{-1} is in excellent agreement with ΔS^0 (expt) = -0.7 cal mol^{-1} K^{-1}.

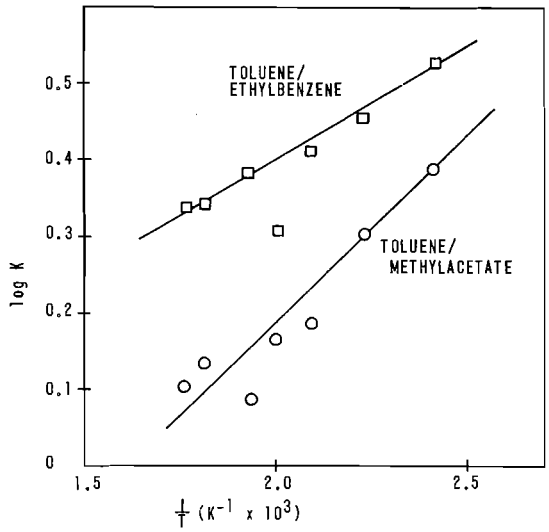

FIG. 8. Van't Hoff plots for the equilibrium $A{\cdot}HgCH_3^+ + B \rightleftharpoons B{\cdot}HgCH_3^+ + A$ for the A/B pairs toluene/ethylbenzene and toluene/methylacetate.

The increase in binding energy from toluene to methylacetate is much greater for H^+ than for CH_3Hg^+ which may signify a decrease in the covalent contribution to the binding energy for the more electronegative oxygen base. The measured change in entropy (-3.0 cal mol^{-1} K^{-1}) is relatively large and is also in the opposite direction to that calculated by neglecting vibrational partition function contributions ($+1.3$ cal mol^{-1} K^{-1}). Obviously the latter must be considered when mercury changes its bonding from carbon to oxygen. The assessment of binding energy differences from experimental free energy differences must therefore be treated with caution for equilibria involving heavy atoms. Initially at least experimental determinations of ΔH^0 will be essential.

Acknowledgements

The authors thank Professor Paul Kebarle for his advice on the design of the high pressure mass

Can. J. Chem. Downloaded from www.nrcresearchpress.com by 210.87.254.42 on 09/06/12
For personal use only.

spectrometer. A research grant from the Natural Sciences and Engineering Research Council of Canada is acknowledged.

1. E. M. ARNETT, E. J. MITCHELL, and T. S. S. R. MURTY. J. Am. Chem. Soc. **96**, 3875 (1974).
2. M. M. KAPPES, J. S. UPPAL, and R. H. STALEY. Proceedings of 28th Conference on Mass Spectrometry and Allied Topics, New York. 1980. p. 239.
3. R. G. PEARSON. J. Chem. Educ. **45**, 581 (1968) and references cited therein.
4. R. S. DRAGO, G. C. VOGEL, and T. E. NEEDHAM. J. Am. Chem. Soc. **93**, 6014 (1971).
5. J. MARCH. Advanced organic chemistry. McGraw-Hill. 1977. p. 238.
6. P. KEBARLE. Ann. Rev. Phys. Chem. **28**, 445 (1977).
7. I. N. TANG, M. S. LIAN, and A. W. CASTLEMAN. J. Chem. Phys. **65**, 4022 (1976).
8. J. A. STONE, R. J. CAMICIOLI, and M. C. BAIRD. Inorg. Chem. **19**, 3128 (1980).
9. A. J. CUNNINGHAM, J. D. PAYZANT, and P. KEBARLE. J. Am. Chem. Soc. **94**, 7627 (1971).
10. K. N. HARTMAN, S. LIAS, P. AUSLOOS, H. M. ROSENSTOCK, S. S. SCHROYER, C. SCHMIDT, D. MARTINSEN, and G. W. A. MILNE. Natl. Bur. Stand. (Tech. Rep.) NBSIR (U.S.) (1979) NBSIR-79-177.
11. J. F. WOLFE, R. H. STALEY, I. KOPPEL, M. TAAGEPERA, R. T. MCIVER, J. L. BEAUCHAMP, and R. W. TAFT. J. Am. Chem. Soc. **99**, 5417 (1977).
12. D. H. AUE and M. T. BOWERS. *In* Gas phase ion chemistry. Vol. 2. *Edited by* M. T. Bowers. Academic Press, New York, 1979. Chapt. 9.
13. G. A. OLAH, S. H. YU, and D. G. PARKER. J. Org. Chem. **41**, 1983 (1976).
14. L. C. DAMUDE and P. A. W. DEAN. J. Organomet. Chem. **181**, 1 (1979).
15. R. H. STALEY and J. L. BEAUCHAMP. J. Am. Chem. Soc. **97**, 5920 (1975).
16. J. B. CUMMING and P. KEBARLE. J. Am. Chem. Soc. **94**, 7627 (1972).
17. S. W. BENSON. Thermochemical kinetics. Wiley-Interscience, New York. 1976.

Can. J. Chem. Downloaded from www.nrcresearchpress.com by 210.87.254.42 on 09/06/12
For personal use only.

Ion–molecule equilibria measurements by high pressure mass spectrometry. Some recent advances in concepts and technique

JAN SUNNER, TOM F. MAGNERA, AND PAUL KEBARLE
Department of Chemistry, University of Alberta, Edmonton, Alta, Canada T6G 2G2

Received November 17, 1980

This paper was presented at a Special Symposium "The Structure and Thermochemistry of Gaseous Ions", held in honour of Dr. F. P. Lossing of the National Research Council of Canada, during the Second Canadian Conference on the Gas Phase Chemistry of Ions, Trent University, June 5–8, 1980, and is dedicated to him on the occasion of his 65th birthday

JAN SUNNER, TOM F. MAGNERA, and PAUL KEBARLE. Can. J. Chem. **59**, 1787 (1981).

Two efforts to improve ion–molecule equilibrium measurement methodology and instrumentation are described. The first part deals with dissociation of ions AB^+ in the mass analysis system of the mass spectrometer. To measure the equilibrium constant of the association equilibrium $A^+ + B = AB^+$ one needs to sample both A^+ and AB^+. The AB^+ ions escaping from the high pressure ion source have a thermal energy distribution. A fraction f_{ex} has internal energy which is higher than the dissociation energy for $AB^+ \rightarrow A^+ + B$. This fraction can dissociate before detection. A theoretical analysis for the system $K^+(H_2O)_n$ is made which is based on calculated vibrational frequencies and geometries of $K^+(H_2O)_n$. From these $f_{n,ex}$ can be evaluated. RRKM calculations also provide rates for the dissociation of the AB^+_{ex}. It is found that severe dissociation during mass analysis can occur if the experimental conditions are not selected carefully. Results for $H^+(H_2O)_2$ and $(C_6H_6^+)_2$ are also presented. Measurements of the association equilibria must be done at low pressures of B in the presence of high pressure of an inert bath gas.

By connecting the repeller to a gated radio frequency source, pulses of RF can be applied in the high pressure ion source. These increase the internal energy of the ions. If the reaction system was at equilibrium a displacement of the equilibrium is produced by the RF pulse. The system relaxes to the original state after the RF has been shut off. Kinetic measurements of the relaxation times provide rate constants form which an equilibrium constant not affected by ion mass discrimination can be determined. Fast reaction kinetics also can be studied with this technique.

JAN SUNNER, TOM F. MAGNERA et PAUL KEBARLE. Can. J. Chem. **59**, 1787 (1981).

On décrit deux essais effectués en vue d'améliorer l'instrumentation et la méthodologie de la mesure de l'équilibre ion–molécule. Le premier essai porte sur la dissociation des ions AB^+ dans le système d'analyse de masse du spectromètre de masse. Pour mesurer la constante d'équilibre d'association $A^+ + B = AB^+$, il faut des échantillons de A^+ et de AB^+. Les ions AB^+ s'échappant d'une source d'ions à haute pression ont une distribution d'énergie thermique. Une fraction f_{ex} a une énergie interne qui est supérieure à l'énergie de dissociation $AB^+ \rightarrow A^+ + B$. Cette fraction peut se dissocier avant d'être détectée. On a effectué une analyse théorique du $K^+(H_2O)_n$ qui se fonde sur les fréquences vibrationnelles et les géométries calculées de $K^+(H_2O)_n$. A partir de ces données on peut évaluer $f_{n,ex}$. Les calculs de RRKM fournissent également la vitesse de dissociation de AB^+_{ex}. On a trouvé qu'il peut se produire une forte dissociation pendant l'analyse de masse si on ne choisit pas convenablement les conditions expérimentales. On présente également les résultats relatifs à $H^+(H_2O)_2$ et à $(C_6H_6^+)_2$. Les mesures de l'équilibre d'association doivent être réalisées à de faibles pressions de B en présence d'une forte pression d'un gaz inerte agissant comme bain.

En reliant la plaque répulsive à une source de fréquence radio, on peut appliquer des impulsions de FR dans la source de haute pression. Ces impulsions augmentent l'énergie interne des ions. L'impulsion FR produit un déplacement de l'équilibre si le système réactionnel est à l'équilibre. Le système se détend et revient à son état initial lorsqu'on élimine la FR. Les mesures cinétiques des temps de relaxation fournissent les constantes de vitesse à partir desquelles on peut déterminer la constante d'équilibre qui n'est pas affectée par la détermination de la masse de l'ion. A l'aide de cette technique on peut également étudier la cinétique des réactions rapides.

[Traduit par le journal]

Introduction

The measurement of ion–molecule equilibria was first initiated in this laboratory some 15 years ago (1, 2). In the intervening years many measurements of ion equilibria have been reported from this and other laboratories. The method has proven to be of extraordinary usefulness since it provides thermochemical information on inorganic and organic ions, gas phase acidities and basicities, ion–ligand binding energies and ion – solvent molecule interactions (3–5). In addition to high pressure mass spectrometry, used in this and other laboratories, flowing afterglow and particularly ion cyclotron resonance have proven to be very valuable instrumental methods (3–5).

The work on ion equilibria by high pressure mass spectrometry from this laboratory had an initial stage in which considerable effort was put into instrumental developments and experiments designed to improve the reliability of the measurements. This stage was followed by a period of extensive utilization of the method for obtaining results of interest to different areas of chemistry. Recently, we have felt that again more effort should be devoted to instrumental and methodology development. In the early measurements, when no

0008-4042/81/121787-10$01.00/0
©1981 National Research Council of Canada/Conseil national de recherches du Canada

Can. J. Chem. Downloaded from www.nrcresearchpress.com by 210.87.254.6 on 09/06/12
For personal use only.

Can. J. Chem. Downloaded from www.nrcresearchpress.com by 210.87.254.6 on 09/06/12
For personal use only.

data whatsoever were available, we considered an accuracy of a few kcal/mol for association equilibrium [1] and a 1 kcal/mol for transfer equilibrium [2]

[1] $A^+ + B = AB^+$

[2] $CD^+ + E = C + DE^+$

as quite sufficient. However as more data accumulate, it is clearly desirable to achieve greater accuracy and reliability. In the present work we will address ourselves to a problem area in the existing technique and to an advance in technique. Part I deals with the problem of unimolecular dissociation of association products AB^+ in the vacuum of the mass analysis region. Part II describes a new ion *T*-jump relaxation method with which the kinetics of ion equilibria can be determined.

I. Unimolecular Dissociation of Ions from Association Equilibria

(a) General

The reverse reaction in the association equilibrium [1] is the thermal decompositon of the adduct AB^+. This decomposition occurs in the high pressure ion source in the course of an equilibrium measurement. At any time a fraction of AB^+ are thermally activated to the dissociation limit, $E_0 \approx -\Delta H_1$. The activation and deactivation of AB^+ is

[1] $A^+ + B \underset{k_r}{\overset{k_f}{\rightleftharpoons}} AB^+$ Lindeman

$$A^+ + B \underset{k_d}{\overset{k_c}{\rightleftharpoons}} AB^+_{ex} \underset{k_a[M]}{\overset{k_s[M]}{\rightleftharpoons}} AB^+$$

[3] Dissociation limit: $E_0 \approx -\Delta H_1$

[4] $f_{ex} = [AB^+_{ex}]/[AB^+]$

represented above through Lindeman's strong collision mechanism. The fraction of molecules AB^+ excited above the dissociation limit E_0 are defined as f_{ex} in eq. [4].

In the ion sampling process used in high pressure mass spectrometry and flowing afterglow, gas and ions effuse through an exit orifice into the evacuated mass analysis region. In our apparatus, molecular flow prevails so that there are few collisions on the vacuum side of the orifice. The initial internal energy distribution of the ions should be very close to thermal. The fraction f_{ex} which has sufficient internal energy to dissociate can do so in the vacuum. However, once these ions have been used up no other ions can dissociate since the thermal population, due to the absence of collisions, is not maintained. Therefore if f_{ex} is small, say $f_{ex} < 0.05$ no serious error will occur in the equilibrium measurements.

The possibility of sampling error due to unimolecular dissociation of AB^+_{ex} in vacuum was considered in the first paper on ion equilibria (1). However, a detailed analysis was not made. In subsequent work (3), in general, conditions were selected which keep f_{ex} as low as possible. f_{ex} is low at low temperature, where the rate of the reverse reaction [1r] is slow. If one is to observe the equilibrium, one needs also to slow down the rate of the forward reaction [1f]. This means one must use a low concentration of B. However, since the ion life-times with regard to discharge to the wall of the ion source should be relatively longer than the the equilibrium halflives, ion diffusion to the wall also must be slowed down. This is achieved by the addition of an inert major gas. Although the advantage of the third gas addition was realized early (6) and used whenever possible (3), in some cases the use of the neat gas B was continued. The ion intensity in the alkali ion clustering equilibria apparatus was low and was adversely affected by the introduction of a third gas. This condition could have been removed by improved design. However, the possible seriousness of unimolecular decomposition in vacuum was not realized and measurements were performed with neat B in this apparatus.

(b) Unimolecular decomposition in $K^+(H_2O)_n$ clusters

The present section provides an analysis of the possible problem due to unimolecular dissociation of AB^+ in the vacuum of the mass analysis system. Most of the work deals with the potassium hydrate equilibria [5]. However, the results are of significance also for any other clustering equilibria measurements.

[5] $K^+(H_2O)_{n-1} + H_2O = K^+(H_2O)_n$

The fraction f_{ex} representing molecules AB^+ excited above the dissociation limit can be calculated from statistical mechanics expressions. These provide the internal thermal energy distribution function $P(E)$ if the normal vibration frequencies and the internal rotations of AB^+ are known. These parameters were evaluated for $K^+(H_2O)_n$, $n = 1$ to 6. Potential energy surfaces for the various normal vibrations were obtained (10) from improved electrostatic calculations, similar to those performed earlier by Davidson and Kebarle (9), but incorporating the ligand–ligand dipole attractions and repulsions. The binding energies i.e. $\Delta E_{0,n}$ (see eq. [5]) for the $K^+(H_2O)_n$ clusters are also obtained with this method. A comparison of the results obtained by the electrostatic calculations (Els) with those from other methods (11) and the experimental results are given in Table 1.

Can. J. Chem. Downloaded from www.nrcresearchpress.com by 210.87.254.6 on 09/06/12
For personal use only.

Third law entropies for the clusters $K^+(H_2O)_n$ can be readily obtained from Els calculated vibrational normal frequencies etc., and standard statistical mechanics expressions. The $\Delta S^0_{n-1,n}$ obtained in this manner are shown as $\Delta S^0_{n-1,n}$ (Els). These data are in substantial agreement with Mruzik's Monte Carlo entropies, ΔS(Monte) (12). The experimental (7) $-\Delta S^0_{n-1,n}$ are fairly close too, but are found to be somewhat higher, particularly for $n = 5$ and 6. As will be seen later, there is reason to believe that the $-\Delta S^0_{4,5}$ and $-\Delta S^0_{5,6}$ (exp) are too high. The general agreement between the $\Delta S^0_{n-1,n}$ Els, Monte, and Exp lends support for the Els predicted frequencies and rotational parameters.

The vibrational frequencies obtained from the electrostatic calculations for the clusters $K^+(H_2O)_n$ ($n = 1$ to 6) were used for the evaluation of the thermal distribution function $P(E)$. From this, f_{ex} was calculated by eq. [6]. The calculated f_{ex} for

$$[6] \qquad f_{n,ex} = \int_{E_0}^{\infty} P_n(E)\, dE$$

$K^+(H_2O)_n$ are shown in Fig. 1 as a function of the temperature. The temperature interval given for each $K^+(H_2O)_n$ corresponds to the range accessible to measurement with the high pressure mass spectrometer. The corresponding equilibrium constants $K_{n-1,n}$ for reaction [5] are also given in the figure. It is evident from Fig. 1 that f_{ex} is less than 10^{-1} for $n = 2$ and $n = 3$, but for higher n, f_{ex} is generally larger than 0.1. The best conditions for measurement, i.e. lowest f_{ex}, are at low temperature. This corresponds to high values of $K_{n-1,n}$. For example if conditions were used to measure $K_{n-1,n}$ where they are larger than 100 $Torr^{-1}$, f_{ex} would have been less than 10^{-1} even for $n = 6$. Conditions for $K_{n-1,n} = 100\ Torr^{-1}$ are generally easily obtained. One uses a third gas as diffusion barrier while the pressure of the clustering gas B (H_2O in the present case) is kept in the 1 to 10 mTorr range. With ions n and $n - 1$ at similar concentrations, this leads to $K_{n-1,n} \approx 1000$ to 100 $Torr^{-1}$.

The fraction of molecules excited above the dissociation limit f_{ex} give the ions AB^+ that have enough energy to dissociate in the vacuum of the analysis system. Whether they will dissociate during the time of flight to the ion detector ($\sim$15 μs) depends on the actual unimolecular decomposition rates. The rate constants for unimolecular decomposition $k_n(E)$ of the $K^+(H_2O)_n$ ions were calculated using RRKM theory (10). The required frequencies were obtained from the electrostatic calculations mentioned earlier. The intensity I_n of an

TABLE 1. Comparison of stabilization energies ΔE, enthalpies ΔH, and entropies ΔS for reactions: $K^+(H_2O)_{n-1} + H_2O = K^+(H_2O)_n$[a]

	$-\Delta E_{0,n}$			R_{K-O}[e]		$-\Delta H^0_{n-1,n}$			$-\Delta S^0_{n-1,n}$				
n	Els[b]	HF[c]	PP[d]	Els[b]	PP[d]	Els[f]	Monte[g]	Exp[h]	Expc[i]	Els[f]	Monte[g]	Exp[h]	Expc[i]	Temp.[h]
1	16.6	17.5	17.5	2.62	2.67	16.4	17.5	17.9	17.9	18.6	19.0	21.6	21.6	550
								16.9	16.9			19.9	19.9	
2	31.7	33.5	34.1	2.65	2.69	14.1	16.2	16.2	16.0	20.2	20.9	24.2	24.1	460
3	44.9	47.5	48.9	2.68	2.72	12.5	14.5	13.2	12.9	20.2	21.4	23.0	22.1	390
4	56.2	—	62.0	2.71	2.74	10.3	12.6	11.8	11.1	23.0	20.9	24.7	22.2	330
5	64.4	—	72.6	2.76	2.79	7.3	11.2	10.7	9.6	22.6	20.4	25.2	21.8	300
6	71.3	—	82.4	2.81	2.84	6.0	10.5	10.0	8.4	23.7	21.3	25.7	19.2	270

[a]All energies in kcal mol^{-1}, entropy in cal deg^{-1} mol^{-1}, stand state 1 atm.
[b]Electrostatic calculations, present work and Sunner and Kebarle (10).
[c]Hartree–Fock calculations by Clementi *et al.* (11).
[d]Clementi *et al.*, pair potential functions (11).
[e]Distance in Angstrom between potassium and oxygen nucleus. The PP distances are for the symmetric clusters.
[f]Based on moments of inertia and vibrational frequencies predicted by electrostatic calculations and evaluation of heat capacities and entropies with use of statistical mechanics.
[g]Monte Carlo calculations by Mruzik *et al.* (12) based on energies provided by potential functions of Clementi, temperature 298 K.
[h]Experimental results Searles and Kebarle (7), lower number given for $n = 1$ from Davidson and Kebarle (9). Temperature given in table correspond to average temperature at which the equilibria measurements were made.
[i]Experimental results as above but approximately corrected for unimolecular dissociation, with use of eq. [7].

Can. J. Chem. Downloaded from www.nrcresearchpress.com by 210.87.254.6 on 09/06/12
For personal use only.

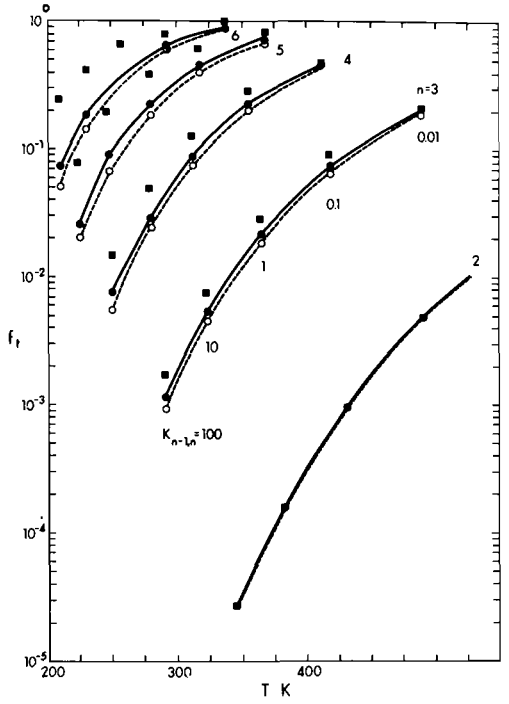

FIG. 1. Results of calculations for system $K^+(H_2O)_{n-1} + H_2O = K^+(H_2O)_n$; ■ $f_{n,ex}$ = fraction of clusters n excited above critical energy $E_0 = -\Delta H_{n-1,n}$, i.e. fraction of clusters n that have sufficient internal energy to dissociate in the vacuum of the mass analysis system; ● $f_{n,b}$ = fraction of clusters n that dissociate before leaving magnetic sector. ○ $f_{n,a}$ = fraction of clusters n that dissociate within 2 μs after entering the vacuum system. For each n, the value of the equilibrium constant $K_{n-1,n}$ in $Torr^{-1}$ is shown on the curves. That value changes from 100 to 0.01 $Torr^{-1}$.

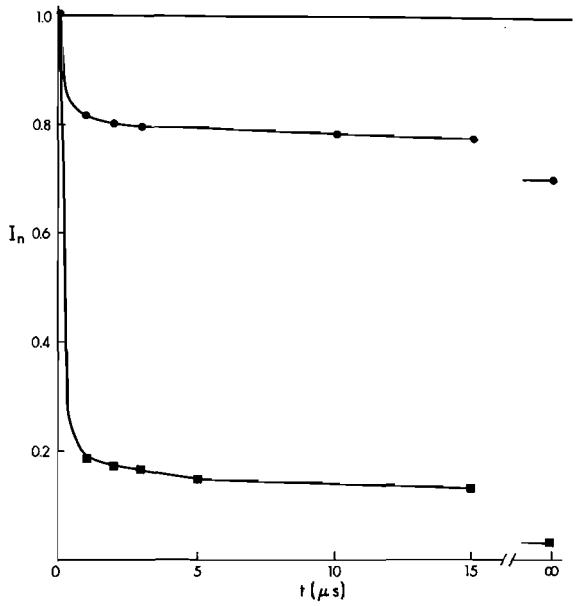

FIG. 2. Calculated unimolecular decay of a thermal population of ions exposed to vacuum. ● $K^+(H_2O)_4$ initially at 354 K ($K_{3,4} \approx 0.1$ $Torr^{-1}$); ■ $K^+(H_2O)_6$ initially at 337 K ($K_{5,6} \approx 0.01$ $Torr^{-1}$). These are examples of severe change of ion intensities due to unimolecular dissociation of the cluster ions.

ion in function of the flight time t (in vacuum) is given by [7].

$$[7] \quad I_n(t) = \int_0^\infty P_n(E)\{\exp[-k_n(E)t]\}\,dE$$

The intensity time dependence for two ions $K^+(H_2O)_4$ and $K^+(H_2O)_6$ calculated with eq. [7] for conditions where quite severe dissociation occurs is shown in Fig. 2. From [7] one can also evaluate $f_{n,a}$ the fraction of ions dissociating within 2 μs and $f_{n,b}$, those dissociating before having left the magnetic sector of the mass analysis system. $f_{n,a}$ gives the fraction of ions n that will be detected as $n - 1$, while $1 - f_{n,b}$ gives the fraction of ions n that will be detected as n. The fractions $f_{n,a}$ and $f_{n,b}$ are shown in Fig. 1. For small n i.e. $n = 2$ and 3, $f_{ex} \approx f_b \approx f_a$ i.e. all ions with energy above the dissociation limit E_0 dissociate rapidly. This is expected for systems that have a small number of degrees of freedom. For higher n the difference between f_{ex}, f_b, and f_a increases. For these systems there are many vibrations which can obtain energy quanta. Therefore considerable time elapses before sufficient energy can collect in the critical mode. It is also observed in Fig. 1 that for a cluster with a given n, the difference between f_{ex}, f_a, and f_b increases as the temperature is decreased. This behavior reflects the different energy distribution in the cluster for different temperatures. At low temperatures the energy distribution above E_0 falls off rapidly with E, therefore it takes a longer average time for this energy poor population of excited clusters to decompose.

Considering that the predicted decomposition (see Figs. 1 and 2) can be so severe for higher n, the question immediately arises: why is there no indication in the experimental results of something being wrong? As will be shown below a cancellation which reduces the error occurs.

The relationship between the true equilibrium constant for the $n - 1,n$ equilibrium $K_{n,tr}$, and the observed equilibrium constant $K_{n,obs}$ is given in eq. [8].

$$[8] \quad \frac{K_{n,obs}}{K_{n,tr}} = \frac{(1 - f_{n,b}) + (f_{n+1,a})(K_{n+1,tr})\,P}{(1 - f_{n-1,b}) + (K_{n,tr})(f_{n,a})\,P}$$

P is the pressure of the clustering gas, i.e. H_2O in the present case. Equation [8] expresses the fact that a fraction $(1 - f_{n,b})$ of clusters n are detected as clusters n and a fraction $f_{n+1,a}$ of clusters $(n + 1)$ are

Can. J. Chem. Downloaded from www.nrcresearchpress.com by 210.87.254.6 on 09/06/12
For personal use only.

also detected as clusters n. Furthermore a fraction $(1 - f_{n-1,b})$ of clusters $(n - 1)$ are detected as $(n - 1)$ and a fraction $f_{n,a}$ of clusters n are detected as clusters $(n - 1)$. An example of the changes due to unimolecular decomposition is given in Fig. 3 for the ions, $n = 5$ and $n = 4$. The value of the observed equilibrium constant $K_{5,obs}$ is not too far from the true value, because both the ion $n = 5$ and $n = 4$ receive a somewhat proportional contribution from fast dissociating ions $n = 6$ and $n = 5$ respectively.

The calculated $K_{n,obs}$ obtained from eq. [8] are compared with the $K_{n,tr}$ in Fig. 4. These results show that the effect of unimolecular dissociation is to introduce some curvature and steepen the experimental van't Hoff plots. The curvature will not be noticed in experimental work unless the measurements extend over a wide range of temperatures. The steeper slopes lead to $-\Delta H_{n-1,n}$(obs) that are larger than the true values. This effect increases with n. A set of corrected $\Delta H^0_{n-1,n}$ and $\Delta S^0_{n-1,n}$ based on this analysis is given in Table 1, where these corrected experimental results are identified as Expc. The largest difference observed for $-\Delta H^0_{5,6}$ is: Exp 10.0 kcal/mol, Expc 8.4 kcal/mol.

An experimental verification for the occurrence of unimolecular decomposition can be obtained by

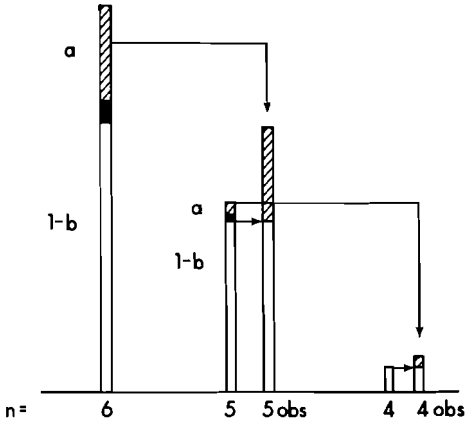

FIG. 3. Illustration of partial cancellation of errors caused by unimolecular decomposition of ion clusters in vacuum. Ion source temperature 250 K. 1 Torr H_2O pressure. Shaded part of ion intensity designated as a, represents clusters n that dissociate rapidly to $n - 1$ and are detected as $n - 1$. Clear part of ion intensity designated $(1 - b)$ represents clusters n which do not decompose until after mass separation and are therefore detected as clusters n. The observed equilibrium constant $K_{4,5}$(obs) = 8.5 (Torr^{-1}) while the true constant is $K_{4,5}$(true) = 10 (Torr^{-1}). Error is reduced because *both observed* ions $n = 5$ and $n = 4$ receive a contribution from the respective rapidly dissociating $n + 1$ ion. Black part of ion intensity are ions that dissociate during acceleration and mass analysis and are not detected.

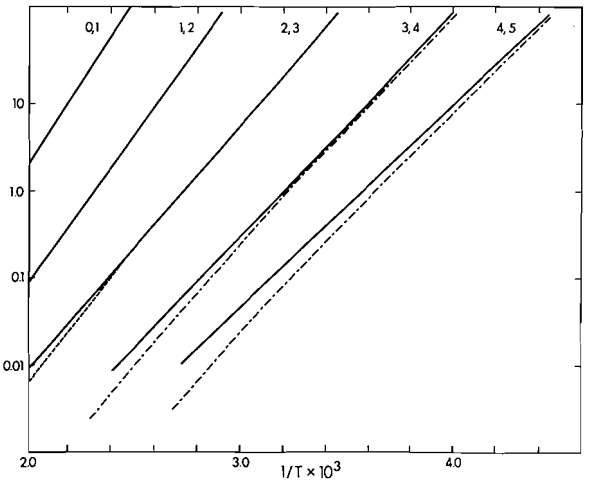

FIG. 4. Effect of unimolecular dissociation of $K^+(H_2O)_n$ to $K^+(H_2O)_{n-1}$ in vacuum, on van't Hoff plots. — $K_{n-1,n} = K_{n,tr}$ = (assumed) true equilibrium constants; -·-·- observed equilibrium constants $K_{n,obs}$ as predicted by eq. [7]. Calculations are for $p(H_2O) = 1$ Torr. The effect of the unimolecular decomposition is to introduce some curvature and steepen the plots. This leads to somewhat larger enthalpies: $-\Delta H_{n-1,n}$.

measurement of metastable ions resulting from dissociations $K^+(H_2O)_n \rightarrow K^+(H_2O)_{n-1}$ in the field-free region before the magnetic field. These experiments are somewhat difficult for two reasons. The abundance of unimolecular decomposition metastables is quite low. For example, an ion like $K^+(H_2O)_4$ of mass 112 enters the metastable region after 8 μs and leaves it after 12 μs. An inspection of the unimolecular decay curves in Fig. 2 shows that most of the decomposition occurs much earlier, and that very little decomposition occurs in the metastable region. On the other hand there is some collision-induced decomposition, with residual gas in the vacuum system, which also produces metastables. Results from experimental measurements of the metastables are shown in Fig. 5. The ratio R_n is defined in the equation below.

$$R_n = \frac{\text{Detected metastables from transition } n \rightarrow n-1}{\text{Ions detected as } n}$$

R_n(RRKM) is the ratio predicted by the calculations, while R_n(exp) is the experimentally observed ratio. Fair agreement is observed in Fig. 5 for the calculated and observed R_5 and R_4. Experiments in which known gas pressures were admitted into the ion flight tube permitted the study of collision induced dissociation. Extrapolation of these data to low tube pressures showed that the R_3(Exp) observed at low temperatures is due to collision induced metastables. The unimolecular decomposition metastables, from the $n = 3$ ion, at that

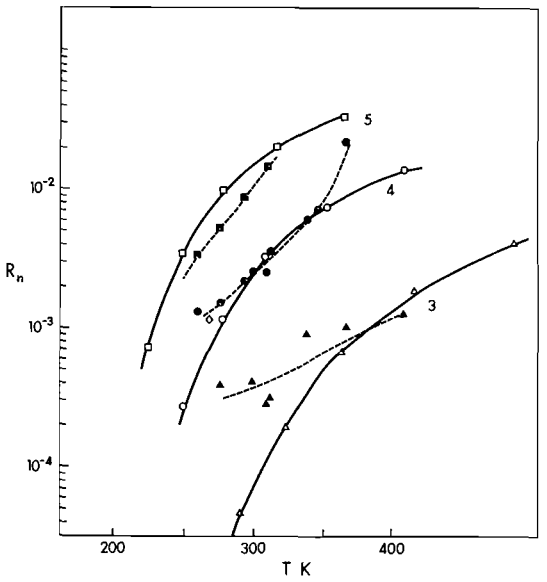

FIG. 5. R_n is ratio of metastables due to decomposition $K^+(H_2O)_n \rightarrow K^+(H_2O)_{n-1}$, over ions detected as $K^+(H_2O)_n$. □, ○, △ experimentally measured R_n; ■, ●, ▲ R_n predicted by calculation, for equilibrium measurement at 1 Torr H_2O ion source pressure. Mass analysis region at 3×10^{-7} Torr. Abscissa gives ion source temperature.

temperature are of such low intensity that they are overshadowed by the collision induced metastables. On the other hand, the R_4(Exp) and R_5(Exp) correspond almost completely to unimolecular metastables.

(c) *Unimolecular decomposition of $H^+(H_2O)_2$ and $(C_6H_6)_2^+$*

Calculations also were performed for the equilibria [9] and [10].

[9] $H_3O^+ + H_2O = H_3O^+ \cdot H_2O$

[10] $C_6H_6^+ + C_6H_6 = (C_6H_6)_2^+$

For these systems use was made of the parameters for internal motion given by Brauman and coworkers (13). The calculated fraction of complexes excited over the threshold energy f_{ex} is given in Table 2. The experimental measurements for the equilibrium constant K_9 were made (14) with K_9 ranging from 100 to 10. Examination of Table 2 shows that even for $K_9 = 1$ Torr^{-1}, f_{ex} is only 1.1×10^{-3}. This means that no error due to unimolecular decomposition in vacuum was present in the K_9 measurements.

Measurements of the equilibrium [10] were made by Field *et al.* (15) in the temperature range 330 to 475 K at 0.5 Torr constant benzene pressure. The upper experimental temperature falls in the region where appreciable dissociation of the dimers is

TABLE 2. Data for $H_3O^+ \cdot H_2O$ and $(C_6H_6)_2^+$

(*a*) $H_3O^+ \cdot H_2O$

T^a (K)	K^a (Torr^{-1})	$f_{ex}{}^b$	$f_{ex}{}^c$	$k_{to} \times 10^{28}$(exp)^d
617	10^3	4.2×10^{-6}	4.0×10^{-6}	2
677.7	10^2	2.9×10^{-5}	2.4×10^{-5}	1.2
750	10	1.9×10^{-4}	1.4×10^{-4}	0.7
843	1	1.1×10^{-3}	1.1×10^{-3}	0.5
960.3	10^{-1}	6.3×10^{-3}	8×10^{-3}	0.5
1115.4	10^{-2}	2.9×10	5.6×10	0.3

(*b*) $(C_6H_6)_2^+$

T (K)	$f_{ex}{}^b$
301	3×10^{-3}
331	1.5×10^{-2}
368	5.5×10^{-2}
414	0.17
474	0.42
554	0.74

[a] Temperatures and corresponding equilibrium constants from Cunningham, Payzant, and Kebarle (14).
[b] f_{ex} calculated from frequencies of Brauman (13).
[c] f_{ex} calculated from eq. [15] and experimentally measured (14) third order rate constant k_{to} given in table. Units for k_{to}: cm^6 molecule^{-2} s^{-1}.
[d] Experimental value for k_{to} from ref. 14.

predicted (Table 2), however most of the van't Hoff plots fall in a region where f_{ex} is small. The experimental $\Delta H^0{}_{10}$ and $\Delta S^0{}_{10}$ probably are affected only little by unimolecular decomposition.

(d) *How to Determine if Unimolecular Decomposition Occurs*

Calculations to determine the extent of unimolecular decomposition such as those described above may be very time consuming. The experimental test consisting of measurements of metastables can be unreliable, because of the collision induced metastables. It is clearly desirable to have some simple rules or experimental tests with which to determine whether danger from unimolecular decomposition does or does not exist. Such a test is presented below. The Lindeman treatment of the reaction [1] leads to eqs. [11]–[13].

$$[11] \quad k_f = \frac{k_c k_s[M]}{k_d + k_s[M]} \qquad k_r = \frac{k_a k_d[M]}{k_d + k_s[M]}$$

$$[12] \quad \frac{[AB^+*]}{[AB^+]} = \frac{k_a}{k_s}$$

$$[13] \quad K_{eq} = \frac{k_c k_s}{k_d k_a}$$

Can. J. Chem. Downloaded from www.nrcresearchpress.com by 210.87.254.6 on 09/06/12
For personal use only.

Can. J. Chem. Downloaded from www.nrcresearchpress.com by 210.87.254.6 on 09/06/12
For personal use only.

Under conditions where the forward reaction is third order

$$k_d \gg k_s[M],$$

such that

$$[14] \quad k_f = \frac{k_c k_s[M]}{k_d} = k_{to}[M]$$

where $k_{to} = k_c k_s / k_d$ is the third order rate constant for the forward direction. Substituting [13] and [14] into [12] one obtains [15].

$$[15] \quad f_{ex} = \frac{[AB^+*]}{[AB]} = \frac{k_{to}}{k_s K_{eq}} \approx \frac{3 \times 10^{25} k_{to}\,(\text{molecule}^{-2}\,\text{cm}^6\,\text{s}^{-1})}{K_{eq}\,(\text{Torr}^{-1})}$$

The numerical factor on the right side of [15] was obtained by assuming: $k_s = 10^{-9}$ cm^3 molecule^{-1} s^{-1}, which is the Langevin rate constant for orbiting collisions, and introducing the proper convervsion factors. f_{ex} calculated from [15] for reaction [9] are given in Table 2. The k_{to} and K_{eq} required for [15] are experimental values taken from our earlier publication (14). The agreement between f_{ex} (eq. [15]) and f_{ex} obtained from vibrational frequencies and statistical mechanics equations is extremely close. The close agreement is obviously fortuitous, however the result supports both [15] and the frequencies used by Brauman and co-workers (13) which enter the calculation of f_{ex}.

Equation [15] can be used when one wishes to examine whether unimolecular decomposition is occurring. Having measured K_{eq} at a given T_{eq} one substitutes K_{eq} and k_{to} (T_{eq}) into [15]. If $f_{ex} < 0.05$ the experiment should not be significantly affected by sampling error due to unimolecular decomposition. The k_{to} will have to be determined in separate kinetic measurements at temperatures below T_{eq}. Plots of log k_{to} versus log T are common practice in ion molecule kinetic measurements and almost always lead to straight lines. Such plots should be used to obtain an extrapolated k_{to} at T_{eq}.

An even simpler condition not requiring the knowledge of k_{to} can be obtained. Combining [12] and [13] one obtains [16].

$$[16] \quad f_{ex} = \frac{[AB^+*]}{[AB]} = \frac{k_c}{k_d K_{eq}}$$

substituting the third order condition $k_s[M] < k_d$ one obtains [17].

$$[17] \quad f_{ex} < \frac{k_c}{k_s[M]K_{eq}} \approx \frac{1}{[M]K_{eq}}$$

The approximate expression on the right is obtained with the assumption $k_c \approx k_s$ (both probably Langevin rate constants). Equation [17] shows that if f_{ex} is to be small, say 10^{-2}, then for a pressure of M in the 1 to 10 Torr range, measured K_{eq} should be in the 100 to 10 (Torr^{-1}) range. It should be noted that [17] is valid also for reactions in which the forward rate is second order but the unequal sign must be reversed. Evidently an even larger K_{eq} should be selected in this case if f_{ex} is to be kept small.

The problem arising from unimolecular decomposition could be solved by instrumental changes. One method eliminating ion sampling errors is the ion T-jump technique discussed in section II. However, this technique will eliminate the problems only if all ions detected as n originate from ions n in the ion source. Another approach is to use controlled adiabatic expansion in the ion exit leak to cool the clusters down before their passage through vacuum. Experiments along these lines are tried presently in our laboratory.

(e) Conclusions

Unimolecular decomposition of ion clusters n or adducts AB^+ can occur in the vacuum region of the mass analysis system. The effect of the decomposition is to increase somewhat $-\Delta H^0_{n-1,n}$ and $-\Delta S^0_{n-1,n}$. The problem occurs for $n > 4$ and is aggravated by ligand molecules which have a large number of internal degrees of freedom.

The problem can be avoided by proper choice of experimental conditions. One must measure equilibrium constants $K_{n-1,n}$ at the lowest experimentally accessible temperature, i.e. the values of the equilibrium constants should be in the range $K = 10^3$ to 10 Torr^{-1}. Such values can be measured with present apparatus by using pressures of the clustering gas in the 1–100 mTorr range and a third gas in the Torr range.

II. An Ion T-jump Technique

The high pressure ion sources used in our laboratory have a repeller which is placed some 5 mm above the ion exit slit. In normal operation this repeller is kept at the same potential as the ion source. The ion T-jump technique consists of applying a radiofrequency (RF) field pulse to the repeller. The normal operating pressure of the ion source is 0.5–4 Torr. At these pressures, the ions accelerated by the RF field suffer collisions with the (nonreacting) major gas. These collisions increase the internal energy of the ions. If the ions are participating in an ion–molecule equilibrium a shift of the equilibrium towards a higher "temperature"

occurs. An experiment illustrating the effect is shown in Fig. 6. The reaction system is the equilibrium between Cl^- and Cl^-(DMSO) as shown in [18].

$$[18] \quad Cl^- + DMSO \underset{r}{\overset{f}{\rightleftharpoons}} Cl^-(DMSO)$$

The results in Fig. 6 were obtained with a mixture having the following ion source pressures: isobutane 0.7 Torr, DMSO 0.8 mTorr, CCl_4 ~ a few mTorr. The chloride ion is produced from dissociative electron capture by CCl_4. The Cl^- then reacts with DMSO according to [18]. The normalized ion intensities shown in Fig. 6 are observed after an electron pulse of some 20 μs duration. The system rapidly approaches equilibrium with Cl^- decreasing and Cl^-(DMSO) increasing in intensity. In the absence of an RF field pulse the system would have followed the dashed lines (see Fig. 6). The application of the RF (700 kHz) 40 V peak-to-peak pulse of duration ~500 μs displaces the system from equilibrium. The reaction reaches a new steady state towards the end of the RF pulse. The reactants relax back to equilibrium after the RF pulse is terminated.

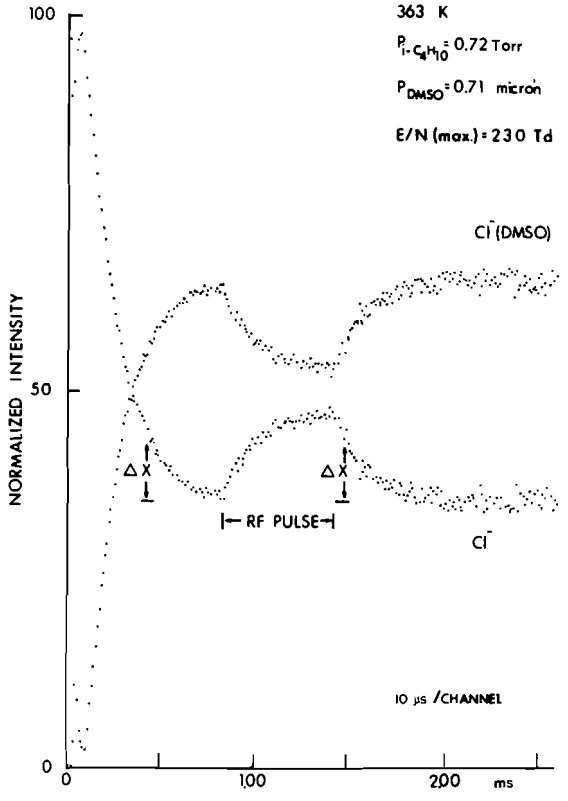

FIG. 6. Time resolved ion intensities obtained with 0.7 Torr *i*-butane, 0.7 mTorr DMSO, and traces of CCl_4. Ion source temperature 363 K. Electron pulse duration 20 μs. The reaction: Cl^- + DMSO = Cl^-(DMSO) rapidly reaches equilibrium. Application of an RF burst displaces the equilibrium to higher temperature. After the RF is terminated, relaxation to the equilibrium occurs.

The "temperature" with the RF field on can be estimated as follows. In separate experiments which are to be published elsewhere (16) the equilibrium constant for [18] was determined by measuring the equilibrium concentration of the ions. Measurements of K_{eq} at different temperatures provided a van't Hoff plot of the equilibrium [18]. The maximum displacement from the equilibrium during the RF pulse in Fig. 6 may be considered as a new position of equilibrium at a higher "temperature". Evaluating an equilibrium constant from the ion concentrations with the RF on, and reading off the temperature from the van't Hoff plot corresponding to the new equilibrium constant gives a "temperature" in the presence of the RF field which is about 10° higher, than the ion source temperature (363 K) in the absence of the field.

The clustering of DMSO to Cl^-, reaction [18], is pseudo first order in the forward and reverse direction. To make the treatment more general we replace [18] with reaction [19]. Calling a displacement from equilibrium, ΔX as defined in [20], it is easy to show that the variation of ΔX with time is given by [21]. The relaxation time τ is equal to the

$$[19] \quad A^{\pm} + B \underset{v_r}{\overset{v_f}{\rightleftharpoons}} C^{\pm}$$

$$[20] \quad \Delta X = [A^{\pm}]_t - [A^{\pm}]_{eq} = [C^{\pm}]_{eq} - [C^{\pm}]_t$$

$$[21] \quad \Delta X = \Delta X_0 e^{-t/\tau}$$

$$\tau = \frac{1}{v_f + v_r}$$

inverse of the sum of the pseudo first order rate constants (reaction frequencies) v_f and v_r. According to [21], a plot of ln (ΔX) versus t should give a straight line with slope $-1/\tau$. Two such plots of the data in Fig. 6 are shown in Fig. 7. The first plot is for the system going to equilibrium at the normal ion source temperature before the RF pulse was applied i.e. during the time interval 0.5 to 0.8 ms after the ionizing electron pulse (see Figs. 6 and 7). The other plot is for the system relaxing to equilibrium after the RF pulse was turned off. The plot starts some 0.1 ms after the RF was turned off, at a time when, presumably, the ions have already become thermalized to the ion source temperature so that the plotted ion concentration changes are due to the kinetic approach to the equilibrium at the ion source temperature. The two slopes lead to relaxation times τ = 0.159 msec and τ = 0.158 ms which are virtually identical. Since τ gives the sum of the

Can. J. Chem. Downloaded from www.nrcresearchpress.com by 210.87.254.6 on 09/06/12
For personal use only.

Can. J. Chem. Downloaded from www.nrcresearchpress.com by 210.87.254.6 on 09/06/12
For personal use only.

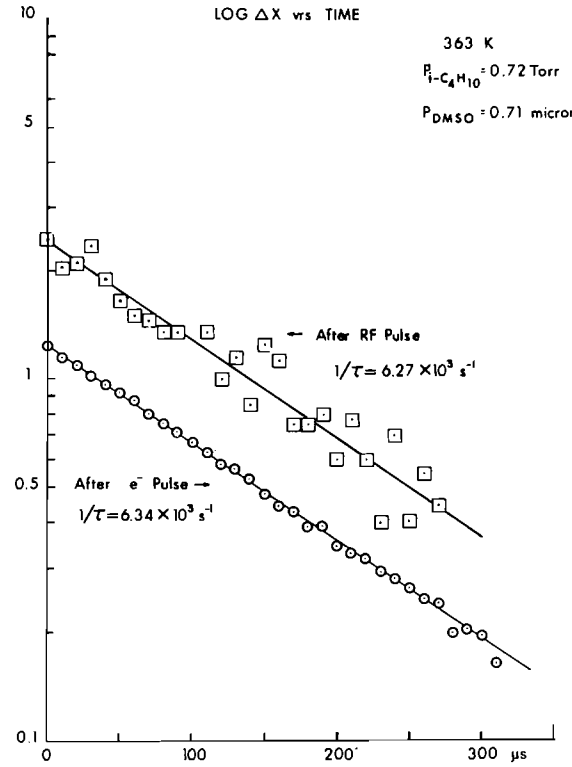

FIG. 7. Plot of ln ΔX versus time t. Slope leads to $-1/\tau = \nu_f + \nu_r$; □ relaxation to equilibrium after RF pulse; ○ approach to equilibrium after electron pulse (see Fig. 6).

forward and reverse reaction frequency, additional experiments must be done in order to obtain separate values for ν_f and ν_r. For reaction [19], ν_f is proportional to the concentration of B. Therefore the reciprocal of τ can be expressed by eq. [22],

$$[22] \quad 1/\tau = \nu_f + \nu_r = k_f[B] + k_r$$

where f_f is a second order and $k_r = \nu_r$ a first order rate constant. In a series of experiments with different pressures of the clustering gas (DMSO in the present case), τ can be obtained in function of the concentration of the clustering gas. A plot of $1/\tau$ versus the concentration of B leads, see [22], to a straight line whose slope equals k_f and intercept equals k_r. The equilibrium constant for the clustering reaction can then be obtained from $K = k_f/k_r$. We are presently engaged in determining k_f, k_r, and K for several systems whose equilibria were determined previously [1] by the conventional way, i.e. by measuring the equilibrium constant eq. [23].

$$[23] \quad K_{eq} = \frac{[C^+]_{eq}}{[A^+]_{eq}[B]}$$

The purpose of these experiments is to discover whether any systematic deviations of the equilibrium constants obtained via the kinetic eq. [22] and eq. [23] exists. It will be noted that the equilibrium constant obtained via the kinetic plots in Fig. 7 and eq. [22] is independent of the values of the ion concentration $[A^\pm]$, $[C^\pm]$, or the ratio $[A^\pm]/[C^\pm]$. Thus these kinetic results are free of problems which can arise from selective losses of ions to the walls of the ion source and selective transmission losses occurring in the passage of the ions out of the ion source and in the mass analysis and detection system. Therefore the measurement of the equilibrium constants with the kinetic and relaxation technique of Fig. 6 and eq. [22] represents an important check of the reliability and accuracy of the previous equilibrium determinations.

As pointed out earlier, the plots of ΔX versus time (see Fig. 4) can be obtained from the ordinary kinetic approach to the equilibrium *and* the relaxation after the RF pulse. In fact the scatter in the points after the RF pulse is considerably larger than that after the e^- pulse. What is then the advantage of using an RF pulse? The point is best explained

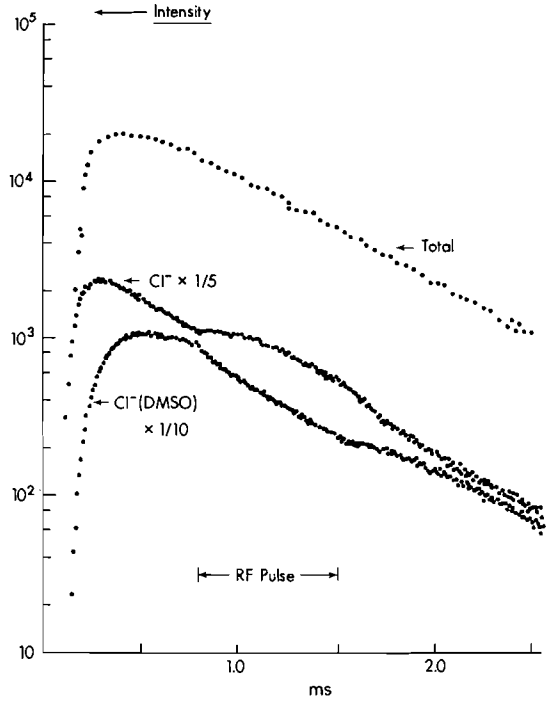

FIG. 8. Total ionization in experiment undertaken at conditions similar to that in Fig. 6. Onset of negative ions is delayed by ~200 μs due to trapping of the positive space charge produced by ambipolar electron – positive ion diffusion. First ~300 μs correspond to rapid positive negative ion changes which may affect measurement of ion molecule reaction kinetics. RF relaxation kinetics can be executed when above phenomena are over.

with reference to Fig. 8 which shows the total ion currents observed in a run for conditions very similar to those used in Fig. 6. The stage of conventional kinetics generally occurs in the range 0 to 0.6 ms. At short reaction times the negative ions are trapped inside the ion source due to the net positive potential in the positive ion–electron ambipolar diffusion stage. The change over from ambipolar electron to ambipolar ion–ion and free ion diffusion is signalled by a rapid drop off of positive ions and a large rapid increase of negative ions. The stage occurs after some 100 μs in Fig. 8. Even after this period up to about 300–400 μs there is a fairly rapid change of total ion concentration. Therefore the kinetic results obtained from plotting the normalized ion intensities are somewhat suspect over the first 200 μs and probably also slightly affected even for somewhat longer reaction times. The application of the RF pulse and the measurement of the relaxation time to the equilibrium can be done some 500 μs after the electron pulse, i.e. at a time where the ion concentration is low and space charge effects and higher than first order ion diffusion modes are minimal. Agreement of the RF relaxation kinetics with the kinetics at short reaction times provides support for the kinetic treatments used in earlier work.

We have recently put in operation a much faster multiscaler (1 μs/channel rather than the 10 μs per channel utilized in Fig. 6). With this more rapid device relaxation times of 100 or even 10 μs are accessible. This allows measurement of faster kinetics and shorter relaxation times, i.e. fast kinetics. Such fast kinetic measurements are not possible without the T-jump technique, because of the rapid changes of positive–negative ion intensities immediately after the electron pulse.

1. A. M. HOGG and P. KEBARLE. J. Chem. Phys. **43**, 449 (1965).
2. A. M. HOGG, R. N. HAYNES, and P. KEBARLE. J. Am. Chem. Soc. **88**, 28 (1966).
3. P. KEBARLE. Ann. Rev. Phys. Chem. **28**, 445 (1977).
4. R. W. TAFT and E. M. ARNETT. *In* Proton transfer reactions. *Edited by* E. F. Caldin and V. Gold. Chapman and Hall. London, 1975.
5. M. T. BOWERS (*Editor*). Gas phase ion chemistry. Academic Press. 1979. (*a*) Chapt. 9; (*b*), Chapt. 11.
6. A. GOOD, D. A. DURDEN, and P. KEBARLE. J. Chem. Phys. **52**, 212 (1970).
7. S. K. SEARLES and P. KEBARLE. Can. J. Chem. **47**, 2620 (1969).
8. I. DZIDIC and P. KEBARLE. J. Phys. Chem. **74**, 1466 (1970).
9. W. R. DAVIDSON and P. KEBARLE. J. Am. Chem. Soc. **98**, 6125 (1976); **98**, 6133 (1976).
10. J. SUNNER and P. KEBARLE. J. Phys. Chem. To be published.
11. H. KISTENMACHER, H. POPKIE, and E. CLEMENTI. J. Chem. Phys. **61**, 799 (1974).
12. M. R. MRUZIK, F. F. ABRAHAM, D. E. SCHRIBER, and G. M. POUND. J. Chem. Phys. **64**, 41 (1976).
13. J. M. JASINSKI, R. N. ROSENFELD, D. M. GOLDEN, and J. I. BRAUMAN. J. Am. Chem. Soc. **101**, 2259 (1979).
14. A. J. CUNNINGHAM, J. D. PAYZANT, and P. KERBARLE. J. Am. Chem. Soc. **94**, 7627 (1972).
15. F. H. FIELD, P. HAMLETT, and W. F. LIBBY. J. Am. Chem. Soc. **91**, 2839 (1969).
16. T. F. MAGNERA, J. SUNNER, and P. KEBARLE. J. Am. Chem. Soc. To be published.

Can. J. Chem. Downloaded from www.nrcresearchpress.com by 210.87.254.6 on 09/06/12
For personal use only.

Ionization energies of metal chelates. Acetylacetonates, trifluoroacetylacetonates, and hexafluoroacetylacetonates of trivalent metals of the first transition series

JOHN B. WESTMORE AND MARK L. J. REIMER

Department of Chemistry, University of Manitoba, Winnipeg, Man., Canada R3T 2N2

AND

CHARLES REICHERT

Alberta Research Council, 11315 87th Avenue, Edmonton, Alta., Canada T6G 2C2

Received November 26, 1980

This paper was presented, in part, at a Special Symposium "The Structure and Thermochemistry of Gaseous Ions", held in honour of Dr. F. P. Lossing of the National Research Council of Canada, during the Second Canadian Conference on the Gas Phase Chemistry of Ions, Trent University, June 5–8, 1980, and is dedicated to him on the occasion of his 65th birthday

JOHN B. WESTMORE, MARK L. J. REIMER, and CHARLES REICHERT. Can. J. Chem. **59**, 1797 (1981).

For several β-diketonate complexes of metals of the first transition series the electron impact ionization efficiency curves obtained using unfiltered electron beams were fitted to empirical post-threshold ionization laws. In the energy region extending to 2–3 V above threshold, fits of high quality were obtained for a second power ionization law (i.e. ion current was proportional to the square of the electron energy in excess of the threshold energy) for complexes of Al(III), Sc(III), Mn(III), Fe(III), and Co(III) (d^0, d^0, d^4, d^5, and d^6, respectively). In the cases of Ti(III), V(III), and Cr(III) complexes (d^1, d^2, and d^3, respectively) the experimental points lay above the "best fit" curves in the immediate post-threshold region. Electron energies were initially calibrated by fitting experimental data points for xenon to its published ionization functions. In later experiments, $Al(tfa)_3$ or $Al(hfa)_3$ was used for calibration purposes. When the electron impact results were compared with published photoelectron spectra of the complexes (where available) it became apparent that, in the threshold region, the strongest ionization processes involved electron removal from ligand dominated π orbitals. In the cases of Ti(III), V(III), and Cr(III) complexes, weaker ionization processes involving electron removal from orbitals of predominantly metal 3*d* character (correlating with t_{2g} in octahedral symmetry) could also be detected at lower electron energies.

JOHN B. WESTMORE, MARK L. J. REIMER et CHARLES REICHERT. Can. J. Chem. **59**, 1797 (1981).

Dans le cas de plusieurs complexes de β-dicétonates des métaux de la première série de métaux de transition, les courbes d'efficacité de l'ionisation par impact électronique obtenues en utilisant un faisceau d'électrons non filtré sont ajustées à des lois empiriques relatives aux ionisations post seuils. Dans la région d'énergie s'étendant jusqu'à 2 à 3 V au-dessus du seuil, on a réalisé des ajustements de haute qualité pour une loi d'ionisation du deuxième ordre (i.e. le courant lionique est proportionnel au carré de l'énergie de l'électron en excès par rapport à l'énergie de seuil pour les complexes de Al(III), Sc(III), Mn(III), Fe(III) et Co(III) (d^0, d^0, d^4, d^5 et d^6 respectivement). Dans le cas des complexes du Ti(III), du V(III) et du Cr(III) (d^1, d^2 et etd^3 respectivement), les points expérimentaux de la loi restent au-dessus des courbes qui assurent une meilleure corrélation dans la région immédiate du post seuil. On a initialement calibré les énergies de l'électron en insérant les données expérimentales du xénon dans ses fonctions d'ionisation déjà connues. Dans des expériences subséquentes, on a tenté d'utiliser les complexes $Al(tfa)_3$ ou $Al(hfa)_3$ pour l'étalonnage. Quand on compare les résultats de l'impact électronique avec les spectres photoélectriques connus des complexes (quand ils sont disponibles), il devient apparent que dans la région du seuil, le processus d'ionisation le plus important fait intervenir l'enlèvement de l'électron des orbitales π dominées par le ligand. Dans les cas des complexes de Ti(III) de V(III) et de Cr(III), des processus d'ionisation plus faibles impliquant l'enlèvement d'un électron des orbitales à caractère 3d métallique prédominant (en accord avec t_{2g} dans une symétrie octaédrique) peuvent aussi être décelés à des plus faibles énergies des électrons.

[Traduit par le journal]

Introduction

Studies of the ionization of many metal β-ketoenolate complexes by electron and photon impact have been summarized in an earlier review (1) which contains the leading references. In the case of electron impact ionization the threshold energies reported by several authors, including ourselves, were determined from ionization efficiency curves by such techniques as semi-logarithmic plot (2), vanishing current (3), critical slope (4), extrapolated voltage difference (5), and energy compensation (6). All involve certain assumptions about threshold ionization behavior in an absolute and/or relative way as compared to reference species (such as xenon) used to calibrate the electron energy and have been criticized on theoretical and practical grounds (7). Successful application of deconvolution methods, i.e. derivative (8–12), "energy distribution difference" (EDD) (13), and double EDD methods (14), to obtain the maximum information from the ionization efficiency curves requires data with a very high signal-to-noise ratio (S/N). Methods of noise removal to improve the S/N have been described (13, 15) which result in some inevitable loss of energy resolution. There is no doubt that the highest quality information would be obtained using energy selected electron beams, or, less ideally, by rapid, repetitive scans of the ion

0008-4042/81/121797-08$01.00/0

©1981 National Research Council of Canada/Conseil national de recherches du Canada

Can. J. Chem. Downloaded from www.nrcresearchpress.com by 210.87.254.105 on 09/06/12
For personal use only.

Can. J. Chem. Downloaded from www.nrcresearchpress.com by 210.87.254.105 on 09/06/12
For personal use only.

yield vs. electron energy through interfacing the mass spectrometer to a data acquisition system. Nevertheless, we demonstrate here, using data of insufficiently high S/N for successful application of the deconvolution methods, that reliable threshold energies can be determined by a least squares curve fitting procedure using only a programmable pocket calculator as the most sophisticated computing instrument. The method was successful even when the threshold ionization laws for the molecule of interest and the calibrating species (in this case xenon) were very different. The general approach could therefore be considered by the many workers lacking the specialized instrumentation referred to above.

The method was applied to the electron impact ionization data for the title compounds, for which the origin of the electron removed at the ionization threshold has been the subject of debate (1). For some of these compounds the results can be compared with published photoelectron spectra.

Results and Discussion

Theory

When an unfiltered electron beam is used the observed ion current will be given by a convolution of the electron energy distribution with the post-threshold ionization law. In the general case, we may assume the ionization probability to depend upon the nth power of the energy (E) of the electron in excess of the threshold value (IE); that is

$$p(E) \propto (E - \mathrm{IE})^n$$

For electron impact ionization of a neutral molecule in its ground state to a single electronic state of the molecular ion the value of n is theoretically expected to equal unity, and experimental evidence to support this has been cited (16). However, in the development of the critical slope method Honig (4) assumed $n = 2$. This may well be a better assumption for polyatomic molecules containing several atoms and many rotational–vibrational energy levels. As will be shown, the ionization of the title compounds gives excellent agreement with the assumption that $n = 2$.

The thermal energy distribution of the electron beam was assumed to be Maxwellian, that is:

$$\mathrm{d}N_U = \frac{4\pi mA}{h^3} U \exp\left(-\frac{(\phi + U)}{kT}\right) \mathrm{d}U$$

where $\mathrm{d}N_U$ is the number of electrons with energies between U and $U + \mathrm{d}U$ leaving the filament per second; m is the electron mass; h and k are the Planck and Boltzmann constants, respectively; and A, ϕ, and T are the area, work function, and absolute temperature, respectively, of the filament. At an electron accelerating voltage V the total electron energy is $E = U + V$. When convoluted with empirical post threshold ionization laws standard mathematical methods lead to the following expressions for the ion current as a function of V:

First power post threshold ionization law, i.e. $p(E) \propto (E - \mathrm{IE})$

$$[1a] \quad I_V = B(2kT - V + \mathrm{IE}) \times \exp\left(\frac{V - \mathrm{IE}}{kT}\right) \qquad \text{for } V \leq \mathrm{IE}$$

$$[1b] \quad I_V = B(2kT + V - \mathrm{IE}) \qquad \text{for } V \geq \mathrm{IE}$$

Second power post threshold ionization law, i.e. $p(E) \propto (E - \mathrm{IE})^2$

$$[2a] \quad I_V = 2kTC(3kT - V + \mathrm{IE}) \times \exp\left(\frac{V - \mathrm{IE}}{kT}\right) \qquad \text{for } V \leq \mathrm{IE}$$

$$[2b] \quad I_V = C[6(kT)^2 + 4kT(V - \mathrm{IE}) + (V - \mathrm{IE})^2] \qquad \text{for } V \geq \mathrm{IE}$$

B and C are scaling constants. Although presented in a different way, convenient for the present studies, these equations are really the same as those given by other authors (17, 18). Non-integral values of n were not investigated because in the present work satisfactory results were obtained using $n = 1$ or 2. We will return to this point later.

Rationale

We had observed when studying ionization efficiency curves of β-diketonate complexes of several metals that an extended linear portion occurred when the square root of the ion current was plotted versus the electron energy, thus implying that $p(E) \propto (E - \mathrm{IE})^2$. Consequently, if a simple relationship such as this extended downward to the ionization threshold then the curved "foot" of the ionization efficiency curve would be defined by convolution of this function with the high energy portion of the electron energy distribution. The contribution of any weak ionization processes at lower energies, should they be present, can then be detected by positive deviations of the experimental points from the "defined" foot of the curve.

A second reason for trying to establish the nature of the ionization probability functions was to compare the results for closely related complexes of non-transition and transition metals to attempt to evaluate the contribution of d electrons in the ionization threshold region.

Can. J. Chem. Downloaded from www.nrcresearchpress.com by 210.87.254.105 on 09/06/12
For personal use only.

Curve Fitting and Electron Energy Calibration

The expressions $[1a, 1b]$ and $[2a, 2b]$ for the ion currents contain three variable parameters, namely, IE, kT, and B or C. Attempts were made to fit the expressions to experimental data points obtained for the metal complexes. The least squares method (see Experimental section) was used to fit the expressions in two alternative ways, viz.

(*a*) $\sqrt{[1a, 1b]}$ or $\sqrt{[2a, 2b]}$ to $\sqrt{I_V/I_{50}}$

(*b*) $[1a, 1b]$ or $[2a, 2b]$ to I_V/I_{50}

where I_V and I_{50} are the ion currents at V and 50 volts respectively. These methods weight the upper data points more heavily than the lower ones, method (*b*) more so than method (*a*). In fact, this is desirable because the upper points are used to define the contribution to the lower part of the ionization efficiency curve which results from ionization caused by the high energy tail of the electron energy distribution. Consequently, weak ionization processes occurring at lower thresholds should be more readily observable. Although there was no theoretical basis for different methods of weighting the data points it was found that when good fits between test expressions and data points were obtained that methods (*a*) and (*b*) led to virtually identical values of IE, kT, and B or C.

For none of the metal complexes could expressions $[1a, 1b]$ be fitted satisfactorily to the experimental data points. However, for several complexes expressions $[2a, 2b]$ gave excellent fits, as illustrated in Fig. 1 for Al(III) complexes (where attempted fits to $[1a, 1b]$ are also shown for comparison). We have judged this visual presentation of the results to be a more effective way of presenting the quality of the fit than a statistical method. The electron energy scale has been calibrated with reference to xenon also present in the ion source as will now be described.

Attempts to fit expressions $[1a, 1b]$ or $[2a, 2b]$ to experimental data points for xenon were unsuccessful. This was not surprising in view of the known complexity of the ionization efficiency curve for xenon in the threshold region. Several authors have identified additional ionization processes (including, in some cases, autoionization) lying slightly above the lowest ionization threshold. These results are summarized in Table 1. For each ionization process a function of the type $p(E) \propto (E - \mathrm{IE}_n)$ was valid, where IE_n was the threshold value for the particular process. The ionization efficiency curve for xenon in the threshold region was thus a summation of the individual processes. Consequently, in the present work, the parameters from

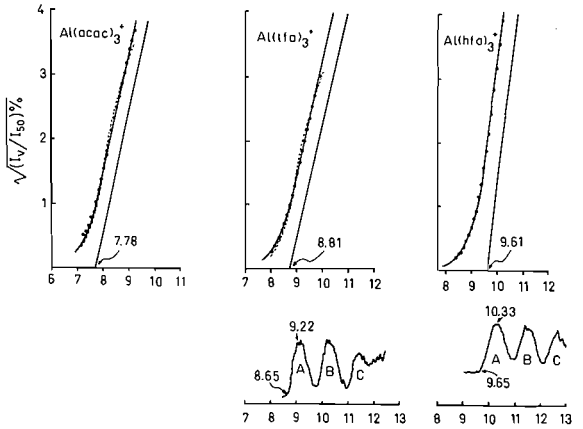

FIG. 1. Threshold ionization efficiency curves and photoelectron spectra of Al(III) complexes. Solid lines, $n = 2$ fit; broken lines, $n = 1$ fit. The straight line representing the ionization probability function is drawn from the ionization energy intercept with a slope arbitrarily made parallel to the nearly straight portion of the "best fit" $n = 2$ curve.

Table 1 were used to generate test functions for fitting to our experimental data points. Composite expressions $[1a', 1b']$ given by $I_V = I_{V,0} + I_{V,1} + \ldots + I_{V,n}$ (where each term has its own threshold IE ($= \mathrm{IE}_0 + \Delta\mathrm{IE}_n$) with relative weighting according to Table 1) were fitted to experimental data points for xenon. The fits to one set of experimental data are shown in Fig. 2. With the exception of the parameters of Melton and Hamill fits of high quality were obtained (in spite of the apparent diversity of the parameters used) and the values of the lowest ionization threshold, IE_0, were nearly the same (11.04 ± 0.02 eV). Because of this, and because they gave the best fit (though the other fits were nearly as good), the parameters of Foner and Nall were used to generate the composite function $[1a', 1b']$ for fitting to experimental data points for xenon. When this had been done, the difference between the fitted ionization energy and the spec-

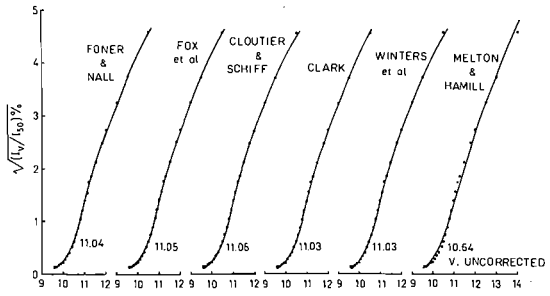

FIG. 2. "Best fit" threshold ionization efficiency curves to the same set of experimental data points for xenon, using parameters from the work of several authors. The values shown are for the resulting lowest ionization threshold.

TABLE 1. Structure observed in ionization data for xenon

Method	Onsets, volts above threshold (probability relative to the initial process)		
RPD; Fox, Hickam, and Kjeldaas (19)	1.27[a](0.36)[b]		
Electron energy selector; Clark (20)	0.82 (0.26)[b]	1.11 (0.27)[b]	
RPD; Cloutier and Schiff (21)	1.31[a](0.27)[b]		
Electron energy selector; Foner and Nall (22)	0.70 (0.16)	1.33 (0.13)	2.05 (0.16)
RPD; Melton and Hamill (23)	0.37 (0.80)[b]	0.75 (2.61)[b]	1.15 (2.98)[b]
EDD; Winters, Collins, and Courchene (13)	0.33 (0.56)	1.27 (0.33)	

[a] $^2P_{1/2}$ energy level.
[b] Estimates made from a study of the published data.

troscopic value (12.13 eV) was used to correct the energy values for the particular complex studied concurrently.

Although xenon was used as a standard to calibrate the electron energy its use was not without problems. In particular, there was always the possibility that a fragment ion from the metal complex would have the same m/z value as Xe^+. Fortunately, xenon has a variety of isotopes which can be selected to minimize this problem. In some of the later experiments Al(III) complexes were used to calibrate the electron energy.

The least squares method was applied to both the sample ion and reference ion using three variable parameters, i.e. IE, kT, and B or C. At a filament temperature of 2500 K the value of kT is 0.215 eV. Although the values of kT for which the sum of the squares of the deviations were minimized were generally within ±0.02 eV of this result the values were usually not exactly the same for sample and reference ion. This was not a serious difficulty because the resulting values for the IE were relatively insensitive to kT, and varied with kT by almost exactly equal amounts for sample and reference ion. Consequently, the value of IE for the sample was calculated using the same value of kT for both sample and reference ion.

Ionization Efficiency Curves for the Metal Complexes

The results of fitting expression [2*a*, 2*b*] to experimental data points obtained for electron impact ionization of complexes of Sc(III), Ti(III), V(III), Cr(III), Mn(III), Fe(III), and Co(III) are shown in Figs. 3–9. Like Al(III), fits of high quality were given by the complexes of Sc, Mn, Fe, and Co, while for the complexes of Ti, V, and Cr the experimental points lie above the "best fit" curve in the low energy regions. Also shown in Figs. 1 and 3–9 are available photoelectron spectra for the complexes. These spectra were redrawn and positioned to the same energy scale as the ionization efficiency curves from photographic enlargements of the published PE spectra (24).

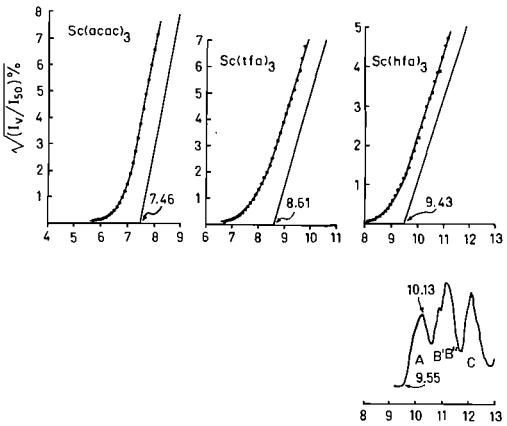

FIG. 3. Threshold ionization efficiency curves and photoelectron spectra of Sc(III) complexes. For explanation see Fig. 1.

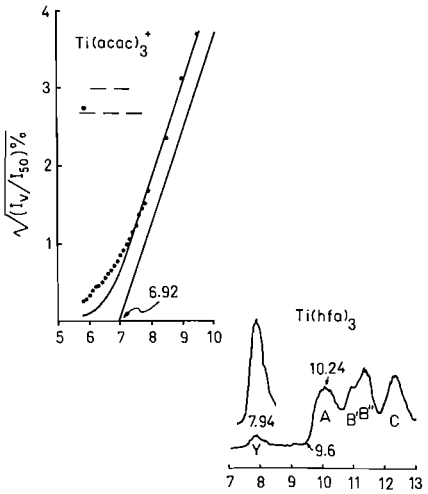

FIG. 4. Threshold ionization efficiency curves and photoelectron spectra of Ti(III) complexes. For explanation see Fig. 1.

In their interpretation of the PE spectra the authors assigned bands A, B, and C to ionization by electron removal from ligand dominated π orbitals, and band Y to ionization by electron removal from metal 3*d* dominated orbitals ($a_1 + e_a$ in the D_3 point group, correlating with t_{2g} in octahedral symmetry).

Can. J. Chem. Downloaded from www.nrcresearchpress.com by 210.87.254.105 on 09/06/12
For personal use only.

Can. J. Chem. Downloaded from www.nrcresearchpress.com by 210.87.254.105 on 09/06/12
For personal use only.

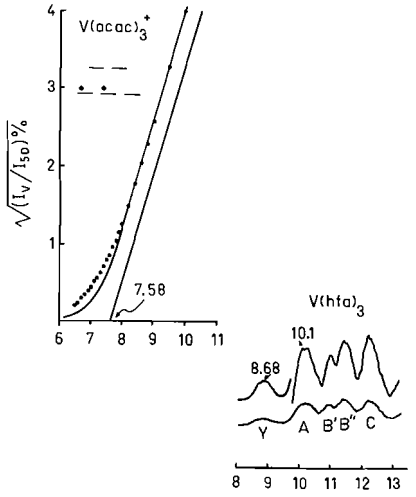

FIG. 5. Threshold ionization efficiency curves and photoelectron spectra of V(III) complexes. For explanation see Fig. 1.

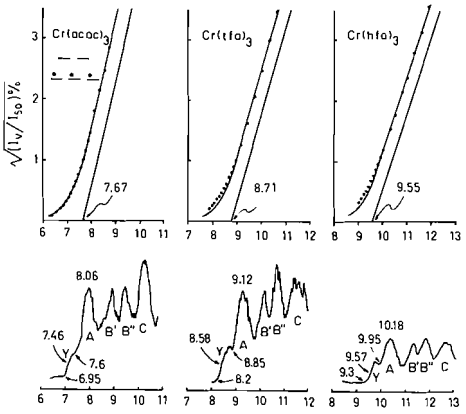

FIG. 6. Threshold ionization efficiency curves and photoelectron spectra of Cr(III) complexes. For explanation see Fig. 1.

Assignments of bands K, L, and M, observed in some spectra, were more tentative. They arise when the ligand π and metal $3d$ orbitals are close in energy and substantial interaction between the orbitals occurs. The preferred assignment of the leading band K was to ionization by electron removal from an orbital of mainly ligand π type. The authors tabulated values of band maxima (vertical ionization energies). These values are shown for the leading band(s) in Table 2, together with values of band onsets ($\geq$ adiabatic ionization energies) that we have estimated from their published spectra.

It was noted earlier in this paper that electron impact ionization of a neutral molecule in its ground state to a single electronic state of the molecular ion should yield an ionization probability of the form $p(E) \propto (E - \mathrm{IE})$. The fitted portions of

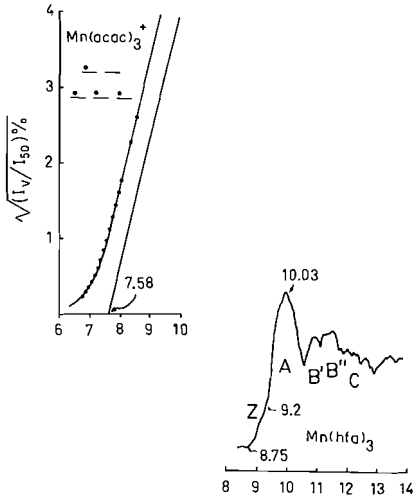

FIG. 7. Threshold ionization efficiency curves and photoelectron spectra of Mn(III) complexes. For explanation see Fig. 1.

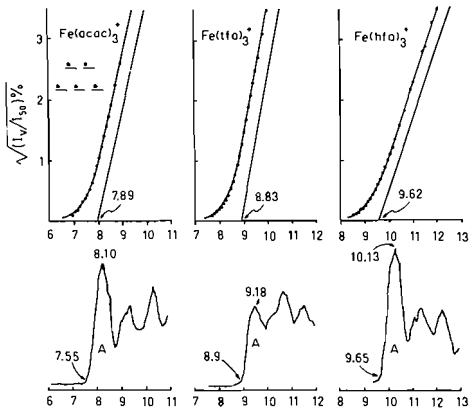

FIG. 8. Threshold ionization efficiency curves and photoelectron spectra of Fe(III) complexes. For explanation see Fig. 1.

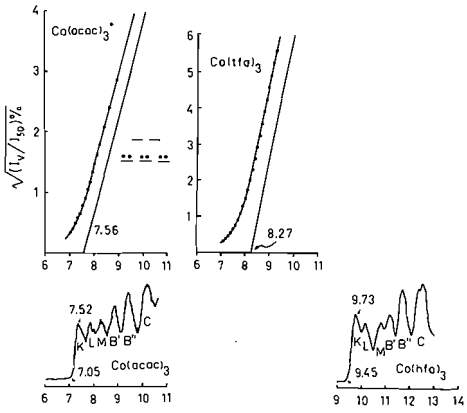

FIG. 9. Threshold ionization efficiency curves and photoelectron spectra of Co(III) complexes. For explanation see Fig. 1.

TABLE 2. Ionization energies (eV) of metal acetylacetonates, trifluoroacetylacetonates, and hexafluoroacetylacetonates

Complex	This work[a] IE (rel. prob.)	PE spectra[b] Band onset[c]	PE spectra[b] Band max.	Previous value[d]	Other literature values[e]
$Al(acac)_3$	7.78	—	—	7.95 ± 0.05(25)	8.27 ± 0.13(26,VC[Hg])
$Sc(acac)_3$	7.46	—	—	—	—
$Ti(acac)_3$	5.45 ± 0.2(0.068)	—	—	7.1 ± 0.1 (25)	—
	6.92				
$V(acac)_3$	6.45 ± 0.2(0.066)	—	—	7.9 ± 0.1 (25)	7.72 ± 0.10(26,VC[Hg])
	7.58				
$Cr(acac)_3$	[f]	6.95(Y)	7.46(Y)	8.1 ± 0.05(25)	7.87 ± 0.12(26,VC[Hg])
	7.67	7.6 (A)	8.06(A)		7.40(27,EC[Xe, C_6H_6, $C_{14}H_{10}$])
$Mn(acac)_3$	7.58	[g]	(7.32)[h]	7.85 ± 0.05(25)	7.95 ± 0.10(26,VC[Hg])
			8.14		
$Fe(acac)_3$	7.89	7.55(A)	8.10(A)	8.45 ± 0.05(25)	8.64 ± 0.11(26,VC[Hg])
$Co(acac)_3$	7.56	7.05(K)	7.52(K)	7.80 ± 0.05(25)	7.81 ± 0.10(28,NS)
$Al(tfa)_3$	8.81	8.65(A)	9.22(A)	9.05 ± 0.05(29)	—
$Sc(tfa)_3$	8.61	—	—	—	—
$Cr(tfa)_3$	[f]	8.2 (Y)	8.58(Y)	9.09 ± 0.05(30)	—
	8.71	8.85(A)	9.12(A)		
$Fe(tfa)_3$	8.83	8.9 (A)	9.18(A)	9.10 ± 0.05(29)	9.38 ± 0.11(26,VC[Hg])
$Co(tfa)_3$	8.27	—	—	—	—
$Al(hfa)_3$	9.61	9.65(A)	10.33(A)	9.80 ± 0.1 (29)	10.30 ± 0.11(26,VC[Hg])
$Sc(hfa)_3$	9.43	9.55(A)	10.13(A)	—	—
$Cr(hfa)_3$	[f]	9.3 (Y)	9.57(Y)	10.13 ± 0.05(30)	9.97 ± 0.08(26,VC[Hg])
	9.55	9.95(A)	10.18(A)		9.21(24,PI)
$Fe(hfa)_3$	9.62	9.65(A)	10.13(A)	10.2 ± 0.1 (29)	10.34 ± 0.10(26,VC[Hg])

[a] Electron energy calibrated with xenon except for $Sc(acac)_3$, $Sc(tfa)_3$, and $Co(tfa)_3$ for which $Al(tfa)_3$ was used, and for $Sc(hfa)_3$ for which $Al(hfa)_3$ was used. Reproducibility was within ±0.05 eV (except as noted) for replicate determinations when good fits were obtained. Probability of the weak ionizations is given relative to the main threshold process.
[b] Band assignments shown in parentheses.
[c] Estimated from published spectra; uncertainty may be ±0.2 eV.
[d] "Semi-log plot" or "extrapolated voltage difference" methods using xenon to calibrate electron energy.
[e] VC = vanishing current, EC = energy compensation, NS = not specified, PI = photoionization methods (calibrating species in parentheses).
[f] Reliable value could not be extracted from the data.
[g] Spectra not published.
[h] Shoulder.

the $\sqrt{I}$ versus electron energy plots for the chelates of Al(III), Sc(III), Mn(III), Fe(III), and Co(III) extend upward from the ionization threshold by at least 3 eV in some cases, indicating that $p(E) \propto (E - \text{IE})^2$. This result implies a linear progression of excited states for the ion. Such a condition may be approximately true while ascending the steeply rising portion of the leading edge of the rotation–vibration envelope of an electronically excited state. In the PE spectra this region extends typically over not more than 0.5 eV. However, electron impact ionization is not subject to the selection rule restrictions of photon impact with the result that many more rotation–vibration levels of the excited ion should be accessible over a more extended energy range.

It is apparent from the foregoing that the optimum value of n to be used in the ionization probability function $p(E) \propto (E - \text{IE})^n$ will depend upon the structure of the rotation–vibration envelopes of the electronically excited states involved. Fine structural details cannot, of course, be detected by the methods we have used and the optimum value of n will be a "smoothed" value. One approach to finding this optimum value would be to treat n as a variable parameter in the curve fitting procedures (with a concomitant great increase in complexity). This approach was not attempted in this work because the results for the metal complexes using $n = 2$ were very satisfactory and would not have been significantly better for other values of n.

The values of the ionization energies obtained in this work are consistently lower than the previously reported values, usually by 0.2–0.6 eV (Table 2). (They are also lower than the IE values extracted from the poor $n = 1$ fits by similar amounts.) The "semi-log" plot method was recommended only for situations in which the sample and reference ions had log I plots closely parallel in the 1% region of the I_{50} value (2), a condition not achieved for the metal chelates when xenon was the calibrating species. A further complication in the case of the metal chelates arises from the much more extensive fragmentation of the molecular ions of some complexes than of others (i.e. there are

Can. J. Chem. Downloaded from www.nrcresearchpress.com by 210.87.254.105 on 09/06/12
For personal use only.

Can. J. Chem. Downloaded from www.nrcresearchpress.com by 210.87.254.105 on 09/06/12
For personal use only.

wide variations in relative I_{50} values). The "extrapolated voltage difference" method attempts to overcome these complications but even here there may be difficulties in making a reliable extrapolation.

We believe that the curve fitting procedure (which is not subject to the restrictions above) yields more reliable ionization energies than reported previously for the metal chelates, a viewpoint supported by comparisons with available PE spectra. These comparisons show that the electron impact ionization energy of a complex normally lies between the band maximum and band onset of the leading band, i.e. between the vertical and adiabatic ionization energies.

The chelates of Sc(III) (electron impact data reported for the first time) and Al(III) illustrate the variation in ionization energy with CF_3 for CH_3 substitution for complexes having no *d* electrons. The variations, which have been summarized in more detail elsewhere (1), are similar whether or not low lying *d* orbitals are available.

The PE spectra of $Ti(hfa)_3$, d^1, and $V(hfa)_3$, d^2, contain a weak band (band Y) appearing at lower energies than the stronger band A. Band Y was assigned to ionization by electron removal from orbitals of mainly 3*d* character. On the assumption that for the $Ti(acac)_3$ and $V(acac)_3$ complexes the deviations of the low energy data points from the "best fit" curves are caused by similarly assigned weak ionizations it is possible to estimate the threshold values for these processes. This was done by subtracting the extrapolated contribution of the "best fit" results from the experimental points, and fitting the resulting values to an expression of the type [2*a*, 2*b*]. The threshold values, and the ionization probability relative to the main threshold processes, are given in Table 2. The uncertainty in the thresholds for these weak processes is greater than for the main thresholds because of the smaller number of data points and the higher signal-to-noise ratio for the low ion currents involved. Even though comparison PE spectra are not available for these complexes the extracted values are reasonable when compared with observed changes in energies of metal and ligand orbitals as CH_3 is replaced by CF_3. The energies of metal dominated orbitals are shifted by slightly less than those of ligand dominated π orbitals (as illustrated very well by the PE spectra of the Cr(III) complexes) and also band Y moves closer to band A as the number of *d* electrons increases (24). The weak processes should influence the values of the ionization energies extracted from the "best fit" curves for $Ti(acac)_3$ and $V(acac)_3$. More satisfactorily, a composite function involving two threshold values should be used in an approach similar to that adopted for xenon. This was not attempted since we do not know what form the ionization probability function for these weak processes would take at values 1–3 V above their thresholds. We anticipate that the corrections to the IE values reported in Table 2 would be small.

The PE spectra of the Cr(III) complexes (d^3) show that as CF_3 replaces CH_3, the separation between the bands A and Y increases slightly. Correspondingly, the low energy electron impact ionization data points lie above the "best fit" curves in the cases of the $Cr(tfa)_3$ and $Cr(hfa)_3$ complexes. It was not possible to obtain reliable threshold values for assumed weak ionizations in these regions because they are too close to the main threshold. The signal-to-noise ratio became too difficult to handle when the weak ionization contributed only a small proportion of the total ion current. The "best fit" curve for the $Cr(acac)_3$ complex shows no detectable deviation from the experimental points, even in the low energy region, perhaps because, as shown by the PE spectra, in this case band Y is largely unresolved from band A.

The "best fit" curves for the Mn(III), Fe(III), and Co(III) chelates (d^4, d^5, and d^6 respectively) all fit the experimental data points very well. In agreement with this, the PE spectra show no weak, low energy bands that are well resolved from the main bands. The results for the Mn(III) and Fe(III) chelates show no obvious evidence, in either electron or photon impact, for ionization by electron removal from an e_b orbital (correlating with e_g^* in octahedral symmetry) of mainly metal 3*d* character. Although the barely discernible shoulder Z in the PE spectrum of $Mn(hfa)_3$ was suggested to arise in this way (24) we believe other assignments are possible and regard the energies of the e_g^* orbitals as a currently unsolved problem.

Experimental

The acetylacetonates (25), tri- and hexafluoroacetylacetonates (29) of Al(III), Ti(III), V(III), Cr(III), Mn(III), Fe(III), and Co(III) were prepared as described previously. The Sc(III) complexes were prepared by reacting slightly more than the stoichiometric quantity of the β-diketone with scandium nitrate in methanol buffered with ammonium acetate. After removal of solvent with a stream of air under partial vacuum, the wet residue was extracted with chloroform. The residue of ammonium salts was removed by filtration. Evaporation of the chloroform left a sticky residue which on treatment with hexane yielded the desired product as a dry white powder. $Co(tfa)_3$ was prepared by electrochemical oxidation at a platinum electrode of a methanolic solution containing cobalt(II) nitrate and trifluoroacetylacetone buffered with potassium acetate. It was recovered from the solution as dark green crystals.

Can. J. Chem. Downloaded from www.nrcresearchpress.com by 210.87.254.105 on 09/06/12
For personal use only.

Ionization efficiency curves were measured using a Hitachi RMU-6D single focussing mass spectrometer. Metal chelates were introduced to the ion source through the direct insertion probe and heated carefully until the vaporization rate (as determined by the mass spectral peaks) was steady. The temperature of the ion source was about 150°C. In the early work a Hewlett-Packard Model 3459A digital voltmeter was used to monitor both the amplified ion current and the chamber voltage (electron accelerating voltage) when ionization efficiency curves were being measured. The chamber voltage was stable to within ±0.001 V. Ion current readings for a particular ion were taken at 0.100 V intervals upward from the ionization threshold and also at a chamber voltage of 50 V before and after these readings. To calibrate the electron energy, ionization efficiency curves for xenon admitted to the ion source simultaneously were similarly measured. In the recent studies the DC amplifier was replaced by an ion counting system comprised of a Galileo CEM4039 Channeltron electron multiplier, SSRI model 1120 amplifier discriminator, SSRI model 1127 NIM adaptor, Ortec model 776 counter and timer, and Ortec model 777A line printer (the last three items installed in an Ortec model 401A bin). This system greatly improved both sensitivity and signal-to-noise ratios. Calibration of the electron energy was accomplished by similar measurements on a metal chelate ($Al(tfa)_3$ or $Al(hfa)_3$ in these studies) of previously determined ionization energy, admitted to the ion source simultaneously via the gas inlet system.

Initially, curve fitting was achieved using a Hewlett-Packard HP-67 programmable pocket calculator. The sum of the squares of the deviations (χ^2) was minimized for the three parameters IE, B or C, and kT by an iterative method. After it was established that the value of IE extracted by this procedure varied for the sample and reference by almost exactly the same amount (the change in the difference was within 0.02 eV in most cases) as kT was varied, then for subsequent fittings kT was put equal to 0.215 eV (T = 2500 K). This resulted in significant reductions in time taken to find the "best fit" values of IE and B or C. With experience these values could be found quite quickly (usually within 30 min) by manual control of the iterations, which required only minimal attention of the operator (i.e. entering test values of IE and B or C).

In the later stages of the work the Hewlett-Packard HP-41C programmable pocket calculator became commercially available. With its much more extensive memory and programming capabilities the iterations were controlled by the calculator. The value of χ^2 was minimized using a parabolic extrapolation method (31).

Acknowledgement

We thank the Natural Sciences and Engineering Research Council of Canada for financial support of this work.

1. J. B. Westmore. Chem. Rev. **76**, 695 (1976).
2. F. P. Lossing, A. W. Tickner, and W. A. Bryce. J. Chem. Phys. **19**, 1254 (1951).
3. H. D. Smyth. Proc. R. Soc. London, Ser. A, **102**, 283 (1922).
4. R. E. Honig. J. Chem. Phys. **16**, 105 (1948).
5. J. W. Warren. Nature, London, **164**, 810 (1950).
6. R. W. Kiser and E. J. Gallegos. J. Phys. Chem. **66**, 947 (1962).
7. B. N. McMaster. Specialist Periodical Reports; Mass Spectrometry, **3**, 1 (1975).
8. J. D. Morrison. J. Chem. Phys. **19**, 1305 (1951).
9. J. D. Morrison. J. Chem. Phys. **21**, 1767 (1953).
10. J. D. Morrison. J. Chem. Phys. **22**, 1219 (1954).
11. J. D. Morrison. J. Chem. Phys. **22**, 2090 (1954).
12. J. D. Morrison. J. Chem. Phys. **39**, 200 (1963).
13. R. E. Winters, J. H. Collins, and W. L. Courchene. J. Chem. Phys. **45**, 1931 (1966).
14. J. Vogt and C. Pascual. Internat. J. Mass Spectrom. Ion Phys. **9**, 441 (1972).
15. R. G. Dromey, J. D. Morrison, and J. C. Traeger. Internat. J. Mass Spectrom. Ion Phys. **6**, 57 (1971).
16. J. E. Collin. *In* Mass spectrometry. *Edited by* R. I. Reed. Academic Press, New York. 1965. p. 201 and references therein.
17. F. H. Field and J. L. Franklin. Electron impact phenomena. Academic Press, New York. Rev. ed. 1970. p. 15.
18. C. G. Pitt and D. Rosenthal. J. Chem. Soc. Faraday Trans. II, **69**, 332 (1973).
19. R. E. Fox, W. M. Hickman, and T. Kjeldaas. Phys. Rev. **89**, 555 (1953).
20. E. M. Clarke. Can. J. Phys. **32**, 764 (1954).
21. G. G. Cloutier and H. I. Schiff. J. Chem. Phys. **31**, 793 (1954).
22. S. N. Foner and B. H. Nall. Phys. Rev. **122**, 512 (1961).
23. C. E. Melton and W. H. Hamill. J. Chem. Phys. **41**, 546 (1964).
24. S. Evans, A. Hamnett, A. F. Orchard, and D. R. Lloyd. Faraday Discuss. Chem. Soc. **54**, 227 (1972).
25. G. M. Bancroft, C. Reichert, and J. B. Westmore. Inorg. Chem. **7**, 870 (1968).
26. S. M. Schildcrout, R. G. Pearson, and F. E. Stafford. J. Am. Chem. Soc. **90**, 4006 (1968).
27. M. M. Bursey and P. F. Rogerson. Inorg. Chem. **9**, 676 (1970).
28. R. W. Kiser, R. M. Teeter, and E. J. Gallegos. Private communication.
29. C. Reichert, G. M. Bancroft, and J. B. Westmore. Can. J. Chem. **48**, 1362 (1970).
30. G. M. Bancroft, C. Reichert, J. B. Westmore, and H. D. Gesser. Inorg. Chem. **8**, 474 (1969).
31. P. R. Bevington. Data reduction and error analysis for the physical sciences. McGraw-Hill, New York. 1969.

Water elimination from the keto and enol tautomers of ionised ethylacetate

J. L. HOLMES AND P. C. BURGERS
Chemistry Department, University of Ottawa, Ottawa, Ont., Canada K1N 9B4
AND
J. K. TERLOUW
Analytical Chemistry Laboratory, University of Utrecht, Croesestraat 77A, 3522AD, Utrecht, The Netherlands

Received November 24, 1980

This paper is dedicated to Dr. F. P. Lossing of the National Research Council of Canada on the occasion of his 65th birthday

J. L. HOLMES, P. C. BURGERS, and J. K. TERLOUW. Can. J. Chem. **59**, 1805 (1981).

The keto and enol forms of ionised ethylacetate both lose H_2O to generate the keto and enol ions of methylvinylketone, probably via common reacting configurations. All hydrogen atoms and both oxygen atoms participate in this mechanistically complex reaction; the degree of their involvement depends upon the internal energy content of the fragmenting ions.

J. L. HOLMES, P. C. BURGERS et J. K. TERLOUW. Can. J. Chem. **59**, 1805 (1981).

Les formes cétoniques et énoliques de l'acétate d'éthyle ionisé perdent H_2O et conduisent aux ions de formes cétonique et énolique de la méthylvinylcétone, probablement par l'intermédiaire de configurations réactionnelles communes. Tous les atomes d'hydrogène et les deux atomes d'oxygène prennent part à cette réaction dont le mécanisme est complexe; le taux de leur participation dépend de l'énergie interne des ions qui subissent la fragmentation.

[Traduit par le journal]

Introduction

The unimolecular reaction of lowest energy requirement for ionised ethylacetate is the elimination of H_2O. This reaction is the predominant process observed in the μs time-frame; loss of $CH_3^{\bullet}$ and $C_2H_3^{\bullet}$ compete unfavorably with H_2O elimination and only produce weak metastable peaks. The elimination of H_2O was last studied by Yeo (1) in 1970. He concluded that the metastable molecular ions (species having little internal energy in excess of the fragmentation threshold) underwent appreciable positional mixing of all H-atoms (but not to the statistical limit), whereas for ion-source reactions only H atoms within the C_2H_5 group extensively lost their positional identity. The chosen daughter ion structure was the four-membered ring-closed form of ionised methylvinylketone, $[CH_3C(O)CH—CH_2]^{+\bullet}$.

It has been shown previously that ionised α–β unsaturated methyl and ethyl esters (2) such as $CH_2=CH—C(O)O—CH_3$, also fragment by the loss of H_2O, a reaction of minor importance in the ion source but prominent in the field-free regions. From analyses of metastable peak shapes it was concluded that although this reaction could result from an interchange of the alkyl group with a β-vinylic hydrogen atom (ester → acid rearrangement), it actually involved a facile 1,4-hydrogen migration followed by cyclization to yield the enol form of ionized γ-butyrolactone. For α–β unsaturated benzylesters (3) the reaction appeared to have structure diagnostic value in the normal mass spectra.

In contrast to the above, the saturated isomers ethylacetate and the $[C_4H_8O_2]^{+\bullet}$ acids do not have loss of H_2O as a common fragmentation pathway and so their interchange does not take place.

The present paper reports our investigation of the H_2O loss from ethylacetate, using metastable ion (MI) characteristics (MI spectra and peak shapes), collisional activation (CA) spectra, appearance energy (AE) measurements, thermochemical data and measurements performed with labelled compounds. This paper also forms part of our continuing study of the thermochemistry and reactions of isomeric keto and enol ions (4–6). Thus it will be shown here that the enol ion of ethylacetate, which is thermodynamically much more stable than its keto counterpart, also loses H_2O abundantly in the μs time frame, probably via the same reacting configuration as for the keto tautomer.

Results and Discussion

In order to establish the structure of the $[C_4H_6O]^{+\bullet}$ daughter ions produced from each tautomer, the following experiments were performed.

(1) The appearance energies (AE) of the daughter ions were measured using energy selected electrons and the results were compared with established thermochemical data. The AE for *m/z* 70 from $CH_3COOCH_2CH_3$ was found to be 10.32 ±

0008-4042/81/121805-05$01.00/0
©1981 National Research Council of Canada/Conseil national de recherches du Canada

Can. J. Chem. Downloaded from www.nrcresearchpress.com by 210.87.254.42 on 09/06/12
For personal use only.

Can. J. Chem. Downloaded from www.nrcresearchpress.com by 210.87.254.42 on 09/06/12
For personal use only.

0.05 eV, leading to $\Delta H_f[C_4H_6O]^{+\cdot}$ = 190 kcal mol^{-1} ($\Delta H_f[CH_3COOCH_2CH_3]$ = −106.3 kcal mol^{-1} (4); $\Delta H_f[H_2O]$ = −57.8 kcal mol^{-1} (7)). AE *m/z* 70 from $CH_3CH_2CH_2CH_2COOCH_2CH_3$ (4) = 11.00 ± 0.05 eV, leading to $\Delta H_f[C_4H_6O]^{+\cdot}$ = 185 kcal mol^{-1} ($\Delta H_f[CH_3(CH_2)_3COOCH_2CH_3]$ = −121.3 kcal mol^{-1} (4); $\Delta H_f[CH_2{=}CHCH_3]$ = +4.9 kcal mol^{-1} (7)). Now $\Delta H_f[CH_3COCH{=}CH_2]^{+\cdot}$ = 195 kcal mol^{-1} (8). Of the $[C_4H_6O]^{+\cdot}$ ions studied in this work, five have energies which (with $\Delta H_f[H_2O]$) lie close to or below the threshold for the ethylacetate fragmentation. These are $[CH_2{=}C(OH)CH{=}CH_2]^{+\cdot}$, ΔH_f = 182 kcal mol^{-1} (8); $[CH_2{=}CHCH{=}CH(OH)]^{+\cdot}$, ΔH_f = 176 kcal mol^{-1} (8); $[(CH_3)_2CCO]^{+\cdot}$, ΔH_f = 163 kcal mol^{-1} (from IE = 8.38 eV (9), $\Delta H_f[(CH_3)_2CCO]$ = −30.7 kcal mol^{-1} (10)); $[\overbrace{CH_2CH{=}CHCH_2O}]^{+\cdot}$, ΔH_f = 194 kcal mol^{-1} (IE = 9.14 eV, energy selected electrons, $\Delta H_f[\overbrace{CH_2CH{=}CHCH_2O}]$ = 17 kcal mol^{-1} (10)). Of the above, ionised dimethylketene is unlikely to be generated on mechanistic grounds and as will be described below, the dihydrofuran molecular ions have characteristic collisional activation mass spectra which permits their being ruled out. It can be concluded therefore that *at threshold* the $[C_4H_6O]^{+\cdot}$ daughter ions from both tautomers are not ionised methylvinylketone. These results are also presented in the energy diagram, Fig. 1; it should be noted that ionised ethyl acetate is "hot" with respect to the above enol product ions at its ionisation threshold whereas an appreciable activation energy exists for their generation from the ionised enol ester.

Note (Fig. 1) that the second least energy demanding fragmentation of ethyl acetate, loss of $C_2H_3^{\cdot}$, producing $[\overset{+}{C}H_3C(OH)_2]$, also takes place in the μs time frame (AE *m/z* 61 = 10.62 ± 0.05 eV, $\Delta H_f[C_2H_3^{\cdot}]$ = 64 kcal mol^{-1} (average value from ref. 11) $\Delta H_f[\overset{+}{C}H_3C(OH)_2]$ = 74 kcal mol^{-1}). The metastable peak, however, is only ca. 0.02 as intense as that for the H_2O loss process.

(*2*) The MI and CA characteristics of the daughter ions were compared with those of selected $[C_4H_6O]^{+\cdot}$ ions of known structure.

The $[C_4H_6O]^{+\cdot}$ daughter ions from ethyl acetate and its tautomer produced only very weak MI spectra, too weak to be of value in ion structure identification. The CA results are presented in Table 1 where it can be seen that the major portion of the $[C_4H_6O]^{+\cdot}$ ions derived from either *metastable* ester ions or those fragmenting in the ion source consist of $[CH_3COCH{=}CH_2]^{+\cdot}$, but the enhanced intensity of *m/z* 69 in the CA spectra (and that obtained from the $[M - H_2O]^{+\cdot}$ ion from the enol

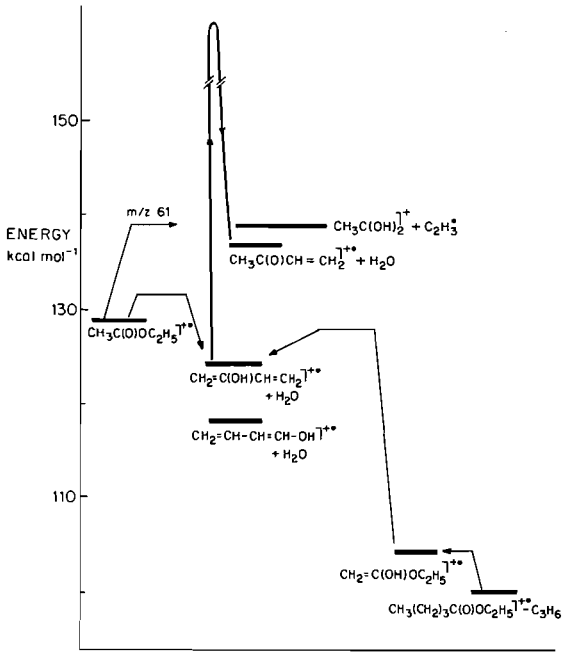

FIG. 1. Energy diagram for the primary fragmentations of the keto and enol forms of ionised ethyl acetate. The broken line indicates that there is a large barrier (at least 53 kcal mol^{-1} (8)) for the isomerisation of methylvinylketone to its enol.

ion of ethylacetate), compared with that from $[CH_3COCH{=}CH_2]^{+\cdot}$, may arise from contributions from other ion structures. Note that a very small amount of $[CH_2{=}CHCH{=}CHOH]^{+\cdot}$ ions in admixture with $[CH_3COCH{=}CH_2]^{+\cdot}$ would only be observable by an enhanced abundance at *m/z* 69 in CA spectra. The possible formation of ionised dihydrofuran, although energetically and mechanistically feasible, can be ruled out by virtue of its CA spectrum (Table 1). The possible presence of the ether ion $[CH_2{=}CH{-}O{-}CH{=}CH_2]^{+\cdot}$ must also be considered on energetic and mechanistic grounds; $\Delta H_f[CH_2{=}CH{-}O{-}CH{=}CH_2]^{+\cdot}$ = 197 kcal mol^{-1} (IE = 8.68 ± 0.05 eV, $\Delta H_f[CH_2{=}CH{-}O{-}CH{=}CH_2]$ = −3.1 kcal mol^{-1} (10)), but it too need not be considered further in view of its significantly different CA spectrum, see Table 1.

Labelling Experiments

The metastable peaks for loss of H_2O from the tautomeric molecular ions $[CH_3COOCH_2CH_3]^{+\cdot}$, *a*, and $[CH_2{=}C(OH)OCH_2CH_3]^{+\cdot}$, *b*, (produced by C_3H_6 loss from ionised ethyl pentanoate (4)) are of simple Gaussian shape (n = 1.8 and 1.9 (12)) respectively and have very closely similar profiles indicating that the same reacting configuration may well be involved. However, the kinetic energy releases evaluated from the peak widths at half-height, $T_{0.5}$, depended upon the timescale of the

Can. J. Chem. Downloaded from www.nrcresearchpress.com by 210.87.254.42 on 09/06/12
For personal use only.

observations; in increasing times, MS902 (first field-free region) $T_{0.5}(a)$ = 13.5 meV, (second ffr) $T_{0.5}(a)$ = 10.6 meV and ZAB-2f (second ffr) $T_{0.5}(a)$ = 9.2 meV. This systematic change of kinetic energy release can arise from either the relationship between energy partitioning and the internal energy content for a single reacting configuration or from the presence of more than one reacting configuration (12). The MI spectra of ^{18}O labelled ionised ethyl acetate and its enol were also investigated and the results are shown in Table 2. For ion source decompositions and all metastable ion observation times the keto and enol O atoms are similarly preferentially lost and it appears that this process has a lower energy requirement than the H_2O loss which involves the ester O atom because (*i*) the $T_{0.5}$ value (keto, enol) is lower than that for the ester O atom and (*ii*) the former process becomes increasingly more important at longer ion lifetimes. Thus both oxygen atoms participate in H_2O loss and the similarity of the results for both tautomers again indicates that common reacting configurations are involved. (It must be noted that keto and ester O atoms do not readily exchange in the *neutral* ester (13).)

The results of observations on deuterium labelled compounds are presented in Table 3.

For the keto ions, ion source fragmentations largely involve the H atoms in the ethyl group but at the longest times the observations indicate that all H atoms participate in water loss, tending towards their complete loss of positional identity. These observations agree with those previously reported by Yeo (1). The metastable peaks for the various labelled water losses had a common shape.

In the case of the labelled enol ions, the methylene hydrogen atoms barely participate in ion-source reactions and a trend towards positional randomisation at long ion lifetimes similar to but not identical with that for the keto ions was observed.

We have also compared the CA mass spectra of the $[M - D_2O]^{+\cdot}$ and $[M - HDO]^{+\cdot}$ daughter ions produced from $[CH_2{=}C(OH)OC_2D_5]^{+\cdot}$. The feature that should be emphasized is that *both* CA spectra showed mostly loss of $CH_2D^{\cdot}$ from the daughter ions. These results are shown in Table 4 where it can also be seen that the $[M - D_2O]^{+\cdot}$ ion clearly contains some enol-characteristic fragments in its CA spectrum by virtue of the enhanced peak for $H^{\cdot}$ loss.

It may therefore be concluded that prior to loss of both HDO and D_2O from the enol ion in the ion source, deuterium is transferred irreversibly to the CH_2 group. Although observations from the deu-

TABLE 1. Collisional activation spectra of $[C_4H_6O]^{+\cdot}$ ions

$C_4H_6O^{+\cdot}$ isomer	*m/z* of daughter ion[a,b]																					
	69	68	67	55	54	53	52	51	50	49	44	43	42	41	40	39	38	37	31	29	27	26	25	15
$CH_3C(O)OCH_2CH_3 - H_2O$ (S)[c]	6	—	—	100	2	1	—	—	1	—	—	17	5	2	—	2	—	—	—	—	4	2	—	1
(M*)	4			100	2	1	—	1	1	—	—	20	6	2	1	2	—	—	—	—	6	3	1	1
$CH_2{=}\dot{C}(OH)OCH_2CH_3 - H_2O$	7			100	1	1	—	1	1	—	—	18	6	3	1	4	1	—	1	—	6	4	—	1
$CH_3\dot{C}(O)CH{=}CH_2$	1			100	2	1	—	—	—	1	—	16	5	1	—	3	—	—	—	—	4	2	—	1
$CH_2{=}C(OH)CH{=}CH_2$	(100)	5	3	100	3	13	14	28	30	8	8	91	86	50	17	55	13	10	6	12	46	16	4	6
$CH_2{=}CH{-}CH{=}CH{-}OH$	(670)	30	4	33	2	6	9	26	23	7	11	20	49	87	22	100	24	14	8	22	22	10	2	2
$CH_2{=}CH{-}O{-}CH{=}CH_2$	40	7	—	2	—	—	—	—	—	—	50	80	100	38	4	10	3	2	12	2	62	12	2	10
$CH_2CHCHCH_2O$	(150)	25	—	1	—	—	—	1	2	—	1	1	100	41	15	56	11	5	—	10	6	3	—	1

[a]Abundances (average of three runs) relative to the base peak = 100%; peaks of low intensity at *m/z* 66, 56, 36, and 16 have been omitted; estimated accuracy ±1%. Electron energy, 70eV.
[b]Apart from the *m/z* 69 peak (intensities in parentheses), all peak intensities have been corrected for contributions of unimolecular decompositions as described in ref. 14.
[c]S stands for $[C_4H_6O]^{+\cdot}$ ions derived from ester ions fragmenting in the ion source and M* for metastable ester ions.

TABLE 2. Relative abundance[a] for loss of $H_2{}^{16}O$ and $H_2{}^{18}O$ from $[CH_3C(^{18}O)OCH_2CH_3]^{+\cdot}$ and $[CH_2{=}C(^{18}OH)OCH_2CH_3]^{+\cdot}$ ions

	$CH_3{-}C(=^{18}O){-}O{-}CH_2CH_3$		$CH_2{=}C(^{18}OH){-}O{-}CH_2CH_3$	
	$H_2{}^{16}O$	$H_2{}^{18}O$	$H_2{}^{16}O$	$H_2{}^{18}O$
Ion source	35	65	34	66
1st ffr MS902	30	70	29	71
2nd ffr MS902	18	82	19	81
2nd ffr ZAB-2f	13(13.0)[b]	87(8.6)	15(14.4)	85(10.0)

[a]Intensities normalized to sum = 100%, all values ± 1.
[b]Values in parentheses refer to kinetic energy release (meV) evaluated from the half-height widths of the metastable peaks.

TABLE 3. Relative abundances[a] for water losses from some D-labelled $[CH_3C(O)OC_2H_5]^{+\cdot}$ and $[CH_2{=}C(OH)OC_2H_5]^{+\cdot}$ ions

	$CH_3{-}C(=O){-}OC_2D_5$			$CH_2{=}C(OH){-}O{-}C_2D_5$			$CD_2{=}C(OH){-}O{-}C_2H_5$		
	H_2O	HDO	D_2O	H_2O	HDO	D_2O	H_2O	HDO	D_2O
Ion source	—	13	86	2	56	44	95	5	—
1st ffr MS902	2	27	71	4	51	45	88	12	—
2nd ffr MS902	5	44	51	7	51	42	77	23	1
2nd ffr ZAB-2f	6	44	50	7	51	42	73	26	1
Calculated[b]	11	54	36	11	54	36	54	43	4

[a]Intensities normalized to sum = 100%, all values ± 1.
[b]Assuming complete loss of positional identity.

TABLE 4. Partial collisional activation spectra of the $[M - HDO]^{+\cdot}$ and $[M - D_2O]^{+\cdot}$ ions generated from $[CH_2{=}C(OH)OC_2D_5]^{+\cdot}$

	m/z of daughter ion[a]										
Ion	73	72	58	57	56	45	44	43	42	30	29
$[M - HDO]^{+\cdot}$ $m/z = 74$	1	2	100	11	2	4	17	3	2	9	2
$[M - D_2O]^{+\cdot}$ $m/z = 73$		11	11	100	11	11	21	17	5	2	11

[a]Abundances relative to the base peak = 100%, all values ± 1. Electron energy 70eV.

terium labelling experiments can most simply be interpreted as resulting from enol → keto tautomerisation preceding the loss of water from the enol ion, we cannot unequivocally distinguish this from among other potential reaction paths. Note that the CA mass spectra of the keto and enol ester ions are not the same, Table 5. The observations however do not imply that keto ions cannot partially tautomerize, i.e., there is no evidence that the CA spectrum of the keto ions is that of a *single* ionic species; the very small energy difference between ionisation and fragmentation precludes any experiment designed to show energy dependence in the CA mass spectrum. For the enol ion, the CA mass spectrum was found to be unaffected by reduction of the ionising electron energy to a level compatible with maintaining the signal strength. For the longer-lived ions which fragment in the field-free regions, the results tend towards complete loss of positional identity of H/D atoms at the longest observation times. For such ions the tautomerisation possibly is reversible; this too is in keeping with the observation (Table 3) that label randomisation is more complete for keto ions in any given field-free region than for the enol species (compare the first and third columns in Table 3). This latter effect cannot readily be attributed to internal energy differences because the metastable peak shapes for water loss from ions initially having keto or enol configurations are so very closely similar.

It is tempting to try to write mechanistic pathways for this water elimination reaction; however, the experiments give no clear indication as to what the reacting configuration(s) might be. Note for example that although the loss of keto oxygen becomes nearly specific among ions of lowest internal energy, these are the very ions in which loss of positional identity of H atoms becomes maximal — and vice-versa for the ions fragmenting in the ion source.

Two other experimental observations deserve brief mention. Whereas the isomeric ionised mole-

Can. J. Chem. Downloaded from www.nrcresearchpress.com by 210.87.254.42 on 09/06/12
For personal use only.

TABLE 5. Collisional activation mass spectra of $[CH_3C(O)OC_2H_5]^{+\cdot}$ and $[CH_2{=}C(OH)OC_2H_5]^{+\cdot}$ ions

	m/z of daughter ion [a,b]																	
Ion	87	73	70	69	61	60	55	45	44	43	42	41	39	31	29	28	27	26
$CH_3C(O)OC_2H_5$	—	7	60	—	100	49	2	46	6	31	11	—	—	1	5	3	4	2
$CH_2{=}C(OH)OC_2H_5$	1	6	40	3	95	100	3	44	4	30	30	3	2	3	17	5	9	2

[a]Abundances relative to the base peak = 100%, all values ± 1. Electron energy 70 eV.
[b]Peak intensities at *m/z* 70 have been corrected for MI contributions.

cule, $CH_3COCH(OH)CH_3$, does not lose H_2O, or generate *m/z* 61 (the second most intense peak in the mass spectrum of ethyl acetate); the related keto-alcohol $[CH_3COCH_2CH_2OH]^{+\cdot}$ eliminates H_2O producing an intense metastable peak, ($T_{0.5}$ = 6.9 meV) and also generates *m/z* 61 in its mass spectrum. It is possible therefore that 4-hydroxybutan-2-one is a participating structure in the complex behaviour of the keto and enol ions of ethyl acetate.

Conclusions

The investigation described in this paper employed most of the presently available techniques for the detailed study of unimolecular ionic fragmentations. Disappointingly few firm conclusions can be drawn from this study (see abstract). The acquisition of more detailed information, which might for example permit the reaction mechanism to be elucidated, probably could be achieved if ions having known, sharply defined, internal energy contents were studied. Note for example (Fig. 1) the small energy range between the fragmentation threshold for ethylacetate and the thermochemical threshold for [methylvinylketone]$^{+\cdot}$ + H_2O. Although metastable ion phenomena relate to a small range of rate constants, ca. 10^5–10^6 s^{-1}, normal electron impact ion sources produce ions having broad, ill-defined energy contents.

Experimental

CA mass spectra and metastable peak observations were recorded on a VG-Micromass ZAB 2f mass spectrometer as described in ref. 14. For metastable peak observations the main beam width at half height was reduced to 0.1 V at an electric sector potential of 422.1 V. Metastable peak shapes were also recorded on a AEI-MS902S mass spectrometer with a main beam width of 1.8 V at 6300 V accelerating voltage. Kinetic energy release values were calculated in the usual way with correction for the main beam width (12).

Ethylacetate, methylvinylketone, and methylacetyl carbinol were purchased from Aldrich Europe and used without further purification. Divinyl ether was prepared as described in ref. 15. 4-Hydroxy-2-butanone was synthesized by the method Hays *et al.* (16).

The OC_2D_5-labelled esters were prepared by esterification of acetic acid or pentanoic acid with C_2D_5OD (Merck, Sharpe and Dohme, 99.5 atom %D). The methylene-labelled esters were prepared as follows:

To a solution of butyldiisopropylamine (0.1 mol) in dry ether (80 cm^3) was slowly added (N_2 atmosphere), 0.1 mol of acetonitrile-d_3 (Aldrich, Europe) at −40°C. After raising the temperature to −20°C, C_3H_7I (10.5 cm^3) in ether (50 cm^3) was slowly added. The mixture was agitated for 2 h and subsequently poured into ice-water (100 cm^3). The mixture was extracted five times with ether (50 cm^3), and the combined organic layers were dried over calcium chloride. Distillation yielded 3.0 g (30%) $CH_3CH_2CH_2CD_2C{\equiv}N$ (95%D). The corresponding acid was made as described in ref. 17 and the esters were prepared therefrom using C_2H_5OH or C_2D_5OD.

The ^{18}O-labelled esters were synthesized on a microscale by converting the purified acid chlorides to the ^{18}O-labelled acids with $H_2{}^{18}O$ (Prochem 90 atom%) in a small Pyrex tube at room temperature and subsequently adding C_2H_5OH.

Acknowledgements

J.H. thanks the Natural Sciences and Engineering Research Council of Canada for continuing financial support. The authors thank Dr. F. P. Lossing for AE measurements and many stimulating discussions.

1. A. N. H. YEO. Chem. Commun. 1154 (1970).
2. P. C. BURGERS, J. K. TERLOUW, P. C. VIJFHUIZEN, and J. L. HOLMES. Org. Mass. Spectrom. **13**, 470 (1978).
3. P. C. BURGERS, J. K. TERLOUW, and P. C. VIJFHUIZEN. Org. Mass Spectrom. **13**, 658 (1978).
4. J. L. HOLMES and F. P. LOSSING. J. Am. Chem. Soc. **102**, 1591 (1980).
5. J. L. HOLMES and F. P. LOSSING. J. Am. Chem. Soc. **102**, 3732 (1980).
6. J. L. HOLMES and F. P. LOSSING. Org. Mass Spectrom. **14**, 512 (1979).
7. H. M. ROSENSTOCK, K. DRAXL, B. W. STEINER, and J. T. HERRON. J. Phys. Chem. Ref. Data, Suppl. 1, 6 (1966).
8. J. K. TERLOUW, W. HEERMA, J. L. HOLMES, and P. C. BURGERS. Org. Mass. Spectrom. **15**, 582 (1980).
9. H. BOCK, T. HIRABAYASHI, S. MOHMAND, and B. SOLOUKI. Angew. Chem. Int. Ed. Engl. **16**, 105 (1977).
10. S. W. BENSON, F. R. CRUIKSHANK, D. M. GOLDEN, G. R. HAUGEN, H. E. O'NEAL, A. S. RODGERS, R. SHAW, and R. WALSH. Chem. Rev. 279 (1969).
11. F. P. LOSSING. Can. J. Chem. **49**, 357 (1971); D. M. GOLDEN and S. W. BENSON. Chem. Rev. **69**, 125 (1969).
12. J. L. HOLMES and J. K. TERLOUW. Org. Mass Spectrom. **15**, 383 (1980).
13. G. G. SMITH, K. J. VOORHEES, and F. M. KELLY. Chem. Commun. 709 (1971).
14. J. K. TERLOUW, P. C. BURGERS, and H. HOMMES. Org. Mass Spectrom. **14**, 387 (1979).
15. L. BRANDSMA and J. F. ARENS. Rec. Trav. Chim. Pays-Bas, **81**, 33 (1962).
16. J. T. HAYS, G. F. HAGER, H. M. ENGELMANN, and H. M. SPURLIN. J. Am. Chem. Soc. **73**, 5369 (1951).
17. A. I. VOGEL. Textbook of practical organic chemistry. Longmans, Green and Co., New York. 1940. p. 353.

Can. J. Chem. Downloaded from www.nrcresearchpress.com by 210.87.254.42 on 09/06/12
For personal use only.

Flame-ion probe of the reaction zone in a CH_4–O_2–Ar flame with added HCN, NH_3 and NO

JOHN M. GOODINGS, GARY B. DE BROU,[1] AND DIETHARD K. BOHME

Department of Chemistry, York University, 4700 Keele Street, Downsview, Ont., Canada M3J 1P3

Received October 22, 1980

This paper was presented at a Special Symposium "The Structure and Thermochemistry of Gaseous Ions," held in honour of Dr. F. P. Lossing of the National Research Council of Canada, during the Second Canadian Conference on the Gas Phase Chemistry of Ions, Trent University, June 5–8, 1980, and is dedicated to him on the occasion of his 65th birthday

JOHN M. GOODINGS, GARY B. DE BROU, and DIETHARD K. BOHME. Can. J. Chem. **59**, 1810 (1981).

The addition of 0.3% of the fuel-nitrogen (fuel-N) compounds HCN, NH_3, or NO to a premixed, fuel-rich, CH_4–O_2–Ar flame burning at atmospheric pressure demonstrated the rapid interconversion of nitrogenous intermediates in the reaction zone. The nitrogenous species (HCN/CN, HNCO/NCO, NH_3, NH_2, NH, NO, NO_2) were observed as ions (CN^-, H_2CN^+, NCO^-, H_2NCO^+, NH_4^+, NH_3^+, NH_2^+, NO^+, NO_2^-, and hydrate ions) formed in chemical ionization processes discussed previously (1). The ions were sampled directly into a flame-ion mass spectrometer which had sufficient spatial resolution for the measurement of ion concentration profiles through the reaction zone. The study bears on Fenimore's suggestion for the formation of "prompt NO" in fuel-rich hydrocarbon flames. These additive results were compared with previous results involving nitrogenous species present in a similar CH_4–O_2 flame doped with 10% N_2. The increased sensitivity of the additive approach confirmed many of the mass assignments and mechanisms involved in the N_2 study. Reasonably good evidence was obtained for the elusive intermediate HNCO (and possibly isomeric HCNO as well) in protonated form, and also formamide, NH_2CHO, which had not been detected previously. Similarities in profile peak positions and magnitudes observed for many ions, irrespective of the nature of the fuel-N additive, indicated that the nitrogenous species were linked by a network of fast bimolecular reactions, many of which appeared to be balanced in the reaction zone.

JOHN M. GOODINGS, GARY B. DE BROU et DIETHARD K. BOHME. Can. J. Chem. **59**, 1810 (1981).

L'addition de 0,3% de combustibles azotés (combustible-N) HCN, NH_3 ou NO à la flamme de CH_4–O_2–Ar riche en combustible, prémélangée et brûlant à pression atmosphérique démontre qu'il se produit une interconversion rapide des intermédiaires azotés dans la zone de réaction. On a observé que les espèces azotées (HCN/CN, HNCO/NCO, NH_3, NH_2, NH, NO, NO_2) sont présentes sous forme d'ions (CN^-, H_2CN^+, NCO^-, H_2NCO^+, NH_4^+, NH_3^+, HN_2^+, NO^+, NO_2^- et sous forme d'ions hydratés) formés selon un processus d'ionisation chimiques discuté antérieurement (1). Les échantillons d'ions sont injectés directement dans un spectromètre de masse à ionisation par flamme qui a une résolution spatiale suffisante pour mesurer les profils de concentrations en ions dans la zone de réaction. L'étude est reliée à la suggestion de Fenimore relative à la formation "rapide de NO" dans des flammes d'hydrocarbures riches en combustibles. On a comparé ces résultats additifs aux résultats antérieurs impliquant des espèces azotées présentes dans un flamme semblable de CH_4–O_2 dopée avec 10% de N_2. L'augmentation de la sensibilité dans l'approche additive confirme plusieurs des attributions de masse et des mécanismes impliqués dans l'étude du N_2. Les données obtenues sont suffisantes pour justifier la présence de l'intermédiaire insaisissable HNCO (et peut être aussi de son isomère HCNO) sous forme protonée ainsi que du formamide NH_2CHO, qui n'avait pas été décelé antérieurement. Des ressemblances dans les profils des positions des pics, dans les amplitudes observées pour plusieurs ions, indépendamment de la nature de l'additif combustible-N indiquent que les espèces azotées sont liées par un réseau de réactions bimoléculaires rapides dont plusieurs semblent être balancées dans la zone de réaction.

[Traduit par je journal]

Introduction

In a previous paper (1), we discussed how flame ionization can be employed as a probe for nitrogenous intermediates leading to NO_x formation in the reaction zone and burnt gas of CH_4–O_2–N_2 flames. Ion concentration profiles along the axis of a fuel-rich flame indicated the presence of nitrogenous ions (CN^-, H_2CN^+, NCO^-, NH_2^+, NH_3^+, NH_4^+, NO^+, NO_2^-) formed in chemical ionization (CI) processes of nitrogenous neutral species (CN/HCN, NCO/HNCO, NH, NH_2, NH_3, NO, NO_2). The relevant ion chemistry was discussed in detail. The nitrogenous neutral chemistry based on Fenimore's initial concept of "prompt NO" (2) in fuel-rich hydrocarbon combustion was briefly summarized, involving a sequence of nitrogenous intermediates N_2–HCN–HNCO–NH_i (i = 0–3)–NO_x; a recent and detailed review is available (3).

The experiments to be described here involve stepping into this sequence at various stages by the addition of 0.3% of fuel-nitrogen (fuel-N) in the form of HCN, NH_3, and NO to essentially the same methane–oxygen flame discussed previously (1). In similar experiments involving a variety of fuel-N additives, Morley (4) used a flame-ion mass spectrometer to sample the nitrogenous ions present in hydrocarbon flames. His published data pertain to the region downstream of the reaction zone in the

[1]Present address: Ministry of the Environment, Air Resources Branch, 880 Bay Street, Toronto, Ont., Canada M5S 1Z8.

0008-4042/81/121810-09$01.00/0

©1981 National Research Council of Canada/Conseil national de recherches du Canada

Can. J. Chem. Downloaded from www.nrcresearchpress.com by 210.87.254.5 on 09/06/12
For personal use only.

Can. J. Chem. Downloaded from www.nrcresearchpress.com by 210.87.254.5 on 09/06/12
For personal use only.

burnt gas. In our case, we emphasize nitrogenous ions present in the reaction zone of conical flames where the chemistry is initiated, taking advantage of good spatial resolution. Flame-ion sampling is one of a very few techniques available for probing the reaction zone of a flame and, while possibly causing some distortion of the ion concentrations, is unlikely to falsify the result in any qualitative sense.

The high concentrations of available nitrogen from the addition of HCN, NH_3, and NO clarify the identities of the nitrogenous species present in the reaction zone which were reported in our previous study of N_2-doped flames (1). The data also offer confirmation of the kinds of CI processes which are dominant. Perhaps most important, however, is the demonstration of the rapid interconversion of the nitrogenous neutral intermediates within the confines of the reaction zone, a distance ca. 0.3 mm corresponding to a residence time <300 μs.

Experimental

The results will be presented for five variations of essentially the same fuel-rich, premixed, CH_4–O_2-diluent flame burning at atmospheric pressure. The CH_4 and O_2 flow rates were always maintained at 8.00 and 7.90 mL s^{-1}, respectively, amounting to an equivalence ratio $\phi = 2.03$. Flame 1 had a diluent flow rate of Ar of 2.15 mL s^{-1}. Flame 2 had a diluent flow rate of N_2 of 1.69 mL s^{-1}, amounting to a molar dilution of the unburnt gas of roughly 10%. The Ar flow rate for flame 1 was chosen so that flames 1 and 2 had the same adiabatic flame temperature of 2510 ± 20 K. These are the two flames which have been described and studied previously (1). Flames 3, 4, and 5 are the same as flame 1 with the addition of 0.3 mol% of HCN, NH_3, and NO, respectively. Such a small amount of an additive is not expected to have any appreciable effect on the physical flame characteristics (5). The constancy of the measured sampling temperature was checked for flame 4 (NH_3 additive) and flame 1 using a pneumatic probe consisting of two critical-flow (i.e., choked-flow) orifices in series described previously (1, 6). The compressed gases used were all of CP grade ($CH_4 > 99.6\%$, $O_2 > 99.6\%$, $N_2 > 99.9\%$, Ar > 99.9%). The HCN was added as a 2.7 ± 0.1% mixture of HCN in Ar. The NH_3 (anhydrous, >99.99%) and NO (CP grade, >99.0%) were added directly from lecture bottles into the premixed gas stream.

All flames were laminar with conical luminous reaction zones (height ~5 mm, base diameter ~3 mm, thickness ~0.3 mm) to facilitate ionic sampling along the flame axis into a mass spectrometer. The burnt gas velocity was approximately 1 m s^{-1}. The flames were stabilized on a simple, tubular, quartz burner (2.3 mm id) surrounded by a flowing argon shield to minimize the entrainment of atmospheric air. The burner was mounted on a motor-driven carriage with accurate axial alignment and calibrated drive providing spatial resolution of ±0.02 mm along the flame axis (designated z) for both positive and negative ion profiles.

The flame-ion mass spectrometer has been described previously in detail (7) and in summary form (1). For these additive studies, the flame burned against a 60°, conical, chromium, sampling nozzle of orifice diameter ca. 0.1 mm mounted in a water-cooled flange. The sampled ions pass through two stages of differential pumping into a quadrupole mass filter. The mass-analyzed ions are detected with a parallel-plate Faraday cage connected to a vibrating reed electrometer having a grid-leak resistance of 10^{11} ohms. The ion signal magnitudes in Figs. 2, 3, and 5 are quoted in mV based on the detected ion current passing through 10^{11} ohms. Profiles can be drawn for ion species having a peak concentration as low as 5×10^5 ions mL^{-1}, corresponding to a signal magnitude of about 0.5 mV. A method has been described (1, 7) for locating a reproducible origin ($z \equiv 0$) in the *flame* (not referred to the burner) corresponding to the downstream edge of the luminous reaction zone on the flame axis. In this way, a family of ion profiles at different mass numbers (m/e), can be accurately overlaid on the distance scale z.

Results and Discussion

Total Ion Profiles

In order to appreciate the behaviour of individual ion signals, it is first necessary to recognize the effects of the additives on the total ionization characteristics of the flames. Total ion profiles, both positive and negative, are shown in Fig. 1 for each of the five flames. The total positive profiles are shown normalized to unity at the profile maxima. This constancy of peak signal corresponding to approximately 10^{10} ion mL^{-1} was observed to be true within an experimental error of ±10%. It reflects the basic chemi-ionization process responsible for the formation of flame ions in the reaction zone (8, 9)

[1] $CH + O \rightarrow HCO^+ + e^-$

whose rate will be approximately constant for all five flames at the same temperature. An appreciable upstream shoulder is apparent for flame 4 (NH_3 additive), and a smaller one for flame 5 (NO), but is absent in flames 3 (HCN) and 2 (N_2). These shoulders are indicative of an additional chemi-ionization source term. One such process deduced by other workers (10) to be responsible for the ions observed in an NH_3–O_2–N_2 flame

[2*a*] $N(2^2D) + O(^3P) \rightarrow NO^+ + e^-$

might be applicable here, particularly if the order of availability for excited N atoms in the chemical decomposition of the nitrogen additives is $NH_3 > NO > HCN, N_2$. A second reaction which has been considered as a source of ions in CO–O_2–N_2 (11) or H_2 – air diffusion (12) flames, both with added cyanogen, C_2N_2

[2*b*] $CN + O + O \rightarrow NO^+ + e^- + CO$

is less likely to be significant in the fuel-rich flames employed in this study; in any case, it is of little help in explaining the absence of a shoulder with the HCN additive (flame 3).

In contrast, a considerable enhancement of the

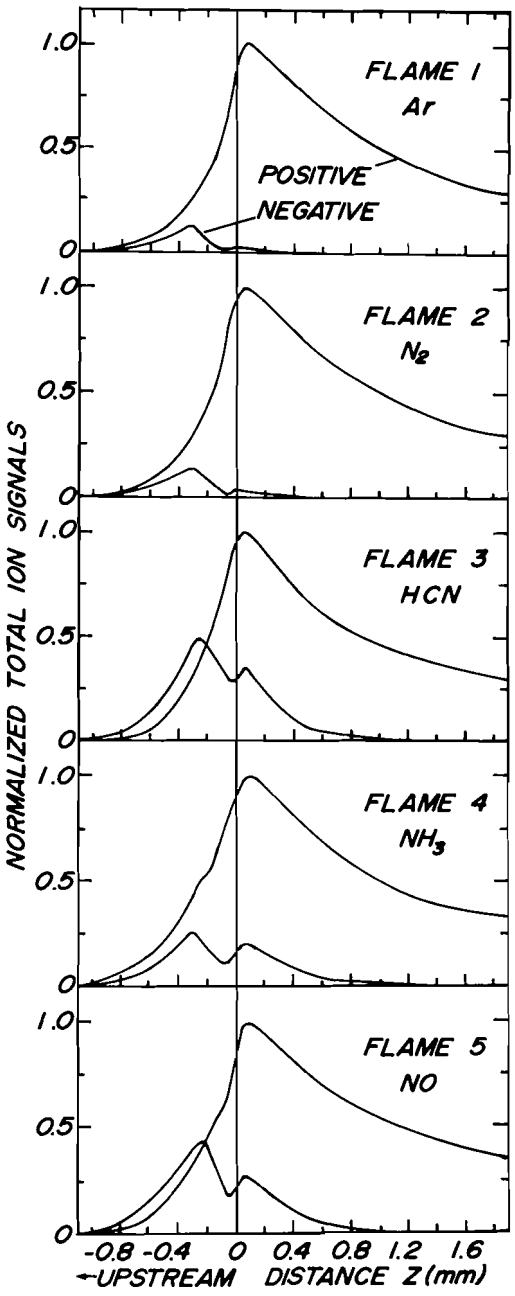

FIG. 1. Positive and negative total ionization profiles for flames 1–5 with added Ar, N_2, HCN, NH_3, and NO, respectively. The curves are normalized to unity at the peaks of the positive ion profiles.

peak negative ion signal in the reaction zone is apparent for each of the fuel-N additives (HCN > NO > NH_3) compared with the signals observed for flames 1 (Ar) and 2 (N_2). In flames 1 and 2, the primary negative ion formation process is three-body electron attachment to oxygen (13)

[3] $e^- + O_2 + M \rightleftharpoons O_2^- + M \qquad \Delta G^0_{1800} = 16.8$

(Standard free energies and enthalpies of reaction are quoted in kJ mol^{-1} based on data from JANAF Tables (14). The subscript temperature of 1800 K is typical in these flames for a region near the middle of the reaction zone.) Secondary negative ions are formed rapidly in the reaction zone; e.g., by charge transfer from O_2^-. The negative ion spectrum for each of flames 3 and 4 is dominated by CN^- (given later in Fig. 3), arising from proton abstraction from HCN by a basic source ion

[4] $X^- + HCN \rightarrow CN^- + HX$

or possibly three-body attachment to CN radicals

[5] $e^- + CN + M \rightarrow CN^- + M \qquad \Delta H^0_{1800} = -406$

or, probably to a much smaller extent, dissociative electron attachment to HCN

[6] $e^- + HCN \rightarrow CN^- + H \qquad \Delta H^0_{1800} = 118$

which is quite endothermic. The high electron affinity of CN (EA = 3.8 eV) and moderate base strength of CN^- (proton affinity PA = 1468 kJ mol^{-1} at 1800 K) cause CN^- to be a comparatively stable species in the chemical environment of the reaction zone, resulting in the negative ion enhancement observed for flames 3 and 4. That the peak signal for flame 4 is lower is not surprising: the added NH_3 must first react to form HCN (or perhaps CN) before CN^- can be formed. The data indicate that roughly half of the NH_3 is converted to HCN at a point midway through the reaction zone.

On the other hand, the negative ion spectrum for flame 5 is dominated by approximately equal contributions from CN^- and NO_2^- (given later in Fig. 3). The large CN^- signal indicates a rapid chemical conversion of nearly half the NO additive to HCN halfway through the reaction zone. Presumably NO_2^- is formed by three-body electron attachment to NO_2, or by charge transfer to NO_2 from O_2^-. Evidently an appreciable amount of NO is oxidized to NO_2 in the reaction zone of this fuel-rich flame before the molecular oxygen is exhausted downstream. The important point demonstrated is the rapid conversion of NH_3 (flame 4) and NO (flame 5) to HCN; this is consistent with Morley's statement (4) that the chemical "route passes through HCN and this compound is formed quantitatively from fuel nitrogen irrespective of its chemical nature".

Finally, the observation that the total negative ion signal appears to exceed the positive ion signal upstream in flames 3 and 5 is, at first, surprising for a quasi-neutral flame plasma. The phenomenon was encountered previously for fuel-lean, CH_4–O_2 (13) and CH_3OH–O_2 (15) flames. An explanation was offered in terms of the back-diffusion of elec-

Can. J. Chem. Downloaded from www.nrcresearchpress.com by 210.87.254.5 on 09/06/12
For personal use only.

Can. J. Chem. Downloaded from www.nrcresearchpress.com by 210.87.254.5 on 09/06/12
For personal use only.

trons a distance of the order of a Debye length followed by three-body attachment to electronegative O_2 molecules in the cooler unburnt gas upstream where the O_2 concentration is highest. The [negative ion]/[free electron] concentration ratio is shifted in favour of negative ions if an additive results in the formation of negative ions more stable than O_2^- in the flame environment. As described above, these are CN^- in flame 3, NO_2^- and CN^- in flame 5 and, to a lesser extent, CN^- in flame 4.

Individual Ion Profiles

Nearly all profiles observed for nitrogenous ion species, both positive and negative (and many non-nitrogenous ones also), exhibit the same basic double-peaked structure illustrated in Fig. 2 at +16 amu ($\sim NH_2^+$) for flame 4 with added NH_3; the ratio of the upstream/downstream peak magnitudes can vary considerably, however. The reasons for this profile structure encountered in fuel-rich flames have been discussed previously (1, 7, 13). Although the reaction zone is only about 0.3 mm thick extending back from $z = 0$, it appears thicker in profiles such as Fig. 2 because the distance scale is spread out upstream when a conical flame is sampled along its axis; even when the mass-spectrometer sampling probe is inserted well upstream of $z = 0$, ions can still diffuse through the orifice from the inside surface of the truncated luminous cone.

We shall confine our attention here to the profile peaks occurring upstream in the reaction zone. The presentation of profiles at all relevant mass numbers (m/e) would constitute an overwhelming body of data. Instead, we shall characterize the upstream peaks in terms of two simple parameters: the peak height, and the peak position on the distance scale z. The peak heights are presented in Fig. 3 for each mass number as a "histogram" giving the peak magnitudes of the ion signals for flames 1–5 (with added Ar, N_2, HCN, NH_3, and NO, in order). Similarly, a peak position plot is given in Fig. 4 where the horizontal lines indicate an uncertainty in peak position of ± 0.02 mm; the uncertainty can be larger for small, broad peaks, however. In both Figs. 3 and 4, selected ionic species are placed into one of six groups depending upon the role played by the species.

In general, the nitrogenous ions in the reaction zone are formed by chemical ionization (CI) processes involving a source ion reacting with a nitrogenous neutral. The first group in Fig. 3, labelled positive source ions, consists of the major protonated species in the reaction zone which can

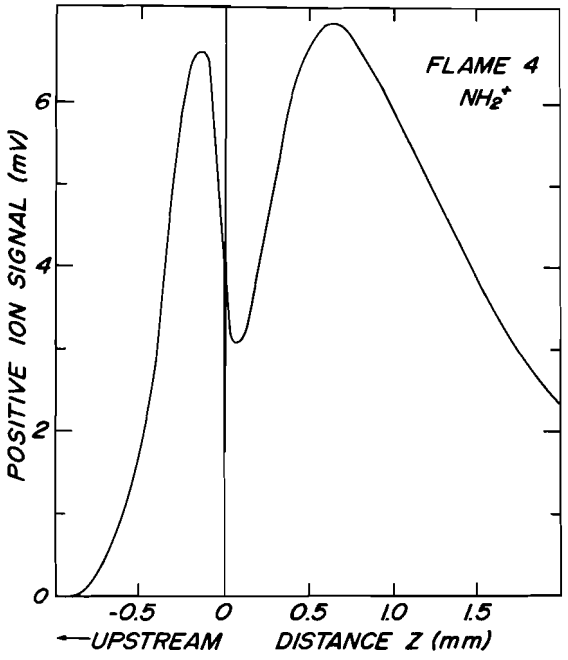

FIG. 2. Typical double-peaked profile structure observed for most individual ionic species, both positive and negative. The curve shown was recorded at +14 amu in flame 4 with the NH_3 additive. The reaction zone is located upstream of $z = 0$.

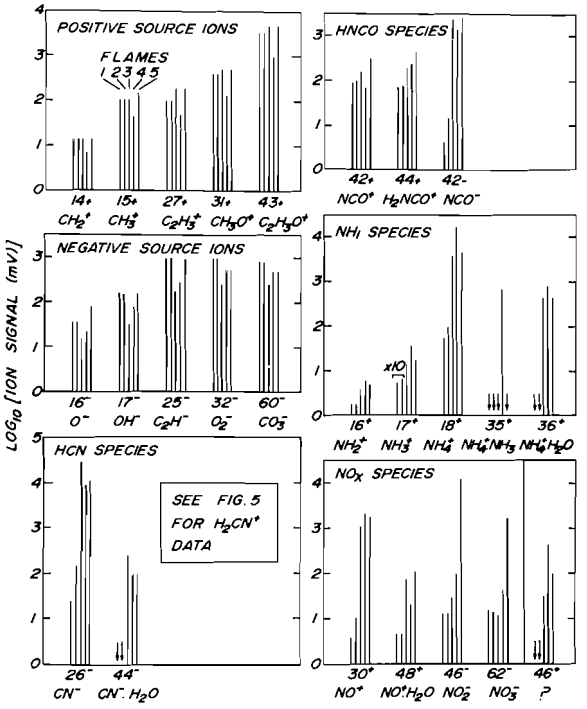

FIG. 3. Histograms for individual mass numbers m/e giving the profile magnitudes of the upstream peaks occurring in the reaction zone. Each histogram consisting of five vertical lines, from left to right, represents the peak heights measured in flames 1–5 with added Ar, N_2, HCN, NH_3, and NO, respectively.

Can. J. Chem. Downloaded from www.nrcresearchpress.com by 210.87.254.5 on 09/06/12
For personal use only.

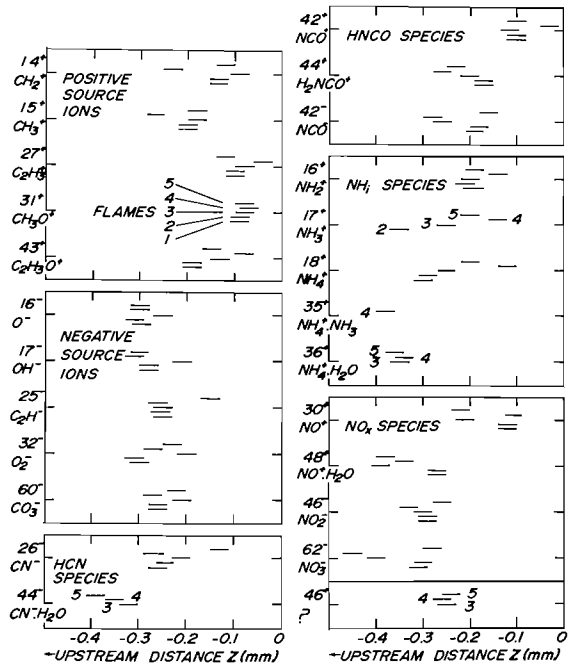

FIG. 4. Profile peak position plot for individual mass numbers *m/e* giving the peak positions on the flame axis of the upstream peaks occurring in the reaction zone. Each group of five horizontal lines, from bottom to top, represents the peak positions measured with an uncertainty of ±0.02 mm in flames 1–5 with added Ar, N_2, HCN, NH_3, and NO, respectively.

chemically ionize neutrals by proton transfer. The striking similarity of the histograms is evident. The very high proton affinity of ammonia causes all five source ions to be depleted in flame 4. The histograms of the second group, labelled negative source ions, again show a basic similarity to each other. All five source ions are depleted by proton transfer reactions with HCN to form CN^- in flames 3 and 4; flame 4 requires the prior conversion of NH_3 to HCN as mentioned above in the discussion of total ion profiles. The least regular behaviour is evident for the NO addition in flame 5. The net reaction of OH^- and C_2H^- is very small. The reaction

[7] $O_2^- + NO \rightarrow O^- + NO_2$

could account for the decrease of O_2^- and increase of O^-. The CO_3^- peak will be depleted by the known reaction (16)

[8] $CO_3^- + NO \rightarrow NO_2^- + CO_2$

With regard to the peak position plot given in Fig. 4, the actual peak position of a given ion signal is a less meaningful parameter than the peak magnitude. Downstream in the burnt gas, the peak positions provide some evidence for a chemical sequence of the nitrogenous species N_2–HCN/CN–HNCO/NCO–NH_i (i = 0–3)–NO_x (1, 4). No such sequence is evident in the spatially-limited reaction zone. In fact, the peak position of a nitrogenous ion is more revealing of its source ion than the nitrogenous neutral from which it is made. This situation can sometimes be used to advantage to clarify the dominant CI process. Figure 4 is also useful for the identification of cluster ions which tend to peak far upstream at lower temperature.

In addition to the positive and negative source ions given in Figs. 3 and 4, the remaining four groups of ions provide evidence for particular nitrogenous neutrals in the reaction zone of the flame doped with various additives. These four groups designated as HCN species, HNCO species, NH_i species, and NO_x species will be discussed in turn.

HCN Species

Evidence for HCN and /or CN radicals is obtained from ion signals corresponding to CN^- and its hydrate $CN^-.H_2O$, and also from the H_2CN^+ profiles given in Fig. 5. The CN^- ions can be formed by proton transfer from HCN; e.g.

[9] $C_2H^- + HCN \rightleftharpoons CN^- + C_2H_2$

or by charge transfer to CN radicals from negative ions such as O^-, OH^-, C_2H^-, and O_2^-. This am-

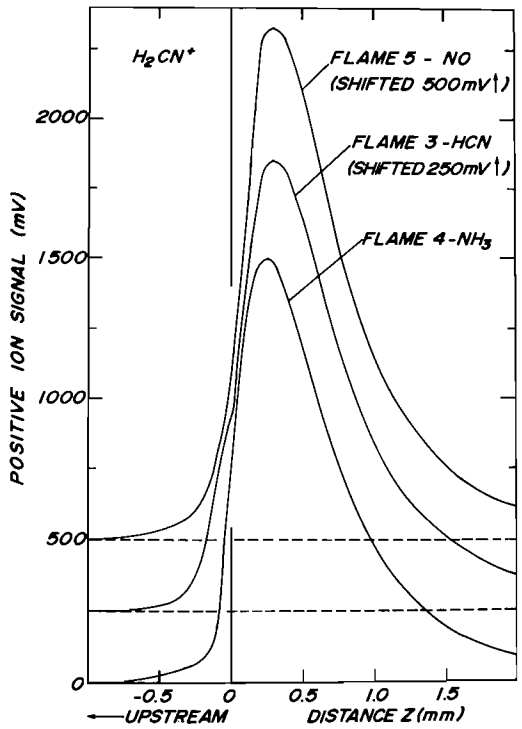

FIG. 5. Single-peaked profiles for H_2CN^+ at +28 amu in flames 3–5 with added HCN, NH_3, and NO, respectively. The peaks are displaced vertically to avoid overlapping.

Can. J. Chem. Downloaded from www.nrcresearchpress.com by 210.87.254.5 on 09/06/12
For personal use only.

biguity concerning the identity of the dominant source, neutral stable molecule or free radical, has occurred frequently in these studies (1). In an attempt to resolve the dilemma, consider the behaviour of flame 3 with 0.3% HCN additive. The HCN molecules will be attacked to form CN radicals by reactions such as (17, 18)

[10] $HCN + H \rightleftharpoons CN + H_2 \quad \Delta G^0_{1800} = 58.6$

or its OH/H_2O counterpart. In these fuel-rich flames, however, reaction [10] will tend to dominate. Assuming a forward rate constant k_{10} of 10^{-10} cm^3 molecule^{-1} s^{-1}, reaction [10] has a relaxation time $\tau \simeq 1/k_{10}[HCN] = 0.1$ μs in the forward direction and considerably smaller in the reverse direction. The forward relaxation time corresponds to 5×10^{-5} mm on the flame axis, assuming a velocity midway in the reaction zone of 500 mm s^{-1} (downstream velocity $\simeq 1$ m s^{-1}), so that reaction [10] will be locally balanced. Using mole fractions for H of 0.009 and H_2 of 0.25 obtained by Hastie (19) in the middle of the reaction zone of a very similar CH_4–O_2 flame and an equilibrium constant $K = 0.02$ at 1800 K, the equilibrium ratio $[CN]/[HCN] = K_{1800}[H]/[H_2] = 7 \times 10^{-4}$. Even if [CN] were to overshoot its local equilibrium value considerably, CN will still be a minor species compared with HCN. Thus, the formation of CN^- by proton transfer from HCN should dominate its formation by charge transfer to CN radicals. Even for the flames 2, 4, and 5 involving nitrogenous additives other than HCN, the same considerations should apply. Therefore, the high CN^- peak magnitudes in Fig. 3 for flames 4 and 5, only slightly less than that for flame 3, illustrate the rapid conversion of NH_3 and NO to HCN.

If a reaction such as [10] is locally balanced in the reaction zone, the same should be true for the proton transfer reactions like [9] or

[11] $OH^- + HCN \rightleftharpoons CN^- + H_2O$

since their relaxation times involve ion–molecule rate constants which are even larger than k_{10}. Not surprisingly, the CN^- peak shapes follow those of the major negative source ions as indicated in Fig. 4; the corresponding peak positions of CN^- and C_2H^- are remarkably similar.

The relative magnitudes of the $CN^-.H_2O$ peaks in Fig. 3 are very nearly 1% of the corresponding CN^- peaks in flames 3, 4, and 5. The signals at −44 amu are assigned to the CN^- hydrate on the basis of the peak position plot in Fig. 4; the hydrate signals peak considerably upstream of CN^- where the lower flame temperature favours hydrate formation.

The H_2CN^+ profiles are shown separately in Fig. 5 for flames 3, 4, and 5 since they represent one of the few cases where single-peaked profiles were observed. Nevertheless, the upstream tails through the reaction zone are considerable. The large positive source ions in the reaction zone involve species with proton affinities (PA's) > PA(HCN). The formation of appreciable H_2CN^+ must await the rise of H_3O^+ since PA(HCN) > PA(H_2O) (20). Once again, a rough calculation of the relaxation times for the forward and reverse directions of

[12] $H_3O^+ + HCN \rightleftharpoons H_2CN^+ + H_2O$

indicates that reaction [12] is locally balanced. Thus, the shapes of the H_2CN^+ profiles are dominated by the corresponding H_3O^+ profiles in the reaction zone and for some distance downstream. The slight upstream shoulder apparent for the HCN additive profile in Fig. 5 is explicable in terms of the production of H_2CN^+ via an exothermic proton transfer reaction such as

[13] $C_2H_3^+ + HCN \rightleftharpoons H_2CN^+ + C_2H_2$

where PA(HCN) > PA(C_2H_2) at room temperature (20, 21).

It should also be mentioned that the profiles at +45 amu for flames 1–5 (not presented in the figures) showed the usual double-peaked structure except that flame 4 with the NH_3 additive had a third peak relatively far upstream at $z = -0.30$ mm indicative of NH_4^+.HCN cluster ions. As a final observation concerning the HCN species, no clear evidence was obtained for either CN^+ or HCN^+. This is not surprising in view of the fact that the CN radical has a high ionization energy and a low proton affinity.

In summary, these ion data show the rapid conversion of NH_3 and NO to HCN. At a given point z in the reaction zone, the signal magnitudes for each of CN^-, $CN^-.H_2O$, and H_2CN^+ invariably exhibit the order flame 3 (HCN) > flame 5 (NO) > flame 4 (NH_3) for 0.3% of these three fuel-N additives. The results suggest the existence of a direct chemical path linking HCN and NO involving CH_i radicals

[14a] $CH_i(i = 1\text{–}3) + NO \rightleftharpoons HCN + H_{i-1}O(i = 1\text{–}3)$

[14b] $\rightleftharpoons CN + H_iO(i = 1, 2)$

All five reactions [14] are exothermic in the forward direction.

HNCO Species

The large NCO^- signals observed at −42 amu in flames 3, 4, and 5 may be formed by proton transfer from HNCO or charge transfer to NCO radicals. Several authors have postulated the oxidation of HCN/CN to form HNCO/NCO (4, 22–24) although direct evidence of the latter species is lacking. Pre-

TABLE 1. Structural features of profiles at −42 amu in the reaction zone

		Upstream		Downstream	
Flame	Additive	z(mm)	Feature	z(mm)	Feature
2	N_2	−0.32	Slight shoulder	−0.18	Main peak
3	HCN	−0.26	Main peak	−0.10	Second peak, barely resolved
4	NH_3	−0.28	Single peak		
5	NO	−0.25	Slight shoulder	−0.16	Main peak

sumably the species are linked by fast balanced reactions

[15a] $HNCO + H \rightleftharpoons NCO + H_2$ $\Delta G^0_{1800} = 25.2$

[15b] $HNCO + OH \rightleftharpoons NCO + H_2O$ $\Delta G^0_{1800} = -15.8$

Using Hastie's concentration values (19) and data from JANAF Tables (14), the equilibrium ratio [NCO]/[HNCO] = 7×10^{-3} at 1800 K. Although this ratio is an order of magnitude larger than [CN]/[HCN], a similar conclusion seems justified. That is, NCO is a relatively minor species compared with HNCO, so that the formation of NCO^- by proton transfer from HNCO will dominate its formation by charge transfer to NCO radicals in the reaction zone.

Although the profiles at −42 amu have the usual double-peaked shape, the peak in the reaction zone of flames 2, 3, and 5 shows further structure in addition to the main peak position given in Fig. 4; these details are listed in Table 1. One possible interpretation involves the two isomeric forms HNCO/NCO (designated form A, having a CO bond) and HCNO/CNO (form B, with an NO bond). However, it is difficult to associate one particular isomeric form with the upstream or downstream position of the features. Perhaps the rising concentration of CO favours form A in the downstream position. In any case, the similar magnitude of the major peaks in flames 3, 4, and 5 again illustrates the rapid interconversion of the fuel-N additives in the reaction zone.

The histogram at +42 amu in Fig. 3 is similar to those designated as positive source ions with one difference; the enhanced peak height for flame 5 provides possible evidence for ionized NCO radicals. Also, the enhanced signals in flames 3–5 at +44 amu provide reasonably good evidence for protonated HNCO. The peak heights are not consistent with an assignment as $^{13}C^{12}CH_3O^+$ stemming from the large source ion signals at +43 amu representing protonated ketene. Nor is N_2O^+ a likely contender in view of the high ionization energy of $N_2O \sim 13$ eV; the preferred source reaction involving charge transfer from O^+ (1, 25) is highly unlikely in a fuel-rich flame where O^+ was not detected.

NH_i Species

The histograms in Fig. 3 at +16, 17, and 18 amu are distinctly different from those at +14 and 15 amu. Major contributions to the former arise from protonated NH_i (i = 1–3) species whereas the latter represent CH_2^+ and CH_3^+, respectively. No evidence was obtained for NH^+ at +15 amu. From Fig. 4, the peak positions of the NH_i^+ ions in flames 3–5 are similar. If the NH_i species are protonated by the same source ions, the evidence is indicative of a rapid interconversion of the NH_i species

[16] $NH_i + H(OH) \rightleftharpoons NH_{i-1} + H_2(H_2O)$

for i = 2, 3. Presumably the very high proton affinity of NH_3 leading to the very large NH_4^+ signal detected in flame 4 accounts for the depression of all of the positive source ions in flame 4 as shown in Fig. 3. In conclusion, it is again worth emphasizing the evidence presented by this data for the rapid interconversion of the fuel-N additives; in this case, the conversion of HCN and NO to NH_3, NH_2, and NH.

Of minor interest are a number of cluster ions assigned on the basis of their peak positions shown relatively far upstream in Fig. 4. These include $NH_4^+.NH_3$ at +35 amu which was observed only in flame 4 with the NH_3 additive, and $NH_4^+.H_2O$ at +36 amu for flames 3–5.

NO_x Species

From Fig. 3, the NO^+ signals at +30 amu in flames 3–5 are of comparable magnitude. At first glance it is somewhat surprising to find the largest signal in flame 4 with the NH_3 additive. The probable explanation offers some confirmation of a mechanism discussed previously (1), involving a contribution from $CH_2NH_2^+$, also at +30 amu, by condensation reactions of $NH_i^+ + CH_j$ or $CH_j^+ + NH_i$ (26). This explanation is reinforced by the peak position in Fig. 4, since the signals at +30 amu in flames 3 and 5 peak upstream of the flame 4 peak; the latter occurs in close proximity to those of the NH_i^+ ions. Presumably the major portion of the signals in flames 3 and 5 is due to NO^+ produced by exothermic charge transfer to NO by source ions such as CH_3^+ and CH_2^+. Similar *relative* peak posi-

Can. J. Chem. Downloaded from www.nrcresearchpress.com by 210.87.254.5 on 09/06/12
For personal use only.

Can. J. Chem. Downloaded from www.nrcresearchpress.com by 210.87.254.5 on 09/06/12
For personal use only.

tions at +48 amu occurring considerably further upstream are indicative of hydrate ions. However, the depressed peak height for flame 4 shown in Fig. 3 is consistent with $CH_2NH_2^+.H_2O$ being less stable than $NO^+.H_2O$.

The NO_2^- ions at −46 amu can be produced by exothermic charge transfer to NO_2 by O^-, OH^-, and O_2^-. However, NO_2 is not expected to be abundant in these fuel-rich flames. A probable major formation mechanism involving NO directly, particularly in flame 5, is

[8] $CO_3^- + NO \rightarrow NO_2^- + CO_2$

as discussed previously (1). Certainly the signals at −46 amu peak together in a group in proximity to the CO_3^- peaks, as shown in Fig. 3. The peaks at −46 amu in flames 1 and 2 are due to isotopic $^{13}CHO_2^-$ from the very large $^{12}CHO_2^-$ signals detected at −45 amu. Data at −45 amu have not been included as source ions because the profiles are remarkably constant over the range of flames 1–5. Nevertheless, they provide a useful internal "calibration standard" for comparing other negative ion profile magnitudes in the various flames.

The signals observed at −62 amu cover a wide range on the peak position plot, Fig. 4. In these fuel-rich flames, it is probable that the signal represents NO_3^- only in flame 5, formed by the known reaction (16)

[17] $CO_3^- + NO_2 \rightarrow NO_3^- + CO_2$

The peak positions for flames 3 and 4 located very far upstream are indicative of hydrates, most probably $CN^-.2H_2O$; another possibility for flame 4 is $CHO_2^-.NH_3$ since an additional shoulder is observed on the profile at $z = -0.30$ mm.

Finally, the nitrogenous ions at +46 amu in flames 3–5 shown at the lower right of Figs. 3 and 4 present a problem of assignment; all of NO_2^+, $H_2CN^+.H_2O$, $NH_4^+.CO$, and CH_4NO^+ have the right mass number (m/e). However, the signal is largest for the NH_3 additive, and the peak positions given in Fig. 4 are not indicative of cluster ions. We believe the most logical candidate to be CH_4NO^+, interpreted as protonated formamide $NH_2CHO.H^+$. The parent molecule can be formed from the reaction of NH_3 with formaldehyde.

[18] $NH_3 + HCHO \rightarrow NH_2CHO + H_2$

and considerable formaldehyde is present in the reaction zone of these flames (detected as the source ion CH_3O^+).

Conclusions

These studies in the reaction zone of a fuel-rich hydrocarbon flame with fuel-N additives provide confirmation of many of the mass assignments and mechanisms discussed previously for N_2 addition (1). The nitrogenous chemistry, both neutral and ionic, is much easier to sort out using the fuel-N additives, however. The present results also indicate the presence of formamide, a new species not previously detected. When ions are used to probe the neutral chemistry, a question frequently arises: is a given nitrogenous ion representative of a related nitrogenous neutral (e.g., NO^+ from NO), formed in a simple chemical ionization process such as proton transfer or charge transfer? Or, is the identity obscured by a more complicated ion–molecule source reaction involving rearrangement or condensation (e.g., NO_2^- from NO, not NO_2; $CH_2NH_2^+$ as well as NO^+ at +30 amu)? The present experiments answer this question in a number of important cases.

The picture emerging from these studies is that of a spatially limited reaction zone containing a wide variety of nitrogenous neutral intermediates intermingled together, temporally independent of the nitrogen source. The main value of the additive approach is realized when one adds a neutral species (HCN, NH_3, NO) and observes a nitrogenous ion signal which cannot reasonably result from a direct ion–molecule reaction of the neutral flame ions. In this circumstance, rapid interconversion of the nitrogenous neutrals can be demonstrated, the ions merely functioning as a probe of the neutral chemistry.

Acknowledgements

Support of this work by the Natural Sciences and Engineering Research Council of Canada under Grant Numbers A1604 (J.M.G.) and A6258 (D.K.B.) is acknowledged.

1. G. B. De Brou, J. M. Goodings, and D. K. Bohme. Combust. Flame, **39**, 1 (1980).
2. C. P. Fenimore. Thirteenth Symposium (International) on Combustion. The Combustion Institute, Pittsburgh, PA. 1971. p. 373.
3. A. N. Hayhurst and I. M. Vince. Prog. Energy Combust. Sci. **6**, 35 (1980).
4. C. Morley. Combust. Flame, **27**, 189 (1976).
5. E. M. Bulewicz and P. J. Padley. Ninth Symposium (International) on Combustion. Academic Press, New York. 1963. p. 638.
6. Chun-Wai Ng. M.Sc. Thesis, York University, Downsview, Ont., Canada M3J 1P3. 1977.
7. J. M. Goodings, Chun-Wai Ng, and D. K. Bohme. Combust. Flame, **36**, 27 (1979).
8. H. F. Calcote. Eighth Symposium (International) on Combustion. Williams & Wilkins, Baltimore, MD. 1962. p. 184.
9. K. N. Bascombe, J. A. Green, and T. M. Sugden. Adv. Mass Spectrom. **2**, 66 (1962).
10. C. Bertrand and P. J. Van Tiggelen. J. Phys. Chem. **78**, 2320 (1974).
11. A. van Tiggelen, J. Peeters, and C. Vinckier. Thir-

teenth Symposium (International) on Combustion. The Combustion Institute, Pittsburgh, PA. 1971. p. 311.
12. B. L. CHAWNER and A. T. BLADES. Can. J. Chem. **56**, 2278 (1978).
13. J. M. GOODINGS, CHUN-WAI NG, and D. K. BOHME. Combust. Flame, **36**, 45 (1979).
14. JANAF Thermochemical Tables. (*a*) D. R. STULL, H. PROPHET *et al.* NSRDS-NBS 37, 2nd ed. U.S. Government Printing Office, Washington, DC. 1971; (*b*) M. W. CHASE, J. L. CURNUTT, A. T. HU, H. PROPHET, A. N. SYVERUD, and L. WALKER. 1974 Supplement, J. Phys. Chem. Ref. Data, **3**, 311 (1974); (*c*) M. W. CHASE, J. L. CURNUTT, H. PROPHET, R. A. MCDONALD, and A. N. SYVERUD. 1975 Supplement, J. Phys. Chem. Ref. Data, **4**, 1 (1975).
15. J. M. GOODINGS, CHUN-WAI NG, and D. K. BOHME. Int. J. Mass Spectrom. Ion Phys. **29**, 57 (1979).
16. F. C. FEHSENFELD and E. E. FERGUSON. J. Chem. Phys. **61**, 3181 (1974).
17. P. M. RENZEPIS and T. M. SUGDEN. Nature, **202**, 448 (1964).
18. J. C. BODEN and B. A. THRUSH. Proc. R. Soc. London Ser. A, **305**, 107 (1968).
19. J. W. HASTIE. Combust. Flame, **21**, 187 (1973).
20. K. TANAKA, G. I. MACKAY, and D. K. BOHME. Can. J. Chem. **56**, 193 (1978).
21. W. A. CHUPKA, J. BERKOWITZ, and K. M. A. REFAEY. J. Chem. Phys. **50**, 1938 (1969).
22. B. HAYNES, D. IVERACH, and N. Y. KIROV. Fifteenth Symposium (International) on Combustion, The Combustion Institute, Pittsburgh, PA. 1975. p. 1103.
23. J. MULVIHILL and L. F. PHILLIPS. Fifteenth Symposium (International) on Combustion, The Combustion Institute, Pittsburgh, PA. 1975. p. 113.
24. C. P. FENIMORE. Combust. Flame, **26**, 249 (1976).
25. G. B. DE BROU. M.Sc. Thesis, York University, Downsview, Ont., Canada M3J 1P3. 1980.
26. D. SMITH and N. G. ADAMS. Chem. Phys. Lett. **47**, 145 (1977).

Can. J. Chem. Downloaded from www.nrcresearchpress.com by 210.87.254.5 on 09/06/12
For personal use only.

Ionization of nitromethane in the flame ionization detector

T. McALLISTER AND A. J. C. NICHOLSON
C.S.I.R.O. Division of Chemical Physics, P.O. Box 160, Clayton, Victoria, Australia 3168
AND
J. D. SCOTT
Swinburne College of Technology, P.O. Box 218, Hawthorn, Victoria, Australia 3122

Received October 28, 1980

This paper is dedicated to Dr. F. P. Lossing of the National Research Council of Canada on the occasion of his 65th birthday

T. McALLISTER, A. J. C. NICHOLSON, and J. D. SCOTT. Can. J. Chem. **59**, 1819 (1981).

The mass spectra observed on sampling the unburnt gases of a flame ionization detector to which nitromethane has been added are due mostly to proton transfer reactions of NH_4^+ and H_3O^+. These are formed in the reaction zone from the primary ion HCO^+, and pass through the unburnt gases to the sampling orifice. The ions which are detected may be attributed to pyrolysis (CH_4NO^+ and NO^+) or hydrogenation products ($CH_2NH_2^+$ and $CH_3NH_2^+$) of nitromethane. The small amount of NO^+ observed in the unburnt gases is attributed either to a primary ionization mechanism which produces NO^+ from excited nitrogen atoms or molecules in the reaction zone, or to a reaction of H_3O^+ with HNO_2, a pyrolysis product of nitromethane. Observations of $CH_2NH_2^+$ in the flame and in double resonance experiments performed in an ion cyclotron resonance mass spectrometer give limits on the proton affinity of methanimine (CH_2NH) of 847.6–862.3 kJ mol^{-1}.

T. McALLISTER, A. J. C. NICHOLSON et J. D. SCOTT. Can. J. Chem. **59**, 1819 (1981).

Les spectres de masse d'échantillons de gaz qui n'ont pas brulé dans un détecteur par ionisation à flamme auxquels on a ajouté du nitrométhane sont dus principalement aux réactions de transfert de proton du NH_4^+ et du H_3O^+. Ceux-ci se forment dans la zone de réaction à partir de l'ion primaire HCO^+ et sont véhiculés, par les gaz qui n'ont pas brulé, dans l'orifice d'échantillonnage. Les ions qui sont détectés peuvent être attribués à la pyrolyse (CH_4NO^+ et NO^+) ou aux produits d'hydrogénation ($CH_2NH_2^+$ et $CH_3NH_2^+$) du nitrométhane. On attribue les faibles quantités de NO^+ observées dans les gaz qui n'ont pas brulé soit à un mécanisme d'ionisation primaire qui produit du NO^+ à partir des atomes d'azote excités ou des molécules présentes dans la zone de réaction, soit à une réaction de H_3O^+ avec HNO_2, un produit de pyrolyse du nitrométhane. Les ions $CH_2NH_2^+$ observés dans la flamme ou dans des expériences de double résonance réalisées dans un spectromètre de masse à résonance d'ion dans un cyclotron donnent des limites de l'affinité de la méthanimine (CH_2NH) pour le proton de 847,6–862,3 kJ mol^{-1}.

[Traduit par le journal]

Introduction

Studies of ions in flames have tended to concentrate on premixed flames of hydrocarbons (1–6), although some work has been done on ammonia and cyanogen flames (7, 8). The flame ionization detector (FID) operates with a wide range of organic compounds and uses a small, conical, diffusion flame, in contrast to the large, flat, premixed flames employed in most of the recent studies. Investigations of the FID type of flame (9, 10) have shown the ionization mechanism is similar to that suggested for premixed flames (3), namely the reactions:

[A] $CH + O \rightarrow HCO^+ + e$,

[B] $HCO^+ + H_2O = H_3O^+ + CO$.

In flames containing inorganic nitrogen compounds, it is possible that the ionization reaction is either (7, 8)

[C] $N(^2P) + O \rightarrow NO^+ + e$

or (11)

[D] $N_2(A\,^3\Sigma_u^+) + NO(a\,^4\Pi) \rightarrow NO^+ + N_2 + e$

but, with organic nitrogen compounds in an FID type flame, both HCO^+ and NO^+ mechanisms should be possible.

A feature of conical flames, first noted by Bascombe *et al.* (12), is that ions can be sampled in such a way as to detect the products of their reactions with the constituents of the unburnt gases (see Fig. 1): oxonium ions (H_3O^+), for example, may undergo proton transfer with the organic additive, or with its pyrolysis and (in the case of the FID) its hydrogenation products. Such effects have already been noted in the FID flames of benzene, toluene, and cyclohexane (10). This paper presents observations on the unburnt gases of an FID-type flame containing nitromethane, which are relevant to the pyrolysis (13–15) and hydrogenation of that compound, as well as to the mechanism of secondary ionization in cyanogen/hydrogen flames (8).

Experimental

Our FID-type flame burns a mixture of 1.5 mL s^{-1} of hydrogen with 0.6 mL s^{-1} of argon containing approximately 1% of the

0008-4042/81/121819-05$01.00/0
©1981 National Research Council of Canada/Conseil national de recherches du Canada

Can. J. Chem. Downloaded from www.nrcresearchpress.com by 210.87.254.42 on 09/06/12
For personal use only.

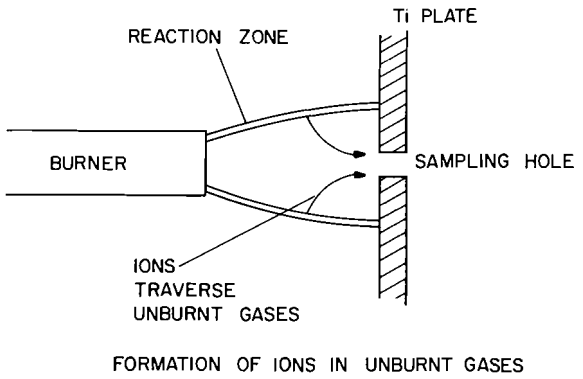

FIG. 1. Formation of ions in unburnt gases.

additive. For these experiments, a moveable burner of 0.75 mm id was positioned horizontally on an axis coincident with the axis of the entrance hole (0.1 mm diameter in a titanium plate) of the mass spectrometer sampling system. This gave a flame with a conical-shaped luminous reaction zone of about 1 mm base diameter and 3–4 mm apex height. The mass spectrometer, the three-stage sampling system, and the electric potentials required for the detection of ions have been described previously (9, 10). Deuterium flames were also investigated, in order to elucidate the formulas of ions which were not clearly identified by the *m/z* values in hydrogen flames.

Proton affinities were determined by means of an ion cyclotron resonance (icr) mass spectrometer (16).

The FID sensitivity of nitromethane was determined by gas chromatography of solutions of nitromethane and hexane in di-*tert*-butyl ketone.

Results

The identification of ions found in the unburnt gases is illustrated by Fig. 2, in which typical mass spectra from the hydrogen and deuterium flames are compared. H_3O^+, NH_4^+, and their hydrates, $H_3O^+ \cdot H_2O$ and $NH_4^+ \cdot H_2O$, and protonated nitromethane ($CH_3NO_2H^+$) were clearly identified. It appears that the ion of *m/z* 30 is mostly $CH_2NH_2^+$ with a minor proportion being NO^+, but there remains an ambiguity concerning a proportion of the ions at *m/z* 30 and 32 in the hydrogen flame; a deuterium shift to *m/z* 34 may be explained by the presence of both protonated methanimine ($CH_2NH_2^+$) and nitroxide ion (NH_2O^+). The protonated imine (or its isomer, vinylamine) is also a possible structure for the ions of *m/z* 44 and 58, with formulas $C_2H_4NH_2^+$ and $C_3H_6NH_2^+$. Shifts of *m/z* 32 to 38 and 46 to 54 may be explained by the presence of protonated methylamine ($CH_3NH_3^+$) and ethylamine ($C_2H_5NH_3^+$); for *m/z* 46, also, a shift to *m/z* 50 indicates the presence of protonated nitrosomethane (CH_3NOH^+) or perhaps formamide (NH_2CHOH^+).

It has been shown (3, 5) that the hydrates observed when a flame is sampled by a mass spectrometer are usually formed in the cool boundary layer next to the orifice or the expansion region inside the orifice. The temperature dependence of the equilibrium constants obtained by Kebarle *et al.* (17) for the oxonium hydrates also suggests that only negligible amounts of hydrate will be present in flames at temperatures > 1000 K. Therefore profiles of ion intensity (expressed as a percentage of total ion current) with varying burner to orifice distance were plotted, in which the intensities of all members of a hydrate series, e.g. NH_4^+, $NH_4^+ \cdot H_2O$, etc., were summed. The profiles of NH_4^+ thus obtained peaked a few tenths of a mm downstream of the luminous reaction zone; this was made the zero of the distance scales of the profiles, to facilitate comparison between the hydrogen and deuterium flames (see Figs. 3 and 4).

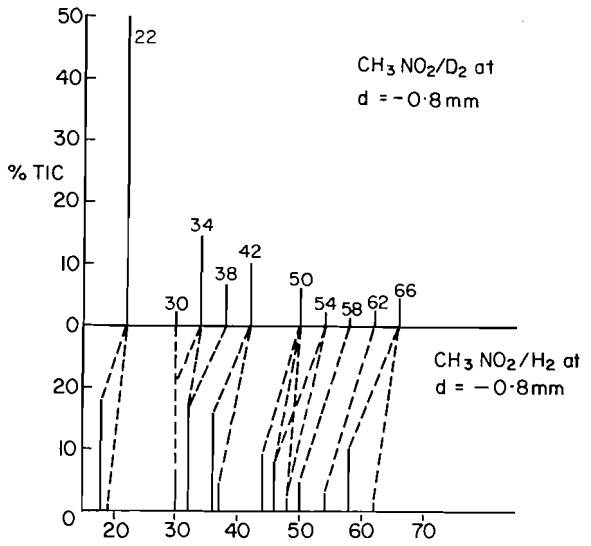

FIG. 2. Deuterium shifts in a nitromethane/FID flame.

Double resonance experiments in the icr mass spectrometer on mixtures of ethylene diamine with diethyl ether and acetone, in which the $CH_2NH_2^+$ ion was observed to undergo proton transfer to diethyl ether, but not to acetone, established that the proton affinity of methanimine (CH_2NH) lies between 847.6 and 862.3 kJ mol^{-1} on the scale given by Kebarle *et al.* (18), and modified by the recent redetermination of the proton affinity of isobutene (19) which sets proton affinity of ammonia at 873.2 kJ mol^{-1}. This is compatible with an unpublished observation of Huntress and Beauchamp (see ref. 23).

The FID sensitivity of nitromethane was found to be 0.7 of that expected from the equal-per-carbon response scale, on which the sensitivity of hexane is 6.0. The sensitivities of NH_3 and NO on this scale are about 10^{-3} (20).

Can. J. Chem. Downloaded from www.nrcresearchpress.com by 210.87.254.42 on 09/06/12
For personal use only.

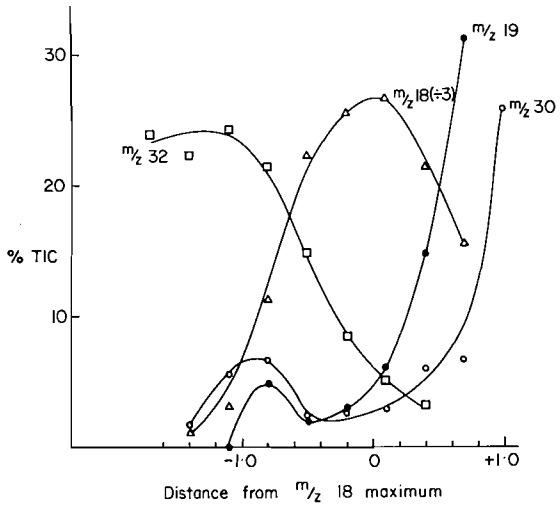

FIG. 3. Ion profiles in $H_2/Ar/CH_3NO_2$ flame.

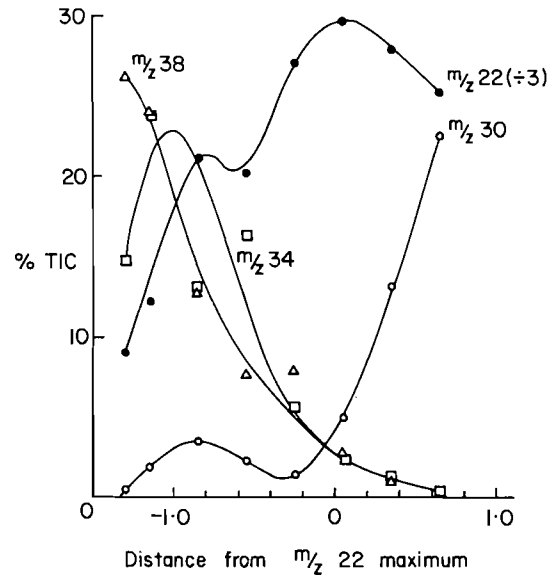

FIG. 4. Ion profiles in $D_2/Ar/CH_3NO_2$flame.

Discussion

Only tentative conclusions may be drawn on the mechanisms which produce the observed flame ions. Although proton transfer reactions appear to be important in many flames, it is possible to write more complicated alternative mechanisms. Where there are no absolute criteria for deciding between these alternatives, we prefer the simpler mechanism.

Most of the ions found in the unburnt gases may be grouped into three sets for discussion: those which originate in the reaction zone, those apparently derived from pyrolysis products of nitromethane, and those apparently derived from reduction products of nitromethane. NO^+ is an exception to this classification, as it may be considered both as a reaction zone ion and as a pyrolysis-derived ion.

(a) *Ions Originating in the Reaction Zone: NH_4^+, H_3O^+, and NO^+*

The FID sensitivity of nitromethane, combined with the preponderance of NH_4^+ and H_3O^+ over NO^+ in the unburnt gases and reaction zone, in comparison with that observed by Bertrand and Van Tiggelen in ammonia flames (7) where NO^+ is the major ion, suggests that most of the flame ionization is from reaction [A]. An ionization scheme with NO^+ as the primary ion, from reactions [C] and [D], would be expected to give a much lower sensitivity as well as a greater intensity of NO^+ in relation to NH_4^+ and H_3O^+. Apart from this, there is the difficulty of the reaction mechanism whereby NO^+ gives H_3O^+. One suggestion is that an intermediate HNO^+ is formed, which undergoes rapid proton transfer reactions so that its concentration is too low to detect (7). Another (7) is that the reactions suggested by Fehsenfeld *et al.* for the formation of oxonium hydrates from nitrosyl hydrates in the ionosphere (21) are also applicable to flames:

$$NO^+(H_2O)_n + H_2O = H_3O^+(H_2O)_{n-1} + HNO_2$$

In this case, it should be noted that the relevant reaction in flames would be of unhydrated ions, because of the flame temperature:

[E] $NO^+ + 2H_2O = H_3O^+ + HNO_2$

$\Delta H = +8.2\,kJ\,mol^{-1}$ at 2000 K (22).

NH_4^+ and H_3O^+ are formed by proton transfer from the primary ion HCO^+:

$$HCO^+ + NH_3 = NH_4^+ + CO$$

$$HCO^+ + H_2O = H_3O^+ + CO$$

The strongly reducing conditions in the unburnt gases of the FID flame are expected to produce ammonia from nitromethane. The equilibrium constants, K, for these proton transfer reactions are largely determined by the relative proton affinities of the neutral species, as the entropy of proton transfer is relatively small (23). Approximate calculations of K_p using the proton affinity table (18) indicate that the ratios of NH_4^+ and H_3O^+ to HCO^+ will be of the order of 10^3 or 10^4, where the concentrations NH_3, H_2, and CO are similar. NH_4^+ and H_3O^+ may participate in further proton transfer

Can. J. Chem. Downloaded from www.nrcresearchpress.com by 210.87.254.42 on 09/06/12
For personal use only.

Can. J. Chem. Downloaded from www.nrcresearchpress.com by 210.87.254.42 on 09/06/12
For personal use only.

reactions in the unburnt gases and, because of the higher proton affinity of NH_3 (134 kJ mol^{-1} greater than that of H_2O), it will be the reactions with NH_4^+ which will determine the relative intensities of the ions derived from the unburnt gas constituents.

(b) *Ions Derived from Nitromethane and its Pyrolysis Products: $CH_3NO_2H^+$, CH_3NOH^+, NO^+, and the Problem of NH_2O^+*

A weak signal was observed for the protonation of undecomposed nitromethane to give *m/z* 62. This is to be expected because the proton affinity of nitromethane is 84 kJ mol^{-1} less than that of ammonia (23, 24). The stronger signal observed for CH_3NOH^+ and/or NH_2CHOH^+ is an indication that the proton affinity of these products is greater than that of nitromethane (assuming that their concentrations are no greater than that of nitromethane).

NO is a pyrolysis product of nitromethane, and the possibility exists that some of the NO^+ observed in the unburnt gas is of secondary rather than primary origin. The formation of NO^+ in the *burnt* gases of flames has been noted since the earliest work on flame ionization (2), and recently it has been closely associated with H_3O^+ (25). It may be that the reverse of the reaction [E] is significant in the unburnt gases, with the HNO_2 being supplied from the nitromethane pyrolysis (13–15).

The presence of NH_2O^+ is one explanation of the deuterium shifts observed for *m/z* 30 and 32 to 34 (see Fig. 2). It could be produced by proton transfer to the pyrolysis product HNO (13–15), the proton affinity of which is calculated to be 757.3 kJ mol^{-1} (26, 27). This is, however, very similar to the proton affinity for nitromethane, for which, as we have seen, there is only a weak signal because of the unfavourable equilibrium constant for proton transfer with NH_4^+. The amount of HNO present is unlikely to be sufficiently large to overcome this disadvantage, and we conclude that NH_2O^+ will be present in only negligible intensity. This conclusion is reinforced by the absence of other ions which could be derived from pyrolysis products of comparatively low proton affinity: CH_3OH^+ from CH_3O, CH_3O^+ from CH_2O, and H_2CN^+ from HCN (28, 29).

(c) *Ions Derived from Reduction Products of Nitromethane: $CH_2NH_2^+$ and $CH_3NH_3^+$*

These ions may be produced by proton transfer to methanimine and methylamine. The reduction of nitromethane to methylamine by catalytic methods at lower temperatures is known, but there have been no high-temperature, homogeneous studies. It is possible that methylamine is the precursor of methanimine, which may be formed from it by pyrolysis (30). On the other hand, the possibility that HCN is present, although H_2CN^+ is not detected (see previous section), suggests also that a stepwise reduction of HCN by H_2 may be taking place:

$$HCN \rightarrow CH_2NH \text{ (methanimine)} \rightarrow CH_3NH_2.$$

The proton affinity of methylamine is 929 kJ mol^{-1}, 55.8 kJ mol^{-1} greater than that of ammonia, so that the proton transfer equilibrium will favour its detection. The proton affinity of methanimine is less (by 9–16 kJ mol^{-1}) than that of ammonia, but still sufficiently close to allow detectable quantities of CH_2NH_2 in the presence of NH_4^+, given similar amounts of CH_2NH and NH_3. The lower intensity of $CH_2NH_2^+$ in comparison with $CH_3NH_3^+$ is in keeping with the known order of proton affinities of the neutrals.

A stepwise reduction mechanism for the formation of ions of *m/z* 28, 30, and 32 in C_2N_2/H_2 flames has been suggested by Bredo *et al.* (8). In their case they suggest a form of association reaction of the ions, e.g.

$$H_2CN^+ + H_2 \rightarrow H_4CN^+$$

This is very unlikely. Association reactions of this kind have been postulated for interstellar clouds by Herbst (31) but would not apply to flames at 2000 K. It is much more likely that the ions which they observe are, as in our experiments, formed by protonation of neutral substances. Such a mechanism would give a dependence of ion intensity on cyanogen concentration similar to the one which they have adopted.

A further alternative to the proton transfer mechanism is provided by the reactions of CH_3^+ and CH_2^+ with NH_3, investigated by Smith and Adams (32):

$$CH_2^+ + NH_3 \rightarrow CH_2NH_2^+ + H,$$

$$CH_3^+ + NH_3 \rightarrow CH_3NH_3^+.$$

In this case the rate coefficients are suitable for our system ($\sim 10^{-9}$ cm^3 s^{-1}) but we did not detect the precursor ions. Therefore it must be assumed that the reactions go to completion, as significant amounts of CH_2^+ and CH_3^+ are required to produce the observed signals for $CH_2NH_2^+$ and $CH_3NH_3^+$. Such amounts have not been detected by us in other nonnitrogenated FID-type flames (9, 10). We therefore conclude that these reactions are less important than the protonation of methanimine and methylamine.

The very likely presence of methanimine and its

relatively high proton affinity lead us to conclude that ND_2O^+ contributes at most only a minor proportion of the peak at m/z 34 observed in the deuterium flame (see Fig. 4), and reinforces the argument of section (b) against the presence of NH_2O^+ in the hydrogen flame (see Fig. 3).

1. P. F. KNEWSTUBB and T. M. SUGDEN. Nature, **181**, 474 (1958).
2. P. F. KNEWSTUBB and T. M. SUGDEN. Proc. R. Soc. London, Ser. A, **255**, 520 (1960).
3. J. A. GREEN and T. M. SUGDEN. Ninth International Symposium on Combustion, Academic Press, New York. 1963. p. 607.
4. J. PEETERS, C. VINCKIER, and A. VAN TIGGELEN. Oxid. Combust. Rev. **4**, 93 (1969).
5. A. N. HAYHURST and N. R. TELFORD. Combust. Flame, **28**, 67 (1977).
6. D. K. BOHME, J. M. GOODINGS, and C.-W. NG. Int. J. Mass Spectrom. Ion Phys. **24**, 335 (1977).
7. C. BERTRAND and P. J. VAN TIGGELEN. J. Phys. Chem. **78**, 2320 (1974).
8. M. A. BREDO, P. J. GUILLIAUME, and P. J. VAN TIGGELEN. Fifteenth International Symposium on Combustion, Combustion Institute, Pittsburg, PA. 1975. p. 1003.
9. H. C. BOLTON, J. GRANT, I. D. MCWILLIAM, A. J. C. NICHOLSON, and D. L. SWINGLER. Proc. R. Soc. London, Ser. A, **360**, 265 (1978).
10. T. MCALLISTER and J. SCOTT. Int. J. Mass Spectrom. Ion Phys. **33**, 63 (1980).
11. J. N. BRADLEY and E. METCALFE. J. Chem. Soc. Faraday Trans. I, 1301 (1979).
12. K. N. BASCOMBE, J. A. GREEN, and T. M. SUGDEN. Adv. Mass Spectrom. **2**, 66 (1963).
13. A. MAKOVKY and T. B. GRUENWALD. Trans. Faraday Soc. **54**, 952 (1958).
14. C. G. CRAWFORTH and C. J. WADDINGTON. Trans. Faraday Soc. **65**, 1334 (1969).
15. K. GLANZER and J. TROE. Helv. Chim. Acta, **55**, 2884 (1972).
16. T. MCALLISTER and P. PITMAN. Int. J. Mass Spectrom. Ion Phys. **19**, 241 (1976).
17. P. KEBARLE, S. K. SEARLES, A. ZOLLA, J. SCARBOROUGH, and M. ARSHADI. J. Am. Chem. Soc. **89**, 6393 (1967).
18. P. KEBARLE, R. YAMDAGNI, K. HIRAOKA, and T. B. MCMAHON. Int. J. Mass Spectrom. Ion. Phys. **19**, 71 (1976).
19. R. G. MCLOUGHLIN and J. C. TRAEGER. J. Am. Chem. Soc. **101**, 5791 (1979).
20. A. T. BLADES. J. Chromatogr. Sci. **10**, 693 (1972).
21. F. C. FEHSENFELD, M. MOSESMAN, and E. E. FERGUSON. J. Chem. Phys. **55**, 2120 (1971).
22. JANAF. Thermochemical Tables, 2nd ed. NSRDS–NBS 37, U.S. Dept. of Commerce (1971).
23. J. F. WOLF, R. H. STALEY, I. KOPPEL, M. TAAGEPERA, R. T. MCIVER, JR., J. L. BEAUCHAMP, and R. W. TAFT. J. Am. Chem. Soc. **99**, 5417 (1977).
24. P. KREIMLER and S. E. BUTTRIL, JR. J. Am. Chem. Soc. **95**, 1365 (1973).
25. N. A. BURDETT and A. N. HAYHURST. 16th International Symposium on Combustion, Combustion Institute, Pittsburg, PA. 1977. p. 903.
26. G. H. LOEW, D. S. BERKOWITZ, and S. CHANG. Astrophys. J. **219**, 458 (1978).
27. M. Y. CLEMENT and D. A. RAMSEY. Can. J. Phys. **39**, 205 (1961).
28. H. M. ROSENSTOCK, K. DRAXL, B. W. STEINER, and J. T. HERRON. J. Phys. Chem. Ref. Data 6, Suppl. 1 (1977).
29. J. L. BEAUCHAMP. Ann. Rev. Phys. Chem. **22**, 527 (1971).
30. D. R. JOHNSON and F. J. LOVAS. Chem. Phys. Lett. **15**, 65 (1972).
31. E. HERBST. Astrophys. J. **205**, 94 (1976).
32. D. SMITH and N. G. ADAMS. Chem. Phys. Lett. **47**, 145 (1977).

Can. J. Chem. Downloaded from www.nrcresearchpress.com by 210.87.254.42 on 09/06/12
For personal use only.

A note on mass spectrometric studies concerning a role of free radicals in catalytic reactions

ZDENEK DOLEJŠEK AND JANA NOVÁKOVÁ

J. Heyrovský Institute of Physical Chemistry and Electrochemistry, Czechoslovak Academy of Sciences, 121 38 Prague, Czechoslovakia

Received November 13, 1980

This paper is dedicated to Dr. F. P. Lossing of the National Research Council of Canada on the occasion of his 65th birthday

ZDENEK DOLEJŠEK and JANA NOVÁKOVÁ. Can. J. Chem. **59**, 1824 (1981).

Free radicals were detected by means of mass spectrometry in the low pressure interaction of reactants with solid catalysts. The same radicals were also prepared by very low pressure pyrolysis and their reactivity studied both with a catalyst (as a model study of the radicals' role on the catalyst surface) and with other gas phase components present in the system, with the aim to observe a possible shift of the reaction to the gas phase.

ZDENEK DOLEJŠEK et JANA NOVÁKOVÁ. Can. J. Chem. **59**, 1824 (1981).

Au cours de l'interaction des corps réagissants à pression basse avec des catalyseurs on a observé la présence des radicaux libres par la spectrométrie de masse. Les mêmes radicaux furent aussi préparés par la pyrolyse à pression très basse et on a étudié leur réactivité avec un catalyseur (pour modeler leur rôle sur la surface du catalyseur) ainsi qu'avec d'autres composants de la phase gazeuse pour pouvoir étudier le transport possible de la réaction en phase gazeuse.

Considerable evidence, especially of an indirect nature, suggests that a reaction may shift from a catalytic surface to the gas phase (e.g. refs. 1, 2). It is assumed that such hetero–homogeneous reactions proceed by a radical mechanism initiated on the catalyst surface. In only a few cases (3, 4) was the presence of radicals in the gas phase confirmed directly following the catalytic interaction. The question whether the observed radicals are merely reaction by-products or whether they play a more important role in further steps of the reaction remains unanswered thus far. For this reason it is important not only to detect the free radicals if present but also to check simultaneously for their reactivity with all potential reactants in the system. We have tried to use mass spectrometry for this purpose.

Experimental

A cylindrical quartz tube reactor similar to the one used by Lossing and co-workers (5) for measurements of the ionization potential of free radicals was placed close to the ionization chamber of a modified MI 1305 sector field mass spectrometer. The reactor was loosely packed with several grains of a catalyst. In this way we were able to study catalytic reactions under molecular flow conditions at pressures $1–10^{-3}$ Pa. Both the reaction products and unstable intermediates of radical character could be followed simultaneously using ionization with low energy electrons in the latter case. In the second part of the experiments, where radicals in the gas phase were prepared by pyrolysis (~1 Pa), a reactor with two separately heated sections was used. The radicals prepared in the first section passed through the second section over a catalyst and thence directly to the detection region.

With these two experimental arrangements (the single or double section reactor) the following reactions were studied: (*i*) selective oxidation of propylene to acrolein on bismuth molybdate (6, 7); (*ii*) oxidation of methanol to formaldehyde on a silver catalyst (8). In the first case a shift of the reaction to the gas phase, with participation of allyl and allylperoxyl radicals has been assumed (1, 2). In the second case the presence of RO, RO_2, and HO_2 radicals in the gas phase was proven by epr at atmospheric pressure (4).

Results and Discussion

In order to check our instrument's ability to detect free allyl radicals in a catalytic reaction we have repeated Hart and Friedli's experiments (3) involving the interaction of propylene with manganous oxide. In an extension of this work we have detected allyl radicals in the gas phase also in the ZnO/propylene interaction (9). On the other hand no allyl radicals were found with bismuth molybdate/propylene, where the appearance of free allyl radicals as a first step in the transfer of the reaction in the gas phase had been expected (9). Due to the presence of a large amount of unreacted propylene the increase of the ratio of the peaks at the mass-to-charge ratios 41/42 had to be used as an evidence for the free allyl radical formation on the heated oxide catalysts (Table 1).

In order to check for the possibility that even with bismuth molybdate/propylene allyl radicals are formed on the catalyst surface but that they quickly react with lattice oxygen, in which case they would probably appear in the gas phase as oxygen-containing species, additional experiments aimed to study the reactivity of allyl radicals were carried out. Allyl radicals were prepared by pyrolysis of 1,5-hexadiene in the first part of the two section reactor and allowed to react with a catalyst in the second section. With a catalyst kept at moderate temperature (370 K), acrolein was

0008-4042/81/121824-03$01.00/0

©1981 National Research Council of Canada/Conseil national de recherches du Canada

Can. J. Chem. Downloaded from www.nrcresearchpress.com by 210.87.254.42 on 09/06/12
For personal use only.

TABLE 1. Ratio of 41/42 peak intensities[a] at some different catalyst temperatures obtained with 13.5 eV electron beam energy

	Temperature (K)						
Catalyst[b]	290	400	600	700	800	850	900
I	0.10	0.10	0.12	0.13	0.17	0.19	[c]
II	0.10	0.10	0.12	0.13	0.18	0.22	0.28
III or IV	0.10	0.10	0.10	0.10	0.10	0.10	0.10

[a]In %.
[b]I, ZnO; II, Mn(II)Mn(III) oxide; III, bismuth molybdate; IV, quartz wool (blank experiment).
[c]Volatile.

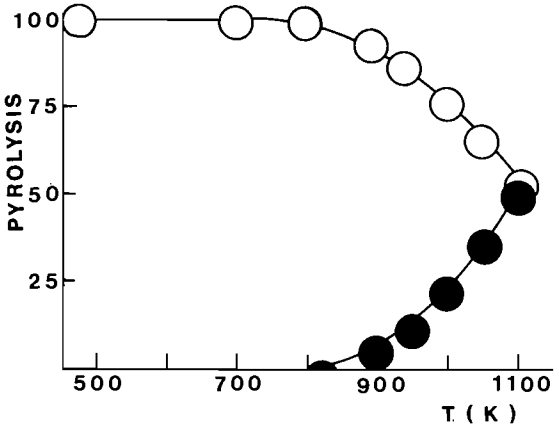

FIG. 1. Decomposition of 1,5 hexadiene (○) and formation of allyl radicals (●) plotted against temperature of pyrolyzer.

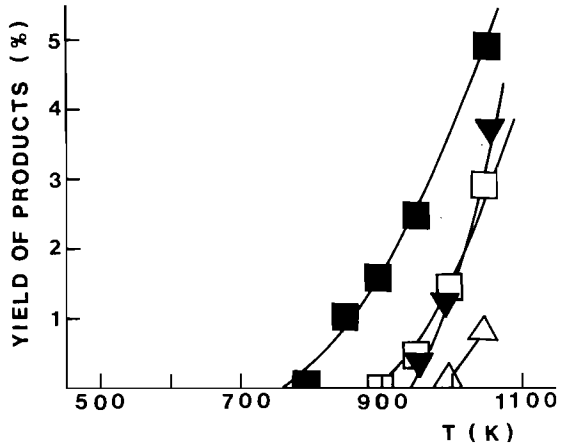

FIG. 2. Products of allyl radical interaction with MoO_3 catalyst plotted against temperature of pyrolyzer, reactor temperature ≤ 470 K: acrolein (■), propylene (□), CO (▼), CO_2 (△). (At 1000 K only one third of the allyl radicals formed passed through catalyst region without reaction.)

found as a product not only with catalysts generally used for acrolein production, but also with other oxides, e.g. MoO_3, ZnO, Co_3O_4 (6, 7). It is evident that the allyl radical, once formed, could be easily oxidized to acrolein by lattice oxygen. In an experiment with a very active oxidation catalyst, Co_3O_4, allyl radicals were easily overoxidized to CO and CO_2 by a relatively moderate warming of the catalyst to 500 K. These experiments with the two section reactor are illustrated for the case of MoO_3 in Figs. 1 and 2. Figure 1 shows the formation of allyl radicals by pyrolysis of 1,5-hexadiene in the first section of the quartz tube (pyrolyzer); Fig. 2 gives the products of the allyl radical-catalyst interaction in the second section (reactor).

Further experiments concerned the possible interaction of allyl radicals in the gas phase. At our low pressure conditions (~1 Pa) allyl radicals were not oxidized by molecular oxygen in the absence of a catalyst (see also ref. 10). When the residence time in the reactor was increased by a quartz wool plug inserted into the reactor exit, only increased recombination of allyl radicals was observed. Under comparable conditions (in the absence of a catalyst and the quartz wool plug) oxidation of benzyl radicals after admission of molecular oxygen was clearly observed. Thus, in our conditions we were unable to verify the role of allyl radicals as an active intermediate in the shift of the reaction into the gas phase. On the other hand, allyl radicals were found to react easily with lattice oxygen to yield acrolein as a product.

In the more recent experiments on the reaction of methanol vapour with a heated silver wire we observed, using low energy electrons (14 eV), a very small amount of a product contributing to the peak at mass-to-charge ratio $m/e = 15$ (8). Because of large concentration differences we were unable to obtain a reliable ionization potential of this product and to assign it unambiquously to the methyl radical. As the concentration of this species decreased with addition of oxygen while the concentration of the main product, formaldehyde, rose at the same time, it seems likely that the observed additional product at $m/e = 15$ acts as an intermediate in the mechanism of the main product formation (Table 2).

Can. J. Chem. Downloaded from www.nrcresearchpress.com by 210.87.254.42 on 09/06/12
For personal use only.

TABLE 2. Influence of oxygen addition on formation of the unstable product (m/e = 15) and formaldehyde (m/e = 30) from methanol on silver wire at 690 K[a]

	Mass-to-charge m/e peak intensities	
	$m/e = 30$ (690 K)	$m/e = 15$ (690 K)
Ag + methanol	47	9
Ag + (methanol + oxygen) 1 : 1 mixture	147	5

[a]14.0 eV electron beam energy.

From the experiments described it follows that low pressure mass spectrometry can provide information on primary reaction products as well as, in special cases, on radical intermediates in interactions of reactants with catalysts. Comparative studies concerning the reactivity of these radicals with other components in the gas phase probably will require measurements at rather higher pressures, which we were unable to carry out with the present simple apparatus.

1. L. YA. MARGOLIS. Heterogeneous catalytical oxidation of hydrocarbons in Russian, Chimiya, Leningrad. 1967. pp. 151–163.
2. C. DANIEL and C. W. KEULKS. J. Catal. **24**, 529 (1972).
3. P. J. HART and H. R. FRIEDLI. J. Chem. Soc. D, Chem. Commun. 621 (1970).
4. T. A. GARIBYAN, R. R. GRIGORYAN, L. YA. MARGOLIS, and A. B. NALBANDYAN. Dokl. Akad. Nauk. **234**, 90 (1977).
5. R. F. POTTIE, A. G. HARRISON, and F. P. LOSSING. J. Am. Chem. Soc. **83**, 3204 (1961).
6. Z. DOLEJŠEK and J. NOVÁKOVÁ. Coll. Czech. Chem. Commun. **44**, 673 (1979).
7. J. NOVÁKOVÁ and Z. DOLEJŠEK. Coll. Czech. Chem. Commun. **44**, 2009 (1979).
8. Z. DOLEJŠEK, J. NOVÁKOVÁ, and F. TUREČEK. React. Kinet. Catal. Lett. To be published.
9. Z. DOLEJŠEK and J. NOVÁKOVÁ. J. Catal. **37**, 540 (1975).
10. D. M. GOLDEN, G. N. SPOKES, and S. W. BENSON. Angew. Chem. **85**, 602 (1973).

Can. J. Chem. Downloaded from www.nrcresearchpress.com by 210.87.254.42 on 09/06/12
For personal use only.

Gas phase photochemical decomposition of 1-bromopropane

STUART G. BAYLISS, ROBERT L. FAILES, AND JACOB S. SHAPIRO[1]

School of Chemistry, Macquarie University, North Ryde, N.S.W., Australia

Received December 30, 1980

This paper is dedicated to Dr. F. P. Lossing of the National Research Council of Canada on the occasion of his 65th birthday

STUART G. BAYLISS, ROBERT L. FAILES, and JACOB S. SHAPIRO. Can. J. Chem. **59**, 1827 (1981).

The gas phase photochemical decomposition of 1-bromopropane (1bp) was studied over the temperature range 374–483 K and the pressure range 10–95 kPa. Within these ranges the overall kinetics are expressed by:

$$\frac{-d[1bp]}{dt} = k[1bp]^{3/2}\frac{[HBr]^{1/2}}{[C_3H_6]^{1/2}}I_0^{1/2}$$

where I_0 is the incident light intensity. The principal propagation step involves the abstraction of the secondary hydrogen by a bromine atom leading to two major products: propene and hydrogen bromide. Termination involving allyl radical is postulated, a feature that sets this photolysis apart from those of ethyl and neopentyl bromides. The overall activation energy is 33.8 ± 0.8 kJ mol^{-1} and it leads to Arrhenius parameters for the propagation step [3] of $E_a = 29.7$ kJ mol^{-1} and $\log_{10}A = 9.1$ (A in dm^3 mol^{-1} s^{-1}).

[3] $Br^{\cdot} + CH_3CH_2CH_2Br \rightarrow CH_3\dot{C}HCH_2Br + HBr$

STUART G. BAYLISS, ROBERT L. FAILES et JACOB S. SHAPIRO. Can. J. Chem. **59**, 1827 (1981).

On a étudié la décomposition photochimique en phase gazeuse du bromo-1 propane (1bp) dans des intervalles de température et de pression allant de 374 à 483 K et de 10 à 95 kPa respectivement. A l'intérieur de ces limites, on peut exprimer la cinétique globale par le relation

$$\frac{-d[1bp]}{dt} = k[1bp]^{3/2}\frac{[HBr]^{1/2}}{[C_3H_6]^{1/2}}I_0^{1/2}$$

où I_0 est l'intensité de la lumière incidente. L'étape principale de la propagation fait intervenir l'enlèvement d'un hydrogène secondaire par l'atome de brome, conduisant ainsi à deux produits principaux: le propène et le bromure d'hydrogène. On envisage la présence de radicaux allyles pour expliquer l'arrêt de la réaction. C'est une caractéristique qui convient parfaitement à cette photolyse à l'exception de celle des bromures d'éthyle et de néopentyle. L'énergie d'activation globale est de 33,8 ±0,8 kJ mol^{-1} et elle conduit à des paramètres d'Arrhénius pour l'étape de propagation [3] de E_a = 29,7 kJ mol^{-1} et $\log_{10} A$ = 9,1 (A en dm^3 mol^{-1} s^{-1}).

[3] $Br^{\cdot} + CH_3CH_2CH_2Br \rightarrow CH_3\dot{C}HCH_2Br + HBr$

[Traduit par le journal]

Introduction

Photochemically initiated decompositions of alkyl bromides in the gas phase have received little attention, possibly because of their complexity. In bromides possessing more than one type of hydrogen atom several kinds of free radical intermediates may be formed. When both α- and β-bromoalkyl radicals may be formed (1*a*), the former are incapable of propagating kinetic chains. In other cases facile isomerisation of bromoalkyl radicals via bridged transition states (2, 3) obscures the identity and relative importance of the initially formed radical. Nevertheless in the case of some primary alkyl bromides, e.g. ethyl (4, 17) and neopentyl (5) bromides, it has been found possible to use the results of the photolyses to examine Arrhenius parameters of individual elementary steps including that for dissociation of the bromoalkyl radical into a molecule and a bromine atom for which information is still scant.

In view of the above considerations we have started a systematic examination of some alkyl bromide photolyses in an attempt to examine the effect of variation of molecular structures on their kinetics and mechanism. The choice of 1-bromopropane arose from its relationship to the corresponding pyrolysis of the compound for which it has been proposed (8) that the experimentally observed 3/2-order kinetics (6, 7) result from a combination of 1st-order unimolecular reaction and a 2nd-order radical chain reaction.

Experimental

1-Bromopropane, 1bp, was dried over P_2O_5 and distilled through a packed column. The fraction boiling at 70–72°C (71.0°C) (9), n_D^{22} 1.4336 (n_D^{20} 1.4343) (9) was used. Allyl bromide (May and Baker, Dagenham, England) was freshly distilled prior to use and the fraction boiling at 71.0°C (70°C[753]) (9) was used. The purity of the bromoalkanes, checked by gas chromato-

[1]To whom all correspondence should be addressed.

0008-4042/81/121827-07$01.00/0

©1981 National Research Council of Canada/Conseil national de recherches du Canada

Can. J. Chem. Downloaded from www.nrcresearchpress.com by 210.87.254.40 on 09/06/12
For personal use only.

Can. J. Chem. Downloaded from www.nrcresearchpress.com by 210.87.254.40 on 09/06/12
For personal use only.

graphic analysis using a flame ionization detector showed no observable impurities. Propane and propene (Matheson research grade) were used directly for identification by glc. Neopentane (Matheson research grade) was used as an internal standard in the quantitative analysis of the hydrocarbon products.

Hydrogen bromide (Matheson research grade) was purified by trap-to-trap distillations at −77°C then stored in a darkened bulb attached to a vacuum line.

Photolyses were carried out in a cylindrical fused quartz cell, 5 cm long and 89.6 cm^3 in volume, with flat quartz windows, joined to a mercury-free high vacuum line. The pressure and temperature measurement systems, the glc analysis, and the photolysis equipment have been described in a previous publication (5). Two lamps were used in the study over a period of four years, their output at 254 nm was measured and was found to be similar (9.7 and 8.9 × 10^{13} photons s^{-1} for lamps I and II, respectively). The fraction of light absorbed did not exceed 6%, leading to errors of less than 2% in the measured values of I_0 with the HBr actinometer (31).

It was possible to follow the progress of the reaction by the pressure increase which was shown to be directly proportional to the amounts of hydrogen bromide and propene evolved, confirming the stoichiometric relationship to be

$$C_3H_7Br \rightarrow C_3H_6 + HBr$$

Such a relationship was shown to be valid at least up to 6% reaction for C_3H_6 and up to 20% reaction for HBr. However, kinetic data were collected from runs restricted to only 2% decomposition or less.

Results

The major chemical process occurring during the photolysis was shown to be the formation of hydrogen bromide and propene in equimolar yields. Propane was formed with a quantum yield of 0.9 ± 0.1 but represented only between 0.1 and 2% of the propene yield depending on experimental conditions, as displayed in Table 1.

Low temperatures, long photolysis times, and low reactant pressures are seen to increase the proportion of propane. Traces of 2-bromopropane were observed in runs carried out to high conversion (>40% reaction and photolysis times >5 × 10^4 s). Examination of reaction products by combined gas chromatography – mass spectrometry failed to detect high boiling products such as 1,5-hexadiene or allyl bromide. No evidence was found for noncondensible products such as methane or hydrogen.

The pressure–time plots in Fig. 1 exhibited an almost imperceptible induction period, which became somewhat longer at the lower temperatures. This was followed by an approximately linear region with the rate of pressure increase slowly falling off as the reaction proceeded. The pressure–time data for the first 2% of the reaction were fitted to a second order polynomial equation (10) from which the initial photolysis rate, $\Delta P/\Delta t$, was determined. The initial rate, given by the first coefficient of the fitted equation, was shown to be independent of the extent of reaction considered for 1 to 5% conversion. A correction (up to 15% maximum) was made in each run to individual rates to allow for the reactor dead space (11) (ca. 10% of reactor volume).

TABLE 1. Relative yields of C_3H_6 to C_3H_8 for different conditions in the photolysis of 1-bromopropane

(*a*) Effect of 1-bromopropane pressure at 373.8 K

P_{1bp}/kPa	Photolysis time/s	$Y_{C_3H_6}/Y_{C_3H_8}$
55.69	5300	124
48.36	5650	92
13.86	5400	62

(*b*) Effect of photolysis time

T/K	P_{1bp}/kPa	Photolysis time/s	$Y_{C_3H_6}/Y_{C_3H_8}$
373.8	41.20	320	231
	39.98	504	115
	38.39	2000	104
	40.23	4750	122
	41.10	6550	120
	39.38	16600	101
482.7	54.81	1504	981
	51.43	2376	979
	42.19	5680	815
	40.74	45000	393
	41.48	83400	315

(*c*) Effect of temperature

P_{1bp}/kPa	Photolysis time/s	Temperature/K	$Y_{C_3H_6}/Y_{C_3H_8}$
48.69	2500	373.8	126
48.36	5650	373.8	102
51.43	2376	482.7	979
42.19	5680	482.7	815

Kinetic data were found to be best interpreted in terms of a 1.5-order process:

$$(\Delta P/\Delta t)_{initial} = k_{1.5}P_{1bp}^{3/2}I_0^{1/2} = k_{1.5}^1 P_{1bp}^{3/2}$$

where

$$k_{1.5}^1 = k_{1.5}I_0^{1/2}$$

The 1.5-order rate constant, $k_{1.5}^1$, was independent of pressure in the range 10–95 kPa and over the temperature range 373–483 K as shown in Fig. 2. The rate was proportional to I_0^n where $n = 0.5 \pm 0.05$ over a tenfold range of I_0.

Least-squares treatment of the data obtained at different temperatures and a range of initial pressures, 30–70 kPa (40 runs with a constant light intensity), yielded

$$k_{1.5}^1 = 10^{0.307\pm0.84} \times \exp(-33\,800 \pm 800/RT)\ L^{1/2}\ mol^{-1/2}\ s^{-1}$$

Can. J. Chem. Downloaded from www.nrcresearchpress.com by 210.87.254.40 on 09/06/12
For personal use only.

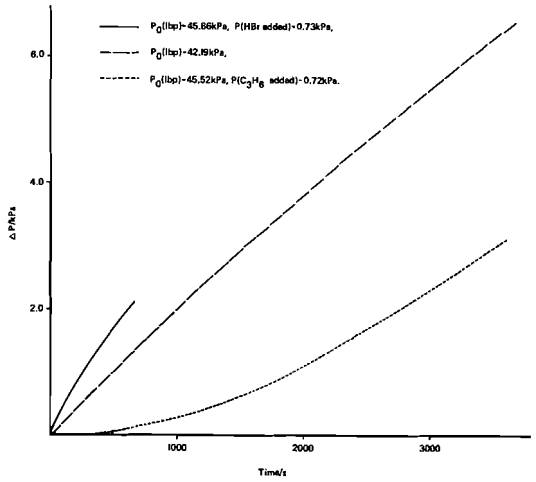

FIG. 1. Typical pressure–time plots, 482.7 K.

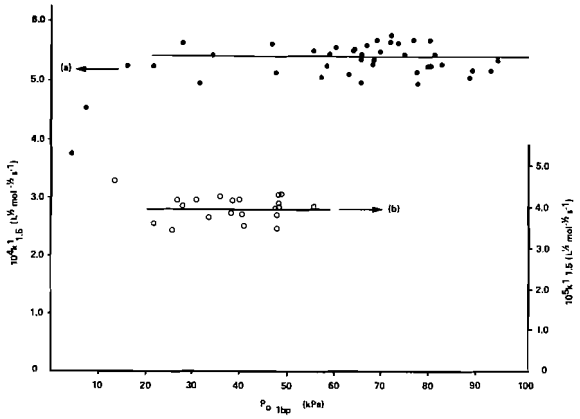

FIG. 2. Variation of $k^1_{1.5}$ with initial pressure of 1-bromopropane; (*a*) ● 482.7 K, (*b*) ○ 373.8 K.

and

$$k_{1.5} = 10^{-6.67\pm0.84} \times \exp(-33\,800 \pm 800/RT)\ \mathrm{L^{1/2}\ mol^{-1/2}\ s^{-1/2}}$$

with

$$R = 8.314\ \mathrm{J\ K^{-1}\ mol^{-1}}$$

The effects of added hydrogen bromide and propene, seen in Fig. 1, illustrate the profound effect of the reaction products on the rate even at low levels of addition. In the case of propene addition, while the effect is particularly marked, after a long photolysis time the pressure–time plot for the propene-added photolysis becomes almost parallel to that of the normal photolysis indicating that the propene acts as a retarder rather than an inhibitor (12). Runs without added hydrogen bromide or propene display only a slight fall off in rate up to 10% reaction even though both hydrogen bromide and propene are formed in the reaction.

The pressure–time data for runs in the presence of added propene or hydrogen bromide could no longer be satisfactorily fitted to a parabolic equation. With added HBr the initial slope is steep but falls off rapidly as the reaction proceeds and is therefore highly dependent on the first few data points. A plot (not shown) of log (initial rate) versus log (pressure added HBr), at constant P_{1bp}, gives scattered results but the order is close to 0.5 with respect to P_{HBr}. For experiments with added C_3H_6 the rate is extremely slow initially but increases as the reaction proceeds (and hydrogen bromide is produced). Meaningful interpretation in terms of initial rates, however, is not possible.

Analysis of runs with added HBr and propene becomes possible in terms of a rate equation of the form

$$[\mathrm{I}]\quad \frac{\mathrm{d}(\Delta P)}{\mathrm{d}t} = k^1_{1.5} P_{1bp}{}^{3/2} \left[\frac{P_{HBr}}{P_{C_3H_6}}\right]^{1/2}$$

In the presence of added HBr, eq. [I] becomes

$$\frac{\mathrm{d}(\Delta P)}{\mathrm{d}t} = k^1_{1.5} P_{1bp}{}^{3/2} \left(\frac{C + \Delta P}{\Delta P}\right)^{1/2}$$

where $C = P_{HBr}$ added and ΔP = observed pressure increase. Over the first few percent of photolysis P_{1bp} is approximately constant and is equal to $(P_{1bp})_0$. On integrating the above expression the following result is obtained:

$$\sqrt{\Delta P(C+\Delta P)} + \frac{C}{2} \ln\left[\frac{\sqrt{\Delta P(C+\Delta P)} - \Delta P}{\sqrt{\Delta P(C+\Delta P)} + \Delta P}\right] = k^1_{1.5}(P_{1bp})_0{}^{3/2}(t - t_0)$$

For runs of 1-bromopropane with added HBr a plot of the left hand side of the equation (= F_{HBr}) against time is found to be almost linear with only a small amount of fall off, as seen in Fig. 3. Values of $k^1_{1.5}$ calculated from these plots are independent of $(P_{1bp})_0$ between 25 kPa and 63 kPa and of $P_{HBr\,added}$, up to 10 kPa at 482.7 K. The light intensity dependence (graph not shown) is close to half-order (exponent is 0.57). Rate constants calculated in this manner are approximately the same as those without added HBr, e.g. 4.89×10^{-4} and 4.65×10^{-4} $\mathrm{L^{1/2}\ mol^{-1/2}\ s^{-1}}$, respectively at 482.7 K.

For the photolysis with added propene the corrected rate expression, [I], becomes

$$\frac{\mathrm{d}(\Delta P)}{\mathrm{d}t} = k^1_{1.5}(P_{1bp})^{3/2} \left[\frac{\Delta P}{g + \Delta P}\right]^{1/2}$$

where $g = P_{C_3H_6}$ added. On integration (with the

Can. J. Chem. Downloaded from www.nrcresearchpress.com by 210.87.254.40 on 09/06/12
For personal use only.

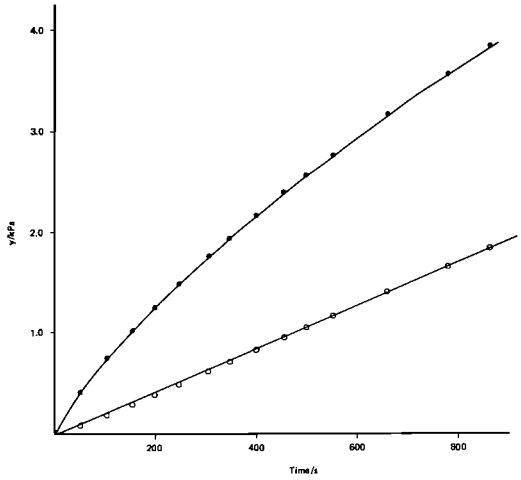

FIG. 3. Integrated plot for typical run with added hydrogen bromide at 482.7 K with P_{1bp} = 45.96 kPa and P_{HBr} added = 5.40 kPa. Plots of y = (*a*) ΔP (●), (*b*) F_{HBr} (○).

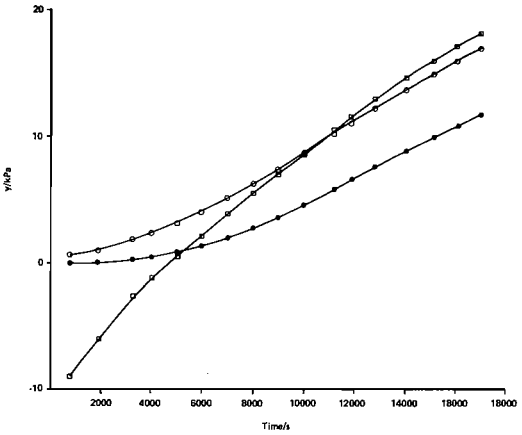

FIG. 4. Integrated plots for typical run with added propene at 482.7 K with P_{1bp} = 46.31 kPa and $P_{C_3H_6}$ added = 2.60 kPa. Plots of y = (*a*) ΔP (●), (*b*) $F_{C_3H_6}$ (○), (*c*) $\Delta P + 2.60 \ln(\Delta P)$ (□).

assumption that P_{1bp} is essentially constant) the following equation is obtained:

$$\sqrt{\Delta P(g + \Delta P)} - \frac{g}{2} \ln\left[\frac{\sqrt{\Delta P(g + \Delta P)} - \Delta P}{\sqrt{\Delta P(g + \Delta P)} + \Delta P}\right] = k_{1.5}^{\dagger}(P_{1bp})_0^{3/2}(t - t_0)$$

Plots of the left hand side of the equation, $F_{C_3H_6}$, versus time, shown in Fig. 4, display a significant "induction" period, the duration of which increases with pressure of added C_3H_6. This is followed by an approximately linear region. The values of $k_{1.5}^{\dagger}$ determined from the slope of this linear region, however, fall off with increasing pressure of added propene.

It is likely, however, that large added pressures of propene lead to a change in termination (Step 7 replacing Step 6 in the mechanism given later) leading to the rate expression

$$d(\Delta P)/dt = k_x P_{1bp}^{3/2} P_{HBr}/P_{C_3H_6}$$

Integration (with $P_{C_3H_6 added} = g$) yields

$$k_x P_{1bp}^{3/2}(t - t_0) = \Delta P + g \ln \Delta P$$

Plots of ($\Delta P + g \ln \Delta P$) against time are found to be reasonably linear (Fig. 4) and values of k_x derived from the slope do not now vary with pressure of added propene ($P_{HBr} < 20$ kPa). For example $k_{1.5}^{\dagger}$ in the absence of added C_3H_6 at 482.7 K is 5.00 × 10^{-4} $L^{1/2}$ $mol^{-1/2}$ s^{-1} while k_x (P_{1bp} = 46–54 kPa, $P_{C_3H_6}$ = 0.05–2.6 kPa, 6 runs) ranges from (4.02–4.20) × 10^{-4} $L^{1/2}$ $mol^{-1/2}$ s^{-1}.

Discussion

A mechanism, consistent with the above experimental results, is described below.[2]

Initiation

$$C_3H_7Br + h\nu \xrightarrow{[1]} C_3H_7^{\cdot} + Br$$

$$C_3H_7^{\cdot} + C_3H_7Br \xrightarrow{[2]} C_3H_6Br^{\cdot} + C_3H_8$$

$$C_3H_7^{\cdot} + HBr \xrightarrow{[2a]} Br^{\cdot} + C_3H_8$$

Propagation

$$Br^{\cdot} + C_3H_7Br \underset{[-3]}{\overset{[3]}{\rightleftharpoons}} CH_3\dot{C}HCH_2Br + HBr$$

$$Br^{\cdot} + C_3H_7Br \underset{[-3a]}{\overset{[3a]}{\rightleftharpoons}} CH_3CH_2\dot{C}HBr + HBr$$

$$CH_3\dot{C}HCH_2Br \overset{[4]}{\rightleftharpoons} CH_3CH{=}CH_2 + Br^{\cdot}$$

$$CH_3CH_2\dot{C}HBr + C_3H_7Br \underset{[-4a]}{\overset{[4a]}{\rightleftharpoons}} CH_3\dot{C}HCH_2Br + C_3H_7Br$$

$$CH_3CH{=}CH_2 + Br^{\cdot} \underset{[-5]}{\overset{[5]}{\rightleftharpoons}} CH_2{=}CH{-}\dot{C}H_2 + HBr$$

Termination

$$CH_2{=}CH{-}\dot{C}H_2 + Br^{\cdot} \xrightarrow{[6]} C_3H_5Br$$

$$2CH_2{=}CH{-}\dot{C}H_2 \xrightarrow{[7]} C_6H_{10}$$

Since propene and propane are products of propagation and initiation respectively, their ratio $Y_{C_3H_6}/Y_{C_3H_8}$ serves as a measure of the kinetic chain length. As seen from Table 1, the kinetic chain length varies from 60 to 980 depending on experi-

[2]Computer simulation of the reaction mechanism has been carried out along lines similar to those applied by Frank and Hanrahan (17) to ethyl bromide photolysis. Results in complete agreement with experimental data were obtainable for runs with and without added HBr and C_3H_6. These results will be published separately.

Can. J. Chem. Downloaded from www.nrcresearchpress.com by 210.87.254.40 on 09/06/12
For personal use only.

mental conditions. This large chain length, coupled with the fact that this study was performed at large reactant pressures, tends to rule out the possibility of direct formation of HBr and C_3H_6 via a unimolecular mechanism which would be expected to occur with a quantum yield of unity. Another possible initiation process believed to occur thermally (8), i.e. RX + HX → RH + 2X, is not evident in this case, since there is no dark reaction at 373 K and only a very slight one at 483 K.

The three major carbon-containing radicals in the mechanism are the bromopropyl radicals, $CH_3CH_2\dot{C}HBr$ and $CH_3\dot{C}HCH_2Br$ and the allyl radical, $CH_2{=}CH{-}\dot{C}H_2$. Termination steps involving the μ radical $CH_3\dot{C}HCH_2Br$ lead to ${}^1\mu\mu_{1/2}$ or ${}^1\beta\mu_1$ mechanisms (30) and can be excluded since they do not lead to 3/2-order kinetics. Termination steps involving the α-bromopropyl radical,

$$CH_3CH_2\dot{C}HBr + Br^{\cdot} \rightarrow C_3H_6Br_2$$

or

$$2CH_3CH_2\dot{C}HBr \rightarrow C_6H_{12}Br_2$$

while giving 3/2-order kinetics (they lead to ${}^1\beta\beta_{3/2}$ mechanisms) can be excluded on the grounds of low concentration of that radical relative to the allyl radical. An upper limit to this ratio can be calculated simply by neglecting reactions [4*a*] and [−4*a*] (reaction [4*a*] can only reduce the concentration and reaction [−4*a*] would be so much slower than reaction [−3*a*] — even at low [HBr] — as to be negligible). The steady-state ratio is

$$\frac{[CH_3CH_2\dot{C}HBr]}{[CH_2{=}CH\dot{C}H_2]} = \left(\frac{k_{3a}}{k_{-3a}}\right)\left(\frac{k_{-5}}{k_5}\right)\left(\frac{[C_3H_7Br]}{[CH_3CH{=}CH_2]}\right)$$

Now the factor (k_{3a}/k_{-3a}) is the equilibrium constant for reactions [3*a*], [−3*a*], and estimated from $\Delta H^0 = 9.2\,\text{kcal mol}^{-1}$ and $\Delta S^0 = 8.0\,\text{cal mol}^{-1}\,\text{K}^{-1}$ (themselves calculated from estimated ΔH_f^0 and S^0 values by Benson's method (1)), it has a value of approximately $10^{-3.6}$ at 373 K and $10^{-2.4}$ at 482 K. Similarly, the factor (k_{-5}/k_5) is the equilibrium constant for reactions [−5], [5], and estimated from $\Delta H^0 = -1.3\,\text{kcal mol}^{-1}$ and $\Delta S^0 = -5.6\,\text{cal mol}^{-1}\,\text{K}^{-1}$ it has a value of approximately $10^{-0.4}$ at 373 K and $10^{-0.6}$ at 482 K. Hence, the expression $(k_{3a}/k_{-3a})\,(k_{-5}/k_5)$ is approximately $10^{-4.0}$ at 373 K and $10^{-3.0}$ at 482 K and after a very small amount of reaction the relative concentration of the α-bromopropyl radical would be too small for it to be involved in termination. Thus, of the possible propagation steps only [3], [4], [5], and [−5] are important in this photolysis.

It is difficult to confirm experimentally the actual intermediacy of the allyl radical in the photolysis since allyl bromide and 1,5-hexadiene were not found among the minor products even on examination by gc–ms analysis. A control experiment at 482.7 K in which 0.53 kPa of allyl bromide and 40.22 kPa of 1-bromopropane were photolysed for 8.1×10^4 s showed that the former disappears many times faster than the latter. Hence it is not unreasonable not to find evidence of the end products of the allyl radicals during the photolysis of 1-bromopropane.

Termination steps involving allyl radicals were included in a kinetic scheme proposed by Cross and Stimson (8) for the thermal decomposition of 1-bromopropane and by Field and Abell (14) for the photoaddition of hydrogen bromide to propene.

Benson (1*b*) has also postulated that any free radical mechanism of the pyrolysis of *t*-butyl bromide would involve termination through the combination of a methylallyl radical and a bromine atom.

The prospect of the reverse overall reaction merits a brief consideration, i.e. the photoaddition of hydrogen bromide to propene (14), despite the fact that the kinetics of the photolysis in this study are determined from very low conversion runs. Unfortunately the work of Field and Abell (14) is not completely comparable with the experimental conditions of the present study. Their study was conducted at temperatures from 324 to 423 K, much lower pressures, and for $[HBr]:[C_3H_6] > 1$. High reactant pressures used in the current study permit omission of consideration of excited bromoalkyl radicals as intermediates (14). The only yard stick for estimating the extent of the reverse reaction—the formation of 2-bromopropane (which itself photolyses at a slower rate than the 1-bromopropane)—suggests that the reverse reaction in the normal photolysis is not worthy of serious consideration in the early stages of the decomposition.

Assuming long chains ($\phi C_3H_6 \simeq 10^2$–10^3) and applying the steady state approximation the following rate expression is obtained:

$$\frac{-d[C_3H_7Br]}{dt} = k_3\left[\frac{k_1}{k_6K_5 + k_7K_5^2([C_3H_6]/[HBr])}\right]^{1/2} \times I_0^{1/2}\left[\frac{[HBr]}{[C_3H_6]}\right]^{1/2}[C_3H_7Br]^{3/2}$$

For runs in the absence of added HBr and C_3H_6, since HBr and C_3H_6 are formed in equal amounts, their ratio is unity, hence the rate should appear to be independent of both products, which is the case at low conversions. The derived rate equation is

TABLE 2. Arrhenius parameters for elementary reactions

Reaction	E/kJ mol^{-1}	log A*	Comments
[1]	~8.4	†	A and E_a were estimated from the temperature dependence of the extinction coefficients of alkyl bromides (28, 29)
[6]	~0	10.9	$k_6 \simeq 10k_7$
[7]	~0	9.9	References 25, 26
Equilibrium [5]: at 373.6 K $\log_{10} K_5 = 1.06 \pm 1.76$‡ at 482.7 K $\log_{10} K_{-5} = 1.04 \pm 1.36$§			

*Units for A and k are either dm^3 mol^{-1} s^{-1}, s^{-1}, or dm^6 mol^{-2} s^{-1}.
†Reaction [1] n-$C_3H_7Br + h\nu \rightarrow n$-$C_3H_7^{\cdot} + Br^{\cdot}$.
For k_1 defined by rate = $k_1 I_0(C_3H_7Br)$ k_1 and the extinction coefficient, ε, for absorption of light by C_3H_7Br are related (31) by

[I] $k_1 = 2.3\varepsilon b\phi/N_a V_{Rv}$

where b is the path length, ϕ is the quantum yield, and V_{Rv} is the volume of the reaction vessel. Substitution of $\varepsilon_{253.7\,nm} = 1.2\,cm^3\,mol^{-1}\,cm^{-1}$ at 298 K (our measurements) and activation energy of 8.4 kJ mol^{-1} for temperature dependence of extinction coefficients of alkyl bromides (28, 29) give

$$k_1 = 10^{-20.06} \exp(-8.4 \times 10^3/RT)$$

(The expression for k_1 given by eq. [I] will be in error when the fraction of light absorbed becomes large (31). At the highest temperatures and pressures used this fraction may be as large as 40%. Uncorrected values are reported however since the errors involved amount to only 0.2 in log A and 1 kJ in E_a.)
‡From values of $(\Delta H_f^0)_g$, S^0, and C_p^0 at 300–500 K for Br (20), C_3H_6 (21), HBr (20), and CH_2CHCH_2 (22–26), $\log_{10} K_5 = 1.06$ and 1.04 at 373.8 K and 482.7 K, respectively.
§References 20–26.

also consistent with the effect of added HBr where the very rapid initial rate falls off quickly as propene is formed and with the effect of added propene where the initial rate is extremely small but increases as reaction proceeds.

From the overall rate constant, it is possible to evaluate k_3, i.e. the rate constant for secondary hydrogen abstraction from 1-bromopropane. Thus from the overall kinetics it follows that,

$$k_{1.5} = k_3 \left[\frac{k_1}{k_6 K_5 + k_7 K_5^2}\right]^{1/2}$$

Upon substituting the appropriate Arrhenius equations for rate constants, k_1, k_6, k_7, and a numerical value for K_5 (these are discussed in Table 2), the rate constant k_3 is then found to be expressible by the equation:

$$k_3 = 10^{9.1} \exp(-29\,700/RT)\ \text{L mol}^{-1}\ \text{s}^{-1} \qquad (R \text{ in J K}^{-1}\ \text{mol}^{-1})$$

Arrhenius factors reported for the abstraction of secondary hydrogen atoms from propane (15) by bromine atoms are log A/M^{-1} s^{-1} = 10.96 and E_a = 43.6 kJ mol^{-1} and those for abstraction from n-butane are similar (15, 16). Thus log A and E_a are less for abstraction from bromosubstituted alkanes than from unsubstituted alkanes by 1.4 and 13.9 kJ mol^{-1}, respectively (13, 27). These decreases are almost identical to those observed in the case of the corresponding liquid phase reactions (decreases of 1.5 in log A and 13.0 kJ mol in E_a, observed in this study and in ref. 15) supporting the statement by Pryor (18) and Poutsma (19) regarding the applicability of liquid phase results to gas-phase bromination studies. The faster abstraction of hydrogen atoms in bromoalkanes can be attributed to the anchimeric assistance of the bromine substituent (27).

A number of publications have considered the relative ease of β- versus α-hydrogen abstraction from bromoalkanes (13, 27). The most recent and definitive report is one by Tanner *et al.* (27) for the vapour phase bromination of 1-bromobutane at 296 K under which conditions the rate for β- relative to α-hydrogen abstraction is found to be 34.6:1. This value may possibly vary at the higher temperatures (i.e. up to 483 K) employed in the present study, nevertheless it is not expected to change so significantly as to alter the conclusions that follow.

Finally, it is noteworthy that whereas the 1-bromopropane photolysis is a 3/2-order process the only other bromide photolyses so far studied (those of ethyl (4) and neopentyl (5) bromides) are found to be predominantly 1st-order processes. For these the prospect of termination involving allylic type radicals does not arise and chain termination appears to involve combination of bromine atoms with μ-type radicals (the γ-bromoalkyl radical in the case of neopentyl bromide and the β-bromoalkyl radical in the case of ethyl bromide).

1. S. W. BENSON. Thermochemical kinetics. 2nd ed. Wiley, New York. 1976. (*a*) pp. 234–236, (*b*) p. 246.
2. P. S. SKELL, R. R. PAVLIS, D. C. LEWIS, and K. J. SHEA. J. Am. Chem. Soc. **95**, 6735 (1973).
3. P. S. SKELL and K. J. SHEA. Israel J. Chem. **10**, 493 (1972).
4. R. BARKER and A. MACCOLL. J. Chem. Soc. 2839 (1963).
5. S. G. BAYLISS, R. L. FAILES, J. S. SHAPIRO, and E. S. SWINBOURNE. J. Chem. Soc. Faraday Trans. I, **74**, 776 (1978).
6. P. J. AGIUS and A. MACCOLL. J. Chem. Soc. 973 (1955).
7. N. N. SEMENOV, G. B. SERGEEV, and C. A. KAPRALOVA. Dokl. Akad. Nauk SSSR, **105**, 301 (1955).
8. J. T. D. CROSS and V. R. STIMSON. Aust. J. Chem. **21**, 973 (1968).
9. R. C. WEAST (*Editor*). CRC handbook of chemistry and physics. 55th ed. CRC Press, Cleveland. 1974. pp. C440–C457.
10. K. J. HALL, T. I. QUICKENDEN, and D. W. WATTS. J. Chem. Ed. **53**, 493 (1976).
11. E. S. SWINBOURNE. Analysis of kinetic data. Nelson, London. 1971. p. 92.
12. J. M. G. COWIE. Polymers: chemistry and physics of modern materials. Intertext Book, Great Britain. 1973. p. 59.
13. K. J. SHEA, D. C. LEWIS, and P. S. SKELL. J. Am. Chem. Soc. **95**, 7768 (1973).
14. R. J. FIELD and P. I. ABELL. J. Am. Chem. Soc. **91**, 7226 (1969).
15. J. C. AMPHETT and E. WHITTLE. Trans. Faraday Soc. **64**, 2130 (1968).
16. K. C. FERGUSON and E. WHITTLE. Trans. Faraday Soc. **67**, 2618 (1971).

Can. J. Chem. Downloaded from www.nrcresearchpress.com by 210.87.254.40 on 09/06/12
For personal use only.

17. A. J. FRANK and J. HANRAHAN. J. Phys. Chem. **82**, 2194 (1978).
18. W. A. PRYOR. Free radicals. McGraw-Hill, New York. 1966. p. 189.
19. M. L. POUTSMA. *In* Free radicals. Vol. 2. *Edited by* J. K. Kochi. Wiley, New York. 1973. p. 174.
20. JANAF. Thermochemical tables. 2nd ed. *Edited by* D. R. Stull *et al.* NSRDS-NBS-37, U.S. Govt. Printing Off., Washington DC. 1971.
21. D. R. STULL, E. F. WESTRUM, and G. C. SINKE. The chemical thermodynamics of organic compounds. Wiley, New York. 1969.
22. H. E. O'NEAL and S. W. BENSON. Int. J. Chem. Kinet. **I**, 217 (1969).
23. W. TSANG. J. Chem. Phys. **46**, 2817 (1967).
24. D. M. GOLDEN and S. W. BENSON. Chem. Rev. **69**, 125 (1969).
25. M. ROSSI, K. D. KING, and D. M. GOLDEN. J. Am. Chem. Soc. **101**, 1223 (1979).
26. M. ROSSI and D. M. GOLDEN. J. Am. Chem. Soc. **101**, 1230 (1979).
27. D. D. TANNER, Y. KOSUGI, R. ARHART, N. WADA, T. PACE, and T. RUO. J. Am. Chem. Soc. **98**, 6275 (1976).
28. H. L. FRIEDMAN, R. B. BERNSTEIN, and H. E. GUNNING. J. Chem. Phys. **26**, 528 (1957).
29. P. FINKE and C. F. GOODEVE. Proc. R. Soc. London, A**163**, 592 (1937).
30. P. GOLDFINGER, M. LETORT, and M. NICLAUSE. Contribution a l'étude de la structure moleculaire. Victor Henri Commemorative Volume. Desoer, Liege. 1948. p. 283.
31. J. G. CALVERT and J. N. PITTS, JR. Photochemistry. John Wiley, New York. 1966.

Can. J. Chem. Downloaded from www.nrcresearchpress.com by 210.87.254.40 on 09/06/12
For personal use only.

Interfacial excess entropies and solvent structures

GRAHAM HILLS AND FERNANDO SILVA
Department of Chemistry, The University, Southampton S09 5NH, England
Received October 15, 1980

This paper is dedicated to Dr. Sam Levine on the occasion of his 70th birthday

GRAHAM HILLS and FERNANDO SILVA. Can. J. Chem. **59**, 1835 (1981).

Detailed consideration is given to thermodynamic relationships describing the temperature dependence of the properties of electrified interfaces. Excess entropies are derived for multicomponent systems and in particular it is shown that the effect on the residual excess entropy, S^*, of the specifically adsorbed organic species can be directly determined by experiment. Values of S^* in the presence of thiourea (TU) can be understood in terms of the surface excesses of TU and the degree of solvent orientation. The preferred orientation of water is shown to be charge-dependent, under all conditions to be zero at $-3\,\mu C\ cm^{-2}$, and largely determined by its molecular polarisability. Temperature-invariant capacities are shown to occur widely and are not easily explained in terms of cluster models or time-dependent solvent orientation.

GRAHAM HILLS et FERNANDO SILVA. Can. J. Chem. **59**, 1835 (1981).

On considère en détail les relations thermodynamiques qui décrivent l'influence de la température sur les propriétés des interfaces électrifiées. On décrit les entropies d'excès pour des systèmes à plusieurs constituants et on démontre en particulier que l'effet sur l'entropie d'excès résiduelle, S^*, d'une espèce organique adsorbée peut être mesuré directement par expérimentation. On peut interpréter les valeurs de S^* que l'on obtient en présence de la thiourée (TU) en termes de l'excès de TU en surface et du dégré d'orientation du solvant. L'orientation préférée de l'eau dépend de la charge, est zéro à $-3\,\mu C\ cm^{-2}$ pour toutes conditions, et est déterminée en grande mesure par la polarisabilité moléculaire de l'eau. Il existe souvent des capacités indépendantes de la température mais on ne peut pas les expliquer en termes de modèles "cluster" ou de variations dans l'orientation du solvant.
[Traduit par le journal]

Introduction

This paper is dedicated to Sam Levine who stimulated the authors to examine more closely the evidence for orientational states of the solvent at the mercury/aqueous electrolyte interface.

The story is told of a research seminar by Sir Eric Rideal on the subject of double layers after which an earnest young man persisted in questioning the lecturer about certain aspects of the theory. In desperation, Rideal is said to have replied "That is too difficult a question for me, you will have to ask a Dr. Levine about that", to which the questioner replied "But I am Levine". That story, hopefully not too apocryphal, describes at least two things about Sam Levine, (1) his persistent thrusts into the fundamentals of double layer theory and (2) his cheerful North American assertiveness which enlivened any discussion.

His contributions to the theory of the double layer have been noteworthy throughout two or more decades when effectively there was no theory. The marvellous thermodynamic analyses of Grahame, Frumkin, and Parsons had invited all sorts of imaginative improper microscopic interpretations requiring for their quantitative evaluation the best of statistical mechanical treatments of condensed phases, all beyond the ability, not to say the comprehension, of but a handful of chemical physicists. Sam Levine had that ability since he was by nature and by training a mathematician. His analytical treatments of the electrical state of the interface and later of its structural state were milestones in the conceptual description of the interface and the latter led to the firm suggestion that the capacity maximum, so charmingly described as the "hump", was due to reorientation of the solvent. The fact that one or two systems displayed more than one maximum was neither here nor there but Sam Levine's (1) treatment of the Watts–Tobin's proposals (2) stimulated a more detailed thermodynamic study of the interface and the paper which follows is a further step in that direction.

Excess Entropies of the Charged Interface

A number of formal descriptions have been given of the temperature coefficients of the electrical and compositional state of the metal solution interface. The Gibbs equation for the equilibrium interfacial free energy per unit area can be written as

$$[1] \qquad d\sigma = -\Gamma_s\,dT + \Gamma_v\,dP - \sum \Gamma_i\,d\mu_i - q\,d\varepsilon_\pm$$

where $\varepsilon_\pm$ is the electrochemical potential and the other terms have their usual significance. The important term here is Γ_s, the excess entropy, and it is evidently defined as

$$[2] \qquad \Gamma_s = -\left(\frac{\partial\sigma}{\partial T}\right)_{P,\mu,\varepsilon_\pm}$$

0008-4042/81/131835-09$01.00/0
©1981 National Research Council of Canada/Conseil national de recherches du Canada

Can. J. Chem. Downloaded from www.nrcresearchpress.com by 210.87.254.40 on 09/06/12
For personal use only.

Can. J. Chem. Downloaded from www.nrcresearchpress.com by 210.87.254.40 on 09/06/12
For personal use only.

where σ is simply the interfacial tension but where, because both μ and $\varepsilon_\pm$ are not necessarily independent of temperature even though the composition remains unchanged, care must be given to the exact evaluation of the partial derivative. By implication, the system described by eq. [1] contains a reference electrode reversible to one of the constituent ions and it is a straightforward matter to show (3) that Γ_s is given by

$$[3] \qquad \Gamma_s = \int\int \left(\frac{\partial \frac{1}{C}}{\partial T}\right)_{m,q}$$

where m is the molality of the solution components and where the two constants of integration are, in order,

$$\left(\frac{\partial E_\pm}{\partial q}\right)_\mu \quad \text{and} \quad \left(\frac{\partial \sigma}{\partial T}\right)_{q,\mu}$$

at $q = 0$. In all the equations subsequent to [2] the subscript P denoting constant pressure has been omitted for the sake of clarity.

The excess entropy contains contributions from all the components present in the interface although it is believed that its charge dependence is largely determined by the reorganisation of the solution side. This is likely to be so if the metallic phase is a one component system and, in any case, interest principally attaches to variations in Γ_s with solution composition. The contribution to the excess entropy from species adsorbed into the interface can be resolved if their relative excesses and partial molar entropies are known. Thus, it is possible (4) to define a residual excess entropy, S^*, as

$$[4] \qquad S^* = \Gamma_s - \sum_i \Gamma_i \bar{S}_i$$

If the adsorbed components are ions, then a non-thermodynamic assumption intervenes in that single ion entropies are not known. However, seemingly reasonable estimates have been made of partial molar ionic entropies in aqueous solution and their use in this context leads to consistent values of S^*.

The complete route to S^* is a slightly complex one and needs to be firmly established, especially in the presence of several adsorbed components. Alternative but equivalent routes to S^* are given here and are extensions of previous formulations (5) in that they allow its straightforward determination in the presence of adsorbed organic compounds.

Thus, for a system of a single uni-univalent electrolyte, eq. [4] becomes

$$[5] \qquad S^* = \Gamma_s - \Gamma_- \bar{S}_- - \Gamma_+ \bar{S}_+$$

or, because of the electroneutrality condition,

$$[6] \qquad \begin{aligned} S^* &= \Gamma_s - \left(\Gamma_+ + \frac{q}{F}\right)\bar{S}_- + \Gamma_+ \bar{S}_+ \\ &= \Gamma_s - \Gamma_\mp \bar{S}_{\text{salt}} \pm \frac{q}{F}\bar{S}_\pm \end{aligned}$$

The $\bar{S}_\pm$ terms are the separate partial molar ionic entropies and $\bar{S}_{\text{salt}}$ is the readily determinable partial molar entropy of the salt. The total relative excess entropy is thus redefined by re-arrangement of eq. [6] as

$$[7] \qquad \Gamma_s = S^* + \Gamma_\mp \bar{S}_{\text{salt}} \pm \frac{q}{F}\bar{S}_\pm$$

and this can be substituted into the alternative form of [1], namely

$$[8] \qquad -d\xi_\pm = +\Gamma_s\, dT + \sum \Gamma_i\, d\mu_i - \varepsilon_\pm\, dq$$

where ξ is the Parsons auxiliary variable. Thus, at constant composition,

$$[9] \qquad -d\xi_\pm = \left(S^* + \Gamma_\mp \bar{S}_{\text{salt}} \mp \frac{q}{F}\bar{S}_\pm\right) dT - \varepsilon_\pm\, dq + \Gamma_\mp\, d\mu_{\text{salt}}$$

and because at constant composition

$$[10] \qquad d\mu_{\text{salt}} = -\bar{S}_{\text{salt}}\, dT$$

eq. [9] simplifies to

$$[11] \qquad -d\xi_\pm = \left(S^* \mp \frac{q}{F}\bar{S}_\pm\right) dT - \varepsilon_\pm\, dq$$

Because $\xi_\pm$ is a total differential, cross-differentiation leads to

$$[12] \qquad \frac{d}{dq}\left(S^* \mp \frac{q}{F}\bar{S}_\pm\right)_{m,T} = -\left(\frac{\partial \varepsilon_\pm}{\partial T}\right)_{m,q}$$

and therefore

$$[13] \qquad \left(\frac{\partial S^*}{\partial q}\right)_{m,T} = -\left(\frac{\partial \varepsilon_\pm}{\partial T}\right)_{m,q} \pm \frac{\bar{S}_\pm}{F}$$

The temperature coefficient of the electrochemical potential is related to the temperature coefficient of the potential, $E_\pm$ of the metallic interface with respect to a reversible reference electrode. Changes in temperature of the cell (even at constant $E_\pm$) must take account of the entropies of the reference components not directly related to the compositional dependence of the potential, e.g. of the solid Hg_2Cl_2 and liquid mercury in a directly reversible calomel reference electrode.

In general terms,

Can. J. Chem. Downloaded from www.nrcresearchpress.com by 210.87.254.40 on 09/06/12
For personal use only.

$$[14] \quad \left(\frac{\partial \varepsilon_{\pm}}{\partial T}\right)_{m,q} = \left(\frac{\partial E_{\pm}}{\partial T}\right)_{m,q} + \frac{1}{F}\frac{dk}{dT}$$

where k is a sum of known free energy terms independent of composition and electric potential.

Since

$$[15] \quad \left(\frac{\partial E_{\pm}}{\partial T}\right)_{m,q} = \left(\frac{\partial E_{\pm}}{\partial T}\right)_{m,q=0} + \int_0^q \left[\frac{\partial\left(\frac{1}{C}\right)}{\partial T}\right]_{m,q} dq$$

eq. [13] can be rewritten to include [14] and [15] and then integrated to give

$$[16] \quad S_q^* - S_{q_r}^* = -\int_{q_r}^q \left[\int_0^q \left(\frac{\partial\left(\frac{1}{C}\right)}{\partial T}\right)_{m,q} dq + \left(\frac{\partial E_{\pm}}{\partial T}\right)_{m,q=0}\right] dq - \left[\frac{1}{F}\frac{\partial k}{\partial T} \mp \frac{\bar{S}_{\pm}}{F}\right](q - q_r)$$

where q_r refers to any reference state of the system and which might well be but not necessarily that of $q = 0$. The principal variables on the right hand side of [16] are directly obtainable from the routine measurement of differential capacity as a function of charge and temperature at a series of different compositions. The last bracketted term contains only constants.

Equation [16] can also be obtained from the cross-differentiation of eq. [8] at constant composition, i.e.

$$[17] \quad \left(\frac{\partial \Gamma_s}{\partial q}\right)_{\mu,T} = -\left(\frac{\partial \varepsilon_{\pm}}{\partial T}\right)_{\mu,q}$$

where, as before,

$$[18] \quad \left(\frac{\partial \varepsilon_{\pm}}{\partial T}\right)_{\mu,q} = \left(\frac{\partial E_{\pm}}{\partial T}\right)_{\mu,q} + \frac{1}{F}\frac{dk}{dT}$$

But

$$[19] \quad \left(\frac{\partial E_{\pm}}{\partial T}\right)_{\mu,q} = \left(\frac{\partial E_{\pm}}{\partial T}\right)_{m,q} - \left(\frac{\partial E_{\pm}}{\partial \mu}\right)_q \left(\frac{\partial \mu}{\partial T}\right)_m$$

where also from eq. [1]

$$\left(\frac{\partial E_{\pm}}{\partial \mu}\right)_q = -\left(\frac{\partial \Gamma_{\pm}}{\partial q}\right)_{\mu}$$

and where

$$\left(\frac{\partial \mu}{\partial T}\right)_m = -\bar{S}_{salt}$$

Thus

$$[20] \quad \left(\frac{\partial E_{\pm}}{\partial T}\right)_{\mu,q} = \left(\frac{\partial E_{\pm}}{\partial T}\right)_{m,q} - \left(\frac{\partial \Gamma_{\pm}}{\partial q}\right)_{\mu} \bar{S}_{salt}$$

and substitution of eqs. [18], [19], and [20] into [17] followed by integration then gives eq. [16], as indeed it must.

The first route to eq. [16] is, however, preferred because of the ease with which it can be extended to systems of several components. In this work, the full details of which will be given elsewhere (6), we were concerned with the adsorption of thiourea at a mercury interface and with the competition between the organic adsorbate and anions and between both and the solvent water. The effect on the solvent is well reflected in S^* which is strongly affected by the presence of adsorbed thiourea.

Thus, it is a straightforward matter to include appropriate terms for this molecule (here denoted by TU) into eq. [9], such that

$$[21] \quad -d\xi_{\pm} = \left(S^* \mp \frac{q}{F}\bar{S}_{\pm} + \Gamma_{\mp}\bar{S}_{salt} + \Gamma_{TU}\bar{S}_{TU}\right) dT + \Gamma_{\mp}\, d\mu_{salt} + \Gamma_{TU}\, d\mu_{TU} - \varepsilon_{\pm}\, dq$$

But at constant composition,

$$[22a] \quad d\mu_{salt} = -\bar{S}_{salt}\, dT$$

and

$$[22b] \quad d\mu_{TU} = -\bar{S}_{TU}\, dT$$

and substitution for $d\mu_{salt}$ and $d\mu_{TU}$ in eq. [21] gives simply

$$[23] \quad -(d\xi_{\pm})_{m_{salt},m_{TU}} = \left(S^* \mp \frac{q}{F}\bar{S}_{\pm}\right) dT - \varepsilon_{\pm}\, dq$$

which is identical to eq. [11], except for the condition that the concentration of TU is also constant. The same sequence of equations then follows to give again eq. [16] which contains only observable quantities and $\bar{S}_{\pm}$ but *no* term directly related to thiourea. The influence of the strongly adsorbed thiourea is of course manifested in the experimental values of $d(1/C)/dT$ and $(dE_{\pm}/dT)_{q=0}$ determined at constant composition but dependent on the concentration and surface excess of TU. Thus if we label S^* in the presence and absence of TU as S_{TU}^* and S_b^*

Can. J. Chem. Downloaded from www.nrcresearchpress.com by 210.87.254.40 on 09/06/12
For personal use only.

respectively (b denotes base electrolyte) and so on for the other terms, then

$$[24]\quad \frac{\partial}{\partial q}(S_{TU}^* - S_b^*) = -\left(\frac{\partial E_{\pm,TU}}{\partial T}\right)_{q=0} - \int_0^q \left(\frac{\partial \frac{1}{C_{TU}}}{\partial T}\right)_{q,m_{TU}} + \frac{\bar{S}_{\pm,TU}}{F} + \left(\frac{\partial E_{\pm,b}}{\partial T}\right)_{q=0} + \int_0^q \left(\frac{\partial \frac{1}{C_b}}{\partial T}\right)_{q,m_b} - \frac{\bar{S}_{\pm,b}}{F}$$

If the reasonable assumptions are then made (*i*) that the degree of ionic adsorption is independent of the concentration of thiourea and (*ii*) that $\bar{S}_\pm$ is also independent of the presence of the thiourea (see ref. 7), the difference $\bar{S}_{\pm,TU} - \bar{S}_{\pm,b}$ can be equated to zero and the integration of eq. [24] then gives $S_{TU}^* - S_b^*$ irrespective of the nature of the base electrolyte or the reference electrode, i.e. determined solely by the experimental quantities, C and $E_\pm$. The resultant integral,

$$[25]\quad S_{TU}^* - S_b^* = \int_{q_r}^q \left[\int_0^q \left(\frac{\partial \frac{1}{C_b}}{\partial T}\right)_{m_b,q} - \int_0^q \left(\frac{\partial \frac{1}{C_m}}{\partial T}\right)_{m_{TU},q} + \left(\frac{\partial E_{\pm,b}}{\partial T}\right)_{m_b,q=0} - \left(\frac{\partial E_{\pm,m}}{\partial T}\right)_{m_{TU},q=0}\right]$$

is therefore the basis of the direct determination of the effect of adsorbed molecules, especially organic molecules, on the residual interfacial entropy and hence on the configuration of the solvent in the interface. The same procedure could be followed in studying the adsorption of an additional ionic component but it would be necessary to involve an indifferent base electrolyte, e.g. NaF, and to carry out the measurements at constant total ionic strength.

The Charge Dependence of Γ_s and S*

Values of Γ_s and S^* were obtained from a range of aqueous solutions of KCl and for the same solutions containing a wide concentration range of thiourea (6). The number of results from such a multivariate system was very large and only a sample can be presented here. The new capacitance–potential data were recorded on paper tape and processed off-line. Potentials of zero charge were determined using either a streaming electrode or the method of back integration. The details of these and other related studies will be given elsewhere (6). The data were processed to give the interfacial tension, σ, and also q, Γ_{Cl^-}, Γ_{TU}, Γ_s, and S^*.

Figure 1 shows a typical set of capacity – surface charge density curves as a function of temperature for one composition, namely 0.04 *M* thiourea in 0.1 *M* KCl. The first aspect to note is the temperature invariant point characteristic of many if not all capacitance charge curves in aqueous solutions; this will be referred to later. Values of ΔS^* (i.e. $S_{TU}^* - S_b^*$) for a range of thiourea concentrations in 0.1 *M* KCl and at 25°C are shown in Fig. 2 as a function of surface charge density. The falling curves reflect the change in interfacial composition. The effect of the specific adsorption of the chloride ions is already taken into account in the evaluation of ΔS^*, subject only to the assumption that $\bar{S}_{Cl^-}$ is independent of its own surface coverage and that of other species. The fall in ΔS^* is therefore predominantly due to the change in the relative surface excess of thiourea. That this is so is evident from Fig. 3 which shows the dependence of ΔS^* on Γ_{TU} for different concentrations of thiourea. The lines have similar slopes and the systematic difference in the absolute values of ΔS^* even at constant Γ_{TU} result solely from the

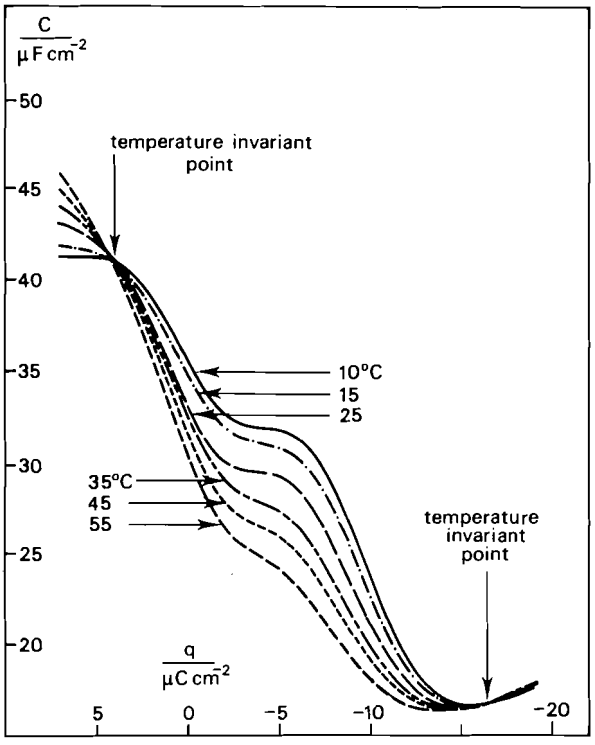

FIG. 1. Differential capacity of Hg/0.1 *M* KCl, 0.04 *M* thiourea as a function of charge and temperature.

Can. J. Chem. Downloaded from www.nrcresearchpress.com by 210.87.254.40 on 09/06/12
For personal use only.

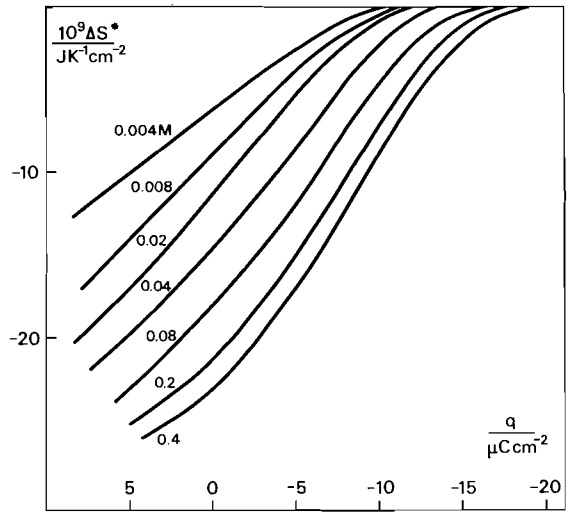

FIG. 2. ΔS^* as a function of surface charge density for seven concentrations of thiourea.

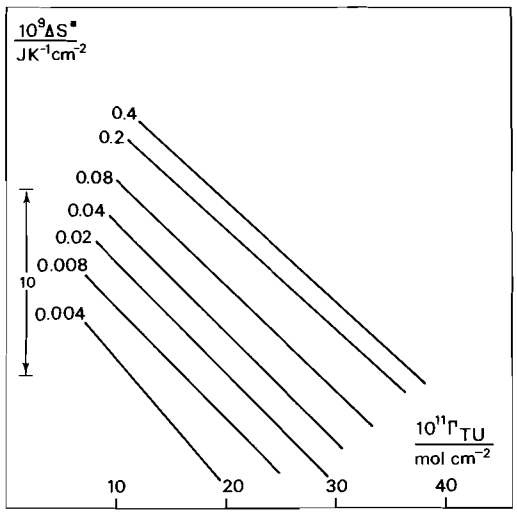

FIG. 3. ΔS^* as a function of the surface excess of thiourea at different bulk concentrations of thiourea in 0.1 M aqueous KCl at 25°C.

choice of integration constant which was conveniently but arbitrarily made zero for all concentrations at $q = 0$. A knowledge of the variation of the absolute values is not essential to this paper but to clarify the complex interdependence of ΔS^*, Γ_{TU}, and q, values of S^* were calculated as a function of charge density but at constant molality of thiourea. The derived relationships shown in Fig. 4 as the full lines are all parabolic in nature and have been adjusted here to a common value at extreme cathodic potentials where the differential capacity is no longer temperature dependent and where, therefore, ΔS^* is effectively zero. The important feature of all these curves is that

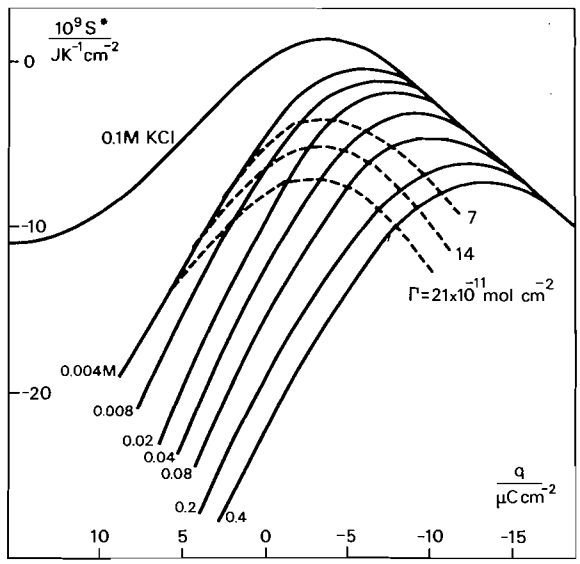

FIG. 4. S^* (full lines) and $S^* - \Gamma_{TU}(d\Delta S^*/d\Gamma_{TU})$ (dashed lines) as a function of q and of the bulk concentration of thiourea at 25°C.

each shows a maximum but the height and, more importantly, the position on the charge axis are systematically dependent on the composition of the solution and therefore of the interface, i.e. on the value of m_{TU}. The decrease of S^* with Γ_{TU} at constant solution composition is evidence of the significant contribution to ΔS^*made by the solvent water which has been the principal conclusion of all previous studies (3–5, 8, 9). The lateral displacement of the maxima to more cathodic potentials is evidence that reorganisaton of the complex interface still occurs as the charge density is varied.

The forced fit of the parabolas in Fig. 4 can also be applied to the lines in Fig. 3. Figure 5 shows them stemming from a common origin at $\Gamma_{TU} = 0$. The slopes are essentially the same and certainly no significant dependence on m_{TU} was observed. It is easy to show (4) that ΔS^*, as operationally defined by eq. [25], is also given by

$$[26] \quad \Delta S^* = \left[\sum_i m_i^\sigma(\bar{S}_i^\sigma - \bar{S}_i)\right] - \left[\sum_j m_j^\sigma(\bar{S}_j^\sigma - \bar{S}_j)\right]_r$$

where r denotes a convenient reference state, in this case where $m_{TU} = 0$, and where m_i^σ and m_j^σ are the number of moles of each component in the same arbitrary volume of interface for the given and reference states respectively. Since the surface excess is closely related to the surface composition, it follows from eq. [26] that

Can. J. Chem. Downloaded from www.nrcresearchpress.com by 210.87.254.40 on 09/06/12
For personal use only.

$$[27]\quad \frac{d\Delta S^*}{d\Gamma_{TU}} = \frac{dS^*}{d\Gamma_{TU}} \approx \frac{dS^*}{dm_{TU}^{\sigma}} = -(\bar{S}_{TU}^{\sigma} - \bar{S}_{TU}) + n(\bar{S}_{H_2O}^{\sigma} - \bar{S}_{H_2O})$$

where n is the number of water molecules displaced or replaced by adsorption or desorption of a thiourea molecule. The linearity of the slopes in Fig. 3 and 5 suggests (*i*) that the partial molar entropy of adsorption of thiourea into the interface is not significantly dependent on its surface coverage and (*ii*) that the predominant term in eq. [27] is $(\bar{S}_{TU}^{\sigma} - \bar{S}_{TU})$ which in fact is large and negative.

Given the observed dependence of ΔS^* on Γ_{TU}, it is now possible to refine ΔS^* still further by deconvoluting from the lines in Fig. 4, the contribution due to Γ_{TU} thus leaving the residual contribution due solely to the remaining component, namely water. Thus, at each value of q, the quantity $\Delta S^* - \Gamma_{TU}(d\Delta S^*/d\Gamma_{TU})$ was evaluated and the new relationships are shown as the dashed lines on the same figure. These parabolic curves corresponding to the variation with surface charge density of the residual excess entropy at constant surface excess of thiourea are remarkable in that their maxima occur at the same value of q as for solutions containing no thiourea, i.e. where $\Gamma_{TU} = 0$. The charge density at zero preferred solvent orientation is therefore, as before, -3 ± 1 μC/cm^2. The electric potential at that point is a reference potential probably no less important than the potential of zero charge, but the more important conclusion here is that it depends on the preferred orientation of *individual* solvent molecules (see refs. 8–15).

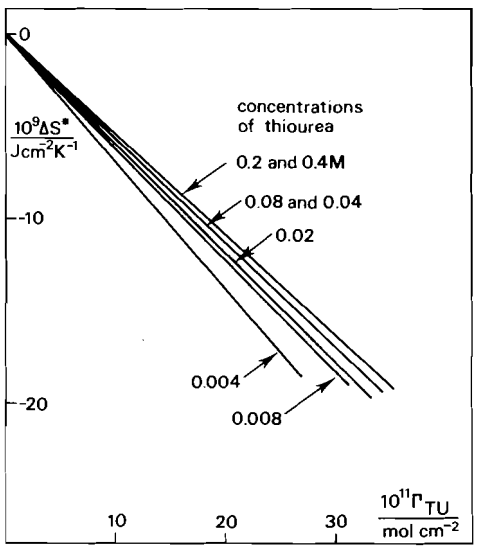

FIG. 5. ΔS^* as a function of Γ_{TU} for different concentrations of thiourea in 0.1 *M* KCl.

It is also clearly evident that the entropic nature of water in the interface, at least as it depends on charge density, is independent of its molecular number density even up to higher coverages of thiourea, in this case ~50%. This casts doubt, to say the least, on suggestions that the clustering of water molecules is an important feature of their interfacial state, particularly as it affects their electrical properties.

The dashed lines in Fig. 4 appear to be parallel and this is also to be expected from thermodynamic argument. Thus, their slopes are given by $(d\Delta S/\partial q)_\Gamma$ and it follows that this can be rewritten as

$$[28]\quad \left(\frac{d\Delta S^*}{dq}\right)_\Gamma = \left(\frac{d\Delta S^*}{dq}\right)_m - \left(\frac{d\Delta S^*}{d\Gamma}\right)_q \left(\frac{d\Gamma}{dq}\right)_m$$

From considerations of congruence (6) it can be shown that

$$[29]\quad \left(\frac{\partial S^*}{\partial \Gamma}\right)_m = \left(\frac{\partial S^*}{\partial \Gamma}\right)_q$$

and experimentally it was observed (Figs. 3 and 5) that

$$[30]\quad \left(\frac{d\Delta S^*}{\partial \Gamma_{TU}}\right)_m = \text{constant} = k'$$

Substitution of [29] and [30] into [28] and integration with respect to q, gives

$$[31]\quad \Delta S^*_{\Gamma_{TU}} = \Delta S^*_{m_{TU}} - k'\Gamma_{TU}$$

so that the dashed lines in Fig. 4 should be parallel.

It is unlikely that the thiourea undergoes any orientation over the range of charge densities used here because (*1*) the Hg–S linkage is evidently very strong and (*2*) the near constancy of the slopes of $(d\Delta S^*/\partial\Gamma_{TU})$ for all conditions of composition and charge density indicate that $(\bar{S}_{TU}^{\sigma} - \bar{S}_{TU})$ and therefore the polarisability of the molecule remains constant so far as $\bar{S}_{TU}^{\sigma}$ is concerned.

The fact remains that the entropic nature of interfacial water as a function of charge density is not dependent on *its* molecular number density. It follows that its smooth, monotonic entropy–charge density dependence is adequately explained in terms of a simple two state model of the kind put forward by Conway and Gordon (10) and by Bockris and Habib (11). The intensive property of the interfacial water is its preferred state of orientation and the corresponding extensive property is the surface number density of individual water molecules.

Solvent Orientation and Temperature Invariant Capacities

The state of the solvent in the interface is not only a necessary aspect of the explanation of the observed

Can. J. Chem. Downloaded from www.nrcresearchpress.com by 210.87.254.40 on 09/06/12
For personal use only.

excess entropies, it is also a vital ingredient of the understanding of the much more widely observed electrical capacity – potential relationships and, in particular, of the striking points of temperature invariant capacity these curves display as a function of temperature.

The word individual used in the last paragraph of the previous section was intended to stress that the present work offers no evidence of co-operative phenomena involving many-state models. It follows that the electrical response of individual molecules is likely to be that of their individual polarisabilities and that would at once explain the first order difference between inner layer differential capacities on either side of the charge or potential of zero preferred orientation. On the far cathodic side, the lower polarisability of the misfit configuration and the

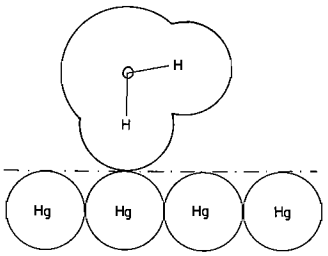

The misfit configuration.

saturation coverage of water molecules leads to the low, charge and temperature independent capacities that are invariably recorded. On the anodic side of the charge of zero preferred orientation, the higher capacity reflects the higher polarisability of the better

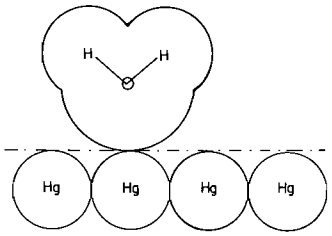

The better fit configuration.

fit configuration and the competition between water molecules and electrostatically attracted anions.

The nature and values of the two extreme polarisabilities, $\alpha_\uparrow$ and $\alpha_\downarrow$, are not known. They are unlikely to be satisfactorily explained in terms of "homogeneous" interactions between multipoles in the solvent molecule and their images in the metal. Were this not so, it would be difficult to explain the first order sensitivity of the differential capacity to metal type as well as to solvent type. In other words, statistical mechanical *molecular* calculations are likely to be less important than equivalent calculations involving site–site interactions, i.e. of constituent atoms, each determined by the particular quantum mechanical interactions of the atom pair in question. These speculations are necessary to direct attention away from macroscopic considerations of dielectric constant and of time-dependent orientational contributions to the capacity which are not easily reconciled with the precise invariance of the isosbestic point on the anodic side of the potential or charge of zero preferred orientation.

Figure 1 is a direct descendent of an earlier famous figure by Grahame reproduced here for convenience as Fig. 6(*a*). Such isosbestic points are commonly found with many other systems but are not so well defined on a normal inner layer capacity–potential plot. The lack of definition arises because the potential scale itself is temperature dependent for the reasons touched on in the earlier part of this paper. If, however, at each temperature the electric potential is re-expressed on a rational scale, cf. Fig. 6(*b*), then the convergence of the intersections also occurs, confirming that we are dealing with a single electrical state of the system at each temperature, the result of which is independent of whether it is expressed as charge or potential. The result of that electric state is to determine and to be determined by the relative populations of solution species in the interface, i.e. the degrees of adsorption. The temperature invariant capacity simply corresponds to an electric state of the system no longer temperature dependent.

Now, it is in the nature of thermodynamics that the simple statement

$$[32] \quad \left(\frac{dC}{dT}\right)_{q,m} = 0 = \left(\frac{d\frac{1}{C}}{dT}\right)_{q,m} \text{ etc.}$$

can be re-expressed in many ways, e.g. as to involve Γ_s or S^* at the point in question. The arguments are, of course, circular in nature and most re-statements of eq. [32] offer little further insight than [32] itself. It is, however, worth noting that

$$[33] \quad \frac{1}{C} = \left(\frac{dE_\pm}{dq}\right)_m$$

and that

$$[34] \quad \left(\frac{d\frac{1}{C}}{dT}\right)_{m,q} = \frac{d}{dT}\left(\frac{dE_\pm}{dq}\right) = \frac{d}{dq}\left(\frac{dE_\pm}{dT}\right)$$

A typical plot for this system of (dE_-/dT) vs. q is shown in Fig. 7. Not surprisingly, the temperature invariant point is now defined by the maximum in dE_-/dT and this has been noted previously (4). A feature not noted previously is that the potential of

Can. J. Chem. Downloaded from www.nrcresearchpress.com by 210.87.254.40 on 09/06/12
For personal use only.

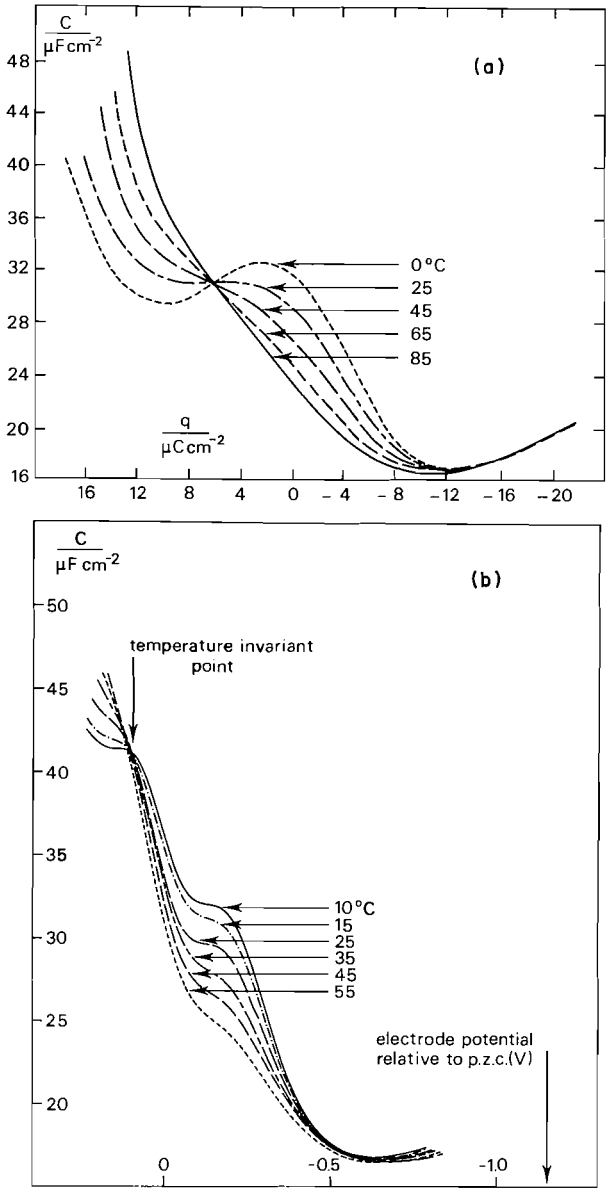

FIG. 6(a). Calculated capacity C_{M-2} of the compact double layer for mercury in 0.8 M sodium fluoride at several temperatures; (b) Differential capacity of 0.04 M thiourea in 0.1 M KCl as a function of temperature and rational potential.

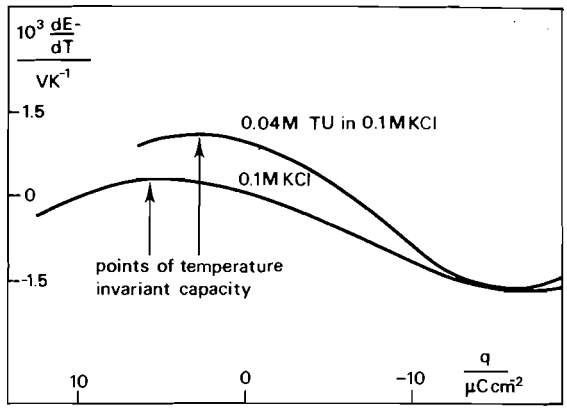

FIG. 7. Charge dependence of $(dE_-/dT)_c$ for aqueous 0.1 M KCl and 0.04 M thiourea in 0.1 M KCl.

zero preferred solvent orientation (when ΔS^* is a maximum) coincides with the value of $d\varepsilon_-/dT = 0$. At far cathodic values of E_- or q, dE_-/dT passes through a minimum indicating another isosbestic point.

The general symmetry of the dE_-/dT vs. q relationship about the potential or charge of zero preferred solvent orientation is satisfying and will no doubt be explained in terms of changing interfacial composition and changing degree of solvent orientation. Both the maxima in dE_-/dT and the isosbestic points beg for an elegant explanation which, unfortunately, is unlikely to come from further thermodynamic argument or statistical mechanical modelling. Given the simple fact that at a particular state of the system $C \neq f(T)$, it is difficult to escape the conclusion that the composition of the interface and its electrical state are also temperature invariant, i.e. that it is improbable that, as argued previously (16), there should be some fortuitous intersection of two equivalently temperature dependent processes, i.e. the temperature analogue of the normal explanation of an isosbestic point. The capacity can be written in general terms as

$$[35] \quad C = \sum_i m_i^\sigma \alpha_i$$

where the m_i^σ terms represent the surface composition and the α_i terms the corresponding polarisabilities. Because of the extreme sensitivity of the capacity to the nature of metallic phase, the polarisabilities are assumed to be wholly electronic and intramolecular in character, i.e. any contribution from time-dependent dipolar or even quadrupolar re-orientation is assumed to be negligible. As such, they *will* be temperature independent and the fact that *both* the m_i amd α_i values must be temperature invariant for C to be constant, is taken as *prima facie* evidence this is so.

The compositional invariance is slightly harder to live with especially for multicomponent systems, but there will be values of m and q at which the individual partial molar free energies of adsorption or, more correctly, of their interchange, will each and all be zero. It could further be argued that the composition and state relating to this invariant condition might be unique for a particular system. Thus to maintain the temperature invariant state an increase in the bulk concentration of thiourea would need to be com-

TABLE 1. The dependence of the temperature invariant point on concentration (*i*) of thiourea in 0.1 *M* KCl and (*ii*) of KCl in aqueous solution

Concentration of thiourea (mol/dm³)	$q_{dC/dT=0}$ (μC cm⁻²)	Concentration of KCl (mol/dm³)	$q_{dC/dT=0}$ (μC cm⁻²)
0.04	+3.0	0.1	5.8
0.08	+2.0	0.5	5.5
0.20	+1.2	1.0	5.5
0.40	+1.0		
0.60	+0.8		

pensated by a decrease in the positive charge density on the mercury surface. The results obtained here (Table 1) indicate that this is so both for the thiourea system and for the simple two component water – potassium chloride system. However, derived values of Γ_{TU} for the range of temperature invariant points corresponding to different bulk concentrations of thiourea and different values of q are not constant, so that the notion of a unique composition is too simple.

Equation [35] may nonetheless describe the best model along which the physics of the temperature invariant points can be further explored. Certainly, the points themselves deserve to be looked for in many other systems and their characteristic values q, Γ, Γ_s, S^*, etc, examined in detail. Some results of such further studies will be reported on at a later date.

Acknowledgements

One of us (F.S.) wishes to thank the Gulbenkian Foundation (Portugal) and the Instituto Nacional de Investigacao Cientifica (Lisbon) for their generous assistance.

1. S. LEVINE, G. M. BELL, and A. L. SMITH. J. Phys. Chem. **73**, 3534 (1969).
2. R. J. WATTS-TOBIN. Phil. Mag. **6**, 133 (1961).
3. G. J. HILLS and R. PAYNE. Trans. Faraday Soc. **61**, 326 (1965).
4. J. A. HARRISON, J. E. B. RANDLES, and D. J. SCHIFFRIN. J. Electroanal. Chem. **48**, 359 (1973).
5. G. J. HILLS and S. HSIEH. J. Electroanal. Chem. **58**, 289 (1975).
6. A. F. SILVA. Ph.D. Thesis, Southampton. 1980.
7. J. H. STERN and J. D. KORLUK. J. Phys. Chem. **73**, 2795 (1969).
8. H. HURWITZ and C. V. D'ALKAINE. J. Electroanal. Chem. **42**, 77 (1973).
9. R. REEVES. *In* Modern aspects of electrochemistry. Vol. 9. *Edited by* B. E. Conway and J. O'M. Bockris. Plenum Press, New York. 1974. p. 239.
10. B. E. CONWAY and L. G. M. GORDON. J. Phys. Chem. **73**, 3609 (1969).
11. J. O'M. BOCKRIS and M. A. HABIB. J. Electroanal. Chem. **65**, 473 (1975).
12. R. PARSONS. J. Electroanal. Chem. **59**, 229 (1975).
13. B. B. DAMASKIN. J. Electroanal. Chem. **75**, 359 (1977).
14. W. R. FAWCETT. J. Phys. Chem. **82**, 1385 (1978).
15. R. GUIDELLI. J. Electroanal. Chem. **110**, 205 (1980).
16. G. J. HILLS. J. Phys. Chem. **73**, 308 (1969).

Can. J. Chem. Downloaded from www.nrcresearchpress.com by 210.87.254.40 on 09/06/12
For personal use only.

The location of the reaction site and discreteness-of-charge effects in electrode kinetics

W. R. FAWCETT

The Guelph-Waterloo Centre for Graduate Work in Chemistry (Guelph Campus), Department of Chemistry, University of Guelph, Guelph, Ont., Canada N1G 2W1

Received August 26, 1980

This paper is dedicated to Dr. Sam Levine on the occasion of his 70th birthday

W. R. FAWCETT. Can. J. Chem. **59**, 1844 (1981).

Discreteness-of-charge effects for simple heterogeneous electron transfer reactions, namely, the self-image effect, the exclusion disc effect, and the effect of local attractive ion–ion interactions, are considered for a variety of reaction sites in the double layer, both in the presence and in the absence of ionic specific adsorption. An expression is derived for the local activity coefficient of the activated complex; this quantity is shown to be a function of both the potential drop across the inner layer and the adsorbed charge density due to specifically adsorbed ions when the standard state is chosen on the basis of the reaction conditions considered in the classical Frumkin theory (reaction site at the outer Helmholtz plane). The consequences of discreteness-of-charge effects for reactions occuring in three different double layer environments of increasing complexity are described. These effects are discussed on the basis of data obtained earlier for the electroreduction of periodate anion in the presence of specifically adsorbed anions.

W. R. FAWCETT. Can. J. Chem. **59**, 1844 (1981).

On a examiné les effets du caractère discret des charges lors de réactions simples de transfert hétérogène d'électron, en particulier l'effet d'auto-image, l'effet d'exclusion du disque et l'effet des interactions locales ion–ion attractives sur divers sites réactionnels de la couche double en présence ainsi qu'en l'absence d'adsorption ionique spécifique. On a déduit une expression pour le coefficient d'activité locale du complexe activé; on montre que cette quantité est une fonction de la chute de potentiel à travers la couche interne et de la densité de charge adsorbée provenant d'ions spécifiquement adsorbés quand l'état normal est choisi en fonction des conditions de la réaction considérée dans la théorie classique de Frumkin (site réactionnel au plan extérieur de Helmholtz). On décrit les conséquences des effets du caractère discret de la charge de la couche double pour des réactions qui ont lieu dans trois environnements différents de complexité croissante. On discute de ces effets en fonction de données relatives à l'électro-réduction de l'anion périodate en présence d'anions spécifiquement adsorbés que nous avons obtenus antérieurement.

[Traduit par le journal]

Introduction

In a recent discussion of discreteness-of-charge effects in electrode kinetics (1), it was pointed out that most theoretical treatments (2–7) assume that the reaction site for the electron transfer process is located on the inner Helmholtz plane (i.H.p.), that is, on the plane through the charge centres of specifically adsorbed non-reacting ions. The treatment of discreteness-of-charge effects in these papers is based on the work of Levine and co-workers first presented in this Journal nineteen years ago (8) and subsequently developed in a series of papers (9–17). On the basis of Levine's theory one may estimate the discreteness-of-charge effect for any reaction site in the inner layer (10, 17). This is especially important in understanding discreteness-of-charge effects in electrode kinetics since, in general, ionic reactants have different sizes and different locations in the double layer depending on the nature of the reaction.

It has also been suggested (1) that to improve the understanding of double layer effects in electrode kinetics one should distinguish three types of reactions. The double layer effect is called Type I in the case of a simple redox reaction occuring in an environment composed chiefly of ions of the same sign. A simple example is the electroreduction of $Cr(H_2O)_6^{3+}$ to $Cr(H_2O)_6^{2+}$ at a negatively charged inert electrode at which the region of the double layer near the electrode is predominantly populated by cations. A Type II effect holds when the reaction occurs in an environment composed chiefly of ions of the opposite sign. This situation arises when anions are reduced at negatively charged electrodes in the absence of specific adsorption. The Type III effect is the most complex and is present for reactions occurring in ionic atmospheres with both cations and anions in close proximity. Both of the above systems involve Type III double layer effects when specifically adsorbed non-reacting anions are present on the i.H.p.

The purpose of this paper is to present a general model for discreteness-of-charge effects applicable to situations in which the reaction plane (r.p.) is not coincident with either the i.H.p. or outer Helmholtz plane (o.H.p.). Examples of data from the literature are discussed within the context of the theory and methods of data analysis to determine the extent of the discreteness-of-charge effects are presented.

Estimation of the Discreteness-of-Charge Effect

According to the generally accepted convention (1), the electrochemical potential of ion i at a

0008-4042/81/131844-10$01.00/0

©1981 National Research Council of Canada/Conseil national de recherches du Canada

Can. J. Chem. Downloaded from www.nrcresearchpress.com by 210.87.254.105 on 09/06/12
For personal use only.

Can. J. Chem. Downloaded from www.nrcresearchpress.com by 210.87.254.105 on 09/06/12
For personal use only.

reaction site near a polarizable inert electrode may be written

$$[1] \quad \tilde{\mu}_i = \mu_i^0 + RT \ln \gamma_i^r c_i^r + z_i F \phi^r$$

μ_i^0 is the standard chemical potential, c_i^r, the local concentration of ion i, γ_i^r, its local activity coefficient, z_i the charge on the ion, and ϕ^r, the average potential on the plane which is parallel to the interface and a distance x_r from it. In the following it is assumed that the reacting system interacts weakly with the electrode. In this case, and for reactants which can be represented as point charges, the local activity coefficient is associated with discreteness-of-charge effects:

$$[2] \quad RT \ln \gamma_i^r = N_0 \int_0^{z_i e_0} \zeta_i^r de = \xi_i^r$$

ζ_i^r is the discreteness-of-charge potential and ξ_i^r, the corresponding energy (3, 5). When the reactant interacts strongly with the electrode or when interfacial solvent molecules are involved in the reaction mechanism, an entropic term must be considered in estimating the local activity (1, 3). On the basis of Flory–Huggins statistics (18, 19), this term is given by

$$p_i \ln \left(1 - \sum_j p_j \theta_j\right)$$

were p_i is the number of solvent molecules displaced by species i, and $p_j\theta_j$, the fraction of the surface covered by species j. One should also consider the non-electrostatic work w_i associated with removal of solvent molecules from the inner layer. The expression for γ_i^r is then

$$[3] \quad RT \ln \gamma_i^r = \xi_i^r + w_i + p_i RT \ln \left(1 - \sum_j p_j \theta_j\right)$$

Three contributions to the discreteness-of-charge energy may be distinguished, namely, the self-image energy, $\xi_{i,s}^r$, the exclusion disc energy, $\xi_{i,d}^r$, and the contribution due to local ion pairing, $\xi_{i,p}^r$. In order to estimate these energies, a fairly detailed model of the dielectric properties of the double layer must be specified. These models have been described in detail in previous papers (6, 10–14, 17) and are only briefly discussed here. It is generally recognized that the average dielectric permittivity ε_i of the inner layer is less than that of the bulk of the solution. The simplest model for the spatial variation in ε with distance from the interface x is to assume that it is constant in the inner layer and changes sharply from its value ε_i in this region to its value in the bulk ε_s at the o.H.p. A value for ε_i may be estimated from data for the integral capacity of the inner layer K_i on the basis of an assumed inner layer thickness x_d. In a more detailed model, it is assumed that the dielectric permittivity increases in two steps, from its lowest average value ε_1 in the inner part of the inner layer, to a value ε_2 in the outer zone, and then to the bulk value ε_s (Fig. 1*a*). The plane dividing the inner layer into inner and outer zones is the i.H.p. If one assumes values for the thickness of these regions, one may estimate ε_1 and ε_2 from the corresponding integral inner layer capacities K_1 and K_2; the latter quantities can be determined from experiment in the presence of significant ionic specific adsorption (20). The most detailed model used until now requires that ε change in a continuous and smooth manner with distance from the interface (Fig. 1*b*). Although the last approach is necessary if one wishes to avoid physically meaningless infinities in the estimation of the discreteness-of-charge potential due to the self-image effect (17), it cannot be tested experimentally at present. In fact, introduction of a molecular approach to this problem would be much more preferable to the presently used continuum concepts in a region of space whose thickness corresponds to that for several molecules.

The present paper is concerned mainly with the role of the exclusion disc term in the discreteness-of-charge energy. On the basis of previous theoretical work in which a continuous variation in ε with distance in the inner layer was assumed (Fig. 1*b*), it has been shown that the self-image contribution is small provided the reactant and/or product are not closer to the electrode than the i.H.p. in the transition state (14, 17). When an ion enters the region of lower dielectric permittivity near the electrode it experiences the stabilizing effect of the images formed in the electrode and in the diffuse layer. On the other hand, work must be done to take the ion from a region of higher dielectric permittivity to a region where it is lower. On the basis of reasonable models, these two effects cancel one another, and $\xi_{i,s}^r$ may be neglected for a reacting system which interacts weakly with the electrode. Estimation of the contribution to discreteness-of-charge energy due to ion pairing also requires a detailed knowledge of the dielectric properties of the region of the double layer near the electrode and of the sizes of the interacting ions (6, 7). This contribution is definitely not negligible but will be treated here in a qualitative manner only. In conclusion, the total discreteness-of-charge energy is approximately given by the relation

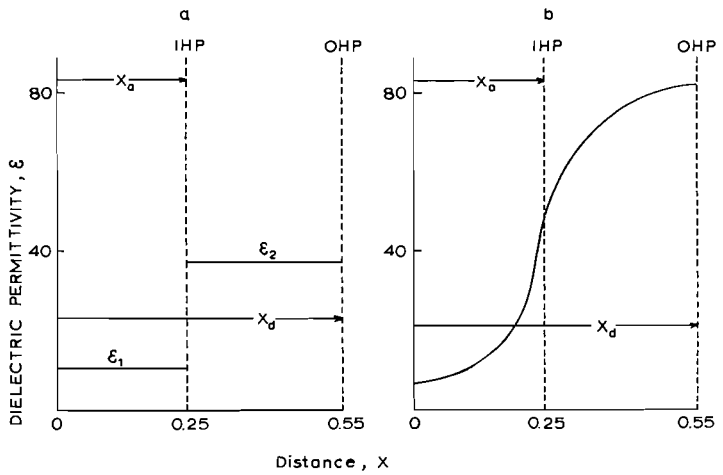

FIG. 1. Dielectric permittivity of the inner layer according to the discontinuous model (*a*) with dielectric constants ε_1 and ε_2 in the inner and outer zones, respectively, and according to the continuous model (*b*). The positions of the i.H.p. and o.H.p. are arbitrarily set at 0.25 and 0.55 nm respectively.

[4] $\xi_i^r = \xi_{i,d}^r + \xi_{i,p}^r$

The important result of the exclusion disc effect is that the neglect of the discrete nature of ions near the electrode leads to a serious overestimation of ion–ion interactions when these are estimated on the basis of the electrostatic potential calculated from a one-dimensional solution of the Poisson–Boltzmann equation. This effect has most often been treated for the case that all ions near the electrode are located on the i.H.p. (3, 4). However, the necessary electrostatic relations have been given for the case that all ions are not located on one plane (10), and the consequences considered for the case of simple electrode kinetics (1). These consequences are examined in more detail below.

When the r.p. is coincident with the i.H.p., the average potential on this plane is given by

[5] $$\phi^r = \phi^d + \frac{\sigma_m + \sigma_a}{K_2}$$

where ϕ^d is the average potential on the o.H.p., σ_m, the charge density on the metal electrode, and σ_a, that due to ions adsorbed on the i.H.p. It is more convenient to express ϕ^r in terms of the potential drop across the inner layer, $\phi^m - \phi^d$ rather than the electrode charge density σ_m. Using the relationship (see Fig. 1)

[6] $$\phi^m - \phi^d = \frac{\sigma_m}{K_i} + \frac{\sigma_a}{K_2}$$

it is easily shown that

[7] $$\phi^r = \phi^d + \lambda(\phi^m - \phi^d) + \frac{(1 - \lambda)\sigma_a}{K_2}$$

where $\lambda = K_i/K_2$. From the work of Levine *et al.* (8, 10, 12), the exclusion disc potential ζ_d^r on the basis of the discontinuous model (Fig. 1*a*) is given by

[8] $$\zeta_d^r = \frac{-K_i}{K_1 K_2} g\sigma_a$$

where g is a dimensionless factor close to unity and given by

[9] $$g = \frac{C_d + K_2}{C_d + K_i}$$

C_d being the differential capacity of the diffuse layer. Robinson and Levine (13) have shown that the estimate of ζ_d^r is not sensitive to the model chosen for ε in the inner layer. Thus, the discontinuous description of ε is assumed to suffice for the estimation of ζ_d^r. The discreteness-of-charge potential on the i.H.p. neglecting ion pairing is given by

[10] $$\psi^r = \phi^r + \zeta^r = \phi^d + \lambda(\phi^m - \phi^a) + \frac{(1 - \lambda)(1 - g)\sigma_a}{K_2}$$

Since g is close to unity the last term on the right-hand side of eq. [10] is approximately zero. It follows that the influence of the exclusion disc potential is to reduce greatly the effect of the adsorbed charge density σ_a on the local potential ψ^r.

When the r.p. is located in the inner region of the inner layer ($0 < x_r \leq x_a$), the average potential on the r.p. is given by

Can. J. Chem. Downloaded from www.nrcresearchpress.com by 210.87.254.105 on 09/06/12
For personal use only.

Can. J. Chem. Downloaded from www.nrcresearchpress.com by 210.87.254.105 on 09/06/12
For personal use only.

[11] $$\phi^r = \frac{\sigma_m}{K_{ra}} + \frac{\sigma_m + \sigma_a}{K_2} + \phi^d = \phi^d + \frac{\sigma_m}{K_{rd}} + \frac{\sigma_a}{K_2}$$

K_{ra} is the integral capacity of the region between the r.p. and i.H.p., and K_{rd}, that between the r.p. and o.H.p. ($1/K_{rd} = 1/K_{ra} + 1/K_2$). Making use of eq. [6], eq. [11] may be rewritten

[12] $$\phi^r = \phi^d + \lambda'(\phi^m - \phi^d) + \frac{(1 - \lambda')\sigma_a}{K_2}$$

where $\lambda' = K_i/K_{rd}$. Equation [12] is identical with eq. [7] once it is realized that λ' is identical to λ when K_{rd} equals K_2. This is indeed the case when the r.p. is coincident with i.H.p. In the inner region the exclusion disc potential is given by (1, 10)

[13] $$\zeta_d^r = \frac{-K_i g}{K_{mr} K_2}\sigma_a = \frac{-(1 - \lambda')g}{K_2}\sigma_a$$

and the discreteness-of-charge potential by

[14] $$\psi^r = \phi^d + \lambda'(\phi^m - \phi^d) + \frac{(1 - \lambda')(1 - g)}{K_2}\sigma_a$$

When the r.p. is located in the outer region of the inner layer ($x_a < x_r \leq x_a$), ϕ^r is given by

[15] $$\phi^r = \phi^d + \frac{\sigma_m + \sigma_a}{K_{rd}}$$

On the basis of the same transformation used above, this may be rewritten

[16] $$\phi^r = \phi^d + \lambda'(\phi^m - \phi^d) - \frac{\lambda'\sigma_a}{K_2} + \frac{\sigma_a}{K_{rd}}$$

In this region, the exclusion disc potential is given by (1, 10)

[17] $$\zeta_d^r = \frac{-(1 - \lambda')g}{K_2}\sigma_a + \frac{\sigma_a}{K_{ar}}$$

When eqs. [16] and [17] are added, the expression obtained for ψ^r is

[18] $$\psi^r = \phi^d + \lambda'(\phi^m - \phi^d) + \frac{(1 - \lambda')(1 - g)\sigma_a}{K_2}$$

On comparing eqs. [11], [14], and [18] it is apparent that the same expression for ψ^r holds for all reaction sites within the inner layer provided $\lambda' = \lambda$. Since the case that the r.p. is coincident with the i.H.p. is a special case in the general problem being treated, the distinction between them is dropped in the following, λ being now defined as K_i/K_{rd}.

The final contribution due to attractive ion–ion interaction in the vicinity of the reaction site results in an increase in the activity of the reactant at the reaction site. Although detailed models have been developed for this effect (6, 7), it will simply be assumed in the present paper that the corresponding contribution to the discreteness-of-charge energy $\xi_{i,p}^r$ is proportional to the charge density of the oppositely charged ion on a plane or planes sufficiently close to the r.p. that ion pair formation is possible. Thus, one may write

[19] $$\xi_{i,p}^r = a_{ij}\sigma_j$$

where σ_j is the charge density of the oppositely charged ion in the vicinity of the r.p., and a_{ij}, the interaction parameter which depends on the dielectric properties of the inner layer, and thus, on electrode potential. In the case that the ion involved in attractive ion–ion interactions is adsorbed, then $\sigma_j = \sigma_a$. On the other hand, the ion involved may be the predominant ion in the region of the o.H.p. in which case $\sigma_j = \sigma_d$; σ_d represents the number density of these ions in a region close to the o.H.p. in which attractive ion–ion interactions are important for the ions of the reaction couple (Fig. 2). Estimation of σ_d is difficult but a reasonable approximate value may be calculated from Gouy-Chapman theory. Accordingly, the potential in the diffuse layer as a function of distance from the interface, x, for a 1-1 electrolyte is given by

[20] $$\phi = \frac{2}{f}\ln\left[\frac{1 + t\exp\left[-\kappa(x - x_d)\right]}{1 - t\exp\left[-\kappa(x - x_d)\right]}\right]$$

where $t = \tanh(f\phi^d/4)$, x_d is the distance of the o.H.p. from the interface, κ is the reciprocal Debye–Hückel length, and $f = F/RT$. The charge density σ_d may be estimated using the equation

[21] $$\sigma_d = z_i F c_s \int_{x_d}^{x} \exp\left(-z_i f\phi\right) dx$$

where c_s is the concentration of the 1-1 electrolyte. When ϕ^d is negative and cations predominate at the o.H.p. ($z_i = 1$), solution of eq. [21] using the Gouy–Chapman expression for ϕ (eq. [20]) gives the following result:

[22] $$\sigma_d = A\left[\frac{\kappa r}{2} + \coth\left(-\frac{\ln t}{2}\right) - \coth\left(\frac{\kappa r}{2} - \frac{\ln t}{2}\right)\right]$$

where $A = (2RT\varepsilon\varepsilon_0 c_s)^{1/2}$ and $r = x - x_d$, ε being the dielectric constant of the solvent and ε_0, the permittivity of free space. Plots of σ_d against the potential drop across the inner layer, $\phi^m - \phi^d$ for various values of r and c_s are illustrated in Fig. 3. It is clear that σ_d is not a linear function of $\phi^m - \phi^d$ but no potential regions are found where σ_d changes sharply with $\phi^m - \phi^d$. On the other hand, the value

Can. J. Chem. Downloaded from www.nrcresearchpress.com by 210.87.254.105 on 09/06/12
For personal use only.

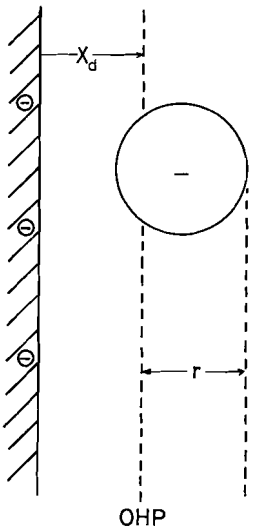

FIG. 2. Schematic diagram showing an anion at its reaction site in the double layer and indicating the thickness of the inner layer (position of o.H.p.) and effective distance for ion pairing in the diffuse layer, r.

of σ_d changes greatly with ϕ^d at constant salt concentration (Fig. 4). As will be seen below, this result has important consequences in the interpretation of the effects of ion–ion interactions on kinetic parameters.

As pointed out previously (1), it is much more convenient to define an effective local activity coefficient γ_i^e which accounts for the departure of the local potential at the reaction site from the average potential on the o.H.p. This choice is made in view of the traditional treatment of double layer effects which dates from the work of Frumkin (21) and which assumes that the r.p. is coincident with the o.H.p. In addition, reasonable estimates of the average potential drop across the diffuse layer may be made using the Gouy–Chapman theory. Accordingly, one writes the electrochemical potential of species i as

$$[23] \quad \tilde{\mu}_i = \mu_i^0 + RT \ln \gamma_i^e c_i^r + z_i F \phi^d$$

where

$$[24] \quad \ln \gamma_i^e = \ln \gamma_i^r + z_i f(\phi^r - \phi^d)$$

$$= z_i f \lambda (\phi^m - \phi^d) + \frac{z_i f (1-\lambda)(1-g)}{K_2} \sigma_a + \frac{a_{ij}\sigma_j}{RT} + \frac{w_i}{RT} - p_i \ln \left(1 - \sum_j p_j \theta_j\right)$$

In conclusion, on the basis of the above derivation, it is clear that one expression applies to the discreteness-of-charge effect in the inner layer, independent of the position of the r.p. with respect to the i.H.p. and o.H.p. Changes in the dielectric properties of the inner region, and of the relative positions of the r.p., i.H.p., and o.H.p. due to change in the nature of the non-reacting ions in the double layer will result in changes in λ, a_{ij}, and to a lesser extent, g. Thus, the activity coefficient γ_i^e is a complex function of electrode potential. However, in certain limiting cases where simplifying assumptions can be made, it is possible to neglect variation in one or more of the contributions to γ_i^e and thus, analyze one aspect of the discreteness-of-charge effect in more detail.

Analysis of Kinetic Data for Simple Electrode Reactions

In the case of the simple electrode reaction

$$[25] \quad A + e \longrightarrow B$$

the expression for the rate of the forward reaction with consideration of local activity coefficients is (1)

$$[26] \quad \ln \vec{v} = \ln k_c + \ln (\gamma_A^s c_A^s) - \ln \gamma_{\pm}^e + (\alpha - z_A) f \phi^d - \alpha f \phi^m$$

where k_c is the potential independent part of the rate contant, γ_A^s, the activity coefficient for reactant A in the bulk of the solution, c_A^s, its bulk concentration, $\gamma_{\pm}^e$, the local effective activity coefficient of the activated complex, and α, the intrinsic transfer coefficient. On the basis of the Bronsted relation, the activity coefficient $\gamma_{\pm}^e$ is given by

$$[27] \quad \ln \gamma_{\pm}^e = (1 - \alpha) \ln \gamma_A^e + \alpha \ln \gamma_B^e$$

Defining the forward rate constant $\vec{k}$ with respect to the bulk reactant concentration ($\vec{k} = \vec{v}/c_A^s$), the logarithm of the rate constant corrected for the effect of the diffuse layer on reactant concentration may be written

$$[28] \quad \ln \vec{k} + z_A f \phi^d = \ln k_c + \ln (\gamma_A^s/\gamma_{\pm}^e) + \alpha f (\phi^d - \phi^m)$$

From eq. [28], the slope of a corrected Tafel plot, that is, a plot of $\ln \vec{k} + z_A f \phi^d$ against $\phi^d - \phi^m$ gives the apparent transfer coefficient defined as

$$[29] \quad \alpha_a = \frac{\partial(\ln \vec{k} + z_A f \phi^d)}{f \partial(\phi^d - \phi^m)} = \alpha - \frac{\partial \ln \gamma_{\pm}^e}{f \partial(\phi^d - \phi^m)}$$

It is of interest to examine the difference in the apparent and intrinsic transfer coefficients in more detail insofar as discreteness-of-charge effects are concerned.

For Type I reactions occuring in the absence of ionic specific adsorption, local ion pairing is negli-

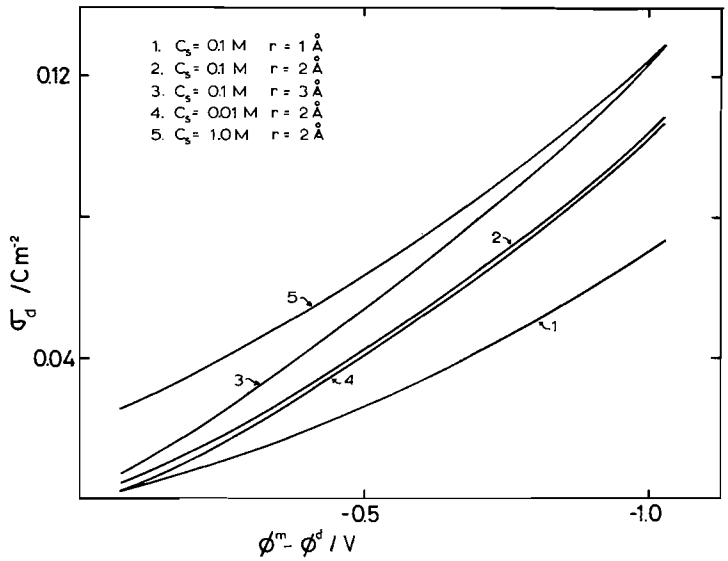

FIG. 3. Plot of the charge density σ_d in the diffuse layer adjacent to an ion at its reaction site which is positioned such that it can interact with ions in the diffuse layer a distance r from the outer Helmholtz plane. The values of r are 1 Å (*1*), 2 Å (*2*, *4*, *5*), and 3 Å (*3*). The concentration of the base electrolyte is 0.01 *M* for (*4*), 0.1 *M* for (*1*, *2*, *3*) and 1.0 *M* for (*5*).

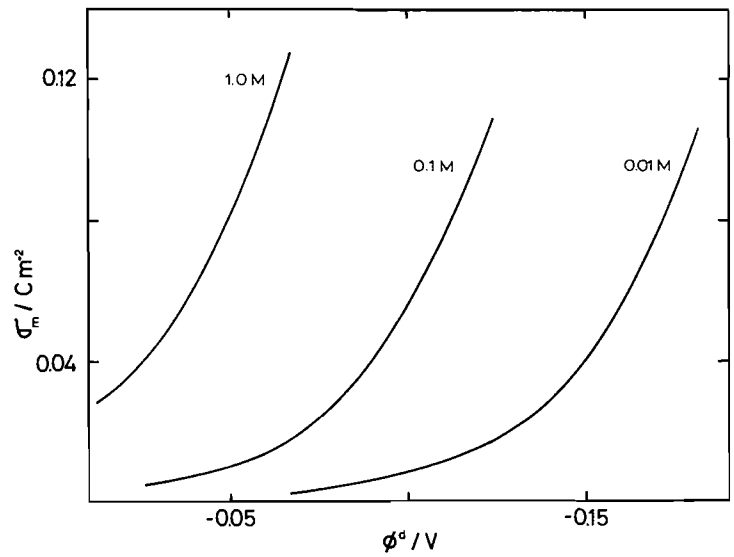

FIG. 4. Plot of the charge density σ_d in the diffuse layer adjacent to an ion at its reaction site which is positioned such that it can interact with ions in the diffuse layer a distance r (r = 2 Å) from the outer Helmholtz plane, as a function of the potential drop across the diffuse layer ϕ^d. The concentration of the electrolyte is indicated on the figure.

gible and the local activity complex in the case of weak interaction is given by

$$[30] \quad \ln \gamma_{\pm}^{e} = z_{\pm} f\lambda(\phi^m - \phi^d)$$

Within the context of the transition state model of electron transfer kinetics, $z_{\pm} = z_A - \alpha$ for a one electron reduction process. Then, from eq. [29], the apparent transfer coefficient may be written

$$[31] \quad \alpha_a = \alpha + \lambda(z_A - \alpha)$$

This expression was first derived by Frumkin in connection with the analysis of data for the electroreduction of H^+ at Hg (22) and can be used to explain the dependence of α_a on the nature of the inert cation in this reaction system (23). The effects of the nature of the alkali metal cation on the kinetic parameters for the electroreduction of H^+ have been discussed in more detail elsewhere (1, 23).

Can. J. Chem. Downloaded from www.nrcresearchpress.com by 210.87.254.105 on 09/06/12
For personal use only.

Can. J. Chem. Downloaded from www.nrcresearchpress.com by 210.87.254.105 on 09/06/12
For personal use only.

For a Type II reaction, for instance, the electroreduction of anions at negatively charged electrodes, the local activity coefficient is given by

$$[32] \quad \ln \gamma_{\pm}^{e} = z_{\pm} f \lambda (\phi^{m} - \phi^{d}) + \frac{a_{\pm}\sigma_{d}}{RT}$$

where $a_{\pm}$ is the interaction parameter for the activated complex. Because attractive ion–ion interactions occur between the reacting anion and surrounding cations in the diffuse layer, $a_{\pm}$ is negative. The apparent transfer coefficient in this case is

$$[33] \quad \alpha_{a} = \alpha + \lambda(z_{A} - \alpha) + \frac{\partial(a_{\pm}\sigma_{d})}{F\partial(\phi^{d} - \phi^{m})}$$

Both the size term and interaction term in this expression are negative and result in values of α_a which are less than α. Since $\partial\sigma_d/\partial(\phi^d - \phi^m)$ is not constant, it is highly probable that the interaction term results in some potential dependence of the apparent transfer coefficient α_a. Potential dependence of α_a is clearly seen with data for the electroreduction of peroxydisulphate anion (24). It was previously suggested that curvature of the corrected Tafel plots could be attributed to an electrostrictive effect (change in λ with electrode potential) (25). However, this effect cannot explain the observed dependence of the heat of activation on the nature of the non-reacting cation (26) and probably is not quantitatively important. In conclusion, the large cation effects observed for kinetic data involving the electroreduction of anions can be attributed largely to the interaction term as suggested earlier by Frumkin (24, 26).

When non-reacting anions are adsorbed at the electrode under conditions for which the potential drop across the inner layer remains negative, the double layer conditions correspond to those for Type III reactions. In the case of a cation reacting in such an atmosphere (Type IIIA), the local activity coefficient is

$$[34] \quad \ln \gamma_{\pm}^{e} = z_{\pm} f \lambda (\phi^{m} - \phi^{d}) + \frac{z_{\pm} f (1 - \lambda)(1 - g)}{K_{2}} \sigma_{a} + \frac{a_{\pm}\sigma_{a}}{RT} + \frac{w_{\pm}}{RT} - p_{\pm} \ln (1 - \sigma_{a}/\sigma_{am})$$

where σ_{am} is the maximum charge density due to the adsorbed non-reacting ions. Although the expression for $\gamma_{\pm}^{e}$ is rather complex, it is clear that this quantity is a function of two variables, namely, $\phi^m - \phi^d$ and σ_a. When the reacting system interacts weakly with the electrode, or when interfacial solvent molecules are not involved in the reaction mechanism, the last two terms in eq. [34] are negligible. The interaction coefficient $a_{\pm}$ for the cationic system in the presence of adsorbed anions (σ_a is negative) is a positive number indicating that $\gamma_{\pm}^{e}$ decreases with increase in adsorbed anion charge density, and the reaction rate increases.

The analysis of the effects of specifically adsorbed ions is facilitated if a comparison is made between the rates of a given reaction in the absence and presence of the adsorbed species, the ionic strength of the solution, or more precisely, the bulk activities of the ions in the reaction couple, being maintained constant. From the above, the difference between the logarithms of the rate constants corrected for the diffuse layer effect at constant $\phi^m - \phi^d$ is given by

$$[35] \quad \Delta = [(\ln \vec{k} + z_{A} f \phi^{d}) - (\ln \vec{k} + z_{A} f \phi^{d})_{0}]_{\phi^{m} - \phi^{d}} = [(\ln \gamma_{\pm}^{e})_{0} - (\ln \gamma_{\pm}^{e})]_{\phi^{m} - \phi^{d}}$$

where the subscript 0 refers to the system with no adsorbing ions. On the basis of eqs. [30] and [34], Δ is given by

$$[36] \quad \Delta = -\frac{z_{\pm} f (1 - \lambda)(1 - g)}{K_{2}} \sigma_{a} - \frac{a_{\pm}\sigma_{a}}{RT} + p_{\pm} \ln (1 - \sigma_{a}/\sigma_{am})$$

and is a function of σ_a only. The comparison described here was first suggested by Parsons (27) in a somewhat different manner, that is, without consideration of diffuse layer effects. Parsons showed that the acceleration of the electroreduction of hydrogen at Hg by adsorbed halide ions is a function of adsorbed anion charge density when kinetic data are compared at constant electrode potential. The accelerating effect increases in the order $I^- < Br^- < Cl^-$ which suggests that the interaction term involving $a_{\pm}$ is the most important; as the radius of the adsorbed anion decreases, its ability to influence the local potential at the reaction site becomes stronger.

Detailed studies of the effects of ionic specific adsorption on the electroreduction of hexaquochromium(III) (28, 29) and a variety of other cationic complexes of Cr(III) (30–32) have been described in the literature. In the case of hexaquochromium(III), the accelerating effect of adsorbed anions is accounted for by the classical double layer correction which suggests that the reaction site is at the o.H.p. or further away in the diffuse layer (28, 32). In the case of hexamminochromium(III), the accelerating effect of adsorbed anions is significantly larger than that for $Cr(H_2O)_6^{3+}$ which suggests that the reaction site is closer to the electrode and that discreteness-of-charge effects may be important (32). In the case that the complex

Can. J. Chem. Downloaded from www.nrcresearchpress.com by 210.87.254.105 on 09/06/12
For personal use only.

cation contains an anionic ligand which is adsorbable at the electrode, the effects of specifically adsorbed non-reacting ions result in deceleration of the reaction rather than acceleration (30–32). These results clearly show that models in which the components of the reaction system are treated as point charges are unable to describe the observed double layer effects. One method of treating this result is to consider the reactant as two contiguous charged spheres, the adsorbed anionic ligand being one and the central transition metal cation the other. Since the anion is closer to the electrode, it experiences a larger repulsion effect from coadsorbed non-reacting anions; the more distant cation correspondingly experiences less attraction from the same species (30). Alternatively, the reacting system may be treated as a point charge and dipole, the electrostatic effects on these components acting in opposite directions (33).

The reduction of anions in the presence of adsorbed non-reacting anions is the most complex double layer effect to be considered here (Type IIIB). In this case the local activity coefficient is given by

$$[37]\quad \ln \gamma_{\pm}^{e} = z_{\pm} f\lambda(\phi^{m} - \phi^{d}) + \frac{z_{\pm} f(1-\lambda)(1-g)\sigma_{a}}{K_{2}} + \frac{a_{\pm}\sigma_{d}}{RT} + \frac{w_{\pm}}{RT} - p_{\pm}\ln(1-\sigma_{a}/\sigma_{am})$$

$\gamma_{\pm}^{e}$ is now a function of three variables, namely, $\phi^{m} - \phi^{d}$, σ_{a} and σ_{d}. The advantages of comparing reaction rates in the presence and absence of adsorbed non-reacting ions discussed above for Type IIIA reactions no longer hold; since ϕ^{d}, and thus, σ_{d} change significantly with changes in σ_{a} at constant $\phi^{m} - \phi^{d}$, quantitative separation of the factors contributing to the change in the local activity coefficient is difficult to make. On the basis of eqs. [32] and [37],

$$[38]\quad \Delta = -z_{\pm} f(1-\lambda)(1-f)\sigma_{a} + \frac{(a_{\pm}\sigma_{d})}{RT} - \frac{a_{\pm}\sigma_{d}}{RT} + p_{\pm}\ln(1-\sigma_{a}/\sigma_{am})$$

The role of discreteness-of-charge effects in the kinetics of electroreduction of periodate ion at high pH

$$[39]\quad H_{3}IO_{6}^{2-} + 2e \longrightarrow IO_{3}^{-} + 3OH^{-}$$

has been discussed previously (34) and is reassessed here on the basis of the above analysis. As one would expect, the adsorption of anions, in this particular case, toluene-*p*-sulphonate (TPS), lowers the rate of reaction at constant electrode potential when the bulk concentration of the adsorbing anion is increased at constant ionic strength (34). The variation in the logarithm of the rate constant corrected for the diffuse layer effect, $\ln \vec{k} + z_{A} f\phi^{d}$, is shown as a function of the adsorbed charge density σ_{a} in Fig. 5. It is clear that the corrected rate constant *increases* with increase in σ_{a} at lower coverages; as coverage increases, the entropic term which accounts for the loss in interfacial water molecules becomes dominant and the corrected rate constant decreases at high coverage. When the logarithm of the rate constant is corrected for both the diffuse layer and the entropic terms (Fig. 6), a continuous increase in the function $\ln \vec{k} + z_{A} f\phi^{d} - p_{A}\ln(1-\sigma_{a}/\sigma_{am})$ is observed. On the basis of the analysis of the equilibrium double layer data for the TPS system, σ_{am} is assumed to be -0.17 C m^{-2} and $p_{A} = 1$.[1] The increase in the corrected rate constant can be attributed to two factors. Firstly, since the parameter g is slightly greater than unity (34), the local potential at the reaction site is slightly more positive than the value estimated on the assumption that the potential in the inner layer changes linearly with the *average* potential drop in that region, $\phi^{m} - \phi^{d}$. In assessing this conclusion, one should keep in mind that if discreteness-of-charge effects were ignored, one would conclude that the potential at the reaction site should be considerably more negative in the presence of specifically adsorbed anions than it is in their absence. It follows that the decelerating effect of adsorbed anions on an anionic reacting system would be much greater than that observed if the charged species near the interface were not discrete. The second effect resulting in reaction acceleration with increase in σ_{a} at constant $\phi^{m} - \phi^{d}$ follows from the fact that ϕ^{d}, and thus, σ_{d} also increase; for example, at $\phi^{m} - \phi^{d} = -0.7$ V, ϕ^{d} changes from -0.035 V in the absence of specific adsorption to -0.074 V when $\sigma_{a} = -0.125$ C m^{-2}. If the interaction parameter $a_{\pm}$ is sufficiently large, a concomitant increase occurs in the rate of the electrode reaction. The best evidence for the presence of an attractive interaction effect is the large change in the corrected rate constant between the system with no TPS and that with the lowest bulk concentration where the change in ϕ^{d} is greatest. For this reason the data for the system

[1] In the previous analysis σ_{am} was assumed to be -0.25 C m^{-2}. Because of the complexities of the TPS system due to reorientation of the anion (35), the method of analysis used earlier can be questioned. The value used in the present analysis is simply the apparent limiting adsorbed charge density at low bulk concentration of TPS under conditions where the adsorbed anion may be assumed to lie flat on the electrode (34, 35)

Can. J. Chem. Downloaded from www.nrcresearchpress.com by 210.87.254.105 on 09/06/12
For personal use only.

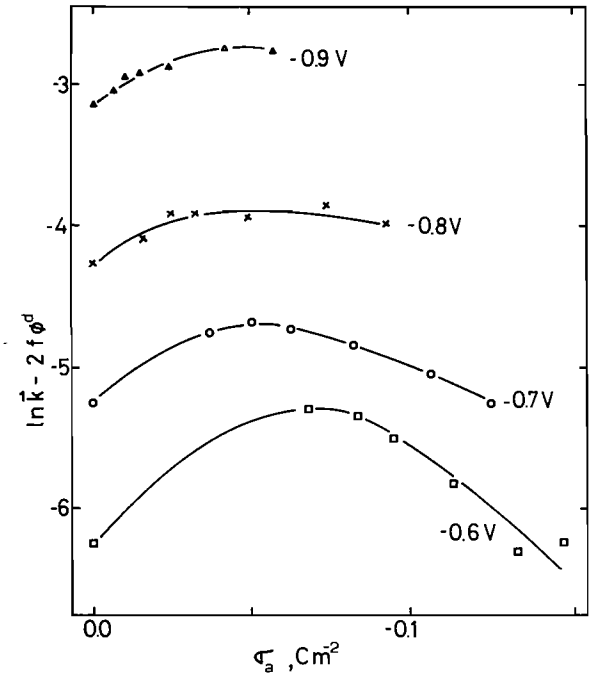

FIG. 5. Plot of the logarithm of the rate constant for the electroreduction of periodate ion corrected for the potential drop across the diffuse layer against charge density due to adsorbed toluene-*p*-sulphonate anion for constant potential drop across the inner layer ($\phi^m - \phi^d$) as indicated.

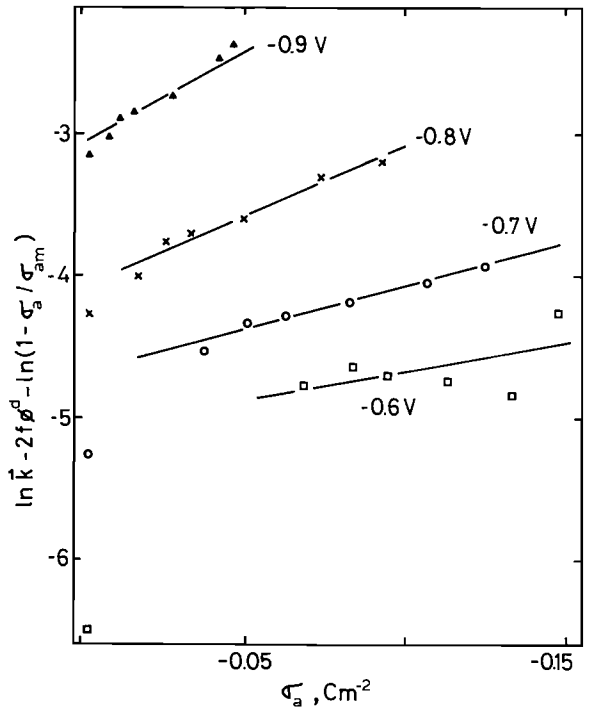

FIG. 6. The data presented in Fig. 5 also corrected for coverage of the electrode by adsorbed toluene-*p*-sulphonate anion.

without TPS were not considered when the straight lines shown in Fig. 6 were constructed. The slope of these lines vary from 4 $m^2\ C^{-1}$ at $\phi^m - \phi^d = -0.6$ V to13 $m^2\ C^{-1}$ at $\phi^m - \phi^d = -0.9$ V. On the basis of the double layer data (34), $f(1 - g)/K_2 \simeq -4\ m^2\ C^{-1}$. Thus, the observed acceleration is of the correct order of magnitude on the basis of the Levine model for discreteness-of-charge effects (8–13). Because of the complexity of this system, no attempt is made here to separate the exclusion disc term from the ion–ion interaction term.

Other studies of the effects of specifically adsorbed anions on the rate of reduction of anions have been carried out by Guidelli and co-workers (36–38). Unfortunately, these experiments were carried out at varying ionic strength so that the role of ion–ion interactions at the reaction site is more complex than that discussed above. In addition, the effect of change in ionic strength on reactant activity was not accounted for. However, the chief criticism which can be made of the previous work (34, 36–38) is that the discreteness-of-charge effects were interpreted assuming that the reaction site is coincident with the i.H.p. This leads to parameters for the inner layer estimated from analysis of the kinetic data which are unrealistic in comparison with similar parameters obtained from analysis of equilibrium data for the interface in the presence of adsorbed anions only.

Discussion

The important conclusion of the above analysis is that the expression derived earlier for the micropotential on the i.H.p. (3) is valid for any location in the inner layer provided that the position parameter λ is recognized to equal the ratio of the total integral capacity of the inner layer to that between the r.p. and o.H.p. The treatment of discreteness-of charge effects discussed earlier (3, 4) in which the r.p. and i.H.p. were assumed to be coincident is therefore a special case of the general problem outlined in this paper. It is also very important to consider the effects of ion–ion interactions separately from the estimation of the exclusion disc contribution to the micropotential (6) and not as part of the exclusion disc contribution (3). Although a quantitative estimate of the ion–ion interaction term cannot be made on the basis of the theory presented in this paper, it is quite clear that this contribution to the total double layer effect is quite important.

Further improvement in the theory of discreteness-of-charge effects must await the development of molecular models of the double layer such as those discussed recently by Blum and Henderson (39) and Carnie and Chan (40). It is obvious that one

of the limitations of the above treatment is that it relies on continuum concepts such as the dielectric permittivity in a region of the double layer a few molecules thick. The availability of these more sophisticated descriptions of the structure of the interfacial region will certainly improve the quantitative description of the effects discussed in this paper. Examination of the literature reveals far too few data which can be effectively tested by the existing theory. The acquisition of more kinetic data illustrating double layer effects would help considerably in improving the present state of understanding.

Acknowledgement

The financial support of the Natural Science and Engineering Research Council of Canada is gratefully acknowledged.

1. W. R. FAWCETT. Proceedings of the Third Symposium on Electrode Processes, 1979. *Edited by* S. Bruckenstein, J. D. E. McIntyre, B. Miller, and E. Yeager. The Electrochemical Society, 1980. p. 213.
2. R. GUIDELLI and M. L. FORESTI. Electrochim. Acta, **18**, 301 (1973).
3. W. R. FAWCETT and S. LEVINE. J. Electroanal. Chem. **43**, 175 (1973).
4. R. GUIDELLI. J. Electroanal. Chem. **53**, 205 (1974).
5. W. R. FAWCETT. J. Chem. Phys. **61**, 3842 (1974).
6. W. R. FAWCETT and S. LEVINE. J. Electroanal. Chem. **65**, 505 (1975).
7. R. GUIDELLI. J. Electroanal. Chem. **74**, 347 (1976).
8. S. LEVINE, G. M. BELL, and D. CALVERT. Can. J. Chem. **40**, 518 (1962).
9. S. LEVINE, J. MINGINS, and G. M. BELL. Can. J. Chem. **43**, 2834 (1965).
10. S. LEVINE. J. Colloid Interfac. Sci. **37**, 619 (1971).
11. S. LEVINE, K. ROBINSON, G. M. BELL, and J. MINGINS. J. Electroanal. Chem. **38**, 253 (1972).
12. S. LEVINE and K. ROBINSON. J. Electroanal. Chem. **41**, 159 (1973).
13. K. ROBINSON and S. LEVINE. J. Electroanal. Chem. **47**, 395 (1973).
14. S. LEVINE, K. ROBINSON, and W. R. FAWCETT. J. Electroanal. Chem. **54**, 237 (1974).
15. G. FEAT and S. LEVINE. J. Chem. Soc. Faraday Trans. II, **73**, 1345 (1977).
16. S. LEVINE and G. FEAT. J. Chem. Soc. Faraday Trans. II, **73**, 1359 (1977).
17. S. LEVINE and W. R. FAWCETT. J. Electroanal. Chem. **99**, 265 (1979).
18. P. J. FLORY. J. Chem. Phys. **10**, 51 (1942).
19. M. L. HUGGINS. J. Chem. Phys. **46**, 151 (1942); Ann. N.Y. Acad. Sci. **43**, 1 (1942).
20. P. DELAHAY. Double layer and electrode kinetics. Wiley-Interscience, New York. 1965. Chapt. 4.
21. A. N. FRUMKIN. Z. Phys. Chem. **164**, 121 (1933).
22. A.N. FRUMKIN. Adv. Electrochem. Electrochem. Eng. **1**, 65 (1961).
23. B. G. CHAUHAN, W. R. FAWCETT, and T. A. MCCARRICK. J. Electroanal. Chem. **58**, 275 (1975).
24. A. N. FRUMKIN, O. A. PETRY, and N. V. NIKOLAEVA-FEDOROVICH. Electrochim. Acta, **8**, 177 (1963).
25. W. R. FAWCETT. J. Electroanal. Chem. **22**, 19 (1969).
26. A. N. FRUMKIN, N. V. NIKOLAEVA-FEDEROVICH, N. P. BEREZINA, and KH. E. KEIS. J. Electroanal. Chem. **58**, 189 (1975).
27. R. PARSONS. J. Electoanal. Chem. **21**, 35 (1969).
28. K. ALIAS and W. R. FAWCETT. Can. J. Chem. **52**, 3165 (1974).
29. M. J. WEAVER and F. C. ANSON. J. Electroanal Chem. **65**, 737 (1975).
30. M. J. WEAVER and F. C. ANSON. Inorg. Chem. **15**, 1871 (1976).
31. F. C. ANSON, M. G. FINN, and A. YAMADA. Inorg. Chem. **16**, 2124 (1977).
32. M. J. WEAVER and T. L. SATTERBERG. J. Phys. Chem. **81**, 1772 (1977).
33. W. R. FAWCETT and C. L. GARDNER. J. Electroanal. Chem. **82**, 303 (1977).
34. K. ALIAS, W. R. FAWCETT, and R. PARSONS. J. Chem. Soc. Faraday Trans. I, **70**, 1046 (1974).
35. J. M. PARRY and R. PARSONS. J. Electrochem. Soc. **113**, 992 (1966).
36. M. L. FORESTI and R. GUIDELLI. J. Electroanal. Chem. **53**, 219 (1974).
37. M. L. FORESTI, D. COZZI, and R. GUIDELLI. J. Electroanal. Chem. **53**, 235 (1974).
38. R. GUIDELLI and M. L. FORESTI. J. Electroanal. Chem. **67**, 231 (1976).
39. L. BLUM and D. HENDERSON. J. Chem. Phys. **74**, 1902 (1981).
40. S. L. CARNIE and D. Y. C. CHAN. J. Chem. Phys. **73**, 2949 (1980).

Can. J. Chem. Downloaded from www.nrcresearchpress.com by 210.87.254.105 on 09/06/12
For personal use only.

A preliminary treatment of solute and solvent interactions in the diffuse part of the electric double layer

C. W. OUTHWAITE

Department of Applied Mathematics and Computing Science, The University, Sheffield S10 2TN, England

Received April 17, 1980

This paper is dedicated to Dr. Sam Levine on the occasion of his 70th birthday

C. W. OUTHWAITE. Can. J. Chem. **59**, 1854 (1981).

The electrolyte in the diffuse layer is modelled by a system of charged hard spheres and dipolar hard spheres. Poisson's equation and integral equations for the mean electrostatic potential are derived and the implications worked out for a mean field approximation.

C. W. OUTHWAITE. Can. J. Chem. **59**, 1854 (1981).

On a développé un modèle de l'électrolyte dans la couche diffuse à l'aide d'un système de sphères dures chargées et dipolaires. On a déduit l'équation de Poisson et des équations intégrales du potentiel électrostatique moyen et on en a examiné les implications dans une approximation du champ moyen.

[Traduit par le journal]

Can. J. Chem. Downloaded from www.nrcresearchpress.com by 210.87.254.5 on 09/06/12
For personal use only.

1. Introduction

The aqueous electric double layer is an extremely complex system so that its theoretical understanding is based on fairly simple models. Usually the double layer is divided into a compact part adjacent to the interface and a diffuse part extending into the electrolyte bulk. The regions are conventionally treated using modifications of the classical Gouy–Chapman–Stern theory (1–3). Gouy and Chapman initiated the theory of the diffuse double layer and they sought to calculate the mean electrostatic potential ψ for a system of point ions in a dielectric continuum. Numerous attempts have since been made to calculate ψ in the diffuse layer using this electrolyte model (4) and the primitive model electrolyte (charged hard spheres moving in a continuous dielectric medium) (5). The compact layer is perhaps more difficult to treat because of the adsorbed solvent and solute molecules which require a detailed treatment of polarisation and structural effects (6–11). Here we consider the effect of modelling the electrolyte by a system of charged hard spheres and dipolar hard spheres. The interface is chosen to be a semi-infinite charged plane wall so that important compact layer effects are neglected. Since the ions and dipoles have a finite size they are restricted in how close they can approach the wall so that there is a simple Stern layer. The chosen electrolyte model is the simplest model of an aqueous electrolyte solution which gives structure to both the solute and solvent molecules. This electrolyte model has been studied in the bulk situation by various authors (12–20).

We follow the bulk idea of ref. 15 and attempt to calculate the properties of the double layer via the mean electrostatic potential ψ. A possible alternative potential approach is suggested by the bulk work of Adelman and Chen (18). Our first step is the formulation of the integral equation and Poisson equation satisfied by ψ. To obtain a closed system of equations a mean field approximation is used which is analogous to that used by Gouy and Chapman. A systematic way of implementing a higher order closure in bulk is given in ref. 15 but we do not consider this extension. Within this mean field approximation the full set of non-linear equations for ψ cannot be completely solved analytically. However the linear equations can be solved and hence the relationship to the Gouy–Chapman theory studied. The dielectric constant ε of the electrolyte solution arises naturally out of the linear theory but unfortunately its value is only applicable to a very dilute dipolar system. The linear theory also predicts the expected Debye shielding in the singlet ion and singlet dipole potential of mean force.

2. Equations Satisfied by ψ

At an arbitrary point $\boldsymbol{r}_1$ in the electric double layer for a fixed surface distribution of molecules the mean electrostatic potential $\psi(1)$ can be expressed as

$$[1] \quad \psi(1) = \psi_m(1) + \sum_t \int [v_t(p, 1) + v_t^*(p, 1)] n^t(p)\, \mathrm{d}(p)$$

0008-4042/81/131854-06$01.00/0

©1981 National Research Council of Canada/Conseil national de recherches du Canada

Can. J. Chem. Downloaded from www.nrcresearchpress.com by 210.87.254.5 on 09/06/12
For personal use only.

Here $v_t(p, 1)$ is the electrostatic potential at $\boldsymbol{r}_1$ due to the charge distribution of a molecule of species t at $\boldsymbol{r}_p$, $v_t^*(p, 1)$ is the corresponding image potential at $\boldsymbol{r}_1$ due to the molecule of species t at $\boldsymbol{r}_p$, $n^t(p)$ is the mean number density of molecules of type t at $\boldsymbol{r}_p$, the sum in t is over the molecular species while $\mathrm{d}(p) = \mathrm{d}\boldsymbol{r}_p\,\mathrm{d}\boldsymbol{\omega}_p$ where $\mathrm{d}\boldsymbol{r}_p$ denotes the positional elements and $\mathrm{d}\boldsymbol{\omega}_p$ the rotational elements. The electrostatic potential $\psi_m(1)$ comes from the fixed surface distribution and any arbitrary constant is determined by requiring that $\psi(1) \to 0$ at large distances from the interface. For a mobile surface distribution of molecules $\psi_m(1)$ needs to be replaced by an appropriate surface average.

Taking the Laplacian of [1] we obtain the generalised Poisson equation

$$[2] \quad \nabla^2\psi(1) = -4\pi \sum_t \int \left\{ e_t + \sum_{l=1}^{\infty} q_{lt} \left[\prod_{i=1}^{l} (-\hat{\boldsymbol{n}}_{it} \cdot \nabla) \right] \right\} n^t(1, \omega)\,\mathrm{d}\omega$$

since $\nabla^2\psi_m(1) = \nabla^2 v_t^*(p, 1) = 0$. Here e_t is the charge of a molecule of species t, q_{lt} the moment of the multipole of order l of species t and $\hat{\boldsymbol{n}}_{it}$ a unit vector associated with displacing a multipole of order i to obtain a multipole of order $i + 1$. The first term on the right hand side of [2] is simply $-4\pi \times$ (mean charge at $\boldsymbol{r}_1$) while the remaining averaged multipole terms give $-4\pi \times$ (mean apparent charge due to multipole distribution) which is a polarisation term.

For simplicity we now consider the aqueous electrolyte to be modelled by a system of charged hard spheres (the solute) and dipolar hard spheres (the solvent). We denote the charge on an ion of species s by e_s and the dipole moment of the dipole species α by $\boldsymbol{\mu}_\alpha$. The non-aqueous medium forming the interface is assumed to be uniform with the interface being a semi-infinite plane carrying a fixed surface charge density σ. In this situation eqs. [1] and [2] reduce to

$$[3] \quad \psi = \psi_m + \sum_s e_s \int \left(\frac{1}{r_{p_1}} + \frac{f}{r_{p_1}^*} \right) n^s(p)\,\mathrm{d}\boldsymbol{r}_p + \sum_\alpha \int \left(\frac{\boldsymbol{\mu}_\alpha \cdot \boldsymbol{r}_{p_1}}{r_{p_1}^3} + \frac{\boldsymbol{\mu}_\alpha^* \cdot \boldsymbol{r}_{p_1}^*}{r_{p_1}^{*3}} \right) n^\alpha(p)\,\mathrm{d}(p)$$

$$[4] \quad \nabla^2\psi = -4\pi \sum_s e_s n^s(1) + 4\pi \sum_\alpha \int \boldsymbol{\mu}_\alpha \cdot \nabla n^\alpha(1, \omega)\,\mathrm{d}\omega$$

where ψ and ψ_m are functions only of the perpendicular distance x_1 from the wall into the electrolyte, the sums in s and α are over the ion and dipole species respectively, fe_s is the image charge of e_s, $\boldsymbol{\mu}_\alpha^*$ the image dipole of $\boldsymbol{\mu}_\alpha$, $\boldsymbol{r}_{p_1}^*$ the distance of the image point in the wall from $\boldsymbol{r}_1$ and $n^s(p)$, $n^\alpha(p)$ the mean number density of ions and dipoles at $\boldsymbol{r}_p$ respectively. Also from symmetry considerations we have that $n^s(1) = n^s(x_1)$ and $n^\alpha(1, \omega) = n^\alpha(x_1, \omega)$.

The wall charge σ gives rise to an equal and opposite double layer charge so that we also have the overall neutrality condition

$$[5] \quad \sum_s e_s \int_0^\infty n^s(x)\,\mathrm{d}x = -\sigma$$

Note that this does not contradict the Poisson equation [4] as the integral over the apparent charge vanishes.

We now introduce cylindrical polar coordinates to simplify the integrals occurring in eq. [3]. Noting that $r_{p_1}^{*2} = 4x_1x_p + r_{p_1}^2$, $\mathrm{d}\boldsymbol{r}_p = r_p\,\mathrm{d}r_p\,\mathrm{d}\phi\,\mathrm{d}x_p$ and integrating with respect to ϕ and r_p leads to

$$[6] \quad \psi = \psi_m - \lim_{R\to\infty} 2\pi \sum_s e_s \int_0^\infty n^s(x)[|x_1 - x| + f(x + x_1) - \sqrt{(x_1 - x)^2 + R^2}$$
$$- f\sqrt{(x + x_1)^2 + R^2}]\,\mathrm{d}x - \lim_{R\to\infty} 2\pi \sum_\alpha \int\int_0^\infty n^\alpha(x, \omega) \left\{ \mu_{\alpha x} \left[\frac{x - x_1}{|x_1 - x|} - \frac{1}{\sqrt{(x_1 - x)^2 + R^2}} \right] \right.$$
$$\left. + \mu_{\alpha x}^* \left[1 - \frac{1}{\sqrt{(x + x_1)^2 + R^2}} \right] \right\} \mathrm{d}x\,\mathrm{d}\omega$$

where $x = x_p$, $\mu_{\alpha x}$ is the component of $\boldsymbol{\mu}_\alpha$ in the x-direction and $\mu_{\alpha x}^*$ is the component of $\boldsymbol{\mu}_\alpha^*$ in the x-direction.

Now for large R,

$$[7]\quad 2\pi\sum_s e_s\int_0^\infty n^s(x)[\sqrt{(x_1-x)^2+R^2}+f\sqrt{(x+x_1)^2+R^2}]\,dx \sim 2\pi R(1+f)\sum_s e_s\int_0^\infty n^s(x)\,dx = -2\pi R\sigma(1+f)$$

so we can discard this term in [6] as it is simply an additive (although infinite) constant. The other limit in the dipole term of [6] containing R vanishes and so

$$[8]\quad \psi = \psi_m - 2\pi\sum_s e_s\int_0^\infty n^s(x)[|x_1-x|+f(x+x_1)]\,dx - 2\pi\sum_\alpha\int\int_0^\infty n^\alpha(x,\boldsymbol{\omega})\left[\mu_{\alpha x}\frac{(x-x_1)}{|x_1-x|}+\mu_{\alpha x}^*\right]dx\,d\boldsymbol{\omega}$$

To determine ψ_m we use the condition that $\psi \to 0$ as $x_1 \to \infty$. This yields the expected linear form

$$[9]\quad \psi_m = 2\pi(f-1)\sum_s e_s\int_0^\infty xn^s(x)\,dx + 2\pi\sum_\alpha\int\int_0^\infty(-\mu_{\alpha x}+\mu_{\alpha x}^*)n^\alpha(x,\boldsymbol{\omega})\,dx\,d\boldsymbol{\omega} - 2\pi\sigma(1+f)x_1$$

Hence the integral equation for ψ can be written as

$$[10]\quad \psi = -2\pi\sum_s e_s\int_0^\infty n^s(x)[|x_1-x|-x_1+x]\,dx - 2\pi\sum_\alpha\int\int_0^\infty \mu_{\alpha x}n^\alpha(x,\boldsymbol{\omega})\left[\frac{(x-x_1)}{|x_1-x|}+1\right]dx\,d\boldsymbol{\omega}$$

which does not explicitly contain the image terms.

If the ions of species s have radii a_s and the dipoles of species α have radii a_α, then

$$[11]\quad \psi = -4\pi\sum_s e_s\int_{\max(a_s,x_1)}^\infty (x-x_1)n^s(x)\,dx - 4\pi\sum_\alpha\int\int_{\max(a_\alpha,x_1)}^\infty \mu_{\alpha x}n^\alpha(x,\boldsymbol{\omega})\,dx\,d\boldsymbol{\omega}$$

The formulae corresponding to the primitive model electrolyte are found by neglecting the dipole terms and dividing the right hand side of eqs. [4], [9]–[11] by the dielectric constant. In calculating ψ we may either use the integral equation [11] or the Poisson equation [4]. The Poisson equation [4] is the usual starting point in the Gouy–Chapman theory and to use it here we have to derive the boundary conditions on ψ. The mean potential is continuous everywhere but considering the derivative of [11]

$$[12]\quad \psi' = 4\pi\sum_s e_s\int_{\max(a_s,x_1)}^\infty n^s(x)\,dx + 4\pi\sum_\alpha H(x_1-a_\alpha)\int\mu_{\alpha x}n^\alpha(x_1,\boldsymbol{\omega})\,d\boldsymbol{\omega}$$

where $H(x)$ is the Heaviside (unit step) function so that ψ' is discontinuous at the distances of nearest approach of the dipoles to the wall. This is expected for at a macroscopic level we have regions of different solvent which could be characterised by different dielectric constants. At a point of discontinuity a_D,

$$[13]\quad \psi_+'(a_D) = \psi_-'(a_D) + 4\pi\sum_\alpha\int\mu_{\alpha x}n^\alpha(a_D,\boldsymbol{\omega})\,d\boldsymbol{\omega}$$

where the sum is over those species with radius a_D. We also see from [12] that $\psi_+'(0) = -4\pi\sigma$.

3. The Mean Field Approximation

To determine ψ through either the integral equation [11] or the Poisson equation [4] requires a knowledge of the functional dependence of $n^s(x)$ and $n^\alpha(x,\boldsymbol{\omega})$ upon ψ. This is a very difficult problem which requires recourse to statistical mechanical considerations. We shall simply consider here the mean field approximation

$$[14]\quad n^s(x) = \begin{cases}0 & x < a_s\\ n_s^0\exp(-\beta e_s\psi) & x > a_s\end{cases}$$

$$[15]\quad n^\alpha(x,\boldsymbol{\omega}) = \begin{cases}0 & x < a_\alpha\\ (n_\alpha^0/4\pi)\exp(-\beta\boldsymbol{\mu}_\alpha\cdot\nabla\psi) & x > a_\alpha\end{cases}$$

which is analogous to that used by Gouy and Chapman. Here n_s^0, n_α^0 are the bulk number densities of the ions and dipoles respectively and $\beta = 1/kT$. From bulk work (15) the approximations in this closure relate

Can. J. Chem. Downloaded from www.nrcresearchpress.com by 210.87.254.5 on 09/06/12
For personal use only.

to the neglect of exclusion volume and fluctuation terms. We further suppose that all the ion species have the same radius a_I and all the dipole species the same radius a_D. With the mean field closure [14], [15], the integration over the dipole orientations can be performed so that the integral equation [11] for ψ is

$$[16]\quad \psi = 4\pi \sum_s e_s n_s^0 \int_{\max(a_I,x_1)}^{\infty} (x_1 - x) \exp(-\beta e_s \psi)\, dx - 4\pi \sum_\alpha n_\alpha^0 \mu_\alpha \times \int_{\max(a_D,x_1)} \left[\frac{\sinh\theta_\alpha - \theta_\alpha \cosh\theta_\alpha}{\theta_\alpha^2}\right] dx \qquad x_1 > 0$$

where $\theta_\alpha = \beta\mu_\alpha\psi'$. Unfortunately we cannot analytically solve this equation for ψ, but we can make some progress in determining ψ via the Poisson equation [4] which is

$$[17]\quad \psi'' = -4\pi H(x_1 - a_I) \sum_s e_s n_s^0 \exp(-\beta e_s\psi) - 4\pi H(x_1 - a_D) \sum_\alpha n_\alpha^0 \mu_\alpha \frac{d}{dx_1}\left[\frac{\theta_\alpha \cosh\theta_\alpha - \sinh\theta_\alpha}{\theta_\alpha^2}\right] \qquad x_1 > 0$$

A first integral of eq. [17] can be readily obtained, so using the conditions that $\psi, \psi' \to 0$ as $x_1 \to \infty$ we have

$$[18]\quad \tfrac{1}{2}\psi'^2 + (4\pi/\beta) \sum_\alpha n_\alpha^0 [(\theta_\alpha \cosh\theta_\alpha - 2\sinh\theta_\alpha + \theta_\alpha)/\theta_\alpha] = (4\pi/\beta) \sum_s n_s^0 [\exp(-\beta e_s\psi) - 1] \qquad x_1 \geq \max(a_I, a_D)$$

If $a_D < x_1 < a_I$ then from the general result [12] or integrating [17]

$$[19]\quad \psi'^3 + 4\pi\sigma\psi'^2 + (4\pi/\beta^2) \sum_\alpha (n_\alpha^0/\mu_\alpha)(\theta_\alpha \cosh\theta_\alpha - \sinh\theta_\alpha) = 0$$

The solution of this equation is $\psi = \eta x_1 + \gamma$ where η is the real root of the transcendental equation for ψ' corresponding to the linear solution and γ is a constant.

Alternatively if $a_I < x_1 < a_D$ then

$$[20]\quad \psi'^2 = (8\pi/\beta) \sum_s n_s^0 [\exp(-\beta e_s\psi) - \exp(-\beta e_s\psi(a_I))] + 16\pi^2\sigma^2$$

which can be formally solved for x_1 in terms of an integral over ψ. In the region next to the wall ψ has the linear form

$$[21]\quad \psi = -4\pi\sigma x_1 + \psi_+(0) \qquad x_1 < \min(a_I, a_D)$$

Thus the solution for ψ devolves upon the integration of eq. [18] and the subsequent fitting of the boundary conditions across a_D and a_I (remembering that $\psi'(a_D)$ is discontinuous, eq. [13]).

Consider now the effect of linearising terms incorporating θ_α. Poisson's equation [17] becomes

$$[22]\quad [1 + H(x_1 - a_D)(4\pi\beta/3) \sum_\alpha \mu_\alpha^2 n_\alpha^0]\psi'' = -4\pi H(x_1 - a_I) \sum_s e_s n_s^0 \exp(-\beta e_s\psi) \qquad x_1 > 0$$

or writing

$$[23]\quad \varepsilon(x_1) = 1 + H(x_1 - a_D)(4\pi\beta/3) \sum_\alpha \mu_\alpha^2 n_\alpha^0$$

we have

$$[24]\quad \psi'' = -[4\pi/\varepsilon(x_1)] \sum_s e_s n_s^0 \exp(-\beta e_s\psi) H(x_1 - a_I)$$

which is simply the Gouy–Chapman equation with dielectric constant $\varepsilon(x_1)$ given by [23]. The expression for $\varepsilon(x_1)$ depends solely upon the parameters of the hard dipolar solvent and in $0 < x_1 < a_D$ takes its vacuum value of unity. Writing $\varepsilon = \varepsilon(x_1)$ for $x_1 > a_D$, we note that this value of ε is the same as that found at the appropriate bulk closure (15) and is unfortunately only applicable to dilute gases. From [13] we have that the boundary condition for ψ' at $x_1 = a_D$ is

Can. J. Chem. Downloaded from www.nrcresearchpress.com by 210.87.254.5 on 09/06/12
For personal use only.

[25] $\varepsilon\psi_+'(a_D) = \psi_-'(a_D)$

Hence in this linearisation approximation ψ can be determined analytically provided (*i*) the Gouy–Chapman equation can be solved and (*ii*) for $a_I < a_D$ eq.[20] is analytically solvable.

If we also linearise the charge terms then ψ can be found in all the cases. In particular if $a_D \leq a_I$ the Poisson equation becomes

[26] $\psi'' = 0$ $\qquad 0 < x_1 < a_I$

[27] $\psi'' = \kappa_1^2\psi$ $\qquad x_1 > a_I$

with the boundary conditions $\psi_+'(0) = -4\pi\sigma$, ψ and $\psi' \to 0$ as $x_1 \to \infty$, ψ continuous everywhere and ψ' continuous everywhere except at $x_1 = a_D$ where [25] holds. Here

[28] $\kappa_1^2 = \kappa_0^2/\varepsilon = (4\pi\beta/\varepsilon)\sum_s e_s^2 n_s^0$

so that κ_1 is the bulk Debye–Hückel constant with ε given by [23]. The solution of [26], [27] satisfying the boundary conditions is

[29] $\psi = -4\pi\sigma x_1 + (4\pi\sigma/\kappa_1\varepsilon)[1 - \kappa_1 a_D + \kappa_1 a_I + \varepsilon\kappa_1 a_D]$ $\qquad 0 < x_1 < a_D$

[30] $\psi = -(4\pi\sigma/\varepsilon)x_1 + (4\pi\sigma/\kappa_1\varepsilon)(1 + \kappa_1 a_I)$ $\qquad a_D < x_1 < a_I$

[31] $\psi = (4\pi\sigma/\varepsilon\kappa_1)\exp[-\kappa_1(x_1 - a_I)]$ $\qquad x_1 > a_I$

As expected the solution for ψ changes in the region close to the wall reflecting the distances of nearest approach of the solute and solvent molecules to the interface. The solution is linear in $0 < x_1 < a_D$ and $a_D < x_1 < a_I$ because of the absence of ionic charge in these regions, while for $x_1 > a_I$ the solution has the familiar damped form. Overall ψ has a monotonic decreasing behaviour for $\sigma > 0$. In the continuum limit ($a_D \to 0$), the solution for ψ is completely equivalent to the linear Gouy–Chapman theory with an effective Stern layer of thickness a_I and dielectric constant ε.

The solution for $a_I \leq a_D$ is of the form

[32] $\psi = -4\pi\sigma x_1 + \delta$ $\qquad 0 < x < a_I$

[33] $\psi = \beta\exp(\kappa_0 x_1) + \gamma\exp(-\kappa_0 x_1)$ $\qquad a_I < x_1 < a_D$

[34] $\psi = \alpha\exp(-\kappa_1 x_1)$ $\qquad x_1 > a_D$

where α, β, γ, δ are somewhat complex constants and nothing is gained by presenting them. The main difference with the solution for $a_D < a_I$ is in the intermediate region $a_I < x_1 < a_D$ where the solution is not linear but a linear combination of exponentials. In this region the interaction between the ions is not reduced by any solvent so that the exponential arguments are functions of κ_0. Again the solution has an overall monotonic behaviour. In the point ion limit ($a_I \to 0$), the linear solution in $0 < x < a_I$ vanishes.

The potentials of mean force W_s, W_α for an ion or dipole respectively in the diffuse layer are

[35] $W_s = e_s\psi = (4\pi\sigma e_s/\varepsilon\kappa_1)\exp(-\kappa_1 x_1)$

[36] $W_\alpha = \boldsymbol{\mu}_\alpha\cdot\nabla\psi = -(4\pi\sigma\mu_{\alpha x}/\varepsilon)\exp(-\kappa_1 x_1)$

on neglecting the hard sphere radii. The potentials of mean force display Debye shielding as in the equivalent bulk analysis (15). Also there is no contribution to the damping from the dipoles since $\kappa_1 = 0$ when all the ions are uncharged. In the bulk analysis a polynomial factor is found in the ion-dipole potential of mean force (15, 17) but no such polynomial (in x_1) occurs in W_α.

4. Conclusion

A preliminary attempt has been made to treat on an equal footing the solute and solvent molecules in the double layer. The theory is based on calculating the mean electrostatic potential ψ in the vicinity of a plane charged wall for a hard sphere ion-dipole system. The implications of a mean field approximation, analogous to that of Gouy and Chapman, have been considered. For the full non-linear system of equations only a first integral of Poisson's equation can be found while on linearising the dipole term the theory reduces to a non-linear theory similar to

Can. J. Chem. Downloaded from www.nrcresearchpress.com by 210.87.254.5 on 09/06/12
For personal use only.

that of Gouy and Chapman. The full set of linear equations are solved and ψ is found to take different forms close to the wall because of the different distances of nearest approach of the ions and dipoles. The dielectric constant ε of the dipolar fluid arises naturally out of the linear theory. Discontinuities occur in ε in the vicinity of the wall due to the finite size of the dipoles, these discontinuities indicating the boundaries of different dielectrics. Regrettably ε is too small because of an inadequate treatment of dipole–dipole interactions.

The value of a numerical solution of the full set of non-linear equations is difficult to assess. We expect the non-linear theory to be inconsistent (in the thermodynamic properties) although a better value of ε may be obtained and perhaps a dependence of ε upon charge found. Any basic progress in the theory must come from a more accurate closure. A method of improving upon the mean field approximation has been given in the bulk (15) where a treatment of the fluctuation potential led to Onsager's ε and a damped oscillatory behaviour in the mean electrostatic potential. We hope to consider corrections along these lines in the future. Many other points need to be considered, for example higher order multipoles or more importantly a treatment of the compact layer. However, we hope that we have indicated a possible way in which the potential approach may be adapted to treat realistically both solute and solvent interactions.

1. G. Gouy. J. Phys. **9**, 457 (1910).
2. D. L. Chapman. Phil. Mag. **25**, 475 (1913).
3. O. Stern. Z. Electrochem. **30**, 508 (1924).
4. E. J. Verwey and J. Th. G. Overbeek. Theory of the stability of lyophobic colloids. Elsevier Pub. Co. 1948.
5. S. Levine and C. W. Outhwaite. J. Chem. Soc. Faraday II, **74**, 1670 (1978).
6. S. Levine, J. Mingins, and G. M. Bell. J. Electroanal. Chem. **13**, 280 (1967).
7. C. A. Barlow and J. R. MacDonald. Adv. Electrochem. Electrochem. Eng. **6**, 1 (1967).
8. R. M. Reeves. Mod. Aspects Electrochem. **9**, 239 (1974).
9. M. A. Habib. Mod. Aspects Electrochem. **12**, 131 (1977).
10. B. E. Conway. Adv. Colloid Interface Sci. **8**, 91 (1977).
11. W. R. Fawcett. Israel J. Chem. **18**, 3 (1979).
12. L. Blum. Chem. Phys. Lett. **26**, 200 (1974); J. Chem. Phys. **61**, 2129 (1974).
13. S. A. Adelman and J. M. Deutch. J. Chem. Phys. **60**, 3935 (1974).
14. G. N. Patey and J. P. Valleau. J. Chem. Phys. **63**, 2334 (1975).
15. C. W. Outhwaite. Mol. Phys. **31**, 1345 (1976).
16. C. W. Outhwaite. Mol. Phys. **33**, 1229 (1977).
17. J. S. Høye and G. Stell. J. Chem. Phys. **68**, 4145 (1978); **71**, 1985 (1979); Discuss. Faraday Soc. **64**, 16 (1977).
18. S. A. Adelman and J. H. Chen. J. Chem. Phys. **70**, 4291 (1979).
19. D. Y. C. Chan, D. J. Mitchell, and B. W. Ninham. J. Chem. Phys. **70**, 2946 (1979).
20. D. Levesque, J. J. Weis, and G. N. Patey. J. Chem. Phys. **72**, 1887 (1980).

Can. J. Chem. Downloaded from www.nrcresearchpress.com by 210.87.254.5 on 09/06/12
For personal use only.

The interaction of two charged spheres in the Poisson–Boltzmann equation

JOSEPH E. LEDBETTER, THOMAS L. CROXTON, AND DONALD A. MCQUARRIE[1]

Department of Chemistry, University of California, Davis, CA 95616, U.S.A.

Received May 22, 1980

This paper is dedicated to Dr. Sam Levine on the occasion of his 70th birthday

JOSEPH E. LEDBETTER, THOMAS L. CROXTON, and DONALD A. MCQUARRIE. Can. J. Chem. **59**, 1860 (1981).

The Poisson–Boltzmann equation for two large charged spheres immersed in an ionic solution with either constant surface charge density or constant surface potential is solved numerically. The repulsion between the spheres is calculated from the electrostatic potential in the double layer surrounding the spheres. Good agreement between this numerically calculated force and the force computed using the Derjaguin formula for spheres with constant surface charge density is found at small separations of the spheres.

JOSEPH E. LEDBETTER, THOMAS L. CROXTON et DONALD A. MCQUARRIE. Can. J. Chem. **59**, 1860 (1981).

On a résolu numériquement l'équation de Poisson–Boltzmann relative à deux grosses sphères chargées immergées dans une solution ionique ayant soit une densité constante de charge superficielle soit un potentiel de surface constant. On a calculé la répulsion entre les sphères à partir du potentiel électrostatique de la double couche entourant les sphères. Lorsque les distances séparant les sphères sont courtes, on a trouvé un bon accord entre la force calculée numériquement et celle calculée en utilisant la formule de Derjaguin pour les sphères ayant une densité constante de charge superficielle.

[Traduit par le journal]

Introduction

The interaction between large charged particles in an aqueous ionic solution is a problem of central concern in colloid science (1). In particular, it is important to be able to calculate the forces acting between such colloid particles since these forces determine the stability of colloidal suspensions. A knowledge of the electrostatic potential in the double layer surrounding charged colloid particles allows one to calculate the electrostatic component of the force between such particles.

In this paper we consider a model system composed of two charged spheres immersed in a solution of point ions in a uniform dielectric medium. With the usual assumption of a Boltzmann distribution of ions (2), Poisson's equation becomes the well-known Poisson–Boltzmann equation for electrostatic potential in this model. Application of the Poisson–Boltzmann equation to the geometry considered here then becomes a boundary value problem of a second order non-linear partial differential equation. For the geometry of two charged spheres, however, an analytical solution to the Poisson–Boltzmann equation is not possible. We thus present in this paper a numerical solution of the Poisson–Boltzmann equation as applied to two identical large charged spheres in an ionic solution. Surface boundary conditions of constant charge density and constant potential are treated. The electrostatic repulsion between the spheres is calculated from the numerical solution of the potential in the double layer surrounding the particles.

A numerical solution to the Poisson–Boltzmann equation for this problem was first presented by Hoskin and Levine (3) for a constant surface potential boundary condition on the spheres. The accuracy of these calculations was later improved by McCartney and Levine (4). We present here a somewhat different approach to the numerical solution of the Poisson–Boltzmann than has been previously considered. Instead of solving for the total electrostatic potential we solve a differential equation for the correction to an approximate solution to the Poisson–Boltzmann equation. This approach not only results in a simpler numerical problem since the correction to the potential is often a slowly varying function, but it also shows directly the inadequacy of the approximate solution used in the method. Whereas previous numerical solutions have only considered the boundary condition of constant surface potential, our method allows us to also solve the Poisson–Boltzmann equation for spheres of constant surface charge density. These two different boundary conditions yield quite different results, and it is important to have definitive numerical calculations for both cases so that a comparison with approximate solutions to the Poisson–Boltzmann equation can be made. The choice of a particular boundary condition is dependent on the physical system which is to be modeled.

Due to its importance in colloid science, the

[1]To whom all correspondence should be addressed.

0008-4042/81/131860-05$01.00/0

©1981 National Research Council of Canada/Conseil national de recherches du Canada

Can. J. Chem. Downloaded from www.nrcresearchpress.com by 210.87.254.6 on 09/06/12
For personal use only.

Can. J. Chem. Downloaded from www.nrcresearchpress.com by 210.87.254.6 on 09/06/12
For personal use only.

Poisson–Boltzmann equation has been well studied and many approximate solutions have been presented (5, 6). It is interesting to note that the linearized Poisson–Boltzmann equation applied to the problem of two interacting charged spheres can be solved exactly (7), but for large surface potentials, this linearized form is no longer valid. For small separations between the interacting spheres, a well-known approximation to the electrostatic force is the Derjaguin formula (8). At larger separations, a common approximation to the potential is the so-called linear superposition approximation (5). Bell *et al.* (5, 6) have combined these two approximations and have shown that the electrostatic repulsion calculated with these approximate methods agrees quite well with the numerical calculations of McCartney and Levine (4) for spheres with constant surface potential. We make a similar comparison at small particle separations of the Derjaguin formula appropriate to spheres of constant surface charge density with our numerical calculation of the force between the particles.

Theory

Consider two identical rigid spherical colloid particles of radius A, whose centers are separated by a distance R, immersed in a solution of point ions of uniform dielectric constant ε. This geometry is shown in Fig. 1*a*. The colloid particles are also assumed to be of uniform dielectric constant equal to that of the electrolyte so that image effects can be ignored. With this model, the mean electrostatic potential in the surrounding double layer is given approximately by the Poisson–Boltzmann equation

$$[1] \quad \nabla^2\psi(r_1, r_2) = (8\pi nze/\varepsilon) \sinh (ze\psi/kT)$$

with the appropriate boundary conditions. In this equation we have assumed a symmetric electrolyte where n is the number density of one type of ion, T is the absolute temperature, k is Boltzmann's constant, and ze is the magnitude of the charge of one ion. Defining the reduced potential and the Debye–Hückel screening constant

$$[2] \quad y = ze\psi/kT$$

$$[3] \quad \kappa = (8\pi nz^2e^2/\varepsilon kT)^{1/2}$$

we can rewrite eq. [1] in reduced form

$$[4] \quad \nabla^2 y = \sinh y$$

In this equation and in all following equations we have reduced all distances by κ. Thus A, R, and r_i are now all reduced by κ.

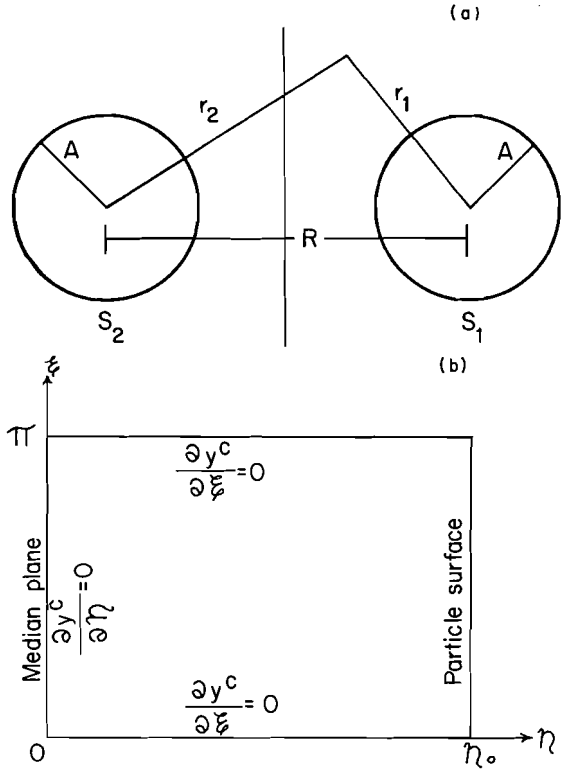

FIG. 1. (*a*) Geometry of two interacting spheres; (*b*) boundary conditions for the correction potential y^c on the half-plane in bispherical coordinates.

Equation [4] could be solved numerically for the total potential y, but we choose instead to formally divide this potential into the sum

$$[5] \quad y(r_1, r_2) = y_1(r_1) + y_2(r_2) + y^c(r_1, r_2) = y^s + y^c$$

The functions $y_i(r_i)$ are arbitrary, but a reasonable approximation to the Poisson–Boltzmann equation is a linear superposition of the potentials due to each sphere (5). We are thus led to choose $y_i(r_i)$ to be the potential due to a single sphere. The correction term $y^c(r_1, r_2)$ clearly goes to zero as the particle separation becomes very large, since the superposition solution $y^s(r_1,r_2)$ better approximates the total potential as the particle separation increases (5, 6). Substitution of eq. [5] into eq. [4] yields a differential equation for $y^c(r_1, r_2)$

$$[6] \quad \nabla^2 y^c = \sinh (y^s + y^c) - [\nabla_{r_1}^2 y_1(r_1) + \nabla_{r_2}^2 y_2(r_2)]$$

where

$$[7] \quad \nabla_{r_i}^2 y_i = r_i^{-2}\, \mathrm{d}(r_i^2\, \mathrm{d}y_i/\mathrm{d}r_i)/\mathrm{d}r_i$$

since $y_i(r_i)$ is spherically symmetric.

Can. J. Chem. Downloaded from www.nrcresearchpress.com by 210.87.254.6 on 09/06/12
For personal use only.

Since the electrostatic potential due to a single colloid particle is not known analytically, we choose the excellent approximation to this potential given by Brenner and Roberts (9)

$$[8] \quad y_i(r_i) = y_{DH}/(a_0 - a_3 y_{DH}^3)$$

In this approximation, the parameters a_0 and a_3 are determined by a variational principle associated with the free energy of the single sphere system. y_{DH} is the familiar Debye–Hückel potential

$$[9] \quad y_{DH}(r_i) = y_0 A\{\exp[-(r_i - A)]\}/r_i$$

where y_0 is the (constant) potential on the sphere. Although it is not obvious because we have not written out the forms of a_0 and a_3, if $y_{DH}(A)$ is substituted into eq. [8], we find that $y_i(A) = y_0$. Substitution of the $y_i(r_i)$ given by eq. [8] into eq. [6] gives the differential equation to be solved for $y^c(r_1, r_2)$ once the surface boundary conditions are given.

In the geometry of two charged spheres, it is convenient first to transform the problem into bispherical coordinates. In this system, surfaces of constant η are spheres, and surfaces of constant ξ are either spindles or dimples on the z-axis. For spheres of the same size, it is sufficient to consider the half-space including the median plane ($\eta = 0$) and excluding one sphere (S_1). This space is defined by the rectangle shown in Fig. 1*b*. The particle surface is defined by the spherical surface given by

$$[10] \quad \eta_0 = \cosh^{-1}(r/2A)$$

Also shown in Fig. 1*b* are the boundary conditions on $y^c(\xi,\eta)$ which are required by the symmetry of the problem.

In order to complete the description of this problem, the boundary condition on the sphere ($\eta = \eta_0$) must be given. A fixed surface potential requires

$$[11] \quad y^c(\xi,\eta = \eta_0) = -y_2(r_2)$$

A fixed surface charge density requires that the normal derivative of the potential on the surface of the sphere be proportional to the charge density

$$[12] \quad (\partial y/\partial r_1)_{\eta_0} = -4\pi z e\sigma/\kappa\varepsilon kT = -\sigma^*$$

Using eq. [5] this condition becomes

$$[13] \quad (\partial y^c/\partial r_1)_{\eta_0} = -\sigma^* - [\partial y_1/\partial r_1 + (\partial y_2/\partial r_2)(\partial r_2/\partial r_1)]_{\eta_0}$$

Evaluation of the partial derivatives in this equation yields

$$[14] \quad (\partial y^c/\partial r_1)_{\eta_0} = y_{DH}\left[\frac{r_2 + 1}{r_2}\right] \times \left[\frac{a_0 + 2a_3 y_{DH}^3}{(a_0 - a_3 y_{DH}^3)^2}\right]\left[\frac{r_2^2 + A^2 - R^2}{2r_2 A}\right]$$

where $y_{DH} = y_{DH}(r_2)$, and where we have identified the (uniform) reduced charge density

$$[15] \quad \sigma^* = y_0\left[\frac{A + 1}{A}\right]\left[\frac{a_0 + 2a_3 y_0^3}{(a_0 - a_3 y_0^3)^2}\right]$$

The boundary condition given by eq. [14] may be manipulated to yield a boundary condition for $(\partial y^c/\partial\eta)_{\eta_0}$ in bispherical coordinates.

After expressing the Laplacian in bispherical coordinates, eq. [6] may then be replaced by a standard set of finite difference equations (3, 10). Such a replacement assumes that third and higher order differences are negligible, which is justifiable since $y^c(\xi,\eta)$ is a rather smooth surface. The spherical surface boundary condition is incorporated into this scheme by using a finite difference equation which is appropriate along the $\eta = \eta_0$ line. Alternate line-by-line matrix inversion is performed over lines of constant η and over lines of constant ξ, and this procedure is iterated to a convergent solution.[2] In the calculations presented here, $y^c(\xi,\eta)$ is represented by a grid of 50 × 50 points. Previous numerical solutions (3, 4) have used fewer points.

Once the electrostatic potential is known, the force between the colloid particles may be obtained by an integration of the Maxwell stress over the median plane (3). This reduced force is given by

$$[16] \quad f^* = (8\pi/\varepsilon)(ze/kT)^2 f = 2\pi\int_0^\infty \left[(\partial y/\partial\xi)_{\eta=0} + \frac{2c^2(\cosh y - 1)}{(1 - \cos\xi)^2}\right]\sin\xi\, d\xi$$

where c is a parameter given by

$$[17] \quad c = A\sinh\eta_0$$

It is also convenient to define another reduced force

$$[18] \quad f^{**} = f^*/2\pi A y_0^2$$

A common and apparently successful approximation to the force between two spherical colloid particles which is good only at small separations is

[2]A copy of the computer program used is available from the authors upon request.

Can. J. Chem. Downloaded from www.nrcresearchpress.com by 210.87.254.6 on 09/06/12
For personal use only.

the Derjaguin formula. In this method, the interacting spheres are essentially replaced by sections of charged parallel plates, and the force between the spheres is found to be proportional to the interaction free energy of this sum of parallel plates. For plates with constant surface charge density, the potential of these interacting plates at infinite separation can be related to the charge density by integrating the Poisson–Boltzmann equation for this one-dimensional geometry. The result is

$$[19] \quad \cosh y_\infty = 1 + (\sigma_p^*)/2$$

Derjaguin's method has been used by Bell and Peterson (6) to calculate interaction forces at small separations between spheres of different sizes and different surface boundary conditions. We compare our numerical calculations of the force between spheres with constant surface charge density with the force calculated from the expressions given by Bell and Peterson.

Results and Discussion

Graphs of the reduced force f^{**} versus the separation $\kappa(R - 2A)$ between the two spheres are given in Figs. 2 and 3. Results for both constant charge and constant potential spheres with reduced potentials of 2 and 4 and reduced radii of 5 and 15 are presented. The forces given here for constant potential spheres agree to within 1% with the force calculations of McCartney and Levine (4). For each radius the charge density is related to the constant surface potential through eq. [15]. Although not shown by the data presented here, the surface potential of the spheres with constant surface charge density does approach the corresponding constant potential y_0 in each case to within a few percent at a separation of approximately $\kappa(R - 2A) = 5$. As expected, the force between the spheres of constant charge is always greater than the force between particles of the corresponding constant potential, and the two force curves approach one another with increasing separation.

In the Derjaguin formula, the reduced force f^{**} is independent of the particle radius (6), and Bell *et al.* (5) have noted that the numerical calculations for spheres with constant surface potential (4) support this approximation. A similar comparison of the force curves in Figs. 2 and 3 for different radii reveals that this approximation is also reasonable for spheres of constant surface charge density.

In Fig. 4 the force curve calculated using Derjaguin's formula is compared with the numerical results for $\kappa A = 5$ and a surface charge density on the sphere of $\sigma^* = 2.78$. This charge density

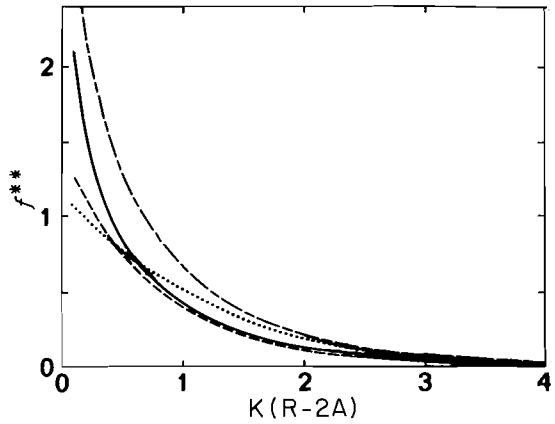

FIG. 2. Force–separation curves plotted as f^{**} versus $\kappa(R - 2A)$ from our numerical solution, for identical spheres with $\kappa A = 5$. The lines ---, —, ···, and ——— are for $y_0 = 4, \sigma^* = 7.91$, $y_0 = 2$, $\sigma^* = 2.78$, respectively. Data with y_0 = constant are for constant surface potential spheres, while data with σ^* = constant are for spheres with constant surface charge density.

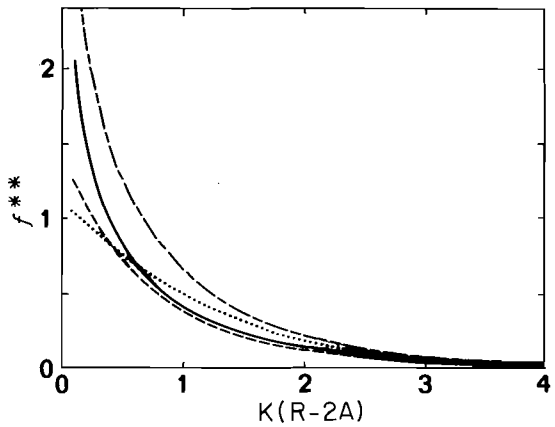

FIG. 3. Similar curves as in Fig. 2 for $\kappa A = 15$. The lines ---, —, ···, and ——— are for $y_0 = 4, \sigma^* = 7.42$, $y_0 = 2$, and $\sigma^* = 2.51$, respectively.

corresponds to a potential at infinite separation of $y_0 = 2$. In the Derjaguin approximation one must use the potential of the plates at infinite separation y_∞, which is related to the constant charge density on the plates by eq. [19]. For a *sphere* of a constant charge density, however, the potential at infinite separation is dependent on the size of the sphere. One must therefore decide whether to use $y_\infty = y_0$, or y_∞ obtained from eq. [19] by setting $\sigma_p^* = \sigma^*$ (constant charge density on the sphere). Figure 4 clearly shows that the correct choice for the potential at infinite separation of the plates is y_0 since good agreement with the numerical calculations of the force is achieved with this identification. Good agreement between Derjaguin's formula

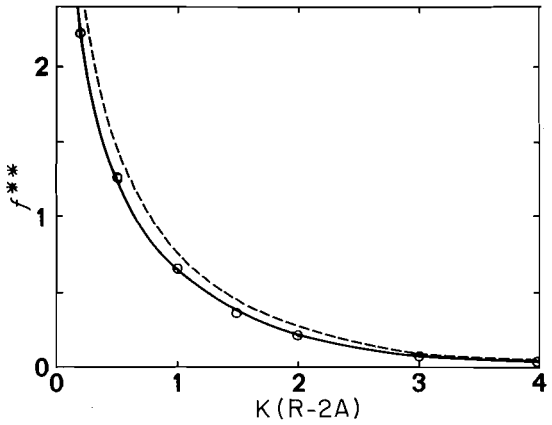

FIG. 4. Comparison of f^{**} calculated from Derjaguin's formula (ref. 6) with our numerical results for $\kappa A = 5$ and $\sigma^* = 2.78$. The lines — and --- are for spheres of constant surface charge density as calculated from Derjaguin's formula with $y_\infty = 2.00$ ($\sigma_p^* = 2.35$) and $y_\infty = 2.26$ ($\sigma_p^* = \sigma^*$), respectively. Circles are the numerical calculations from this work.

and the numerical results for higher reduced potentials and larger spheres is obtained as well with proper choice for y_∞.

In summary, we have presented calculations of the electrostatic repulsion between identical spheres with either constant surface charge density or constant surface potential by numerically solving the Poisson–Boltzmann equation. Forces calculated using the well-known Derjaguin formula appropriate to spheres with constant surface charge density are compared with numerically calculated forces. Good agreement is obtained provided the correct input is used in the Derjaguin method.

Acknowledgement

This work was supported by a grant from the National Institutes of Health, GM 26864-02.

1. E. J. W. VERWEY and J. TH. G. OVERBEEK. Theory of stability of lyophobic colloids. Elsevier, Amsterdam. 1948.
2. D. A. MCQUARRIE. Statistical mechanics. Harper and Row, New York. 1976.
3. N. E. HOSKIN and S. LEVINE. Trans. R. Soc. Sec. A, 248 (1956); 433 (1956); 449 (1956).
4. L. N. MCCARTNEY and S. LEVINE. J. Colloid Interface Sci. **30**, 345 (1969).
5. G. M. BELL, S. LEVINE, and L. N. MCCARTNEY. J. Colloid Interface Sci. **33**, 335 (1970).
6. G. M. BELL and G. C. PETERSON. J. Colloid Interface Sci. **41**, 542 (1972).
7. B. ENOS, D. MCQUARRIE, and P. COLONOMOS. J. Colloid Interface Sci. **52**, 289 (1975).
8. B. V. DERJAGUIN. Kolloid-Z. **69**, 155 (1934).
9. S. L. BRENNER and R. E. ROBERTS. J. Phys. Chem. **77**, 2367 (1973).
10. W. F. AMES. Numerical methods for partial differential equations. Academic Press, New York. 1977.

Can. J. Chem. Downloaded from www.nrcresearchpress.com by 210.87.254.6 on 09/06/12
For personal use only.

Thermodynamics of micellar systems: activity and entropy of sodium decanoate and *n*-alkylamine hydrobromides in water

ROSARIO DE LISI[1], GÉRALD PERRON, JEAN PAQUETTE[2], AND JACQUES E. DESNOYERS[3]

Department of Chemistry, Université de Sherbrooke, Sherbrooke (Que.), Canada J1K 2R1

Received June 16, 1980

This paper is dedicated to Dr. Sam Levine on the occasion of his 70th birthday

ROSARIO DE LISI, GÉRALD PERRON, JEAN PAQUETTE, and JACQUES E. DESNOYERS. Can. J. Chem. **59**, 1865 (1981).

The freezing-point depressions of aqueous solutions of the homologous series RNH_3Br, where R varies from ethyl to *n*-octyl, and of sodium decanoate were determined and used to calculate osmotic and mean activity coefficients. In the case of the surfactants octylamine hydrobromide and sodium decanoate, the pre- and post-micellar regions were covered. Activity data at higher temperatures were calculated using previously published thermochemical data. Some difficulties arise in the critical micellar region of sodium decanoate at high temperatures as a result of the large concentration and temperature dependence of the heat capacity data. The activities from freezing point data are compared with those obtained from specific electrodes.

ROSARIO DE LISI, GÉRALD PERRON, JEAN PAQUETTE et JACQUES E. DESNOYERS. Can. J. Chem. **59**, 1865 (1981).

Les abaissements du point de congélation des solutions aqueuses des sels de la série homologue RNH_3Br, où R varie de méthyl à *n*-octyl, et du décanoate de sodium ont été mesurés et utilisés pour calculer les coefficients osmotiques et les coefficients d'activité moyenne. Dans le cas du bromhydrate d'octylamine et du décanoate de sodium, les régions pré- et post-micellaires ont été couvertes. Les fonctions d'activité aux températures plus élevées ont été calculées à partir de données thermochimiques. Certaines difficultés sont survenues avec le décanoate de sodium dans la région de micellisation à cause de la très grande variation de la capacité calorifique avec la température et avec la concentration. Les activités obtenues par cryoscopie ont été comparées avec celles venant de mesures de forces électromotrices.

Introduction

This paper is part of a series on the measurement of the complete excess thermodynamic properties of typical cationic, anionic, and nonionic surfactants. The thermodynamic properties of nonyl and decyltrimethylammonium bromides (1, 2), the thermochemical and volumetric properties of sodium decanoate (3), and of the homologous series alkylamine hydrobromides (3–5) have already been published. We will now present activity data for alkylamine hydrobromides and sodium decanoate. From these and the corresponding thermochemical data, the excess free energies and entropies can be calculated as a function of temperature. Our aim is to provide accurate data covering the micellar region for quantitative testing of various models or theories.

In recent years, most of the activity data on surfactants were obtained with the EMF method using various types of specific electrodes (see for example Sasaki *et al.* (6), Cutler *et al.* (7), Kale *et al.* (8), and Vikingstad (9)). The advantage of this approach is that individual ionic activity coefficients can be calculated and thus the degree of counterion binding can be evaluated. However, some questions remain on the absolute accuracy of these techniques in view of the non-Nernstian response of many of these electrodes. With the present surfactants, the critical micelle concentrations are all relatively high and the Krafft temperatures are all below the freezing temperature of water. We therefore felt that the freezing point technique would offer a simple method of evaluating the mean activity data in the pre- and post-micellar regions. This method has been used successfully with alkyltrimethylammonium bromides (2).

While these systems were being investigated it came to our knowledge that Vikingstad (9) had also investigated sodium decanoate with the EMF method. This therefore offered the possibility of comparing activities of surfactants obtained by very different methods.

Experimental

Two techniques were used for freezing point measurements. The homologous series RNH_3Br was investigated with a model 3R Advanced Instruments Osmometer. This technique, which supercools a liquid sample by several degrees, initiates ice nucleation, and measures the temperature at which the change of state takes place, is simple and rapid. It was used successfully to measure the salting out and salting in of alcohols by electrolytes (10, 11). However, it is a relative technique, and these studies (10, 11) have suggested that some error can be introduced in determining osmotic coefficients of solutions of organic ions or molecules. This systematic error cancels with ternary systems but not with binary ones. Measurements with the surfactants octylamine hydrobromide (OABr) and sodium de-

[1]On leave of absence from Istituto di Chimica Fisica, Università di Palermo, Palermo, Italy.

[2]Present address: AECL, WNRE, Research Chemistry Branch, Pinawa, Man., Canada R0E 1L0.

[3]Author whom correspondence should be addressed.

0008-4042/81/131865-07$01.00/0

©1981 National Research Council of Canada/Conseil national de recherches du Canada

Can. J. Chem. Downloaded from www.nrcresearchpress.com by 210.87.254.40 on 09/06/12
For personal use only.

Can. J. Chem. Downloaded from www.nrcresearchpress.com by 210.87.254.40 on 09/06/12
For personal use only.

canoate (NaDec) were therefore made with the equilibrium method using a flow densimeter as analytical device, as previously described (12). A comparison of two sets of measurements with OABr can give some idea of the error introduced with the osmometer with these systems.

The origin of chemicals and the purification procedure are the same as in previous studies (3–5). For the osmometric measurements all solutions were prepared by weight. For the equilibrium technique the molality of samples of the solution in equilibrium with ice, prepared with distilled water, were obtained by comparing the density at 25°C with those previously published (3, 4). A few extra density data were obtained to get a good calibration curve and to check the purity of the present salt samples with those used in our previous studies. The data agree inside the expected experimental error.

Results and Discussion

The freezing point data can be used to calculate the osmotic coefficients ϕ, the mean activity coefficients $\gamma_\pm$, and the nonideal free energies $\bar{G}_2^{ni}$ through the following well-known relations (12–14)

$$[1]\quad \phi = \frac{55.51}{\nu m}(0.0042070\theta + 2.1 \times 10^{-6}\theta^2) \times 2.303$$

$$[2]\quad \ln \gamma_\pm = \phi - 1 + \int_0^m (\phi - 1)\, d \ln m$$

$$[3]\quad \bar{G}_2^{ni} = \nu RT \ln \gamma_\pm$$

where θ is the freezing-point depression and ν is the number of ions into which the electrolyte dissociates.

With these relations, the free energy data are obtained at the freezing temperature and can be calculated at any other constant temperature from the known enthalpies of dilution and excess heat capacities (3). The procedure to calculate $\ln \gamma_\pm$ in the micellar region has been reported previously (13). Some of the difficulties encountered should be stressed. Essentially, the integral in eq. [2] has been resolved by splitting it into two contributions and assuming that the Debye–Hückel limiting law (DHLL) was valid up to the lower experimental concentration at which the freezing temperature has been measured (generally about 0.01 m). Use of this approximation can lead to a small difference between the experimental ϕ and the theoretical one, and consequently a discontinuity in the behaviour of $\ln \gamma_\pm$ as a function of m can be obtained at this concentration. The trends observed for the $\ln \gamma_\pm$ of NaDec and other surfactants can be slightly in error due to this approximation.

The nonideal entropies can readily be calculated from the partial molal relative enthalpies $\bar{L}_2$ and $\bar{G}_2^{ni}$

$$[4]\quad \bar{S}_2^{ni} = (\bar{L}_2 - \bar{G}_2^{ni})/T$$

The relative enthalpies can be calculated at any temperature from the heat capacity data (3, 5).

The original freezing-point data are given elsewhere,[4] but a summary of the data for OABr and NaDec at rounded molalities for various temperatures is given in Table 1.

The osmotic coefficients of the homologous series RNH_3Br are shown at 25°C in Fig. 1. All data were obtained with the osmometer with the exception of those of OABr which were determined by both techniques. There is only a small difference between both sets of data for OABr above 0.1 mol kg^{-1} but the difference becomes appreciable at low concentrations.

There is not much difference between the concentration dependence of ϕ for the different homologs but when micellization occurs, as in the case of OABr, ϕ decreases sharply. Similar observations were made in the case of interactions between Bu_4NBr and *tert*-butanol (11). The relative independence of the trends in ϕ on the chain length of the homologs in the pre-micellar region suggests that the important parameter here is the distance of closest approach between Br^- and the ionic head $-NH_3^+$.

The total and nonideal partial molal free energies of OABr were also calculated and are shown at three temperatures in Fig. 2. Beyond the critical micelle concentration (CMC), the mean activity $a_\pm$ increases only slowly with m. This behavior is typical of most ionic surfactants (2, 6–9). The mean activity coefficient $\gamma_\pm$ becomes smaller and the transition less sharp at higher temperatures. This is again typical of hydrophobic solutes. The negative sign of the excess free energy may come from nonstructural interactions but hydrophobic interactions are largely responsible for the temperature dependence of $\ln \gamma_\pm$. In fact, as can be seen in Fig. 2, in the case of $MeNH_3Br$ where the hydrophobic interactions are negligible, the activity coefficient is very nearly temperature independent.

The nonideal contributions to the partial molal entropies of OABr and NaDec were calculated at several temperatures and from these the excess partial molal entropies $(\bar{S}_2 - \bar{S}_2^0)$ were evaluated by addition of the mixing contribution $(-\nu R \ln m)$. These data are shown in Fig. 3 for OABr at 5, 15, and 25°C. The particular shape of the concentration dependence of $\bar{S}_2 - \bar{S}_2^0$ makes it difficult to extract the change in entropy during micellization (2). Since the system is at equilibrium, $\Delta G_m = 0$ and

$$[5]\quad \Delta S_m = \Delta H_m/T$$

[4] A complete set of the actual experimental data is available, at a nominal charge, from the Depository of Unpublished Data, CISTI, National Research Council of Canada, Ottawa, Canada K1A 0S2.

TABLE 1. Activity data and nonideal entropies of *n*-octylamine hydrobromide and sodium decanoate in water

OABr									
	5°C			15°C			25°C		
m^a	ϕ	$-\ln \gamma_\pm$	$\bar{S}_2^{ni\,b}$	ϕ	$-\ln \gamma_\pm$	$\bar{S}_2^{ni}$	ϕ	$-\ln \gamma_\pm$	$\bar{S}_2^{ni}$
0.02	0.9458	0.1589	3.9	0.9448	0.1638	4.1	0.9438	0.1666	4.2
0.04	0.9255	0.2249	5.8	0.9236	0.2317	6.1	0.9217	0.2364	6.3
0.06	0.9165	0.2665	7.4	0.9135	0.2753	7.8	0.9105	0.2821	8.1
0.08	0.9130	0.2948	8.9	0.9089	0.3057	9.3	0.9049	0.3145	9.6
0.10	0.9102	0.3174	10.3	0.9050	0.3305	10.7	0.8999	0.3414	11.1
0.12	0.9072	0.3371	11.7	0.9008	0.3525	12.2	0.8945	0.3656	12.6
0.14	0.9037	0.3552	13.2	0.8959	0.3731	13.7	0.8883	0.3885	14.1
0.16	0.9006	0.3714	14.7	0.8912	0.3920	15.3	0.8821	0.4101	15.7
0.18	0.8970	0.3870	16.4	0.8859	0.4105	16.9	0.8752	0.4313	17.4
0.20	0.8938	0.4012	18.0	0.8808	0.4279	18.8	0.8682	0.4518	19.2
0.21	0.8922	0.4150	18.9	0.8781	0.4364	19.8	0.8643	0.4622	20.3
0.22	0.8903	0.4080	19.9	0.8773	0.4429	20.6	0.8631	0.4698	21.3
0.23	0.8885	0.4217	21.1	0.8731	0.4527	22.8	0.8575	0.4816	22.5
0.24	0.8867	0.4283	22.3	0.8645	0.4669	26.1	0.8443	0.5011	23.8
0.25	0.8829	0.4368	24.9	0.8532	0.4839	29.9	0.8278	0.5243	25.3
0.26	0.8725	0.4520	28.8	0.8363	0.5069	33.3	0.8081	0.5512	27.0
0.27	0.8488	0.4809	38.6	0.8017	0.5483	37.2	0.7708	0.5964	28.7
0.28	0.8261	0.5095	45.3	0.7742	0.5835	39.1	0.7425	0.6335	30.0
0.29	0.8069	0.5352	48.0	0.7540	0.6120	40.3	0.7224	0.6630	30.8
0.30	0.7841	0.5649	50.5	0.7308	0.6439	41.3	0.6996	0.6956	31.5
0.31	0.7612	0.5952	52.4	0.7080	0.6759	42.2	0.6773	0.7281	32.2
0.32	0.7401	0.6243	53.6	0.6876	0.7059	43.0	0.6575	0.7585	32.8
0.33	0.7210	0.6516	54.5	0.6694	0.7340	43.6	0.6400	0.7868	33.2
0.35	0.6847	0.7054	55.8	0.6355	0.7883	44.7	0.6078	0.8411	34.0
0.40	0.6089	0.8282	57.4	0.5674	0.9095	45.8	0.5451	0.9602	34.9
0.45	0.5451	0.9417	58.5	0.5098	1.0214	46.8	0.4918	1.0702	35.8

NaDec									
	5°C			15°C			25°C		
m^a	ϕ	$-\ln \gamma_\pm$	$\bar{S}_2^{ni\,b}$	ϕ	$-\ln \gamma_\pm$	$\bar{S}_2^{ni}$	ϕ	$-\ln \gamma_\pm$	$\bar{S}_2^{ni}$
0.01	0.9663	0.1077	3.3	0.9649	0.1119	3.5	0.9635	0.1145	3.7
0.02	0.9634	0.1366	4.9	0.9608	0.1433	5.3	0.9581	0.1487	5.6
0.03	0.9603	0.1551	6.3	0.9565	0.1646	6.9	0.9526	0.1722	7.2
0.04	0.9575	0.1698	7.7	0.9524	0.1820	8.4	0.9472	0.1921	8.8
0.05	0.9546	0.1825	9.0	0.9482	0.1973	9.9	0.9417	0.2099	10.3
0.06	0.9514	0.1943	10.4	0.9438	0.2115	11.4	0.9360	0.2267	11.9
0.07	0.9485	0.2049	11.7	0.9395	0.2248	12.9	0.9303	0.2427	13.4
0.08	0.9457	0.2147	13.0	0.9357	0.2370	14.2	0.9242	0.2585	14.8
0.09	0.9430	0.2240	14.3	0.9322	0.2482	15.7	0.9170	0.2751	19.0
0.10	0.9404	0.2327	15.6	0.9283	0.2595	18.5	0.9021	0.2994	26.1
0.11	0.9374	0.2415	17.7	0.9106	0.2847	29.8	0.8740	0.3381	32.8
0.12	0.9325	0.2521	27.2	0.8867	0.3174	40.4	0.8371	0.3876	40.0
0.13	0.9252	0.2651	36.6	0.8649	0.3491	48.3	0.8086	0.4302	44.2
0.14	0.9138	0.2824	46.7	0.8429	0.3820	53.8	0.7846	0.4693	46.1
0.15	0.8839	0.3191	55.9	0.8064	0.4303	57.7	0.7485	0.5212	47.7
0.16	0.8371	0.3749	67.2	0.7535	0.4975	61.5	0.6965	0.5912	49.5
0.17	0.7978	0.4253	74.3	0.7111	0.5562	64.4	0.6554	0.6519	50.9
0.18	0.7617	0.4739	78.8	0.6762	0.6086	66.1	0.6227	0.7052	52.0
0.19	0.7297	0.5196	81.1	0.6470	0.6560	67.4	0.5957	0.7534	52.9

[a] m in mol kg^{-1}.
[b] $\bar{S}^{ni}$ in J K^{-1} mol^{-1}.

The enthalpy of micellization ΔH_m is available experimentally as a function of temperature (3, 5). The function $\Delta H_m/T$ is shown at 5 and 15°C in Fig. 3 and seems reasonable with respect to the change in entropy in the micellar region. At 25°C $\Delta H_m/T$ for OABr (not shown) is somewhat smaller than the difference between the extrapolated $\bar{S}_2 - \bar{S}_2^0$ at the CMC, suggesting that the $\bar{S} - \bar{S}_2^0$ data in the post-

Can. J. Chem. Downloaded from www.nrcresearchpress.com by 210.87.254.40 on 09/06/12
For personal use only.

Can. J. Chem. Downloaded from www.nrcresearchpress.com by 210.87.254.40 on 09/06/12
For personal use only.

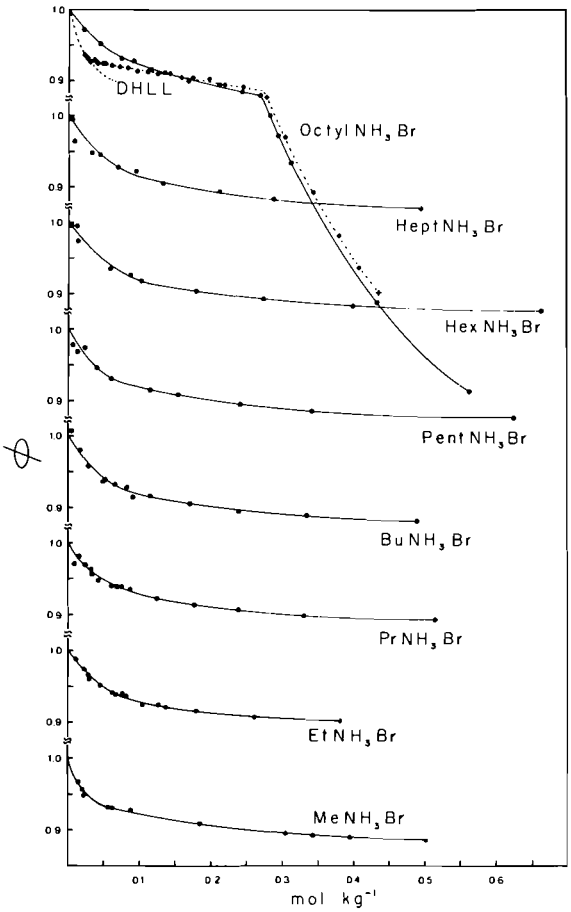

FIG. 1. Osmotic coefficients of the alkylamine hydrobromides at the freezing temperature: ◆ data obtained by the equilibrium technique; ● data from osmometer.

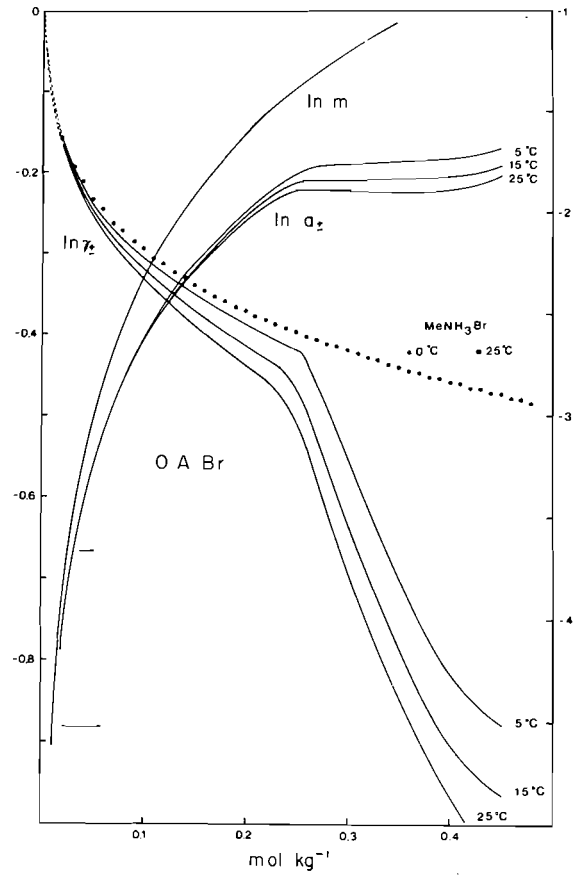

FIG. 2. Mean activity coefficients and activities of octylamine hydrobromide at 5, 15, and 25°C.

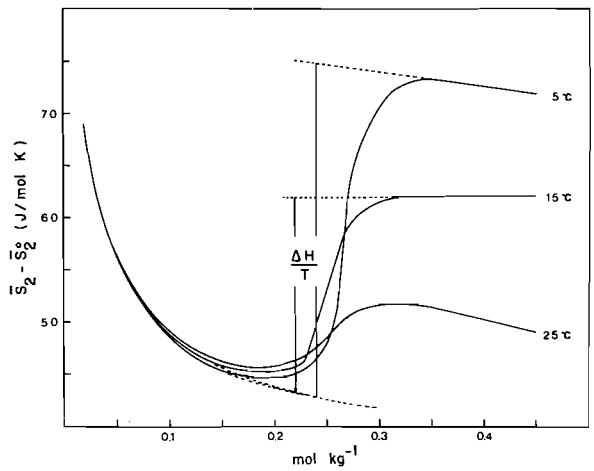

FIG. 3. Excess partial molal entropies of octylamine hydrobromide at 5, 15, and 25°C; comparison with enthalpies of micellization (2, 5).

micellar region would have to be extrapolated to the CMC with a positive slope for self-consistency.

The osmotic coefficients of ϕ of NaDec are shown for various temperatures in Fig. 4. Near the freezing temperature the trends are similar to those of OABr and of alkyltrimethylammonium bromides (2). There is a single break near the CMC. At higher temperatures, however, there seem to be double breaks which sharpen as the temperature is increased. We thought (13) that we finally had thermodynamic evidence for the second CMC that had been reported by numerous authors. However, it turns out that it is rather difficult to calculate excess free energies of NaDec as a function of temperature since the excess partial molal heat capacities show such large concentration and temperature dependence in the CMC region (3) at low temperatures. Calculations of ϕ of NaDec as a function of temperature, but based on only two sets of data for $\bar{C}_{P,2}$, have already been reported (13). These results at 25°C are shown as a dotted line in Fig. 4.

Thus, the breaks in ϕ tend to merge as better values for the temperature dependence of the partial molal heat capacity $\bar{C}_{P,2}$ are taken.

Can. J. Chem. Downloaded from www.nrcresearchpress.com by 210.87.254.40 on 09/06/12
For personal use only.

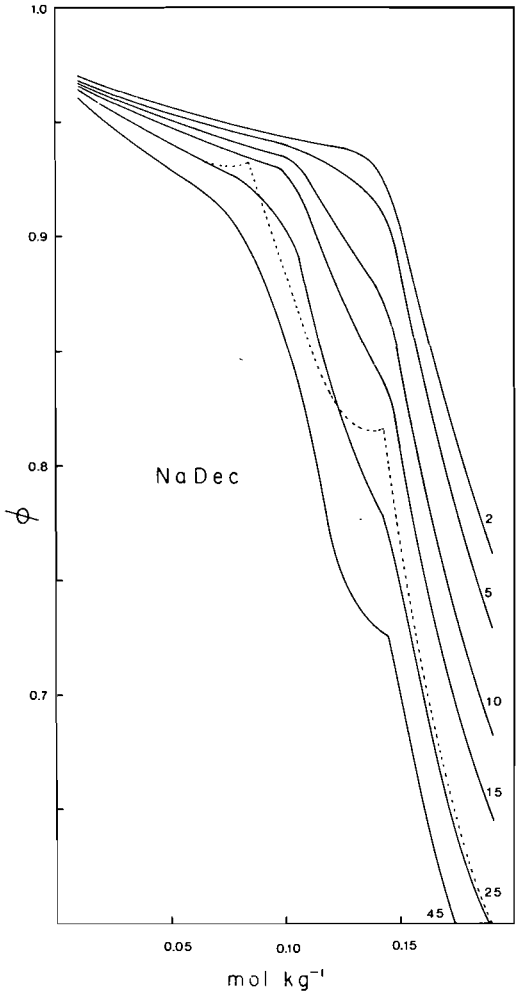

FIG. 4. Osmotic coefficients of sodium decanoate in water at various temperatures; ... data based on heat capacities measured at two temperatures only (13).

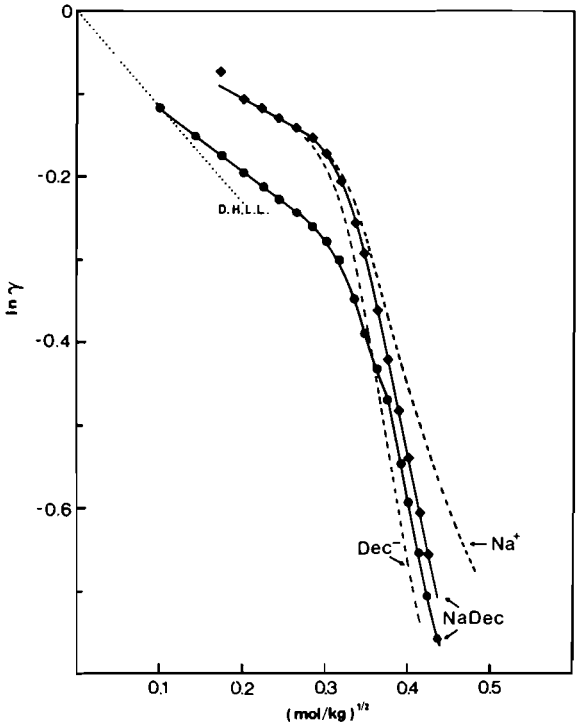

FIG. 5. Comparison of activity coefficients of sodium decanoate at 25°C obtained from freezing-point and EMF data (9).

Vikingstad (9) has recently measured the activity of NaDec at 25°C using a sodium and a Ag/AgDec electrode pair. His results are compared with ours in Fig. 5. Although there is a significant difference between the two sets of data, the EMF values do not show two breaks. Kale and Evans[5] have also investigated NaDec by an EMF method using a membrane decanoate electrode and find only one break. This therefore strongly suggests that the appearance of two breaks in the ϕ curve is most probably an artifact. On the other hand, the large difference between ln $\gamma_\pm$ of Vikingstad and ours is intriguing at first sight. As mentioned earlier, a small error can be introduced in our calculations of ln $\gamma_\pm$ from ϕ due to the method of application of the Gibbs–Duhem equation. Therefore, it is not certain if our ln $\gamma_\pm$ crosses the Debye–Hückel limiting law or if it simply tends to merge with it. On the other hand ln $\gamma_\pm$ from EMF tends to zero but not to the Debye–Hückel limiting law (DHLL).

The main difficulty with activity measurements using the EMF method is the non-Nernstian behavior of these specific electrodes. The method used in estimating the standard EMF, ε^0, in such cases can have a major effect on the trends of ln $\gamma_\pm$ as a function of m. This is best illustrated with decyltrimethylammonium bromide which has been investigated carefully with both the freezing point (2) and EMF (8) techniques. With specific membrane electrodes reversible to both cations and anions

$$[6]\quad \varepsilon = \varepsilon^0 - A \log a_\pm{}^2 = \varepsilon^0 - A \log m^2 - A \log \gamma_\pm{}^2$$

where A is not always equal to the theoretical Nernst slope of 0.059 volt. Different methods exist to derive ε^0 and A; ε can be plotted against log m^2 at low molalities, the slope giving A and the intercept ε^0. With this surfactant ε is not a linear function of log m^2, even at low concentrations. If average values for A and ε^0 are taken from the data at low concentrations then the top curve in Fig. 6 is obtained for ln $\gamma_\pm$. If ln $\gamma_\pm$ is assumed equal to the limiting Debye–Hückel law and again average

[5]K. M. Kale and D. F. Evans, unpublished results.

Can. J. Chem. Downloaded from www.nrcresearchpress.com by 210.87.254.40 on 09/06/12
For personal use only.

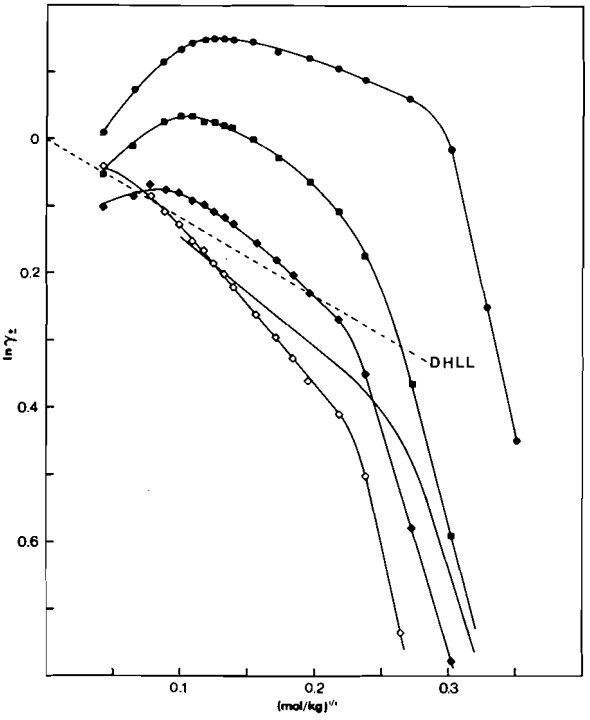

FIG. 6. Comparison of mean activity coefficients of decyltrimethylammonium bromide at 25°C obtained from freezing-points and from EMF data using various assumptions: ●, mean ε^0 and slope A assuming $\gamma = 1$ at low concentration; ■, mean ε^0 and A values assuming that in $\gamma = -Bm^{1/2}$ at low concentration; ◆, mean ε^0 and A values assuming that $\ln \gamma = -Bm^{1/2}/(1 + m^{1/2})$; ○, values of ε^0 and A extrapolated to $m = 0$ if $\ln \gamma = -Bm^{1/2}/(1 + m^{1/2})$ at low concentration.

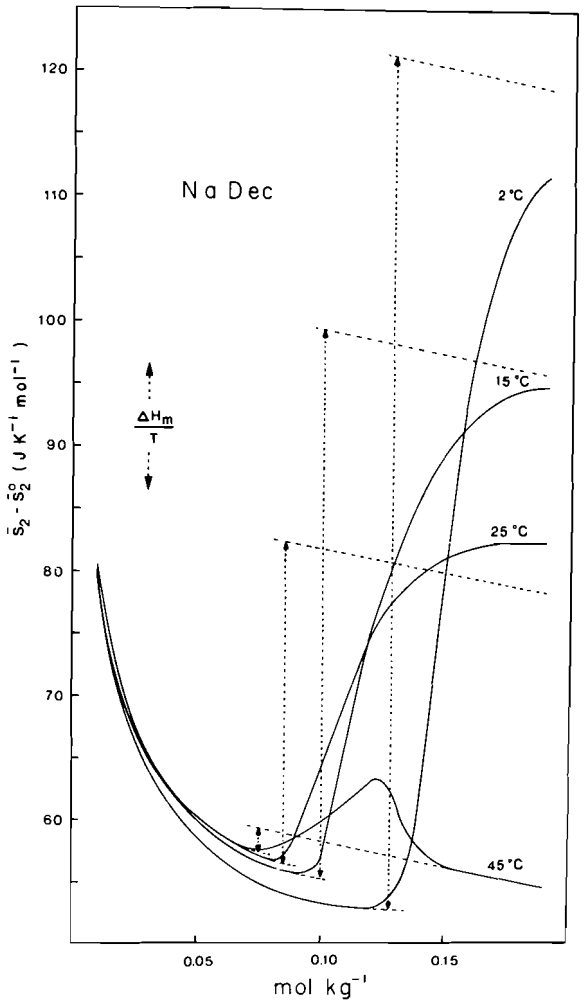

FIG. 7. Partial molal entropies of sodium decanoate in water at various temperatures; the entropies of micellization, $\Delta H_m/T$, were calculated from thermochemical data (2).

values for ε^0 and A are derived, then the new $\ln \gamma_\pm$ values are closer to the freezing point data. Still better agreement is obtained if $\ln \gamma_\pm$ in eq. [6] is taken as $-0.51\, m^{1/2}/(1 + m^{1/2})$. Finally if, instead of taking average values for ε^0 and A, values extrapolated to $m = 0$ are taken, still another curve is obtained for $\ln \gamma_\pm$. This shows that the absolute values of $\ln \gamma_\pm$ of ionic surfactants obtained by the EMF method can be seriously in error. On the other hand, the trends at higher concentrations should be correct.

We therefore have to conclude that the gradual appearance of a double break in the activity of NaDec as the temperature is increased is an artifact related to the difficulty in the analytical treatment of the heat capacity data in the CMC region at low temperature. The same difficulty would arise if we would try to calculate activity data at low temperatures from EMF measurements at 25°C using the thermochemical data.

The Krafft temperature for NaDec is probably just below the freezing temperature. As a result, it is not possible to measure activity data much above the CMC, since the solubility limit is rapidly reached. This limits seriously the data for the calculation of excess entropies. These are shown as a function of temperature in Fig. 7. It is not possible to extract entropies of micellization from these data but, as with OABr, $\Delta H_m/T$ calculated from thermochemical data (3) is shown and appears to be consistent with the entropy data.

Conclusion

It is generally true that it is better to calculate the temperature dependence of excess free energies from good thermochemical data than to try to derive excess heat capacities from the temperature dependence of activity data. Systems like NaDec which show very sharp changes in $\bar{C}_{P,2}$ near the CMC are to some extent exceptions to this rule.

Here both $\bar{C}_{P,2}$ and the activity data need to be measured as a function of temperature. The freezing point technique is probably the most accurate one for activity measurements but is unfortunately limited to the freezing temperature and is usable only with systems which have very low Krafft temperatures.

Acknowledgements

We are grateful to the Natural Sciences and Engineering Research Council of Canada for financial support. We would also like to thank Dr. Vikingstad and Dr. Evans for making some of their data available to us prior to publication.

1. G. M. MUSBALLY, G. PERRON, and J. E. DESNOYERS. J. Colloid Interface Sci. **54**, 80 (1976).
2. R. DE LISI, C. OSTIGUY, G. PERRON, and J. E. DESNOYERS. J. Colloid Interface Sci. **71**, 147 (1979).
3. R. DE LISI, G. PERRON, and J. E. DESNOYERS. Can. J. Chem. **58**, 959 (1980); J. E. DESNOYERS, R. DE LISI, and G. PERRON. Pure Appl. Chem. **52**, 433 (1980).
4. J. E. DESNOYERS and M. AREL. Can. J. Chem. **45**, 359 (1967).
5. P. A. LEDUC, J. L. FORTIER, and J. E. DESNOYERS. J. Phys. Chem. **78**, 1217 (1974).
6. T. SASAKI, M. HATTORI, J. SASAKI, and K. NAKINA. Bull. Chem. Soc. Jpn. **48**, 1397 (1975).
7. S. G. CUTLER, P. MEARES, and D. G. HALL. J. Electroanal. Chem. **85**, 145 (1977); J. Chem. Soc. Faraday Trans. I, **74**, 1758 (1978).
8. K. M. KALE, E. L. CUSSLER, and D. F. EVANS. J. Phys. Chem. **84**, 593 (1980).
9. E. VIKINGSTAD. J. Colloid Interface Sci. **72**, 68 (1979).
10. J. E. DESNOYERS, M. BILLON, S. LÉGER, G. PERRON, and J. P. MOREL. J. Solution Chem. **5**, 681 (1976).
11. J. E. DESNOYERS, G. PERRON, S. LÉGER, B. Y. OKAMOTO, T. H. LILLEY, and R. H. WOOD. J. Solution Chem. **7**, 165 (1978).
12. J. E. DESNOYERS, C. OSTIGUY, and G. PERRON. J. Chem. Educ. **55**, 137 (1978).
13. J. E. DESNOYERS, R. DE LISI, C. OSTIGUY, and G. PERRON. *In* Solution chemistry of surfactants. *Edited by* K. L. Mittal. Plenum Press, New York. 1979. p. 221.
14. J. E. DESNOYERS. *In* Activity coefficients in electrolyte solutions. Vol. 1. *Edited by* R. M. Pytkowicz. CRC Press, Boca Raton, FL. 1979. Chapt. 6.

Can. J. Chem. Downloaded from www.nrcresearchpress.com by 210.87.254.40 on 09/06/12
For personal use only.

Effect of organic compounds on electrolyte chemical potential in aqueous solutions at various temperatures

DAVID M. MOHILNER, TAKASHI KAKIUCHI,[1] AND JOANNA TARASZEWSKA[2]

Department of Chemistry, Colorado State University, Fort Collins, CO 80523, U.S.A.

Received July 2, 1980

This paper is dedicated to Dr. Sam Levine on the occasion of his 70th birthday

DAVID M. MOHILNER, TAKASHI KAKIUCHI, and JOANNA TARASZEWSKA. Can. J. Chem. **59**, 1872 (1981).

Data are reported on the concentration of Na_2SO_4 required to hold its chemical potential equal to its value in a 0.10045 *m* solution in pure water for aqueous solutions containing 2-butanol and 1-propanol at six different temperatures. The data were obtained from emf measurements on a galvanic cell without liquid junction containing a sodium reversible glass electrode and a 2-phase lead amalgam – lead sulfate electrode. The results of the measurements are interpreted in terms of the water structure making properties of the organic compound.

DAVID M. MOHILNER, TAKASHI KAKIUCHI et JOANNA TARASZEWSKA. Can. J. Chem. **59**, 1872 (1981).

On a déterminé la concentration du Na_2SO_4 requise dans des solutions aqueuses de butanol-2 et de propanol-1 à températures différentes pour maintenir son potentiel chimique au niveau qui est le sien dans une solution dans l'eau pure à une concentration de 0,10045 *m*. On a obtenu les données à partir de la mesure de fem d'une pile galvanique sans jonction liquide contenant une électrode de verre réversible au sodium et une électrode à 2 phases au sulfate de plomb amalgame de plomb. On a interprété les résultats des mesures en fonction de la structure de l'eau responsable des propriétés du composé organique.

[Traduit par le journal]

Introduction

Previously we showed (1, 2) experimentally that the additional of 2-butanol to an aqueous sodium sulfate solution could seriously alter the chemical potential of the electrolyte. Our method was to measure the emf of a galvanic cell without liquid junction in which one electrode was reversible to the cation and the other electrode was reversible to the anion. We showed how it was possible from such emf measurements to determine the recipe for preparing a series of solutions in which the chemical potential of the organic compound varies but in which the chemical potential of the electrolyte remains constant.

We are now engaged in a study of the effects of temperature on organic electrosorption (3) in order to determine the excess electrochemical entropy of mixing $\Delta\bar{S}^{E}$ of water and organic compound in the inner layer. For these studies it is necessary to measure the electrosorption isotherm of the organic compound at a series of temperatures. Therefore, at each temperature it is necessary to determine the recipe for preparing a series of solutions with varying organic chemical potential but with constant electrolyte chemical potential. We have now completed these measurements for two compounds, 2-butanol and 1-propanol, at 5°, 10°, 15°, 20°, 25° and 30°C. The purpose of this paper is to report the results of these measurements and to offer some explanation of the results in terms of the water structure making properties of the organic compound.

Experimental

The measurements carried out were emf measurements on a galvanic cell without liquid junction in which one electrode was a glass sodium ion electrode made with NAS11-18 glass (4) (Orion 94-11A) and the other was a two phase lead amalgam – lead sulfate electrode (5). These measurements were carried out in a cell of different design from that which we had employed previously (1, 6) in order to minimize the time required to reach equilibrium. In our previous work we had found that the emf of the cell always drifted slowly and usually reached a steady value only after waiting 12 h or more. Our old procedure was simply to flood the cell with a flow of argon and then pour in the amalgam and the solution. We decided that the reason for the slow drift of emf was that with this procedure some oxidation of the amalgam inevitably still occurred and therefore the electrode initially prepared was a mixed lead oxide – lead sulfate electrode. The waiting time was probably that required for the small amount of lead oxide to dissolve. Therefore a new cell was designed which would completely eliminate the possibility of the lead amalgam coming into contact with any atmospheric oxygen. A photograph of this new cell is shown in Fig. 1. The cell tops of the two amalgam compartments (left) in this new cell are No. 40 "O" ring joints and all stopcocks are No. 4 Kontes Kel F high vacuum stopcocks. Other connections into the cell are made with No. 5 "O" ring joints and all "O" ring joints are clamped tight with Thomas Clamps for "O" ring joints. The glass electrode compartment (right) is connected to the pair of amalgam electrode compartments by a V-shaped tube with fine frit at its apex by means of No. 9 "O" ring joints. Initially the glass electrode compartment is removed and the V-shaped tube is sealed with a No. 9 "O" ring stopper. The cell is then evacuated, filled with argon, and reevacuated three times. Then

[1]Postdoctoral research associate, on leave from Department of Agricultural Chemistry, Kyoto University, Kyoto, Japan.

[2]Postdoctoral research associate, on leave from Institute of Physical Chemistry, Polish Academy of Sciences, Warsaw, Poland.

0008-4042/81/131872-06$01.00/0

©1981 National Research Council of Canada/Conseil national de recherches du Canada

Can. J. Chem. Downloaded from www.nrcresearchpress.com by 210.87.254.40 on 09/06/12
For personal use only.

Can. J. Chem. Downloaded from www.nrcresearchpress.com by 210.87.254.40 on 09/06/12
For personal use only.

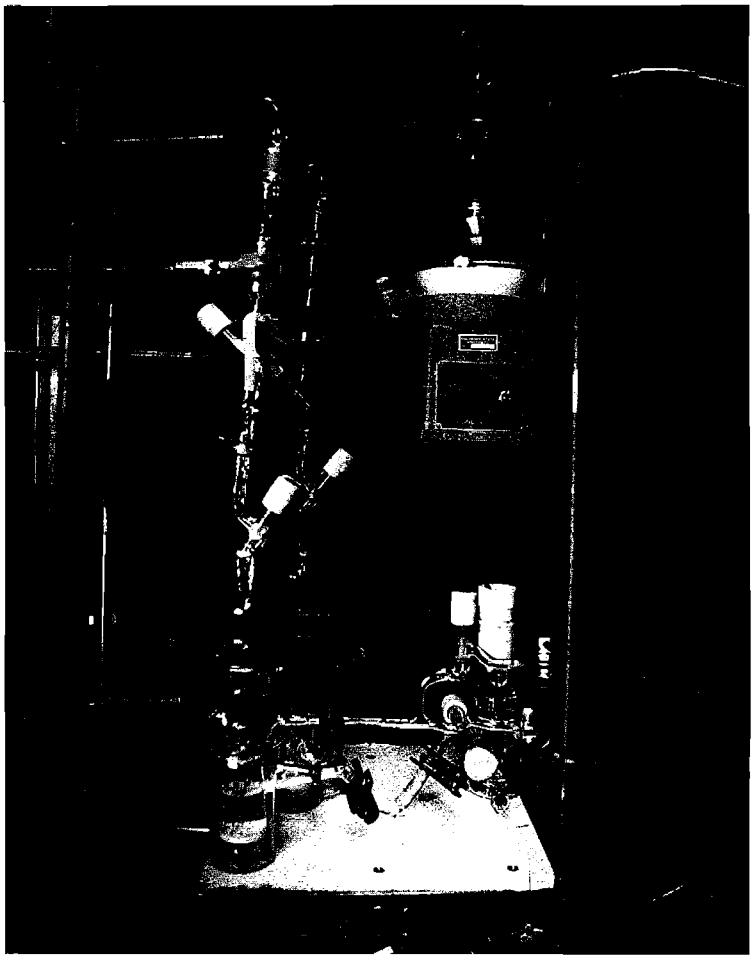

FIG. 1. Photograph of the cell used for the emf measurements.

the two-phase lead amalgam (reservoirs upper left) is admitted into each of the two evacuated amalgam electrode compartments through the high vacuum stopcocks until the platinum electrode contact is covered. (The cell interior is first dewetted with trimethylchlorosilane to prevent any creepage of solution to the platinum contact which would cause drift of the emf.) Then the cell is filled with argon and a slurry of lead sulfate, freshly prepared according to the method of Harned and Hecker (5), in the solution to be studied is admitted to the cell through the high vacuum stopcock. This slurry is kept in suspension by magnetic stirring in a flask (top of picture) which is provided with a bubbler to deaerate the solution. The solution flows down to the frit at the apex of the V-shaped tube and wets the frit. Then the glass electrode compartment is connected to the V-shaped tube at the No. 9 "O" ring joint, filled with deaerated solution, and the glass electrode inserted. This method of preparing the cell completely prevents the formation of any lead oxide on the lead amalgam electrode. The three electrode compartments are jacketed and thermostated water is pumped through the jackets during measurements. The emf is measured by a Keithley 610CR electrometer which has an input impedance in excess of 10^{14} ohms. The glass electrode and the lead amalgam – lead sulfate electrode are connected to the electrometer through a Keithley 6107 pH electrode adapter. The emf is read at the unity gain output of the electrometer on a Fluke 8300A digital voltmeter to the nearest 10 μV.

The electrolyte chosen was sodium sulfate because this compound exhibits no specific ionic adsorption at negative values of the excess charge density on the metal (7). It was decided to hold the chemical potential of the sodium sulfate in each solution containing organic compound at each temperature equal to its value at the same temperature in a solution of Na_2SO_4 at a concentration of 0.1 *M* (prepared at 25°C) which is 0.10045 *m* (6) in pure water. Therefore the emf of the cell containing 0.10045 *m* Na_2SO_4 solution was first measured at each temperature. Then for each concentration of the organic compound four solutions containing different concentrations of Na_2SO_4 were prepared, two of which gave emf values greater and two of which gave emf values less than the value obtained at the same temperature in the 0.10045 *m* Na_2SO_4 solution in pure water. The concentration–emf data at each fixed value of the organic concentration were then fitted to a least-squares quadratic equation in emf and interpolated to the value of emf obtained with the 0.10045 *m* sodium sulfate in pure water. The interpolated value of Na_2SO_4 concentration was thus the needed value to maintain the chemical potential of sodium sulfate in the

Can. J. Chem. Downloaded from www.nrcresearchpress.com by 210.87.254.40 on 09/06/12
For personal use only.

organic solution equal to its value in 0.10045 *m* sodium sulfate in pure water at the given temperature.

In the measurements the emf values of the cell consisting of the glass electrode and each of the two amalgam electrodes were measured. A value of emf was not accepted until the difference of these two emf's was less than 100 μV. The time required to obtain this condition varied with temperature. At 25°C it usually required only about 40 min. At 5°C, however, it usually required about 6 h. The sodium glass electrode was always stored in 0.1 *M* Na_2SO_4, and one hour before beginning the emf measurements it was put into the solution to be studied.

Results and Discussion

In our experimental study (6) of the electrosorption of 2-butanol at 25°C we included solutions with organic concentrations as high as 1.4 *M* (a_A = 0.5652). We found that in the high concentration region there was evidently a reorientation of the 2-butanol molecules on the electrode surface. Since our theory of noncongruent electrosorption (3) cannot accommodate molecular reorientation, it was unnecessary for the temperature dependence studies to include solutions with high concentrations. Therefore it was decided to have the concentration of 2-butanol in these solutions no higher than 0.4 *M* (measured at 25°C). Figure 2 shows the results of the emf measurements for 2-butanol at the six temperatures selected for study. The numerical data for this figure are given in Table 1. The ordinates on this graph are the needed molarity of Na_2SO_4 (measured at 25°C) required to hold the chemical potential of the Na_2SO_4 equal to its value in a 0.10045 *m* solution in pure water at the same temperature. The abcissae on this figure are the values of the molarity of the 2-butanol (measured at 25°C) in the solution. As expected from our previous studies (1) at 25°C covering concentrations up to 1.4 *M* (measured at 25°C) the data all fall on straight lines. The lines shown on the figure are least-squares straight lines constrained to pass through a Na_2SO_4 concentration of 0.1 *M* (measured at 25°C), i.e., 0.10045 *m*, when the 2-butanol concentration is zero. It can be noted from the figure that the slopes of the lines at all temperatures appear to be the same. The actual values of the slopes of these lines and the 95% confidence limits of these slopes are plotted in Fig. 3. It can be seen from the overlap of these 95% confidence limits that statistically these slopes really are the same. This fact has an important practical implication for the electrocapillary measurements, namely, regardless of the temperature, the needed concentration of Na_2SO_4 for a given concentration of 2-butanol is the same. Therefore the electrocapillary curves for all of the different temperatures can be measured on the same set of solutions.

As we stated in our first publication on this subject (1), we believe that the explanation of this effect of the organic compound on the electrolyte chemical potential is the structure making properties of the organic compound. The data are consistent with the following explanation. When an organic molecule is dissolved in the aqueous solution it induces the water molecules in its immediate neighborhood to become more highly structured,

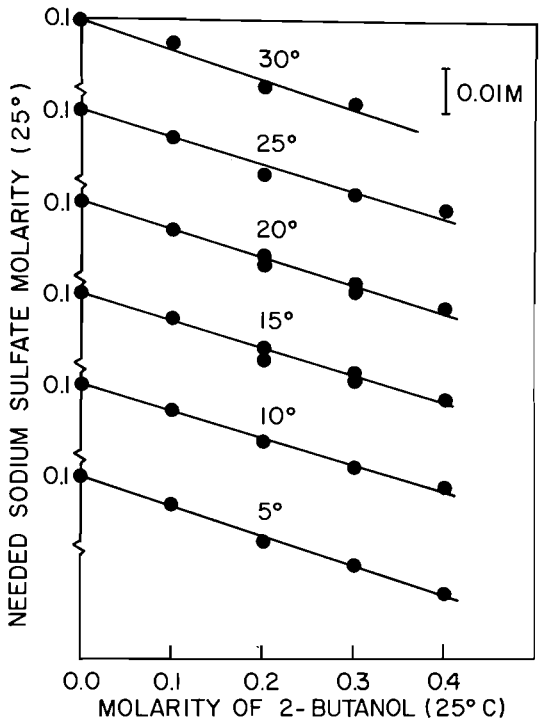

FIG. 2. Sodium sulfate concentration required to hold electrolyte chemical potential in 2-butanol solutions equal to its value in 0.10045 *m* solution in pure water.

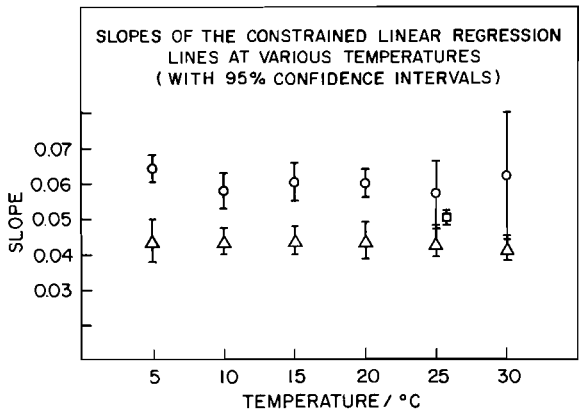

FIG. 3. Slopes of lines in Fig. 2 and their 95% confidence limits for 2-butanol, ○. Slopes and their 95% confidence limits for lines in Fig. 5 for 1-propanol, △. Slopes and its confidence limits for 2-butanol at 25°C determined in ref. 2, □.

TABLE 1. Needed molarity of Na_2SO_4 to keep its chemical potential constant and equal to that in 0.1 M aqueous solution, at the specified temperatures, as a function of the molarity of the alcohol

2-Butanol molarity at 25°C	Needed Na_2SO_4 molarity at 25°C					
	5°C	10°C	15°C	20°C	25°C	30°C
0.1	0.0937	0.0944	0.0947	0.0940	0.0945	0.0947
0.2	0.0863	0.0875	0.0870	0.0875	0.0865	0.0857
0.3	0.0809	0.0819	0.0817	0.0815	0.0818	0.0822
0.4	0.0743	0.0777	0.0769	0.0772	0.0786	—
1-Propanol molarity at 25°C	**Needed Na_2SO_4 molarity at 25°C**					
	5°C	10°C	15°C	20°C	25°C	30°C
0.2	0.0929	0.0914	0.0912	0.0901	0.0896	0.0836
0.3	0.0868	0.0884	0.0864	0.0857	0.0866	0.0869
0.5	0.0727	0.0752	0.0752	0.0755	0.0764	0.0773
0.7	0.0684	0.0689	0.0677	0.0684	0.0694	0.0702
1.0	0.0582	0.0577	0.0588	0.0596	0.0595	0.0603
1.2	0.0518	0.0517	0.0525	0.0530	0.0539	0.0546
1.5	0.0439	0.0446	0.0448	0.0456	0.0463	0.0459
2.0	0.0296	0.0316	0.0338	0.0347	0.0358	0.0361

probably in the form of a clathrate-like cage of water molecules surrounding the organic molecule. If we assume that the effective molality of the Na_2SO_4 in the remaining unstructured water is the same as in the original 0.10045 m solution in pure water, we can calculate how many water molecules are associated with each organic molecule. The calculation is made using the following formula

$$[1] \quad n = [x_W - (55.51/m_0)x_e)]/x_A$$

where n is the number of water molecules in the cage around each organic molecule, x_W, x_e, and x_A are the mole fractions of the water, the electrolyte, and the organic compound, respectively, in the solution, and m_0 is the molality of the electrolyte in the solution containing no organic compound which produces the desired electrolyte chemical potential. The mole fractions of the three components can be calculated from the composition data if the density of the solution is measured. The densities of all of the solutions were measured and the mole fractions of the three components were calculated. The data in Fig. 2 are consistent with a cage of 28 water molecules surrounding each 2-butanol molecule. This would be consistent with a clathrate in the form of a hexakaidecahedron with 12 pentagonal and four hexagonal sides which is one of the structures actually found by X-ray diffraction studies on crystalline hydrates (8). Our previous data on 2-butanol obtained at 25°C covering a range of concentration of up to 1.4 M had indicated a clathrate in the shape of a tetrakaidecahedron containing 24 water molecules. The 95% confidence limits of the slope of the line for that study are also indicated in Fig. 3. It will be noted that these confidence limits are considerably smaller than those we obtained in the present study. The explanation is simply that a better straight line is bound to be obtained when a larger concentration range is used. Actually we do not believe that the organic molecules are surrounded all of the time by a clathrate-like cage. Due to thermal fluctuations the clathrate will be continually broken up and reformed, i.e., any actual framework structure of the water molecules must be a "flickering structure" as originally described by Frank and Quist (9). Very likely at any instant in time an organic molecule is not completely enclosed in a complete clathrate cage but only partly surrounded by the beginnings of such a cage. Our thermodynamic data, of course, give an indication only of the long-time average situation. These data provide no direct information on the structural situation in the solution but they are consistent with the formation of clathrates. There is other thermodynamic evidence in the literature (10) for aqueous alcohol solutions which is consistent with the idea of an enhanced structure produced by the introduction of an alcohol molecule into water. This evidence is that although in dilute solutions the enthalpy of mixing is negative, the excess Gibbs free energy of mixing, ΔG^E, is positive, i.e., the solutions exhibit positive deviations from Raoult's law because the excess entropy of mixing, ΔS^E, is so large and negative that

$$[2] \quad T|\Delta S^E| > |\Delta H^E|$$

Can. J. Chem. Downloaded from www.nrcresearchpress.com by 210.87.254.40 on 09/06/12
For personal use only.

Can. J. Chem. Downloaded from www.nrcresearchpress.com by 210.87.254.40 on 09/06/12
For personal use only.

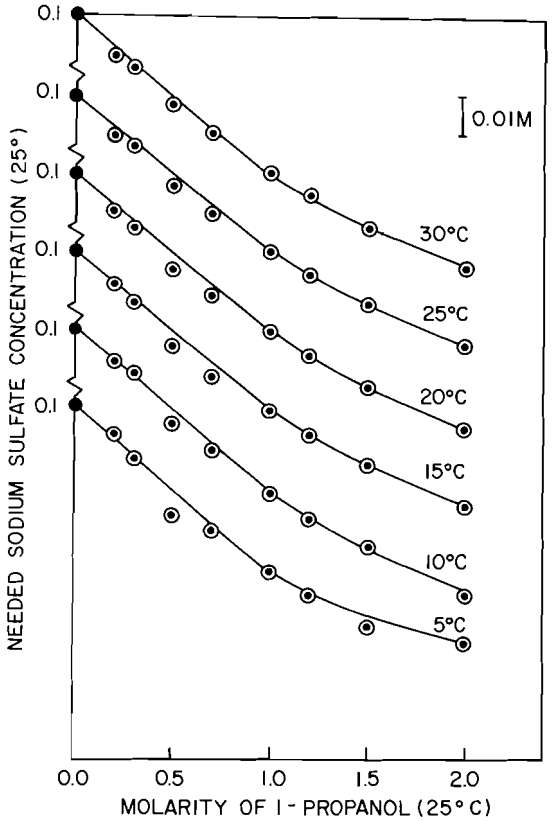

FIG. 4. Sodium sulfate concentration required to hold electrolyte chemical potential in 1-propanol solutions equal to its value in 0.10045 *m* solution in pure water.

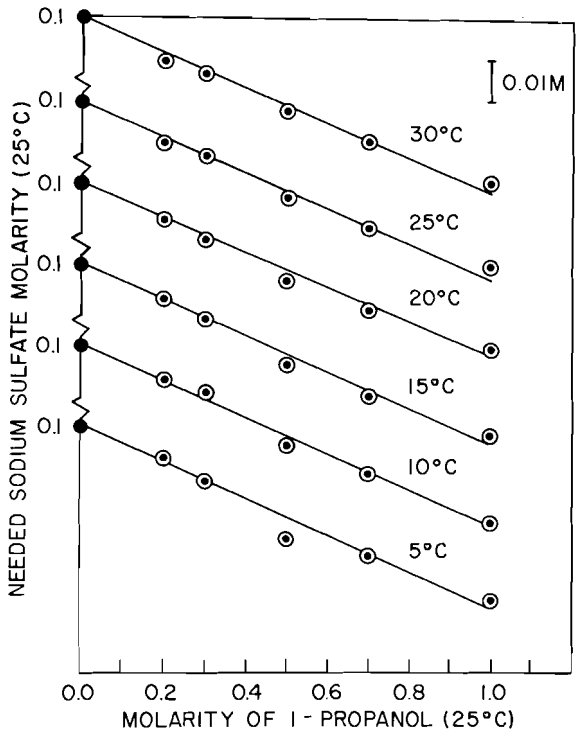

FIG. 5. Data from Fig. 4 fitted to constrained least-squares straight lines.

As Franks has said (11), the thermodynamic properties of aqueous solutions of organic compounds are under entropy control. We have predicted (3) that the thermodynamic properties of the inner layer in the case of organic electrosorption are also under entropy control and the present work was undertaken as a first step required to experimentally test this prediction.

Figure 4 shows the results of our measurements for 1-propanol. The numerical data for this figure are given in Table 1. In the case of this compound we have extended the measurements up to a concentration of 2.0 *M* (measured at 25°C) because we wish in our electrocapillary studies to test for evidence of molecular reorientation. These curves are linear up to a concentration of 1.0 *M* and the corresponding constrained least-squares straight lines are shown in Fig. 5. It will be noted that the slopes of these lines also appear to be all the same. The 95% confidence limits of the slopes of these lines are also shown in Fig. 3. It can be seen by the overlap of these confidence limits that statistically a single slope suffices to describe all the data at all temperatures. Therefore, as in the case of 2-butanol, it will be legitimate to use the same solutions in the electrocapillary measurements at all temperatures. The data for 1-propanol are actually consistent with a clathrate-like cage in the shape of a pentagonal dodecahedron with 20 water molecules, which is the same result we obtained earlier (2) for 2-methyl-2-propanol. As in the case of 2-butanol we do not believe that the molecules are actually all contained in such cages. Rather the true situation at any instant in time is probably a partial cage around any one organic molecule. The thermodynamic data merely indicate the long-time average.

Changes in the emf of the cell as a function of temperature and time for aqueous 0.10045 *m* Na_2SO_4 are shown in Fig. 6. Similar dependence on temperature was also observed in solutions containing 2-butanol and 1-propanol. The plot of emf against temperature is strongly curved. The reason for such behavior is complex because with change of temperature the potentials of both electrodes change due to the change of activity of sodium sulfate, the change of the standard potential of the lead amalgam – lead sulfate electrode, and the change of the asymmetry potential of the sodium glass electrode.

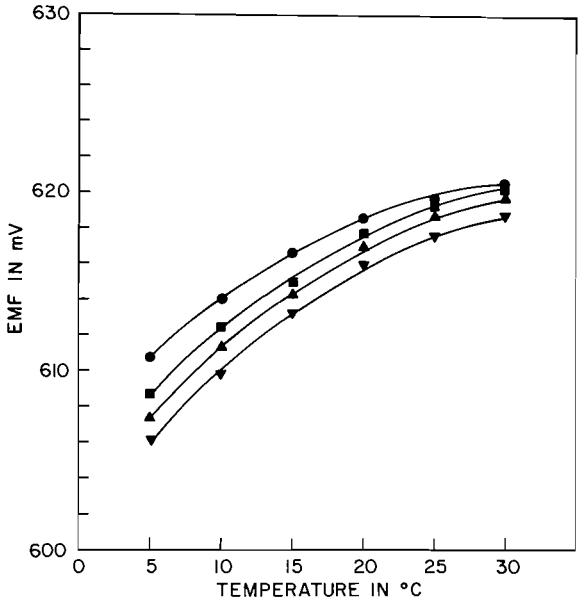

FIG. 6. Electromotive force of cell containing 0.10045 *m* in Na_2SO_4 in pure water as a function of temperature and time. Time of measurements: ●, 4 October 1979; ■, 31 October 1979; ▲, 30 November 1979, ▼, 11 January 1980.

To separate and to estimate these factors individually is not possible at the present time. However, a variation of the emf with time, especially significant at lower temperatures, is most likely due to the change of potential of the sodium glass electrode. As was pointed out by Eisenman and co-workers (12), the glass electrode is a perfect cation exchange membrane, whose standard potential represents a sum of contributions from both diffusion and phase boundary processes. If the properties of the ion exchange sites are modified as a result of the ion exchange, time variations of potential can arise. In the case of the sodium glass electrode the main reason for these variations seems to be the swelling of the glass membrane due to the exchange of some sodium ions for hydrogen ions which can bind water and alcohol molecules (13). This swelling process seems to be an irreversible one leading to a decrease of the measured emf values with time. It will be noted from Fig. 6 that our data are consistent with such behavior. Therefore in precise measurements of sodium activities, especially as a function of temperature where the measured results are small, frequent recalibration of the sodium glass electrode is necessary.

Acknowledgements

This work was supported by the National Science Foundation under grant No. CHE76-83432. Acknowledgement is also made to the donors of the Petroleum Research Fund, administered by the American Chemical Society for partial support of this research. This work constitutes a portion of the research in a collaborative international program on thermodynamic studies of the inner part of the electrical double layer supported in part by the North Atlantic Treaty Organization (NATO).

1. D. M. MOHILNER and H. NAKADOMARI. J. Phys. Chem. **77**, 1698 (1973).
2. D. M. MOHILNER and H. NAKADOMARI. J. Electroanal. Chem. **65**, 843 (1975).
3. D. M. MOHILNER, H. NAKADOMARI, and P. R. MOHILNER. J. Phys. Chem. **81**, 244 (1977).
4. G. EISENMAN. Adv. Anal. Chem. Instrum. **4**, 213 (1965).
5. H. S. HARNED and J. C. HECKER. J. Am. Chem. Soc. **56**, 650 (1934).
6. H. NAKADOMARI, D. M. MOHILNER, and P. R. MOHILNER. J. Phys. Chem. **80**, 1761 (1976).
7. R. PAYNE. J. Electroanal. Chem. **60**, 183 (1975).
8. G. A. JEFFREY. Proc. Conf. Desalination Research, Woods Hole, MA. 1961; Publ. 942, NAS-NRC, Washington, DC. 1963.
9. H. S. FRANK and A. S. QUIST. J. Chem. Phys. **34**, 604 (1961).
10. F. FRANKS and D. J. G. IVES. Q. Rev. Chem. Soc. London, **20**, 1 (1966).
11. F. FRANKS and D. S. REID. Water Compr. Treat. **2**, Chapter 5 (1973).
12. G. EISENMAN (*Editor*). Glass electrodes for hydrogen and other cations. Marcel Dekker, New York. 1967.
13. G. HAUGAARD. J. Phys. Chem. **45**, 148 (1941).

Can. J. Chem. Downloaded from www.nrcresearchpress.com by 210.87.254.40 on 09/06/12
For personal use only.

The electrophoretic mobility of large colloidal particles

RICHARD WYNDHAM O'BRIEN

Department of Theoretical and Applied Mechanics, School of Mathematics, University of New South Wales, Sydney, New South Wales 2033, Australia

AND

ROBERT JOHN HUNTER

School of Chemistry, University of Sydney, Sydney, New South Wales 2006, Australia

Received July 4, 1980

This paper is dedicated to Dr. Sam Levine on the occasion of his 70th birthday

RICHARD WYNDHAM O'BRIEN and ROBERT JOHN HUNTER. Can. J. Chem. **59**, 1878 (1981).

Analytical approximation formulae linking ζ potential and electrophoretic mobility have been derived for a variety of limiting conditions. In this paper we present a simplified derivation of an equation first established by Dukhin and his collaborators for a large spherical particle with a thin double layer. Although potentially a very useful expression it has been little used to date, partly because of the complicated nature of Dukhin's derivation and partly because of the lack of a reliable method of testing its validity. The expression compares very favourably with the computer calculations of O'Brien and White, provided κa is sufficiently large.

RICHARD WYNDHAM O'BRIEN et ROBERT JOHN HUNTER. Can. J. Chem. **59**, 1878 (1981).

On a mis au point une formule d'approximation analytique reliant dans diverses conditions limites le potentiel zeta et la mobilité dans des conditions d'électrophorèse. Dans cet article, nous avons simplifié une équation établie pour la première fois par Dukhin et ses collaborateurs pour une grosse particule sphérique ayant une double couche mince. Cette équation pourrait être très utile, mais elle a été peu utilisée jusqu'à maintenant; cet état de fait est dû en partie à la nature compliquée de l'équation mise au point par Dukhin et en partie à l'absence d'une méthode sûre pour en vérifier la validité. A condition que ka soit suffisamment grand, l'expression se compare favorablement aux calculs faits par ordinateur par O'Brien et White.

[Traduit par le journal]

I. Introduction

Most students of colloid science are familiar with Smoluchowski's formula (1):

$$[1.1] \quad \mu = \varepsilon\zeta/4\pi\eta$$

for the electrophoretic mobility, μ, of a particle of arbitrary shape with uniform electrokinetic potential ζ, immersed in an electrolyte with viscosity η and permittivity ε. This formula, which is valid for particles whose dimensions are much greater than the double layer thickness, is based on the assumption that the double layer is not distorted by the application of the electric field; the ions are of course set into motion by the field, but for thin double layers they move parallel to the surface and since the double layer is approximately flat, the ionic densities do not alter.

This assumption is not valid for large ζ-potentials, for the density of counter-ions in the double layer is then so large that the ionic fluxes due to the small components of the applied electric field and fluid velocity normal to the surface become significant, and the double layer distorts. Thus Smoluchowski's formula breaks down at large ζ-potentials.

For spherical particles we can determine the range of validity of Smoluchowski's formula by comparing the formula with the computer calculated mobilities given in O'Brien and White's paper (2). In Fig. 1 the mobility of particles in KCl solution is plotted as a function of $e\zeta/kT$ for a number of κa values, where as usual e is the electronic charge, kT is the temperature in energy units, κ^{-1} is the double layer thickness, and a is the particle radius. From this figure it can be seen that the Smoluchowski formula ($\kappa a = \infty$) is invalid for $e\zeta/kT \gtrsim 4$ if κa is of the order of 150 or so. The range of validity of the Smoluchowski formula increases with κa, but only slowly.

In order to derive a formula for the mobility of a large particle which is valid for all ζ-potentials it is necessary to take the distortion of the double layer into account.

In 1965 Dukhin (3) solved this difficult problem for the case of a spherical particle in a symmetric electrolyte with two ionic species. Dukhin's mobility formula, which is valid for all ζ-potentials, is based on the observation that the ion densities and electrical potential in the double layer vary on a length scale of order κ^{-1} in the direction normal to the particle surface, while the variations in the tangential direction occur on a length scale of order a, the particle radius. Thus at large κa, the gradients in the electric field and ion densities in the double layer normal to the particle surface will be much larger

0008-4042/81/131878-10$01.00/0

©1981 National Research Council of Canada/Conseil national de recherches du Canada

Can. J. Chem. Downloaded from www.nrcresearchpress.com by 210.87.254.5 on 09/06/12
For personal use only.

Can. J. Chem. Downloaded from www.nrcresearchpress.com by 210.87.254.5 on 09/06/12
For personal use only.

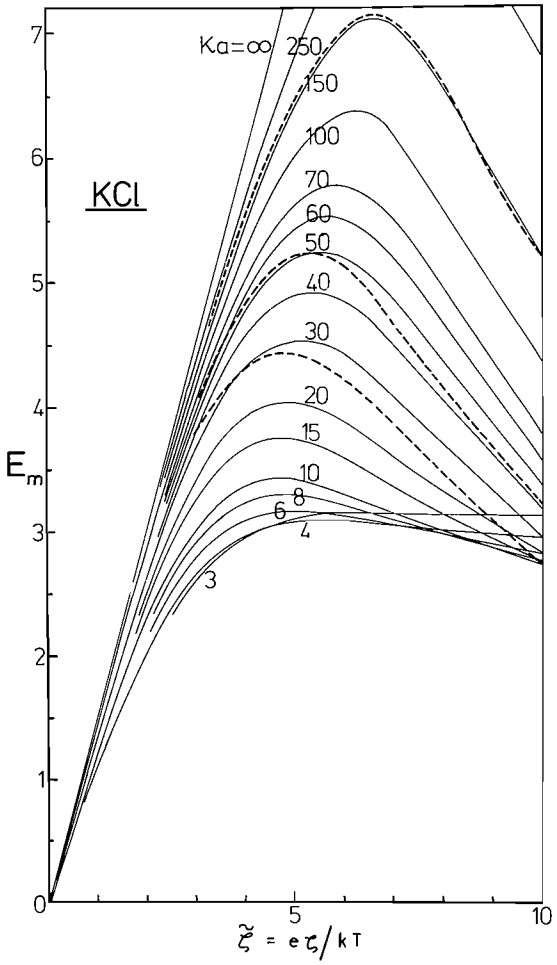

FIG. 1. Comparison of values of the reduced mobility, E_m, as a function of reduced zeta potential ($= ze\zeta/kT$). Full lines: computer solution of O'Brien and White (2). Broken lines: calculated from eq. [5.1] for κa = 150, 50, and 30 respectively (m = 0.184 in all cases).

than the gradients tangential to the surface; as a result there will be a local balance between diffusive flux and the flux of ions due to the component of the electric field normal to the surface. From this it follows that the ions in the double layer are distributed according to a Boltzmann-type expression (eq. [59] of ref. 4, p. 298) which may be written in the form

$$[1.2] \quad n_i(\boldsymbol{r}) = n_i(\infty)(1 - A_i) \exp\left(-\frac{z_i e\psi(\boldsymbol{r})}{kT}\right)$$

where $n_i(\boldsymbol{r})$ is the density of the ith ionic species, $n_i(\infty)$ is the density at large distances from the double layer, z_i is the valency, and ψ is the electrical potential. The quantity A_i is assumed to be approximately constant over distances of order κ^{-1}. This quantity, which is determined in the subsequent analysis, may be related to the local ion density and electrical potential just beyond the double layer. A full discussion of this point is given by Dukhin (5) and by Dukhin and Shilov (6).

In this paper we provide a simplified derivation of Dukhin's formula for the electrophoretic mobility. In sections 2 and 3 below we set out the equations which must be solved in order to calculate the mobility of a spherical particle, and in section 4 we solve these equations in the double layer, using Dukhin's formula [1.2] for the ion densities. By matching this inner solution to a solution which is valid beyond the double layer we obtain the required formula for the mobility. Coincidentally, Dr. Samuel Levine also studied the "polarised double layer" in collaboration with another member of the O'Brien clan (7) in connection with the motion of a liquid droplet in an electric field.

2. The Governing Equations

The problem of calculating the electrophoretic mobility is considerably simplified by the introduction of a set of quantities $\Phi_i(\boldsymbol{r})$, defined by the Boltzmann-type formula[1]

$$[2.1] \quad n_i(\boldsymbol{r}) = n_i(\infty) \exp\left(-\frac{z_i e}{kT}(\psi + \Phi_i)\right)$$

for the density of the ith ionic species. To determine the mobility of a particle we must solve a set of partial differential equations for the quantities $\Phi_i(\boldsymbol{r})$ and the velocity field $\boldsymbol{u}(\boldsymbol{r})$ in the electrolyte surrounding the particle.

In this section we briefly outline the derivation of these equations and the associated boundary conditions; a more complete derivation is given in ref. 2.

In a frame of reference moving with the particle the ionic densities do not vary with time, and consequently the net flux of ions through any closed surface is zero:

$$[2.2] \quad \nabla\cdot(z_i e n_i^0 \nabla\Phi_i) + \lambda_i \nabla n_i^0 \cdot \boldsymbol{u} = 0$$

there being one such equation for each type of ion. The quantity n_i^0 in this equation denotes the density of type i ions in the absence of an applied field, and λ_i is the ionic drag coefficient.

The remaining equations, which are obtained from

[1] In ref. 2 the quantities Φ_i are defined with the potential ψ in the exponent of [2.1] replaced by $\psi + \boldsymbol{E}\cdot\boldsymbol{r}$. For this reason our equations and boundary conditions for Φ_i are slightly different from those given in that paper.

Can. J. Chem. Downloaded from www.nrcresearchpress.com by 210.87.254.5 on 09/06/12
For personal use only.

the laws of conservation of momentum and mass are

$$[2.3] \quad \eta\nabla^2(\nabla \times \boldsymbol{u}) = \sum_{i=1}^{N} z_i e \nabla\Phi_i \times \nabla n_i^0$$

and

$$[2.4] \quad \nabla\cdot\boldsymbol{u} = 0$$

where N is the number of ionic species.

To determine the electrophoretic mobility we must solve eqs. [2.2], [2.3], and [2.4] subject to the following boundary conditions:
On the surface of the particle,

$$[2.5] \quad \boldsymbol{u} = 0$$

and

$$[2.6] \quad \nabla\Phi_i\cdot\hat{n} = 0$$

where $\hat{n}$ is the unit normal to the particle surface; and far from the particle,

$$[2.7] \quad \boldsymbol{u} \approx -\mu\boldsymbol{E}$$

and

$$[2.8] \quad \Phi_i \approx \boldsymbol{E}\cdot\boldsymbol{r}$$

where $\boldsymbol{E}$ is the electric field strength far from the particle and the position vector $\boldsymbol{r}$ is assumed to have its origin at a point in the particle. Since we are mainly concerned here with spherical particles we have assumed in formulating the boundary condition [2.7] that the particle moves in the direction of the applied field; for more complicated particle shapes this boundary condition must be modified.

In addition to these boundary conditions we must satisfy the constraint that the net force on the particle and double layer is zero. In section 8 of ref. 2 it is shown that the disturbance in the velocity field caused by a particle and double layer decays like F/r with increasing distance r from the particle, where F is the net force on the particle and double layer. In this case F is zero, and consequently the velocity disturbance decays to zero more rapidly than $1/r$ as $r \to \infty$; in fact it can be shown that the disturbance decays like $1/r^2$ in this case.

Hence by using the fact that the particle and double layer is force-free we may rewrite the outer boundary condition [2.7] as

$$[2.9] \quad \boldsymbol{u} = -\mu\boldsymbol{E} + O(1/r^2) \qquad \text{as } r \to \infty$$

where the symbol $O(1/r^2)$ denotes a term which decays in proportion to $1/r^2$. By replacing the boundary condition [2.7] by the requirement that $\boldsymbol{u}$ has the above asymptotic form we automatically ensure that the force-free condition is satisfied.

To determine the quantities $\boldsymbol{u}$, Φ_i, and μ we must solve eqs. [2.2] to [2.4] subject to the boundary conditions [2.5], [2.6], [2.8], and [2.9].

3. The Electrophoresis Problem for a Spherical Particle

For a spherical particle it can be shown by symmetry arguments (ref. 2, section 6) that the functions $\Phi_i(r)$ have the form

$$[3.1] \quad \Phi_i(r) = \phi_i(r)E\cos\theta$$

where E is the magnitude of the applied field, and the spherical polar coordinates r and θ are defined in Fig. 2. For a given particle and electrolyte the functions $\phi_i(r)$ depend only on distance from the centre of the sphere.

Similarly, the components of the fluid velocity may be written in the form[2]

$$[3.2] \quad u_r = -\frac{2}{r}g(r)E\cos\theta$$

and

$$[3.3] \quad u_\theta = \frac{1}{r}\frac{d}{dr}(rg(r))E\sin\theta$$

where u_r and u_θ are the components of $\boldsymbol{u}$ in the direction of increasing r and θ; the azimuthal component of the velocity is zero in this case.

The forms [3.2] and [3.3] for u_r and u_θ automatically satisfy the continuity equation [2.4]. By substituting these forms and the expression [3.1] for Φ_i in the remaining equations [2.2] and [2.3], we obtain

$$[3.4] \quad \frac{d^2\phi_i}{dr^2} + \left(\frac{2}{r} - \frac{z_i e}{kT}\frac{d\psi^0}{dr}\right)\frac{d\phi_i}{dr} - \frac{2\phi_i}{r^2} = -\frac{2\lambda_i}{kT}\frac{d\psi^0}{dr}\frac{g}{r}$$

and

$$[3.5] \quad \frac{d^4g}{dr^4} + \frac{4}{r}\frac{d^3g}{dr^3} - \frac{4}{r^2}\frac{d^2g}{dr^2} = \frac{1}{\eta r}\sum_{i=1}^{N} z_i e\frac{dn_i^0}{dr}\phi_i$$

where ψ^0 is the equilibrium potential in the absence of an applied field.

Similarly, the boundary conditions [2.5], [2.6], [2.8], and [2.9], when written in terms of the functions g and ϕ_i, become

$$[3.6] \quad g = 0, \quad dg/dr = 0$$

and

$$[3.7] \quad d\phi_i/dr = 0 \qquad \text{at } r = a$$

[2]These expressions are obtained by writing the formula [6.4] in ref. 2 in component form and replacing the symbol df/dr by $g(r)$.

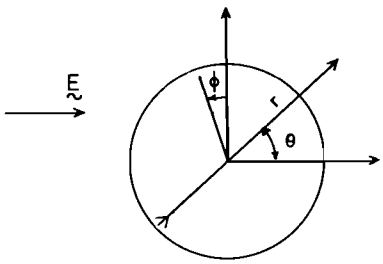

FIG. 2. The spherical polar coordinate system used in sections 3 and 4 in the calculation of the mobility of a sphere. The origin lies at the centre of the sphere and the polar axis ($\theta = 0$) is parallel to the applied electric field.

and

$$[3.8] \quad \phi_i \sim r$$

$$[3.9] \quad g = \frac{\mu r}{2} + O\left(\frac{1}{r}\right) \qquad \text{as } r \to \infty$$

To obtain g, ϕ_i, and μ we must solve the ordinary differential equations [3.4] and [3.5] subject to the above boundary conditions.

The form of the functions ϕ_i and g beyond the double layer may be obtained by using the fact that the coefficients $d\psi^0/dr$ and dn_i^0/dr in eqs. [3.4] and [3.5] are approximately zero in this region. Putting these coefficients to zero and solving the resulting equations subject to the outer boundary conditions [3.8] and [3.9] we find

$$[3.10] \quad \phi_i(r) = r + \frac{c_i}{r^2} \qquad i = 1, 2, ..., N$$

and

$$[3.11] \quad g(r) = \frac{\mu r}{2} + \frac{c_{N+1}}{r^2}$$

beyond the double layer. To determine the quantities μ and c_i in these expressions we must solve the problem for ϕ_i and g in the double layer and match the resulting formulae to the "outer forms" [3.10] and [3.11].

4. The Solution of the Equations for ϕ_i and g in the Double Layer

As we mentioned in the Introduction, the key to the solution of this problem lies in Dukhin's observation (5, 6) that the ions in the double layer are distributed according to the Boltzmann-type formula [1.2]. Comparing this formula with the expression [2.1] defining Φ_i, we see that

$$A_i = 1 - \exp\left(-\frac{z_i e \Phi_i}{kT}\right)$$

Replacing Φ_i in the exponent by the form [3.1] for a spherical particle and neglecting terms of order $(E)^2$ we find[3]

$$[4.1] \quad A_i = \frac{z_i e}{kT} \phi_i E \cos\theta$$

Since we are assuming that the quantity A_i is approximately constant over distances of order κ^{-1}, we may take ϕ_i to be approximately uniform over the double layer. Our analysis is based on this assumption.

By using simple order of magnitude estimates of the terms in the governing equations [3.4] and [3.5] for ϕ_i and g we may eliminate a number of terms from these equations. To begin with, consider the equation [3.5] for g in the double layer:

Let $\bar{g}$ denote the value of g at a distance of order κ^{-1} from the particle surface. Since g is zero at the surface (see [3.6]) g changes by an amount of order $\bar{g}$ over the double layer; hence the derivative dg/dr must rise to a value of order $\bar{g}\kappa$ in the double layer. Similarly d^2g/dr^2 is of order $\bar{g}\kappa^2$, and so on for higher derivatives. By comparing the magnitude of the various terms in eq. [3.5] and neglecting $O(1/\kappa a)$ terms we find that the equation reduces to

$$[4.2] \quad \frac{d^4g}{dx^4} = \frac{1}{\eta a} \sum_{i=1}^{N} z_i e \frac{dn_i^0}{dx} \phi_i$$

where $x = r - a$. This equation is only valid in the double layer, the relative error being of order $1/\kappa a$ in that region.

Integrating eq. [4.2] with respect to x, we obtain

$$[4.3] \quad \frac{d^3g}{dx^3} = \frac{1}{\eta a} \sum_{i=1}^{N} z_i e n_i^0(x) \phi_i + A$$

where A is a constant of integration.

To integrate eq. [4.3], we require expressions for the equilibrium ion densities $n_i^0(x)$. These quantities are related to the equilibrium potential $\psi^0(x)$ in the absence of the field by the Boltzmann formula:

[3]The assumed linear relation between particle velocity and applied field is only valid in the limit as $E \to 0$; hence we may neglect terms of $O(E^2)$ in the analysis.

Can. J. Chem. Downloaded from www.nrcresearchpress.com by 210.87.254.5 on 09/06/12
For personal use only.

$$[4.4] \quad n_i^0(x) = n_i(\infty) \exp\left(-\frac{z_i e\psi^0(x)}{kT}\right)$$

Neglecting terms of order $(\kappa a)^{-1}$ corresponds to treating the double layer as being locally flat, so that, for a symmetric electrolyte, the potential is given by (8):

$$[4.5] \quad \frac{ze\psi^0}{kT} = 2 \ln\left(\frac{1 + \alpha e^{-\kappa x}}{1 - \alpha e^{-\kappa x}}\right)$$

where

$$[4.6] \quad \alpha = \tanh\left(\frac{ze\zeta}{4kT}\right), \qquad \kappa^2 = \frac{8\pi e^2 z^2 n(\infty)}{\varepsilon kT}$$

and

$$z = z_1 = -z_2$$

Replacing $n_i^0(x)$ in [4.3] by the Boltzmann formula [4.4] and using the formula [4.5] for the potential we get

$$[4.7] \quad \frac{d^3g}{dx^3} = \frac{zen}{a\eta}\left\{\phi_1\left[\frac{1 - \alpha e^{-\kappa x}}{1 + \alpha e^{-\kappa x}}\right]^2 - \phi_2\left[\frac{1 + \alpha e^{-\kappa x}}{1 - \alpha e^{-\kappa x}}\right]^2\right\} + A$$

where

$$n = n_1(\infty) = n_2(\infty)$$

Integrating the expression [4.7] twice with respect to x and using the fact that dg/dx is zero on the particle surface $x = 0$ (see [3.6]) we obtain

$$[4.8] \quad \frac{dg}{dx} = \frac{\varepsilon kT}{2\pi a\eta ze}\left\{\phi_2 \ln\left(\frac{1 - \alpha e^{-\kappa x}}{1 - \alpha}\right) - \phi_1 \ln\left(\frac{1 + \alpha e^{-\kappa x}}{1 + \alpha}\right)\right\} + Ax^2 + Bx$$

where A and B are constants of integration.

From [4.8] we see that

$$[4.9] \quad \frac{dg}{dx} \approx \frac{\varepsilon kT}{2\pi a\eta ze}\{\phi_1 \ln(1 + \alpha) - \phi_2 \ln(1 - \alpha)\} + Ax^2 + Bx$$

at distances of more than a few double layer thicknesses from the surface. In this region the outer form [3.11] for g is also valid. On differentiating this formula and replacing r by $x + a$ we get

$$[4.10] \quad \frac{dg}{dx} = \frac{\mu}{2} - \frac{2c_3}{(a + x)^3} = \frac{\mu}{2} - \frac{2c_3}{a^3}\left(1 + O\left(\frac{1}{\kappa a}\right)\right)$$

Thus the "inner form" [4.9] for dg/dx approaches the constant value given by [4.10] as x increases, and hence A and B are approximately zero and

$$[4.11] \quad \frac{\mu}{2} - \frac{2c_3}{a^3} = \frac{\varepsilon kT}{2\pi a\eta ze}\{\phi_1 \ln(1 + \alpha) - \phi_2 \ln(1 - \alpha)\}$$

To determine μ and c_3 in terms of ϕ_1 and ϕ_2 we require another equation involving these quantities. It was noted earlier that the ratio $g(dg/dr)^{-1}$ is of order κ^{-1} in the double layer. This estimate is also valid just beyond the double layer where g is given by the outer form [3.11]. Hence, neglecting terms of order $(\kappa a)^{-1}$, we find that

$$c_3 = -a^3\mu/2$$

and thus the expression [4.11] reduces to:

$$\mu = \frac{\varepsilon kT}{3\pi a\eta ze}\{\phi_1 \ln(1 - \alpha) - \phi_2 \ln(1 + \alpha)\}$$

Can. J. Chem. Downloaded from www.nrcresearchpress.com by 210.87.254.5 on 09/06/12
For personal use only.

Can. J. Chem. Downloaded from www.nrcresearchpress.com by 210.87.254.5 on 09/06/12
For personal use only.

In terms of the non-dimensional mobility E_m, defined by

$$E_m = \frac{6\pi\eta e\mu}{\varepsilon kT}$$

this expression becomes

$$[4.12] \quad E_m = \frac{2}{za}\{\phi_1 \ln(1+\alpha) - \phi_2 \ln(1-\alpha)\}$$

To calculate E_m we must therefore determine the values of the functions ϕ_1 and ϕ_2 in the double layer. These quantities are obtained by solving eq. [3.4] in the double layer subject to the boundary condition [3.7] and matching the solution to the outer forms [3.10] for ϕ_i. To facilitate this matching we rewrite these outer forms as

$$\phi_i = \frac{3r}{2} - \frac{r}{2}\frac{d\phi_i}{dr}$$

obtained by differentiating [3.10] with respect to r and eliminating c_i. At a distance of a few double layer thicknesses from the particle surface the above expression takes the approximate form

$$[4.13] \quad \phi_i = \frac{3a}{2} - \frac{a}{2}\frac{d\phi_i}{dr}$$

By solving the equation [3.4] in the double layer we shall now obtain an expression for $d\phi_i/dr$ at a distance of a few double layer thicknesses from the surface. By substituting this expression for $d\phi_i/dr$ in [4.13] we will then obtain the values of ϕ_1 and ϕ_2, which appear in the formula [4.12] for E_m.

The term $a\,d\phi_i/dr$ in [4.13] is of order $\kappa a\delta\phi_i$, where $\delta\phi_i$ is the variation in ϕ_i over the double layer; although $\delta\phi_i$ is small the product $\kappa a\delta\phi_i$ may well be of order one since κa is large, and thus in order to determine the (approximately uniform) value of ϕ_i in the double layer using [4.13] we must now take into account the small variation in ϕ_i over the double layer. Since the term ϕ_i/r^2 in eq. [3.4] is approximately uniform over the double layer we may replace this equation by a simple first order differential equation for $d\phi_i/dx$, namely

$$[4.14] \quad \frac{d^2\phi_i}{dx^2} - \frac{z_i e}{kT}\frac{d\psi^0}{dx}\frac{d\phi_i}{dx} = \frac{2\phi_i}{a^2} - \frac{2\lambda_i}{akT}\frac{d\psi^0}{dx}g$$

where, as before, x denotes distance from the shear plane and we have dispensed with the small term $(2/r)(d\phi_i/dr)$.

Solving eq. [4.14] subject to the boundary condition [3.7], we obtain an expression for $d\phi_i/dx$ which at distances of more than a few double layer thicknesses from the particle surface reduces to:

$$[4.15] \quad \frac{d\phi_i}{dx} = \frac{2\phi_i}{a^2}\left[x + \int_0^\infty \left(\exp\left(-\frac{z_i e\psi^0}{kT}\right) - 1\right)dy\right] - \frac{2\lambda_i}{kT}\int_0^\infty g\exp\left(-\frac{z_i e\psi^0}{kT}\right)\frac{d\psi^0}{dy}dy$$

(The upper limits of integration have been extended to ∞ on the grounds that these integrals are dominated by the contributions from the double layer.)

Performing integration by parts on the second integral in [4.15] and using the expression [4.8] for dg/dx (with A and B set to zero), we find

$$[4.16] \quad \begin{cases} \dfrac{d\phi_1}{dx} = \dfrac{2\phi_1}{a}\left\{\dfrac{x}{a} - \dfrac{4\alpha}{\kappa a(1+\alpha)}\right\} - \dfrac{24m_1}{\kappa az^2}\left\{\dfrac{\phi_2}{2a}\ln(1-\alpha^2) - \dfrac{\phi_1}{a}\left[\ln(1+\alpha) - \dfrac{\alpha}{1+\alpha}\right]\right\} \\ \text{and} \\ \dfrac{d\phi_2}{dx} = \dfrac{2\phi_2}{a}\left\{\dfrac{x}{a} + \dfrac{4\alpha}{\kappa a(1-\alpha)}\right\} + \dfrac{24m_2}{\kappa az^2}\left\{\dfrac{\phi_2}{a}\left[\ln(1-\alpha) + \dfrac{\alpha}{1-\alpha}\right] - \dfrac{\phi_1}{2a}\ln(1-\alpha^2\right\} \end{cases}$$

where

$$m_i = \frac{\varepsilon kT\lambda_i}{6\pi\eta e^2}$$

is the usual non-dimensional ionic drag coefficient.

Can. J. Chem. Downloaded from www.nrcresearchpress.com by 210.87.254.5 on 09/06/12
For personal use only.

The formulae [4.16] and [4.13] (obtained from the outer form for ϕ_i) are valid at distances from the surface which are large compared to the double layer thickness but small compared to the particle radius. Replacing $d\phi_i/dr$ in [4.13] by the expressions [4.16] for $i = 1$ and 2 and neglecting terms of order $(\kappa a)^{-1}$, we obtain a pair of simultaneous linear equations for ϕ_1 and ϕ_2, viz.

$$[4.17]\quad \begin{cases} \phi_1 - \dfrac{6m_1\phi_2}{\kappa a z^2}\ln(1-\alpha) = \dfrac{3a}{2} \\ \text{and} \\ -\dfrac{6m_2}{\kappa a}\ln(1-\alpha)\phi_1 + \phi_2\left\{1 + \dfrac{4\alpha}{\kappa a(1-\alpha)} + \dfrac{12m_2}{\kappa a z^2}\left[\ln(1-\alpha) + \dfrac{\alpha}{1-\alpha}\right]\right\} = \dfrac{3a}{2} \end{cases}$$

The terms in these equations which have κa in the denominator are negligible unless α is close to unity, which means $\exp ze\zeta/kT$ must be large, in which case [4.6] becomes:

$$[4.18]\quad \alpha \approx 1 - 2\exp\left(\frac{-ze\zeta}{2kT}\right)$$

We may then replace α in these equations by the approximate expression [4.18] for *all* values of ζ. The solution of the equations for ϕ_1 and ϕ_2 is then found by straightforward elimination to be

$$[4.19]\quad \phi_1 = \frac{3a}{2} \qquad \text{and} \qquad \phi_2 = \frac{3a}{2}\left[1 + \frac{2\exp\left(\dfrac{ze\zeta}{2kT}\right)}{\kappa a}\left(1 + 3\frac{m_2}{z^2}\right)\right]^{-1}$$

Thus the function ϕ_1 has the value $3a/2$ in the double layer for all ζ while ϕ_2 decreases monotonically to zero from $3a/2$ as ζ increases. The reason for the decrease in ϕ_2 is that at large values of $\exp ze\zeta/kT$ the density of counterions in the double layer is so great that the flux of ions around the surface due to tangential gradients in Φ_2 will be very large unless the gradient of Φ_2 is itself small; such large fluxes could not be balanced by the flow of ions from beyond the double layer and thus the tangential gradient of Φ_2 around the surface approaches zero as ζ increases. Thus Φ_2 becomes uniform over the surface, and from [3.1] it follows that ϕ_2 approaches zero at the surface as ζ increases.

The required formula for the mobility is obtained by substituting the formulae [4.19] for ϕ_1 and ϕ_2 in the expression [4.12] for E_m, which becomes, after some simple manipulations

$$[4.20]\quad E_m = \frac{3}{2}\frac{e\zeta}{kT} - \frac{\left[3\dfrac{e\zeta}{kT} - \dfrac{6\ln 2}{z}\left\{1 - \exp\left(-\dfrac{ze\zeta}{kT}\right)\right\}\right]}{\left\{2 + \left[\kappa a \exp\left(-\dfrac{ze\zeta}{2kT}\right)\right] \Big/ (1 + 3m_2/z^2)\right\}}$$

In deriving this expression we have used the formula

$$\ln\left[\frac{1+\alpha}{1-\alpha}\right] = \frac{ze\zeta}{2kT}$$

obtained by putting $x = 0$ in the expression [4.5] for ψ^0, and we have simplified the numerator of the second term of the right hand side of [4.20] by neglecting terms of order $(\kappa a)^{-1}$.

5. Comparison with Dukhin's Result

The relation derived by Dukhin (4) reads:[4]

$$[5.1]\quad E_m = \frac{3}{2}\frac{e\zeta}{kT} - 6\left\{\frac{\tilde{\zeta}M\sinh^2 Z + [2z^{-1}\sinh 2Z - 3m\tilde{\zeta}]\ln\cosh Z}{\kappa a + 8M\sinh^2 Z - (24m/z^2)\ln\cosh Z}\right\}$$

[4]Note that the term z^{-1} in the numerator of [5.1] is in-correctly rendered as z in ref. 4, p. 307.

Can. J. Chem. Downloaded from www.nrcresearchpress.com by 210.87.254.5 on 09/06/12
For personal use only.

TABLE 1. Comparison of computer solution of mobility equations (2) with eqs. [4.20] and [5.1]. The table shows values of E_m (= 7520 μ for μ in $cm^2\ V^{-1}\ s^{-1}$) for KCl solutions (with m = 0.184) for various values of $\tilde{\zeta} = \zeta$ (mV)/25.7 at 298 K

	E_m				
$\tilde{\zeta}$	Computer	Eq. [4.20]	% error	Eq. [5.1]	% error
$\kappa a = 150$					
9.9997	5.2194	5.2532	+0.6	5.1845	−0.7
6.8705	7.1103	7.0875	−0.3	7.1394	+0.4
5.6589	6.8490	6.8232	−0.4	6.9070	+0.8
4.8761	6.3229	6.3083	−0.2	6.3932	1.1
4.2880	5.7764	5.7744	−0.03	5.8514	1.3
3.8109	5.2577	5.2666	+0.2	5.3333	1.4
3.4054	4.7747	4.7921	+0.4	4.8485	1.5
3.0497	4.3253	4.3494	+0.6	4.3960	1.6
2.7303	3.9054	3.9341	+0.7	3.9720	1.7
2.4385	3.5105	3.5426	+0.9	3.5725	1.8
$\kappa a = 100$					
10.000	4.3574	4.3837	+0.6	4.2862	−1.6
5.6640	6.3045	6.2788	−0.4	6.3557	+0.8
4.2927	5.5166	5.5184	−0.03	5.6104	1.7
3.4096	4.6335	4.6618	+0.6	4.7352	2.2
2.7340	3.8200	3.8668	1.2	3.9184	2.6
2.1712	3.0849	3.1377	1.7	3.1699	2.8
1.6776	2.4077	2.4611	2.2	2.4778	2.9
1.2267	1.7722	1.8200	2.7	1.8254	3.0
0.8036	1.1657	1.2029	3.2	1.2013	3.1
0.3980	0.5785	0.6001	3.7	0.5965	3.1
$\kappa a = 50$					
9.9995	3.3835	3.3446	−1.1	3.2074	−5.2
6.8894	4.9304	4.8807	−1.0	4.7948	−2.7
5.6790	5.2567	5.1984	−1.1	5.2056	−1.0
4.8960	5.1815	5.1373	−0.9	5.1994	0.3
4.3070	4.9455	4.9241	−0.4	5.0124	1.4
3.8289	4.6417	4.6442	+0.05	4.7411	2.1
3.4224	4.3105	4.3351	+0.6	4.4301	2.8
3.0655	3.9709	4.0141	1.1	4.1015	3.3
2.7451	3.6320	3.6904	1.6	3.7669	3.7
2.4521	3.2979	3.3677	2.1	3.4321	4.1
$\kappa a = 30$					
9.9993	2.9788	2.8695	−3.7	2.7124	−8.9
6.9078	4.1057	4.0165	−2.2	3.8356	−6.6
5.6987	4.4866	4.3954	−2.0	4.2997	−4.2
4.9153	4.5426	4.4682	−1.6	4.4490	−2.1
4.3256	4.4334	4.3872	−1.0	4.4212	−0.3
3.8466	4.2356	4.2216	−0.3	4.2876	+1.3
3.4390	3.9892	4.0068	+0.4	4.0889	+2.5
3.0811	3.7164	3.7627	+1.2	3.8494	3.6
2.7595	3.4301	3.5007	2.1	3.5842	4.5
2.4653	3.1375	3.2277	2.9	3.3029	5.3

where $\tilde{\zeta} = e\zeta/kT$, $Z = z\tilde{\zeta}/4$, and $M = 1 + 3m/z^2$. Values of E_m calculated from this relation as a function of $\tilde{\zeta}$ are shown in Fig. 1 for various (large) values of κa and for $m_1 = m_2 = m = 0.184$, an appropriate figure for KCl as electrolyte. The agreement with the computer calculation of O'Brien and White (2) is excellent, especially at the higher κa values.

Equation [5.1] may be reduced to eq. [4.20] by eliminating terms of order $(1/\kappa a)$. Rather surprisingly, a comparison of eq. [4.20] with [5.1] shows that in most cases formulation [4.20] is closer to the computer result. Table 1 shows this comparison for $z = 1$ and $m = 0.184$ whilst Table 2 shows it for $z = 2$ and $\lambda_{\pm}^{0} = 60$ ohm^{-1} cm^2 equiv.$^{-1}$ (i.e. $m_{\pm} = 0.4287$). Only at $z = 2$ and very low values of the ζ-potential is the more elaborate relation [5.1] superior and under these conditions it can be

TABLE 2. Comparison of exact computer solution of mobility equations (2) with eqs. [4.20] and [5.1] for $z_\pm = 2$ and $\Lambda_\pm^0 = 60$ ohm^{-1} cm^2 equiv.$^{-1}$ ($m_\pm = 0.4287$)

	E_m				
$\tilde{\zeta}$	Computer	Eq. [4.20]	% error	Eq. [5.1]	% error
$\kappa a = 150$					
0.1335	0.1965	0.2011	2.3	0.2002	+1.9
0.4054	0.5956	0.6073	2.0	0.6072	+1.9
0.6929	1.0143	1.0305	1.6	1.0346	+2.0
1.0107	1.4698	1.4877	1.2	1.5001	+2.1
1.3841	1.9875	2.0038	0.8	2.0306	+2.2
2.1879	2.9742	2.9756	0.05	3.0450	+2.4
3.3266	3.7150	3.6893	−0.7	3.8053	+2.4
6.4102	1.7909	1.7718	−1.1	1.8026	+0.6
$\kappa a = 100$					
0.1335	0.1947	0.2016	3.5	0.2002	+2.9
0.4054	0.5897	0.6069	2.9	0.6067	+2.9
0.6927	1.0026	1.0261	2.3	1.0320	+2.9
1.0103	1.4484	1.4740	1.8	1.4918	+3.0
1.3830	1.9471	1.9696	1.2	2.0075	+3.1
1.8635	2.5250	2.5360	0.4	2.6060	+3.2
2.1834	2.8475	2.8478	0.01	2.9397	+3.2
3.3073	3.3504	3.3165	−1.0	3.4437	+2.8
6.0117	1.7457	1.7165	−1.7	1.7552	+0.5
$\kappa a = 50$					
0.1335	0.1899	0.2028	6.8	0.2002	+5.4
0.4053	0.5740	0.6057	5.5	0.6052	5.4
0.6923	0.9715	1.0138	4.4	1.0244	5.5
1.0091	1.3919	1.4361	3.2	1.4677	5.5
1.3798	1.8438	1.8795	1.9	1.9432	5.4
1.8555	2.3244	2.3363	0.5	2.4443	5.2
2.1702	2.5572	2.5498	−0.3	2.6821	4.9
3.2529	2.7168	2.6608	−2.1	2.8085	3.4
5.3391	1.6784	1.6198	−3.5	1.6751	−0.2

replaced by the Smoluchowski equation with no loss of accuracy.

6. Discussion

It is clear that eq. [4.20] is a very considerable improvement on the Smoluchowski formula for large κa and that it is a useful approximation formula even at modest values of κa, below those at which its assumptions could be expected to remain strictly valid. This is not an uncommon occurrence in colloid science where the many assumptions and idealisations which are forced on the theoretical analysis are often mutually compensating to some extent.

The result obtained in this case is of some consequence on two counts. Firstly, it provides valuable confirmation of the validity of the notion of the "polarised double layer" as used by Dukhin and co-workers. Although Semenikhin and Dukhin (9) make a passing reference to a comparison of their analytical approach with results obtained by computer analysis, this is the first detailed comparison to be published. Apart from the electrophoresis problem this concept can be applied to a variety of other problems to generate approximate analytical solutions which should be useful for systems with thin double layers.

Secondly, it provides a very practical alternative to the use of the complete computer solution for calculating the mobility/ζ relation for particles with thin double layers. Although the O'Brien and White (2) computer solution is a significant improvement over its predecessor (10) it requires access to a fairly sophisticated computer and the expenditure of significant computation time. Not only does eq. [4.20] provide a reliable alternative in appropriate cases, but Tables 1 and 2 give an estimate of the likely correction which should be applied. It is also worth noting that the computer comparison referred to above (9) was not to eq. [5.1] but to a much more elaborate set of equations which are claimed to be valid for lower values of κa. The great merit of eq. [4.20] is, of course, its relative simplicity.

7. Summary

An analysis of the "polarised double layer" reveals that a very simple analytical approximation

Can. J. Chem. Downloaded from www.nrcresearchpress.com by 210.87.254.5 on 09/06/12
For personal use only.

formula can be derived to correct the Smoluchowski equation for the electrophoretic mobility of a large spherical particle with a thin double layer. The equation is a simplification of the earlier result of Dukhin and is in excellent agreement with detailed computer calculations for $\kappa a \geq 150$; even at $\kappa a \approx 30$, the error is tolerable and could easily be allowed for, most values of the ζ-potential.

Acknowledgements

We thank Dr. Lee White of the Australian National University and Colin N. Bensley of the University of Sydney for running the computer calculations for $z = 1$ and $z = 2$ respectively.

1. J. TH. G. OVERBEEK. *In* Colloid science. Vol. 1. *Edited by* H. R. Kruyt. Elsevier, Amsterdam. 1952. p. 202.
2. R. W. O'BRIEN and L. R. WHITE. J. Chem. Soc. Faraday II, **74**, 1607 (1978).
3. S. S. DUKHIN. *In* Research in surface forces. Vol. 2. *Edited by* B. V. Deryaguin. Consultants Bureau, New York. 1966. p. 54.
4. S. S. DUKHIN and B. V. DERYAGUIN. *In* Surface and colloid science, Vol. 7. *Edited by* E. Matijevic. John Wiley, New York. 1974.
5. S. S. DUKHIN. *In* Research in surface forces. Vol. 3. *Edited by* B. V. Deryaguin. Consultants Bureau, New York. 1966. p. 287.
6. S. S. DUKHIN and V. N. SHILOV. Colloid J. USSR, **31**, 564 (1969).
7. S. LEVINE and R. N. O'BRIEN. J. Colloid Interface Sci. **43**, 616 (1973).
8. E. J. W. VERWEY and J. TH. G. OVERBEEK. Theory of stability of lyophobic colloids. Elsevier, Amsterdam. 1948. p. 27.
9. N. M. SEMENIKHIN and S. S. DUKHIN. Colloid J. USSR, **37**, 1017 (1975).
10. P. H. WIERSEMA, A. L. LOEB, and J. TH. G. OVERBEEK. J. Colloid Interface Sci. **22**, 78 (1966).

Can. J. Chem. Downloaded from www.nrcresearchpress.com by 210.87.254.5 on 09/06/12
For personal use only.

Forces between dissimilar colloidal plates for various surface conditions. II. Equilibrium adsorption effects[1]

G. M. BELL

Mathematics Department, Chelsea College (University of London), Manresa Road, London, SW3 6LX, England

AND

G. C. PETERSON

Unilever Research, Port Sunlight Laboratory, Quarry Road East, Bebington, Wirral, Merseyside, L63 3JW, England

Received July 7, 1980

This paper is dedicated to Dr. Sam Levine on the occasion of his 70th birthday

G. M. BELL and G. C. PETERSON. Can. J. Chem. **59**, 1888 (1981).

A method previously developed by the authors is used to study the effects of adsorption of ions on the electric double layer interaction between dissimilar colloidal plates immersed in 1:1 electrolyte. For adsorption models which permit the total charge on a plate to change sign, the double layer force remains finite at all plate separations, including zero. For weak adsorption of the ions on the plates the force between two dissimilar plates tends to be repulsive at small separations, looking rather like a weakened constant surface charge density model. Conversely for strong ionic adsorption the force tends to be attractive at small separations, rather as in the constant surface potential model. In this paper we discuss three adsorption models: (*1*) fixed primary charge density on the plates with secondary adsorption of both counter-ions and co-ions; (*2*) fixed primary charge density on the plates with secondary adsorption of the counter-ions only, but including the effects of a Stern layer and self-atmosphere potentials; (*3*) zero primary charge on both plates with equilibrium adsorption of both anions and cations from solution, the net charge density on the plates arising from differential adsorption of the ion types.

G. M. BELL et G. C. PETERSON. Can. J. Chem. **59**, 1888 (1981).

On utilise une méthode que l'on a mise au point antérieurement pour étudier les effets d'adsorption d'ions sur l'interaction électrique de la double couche entre des plaques colloidales dissemblables immergées dans un électrolyte de type 1:1. Dans le cas des modèles d'adsorption qui permettent à la charge totale sur une plaque de changer de signe, la force de la double couche demeure finie pour toutes les séparations de plaque, y compris zéro. Pour l'adsorption faible d'ions sur les plaques, la force entre deux plaques dissemblables tend à être répulsive pour de petites séparations et se comporte comme un modèle de densité de charge superficielle constante faible. Dans le cas d'une adsorption ionique forte, la force devient au contraire attractive pour de petites séparations et elle se comporte plutôt comme un modèle de potentiel superficiel constant. Dans cet article nous discutons de trois modèles: (*1*) un modèle de densité de charge primaire fixe sur les plaques avec une adsorption secondaire à la fois des ions opposés et des co-ions; (*2*) un modèle de densité de charge primaire fixe sur les plaques avec seulement une adsorption secondaire des ions opposés mais incluant les effets d'une couche de Stern et des potentiels d'auto-atmosphère; (*3*) un modèle de charge primaire égale à zéro sur les deux plaques avec une adsorption équilibrée des anions et des cations à partir de la solution; la densité de charge nette sur les plaques provient d'une adsorption différentielle des deux types d'ions.

[Traduit par le journal]

1. Introduction

We consider the electrical double-layer forces between dissimilar parallel plates, the left and right hand plates being labelled 1 and 2 respectively. The term "dissimilar" means here that when the width H of the diffuse region between the plates is infinite the reduced potential $\Phi_{1\infty}$ at the diffuse region boundary adjacent to plate 1 is unequal to the corresponding potential $\Phi_{2\infty}$ at plate 2. It has often been assumed that the plate potentials Φ_1 and Φ_2 remain equal to $\Phi_{1\infty}$ and $\Phi_{2\infty}$ for all values of H. However the "constant potential" assumption implies that the electrical force approaches an infinite attractive value as $H \to 0$, except when $\Phi_{1\infty} = \Phi_{2\infty}$. This occurs because the electric field and hence the Maxwell tension term in the force must become indefinitely large if Φ_1 and Φ_2 remain unequal as $H \to 0$. An alternative assumption that the plate charge densities, σ_1 and σ_2 respectively, remain constant implies that the electrical force approaches an infinite repulsive value as $H \to 0$, except when $\sigma_1 = -\sigma_2$. This happens because the total charge in the diffuse region per unit plate area is $-(\sigma_1 + \sigma_2)$ and hence if the latter remains non-zero as $H \to 0$ the ionic concentrations in the diffuse region and the osmotic term in the force become infinitely large. Double layer models are hardly realistic for very small H since, for instance, real ions have a finite size. Nevertheless an indefinite increase in force is unphysical and it seems likely that some mechanism operates to moderate the force by reduc-

[1]The authors much appreciate being able to participate in this issue in honour of Dr. Sam Levine's devoted work and many important contributions to theoretical chemistry. G.M.B. has had the privilege of collaboration with him over many years and would like to express his grateful thanks.

0008-4042/81/131888-10$01.00/0

©1981 National Research Council of Canada/Conseil national de recherches du Canada

Can. J. Chem. Downloaded from www.nrcresearchpress.com by 210.87.254.5 on 09/06/12
For personal use only.

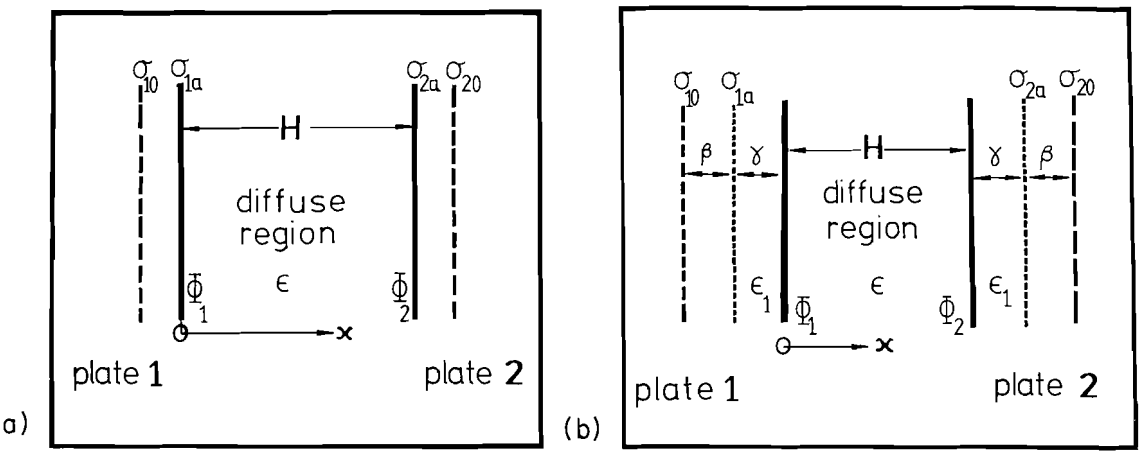

FIG. 1. Surface charges and diffuse layer.

ing the magnitude of the double-layer free energy. One possible mechanism is equilibrium specific adsorption of ions from the diffuse layer onto a plane at or near the diffuse layer boundary. In this paper we shall use several models to study the effect of such adsorption. For definiteness and comparability we fix the values of $\Phi_{1\infty}$ and $\Phi_{2\infty}$ in most of our illustrations of the theory at 2 and ± 0.8 respectively. The methods used here were developed in Bell and Peterson (1), which will henceforth be referred to as I, where they were applied mainly to plates with unequal constant charge densities.

Interactions between similar plates with a fixed primary charge and equilibrium adsorption of counter-ions were first considered by Bierman (2) and then by Levine and Bell (3, 4) and Melville and Smith (5). Models of this type are considered in § 3 and § 4 below. Stern layer and self-atmosphere effects are discussed in § 4. Melville and Smith (5) also considered the assumption that the potential stays constant at the plane of primary charge rather than the diffuse region boundary. Chan *et al.* discussed the interaction between similar (6) and dissimilar (7) "amphoteric" surfaces in which all surface ions are in equilibrium with the medium by way of association–dissociation reactions and gave a comprehensive survey of possible cases. The model we introduce in § 5 yields a similar adsorption isotherm to theirs and we discuss its relation to the results deriving from the other models.

2. Definitions and Method

We define a reduced (dimensionless) potential ϕ and distance ξ by

[1] $\phi = e_0\psi/kT \qquad \xi = \kappa x$

Here ψ is the potential in V, e_0 is the proton charge, k Boltzmann's constant, T the absolute temperature, κ the Debye–Hückel constant for the bulk electrolyte while the x-coordinate is perpendicular to the plates (see Fig. 1). We assume throughout that the electrolyte is of the 1–1 type and the Poisson–Boltzmann equation for the diffuse region can then be expressed as

[2] $d^2\phi/d\xi^2 = \sinh \phi$

A first integral of [2] can be immediately obtained and expressed in the physically perspicuous form

[3] $\mathscr{F}^+ = \cosh \phi - 1 - \frac{1}{2}(d\phi/d\xi)^2$

Here $\mathscr{F}^+$ is the reduced force per unit plate area defined for a 1–1 electrolyte by

[4] $\mathscr{F}^+ = \mathscr{F}/(2nkT)$

$\mathscr{F}$ being the electrical double-layer force per unit area and n the number of ions of each type per unit volume in the bulk electrolyte medium. In [3] the term $\cosh \phi - 1$ represents the repulsive osmotic pressure term in the force while $-\frac{1}{2}(d\phi/d\xi)^2$ represents the attractive Maxwell tension term. Equation [3] can also be expressed as

[5] $d\phi/d\xi = \pm g(\phi)$

where

[6] $g(\phi) = (2 \cosh \phi - 2 - 2\mathscr{F}^+)^{1/2} > 0$

To obtain the diffuse layer width H a second integration is necessary. This yields the relations

[7] $\kappa H = \left| \int_{\Phi_1}^{\Phi_2} \frac{d\phi}{g(\phi)} \right|$

Can. J. Chem. Downloaded from www.nrcresearchpress.com by 210.87.254.5 on 09/06/12
For personal use only.

$$[8] \quad \kappa H = \left| \int_{\phi_m}^{\Phi_1} \frac{d\phi}{g(\phi)} \right| + \left| \int_{\phi_m}^{\Phi_2} \frac{d\phi}{g(\phi)} \right|$$

The form [8] is to be used when the curve of ϕ against ξ has a turning point between the plates, the value of ϕ at the turning point being denoted by ϕ_m. This can only occur when $\mathscr{F}^+ > 0$. For $\mathscr{F}^+ < 0$ and when $\mathscr{F}^+ > 0$ but there is no turning point the alternative form [7] must be used. The reduced width κH can be obtained in terms of elliptic integrals, different formulas being necessary for different conditions. These are given in forms suitable for the dissimilar plate problem in the Appendix to I. However the results given in the present paper were all obtained by numerical integration.

We now consider conditions on the plates. It is assumed that the plate surface charge densities σ_1 and σ_2 are functions of the diffuse layer boundary potentials Φ_1 and Φ_2 respectively. Reduced densities f_1 and f_2 are defined by the relations

$$[9] \quad f_1(\Phi_1) = \frac{e_0}{\varepsilon \kappa k T} \sigma_1, \qquad f_2(\Phi_2) = \frac{e_0}{\varepsilon \kappa k T} \sigma_2$$

where ε denotes the dielectric permittivity of the diffuse layer aqueous medium and is assumed to be uniform. Bearing in mind that the left and right hand plates are labelled 1 and 2 respectively the electrostatic boundary conditions can now be written in dimensionless form as

$$[10] \quad (d\phi/d\xi)_1 = -f_1(\Phi_1) \qquad (d\phi/d\xi)_2 = f_2(\Phi_2)$$

For any given $\mathscr{F}^+$ the possible values of the boundary potentials can be obtained by combining [5] with [10] to yield

$$[11] \quad f_1(\Phi_1) = \pm g(\Phi_1) \qquad f_2(\Phi_2) = \pm g(\Phi_2)$$

At $\kappa H = \infty$ the signs are unambiguous since $(d\phi/d\xi)_2$ and Φ_2 have the same sign while $(d\phi/d\xi)_1$ and Φ_1 have opposite signs. Hence putting $\mathscr{F}^+ = 0$ in [11] we obtain

$$[12] \quad \begin{aligned} 2 \sinh (\Phi_{1\infty}/2) &= f_1(\Phi_{1\infty}) \\ 2 \sinh (\Phi_{2\infty}/2) &= f_2(\Phi_{2\infty}) \end{aligned}$$

It can be assumed without loss of generality that

$$\Phi_{1\infty} > 0 \qquad \Phi_{1\infty} \geq |\Phi_{2\infty}|$$

For definiteness we shall in most of our calculations adjust the parameters in f_1 and f_2 to make [12] yield $\Phi_{1\infty} = 2$, $\Phi_{2\infty} = \pm 0.8$.

In order to obtain force–separation curves we thus have to solve the non-linear differential equation [2] and, for adsorption models, the boundary conditions [10] are also nonlinear. For each case we have to pick the correct signs in [11] and, if $\mathscr{F}^+ > 0$, decide between [7] and [8]. This can be done during the whole process of taking the plates from infinite to zero separation with the aid of a graph of the type introduced in I, in which the ordinate is $-d\phi/d\xi$ and the abscissa is ϕ. It should be stressed that the aim of this graphical method is to give a general picture of the behaviour of the plate potentials and the electrical force $\mathscr{F}^+$ during this process and is not intended as a substitute for accurate calculation. Indeed either numerical techniques or tables are always essential to evaluate the integrals [7] or [8]. In this method it is necessary to plot the curves of $f_1(\phi)$ and $-f_2(\phi)$, which by [10] give the values of $-d\phi/d\xi$ at the diffuse region boundaries, against ϕ. These are termed "plate curves" and if they intersect this corresponds to a solution of the equation

$$[13] \quad f_1(\Phi_0) + f_2(\Phi_0) = 0$$

and gives the potential $\Phi_1 = \Phi_2 = \Phi_0$ in the mathematical limiting case of zero separation $\kappa H = 0$. Since it corresponds to finite values of the boundary potential and the electrical field at zero separation the existence of a solution to [13] is necessary if the force is to have a finite limit. If the charge densities on both plates are positive at $\kappa H = \infty$ then a solution of [13] implies that either (*i*) f_1 or f_2 changes sign during the approach of the plates or (*ii*) $f_1(\Phi_0) = f_2(\Phi_0) = 0$. Condition (*ii*) must occur for symmetrical plates since $f_1(\Phi_0)$ is then equal to $f_2(\Phi_0)$. However if $f_i(\phi)$ is a continuous monotonic function of ϕ then $f_i(\Phi_0) = 0$ implies that $f_i(\phi)$ changes sign at $\phi = \Phi_0$. The only other possibility for a continuous function is that $f_i(\phi)$ has both a zero and a turning point at $\phi = \Phi_0$ but this is unlikely for any physically reasonable isotherm. Hence for a solution of [13] to exist for all initial values $\Phi_{1\infty}$ and $\Phi_{2\infty}$ it must be possible to change the sign of the charge on at least one plate by an appropriate change of the potential at the diffuse layer boundary adjacent to the plate. This places some restriction on the type of adsorption model which will give a finite force at $\kappa H = 0$. If it is assumed that the primary ions are all of the same sign and that the number of adsorption sites is equal to the number of primary ions then the plate charge density cannot change sign under any circumstances. This implies that the limiting force is infinite even in the case of similar plates.

The other element of the graphical method is to draw isodynamic slope curves which are plots of $\pm g(\phi)$ against ϕ for fixed $\mathscr{F}^+$. By [5], these show the variation of reduced electric field $-d\phi/d\xi$ with reduced potential ϕ in the medium. By [11], the intersections of the plate and isodynamic slope curves give the possible values of the boundary potential for

Can. J. Chem. Downloaded from www.nrcresearchpress.com by 210.87.254.5 on 09/06/12
For personal use only.

Can. J. Chem. Downloaded from www.nrcresearchpress.com by 210.87.254.5 on 09/06/12
For personal use only.

given $\mathscr{F}^+$. The segment of an isodynamic slope curve between its intersections with two plate curves represents the behaviour of the reduced field $-d\phi/d\xi$ and the reduced potential ϕ between the two plates at the given $\mathscr{F}^+$ value. The most important isodynamic slope curves are those for $\mathscr{F}^+ = 0$ which, by [6], are in fact plots of $\pm 2 \sinh(\phi/2)$ against ϕ. These are the only isodynamic slope curves which pass through the origin and they divide the plane into regions of positive and negative $\mathscr{F}^+$ (see Figs. 2, 6, 8, and 10). The two regions containing the ϕ-axis correspond to positive $\mathscr{F}^+$ while the two containing the $-d\phi/d\xi$ axis correspond to negative $\mathscr{F}^+$. By [12] the intersection of an f_1 plate curve with the $2 \sinh \phi/2$ plot gives the potential $\Phi_{1\infty}$ at $\kappa H = \infty$ and that of a $-f_2$ plate curve with the $-2 \sinh \phi/2$ plot gives $\Phi_{2\infty}$. The general behaviour of $\mathscr{F}^+$ can be deduced from the regions through which the plate curves pass from the $\kappa H = \infty$ points to the intersection corresponding to $\kappa H = 0$. Generally this can be seen most easily from the curve for the plate with the lowest potential at infinity. Examples will be found in subsequent sections while I may be consulted for further details.

An alternative graphical approach of Chan *et al.* (7) depends on the square of the charge density function. We believe our method to be better than that of Chan *et al.* since by using σ rather than σ^2 as ordinate the plate curves assume a simpler form and the signs of the plate charges are clearly displayed. The simultaneous states of the two plate surfaces can be seen for any $\mathscr{F}^+$ value by using the appropriate isodynamic slope curve and it is easy to deduce the succession of $\mathscr{F}^+$ values and plate states between infinite and zero separation.

3. Constant Primary Charge with Adsorption

We assume that a plate surface carries a fixed charge density σ_0 of primary ions and a charge σ_a of ions adsorbed from the 1–1 electrolyte onto an adsorption plane coincident with the diffuse layer boundary or outer Helmholtz plane (see Fig. 1*a*). Each unit area of surface carries ν_+ and ν_- positive and negative adsorbed ions respectively randomly distributed over N_s adsorption sites (Langmuir isotherm). The adsorbed ions remain in equilibrium with the electrolyte medium for all plate separations and the equilibrium equations can be written

$$[14] \quad \ln \nu_+/(N_s - \nu_+ - \nu_-) + \Phi = \ln C_+$$

$$[15] \quad \ln \nu_-/(N_s - \nu_+ - \nu_-) - \Phi = \ln C_-$$

Here Φ denotes the diffuse-layer boundary potential while $\ln C_+$ and $\ln C_-$ are constants which include the chemical free energy of adsorption and the bulk electrolyte chemical potential, divided by kT. It can be shown from [14] and [15] that the adsorbed charge density is given by

$$[16] \quad \sigma_a = e_0(\nu_+ - \nu_-) = e_0 N_s \frac{C_+ e^{-\Phi} - C_- e^{\Phi}}{1 + C_+ e^{-\Phi} + C_- e^{\Phi}}$$

In this section we now specialise to the case $C_+ = C_- = C$ which means that co-ions are not hindered chemically from adsorption although they are less favoured than counter-ions by the electrical potential, at least at large plate separations where Φ has the same sign as the charge on the primary ions. Equation [16] now becomes

$$[17] \quad \sigma_a = 2e_0 N_s C \sinh \Phi/(1 + 2C \cosh \Phi)$$

It is convenient to introduce a primary charge parameter q defined by

$$[18] \quad \sigma_0 = e_0 N_s q$$

The sign of q is that of the primary charge while the magnitude $|q|$ is the number of primary ions per adsorption site. The value $|q| = 1$ means that there is one adsorption site per primary charge. Since $|\sigma_a| < N_s e_0$ for all finite positive or negative values of Φ it follows that the resultant charge density $\sigma_0 + \sigma_a$ cannot change sign. Hence, as remarked in § 2 above, it is necessary that the number of adsorption sites exceed the number of primary ions if the limiting force $\mathscr{F}^+$ at $H = 0$ is to remain finite, which implies $|q| < 1$.

We now reintroduce the labels 1 and 2 to distinguish the two plates. It will be assumed that the adsorption constant C and the density of adsorption sites N_s are the same for the two plates but that the primary charges are unequal. Combining [9] with [17] and [18] the following relations for the reduced plate charge densities f_1 and f_2 are obtained:

$$[19] \quad \begin{aligned} f_1(\Phi_1) &= \lambda\left(q_1 - \frac{2C \sinh \Phi_1}{1 + 2C \cosh \Phi_1}\right) \\ f_2(\Phi_2) &= \lambda\left(q_2 - \frac{2C \sinh \Phi_2}{1 + 2C \cosh \Phi_2}\right) \end{aligned}$$

where $\lambda = e_0^2 N_s/(\kappa \varepsilon kT)$ is a dimensionless constant. We now consider a specific example by supposing that the bulk medium contains 0.1 mol L^{-1} of electrolyte and that there are 10^{19} adsorption sites per square metre (i.e. the area per adsorption site is 10 Å^2) which gives $\lambda = 86.2$ at 25°C. (The same value of λ would correspond to a bulk electrolyte concentration of 0.01 mol L^{-1} if the area per adsorption site were changed to 31.6 Å^2.) Taking the adsorption constant C as 0.01 we use [12] to adjust the primary charge parameters q_1 and q_2 to give $\Phi_{1\infty} = 2$, $\Phi_{2\infty} = \pm 0.8$. This

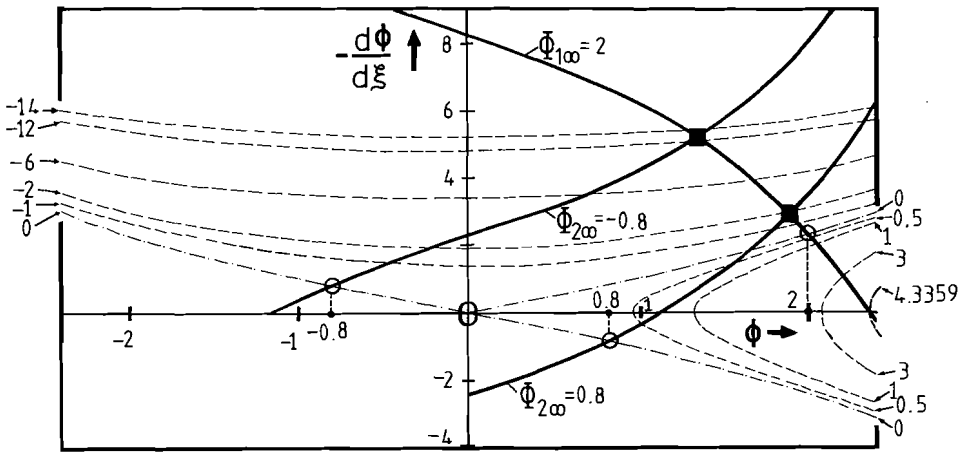

FIG. 2. Isodynamic slope diagram for primary charge with adsorbed counter-ions and co-ions. The plate curves are shown as full lines and the constant force curves as broken lines labelled with the force values. The points representing the plates at $\kappa H = \infty$ are circled while the points representing them at $\kappa H = 0$ are indicated by squares. Parameter values are $\lambda = 86.2$, $C = 0.01$ while for $\Phi_{1\infty} = 2$ the primary charge parameter $q_1 = 0.09473$ and for $\Phi_{2\infty} = \pm 0.8$, $q_2 = \pm 0.02683$.

corresponds to one primary ion per 105.6 Å^2 on plate 1 and one per 372.7 Å^2 on plate 2. Figure 2 is the isodynamic slope diagram for the plate interactions with these parameter values. For the (+ve,+ve) interaction the general force behaviour can be seen by following the segment of the $\Phi_{2\infty} = 0.8$ plate curve which starts at the $\kappa H = \infty$ point (i.e. its intersection with the $-2\sinh(\phi/2)$, $\mathscr{F}^+ = 0$, curve) and ends at the $\kappa H = 0$ point (i.e. its intersection with the $\Phi_{1\infty} = 2$ plate curve). Initially the plate point is in the positive $\mathscr{F}^+$ region. Then, after passing through a maximum $\mathscr{F}^+$ value between 0.5 and 1, it crosses into the negative region to reach the intersection with the $\Phi_{1\infty} = 2$ plate curve. Thus the force is positive (repulsive) at large κH but, after reaching a maximum, it becomes negative (attractive) at small κH. The force/distance curve itself, labelled "adsorbed charge", is shown in Fig. 3. For the (+ve,−ve) plate interaction the relevant segments of the $\Phi_{2\infty} = -0.8$ and the $\Phi_{1\infty} = 2$ plate curves can be seen in Fig. 2 to lie entirely in the negative $\mathscr{F}^+$ region. The force/distance curve is shown in Fig. 4.

In Figs. 3 and 4 the force/distance curves for the present model are compared with those calculated on the assumptions of constant potential and constant total plate charge respectively for the same values of $\Phi_{1\infty}$ and $\Phi_{2\infty}$. The "adsorbed charge" curves go to finite $\mathscr{F}^+$ values as κH decreases to zero while the "constant potential" and "constant charge" curves go to infinity. At non-zero κH values, the "constant potential" behaviour is qualitatively closer to that of the present model than is the "constant charge" behaviour. However, the behaviour of the force at small κH is highly sensitive to the parameter values

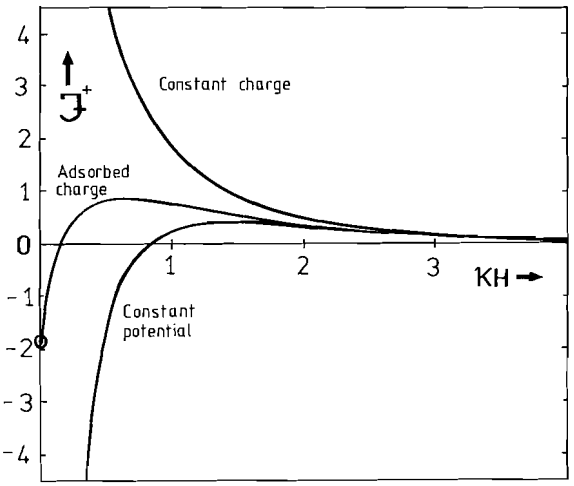

FIG. 3. Force/separation plots for $\Phi_{1\infty} = 2, \Phi_{2\infty} = 0.8$. The curve labelled "adsorbed charge" corresponds to the model of Fig. 2 and is compared with curves calculated on the constant potential and constant plate charge assumptions.

assumed in the model. This can be seen from Fig. 5 where the limiting value $\mathscr{F}_0{}^+$ of the force as $\kappa H \rightarrow 0$ is plotted against the logarithm of the adsorption constant C. The primary charge densities are kept constant on each curve at the values used in the previous calculations, which give $\Phi_{1\infty} = 2$, $\Phi_{2\infty} = \pm 0.8$ at $C = 0.01$. The labels (+ve,+ve) and (+ve,−ve) refer to the signs of the potentials and plate charges at large κH. For small values of C, the limiting force $\mathscr{F}_0{}^+$ is positive whatever the sign of the force at large κH. As $C \rightarrow 0$ ($\log_{10} C \rightarrow -\infty$) $\mathscr{F}_0{}^+$ rapidly approaches infinity. Physically this means that for very weak adsorption the behaviour is similar to that found with constant total plate

Can. J. Chem. Downloaded from www.nrcresearchpress.com by 210.87.254.5 on 09/06/12
For personal use only.

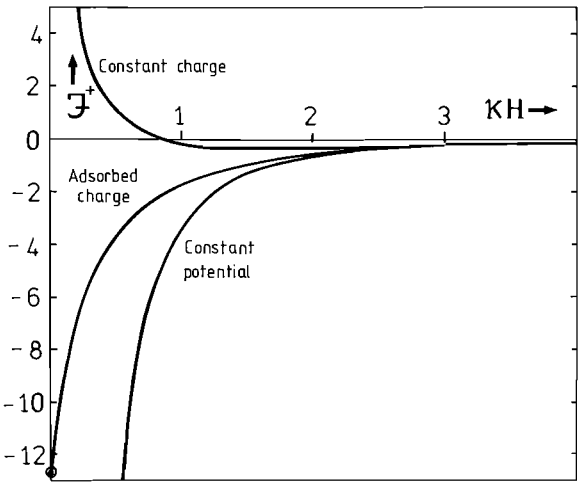

FIG. 4. As Fig. 3 for $\Phi_{1\infty} = 2, \Phi_{2\infty} = -0.8$.

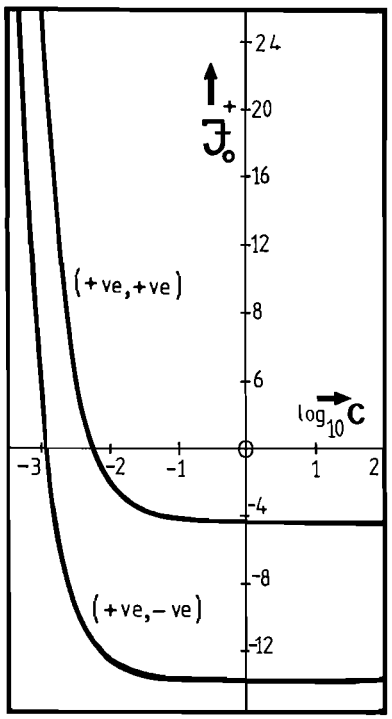

FIG. 5. Primary charge with adsorbed counter-ions and co-ions. Primary charge parameters $q_1 = 0.09473$, $q_2 = \pm 0.02683$. The limiting force $\mathscr{F}_0^+$ at $\kappa H = 0$ is plotted against the logarithm of the adsorption parameter.

charges. As C increases $\mathscr{F}_0^+$ becomes negative on both curves, which is the situation illustrated in Figs. 2, 3, and 4. For $C > 0.1$, $\mathscr{F}_0^+$ is nearly constant on both curves. It is noteworthy that even for very large C the "constant potential" situation of infinite attractive limiting force is not approached. There is a small intermediate range of C ($-2.992 < \log_{10} C < -2.204$) where the sign of $\mathscr{F}_0^+$ is the same as that of $\mathscr{F}^+$ at large separations for both the (+ve,+ve) and the (+ve,−ve) cases.

4. Counter-ion Adsorption: Stern Layer and Self-atmosphere Effects

Our main aim in this section is to investigate how Stern layer and self-atmosphere contributions to the potential at an adsorbed ion affect the inter-plate electrical force. However, we first consider a modification to the model of the last section which consists in assuming that only ions of opposite sign to the primary ions can be adsorbed. We must thus put $C_+ = 0$ in eq. [16] for the adsorbed charge density if the primary charge is positive and $C_- = 0$ if it is negative. Introducing indices 1 and 2 to distinguish the plates and taking q_1 as always positive, the reduced charge densities f_1 and f_2 are given by

$$f_1(\Phi_1) = \lambda\left[q_1 - \frac{C_{1-}\exp(\Phi_1)}{1 + C_{1-}\exp(\Phi_1)}\right]$$

$$[20]\quad f_2(\Phi_2) = \lambda\left[q_2 - \frac{C_{2-}\exp(\Phi_2)}{1 + C_{2-}\exp(\Phi_2)}\right] \quad q_2 > 0$$

$$f_2(\Phi_2) = \lambda\left[q_2 + \frac{C_{2+}\exp(-\Phi_2)}{1 + C_{2+}\exp(-\Phi_2)}\right]$$

$$q_2 < 0$$

It has been assumed that the adsorption site density is the same for both plates and that λ is defined as in § 3.

We now consider a specific example. We take $\lambda = 43.1$, corresponding to an area 20 Å^2 per adsorption site if the bulk electrolyte is 0.1 normal and for simplicity put $C_{1-} = C_{2-} = C_{2+} = C$, giving these adsorption constants the common value of 10^{-3}. As before, the primary charge parameters are adjusted to make $\Phi_{1\infty} = 2$, $\Phi_{2\infty} = \pm 0.8$. In the isodynamic slope diagram (Fig. 6) the plate curve intersection points both lie in the $\mathscr{F}^+ > 0$ region and the relevant segment of the $\Phi_{2\infty} = 0.8$ plate curve lies entirely in this region. On the other hand the corresponding segment of the $\Phi_{2\infty} = -0.8$ curve passes from the $\mathscr{F}^+ < 0$ region to the $\mathscr{F}^+ > 0$ region. Thus in the force/distance plots shown in Fig. 7, $\mathscr{F}^+$ is monotonic for the (+ve,+ve) case but passes through a minimum, changes sign and becomes positive at small κH for the (+ve,−ve) case.

We now suppose that the plane of adsorbed charge is separated by a distance γ from the diffuse layer boundary and that the region between these two planes has a dielectric permittivity ε_1 which is less than ε (see Fig. 1*b*). This region is known as the

Can. J. Chem. Downloaded from www.nrcresearchpress.com by 210.87.254.5 on 09/06/12
For personal use only.

Can. J. Chem. Downloaded from www.nrcresearchpress.com by 210.87.254.5 on 09/06/12
For personal use only.

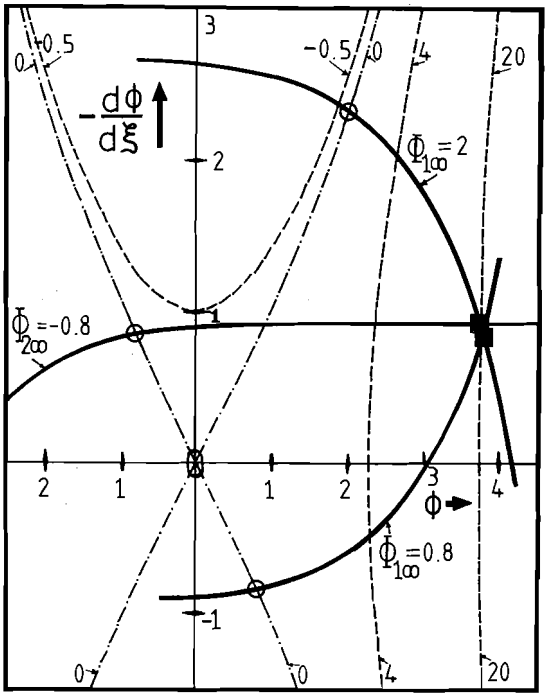

FIG. 6. Primary charge with adsorbed counter-ions. As Fig. 2. Parameter values are $\lambda = 43.1$, $C = 10^{-3}$ while for $\Phi_{1\infty} = 2, q_1 = 0.06189$ and for $\Phi_{2\infty} = \pm 0.8, q_2 = \pm 0.02188$.

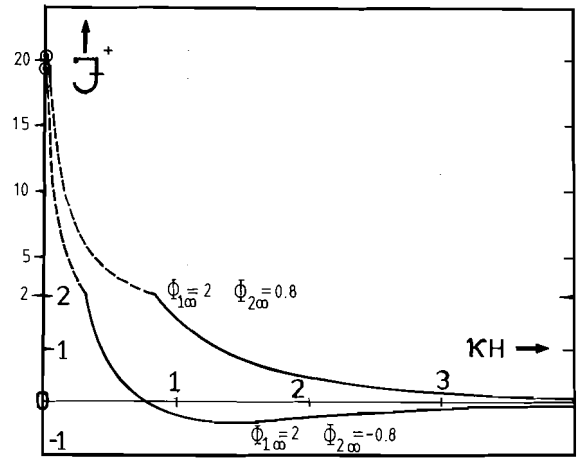

FIG. 7. Force/separation plots for model and parameter values of Fig. 6. Note change of scale at $\mathcal{F}^+ = 2$. Curves for $\mathcal{F}^+ > 2$ are shown as broken lines.

Stern layer and its introduction is intended to allow for finite ion size and decreased polarisability near the plate surface. The potential at the adsorption plane is denoted by Φ_γ and is related to the potential Φ at the diffuse layer boundary by

$$[21] \quad \Phi_\gamma = \Phi + \frac{e_0\gamma}{kT\varepsilon_1}(\sigma_0 + \sigma_a)$$

In a comprehensive theory allowance must be made for the "self-atmosphere" which each adsorbed ion creates by repelling other adsorbed ions and modifying the diffuse layer charge in its vicinity. Hence to obtain the potential at an adsorbed ion charge a self-atmosphere term $\Phi_{s.a.}$ must be added to the adsorption plane mean potential. We shall use a simple expression obtained by Levine *et al.* (8) and used in refs. 3 and 4, which is

$$[22] \quad \Phi_{s.a.} = -\frac{\beta\gamma g}{\varepsilon_1 d}\frac{e_0}{kT}\sigma_a$$

where β is the depth of the layer of permittivity ε_1 behind the adsorption plane (see Fig. 1*b*), $d = \beta + \gamma$ and g is a positive parameter depending on β, γ, the electrolyte concentration and the permittivities. Combining [21] with [22],

$$[23] \quad \Phi_\gamma + \Phi_{s.a.} = \Phi + \frac{e_0\gamma}{kT\varepsilon_1}\left\{\sigma_0 + \left(1 - \frac{\beta g}{d}\right)\sigma_a\right\}$$

It can be seen that the σ_a terms in the Stern layer effect and the self-atmosphere effect tend to cancel out. There is some simplification if $\varepsilon/\varepsilon_1$ and the electrolyte concentration are large enough for the diffuse layer boundary to act as a perfect conductor in relation to the inner layer and if the effective adsorption plane self-atmosphere radius is considerably larger than γ and β. Then $g = 1$ if the plate is metallic while if, on the other hand, it is of low dielectric permittivity and adsorbed ion image effects in the plate are neglected we can put $\beta g/d = 1$ (8). We shall make the latter assumption and then, using eq. [18] for the primary charge density parameter q, eq. [23] becomes

$$[24] \quad \Phi_\gamma + \Phi_{s.a.} = \Phi + \lambda\frac{\varepsilon}{\varepsilon_1}\kappa\gamma q$$

More refined theories of the self-atmosphere effect have been developed (9, 10) but their incorporation in the present formalism would be difficult.

We now introduce a specific example. Putting $\kappa\gamma = 0.2$ and $\varepsilon/\varepsilon_1 = 5$ we replace Φ_1 and Φ_2 in eq. [20] by $\Phi_1 + \lambda q_1$ and $\Phi_2 + \lambda q_2$ respectively. We take $\lambda = 43.1$ as before but modify C to 10^{-4} and adjust q_1 and q_2 to make $\Phi_{1\infty} = 2$ and $\Phi_{2\infty} = \pm 0.8$. Figure 8 is the isodynamic slope diagram for this case and it can be seen that the plate curve intersections are in the $\mathcal{F}^+ > 0$ region, just as they were before Stern and self-atmosphere effects were introduced into the adsorbed counter-ion model. One interesting feature is that for the (+ve,+ve) interaction it is the charge on the plate originally at the higher potential ($\Phi_{1\infty} = 2$) which changes sign. However, this makes little difference to the force/distance curves shown in Fig. 9 which are very

Can. J. Chem. Downloaded from www.nrcresearchpress.com by 210.87.254.5 on 09/06/12
For personal use only.

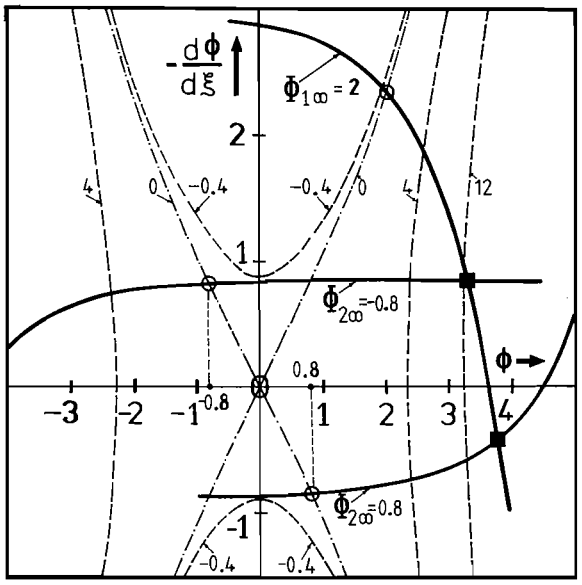

FIG. 8. Primary charge with adsorbed counter-ions: Stern layer and self-atmosphere effects incorporated. As Fig. 2. Parameter values are $\lambda = 43.1$, $C = 10^{-4}$ while for $\Phi_{1\infty} = 2$, $q_1 = 0.06847$ and for $\Phi_{2\infty} = \pm 0.8$, $q_2 = \pm 0.01958$.

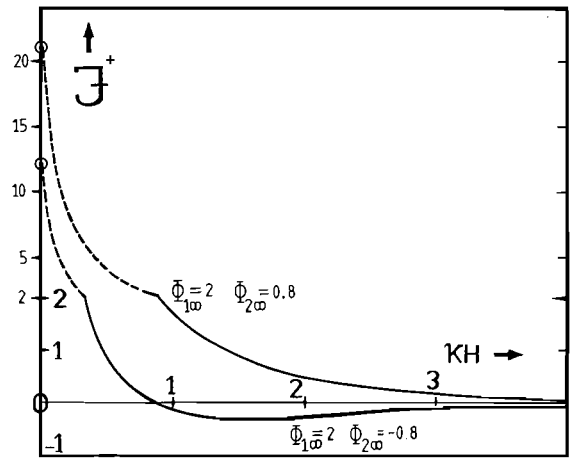

FIG. 9. Force/separation plots for model and parameter values of Fig. 8. Change of scale as on Fig. 7.

similar to those of Fig. 7. However, it should be noted that the adsorption constant C has been reduced by a factor of 10. This indicates that the main effect of introducing the Stern and self-atmosphere potentials is to produce similar behaviour with a smaller adsorption constant. In other words, they increase the effective adsorption strength for counter-ions.

5. Complete Adsorption Equilibrium

The theory of § 3 is now modified in another way. We assume that there is no fixed primary charge and that all the plate charge is adsorbed from the electrolyte medium and in equilibrium with it. Equation [16] now gives the total plate charge density and it follows that

$$f_1(\Phi_1) = \lambda \frac{C_{1+}\exp(-\Phi_1) - C_{1-}\exp(\Phi_1)}{1 + C_{1+}\exp(-\Phi_1) + C_{1-}\exp(\Phi_1)}$$

$$f_2(\Phi_2) = \lambda \frac{C_{2+}\exp(-\Phi_2) - C_{2-}\exp(\Phi_2)}{1 + C_{2+}\exp(-\Phi_2) + C_{2-}\exp(\Phi_2)} \quad [25]$$

For positive potentials at infinite separation

$$C_{1+} > C_{1-}\exp(2\Phi_{1\infty})$$

$$C_{2+} > C_{2-}\exp(2\Phi_{2\infty})$$

while if the potential $\Phi_{2\infty}$ is negative

$$C_{2-} > C_{2+}\exp 2|\Phi_{2\infty}|$$

In a specific example we put the larger adsorption constants equal to 0.3 and adjust the others till, again, $\Phi_{1\infty} = 2$, $\Phi_{2\infty} = \pm 0.8$. Figure 10 is the isodynamic slope diagram and it can be seen that as in the "strong adsorption" example given in § 3 above, the plate curve intersections are both in the $\mathcal{F}^+ < 0$ region. However, as would be expected, the range of variation of the plate charge densities is much larger, especially in the (+ve,−ve) interaction. The corresponding force/distance curves are given in Fig. 11 and resemble those given for the adsorbed charge model in Figs. 3 and 4 except that the limiting force magnitudes at $\kappa H = 0$ are much larger, due to the greater variation of plate charge.

A similar form of charge density function to [25] was derived by Chan *et al.* (6, 7) from association/dissociation surface equilibria. However, it may be noted that mathematically [25] is not as different as it first appears to be from the charge density function [19] based on constant primary charge plus equilibrium adsorbed charge. Both are monotonically decreasing functions of the diffuse layer boundary potential. Also, after some manipulation, $f_1(\Phi_1)$ as given by [25] can be transformed to

$$f_1(\Phi_1) = \frac{\lambda}{1 + C_{1+} + C_{1-}} \times \left\{ C_{1+} - C_{1-} - 2\sinh\frac{\Phi_1}{2} \frac{C_{1-}(1 + 2C_{1+})\exp(\tfrac{1}{2}\Phi_1) + C_{1+}(1 + 2C_{1-})\exp(-\tfrac{1}{2}\Phi_1)}{1 + C_{1+}\exp(-\Phi_1) + C_{1-}\exp(\Phi_1} \right\} \quad [26]$$

Can. J. Chem. Downloaded from www.nrcresearchpress.com by 210.87.254.5 on 09/06/12
For personal use only.

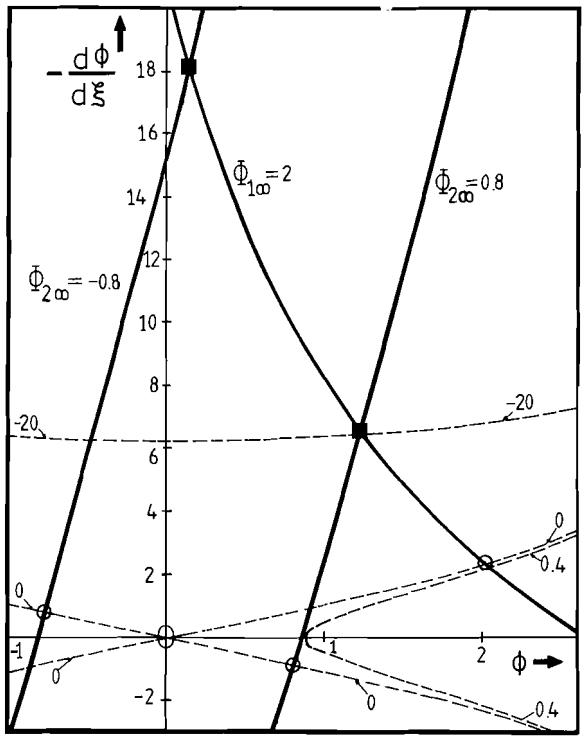

FIG. 10. Equilibrium adsorption of all plate charge. As Fig. 2. Parameter values are $\lambda = 86.2$ and for $\Phi_{1\infty} = 2$, $C_+ = 0.3$, $C_- = 0.001611$; for $\Phi_{2\infty} = 0.8$, $C_+ = 0.3$, $C_- = 0.05518$; for $\Phi_{2\infty} = -0.8$, $C_+ = 0.05518$, $C_- = 0.3$.

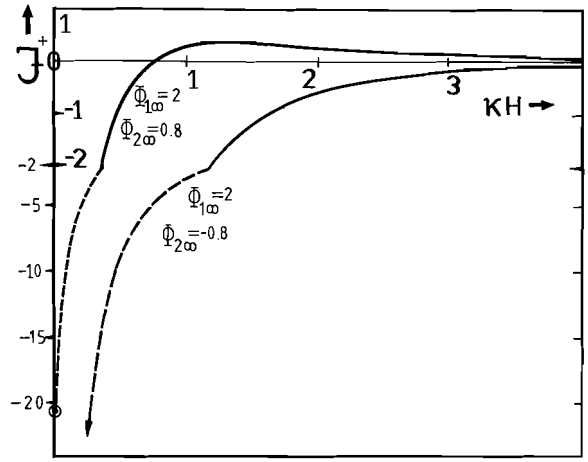

FIG. 11. Force/separation plots for model and parameter values of Fig. 10. Change of scale as in Fig. 7. The $\Phi_{1\infty} = 2$, $\Phi_{2\infty} = -0.8$ plot goes to a limiting value $\mathscr{F}^+ = -161.5$ as $\kappa H \to 0$.

and similarly, of course for $f_2(\Phi_2)$. Thus, as in the model of § 3 above, the charge density can be expressed as a constant term minus an increasing function of the diffuse region boundary potential Φ_1 which becomes zero at $\Phi_1 = 0$.

6. Discussion

The electrical forces between two parallel plates in a 1–1 electrolyte have been investigated for several adsorption models in cases where the plate potentials at large separation differ considerably in magnitude. Some attention has been given to the limiting value of the electrical force as the width of the diffuse layer between the plates approaches zero. Although the models treated can hardly be regarded as realistic at "zero separation" this attention is justified for two reasons. One is that the existence of a finite value for the force limit affords a test of the physical reasonableness of the model and the other is that the sign of the force limit provides valuable evidence for the behaviour of the force at non-zero separations. It has been found that at small κH all the adsorption mechanisms treated reduce the interaction free energy magnitude sufficiently to give a finite force limit. An essential condition is that it should be possible for the plate charge to change sign for a sufficiently large change of potential.

The behaviour of the electrical force at medium and small separations depends quite sensitively on the details of the model and the parameter values. There is some interaction between the two and it is found, for instance, that in the adsorbed counter-ion model the incorporation of Stern and self-atmosphere potentials has the same effect as decreasing the free energy of adsorption. Two main patterns of force behaviour have emerged for the dissimilar plates studied here. In what may be termed the "weak adsorption" situation there is no change in the sign of the force when it is repulsive at large separations and its magnitude increases steadily as the separation decreases. On the other hand, when the force is attractive at large separations it passes through a turning point and then changes sign to become repulsive at small separations. In the "strong adsorption" situation the opposite occurs. The force which is repulsive at large separations passes through a turning point and then becomes attractive at small separations while the originally attractive force remains attractive at all separations. There can be an intermediate adsorption parameter range where neither the originally repulsive nor the originally attractive force changes sign but in the case considered here this range is small. It might be larger if the ratio between the potentials at infinity were nearer to 1. We have not attempted here to incorporate the dispersive forces which are necessary for a consideration of colloidal stability. However in the "strong adsorption" case it seems unlikely that there is an effective energy barrier to the approach of two particles.

1. G. M. BELL and G. C. PETERSON. J. Colloid Inter. Sci. **60**, 376 (1977).
2. A. BIERMAN. J. Colloid Sci. **10**, 231 (1955).
3. S. LEVINE and G. M. BELL. J. Colloid Sci. **17**, 838 (1962).
4. S. LEVINE and G. M. BELL. J. Phys. Chem. **67**, 1408 (1963).
5. J. B. MELVILLE and A. L. SMITH. J. Chem. Soc. Faraday Trans. I, **70**, 1551 (1974).
6. D. CHAN, J. W. PERRAM, L. R. WHITE, and T. W. HEALY. J. Chem. Soc. Faraday Trans. I, **71**, 1046 (1975).
7. D. CHAN, T. W. HEALY, and L. R. WHITE. J. Chem. Soc. Faraday Trans. I, **72**, 2844 (1976).
8. S. LEVINE, G. M. BELL, and D. CALVERT. Can. J. Chem. **40**, 518 (1962).
9. S. LEVINE, K. ROBINSON, G. M. BELL, and J. MINGINS. J. Electroanal. Chem. **38**, 253 (1972).
10. S. LEVINE and K. ROBINSON. J. Electroanal. Chem. **41**, 159 (1973).

Can. J. Chem. Downloaded from www.nrcresearchpress.com by 210.87.254.5 on 09/06/12
For personal use only.

The contribution to the capacity of an electrode from a species adsorbed with partial charge transfer[1]

ROGER PARSONS

Laboratoire d'Electrochimie Interfaciale du C.N.R.S., 1, Place Aristide Briand, 92190 Meudon, France

Received July 7, 1980

This paper is dedicated to Dr. Sam Levine on the occasion of his 70th brithday

ROGER PARSONS. Can. J. Chem. **59**, 1898 (1981).

The effect of partial charge transfer on the observed capacity of an electrode adsorbing a species from solution is discussed in a general way for the condition of constant fraction of charge transferred. It is confirmed that the width of the peaks is primarily determined by the interaction between adsorbed species. A simple model in which the degree of charge transfer changes rapidly with electrode potential is suggested. This may account for some of the sharp peaks observed experimentally.

ROGER PARSONS. Can. J. Chem. **59**, 1898 (1981).

On présente une discussion générale de l'effet du transfert partiel de charge sur la capacité observée pour une électrode adsorbant une espèce de la solution lorsque la fraction de charge transférée est constante. On confirme que la largeur des pics est déterminée premièrement par l'interaction entre les espèces adsorbées. On suggère un modèle simple dans lequel le taux de transfert de charge change rapidement avec le potentiel d'électrode. Ce modèle pourrait expliquer les quelques pics fins observés expérimentalement.
[Traduit par le journal]

Can. J. Chem. Downloaded from www.nrcresearchpress.com by 210.87.254.40 on 09/06/12
For personal use only.

1. Introduction

Since Lorenz (1) introduced the concept of partial charge transfer into the consideration of adsorption and kinetics at electrodes, there has been a great deal of discussion of the effect of this possibility on the observed behaviour. Rather little has been said directly about the effect on capacity measurements and this paper is an attempt to treat this problem in a fairly general way. Since this work was first presented Conway and Angerstein-Kozlowska (2) have discussed interaction effects in adsorbed layers from this point of view and their work partially overlaps with the work presented here.

2. The Electrode Capacity

The observed charge dq which flows into unit area of an electrode interphase for a given change of potential dE may be regarded as the sum of dσ, the physical charge on the metal and the charge required in partial neutralisation of the adsorbed species λedΓ, where Γ is the surface excess of the species adsorbed (it is assumed that only one species undergoes charge transfer with the electrode), λ is the (fractional) number of electrons transferred to the electrode per ion adsorbed, and e is the unit charge. That is

$$[1] \quad dq = d\sigma + \lambda e d\Gamma$$

Hence the observed capacity is

$$[2] \quad C = \left(\frac{\partial q}{\partial E}\right)_\mu = \left(\frac{\partial \sigma}{\partial E}\right)_\mu + \lambda e \left(\frac{\partial \Gamma}{\partial E}\right)_\mu$$

which may be considered as a parallel combination of two capacities. Such a division is of course subject to the uncertainty in the determination of λ.

The first component $(\partial\sigma/\partial E)_\mu$ will be called the double layer capacity and can be analysed in a familiar way (3) by writing the potential across the inner layer (ϕ^{M-2}) as a function of the electrode charge and the charge on the specifically adsorbed ions (σ^1)

$$[3] \quad d\Phi^{M-2} = \left(\frac{\partial \Phi^{M-2}}{\partial \sigma}\right)_{\sigma^1} d\sigma + \left(\frac{\partial \Phi^{M-2}}{\partial \sigma^1}\right)_\sigma d\sigma^1$$

Note that σ and σ^1 are the charges supposed to be actually present in the double layer. These may be written

$$[4] \quad \sigma = q - \lambda e \Gamma$$

following [1] and

$$[5] \quad \sigma' = (z + \lambda) e \Gamma$$

where ze is the charge on the adsorbing ion when it is in the bulk solution.

Hence in the limit $\lambda \to -z$ (complete charge transfer) $\sigma^1 \to 0$ and the double layer capacity is simply

$$[6] \quad C^i = {}_\sigma C^i = \left(\frac{\partial \sigma}{\partial \phi^{M-2}}\right)_\mu = \left(\frac{\partial (q - ze\Gamma)}{\partial \phi^{M-2}}\right)_\mu$$

This is in parallel with the adsorption capacity.

In the opposite limit when $\lambda = 0$ only the double

[1]The main part of this article was presented at a Dechema Symposium in Tutzing, Germany, on February 13, 1979.

0008-4042/81/131898-05$01.00/0

©1981 National Research Council of Canada/Conseil national de recherches du Canada

Can. J. Chem. Downloaded from www.nrcresearchpress.com by 210.87.254.40 on 09/06/12
For personal use only.

layer capacity exists and it has the well-known form (3).

For any value of λ, eqs. [2] and [3] may be combined, taking account of [4] and [5], to obtain

$$[7]\quad \left(C - \lambda e \frac{d\Gamma}{dE}\right)^{-1} = {}_{\sigma}C^{-1} + {}_{\sigma^1}C^{-1}(z + \lambda)e \frac{d\Gamma}{d(q - \lambda e\Gamma)}$$

$$= {}_{\sigma}C^{-1} + {}_{\sigma^1}C^{-1}(z + \lambda)e \left[\frac{dq}{d\Gamma} - \lambda e\right]^{-1}$$

$$[8]\quad = {}_{\sigma}C^{-1} + {}_{\sigma^1}C^{-1}\left[\frac{1}{(z + \lambda)e}\frac{dq}{d\Gamma} - \frac{\lambda}{z + \lambda}\right]^{-1}$$

Hence we can calculate the observed capacity C from a model which gives the geometric capacities ${}_{\sigma}C$ and ${}_{\sigma^1}C$, as well as λ, and Γ as a function of E (or q). This last relation is of course dependent on the adsorption isotherm.

3. The Adsorption Isotherm

The equilibrium condition for adsorption may be written (cf. ref. 4)

$$[9]\quad \tilde{\mu}^{soln} = \tilde{\mu}^{ads} + \lambda\tilde{\mu}_e{}^M$$

where $\tilde{\mu}^{soln}$ and $\tilde{\mu}^{ads}$ are the electrochemical potentials of the adsorbing species in the solution and adsorbed states respectively and $\tilde{\mu}_e{}^M$ is the electrochemical potential of electrons in the metal electrode. This equilibrium condition may be expanded in terms of local electrical potentials and local concentrations to obtain

$$\mu^{0,s} + ze\phi + kT\ln a_s = \mu^{0,a} + (z + \lambda)e\phi_1 + kT\ln f(\Gamma) + \lambda\mu_e{}^M - \lambda e\phi^M$$

or

$$[10]\quad kT\ln\{a_s/f(\Gamma)\} = \Delta G^{\theta} + ze(\phi_1 - \phi) - \lambda e(\phi^M - \phi_1)$$

where

$$\Delta G^{\theta} = \mu^{0,a} + \lambda\mu_e{}^M - \mu^{0,s}$$

is the standard Gibbs energy of adsorption and $f(\Gamma)$ is a function of the amount adsorbed deriving from the configuration of the monolayer and its short range interactions.

Vetter and Schultze (4) assumed that ϕ_1 was related to the total potential drop across the inner region of the double layer (ϕ^{M-2}) by a geometric factor g. They also included an energy due to the replacement of solvent dipoles by adsorbate dipoles. We neglect the latter for simplicity and use a method for the calculation of ϕ_1 which allows for the discreteness of charge effect [3].

$$[11]\quad \phi_1 - \phi = g\frac{\sigma}{{}_{\sigma}K} + \frac{h\sigma^1}{{}_{\sigma^1}K}$$

Here, we have neglected the difference between ϕ_2 and ϕ, the potential of the solution; g is the geometric factor $(x_2 - x_1)/x_2$ equal to that of Vetter and Schultze, with x_1 the distance of the charge centers of the adsorbed ion from the metal surface and x_2 the thickness of the inner region. The first term in [11] represents the constant field due to the smeared-out charge σ (a uniform permittivity being assumed), h is a factor, previously called $\gamma/(\beta + \gamma)$ which represents the distribution of the part of the potential due to the adsorbed charge. In the low density limit, $h \to g$ as originally shown by Ershler (5). In the high density limit or if the charge σ^1 is regarded as a uniformly smeared-out charge, $h \to 1$.

The integral capacity of the whole double layer K is defined as

$$[12]\quad K = \sigma/(\phi^M - \phi)$$

that is, it is the integral capacity related to the differential capacity which is the reciprocal of the right-hand side of [7]. Thus, from [11] and [12]

$$[13]\quad \phi_1 - \phi = g\frac{K}{\sigma K}(\phi^M - \phi) + \frac{h\sigma^1}{{}_{\sigma^1}K}$$

and obviously

$$[14]\quad \phi^M - \phi_1 = (1 - g)\frac{K}{\sigma K}(\phi^M - \phi) + (1 - h)\frac{\sigma^1}{{}_{\sigma^1}K}$$

Consequently eq. [10] may be written

$$[15]\quad kT\ln\frac{a_s}{f(\Gamma)} = \Delta G^{\theta} + e(\phi^M - \phi)[gz - \lambda(1 - g)]\frac{K}{{}_{\sigma}K} + \frac{e\sigma^1}{{}_{\sigma^1}K}[zh - \lambda(1 - h)]$$

In the limit of complete charge transfer $\sigma^1 \to 0$, [15] becomes

$$[16]\quad kT\ln\frac{a_s}{f(\Gamma)} = \Delta G^{\theta} + ze(\phi^M - \phi)$$

since it follows from [8] that $K/{}_{\sigma}K \to 1$. Equation [16]

Can. J. Chem. Downloaded from www.nrcresearchpress.com by 210.87.254.40 on 09/06/12
For personal use only.

is the form used by Conway and Gileadi (6) and later by Bewick and Thomas (7) with

$$[17] \quad f(\Gamma) = \frac{\theta}{1-\theta}\exp A\theta$$

where $\theta = \Gamma/\Gamma_m$ and Γ_m is the maximum coverage.

On the other hand, in the limit of zero charge transfer ($\lambda \to 0$) eq. [15] becomes

$$[18] \quad RT \ln \frac{a_s}{f(\Gamma)} = \Delta G^\theta + egz\frac{K}{{}_\sigma K}(\phi^M - \phi) + \frac{zhF\sigma_1}{{}_{\sigma^1}K}$$

This is the same form as used by Parry and Parsons (3) with the second term on the right-hand side, expressed in terms of σ, giving the linear dependence of the standard Gibbs energy of adsorption on charge and the third term on the right-hand side giving the ionic interaction energy. Note that, in fact, this term adds to the interaction energy $A\theta$ of the uncharged species in [17]; the latter may be regarded as the short range contribution and may well be attractive.

4. The Origin of Large Capacity Peaks

If we consider the general equation [7] it is evident that large variations in the magnitude of the capacity can arise from the change in the amount adsorbed with potential or charge, that is from the magnitude of the term $\partial\Gamma/\partial E$, for example. It is evident from eq. [18] that variations in this term can arise as a result of the variations in the second or third terms on the right-hand side.

We consider the second term in its form with charge replacing potential i.e. $e[gz - \lambda(1-g)]\sigma$. It is evident from this that no large change in capacity can arise from this term when charge transfer occurs since the term in square brackets changes from gz to z as λ varies from 0 to $-z$. This is normally a change by a factor of 2 or so.

Consequently it must be concluded that the principal cause of the change in magnitude of the capacity must arise from the third term, that is the interaction term. If we add the interaction term from [17] to that in [18], we may write a general form of interaction term

$$[19] \quad A'\theta = A''\Gamma = \{(AkT/\Gamma_m) + (e/{}_{\sigma^1}K) \times [zh - \lambda(1-h)](z+\lambda)\}\lambda$$

Since the electrostatic (long range) interactions are included in the second part of the coefficient A'', the first part AkT/Γ_m is likely to be small and A may well be negative having a value around the critical value of -4. It is interesting to see whether the electrostatic contribution to [19] has a value large in comparison with this. When $\lambda = 0$ the quantity to be compared with A is $zhe\,\sigma^1{}_m/{}_{\sigma^1}KkT$. For a univalent ion with $h = \frac{1}{2}$, ${\sigma_m}^1 = 100\ \mu C\ cm^{-2}$ and ${}_{\sigma^1}K = 100\ \mu F\ cm^{-2}$ this term amounts to about 20. Consequently the repulsion is strong and the peaks are broad and low. For less highly charged ions (i.e. ones which have undergone partial charge transfer) the repulsion decreases and the peaks become higher and narrow. This is probably the strongest argument that submonolayer deposits of metals consist essentially of neutral atoms, as pointed out by Conway *et al.* (8). The consequences of this change in interaction parameter have been explored in detail (2).

Here we may simply note that with the definition [19] of the interaction coefficient and the allowance for adsorption of particles of a different size from the solvent they replace, we may write the adsorption isotherm in the forms:

$$[20] \quad \ln \theta(1-\theta)^{-r} + A'\theta = \ln a_s - \frac{\Delta G^0}{RT} - \frac{e}{{}_\sigma KkT}[gz - \lambda(1-g)]\sigma$$

$$[21] \quad = \ln a_s - \frac{\Delta G^0}{RT} - \frac{eK}{{}_\sigma KkT}[gz - \lambda(1-g)]\phi^{M-2}$$

$$[22] \quad = \ln \beta a_s$$

where one adsorbing particle replaces r solvent molecules.

Hence we may derive the coefficients:

$$[23] \quad \left(\frac{\partial \ln \beta}{\partial\theta}\right)_{a_s,\sigma} = \frac{1}{\theta} + \frac{r}{1-\theta} + A'$$

$$[24] \quad \left(\frac{\partial \ln \beta}{\partial\sigma}\right)_{a_s} = \frac{e}{{}_\sigma KkT}[gz - \lambda(1-g)]$$

$$[25] \quad \left(\frac{\partial \ln \beta}{\partial\phi^{M-2}}\right)_{a_s} = \frac{eK}{{}_\sigma KkT}[gz - \lambda(1-g)]$$

which are valid provided that ${}_\sigma K$, K, λ, and g are constant.

From [23] and [25] the coefficient $\partial\theta/\partial E$ required for the left-hand side of (8) is obtained if $d\phi^{M-2} = dE$ while from [23] and [24] the coefficient $\partial\theta/\partial\sigma$ is found. This must be combined with the relation

$$[26] \quad \partial q/\partial\sigma = 1 + \lambda e(\partial\Gamma/\partial\sigma)$$

obtained from [1] to find the coefficient $\partial q/\partial\Gamma$ required for the right-hand side of [8]. Hence the

Can. J. Chem. Downloaded from www.nrcresearchpress.com by 210.87.254.40 on 09/06/12
For personal use only.

capacity C may be found knowing the adsorption isotherm.

As already shown (9) the capacity peak found for a species with attractive interaction will be higher and narrower than that for a species with repulsive interaction and this is qualitatively in agreement with experimental results for submonolayer metal deposition (8, 10). Nevertheless it is frequently observed in such systems as well as in the adsorption of hydrogen (11) and of halides on solid metals (12) that there are sharp peaks which correspond to the adsorption of substantially less than a monolayer of adsorbate and that these are surrounded by broader peaks. While there may be an explanation of these in terms of adsorption on defects, it is also interesting to consider whether they could be explained in terms of the transfer of charge from the adsorbate to the metal.

5. A Simple Model for a Variation in the Amount of Charge Transfer

In contrast to the previous sections where λ has been assumed to be constant, it is here assumed that this quantity depends on the electrode potential. Some suggestion that this might be so comes from the model proposed by Schmickler (13). However, very little evidence is available as to the extent to which such a variation may occur. This section is therefore only a speculation and further evidence may lead to extensive modification of the proposals made here.

It will be assumed that the adsorbed species transfers its charge over a rather narrow region of potential, that is λ/z changes quite rapidly from 0 to 1. In the absence of any knowledge of the functional dependence of this change it will simply be assumed that it follows a Fermi–Dirac-like function

$$[27] \quad \frac{\lambda}{z} = \frac{\exp(E - E_p)/\varepsilon}{1 + \exp(E - E_p)/\varepsilon}$$

where the parameter ε characterizes the range of potential over which λ/z changes. Clearly E_p is the potential at which $\lambda/z = \frac{1}{2}$.

It will be further assumed that if ε is sufficiently small, the change in Γ, the amount adsorbed, and σ, the physical charge on the metal electrode, is small and may be neglected. The latter assumption is perhaps the most questionable, because it is not known how the redistribution of charge takes place. It could also be assumed that as the charge on the adsorbed species changed by λe the charge on the electrode changed by $-\lambda e$ so that no external charge flowed. In the latter case only the effects due to changes in Γ and σ would be observable, so that it seems more interesting to investigate the limiting case of constant Γ and σ. However, it must be remembered that intermediate cases are also possible.

With the assumption of constant Γ and σ, it follows that the external charge flow is given by

$$[28] \quad dq = e\Gamma d\lambda$$

Or with the aid of [27]

$$[29] \quad dq = e\Gamma \frac{z}{\varepsilon} \frac{\exp(E - E_p)/\varepsilon}{\{1 + \exp(E - E_p)/\varepsilon\}^2}$$

Consequently the observed capacity is

$$[30] \quad C = \frac{ze\Gamma}{\varepsilon} \frac{\exp(E - E_p)/\varepsilon}{\{1 + \exp(E - E_p)/\varepsilon\}^2}$$

$$[31] \quad = \frac{ze\Gamma}{\varepsilon} \frac{\lambda}{z} \left(1 - \frac{\lambda}{z}\right)$$

The peak capacitance occurs at $E = E_p$ or $\lambda/z = \frac{1}{2}$ and has the value

$$[32] \quad C_p = ze\Gamma/4\varepsilon$$

It is thus proportional to the amount adsorbed and inversely proportional to the parameter ε. The width at half height of this capacity peak is readily shown to be 3.52ε. (The analogy with a Langmuirian adsorption peak should be obvious.)

If ε is given the value kT/e for a singly charged species and $ze\Gamma$ is taken as 100 μC cm^{-2} for an almost saturated monolayer of small ions, the peak height is 975 μF cm^{-2} and the peak width is 90 mV. This is rather more than twice the height observed for the sharp peaks in the adsorption of halide ions on silver single crystals and rather broader. If the model is correct this may result from a smaller value of Γ or from the lack of constancy of σ (or less probably of Γ).

If σ is constant, or nearly constant, then the external flow of charge q involves the flow of electrons in the metal and of ions in the solution to adjust the charge in the diffuse layer. This rapid change in the diffuse layer charge over a narrow potential range is likely to lead to a contribution to the measured impedance from the mass transport (see for example ref. 4) and this is in fact observed (12).

This suggestion for the origin of the sharp peaks in the adsorption of halide ions on silver and perhaps for some of the other sharp peaks observed in systems like those of the submonolayer deposition of metals is certainly oversimplified but it may suggest a route to a more detailed explanation.

1. W. Lorenz and G. Salié. Z. Phys. Chem. **218**, 259 (1961).

2. B. E. CONWAY and H. ANGERSTEIN-KOSLOWSKA. J. Electroanal. Chem. **113**, 63 (1980).
3. R. PARSONS and J. M. PARRY. Trans. Faraday Soc. **59**, 241 (1963).
4. K. J. VETTER and T. W. SCHULTZE. Ber. Bunsenges. Phys. Chem. **76**, 920 (1972); **76**, 927 (1972).
5. B. V. ERSHLER. Zhur. Fiz. Khim. **20**, 679 (1946).
6. B. E. CONWAY and E. GILADI. *In* Modern aspects of electrochemistry. *Edited by* B. E. Conway and J. O'M. Bockris. Vol. 3. Butterworths, London. 1964. Chapt. 5.
7. A. BEWICK and B. THOMAS. J. Electroanal. Chem. **85**, 321 (1977).
8. B. E. CONWAY, H. ANGERSTEIN-KOZLOWSKA, and W. B. A. SHARP. Z. Phys. Chem. NF, **98**, 61 (1975).
9. R. PARSONS. J. Electroanal. Chem. **5**, 397 (1963); 7, 136 (1964).
10. D. M. KOLB. Advances in electrochemistry and electrochemical engineering. Vol. 6. *Edited by* H. Gerischer and C. W. Tobias. Wiley–Interscience, New York. 1979. p. 125.
11. J. CLAVILIER, R. FAURE, G. GUINET, and R. DURAND. J. Electroanal. Chem. **107**, 205 (1980).
12. G. VALETTE, A. HAMELIN, and R. PARSONS. Z. Phys. Chem. **113**, 71 (1978).
13. W. SCHMICKLER. J. Electroanal. Chem. **100**, 533 (1979).
14. G. C. BARKER. J. Electroanal. Chem. **12**, 495 (1966).

Can. J. Chem. Downloaded from www.nrcresearchpress.com by 210.87.254.40 on 09/06/12
For personal use only.

Perturbation theory, the mean spherical approximation, and the electrical double layer[1]

DOUGLAS HENDERSON
IBM Research Laboratory, San Jose, CA 95193, U.S.A.
AND
LESSER BLUM
Department of Physics, University of Puerto Rico, Rio Piedras, PR 00911, U.S.A.

Received July 15, 1980

This paper is dedicated to Dr. Sam Levine on the occasion of his 70th birthday

DOUGLAS HENDERSON and LESSER BLUM. Can. J. Chem. **59**, 1903 (1981).

Simple arguments, based on perturbation theory, are used to derive expressions for the energy of a bulk ionic fluid and the potential difference in an electric double layer. These expressions are identical to those obtained from the much more elaborate mean spherical approximation.

DOUGLAS HENDERSON et LESSER BLUM. Can. J. Chem. **59**, 1903 (1981).

On a utilisé des arguments simples, fondés sur la théorie de perturbation, pour déduire les expressions de l'énergie de l'ensemble d'un fluide ionique et la différence de potentiel d'une double couche électrique. Ces expressions sont identiques à celles obtenues à partir de l'approximation sphérique moyenne beaucoup plus compliquée.

[Traduit par la journal]

Can. J. Chem. Downloaded from www.nrcresearchpress.com by 210.87.254.6 on 09/06/12
For personal use only.

Introduction

For somewhat more than a decade, perturbation theory (1, 2) has been recognized as one of the most tractable, yet most useful, theories of simple liquids, such as argon. Until recently, it has been thought that perturbation theory does not have a similar utility in theory of ionic fluids because, due to the long range Coulomb forces in such systems, many of the terms in a perturbation expansion diverge. The purpose of this note is to demonstrate that, because of electroneutrality and screening, these divergent terms can be resumed and that perturbation theory is at least as useful for ionic fluids as for simple fluids. Perturbation theory yields results which are comparable in accuracy with those of other theories of ionic fluids. In particular, we show that perturbation theory can be used in a very simple, although nonrigorous, way to derive the mean spherical approximation (MSA) expressions for thermodynamic quantities both for bulk ionic fluids and for ionic fluids near an electrified interface (i.e., for the electrical double layer).

Perturbation Theory

Using the expressions of Barker and Henderson (3) the energy of a mixture of molecules, whose pair interactions are described by

$$[1] \quad u_{ij}(r) = \begin{cases} \infty & r < \sigma_{ij} \\ w_{ij}(r), & r > \sigma_{ij} \end{cases}$$

where $\sigma_{ij} = (\sigma_{ii} + \sigma_{jj})/2$ are the hard-sphere diameters of molecules, is

$$[2] \quad U = \frac{3}{2}NkT + \frac{1}{2}N\rho \sum_{ij} x_i x_j \int w_{ij}(r) g_{ij}{}^0(r)\, d\boldsymbol{r} - \frac{1}{2}N\rho\beta \sum_{ij} x_i x_j \int w_{ij}{}^2(r) g_{ij}{}^0(r)\, d\boldsymbol{r} + \ldots$$

where $\rho = N/V$, $\beta = 1/kT$, N is the number of hard spheres, V is the volume, T is the temperature, and $g_{ij}{}^0(r)$ are the radial distribution functions of a system of hard spheres (i.e., $w_{ij}(r) = 0$).

Bulk Ionic Fluids

Consider a fluid of charged hard spheres in a medium of dielectric constant ε. If the charge of the hard spheres is $z_i e$ then

$$[3] \quad w_{ij}(r) = z_i z_j e^2/r\varepsilon$$

For the moment assume that $\sigma_{ij} = \sigma$. If eq. [2] is applied to this system, the two integrals diverge. The first divergence is not troublesome. Because of electroneutrality

$$[4] \quad \sum_i z_i x_i = 0$$

and the net contribution of these terms vanishes.

The second set of integrals is slightly more difficult. Setting

$$g_{ij}{}^0(r) = h_0(r) + 1$$

and substituting eq. [3] into eq. [2] gives

[1]Supported in part by NSF Grant No. CHE80-01969.

0008-4042/81/131903-03$01.00/0
©1981 National Research Council of Canada/Conseil national de recherches du Canada

$$[5] \quad U_i/NkT = -\frac{\kappa^4}{8\pi\rho}\int_0^\infty dr - \frac{\kappa^4}{8\pi\rho}\int_0^\infty h_0(r)\,dr + \ldots$$

where

$$\kappa^2 = 4\pi\beta e^2\rho\sum_i x_i z_i^2/\varepsilon$$

The factor $3NkT/2$ has been subtracted from U to define U_i. The first integral is divergent. However, this integral is the first term in a "ring sum". Because of screening, this ring sum converges. Replacing the integral in [5] by its chain sum gives an integral over $e^{-\kappa r}$ rather than unity. This resummation of a ring sum and resultant screening is already familiar in the Debye–Hückel theory. Thus,

$$[6] \quad U_i/NkT = -\frac{\kappa^3}{8\pi\rho} - \frac{\kappa^4}{8\pi\rho}\int_0^\infty h_0(r)\,dr + \ldots = -\frac{\kappa^3}{8\pi\rho} + \frac{\kappa^4\sigma}{8\pi\rho} + \ldots$$

where the low concentration approximation, $h_0(r) = -1$, $r < \sigma$, and zero otherwise, has been used. The above series is due to Stell and Lebowitz (4). Brout and Carruthers (5) give a derivation in the context of an electron gas.

It is convenient to introduce the normalized screening parameter, Γ, defined by

$$[7] \quad \kappa = 2\Gamma(1 + \Gamma\sigma)$$

If [7] is substituted into [6] then, to order Γ^4,

$$[8] \quad U_i/NkT = -\frac{(2\Gamma)^3(1 + \Gamma\sigma)}{8\pi\rho}$$

Equation [8] is *exactly* the mean spherical approximation (MSA) for a system of charged hard spheres (6–9). Although the above derivation is nonrigorous, it is considerably simpler than the arguments involved in the MSA. Also as we shall see, this same procedure yields this MSA result for potential difference in an electric double layer.

Even if higher-order terms in κ are included in [6], eq. [8] still results provided that only MSA type terms (i.e., nodal diagrams of order κ^n/ρ) are included and evaluated using the low concentration limit of the correlation functions.

Electric Double Layer

Now let us apply perturbation theory to a system of N charged hard spheres of diameter σ and charged $z_i e$ and two charged hard spheres of diameter $R \gg \sigma$ and charge $\pm Q$. We choose two hard spheres of diameter R so that *both* sets of spheres satisfy charge neutrality. However, in every other way we regard the concentration of the spheres to be so small that each sphere of diameter R is independent of the other sphere of diameter R. That is, the concentration of each sphere of diameter R is $1/N$ and terms of order $1/N^2$ can be neglected.

Returning to eq. [2] we see that the excess energy due to the presence of each of the hard spheres of diameter R is

$$[9] \quad \Delta U = -\frac{\kappa^2 Q^2}{2\varepsilon}\int_{(R+\sigma)/2}^\infty g_0^w(r)\,dr + \ldots = -\frac{\kappa^2 Q^2}{2\varepsilon}\int_0^\infty dr - \frac{\kappa^2 Q^2}{2\varepsilon}\int_0^\infty h_0^w(r)\,dr + \ldots$$

where

$$g_0^w(r) = 1 + h_0^w(r)$$

is the radial distribution function for pairs of the large and small spheres. Equation [9] is obtained by applying eq. [2] to the above mixture of charged hard spheres of diameter σ and R, taking the difference between that result and eq. [5], and neglecting terms of order $1/N^2$. Replacing the divergent integral in [9] by the ring sum of which it is the first member and using the low concentration limit for $h_0^w(r)$ gives

$$[10] \quad \Delta U = -\frac{\kappa Q^2}{2\varepsilon} + \frac{\kappa^2 Q^2}{2\varepsilon}\left(\frac{R+\sigma}{2}\right) + \ldots$$

Introducing Γ gives

$$[11] \quad \Delta U = -\frac{Q^2}{\varepsilon}\Gamma(1 - \Gamma R) + \ldots = -\frac{Q^2}{\varepsilon}\frac{\Gamma}{1 + \Gamma R}$$

For large R, eq. [11] becomes

$$[12] \quad \Delta U = -\frac{Q^2}{\varepsilon R} + \frac{Q^2}{\varepsilon\Gamma R^2} + \ldots$$

The first term in [12] is the energy of a sphere and the second term is the energy of the double layer.

The potential difference across the double layer is

$$[13] \quad V = \partial(\Delta U')/\partial Q$$

where $\Delta U'$ is the second term in eq. [12]. Strictly speaking the potential difference is the derivative of the free energy. However, it is more convenient to use the energy because the summation of the ring diagrams is more straightforward. In any case, for the terms considered here, differentiating the energy

Can. J. Chem. Downloaded from www.nrcresearchpress.com by 210.87.254.6 on 09/06/12
For personal use only.

yields the same potential as differentiating the free energy.

Thus,

$$[14] \quad V = 2Q/\varepsilon\Gamma R^2$$

If E is the electric field at the surface of the sphere, the surface charge density is $\varepsilon E/4\pi$ and $Q = \varepsilon E R^2/4$. Thus,

$$[15] \quad V = E/2\Gamma$$

which is the MSA result (10).

Again we see that we have obtained exactly the MSA result by a nonrigorous, but fairly simple, argument based upon perturbation theory.

Summary

Perturbation theory can provide a simple formalism for the development of the MSA expressions both for the bulk fluid thermodynamics and for the double layer potential difference.

These arguments can be extended to fluids in which the solvent consists of discrete molecules. However, in this case, they should not be expected to give results which are identical to those of the MSA since for such fluids the MSA does not yield explicit expressions. In any case, discreteness of the solvent leads to ring sums involving renormalized bonds and so the situation is much more complex. These questions will be treated in a later publication.

1. J. A. Barker and D. Henderson. J. Chem. Phys. **47**, 2856 (1976).
2. J. A. Barker and D. Henderson. J. Chem. Phys. **47**, 4714 (1976).
3. J. A. Barker and D. Henderson. Rev. Mod. Phys. **48**, 587 (1976).
4. G. Stell and J. L. Lebowitz. J. Chem. Phys. **49**, 3706 (1968).
5. R. Brout and P. Carruthers. Lectures on the many electron problem. Gordon and Breach, New York. 1969. Section 1.3.
6. E. Waisman and J. L. Lebowitz. J. Chem. Phys. **56**, 3086 (1972).
7. E. Waisman and J. L. Lebowitz. J. Chem. Phys. **56**, 3093 (1972).
8. L. Blum. Mol. Phys. **30**, 1529 (1975).
9. L. Blum and J. S. Høye. J. Phys. Chem. **81**, 1311 (1977).
10. L. Blum. J. Phys. Chem. **81**, 136 (1977).

Can. J. Chem. Downloaded from www.nrcresearchpress.com by 210.87.254.6 on 09/06/12
For personal use only.

The application of the generalized mean spherical approximation to the theory of the diffuse double layer[1]

DOUGLAS HENDERSON
IBM Research Laboratory, San Jose, CA 95193, U.S.A.
AND
LESSER BLUM
Department of Physics, University of Puerto Rico, Rio Piedras, PR 00931, U.S.A.
Received October 7, 1980

This paper is dedicated to Dr. Sam Levine on the occasion of his 70th birthday

DOUGLAS HENDERSON and LESSER BLUM. Can. J. Chem. **59**, 1906 (1981).

A system of charged hard spheres near a uniformly charged hard wall is considered. An approximation is established by postulating a closure for the Ornstein–Zernike (OZ) equations for this system. In this paper these OZ equations are solved for a closure in which the direct correlation functions are equal to the wall-ion potentials plus a sum of exponential functions. As a specific application of this solution we use one exponential and adjust two parameters to satisfy an approximate contact value theorem and give the same diffuse layer potential as is obtained using the hypernetted chain (HNC) approximation. Once this fit is made, the density, charge, and potential profiles can be easily calculated. The agreement with the corresponding HNC results is good. Comparison with the simpler Poisson–Boltzmann theory of Gouy and Chapman (GC) shows the GC theory to be better than one would expect. However, appreciable differences between the present results and the GC results for the diffuse layer potential are found.

DOUGLAS HENDERSON et LESSER BLUM. Can. J. Chem. **59**, 1906 (1981).

On a fait une étude d'un système de sphères dures chargées situées près d'un mur solide chargé d'une façon uniforme. On a établi une approximation en faisant l'hypothèse que les équations de Ornstein–Zernike (OZ) de ce système sont fermées. Dans le cadre de ce travail, nous avons résolu ces équations de corrélation OZ par le biais d'une fermeture dans laquelle les fonctions de corrélation directe sont égales aux potentiels mur-ions auxquels on ajoute une fonction exponentielle. Une application spécifique de cette solution a été faite; utilisant une exponentielle et ajustant deux paramètres afin de trouver des valeurs satisfaisantes pour le théorème de valeur de contact approximative, nous avons trouvé pour le potentiel de couche diffuse la même valeur que celle obtenue en faisant appel à l'équation d'hyperchaîne (EHC). Lorsque cette corrélation est établie, on peut facilement calculer les profils de densité, de charge et de potentiel. Il existe un bon accord avec les résultats correspondants obtenus par l'équation (EHC). Une comparaison avec la théorie plus simple de Poisson–Boltzmann développée par Gouy et Chapman (GC) révèle que cette théorie de GC est meilleure que prévue. Cependant on trouve que les différences appéciables entre les résultats actuels et les résultats de GC sont dues au potentiel de couche diffuse.

[Traduit par le journal]

Introduction

Henderson *et al.* (1) have formulated the Ornstein–Zernike equation in a form appropriate for the study of surfaces near a wall. Probably the most interesting applications of these equations is to the study of an ionic fluid near a charged wall both because the study of long range forces is of considerable theoretical interest and because this electrolyte–electrode system is of practical importance.

In this paper we consider the so-called restricted primitive fluid (a symmetric electrolyte of charged hard spheres all of equal diameter) near a uniform, hard, charged wall. This system is admittedly a gross simplification of a real electrolyte–electrode system. In particular by treating the solvent as a continuous dielectric medium, the explicit contributions of the solvent to the interfacial properties are lost. This is a serious loss since at high charge densities on the wall, and also at high electrolyte concentrations, these contributions dominate. Nonetheless, calculations based upon this primitive model are of interest for two reasons. Firstly, the development of theories which can adequately describe this relatively simple model is a necessary first step in the more general program of studying the full ion–solvent system. Secondly, the conventional method of determining the explicit contributions of the solvent to the interfacial properties is to subtract from experimental results the corresponding values calculated by the theory of Gouy (2) and Chapman (3) which is based upon this primitive model together with the additional assumption that the ions are point charges. Clearly, any errors in the Gouy–Chapman (GC) theory will lead to errors in the estimates of the solvent contributions.

This primitive model has been extensively studied

[1]Work supported in part by NSF Grant No. CHE80-01969.

0008-4042/81/131906-12$01.00/0
©1981 National Research Council of Canada/Conseil national de recherches du Canada

Can. J. Chem. Downloaded from www.nrcresearchpress.com by 210.87.254.40 on 09/06/12
For personal use only.

Can. J. Chem. Downloaded from www.nrcresearchpress.com by 210.87.254.40 on 09/06/12
For personal use only.

in recent years. Blum (4) and Henderson and Blum (5) have used the mean spherical approximation (MSA). Henderson *et al.* (6), Henderson and Blum (7), and Carnie *et al.* (8) have used the hypernetted chain (HNC) approximation. Levine and Outhwaite (9), Outhwaite *et al.* (10), and Bhuiyan *et al.* (11, 12) have used the modified Poisson–Boltzmann (MPB) approximation. In addition, Croxton and McQuarrie (13, 14) have used the Born–Green–Yvon (BGY) approximation. Each of these approximations reduces the GC theory if the diameter of the charged hard spheres is set equal to zero.

The most meaningful test of these calculations is comparison with the computer simulations of Torrie and Valleau (15, 16). In a direct test with experiment one is faced with the problem of disentangling the effects due to the model from those due to the approximation. Since the simulations are based upon the same model as the approximate theories, comparison with the computer simulations permits an unambiguous assessment of the validity of the theories. However, it is to be emphasized that comparison with computer simulations is not a goal in and of itself. The ultimate goal is the development of an accurate theory which can be generalized to a more realistic model and so can be fruitfully compared with experiment.

The MSA gives analytical results and so is easy to use. However, it is a linearized theory and is useful only in the limiting case of small charge on the wall. The other theories give rise to integral equations which must be solved analytically and so are difficult to use. One means of simplifying the calculation is to use the noniterative scheme of Henderson and Blum (7). Henderson and Blum used this scheme in the HNC approximation. However, the scheme is more widely applicable. This scheme is simple but has the drawback of yielding only the potential difference across the interface. Fortunately, this drawback can be overcome through the use of the generalized mean spherical approximation (GMSA) which we present here. In the GMSA, a solution of the OZ equations is obtained in terms of some adjustable parameters which can be chosen so as to yield the potential difference calculated by the noniterative procedure. The profiles calculated by this procedure agree well with those obtained from a full numerical solution of the integral equations but are much more easily obtained.

In the application considered here, we use the potential difference calculated by means of the noniterative scheme when applied to the HNC integral equations using the MSA to describe the bulk fluid (the so-called HNC/MSA, or more simply H/M, equations). Some of the other theories have advantages. However, HNC/MSA results agree with the computer simulations as well as, if not better than, those of the other theories. Also we believe that the HNC/MSA theory is the one most likely to be generalized to more realistic models.

Generalized Mean Spherical Approximation

Consider the general case of a system of charged hard spheres near a charged wall. The OZ equation for this system is (5)

$$[1]\quad h_{wi}(x) - c_{wi}(x) = 2\pi \sum_j \rho_i \int_{-\infty}^{\infty} h_{wj}(t)\,dt \int_{|x-t|}^{\infty} sc_{ij}(s)\,ds + 2\pi\beta z_i \sum_j \rho_j z_j \int_0^{\infty} h_{wj}(t)\,\{|x-t| + x + t\}\,dt$$

where $h_{wi}(x) = g_{wi}(x) + 1$, ρ_i, and z_i are the correlation function, bulk number density, and charge of a hard sphere of species i. Further, x is the distance of the center of the hard sphere from the wall and $\beta = 1/k_B T$ is the Boltzmann factor (k_B is Boltzmann's constant).

The bulk direct correlation functions, $c_{ij}(r)$, are assumed to be known. In this paper we assume them to be those obtained from the MSA when applied to the bulk. The interfacial direct correlation functions, $c_{wi}(x)$, are specified by some approximation. One purpose of this note is to give an explicit solution of [1] when the $c_{wi}(x)$ are given by

$$[2]\quad c_{wi}(x) = \sum_n A'_{ni} \exp[-\mu_{ni}x] + \sum_n B''_{ni} \exp[-\nu_{ni}x] - z_i B_0 x, \quad x > \sigma/2$$

for Re $\mu_{ni} > 0$, Re $\nu_{ni} > 0$, and the $g_{wi}(x) = 0$, $x < \sigma/2$.

If $A'_{ni} = B''_{ni} = 0$ and $B_0 = \beta E$, this is the MSA for charged hard spheres near a charged wall whose charge density is $\varepsilon E/4\pi$, where ε is the dielectric constant. If this is not the case, there are at least three ways of using

Can. J. Chem. Downloaded from www.nrcresearchpress.com by 210.87.254.40 on 09/06/12
For personal use only.

[2]. Firstly, the parameters A'_{ni}, B''_{ni}, μ_{ni}, and ν_{ni} can be regarded as potential parameters specifying some non-Coulomb interaction, perhaps a short range potential describing specific adsorption. As before, $B_0 = \beta E$ would describe the Coulomb interactions for the charged hard sphere/charged hard wall system. In this case, [2] is the MSA for this system.

Secondly, these parameters can be regarded as parameters which may be adjusted to fit some theoretical criteria for the charged hard sphere/charged hard wall system. When used in this manner, [2] is referred to as the GMSA. An example of this type of application has been given by Henderson and Blum (17) who chose 4 parameters to fit some contact value theorems (18) for the $g_{wi}(x)$ when the spheres are in contact with the wall and some approximate expressions for the derivatives of the $g_{wi}(x)$ at contact.

Thirdly, these parameters can be varied to satisfy some approximation for the $c_{wi}(x)$ to some level of accuracy. Used in this way, [2] becomes a numerical method for solving [1]. An example of this type of application has been given by Henderson *et al.* (19) who varied 16 parameters so that [2] satisfied, as well as possible, the extended mean spherical approximation (EMSA).

In this note we return to the second type of approximation, the GMSA. We adjust 2 parameters. One is adjusted to satisfy a contact value theorem and the other is adjusted to fit the potential difference calculated from the HNC/MSA by means of our noniterative scheme (7). We feel that this is preferable to our earlier GMSA calculation (18) because our approximate expressions for the derivatives of $g_{wi}(x)$ at contact are of uncertain accuracy. In addition, when used in this manner the GMSA gives a means of extending our non-iterative technique so that the $g_{wi}(x)$ are obtained. We assume that the charge density on the electrode is $\varepsilon E/4\pi$ and that this charge is positive. Thus $B_0 = \beta E$. Further we assume that the ions of species 1 are anions and the ions of species 2 are cations.

Solution of [1] and [2]

We now proceed to outline the solution of [1] and [2]. This section is of necessity somewhat abstract. Readers uninterested in the mathematical detail may go directly to the next section.

The general solution to this problem is given by [30] of Blum and Stell (20)

$$[3]\quad \Delta\tilde{g}_{wi}(s) = \sum_j \exp[-s\sigma_j/2]\left[\sum_l \frac{1}{s}\tilde{Q}_{lj}(0) - \tilde{F}_j(s)\right][\tilde{Q}(is)]^{-1}_{ji}$$

where $\Delta\tilde{g}_{wi}(s)$ is the Laplace transform of the distribution function $\Delta g_{wi}(x)$ which is the difference between $g_{wi}(x)$ and the corresponding distribution for the hard sphere/hard wall system. Thus,

$$[4]\quad \Delta\tilde{g}_{wi}(s) = \int_{\sigma_i/2}^{\infty} [\exp(-sx)]\,\Delta g_{wi}(x)\,dx$$

Further $\tilde{Q}_{lj}(k)$ is the Fourier transform of the Baxter function (21) $Q_{lj}(r)$,

$$[5]\quad \tilde{Q}_{lj}(k) = \delta_{lj} - \rho_j \int_{\lambda_{ji}}^{\infty} [\exp(ikx)]\,Q_{lj}(x)\,dx$$

$$[6]\quad \lambda_{ji} = \tfrac{1}{2}(\sigma_j - \sigma_i)$$

We have also used

$$[7]\quad \tilde{F}_j(s) = \frac{1}{2\pi}\sum_l \int_{-\infty}^{\infty} \frac{\exp(-ik\sigma_j/2)}{s + ik}\,\tilde{\phi}_l(k)[\tilde{Q}^{T}(-k)]^{-1}_{lj}\,dk$$

with

$$[8]\quad \tilde{\phi}_l(k) = \int_{\sigma_l/2}^{\infty} \exp(ikx)\left[\sum_n A'_{nl}\exp[-\mu_{nl}x] + \sum_n B''_{nl}\exp[-\nu_{nl}x] + z_l B_0 x\right]dx$$

$$= z_l B_0 \lim_{\nu_0 \to 0} \frac{\exp[(ik - \nu_0)\sigma_l/2]}{(\nu_0 - ik)^2}\left[1 - \frac{\sigma_l}{2}(ik - \nu_0)\right]$$

$$+ \sum_n \exp(ik\sigma_l/2)\left[\frac{A'_{nl}\exp(-\mu_{nl}\sigma_l/2)}{\mu_{nl} - ik} + \frac{B''_{nl}\exp(-\nu_{nl}\sigma_l/2)}{\nu_{nl} - ik}\right]$$

Can. J. Chem. Downloaded from www.nrcresearchpress.com by 210.87.254.40 on 09/06/12
For personal use only.

Substitution of this expression into [7] gives

$$[9] \quad \tilde{F}_j(s) = \tilde{F}_j^{(0)}(s) + \tilde{F}^{(1)}(s)$$

where

$$[10] \quad \tilde{F}_j^{(0)}(s) = \frac{B_0}{2\pi}\sum_l \int_{-\infty}^{\infty} \frac{\exp(-ik\sigma_j/2)}{s+ik}\left\{z_l \lim_{\nu_0\to 0} \frac{\exp[i(k-\nu_0)\sigma_l/2]}{(\nu_0 - ik)^2}\left[1 - \frac{\sigma_l}{2}(ik-\nu_0)\right]\right\}[\tilde{Q}^{\mathrm{T}}(-k)]_{lj}^{-1}\,dk$$

and

$$[11] \quad \tilde{F}_j^{(1)}(s) = \frac{1}{2\pi}\sum_l \int_{-\infty}^{\infty} \frac{\exp(-ik\sigma_j/2)}{s+ik}\sum_n \exp(ik\sigma_l/2)\left[\frac{A'_{nl}\exp(-\mu_{nl}\sigma_l/2)}{\mu_{nl}-ik} + \frac{B''_{nl}\exp(-\nu_{nl}\sigma_l/2)}{\nu_{nl}-ik}\right] \times [\tilde{Q}^{\mathrm{T}}(-k)]_{lj}^{-1}\,dk$$

The integrals in [10] and [11] can be evaluated by choosing a contour around the lower complex k plane, where $\tilde{Q}^{\mathrm{T}}(-k)$ is a nonsingular matrix (21). Furthermore, it can be shown (20, 21) that for $\mathrm{Im}\, k = k' \to \infty$,

$$[12] \quad [\tilde{Q}^{\mathrm{T}}(-k)]_{lj}^{-1} \to O[\exp(-k'\lambda_{lj})]$$

and for $|k| \to \infty$ the integrand is $O(1/|k|^2)$. Hence the only contributions to the integrals are those from the poles in the lower half-plane

$$[13] \quad k = i\mu_{nl};\quad -i\nu_{nl};\quad -i\nu_0$$

Using Cauchy's residue theorem we get for the ionic part

$$[14] \quad \tilde{F}_j^{(0)} = -\frac{B_0}{2\pi}\sum_l z_l \lim_{\mu_0\to 0} 2\pi i\ \mathrm{Res}\left\{\frac{\exp[i(k-\nu_0)\sigma_l/2]\exp(-ik\sigma_j/2)}{(\nu_0-ik)^2}\left[1-\frac{\sigma_l}{2}(ik-\nu_0)\right]\right\} \times [\tilde{Q}^{\mathrm{T}}(-k)]_{lj}^{-1}\Big|_{k\to -i\mu_0} = -\frac{B_0}{s}\sum_l z_l \lim_{\nu_0\to 0}\frac{\partial}{\partial\nu_0}[\tilde{Q}^{\mathrm{T}}(i\nu_0)]_{lj}^{-1}$$

Similarly, the other term, $\tilde{F}_j^{(1)}$, yields

$$[15] \quad \tilde{F}_j^{(1)}(s) = \sum_l\sum_n \left\{A'_{nl}\frac{\exp(\mu_{nl}\lambda_{lj})}{s+\mu_{nl}}[\tilde{Q}^{\mathrm{T}}(i\mu_{nl})]_{lj}^{-1} + B''_{nl}\frac{\exp(\nu_{nl}\lambda_{lj})}{s+\nu_{nl}}[\tilde{Q}^{\mathrm{T}}(i\nu_{nl})]_{lj}^{-1}\right\}$$

which together with [3] yields $\Delta\tilde{g}_i(s)$.

More explicit relations can be obtained if the sizes of the ions in the bulk are equal, and if also some reasonable assumptions are made about the coefficients A'_{nl} and B''_{nl}. From Blum (4) we have

$$[16] \quad [\tilde{Q}^{\mathrm{T}}(is)]_{kj}^{-1} = \delta_{kj} + \rho_k\tilde{P}^{(0)}(s)/\rho + z_k z_j \rho_k \tilde{P}^{\pm}(s)/\xi_0$$

where

$$[17] \quad \rho = \sum_{i=1}^{n}\rho_i$$

$$[18] \quad \xi_0 = \sum \rho_i z_i^2$$

$$[19] \quad \tilde{P}^0(s) = \rho\tilde{Q}_0(s)/[1-\rho\tilde{Q}_0(s)]$$

$$[20] \quad \tilde{P}^{\pm}(s) = \frac{-2\Gamma(s+\Gamma-\Gamma e^{-s\sigma})}{[s^2+2\Gamma s+2\Gamma^2(1-e^{-s\sigma})]}$$

with

$$[21] \quad \Gamma = \frac{1}{2\sigma}[-1+\sqrt{1+2\kappa\sigma}]$$

Can. J. Chem. Downloaded from www.nrcresearchpress.com by 210.87.254.40 on 09/06/12
For personal use only.

and

$$[22]\quad \kappa^2 = 4\pi\beta \sum_i \rho_i z_i^2/\varepsilon$$

The parameter κ is the Debye screening constant. Further we recall that

$$[23]\quad \tilde{P}^0(s) = \frac{-m_0 - m_1 s - m_2 s^2 - N(s)\, e^{-s\sigma}}{M(s) + N(s)\, e^{-s\sigma}}$$

with

$$[24]\quad M(s) = s^3 + s^2 m_2 + s m_1 + m_0$$

$$[25]\quad N(s) = s n_1 + n_0$$

$$[26]\quad m_0 = -\frac{2\pi\rho}{\Delta^2}\left(1 + \frac{\pi\rho\sigma^3}{3}\right)$$

$$[27]\quad m_2 = \pi\rho\sigma^2/\Delta$$

$$[28]\quad m_1 = m_2^2/2$$

$$[29]\quad n_1 = \frac{2\pi\rho\sigma}{\Delta}\left(1 + \frac{\pi\rho\sigma^3}{4\Delta}\right)$$

$$[30]\quad n_0 = m_0\sigma$$

From [16] and [20] we have

$$[31]\quad \sum_l z_l \left[\frac{\partial}{\partial\nu}[\tilde{Q}^{\mathrm{T}}(i\nu)]^{-1}_{lj}\right]_{\nu=0} = z_j \lim_{s\to 0}\frac{\partial}{\partial s}\left[\frac{s^2}{s^2 + 2\Gamma s + 2\Gamma^2(1 - e^{-s\sigma})}\right] = z_j \frac{1}{2\Gamma(1 + \Gamma\sigma)} = \frac{z_j}{\kappa}$$

Substitution of [31] into [3] and [14] gives

$$[32]\quad \Delta\tilde{g}_{wi}(s) = -\frac{z_i B_0}{\kappa} e^{-s\sigma/2}\left[\frac{1 + \tilde{P}^{\pm}(s)}{s}\right] + \sum_{j,n}\frac{\exp[-(s + \mu_n)\sigma_j/2]}{s + \mu_n}\left\{\sum_l A'_{nl}[\tilde{Q}^{\mathrm{T}}(i\mu_n)]^{-1}_{lj}\right\}[\tilde{Q}(is)]^{-1}_{ji} + \sum_{j,n}\frac{\exp[-(s + \nu_n)\sigma_j/2]}{s + \nu_n}\left\{\sum_l B''_{nl}[\tilde{Q}^{\mathrm{T}}(i\nu_n)]^{-1}_{lj}\right\}[\tilde{Q}(is)]^{-1}_{ji}$$

Further, suppose that the coefficients are of the form

$$[33]\quad A'_{nl} = A'_n$$

$$[34]\quad B''_{nl} = z_n B'_n$$

Hence,

$$[35]\quad \Delta\tilde{g}_{wi}(s) = -\frac{z_i B_0}{\kappa} e^{-s\sigma/2}\left[\frac{1 + \tilde{P}^{\pm}(s)}{s}\right] + \sum_n A'_n \frac{\exp[-(s + \mu_n)\sigma/2]}{s + \mu_n}[1 + \tilde{P}^0(\mu_n)][1 + \tilde{P}^0(s)] - z_i \sum_n B'_n \frac{\exp[-(s + \nu_n)\sigma/2]}{s + \nu_n}[1 + \tilde{P}^{\pm}(\nu_n)][1 + \tilde{P}^{\pm}(s)]$$

If we recall that

$$[36]\quad 1 + \tilde{P}^{\pm}(s) = \frac{s^2}{s^2 + 2\Gamma s + 2\Gamma^2(1 - e^{-s\sigma})}$$

and

$$[37]\quad 1 + \tilde{P}^{(0)}(s) = \frac{s^3 e^{s\sigma}}{L(s) + S(s) e^s}(1 - \eta)^2$$

where $\eta = \pi\rho\sigma^3/6$ and $L(s)$ and $S(s)$ are polynomials defined by Wertheim (22, 23), we have an explicit expression for $\Delta\tilde{g}_{wi}(s)$.

Can. J. Chem. Downloaded from www.nrcresearchpress.com by 210.87.254.40 on 09/06/12
For personal use only.

Summary of Solution

It is convenient to define

$$[38]\quad A_n = A'_n \frac{\mu_n^3 \exp(\mu_n\sigma)}{L(\mu_n) + S(\mu_n)\exp(\mu_n\sigma)}$$

and

$$[39]\quad B_n = B'_n \frac{\nu_n^2}{\nu_n^2 + 2\Gamma\nu_n + 2\Gamma^2[1 - \exp(-\nu_n\sigma)]}$$

where $A'_n = A'_{nl}$, $B'_n = B''_{nl}/z_n$, $L(s)$, and $S(s)$ are polynomials defined by Wertheim (22, 23), and Γ is defined by [21] and [22]. Equation [35] simplifies somewhat if [38] and [39] are used. A further simplification is obtained if $x = 0$ is chosen to be the center of the spheres at their distance of closest approach to the wall. Thus,

$$[40]\quad \tilde{g}_{ws}(s) = \frac{a}{s}(1-\eta)^2 e^s f(s,\eta) + (1-\eta)^4 e^s f(s,\eta)\sum_n \frac{A_n}{s+\mu_n}$$

and

$$[41]\quad \tilde{g}_{wd}(s) = \frac{zB_0}{\kappa}\tilde{F}(s) + zs\tilde{F}(s)\sum_n \frac{B_n}{s+\nu_n}$$

where $g_{ws}(x) = [g_{w1}(x) + g_{w2}(x)]/2$ is the normalized density profile, $\rho(x)/\rho$ where ρ is the bulk density, and $g_{wd}(x) = [g_{w1}(x) - g_{w2}(x)]/2$ is the normalized charge profile, $-q(x)/z\rho$, $\eta = \pi\rho\sigma^3/6$, $a = (\beta\partial p/\partial\rho)^{1/2}$, the square root of the bulk fluid compressibility,

$$[42]\quad f(s,\eta) = \frac{s^3}{L(s) + S(s)e^s}$$

$z = |z_i|$, and

$$[43]\quad \tilde{F}(s) = \frac{s}{s^2 + 2\Gamma s + 2\Gamma^2(1 - e^{-s\sigma})}$$

The first term in [40] is the hard sphere/hard wall distribution function. Equation [40] has been given before by Waisman *et al.* (24) and Henderson *et al.* (25). The first term in [14] has been given before by Blum (4) in his solution of the MSA for charged hard spheres near a charged hard wall.

Inverting gives

$$[44]\quad g_{ws}(x) = \left[1 + \frac{(1-\eta)^2}{a}\sum_n A_n\right] g_0(x) - \frac{(1-\eta)^2}{a}\sum_n \mu_n A_n \int_0^x \exp[-\mu_n(x-t)]\, g_0(t)\, dt$$

and

$$[45]\quad g_{wd}(x) = \left[b + z\sum_n B_n\right] F(x) - z\sum_n \nu_n B_n \int_0^x \exp[-\nu_n(x-t)]\, F(t)\, dt$$

where $g_0(x)$ is the hard sphere/hard wall distribution function, $b = \beta zE/\kappa = zB_0/\kappa$, where κ is defined by [22], and $F(x)$ is the inverse of $\tilde{F}(s)$. Explicit expressions for $g_0(x)$ and $F(x)$ have been given by Henderson and Smith (26). Explicit expressions can be obtained for $g_{ws}(x)$ and $g_{wd}(x)$. However, they are complex. For most situations we found it more convenient to perform the integrations in [44] and [45] numerically.

From [44] and [45] we see immediately that

$$[46]\quad g_{ws}(0) = a + (1-\eta)^2\sum_n A_n$$

and

$$[47]\quad g_{wd}(0) = b + z\sum_n B_n$$

since $g_0(0) = a$ and $F(0) = 1$. Differentiating [44] and [45] gives

Can. J. Chem. Downloaded from www.nrcresearchpress.com by 210.87.254.40 on 09/06/12
For personal use only.

[48] $$g'_{ws}(0) = -(1-\eta)^2 \sum_n \mu_n A_n - \frac{6\eta}{1-\eta} g_{ws}(0)$$

and

[49] $$g'_{wd}(0) = -z \sum_n \nu_n B_n - 2\Gamma g_{wd}(0)$$

since

$$g'_0(0) = -\frac{6\eta}{1-\eta} a$$

and

$$F'(0) = -2\Gamma$$

Finally we can obtain, by expansion of [44] and [45] in powers of s, explicit expressions for the integrals

[50] $$\int_0^\infty [g_{ws}(x) - 1]\,dx = \frac{3\eta}{2(1+2\eta)} + \frac{(1-\eta)^4}{(1+2\eta)} \sum_n \frac{A_n}{\mu_n}$$

[51] $$\int_0^\infty g_{wd}(x)\,dx = \frac{b}{\kappa}$$

and

[52] $$\int_0^\infty x g_{wd}(x)\,dx = \frac{b}{\kappa^2}(1-\Gamma^2) - \frac{z}{\kappa} \sum_n \frac{B_n}{\nu_n}$$

The first and third integrals are, apart from numerical factors, the excess charge adsorbed by the electrode and the diffuse layer potential. The second integral is the charge neutrality condition

[53] $$\int_0^\infty q(x)\,dx = -\frac{\varepsilon E}{4\pi}$$

Setting $A_n = B_n = 0$ gives the MSA results for the charged hard sphere/charged hard wall system (4). Setting $B_0 = B_n = 0$ gives the results of Waisman *et al.* (24) for hard spheres near a hard wall.

Choice of the Parameters

Henderson *et al.* (27) have obtained the exact result

[54] $$g_{ws}(0) = \beta p/\rho + b^2/2$$

Thus, one possibility would be to retain only one term in the sums in [40], [44], [46], [48], and [50] and choose A so that [54] is satisfied. However, this leaves μ undetermined. In principle, μ could be determined by requiring that [50] be equal to its value calculated from the HNC theory. Unfortunately, this requires a full solution of the HNC equation. If the GMSA is to be useful it must be easy to use. Hence, the above procedure is not attractive.

Instead we use the result

[55] $$g_{wd}(0) = b\sqrt{1 + (b^2/4)}$$

Equation [55] is not exact. However, it is satisfied rather closely by the HNC $g_{wd}(x)$. Retaining only one term in the sums in [45], [47], [49], and [52] we have

[56] $$zB = b\sqrt{1 + (b^2/4)} - b$$

The parameter ν is chosen so that the diffuse layer potential,

[57] $$\phi = \frac{E(1-\Gamma^2)}{\kappa} - \frac{zE}{b}\frac{B}{\nu}$$

is equal to that calculated from the HNC approximation (in the HNC/MSA version). Since ϕ can be calculated rather easily by means of the noniterative scheme of Henderson and Blum (7), this procedure is attractive.

The function $g_{wd}(x)$ is now specified. All that remains is the determination of $g_{ws}(x)$. In the HNC approximation

[58*a*] $$g_{ws}(x) = \exp\{\xi(x)\} \cosh\{\eta(x) + \beta z e \phi(x)\}$$

and

[58*b*] $$g_{wd}(x) = \exp\{\xi(x)\} \sinh\{\eta(x) + \beta z e \phi(x)\}$$

where

[59] $$\xi(x) = 2\pi\rho \int_{-\infty}^{\infty} \{g_{ws}(t) - 1\}\,dt \times \int_{|x-t|}^{\infty} s c_s(s)\,ds$$

[60] $$\eta(x) = 2\pi\rho \int_0^\infty g_{wd}(t)\,dt \int_{|x-t|}^{\infty} s c_s^{sr}(s)\,ds$$

and

[61] $$\beta z \phi(x) = \kappa^2 \int_x^\infty (t-x) g_{wd}(t)\,dt$$

In [59] and [60], $c_s(r) = [c_1(r) + c_2(r)]/2$ and $c_d^{sr}(r) = [c_1(r) - c_2(r)] + \beta z^2/\varepsilon r$. Thus, $\xi(x)$ and $\eta(x)$ are contributions arising from the cores of the ions. For point ions, $\xi(x) = \eta(x) = 0$ and the HNC approximation reduces to the GC theory (28). For ions with a nonvanishing core, $\xi(x)$ is small and to a good approximation $g_{ws}(x)$ and $g_{wd}(x)$ are hyperbolic functions but with a different argument than that used in the GC theory. This suggests that $g_{ws}(x)$ be calculated from

[62] $$g_{ws}(x) = \cosh[\sinh^{-1} g_{wd}(x)] = \sqrt{1 + g_{wd}^2(x)}$$

Now both $g_{ws}(x)$ and $g_{wd}(x)$ are specified.

Can. J. Chem. Downloaded from www.nrcresearchpress.com by 210.87.254.40 on 09/06/12
For personal use only.

Results

Inasmuch as we use the HNC/MSA values of $\phi = \phi(0)$ to determine ν, it is important to establish the accuracy of these values of ϕ. In Fig. 1 it is seen that the HNC/MSA values of ϕ are in good agreement with the computer simulation values of Torrie and Valleau (16). The HNC/HNC values are poor and are not plotted. At low concentrations the HNC/HNC values of ϕ pass through a maximum at low charge densities. Blum *et al.* (29) have shown that the *total* potential must be monotonic. Although there seems to be no general theorem for ϕ (the *diffuse layer* potential) it seems probable that it too must be monotonic since there is no sign of nonmonotonic behaviour of ϕ in the computer simulations of Torrie and Valleau. At very high charge densities the HNC/MSA values of ϕ also exhibit a maximum. However, the charge densities at which this occurs are much higher than are experimentally accessible so that this behaviour of the HNC/MSA ϕ at high charge densities is of no practical interest. Some refined versions of the MPB and BGY theories predict a monotonic ϕ and are qualitatively superior to the HNC/MSA approximation. However, for values of the charge density which are of experimental interest, the HNC/MSA ϕ is quantitatively better than that of either of these refined approximations.

As seen in Fig. 1, the GC results for ϕ are considerably less satisfactory than the HNC/MSA results. In the GC theory, at high charge densities ϕ is a linear function of log c (where c is the concentration). There is indirect experimental evidence supporting this prediction. This is often taken to be an experimental confirmation of the GC theory. However, as is seen in Fig. 2, the HNC/MSA values of ϕ are also a linear function of log c at high charge densities.

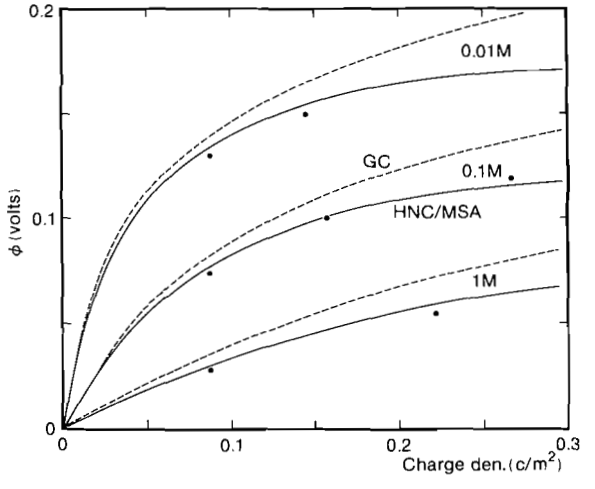

FIG. 1. Diffuse layer potential as a function of charge density on the electrode for a model monovalent ionic fluid (σ = 0.425 nm, T = 298 K, ε = 78.5). The points are the simulation values of Torrie and Valleau (16). The broken curve gives the Gouy–Chapman (GC) results and the solid curve gives the HNC/MSA results.

In Figs. 3 and 4 the distribution functions which result from the GMSA are compared with those resulting from a full HNC/MSA calculation. The agreement is good and indicates that the GMSA procedure is satisfactory.

Although the HNC/MSA ϕ is appreciably different from the GC result, it is insensitive to changes in ionic diameter. However, as is seen from Figs. 5 and 6 there is a diameter dependence in the distribution functions. In general in the GMSA, more counterions are found near the electrode (and consequently fewer further from the electrode, as required by charge neutrality) than is the case in the GC theory. However, as the diameter of the ions is increased, the number of counterions in the immediate vicinity of the electrode decreases. This, presumably, is due to the packing of the spheres right at the electrode. Somewhat further out there is a bulge in the counterion distribution function of the larger spheres so that ϕ is fairly insensitive to the size of the ions. At high charge densities this bulge becomes more pronounced but does not become as pronounced as in the computer simulations where a second layer of

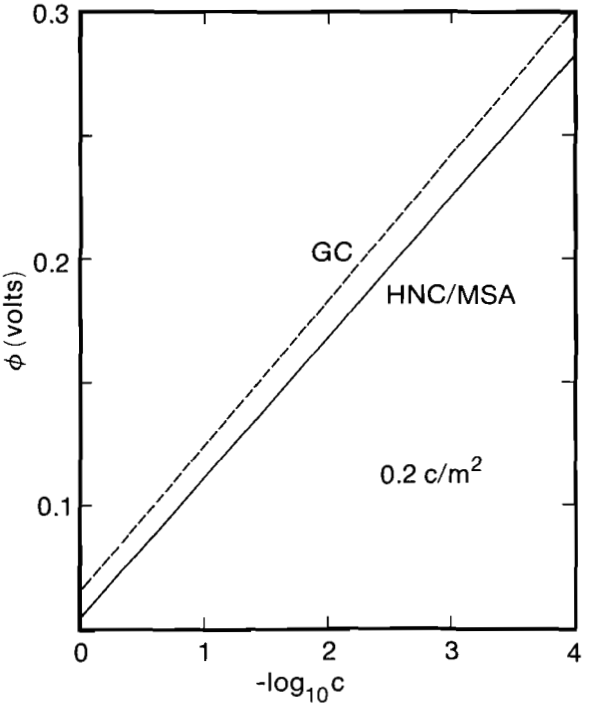

FIG. 2. Diffuse layer potential as a function of concentration for a model monovalent ionic fluid (σ = 0.425 nm, T = 298 K, ε = 78.5). The curves have the same meaning as in Fig. 1.

Can. J. Chem. Downloaded from www.nrcresearchpress.com by 210.87.254.40 on 09/06/12
For personal use only.

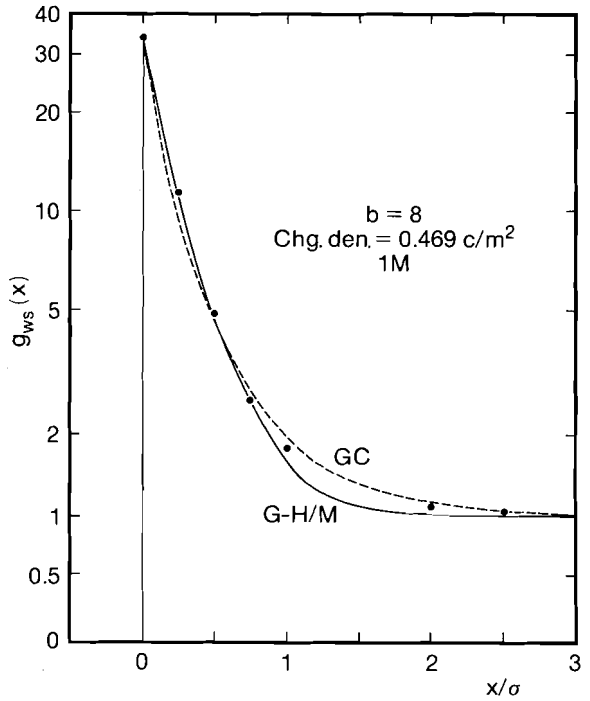

FIG. 3. The density profile of a model monovalent ionic fluid ($\sigma = 0.276$ nm, $T = 298$ K, $\varepsilon = 78.4$). The points are the results of full HNC/MSA calculation, whereas the solid curve gives the GMSA values when v is fitted to the HNC/MSA diffuse layer potential. This latter calculation is designated G-H/M.

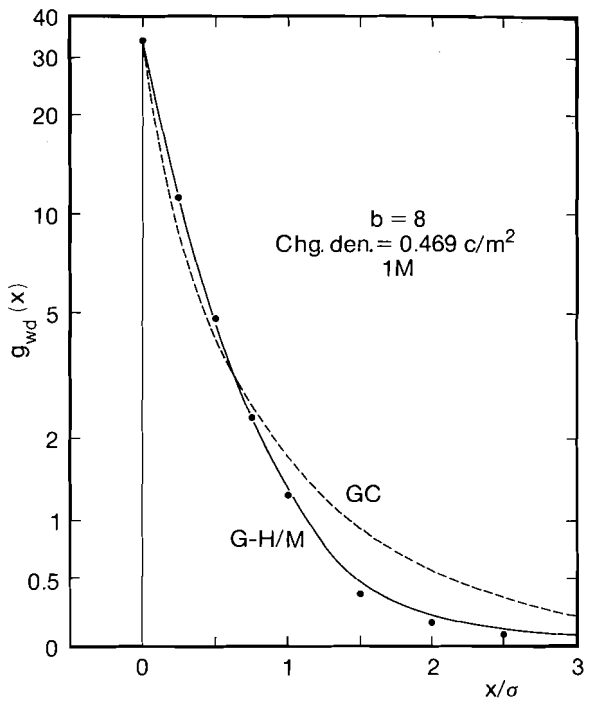

FIG. 4. The charge profile of a model monovalent ionic fluid ($\sigma = 0.276$ nm, $T = 298$ K, $\varepsilon = 78.4$). The points and curves have the same meaning as in Fig. 3.

counterions is formed. However, we note that this formation of a second layer occurs at higher charge densities than is of experimental interest. At the charge densities of practical interest, the GMSA distribution functions are reasonable.

The GMSA values of $g_{wd}(x)$ and $\phi(x)$ for a 1 M solution are plotted in Figs. 7 and 8. In Figs. 9–11 we have plotted $g_{wi}(x)$, $g_{wd}(x)$, and $\phi(x)$ for a 10^{-2} M solution. At both concentrations, errors in the GC profiles are seen. However, given the rapid rate of change of the counterion profile, the GC results for $g_{wi}(x)$ are reasonably good. In looking at Figs. 5–7 and 9–10 it should be kept in mind that the scale is nonlinear and magnifies differences where the distribution functions are small. The agreement of the GC and GMSA results would look better on a linear scale. Despite the fairly good agreement of the GC and GMSA charge profiles, the potential profiles of the two theories, plotted in Figs. 8 and 11, are appreciably different.

Finally, the excess charge adsorbed by the electrode is plotted in Fig. 12. The results of the GC theory and MSA are virtually identical. Of all the quantities considered here, this is the least sensitive.

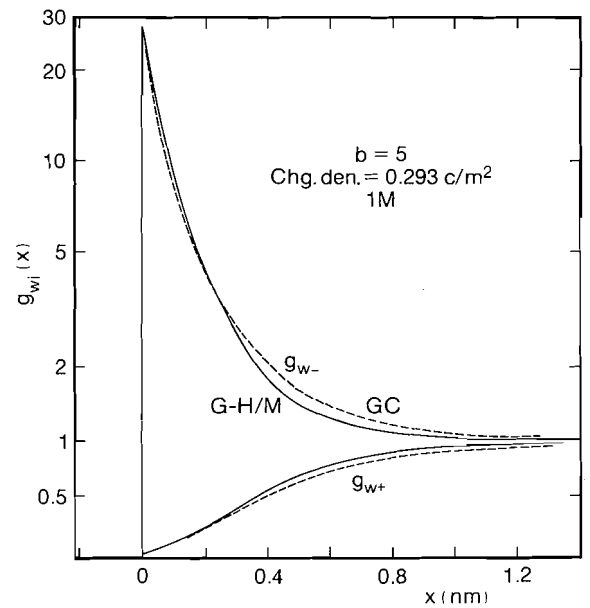

FIG. 5. Ionic distribution functions of a 1 M model monovalent ionic fluid ($\sigma = 0.276$ nm, $T = 298$ K, $\varepsilon = 78.4$). The broken curve gives the Gouy–Chapman (GC) results and the solid curve gives the GMSA results when v is chosen to fit the HNC/MSA results. This latter calculation is designated G-H/M.

Can. J. Chem. Downloaded from www.nrcresearchpress.com by 210.87.254.40 on 09/06/12
For personal use only.

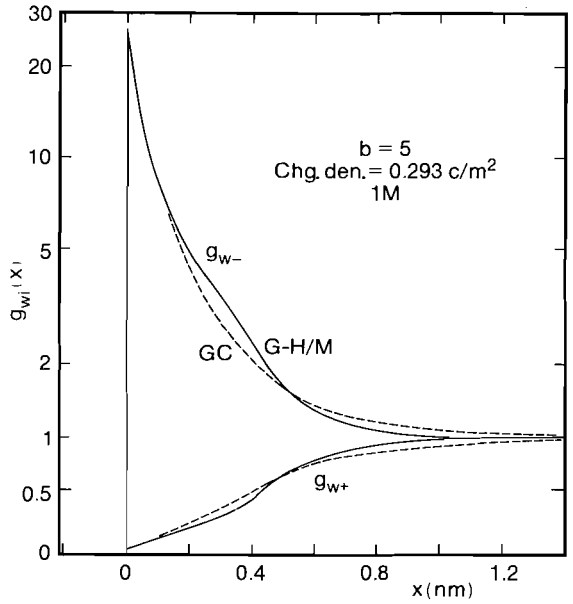

FIG. 6. Ionic distribution functions of a 1 M model monovalent ionic fluid ($\sigma = 0.425$ nm, $T = 298$ K, $\varepsilon = 78.5$). The curves have the same meaning as in Fig. 5.

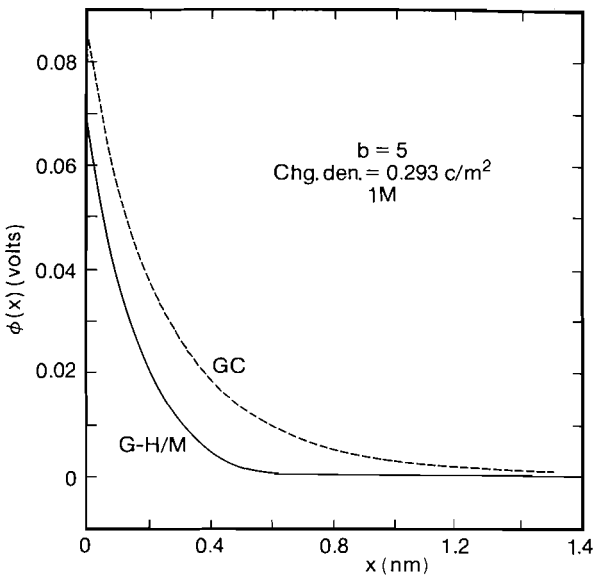

FIG. 8. Potential profile of a 1 M model monovalent ionic fluid ($\sigma = 0.425$ nm, $T = 298$ K, $\varepsilon = 78.5$). The curves have the same meaning as in Fig. 5.

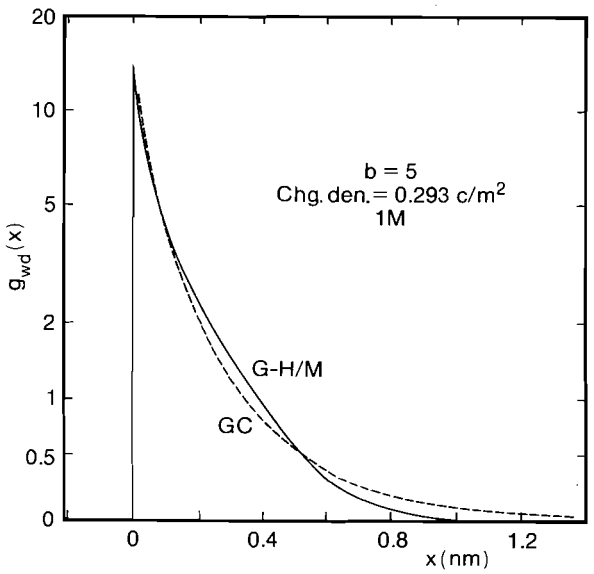

FIG. 7. Charge profile of a 1 M model monovalent ionic fluid ($\sigma = 0.425$ nm, $T = 298$ K, $\varepsilon = 78.5$). The curves have the same meaning as in Fig. 5.

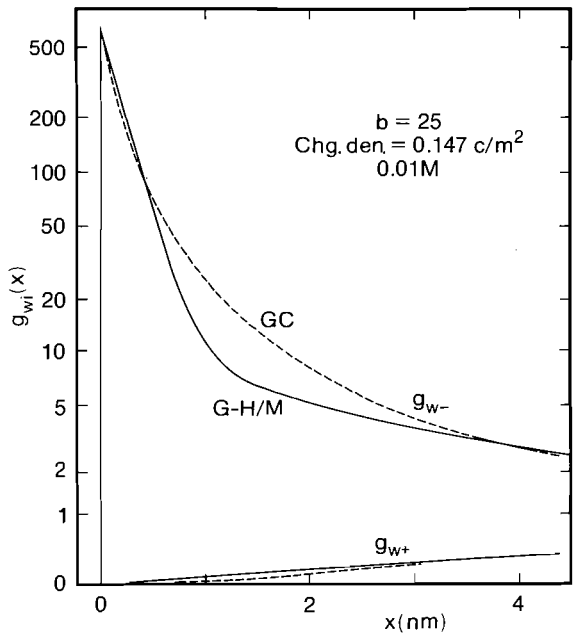

FIG. 9. Ionic distribution functions of 10^{-2} M model monovalent ionic fluid ($\sigma = 0.425$ nm, $T = 298$ K, $\varepsilon = 78.5$). The curves have the same meaning as in Fig. 5.

Summary

We have made a GMSA calculation of the distribution functions of a system of charged hard spheres near a hard charged wall. We find that the distribution functions, and thus the density and charge profiles, are given fairly accurately by the GC theory. However, errors in the GC theory can be seen. Specifically, there are more counterions near the electrode than in the GC theory. Also at higher concentrations and high charge densities on the electrode there is charge oscillation. That is after the

Can. J. Chem. Downloaded from www.nrcresearchpress.com by 210.87.254.40 on 09/06/12
For personal use only.

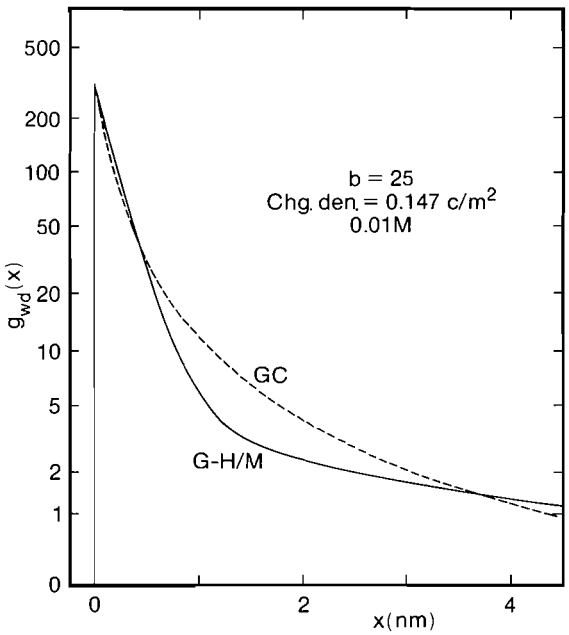

FIG. 10. Charge profile of a 10^{-2} M model monovalent ionic fluid (σ = 0.425 nm, T = 298 K, ε = 78.5). The curves have the same meaning as in Fig. 5.

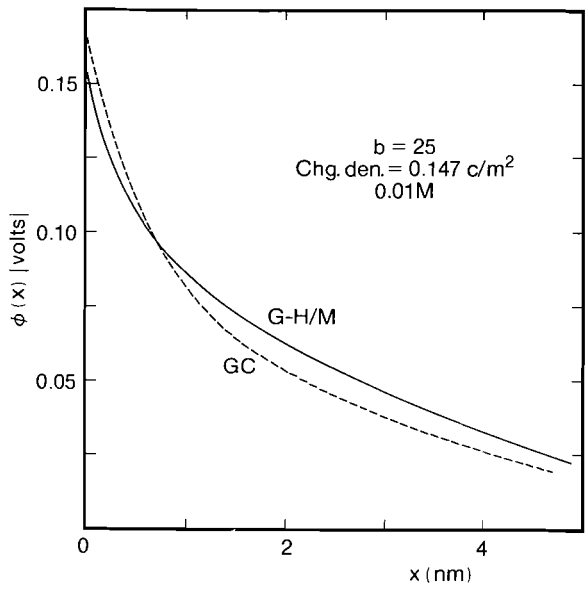

FIG. 11. Potential profile of a 10^{-2} M model monovalent ionic fluid (σ = 0.425 nm, T = 298 K, ε = 78.5). The curves have the same meaning as in Fig. 5.

layer of counterions near the electrode there is a small "layer" of ions of the same charge as the electrode. However, it occurs under extreme conditions and is probably not of practical importance. Given the rapid rate of change of the counterion profile, the GC profiles are fairly good.

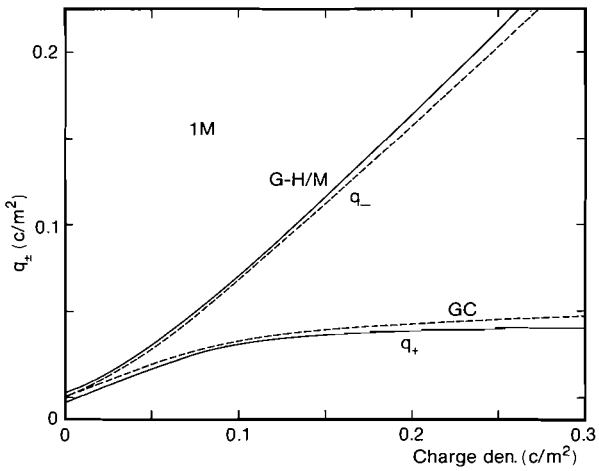

FIG. 12. Excess charge adsorbed by the electrode in a model monovalent ionic fluid (σ = 0.425 nm, T = 298 K, ε = 78.5). The curves have the same meaning as in Fig. 5.

The errors in the GC diffuse layer potentials and potential profiles are relatively more important. This is because the integrand in integral [52] is weighted towards larger values of $g_{wd}(x)$ where the GC values are too large. The integrands in [50] and [51] are unweighted and as a result more accurate values are obtained for these integrals.

The major defect in this calculation is the fact that the GMSA, in common with the HNC, BGY, and MGC approximations, does not adequately treat the excluded volume effects among the ions near the wall. As a result, at higher charge densities, too many counterions are allowed near the wall and the GMSA diffuse layer potential will be too small. However, this effect does not become serious until the charge density on the wall is greater than is experimentally relevant. For charge densities of experimental interest, the GMSA and the HNC approximations are satisfactory.

Since the number of counterions near the wall is small, it seems likely that the GMSA and the HNC approximations give better results for the co-ion distribution functions than for the counterion distribution functions.

Acknowledgments

The authors are grateful to Drs. G. Torrie and J. Valleau for sending them a preprint of their work.

1. D. HENDERSON, F. F. ABRAHAM, and J. A. BARKER. Mol. Phys. **31**, 1291 (1976).
2. G. GOUY. J. Phys. **9**, 457 (1910).
3. D. L. CHAPMAN. Philos. Mag. **25**, 475 (1913).
4. L. BLUM. J. Phys. Chem. **81**, 136 (1977).
5. D. HENDERSON and L. BLUM. J. Chem. Phys. **69**, 5441 (1978).
6. D. HENDERSON, L. BLUM, and W. R. SMITH. J. Phys. Lett. **63**, 381 (1979).

7. D. HENDERSON and L. BLUM. J. Electroanal. Chem. **111**, 217 (1980).
8. S. L. CARNIE, D. Y. C. CHAN, D. J. MITCHELL, and B. W. NINHAM. J. Chem. Phys. **74**, 1472 (1981).
9. S. LEVINE and C. W. OUTHWAITE. J. Chem. Soc. Faraday Trans. II, **74**, 1670 (1978).
10. C. W. OUTHWAITE, L. B. BHUIYAN, and S. LEVINE. Chem. Phys. Lett. **64**, 150 (1979).
11. L. B. BHUIYAN, C. W. OUTHWAITE, and S. LEVINE. Chem. Phys. Lett. **66**, 321 (1979).
12. C. W. OUTHWAITE, L. B. BHUIYAN, and S. LEVINE. J. Chem. Soc. Faraday Trans. II, **76**, 1388 (1980).
13. T. L. CROXTON and D. A. MCQUARRIE. Chem. Phys. Lett. **68**, 489 (1979).
14. T. L. CROXTON and D. A. MCQUARRIE. Mol. Phys. **42**, 141 (1981).
15. G. M. TORRIE and J. P. VALLEAU. Chem. Phys. Lett. **65**, 343 (1979).
16. G. M. TORRIE and J. P. VALLEAU. J. Chem. Phys. **73**, 5807 (1980).
17. D. HENDERSON and L. BLUM. Surf. Sci. **101**, 189 (1980).
18. D. HENDERSON, L. BLUM, and J. L. LEBOWITZ. J. Electroanal. Chem. **102**, 315 (1979).
19. D. HENDERSON, L. BLUM, D. A. MCQUARRIE, and W. OLIVARES. Chem. Phys. Lett. **71**, 569 (1980).
20. L. BLUM and G. STELL. J. Stat. Phys. **15**, 439 (1976).
21. R. J. BAXTER. J. Chem. Phys. **52**, 4559 (1970).
22. M. WERTHEIM. Phys. Rev. Lett. **10**, 321 (1963).
23. M. WERTHEIM. J. Math. Phys. **5**, 643 (1964).
24. E. WAISMAN, D. HENDERSON, and J. L. LEBOWITZ. Mol. Phys. **32**, 1373 (1976).
25. D. HENDERSON, J. L. LEBOWITZ, L. BLUM, and E. WAISMAN. Mol. Phys. **39**, 47 (1980).
26. D. HENDERSON and W. R. SMITH. J. Stat. Phys. **19**, 191 (1978).
27. D. HENDERSON, L. BLUM, and J. L. LEBOWITZ. J. Electroanal. Chem. **102**, 315 (1979).
28. D. HENDERSON and L. BLUM. J. Electroanal. Chem. **93**, 151 (1978).
29. L. BLUM, J. L. LEBOWITZ, and D. HENDERSON. J. Chem. Phys. **72**, 4249 (1980).

Can. J. Chem. Downloaded from www.nrcresearchpress.com by 210.87.254.40 on 09/06/12
For personal use only.

Adsorption of phthalic acid on mercury electrodes

MARCIN OPALLO,[1] JADWIGA DOJLIDO, AND ZBIGNIEW GALUS

Department of Chemistry, University of Warsaw, 02093 Warsaw, Pasteura 1, Poland

Received July 18, 1980

This paper is dedicated to Dr. Sam Levine on the occasion of his 70th birthday

MARCIN OPALLO, JADWIGA DOJLIDO, and ZBIGNIEW GALUS. Can. J. Chem. **59**, 1918 (1981).

The adsorption of *o*-phthalic acid (H_2Pht) on mercury electrodes was studied in the pH range 0.5–11.5 using surface tension, double layer capacity, and zero charge potential measurements. The calculated adsorption isotherms indicate a reorientation of H_2Pht molecules from flat to vertical orientation with increase of H_2Pht concentration in the solution. These results combined with the change of the zero charge potentials suggest that in the vertical position —COOH groups are directed to the surface of the metal. The change in the adsorption of phthalic acid at different pH's was explained by the different adsorbability of free acid H_2Pht and its ions $HPht^-$ and Pht^{2-}.

MARCIN OPALLO, JADWIGA DOJLIDO et ZBIGNIEW GALUS. Can. J. Chem. **59**, 1918 (1981).

On a étudié l'adsorption de l'acide *o*-phtalique (H_2Pht) sur des électrodes de mercure dans l'intervalle de pH 0,5–11,5 en utilisant des mesures de tension superficielle, de capacité de la double couche et de potentiel de charge zéro. Les isothermes d'adsorption calculées indiquent qu'il se produit une réorientation des molécules de H_2Pht d'une orientation plane vers une orientation verticale lorsque la concentration de H_2Pht augmente dans la solution. Ces résultats, combinés aux changements du potentiel de charge zéro, suggèrent que dans la position verticale les groupes COOH sont dirigés vers la surface du métal. La variation de l'adsorption de l'acide phtalique à différents pH s'explique par l'adsorbabilité différente de l'acide libre H_2Pht et de ses ions $HPht^-$ et Pht^{2-}.

[Traduit par le journal]

Introduction

In a previous investigation we studied the adsorption of benzoic acid (1). From this and other studies (2–5) of the adsorption of monosubstituted benzene derivatives it follows that the substituent has an important role in the modification of the equilibrium constant and the mechanism of adsorption. These parameters are changed also by introducing a second substituent in the benzene ring (6, 7).

In the present investigation the adsorption of *o*-phthalic acid (H_2Pht) was studied in order to look for a correlation between the adsorption mechanism and the structure of the adsorbate. Inspection of the literature reveals that there is no paper on the adsorption of phthalic acid on mercury electrodes. Only the adsorption of phthalate ion was studied (8). However, this work was carried out under special conditions, with a high concentration of potassium phthalate without addition of an indifferent electrolyte.

We studied the adsorption of H_2Pht using three independent methods, namely, double layer capacity, surface tension, and potential of the zero charge measurements. Since these studies were carried out at different pH's, a knowledge of the distribution of H_2Pht and its anions in such solutions was important. The protolytic equilibrium of phthalic acid in aqueous solutions was previously described in the literature (9). The pK values of two dissociation steps are equal to 2.95 and 5.40. It should be emphasized that a protolytic equilibrium in the bulk of the solution of many organic compounds influences to a large extent the double layer capacity and zero charge potentials of mercury electrodes. This was illustrated in our earlier works (1, 10, 11).

[1]Present address: Institute of Physical Chemistry of the Polish Academy of Sciences, 01224 Warsaw, Kasprzaka 44/52, Poland.

Experimental

Reagent and Solutions

Phthalic acid, NaOH, Na_2SO_4, and KCl were reagent grade chemicals, H_2SO_4 was Merck for spectroscopy; Na_2SO_4 was additionally purified by recrystallization from thrice distilled water. Water of the same purity was used for preparation of all solutions. The second distillation of water was carried out from an alkaline solution of permanganate and a third one from an all-quartz still. Mercury was chemically purified by prolonged shaking with a solution of $Hg_2(NO_3)_2$ acidified with HNO_3 and then distilled under vacuum. Purity of all reagents was tested polarographically. Before measurements all solutions were deoxygenated with a stream of argon presaturated with the investigated solution.

Apparatus

The double layer capacity of the mercury electrode was measured using an impedance bridge type R 565 manufactured in the Soviet Union. The capacities were measured at different frequencies. Above pH 2 no frequency dispersion was found at potentials close to the capacity minimum and in its vicinity, in solutions of different phthalic acid concentration. At lower pH some frequency dispersion of the measured capacity was observed, also at the capacity minimum, both in presence of phthalic acid and for the background electrolyte alone, being, however, larger in the former case. Since it was difficult to linearize the capacities at the low frequency range, we selected on the basis of our experience the frequency 500 Hz hoping that this approach would result in smaller error. Such a procedure could influence the isotherm calculated on the basis of the

0008-4042/81/131918-07$01.00/0

©1981 National Research Council of Canada/Conseil national de recherches du Canada

Can. J. Chem. Downloaded from www.nrcresearchpress.com by 210.87.254.105 on 09/06/12
For personal use only.

Can. J. Chem. Downloaded from www.nrcresearchpress.com by 210.87.254.105 on 09/06/12
For personal use only.

capacity measurements; however, since there is a similar deviation of the capacity from the equilibrium value in the different solutions considered in calculating θ, the calculated θ values should not be much different from the true values. The bridge was balanced after 3 s of drop growth. The precision of capacity measurement was ±0.1% and the reproducibility of results was about ±0.5%.

Surface tension was measured with the use of a capillary electrometer applying the maximum bubble pressure method (12). A simple drawn out nonsiliconized capillary dipping vertically into the solution was used. In preliminary experiments a U-shaped capillary was used; however, no improvement in the precision and accuracy of measurements was found. The level of the mercury meniscus in the tube was read by means of a KM 6 cathetometer (Soviet production) with a precision of 0.01 mm. This apparatus was calibrated with a 0.05 *M* solution of Na_2SO_4 taking the maximum value of surface tension to be 426.2 mN m^{-1} (13). The precision of these measurements was ±0.1 mN m^{-1} and the accuracy was about 0.5 mN m^{-1}. Zero charge potentials were measured using the streaming mercury electrode. The precision of these measurements was ±0.5 mV and the accuracy was about 2 mV.

All potentials in electrocapillary experiments were measured with respect to a calomel electrode with 1 *M* NaCl. Double layer capacity and zero charge potential (pzc) measurements were carried out with respect to a calomel electrode with 1 *M* KCl. According to Grahame (in ref. 14) the 1 *M* NaCl calomel electrode has a potential 5 mV more positive than the 1 *M* KCl calomel electrode. Numerical values of E^z in Fig. 6a were corrected for the liquid junction potential estimated using the Henderson formula. All measurements were carried out at 298 ± 0.5 K.

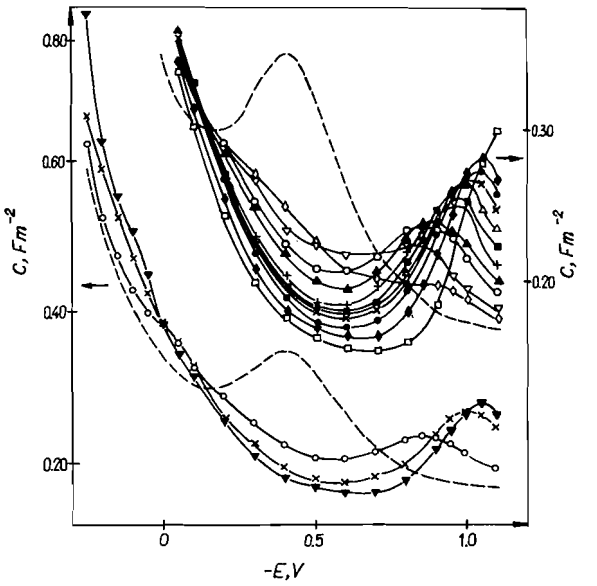

FIG. 1. The dependence of the differential capacity of the mercury electrode on the potential in 0.5 *M* H_2SO_4 containing the following molar concentrations of phthalic acid: (---) 0, (◇) 0.0005, (▽) 0.001, (○) 0.002, (▲) 0.003, (+) 0.005, (■) 0.006, (△) 0.008, (×) 0.010, (●) 0.012, (◆) 0.015, (▼) 0.017, (□) saturated solution.

Results

Protolytic equilibria of phthalic acid in the bulk of the solution suggest that different forms of this compound may be adsorbed on the mercury surface. The distribution of H_2Pht, $HPht^-$, and Pht^{2-} as a function of pH is shown in Fig. 6b. It should be emphasized that these equilibria at the electrode surface may be changed to some extent (see for instance ref. 1). Values of pH equal to 0.5 and 8.0 were chosen to study the adsorption of H_2Pht and Pht^{2-} respectively. Under such conditions the influence of adsorption of other forms was practically eliminated. The maximum mole fraction of $HPht^-$ in aqueous solution is equal to 0.89 (see Fig. 6b); as a consequence there is no pH at which the adsorption of this species could be studied neglecting the other forms.

Measurements in Acidic Solutions

The measured double layer capacities and surface tensions as a function of the mercury electrode potential for 5 × 10^{-4} *M* to saturated solution of H_2Pht in 0.5 *M* H_2SO_4 are given in Figs. 1 and 2. Zero charge potentials for the same H_2Pht concentration range are shown in Fig. 3.

The range of potentials was limited to +250 to −1100 mV and 0 to −1100 mV in double layer

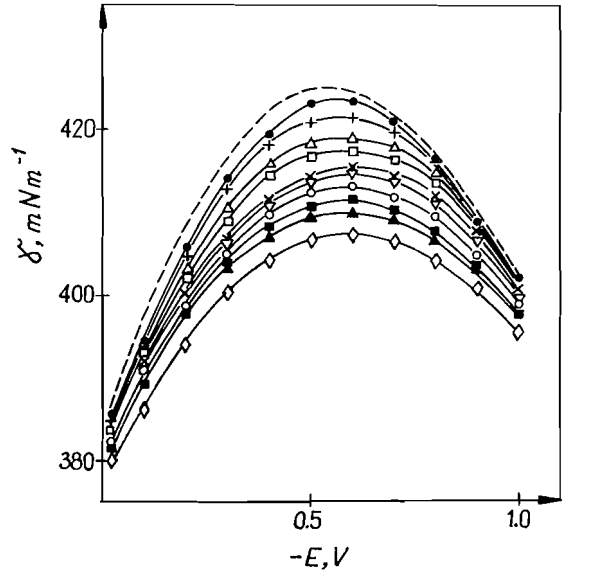

FIG. 2. The dependence of the interfacial tension on the potential in 0.5 *M* H_2SO_4 containing the following molar concentrations of phthalic acid: (---) 0, (●) 0.0005, (+) 0.001, (△) 0.002, (□) 0.003, (×) 0.005, (▽) 0.006, (○) 0.008 and 0.010, (■) 0.012, (▲) 0.015, (◇) saturated solution.

Can. J. Chem. Downloaded from www.nrcresearchpress.com by 210.87.254.105 on 09/06/12
For personal use only.

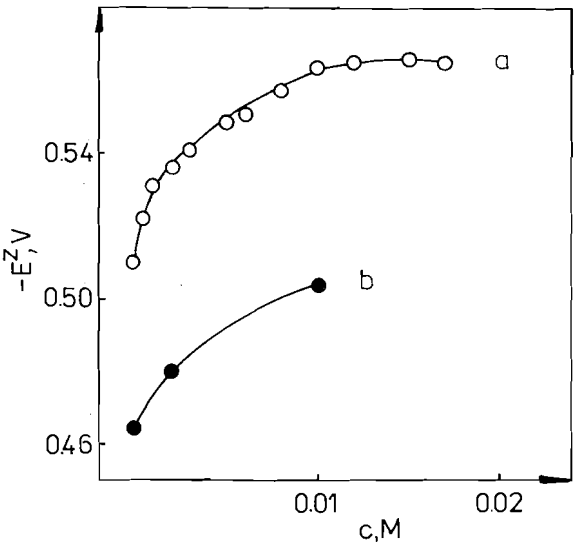

FIG. 3. The dependence of pzc (E^z) of the mercury electrode on the concentration of phthalic acid: (a) 0.5 *M* H_2SO_4 and (*b*) 0.5 *M* Na_2SO_4 with pH = 8.

capacity and electrocapillary measurements, respectively. A significant increase of capacity at potentials near to 0 V was caused by mercury oxidation. At potentials more negative than −1100 mV the measurements were difficult due to electroreduction of phthalic acid (15).

The surface tension decreases significantly with increase in the surfactant concentration. Even at low H_2Pht concentrations both surface tensions and differential capacities are considerably lower with respect to those for the pure background electrolyte. The electrocapillary curves do not coincide with that of the background electrolyte at a potential of −1100 mV. Probably phthalic acid desorbs completely from the electrode surface at more negative potentials not accessible to the experimental measurements.

The decrease in the minimum of the capacity is proportional to surfactant concentration. However, in the concentration range 0.005 to 0.010 *M*, the capacity changes only by 0.09 F m^{-2}, decreasing more significantly at concentrations exceeding 0.010 *M*. This effect may indicate reorientation of H_2Pht on the electrode surface and will be discussed later in this paper. The value of the capacity minimum in H_2Pht saturated solution is equal to 0.156 F m^{-2}.

At a lower H_2Pht concentration range, the pzc shifts to more negative values with increase in phthalic acid concentration. In the concentration range 0.010 to 0.017 *M* it attains a constant value. The maximum of this shift is equal to −55 mV.

Measurements in Alkaline Solutions

These measurements were carried out at pH = 8. As a background electrolyte 0.50 *M* Na_2SO_4 was used; pH was adjusted by addition of NaOH.

The dependence of the capacity on the potential for three concentrations of phthalic acid is shown in Fig. 4. Phthalate ion causes a decrease of the capacity of the mercury electrode at potentials near to 0 V but this effect is much smaller than in acidic solutions. At more negative potentials, the differential capacities were larger in comparison to that in the background electrolyte alone. A similar observation was made by Tilak and Devanathan (8) in their studies on phthalate ion adsorption in the absence of the background electrolyte.

It seems that in our case, at potentials positive with respect to the zero charge potential, the larger capacity is due to pseudo-capacity effects.

At potentials cathodic to E^z the reason for higher capacity in the presence of phthalates is not well understood, but the experimental data in Fig. 4 were confirmed in careful measurements.

It follows from Fig. 3 (curve b) that the pzc is shifted to more negative values with increasing phthalic acid concentration under the above conditions.

It was also found that phthalic acid in alkaline solution causes a small decrease of surface tension on the positive branch of the electrocapillary curve. For instance, this decrease amounts to about 5 mN m^{-1} at −450 mV in a solution saturated with H_2Pht. However, it must be emphasized that the reproducibility of the measurement was not satisfactory.

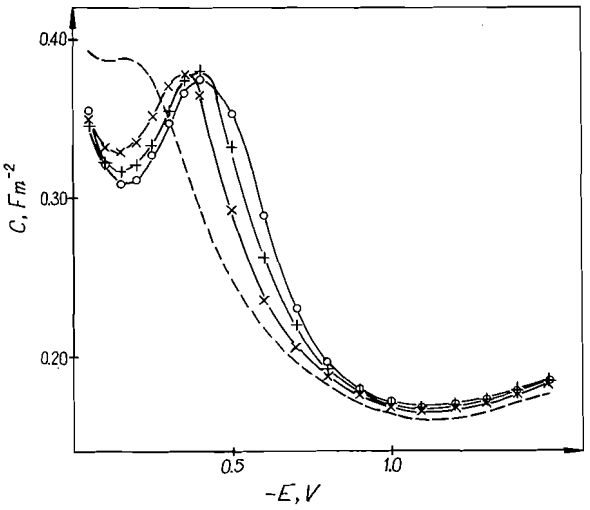

FIG. 4. The dependence of the differential capacity of the mercury electrode on potential in 0.5 *M* Na_2SO_4 at pH = 8, containing the following molar concentrations of phthalic acid (---) 0, (x) 0.002, (+) 0.010, (○) saturated solution.

Can. J. Chem. Downloaded from www.nrcresearchpress.com by 210.87.254.105 on 09/06/12
For personal use only.

Measurements at other pH's

The dependence of the differential capacity on the electrode potential at different pHs is presented in Fig. 5. The differential capacity and pzc were measured for 0.01 *M* H_2Pht solution with the pH changing from 0.45 to 11.60. A concentration of H_2Pht equal to 0.01 *M* was found to be the most appropriate in these experiments. The pH was adjusted by addition of the appropriate amount of H_2SO_4 or NaOH to the Na_2SO_4 solution. The total electrolyte concentration was kept constant and equal to 0.50 *M*.

Discussion

The results of the electrocapillary, differential capacity, and zero charge potential measurements in acidic solution indicate the adsorption of phthalic acid molecules at the mercury electrode.

Since our studies were carried out over a wide range of pH, fluorides could not be used as background electrolyte. Under such conditions the selection of sulphates was justified. However, these anions are adsorbed to some extent on mercury electrodes as was shown by Payne (16). Consequently our results are influenced to some extent by this adsorption especially at positive potentials with respect to E^z. Since the pK_2 value for H_2SO_4 is equal to 2.0, at lower pH, the HSO_4^- ion exists in solution, and is also adsorbed to some extent on the mercury electrode. This adsorption was studied by us, and it will be presented elsewhere, since its influence on results presented in the present paper is rather small.

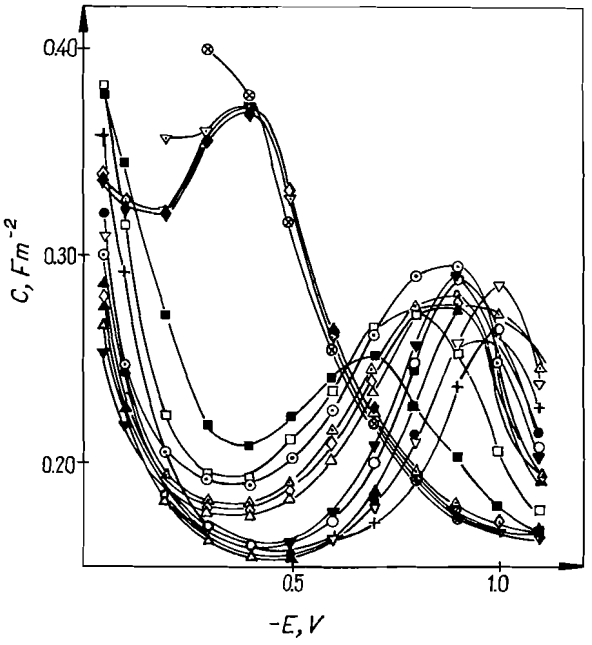

FIG. 5. The dependence of the differential capacity of the mercury electrode on the potential in solution of 0.01 *M* phthalic acid in 0.5 *M* Na_2SO_4 at following pH's: (+) 1.33, (○) 1.85, (▽) 2.02, (▲) 2.26, (○) 2.80, (▼) 3.02, (△) 3.45, (◇) 3.72, (▲) 4.01, (⊙) 4.32, (□) 4.60, (■) 5.02, (◇) 5.72, (◆) 8.05, (▽) 11.40, (⊗) 11.62.

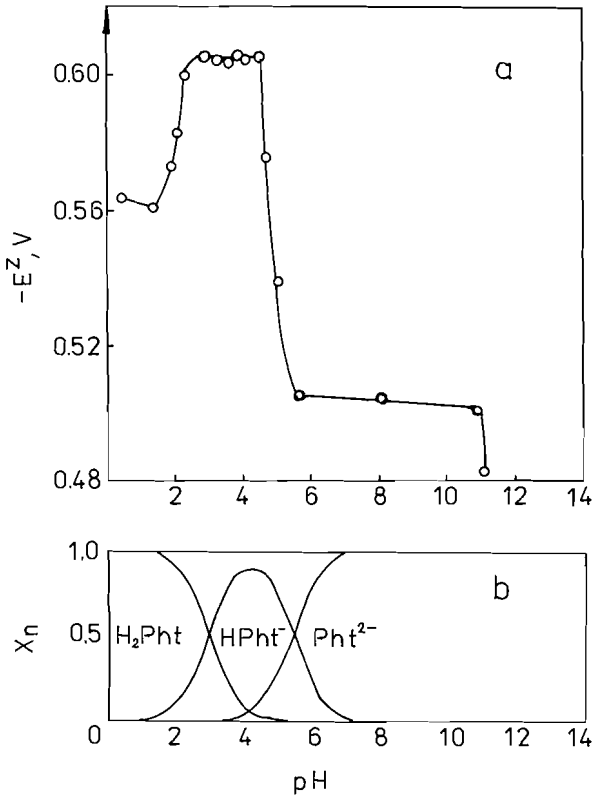

FIG. 6. (a) The dependence of pzc (E^z) of the mercury electrode on pH in a solution of 0.01 *M* phthalic acid in 0.5 *M* Na_2SO_4; (b) The distribution of H_2Pht, $HPht^-$, and Pht^{2-} as a function of pH in the bulk of the solution.

Adsorption isotherms (Fig. 7) determined on the basis of electrocapillary measurements can precisely describe the extent of adsorption. At potentials −500 to −700 mV the surface excess attains a constant value in the concentration range 0.003 to 0.01 *M* and is equal to about 1.6×10^{-6} Mm^{-2}. However, for concentrations of phthalic acid higher than 0.01 *M*, the value of the surface excess strongly increases. It may point to a change of adsorption mechanism. The surface of projection of the phthalic acid molecule with the benzene ring perpendicular to the electrode surface calculated from crystallographic data (17) is equal to 62 $Å^2$. The calculated value of the maximum surface excess on the basis of flat oriented molecules on the electrode is equal to 2.7×10^{-6} Mm^{-2}. This value is higher by 1.1×10^{-6} Mm^{-2} than the value corre-

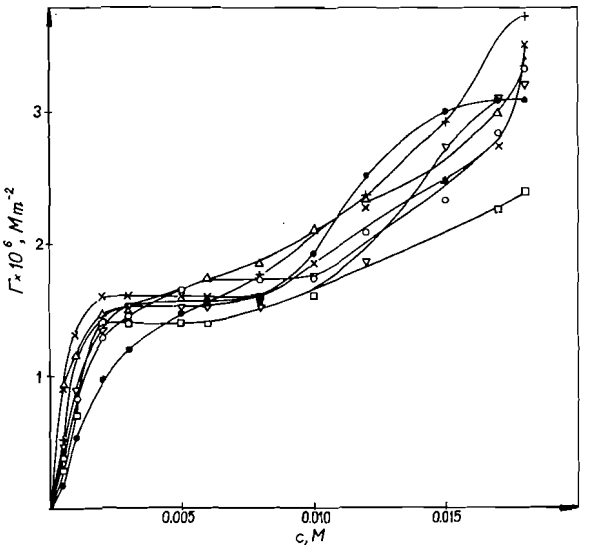

FIG. 7. The dependence of the surface excess concentration of phthalic acid on a mercury electrode on its bulk concentration in 0.5 M H_2SO_4 at the following potentials: (□) 200, (▽) 300, (+) 400, (×) 500, (△) 600, (○) 700, (●) 800 mV.

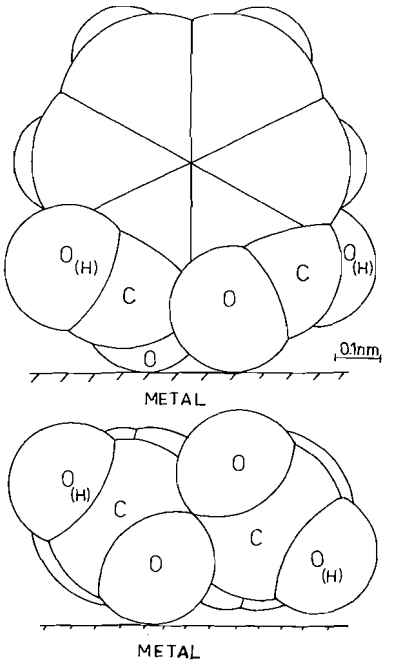

FIG. 8. Model for the adsorption of a phthalic acid molecule in vertical (a) and flat (b) orientation on mercury. Hydrogen atoms of carboxylic groups are not shown in the figure.

sponding to the plateau of the adsorption isotherms given in Fig. 7. In estimating the maximum surface excess in a vertical orientation, the model presented in Fig. 8 was used. Close-packed orientation and no hydration of H_2Pht was assumed in the calculation of Γ_m in both orientations.

The above conclusions are confirmed also by differential capacity data. The minimum value of capacity is much higher than those for various aromatic compounds of structure similar to that of phthalic acid (1–4) but in the minimum capacity range, vertical orientation of these molecules was proved. The small change of capacity in the concentration range 0.005 to 0.01 M (Fig. 1) also points to saturation of the electrode surface by phthalic acid molecules in the flat orientation (Fig. 8). The value of the minimum capacity for the 0.01 M phthalic acid solution ± 0.180 Fm^{-2}, is equal to the capacity corresponding to flat oriented adsorbed benzoic acid molecules (1). Our isotherms up to 0.01 M phthalic acid concentration show qualitative agreement with the isotherms of several flat oriented aromatic compounds in this concentration range, given by Bockris and co-workers (2).

At concentrations lower than 0.01 M of H_2Pht, where we postulate that the adsorption of this substance occurs in a flat orientation, the adsorption isotherm could also be calculated on the basis of the capacity measurements. As the most optimal potential, −600 mV was chosen, at which the adsorption–desorption effects should be the lowest and the measured capacity should be near to the equilibrium value. At this potential as well as at −500 mV a plot of $E_\theta^z - E_{\theta=0}^z$ against θ was nonlinear (with a shape similar, for instance, to that observed in the case of caproic acid (18)), pointing to the congruence of H_2Pht electrosorption with respect to potential.

The surface coverage calculation was based on the decrease of the differential capacity at a given potential using the well-known formula

$$\theta = \frac{C_0 - C}{C_0 - C_M}$$

where C_0 and C_M are capacities in the base electrolyte alone and at $\theta = 1$, respectively, and C stands for the capacity at a given θ. The determination of the capacity corresponding to maximum coverage of the electrode by phthalic acid could not be done simply by experiment due to the reorientation effect at higher bulk concentrations of acid. This problem was solved by determining C_M from a plot of the reciprocal of the measured capacity versus the reciprocal of phthalic acid concentration. This plot is shown in Fig. 9; the linear part at higher 1/C values corresponds to capacities for flat H_2Pht orientation. From extrapolation C_M equals 0.169 Fm^{-2}. This value is different from C_M found for other aromatic compounds of a similar structure, 0.070 for phenol, 0.070 for cresol, 0.050 for

Can. J. Chem. Downloaded from www.nrcresearchpress.com by 210.87.254.105 on 09/06/12
For personal use only.

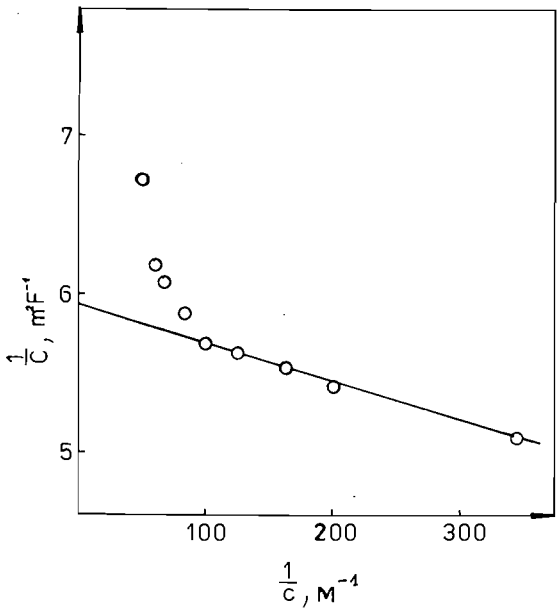

FIG. 9. The plot of reciprocal of the measured capacity versus reciprocal of phthalic acid concentration.

pyridine, and 0.063 Fm^{-2} for benzoic acid. These much lower values of the differential capacity correspond, however, to a vertical orientation of the adsorbed molecules. The strong deviation of 1/c from linearity at higher H_2Pht concentrations (Fig. 9) may point to reorientation of the phthalic acid molecules.

The calculated θ values as a function of concentration of H_2Pht are given in Fig. 10. Using the Frumkin isotherm the following values of the equilibrium adsorption constant and interaction coefficient, 295 M^{-1} and 0.7, respectively, were obtained. Attempts to get reliable values of the interaction coefficient at other potentials were not successful.

It follows from these considerations that for phthalic acid concentrations up to 0.01 *M*, the adsorption of this substance may be described by a model of two parallel condensers. The interior of the capacitors is filled by water and flat oriented phthalic acid molecules. For concentrations higher then 0.01 *M* the three-condenser model elaborated by Damaskin is valid (19). This conclusion is supported by the form of the isotherm shown in Fig. 7 as well as the change of capacity at higher H_2Pht concentrations presented in Fig. 9. However, the quantitative analysis of the adsorption according to the three-condenser model can not be carried out in the context of the Damaskin theory with satisfactory precision, in view of the number of parameters which should be known precisely in order to get meaningful results. In our case parameters such as $\theta_{vertical}$ or $E^z_{vertical}$ could only be estimated because full coverage of the surface in the vertical position is not attained due to the limited solubility of H_2Pht. Qualitative use of the Damaskin concept leads to the conclusion that there is an interaction of H_2Pht molecules in two different positions, because of the absence of the reorientation peak. Such interaction is possible in view of the model proposed in Fig. 8, where carboxylic groups in both orientations may not be too distant.

The estimated value of maximum surface excess corresponding to vertical orientation of H_2Pht on the electrode surface is equal to 5.4×10^{-6} Mm^{-2}. There is some difference in behaviour of phthalic acid in comparison to other aromatic compounds such as phenol (2, 3, 20) and benzoic acid (1). The influence of potential on reorientation of molecules is not evident in the present case of H_2Pht, though the disappearance of a plateau on the isotherm at −800 mV (Fig. 7) suggests that surface saturation by flat oriented molecules was not attained and that there is a progressive reorientation process with increase of H_2Pht concentration. It should be pointed out that our conclusion concerning the reorientation of H_2Pht on the electrode surface was based mainly on electrocapillary measurements. The differential capacity data were not so useful in view of the pseudocapacity peaks occurring over a large potential range. Moreover the charge vs. potential dependence obtained by the integration of the capacity curves was also studied. These dependences were grouped in two families of curves for lower and higher H_2Pht concentrations, eventually pointing also to reorientation.

When considering the independence of the zero charge potentials on H_2Pht concentration in the region of the change of orientation from flat to vertical, one may arrive at the conclusion that it is due to compensation of two effects acting in different directions. The interaction of the π-electrons of the benzene ring in the flat orientation is reflected in the change of the pzc to more negative potentials with increase of H_2Pht concentration. The influence of the reorientation process on E^z may be then expressed as (*i*) a shift of pzc to less negative values as a result of a decrease of the surface coverage of the electrode by H_2Pht in the flat orientation, and (*ii*) a shift of pzc to more cathodic values with an increase of the surface coverage of H_2Pht in the vertical orientation. Since the negative charge of the H_2Pht dipole should be localized on —COOH groups, the shift of pzc to negative values may indicate that these groups are directed to the electrode surface in the vertical orientation of H_2Pht.

Can. J. Chem. Downloaded from www.nrcresearchpress.com by 210.87.254.105 on 09/06/12
For personal use only.

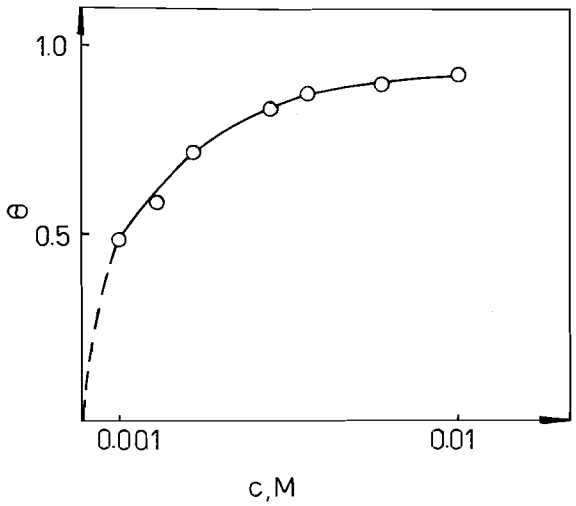

FIG. 10. The dependence of the surface coverage of the mercury electrode on the concentration of phthalic acid in 0.5 *M* H_2SO_4.

The proposed orientation is different from that observed for the aliphatic alcohols and acids (21) and probably also benzoic acid (1).

H_2Pht molecules interact with water by hydrogen bonding. As it follows from the model (Fig. 10b) there should exist also an internal hydrogen bond between two —COOH groups of H_2Pht molecule. Such interaction should decrease the hydrophilic nature of this part of the H_2Pht molecule and at least may explain the tendency of *o*-phthalic acid to have —COOH groups directed to the electrode surface when adsorbed in the vertical position.

Significant changes of the double layer capacity and of zero charge potential with pH (Figs. 5 and 6) at constant analytical concentration of phthalic acid make it possible to describe phthalic acid adsorption more precisely.

Adsorption of hydrogen phthalate ion was studied by Tilak and Devanathan (8). The flat orientation of this ion, with the COO^- group interacting through oxygen with the surface and the benzene ring parallel to the metal surface, was assumed, similar to that proposed by us for the neutral molecules at low bulk concentrations. While this assumption seems to be justified, the assumption that the second carboxylic acid group of the phthalate ion is ionized due to the intense electric field across the interface is questionable.

In Fig. 6a the dependence of the pzc on pH of the solution is shown. Three parts of this dependence at pH 0.5–1.5, 2.5–4.5, and 5.5–10.5 correspond, according to us, to the adsorption of the H_2Pht, $HPht^-$, and Pht^{2-} species, respectively. This view is based on the distribution curves of these species with pH given in part (b) of Fig. 6. By comparing both parts of this figure one may suggest a small influence of the electrical field on the increase of acidity of H_2Pht and $HPht^-$. One may mention that the dependence of the differential capacity at a constant potential (e.g. −0.40 V) on pH has a similar shape. Small changes in capacity and the flat part of the dependence of E^z on pH around pH 4 point to the predominance of $HPht^-$ on the electrode surface.

Acknowledgements

The authors are greatly indebted to Professor T. M. Krygowski and K. Suwińska, M. Sc. for discussions concerning the model of *o*-phthalic acid.

1. J. DOJLIDO, M. DMOWSKA-STAŃCZAK, and Z. GALUS. J. Electroanal. Chem. **94**, 107 (1978).
2. E. BLOMGREN, J. O'M. BOCKRIS, and C. JESCH. J. Phys. Chem. **65**, 2000 (1961).
3. R. S. HANSEN, D. J. HELSH, and D. H. GRANTHAM. J. Phys. Chem. **67**, 2316 (1963).
4. B. B. DAMASKIN, V. M. GEROVICH, I. P. GLADKIH, and R. I. KAGANOVICH. Zh. Fiz. Khim. **38**, 2495 (1965).
5. R. I. KAGANOVICH, V. M. GEROVICH, and O. J. GUSAKOVA. Elektrokhimiya, **3**, 946 (1967).
6. G. MANOHAR and S. SATHYANARAYANA. J. Electroanal. Chem. **70**, 301 (1971).
7. K. M. JOSHI and S. RAJAGOPALAN. Electrochim. Acta, **17**, 479 (1972).
8. B. V. K. S. R. A. TILAK and M. A. V. DEVANATHAN. J. Phys. Chem. **73**, 3582 (1969).
9. D. DOBOS. Electrochemical data. Akademiai Kiadó, Budapest. 1975. p. 149.
10. Z. GALUS, J. DOJLIDO, and G. CHOJNACKA-KALINOWSKA. Electrochim. Acta, **17**, 265 (1972).
11. J. DOJLIDO, Z. GALUS, and L. JEFTIĆ. J. Electroanal. Chem. **62**, 433 (1975).
12. D. J. SCHIFFRIN. J. Electroanal. Chem. **23**, 168 (1969).
13. C. A. SMOLDERS and E. M. DUYVIS. Recl. Trav. Chim. Pays-Bas, **80**, 635 (1961).
14. B. E. CONWAY (*Editor*). Electrochemical data. Elsevier, Amsterdam. 1952. p. 223.
15. N. H. FURMAN and C. E. BRICKER. J. Am. Chem. Soc. **64**, 660 (1942).
16. R. PAYNE. J. Electroanal. Chem. **60**, 183 (1975).
17. R. W. G. WYCKOFF. Crystal structures. Vol. 6. Interscience Publishers, New York, London. 1969. p. 174.
18. B. B. DAMASKIN, O. A. PETRII, and V. V. BATRAKOV. Adsorption of organic compounds on electrodes. Vol. 3. Plenum Press, New York 1971.
19. B. B. DAMASKIN. J. Electroanal. Chem. **21**, 149 (1969).
20. K. NIKI. Bull. Chem. Soc. Jpn. **48**, 997 (1975).
21. A. N. FRUMKIN. Potentials of zero charge. Izdatelstvo Nauka, Moskow. 1979. p. 156.

Can. J. Chem. Downloaded from www.nrcresearchpress.com by 210.87.254.105 on 09/06/12
For personal use only.

Determination of single ion activities by relying on the electrical double layer model: NaF aqueous solutions[1]

ANNA DAGHETTI AND SERGIO TRASATTI

Laboratory of Electrochemistry, University of Milan, Via Venezian 21, 20133 Milan, Italy

Received July 21, 1980

This paper is dedicated to Dr. Sam Levine on the occasion of his 70th birthday

ANNA DAGHETTI and SERGIO TRASATTI. Can. J. Chem. **59**, 1925 (1981).

Single ion activity coefficients for aqueous solutions of NaF in the range $m = 0.1$ up to $m = 0.9$ mol kg^{-1} have been derived by measuring the potential difference of the cell Hg (σ = const)/NaF(m)/F$^-$-selective electrode. The approach rests on the assumption that the electric potential drop across the Hg/solution interface is independent of the electrolyte concentration once the diffuse layer effects are accounted for by the Gouy–Chapman theory, provided specific adsorption of ions is absent. The derived γ_- values have been compared with the "real" activity coefficients as determined by Rabinovich and Titov and with the predictions of the hydration theory of Bates and Robinson. It is shown that the latter do not agree with the present experimental observations. Possible reasons for this apparent discrepancy are discussed.

ANNA DAGHETTI et SERGIO TRASATTI. Can. J. Chem. **59**, 1925 (1981).

La mesure de la différence de potentiel d'une cellule Hg (σ = const/NaF(m)/F$^-$ une électrode sélective, a permis de déduire les coefficients d'activité d'un ion unique dans des solutions aqueuses de NaF pour des molalités variant de $m = 0{,}1$ à $m = 0{,}9$ mol kg^{-1}. Cette approche est fondée sur le fait que la chute de potentiel au niveau de l'interface Hg/solution est indépendante de la concentration de l'électrolyte quand les effets de diffusion de couche sont interprétés selon la théorie de Gouy–Chapman relative à l'absence de l'absorption spécifique de l'ion. On a comparé les valeurs de γ obtenues avec celles des coefficients "réels" d'activités tels que déterminés par Rabinovich et Titov et avec les prévisions de la théorie d'hydratation de Bates et Robinson. On montre que les résultats de ces derniers ne s'accordent pas avec les observations expérimentales. On discute des raisons probables de cette différence.

[Traduit par le journal]

Introduction

It is well known on the basis of strictly thermodynamic arguments (1–4) that single ion activities are not amenable to direct experimental determination, the resulting quantities being mean ionic activities. Even the concept of the former quantity is difficult to assess properly since "single-ion" activities are unavoidably related to the nature of the co-ions. Single ion activities are however much more significant than mean ionic activities for the investigation of the structure of solutions. Therefore, various methods have been proposed to derive single ion activities from measurable experimental quantities. All these approaches obviously imply some non-thermodynamic arguments and approximations. In other words, the necessary step to be taken to arrive at single ion activities is the introduction of some model assumptions.

The simplest experimental arrangement makes use of an electrochemical cell consisting of the electrode under study and a "constant" potential reference electrode (for instance, a saturated calomel electrode). Single ion activity coefficients (γ_i) can then be derived from the measured cell potential difference E by correcting for the unknown contribution due to the solution/reference electrode junction (5, 6). In such a case the model introduced is that for the liquid junction potential calculation.

Another experimental route, originally proposed by Szabo (7) and developed by Milazzo and Defay (8), involves the measurement of the emf for a non-isothermal system constituted by two equal electrodes. Assumptions and approximations are necessary in this case as well (9).

A further experimental method consists in measuring the potential difference for a cell of the type (10–13)

[1] $\quad Pt(H_2)/HCl(m)/air/HCl(m_{ref})/(H_2)Pt$

where m_{ref} is a reference solution. This method provides single ion activities directly, but these are related to *real* rather than to *chemical* potentials (14). This implies that the γ values are affected by some contribution from the surface potential of the solution.

[2] $\quad \ln \gamma_i^* = \ln \gamma_i + (F/RT)(\Delta\chi)$

where γ_i^* is the "real" activity coefficient and $\Delta\chi$ is the change in surface potential of the solution with

[1]From a paper presented at the 5th International Symposium on Ion–Ion–Solvent Interaction, Florence, Italy, June 2–6, 1980. First presented in part at the 2nd Meeting of the Electrochemical Division of the Italian Chemical Society, Padua, October 1977.

0008-4042/81/131925-08$01.00/0

©1981 National Research Council of Canada/Conseil national de recherches du Canada

Can. J. Chem. Downloaded from www.nrcresearchpress.com by 210.87.254.40 on 09/06/12
For personal use only.

Can. J. Chem. Downloaded from www.nrcresearchpress.com by 210.87.254.40 on 09/06/12
For personal use only.

respect to the pure solvent. Beyond this point, a model must necessarily be introduced to derive the desired quantity γ_i (15, 16).

A proposed non-experimental route rests on the assumption (17) that for not very dissimilar ions the difference in γ_i is mainly related to the difference in solvation. The following equation has been proposed (18) for 1–1 electrolytes:

$$[3] \quad \ln \gamma_{+(-)} = \ln \gamma_{\pm} + 0.00782[h_{+(-)} - h_{-(+)}]m\phi$$

where h_+ and h_- are single ion hydration numbers, and ϕ is the osmotic coefficient. A number of factors which may make γ_+ differ from γ_- has been discussed by Frank (19).

The basic prerequisite for emf measurements to determine single ion activity coefficients is to reproduce possible conditions of constancy in potential for one of the two electrodes of the electrochemical cell. In this work, we propose to adopt the model of the electrical double layer at the electrode/solution interface in the absence of specific adsorption as the one best meeting the above requirement.

The Model

Presently accepted views on the structure of the electrical double layer at the electrode/solution interface (20) rest on the concepts introduced by Gouy, Chapman, and Stern and developed by Grahame. The interphase is assumed to consist of two adjacent regions, an inner layer and a diffuse layer. The electric potential drop across the whole interfacial region thus consists of two contributions: the potential drop across the diffuse layer is a function of the ionic concentration in solution, while the potential drop across the inner layer does not depend on the ionic concentration provided specific adsorption is absent. The potential drop across the diffuse layer can be calculated by means of the Gouy–Chapman theory; it vanishes as the charge on the metal vanishes (potential of zero charge). It ensues that an ideally polarizable electrode in the absence of specific adsorption, kept at the potential of zero charge, or at constant inner layer potential drop (which implies constant charge on the metal) is expected to work as a constant potential electrode insensitive to the activity of any of the species in solution.

The above feature is implicit in the original theory (21) and has been verified independently by Grahame (22) in terms of differential capacity. The possibility that such an electrode may work as a constant potential electrode also ensues (23, 24) from the analysis of the Esin and Markov effect. Thus far only one experimental approach (25) has however been attempted along the lines proposed in this work. Šťastný and Štráfelda (25) have stressed the possibility of determining single ion activity coefficients by measuring the zero charge potential of Hg. However, the difficult point in their work is that for the only electrolyte known (21) not to be specifically adsorbed (F^-) no reversible electrode was available at that time, while the reference electrode they used (Ag/AgCl) is reversible to Cl^- which is specifically adsorbed on Hg. Thus, their data are "vitiated" by the use of the Henderson equation to estimate some liquid junction potential. The present availability of electrodes reversible to the fluoride ion (26) makes it possible to set up electrochemical cells without any liquid junction.

Experimental

The following electrochemical system has been used

$$[4] \quad \mathrm{Hg}(\sigma = \text{const})/\mathrm{NaF}(m)/\mathrm{F^-}\text{-selective electrode}$$

Although KF is recommended (27) as the best reference standard for fluoride ion activity in that it is unassociated, NaF was used in this work because most of the experimental data with Hg electrodes were obtained with this electrolyte. Fluoride ions are probably adsorbed on Hg at positive charges, but adsorption can be ruled out at the potential of zero charge and at negative charges (28). In this region the potential difference for cell [4] is given by

$$[5] \quad E = \text{constant} - (RT/F) \ln \gamma_- m$$

where the constant term includes the electric potential drop across the Hg/solution inner layer.

A LaF_3-based Orion electrode was used as the F^--selective electrode. The potential of zero charge of Hg was determined directly by means of the jet electrode technique (29), while the potential at other charges was calculated by integrating differential capacity/potential curves from the potential of zero charge and correcting for the effect of the diffuse layer on the basis of the Gouy–Chapman theory.

The reliability of the response of the F^--selective electrode was checked by measuring the emf of the cell

$$[6] \quad \mathrm{F^-}\text{-selective electrode}/\mathrm{NaF}(m)/\mathrm{Na^+}\text{-selective electrode}$$

$\gamma_\pm$ values for NaF were then calculated and compared to published values (30). An Ingold glass electrode was used as the Na^+-selective electrode.

The potential of zero charge of Hg was in practice measured against a saturated calomel electrode, and the potential difference for cell [4] was obtained by adding the potential difference of the cell

$$[7] \quad \mathrm{F^-}\text{-selective electrode}/\mathrm{NaF}(m)/\text{saturated calomel electrode}$$

The design of the saturated calomel electrodes was such as to ensure the reproducibility of the liquid junction potential to better than 0.1 mV. The drift (31) in the potential of the ion-selective electrodes was accounted for by measuring the emf of cells [6] and [7] in a 0.1 *m* NaF solution before and after each run of measurements (practically, at the beginning and at the end of each day). In all experiments, the temperature of the solution was kept constant at 25 ± 0.1°C.

The experimental technique to measure capacity curves has

Can. J. Chem. Downloaded from www.nrcresearchpress.com by 210.87.254.40 on 09/06/12
For personal use only.

been described elsewhere (32). The integration of the capacity data was carried out with the aid of a computer. All measurements of cell potential difference were repeated several times to check reproducibility and accuracy. The concentration range investigated was from 0.01 to 0.9 m NaF. All values of m in text and in figures are quoted in mol kg^{-1}.

Results

The data of potential difference for both cell [4] and cell [6] have been analyzed (33) by means of the extended Hückel equation (34) for the activity coefficients of 1–1 electrolytes

$$[8] \quad \log \gamma_i = bm - (A\sqrt{m})/(1 + aB\sqrt{m}) - \log (1 + 0.036m)$$

where γ_i may be either $\gamma_\pm$ or single ion activity coefficients, A and B are constants, b accounts for short-range interactions, and a is the cation–anion distance of closest approach. For NaF this parameter has been taken as 0.4 nm according to literature data (18).

In the particular case of cell [4], from eq. [8] and eq. [5], it results in

$$[9] \quad E + k \log m - (kA\sqrt{m})/(1 + aB\sqrt{m}) - k \log (1 + 0.036m) = \Psi = \text{constant} - kbm$$

where $k = 2.3(RT/F)$. All terms in the left-hand side of eq. [9] are known so that Ψ can be calculated for any value of m. A plot of Ψ against m is thus expected to yield a straight line whose slope determines the value of b. Once b is known, values of γ_i can be obtained by eq. [8] for any value of m. This procedure gives "smoothed" γ_i values. Alternatively, the intercept in the plot of Ψ vs. m (the "constant" term) may be introduced into eq. [5] to calculate "not smoothed" γ_i values. The linearization of eq. [9] was performed by the least square method.

Figure 1 shows a typical linearization of eq. [9] with the data of cell [4]. The mean square deviation is equal to 0.0004 V which points to the satisfactory accuracy of the experimental results.

Values of $\gamma_\pm$ were derived by applying the same procedure to the data of cell [6]. Figure 2 shows that the $\gamma_\pm$ values for NaF as obtained in this work are in good agreement with data reported in the literature (30) (solid line) obtained by the isopiestic method. The scatter of points is within the expected uncertainty as can also be seen in previous data reported by Bates (35) and obtained with a similar experimental set up.

Figure 3 shows the concentration dependence of the potential of zero charge of Hg in NaF aqueous solutions as obtained by the streaming electrode technique and measured against a saturated calomel electrode. The accuracy of this method is given as ± 0.5 mV. The different points refer to different measurements carried out by different operators with different electrodes not only in connection with the present work. The accuracy is in general within the limits claimed. A definite trend for the potential of zero charge to decrease as the NaF concentration increases can be recognized. At low m values E levels off at -432 to -433 mV. The change in potential with m is observed also in the original data of Grahame (22). The ΔE between low and high concentrations was of the order of 2 mV, in good agreement with the present data. The absolute values of the potential of zero charge are, however, about 1 to 2 mV more negative in Grahame's work over the entire concentration range. This may be due to the introduction of a calculated value for the liquid junction potential in Grahame's data, but an effect of the design of the jet electrode cannot be ruled out (28). However, in this work the relative values of the potential of zero charge as a function of m are more relevant than the absolute values. In this respect, our data and Grahame's run parallel.

Figure 4 displays the final picture of the results. The present approach is possible only with electrolytes which are not specifically adsorbed at $\sigma = 0$. Only F^- and perhaps SO_4^{2-} are known to meet this requirement (21, 28). In order to explore the possibility of using this method with electrolytes which are specifically adsorbed at $\sigma = 0$, γ_- values have also been calculated by using values of potential difference of cell [4] corresponding to Hg at negative charges, where specific adsorption of anions is expected to vanish. The procedure followed for the data with Hg at $\sigma = 0$ was thus extended to data of potential with Hg at $\sigma < 0$, in particular $\sigma = -10\ \mu C\ cm^{-2}$.

In Fig. 4 the γ_- values obtained with Hg at negative charges exhibit the same trend as those with Hg at $\sigma = 0$. The scatter of points is somewhat larger and this is very likely to be related to the fact that the accuracy in the measured differential capacity is of the order of 0.2 to 0.3% (36). Due to the integration procedure, the inaccuracy bears increasingly on the results as the charge becomes more negative. The inaccuracy which is probably small for double layer problems is significant for the present treatment of the data. The important point is to verify if the concentration dependence of E for cell [4] may be a function of the amount of charge on the Hg electrode.

Figure 5 shows that between 0.1 and 1 mol kg^{-1} the plot of E against $\log a_-$ (a_- is calculated from the data with Hg at $\sigma = 0$) gives straight lines with the same 0.059 mV slope. This indicates that in this concentration range the basic assumptions behind

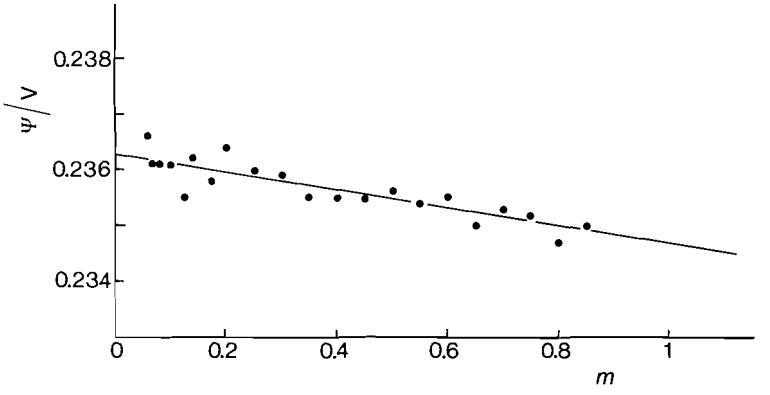

FIG. 1. Typical linearization of eq. [9] in the text. Data refer to cell Hg ($\sigma = 0$)/NaF(m)/F^--selective electrode. The straight line has been drawn by means of the least square method.

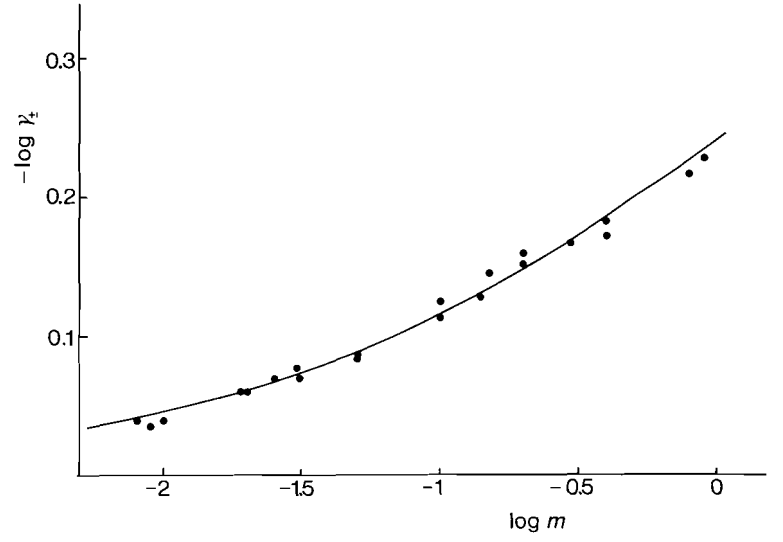

FIG. 2. Mean ionic activity coefficients for NaF in water as a function of electrolyte molality. (—) Literature data as obtained by the isopiestic method; (●) Data as obtained in this work by emf measurements for cell (*b*) in Fig. 1.

the method hold at any charge on Hg. This may also be taken as an indirect proof that the corrections for the diffuse layer as calculated by the Gouy–Chapman theory are probably accurate within the limit of validity of the present approach.

Scrutiny of Fig. 5 however reveals that some deviation from the linearity is increasingly apparent in the low concentration range as the charge becomes more negative. This can be better seen in Fig. 6 where the data on E are plotted against $\log a_-$ all over the range from 0.01 to 1 mol kg^{-1}. Whereas the points fit on the straight line of 0.059 mV slope when the charge on Hg is zero, a deviation from linearity is observed when the charge is $-10\ \mu C\ cm^{-2}$. This may be due to an incorrect compensation of the diffuse layer potential drop by the Gouy–Chapman theory. Actually, this effect is observed at concentrations below 0.1 m where the difference between γ_- and $\gamma_\pm$ are unimportant, and could be neglected for the purpose of this work. But it is important to try to understand whether the method itself is inapplicable because of failure of the basic assumptions or other causes are responsible for the observed behaviour.

In order to look at the same phenomena from a different point of view, the data published by Grahame (22) on the capacity of Hg in NaF aqueous solutions have been used. The available concentrations are in this case only 0.001, 0.01, 0.1, 0.66, and 0.916 mol dm^{-3}. Figure 6 shows that Grahame's data satisfy the linearity of the plot both at $\sigma = 0$ and $\sigma = -10\ \mu C\ cm^{-2}$. In the latter case the linearity is probably observed down to 0.001 mol dm^{-3}. Thus, it appears that the deviation from the linearity is probably related to the accuracy of the capacity data in the low concentration range. In

Can. J. Chem. Downloaded from www.nrcresearchpress.com by 210.87.254.40 on 09/06/12
For personal use only.

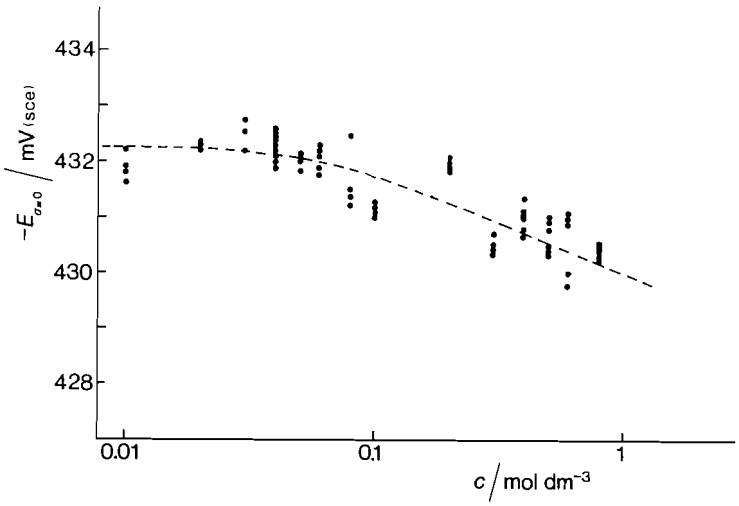

FIG. 3. Potential of zero charge of a Hg electrode in NaF aqueous solutions. The dashed line emphasizes the general trend of the plot.

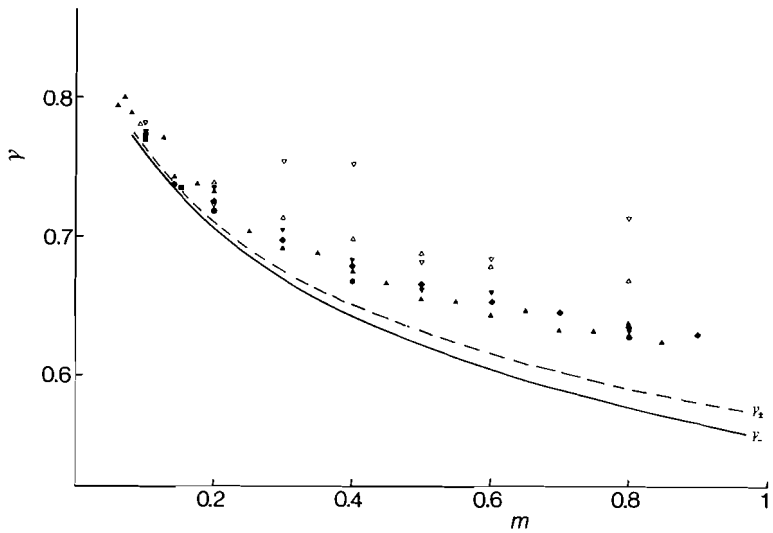

FIG. 4. Summary of experimental results. (---) Mean ionic activity coefficients of NaF in water; (—) Activity coefficients of F^- in NaF as calculated by the hydration theory. Symbols refer to different sets of data for the cell Hg (σ = constant)/NaF (m)/F^--selective electrode. Solid symbols, $\sigma = 0$. Open symbols, $\sigma = -10\,\mu C\,cm^{-2}$; (△) from data of Grahame; (▽) our data.

fact some difference with respect to Grahame's data was also observed by Parsons and Trasatti (37) at low concentrations of KCl (around 0.01 mol dm^{-3}). The design of the measuring apparatus (the same basic bridge and the same cell were used in this work and in the work of ref. 37) might be responsible for the observed deviation as a consequence of the high impedance of the interface. This effect can be neglected in double layer studies but may become significant in this particular way of treating the experimental data. If the above explanation is correct, the data indicate substantially that the present approach can be used also with electrolytes which are specifically adsorbed at the potential of zero charge but not at moderate negative charges. This is an interesting possibility to check the basic assumptions of this approach in that most of the determinations of single ion activity coefficients by other methods are in particular carried out with chlorides.

Grahame's data can be used independently to derive γ_- values. Figure 4 shows that the resulting (smoothed) values agree reasonably well with those derived with our data. Of course, the same values are obtained in this case with $\sigma = 0$ and $\sigma = -10\,\mu C\,cm^{-2}$. However, when Grahame's data are used independently, a slight deviation in the γ_- values can in fact be observed with respect to our

Can. J. Chem. Downloaded from www.nrcresearchpress.com by 210.87.254.40 on 09/06/12
For personal use only.

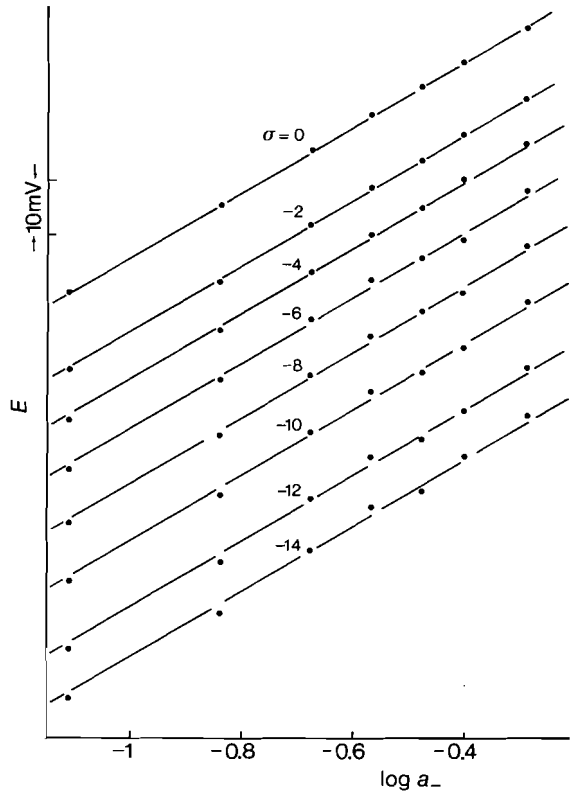

FIG. 5. Plot of the potential difference of cell (4) in the text against the fluoride ion activity (calculated at $\sigma = 0$) with the Hg electrode at various negative charges.

values. It is thought that this may be due to the fact that the original data on the potential of zero charge contain an estimated correction for the liquid junction potential which is not present in our data.

Discussion

The results in Fig. 4 indicate that γ_- is possibly higher than $\gamma_\pm$ for NaF in water. In order to appraise the significance of this observation, it is necessary to compare the present results with the predictions of theories or with the results by other methods.

Rabinovich and Titov (38, 39) have reported the values of the "real" activity coefficients of the single ions for NaF, KF and CsF.[2] Table 1 compares their results with ours. The agreement is reasonably good. In principle, our γ_- values are "real" activity coefficients in that the measurements include the surface potential contribution from the solution. However, whereas the double layer model for the metal/solution interface assumes explicitly that the surface potential of the solution does not vary with the electrolyte concentration (20, 23), the possibility that the surface potential at the free surface of the solution may change with the electrolyte concentration is concretely considered by Rabinovich *et al.* (11, 12). There are experimental results showing that this may well be the case (40, 41). If some correction is attempted by means of eq. [2], Rabinovich and Titov's results show that γ_- may become almost equal to γ_+ in KF (38). No data are available for NaF but the same effect may be expected also for this electrolyte, even though to a different extent. The agreement in Table 1 may thus be only apparent and not real. Some experimental results however show that the term $\Delta\chi$ may become significant only at higher concentrations than 0.5–1 mol dm^{-3}. Such a range of concentration cannot be explored with NaF because of the limited solubility.

TABLE 1. Comparison of activity coefficients for F^- in NaF aqueous solutions from this work with "real" activity coefficients as obtained by Rabinovich and Titov (38)

	γ_{F^-}	
m/mol kg^{-1}	Ref. 38	This work
0.1	0.760	0.765
0.2	0.719	0.720
0.5	0.641	0.655
0.7	0.618	0.633
1.0	0.591	0.615

Stokes and Robinson (17) have developed a hydration theory to calculate mean ionic activity coefficients which has then been extended by Bates *et al.* (18) to the calculation of single ion activity coefficients. According to the latter treatment, γ_- is expected to differ from γ_+ when the hydration number of the anion, h_-, differs from that of the cation, h_+. For 1–1 electrolytes, the resulting relationship between γ_i and $\gamma_\pm$ is given by eq. [3]. Once h_+ and h_- are known, γ_- can be derived from $\gamma_\pm$. Single ion hydration numbers are not amenable to direct experimental determination, but analysis of estimated data available in the literature (42) suggests that, for NaF, it is probably

$$[10] \quad h_+ - h_- = 1 \pm 2$$

More precise values for h_+, h_-, and h ($= h_+ + h_-$) have been suggested by Robinson *et al.* (27). According to Bates and Robinson (43) h can be derived by fitting the calculated curve containing the hydration number as the variable to the experimental points for the mean ionic activity coefficients. They suggest that $h = 5.37$ with $h_+ = 3.5$ and $h_- = 1.87$. Although the hydration theory has

[2]The authors are grateful to V. A. Rabinovich for making the original data available.

Can. J. Chem. Downloaded from www.nrcresearchpress.com by 210.87.254.40 on 09/06/12
For personal use only.

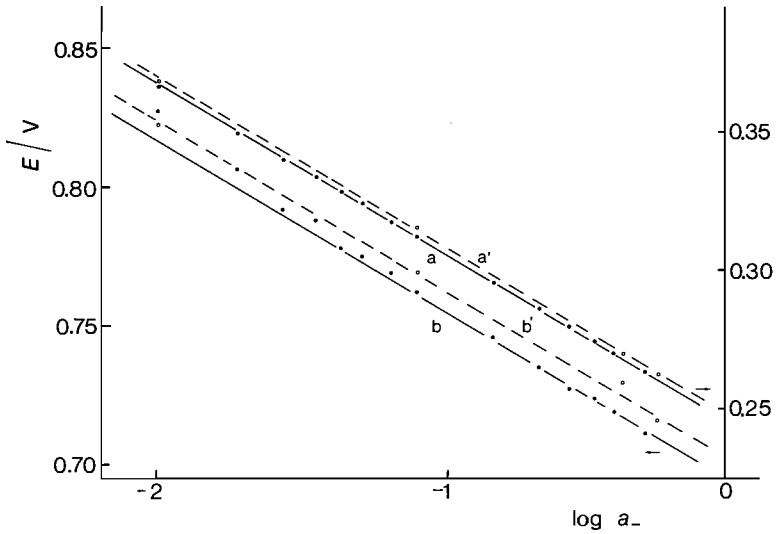

FIG. 6. Plot of the potential difference of cell (4) in the text against the fluoride ion activity. (a,b) Our data: (a',b') From Grahame's data. (a,a') Hg at $\sigma = 0$; (b,b') Hg at $\sigma = -10\,\mu C\,cm^{-2}$. (—) Straight line of 0.059 mV slope through our points; (---) straight line of 0.059 mV slope through Grahame's points.

been developed for unassociated electrolytes (NaF is probably somewhat associated in solution (27)), eq. [3] is expected to enable the calculation of γ_- if the experimental $\gamma_\pm$ (including the effect of ion pairing) is used.

The solid line in Fig. 4 has been obtained by calculating γ_- for NaF according to the hydration theory. This of course predicts that the ion with the higher hydration number should exhibit the higher activity coefficient. The predictions of the hydration theory are therefore at variance with our experimental results, but it is not yet clear if the two sets of data depend on the same factors which may be responsible for the difference between γ_+ and γ_-. Also taking into account Table 1, the observed discrepancy may be due to one or more of the following reasons: (*i*) The hydration theory does not include other factors which may be important; (*ii*) The estimated values of h_+ and h_- do not correspond to the true values, although it appears unlikely that h_- may be higher than h_+; (*iii*) The assumed concentration independence of the inner layer potential drop at constant charge on the electrode may be a good approximation in double layer studies but not in this case when as high an accuracy as 1 mV is required; (*iv*) Absence of specific adsorption is only an approximation. Work is in progress with other electrolytes to try to elucidate the role of the various factors.

1. E. A. GUGGENHEIM. J. Phys. Chem. **33**, 842 (1929); **34**, 1540 (1930); **34**, 1758 (1930).
2. P. T. TAYLOR. J. Phys. Chem. **31**, 1478 (1927).
3. H. S. HARNED. J. Phys. Chem. **30**, 433 (1926).
4. I. W. GIBBS. Collected works. Vol. 1. Longmans, New York. 1928. p. 429.
5. J. BRAGG and G. A. RECHNITZ. Anal. Chem. **45**, 271 (1973).
6. A. SHATKAY and A. LERMAN. Anal. Chem. **41**, 514 (1969).
7. Z. G. SZABO. Z. Phys. Chem. A **181**, 169 (1938).
8. G. MILAZZO and R. DEFAY. J. Electroanal. Chem. **4**, 419 (1962).
9. G. MILAZZO, N. BONCIOCAT, and M. BORDA. Electrochim. Acta, **21**, 349 (1976).
10. V. A. RABINOVICH, T. E. ALEKSEEVA, and L. A. VORONINA. Elektrokhimiya, **9**, 1434 (1973).
11. V. A. RABINOVICH and T. E. ALEKSEEVA. Elektrokhimiya, **10**, 521 (1974).
12. V. A. RABINOVICH, T. E. ALEKSEEVA, and R. V. DROZDOVA. Electrokhimiya, **12**, 142 (1976).
13. V. A. RABINOVICH and V. E. TITOV. Electrokhimiya, **13**, 306 (1977).
14. V. A. RABINOVICH, A. E. NIKEROV, and V. P. ROTSTEIN. Electrochim. Acta, **12**, 155 (1967).
15. YU. F. RYBKIN and N. F. SHEVCHENKO. Elektrokhimiya, **1**, 46 (1965).
16. YU. F. RYBKIN and T. N. SEREDENKO. Elektrokhimiya, **10**, 1566 (1974).
17. R. H. STOKES and R. A. ROBINSON. J. Am. Chem. Soc. **70**, 1870 (1948).
18. R. G. BATES, B. R. STAPLES, and R. A. ROBINSON. Anal. Chem. **42**, 867 (1970).
19. H. S. FRANK. J. Phys. Chem. **67**, 1554 (1963).
20. S. TRASATTI. *In* Modern aspects of electrochemistry. Vol. 13. *Edited by* B. E. Conway and J. O'M. Bockris. Plenum, New York. 1979.
21. D. C. GRAHAME. Chem. Rev. **47**, 441 (1947).
22. D. C. GRAHAME. J. Am. Chem. Soc. **76**, 4819 (1954).
23. R. PARSONS. Proc. 2nd Int. Congr. Surf. Act. London, 1956; 38 (1957).
24. D. G. HALL. J. Chem. Soc. Faraday II, **74**, 405 (1978).
25. M. ŠŤASTNÝ and F. STRÁFELDA. Coll. Czech. Chem. Commun. **37**, 37 (1972).
26. M. S. FRANT and J. W. ROSS. Science, **154**, 1553 (1966); J. Koryta. Anal. Chim. Acta, **91**, 1 (1977).

Can. J. Chem. Downloaded from www.nrcresearchpress.com by 210.87.254.40 on 09/06/12
For personal use only.

27. R. A. ROBINSON, W. C. DUER, and R. G. BATES. Anal. Chem. **43**, 1862 (1971).
28. D. J. SCHIFFRIN. Trans. Faraday Soc. **67**, 3318 (1971).
29. D. C. GRAHAME, E. M. COFFIN, J. I. CUMMINGS, and M. A. POTH. J. Am. Chem. Soc. **74**, 1207 (1952).
30. R. PARSONS. Handbook of electrochemical constants. Butterworths, London. 1959.
31. IUPAC Commission on Analytical Nomenclature. Pure Appl. Chem. **48**, 127 (1976).
32. A. DE BATTISTI and S. TRASATTI. J. Electroanal. Chem. **48**, 213 (1973).
33. A. DE BATTISTI and S. TRASATTI. J. Chim. Phys. **70**, 395 (1973).
34. E. HUECKEL. Phys. Z. **26**, 93 (1925).
35. R. G. BATES. Pure Appl. Chem. **36**, 407 (1973).
36. G. J. HILLS and R. PAYNE. Trans. Faraday Soc. **61**, 316 (1965).
37. R. PARSONS and S. TRASATTI. Trans. Faraday Soc. **65**, 3314 (1969).
38. V. A. RABINOVICH and V. E. TITOV. Deposited Doc. 1976. VINITI 1357-76, 19 p.
39. V. E. TITOV and V. A. RABINOVICH. XXX Gertsenovsk. Chteniya. Khimiya 1977, 18. Chem. Abstr. **88**, 111372*j* (1978).
40. J. E. B. RANDLES. Adv. Electrochem. Electrochem. Eng. **3**, 1 (1963).
41. B. E. CONWAY. J. Solut. Chem. **7**, 721 (1978).
42. B. E. CONWAY and J. O'M. Bockris. *In* Modern aspects of electrochemistry. *Edited by* J. O'M. Bockris and B. E. Conway. Butterworths, London. 1954.
43. R. G. BATES and R. A. ROBINSON. Conference on ion-selective electrodes. Akadémiai Kiadó, Budapest. 1977. p. 3.

Can. J. Chem. Downloaded from www.nrcresearchpress.com by 210.87.254.40 on 09/06/12
For personal use only.

Steady state concentration polarization by laser interferometry

R. N. O'BRIEN, B. B. KULKARNI,[1] W. MICHALIK,[2] AND K. S. V. SANTHANAM[1]

Department of Chemistry, University of Victoria, Victoria, B.C., Canada V8W 2Y2

Received August 6, 1980

This paper is dedicated to Dr. Sam Levine on the occasion of his 70th birthday

R. N. O'BRIEN, B. B. KULKARNI, W. MICHALIK, and K. S. V. SANTHANAM. Can. J. Chem. **59**, 1933 (1981).

A laser interferometry study was done on the $Cu/CuSO_4/Cu$ system at natural pH to investigate the effects of natural convection with plane-parallel horizontal electrodes in the anode over cathode position. A constant concentration profile is established where migration is just equal to diffusion plus convection at cd's less than 0.2 mA cm^{-2} and electrode separations less than 1 mm. Above these values convective or roll cells reminiscent of Bénard cells always develop.

R. N. O'BRIEN, B. B. KULKARNI, W. MICHALIK et K. S. V. SANTHANAM. Can. J. Chem. **59**, 1933 (1981).

On a réalisé une étude par interférométrie au laser sur le système $Cu/CuSO_4/Cu$ à un pH naturel dans le but de trouver les effets de convection naturelle, avec des électrodes horizontales dans des plans parallèles alors que l'anode est dans la position au-dessus de la cathode. On a établi un profil de concentration constante où la migration est exactement égale à la diffusion plus la convection à des cd inférieurs a 0,2 mA cm^{-2} et pour des électrodes dont la distance de séparation est inférieure à 1 mm. Au-dessus de ces valeurs, il se développe toujours des convections ou des cellules en spirale qui rappellent les cellules de Bénard.

[Traduit par le journal]

Introduction

It has long been known that at vertical electrodes natural convection limits the extent of both thickness and concentration change in the diffusion layer. Optical methods have produced convincing visible evidence (1–3) of this. Electrochemical systems where the electrodes are not perfectly horizontal, plane-parallel, or do not intersect the total area of the electrolytic conduction path will usually within a short period of time show a constant concentration polarization. The assumption is also made that all other sources of polarization are small or absent as in, for example, the deposition of copper or zinc.

Recently another mode of stabilization of concentration polarization has been observed, the condition where migration is just equal to diffusion in horizontal plane-parallel electrodes (4). With no convection present this is the expected result. Considering the cathode, the attraction of cations to the cathode and their discharge (and the simultaneous replulsion of anions) will lower the concentration near the electrode giving rise to a concentration gradient and hence diffusion down that gradient. Interferometric evidence for the early part of such a process is difficult to obtain, but the process at a working electrode can be inferred from an electret immersion experiment. In this experiment on the formation of a double-layer at the electret surface, the straight-line dependence of concentration with distance expected for the effect of a field on an ion was observed, followed by the curved (error function) form characteristic of diffusion (5).

This work reports an interferometric study of another case of a stable or equilibrium concentration polarization. Plane-parallel horizontal electrodes where the anode is above the cathode (A/C) produce a type of convection cell analogous to Bénard cells but probably more consistent with the original Rayleigh theory than those investigated by Bénard (6). Tobias and Hickman (7) studied an A/C system under forced and natural convection and referred to the convection cells that formed as "roll cells". Their study was done with the acidified $Cu/CuSO_4/Cu$ system. Optical evidence for convective cell formation will be presented for the system $Cu/CuSO_4/Cu$ at natural pH.

Experimental

The electrolysis cell used was also a Fabry–Perot interferometer with 90% reflecting glass flats giving a finesse of about 7 with He–Ne laser light. The details of construction of this type of cell have been published elsewhere (8–10). The critical data are that the electrodes were of 99.999% polycrystalline Cu with exposed active surfaces of about 0.9 cm^2, and were three mm thick along the line of light propagation. The general cell construction was of Teflon and Teflon was used to space the electrodes at selected values between about 0.2 mm to 3 mm. The actual spacing was measured with a micrometer and then optically against a grid placed in the optical system for this purpose.

Wedge-type interference fringes were recorded on videotape and a running voice commentary was made in the audio mode on the tape. The video camera recorded the complete experiment through the view finder of a Nikon 35 mm camera with which interferograms were recorded at selected intervals and at other

[1]Permanent address: Chemical Physics Group, Tata Institute of Fundamental Research, Bombay 400 005, India.

[2]Permanent address: Akademia Garniczo-Hutnicza, Al Mickiewicza 30, Krakow, Poland.

0008-4042/81/131933-05$01.00/0

©1981 National Research Council of Canada/Conseil national de recherches du Canada

Can. J. Chem. Downloaded from www.nrcresearchpress.com by 210.87.254.40 on 09/06/12
For personal use only.

Can. J. Chem. Downloaded from www.nrcresearchpress.com by 210.87.254.40 on 09/06/12
For personal use only.

times when other events of interest appeared on the monitor. The optical train was arranged to give magnifications on the monitor varying from about 30 to 100 as appropriate.

Electrolysis runs were generally limited to three minutes although a few were carried on to 10 min. The solution was 0.1 *N* $CuSO_4$ in all cases. Current densities were varied from 1 mA cm^{-2} to 56 μA cm^{-2}. In all cases the electrodes were plane-parallel and horizontal with the anode over the cathode.

The solution was used at the natural pH of 4.7. A stock solution was made up from AnalaR grade $CuSO_4 \cdot 5H_2O$. After each run, the solution was withdrawn by syringe and replaced. The interferometer was opened and the electrodes removed and polished after each set of runs, usually consisting of seven or eight at a given electrode separation.

The interferograms were hand measured in the usual way by projection onto a plotting table. Fringe displacements were converted to concentration by the modified Bragg equation, $2nt \cos\theta = N\lambda$, where θ must be near zero angle of incidence of light and hence $\cos\theta = 1$, n is the refractive index (~ 1.32950), t is the thickness of the electrodes (3 mm), N is the order of interference (~ 12 500), and λ is the He–Ne laser wavelength (632.8 nm). Distances from the electrode surfaces were calculated from the magnification.

Because, for even the highest current density runs, less than one atomic layer was anodically dissolved or deposited, electrode polishing did not seem necessary. However, in some cases at the higher cd runs, discoloration of the electrode surface was noticed. No increase or decrease of fringes within the field of view was evident, or the electrolyte solution retained its original concentration, although in the smallest separations less than 1.5×10^{-2} mL of solution were used with less than 1.5×10^{-6} equivalents of cupric ion present. All runs were at room temperature of 22.0°C ± 0.5.

Results and Discussion

Figure 1 is a series of interferograms showing a stable S-curve concentration profile between the two electrodes (the black edges, top and bottom) in the A/C configuration. Certain imperfections in the glass flat coatings should be ignored, as, for example, a scratch concave upwards just above the fringe bends at the cathode. Panels (a) and (b) were taken at 120 s and 180 s of electrolysis and show a concentration profile that is more characteristic of a far lower current density (~ 0.01 mA cm^{-2}) when no convection is occurring. Panels (c) and (d) at 5 s and 30 s after current off are included to show that when electrolysis ceases, convective relaxation occurs. The evidence of convection is distortion and uneven spacing of the fringes and (not shown) that relaxation was essentially complete at 50 s, whereas for nonconvective relaxation the usual time required is in excess of 5 min. Table 1 gives a comparison of the values for diffusion only, calculated using the expression for the solution by Laplace transform of Fick's Second Law and the value found in the A/C configuration with concentration profiles present similar to those in Fig. 1. The observed values of the change of concentration as close to the electrode as possible (<0.02 mm) are greater than the calculated values for times less

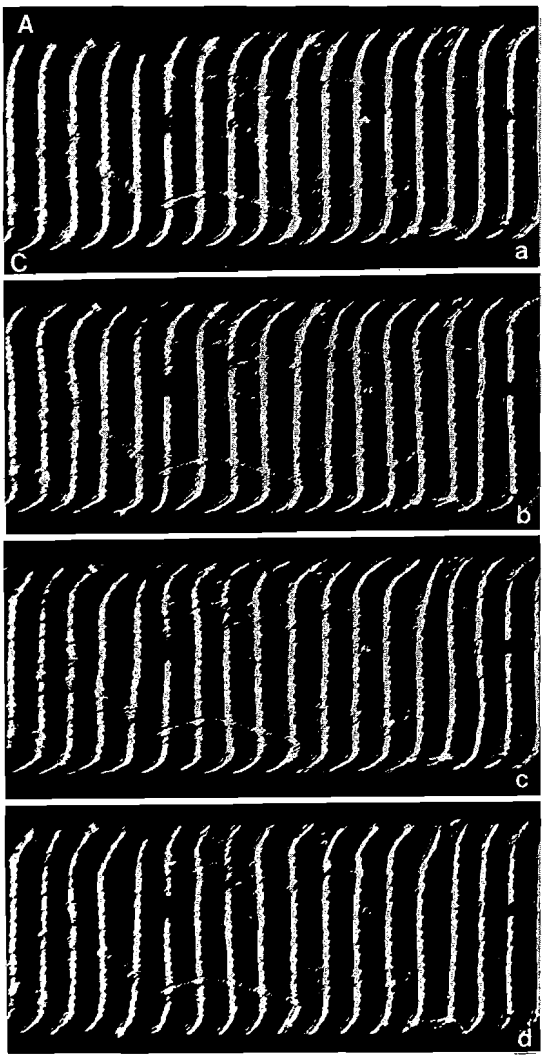

FIG. 1. Interferograms with the anode above the cathode (as shown) at 120 and 180 s of electrolysis in frames (a) and (b) at 0.1 mA cm^{-2}. Frames (c) and (d) are 5 and 30 s after current off, all with electrode separation of 2.3 mm.

TABLE 1. Electrode separation 1.651 mm at 0.238 mA cm^{-2}

	Concentration change (*M*)		
Time (s)	Calculated	Cathode	Anode
15	—	0.0082	0.00739
30	0.000417	0.00903	0.00903
45	0.00431	0.0123	0.0115
60	0.009703	0.0215	0.0115
90	0.03782	0.00239	0.00903
120	0.08699	0.00739	0.00903
180	0.19934	0.00739	0.00739

Can. J. Chem. Downloaded from www.nrcresearchpress.com by 210.87.254.40 on 09/06/12
For personal use only.

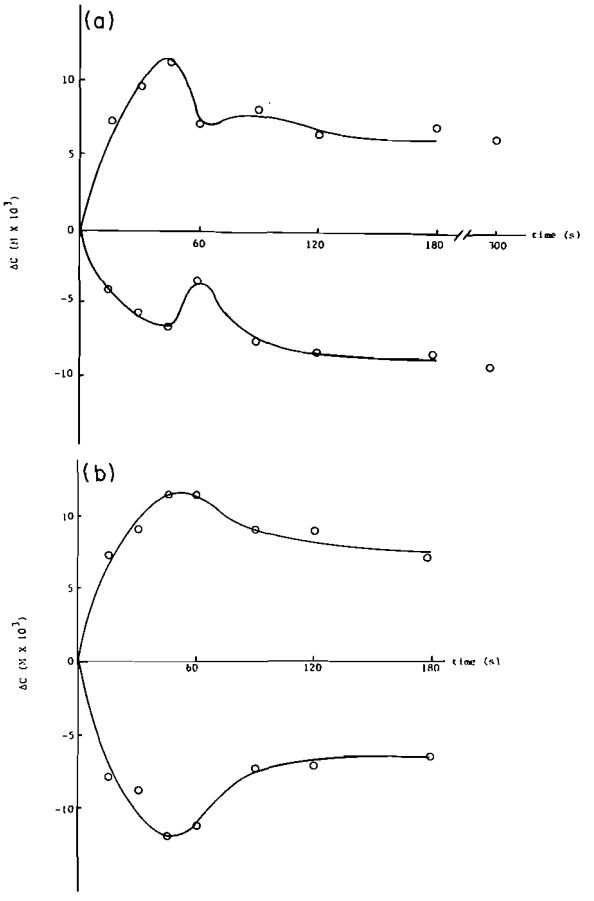

FIG. 2. Plots (a) and (b), change of concentration at the anode and cathode at the electrode surface vs. time in seconds (A/C) at 3.3 mm electrode separation at 0.1 mA cm^2 and 0.2 mA cm^2 respectively.

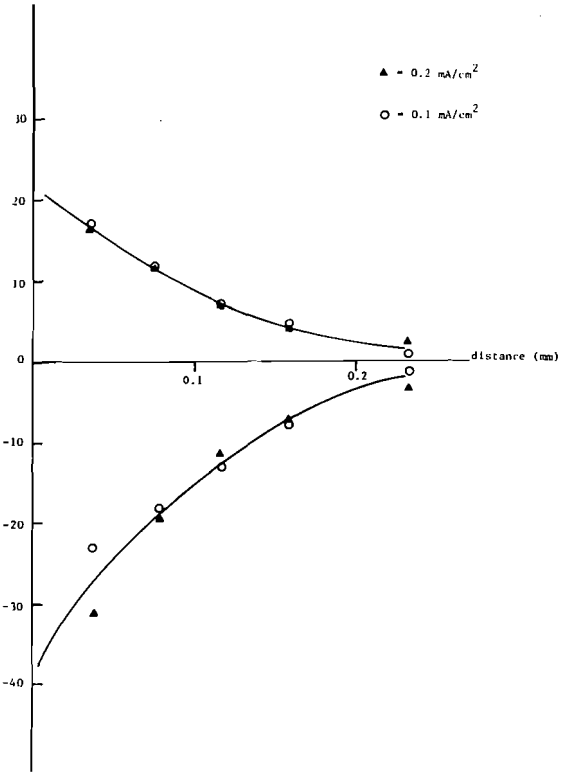

FIG. 3. The data from Fig. 2 with change in concentration plotted against time at 300 s of electrolysis.

than one minute but, at and after one minute, the calculated values (which are close to those observed for convectionless, cathode over anode systems (4, 8)) the measured values go through a maximum and decline to a reasonably constant value much lower than the calculated. Figures 2 (a) and (b) show this effect graphically for (a) a run at 0.1 mA cm^{-2} with electrode separation of 0.3302 mm and (b) 0.2 mA cm^{-2} at the same separation. Figure 3 shows these runs analysed at 300 s of electrolysis for concentration change vs. distance. The calculated value, ignoring convection, would be at least an order larger and the relatively flat curves would be the much more steeply formed asymptotes to the abscissa of the error-function type. Data point sizes approximate estimated measurement errors.

When conditions are more severe, that is at higher current densities and smaller electrode separations, the smooth convective–diffusive system breaks down into roll cells as shown in Fig. 4 (a)–(d). In panel (d) at 45 s there are large distortions of 1 or 2 fringes next to 2–3 fringes which are very little distorted (more obvious in Fig. 5). These distorted areas show the central part of a roll cell,

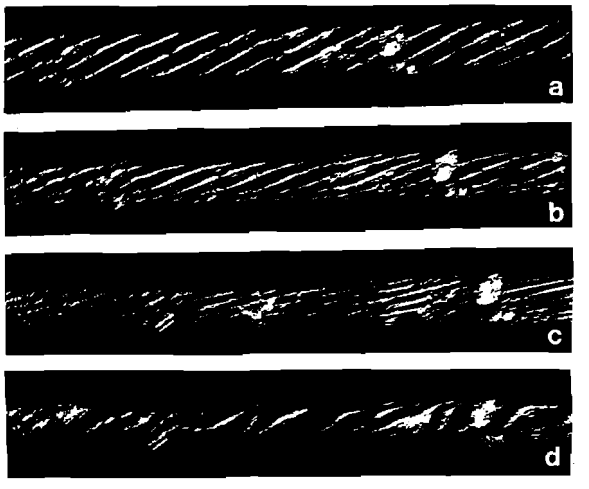

FIG. 4. Four interferograms taken at 10, 15, 25, and 45 s showing the onset of roll cells at 40–45 s A/C at 0.1 mA cm^{-2} with electrode separation of 0.46 mm.

Can. J. Chem. Downloaded from www.nrcresearchpress.com by 210.87.254.40 on 09/06/12
For personal use only.

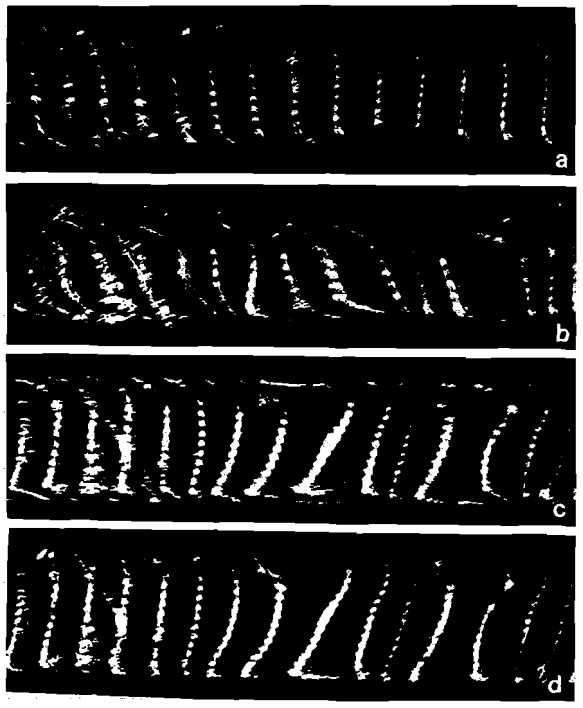

FIG. 5. Panels (a) and (b) are during electrolysis, 30 and 40 s respectively at 1.0 mA cm^{-2} at 1.15 mm electrode separation showing a transition from an S-curve to roll cells. Panels (c) and (d) are 5 and 15 s after switch-off showing persistence in the relaxation of concentration polarization. Relaxation was complete at 55 s.

the straight close-packed ones the areas of contact between rising and falling streams at the boundaries between cells. Figure 5 shows a well-developed set of roll cells. According to Normand and Pomeau (6) they should have their height equal to their width. We did not always find it so. Table 2 gives a list of conditions where roll cells developed at 40–45 s of electrolysis. From this list it can be seen that, for the $Cu/CuSO_4/Cu$ system, roll cell development occurs at approximately 0.2 mA cm^{-2} for electrode separations of greater than 1 mm, and at 0.46 mA cm^{-2} for lower cd's.

The regime of interest then, the smooth S-curve concentration polarization curve which becomes constant with time, is bounded by higher current densities and greater electrode separations. The regime itself resembles in character but not physical set-up the convective diffusion regime described by Levich at the rotating disc electrode (11) and is, to the best of our knowledge, the first report of this phenomenon.

TABLE 2. Occurrence of roll cells

Electrode separation (mm)	Current density (mA cm^{-2})
0.46	0.1
1.15	<0.2
1.55	0.2
1.94	0.2
2.28	0.2
3.30	>0.2

Conclusions

When plane-parallel horizontal electrodes in an electrolysis cell have the anode above the cathode, natural convection has always been found to be an important transport mechanism, limiting the diffusion layer thickness and therefore concentration polarization. The optical evidence obtained from laser interferometry suggests that there are two regimes, one in which an obvious equilibrium is set up to give a constant concentration profile of the S-curve variety, superficially resembling that in a nonconvecting system. This results in a system where migration is just equal to the combined diffusion and convection transport of ions. The second is one in which roll or Bénard type convective cells are set up. The appearance is of some turbulence and hence some possibility of local concentration polarization differences not due to electrode surface influences. Tobias and Hickman (7) found striations along the line of their roll cells.

The regime of smooth S curves and constant concentration polarization with convection is limited in extent by cd and electrode separation. It resembles Levich's convective diffusion except that the phenomenon he describes is a general, smooth flow of electrolyte over a spinning disc. In the present process convective transport must be in both directions, upward to the anode and downward to the cathode. The only explanation for the appearance of a smooth S-curve that presently seems reasonable is that convective cells of very small size (more than 10 across the electrode width of 3 mm or of less than 0.3 mm in diameter) are formed. We cannot at present give an explanation of why they should grow to approximately those predicted by Bénard theory very suddenly on slight increase in current density or electrode separation or why this occurs as soon as the current is switched off (open circuit conditions) after electrolysis. Relaxation by turbulent (large cell) convection is almost an order of magnitude faster than cathode over anode relaxation or at vertical electrodes.

Because the presence of roll cells seemed to result in surfaces that were not smooth, the implications for electromachining seem to be to use the A/C configuration where possible and attempt to stay in the smooth S-curve concentration polarization regime. Since electromachining uses hot con-

centrated electrolyte at very high cd's and forced convection, a further refining of the size of turbulent structures may help to produce the close tolerances the technique is noted for.

Acknowledgment

We wish to acknowledge support for this work by the Natural Sciences and Engineering Research Council of Canada to whom we are grateful for an operating grant.

1. R. MULLER. Double beam interferometry for electrochemical studies. *In* Advances in electrochemistry and electrochemical engineering. Vol. 9. *Edited by* Paul Delahay and Charles Tobias. Wiley, New York. 1973; V. SRINIVASAN. Holography and holographic interferometry. *In* Advances in electrochemistry and electrochemical engineering. Vol. 9. *Edited by* Paul Delahay and Charles Tobias. Wiley, New York. 1973.
2. R. N. O'BRIEN. J. Electrochem. Soc. **119**, 489 (1972).
3. A. TVARUSKO and L. S. WATKINS. Electrochim. Acta, **13**, 891 (1968).
4. R. N. O'BRIEN and H. KOLNY. Can. J. Chem. **56**, 591 (1978).
5. R. N. O'BRIEN and K. J. LUSHINGTON. Nature (London) Phys. Sci. **243**, 117 (1978).
6. C. NORMAND and Y. POMEAU. Rev. Mod. Phys. **49**, 581 (1977).
7. C. W. TOBIAS and R. G. HICKMAN. Z. Phys. Chem. Leipzig, **229**, 145 (1965).
8. R. N. O'BRIEN. J. Electrochem. Soc. **113**, 289 (1966).
9. R. N. O'BRIEN. Rev. Sci. Instrum. **35**, 803 (1964).
10. R. N. O'BRIEN. Interferometry. *In* Techniques of chemistry, physical methods. Vol. I. Part IIIA. *Edited by* A. Weissberger and B. Rossiter. Wiley–Interscience, New York, NY. 1972. Chapt. I.
11. V. G. LEVICH. Physicochemical hydrodynamics. Prentice-Hall, Englewood Cliffs, NJ. 1962.

Can. J. Chem. Downloaded from www.nrcresearchpress.com by 210.87.254.40 on 09/06/12
For personal use only.

Importance of lignosulfonates in petroleum recovery operations

GRAHAM NEALE, VLADIMIR HORNOF, AND CHRISTOPHER CHIWETELU
Chemical Engineering Department, University of Ottawa, Ottawa, Ont., Canada
Received August 12, 1980

This paper is dedicated to Dr. Sam Levine on the occasion of his 70th birthday[1]

GRAHAM NEALE, VLADIMIR HORNOF, and CHRISTOPHER CHIWETELU. Can. J. Chem. **59**, 1938 (1981).

This paper reviews the potential importance of aqueous lignosulfonate solutions in the recovery of petroleum from existing partially depleted oil fields. The surfactant qualities of lignosulfonates are described and their ability to interact synergistically with petroleum sulfonate surfactants (which are currently popular in the industry) to produce ultra-low interfacial tensions with crude oil is discussed. The phase behaviour characteristics and oil recovery efficacies of these mixed surfactant systems are also examined.

GRAHAM NEALE, VLADIMIR HORNOF et CHRISTOPHER CHIWETELU. Can. J. Chem. **59**, 1938 (1981).

Dans ce travail, on présente une revue sur l'importance potentielle de solutions aqueuses de lignosulfonates pour la récupération du pétrole de champs existants mais partiellement épuisés. On décrit les propriétés des lignosulfonates comme agent de surface et on discute de leur possibilité d'avoir un effet synergétique sur les sulfonates dérivés du pétrole (qui sont des agents de surface populaire dans l'industrie) pour produire des tensions interfaciales très faibles avec l'huile brute. On a également étudié les caractéristiques du comportement de phase de ces systèmes d'agents de surface mixtes ainsi que leur efficacité dans la récupération du pétrole.

[Traduit par le journal]

Introduction

Petroleum occurs in nature within the pores of certain underground rock formations. Once an oil well has been drilled, a proportion of the oil originally in place (usually between 10% and 30%) flows naturally to the surface as a result of the very high pressure of the oil; this process is called "primary recovery". A further 10–30% of the original oil can usually be recovered by pumping water into the reservoir formation through a set of injection wells and retrieving the displaced oil at the surface via a central production well. This operation is known as "secondary recovery" and has been used successfully in the field for many years. Because of the very high current cost of oil it has now become economically feasible to attempt to recover the still remaining 40–80% of original oil using "tertiary recovery" schemes.

The basis for many tertiary recovery processes is the extremely low interfacial tension which can be obtained between petroleum and a displacing aqueous solution of certian surfactants, such as petroleum sulfonates (1, 2). Small quantities of a co-surfactant (usually alcohols) and an electrolyte (usually sodium chloride) are incorporated because these additives serve to improve the displacement efficiency. The co-surfactant assists in the adjustment of viscosity, permits the surfactant micelles to solubilize more oil and, in particular, helps to reduce the adsorption of the expensive petroleum sulfonate on the reservoir rock surface. The electrolyte also aids in viscosity adjustment.

The present paper reviews the use of a new class of surfactant known as lignosulfonates as possible alternatives to the more conventional petroleum sulfonates. Lignosulfonates are wood-based chemicals manufactured from the sulfite liquor effluents of pulp and paper plants. These effluents contain sulfonated lignin, polysaccharides and wood sugars dissolved in water. The sulfonated lignin, upon purification, yields lignosulfonate products, many of which possess important surfactant and emulsion stabilizing properties (3). Lignosulfonates can alternatively be obtained by the sulfonation of kraft lignin. The great appeal of lignosulfonates is that they are at least four times cheaper than petroleum sulfonates and are available in large quantities as by-products from the Canadian pulp and paper industry.

Characteristics of Lignosulfonates

Lignosulfonates are water soluble, anionic surface active derivatives of lignin and their properties can be adjusted with respect to sulfonate content, molecular weight, kind and amount of cation and surface activity. The Marasperse® products used in

[1]This paper is dedicated by G. N. to Sam Levine, who has been a friend, co-worker, and constant inspiration for the last ten years. It was written in recognition of his life-long committment to obtaining a better understanding of physical phenomena, which in recent years has included valuable studies concerned with the recovery of oil from the Alberta Tar Sand deposits.

0008-4042/81/131938-06$01.00/0
©1981 National Research Council of Canada/Conseil national de recherches du Canada

this work are manufactured by the American Can Company and are amongst the purest available. The basic functional constituent of these products is lignosulfonate, an anionic polyelectrolyte of molecular weight between 1 000 and 20 000. The structure of the lignosulfonate molecule is not completely known, but the basic lignin monomer unit is a substituted phenyl propane. This complex structure renders lignosulfonates completely insoluble in oils. The type of metallic ions in the lignosulfonate molecule affects its properties to some degree, while the degree of sulfonation controls the magnitude of its electrical charge when in aqueous solution.

Emulsification Properties of Lignosulfonates

Emulsions stabilized by Marasperse lignosulfonates are quite resistant to pH variations and to the presence of electrolytes such as sodium chloride, sodium sulfate, and sodium phosphate (3, 4). However, sodium hydroxide enhances the activity of aqueous lignosulfonate solutions, tending to lower the interfacial tension in an oil–water emulsion thereby rendering it more stable. Lignosulfonate-stabilized emulsions are not adversely affected by mechanical agitation (in fact such action tends to stabilize them further) or by large temperature variations.

As lignosulfonate-stabilized emulsions are extremely stable, the conventional methods of breaking emulsions are not entirely effective. The most effective way of nullifying the action of lignosulfonate is by adding a cationic surface active agent; in this work small quantities of hexadecyl trimethyl ammonium bromide were found to be effective in breaking lignosulfonate-stabilized emulsions.

Stabilization Mechanisms in Lignosulfonate-based Emulsions

Aqueous solutions of lignosulfonates are subcolloidal, high molecular weight polyelectrolytes (3, 4). They do not show any marked tendency to form micelles and do not possess a hydrophobic–hydrophilic molecular structure. The mechanisms of emulsification and stabilization are therefore different from those of conventional surfactants. The stabilization is the result of adsorption of lignosulfonate at the oil–water interface, which establishes an electrokinetic charge and a semi-rigid film. The highly charged lignosulfonate molecules in the solution then cover the entire oil–water interface. This separation of charge leads to stabilization of the dispersed oil droplets in the aqueous phase. At higher lignosulfonate concentrations, its molecules are packed closer together and are forced into the interface, resulting in a decreased interfacial tension and more stable emulsion.

Previous Work involving Lignosulfonates

Very little work involving lignosulfonates in the tertiary recovery of petroleum has been reported, although the use of sulfite spent liquors in secondary waterflooding was first proposed in 1931 (5). However, Kalfoglou (6) recently patented a process involving the use of lignosulfonates as a "sacrificial" agent during tertiary oil recovery operations. His results indicated that the presence of lignosulfonates in admixture with petroleum sulfonate surfactants increased oil recovery through reduced loss by adsorption of the costly petroleum sulfonate. It was asserted that since lignosulfonates possess strongly ionized sulfonate groups they were capable of covering the potential adsorption sites of the rock by means of electrostatic attraction or hydrogen bonding, thereby imparting a negative charge to them. The surface would therefore have no affinity for anionic surfactants such as petroleum sulfonates. However, Kalfoglou did not consider that some part of the increased oil recovery could have been due to the favourable surfactant and emulsion stabilizing properties of the lignosulfonate itself.

Work has been continuing in our laboratories on ways of improving the oil recovery efficacy of lignosulfonate solutions. In an earlier paper (3), interfacial tensions as low as 10 mN/m were reported between commercial Fuel Oil No. 4 and Marasperse N-22 lignosulfonate solution. In displacement tests conducted using unconsolidated Ottawa sand packs additional recoveries of 1.3% and 8.5% (relative to those obtained with pure waterflooding) were obtained at 1% and 10% lignosulfonate concentrations respectively. The next phase of the study involved the screening of a number of organic and inorganic reagents as co-surfactants. These results have been reported elsewhere (2). The lowest interfacial tensions obtained were about 1 mN/m, upon the addition of small quantities of caustic soda and butanol-1 into lignosulfonate solutions. However, neither of the preceding studies (2, 3) produced interfacial tensions low enough (i.e. $\lesssim 0.001$ mN/m) for practical tertiary oil recovery operations.

More recent work has focused on the study of mixtures of lignosulfonates with petroleum sulfonates, since lignosulfonates alone are evidently not satisfactory. This work has produced some extremely encouraging results, in the form of interfacial tensions (IFT) as low as 10^{-4} mN/m with real

crude oils. Within this framework, the following parameters are of particular interest: (*a*) degree of mutual compatibility of lignosulfonates and petroleum sulfonates; (*b*) phase behaviour and interfacial activity of such mixtures; (*c*) optimization of a surfactant solution for the establishment of a minimum IFT with any given crude oil. In connection with item (*c*) above, Cayias *et al.* (7) have developed the important "Equivalent Alkane Carbon Number" (EACN) concept for characterizing crude oils and matching them to optimum petroleum sulfonate surfactant formulations for the attainment of minimum interfacial tensions. It is shown later in this article that the EACN concept appears also to be valid for lignosulfonate-based surfactant mixtures.

The EACN Concept

It is now accepted that the mechanisms involved in tertiary oil recovery are extremely complex and that the optimum composition of a displacing surfactant solution has to be determined in the laboratory for each prospective oil reservoir, with due consideration being given to the nature of the reservoir fluids, temperature, pressure, rock structure, etc.

Recently, work by Cayias *et al.* (7) and Wade *et al.* (8) has produced a model capable of relating the suitability of any particular surfactant system to any given crude oil. Their research has given rise to the "Equivalent Alkane Carbon Number" (EACN) concept for pure hydrocarbons and their mixtures. The EACN is determined in the following manner for pure compounds:

For *n*-alkanes

EACN = number of carbon units.

For *n*-alkylcyclohexanes

EACN = number of carbon units in alkyl side chain, plus 4.

For *n*-alkylbenzenes

EACN = number of carbon units in alkyl side chain.

For example, heptane, propylcyclohexane, and heptyl benzene each possess an EACN of 7. For mixtures of hydrocarbons the EACN is determined using the formula:

$$(\text{EACN})_{\text{mixture}} = \sum_i (\text{EACN})_i X_i$$

where X_i denotes the mole fraction of the ith component present. For example, an equimolar mixture of butylcyclohexane (EACN = 8) and propylbenzene (EACN = 3) would have an EACN of 5.5. This mixture, according to the EACN concept, would then be predicted to yield a minimum interfacial tension against any surfactant solution which provides ultra-low tensions against pure alkanes intermediate between pentane and heptane. The above equation has been verified for a wide range of binary mixtures using petroleum sulfonate and related surfactants (7). Moreover, the EACN concept has been successfully verified using a complicated synthetic crude oil made up from 29 different aliphatic, alicyclic, and aromatic hydrocarbons (7). Hence, its applicability to real crude oils (for which the EACN cannot usually be determined directly on account of their unknown composition) can be inferred. Preliminary data presented here confirms that the EACN concept is also valid for lignosulfonate-based surfactants. This is to be expected since, according to the theory, the EACN of a given mixture of oils is an inherent characteristic of the oil, being independent of the surfactant solution in question.

Results

The crude oil used was a light oil from the Gosfield South Field near Chatham, Ontario, having a specific gravity of 0.82 and viscosity of 5.3 mPa s at 25°C. The lignosulfonate used was calcium based Marasperse C-21, a brown powder of bulk density 600 kg/m^3 which is 100% soluble in water and completely insoluble in oils. The petroleum sulfonates used were Petrostep 420 and Petrostep 450 (manufactured by Stepan Chemical Co.), each containing approximately 61% sulfate, 15% free oil, 19% free water, and 5% inorganic salts. The numbers 420 and 450 refer to the equivalent weights of the two materials.

Two distinct aspects of the mixed lignosulfonate – petroleum sulfonate surfactant systems were investigated. Firstly, formulations of these two surfactants were prepared and their physicochemical properties (i.e. viscosity, density, pH, surface and interfacial tensions) were measured. Secondly, the most successful formulations were evaluated for their oil recovery efficacies by means of simulated oil displacement tests using packed sand beds. Fuller details of the experimental procedures and techniques are presented elsewhere (2, 3, 9).

A salinity level of 1.5% NaCl was maintained in all formulations, and various concentrations within the ranges 0–4% lignosulfonate and 0–5% petroleum sulfonate were employed. The oil displacement tests were conducted by displacing the oil from previously saturated sand packs of porosity 0.34. One pore-volume of pure 1.5% NaCl solution was first introduced (in order to simulate a conventional secondary recovery process) followed by two pore-volumes of surfactant solution (to simu-

TABLE 1. Effects of interfacial tension and viscosity on oil recovery

Run No.	Surfactant solution (all include 1.5% NaCl) Petrostep petroleum sulfonate	Marasperse lignosulfonate	Viscosity at 25°C (mPa s)	IFT at 25°C (mN/m)	Final oil recovery (%)
1	2% 420	0% C-21	1.54	0.114	88.2
2	2% 420	0.5% C-21	2.44	7.72×10^{-2}	88.6
3	2% 420	1.0% C-21	6.42	8.22×10^{-3}	98.8
4	3% 420	0% C-21	2.00	0.115	90.9
5	3% 420	1% C-21	5.50	4.57×10^{-2}	100.0
6	3% 420	2% C-21	4.30	3.89×10^{-2}	80.4
7	4% 450	0% C-21	2.30	0.120	98.2
8	4% 450	1% C-21	9.65	4.44×10^{-2}	100.0
9	4% 450	2% C-21	62.0	1.88×10^{-2}	83.7
10	0%	0%	1.01	4.55	85.3

late a tertiary recovery process). The recovered oil was usually in emulsified form; separation was effected by centrifugation followed by addition of the emulsion breaker hexadecyltrimethyl ammonium bromide. Representative surfactant solution properties and final oil recoveries are summarized in Table 1. The final oil recoveries represent the percentage of original oil recovered at the end of the displacement process. More detailed data showing the production history during each of the secondary and tertiary stages is available elsewhere (9).

Stable single phases were observed at all concentrations of Petrostep 420 and 450 when used alone (up to 4%) as well as for these systems when containing up to 1% C-21 lignosulfonate. However, increasing instability and phase separation was observed at higher lignosulfonate concentrations. At 2% petroleum sulfonate concentration the maximum tolerable lignosulfonate concentration was about 2%, while at 3% and 4% petroleum sulfonate precipitation occurred at about 3% lignosulfonate.

As displayed in Fig. 1, the surface tension of the Petrostep solutions drops to a minimum as lignosulfonate is added. Beyond a certain C-21 concentration the surface tension increases due to the appearance of multiple phases. The trend towards a minimum was similar but less pronounced with Petrostep 450 (not shown here). The pH of all solutions decreases with increasing lignosulfonate concentration.

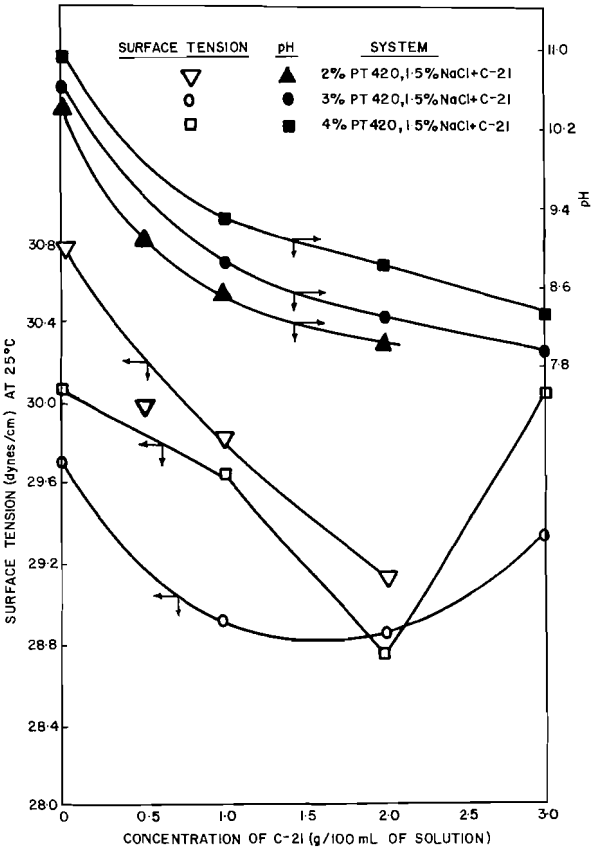

FIG. 1. Surface tension and pH plots for mixed surfactant systems containing Petrostep-420 and Marasperse C-21.

The significant changes in IFT and viscosity with increasing lignosulfonate concentration are clearly seen in Fig. 2. Beyond the mutual tolerance limits, further addition of lignosulfonate leads to an increase in IFT and decrease in viscosity, due to precipitation and consequent decreased synergistic action between the lignosulfonate and petroleum sulfonate. These effects are manifested in lower final oil recoveries in Table 1 (for example, compare Run 6 with Run 5 and Run 9 with Run 8). Under prolonged observation of the most highly viscous formulations, the viscosity was observed

TABLE 2. Effects of EACN on interfacial tension

Organic phase	EACN	IFT (mN/m) Without lignosulfonate	IFT (mN/m) With lignosulfonate
Hexane	6	1.393×10^{-1}	3.170×10^{-3}
Heptane	7	7.066×10^{-2}	6.564×10^{-4}
Octane	8	8.195×10^{-2}	3.021×10^{-3}
Dodecane	12	1.804×10^{-1}	3.613×10^{-2}
Hexadecane	16	2.260×10^{-1}	7.458×10^{-2}
Chatham crude	—	8.143×10^{-2}	2.435×10^{-3}

to vary with the age of the system, with the shearing rate, and with the duration of shearing at a fixed shear rate. Newly prepared systems were thixotropic, tending to become increasingly rheopectic with age.

Table 1 provides a summary of the 10 separate displacement runs conducted, and demonstrates very vividly the pronounced effect which ultra-low IFT's have on final oil recovery. Run 10, a 3 pore-volume pure brine (1.5% NaCl) displacement, served as the reference run for the other 9 runs conducted. The oil recoveries at the termination of the secondary displacements (of 1 pore-volume) all varied between 53 and 57%. It is clear from Table 1, therefore, that much additional oil was recovered during the ensuing 2 pore-volume tertiary displacements using surfactant solutions (compare with the recovery for Run 10 using only brine during the tertiary phase). The exceptions to this are Runs 6 and 9 in which the mutual tolerance limit was exceeded and precipitation occurred, thereby decreasing the surfactant solution effectiveness (resulting in reduced final oil recoveries).

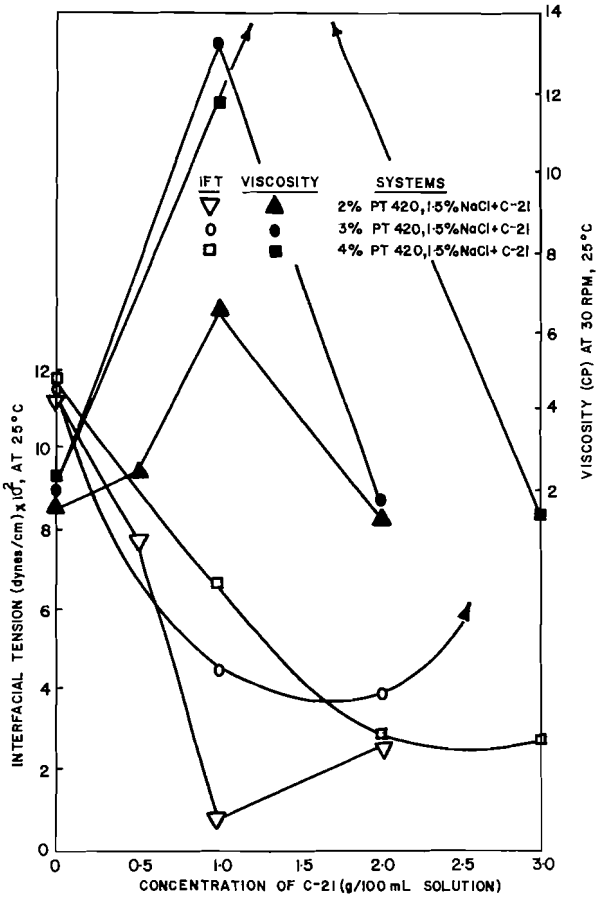

FIG. 2. Interfacial tension and viscosity plots for mixed surfactant systems containing Petrostep-420 and Marasperse C-21.

EACN Concept Results

In this very preliminary work the IFT's of the Chatham crude oil and pure hydrocarbons shown in Table 2 were measured against two surfactant solutions, the first containing 1% C-21 lignosulfonate, 5% Petrostep 420, and 1.5% NaCl, the second containing 5% Petrostep 420 and 1.5% NaCl with *no* lignosulfonate present. As usual, the organic liquids were pre-equilibrated for 48 h with the surfactant solutions (9) in order to attain mutually saturated phases and interfacial tensions were then measured using a spinning drop tensiometer. The results are summarized in Table 2.

From Table 2 it is apparent that, for both surfactant systems, a minimum IFT is observed at an EACN of about 7, in general agreement with the findings of Cayias *et al.* (7) of a minimum (for crude oils) within the 7–8 range. The EACN at which the minimum occurs is of course a function of the surfactant solution composition. The EACN of the natural crude oil cannot be accurately determined directly (since its composition is unknown) but it can be estimated by interpolation of the above data. For both surfactant mixtures, the extrapolated value would be approximately 8, again in good agreement with previous work on real crude oils (7, 8). The optimum surfactant for producing an ultra-low IFT against Chatham crude oil would therefore

be one which gives low tensions against alkanes intermediate between heptane and decane. The above data, although very preliminary, do seem to confirm that the EACN concept is valid for lignosulfonate-based surfactant solutions (in addition to the petroleum sulfonate and other surfactant solutions for which it was originally devised).

Discussion

Although the displacement experiments reported in this paper do not simulate exact conditions in real oil reservoirs, the conditions were unchanged from one run to another, thereby enabling a meaningful comparison of the individual runs to be made. By inspection of Table 1 it is clear that the high oil recovery obtained in Run 3 (compared with that of Run 1) can only be attributed to the much lower IFT and, to a lesser degree, to the improved system viscosity. This same conclusion applies also to Run 5 (when compared with Run 4) and, to a reduced extent, to Run 8 (when compared with Run 7). The recoveries in Runs 6 and 9 are low because of the incompatibility of the lignosulfonate and petroleum sulfonate at the prevailing concentrations. The phase behaviour of these mixed surfactant systems, corresponding to increasing lignosulfonate concentration, may be represented schematically as follows:

$$\text{Isotropic} \rightleftarrows \text{birefringent} \rightarrow \text{phase separation}$$

with the critical concentration ratio, C^*_{crit}, for mutual compatibility of the two surfactants being given approximately by:

$$C^*_{crit} = C_{Pet}/C_{lig} \gtrsim 1.5$$

This limiting concentration ratio is expected to depend upon the type and composition of both surfactants present. Work in this area is currently being pursued.

Shah *et al.* (10) have observed that at low surfactant concentrations, micro-emulsions consist of isotropic and spherical micelles, regardless of phase-externality. With increasing surfactant concentration anisotropic liquid crystalline structures appear. The appearance of such aggregates results in changes in the optical properties as well as in the electrical and rheological properties of the micellar systems. Although optical measurements have not been performed in this work, the rheology of the mixed surfactant systems does appear to indicate the presence of liquid crystalline structures. The variation in viscosity of these systems with age and with time of shear is consistent with the observations of Bansal and Shah (11), who identified such phenomena with liquid crystalline structures.

The problem of surfactant loss by adsorption onto the rock surface has not been investigated here. However, as Kalfoglou (6) has claimed, adsorption losses of petroleum sulfonates can be reduced in the presence of sacrificial agents, such as lignosulfonates. Another problem which has not been explicitly examined here concerns the mechanisms of oil displacement by aqueous solutions at the microscopic level, as discussed in some depth by Levine *et al.* (12). However, the present work does strongly affirm the great potential which lignosulfonates possess in the enhanced recovery of oil from existing, partially depleted oil fields.

1. R. L. Reed and R. N. Healy. *In* Improved oil recovery by surfactant and polymer flooding. *Edited by* D. O. Shah and R. S. Schecter. Academic Press, New York. 1977.
2. C. Chiwetelu, G. Neale, and V. Hornof. J. Can. Pet. Tech. **19**, No. 3 (1980).
3. B. B. Bansal, V. Hornof, and G. Neale. Can. J. Chem. Eng. **57**, 203 (1979).
4. Chemicals from wood. Bulletin No. 131, American Can Co., Greenwich, Conn., U.S.A.
5. M. de Groote and L. T. Monson. U.S. Patent No. 1,823,440 (1931).
6. G. Kalfoglou. U.S. Patent No. 4,006,779 (1977).
7. J. L. Cayias, R. S. Schecter, and W. H. Wade. Soc. Pet. Eng., J. **16**, 351 (1976).
8. W. H. Wade, J. C. Morgan, J. K. Jacobson, and R. S. Schecter. Soc. Pet. Eng. J. **17**, 122 (1977).
9. C. Chiwetelu. M.A.Sc. Thesis, University of Ottawa. Ottawa, Ont. 1979.
10. D. O. Shah, V. K. Bansal, K. Chan, and W. C. Hsieh. *In* Improved oil recovery by surfactant and polymer flooding. *Edited by* D. O. Shah and R. S. Schecter. Academic Press, New York. 1977. p. 293.
11. V. K. Bansal and D. O. Shah. *In* Microemulsions – theory and practice. *Edited by* L. M. Prince. Academic Press, New York. 1977.
12. S. Levine, P. Reed, G. Shutts, and G. Neale. Powder Tech. **17**, 163 (1977).

The role of the supporting electrolyte cation in the kinetics of outer-sphere electrochemical redox processes involving metal complexes

MICHAEL J. WEAVER,[1] H. Y. LIU, AND YONGJOO KIM

Department of Chemistry, Michigan State University, East Lansing, MI 48824, U.S.A.

Received August 12, 1980

This paper is dedicated to Dr. Sam Levine on the occasion of his 70th birthday

MICHAEL J. WEAVER, H. Y. LIU, and YONGJOO KIM. Can. J. Chem. **59**, 1944 (1981).

The electroreduction rates of $Cr(OH_2)_6^{3+}$ and $Cr(NH_3)_6^{3+}$ at the mercury–aqueous interface were monitored as a function of electrode potential in electrolytes containing univalent, divalent, or trivalent cations with systematically varying atomic number in order to scrutinize the role of the supporting electrolyte cation in the kinetics of these simple one-electron outer-sphere electrode reactions. The comparison between the corresponding rate responses for $Cr(OH_2)_6^{3+}$ and $Cr(NH_3)_6^{3+}$ reduction brought about by changing the supporting electrolyte cation is expected to provide information on the influence of the cation upon the potential profile in the double layer; despite the close structural and mechanistic similarity of the reactants, the transition state for the latter reaction appears to lie significantly closer to the electrode than that for the former process. The virtues of comparing rate responses at a constant electrode charge density rather than at a constant electrode potential are pointed out. It was found that the variations in the effective average potential at constant charge $(\Delta\phi_r)_{q^m}$ for the two reactants are closely similar but noticeably smaller than the corresponding changes in the electrode potential $(\Delta E)_{q^m}$ derived from thermodynamic double-layer measurements. These results, along with the observed variations in the transfer coefficients for the two reactions, are semiquantitatively consistent with a model involving changes in the position of the oHp as the supporting electrolyte cation is altered, but are inconsistent with a model attributing the rate variations to cation specific adsorption.

MICHAEL J. WEAVER, H. Y. LIU et YONGJOO KIM. Can. J. Chem. **59**, 1944 (1981).

On a enregistré les vitesses d'électroréduction du $Cr(OH_2)_6^{3+}$ et du $Cr(NH_3)_6^{3+}$ au niveau de l'interface mercure–eau en fonction du potentiel d'électrode dans des électrolytes contenant des cations uni, di et trivalents en faisant varier systématiquement le numéro atomique dans le but d'étudier le rôle du cation de l'électrolyte de support dans la cinétique de ces réactions simples faisant intervenir un seul électron dans la couche extérieure de l'électrode. On s'attend à ce que les variations, dues au changement du cation de l'électrolyte de support, dans les taux de réponse lors des réductions du $Cr(OH_2)_6^{3+}$ et du $Cr(NH_3)_6^{3+}$ fournissent des informations relatives à l'influence du cation sur le profil du potentiel de la couche double; malgré les ressemblances des réactifs tant du point de vue structural que du point de vue mécanistique, l'état de transition de la dernière réaction semble se produire plus près de l'électrode que dans la première réaction. On signale l'utilité de comparer les taux de réponse à une densité constante de la charge de l'électrode plutôt qu'à un potentiel constant de l'électrode. On a trouvé que les variations du potentiel moyen efficace à charge constante $(\Delta\phi_r)_{q^m}$ des deux réactifs sont assez semblables mais nettement plus faibles que les variations correspondantes du potentiel d'électrode $(\Delta E)_{q^m}$ obtenu à partir de mesures thermodynamiques de la couche double. Ces résultats ainsi que les variations observées dans les coefficients de transfert des deux réactions sont semi-quantitativement en accord avec un modèle impliquant des variations dans la position pHo lorsqu'on modifie le cation de l'électrolyte de support mais ils ne correspondent pas avec un modèle dans lequel on attribue les variations de vitesse à l'adsorption spécifique du cation.

[Traduit par le journal]

Introduction

The various influences of the ionic double-layer composition upon the kinetics of electrode reactions at the mercury–aqueous interface have received extensive scrutiny over the years. Most early studies were concerned with testing the applicability of the Frumkin model in conjunction with the Gouy–Chapman–Stern theory of the double layer (GCSF approach) at potentials well negative of the potential of zero charge (pzc) where specific ionic adsorption is most likely to be weak or absent (1, 2). Broadly speaking, the GCSF model has been found to be surprisingly successful under these conditions, although unexpectedly large rate variations have been found when the nature of the supporting electrolyte cation is altered. These have been ascribed to cation specific adsorption, ion-pairing influences, and variations in the position of the outer Helmholtz plane (oHp) relative to the reaction plane (1, 2). More recently, there has been considerable interest in testing the GCSF model under conditions where there is extensive specific adsorption of the supporting electrolyte anions. Significant deviations from the GCSF predictions have been reported, which have been ascribed variously to deficiencies of the Gouy–Chapman theory, the noncoincidence of the reaction plane and the oHp, and discreteness-of-charge effects (e.g. refs. 3–5). However, the majority of these studies have employed reactions for which the chemical structure and spatial position of the transition state for electron transfer is unknown or ill-defined, particularly oxyanion reductions and hydrogen evolution. We have suggested (5–7) that

[1]Author to whom correspondence should be addressed.

0008-4042/81/131944-10$01.00/0

©1981 National Research Council of Canada/Conseil national de recherches du Canada

Can. J. Chem. Downloaded from www.nrcresearchpress.com by 210.87.254.40 on 09/06/12
For personal use only.

Can. J. Chem. Downloaded from www.nrcresearchpress.com by 210.87.254.40 on 09/06/12
For personal use only.

an attractive class of model reactants is provided by substitutionally inert transition-metal complexes containing aquo or ammine ligands that can be reduced (or oxidized) via a *single* electron transfer step. No metal–ligand bond cleavage or formation takes place prior to electron transfer so that the structure of the transition states is well defined, being approximately midway between those of the oxidized and the reduced forms. Moreover, we have found that the electroreduction kinetics of substitutionally inert Cr(III) and Co(III) complexes containing aquo or ammine ligands are uniformly in reasonable accordance with the predictions of the Frumkin model both in the absence and the presence of specific anionic adsorption, once the likely noncoincidence of the reaction planes and the oHp is taken into account (5–9) (*vide infra*).[2]

In view of these appealing features, it seems worthwhile to employ such reactions to examine further the effects of varying the supporting electrolyte cation upon electrode kinetics. In particular, $Cr(NH_3)_6^{3+}$ and $Cr(OH_2)_6^{3+}$ are both reduced irreversibly at negative potentials (ca. −800 to −1000 mV vs. sce) where the supporting electrolyte cation forms the predominant component of the diffuse layer. Moreover, both reactions probably proceed via outer-sphere pathways, i.e., where the "primary inner layer" of water adjacent to the electrode surface is not penetrated by the reacting species in the transition state for electron transfer (5, 7) so that the double-layer effects upon these reactions should be predominantly electrostatic in origin. Both reactants are spherical and of comparable size to the aquo cations that commonly form the supporting electrolyte. However, the reaction planes for the reduction of $Cr(NH_3)_6^{3+}$ and other Cr(III) and Co(III) ammines appear to lie significantly closer to the electrode surface than for the reduction of $Cr(OH_2)_6^{3+}$ and other aquo complexes, as deduced from the markedly larger double-layer effects observed for the former reactions (5–7). These differences appear to rise from the larger effective size of the aquo reactants; although the crystallographic radii of corresponding ammine and aquo complexes are closely similar, the hydrated radii of the latter reactants are significantly (~1 Å) larger as a result of hydrogen bonding between the aquo ligands and surrounding water molecules ("solvent structure-making") (5, 11, 12). Similarly, the increases in the inner-layer capacitance seen at electrode potentials negative of the pzc for supporting electrolytes with cations of increasing atomic number and charge arise from decreases in the inner-layer thickness due to decreases in the effective hydrated radii of the cations that form the oHp (13–15). However, some of these capacitance variations have also frequently been ascribed to specific adsorption of the heavier cations, particularly cesium (16). Distinction between these two possibilities has proved to be difficult purely on the basis of thermodynamic data since both models lead to predictions that are broadly in accordance with experiment (15, 16).

The comparison of the influence of varying the nature of the supporting electrolyte cation upon the reduction kinetics of $Cr(OH_2)_6^{3+}$ and $Cr(NH_3)_6^{3+}$ is anticipated to shed light on this question since the relative rate responses obtained for these two similar reactants having the same charge yet different reaction planes to changes in the supporting electrolyte cation should be sensitive to the potential profile within the double layer. Such a study is reported in the present paper.

Experimental

Stock solutions of $Cr(OH_2)_6^{3+}$ and $Cr(OH_2)_5F^{2+}$ in excess perchloric acid were prepared essentially as described in refs. 17 and 18, respectively. Solid $Cr(NH_3)_6\cdot(ClO_4)_3$ was synthesized as outlined in ref. 19; $Ru(NH_3)_6\cdot(ClO_4)_3$ was obtained by recrystallizing samples of $Ru(NH_3)_6\cdot Cl_3$ (Alfa Inorganics) from solutions containing perchloric acid. Analytical grade reagents were often used without further purification, although they were recrystallized from water in a number of cases. Water for electrode kinetics experiments was either purified by a Milli-Q water purification system (Millipore Corp) or by distillation from alkaline permanganate followed by pyrodistillation (11), with identical results.

The apparatus employed was substantially the same as described in ref. 5. The apparent heterogeneous rate constants k_{app} were determined as a function of electrode potential E using either normal pulse or dc polarography, employing a PAR 174 Polarographic Analyzer (Princeton Applied Research Corp) coupled with a Hewlett-Packard 7045A X-Y recorder. A dropping mercury electrode having flow rates in the range 1.5–2 mg s^{-1} was used with a mechanically controlled drop time of 2 s. The analyses of the irreversible polarographic waves employed the methods due to Oldham and Parry (20). Normal pulse polarography was preferred to dc polarography for most measurements since larger rate constants (up to ca. 4×10^{-2} cm s^{-1}) could be obtained with the former technique and it is also less susceptible to polarographic maxima.

Since relatively small differences (often less than a factor of 2–3) in k^E_{app} for a given electrode reaction between the various electrolytes at a given electrode potential were required to be measured, a good deal of attention was paid to the optimization of experimental precision and accuracy. It was found that although noticeable discrepancies in the values of k^E_{app} (up to ca. 50%) for a given system could be obtained by different workers using different capillaries, etc., much better precision (values of k^E_{app} within 5%) could be obtained by a given worker using the

[2]Note that the apparent breakdown of the Frumkin model for Eu^{2+} oxidation in perchlorate electrolytes reported in ref. 10 now appears instead to be an artifact of the data analysis (9).

Can. J. Chem. Downloaded from www.nrcresearchpress.com by 210.87.254.40 on 09/06/12
For personal use only.

same experimental setup, especially if a series of electrolytes was run consecutively so that the mercury flow rate, cell temperature, etc., remained essentially constant. As much kinetic data as possible were therefore obtained in this manner. The precision in k_{app} achieved was limited at the bottom and the top of the polarographic waves by the corrections for the background currents and the inevitable errors in the assignment of the diffusion-limited current i_{lim}, respectively. The polarographic analyses were therefore restricted to measured currents i such that $0.08 \lesssim i/i_{lim} \lesssim 0.92$. Reactant concentrations were usually between 0.5–1 mM to avoid polarographic maxima yet to allow currents at the foot of the wave to be separated from the background. Using these conditions, values of the apparent transfer coefficients α_{app} were usually reproducible to within 1–2%. All kinetic measurements were made at 25.0° ± 0.1°C, using a jacketed cell through which water was circulated from a Braun Melsungen thermostat.

Formal potentials for $Fe(OH_2)_6^{3+/2+}$ and $Ru(NH_3)_6^{3+/2+}$ in the various electrolytes were evaluated as described in ref. 11 by means of cyclic voltammetry using platinum "flag" and hanging mercury drop electrodes, respectively. Small concentrations of chloride ions (1–2 mM) were added to the solutions containing Fe^{3+} in order to enhance the electrochemical reversibility of the $Fe(OH_2)_6^{3+/2+}$ couple. All electrode potentials are reported with respect to the saturated (KCl) calomel electrode (sce), although measurements in concentrated perchlorate media employed an sce containing saturated NaCl in order to eliminate spurious liquid junction potentials caused by precipitation of $KClO_4$ in the fiber junction.

Results

Table 1 contains a summary of rate–potential data obtained for the electroreduction of $Cr(OH_2)_6^{3+}$ and $Cr(NH_3)_6^{3+}$ in various supporting electrolytes containing univalent, divalent, and trivalent cations of systematically varying atomic number. The choice of electrolytes was determined partly by the conditions employed previously to study double-layer effects with these reactants (5, 17, 21–23), and partly by availability of accurate capacitance measurements. Grahame has reported capacitance–potential data for 0.1 M chloride salts with a wide range of cations (24). In view of the significant ion-pairing between the Cr(III) reactants and Cl^- at these high ionic strengths (21), the corresponding perchlorate or nitrate salts were used instead. At the negative electrode potentials of interest here ($-E > 800$ mV vs. sce) specific adsorption of nitrate, perchlorate, or chloride is negligible and the supporting electrolyte cation therefore provides the dominant contribution to the ionic charge in the double layer. For the divalent cation series Mg^{2+}, Ca^{2+}, Sr^{2+}, Ba^{2+}, and the trivalent series Al^{3+}, Yb^{3+}, La^{3+}, 0.1 M perchlorate salts were employed since Grahame's capacitance data could then be used directly. For the univalent cation series Li^+, Na^+, K^+, Rb^+, Cs^+, and NH_4^+, 0.5 M solutions of the nitrate salts were used instead. This is because the Gouy–Chapman diffuse-layer potentials ϕ_d^{GCS} in 0.1 M MX salts (where M is a metal cation or NH_4^+), are sufficiently negative at the electrode charge densities q^m encountered here ($7 < -q^m \lesssim 10\,\mu C\ cm^{-2}$) so that the tripositive Cr(III) reactants are calculated to provide a significant influence on ϕ_d even for small bulk reactant concentrations (~0.5–1 mM). For 0.5 M MX salts (as well as for 0.1 M MX_2 and MX_3 salts), ϕ_d^{GCS} is estimated to be sufficiently small ($-\phi_d^{GCS} < 50$ mV) to render this effect negligible. Although nitrate is expected to have a greater tendency than perchlorate to form ion pairs with the Cr(III) reactants, $Cr(NH_3)_6^{3+}$ is insufficiently soluble in 0.5 M perchlorate solutions (<0.5 mM); also the use of nitrate rather than perchlorate salts allowed 0.5 M K^+, Rb^+, and Cs^+ solutions to be studied. Nevertheless, similar rate data were obtained for a given reactant in corresponding alkali nitrate and perchlorate media (Table 1).

The kinetic data in Table 1 are summarized as observed (apparent) rate constants k_{app} at −900 mV vs. sce together with the apparent transfer coefficient α_{app} ($= -(RT/F)(\partial \ln k_{app}/\partial E)_\mu$) obtained from the slope of the Tafel plot in a given electrolyte μ at the same potential. This potential was chosen since the most trustworthy rate data for both reactants were obtained in the potential region −850 to −950 mV. Essentially linear Tafel plots (i.e., potential-independent values of α_{app} were uniformly obtained for $Cr(NH_3)_6^{3+}$ reduction over the relatively narrow (ca. 150–200 mV) range of overpotentials that were conveniently accessible due to the large values of α_{app} (~0.8). The reduction of $Cr(OH_2)_6^{3+}$ yielded essentially linear Tafel plots in 0.5 M MNO_3 and $MClO_4$ electrolytes in the observable potential range −750 to −1100 mV vs. sce, as previously noted for concentrated $NaClO_4$ (17, 22). Small yet significant decreases in α_{app} with increasing overpotential (ca. 0.02–0.03 over the ~250 mV observable potential range) were seen in the dipositive and especially tripositive supporting electrolytes, as noted previously with $La(ClO_4)_3$ electrolytes (17, 22).

The reduction kinetics of $Cr(OH_2)_5F^{2+}$ were monitored for the divalent cation series 0.1 M $Mg(ClO_4)_2 \rightarrow$ 0.1 M $Ba(ClO_4)_2$. Decreases in k_{app} were again observed with increasing cation atomic number, although they were noticeably (40–50%) less than those for $Cr(OH_2)_6^{3+}$ reduction, as expected in view of the smaller charge of the fluoro complex (23).

Inspection of the rate data in Table 1 reveals that for a given series of electrolytes having the same concentration and cation charge there are progressive decreases in k_{app} and also α_{app} at a given electrode potential as the atomic number of the supporting electrolyte cation increases. The sim-

TABLE 1. Rate constants and transfer coefficients for the reduction of $Cr(OH_2)_6^{3+}$ and $Cr(NH_3)_6^{3+}$ at −900 mV vs. sce in electrolytes containing various cations

Electrolyte[a]	$Cr(OH_2)_6^{3+}$ reduction				$Cr(NH_3)_6^{3+}$ reduction			
	$-\log k_{app}$[b]	α_{app}[c]	$-\log k_{corr}^{GCS}$[d]	α_{corr}^{GCS}[e]	$-\log k_{app}$[b]	α_{app}[c]	$-\log k_{app}^{GCS}$[d]	α_{corr}^{GCS}[e]
0.5 *M* $LiNO_3$	2.26	0.65	4.36	0.48	2.83	0.81	4.93	0.66
0.5 *M* $NaNO_3$	2.41	0.63	4.53	0.46	3.03	0.79	5.17	0.63
0.5 *M* KNO_3	2.44	0.62	4.57	0.45	3.06	0.78	5.19	0.62
0.5 *M* $RbNO_3$	2.48	0.61	4.63	0.43	3.10	0.77	5.25	0.60
0.5 *M* $CsNO_3$	2.69	0.58	4.89	0.39	3.29	0.76	5.49	0.58
0.5 *M* NH_4NO_3	2.53	0.61	4.67	0.43	3.12	0.78	5.26	0.61
0.5 *M* $LiClO_4$[f]	2.30	0.65	4.40	0.48				
0.5 *M* $NaClO_4$[f]	2.40	0.63	4.52	0.46				
0.5 *M* NH_4ClO_4[f]	2.50	0.61	4.64	0.43				
0.1 *M* $Mg(ClO_4)_2$[g]	2.37	0.64	4.17	0.54	2.93	0.81	4.73	0.71
0.1 *M* $Ca(ClO_4)_2$	2.39	0.63	4.20	0.53	2.95	0.80	4.76	0.70
0.1 *M* $Sr(ClO_4)_2$	2.47	0.62	4.29	0.52	3.03	0.79	4.85	0.69
0.1 *M* $Ba(ClO_4)_2$	2.65	0.61	4.48	0.51	3.12	0.78	4.95	0.68
0.1 *M* $Al(ClO_4)_3$	2.87	0.58	4.10	0.51	3.20	0.80	4.43	0.74
0.1 *M* $La(ClO_4)_3$	2.95	0.56	4.19	0.49	3.29	0.79	4.53	0.73
0.04 *M* $Al(ClO_4)_3$	2.51	0.59	4.04	0.51	2.87	0.81	4.40	0.74
0.04 *M* $Yb(ClO_4)_3$	2.60	0.57						
0.04 *M* $La(ClO_4)_3$	2.67	0.56	4.21	0.49	3.02	0.80	4.56	0.73

[a] Electrolytes contained 5 m*M* $HClO_4$ in order to suppress hydrolysis of $Cr(OH_2)_6^{3+}$ and some supporting electrolyte cations and to prevent precipitation of $Cr(OH)_2$ resulting from spurious pH changes in vicinity of electrode (5).

[b] k_{app} is measured (apparent) rate constant at electrode potential of −900 mV vs. sce. Experimental precision in log k_{app} is ca. ±0.02 (see text).

[c] α_{app} is apparent transfer coefficient (= $-(2.303\ RT/F)(\partial \log k_{app}/\partial E)_\mu$) at −900 mV vs. sce. Experimental precision ca. ±0.01 (see text).

[d] k_{corr}^{GCS} is double-layer corrected rate constant at −900 mV vs. sce; obtained from corresponding value of k_{app} using eq. [1] and assuming that $\phi_r = \phi_d^{GCS}$, where ϕ_d^{GCS} is the potential drop across the diffuse layer calculated from the Gouy–Chapman–Stern theory. The required value of the electrode charge q^m for each electrolyte was obtained from data in ref. 24 (see text).

[e] α_{corr}^{GCS} is double-layer corrected rate constant at −900 mV vs. sce; obtained from corresponding value of α_{app} using eq. [2] and assuming that $(\partial\phi_r/\partial E)_\mu = (\partial\phi_d^{GCS}/\partial E)_\mu$. Values of $(\partial\phi_d^{GCS}/\partial E)_\mu$ were obtained from Gouy–Chapman–Stern estimates of diffuse-layer capacitance coupled with values of electrode capacitance taken from ref. 24.

[f] Studies of $Cr(NH_3)_6^{3+}$ reduction precluded due to insufficient solubility of $Cr(NH_3)_6(ClO_4)_3$ in these media.

[g] Identical kinetic parameters within experimental error also were obtained for both reactions in 0.1 *M* $Mn(ClO_4)_2$ and 0.1 *M* $Co(ClO_4)_2$.

plest possibility is that these rate variations may be due to differences in the diffuse-layer potentials between the various electrolytes. We can write for a one-electron reduction at a given electrode potential E (e.g. ref. 8)

$$[1]\quad \log k_{app} = \log k_{corr} + \log(\gamma_r/\gamma_\pm) - \frac{F}{2.303RT}(Z_r - \alpha_{corr})\phi_r$$

where k_{corr} and α_{corr} are the ("double-layer corrected") rate constant and transfer coefficient, respectively, that would be observed in the absence of the ionic double layer, Z_r is the reactant charge, γ_r and $\gamma_\pm$ are the activity coefficients for the bulk reactant and the transition state, respectively, and ϕ_r is the average potential on the reaction plane. Similarly, we can relate the apparent and corrected transfer coefficients by

$$[2]\quad \alpha_{corr} = \frac{\alpha_{app} - Z_r(\partial\phi_r/\partial E)_\mu}{1 - (\partial\phi_r/\partial E)_\mu}$$

In the GCSF approach ϕ_r is assumed to equal the potential drop across the diffuse layer as calculated from the Gouy–Chapman–Stern (GCS) theory (ref. 1*b*, Chapt. 3), ϕ_d^{GCS}, and $\gamma_r/\gamma_\pm = 1$. Values of ϕ_d^{GCS} and $(\partial\phi_d^{GCS}/\partial E)_\mu$ were obtained for each electrolyte at the required electrode potential by reading off the corresponding values of the excess electrode charge density q^m and the electrode capacitance $(\partial q^m/\partial E)_\mu$ from the appropriate q^m–E plots, and then employing the GCS theory assuming that cation specific adsorption is absent (*vide infra*). These plots for the corresponding 0.1 *M* salts were extracted directly from Grahame's published data for the corresponding 0.1 *M* chloride electrolytes (24). The q^m–E plots for electrolytes at other ionic strengths were obtained by assuming that the displacement of E at each q^m is given by the difference in ϕ_d^{GCS} between 0.1 *M* and the desired salt concentration.

The resulting values of log k_{corr}^{GCS} and α_{corr}^{GCS} determined in this manner for $E = -900$ mV vs. sce are also given in Table 1. It is seen that there is a considerable variation in log k_{corr}^{GCS} as well as in log k_{app}^{GCS} with the nature of the supporting electrolyte cation; indeed the diffuse-layer correction acts to magnify the rate differences within each series of electrolytes containing cations of the same charge and concentration.

Since qualitative changes in the supporting elec-

Can. J. Chem. Downloaded from www.nrcresearchpress.com by 210.87.254.40 on 09/06/12
For personal use only.

Can. J. Chem. Downloaded from www.nrcresearchpress.com by 210.87.254.40 on 09/06/12
For personal use only.

trolytes are involved, it is possible that part of the observed rate variations arises from changes in the bulk activity coefficients of the reactants and/or liquid junction potentials. These possibilities can be checked by measuring the formal potentials E_f for the reactant redox couples in the various electrolytes. However, it is extremely difficult to determine E_f for the $Cr(OH_2)_6^{3+/2+}$ couple to the desired accuracy (±2 mV) in view of its extremely small standard rate constants in these media (ca. 1×10^{-5} cm s^{-1}); also values of E_f for $Cr(NH_3)_6^{3+/2+}$ cannot be measured due to the kinetic and thermodynamic instability of $Cr(NH_3)_6^{2+}$. Instead, values of E_f in each electrolyte were obtained for $Fe(OH_2)_6^{3+/2+}$ and $Ru(NH_3)_6^{3+/2+}$. Since these couples have the same charge and ligand composition and are of similar size to $Cr(OH_2)_6^{3+/2+}$ and $Cr(NH_3)_6^{3+/2+}$, respectively, it is likely that the observed variations in E_f for the former couples will mimic those for the latter systems. Table 2 contains a summary of the observed formal potentials. It is seen that only small variations in E_f (ca. $\lesssim$ 5 mV) were obtained for $Fe(OH_2)_6^{3+/2+}$ in the various perchlorate electrolytes, even between electrolytes with cations of different charges. Larger variations in E_f (up to 20 mV) were seen for $Ru(NH_3)_6^{3+/2+}$. In particular, the values of E_f in the heavier alkali nitrate media are significantly more negative than those in the perchlorate electrolytes.

TABLE 2. Formal potentials for $Fe(OH_2)_6^{3+/2+}$ and $Ru(NH_3)_6^{3+/2+}$ in electrolytes containing various cations

	Formal potential, mV vs. sce[b]	
Electrolyte[a]	$Fe(OH_2)_6^{3+/2+}$	$Ru(NH_3)_6^{3+/2+}$
0.5 *M* $LiNO_3$	485	−188
0.5 *M* $NaNO_3$	486	−194
0.5 *M* KNO_3	488	−198
0.5 *M* $RbNO_3$	486	−198
0.5 *M* $CsNO_3$	486	−198
0.5 *M* NH_4NO_3	488	−198
0.5 *M* $LiClO_4$	490	−184
0.5 *M* $NaClO_4$	490	−186
0.5 *M* NH_4ClO_4	486	−187
0.1 *M* $Mg(ClO_4)_2$	484	−181
0.1 *M* $Ca(ClO_4)_2$	487	−179
0.1 *M* $Sr(ClO_4)_2$	489	−179
0.1 *M* $Ba(ClO_4)_2$	487	−180
0.04 *M* $Al(ClO_4)_3$	486	−180
0.04 *M* $La(ClO_4)_3$	484	−178
0.1 *M* $Al(ClO_4)_3$	485	−182

[a]Electrolytes contained 10 m*M* $HClO_4$ to suppress hydrolysis of $Fe(OH_2)_6^{3+}$; 1–2 m*M* of Cl^- was also added to enhance electrochemical reversibility of $Fe(OH_2)_6^{3+/2+}$.

[b]Obtained using cyclic voltammetry from mean of forward (cathodic-going) and backward (anodic-going) peak potentials (11). Solutions contained 1 m*M* of either $Fe(OH_2)_6^{3+}$ or $Ru(NH_3)_6^{3+}$. Electrodes used were a platinum flag for $Fe(OH_2)_6^{3+/2+}$ and a hanging mercury drop for $Ru(NH_3)_6^{3+/2+}$. Experimental reproducibility of E_f is ca. ±1–2 mV in each case.

Discussion

The variations in k_{app} and k_{corr}^{GCS} for $Cr(OH_2)_6^{3+}$ and $Cr(NH_3)_6^{3+}$ reduction summarized in Table 1 are qualitatively similar to those seen previously with a more limited range of supporting electrolyte cations for the reduction of protons (25, 26) and several other cations (2) in that rate decreases are seen with increasing cation atomic number. On the basis of eq. [1], these rate variations seem most likely to be due to alterations in ϕ_r caused by either (*i*) changes in the extent of cation specific adsorption, and/or (*ii*) changes in the position of the oHp as the supporting electrolyte cation is varied.

When analyzing electrode kinetic data for the effects of specific adsorption (model (*i*)) it has become conventional to monitor the change in the measured rate constant k_{app} at a given electrode potential, $(\Delta \log k_{app})_E$, and to compare the resulting variations in ϕ_r, $(\Delta\phi_r)_E$, obtained using eq. [1] with the corresponding estimates obtained from double-layer compositional data using the GCS model or other approaches (e.g. refs. 5, 8, 28). However, for the present purposes involving the comparison of both models (*i*) and (*ii*) with the kinetic data it is more convenient to monitor instead the change in k_{app} in response to an alteration in electrolyte composition at a *constant electrode charge density* q^m, $(\Delta \log k_{app})_{q^m}$. This quantity is related to the corresponding change in ϕ_r, $(\Delta\phi_r)_{q^m}$, by

$$[3] \quad (\Delta \log k_{app})_{q^m} = \Delta \log (\gamma_r/\gamma_\pm) - \frac{F}{2.303RT} \times [(Z_r - \alpha_{corr})(\Delta\phi_r)_{q^m} + \alpha_{corr}(\Delta E)_{q^m}]$$

where $(\Delta E)_{q^m}$ is the difference in the electrode potential between the two supporting electrolytes at the same value of q^m, and $\Delta\log(\gamma_r/\gamma_\pm)$ is the corresponding change in the activity coefficients. The values of $(\Delta E)_{q^m}$ were read from the appropriate q^m–E plots obtained from ref. 24. The virtue of computing estimates of $(\Delta\phi_r)_{q^m}$ rather than $(\Delta\phi_r)_E$ is that the diffuse-layer potential will very likely remain constant at constant q^m for a series of electrolytes containing different cations of equal charge and concentration, providing that cation specific adsorption is negligible. The comparison of $(\Delta\phi_r)_{q^m}$ for a series of such electrolytes with the corresponding changes in the potential drop across the entire metal–solution interface $(\Delta E)_{q^m}$ therefore provides an incisive way of comparing the kinetic data with the predictions of model (*ii*).

Table 3 contains a summary of the values of $(\Delta\phi_r)_{q^m}$ for $Cr(OH_2)_6^{3+}$ and $Cr(NH_3)_6^{3+}$, labeled

TABLE 3. Changes in potential at reaction planes for $Cr(OH_2)_6^{3+}$ and $Cr(NH_3)_6^{3+}$ reductions resulting from variations in supporting electrolyte cation compared with corresponding changes in electrode potential

	$q^m = -8\,\mu C\,cm^{-2}$				$q^m = -10\,\mu C\,cm^{-2}$			
Electrolyte	$-E^a$ mV vs. sce	$(\Delta E)_{q^m}{}^b$ mV	$(\Delta\phi_r)_{q^m}{}^{OH_2c}$ mV	$(\Delta\phi_r)_{q^m}{}^{NH_3d}$ mV	$-E^a$ mV vs. sce	$(\Delta E)_{q^m}{}^b$ mV	$(\Delta\phi_r)_{q^m}{}^{OH_2c}$ mV	$(\Delta\phi_r)_{q^m}{}^{NH_3d}$ mV
0.5 *M* $LiNO_3$	819.5				940.5			
0.5 *M* $NaNO_3$	815.0	4.5	3	3.5	933.5	7	4.5	6
0.5 *M* KNO_3	814	5.5	3.5	4.5	931	9.5	4.5	6.5
0.5 *M* $RbNO_3$	808	9.5	4.5	5.5	922.5	18	6	9
0.5 *M* $CsNO_3$	795.5	24	9	11	904.5	36	12	15.5
0.5 *M* NH_4NO_3	809.5	10	7.5	7.5	924.5	16	8.5	10
0.5 *M* $LiClO_4$	819.5				940.5			
0.5 *M* $NaClO_4$	815	4.5	3		933.5	7	3	
0.5 *M* NH_4ClO_4	809.5	10	6		924.5	16	6	
0.1 *M* $Mg(ClO_4)_2$	828				946			
0.1 *M* $Ca(ClO_4)_2$	818	10	0.5	2	935	11	1.5	2.5
0.1 *M* $Sr(ClO_4)_2$	814	14	3	3.5	929.5	16.5	3.5	4
0.1 *M* $Ba(ClO_4)_2$	813	15	6	6	928.5	17.5	7	7
0.1 *M* $Al(ClO_4)_3$	808	20	9	8.5	923.5	22.5	12	9
0.1 *M* $La(ClO_4)_3$	800	28	12	11.5	912	34	16	12.5

[a] Electrode potential for stated electrolyte corresponding to electrode charge density q^m of -8 or $-10\,\mu C\,cm^{-2}$, as noted. Obtained from data in ref. 24 as described in the text.

[b] Change in electrode potential at a constant electrode charge density q^m of -8 or -10 $\mu C\,cm^{-2}$, as noted, for listed electrolyte relative to "parent" electrolytes 0.5 *M* $LiNO_3$ (for 0.5 *M* MNO_3 series), 0.5 *M* $LiClO_4$ (for 0.5 *M* $MClO_4$ series), or 0.1 *M* $Mg(ClO_4)_2$ (for 0.1 *M* $M(ClO_4)_2$ and 0.1 *M* $M(ClO_4)_3$ series).

[c] Change in average potential on reaction plane for $Cr(OH_2)_6^{3+}$ reduction at $q^m = -8$ or $-10\,\mu C\,cm^{-2}$, as noted, for listed electrolyte relative to "parent" electrolytes given in *b*. Obtained from kinetic data in Table 1 using eq. [3], as outlined in text.

[d] Change in average potential on reaction plane for $Cr(NH_3)_6^{3+}$ reduction at $q^m = -8$ or $-10\,\mu C\,cm^{-2}$, as noted, for listed eleetrolyte relative to "parent" electrolytes given in *b*. Obtained from kinetic data in Table 1 using eq. [3], as outlined in text.

$(\Delta\phi_r)_{q^m}{}^{OH_2}$ and $(\Delta\phi_r)_{q^m}{}^{NH_3}$, respectively, which result from the rate data given in Table 1 using eq. [3], assuming that $\alpha_{corr} = 0.5$ (5, 17, 22) and that $\Delta\log \gamma_r/\gamma_{\pm} = 0$ (8).[3] For the alkali metal series 0.5 *M* MNO_3 and 0.5 *M* $MClO_4$, the values of $(\Delta\phi_r)_{q^m}$ were calculated with respect to 0.5 *M* $LiNO_3$ and 0.5 *M* $LiClO_4$, respectively. Values of $(\Delta\phi_r)_{q^m}$ for the divalent and trivalent electrolytes were referred to 0.1 *M* $Mg(ClO_4)_2$ as the parent system. The corresponding values of $(\Delta E)_{q^m}$ are also listed in Table 3. Values of $(\Delta\phi_r)_{q^m}$ and $(\Delta E)_{q^m}$ are given for each system for the electrode charge densities $q^m = -8$ and $-10\,\mu C\,cm^{-2}$.

Inspection of Table 3 reveals that the corresponding values of $(\Delta\phi_r)_{q^m}{}^{OH_2}$ and $(\Delta\phi_r)_{q^m}{}^{NH_3}$ for most electrolytes are similar, although there is a tendency for $(\Delta\phi_r)_{q^m}{}^{NH_3}$ to be slightly (~10–20%) larger.[3] This similarity in the rate responses for the aquo and ammine reactants at constant electrode charge density is also seen at constant potential (Table 1) in that the differences in $\log k_{app}$ between the various electrolytes at -900 mV vs. sce, $\Delta\log k_{app}$, for the two reactants are often within 10–20% of each other. These results contrast those from our previous comparison of double-layer effects upon the reduction kinetics of Cr(III) ammine and aquo complexes (5). It was found that the corresponding values of $(\Delta\log k_{app})_E$ and hence $(\Delta\phi_r/\Delta q')_E$ resulting from the specific adsorption of a given charge density q' of anions at a constant ionic strength were both *three- to fourfold larger* for $Cr(NH_3)_6^{3+}$ compared with $Cr(OH_2)_6^{3+}$ reduction (5). Using the analysis at constant charge (eq. [3]), it is simple to show that the values of $(\Delta\phi_r)_{q^m}{}^{NH_3}$ are also about three- to fourfold larger than the corresponding values of $(\Delta\phi_r)_{q^m}{}^{OH_2}$ under these conditions. As noted above, these behavioral differences were traced to the ability of the more weakly hydrated $Cr(NH_3)_6^{3+}$ reactant to approach the surface more closely than $Cr(OH_2)_6^{3+}$, so that the former reactant will experience a greater fraction of the changes in the potential at the inner Helmholtz plane (iHp) induced by anion specific adsorption (5). Similarly, larger values of $(\Delta\phi_r/\Delta q^m)_\mu$ induced by changes in electrode potential in the absence of specific ionic adsorption were also seen for $Cr(NH_3)_6^{3+}$ compared to $Cr(OH_2)_6^{3+}$ reduction (5). For a given reaction in a given base electrolyte, the values of $(\Delta\phi_r/\Delta q^m)_\mu$ and $(\Delta\phi_r/q')_E$ were found to be consistently similar (5); this simple result was

[3] The likely negative shift in E_f for the ammine couple within the electrolyte series 0.5 *M* $LiNO_3 \rightarrow CsNO_3$ from the data in Table 2 suggests that $\Delta\log(\gamma_r/\gamma_{\pm})$ is negative; this would tend to make the actual values of $(\Delta\phi_r)_{q^m}$ for $Cr(NH_3)_6^{3+}$ reduction smaller for these electrolytes than the values listed in Table 3. Although the magnitude of this correction is difficult to estimate quantitatively, since $\Delta E_f = (2.303RT/F)\log(\gamma_r/\gamma_P)$, where γ_P is the coefficient of the bulk product, then if $\gamma_r/\gamma_{\pm} \sim 0.5$ (γ_r/γ_P) it follows that the actual values of $(\Delta\phi_r)_{q^m}$ for $Cr(NH_3)_6^{3+}$ reduction are smaller by up to 5 mV than the listed values; i.e., closer to or smaller than the corresponding values of $(\Delta\phi_r)_{q^m}$ for $Cr(OH_2)_6^{3+}$ reduction.

Can. J. Chem. Downloaded from www.nrcresearchpress.com by 210.87.254.40 on 09/06/12
For personal use only.

Can. J. Chem. Downloaded from www.nrcresearchpress.com by 210.87.254.40 on 09/06/12
For personal use only.

also seen for the outer-sphere electroreduction of various Co(III) ammines (6).

It would therefore be expected that if the observed cation effects upon the reduction kinetics of $Cr(OH_2)_6^{3+}$ and $Cr(NH_3)_6^{3+}$ were due predominantly to cation specific adsorption (model (*i*)), markedly larger rate decreases should be obtained for the latter reaction, either at constant electrode potential or charge, as the extent of cation specific adsorption increases. This point is illustrated in Fig. 1*a*, which consists of a pair of schematic plots of the average potential ϕ against distance x from the electrode surface D. Curve I is such a profile as would be expected at negative electrode charges in the absence of specific cation adsorption. It contains three regions: the diffuse layer AB bounded by the oHp which is the plane of closest approach of the supporting electrolyte cations; the region BC between the oHp and the monolayer of water molecules adjacent to the electrode; these form the "primary inner layer" CD. (Although the shape of this profile is undoubtedly oversimplified, the use of more complicated double-layer models does not alter the qualitative treatment considered here.) Curve II is a corresponding potential profile at the same electrode charge resulting from significant cation specific adsorption at the site C′. Inspection of Fig. 1*a* shows that the vertical displacement $\Delta\phi$ between curves I and II increases with decreasing x for $x >$ C′D. Thus the values of $(\Delta\phi_r)_{q^m}$ for ammine reactants are expected to be noticeably larger than those for aquo reactants if the latter indeed react farther from the electrode surface. This prediction is in direct contrast to the experimental observations (Table 3).

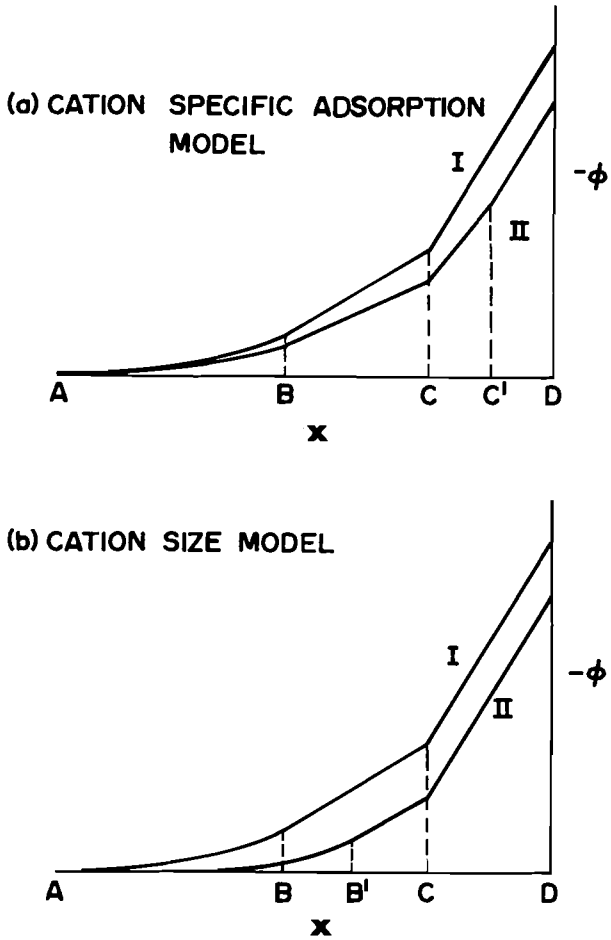

FIG. 1. Effect of varying supporting electrolyte cation at constant electrode charge density upon schematic potential profile within double layer.

Figure 1*b* consists of a corresponding pair of ϕ–x plots at a fixed electrode charge for two supporting electrolytes differing only in the effective cation size, specific adsorption being absent in both cases (i.e., model (*ii*)). The substitution of the smaller for the larger cation results in a shift of the oHp from B to B′. Providing that the inner-layer water structure is unaffected by this change, the smaller cation will yield a ϕ–x profile (curve II) which parallels that for the larger cation (curve I) but displaced vertically by an amount $(\Delta\phi)_{q^m}$ which is *independent* of x for $x <$ B′. Such a model is therefore able to account for the observation that $(\Delta\phi_r)_{q^m}$ for $Cr(OH_2)_6^{3+}$ and $Cr(NH_3)_6^{3+}$ reduction are similar, provided that the reaction planes for these processes are inside, or within the vicinity, of the oHp for the various electrolytes scrutinized.

Estimates of the positions of these reaction planes with respect to the oHp can be obtained from a consideration of the relative hydrated radii of the transition state species and the supporting electrolyte cations. To a first approximation it might be expected that the distance between the oHp and the primary inner layer (BC in Fig. 1) would equal the effective hydrated radius of the supporting electrolyte cation (15, 27). Some direct evidence supporting this notion has been obtained from estimates of the thickness of the cation-free region derived from electrocapillary measurements (14, 29). Table 4 lists values of hydrated radii for the cations of interest here according to two commonly used scales: those from the compilation of Monk (r_h) derived from ionic molar volume data (30), and the "Stokes radii" (r_s) obtained from ion transport data. Table 4 also contains estimates of r_h and r_s for the two transition state species ($Cr(OH_2)_6^{2.5+}$ and $Cr(NH_3)_6^{2.5+}$) that will presumably determine the effective plane of closest approach and hence ϕ_r for the reduction of $Cr(OH_2)_6^{3+}$ and $Cr(NH_3)_6^{3+}$, re-

Can. J. Chem. Downloaded from www.nrcresearchpress.com by 210.87.254.40 on 09/06/12
For personal use only.

TABLE 4. Estimates of effective hydrated radii of various cations

Cation	Hydrated radius (Monk)[a] r_h, Å	Stokes radius[b] r_s, Å
Li^+	2.50	2.37
Na^+	2.17	1.83
K^+	1.75	1.25
Rb^+	1.53	1.18
Cs^+	1.47	1.19
NH_4^+	1.88	1.25
Mg^{2+}	2.96	3.45
Ca^{2+}	2.72	3.08
Sr^{2+}	2.74	3.08
Ba^{2+}	2.48	2.88
Co^{2+}	—	3.42
Mn^{2+}	—	3.45
Al^{3+}	—	4.39[d]
La^{3+}	3.19	3.96[d]
Cr^{3+}	—	4.12[d]
$Cr(NH_3)_6^{3+}$	—	2.80[e]
$[Cr(OH_2)_6^{2.5+}]$	~3.3[c]	~3.8[c]
$[Cr(NH_3)_6^{2.5+}]$	~2.8[f]	~2.8[c,f]

[a]Hydrated radii estimated by Monk (30) from ionic molar volume data.
[b]Hydrated ("Stokes") radii quoted by Monk (30) unless otherwise indicated; estimated from equivalent conductance, diffusion coefficient, and solvent viscosity using Stokes–Einstein relations.
[c]Estimates of r_h and r_s for transition states for the outer-sphere one-electron reduction of $Cr(OH_2)_6^{3+}$ and $Cr(NH_3)_6^{3+}$; obtained by taking an average of the estimated hydrated radii for the oxidized (Cr^{III}) and reduced (Cr^{II}) species (see text).
[d]From ref. 31.
[e]From ref. 32.
[f]Obtained from average of estimated crystallographic radii of $Cr(NH_3)_6^{3+}$ and $Cr(NH_3)_6^{2+}$.

spectively.[4] These were obtained from the average of the corresponding estimates of r_h and r_s for the reactant and product species. On the basis of the relative values of both r_h and r_s for the transition states versus those for the supporting electrolyte cations, the transition state for $Cr(NH_3)_6^{3+}$ reduction is expected to be situated within the oHp except when this is formed by univalent cations, whereas that for $Cr(OH_2)_6^{3+}$ reduction is anticipated to lie outside the oHp except when this consists of trivalent cations. On the basis of Fig. 1*b*, it is therefore somewhat surprising that the values of $(\Delta\phi_r)_{q^m}^{OH_2}$ tend to approach those for $(\Delta\phi_r)_{q^m}^{NH_3}$ even for pairs of univalent electrolytes (Table 3). The simplest explanation is that the fields in the diffuse layer close to the oHp are comparable to those within the "secondary inner layer" BC (Fig. 1*b*), so that $(\Delta\phi_r)_{q^m}$ will remain independent of x even for $x > B'D$.

The simple cation size model embodied in Fig. 1*b* also predicts that $(\Delta\phi_r)_{q^m}$ will equal $(\Delta E)_{q^m}$ for $x < B'D$, whereas it is seen in Table 3 that $(\Delta\phi_r)_{q^m}^{OH_2}$ and $(\Delta\phi_r)_{q^m}^{NH_3}$ are both typically a factor of two or so smaller than $(\Delta E)_{q^m}$. Two explanations can most readily account for this discrepancy. Firstly, ϕ_r appearing in eqs. [1]–[3] is really the micropotential at the reaction site which may differ from the average (macro-) potential on the reaction plane ϕ_{rp} due to discreteness-of-charge effects (3), whereas $(\Delta E)_{q^m}$ is a difference between average potentials. Secondly, the assumption that the potential profile inside the oHp (the region BD) is unaffected by the substitution of different cations at the oHp at constant q^m may be a serious oversimplification in that the water structure and hence the potential profile of the inner-layer, in particular the region BC, may well be influenced significantly by the nature of these cations.

In addition to analyzing the cation dependence of k_{app}, it is also instructive to examine the corresponding influences upon the transfer coefficients. As expected from the cation size model, both α_{app} and α_{corr}^{GCS} tend to decrease for cations of decreasing hydrated radius, these variations being similar for $Cr(OH_2)_6^{3+}$ and $Cr(NH_3)_6^{3+}$ reduction (Table 1). This is also seen in Fig. 2, which contains plots of α_{corr}^{GCS} for $Cr(OH_2)_6^{3+}$ (open symbols) and $Cr(NH_3)_6^{3+}$ reduction (closed symbols) at −900 mV vs. sce (Table 1) in each supporting electrolyte against the hydrated cation radii r_h (Table 4). The interesting feature of this figure is that although the slopes of the two plots are similar, the values of α_{corr}^{GCS} for $Cr(NH_3)_6^{3+}$ reduction at a given value of r_h are displaced by almost 0.2 above those for $Cr(OH_2)_6^{3+}$ reduction. If the only factor aside from the diffuse-layer influencing ϕ_r and hence $(\partial\phi_r/\partial E)_\mu$ is the position of the reaction plane relative to the oHp, then equal values of α_{corr}^{GCS} for the two reactions should be obtained for equal values of $r_h - r_\neq$, where $r_\neq$ is the hydrated radius of the transition state species. In particular, α_{corr}^{GCS} should equal the "true" value of α_{corr} (i.e., the "intrinsic" transfer coefficient α_I (33), normally taken as 0.5) when $r_h = r_\neq$. However, this expectation is not entirely borne out by the data in Fig. 2. Thus using the estimates of $r_\neq$ given in Table 4, the value of α_{corr}^{GCS} found from Fig. 3 for $r_h = r_\neq$ equals about 0.55 for $Cr(OH_2)_6^{3+}$ reduction but about 0.7 for $Cr(NH_3)_6^{3+}$ reduction. Similar results are obtained using Stokes radii r_s in place of r_h. Although it is possible that the GCS model may yield incorrect estimates of the diffuse-layer effect upon α_{app}, this is unlikely to account for

[4]According to the conventional theoretical treatment of outer-sphere (weak adiabatic) electron transfer processes, each transition state for these simple symmetrical one-electron reactions will have a structure, including that of the surrounding solvent and ionic atmosphere, appropriate to that for a hypothetical ground-state cation with the same ligand composition yet having a charge midway between that for the reactant and the product. (For example, see ref. 39.) The plane of closest approach and hence the values of ϕ_r will therefore be determined by the transition state rather than the ground state reactant structure.

Can. J. Chem. Downloaded from www.nrcresearchpress.com by 210.87.254.40 on 09/06/12
For personal use only.

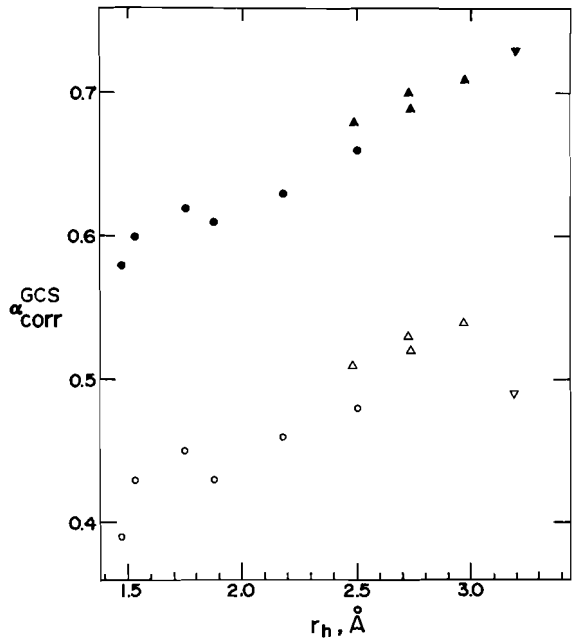

FIG. 2. Plot of the diffuse-layer corrected transfer coefficient α_{corr}^{GCS} at −900 mV vs. sce for $Cr(OH_2)_6^{3+}$ reduction (open symbols) and $Cr(NH_3)_6^{3+}$ reduction (closed symbols) (Table 1) in various electrolytes against the hydrated radius r_h of the supporting electrolyte cation (Table 4). Circles, univalent cations; upright triangles, divalent cations; inverted triangles, trivalent cations.

the unexpected large differences in α_{app} and α_{corr}^{GCS} between the two reactions. Also, the fact that the values of α_{corr}^{GCS} for a given reaction in electrolytes with uni-, di-, and trivalent cations all fall roughly on a common line (Fig. 2) indicates that the GCS model provides a consistent diffuse-layer correction. Some of the observed deficiencies of the GCSF model that were previously attributed to failures of GCS theory (17, 21) could well be due instead to a noncoincidence of the reaction plane and the oHp.

Three possibilities seem most likely to account for the unexpectedly large values of α_{corr}^{GCS} for $Cr(NH_3)_6^{3+}$ reduction. Firstly, α_1 for this reaction could be significantly larger than 0.5 as a result of the higher force constants expected for the reactant Cr^{III}—NH_3 bonds compared with the product Cr^{II}—NH_3 bonds. (This effect is likely to be smaller for the $Cr(OH_2)_6^{3+/2+}$ couple in view of the lower ligand field strength of OH_2 versus NH_3 ligands.) However, model calculations (34, 35) indicate that α_1 for such systems is likely to lie in the range ca. 0.45–0.55 at the small to moderate cathodic overpotentials considered here (22). Secondly, the reaction plane for $Cr(NH_3)_6^{3+}$ reduction may lie closer to the electrode than expected on the basis of the estimates of cation size given in Table 4; from Fig. 2 the reaction plane is estimated to lie about 1.5 Å closer than anticipated. Such a breakdown of the simple model may arise from a partial penetration of the primary inner layer of water molecules by the ammine ligands. Thirdly, for such reaction sites close to the electrode it is quite likely that discreteness-of-charge effects will be significant, in particular the "self-image" potential generated by the interaction of the reacting ion with its image in the electrode (36). Although the magnitude of this influence upon α_{corr} is uncertain, it is likely that the self-image effect would act to increase α_{corr} for cation reduction in the potential range of interest here (5, 36), and more so for an ion reacting closer to the electrode (37), in accordance with the present observations. A similar self-image effect was also invoked recently to explain the unexpectedly large rate constants seen for heterogeneous outer-sphere electron transfer reactions involving ammine versus aquo complexes in comparison with the rate constants for the corresponding homogeneous reactions (38).

Nevertheless, the simple average potential approach embodied in eqs. [1]–[3] is able to account at least semiquantitatively for the observed cation effects upon the electrode kinetics of these archetypically simple outer-sphere reactions, once the noncoincidence of the reaction plane with the oHp is taken into account using a simple cation size model. It seems that at least part of the disparate and frequently larger cation effects seen upon the electroreduction kinetics of various anions (1, 2, 16) arises from specific reactant–cation interactions at the reaction site (2) in addition to the average potential effects seen with the present cationic reactants. Although it is quite likely that cation specific adsorption is significant and even substantial at large negative electrode charges for weakly solvated cations such as cesium, the present results support the point of view (15) that such adsorption is minor at moderate electrode charges ($-q^m \lesssim 10\ \mu C\,cm^{-2}$). However, it is important to note that even the conceptual distinction between specific ion effects due to specific adsorption and variations in the planes of closest approach becomes clouded when the center of the adsorbed charge (iHp) lies outside the primary inner layer, as expected for large adsorbates or if the primary hydration sheath remains intact upon adsorption. Thus the discrimination between these two alternatives may ultimately prove to be illusory in some cases.

Acknowledgement

The work is supported by the U.S. Air Force Office of Scientific Research.

1. (*a*) R. PARSONS. *In* Advances in electrochemistry and electrochemical engineering. Vol. 1. *Edited by* P. Delahay and C. W. Tobias. Interscience, New York. 1961. Chapt. 1; (*b*) P. DELAHAY. Double layer and electrode kinetics. Interscience, New York. 1961. Chapt. 9.
2. L. GIERST, E. NICOLAS, and L. TYTGAT-VANDERBERGHEN. Croat. Chem. Acta, **42**, 117 (1970).
3. W. R. FAWCETT and S. LEVINE. J. Electroanal. Chem. **43**, 175 (1973).
4. R. GUIDELLI. J. Electroanal. Chem. **74**, 347 (1976).
5. M. J. WEAVER and T. L. SATTERBERG. J. Phys. Chem. **81**, 1772 (1977).
6. T. L. SATTERBERG and M. J. WEAVER. J. Phys. Chem. **82**, 1784 (1978).
7. M. J. WEAVER. Isr. J. Chem. **18**, 35 (1979).
8. M. J. WEAVER. J. Electroanal. Chem. **93**, 231 (1978).
9. P. D. TYMA and M. J. WEAVER. J. Electroanal. Chem. **111**, 195 (1980).
10. M. J. WEAVER and F. C. ANSON. J. Electroanal. Chem. **84**, 47 (1977).
11. E. L. YEE, R. J. CAVE, K. L. GUYER, P. D. TYMA, and M. J. WEAVER. J. Am. Chem. Soc. **101**, 1131 (1979).
12. M. J. WEAVER and S. M. NETTLES. Inorg. Chem. **19**, 1641 (1980).
13. N. F. MOTT, R. PARSONS, and R. J. WATTS-TOBIN. Philos. Mag. Ser. 8, **7**, 483 (1962).
14. J. A. HARRISON, J. E. B. RANDLES, and D. J. SCHRIFFRIN. J. Electroanal. Chem. **25**, 197 (1970).
15. W. R. FAWCETT. J. Electroanal. Chem. **39**, 474 (1972).
16. B. B. DAMASKIN. J. Electroanal. Chem. **65**, 799 (1975).
17. M. J. WEAVER and F. C. ANSON. J. Electroanal. Chem. **65**, 711 (1975).
18. T. W. SWADDLE and E. L. KING. Inorg. Chem. **4**, 532 (1965).
19. G. BRAUER (*Editor*). Handbook of preparative inorganic chemistry. Vol. 2. 2nd ed. Academic Press, New York 1965. p. 1351.
20. K. B. OLDHAM and E. P. PARRY. Anal. Chem. **40**, 65 (1968).
21. M. J. WEAVER and F. C. ANSON. J. Electroanal. Chem. **65**, 737 (1975).
22. M. J. WEAVER and F. C. ANSON. J. Phys. Chem. **80**, 1861 (1976).
23. M. J. WEAVER and F. C. ANSON. Inorg. Chem. **15**, 1871 (1976).
24. D. C. GRAHAME. J. Electrochem. Soc. **98**, 343 (1951).
25. E. A. MAZNICHENKO, B. B. DAMASKIN, and Z. A. IOFA. Dokl. Akad. Nauk SSSR. **138**, 1377 (1961).
26. A. N. FRUMKIN. *In* Advances in electrochemistry and electrochemical engineering. Vol. 1. *Edited by* P. Delahay and C. W. Tobias. Interscience, New York. 1961. Chapt. 2.
27. W. R. FAWCETT. J. Electroanal. Chem. **22**, 19 (1969).
28. R. PARSONS. J. Electroanal. Chem. **21**, 35 (1969).
29. R. PARSONS and F. G. R. ZOBEL. J. Electroanal. Chem. **9**, 333 (1965).
30. C. B. MONK. Electrolyte dissociation. Academic Press, New York. 1961. p. 271.
31. E. R. NIGHTINGALE. J. Phys. Chem. **63**, 1381 (1959).
32. T. TAKAHASHI and T. KOISO. Bull. Chem. Soc. Jpn. **49**, 2784 (1976).
33. R. PARSONS. Croat. Chem. Acta, **42**, 281 (1970).
34. R. A. MARCUS. J. Chem. Phys. **43**, 691 (1965).
35. W. SCHMICKLER. Ber. Bunsenges. Phys. Chem. **77**, 991 (1973).
36. W. R. FAWCETT. J. Chem. Phys. **61**, 3842 (1974).
37. S. LEVINE and W. R. FAWCETT. J. Electroanal. Chem. **99**, 265 (1979).
38. M. J. WEAVER. J. Phys. Chem. **84**, 568 (1980).
39. W. J. ALBERY. Electrode kinetics. Oxford. 1975. Chapt. 4.

Can. J. Chem. Downloaded from www.nrcresearchpress.com by 210.87.254.40 on 09/06/12
For personal use only.

Tensiometric studies on wetting. I. Some effects of surface roughness (theoretical)

ERDAL BAYRAMLI, THEODORE G. M. VAN DE VEN, AND STANLEY G. MASON

Pulp and Paper Research Institute of Canada, and Department of Chemistry, McGill University, Montreal, P.Q., Canada H3A 2A7

Received August 15, 1980

This paper is dedicated to Dr. Sam Levine on the occasion of his 70th birthday

ERDAL BAYRAMLI, THEODORE G. M. VAN DE VEN, and STANLEY G. MASON. Can. J. Chem. **59**, 1954 (1981).

The effect of roughness on the wettability of an axisymmetric cylinder is investigated theoretically by making use of equilibrium meniscus shapes on solid surfaces analogously to previous studies for drops on horizontal surfaces. Employing circumferential sinusoidal and saw-toothed grooved structure, and using mechanistic arguments, one can explain wetting hysteresis, the formation of composite surfaces, and the presence of non-equilibrium jumps during contact line motion.

On unidirectionally random surfaces the maximum surface slopes mainly determine the value of the advancing, and the minimum slopes of the receding contact angle. These effects of surface slopes diminish with decreasing roughness size. Diminishing roughness size also gives rise to numerous small non-equilibrium jumps imposed upon larger jumps during wetting. The contact angle hysteresis is found to show a nearly linear relationship with the spread in the distribution of solid surface slopes.

ERDAL BAYRAMLI, THEODORE G. M. VAN DE VEN et STANLEY G. MASON. Can. J. Chem. **59**, 1954 (1981).

Comme on l'a fait d'une façon analogue lors d'études antérieures relatives à des chutes sur des surfaces horizontales, on a effectué une étude théorique de l'effet de la rugosité sur les propriétés de mouillage d'un cylindre de symétrie axiale qui est basé sur l'équilibre des formes du ménisque sur les surfaces solides. On peut expliquer l'hystérésis de mouillage, la formation de surfaces composites et la présence d'un saut non équilibré pendant le mouvement de la ligne de contact en faisant appel à des arguments mécanistiques et à des structures sinusoidales circonférentielles et à gorge en dents de scie.

Sur des surfaces unidirectionnelles, distribuées au hasard, ce sont principalement les pentes maximales des surfaces qui déterminent la valeur et l'angle de contact de l'avance et les pentes minimales de l'angle de contact de recul. Ces effets des pentes de surface diminuent avec la taille de la rugosité. La diminution de la taille de la rugosité donne également lieu à plusieurs petits sauts non équilibrés superposés à de plus grands sauts durant le mouillage. On a trouvé que l'angle de contact d'hystérésis présente une relation presque linéaire avec l'étalement dans la distribution des pentes de surface du solide.

[Traduit par le journal]

Introduction

The effect of regular surface roughness on the wetting of solid surfaces was recently investigated experimentally by Oliver, Huh, and Mason (1) by a method in which liquid drops were formed in a well defined manner on horizontal solid surfaces. In general, their results were in agreement with a theory developed by Huh and Mason (2) according to which the wetting hysteresis due to roughness depends strongly on the geometrical nature of the roughness. Whereas results obtained on wetting of mathematically well-defined surfaces may not be directly applicable to real surfaces, nevertheless the simple models used in these studies revealed information which is not easy to obtain from theoretical or experimental investigations of complex surface morphologies.

In this study we extend the theoretical work on horizontal solid surfaces to vertical axisymmetric cylindrical solid surfaces penetrating a liquid interface which exhibit fewer mathematical difficulties than drops on a horizontal surface. Also, experimentally such surfaces can be investigated to a higher degree of accuracy and detail with a tensiometric technique called capillarography (3) where the formation of the meniscus on the solid surface is controlled with precision. Use is made of this tensiometric technique in experiments designed to test the present theory, which will be discussed in the following paper (4). Also, the wetting of such surfaces is basic to problems of wetting of fibrous structures.

In Section A we consider the general characteristics of wetting of cylindrical axisymmetric solid bodies which will be followed by studies of specific surface geometries.

The work of Oliver, Huh, and Mason (5) and Bayramli and Mason (6) has shown the importance of sharp edges in wetting. In Sections B and C the effects of circumferential saw-tooth shaped and of circumferential sinusoidal grooves are studied. The multiplicity of equilibrium states for the liquid meniscus, contact angle hysteresis, conditions for the formation of composite surfaces, and the mechanism of the non-equilibrium jumps between equilibrium states and its dependence on groove wavelength are investigated.

As an example of a surface which represents a more realistic surface more closely, we studied the wetting of an axisymmetric rod which has a random

0008-4042/81/131954-08$01.00/0

©1981 National Research Council of Canada/Conseil national de recherches du Canada

Can. J. Chem. Downloaded from www.nrcresearchpress.com by 210.87.254.6 on 09/06/12
For personal use only.

Can. J. Chem. Downloaded from www.nrcresearchpress.com by 210.87.254.6 on 09/06/12
For personal use only.

distribution of roughness along its axis of symmetry. This is done in Section D where we investigate the wetting of a cylinder surface which has unidirectionally random roughness. We show the influence of roughness dimensions and solid surface slope distribution in observed contact angles and non-equilibrium jumps for a moving contact line.

Axisymmetric Roughness

A. General

Huh and Scriven (7) have studied liquid meniscus shapes around vertical cylindrical rods by numerically solving the Young–Laplace equation with specific boundary conditions, presenting the solutions in extensive numerical tables. In their analysis the angle of inclination of the liquid–fluid interface, ϕ, is employed as the main parameter.

When the cylinder radius, r_0, or the density difference between the phases 1 and 2, $\Delta\rho$, is small, or the interfacial tension σ_{12} very large, the approximate solution of James (8) can be used to calculate the meniscus shape without any significant error (a similar derivation was also made by Deryaguin (9)). The maximum height z_c (Fig. 1*a*) of the meniscus on the cylinder surface is, in this case, given by

$$[1] \quad \frac{z_c}{r_0} = \cos\theta \left[\ln\left\{ \frac{4}{ar_0}(1 + \sin\theta) \right\} - \gamma \right]$$

where θ is the apparent contact angle with $\phi = \theta$ at $r = r_0$; $\gamma = 0.57721$ is Euler's constant, $a = [g\Delta\rho/\sigma_{12}]^{1/2}$, and g the gravitational constant.

The experimentally measurable vertical capillary force is given by

$$[2] \quad F^* = 2\pi r_0 \sigma_{12} \cos\theta - F_B$$

where F_B is the buoyancy force. We define a dimensionless parameter F as

$$[3] \quad F = \frac{F^* + F_B}{2\pi r_0 \sigma_{12}} = \cos\theta$$

The buoyancy force is easily calculated for smooth cylindrical rods, but for a more general axisymmetric geometry a certain amount of care is required. Figure 1*b* shows a vertical axisymmetric solid body partially submerged at a liquid–fluid interface. Here F_B is equal to the pressure integral over the solid–liquid interface, S_1.

$$[4a] \quad F_B = -\int_{S_1} p\,dS$$

$$[4b] \quad F_B = -\int_{S_1+S_2} p\,dS + \int_{S_2} p\,dS$$

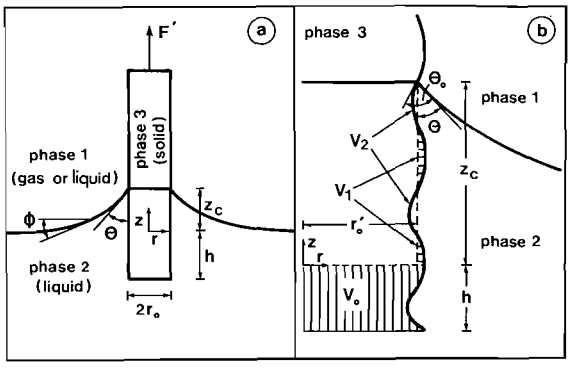

FIG. 1. (*a*) Diagram of a solid cylinder at a liquid-fluid interface. (*b*) Schematic geometry of a meniscus on a cylinder whose surface topography is given by a general function $f(r_0, z)$. V_1 is the portion of the rod volume where $r_0 > r_0'$ and V_2 shows the liquid volume where $r_0 < r_0'$ between $0 < z < z_c$, V_0 designates the solid volume below $z = 0$.

where S_2 is the cross sectional area of the rod at $z = z_c$. Using the divergence theorem, [4*b*] can be written as:

$$[4c] \quad F_B = -\int_V \nabla p\,dV + \int_{S_2} p\,dS$$

where V is the volume of the solid body submerged in phase 2. The pressure at z is

$$[5] \quad p = -\Delta\rho g z$$

Performing the integrations in [4*c*], using [5], yields

$$[6] \quad F_B = \Delta\rho g(V_0 + V_1 - V_2)$$

The volumes V_0, V_1, and V_2 are shown in Fig. 1*b* where r_0' is the distance of the contact line position from the fiber center. It is seen that for the calculation of the buoyancy factor, the portion of the solid volume V_1 where $r_0 > r_0'$ and $0 < z < z_c$ must be added and the liquid volume V_2 where $r_0 < r_0'$ and $0 < z < z_c$ must be subtracted from the solid volume V_0 below the hydrostatic zero level ($z = 0$). V_0, V_1, and V_2 are to be calculated from the explicit expression, $f(r_0, z)$, of a given solid surface geometry.

B. Concentric Saw-toothed Grooves

For a geometry of parallel circumferential grooves of triangular cross-section with angles θ_1, θ_2, θ_3 and minimum cylinder radius r_0^* (Fig. 2, inset), the cylinder radius r_0 located at the 1–2 interface depends on the inclination of the grooves and is given by

$$[7a] \quad r_0 = r_0^* + \frac{1}{g_0}[\varepsilon l(z_c - h - nl)] \quad \text{if } (z_c - h - nl) \leq g_0$$

Can. J. Chem. Downloaded from www.nrcresearchpress.com by 210.87.254.6 on 09/06/12
For personal use only.

$$[7b] \quad r_0 = r_0^* + \frac{1}{(l - g_0)}[\varepsilon l\{(n+1)l - (z_c - h)\}] \quad \text{if } (z_c - h - nl) > g_0$$

where

$$[7c] \quad g_0 = \varepsilon l/\tan\theta_2$$

Here $(z_c - h)$ is the length of the grooved surface submerged in phase 2, l and εl are the wavelength and the height of grooves respectively and n is an integer denoting the number of complete grooves below the contact line at $z = z_c$.

The macroscopically observed contact angle θ is given by

$$[8] \quad \theta = \theta_0 - \tan^{-1}(dr_0/dz)$$

where θ_0 is the intrinsic contact angle; from simple geometry we have $\theta = \theta_0 - \theta_2$ for the case [7*a*] and $\theta = \theta_0 + \theta_1$ for [7*b*].

A surface such as the one described above has a multiplicity of equilibrium states at a constant immersion depth, h, of the cylinder. We now investigate the wetting of a given geometry in more detail; as an example we choose $\theta_1 = \theta_2 = 30°$, $r_0^* = 0.025$ cm, $l = 0.1r_0$, and $ar_0^* = 0.1$. Figure 2 shows the permissible apparent contact angles on the cylinder surface for $\theta_0 = 40°$. For $h = 0$ many equilibrium sites exist on the grooved surface, indicated by the numerous intersections of $z_c(\theta)$ with the permissible contact line locations. In this calculation the meniscus height z_c was calculated using James' approximation [1] and [8]. As h is increased or decreased gradually, it is possible to construct a wetting hysteresis loop, due to the grooves as shown

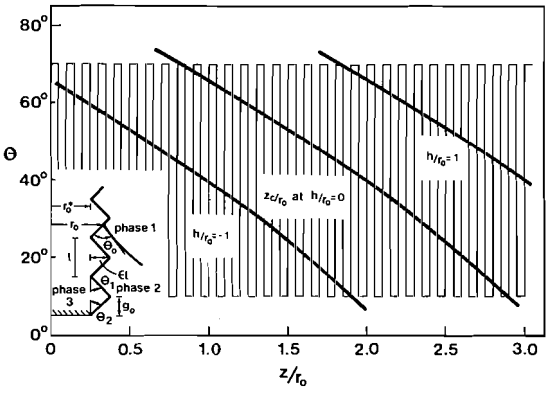

FIG. 2. The possible apparent contact angles on a saw-toothed cylinder surface with $r_0^* = 0.025$ cm, $l/r_0^* = 0.1$, $\theta_0 = 40°$, $\theta_1 = \theta_2 = 30°$, and $ar_0 = 0.1$. The continuous lines show the meniscus height on the cylinder as a function of θ at constant h. The numerous intersections are the available equilibrium positions for the contact line. Inset shows the surface geometry of the cylinder.

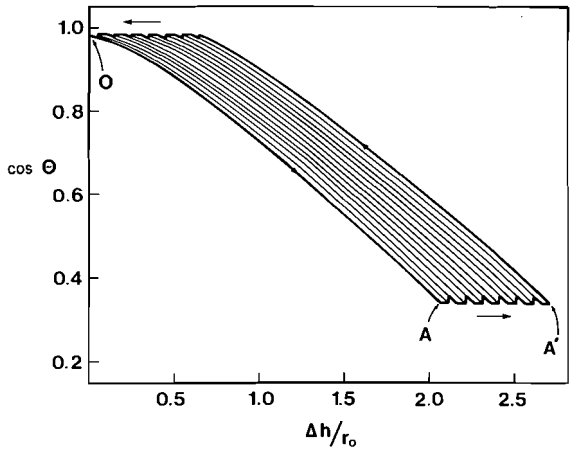

FIG. 3. cos θ as a function of displacement $(\Delta h/r_0)$ for system in Fig. 2. The bold line indicates the path followed by an advancing and receding contact line on the grooved surface.

in Fig. 3. The bold lines in Fig. 3 are for the path followed by an advancing and receding meniscus assuming the contact line jumps to the nearest equilibrium position. First, starting at O, the contact line hinges at a single groove as the contact angle changes from a receding to an advancing one until reaching A; it must then make non-equilibrium jumps from one stable position to another as Δh continuously increases. When the motion of the contact line is reversed at A', the advancing contact angle decreases until $\theta = 10°$ while hinging at a single groove, and then moves in a stick-jump fashion when Δh is decreased further. The difference in h values, Δh, is defined here as being positive in the $-z$ direction measured from an arbitrary reference height h_0. This result is analogous to the Haines' jumps across radial grooves considered by Huh and Mason (2).

The geometric constraints of a saw-toothed concentric groove exclude certain parts of the surface to an advancing or receding meniscus causing the formation of composite surfaces. For a receding contact line a composite surface in which liquid pockets are left behind is formed when $\theta_0 < (\theta_1 + \theta_2)$. For an advancing meniscus pockets of phase 1 are left behind the contact line when $\theta_0 > 2\pi - (\theta_1 + \theta_2)$. Therefore the condition of preventing the formation of a composite surface during a hysteresis loop is $(2\pi - (\theta_1 + \theta_2)) > \theta_0 > (\theta_1 + \theta_2)$. The schematic diagrams in Fig. 4 show the formation of composite surfaces during advancing and receding contact line motion.

A closer investigation of non-equilibrium jumps of the contact line shows that three possibilities exist: (*i*) the contact line jumps from O to O' (Fig.

Can. J. Chem. Downloaded from www.nrcresearchpress.com by 210.87.254.6 on 09/06/12
For personal use only.

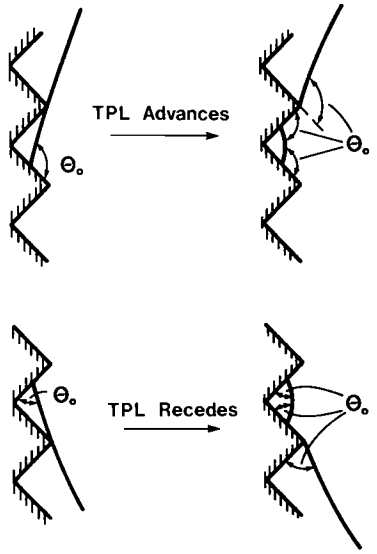

FIG. 4. Schematic diagram showing the formation of composite surfaces during advancing and receding of the three phase contact line (TPL). While advancing pockets of phase 1, and while receding of phase 2 are left behind a moving TPL.

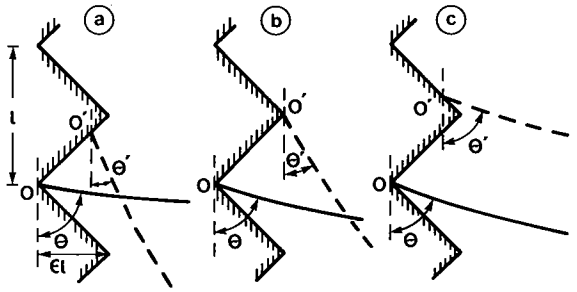

FIG. 5. Schematic diagram showing the three possible cases of non-equilibrium jumps of an advancing contact line on a cylinder surface with parallel circumferential saw-toothed shaped grooves.

5*a*) which may occur if $\varepsilon l \ll l$ or $l \simeq O(r_0)$; here $\theta > \theta'$; (*ii*) it may jump from one valley to the peak of the next groove when $\varepsilon l \simeq O(l)$ with $\theta > \theta'$ (Fig. 5*b*); (*iii*) a jump from a valley over a peak onto the next groove surface ($\theta = \theta'$), since it is possible that no equilibrium position at the sharp edge of the groove exists (Fig. 5*c*).

C. Sinusoidal Grooves

The surface shape of circumferential sinusoidal grooves on a cylinder surface is given by

$$[9] \quad r_0 = r_0^* + \varepsilon l \sin(2\pi z/l)$$

where l and εl are the wavelength and the amplitude of the grooves respectively and r_0^* is defined as the median position of the grooves (Fig. 6, inset). The slope angle of the surface is given by

$$[10] \quad \phi_0 = \tan^{-1}[2\pi\varepsilon \cos(2\pi z/l)]$$

from which the apparent contact angle θ ($\equiv \theta_0 - \phi_0$) can be calculated.

As in the case of parallel saw-toothed grooves we have a multiplicity of equilibrium states for a given immersion depth of the cylinder into the liquid phase. For a system where $\theta_0 = 70°$, $\varepsilon = 0.2$, $l/r_0^* = 0.1$, $r_0^* = 0.025$ cm, and $ar_0^* = 0.1$ we obtain a hysteresis loop as shown in Fig. 6, in which we used James' approximation [1] and [8] to calculate the equilibrium mensicus height on the cylinder surface starting from O. As the cylinder is immersed into the phase 2, with Δh increasing continuously, the contact line moves slowly on a single groove till it reaches A. From A to A′ the contact line moves with regular jumps. For the receding contact line, which is obtained by gradually withdrawing the rod vertically from phase 2, the contact line will remain (i.e. sticks) on the same groove until it reaches A″ where it starts to make non-equilibrium jumps while receding.

The formation of composite surfaces due to the constraints arising from surface geometry is shown in Fig. 7. The shaded area shows the region in which no composite surface formation occurs. Above and below the shaded area there is always a composite formation during wetting of the solid surface.

D. Randomly Rough Surfaces with Axial Symmetry

Randomly rough surfaces without axial symmetry are difficult to treat mathematically, not only because the capillarity equations become very complicated to solve, but also because the exact location of the contact line is not known *a priori* (2). Here we investigate the more tractable problem of wetting of a surface with one-dimensional random roughness.

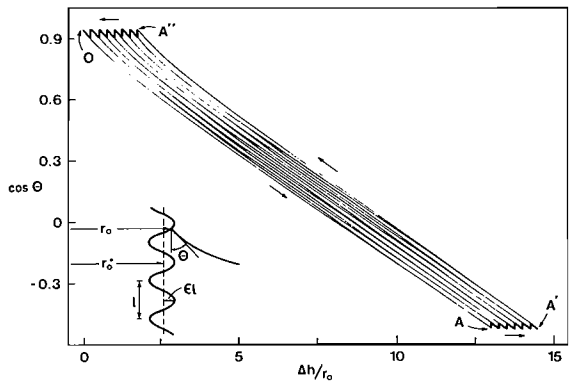

FIG. 6. cos θ vs. $\Delta h/r_0$ for sinusoidal circumferential grooves on a cylinder with $r_0^* = 0.025$ cm, $\varepsilon = 0.2$, $\theta_0 = 70°$, $l/r_0^* = 0.1$ and $ar_0 = 0.1$; starting from O a hysteresis loop is obtained by vertically immersing the cylinder into phase 2 from O to A′ and withdrawing from A′ to O.

Can. J. Chem. Downloaded from www.nrcresearchpress.com by 210.87.254.6 on 09/06/12
For personal use only.

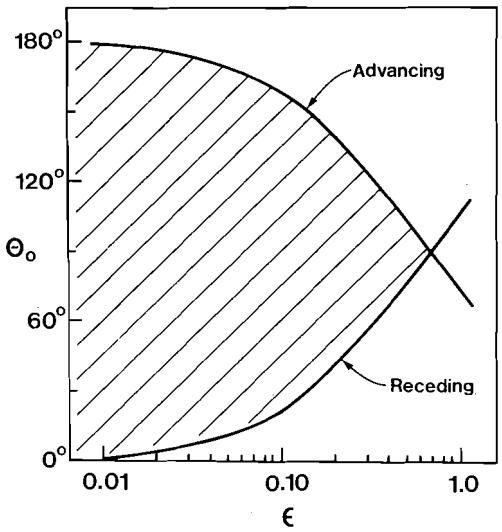

FIG. 7. The intrinsic contact angle θ_0 vs. ε; configurations below the advancing and above the receding line do not result in composite surface formation during advancing and receding contact line motions respectively and hence, in the shaded area no composite surface will be found during a hysteresis loop.

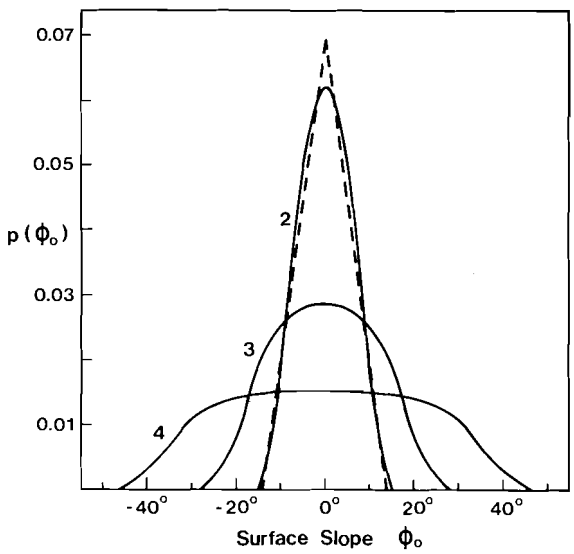

FIG. 8. Distribution of surface slopes for systems 2, 3, and 4 (Table 1). The dashed line shows the distribution for system 2 as calculated from ref. 11.

A unidirectional randomness on a cylinder surface is generated as follows: a uniformly distributed set of random points between r_0^* and $(r_0^* + \delta r_0^*)$ is generated by a computer subroutine at regular intervals Δz, along the z-axis with $0.01 \leq \delta \leq 0.1$ keeping δ constant for each surface generation. Here, δ can be defined as the roughness size. The set of points, $((r_{0i}, z_i), i = 1, 2, \ldots, n)$, is used to produce a surface numerically, making use of a cubic spline interpolation scheme. In each interval the surface is represented by a spline (a polynomial), the coefficients of which are chosen such that consecutive intervals are smoothly connected.

The slope of the generated surface is calculated analytically from the coefficients of the splines used in each interval. Details of the generated surfaces are summarized in Table 1 and Fig. 8, which shows the distribution of solid surface slopes ϕ_0 of systems 2, 3, and 4. Systems 1 and 5 have the same surface slope distribution as system 3 since $\delta/\Delta z$ is the same for systems 1, 3, and 5. Figure 8 is calculated by grouping ϕ_0 in 1° intervals and smoothing the final population distribution for a total of 1500 points for each curve.

Neglecting the smoothing, the probability distribution for the slopes can be readily determined from the set of points (r_{0i}, z_i) by connecting them with straight lines. In this case the probability, $p(\phi_0)d\phi_0$, of finding a slope between ϕ_0 and $\phi_0 + d\phi_0$ is given by

$$[11] \quad p(\phi_0) = \alpha(S - \tan|\phi_0|)$$

where $S = \delta/\Delta z$ and α is a normalization constant determined by

$$[12] \quad \int_{-\tan^{-1}S}^{\tan^{-1}S} \alpha(S - \tan|\phi_0|)d\phi_0 = 1$$

From eq. [12] we have

$$[13] \quad \alpha = [2S\tan^{-1}S - \ln(S^2 + 1)]^{-1}$$

Due to our method of generating surfaces by smoothly connecting the generated random points, a more gradual change of slopes occurs in the vicinity of $\phi_0 = 0$. Also, slopes with $\tan\phi_0 > S$ exist as indicated by the slight tail near $p(\phi_0) = 0$ (Fig. 8). In the limit $S \to 0$, the probability distribution of solid surface slopes will be given by [11]. Already, at $S = 1/4$, [11] is a close approximation of the numerically calculated $p(\phi_0)$ as shown by the dashed line in Fig. 8.

The autocorrelation function of the solid surface profiles indicated that the correlation length was approximately equal to Δz_i, and the Fourier transform of the autocorrelation function showed no dominant frequency, from which we can deduce that the surface profiles were unidirectionally random.

We now investigate the wetting behavior of our numerically generated surfaces. In the following calculations we chose $r_0^* = 0.025$ cm and $ar_0^* = 0.1$; [1] is used to find the equilibrium meniscus height z_e. A portion of the numerically generated surface profile for system 5 is shown in Fig. 9*a*. Figure 9 *b* and *c* show the apparent contact angles

TABLE 1. Summary of calculations on filaments with unidirectionally random roughness ($\theta_0 = 70°$, $ar_0{}^* = 0.1$)

System	δ	S[a]	σ[b] (deg)	$\bar{\theta}_A \pm \sigma_A$[c] (deg)	$\bar{\theta}_R \pm \sigma_R$[c] (deg)	$\Delta\theta$ (deg)
1	0.1	0.50	11.6	85.6±6.4	56.6±5.3	29.0
2	0.03	0.25	6.0	77.0±3.4	63.8±3.1	13.2
3	0.03	0.50	11.6	88.0±4.7	52.8±4.3	35.2
4	0.03	1.00	21.5	110.2±4.8	35.2±5.4	75.0
5	0.01	0.50	11.6	95.1±4.4	47.9±3.9	47.2

[a] $S = \delta/\Delta z$.
[b] Spread in distribution of surface slopes.
[c] Standard deviation from the mean advancing or receding apparent contact angle.

on the solid surfaces, calculated from [8], for system 5 and system 1 respectively when $\theta = 70°$. The intersections of the lines $\theta(z_c/r_0)$ at a constant immersion depth h with $\theta(z/r_0)$ indicate the possible equilibrium positions for the contact line. As h/r_0 increased or decreased it is possible to obtain a hysteresis loop similar to the case of saw-toothed or sinusoidal grooves (Figs. 3 and 6).

We immediately notice that as the magnitude of roughness decreases (everything else being the same) only higher and lower surface slope sites for advancing and receding contact lines become accessible.

Using Fig. 9 one can construct theoretical wetting hysteresis loops by gradually increasing and decreasing the immersion depth from, say, $h = 0$. Figure 10 *a* and *b* are the hysteresis loops for the systems in Fig. 9 *b* and *c* respectively. Conceptually it is easier to form Fig. 10 using Fig. 9, but in numerical calculations it is much more practical to calculate the equilibrium meniscus heights at regular Δz_i intervals on the solid surface and search for the locations of non-equilibrium jumps to the nearest equilibrium positions as h continuously increases for advancing and decreases for receding contact lines. At smaller roughness dimension (Fig. 10*a*) we obtain more frequent smaller three phase contact line (TPL) jumps together with larger non-equilibrium jumps. Also the contact angle hysteresis ($\Delta\theta = \bar{\theta}_a - \bar{\theta}_r$) is larger at smaller roughness dimensions (Table 2).

The mean advancing contact angle $\bar{\theta}_a$ and the mean receding contact angle $\bar{\theta}_r$ are shown in Fig. 11 as a function of the roughness size of the solid surface when the standard deviation of the surface slope distribution $\sigma = 11.65$. The bars indicate the standard deviation from the mean apparent contact angle; they are slightly larger for larger roughness sizes (Table 1). For smaller roughness dimensions only the extreme surface slope values contribute to

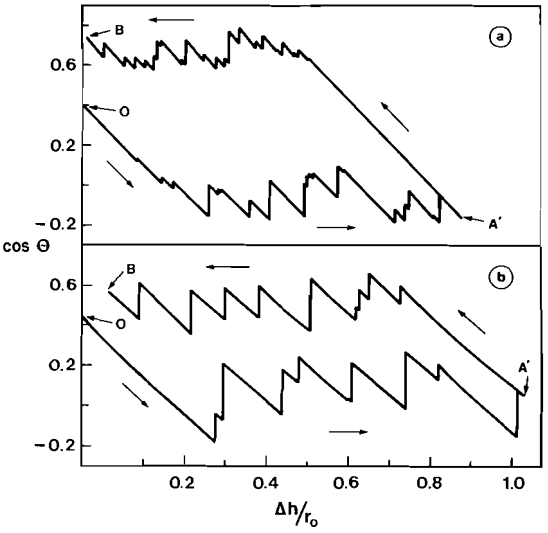

FIG. 10. cos θ vs. $\Delta h/r$ obtained by immersing the cylinder into phase 2 from O to A′ and withdrawing from A′ to B with $\theta_0 = 70°$. (*a*) For system 5 and (*b*) for system 1.

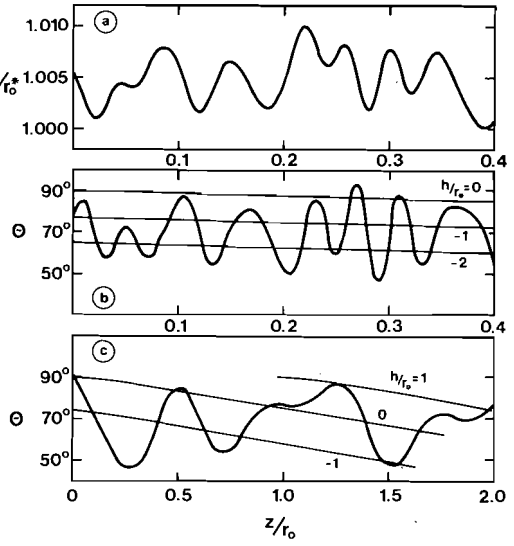

FIG. 9. (*a*) A section of the numerically generated surface profile for system 5. (*b*) The possible apparent contact angles ($\theta_0 = 70°$) on a unidirectionally random cylinder surface for system 5, and (*c*) for system 1. The lines indicate the meniscus height, z_c, at a constant h/r_0 with varying θ; the intersections are the available equilibrium positions for the contact line.

Can. J. Chem. Downloaded from www.nrcresearchpress.com by 210.87.254.6 on 09/06/12
For personal use only.

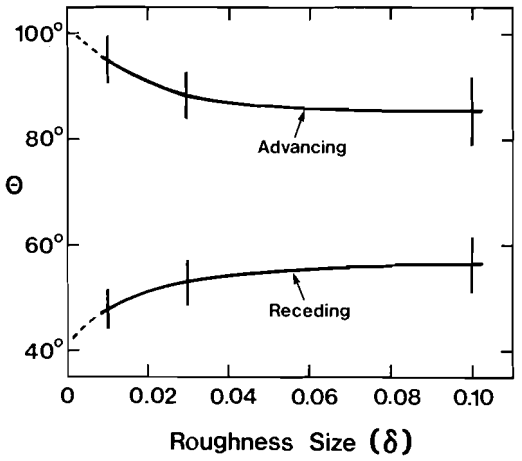

FIG. 11. Effect of roughness size δ on apparent contact angle for $\theta_0 = 70°$ and $S = 0.5$ (systems 1, 3, 5).

the hysteresis; at larger rough dimensions the hysteresis asymptotically approaches a constant value.

Figure 12 shows the dependence of contact angle hysteresis on the solid surface slope distribution for $\delta = 0.03$. The bars show the standard deviation from the mean advancing and receding contact angles. There is an almost linear relationship between σ and the amount of hysteresis in the range $5° < \sigma < 25°$.

Discussion

The effect of circumferential axisymmetric roughness on wetting hysteresis has been investigated by considering a cylindrical rod being immersed into or withdrawn from a flat liquid–fluid interface at very slow contact line velocities in order to approach equilibrium conditions. A general feature of contact line motion is jumps between equilibrium meniscus configurations, thus demonstrating that wetting of these surfaces is basically an irreversible phenomenon (2). We believe that treatments of wetting based on equilibrium thermodynamics should be extended to cover the irreversible aspects of contact line motion. Also the formation of composite surfaces during wetting due to constraints arising from solid surface geometry is a cause of irreversibility during wetting.

For axisymmetric unidirectionally random roughness, the reduction in absolute dimension of roughness produces a more distinct and larger hysteresis loop with smaller non-equilibrium jumps. The number of rugosities skipped over during non-equilibrium jumps increases with decreasing roughness dimensions. At the same time the contribution of large and small solid surface slopes ϕ_0 during advancing and receding of the contact line becomes more pronounced. It may be speculated that as the dimensions of roughness are progressively reduced, one will eventually observe a smooth motion of the contact line where, at a microscopic level, the contact line advances or recedes with very small jumps from one equilibrium site to the next. The question of the minimum roughness dimension which can be considered as a cause of wetting hysteresis seems to be a basic one. It has been claimed that surface roughnesses below 0.1–1 μm do not cause any significant hysteresis (10, 11), whereas the work of Oliver *et al.* (5) indicates that 0.05 μm high steps on a mica surface inhibit spreading. It seems that the nature of the roughness (surface texture (2)) rather than its absolute size is a determining factor as well (12).

At smaller roughness scales (~1 μm) we obtain many small jumps coupled with larger non-equilibrium jumps; this may prove to be significant in studies of contact line motion. Studies by Dussan (13), Hocking (14), Huh and Mason (15), and Levine *et al.* (16) indicate the importance of the mechanism(s) by which a meniscus moves on a solid surface. Most of the workers in this field assign a slip parameter at the contact line (10^{-6} to 10^{-9} cm) to overcome the infinite amount of force required to move a contact line (an unrealistic consequence of the no-slip boundary condition). It may be possible that at a submicroscopic level the contact line moves with non-equilibrium jumps rather than with continuous slippage of the leading edge of the meniscus. Again, the problem posed by the minimum roughness dimensions which can affect wetting needs to be answered.

In the following papers we investigate experimentally the influence of roughness shapes and dimensions, and of contact line velocities on wetting (4, 17).

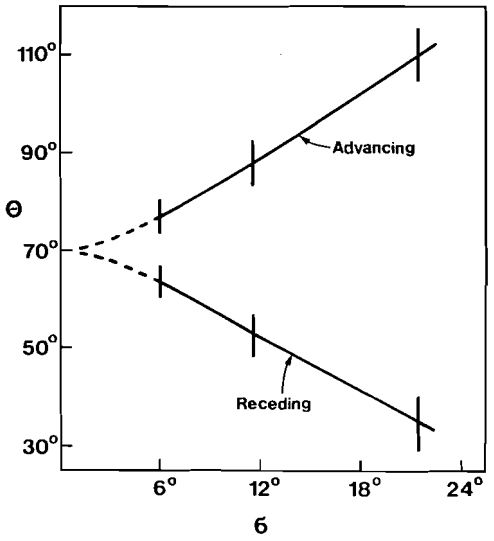

FIG. 12. Effect of standard deviation in solid surface slope distribution σ on the apparent contact angle; $\theta_0 = 70°$.

Can. J. Chem. Downloaded from www.nrcresearchpress.com by 210.87.254.6 on 09/06/12
For personal use only.

1. J. F. OLIVER, C. HUH, and S. G. MASON. Colloids and Surfaces, **1**, 79 (1980).
2. C. HUH and S. G. MASON. J. Colloid Interface Sci. **60**, 11 (1977).
3. A. OKAGAWA and S. G. MASON. Fibre water interactions in paper-making. Proceedings of 1977 Oxford Symposium. Technical Section, British Paper and Board Federation, 1978. pp. 581–586.
4. E. BAYRAMLI and S. G. MASON. Can. J. Chem. **59**, 000 (1981).
5. J. F. OLIVER, C. HUH, and S. G. MASON. J. Colloid Interface Sci. **59**, 1568 (1977).
6. E. BAYRAMLI and S. G. MASON. J. Colloid Interface Sci. **66**, 200 (1978).
7. C. HUH and L. E. SCRIVEN. J. Colloid Interface Sci. **30**, 323 (1969).
8. D. H. JAMES. J. Fluid Mech. **63**, 657 (1974).
9. B. DERYAGUIN. Dokl. Akad. Nauk. SSSR, **51**, 517 (1946).
10. R. E. JOHNSON and R. H. DETTRE. Adv. Chem. Ser. Am. Chem. Soc. **43**, 136 (1964).
11. A. W. NEUMANN, D. RENZOW, H. REUMUTH, and I. E. RICHTER. Fortschrittsber, Kolloide Polym. **55**, 49 (1971).
12. S. G. MASON. Wetting, spreading and adhesion. *Edited by* J. F. Padday. Academic Press, New York. 1978. p. 384.
13. E. B. DUSSAN. V. J. Fluid Mech. **77**, 65 (1976).
14. L. M. HOCKING. J. Fluid Mech. **79**, 209 (1977).
15. C. HUH and S. G. MASON. J. Fluid Mech. **81**, 401 (1977).
16. S. LEVINE, J. LOWNDES, E. J. WATSON, and N. GRAHAM. J. Colloid Interface Sci. **73**, 136 (1980).
17. E. BAYRAMLI, T. G. M. VAN DE VEN, and S. G. MASON. Colloids Surfaces, In Press.

Can. J. Chem. Downloaded from www.nrcresearchpress.com by 210.87.254.6 on 09/06/12
For personal use only.

Tensiometric studies on wetting. II. Some effects of surface roughness (experimental)

ERDAL BAYRAMLI AND STANLEY G. MASON

Pulp and Paper Research Institute of Canada and Department of Chemistry, McGill University, Montreal, P.Q., Canada H3A 2A7

Received August 15, 1980

This paper is dedicated to Dr. Sam Levine on the occasion of his 70th birthday

ERDAL BAYRAMLI and STANLEY G. MASON. Can. J. Chem. **59**, 1962 (1981).

The wetting of regularly rough solid bodies was investigated by means of capillarography. In this technique solid probes are immersed and withdrawn from liquid–fluid interfaces with steady velocities. Continuous observation of the three phase contact line (TPL) motion and recording of the capillary force are possible simultaneously. The effect of regular axisymmetric grooves on cylindrical rods on wetting hysteresis was found to follow theoretical predictions closely at large roughness dimensions (~86 μm) in which case the TPL makes jumps from one equilibrium position to another while advancing. At lower rugosities (~1 μm) the effect of regular roughness for a given concentric groove geometry is complicated by effects attributed to the dominant influence of chemical heterogeneity of the solid surface.

ERDAL BAYRAMLI et STANLEY G. MASON. Can. J. Chem. **59**, 1962 (1981).

On a étudié la capacité de mouillage de corps solides ayant une rugosité au moyen de la capillarographie. Dans cette technique, on immerge et on retire des sondes solides des interfaces liquide–fluide avec des vitesses constantes. On peut observer simultanément et d'une façon continue le mouvement des trois lignes de contact de phase (LCP) tout en enregistrant la force capillaire. On a trouvé que des gorges axio-symétriques régulières présentes sur des barres cylindriques provoquent sur l'hystérésis de mouillage des effets qui suivent de très près les prédictions théoriques pour les rugosités de grandes dimensions (~86 μm). Toutefois les LCP sautent d'une position d'équilibre à une autre lorsqu'elles avancent. A de plus faibles rugosités (~1 μm), l'effet d'une rugosité régulière pour une géométrie à gorge concentrique donnée est compliqué par des effets attribués à l'influence dominante de l'hétérogénéité chimique de la surface solide.

[Traduit par le journal]

Introduction

In the preceding study we theoretically investigated some effects of surface roughness on wetting of axisymmetric circular cylinders (1), which was the continuation of the theoretical and experimental work initiated by Huh and Mason (2) and Oliver *et al.* (3) for drops on horizontal solid surfaces. In this study a tensiometric technique called capillarography (4) is used to investigate the wetting of small solid bodies with regular roughness features. The technique is well-suited for the study of the envisaged mechanism of non-equilibrium jumps of the meniscus, the nature of wetting hysteresis and the effect of roughness shape and dimensions on wetting.

Among the surfaces investigated are a cylindrical rod with 1 μm parallel circumferential grooves of saw-tooth shape (the microgrooved cylinder, μgc) which has a roughness scale smaller than hitherto investigated regular roughnesses. Another cylinder with about 86 μm wavelength of saw-toothed grooves (the macrogrooved cylinder, Mgc) is used along with other surfaces with regular physical roughnesses to explore the effects of regular roughness of varying length scales on wetting of solids.

In actual experimental conditions, the effects of regular roughness on wetting coexist with those of the intrinsic chemical heterogeneity and the physical roughness of the surfaces. Therefore, with both the μgc and the Mgc two different hysteresis loops are obtained on the grooved and ungrooved parts of the same cylindrical rod (Fig. 1).

Experimental Part

1. Apparatus

Use was made of a micro- and macrocapillarograph (abbreviated as μc and MC) designed for small (e.g. 10 μm diameter fibers) and large solid bodies travelling respectively over small and large distances through an interface. Details of the experimental technique are given elsewhere (5). In each apparatus a platform holding the vessel containing the wetting liquid is moved vertically by means of a motor-powered hydraulic drive, whose speed can be varied sensitively and continuously. The vertical force F' is measured by an electrobalance (capacity up to 10^{-2} N, sensitivity down to 2×10^{-7} N), and the vertical displacement h of the platform by a magnetic transducer; F' versus h is plotted on an X–Y recorder. A plot obtained in this manner is called a capillarogram. In the μc, platform velocities (5×10^{-3} to 0.4 μm s^{-1} for a total vertical displacement of 0.3 cm) are obtained by a variable speed hydraulic drive which is mounted independently of the main electric driving motor to reduce vibration. The assembly is securely mounted on four pressurized air supports to reduce the ambient vibrations. The MC has higher stage velocities and a larger travel distance (2–14 μm s^{-1} over a distance of 5 cm) and is placed atop a large cement block on anti-vibration pads; again, the hydraulic drive for the platform is mounted separately. Both instruments provide platform velocities constant to ±0.5%.

The platform of the μc has a vertical displacement resolution of about 25 Å, i.e. of the same order as a low resolution electron microscope; this, of course, was vastly exceeded by vibration displacements (rms movement of 0.15 μm at a dominant frequency of 28.6 Hz no matter where located and independent of the speed of the hydraulic drive motors (15)); as a result this resolution cannot yet be realized. In addition there is an uncer-

0008-4042/81/131962-07$01.00/0

©1981 National Research Council of Canada/Conseil national de recherches du Canada

Can. J. Chem. Downloaded from www.nrcresearchpress.com by 210.87.254.6 on 09/06/12
For personal use only.

TABLE 1. Systems used

Solid surfaces	$2r_0$ (cm)	λ (μm)	εl (μm)	θ_1 (deg)	θ_2 (deg)	θ_3 (deg)
μgc[a]	0.3971	1±0.2	0.4	50	30	100
Mgc[b]	0.2830	86±4	16	13.6	38.7	127.7
Jeweller's saw[c]	—	300	—	—	—	—
Guitar string[d]	—	180	—	—	—	—
Plane grating	—	10±0.5	—	20	60	100

Wetting liquids	σ_{12} (mN m^{-1})	$\Delta\rho$ (g cm^{-3})
Water	72.4±0.3[g]	0.9975
Tetrabromoethane (TBE)	49.9±0.2[h]	2.9656
Decane	23.9±0.1[h]	0.7300
Silicone oil (1 cPa s)	20.6±0.1[h]	0.9550

[a]Dimensions specified by the manufacturer.
[b]Dimensions measured by Nikon Shadograph; θ_1, θ_2, θ_3 calculated geometrically from measured groove dimensions.
[c]Teeth on one side only (see Fig.2).
[d]Spirally wound.
[e]Temperature = 23.5 ± 0.5°C.
[f]By pycnometry.
[g]By pendant drop shape method.
[h]By Pt ring tensiometry.

tainty in the location of the contact line due to evaporation of the wetting liquid during the course of an experiment (~5×10^{-3} μm s^{-1} for water depending on the relative humidity, considerably less for the other, less volatile, liquids). For the MC, the displacement resolution is about 1 μm.

2. *Materials*

Solid Bodies

The microgrooved cylinder (μgc) was an aluminium-coated sapphire rod grating having parallel circumferential grooves 1 μm apart (made by Diffraction Products Inc., Woodstock, IL, USA). The polished sapphire rod was coated with aluminium by vacuum evaporation and a 1 cm long portion of the Al surface was grooved by a diamond tip one groove at a time, yielding the angles θ_1, θ_2, and θ_3 in phase 3 (Fig. 1) for the triangular cross-section of the grooves (Table 1). To prevent peeling of the Al coating, the surface was cleaned by washing in benzene, methanol, and then with copious quantities of distilled water, and followed by vacuum drying for 6 h at 50°C. The sensitive nature of the grooved surface precluded the use of oily or viscous liquids as wetting phases because of difficulties in subsequent cleaning.

The macrogrooved cylinder (Mgc) was similarly made on a 1 cm section of a 1.5 cm length of a polished bronze rod 0.3 cm diameter with groove dimensions listed in Table 1. The groove shape was analyzed in a Nikon Shadograph with a linear resolution ± 1 μm.

Other axisymmetric surfaces with regular macroscopic roughness were a jeweller's saw and a guitar string. The saw was a thin blade of steel with sharp teeth on one side; the guitar string was made of spirally wound steel wire on an iron wire core (see Table 1 and Fig. 2).

The plane grating, on which the drop shape observations were made, with parallel saw-tooth shaped grooves (Diffraction Products Inc., Woodstock, IL, USA), was a thin polymethylmethacrylate (PMMA) surface on a glass support, replicated from a master grating (Table 1).

Wetting Liquids

Purified water (conductivity 10^{-4} Ω^{-1} m^{-1}) was prepared by passing tap water through ion-exchange columns and then triply distilling it (single stage, from permanganate, and finally through a multistage unit), and then using it within 24 h. As non-aqueous liquids analytical grade tetrabromoethane (TBE), decane, and silicone oil (Dow Corning 200D series, 10cs.) were used as supplied.

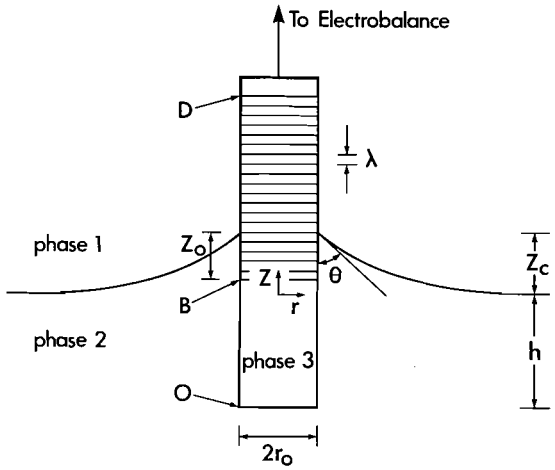

FIG. 1. Diagram of the grooved cylinder and the liquid meniscus; the region O to B designates the ungrooved part and B to D the grooved part of the cylinder; λ is the wavelength of the grooves. Other important parameters are shown.

The surface tension of the water was determined by the pendant drop shape method; and that of TBE, decane, and silicone oil by Pt ring tensiometry (Table 1). The MC with its recording microbalance and smooth displacement capability is ideally suited for the measurement of maximum force in ring tensiometry where a receding contact line was obtained in order to have the intrinsic contact angle $\theta_0 \simeq 0°$. Also the advancing and receding tensiograms were nearly identical, from which we can deduce that $\theta_0 \simeq 0$ in all cases (6). The cited values are well within the experimental accuracy required for the present work.

The liquid densities were determined pycnometrically; all measurements and experiments were performed in a room controlled at 23 ± 0.5°C.

Can. J. Chem. Downloaded from www.nrcresearchpress.com by 210.87.254.6 on 09/06/12
For personal use only.

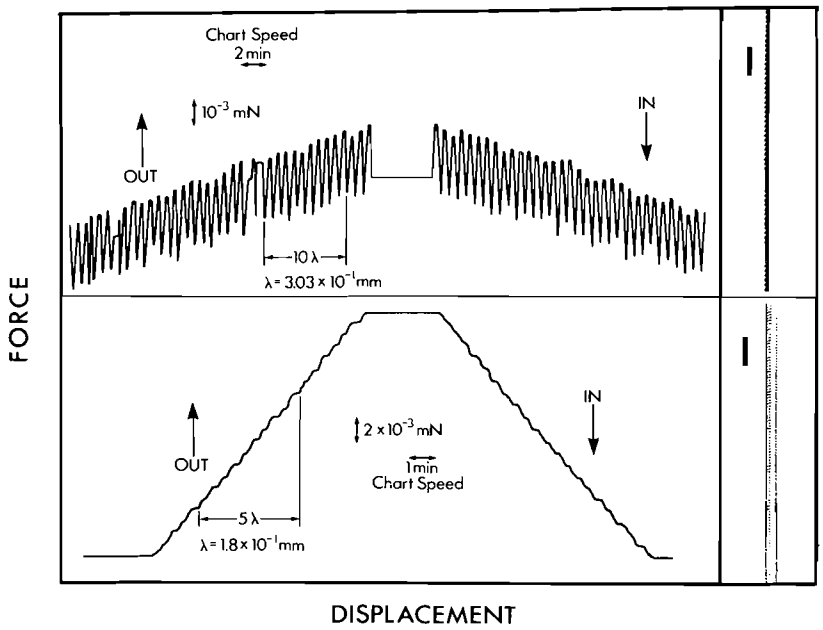

FIG. 2. Capillarograms of the jeweller's saw (upper) and the guitar string (lower) with silicone oil (10 cs) as the wetting liquid. The motion of the platform was reversed after stopping it about 4 min at the mid-point. The general increase in force while receding and decrease while advancing is due to buoyancy. The length scales on the photographs on the right, represented by the solid bars, indicate 2 mm.

3. Methods

In recording most capillarograms, a hysteresis loop was first obtained on the ungrooved portion of the rods and then on the grooved portion by moving the platform up and down at 0.30 μm s^{-1} in the μc and at 4 μm s^{-1} in the MC. Making use of the independent measurements of apparent receding contact angles measured photographically (normal to the cylinder axis), the force-displacement capillarograms were evaluated in terms of the apparent contact angle θ (7).

Results and Discussion

Large Solid Bodies

As a qualitative demonstration of the effect of macroscopic roughness on the apparent contact angle, we recorded capillarograms in the MC of the jewller's saw and the guitar string (Fig. 2) using silicone oil as the wetting phase for which $\theta \simeq 0°$. Figure 6 (upper) shows that at this scale of roughness (~0.3 mm) the apparent contact angle varied considerably as the three phase contact line (TPL) advanced or receded at 8 μm s^{-1} on the saw surface. Similarly, on the guitar string we observe from Fig. 2 (lower) that the TPL slope varied with respect to the vertical axis due to the spiral grooves, but in a less pronounced way; the sharp edges were more effective in inhibiting spreading (8). From the close symmetry of Fig. 2 we can deduce that the intrinsic contact angle was nearly constant (~0°) during advancing and receding of the TPL.

Macrogrooved Cylinder

The well defined geometry of the Mgc allows the theoretical predictions in ref. 1 to be tested. For an advancing TPL the apparent contact angle should be $\theta = \theta_0 + \theta_1$. The observed increase in θ when $\theta_1 = 13.6°$ is 13.1° ± 0.5° (Fig. 3) with TBE as the wetting phase and using the MC at 4 μm s^{-1} stage velocity, in good agreement with the theory. Here, r_0* is the minimum radius of the cylinder and Δh is the change in the downward vertical displacement h of the cylinder with respect to the horizontal level of the 12 interface (Fig. 1). For the ungrooved part of the surface, $\theta = 47.9°$ and 0° for the advancing and receding TPL's respectively. The periodicity of the advancing TPL 86 ± 4 μm matches well with the wavelength of the grooves measured using a Nikon Shadograph. The only discrepancy is that larger non-equilibrium jumps were observed than the expected jump value, calculated using Huh and Scriven's tables (7) of meniscus shapes around a cylinder, which corresponds to jumps from a valley to the nearest equilibrium position on the neighbouring peak of the grooves. Rather, the jump occurred from one valley to the next one which corresponded to a 6.0° (55.0°–61.0°) change in the observed contact angle. The dotted line (Fig. 3) indicates the capillarogram expected from a valley to peak jump with no change in intrinsic contact angle. This result is most probably due to experi-

Can. J. Chem. Downloaded from www.nrcresearchpress.com by 210.87.254.6 on 09/06/12
For personal use only.

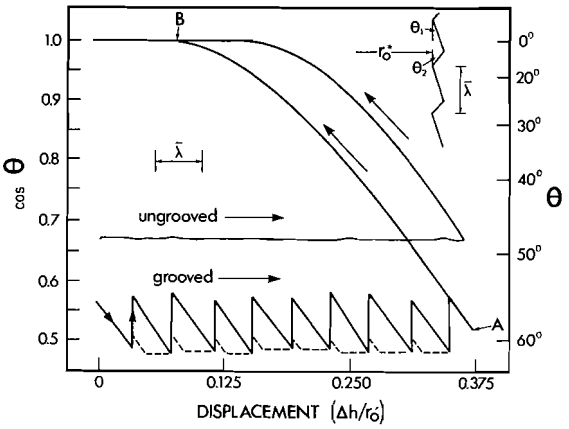

FIG. 3. cos θ vs. $\Delta h/r_0^*$ for the Mgc with tetrabromoethane, first on the ungrooved and then on the grooved part of the cylinder. The broken line shows an approximation of the expected capillarogram which can be calculated from Huh and Scriven's tables (7) assuming that the contact line makes a non-equilibrium jump from a groove valley to a neighbouring peak. The inset (upper right) shows the groove geometry.

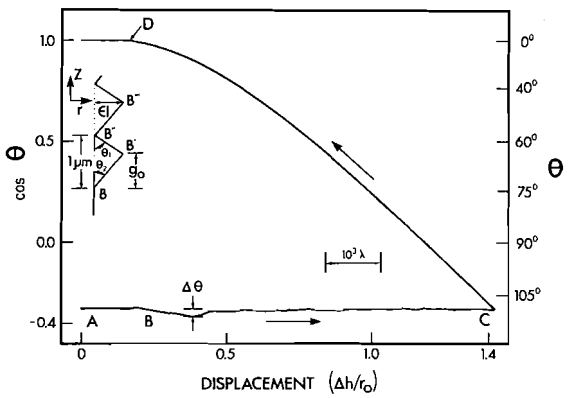

FIG. 4. cos θ vs. $\Delta h/r_0^*$ for the μgc with water as the wetting liquid. The slight increase Δθ at the start of grooved portion of the cylinder at B corresponds to an increase of 2.3°. Note the smooth section where (starting at C) the receding contact line sticks and hinges until it reaches θ_R which is very close to zero. The groove geometry is shown in the inset.

mental limitations because for sudden changes in capillary force, such as during the jumps, the arm of the microbalance overshoots its equilibrium position before coming to rest (5). Since hysteresis is present in the system even in the absence of grooves (due to surface chemical heterogeneity), the TPL can come to rest on the next valley after overshooting its equilibrium position (i.e. at the peak where $\theta_0 = 47.9°$).

For the receding TPL no effect of the grooves was observed due to liquid bridges filling the grooves left behind, creating a composite surface. This occurs because $\theta_0 \simeq 0°$ and $\theta_0 < (\theta_1 + \theta_2)$ is the condition for formation of a composite surface for a receding TPL (1).

Microgrooved Cylinder

For the μgc where the wavelength $\lambda \simeq 1$ μm and θ_1, θ_2 are equal to 50° and 30° respectively, an increase of about 50° can be expected on the grooved part of the cylinder compared to that of the ungrooved part for an advancing TPL. The jumps of the TPL from one groove to another are too small to be recorded since the force change for this effect will be of the order of $\lambda\varepsilon l 2\pi r_0 \Delta\rho g \simeq 10^{-9}$ N, εl being the height and λ the wavelength of the grooves, g denotes the gravitational constant and Δρ the density difference between phases 1 and 2 respectively. The change in advancing contact angle is a macroscopic effect and should be readily observable.

Figure 4 shows a typical experiment in the μc using the μgc with water as the wetting liquid at 0.3 μm s^{-1} stage velocity. When the TPL encountered the grooved portion of the μgc at B the decrease in tension corresponded to a 2.3° increase in θ. The final contact angle θ at C was the same as the one at A within experimental accuracy; the tension difference measured on ungrooved and grooved parts did not show any systematic difference; it was found to be 112.7° ± 4.0° for grooved and 112.2° ± 4.0° for ungrooved portions (Table 2). It seems that the first groove at B had some effect on the TPL motion, but subsequent motion was unaffected. On both surfaces (grooved and ungrooved), the contact line stuck between C and D while the contact angle changed from the advancing contact angle, θ_A, to the receding angle, θ_R, and the receding contact line was much smoother than the advancing TPL. The receding angle $\theta_R \simeq 0°$ was measured by photographs of the TPL.

A similar situation was observed when TBE was used instead of water as the liquid phase; there was no systematic difference in the magnitude of hysteresis loops over grooved and ungrooved portions of the μgc with $\theta_A = 47.6° \pm 6°$ and, as in the case of water, θ_R was very close to zero. The differences between the various runs were mainly due to the difficulty in reproducing the same Al surface given the limitations of the cleaning procedures. Still, it can be said that, on the μgc surface, no macroscopic contact angle variation was observed due to grooves, except a small change at the first groove while advancing.

Figure 5(*a*) and (*b*) shows SEM-graphs of the μgc surface. The experiments were made on a surface which was in a better condition than Fig. 5 suggests because an attempt for a more rigorous cleaning was made with dilute chromic acid solution which was terminated when the Al-coating started to peel

Can. J. Chem. Downloaded from www.nrcresearchpress.com by 210.87.254.6 on 09/06/12
For personal use only.

Can. J. Chem. Downloaded from www.nrcresearchpress.com by 210.87.254.6 on 09/06/12
For personal use only.

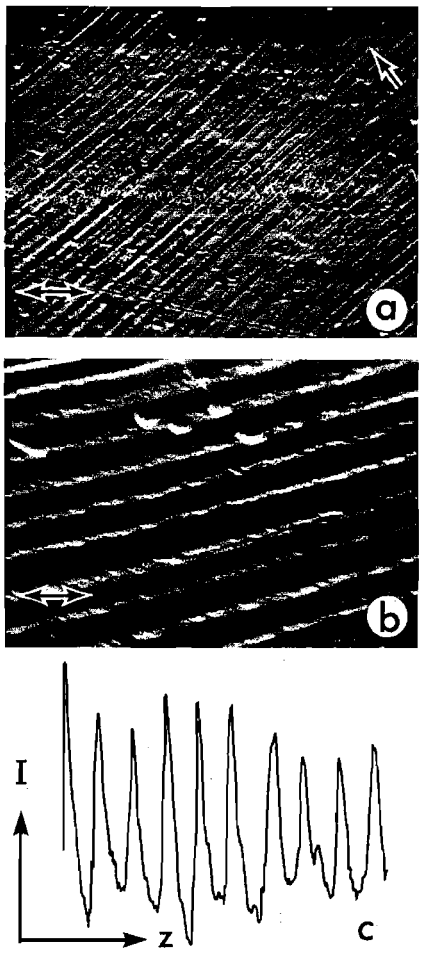

FIG. 5. SEM-graphs of the μgc. The arrows indicate the direction of the cylinder axis (ignore the faint signals in (*a*) which are artifacts). The length scales show 4 μm in (*a*) and 0.8 μm in (*b*). The light intensity I that passes through the negative of (*b*) which was obtained by a microdensitometer scanning in the Z-direction of the μgc is shown in (*c*); the intensity I is linearly proportional to the image density.

off from the smooth surface of the sapphire. The S.E.M. photograph in Fig. 5 shows the condition of the grooves after this attempt on which no experiments were performed. Nevertheless, the analysis of the negative of Fig. 5(*b*) by a recording densitometer indicates that groove spacings were quite regular, Fig. 5(*c*). A single scanning line in the Z-direction shows that the grooves are quite sharp and uniform as indicated by the intensity I of the scanning light source which passes through the negative of Fig. 5(*b*) and which is linearly proportional to the image density.

The most probable explanation of the lack of hysteresis due to the regular grooves is that the effect of chemical heterogeneity may overshadow the effects of regular roughness. If there are large differences in solid surface free energy the TPL may not be horizontal but traverse several grooves, as shown schematically by the broken line in Fig. 6, conforming to the variations in surface free energy of the solid. If the effect of groove edges (8) is neglected, one can make the following simplifications assuming the contact line traverses many grooves, so that statistically we have

$$[1] \quad t \simeq \frac{\varepsilon l}{\sin \theta_1} 2\pi r_0$$

$$[2] \quad d - t \simeq \frac{\varepsilon l}{\sin \theta_2} 2\pi r_0$$

where t is the area of one groove surface where $\tan^{-1}(dr/dz) = -\theta_1$ and $d - t$ is the area of groove surface where $\tan^{-1}(dr/dz) = \theta_2$. Then the average apparent contact angle, $\bar{\theta}$, is given by

$$[3] \quad \bar{\theta} = \theta + \frac{t}{d}\theta_1 - \frac{d-t}{d}\theta_2$$

Therefore for groove geometries where $t = (1/2)\,d$, effects of regular roughness cannot be observed due to traversing of the contact line over several grooves but, if $(1/2)\,d \neq t$, small changes in contact angle may be observable in accordance with [3]. For the μgc we have $t/d = 0.605$ and $(d - t)/d = 0.395$, therefore from [3], $\bar{\theta}_A = \theta_A + 1.6°$, i.e. little change in hysteresis due to regular roughness is expected. (The μc is capable of detecting contact angle changes to better than 0.1°, depending on the cylinder diameter and value of θ, but reproducibility of the runs in our experiments was about ±4° which is much larger than the expected change in contact angle.)

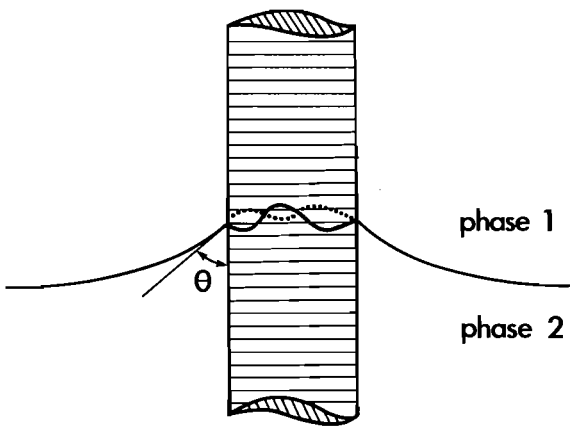

FIG. 6. Schematic of the meniscus on the grooved surface showing the contact line traversing several microgrooves.

TABLE 2. Data from microcapillarograms for microgrooved cylinder (μgc)

	Ungrooved part		Grooved part	
	θ_A[c]	θ_R[d]	θ_A[c]	θ_R[d]
Water[a]	112.2±4.0°	0°	112.7±4.0°	0°
Tetrabromoethane[b]	47 ±6°	0°	47 ±6°	0°

[a]Average of 6 experiments.
[b]Average of 3 experiments.
[c]Calculated from tension differences.
[d]Photographic observation.

Another explanation is the presence of capillary waves caused by ambient vibrations which were measured using an accelerometer and were found to have a maximum vertical displacement of about 0.5 μm (5). If there is no resonance in the system it is reasonable to assume that capillary waves in the liquid surface are of the same order of magnitude and frequency as the instrument vibrations. A crude calculation, assuming waves are transmitted with major frequency of vibrations (28.6 Hz) with amplitude 0.3 μm (5), yields a wave velocity of 35.9 cm s^{-1} and 1.25 cm wavelength (9). It should be added that the surface vibrations alone do not suffice to explain the observations. The vibrations have to be considered in connection with the slip boundary condition of a moving TPL (10, 11). If the length scales involved in surface vibrations and slip boundary conditions are of the same order of magnitude as surface roughness, it would not be meaningful to make predictions about the magnitude of hysteresis due to either physical or chemical heterogeneity. Most probably the slippage phenomenon is operative at length scales smaller than 1 μm, and in our experiments both effects contribute to the lack of hysteresis due to regular grooves.

For a qualitative demonstration of the effects of regular roughness in the range of 1 μm < λ < 100 μm on liquid spreading, a drop formation experiment was carried out on a planar PMMA surface with parallel saw-tooth shaped grooves (Table 1). The TBE drops were formed using a slowly moving infusion pump with a fine syringe needle almost touching the surface. The final shape of the drop which is elongated in the direction of the grooves (Fig. 7) dramatically shows their effect.

In a wider context the results may be related to Wenzel's equation (12, 13)

$$[4] \quad \cos\theta = \bar{\sigma}\cos\theta_0$$

where $\bar{\sigma}$ is the ratio of the true to the geometric solid surface area which is derived thermodynamically from the minimization of total free energy of a system. The relationship between θ and θ_0 on regular grooves is easily visualized as shown by the experiments with the Mgc. In experiments with the μgc, the increase in surface area due to grooves did not have an observable effect on θ_0 which may indicate that the order of magnitude of roughness has to be much smaller than 1 μm in order to attach a thermodynamic meaning to Wenzel's equation.

FIG. 7. Photograph of a TBE drop on PMMA plane grating with λ = 10 μm. The groove direction is along the elongated axis of the drop.

Another relevant observation is that the contributions of chemical heterogeneity and physical roughness are not additive; this follows from the experiments with the μgc. The exact nature of this interaction requires further study.

In a subsequent paper (14), dealing with wetting of solid surfaces, we investigate thin fibers of high and low surface energies using the μc at very low and medium TPL velocities. Study of these fibers, made of commonly used materials such as glass, platinum, Teflon, reveals interesting observations relevant to the nature of contact angle hysteresis on more realistic solid surfaces.

Acknowledgement

The authors wish to thank Dr. T. G. M. van de Ven for constructive criticism and suggestions.

1. E. BAYRAMLI, T. G. M. VAN DE VEN, and S. G. MASON. Can. J. Chem. **59**, 1954 (1981).
2. C. HUH and S. G. MASON. J. Colloid Interface Sci. **60**, 11 (1977).

Can. J. Chem. Downloaded from www.nrcresearchpress.com by 210.87.254.6 on 09/06/12
For personal use only.

3. J. F. OLIVER, C. HUH, and S. G. MASON. Colloids and Surfaces, **1**, 79 (1980).
4. A. OKAGAWA and S. G. MASON. Fibre Water Interactions in Paper-making, Proceedings of 1977 Oxford Symposium. Technical Section, British Paper and Board Industry Federation, 1978. pp. 581–585.
5. E. BAYRAMLI. Ph.D. Thesis. McGill University, Montreal, P.Q. 1980. Appendix I.
6. E. BAYRAMLI, C. HUH, and S. G. MASON. Can. J. Chem. **56**, 818 (1978).
7. C. HUH and L. E. SCRIVEN. J. Colloid Interface Sci. **30**, 323 (1969).
8. J. F. OLIVER, C. HUH, and S. G. MASON. J. Colloid Interface Sci. **39**, 568 (1977).
9. C. A. COULSON. Waves in liquids. Oliver and Boyt, London. 1955. p. 86.
10. E. B. V. DUSSAN. J. Fluid Mech. **77**, 665 (1976).
11. C. HUH and S. G. MASON. J. Fluid Mech. **81**, 401 (1977).
12. R. N. WENZEL. Ind. Eng. Chem. **28**, 988 (1936).
13. R. N. WENZEL. J. Phys. Colloid Chem. **53**, 1466 (1949).
14. E. BAYRAMLI, T. G. M. VAN DE VEN, and S. G. MASON. To be published.

Can. J. Chem. Downloaded from www.nrcresearchpress.com by 210.87.254.6 on 09/06/12
For personal use only.

Patchwise interfacial dipole layers on solids. Application to the silver iodide – aqueous solution interface

ARIE DE KEIZER AND JOHANNES LYKLEMA

Laboratory for Physical and Colloid Chemistry, Agricultural University, De Dreijen 6, 6703 BC Wageningen, The Netherlands

This paper is dedicated to Dr. Sam Levine on the occasion of his 70th birthday

Received September 8, 1980

Can. J. Chem. Downloaded from www.nrcresearchpress.com by 210.87.254.5 on 09/06/12
For personal use only.

ARIE DE KEIZER and JOHANNES LYKLEMA. Can. J. Chem. **59**, 1969 (1981).

The hydration of solid particles in aqueous solution is treated as a patchwise phenomenon, in which the orientation of water dipoles varies in a patchwise fashion along the surface. The idea is applied to the AgI system where besides the neutral surface Ag^+ patches and I^- patches are distinguished. A first-order elaboration is offered, including an analysis of the relation between overall macroscopic quantities and local properties. The model offers an interpretation of two characteristics of double layers on silver iodide: the asymmetry of its p.z.c. and the conspicuous capacitance rise on the positive side and may serve as a starting point for a better description of the typical differences between the double layers on AgI and Hg.

ARIE DE KEIZER et JOHANNES LYKLEMA. Can. J. Chem. **59**, 1969 (1981).

On considère l'hydratation des particules solides en solution aqueuse comme un phénomène impliquant des blocs dans lesquels l'orientation des dipôles de l'eau varie avec les blocs présents à la surface. On a appliqué ce concept à un système de AgI dans lequel en plus du bloc neutre, on peut distinguer des blocs de Ag^+ et d'autres de I^-. On présente une étude approfondie de premier ordre comportant une analyse de la relation entre les quantités macroscopiques globales et les propriétés locales. Le modèle propose une interprétation pour deux caractéristiques de la couche double sur l'iodure d'argent: l'asymétrie de son c.z.p. et l'augmentation manifeste de la capacité de la partie positive; ce modèle peut servir de point de départ pour une meilleure description des différences caractéristiques entre les couches doubles sur AgI et Hg.

[Traduit par le journal]

Introduction

The description of the orientation of water (and other) dipoles near a phase boundary remains one of the most difficult problems of interfacial electrochemistry. The majority of models refer to the metal–water interface. The state-of-art in this field has been covered in an excellent review by Trasatti (1). However, it is questionable whether the results obtained for metal–water interfaces are of immediate applicability to non-metal solid–water interfaces, as occurring in many disperse systems. More often than not the charge on the surface is localized, while in addition solid surfaces are often heterogeneous. It follows that the state of hydration, or, for that matter, the interfacial polarization, varies along the surface. For instance, with negatively charged AgI-sols one would expect a mode of orientation of the water dipoles near an adsorbed I^- ion differing from that near an uncharged part of the surface: the adsorbed I^- ion would create a small hydrophilic patch in an otherwise hydrophobic surface. Similar reasoning would apply to, say, negatively charged polystyrene latex particles.

Below we shall refer to models, based on interfacial water molecules treated as if their orientation is due to a homogeneous electrical field as "*homogeneous interfacial hydration models*", in contradistinction to "*patchwise interfacial hydration models*", in which the existence on the surface of loci or patches of differing hydration properties is explicitly accounted for. The first category encompasses the main body of what has hitherto been studied, but here we intend to emphasize the second. "Interfacial hydration" is interpreted here in the general sense as including *all* variations of the properties of water due to an adjacent phase, including those near water-rejecting surfaces, giving rise to hydrophobic hydration.

In this paper we will emphasize the orientational properties of the solvent molecules. The model to be developed will be applied to the silver iodide – aqueous solution interface (2) and incorporated in a theory of the AgI–electrolyte interface, which is based on the individual adsorptions of the potential determining (p.d.) ions. It will be shown that the proposed picture is entirely compatible with experimental charge–potential curves.

Patchwise Interfacial Hydration, Some Basic Aspects

The discrimination between systems, where a homogeneous hydration model applies and those in which a patchwise treatment is indicated, is not always obvious. Clearly, air in contact with water is homogeneous, so are other fluids, including mercury. If the mercury bears a charge, due to, say, an excess of electrons, these electrons move very rapidly along the surface, so that the surface charge density σ is really smeared-out and the electrical field near the

0008-4042/81/131969-09$01.00/0

©1981 National Research Council of Canada/Conseil national de recherches du Canada

Can. J. Chem. Downloaded from www.nrcresearchpress.com by 210.87.254.5 on 09/06/12
For personal use only.

surface is homogeneous. A patchwise model is obvious for most heterogeneous surfaces. Heterogeneity can arise if the surface consists of a collection of different but homogeneous patches or if it carries a number of fixed charges (of one or more types) on an otherwise uncharged area. For instance, polystyrene latex spheres negatively charged by immobile covalently bound, completely dissociated sulphate groups clearly belong to the patchwise category because the charged groups cannot move at all. An intermediate situation exists for homogeneous surfaces on which the surface charges have a limited tangential mobility. The discriminating question is then whether or not the relaxation rate of the lateral motion of these ions exceeds that of the adjustment of water dipoles. Silver iodide is intermediate because the adsorbed p.d. ions (Ag^+ and I^-) have a certain tangential mobility, either inside the solid, or by desorption and readsorption at a different site.

Some indication of the applicability of the patchwise model can be obtained from different kinetic interfacial parameters. For the AgI – aqueous solution interface, the rotational relaxation time of water, as obtained from nmr-measurements, is of order 10^{-9} s or faster. The relaxation time for the adjustment of surface charges can be inferred from recent work by Peverelli and van Leeuwen (3), who found a relaxation time order of 10^{-3} s. Although the latter is related to the transfer of charges across the interface and is probably controlled by the dehydration process of p.d. ions, it is so much slower than the relaxation time for the adjustment of an interfacial water molecule that for the purpose of description of the properties of the interfacial water layer the distribution of adsorbed Ag^+ and I^- ions is virtually fixed. In other words, in this case a patchwise approach is indicated.

In a patchwise hydration model, the electrical interfacial properties due to free and induced charges will be locally dependent on the surface properties of the patch. We intend to evaluate the total Galvani-potential difference $\phi^S - \phi^L$ between the interior of the (homogeneous) solid and that of the liquid in terms of its components. To be rigorous, one should take into account both the discreteness of the surface charge (and counter charge), as well as the patchwise behaviour of interfacial hydration. However, for the present purpose, we will use the following first order approximation: (*i*) The Galvani potential is considered a statistical mean of the local properties. (*ii*) The charges will also be taken as smeared out except for their effect on interfacial hydration. (*iii*) Local solvent properties are calculated with a patchwise model, but in a later stage these properties will be averaged over the surface.

It is not always meaningful to average or to smear out the local hydration properties in the patchwise interfacial hydration model. This can be illustrated by considering the orientation of solvent dipoles and the dipolar potential. For reversible interfaces, like that between AgI and an electrolyte solution, the dipolar potential is part of the Galvani potential difference $\phi^S - \phi^L$. It is likely that adsorption of p.d. ions will be related to the dipolar (macro) potential. However, for systems consisting of a non-conducting solid and fixed surface groups chargeable by a dissociation equilibrium only the effect of hydration on the micropotential is meaningful. This local hydration can be incorporated in the equilibrium constant or the adsorption free energy.

Interfacial Dipole Potentials, In First Order Approximation

Assume a surface to be composed of a collection of patches of differing properties denoted by $i, j, k \ldots$. Patches i are characterized by a surface charge density σ_i, a relative dielectric constant in the fluid ε_i, and an effective number of normally oriented water molecules $n_i^\perp$. The sign of $n_i^\perp$ denotes the direction of the oriented dipoles. We will simplify our treatment by assuming σ_i, ε_i, and $n_i^\perp$ to be independent of the total surface charge density σ. This limits our treatment either to heterogeneous surfaces with a fixed surface charge, or to homogeneous surfaces with localized charges determining surface hydration. It is our aim to evaluate the dipolar potential difference of the entire interface $\Delta\phi(\text{dip})$ from local properties.

The electrical potential difference across a homogeneous layer of surface dipoles is given by the Helmholtz-equation [1].

$$[1] \quad \Delta\phi(\text{dip}) = \frac{n^\perp \mu}{\varepsilon_0 \varepsilon^H}$$

Rational units are used throughout, thus ε_0 is the dielectric permittivity of vacuum (8.854×10^{-12} C/V m). As discussed by Trassatti (1) difficult points in the application of [1] are assigning values to the effective dipole moment of water μ and to the relative dielectric constant ε^H. For μ we take the value for isolated water molecules, i.e. 1.84 D ($= 6.13 \times 10^{-30}$ C m). This choice automatically implies a choice on the value of ε^H, a point to which we return below. Before discussing ε^H it is useful to analyse the overall behaviour of the dielectric constant near the surface.

It is assumed that the region between the homogeneous surface and the Outer Helmholtz Plane (OHP), the inner or Stern layer, has a uniform dielectric constant ε^S. In the absence of specific adsorption the Stern layer can be considered as a

Can. J. Chem. Downloaded from www.nrcresearchpress.com by 210.87.254.5 on 09/06/12
For personal use only.

molecular condenser for which the potential difference is written as

$$[2] \quad \Delta\phi(\text{Stern}) = \frac{\sigma d}{\varepsilon_0 \varepsilon^S}$$

where d is the thickness of the Stern layer. This potential difference is a function of the charge of the surface and the orientation of permanent dipoles at the surface and can thus formally be separated in two components, a dipolar contribution $\Delta\phi(\text{dip})$ and another one $\Delta\phi(\text{mol})$, to be discussed later:

$$[3] \quad \Delta\phi(\text{Stern}) = \Delta\phi(\text{mol}) + \Delta\phi(\text{dip})$$

Also formally, this separation can be extended to the right hand side of [2]. Assuming σ and d to be equal for the two components, we can write

$$[4] \quad \Delta\phi(\text{Stern}) = \frac{\sigma d}{\varepsilon_0 \varepsilon^M} - \frac{\sigma d}{\varepsilon_0 \varepsilon^O}$$

which is equivalent with a splitting-up of the reciprocal Stern permittivity ε^S according to

$$[5] \quad \frac{1}{\varepsilon^S} = \frac{1}{\varepsilon^M} - \frac{1}{\varepsilon^O}$$

Here, ε^M is the apparent dielectric constant due to molecular polarization only and ε^O is the same due to the orientational effect of the water dipoles only. The minus sign follows from the fact that the orientation of permanent dipoles is opposite to the field vector. The parameter ε^M is the dielectric constant at fixed orientation of the dipoles and will be close to the high-frequency value ε_∞. It is assumed that ε^M is isotropic and thus independent of $\Delta\phi(\text{dip})$. It follows also, that for different patches i, ε_i^M is independent of the patch properties ($\varepsilon_i^M = \varepsilon^M$). The quintessence of the separation of ε^S is that all variations of ε^S with surface charge are ascribed to ε^O and hence to $\Delta\phi(\text{dip})$. The dipolar potential dependence on surface charge follows from model considerations.

Let us now return to the choice of the value for dielectric permittivity of the Helmholtz layer, ε^H. First, it is noted that in [2], ε^S applies over the entire region between the centres of the surface charges and the OHP, whereas in [1] ε^H applies only to a monolayer of water molecules. Strictly speaking ε^H could well be unity, but we have to account for the approximation made above that for μ the value of isolated water dipoles has been substituted. This is an overestimation because of the lateral interaction of the dipoles (4, 5) and a correction factor is needed in the denominator of [1], which, in our formalism is included in ε^H. The precise resulting value of ε^H is difficult to assess, the actual choice has no influence on our line of reasoning although it affects the values of the parameters to be substituted.

Let the fraction of the surface covered with patches i be denoted by θ_i. The total surface charge density and the total effective number of normally oriented water molecules per unit area can be written as

$$[6] \quad \sigma = \sum_{i=1}^{N_p} \sigma_i \theta_i$$

$$[7] \quad n^\perp = \sum_{i=1}^{N_p} n_i^\perp \theta_i$$

where N_p is the number of patches. From the previous discussion it follows that ε^M, μ, and d are independent of the specific patch properties. In our first order approximation the density of the patchwise oriented dipoles and the surface charge density on the different patches can be taken as smeared out. The additivity of the components of the dipolar potentials and those of the molecular polarizability part of the Stern layer potential ([8], [9]) can be derived from [1], [4], [6], and [7].

$$[8] \quad \Delta\phi(\text{mol}) = \frac{\left(\sum_{i=1}^{N_p} \sigma_i \theta_i\right) d}{\varepsilon_0 \varepsilon^M} = \sum_{i=1}^{N_p} \Delta\phi_i(\text{mol})$$

$$[9] \quad \Delta\phi(\text{dip}) = \frac{\left(\sum_{i=1}^{N_p} n_i^\perp \theta_i\right) \mu}{\varepsilon_0 \varepsilon^H} = \sum_{i=1}^{N_p} \Delta\phi_i(\text{dip})$$

The potential differences $\Delta\phi_i(\text{mol})$ and $\Delta\phi_i(\text{dip})$ are considered as components of a total potential difference and analyzed, regarding the charge density and the density of oriented dipoles at the patches i respectively as smeared out over the whole surface.

If the origin of a patch on a surface is the adsorption of localized surface charges on a homogeneous neutral surface, the degree of occupation θ_i is mostly not well defined. However, we can eliminate θ_1, the surface fraction of neutral patches, from [9], because the condition [10] is valid.

$$[10] \quad \sum_{i=1}^{N_p} \theta_i = 1$$

Moreover, the surface fractions of the charged patches are proportional to the surface excesses of the corresponding ions, expressed in eq/unit area, according to [11].

$$[11] \quad \theta_i = k_i' F \Gamma_i$$

Here F is the Faraday constant and k_i' is a measure for the effective patch area per adsorbed ion. If we introduce [10] and [11] in [9] the surface fractions θ_i are eliminated.

$$[12]\quad \Delta\phi(\text{dip}) = \frac{n_1^{\perp}\mu}{\varepsilon_0\varepsilon^{H}} + \sum_{i=2}^{N_p}\frac{(n_i^{\perp} - n_1^{\perp})\mu}{\varepsilon_0\varepsilon^{H}}k_i'F\Gamma_i$$

$$= \Delta\phi_N(\text{dip}) + \sum_{i=2}^{N_p} k_iF\Gamma_i$$

$$= \Delta\phi_N(\text{dip}) + \sum_{i=2}^{N_p}\Delta\phi_i^{R}(\text{dip})$$

Application of the same procedure to [8] is not meaningful because σ_1 is zero. The value of $\Delta\phi_N(\text{dip})$ is a constant (independent of the surface charge) and applies to the neutral surface. On the other hand, the dipolar potential components $\Delta\phi_i^R$ are proportional to the surface excesses of the ions.

The Local Interfacial Hydration Model Applied to AgI

On silver iodide the surface charge σ is related to the surface excesses of silver and iodide ions according to [13].

$$[13]\quad \sigma = F(\Gamma_{Ag^+} - \Gamma_{I^-})$$

Physically, the charge may be a real surface excess of the p.d. ions (relative to AgI) or a surface vacancy or a space charge in the solid. In our model, all charges are attributed to local positive excesses on the surface.

As explained before, it is likely that the relaxation of water molecules near adsorbed p.d. ions is much faster than the lateral movement of these ions. Moreover, the absolute value of the charge density σ never exceeds 5 $\mu C/cm^2$ in experimental situations. This surface charge corresponds with mutual distances between the charges of minimally 1.8 nm. Hence, the charges are sufficiently well separated and localized on the timescale of the reorientation of water, and, therefore for the purpose of our analysis they may be treated as individual sites.

We distinguish three kinds of randomly distributed patches, Ag^+ patches, I^- patches, and the remaining uncharged AgI patch. The resulting expression for the dipolar potential according to [12] reads for this case

$$[14]\quad \Delta\phi(\text{dip}) = \Delta\phi_{Ag^+}^{R}(\text{dip}) + \Delta\phi_{I^-}^{R}(\text{dip}) + \Delta\phi_{AgI}(\text{dip})$$

$$= k_{Ag^+}F\Gamma_{Ag^+} + k_{I^-}F\Gamma_{I^-} + \Delta\phi_{AgI}(\text{dip})$$

The coefficients k_{Ag^+} and k_{I^-} are parameters related to the net degree of orientation of water molecules at an Ag^+ and an I^- patch respectively.

On the neutral part of an AgI surface the silver and iodide atoms are only partly charged, because the silver iodide lattice is essentially covalent. Here, the orientation is determined by a competitive effect of the solid *and* the solution phase. As silver iodide behaves as a hydrophobic solid, it is not unlikely that on the neutral part of the surface the orientation of H_2O dipoles (and hence the potential difference $\Delta\phi_{AgI}(\text{dip})$ is mainly determined by the solution side. Consequently, it is not very different from that at the air–solution interface. At the air–solution interface water molecules are oriented with the O-atom outwards. The surface or χ-potential amounts to ca. 0.13 V (1).

It may be a good first approximation that the hydration of the water molecules on the Ag^+ and I^- patches is similar (or at least related) to that of the corresponding ions in solution. The hydration free energies $G_{Ag^+}^{h,L}$ and $G_{I^-}^{h,L}$ of the silver and iodide ions in solution are very different and amount to -479.4 kJ/mol and -257.1 kJ/mol respectively (6). It appears that $G_{Ag^+}^{h,L}$ is very high compared to the same quantity for an alkali ion of the same radius. This fact points to a specific interaction between the Ag^+ ion and the surrounding water molecules. We assume that the high hydration free energy of Ag^+ corresponds to a relatively high degree of radial orientation of water molecules around the ion. If this behaviour is similar at the surface the effective orientation of water molecules on Ag^+ patches will be stronger than that on I^- patches. As a consequence k_{Ag^+} will exceed k_{I^-} and this fact is probably the main reason for the asymmetry of the charge–potential curve of AgI in 0.1 *M* KNO_3 as will be shown later.

The effective number of oriented water molecules of a given kind of patch can be estimated from the Helmholtz-equation [1] or [12]. To that end we will use some parameters obtained by anticipating the fitting of an experimental charge–potential curve to an electrical double layer model including patchwise interfacial hydration. The origin of the data will be given below. The data used are the values obtained in the p.z.c. For $\Delta\phi_{Ag^+}^{R}(\text{dip})$, $\Delta\phi_{I^-}^{R}(\text{dip})$, and $\Delta\phi_{AgI}(\text{dip})$ we have introduced -94 mV, $+34$ mV, and -140 mV respectively. $F\Gamma_{Ag^+}$ and $F\Gamma_{I^-}$ are both 1 $\mu C/cm^2$, whereas the relative dielectric constant ε^H was given a value of 6. Substituting these parameters into the Helmholtz-equation [1] the averaged number of oriented water dipoles nm^{-2} (inclusive sign indicating polarity) $\bar{n}_{Ag^+}^{\perp}$, $\bar{n}_{I^-}^{\perp}$, and $\bar{n}_{AgI}^{\perp}$ can be calculated as -0.81, $+0.29$, and -1.21 respectively. For Ag^+ and I^- patches this corresponds to a number of 11 and 5 effectively oriented water molecules per adsorbed p.d. ion respectively. These values seem rather high for half the hydration of a single ion. Although effectively the number of

Can. J. Chem. Downloaded from www.nrcresearchpress.com by 210.87.254.5 on 09/06/12
For personal use only.

Can. J. Chem. Downloaded from www.nrcresearchpress.com by 210.87.254.5 on 09/06/12
For personal use only.

oriented water molecules are not only in contact with an adsorbed ion, but also with neighbouring (partly charged) atoms of the same kind, it is likely that a number of 11 water molecules on an Ag^+ patch is too high. Other values for $\Delta\phi^R_{Ag^+}$(dip) and $\Delta\phi^R_{I^-}$(dip) as resulting from a different parameter choice give a worse correspondence of calculated and experimental charge–potential curves. However, it must always be realized that assignment of reliable hydration numbers is thwarted by the uncertainty inherent in the choice of ε^H, as discussed above.

Adsorption of p.d. Ions and the Nernst Equation

Unlike the surface charge, given in [13], the individual surface excesses Γ_{Ag^+} and Γ_{I^-} are experimentally inaccessible. However, in order to obtain $\Delta\phi$(dip) these individual values are needed. They can be obtained by assuming some adsorption model and by making a proper choice of the isotherm parameters.

The adsorption of p.d. ions is an equilibrium process. This means that the electrochemical potentials ($\tilde{\mu}$) of these ions in the bulk of the solid (S), the interface (I), and the bulk of the solution (L) must be equal.

$$[15]\quad \tilde{\mu}^S_{Ag^+} = \tilde{\mu}^I_{Ag^+} = \tilde{\mu}^L_{Ag^+}$$

$$[16]\quad \tilde{\mu}^S_{I^-} = \tilde{\mu}^I_{I^-} = \tilde{\mu}^L_{I^-}$$

To split the electrochemical potentials of the interface into an electrical and a chemical contribution the position of the interface has to be fixed. The electrochemical potentials of p.d. ions in the two bulk phases are readily given by [17] to [20].

$$[17]\quad \tilde{\mu}^S_{Ag^+} = \tilde{\mu}^{S0}_{Ag^+}(T) + F\phi^S$$

$$[18]\quad \tilde{\mu}^S_{I^-} = \tilde{\mu}^{S0}_{I^-}(T) - F\phi^S$$

$$[19]\quad \tilde{\mu}^L_{Ag^+} = \tilde{\mu}^{L0}_{Ag^+}(T) + RT\ln c_{Ag^+} + F\phi^L$$

$$[20]\quad \tilde{\mu}^L_{I^-} = \tilde{\mu}^{L0}_{I^-}(T) - RT\ln c_{I^-} - F\phi^L$$

The potentials ϕ^S and ϕ^L are unmeasurable in principle, but variations of $\Delta\phi = \phi^S - \phi^L$ are accessible because they are related to changes of cell potentials. If the indifferent electrolyte concentration is much higher than c_{Ag^+} and c_{I^-}, the ionic strength is approximately constant during variations of c_{Ag^+} and c_{I^-}. The (constant) activity coefficients are then included in $\tilde{\mu}^{L0}_{Ag^+}$ and $\tilde{\mu}^{L0}_{I^-}$.

Equating [17] and [19] or [18] and [20] leads to the *Nernst equation.*

$$[21]\quad \Delta\phi = \tilde{\mu}^{L0}_{Ag^+}(T) - \tilde{\mu}^{S0}_{Ag^+}(T) + (RT/F)\ln c_{Ag^+}$$

$$[22]\quad \Delta\phi = \tilde{\mu}^{L0}_{I^-}(T) - \tilde{\mu}^{S0}_{I^-}(T) - (RT/F)\ln c_{I^-}$$

The Nernst equation is a relation between bulk properties of the system. Interfacial quantities, particularly interfacial potentials, are only obtainable by introducing model assumptions for the adsorption of p.d. ions. In our picture, it is assumed, that the adsorption of p.d. ions occurs on a lattice consisting of a finite number of adsorption sites. Let ϕ^A be the electrical potential in the adsorption plane. The potential ϕ^A will be equal for the adsorption of Ag^+ and I^- ions. This is so because for ϕ^A we substitute the average electrostatic macropotential, which is the same for each site by definition. Local deviations due to the discreteness of the charges are in first instance independent of Γ_{Ag^+} and Γ_{I^-} and are incorporated in $\tilde{\mu}^{I0}_{Ag^+}$ and $\tilde{\mu}^{I0}_{I^-}$. For a p.d. ion to become adsorbed from the solution, it must pass through the diffuse layer, the Stern layer, and the hydration layer successively. Hence, $\Delta\phi$(ads) can be written as [23].

$$[23]\quad \Delta\phi(\text{ads}) \equiv \phi^A - \phi^L = \Delta\phi(\text{diff}) + \Delta\phi(\text{mol}) + \Delta\phi(\text{dip})$$

Potential differences due to volume charges in or polarization of the solid phase are not included in [23], because we assumed positive excess adsorption values of p.d. ions being present *on* the solid surface.

We assume, that the adsorption of p.d. ions satisfies a *Langmuir equation.* The interfacial electrochemical potentials can then be written as

$$[24]\quad \tilde{\mu}^I_{Ag^+} = \tilde{\mu}^{I0}_{Ag^+} + RT\ln\frac{\Gamma_{Ag^+}}{\Gamma^{max}_{Ag^+} - \Gamma_{Ag^+}} + F\phi^A$$

$$[25]\quad \tilde{\mu}^I_{I^-} = \tilde{\mu}^{I0}_{I^-} + RT\ln\frac{\Gamma_{I^-}}{\Gamma^{max}_{I^-} - \Gamma_{I^-}} - F\phi^A$$

Our ultimate aim is to establish a relation between σ and $\Delta\phi$ (or between σ and c_{Ag^+} or c_{I^-}). To that end we have to express Γ_{Ag^+} and Γ_{I^-} as a function of σ. The values of Γ_{Ag^+} and Γ_{I^-} can be related with [15], [16], [17], [18], [24], and [25].

$$[26]\quad RT\ln\frac{\Gamma_{Ag^+}}{\Gamma^{max}_{Ag^+} - \Gamma_{Ag^+}}\frac{\Gamma_{I^-}}{\Gamma^{max}_{I^-} - \Gamma_{I^-}} = \tilde{\mu}^{S0}_{Ag^+} + \tilde{\mu}^{S0}_{I^-} - \tilde{\mu}^{I0}_{Ag^+} - \tilde{\mu}^{I0}_{I^-} = K$$

Hence, $\Gamma_{Ag^+}(\sigma)$ and $\Gamma_{I^-}(\sigma)$ can be solved from [13] and [26]. The value of K is related to the adsorption values of Ag^+ and I^- in the p.z.c. ($\sigma = 0$ and $\Gamma_{Ag^+} = \Gamma_{I^-}$) and hence to the molecular partial free energies of adsorbed ions. It is interesting to note, that [26] resembles an expression for the "solubility product in the interface", analogous to the solubility product in solution, which follows from [19] and [20].

Finally, the equations presented in this section enable the calculation of the potential difference between the bulk of the solid and the adsorption

plane. The value of $\Delta\phi$(solid) follows from equating [17] and [24] (or alternatively from [18] and [25]).

$$[27]\quad \Delta\phi(\text{solid}) \equiv \phi^S - \phi^A = \frac{\mu^{IO}_{Ag^+} + \mu^{SO}_{Ag^+}}{F} + \frac{RT}{F}\ln\frac{\Gamma_{Ag^+}}{\Gamma^{max}_{Ag^+} - \Gamma_{Ag^+}}$$

The necessity of a non-zero potential difference in the solid is thus a consequence of thermodynamic equilibrium within the theoretical framework presented. However, the molecular interpretation of $\Delta\phi$(solid) is not so clear. It may be due either or both to free space charges (Frenkel defects) and molecular polarization of the solid. We recall, that in our picture we neglect the presence of a space charge in the solid phase attributing the surface charge entirely to p.d. ions adsorbed at the interface proper.

It may be repeated, that for the purpose of our analysis only those components of the potential differences have to be accounted for, that are dependent on the surface charge or on the adsorption of ions or molecules. Other contributions, such as a constant dipolar potential inside the solid, may be included in the standard electrochemical potentials (e.g. $\tilde{\mu}^{IO}_{Ag^+}$).

The Point of Zero Charge

In the absence of specific adsorption the p.z.c. of AgI (pAg = 5.67) does not coincide with its stoichiometric equivalence point (pAg = 8.1). It is possible to interpret this fact within the theoretical framework of the previous section. In addition a more quantitative explanation can be offered by application of the principles of the patchwise hydrated interface model.

We assume, that the covalent part of the free energies of bonding for Ag^+ and I^- ions to the AgI surface is equal on the argument that bonding of each of these ions involves the forming of an AgI bond. Let this contribution be G^{cov}_{AgI}. Then the difference in affinity of the adsorption from solution is only a function of the difference of the hydration free energy in the surface ($G^{h,I}_{Ag^+}$, $G^{h,I}_{I^-}$) and in the solution ($G^{h,L}_{Ag^+}$, $G^{h,L}_{I^-}$). As silver ions are more difficult to dehydrate than iodide ions, they have a lower adsorption in the stoichiometric equivalence point. From this it follows immediately that the p.z.c. is to the positive side of the stoichiometric equivalence point, that is: at lower pAg.

The standard affinities of the p.d. ions for the AgI surface may be defined as

$$[28]\quad \Delta G^0_{Ag^+} = G^{cov}_{AgI} + G^{h,I}_{Ag^+} - G^{h,L}_{Ag^+} \quad (= \tilde{\mu}^{IO}_{Ag^+} - \tilde{\mu}^{LO}_{Ag^+})$$

$$[29]\quad \Delta G^0_{I^-} = G^{cov}_{AgI} + G^{h,I}_{I^-} - G^{h,L}_{I^-} \quad (= \tilde{\mu}^{IO}_{I^-} - \tilde{\mu}^{LO}_{I^-})$$

Considering that

$$\Gamma_{Ag^+}(\text{p.z.c.}) \ll \Gamma^{max}_{Ag}$$

and

$$\Gamma_{I^-}(\text{p.z.c.}) \ll \Gamma^{max}_{I^-},$$

the difference in standard affinities can be directly related to the position of the p.z.c. by application of [19], [20], [24], [25], [28], and [29].

$$[30]\quad \Delta G^0_{Ag^+} - \Delta G^0_{I^-} = 2.30RT[\text{pL} - 2(\text{pAg})_{pzc}] - 2F\Delta\phi\,(\text{dip})_{pzc} - RT\ln\frac{\Gamma^{max}_{Ag^+}}{\Gamma^{max}_{I^-}}$$

We have assumed the absence of any specifically adsorbing electrolyte in the p.z.c. Further, we used $\Delta\phi(\text{ads})_{pzc} = \Delta\phi(\text{dip})_{pzc}$ and the following expression for the solubility product of AgI in solution.

$$[31]\quad \text{pL} = -\log(c_{Ag^+}c_{I^-}) = \text{pAg} + \text{pI}$$

The last term in [30] is comparatively small and we shall neglect it in the following.

Equation [30] can be applied after making proper choices of the parameters. The value of $\Delta\phi(\text{dip})_{pzc}$ can be estimated from the maximum shift of the p.z.c. upon adsorption of non-polar or weakly polar organic molecules (7, 8). A value of -200 mV appears to be a good estimation. Using for the p.z.c. and pL the familiar values of 5.67 and 16.11 respectively, we find

$$[32]\quad \Delta G^0_{Ag^+} - \Delta G^0_{I^-} = 26.9RT = 65.6\ \text{kJ/mol}$$

If the AgI were structureless and the adsorbed Ag^+ and I^- ions were halfway immersed in the solid then upon adsorption the Ag^+ and I^- ions would be halfway dehydrated. In this case the difference in adsorption free energy would be half the difference of the bulk Gibbs energies of hydration, i.e. (479.4 − 257.1)/2 = 111 kJ/mol. The actual difference is lower, indicating that the effective dehydration is less than half. This is in accordance with the picture, that each adsorbed Ag^+ and I^- ion is surrounded by a number of ions of the same kind, giving a reinforcement of the hydration effect at the interface.

It must be realized that the shift of the p.z.c. upon adsorption of organic molecules is due to the variation of both the electrical and the chemical part of the difference in adsorption free energy of the two p.d. ions. If upon adsorption of the p.d. ions from a (dilute) aqueous solution of organic molecules the ions are more strongly dehydrated than they are from pure aqueous electrolyte, $\Delta G^0_{Ag^+} - \Delta G^0_{I^-}$ will be larger and consequently, a larger shift of the p.z.c. to more posi-

Can. J. Chem. Downloaded from www.nrcresearchpress.com by 210.87.254.5 on 09/06/12
For personal use only.

Can. J. Chem. Downloaded from www.nrcresearchpress.com by 210.87.254.5 on 09/06/12
For personal use only.

tive potentials is expected. Hence, the interpretation of the shift of the p.z.c. in terms of a dipolar potential on a neutral surface is thwarted by the lack of information of the separation of the electrical and chemical part. Consequently, one must be aware, that conclusions on the net orientation of water molecules at the silver iodide surface based on the shift of the p.z.c. must be taken with due care.

The Charge–Potential Relation

The model developed enables us to evaluate the relation between the surface charge σ and the Galvani potential difference $\Delta\phi = \phi^S - \phi^L$ or the pAg. To that end the components of ϕ are calculated as a function of σ.

$$[33] \quad \Delta\phi = \Delta\phi(\text{solid}) + \Delta\phi(\text{dip}) + \Delta\phi(\text{mol}) + \Delta\phi(\text{diff})$$

Expressions for the first three terms have already been given. The potential in the diffuse layer follows from the Poisson–Boltzmann equation for a flat surface.

$$[34] \quad \Delta\phi(\text{diff}) = \frac{2RT}{F} \sinh^{-1}\left(\frac{\sigma F}{2\varepsilon_0 \varepsilon^L RT\kappa}\right)$$

$$[35] \quad \kappa^2 = 2cF^2/\varepsilon_0\varepsilon^L RT$$

Here ε^L is the relative dielectric constant of the solution containing a (1–1) electrolyte of concentration c. The parameter κ is usually called the reciprocal thickness of the diffuse double layer. In our picture, for σ the surface charge is substituted, as specific adsorption is neglected.

We are now in a position to calculate the charge–potential curves theoretically by assigning proper values to the different parameters. The parameters are chosen so as to obtain an optimal fit to the experimental charge–potential curve.

The relative dielectric constant ε^M and the thickness of the Stern layer, d, are chosen as 6 and 0.5 nm respectively. These values are close to those obtained in earlier work (9). The apparent relative dielectric constant for the Stern layer at mercury is frequently (1) also taken as 6, whereas the thickness of the Stern layer at AgI is expected to exceed the corresponding value at mercury (ca. 0.3 – 0.4 nm) due to the radii of the silver and iodide ions of the crystal lattice.

We have estimated the value of $\Delta\phi(\text{dip})_{\text{pzc}}$ as -200 mV. This is almost identical to the value of -192 mV derived from the butanol work (2). This value is split up into -140 mV for $\Delta\phi_{\text{AgI}}(\text{dip})$ and -60 mV for $\Delta\phi^R_{\text{Ag}^+}(\text{dip}) + \Delta\phi^R_{\text{I}^-}(\text{dip})$. This choice followed from the optimization considering the fact that the number of water molecules to be oriented by Ag^+ and I^- ions is limited.

$F\Gamma^{\max}_{\text{Ag}^+}$ and $F\Gamma^{\max}_{\text{I}^-}$ were rather arbitrarily chosen as 15 μC/cm^2, which was considered as realistic. However, this choice is not critical at all, as long as the value exceeds 1.5 times the surface charge.

Finally, two adjustable parameters are left, i.e. the surface excesses of the two p.d. ions at the p.z.c. and the ratio $k_{\text{Ag}^+}/k_{\text{I}^-}$.

The values of Γ_{Ag^+} and Γ_{I^-} are solved from [13] and [26] as explained above. The potentials $\Delta\phi$(Stern), $\Delta\phi$(dip), $\Delta\phi$(solid), and $\Delta\phi$(diff) follow from [2], [14], [27], and [34], realizing that $\Delta\phi$(solid) at the p.z.c. is set equal to zero. Further, $\Delta\phi$ follows from [33] and the pAg is then calculated according to the Nernst equation. Following the procedure given, an optimal correspondence between the calculated and experimental charge potential was obtained, if the surface excesses of the two p.d. ions at the p.z.c. would correspond to $+1.0$ and -1.0 μC/cm^2 respectively and if the ratio $k_{\text{Ag}^+}/k_{\text{I}^-}$ amounts to 2.75. The agreement between the two curves is illustrated in Fig. 1. The correspondence between the calculated and experimental curve is excellent, except at the extreme negative side where the calculated curve somewhat exceeds the experimental one. A likely reason for this discrepancy is that at extreme negative surfaces specific adsorption of counter ions may not be neglected. Some numerical results obtained with these data are summarized in Table 1.

The effect of the various input parameters on the final outcome is quite different. It appears that ε^M, d, and $k_{\text{Ag}^+}/k_{\text{I}^-}$ do not affect the curvature of the charge–potential curve. Neither do the parameters $\Delta\phi_{\text{AgI}}(\text{dip})$, $\Gamma^{\max}_{\text{I}^-}$, and $\Gamma^{\max}_{\text{Ag}^+}$ affect the results significantly. However, the curvature is sensitive to the choices of $\Delta\phi^R_{\text{Ag}^+}(\text{dip})$, $\Delta\phi^R_{\text{I}^-}(\text{dip})$ and the surface excesses of the p.d. ions at the p.z.c. Other

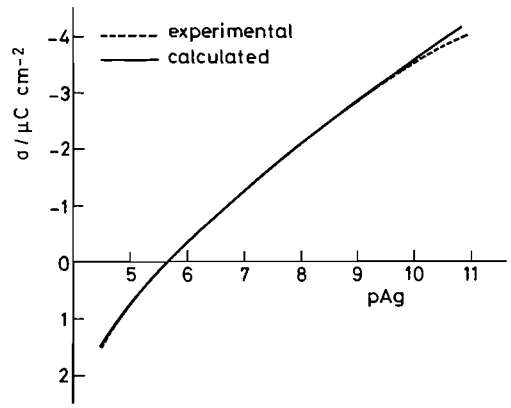

FIG. 1. Comparison of the calculated and experimental relation between charge and potential for the double layer on AgI. Electrolyte 0.1 M KNO_3, $T = 25$°C.

TABLE 1. Calculated composition of the double layer on AgI[a]

σ	$F\Gamma_{Ag^+}$	$F\Gamma_{I^-}$	Δφ (solid)[b]	Δφ (dip)	Δφ (mol)	Δφ (diff)	Δφ	pAg	pAg-exp[c]
−4.0	0.19	4.19	−43	−15	−376	−48	−482	10.50	10.95
−3.5	0.23	3.73	−39	−34	−329	−44	−445	9.87	10.02
−3.0	0.27	3.27	−34	−53	−282	−38	−408	9.23	9.25
−2.5	0.32	2.82	−30	−74	−235	−33	−371	8.60	8.57
−2.0	0.39	2.39	−25	−95	−188	−27	−335	7.97	7.90
−1.5	0.49	1.99	−19	−118	−141	−21	−299	7.34	7.28
−1.0	0.61	1.61	−13	−142	−94	−14	−263	6.74	6.70
−0.5	0.78	1.28	−7	−170	−47	−7	−230	6.17	6.12
0.0	1.00	1.00	−0	−200	0	0	−200	5.65	5.65
0.5	1.28	0.78	7	−234	47	7	−173	5.19	5.25
1.0	1.61	0.61	13	−271	94	14	−150	4.79	4.83
1.5	1.99	0.49	19	−311	141	21	−130	4.44	4.50

[a]The following units are used: σ (μC cm^{-2}), $F\Gamma$ (μC cm^{-2}), Δφ (mV).
[b]Δφ(solid) is given relative to its value at the p.z.c.
[c]Experimental data from ref. 2. The reproducibility of the experimental curve is ca. 0.05 μC/cm^2 but deteriorates at the ends of the curve. The absolute accuracy depends mainly on the uncertainty of the specific surface area, which is much higher but of no consequence for the present analysis because it would affect the entire curve by a constant factor.

assignments of values to these parameters may mathematically appear equally successful but they are in the author's opinion physically less realistic.

The calculations are performed for a concentration of indifferent electrolyte of 0.1 *M*. As is shown by Lijklema (9) the differences between curves at different salt concentrations are completely accounted for by the different contribution of the diffuse part of the double layer. Hence, our model is also compatible with the behaviour of charge–potential curves at other salt concentrations.

Comparison with Previous Work

Mackor (10) has already interpreted charge–potential curves on AgI qualitatively by assuming a constant Stern layer capacitance and a variable dipolar potential. The behaviour of the dipolar potential on mercury and AgI were assumed to be equivalent. In later studies with the AgI system little attention has been paid to the dependence of the dipolar potential on the surface charge.

The steep rise in capacitance at the positive side of the p.z.c. is typical for the AgI system. In previous work, this has been explained by assuming that silver ions are adsorbed as $AgNO_3$ (9, 11). However, to this explanation some objections can be raised. The capacitance rise is also quite pronounced for the fluoride ion, although with this ion the p.z.c. is not shifted at all, indicating absence of specific adsorption, at least at the p.z.c.

Comparison with Other Models

Apart from the solute and solvent orientation, the given model is equivalent with the ionizable surface group model as described by Healy and White (12). Introduction of surface equilibria is equivalent to using the Langmuir model for the adsorption of p.d. ions. However, in the Healy and White model the charge–"potential" relation is almost linear over the same experimental range of charges as encountered in the AgI case, i.e. this picture implies a constant capacitance.

Trasatti (1) has reviewed the various models for the mercury–electrolyte interface in some detail. All these models predict an almost linear relationship of the potential with surface charge for charge-densities between +4 and −4 μC/cm^2, contrary to our model. It can be inferred from Table 1 that in our model the variation of dipolar potential with surface charge is in the order of 50–100 mV/μC cm^{-2}. For mercury Bockris and Habib (13) calculate 8 mV/μC cm^{-2}, whereas on the other extreme Levine *et al.* (14) find 360 mV/μC cm^{-2}. The other models discussed by Trasatti predict potential drops in the order of 30–50 mV/μC cm^{-2}. This is also the case for Parsons' model (15) in which a four-state water orientation was assumed with single water molecules and clusters. It is interesting, that in Parsons' model also an asymmetry of the charge–potential curves can arise around the p.z.c. dependent on a difference in free energy of the water clusters in the two orientations.

Conclusions

In this article we offered a patchwise hydration model for the interface between silver iodide particles and aqueous electrolyte solutions. Although several simplifying assumptions were made it was shown that with the present picture some typical properties of the AgI system, such as the asymmetry of the capacitance curve and that of the p.z.c. could be accounted for. Therefore, the model holds promises

Can. J. Chem. Downloaded from www.nrcresearchpress.com by 210.87.254.5 on 09/06/12
For personal use only.

for further quantitative analysis of other hydration-sensitive properties, such as the adsorption maximum of organic substances. In addition, it can be helpful in better understanding the quantitative differences between the double layers on mercury, silver iodide, and other systems.

1. S. TRASATTI. *In* Modern aspects of electrochemistry. Vol. 13. *Edited by* B. E. Conway and J. O'M. Bockris. Plenum Press, London. 1979. p. 81.
2. B. H. BIJSTERBOSCH and J. LYKLEMA. Adv. Colloid Interface Sci. **9**, 147 (1978).
3. K. J. PEVERELLI and H. P. VAN LEEUWEN. J. Electroanal. Chem. **110**, 137 (1980).
4. S. LEVINE, G. M. BELL, and A. L. SMITH. J. Phys. Chem. **73**, 3534 (1969).
5. S. LEVINE and A. L. SMITH. Discuss. Faraday Soc. **52**, 290 (1971).
6. H. L. FRIEDMAN and C. V. KRISHNAN. *In* Water, a comprehensive treatise. Vol. 3. *Edited by* F. Franks. Plenum Press, London. 1973. Chapt. 1.
7. B. H. BIJSTERBOSCH and J. LYKLEMA. J. Colloid Sci. **20**, 665 (1965).
8. A. DE KEIZER and J. LYKLEMA. J. Colloid Interface Sci. **75**, 171 (1980).
9. J. LIJKLEMA. Thesis. State Univ. Utrecht, Netherlands. 1957.
10. E. L. MACKOR. Rec. Trav. Chim. **70**, 763 (1951).
11. B. VINCENT, J. LYKLEMA. Special Discuss. Faraday Soc. **1**, 148 (1970).
12. T. W. HEALY and L. R. WHITE. Adv. Colloid Interface Sci. **9**, 303 (1978).
13. M. A. HABIB. *In* Modern aspects of electrochemistry. Vol. 12. *Edited by* J. O'M. Bockris and B. E. Conway. Plenum Press, London. 1979. p. 131.
14. S. LEVINE, K. ROBINSON, A. L. SMITH, and A. C. BRETT. Discuss. Faraday Soc. **59**, 133 (1976).
15. R. PARSONS. J. Electroanal. Chem. **59**, 229 (1975).

Can. J. Chem. Downloaded from www.nrcresearchpress.com by 210.87.254.5 on 09/06/12
For personal use only.

Solvent accessibility and hydrophobicity in the adsorption of alkylammonium cations at air/water and Hg/water interfaces. Part 1. Behavior at the air/water interface in relation to hydration properties

R. BENNES[1] AND B. E. CONWAY

Chemistry Department, University of Ottawa, Ottawa, Ont., Canada K1N 9B4

Received September 18, 1980

This paper is dedicated to Dr. Sam Levine on the occasion of his 70th birthday

R. BENNES and B. E. CONWAY. Can. J. Chem. **59**, 1978 (1981).

By means of adsorption and surface-potential studies on a series of $R_{4-n}N^+H_n$ perchlorates at the air/water interface, the role of hydrophobic and hydrophilic interaction in the adsorption and ion distribution of these salts near the air/water interface is examined. While the adsorption of the alkylamine ions increases as n decreases from three to zero, inclusive, the surface-potential change accompanying the adsorption decreases. This effect is interpreted in terms of opposing hydrophilic, electrostatic and hydrophobic interactions between the organic ion and water near the liquid surface, leading to a progressive change of double-layer ion distribution. In Part II, comparative studies of the same series of compounds at the Hg/water interface are reported.

R. BENNES et B. E. CONWAY. Can. J. Chem. **59**, 1978 (1981).

Faisant appel à des études d'adsorption et de potentiel de surface d'une série de perchlorate de $R_{4-n}N^+H_n$ à l'interface air/eau, on étudie le rôle de l'interaction hydrophobe et hydrophile lors de l'adsorption et de la distribution de l'ion de ces sels près de l'interface air/eau. Alors que l'adsorption des ions alkylamines augmente lorsque n décroît de trois à zéro inclusivement, le changement de potentiel de surface qui accompagne l'adsorption diminue. On interprète cet effet en fonction d'interactions hydrophiles électrostatiques et hydrophobes opposées entre l'ion organique et l'eau au voisinage de la surface du liquide, conduisant ainsi à un changement progressif de la distribution de l'ion dans la couche double. On rapporte dans une deuxième partie, des études comparatives portant sur les mêmes séries composés à l'interface Hg/eau.

[Traduit par le journal]

Introduction[2]

The R_4N^+ and related $R_{4-n}NH_n^+$ ($1 < n \leq 3$) series of ions have attracted much attention in recent years (e.g. refs. 1, 2) from the ionic solvation and solution-structure point of view, and the individual cation properties have been well characterised (3). The properties of individual ions are of special interest in adsorption at interfaces, particularly at charged surfaces where predominantly one type of ion of an electrolyte is preferentially adsorbed so that its individual properties are manifested in the interfacial behavior.

The surface activity of primary to quaternary alkylammonium cations is thus of interest in detergency, mineral flotation, corrosion inhibition (4), and in some electrochemical syntheses (5) where a local hydrophobic double-layer is required. Previous studies at electrodes have been concerned with super-equivalent adsorption of symmetrical (6–8) and unsymmetrical (9) tetraalkylammonium (R_4N^+) salts with varying chain length of R while corresponding alkylpyridinium ions have also been examined (10, 11). The structure of the double-layer in the presence of R_4N^+ ions is of particular interest (cf. refs. 6, 12), since the ionic radii of the higher R_4N^+ ions are larger than those of most anions, thus changing the usual situation (13) where an inner Helmholtz plane is populated by anions and outer one by hydrated cations. Recently interest has centered on R_4N^+ ions as "phase-transfer" agents (14) and on the question of the double-layer at interfaces of immiscible liquids other than Hg and water (15, 16).

Restriction of hydration of an ion near an interface of water with air or its vapor is a major factor in determining the generally observed (17, 24) negative adsorption of simple ions at air/water interfaces. This effect has been treated theoretically in terms of the image effect by Wagner (17), Onsager and Samaras (18), Bell and Rangescroft (19), and by Conway (20) in terms of restriction of Born polarization energy. Useful reviews have been given by Llopis (21) and by Randles (22). With alkylammonium ions, opposing effects due to hydrophobicity arise and lead to a tendency for positive adsorption, depending on the length and number of R groups coordinating the N^+ charge center.

Some aspects of alkylammonium adsorption at the Hg electrode interface with water have previously been studied by Piro, Bennes and Bon Karam (6), and by Kimmerle *et al.* (9), while earlier work of Conway *et al.* (10, 11) was concerned

[1]On leave of absence from the Research Group: "Physicochimie des Interfaces", C.N.R.S., B.P. 505, 34033 Montpellier, France.

[2]This Introduction serves, in the main, for both Parts I and II.

0008-4042/81/131978-09$01.00/0

©1981 National Research Council of Canada/Conseil national de recherches du Canada

Can. J. Chem. Downloaded from www.nrcresearchpress.com by 210.87.254.42 on 09/06/12
For personal use only.

Can. J. Chem. Downloaded from www.nrcresearchpress.com by 210.87.254.42 on 09/06/12
For personal use only.

with the adsorption of quaternary pyridinium and related cyclic N^+ ions at the Hg/water interface. More recently, the interesting question of the relation between the adsorption of $R_{4-n}N^+H_n$ ions at the Hg/water interface and their entropies of hydration was examined by Ikeda *et al.* (30). The adsorption behavior of R_4N^+ ions at the air/water interface was also studied by Krylov (34) and Gurenkov (35).

Alkylammonium ions are of interest (25) because they present situations of systematically varying accessibility of the N^+ centre to solvating H_2O dipoles. Related measurements previously carried out in this laboratory have led to useful information on the hydration and ionization behavior of these species with respect to steric effects in hydration (25, 26). The partial molal volumes (27) and compressibilities (28) of a series of $R_{4-n}NH_n^+$ ($n = 0 \rightarrow 4$) salts were studied, as well as the H_2O–D_2O solvent isotope effects (26) on these thermodynamic properties, giving the transfer functions for $H_2O \rightarrow D_2O$. Thus, a considerable volume of information exists on the hydration behavior of these ions and on the role of hydrophobicity and hydrophobic interactions (1, 29) which can arise in their solutions at finite concentrations.

In the present papers (Parts I and II), we report investigations on the adsorption behavior and associated surface potential changes for aqueous solutions of $R_{4-n}N^+H_n$ perchlorates (where $n = 0 \rightarrow 4$) at both the air/water and the Hg/water interfaces.

Surface-potential and surface-tension measurements at the air–water interface enable the changes of surface potential, $\Delta\chi$, to be related to the surface excess, Γ, of the salt and to effects on the orientation of water molecules at the solution surface (31). The use of a series of salts with a common anion and with cations having varying accessibility to water solvent dipoles enables the relation between the opposing effects of hydrophobicity and hydration in adsorption to be explored.

Surface-tension measurements at the Hg/water interface enable a more detailed study to be made of the adsorption of the $R_{4-n}NH_n^+$ ions since the behavior as a function of surface charge density or electrode potential is thermodynamically accessible. At the Hg/water interface, similar hydrophobic adsorption effects will arise as at the air/water interface but, in addition, coulombic interaction between the charged Hg surface and the $R_{4-n}N^+N_n$ cations in the double-layer will be involved as well as image interactions of a different sign (17, 20) to those of the air/water interface.

The combined results enable some useful comparisons to be made on the *same type of ions* at the air/water and Hg/water interfaces.

Experimental

(1) Choice of Systems

$R_{4-n}N^+H_n$–perchlorates were used in order to compare the adsorption behavior at the air/water interface with that at Hg (Part II) where use of ClO_4^- as a counter anion minimizes specific adsorption of the anion (F^- could also have been used but was avoided for reasons connected with obvious difficulties in the preparation of impurity-free solutions of $R_{4-n}N^+H_n$-fluorides). Measurements were made in an excess of aq. $HClO_4$ (1 *M*) as supporting electrolyte (*a*) in order to make comparisons with the present and other results obtained at the Hg electrode in a similar supporting electrolyte; (*b*) in order to minimize concentration-dependent diffuse-layer effects (18, 19) at the air/water interface due to preferential adsorption of cations or anions, and (*c*) to ensure (cf. refs. 10, 32) that the alkylamine species in solution is predominantly in the cationic form.

(2) Surface Potential Measurements

$\Delta\chi$ values at the air/water interface were measured by the Kelvin–Volta method using a vibrating plate capacitor. The principles of this method have been fully described elsewhere (33, 36). The test solution was contained in a water-jacketed cell, thermostatted at 298 ± 0.1 K and provided with a solution bridge to a Ag/AgCl reference electrode. The whole cell was maintained in a small Faraday cage inside a thermostatted closet (±1°C) and mounted on a basement floor in order to minimize vibration. The solution meniscus was 7 cm in diameter to ensure a flat surface. The vibrating capacitor plate could be adjusted by means of a micrometer mounted on a rigid frame and reproducibility of its position with respect to the solution meniscus was achieved by lowering the plate and vibrator by means of the micrometer until an auxiliary point contact indicated electrical connection with the conducting solution. Measurements were made at low vibration amplitudes with the plate as close to the surface as possible. $\Delta\chi$ values are then independent of the position of the plate at close proximities to the surface.

The electronic instrumentation included a Tinsley highly tuned detector amplifier and a high impedance cathode follower (Keithley Instruments), as described by Pethica *et al.* (36). Null-point detection, in which the potential supplied from a potentiometer exactly opposed the solution surface potential, $\Delta\chi$, was achieved by observing the form of the elliptical Lissajous figure generated on an oscilloscope by combining the ac driving signal to the vibrator and the ac signal generated by the vibrating plate at the liquid surface on the X- and Y-plates of an oscilloscope, after the latter signal had been communicated to the oscilloscope by means of the cathode follower.

(3) Surface Tension Measurements

The surface tension of pure water (see below) and the test solutions was measured by the de Noüy ring method (37–41) using a Fisher-Cahn electrobalance. The liquid surface was maintained in a cell thermostatted at 298 ± 0.1 K and situated in a closed box in the electrobalance chamber. The whole system was set up in the thermostatted closet mentioned above. The surface tension values were derived from recorder plots of the maximum force required to withdraw the Pt ring from the surface using the calibration corrections tabulated by Harkins and Jordan (38). The surface tension values were reproducible

Can. J. Chem. Downloaded from www.nrcresearchpress.com by 210.87.254.42 on 09/06/12
For personal use only.

to ca. 0.2 dyn cm^{-1} and their absolute accuracy was estimated at 0.5 dyn cm^{-1}, referred to pure water as the calibrating material.

(4) Water and Electrolyte Solutions

Pyrodistilled water, specially prepared as described recently (42), was used for the surface tension and surface potential measurements on the salt solutions. This water had been previously shown (42) by sensitive electrochemical measurements at Pt to be free of organic surface-active impurities. Salt solutions were made up from the redistilled amines by titrating them into $HClO_4$ (Fisher ACS grade) solutions in the purified water. *n*-$Pr_4N^+ClO_4^-$ was prepared by titrating a solution of the tetra-*n*-propylammonium hydroxide (Aldrich Chemical Co.) into the aq. $HClO_4$. Measurements were also made on the aq. $HClO_4$ supporting electrolyte itself at various concentrations.

Results

The changes of surface tension, $\Delta\gamma$, of 1 *M* aq. $HClO_4$ solution due to various concentrations, *c*, of $R_{4-n}N^+H_n$ as perchlorates are shown in Fig. 1. The concentration range for the salts with $n > 2$ is limited by the restricted solubility of the ClO_4^- salts, especially the $(n\text{-Pr})_4N^+$ salt. The corresponding surface excess data, Γ, derived from the Gibbs equation[3] are shown in Fig. 2. The $\Delta\chi$ values, are plotted in Fig. 3 (*a*), (*b*), vs. *c* and Γ, respectively. While *n*-$Pr_4N^+ClO_4^-$ is the most strongly adsorbed salt (Figs. 1, 2), it is evident from Fig. 3 that it produces the *smallest* relative $\Delta\chi$. Thus, $\Delta\chi$ *increases* with decreasing hydrophobicity while the adsorbability, as measured by positive Γ values, decreases in this direction.

The relative effects are demonstrated by plotting $\Delta\chi$ vs. log *c* and evaluating the slopes which are analogous to Esin and Markov coefficients (43) in electrochemical studies of adsorption at the Hg electrode.Fig. 4 shows such plots while Fig. 5 shows the slopes, $d\Delta\chi/2.3d \log c$, vs. the number of *n*-Pr chains or total number of C atoms (as CH_2 or CH_3).

Figures 1, 2, and 4 show that $\Delta\chi$ is displaced to more positive values as the concentration of *n*-$Pr_{n-4}N^+H_n$ is increased but the displacement is less in the order $PrNH_3^+ > Pr_2NH_2^+ > Pr_3NH^+ > Pr_4N^+$. The relations between $\Delta\chi$ and log *c* are linear and have the following slopes, expressed in units of RT/F: *n*-$PrNH_3^+$, 3.97; $(n\text{-Pr})_2NH_2^+$, 2.66; $(n\text{-Pr})_3NH^+$, 1.0; and $(n\text{-Pr})_4N^+$, 0.3. For aq. $HClO_4$, the slope is 1.66. However, for the alkylammonium ions, it is to be

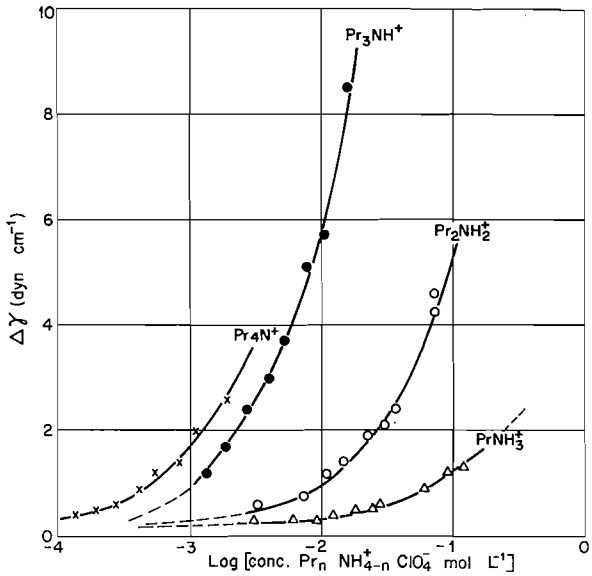

FIG. 1. Surface-tension change, $\Delta\gamma$, of the air/water interface as a function of log [concentration] of *n*-propylammonium perchlorates in 1 *M* aq. $HClO_4$ at 298 K.

remembered that all the results are obtained in an excess (1 *M*) of $HClO_4$ as supporting electrolyte so that the Debye parameter κ is constant with $1/\kappa \doteqdot 0.5$ nm, giving a constant shielding effect (18, 19) in the interphase region. Since ClO_4^- is a common anion between the supporting electrolyte and the added alkylammonium salt, the changes of γ and $\Delta\chi$ are due predominantly (apart from activity coefficient effects) to the adsorption of the organic cation, including any effects it has on the orientation of water dipoles at the air/water interface (cf. refs. 20, 31).

Discussion

(1) Relation between $\Delta\chi$ and Extent of Adsorption

In order to provide a basis for interpretation of the electrical aspects of adsorption behavior of the alkylammonium salts at the air/water interface, it is first necessary to state the main factors which give rise to changes of χ. These are (*a*) differential distribution of cations and anions near the interface due to different distances of closest approach connected with different radii of primary solvation shells of cations and anions. This gives rise to a double-layer p.d. near the interface; (*b*) differential distribution of cations and anions near the interface due to different charges on the ions (19) (inapplicable to the conditions of the present experiments); (*c*) effects of the ion on the intrinsic surface dipole p.d. at the water interface which arises from residual net orientation of H_2O dipoles (20, 21); and

[3]Unfortunately, the Γ values are not strictly thermodynamic due to the lack of activity coefficient data for salts of the type studied here. This has been a problem also in other work (6–12). Mohilner *et al*. (ref. 18 in Part II which follows) have discussed this problem in some detail and obtained some activity coefficient data for neutral molecules of interest in adsorption studies at Hg but reliable data are lacking for R_4N^+ types of adsorbates.

Can. J. Chem. Downloaded from www.nrcresearchpress.com by 210.87.254.42 on 09/06/12
For personal use only.

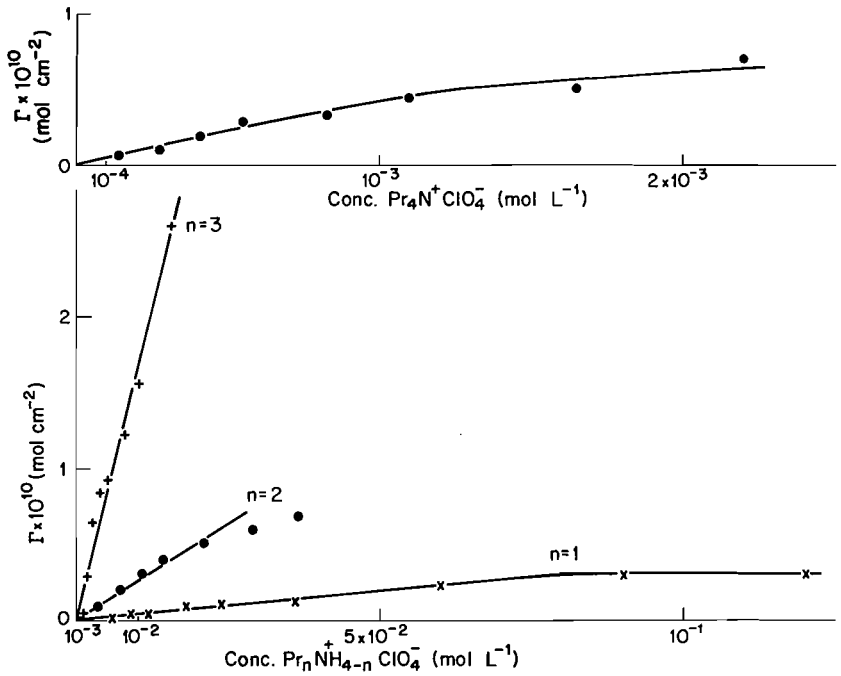

FIG. 2. Surface excess, Γ, of *n*-propylammonium perchlorates at the air/water interface (1 *M* aq. $HClO_4$) as a function of concentration of the organic salt (298 K).

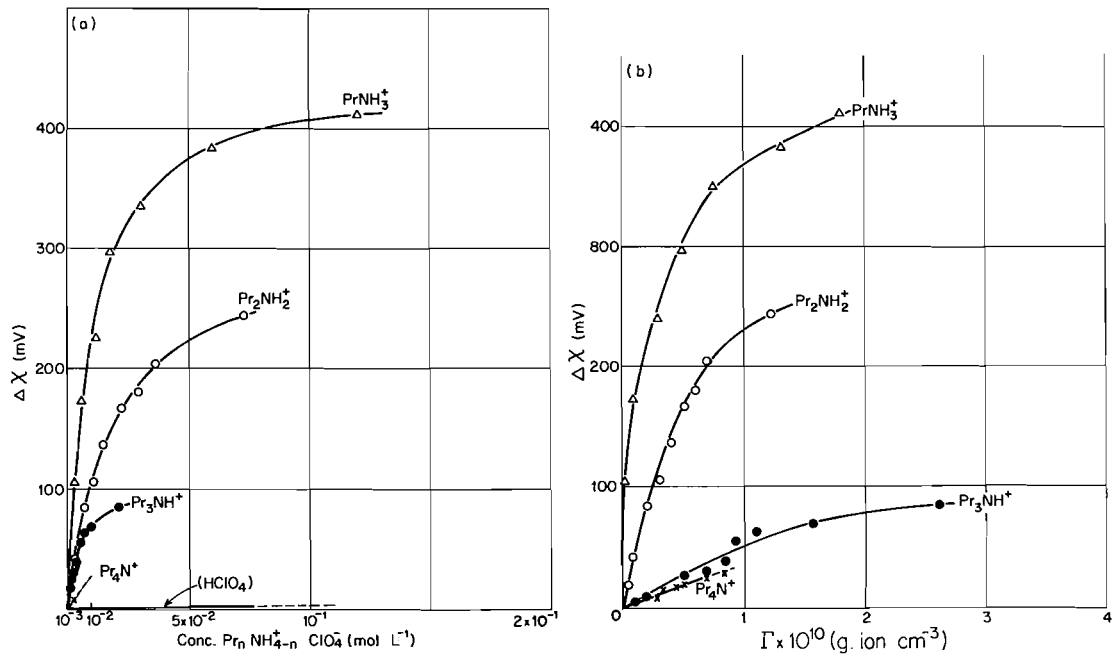

FIG. 3. (*a*) Surface-potential change, Δχ, at the air/water interface (1 *M* aq. $HClO_4$, 298 K), due to adsorption of *n*-propylammonium perchlorates, as a function of their respective concentrations; (*b*) Surface-potential change, Δχ, at the air/water interface (1 *M* aq. $HClO_4$, 298 K), due to adsorption of *n*-propylammonium perchlorates, as a function of their respective surface excesses, Γ.

Can. J. Chem. Downloaded from www.nrcresearchpress.com by 210.87.254.42 on 09/06/12
For personal use only.

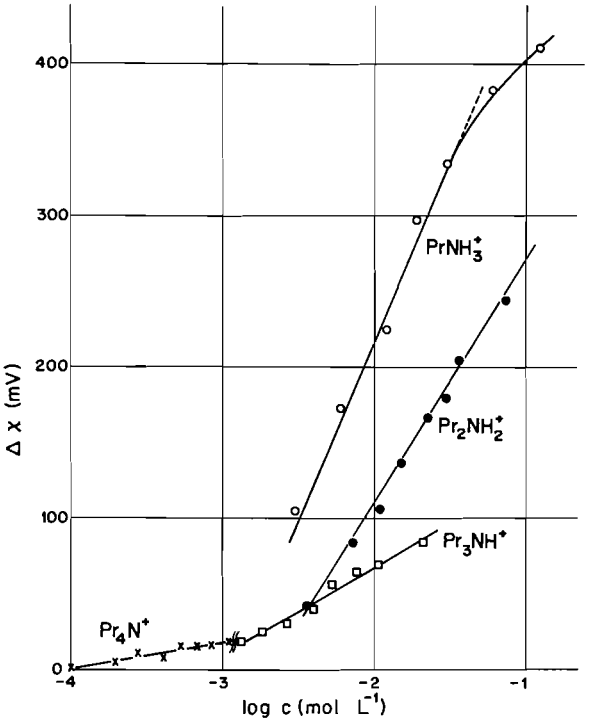

FIG. 4. Surface-potential changes, $\Delta\chi$, due to adsorption of n-propylammonium perchlorates as a function of the *log* of their concentrations.

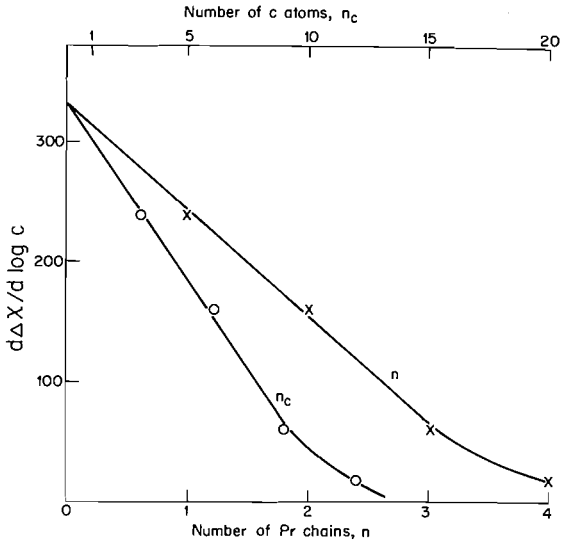

FIG. 5. Slopes, $d\Delta\chi/d \log c$, of the lines of Fig. 4 plotted against the numbers, n, of n-Pr chains or the number n_c of C atoms in the molecule, for the series of n-propylammonium perchlorates.

(d), connected with (c) above, any interaction (20) of the hydration co-sphere of the ion with the region of net orientation of water dipoles near the water interface. Factors (a) and (c) are probably the most important ones in the adsorption behavior of the alkylammonium ions.

The values of $\Delta\chi$ for n-$PrNH_3^+$ and $(n\text{-Pr})_2NH_2^+$ are relatively large[4] in comparison with those generated by simple salts. Large values, but at higher concentrations, were also found by Frumkin (46), Randles (22), and by Zagorska and Koczorowski (23) in the case of Me_4N^+ and Et_4N^+ salts. However, these $\Delta\chi$ values are opposite in sign from those for simple salts and for the present alkylamine salts.

Comparison of the behavior in Figs. 1 and 3 shows that the ions which are most strongly (positively) adsorbed give the least change of surface potential. This trend, shown in Table 1, is closely connected with the extent of hydration of the alkylammonium ion as measured e.g. by the electrostriction (27) or the partial molal adiabatic compressibility (28). Thus, Fig. 6 shows how $d\Delta\chi/2.3$ d log c for the n-Pr series of salts varies with the partial molal compressibility and electrostriction (relative to n-Pr_4N^+) of a corresponding series of methylammonium or n-propylammonium salts. It is clear from this type of relation that the stronger the cation–water interaction, the less is the cation adsorbed but the greater is the relative change of surface potential, a situation of some considerable interest.

The data on which Fig. 6 is based are the additivity relations w.r.t. CH_2-groups in R chains in R_4N^+ and $R_{4-n}N^+H_n$ salts for partial molal volume and adiabatic compressibility measurements derived by Conway and Verrall (27, 28) and by Conway, Desnoyers, and Verrall (44).

This trend of the data in Fig. 6 may be rationalized by noting (a) that the more strongly an ion is

TABLE 1. Molecular areas* and Γ_{max} values for the alkylammonium ions

	Area (Å²)		$\Gamma_{max} \times 10^{10}$ (mol cm^{-2})	
Ion	⊥	∥	⊥	∥
n-$PrNH_3^+$	~19	27.2	~8.7	6.1
$(n\text{-Pr})_2NH_2^+$	~19	40.4	~8.7	4.1
$(n\text{-Pr})_3NH^+$	39.6	56.3	4.2	3.0
$(n\text{-Pr})_4N^+$	43.7	51.4	3.8	3.2

*These values differ appreciably from those of Kimmerle and Menard (7) for the corresponding amines which seem too large. Although the apparent projected areas can depend somewhat on the conformations of the n-Pr chains assumed, this cannot account for the discrepancies.

[4]Separate experiments on $HClO_4$ solutions up to 5.0 M in water showed that $\Delta\chi$ due to $HClO_4$ is 7 ± 2 mV at 1.0 M concentrations. All the results obtained with the alkylammonium salts represent changes of χ due to the added organic salt since the supporting electrolyte (1 M $HClO_4$) was kept at constant concentration of 1.0 M.

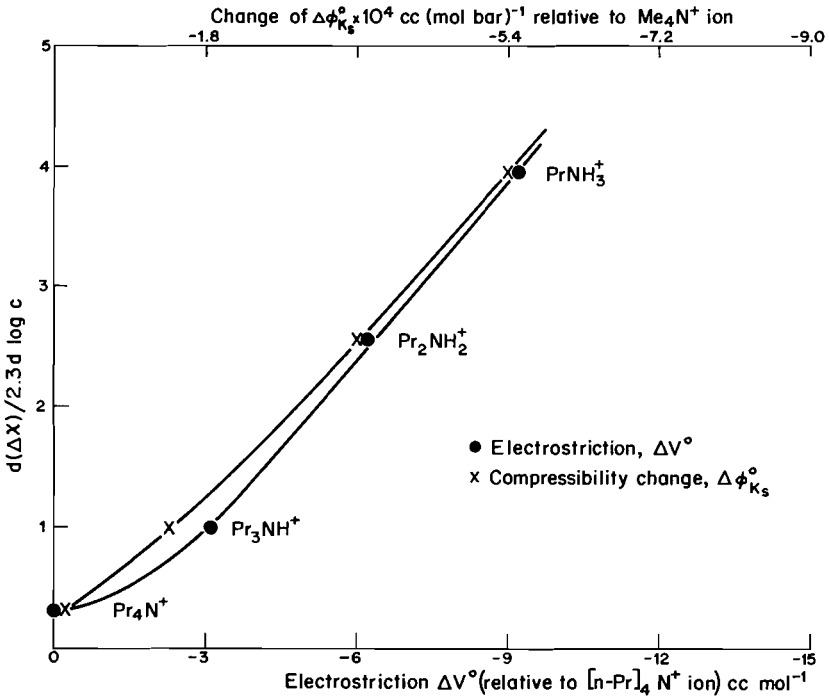

FIG. 6. Slopes, $d\Delta\chi/2.3\ d\log c$, in units of RT, for the effects of n-propylammonium perchlorates on $\Delta\chi$ at the air/water interface (1 M aq. $HClO_4$) plotted against two thermodynamic solution properties of these salts: $-\Delta V^0$, the electrostriction and $\Delta\phi_{K_s}{}^0$, the partial molar compressibility change at infinite dilution.

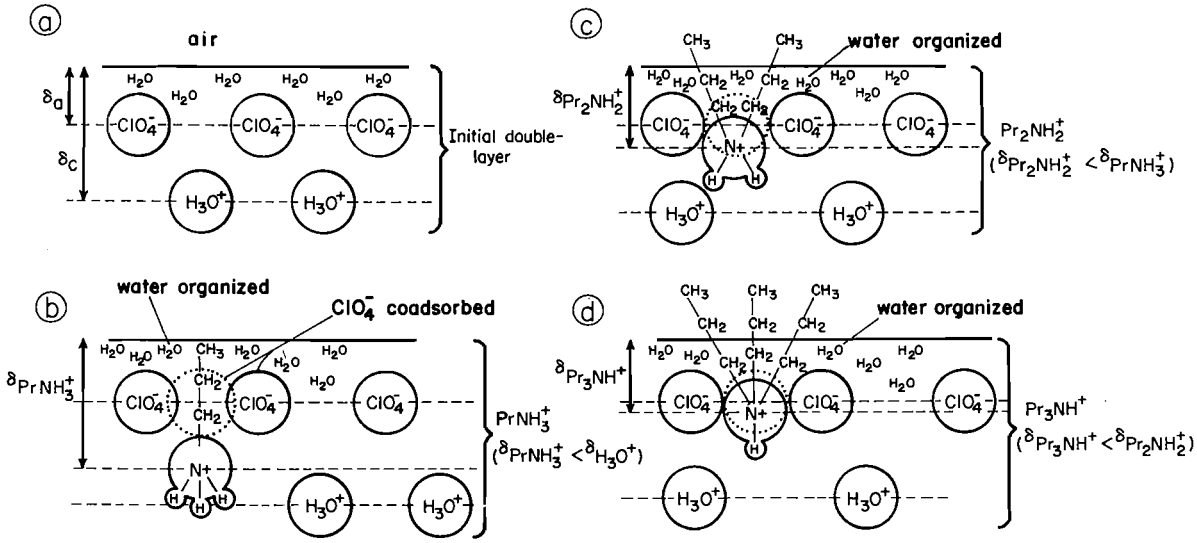

FIG. 7. Schematic model for cation/anion distribution with H_3O^+ and n-propylammonium cations in the air/water interphase.

hydrated, the greater is the tendency for it to be repelled[5] from the surface in order to minimize restriction of its interaction with the solvent dielectric; and (*b*) that the more hydrophobic is the ion (n decreasing in value from 4 → 0) the greater will be the tendency for it to be displaced out of the bulk water medium into the surface layer region where energetically unfavorable hydrocarbon–water interactions (47) are minimized. Thus, two opposing

[5]A distribution of ions repelled from the surface in fact arises, giving a diffuse-charge region (18, 19) over a distance dependent on the Debye κ parameter, as at electrode interfaces.

Can. J. Chem. Downloaded from www.nrcresearchpress.com by 210.87.254.42 on 09/06/12
For personal use only.

Can. J. Chem. Downloaded from www.nrcresearchpress.com by 210.87.254.42 on 09/06/12
For personal use only.

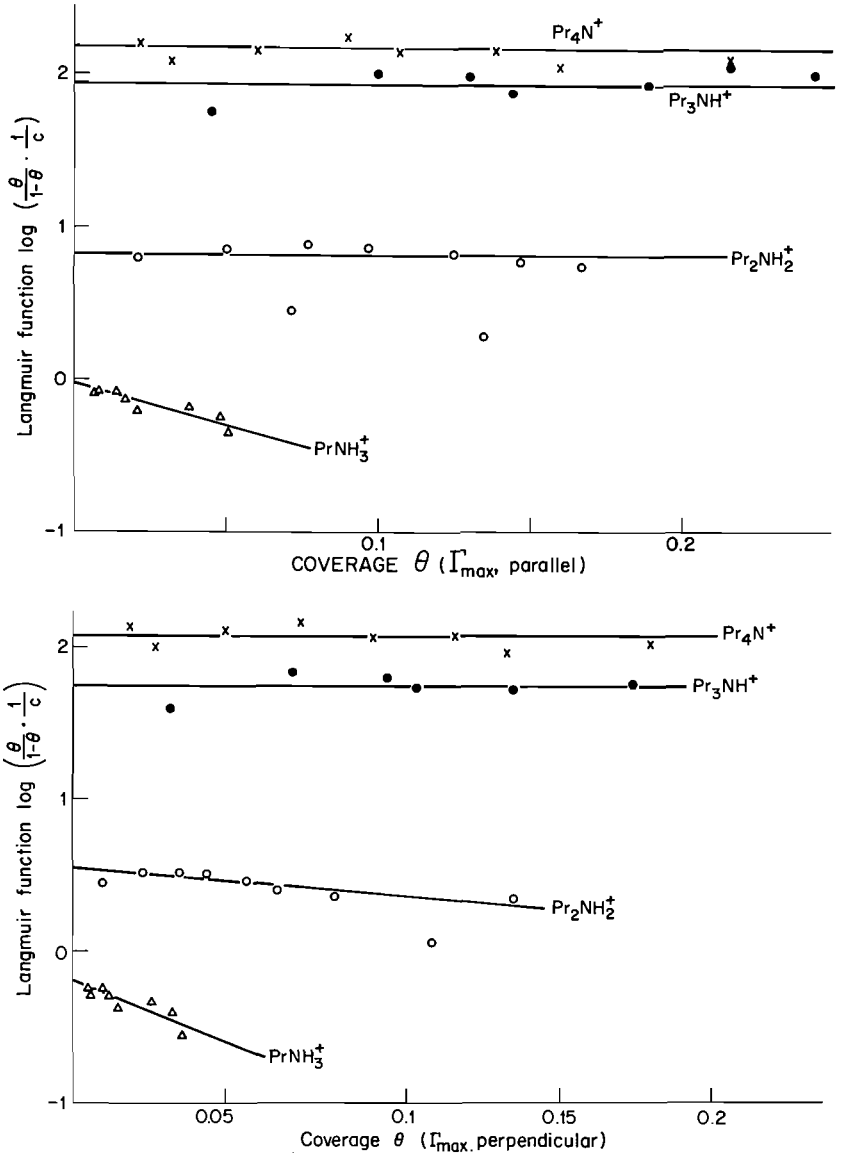

FIG. 8. Plot of the Langmuir adsorption function, $\log [\theta/(1-\theta)][1/c]$ vs. coverage θ for two estimates of Γ_{max}, giving the variation of $-\Delta G^0/RT$ for the adsorption process with coverage.

effects generate the trend of adsorption and surface potential behavior shown in Figs. 1–5.

The hydrophobic effect diminishes, as expected in the case of R_4N^+ salts, when the adsorption and $\Delta\chi$ measurements are made in progressively more methanolic solutions in CH_3OH–H_2O mixtures (23). This is consistent with the observed (45) lack of lyophobic interaction behavior of R_4N^+ salts in methanol.

In the behavior of this series of salts, the positive values of Γ do not uniquely signify that the alkyl chain resides above the surface in the air phase or the hydrophilic N^+ group just below the surface in the water phase that would otherwise be depleted of simple ions. The measured surface excess is one of cations and anions. Normally a large anion will be distributed up to a plane of closest approach to the interface which is nearer to the interface than that for simple cations which are relatively more hydrated (13, 20). As the number of chains is increased on the N^+ center, probably the cation would tend to be adsorbed progressively nearer to the surface of separation of the phases, so that the difference of position of the planes of approach of

Can. J. Chem. Downloaded from www.nrcresearchpress.com by 210.87.254.42 on 09/06/12
For personal use only.

added alkylammonium cations and the solution anions tends to be reduced. The surface potential due to such an ionic double-layer would then tend to become diminished.

Since the alkyl chains may be supposed to be directed towards, or reside partly in, the air phase, an additional factor leading to a change of surface potential can arise, viz. an influence on the H_2O dipole contribution (cf. 31) to χ due to the effects of alkyl chains on the water structure at the surface on its local dielectric constant. This contribution to $\Delta\chi$ cannot, however, be separately evaluated.

The supposed progressive change of the distribution of cations and anions in the interphase near the air–water interface is shown schematically in Fig. 7 which illustrates how the double-layer ionic separation and consequent p.d. can diminish with increasing positive adsorption of the alkylammonium ion. The situation with the $(n\text{-Pr})_3N^+$ ion in Fig. 7*d*, or ultimately with the $(n\text{-Pr})_4N^+$ ion, is like that envisaged by Hayter and Hunter (12) for $R_3R'N^+$ ions at the Hg/water interface where adsorbed anions exist amongst the layer of adsorbed hydrophobic cations. This is consistent with the fact that it is found (6) that the Langmuir isotherm apparently applies (i.e. the apparent standard free energy of adsorption is independent of coverage θ up to $\theta = 0.8$) to the adsorption of Et_4N^+ at the Hg electrode. This means that repulsive coulombic interaction between Et_4N^+ ions must be attenuated by attractions between the Et_4N^+ ions and co-adsorbed anions and/or by hydration co-sphere sharing (see Part II).

(2) Coverage Dependence of the Free Energy of Adsorption, and Interaction Effects

Such effects are revealed by evaluation of the coverage-dependence of the apparent standard free energy of adsorption from a Langmuir type configurational free energy function $\ln [\theta/(1 - \theta)]$ for the adlayer. Thus, the standard free energy of adsorption ΔG^0 may be calculated in the usual way (6, 10, 11) from a Langmuir type isotherm function and its constancy examined with respect to coverage θ. Variation of ΔG^0 with θ indicates interaction and/or size effects not included in the isotherm expression.

In order to derive ΔG^0 values, some estimates of θ are required. Since $\theta = \Gamma/\Gamma_{max}$, where Γ_{max} is the surface excess at geometrical saturation of the surface, an evaluation of the molecular size of the adsorbate must be made to provide some estimates of Γ_{max}. These were obtained with the aid of Courtauld space-filling models which give the molecular areas and corresponding Γ_{max} values

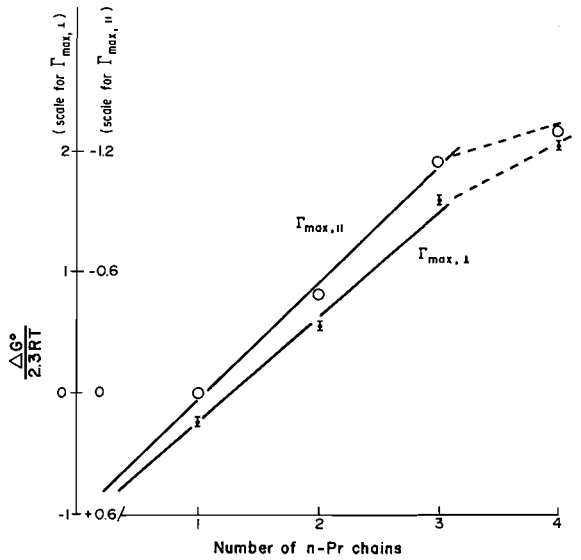

FIG. 9. Dependence of the apparent standard free energy of adsorption, ΔG^0, (as $\Delta G^0/2.3RT$) of the *n*-propylammonium perchlorates as a function of the number of *n*-Pr chains in the molecule.

shown in Table 1. Two mean orientations of the $R_{4-n}N^+H_n$ ions are possible giving two limiting Γ_{max} values for "perpendicular" ($\perp$) or "parallel" ($\parallel$) orientation at the surface, i.e. for the ions sitting "flat" or "standing up" at the surface — this difference is significant, of course, only for the ions for which $n > 0$. Of course, there will be molecular rotations or libration in the interphase, which averages out these differences.

Evaluations of ΔG^0 were made for both limiting values of Γ_{max} in Table 1. Figure 8 shows that ΔG^0 is surprisingly constant with increasing θ for $(n\text{-Pr})_4N^+$ and $(n\text{-Pr})_3NH^+$, while there is some evidence for $-\Delta G^0$ to become smaller with θ for $(n\text{-Pr})_2NH_2^+$ and $n\text{-PrNH}_3^+$ ions. This is consistent with the more separated layers of cations and anions in the interphase shown in Fig. 7. ΔG^0 also progressively becomes more negative with increasing number of *n*-Pr chains in an almost linear way (Fig. 9), paralleling the trend of decreasing $\Delta\chi$ with increasing ionic size (Fig. 6) and hydrophobicity. Similar effects are found for adsorption at the Hg electrode (Part II).

(3) Comparison with the Behavior at the Hg/Water Interface

It is of interest to compare the adsorption behavior of these salts at the air/water interface reported here with that at the Hg/water interface where the surface charge can be independently controlled. This forms the basis of Part II of this work, described in the following paper.

Can. J. Chem. Downloaded from www.nrcresearchpress.com by 210.87.254.42 on 09/06/12
For personal use only.

Acknowledgements

Grateful acknowledgement is made to the Natural Sciences and Engineering Research Council of Canada and to Environment Canada for support of this work. One of us (R.B.) acknowledges the award of a C.N.R.S. Exchange Fellowship.

1. W. Y. WEN. J. Solution Chem. **2**, 253 (1973).
2. H. G. HERTZ and M. D. ZEIDLER. Ber. Bunsenges. Phys. Chem. **68**, 821 (1964); H. G. HERTZ, B. LINDMAN, and V. SIEPE. Phys. Chem. **73**, 542 (1969); H. G. HERTZ. J. Solution Chem. **2**, 239 (1973).
3. B. E. CONWAY. J. Solution Chem. **7**, 721 (1978); Ionic hydration in chemistry and biophysics. Elsevier Publishing Co., Amsterdam. 1981.
4. R. J. MEAKINS. J. Appl. Chem. **15**, 416 (1965).
5. M. M. BAIZER. J. Electrochem. Soc. **111**, 215 (1964); M. M. BAIZER. J. Electrochem. Soc. **124**, 185*c* (1977).
6. J. PIRO, R. BENNES, and E. BOU KARAM. J. Electroanal. Chem. **57**, 399 (1974).
7. E. VERDIER, G.-H. NAFICY, and P. VANEL. J. Chim. Phys. **70**, 160 (1973).
8. R. BENNES. To be published.
9. F. KIMMERLE and H. MENARD. J. Electroanal. Chem. **47**, 375 (1973).
10. B. E. CONWAY and R. G. BARRADAS. Coll. Czeck. Chem. Commun. **32**, 1790 (1967).
11. B. E. CONWAY, R. G. BARRADAS, P. G. HAMILTON, and J. M. PARRY. J. Electroanal. Chem. **10**, 485 (1965).
12. J. B. HAYTER and R. J. HUNTER. J. Electroanal. Chem. **37**, 71 (1972); **37**, 81 (1972).
13. D. C. GRAHAME. Chem. Rev. **47**, 447 (1947).
14. VON E. V. VON DEHMLOW. Angew. Chim. **89**(8), 521 (1977).
15. J. KORYTA, P. VANYSEK, and M. BREZINA. J. Electroanal. Chem. **75**, 211 (1977); M. ZEMBALA. J. Electroanal. Chem. **66**, 45 (1975); Z. SAMEC. J. Electronal. Chem. **103**, 1 (1979).
16. G. GAVACH, P. SETA, and B. D'EPENOUX. J. Electroanal. Chem. **83**, 225 (1977); M. GROS, S. GROMB, and C. GAVACH. J. Electroanal. Chem. **29**, 89 (1978).
17. C. WAGNER. Phys. Z. **25**, 474 (1924).
18. L. ONSAGER and N. N. T. SAMARAS. J. Chem. Phys. **2**, 528 (1934).
19. G. M. BELL and P. D. RANGECROFT. Trans. Faraday Soc. **67**, 649 (1971).
20. B. E. CONWAY. J. Electroanal. Chem. **65**, 491 (1975).
21. J. LLOPIS. *In* Modern aspects of electrochemistry. Vol. 6. *Edited by* J. O'M. Bockris and B. E. Conway. Plenum Publishing. Corp. New York. 1971. Chapt. 2.
22. J. E. B. RANDLES. Adv. Electrochem. and Electrochem. Eng. **3**, 1 (1963); Discuss. Faraday Soc. **24**, 194 (1957).
23. I. ZAGORSKA and Z. KOCZOROWSKI. Rocz. Chem. **48**, 57 (1974).
24. N. L. JARVIS and M. A. SCHIEMAN. J. Phys. Chem. **72**, 74 (1968).
25. B. E. CONWAY and L. LALIBERTÉ. *In* Hydrogen bonded solvent systems. *Edited by* A. K. Covington and P. Jones. Taylor and Francis, London. 1968.
26. J. G. MATHIESON and B. E. CONWAY. J. Chem. Soc. Faraday Trans. I. **70**, 752 (1974).
27. B. E. CONWAY and R. E. VERRALL. J. Phys. Chem. **70**, 3952 (1966).
28. R. E. VERRALL and B. E. CONWAY. J. Phys. Chem. **70**, 3961 (1966).
29. J. E. DESNOYERS, M. AREL, G. PERRON, and C. JOLICOEUR. J. Phys. Chem. **73**, 3347 (1969).
30. O. IKEDA, Y. MATSUDA, H. YONEYAMA, and H. TAMURA. Electrochim. Acta, **21**, 519 (1976).
31. W. H. MADDEN, R. GOMER, and M. J. MANDELL. J. Phys. Chem. **81**, 2652 (1977).
32. E. BLOMGREN and J. O'M BOCKRIS. J. Phys. Chem. **63**, 1475 (1959).
33. S. MINC, I. ZAGORSKA, and Z. KOCZOROWSKI. Rocz. Chem. **41**, 1983 (1967).
34. V. S. KRYLOV. Electrochim. Acta, **9**, 679 (1964).
35. Y. GURENKOV. Zhur. Fiz Khim. **30**, 1830 (1956).
36. B. A. PETHICA, M. M. STANDISH, J. MINGINS, C. SMART, D. H. ILES, M. E. FEINSTEIN, S. A. HOSSAIN, and J. B. PETHICA. Adv. Chem. Ser. In press.
37. R. DU NOÜY. J. Gen. Physiol. **1**, 521 (1918/19).
38. W. D. HARKINS and H. F. JORDAN. J. Am. Chem. Soc. **52**, 1751 (1930).
39. B. B. FREUD and H. Z. FREUD. J. Am. Chem. Soc. **52**, 1772 (1930).
40. A. C. ZETTLEMOYER and V. V. SUBRA RAO. J. Coll. Interface Sci. **29**, 172 (1969).
41. E. A. BOUCHER, T. M. GRINCHUK, and A. C. ZETTLEMOYER. J. Coll. Interface Sci. **23**, 600 (1967).
42. B. E. CONWAY, W. B. A. SHARP, H. ANGERSTEIN-KOZLOWSKA, and E. CRIDDLE. Anal. Chem. **45**, 1331 (1973).
43. R. PARSONS. Modern aspects of electrochemistry. Vol. 1. *Edited by* J. O'M. Bockris. Butterworths, London. 1954. Chapt. 3.
44. B. E. CONWAY, J. E. DESNOYERS, and R. E. VERRALL. J. Phys. Chem. **75**, 3031 (1971).
45. A. BEN-NAIM. J. Chem. Phys. **54**, 1387 (1971); J. Phys. Chem. **77**, 95 (1973).
46. A. N. FRUMKIN. Trans. Faraday Soc. **55**, 156 (1959).
47. G. NEMETHY and H. A. SCHERAGA. J. Chem. Phys. **36**, 3382 (1962); **36**, 3401 (1962).

Solvent accessibility and hydrophobicity in the adsorption of alkylammonium cations at air/water and Hg/water interfaces. Part II. Behavior at the Hg/water interface in relation to hydrophobic interactions

B. E. CONWAY AND F. ROCHELEAU

Chemistry Department, University of Ottawa, Ottawa, Ont., Canada K1N 6N5

Received September 18, 1980

This paper is dedicated to Dr. Sam Levine on the occasion of his 70th birthday

B. E. CONWAY and F. ROCHELEAU. Can. J. Chem. **59**, 1987 (1981).

The adsorption behavior of a series of *n*-propylammonium ions in which the N^+ center has varying accessibility to the solvent, and hence the ions exhibit varying hydrophobicity, is examined at the Hg/H_2O interface at various electrode potentials. With the most hydrophobic ion, $(n\text{-}Pr)_4N^+$, attractive interactions arise in the interphase. An attempt is made to explain this behavior in terms of Gurney hydration co-sphere sharing effects which are significant in 3-dimensional aqueous solutions of R_4N^+ salts.

The surface pressure behavior and Esin and Markov effects are also evaluated.

Comparisons are made with the adsorption and surface potential results reported in Part I for the air/water interface.

B. E. CONWAY et F. ROCHELEAU. Can. J. Chem. **59**, 1987 (1981).

Opérant à l'interface Hg/H_2O et à divers potentiels d'électrode, on étudie le comportement, lors de l'adsorption d'une série d'ions *n*-propylammonium dans lesquels le N^+ central est plus ou moins accessible au solvant et qui ont dans ce cas des caractères hydrophobes variés. Avec l'ion le plus hydrophobe $(n\text{-}Pr)_4N^+$ il se développe des interactions attractives à l'interface. On essaie d'expliquer ce comportement en fonction des effets de partage de la cosphère d'hydratation de Gurney tels qu'il en existe d'une façon importante en trois dimensions de sels R_4N^+.

On a également évalué le comportement de la pression de surface et les effets de Esin et Markov.

On a établi des comparaisons avec les résultats d'adsorption et de potentiel de surface relatifs à l'interface air/eau publiés dans la première partie de ce travail.

[Traduit par le journal]

Introduction

A general introduction was given in Part I (see preceding paper) where previous work both at the air/water and Hg electrode/water interfaces was referred to. In comparison with the situation at the air/water interface, studies at the Hg electrode enable the adsorption of the $R_{4-n}NH_n^+$ ions to be evaluated as a function of electrode potential or surface charge density, q. This has the effect of (*a*) changing the electrostatic attraction or repulsion between the $R_{4-n}N_n^+$ cations and the Hg surface and (*b*) changing the state of water structure (1, 2) and H_2O-dipole orientation (refs. 1, 3, 4*a*, see also ref. 4*b* for a 4-state model of H_2O adsorption) in the interphase and thus indirectly influencing the alkylammonium ion adsorption. Analysis of the results according to previously described procedures (5–7) enables standard free energies of adsorption to be derived as a function of coverage by the $R_{4-n}NH_n^+$ ions and of q, and the surface pressure behavior to be investigated. Special mention should be made of the work by Kimmerle and Menard (3) who made a thorough study of the adsorption of Me_4N^+ halides (F^- to I^-) at Hg with particular reference to the effects of the co-anions.

While changes of surface potential, $\Delta\chi$, cannot be directly measured as they can at the air/water interface (Part I), an equivalent quantity, the change of electrode potential, ΔE_q, evaluated for constant surface charge density (5), is of interest in relation to the ionic double-layer potential difference and the potential difference due to H_2O-dipole orientation as treated previously (2, 7, 8) for neutral molecule adsorption at the Hg electrode.

Finally, the results enable some interesting conclusions to be reached regarding lateral interactions between adsorbed alkylammonium ions, especially the most hydrophobic one of the present series $(n\text{-}Pr)_4N^+$, where Gurney hydration cosphere sharing effects (9) lead to attractive interactions between the cations in the interphase.

Experimental

(1) The Surface Tension Measurements

The surface tension of the Hg/water interface was determined at various potentiostatically controlled potentials by means of a drop-time tensiometer of the type recently described in the literature (10, 11). Drop-times were recorded electrically by interruption of a thin light beam incident on a photo cell. The signal from the photo-cell was shaped by a Schmidt trigger and communicated to a Hewlett-Packard electronic timer. All measurements were made at 298 ± 0.1 K in a thermostatted cell.

The precision of drop-timing depends largely on keeping the capillary free from mechanical vibrations; in order to minimize

0008-4042/81/131987-11$01.00/0

©1981 National Research Council of Canada/Conseil national de recherches du Canada

Can. J. Chem. Downloaded from www.nrcresearchpress.com by 210.87.254.5 on 09/06/12
For personal use only.

Can. J. Chem. Downloaded from www.nrcresearchpress.com by 210.87.254.5 on 09/06/12
For personal use only.

vibrations, the cell, the mercury column, the lamp, and the photoelectric cell were fixed to a metal framework suspended from the ceiling by means of springs attached to a platform resting on a semi-inflated "inner tube" as recommended by Kimmerle and Menard (10). This system proved to be very satisfactory. Experimental runs gave a standard deviation of ±0.02% or better, i.e. ±0.1 dyn cm^{-1} in the surface tension, γ, over a range of ten drop-times for each potential. Most data were subsequently collected from three drop-time measurements at each potential. Other factors which are important in obtaining accurate and reproducible results have been discussed elsewhere (11) and in a thesis (12). γ-Data obtained by drop-time and capillary electrometer methods were shown to be in good agreement (13) for simple organic substances. γ-Values were derived from drop-times by procedures previously discussed in the literature (11, 14).

It should be mentioned that the drop-time method employed in the present work is a dynamic one so that problems of non-equilibrium in the adsorption at the Hg drops can arise. However, the direct comparison made in previous work (13) between the drop-time and electrocapillary method (in which equilibrium conditions more or less obtain), using compounds rather similar to those employed in the present work, gave good agreement between results obtained by the two methods. This implies that non-equilibrium in the present work is not a serious problem.

All measurements were made in a $NaClO_4$ or $HClO_4$ supporting electrolyte to minimize effects due to specific adsorption of anions. Since ClO_4^- does not form a reference electrode of the "second kind", a Ag/AgCl electrode in 0.1 *M* KCl, prepared by a method described by Ives and Janz (15), was employed. The liquid junction, which is unavoidable under the above conditions, was formed at a closed wetted stopcock between the reference electrode and the dropping Hg electrode compartments of the cell.

(2) Substances Employed in the Experiments

(*a*) *Sodium perchlorate*: Anachemia $NaClO_4$ was used.

(*b*) *Perchloric acid*: BDH "Aristar" grade $HClO_4$ was used without further purification in the experiments on alkylammonium ion adsorption. Its initial strength was determined by titration.

(*c*) *Hydrochloric acid*: BDH "Aristar" grade hydrochloric acid was used without further purification.

(*d*) *Sodium chloride*: ACS analytical grade reagent was used.

(*e*) *Potassium chloride*: BDH "analytical reagent" grade potassium chloride was dried under vacuum at 333 K for 12 h and used without further purification since the same results were shown to be obtained when a sample of KCl, doubly-recrystallized from water, was used. Potassium chloride was used for standardization of capillaries in terms of the published surface tension for the Hg/aq.KCl interface at various potentials (16).

(*f*) n-*Propylamines*: Mono-, di-, and tri-*n*-propylamines (Matheson, Coleman and Bell) were purified by distillation under dry N_2 at atmospheric or reduced pressure as required.

(*g*) *Tetra*-n-*propylammonium hydroxide*: The Eastman Kodak material (10% aq. solution) was used without further purification to prepare $(n\text{-Pr})_4N^+ClO_4^-$ solutions by titration with the $HClO_4$ mentioned above.

In the work at Hg, solutions of various concentrations of the amines in excess (1 *M*) aq. $HClO_4$ were used in order that the anion and total ionic concentrations remained constant. Each of the propylamine bases is sufficiently strong that virtually all the organic compound is in the form of the $R_{4-n}NH_n^+$ ($1 \leq n \leq 3$) ion under these conditions. Variation of the concentration of amine in excess $HClO_4$ is then almost quantitatively equivalent to variation of the alkylammonium ion concentration.

Results

(i) Derived Quantities

The electrocapillary curves obtained from the drop-time measurements at various potentials and concentrations were fitted to a polynomial function and treated in the manner described in previous publications (5, 7, 10), using appropriate computer programs, in order to obtain the surface excess values, Γ_q, at constant charge-density, q, and the q values themselves. Evaluation of strictly thermodynamic values of $\Gamma_q = -[(1/RT)(\partial\gamma/\partial \ln a)]_q$ presents some problems (as with other types of organic solutes in water) as the activity coefficients for the alkylammonium salts we have used are unavailable (some activity coefficient data for R_4N^+ salts were given in ref. 17*a*, but the derivation of these data has been criticized by Frank (17*b*)) except for some data recently published by Leyendekkers and Hunter (28) for the symmetrical R_4N^+ ions. Their data for $(n\text{-Pr})_4N^+$ (as Br^- salt) have been used here in the absence of any data for salts with other anions, in particular ClO_4^-.

The problem with activity coefficients for the other alkylammonium ions studied in the present work is diminished significantly since for all varying concentrations of $R_{4-n}N^+H_n$ ions, the total ionic strength was kept constant. Both Mohilner *et al.* (18) and one of the present authors in an earlier paper (19) on the adsorption of alkaloid cations at Hg have recognized this problem but adequate activity data are still lacking for most salts of organic ions. In the present work, these problems are diminished somewhat, in a relative sense, because the main purpose of the investigation is to make comparisons between the adsorption of the series of *n*-Pr ammonium ions at Hg and to compare the behavior at Hg with that at the air/water interface (Part I).

Free energies of adsorption, ΔG_q^0, at given values of q were obtained using the Flory–Huggins type of isotherm as in previously published papers (6, 20), viz.

$$[1] \quad \frac{\theta}{e^{x-1}(1-\theta)^x} = Kc$$

where x is the relative size of adsorbate and water molecules and $\theta = \Gamma/\Gamma_{max}$. Γ_{max}, the saturation coverage, cannot normally be determined reliably as the isotherms do not approach a well defined saturation limit over the accessible concentration ranges. Γ_{max} values were therefore estimated as shown in Table 1, from projection of Courtauld space-filling models (21) in various orientations, as in previous work (6, 22) and in Part I.

Can. J. Chem. Downloaded from www.nrcresearchpress.com by 210.87.254.5 on 09/06/12
For personal use only.

TABLE 1. Calculated maximum surface excess (Γ_{max}) values (10^{-10} mol cm^{-2}), figures in parentheses, and areas in Å^2 of *n*-propylammonium ions derived from measurements on Courtauld models*

Ion	"Perp." orientation	"Parallel" orientation	Expt.
$(n\text{-Pr})NH_3^+$	19.2 (8.7)	27.2 (6.1)	<57 (>2.9)
$(n\text{-Pr})_2NH_2^+$	18.5[a] (9.0) 33.8–40.4[b] (4.93 ~ 4.13)	40.4 (4.1)	<24 (>6.8)
$(n\text{-Pr})_3NH^+$	39.6 (4.2)	56.3[c] (2.96) 66.3[d] (2.50)	70 (2.4)
$(n\text{-Pr})_4N^+$	43.7 (3.8)	51.4 (3.2)	<36 (>4.6)

*Rather different values were estimated by Kimmerle and Menard (10) based on unspecified molecular models. It was not possible to reproduce their estimates using the Courtauld models. Shape basis of area measurement: (*a*) linear; (*b*) angular (30–180°); (*c*) triangular, (*d*) circular area swept out by rotational motion.

It is useful to derive apparent values of K and hence of ΔG^0 at various Γ values. They usually (6, 22, 23) depend on Γ due to coverage-dependent interactions in the interphase and to the coverage-dependent state of co-adsorbed water dipoles (1–4). The variation of apparent values of ΔG^0 then gives useful information about interaction effects in the interphase, with a rationally chosen value of x in eq. [1], as has been shown in various earlier publications (6, 7, 20, 22) on other systems, using this procedure. This method seems preferable to arbitrarily choosing an isotherm with an interaction term and then fitting the data to it, as we have argued previously (6).

The surface pressure, Φ, at constant q was also obtained in the usual way (cf. refs. 5, 7) as a function of Γ or relative free area, from the decrease of γ with increasing adsorbate concentration. Since the experiments were carried out at constant and large (1 M) ionic strength, there is virtually no diffuse-layer contribution to Φ_q, so that Φ_q derived from changes of γ due to alkylammonium ion adsorption represents, to a good approximation, the surface pressure exerted by the alkylammonium ions in the monolayer interphase at the Hg surface (cf. ref. 5).

(ii) Free Energies of Adsorption and Surface Charge

Figures 1 and 2 show the variation of the apparent ΔG_q^0, calculated for various Γ values, with surface charge density, q, for two of the alkylammonium ions $(n\text{-Pr})_2NH_2^+$ and $(n\text{-Pr})_4N^+$. There is a general trend for $-\Delta G_q^0$ to become larger with increasing negative q but there is some indication of a minimum in the curves around $q = -4 \sim -6\ \mu C\ cm^{-2}$, reminiscent of neutral molecule adsorption. The results shown in Figs. 1 and 2 have been calculated for several values of the size factor x in eq. [1] since it is (*a*) difficult to assign an *a priori* value to x and (*b*) desirable to show how the trend of ΔG^0 values depends on x. On the basis of geometrical considerations alone, x would be 3–4 but it may well be effectively less than this due to flexibility of the alkyl chains.

The general trend of ΔG_q^0 values with q is similar for various assumed values of x but the spread of ΔG_q^0 values with Γ is larger at a given q (see below), as x is taken larger.

(iii) Free Energies of Adsorption and Number, N_c, of Carbon Atoms in the $(n\text{-Pr})_{4-n}N^+H_n$ Series

ΔG_q^0 generally involves several contributions. That due to direct electrostatic interactions with the surface can be eliminated by considering ΔG_q^0 values for $q = 0$. Figure 3 shows the dependence of ΔG_q^0 on N_c for each cation, taken for $\theta \simeq 0.2$ in order to include the value of ΔG_q^0 for $n\text{-}PrNH_3^+$. It is seen that the relation ΔG_q^0 vs. N_c follows Traube's rule (1891) which relates strength or extent of adsorption of molecules in an homologous series of (aliphatic) organic substances to the length and the number of alkyl chains. From Fig. 3, it is seen that the decrease of ΔG_q^0 per C atom is approximately constant at about -380 cal mol^{-1}, a trend which reflects both the increasing hydrophobicity in the series of ions and the Van der Waals component of the adsorption energy. The figure of -380 cal mol^{-1} is about $0.66\,kT$, i.e., significantly less than the energy involved in complete removal of a CH_2 group from water. Figure 3 also shows the ΔG^0 values for adsorption at the air/water interface from Part I, for comparison.

(iv) Free Energies of Adsorption and Coverage

The dependence of ΔG_q^0 on Γ is of interest in relation to (*a*) direct coulombic interaction effects; (*b*) modification of the water structure in the electrode/solution interphase, and (*c*) Gurney co-sphere interaction (9) in the interphase (6). Plots of ΔG_q^0 for various q values vs. Γ for the four types of propylammonium ions are shown in Fig. 4. The predominant trend of ΔG_q^0 is to more *negative* values with increasing Γ when Γ is largest at appreciable negative q values (Fig. 4 *b*, *c*, *d*). For such conditions, co-anion adsorption will be minimal so that this decrease of ΔG_q^0 is unlikely to be associated with attractive lateral cation/anion in-

Can. J. Chem. Downloaded from www.nrcresearchpress.com by 210.87.254.5 on 09/06/12
For personal use only.

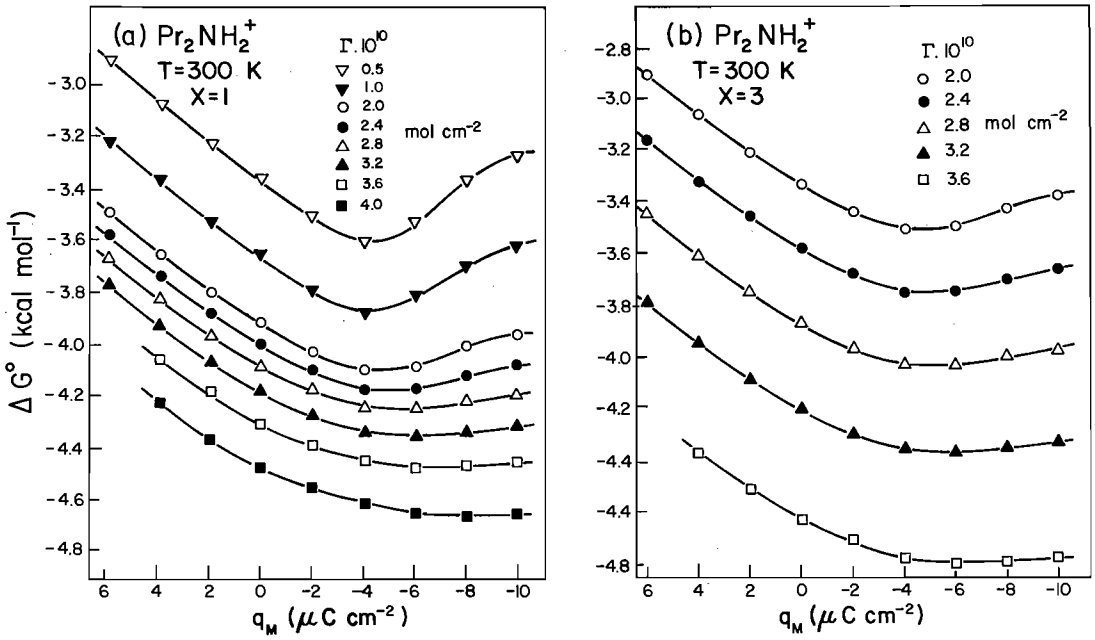

FIG. 1. Values of ΔG_q^0 calculated for various Γ values plotted against metal surface charge, q, for the adsorption of $(n\text{-Pr})_2NH_2^+$ at Hg (300 K). ΔG_q^0 is derived using eq. [1] for the indicated values of the size factor x.

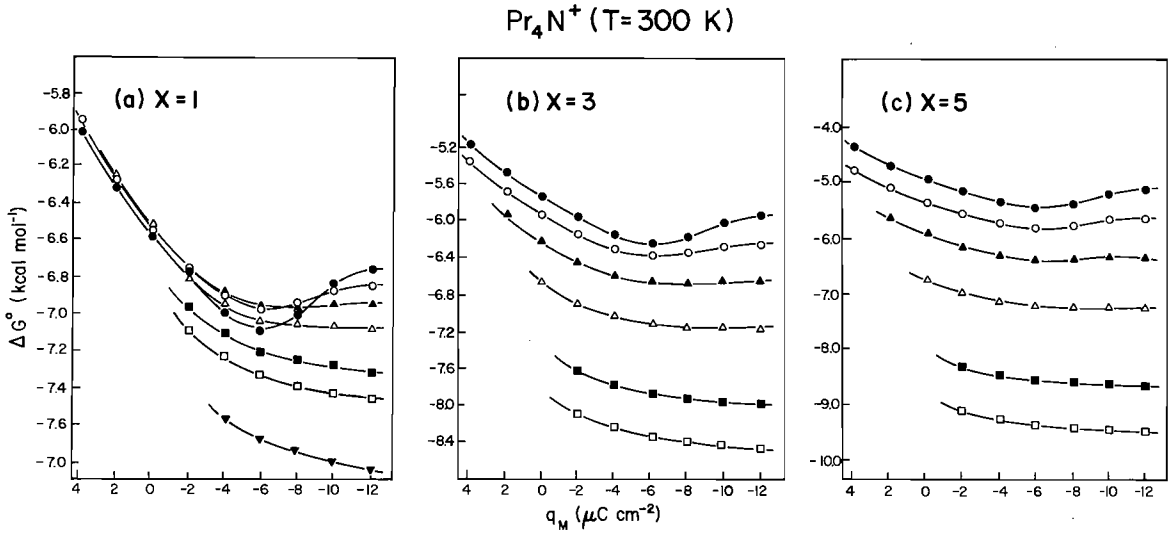

FIG. 2. As in Fig. 1, but for adsorption of $(n\text{-Pr})_4N^+$ at Hg for three values of the size factor, x.

teractions in the double layer. The effect is largest with the $(n\text{-Pr})_4N^+$ ion (Fig. 4*d*). Obviously it cannot arise from coulombic repulsions which would lead (cf. refs. 22, 23) to opposite dependence of ΔG_q^0 on Γ. The behavior found, especially with the $(n\text{-Pr})_nN^+$ ion, suggests that hydrophobic attractive interactions of the kind that have been postulated (9) for ions of this type in homogeneous aqueous solutions may be important. The effect arises through sharing of the Gurney co-spheres of the ions and leads to a minimization of free energy due to the diminished unfavorable interaction with water which can arise when two or more previously separate hydrophobic groups can passively (24) associate together. This point may be developed further in a more quantitative way, as follows.

Can. J. Chem. Downloaded from www.nrcresearchpress.com by 210.87.254.5 on 09/06/12
For personal use only.

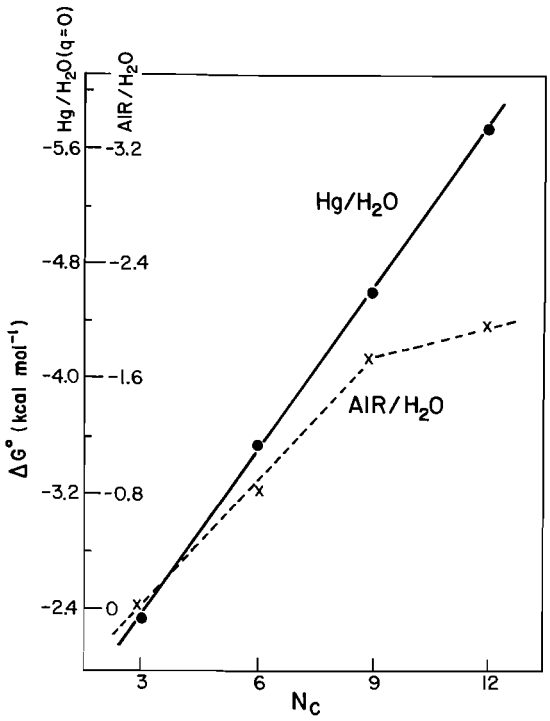

FIG. 3. Relation between ΔG_q^0 and the number of C atoms in each of the *n*-propylammonium ions studied at Hg in relation to the corresponding ΔG^0 values at the air/water interface (from Part I) for "||" orientation (size factor $x = 1$).

(v) Gurney Co-sphere Interaction Effects and ΔG^0 *as* $f(\Gamma)$

Co-sphere repulsive interactions due to overlap of dielectric polarization co-spheres, between hydrophilic ions in the double-layer were treated by Conway and Dhar (6) as a basis for explaining increases of ΔG_q^0 with Γ which can arise in addition to those due to simple coulombic repulsions between ions of like sign. The basis of evaluation of lateral co-sphere interactions is the model of Ramanathan and Friedman (25) for homogeneous solutions where such factors are important in the activity and osmotic coefficient behavior of salts at elevated concentrations (>1 *M*).

The Gurney co-sphere overlap free energy for two ions, *i* and *j*, is expressed by the relation (25)

$$[2]\quad \mathrm{GUR}_{ij} = A_{ij} V_{\mathrm{H_2O}}^{-1}\, V_c(r_i + r_{c,i}, r_j + r_{c,j}, r)$$

where A_{ij} is an empirical interaction free energy parameter, $V_{\mathrm{H_2O}}$ is the molar volume of water, and V_c is the volume of ion-influenced solvent which is returned to a normal bulk state with a resulting free energy change GUR_{ij} when two ions come together to a mean distance r. In eq. [2], $r_{c,i}$ or $r_{c,j}$ are the thicknesses of the co-spheres around ions *i* or *j*, and r_i and r_j are the ionic radii. The overlap volume, V_c, is given geometrically by the formula for the volume of spherical segments:

$$[3]\quad V_c = \pi\left[-\frac{(a^2-b^2)^2}{4r} + \frac{2}{3}(a^3+b^3) - \frac{1}{2}r(a^2+b^2) + \frac{r^3}{12}\right]$$

where a and b are the co-sphere radii $r_i + r_{c,i}$ and $r_j + r_{c,j}$ of the two ions. For lateral interaction in the double-layer between two identical R_4N^+ cations, the case of interest here, obviously $a = b$ so that

$$V_c = \pi((4/3)a^3 - ra^2 + r^3/12)$$

Some values of the A_{ij} parameters for various pairs of ions have been given by Ramanathan and Friedman (25) for aqueous electrolyte solutions. V_c is shown in Fig. 5 as a function of mean interionic separation, r, expressed in terms of Γ through the following relation:

$$[4]\quad r = (1/N_A\Gamma)^{1/2}$$

where N_A is Avogadro's number and a square lattice is assumed in eq. [4].

For R_4N^+ ions in aq. solution, there arise *attractive* cation–cation interactions which can be represented by the Gurney A_{ij} values given by Streng and Wen (26). These A_{ij} parameters (A_{++} for cations) can be used to estimate the (attractive) interaction effects that can arise in the double-layer (as in bulk water solution) due to sharing of structure-promoted regions of the solvent about such cations.

The volume of the water molecule to be taken in eq. [2] is ca. 30 $(Å)^3$ so that an attractive energy of the order of -85 to -300 cal mol^{-1} arises with increasing coverage of an electrode surface by R_4N^+ ions due to hydration shell sharing in the Gurney co-sphere. This energy adds (cf. ref. 25) to the coulombic repulsion (small with the larger R_4N^+ ions) and Van der Waals attraction contributions (23). Co-sphere "contact" for 1-H_2O thickness occurs at the following mean ionic charge densities in the double-layer for R_4N^+ ions: Me 13.1, Et 10.6, *n*-Pr 9.1, and *n*-Bu, 8.2 μC cm^{-2}. Significant contacts will, of course arise statistically below these limiting surface concentrations due to thermal fluctuations and be determined by the two-dimensional pair (++) distribution function for cation–cation encounters.

Figures 4 *c* and *d* showed the experimentally determined standard free energies of adsorption of

Can. J. Chem. Downloaded from www.nrcresearchpress.com by 210.87.254.5 on 09/06/12
For personal use only.

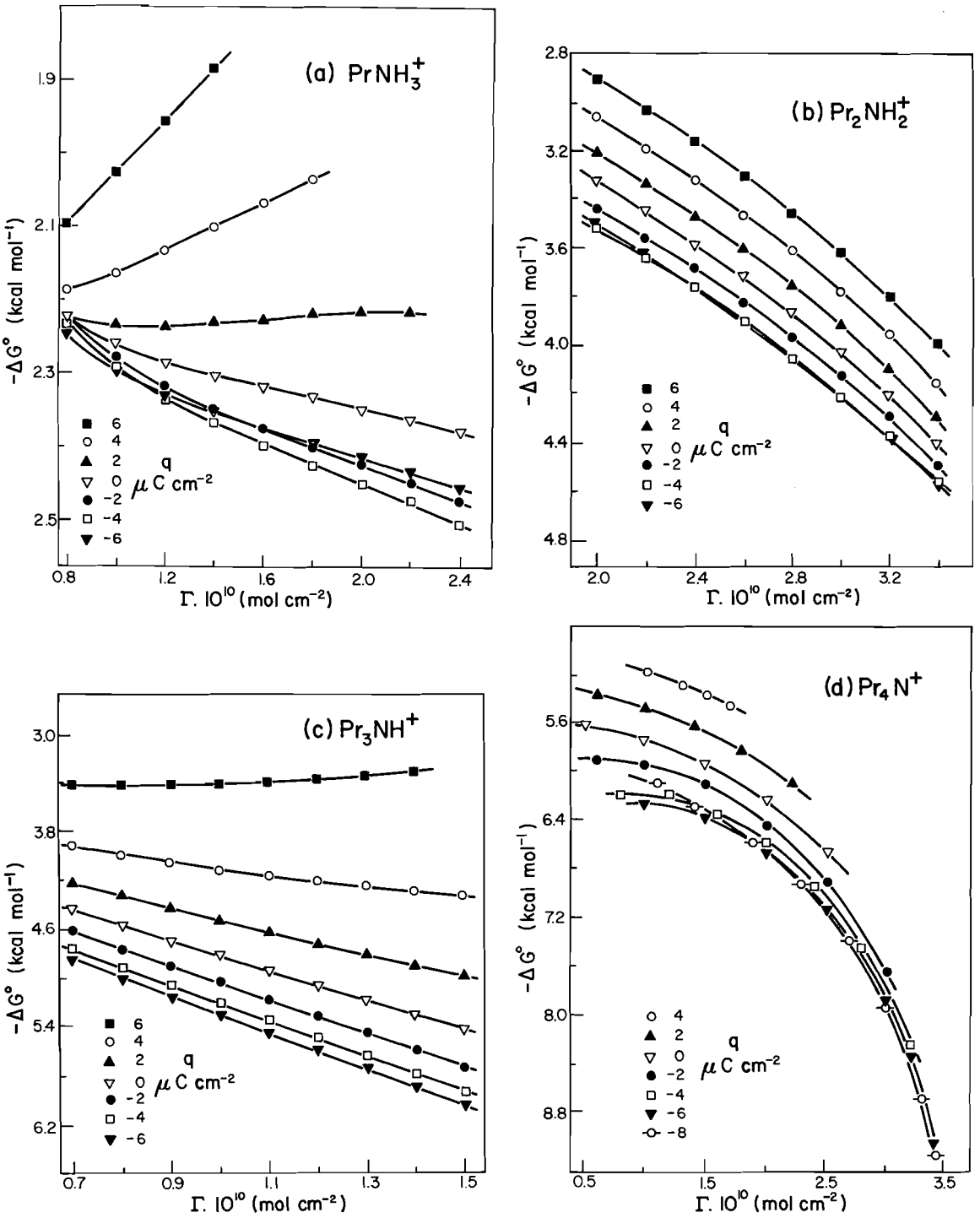

FIG. 4. Plots of the variation of ΔG_q^0 against surface excess, Γ, at various constant q values, for adsorption of the series (a–d) of n-propylammonium perchlorates at a Hg electrode at 300 K.

Can. J. Chem. Downloaded from www.nrcresearchpress.com by 210.87.254.5 on 09/06/12
For personal use only.

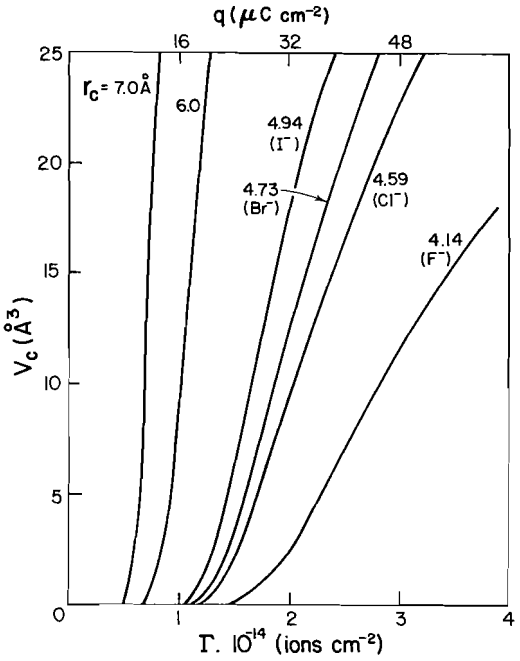

FIG. 5. Hydration co-sphere overlap volume, V_c, for ions with a single H_2O co-sphere hydration shell of radius, r_c, as a function of the surfaces excess Γ or corresponding charge q for univalent ions (as indicated) or larger ions with indicated r_c values.

$(n\text{-Pr})_4N^+$ and $(n\text{-Pr})_3NH^+$ ions in excess (1 *M*) $HClO_4$ from aqueous solution at Hg at 300 K as a function of Γ. As was shown in Fig. 4*d*, the $-\Delta G_q^0$ values *increase* with increasing coverage, i.e. apparent *attractive* interactions are predominant and the effect is greater with the tetra- than with the tri-*n*-propylammonium ion. Normally (22, 23) coulombic ionic repulsions lead, in the first order approximation, to $-\Delta G_q^0$ decreasing with coverage. The $-\Delta G_q^0$ values actually *increase* by ca. 2.5 kcal mol^{-1} which is of the correct order of magnitude for the quasi-attractive interaction effects which can evidently arise in this case due to the co-sphere overlap effects determined by A_{ij} values. In Table 2 are shown free energy changes, GUR_{ij}, for $(n\text{-Pr})_4N^+$, as calculated from eq. [2] for $A_{++} = -0.12$ kcal mol^{-1}, $V_{H_2O} = 30$ (Å)^3, and $r_c = 6.76$ Å (for 1 H_2O) for various Γ values. Also tabulated are the relative experimental free energy values, $\Delta G^0_{\Gamma\to 0} - \Delta G^0_{\Gamma}$, taken from Fig. 4*d*. The experimental relative energy values and the calculated GUR_{++} values for $(n\text{-Pr})_4N^+$ are plotted against Γ as shown in Fig. 6.

Quite good agreement with experiment is evidently obtained indicating that the co-sphere overlap effect is a major factor in the attractive interactions for this case. By contrast, for $(n\text{-Pr})_3NH^+$, the

TABLE 2. Comparison between relative values of experimental free energies of adsorption of $(n\text{-Pr})_4N^+$ and calculated Gurney co-sphere overlap energies at various surface concentrations

$\Gamma \times 10^{10}$ (mol cm^{-2})	r (Å)	V_c (Å^3)	GUR_{++} (kcal mol^{-1})	ΔG^0 (kcal mol^{-1})
1.0	12.9	0.97	~0	−0.06
1.5	10.5	83.6	−0.33	−0.16
2.0	9.10	181.6	−0.72	−0.40
2.5	8.19	260	−1.04	−0.86
3.0	7.46	329	−1.32	−1.54
3.5	6.93	383	−1.53	−3.32

effects are smaller owing to the greater hydrophilic character of this ion in comparison with $(n\text{-Pr})_4N^+$, and the anticipated co-sphere repulsion contribution (6) due to solvent polarization at the NH^+ centre (29). The coulombic repulsion effect will be almost the same at a given coverage (depending on the local dielectric properties of the interphase) and the Van der Waals interaction approximately 25% smaller.

(vi) Surface Pressure Behavior

Plots of Φ_q vs. Γ are shown in Fig. 7 *a–d*. For an ideal 2-dimensional surface gas, $\Phi = RT\Gamma$. The line of slope RT corresponding to this limiting relation is shown in Fig. 7 by the dotted lines. Normally (5, 27), deviations from this relation are observed due to (*a*) finite size of the adsorbate molecules and (*b*) their mutual interactions. In the case of ions in the double-layer, the interactions are complex, as has

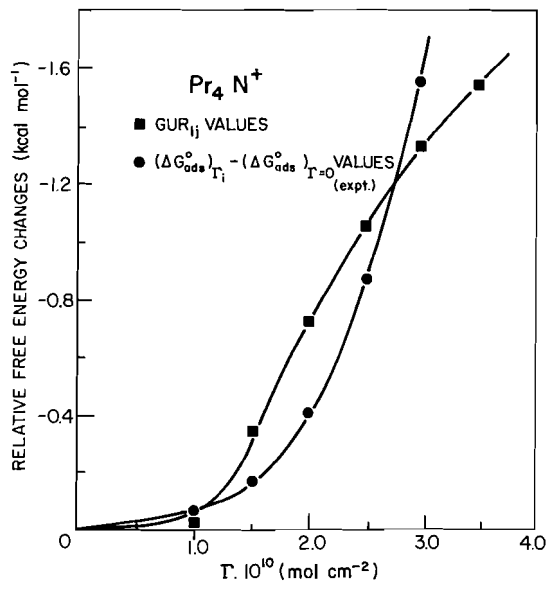

FIG. 6. Comparison of the experimental relative variation of $\Delta G_{q=0}^0$ with Γ for $n\text{-Pr}_4N^+$ adsorption at Hg with that calculated using Wen and Streng's solution Gurney A_{++} parameters.

Can. J. Chem. Downloaded from www.nrcresearchpress.com by 210.87.254.5 on 09/06/12
For personal use only.

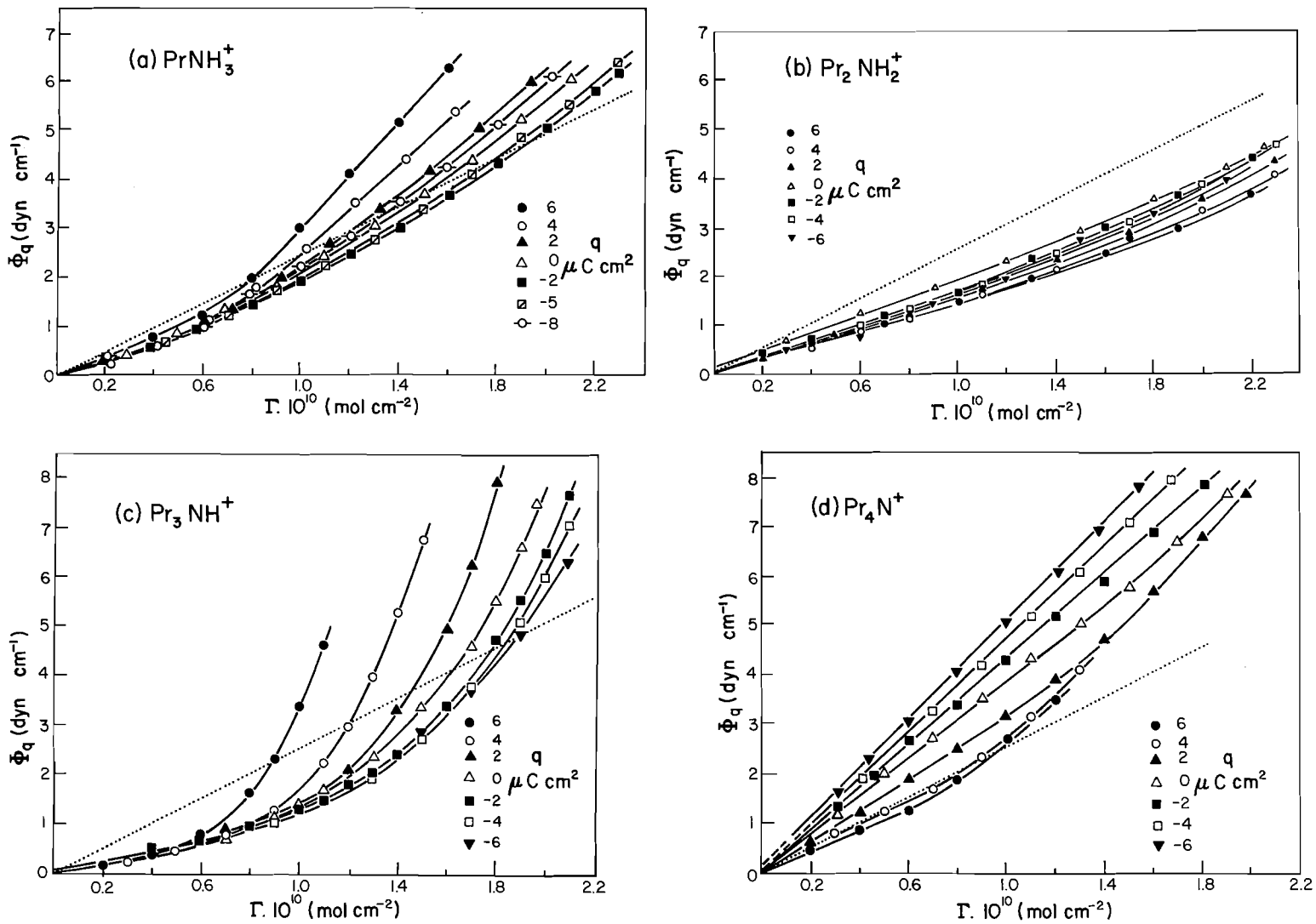

FIG. 7. Plots of surface pressure, Φ, against surface excess, Γ, for the series (*a*–*d*) of 4 *n*-propylammonium salts adsorbed at a mercury electrode at constant charges, q, as indicated (dashed line shows hypothetical ideal 2-dimensional gas law behavior).

TABLE 3. Esin and Markov slopes as a function of surface charge density, q, in $\mu C\ cm^{-2}$ for the n-propylammonium salt series in 1 M $HClO_4$

	$(\partial E/\partial\Gamma)_q$ (V cm² mol⁻¹ × 10⁷)				
			$(n\text{-Pr})_3NH^+$		
q	$(n\text{-Pr})NH_3^+$	$(n\text{-Pr})_2NH_2^+$	Initial (20%)	Final (10%)	$(n\text{-Pr})_4N^+$
−12	—	—	—	—	4.0
−8	−12.3	3.2	3.9	140	—
−6	−5.2	8.4	17.0	150	16.0
−4	3.3	10.0	39.0	145	22.0
−2	—	17.0	—	—	—
0	7.6	22.0	47.0	170	50.0
4	15.0 (20%)	31.0	51.0	195	73.0
8	24.6 (20%)	39.0	71.0	265	94.0

been discussed in relation to the coulombic and ion hydration effects. Both positive and negative deviations from the ideal relation arise, depending on ion size and charge q. The largest positive deviations arise for the $(n\text{-Pr})_4N^+$ ion (Fig. 7*d*). It is difficult to make a quantitative analysis of the observed behavior as obviously several effects to do with coulombic, solvent structure, and ion hydration effects will be involved. The co-area factor b (Volmer equation; $\phi(1/\Gamma - b) = RT$), will be important for the appreciable coverages that are reached, particularly because the areas of the ions in the $(n\text{-Pr})_{4-n}N^+H_n$ series are quite large. This factor would be allowed for by plotting Φ vs. $\Gamma/(1 - b\Gamma)$ instead of vs. Γ.

In concluding this section, it should be stated that we recognize that not all of the features of the surface pressure relations can be consistently reconciled with the variations of ΔG_q with coverage shown in section *iv*. This is probably due to the complexities of combined hydrophilic and hydrophobic interactions of these alkylammonium ions at the Hg/H_2O interface.

(vii) Effects on the Potential of Zero Charge and on the Potentials for Other Charges (Esin and Markov Coefficients)

The variation of E_q, the potential at which a given q is attained, with log [concentration] (or activity) of adsorbate is of interest in relation to (*a*) specific adsorption of ions (16) and (*b*) substitution of adsorbed oriented solvent dipoles at the Hg/water interface (4, 7) by the adsorbate. Both effects can contribute to changes, ΔE_q, in E_q when adsorption of organic species occurs.

Figure 8 shows how $\Delta E_{q=0}$, for the potential of zero charge, varies with log c of the four types of cations. The shifts arise at lower concentrations for the more adsorbable ions, as expected. Fig. 9, *a–d* show ΔE_q values as a function of Γ for various q. The simplest ion $n\text{-}PrNH_3^+$ exhibits behavior

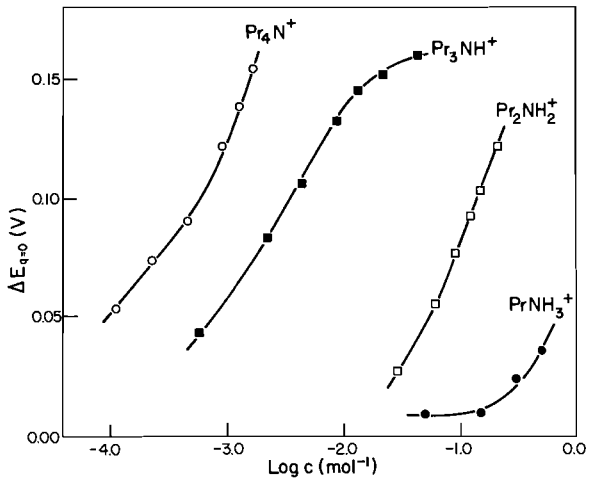

FIG. 8. Variation of shift, $\Delta E_{q=0}$, of potential of zero charge with log [concentration] of the 4 n-propylammonium perchlorates at the Hg electrode at 300 K.

similar to that of a simple neutral symmetrical molecule, e.g. pyrazine, where positive and negative changes of E_q occur depending on q. This type of effect is observed when the adsorbate replaces solvent dipoles whose orientation at the interface depends on q. For the other cations, ΔE_q is positive for all q values and increases with Γ in the expected way. This type of behavior is characteristic of the accumulation of strongly adsorbed positive ion charge and seems, unexpectedly, larger with $(n\text{-Pr})_3NH^+$ than with $(n\text{-Pr})_4N^+$ and may be connected with the greater electrical asymmetry of the former than the latter ion. The slopes $(\partial E/\partial\Gamma)_q$ of the lines in Fig. 9, *a–d* are recorded in Table 3.

The trends of the plots of ΔE_q as a function of Γ (Fig. 9) for various constant q values are rather unusual. At the pzc, ΔE_q shows expected positive values, increasing with Γ. However, for $Pr_2NH_2^+$, Pr_3NH^+, and Pr_4N^+, the slope $d\Delta E_q/d\Gamma$ becomes much diminished as q goes from 0 to −8 or

Can. J. Chem. Downloaded from www.nrcresearchpress.com by 210.87.254.5 on 09/06/12
For personal use only.

Can. J. Chem. Downloaded from www.nrcresearchpress.com by 210.87.254.5 on 09/06/12
For personal use only.

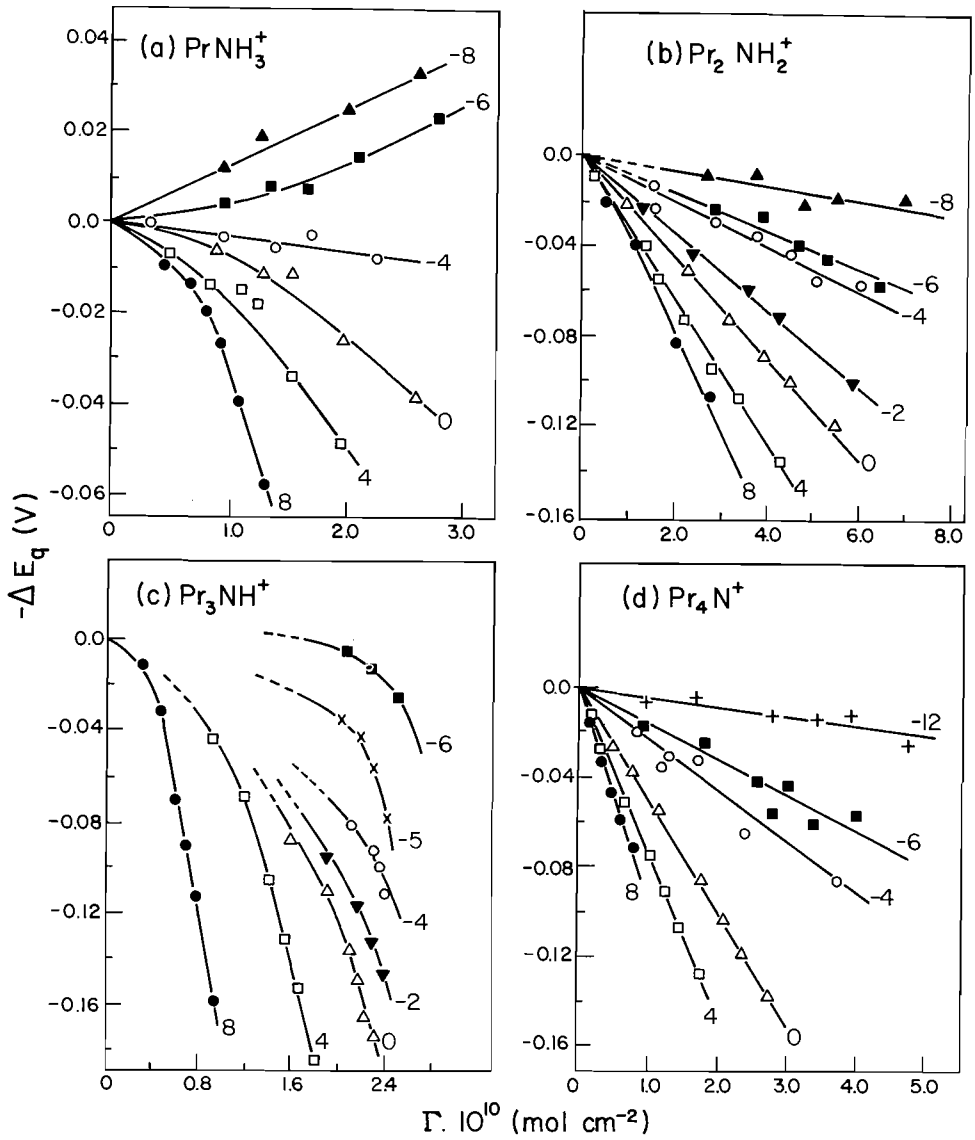

FIG. 9. Series of plots (*a*–*d*) for shift of potential at constant q due to adsorption of the series of *n*-propylammonium perchlorates at Hg, for various constant q values as a $f(\Gamma)$.

$-12\ \mu C\ cm^{-2}$ or, conversely, increases as q becomes positive. For $PrNH_3^+$, $d\Delta E_q/d\Gamma$ becomes negative as q becomes negative. Inspection of the raw data in terms of the electrocapillary curves shows that this effect is due to γ for $Pr_2NH_2^+$, Pr_3NH^+, and Pr_4N^+ solutions being less sharply curved with changing potential at large negative potentials and for the higher concentrations than are the curves for the base solution or for the solutions having low organic ion concentrations; that is, the capacity of the interface is diminished with increasing concentration, especially on the "negative branches" of the electrocapillary curves.

In contrast to the case with adsorbable simple ions, where $(\partial E/\partial\Gamma)_q$ tends to be larger at numerically increasing q values of opposite sign to that of the charge on the ion being adsorbed, e.g. as found in the case of $Me_4N^+F^-$ in the series of tetramethylammonium salts studied by Kimmerle and Menard (3), the present results with Pr-ammonium ions show a surprising opposite trend. The only reasonable, but speculative, rationalization we can offer for this interesting result is that adsorption of these large alkylammonium ions requires solvent displacement from the Hg surface to a much greater extent than does adsorption of simple specifically adsorbed ions, e.g. Cl^-. The adsorption of the

organic ions would be accompanied by a substantial $(\partial E/\partial \Gamma)_q$ component due to diminution of the dipole surface potential of oriented water dipoles, as is found in the case of neutral molecule adsorption, e.g. with pyrazine (7), pyridine (7), or thiourea (27). This effect, due to displacement of oriented solvent dipoles, tends to be greater at higher electrode/solution fields and gives rise to a larger $(\partial E/\partial \Gamma)_q$ contribution at larger negative q values but of *opposite sign* (cf. ref. 7) to the "normal" $(\partial E/\partial \Gamma)_q$ due to charge separation across the double-layer brought about by accumulation of specifically adsorbed (small) ion charge in the interphase. The solvent displacement effect is characteristic of adsorption of organic substances and reflects the hydrophobic behavior of the *n*-Pr chains.

Relation to $\Delta\chi$ Behavior at the Air/Water Interface

Finally, it is interesting to observe that the ΔE_q values at the Hg/water interface are substantially larger than the $\Delta\chi$ values at the air/water interface (Part I), for the same organic ions. This may be the result of the situation at the air/water interface where hydrophobic ions can have part or all of their organic residues "out" of the water phase while at the Hg/water interface, accommodation of alkyl groups of the ions can only be realized by displacement of previously adsorbed and oriented solvent molecules.

Acknowledgements

Grateful acknowledgement is made to the National Research Council of Canada and later the Natural Sciences and Engineering Research Council of Canada for support of this work.

1. B. B. Damaskin and A. N. Frumkin. Electrochim. Acta, **19**, 137 (1974).
2. B. E. Conway. Adv. Coll. Interface Sci. **8**, 91 (1977); Ionic hydration in chemistry and biophysics. Elsevier Publishing Co., Amsterdam. 1981.
3. F. M. Kimmerle and H. Menard. J. Electroanal. Chem. **54**, 101 (1974).
4. (*a*) J. O'M. Bockris, M. A. V. Devanathan, and K. Müller. Proc. R. Soc. London, A**274**, 55 (1963); R. Parsons. J. Electroanal. Chem. **59**, 229 (1975).
5. R. Parsons. Trans. Faraday Soc. **51**, 1518 (1955).
6. B. E. Conway and H. P. Dhar. J. Coll. Interface Sci. **48**, 73 (1974).
7. B. E. Conway, J. G. Mathieson, and H. P. Dhar. J. Phys. Chem. **78**, 1226 (1974); Croat. Chem. Acta, **45**, 109 (1973).
8. S. Trasatti. J. Chem. Soc. Faraday Trans. I, **68**, 229 (1972); J. Electroanal. Chem. **39**, 163 (1972); Surface Sci. **32**, 735 (1972).
9. J. E. Desnoyers, M. Arel, A. Perron, and C. Jolicoeur. J. Phys. Chem. **73**, 3347 (1969).
10. F. M. Kimmerle and H. Menard. J. Electroanal. Chem. **47**, 375 (1973).
11. R. G. Barradas and F. M. Kimmerle. J. Electroanal. Chem. **9**, 483 (1965); **11**, 128 (1966).
12. F. Rocheleau. M.Sc. Thesis, University of Ottawa. Ottawa, Ont. 1978.
13. F. Kimmerle, H. Menard, B. E. Conway, and H. P. Dhar. Electrochim. Acta, **19**, 883 (1974).
14. P. Corbusier and L. Gierst. Anal. Chim. Acta, **15**, 254 (1956).
15. D. J. G. Ives and G. J. Janz. Reference electrodes. Academic Press, New York. 1961. Chapt. 3. p. 133.
16. D. C. Grahame, R. P. Larsen, and M. A. Poth. J. Am. Chem. Soc. **71**, 2975 (1949).
17. (*a*) M. A. V. Devanathan and M. J. Fernando. Trans. Faraday Soc. **58**, 784 (1962); (*b*) H. S. Frank. J. Phys. Chem. **67**, 1554 (1963).
18. D. M. Mohilner, L. M. Bowman, S. J. Freeland, and H. Nakadomari. J. Electrochem. Soc. **120**, 1658 (1973); D. M. Mohilner and H. Nakadomari. J. Electroanal. Chem. **65**, 843 (1975).
19. B. E. Conway and J. O'M. Bockris. Proc. 6th C.I.T.C.E. Meeting, Poitiers 1954, Publ. Butterworths, London. 1955. p. 207.
20. B. E. Conway and H. P. Dhar. Electrochim. Acta, **19**, 445 (1974).
21. G. S. Hartley and C. Robinson. Trans. Faraday Soc. **48**, 847 (1952).
22. B. E. Conway and R. G. Barradas. Electrochim. Acta, **5**, 319 (1961); **5**, 349 (1961).
23. E. Blomgren and J. O'M. Bockris. J. Phys. Chem. **63**, 1475 (1959).
24. A. Ben-Naim. *In* Water and aqueous solutions. *Edited by* R. A. Horne. Wiley-Interscience, New York. 1972. Chapt. 11.
25. P. S. Ramanathan and H. L. Friedman. J. Chem. Phys. **54**, 1086 (1971); See also P. S. Ramanathan, C. V. Krishnan, and H. L. Friedman. J. Solution Chem. **1**, 237 (1972).
26. W. H. Streng and W-Y. Wen. J. Solution Chem. **3**, 865 (1974).
27. R. Parsons. Proc. R. Soc. London, A**179**, 261 (1961).
28. J. V. Leyendekkers and R. J. Hunter. J. Electroanal. Chem. **81**, 123 (1977).
29. B. E. Conway. Ionic hydration in chemistry and biophysics. Elsevier Publ. Co., Amsterdam. 1981.

Can. J. Chem. Downloaded from www.nrcresearchpress.com by 210.87.254.5 on 09/06/12
For personal use only.

Ionic solution near an uncharged surface with image forces

T. CROXTON AND D. A. MCQUARRIE
Department of Chemistry, University of California, Davis, CA 95616, U.S.A.

G. N. PATEY
Department of Chemistry, University of British Columbia, Vancouver, B.C., Canada V6T 1W6

G. M. TORRIE
Department of Mathematics, Royal Military College, Kingston, Ont., Canada K7L 2W3

AND

J. P. VALLEAU
Department of Chemistry, University of Toronto, Toronto, Ont., Canada M5S 1A1

Received September 29, 1980

This paper is dedicated to Dr. Sam Levine on the occasion of his 70th birthday

T. CROXTON, D. A. MCQUARRIE, G. N. PATEY, G. M. TORRIE, and J. P. VALLEAU. Can. J. Chem. **59**, 1998 (1981).

We studied the ion density in a dilute electrolyte solution which is next to an uncharged surface at which there is a discontinuity in the dielectric constant. In particular, we treated the restricted primitive model of a 1–1 aqueous solution next to a pure phase of unit dielectric constant. This served as a primitive model of the interface between an electrolytic solution and the air. Monte Carlo data are presented: the image forces are included and treated exactly. The model was also treated using the Born–Green–Yvon (BGY) integral equation approach; a modification of BGY theory which ensures electroneutrality is in very good agreement with the Monte Carlo data. The use of a "screened self-image" approximation to the potential energy has been tested using Monte Carlo computation and is found to be inadequate for the present model. Hypernetted-chain equation results using this approximation are also reported.

T. CROXTON, D. A. MCQUARRIE, G. N. PATEY, G. M. TORRIE et J. P. VALLEAU. Can. J. Chem. **59**, 1998 (1981).

Nous avons étudié la densité ionique d'une solution d'électrolyte diluée voisine d'une surface non chargée où se trouve une discontinuité dans la constante dielectrique. Nous traitons en particulier du modèle primitif restrient d'une solution aqueuse 1–1 au voisinage d'une phase pure de constante diélectrique égale à un. Ceci sert de modèle primitif de l'interface entre une solution d'électrolyte et l'air. On présente des données de Monte Carlo: on y inclut les images électrique et on les traite d'une façon exacte. On traite également le modèle en utilisant l'approche de l'équation intégrale de Born-Green-Yvon; une modification de la théorie BGY, qui assure une neutralité électrique, est en bon accord avec les données de Monte Carlo. Faisant appel à des calculs de type Monte Carlo, on a étudié l'approximation "auto-image tamisée" pour l'énergie potentielle et on a trouvé que cette approximation n'est pas utile pour le présent modèle. On rapporte également des résultats basés sur l'équation HNC qui font appel à cette approximation.

Introduction

This paper is concerned with the structure of an ionic solution next to an uncharged planar surface at which there is a discontinuity in the dielectric constant. The resulting electrostatic effects cause distortion of the ionic density near the surface; this is studied here using Monte Carlo and integral equation techniques.

Most studies of electrolytes next to surfaces have focussed on the classic "double-layer" problem of the ion distributions next to a *charged* surface. For real double layers there will be in addition a change of dielectric constant at the surface, the effects of which should be combined with those of the surface charge in a thorough theoretical treatment. Most commonly, however, the surface-charge effects have been examined in isolation, as in theoretical work based on the Gouy–Chapman theory. This paper reverses the procedure by examining in isolation the effects of a dielectric discontinuity. This allows us to examine the magnitude and character of the dielectric effects. A further purpose is to evaluate the ability of various approximate theories to handle accurately such effects. The classic Poisson–Boltzmann theory of Gouy and Chapman is not designed to take any account of them, and therefore does not predict any nonuniformity of ion density for the present model. This paper examines instead two versions of an approach based on the Born–Green–Yvon integral equation, and they are evaluated using Monte Carlo results.

We examine the particular case of a dielectric constant of unity outside the solution. The work may, therefore, be regarded as a study of the struc-

0008-4042/81/131998-06$01.00/0
©1981 National Research Council of Canada/Conseil national de recherches du Canada

Can. J. Chem. Downloaded from www.nrcresearchpress.com by 210.87.254.40 on 09/06/12
For personal use only.

Can. J. Chem. Downloaded from www.nrcresearchpress.com by 210.87.254.40 on 09/06/12
For personal use only.

ture of the "free" surface of an ionic solution open to the air. The ion density distribution is then related to the surface tension of the solution. While the present results can be so interpreted we have not done this since such an interpretation could not likely be taken very seriously, due to the limitations of the model.

We consider the restrictive primitive model of an aqueous 1–1 ionic solution. That is, the solvent is represented only as a continuum of dielectric constant 78.5, and the ions are hard spheres, all of the same diameter d. The discontinuity in the dielectric constant occurs at $z = 0$, and it has values ε_0 for $z < 0$, outside the solution, and ε_1 for $z > 0$, within the solution. (For the results reported here $\varepsilon_0 = 1$ and $\varepsilon_1 = 78.5$.) The centres of the ions are allowed to approach to within one ionic radius of the surface, so they lie in $z \geq d/2$.

The electrostatic effects of the dielectric discontinuity are equivalent to those of a set of "images" of the ions located behind the surface of discontinuity, as shown in Fig. 1. For the reported results $\varepsilon_0 < \varepsilon_1$, so that each image charge is of the same sign as that of the ion which generates it. The average effect is therefore to repel the ions from the surface.

Following Buff and Stillinger (1) we write the potential energy as

$$[1] \quad u = \sum_i u_i^{(1)} + \frac{1}{2}\sum_{i,j} u_{ij}^{(2)}$$

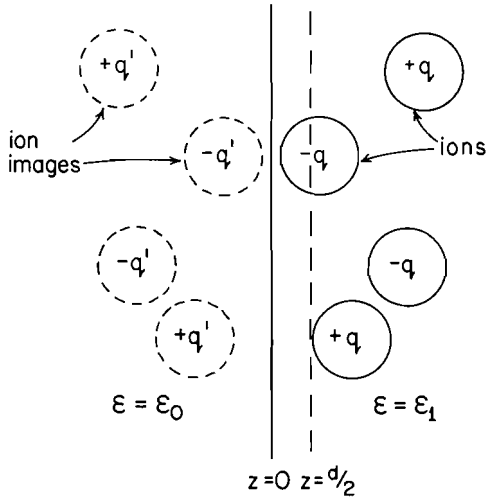

FIG. 1. Ions next to a discontinuity of the dielectric constant at $z = 0$. Each ion and its image are equidistant from $z = 0$, and $q'/q = (\varepsilon_1 - \varepsilon_0)/\varepsilon_1 + \varepsilon_0)$. Note that $z = d/2$ is the plane one radius from $z = 0$ and in the present model represents the closest allowed approach of the center of the ions to the surface.

expressing it in terms of a one-particle potential $u_i^{(1)}$ and a two-particle potential $u_{ij}^{(2)}$. Then

$$u_i^{(1)}(z_i) = u_i^{\text{elec}}(z_i) + u_i^{\text{hw}}(z_i)$$

$$[2] \quad u_i^{\text{elec}}(z_i) = \lambda q_i^2/4\varepsilon_i z_i$$

$$u_i^{\text{hw}}(z_i) = 0, \quad z_i \geq d/2$$

$$= \infty, \quad z_i < d/2$$

and

$$u_{ij}^{(2)}(r_i, r_j) = u_{ij}^{\text{elec}}(r, r_{\text{im}}) + u_{ij}^{\text{hs}}(r)$$

$$[3] \quad u_{ij}^{\text{elec}}(r, r_{\text{im}}) = \frac{q_i q_i}{\varepsilon_1 r} + \frac{\lambda q_i q_j}{\varepsilon_1 r_{\text{im}}}$$

$$u_{ij}^{\text{hs}}(r) = 0, \quad r \geq d$$

$$= \infty, \quad r < d$$

In these equations, q_i and $\boldsymbol{r}_i$ are the charge and position of ion i, and we define

$$\lambda \equiv \frac{\varepsilon_1 - \varepsilon_0}{\varepsilon_1 + \varepsilon_0}$$

$$[4] \quad r \equiv |\boldsymbol{r}_j - \boldsymbol{r}_i|$$

$$r_{\text{im}} = \sqrt{(r^2 + 4z_i z_j)}$$

These potential energy functions are used below in conjunction with Monte Carlo computations (MC) and with two versions of the Born–Green–Yvon theory (BGY).

In an early examination of the electrolyte surface problem Onsager and Samaras (2), following Wagner (3), began with the linearized form of the Poisson–Boltzmann equation, familiar in Debye–Hückel theory. To incorporate the image effects they solved that approximate equation for the electrostatic potential in the presence of an ion fixed in the solution and of the image of that ion. (The solution was simplified by the two further approximations that ε_0 (in our notation) can be neglected compared with ε_1, and that the Debye shielding constant $\kappa(\boldsymbol{r})$, which should depend on the local concentration at the field point $\boldsymbol{r}$, can be replaced by the constant value of κ appropriate to the bulk concentration of the electrolyte.) The resulting electrostatic potential was used to estimate the potential of mean force on an ion near the surface of the electrolyte, which is given by

$$[5] \quad \frac{q_i^2}{4\varepsilon_1 z_i} \exp(-2\kappa z_i)$$

This has the form of the repulsive potential of the ion's own image, screened by an exponential factor

Can. J. Chem. Downloaded from www.nrcresearchpress.com by 210.87.254.40 on 09/06/12
For personal use only.

typical of Debye–Hückel theory. In approximate double-layer theories based on versions of the Poisson–Boltzmann equation a generalized form of this result again emerges (4–8). It should be correct asymptotically at low concentrations. The predictions of [5] for the present model are compared below with MC computations at finite concentrations.

A different use of this result has been suggested (9). In the model, as summarized in [1]–[4], each ion interacts explicitly with its own electrostatic image and with the images of each of the other ions. This is electrostatically correct, but inclusion of this exact form of the potential energy in modern integral equation theories can lead to extremely difficult equations (10). The suggestion has therefore been made that the Poisson–Boltzmann result [5] be used to represent the effect of images in an approximate "effective potential energy" for insertion into modern theories. This would mean replacing the electrostatic terms of [2] and [3] by

$$[6]\qquad u_i^{\text{elec}}(z_i) = \frac{\lambda q_i^2}{4\varepsilon_1 z_i}\exp(-2\kappa z_i)$$

$$u_{ij}^{\text{elec}}(r) = q_i q_j/\varepsilon_1 r$$

The effects on an ion of images other than its own enter only through the screening of the self-image term. If it were adequate this "screened self-image approximation" (SSI) would be most useful, since it can be incorporated into various theories much more easily than the exact potential energy given by [1]–[3]. A secondary purpose of the present study is therefore to test this approximation for the potential energy. This has been done by direct comparison of Monte Carlo results generated for *both* the exact and the SSI potential energies.

The SSI approximation has been used to allow solution of the hypernetted-chain theory (HNC) for double-layer problems (11), and some results of this HNC–SSI approximation for the present model are also reported below.

In the following sections the Monte Carlo and theoretical techniques are briefly described, after which we present MC and BGY results for the exact treatment of the model, as well as a modification, BGY + EN, of BGY theory. The MC and HNC results are given for the SSI approximations as well, and the various results compared and discussed.

Monte Carlo Calculations

The Monte Carlo computations were carried out in the grand canonical ensemble, using ionic activity coefficients determined previously (12). The details of the Monte Carlo techniques are described elsewhere (11, 12). The ions included explicitly in the MC computation are enclosed in a rectangular box of dimensions $L \times W \times W$ between the surface under study, at $z = 0$, and a second hard wall, at $z = L$. The second wall is inert, in the sense that its dielectric constant is supposed equal to that of the liquid so there are no image forces there. The system is periodic in the x and y directions, i.e., parallel to the surface.

Around each ion may be pictured its own "central" box (such that the box is centered on the ion in the x and y directions) which contains just one of the periodic replications of each ion. In the "exact" computation the potential energies corresponding to all interactions with ions within this central box and with their images were calculated explicitly. Interactions with more distant parts of the system were calculated using a method described elsewhere (11, 13, 14) (but were anyway negligible for this problem involving no charge separation).

Convergence of the Monte Carlo Markov chains for the structure near the surface is rather slow for this field-free problem. Runs of roughly 10 000 configurations per particle were required to obtain the results reported below (in Figs. 2–4). The box dimensions L and W were chosen so that L was substantially greater than the thickness of the surface layer, and so that other boundary effects were negligible. Roughly 180 particles were involved.

To test the SSI approximation a second MC computation was carried out for the 1.0 M solution using [6] with the value of κ corresponding to the bulk concentration. The corresponding density profile is compared with that of the exact treatment in Fig. 4.

The BGY and BGY + EN Theories

The first member of the BGY hierarchy,

$$[7]\qquad -kT\frac{\partial \ln \rho_i^{(1)}(z_1)}{\partial z_1} = \frac{\partial u_i^{(1)}(z_1)}{\partial z_1} + \sum_{j=1}^{\omega}\int d\boldsymbol{r}_2 \frac{\partial u_{ij}^{(2)}(\boldsymbol{r}_1, \boldsymbol{r}_2)}{\partial z_1}\frac{\rho_{ij}^{(2)}(\boldsymbol{r}_1, \boldsymbol{r}_2)}{\rho_i^{(1)}(z_1)}$$

where ω is the number of components, is an exact equation relating the singlet and doublet density distribution functions $\rho_i^{(1)}$ and $\rho_{ij}^{(2)}$. Croxton and McQuarrie (15) have suggested as an approximate closure for this

$$[8]\qquad \rho_{ij}^{(2)}(\boldsymbol{r}_1, \boldsymbol{r}_2) \approx \rho_i^{(1)}(z_1)\rho_j^{(1)}(z_2)g_{ij}(r)\,[\exp(-\beta w_{ij}^{\text{im}}(r_{\text{im}}))]$$

Can. J. Chem. Downloaded from www.nrcresearchpress.com by 210.87.254.40 on 09/06/12
For personal use only.

where $g_{ij}(r)$ is the radial distribution function in bulk solution and w_{ij}^{im} is the low density limiting expression for the image contribution to the potential of mean force given by

$$[9] \quad w_{ij}^{\text{im}}(r_{\text{im}}) = \lambda \frac{q_i q_j}{\varepsilon_1} \frac{\exp(-\kappa r_{\text{im}})}{r_{\text{im}}}$$

In this equation κ is the usual Debye–Hückel parameter. Solution of [7] under this approximation will be called the BGY theory.

When applied to the charged-wall system for which $w_{ij}^{\text{im}} \equiv 0$, this approximation was found to yield poor results (16). However, much improvement could be obtained by introducing a more flexible form for $\rho_{ij}^{(2)}$ including z_1 and z_2 dependence explicitly and requiring $\rho_{ij}^{(2)}$ to satisfy electroneutrality. In analogy to the expression used by Croxton and McQuarrie (16) in that work, we suggest the approximation

$$[10] \quad \rho_{ij}^{(2)}(r_1, r_2) \approx \rho_i^{(1)}(z_1)\rho_j^{(1)}(z_2)\{1 + f_i(z_1)f_j(z_2)[g_{ij}(r)\exp(-\beta w_{ij}^{\text{im}}(r_{\text{im}}))] - 1]\}$$

where the f_i's are arbitrary unknown functions. If this $\rho_{ij}^{(2)}$ is required to satisfy electroneutrality, we obtain an integral equation involving $\rho^{(1)}$ and f:

$$[11] \quad f(z_1) = -\left[\pi\rho\int_0^\infty dz_2 g^{(1)}(z_2)f(z_2)\int_{|z_1-z_2|}^\infty dr\, r \sum_{j=1}^{2}\frac{q_j}{q_1}\left(g_{1j}(r)\exp\left[-\lambda\frac{q_1 q_j}{\varepsilon KT}\frac{\exp(-\kappa r_{\text{im}})}{r_{\text{im}}}\right] - 1\right)\right]^{-1}$$

In writing [11], we have used the fact that $f_i = f$ and $\rho_i^{(1)} = \rho^{(1)}$ are the same for each species i for this system. Simultaneous solution of [7] and [11] for f and $\rho^{(1)}$ will be called the BGY + EN theory.

If we define $g_i^{(1)}(z)$ and $g_{ij}^{(2)}(r_1, r_2)$ by

$$[12] \quad \rho_{ij}^{(2)}(r_1, r_2) = \rho_i^{(1)}(z_1)\rho_j^{(1)}(z_2)g_{ij}^{(2)}(r_1, r_2)$$

$$[13] \quad \rho_i^{(1)}(z_1) = \rho_i g_i^{(1)}(z_1)$$

where $\rho = (\rho_1 + \rho_2)d^3$ and ρ_i is the bulk number density of species i, the BGY equation for this system may be written as

$$[14] \quad \ln g^{(1)}(z) = -\frac{u^{(1)}(z)}{kT} + \pi\rho\int_0^\infty dz_2 g^{(1)}(z_2)\int_z^\infty dz_1\int_{|z_1-z_2|}^\infty dr\, r\sum_{j=1}^{2}\frac{\partial}{\partial z_1}\left(\frac{u_{ij}^{(2)}}{kT}\right)g_{ij}^{(2)}(r_1, r_2)$$

As in [11] we have used the fact that $g_i^{(1)}(z) = g^{(1)}(z)$. After a considerable amount of manipulation, [14] may be brought into the more convenient computational form

$$[15] \quad \ln g^{(1)}(z) = F(z) + \pi\rho\int_0^\infty dz_2[g^{(1)}(z_2) - 1]K(z, z_2)$$

where

$$[16] \quad F(z) = -\frac{\lambda}{2}\frac{\beta^*}{z} + \frac{\pi\rho}{3}(m^2 - 3m + 2) - 2\pi\rho\int_0^\infty dz_1\left[\int_{M_1}^{z_1+d} dz_2(z_1 - z_2)h_s^{(2)}(r = d) - 2\beta^*\int_0^\infty dz_2\int_{|z_1-z_2|}^\infty dr\, r\left(\frac{z_1 - z_2}{r^3} + \lambda\frac{z_1 + z_2 + d}{r_{\text{im}}^3}\right)h_d^{(2)}\right]$$

$$[17] \quad K(z, z_2) = (m_2^2 - 1) + 2\int_z^\infty dz_1\left[-(z_1 - z_2)h_s^{(2)}(r = d)\Theta(d - |z_1 - z_2|) + 2\beta^*\int_{|z_1-z_2|}^\infty dr\, r\left(\frac{z_1 - z_2}{r^3} + \lambda\frac{z_1 + z_2 + d}{r_{\text{im}}^3}\right)h_d^{(2)}\right]$$

and where $\beta^* = q^2/\varepsilon_1 kTd$, $m = \min(z, \frac{1}{2}d)$, $M_1 = \max(0, z - \frac{3}{2}d)$, $h_s^{(2)} = (h_{12}^{(2)} + h_{11}^{(2)})/2$, $h_d^{(2)} = (h_{12}^{(2)} - h_{11}^{(2)})/2$, $m_2 = \min(d, |z - z_2|)$, and $\Theta(X)$ is the unit step function.

The numerical procedure used was first to calculate $g^{(1)}(z)$ from [15] with $f(z) = 1$ and then to use $g^{(1)}(z)$ to obtain $f(z)$ from [11]. This $f(z)$ was used to evaluate and store $F(z)$ and $K(z, z_2)$ and [15] is solved for $g^{(1)}(z)$ by direct iteration. This entire process was repeated until f and $g^{(1)}$ were stable. The bulk radial distribution functions used were those obtained from the second BGY equation

Can. J. Chem. Downloaded from www.nrcresearchpress.com by 210.87.254.40 on 09/06/12
For personal use only.

under superposition (17). The BGY theory is solved similarly but with the constraint $f(z) \equiv 1$ and so requires only one master iteration. The results presented here were obtained using 61 points uniformly spaced over an interval of length L with L equal to about 5 D lengths. The infinite integrals required were evaluated as finite integrals with upper limits ranging from $2L$ to $4L$. An asymptotic tail was also added to the triple integral of $F(z)$ which exactly cancels the asymptotic contribution of the first, z^{-1}, term. The procedure described is quite stable numerically.

The HNC Theory in the SSI Approximation

The hypernetted-chain approximation (HNC) has recently been extended by Blum and Henderson (9, 18) and others to include electrolytes next to a charged surface. Inclusion of the exact forms of the one- and two-particle potential energies due to image forces (cf. eqs. [2]–[4]) leads to extremely difficult equations (10). It is relatively easy, however, to include the effects of image forces in the "screened self-image" approximation (SSI) since they appear only in the one-particle energy (cf. eqs. [5], [6]). This is described in detail elsewhere (11), and numerical solution of the equations has been carried out. Results for the present model are reported below for a bulk concentration of 1.0 M.

Results and Discussion

Figures 2–4 show the Monte Carlo results for the ion density profiles near the surface, along with theoretical results. We first consider results for the exact treatment of the model. At 0.1 M, BGY and BGY + EN are not very different, and both give

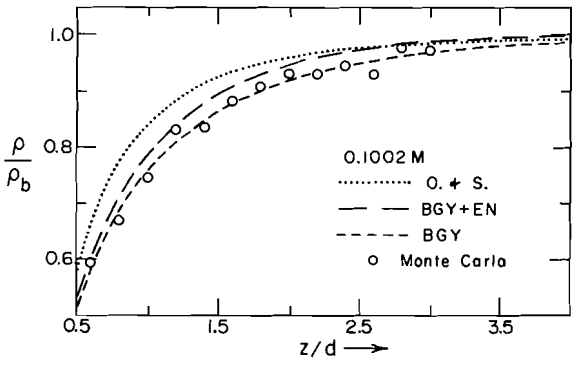

FIG. 2. Ionic density $\rho(z)$ near a planar dielectric interface, relative to the bulk density ρ_b, for a 0.1002 M 1–1 restricted primitive electrolyte. The parameters are $d = 4.25$ Å, $T = 298$ K, $\varepsilon_1 = 78.5$, and $\varepsilon_0 = 1$. The lines of short and long dashes are for the BGY and BGY + EN theories while the dotted line corresponds to that of Onsager and Samaras. The circles show Monte Carlo data, for which the uncertainty in ρ/ρ_b (one standard deviation) is about 0.015.

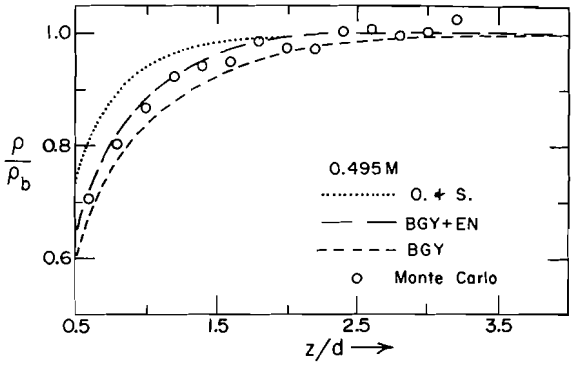

FIG. 3. Ionic density near the interface at 0.495 M. The other parameters and the symbols are described in the caption to Fig. 2. The Monte Carlo points have again an uncertainty of ± 0.015.

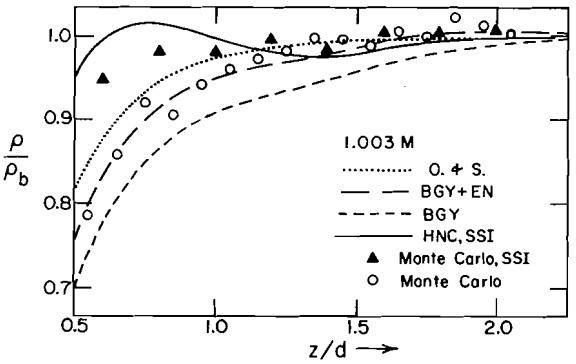

FIG. 4. Ionic density near the interface at 1.003 M. The other parameters and the symbols described for Fig. 2 apply here. This figure shows as well results using the SSI approximation to the potential energy: the triangles show Monte Carlo data and the solid line the result of using the approximation in the hypernetted-chain theory. The uncertainty in the Monte Carlo points is ± 0.02.

satisfactory descriptions of the MC results. As the concentration increases, however, BGY itself becomes rather unsatisfactory. It predicts a too-great repulsion of the ions from the surface, and a layer of surface distortion which is much too thick (cf. Fig. 4). BGY + EN, by contrast, continues to give a good description of the density profiles at the concentrations studied. In conjunction with the results of BGY + EN theory for the charged-wall system (16), the present results suggest that this may prove to be an accurate approximate theory for ion distributions near surfaces.

The figures show the ion density profiles predicted by the potential of mean force [5] in the theory of Onsager and Samaras (2). They are fairly successful, but evidently underestimate the ion depletion (and therefore underestimate the increase of surface tension caused by the ions). In particular the *thickness*

of the layer of ion depletion is substantially underestimated at finite concentrations. At 1.0 M the errors of [5] are being partially compensated by enhanced ion density due to volume exclusion effects ignored in the theory of Onsager and Samaras. It will be interesting to see the predictions of more sophisticated Poisson–Boltzmann theories such as that of Levine and Outhwaite (8).

Figure 4 contains results bearing on the use of the SSI approximation [6] in the potential energy. The MC results are shown for this SSI potential as well as for the exact potential energy [1]–[3] of the model. It is evident that they lead to very different behaviour. The error is in the direction of grossly underestimating the effect of the image forces. It appears therefore that for at least some regimes, such as this zero-field case, the SSI approximation is unreliable.

The SSI calculations have used in [6] the value of κ appropriate to the bulk concentration. In some applications of SSI a *local* value of κ has been used instead ((11), cf. refs. (3), (5)), corresponding to that of the local concentration at the position of the ion. In the present case the local concentrations differ so little from the bulk concentration that this modification would have little effect. This is confirmed by comparing HNC calculations, which have been carried out using *both* bulk and local values of κ. In typical double layer problems with charged surfaces the local concentrations will, however, exceed the bulk concentrations, and often substantially. Use of the SSI approximation with the local κ would then mean a still greater underestimate by SSI of the effects of images.

This failure of the SSI approximation seems doubly unfortunate in view of the relative success of the HNC theory in predicting the behaviour of the SSI system itself. The HNC density results are slightly higher than the MC results and show an oscillatory structure that at least is not obvious in the rather noisy MC data, but overall the agreement is very satisfactory. This means though that HNC, using SSI, fails completely to describe the model system itself, and this is due largely to the failure of the SSI approximation.

Acknowledgement

We acknowledge with thanks the financial support of the Natural Sciences and Engineering Research Council of Canada and a grant from the U.S. National Institutes of Health, GM 26864-02.

1. F. P. Buff and F. H. Stillinger. J. Chem. Phys. **25**, 312 (1956).
2. L. Onsager and N. N. T. Samaras. J. Chem. Phys. **2**, 528 (1934).
3. C. Wagner. Phys. Z. **25**, 474 (1924).
4. A. L. Loeb. J. Colloid Sci. **6**, 75 (1951).
5. S. Levine and G. M. Bell. J. Phys. Chem. **64**, 1188 (1960).
6. S. L. Brenner, V. A. Parsegian, and D. Gingell. J. Phys. Chem. **82**, 1727 (1978).
7. G. M. Bell and P. D. Rangecroft. Mol. Phys. **24**, 255 (1972).
8. S. Levine and C. W. Outhwaite. J. Chem. Soc. Faraday Trans. II, **74**, 1670 (1978).
9. L. Blum. J. Phys. Chem. **81**, 136 (1977).
10. S. Carnie. Private communication.
11. G. M. Torrie, J. P. Valleau, and G. Patey. In preparation.
12. J. P. Valleau and L. K. Cohen. J. Chem. Phys. **72**, 5925 (1980).
13. G. M. Torrie and J. P. Valleau. J. Chem. Phys. **73**, 5807 (1980).
14. J. P. Valleau and G. M. Torrie. Proceedings of NRCC workshop on the problem of long-range forces in the computer simulation of condensed media. *Edited by* D. Ceperly. Lawrence Berkeley Laboratory (1980).
15. T. L. Croxton and D. A. McQuarrie. Chem. Phys. Lett. **68**, 489 (1979).
16. T. L. Croxton and D. A. McQuarrie. Mol. Phys. In press.
17. T. L. Croxton and D. A. McQuarrie. J. Phys. Chem. **83**, 1840 (1979).
18. D. Henderson and L. Blum. J. Chem. Phys. **69**, 5441 (1978).

Can. J. Chem. Downloaded from www.nrcresearchpress.com by 210.87.254.40 on 09/06/12
For personal use only.

London – van der Waals forces and torques exerted on an ellipsoidal particle by a nearby semi-infinite slab

HOWARD BRENNER[1] AND LAWRENCE J. GAJDOS[2]

Department of Chemical Engineering, University of Rochester, Rochester, NY 14627, U.S.A.

Received October 7, 1980

This paper is dedicated to Dr. Sam Levine on the occasion of his 70th birthday

HOWARD BRENNER and LAWRENCE J. GAJDOS. Can. J. Chem. **59**, 2004 (1981).

A Hamaker-type integration of the pairwise *en vacuo* intermolecular forces is performed for a homogeneous triaxial ellipsoidal particle in proximity to a homogeneous semi-infinite slab bounded by a plane wall. The orientation of the ellipsoid relative to the plane is taken to be arbitrary, as too is its distance from the plane. The integrated potential energy function of the ellipsoid with respect to the slab is found to possess nonadditive positional and orientational contributions. This macroscopic potential is employed to compute the force and torque on the ellipsoid as functions of both its position and orientation relative to the plane.

The novel integration scheme pertains to centrally-symmetric pairwise intermolecular potentials of arbitrary functional form. Specific results are derived for classical inverse-power intermolecular potentials possessing both attractive (r^{-n}) and repulsive ($-r^{-m}$) additive components (with $n > m$). In stable equilibrium the ellipsoid aligns itself with the shortest of its three principal axes perpendicular to the bounding wall, and at a separation distance comparable to the length scale of the intermolecular potential itself.

HOWARD BRENNER et LAWRENCE J. GAJDOS. Can. J. Chem. **59**, 2004 (1981).

On a effectué une intégration du type Hamaker des forces intermoléculaires *en vacuo* prises deux à deux pour une particule éllipsoidale triaxiale homogène au voisinage d'une plaque homogène semi-infinie reliée à un mur plan. On considère que l'orientation de l'ellipsoide par rapport au plan ainsi que sa distance par rapport à ce plan sont arbitraires. On a trouvé que la fonction d'énergie potentielle intégrée de l'ellipsoide par rapport à la plaque possède des contributions de position et d'orientation qui ne sont pas additives. On a employé cette propriété macroscopique pour calculer la force et la torsion appliquée à l'ellipsoide en fonction à la fois de sa position et de son orientation par rapport au plan.

Le nouveau schéma d'intégration s'applique à des potentiels intermoléculaires centro-symétriques considérées sous forme de paire dont la forme fonctionnelle est arbitraire. On a déduit des résultats spécifiques pour des potentials intermoléculaires de puissance inverse classique possédant à la fois des composantes additives (r^{-n}) et répulsives ($-r^{-m}$) (avec $n > m$). En équilibre stable, l'ellipsoide s'aligne lui-même avec le plus court de ses trois axes perpendiculaires principaux par rapport au mur plan liant et la distance qui le sépare d'un mur se compare à l'échelle de longueur du potentiel intermoléculaire lui-même.

[Traduit par le journal]

1. Introduction

Many areas within the field of colloid science are concerned with the interaction between a particle and a nearby boundary. The interaction may be *indirect*, through the agency of an intervening hydrodynamic field (1) — arising as a consequence of the motion of the particle through the viscous fluid in which it is suspended; or it may derive from *direct*, short-range interactions between the particle and surface — as in the case of dispersion forces (2, 3). The latter type of interaction constitutes the focus of the present contribution.

Our interest in this problem derives from questions relating to the boundary conditions to be imposed upon the solutions of the convective-diffusion equation involving the transport of orientable, i.e., nonspherical, Brownian solute particles (4–6) moving in proximity to surfaces (7–10). In attempting to solve the relevant particle continuity equation in bounded systems it is a nontrivial matter to explicitly account for the constraints imposed upon the translational and rotational particle motions by the presence of a nearby bounding wall (9).

This problem is largely avoided when attention is restricted to spherical particles, since particle orientation effects are physically irrelevant for such shapes. When, however, the arena of interest is enlarged to include nonspherical particles, the physico-mathematical description of such common boundary conditions as "adsorption" of the particle at the surface, or "impenetrability" of the surface to the particle, acquires a more complex character owing to the need to supplement the usual positional variables with orientational ones. Geometrically, hydrodynamically, and dynamically, "coupling" (7, 9, 11) between translational and rotational particle motions invariably occurs in proximity to a boundary, even for spherical particles.

These considerations may be recast and postponed by viewing the particle/boundary interaction on a finer length scale than is common in the usual macroscopic theory of transport processes. By

[1]To whom all correspondence should be addressed.

[2]Current address: Box 164, Mellon Institute, Carnegie-Mellon University, Pittsburgh, PA 15213.

0008-4042/81/132004-15$01.00/0

©1981 National Research Council of Canada/Conseil national de recherches du Canada

Can. J. Chem. Downloaded from www.nrcresearchpress.com by 210.87.254.6 on 09/06/12
For personal use only.

Can. J. Chem. Downloaded from www.nrcresearchpress.com by 210.87.254.6 on 09/06/12
For personal use only.

recognizing the boundary as the seat of short-range forces and torques external to the particle it is possible to incorporate these forces and torques directly into the continuity (i.e., conservation) equation itself (via the addition of Smoluchowski-type external force and torque contributions to the conventional constitutive equations for the translational and rotational particle fluxes) (5, 9, 10, 12). Such constitutive relations normally entail only diffusive and "piggy-back"-type fluid-convective contributions.

If the external force possesses a short-range repulsive component that tends to infinity sufficiently rapidly with diminishing distance of the particle from the boundary, intuition suggests that no boundary condition need be imposed. Rather, the repulsive force itself suffices to prevent penetration of the boundary by the particle. Furthermore, the variation of the resulting repulsive potential with particle orientation relative to the boundary provides an external torque on the particle, which then figures as a Smoluchowski-type contribution to the rotary particle flux (9) (in addition to the usual rotary diffusive and convective fluid contributions).

Thus, by modelling the bounding surface as the source of an external potential field acting upon the suspended particles, the continuity equation — supplemented by constitutive expressions for the flux densities appearing therein, including the Smoluchowski force and torque contributions — can be regarded as a self-contained descriptor of particle behavior in proximity to a boundary. Passage from this fine-scale view, which incorporates the short-range forces directly into its formulation, to a more conventional macroscopic view, can be accomplished by the methods of singular perturbation theory. This involves utilizing the ratio of short-range length scale to macroscopic boundary-length scale as a small perturbation parameter (10, 13). Matching of the inner and outer expansions then serves to furnish the proper macroscopic "boundary conditions" in a wholly rational manner (10, 13).

Though surface-derived particle forces have been extensively employed in the prior literature to describe the behavior of macroscopic particles moving near boundaries, the emphasis has been almost exclusively on the case of particle attraction towards the surface. Little consideration has been given to the effects of repulsion, except perhaps implicitly in the degenerate, infinitely-repulsive case of point contact between a rigid particle and rigid boundary. This unfortunately provides no repulsive length scale analogous to the length scale of the attractive forces. Moreover, the particles studied have almost invariably been taken to be spherical in shape, thus bypassing fundamental orientational issues involved in the present paper.

In the context of the above remarks Spielman *et al.* (14–16) have considered the capture of spheres on the surfaces of various collector geometries via London forces, including repulsive double-layer forces. Limiting themselves to non-Brownian particles they derived the deterministic particle trajectories followed by the suspended particles migrating towards the collecting surfaces. Spielman and Friedlander (17) and Ruckenstein and Prieve (18) extended this analysis to Brownian particles by replacing the particle-trajectory equation with a convective-diffusion equation. By specifying a boundary condition of zero particle concentration at the collector surface, corresponding to complete particle adsorption, each independently showed that (beyond a surface boundary layer) the macroscopic or bulk behavior could be modelled as an apparent first-order irreversible chemical reaction occurring at the collector surface.

In yet another application, Dahneke (19) studied the escape rates of adsorbed particles; that is, he considered the reversibility of the particle deposition process. This was accomplished by using a surface potential containing both attractive and repulsive components.

These applications indicate that short-range surface forces may indeed serve as the precursors of boundary conditions imposed upon the bulk properties of the fluid/particle system when the latter is viewed at the conventional macroscopic continuum level. Indeed, the classical reflection (zero normal flux) and adsorption (zero concentration) boundary conditions can immediately be deduced by assuming that the surface force is an infinitely repulsive or attractive step function. More realistic and rigorous physical modelling of such surface forces incorporates London – van der Waals forces (3), retardation effects (3, 20), and double-layer forces (3, 21). Dahneke (22) and others (23, 24) even go so far as to include Hertzian particle deformation upon contact.

The remainder of this paper is devoted to the exposition of a prototype "boundary potential" for an orientable particle — specifically, an ellipsoid in proximity to the plane surface of a semi-infinite slab. A summary outline of the subsequent analysis now follows.

In Section 2 we begin by writing the external boundary potential as the double integral of a continuous centrally-symmetric pairwise intermolecular potential. The latter expresses the interaction of the

Can. J. Chem. Downloaded from www.nrcresearchpress.com by 210.87.254.6 on 09/06/12
For personal use only.

material in the neighborhood of a point within the ellipsoid with the matter in the neighborhood of another point located in the slab. In order to utilize available results insofar as possible, the slab is modelled as a sphere whose radius is eventually allowed to become infinite. A geometric transformation of the resulting volume integral over the ellipsoid provides the *ansatz* by means of which the requisite integration can be effected. This transformation has the effect of replacing the ellipsoid by an equivalent sphere of appropriate radius. The resulting expression for the potential of the ellipsoid relative to the slab is then reduced from a two- to a one-dimensional quadrature of the intermolecular potential via a second transformation. Though the intermolecular potential appearing in the integrand of this remaining one-dimensional integral may be of arbitrary form, convergence requires that it tend to zero at infinity faster than r^{-3}.

In Section 3 the potential energy of the ellipsoid is explicitly calculated for inverse-power intermolecular potentials of the form r^{-q} ($q > 3$). Both attractive and repulsive potentials are included by an appropriate choice of the algebraic sign preceding r^{-q}. Additivity permits both attractive and repulsive contributions to be simultaneously considered within the same formulation.

The integrated, macroscopic attractive/repulsive potential is utilized in Section 4 to obtain the force and torque exerted by the slab on the ellipsoid. Each of these dynamical quantities is a function of the distance of the ellipsoid center from the plane and the orientation of the principal axes of the ellipsoid relative to the unit normal vector to the plane bounding the slab. These results are utilized to calculate the positions and orientations of the ellipsoid at which it experiences neither a net force nor torque (as a result of the cancellation of the separate attractive and repulsive components). These constitute necessary, but insufficient, conditions for equilibrium. Three pairs of positions and (symmetrical) orientations are found for which *both* the force and torque vanish simultaneously. Stability theory, involving minimization of the ellipsoid's potential energy, is then invoked to establish which of these three pairs corresponds to the *stable* equilibrium configuration. A close analogy is drawn between the present problem and that of a gravitating ellipsoidal particle in point contact with a horizontal plane. This analogy is used to conjecture that our calculations for ellipsoidal particles can, in fact, be extended to nonreentrant particles of any shape. Such more general considerations are, however, left for a future study.

It is shown in Section 5 that the ellipsoid positions itself at virtually molecular separation distances from the slab surface (with the shortest of the three principal axes of the ellipsoid lying normal to the plane). Available experimental data on the orientations of small spheroidal bacterial spores on a plane surface are shown to be not inconsistent with the present theory — though the inference can hardly be described as conclusive.

Finally, three appendices supporting and otherwise supplementing the calculations of the main text complete the presentation.

2. Ellipsoid/Slab System

The general theory underlying the calculations of the present section are summarized by Mahanty and Ninham (3), who also review all of the currently known two-body results for various geometrical configurations.

Let ξ denote the intermolecular potential energy shared between any pair of molecules located in bodies 1 and 2, respectively. Following Hamaker (25) it will be assumed that the net potential between the two ponderable bodies 1 and 2 may be obtained by summation over all such molecular pairs, and that the requisite summation may be effected by integrating over the volumes V_1 and V_2 of the bodies (assuming spatially continuous molecular number densities n_1 and n_2, respectively). In this work n_1 and n_2 will each be taken as constants, corresponding to homogeneous bodies. The net potential E is thus given by

$$[2.1] \quad E = \int_{V_1} \mathrm{d}V_1 \int_{V_2} \mathrm{d}V_2 \, \xi n_1 n_2$$

Alternatively, with E' the net potential of body 2 due to an arbitrary point P in V_1, such that

$$[2.2] \quad E' = \int_{V_2} \mathrm{d}V_2 \, \xi$$

there obtains

$$[2.3] \quad E = \int_{V_1} \mathrm{d}V_1 \, E' n_1 n_2$$

The volume V_2 will be assumed to be a sphere of radius a_s. After using an existing lemma to effect a partial integration of [2.2], the radius a_s will be allowed to become infinite, rendering the resulting calculation appropriate to that for a semi-infinite slab.

Following Chu (26), the sphere volume element $\mathrm{d}V_2$ can be twice integrated to give

$$[2.4] \quad \mathrm{d}V_2 = (\pi\bar{r}/R)[a_s^2 - (R - \bar{r})^2]\mathrm{d}\bar{r}$$

where R is the distance from the center of the sphere

Can. J. Chem. Downloaded from www.nrcresearchpress.com by 210.87.254.6 on 09/06/12
For personal use only.

V_2 to an arbitrary point P in V_1. Additionally, the remaining variable of integration $\bar{r}$ spans V_2, such that $\bar{r}$ = constant represents the open surface (a spherical cap) in V_2 formed by the intersection with V_2 of a sphere of radius $\bar{r}$ centered at P. Consequently, $\bar{r}$ takes on the range of values

$$[2.5] \quad R - a_s \leq \bar{r} \leq R + a_s$$

This is illustrated in Fig. 1.

Observe that the position vector $\boldsymbol{R}$ drawn from the center of V_2 to point P in V_1 possesses a magnitude R consistent with the above definition. This vector can be expressed as

$$[2.6] \quad \boldsymbol{R} = \boldsymbol{n}(a_s + d) + \boldsymbol{r}$$

where $\boldsymbol{n}$ is a unit vector from the center of V_2 directed towards an arbitrary, but fixed, reference point O in V_1. Further, d is the distance from the surface of V_2 to point O, and $\boldsymbol{r}$ is a position vector, locating point P relative to point O. Note that $\boldsymbol{n}$ is also the outward normal from V_2, a status that it will retain even in the limit as $a_s \to \infty$.

From eq. [2.6] the magnitude of $\boldsymbol{R}$ expressed in terms of these new variables is

$$[2.7] \quad R^2 = a_s^2 + 2a_s(d + \boldsymbol{n}\cdot\boldsymbol{r}) + (\boldsymbol{n}d + \boldsymbol{r})^2$$

so that

$$[2.8] \quad R = a_s + (d + \boldsymbol{n}\cdot\boldsymbol{r}) + O(a_s^{-1})$$

Hence, from [2.5], the range spanned by $\bar{r}$ becomes

$$[2.9] \quad (d + \boldsymbol{n}\cdot\boldsymbol{r}) + O(a_s^{-1}) \leq \bar{r} \leq 2a_s + O(1)$$

Furthermore, the volume element dV_2, given by [2.4], may be expressed as

$$[2.10] \quad dV_2 = 2\pi\bar{r}[\bar{r} - (d + \boldsymbol{n}\cdot\boldsymbol{r}) + O(\bar{r}^2/a_s)]d\bar{r}$$

Thus, from [2.2],

$$[2.11] \quad E' = 2\pi \int_{d+\boldsymbol{n}\cdot\boldsymbol{r}+O(a_s^{-1})}^{2a_s+O(1)} \bar{r}[\bar{r} - (d + \boldsymbol{n}\cdot\boldsymbol{r}) + O(\bar{r}^2/a_s)]\xi(\bar{r})d\bar{r}$$

Let E_∞' denote the limit of E' as $a_s \to \infty$. It is apparent that so long as

$$[2.12] \quad \xi(\bar{r}) = o(\bar{r}^{-3})$$

this limit is given by

$$[2.13] \quad E_\infty' = 2\pi \int_{d+\boldsymbol{n}\cdot\boldsymbol{r}}^{\infty} \bar{r}[\bar{r} - (d + \boldsymbol{n}\cdot\boldsymbol{r})]\xi(\bar{r})d\bar{r}$$

From this equation derives the important conclusion that E_∞' is a function of the single entity $d + \boldsymbol{n}\cdot\boldsymbol{r}$. (This quantity is the distance of the point P, as described by $\boldsymbol{r}$, from the surface of the plane; cf. Fig. 2 in Appendix A.) Consequently, with the functional dependence

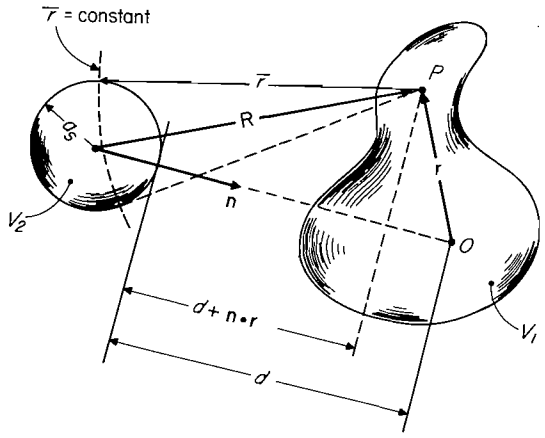

FIG. 1. Definition of variables for the interaction between a sphere of radius a_s (V_2) and another body (V_1).

$$[2.14] \quad E_\infty' = E_\infty'(d + \boldsymbol{n}\cdot\boldsymbol{r})$$

eq. [2.3] shows that

$$[2.15] \quad E_\infty = \lim_{a_s\to\infty} E = \int_{V_1} dV_1\, E_\infty'(d + \boldsymbol{n}\cdot\boldsymbol{r})n_1n_2$$

Henceforth we shall specialize the body V_1 to be ellipsoidal in shape. With the particle locator point O in V_1 chosen to lie at the center of the ellipsoid, the interior of the ellipsoid is described in invariant vector/dyadic form by the inequality

$$[2.16] \quad \mathbf{D}^{-2}:\boldsymbol{rr} \leq 1 \text{ (defines } V_1)$$

(The equality sign describes those points $\boldsymbol{r}$ lying on the surface of the ellipsoid.) In this relation $\mathbf{D}$ is the symmetric, positive-definite dyadic

$$[2.17] \quad \mathbf{D} = \boldsymbol{e}_1\boldsymbol{e}_1a_1 + \boldsymbol{e}_2\boldsymbol{e}_2a_2 + \boldsymbol{e}_3\boldsymbol{e}_3a_3$$

with (a_1,a_2,a_3) the semi-lengths of the principal axes of the ellipsoid, and $(\boldsymbol{e}_1,\boldsymbol{e}_2,\boldsymbol{e}_3)$ a trio of mutually perpendicular unit vectors colinear with each of the three principal axes. The notation in [2.16] is standard (27); namely, for $\boldsymbol{\Psi}$ any dyadic, $\boldsymbol{\Psi}^{-1}$ denotes the inverse dyadic; furthermore, $\boldsymbol{\Psi}^2 = \boldsymbol{\Psi}\cdot\boldsymbol{\Psi}$.

Observe that the position and orientation of the ellipsoid with respect to the plane, though arbitrary, are each to be held fixed during the integration of [2.15]. The position of the ellipsoid is completely specified by the distance d of its center O from the surface of the plane boundary, whereas its orientation is completely specified by the orientations of each of the unit vectors $(\boldsymbol{e}_1,\boldsymbol{e}_2,\boldsymbol{e}_3)$ with respect to the unit vector $\boldsymbol{n}$ drawn normal to the plane towards the ellipsoid.

Can. J. Chem. Downloaded from www.nrcresearchpress.com by 210.87.254.6 on 09/06/12
For personal use only.

It is convenient to define a new variable of integration,

$$[2.18] \quad \boldsymbol{r}_* = \mathbf{D}^{-1}\cdot\boldsymbol{r}\alpha$$

in place of $\boldsymbol{r}$ in [2.15]. For the time being the scalar α will be regarded as arbitrary. Inverse to [2.18] is the relation

$$[2.19] \quad \boldsymbol{r} = \mathbf{D}\cdot\boldsymbol{r}_*/\alpha$$

Equation [2.16] implies that the integration of $\boldsymbol{r}$ over V_1 in [2.15] is formally equivalent to integrating the integrand $dV_1{}^*E_\infty'(d + \mathbf{D}:\boldsymbol{n}\boldsymbol{r}_*/\alpha)$ over the volume $V_1{}^*$ of the sphere

$$[2.20] \quad \boldsymbol{r}_*\cdot\boldsymbol{r}_*/\alpha^2 \leq 1 \text{ (defines } V_1{}^*)$$

of radius α. Here,

$$dV_1 = dx_1dx_2dx_3 = a_1dx_1{}^*a_2dx_2{}^*a_3dx_3{}^*$$

whence

$$[2.21] \quad dV_1 = \alpha^{-3}\det\mathbf{D}\, dV_1{}^*$$

where $\boldsymbol{r} \equiv (x_1, x_2, x_3)$ and $\boldsymbol{r}_* \equiv (x_1{}^*, x_2{}^*, x_3{}^*)$. In addition,

$$[2.22] \quad \det\mathbf{D} = a_1a_2a_3$$

is a constant.

Define the positive scalar α as the magnitude of the vector $\boldsymbol{\alpha}$ defined as[3]

$$[2.23] \quad \boldsymbol{\alpha} = \hat{\boldsymbol{\alpha}}\alpha = \boldsymbol{n}\cdot\mathbf{D}$$

with $\hat{\boldsymbol{\alpha}}$ a unit vector along $\boldsymbol{\alpha}$. Thus,

$$[2.24] \quad \alpha = |\boldsymbol{n}\cdot\mathbf{D}|$$

or, equivalently,

$$[2.25] \quad \alpha^2 = \mathbf{D}^2{:}\boldsymbol{n}\boldsymbol{n}$$

In addition,

$$[2.26] \quad \hat{\boldsymbol{\alpha}} = \boldsymbol{n}\cdot\mathbf{D}/|\boldsymbol{n}\cdot\mathbf{D}|$$

Note that since $\mathbf{D}$ is a symmetric dyadic no difference exists between the vectors $\boldsymbol{n}\cdot\mathbf{D}$ and $\mathbf{D}\cdot\boldsymbol{n}$.

These transformations lead to a functional dependence of the potential E_∞' upon the following combination of variables:

$$[2.27] \quad d + \boldsymbol{n}\cdot\boldsymbol{r} = d + \mathbf{D}:\boldsymbol{n}\boldsymbol{r}_*/\alpha \equiv d + \boldsymbol{\alpha}\cdot\boldsymbol{r}_*$$

Equations [2.15], [2.20], and [2.21] combine with the latter to yield

$$[2.28] \quad E_\infty = \int_{\boldsymbol{r}_*\cdot\boldsymbol{r}_*\leq\alpha^2} dV_1{}^*\, E_\infty'(d + \hat{\boldsymbol{\alpha}}\cdot\boldsymbol{r}_*)n_1n_2 \times \alpha^{-3}\det\mathbf{D}$$

By comparing [2.15] with the above it is clear that the effect of the transformation of variables is such that the integrated potential for an ellipsoid (described by the dyadic $\mathbf{D}$, and whose center is at a distance d from a plane whose unit outer normal is $\boldsymbol{n}$) differs only by the scalar factor[4] $\alpha^{-3}\det\mathbf{D}$ from the integrated potential for a sphere (of radius α, whose center is at a distance d from a plane whose unit outer normal is $\hat{\boldsymbol{\alpha}}$). This theorem applies for all pairwise potentials ξ satisfying the restriction [2.12]. (Thus, for example, it would not be applicable to the potential between a uniformly charged plane and a uniformly charged ellipsoid, since such a case would result in $\xi = O(r^{-2})$, in violation of [2.12].)

Partial integration of [2.28] can be effected by defining a circular cylindrical coordinate system (ρ,ϕ,z) with unit vectors $(\hat{\boldsymbol{\rho}},\hat{\boldsymbol{\phi}},\hat{\boldsymbol{z}} = \hat{\boldsymbol{\alpha}})$ and with origin at O, the center of the ellipsoid V_1. In this coordinate system, $\boldsymbol{r}_* = \hat{\boldsymbol{\rho}}\rho + \hat{\boldsymbol{\alpha}}z$, whence $d + \hat{\boldsymbol{\alpha}}\cdot\boldsymbol{r}_* = d + z$. Consequently, the domain [2.20] corresponds to $\boldsymbol{r}_*\cdot\boldsymbol{r}_* = \rho^2 + z^2 \leq \alpha^2$. The volume element dV_1 is now $\rho d\rho d\phi dz$. Upon integration over the ranges $0 \leq \rho \leq (\alpha^2 - z^2)^{1/2}$ and $0 \leq \phi \leq 2\pi$, eq. [2.28] becomes

$$E_\infty = \pi n_1n_2\alpha^{-3}\det\mathbf{D}\int_{-\alpha}^{\alpha}(\alpha^2 - z^2) \times E_\infty'(d + z)dz$$

Explicitly,

$$[2.29] \quad E_\infty = 2\pi^2n_1n_2\alpha^{-3}\det\mathbf{D}\int_{z=-\alpha}^{\alpha}(\alpha^2 - z^2) \times \int_{\bar{r}=d+z}^{\infty}\bar{r}[\bar{r} - (d + z)]\xi(\bar{r})d\bar{r}dz$$

The latter follows from [2.13], [2.27], and the above definitions of the circular cylindrical coordinate system. It is convenient to scale distances with the body-dimension parameter α, in which case the integration variables appearing in [2.29] may be transformed via the definitions

$$[2.30] \quad u = \bar{r}/\alpha,\ \zeta = (z + d)/\alpha$$

and

[3]It is shown in Appendix A that the scalar $\alpha \equiv d - s$, where d is the distance of the ellipsoid center from the plane and s is the minimum separation distance between the ellipsoid and plane, i.e., the distance of the closest point on the ellipsoid surface from the plane. As such, α may be regarded as a body-size parameter whose value depends upon the ellipsoid's orientation.

[4]Note that this scalar factor is dimensionless and, hence, independent of the *size* of the ellipsoid. It depends only upon the *shape* $a_1 : a_2 : a_3$ of the ellipsoid and its orientation with respect to $\boldsymbol{n}$.

Can. J. Chem. Downloaded from www.nrcresearchpress.com by 210.87.254.6 on 09/06/12
For personal use only.

[2.31] $\delta = d/\alpha$

Consequently,

$$[2.32] \quad E_\infty = 2\pi^2 n_1 n_2 \alpha^3 \det \mathbf{D} \int_{\zeta=\delta-1}^{\delta+1} [1 - (\zeta - \delta)^2] \times \int_{u=\zeta}^{\infty} u(u - \zeta)\xi(\alpha u)\mathrm{d}u\mathrm{d}\zeta$$

Upon reversing the order of the integrations appearing in [2.32], it is possible to reduce the two-dimensional integral to the sum of two one-dimensional integrals (over u):

$$[2.33] \quad E_\infty = 2\pi^2 n_1 n_2 \alpha^3 \det \mathbf{D} \times \left[\int_{\delta-1}^{\delta+1} u\xi(\alpha u)H(u; u)\mathrm{d}u + \int_{\delta+1}^{\infty} u\xi(\alpha u)H(u; \delta + 1)\mathrm{d}u \right]$$

in which

$$[2.34] \quad H(u; x) = \int_{\delta-1}^{x} (u - \zeta)[1 - (\zeta - \delta)^2]\mathrm{d}\zeta$$

The H integration is readily performed in closed form. However, we shall not bother to give the explicit result since, for the inverse-power potentials of interest to us here, the original two-dimensional integral [2.32] is actually algebraically easier to evaluate.[5]

3. Inverse-power Functions

In this section we perform the integration of [2.32] for inverse-power functions of the form

$$[3.1] \quad \xi(r) = K_q r^{-q} \quad (q > 3)$$

where K_q is a constant that may depend upon q. The restriction $q > 3$ is imposed by [2.12].

The intermediate result obtained after performing the u integration in [2.32] is

$$[3.2] \quad E_q = \frac{2\pi^2 n_1 n_2 K_q \alpha^{3-q} \det \mathbf{D}}{(q - 2)(q - 3)} \times \int_{\delta-1}^{\delta+1} [1 - (\zeta - \delta)^2]\mathrm{d}\zeta/\zeta^{q-3}$$

We have supressed the subscript ∞ (since it is no longer relevant), and introduced in its stead the subscript q, which denotes the inverse power of the intermolecular potential. After much algebra the remaining integral yields

$$[3.3] \quad E_q = 4\pi^2 n_1 n_2 K_q (\det \mathbf{D})\alpha^{3-q} f_q(\delta)$$

with

$$[3.4] \quad f_q(\delta) = \frac{1}{(q - 2)(q - 3)(q - 4)(q - 5)(q - 6)} \times \left\{ \frac{[\delta + (q - 5)](\delta - 1)^{q-5} - [\delta - (q - 5)](\delta + 1)^{q-5}}{(\delta^2 - 1)^{q-5}} \right\}$$

provided that $q \neq 4, 5, 6$ (and $q > 3$). An alternative, but perhaps simpler, form is

$$[3.5] \quad f_q(\delta) = \frac{1}{(q - 2)(q - 3)(q - 4)(q - 5)(q - 6)} \times \left[\frac{\delta + (q - 5)}{(\delta + 1)^{q-5}} - \frac{\delta - (q - 5)}{(\delta - 1)^{q-5}} \right]$$

The additional restrictions upon q are not intrinsic; that is, $q = 4$, 5, and 6 merely define special cases for which [3.4] or [3.5] are not valid due to the generation of a logarithmic term. Each of these three cases must be evaluated, one-by-one, directly from [3.2]. For example, in the physically important case $q = 6$, we obtain

$$[3.6] \quad f_6(\delta) = \frac{1}{4}\left[\frac{\delta}{3(\delta^2 - 1)} - \frac{1}{6}\ln\left(\frac{\delta + 1}{\delta - 1}\right) \right]$$

When the ellipsoid degenerates to a sphere of radius a, such that $\alpha = a_1 = a_2 = a_3 = a$, the above reduces to the classical result originally obtained by Hamaker (25).

The form of the intermolecular potential V_{12} between a pair of molecules within the ellipsoid and slab, respectively, when separated by a distance r_{12} will be assumed to be given by (28, 29)

$$[3.7] \quad V_{12} = 4\varepsilon[(\sigma/r_{12})^n - (\sigma/r_{12})^m] \qquad (n > m)$$

with σ the collision diameter (2 to 10 Å) and ε the interaction energy (ε/k = 10 to 1000 K, in which k is Boltzmann's constant). The first term corresponds to a short-range repulsion and the second to a long-range attraction. Such a potential was used by Bradley (30). Although Dahneke (22) is critical of the repulsive term — presenting sound arguments for particle flattening and the concomitant use of Hertz's theory of repulsion via the compressive stresses generated within the particle — we shall nevertheless utilize the repulsive term in [3.7]. All we really seek here is an illustrative example applicable to a prototype nonspherical particle. For this

[5] The utility of [2.33] would appear only for potentials where the inner integration in [2.32] could not be accomplished in closed form, thereby requiring numerical quadrature. It is obviously far easier to perform a one-dimensional numerical integration than a two-dimensional one.

Can. J. Chem. Downloaded from www.nrcresearchpress.com by 210.87.254.6 on 09/06/12
For personal use only.

reason also, retardation effects, explained by the Lifshitz field theory, will also be ignored — although they are known to increase the exponent of the classical attractive potential from $m = 6$ to $m = 7$ at intermolecular distances $r_{12} > \sim 50$ nm (3, 23).

The potential energy E of the ellipsoid corresponding to the intermolecular potential [3.7] can be derived from the relation $E = E_n - E_m$ where E_n and E_m are given by [3.3] with the choice of the constants $K_n = 4\varepsilon\sigma^n$ and $K_m = 4\varepsilon\sigma^m$. In this manner there results

$$[3.8] \quad E = 4A\alpha^{-3} \det \mathbf{D} \left[-\left(\frac{\sigma}{\alpha}\right)^{m-6} f_m(\delta) + \left(\frac{\sigma}{\alpha}\right)^{n-6} f_n(\delta) \right]$$

where

$$[3.9] \quad A = 4\pi^2 n_1 n_2 \varepsilon \sigma^6$$

is Hamaker's "constant". Typical numerical values of A lie in the range 5×10^{-13} to 5×10^{-12} ergs (19).

Precedent exists for using a Leonard-Jones 6-12 potential ($m = 6$, $n = 12$). However, since the exponent of the repulsive term is not very well quantified, we will choose $n = 8$ in the interests of simpler algebra. Thus, [3.8] becomes

$$[3.10] \quad E = A\alpha^{-3} \det \mathbf{D} \left[\frac{1}{6} \ln\left(\frac{\delta + 1}{\delta - 1}\right) - \frac{\delta}{3(\delta^2 - 1)} + \frac{4}{45}\left(\frac{\sigma}{\alpha}\right)^2 \frac{\delta}{(\delta^2 - 1)^3} \right]$$

for the 6-8 intermolecular potential.

4. Force and Torque on the Ellipsoid

The results of the preceding section will now be used to illustrate how dispersion forces contribute to the *en vacuo* interaction between an ellipsoidal particle and a semi-infinite solid bounded by a plane. Of particular interest is the calculation of the equilibrium orientation and separation distance of the ellipsoid from the plane.

As regards possible applications to the class of boundary-layer problems outlined in the Introduction, the calculation to be performed should be regarded as purely expository with respect to the physics. Although double-layer forces are often important in liquid systems (3, 21), they do not give rise to an infinite repulsion. Since they do not provide qualitatively "correct" behavior they will not be further considered. Rather, the particle/boundary potential will be assumed to be the net effect only of the pairwise intermolecular interactions, which constitutes the sole theoretical thrust of the present paper.

The potential energy E of the ellipsoid may be regarded as a function of the location[6] $\boldsymbol{R}$ of its center and of its orientation $\boldsymbol{\phi}$. Thus,

$$[4.1] \quad E = E(\boldsymbol{R}, \boldsymbol{\phi})$$

The notation is that of Brenner and Condiff (5, 12). In terms of these variables the external force $\boldsymbol{F}$ and torque $\boldsymbol{T}$ (about the center O of the ellipsoid) exerted on the ellipsoid by the slab are, respectively,

$$[4.2a,b] \quad \boldsymbol{F} = -\partial E/\partial \boldsymbol{R})_{\boldsymbol{\phi}}, \quad \boldsymbol{T} = -\partial E/\partial \boldsymbol{\phi})_{\boldsymbol{R}}$$

It is convenient to choose the origin from which $\boldsymbol{R}$ is to be measured to lie on the bounding plane of the slab. With this choice,

$$[4.3] \quad d = \boldsymbol{R}\cdot\boldsymbol{n}$$

Relative to space-fixed axes locked into the slab, the body-fixed ellipsoidal unit vectors $\boldsymbol{e}_j$ ($j = 1, 2, 3$) appearing in the definition [2.17] of $\mathbf{D}$ are each functions of the orientation $\boldsymbol{\phi}$ of the ellipsoid. While the $\boldsymbol{e}_j$ can be expressed in terms of space-fixed unit vectors (of which $\boldsymbol{n}$ is one) via a system of Eulerian angles (5), such an explicit representation will not be required for our purposes. Rather, all the requisite calculations can be brought to fruition in invariant form. It will suffice in this respect merely to note that $\mathbf{D} = \mathbf{D}(\boldsymbol{\phi})$, whence [2.24] or [2.25] may be regarded as giving α as a function of $\boldsymbol{\phi}$ and $\boldsymbol{n}$. Thus, with these choices we have that

$$[4.4a,b] \quad d = d(\boldsymbol{R},\boldsymbol{n}), \qquad \alpha = \alpha(\boldsymbol{\phi},\boldsymbol{n})$$

where the former is given explicitly by [4.3]. In our space-fixed view, $\boldsymbol{n}$ is, of course, to be regarded as a given constant vector.

The results of Section 3 give E explicitly in the functional form

$$[4.5] \quad E = E(d,\alpha)$$

rather than in the form [4.1]. The transformations of partial derivatives between the (d,α) and $(\boldsymbol{R},\boldsymbol{\phi})$ systems, required to calculate $\boldsymbol{F}$ and $\boldsymbol{T}$ via [4.2], are readily effected by standard methods to obtain

$$[4.6] \quad \left(\frac{\partial E}{\partial \boldsymbol{R}}\right)_{\boldsymbol{\phi}} = \left(\frac{\partial d}{\partial \boldsymbol{R}}\right)_{\boldsymbol{n}} \left(\frac{\partial E}{\partial d}\right)_{\alpha} = \boldsymbol{n}\left(\frac{\partial E}{\partial d}\right)_{\alpha}$$

and

$$[4.7] \quad \left(\frac{\partial E}{\partial \boldsymbol{\phi}}\right)_{\boldsymbol{R}} = \left(\frac{\partial \alpha}{\partial \boldsymbol{\phi}}\right)_{\boldsymbol{n}} \left(\frac{\partial E}{\partial \alpha}\right)_{d}$$

[6]This position vector should not be confused with the vector $\boldsymbol{R}$ appearing in [2.6].

Can. J. Chem. Downloaded from www.nrcresearchpress.com by 210.87.254.6 on 09/06/12
For personal use only.

Equation [4.3] has to be utilized in the former of these relations. Upon differentiation, [2.25] yields

$$[4.8]\quad \left(\frac{\partial\alpha}{\partial\phi}\right)_n = \frac{1}{2\alpha}\left(\frac{\delta\mathbf{D}^2}{\delta\phi}\right):\boldsymbol{nn}$$

However, for any body-fixed dyadic, $\Psi = \Psi(\phi)$, Brenner and Condiff (5) show that

$$[4.9]\quad \frac{\delta\Psi}{\delta\phi} = -[\boldsymbol{\varepsilon}:\Psi + (\boldsymbol{\varepsilon}:\Psi^{\dagger})^{\dagger}]$$

in which $\boldsymbol{\varepsilon}$ is the unit alternating pseudoisotropic triadic ($\boldsymbol{\varepsilon} = -\mathbf{I}\times\mathbf{I}$, with $\mathbf{I}$ the unit dyadic). The dagger denotes a dyadic transposition operator. A straightforward calculation utilizing the symmetry properties of $\mathbf{D}^2$ (and $\boldsymbol{nn}$) eventually yields

$$[4.10]\quad \frac{\delta\mathbf{D}^2}{\delta\phi}:\boldsymbol{nn} = 2(\boldsymbol{\varepsilon}\cdot\boldsymbol{n})\cdot\mathbf{D}^2\cdot\boldsymbol{n} \equiv -2(\boldsymbol{n}\times\mathbf{D})\cdot(\mathbf{D}\cdot\boldsymbol{n})$$

Substitution of the latter into [4.8] followed by use of [2.24] and [2.26] thereby gives

$$[4.11]\quad \left(\frac{\partial\alpha}{\partial\phi}\right)_n = -\boldsymbol{n}\times\mathbf{D}\cdot\hat{\boldsymbol{\alpha}}$$

In this manner [4.7] becomes

$$[4.12]\quad \left(\frac{\partial E}{\partial\phi}\right)_R = -\boldsymbol{n}\times\mathbf{D}\cdot\hat{\boldsymbol{\alpha}}\left(\frac{\partial E}{\partial\alpha}\right)_d$$

Equation [4.2] for the force and torque may now be written as

$$[4.13]\quad \boldsymbol{F} = -\boldsymbol{n}\left(\frac{\partial E}{\partial d}\right)_\alpha$$

$$[4.14]\quad \boldsymbol{T} = \boldsymbol{n}\times\mathbf{D}\cdot\hat{\boldsymbol{\alpha}}\left(\frac{\partial E}{\partial\alpha}\right)_d$$

Alternatively, in terms of the vector defined as

$$[4.15]\quad \boldsymbol{r}_s = -\mathbf{D}\cdot\hat{\boldsymbol{\alpha}}$$

the torque may be expressed in the form

$$[4.16]\quad \boldsymbol{T} = -\boldsymbol{n}\times\boldsymbol{r}_s\left(\frac{\partial E}{\partial\alpha}\right)_d$$

It is demonstrated in Appendix A (see Fig. 2) that, for a fixed position and orientation of the ellipsoid, the vector $\boldsymbol{r}_s$ is the vector drawn from the center of the ellipsoid to that point on its surface which lies closest to the plane. The tendency of the torque is thus to rotate the body about an axis which is perpendicular to the plane formed from the vectors $\boldsymbol{n}$ and $\boldsymbol{r}_s$.[7]

Equation [4.13] shows that the direction of the force on the ellipsoid is always normal to the plane of the slab, while [4.16] shows that the torque possesses no component about an axis normal to the wall ($\boldsymbol{n}\cdot\boldsymbol{T} = 0$) that would otherwise tend to rotate the ellipsoid about such an axis. Both of these conclusions are obviously consistent with the transversely isotropic nature of the (homogeneous) slab with respect to the $\boldsymbol{n}$ axis. For there exists no mechanism by which the different perspectives offered by the body as it is rotated about the $\boldsymbol{n}$ axis can be physically distinct from one another. Rather, rotation of the body about such an axis cannot be physically distinguished from a rotation of the observer, and such a rotation clearly cannot result in any force or torque on the body.

We note also that in the special case where the ellipsoid degenerates to a sphere, $a_1 = a_2 = a_3 = a$, say, that $\mathbf{D} = \mathbf{I}a$. For this situation $\hat{\boldsymbol{\alpha}} = \boldsymbol{n}$, whence $\boldsymbol{T} = 0$. The vanishing of the torque under these circumstances is obviously consistent with the geometry symmetry of the sphere/slab system.

Of particular interest are the position(s) and orientation(s) for which the ellipsoid experiences no net force or torque. These states will be denoted by the superscript 0. Hence, d^0 (or $\boldsymbol{R}^0$) will denote the force-free position of the ellipsoid (which value will be shown generally to vary with the "orientation" α of the ellipsoid). Similarly, $\boldsymbol{e}_j{}^0 (j = 1, 2, 3)$ or ϕ^0 or $\mathbf{D}^0$ or α_0 will denote the torque-free state. (This state will be shown to be independent of the "position" d of the ellipsoid.) Double superscript notation, e.g. d^{00}, will represent the combined force- and torque-free states.

From [4.13], for a fixed orientation α, the condition $\boldsymbol{F} = 0$ corresponds to that value of $d = d^0$ for which $(\partial E/\partial d)_\alpha = 0$, i.e.

$$[4.17]\quad (\partial E/\partial d)_\alpha^0 \overset{\text{def.}}{=} (\partial E/\partial d)_\alpha|_{d=d^0} = 0$$

From [3.10] there follows

$$[4.18]\quad (\partial E/\partial d)_\alpha = A\alpha^{-4}\det\mathbf{D}\left[\frac{2}{3(\delta^2-1)^2} - \frac{4}{45}\left(\frac{\sigma}{\alpha}\right)^2\frac{5\delta^2+1}{(\delta^2-1)^4}\right]$$

[7] It is also demonstrated in Appendix A that $\boldsymbol{n}\cdot\boldsymbol{r}_s = -\alpha$. Thus, if $\boldsymbol{r}_s$ rather than α is used as the orientational variable, eq. [4.16] may be expressed in the interesting invariant form

$$\boldsymbol{T} = (\boldsymbol{n}\times\boldsymbol{r}_s)\boldsymbol{n}\cdot(\partial E/\partial\boldsymbol{r}_s)_{n,d}$$

directly in terms of the physically observable vectors $\boldsymbol{n}$ and $\boldsymbol{r}_s$.

Can. J. Chem. Downloaded from www.nrcresearchpress.com by 210.87.254.6 on 09/06/12
For personal use only.

The value

[4.19] $\delta^0 = d^0/\alpha$

corresponding to the vanishing of the term in square brackets in [4.18] is easily found to be

[4.20] $$\delta^0 = \left[1 + \frac{2}{\sqrt{5}}\left(\frac{\sigma}{\alpha}\right)\left\{1 + \frac{5}{36}\left(\frac{\sigma}{\alpha}\right)^2\right\}^{1/2} + \frac{1}{3}\left(\frac{\sigma}{\alpha}\right)^2\right]^{1/2}$$

Now σ is of molecular dimensions, whereas α — which is of the order of the size of the ellipsoid — is of macroscopic dimensions. Thus, $\sigma/\alpha \ll 1$. Hence, by the binomial theorem

[4.21] $$\delta^0 \simeq 1 + \frac{1}{\sqrt{5}}\left(\frac{\sigma}{\alpha}\right) + \frac{1}{15}\left(\frac{\sigma}{\alpha}\right)^2 + O\left(\frac{\sigma}{\alpha}\right)^3$$

In conjunction with [4.19] this equation yields the distance d^0 (for each orientation α) at which $\boldsymbol{F} = 0$. To establish whether, for a fixed orientation α, the condition [4.17] corresponds to a (local) minimum or maximum (if either), we calculate

$$\left(\frac{\partial^2 E}{\partial d^2}\right)_\alpha^0 \overset{\text{def.}}{=} \left(\frac{\partial^2 E}{\partial d^2}\right)_\alpha\Bigg|_{\delta=\delta^0} = \frac{8A(\det \mathbf{D})}{45\alpha^5}\left(\frac{\sigma}{\alpha}\right)^2 \frac{\delta^0[5(\delta^0)^2 + 7]}{[(\delta^0)^2 - 1]^5}$$

Inasmuch as $\delta^0 > 1$ this shows that

[4.22] $(\partial^2 E/\partial d^2)_\alpha^0 > 0$

whence the condition [4.21] corresponds to a minimum for each α. Equivalently, if we write $\boldsymbol{F} = \boldsymbol{n}F(d,\alpha)$ then $F < 0$ for $d > d^0$ and $F > 0$ for $d < d^0$. In words, (for each orientation) the force exerted on the ellipsoid by the slab is attractive if the ellipsoid center is further away from the plane than d^0, and repulsive if closer than d^0.

From [4.14] the condition that $\boldsymbol{T} = 0$ requires that the right-hand side be zero. By the chain rule,

$$(\partial E/\partial\alpha)_d = (\partial E/\partial\alpha)_\delta + (\partial\delta/\partial\alpha)_d(\partial E/\partial\delta)_\alpha$$

However, from the definition [2.31] of δ, we have $(\partial E/\partial\delta)_\alpha = (\partial E/\partial d)_\alpha$. The latter vanishes in the force-free state as a consequence of [4.17]. Hence, $(\partial E/\partial\alpha)_d^0 = (\partial E/\partial\alpha)_\delta^0$. Upon differentiating [3.10] with respect to α at constant δ and evaluating the result at the value of δ^0 given by [4.21] we eventually obtain

[4.23] $$\left(\frac{\partial E}{\partial\alpha}\right)_d^0 = \frac{A \det \mathbf{D}}{\alpha^4}\left(\frac{\sigma}{\alpha}\right)\left[\frac{2\sqrt{5}}{9} + O\left(\frac{\sigma}{\alpha}\ln\frac{\sigma}{\alpha}\right)\right]$$

It is a consequence of this that

[4.24] $(\partial E/\partial\alpha)_d^0 \overset{\text{def.}}{=} (\partial E/\partial\alpha)_{d=d^0} > 0$

for all orientations α.

Equation [4.14] thereby shows that the force- and torque-free condition requires that the vector $\mathbf{D}\cdot\hat{\boldsymbol{\alpha}}^0$ be colinear with $\boldsymbol{n}^0$,[8] whence it is required that

[4.25] $\mathbf{D}\cdot\hat{\boldsymbol{\alpha}}^0 = \lambda\boldsymbol{n}^0$

wherein (cf. [2.26])

[4.26] $\hat{\boldsymbol{\alpha}}^0 = \mathbf{D}\cdot\boldsymbol{n}^0/|\mathbf{D}\cdot\boldsymbol{n}^0|$

and λ is a scalar to be determined. Explicitly, the latter two equations necessitate that

[4.27] $\mathbf{D}^2\cdot\boldsymbol{n}^0/\alpha_0 = \lambda\boldsymbol{n}^0$

in which

[4.28] $\alpha_0 = (\boldsymbol{n}^0\cdot\mathbf{D}^2\cdot\boldsymbol{n}^0)^{1/2} \equiv |\mathbf{D}\cdot\boldsymbol{n}^0|$

Dot multiply [4.27] by $\boldsymbol{n}^0$ and use the definition of α_0 to obtain $\lambda = \alpha_0$. Consequently, [4.27] shows that the zero torque condition corresponds to those values of $\boldsymbol{n}^0$ for which

[4.29] $\mathbf{D}^2\cdot\boldsymbol{n}^0 = \alpha_0{}^2\boldsymbol{n}^0$

The preceding relation requires that the zero-torque orientation $\boldsymbol{n}^0$ be an eigenvector of $\mathbf{D}^2$ (and that $\alpha_0{}^2$ be an eigenvalue). However, [2.17] shows that, in general,

[4.30] $\mathbf{D}^2\cdot\boldsymbol{e}_j = a_j{}^2\boldsymbol{e} \qquad (j = 1, 2, 3)$

Comparison with [4.29] thereby yields[9]

[4.31] $\boldsymbol{n}^0 = \boldsymbol{e}_j \qquad (j = 1, 2, 3)$

with corresponding eigenvalues

[4.32] $\alpha_0{}^2 = a_j{}^2 \qquad (j = 1, 2, 3)$

Equation [4.31] is equivalent to the conclusion that the ellipsoid will experience no net torque when it is oriented in such a manner that one of its three

[8]Since we are concerned only with the *relative* orientations of the ellipsoid and plane, we have altered our notation here so as to regard the ellipsoid as being fixed and the plane as being rotated; that is, in place of the notation $(\mathbf{D}^0, \boldsymbol{n})$ we prefer to use $(\mathbf{D}, \boldsymbol{n}^0)$. The *relative* orientation is, of course, the same in both views. This is an algebraically simpler view than the prior one, in which in place of equation [4.25] there would arise the more complex-appearing equation $\mathbf{D}^0\cdot\hat{\boldsymbol{\alpha}}^0 = \lambda\boldsymbol{n}$, wherein $\hat{\boldsymbol{\alpha}}^0 = \mathbf{D}^0\cdot\boldsymbol{n}/|\mathbf{D}^0\cdot\boldsymbol{n}|$.

[9]If we revert back to our previous perspective, where the plane is regarded as fixed, and the ellipsoid free to rotate, the three zero-torque orientations of the ellipsoid $(\boldsymbol{e}_1{}^0, \boldsymbol{e}_2{}^0, \boldsymbol{e}_3{}^0)$ are those for which $\boldsymbol{e}_j{}^0 = \boldsymbol{n}$ $(j = 1, 2, 3)$.

Can. J. Chem. Downloaded from www.nrcresearchpress.com by 210.87.254.6 on 09/06/12
For personal use only.

principal axes is perpendicular to the wall. The other two principal axes will, of course, lie in a plane parallel to the wall.

In terms of the body-fixed vector $\boldsymbol{r}_s$ defined in [4.15], whose physical significance is described in Appendix A, these zero-torque orientations correspond to the three orientations

$$[4.33] \quad \boldsymbol{r}_s^0 = a_j \boldsymbol{e}_j \equiv a_j \boldsymbol{n} \qquad (j = 1, 2, 3)$$

In deriving [4.31] we have not actually used the explicit form of $E(d,\alpha)$ given in [3.10], except insofar as the inequality [4.24] is concerned. Thus, the orientational result is much more general than might otherwise be implied. Indeed, it is obviously a pure symmetry result, demanded by the geometric symmetry of the ellipsoid and the slab, and is quite independent of the explicit form of the potential.

Of the three possible orientations of the ellipsoid that result in no torque it remains yet to establish which of these is the stable, equilibrium orientation. The equilibrium position and orientation necessarily correspond to a minimum potential energy for the ellipsoid; that is, $(\partial E/\partial \boldsymbol{R})^*_\phi = 0$ and $(\partial E/\partial \phi)^*_R = 0$, where the asterisk denotes the equilibrium state. From [4.2] these correspond to a force- and torque-free state. While these conditions are necessary for a stable equilibrium, they are by themselves insufficient (31). Sufficient conditions require that the second variation

$$[4.34] \quad \Delta^2 E = \Delta \boldsymbol{R} \cdot \partial^2 E/\partial \boldsymbol{R} \partial \boldsymbol{R} \cdot \Delta \boldsymbol{R} + 2\Delta \boldsymbol{R} \cdot (\partial^2 E/\partial \phi \partial \boldsymbol{R})_{sym} \cdot \Delta \phi + \Delta \phi \cdot \partial^2 E/\partial \phi \partial \phi \cdot \Delta \phi$$

satisfy the inequality (31)

$$[4.35] \quad \Delta^2 E^* > 0$$

for arbitrary displacements $(\Delta \boldsymbol{R}, \Delta \phi)$ from the equilibrium state E^*. Here, "sym" denotes the symmetric portion of the dyadic. It is shown in Appendix B that [4.34] reduces in the state E^{00} of zero force and torque to

$$[4.36] \quad \Delta^2 E^{00} = (\boldsymbol{n} \cdot \Delta \boldsymbol{R})^2 \left(\frac{\partial^2 E}{\partial d^2}\right)^0_\alpha - \Delta \phi \cdot \left(\frac{\partial^2 \alpha}{\partial \phi \partial \phi}\right)^0 \cdot \Delta \phi \left(\frac{\partial E}{\partial \alpha}\right)^0_d$$

in which

$$[4.37] \quad \left(\frac{\partial^2 \alpha}{\partial \phi \partial \phi}\right)^0 = -\frac{1}{\alpha_0}[\alpha_0^2(\mathbf{I} - \boldsymbol{n}^0\boldsymbol{n}^0) + \boldsymbol{n}^0 \times \mathbf{D}^2 \times \boldsymbol{n}^0]$$

As regards the first term of [4.36], we have from [4.3] that

$$\Delta d = \boldsymbol{n} \cdot \Delta \boldsymbol{R}$$

Into [4.37] introduce the expressions [4.31] and [4.32]. In addition, write

$$\mathbf{I} = \boldsymbol{e}_j\boldsymbol{e}_j + \boldsymbol{e}_k\boldsymbol{e}_k + \boldsymbol{e}_l\boldsymbol{e}_l$$

and

$$\mathbf{D}^2 = \boldsymbol{e}_j\boldsymbol{e}_j a_j^2 + \boldsymbol{e}_k\boldsymbol{e}_k a_k^2 + \boldsymbol{e}_l\boldsymbol{e}_l a_l^2$$

in which (j,k,l) is a cyclic permutation of the indices 1, 2, and 3 (so that $j \neq k \neq l$). In this manner [4.37] becomes

$$\left(\frac{\partial^2 \alpha}{\partial \phi \partial \phi}\right)^0 = \frac{1}{a_j}[\boldsymbol{e}_k\boldsymbol{e}_k(a_l^2 - a_j^2) + \boldsymbol{e}_k\boldsymbol{e}_k(a_k^2 - a_j^2)]$$

with $\boldsymbol{e}_j$ the zero-torque orientation (cf. [4.31]) and $j \neq k \neq l$. An arbitrary infinitesimal rotation $\Delta\phi$ can be expressed as (5)

$$\Delta \phi = \boldsymbol{e}_j \Delta\phi_j + \boldsymbol{e}_k \Delta\phi_k + \boldsymbol{e}_l \Delta\phi_l$$

With these substitutions [4.36] becomes

$$[4.38] \quad \Delta^2 E^{00} = (\Delta d)^2 (\partial^2 E/\partial d^2)^0_\alpha + a_j^{-1}[(\Delta\phi_k)^2(a_l^2 - a_j^2) + (\Delta\phi_l)^2(a_k^2 - a_j^2)](\partial E/\partial\alpha)^0_d$$

The combined zero-force and zero-torque state (00) corresponds to a special case of the equilibrium state (*). Thus, in view of [4.22] and [4.24], the inequality [4.35] will be satisfied if, and only if, simultaneously,

$$a_l > a_j \text{ and } a_k > a_j$$

This is equivalent to the requirement that

$$[4.39] \quad a_j = \min(a_1, a_2, a_3)$$

since $j \neq k \neq l$. Inasmuch as $\boldsymbol{e}_j$ has been established to lie parallel to $\boldsymbol{n}$, it may be concluded that the stable equilibrium orientation of the ellipsoid is such that the shortest principal axis of the ellipsoid lies normal to the plane of the slab. Thus, for example, an oblate spheroid will be at equilibrium when its axis of revolution lies normal to the plane, whereas a prolate spheroid will be equilibrated with its axis of revolution parallel to the plane.

Though these conclusions may appear to be limited to situations for which the potential is specifically given by [3.10] ($m = 6$, $n = 8$), the result is clearly true for any attractive/repulsive potential for which the inequalities [4.22] and [4.24]

Can. J. Chem. Downloaded from www.nrcresearchpress.com by 210.87.254.6 on 09/06/12
For personal use only.

are valid. And these inequalities can be shown[10] to obtain whenever $m > n$ in [3.8]. In this sense the stable equilibrium orientational conclusion may be regarded as arising essentially as a result of geometric symmetry rather than from the specific nature of the intermolecular potential energy function [3.7] (with $m = 6$ and $n = 8$).

A homogeneous ellipsoidal particle at rest under the influence of gravity on a horizontal plane wall would do so with its center (of mass) as close to the wall as possible (see Appendix C). This corresponds to the same stable orientation as was found for the attractive/repulsive potential. As such, it reinforces the view that the result may be attributed solely to the geometric symmetry of the ellipsoid/plane wall configuration. Note that in this analogy the short-range repulsive force exerted on the ellipsoid by the wall (i.e., the reaction force at the contact point) has an infinite step function character, rather than deriving from a "soft" potential.

The advantage of our method of calculating the stable equilibrium orientation of the ellipsoid over alternative methods lies in the fact that it shows that the conclusions are independent of the particular potential selected. However, it is also possible to arrive at this orientational conclusion by more elementary means for any specific potential, e.g. [3.10]. Let $d^0 \equiv d^0(\alpha)$ [or, equivalently, $\delta^0(\alpha) = d^0/\alpha$] represent the distance at which the ellipsoid experiences no force. This distance varies, of course, with each orientation α, and corresponds to those values of d for which $(\partial E/\partial d)^0_\alpha = 0$ (and $(\partial^2 E/\partial d^2)^0_\alpha > 0$). The function

$$[4.40] \quad E^0(\alpha) \overset{\text{def.}}{=} E(d = d^0, \alpha)$$

gives the potential energy as a function of α for this zero-force condition. Since the stable equilibrium configuration corresponds to the minimum value of the potential energy function, the stable equilibrium orientation α^* may then be found by establishing the value of α which minimizes $E^0(\alpha)$:

$$[4.41] \quad \alpha^* = \min_\alpha E^0(\alpha)$$

(for which orientation the minimum potential energy E^* is, in fact, $E^* = \min_{d,\alpha} E(d,\alpha) \equiv E^0(\alpha^*)$).

From its definition, [2.24], α spans the bounded range

$$[4.42] \quad a_{\min} \leq \alpha \leq a_{\max}$$

where $a_{\min}$ and $a_{\max}$ are, respectively, the minimum and maximum values of the three lengths (a_1,a_2,a_3). In conducting the search for the value of α which minimizes $E^0(\alpha)$ two possibilities (31) need be considered: (*i*) the point α^* is an interior point — that is, the end points $a_{\min}$ and $a_{\max}$ of the interval [4.42] are not included (in which case the minimum corresponds to the value of α for which $\partial E^0/\partial\alpha|_{\alpha=\alpha^*} = 0$ with $\partial^2 E^0/\partial\alpha^2|_{\alpha=\alpha^*} > 0$); or (*ii*) the point α^* satisfying [4.41] is one of the two boundary points, $a_{\min}$ or $a_{\max}$.

We carried out this search procedure (numerically) for the potential [3.10], for which case the function $E^0(\alpha)$ is given by [3.10] with δ replaced by the expression for δ^0 appearing in [4.20]. It was found that case (*ii*) applied, and that the $\alpha^* = a_{\min}$. This nonvectorial calculation confirms, albeit in a specific case, the more general geometrical conclusions arrived at earlier.

5. Discussion

Having established the stable equilibrium orientation such that $\alpha^* = a_{\min}$, with $a_{\min} = \min(a_1,a_2,a_3)$, eq. [4.21] (or, more accurately, [4.20]) yields the equilibrium distance

$$[5.1] \quad d^* \simeq a_{\min}\left(1 + \frac{1}{\sqrt{5}}\frac{\sigma}{a_{\min}}\right)$$

of the ellipsoid center from the plane. Alternatively, from [A.1], the minimum clearance distance s^* between the ellipsoid and the wall is

$$[5.2] \quad s^* \simeq \sigma/\sqrt{5}$$

Interestingly, this distance is independent of the actual dimensions of the ellipsoid, though such dependence would arise in the next order approximation, involving a term of $O(\sigma^2/a_{\min})$ in s^*. Since, typically, σ lies between 2 and 10 Å, the equilibrium gap width s^* is of the order of molecular dimensions. Considering the roughness of real surfaces, the effect of Hertzian flattening (22, 23), and the implicit approximations of the pairwise additive continuum model, such a result cannot be taken literally. However, the orientational result is likely to remain valid provided that $\boldsymbol{n}$ is interpreted as representing the normal to the *mean* or *projected* area of the rough

[10]Such proofs may be formulated by utilizing the definition $E = E_n - E_m$ $(n > m)$ in conjunction with the monotonicity condition $(\partial E_q/\partial d)_\alpha > 0$ applicable for all q. The zero-force condition then corresponds to $(\partial E_n/\partial d)^0_\alpha = (\partial E_m/\partial d)^0_\alpha$ at $d = d^0$, in addition to which the inequalities, $(\partial E_n/\partial d)_\alpha > (\partial E_m/\partial d)_\alpha$ for $d > d^0$ (and conversely), are readily established. Use of the Taylor series expansions about the zero-force point,

$$(\partial E_q/\partial d)_\alpha = (\partial E_q/\partial d)^0_\alpha + (\partial^2 E_q/\partial d^2)^0_\alpha(d - d^0) + \ldots$$

applied to $q = m$ and $q = n$ may then be employed to establish the general nature of the inequality [4.22]. Similar methods, utilizing the specific functional form [3.3] in conjunction with the fact that $\delta = d/\alpha$, may also be used to establish the general nature of the orientational inequality [4.24].

Can. J. Chem. Downloaded from www.nrcresearchpress.com by 210.87.254.6 on 09/06/12
For personal use only.

and/or deformed surface,

$$[5.3] \quad \boldsymbol{n} = \int d\boldsymbol{s}/|\int d\boldsymbol{s}|$$

where $d\boldsymbol{s}$ represents the "true" directed element of surface area at a point on the "true" surface of the rough slab (32).

Gallily (33) photographed bacterial spores deposited on a plate. These spores were approximately 1 μm in size, and resembled prolate spheroids with an axis ratio of approximately 2:1. His experiments revealed that spores deposited from a liquid medium (which had subsequently been evaporated) do tend to lie flat on the surface, in agreement with the conclusions drawn here. However, for deposition from a gaseous medium he found a distribution of angles θ (between the normal to the plane and the symmetry axis of the spheroid), with a median angle of 30°, instead of the 90° angle predicted by the present theory. In both cases Gallily expected a completely random distribution of angles, for which the orientational probability density function would be sin θ. Thus, his results did not confirm his prediction in either case. He concluded that the liquid-deposited spores had been pulled flat by surface tension during the evaporation process, and that the gas-deposited spores showed deviations from the sin θ density distribution due to their being permanently charged, resulting in an electrostatic interaction with the metal plate upon which they were deposited. Were such the case the nature of the ellipsoid/plane interaction would be different from that considered here.

To the extent that the *en vacuo* ellipsoid/plane potential may be employed even in the presence of an intervening fluid (3), the potential energy function E gives rise to a Boltzmann probability density $P(\boldsymbol{R}, \phi)$ for the position $\boldsymbol{R}$ of the center of the ellipsoid and its orientation ϕ of the form

$$[5.4] \quad P(\boldsymbol{R},\phi) = P_{\max} \exp\left[\frac{E_{\min} - E(\boldsymbol{R},\phi)}{kT}\right]$$

The normalization constant $P_{\max}$ is determined by the requirement that (5)

$$[5.5] \quad \int_{\boldsymbol{R}} \int_{\phi} P \, d^3\phi \, d^3\boldsymbol{R} = 1$$

where the integration is over all positions and orientations. In the simple case of ellipsoids of revolution, [2.17] becomes

$$[5.6] \quad \mathbf{D} = \boldsymbol{ee}a_{\parallel} + (\mathbf{I} - \boldsymbol{ee})a_{\perp}$$

where $\boldsymbol{e}$ is a body fixed unit vector (5) along the symmetry axis and $a_{\parallel}$ and $a_{\perp}$ are, respectively, the semilengths parallel and perpendicular to the axis of revolution of the spheroid. With the cone angle θ between $\boldsymbol{n}$ and $\boldsymbol{e}$ defined as $\cos\theta = \boldsymbol{e}\cdot\boldsymbol{n}$, this yields

$$[5.7] \quad \alpha = [(a_{\parallel}^2 - a_{\perp}^2)\cos^2\theta + a_{\perp}^2]^{1/2}$$

In this manner [5.4] becomes

$$[5.8] \quad P(d,\theta) = P_{\max} \exp\left[\frac{E_{\min} - E(d,\theta)}{kT}\right]$$

with $P_{\max}$ chosen such that

$$[5.9] \quad 2\pi \int_0^{\infty} \int_0^{\pi} P(d,\theta) \sin\theta \, d\theta dd = 1$$

In this expression $E(d,\theta)$ is given by [3.10] with the value of $\alpha \equiv \alpha(\theta)$ cited in [5.7], and $\det \mathbf{D} = a_{\parallel}a_{\perp}^2$.

Integration of [5.8] over all positions defines the conditional probability density

$$[5.10] \quad p(\theta) = \int_0^{\infty} P(d,\theta) dd$$

that the spheroid will possess an orientation θ irrespective of its position. It is this type of quantity that was presumably measured in Gallily's (33) liquid-phase experiments, since the distances s^* are so small as to be unmeasurable.

In effect, these considerations show how the Brownian motion may be expected to influence the observed orientations of nonspherical particles in proximity to boundaries. Gravitational effects arising from different particle and fluid densities could be incorporated into the calculation by adding to the London – van der Waals potential E the appropriate gravitational potential (cf. Appendix C).

Acknowledgement

This work was supported by the United States Public Health Service under Grant No. 2P01 HL 18208-06.

1. R. G. Cox and H. Brenner. J. Fluid Mech. **28**, 391 (1967).
2. D. Langbein. Theory of van der Waals attraction. Springer Tracts in Modern Physics, Vol. 72. Springer-Verlag, Berlin. 1974.
3. J. Mahanty and B. W. Ninham. Dispersion forces. Academic Press, New York. 1976.
4. D. W. Condiff and H. Brenner. Phys. Fluids, **12**, 539 (1969).
5. H. Brenner and D. W. Condiff. J. Colloid Interface Sci. **41**, 228 (1972).
6. H. Brenner and D. W. Condiff. J. Colloid Interface Sci. **47**, 199 (1974).
7. H. Brenner and L. J. Gajdos. J. Colloid Interface Sci. **58**, 312 (1977).
8. H. Brenner and L. G. Leal. J. Colloid Interface Sci. **62**, 238 (1977).
9. L. J. Gajdos and H. Brenner. Sep. Sci. Technol. **13**, 215 (1978).
10. H. Brenner and L. G. Leal. J. Colloid Interface Sci. To be published.

11. A. J. GOLDMAN, R. G. COX, and H. BRENNER. Chem. Eng. Sci. **22**, 637 (1967); **22**, 653 (1967).
12. H. BRENNER. J. Colloid Interface Sci. **23**, 407 (1967).
13. L. G. LEAL and H. BRENNER. *In* Physicochemical hydrodynamics. Vol. II. *Edited by* D. B. Spalding. Advance Publications, London. 1977. p. 667.
14. L. A. SPIELMAN and S. L. GOREN. Env. Sci. Tech. **4**, 135 (1970).
15. L. A. SPIELMAN and J. A. FITZPATRICK. J.Colloid Interface Sci. **42**, 607 (1973).
16. L. A. SPIELMAN and P. M. CUKOR. J. Colloid Interface Sci. **43**, 51 (1973).
17. L. A. SPIELMAN and S. K. FRIEDLANDER. J. Colloid Interface Sci. **46**, 22 (1974).
18. E. RUCKENSTEIN and D. C. PRIEVE. J. Chem. Soc. Faraday Trans. II, **69**, 1522 (1973).
19. B. DAHNEKE. J. Colloid Interface Sci. **50**, 89 (1975).
20. I. E. DZYALOSHINSKI, E. M. LIFSHITZ, and L. P. PITAEVSKII. Adv. Phys. **10**, 165 (1961).
21. C. J. BARNES. Proc. R. Soc. London, A**368**, 177 (1979).
22. B. DAHNEKE. J. Colloid Interface Sci. **40**, 1 (1972).
23. J. N. ISRAELACHVILI. Contemp. Phys. **15**, 159 (1974).
24. J. N. ISRAELACHVILI. Q. Rev. Biophys. **6**, 341 (1974).
25. H. C. HAMAKER. Physica, **4**, 1058 (1937).
26. B. CHU. Molecular forces. Interscience, New York. 1967. p. 51.
27. J. W. GIBBS and E. B. WILSON. Vector analysis. Dover, New York. 1960.
28. J. O. HIRSCHFELDER, C. F. CURTISS, and R. B. BIRD. Molecular theory of gases and liquids. John Wiley, New York. 1954.
29. S. CHAPMAN and T. G. COWLING. The mathematical theory of non-uniform gases. 3rd ed. Cambridge University Press, London. 1970.
30. R. S. BRADLEY. Trans Faraday Soc. **32**, 1088 (1936).
31. G. A. KORN and T. M. KORN. Mathematical handbook for scientists and engineers. 2nd ed. McGraw-Hill, New York. 1968. p. 333.
32. H. BRENNER. Ann. Rev. Fluid Mech. **2**, 137 (1970).
33. I. GALLILY. J. Colloid Interface Sci. **37**, 403 (1971).

Appendix A. Separation Distance between an Ellipsoid and a Plane

In this appendix it will be demonstrated that the physical significance of the parameter α defined in [2.24] is such that (see Fig. 2)

[A.1] $\alpha = d - s$

where, for a fixed orientation of the ellipsoid relative to the plane, s is the minimum separation distance between a point on the surface of the ellipsoid and the plane.

To prove this relation let $\boldsymbol{r}$ be a position vector drawn from the center O of the ellipsoid to an arbitrary point P lying upon its surface; that is, $\boldsymbol{r}$ is a solution of the equation

[A.2] $\boldsymbol{r}\cdot\mathbf{D}^{-2}\cdot\boldsymbol{r} = 1$

Let l be the distance from the plane to the terminus of $\boldsymbol{r}$. Then

[A.3] $l = d + \boldsymbol{n}\cdot\boldsymbol{r}$

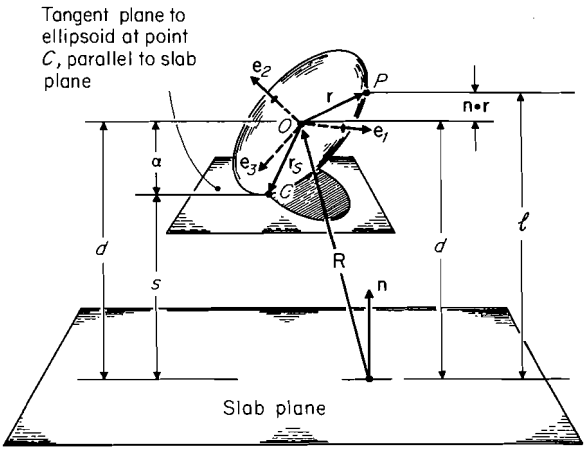

FIG. 2. Ellipsoid near a plane wall bounding a semi-infinite slab.

By definition

[A.4] $s = \min_{\boldsymbol{r}} l$

in which the minimization is to be accomplished subject to the constraints that

[A.5] d, $\boldsymbol{n}$, $\mathbf{D}$ are fixed

That $\mathbf{D}$ is fixed is, of course, a consequence of the fact that the ellipsoid orientation is fixed. From [A.3] and [A.4] there follows

[A.6] $s = d + \boldsymbol{n}\cdot\boldsymbol{r}_s$

where $\boldsymbol{r}_s$ is the particular vector $\boldsymbol{r}$ which minimizes (in an algebraic sense) the scalar $\boldsymbol{n}\cdot\boldsymbol{r}$, subject to the constraints [A.5]. That is,

[A.7] $\boldsymbol{n}\cdot\boldsymbol{r}_s = \min_{\boldsymbol{r}} (\boldsymbol{n}\cdot\boldsymbol{r})$

By identity,

[A.8] $\boldsymbol{n}\cdot\boldsymbol{r} = (\boldsymbol{n}\cdot\mathbf{D})\cdot(\mathbf{D}^{-1}\cdot\boldsymbol{r})$

From the definition of the dot product of the two vectors $\boldsymbol{n}\cdot\mathbf{D}$ and $\mathbf{D}^{-1}\cdot\boldsymbol{r}$, this yields

[A.9] $\boldsymbol{n}\cdot\boldsymbol{r} = |\mathbf{D}\cdot\boldsymbol{n}|\ |\mathbf{D}^{-1}\cdot\boldsymbol{r}| \cos(\mathbf{D}\cdot\boldsymbol{n}; \mathbf{D}^{-1}\cdot\boldsymbol{r})$

where $\cos(\boldsymbol{\beta};\boldsymbol{\gamma})$ denotes the cosine of the angle between the vectors $\boldsymbol{\beta}$ and $\boldsymbol{\gamma}$. Now, eq. [A.2] may be written alternatively as

$$(\mathbf{D}^{-1}\cdot\boldsymbol{r})\cdot(\mathbf{D}^{-1}\cdot\boldsymbol{r}) = 1$$

This shows that the vector $\mathbf{D}^{-1}\cdot\boldsymbol{r}$ is a unit vector:

[A.10] $|\mathbf{D}^{-1}\cdot\boldsymbol{r}| = 1$

Introduce the latter along with [2.24] into [A.9] and substitute the resulting expression into [A.7] to obtain

Can. J. Chem. Downloaded from www.nrcresearchpress.com by 210.87.254.6 on 09/06/12
For personal use only.

[A.11] $\boldsymbol{n}\cdot\boldsymbol{r}_s = \alpha \min_{r} \cos(\mathbf{D}\cdot\boldsymbol{n}; \mathbf{D}^{-1}\cdot\boldsymbol{r})$

The cosine function attains its minimum algebraic value of -1 when the vectors $\mathbf{D}\cdot\boldsymbol{n}$ and $\mathbf{D}^{-1}\cdot\boldsymbol{r}$ are antiparallel. Consequently,

[A.12] $\boldsymbol{n}\cdot\boldsymbol{r}_s = -\alpha$

and

[A.13] $\mathbf{D}^{-1}\cdot\boldsymbol{r}_s = -\lambda\mathbf{D}\cdot\boldsymbol{n}$

with λ a positive scalar. This scalar is easily determined by forming the magnitude of both sides of the latter equation and invoking eqs. [A.10] and [2.24]. In this manner we obtain $\lambda = 1/\alpha$. Thus, the solution $\boldsymbol{r}_s$, obtained from [A.13], is

[A.14] $\boldsymbol{r}_s = -\mathbf{D}\cdot\hat{\boldsymbol{\alpha}}$

with $\hat{\boldsymbol{\alpha}}$ the unit vector defined in [2.26]. Finally, substitution of [A.12] into [A.6] provides the requisite proof of [A.1].

The proof may be carried out in an alternative, and perhaps simpler, manner. As is well known (27), the unit normal vector $\boldsymbol{N}$ to any surface $f(\boldsymbol{r}) =$ constant and pointing in the direction of increasing f is $\nabla f/|\nabla f|$. This may be applied to the ellipsoidal surface [A.2], thereby obtaining

$$\boldsymbol{N} = \boldsymbol{r}\cdot\mathbf{D}^{-2}/|\boldsymbol{r}\cdot\mathbf{D}^{-2}|$$

for the direction of the *outer* normal unit vector at any point $\boldsymbol{r}$ on the surface of the ellipsoid. It is clear from Fig. 2 that when $\boldsymbol{r} = \boldsymbol{r}_s$, $\boldsymbol{N}$ must be identical to $-\boldsymbol{n}$. Thus we obtain

$$\boldsymbol{r}_s\cdot\mathbf{D}^{-2}/|\boldsymbol{r}_s\cdot\mathbf{D}^{-2}| = -\boldsymbol{n}$$

When solved for $\boldsymbol{r}_s$ subject to the constraint that $\boldsymbol{r}_s$ satisfy [A.2] this yields both [A.14] and [A.12].

Appendix B. Derivation of Equation [4.36]

A second application of the operator $(\partial/\partial\boldsymbol{R})_\phi$ to [4.6] gives the identity

[B.1] $\partial^2 E/\partial\boldsymbol{R}\partial\boldsymbol{R} = \boldsymbol{nn}(\partial^2 E/\partial d^2)_\alpha$

As in the derivation of [4.13] and [4.16],

$$\frac{\partial^2 E}{\partial\phi\partial\boldsymbol{R}} = \frac{\partial}{\partial\phi}\left[\boldsymbol{n}\left(\frac{\partial E}{\partial d}\right)_\alpha\right] = (\boldsymbol{n}\times\boldsymbol{r}_s)\boldsymbol{n}\frac{\partial^2 E}{\partial\alpha\partial d}$$

Symmetrization thereby yields

$$\left(\frac{\partial^2 E}{\partial\phi\partial\boldsymbol{R}}\right)_{\text{sym}} = \frac{1}{2}[(\boldsymbol{n}\times\boldsymbol{r}_s)\boldsymbol{n} + \boldsymbol{n}(\boldsymbol{n}\times\boldsymbol{r}_s)]\frac{\partial^2 E}{\partial\alpha\partial d}$$

Upon utilizing the zero-torque condition given in [4.33] it follows immediately that

[B.2] $(\partial^2 E/\partial\phi\partial\boldsymbol{R})^0_{\text{sym}} = 0$

Inasmuch as $\partial/\partial\phi = (\partial\alpha/\partial\phi)\partial/\partial\alpha$ (with $\boldsymbol{n}$ fixed), application of the chain rule gives

$$\frac{\partial^2 E}{\partial\phi\partial\phi} = \left(\frac{\partial^2\alpha}{\partial\phi\partial\phi}\right)\left(\frac{\partial E}{\partial\alpha}\right)_d + \left(\frac{\partial\alpha}{\partial\phi}\right)\left(\frac{\partial\alpha}{\partial\phi}\right)\left(\frac{\partial^2 E}{\partial\alpha^2}\right)_d$$

However, from [4.11] and [4.14] the zero-torque condition corresponds to $(\partial\alpha/\partial\phi)^0 = 0$. Consequently,

[B.3] $\left(\frac{\partial^2 E}{\partial\phi\partial\phi}\right)^0 = \left(\frac{\partial^2\alpha}{\partial\phi\partial\phi}\right)^0\left(\frac{\partial E}{\partial\alpha}\right)^0_d$

From [4.11] and [2.23] we have

$$\left(\frac{\partial\alpha}{\partial\phi}\right)_n = \frac{(\mathbf{D}^2\cdot\boldsymbol{n})\times\boldsymbol{n}}{\alpha}$$

A second differentiation gives

$$\frac{\partial^2\alpha}{\partial\phi\partial\phi} = \left[\frac{\partial}{\partial\phi_n}\left(\frac{1}{\alpha}\right)\right](\mathbf{D}^2\cdot\boldsymbol{n})\times\boldsymbol{n} + \frac{1}{\alpha}\left(\frac{\delta\mathbf{D}^2}{\delta\phi}\cdot\boldsymbol{n}\right)\times\boldsymbol{n}$$

However, from [4.29], $(\mathbf{D}^2\cdot\boldsymbol{n}^0)\times\boldsymbol{n}^0 = 0$, whence the first term vanishes in the zero-torque state. Hence, with use of [4.9], there follows

[B.4] $$\left(\frac{\partial^2\alpha}{\partial\phi\partial\phi}\right)^0 = -\frac{1}{\alpha_0}[(\boldsymbol{\varepsilon}\cdot\mathbf{D}^2\cdot\boldsymbol{n}^0)\times\boldsymbol{n}^0 + \{(\boldsymbol{\varepsilon}\cdot\mathbf{D}^2)^\dagger\cdot\boldsymbol{n}^0\}\times\boldsymbol{n}^0]$$

With the aid of [4.29] the first term in brackets in the above expression becomes

[B.5] $$(\boldsymbol{\varepsilon}\cdot\mathbf{D}^2\cdot\boldsymbol{n}^0)\times\boldsymbol{n}^0 = \alpha_0^2(\boldsymbol{\varepsilon}\cdot\boldsymbol{n}^0)\times\boldsymbol{n}^0 = \alpha_0^2(\mathbf{I} - \boldsymbol{n}^0\boldsymbol{n}^0)$$

Furthermore, by identity,

[B.6] $(\boldsymbol{\varepsilon}\cdot\mathbf{D}^2)^\dagger\cdot\boldsymbol{n} = -\boldsymbol{n}\cdot\boldsymbol{\varepsilon}\cdot\mathbf{D}^2 = \boldsymbol{n}\times\mathbf{D}^2$

since $\boldsymbol{\varepsilon} = -\mathbf{I}\times\mathbf{I}$. Substitution of [B.5] and [B.6] into [B.4] thereby yields the relation cited in [4.37]. In conjunction with [B.1] and [B.2] this thereby furnishes a proof of [4.36].

Appendix C. Ellipsoid in a Gravity Field in Contact with a Horizontal Plane Wall

That the equilibrium orientational gravity results are similar to those for a general attractive/repulsive potential is not coincidental. Rather, it is a manifestation of a much deeper, and potentially fruitful, analogy. Consider the case of an ellipsoid in contact with a horizontal plane, as in Fig. 3. As a result of gravity the ellipsoid experiences an external gravitational body force,

[C.1] $\boldsymbol{F} = -\boldsymbol{n}F$

with

Can. J. Chem. Downloaded from www.nrcresearchpress.com by 210.87.254.6 on 09/06/12
For personal use only.

Can. J. Chem. Downloaded from www.nrcresearchpress.com by 210.87.254.6 on 09/06/12
For personal use only.

[C.2] $F = \rho g(4\pi/3) \det \mathbf{D}$

The former is parallel to the direction of the gravity force. Here, ρ is the density of the (homogeneous) ellipsoid and g is the strength of the gravity field. The action of this external force is to cause the center (of mass) of the ellipsoid to move in the direction of gravity, towards the plane.

Since the ellipsoid is homogeneous, no direct gravitational body-force couple exists with respect to an origin through its center. However, due to the action/reaction forces at the contact point (point C in Fig. 3) there does exist an external torque $\boldsymbol{T}$ about O which is the moment of the reaction force $-\boldsymbol{F}$. Thus, since $\boldsymbol{r}_s$ is the moment arm of this force,

[C.3] $\boldsymbol{T} = \boldsymbol{r}_s \times (-\boldsymbol{F}) = -\boldsymbol{n} \times \boldsymbol{r}_s F$

Since $F > 0$ the action of this torque is to cause the ellipsoid to rotate about an axis (through O) which lies perpendicular to the plane formed by the vectors $\boldsymbol{r}_s$ and $\boldsymbol{n}$, and in a sense such that a right-handed screw turned from $\boldsymbol{r}_s$ towards $\boldsymbol{n}$ would advance in the direction in which the axis of rotation points. Of course this axis of rotation lies in a plane parallel to the wall, and tends to cause the fixed point on the surface of the ellipsoid which lies closest to its center (i.e., the point at the intersection of the shortest principal axis and the ellipsoid surface; point M in Fig. 3) to move closer to the plane.

The important points to observe here are that the *directions* (i.e., the vector portions) of [C.1] and [C.3] are precisely those that appear in [4.13] and [4.16] respectively. This affords a simple explanation as to why the stable orientation of the ellipsoid is the same for the gravity case as it is for the London – van der Waals case.

The analogy can be pursued even further by expressing the preceding results in terms of the potential energy function

[C.4] $E = \rho g(4\pi/3)(\det \mathbf{D})\boldsymbol{n}\cdot\boldsymbol{R}$

where $\boldsymbol{R}$ is measured from a point on the surface of the plane.[11] Equivalently, from [4.3],

[C.5] $E = \rho g(4\pi/3)(\det \mathbf{D})d$

with $a_{min} \leq d < \infty$. While superficially this potential may appear to be independent of the orientation of the ellipsoid, this is not true since eq. [A.1] (with $s = 0$) shows that $d = \alpha$, owing to the constraint that the surface of the ellipsoid be in contact with the plane. Thus, [C.5] is also equivalent to

[C.6] $E = \rho g(4\pi/3)(\det \mathbf{D})\alpha$

[11] In addition, $E = \infty$ if any point of the ellipsoid lies below the plane, i.e. $\boldsymbol{n}\cdot\boldsymbol{R} < a_{min}$.

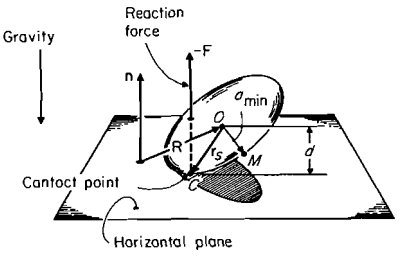

FIG. 3. Ellipsoidal particle in point contact with a horizontal plane.

In terms of this potential, eqs. [C.1] and [C.3] are equivalent to

[C.7a,b] $\boldsymbol{F} = -\boldsymbol{n}\dfrac{dE}{dd}, \quad \boldsymbol{T} = -\boldsymbol{n} \times \boldsymbol{r}_s \dfrac{dE}{d\alpha}$

These are identical to [4.13] and [4.16] except for the fact that the derivatives appearing in [C.7] are total, rather than partial, owing to the fact that d and α are no longer independent.

This analysis of a gravitating ellipsoid clearly applies to a (nonreentrant) body of any shape, provided that we simply replace the factor $(4\pi/3)$ det $\mathbf{D}$ by the volume of the body. On the basis of the analogy that we have pointed out, it would therefore appear that the attractive/repulsive potential results that we have obtained are essentially purely geometrical in nature, and that the attractive/repulsive potential energy E of *any* nonreentrant body near a slab can be expressed in the form

[C.8] $E = f(d, \alpha)$

where $\alpha = -\boldsymbol{n}\cdot\boldsymbol{r}_s$ is the orientational variable and $d = \boldsymbol{n}\cdot\boldsymbol{R}$ is the positional variable.[12] Concomitantly, these suggest that the force on any body will always be colinear with $\boldsymbol{n}$, and that the stable equilibrium orientation of any nonreentrant body will always be such that the body-fixed vector drawn from its centroid to the nearest point lying on its surface is antiparallel to $\boldsymbol{n}$. This is certainly true in the gravitational case, where the equilibrium orientation is such that the center (of mass) of the body is as close to the plane as is possible.

Exploration of these conjectures will form the subject matter of a future study.

[12] In this context we note from the arguments given at the end of Appendix A that if $f(\boldsymbol{r}) =$ constant defines the surface of the body from the viewpoint of a body-fixed observer (with $\boldsymbol{r}$ a position vector drawn from the centroid O to a point on the surface), then $\boldsymbol{r}_s$ as a function of the orientation of the body is given implicitly by the solution $\boldsymbol{r} = \boldsymbol{r}_s$ of the vector equation

$$(\nabla f)_{f=\text{const}}/|\nabla f|_{f=\text{const}} = -\boldsymbol{n}$$

This serves to define $\boldsymbol{r}_s$ in terms of $\boldsymbol{n}$ and of the geometry f of the body (27).

Effect of the crystallographic inhomogeneity of a polycrystalline electrode surface on the kinetics of the cathodic reduction of anions

M. D. Levi, N. V. Fedorovich, and B. B. Damaskin

Department of Electrochemistry, Faculty of Chemistry, Moscow State University, Lenin Hills, Moscow V 234, U.S.S.R.

Received July 2, 1980[1]

This paper is dedicated to Dr. Sam Levine on the occasion of his 70th birthday

M. D. Levi, N. V. Fedorovich, and B. B. Damaskin. Can. J. Chem. **59**, 2019 (1981).

The effect of crystallographic surface inhomogeneity of a polycrystalline electrode on the kinetics of the electroreduction of anions was investigated. It was established theoretically that corrected Tafel plots for the reduction of anions of $S_2O_8^{2-}$ type should not coincide for different polycrystalline electrodes with a noticeable crystallographic inhomogeneity of the surface. The analysis of experimental data for a polycrystalline silver electrode fully confirms this conclusion.

M. D. Levi, N. V. Fedorovich et B. B. Damaskin. Can. J. Chem. **59**, 2019 (1981).

On étudie l'influence de l'hétérogénéité de la surface cristallographique d'une électrode polycristalline sur la cinétique de l'électroréduction des anions. On a établi théoriquement que les courbes corrigées de Tafel relatives à la réduction des anions du type $S_2O_8^{2-}$ ne doivent pas coincider dans les cas d'électrodes polycristallines différentes dont l'hétérogénéité de la surface cristallographique est apparente. L'analyse des données expérimentales relatives à une électrode polycristalline d'argent confirme tout à fait cette conclusion.

[Traduit par le journal]

Introduction

One of the most important problems in the kinetics of electrode processes is that of investigating the dependence of the rate of electrochemical reactions on the nature of the electrode. The reaction of the cathodic reduction of anions of $S_2O_8^{2-}$ type (anions of the first group (1)) can be regarded as a convenient model for establishing the causes of this dependence. The quantitative theory was proposed by Frumkin and co-workers (2–5) and is based on the assumption that the elementary act of the reaction proceeds at a certain finite rate. According to this theory, reaction rate i is related to the electrode potential E by the equation

$$[1] \quad i = KC_A \exp\left[\frac{\alpha F}{RT}\left(-E + \frac{n_1 + \alpha}{\alpha}\psi_1\right)\right]$$

where K is the constant of the reaction rate, C_A and n_1 are the concentration and charge of the reacting particles in the bulk solution, α is the transfer coefficient, ψ_1 is the mean value of the potential in the plane in which are located the centres of the charges of the reacting particles in the transition state of the reaction.

The theory is based on the following assumptions: during the flow of current, the steady-state concentration of all ions in the diffuse layer and, therefore, the electrode potential are maintained constant, the ionic concentrations being given by the Gouy–Chapman theory; the structure of the double layer at the electrode conforms to the Grahame model; the non-Coulombic interaction of reacting particles and reaction products, both with the electrode surface and with the ions of the double layer, does not depend on electrode potential; the anions are discharged from the outer Helmholtz plane, i.e. $\psi_1 = \psi_0$ (ψ_0 is the potential of the outer Helmholtz plane) and, therefore, the discreteness-of-charge effect in the diffuse part of the double layer is not taken into account; the dependence of the rate of the reaction in which the adsorbed particle takes part, expressed as ($\ln i + n_1F/RT$), on the potential difference ($E - \psi_0$) is described by the classical Tafel equation with a constant transfer coefficient α. As was shown for a large number of reduction reactions of anions of the first group (5–12), the dependence of the rate of the reaction on the electrode potential, and nature and concentration of the supporting electrolyte can be described quantitively by the theory of slow discharge. The dependence of the rate of the reaction on the nature of the metal was analysed in detail in a number of papers (13, 14), and it was established that the rate constant of electrochemical reactions for which the Brønsted relationship is applicable does not depend on the nature of the electrode if the potential is measured against a given standard reference electrode. This result is due to the fact that at constant electrode potential E, the difference between the chemical potentials of the electron in two different metals is balanced by the

[1]Revision received March 24, 1981.

0008-4042/81/132019-07$01.00/0

©1981 National Research Council of Canada/Conseil national de recherches du Canada

Can. J. Chem. Downloaded from www.nrcresearchpress.com by 210.87.254.6 on 09/06/12
For personal use only.

Can. J. Chem. Downloaded from www.nrcresearchpress.com by 210.87.254.6 on 09/06/12
For personal use only.

difference between the Galvani potentials at the interface of the two metals with the solution. The energy level of the electron with respect to the solution, and, consequently, the real activation energy of the reaction proves to be the same for different electrodes (15). In this case the difference in the rate of anion discharge on different metals, just as on different crystallographic faces of one and the same metal, is connected only with the corresponding changes in the structure of the double layer, i.e. with changes in the ψ_0-potential, the value and sign of which are determined by the position of the potential of zero charge (p.z.c.) of the electrode and the values of the capacity of the Helmholtz double layer.

If eq. [1] is re-written as:

$$[2] \quad \ln i + \frac{n_1 F}{RT}\psi_0 = \ln KC_A - \frac{\alpha F}{RT}(E - \psi_0)$$

it then follows that the dependence of the reaction rate on the potential in the coordinates ($\log i + n_1F/2{\cdot}3RT$) against ($E - \psi_0$), which are called corrected Tafel plots (c.T.p.) is linear; moreover c.T.p. for different concentrations of the supporting electrolyte and for different electrodes coincide.

This conclusion was confirmed quantitively when studying the cathodic reduction of the anions $S_2O_8^{2-}$, $S_4O_6^{2-}$, $Fe(CN)_6^{3-}$ both on electrodes with a homogeneous surface (liquid and single crystal faces) and on polycrystalline electrodes in aqueous and non-aqueous solutions (5–12). The sole exception proved to be the data for the reduction of the $S_2O_8^{2-}$ anion on polycrystalline silver (16). In this case, the c.T.p. did not coincide with the c.T.p. for silver single crystal faces (111), (100), and with those obtained for other solid polycrystalline electrodes.

It was suggested in ref. 16 that the different nature of the c.T.p in the case of polycrystalline silver could be due to a marked crystallographic inhomogeneity (17, 18) of the electrode surface caused by substantial differences in the values of the pzc of the individual silver single crystal faces. A detailed analysis of the effect of the crystallographic inhomogeneity of the surface and its influence on the structure of the electric double layer at polycrystalline electrodes in ref. 19 makes it possible to propose a quantitative criterion for its influence on the kinetics of the cathodic reduction of anions.

Within the framework of a model describing the structural properties of the surface of these electrodes, which are aggregates of individual single crystal faces, two possible ways in which the

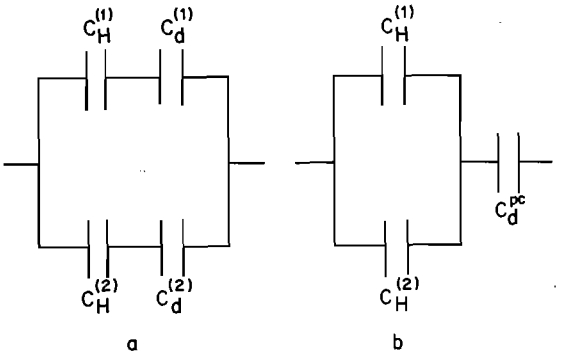

FIG. 1. Equivalent circuits for the double layer according to model I (*a*) and model II (*b*)

capacity of the diffuse part of the double layer are included have been examined (19): (*1*) each of the faces is assigned its own Helmholtz and diffuse double layer (model I) and (*2*) the faces retain the Helmholtz layers typical to them, while the diffuse double layer is common to both faces (model II) (Fig. 1). It can be easily seen that in model I, the charges in the diffuse double layer are distributed discretely and, consequently, the outer Helmholtz plane is non-equipotential.[2] Conversely, in model II the polycrystalline electrode, just like electrodes with a homogeneous surface, has an equipotential outer Helmholtz plane.

It follows from eq. [1] that a decrease in rate of anion discharge on the negatively charged surface of the electrode is, in the first approximation, connected with the dependence of the ψ_0-potential on the polarization and concentration of the inactive electrolyte in the solution (1, 5–12). Therefore, the ratio of the reaction rates on polycrystalline electrodes follow model II, and, on electrodes with a homogeneous surface, will be determined only by the difference in the mean values of the capacity of the Helmholtz layer at constant $E - \psi_0$, and the difference in the potentials of zero charge. The constant of the reaction rate K and the transfer coefficient α remain unchanged.

An entirely different effect can be expected for the discharge of anions on the surface of a polycrystalline electrode if the structure of its double layer follows the relationships of model I. Indeed, at a given value of the electrode potential E with respect to the reference electrode, the outer Helmholtz plane in the vicinity of which the electric

[2]The non-equipotential state of the outer Helmholtz plane arising from the discrete nature of the distribution of the ions in the diffuse layer was not taken into account. However, that does not affect the subsequent conclusions, since a certain analogy is observed in the dependence of the local value of the ψ_1-potential and mean value of the ψ_0-potential on the electrode potential E and concentration of the supporting electrolyte (8).

Can. J. Chem. Downloaded from www.nrcresearchpress.com by 210.87.254.6 on 09/06/12
For personal use only.

centres of the discharging particles are to be found is non-equipotential and, therefore, the rate of the reaction on different sections of the surface is not the same. Under these circumstances when passing from the homogeneous to the polycrystalline structure of the electrode surface the values K and α could formally change greatly; this would lead to the c.T.p. for the anion reduction reaction not coinciding on different polycrystalline electrodes.

Method of Data Analysis

The computations were conducted on the assumption that two faces (1) and (2) in thermodynamic equilibrium are present on the surface of the polycrystalline electrode. Changes in the properties of the boundary regions were disregarded. Face (2) has more pronounced hydrophilic properties than face (1), i.e. $(C_H^{(2)})_{q=0} > (C_H^{(1)})_{q=0}$ where C_H is the capacity of the Helmholtz layer of the corresponding face. At large negative potential drops in the Helmholtz layer, $C_H^{(2)} = C_H^{(1)}$ and does not change when the cathodic polarization is further increased. The potential of zero charge of face (1), $E_{q=0}^{(1)}$ is less negative by 0.233 V than that of face (2), $E_{q=0}^{(2)}$ which is the result of their different hydrophilic properties.[3] The crystallographic inhomogeneity of the electrode is taken to be the maximum, i.e. $\theta^{(1)} = \theta^{(2)} = 0.5$, where $\theta^{(1)}$ and $\theta^{(2)}$ are the surface fractions of face (1) and face (2), respectively.

Initially, partial C_H, q curves for faces (1) and (2) were preset with parameters close to those observed experimentally in aqueous solutions. In keeping with the equivalent circuit of model I (Fig. 1*a*) at constant E, the capacity of the polycrystalline electrode C^{pc}

$$[3] \quad C^{pc} = 0.5(C^{(1)} + C^{(2)})$$

To find the dependence of the capacity of the Helmholtz double layer of the polycrystalline electrode C_H^{pc} on the potential drop in the Helmholtz layer $(E - \psi_0)$ it is necessary to know the values of $C_H^{(1)}$ and $C_H^{(2)}$ at the same potentials. For face (1) the potential $(E - \psi_0)$ corresponding to charge q is determined by the formula

$$[4] \quad (E - \psi_0) = \int_0^q (1/C_H^{(1)})\, dq$$

and for face (2)

$$[5] \quad (E - \psi_0) = (E - \psi_0)^* - \int_{q^*}^q (1/C_H^{(2)})\, dq$$

where $(E - \psi_0)^*$ is the potential drop in the Helmholtz layer corresponding to a charge q^* where the partial C_H, q-curves coincide.

To compute the dependence of the differential capacity of the polycrystalline electrode on electrode potential in solutions of different concentrations it is essential to know the dependence of $C^{(1)}$ and $C^{(2)}$ on E at constant q in the same solutions. To this end, in keeping with the main relationship of the Grahame theory

$$[6] \quad 1/C = 1/C_H + 1/C_d$$

where $C_d = 19.45\sqrt{137.8C + q^2}$. The values of $C^{(1)}$ and $C^{(2)}$ were found at constant q. Transformation from charge to potential for the faces was accomplished using equations similar to [4] and [5]. For face (1)

$$[7] \quad E = \int_0^q (1/C^{(1)})\, dq$$

And for face (2)

$$[8] \quad E = E^* - \int_{q^*}^q (1/C^{(2)})\, dq$$

where

$$[9] \quad E^* = \int_0^q (1/C^{(1)})\, dq$$

The dependence of the capacity of the polycrystalline electrode on potential in solutions of different concentrations was found using eq. [3]. To calculate the ψ_0-potential the value of the charge q corresponding to the electrode potential E was calculated from the following equation:

$$[10] \quad q^{pc} = q^* - \int_{E^*}^E C^{pc}\, dE$$

When analysing the experimental dependence of the capacity of the double layer on the polycrystalline electrode potential, it is usually assumed that, in dilute solutions the surface charge equals zero[4] at the minimum on the C against E-curve. Consequently in the computations used in this work, the electrode charge was also calculated from the charge corresponding to E_{min}.

The mean value of the ψ_0-potential at $q < 0$ was calculated in keeping with the theory of the diffuse double layer

$$[11] \quad \psi_0 = -0.0513 \sinh^{-1}(q/11.72\sqrt{c})$$

The numerical values in eq. [11] correspond to

[3]Neglect of the difference in the work functions of faces (1) and (2) does not affect the subsequent results, if the electrode charge is calculated from the charge corresponding to the potential of the minimum (E_{min}) on the C^{pc} against E curve.

[4]In reality, as was first noted in ref. 18, at E_{min} the mean charge of the polycrystalline electrode surface conforming to model I is not equal to zero and can have considerably negative values (19).

aqueous solutions with a non-adsorbing electrolyte at $T_0 = 25°C$.

The mean values of the reaction rate on the polycrystalline electrode at constant E were calculated from the equation

[12] $i^{pc} = 0.5(i^{(1)} + i^{(2)})$

where $i^{(1)}$ and $i^{(2)}$ are the partial discharge currents on the corresponding faces, the discharge currents on the individual faces being calculated according to [1] with $n_1 = -2$.

Results and Discussion

The initial c.T.p. was linear for the cathodic reduction of a hypothetical divalent anion (Fig. 2, line 1) for which the transfer coefficient α was assumed to be 0.23 (1, 5). Then, using eq. [11] for three concentrations, namely, 0.1 *M*, 0.01 *M*, and 0.001 *M*, the ψ_0 against E curves were calculated for individual crystal faces (Fig. 3, curves *1*, *2*, and *3* for face (2), and curve *4* for face (1).) To calculate the dependence of the partial discharge currents $i^{(1)}$ and $i^{(2)}$ on electrode potential E (Fig. 4, curve *1* and *2* for a solution concentration of 0.001 *M*) the calculated values of the ψ_0-potential were substituted into eq. [1]. Figure 4 also shows the dependence of the discharge rate on the potential E at the polycrystalline electrode calculated according to eq. [12].

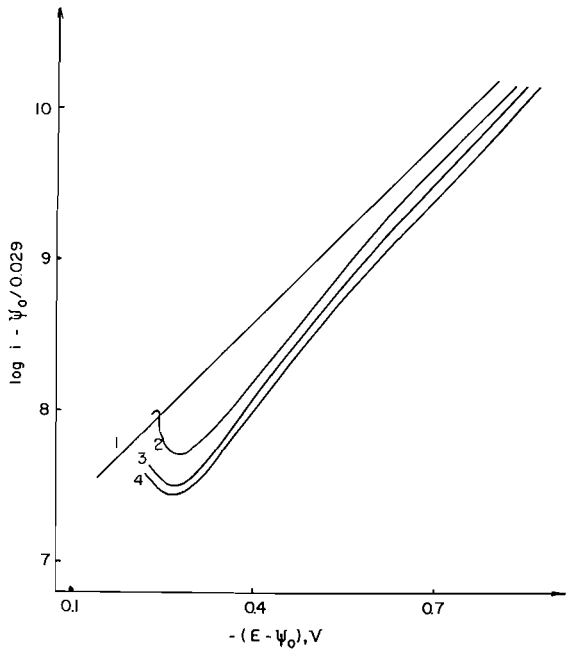

FIG. 2. Corrected Tafel plots for the reduction of a divalent anion: *1*, on faces (1) and (2) and *2–4* on a polycrystalline electrode in the presence of various concentrations of an inactive supporting electrolyte, *2*, 0.001 *M*, *3*, 0.01 *M*, *4*, 0.1 *M*.

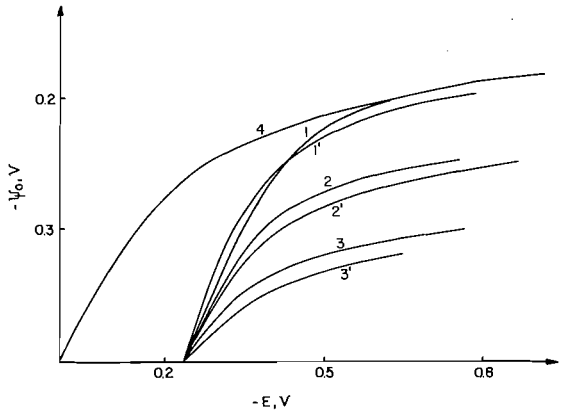

FIG. 3. Dependence of the ψ_0-potential on the electrode potential E: *1–3* and *1'–3'* on face (2) and on the polycrystalline electrode, respectively for different concentrations of the base electrolyte, *1*, *1'*, 0.001 *M*; *2*, *2'*, 0.01 *M*; *3*, *3'*, 0.1 *M*; and *4* on face (1) for a 0.001 *M* electrolyte concentration.

The rates of the electroreduction of anions found in this way were corrected by the effective values of the ψ_0^{pc}-potential calculated from eq. [11] for a polycrystalline electrode. The calculated ψ_0^{pc} against E curves are shown in Fig. 3. It can be seen from this figure that only when $E_{q=0}^{(2)} = -0.233$ V, in keeping with the accepted method of estimating the charge on the polycrystalline electrode, does $\psi_0^{pc} = \psi_0^{(2)} = 0$. At all other values of E $|\psi_0^{pc}| < |\psi_0^{(2)}|$ with the exception of highly dilute solutions (0.001 *M*) for which $|\psi_0^{pc}| > |\psi_0^{(2)}|$ at small negative departures from $E_{q=0}^{(2)}$. The reversal of the inequality is due to the fact that as the solution is made more dilute, the capacity of the polycrystalline electrode in the vicinity of $E_{q=0}^{(2)}$ moves not in the direction of zero, as on electrodes with a homogeneous surface, but to a certain finite value depending in general on the relative fractions of the two faces on the surface, and on the differential capacity at face (1) at p.z.c. of face (2) (18, 19). In more concentrated solutions at constant E, C^{pc} is always less than $C^{(2)}$; it also follows that $|q^{pc}| < |q^{(2)}|$ and, in keeping with eq. [11] that $|\psi_0^{pc}| < |\psi_0^{(2)}|$. The c.T.p. for the cathodic reduction of a hypothetical divalent anion calculated for three concentrations are shown in Fig. 2 (curves *2*, *3*, *4*). An analysis of the shapes of these curves and their dependence on the concentration of the supporting electrolyte leads to the conclusion that, on the c.T.p. for the polycrystalline electrode, unlike those for electrodes with a homogeneous surface, there are three regions with substantially different values of the apparent transfer coefficient α^{pc}.

In the vicinity of $E_{q=0}^{(2)}$, the transfer coefficient α^{pc} assumes negative values. This result is explained in Fig. 5 which shows the C against

Can. J. Chem. Downloaded from www.nrcresearchpress.com by 210.87.254.6 on 09/06/12
For personal use only.

Can. J. Chem. Downloaded from www.nrcresearchpress.com by 210.87.254.6 on 09/06/12
For personal use only.

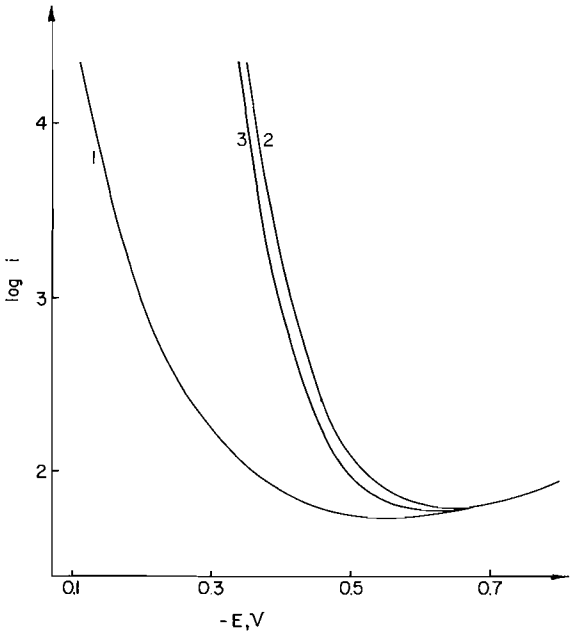

FIG. 4. Dependence of rate of reduction of a divalent anion on the electrode potential: *1*, at face (1); *2*, at face (2); and *3* at a polycrystalline electrode.

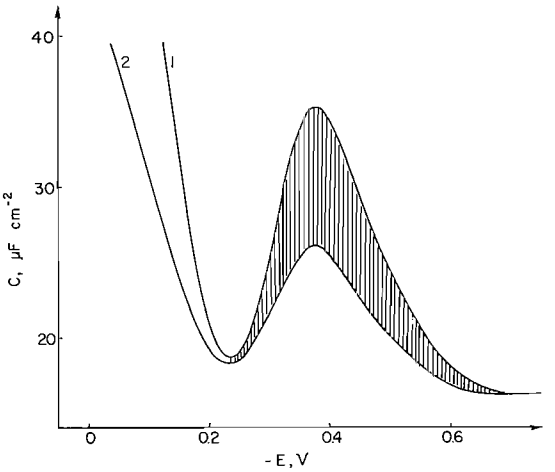

FIG. 5. Dependence of differential capacity on the electrode potential in a 0.01 *M* solution of a non-adsorbing electrolyte: *1*, at face (2) and *2*, at a polycrystalline electrode.

E-curves on face (2) and on a polycrystalline electrode in a 0.01 *M* solution of a surface inactive supporting electrolyte. The cross-hatched area corresponds to the difference in the surface charges of the two electrodes at E = constant. When the potential shifts from $E_{q=0}^{(2)}$ towards more negative values, the absolute value of $|q^{(2)}|$ increases more quickly than $|q^{pc}|$ (Fig. 6). In other words, the effective repulsion of anions from the negatively charged surface of the polycrystalline electrode is

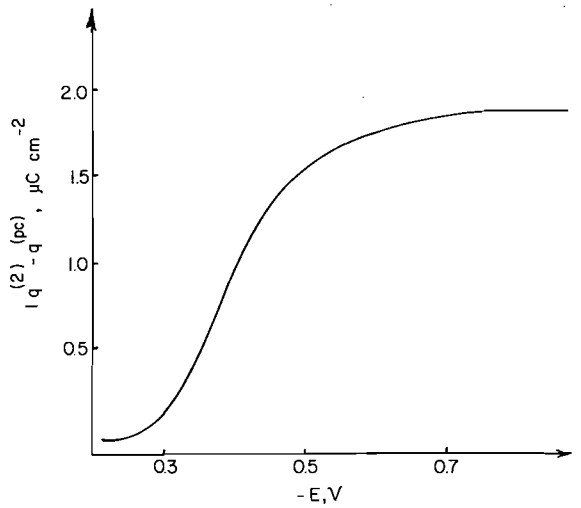

FIG. 6. Dependence of the absolute value of difference in surface charge on face (2) and on a polycrystalline electrode, $|q^{(2)} - q^{(pc)}|$ on electrode potential E.

less than on face (2), and the value of log i corresponding to the polycrystalline electrode remains "undercorrected" by the ψ_0-potential.

Starting from $E = -0.353$ V (where a minimum is observed on the c.T.p. of the polycrystalline electrode in a 0.01 *M* solution), the rate of growth of the absolute value of the difference in charges $|q^{(2)} - q^{pc}|$ decreases (Fig. 6) and the surface of the polycrystalline electrode begins formally to repulse the anions more strongly. In other words, in the examined region of potentials the value log i could be said to be "overcorrected" by the ψ_0-potential, which leads to the appearance in the middle part of the c.T.p. of a roughly linear section with a considerably larger value of α^{pc} than for the single crystal faces.

At potentials more negative than the potential at which the C against E-curves for faces (1) and (2) merge, the difference in the value of the charge on face (2) and on the polycrystalline electrode attains a constant value and, correspondingly, the c.T.p. for the polycrystalline electrode runs parallel to the c.T.p. for the single crystal faces. The formal decrease in the reaction rate constant on passing from a single crystal to a polycrystalline electrode is due to the method chosen for evaluating the charge on the crystallographic inhomogeneous surface.

Unlike the case of single crystal faces, the c.T.p. on a polycrystalline electrode depends on the concentration of the inactive electrolyte (see Fig. 2). This result stems from the fact that the concentration of ions in the diffuse double layer changes not only with distance from the surface of the

Can. J. Chem. Downloaded from www.nrcresearchpress.com by 210.87.254.6 on 09/06/12
For personal use only.

polycrystalline electrode, but also in a direction parallel to this surface. It follows that the one-dimensional model of the diffuse layer proposed by Gouy and Chapman is inapplicable for a polycrystalline electrode (19).

It was shown in ref. 19 that the crystallographic inhomogeneity of the surface is inherent in one degree or another to all polycrystalline electrodes, but in the case of gold and, particularly, silver, this effect reaches its maximum. From this point of view, let us analyse the kinetics of the cathodic reduction of persulphate anions on single crystal faces of silver with Miller indices (111), (100)[5] and on polycrystalline silver. These data were reported earlier (16). Figure 7 shows c.T.p. for the reduction of a persulphate anion on a number of polycrystalline electrodes, at silver single crystal faces and at polycrystalline silver. In ref. 16 the corresponding ψ_0^{pc} against E needed to obtain c.T.p. were calculated from the C^{pc} against E data (20) using a roughness factor $f = 1.3$.[6] However, in a later paper (21) it was shown that $f = 1.5$. That f cannot be equal to 1.3 is also evident from the analysis cited below. It can be seen from Fig. 2 that on the negatively charged surface of the polycrystalline electrode the rate of the cathodic reduction of anions corrected by the ψ_0-potential is always less than that on the single crystal face while the c.T.p. at a polycrystalline electrode calculated on the basis of $f = 1.3$ intersects the c.T.p. of the single crystal faces (Fig. 4 in ref. 16).

Figure 7 gives the c.T.p. for polycrystalline silver calculated on the basis of $f = 1.5$. This figure shows that for silver single crystal faces and polycrystalline electrodes of bismuth, tin, and lead, their c.T.p. coincide. The absence of any noticeable influence of surface crystallographic inhomogeneity for these electrodes on the reaction kinetics is, apparently, due to the small anisotropy of the p.z.c. of the single crystal faces of these metals. At the same time, the experimental data for polycrystalline silver can be rationalized on the basis of the analysis given in this paper.

A comparison of Figs. 2 and 7 shows that the c.T.p. of polycrystalline silver can be identified with the middle section of the calculated curve where the value of α^{pc} typically increases and a gradual transition occurs to that region of potentials in which the c.T.p. for the polycrystalline

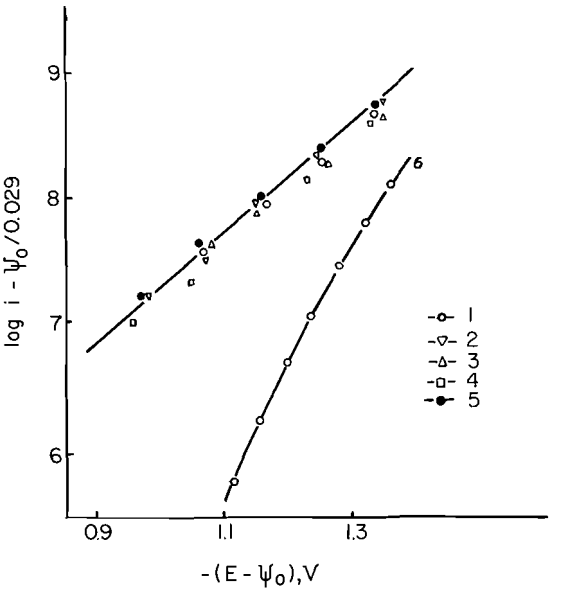

FIG. 7. Corrected Tafel plot of reduction of 10^{-3} N $K_2S_2O_8$ + 0.9×10^{-2} N KF on electrodes: *1*, Bi; *2*, Sn; *3*, Pb; *4*, Ag(111), *5*, Ag(100), *6*, Ag polycrystalline.

electrode and single crystal faces are parallel to each other.[7]

The absence of a section with a minimum ($\alpha^{pc} < 0$) on the experimental curve can be explained by the fact that the real rate of the reaction on a polycrystalline electrode in the vicinity of the potential minimum on the C^{pc} against E-curve is lower, apparently as a result of oxidation, than it should be according to the above model. The coincidence, within the limits of error of the experiment, of the c.T.p. for the reduction of persulphate anions on polycrystalline silver for different concentrations of a non-adsorbed electrolyte also becomes understandable, if it is remembered that the interval in changes in concentration amounts to only one-half of one order of magnitude.

Thus, in the case of electrodes with sharply differing values of potentials of zero charges for individual crystal faces, the c.T.p. for the discharge of anions should not coincide, since the structure of the electric double layer does not conform to the Grahame model. In order to establish the dependence of the reaction rate on the nature of the metal, it is necessary to conduct investigations on individual crystal faces.

[5]No study was made of the kinetics of the electroreduction of the persulphate anion on the silver single crystal face (110).

[6]In reality for a polycrystalline electrode the reciprocal of the slope of the Parsons–Zobel plot is $f = f_r \cdot f_{ci}$ where f_r is the roughness factor, and f_{ci} the coefficient of the crystallographic surface inhomogeneity (17, 19).

[7]The changes in the value of α with the electrode potential, as follows from the analysis, are connected with the crystallographic inhomogeneity of the surface of polycrystalline electrodes and cannot serve as proof of the dependence of α on E (22), as predicted by the quantum theory of the elementary act of discharge.

1. N. V. FEDOROVICH. Itogi Nauki Tekh. Ser. Electrokhim. v. 14, Viniti, Moscow. 1979. p. 5.
2. A. N. FRUMKIN. Usp. Khim. **4**, 88 (1935).
3. A. N. FRUMKIN and G. M. FLORIANOVICH. Dokl. A.N. SSSR, **80**, 907 (1951).
4. A. FRUMKIN, N. NIKOLAYEVA-FEDOROVICH. Progress in polarography. Interscience, New York. 1962. p. 223.
5. A. N. FRUMKIN, N. V. NIKOLAYEVA-FEDOROVICH, N. P. BERESINA, and KH.E. KEIS. J. Electroanal. Chem. **58**, 189 (1975).
6. A. FRUMKIN, O. PETRY, and N. NIKOLAYEVA-FEDOROVICH. Electrochim. Acta, **8**, 177 (1963).
7. N. FEDOROVICH, A. FRUMKIN, and KH. KEIS. Coll. Czech. Chem. Commum. **36**, 722 (1971).
8. A. N. FRUMKIN, N. V. FEDOROVICH, S. I. KULAKOVSKAYA, and M. D. LEVI. Elektrokhimiya, **10**, 130 (1974).
9. A. N. FRUMKIN, N. V. FEDOROVICH, and S. I. KULAKOVSKAYA. Elektrokhimiya, **10**, 330 (1974).
10. A. N. FRUMKIN, S. I. KULAKOVSKAYA, and N. V. FEDOROVICH. Elektrokhimiya, **10**, 837 (1974).
11. N. V. FEDOROVICH, M. D. LEVI, and A. V. SHLEPAKOV. Elektrokhimiya, **13**, 89 (1977).
12. M. D. LEVI, N. V. FEDOROVICH, and A. V. SHELPAKOV. Elektrokhimiya, **12**, 1846 (1976).
13. M. I. TEMKIN and A. N. FRUMKIN. Zh. Fiz. Khim. **29**, 1513 (1955).
14. A. N. FRUMKIN. Elektrokhimiya, **1**, 394 (1965).
15. L. I. KRISHTALIK. Electrode reactions, mechanism of the elementary act. Nauka Publ. House, Moscow. 1979. p. 24.
16. N. V. FEDOROVICH, M. D. LEVI, and S. I. KULAKOVSKAYA. Elektrokhimiya, **13**, 904 (1977).
17. G. VALETTE and A. HAMELIN. J. Electroanal. Chem. **45**, 301 (1973).
18. N. B. GRIGORYEV. Dokl. AN SSSR, **229**, 647 (1978).
19. I. BAGOTSKAYA, B. DAMASKIN, and M. LEVI. J. Electroanal. Chem. To be published.
20. E. S. SEVASTYANOV. Double layer and adsorption on solid electrodes. Vol. IV. Tartu University Press. 1975. p. 281.
21. A. V. SHLEPAKOV and E. S. SEVASTYANOV. Elektrokhimiya, **14**, 287 (1978).
22. R. R. DOGONADZE and A. M. KUZNETSOV. Itogi Nauki Tekh. Ser. Fiz. Khim. Kinet. Vol. 2, Viniti, Moscow. 1973.

Can. J. Chem. Downloaded from www.nrcresearchpress.com by 210.87.254.6 on 09/06/12
For personal use only.

Kinetics of electrode processes in the presence of a discrete layer of a specifically adsorbed organic substance

V. S. KRYLOV AND I. F. FISHTIK

Institute of Electrochemistry, Academy of Sciences of the USSR, Moscow, USSR

Received July 2, 1980

This paper is dedicated to Dr. Sam Levine on the occasion of his 70th birthday

V. S. KRYLOV and I. F. FISHTIK. Can. J. Chem. **59**, 2026 (1981).

The problem of an adequate statistical mechanical approach to the transition from the description of the elementary act of an electrochemical process occurring in the presence of electrochemically inactive specifically adsorbed species to the description of the resulting heterogeneous process for which the rate is measured in experiments is discussed. The analysis of the electrode kinetics is given for the particular case where the irreversible electron transfer reaction at the metal/solution takes place in the presence of a fixed discrete layer of specifically adsorbed dipole molecules. The theoretical results are compared with the available experimental data on the influence of adsorbed organic substances on the electrochemical reaction rate.

V. S. KRYLOV et I. F. FISHTIK. Can. J. Chem. **59**, 2026 (1981).

On discute d'une approche appropriée, par le biais de la mécanique statistique, au problème de la transition entre la description d'un acte élémentaire d'un processus électrochimique se produisant en présence d'espèces inactives électrochimiquement et spécifiquement adsorbées et la description de la réaction hétérogène résultante dont on a mesuré expérimentalement la vitesse. Dans le cas particulier où une réaction irréversible de transfert d'électron a lieu au niveau métal/solution en présence d'une couche discrète mixte de molécules polaires spécifiquement adsorbées, on présente l'analyse de la cinétique à l'électrode. On a comparé les résultats théoriques aux données expérimentales disponibles relatives à l'influence de substances organiques adsorbées sur la vitesse de la réaction électrochimique.

[Traduit par le journal]

The problem of decoding the mechanism of interaction between the elementary act of an electrochemical process and adsorption phenomena at a metal/solution interface is of principal interest because this problem is directly connected with the interpretation of electrochemical kinetic data as well as with the correct mathematical description of the effect of the electrical double layer on the electrode process rate. Because of this a fundamental problem arises, namely, the problem of an adequate statistical mechanical approach to the transition from the description of the elementary act of an electrochemical process occurring in the presence of electrochemically inactive specifically adsorbed species (ions and dipole molecules) to the description of the resulting electrode process for which the rate is experimentally measurable. The no less important aspect of the theory of heterogeneous processes at polarizable interfaces is related to consideration of the discrete nature of reactants and specifically adsorbed indifferent particles. One of the most significant achievements in recent years in the field of interpretation of electrochemical kinetic data was in substantiation of the role of the discreteness effects. A remarkable contribution to this work was made by Levine and co-workers (1–4). The local electric field acting near the interface on discrete particles possessing electric charge or dipole moment, due to polarization of the interface by these particles, differs from the average field described by the macroscopic equations of electrodynamics with a continuous charge and dipole moment distribution. The characteristic relaxation times of "the electrostatic image" forces, i.e., the redistribution times of free and bound charges at the interface due to its polarization by discrete particles present in solution, are of the order of 10^{-15}–10^{-14} s. The characteristic times of many types of electrochemical reactions, however, are comparable with the fluctuation reorientation time of dipole molecules of the solvent in the solvation shells of reactants (10^{-11} s), i.e., they are by 3–4 orders higher than the relaxation times of "the electrostatic self-image" forces. For this reason, the discrete nature of charges and dipole moments should affect the probability of the elementary act of electrochemical processes. Moreover, the local electric field associated with the discreteness effect can influence the rate of electrochemical processes by changing the concentration of reactants and reaction products in the layer adjacent to the electrode. Another aspect of the problem of taking into consideration the fine structure of the double layer in electrochemical kinetics is a correct, from the point of view of quantum mechanics and statistical physics, derivation of an equation for the electrochemical reaction rate taking into account the local electric field (5, 6).

In the present paper the problem of the statistical mechanical averaging of the probability of the elementary act of an irreversible electron transfer reaction occurring at a metal/solution interface in the presence of specifically adsorbed electrochem-

0008-4042/81/132026-05$01.00/0

©1981 National Research Council of Canada/Conseil national de recherches du Canada

Can. J. Chem. Downloaded from www.nrcresearchpress.com by 210.87.254.40 on 09/06/12
For personal use only.

Can. J. Chem. Downloaded from www.nrcresearchpress.com by 210.87.254.40 on 09/06/12
For personal use only.

ically inert dipole molecules is considered for the particular case when the positions of all the molecules inside the adsorption layer are fixed and when the electrochemical process does not disturb the statistical equilibrium with respect either to ionic reactants or to supporting electrolyte ions.

Let us consider an irreversible electrochemical reaction

$$A^z + e \rightarrow B^{z-1}$$

occurring at an electrode partly covered by specifically adsorbed electroinactive dipole molecules. We shall assume for simplicity that the molecules are point-like dipoles the centers of which are located in the plane $x = 0$ inside the Helmholtz layer, $-\beta \leq x \leq \gamma$, at a distance β from the electrode surface, $x = -\beta$. Let us suppose that the positions of the adsorbed molecules in the plane $x = 0$ are strictly fixed and let us denote them by $\boldsymbol{r}_1, \boldsymbol{r}_2, ..., \boldsymbol{r}_M$, where M is the total number of molecules. The positions of ions which are present in the system (including the reactant ones) will be denoted by $\boldsymbol{R}_1, \boldsymbol{R}_2, ..., \boldsymbol{R}_N$. The probability, w, of electron transfer from the electrode to the reactant ion A^z is an exponential function of the activation energy, E_a:

$$[1] \quad w(\boldsymbol{R}_1, ..., \boldsymbol{R}_N, \boldsymbol{r}_1, ..., \boldsymbol{r}_M) = A(\boldsymbol{R}_1) \exp \{-E_a(\boldsymbol{R}_1, ..., \boldsymbol{R}_N, \boldsymbol{r}_1, ..., \boldsymbol{r}_M)/kT\}$$

where the factor $A(\boldsymbol{R}_1)$ is temperature independent. The density, i, of the current generated in the electrochemical reaction is connected with the probability w by the expression

$$[2] \quad i = eN_R f\langle w \rangle$$

where N_R is the total number of the reactant ions in the system, f is a factor accounting for the part of the electrode surface available for the electrochemical reaction to occur, and the symbol $\langle\ \rangle$ stands for the statistical averaging operation over the whole system of particles present in solution including the specifically adsorbed molecules.

In further consideration we shall treat the subsystem of the specifically adsorbed molecules as a factor providing a fixed external force field for the remaining, nonadsorbed particles and, accordingly, shall carry out the statistical averaging over only nonadsorbed particles. Furthermore, we shall assume that the electrochemical process under consideration does not disturb the statistical equilibrium for either reactant or supporting electrolyte ions. It means that the statistical averaging should be carried out using the Gibbs equilibrium distribution function $D_N(\boldsymbol{R}_1, ..., \boldsymbol{R}_N, \boldsymbol{r}_1, ..., \boldsymbol{r}_M)$ dependent on the coordinates of the specifically adsorbed molecules as on parameters. Thus we have

$$[3] \quad \langle w \rangle = \int A(\boldsymbol{R}_1) \exp [-E_a(\boldsymbol{R}_1, ... \boldsymbol{R}_N, \boldsymbol{r}_1, ... \boldsymbol{r}_M)/kT] \times D_N d\boldsymbol{R}_1, ..., d\boldsymbol{R}_N$$

where the function D_N is defined by the expression

$$[4] \quad D_N(\boldsymbol{R}_1, ..., \boldsymbol{R}_N, \boldsymbol{r}_1, ..., \boldsymbol{r}_M) = Q_N^{-1} \exp \left\{ -\frac{1}{kT} [V_Z(\boldsymbol{R}_1, ..., \boldsymbol{R}_N) + W_Z(\boldsymbol{R}_1, \boldsymbol{r}_1, ..., \boldsymbol{r}_M) + U_Z(\boldsymbol{R}_1) + U_{N-1}(\boldsymbol{R}_2, ..., \boldsymbol{R}_N) + U_{N-1,M}(\boldsymbol{R}_2, ..., \boldsymbol{R}_N, \boldsymbol{r}_1, ..., \boldsymbol{r}_M)] \right\}$$

Here V_Z is the energy of interaction between the ion A^Z and the remaining ions; W_Z is the corresponding energy of interaction with the adsorbed dipoles; the energy $V_Z(\boldsymbol{R}_1)$ accounts for the interaction of the ion A^Z with the electrostatic self-image forces; U_{N-1} is the energy of interaction of the ions located at the positions $\boldsymbol{R}_2, ..., \boldsymbol{R}_N$ with one another (including the interactions with the corresponding image forces); $U_{N-1,M}$ is the interaction energy of the same ions with the adsorbed dipoles and their "images" in metal; Q_N is the configuration integral. The methods of calculation of the energies V_Z, U_Z, and U_{N-1} were developed in refs. 7–9. For the function $U_{N-1,M}$, according to its definition, the expression

$$U_{N-1,M} = \sum_{k=2}^{N} W_Z(\boldsymbol{R}_k, \boldsymbol{r}_1, ..., \boldsymbol{r}_M)$$

is valid. Therefore the problem consists in calculating the functions E_a and W_Z and in carrying out the statistical averaging in [3].

According to the Brönsted equation the activation energy is a linear function of the thermal effect of reaction, ΔJ:

$$[5] \quad E_a = E_a^{(0)} + \alpha \Delta J$$

where $E_a^{(0)}$ is the term independent of coordinates and α is the electron transfer coefficient. The thermal effect ΔJ may be split into the following contributions:

$$[6] \quad \Delta J = E_0 - E_m + E_B^{(s)} - E_A^{(s)} + e\varphi_0 + U_{Z-1}(\boldsymbol{R}_1) - U_Z(\boldsymbol{R}_1) + V_{Z-1}(\boldsymbol{R}_1, ..., \boldsymbol{R}_N) - V_Z(\boldsymbol{R}_1, ..., \boldsymbol{R}_N) + W_{Z-1}(\boldsymbol{R}_1, \boldsymbol{r}_1, ..., \boldsymbol{r}_M) - W_Z(\boldsymbol{R}_1, \boldsymbol{r}_1, ..., \boldsymbol{r}_M)$$

Can. J. Chem. Downloaded from www.nrcresearchpress.com by 210.87.254.40 on 09/06/12
For personal use only.

Here $E_B^{(s)}$ and $E_A^{(s)}$ are the solvation energies of ions B^{Z-1} and A^Z; φ_0 is the electrode potential relative to the bulk of solution; E_0 and E_m are the energy levels of the electron transferred, respectively, in ion A^Z and in metal; the subscripts Z and $Z-1$ refer to ions A^Z and B^{Z-1}.

Now we can proceed to performing the integration in [3]. Using the definition of the one-particle distribution function, $g_Z(x_1)$, for ions with valence Z, namely,

$$g_Z(x_1) = \frac{1}{V}\int D_N(\boldsymbol{R}_1, ..., \boldsymbol{R}_N, \boldsymbol{r}_1, ..., \boldsymbol{r}_M)\, d\boldsymbol{R}_2, ..., d\boldsymbol{R}_N$$

where V is the total volume of solution, after simple transformations we arrive at the following equation:

$$[7]\quad i = eN_R\delta^* A^* f \exp\left\{-\frac{\alpha}{kT}[e\varphi_0 + U_{Z-1}(x_1^*) - U_Z(x_1^*)] - \frac{E_a^{(0)}}{kT} - \frac{1}{kT}[U_Z(x_1^*) - U_{Z-\alpha}(x_1^*) + W_{Z-\alpha}(x_1^*)]\right\} g_{Z-\alpha}(x_1^*)$$

Here the quantities marked with the asterisk are to be calculated at the point $\boldsymbol{R}_1^* = (x_1^*, 0, 0)$ in the plane $x_1 = x_1^*$ corresponding to the distance of the most probable place of ion discharge from the electrode; δ^* denotes the width of the region near the plane $x_1 = x_1^*$ which makes the main contribution to the integral over $\boldsymbol{R}_1$. The preferential distance x_1^* arises in the course of integration due to the fact that the integrand contains two factors, one of which, $A(\boldsymbol{R}_1)$, decreases sharply with the distance from the electrode while the other increases.

It is worthwhile to point out that the distribution function, $g_{Z-\alpha}(x_1^*)$, and the energy of interaction of a discharging ion with adsorbed dipoles, $W_{Z-\alpha}(x_1^*)$, correspond to a transition state of a discharging ion in which all the neighbouring ions and dipoles around the given ion would be in statistical equilibrium with the ion if the charge of the latter had been equal to $e(Z-\alpha)$. The ion with the charge $e(Z-\alpha)$ is, in some sense, an analog of the activation complex involved in the absolute reaction rate theory. However, in contrast with predictions given by that theory, the resulting rate of an electrode process is determined by the local electrical field rather than by the average field corresponding to continuously spread ionic charges and molecular dipole moments. In application to the case of specific adsorption of ions the equation analogous to [7] was obtained in ref. 10.

As was shown elsewhere (11) for the function $g_{Z-\alpha}(x_1)$, the expression

$$[8]\quad g_{Z-\alpha}(x_1) = \exp\{-[e(Z-\alpha)\varphi(x_1) + U_{Z-\alpha}(x_1) + V_{atm}(Z-\alpha, x_1)]/kT\}$$

is valid where $\varphi(x_1)$ is the average potential in the plane $x = x_1$ and the term $V_{atm}(Z-\alpha, x_1)$ accounts for interaction of an ion having the charge $e(Z-\alpha)$ with its own ionic atmosphere distorted by the image forces. Using [8] we can rewrite [7] in the following manner:

$$i = Kf(\theta)c_s \exp\left\{\frac{\alpha}{kT}[U_Z(x_1) - U_{Z-1}(x_1) - e\varphi_0 + e\varphi(x_1)] + \frac{1}{kT}[V_{atm}(Z, x_1) - V_{atm}(Z-\alpha, x_1) + U_{Z-\alpha}(x_1) - U_z(x_1) - W_{Z-\alpha}(x_1)]\right\}$$

where K is a constant independent of θ, the degree of coverage of the electrode surface by adsorbed molecules, c_s being the local concentration of the reactant ions at the plane $x = x_1$. Generally, all the energies entering the exponent in the last equation depend on θ, even the self-image terms, U_Z and $U_{Z-\alpha}$, because all of them contain the compact layer parameters, β, γ, and ε_1 which can change in the presence of adsorbed molecules. In the case of the compact layer parameters being independent of θ it is possible to present the kinetic equation in the form

$$[9]\quad i = K^* f(\theta)c_s \times \exp\left\{-\frac{\alpha e[\varphi_0 - \varphi(x_1)] + W_{Z-\alpha}(x_1, \theta)}{kT}\right\}$$

In order to calculate the energy $W_{Z-\alpha}(x_1, \theta)$ one must first specify the part of the double layer (either the compact or the diffuse one) into which the electron is transferred in the course of the reaction. In the case when the centers of discharging ions in the reaction state are located in the diffuse part of the double layer the following electrostatic problem must be solved:

$$[10]\quad \begin{aligned} \Delta\varphi_1 &= 0, && -\beta \le x < 0 \\ \Delta\varphi_2 &= 0, && 0 \le x \le \gamma \\ \Delta\varphi_3 &= -\frac{4\pi eZ}{\varepsilon_0}\delta(\boldsymbol{r} - \boldsymbol{R}_1) && \gamma \le x < \infty. \end{aligned}$$

where $\delta(x)$ is the Dirac delta-function, with the boundary conditions

$$\varphi_1 = 0 \quad \text{at} \quad x = -\beta$$

$$\varphi_1 - \varphi_2 = \frac{4\pi\mu}{\varepsilon_1}\sum_{m,n}\delta(y - y_{mn})\delta(z - z_{mn});$$

[11] $$\frac{\partial\varphi_1}{\partial x} = \frac{\partial\varphi_2}{\partial x} \quad \text{at} \quad x = 0$$

$$\varphi_2 = \varphi_3, \quad \varepsilon_1\frac{\partial\varphi_2}{\partial x} = \varepsilon_0\frac{\partial\varphi_3}{\partial x} \quad \text{at} \quad x = \gamma$$

$$\varphi_3 = 0 \quad \text{at} \quad x \to \infty$$

Here the quantity μ is the projection of the dipole moments of the adsorbed molecules on the x axis; ε_0 and ε_1 are the dielectric permittivities, respectively, of the diffuse and the compact parts of the double layer; y_{mn} and z_{mn} are the coordinates of the centers of the adsorbed molecules.

In the case of location of the discharging ions inside the compact layer ($-\beta \le x_1 \le \gamma$), one should solve one of the following electrostatic problems:

[12] $$\Delta\varphi_1 = -\frac{4\pi eZ}{\varepsilon_1}\delta(\boldsymbol{r} - \boldsymbol{R}_1); \Delta\varphi_2 = 0; \Delta\varphi_3 = 0$$

[13] $$\Delta\varphi_1 = 0; \Delta\varphi_2 = -\frac{4\pi eZ}{\varepsilon_1}\delta(\boldsymbol{r} - \boldsymbol{R}_1); \Delta\varphi_3 = 0$$

$$-\beta \le x < 0; \quad 0 < x \le \gamma; \quad \gamma \le x < \infty$$

depending on the location of the plane $x = x_1$. The boundary conditions [11] are the same for all the cases.

The solution of the system [10] with the boundary conditions [11] allows calculation of the so-called micropotential, φ_m, which is determined by the equation

$$\varphi_m = \lim_{\boldsymbol{r}\to\boldsymbol{R}_1}\left\{\varphi_3(\boldsymbol{r}, \boldsymbol{R}_1) - \frac{eZ}{\varepsilon_0|\boldsymbol{r} - \boldsymbol{R}_1|}\right\}$$

and then to find the energy W_Z using the simple relation $W_Z = eZ\varphi_m$. After calculations we obtain

[14] $$W_z(x_1) = \frac{eZ\mu}{\varepsilon_1}\sum_{m,n}\int_0^\infty (\exp -\lambda x_1)\,\chi(\lambda)J_0(\lambda R_{mn})\,d\lambda$$

where $J_0(\lambda R_{mn})$ is the Bessel function of the first kind; R_{mn} and $\chi(\lambda)$ are determined by the expressions

$$R_{mn} = \sqrt{y_{mn}^2 + z_{mn}^2}; \quad \chi(\lambda) = \frac{2\varepsilon_1\lambda}{\varepsilon_1 + \varepsilon_0}\frac{\omega - \xi}{1 - \xi}$$

$$\omega = \frac{\varepsilon_1 + \varepsilon_0}{\varepsilon_1 - \varepsilon_0}e^{2\lambda\gamma}; \quad \xi = \omega\frac{\tanh\lambda\beta + 1}{\tanh\lambda\beta - 1}$$

In the case of location of the plane $x = x_1$ inside the interval $-\beta \le x_1 < 0$ the solution of the system [12] leads to the Fourier–Bessel integral of the same form as [14], only one must substitute the expression

$$\left(\frac{\varepsilon_1 + \varepsilon_0}{\omega\varepsilon_1}\chi - 2\lambda\right)\frac{\sinh[\lambda(\beta + x_1)]}{\sinh\lambda\beta + \cosh\lambda\beta}$$

for $\exp(-\lambda x_1)\chi(\lambda)$. In the case of $0 < x_1 \le \gamma$ again one obtains [14] in which the product $\exp(-\lambda x_1)\chi(\lambda)$ must be substituted by

$$\frac{\varepsilon_1 + \varepsilon_0}{2\varepsilon_1}\left\{\exp(-\lambda x_1) + \frac{1}{\omega}\exp(\lambda x_1)\right\}$$

The effect of specifically adsorbed dipole molecules on the electrode kinetics can be characterized by the ratio of the current density, i, determined by [9] to the current density, i_0, in the absence of adsorbed molecules. The value i_0 is described by the equation

[15] $$i_0 = K_0 c_s^{(0)} \exp\left\{-\frac{\alpha e}{kT}[\varphi_0 - \varphi^{(0)}(x_1)]\right\}$$

Here the local concentration $c_s^{(0)}$ and the average potential $\varphi^{(0)}(x_1)$ are related to the electrode potential, φ_0, and the bulk concentration of the reactant ions, c_0, by the expressions

$$c_s^{(0)} = c_0 \exp\{-[eZ\varphi^{(0)}(x_1) + U_Z(x_1) + V_{atm}(Z, x_1)]/kT\}$$

$$\varphi^{(0)}(x_1) = \varphi_0\left(1 - \frac{x_1}{\beta + \gamma}\right)$$

From [9] and [15] we obtain

[16] $$i/i_0 = K^* f(\theta) \exp\{-[e(Z - \alpha)[\varphi(x_1, \theta) - \varphi^{(0)}(x_1)] + W_{Z-\alpha}(x_1, \theta)]/kT\}$$

where the average potential, $\varphi(x_1, \theta)$, in the presence of adsorbed molecules is determined by the relations

[17] $$\varphi(x_1,\theta) = \begin{cases} \varphi_0\left(1 - \dfrac{x_1}{\beta + \gamma}\right) - \dfrac{4\pi\mu x_1\Gamma_\infty\theta}{\varepsilon_1(\beta + \gamma)} & -\beta \le x_1 < 0 \\ \varphi_0\left(1 - \dfrac{x_1}{\beta + \gamma}\right) + \dfrac{4\pi\mu(\beta + \gamma - x_1)\Gamma_\infty\theta}{\varepsilon_1(\beta + \gamma)} & 0 < x_1 \le \gamma \end{cases}$$

the value Γ_∞ being the limiting number of adsorbed molecules per unit area.

Equation [16] describes the so-called inhibition effect of surface-active substances on electrochemical

Can. J. Chem. Downloaded from www.nrcresearchpress.com by 210.87.254.40 on 09/06/12
For personal use only.

Can. J. Chem. Downloaded from www.nrcresearchpress.com by 210.87.254.40 on 09/06/12
For personal use only.

kinetics. In ref. 12 this effect was estimated taking into account the phenomena of fractional charge transfer and formation of donor–acceptor complexes between metal and adsorbed molecules. However, calculations were carried out using [16] in which the term $W_{Z-\alpha}$ responsible for interaction between discrete charges and dipole moments in the adsorption layer was discarded. Our calculations, the details of which will be given below, show that in many real systems the contribution of the term $W_{Z-\alpha}$ into the inhibition effect is dominating.

The inhibition effect of surface-active substances was calculated for the cases of discharge of zinc and cadmium cations on mercury in the presence of specifically adsorbed *n*-butanol. Equations [16] and [17] were used in which the values of the parameters were chosen as follows: $\alpha = 0.5$; $\beta = 4$ Å; $\gamma = 1$ Å; $\varepsilon_1 = 8$; $\mu = -1.6$ D; $K^* = 1$. The negative value of μ means that the adsorbed alcohol molecules are oriented by their positive poles towards metal. The function $f(\theta)$ was approximated by the expression $f(\theta) = 1 - \theta$ that means that we take into account the simple effect of partial blockage of the electrode surface by the adsorbed molecules. For the case of zinc the values of x_1 and Γ_∞ were put equal to -3.17 Å and 1.2×10^{14} cm^{-2} (the value $x_1 = -3.17$ Å corresponds to the distance 0.83 Å from the electrode surface, and this distance is equal to the crystallochemical radius of zinc). In the case of cadmium the corresponding values were -3.08 Å and 1.5×10^{14} cm^{-2}. The results of calculation are presented in Figs. 1 and 2. In the same figures the experimental data on electroreduction of Zn^{2+} and Cd^{2+} in the presence of *n*-butanol are shown. The

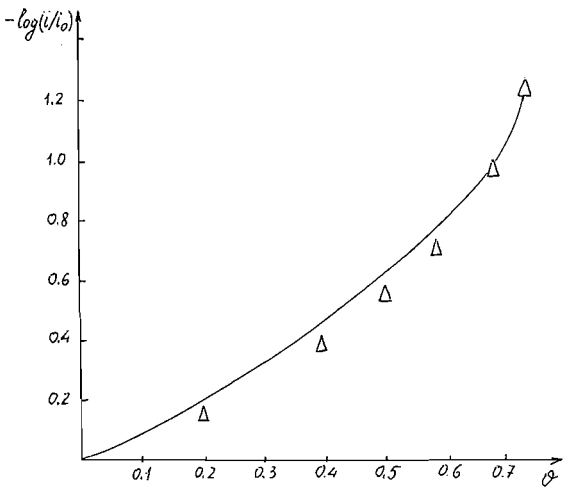

FIG. 1. Theoretical (solid line) and experimental (triangles) dependences characterizing the inhibition effect of *n*-butanol adsorbed on mercury for the reaction of discharge of zinc cations.

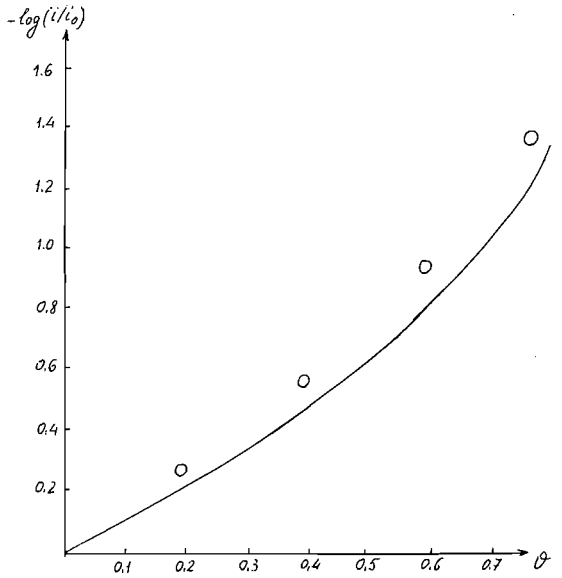

FIG. 2. The inhibition effect for the process of discharge of cadmium cations on mercury in the presence of specifically adsorbed molecules of *n*-butanol (solid line—the result of theoretical calculation; circles—the experimental data).

triangles in Fig. 2 correspond to the data obtained in ref. 13 for the system $Zn^{2+} + n\text{-}C_4H_{10}OH + 0.2\ N\ H_2SO_4 + 1.0\ N\ Na_2SO_4$. The data (14) on inhibition of discharge of Cd^{2+} ions by adsorbed molecules of *n*-butanol in the system $Cd^{2+} - n\text{-}C_4H_{10}OH + 0.1\ M\ HClO_4 + 0.9\ M\ NaClO_4$ are indicated by circles in Fig. 2. As can be seen from the figures there is quite good agreement between theoretical results and experimental data at reasonable values of the parameters.

1. W. R. FAWCETT and S. LEVINE. J. Electroanal. Chem. **43**, 175 (1973).
2. K. ROBINSON and S. LEVINE. J. Electroanal. Chem. **47**, 375 (1973).
3. S. LEVINE, K. ROBINSON, and W. R. FAWCETT. J. Electroanal. Chem. **54**, 237 (1974).
4. W. R. FAWCETT and S. LEVINE. J. Electroanal. Chem. **65**, 505 (1975).
5. R. R. DOGONADZE and A. M. KUZNETZOV. Elecktrokhimia, **11**, 3 (1975).
6. R. R. DOGONADZE and A. M. KUZNETZOV. Elektrokhimia, **13**, 1268 (1977).
7. V. S. KRYLOV and V. A. KIRYANOV. Elektrokhimia, **12**, 536 (1976).
8. M. A. VOROTYNTZEV. Elektrokhimia, **14**, 1274 (1978).
9. V. S. KRYLOV. Elektrokhimia, **14**, 1274 (1978).
10. V. S. KRYLOV, V. A. KIRYANOV, and I. F. FISHTIK. Elektrokhimia, **16**, 340 (1980).
11. V. S. KRYLOV, W. R. FAWCETT, and V. A. KIRYANOV. Elektrokhimia, **12**, 424 (1976).
12. S. F. TIMASHEV. Elektrokhimia, **15**, 333 (1979).
13. S. SATHYANARAYANA. J. Electroanal. Chem. **10**, 119 (1965).
14. T. BIEGLER and H. A. LAITINEN. J. Electrochem. Soc. **113**, 852 (1966).

Nonlocal dielectric response of the electrode/solvent interface in the double layer problem

A. A. KORNYSHEV AND M. A. VOROTYNTSEV

Institute of Electrochemistry, Academy of Sciences of the USSR, Moscow V-71, Leninskii prosp. 31, USSR

Received July 2, 1980

This paper is dedicated to Dr. Sam Levine on the occasion of his 70th birthday

A. A. KORNYSHEV and M. A. VOROTYNTSEV. Can. J. Chem. **59**, 2031 (1981).

A theory of the double layer in the electrolyte solution near the electrode surface is formulated in terms of the most general description of the electrode/solvent interface, the ionic plasma being treated in the Poisson–Boltzmann approximation. As a result, the differential capacitance of the electrochemical contact is calculated. In the case of low ionic concentrations ($\lesssim 0.1\ M$) it takes the form: $C^{-1} = C_{GC}^{-1} + C_*^{-1}$, where the C_{GC} is the Gouy–Chapman nonlinear differential capacitance and C_* is a "constant" capacitance, not depending on the concentration, but possessing a possible dependence on the charge of the electrode. The "compact layer" capacitance C_* is expressed through a unified nonlocal dielectric function of the electrode–solvent system. This may be considered as a formal approval of Grahame's parametrization of experimental data. But the physical meaning of the compact layer capacity is reconsidered subject to the relation obtained with the nonlocal dielectric function. The latter reflects the electronic structure of the metal and the structure of the solvent in contact. Thereby, the possible reasons for the dependence of the "compact layer" capacity on the nature of the electrode, solvent, and the interaction between them are revealed. A generalization of the results on the case of a more general description of ionic plasma is discussed.

A. A. KORNYSHEV et M. A. VOROTYNTSEV. Can. J. Chem. **59**, 2031 (1981).

On formule une théorie de la double couche dans une solution électrolytique au voisinage de la surface d'une électrode en fonction de la description la plus générale de l'interface électrode/solvant alors qu'on traite le plasma ionique par l'approximation de Poisson-Boltzmann. Il en résulte que l'on peut calculer la capacité différentielle du contact électrochimique. Dans le cas des faibles concentrations ioniques ($\lesssim 0{,}1\ M$), elle prend la forme $C^{-1} = C_{GC}^{-1} + C_*^{-1}$ où C_{GC} est la capacité différentielle non linéaire de Gouy–Chapman et C_* est une capacité constante indépendante de la concentration qui peut éventuellement dépendre de la charge sur l'électrode. On exprime la capacité de la "couche compacte" C_* au moyen d'une fonction diélectrique non locale unifiée du système électrode–solvant. On peut considérer ceci comme une confirmation formelle de la transposition des données expérimentales en paramètre qui a été faite par Grahame. Toutefois, on a reconsidéré la signification physique de la capacité de la couche compacte, en fonction de la relation obtenue avec la fonction diélectrique non locale. Cette dernière reflète la structure électronique du métal et la structure du solvant qui est en contact. On trouve aussi les diverses raisons qui pourraient expliquer pourquoi la capacité de la "couche compacte" dépend de la nature de l'électrode, du solvant et de l'interaction entre-eux. On discute de la généralisation des résultats dans le cas d'une description plus générale d'un plasma ionique.

[Traduit par le journal]

Introduction

Much attention has been recently paid to the research and development of new methods for the investigation of the electrochemical interface *in situ*, based on the modern advances in surface science (see, e.g., papers in ref. 1). However, classical capacity measurements remain one of the major tools for studying the interfacial properties. Indeed, the capacitance and related characteristics are sensitive to the specific properties of the contact region when the electric potential changes in a distance comparable with its "thickness". It is difficult to realize such a rapid variation of the potential in electrode–vacuum systems (in order to do this, one should, e.g., place the second electrode at a microscopic distance from the first one). The rapid drop of the potential near the electrochemical interface is provided by the screening of the field in the electrolyte. For typical ionic concentrations the depth of the field penetration into the electrolyte solution is comparable with the dimensions of the interfacial region. Thus, the electrical properties of the electrochemical interface (the capacitance, in the equilibrium case) are sensitive to its structure. An adequate interpretation of capacitance data is one of the central points in electrochemistry.

Grahame's Hypothesis

In this paper we shall discuss systems without specific adsorption of electrolyte ions onto the electrode surface. A parametrization of capacitance data for such systems was proposed by Grahame (2, 3) which has been widely used during the last 30 years. According to Grahame's hypothesis, the total capacitance of the metal–electrolyte contact has the form of two capacitors in series

$$[1] \quad 1/C = 1/C_i + 1/C_d$$

Here C_d is the capacitance of the diffuse layer in the solution, depending on the electrode charge and electrolyte concentration; C_i is the, so called, inner layer (or compact layer) capacitance depending on the charge of the electrode but *not depending* on the concentration. Furthermore, Grahame assumed that

0008-4042/81/132031-12$01.00/0

©1981 National Research Council of Canada/Conseil national de recherches du Canada

Can. J. Chem. Downloaded from www.nrcresearchpress.com by 210.87.254.5 on 09/06/12
For personal use only.

Can. J. Chem. Downloaded from www.nrcresearchpress.com by 210.87.254.5 on 09/06/12
For personal use only.

the dependence of C_d on the electrode charge σ (calculated per unit contact area) and on the total concentration of ionic species in the solution, c, can be described by the Gouy–Chapman theory. In the case of a binary symmetric electrolyte, the latter gives:

$$[2] \quad C_d = C_{GC} = \frac{\varepsilon}{4\pi}\sqrt{\kappa^2 + 4\pi\frac{L_B^2\sigma^2}{e^2}}$$

where κ^{-1} is the Gouy (Debye) length,

$$[3] \quad \kappa = \sqrt{\frac{4\pi e^2 c \sum_i Z_i^2 \nu_i}{\varepsilon\theta}}$$

and L_B is the Bjerrum length

$$[4] \quad L_B = e^2/\varepsilon\theta$$

(ε is the macroscopic dielectric constant of the solvent; Z_i and ν_i are the valencies and the stoichiometric coefficients for electrolyte ions and θ, the temperature in energetic units).

Testing Grahame's Assumption

By plotting the measured values of C^{-1} versus C_d^{-1} calculated via [2] for different values of the concentration c, one may check Grahame's hypothesis. This was first done by Parsons and Zobel (4) and later used for the interpretation of the capacitance of various electrochemical systems. The data obtained for systems without specific adsorption give a straight line with unit slope, thus supporting Grahame's assumption. In the light of the success of the Grahame's parametrization, the data are frequently presented in the "resolved form" of the dependence of C_i upon the charge of the electrode, the nature of the electrode, the solvent, temperature, etc. (for reviews see refs. 5–7).

The applicability of Grahame's assumption is frequently discussed in terms of whether C_i depends on the value of the concentration for which it was evaluated. It was proposed, in particular, to use the data obtained at low concentrations $c \lesssim 0.01\ N$ where the Gouy–Chapman theory is supposed to give the most reliable results (40). The values thereby obtained might differ slightly from $C_i(\sigma)$ evaluated by Grahame. At the same time, it is evident that the lowering of the experimental accuracy in the range of small concentrations and the increase in the contribution of the diffuse layer capacitance would enhance the inaccuracy in the determination of $C_i(\sigma)$. So, the question is then whether the results for $C_i(\sigma)$ obtained for different concentrations are in agreement *within the accuracy of its determination.*

A natural way to check it is as follows. The measured value of the inverse capacitance minus the inverse Gouy–Chapman capacitance is plotted versus concentration for fixed values of the charge σ. For each concentration the inaccuracy in the determination of the ordinate is indicated. If a horizontal line can be drawn through all the points within the range of accuracy, then Grahame's assumption is supported. The values thus obtained for $C_i(\sigma)$ are fitted to all concentrations, which may be regarded as an additional advantage of this method. Another, more decisive test is in plotting $[C^{-1}(\text{measured}) - C_d^{-1}(\text{calculated})]$ versus σ for different fixed values of concentration. If these $C_i(\sigma)$ curves, obtained for different c, coincide within the range of established accuracy, then Grahame's assumption does not contradict the experimental data. Examples of the application of both methods are given in the Appendix.

Physics of Grahame's Parametrization

The following two questions are usually the matter of discussion in the interpretation by Grahame. (*1*) What is the exact physical meaning of the concentration independent contribution to the inverse capacitance, C_i^{-1}, and what is the mechanism of the dependence on the charge of the electrode, the type of contact, and the thermodynamic parameters? (*2*) The expression [2] is a consequence of the nonlinear Gouy–Chapman theory. One is accustomed in literature to seeing criticism of it on statistico-mechanical grounds (8). Why then does [2] work so satisfactorily in the calculation of the diffuse layer capacity in Grahame's interpretation?

Let us discuss initially the second question which is less central for the aims of this paper than the first one. Computer simulation tests (9) and some other studies (10, 11) suggest an idea that a result similar to that of Gouy–Chapman may hold in a statistically justified theory (due to a compensation of corrections of different origins) even in a wide range of c and charges σ. However, even if the concrete form of [2] may only pretend to semiquantitatative results,[1] the interpretation of the data with its help possesses an "interpolation" accuracy. In fact, the contribution of C_d to the total capacitance [1] dominates in the vicinity of the zero charge point for small concentrations. Here,

$$[5] \quad C_d = \frac{\varepsilon\kappa}{4\pi}\cosh\left\{\frac{eV}{2\theta}\right\}$$

When the rationalized potential drop V tends to

[1]For not too large charges and concentrations, [2] predicts reasonable qualitative behaviour: before the beginning of the lattice effects (12) the characteristic thickness of the diffuse layer should decrease with the rise of the potential drop.

Can. J. Chem. Downloaded from www.nrcresearchpress.com by 210.87.254.5 on 09/06/12
For personal use only.

zero, this result has a rigorous statistical foundation (13). With the increase of the charge and concentration the limiting form [5] no longer holds, but at the same time, C_d increases, and its contribution to the total capacitance diminishes. So, the latter is determined in this range mainly by the value of C_i, and the difference in the form of C_d predicted by different theories will be revealed but weakly in the experiment.

A variety of papers has been devoted to a physical interpretation of C_i (14). The Helmholtz idea that a plane condenser is arranged at the metal–electrolyte interface, the inner plane of which is the "metal surface" and the outer plane is determined by the distance of the closest approach of ions to the electrode, was utilized by Stern (15). He matched this inner layer condenser with the space charge in the electrolyte. The proper development of Stern's picture, given in an early paper by Grahame (2), attributed C_i just to this inner layer capacitor. A formula of macroscopic electrostatics was used to estimate C_i:

$$[6] \quad C_i = \varepsilon_i/4\pi L_i$$

where ε_i and L_i are the dielectric constant and the thickness of the inner layer. A reduced value of ε_i with respect to ε and its dependence on the voltage was discussed by Grahame (16) on the basis of Malsch's (17) observation of the bulk dielectric saturation effect. This approach was developed by Macdonald (18) and in some other publications (for review see refs. 8 and 9).

Later, microscopic molecular models were proposed for the inner layer structure. On the basis of these models, the capacitance was calculated and its dependence on charge analyzed (see reviews in refs. 14, 19–21). One common feature of these works, recognized in literature (10), is that the properties of the inner layer are considered spearately from the diffuse layer. The critical attitude to the description of an interfacial monolayer or bilayer of solvent molecules as a separate phase is evident: due to the structure of the solvent, the molecules of the "inner layer" are coupled with the outer solvent molecules (22, 23).

Electric Field Penetration into the Metal

Another group of papers discusses a contribution of the space charge in the metal. It originates in the paper by Rice (24). He utilized the Sommerfeld quantum theory of metals and applied it to the problem of the capacitance of an electrochemical interface prior to its development and application in the physics of metal surfaces. Different views on the role of the space charge in the metal were presented in the subsequent electrochemical literature. To put in order this controversial picture, it is worth discussing the question in more detail.

Rice's approach was analogous to a simple linearized Thomas–Fermi model with a sharp boundary for electrons at the surface. In modern terms this model prescribes for the capacitance of space charge in the metal:

$$[7] \quad C_M = \varepsilon_M \kappa_{TF}/4\pi$$

Here $\kappa_{TF} = (6\pi n_0 e^2/\varepsilon_M E_F)^{1/2}$ is the inverse Thomas–Fermi length (n_0, the average concentration of electrons; E_F, the Fermi energy); ε_M is the background dielectric constant due to the polarizability of the degrees of freedom having higher frequencies than the motion of free charge carriers (25). For instance, this might be the polarizability due to interband transitions, so that ε_M can be much greater than unity in semi-metals (e.g. Bi) and semiconductors, and close to one in simple metals like Hg. At Rice's time the band theory did not exist and he proposed a naive picture of the "solvent" composed of skeleton ions in which the electrons are dissolved. In the case of mercury, he attributed $\varepsilon_M \simeq 8$ to this "solvent". It seems hardly realistic now because the band gap in mercury is large enough and interband transitions cannot give a large contribution to the background polarizability, i.e., $\varepsilon_M \simeq 1$. After Grahame's measurements of the capacitance of the Hg/NaF–H_2O contact the value of C_i became known: $C_i = 29$ μF/cm^2, i.e., $1/4\pi C_i = 0.3$ Å. The metal capacitance is supposed to give a contribution in series with the contribution from the electrolyte side. The modern estimate with $\varepsilon_M \simeq 1$ and $\kappa_{TF}^{-1} = 0.5$ Å gives $1/4\pi C_M = 0.5$ Å which exceeds the experimental value of 0.3 Å (and, thus, does not allow any other contribution to the constant capacitance), while Rice's estimate is half that.

Attributing C_i to the metal capacitance only was criticized by Watts-Tobin and Mott (26, 27). They indicated a remarkable dependence of the experimental values of C_i on the temperature and the increase of C_i with anodic polarization. These cannot be provided by the metal, so that the solvent *must* take an important part. It should be emphasized that nowhere did they conclude that the inverse metal/vacuum capacitance is small compared to the experimental C_i^{-1}. They only argued against simply adding the vacuum value of the metal capacitance in series with a contribution from the solution part — otherwise the "pure metal" effect will be *too large*, in contradiction with experimental data! One cannot simply throw away the metallic space charge effect, but it must be somehow diminished. Thus, Mott and Watts-Tobin (27) argued against the model of a

Can. J. Chem. Downloaded from www.nrcresearchpress.com by 210.87.254.5 on 09/06/12
For personal use only.

sharp interface. They presumed that the "field does not jump sharply at the interface", implying that the metal electron cloud near the boundary is mixed with the solvent. That means, in other words, that the interfacial layer should be characterized by a unified background dielectric polarizability. A very rough estimate is appropriate for an illustration of this statement:

$$\frac{1}{4\pi C_i} \sim \frac{1}{4\pi C_M^{interf}} + \frac{1}{4\pi C_H}$$

where C_M^{interf} and C_H are the interfacial electronic gas and the Helmholtz layer contributions. Introducing some effective dielectric constant of the interfacial region $\tilde{\varepsilon}$ one may evaluate $C_M^{interf} \sim \tilde{\varepsilon}\kappa_{TF}/4$, $C_H \sim \tilde{\varepsilon}/4\pi L$ where L is the Helmholtz layer effective thickness. Then $1/4\pi C_i \sim (\kappa_{TF}^{-1} + L)/\tilde{\varepsilon}$, and one may speak about the metallic effect as a small distance added to L.[2] However more accurate estimates take into account $\tilde{\varepsilon}$ in the Thomas–Fermi length $\kappa_{TF}^{-1} \sim \sqrt{\tilde{\varepsilon}}\kappa_{TF_0}^{-1}$ ($\kappa_{TF_0}^{-1}$, the isolated metal value):

$$1/4\pi C_i \sim (\kappa_{TF_0}^{-1}\sqrt{\tilde{\varepsilon}} + L)/\tilde{\varepsilon}$$

Thus, the electric field penetration adds to L not 0.5 Å but rather more than 1 Å, which gives about 20% to the total result. So, Mott and Watts-Tobin's qualitative arguments (in contrast to their misleading quotes in some subsequent publications) mean only that a rigorous theory must be developed to justify why the metal effect is not large enough to cover the whole value of C_i^{-1}.

Quantum-mechanical Approach to the Structure of the Interface

Recent advances in the quantum self-consistent theory of metal surfaces (29, 30) demonstrate that the electronic "tails" are spread outside the metal skeleton edge into the vacuum. However, a simple matching of the vacuum–metal capacitance, calculated without an assumption of an infinite barrier for electrons at the surface, to the electrolyte capacitance in series would not lead to a resolution of the problem. Indeed it is natural to expect that the effective screening length in the surface region should be greater than the bulk value. A treatment of this kind was proposed by Kuklin (31) and, in fact, it does not agree with experimental data.[3]

Quantum self-consistent theory of the metal–insulator contact is not yet developed. Only the first steps have been made in purely electrostatic estimates of the effect of the bounding dielectric polarizability on the character of electronic distribution near the interface (32). The effect is, in addition, spread out inside the insulator. A proper treatment of the metal – polar solvent interface should also take into account the quantum interaction of the metallic electrons with the electronic orbitals of solvent molecules. In the case of chemisorption of the solvent, a corresponding exchange term would be involved in the Hamiltonian. These effects taken together will determine the resulting character of the electronic distribution in the interfacial region and the contact dielectric response. In the light of this general view, various data for the dependence of C_i on the nature of the metal, solvent, and their interaction may be understood. However, the quantitative explanation of the data can be given only by a model quantum treatment of the problem.

Phenomenological Approach

Prior to the creation of a theory of this kind, a "modelless" phenomenological analysis of the potential distribution in the system is relevant in order to reveal which properties of the capacitance depend on the model of the contact and which are general for any system. In particular, such an approach would permit one to investigate to what extent Grahame's parametrization is justified and, in the case of its validity, to express the "compact layer capacitance" C_i through the dielectric response of the system. For the potentials close to the zero charge point, such a problem has been solved by Schmickler and the authors of this paper (33) (for a discussion of these results, see also the review article by A. A. Kornyshev and M. A. Vorotyntsev in ref. 1).

[2]This would not be true, if the *vacuum* metal capacitance is added in series: $1/4\pi C_i = \kappa_{TF_0}^{-1} + L/\tilde{\varepsilon}$. Here the first term is of the same order as the second one, in contrast to the statement made in ref. 28.

[3]An apparent agreement with experimental data drawn in Fig. 3 of ref. 31 is caused by two circumstances. (*1*) For $c = 10^{-3}$ *M*, 10^{-2} *M* the compact layer contribution is negligible with respect to that of the diffuse layer. So, for low concentrations any mistake in the expression for the compact layer capacity is not observable in the plots of the charge dependence of the total capacitance. (*2*) At $c = 10^{-1}$ *M*, the results start to be sensitive to the description of the compact layer contribution. Therefore, a discrepancy between the experimental data and predictions of Kuklin's model should be expected. However, the theoretical point given in Fig. 3 for $c = 10^{-1}$ *M* lies rather close to the experimental curve, too close, probably, due to an arithmetical mistake. Indeed, from the formulae [32′], [34], [34′], [34″] of ref. 31 it follows that $C < C_M$. At the same time, C_M should be equal to 16 μF/cm² for the Thomas–Fermi model if one uses the estimate of ref. 31 for Thomas–Fermi parameter $K_s = 1.8 \times 10^{-8}$ cm^{-1} (p. 388), and be smaller for other models. This is in obvious contradiction to $C = 18$ μF/cm² obtained by the author for the total capacity. The discrepancy between the Kuklin's model of matching the metal and electrolyte contributions and the experimental data will be even more drastic for higher concentrations.

Can. J. Chem. Downloaded from www.nrcresearchpress.com by 210.87.254.5 on 09/06/12
For personal use only.

This phenomenological analysis enabled one to come to a qualitative conclusion concerning the microscopic structure of the interface: it has been unambiguously shown that no quantum model of the metal with an infinite potential barrier for electrons at the interface can be consistent with the capacitance data for mercury (and a set of simple metals) – sodium fluoride aqueous solution contact. That means that the electronic "tails", presumably, penetrate into the interfacial solvent region.

In the present paper we shall extend this theory to the case of a moderate deviation of the electrode potential from the zero charge point. It will be seen from its results that (*1*) Grahame's parametrization is valid for any model of the contact and has a rigorous foundation at moderate electrolyte concentrations and charges at the electrode. (*2*) The value of C_i is expressed through a unified dielectric function of the electrode–solvent system. (*3*) This expression provides the possibility for studying the dependence of C_i on the nature of the metal, solvent, electrode charge, temperature, etc., on the basis of models for this function.

Poisson–Boltzmann Equation with an Account of Spatial Dispersion of the Dielectric Permittivity of the Electrode–Solvent System

Let us consider firstly the potential distribution at the zero charge point (zcp), $\phi^0(z)$. It obeys the Poisson equation

$$\frac{d^2}{dz^2}\phi^0(z) = -4\pi(\rho_{ion}{}^0 + \rho_{ms}{}^0)$$

Here, $\rho_{ion}{}^0$ is the charge density for ions in the diffuse layer; $\rho_{ms}{}^0$ is the combined induced charge density due to the electrons of the metal and the bound charge of the solvent polarization; z is the coordinate normal to the interface which we consider being plane in this paper.[4] Within the classical theory of the compact layer, $\phi^0(z)$ is equal to zero in the diffuse layer region because $\rho_{ion}{}^0 = 0$. However, this is not true if the electron tails of the metallic electron density penetrate inside the solvent with nonlocal dielectric properties. In this case, the information about the nonzero field in the range of electron tails is spread into the solvent, inducing a nonzero field in a layer of a characteristic thickness associated with the correlation length for the fluctuations of the solvent polarization. The correlation is determined by the short-range dynamic structure of the solvent (for a detailed discussion see review, ref. 41). In associated liquids it may come to several molecular diameters. Thus, up to such distances the field is nonzero and, thereby, $\rho_{ion}{}^0 \neq 0$, strictly speaking.

When the interface is charged, the Poisson equation takes the form

$$\frac{d^2\phi^\sigma(z)}{dz^2} = -4\pi(\rho_{ion}{}^\sigma + \rho_{ms}{}^\sigma)$$

where the superscript σ indicates the value of the charge, calculated per unit area of the interface. Then, the deviation of the electric potential from that of zcp

$$\phi(z) \equiv \phi^\sigma(z) - \phi^0(z)$$

obeys the equation

$$\frac{d^2}{dz^2}\phi(z) = -4\pi(\rho_{ms} + \rho_{ion}{}^\sigma - \rho_{ion}{}^0)$$

where $\rho_{ms} = \rho_{ms}{}^\sigma - \rho_{ms}{}^0$.

Let us introduce a nonlocal dielectric permeability of the metal–solvent system, $\chi(z, z')$. It relates the change in the density of the metal electrons and the solvent bound charge, ρ_{ms}, with the change of the electric field due to the charging

$$[8] \qquad \rho_{ms}(z) = \frac{d}{dz}\int_{-\infty}^{\infty} dz'[\chi(z, z')]\frac{d\phi(z')}{dz'}$$

Then the equation for $\phi(z)$ takes the form:

$$\frac{d}{dz}\int_{-\infty}^{\infty} dz'[\varepsilon(z, z')]\frac{d\phi(z')}{dz'} = -4\pi[\rho_{ion}{}^\sigma(z) - \rho_{ion}{}^0(z)]$$

where

$$\varepsilon(z, z') = \delta(z - z') + 4\pi\chi(z, z')$$

is the *nonlocal dielectric function of the metal–solvent system.*[5]

In order to make the equation closed, we use the Boltzmann form, relating the electrolyte ionic density and the potential[6]

[4]The one-dimensional picture breaks down in the absence of translational invariance along the interfacial plane. These are the cases of (*a*) discrete translational invariance (single-crystalline electrodes), (*b*) inhomogeneous interface (polycrystalline electrodes), (*c*) microroughness of the electrode surface (solid metals, oxide covered metals with island formation, etc.). Here, the induction and potential would depend upon the coordinates along the interface. This case requires a special consideration and is not considered in this paper.

[5]The physical meaning and basic properties of this function are reviewed in ref. 34, (see also ref. 33). To ensure the smooth reading of this paper, we summarize them in Appendix 2.

[6]The case of a relation of an arbitrary form, $\rho_{ion}{}^\sigma(z) = \rho(\phi)$ is considered in one of the subsequent sections.

$$\rho_{ion}{}^{\sigma}(z) = ec \sum_i z_i \nu_i \theta(z - L_i) \times \exp\left\{-ez_i \frac{\phi^{\sigma}(z)}{\theta}\right\}$$

Here, the Heaviside step function $\theta(z - L_i)$ takes into account (for generality) the finite distance of the closest approach of ions of i-kind to the electrode. Assuming for simplicity L_i being the same for all species ($L_i = L$), we then arrive at the following nonlinear integro-differential equation

$$[9] \quad \frac{d}{dz}\int_{-\infty}^{\infty} dz'[\varepsilon(z, z')]\frac{d\phi(z')}{dz'} = -4\pi\theta(z - L)ec \times \sum_i z_i \nu_i \left\{\exp\left[-ez_i \frac{\phi^0(z) - \phi(z)}{\theta}\right] - \exp\left[-ez_i \frac{\phi^0(z)}{\theta}\right]\right\}$$

It is convenient to rewrite [9] in the equivalent form by introducing the induction $D(z)$:

$$[10] \quad D(z) = \int_{-\infty}^{\infty} dz'[\varepsilon(z, z')]\left[-\frac{d\phi(z')}{dz'}\right]$$

then

$$[9'] \quad \frac{dD}{dz} = 4\pi\theta(z - L)ec \sum_i z_i \nu_i \times \left\{\exp\left[-ez_i \frac{\phi^0(z) + \phi(z)}{\theta}\right] - \exp\left[-ez_i \frac{\phi^0(z)}{\theta}\right]\right\}$$

Since the electrode–solvent system is described by a unified dielectric function, the approach based on (9) includes any variants of the interaction between the electrode and the solvent. At the same time, the charge of the electrolyte plasma is extracted in the right-hand side of [9]. Thus, [9] (and [9']) are inapplicable in the case when chemisorption of ions onto the electrode surface is possible.

The Solution of [9] in the Range of Moderate Electrolyte Concentrations and Electrode Charges

In general, to solve the integro-differential equation [9], it is necessary to specify an analytical form of the kernel $\varepsilon(z, z')$, corresponding to each concrete model of the contact. However, in the case of a solution of a low concentration (when the effective screening length in the electrolyte is much greater than the characteristic scales of $\varepsilon(z, z')$ variation), it is possible to express the solution for the potential $\phi(z)$ through $\varepsilon(z, z')$ of an arbitrary form.

In order to do this we use the singular perturbation technique (the method of matching asymptotic expansions) (35). Since it has been considered rigorously and in detail for the case of the linearized Poisson–Boltzmann integro-differential equation (33), we shall give here only a schematic derivation, retaining the major terms in the asymptotic expansions.

Let us denote the characteristic distance of $\varepsilon(z, z')$ variation by z^*, and consider the case $z^* \ll \kappa^{-1}$. The solution for ϕ is represented in two different forms for the "internal" and "external" regions:

$$[11] \quad \phi(z) = \begin{cases} \phi_{int}(z), & z \ll \kappa^{-1} \\ \phi_{ext}(z), & z \gg z^* \end{cases}$$

with $\phi_{int}(z) = \phi_{ext}(z)$ for $z^* \ll z \ll \kappa^{-1}$. The boundary conditions then take the form

$$[12] \quad \phi_{int}(z \to -\infty) = V\,(=\phi^{\sigma}(-\infty) - \phi^0(-\infty)) \quad \phi_{ext}(z \to +\infty) = 0$$

$$[13] \quad \phi_{int}(z \to \infty) = \phi_{ext}(z \to L)$$

In [12], V is the change of the total potential drop between the bulk of the metal and solution with the charging of the electrode (i.e., the rationalized potential). Equation [13] is the matching condition for asymptotic expansions.

In the range of $z \ll \kappa^{-1}$ and for not too large deviations from the zero charge point, the leading term of the asymptotic expansion corresponds to the limit of $c \to 0$, i.e., to obtain it one may simply omit the right-hand side of [9]:

$$[14] \quad \frac{d}{dz}\int_{-\infty}^{\infty} dz'[\varepsilon(z, z')]\frac{d\phi_{int}(z')}{dz'} = 0$$

Other aspects of [9] are simplified in the range of $z \gg z^*$. In this region, $\phi^0(z) \simeq 0$, and, thereby, $\rho_{ion}{}^0 \simeq 0$. Furthermore, $\varepsilon(z, z')$ is a rapidly varying function. Therefore, $d\phi(z')/dz'$ in the integrand may be expanded in a power series near $z' = z$. If only the major term in the expansion is considered, the left-hand side is reduced to

$$\frac{d}{dz}\left\{\frac{d\phi_{ext}}{dz}\int_{-\infty}^{\infty} dz'[\varepsilon(z, z')]\right\}$$

Taking into account that $\varepsilon(z, z')$ coincides in this range with the bulk dielectric function of the solvent, $\varepsilon_s(z - z')$, and using the identity $\int dz'[\varepsilon_s(z - z')] = \varepsilon_S$ (ε_S is the macroscopic dielectric constant of the solvent) we obtain

$$[15] \quad \varepsilon_S \frac{d^2\phi_{ext}}{dz^2} = -4\pi ec\theta(z - L)\sum_i z_i \nu_i \times \exp\{-ez_i\phi_{ext}(z)/\theta\}$$

Can. J. Chem. Downloaded from www.nrcresearchpress.com by 210.87.254.5 on 09/06/12
For personal use only.

Can. J. Chem. Downloaded from www.nrcresearchpress.com by 210.87.254.5 on 09/06/12
For personal use only.

The integration of [14] gives

$$[16]\quad \int_{-\infty}^{\infty} dz'\,[\varepsilon(z, z')]\frac{d\phi_{int}(z')}{dz'} = -D$$

D is a constant of integration equal to the induction [10] in the range where ions are absent. Let us introduce the inverse function of $\varepsilon(z, z')$:

$$[17]\quad \int_{-\infty}^{\infty} dz''[\varepsilon(z, z'')][\varepsilon^{-1}(z'', z')] = \delta(z - z')$$

Using it, we may rewrite [17] as

$$[18]\quad \frac{d}{dz}\phi_{int}(z) = -D\int_{-\infty}^{\infty} dz'[\varepsilon^{-1}(z, z')]$$

Integrating [18] and taking [12] into account, gives

$$[19]\quad \phi_{int}(z) = V - D\int_{-\infty}^{z} dz''\int_{-\infty}^{\infty} dz'[\varepsilon^{-1}(z'', z')]$$

The integral in [19] diverges with $z \to \infty$. Therefore, it is convenient to rewrite [19] by adding and subtracting the asymptotic behaviour of this integral at $z \to \infty$:

$$[20]\quad \phi_{int}(z) = V - \frac{D}{\varepsilon}\theta(z - L)(z - L) - D \times \int_{-\infty}^{z} dz''\left[\int_{-\infty}^{\infty} dz'\,[\varepsilon^{-1}(z'', z')] - \frac{\theta(z'' - L)}{\varepsilon}\right]$$

The integral in [20] approaches the finite value[7]

$$[21]\quad l = \int_{-\infty}^{\infty} dz\left\{\int_{-\infty}^{\infty} dz'[\varepsilon^{-1}(z, z')] - \frac{1}{\varepsilon}\theta(z - L)\right\}$$

as $z \to \infty$.

The solution of the external region equation [15] coincides with that of the classical local Poisson–Boltzmann equation. Integrating it in a standard way we have

$$[22]\quad -[\operatorname{sgn}\phi_0]\sqrt{\frac{\varepsilon}{8\pi\theta c}} \times \int_{\phi_0}^{\phi_{ext}} \frac{d\psi}{\sqrt{\sum_i \nu_i\left[\exp\left(\frac{-ez_i\psi}{\theta}\right) - 1\right]}} = z - L$$

where the constant of integration $\phi_0 = \phi_{ext}(z)$ should be obtained from condition [13]. To do this we rewrite [22] in the range of $z \to L(z \ll \kappa^{-1})$, i.e., for $\phi_{ext} \to \phi_0$:

$$[23]\quad \underset{z\to L}{\phi_{ext}} = \phi_0 - (z - L) \times \sqrt{\frac{8\pi\theta c}{\varepsilon}\sum_i \nu_i\left[\exp\left(-\frac{ez_i\phi_0}{\theta}\right) - 1\right]} \times \operatorname{sgn}\phi_0$$

On the other hand, it follows from (20) that

$$[24]\quad \underset{z\to\infty}{\phi_{int}} = V - Dl - (z - L)D/e$$

The substitution of [23] and [24] into [13] leads to a pair of equations

$$[25]\quad \phi_0 = V - Dl$$

$$[26]\quad D = \sqrt{8\pi\varepsilon\theta c\sum_i \nu_i\left[\exp\left(-\frac{ez_i\phi_0}{\theta}\right) - 1\right]} \times \operatorname{sgn}\phi_0$$

Let us insert [25] into [26] and use the expression for D through the charge separated in the system per unit contact area,

$$[27]\quad D = 4\pi\sigma$$

We then have

$$[28]\quad \sigma = \sqrt{\frac{\varepsilon\theta c}{2\pi}\sum_i \nu_i\left\{\exp\left[-\frac{ez_i}{\theta}(V - 4\pi l\sigma)\right] - 1\right\}} \times \operatorname{sgn}\phi_0$$

We limit the subsequent discussion to a binary symmetric electrolyte. In this case, [28] can be rewritten as an explicit equation

$$[29]\quad V = 4\pi l\sigma - \frac{2\theta}{e}\operatorname{arcsh}\left\{\sqrt{\frac{\pi}{\varepsilon\theta c}}\sigma\right\}$$

Equation [8] has a form of a linear relationship between the induced charge density ρ_{ms} and the change in the electric field $(-d\phi/dz)$ with the charging of the contact from the zcp up to σ. At large values of σ, the linearity of this relationship starts to break down. However, this can be formally taken into account by the introduction of a parametric dependence of $\varepsilon(z, z')$ on σ. Such a possibility is

[7]We note that normally the existence and uniqueness of the inverse function $\varepsilon^{-1}(z, z')$, determined by [17] for a given $\varepsilon(z, z')$, take place. Indeed, $\varepsilon(z, z')$ contains a local part: $\varepsilon(z, z') = \delta(z - z') + \chi(z, z')$. Rewriting the solution of [17] in the form $\varepsilon^{-1}(z, z') = \delta(z - z') + \chi^{-1}(z, z')$, we reduce [17] to $\chi^{-1}(z, z') + \int dz''[\tilde{\chi}(z, z'') \cdot \tilde{\chi}^{-1}(z'', z')] = -\tilde{\chi}(z, z')$. This is the Fredholm inhomogeneous equation of the second kind. It possesses a unique solution except for the case when (-1) is an eigenvalue of the kernel $\tilde{\chi}(z, z')$. We are not aware of physical models for which the latter takes place.

Can. J. Chem. Downloaded from www.nrcresearchpress.com by 210.87.254.5 on 09/06/12
For personal use only.

caused by the following circumstance. The nonlinear dielectric properties are dominant in the range of z where the effect of electrolyte ions on the distribution of electric field is small. So, the form of the function $\varepsilon(z, z')$ is unambiguously determined by the value of σ and the properties of the uncharged metal–solvent contact, but is independent of the structure of the solution. Hence, l is a function of σ, independent of the concentration of electrolyte.

Differentiating [29] with respect to σ we obtain for the differential capacitance

$$[30] \quad C \equiv d\sigma/dV$$

the expression

$$[31] \quad \frac{1}{4\pi C} = l + \sigma\frac{dl}{d\sigma} + \frac{1}{4\pi C_{GC}}$$

where C_{GC} is given by [2]. This result supports the Grahame hypothesis [1], giving the expression for C_i

$$[32] \quad \frac{1}{4\pi C_i} = l + \frac{dl}{d\sigma}$$

One can obtain the integral capacitance

$$[33] \quad K \equiv \frac{\sigma}{V} \equiv \left\{\frac{1}{\sigma}\int_0^\sigma \frac{d\sigma}{C}\right\}^{-1}$$

by dividing [29] by σ:

$$[34] \quad 1/4\pi K = l + 1/4\pi K_{GC}$$

where K_{GC} is the Gouy–Chapman integral capacitance. Thus, the integral capacitance of the inner layer, K_i, is simply related to l:

$$[35] \quad l = \frac{1}{4\pi K_i} = \frac{1}{\sigma}\int_0^\sigma \frac{d\sigma}{4\pi C_i}$$

Expression [35] shows how to evaluate the characteristic length l via the data for the integral or differential inner layer capacity.[8]

On the Criterion of the Validity of [31]

The result [34] is rigorous if the matching of asymptotic expansions and their form are valid. Accurate criteria for the approximations used can be obtained if the next order terms of the asymptotic expansions are found. However, in order to get a semiquantitative estimate, we shall make a simple verification.

The result was achieved primarily by means of omitting the right-hand side of [9] in the internal solution. Evidently, this approximation is reasonable when the portion of the charge in the electrolyte layer of thickness z^* (the characteristic scale of $\varepsilon(z, z')$ variation) neighbouring the electrode is much smaller than the total charge in the double layer as a whole:

$$[36] \quad ec\sum_i z_i\nu_i \int_L^{z^*+L} dz \exp\left\{-\frac{ez_i\phi_{int}(z)}{\theta}\right\} \ll \sigma$$

From [20], let us estimate $\phi_{int}(z)$ in this interval by $(V - Dl)$. Inserting this into [36] we obtain the condition

$$[37] \quad z^*ec\sum_i \nu_i z_i \exp\left\{-\frac{ez_i}{\theta}(V - 4\pi\sigma l)\right\} \ll \sigma$$

For $\sigma \to 0$ the left-hand side of this inequality tends to $(z^*\kappa_0^2/4\pi C_{GC})\sigma$ so that we arrive at

$$[38] \quad z^*\kappa^2 \ll \sqrt{\kappa^2 + 4\pi L_B^2\sigma^2/e^2}$$

i.e.,

$$[39] \quad z^* \ll \kappa^{-1}$$

For larger σ, the sum in [37] can be estimated in the light of [28] by

$$1 + \frac{2\pi}{\varepsilon\theta c}\sigma^2 \sim \frac{2\pi}{\varepsilon\theta c}\sigma^2$$

Thus [37] is reduced to

$$[40] \quad |\sigma| \ll \frac{1}{2\pi}\frac{e}{L_B z^*}$$

At the same time the simplification of the external solution also implied the inequality [39].

Thus the obtained solution of [9] (which justifies Grahame's parametrizations) is appropriate for moderate concentration [39] and in the range around zcp determined by [40]. Taking for estimates an aqueous solution ($z_* \sim 5$ Å, $L_B \simeq 7$ Å) of 1–1 electrolyte, we come to the restrictions $|\sigma| \ll 10\ \mu C/cm^2$, $c \ll 1\ M$. These values belong to the typical range of charges and concentrations in electrochemical experiments.

Some Generalizations

We considered above the electrode–electrolyte solution system within a most general description of an electrode–solvent interface, while using Poisson–Boltzmann approximation (PBA) for ionic plasma. However, it is possible to go out of the framework of PBA.

Let us consider an equation

$$[41] \quad \frac{d}{dz}\int_{-\infty}^{\infty} dz'[\varepsilon(z, z')]\frac{d\phi(z')}{dz'} = -4\pi\rho[\phi]$$

[8]The quantities χ and ε in [8]–[10] characterize the response of the system to the charging from zcp to σ. Therefore, $l(\sigma)$ is naturally related with such an integral response characteristic of the integral capacitance. We could have introduced by analogy the "differential response" functions, prescribing how the metal–solvent system reacts to the charging from σ to $\sigma + d\sigma$, which can be strictly related to the differential capacitance.

Can. J. Chem. Downloaded from www.nrcresearchpress.com by 210.87.254.5 on 09/06/12
For personal use only.

where $\rho[\phi]$ is a function of the potential ϕ. The concrete form of this functional can be specified for a model of electrolyte plasma, i.e., for a given statistical description of the diffuse layer (c.f. ref. 10). For instance, in a particular case of PBA, $-4\pi\rho[\phi]$ coincides with the right-hand side of [9]. We further assume that the form of $\rho[\phi]$ provides the existence and uniqueness of the solution of [41].

Let

$$[42] \quad \int_0^{z^*} dz\, \rho[\phi(z)] \ll \sigma$$

Then again we may use the concept of internal and external solutions [11]. Here the internal solution is valid in the range of z much smaller than the characteristic thickness of the diffuse layer. Boundary conditions [12] and the matching condition [13] (with $L = 0$)[9] can be used. The internal solution is given by [20] ($L = 0$). If the scales of variation of the potential in the outer region are much greater than z^*, one obtains by analogy to [15] the equation for the external solution:

$$[43] \quad \varepsilon \frac{d^2\phi_{ext}}{dz^2} = -4\pi\rho[\phi_{ext}]$$

Let us assume that the general solution of [43] is known. Then the matching of

$$[44] \quad \phi_{\substack{ext \\ z\to 0}} = \phi_{ext}(0) - z\left.\frac{d\phi_{ext}}{dz}\right|_{z=0}$$

and

$$[45] \quad \phi_{\substack{int \\ z\to\infty}} = V - Dl - zD/\varepsilon$$

gives

$$[46] \quad \phi_{ext}(0) = V - Dl$$

$$[47] \quad D = -\varepsilon\left.\frac{d\phi_{ext}}{dz}\right|_{z=0}$$

Equation [47] means that the charge at the "metal boundary of the classical diffuse layer" of the external solution is equal to charge at the electrode $\sigma = (D/4\pi)$. Thus, differentiating [46] with respect to σ we have

$$d\phi_{ext}(0)/d\sigma = 1/C - 4\pi(l + \sigma dl/d\sigma)$$

Since the meaning of $d\phi_{ext}(0)/d\sigma$ is the inverse capacitance $1/C_d$ of the diffuse layer, which is described by [43], we come finally to [1], where C_i is determined by [32], and C_d is determined by the "diffuse" layer theory [43].

[9]Below, we shall not introduce L, implying that all the information concerning the short-range effects is included in $\rho[\phi]$.

This is a remarkable result. Indeed the theoretical analysis of the distribution of the potential and charge density in an "academic" system of charges immersed in a continuum of a dielectric constant ε near a plane charged boundary was a subject of many papers (10). We see now that the expressions for the capacity obtained in these theories can be matched with the compact layer contribution in series, the compact layer capacity being expressed independently via [32] through the properties of the electrode and solvent in contact. However, such a simple procedure is justified only when the inequality [42] holds. Corresponding numerical criteria can be established for a given form of $\rho[\phi]$. Strictly speaking, this approach becomes inappropriate when the characteristic length of spatial dispersion of $\varepsilon(z, z')$ in the solvent is comparable with the characteristic thickness of the diffuse layer. In this case [41] should be solved exactly for specified $\varepsilon(z, z')$ and $\rho[\phi]$.

Concluding Remarks

Experimental data for the capacitance C_i (including dependencies on the charge, electrode material, solvent, temperature, etc., can be used in [35] to plot the values of the characteristic integral l [21]. This is done, e.g., in Figs. 1 and 2. Plots of this kind are valuable from two points of view. (*1*) The characteristic integral l arises in some other inter-

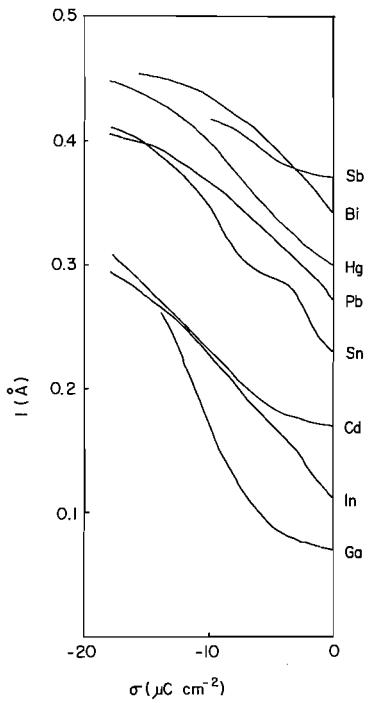

FIG. 1. Dependencies of l on σ, integrated via [36]. $l(\sigma)$ for aqueous solution of NaF on different metals at $T = 25°C$ (after the data for C_i taken from the review article ref. 5).

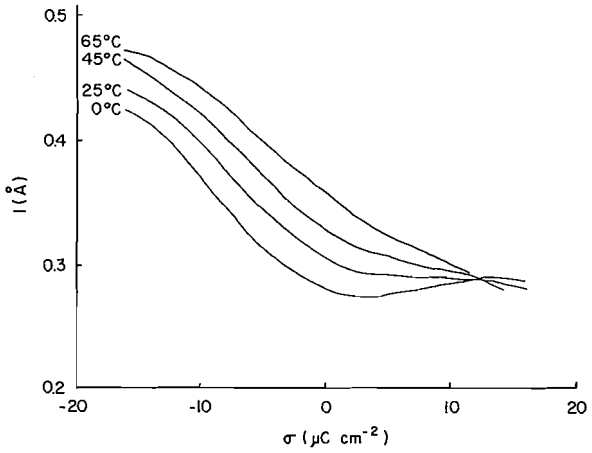

FIG. 2. $l(\sigma)$ for the aqueous solution of NaF on mercury at different temperatures via the Grahame's data for C_1 (2).

facial problems. In particular, it seems to be a basic parameter in the interaction of ions adsorbed at the interface (this will be shown in a subsequent publication). So, the experimental data for l enables one to analyze these problems with no relation to model calculation of l. (2) Approximations for $\varepsilon(z, z')$ and, thereby, $\varepsilon^{-1}(z, z')$ should be in accordance with the experimental data for l. The result of integration [21] would depend on the parameters involved in these approximations. Comparing these dependencies with the observed tendencies one may judge the adequacy of the approximation. The trends in these parameters with the variation of the charge, temperature, solvent, and electrode can be established. The same can be said about first-principle or micro-model calculations. For instance, Partenskii and Smorodinskii (36) extended Smith's version (37) of the self-consistent density-functional treatment of a neutral metal–vacuum interface to the study of the system properties in an external electric field. They arrived at some reconstruction of the electron density near the edge of the ionic skeleton (assumed to be a uniform rigid background) with the variation of applied field. Their numerical data revealed 10% variation of the "electronic tail" decay length for the fields of the order of 10^6–10^7 V/cm with respect to the zero field value. In higher fields (actual for the electrochemical interface) the reconstruction via this mechanism will be more considerable. The field (or charge) dependence of K_i or l may be in some way associated with such a reconstruction. Unfortunately, the results of ref. 36 cannot be applied immediately for the metal–solvent interface. *The simultaneous rearrangement of the structure of the solvent layer, adjacent to the metal, together with the solvent effect on the electron density must be taken into account.* The discrete ionic structure of the metal, shown to be important for the metal–vacuum systems (38), should be involved as well. The theory considering these effects will form the subject of future investigations. However, some qualitative conclusions on the possible physical effects can be already drawn from the curves of Figs. 1 and 2. They will be discussed in a paper to follow.

Acknowledgements

The authors thank I. A. Bagotskaya, L. I. Krishtalik, and M. Levi for stimulating discussions. Kind assistance of V. Izotov and A. A. Kulikovsky in numerical computations is appreciated.

1. Proc. International conference on the nontraditional approaches to the study of solid–electrolyte interface. Snowmass, CO. U.S.A. 1979. Surf. Sci. **101**. 1980.
2. D. C. GRAHAME. Chem. Rev. **41**, 441 (1947).
3. D. C. GRAHAME. J. Am.Chem. Soc. **79**, 393 (1957).
4. R. PARSONS and F. G. R. ZOBEL. J. Electroanal. Chem. **9**, 333 (1965).
5. D. I. LEIKIS and R. V. RYBALKA. *In* Adsorption and double layer in electrochemistry. A special issue of Elektrokhimiya. *Edited by* A. N. Frumkin and B. B. Damaskin. 1972. p. 5.
6. B. B. DAMASKIN and A. N. FRUMKIN. Electrochim. Acta, **19**, 173 (1974).
7. R. PAYNE. Adv. Electrochem. Electrochem. Eng. **7**, 1 (1970).
8. A. SANFELD. Introduction to the thermodynamics of charged and polarized layers. J. Wiley, London, Engl. 1968.
9. G. M. TORRIE and J. P. VALLEAU. Chem. Phys. Lett. **65**, 343 (1979).
10. S. LEVINE and C. W. OUTHWAITE. J. Chem. Soc. Faraday Trans. II, **74**, 1670 (1978).
11. D. HENDERSON and L. BLUM. J. Chem. Phys. **69**, 5441 (1978); J. Electroanal. Chem. **93**, 151 (1978).
12. A. A. KORNYSHEV and M. A. VOROTYNTSEV. Electrochim. Acta, **23**, 267 (1978).
13. F. H. STILLINGER and J. G. KIRKWOOD. J. Chem. Phys. **33**, 1282 (1960).
14. R. M. REEVES. Mod.Aspects Electrochem. **9**, 239 (1974).
15. O. STERN. Z. Electrochem. **30**, 508 (1924).
16. D. G. GRAHAME. J. Chem. Phys. **18**, 903 (1950).
17. F. MALSCH. Phys. Z. **29**, 770 (1928); **30**, 837 (1929).
18. J. R. MACDONALD. J. Chem. Phys. **22**, 1857 (1954).
19. A. N. FRUMKIN. Zero charge potentials. Nauka, Moscow, U.S.S.R. 1979.
20. S. LEVINE, G. M. BELL, and A. L. SMITH. J. Phys. Chem. **73**, 3534 (1969).
21. C. A. BARLOW and J. R. MACDONALD. Adv. Electrochem. Electrochem. Eng. **6**, 1 (1967).
22. L. I. KRISHTALIK. Elektrokhimiya, **13**, 1890 (1977).
23. M. A. VOROTYNTSEV and A. A. KORNYSHEV. Elektrokhimiya, **15**, 660 (1979).
24. O. K. RICE. Phys. Rev. **31**, 1051 (1928).
25. P. M. PLATZMAN and P. A. WOLFF. Waves and interactions in solid state plasmas. Solid state physics. Suppl. 13. Academic Press, New York, NY. 1973.
26. R. J. WATTS-TOBIN. Philos. Mag. **6**, 133 (1961).
27. N. F. MOTT and R. J. WATTS-TOBIN. Electrochim. Acta, **4**, 79 (1961).
28. J. R. MACDONALD and C. A. BARLOW. J. Chem. Phys. **36**, 3062 (1962).

Can. J. Chem. Downloaded from www.nrcresearchpress.com by 210.87.254.5 on 09/06/12
For personal use only.

29. N. D. LANG. Solid State Phys. **28**, 225 (1973).
30. M. B. PARTENSKII. Usp. Fiz. Nauk, **128**, 69 (1979).
31. R. N. KUKLIN. Electrokhimiya, **14**, 381 (1978).
32. M. B. PARTENSKII and B. E. KUZEMA. Fiz. Tverd. Tela, **21**, 2842 (1979).
33. A. A. KORNYSHEV, W. SCHMICKLER, and M. A. VOROTYNTSEV. Phys. Rev. B. In press.
34. A. A. KORNYSHEV. Electrochim. Acta, **26**, 1 (1981).
35. I. D. COLE. Perturbation methods in applied mathematics. Plaisdell, Waltham, MA. 1968.
36. M. B. PARTENSKII and YA. G. SMORODINSKII. Fiz. Tverd. Tela, **16**, 644 (1974).
37. J. R. SMITH. Phys. Rev. **181**, 522 (1969).
38. R. M. KOBELEVA, B. R. GELCHINSKII, and V. F. UKHOV. Fiz. Met. Metalloved. **45**, 25 (1978).
39. D. C. GRAHAME. J. Am. Chem. Soc. **76**, 4819 (1954).
40. V. S. KRYLOV. Private communication.

Appendix 1

New Tests of Grahame's Parametrization

As discussed in the Introduction, it is relevant to plot the dependence of the experimental value of the inverse capacitance of the contact minus the inverse of the Gouy–Chapman capacitance versus concentration c for fixed values of the charge at the electrode, σ. For brevity, we call this difference the inverse compact later capacitance. We shall do it here for the integral capacitances, c.f. [35]. Then, for aqueous solution of 1–1 electrolyte at $T = 25°C$ one has

$$[A.1] \quad l = \frac{1}{4\pi K_i} = \frac{8.84}{\sigma}\left\{V - 0.051 \ln\left[0.085\frac{\sigma}{\sqrt{c}} + \sqrt{1 + \left(\frac{0.085\sigma}{\sqrt{c}}\right)^2}\right]\right\}$$

Here, σ is given in $\mu C/cm^2$, the rationalized potential V in V, c in N.

The plots of $l(c)$ at two values of σ are given in Fig. 3 for the Hg/H_2O–NaF system. The experimental data due to Grahame (39) (Table 1 for the dependence of σ on V and c) were used. We see that within the indicated accuracy one may draw the horizontal through the points corresponding to all the concentrations used. The values of l thereby evaluated are:

$$\sigma = -15, \; l = 0.440 \pm 0.001$$
$$\sigma = +10, \; l = 0.288 \pm 0.002$$

They are in very good agreement with the results obtained by the numerical integration of the curves of the compact layer differential capacitance versus σ (see Fig. 2: $l = 0.436$ ($\sigma = -15$) and $l = 0.288$ ($\sigma = +10$)).

Generally the inaccuracy in the determination of ordinates in Fig. 3 is associated not only by the dispersion in the experimental data for the capacitance C, but also due to the inaccuracy arising in plotting

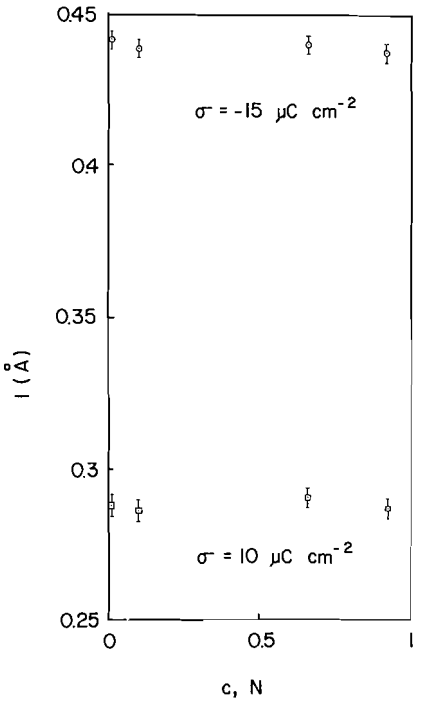

FIG. 3. Values for l estimated via [A.1] using Grahame's data (39). Values of charge are fixed, concentration is varied.

V versus σ at fixed c. The dispersion marked in Fig. 3 is determined by this latter source since we were limited by the data (39) tabulated with 100 mV interval. For this reason we presented the curves for large σ, for which the inaccuracy due to a numerical recalculation is not too high.

The accuracy of the proposed method can be essentially increased when using more detailed data.

The difficulty above is avoided in another test. This is simple plotting l via [A.1] versus the data for σ. In the classical Grahame's paper (39) just the data for σ and V are tabulated for different fixed c. Using these we plot $l(\sigma)$ in Fig. 4 for four concentrations employed by Grahame. The indicated dispersion was calculated via the formula

$$\sigma_{\substack{max \\ min}} = o(c) \pm \Delta(c) \, V$$

and the points $l(\sigma_{max})$ and $l(\sigma_{min})$ are calculated via [A.1]. The inaccuracy coefficient is estimated as (41): $\Delta(c) = 0.1$ at $c \gtrsim 10^{-1} M$, $\Delta(c) = 0.2$ at $c \sim 10^{-2} M$. From Fig. 4 we see that the $l(\sigma)$ curves obtained for different concentrations lie very close to each other within the range of scatter of experimental points $l(\sigma_{min})$, $l(\sigma_{max})$. Noticeably, the results of the preceding test (Fig. 3) are in excellent agreement with the data of Fig. 4.

Can. J. Chem. Downloaded from www.nrcresearchpress.com by 210.87.254.5 on 09/06/12
For personal use only.

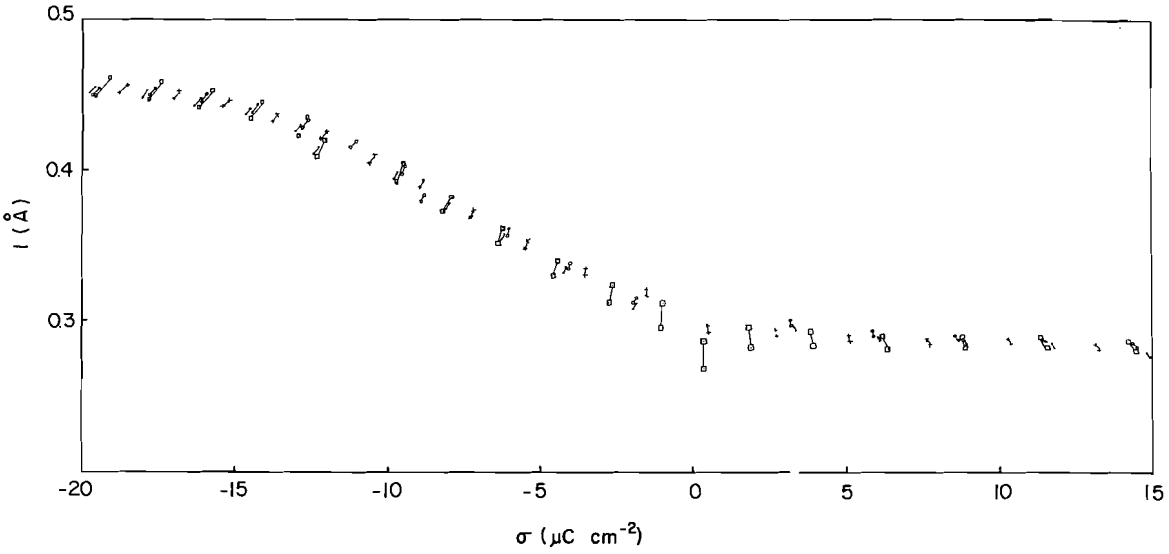

FIG. 4. $l(\sigma)$ dependence estimated for four fixed concentrations: ●, $c = 0.916$; ○, $c = 0.66$; +, $c = 0.1$; ⊡, $c = 0.01$ (N).

Appendix 2

The nonlocal character of the relation [8], i.e. the dependence of the dielectric permeability χ and permittivity ε on two variables z, z' reflects the structure of the system. The latter manifests itself in the correlation of the bound charge density in space. Due to this correlation, σ_{ms} in a point z is determined not only by the gradient of potential in the point z but also by its values in points z', belonging to a certain region which we may call the correlation range. In the case of a simple metal in contact with vacuum, such a correlation would be caused by the electron gas structure (see reviews in refs. 29, 30). In a semi-infinite solvent the nonlocal response is a consequence of the correlation in the dipoles bound charge near the surface and in the bulk, determined by the polar liquid structure (ref. 1, p. 23, 23, 34).

In the bulk of the metal or of the solvent, the system may be regarded as translationally invariant if the discrete translational invariance of the solid crystal metal is neglected. Both χ and ε are then the functions of $z - z'$. The limiting behaviour of $\varepsilon(z, z')$ at z, z' tending to $+\infty$ (into the bulk of the solvent) is: $\lim \varepsilon(z, z') = \varepsilon_{solv}(z - z')$. The special properties of the interfacial region lead to a breakdown of the translational invariance in the direction normal to the interface, so that ε becomes a function both of z and z' separately.

The unidimensional dielectric function of the bulk solvent is simply related with the so called (41) wave number dependent dielectric function of a uniform unbounded solvent $\varepsilon_s(k)$:

$$\varepsilon_s(z - z') \equiv \varepsilon_s(z - z', \kappa = 0)$$

$$\varepsilon_s(z - z', \kappa) = \frac{1}{2\pi} \int_{-\infty}^{\infty} dA[\exp(iA)(z - z')] \times [\varepsilon_s(k = \sqrt{A^2 + \kappa^2})]$$

Hence

$$\int_{-\infty}^{\infty} d(z - z')[\varepsilon_s(z - z')]\{\exp[-iA(z - z')]\} = \varepsilon_s(k = A)$$

$$\int d(z - z')[\varepsilon_s(z - z')] = \varepsilon_s(k = 0)$$

The value $\varepsilon_s(k = 0)$ characterizes the response of the medium to a long wavelength electric field. In the systems without free charge carriers, $\varepsilon_s(k = 0)$ equals, by definition, the macroscopic dielectric constant ε_s. Since $\varepsilon_s(z - z')$ is symmetric with respect to z and z', $\varepsilon_s(z - z') = \varepsilon_s(z' - z)$, we may also write

$$\int dz'[\varepsilon_s(z - z')] = \int dz[\varepsilon_s(z - z')] = \varepsilon_s.$$

Can. J. Chem. Downloaded from www.nrcresearchpress.com by 210.87.254.5 on 09/06/12
For personal use only.

Medium effect. Adsorption of *N*-methylformamide (NMF) at the Hg electrode from H_2O + NMF + NaCl solutions

D. KOŹMIŃSKA, Z. BORKOWSKA, AND B. BEHR

Institute of Physical Chemistry, Polish Academy of Sciences, Kasprzeka 44/52, 01-224-Warszawa, Poland

Received July 24, 1980

This paper is dedicated to Dr. Sam Levine on the occasion of his 70th birthday

D. KOŹMIŃSKA, Z. BORKOWSKA, and B. BEHR. Can. J. Chem. **59**, 2043 (1981).

The adsorption of NMF from H_2O + NMF + NaCl solutions has been studied in two series of experiments, one in which μ_{NaCl} was kept constant over the whole H_2O + NMF composition range and another in which constant concentration of NaCl was maintained. The results are compared and the medium effect discussed.

D. KOŹMIŃSKA, Z. BORKOWSKA et B. BEHR. Can. J. Chem. **59**, 2043 (1981).

On a étudié l'adsorption du NMF à partir de solutions de H_2O + NMF + NaCl dans deux séries d'expériences; dans l'une μ_{NaCl} est maintenu constant sur toute l'étendue de composition en H_2O + NMF alors que dans l'autre on a maintenu la concentration en NaCl constante. On compare les résultats et on discute de l'effet du milieu.

[Traduit par le journal]

Introduction

N-Methylformamide (NMF) is one of the hydrogen bonded solvents with high dielectric constant equal to 182. As a highly structured liquid and good solvent for electrolytes it is of wide interest. This solvent has unusual surface properties, e.g., a broad "hump" on the double layer capacity curve at the negatively charged mercury electrode (1). This hump has been attributed to the reorientation of the solvent dipoles by the electrical field in the inner layer. According to simple models of the solvent dipoles at electrified interfaces this implies a pronounced preferential orientation with the negative end of the dipole towards the electrode at the potential of zero charge (pzc) (2–4). Considerable data concerning the double layer in NMF solutions exist, especially concerning the adsorption of anions (5–7).

The adsorption of NMF from aqueous solutions up to 6.59 *M* was studied by Payne (8) who concluded that at the pzc specific orientation with the negative end of the dipole towards the electrode is negligible. This does not allow one to draw conclusions concerning the double layer structure in pure NMF. More information could be obtained by studying the adsorption of NMF from its mixtures with water over the whole concentration range of both solvents.

According to the electrocapillary equation [1], a strictly thermodynamic study of the adsorption from mixed solvents demands constant chemical potential of an electrolyte in solutions of varying chemical potential of the solvent (9–15). At constant T and p

$$[1] \quad -d\gamma = \sigma_M dE_{\pm} + \Gamma_{2(1)} d\mu_2 + \Gamma_{\mp} d\mu_{salt}$$

and

$$[2] \quad \Gamma_{2(1)} = -(\partial\gamma/\partial\mu_2)_{E_{\pm},\mu_{salt}} = -(\partial\xi/\partial\mu_2)_{\sigma_M,\mu_{salt}}$$

where γ is the surface tension, σ_M is the charge density on the metal, $E_{\pm}$ is the potential of the electrode with respect to the reference electrode reversible towards cations or anions of the salt, $\Gamma_{2(1)}$ is the relative surface excess of solvent 2 with respect to solvent 1, $\Gamma_{\mp}$ is the relative surface excess of anion or cation with respect to solvent 1, μ is the chemical potential, and $\xi = \gamma + \sigma_M E$.

Unfortunately, thermodynamic data for electrolyte solutions in mixed solvents are scarce. Therefore many authors use a constant concentration of the electrolyte and a constant potential reference electrode with liquid junction. This procedure, called by Battisti and Trasatti (12) "customary", introduces two sources of errors:

(*i*) $\mp(\partial\mu_{salt}/\partial\mu_2)_{c_{salt}}$ (see refs. 12 and 13)

(*ii*) $(\sigma_M/F)(\partial\mu_{\pm}/\partial\mu_2)_{c_{salt}}$

where (*i*), which is due to the change of the chemical potential of the electrolyte with the mixed solvent composition, the so-called medium effect, can be determined by independent thermodynamic measurements, but where (*ii*), which is due to the change of the potential of the reference electrode reversible to cation or anion with the mixed solvent composition, cannot be determined.

Although it is obvious that one should use the strictly thermodynamic procedure it seemed to us interesting to compare the former results with those obtained with the "customary" one. Such a comparison was made by Trasatti (12) and Mohilner and Nakadorami (11) for the adsorption of

0008-4042/81/132043-10$01.00/0

©1981 National Research Council of Canada/Conseil national de recherches du Canada

Can. J. Chem. Downloaded from www.nrcresearchpress.com by 210.87.254.105 on 09/06/12
For personal use only.

organic substances within a limited range of concentrations. The aim of the present work was to study the adsorption of NMF from H_2O + NMF + NaCl solutions over the whole composition range of H_2O + NMF at constant chemical potential or at constant concentration of NaCl. This electrolyte has been chosen, because its solubility in both water and NMF is good and also because it is comparatively easy to determine the chemical potential of NaCl in the solvent mixtures under study from emf measurements (14).

Experimental

Reagents

NMF (Flukà or Merck-Schuchardt) was dried over 4 Å molecular sieves and purified by twofold distillation under nitrogen at low pressure. In the final product gas chromatography showed ca. 0.02% impurities other than water and ca. 0.01% water.

Analytical grade NaCl was purified by crystallization from triply distilled water and dried at 150°C. The purity of aqueous solutions of NaCl in triply distilled water was checked for electroactive impurities by dc polarography and for surface active impurities by ac polarography. The solutions were deaerated by the flow of hydrogen presaturated with the investigated solution.

Apparatus and Technique of Measurement

The chemical potentials and activity coefficients of NaCl were determined from the electromotive force (emf) of the following reversible cell:

[I] $\mathrm{Ag|AgCl|}x\mathrm{NMF} + (1-x)\mathrm{H_2O} + y\ M\ \mathrm{NaCl}\ \mathrm{Na^+|glass\ electrode}$

where x is the mole fraction of NMF and y is the molarity of NaCl ($10^{-3} \leq y \leq 10^{-1}$).

The emf was measured with a Radiometer PHM 4p pH meter. Sodium glass electrodes were produced by the M.Curie-Skłodowska University in Lublin (16). Silver chloride electrodes were prepared as described in the literature (17) and were stable in solutions up to ca. 0.41 mole fraction NMF (70 vol.%). In NMF solutions slow decomposition of the electrodes was observed due to the dissolution of the AgCl deposit (18). However, reproducible results were obtained using freshly prepared electrodes kept in contact with NMF not longer than 30 min. The performance of the electrodes was checked by measuring the emf of the cell given above with the saturated NaCl solutions in all solvent mixtures. The results were satisfactory, the emf values being constant within 1 mV. The equilibrium emf values were reached after ca. 3 or 15 min, in dilute or concentrated NMF solutions respectively.

The double layer capacity was measured with an ac Schering-type impedance bridge at 220 Hz using a thin walled glass capillary according to Randles (19) for the dropping mercury electrode and a Pt cylinder as auxilary elecrode. Two series of solutions were studied, the first at constant chemical potential of NaCl, fulfilling the thermodynamic requirements. The potentials should be referred to an electrode reversible towards Na^+ or Cl^- without liquid junction. As the Ag|AgCl electrodes were not very stable during the time-consuming impedance measurements, the potentials were fixed with respect to a mercury pool which should act as a calomel electrode under these circumstances.

However, the mercury pool electrode did not fulfil the thermodynamic conditions (the test of constant emf, independent of solvent composition, in saturated NaCl solutions). Therefore the potentials were recalculated using the data from a separate experiment and the potential scale referred to a Ag|AgCl electrode was found. The second series of solutions was with 0.1 M NaCl in all H_2O + NMF mixtures. In this case the aqueous 0.1 M NaCl calomel electrode was used as reference.

The capacity was independent of frequency in the range 100–500 Hz. The reliability of the results was additionally checked by replacing the cell with an equivalent circuit of the same impedance as that found from measurements. At higher frequencies or with thick walled capillaries the values measured in the solutions with $x_{NMF} > 0.41$ and $c_{NaCl} < 5 \times 10^{-2}$ were erroneous.

Zero charge potentials (pzc) and the maximum surface tensions γ_{max} were measured using a streaming mercury electrode (8) and a capillary electrometer respectively. Electrocapillary measurements were carried out by the maximum bubble pressure method (20), using "pipe type" thin walled capillaries, with an accuracy of ± 0.2 mN m^{-1}. The electrometer was calibrated with aqueous 0.05 M Na_2SO_4 solution using the value 426.2 $\pm$ 0.2 mN m^{-1} as γ_{max} at 25°C (21). Charge density and surface tension versus potential curves were calculated by numerical integration of the double layer capacities using the pzc and γ_{max} as integration constants. The interfacial tension at the free surface of H_2O + NMF solutions was measured by the maximum bubble pressure method. All measurements were carried out at 25 $\pm$ 0.2°C.

Results and Discussion

Thermodynamic Properties of NaCl + NMF + H_2O Solutions

Activity coefficients and some other thermodynamic data for NaCl solutions in NMF are reported in the literature (22, 23); however, no data are available for H_2O + NMF mixtures.

The chemical potentials of NaCl in H_2O + NMF mixtures were determined by means of cell [I]. The results of the emf measurements are presented in Fig. 1. The concentrations of NaCl which correspond to the constant emf of cell [I] (dashed line in Fig. 1) are those at which the chemical potential of NaCl is constant and equal to μ_{NaCl} in 0.1 M aqueous solution.

The free enthalpies of transfer of NaCl from 0.1 M aqueous solution to a given mixed solvent ${}^{s}_{w}\Delta\mu_{NaCl}$ are shown in Fig. 2 (full curve). The maximum value of ${}^{NMF}_{w}\Delta\mu_{NaCl}$ equal to 2.95 kcal mol^{-1} is in good agreement with that given by Povarov *et al.* (23). According to Trasatti, it is possible to neglect $\pm d\mu_{salt}$ if $\Delta\mu_{salt}$ is smaller than 1 kcal mol^{-1} for charge densities $-5 < \sigma < 5$ μC cm^{-2}. In H_2O + NMF + NaCl solutions this condition is met for $x_{NMF} < 0.2$ (45 vol.%). Therefore the results obtained by Payne (8), who investigated the adsorption of NMF from aqueous 0.1 M NaF solutions up to 30 vol.% are correct within the limited range of charge density in spite of the "customary" procedure used.

Can. J. Chem. Downloaded from www.nrcresearchpress.com by 210.87.254.105 on 09/06/12
For personal use only.

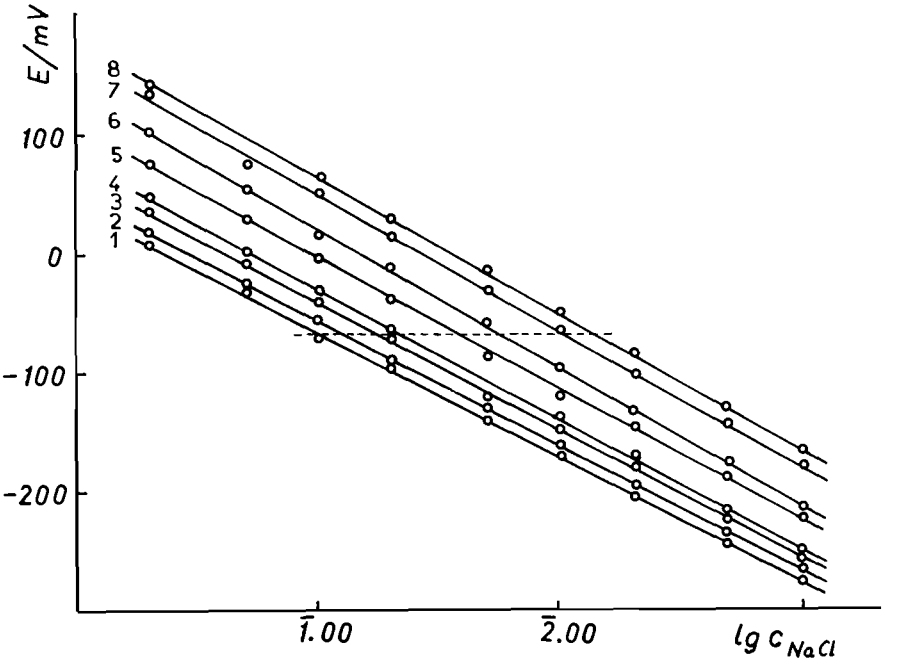

FIG. 1. The electromotive force E of the cell with NaCl solution in the mixed solvent: Ag|AgCl|xNMF + $(1 - x)H_2O$ + y M NaCl|Na^+ glass electrode, as a function of NaCl concentration: x, the mole fraction of NMF, is equal to: (1) 0; (2) 0.03(10); (3) 0.068(20); (4) 0.115(30); (5) 0.235(50); (6) 0.415(70); (7) 0.735(90); (8) 1.0 (the vol.% is given in parentheses). The dotted line indicates the concentrations of NaCl to be chosen at various x_{NMF} in order to prepare the solutions of chemical potential of NaCl equal to that of 0.1 M NaCl in aqueous solution.

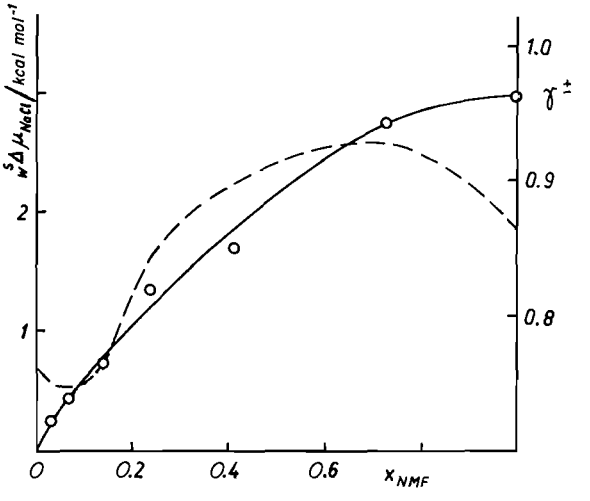

FIG. 2. The change of chemical potential of NaCl on transfer from 0.1 M solution in H_2O to 0.1 M solution in the mixed solvent xNMF + $(1 - x)H_2O$ (full curve) and of the activity coefficient of 0.1 M NaCl in these mixtures (dotted curve) as a function of mole fraction of NMF.

The activity coefficients for 0.1 M NaCl in investigated solutions are given in Fig. 2 (dotted curve). The $f_\pm$ values for aqueous and NMF solutions are in good agreement with the literature (22, 23). Up to $x_{NMF} = 0.165$ (40 vol.%) $f_\pm$ is practically equal to that in aqueous solution within the experimental error ± 0.02. It increases with increasing concentration of NMF, reaching the maximal value at ca. 0.7 mole fraction NMF (85 vol.%). This maximum on the $f_\pm$ versus x_{NMF} relationship may be related to the reinforcement or destruction of the solvent structure depending on the ratio of NMF to H_2O which was found by nmr measurements in H_2O + NMF solutions (24). Also, the viscosity and density of H_2O + NMF mixtures go through maxima at intermediate concentrations of NMF (Fig. 3). Activity coefficients for H_2O and NMF in solvent mixtures used here were estimated from the isobaric data given in the literature (25, 26). The activities of H_2O and NMF as a function of mole fraction of NMF are presented in Fig. 4.

Taking into account the approximations involved in the calculation procedure (30), the shape of the activity vs. mole fraction curves have no quantitative meaning. However, one may conclude that the deviation from ideal behaviour in this system, indicated by diagonal lines in Fig. 4, is small and positive.

Double Layer Measurements

The double layer capacity, charge density, and surface tension curves for the NMF + H_2O +

Can. J. Chem. Downloaded from www.nrcresearchpress.com by 210.87.254.105 on 09/06/12
For personal use only.

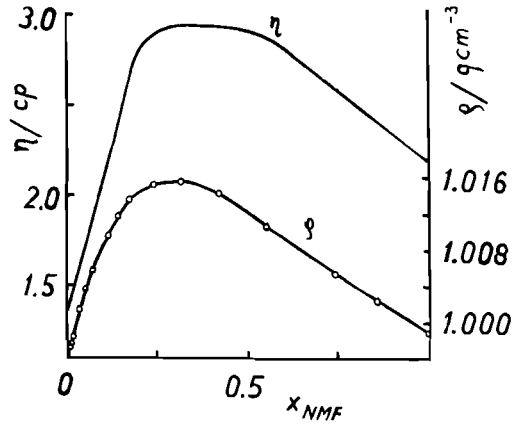

FIG. 3. The viscosity η (29) and density ρ of H_2O + NMF mixtures as a function of the mole fraction of NMF.

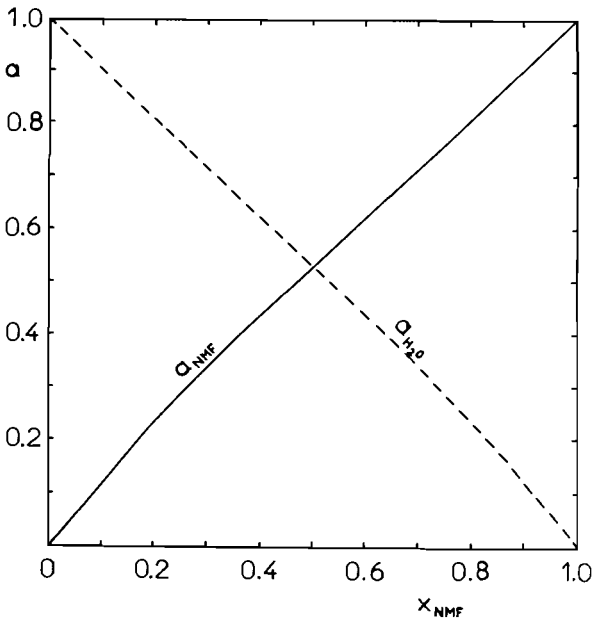

FIG.4. The activities of NMF and of H_2O in their mixtures as a function of the mole fraction of NMF.

NaCl|Hg interface are presented in Fig. 5. Series (*a*) corresponds to the solutions with constant chemical potential of NaCl equal to that of 0.1 *M* aqueous solution. The potential scale is referred to a Ag|AgCl electrode in the working solution. Series (*b*) corresponds to solutions of constant concentration of NaCl equal to 0.1 *M* and in this case the potential scale is referred to aqueous Ag|AgCl in 0.1 *M* NaCl.

The coordinates of the electrocapillary maximum and of the capacity hump are given in Tables 1 and 2.

The double layer capacity curve for 0.1 *M* NaCl solution in NMF is in good agreement with that given by Damaskin and Ivanova (5). The results obtained in both series (*a*) and (*b*) are similar up to ca. 0.165 mole fraction NMF (40 vol.%), which was to be expected according to the thermodynamic measurements. The hump is clearly visible on the double layer capacity curves measured in the solutions containing 20 or more vol.% NMF ($x \geq 0.068$) as was stated previously in the literature (1, 5). The hump becomes more pronounced with increasing NMF concentrations, but its potential is almost constant.

Charge–potential curves shown in the enlarged scale for NMF concentrations of 0–20 vol.% exhibit features typical for the adsorption of organic compounds. The potential of zero charge shifts towards more positive values as compared with aqueous solutions, and the parameters of the intersection point are 0.6 or 0.62 V and 0.025 or 0.027 C m^{-2} for the series μ_{NaCl} = const. and c_{NaCl} = const., respectively. This point corresponds to the maximum adsorption of NMF if Γ_{NMF} is plotted vs. charge or potential. At higher concentrations the charge–potential curves are no longer typical. At negative electrode charge they are almost parallel, or even overlap within a wide range and the potential of maximum adsorption can hardly be found, although it is rather certain that maximum adsorption for concentrated solutions occurs at more negative potentials (see Fig. 6). At these concentrations the electrocapillary curves obtained by integration are displaced, though still parallel, with increasing NMF concentration.

The charge density – potential curves for aqueous and 100% NMF solutions almost overlap from −0.9 to −1.3 V. This can be interpreted in terms of a simple model of the inner layer in both cases with a similar ratio of ε/d, i.e., of the dielectric permittivity to the distance of the Helmholtz plane from the electrode. It is possible that in NMF solutions the distance d is higher than in water, but that ε is also higher. In the case of less polar organic solvents the double layer capacity is as a rule much lower and has a minimum at the potentials at which in NMF solutions the hump is formed.

The comparison of both series μ_{NaCl} = const. and c_{NaCl} = const. shows that distinct differences are observed only at positively charged electrodes. The double layer capacity and charge density are much lower for solutions of high NMF content in the case of μ_{NaCl} = const. This fact can be explained when one considers the specific adsorption of chloride ions. In the μ_{NaCl} = const. series the solutions contain NaCl in lower concentrations (cf. Table 1) and therefore the adsorption of Cl^- is smaller.

It is not possible to compare the shift of zero

Can. J. Chem. Downloaded from www.nrcresearchpress.com by 210.87.254.105 on 09/06/12
For personal use only.

Can. J. Chem. Downloaded from www.nrcresearchpress.com by 210.87.254.105 on 09/06/12
For personal use only.

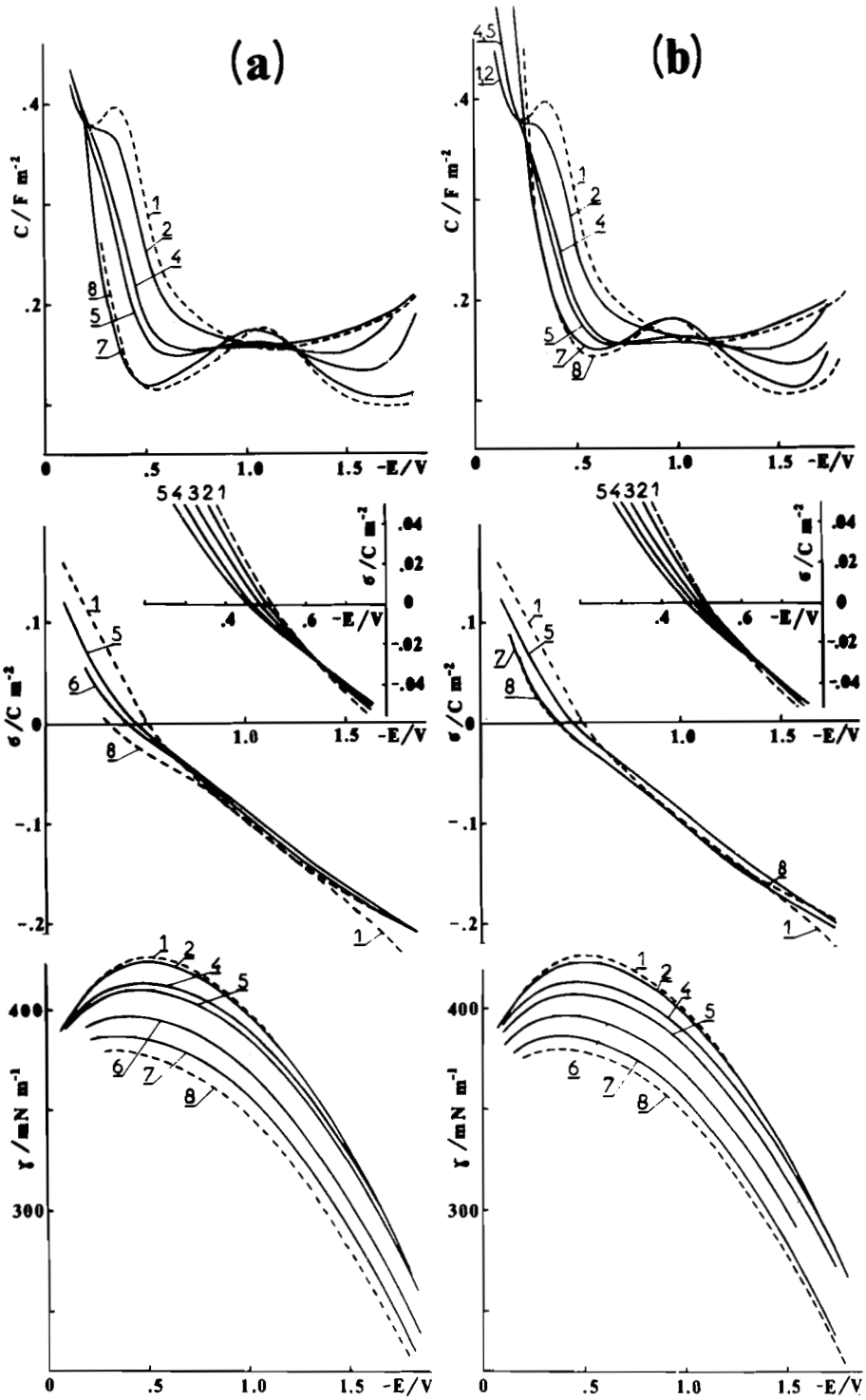

FIG. 5. The dependence of the double layer capacity C, charge density σ, and surface tension γ of the Hg electrode on potential in the solutions of NaCl in xNMF + $(1 - x)H_2O$ where x is equal to (1) 0; (2) 0.003(1); (3) 0.015(5); (4) 0.03(10); (5) 0.068(20); (6) 0.235(50); (7) 0.550(80); (8) 1.0 (the vol.% is given in parentheses). Left side: constant chemical potential of NaCl (concentrations are given in Tables 1 and 2). Right side: the concentration of NaCl equal to 0.1 M in all solutions. A fragment of charge density – potential curves is shown in an enlarged scale for small concentrations of NMF.

Can. J. Chem. Downloaded from www.nrcresearchpress.com by 210.87.254.105 on 09/06/12
For personal use only.

TABLE 1. The coordinates of electrocapillary maximum for a Hg electrode in NMF + H_2O + NaCl solutions

NMF concentration			μ_{NaCl} = const.			c_{NaCl} = 0.1 mol L^{-1}		
Mole fraction x	Vol.%	c_{NaCl} (mol L^{-1})	$-E^*$ (V)	C (μF cm^{-2})	γ (mN m^{-1})	$-E^\dagger$ (V)	C (μF cm^{-2})	γ (mN m^{-1})
0	0	10×10^{-2}	0.513	29.90	426	0.513	29.90	426
0.003	1	9.8×10^{-2}	0.506	26.03	423	0.506	26.40	423_5
0.009	3	9.5×10^{-2}	0.495	23.68	419_5	—	—	—
0.015	5	9.0×10^{-2}	0.490	22.95	417_5	0.492	23.22	417_5
0.030	10	8.2×10^{-2}	0.479	20.82	413_5	0.477	21.70	413_5
0.051	15	7.5×10^{-2}	0.467	19.93	410	0.471	21.68	410
0.068	20	6.7×10^{-2}	0.459	19.10	409_5	0.463	20.64	407_5
0.115	30	5.4×10^{-2}	0.444	18.8	403_5	0.445	20.06	403_5
0.165	40	4.3×10^{-2}	0.427	17.6	400	—	—	—
0.235	50	3.0×10^{-2}	0.408	17.4_5	396_5	0.424	19.7	396_5
0.415	70	2.0×10^{-2}	0.363	17.9	390	—	—	—
0.550	80	1.4×10^{-2}	0.346	17.8	387	0.396	20.7	387
0.735	90	1.1×10^{-2}	0.325	20.0	384	0.396	20.2	383
1.0	100	1.0×10^{-2}	0.315	22.2	380	0.386	21.2	380

*Potentials vs. inner Ag|AgCl electrode without liquid junction.
†Potentials vs. aqueous 0.1 *M* NaCl Ag|AgCl elecrode with liquid junction.

charge potential in both series because of the noncomparable potential scales, although it seems that the more negative value of the pzc in the c_{NaCl} = const. series is in accord with specific adsorption of chloride ions. Otherwise the similarity of both series is rather striking; the subtle differences can be found only with the double layer capacity measurements in the solutions containing more than 20% NMF.

One could conclude that in the particular case of the H_2O + NMF mixture, where both components are highly structured liquids of high dielectric permittivity, the "customary" procedure can be applied in the whole composition range, although the adsorption of Cl^- ions should be taken into account.

Relative Surface Excess of NMF

The surface tension data in the series μ_{NaCl} = const. were used to calculate the adsorption isotherms.

The relative surface excess of NMF, $\Gamma_{2(1)}$, is given by [2] which can be rearranged as follows:

$$[3] \quad \Gamma_{2(1)} = \frac{1}{2.3RT}\left(\frac{\partial \xi}{\partial \log a_2}\right)_{\mu_{NaCl},\sigma_M} = \frac{1}{2.3RT}\left(\frac{\partial \xi}{\partial \log x_2}\right)_{c_{NaCl},\sigma_M} \frac{\log x_2}{\log a_2}$$

where subscript 2 refers to NMF and subscript 1 refers to water.

The factor $\partial \log x_2/\partial \log a_2$ accounts for non-

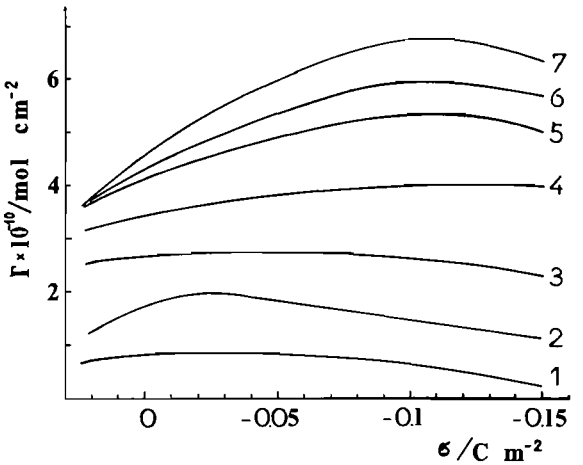

FIG. 6. The relative surface excess of NMF, Γ, as a function of charge density of Hg electrode in NaCl solutions of const. μ_{NaCl} in xNMF + $(1 - x)H_2O$ at various NMF concentrations: x is equal to: (1) 0.003(1); (2) 0.009(3); (3) 0.03(10); (4) 0.068(20); (5) 0.165(40); (6) 0.235(50); (7) 0.415, 0.55, 0.735(70, 80, 90) (the vol.% is given in parentheses).

TABLE 2. The coordinates of "capacity hump" for NMF + H_2O + NaCl solutions

NMF (vol.%)	μ_{NaCl} = const. $-E$ (V)	$-\sigma \times 10^2$ (C m^{-2})	$C \times 10^2$ (F m^{-2})	γ (mN m^{-1})	c_{NaCl} = 0.1 mol L^{-1} $-E$ (V)	$-\sigma \times 10^2$ (C m^{-2})	$C \times 10^2$ (F m^{-2})	γ (mN m^{-1})
0	0.41	5.5	39.8	422	0.41	5.5	39.8	422
20	1.04_5	9.3	16.25	381.7	1.06	9.0	16.25	382
30	1.00	8.9	16.98	378.7	1.05	9.1	16.86	387.4
40	1.02	9.5	17.09	372.0				
50	1.03	9.6	17.18	367.7	1.02_5	9.1	17.12	371.3
70	1.03_5	10.1	17.3	357.4				
80	1.04_5	10.2	17.5	353.2	1.02_5	9.7	18.02	358.5
90	1.07	11.0	17.66	344.8	1.02_5	9.6	18.32	355.5
100	1.09	11.2	17.73	338	1.02_5	9.6	18.05	351.7

ideality of NMF + H_2O mixtures. Depending on the detailed shape of the a vs x relationship (Fig. 4) this factor could become quite significant at ca. 0.3 mole fraction of NMF. However, as has been pointed out earlier, all one can tell from Fig. 4 is that the deviation from ideality is small. Therefore we felt justified in assuming that $f_{NMF} = f_{H_2O} = 1$ and $a_{NMF} = x_{NMF}$ over the whole concentration range of H_2O + NMF mixtures.

Relative surface excesses of NMF found by differentiation from the ξ vs. log x relationship are presented in Fig. 6 as a function of charge at constant x_{NMF}, and in Fig. 7 as a function of x_{NMF} at constant charge.

It can be seen in Fig. 7 that the adsorption isotherms reach a plateau at $x_{NMF} = 0.5$ or earlier, but the values of the maximum relative excesses are different at various charge densities. This plateau has no physical meaning since at high NMF concentrations relative surface excesses $\Gamma_{2(1)}$ may differ considerably from surface concentrations, Γ_2. Also, the approximation made concerning solvent activities could distort the adsorption isotherm at the concentrations corresponding to plateau.

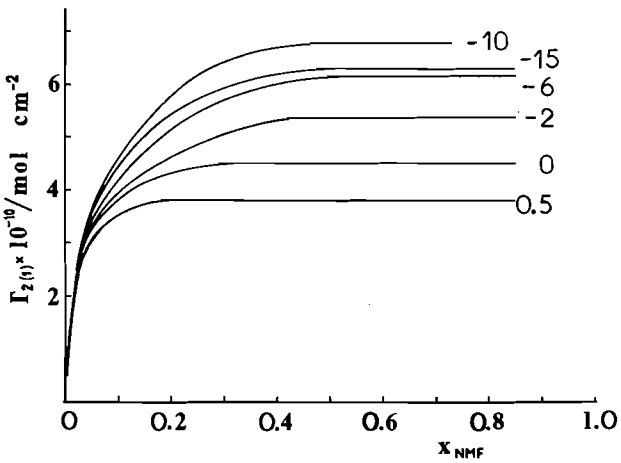

FIG. 7. The relative surface excess of NMF, Γ, at a Hg electrode in NaCl solutions of const. μ in xNMF + $(1-x)H_2O$ as a function of mole fraction of NMF at various charge densities indicated in the figure (σ in C m^{-2} × 100).

The highest value of $\Gamma_{2(1)}$ is reached at $\sigma = -0.1$ cm^{-2}. This can be seen also in Fig. 6, which also shows that the strongest adsorption at low NMF concentrations occurs at a different charge $\sigma = -0.025$ cm^{-2}. This change of the character of adsorption with increasing NMF concentration is accompanied by the development of the hump on the double layer capacity curves.

The $\Gamma_{2(1)}$ values in Fig. 6 can be compared with those given by Payne (8). These data were transformed from units of molecule cm^{-2} to mol cm^{-2}, and the concentrations of NMF from mol L^{-1} to mole fractions or vol.%. After doing so the surface excesses at low concentrations of NMF (< 10 vol.%) were in good agreement with our values.

At higher NMF concentrations there were discrepancies. There are differences in both the values and in the shape of the curves. The values of Payne for $\sigma = 0$ are higher than ours, which can be explained by the different concentration scale used. The derivative in [3] can be expressed using a different concentration scale as follows:

$$[4]\quad 2.3RT\Gamma_{2(1)} = \frac{\partial \xi}{\partial \log x} = \frac{\partial \xi}{\partial \log x}\frac{\partial \log c}{\partial \log x} = 2.3RT\Gamma_{\text{Payne}}\frac{\partial \log c}{\partial \log x}$$

As long as c is proportional to x the concentration scale used has no influence on the results. However, above 10 vol.% the relationship between c and x is no longer linear and $\partial \log c/\partial \log x < 1$. Thus, the value of Payne must be reduced to get the thermodynamic value $\Gamma_{2(1)}$, and the more so, the higher is the concentration.

Can. J. Chem. Downloaded from www.nrcresearchpress.com by 210.87.254.105 on 09/06/12
For personal use only.

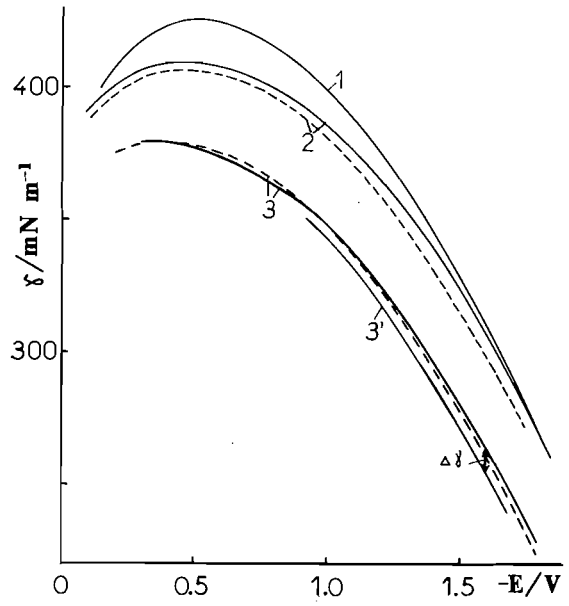

FIG. 8. The comparison of the surface tension of Hg vs. potential curves from series (*a*) (μ_{NaCl} = const., potential referred to Ag|AgCl electrode without liquid junction, full lines) with those from series (*b*) (c_{NaCl} = const., potential referred to aq. Ag|AgCl electrode in 0.1 *M* NaCl, dotted lines): x_{NMF} is equal to: (1) 0; (2) 0.068(20); (3) 1.0(100); (the vol.% is given in parentheses). The section of the curve 3′ shows how the change of potential scale $E^{\pm}$ corresponding to the change of NaCl concentration from 0.01 to 0.1 *M* would affect the γ value used for calculation of $RT\Gamma = (\partial\gamma/\partial \ln x)_{E^{\pm}}$.

The shapes of the curves different from ours can be explained by the different potential scale used. The problem of the potential scales is demonstrated in Fig. 8. Dotted curves from the c_{NaCl} = const. series are compared with those from the μ_{NaCl} = const. series. It can be seen that a small shift along the potential scale would result in an overlap of the cathodic branches, or, to the contrary, in increased differences of γ at constant potential. These changes would affect the calculated surface excess more as the γ–*E* curve becomes steeper because: $\Delta\gamma = (\partial\gamma/\partial E)\Delta E = q_M\Delta E$. The contribution of this uncertainty of potential scale, ΔE, can be quite significant at a highly charged electrode. If it is assumed that the shape of the cathodic branch of the electrocapillary curve in NMF does not depend on the NaCl concentration, one should expect that the change of NaCl concentration from 0.1 to 0.01 *M* should produce a shift of the cathodic branch of the electrocapillary curve by 60 mV if the Ag|AgCl electrode in the working solution were used as reference, which would give at 0.17 C cm^{-2} a difference of ca. 10 mN m^{-1}. The part of the curve, as measured in 0.1 NaCl, instead of the required 0.01 *M* NaCl vs. Ag|AgCl in the same solution, is shown in Fig. 8, curve 3′.

Thus, the "customary" procedure if the electrode without liquid junction were used would lead to too high surface excesses.

Generally one should keep in mind that the medium effect producing the change in chemical potential of the salt $\Delta\mu$ will result in a shift of the potential scale $\Delta E = \Delta\mu/nF$, and this can be quite large.

If, therefore, the proper concentrations of the salt cannot be used, e.g., because of the lack of information regarding μ, it is probably better to use a constant potential electrode, with liquid junction, as can be noted from the comparison of series (*a*) and (*b*) in Figs. 5 and 8.

The Composition of the Surface Phase

To calculate the composition of the heterogeneous region at the electrode surface the quasi-thermodynamic model of Randles and co-workers (27, 28) has been adopted. The surface layer is regarded as a surface phase of thickness τ and of determined thermodynamic properties related to those of the bulk of the solution at the same composition. Another assumption is that the molecules occupy constant areas, $A_1 = V_1/N\tau$ and $A_2 = V_2/N\tau$, where V_1 and V_2 are partial molar volumes assumed to be equal to the molar volumes of the pure components and *N* is Avogadro's number.

The adsorption isotherm has the following form:

$$[5]\quad \frac{a_2^s}{(a_1^s)^r} = \frac{a_2}{(a_1)^r}\exp\left[\frac{-V_2(\gamma_2 - \gamma_1)}{\tau RT}\right]$$

a_1^s and a_2^s are the activities in the surface phase averaged over the thickness τ, and γ_1 and γ_2 are the surface tension of the pure components water and NMF respectively.

The isotherm involves two adjustable parameters: one is the thickness τ; the other relates the activity coefficients in the surface phase to those in the bulk phase. In view of the approximation $a = x$ adopted in this work for H_2O + NMF solutions in the bulk phase, the same is assumed for the surface phase and only one parameter is needed.

In Fig. 9 the experimental γ values for Hg at the pzc and for the free surface are given, and the theoretical curves composed of two sections are indicated. It was impossible to fit the experimental data with the use of one value of τ in the whole composition range. The two segments correspond to τ = 4.6 Å at low NMF concentrations and τ = 5.36 Å at higher concentrations. If the change in τ has a physical meaning, it should support the view that

Can. J. Chem. Downloaded from www.nrcresearchpress.com by 210.87.254.105 on 09/06/12
For personal use only.

Can. J. Chem. Downloaded from www.nrcresearchpress.com by 210.87.254.105 on 09/06/12
For personal use only.

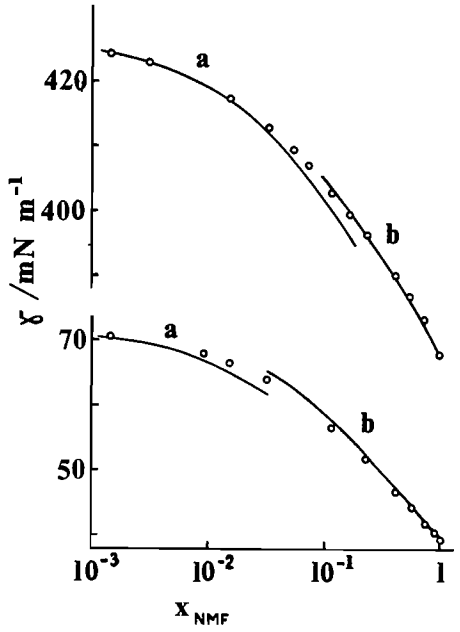

FIG. 9. The relationship between the surface tension of a Hg electrode at pzc in H_2O + NMF + NaCl (μ_{NaCl} = const.) (upper curve) or of the free surface of corresponding solutions (lower curve) and mole fraction of NMF. Points: experimental values; lines: the calculated values using the model of Randles and Behr (27) with $\tau = 4.6$ Å (section *a*) and $\tau = 5.36$ Å (section *b*); $a_{NMF} = x_{NMF}$; $a_{H_2O} = x_{H_2O}$.

the orientation of NMF at low bulk concentration when it behaves like a typical aliphatic solvent is different from that at higher concentrations. The thicker layer at higher concentrations should indicate an orientation at the surface close to perpendicular. The postulated change of τ is certainly not a result of the approximation $a_{NMF} = x_{NMF}$, because up to $x_{NMF} = 0.1$ the system obeys Henry's law (Fig. 4) and therefore the value of the activity coefficient does not affect the calculated γ values since $\partial\gamma/\partial \log a = \partial\gamma/\partial \log x$. The reorientation of NMF molecules at the Hg electrode as a function of the electrical variable σ or E was postulated in the literature (1) in order to explain the hump on the double layer capacity curve. The reorientation with increasing bulk concentration and with the electrical potential or charge are related to each other; thus our hypothesis is compatible with the general picture of NMF adsorption.

The surface concentrations of water and NMF, Γ_1 and Γ_2 respectively, were calculated from the experimentally found surface excess $\Gamma_{2(1)}$ (Fig. 7) using two equations: $\Gamma_{2(1)} = \Gamma_2 - \Gamma_1 x_2/x_1$, which is the definition of the relative surface excess, and $V_1\Gamma_1 + V_2\Gamma_2 = \tau$ which is related to the model. τ was equal to 5.36 Å for $x_{NMF}^s \geq 0.1$ and 4.6 Å for $x_{NMF}^s < 0.1$, as found from the γ vs. $\log x$ fit (Fig. 9). Surface concentrations of NMF, Γ_2 at constant electrode charge are presented in Fig. 10. Γ_2 increases continuously with the concentration of NMF in the bulk. In contrast to the $\Gamma_{2(1)}$ vs. x_{NMF} relationships (Fig. 7), a plateau is formed. However, as has been stated before, maximum adsorption from concentrated NMF solutions is observed at -0.1 C m^{-2}.

The composition of the solvent in the surface phase at uncharged Hg and at the free surface are compared in Fig. 11. The adsorption at both interfaces is similar but slightly stronger at the mercury–solution interface.

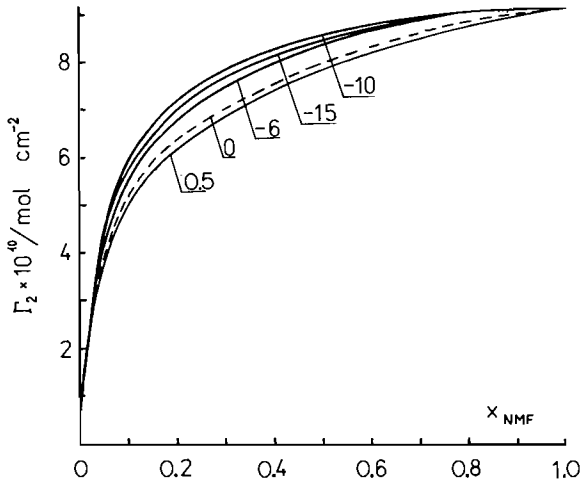

FIG. 10. The surface concentration of NMF, Γ_2, as function of mole fraction of NMF in the bulk solution, x_{NMF}, at various charge densities as indicated in the figure (σ in C m^{-1} × 100). Γ_2 calculated from the data in Fig. 7 using the surface phase model.

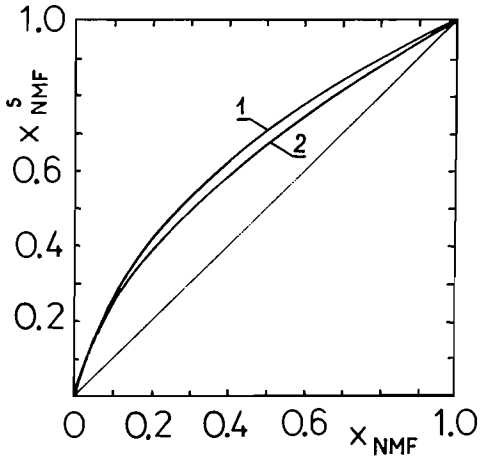

FIG. 11. Adsorption isotherms of NMF, $x_2^s = f(x_{NMF})$ at $Hg_{\sigma=0}$: (1) at the free surface and (2) according to the surface phase model.

Can. J. Chem. Downloaded from www.nrcresearchpress.com by 210.87.254.105 on 09/06/12
For personal use only.

According to [5], free enthalpies of adsorption are defined as follows:

$$[6] \quad -\Delta G_{ads} = (V_2/\tau)(\gamma_2 - \gamma_1)$$

The calculation with τ equal to 4.6 Å or 5.36 Å gives ΔG_{ads} equal to 1.4 or 1.22 kcal mol^{-1} for the Hg–solution interface and 1.03 or 0.88 kcal mol^{-1} for the air–solution interface. The higher ΔG_{ads} for uncharged mercury as compared with the free surface is in accordance with the lowering of the surface tension by NMF at both surfaces (45 mN m^{-1} and 32.5 mN m^{-1}) respectively. The adsorption energy at uncharged Hg is slightly higher than that for methanol and lower than that for acetone.

Conclusions

Adsorption of NMF from H_2O + NMF + NaCl solutions can be considered in two concentration regions. From dilute NMF solutions $c \leq 20$ vol.%, the adsorption of NMF is similar to that of other aliphatic solvents with the maximum at ca. 0.02 C m^{-2}. In this concentration range, no NMF hump is visible on the capacity curves. For more concentrated NMF solutions, maximum adsorption occurs at ca. -0.1 C m^{-2}, which is close to the NMF hump on the capacity curves.

The thickness of the adsorbed layer at uncharged Hg increases with increasing NMF concentration which may be caused by reorientation of the dipoles.

Comparison of the results obtained when strictly thermodynamic and "customary" procedures have been used shows that the "customary" procedure is satisfactory over the whole concentration range of NMF + H_2O mixtures. However, at higher NMF concentrations the adsorption of Cl^- ions must be taken into account.

Acknowledgements

We should like to thank Dr. T. Kubala from Jagiellonian University in Kraków for performing the measurements of surface tensions at the H_2O + NMF–air interface.

We are greatly indebted to Dr. St. Malanowski from the Institute of Physical Chemistry, Polish Academy of Sciences, for evaluating the activity coefficients of H_2O and NMF in their mixtures at 25°C from the isobaric literature data.

This work has been performed as a part of research project 03.10 and was also partly financed by research project MR I-11.

1. R. Payne. Adv. Electrochem. Electrochem. Eng. **7**, 1 (1970).
2. R. M. Reeves. Mod. Aspects Electrochem. **9**, 239 (1974).
3. R. Parsons. Trans. Soc. Adv. Electrochem. Sci. Technol. **13**, 239 (1978).
4. W. R. Fawcett and R. O. Loutfly. J. Electroanal. Chem. **39**, 185 (1972).
5. B. B. Damaskin and R. V. Ivanova. Zh. Fiz. Khim. **38**, 176 (1964).
6. S. Minc and M. Brzostowska. Rocz. Chem. **38**, 301 (1964).
7. R. V. Ivanova, L. N. Kuzniecova, and B. B. Damaskin. Rocz. Chem. **15**, 1267 (1979).
8. R. Payne. J. Electroanal. Chem. **47**, 265 (1973).
9. R. Parsons and A. M. Devanathan. Trans. Faraday Soc. **49**, 673 (1953).
10. R. S. Majzlish, J. P. Twardowskiy, and A. N. Frumkin. Zh. Fiz. Khim. **28**, 87 (1954).
11. D. M. Mohilner and H. Nakadomari. J. Phys. Chem. **77**, 1549 (1973).
12. A. Battisti and S. Trasatti. J. Electroanal. Chem. **54**, 1 (1974).
13. D. M. Mohilner and H. Nakadomari. J. Electroanal. Chem. **65**, 843 (1975).
14. Z. Borkowska. J. Electroanal. Chem. **63**, 379 (1975).
15. J. Taraszewska. J. Electroanal. Chem. In press.
16. K. Sykut and A. Kusak. Ann. Univ. Marie Curie Sklodowska Sect. AA, **23**, 16 (1978).
17. D. J. G. Ives and G. J. Janz. Reference electrodes. Academic Press, New York and London. 1961.
18. J. M. Povarov, W. E. Kazarinov, J. M. Kessler, and A. J. Gorbaniev. Zh. Neorg. Khim. **9**, 1008 (1964).
19. J. E. B. Randles. Trans. Symposium on Electrode Processes, Philadelphia 1959. Wiley, New York, NY. 1961.
20. D. J. Schiffrin. J. Electroanal. Chem. **23**, 168 (1968).
21. E. M. Duyvies and C. A. Smolders. Rec. Trav. Chim. **80**, 636 (1961).
22. E. Luksha and C. M. Criss. J. Phys. Chem. **70**, 1496 (1966).
23. J. M. Povarov, J. M. Kessler, and A. J. Gorbaniev. Izv. Akad. Nauk SSSR, **10**, 1895 (1964).
24. D. N. Glew, H. D. Mak, and N. S. Roth. *In* Hydrogen bonded solvent systems. *Edited by* A. K. Covington and P. Jones. Taylor and Francis, London. 1968.
25. W. B. Kogan, W. M. Fridman, and W. W. Kafanov. Equilibria between liquid and gas. Moskva. p. 274.
26. G. Kortüm and H. v. Bierdersee. Chem. Ing. Tech. **42**, 552 (1970).
27. J. E. B. Randles and B. Behr. J. Electroanal. Chem. **35**, 389 (1972).
28. J. E. B. Randles, B. Behr, and Z. Borkowska. J. Electroanal. Chem. **65**, 775 (1975).
29. J. M. Hale and R. Parsons. Adv. Polarogr. **3**, 829 (1960).
30. S. Malanowski. Liquid–vapour equilibrium. Polsk. Wyd. Nauk. 1974.

The surface phase at the ideal polarized mercury electrode. IV. Determination of molar entropies of adsorption of specifically adsorbed halide ions

M. H. CHARLES, M. MULENGA, A. JENARD, AND H. D. HURWITZ[1]

Faculty of Sciences, Université Libre de Bruxelles, C.P. 160, 50, av. F. D. Roosevelt, 1050 Brussels, Belgium

Received September 29, 1980

This paper is dedicated to Dr. Sam Levine on the occasion of his 70th birthday

M. H. CHARLES, M. MULENGA, A. JENARD, and H. D. HURWITZ. Can. J. Chem. **59**, 2053 (1981).

Differential capacitances are measured as a function of temperature at the ideal polarized Hg electrode in systems of mixed sodium halides at ionic strength $J = 10^{-1}$ mol kg^{-1}. A quasi-thermodynamic treatment is presented according to which excess entropies of adsorption in the inner layer are determined. The formation entropy of the inner layer and the water and ion molar entropies of adsorption are presented for a range of moderate and small ionic surface coverages.

M. H. CHARLES, M. MULENGA, A. JENARD et H. D. HURWITZ. Can. J. Chem. **59**, 2053 (1981).

Utilisant des systèmes mixtes d'halogénures de sodium de force ionique $J = 10^{-1}$ mol kg^{-1}, on a mesuré, en fonction de la température, les capacités différentielles au niveau d'une électrode à Hg polarisée idéale. On présente un traitement quasi-thermodynamique selon lequel on détermine les entropies d'adsorption en excès de la couche interne. On rapporte l'entropie de formation de la couche interne et les entropies molaires d'adsorption de l'eau et de l'ion pour un certain nombre de surfaces ioniques moyennes et petites.

[Traduit par le journal]

I. Introduction

The problem of ionic specific adsorption at the electrode surface remains a crucial and largely unsettled subject of electrochemistry. Many theoretical attempts have been made in order to describe the adsorption process of inorganic anions. The Stern–Grahame–Devanathan theory of the electrochemical double layer was modified by introducing the so-called discreteness of charge effect. This concept was invoked initially by Esin and Markov (1). Later on it was developed within a model of ions distributed on the surface at the lattice points of an hexagonal array (2–5). One of the merits of Levine's work (6, 7) was to reconsider totally this approach and to propose a different expression of the discreteness-of-charge effect essentially in terms of cavity potential in the inner layer and self atmosphere potential in the inner and diffuse layer. In that way, his model led to a consistent statistical mechanical calculation of the free energy of adsorption, making allowance for the thermal motion of the adsorbed species and for the redistribution of the adsorbed particles upon adsorption of one ion. Further decisive improvements of the theory of ionic specific adsorption were, however, particularly impaired by our lack of knowledge of the role of the adsorbed solvent at the electrode. Accordingly, it was recognized for a few years that electrocapillary measurements as a function of temperature and pressure (8) might yield some fundamental thermodynamic criteria, with respect to the behaviour of the solvent, for defining new models of ionic specific adsorption. Nowadays, several electrocapillary studies of temperature effects at the ideal polarized Hg – aqueous electrolyte solution interface have already led to the evaluation of thermodynamic or quasi-thermodynamic quantities like the surface excess entropy (8), the interphase or inner layer entropy of formation (9–11), and the partial molar adsorption entropy of the solvent (12, 13).

In presence of fluoride anions, which are considered to be unspecifically adsorbed at 25°C, the thermodynamic data have provided some important characterization of the water adsorption at the electrode surface. Hills and Payne (8) gave particular consideration to the systematic use of temperature and pressure coefficients of the surface tension in the investigation of the water in the inner layer. Combining the thermodynamic deduction with previous assertion based on dielectric models of the interface, they envisioned a model of water adsorption based on the competitive influence of the changes of the inner layer ionic concentration and of the changes of the dielectric permittivity of the adsorbed water molecules. Later on, careful thermodynamic investigations as a function of temperature were carried out by Harrison *et al.* (9), Nguyen Huu *et al.* (12), and Hills and Hsieh (11). These measurements have contributed to bring out the following features pertaining to the water monolayer adsorbed at the Hg electrode: (*a*) there exists a maximum of entropy of adsorption of water at about -4×10^{-2} C m^{-2}; (*b*) the water molecules

[1]To whom all correspondence should be addressed.

0008-4042/81/132053-19$01.00/0

©1981 National Research Council of Canada/Conseil national de recherches du Canada

Can. J. Chem. Downloaded from www.nrcresearchpress.com by 210.87.254.5 on 09/06/12
For personal use only.

Can. J. Chem. Downloaded from www.nrcresearchpress.com by 210.87.254.5 on 09/06/12
For personal use only.

are preferentially adsorbed at the p.z.c. with their negative poles pointing to the electrode; (*c*) even at the maximum of entropy of adsorption, the configuration of adsorbed water is slightly more ordered than that of bulk water; (*d*) the density of water dipoles in the inner monolayer changes only slightly within the experimental range of the electrode charge densities. Consequently, the orientational changes of the adsorbed water dipoles determine essentially the physical properties of the inner layer.

Temperature coefficients of surface tension were also determined in presence of specifically adsorbed anions. Attempts to relate these data to molecular models of the interface were largely frustrated by the inadequacies of the quasi-thermodynamic treatments used so far for the system of ionic surfactant and water co-adsorption. For example, the approaches used failed to present the relevant thermodynamic quantities like the inner layer entropy of formation in terms of the composition of the interphase. Furthermore, the formulation adopted for the derived surface excess entropies (8, 14) made it difficult to distinguish between the contributions of the various species involved in the adsorption process, namely the anion and water in the inner layer and the electrolyte in the diffuse layer. Accordingly, in presence of ionic specific adsorption, the numerous attempts to correlate the measurements involving the variable temperature with microscopic properties of the interface were rather contradictory. Hills and Payne (8) and Hills and Hsieh (11) concluded that the change of surface excess entropy is essentially dominated by the adsorption of water. The increase of this entropy in presence of Cl^-, NO_3^-, and SO_4^{2-} ions is therefore associated with the number of water molecules released from the inner layer by the adsorption of each ion. The observation of a decrease of the inner layer entropy of formation in presence of PF_6^-, NO_3^-, Cl^-, I^- led Harrison *et al.* (9) to the opposite suggestion. They assumed that the adsorption of the anion and its effect on the solvent is the overriding factor.

We endeavour in this paper to treat the system of halide specific adsorption by using a consistent quasi-thermodynamic frame-work. We expect to speculate, on this basis, about the microscopic properties of the inner monolayer. The first part of this work deals with the thermodynamic formulation.

II. Theoretical Derivation of Entropies of Adsorption

1. *General Thermodynamic Considerations*

The case corresponding to an isothermal electrochemical cell with an ideal polarized mercury electrode (in the absence of an amalgam) was treated previously (10) with respect to the condition of keeping at constant ionic strength a solution of a mixture of two symmetrical electrolytes with one common ion.

For clarity, in this article we are replacing A^{Z_a} by **A**, B^{Z_b} by **B**, and C^{Z_c} by **C**. For the electrolytes AB and AC with the common ion A^{Z_a} (**A**) at ionic strength $J = Z_a^2(m_{AB} + m_{AC}) = Z_a^2 m_{\mathbf{A}}$ where the m represents the molalities in the bulk phase β, the suggested treatment leads to write the Gibbs equation at constant pressure P and constant J in the following form:

$$[1] \quad (d\xi)_{J,P} = -[\Gamma_s^\sigma - q^\alpha E_T^{\beta,Hg}]\, dT - RT\Gamma_{i_C}\, d \ln m_{AC} + E\, d\, q^\alpha$$

The quantities ξ, Γ_s^σ, and Γ_{i_C} are taken as

$$[2] \quad \xi = \gamma + q^\alpha E$$

$$[3] \quad \Gamma_s^\sigma \equiv \frac{S^\sigma}{\Omega^\sigma} - \sum_{j^\alpha} \Gamma_{j^\alpha} \dot{s}_{j^\alpha}^{\alpha} - \sum_{j^\beta} \Gamma_{j^\beta} \dot{s}_{j^\beta}^{\beta} \qquad (j^\alpha = Hg^+, e^-;\ j^\beta = \mathbf{A}, \mathbf{B}, \mathbf{C}, w)$$

$$[4] \quad \Gamma_{i_C} \equiv \Gamma_C - \frac{m_{AC}}{m_{AB}} \Gamma_B$$

where γ, q^α, and E are respectively the surface tension, the charge density on Hg surface and the potential of mercury with respect to a constant reference electrode. The entropy of formation Γ_s^σ of the ideal polarized interphase of surface area Ω^σ is expressed as the difference between two entropies: the overall entropy of the surface phase S^σ and the entropy obtained as if the adsorbed components kept the same partial molar entropy at the surface as in their respective bulk phases (e.g. Hg^+ and electrons e^- in the metallic phase α and **A**, **B**, **C**, and the water w in the aqueous electrolyte solution β). These partial molar entropies in bulk phases α and β are respectively written as $\dot{s}_{j^\alpha}^{\alpha}$ and $\dot{s}_{j^\beta}^{\beta}$. The corresponding molar surface excesses of the species are indicated by Γ_{j^α} and Γ_{j^β}. By means of these quantities, the electroneutrality condition becomes:

$$[5] \quad q^\alpha = F \sum_{j^\alpha} \Gamma_{j^\alpha} Z_{j^\alpha} = -F \sum_{j^\beta} \Gamma_{j^\beta} Z_{j^\beta} \qquad (j^\alpha = Hg^+, e^-;\ \ j^\beta = \mathbf{A}, \mathbf{B}, \mathbf{C})$$

Let us stress that the validity of eq. [1] relies further on the assumptions that: (*1*) the values of the temperature coefficient of the KCl calomel electrode $E_T^{\beta,Hg}$ is correctly approached by means of experimental and quasi-thermodynamic determinations (15, 16). ($FE_T^{\beta,Hg} \equiv -\dot{s}_{Hg}^{\alpha} + \frac{1}{2}\dot{s}_{Hg_2Cl_2} - \dot{s}_{Cl^-}^{\beta} + \dot{s}_{e^-}^{Cu} = -0.581$ mV deg^{-1} at 25°C for 1 *M* KCl calomel electrode); (*2*) the temperature coefficients

Can. J. Chem. Downloaded from www.nrcresearchpress.com by 210.87.254.5 on 09/06/12
For personal use only.

of contact potentials ($\dot{s}_{e^-}{}^{\alpha} - \dot{s}_{e^-}{}^{Cu}$) in the circuit are negligible; (*3*) the changes of activity coefficients with salt concentration are very small in binary mixtures of strong electrolytes kept at constant ionic strength.

It is assumed that Γ_{i_C} represents the total amount of specifically adsorbed ions of species **C** per unit area. In connection with eq. [4], we have already pointed out that thereby the validity of the treatment is restricted to systems of electrolytes and to potential and temperature ranges chosen such as to let the ion **C** be the only ion of phase β involved in specific adsorption at the electrode (thus present in the inner Helmholtz layer). Consequently, the diffuse part of the double layer appears as the region of purely unspecific interactions with regard to the nature of ions B and C, which is consistent with the model of Gouy–Chapman. The ionic overall composition of the diffuse part of the double layer is therefore $N_{\mathbf{A}}{}^{\sigma}$, $N_{\mathbf{B}}{}^{\sigma}$, $N_{d_{\mathbf{C}}}{}^{\sigma} = (m_{AC}/m_{AB})N_{\mathbf{B}}{}^{\sigma}$.

Using simple mathematical analysis, we get from eq. [1]:

$$[6] \qquad \frac{1}{RT}\left(\frac{\partial \xi}{\partial \ln m_{AC}}\right)_{T,P,J,q^{\alpha}} = -\Gamma_{i_C}$$

$$[7] \qquad \left(\frac{\partial \xi}{\partial T}\right)_{P,J,q^{\alpha},m_{AC}} = -\left(\Gamma_s{}^{\sigma} - q^{\alpha}E_T{}^{\beta,Hg}\right)$$

$$[8] \qquad \left(\frac{\partial \xi}{\partial T}\right)_{P,J,q^{\alpha},\Gamma_{i_C}} = -\left[\Gamma_s{}^{\sigma} - \Gamma_{i_C}\left(\frac{\partial \Gamma_s{}^{\sigma}}{\partial \Gamma_{i_C}}\right)_{T,P,J,q^{\alpha}}\right] + q^{\alpha}E_T{}^{\beta,Hg}$$

2. Definition of the Surface Layer System

By carrying out some further thermodynamics on the system, we have to select two complementary conditions regarding the interphase. We have emphasized, in our previous work (10), that these conditions are completely conventional. Obviously, the values of the quantities so far defined, $\Gamma_s{}^{\sigma}$, q^{α}, Γ_{i_C} are independent of these conditions. But the relevancy of quantities such as $\Gamma_{j\alpha}$, $\Gamma_{j\beta}$, S^{σ} and of partial molar surface quantities such as:

$$\left(\frac{\partial S^{\sigma}}{\partial N_{j^{\beta}}{}^{\sigma}}\right)_{T,P,N_{j'^{\beta}\neq j^{\beta}}{}^{\sigma}} = \dot{S}_{j^{\beta}}{}^{\sigma}$$

$$\left(\frac{\partial \Omega^{\sigma}}{\partial N_{j^{\beta}}{}^{\sigma}}\right)_{T,P,N_{j'^{\beta}\neq j^{\beta}}{}^{\sigma}} = \dot{\Omega}_{j^{\beta}}{}^{\sigma}$$

$$\left(\frac{\partial V^{\sigma}}{\partial N_{j^{\beta}}{}^{\sigma}}\right)_{T,P,N_{j'^{\beta}\neq j^{\beta}}{}^{\sigma}} = \dot{V}_{j^{\beta}}{}^{\sigma}$$

is strictly assessed only by the choice of these two conditions. Regardless of which particular condition we select, we are then intrinsically led to define an arbitrary location and thickness of the interphase. Thus to this region will be assigned the set of independent extensive surface phase variables $N_{j\alpha}{}^{\sigma}$, $N_{j\beta}{}^{\sigma}$ (which are respectively the total number of particles of species j^{α} and j^{β} in the surface phase) and of extensive surface state functions Ω^{σ}, V^{σ}, and S^{σ} (which are respectively the overall surface area, volume, and entropy). We have also stressed the fact (10) that the convention adopted by Gibbs ($V^{\sigma} = 0$ and $\Gamma_w{}^{\sigma} = 0$) is by no means the most convenient, when the thermodynamic properties have to serve in conjunction with a theoretical interpretation in terms of the double layer model of Grahame. To this end we have advocated a more suitable convention. It amounts to select the functions:

$$[9a] \qquad \Gamma_{Hg^+} = \Gamma_{Hg^+}(T,P,J,q^{\alpha},m_{AC})$$

$$[9b] \qquad \Gamma_w = \Gamma_w(T,P,J,q^{\alpha},m_{AC})$$

in order to generate a surface phase equivalent to a monomolecular layer. Therefore, the value

$$[10a] \qquad \Gamma_{Hg^+} = 0$$

is given to eq. [9*a*] and eq. [9*b*] is taken as

$$[10b] \qquad \Sigma_{j\beta}\,\dot{\Omega}_{j\beta}\Gamma_{j\beta} = 1$$

in combination with the following set of partial molar surface phase areas.

$$[10c] \qquad \Omega_w{}^{\sigma} = a_w(T,P,J,q^{\alpha},m_{AC})$$

$$[10d] \qquad \Omega_{i_C}{}^{\sigma} = a_{i_C}(T,P,J,q^{\alpha},m_{AC})$$

$$[10e] \qquad \Omega_{\mathbf{B}}{}^{\sigma} = \Omega_{\mathbf{A}}{}^{\sigma} = 0$$

In view of this choice, the condition [10*b*] becomes

$$[10f] \qquad a_w\Gamma_w + a_{i_C}\Gamma_{i_C} = 1$$

The parameters a_w and a_{i_C} are assumed to represent approximately the areas occupied, under given conditions of T,P,J,q^{α},m_{AC} by one mole of each constituent w and **C** in a monolayer supposedly a two-dimensional rather close-packed liquid composed exclusively of Γ_w and Γ_{i_C} particles per unit area in direct contact with the electrode.

Having thus retained the conditions [10*a*] and [10*f*], it becomes evident that the surface phase to which we refer is bound on the metal side by the plane of zero adsorption of Hg^+ and extends towards the solution on an average distance $l^{\sigma} = \theta l_{i_C} + (1-\theta)l_w$ where θ represents $a_{i_C}\Gamma_{i_C}$ and where $\dot{V}_w{}^{\sigma}/a_w = l_w$ and $\dot{V}^{\sigma}/a_{i_C} = l_{i_C}$. Hence, the thickness of the surface phase is confined between the values of l_w and l_{i_C} and, since most frequently $\theta \ll 1$, l^{σ} is near l_w of the solvent.

According to the chosen definition, the set of independent surface composition variables can be

Can. J. Chem. Downloaded from www.nrcresearchpress.com by 210.87.254.5 on 09/06/12
For personal use only.

put as:

$$[11a] \quad \Gamma_{j^\beta}{}^\sigma = \frac{N_{j^\beta}{}^\sigma}{\Omega^\sigma} = \int_{l^\sigma}^{\infty} [n_{j^\beta}{}^\sigma(z) - n_{j^\beta}{}^\beta(\infty)]\, dz \qquad (j^\beta = \mathbf{A}, \mathbf{B})$$

where $n_{j^\beta}{}^\sigma(z)$ and $n_{j^\beta}{}^\beta(\infty)$ denote the local concentration of constituent j^β at distance z from the electrode and in the bulk.

$$[11b] \quad \Gamma_w{}^\sigma = \frac{N_w{}^\sigma}{\Omega^\sigma} = \frac{1-\theta}{a_w}$$

and

$$[11c] \quad \Gamma_{i_C} = \Gamma_{i_C}(T,P,J,q^\alpha,m_{AC})$$

as derived from eq. [6].

3. Entropies of Adsorption in the Surface Layer

The system of surface state variables [11*a*,*b*,*c*] enables the determination of S^σ as follows (see Appendix)

$$[12] \quad S^\sigma = \dot{S}_w{}^\sigma N_w{}^\sigma + \dot{S}_{i_C}{}^\sigma N_{i_C}{}^\sigma + S_d{}^\sigma$$

where $S_d{}^\sigma$ denotes the contribution of non-specific adsorption, thus:

$$[13] \quad S_d{}^\sigma = \dot{S}_A{}^\sigma N_A{}^\sigma + \dot{S}_B{}^\sigma N_B{}^\sigma$$

With the help of eqs. [3], [5], and [12], we are now in position to reformulate eqs. [7] and [8] as follows:

$$[14a] \quad -\left[\left(\frac{\partial \xi}{\partial T}\right)_{P,J,q^\alpha,m_{AC}} - q^\alpha E_T{}^{\beta,Hg}\right] = \Gamma_s{}^\sigma$$

$$[14b] \quad \Gamma_s{}^\sigma = \Gamma_w[\dot{S}_w{}^\sigma - \dot{s}_w{}^\beta] + \Gamma_{i_C}[\dot{S}_{i_C}{}^\sigma - (\dot{s}_{i_C}{}^\beta + Z_C \dot{s}_{e^-}{}^\alpha)] + \Gamma_{s,d}{}^\sigma$$

$$[15] \quad -\left[\left(\frac{\partial \xi}{\partial T}\right)_{P,J,q^\alpha,\Gamma_{i_C}} - q^\alpha E_T{}^{\beta,Hg}\right] = \frac{\dot{S}_w{}^\sigma - \dot{s}_w{}^\beta}{a_w} + F_{s,d}$$

Equations [14*b*] and [15] have been written so that the non-specific ionic effects are isolated in separate terms on the right hand side.

Taking into account our previous results obtained from a complementary analysis of electric forces and stresses at the interphase (10), we can readily deduce the following relations for $\Gamma_{s,d}{}^\sigma$ and $F_{s,d}$.

$$[16] \quad \Gamma_{s,d}{}^\sigma = -\left[\frac{\partial}{\partial T}\left(\int_0^{q^\alpha + Z_c F \Gamma_{i_C}} \psi(\delta^\beta)\, d\sigma\right)\right]_{P,J,q^\alpha,m_{AC}}$$

$$[17] \quad F_{s,d} = -\left[\frac{\partial}{\partial T}\left(\int_0^{q^\alpha + Z_c F \Gamma_{i_C}} \psi(\delta^\beta)\, d\sigma\right)\right]_{P,J,q^\alpha,\Gamma_{i_C}} = -\int_0^{q^\alpha + Z_c F \Gamma_{i_C}} \left(\frac{\partial \psi(\delta^\beta)}{\partial T}\right)_{P,J,\sigma} d\sigma$$

in which the electric potential $\psi(\delta^\beta)$ is taken at the outer Helmholtz plane. It is also appropriate at this stage to express the relationship between $\Gamma_{s,d}{}^\sigma$ and $F_{S,d}$. By simple application of analysis, we have:

$$[18] \quad \Gamma_{s,d}{}^\sigma = F_{s,d}{}^\sigma - \psi(\delta^\beta)\left(\frac{\partial Z_c F \Gamma_{i_C}}{\partial T}\right)_{P,J,q^\alpha,m_{AC}}$$

4. Calculation of Diffuse Layer Contribution

We now describe the distribution $n_{j^\beta}{}^\sigma(Z)$ of non-specific adsorbed ions at the interface by means of the model of diffuse layer of Gouy–Chapman. In this case the value of $\psi(\delta^\beta)$ is known to be (17, 18):

$$[19] \quad \psi(\delta^\beta) = \frac{2RT}{|Z_a|F} \sinh^{-1} \gamma$$

$$\gamma \equiv [(q^\alpha + Z_c F \Gamma_{i_C})/\sqrt{8RT\varepsilon\varepsilon_0 J \rho_d}]$$

where ρ_d is the specific weight of the electrolyte solution and ε the dielectric permittivity in the bulk.

Upon introduction of eq. [19] into eq. [17], the expression for $F_{s,d}$ becomes:

$$[20] \quad F_{s,d} = -R\left(\frac{2RT\varepsilon J \rho_d}{\pi Z_a{}^2 F^2}\right)^{1/2}\left\{2\gamma \cosh^{-1}(1+\gamma^2)^{1/2} - \left[3 + \left(\frac{\partial \ln \varepsilon \rho_d}{\partial \ln T}\right)_{P,J}\right](\{1+\gamma^2\}^{1/2} - 1)\right\}$$

Values computed by means of eq. [20] can be found in ref. 10.

III. Experimental

1. Method and Systems

Systematic differential capacitance measurements were carried out, using a symmetrical Wien Bridge similar to those described by Hills and Payne (8) and Privat and Grand (19). The experimental conditions (temperature, potential, and concentration range) were chosen such as to make the influence of specific adsorption of fluoride ions negligible. The three mixed electrolyte systems NaF–NaCl; NaF–NaBr; NaF–NaI were studied at 15, 25, and 35°C in a potential range included between 0 and +1.5 V versus N.C.E. In all cases, the total ionic strength was kept at 10^{-1} mol kg^{-1}. The following compositions were selected:

$m_{NaF} + m_{NaX} = 10^{-1}$ mol kg^{-1}

m_{NaX}: 0; 10^{-4}; 3×10^{-4}; 10^{-3}; 3×10^{-3}; 10^{-2}; 3×10^{-2}; 10^{-1} mol kg^{-1} (X = Cl^-, Br^-, I^-)

In order to avoid any non-equilibrium effects at low values of m_{NaX}, the balance point of the bridge was taken in all experiments at the 30th s on a drop, the total life of which was 90 s. Furthermore, no significant frequency dependence of the capacitance measurements was observed between 200 and 1200 Hz at all compositions and polarization within the experimental range. In all cases, the frequency effects were of the same order of magnitude as or even lower than the error made on the capacitance measurements, i.e. ~0.15%. The dimension of the tip of the dropping mercury electrode was always small enough to avoid any screening effect. In the absence of any significant frequency influence, all the capacitance measurements were made at 1000 Hz.

Some results obtained at 25°C are shown in Fig. 1. At the most negative potential range, between −1.2 and −1.5 V, capacitance values coincide for each solution with a scattering of less than 0.15%. This error represents the sum of the errors made on the capacity measurement itself as well as on the time, potential, and mercury flow determination.

2. Calculations

(a) Density of Charge, Surface Tension, and ξ Function

The capacitance curves were integrated with respect to the potential in order to obtain the density of charge at the electrode. The required integration constants at each temperature were taken at −1.5 V vs. N.C.E. (Table 1). Those charges were obtained from p.z.c. measurements of 0.1 *m* NaF system, using the streaming electrode. The integration procedure was carried out, using both a graphical method (potential range divided in trapezoids of 10 mV width) and a computation program that fits third degree polynomials to the curves. Both methods provide equally good results.

The constants for the integration of charge versus potential was obtained from direct measurements of surface tension for 0.1 *m* NaF system by means of the maximum bubble pressure method (Table 1). The surface tensions are calculated from integration with a precision of about 0.1 m*N* m^{-1}.

Values of E, γ, for each entire q^α value included in the polarization range, were computed by means of an interpolation programme. Thus values of $\xi = \gamma + q^\alpha E$ versus E were determined at each ionic strength.

(b) Adsorption Isotherms

The equation

$$[21] \quad \Gamma_{i_c}(T, P, q^\alpha, m_{AC}) = -\int_{-20\ \mu C}^{q^\alpha} \left(\frac{\partial \Delta E}{\partial \mu_{AC}{}^\beta}\right)_{q'^\alpha, T, P} dq'^\alpha$$

yields the most suitable method of deriving surface excesses Γ_{i_c} with a good precision (20). We have defined $\Delta E = E - E_0$. The electromotive forces E and E_0 are measured respectively in the system NaF + NaX and NaF at the same q^α and J. Plots of $(\Delta E)_{q\alpha}$ versus ln m_{AC} were drawn for entire q^α values included between -20×10^{-2} C m^{-2} and $+12 \times 10^{-2}$ C m^{-2}. The dispersion of the experimental results never exceeds 2 mV which is comparable with the expected errors arising from capacity measurements and integration. The slopes of these curves were evaluated, using the Lagrange interpolation formula. If one admits an error of about 1 mV on ΔE of the ordinate, one gets a standard deviation of the slopes of 0.7 for about 100 trials using a random generation of simulated experimental results. This represents a relative deviation of about 2% in most cases and reaches 20% only in the case of Cl^- ions at negative densities of charges or very low concentrations of the heteroion.

The values of $(\partial \Delta E/\partial \mu_{AC}{}^\beta)_{q\alpha}$, taken at each value of the selected concentration of NaX were integrated with respect to q^α. Thereby, the curves representing the integrand as a function of q^α were smoothed which reduces again the dispersion, so that the error on Γ_{i_c} lies at maximum within ±2%. As a matter of fact, the internal consistency of the resulting values of $F\Gamma_{i_c}$, as yielded by the dispersion of the computed points, is usually better than 0.3×10^{-2} C m^{-2}. Some adsorption isotherms are given in Fig. 2.

3. Entropy Excesses

Partial molar entropy of water adsorption can be obtained from eq. [15]. The temperature coefficient of 1 *N* calomel electrode reported by de Bethune (15) at 25°C is $E_T{}^{\beta,Hg} = -0.581$ mV K^{-1}. The contribution of the diffuse layer $F_{s,d}$, evaluated on ground of the Gouy–Chapman model, is calculated by means of eq. [20].

The results obtained from capacitance measurements of 0.1 *M* NaF solutions at 25°C are similar to those already published in our previous work using coulostatic techniques (12). In presence of halide adsorption, the partial differentials $-(\partial \xi/\partial T)_{J,P,q^\alpha,\Gamma_{i_c}}$ at 25°C were derived either at some selected values of the molalities $m_{AC}{}^\beta$ or at some selected values of Γ_{i_c}. The temperature coefficients were evaluated using a quadratic relation for ξ.

(i) Adsorption Entropies of the Solvent as a Function of Molalities

The values Γ_{i_c} corresponding to some chosen value of $m_{AC}{}^\beta$ and q^α is deduced from the isotherms at 25°C. The adsorption isotherms at 15°C and 35°C allow to relate this value of Γ_{i_c} to the corresponding molalities at 15 and 35°C. Plots of ξ versus m_{AC} at various q^α and T yield the three values of ξ corresponding to 15, 25, and 35°C which then allow to determine the differential of eq. [15] at 25°C for Γ_{i_c} and q^α constant. By repeating the same procedure at different densities of charges and correcting adequately for the reference electrode temperature coefficient one gets the results depicted in Fig. 3.

(ii) Adsorption Entropies of the Solvent as a Function of Surface Excess

The calculation of $(\partial \xi/\partial T)_{P,J,q^\alpha,\Gamma_{i_c}}$ at given values of Γ_{i_c} occurs quite in a similar way as in (*i*). This time, however, values of Γ_{i_c} and q^α are chosen and the corresponding molalities at each temperature are found. Deduction of the quantities ξ at 15, 25, and 35°C is made from ξ versus 1 g m_{AC} plots. Figure 4 represents the value of the right hand side term of eq. [15] at 25°C for different densities of charges and Γ_{i_c}. The correction for the reference electrode term has been made as previously stated and the contribution of the diffuse layer at the selected values of Γ_{i_c} and q^α is evaluated from eq. [20].

The errors associated with the data here reported in Figs. 3 and 4 have been estimated as follows. Within an error of $\simeq 10^{-3}$ C m^{-2} on Γ_{i_c} and on q^α, the subsequent error on ξ is of about 0.1 m*N* m^{-1}. Then the quantity $((\dot{S}_w{}^\sigma - \dot{s}_w{}^\beta)/a_w)_{T,P,J,q^\alpha,\Gamma_{i_c}}$ is determined within a precision of ±0.01 m*N* K^{-1} m^{-1}. Apparently, the dispersion of calculated results at low Γ_{i_c} does not exceed this value and is even much smaller at larger amounts of anions adsorbed.

(iii) Entropy of Formation of the Interface as a Function of Molalities

The entropy of formation $\Gamma_s{}^\sigma$ has been calculated by means of

Can. J. Chem. Downloaded from www.nrcresearchpress.com by 210.87.254.5 on 09/06/12
For personal use only.

Can. J. Chem. Downloaded from www.nrcresearchpress.com by 210.87.254.5 on 09/06/12
For personal use only.

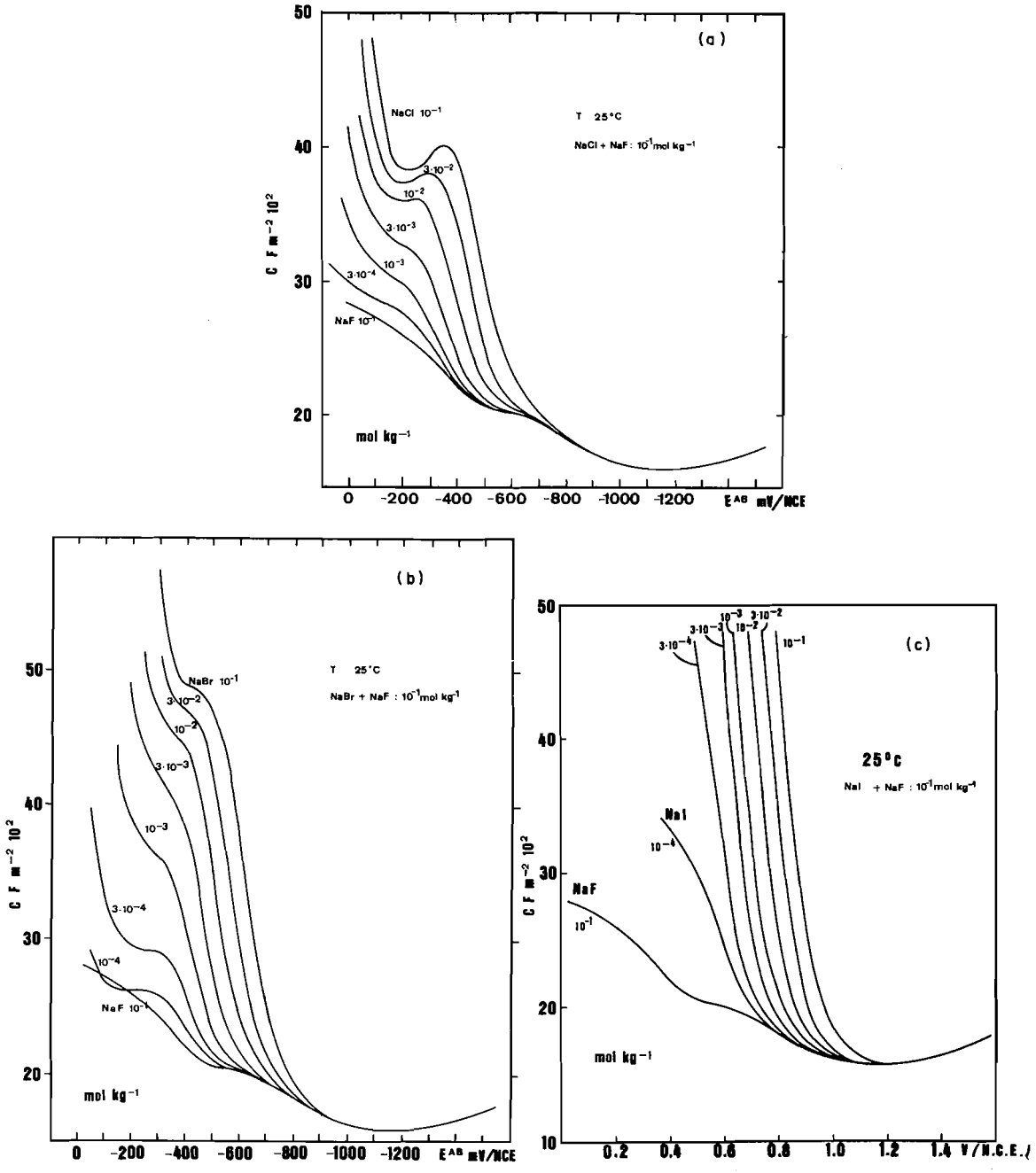

FIG. 1. Differential double layer capacitance of mercury in contact with mixed electrolyte solutions at constant ionic molality. (*a*) The NaF–NaCl system; (*b*) the NaF–NaBr system; (*c*) the NaF–NaI system.

Can. J. Chem. Downloaded from www.nrcresearchpress.com by 210.87.254.5 on 09/06/12
For personal use only.

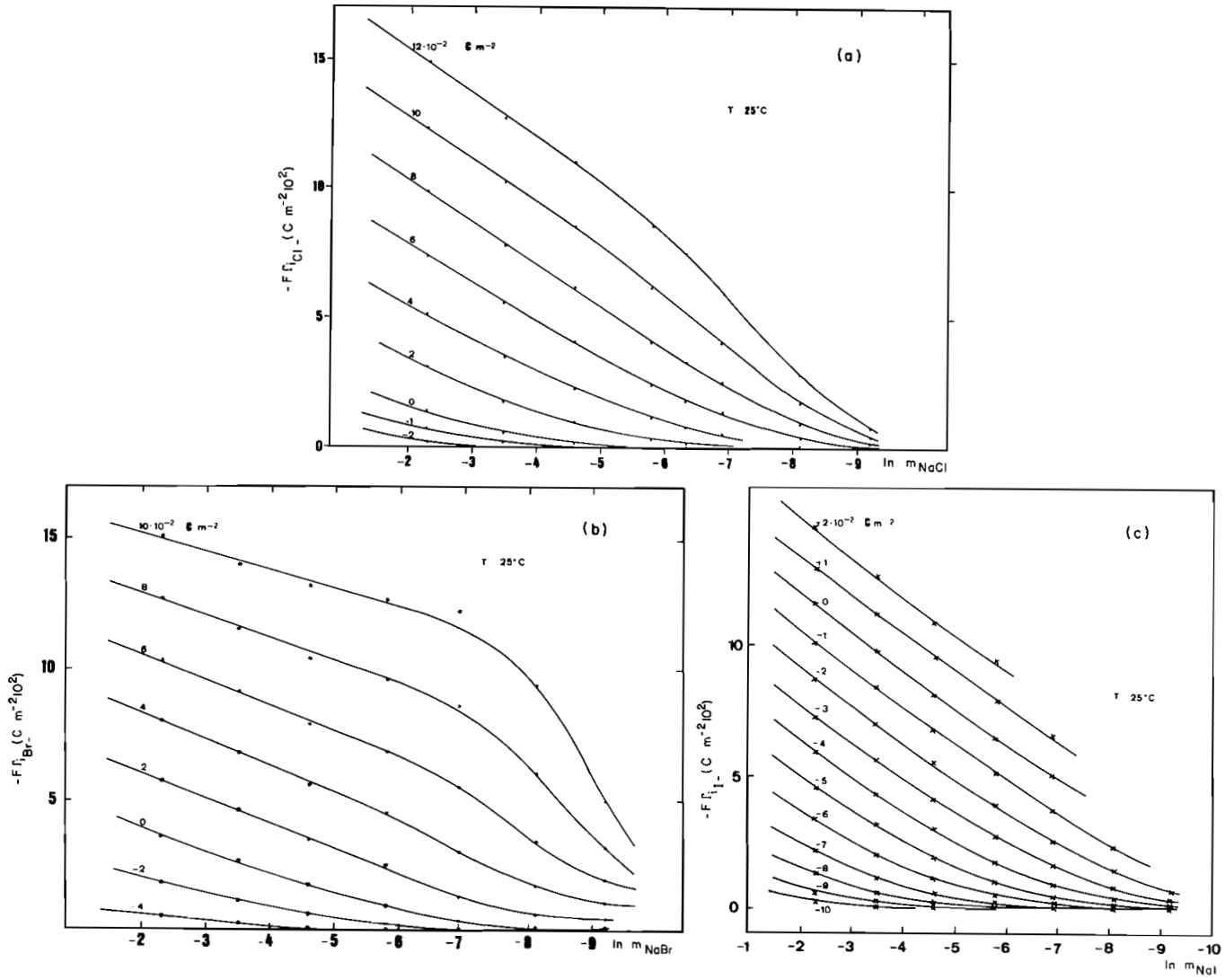

FIG. 2. The adsorption isotherms in the inner Helmholtz layer at different charge densities from mixed electrolyte solutions at constant ionic molality of 10^{-1} M kg^{-1}. (*a*) The NaF–NaCl system; (*b*) the NaF–NaBr system; (*c*) the NaF–NaI system.

Can. J. Chem. Downloaded from www.nrcresearchpress.com by 210.87.254.5 on 09/06/12
For personal use only.

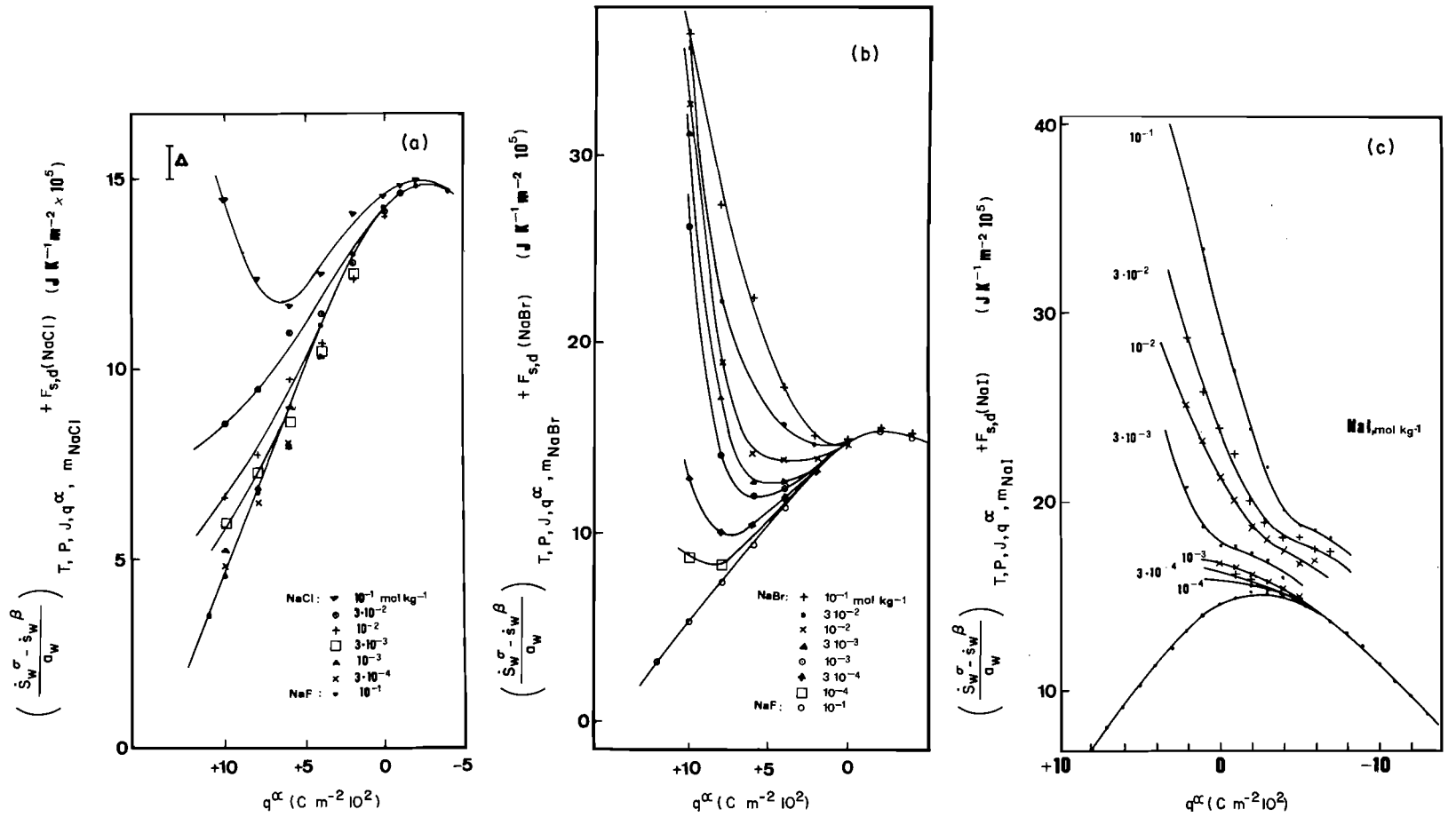

FIG. 3. Adsorption entropies of water at 25°C without correction of the diffuse layer contribution from mixed electrolytic solutions at constant ionic molality of 10^{-1} M kg^{-1}. (*a*) The NaF–NaCl system at different molalities of NaCl; (*b*) the NaF–NaBr system at different molalities of NaBr; (*c*) the NaF–NaI system at different molalities of NaI.

Can. J. Chem. Downloaded from www.nrcresearchpress.com by 210.87.254.5 on 09/06/12
For personal use only.

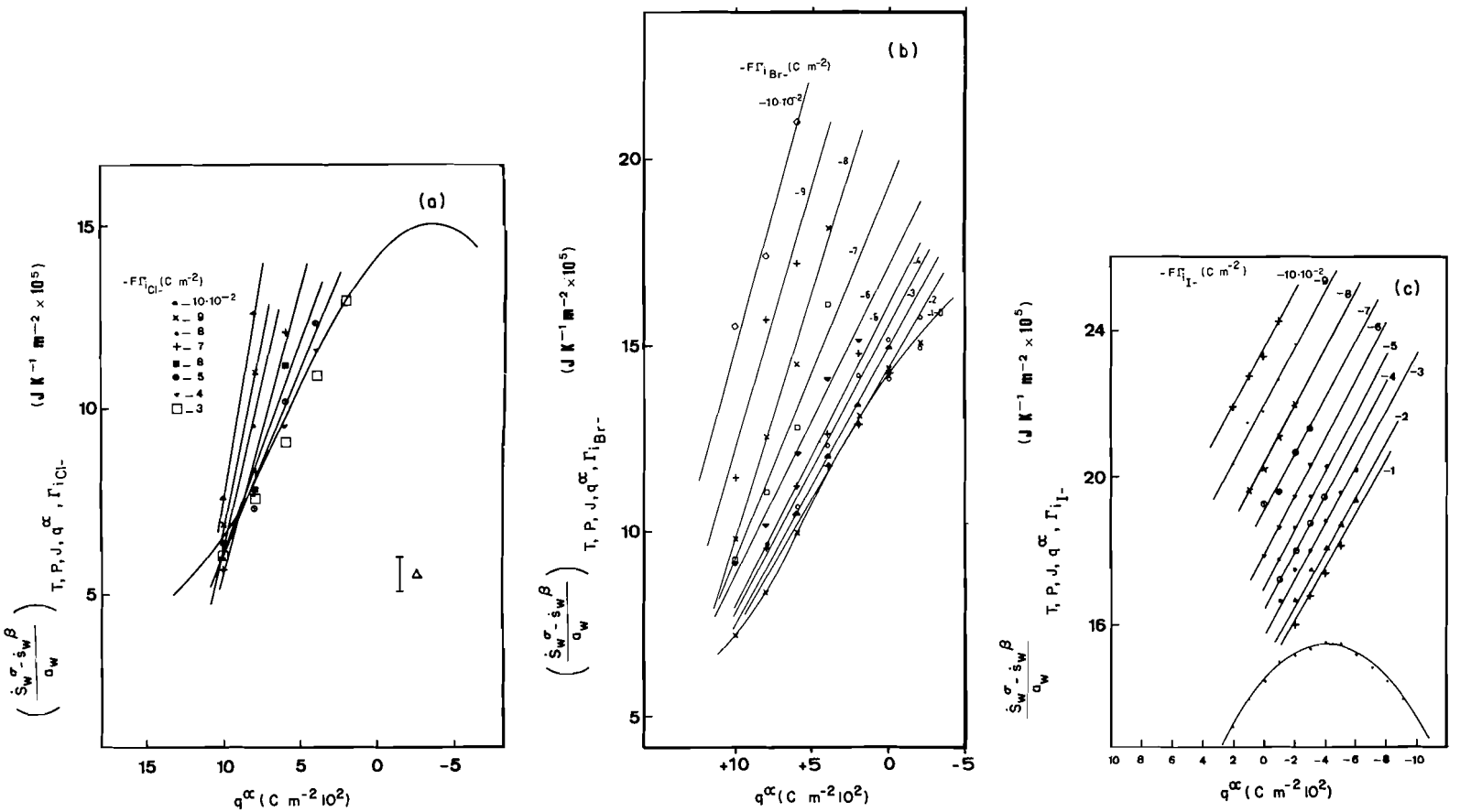

FIG. 4. Adsorption entropies of water in the inner Helmholtz layer at 25°C from mixed electrolytic solutions at constant ionic molality of 10^{-1} M kg^{-1}. The estimated maximum deviation Δ is 0.01 mN m^{-1} K^{-1}. (*a*) The NaF–NaCl system at different molar surface excesses of Cl^- in the inner layer; (*b*) the NaF–NaBr system at different molar surface excesses of Br^- in the inner layer; (*c*) the NaF–NaI system at different molar surface excesses of I^- in the inner layer.

Can. J. Chem. Downloaded from www.nrcresearchpress.com by 210.87.254.5 on 09/06/12
For personal use only.

TABLE 1. Integration constants (for NaF 0.1 M kg^{-1})

Temperature	p.z.c. (mV)	q^{α} at −1.5 V vs. N.C.E. (10^{-2} C m^{-2})	γ at −1.5 V vs. N.C.E. (mN m^{-1})
15°C	−471.0 ± 0.2	−18.22 ± 0.04	328.5 ± 0.1
25°C	−472.1 ± 0.2	−17.97 ± 0.04	329.1 ± 0.1
35°C	−473.1 ± 0.2	−17.72 ± 0.04	329.8 ± 0.1

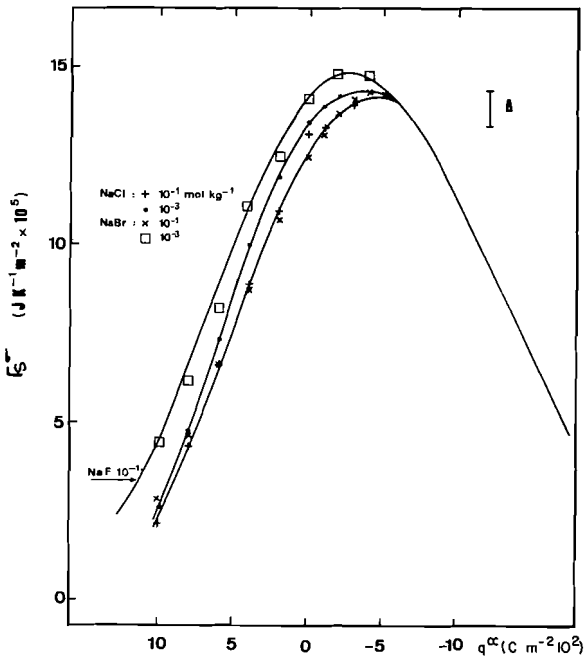

FIG. 5. The overall entropies of formation at 25°C of the double layer (without diffuse layer correction) at the mercury electrode in contact with mixed electrolyte solutions at constant ionic molality of 10^{-1} M kg^{-1}. The systems represented are NaF–NaCl and NaF–NaBr. The maximum indetermination arising from an error of 0.1 mN m^{-1} on ξ is shown in the figure.

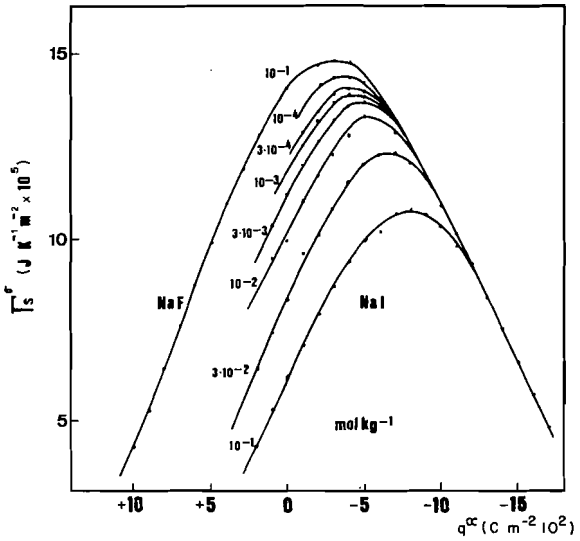

FIG. 6. The overall entropies of formation at 25°C of the double layer (without diffuse layer correction) at the mercury electrode in contact with NaF–NaI solutions kept at constant ionic molality of 10^{-1} M kg^{-1}.

eq. [7] at 25°C and for various values of the molality m_{AC}. These are thermodynamic quantities and thus include the contribution of the diffuse part of the double layer. In Fig. 5 are shown the values of Γ_s^{σ} as a function of q^{α} at $m_{NaX} = 10^{-1}$ and 10^{-3} mol kg^{-1} (X = Cl$^-$, Br$^-$) and in Fig. 6 is depicted the behaviour of Γ_s at various values of m_{NaI}. The indetermination on Γ_s arising from a prior error of 0.1 mN m^{-1} on ξ is represented in each figure. The dispersion of calculated results appears to be much less in most cases.

IV. Discussion

1. *Comparison of Adsorption Isotherms at 25°C with Previous Results*

We can compare directly the differential capacity curves recorded in Fig. 1 at 0.1 M and 25°C with the experimental data already published for single electrolyte systems. Deviations from these values never exceed 0.5% in the case of Cl$^-$ adsorption (21, 22) and are below 1% in the case of Br$^-$ (23) and I$^-$ (24) adsorptions. The capacity data for 0.1 M NaF, although slightly higher than Grahame's values (by about 1%) (25), were shown to be very reproducible over all the experimental range. These measurements have already been thoroughly discussed (12).

There is a large dissimilarity of patterns of adsorption isotherms of halides from single and from mixed alkaline halides solutions at constant J. In the mixed electrolytes system, each of the constant charge isotherms for Cl$^-$ and Br$^-$ ions displays a sharp bending followed by an inflexion point and tends asymptotically to zero amount adsorbed with decreasing m_{AC}. In the corresponding single alkaline halide solutions, the constant charge isotherms present a flattening and, at $q^{\alpha} > 0$, are asymptotic to a finite amount adsorbed which is

Can. J. Chem. Downloaded from www.nrcresearchpress.com by 210.87.254.5 on 09/06/12
For personal use only.

numerically close to q^{α}. Consequently, both types of isotherms cannot be fitted easily to a common curve. This problem has been considered already by several authors (26–30). It has led to the analyses of the systems by means of the fitting of the experimental results to theoretical simple virial adsorption isotherms and by the electrical characterization of the inner layer properties (e.g. inner layer capacitances and potential drop).

The possibility of using the same virial isotherm for the description of the adsorption from single electrolytes and mixed electrolytes systems was attempted without much success in the case of Cl^- and Br^- adsorption (27–29) but provided better results in the case of I^- adsorption at small coverage (20, 29, 30). The following arguments are used to explain these discrepancies between both experimental methods. First, one considers that the most important effect is presumably due to the composition difference of the diffuse layer in the two types of systems. The electrical contribution to the standard free energy of adsorption ΔG^0 should depend: (*i*) on the potential at the outer Helmholtz plane (31, 32); (*ii*) on the effective thickness of the inner layer which is set under control of the countercations adsorbed at the outer Helmholtz plane (31, 34); (*iii*) on the increased efficiency of the image formation in the diffuse layer of the specifically adsorbed anions (33, 34).

Hills and Reeves further stressed the role of F^- specific adsorption (29, 35). It was also shown that the comparison of adsorption isotherms between single electrolytes and mixed electrolytes systems as recorded in Fig. 2, required a careful choice of the log of the bulk ionic activities to be used (20, 36). This problem is raised if no account is made of the buffering effect of the diffuse layer by introducing the potential at the outer Helmholtz plane in ΔG^0. This correction amounts to taking the concentration of the specifically adsorbing ion at the outer Helmholtz plane as a concentration variable.

Thus far all the corrections suggested above have been relatively inadequate in providing a good fit of the adsorption isotherms derived from single electrolytes and from mixed electrolytes systems. It is also noteworthy that the values of $\Gamma_{i_{Cl^-}}$ and $\Gamma_{i_{Br^-}}$ here derived for $10^{-1}\,M$ solution at 25°C are substantially lower than those obtained in refs. (21, 23). Similar discrepancies with the single halides systems were found at the largest **C** bulk concentration by Payne (27) in the mixed KF + KCl system (at $J = 1\,M$), by Sears and Lyons (28) in the mixed KF + KBr system (at $J = 1\,M$) and by Hills and Reeves (29) in the mixed NH_4F + NH_4Br system at ($J = 0.5\,M$). These differences are undoubtedly related to the method of derivation of Γ_{i_C}. In mixed electrolyte systems these values are obtained by differentiation at the end of the experimental range and are probably much in error. However, it is also worth mentioning that the calculations in both types of systems make use of different definitions of the ionic bulk activities. In most electrocapillary measurements with mixed electrolytes at constant J so far published the bulk activity coefficients are assumed to be constant. The influence of these coefficients was already analyzed in refs. (37, 38). In the case of binary mixtures, $\ln \gamma_{AB}$ and $\ln \gamma_{AC}$ can be estimated by means of Harned's rule (39–41). It follows that for most halides systems at constant J, the Harned's coefficients are small and do not affect significantly the data derived from eq. [1]. An attempt has been made more recently by Fawcett *et al.* (33, 34) to estimate the individual ionic activities. These authors consider that the activity coefficients of the anions γ_B and γ_C remain unaffected by the concentration m_C on account of the fact that the atmosphere around a given anion is largely unmodified when the solution composition is changed at J constant. As concerns the activity coefficient of the single cation γ_A, the Hückel–Brönsted–Guggenheim equation was used (39). This expresses $\ln \gamma_A$ as a function of m_c. In our systems, the tabulated activity coefficients in $0.1\,M$ NaF, NaCl, NaBr, and NaI are at 25°C respectively 0.765, 0.778, 0.782, 0.787 (42). These data yield a maximum difference of less than 3% between γ_{NaF} and γ_{NaI}. Under such conditions and upon application of the treatment developed by Fawcett *et al.*, provided that $J = 0.1\,M$, the maximum shift of the potential scale E_A with respect to that measured against a constant reference electrode E is 0.8 mV when the electrolyte is changed from $0.1\,M$ NaF to $0.1\,M$ NaI. The determination of surface excesses from eq. [1] will be affected by a maximum error of 3% in $m_{NaI} = 0.1$ mol kg^{-1}.

The measurements published so far on the degree of specific adsorption of Cl^- (27) and Br^- ions (28, 29), adsorbed from mixed electrolytes solution were performed at $1\,M$ (27, 28) and $0.5\,M$ (29) constant ionic strength. Furthermore, the lowest concentrations reported were 10^{-3}, 5×10^{-3}, and $2.5 \times 10^{-4}\,M$, respectively for KCl, KBr, and NH_4Br. These conditions contrast with ours as much for the concentration range as for the choice of the common cation. A direct comparison is therefore rather difficult. It is observed that our molar surface excesses are systematically lower than those so far reported and that the shapes of the isotherms are different. This is evidently related to

Can. J. Chem. Downloaded from www.nrcresearchpress.com by 210.87.254.5 on 09/06/12
For personal use only.

the influences exerted by the diffuse layer. Damaskin *et al.* (36) have indicated that the buffering effect of the diffuse layer is the larger at $(q^\alpha + Z_c F\Gamma_{ic}) > 0$, the smaller the ionic strength. In our experiments the conditions $(q^\alpha + Z_c F\Gamma_{ic}) > 0$ is fulfilled at concentrations of Cl^- below $3 \times 10^{-2}\,M$ and of concentrations of Br^- below $10^{-3}\,M$. The buffering effect of the diffuse layer is thus expected to be quite different according to systems investigated at $J = 1\,M$ or $0.5\,M$ and at $J = 0.1\,M$ especially in the range of large q^α and low m_{AC}. It is further noticed that the nature of the common countercation might affect the specific adsorption of anions. Fawcett *et al.* (33, 34) suggested that the distance between the inner and outer Helmholtz plane decreases by approximately a factor of two when the countercation is changed from Na^+ to K^+. Consequently, the average potential at the adsorption plane becomes less negative and the screening of the adsorbed anion by the diffuse layer is more effective in presence of K^+ than of Na^+. Hence discreteness of charges contributes to Γ_{ic} being larger in the K^+ system than in the Na^+ system. It is also expected that the adsorption data at $J > 0.1\,M$ are more strongly subjected to the influence of F^- specific adsorption (29, 35, 43). In the worst experimental situation encountered in this respect with our measurements ($m_{AC} = 0$, $J = 10^{-1}\,M$, $q^\alpha = 10^{-1}$ C m^{-2}) a value of $|Z_c F\Gamma_{ic}| < 10^{-2}$ C m^{-2} can be deduced from the results of Hills and Reeves at 25°C (35). Therefore, in the present investigation, the amount of F^- specifically adsorbed will never exceed the absolute precision of the molar excess determination.

Finally, it is noteworthy that Payne (27) derived congruent isotherms with respect to q^α in the system KF + KCl at $J = 1\,M$, that Sears and Lyons (28) did not detect such congruency in the system KF + KBr at $J = 1\,M$ and that Hills and Reeves (29) could find such congruency with the system NH_4Br + NH_4F at $J = 0.1\,M$. We have not observed this property for the Cl^- and Br^- adsorption at any temperature. In the case of Br^- adsorption a change of curvature of the isotherms occurs if q^α is increased above 6×10^{-2} C m^{-2}. A similar change was observed in ref. 28. It might indicate either that some adsorption saturation is being approached or, if expressed in terms of virial isotherms, that the virial B coefficient decreases considerably with increasing q^α. At first approximation, the virial state equation corresponding to the virial adsorption isotherm takes the form:

$$[22] \qquad (\xi_0 - \xi)/RT = \Phi/RT = \Gamma_{ic}[1 + B(q^\alpha)\Gamma_{ic}]$$

where ξ and ξ_0 are measured respectively in the NaF + NaX solution and in NaF solution at the same values of q^α, J, and T.

Plots of the surface pressure Φ have been drawn in Fig. 7. If a state equation with B constant as a function of q^α is obeyed, and if the isotherms are congruent with respect to q^α, the curves should be parallel and linear, hence

$$[23] \qquad \left(\frac{\xi_0 - \xi}{\partial q^\alpha}\right)_{T,P,J,\Gamma_{ic}} = 0$$

According to eq. [22], it is evident from Fig. 7*a* and *b* that B decreases considerably with increasing q^α, especially with Br^- ions, the lowest value being somewhat smaller than that obtained in Fig. 7*c* with I^- ions.

The behaviour of I^- differs considerably from that observed with Cl^- and Br^- ions. The adsorption isotherms, as shown in Figs. 2*c* and 7*c* remain congruent with respect to q^α over the whole experimental range and the values of $\Gamma_{i_{I^-}}$ calculated at $10^{-1}\,M$ and 25°C agree within less than 1.5% with the data derived from a single electrolyte system (24). A plot of $\Gamma_{i_{I^-}}$ versus ΔE is shown in Fig. 8. According to the equation

$$[24] \qquad \Delta E = E - E_0 = RT\left(\frac{\partial \ln m_{AC}}{\partial q^\alpha}\right)_{T,P,J,\Gamma_{ic}} \Gamma_{i_c} = -RT\left(\frac{\partial \ln \beta}{\partial q^\alpha}\right)_{T,P,J} \Gamma_{i_c}$$

which is valid in the case of congruency with respect to q^α (37), the slopes of the plot recorded in Fig. 8 yield the coefficients $(\partial \ln \beta/\partial q^\alpha)_{T,P,J}$ where

$$[25] \qquad \ln \beta = -\Delta G^0/RT$$

It appears that these coefficients depend weakly on q^α. This behaviour reflects the fact that ΔG^0 cannot be represented strictly by a simple linear function of q^α. The values of the coefficients vary between 0.835 and 0.813×10^2 m^2 C^{-1} at respectively $q^\alpha = -8$ and -2×10^{-2} C m^{-2}, the lowest value being about 2.5% higher than the value found by Dutkiewicz and Parsons (20). A constant value of 3.4 (nm^2)/ion is deduced from the plot of Fig. 8 for the second virial coefficient B. This is in perfect agreement with the values derived in the literature which vary between 3.1 and 3.9 (nm)^2/ion over a wide range of charge densities (30, 44). Let us note however in this respect that adsorption isotherms derived by Fawcett and McCarrick (33) in the NaF–NaI and the KF–KI systems at $J = 0.25\,M$ did fit into a simple virial equation.

All the experimental evidence now available suggests that I^- ions manifest a much simpler behaviour in their process of specific adsorption

Can. J. Chem. Downloaded from www.nrcresearchpress.com by 210.87.254.5 on 09/06/12
For personal use only.

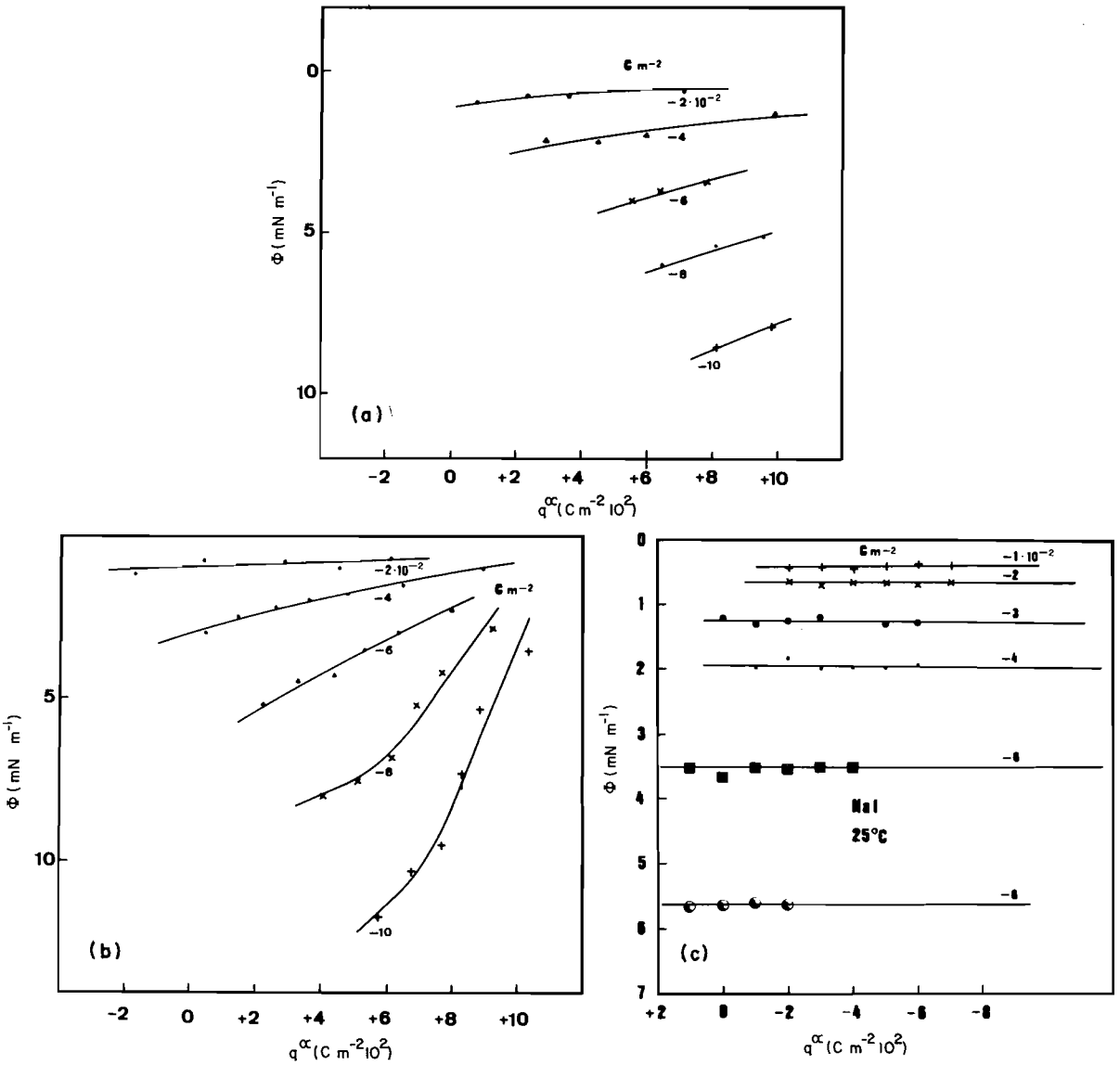

FIG. 7. Surface pressure Φ as a function of the surface charge density at 25°C. (*a*), The NaF–NaCl system at different molar excesses of Cl^- in the inner layer; (*b*), the NaF–NaBr system at different molar excesses of Br^- in the inner layer; (*c*), the NaF–NaI system at different molar excesses of I^- in the inner layer.

than Cl^- and Br^- ions. It happens generally that the *B* coefficient is constant in systems of strong ionic adsorption (30) and that furthermore this coefficient depends on the nature of the solvent (30). Consequently, we are led to assume that the average conformation of the coadsorbed solvent in the inner layer is less affected by the presence of the strongest adsorbed I^- ions than by Br^- and Cl^- ions. This hypothesis is confirmed in the following section on account of the dependence of the entropy of solvent adsorption with q^α and $\Gamma_{i_{I^-}}$. As opposed to the *B* constancy in the I^- system, the variation of *B* with Cl^- and Br^- adsorption might reveal a disturbance of the adsorbed solvent configuration. This might be considered as equivalent to an increase of the free energy of hydration of the Cl^- and Br^- ions at the surface as a function of decreasing q^α. In the case of solvent restructuring effects extending over a sufficiently large distance on the surface, this behaviour will also be formally equivalent to a reinforcement of the lateral repulsion between the adions.

The present investigation is essentially devoted to the thermodynamic analysis of temperature

Can. J. Chem. Downloaded from www.nrcresearchpress.com by 210.87.254.5 on 09/06/12
For personal use only.

effects on electrocapillary data. Accordingly, we do not intend to carry out further detailed and more quantitative computation of the adsorption parameters at the level of a microscopic model of the inner region like, for example, the potential drop and various types of capacities. We leave this important but distinct question to a forthcoming publication.

2. The Entropy of Adsorption of the Solvent in the Inner Layer

The results recorded in Fig. 3 indicate clearly that at 25°C the partial molar entropy of adsorption $\dot{S}_w^\sigma$ of the solvent is a complex function of q^α if plotted at constant m_{AC}. However, if we draw plots of $\dot{S}_w^\sigma$ at constant Γ_{i_C}, the dependence with q^α becomes nearly linear. The values of entropies presented in Fig. 4 decrease with increasing q^α at constant Γ_{i_C} and increase as a function of Γ_{i_C} at constant q^α. In the case of Cl^- and Br^- adsorption, the increment of $\dot{S}_w^\sigma$ with Γ_{i_C} depends on the value of q^α and is not linearly related to the ionic amount specifically adsorbed at constant q^α. In the case of I^-, however, an identical variation of $\dot{S}_w^\sigma$ with $\Gamma_{i_{I^-}}$ occurs at all values of q^α. The property of constant virial B coefficient has the following consequence upon the dependence of $\dot{S}_w^\sigma$ on q^α and on $\Gamma_{i_{I^-}}$. According to eq. [23], one gets within the range of isotherm congruency that

$$[26]\quad \left(\frac{\partial^2}{\partial T \partial q^\alpha}(\Phi)\right)_{P,J,\Gamma_{i_C}} = \left[\frac{\partial}{\partial q^\alpha}\left(\frac{\dot{S}_w^\beta}{a_w} - \frac{S_0^\beta}{a_{w0}}\right)\right]_{T,P,J,\Gamma_{i_C}} + \left[\frac{\partial}{\partial q^\alpha}(F_{s,d} - F_{s,d0})\right]_{T,P,J,\Gamma_{i_C}} = 0$$

where the subscript 0 refers to the system without specific adsorption. A similar equation has already been derived in ref. 10.

In Fig. 9, we have plotted the values of $(\dot{S}_w^\beta/a_w - F_{s,d})$ in presence of I^- as a function of Γ_{i_C}. It appears that good straight lines might be drawn with minor deviations at relatively low coverage. Since the experimental points lie markedly on the lines, these plots support the view that, at constant q^α, the internal accuracy of our results is better than $0.003\ mN\ m^{-1}\ K^{-1}$ although the absolute accuracy has been estimated to lie within $0.01\ mN\ m^{-1}\ K^{-1}$. The dependence on q^α of the extrapolated quantities $[(S_w/a_w)_{0,q^\alpha} - (S_{w0}/a_{w0})_{q^\alpha}]$ in Fig. 9 is illustrated in Fig. 10. The deviations of $(S_w/a_w)_{0,q^\alpha}$ from $(S_{w0}/a_{w0})_{q^\alpha}$ are below the acceptable experimental error and the validity of eq. [26] is thus assessed in the domain of low ionic coverage here considered. Consequently, it might be suggested that the shifts of the lines in Fig. 9 are due to systematic errors on the determination of q^α or Γ_{i_C}. Thus upon application of eq. [26], one gets an expression of the partial molar surface entropy of water as follows:

$$[27]\quad \left(\frac{\dot{S}_w^\sigma}{a_w}\right)_{\Gamma_{i_{I^-}},q^\alpha} = \left(\frac{\dot{S}_{w0}^\sigma}{a_{w0}}\right)_{q^\alpha} - \frac{R}{a_w}\ln a_w\Gamma_w + \int_{q^\alpha}^{q^\alpha + Z_c F \Gamma_{i_{I^-}}} \left(\frac{\partial \phi(\delta^\beta)}{\partial T}\right)_\sigma d\sigma$$

where the second term on the r.h.s. is independent of q^α.

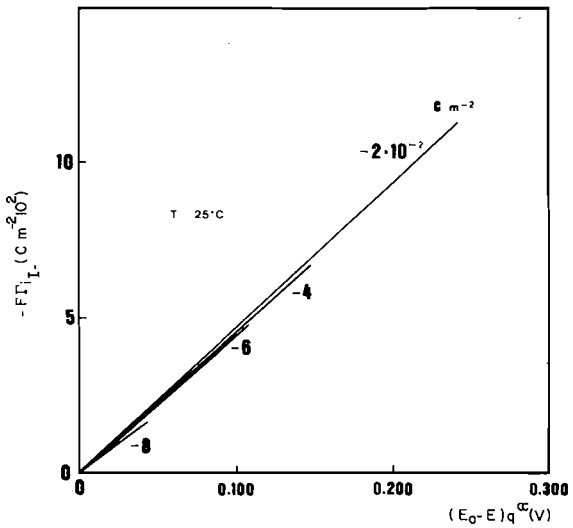

FIG. 8. Molar ionic excess of I^- in the inner layer as a function of the difference of potential $(E - E_0)$ at different densities of charges.

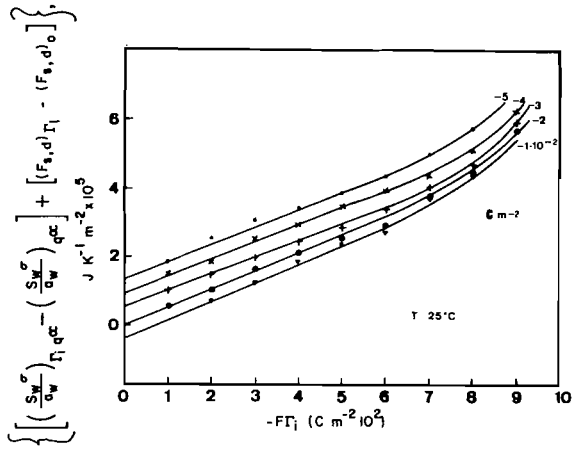

FIG. 9. Ionic molar inner layer excess dependence of the water adsorption entropies uncorrected for the diffuse layer contribution at different densities of charge in the NaF–NaI system at 25°C.

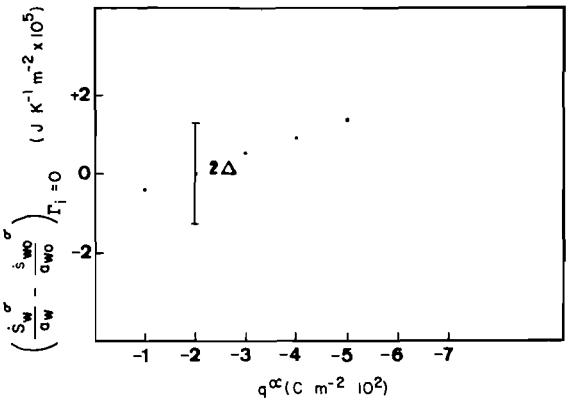

FIG. 10. Values of extrapolated partial molar standard entropies of the adsorbed water in presence of I^- adsorption plotted as a function of density of charge.

Equation [27] expresses the limiting condition of an ideal entropy of mixing as encountered in systems conforming to surface fraction statistics (45). Therefore terms such as the surface equivalent of osmotic or activity coefficients of water do not play any role. Indeed if this had not been the case, one would have to assume that the molecular interactions are independent of the average molecular configurations of water at the surface, which themselves are functions of q^α. This is of course very unlikely. Therefore the term $(\dot{S}_{w0}^\sigma/a_{w0})_{q^\alpha}$ carries alone all the effects resulting from the molecular conformation of adsorbed water as a function of q^α. For its part, the last term on the r.h.s. of eq. [27] bears exclusively the contributions of the diffuse layer. The choice of such simple equations for the partial molar surface entropies of water does not necessarily involve that the free energy expression is of the Langmuirian type. It suggests however that for example the virial B coefficient or some Frumkin coefficient in the isotherm is nearly independent of temperature.

In the experimental range of small surface excesses corresponding at the limit to the Henry's law domain, one has:

$$a_{I^-}\Gamma_{i_{I^-}} \ll a_w\Gamma_w$$

Hence one may approximate the second term of eq. [27] as follows:

$$[28] \qquad -\frac{R}{a_w}\ln \Gamma_w a_w \simeq R\left(\frac{a_{I^-}}{a_w}\right)\Gamma_{i_{I^-}}$$

Under this condition the slopes of the lines in Fig. 9 yield approximately the value $(a_{I^-}/a_w) \simeq 6.3$

Taking the average value of the diameter of one water molecule adsorbed at the surface as between 0.28 nm and 0.37 nm (12), one gets 0.7 to 0.95 nm for the diameter of the adsorbed anionic entity. A way of explaining this large figure is to regard the desolvated iodide adsorption process as involving a strong polarization of the nearest neighbour water molecules around the iodide ion in the inner layer. This amounts to an adsorbed entity made out, at vanishing ionic coverage, of one central ion surrounded by a circular sheet of thickness of the diameter of one water molecule. A similar hypothesis has been proposed by Hills and Payne (8) who suggested also that the ion could be adsorbed with a largely intact solvation shell. However, according to the results presented in Fig. 4, the conformation of the solvent beyond this peripheral solvation sheet should be unaffected.

3. *Formation Entropy of the Inner Layer and Adsorption Entropy of the Ions*

The influence of the adsorbed ion molalities m_{AC} on the surface formation entropies Γ_s^σ is depicted in Fig. 5 in the presence of Cl^- and Br^- ions. Only small deviations are observed from the curve recorded in absence of specific adsorption. The decrease of the surface entropy of formation is much more pronounced with I^-, as illustrated on Fig. 6. A comparison with Fig. 3, which reports the positive deviations of the adsorption entropy of water from the entropy in absence of specific adsorption as a function of m_{AC} bears out any simple explanation of the behaviour of Γ_s^σ and leads roughly to admit that this thermodynamic function is made out of several contributions working in opposite directions: (*a*) a positive deviation increasing with m_{AC} related to the solvent adsorption; (*b*) a negative deviation increasing with m_{AC} related to the specifically adsorbed ions; (*c*) a complex term given by eq. [18] expressing the formation entropy of the diffuse layer.

We shall attempt next a careful interpretation of these data and therefore compute the inner layer formation entropy which is defined as:

$$[29] \qquad \Gamma_{is}^\sigma = \Gamma_w^\sigma(\dot{S}_w^\sigma - \dot{s}_w^\beta) + \Gamma_{ic}^\sigma(\dot{S}_{ic}^\sigma - \dot{s}_{ic}^\beta)$$

Using eqs. [14], [16], [18], we calculate Γ_{is}^σ from the following relation:

$$[30] \qquad \Gamma_{is}^\sigma = \Gamma_s^\sigma - F_{s,d} + \psi(\delta^\beta) \times \left(\frac{\partial Z_c F\Gamma_{ic}}{\partial T}\right)_{P,J,q^\alpha,m_{AC}}$$

The values of the inner layer formation entropies are given in Fig. 11. In their general features, they agree with the results published by Harrison *et al.* (9). Thus, Γ_{is}^σ shows a tendency to decrease at constant q^α and m_{AC} with the increasing adsorbability of the ionic species. Furthermore, the influence of the ionic concentration is amplified by

Can. J. Chem. Downloaded from www.nrcresearchpress.com by 210.87.254.5 on 09/06/12
For personal use only.

Can. J. Chem. Downloaded from www.nrcresearchpress.com by 210.87.254.5 on 09/06/12
For personal use only.

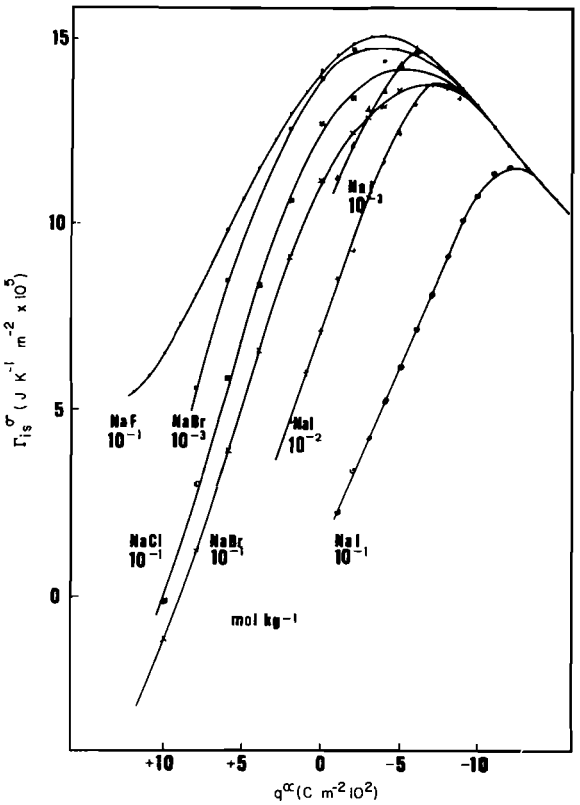

FIG. 11. The inner layer formation entropies at 25°C at the mercury electrode in contact with mixed electrolyte solutions at constant ionic molality of 10^{-1} M kg^{-1} for NaF–NaX systems (X = Cl$^-$, Br$^-$, I$^-$) at different molalities of NaX.

the ionic adsorbability. The reason for the negative deviation from the behavior in absence of specific adsorption can now be attributed to the overriding contribution of the partial molar entropy of specifical adsorption of ions. Denoting this quantity by $\Delta\dot{S}_{i_C}{}^{\sigma}$, we can express it as follows:

$$[31]\quad \Delta\dot{S}_{i_C}{}^{\sigma} = \dot{S}_{i_C}{}^{\sigma} - \dot{s}_C{}^{\beta_o} = \frac{1}{\Gamma_{i_C}}\left\{\Gamma_{is}{}^{\sigma} - \left(\frac{\dot{S}_w{}^{\sigma} - \dot{s}_w{}^{\beta}}{a_w}\right)(1 - \Gamma_{i_C}a_{i_C})\right\} - R\ln m_{AC}$$

where $\dot{s}_C{}^{\beta}$ has been decomposed in such a way as to leave only the standard partial molar bulk entropy $s_C{}^{\beta_o}$ in the definition of $\Delta\dot{S}_{i_C}{}^{\sigma}$. At relatively large ionic coverage, the ionic adsorption entropy depends on the arbitrary choice of a_{i_C}. These values have been selected by taking the ionic radii of Pauling (46). It results that $a_{Cl^-} = 8.4 \times 10^{-2}$ (nm)^2/ion; $a_{Br^-} = 10.2 \times 10^{-2}$ (nm)^2/ion; $a_{I^-} = 13.1 \times 10^{-2}$ (nm)^2/ion. The dependence of $\Delta\dot{S}_{i_C}{}^{\sigma}$ on q^{α} at constant Γ_{i_C} is depicted in Fig. 12. These plots show that satisfactory straight lines are obtained and it seems that within the experimental accuracy, the data can be fitted to a linear function even for chloride. The deviation arising from the limited accuracy of the experimental and computational methods might be estimated to lie roughly within a maximum of ± 8 J K^{-1} mol^{-1} of the value of $\Delta\dot{S}_{i_C}{}^{\sigma}$ and is certainly smaller in presence of iodide. It should be emphasized that the plots of Fig. 12 can be predicted from the strict application of the Gibbs–Duhem equation to the monolayer interphase. According to this condition, it is possible to evaluate the slopes of $\dot{S}_{i_C}$ vs. q^{α} from the slopes of the lines presented in Fig. 4. At equilibrium, the relationship is:

$$[32]\quad \Gamma_{i_C}\left(\frac{\partial\dot{S}_{i_C}{}^{\sigma}}{\partial q^{\alpha}}\right)_{\Gamma_{i_C}} = -\Gamma_w\left(\frac{\partial\dot{S}_w{}^{\sigma}}{\partial q^{\alpha}}\right)_{\Gamma_{i_C}} \simeq -(a_w\Gamma_w)\left(\frac{\partial(\dot{S}_w{}^{\sigma}/a_w)}{\partial q^{\alpha}}\right)_{\Gamma_{i_C}}$$

There is indeed a qualitative agreement between eq. [32] and our measurements. This is reflected by the opposite sign of the slopes computed from Fig. 4 and Fig. 12. In presence of Br$^-$ and I$^-$ adsorption, the graphical determination of the straight lines in Fig. 12 is sufficiently discriminating as to indicate that the slopes are decreasing when Γ_{i_C} is increased. Consequently, the value of the ratio

$$\left(\frac{\partial\dot{S}_{i_C}{}^{\sigma}}{\partial q^{\alpha}}\right)_{\Gamma_{i_C}} \Big/ \left(\frac{\partial(\dot{S}_w{}^{\sigma}/a_w)}{\partial q^{\alpha}}\right)_{\Gamma_{i_C}}$$

as deduced from Figs. 4 and 12 is decreased in function of increasing Γ_{i_C}, which conforms to the theoretical prediction of eq. [32] and further illustrates the internal consistency of our results.

For Cl$^-$ and Br$^-$, the range of variation of $\Delta\dot{S}_{i_C}{}^{\sigma}$ in Fig. 12 overlaps the value zero, the points on the positive side corresponding to the lowest experimental molality ($m_{AC} = 10^{-3}$ mol/kg). Except for these dilute systems, all the points are found at negative adsorption entropies, the values being the more negative, the more the ionic species are adsorbable. At constant charge, an increase of the ionic excess Γ_{i_C} leads to a decrease of $\Delta\dot{S}_{i_C}{}^{\sigma}$. It is likely that the source of the observed decrease in entropy is due, for a small part, to the entropy of mixing and that the main intervention is that of lateral electric repulsion between the ions located in the inner layer.

Since the range of entropy variation realized by a similar change of Br$^-$ and I$^-$ surface concentration is larger for Br$^-$ ions, it can be inferred that the lateral repulsion for Br$^-$ is larger than for I$^-$. There

Can. J. Chem. Downloaded from www.nrcresearchpress.com by 210.87.254.5 on 09/06/12
For personal use only.

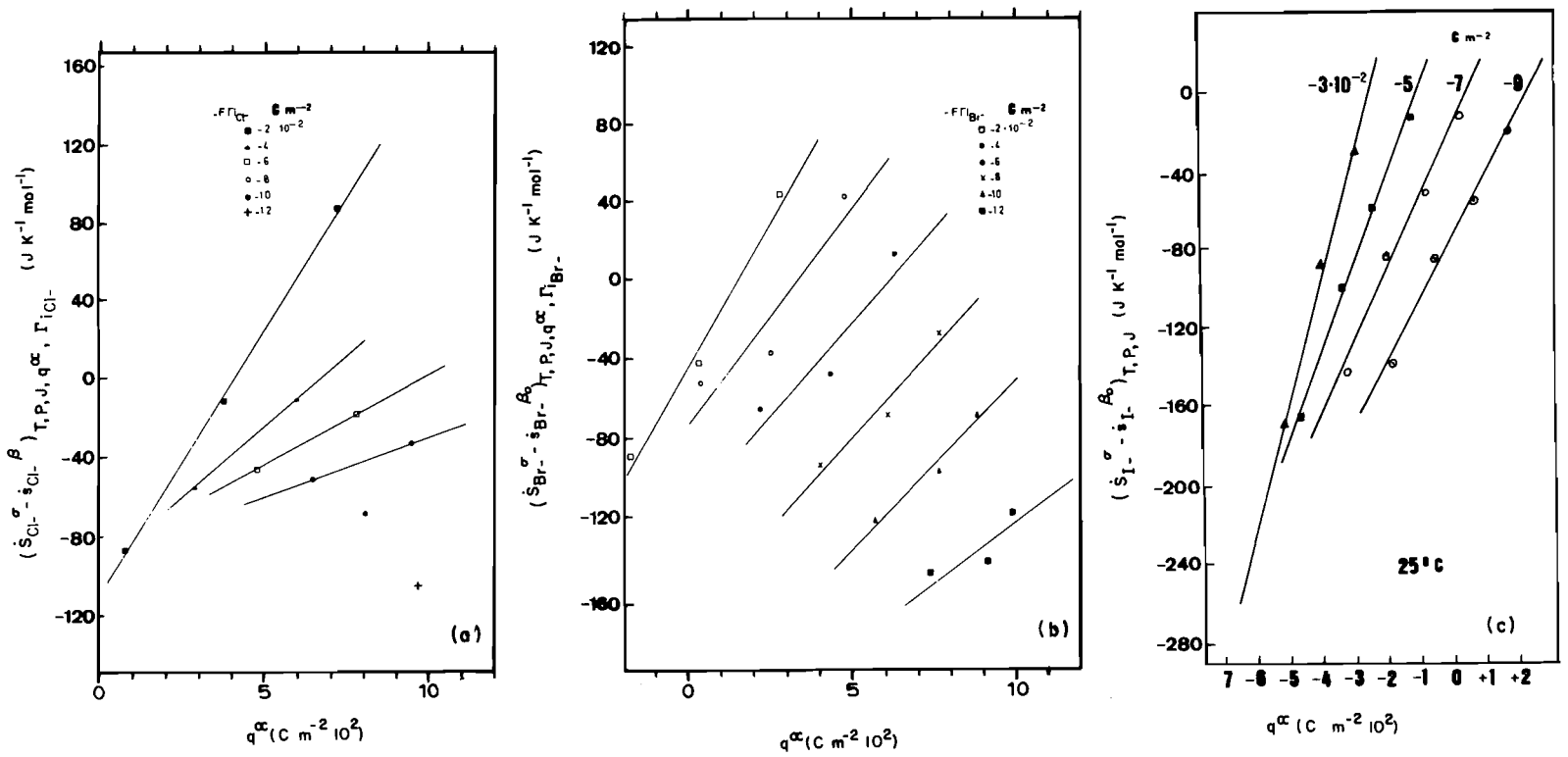

FIG. 12. The adsorption entropies of halide ions in the inner layer at 25°C as a function of the density of charge. (*a*) The case of Cl^- specific adsorption at different molar surface excesses in the inner layer. $a_{Cl^-} = 8.4 \times 10^{-2}$ (nm)²/ion; (*b*) the case of Br^- specific adsorption at different molar surface excesses in the inner layer. $a_{Br^-} = 10.2 \times 10^{-2}$ (nm)²/ion; (*c*) the case of I^- specific adsorption at different molar surface excesses in the inner layer. $a_{I^-} = 13.1 \times 10^{-2}$ (nm)²/ion.

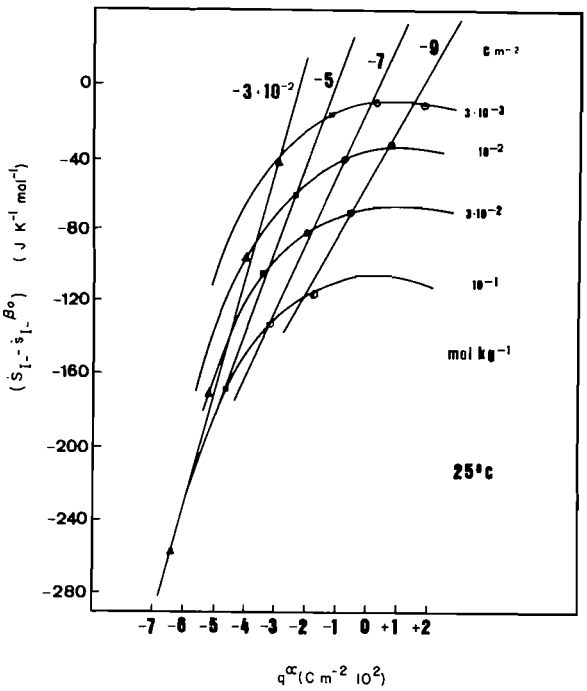

FIG. 13. The adsorption entropy of I^- ion in the inner layer at 25°C as a function of the density of charge. The curves at different molalities m_{NaI} in the mixed electrolytic solution and at different molar surface excesses of I^- in the inner layer are presented. $a_{I^-} = 47 \times 10^4$ m^2 M^{-1}.

is no simple explanation for the charge dependence of $\Delta\dot{S}_{i_C}{}^{\sigma}$ at constant Γ_{i_C}. Several factors might be suggested which could determine the increase of entropy with increasing positive charge. One might assume that an increase of standard entropy of the adions occurs by means of some partial charge transfer with the metal phase (47, 48). The adions Cl^- and Br^- might also act as structure promoting centers for the water dipoles adsorbed at the surface. This process should be all the less efficient as more dipoles are pointing their positive poles to the solution. Alternatively, one might suggest that the electric repulsion between the adions gets weaker under the effect of increased positive charge on the metal. This effect may be caused by the predominant orientation of the water dipoles with their positive poles pointing towards the solution and thereby neutralizing more efficiently the negative ionic charges penetrating in the inner layer. Such explanation has been invoked in the case of ionic adsorption at the Ga electrode where water dipoles are strongly adsorbed (49).

As regards the dependence of $\Delta\dot{S}_{i_C}{}^{\sigma}$ on the choice of the specific area a_C, it is shown in Fig. 13 that a value of $a = 78 \times 10^{-2}$ (nm)^2/ion corresponding to a radius of 0.5 nm does not modify the general features of the plot of Fig. 12. This value has been selected in relation to the determination of a from the initial slope of the function recorded in Fig. 9.

We show furthermore in Fig. 13 the general pattern of changes of $\Delta\dot{S}_{i_C}{}^{\sigma}$ at given ionic molalities. It is observed from this figure that the function increases strongly at constant m_{AC} with increasingly positive q^{α}, reaches a maximum and thereafter is levelled or even somewhat lowered. The lowering is practically controlled by the mechanism of ionic lateral repulsion. The initial rise of the function seems to be determined to a great extent by the overwhelming influence of the mechanism through which $\Delta\dot{S}_{i_C}{}^{\sigma}$ is increased with increasing q^{α} at constant ionic surface excess.

Acknowledgements

We wish to thank the Fonds National de la Recherche Fondamentale Collective and the Fonds National de la Recherche Scientifique of Belgium for having supported this work.

1. O. A. ESIN and B. F. MARKOV. Acta Physicochim. U.R.S.S. **10**, 353 (1959).
2. O. A. ESIN and V. SHIKOV. Zhur. Fiz. Khim. **17**, 236 (1943).
3. B. V. ERSHLER. Zhur. Fiz. Khim. **20**, 679 (1946).
4. V. G. LEVICH, V. A. KINYANOV, and V. S. KRYLOV. Dokl. Akad. Nauk. S.S.S.R. **135**, 1425 (1960).
5. C. A. BARLOW JR. and J. R. MACDONALD. J. Chem. Phys. **40**, 1535 (1964).
6. S. LEVINE, G. M. BELL, and D. CALVERT. Can. J. Chem. **40**, 518 (1962).
7. S. LEVINE, J. MINGINS, and G. M. BELL. Can. J. Chem. **43**, 2843 (1965).
8. G. J. HILLS and R. PAYNE. Trans. Farad. Soc. **61**, 326 (1965).
9. J. A. HARRISON, J. E. B. RANDLES, and D. J. SCHIFFRIN. J. Electroanal. Chem. **48**, 359 (1973).
10. H. D. HURWITZ and C. V. D'ALKAINE. J. Electroanal. Chem. **42**, 77 (1973).
11. G. J. HILLS and S. HSIEH. J. Electroanal. Chem. **58**, 289 (1975).
12. NGUYEN HUU CUONG, C. V. D'ALKAINE, A. JENARD, and H. D. HURWITZ. J. Electroanal. Chem. **51**, 377 (1974).
13. NGUYEN HUU CUONG, A. JENARD, and H. D. HURWITZ. J. Electroanal. Chem. **103**, 399 (1979).
14. G. HILLS. J. Phys. Chem. **6**, 3591 (1969).
15. A. J. DE BETHUNE, H. O. DALEY, N. A. SWENDEMAN, and G. R. SOLVI. J. Electrochem. Soc. **114**, 578 (1967).
16. A. J. DE BETHUNE, T. S. LICHT, and N. A. SWENDEMAN. J. Electrochem. Soc. **106**, 616 (1959).
17. D. C. GRAHAME. J. Chem. Phys. **16**, 1117 (1948).
18. D. M. MOHILNER. *In* Electroanalytical chemistry. Vol. 1. *Edited by* A. J. Bard. Marcel Dekker, New York. 1966. p. 241.
19. M. PRIVAT and R. GRAND. J. Chim. Phys. **70**, 607 (1973).
20. E. DUTKIEWICZ and R. PARSONS. J. Electroanal. Chem. **11**, 100 (1966).
21. D. C. GRAHAME. J. Am. Chem. Soc. **71**, 2975 (1949).
22. D. C. GRAHAME and R. PARSONS. J. Am. Chem. Soc. **83**, 1291 (1961).

Can. J. Chem. Downloaded from www.nrcresearchpress.com by 210.87.254.5 on 09/06/12
For personal use only.

23. J. LAWRENCE, R. PARSONS, and R. PAYNE. J. Electroanal. Chem. **16**, 193 (1968).
24. D. C. GRAHAME. J. Am. Chem. Soc. **80**, 4201 (1958).
25. D. C. GRAHAME. J. Am. Chem. Soc. **79**, 2093 (1957).
26. R. PARSONS. Rev. Pure Appl. Chem. **18**, 91 (1968).
27. R. PAYNE. Trans. Faraday Soc. **64**, 1638 (1968).
28. A. R. SEARS and P. A. LYONS. J. Electroanal. Chem. **42**, 64 (1973).
29. G. J. HILLS and R. M. REEVES. J. Electroanal. Chem. **42**, 355 (1973).
30. J. D. GARNISH and R. PARSONS. Trans. Faraday Soc. **63**, 1754 (1967).
31. R. DE LEVIE. J. Electrochem. Soc. **118**, 184.C (1971).
32. C. V. D'ALKAINE, E. R. GONZALEZ, and R. PARSONS. J. Electroanal. Chem. **32**, 57 (1971).
33. W. R. FAWCETT and T. A. MCCARRICK. J. Electrochem. Soc. **123**, 1325 (1976).
34. W. R. FAWCETT and J. B. SELLAN. Can. J. Chem. **55**, 3871 (1977).
35. G. J. HILLS and R. M. REEVES. J. Electroanal. Chem. **31**, 264 (1971).
36. B. B. DAMASKIN, U. PALM, E. PETYÄRV, and M. SALVE. J. Electroanal. Chem. **47**, 127 (1973).
37. H. D. HURWITZ. J. Electroanal. Chem. **10**, 35 (1965).
38. S. LAKSHMANAN and S. K. RANGARAJAN. J. Electroanal. Chem. **27**, 127 (1970).
39. H. S. HARNED and B. B. OWEN. The physical chemistry of electrolytic solutions. 3rd ed. Reinhold, New York. 1963.
40. J. LAKSHMANAN and S. K. RANGARAJAN. J. Electroanal. Chem. **27**, 170 (1970).
41. D. R. ROSSEINSKY and R. J. HILL. J. Electroanal. Chem. **30**, App. 7 (1971).
42. R. A. ROBINSON and R. H. STOKES. Electrolyte solutions. Butterworths Publ., London. 1959.
43. D. J. SCHIFFRIN. Trans. Faraday Soc. **67**, 3318 (1971).
44. R. PARSONS. Trans. Faraday Soc. **55**, 999 (1959).
45. T. L. HILL. An introduction to statistical thermodynamics. Addison-Wesley Publ. Co., Reading, MA. 1966.
46. L. PAULING. The nature of the chemical bond. Cornell University Press, Ithaca, NY. 1948.
47. W. LORENZ and G. KRÜGER. Z. Phys. Chem. Leipzig, **221**, 231 (1962).
48. W. LORENZ. Z. Phys. Chem. Leipzig, **224**, 145 (1963).
49. V. A. KIRIYANOV, V. S. KRYLOV, and N. B. GRIGORIEV. Elektrokhimiya, **4**, 408 (1968).
50. D. J. SCHIFFRIN. Trans. Faraday Soc. **67**, 3318 (1971).

Appendix

In our previous theoretical publication (10), we have expressed the surface entropy S^σ as follows:

$$[A1] \quad S^\sigma = \sum_{j'\beta} \dot{S}_{j'\beta}{}^\sigma N_{j'\beta}{}^\sigma$$

where $j'\beta$ is a short notation for the set of constituents w (water), **A**, **B**, ^{i}**C** in which ^{i}**C** is heteroion **C** present in the inner layer. From Euler's theorem, we obtain

$$[A2] \quad S^\sigma = \sum_{j'\beta} \dot{S}_{j\beta}{}^\sigma N_{j'\beta}{}^\sigma + \dot{S}_{d_C}{}^\sigma \times \sum_{j'\beta} \left(\frac{\partial N_{d_C}{}^\sigma}{\partial N_{j'\beta}}\right)_{T,P,(N_{j'\beta^\sigma} - N_{j'\beta})} N_{j'\beta}{}^\sigma$$

The partial molar surface entropy $\dot{S}_{j\beta}{}^\sigma$ corresponds to the expression:

$$[A3] \quad \dot{S}_{j\beta}{}^\sigma = \left(\frac{\partial S^\sigma}{\partial N_{j\beta}{}^\sigma}\right)_{T,P,(N_{j\beta^\sigma} - N_{j\beta})}$$

and $j\beta$ refers to the set of constituants w, **A**, **B**, ^{i}**C**, ^{d}**C**, in which ^{d}**C** is the heteroion **C** adsorbed in the diffuse part of the double layer. Taking into account that $N_{d_C}{}^\sigma$ is a function of T, P, $N_{j'\beta}{}^\sigma$, eq. [A2] can be rewritten in the form:

$$[A4] \quad \dot{S}^\sigma = \sum_{j'\beta} \dot{S}_{j\beta}{}^\sigma N_{j'\beta}{}^\sigma + \dot{S}_{d_C}{}^\sigma N_{d_C}{}^\sigma = \sum_{j\beta} \dot{S}_{j\beta}{}^\sigma N_{j\beta}{}^\sigma$$

Therefore

$$[A5] \quad (\mathrm{d}S^\sigma)_{T,P} = \sum_{j\beta} \dot{S}_{j\beta}\, \mathrm{d}N_{j\beta}{}^\sigma$$

and

$$[A6] \quad \Gamma_s{}^\sigma = \sum_{j\beta} \dot{S}_j{}^\sigma \frac{N_{j\beta}{}^\sigma}{\Omega^\sigma} - \sum_{j\beta} \Gamma_{j\alpha} \dot{s}_{j\alpha}{}^\alpha - \sum_{j\beta} \Gamma_{j\beta} \dot{s}_{j\beta} = \sum_{j\beta} \Gamma_{j\beta} [\dot{S}_{j\beta}{}^\sigma - (\dot{s}_{j\beta}{}^\beta + Z_{j\beta} \dot{s}_{e^-}{}^\alpha)]$$

owing to the conditions [5] and [10*a*]. Accordingly, eq. [8] yields:

$$[A7] \quad \left(\frac{\partial \xi}{\partial T}\right)_{P,J,q^\alpha,\Gamma_{i_C}} - q^\alpha E_T{}^{\beta,\mathrm{Hg}} = -(\dot{S}_w{}^\sigma - \dot{s}_w{}^\beta)\left[\Gamma_w - \Gamma_{i_C} \times \left(\frac{\partial \Gamma_w}{\partial \Gamma_{i_C}}\right)_{T,P,J,q^\alpha}\right] - F_{s,d}$$

$$[A8] \quad F_{s,d} = \sum_{d_j} [\Gamma_{d_j} - \tau_{d_j} \Gamma_{i_C}] \times [\dot{S}_{d_j}{}^\sigma - (\dot{s}_{d_j}{}^\beta + Z_d \dot{s}_{e^-})]$$

where the notation $^d j$ stands for the set **A**, **B**, ^{d}**C** of ions present in the diffuse layer, and

$$\tau_{d_j} = \left(\frac{\partial \Gamma_{d_j}}{\partial \Gamma_{i_C}}\right)_{T,P,J,q^\alpha}$$

is the double layer transport number of an ionic species of the set $^d j$ (36, 50). Equation [7] yields:

$$[A9] \quad \left(\frac{\partial \xi}{\partial T}\right)_{P,J,q^\sigma,m_{AC}} - q^\alpha E_T{}^{\beta,\mathrm{Hg}} = -\Gamma_w[\dot{s}_w{}^\sigma - \dot{s}_w{}^\beta] - \Gamma_{i_C}[\dot{S}_{i_C}{}^\sigma - (\dot{s}_i{}^\beta + Z_{e^-} - \dot{s}_{e^-}{}^\alpha)] - \Gamma_{s,d}{}^\sigma$$

$$[A10] \quad \Gamma_{s,d}{}^\sigma \equiv \sum_{d_j} \Gamma_{d_j} [\dot{S}_{d_j}{}^\sigma - \dot{s}_{d_j}{}^\beta + Z_{d_j} \dot{s}_{e^-}]$$

Can. J. Chem. Downloaded from www.nrcresearchpress.com by 210.87.254.5 on 09/06/12
For personal use only.

Microscopic modelling of adsorption and the generalised surface layer hypothesis

M. V. SANGARANARAYANAN AND S. K. RANGARAJAN

Department of Inorganic and Physical Chemistry, Indian Institute of Science, Bangalore 560012, India

Received October 7, 1980

This paper is dedicated to Dr. Sam Levine on the occasion of his 70th birthday

M. V. SANGARANARAYANAN and S. K. RANGARAJAN. Can. J. Chem. **59**, 2072 (1981).

Two- and three-state models for the adsorption of organic compounds at the electrode/electrolyte interface are proposed. Different size requirements, if any, for the neutral molecule and the adsorbing solvent are also considered. It is shown how the empirical, generalised surface layer (GSL) relationship (between the potential difference and the electrode charge) formulated by Damaskin *et al.* can be understood at the molecular level.

M. V. SANGARANARAYANAN et S. K. RANGARAJAN. Can. J. Chem. **59**, 2072 (1981).

On propose des modèles à deux et trois états pour l'adsorption des composés organiques à l'interface électrode/électrolyte. On considère également, s'il y a lieu, les conditions imposées par des différences de grosseurs entre la molécule neutre et le solvant adsorbant. On montre comment on peut comprendre, au niveau moléculaire, la relation empirique de la couche de surface généralisé (entre la différence de potentiel et la charge de l'électrode) qui a été formulée par Damaskin *et al.*

[Traduit par le journal]

1. Introduction

Levine *et al.* have made significant contributions to the molecular modelling of the adsorption at charged interfaces and this report on some aspects of the statistical mechanics of the double layer is a token tribute to Professor Levine.

A primary question in electrical double layer is the relationship between the electrode charge (σ) and the potential difference (φ_{m_2}) existing at the interface. This is closely related to (*i*) the dependence of capacitance on coverage (θ) of the adsorbate (or solvent states); (*ii*) the issue of congruence (σ or φ_{m_2}?), and (*iii*) the nature of isotherms (4).

Earlier phenomenological approaches, notably of Frumkin (7), Hansen (8), and Parsons (9) led to some simple forms of σ vs. φ_{m_2}:

(*a*) Frumkin

$$[1] \qquad \sigma = \sigma_0(1 - \theta) + \sigma_1\theta = [C_0(1 + \theta) + C_1\theta]E - C_1E_N\theta$$

(*b*) Hansen

$$[2] \qquad \sigma = [C_0(1 - \theta) + C_1\theta](E - E_N\theta)$$

(*c*) Parsons

$$[3] \qquad \sigma = (E - E_N\theta)C_0/[(1 - \theta) + \theta C_0/C_1]$$

In the above equations, θ is the coverage by the adsorbate; C_0, C_1 are the capacitances at $\theta = 0$ and $\theta = 1$ respectively; and E_N is the total shift of the potential of zero charge (PZC) while going from $\theta = 0$ to $\theta = 1$. E is the potential difference measured with respect to the PZC at $\theta = 0$.

2. The Generalised Surface Layer Equation

Damaskin *et al.* (1–3) proposed on phenomenological grounds, an empirical equation governing the σ–E behaviour (for the adsorption of a class of organic compounds at the electrode/electrolyte interface) given as:

$$[4] \qquad \sigma = \frac{[C_0(1 - \theta) + nC_1\theta]E - nC_1E_N\theta[k(1 - \theta) + \theta]}{1 + n\theta - \theta}$$

There are two "adjustable parameters", n and k, in the above equation and the other parameters have been defined in Section 1. The motivation for such a hypothesis (4) — termed Generalised Surface Layer (GSL) model — is the failure of the earlier models of Frumkin (7), Hansen *et al.* (8), and Parsons (9) to account for several experimental observations. GSL model also served as a construct, *albeit* heuristic, synthesising the earlier results.

The success of GSL equation (4) in experimental "fits" has prompted us to ask the following questions:

(*a*) Is there any physical (molecular) picture of adsorption that would result in a functional form as [4]? Is the GSL equation an approximate or exact version? What are its limitations?

(*b*) Can the adjustable parameters be understood in terms of "molecular constants" like the dipole

0008-4042/81/132072-08$01.00/0

©1981 National Research Council of Canada/Conseil national de recherches du Canada

Can. J. Chem. Downloaded from www.nrcresearchpress.com by 210.87.254.105 on 09/06/12
For personal use only.

Can. J. Chem. Downloaded from www.nrcresearchpress.com by 210.87.254.105 on 09/06/12
For personal use only.

moment, polarisability etc.? What is the molecular basis for n, k?

(*c*) Do different (n, k) pairs reflect the relative strength of adsorbate–solvent, adsorbate–adsorbate interactions etc.?

(*d*) Is the GSL hypothesis associated with a unique molecular picture?

We demonstrate, in what follows that answers to the above questions are possible. In our analysis of the models, permanent and induced dipole moment effects, discreteness of charge calculations and the substrate interactions are included.

One may take into account the polarisability effects which seem to play an important role in the electrochemical adsorption, following Levine's approach (5, 6). We have derived isotherms and charge potential relationship for the two-state and three-state descriptions. The GSL phenomenology can then be interpreted in this framework and the molecular basis for n and k can be unravelled. Table 1 shows a few typical n, k values. For a more exhaustive list, see refs. 3, 10, 19.

TABLE 1. Values of parameters n and k for the adsorption of various organic substances on mercury electrode (4, 19)

Organic substance	n	k
tert-$C_5H_{11}OH$	1	1.19
n-$C_5H_{11}OH$	1	1.57
iso-$C_5H_{11}OH$	1	1.47
n-C_3H_7OH	1	1.16
n-C_4H_9OH	1.13	1.31
C_2H_5COOH	0.91	0.21
n-C_4H_9COOH	1.12	1.09
n-$C_5H_{11}COOH$	1.25	1.15
n-$C_6H_{13}COOH$	1.45	1.20
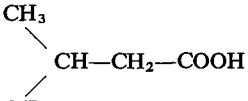	1.10	1.07
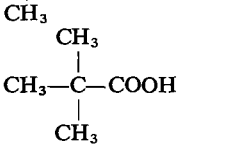	0.6	1.0

3. Principles of Modelling

Adsorption at an electrochemical interface has several facets viz., multicomponent, multiconfigurational, and multisite aspects (11). Hence, *a priori*, one should not expect (except under limiting situations) naive cases of σ or φ_{m_2} congruence. Recent investigations (12–14, 17) have focussed attention on the multiconfigurational aspects of solvent adsorption. As long as site parity[1] is maintained among the various adsorbates including the solvent there is no need to distinguish between the multicomponent and multiconfiguration notions in modelling.

The basic principles in the microscopic modelling of adsorption at charged interfaces have been discussed in detail elsewhere (11, 14). Two important stages in such a modelling are those of the substrate description (cf. homogeneous/heterogeneous, order/disorder, etc.) and the representation of the adsorbate(s) configurations (orientational freedom, multicomponents etc). The simplest models in the hierarchy (*a*) stress on "the lattice" nature of the substrate and (*b*) postulate "a discrete" set of states for the adsorbate(s) — two (15), three (13, 16) or four (17) (ref. 14 for more details).[2] Where more than one adsorbing component is present in the interface, one may identify, on physicochemical grounds, some of the "states" with those of the solvent and the others with the "permitted configurations" of the adsorbates. The two- and three-state pictures outlined below (Sections 4 and 5) proceed on the above principles. For example in the two-state case, the solvent and the adsorbate are assumed to fill all the substrate sites (cf. if a void is to be permitted, the model becomes a "three-state" picture!).

It must be noted here that the classical Frumkin isotherm (4) for organic adsorption *in the presence of a solvent* can also be viewed as a two state version (an approximation of the lattice-gas (11)) *if one relegates the solvent to a continuum background* (ref. 11, Table 1, model A).[3] This obviously is not entirely molecular. A better representation of the solvent is desirable while analysing adsorption phenomena in the condensed phases and the *next* step is to permit *two* configurations for the polar solvent, thus resulting in a three-state model. The corresponding isotherm and other relationships are more complex than the two-state models but the reward is in achieving a more faithful representation of the phenomena!

In the context of adsorption of neutral molecules competing with solvents, multistate versions are not new in the scene — particular mention must be made of the so-called BDM (15) and BGM (16) models.

[1]We use the term "site-parity" to indicate that the several configurations of the same adsorbate or the many adsorbates need one site each of the underlying lattice. This is similar to (but not identical with) a mixture of hard cores of equal radii.

[2]See, in what follows, our comments on refs. 15 and 16.

[3]The fact that originally, the Frumkin isotherm was not based on any molecular model does not deter us from associating one at this stage!

Can. J. Chem. Downloaded from www.nrcresearchpress.com by 210.87.254.105 on 09/06/12
For personal use only.

The former (15) considers solvent adsorption as of two-state and consequently, *by implication*, the adsorption of organic compounds involves three-state (two-states are associated with the solvent and one-state with the organic compound). The latter (16) viz. BGM model is *apparently* a four-state version for adsorption (two each for the organic adsorbate and the solvent), but in reality, is concerned with *three states* (one state only for adsorbate) (ref. 16, Table 2 cases (I)–(V) and the condition $\Delta G_c^A \gg 0$ reducing effectively the permitted orientation of the adsorbate to one!). The analysis and the theory employed therein are not free from criticism and we shall revert to an examination of the BDM and BGM models elsewhere.

4. Results for Two State

We assume one state each for the solvent and the adsorbate. Under meanfield approximation, it can be shown that the isotherm is (Appendix A)

$$[5] \qquad \frac{\theta}{(1-\theta)} = \beta_0' c_{org} \times \exp\left[\Delta\alpha/2kT\left(\frac{c+b\sigma}{a_1+a_2\sigma}\right)^2\right]$$

where β_0' depends on the residual energy of the adsorbate ($U_r^{\uparrow}$) that of the solvent ($U_{r(0)}$) the standard chemical potential of the adsorbate (μ^0_{org}) that of the solvent (μ^0_{wat}) the dipole moment difference (ΔP) between the adsorbate and the solvent, and the polarisability difference ($\Delta\alpha$). c_{org} represents the concentration of the organic adsorbate relative to that of water. The various parameters in the eq. [2] are

$$[6] \qquad \beta_0' = \beta_0 \exp\left[-\Delta P^2/2\Delta\alpha kT\right]$$

$$[7] \qquad \beta_0 = \exp\left[(U_{r(0)} - U_r^{\uparrow} + \mu_{org}{}^0 - \mu_{wat}{}^0)/kT\right]$$

$$[8] \qquad \Delta P = P_{org} - P_0$$

$$[9] \qquad \Delta\alpha = \alpha_{org} - \alpha_0$$

$$[10] \qquad b = 4\pi$$

$$[11] \qquad c = \frac{c_e}{d^3} P_0 - a_1 \frac{\Delta P}{\Delta\alpha}$$

$$[12] \qquad a_1 = 1 + \frac{c_e}{d^3}\alpha_0$$

$$[13] \qquad a_2 = \frac{c_e}{d^3}\Delta\alpha$$

c_e is the coordination number, d is the nearest neighbour distance, P_0 and α_0 are the permanent dipole moment and the polarisability of the solvent respectively.

The relationship between φ_{m_2}, the potential drop across the inner layer and σ, the surface charge also follows as:

$$[14] \qquad \varphi_{m_2} = \frac{4\pi\sigma d}{\varepsilon} + \frac{4\pi N_T}{(a_1+a_2\theta)} \times \left[\Delta P\theta + P_0 - \Delta\alpha\theta\, 4\pi\sigma - \alpha_0 4\pi\sigma\right]$$

where N_T represents the number density of molecules and ε is the dielectric constant (non-orientational contributions)

Comparison with GSL

We note first that GSL hypothesis has phenomenological components like C_0, C_1, E_N and adjustable parameters like n, k. Before we compare our two-state model with GSL it is necessary to obtain molecular representations for such phenomenological components. This is done as follows: The surface charge σ can be written as (Appendix A)

$$[15] \qquad \sigma = \frac{(a_1+a_2\theta)\varphi_{m_2} - 4\pi N_T(\Delta P\theta + P_0)}{(4\pi/\varepsilon)[d(a_1+a_2\theta) - 4\pi N_T(\Delta\alpha\theta + \alpha_0)]}$$

The capacitances C_0 and C_1, defined as

$$[16] \qquad C_0 = \frac{\sigma}{\varphi_{m_2}(\theta=0) - \varphi_{m_2}(\theta=0, \sigma=0)}$$

and

$$[17] \qquad C_1 = \frac{\sigma}{\varphi_{m_2}(\theta=1) - \varphi_{m_2}(\theta=1, \sigma=0)}$$

can be shown to have the following expressions:

$$[18] \qquad C_0 = \frac{1}{4\pi[(d/\varepsilon) - 4\pi N_T\alpha_0/a_1\varepsilon]}$$

$$[19] \quad C_1 = \frac{1}{4\pi[(d/\varepsilon) - 4\pi N_T \alpha_{org}/(a_1 + a_2)\varepsilon]}$$

E_N, the shift of PZC from $\theta = 0$ to $\theta = 1$, can also be shown to be

$$[20] \quad E_N = \frac{4\pi N_T}{a_1} P_0 - \frac{4\pi N_T}{(a_1 + a_2)} P_{org}$$

A comparison of eqs. [4] and [15] indicates that the parameters n and k are written (from the two-state model) as

$$[21] \quad n = \frac{(a_1 + a_2)d - 4\pi N_T \alpha_{org}}{a_1 d - 4\pi N_T \alpha_0}$$

$$[22] \quad k = 1$$

The identification of GSL model with the two-state model is now complete.

The charge-potential equation [15] and the isotherm (eq. [5]) demonstrate how non-trivial consequences follow from even a simple physical representation like the one analysed in Section 4. Apart from obtaining a molecular justification for a particularised version viz $k = 1$ of the GSL equation [4], the two state model as presented here tells us (*a*) why congruence can fail (note the coupling between σ and θ in the r.h.s. of eq. [5]; also see ref. (18)), (*b*) how an inner layer dielectric constant that depends on σ and θ arises. We are also able to see how, as a special case, a pseudo-Frumkin isotherm can be realised with pseudo-interaction constant.

5. A Three-state Model and Comparison with the GSL

We assume here that the solvent has two orientations at the interface ("up" and "down") while the adsorbate has one orientation only. It can be shown in this case that (Appendix B)

$$[23] \quad \frac{R}{(1 - \theta)} = -\tanh\{K_1 + K_2\sigma + K_3 R + K_4\theta\}$$

where $R = (N^{\uparrow} - N^{\downarrow})/N_T$, $N^{\uparrow}$ and $N^{\downarrow}$ denote the number of solvent dipoles in the two orientations; K_1 depends on the difference in residual energies $(U_r^{\uparrow} - U_r^{\downarrow})$ of the two orientations. K_2, K_3, and K_4 are functions of dipole moment, polarisability, coordination number, nearest neighbour distance etc. (see Appendix B).

Writing $R/(1 - \theta) = \mathscr{R}$ an approximate equation for $\mathscr{R}$ is

$$[24] \quad \mathscr{R} \simeq -\tanh K_1 - [K_2\sigma + K_3(1 - \theta)\mathscr{R} + K_4\theta]\,\mathrm{sech}^2 K_1$$

Let us approximate $\mathscr{R}$ as

$$[24a] \quad \mathscr{R} \simeq Z_1 + Z_2\theta$$

where

$$[25] \quad Z_1 = Z_1^{\,0} + (4\pi\sigma/\varepsilon)K_R$$

$Z_1^{\,0}$ represents the value of Z_1 at $\sigma = 0$. The relationship between φ_{m_2} and σ in this case is

$$[25a] \quad \varphi_{m_2} = \frac{4\pi\sigma d}{\varepsilon} + \frac{4\pi N_T}{(a_1 + a_2\theta)}[P_w R + P_{org}\theta - \Delta\alpha\theta 4\pi\sigma - \alpha_0 4\pi\sigma]$$

$$[26] \quad = \frac{4\pi\sigma d}{\varepsilon} + \frac{4\pi N_T}{(a_1 + a_2\theta)}[P_w(Z_1 + Z_2\theta)(1 - \theta) + P_{org}\theta - \Delta\alpha\theta 4\pi\sigma/\varepsilon - \alpha_0 4\pi\sigma/\varepsilon]$$

As in the earlier description of the two-state model, the various phenomenological parameters can be defined consistently and identified with the molecular parameters in following way:

$$[27] \quad C_0 = \frac{a_1}{4\pi/\varepsilon[a_1 d + 4\pi N_T(P_w K_R - \alpha_0)]}$$

Can. J. Chem. Downloaded from www.nrcresearchpress.com by 210.87.254.105 on 09/06/12
For personal use only.

[28] $$C_1 = \frac{a_1 + a_2}{4\pi/\varepsilon[(a_1 + a_2)d - 4\pi N_T\alpha_{org}]}$$

[29] $$E_N = \frac{4\pi N_T}{a_1}P_w Z_1^0 - \frac{4\pi N_T}{(a_1 + a_2)}P_{org}$$

where P_w is the permanent dipole moment of water and K_R is defined in eq. [25].

[30] $$\varphi_{m_2} - \varphi_{m_2}(\theta = 0, \sigma = 0) = \frac{4\pi\sigma d}{\varepsilon} + \frac{4\pi N_T}{a_1}\left[P_w\frac{4\pi\sigma}{\varepsilon}K_R - \frac{4\pi\sigma}{\varepsilon}\alpha_0\right]$$

Now the surface charge σ can be written as

[31] $$\sigma = \frac{(a_1 + a_2\theta)\{\varphi_{m_2} - \varphi_{m_2}(\theta = 0, \sigma = 0)\} + (a_1 + a_2)\theta E_N\left[1 - \frac{P_w Z_2(1 - \theta)}{(a_1 + a_2)P_w Z_1^0/a_1 - P_{org}}\right]}{4\pi/\varepsilon[(a_1 + a_2\theta)d + 4\pi N_T\{(P_w K_R - \alpha_0)(1 - \theta) - \alpha_{org}\theta\}]}$$

Comparison of eqs. [4] and [31] shows that

[32] $$n = \frac{(a_1 + a_2)d - 4\pi N_T\alpha_{org}}{a_1 d + 4\pi N_T(P_w K_R - \alpha_0)}$$

or $$n = (a_1 + a_2)C_0/a_1 C_1$$

[33] $$k = 1 - \frac{Z_2}{(a_1 + a_2)Z_1^0/a_1 - P_{org}/P_w}$$

k can also be written in terms of E_N as

[34] $$k = 1 - \frac{Z_2 4\pi N_T P_w}{(a_1 + a_2)E_N}$$

Substitution of the expressions for C_0, C', E_N, n, and k in eq. [4] leads to eq. [26], thereby showing the complete analogy between this model and the GSL model. While the expression for C_1 remains the same in both two- and three-state models, that for C_0 is different in the two. This is a consequence of the assumption of one more "state" for solvent in the three-state model.

Let us recall that to obtain identity with the GSL model, we have used only an approximate version of eq. [23]. This means that the charge–potential relation appropriate to this three-state model is more general than the GSL. The first approximation of such a σ–E relation (not given here) leads to the GSL equation as a limit. We also note that k is no longer constrained to be equal to unity (can be, in principle even positive or negative) and that the deviation of k from unity is a measure of adsorbate–solvent interactions. This also serves to decide whether a two- or three-state model is desirable. The parameter Z_2 in eq. [26] is the coefficient of $\theta(1 - \theta)$ in the expression for R and is, thus, an index of strength of adsorbate–solvent interactions vis-à-vis ordering of solvent states.

6. Multisite Models

This differs from the two-state picture of Section 4 only in that the solvent and the adsorbate configurations are of different sizes. To be more specific, let us consider the solvent as a cluster occupying n lattice sites. The adsorbate occupies only one site as before. The total number of nearest neighbour interactions experienced by a cluster (17) is

[35] $$qc_e = nc_e - 2n + 2$$

The p.d. across the interface is

[36] $$\varphi_{m_2} = \frac{4\pi\sigma d}{\varepsilon} + 4\pi(M_m + M_c)$$

where M_m and M_c are the mean net dipole moments due to the adsorbate and the cluster respectively. Writing M_m and M_c in terms of reaction fields X_m (see ref. 17) and X_c

Can. J. Chem. Downloaded from www.nrcresearchpress.com by 210.87.254.105 on 09/06/12
For personal use only.

$$[37] \quad \varphi_{m_2} = \frac{4\pi\sigma d}{\varepsilon} + \frac{4\pi N_T}{(A + B\theta)}\{(d^3/c)P_{c1} + k'\theta + k''\theta^2 - E(k_1' + k_2'\theta + k_3'\theta^2)\}$$

where $P_{c1} = P_c q/n^2$; $\alpha_{c1} = \alpha_c q/n^2$; $\Delta P = P_m - P_{c1}$; $\Delta\alpha = \alpha_m - \alpha_{c1}$; P_c and α_c represent the permanent dipole moment and the polarisability of the solvent respectively. The other parameters are as follows:

$$[38] \quad A = (d^3/c_e)(q/n) + \alpha_{c1}q/n$$

$$[39] \quad B = (d^3/c_e) + \alpha_m - A$$

$$[40] \quad k_1' = A\alpha_{c1}n/q - \alpha_{c1}^2$$

$$[41] \quad k_2' = A\alpha_m - A\alpha_{c1}n/q - 2\Delta\alpha\alpha_{c1} + B\alpha_{c1}n/q$$

$$[42] \quad k_3' = B\alpha_m - B\alpha_{c1}n/q - \Delta\alpha^2$$

$$[43] \quad k' = BP_{c1}n/q - \Delta P\alpha_{c1} + AP_m - AP_{c1}n/q - P_{c1}\Delta\alpha$$

$$[44] \quad k'' = BP_m - \Delta P\alpha_m - BP_{c1}n/q + \Delta P\alpha_{c1}$$

From eq. [37]

$$[45] \quad \sigma = \frac{(A + B\theta)\varphi_{m_2} - 4\pi N_T[(d^3/c_e)P_{c1} + k'\theta + k''\theta^2]}{4\pi/\varepsilon[d(A + B\theta) - 4\pi N_T(k_1' + k_2'\theta + k_3'\theta^2)]}$$

We attempt a comparison with the GSL; in the usual manner n in GSL result can then be identified as

$$[46] \quad n(\text{GSL}) = \frac{d/(A + B) - 4\pi N_T(k_1' + k_2' + k_3')}{Ad - 4\pi N_T k_1'}$$

Also,

$$n = C_0(A + B)/C_1A$$

As in the earlier models, C_0, C_1, and E_N can be shown to have the following expressions:

$$[47] \quad C_0 = A/4\pi/\varepsilon[Ad - 4\pi N_T k_1']$$

$$[48] \quad C_1 = (A + B)/(4\pi/\varepsilon)[d(A + B) - 4\pi N_T(k_1' + k_2' + k_3')]$$

$$[49] \quad E_N = \frac{4\pi N_T d^3}{A \quad c_e} P_{c1} - \frac{4\pi N_T}{(A + B)} \times [(d^3/c)P_{c1} + k' + k'']$$

k in GSL can now be found:

$$[50] \quad k = \frac{B(d^3/C_e)P_{c1} - Ak'}{B(d^3/C_e)P_{c1} - A(k' + k'')}$$

The two-state site parity case discussed in Section 4 is a special case of the above treatment. Setting n in eq. [35] to 1, it follows from [35] that $q = 1$. Consequently $k'' = 0$ and k becomes unity, as has indeed been shown earlier (eq. [22]).

The σ–φ_{m_2} relationship [45] is more general than the empirical GSL (4), reducing the latter, at best, to a valid approximation.

Finally, it is not our aim in the above multi-site analysis to assert that the solvent state is always a cluster and is "larger" in size than the adsorbate. The above is only an illustration of possibilities. Other cases, including the four-state models of adsorption have been rigorously analysed and will be reported later.

7. Conclusions

We now turn back to the questions posed in the beginning of this paper (Section 1) and answer them.

(*a*) It is possible to relate a molecular basis for the GSL phenomenological equation. A simple two-state version with site parity leads to the GSL equation except that k is always unity, irrespective of the values chosen for energetics, dipole moments, polarisabilities, etc.! If site parity is relaxed the σ–φ_{m_2} expressions, more general than that of GSL, would follow. Similarly the three-state model leads to the GSL under some approximations. But in the case of the three-state, site-parity need not be relaxed.

(*b*) In all cases where the GSL result is derived from molecular considerations (as exact or approximate), the parameters n and k can be written explicitly in terms of molecular "constants" like the permanent dipole moment, polarisability, the size-ratio etc.

(*c*) As mentioned in the discussion above, the composition of (n, k) and their dependence on the energetic parameters reveal their close connection

Can. J. Chem. Downloaded from www.nrcresearchpress.com by 210.87.254.105 on 09/06/12
For personal use only.

Can. J. Chem. Downloaded from www.nrcresearchpress.com by 210.87.254.105 on 09/06/12
For personal use only.

with the adsorbate–solvent and adsorbate–adsorbate interactions etc. existing at the interface. It should be possible to use these to "classify" adsorbates.

(*d*) Higher-state versions unfold progressively the complex nature of the coupling that exists at the interface and in this process, even the GSL result is reduced to a mere approximation. Thus it is possible for us to look for proper relationships governing σ and φ_{m_2} *with justification*. We have already seen that both the two-state (without site-parity) and the three-state (site-parity) cases lead to the GSL result as approximations! Which model is nearer the "truth"? In our opinion, the issue is to be decided mostly by the appropriateness of parameters needed to obtain agreement with experiments.

We want to reiterate that it is necessary to couple such analysis with explicit molecular details (15, 16) like choosing values for P_{org}, P_{water}, α_{org}, α_{water} etc. More details on the models considered here and their generalisations along with their predictions and experimental fits will be reported in subsequent publications.

1. B. B. Damaskin. Elektrokhimiya, **6**, 1135 (1970).
2. B. B. Damaskin and A. V. Chizhov. Electrokhimiya, **6**, 1140 (1970).
3. B. B. Damaskin, A. Frumkin, and A. Chizhov. J. Electroanal. Chem. **28**, 93 (1970).
4. B. B. Damaskin, V. V. Batratov, and O. Petrii. Adsorption of organic compounds on electrodes. Plenum Press, New York. 1971.
5. S. Levine, G. M. Bell, and A. L. Smith. J. Phys. Chem. **73**, 3534 (1969).
6. S. Levine, K. Robinson, A. L. Smith, and A. C. Brett. Discuss. Faraday. Soc. **59**, 1133 (1975).
7. A. N. Frumkin. Z. Phys. **35**, 792 (1926).
8. R. S. Hansen, D. J. Kelsh, and D. H. Grantham. J. Phys. Chem. **67**, 2316 (1963).
9. R. Parsons. J. Electroanal. Chem. **7**, 136 (1964).
10. B. N. Afans'ev and B. B. Damaskin. Elektrokhimiya, **12**, 307 (1976).
11. S. K. Rangarajan. J. Electroanal. Chem. **82**, 93 (1977).
12. W. R. Fawcett. Isr. J. Chem. **18**, 3 (1979).
13. W. R. Fawcett. J. Phys. Chem. **82**, 1385 (1978).
14. S. K. Rangarajan. Specialist Periodical Reports, Electrochemistry, Vol. 7 The Chemical Society, London, 1980. Chapt. IV.
15. J. O'M. Bockris, M. A. V. Devanathan, and K. Muller. Proc. R. Soc. London. A**274**, 55 (1963).
16. J. O'M. Bockris, E. Gileadi, and K. Muller. Electrochim. Acta, **12**, 1301 (1967).
17. W. R. Fawcett, S. Levine, R. M. De Nobriga, and A. C. Mcdonald. J. Electroanal. Chem. **111**, 163 (1980).
18. S. K. Rangarajan. J. Electroanal Chem. **41**, 279 (1973); **41**, 283 (1973).
19. B. B. Damaskin, Yu. N. Kuryakov, and S. L. Dyatkina. Sov. Electrochem. **12**, 1462 (1976).

Appendix A

Two-state Model Isotherm

The analysis given here closely follows the one given in ref. 13 in a different context.

Let us assume that the electrode is covered by a hexagonally closepacked monolayer of solvent and adsorbate molecules. The total number density of molecules is N_T, the nearest neighbour distance is d and the effective co-ordination number is c_e

$$[A1] \quad N_T = N^{\uparrow} + N_0$$

where $N^{\uparrow}$ and N_0 denote the number densities of the adsorbate and the solvent respectively.

The field acting at any site due to its neighbours must be proportional to $(m_p + m_i)$ where m_p is the net polarisation per site due to permanent dipole moments and m_i that due to induced dipole moments. E is the field due to σ, the charge on the electrode.

$$[A2] \quad x = c_e/Ad^3[P_{org}\theta + P_0(1 - \theta) - qE]$$

$$[A3] \quad q = \alpha_{org}\theta + \alpha_0(1 - \theta)$$

$$[A4] \quad A = 1 + c_e q/d^3$$

The excess internal energy per unit area for dipoles at a charged surface may be written (13)

$$[A5] \quad U = \frac{N_T c_e}{2d^3}(m_p + m_i)^2 + \tfrac{1}{2}N^{\uparrow}\alpha_{org}(E + X)^2 + \tfrac{1}{2}N_0\alpha_0(E + X)^2 + N_T E(m_p + m_c) + N^{\uparrow}U_r^{\uparrow} + N_0 U_{r(0)} - \mu_{org}N^{\uparrow} - \mu_0 N_0$$

where μ_{org} and μ_0 represent the chemical potentials of the adsorbate and the solvent respectively.

Assuming random mixing of dipoles, the configurational entropy is given by

$$[A6] \quad S = -kN^{\uparrow}\ln(N^{\uparrow}/N_T) - kN_0\ln(N_0/N_T)$$

Since $F = U - TS$, the equilibrium condition can be derived from $(\partial F/\partial N^{\uparrow})_{N^{\uparrow}+N_0} = 0$.

$$[A7] \quad N^{\uparrow}/N_0 = \beta_0 c_{org}\exp\{[-2\Delta P(E + X) + \Delta\alpha(E + X)^2]/2kT\}$$

where c_{org} is the concentration of the adsorbate relative to that of water and β_0 has been defined in [9]. If $N^{\uparrow}/N_T$ is defined as θ and N_0/N_T as $(1 - \theta)$,

$$[A8] \quad \frac{\theta}{(1 - \theta)} = \beta_0' c_{org}\exp\left[\left(\frac{\Delta\alpha}{2kT}\right) \times \left(E + X - \frac{\Delta P}{\Delta\alpha}\right)^2\right]$$

It can be shown that

$$\left(E + X - \frac{\Delta P}{\Delta\alpha}\right) = \left(\frac{C + b\sigma}{a_1 + a_2\theta}\right)$$

Therefore the isotherm becomes

$$[A9] \quad \frac{\theta}{(1 - \theta)} = \beta_0' c_{org}\exp\left\{\frac{\Delta\alpha}{2kT}\left(\frac{c + b\sigma}{a_1 + a_2\theta}\right)^2\right\}$$

Can. J. Chem. Downloaded from www.nrcresearchpress.com by 210.87.254.105 on 09/06/12
For personal use only.

where all the parameters have been defined in eqs. [6]–[13]. The potential drop across the monolayer region is

$$[A10] \quad \varphi_{m_2} = \frac{4\pi\sigma d}{\varepsilon} + \frac{4\pi N_T d^3 X}{c_e}$$

Substituting [A2] in [A10],

$$[A11] \quad \varphi_{m_2} = \frac{4\pi\sigma}{\varepsilon(a_1 + a_2\theta)} [d(a_1 + a_2\theta) - 4\pi N_T(\Delta\alpha\theta + \alpha_0)] + \frac{4\pi N_T}{(a_1 + a_2\theta)} (\Delta P\theta + P_0)$$

Hence eq. [15] of the text follows.

Appendix B

A Three-state Model

Next in the hierarchy in modelling, the solvent is assumed to have two different configurations at the interface ("up" and "down"). The adsorbate has still only one configuration. The solvent and the adsorbate are considered as occupying only one site each.

Proceeding as in Appendix A,

$$[B1] \quad N^{\uparrow}/N^{\downarrow} = \exp\{[U_r^{\downarrow} - U_r^{\uparrow} - 2P_w(E + X)]/kT\}$$

P_w is the permanent dipole moment of the solvent; $N^{\uparrow}$ and $N^{\downarrow}$ denote respectively, the number of solvent molecules in the "up" and "down" orientation.

If R is defined as $R = (N^{\uparrow} - N^{\downarrow})/N_T$, it is easy to show that

$$[B2] \quad R = -(1 - \theta)\tanh\left\{\frac{1}{2kT}\left[U_r^{\uparrow} - U_r^{\downarrow} + \frac{2P_w}{A}\left(E + \frac{c_e}{d_3}\overline{P_w R + P_{org}\theta}\right)\right]\right\}$$

This can be written as

$$[B3] \quad R = -(1 - \theta)\tanh\{K_1 + K_2\sigma + K_3 R + K_4\theta\}$$

where

$$K_1 = \frac{U_r^{\uparrow} - U_r^{\downarrow}}{2kT}$$

$$K_2 = \frac{P_w 4\pi}{AkT\varepsilon}$$

$$K_3 = \frac{P_w P_w c_e}{Ad^3 kT}$$

$$K_4 = \frac{c_e P_{org} P_w}{Ad^3 kT}$$

The potential difference across the monolayer region is given as before, by

$$[B4] \quad \varphi_{m_2} = \frac{4\pi\sigma d}{\varepsilon} + \frac{4\pi N_T d^3 X}{c_e}$$

$$[B5] \quad = \frac{4\pi\sigma d}{\varepsilon} + \frac{4\pi N_T}{(a_1 + a_2\theta)}[P_w R + P_{org}\theta - \Delta\alpha\theta E - \alpha_0 E]$$

Writing $R/(1 - \theta)$ as $\mathscr{R}$ and approximating $\mathscr{R}$ as $\mathscr{R} \simeq Z_1 + Z_2\theta$ (see text for the definition of Z_1 and Z_2),

$$[B6] \quad \varphi_{m_2} = \frac{4\pi\sigma d}{\varepsilon} + \frac{4\pi N_T}{(a_1 + a_2\theta)}[P_w(Z_1 + Z_2\theta) \times (1 - \theta) + P_{org}\theta - \Delta\alpha\theta E - \alpha_0 E]$$

From eq. [B3]

$$[B7] \quad \mathscr{R} \simeq -\tanh K_1 - [K_2\sigma + K_3(1 - \theta)\mathscr{R} + K_4\theta]\,\mathrm{sech}^2 K_1$$

$$[B8] \quad \mathscr{R} \simeq \frac{-\tanh K_1}{1 + K_3\,\mathrm{sech}^2 K_1} - \frac{(K_2\sigma + K_4\theta)\,\mathrm{sech}^2 K_1}{1 + K_3\,\mathrm{sech}^2 K_1} = Z_1 + Z_2\theta$$

where

$$[B9] \quad Z_1 = -\frac{(\tanh K_1 + K_2\sigma\,\mathrm{sech}^2 K_1)}{1 + K_3\,\mathrm{sech}^2 K_1}$$

$$[B10] \quad Z_2 = -\frac{K_4\,\mathrm{sech}^2 K_1}{1 + K_3\,\mathrm{sech}^2 K_1}$$

Z_1 can be written as $Z_1^0 + (4\pi\sigma/\varepsilon)K_R$, where Z_1^0 is the value of Z_1 at $\sigma = 0$. Therefore

$$Z_1^0 = -\frac{\tanh K_1}{1 + K_3\,\mathrm{sech}^2 K_1}$$

$$K_R = \frac{K_2\,\mathrm{sech}^2 K_1}{1 + K_3\,\mathrm{sech}^2 K_1}\frac{\varepsilon}{4\pi}$$

Structural studies of the capsular polysaccharide from *Streptococcus pneumoniae* Type 12F

KARIN LEONTEIN, BENGT LINDBERG, AND JÖRGEN LÖNNGREN

Department of Organic Chemistry, Arrhenius Laboratory, University of Stockholm, S-106 91 Stockholm, Sweden

Received February 13, 1981

This paper is dedicated to Prof. Raymond U. Lemieux on the occasion of his 60th birthday

KARIN LEONTEIN, BENGT LINDBERG, and JÖRGEN LÖNNGREN. Can. J. Chem. **59**, 2081 (1981).

The capsular polysaccharide from *Streptococcus pneumoniae* type 12F is composed of D-glucosyl, D-galactosyl, 2-acetamido-2-deoxy-D-galactosyl, 2-acetamido-2,6-dideoxy-L-galactosyl, and 2-acetamido-2-deoxy-D-mannuronic acid residues in the proportions 2:1:1:1:1. The main structural evidence was adduced from nmr spectroscopy, methylation analysis, and specific degradations whereby it could be concluded that the polysaccharide is composed of hexasaccharide repeating-units having the structure:

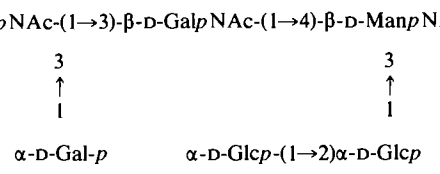

KARIN LEONTEIN, BENGT LINDBERG et JÖRGEN LÖNNGREN. Can. J. Chem. **59**, 2081 (1981).

Le polysaccharide capsulaire provenant du *Streptococcus pneumoniae* de type 12F se compose d'unités D-glucosyle, D-galactosyle, acétamido-2 déoxy-2-D-galactosyle, acétamido-2 didéoxy-2,6 L-galactosyle et acide acétamido-2 déoxy-2 D-mannuronique dans les proportions de 2:1:1:1:1. Les principales preuves de structure sont fournies par la spectroscopie de rmn, par l'analyse de la méthylation et par des dégradations spécifiques qui ont permis de conclure que le monomère du polysaccharide est un hexasaccharide ayant la structure suivante:

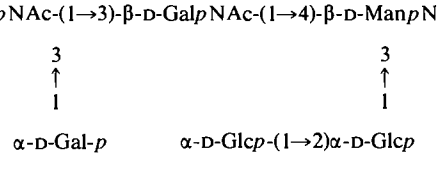

[Traduit par le journal]

Introduction

The capsular polysaccharide from *Streptococcus pneumoniae* type 12F (1) (previously called type 12) has been investigated by different groups (2–4). Sugar analyses revealed that it contains D-glucose, D-galactose, 2-amino-2,6-dideoxy-L-galactose, and 2-amino-2-deoxy-D-galactose in the proportions 2:1:1:1. Immunological and chemical studies showed the presence of terminal kojibiosyl (2-*O*-α-D-glucopyranosyl-D-glucopyranosyl) and α-D-galactopyranosyl groups. In agreement with these results, the polysaccharide was precipitated by concanavalin A. From the combined results it was suggested (4) that the polysaccharide is composed of pentasaccharide repeating-units in which kojibiose and D-galactose are linked to a backbone of amino sugar residues. We now report further structural studies on this polysaccharide, in the following called S 12F.

Results and Discussion

In our preliminary studies crude S 12F was purified by chromatography on a concanavalin A – Sepharose column (3). The purified samples contained the sugars listed above but also some 2-amino-2-deoxy-D-glucose, indicating that the material was not quite pure. As the structural studies gave results which were difficult to interpret, we eventually concluded that S 12F contains a further component. This was subsequently identified as 2-acetamido-2-deoxy-D-mannuronic acid (see below). Having established this, the material was purified by chromatography on a DEAE–Sepharose column. Only traces of 2-amino-2-deoxy-D-glucose were obtained on acid hydrolysis of this material, which showed $[\alpha]_{578}$ − 2°.

In the sugar analyses of S 12F and modified polysaccharides prepared from S 12F, the best yield of monomers was obtained when the hydrolysis was performed with 4 *M* hydrochloric acid at 100°C for 2 h. When the hydrolysate from S 12F was reduced with sodium borohydride, acetylated, and analysed by glc, the alditol acetates of D-glucose, D-galactose, 2-amino-2,6-dideoxy-L-ga-

0008-4042/81/142081-05$01.00/0

©1981 National Research Council of Canada/Conseil national de recherches du Canada

Can. J. Chem. Downloaded from www.nrcresearchpress.com by 210.87.254.105 on 09/06/12
For personal use only.

Can. J. Chem. Downloaded from www.nrcresearchpress.com by 210.87.254.105 on 09/06/12
For personal use only.

lactose, 2-amino-2-deoxy-D-galactose, and a further component were obtained in the proportions 1.9:1.0:0.9:1.2:0.6 (f.i. detector response). The latter component was identified as fully acetylated 1,5-dideoxy-1,5-imino-D-mannitol (**1**). The identification of **1** and its mode of formation will be discussed in a separate communication. When the hydrolysate was *N*-acetylated before the borohydride reduction, no **1** was formed but the alditol acetate of 2-amino-2-deoxy-D-mannose was obtained. The ratio between this component and 2-acetamido-2-deoxy-D-galactitol was 0.7. The results indicate that the hydrolysate contains a lactone of 2-amino-2-deoxy-mannuronic acid. The alditol acetates of 2-amino-2-deoxy-D-glucose, -D-galactose, and -D-mannose were well separated by glc on SP-1000 or SE-30 glass capillary columns. The absolute configurations of the amino sugars were established using the method of Gerwig *et al.* (5) and that of the neutral sugars using the method of Leontein *et al.* (6).

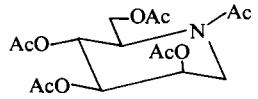

1

The presence of 2-amino-2-deoxy-D-mannuronic acid in the hydrolysate of S 12F was also indicated by paper electrophoresis in molybdate buffer at pH 5 (7). This acid is well separated from the *gluco*- and *galacto*-isomers in this system.

S 12F proved to be resistant to carboxyl reduction according to Taylor *et al.* (8). A product which had been subjected to several reductions yielded on acid hydrolysis only traces of 2-amino-2-deoxy-D-mannose. Modified S 12F, in which the side-chains had been selectively split off, (see below) was easier to reduce, and 2-amino-2-deoxy-D-mannose was identified in the hydrolysate of this material.

The ^{1}Hmr spectrum of S 12F showed, *inter alia*, signals for the methyl protons of the 2-acetamido-2,6-dideoxy-L-galactosyl residue at δ 1.24, $J_{5,6} \sim 5$ Hz (3H), for the methyl protons of three acetamido groups at δ 2.02 (s, 6H) and δ 2.14 (s, 3H), and for the anomeric protons at δ 5.26, $J_{1,2} \sim 2$ Hz (2H) and δ 5.42, $J_{1,2} \sim 2$ Hz (1H). The signals for the other anomeric protons, which were not well resolved, appeared at higher fields (δ < 5).

The ^{13}Cmr spectrum of S 12F showed, *inter alia*, signals for C-6 of the 2-acetamido-2,6-dideoxy-L-galactosyl residue at δ 17.9, for the methyl carbons of *N*-acetyl groups at δ 24.3 (3C), for C-2 of the three amino sugar residues at δ 50.5, 53.7, and 54.1, for unsubstituted C-6 of hexosyl residues at δ ≃ 63 (4C), for one anomeric carbon at δ 97.4, and for five anomeric carbons at δ ≃ 101.5 (not well resolved).

The above results, in conjunction with those from previous studies, indicate that S 12F is composed of hexasaccharide repeating-units, containing two residues of D-glucose and one residue each of D-galactose, 2-acetamido-2,6-dideoxy-L-galactose, 2-acetamido-2-deoxy-D-galactose, and 2-acetamido-2-deoxy-D-mannuronic acid. Further the ^{13}Cmr data also imply that all sugar residues are pyranosidic.

Methylation analysis of S 12F and analysis of the sugars as the alditol acetates (9, 10) (Table 1, column A) confirmed the presence of terminal D-glucopyranosyl and D-galactopyranosyl groups and of 2-linked D-glucopyranosyl residues. The analysis further demonstrated that the 2-acetamido-2,6-dideoxy-L-galactopyranosyl residue is linked through *O*-3 and *O*-4 and that the 2-acetamido-2-deoxy-D-galactopyranosyl residue is linked through *O*-3. No derivative of the 2-acetamido-2-deoxy-D-mannopyranosyluronic acid residue was obtained in this analysis. As the above ethers correspond to two terminals but only to one branching point, the latter sugar should also represent a branching point and be linked through *O*-3 and *O*-4, the only positions available.

The methylation analysis indicates that the D-glucose and D-galactose residues in S 12F, but not the amino sugar residues, should be oxidized by periodate. S 12F was therefore subjected to a Smith degradation (11), i.e. periodate oxidation, borohydride reduction, and mild acid hydrolysis. Methylation analysis of the product (Table 1, column B) showed that the 2-acetamido-2,6-dideoxy-L-galactopyranosyl residues are linked through *O*-4 and confirms that the 2-acetamido-2-deoxy-D-galactopyranosyl residues are linked through *O*-3. Carboxyl reduction of this material yielded a product $[\alpha]_{578}$ −36°, which on hydrolysis yielded 2-amino-2,6-dideoxy-L-galactose, 2-amino-2-deoxy-D-galactose and 2-amino-2-deoxy-D-mannose in the proportions 0.95:1.0:0.64. Nitrous acid deamination (12) of the hydrolysate and conversion of the products to alditol acetates yielded 2,5-anhydro-D-talitol, 2,5-anhydro-6-deoxy-L-talitol, and D-glucose. These compounds derive from D-galactosamine, L-fucosamine, and D-mannosamine, respectively (13). Methylation analysis (Table 1, column C) demonstrated that the 2-acetamido-2-deoxy-D-mannopyranosyluronic acid residue in the degraded product is linked through *O*-4. The amino sugars in S 12F consequently form a linear backbone and the side chains, D-galactopyranosyl and kojibiosyl groups, are linked to the 3-positions of the 2-acetamido-

Can. J. Chem. Downloaded from www.nrcresearchpress.com by 210.87.254.105 on 09/06/12
For personal use only.

TABLE 1. Methylation analyses of original and modified type S 12F capsular polysaccharides of *Streptococcus pneumoniae*

Methylated sugar[a]	T^b	Mol%[c] A	B	C	D
2,3,4,6-Glc	1	28	—	—	28
2,3,4,6-Gal	1.1	26	—	—	—
3,4,6-Glc	1.6	28	—	—	30
2,3-FucNAc	3.9	—	53	46	17
2-FucNAc	5.3	9	—	—	—
2,3,6-ManNAc	8.3	—	—	27	—
2,4,6-GalNAc	8.9	9	47	27	25

[a]2,3,4,6-Glc = 2,3,4,6-tetra-*O*-methyl-D-glucose, 2,3-FucNAc = 3-*O*-methyl-2-*N*-methylacetamido-2,6-dideoxy-L-galactose.
[b]Retention times of the corresponding alditol acetates relative to 1,5-di-*O*-acetyl-2,3,4,6-tetra-*O*-methyl-D-glucitol on an OV-17 column at 180°C.
[c]Polysaccharide: A, original; B, Smith degraded polysaccharide; C, Smith degraded and carboxyl-reduced polysaccharide; D, polysaccharide subjected to modified Smith degradation (see text).

2,6-dideoxy-L-galactopyranosyl and the 2-acetamido-2-deoxy-D-mannopyranosyluronic acid residues, respectively. In the ^{1}Hmr spectrum of the degraded product signals at δ 1.22 (3H), δ 2.02 (6H), and δ 2.10 (3H) confirmed the presence of one 6-deoxysugar and three *N*-acetyl groups. The three low-field signals for anomeric protons in the spectrum of unmodified S 12F had disappeared but the poorly resolved signals at higher fields (δ < 5) remained. This result therefore indicates that the D-glucopyranosyl and D-galactopyranosyl residues are α-linked. In the ^{13}Cmr the C-2 signals of the three acetamidosugars appeared at δ 52.1, 53.5, and 54.2. The anomeric carbons appeared at δ ≃ 101. The signal at δ 97.4 in the spectrum of unmodified S 12F most probably derives from the 2-substituted α-D-glucopyranosyl residue of the kojibiose side chain.

The product from the Smith degradation was carboxyl reduced, acetylated and treated with chromium trioxide in acetic acid (10, 14). The β-linked sugar residues should be oxidized but not the α-linked residues. Sugar analysis of the product showed that the 2-acetamido-2,6-dideoxy-L-galactopyranosyl residues had survived this treatment. These residues are consequently α-linked and the other sugar residues β-linked.

The terminal α-D-galactopyranosyl group with a pair of *cis*-oriented vicinal hydroxyl groups is oxidized more readily by periodate than the kojibiose residue. It was therefore possible to remove the α-D-galactopyranosyl group selectively by a Smith degradation, in which the periodate oxidation was performed under mild conditions. Methylation analysis of this material (Table 1, column D), showed that the α-D-galactopyranosyl group in the original S 12F is linked to *O*-3 of the 2-acetamido-2,6-dideoxy-L-galactopyranosyl residue. The results therefore demonstrate the presence of the structural elements **2**, **3**, and **4** in S 12F.

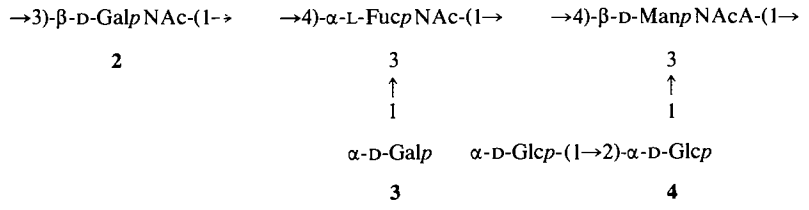

In order to establish the sequence of the three elements, S 12F was treated with liquid hydrogen fluoride. This reagent cleaves glycosidic linkages but leaves amide linkages intact (15). The hydrolysed product of S 12F contained D-glucose, D-galactose, and 2-acetamido-2,6-dideoxy-L-galactose as the only monomeric sugars. In addition an acidic disaccharide was isolated by gel filtration and ion exchange chromatography. Sugar analysis of this disaccharide revealed that it was not pure, but 2-acetamido-2-deoxy-D-galactose and 2-acetamido-2-deoxy-D-mannuronic acid (as **1**) were the main components.

The product was reduced with sodium borodeuteride, methylated, and investigated by glc–ms (16). The spectrum of the main component demonstrated that it derived from a pseudoaldobiouronic acid in which both the aldehyde group and the carboxyl group had been reduced. The material was hydrolysed and transformed into alditol acetates. 2-Deoxy-3,4,6-tri-*O*-methyl-2-*N*-methylacetamido-D-galactose and a 2-deoxy-3,5,6-tri-*O*-methyl-2-*N*-methylacetamido-D-mannitol, deuterium labelled at C-1 and C-6, were obtained. The latter compound was formed by demethylation of the corresponding 1-*O*-methyl ether during the hydrolysis (17). These results, in conjunction with other evidence discussed above, show that the pseudoaldobiouronic acid has structure **5** and the reduced

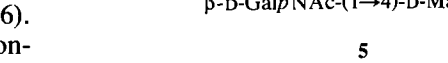

5

Can. J. Chem. Downloaded from www.nrcresearchpress.com by 210.87.254.105 on 09/06/12
For personal use only.

and methylated product structure **6**. (The origin of some pertinent fragments is indicated in the formula.) The identification of **5** defines the sequence of

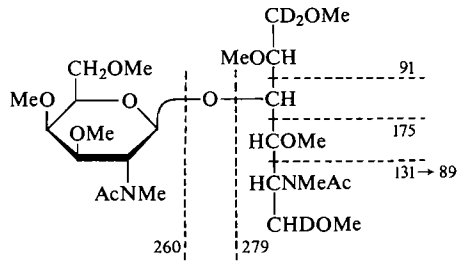

6

the sugar residues in S 12F, the hexasaccharide repeating unit of which has the structure **7**.

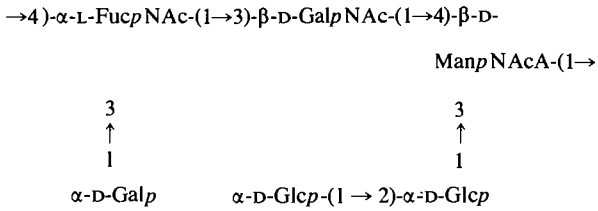

7

The capsular polysaccharide from *Haemophilus influenzae* type e, strain NCTC 8455, is composed of disaccharide repeating units (**8**) (18). The main

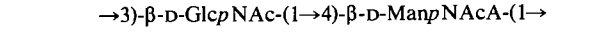

8

product formed on treatment of this polysaccharide with hydrogen fluoride, followed by aqueous acetic acid, reduction with sodium borodeuteride, and methylation, gave a mass spectrum which was superimposable with that of **6**. It thus has structure **9** and the only difference between this substance

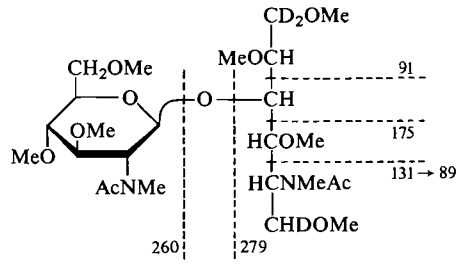

9

and **6** is that the glycosyl group has the D-*gluco* configuration in the former and the D-*galacto* configuration in the latter. The results are consequently analogous for the two polysaccharides. A pseudoaldobiouronic acid derivative is selectively formed on treatment with hydrogen fluoride. On treatment of this product with sodium borohydride, not only the aldehyde group but also the carboxyl group is reduced. These unexpected results merit further studies.

Experimental

For glc, Perkin-Elmer 990 or Hewlett-Packard 5830 A instruments equipped with flame-ionization detectors were used. Separations were performed on glass columns (180 × 0.15 cm, with 100/120 mesh Gas Chrom Q as support material) containing 3% OV-225 or 3% OV-17 (for alditol acetates, partially methylated alditol acetates, and oligosaccharide derivatives). Some separations of alditol acetates, silylated butyl glycosides (5), and acetylated octyl glycosides (6) were performed on SP-1000 or SE-30 glass capillary columns (0.25 mm × 25 m). The alditol acetates of 2-amino-2-deoxy-D-glucose, -D-mannose, and -D-galactose showed T = 3.3, 4.0, 3.9 (retention time relative to glucitol hexaacetate) and T = 1.8, 1.9, 2.0 on SP-1000 (230°C) and SE-30 (170°C) columns, respectively. The glc–ms measurements were performed with a Varian MAT 311-SS 100 ms-computer system fitted with the appropriate glc columns. For nmr a JEOL FX-100 instrument operated in the PFT-mode was used. The spectra were recorded in D_2O at 85°C. Chemical shifts are given in ppm relative to external tetramethylsilane (^{13}C) or internal sodium 1,1,2,2,3,3-hexadeuterio-4,4-dimethyl-4-silapentane-1-sulfonate (^1H), respectively. For treatment with hydrogen fluoride an apparatus (Type II) from Peninsula Laboratories, Inc., P.O. Box 1111, San Carlos, CA 94070, U.S.A. was used.

Purification of the Polysaccharide

Crude polysaccharide samples were obtained from Professor Michael Heidelberger (New York) and Dr D. J. Carlo (New Jersey). Crude material (80 mg) was dialysed, freeze-dried, and dissolved in water (72 mg, 3 mL), applied to a column (1.0 × 40 cm) of DEAE – Sepharose CL 6B and washed with water (200 mL), followed by a linear gradient of ammonium hydrogen carbonate (0–1 M). The separation was monitored with phenol – sulfuric acid assay. S 12F was eluted at a salt concentration of approximately 0.2 M and recovered by freeze-drying. The polysaccharide (66 mg) had $[\alpha]_{578}$ −2° (c 0.6, water) and contained only traces of sulphur and phosphorus.

Sugar and Methylation Analyses

Sugar analyses were performed by hydrolysis of polysaccharide samples (1 mg) for 2 h at 100°C with 4 M aqueous hydrochloric acid. The hydrolysate was concentrated to dryness and codistilled with methanol (3 × 3 mL). The sugars were then transformed into alditol acetates and analysed by glc (19) and glc–ms (20). The acetate of compound **1** showed T_{Glc} = 1.35 (retention time relative to glucitol hexaacetate on an OV-17 column at 180°C). The mass spectrum of this compound was superimposable on that of acetylated deoxynojirimycin (the *gluco*-analog of **1**, see ref 21), and showed, *inter alia*, peaks at *m/e* (relative intensities in brackets): 96(100), 110(12), 138(82), 152(19), 180(19), 198(12), 212(6), 240(16), 254(16), and 313(6). Sugar analysis including deamination was performed essentially as described elsewhere (12). Methylation analyses were performed as described elsewhere (9), except that the hydrolysis steps were performed as described above. Electrophoresis in molybdate buffer (pH 5.0) was performed as described by Mayer and Westphal (7). 2-Amino-2-deoxy-D-mannuronic acid showed M_{Man} = 0.79 (migration relative to mannitol), (lit. (7) M_{Man} = 0.78).

Can. J. Chem. Downloaded from www.nrcresearchpress.com by 210.87.254.105 on 09/06/12
For personal use only.

Carboxyl Reduction

Attempted carboxyl reduction of original S 12F and of Smith degraded S 12F (see below) was performed as described elsewhere (8) except that the reaction mixture was not heated during the treatment with sodium borohydride.

Smith Degradation of S 12F

S 12F (30 mg) was dissolved in 0.1 *M* sodium acetate buffer (pH 3.9, 24 mL), and sodium metaperiodate (350 mg) in the same buffer (8 mL) was added. The solution was kept in the dark at 6°C for 192 h. Excess of sodium metaperiodate was reduced by addition of ethylene glycol (2 mL), the mixture was dialysed and concentrated to 20 mL, and sodium borohydride (160 mg) was added. After stirring for 6 h at room temperature, excess of borohydride was decomposed by adding 50% acetic acid, and the solution was dialysed and freeze-dried (27 mg). Sugar analysis of part of the material (1 mg) showed that only trace amounts of D-galactose and D-glucose remained. The remaining material was hydrolysed under mild conditions (0.5 *M* trifluoroacetic acid, 8 h, room temperature), neutralized with 0.1 *M* sodium hydroxide, dialysed, and freeze-dried. The product (18 mg) showed $[\alpha]_{578}^{25}$ −33° (*c* 0.2, water). Part (2 mg) of the product was subjected to methylation analysis (Table 1, column B). Another part (10 mg) was subjected to carboxyl reduction (3 treatments). The carboxyl-reduced product (7 mg) showed $[\alpha]_{578}^{25}$ −36° (*c* 0.3, water). Part (2 mg) of this material was subjected to methylation analysis (Table 1, column C), part (1 mg) to sugar analysis (see text), and part (1 mg) to sugar analysis including deamination (see text). Another part (3 mg) was dissolved in formamide (4 mL) and acetylated using acetic anhydride (2 mL) and pyridine (2 mL). After work-up by dialysis and freeze-drying, the procedure was repeated once and the acetylated polysaccharide (3 mg) was subjected to chromium trioxide oxidation as described earlier (14). The oxidized material was subjected to sugar analysis; essentially all 2-amino-2,6-di-deoxy-L-galactose was recovered but only traces of 2-amino-2-deoxy-D-mannose and 2-amino-2-deoxy-D-galactose were detected.

Modified Smith Degradation

S 12F (32 mg) was dissolved in water (48 mL) and sodium metaperiodate (274 mg) in water (16 mL) was added. The solution was kept in the dark at 6°C for 1 h and processed as described above. Sugar analysis of the polyalcohol showed less than 15% of the original D-galactose remained. The modified polysaccharide (31 mg) recovered after mild acidic hydrolysis showed $[\alpha]_{578}$ −26° (*c* 0.4, water). A sample (2 mg) was subjected to methylation analysis (Table 1, column D).

Treatment of S 12F with Hydrogen Fluoride

S 12F (30 mg) was treated with liquid hydrogen fluoride (6 mL). After 1 h at room temperature the hydrogen fluoride was evaporated at reduced pressure and the residue was treated with 5% aqueous acetic acid for 16 h at room temperature. The solution was concentrated to dryness and the monomeric sugars were analysed by sodium borohydride reduction, acetylation, and glc. The product was fractionated on a column of Sephadex G-15 (1.5 × 60 cm) and eluted with water. The material eluted in the disaccharide region was further enriched on a DEAE – Sepharose CL 6B column (1.0 × 20 cm) which was irrigated first with water and then with 0.5 *M* ammonium hydrogen carbonate. Part (~2 mg) of this material was used for sugar analysis.

Another sample (20 mg) of S 12F was treated in the same manner with liquid hydrogen fluoride and aqueous acetic acid. The product was reduced with sodium borodeuteride and methylated. Compound **6** showed $T_{\text{Chitobiitol}}$ = 1.01 (retention time relative to methylated chitobiitol on an OV-17 column at 230°C). The mass spectrum of this compound showed, *inter alia*, peaks at *m/e* (relative intensities in brackets and some assignments (16) in square brackets): 89(100), 91(22), 101(80), 129(57) [H], 131(51), 175(19), 228(35) [aA_2], 260(42) [aA_1], 279(40) [bA_1]. The degradation and analysis of *Haemophilus influenzae* type e polysaccharide was performed as described above for S 12F. Compound **9** showed $T_{\text{Chitobiitol}}$ = 0.91.

Acknowledgments

We thank Professor Michael Heidelberger for his interest, and, together with Dr. D. J. Carlo, for generous gifts of polysaccharide material. Professor Hans Paulsen kindly supplied a sample of deoxynojirimycin. The expert assistance of Miss Viveka Eriksson and Mrs. Helena Liedgren is gratefully acknowledged. This work was supported by grants from the Swedish Natural Science Research Council, The Swedish Medical Research Council (B79-03X-02522-11C), and Stiftelsen Sigurd och Elsa Goljes Minne.

1. F. KAUFFMAN, E. LUND, and B. E. EDDY. Int. Bull. Bacteriol. Nomencl. Taxon. **10**, 30 (1960).
2. J. A. CIFONELLI, P. REBERS, M. P. PERRY, and J. K. N. JONES. Biochemistry, **5**, 3066 (1966).
3. I. J. GOLDSTEIN, J. A. CIFONELLI, and J. L. DUKE. Biochemistry, **13**, 867 (1974).
4. J. L. DUKE, I. J. GOLDSTEIN, and J. A. CIFONELLI. Carbohydr. Res. **37**, 81 (1974).
5. G. J. GERWIG, J. P. KAMERLING, and J. F. G. VLIEGENTHART. Carbohydr. Res. **77**, 1 (1979).
6. K. LEONTEIN, B. LINDBERG, and J. LÖNNGREN. Carbohydr. Res. **62**, 359 (1978).
7. H. MAYER and O. WESTPHAL. J. Chromatogr. **33**, 514 (1968).
8. R. L. TAYLOR, J. E. SHIVELY, and H. E. CONRAD. Methods Carbohydr. Chem. **7**, 149 (1976).
9. P.-E. JANSSON, L. KENNE, H. LIEDGREN, B. LINDBERG, and J. LÖNNGREN. Chem. Commun. Univ. Stockholm, **8** (1976).
10. B. LINDBERG and J. LÖNNGREN. Methods Enzymol. C, **50**, 3 (1978).
11. I. J. GOLDSTEIN, G. W. HAY, B. A. LEWIS, and F. SMITH. Methods Carbohydr. Chem. **5**, 361 (1965).
12. B. LINDBERG, J. LÖNNGREN, and D. A. POWELL. Carbohydr. Res. **58**, 177 (1977).
13. J. M. WILLIAMS. Adv. Carbohydr. Chem. **31**, 9 (1975).
14. J. HOFFMAN, B. LINDBERG, and S. SVENSSON. Acta Chem. Scand. **26**, 661 (1972).
15. A. J. MORT and D. T. A. LAMPORT. Anal. Biochem. **82**, 289 (1977).
16. J. LÖNNGREN and S. SVENSSON. Adv. Carbohydr. Chem. Biochem. **29**, 41 (1974).
17. M. CAROFF and L. SZABÓ. Carbohydr. Res. **84**, 43 (1980).
18. P. BRANEFORS-HELANDER, L. KENNE, B. LINDBERG, K. PETERSSON, and P. UNGER. Carbohydr. Res. **88**, 77 (1981).
19. J. S. SAWARDEKER, J. H. SLONEKER, and A. R. JEANES. Anal. Chem. **37**, 1602 (1965).
20. L. S. GOLOVKINA, O. S. CHIZHOV, and N. S. WULFSON. Bull. Acad. Sci. USSR, Div. Chem. Sci. **11**, 1853 (1966).
21. S. INOUYE, T. TSURUOKA, T. ITO, and T. NIIDA. Tetrahedron, **23**, 2125 (1968).

The synthesis and characterization of α- and β-L-fucopyranosyl phosphates and GDP fucose[1]

HERNAN A. NUNEZ, JOHN V. O'CONNOR,[2] PAUL R. ROSEVEAR, AND ROBERT BARKER[3]

Department of Biochemistry, Michigan State University, East Lansing, MI 48824, U.S.A.

Received November 25, 1980

HERNAN A. NUNEZ, JOHN V. O'CONNOR, PAUL R. ROSEVEAR, and ROBERT BARKER. Can. J. Chem. **59**, 2086 (1981).

Guanosine diphosphate fucose (GDPFuc) has been synthesized chemically in an overall yield of 40% from fucose. This synthesis was made possible by increasing the yield of the key intermediate, β-L-fucopyranosyl phosphate, five-fold over that previously reported (Prihar and Behrman. Biochemistry, **12**, 997 (1973)), by utilizing guanosine 5′-phosphoric di-*n*-butylphosphinothioic anhydride (Furusawa *et al.* J. Chem. Soc. Perkin Trans I, 171 (1976)) or GMP morpholdate for the synthesis of GDPFuc, and by improving the method of isolating intermediates and the final product. At pH 3, GDPFuc is degraded to GDP with a half-life of 7 h at 37°C and 52 h at 4°C. At pH values between 5 and 8, less than 10% is degraded after 7 days. Neither 20 m*M* Mn^{2+} nor Mg^{2+} in 0.2 *M* PIPES buffer at pH 7.5 stimulate the hydrolysis of GDPFuc. Heteronuclear, C–P and H–P coupling constants indicate that the preferential position of the phosphate moiety in both β-L-fucopyranosyl phosphate and GDPFuc is *trans* to C-2. In the ribose moiety of GDPFuc, the 5′-phosphate is *trans* to C-4. The ^1H and ^{13}C nmr parameters of intermediates and products are reported.

HERNAN A. NUNEZ, JOHN V. O'CONNOR, PAUL R. ROSEVEAR et ROBERT BARKER. Can. J. Chem. **59**, 2086 (1981).

On a synthétisé chimiquement le fucose diphosphate de guanosine (FucDPG) avec un rendement global de 40% à partir du fucose. Cette synthèse a pu être réalisée en préparant l'intermédiaire principal, le phosphate de β-L-fucopyrannosyle, avec un rendement 5 fois supérieur à celui obtenu antérieurement (Prichar et Behrmann. Biochemistry, **12**, 997 (1973)); pour parvenir à cette fin, on utilise soit l'anhydride mixte de l'acide guanosine phosphorique-5′ et de la di-*n*-butylphosphinothioique (Furusawa *et al.* J. Chem. Soc. Perkin Trans. I, 171, (1976)) ou le morpholybdate de GMP pour la synthèse du FucDPG, et on améliore le mode de séparation des intermédiaires et du produit final. A un pH de 3, le FucDPG se dégrade en DPG dont la demi-vie est de 7 h à 37°C et de 52 h à 4°C. A des pH entre 5 et 8 moins de 10% du produit se dégrade après 7 jours. Ni le MN^{2+} à 20 m*M*, ni le Mg^{2+} dans un tampon de PIPES à 0,2 *M* à pH 7,5 ne stimule l'hydrolyse du FucDPG. Les constantes de couplage hétéronucléaire C–P et H–P indiquent que la position préférentielle de la portion phosphate dans le β-L-fucopyrannosyle et le FucDPG est celle où elle est *trans* par rapport à C-2. Dans la portion ribose du FucDPG, le phosphate-5′ est *trans* par rapport à C-4. On rapporte les donnés de la rmn du ^1H et du ^{13}C des intermédiaires et des produits.

[Traduit par le journal]

Introduction

Guanosine diphosphate fucose (GDPFuc)[4] is the substrate for the fucosyl transferases involved in the biosynthesis of blood group substances and other tissue antigens. The study of these important enzymes is limited by the lack of GDPFuc which is available commercially only in a radioactive form of relatively high specific activity. Previously GDPFuc has been synthesized enzymatically by two different methods. Starting with L-fucose, Heath and co-workers (1–3) described a synthesis using fucokinase and ATP to phosphorylate fucose yielding β-L-fucopyranosyl phosphate which, with guanosine triphosphate pyrophosphorylase and GTP, produces GDPFuc and inorganic pyrophosphate. Ginsburg (4) used an enzyme that reduces the C6 hydroxymethyl of GDPMan to a methyl group, and epimerizes the C3 and C5 positions to convert the α-D-mannopyranosyl moiety to a β-L-fucopyranosyl moiety. Although the enzymatic methods are efficient, purification of the enzymes is difficult. Only small amounts of GDPFuc have been prepared and the products have not been fully characterized.

The chemical synthesis of many nucleotide diphosphate sugars has been achieved by condensation of an activated nucleoside monophosphate and the appropriate glycosyl phosphate (5). However, chemical synthesis of GDPFuc has not been described, probably because β-L-fucopyranosyl phosphate is difficult to prepare and is much more acid labile than most glycosyl phosphates (6).

Behrman and co-workers have reported the synthesis of β-L-fucopyranosyl phosphate in 10% yield from L-fucose by condensation of 2,3,4-tri-*o*-acetyl-β-fucopyranose with *o*-phenylene-

[1]Supported in part by a grant from the Institute of General Medical Sciences (GM21731), National Institutes of Health, Bethesda, MD.

[2]Current address: Department of Biological Chemistry, Hershey Medical Center, Hershey, PA 17033, U.S.A.

[3]To whom correspondence should be addressed at the Division of Biological Sciences, Cornell University, Ithaca, NY 14853, U.S.A.

[4]Abbreviations used: ^{13}C nmr, ^{13}C nuclear magnetic resonance spectroscopy; ^1H nmr, ^1H nuclear magnetic resonance spectroscopy; GDPFuc, guanosine diphosphate fucose; GDPMan, guanosine diphosphate mannose; GDP, guanosine 5′-diphosphate; GMP, guanosine 5′-monophosphate; GTP, guanosine 5′-triphosphate; glc, gas liquid chromatography; hplc, high pressure liquid chromatography; tlc, thin layer chromatography; TEAB, triethylammonium bicarbonate.

0008-4042/81/142086-10$01.00/0

©1981 National Research Council of Canada/Conseil national de recherches du Canada

Can. J. Chem. Downloaded from www.nrcresearchpress.com by 210.87.254.40 on 09/06/12
For personal use only.

Can. J. Chem. Downloaded from www.nrcresearchpress.com by 210.87.254.40 on 09/06/12
For personal use only.

phosphochloridate (7) and in 20% yield from L-fucose orthoacetates (8). Khwaja and Reese (9, 10) and Khwaja *et al.* (11), who developed the phosphorylating reagent used by Prihar and Behrman (7), reported much higher yields of other phosphates that are at least as labile as fucopyranosyl phosphate. Prihar and Behrman (7) used Br_2–H_2O to oxidize the phosphodiester although Khwaja *et al.* (11) had suggested four additional ways of removing the protecting group: hydrogenolysis, periodic acid oxidation, hydrolysis with snake venom phosphodiesterase, and lead tetraacetate oxidation. With the possible exception of periodic acid, these reagents are milder than Br_2–H_2O.

Shibaev *et al.* (12, 13) reported the synthesis of β-L-rhamnopyranosyl phosphate (6-deoxy-β-L-mannopyranosyl phosphate) and 4,6-dideoxy-α- and β-L-lyxopyranosyl phosphate in 50–70% yields using lead tetraacetate to oxidize the *o*-phenylene group. These compounds, especially the *rhamno*-derivative, should be as labile as the *fuco*-derivative because of the methyl group at C6 and the axial hydroxyl group at C2.

In this paper, we describe improved methods for the preparation of β-L-fucopyranosyl phosphate, and from it, of GDPFuc in 40 percent overall yield based on L-fucose. The method is as efficient as the enzymatic methods and is suitable for the preparation of millimolar amounts and for the preparation of isotopically enriched products.

Experimental

GMP and L-fucose were purchased from Sigma, (1-^{14}C)-L-fucose was purchased from New England Nuclear, and *o*-phenylene phosphochloridate was purchased from Aldrich. Silver carbonate was prepared by the method of McCloskey and Coleman (14). Freshly prepared silver carbonate can be kept, in the dark, as a dispersion in the reaction mixture for several hours. Immediately before use, a portion is removed with a wide-bore pipet and filtered on a sintered glass filter in a darkened area. The precipitate is washed on the filter with acetone until, on air drying, it gives a bright yellow powder. This powder forms a fine dipersion when added to reaction mixtures. Di-*n*-butylphosphinothioyl bromide was prepared by the method of Furusawa *et al.* (15), and used immediately. Guanosine 5′-phosphoromorpholidate was prepared according to Moffat (5). All other reagents were ACS Reagent grade or better. Pyridine was boiled under reflux over calcium hydride, distilled, and stored over calcium hydride. Molecular sieves (4 Å, Fisher Scientific) were added to tetrahydrofuran at least 12 h prior to its use in the phosphorylation step.

Thin layer chromatography was performed on Silica gel G plates (250 μM Fisher Scientific). The plates were developed with hexane–ethylacetate (1:1, v/v) and spots were detected by spraying with 2 *N* sulfuric acid and charring. Gas chromatography separations were performed on a 2 m × 3 mm id glass column of HiEFF-3CP (10% on Gas-Chrom Q, 80–100 mesh, Applied Science Laboratories, Inc.). Tetramethylsilyl derivatives of samples were prepared with the standard mixture used by Sweeley *et al.* (16) (hexamethyldisilazene–trimethylchlorosilane–pyridine, 4:1:10, v/v/v). High pressure liquid chromatography was performed on a Partisil-10 SAX column (4.6 mm × 2.5 cm, Anspec, Inc.) in 0.2 *M* potassium phosphate, pH 3.4, at 500 psi.

Paper electrophoresis was performed on Whatman 40 paper in 0.05 *M* TEAB, pH 7.5, for 50 min at 43 V/cm. Picric acid and caffeine were used as standards.

The ^{13}C nmr spectra were obtained on a Bruker WP-60, equipped for Fourier transform operation with quatrature detection, operating at 15.08 MHz, a sweep width of 3000 Hz with 4096 data points and broad band proton decoupling. Probe temperature was 38° ± 1°C. Resonances are reported in ppm from tetramethylsilane. The ^{1}H nmr spectra were obtained either on a Varian HA-100 or on a Bruker WH-180 equipped for Fourier transform operation using sweep width of 1800 Hz and 16K data points. Chemical shifts in D_2O are reported in ppm downfield from internal sodium 3-(trimethylsilyl)-1-propanesulfonate; in deuterochloroform from TMS.

L-Fucopyranosyl Tetraacetates (I)

L-Fucose (5 g, 30.5 mmol) was dissolved in 50 mL of dry pyridine, 35 mL acetic anhydride was added, and the reaction mixture was stored at 4°C for 12 h, at which time 9 mL of water was added. After the reaction mixture was cool (1 h), the volume was reduced to 40 mL *in vacuo* at 40°C and 200 mL of water was added. The solution was extracted with four 100-mL portions of chloroform. The combined chloroform washings were extracted three times with 100 mL of cold 2 *N* H_2SO_4 until the water layer was strongly acidic, and then twice with 100 mL of cold saturated $NaHCO_3$, and once with 100 mL of water. The chloroform layer was dried over calcium chloride for 2 h and evaporated to a thick syrup (11 g, 100%). The tetraacetate gives one spot, R_f = 0.8 on tlc; glc using a temperature program of 180–240°C at 4°/min shows two components corresponding to α:β pyranosyl acetates in the ratio 3:1.

2,3,4-Tri-O-acetyl-α-L-fucopyranosyl Bromide (II)

To a stirred solution of a mixture of α- and β-fucopyranosylacetates (5 g, 15.05 mmol) dissolved in 10 mL of glacial acetic acid, 15 mL of 31–32% HBr in glacial acetic acid was added at 22°C. Stirring was continued for 20 min and then the straw-colored solution was dissolved in 100 mL dichloromethane and extracted twice with 100 mL ice water, with 100 mL of cold 1 *M* $NaHCO_3$, and again with 100 mL of water. The organic layer was dried over powdered anhydrous sodium sulfate for 2 h, filtered, and evaporated *in vacuo* to a light yellow syrup which was stored in a vacuum desiccator over P_2O_5. The yield is essentially quantitative (5.2 g, 14.7 mmol). On tlc, the product gives a single spot R_f = 0.88. The ^{13}C nmr spectrum of the syrup in deuterochloroform has a resonance at 89.8 ppm in the anomeric region corresponding to C1 of α-L-fucopyranosyl bromide.

2,3,4-Tri-O-acetyl-α- and β-L-fucopyranoses (III)

The syrupy acetobromofucose (5.0 g, 14.1 mmol) was dissolved in 27 mL of acetone containing 0.7 mL of water and the solution was cooled to 0°C. Freshly prepared silver carbonate (4 g, 14.5 mmol) was added. The reaction was stirred vigorously for 15 min in the dark, filtered through a sintered glass funnel, washed with acetone, and the combined filtrate and washings evaporated to a syrup (4.4 g, 100%). At this stage more than 95% of the mixture is the β-anomer as determined by glc of the TMS derivatives and by ^{13}C nmr spectroscopy. Separation of the anomers is not necessary for the phosphorylation step since the α and β phosphates can be separated as indicated below. Drying

Can. J. Chem. Downloaded from www.nrcresearchpress.com by 210.87.254.40 on 09/06/12
For personal use only.

TABLE 1. ^{1}H nmr parameters for the intermediates in the synthesis of GDPFuc

Compound	Chemical shifts (ppm) H1	H2	H3	H4	H5	H6	Acetyl	OH
2,3,4-Tri-*O*-acetyl-α-L-fucopyranose[a]	5.33	5.31	5.01	5.18	4.31	1.12	1.95, 2.05, 2.12	3.67
2,3,4-Tri-*O*-acetyl-β-L-fucopyranose[a]	4.59	4.95	4.96	5.14	3.79	1.2	1.95, 2.04, 2.14	3.93
α-L-Fucopyranosyl phosphate[b,c]	5.435	3.721	3.932	3.841	4.270	1.200		
β-L-Fucopyranosyl phosphate[b,c]	4.865	3.548	3.716	3.784	3.843	1.282		
GDP β-L-fucose:[d]								
Guanosine	8.10							
Ribosyl moiety	5.96		4.561	4.374	4.222	4.222[e]		
Fucosyl moiety	4.845				3.745	1.23		

Compound	Coupling constants (Hz) H1–H2	H2–H3	H3–H4	H4–H5	H5–H6	H, OH	P–H1	P–H2	P–H5′
2,3,4-Tri-*O*-acetyl-α-L-fucopyranose	3.5	10.5	3.5	1.0	6.5	3.5			
2,3,4-Tri-*O*-acetyl-β-L-fucopyranose	8.4	8.4	2.0	0.8	6.5	8.8			
α-L-Fucopyranosyl phosphate[c]	3.7	10	3.2	1.0	6.7		7.4	2.6	
β-L-Fucopyranosyl phosphate[c]	7.7	9.8	3.3	1.1	6.6		7.7	0	
GDPFuc:[d]									
Ribosyl moiety	7.6	3.3	5.3						
Fucosyl moiety	7.7			0.8	6.8			0	

[a]Spectra were obtained on a Varian HA-100; chemical shifts are accurate to ±0.1 ppm, coupling constants ±0.5 Hz.
[b]Spectra were obtained on a Bruker WH-180; chemical shifts are accurate to ±0.005 ppm and coupling constants to ±0.1 Hz.
[c]At pH 4.0.
[d]At pH 7.0
[e]"H5" of ribose moiety.

is, however, necessary prior to phosphorylation. To obtain high yields of the β phosphate the syrup should be dried *in vacuo* over P_2O_5 for no longer than 3 h at 22°C. Drying for 24 h gives a mixture containing up to 50% of the α-anomer.

For characterization, the anomeric triacetates were separated by fractional crystallization. The β-anomer was obtained by dissolving the syrup (10 g) in dry diethyl ether (12 mL) and storing the solution at 4°C for 4 h. The crystals were separated by filtration, washed with dry ether, and dried in a desiccator over P_2O_5; mp 121°C; $[\alpha]_{578}^{22}$ −16.8° ± 0.5 (*c* 1, dry ethanol); Prihar and Behrman (7) reported $[\alpha]_D^{22}$ −5.8° for the anomer obtained by this method.

The filtrate from the β-anomer, containing approximately equal amounts of the α- and β-anomers, was treated with a trace of water and stored in a hood for a week. Trituration of the residual syrup with ether and cooling at 6°C for 12 h gave the crystalline 2,3,4-tri-*O*-acetyl-α-L-fucopyranose; mp 103°C; $[\alpha]_{578}^{22}$ −125° ± 1; (*c* 1, dry ethanol); Prihar and Behrman (7) reported $[\alpha]_D^{22}$ −118°; nmr parameters of both anomers are listed in Tables 1 and 2.

α- and β-L-Fucopyranosyl Phosphates (IV)

The 2,3,4-tri-*O*-acetyl-α- and β-fucopyranoses (3 g, 10.3 mmol) dried for no more than 3 h *in vacuo* over P_2O_5 were dissolved in 80 mL of dry tetrahydrofuran. The solution was added gradually (5 min) under anhydrous conditions to a stirred and efficiently cooled (0°C) solution of *o*-phenylene phosphochloridate (freshly distilled at 110°C and 5 Torr; 6.0 g, 32 mmol) and 5 mL of dry *s*-collidine in 100 mL of dry tetrahydrofuran (6, 10). After the addition was complete, stirring was continued for 30 min at 0°C and then the collidinium chloride was removed rapidly by filtration on a sintered glass funnel. Water (1.24 mL) and collidine (5 mL) were added to the cold filtrate. After stirring for 30 min at 22°C, the reaction mixture was cooled to 0°C and filtered. The tetrahydrofuran was removed *in vacuo*. If additional precipitate formed during this manipulation, the mixture was taken up in dry tetrahydrofuran and filtered. After removal of tetrahydrofuran, the residual syrup was dried over magnesium perchlorate under high vacuum for 12 h. The syrup was dissolved in 80 mL of dry dioxane and cooled to 12°C. Lead tetraacetate (13.0 g, 30 mmol) was added with vigorous stirring. The dark brown solution was stirred at 22°C for 30 min and then tested for the presence of lead tetraacetate using a qualitative starch–iodide test. If the test was negative, an additional 1 g of lead tetraacetate was added. After a positive lead tetraacetate reaction had been obtained for 30 min, the solution was added dropwise with stirring to 300 mL of cold 1 *N* NaOH (300 mequiv.) and the reaction mixture stored at 22°C for 2 h. The

Can. J. Chem. Downloaded from www.nrcresearchpress.com by 210.87.254.40 on 09/06/12
For personal use only.

TABLE 2. ^{13}C nmr parameters[a] for the intermediates in the synthesis of GDPFuc

	Chemical shifts ppm						Coupling constants Hz					
Compound	C1	C2	C3	C4	C5	C6	Methyl	Carbonyl	P–C1	P–C2	P–C4′	P–C5′
2,3,4,-Tri-*O*-acetyl-α-L-fucopyranosyl bromide	89.8	68.3	69.9	69.9	67.7	15.3	20.3	170.0 169.7 169.4				
2,3,4-Tri-*O*-acetyl-α-L-fucopyranose	90.4	67.9	68.6	71.1	64.2	15.9						
2,3,4-Tri-*O*-acetyl-β-L-fucopyranose	95.6	70.4	71.2	69.4	71.5	16	20.6	170.3	20.9		170.7	171.1
α-L-Fucopyranosyl phosphate[b]	96.5	69.6	70.9	73.3	69	16.7			6.6	8.8		
β-L-Fucopyranosyl phosphate[b]	99.4	75.8	74.1	72.8	72.8	17.0			3.7	6.0[c]		
GDP β-L-Fucose:[d]												
Guanosine	138.7[e]	155.3		152.8	117.3	160.1					8.8	5.2
Ribosyl moiety	88.2	75.3	71.8	84.9	66.6							
Fucosyl moiety	99.8	70.9	74.1	72.9	72.9	16.9			3.8	8.0[c]		

[a]Chemical shifts are accurate to ±0.1 ppm; coupling constants ±0.7 Hz.
[b]At pH 4.0.
[c]Cannot be determined due to overlapping resonances of C2, C4, and C5.
[d]At pH 7.0.
[e]C8.

Can. J. Chem. Downloaded from www.nrcresearchpress.com by 210.87.254.40 on 09/06/12
For personal use only.

light-brown reaction mixture was cooled in an ice bath, and adjusted to pH 4 with Dowex 50 H^+ (20–50 mesh). The mixture was filtered on a coarse sintered glass funnel and the filtrate adjusted immediately to pH 7.5 with 1 *N* NaOH. The resin was transferred to a beaker, 100 mL of water added, and the mixture sitrred and adjusted to pH 4 with Dowex 50 (H^+) if necessary. The mixture was filtered and the filtrate adjusted to pH 7.5 with 1 *N* NaOH. The combined filtrates were centrifuged for 20 min at 20 000 g. The supernatant, obtained by decantation, was diluted to 4 L with water and applied to a Dowex 1-(HCO_3^-) column (200–400 mesh, 4.5 × 100 cm). The column was developed with a linear gradient of 4 L of 0.05 *M* TEAB buffer and 4 L of 0.3 *M* TEAB buffer, pH 7.5. The eluent was monitored for radioactivity or for acid-labile organic phosphate. α-L-Fucopyranosyl phosphate is eluted at 0.22 *M* TEAB, the β-anomer is eluted at 0.24 *M* TEAB, and a third component, fucose 2-phosphate is eluted with 0.26 *M* TEAB. The fractions containing the β-anomer were pooled and evaporated to a thick syrup. The syrup was dissolved in water and evaporated three times to remove triethylammonium bicarbonate, leaving the triethylammonium salt of the product which can be used for analysis and GDPFuc synthesis. To obtain the cyclohexylammonium salt the product was dissolved in water and 1 mL of cyclohexylamine was added. The solution was evaporated three more times from water to remove triethylamine. The residual white solid was dissolved in warm ethanol and an equal volume of acetone was added in portions over a period of 2 days. The crystalline material was removed by filtration, washed with cold acetone, and dried over P_2O_5 (2.8 g, 50%). The material has $[\alpha]_{578}^{22} -19.4° \pm 1.0$ (*c* 1, water). Prihar and Behrman (7) report $[\alpha]_D^{25} -20.5°$.

*Guanosine 5-Phosphoric Di-*n*-butylphosphinothioic Anhydride*

GMP disodium salt (0.93 g, 2 mmol) was dissolved in 100 mL of water and the solution was adjusted to approximately pH 2.0 with Dowex 50 (H^+). The resin was removed by filtration and washed with water. The acidic filtrate and washings were applied to a 2.8 × 45 cm column of Dower 50 (H^+) which was eluted with 1.8 L of water. Pyridine (10 mL) was added to the acidic eluate and the resulting solution concentrated *in vacuo* to give the pyridinium salt of GMP which was dried by repeated evaporation from 30 mL portions of pyridine. After each evaporation, air was admitted to the apparatus slowly through a drying tube containing magnesium perchlorate to ensure the absence of moisture. Approximately 50 mL of dry *tert*-butanol was added followed by di-*n*-butylphosphinothioyl bromide (15) (1.8 g, 7.0 mmol) and tri-*n*-butylamine (1.5 g, 8 mmol). A clear solution forms after a few min at 35–40°C and the reaction is complete in 2 to 3 h at this temperature. *tert*-Butanol was removed *in vacuo*, 100 mL of water was added, and the excess di-*n*-butylphosphinothioyl bromide was extracted with ether. The water layer was concentrated *in vacuo* to 20 mL and stored at 4°C to produce crystals (white needles) which were removed by filtration, washed with cold water, and dried *in vacuo* over magnesium perchlorate; mp 154–155°C. The crystalline product is homogeneous by electrophoresis in 0.05 *M* triethylammonium bicarbonate, pH 7.5; $R_{GMP} = 0.25$ $\lambda_{max} = 256$ nm.

High pressure liquid chromatography was used to follow the course of this reaction. Samples (10 μL) were evaporated to dryness in a small test tube. The *tert*-butanol-free residue was dissolved in 0.2 *M* potassium phosphate buffer (pH 3.4) and applied to the hplc system. The retention times for GMP and GMP-di-*n*-butylphosphinothioic anhydride are 8.4 and 12.0 min, respectively, at a flow rate of 40 mL/h.

Guanosine Diphosphate Fucose

*A. Using Guanosine 5'-phosphoric Di-*n*-butylphosphiothioic Anhydride*

Dry monotriethylammonium-α-L-fucopyranosyl phosphate (0.5 mmol) and dry guanosine-5 phosphoric-di-*n*-butylphosphinothioic anhydride (0.5 mmol) were dissolved in 10 mL dry pyridine and evaporated to dryness *in vacuo* with care being taken to exclude moisture. Pyridine evaporation was repeated 3 times. The residue was dissolved in 10 mL of dry pyridine and 3.3 g (2 mmol) of dry silver acetate was added with stirring at 22°C. When the reaction was completed (3 to 5 h), 0.5 mL of water was added and the reaction was stirred to complete the hydrolysis of any unreacted di-*n*-butylphosphinothioic anhydride. The mixture was saturated with H_2S to precipitate silver sulfide. The precipitate was removed by filtration and washed with 50% water–pyridine. The filtrate and washings were diluted to 200 mL with water and applied to a 1.8 × 30 cm column of Dowex 1 (Cl^-) 200–400 mesh. The column was washed with 200 mL of water, then developed with a gradient of 0 to 0.4 *M* LiCl or NaCl using 4 L total of eluent. The eluent was monitored at 260 nm and fractions containing GDPFuc, which elutes at 0.2 *M* LiCl, were concentrated to approximately 5 mL and desalted on a 5 × 100 cm column of Bio-Gel P-2 (200–400 mesh), using water as the eluent. Yields based on apparent purity as judged from hplc and $E_{256}^M = 12.2 \times 10^3$ for GMP range from 50 to 80%, averaging 70%.

The course of the reaction was monitored by hplc using the system described above in which the GDPFuc has a retention time of 11.7 min. Samples (20 μL) were evaporated to dryness to remove pyridine, and the dark residue redissolved in buffer. The silver salt of GDPFuc seems to be less soluble in the reaction mixture than that of the di-*n*-butylphosphinothioic anhydride. Therefore, the apparent ratio of starting material to product depends on the amount of supernatant and precipitate in the sample taken for analysis.

B. Using Guanosine 5'-Phosphoromorpholidate

β-L-Fucopyranosyl phosphate bistriethylammonium salt (IV) (195 mg, 0.5 mmol) was dissolved in 10 mL of pyridine and the pyridine evaporated under reduced pressure at 30°C. This process was repeated three times with care to allow only dry air ($CaCl_2$ drying tube) to enter the flask. GMP morpholidate (5) (400 mg, 0.5 mmol) was added. The mixture was evaporated to dryness from 10 mL dry pyridine and the process repeated three times to remove traces of moisture. Finally, the reaction mixture was redissolved in 10 mL dry pyridine, and stored at 22°C under anhydrous conditions. The reaction was monitored by paper electrophoresis ($R_{picrate}$; GMP morpholidate = 0.5, GDPFuc = 1.0, fucopyranosyl phosphate = 1.6) or hplc after removal of pyridine. After three days, the pyridine was removed *in vacuo* at 30°C and the residue was dissolved in 400 mL water and applied to a column of Dowex 1 (Cl^-) and eluted as described previously. Yield based on β-L-fucopyranosyl phosphate was variable and never exceeded 50%.

Results and Discussion

The reaction sequence for the synthesis of GDPFuc is shown in Scheme 1.

*The Synthesis and Characterization of 2,3,4-Tri-*O*-acetyl-α- and β-L-Fucopyranoses*

A mixture of the anomers of 2,3,4-tri-*O*-acetyl-L-fucopyranose is prepared readily in quantitative yield by hydrolysis of the acetobromofucose using silver carbonate as the catalyst. The product mixture contains mostly the β-anomer. The α-anomer can be increased up to 80% by allowing a syrup or a wet pyridine solution to stand at room temperature. Because of the mutarotation process, drying the syrup for the phosphorylation

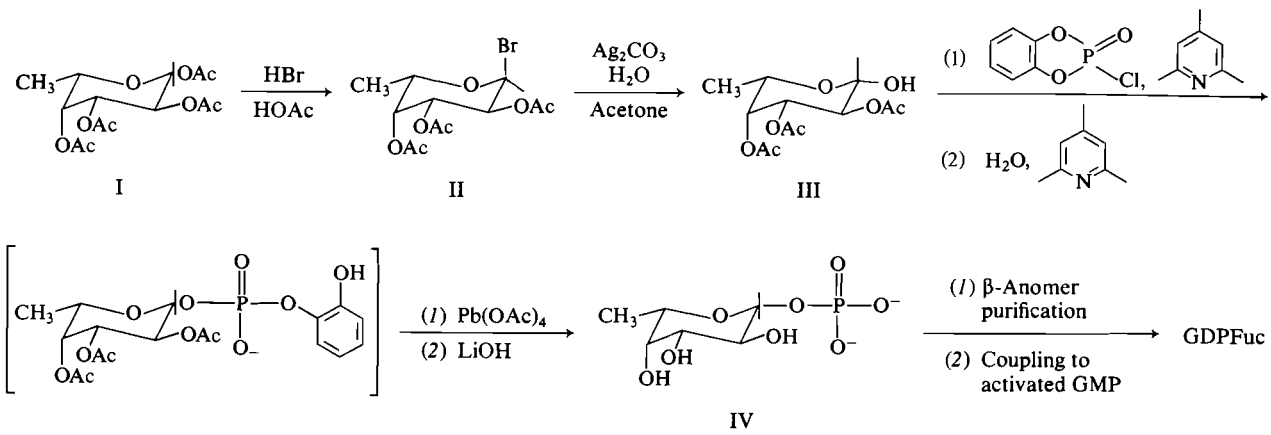

SCHEME 1

step should be limited to two or three hours at 22°C when the β-anomer of the phosphate is desired. The melting points reported for the α- and β-triacetates in the Methods section differ from the values reported by Prihar and Behrman (7). We have assigned anomeric configurations on the basis of the ^{1}H and ^{13}C nmr spectra of the purified compounds. The ^{1}H nmr spectrum of 2,3,4-tri-*O*-acetyl-α-L-fucopyranose is shown in Fig. 1A. The coupling constants and chemical shifts assigned on the basis of a first order analysis are shown in the figure. In Fig. 1B, the spectrum of the same sample after addition of ^2H_2O is shown; in it the hydroxyl resonance at 3.67 ppm is absent, indicating complete exchange of deuterium for hydrogen. The resonance (due to H1) at 5.33 ppm is converted from a triplet to a doublet, since exchange with deuterium removes the coupling between H1 and OH. The doublet has $^3J_{H1-H2} = 3.5$ Hz, indicating a *gauche* arrangement between H1 and H2 (17). This is the arrangement present in α-L-fucopyranose in the $^1C_4$-conformation.

The ^{1}H nmr of 2,3,4-tri-*O*-acetyl-β-L-fucopyranose is shown in Fig. 2. Only the resonances due to H5, H6, and the OH of C1 are first order. On treatment with ^2H_2O the resonance of OH at 3.93 ppm disappears and the multiplet at 4.59 ppm is simplified, indicating that it is due to H1. The coupling constant $^3J_{H1-H2} = 8$ Hz, indicating a *trans* arrangement between H1 and H2, is consistent with this anomer being in the $^1C_4$ conformation as expected. Complete analysis of this spectrum was achieved by computer fitting using the ITRCEL program (18).

The ^{13}C nmr spectra of these compounds also support the anomeric assignment based on ^{1}H nmr. The C1 of the β-anomer resonates further downfield (95.6 ppm) than the α-anomer (90.4 ppm), similar to the anomeric resonances of the galactose analogs.[5] Specific rotations of the two compounds also support the assignments made here. The α-anomer has $[\alpha]_{578}^{22} -125 \pm 1°$ and the β-anomer has $[\alpha]_{578}^{22} -16.8 \pm 0.5$. The β-anomer mutarotates slowly (7 days) in absolute ethanol to give $[\alpha]_{578}^{22} -106.5 \pm 1°$, reflecting the expected greater stability of the α-anomer.

From these data, we conclude that the triacetate with mp 102–103°C is the α-anomer while that with mp 120–121°C is the β-anomer. The values reported by Prihar and Behrman (7) were, for α, mp 117°C, and for β, mp 102–103°C.

Formation of the o-*Hydroxyphenyl Phosphate Diester*

Traces of water interfere with the formation of the phosphodiester by hydrolyzing the phosphorylating reagent. For this reason the reagents were dried and a three-fold excess of *o*-phenylenephosphochloridate was used. (In the ^{13}C nmr spectrum of the reaction mixture the C1 resonance appears as a doublet at 97.5 ppm with $^2J_{P-C} = 5.2$ Hz, consistent with the formation of a β-L-phosphate.)

Tetrahydrofuran was the solvent of choice for this reaction because of its low boiling point and the low solubility of the collidinium chloride formed during the reaction. Dioxane and methylene chloride were not as satisfactory.

s-Collidine is the most satisfactory base for use in this reaction. Khwaja *et al.* (11) used triethylamine and 2,6-lutidine (2,6-dimethylpyridine) in addition to collidine in their preliminary studies with *o*-phenylenephosphochloridate. Prihar and Behrman (7) used triethylamine in attempts to phosphorylate 2,3,4,6-tetra-*O*-acetyl-β-D-mannopyranose with this reagent but found that no reaction occurred.

[5] H. A. Nunez, unpublished observation.

Can. J. Chem. Downloaded from www.nrcresearchpress.com by 210.87.254.40 on 09/06/12
For personal use only.

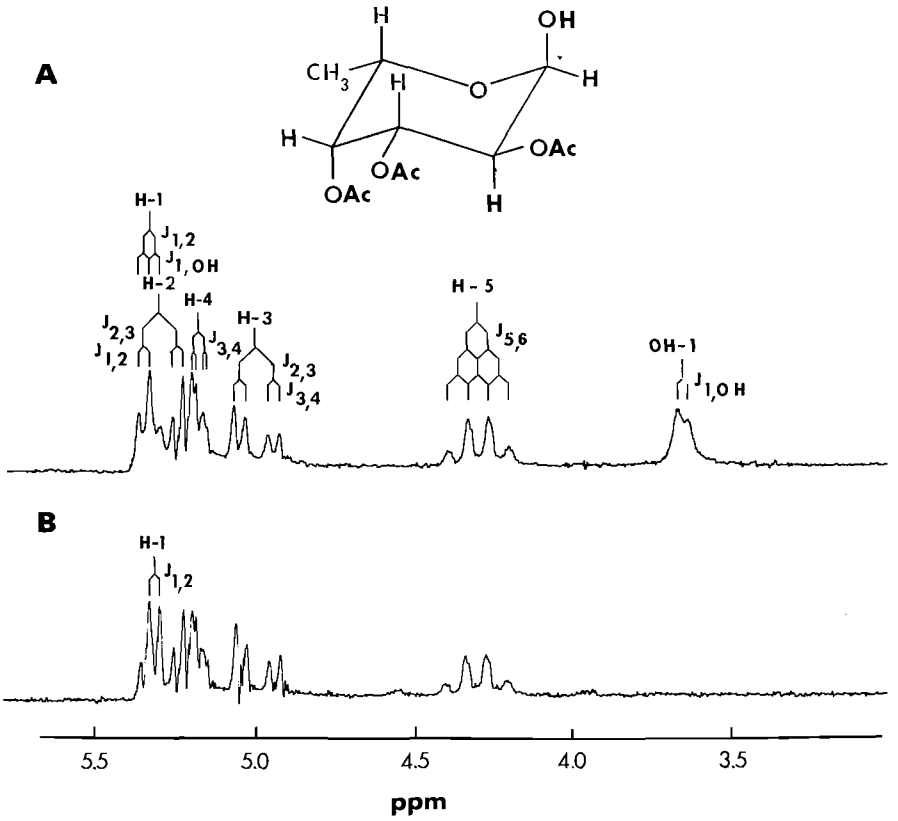

FIG. 1. The 100 MHz ^{1}H nmr spectrum of a 0.2 *M* solution of (A) 2,3,4-tri-*O*-acetyl-α-L-fucopyranose in $CDCl_3$, and (B) the same solution after treatment with D_2O to exchange the H of the OH group on C1. Chemical shifts are in ppm downfield from tetramethylsilane.

Lutidine is not satisfactory because the chloride is somewhat soluble in tetrahydrofuran.

Reaction time is also important. The formation of the phosphodiester bond is very fast at 4°C. Reaction times longer than 30 min at this or higher temperature result in the formation of a side product which seems to be a 1,2-orthoester formed at the expense of the β-phosphate triester intermediate.

Oxidation of the o-*Hydroxyphenyl Group*

At least three methods different from the lead tetraacetate used here for the oxidative removal of the *o*-hydroxyphenyl protecting group have been reported in the literature: catalytic hydrogenation (19), bromine–water oxidation, and periodic acid oxidation (11).

Removal of the *o*-hydroxyphenyl group by lead tetraacetate was first reported for the phosphodiesters of *tert*-butanol, neopentyl alcohol, 2,2,2-trichloroethyl alcohol, and 1,1-dimethylallyl alcohol (9–11). All of these compounds are acid labile and are good models for the labile glycosyl phosphates. In addition, at the same time the present investigation was in progress, Kochetkov and co-workers (12, 13) reported the synthesis of β-L-rhamnopyranosyl-1-phosphate with *o*-phenylenephosphochloridate using lead tetraacetate oxidation. In our hands, lead tetraacetate oxidation of the *o*-hydroxylphenylphosphate group routinely gives yields of glycosyl phosphates greater than 60%, based on starting aldose.

Separation of the Anomeric Fucopyranosylphosphates

Excellent separation of L-fucose 1-phosphate anomers was achieved by the method of MacDonald (20). A small amount of fucose 2-phosphate formed in the process is also well separated. This characteristic makes the separation of the anomeric triacetates unnecessary and at the same time the yield of the β-L-phosphate based on starting aldose is increased. Thus, this method makes practical the synthesis of GDPFuc containing isotopes such as ^{13}C, ^{14}C, ^3H.

Synthesis of GDPFucose.

Two forms of activated GMP were used, guanosine 5′-phosphoric di-*n*-butylphosphinothioic anhydride (15) and GMP morpholidate (5), to

Can. J. Chem. Downloaded from www.nrcresearchpress.com by 210.87.254.40 on 09/06/12
For personal use only.

Can. J. Chem. Downloaded from www.nrcresearchpress.com by 210.87.254.40 on 09/06/12
For personal use only.

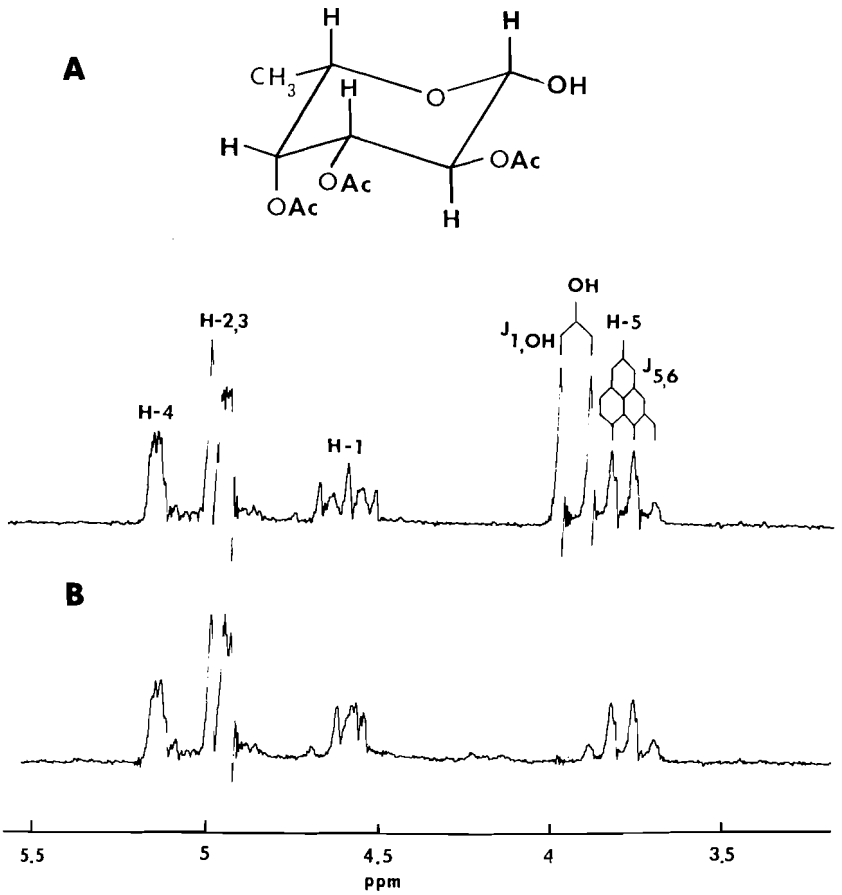

FIG. 2. The 100 MHz ^1H nmr spectrum of a 0.2 *M* solution of (A) 2,3,4-tri-*O*-acetyl-β-L-fucopyranose in $CDCl_3$, and (B) the same solution after treatment with D_2O to exchange the H of the OH group on Cl. Chemical shifts are in ppm downfield from tetramethylsilane.

synthesize GDPFuc. Both require careful elimination of water from the reaction mixture.

The purified GDPFuc can be stored in a frozen neutral solution or after lyophilization as an amorphous white powder for several months at −20°C without noticeable decomposition. The product has the same electrophoretic and hplc properties as the commercially available radioactive GDPFuc. In addition, its ^{13}C nmr (Fig. 3) and ultraviolet spectra were those expected on the basis of the presence of β-L-fucopyranosyl phosphate and guanosine 5′-phosphate in the molecule. The fucose moiety could be transferred to D-galactopyranosyl β(1-4)-2-acetamido-2-deoxy-D-glucopyranosyl-β-hexanolamine by the action of a fucosyl transferase isolated from porcine submaxilary glands. The trisaccharide product was fully characterized as containing an L-fucosyl moiety linked α(1-2) to the galactosyl residue (21).

The Stability of GDPFucose

The stability of GDPFuc over the pH range of 3 to 8 was investigated using hplc. At pH 3 the GDPFuc was degraded to GDP with a half life of 7 h at 37°C and 52 h at 4°C. At pH 5, 6, 7, and 8, there was less than 10% hydrolysis after a week at 37°C.

The effect of Mn^{2+} and Mg^{2+} on the hydrolysis of GDPFuc was studied using concentrations similar to those used in enzyme assays. In agreement with previous findings (2), neither 20 m*M* Mn^{2+} nor Mg^{2+} in 0.2 *M* PIPES buffer at pH 7.5 stimulated the hydrolysis of GDPFuc. During 48 h at 37°C, less than 5% of the GDPFuc is hydrolyzed, a highly desirable property for in vitro enzymatic studies and for manipulations during chemical synthesis.

Because of these findings all the manipulations of the GDPFuc were carried out at near neutral pH. Thus, the chromatography on Dowex 1 (Cl^-) was carried out using a neutral salt gradient rather than the acidic eluent used with other nucleoside diphosphate sugars (5). The high salt concentrations reached during concentration prior to desalting on a BioRad P-2 column does not degrade GDPFuc since only traces of other uv absorbing

Can. J. Chem. Downloaded from www.nrcresearchpress.com by 210.87.254.40 on 09/06/12
For personal use only.

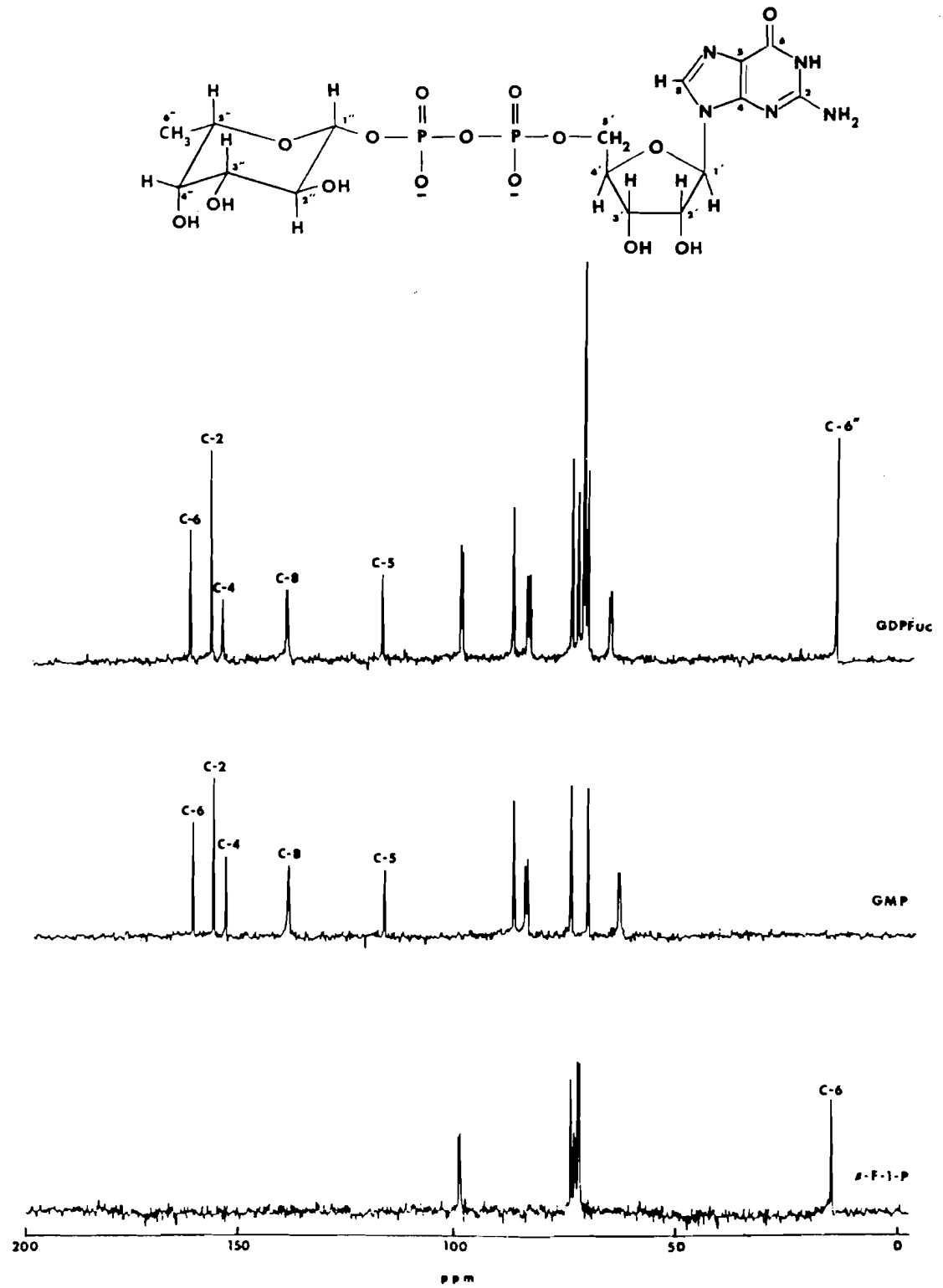

FIG. 3. The 15.08 MHz, proton-decoupled, ^{13}C nmr spectrum of a 0.1 *M* pH 7 solution of the sodium salt of GDPFucose compared to the spectra of GMP and β-L-fucopyranosyl phosphate.

material can be detected in the eluent from the P-2 column and by hplc.

The Conformation of GDPFucose

The solution conformation of GDPFuc was evaluated by ^{13}C and ^{1}H nmr spectroscopy. The fucopyranosyl ring exists in the $^{1}C_4$ conformation as evaluated by ^{1}H–^{1}H coupling constants. The ribofuranosyl ring appears to exist principally in the ^{2}E conformation (70%). Coupling constants between P and C2 of the fucose and P and C4 of the ribose moiety are 9.1 and 8.8 Hz, respectively. From these values it appears that more than 60% of the population of GDPFucose has the pyrophosphate group *trans* to both C4′ of ribose and C2 of fucose (23).

1. H. ISHIHARA and E. C. HEATH. J. Biol. Chem. **243**, 1110 (1968).
2. H. ISHIHARA, D. J. MASSARO, and E. C. HEATH. J. Biol. Chem. **243**, 1103 (1968).
3. H. SCHACHTER, H. ISHIHARA, and E. C. HEATH. Methods Enzymol. **28**, 285 (1972).
4. V. GINSBURG. J. Biol. Chem. **235**, 2196 (1960).
5. J. G. MOFFATT. Methods Enzymol. **8**, 136 (1966).
6. D. H. LEABACK, E. C. HEATH, and S. ROSEMAN. Biochemistry, **8**, 1351 (1969).
7. H. S. PRIHAR and E. J. BEHRMAN. Biochemistry, **12**, 997 (1973).
8. J. H. ISAI and E. J. BEHRMAN. Carbohydr. Res. **64**, 297 (1978).
9. T. A. KHWAJA and C. B. REESE. J. Am. Chem. Soc. **88**, 3446 (1966).
10. T. A. KHWAJA and C. B. REESE. Tetrahedron, **27**, 6189 (1971).
11. T. A. KHWAJA, C. B. REESE, and J. C. H. STEWART. J. Chem. Soc. 2092 (1970).
12. V. H. SHIBAEV, Y. Y. KUSOV, V. A. PENTRENKO, and N. K. KOCHETCOV. Akad. Nauk SSSR, Ser. Khim. 1952 (1974).
13. V. N. SHIBAEV, Y. Y. KUSOV, V. A. PENTRENKO, and N. K. KOCHETCOV. Akad. Nauk SSSR. Ser. Khim. 2485 (1976).
14. C. M. MCCLASKEY and G. H. COLEMAN. Org. Synth. Coll. Vol. III. Wiley and Sons, New York. 1955. p. 434.
15. K. FURUSAWA, M. SEKINE, and T. HATA. J. Chem. Soc. Perkin Trans I, 171 (1976).
16. C. C. SWEELEY, R. BENTLEY, M. MAKITA, and W. W. WELLS. J. Am. Chem. Soc. **85**, 2497 (1963).
17. A. DE BRUYN, M. ANTEUNIS, P. J. GAREGG, and T. NORBERG. Acta Chem. Scand. **830**, 820 (1976).
18. S. CASTELLANO and A. A. BOTHNER-BY. J. Chem. Phys. **41**, 3863 (1964).
19. M. L. TOMAYO and J. CALDEROW. Chem. Abstr. **45**, 7046e (1951).
20. D. L. MACDONALD. Carbohydr. Res. **6**, 376 (1968).
21. P. R. ROSEVEAR, H. A. NUNEZ, and R. BARKER. 178th Am. Chem. Soc. National Meeting BIOL. **145**. (1979).
22. H. A. NUNEZ and R. BARKER. Biochemistry, **15**, 3943 (1976).
23. J. V. O'CONNOR, H. A. NUNEZ, and R. BARKER. Biochemistry, **18**, 500 (1979).

Can. J. Chem. Downloaded from www.nrcresearchpress.com by 210.87.254.40 on 09/06/12
For personal use only.

FOR ERRATA SEE
V 61 1983 P. 640

Protonated cyclopropanes in α-aminoketone deamination[1,2]

OLIVER E. EDWARDS, JOHN DIXON,[3] JOHN W. ELDER,[4] RALPH J. KOLT, AND MAURICE LESAGE
Chemistry Division, National Research Council of Canada, Ottawa, Canada K1A 0R6

Received October 22, 1980

OLIVER E. EDWARDS, JOHN DIXON, JOHN W. ELDER, RALPH J. KOLT, and MAURICE LESAGE. Can. J. Chem. **59**, 2096 (1981).

Deamination of 2-amino-4,4-dideuterio-6,6-dimethylcyclohexanone, 2-*exo*-amino- and 2-*endo*-amino-norbornane-3-one, 2-diazonorbornan-3-one, 2-*exo*-amino-5,6-*exo*-dideuterionorbornan-3-one and the corresponding 5,6-*endo*-dideuterio isomer has been studied. The nature of the products, the deuterium location in them, and the high retention of steric identity in the carbocations are interpreted in terms of σ-bond participation leading to corner- and edge-protonated cyclopropanes as reaction intermediates. Results with other destabilized carbocations are correlated.

OLIVER E. EDWARDS, JOHN DIXON, JOHN W. ELDER, RALPH J. KOLT et MAURICE LESAGE. Can. J. Chem. **59**, 2096 (1981).

On a étudié la désamination de l'amino-2 dideutéro-4,4 diméthyl-6,6 cyclohexanone, des amino-2 *exo* et amino-2 *endo* norbornanones-3, de la diaza-2 norbornanone-3, de l'amino-2-*exo* dideutéro-5,6-*exo* norbornanone-3, ainsi que de son isomère dideutéro-5,6-*endo*. On interprète la nature des produits, la position des deutérium qu'ils contiennent ainsi que le taux élevé de rétention d'identité stérique des carbocations en fonction d'une participation de la liaison σ qui conduit à des intermédiaires du type cyclopropanes protonés au sommet et sur le bord. On établit une corrélation entre ces résultats et ceux obtenus pour d'autres carbocations déstabilisés.

[Traduit par le journal]

We have long been interested in the nature and behaviour of cations generated on carbons attached to carbonyl groups, considered as *destabilized* carbocations (1–3). Related studies have been conducted by Yates (4, 5), Hanack (6), Baumgarten (7), Granger (8), Gassman (9), Levisalles (10*a*), Creary (10*b*), and Charpentier-Morize (11) and their co-workers. In cyclic systems where the carbonyl and the bonds to the electron-deficient carbon are held in a roughly coplanar relationship it has been estimated (11, 12) that such carbonium ions are destabilized relative to the isolated cation by 5 kcal/mol because of proximity to the positive end of the carbonyl dipole. We (see also ref. 10*b*) rationalized our early observations, as did Yates and Crawford (4), in terms of increased σ-bond participation in the ionization to offset this expected destabilization.

Among the most interesting products from these putative α-ketocarbonium ions were cyclopropyl ketones,[5] which we considered (1) to arise via intermediate bridged ions (protonated cyclopropanes) and products of apparent 1,3 hydrogen shift which could also have arisen via protonated cyclopropanes (1). Of great interest also was the cause of the remarkably high retention of steric identity during product formation from these cations (1–5). The present work reports an investigation of the nature of these processes using specific deuterium labelling and comparison of products from deamination of stereoisomeric amines and a diazoketone.

The carbonium ions chosen for study were those produced by nitrous acid deamination of 2-amino-4,4-dideuterio-6,6-dimethylcyclohexanone (**1**), 2-*exo*-amino-5,6-*exo*-dideuterionorbornan-3-one (**2**), 2-*exo*-amino-5,6-*endo*-dideuterionorbornan-3-one (**3**), and 2-*endo*-aminonorbornan-3-one (**4**), and by protonation of 2-diazonorbornan-3-one (**5**). The movement and/or loss of deuterium in product formation occurred in very specific ways, throwing light on the nature of the intermediate ions and suggesting a unified interpretation of the behaviour of these and related carbonium ions.

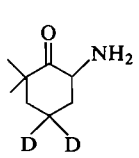

1

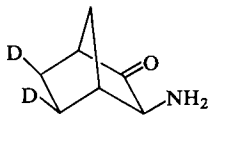

2

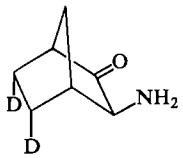

3

Substrate Preparation

2-Amino-4,4-dideuterio-6,6-dimethylcyclohexanone (1)

Scheme 1 outlines the procedure used and aver-

[1]Issued as NRCC No. 19255.

[2]Presented in part at the 55th and 63rd annual meetings of the Chemical Institute of Canada, Quebec, June 4–7 (1972) and Ottawa, June 8–11 (1980).

[3]NRCC Postdoctoral Fellow, 1970–1971.

[4]Visiting Scientist. Present address, Fairfield University, Fairfield, CT., U.S.A.

[5]Cyclopropane formation from carbonium ions is a well known reaction, often occurring in high yield (13).

0008-4042/81/142096-20$01.00/0

©1981 National Research Council of Canada/Conseil national de recherches du Canada

Can. J. Chem. Downloaded from www.nrcresearchpress.com by 210.87.254.6 on 09/06/12
For personal use only.

Can. J. Chem. Downloaded from www.nrcresearchpress.com by 210.87.254.6 on 09/06/12
For personal use only.

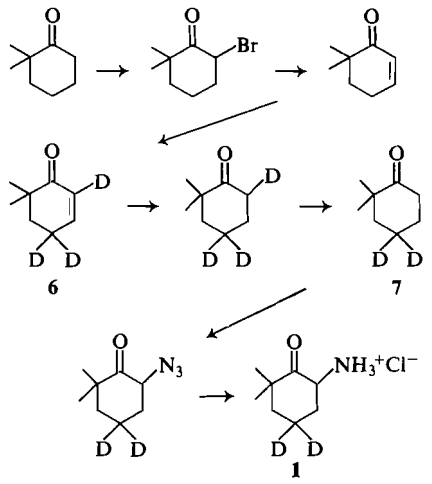

SCHEME 1

age yields starting with 2-methylcyclohexanone.[6] Four methods were attempted for the reduction of the C—C double bond of **6** (see Experimental). Catalytic reduction gave a 70% yield of **7**, but some loss and possible scrambling of deuterium occurred. Lithium in ammonia reduction followed by Jones' oxidation gave the best yields, although some runs gave much polymeric material. Deuterium analysis indicated the presence of 1.95 D per molecule of **7** after exchange of any deuterium α to the carbonyl. The mass spectrum indicated **7** to be a mixture with 8% d_3, 76% d_2, and 16% d_1 species.[7]

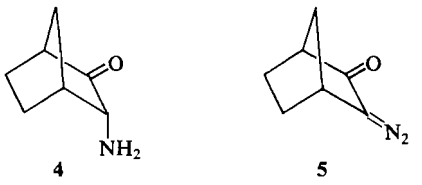

2-exo-*Amino-5,6*-exo-*dideuterionorbornan-3-one (2)*

Norbornadiene was partially reduced using deuterium over 30% Pd/C. The mixture of deuterated norbornene and norbornane was converted following Huisgen *et al* . (14) into the benzoyl aziridine **8** (Scheme 2). This was heated to rearrange it to the phenyloxazoline **9** which was then hydrolysed in aqueous acid to the *N*-benzoyl alcohol **10**. Of the methods tried, only the method of Ratcliffe and Rodehorst (15) gave high yields in the oxidation of **10** to the *N*-benzoyl ketone **11**. A final acid hydrolysis converted this into the desired α-aminoketone isolated as its hydrochloride.

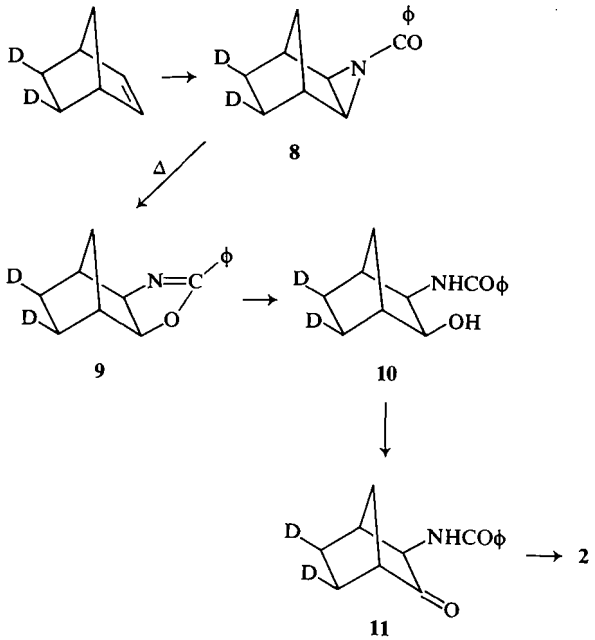

SCHEME 2

2-exo-*Amino-5,6*-endo-*dideuterionorbornan-3-one (3)*

A mixture of 5,6-*exo*-dideuterionorbornene and tetradeuterated norbornane was converted by the method of Werstiuk (16) into 5,6-*endo*-dideuterionorbornene (**12**) (Scheme 3). This was transformed into the desired α-aminoketone by the route described above for the *exo*-dideuterio isomer.

The 2-diazonorbornan-3-one (**5**) was prepared from the mono-*p*-toluenesulfonylhydrazone of 2,3-norbornadione essentially following Wiberg *et al*.

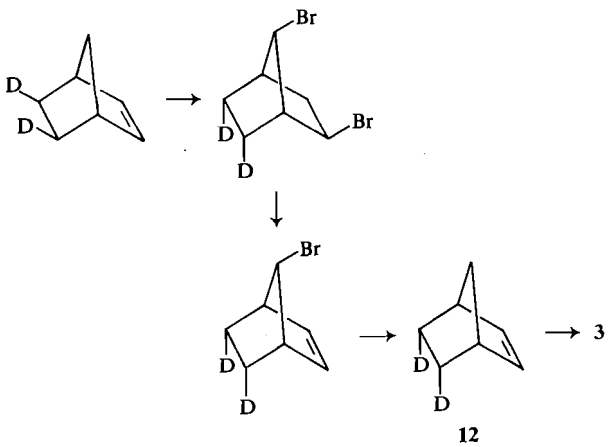

SCHEME 3

[6]We warmly thank Prof. J. W. Apsimon and Dr. C. E. Slemon for providing details of the preparation of 4,4-dimethylcyclohexen-3-one.

[7]See introduction to the Experimental for the method of estimating these values.

Can. J. Chem. Downloaded from www.nrcresearchpress.com by 210.87.254.6 on 09/06/12
For personal use only.

(17). However, the reaction in our hands was complete in around 1.5 h. The product was distilled over a short path at 65°C under 0.05 Torr and used promptly.

A sample of 2-*endo*-aminonorbornan-3-one **4** was prepared by stannous chloride reduction of 2-oximinonorbornan-3-one, an improvement over the published procedure (18).

Reference samples of the ketol acetates **13** and **14** were prepared from the known 2-*exo*-3-*exo* and 2-*endo*-3-*endo* diols, while those of **15**, **16**, and **17** were made following literature procedures. A sample of **18** (R = H) was separated from the products from deamination of **4**, then acetylated.

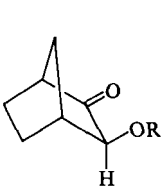

13

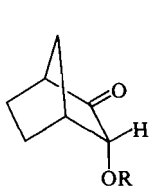

14

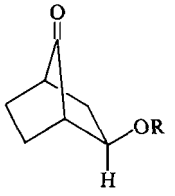

15

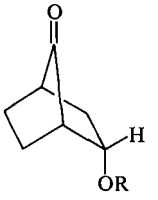

16

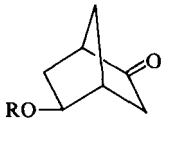

17

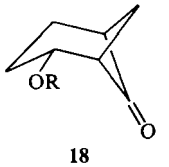

18

Results

The deamination of the deuterated aminocyclohexanone **1** was carried out in dilute aqueous sulfuric acid by addition of sodium nitrite as described earlier (1). Considerable diazoketone (ν_{max} 2080 cm^{-1}) was produced. In order to avoid complication with carbenoid-type reactions, this was destroyed by stirring the ether-extracted products with dilute *p*-toluenesulfonic acid in water. The total extracted products were separated into neutral components and acids, then the neutral ones separated by chromatography on tlc silica gel. The structure **19** was assigned to the trimethylcyclopentenone on the following evidence. Mass spectrometry showed[7] the presence of approximately 73% d_2 and 27% d_1 species. Its ^1H nmr spectrum showed no vinyl hydrogen and approximately equal amounts of CH_2 hydrogens at δ 1.8 and δ 2.47. Its ^2H nmr spectrum had two signals with equal areas at +0.57 (br s) and +5.8 ppm (br t, J = 2.2 Hz) (relative to $CDCl_3$ in hexane).

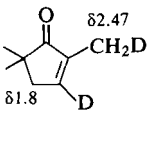

19

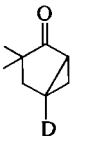

20

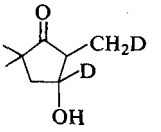

21

The bicyclohexanone was assigned structure **20**. Its mass spectrum[7] showed the presence of 5% d_2, 74% d_1, and 21% d_0 species. Its ^1H nmr spectrum had signals identical to those of the undeuterated molecule except for the absence of a ^1H multiplet near δ 2.0 and a sharpening of the signals between δ 1.7 and 2.1. Its ^2H nmr spectrum had a signal at 5.6 ppm (br s) upfield from deuteriochloroform in cyclohexane.

The more polar products had the same glc retention times as the products identified (1) as two isomers of 3-hydroxy-2,5,5-trimethylcyclopentanone. When a sample of the mixture was absorbed on neutral alumina for 17 h it was largely dehydrated to **19** containing 74% d_2 and 26% d_1 species. We hence conclude that the hydroxy ketone had structure **21**.

The acid fractions were distilled, converted to methyl esters, then these distilled giving essentially pure **21**. Its mass spectrum indicated the presence of 5% d_3, 60% d_2, 29% d_1, and 6% d_0 species.[7]

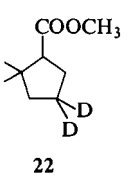

22

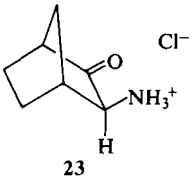

23

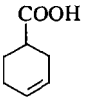

24

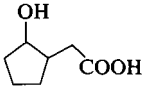

25

The deamination of 2-*exo*-aminonorbornan-3-one (**23**) in aqueous acid gave 3% of nortricyclanone and 15% of 2-*exo*-hydroxynorbornan-7-one. No significant amounts of 2-*exo*-hydroxynorbornan-2-one (**13**, R = H), 2-*exo*-hydroxynorbornan-5-one (**17**, R = H), or 2-*endo*-hydroxynorbornan-3-one (**14**, R = H) could be detected. In addition, 3-cyclohexene-1-carboxylic acid **24** (6%), a hydroxy acid tentatively assigned structure **25** on the basis of analysis and spectra, and a mixture of other unidentified acids were produced.

When the deamination of **23** was conducted in acetic acid containing 1 *M* sodium acetate the yield of nortricyclanone rose to 9%. Eleven other neutral products were evident from glc on column A. The main one, and the only one characterized, was the 2-acetoxy-7-ketone **15** (R = Ac) (12%). Less than 3%, if any, of 2-*exo*-acetoxynorbornan-3-one was present.

Can. J. Chem. Downloaded from www.nrcresearchpress.com by 210.87.254.6 on 09/06/12
For personal use only.

Deamination of 2-diazonorbornan-3-one (**5**) in contact with water (autocatalytic) gave around 1% of nortricyclanone, 50% of 2-*endo*-hydroxynorbornan-3-one (**14**, R = H), 35% of 2-hydroxybicyclo[3.1.1]heptan-6-one (18, R = H), and 17% of readily extracted acid which was mainly 3-cyclohexene-1-carboxylic acid. These results are very comparable to those of Yates and Crawford (4).

The deamination of **5** in 50% acetic acid was rapid and, aside from the production of ketol acetates as well as ketols, the products were similar to those obtained in water. However, the presence of 1 *M* sodium acetate produced striking changes. The rate of reaction dropped considerably, the yield of nortricyclanone rose from 1.5% to 12% and the 2-*exo*-acetoxy-7-one **15** (R = Ac) became a major product (glc peak area three times that of the bicyclo[3.1.1] ketol acetate **18**). When the sodium acetate concentration was increased to 4 *M* in 50% acetic acid the deamination became very slow (45 min for completion), the yield of nortricyclanone rose to 17.5%, and the ratio of **15** to **18** (glc areas) was 4:1. In acetic acid the deamination was very slow (5 min, 0°C) the yield of nortricyclanone was 8.5%, and the ratio of areas (glc) of **15** to **18** was 2.5:1. In this medium 1 *M* sodium acetate had practically no effect on product formation. Deamination of diazo ketone **5** in a slightly acidified aqueous 1.4 *M* sodium nitrite solution gave the same major products as decomposition in water. However, the nortricyclanone yield increased to 3.6%. The yield of recovered neutral product (as ketols) was 71%.

The *endo* aminoketone **4** gave comparable results to the diazoketone (**5**) except that the yield of neutral products was only one-third that from **5**. The yield of nortricyclanone in water was less than 0.2%, in 50% acetic acid 1.5%, and in 1 *M* sodium acetate in 50% acetic acid it was 2.9%. In acetic acid the yield was 2.3% and in 1 *M* sodium acetate in acetic acid it was 3.6%. Without sodium acetate the predominant products were the ketols (acetates) **14** and **18**. Again in the media containing the salt the 7-ketone **15** became a dominant product. The ratio of **15** to **18** in 1 *M* sodium acetate in acetic acid was 3:1.

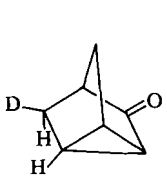

26

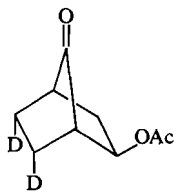

27

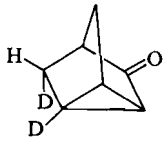

28

Although the ketols **13**, **14**, and **18** (R = H) were rather labile, the samples could be recovered in good yield after exposure to nitrous acid deamination conditions. We conclude that the absence of one or more of these in specific deaminations is not the result of destruction by nitrous acid or oxides of nitrogen, or during work-up.

Deuterium Labelled Aminonorbornanones

The deamination of 2-*exo*-amino-5,6-*exo*-dideuterionorbornan-3-one (**2**) in aqueous acid gave an average of 2.1% of deuterated nortricyclanone. This was shown to be mainly **26** by the following evidence. Its mass spectrum (4% d_2, 93% d_1, and 3% d_0) indicated nearly complete loss of one deuterium. Its ^2H nmr spectrum (Fig. 1) was a doublet 1.1 ppm upfield from external CD_3I with J = 0.9 Hz and its proton decoupled ^{13}C nmr spectrum (Fig. 2) had a peak for C-7 with half the relative intensity of that for the undeuterated molecule (C-6 + C-7) while C-6 gave a triplet centered very close to it.

The most abundant neutral product was a labelled 2-*exo*-hydroxynorbornan-7-one (16%). This

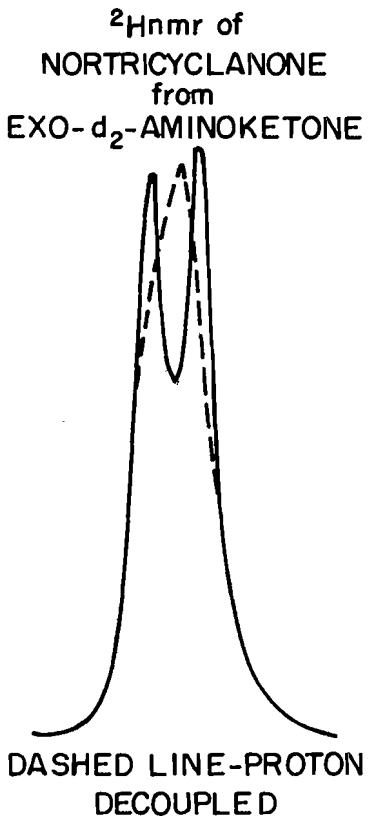

FIG. 1.

Can. J. Chem. Downloaded from www.nrcresearchpress.com by 210.87.254.6 on 09/06/12
For personal use only.

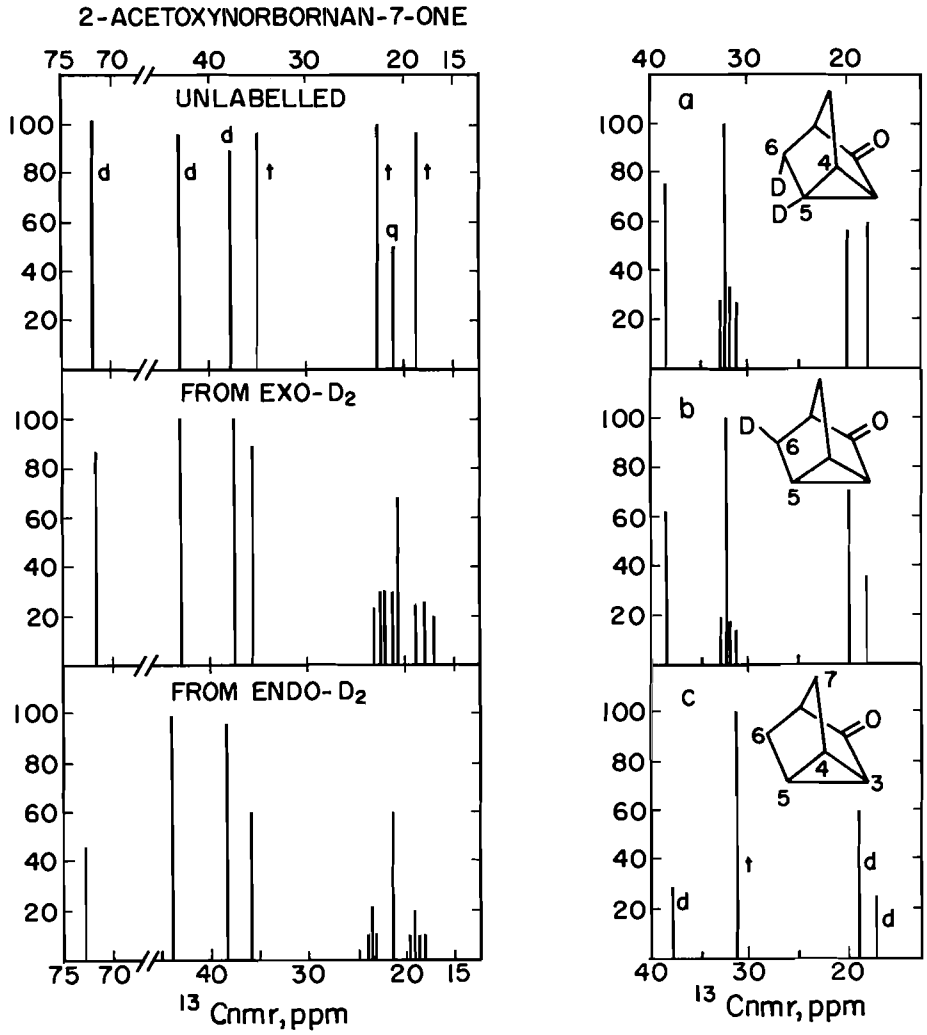

FIG. 2.

was shown to be dideuterated by mass spectrometry of its acetate[7] (6% d_3, 83% d_2, 12% d_1). Its ^{2}H nmr spectrum gave only a broad singlet 1.3 ppm upfield from external CD_3I, which was not resolved on proton decoupling. Its ^{13}C nmr spectrum (Fig. 2) showed the presence of two CHD groups (triplets at 18.1 and 22.3 ppm) and the C-2 signal (72 ppm) was as intense as expected if no deuterium was on this carbon. On this basis we consider its structure to be mainly **27**.

The mixture of readily extracted acids from the deamination of **2** was rich in deuterated 3-cyclohexene-1-carboxylic acid. The mass spectrum of its methyl ester showed a content of 1.5% d_3, 87% d_2, and 12% d_1 species.

The hydroxy ester from **2** analysed for $C_8D_2H_{12}O_3$. The presence of the hydroxyl group was evident from infrared bands at 3450 and 3600 cm^{-1}. This appears identical, except for the labelling, with the main hydroxy acids from **3** and **4** (see Experimental for deamination of **3**). A possible gross structure is **25**.

The deamination products from the *endo*-d_2 isomer **3** were comparable to those from **2**. The yield of deuterated nortricyclanone was higher (average 4.2%). In this case essentially no deuterium was lost[7] (8% d_3, 86% d_2, 6% d_1). Its ^{2}H nmr spectrum (Fig. 3) showed the presence of two types of deuterium giving a broad singlet at 0.65 ppm and a doublet at 0.80 and 0.90 ppm upfield from external CD_3I with relative areas 1:1. The doublet collapsed to a singlet when proton-decoupled. The assignment of deuterium labelling as in **28** was confirmed by its ^{13}C nmr spectrum (Fig. 2). The

Can. J. Chem. Downloaded from www.nrcresearchpress.com by 210.87.254.6 on 09/06/12
For personal use only.

signal for C-4 and C-5 at 18.9 ppm was halved in intensity as expected due to coupling with the deuteron, absence of nuclear Overhauser enhancement, and possible quadrupole broadening of the signal for the deuterated carbon (19).

The deuterium labelling of the 2-acetoxy-7-ketone was revealing. The ^2H nmr spectrum showed the presence of two deuterons at σ 4.6 and 1.6 in the ratio of 1:9. The low-field deuterium was clearly on C-2 as in **29** (20% of the mixture), while the remainder was most probably located as in **30**. The ^{13}C nmr spectrum confirmed this since the peak for C-2 at 73 ppm had only 53% of the relative intensity of the signal at 21 ppm, in comparison with the corresponding signals in the spectrum of **15** (R = Ac) (Fig. 2).

The mass spectrum of the 3-cyclohexen-1-carboxylic acid from the *endo*-d_2 isomer showed retention of most of the deuterium[7] (2% d_3, 89% d_2, 12% d_1). However, the ^2H nmr spectrum of the *p*-bromophenacyl ester of the acid had deuterium signals at δ 5.4 and 1.5 with areas in the ratio 1:25.

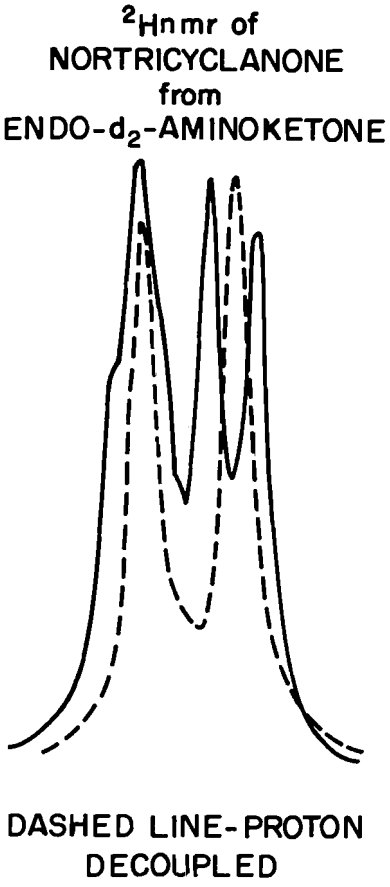

FIG. 3.

This is consistent with the presence of 8% of **31** and 92% of **32**.

The hydroxy ester from the *endo*-d_2 isomer **3** analysed for $C_8D_2H_{12}O_3$ and appeared identical except for labelling with the main hydroxy ester from **2** and **4**. A possible gross structure is **25**.

Discussion

Two explanations for the deuterium labelling pattern in the 5,5-dimethylcyclopenten-2-one **19** seem possible. The first would require the formation of a primary cation as an intermediate as in eq. [1]. This would be around 13 kcal/mol less stable than

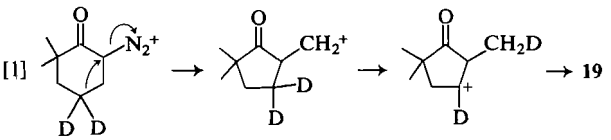

the initial ion.[8] A direct 1,3 deuterium shift has been discredited (20), hence a 1,2-shift on a protonated cyclopropane intermediate would have to be invoked to account for the final product.

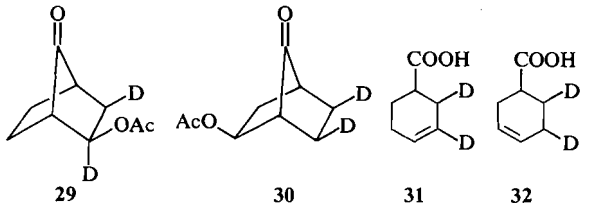

The second alternative (1) would avoid the high energy primary cation by going directly from the initial ion to a corner-protonated cyclopropane. A very specific deuterium shift[9] to give an edge deuteronated cyclopropane (Scheme 4) would then be followed either by loss of a deuteron to give the cyclopropyl ketone or rearrangement to the secondary cation with the charge now remote from the positive end of the carbonyl dipole. Thus all three major neutral products could be accounted for.

The formation of nortricyclanones from norbornyl cations can involve essentially loss of either *exo* hydrogen or deuterium, as in the present results and one of Collins' examples (23), or predominant loss of *endo* deuterium as in one case studied by Collins and Benjamin (24) and one studied by Werstiuk (25). Clearly the simple explanation that *either* the back lobe of the 6-*exo* CH bond (as in **33**) *or* the *endo* CH bond on C-6 (as in **34**) participate in

[8]18 kcal/mol (secondary vs. primary cations) (21) less the 5 kcal/mol destabilization of a cyclic α-ketocarbonium ion (11).

[9]Baird and Aboderin were the first to demonstrate such a migration (22). The reason for the specificity is discussed later in the paper.

Can. J. Chem. Downloaded from www.nrcresearchpress.com by 210.87.254.6 on 09/06/12
For personal use only.

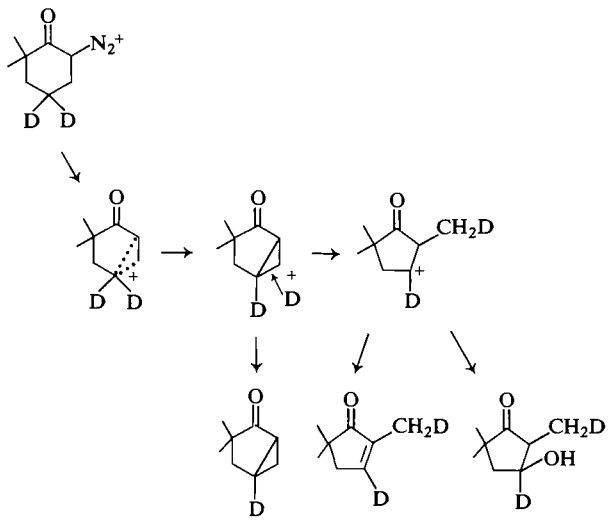

SCHEME 4

the ionization does not account for the facts. However, a mechanism parallel to that outlined in Scheme 4 can account for our observations and, as will be discussed later, those of Collins and Benjamin and Werstiuk also. This is outlined in

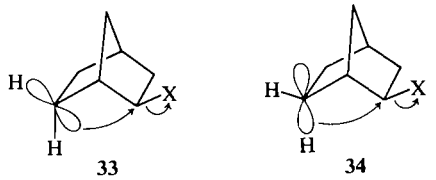

33 34

Scheme 5 for the *endo*-d_2 isomer **3**. By analogy to the aminocyclohexanone case we postulate that a corner-protonated cyclopropane **35** is first formed and that this is converted[9] in part to the edge-protonated cyclopropane **36** and in part directly to the Wagner–Meerwein ion **37**. Since **36** is almost symmetrical, nearly equal proportions of **37** and **38** would form from it. If the activation energy for the transitions **35** → **36** and **35** → **37** is of similar magnitude, it follows, since the amount of nortricyclanone formed is small, that **37** and **38** (and hence **30** and **29**) would be formed in a ratio of roughly 3:1. In actuality the ratio of **30** to **29** was 2.9:1.

We expected to find the same ratio of the two labelled acids **31** and **32** as was found for **29** and **30**. However, the ratio of **32**:**31** estimated from ^{2}H nmr spectrum was 11:1. If the scheme is correct, this must mean that there was an alternate source of **32**. We can only account for this by assuming that considerable diazoketone was formed in the deamination, giving rise to **32** as in eq. [2]. The argument could be advanced against this interpretation that neither of the neutral products expected from the

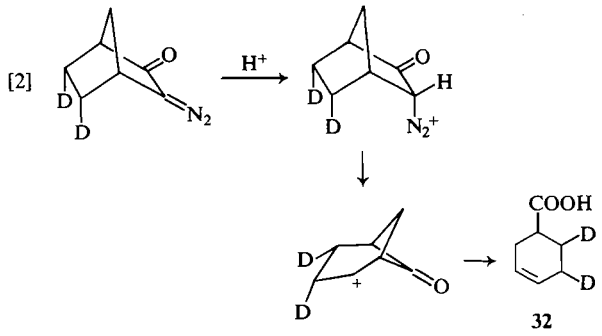

32

diazoketone were observed in deamination of the *exo* amino ketone in water. However, neither is the expected 2-*exo*-hydroxy-3-one (**13**, R = H). Nitrous acid deamination in water gives acids at the expense of neutral products, possibly accounting for this absence.

The deamination of the *exo*-d_2 isomer **2** leading to nearly exclusive loss of one deuterium in the formation of nortricyclanone is consistent with a mechanism parallel to that in Scheme 5.

Schemes 4 and 5 demand two important postulates: (*a*) that mainly one of the two possible edge-protonated cyclopropanes form from the initial corner-protonated cyclopropanes, and (*b*) that proton (deuteron) loss from the intermediate ions is only from the edge-protonated species.

Strong support for these postulates comes from the work of Collins and co-workers (23, 24) and of Werstiuk (25). The former observed mainly loss of *exo* deuterium in the formation of nortricyclene in the solvolysis of **39** (eq. [3]). But in the formation of

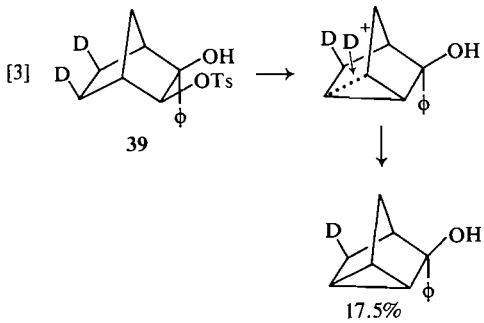

39 17.5%

the substituted nortricyclene from **40**, mainly *endo* deuterium was lost (eq. [4]).

Werstiuk (25) observed predominant loss of

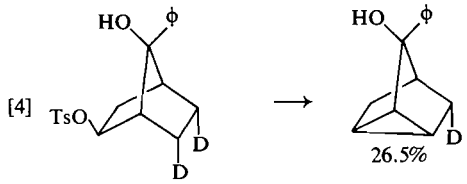

40 26.5%

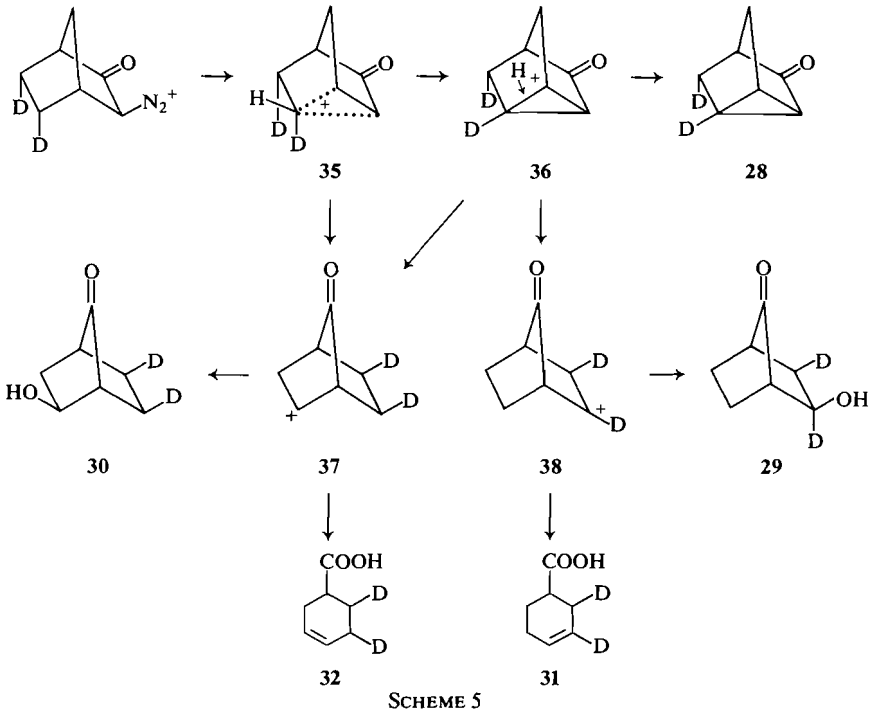

SCHEME 5

endo deuterium in the solvolysis of **41** (eq. [5]). Each of these cases, and our own results, can be rationalized in terms of the two above postulates if the edge-protonated cyclopropane formed has the proton (deuteron) on the *most basic* (electron rich) bond of the *respective cyclopropane*, i.e. the one most remote from the carbonyl or electronegative group (e.g. OH, phenyl).

[5] 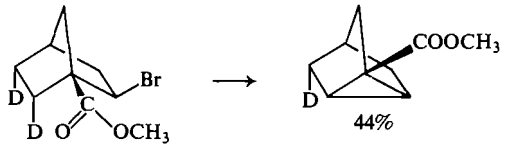

41

Recent work by Nickon *et al.* (26) on cyclopropane ring formation can be rationalized in the same way, with the *p*-anisyl group as the electronegative substituent on the initial corner-protonated cyclopropane.

Collins and Benjamin (24) had postulated involvement of the protonated cyclopropane (as in eq. [3]) as an intermediate or transition state but did not extend the conception to their other example (eq. [4]) or provide an explanation for the specific ion formed. Werstiuk suggested for his cases that the transition state for cyclopropane formation resembled an edge-protonated cyclopropane, but gave no explanation for the specificity (25).

The concept of the proton shift from a corner-protonated cyclopropane to give one with the proton on the most electron rich bond has already been invoked by Hart and Schlosberg (27) to account for isomerization during acylation of cyclopropanes. The validity of this is supported by the evidence of Werstiuk and co-workers (28) that edge-protonation of **42** took place selectively on the bond remote from the chlorine. Since cyclopropyl ketones protonate preferentially on oxygen, the principle of microscopic reversibility cannot be tested in this way for our examples.

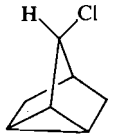

42

Another point of great interest is the high retention of steric identity encountered in the deamination of 2-*endo*- and 2-*exo*-aminonorbornan-3-ones and in protonation of various diazoketones (4, 5). The only common products isolated from the deamination of the two amines in water were nortricyclanone and cyclohex-3-enoic acid. The small amount of nortricyclanone from the *endo* amine most probably arose by *endo* protonation of some diazoketone produced as a transient intermediate. The major neutral product from the *exo* amine, 2-*exo*-hydroxynorbornan-7-one, was not

Can. J. Chem. Downloaded from www.nrcresearchpress.com by 210.87.254.6 on 09/06/12
For personal use only.

Can. J. Chem. Downloaded from www.nrcresearchpress.com by 210.87.254.6 on 09/06/12
For personal use only.

detectable in the products from the *endo* amine or diazoketone in aqueous acid. The acid can arise by different pathways from each developing cation (Scheme 5 and eq. [2]).

Three possible explanations[10] for this retention of steric identity in deamination have been considered:

(A) Configuration holding by tight ion pair formation.

(B) Highly asymmetric solvation of the carbocation, with the solvent closest to the side of the ion from which the nitrogen departs.

(C) Sigma (σ) bond participation as the nitrogen departs, or so rapidly after carbocation formation that no other process intervenes.

An evaluation of these explanations follows:

(A) Collins and co-workers not only considered the location of the initial counter ion to be product determining but considered its position to be held through several molecular rearrangements (30). (An alternate explanation of their results is given in the Appendix.) Much evidence against this postulate for reactions in polar solvents is available. For example, in the 2-diazonorbornan-3-one (5) decompositions reported herein and in the work of Yates and co-workers (4, 5), regardless of the presence of only traces of bicarbonate ions and carboxylate anions, bisulfate anions, or up to 4 *M* sodium acetate, the *unrearranged* product had clean *endo* configuration.

Even with 4 *M* acetate ion present in 50% acetic acid as much of the ketols as ketol acetates were formed, i.e. at least a solvent-separated ion pair was involved.

In the work of Yates and Blattel (5) the presence of chloride or trifluoroacetate ions in 50% acetic acid resulted in no products containing these ions.

Whiting and co-workers (31*a*) showed that in deamination of 1-octylamine only 3% of product derived from the initial counter ion was formed, while 4-octylamine gave 25% of product from the initial counter ion. In our study of medium ring nitrosamides (32) attack of external nucleophiles was favored over that of the internal counter-ion (eq. [6]).

In Collins and Benjamin's own work (33) nearly as much *exo* product **44** (29%) as *endo* product **45** (34.5%) was produced in deamination of **43** in acetic acid. If one adds the other products probably arising from an *exo* cation, the sum of its contribution rises to 62.5%, a clear indication that *initial counter ion control of products is not important in polar solvents*.

[6] 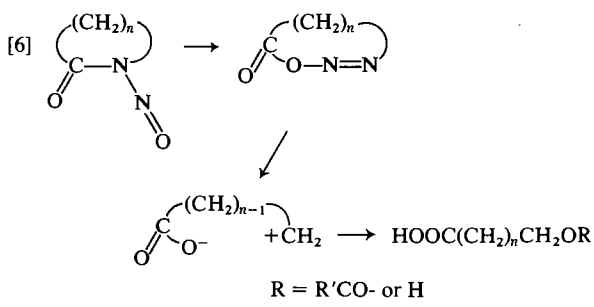

[7] 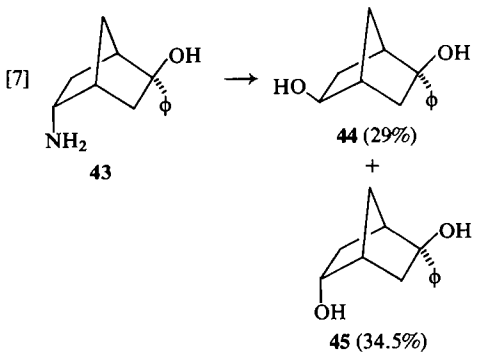

(B) In the deamination of the diazoketone **5** in acetic acid, the departing nitrogen and presumably a solvated acetate ion plus the 5,6 *endo* hydrogens all impede approach to the *endo* face of the presumed classical cation. However, one could argue that the acetic acid solvating the anion would be much more nucleophilic than bulk solvent, so that *endo* capture of acetic acid dominates. However, in the presence of 1 *M* sodium acetate in this solvent, the nucleophilicity of the bulk solvent should be comparable and one would expect major *exo* capture. Actually no 2-*exo* acetate was observed. Hence this explanation is discredited.

(C) The following facts are readily accounted for if bridged ions are formed synchronous with, or very rapidly after, nitrogen loss.

1. The yield of products arising via bridged ion intermediates (Wagner–Meerwein products, cyclopropanes) can be as high as 70%. The yield of cyclopropanes seems directly related to the steric impedance to nucleophilic attack on the cationic centers (5, 13).

2. Sodium acetate acts as a base increasing the cyclopropane yield (present work and that of Yates and Blattel, ref. 5). This can be the result of two effects, (*a*) the catalysis of the equilibrium between the two possible diazonium ions, as illustrated for

[10]Micellar effects are not considered probable for the small rigid polar molecules studied in this work, with concentrations below 1 *M*. The near 100% retention in the absence of acetate ions is strikingly greater than encountered in deaminations in which micelles are important (29).

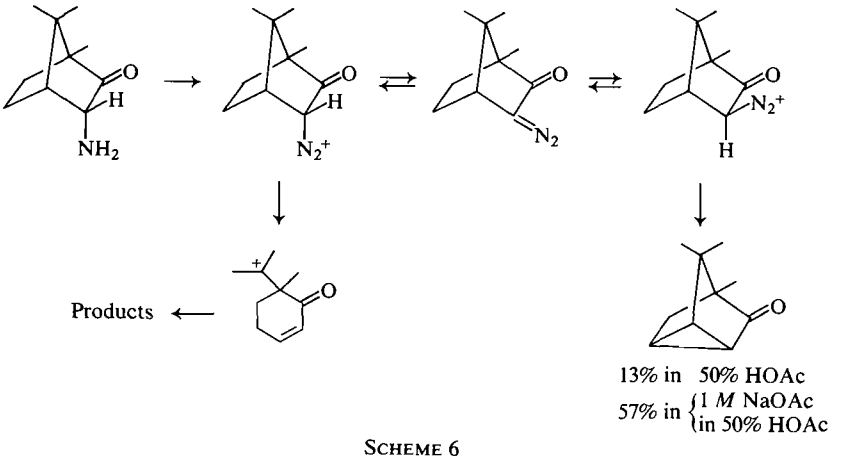

SCHEME 6

3-*endo*-aminocamphor (1, 5) in Scheme 6, and (*b*) action as a base in removing the proton from edge-protonated cyclopropanes. The acetate attack on the carbons of corner- or edge-protonated cyclopropanes derived from 3-*endo*-aminocamphor should be inefficient because of impedance by the methyl groups. Thus the amount of 3-acetoxy-7-one only increases from a trace to 5% when 1 *M* sodium acetate is added (5).

3. Our deuterium labelling studies show that at least 40% of the neutral products from the *exo*-diazonium ion from **3** came from an edge-protonated cyclopropane (Scheme 5) and at least 55% of the products from deamination of **1** arose from protonated cyclopropanes. If our interpretation is correct, Collins' results require at least 26% involvement of protonated cyclopropanes (24) (eq. [4]), and Werstiuk's example requires over 44% of such species (25) (eq. [5]).

Recent support for involvement of protonated cyclopropanes in carbonium ion reactions is found in the work of Lee *et al.* (34), Hudson and co-workers (35), Kirmse and Siegfried (36), and Liu (37). Nuclear magnetic resonance evidence for their existence in superacids is reviewed by Saunders *et al.* (38). Köhler and Lischka (39) have calculated that edge and corner-protonated cyclopropanes in the norbornane series have nearly equal energy in the gas phase, both being more stable than a classical norbornyl cation.

The above work does not enable one to conclude whether σ-bond participation is synchronous with nitrogen departure or whether the participation follows, extremely rapidly, the formation of a classical cation. Indeed the solvolysis studies of Lambert (40) and Brown (41) and their co-workers suggest that the latter is the correct picture. However, the role of acetate ions discussed below leads us to conclude that, at least for α-aminoketone deamination, the participation is synchronous with C—N bond rupture.

Medium Effects

The transition from water to acetic acid as medium for deamination of the diazoketone **5** would be expected to increase the yield of elimination products since acetic acid is a poorer nucleophile. This was indeed observed (increase of nortricyclanone from ca. 1% to 8%). The expectation on adding sodium acetate is less clear since it can act both as a base aiding proton removal, and as a nucleophile capturing intermediate ionic species. In fact, in 50% acetic acid the salt markedly increased the yield of nortricyclanone (0.5% → 17%), hence its role as a base is dominant, which seems totally inconsistent with any tight ion pair concept for the initial cation (see above). In view of our other evidence, the role of acetate can be conceived to be diversion of edge-protonated cyclopropane to cyclopropane at the main expense of Wagner–Meerwein product (see also ref. 11*b*).

The most striking effects of acetate ion are a reduction in reaction rate, and a shift of products from those derived purely from *endo* diazonium ion to those derived from a mixture of *endo* and *exo* ions. We account for this in terms of the equilibria in eq. [8] (42, 11b); without acetate ion the protonation is predominantly *exo* and essentially irreversible. Acetate ion as base makes the process reversible, and permits the few percent of *endo* protonated species to play a role. The key point in our interpretation is that, because of the more favorable overlap of the 1,6 bond, the decomposition of the *exo* diazonium ion is much faster than that of the *endo* ion (1,7 bond overlap) (see ref. 10*b* for a similar conclusion for solvolysis). Thus, despite

Can. J. Chem. Downloaded from www.nrcresearchpress.com by 210.87.254.6 on 09/06/12
For personal use only.

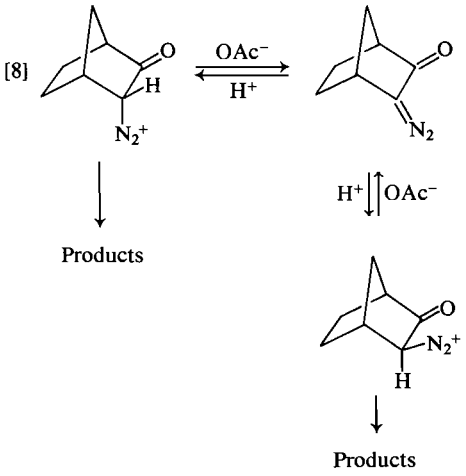

the low ratio of *endo* protonation of the diazoketone, products from the resultant *exo* diazonium ion begin to predominate (more than 50% in 4 *M* sodium acetate in 50% acetic acid) when the equilibration (eq. [8]) is accelerated by the acetate ions.

In the deamination of the *endo* and *exo* aminoketones **2**, **3**, and **4**, nitrite and/or acetate ions were present, hence additional sodium acetate did not have the marked effect on tricyclanone yield that was observed for the diazoketone. The *endo* amine **4** showed an increase in proportion of Wagner–Meerwein product **15** arising from *exo* diazonium ion, when acetate was added, in harmony with the diazoketone observation.

Summary

The following conclusions have been reached.

1. Proton loss from protonated cyclopropanes is from the edge-protonated, not corner-protonated, species; i.e. the principle of microscopic reversibility holds.

2. The bond in a cyclopropane ring most remote from an electronegative substituent on a side chain is the most basic of the three, i.e. is the best proton acceptor. This is the predominant protonated cyclopropane formed (see also ref., 28).

3. Initial counter-ions in deamination are solvent separated, and in the presence of an abundance of ions in polar solvents do not play a major role in product determination.

4. For destabilized carbonium ions, neighboring groups and/or σ-bonds participate either during or very rapidly after C—N bond rupture, resulting in high retention of steric identity at the cationic center.

Experimental

Infrared spectra were for chloroform solutions (s = strong, m = medium and w = weak) and ^{1}H nmr spectra in deuterochloroform unless otherwise indicated. Mass spectra were determined on a Perkin-Elmer-Hitachi R.M.U. 60 instrument at 70 eV. The calculated content of deuterated isomers was estimated as follows: The ratio of $M + 1^+$ and $M - 1^+$ peaks to the M^+ peak was determined for the unlabelled compound, and the corresponding values for the deuterated molecules corrected for these, with M^+ being in this case the main deuterated species. The resultant values were summed, then the percentage of each species relative to the sum calculated. This ignores any possible deuterium isotope effects on the ratio within the cluster. Deuterium nmr spectra were determined on a modified Varian XL-100 instrument, and ^{13}C nmr on a Varian CFT-20 Fourier transform spectrometer. The glc analyses were done using a Victoreen 4000 gas chromatograph with either Column A, 6 ft × 1/4 in. 3% OV-1 (methyl silicone) on acid-washed, DMCS treated 60–80 mesh Chromosorb G, or Column B, 6 ft × 1/4 in. 20% OS-138 (polyphenyl ether) on acid-washed, DMCS treated 80–100 mesh Chromosorb G. Preparative glc was done using a 10 ft × 3/8 in. column with 20% SE-30 (methyl silicone) on 60–80 mesh Chromosorb W or on a 10 ft × 3/8 in. column with 10% OS-138 on gas chromatographic CLA.

High pressure liquid–liquid chromatography was performed on a Waters Assoc. HPLC model ALC-100 instrument using a 4 ft × 3/8 in. Porasil-A column, eluting with 2.5% acetone in hexane (4 mL/min).

2,2-Dimethylcyclohexanone

This was prepared following King and Topliss (43) in 44–50% yield from 2-methylcyclohexanone. It had ν_{max} 1075 cm^{-1} and gave ^{1}H nmr signals at δ 1.15 (6H, s), 1.89 (6H, m, $w_{1/2}$ = 5 Hz), and 2.52 (2H, m, $w_{1/2}$ = 12 Hz).

2-Bromo-6,6-dimethylcyclohexanone[6]

A solution of 50.4 g (0.314 mol) of bromine in 45 mL of acetic acid was added over two hours to a stirred solution of 39.6 g (0.314 mol) of 2,2-dimethylcyclohexanone in 45 mL of acetic acid containing a trace of hydrogen bromide. The reaction mixture was poured into 300 mL of crushed ice – water mixture. The crystalline solid which separated was collected by filtration. It was dissolved in ether, the ether dried, and concentrated. Addition of hexane gave 48 g (0.235 mol) of bromo compound (75%) mp 55–57°C. It had ν_{max} 1728(s) and 1705(m). Its ^{1}H nmr spectrum had signals at 1.24 (6H, s), 1.87 (4H, m), 2.47 (2H, m), 4.99 (1H, m). *Anal.* calcd. for $C_8H_{13}BrO$: Br 38.97%; found: Br 38.77%.

4,4-Dimethylcyclohex-1-en-3-one[6]

A mixture of 2-bromo-6,6-dimethylcyclohexanone (61.5 g, 0.30 mol), 78 g (0.885 mol) of dry lithium bromide, and 21 g (0.29 mol) of lithium carbonate in 400 mL of dry dimethylformamide was heated for 7 h at 130°C. The mixture was cooled, poured into 300 mL of water, then the product extracted into pentane. The residue from evaporation of the pentane was distilled at 77°C, 24 Torr, giving 27 g (72%) of oil with ν_{max} 1670 (s) and 1640 (w) cm^{-1} and λ_{max} 224 nm, ε 10250. Its ^{1}H nmr had signals at δ 1.07 (6H, s), 1.80 (2H, t, J = 6 Hz), 2.36 (2H, m), 5.80 (1H, d of t, J_1 = 2, J_2 = 10 Hz), and 6.82 (1H, d of t, J_1 = 4, J_2 = 10 Hz). *Anal.* calcd. for $C_8H_{12}O$: C 77.37, H 9.79; found: C 77.10, H 9.56%.

6,6-Dideuterio-4,4-dimethylcyclohex-1-en-3-one

A solution of 12.6 g of 4,4-dimethylcyclohex-1-en-3-one in 150 mL of methanol-*d* containing 0.2 *N* sodium methoxide was left for 7 h at room temperature. The solution was neutralized by bubbling in carbon dioxide, then 100 mL chloroform was added. After filtration to remove salts, the solvent was distilled. The

Can. J. Chem. Downloaded from www.nrcresearchpress.com by 210.87.254.6 on 09/06/12
For personal use only.

Can. J. Chem. Downloaded from www.nrcresearchpress.com by 210.87.254.6 on 09/06/12
For personal use only.

residue was distilled under 18 Torr to give 6.4 g, bp 65–78°C, which was mainly trideuterated cyclohexenone **6**. The 2.5 g of higher boiling product was partly the corresponding 3-methoxycyclohexanone (δ 3.23 (s) and 3.6 (m) ppm). The enone still contained a small amount of partially deuterated species (weak ^{1}H nmr signals at 2.2–2.6 and a trace of multiplet centered at δ 5.80). The ratio of the signals at δ 6.8 and 1.8 was 1:2 showing that no exchange of the 3-hydrogen had taken place.

The crude 3-methoxycyclohexanone was heated to 120°C in the presence of 20 mg of *p*-toluenesulfonic acid-*d*. The product was diluted with pentane, then washed with a solution of sodium carbonate in deuterium oxide. The dried pentane solution gave 2.3 g of deuterated enone. Total yield, 8.7 g (70%).

4,4-Dideuterio-6,6-dimethylcyclohexanone (7)

Reduction of the enones was repeatedly attempted, as follows.

(*a*) Sodium borohydride reduction followed by hydroboration and treatment with propionic acid (44). Much polymeric material resulted in most runs. Reoxidation of monomeric product gave good quality deuterated dimethylcyclohexanone but in average yield 14%. After base exchange of α-protons this had 76% d_2 and 18% d_1 by mass spectrometry.

(*b*) Sodium borohydride in pyridine (45) followed by Jones' oxidation also gave much polymer, but 40% of dideuterated ketone was obtained.

(*c*) Catalytic reduction gave a 70% yield of deuterated ketone, but mass spectrometry showed considerable deuterium scrambling. After exchange of the α-hydrogen using base the product had 14% d_3, 54% d_2, 22% d_1, and 17% d_0.

(*d*) The best method proved to be reduction with lithium in ammonia (46). To a solution of 2.0 g of lithium in 100 mL of liquid ammonia was added 36 g of *tert*-butyl alcohol. During 5 min stirring, the mixture turned bronze. A solution of 2.56 g of deuterated enone **6** in 25 mL of dry tetrahydrofuran was added dropwise in the course of one hour. Excess lithium was destroyed by addition of 50% water–tetrahydrofuran mixture, then water. After evaporation of the ammonia the residue was distributed between methylene chloride and water. The methylene chloride extract was oxidized with Jones' reagent (47). The resulting ketone was distilled over a short path at 60–70°C, 10 Torr pressure, giving 1.7 g (68%) of saturated ketone **7**.

The combined ketone from experiments following methods (*a*), (*b*), and (*d*) analysed for 1.97 D. It had ν_{max} 1700 cm^{-1}(s), 2210 (w), 2170 (w), and 2120 (w) cm^{-1}. Its ^{1}H nmr had signals at δ 1.14 (6H, s), 1.69 (2H, br s, $w_{1/2}$ = 3.5 Hz), 1.65–2.04 (2H, m, partly under the signal at δ 1.69), and 2.18–2.61 (2H, m). Its mass spectrum had peaks at *m/e* 129 (0.8), 128 (8.0), and 127 (2.8). The undeuterated ketone had peaks at 126 (8) and 125 (0.9), from which we estimate[7] that the deuterated sample contained 8% d_3, 76% d_2, and 16% d_1 species.

2-Bromo-4,4-dideutero-6,6-dimethylcyclohexanone

To 8.9 g (69.5 mmol) 4,4-dideutero-6,6-dimethylcyclohexanone dissolved in 10 mL glacial acetic acid was added with ice cooling one drop of a solution of hydrobromic acid in glacial acetic acid; then 11.1 g (69.5 mmol) of bromine dissolved in 20 mL glacial acetic acid was added over a period of 45 min. The solution was stirred for 10 min after addition and the reaction mixture was poured into 100 mL of a water – crushed ice mixture. The crude precipitate was filtered, washed with water, pressed dry, and recrystallized from ether–pentane giving 3 crops of crystals, mp 53–55°C, for a total yield of 9.6 g (46.5 mmol, 67%) of deuterated bromo ketone.

Its ^{1}H nmr spectrum had signals at δ 1.22 (6H, s) 1.74 (2H, br s, $w_{1/2}$ = 4 Hz), 1.84–2.7 (2H, m), 4.95 (1H, q, J_1 = 12 Hz, J_2 = 6 Hz).

2-Azido-4,4-dideutero-6,6-dimethylcyclohexanone

A 0.9 *N* methanolic solution of lithium azide was prepared (48) by refluxing for 5 h a mixture of 8.5 g lithium chloride and pulverized sodium azide in 200 mL methanol. After cooling and filtration, 160 mL of this solution was added dropwise with stirring to 9.6 g (46.5 mmol) of deuterated bromo ketone dissolved in 30 mL methanol. The solution was stirred at room temperature for 6 h after addition,and concentrated on a rotary evaporator near room temperature. A 100 mL mixture of crushed ice and water was added and the aqueous layer was extracted 5 times with 100 mL portions of pentane. Evaporation of the pentane near room temperature gave 7.6 g (45 mmol, 97%) of crude 2-azido-4,4-dideutero-6,6-dimethylcyclohexanone. This material was used in the next step without further purification. It had ν_{max} (chloroform) 1715 (s) and 2095 (s) cm^{-1}. The latter signal partially masked some C—D stretching bands.

2-Amino-4,4-dideutero-6,6-dimethylcyclohexanone Hydrochloride (1)

To an ice-cooled solution of 7.6 g (45 mmol) crude deuterated azido ketone in 25 mL 95% ethanol was added dropwise, through a dropping funnel, a solution of 15.8 g of $SnCl_2 \cdot 2H_2O$ in 70 mL of 95% ethanol containing 5 mL concentrated hydrochloric acid. After 3 h stirring, another 5 mL of concentrated hydrochloric acid was added and the reaction was allowed to proceed another 3 h, after which time nitrogen evolution had ceased. The ethanol was removed on a rotary evaporator and hydrogen sulfide was bubbled through an aqueous solution of the residue. A golden yellow precipitate which formed was filtered off through a bed of Celite and the filter cake was washed with water. The procedure was repeated twice until no more precipitate formed upon treatment of the aqueous layer with hydrogen sulfide. Water was removed on a rotary evaporator at 40°C, the residue dissolved in absolute ethanol, then 100 mg of insoluble material removed by filtration. After evaporation of the alcohol, the residue was treated with hot acetone and 3.5 g, mp 170–175°C, which did not dissolve, was collected on a filter. This was recrystallized from absolute ethanol – ethyl acetate yielding 2.3 g of crystals, mp 179–183°C. The mother liquor was combined with the acetone-soluble portion. The mixture was taken to dryness, then the residue triturated with acetone. The acetone-insoluble residue was recrystallized as before, yielding 1.0 g of crystals, mp 179–182°C (total yield 3.3 g, 18.5 mmol, 41%), of deuterated aminoketone hydrochloride **1**. After recrystallization from ethanol – ethyl acetate it had mp 181–184°C. It had ν_{max} 1722 cm^{-1} and its ^{1}H nmr spectrum had signals at δ 1.12 (3H, s), 1.31 (3H, s), 1.76 (2H, br s, $w_{1/2}$ = 5 Hz). *Anal.* calcd.[11] for $C_8D_2H_{14}ClNO$: C 53.48, H 8.97, N 7.80; found: C 53.53, H 9.20, N 7.61%.

Deamination of 2-Amino-4,4-dideuterio-6,6-dimethylcyclohexanone

This was carried out essentially as described earlier (ref. 1, method *b*). The neutral products were first analysed by glc – mass spectrometry[12] on a 10% SE-30 column at 100°C. Five peaks were examined. The first, with M^+ 140, has not been identified. The second was the trimethylcyclopentenone **19** with close to two deuterium atoms. The third was the bicyclic ketone **20** with approximately one deuterium atom. The more strongly retained peaks 4 and 5 appeared to be the isomeric hydroxy ketones rich in d_2 species. These were later shown to be the two isomers of **21** (see below) as expected from our early work (1).

The neutral products from 932 mg of the aminoketone hy-

[11]The gas chromatographic C, H, N determination does not distinguish hydrogen and deuterium, so the calculations are made correcting for this.

[12]We are grateful to Dr. Ross Pottie for help with this work.

Can. J. Chem. Downloaded from www.nrcresearchpress.com by 210.87.254.6 on 09/06/12
For personal use only.

drochloride were separated on a 30-fold ratio of tlc silica gel (flat base column) into two fractions; A (350 mg, pentane–ether) containing the unknown product, **19** and **20**; B (175 mg, ether) containing the ketols (ν_{max} 3450, 1725 cm^{-1}).

Fraction A was chromatographed on a 60-fold ratio of tlc silica gel using 10% ether in pentane for elution. The unknown (6 mg) was followed by 39 mg of a mixture of it and **19**, then 35 mg of pure **19**, 15 mg of a mixture of **19** and **20**, and 145 mg of pure **20**. The two major components were distilled in a chain of bulbs at a bath temperature of 70°C under 30 Torr. These samples were used for mass spectra and ^1H nmr.

Fraction B (67 mg) in 10 mL of 1:1 ether–pentane was stirred with 1 g of neutral alumina, activity III, for 18 h. The suspension was filtered, then the solvents distilled. The residual oil was distilled in a chain of bulbs at a bath temperature of 80°C under 35 Torr giving 35 mg of **19** (identified by glc and infrared spectrum).

3,3-Dimethylbicyclo[3.1.1]hexan-2-one

This gave ^1H nmr signals at δ 1.7–2.15 (4H, m), 1.2 (center of a 1H, m), 1.09 (3H, s), 1.07 (3H, s), 0.89 (center of a 1H, m). It gave *m/e* 125 (4.5), 124 (46), and 123 (0.4).

*5-Deuterio-3,3-dimethylbicyclo[3.1.0]hexane-2-one (**20**)*

The product from deamination of **1** (yield 22%) gave a mass spectrum with *m/e* 126 (8), 125 (46), 124 (13), from which we calculate[7] its deuterium content to be 6% d_2, 74% d_1, and 21% d_0 species. Its ^1H nmr spectrum gave a single peak near δ 1.7 (internal $CDCl_3$ as reference). Its ^1H nmr spectrum had peaks at δ 1.75–2.2 (3H, m), 1.38 (center of a 1H, m), 1.10 (3H, s), 1.05 (3H, s), 0.89 (center of a 1H, m).

2,4,4-Trimethylcyclopenten-3-one

This gave ^1H nmr signals at δ 7.34 (1H, m), 2.46 (2H, m), 1.80 (3H, m), 1.09, 1.11 (3H, singlets). It gave *m/e* 125 (5), 124 (51), 123 (3).

*1-Deuterio-2-monodeuteriomethyl-4,4-dimethylcyclopenten-3-one (**19**)*

(a) Directly Isolated (Yield 10%)

This gave *m/e* 127 (6), 126 (51), and 125 (26). From this we estimate[7] a content of 69% d_2 and 31% d_1 species. Its ^2H nmr spectrum gave two signals at approx δ 7.0 (s) and 1.8(t, J = 2.2 Hz) (internal $CDCl_3$ reference) with relative areas 1:0.92. Its ^1H nmr spectrum (trace of hexane) gave signals at δ 2.47, 1.80, and 1.1 in the ratios 2:2.3:6.2.

*(b) From Dehydration of the Ketol **21** (Yield 23%)*

This had ν_{max} 1690 (5), 1635 (w), and 1620 (w) cm^{-1} and gave *m/e* 127 (5), 126 (51), 125 (19), from which the calculated content[7] was 73% d_2 and 27% d_1 species.

Methyl 2,2-Dimethylcyclopentanecarboxylate

This gave a mass spectrum with peak at *m/e* 157 (17), 156 (M^+, 5.6), 155 (0).

*Methyl 3,3-Dideuterio-5,5-dimethylcyclopentanecarboxylate (**22**)*

The mass spectrum of this ester had peaks at *m/e* 159 (1.2), 158 (M^+, 5.6), 157 (2.7). From this we calculated[6] a content of 63% d_2 and 30% d_1 species. It had ν_{max} (film) 2220, 2180, 2130, 1735 cm^{-1} and gave ^1H nmr signals at δ 0.90 (3H, s), 1.18 (3H, s), 2.51 (1H, q, J_1 = 8.5 Hz, J_2 = 7.5 Hz), 3.78 (3H, s). The methylene signals between δ 1.4 and 2.2 were simplified relative to the undeuterated ester.

2-exo-Benzamidonorbornan-3-one

This was prepared by oxidation of the known benzamido alcohol (14) using the Ratcliffe–Rodehorst reagent (15) (see the *endo-d_2* analogue). It had mp 209°C, and was sparingly soluble in chloroform, but a saturated solution in $CDCl_3$ gave ^1H nmr peaks at δ 7.9–7.25 (aromatic), 6.25 (NH), 3.88 (q, J_1 = 6, J_2 = 3 Hz, 1H), 2.84 (1H), 2.69 (1H), 2.3–1.5 (m, 6H).

*2-exo-Aminonorbornan-3-one Hydrochloride (**23**)*

This was prepared by acid hydrolysis of the benzamido ketone (see the *endo-d_2* analogue). It had mp 145°C and gave ^1H nmr peaks in D_2O–DSS centered at δ 3.43 (d, J = 3 Hz), 3.0, 2.80, and 2.35 representing 1, 0.5, 3, and 1.1 hydrogens respectively. The signal at δ 3.43 had only 58% of the expected intensity for one hydrogen. We attribute this to partial hydration of the carbonyl group in D_2O. Attempts to recrystallize the salt from ethanol – ethyl acetate did not raise the melting point and much was apparently converted to ketal or hemiketal which did not crystallize.

5,6-exo-d_2-Norbornene and 5,6-endo-d_2-Norbornene

Norbornadiene was reduced in methanol over 30% palladium charcoal until an excess of 30% over one mole of deuterium was absorbed. Gas–liquid chromatography on a 20 ft × 3/8 in. column with 30% SE-30 packing at 120°C gave retention times for norbornadiene of 15.5 min, norbornene 16.5 min, and norbornane 20 min. The product from the reduction contained 80% 5,6-*exo*-dideuterionorbornene and 20% of deuterated norbornane. This mixture was used for preparation of the deuterated *N*-benzoyl aziridine or converted by the method of Werstiuk (16) to 5,6-*endo*-dideuterionorbornene.

*N-Benzoyl 6,7-exo-Dideuterio-3-exo-azatricyclo[3.2.1.$0^{2,4}$]octane(**8**)*

A mixture of 10 g of 5,6-*exo*-dideuterionorbornene and 31 g of benzoyl azide was heated at 40°C for four days. Excess azide was destroyed by heating the mixture to 90°C. Isocyanate was removed by distillation in a bath at 50°C under 10 Torr. The residual oil was purified by distillation over a short path at 120°C, 5 × 10^{-3} Torr; ^1H nmr δ: 7.3–8.3 (5H, aromatic), 2.75 (2H), 2.6 (2H), and a set of signals between 1.8 and 0.8 (4H). Its ^2H nmr spectrum gave a single peak near δ 1.6.

*5,6-exo-d_2-Oxazoline (**9**)*

The *N*-benzoyl aziridine **8** was heated at 240°C for 25 min, then the resulting oxazoline distilled over a short path at 110°C, 0.3 Torr. The yield from the norbornene was 14.6 g (69%). It had ν_{max} 2225 (w), 2200 (w shoulder), 2180 (w), 1675 (w shoulder), 1645 (s), 1448 (s), 1355 (s) 1320 (s), 1025 (s), 985 (s) cm^{-1}. Its ^1H nmr spectrum had signals at δ 7.4 to 8.35 (aromatic, 5H), 4.56 (d, J = 7 Hz, 1H), 4.2 (d, J = 7 Hz, 1H) 2.46 (2H), 0.9–1.15 (m, 4H). Its ^2H nmr spectrum gave a single peak near δ 1.6.

*5,6-exo-d_2 Hydroxybenzamide (**10**)*

A suspension of 14.6 g of oxazoline **9** in 50 mL of 2 *N* sulfuric acid was heated under reflux (N_2 atmosphere) for 5 h. The mixture was cooled, neutralized with sodium carbonate, then extracted with methylene chloride. The extracted product crystallized from ethyl acetate giving 11 g, mp 115°C. The mother liquor contained 3.7 g, mainly unchanged oxazoline.

The hydroxybenzamide **10** had ν_{max} 3620 (w), 3420 (m), 2180 (w), 1640 (s), 1602 (w), 1580 (m), 1510 (s), 1485 (s), and 1040 (m) cm^{-1}. Its ^1H nmr spectrum had signals at δ 6.8–8.1 (6H reduced to 5H on exchange with *p*-toluenesulfonic acid in D_2O), 4.6 (1H, exchanged with D_2O), 3.77 (2H), 2.3 (2H, d, J = 9 Hz), and a set of signals between δ 0.66 and 2.0 (4H). Its ^2H nmr gave a single signal near δ 1.5 in trifluoroethanol relative to external TMS.

*5,6-exo-d_2 Ketobenzamide (**11**)*

Dry chromium trioxide (6 g; 60 mmol) was added to a cooled,

Can. J. Chem. Downloaded from www.nrcresearchpress.com by 210.87.254.6 on 09/06/12
For personal use only.

stirred solution of 9.5 g of pyridine (120 mmol) in 150 mL of pure dichloromethane (15). The solution was left at room temperature for 15 min, then a concentrated solution of the hydroxybenzamide **10** (2 g, 10 mmol) was added rapidly. The mixture was stirred for 15 min, then the solution decanted from the dark gum. The gum was washed twice with dichloromethane. The combined CH_2Cl_2 layers were washed with three 100 mL portions of 5% sodium hydroxide solution, 100 mL of 5% hydrochloric acid, 100 mL of 5% aqueous sodium bicarbonate solution, then 100 mL of saturated brine. The product recovered from the CH_2Cl_2 crystallized from a methanol–chloroform mixture to give 1.97 g, mp 207–208°C.

Its ^2H nmr spectrum in chloroform gave a single signal near δ 2.2.

*2-*exo*-Amino-5,6-*exo*-dideuterionorbornan-3-one Hydrochloride (2)*

A suspension of the benzamido ketone **11** (6.95 g) in 400 mL of 1 *N* hydrochloric acid under argon was refluxed for 3 h. The cooled solution was extracted with ether, then the ether back-washed with 1 *N* hydrochloric acid. The aqueous layers were evaporated to dryness in a bath at 50°C under 15 Torr yielding a white crystalline solid. This was purified by suspension in ethyl acetate, then filtration. It had mp 148–152°C dec. (Pyrex capillary). Attempted recrystallizations from ethanol – ethyl acetate led to much amorphous material (hemiketal) and crystals with wider melting range. Its ^1H nmr spectrum in D_2O–DSS gave signals at δ 3.40 (d, J = 3 Hz), 2.97, 2.78, and 2.32 in the ratios 1:0.69:2.2:1.3 respectively. The signal at δ 3.40 had only 60% of the expected intensity. We consider this to be due to partial hydration of the carbonyl (see unlabelled analogue). *Anal.* calcd.[11] for $C_7H_{10}D_2ClNO$: C 52.03, H 7.43, N 8.67; found: C 51.99, H 7.44, N 8.78.

*N-Benzoyl-6,7-*endo*-dideuterio-3-*exo*-azatricyclo-[3.2.1.0^{2,4}]octane (8,* endo-d_2*)*

This was prepared from the 3,6-*endo* deuterated norbornene and benzoyl azide by heating at 40°C for nine days. The *N*-benzoyl aziridine distilled over a short path at 120°C under 4 × 10^{-3} Torr, yield 75%. It had ν_{max} (CCl_4) 2190 (w) and 1679 (s) cm^{-1}. The ^1H nmr spectrum δ: 7.2–8.2 (aromatic, 5H), 2.84 (2H), 2.63 (2H), 1.63, 1.52, 1.23, 0.97, and 0.78 (4H).

*5,6-*endo*-d_2-2,3-*exo*-Oxazoline (9,* endo-d_2*)*

This was prepared by heating the *N*-benzoylaziridine at 245°C for 30 min. It distilled over a short path at 130°C under 0.05 Torr. It gave ^1H nmr signals at δ 7.2–8.3 (aromatic, 5H), 4.58 (d, J = 7 Hz, 1H), 4.20 (d, J = 7 Hz, 1H), 2.45 (2H), 1.5 (m, 2H), 1.23, 1.03 (multiplets, 1H).

*5,6-*endo*-d_2-Hydroxybenzamide (10,* endo-d_2*)*

The oxazoline **9** (*endo-d_2*) was hydrolysed by 2 h refluxing with 2 *N* sulfuric acid. The hydroxybenzamide was surprisingly soluble in acid, so the aqueous solution was neutralized before extraction with chloroform. It crystallized from dichloromethane–hexane mixture, mp 114°C. It had ν_{max} 3620 (w), 3420 (s), 2190 (w), 1642 (s), 1580 (m), 1512 (s), 1470 (s) cm^{-1}. It gave ^1H nmr signals at δ 3.88 (2H), 3.80 (1H, exchanged with D_2O), 2.35 (1H), 2.22 (1H), 1.83, 1.67, 1.46, 1.2, 1.03 (4H). Its ^2H nmr spectrum in chloroform gave a single peak. A small shoulder on the lower-field side of the peak corresponded to approximately 2% of another deuterated species.

*5,6-*endo*-d_2-Ketobenzamide (11,* endo-d_2*)*

The hydroxybenzamide was oxidized in methylene chloride – pyridine (see *exo* isomer for details) giving the sparingly soluble ketone, mp 215°C. It had ν_{max} 3440 (w), 2200 (w), 1703 (s), 1663 (s), 1603 (w), 1593 (w), 1511 (s), and 1485 (s) cm^{-1}. Because of its low solubility its ^1H nmr spectrum was not recorded. Its ^2H nmr spectrum in chloroform gave a single signal near δ 2.2.

*2-*exo*-Amino-5,6-*endo*-dideuterionorbornan-3-one Hydrochloride (3)*

The benzamido ketone (**11**, *endo-d_2*) (3.4 g) was hydrolysed as for the *exo-d_2* isomer. The crystalline solid after evaporation of the water was suspended in dioxane, then collected by filtration. The first crop (1.7 g, 71%) had mp 153°C dec. after drying *in vacuo*. Subsequent crops (297 mg) melted at 150°C dec. Its ^1H nmr spectrum in D_2O–DSS had signals at δ 3.42 (d, J = 3 Hz), 3.02, 2.82, and 2.4 in the ratio of 1.0, 0.5, 1.7, and 1.35 hydrogens respectively. The signal at δ 3.42 (2-hydrogen) had only 59% of the expected intensity. As in the case of the unlabelled and 5,6-*exo* dideuterio analogues we believe this is due to partial hydration of the carbonyl.

*2-*endo*-Aminonorbornane-3-one Hydrochloride (4)*

The mono-oxime of norbornane-2,3-dione (18) (5 g) was added slowly to a stirred cold solution of 15 g of stannous chloride in 20 mL of concentrated hydrochloric acid. The mixture was left at room temperature for 2 h, then diluted with 300 mL of water and extracted with 3 × 100 mL of ether. The aqueous layer was saturated with hydrogen sulfide, then filtered. The filtrate was taken to dryness on a rotary evaporator below 50°C, giving 4.5 g of crude hydrochloride. Quick recrystallization of this from ethanol on addition of ethyl acetate gave 1.5 g of quite pure amine hydrochloride, mp 153–157°C. Its ^1H nmr spectrum had peaks centered near δ 1.78 (8H), a broad signal centered at δ 2.90 (3H), and a doublet centered at δ 3.80 (1H, J = 4 Hz). After 60 h in D_2O the signal at δ 2.9 had reduced to two hydrogens. Addition of *p*-toluenesulfonic acid resulted in a spectrum with signals at δ 1.78 (6H), 2.90 (2H), and 3.80 (1H, d, J = 4 Hz). *Anal.* calcd. for $C_7H_{12}ClNO$: C 52.03; H 7.43, N 8.67; found: C 51.99, H 7.44, N 8.78.

2-Diazonorbornan-3-one (5)

To a stirred suspension of 1.44 g of the monotosylhydrazone of norbornan-2,3-dione (17) in 4 mL of water under 10 mL of pentane, was added 464 mg of sodium hydroxide in 1 mL of water. The pentane layer was separated and replaced at roughly 15 min intervals until no color entered the organic phase (ca. 2 h). The pentane was dried, then distilled. The yellow residue was distilled over a short path at 65°C, 0.05 Torr, giving a yellow oil (389 mg, 62%).

This gave ^1H nmr signals at δ 3.55 (1H, s), 2.78 (1H, s), 2.2–1.3 (6H, m). The diazoketone could be stored for a few days at 0°C in the dark.

*Deamination of 2-*exo*-Amino-5,6-*endo*-dideuterionorbornan-3-one (3)*

A solution of 2.0 g of the hydrochloride of **3**, mp 153°C dec., in 15 mL of 0.5 *N* sulfuric acid was cooled to 15°C. A solution of 3 g of sodium nitrite in 4 mL of water was added slowly to the magnetically stirred solution over the course of 40 min. Another 10 mL of 0.5 *N* sulfuric acid was added in two portions, then the solution stirred for a further 40 min. A layer of pure ether was added, then solid sodium bicarbonate was added cautiously until the solution was neutral. The aqueous layer was extracted with three 25 mL portions of ether. The ether layers were washed with 5 mL of sodium bicarbonate solution, dried, and carefully distilled to a volume of around 8 mL. This was then made up to 10.0 mL for determination of nortricyclanone; glc comparison with a standard showed this to contain 59 mg of deuterated nortricyclanone (4.3%). The ether solution (A) was then concentrated for examination of the nortricyclanone and ketols (see below).

Can. J. Chem. Downloaded from www.nrcresearchpress.com by 210.87.254.6 on 09/06/12
For personal use only.

The aqueous layers were extracted with three 15 mL portions of chloroform, giving 127 mg of oil which was immediately acetylated with acetic anhydride – pyridine (B).

The combined aqueous layers (pH ~ 8) were evaporated to dryness under reduced pressure. Enough 6 *N* sulfuric acid was added to make the suspension strongly acid, then this was extracted successively with methylene chloride and chloroform, finally drying the aqueous layer to a paste, using anhydrous sodium sulfate in the presence of chloroform. The combined extracts were dried and distilled giving 1.23 g of acids (yield calculated as $C_7H_{10}O_4$, 64%).

The ether extract (A) was absorbed on 5 g of neutral alumina, activity I. The nortricyclanone was eluted rapidly with ether. It was pure enough after short path distillation for determination of its ^{2}H nmr, ^{13}C nmr, and mass spectra. The ketols (142 mg) were eluted with 10% methanol in chloroform, then converted to their acetates (C). The total yield of ketol acetates (B + C) was 17% (calcd. as $C_9H_{12}O_3$).

The water soluble acids were converted to methyl esters using diazomethane. A mixture of three hydroxy esters was separated from this by chromatography on a 25-fold ratio of alumina (activity I) eluting with 1:1 ether–chloroform. The 211 mg of hydroxy esters was further purified by hplc. Only one was obtained reasonably pure. It had ν_{max} 3610, 3450, 2175, and 1725 cm^{-1}. Its ^{1}H nmr spectrum had a broad set of signals from δ 0.7–2.7 (7H), 2.9 (OH) (0.8H, s), 3.73 (3H, s) superimposed on a multiplet from 3.2 to 4.3 (0.6H). *Anal.* calcd.[11] for $C_8H_{12}D_2O_3$: C 59.98, H 8.80; found: C 59.32, H 8.75.

Deamination of 2-exo-*Amino-5,6-exo-dideuterionorbornan-3-one*

(a) In Dilute Acid

The *exo*-d_2 was deaminated in dilute sulfuric acid as described for the *endo*-d_2 amine. The yield of nortricyclanone was 2.1% and that of 2-*exo*-hydroxynorbornan-7-one was 15.5%. Preparative runs on a total of 4.0 g of hydrochloride gave a 6.4% yield of pure **27**, 1.8 g of readily extracted acids rich in 3-cyclohexene-1-carboxylic acid, and 1.0 g of very water soluble acids. The latter contained three hydroxy acids of which one was obtained fairly pure by chromatography of the methyl esters on alumina, followed by hplc. The ester had ν_{max} 3620, 3450, 2170, and 1725 cm^{-1}. *Anal.* calcd. for $C_8D_2H_{12}O_3$: C 59.98, H 8.80; found: C 59.70, H 8.55.

(b) In 1 M Sodium Acetate in 50% Aqueous Acetic Acid

Sodium nitrite (195 mg) was added to an ice-cold solution of 457 mg of the hydrochloride of **2** in 4 mL of 50% (v/v) aqueous acetic acid. After four min the cooling bath was removed. A further 150 mg of sodium nitrite was added in portions over the next 2 h. After a total time of 4 h the solution was cooled in ice, a layer of ether added, then neutralized with cooling, using sodium carbonate (pH ca. 8). Ether extraction gave 218 mg of neutral product (containing some cyclohexenoic acid). The nortricyclanone yield was 2.5%.

The neutral product was acetylated yielding 170 mg of acetates (36% calculated as ketol acetate). The yield of 2-*exo*-acetoxynorbornan-7-one was approximately 18%.

Deamination of 2-exo-*Aminonorbornan-3-one*

(a) In Dilute Sulfuric Acid

This was performed as described for the 5,6-*endo*-d_2 aminoketone. The yield of nortricyclanone was 3.1% and that of 2-acetoxynorbornane-7-one was 15.5%. The total yield of neutral product calculated as ketol was 25%. Varying the ratio of sulfuric acid to amine five-fold did not significantly alter the yield of either product. No 2-*endo* or 2-*exo*-acetoxynorbornan-3-one were detected among the products after acetylation. The yield of readily extracted acids was 10% by weight. Of this, the main acid (6% yield) was 3-cyclohexenoic acid. This was converted to its *p*-bromophenacyl ester and methyl ester for identification and spectra. Three hydroxy acids were isolated from the very water-soluble acids, but their structures were not established (see deamination of **3**).

(b) In 50% Aqueous Acetic Acid

(1) Sodium nitrite (284 mg) was added in portions during 22 min to a stirred solution of 262 mg of 2-*exo*-aminonorbornane hydrochloride in 3 mL of 50% acetic acid (v/v) in an ice bath. The mixture was left at room temperature for 1.5 h. After addition of 10 mL of ether, the solution was cooled in an ice-bath, then neutralized by addition of 0.9 g of sodium hydroxide in 3 mL of water, followed by sodium carbonate, then excess sodium hydrogen carbonate (pH ~ 8). Ether extraction (3 × 15 mL) gave an ether solution which was concentrated to ca. 3 mL, then made up to 5.0 mL for glc analysis. The yield of nortricyclanone was 4.1%. The isolated neutral product, which was a mixture of ketols and their acetates, weighed 94 mg.

(c) In 1 M Sodium Acetate in 50% Aqueous Acetic Acid

When 238 mg of amine hydrochloride was deaminated as in (b), but in 3 mL of 1 *M* sodium acetate in 50% (v/v) acetic acid, 92 mg of ether-extracted neutral product was obtained. The yield of nortricyclanone was 4.1%. The neutral compounds from runs (b) and (c) were combined, acetylated, and the main acetate isolated by preparative tlc (10% yield from hydrochloride). It was shown to be 2-*exo*-acetoxynorbornan-7-one by glc and ^{1}H nmr.

(d) In a 1 M Solution of Sodium Acetate in Acetic Acid

A suspension of 435 mg of 2-*exo*-aminonorbornan-3-one hydrochloride in 6 mL of 1 *M* sodium acetate in acetic acid was warmed until the bulk dissolved. Under an argon atmosphere, 600 mg of sodium nitrite was added over a period of 1.5 h to the stirred solution at room temperature. After 4 h a further 110 mg of sodium nitrite was added, then stirring continued for 1 h. Ether and 5 mL of water were added, then the solution was cooled to 0°C and taken to pH 8, first with sodium hydroxide solution, then solid sodium bicarbonate. It was then extracted three times with equal volumes of ether. The dried ether solution was concentrated carefully to ca. 3 mL volume, then made up to 5.0 mL for quantitative glc analysis. The nortricyclanone yield was 9%. The solution was then combined with 18 mg of product extracted by methylene chloride, then made up to 1.0 mL for glc analysis of the 2-acetoxy-7-one **15**. The yield of **15** was 12%.

The total neutral yield (some loss of nortricyclanone) was 273 mg (estimated as ketol acetate, 61%). Besides the 7-ketone and nortricyclanone, nine other products were present in low yield as indicated by glc on column B. If 2-*exo*-acetoxynorbornan-3-one was present it amounted to less than 3% of the total product.

Deamination of 2-endo-*Aminonorbornan-3-one* (*4*)

(a) In Water

A solution of 300 mg of *endo* amine hydrochloride in 2 mL of 0.5 *N* sulfuric acid was cooled to 15°C. A solution of 0.5 g of sodium nitrite in 1 mL of water was added dropwise during 20 min to the stirred acid solution. A further 1 mL of 0.5 *N* sulfuric acid was then added and stirring continued for 15 min. After addition of 5 mL of ether, the mixture was neutralized using sodium bicarbonate. The ether layer was separated, then the aqueous layer washed with 2 × 10 mL of ether. The ether extracts were back-washed with saturated sodium bicarbonate solution. The dried ether extracts were concentrated, then made up to 10.0 mL for quantitative glc analysis. Less than 0.2% of nortricylanone was formed.

The aqueous solutions were acidified and extracted with 3 ×

Can. J. Chem. Downloaded from www.nrcresearchpress.com by 210.87.254.6 on 09/06/12
For personal use only.

10 mL of ether, yielding 50 mg of acid. This was mainly 3-cyclohexene-1-carboxylic acid, identified by the nmr, ir, and mass spectra of its methyl ester.

The water soluble acidic products contained a hydroxy acid with nearly identical spectral properties to the main one described for deamination of 2-*exo*-aminonorbornan-3-one and its deuterated analogues (see deamination of **3**).

(b) In 50% Acetic Acid

A solution of 352 mg of the base hydrochloride in 3 mL of 50% (v/v) acetic acid was cooled in ice, then 150 mg of sodium nitrite added with stirring over 3 min. The solution was removed from the ice bath. After 15 min a further 100 mg of nitrite was added, followed after 20 min by 50 mg of nitrite. After a further 30 min at room temperature the mixture was cooled in ice, 10 mL of ether added, followed by slow addition of a solution of 0.9 g of sodium hydroxide in 3 mL of water. Neutralization was completed using solid sodium carbonate, the final pH being near 8. Three extractions using 15 mL of ether for each gave a solution which was dried, concentrated, then made up to 10.0 mL for quantitative glc analysis. The yield of nortricyclanone was 1.5%. The total neutral product was acetylated. Three ketol acetates were identified by glc. In order of decreasing yield these were 2-*endo*-acetoxynorbornan-3-one (**14**), 2-*exo*-acetoxynorbornan-7-one (**15**), and 2-acetoxybicyclo[3.1.1]heptan-6-one (**18**).

(c) In 1 M *Sodium Acetate in 50% Acetic Acid*

A solution of 351 mg of amine hydrochloride in 3 mL of 1 *M* sodium acetate in 50% (v/v) acetic acid was deaminated as described in (b). The yield of nortricyclanone was 1.5%. The ketol products were formed in similar ratio to those described in (b).

(d) In Acetic Acid

A solution of 350 mg of base hydrochloride in 3 mL of acetic acid was deaminated as in (b), except that the reaction mixture was left for 2 h after the final nitrite addition, and 3 mL of water was added prior to neutralization. The yield of nortricyclanone was 2.3%. Again the same ketols were produced, in similar ratios.

(e) In 1 M *Sodium Acetate in Acetic Acid*

The deamination was carried out as in (d) except that the final reaction period was extended to 3 h. The yield of nortricyclanone was 3.6%. The 2-*exo*-hydroxynorbornan-7-one now became the major ketol product followed by 2-*endo*-hydroxynorbornan-3-one and 2-hydroxybicyclo[3.1.1]heptan-6-one (as alcohols and acetate) in decreasing abundance.

Deamination of 2-Diazonorbornan-3-one (5)

(a) In Very Dilute Sulfuric Acid

Freshly distilled diazoketone (407 mg) was suspended in 5 mL of water containing 0.05 mL of 0.5 *N* sulfuric acid. There was rapid gas evolution. When this ceased the solution was made basic using sodium bicarbonate, then extracted with 3 × 5 mL of methylene chloride. This gave 329 mg (87% calculated as ketol) of neutral product containing some 3-cyclohexene-1-carboxylic acid. The ratio of areas of the two main products was 1.4 (2-*endo*-hydroxynorbornan-3-one **14**) to 1 (2-hydroxybicyclo-[3.1.1]heptan-6-one **18**). The yield of nortricyclanone was in the order of 1%.

(b) In Water

A mixture of 639 mg of diazoketone **5** and 5 mL of water was stirred in a bath at 15°C. Evolution of gas started in less than 1 min and accelerated with time. After 30 min the main reaction was complete. Two drops of 0.6 *N* sulfuric acid were added to ensure complete reaction. The mixture was extracted with ether, then the ether washed with saturated sodium bicarbonate solution. The original aqueous solution was saturated with sodium sulfate, then extracted three times with 10 mL portions of chloroform, which were in turn washed with the bicarbonate solution. The aqueous layers were acidified and extracted with chloroform to give the acidic products.

The ether extract was concentrated to ca. 5 mL, then made up to 10.0 mL for glc analysis. The yield of nortricyclanone was thus estimated by comparison with a standard solution to be 1.3%.

The yield of the various fractions was: (*a*) ether extract, 222 mg; (*b*) chloroform extracted neutrals, 127 mg; (*c*) acids (containing any very water-soluble neutral products), 153 mg. The acid was mainly cyclohexene-3-carboxylic acid, while the neutral extracts were mixtures of **14** (R = H) (approximately 39% yield) and **18** (R = H) (approximately 20% yield).

(c) In 50% Acetic Acid

Freshly distilled diazoketone (ca. 450 mg) was added to ice-cold 50% (v/v) acetic acid with or without added sodium acetate. After disappearance of the yellow color and cessation of nitrogen evolution, the solution was partially neutralized using 0.8 g of sodium hydroxide in 3 mL of water, with ice cooling. A layer of ether was added, and neutralization completed using sodium bicarbonate. The neutral products and some 3-cyclohexene-1-carboxylic acid were extracted into ether (3 × 10 mL). The dried ether solution was concentrated, then made up to 5.0 mL for analysis.

(1) 50% Acetic Acid. Reaction was complete in less than 1 min. The yield of nortricyclanone was 1.5%. The total neutral product was 93% by weight of diazoketone used.

(2) 1 M *Sodium Acetate in 50% Acetic Acid.* Reaction was complete in 5 min. Yield of nortricyclanone 12%. The total neutral product was 82% of the diazoketone used.

(3) 4 M *Sodium Acetate in 50% Acetic Acid.* Reaction was very slow even at room temperature. It was complete in 45 min at 20°C. The yield of nortricyclanone was 17.5%. The neutral products isolated were 65% by weight of diazoketone.

Aside from the increase in nortricyclanone yield, the most striking effects of the sodium acetate were the slowing of reaction and the increase in amount of 2-*exo*-acetoxynorbornan-7-one formed. This was produced in trace amounts in 50% acetic acid, in three times the amount of ketol acetates **14** or **18** when 1 *M* acetate was present, and four times the amount of each of these acetates in the presence of 4 *M* sodium acetate. Even with 4 *M* NaOAc present, the amount of ketols (**14**, **15**, and **18**, R = H) exceeded the amount of ketol acetates (ratio of areas 1.6). For 1 *M* sodium acetate the ratios of areas was 2.9.

(d) In 100% Acetic Acid

Cold glacial acetic acid (3 mL) or 1 *M* sodium acetate in glacial acetic acid was added rapidly to ca. 300 mg samples of freshly distilled diazoketone. When the diazo color had gone and gas evolution ceased, 2 mL of water was added, then during cooling in ice a solution of 1.5 g of sodium hydroxide in 3 mL of water was added. A 10 mL layer of ether was added, then neutralization completed using first sodium carbonate, then sodium hydrogen carbonate (pH taken to near 8). Thorough ether extraction (4 × 15 mL) gave the neutral products and some acid. The dried solutions were concentrated, then made up to 5.0 mL for glc analysis.

(1) Acetic Acid. The reaction time was approximately 5 min. The neutral products weighed 233 mg, of which 16 mg was nortricyclanone. The yield of nortricyclanone was 8.5% and ketols (calcd. as acetates) 66%.

(2) 1 M *Sodium Acetate in Acetic Acid.* The reaction time was approximately 5 min. The yield of nortricyclanone was 8.4% and of ketols and ketol acetates was 67% (calcd. as acetates).

The products from deamination in acetic acid or 1 *M* sodium acetate in acetic acid were nearly identical. The ratio of peak

areas (column B, 190°C) for 2-*exo*-acetoxynorbornane-7-one and the ketol acetates **14** and **18** was 2.5 : 1 : 1. Small amounts of ketols were also present.

To study the action of nitrous acid and nitrogen oxides on the ketols **14** and **18** (R = H), 122 mg of neutral mixture from deamination of diazoketone was dissolved in 1 mL of water plus 1 mL of 0.5 *N* sulfuric acid. To this was added dropwise over 30 min at 10°C a solution of 205 mg of sodium nitrite in 1 mL of water. The solution was then neutralized with sodium bicarbonate and extracted with methylene chloride. The recovered material (115 mg) had very similar composition (glc) to the starting material.

Diazoketone (208 mg) was suspended in 3 mL of water containing 300 mg of sodium nitrite. To the stirred solution was added 0.3 mL of 0.6 *N* sulfuric acid during 10 min. The solution was made basic (pH 8.5) using sodium carbonate, then the neutral products extracted into ether. The dried ether extract was concentrated, then made up to 5.0 mL for glc analysis. The yield of nortricyclanone was 3.6%. On evaporation the ether yielded 78 mg of crystalline ketols (41%). The basic solution yielded 36 mg of 3-cyclohexene-1-carboxylic acid and 50 mg of ketols (30%).

Nortricyclanone

Unlabelled

Authentic nortricyclanone (49) had ν_{max} 1770 (m, shoulder), 1750 (s) cm^{-1}; ^1H nmr signals at δ 2.56–2.06 (2H, m), 2.06–1.75 (3H, m), 1.65 (s, 1H), and 1.22 (t, J = 5 Hz, 2H). Its mass spectrum had *m/e* 109 (5), 108 (40), 107 (5), 81 (9), 80 (75), 79 (100), 8 (10), 77 (32).

From endo-d_2 *Aminoketone 3*

The ether eluates from chromatography of neutral products (extract A) were distilled in a chain of bulbs at 70°C under 13 Torr. Its mass spectrum had *m/e* 111 (7), 110 (34), 109 (7), 83 (8), 82 (69), 81 (100), 80 (34), 79 (21), 78 (20). From this we estimate it to contain 8% d_3, 86% d_2, and 6% d_1 species. Its ^2H nmr spectrum is shown in Fig. 3 and its ^{13}C nmr spectrum in Fig. 2.

From exo-d_2 *Aminoketone 2*

Its mass spectrum had peaks *m/e* 111 (1.0), 110 (12), 109 (87), 108 (13), 82 (23), 81 (100), 80 (99), 79 (48), 78 (51), 77 (24). From this it was estimated to contain 4% d_2, 93% d_1, and 3% d_0 species.

Its ^2H nmr spectrum is shown in Fig. 1 and its ^{13}C nmr spectrum in Fig. 2.

2-exo-*Acetoxynorbornan-3*-exo-*ol*

This was prepared by partial acetylation of the known 2,3-*exo*-diol (50) using 1.2 mol of acetyl chloride in pyridine at 0°C. After purification by chromatography on tlc silica gel using 2% ethanol in chloroform for elution it crystallized as plates from pentane, mp 46–47°C. It had ν_{max} 3595, 3460, and 1728 cm^{-1}, and gave ^1H nmr signals at δ 4.60 (1H, pair of barely resolved doublets, J_1 = 6 Hz), 3.88 (1H, d, J = 6 Hz), 2.13 (3H, s). *Anal.* calcd. for $C_9H_{14}O_3$: C 63.51, H 8.29; found: C 63.68, H 8.19.

2-exo-*Acetoxynorbornan-3-one (13, R = Ac)*

Oxidation of 2-*exo*-acetoxynorbornan-3-ol with Jones' reagent (47) in acetone or Ratcliffe–Rodehorst reagent (15) in methylene chloride gave good yields of the acetoxy ketone as an oil. It was purified by chromatography on 100-fold weight of tlc silica gel using 2% ethanol in chloroform for elution, then distilled over a short path at 115°C, 15 Torr. It had ν_{max} 1763 and 1742 cm^{-1} and ^1H nmr signals at δ 4.60 (1H, d, J = 3 Hz), 2.61 (2H, s), and 2.11 (3H, s). *Anal.* calcd. for $C_9H_{12}O_3$: C 64.27, H 7.19; found: C 64.08, H 7.17.

2-exo-*Hydroxynorbornan-3-one (13, R = H)*

The corresponding acetate could by hydrolysed using 10 mol% of sodium methoxide in methanol at 0°C for 1 h, or a saturated solution of sodium carbonate in 50% aqueous methanol at room temperature for 1 h. The product had mp 146°C and ν_{max} 3580, 3380, and 1700 cm^{-1}. It deteriorated quite rapidly at room temperature in air.

A solution of 48 mg of 2-*exo*-hydroxynorbornan-3-one in 2 mL of 50% acetic acid was prepared. Sodium nitrite (176 mg) was added over 15 min to the stirred solution, then the mixture was left at room temperature for 25 min. The acid was neutralized as in the work-up of comparable deamination and the neutral product recovered (50 mg). This appeared to be essentially pure starting material by glc.

2-endo-*Acetoxynorbornan-3*-endo-*ol*

The known diol (50, 51) was partially acetylated by slowly adding 1.2 mol of acetyl chloride to a solution of the diol in pyridine at 0°C, then leaving for 3 h at room temperature. Purification as for the 2,3-*exo* monoacetate gave the monoacetate as crystals, mp 47–49°C. It had ν_{max} 3590, 3495, and 1725 cm^{-1} and gave ^1H nmr signals at 4.72 (1H, q, J_1 = 9, J_2 = 5 Hz), 4.05 (1H, q, J_1 = 9, J_2 = 5 Hz), 2.79 (1H, s, OH), 2.41 (2H, br s), 2.13 (3H, s). *Anal.* calcd. for $C_9H_{14}O_3$: C 63.51, H 8.29; found: C 63.69, H 8.35.

2-endo-*Hydroxynorbornan-3-one (14, R = H)*

The ketol from deamination of 2-diazonorbornan-3-one **5** had ν_{max} 3450 and 1746 cm^{-1}. Its mass spectrum had peaks at *m/e* 127 (M + 1) (3.5), 126 (12), 124 (3), 99 (3), 98 (13), 97 (3), 86 (6), 84 (9), 80 (5), 79 (3), 70 (3), 69 (4), 68 (5), 67 (12), 66 (3.5), 65 (4), 58 (23), 57 (100), 55 (21).

Its acetate (**14**, R = Ac) was an oil with ν_{max} 1759 cm^{-1} and shoulders at 1745 and 1731 cm^{-1}. Its ^1H nmr spectrum had signals at δ 5.00 (1H, d, J = 5 Hz), 2.93, 2.76 (2H), and 2.17 (3H, s). Its mass spectrum had peaks at *m/e* 168 (33), 126 (15), 125 (100), 99 (24), 97 (34), 79 (3), 71 (4), 67 (21), 57 (15). This proved identical to an authentic sample prepared by oxidation of 2-*endo*-acetoxynorbornan-3-*endo*-ol using Ratcliffe–Rodehorst reagent (15).

2-Hydroxybicyclo[3.1.1]heptan-6-one (18, R = H)

This ketol from deamination of diazoketone **5** (4) had ν_{max} 3600, 3440, and 1768 cm^{-1} and gave ^1H nmr signals at δ 4.6 (1H, m), 3.88 (1H, OH), 3.10 (2H, m). Its mass spectrum had peaks at *m/e* 126 (3), 108 (5), 98 (26), 97 (15), 84 (11), 83 (26), 82 (5), 81 (10), 80 (12), 79 (9), 77 (4), 71 (10), 70 (35), 69 (15), 68 (5), 67 (23), 66 (7), 65 (3), 57 (28), 56 (35), 55 (100), 54 (40), 53 (15).

The corresponding acetate **18** (R = Ac) had ν_{max} 1774 and 1732 cm^{-1} and gave ^1H nmr signals at δ 5.58 (1H, m), 3.21 (2H, br), 2.07 (3H, s). Its mass spectrum had peaks at *m/e* 168 (1.5), 140 (6), 126 (12), 125 (10), 109 (6), 108 (58), 107 (4), 99 (8), 98 (9), 97 (12), 84 (9), 83 (13), 82 (6), 81 (50), 80 (100), 79 (58), 78 (6), 71 (20), 70 (15).

2-exo-*Acetoxynorbornan-5-one (17, R = Ac)*

A sample prepared following ref. 52 had ν_{max} 1740 cm^{-1} and ^1H nmr signals at δ 4.8 (1H, m, $w_{1/2}$ = 13 Hz), 2.63 (2H, $w_{1/2}$ = 18 Hz), and 2.01 (3H, s).

2-exo-*Acetoxynorbornan-7-one (15, R = Ac)*

Authentic **15** (R = Ac) (53) had ν_{max} 1903 (w), 1783 (s), 1770 (s), 1741 (s), 1729 (s), 1375 (m), 1240 (s), 1210 (w), 1139 (w), and 1065 (m) cm^{-1}. Its ^1H nmr spectrum was nearly identical to one kindly sent by Prof. Gassman, with signals at δ 4.83, 4.92, 4.98 (1H), and 2.03 (3H, s). Its mass spectrum had *m/e* 168 (1.6), 108 (78), 81 (58), 80 (100), 79 (30). A more intense spectrum gave *m/e* 175 (5), 169 (18), 168 (100), 167 (10.6). Its ^{13}C nmr spectrum had

Can. J. Chem. Downloaded from www.nrcresearchpress.com by 210.87.254.6 on 09/06/12
For personal use only.

Can. J. Chem. Downloaded from www.nrcresearchpress.com by 210.87.254.6 on 09/06/12
For personal use only.

signals at δ 213, 170.4, 71.7 (d, C-2), 43.2 (d, C-1) 37.8 (d, C-4), 35.1 (t, C-3), 22.9 (t, C-6), 21.1 (q, CH_3CO), 18.7 (t, C-5).

Labelled ***15*** *from* endo-d_2 *Aminoketone* ***3*** *(****29*** *+* ***30****)*

This was purified by hplc on a Porasil-A column using 2.5% acetone in hexane as solvent. It had ν_{max} 2200 (w), 1837 (w), 1775 (s), 1740 (s), 1725 (shoulder), 1375 (m), 1245 (s), 1105 (s) cm^{-1}. Its mass spectrum had signals at *m/e* 170 (1), 142 (4), 141 (1), 129 (1), 128 (12), 127 (8), 126 (2), 114 (1), 113 (2), 112 (4), 111 (7), 110 (43), 109 (57), 108 (6), 100 (15), 99 (15), 98 (13), 97 (5), 86 (11), 85 (13), 84 (28), 83 (89), 82 (100), 81 (99). A more intense spectrum gave *m/e* 171 (17), 170 (100), 169 (17.6) from which we estimate[7] a content of 94% d_2 and 6% d_1 species. Its ^1H nmr spectrum is illustrated in Fig. 3, and its ^{13}C nmr spectrum in Fig. 2.

Labelled ***15*** *from* exo-d_2 *Aminoketone* ***2*** *(****27****)*

This was purified by hplc on a Porasil-A column using 2.5% acetone in hexane as eluant. It had ν_{max} 2200 (w), 1835 (w), 1770 (s), 1740 (s), 1725 (s, shoulder), 1135 (s), 1105 (s) cm^{-1}.Its mass spectrum had peaks at *m/e* 170 (1), 142 (2), 141 (1), 129 (1), 128 (11), 127 (7), 126 (2), 114 (2), 113 (2), 141 (1), 129 (1), 128 (11), 127 (7), 126 (2), 114 (2), 113 (2), 112 (4), 111 (9), 110 (88), 109 (10), 100 (15), 99 (16), 98 (7), 97 (5), 96 (3), 86 (7), 85 (12), 84 (17), 83 (89), 82 (100), 81 (71), 80 (26). A more intense spectrum had *m/e* 171 (25), 170 (100), 169 (25) from which we estimate[7] a content of 5% d_3, 83% d_2, and 12% d_1 species.

Methyl 3-Cyclohexene-1-carboxylate

The unlabelled ester gave a mass spectrum with *m/e* 141 (2.5), 140 (22), 139 (0.8), 125 (15), 111 (5), 109 (18), 108 (38), 82 (8), 81 (100), 80 (93), and 79 (51). It had ν_{max} 1728 (s) and 1650 (w) cm^{-1}.

Methyl Dideuterio-3-cyclohexene-1-carboxylate from ***3***

The readily extracted acid (CH_2Cl_2) from deamination of 2.1 g of *endo-*d_2 aminoketone hydrochloride **3** was esterified using diazomethane. The 463 mg of ester was absorbed from hexane onto 11 g of neutral alumina, activity 1. Hexane eluted 99 mg of nearly pure methyl ester of deuterated acid (**31** + **32**). Ether in hexane eluted 6 mg more (yield 105 mg, 5.8%). The remaining esters were much more polar. The purest ester after distillation over a short path at 100°C, 0.01 Torr, gave a mass spectrum with *m/e* 143 (3), 142 (27), 141 (4.5), 136 (4), 111 (20), 110 (16), 109 (39), 83 (100), 82 (76), 81 (78), 80 (20), 79 (12). The estimated composition is thus:[7] d_3, 0%; d_2, 88%; d_1, 12%.

p-*Bromophenacyl Ester of 3-Cyclohexene-1-carboxylic Acid*

The unlabelled ester had ν_{max} 3020 (wk), 2950 (wk), 2840 (w), 1740 (s), 1588 (s), 1160 (s), 1070 (m), and 1010 (m) cm^{-1}. Its ^1H nmr spectrum gave signals at δ 2.18 (7H), 5.30 (2H, s), 5.75 (2H, s), and 7.76 (4H, m).

p-*Bromophenacyl Esters of* ***31*** *+* ***32***

Deamination of 1.09 g of *endo-*d_2 aminoketone hydrochloride **3** in 0.5 *N* sulfuric acid was conducted as described above. The readily extracted acids (CH_2Cl_2) were converted to their potassium salts, then to the *p*-bromophenacyl esters in refluxing ethanol. The crystalline product (162 mg, 7.5%) gave a ^1H nmr spectrum with signals at δ 7.76 (4H, m), 5.75 (s, 1.4H), 5.30 (2H, s), and a set of signals centered at δ 2.2 (5.5H). This was identical to that of the unlabelled ester except for the diminished intensity of the vinyl hydrogen and high-field signals. Its ^2H nmr spectrum gave a signal near δ 5.8 and a pair near 2.2 and 1.9 with the intensity ratio of 1:25.

Acknowledgements

We are grateful to Drs. I. C. P. Smith and R. Deslauriers and their associates for the ^{13}C and ^2H nmr spectra, Dr. R. W. Retallack for preliminary experiments, Mr. P. Marshall for preparative work, and Mr. H. Seguin for analyses. We thank Professors P. Yates, N. H. Werstiuk, and J. C. Orr for valuable discussions.

1. O. E. Edwards and M. Lesage. Can. J. Chem. **41**, 1592 (1963).
2. O. E. Edwards and T. Sano. Can. J. Chem. **47**, 3489 (1969).
3. O. E. Edwards and Z. Paryzek. Can. J. Chem. **53**, 3498 (1975).
4. P. Yates and R. J. Crawford. J. Am. Chem. Soc. **88**, 1561 (1966).
5. R. A. Blattel and P. Yates. Tetrahedron Lett. 1069 (1972); 1073 (1972).
6. M. Hanack and J. Dolde. Tetrahedron Lett. 321 (1966).
7. H. E. Baumgarten and C. H. Anderson. J. Am. Chem. Soc. **83**, 399 (1961).
8. R. Granger, H. Técher, and A. Massiau. C. R. Acad. Sci. **250**, 4378 (1960).
9. P. G. Gassman and J. G. Macmillan. J. Am. Chem. Soc. **91**, 5527 (1969).
10. (*a*) M. Avaro and J. Levisalles. Bull. Soc. Chim. Fr. 735 (1967); 3166 (1969); 3173 (1969); 3180 (1969); (*b*) X. Creary. J. Org. Chem. **44**, 3938 (1979).
11. (*a*) M. Charpentier-Morize, J. M. Lefour, and N. J. Anh. Tetrahedron Lett. 1729 (1974); (*b*) J.-P. Bégué, M. Charpentier-Morize, C. Pardo, and J. Sansoulet. Tetrahedron Lett. **34**, 293 (1978).
12. J.-P. Bégué and M. Malissard. Tetrahedron, **34**, 2095 (1978).
13. (*a*) J. L. Simonson and L. N. Owen. The terpenes. 2nd ed. Vol. 2. Cambridge University Press, London. 1969. pp. 156–165; (*b*) W. G. Dauben and P. Laug. Tetrahedron, **20**, 1259 (1964); (*c*) J. W. Wilt and W. J. Wagner. J. Am. Chem. Soc. **90**, 6135 (1968); (*d*) J. M. Billy. Ph.D. thesis, University of Montreal, 1960; (*e*) R. M. Coates and J. P. Chen. Chem. Commun. 1481 (1970).
14. R. Huisgen, L. Möbius, G. Müller, H. Stangl, G. Sziemies, and J. M. Vernon. Chem. Ber. **98**, 3992 (1965).
15. R. Ratcliffe and C. R. Rodehorst. J. Org. Chem. **35**, 4000 (1970).
16. N. H. Werstiuk. Can. J. Chem. **48**, 2310 (1970).
17. K. B. Wiberg, B. R. Lowry, and T. H. Colby. J. Am. Chem. Soc. **83**, 3998 (1961).
18. K. Hohenlohe-Oehringen. Monatsh. Chem. **101**, 614 (1970).
19. H. J. Reich, M. Jautelat, M. J. Messe, F. J. Weigert, and J. D. Roberts. J. Am. Chem. Soc. **91**, 7445 (1969); J. B. Stothers, C. T. Tan, A. Nickon, F. Huang, R. Sridhar, and R. Weglein. J. Am. Chem. Soc. **94**, 858 (1972).
20. J. L. Fry and G. J. Karabatsos. *In* Carbonium ions. Vol. II. *Edited by* G. A. Olah and P. von R. Schleyer. Wiley Interscience, New York. 1970. pp. 521–571; W. Kirmse, J. Knist, and H. J. Ratajczak. Chem. Ber. **109**, 2296 (1976); R. Kirchen and T. S. Sorensen. J. Am. Chem. Soc. **101**, 3240 (1979).
21. (*a*) A. E. Evans. The reactions of organic halides in solution. Manchester Univ. Press, Manchester. 1946. p. 15; (*b*) J. L. Franklin. *In* Carbonium ions. Vol. I. *Edited by* G. A. Olah and P. von R. Schleyer. Interscience Publishers, New York. 1968. p. 85.
22. R. L. Baird and A. A. Aboderin. J. Am. Chem. Soc. **86**, 252 (1964); A. A. Aboderin and R. L. Baird. J. Am. Chem. Soc. **86**, 2301 (1964).

23. C. J. COLLINS, I. T. GLOVER, M. D. ECKART, N. J. RAAEN, B. M. BENJAMIN, and B. S. BENJAMINOV. J. Am. Chem. Soc. **94**, 899 (1972).
24. C. J. COLLINS and B. M. BENJAMIN. J. Am. Chem. Soc. **89**, 1652 (1967).
25. N. H. WERSTIUK. Can. J. Chem. **53**, 26 (1975).
26. A. NICKON, J. R. SIMONS, and B. HO. J. Org. Chem. **42**, 800 (1977).
27. H. HART and R. H. SCHLOSBERG. J. Am. Chem. Soc. **88**, 5030 (1966).
28. F. P. CAPPELLI, G. TIMMINS, and N. H. WERSTIUK. Can. J. Chem. **50**, 2163 (1972).
29. R. A. MOSS, C. J. TALKOWSKI, D. W. REGER, and C. E. POWELL. J. Am. Chem. Soc. **95**, 5215 (1973); W. KIRMSE, G. RAULEDER, and H.-J. RATAJCZAK. J. Am. Chem. Soc. **97**, 4141 (1975).
30. C. J. COLLINS. Chem. Soc. Rev. **4**, 251 (1975).
31. (*a*) H. MASKILL, R. M. SOUTHAM, and M. C. WHITING. Chem. Commun. 496 (1965); (*b*) R. A. MOSS. Acc. Chem. Res. **7**, 421 (1974).
32. O. E. EDWARDS and R. S. ROSICH. Can. J. Chem. **45**, 1287 (1967).
33. C. J. COLLINS and B. M. BENJAMIN. J. Org. Chem. **37**, 4358 (1972).
34. C. C. LEE and R. REICHLE. J. Org. Chem. **42**, 2058 (1977); C. C. LEE, R. REICHLE, and U. WEBER. Can. J. Chem. **56**, 658 (1978).
35. W. E. DEPUY, H. R. HUDSON, and P. A. KARAM. Tetrahedron Lett. 3193 (1971); H. R. HUDSON, A. J. KOPLICK, and D. J. POULTON. Tetrahedron Lett. 1449 (1975).
36. W. KIRMSE and R. SIEGFRIED. J. Am. Chem. Soc. **90**, 6564 (1968).
37. K. T. LIU. Tetrahedron Lett. 1129 (1978).
38. M. SAUNDERS, P. VOGEL, E. L. HAGEN, and J. ROSENFIELD. Acc. Chem. Res. **6**, 53 (1973).
39. H. J. KÖHLER and H. LISCHKA. J. Am. Chem. Soc. **101**, 3479 (1979).
40. J. B. LAMBERT, H. W. MARK, A. G. HOLCOMB, and E. S. MAGYAR. Acc. Chem. Res. **12**, 317 (1979).
41. H. C. BROWN. The non-classical ion problem. Plenum Press, New York. 1977.
42. M. AVARO, J. LEVISALLES, and J. M. SOMMER. Chem. Commun. 410 (1968).
43. T. E. KING and J. G. TOPLISS. J. Am. Chem. Soc. **73**, 919 (1957).
44. H. C. BROWN and K. MURRAY. J. Am. Chem. Soc. **81**, 4108 (1959).
45. W. R. JACKSON and A. ZARQIYAH. J. Chem. Soc. 5280 (1965).
46. H. O. HOUSE, R. W. GIESE, K. KRONBERGER, J. P. KAPLAN, and J. F. SIMEONE. J. Am. Chem. Soc. **92**, 2800 (1970).
47. K. BOWDEN, J. M. HEILBRON, E. R. H. JONES, and B. C. L. WEEDON. J. Chem. Soc. 39 (1946).
48. R. HUISGEN and I. UGI. Ber. **90**, 2914 (1957).
49. J. MEINWALD, J. CRANDALL, and W. E. HYMANS. Organic Synth. Coll. Vol. 5, 866 (1973).
50. Y. F. SHEALY and J. D. CLAYTON. J. Am. Chem. Soc. **91**, 3075 (1969).
51. K. ALDER, H. WIRTZ, and H. KOPPELBERG. Ann. **601**, 138 (1956).
52. J. MEINWALD, P. G. GASSMAN, and J. K. CRANDALL. Tetrahedron, **18**, 815 (1962).
53. P. G. GASSMAN and J. L. MARSHALL. J. Am. Chem. Soc. **88**, 2822 (1966).
54. C. J. COLLINS, B. M. BENJAMIN, V. F. RAAEN, I. T. GLOVER, and M. D. ECKART. Ann. **739**, 7 (1970).

Appendix

Collins *et al.* argued (23, 30) that product control in deamination of **A** and **B** was largely determined by retention of the relative position of the *initial* counter ion through Wagner–Meerwein rearrangements and one or more hydride shifts. The carbocations were thus considered to be classical. In the sodium acetate containing medium we consider this to be highly improbable, and find their observations to be internally inconsistent with this hypothesis.

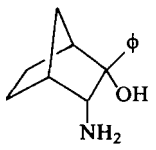

A

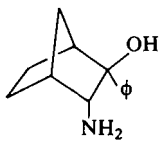

B

The situation pertaining if their hypotheses were correct is illustrated in the following equations:

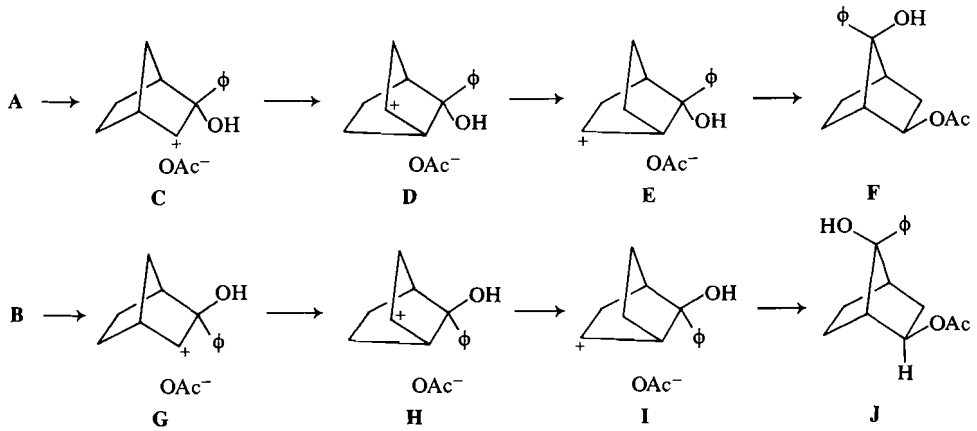

Can. J. Chem. Downloaded from www.nrcresearchpress.com by 210.87.254.6 on 09/06/12
For personal use only.

Can. J. Chem. Downloaded from www.nrcresearchpress.com by 210.87.254.6 on 09/06/12
For personal use only.

However, *no* product from collapse of the supposed initial tight ion pair **G** was observed[13] while only 10% of the *endo* acetate was produced from **C**. Although 29% of **J** was produced from **B**, consistent with their postulate, *37% of **F** was produced by exo* attack of acetate ion on ion **H**. Similarly, 22% of **J** was produced by *exo* attack on ion **D** in violation of their premise.

Their previous work (54) had shown that ions **D** and **I** with an *anti* orientation of the cation and hydroxyl should undergo cleavage to **K** while **E** and **H** should not. In actuality ion **D** did give rise to equal amounts of acetate **F** (22%) and the cleavage product **K**. Therefore since the capture of **D** by external acetate is efficient, as discussed above, the fission must also be an efficient process. However, ion **I** gave *no* fission product, from which we conclude that it did not exist as a classical ion.

No explanation was offered why ion **C** would rearrange to the bicyclo[3.1.1] ion **L** (20%) while ion **G** gave no such rearrangement. Similarly, the classical ion concept cannot account for the 22% of nortricyclene **M** from **B** in contrast to only 8% from **A**.

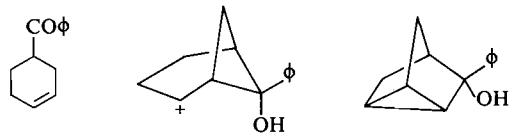

K **L** **M**

[13]It is probable however that the *endo*-phenyl group considerably hinders *endo* attack on C-2 of **G**.

We favor the following explanation of their results. The two electronegative groups on C-3 of **A** and **B** will destabilize the cations **C** and **G**, thus favouring delocalization. In the case of **C** this would be by participation of the 1–7 bond, giving cation **N** which would be the direct precursor of **L** and possibly **K**. Because of its higher energy, **N** could rearrange to the ion **O** which would give the nortricyclanone **M** via the edge-protonated ion **P**. Alternatively the original diazonium ion from **A** could in part rearrange to the *exo* diazonium ion via the diazo compound (see eq. [8], main text), thence to ions **O** and **P**.

In contrast, we suggest that the ion from **B** is delocalized by hydroxyl participation as in **Q**.

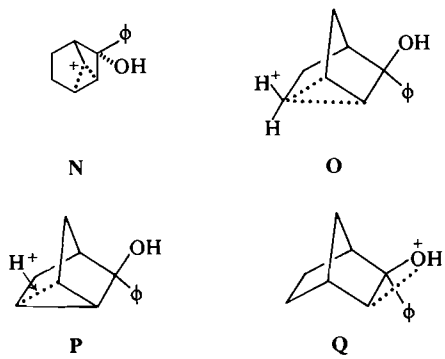

N **O**

P **Q**

Since *endo* attack on this is hindered[13] it would rearrange to ion **O**, then to **P**. These account for 88% of the observed products (**F**, **J**, and **M**).

The excess acidity of aqueous HCl and HBr media. An improved method for the calculation of X-functions and H_0 scales

ROBIN A. COX AND KEITH YATES

Department of Chemistry, University of Toronto, 80 St. George St., Toronto, Ont., Canada M5S 1A1

Received November 3, 1980

ROBIN A. COX and KEITH YATES. Can. J. Chem. **59**, 2116 (1981).

Excess acidity (X-function) scales for 0–40% w/w aqueous HCl and 0–60% w/w aqueous HBr solutions are derived, using ionization ratio data for 29 and 9 weak bases, respectively; in these media the resulting pK_{BH^+} values are quite similar to those obtained by standard acidity function treatments. A generalized derivation of the excess acidity enables the determination of pK_{R^+} values for protonation–dehydration processes, some of which are given, and the study of partially dissociated acids. An improved computer program was used, applicable to smaller data sets (up to 50 bases); this program permitted a determination of the inherent precision of the derived functions, and a more rigorous evaluation of previously derived X-functions and the whole excess acidity method.

ROBIN A. COX et KEITH YATES. Can. J. Chem. **59**, 2116 (1981).

En se basant sur des données de rapport d'ionisation respectivement pour 29 et 9 bases faibles, on a déduit des échelles d'acidité en excès (fonction-X) pour des solutions aqueuses de HCl à 0–40% w/w et de HBr à 0–60% w/w; dans ces milieux les valeurs de pK_{BH^+} obtenues sont tout à fait identiques à celles que donnent les fonctions d'acidité normale. Une dérivation générale de l'acidité en excès permet de déterminer les valeurs de pK_{R^+} pour des réactions de protonation–déshydration, dont quelques-unes sont connues, et d'étudier les acides partiellement dissociés. On a utilisé un programme d'ordinateur amélioré, applicable à des ensembles de données (jusqu'à 50 bases) plus petites; ce programme a permis de déterminer la précision inhérente des fonctions dérivées et d'évaluer d'une façon rigoureuse les fonctions-X dérivées antérieurement ainsi que la méthode totale d'acidité en excès.

[Traduit par le journal]

Introduction

For proton transfer to a weak base B, eq. [1], pK_{BH^+} is defined in terms of molar concentration C and molar activity coefficients f as in eq. [2]; the term C_{BH^+}/C_B, most often measured by uv–visible or nmr spectroscopy, is the ionization ratio I

$$[1] \quad B + H^+ \overset{K_{BH^+}}{\rightleftharpoons} BH^+$$

$$[2] \quad pK_{BH^+} = \log(C_{BH^+}/C_B) - \log C_{H^+} - \log(f_B f_{H^+}/f_{BH^+})$$

(1). The well-tested assumption (2–6) made regarding the activity coefficient term in eq. [2] is that it is linear in an equivalent term for some standard base B*. The latter term is defined as the excess acidity, X, in eq. [3], with slope parameter m^*, and

$$[3] \quad \log(f_B f_{H^+}/f_{BH^+}) = m^* \log(f_{B^*} f_{H^+}/f_{B^*H^+}) = m^* X$$

$$[4] \quad \log I - \log C_{H^+} = pK_{BH^+} + m^* X$$

eq. [2] becomes eq. [4] (6). The term excess acidity is used because X is the difference between the observed acidity and that which the system would have if it were ideal; the standard state at which $X = 0$ is the hypothetical ideal 1 M solution of the acid used, the same as for pH measurements. The above (6) is based on the original analysis due to Bunnett and Olsen (2), and later modifications by Marziano and co-workers (3–5).

X-functions have previously been given for aqueous sulfuric and perchloric acid mixtures (6), and eq. [4] has seen extensive use for extrapolative pK_{BH^+} determinations in these media (4–8). Related kinetic equations based on the excess acidity concept have also been derived (9) and tested (8). In this paper the aqueous HCl and HBr media are studied; due to the smaller amount of ionization ratio data available in these systems, a more statistically rigorous computer program could be used to derive X than the one used before (6). This improved program is used to test some points raised[1] in connection with the previous work, namely: does using different sets of bases in a given medium lead to the same X-function or to different ones; does the implicit definition of B* used before (6) make a difference to the resulting X; and are the initial trial values of m^* and pK_{BH^+} used in the calculation important or not.

Experimental

Computer Program

The program developed for this work is quite different from that used previously (6), although it performs essentially the same operation. The excess acidity X is expressed as a polynomial in the concentration unit involved, percent by weight w here; substitution into eq. [4] gives an eq. [5] for each

$$[5] \quad \log I = \log C_{H^+} + pK_{BH^+} + m^*(a_1 w + a_2 w^2 + a_3 w^3 + \ldots)$$

[1] V. Lucchini, G. Modena, and G. Scorrano, presented at the Fifth IUPAC Conference on Physical Organic Chemistry, Santa Cruz, CA, August, 1980; also personal communications.

0008-4042/81/142116-09$01.00/0

©1981 National Research Council of Canada/Conseil national de recherches du Canada

Can. J. Chem. Downloaded from www.nrcresearchpress.com by 210.87.254.5 on 09/06/12
For personal use only.

Can. J. Chem. Downloaded from www.nrcresearchpress.com by 210.87.254.5 on 09/06/12
For personal use only.

base in the set. Preliminary work showed that the use of z = antilog(w/100), as done before (6), was unnecessary here, and that three polynomial coefficients were sufficient, except for H_2SO_4, where four were used. Equation [5] has no a_0 because $X = 0$ at $w = 0$, i.e. the deviation from ideality in the standard state is zero. The equations are then solved by minimizing the difference d between experimental and calculated log I values. Previously this was done by using trial values of pK_{BH^+} and m^* to estimate X, using this to give new pK_{BH^+} and m^* values, which give a new X, and so on until no further improvement results; essentially d is minimized sequentially, and the method is good for large data sets, i.e. 50 or more compounds (6).

For smaller data sets it is possible to minimize d simultaneously for each coefficient (these being the polynomial coefficients a, and a pK_{BH^+} and m^* for each base). To do this the general-purpose curve-fitting subroutine CURFIT from Bevington (10) was utilized. This requires a subroutine FUNCTN containing the equation to be fitted (the set of eqs. [5] here, with some programming to enable discrimination among them), and another, FDERIV, which computes the derivatives of the fitted equation with respect to each coefficient in it (e.g. $d \log I/da_1 = m^*w$, $d \log I/dpK_{BH^+} = 1$), which are used in the fitting process (10). The difference d (actually a weighted $\sum_i d_i^2$) is calculated in a subroutine FCHISQ, and a matrix inversion subroutine MATINV is also required (10). The size of the matrix involved depends on the number of coefficients; 50 bases, each with its pK_{BH^+} and m^*, plus three polynomial coefficients, minus the defined $m^* = 1$ for B* (see below), needs a 102 × 102 matrix. Since inversion occurs many times during a computer run, 50 compounds represent a practical upper limit to the method, as both the computer time required and the memory storage needed increase rapidly with the size of the matrix. The procedure is iterative insofar as several passes through CURFIT are made until the change in d from the previous pass is negligible, the calculated coefficient values being essentially unchanged (convergence). Further details of the program may be obtained from the authors.

Data and Calculations

Ionization ratio data for 9 primary amines (11–21), 3 secondary amines (12, 18, 22), 8 tertiary amines (14, 23, 24), 7 amides (19, 26), and 2 anions (25) in hydrochloric acid, and 9 primary amines in hydrobromic acid (21, 27), were used. Measurements by different authors on the same compound were amalgamated and treated together. Percent by weight/molarity conversions were performed using available density data (28). An error function given by Kresge and Chen (29) was used to weight the log I values, to reflect their decreasing reliability with increasing distance from 50% ionization. They were also weighted by dividing the weight within each 0.5% acid region by the number of points in that region; this is in order to give equal weight to all acid regions in the calculation. For example, half of the 421 total data points for HCl lie within the range 0–7.5%, leaving the other half for the much larger 7.5–40% range.

The X_0 functions were derived using only primary aromatic amine data; for these the equations fitted are an eq. [5] for each base with m^* set equal to 1.0. For $HClO_4$ the primary amine data used before (30, 31), with some additional log I measurements for 2- and 4-nitroaniline by Kresge *et al.* (11), were analyzed. Straight-line plots according to eqs. [4] and [10] were calculated using a standard weighted line-fitting routine from Bevington (10), as before (6).

Results and Discussion

In comparison to the aqueous H_2SO_4 and $HClO_4$ systems, where ionization ratio data for 165 and 76 compounds, respectively, were available for the calculation of X, other acid media have received less attention. Thus for the systems under consideration here, 29 compounds have been studied in HCl, and only 9 in HBr. This has both advantages and disadvantages. An advantage is that the more statistically rigorous computer program applicable to sets of 50 or fewer bases, described above and discussed below, could be used. This program was used to calculate the X-function for HCl given in Table 1; the 29 primary, secondary, and tertiary amines, amides, and anions for which ionization ratio data were used (11–26), with the pK_{BH^+} and m^* values obtained using this X and eq. [4], are given in Table 2.

For the aqueous HBr system, a disadvantage becomes apparent in that the availablity of data for only primary aromatic amines (21, 27) does not permit the calculation of a full X-function. In cases like this it is best to set $m^* = 1$ for all compounds, and simply use the method to calculate H_0, as was done previously for D_0 in $DClO_4$ (32). Putting $m^* = 1$ for all compounds in eq. [3] leads to cancellation of f_{H^+}; upon rearrangement this becomes $f_B f_{B^*H^+}/f_{B^*} f_{BH^+} = 1$, the original Hammett cancellation assumption (33). Equation [4] then becomes eq. [6],

$$[6] \quad \log I - pK_{BH^+} = \log C_{H^+} + X_0 = -H_0$$

TABLE 1. X and $-H_0$ for aqueous HCl at 25°C

% w/w	C_A, M	X[a]	$-H_0$[a]
0.1	0.0274	0.005±0.000	−1.558±0.000
0.2	0.0547	0.011±0.000	−1.254±0.000
0.5	0.1371	0.027±0.000	−0.844±0.000
1.0	0.275	0.055±0.001	−0.522±0.000
2.0	0.552	0.113±0.001	−0.176±0.001
3.0	0.833	0.175±0.002	0.047±0.001
4.0	1.115	0.240±0.003	0.222±0.002
6.0	1.689	0.381±0.004	0.507±0.002
8.0	2.273	0.534±0.006	0.752±0.003
10	2.868	0.699±0.008	0.980±0.005
12	3.474	0.874±0.010	1.201±0.006
14	4.092	1.058±0.013	1.421±0.007
16	4.720	1.251±0.016	1.642±0.009
18	5.359	1.452±0.019	1.866±0.011
20	6.010	1.660±0.023	2.095±0.013
22	6.673	1.873±0.027	2.329±0.015
24	7.347	2.091±0.032	2.568±0.017
26	8.023	2.313±0.037	2.814±0.020
28	8.728	2.538±0.042	3.067±0.023
30	9.433	2.765±0.048	3.325±0.027
32	10.149	2.993±0.055	3.590±0.030
34	10.874	3.221±0.062	3.862±0.034
36	11.609	3.448±0.070	4.139±0.039
38	12.352	3.673±0.078	4.423±0.043
40	13.106	3.896±0.088	4.714±0.049

[a]Errors are 95% confidence limits.

Can. J. Chem. Downloaded from www.nrcresearchpress.com by 210.87.254.5 on 09/06/12
For personal use only.

TABLE 2. pK_{BH^+} and m^* values for weak bases in hydrochloric acid

Compound[a]	AF[b]	pK_{BH^+}[c]	m^*[c]	r[d]	N[e]	$\pm\sigma_y$	Reference
2-Cl-5-CF_3-An	1.20	1.1983±0.0007	1.05±0.01	0.999	12(1)	0.002	(20)
4-NO_2-An	1.00	1.001±0.002	0.84±0.03	0.965	71(5)	0.010	(11–17)
3,5-di-NO_2-An	0.21	0.222±0.006	0.81±0.03	0.988	21	0.016	(11)
2-NO_2-An	−0.29	−0.239±0.006	0.72±0.01	0.989	63(8)	0.021	(11–14, 18, 19)
4-Cl-2-NO_2-An	−1.06	−1.08±0.02	0.81±0.02	0.997	17(2)	0.024	(14, 18)
5-Cl-2-NO_2-An	−1.40	−1.83±0.03	1.01±0.02	0.999	6	0.015	(21)
2,5-di-Cl-4-NO_2-An	−1.82	−1.82±0.02	0.81±0.02	0.998	12	0.022	(14)
2,4-di-Cl-6-NO_2-An	−3.26	−3.69±0.06	1.01±0.02	0.997	15	0.035	(14, 21)
2,4-di-NO_2-An	−4.50	−5.64±0.17	1.25±0.05	0.999	4	0.021	(21)
DPA	0.78	0.774±0.005	1.25±0.06	0.988	13	0.012	(12, 22)
N-Et-2-NO_2-An	−0.11	−0.050±0.009	1.06±0.03	0.997	7	0.010	(22)
4-NO_2-DPA	−2.35	−2.87±0.04	1.07±0.02	0.998	21(1)	0.025	(18)
N,*N*-di-Me-4-NO_2-An	0.66	0.665±0.005	1.50±0.07	0.984	18(2)	0.014	(14, 23)
N-(2,4-di-NO_2-Ph)-piperidine	−0.46	−0.43±0.02	1.48±0.07	0.992	10	0.032	(14)
N,*N*-di-Me-2,4-di-NO_2-An	−1.65	−1.34±0.04	1.16±0.05	0.992	12(2)	0.052	(24)
N,*N*-di-Me-2,6-di-NO_2-4-Me-An	−1.81	−1.61±0.07	1.22±0.07	0.986	10	0.066	(14)
N,*N*-di-Me-2,4-di-NO_2-l-NpAm	−2.74	−2.48±0.08	1.16±0.05	0.992	10	0.057	(14)
N-Me-4-NO_2-DPA	−3.31	−3.22±0.07	1.26±0.04	0.997	9	0.033	(14)
N-Me-4′-Br-4-NO_2-DPA	−4.16	−4.37±0.18	1.41±0.07	0.992	8	0.056	(14)
N,*N*-di-Et-2,4,6-tri-NO_2-An	−6.02	−6.05±0.25	1.33±0.07	0.996	5	0.035	(14)
Acetanilide	−1.23	−0.97±0.09	0.54±0.10	0.908	8	0.103	(26)
2-Pyrrolecarboxamide	−1.23	−1.13±0.01	0.66±0.02	0.997	11	0.019	(19)
4-OMe-Bz	−1.46	−1.36±0.02	0.67±0.02	0.997	13(1)	0.025	(19)
3,4,5-tri-OMe-Bz	−1.86	−1.82±0.05	0.72±0.03	0.995	9(1)	0.039	(19)
3-NO_2-Bz	−2.25	−2.28±0.06	0.75±0.03	0.995	9	0.032	(19)
3,5-di-NO_2-4-Me-Bz	−2.77	−2.78±0.10	0.73±0.04	0.989	10	0.048	(19)
2,3,6-tri-Cl-Bz	−3.10	−3.43±0.15	0.87±0.06	0.988	8	0.054	(19)
4-(tricyanovinyl)-PDCM anion	0.36	0.35±0.02	1.09±0.18	0.929	8	0.046	(25)
Picrate ion	−0.02	0.03±0.02	0.52±0.12	0.911	6	0.032	(25)

[a]An = aniline; DPA = diphenylamine; NpAm = naphthylamine; PDCM = phenyldicyanomethane; Bz = benzamide.
[b]Acidity function pK_{BH^+} value; from reference cited.
[c]Using eq. [4]; given with standard deviation.
[d]Correlation coefficient.
[e]Number of points. Any rejected as too far off the line by the program used are indicated by parentheses.

Can. J. Chem. Downloaded from www.nrcresearchpress.com by 210.87.254.5 on 09/06/12
For personal use only.

in which the zero subscript on X_0 indicates this *different and less valid* assumption (6). Despite the fact that, essentially, H_0 is being calculated, the advantages of the X-function calculation method are still present in that anchoring is not necessary, since $X_0 = X = 0$ in the aqueous standard state, and that overlap between adjacent indicators is not required (6). The resulting X_0 scale for HBr is given in Table 3; the bases used, with their pK_{BH^+} values, are in Table 4. Even though $m^* = 1$ has been assumed in the calculation, the m^*_0 values that result when data for the individual compounds are plotted against the derived X_0 sometimes differ considerably from unity, which means that the Hammett cancellation assumption (33) is not in fact very good even for these supposedly very similar compounds (6). In Fig. 1. the variation of excess acidity with percent by weight composition for the HCl and HBr systems is illustrated.

The computer program used in this work, described in the Experimental, is different from that used before (6). Although practically limited to data sets of 50 or fewer bases, it is more statistically rigorous, and gives standard deviations on the calculated coefficients. Tables 1 and 3 include 95% confidence limits on X obtained from these using error propagation (10) and statistical formulae (34). This program could not be used to derive X for sulfuric or perchloric acids using the full data set used before (165 and 76 bases) (6), but it can be used to calculate X-functions based on smaller subsets

TABLE 3. X_0 for aqueous HBr at 25°C

% w/w	C_A, M	X_0[a]
0.1	0.0123	0.002±0.000
0.2	0.0247	0.003±0.000
0.5	0.0618	0.008±0.001
1.0	0.124	0.016±0.001
2.0	0.250	0.033±0.002
3.0	0.378	0.051±0.003
4.0	0.507	0.070±0.004
6.0	0.771	0.109±0.007
8.0	1.043	0.153±0.009
10	1.323	0.202±0.012
14	1.909	0.314±0.017
18	2.531	0.450±0.024
22	3.193	0.613±0.031
26	3.899	0.807±0.040
30	4.654	1.037±0.050
35	5.674	1.379±0.065
40	6.790	1.789±0.082
45	8.011	2.27±0.10
50	9.347	2.84±0.13
55	10.809	3.50±0.15
60	12.406	4.26±0.18

[a]Errors are 95% confidence limits.

TABLE 4. pK_{BH^+} values for primary aniline bases in hydrobromic acid

Compound[a]	AF[b]	pK_{BH^+}[c]	m^*_0[c]	r[d]	N[e]	$\pm\sigma_y$	Reference
4-NO_2-An	1.11	0.951±0.008	1.27±0.21	0.845	18(1)	0.016	(21)
2-NO_2-An	−0.17	−0.233±0.003	1.03±0.01	0.999	11	0.004	(21)
4-Cl-2-NO_2-An	−1.03	−0.89±0.05	0.96±0.06	0.975	16(1)	0.039	(27)
5-Cl-2-NO_2-An	−1.40	−1.46±0.02	1.01±0.02	0.997	11	0.022	(21)
2,5-di-Cl-4-NO_2-An	−1.77	−1.76±0.04	1.03±0.03	0.994	17(1)	0.039	(27)
2,4-di-Cl-6-NO_2-An	−3.14	−3.13±0.07	1.00±0.03	0.992	18(1)	0.038	(21, 27)
2,6-di-Cl-4-NO_2-An	−3.25	−2.94±0.10	0.91±0.05	0.980	18	0.050	(27)
2,4-di-NO_2-An	−4.30	−4.62±0.22	1.15±0.07	0.972	18(1)	0.092	(21, 27)
2,6-di-NO_2-An	−5.26	−4.07±0.18	0.75±0.05	0.994	5	0.026	(27)

[a–e]As in Table 2.

Can. J. Chem. Downloaded from www.nrcresearchpress.com by 210.87.254.5 on 09/06/12
For personal use only.

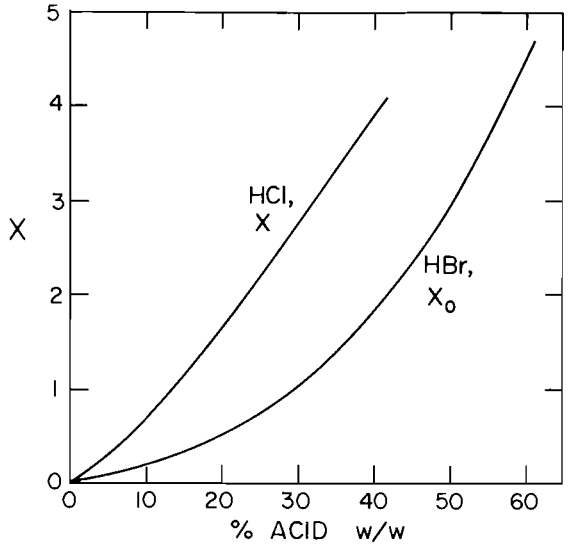

FIG. 1. Excess acidities of aqueous HCl and HBr as a function of percent acid.

of these, to see how well they compare among one another and with previously reported excess acidities. X-functions derived using different data sets, although broadly similar (6), differ in detail, and the point as to whether these differences are important or not has been raised.[1] In other words, a decision must be made as to whether using different data sets leads to the same function or to different ones. This can be done using the well-established (34) statistical test for significant differences, based on the confidence limits.

The ionization ratio data used before (see ref. 6, where the original references may be located), together with some additional primary (11, 13, 20, 35), secondary (14, 22), and tertiary (14, 24, 36) amine measurements, were used to calculate five X-functions for sulfuric acid based on: (A) primary and secondary amines only; (B) tertiary amines, amides, alkoxybenzenes, and α,β-unsaturated ketones; (C) alkenes, cations, anions, the H_S thiocompounds, benzophenones, and azobenzene (37); (D) indoles, carbonyl compounds, and other thiocompounds; and (E) the 50 compounds which have been measured in both H_2SO_4 and $HClO_4$ media. Scale E is compared to X (6) and $M_Cf(x)$ (5) in Fig. 2, which illustrates the differences in detail among X-functions under discussion.

The overall accuracy of the excess acidity method is good, as can be seen from the confidence limits and standard deviations in the tables. Illustrating the confidence limits on the sulfuric acid scales A–E is not easy, diagrams like Fig. 2 rapidly becoming too crowded to be useful, but an attempt to do this is presented in Fig. 3. This shows

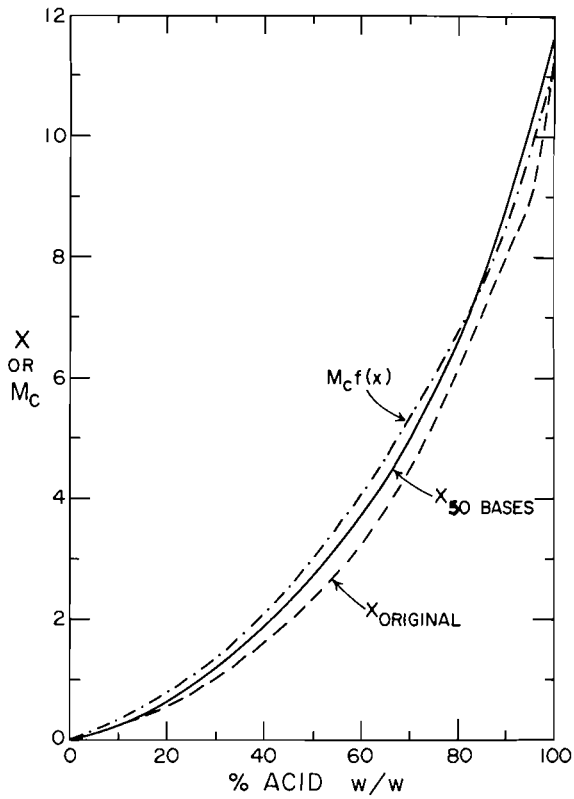

FIG. 2. The excess acidity of aqueous H_2SO_4 at 25°C. $M_Cf(x)$, ref. 5; $X_{original}$, ref. 6; $X_{50\ bases}$, this work.

the confidence limits in 98% sulfuric acid for the functions A–E above, together with X (6) (F), M_C (4) (G), and $M_Cf(x)$ (5) (H) at the same acidity, for comparison. 98% Acid is chosen as an example simply because the spread of the different functions is most noticeable at high acidity, and the accuracy is lowest, providing the most severe test for any significant differences between the scales. The conclusions are the same at any acidity.

Now if the confidence limits of any two scales in Fig. 3 overlap, the difference between them is not significant at the 95% confidence level (34), i.e. they are the same scale within the experimental uncertainties in the data used to calculate them. Amongst scales A–E, only scale C could be regarded as being significantly different from most of the rest. Comparisons with X, M_C, and $M_Cf(x)$ cannot be made with rigor; X was derived using six polynomial coefficients (6) as against four for A–E, the number used for $M_Cf(x)$ is not given (5), and M_C was derived using the older overlap method (4). Nevertheless it would seem probable that only M_C (G in Fig. 3) is really different from all of the others, and is in any case now superceded by $M_Cf(x)$ (5). With this exception, any of the scales

Can. J. Chem. Downloaded from www.nrcresearchpress.com by 210.87.254.5 on 09/06/12
For personal use only.

can be used with equal facility for extrapolative pK_{BH^+} measurements (6) and the analysis of kinetic data (9). This confirms and reinforces the conclusions reached by Marziano *et al.* (5) We will continue to use X, because of the large data set used in its derivation (6), and because the slope change at ~85% H_2SO_4 which X exhibits (see Fig. 2) is likely to be real, since 0–85% and 85–100% H_2SO_4 are quite different media (38). $M_C f(x)$ is a perfectly valid alternative, however; it is very similar to the scales A–E derived in this work.

The excess acidity is calculated using initial trial pK_{BH^+} and m^* values, which the computer iterates until convergence to the unchanging final ones occurs, as described in the Experimental. The question has been raised[1] as to whether or not this is important, insofar as the computer may in some way be "forced" by this choice of initial values. The improved program used here enables this question to be addressed because it gives standard deviations on the calculated coefficients. In general the CURFIT routine used converges rapidly and reliably from quite divergent initial values, because it consists of a combination of the gradient search and fitting function linearization procedures (10). For the X-function calculation for HCl the initial pK_{BH^+} values specified were the acidity function (AF) ones in Table 2, with initial m^* slopes of 1.0 for primary and secondary amines, and anions, 1.3 for tertiary amines, and 0.6 for amides; convergence occurred within 4 iterations. Convergence to the *same* values (i.e. well within the calculated standard deviations), also within 4 or 5 iterations, was found with initial coefficients consisting of the Table 2 AF values plus 1, all $m^* = 1.0$; the AF values plus 2, all $m^* = 1.3$; and the AF values minus 1, all $m^* = 0.5$.

In order to obtain an unambiguous set of m^* and a values, one m^* must be defined for the reference compound B*. Previously (6) this definition was implicit; the more rigorous program used here requires an explicit definition. Rather than arbitrarily choosing the first base in the set (or any single compound) as the reference, the definition used here was that the *average* of all the m^*'s for the set of bases used must be 1.0; this is closest to the previous implicit definition. This is a limitation on the generality of X, since this definition leads to an excess of compounds with large m^*'s producing a steep X-function, and an excess with low m^*'s producing a shallow one (see eq. [4]). Thus X will only be a unique function of the medium if a reasonably large and representative set of bases is available (i.e. some with low and some with high m^*'s), such as the 29 compounds used for HCl in this study (Table 2). Failing this, it is probably best to calculate an X_0 function and H_0 scale, as we have done for HBr. In deriving the H_2SO_4 scales A–E discussed above, a reasonable balance of compound types was attempted; however, the comparison in Fig. 3 is probably less good than it might be because of small differences caused by this factor.

To enable comparisons among the acidity function, X-function, and X_0 scale pK_{BH^+} values, X_0 for HCl was also calculated, using only the primary aromatic amine data. The AF values and those extrapolated using X (eq. [4]) are quite similar, the average deviation between them being $\pm 0.16 pK$ units (Table 2). This, however, is three times as large as the average of the standard deviations of the X-function values in the table. The values obtained using X_0 also differ from the AF ones by ± 0.16, but are otherwise slightly worse; X gives better linear plots than X_0 (lower σ_y, higher correlation coefficient) in 14 cases, worse in 11, and unchanged in 4. Interestingly, 7 of the 9 primary amines used in deriving X_0 give worse plots. However, the differences are very small, and the Bunnett–Olsen extrapolation (2), eq. [7], should

$$[7] \quad \log I + H_0 = \phi(-X_0) + pK_{BH^+}$$

give almost the same results as the X-function extrapolation of eq. [4], in this case. The situation for HBr is similar.

The polynomial coefficients used to calculate X and X_0 are given in Table 5. These can be used to calculate X and $-H_0$ at any percent by weight acid composition w by using X (or X_0) $= a_1w + a_2w^2 + a_3w^3$, and $-H_0 = X_0 + \log C_{H^+}$. The $-H_0$ scale for HCl obtained in this way is given in Table 1. Included in Table 5 is an X_0 scale for $HClO_4$; X for this system is already available (6). This recalculated $HClO_4$ scale is presented (*a*) because it is more accurate than the previous H_0 scale (30) (see below), and (*b*) in the expectation that better results may be obtained with it when using

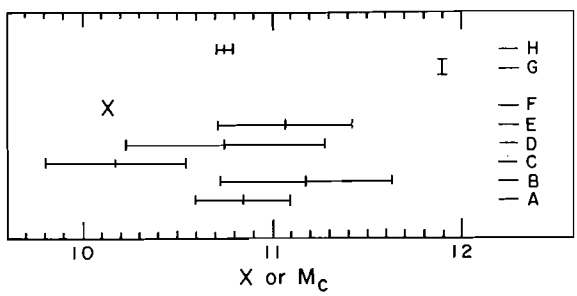

FIG. 3. 95% confidence limits on the excess acidity of 98% sulfuric acid, calculated for the different X-functions. For letter identifications see text.

TABLE 5. Polynomial coefficients for X and X_0

Acid	a_1	a_2	a_3
HCl, X	5.27767×10^{-2}	1.90497×10^{-3}	-1.97423×10^{-5}
HCl, X_0	3.76697×10^{-2}	1.50584×10^{-3}	-4.99680×10^{-6}
HBr, X_0	1.59513×10^{-2}	3.23181×10^{-4}	9.90298×10^{-6}
$HClO_4$, X_0	3.35096×10^{-2}	-7.45044×10^{-4}	2.22391×10^{-5}

the Bunnett–Olsen method (2). However, the X-function method is definitely to be preferred for $HClO_4$, as primary aromatic amines do not appear to be "well-behaved" in this system (6).

The H_0 scales given by Table 5, one of which is in Table 1, are undoubtedly the best available to date, being derived using *all* of the available log I data on primary aromatic amines, each value being properly weighted (29). They can be used for all applications requiring the use of H_0, always remembering the drawbacks associated with acidity functions, which we will not repeat here (6, 9). For HCl the H_0 scale averages 0.05 units more positive than the scale given by Rochester (1), and for HBr it is 0.07 units more positive than Rochester's (1) and 0.07 units more negative than Vinnik's (21) scales below about 45% w/w. This undoubtedly represents anchoring inaccuracies, avoided here because X_0 has to be zero in the standard state, water. Above about 45% the Table 5 HBr scale deviates from Vinnik's and Rochester's H_0 scales and approaches that of Marcus *et al.* (27); between 7.5% and 60% it averages 0.17 units more positive than the latter. (The polynomial coefficients given by Marcus are apparently not applicable below 7.5% w/w (27).) For $HClO_4$, up to 60% the scale averages 0.07 units more positive than that of Attiga and Rochester (31), and 0.08 more than that of Yates and Wai (30); above 60%, however, it averages 0.35 units more positive than the latter, a considerable difference. Aqueous HCl and HBr are quite strong acids; for instance the $-H_0$ values of 10 M $HClO_4$, HBr, HCl, and H_2SO_4 (16) are 5.82, 4.14, 3.53, and 4.89, respectively, and at a mole fraction of 0.25 are 6.16. 5.35, 4.75, and 4.97.

Values of log C_{H^+} for use in eq. [4] are obtained as follows. The stoichiometric acid concentration C_A is related to C_{H^+} via the degree of dissociation α:

$$\begin{array}{ccccc} HA & \rightleftharpoons & H^+ & + & A^- \\ C_A(1-\alpha) & & C_A\alpha & & C_A\alpha \end{array}$$

The acids HCl and HBr can be assumed to be fully dissociated[2] in the range accessible to study, like $HClO_4$ (see the discussion in ref. 6), i.e. $\alpha = 1$ and $C_{H^+} = C_A$. Values of C_A were calculated from listed densities (28) and are included in Tables 1 and 3. For acids which are not fully dissociated, $C_{H^+} = C_A\alpha$, $C_A\alpha_1(1 + \alpha_2)$, and $C_A\alpha_1(1 + \alpha_2 + \alpha_2\alpha_3)$ for mono-, di-, and tribasic acids, and the degrees of dissociation must be known. Values of C_{H^+} for H_2SO_4 derived in this way have already been reported (6); other partially dissociated acids, CF_3CO_2H, HNO_3, etc., will be studied in a future paper.

The α terminology is also useful in the analysis of protonation–dehydration processes, eq. [8]; the definition of pK_{R^+} leads to eq. [9]. In this case I is

$$[8] \quad ROH + H^+ \overset{K_{R^+}}{\rightleftharpoons} R^+ + H_2O$$

$$[9] \quad pK_{R^+} = \log (C_{R^+}/C_{ROH}) - \log (C_{H^+}/C_{H_2O}) - \log (f_{ROH}f_{H^+}/f_{R^+}f_{H_2O})$$

C_{R^+}/C_{ROH}, and the stoichiometric water concentration C_{H_2O} is related to C_A and the mole fraction of acid x_A via $C_{H_2O} = C_A(1 - x_A)/x_A$, so C_A cancels; $\alpha = 1$ here. It is customary not to include the water concentration in definitions of pK_{R^+}, and log(55.346) can be subtracted to account for this; eq. [10] results if the assumption is made that the

$$[10] \quad \log I - \log(x_A/(1 - x_A)) - 1.743 = pK_{R^+} + m^*X$$

activity coefficient term is linear in X, slope m^* as before. This assumption seems reasonable and is easily tested; in Fig. 4 the left-hand side of eq. [10] is plotted against X for some triarylcarbinols in aqueous HCl (14). The good linearity, particularly in the region log $I = \pm 1$, amply justifies the assumption made and the use of eq. [10]; the resulting pK_{R^+} and m^* values are given with statistical information in Table 6. The pK_{R^+} values are within two standard deviations of the AF ones, for all except the most basic compound. This is indicative of the good results to be obtained using the excess acidity method, even for compounds not used in deriving X.

Excluding the first compound, the average m^* in Table 6 is 1.80 ± 0.10, a steep acidity dependence, as expected (6). No particular consistency is evident among the m^* values in Table 2. Primary

[2]This seems reasonable, but hard evidence is difficult to find, e.g. see ref. 27.

Can. J. Chem. Downloaded from www.nrcresearchpress.com by 210.87.254.5 on 09/06/12
For personal use only.

TABLE 6. pK_{R^+} and m^* values for some triphenylcarbinols in hydrochloric acid at 25°C

Compound[a]	AF[b]	pK_{R^+}[c]	m^*[c]	r[d]	N[e]	$\pm\sigma_y$
4,4′,4″-tri-OMe-TPC	0.82	0.692±0.007	2.44±0.13	0.990	10(1)	0.014
4,4′-di-OMe-TPC	−1.06	−1.01±0.03	1.76±0.06	0.995	11	0.034
4-OMe-TPC	−3.08	−3.02±0.08	1.74±0.06	0.996	10	0.041
4-Me-TPC	−4.93	−5.17±0.12	1.95±0.05	0.996	13(1)	0.036
TPC	−6.12	−5.85±0.15	1.76±0.05	0.997	9(1)	0.033

[a]Data from ref. 14. TPC = triphenylcarbinol.
[b]Acidity function pK_{R^+} value from ref. 14.
[c]Using eq. [10]; given with standard deviation.
[d,e]As in Table 2.

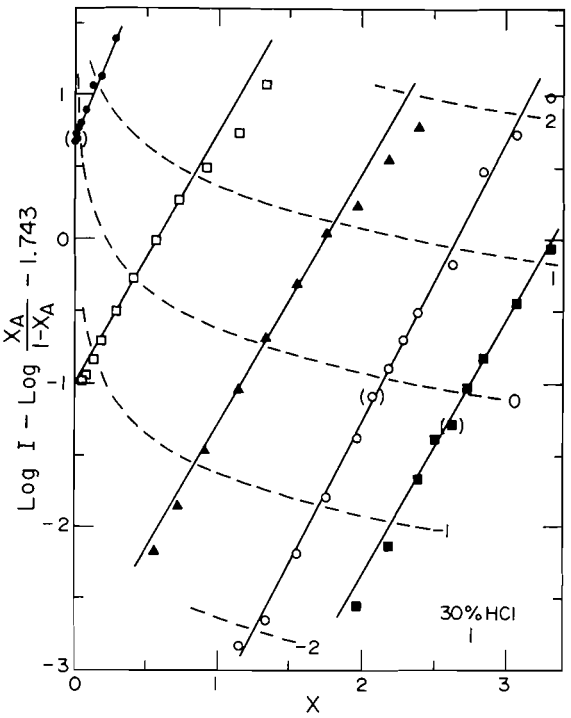

FIG. 4. Plots according to eq. [10] for some triphenylcarbinols (TPC) in aqueous HCl at 25°C; 4,4′,4″-trimethoxy-TPC (●), 4,4′-dimethoxy-TPC (□), 4-methoxy-TPC (▲), 4-methyl-TPC (○), and TPC (■). Data from ref. 14; numbers to the right of the dashed lines are log I values.

amines average at 0.92 ± 0.17, secondary amines 1.13 ± 0.11, tertiary amines 1.32 ± 0.14, and amides 0.71 ± 0.10; the trend is similar to that found in H_2SO_4 and $HClO_4$ (6).

Acknowledgements

We thank Professor E. M. Arnett for providing the ionization data from ref. 14, and Professors Scorrano, Modena, and Lucchini for valuable exchanges of views. Financial support of this research is by the Natural Sciences and Engineering Research Council of Canada.

1. C. H. ROCHESTER. Acidity functions. Academic Press, London. 1970.
2. J. F. BUNNETT and F. P. OLSEN. Can. J. Chem. **44**, 1899 (1966).
3. R. PASSERINI, N. C. MARZIANO, and P. TRAVERSO. Gazz. Chim. Ital. **105**, 901 (1975); N. C. MARZIANO, P. G. TRAVERSO, and R. C. PASSERINI. J. Chem. Soc. Perkin Trans. II, 306 (1977).
4. N. C. MARZIANO, G. M. CIMINO, and R. C. PASSERINI. J. Chem. Soc. Perkin Trans. II, 1915 (1973).
5. N. C. MARZIANO, P. G. TRAVERSO, A. TOMASIN, and R. C. PASSERINI. J. Chem. Soc. Perkin Trans. II, 309 (1977).
6. R. A. COX and K. YATES. J. Am. Chem. Soc. **100**, 3861 (1978).
7. J. T. EDWARD and S. C. WONG. Can. J. Chem. **57**, 1980 (1979).
8. R. A. COX, C. R. SMITH, and K. YATES. Can. J. Chem. **57**, 2952 (1979); R. A. COX, M. F. GOLDMAN, and K. YATES. Can. J. Chem. **57**, 2960 (1979).
9. R. A. COX and K. YATES. Can. J. Chem. **57**, 2944 (1979).
10. P. R. BEVINGTON. Data reduction and error analysis for the physical sciences. McGraw-Hill, New York. 1969.
11. A. J. KRESGE, H. J. CHEN, and Y. CHIANG. J. Chem. Soc. Chem. Commun. 969 (1972); H. J. CHEN. Ph.D. Thesis, Illinois Institute of Technology. 1970.
12. M. A. PAUL. J. Am. Chem. Soc. **76**, 3236 (1954).
13. B. TORCK, M. HELLIN, and F. COUSSEMANT. Bull. Soc. Chim. Fr. 1657 (1962).
14. E. M. ARNETT and G. W. MACH. J. Am. Chem. Soc. **88**, 1177 (1966); G. W. MACH. Ph.D. Thesis, University of Pittsburgh. 1964.
15. R. H. BOYD and C.-H. WANG. J. Am. Chem. Soc. **87**, 430 (1965).
16. C. D. JOHNSON, A. R. KATRITZKY, and S. A. SHAPIRO. J. Am. Chem. Soc. **91**, 6654 (1969).
17. P. SALOMAA. Acta Chem. Scand. **11**, 125 (1957).
18. R. P. BELL, A. L. DOWDING, and J. A. NOBLE. J. Chem. Soc. 3106 (1955).
19. K. YATES and J. C. RIORDAN. Can. J. Chem. **43**, 2328 (1965).
20. K. YATES and S. A. SHAPIRO. Can. J. Chem. **50**, 581 (1972).
21. M. I. VINNIK, R. N. KRUGLOV, and N. M. CHIRKOV. Zh. Fiz. Khim. **30**, 827 (1956).
22. J.-M. CARPENTIER and P. LEMETAIS. Can. J. Chem. **56**, 954 (1978).
23. E. M. ARNETT and G. W. MACH. J. Am. Chem. Soc. **86**, 2671 (1964).
24. N. B. LIBROVICH, YU. K. KARASEVICH, and M. I. VINNIK. Zh. Fiz. Khim. **46**, 2343 (1336 in Engl. ed.) (1972).
25. R. H. BOYD. J. Phys. Chem. **67**, 737 (1963).
26. J. W. BARNETT and C. J. O'CONNOR. J. Chem. Soc. Perkin Trans. II, 220 (1973).

Can. J. Chem. Downloaded from www.nrcresearchpress.com by 210.87.254.5 on 09/06/12
For personal use only.

27. Y. MARCUS, E. PROSS, and N. SOFFER. J. Phys. Chem. **84**, 1725 (1980).
28. International critical tables. Vol. 3. McGraw-Hill. New York. 1930. pp. 54–55.
29. A. J. KRESGE and H. J. CHEN. Anal. Chem. **41**, 74 (1969).
30. K. YATES and H. WAI. J. Am. Chem. Soc. **86**, 5408 (1964); H. WAI. Ph.D. Thesis, University of Toronto. 1968.
31. S. A. ATTIGA and C. H. ROCHESTER. J. Chem. Soc. Perkin Trans. II, 1624 (1974).
32. R. A. COX, S.-O. LAM, R. A. MCCLELLAND, and T. T. TIDWELL. J. Chem. Soc. Perkin Trans. II, 272 (1979).
33. L. P. HAMMETT and A. J. DEYRUP. J. Am. Chem. Soc. **54**, 2721 (1932).
34. D. A. SKOOG and D. M. WEST. Fundamentals of analytical chemistry. 3rd. ed. Holt, Rinehart and Winston, Toronto. 1976. Chapt. 4.
35. R. H. BOYD. J. Am. Chem. Soc. **85**, 1555 (1963); J. C. D. BRAND. J. Chem. Soc. 997 (1950); M. I. VINNIK and R. S. RYABOVA. Zh. Fiz. Khim. **38**, 606 (320 in Engl. ed.) (1964); R. S. RYABOVA, I. M. MEDVETSKAYA, and M. I. VINNIK. Zh. Fiz. Khim. **40**, 285 (182 in Engl. ed.) (1966).
36. I. S. KISLINA, N. B. LIBROVICH, and M. I. VINNIK. Zh. Fiz. Khim. **53**, 1523 (858 in Engl. ed.) (1979).
37. N. B. LIBROVICH, YU. K. KARASEVICH, and M. I. VINNIK. Zh. Fiz. Khim. **46**, 2346 (1338 in Engl. ed.) (1972).
38. R. A. COX. J. Am. Chem. Soc. **96**, 1059 (1974).

Can. J. Chem. Downloaded from www.nrcresearchpress.com by 210.87.254.5 on 09/06/12
For personal use only.

Effect of reaction exothermicity on the proton transfer chemical ionization mass spectra of isomeric C_5 and C_6 alkanols

JAN A. HERMAN[1] AND ALEX. G. HARRISON

Department of Chemistry, University of Toronto, Toronto, Ont., Canada M5S 1A1

Received November 20, 1980

JAN A. HERMAN and ALEX G. HARRISON. Can. J. Chem. **59**, 2125 (1981).

The chemical ionization mass spectra of eight C_5 alkanols and fourteen C_6 alkanols have been obtained using H_3^+, N_2H^+, CO_2H^+, N_2OH^+, and HCO^+ as reactant ions. This choice of reactant ions allows the exothermicity of the protonation reaction to be varied from ~90 kcal mol^{-1} (H_3^+) to ~50 kcal mol^{-1} (HCO^+). The major fragmentation reaction in all cases was H_2O elimination from the protonated alcohol forming the appropriate $C_5H_{11}^+$ or $C_6H_{13}^+$ alkyl ion. The extent of further fragmentation of the alkyl ions decreased with decreasing exothermicity of the protonation reaction and was greatest for alkyl ions derived from primary alcohols, less for alkyl ions derived from secondary alcohols, and very small for alkyl ions derived from tertiary alcohols. The results indicate that there is negligible rearrangement to more stable alkyl ions prior to attaining the critical configuration which determines the energy partitioning between R^+ and H_2O in the fragmentation of ROH_2^+. Other less important reaction modes in the CI spectra involved formation of $(M - H)^+$ ions and formation of oxycarbonium ions by alkane elimination from protonated alcohols.

JAN A. HERMAN et ALEX. G. HARRISON. Can. J. Chem. **59**, 2125 (1981).

Les spectres de masse de chimiionisation de huit pentanols aliphatiques et quatorze hexanols aliphatiques ont été obtenus en utilisant les ions réactifs H_3^+, N_2H^+, CO_2H^+, N_2OH^+ et HCO^+. Ces divers ions réactifs permettent de faire varier l'exothermicité de la réaction de protonation de ~90 kcal mol^{-1} avec H_3^+ à ~50 kcal mol^{-1} avec HCO^+. Dans chaque cas, la principale réaction de fragmentation de l'alcool protoné est une élimination d'eau conduisant à l'ion alkyl $C_5H_{11}^+$ ou $C_6H_{13}^+$ approprié. Le degré de fragmentation ultérieure des ions alkyls décroît avec la diminuation de l'exothermicité de la réaction de protonation; il est maximal pour les ions alkyls dérivés d'alcools primaires, moindre pour ceux provenant d'alcools secondaires et le plus petit si l'alcool était tertiaire. D'après les résultats, l'atteinte de la configuration critique déterminant la répartition de l'énergie entre R^+ et H_2O lors de la fragmentation de ROH_2^+ n'implique aucun réarrangement important conduisant à des ions alkyls plus stables. D'autres modes de réaction moins importants dans les spectres CI impliquent la formation d'ions $(M - H)^+$ et celle d'ions oxycarbonium par élimination d'alcane des alcools protonés.

Introduction

The isobutane chemical ionization (CI) mass spectra of saturated monohydroxylic alcohols with five or more carbons are dominated (1) by the alkyl ion R^+, presumably derived by loss of H_2O from the protonated alcohol ROH_2^+. This observation suggested the possibility that by varying the exothermicity of the protonation reaction one could produce alkyl ions with varying amounts of internal energy and observe the fragmentation of the alkyl ions as a function of internal energy. This possibility is explored in the present work for isomeric C_5 and C_6 alkanols using H_3^+ ($PA(H_2)$ = 101 kcal mol^{-1}), N_2H^+ ($PA(N_2)$ = 117 kcal mol^{-1}), CO_2H^+ ($PA(CO_2)$ = 129 kcal mol^{-1}), N_2OH^+ ($PA(N_2O)$ = 137 kcal mol^{-1}), and HCO ($PA(CO)$ = 141 kcal mol^{-1}) as protonating reagents. The proton affinities given in brackets are derived from the work of Bohme *et al.* (2) and when compared with the estimate (3) of a proton affinity of ~190 kcal mol^{-1} for the higher alcohols, result in a protonation exothermicity ranging from ~90 kcal mol^{-1} to approximately 50 kcal mol^{-1}. As will be shown in the following, this variation in the protonation exothermicity does produce significant changes in the internal energy of the alkyl ions produced, which is reflected by the extent of further fragmentation of the ions resulting from the initial water loss from ROH_2^+. The results obtained will be compared, where possible, with the results obtained from fragmentations of alkyl ions produced by electron impact methods.

Experimental

The chemical ionization mass spectra were obtained using a DuPont 21-490 mass spectrometer equipped with a high pressure chemical ionization source. The source temperature was 60°C and the ionizing electron energy 70 eV with the repellers held at cage potential. The liquid samples were introduced through a heated inlet system held below 100°C. Reagent gas pressures were not measured directly but were estimated to be 0.2–0.3 Torr.

The H_3^+ reactant ion was produced in pure H_2. As discussed elsewhere (4), the N_2H^+, CO_2H^+, and HCO^+ reactant ions were produced by electron impact ionization of the appropriate gas N_2, CO_2, or CO (~10%) in H_2, giving in all cases the relevant ion as the dominant species. In the present work a similar mixture of 10% N_2O in H_2 was found to give largely N_2OH^+ as reactant ion, but, in this case, a significant (10–15%) fraction of the total ionization was observed as NO^+.

Reagent gases were of the highest possible purity (Matheson and Company) while the C_5 and C_6 alcohols were commercial samples of high purity.

[1]Visiting Professor 1979–1980. Permanent address: Département de Chimie, Université Laval, Québec (Qué.).

0008-4042/81/142125-08$01.00/0

©1981 National Research Council of Canada/Conseil national de recherches du Canada

Can. J. Chem. Downloaded from www.nrcresearchpress.com by 210.87.254.6 on 09/06/12
For personal use only.

Can. J. Chem. Downloaded from www.nrcresearchpress.com by 210.87.254.6 on 09/06/12
For personal use only.

Results and Discussion

Chemical Ionization Mass Spectra of Isomeric C_5 Alkanols

The chemical ionization mass spectra of the eight C_5 alcohols investigated are presented in Table 1 for the five reagent gases utilized. Several points deserve comment. First, in agreement with isobutane CI spectra (1), the major fragmentation route of the protonated alcohol is by loss of H_2O to give $C_5H_{11}^+$ alkyl ions. The $C_5H_{11}^+$ ions appear to fragment by three routes [1] to [3]

$$[1] \quad C_5H_{11}^+ \longrightarrow C_3H_7^+ + C_2H_4$$

$$[2] \quad \longrightarrow C_4H_7^+ + CH_4$$

$$[3] \quad \longrightarrow C_5H_9^+ + H_2$$

The first fragmentation reaction is known from metastable ion studies (5, 6) while the latter two have been proposed (5) for higher energy fragmenting ions. The extent of fragmentation of $C_5H_{11}^+$ decreases as the exothermicity of the protonation step decreases and also decreases in the order primary > secondary > tertiary alcohol. These observations will be discussed in more detail below.

Second, all alcohols, with the exception of the tertiary alcohol, 2-methylbutan-2-ol, show moderately abundant $(M - H)^+$ ions, presumably originating primarily from H^- abstraction from the alcohol. The abundance of this fragment ion decreases from the H_2 CI through the CO/H_2 CI (i.e. as the reaction exothermicity decreases). The exception to this trend is observed in the N_2O/H_2 CI spectra where, except for the tertiary alcohol, the $(M - H)^+$ ion intensity is enhanced as a result of H^- abstraction by NO^+, present as one of the reactant ions. Hydride ion abstraction from alcohols by NO^+ has been observed, as has the inability of NO^+ to abstract H^- from tertiary alcohols (7). It should be noted that a significant fraction of the $C_5H_9^+$ ion signal may originate by H_2O loss from the $(M - H)^+$ ion rather than by reaction [3]. In a related study (8) of the CI spectra of pentyl acetates, where hydride abstraction is of lesser importance, we have observed lower yields of $C_5H_9^+$ relative to $C_5H_{11}^+$.

Third, those alcohols containing the —CH(OH)-CH_3 moiety show ion signals at *m/z* 45 and *m/z* 73 corresponding, respectively, to the $CH_3CH{=}OH^+$ and $C_3H_7CH{=}OH^+$ ions. Similarly, pentan-3-ol and 2-methylbutan-2-ol both show ion signals at *m/z* 59 corresponding nominally to the CH_3CH_2-$CH{=}OH^+$ and $(CH_3)_2C{=}OH^+$ structures respectively. The abundances of these oxygen-containing fragments, which reflect the structures of the original alcohol, are particularly pronounced in the H_2 CI mass spectra; however, they do persist through the remaining spectra. They most likely represent alternative modes of fragmentation of the protonated alcohol, i.e.

$$[4] \quad R^1{-}\overset{\overset{+OH_2}{|}}{CH}{-}R^2 \longrightarrow \begin{cases} R^1CH{=}OH^+ + R^2H \\ R^2CH{=}OH^+ + R^1H \end{cases}$$

By far the most interesting observations are that the extent of fragmentation of the $C_5H_{11}^+$ ions depends not only on the exothermicity of the initial protonation reaction but also on the structure of the alcohol, being greatest for primary alcohols, less for secondary alcohols, and least for the tertiary alcohol. This is shown most clearly by the H_2 CI mass spectra presented in Fig. 1. The energetics of the CI systems are presented graphically in Fig. 2, with the energy scale being referenced to the protonated alcohol. The heats of formation of $C_3H_7^+$ (isopropyl) and the $C_5H_{11}^+$ ions were taken from Lossing and Maccoll (9) or calculated from their data by the method outlined by Bowen and Williams (6). The remaining thermochemical data were taken from standard sources (10, 11). The data used are summarized in the Appendix.

Thermochemically, fragmentation of $C_5H_{11}^+$ to $C_4H_7^+ + CH_4$ or $C_5H_9^+ + H_2$ is more favourable than fragmentation to $C_3H_7^+ + C_2H_4$. However, as pointed out by Bowen and Williams (6), the fragmentation route of lowest activation energy (and that observed in metastable ion fragmentations) is the latter, indicating that reactions [2] and [3] have activation energy barriers sufficient to make these routes noncompetitive for decomposing ions of low internal energies. Their occurrence for ions of high internal energy, such as are examined in the present work, must mean that the energy independent term (frequency factor) in the rate expression is more favourable for these reaction modes than for ethylene loss.

As Fig. 2 shows, protonation of $C_5H_{11}OH$ by any of the reagent ions used in the present study is sufficiently exothermic to lead to rapid H_2O elimination in all cases; consequently, it is not surprising that the $C_5H_{11}OH_2^+$ ion intensities are extremely small. Further, if all of the protonation exothermicity were retained by the product $C_5H_{11}^+$ ion, this ion should have sufficient energy to fragment further. In fact, the extent of fragmentation of $C_5H_{11}^+$ is small for the weaker protonating agents and, as noted above, for the stronger protonating agents is dependent on the original structure of the alcohol (primary > secondary > tertiary). The

Can. J. Chem. Downloaded from www.nrcresearchpress.com by 210.87.254.6 on 09/06/12
For personal use only.

TABLE 1. Chemical ionization mass spectra of pentanols

m/z	Ion	Relative abundance H_2 CI	N_2/H_2 CI	CO_2/H_2 CI	N_2O/H_2 CI	CO/H_2 CI
Pentanol-1						
87	$C_5H_{11}O^+$	9	6	4	19	2
71	$C_5H_{11}^+$	69	100	100	100	100
69	$C_5H_9^+$	84	33	12	8	8
55	$C_4H_7^+$	25	14	14	7	5
43	$C_3H_7^+$	100	92	42	15	20
41	$C_3H_5^+$	9	6	1	—	—
3-Methylbutan-1-ol						
87	$C_5H_{11}O^+$	14	8	4	19	3
71	$C_5H_{11}^+$	86	100	100	100	100
69	$C_5H_9^+$	62	16	5	4	3
57	$C_4H_9^+$	7	5	3	3	3
55	$C_4H_7^+$	40	28	14	6	4
43	$C_3H_7^+$	100	75	32	10	14
41	$C_3H_5^+$	7	5	—	—	—
2-Methylbutan-1-ol						
87	$C_5H_{11}O^+$	25	9	5	20	4
71	$C_5H_{11}^+$	100	100	100	100	100
69	$C_5H_9^+$	30	7	3	2	1
57	$C_4H_9^+$	10	7	5	4	4
55	$C_4H_7^+$	33	17	9	4	3
43	$C_3H_7^+$	100	75	32	10	14
41	$C_3H_5^+$	8	4	—	—	—
2,2-Dimethylpropan-1-ol						
87	$C_5H_{11}O^+$	18	6	4	19	3
73	$C_4H_9O^+$	42	21	10	4	4
71	$C_5H_{11}^+$	73	100	100	100	100
69	$C_5H_9^+$	15	2	—	—	—
57	$C_4H_9^+$	15	8	10	6	8
55	$C_4H_7^+$	9	4	—	—	—
43	$C_3H_7^+$	100	46	15	4	9
41	$C_3H_5^+$	9	4	—	—	—
Pentan-2-ol						
87	$C_5H_{11}O^+$	12	5	4	25	3
73	$C_4H_9O^+$	15	9	7	3	3
71	$C_5H_{11}^+$	100	100	100	100	100
69	$C_5H_9^+$	15	3	1	1	1
55	$C_4H_7^+$	12	5	3	1	1
45	$C_2H_5O^+$	39	21	R[a]	R[a]	11
43	$C_3H_7^+$	42	21	8	4	4
41	$C_3H_5^+$	2	—	—	—	—
Pentan-3-ol						
87	$C_5H_{11}O^+$	15	5	4	21	3
73	$C_4H_9O^+$	5	3	1	—	—
71	$C_5H_{11}^+$	100	100	100	100	100
69	$C_5H_9^+$	10	3	1	1	1
59	$C_3H_7O^+$	21	12	14	7	13
55	$C_4H_7^+$	17	7	4	1	1
43	$C_3H_7^+$	56	24	8	3	5
41	$C_3H_5^+$	4	2	—	—	—
3-Methylbutan-2-ol						
87	$C_5H_{11}O^+$	17	5	5	20	4
73	$C_4H_9O^+$	32	16	10	5	4
71	$C_5H_{11}^+$	100	100	100	100	100
69	$C_5H_9^+$	9	2	1	1	1
55	$C_4H_7^+$	6	7	1	1	1
45	$C_2H_5O^+$	15	7	R[a]	R[a]	4
43	$C_3H_7^+$	32	12	5	2	2
41	$C_3H_5^+$	2	—	—	—	—
2-Methylbutan-2-ol						
87	$C_5H_{11}O^+$	9	2	1	1	1
73	$C_4H_9O^+$	26	18	14	6	9
71	$C_5H_{11}^+$	100	100	100	100	100
69	$C_5H_9^+$	10	1	1	1	1
59	$C_3H_7O^+$	7	7	10	4	7
55	$C_4H_9^+$	7	3	1	1	1
43	$C_3H_7^+$	16	5	3	2	2
41	$C_3H_5^+$	2	—	—	—	—

[a]Fragment ion masked by reagent ion peak.

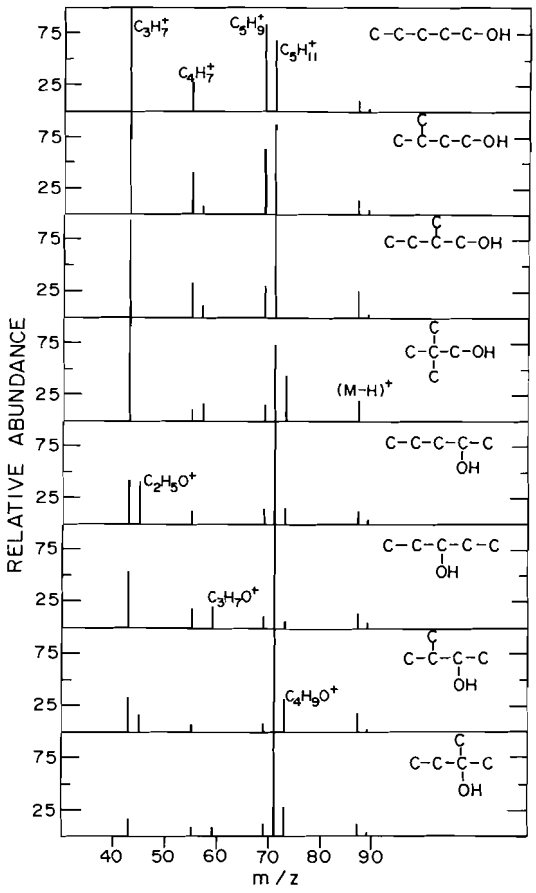

FIG. 1. H_2 CI mass spectra of pentanols.

Can. J. Chem. Downloaded from www.nrcresearchpress.com by 210.87.254.6 on 09/06/12
For personal use only.

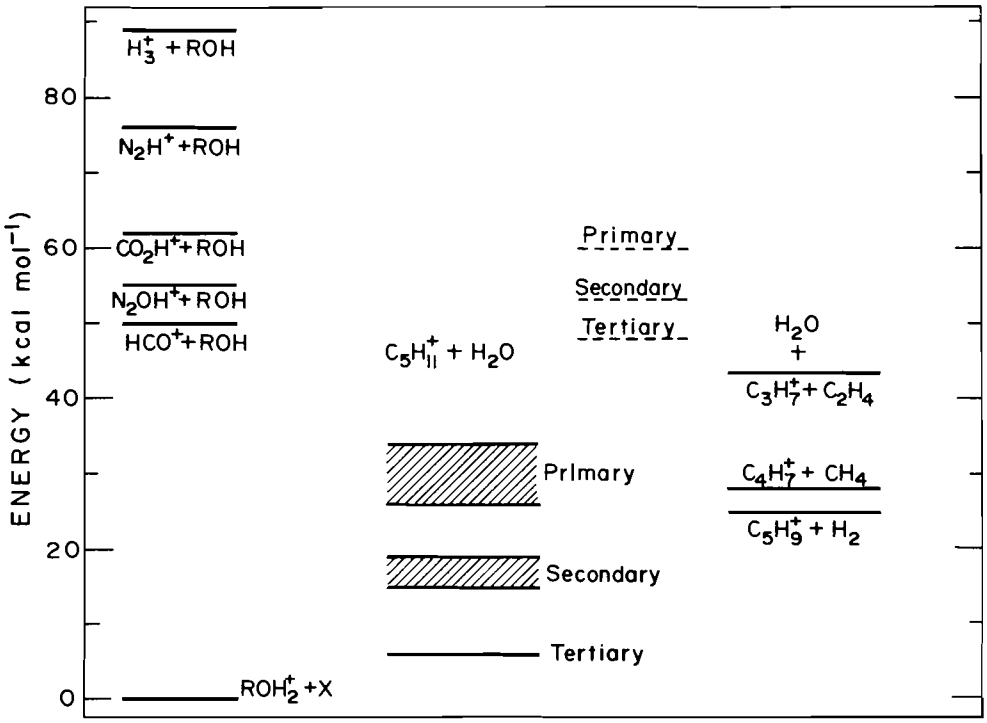

FIG. 2. Energetics of protonation and fragmentation of pentanols.

simplest rationalization of this latter observation is as follows. The enthalpy change for the overall reaction

[5] $H_3^+ + C_5H_{11}OH \longrightarrow C_5H_{11}^+ + H_2O + H_2$

is ~ -60 kcal mol^{-1} for primary alcohols, ~ -73 kcal mol^{-1} for secondary alcohols, and ~ -80 kcal mol^{-1} for the tertiary alcohol, assuming no rearrangement of the alkyl function. If, on average, the same fraction of this exothermicity is retained by the $C_5H_{11}^+$ ion, in all cases, the average energy content of the $C_5H_{11}^+$ ions, relative to their fragmentation products, will be greatest for primary ions and least for tertiary ions. (For example, the levels shown as dotted lines in Fig. 2 assume 50% of the exothermicity is retained by the alkyl ion.) Clearly, if this is the situation, a greater fraction of the $C_5H_{11}^+$ ions derived from primary alcohols will have internal energies sufficient to undergo fragmentation before they are collisionally deactivated to below the decomposition threshold. As has been discussed previously (4), fragmentation following chemical ionization is in competition with collisional deactivation, Scheme 1. At the pressures used in the present work $k_2[M] \simeq 10^7$ s^{-1} with the result that significant fragmentation will be observed only for ions which have an internal energy sufficient to give $k_1 \geq 10^7$ s^{-1}.

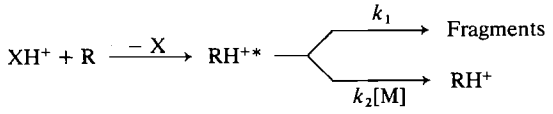

SCHEME 1

If this picture is correct, the extent of fragmentation should be greatest for $C_5H_{11}^+$ ions derived from primary alcohols and least for $C_5H_{11}^+$ ions derived from tertiary alcohols. An essential feature of this rationalization is that the alkyl function does not rearrange to a more stable structure during H_2O elimination from the protonated alcohol or, if it does so, that rearrangement occurs at a sufficiently late stage in the decomposition process that it does not influence the energy partitioning between the neutral H_2O and the $C_5H_{11}^+$ ion. If rearrangement were to occur at an early stage in the decomposition process the distinction between the alcohols should be lost and the extent of further fragmentation should be the same for the isomeric alcohols. This clearly is not the case. In a related study of the CI of pentyl acetates, reported in the following paper, we have observed that the competition between fragmentation reaction channels suggests rearrangement to more stable alkyl ions by (1,2)-H shifts, while the extent of further fragmentation of $C_5H_{11}^+$ reflects the original structure (primary or second-

Can. J. Chem. Downloaded from www.nrcresearchpress.com by 210.87.254.6 on 09/06/12
For personal use only.

ary) of the acetate. These results suggest that the critical activation energy for decomposition of MH^+ reflects the original structure of the alkyl group and determines the partitioning of the excess energy between neutral and ionic species but that the competition between fragmentation reaction channels is determined at a later stage in the decomposition process.

The conclusion that rearrangement in the alcohols does not occur to a significant extent is particularly interesting for 2-methylbutan-1-ol and 3-methylbutan-2-ol where, in each case, a relatively simple (1,2)-H shift would lead to the very stable tertiary carbonium ion. A close examination of the CI mass spectra shows that the extent of fragmentation of $C_5H_{11}^+$ derived from 2-methylbutan-1-ol is less than that observed for any other primary alcohol. Similarly the extent of fragmentation of $C_5H_{11}^+$ from 3-methylbutan-2-ol is less than $C_5H_{11}^+$ derived from other secondary alcohols. These results suggest that rearrangement may be occurring but that the effect on the partitioning of the excess energy between the neutral and ionic fragment is small.

Chemical Ionization Mass Spectra of C_6 Alkanols

The observation that the extent of fragmentation of the $C_5H_{11}^+$ ions produced from the isomeric C_5 alkanols reflected the structure (i.e., primary, secondary, or tertiary) of the carbonium ion initially formed by H_2O elimination encouraged us to extend the study to the isomeric C_6 alkanols. The fragmentation of $C_6H_{13}^+$ alkyl ions has been discussed in detail by Bowen and Williams (6). In the metastable ion region two competing fragmentation reactions are observed, leading to formation of $C_4H_9^+ + C_2H_4$ and to formation of $C_3H_7^+ + C_3H_6$. This has been rationalized in terms of the energy diagram shown in Fig. 3 which assumes that the reacting configuration leading to ethylene elimination is the 3,3-dimethyl-1-butyl carbonium ion which has an energy similar to that of the $C_3H_7^+ + C_3H_6$ products; thus, in the absence of any additional activation barriers the two reaction modes would be competitive. The ratio of metastable abundances for C_2H_4 and C_3H_6 losses are 1:1.6 (12). The reacting configuration leading to loss of C_3H_6 was assumed to be the 4-methyl-2-pentyl carbonium ion. It appeared of interest to attempt the preparation of specific $C_6H_{13}^+$ ion structures by dissociative protonation of the C_6 alcohols to examine the competition between the two major reaction channels as a function of structure. In particular, preparation of the two ions depicted in Fig. 3 might be expected to lead to preferential loss

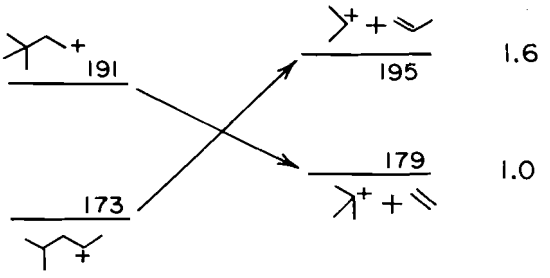

Bowen and Williams, J.C.S. Perk II 1479 (1976)

FIG. 3. Fragmentation mechanisms, $C_6H_{13}^+$ ions.

of C_2H_4 for the primary ion and C_3H_6 for the secondary ion under the higher energy CI induced fragmentation conditions, since these reactions involve only simple bond cleavage reactions and should be favoured over the alternative reaction(s) requiring skeletal rearrangement.

The CI mass spectra of the 14 C_6 alkanols studied are presented in Table 2. The main features of the spectra are essentially the same as described for the C_5 alcohols. The major fragmentation reaction of the protonated alcohol involves H_2O elimination. The resulting $C_6H_{13}^+$ ions fragment further by the following paths.

[6] $C_6H_{13}^+ \longrightarrow C_3H_7^+ + C_3H_6$
[7] $\longrightarrow C_4H_9^+ + C_2H_4$
[8] $\longrightarrow C_5H_9^+ + CH_4$
[9] $\longrightarrow C_6H_{11}^+ + H_2$

Reactions [6] and [7] are the lowest energy fragmentation routes (Fig. 3) while reactions [8] and [9], analogous to reactions [2] and [3] for $C_5H_{11}^+$, have been reported earlier (5) as higher energy fragmentation routes. In agreement with the results for the $C_5H_{11}^+$ ions, the extent of fragmentation of the $C_6H_{13}^+$ ions decreases as one proceeds from primary to secondary to tertiary alcohols. This structural dependence provides additional evidence that structural rearrangement of the alkyl ion does not occur prior to achievement of the critical configuration which determines the energy partitioning between the alkyl ion and neutral H_2O.

As for the C_5 alkanols, $(M - H)^+$ ions are observed for primary and secondary alcohols and show enhanced abundances in the N_2O/H_2 CI spectra due to H^- abstraction by NO^+. In addition, formation of the oxycarbonium ions corresponding to $(M - CH_3)^+$, $(M - C_2H_5)^+$, and $(M - C_3H_7)^+$, as well as formation of $CH_3CH{=}OH^+$, is observed when the neutral structure permits formation of these products without skeletal rearrangement.

Can. J. Chem. Downloaded from www.nrcresearchpress.com by 210.87.254.6 on 09/06/12
For personal use only.

TABLE 2. Chemical ionization (CI) mass spectra of C_6 alkanols

m/z	Ion	H_2 CI	N_2/H_2 CI	CO_2/H_2 CI	N_2O/H_2 CI	CO/H_2 CI
Hexan-1-ol						
101	$C_6H_{13}O^+$	7	3	3	28	4
85	$C_6H_{13}^+$	48	44	100	100	100
83	$C_6H_{11}^+$	74	33	16	14	14
69	$C_5H_9^+$	33	33	22	12	6
57	$C_4H_9^+$	26	22	16	10	14
56	$C_4H_8^+$	11	11	8	4	4
55	$C_4H_7^+$	48	22	5	4	6
43	$C_3H_7^+$	100	100	54	22	37
41	$C_3H_5^+$	7	4	—	—	—
2-Methylpentan-1-ol						
101	$C_6H_{13}O^+$	14	5	4	20	5
85	$C_6H_{13}^+$	61	100	100	100	100
83	$C_6H_{11}^+$	50	18	8	7	7
71	$C_5H_{11}^+$	7	5	6	4	3
69	$C_5H_9^+$	32	21	13	5	5
59	$C_3H_7O^+$	11	3	—	—	—
57	$C_4H_9^+$	25	13	8	5	8
55	$C_4H_7^+$	25	5	2	2	3
43	$C_3H_7^+$	100	66	26	16	22
41	$C_3H_5^+$	7	2	—	—	—
3-Methylpentan-1-ol						
101	$C_6H_{13}O^+$	10	4	2	20	2
85	$C_6H_{13}^+$	75	100	100	100	100
83	$C_6H_{11}^+$	90	29	9	7	11
69	$C_5H_9^+$	85	50	28	5	11
57	$C_4H_9^+$	60	36	17	5	17
56	$C_4H_8^+$	10	6	6	—	—
55	$C_4H_7^+$	40	11	4	2	6
43	$C_3H_7^+$	100	75	36	16	28
41	$C_3H_5^+$	10	11	—	—	—
4-Methylpentan-1-ol						
101	$C_6H_{13}O^+$	8	3	4	25	5
85	$C_6H_{13}^+$	60	53	100	100	100
83	$C_6H_{11}^+$	80	31	9	9	8
69	$C_5H_9^+$	60	60	36	19	9
57	$C_4H_9^+$	32	25	16	9	6
56	$C_4H_8^+$	12	16	11	4	3
55	$C_4H_7^+$	28	9	—	—	—
43	$C_3H_7^+$	100	100	44	23	16
41	$C_3H_5^+$	8	9	—	—	—
2-Ethylbutan-1-ol						
101	$C_6H_{13}O^+$	21	8	4	23	3
85	$C_6H_{13}^+$	83	44	100	100	100
83	$C_6H_{11}^+$	46	14	4	4	3
71	$C_5H_{11}^+$	8	6	9	2	3
69	$C_5H_9^+$	42	33	19	7	5
57	$C_4H_9^+$	25	25	15	5	6
55	$C_4H_7^+$	29	14	4	—	—
43	$C_3H_7^+$	100	100	50	14	17
41	$C_3H_5^+$	4	3	—	—	—
3,3-Dimethylbutan-1-ol						
101	$C_6H_{13}O^+$	3	3	3	32	2
87	$C_5H_{11}O^+$	6	8	13	8	5
85	$C_6H_{13}^+$	27	27	70	100	100
83	$C_6H_{11}^+$	35	14	3	2	2
69	$C_5H_9^+$	47	43	23	13	12
57	$C_4H_9^+$	100	100	100	63	70
55	$C_4H_7^+$	12	3	—	—	—
43	$C_3H_7^+$	41	51	33	8	12
41	$C_3H_5^+$	6	5	—	—	—
Hexan-3-ol						
101	$C_6H_{13}O^+$	22	8	5	26	4
85	$C_6H_{13}^+$	100	100	100	100	100
83	$C_6H_{11}^+$	19	8	2	2	1
73	$C_4H_9O^+$	19	14	6	3	3
69	$C_5H_9^+$	19	14	5	2	1
59	$C_3H_7O^+$	63	36	14	5	6
57	$C_4H_9^+$	19	19	5	2	1
55	$C_4H_7^+$	19	11	3	2	1
43	$C_3H_7^+$	63	50	14	3	4
3-Methylpentan-2-ol						
101	$C_6H_{13}O^+$	10	6	4	27	4
87	$C_5H_{11}O^+$	15	10	6	3	1
85	$C_6H_{13}^+$	100	100	100	100	100
83	$C_6H_{11}^+$	7	2	1	1	1
73	$C_4H_9O^+$	5	2	1	1	—
69	$C_5H_9^+$	7	6	3	1	1
57	$C_4H_9^+$	17	12	4	1	3
55	$C_4H_7^+$	5	2	3	1	—
45	$C_2H_5O^+$	42	28	R[a]	R[a]	5
43	$C_3H_7^+$	27	24	5	3	3
4-Methylpentan-2-ol						
101	$C_6H_{13}O^+$	8	2	3	23	3
87	$C_5H_{11}O^+$	11	9	6	3	3
85	$C_6H_{13}^+$	100	100	100	100	100
83	$C_6H_{11}^+$	19	7	1	1	1
69	$C_5H_9^+$	14	11	5	3	3
57	$C_4H_9^+$	31	18	4	1	3
55	$C_4H_7^+$	5	2	—	—	—
45	$C_2H_5O^+$	44	34	R[a]	R[a]	5
43	$C_3H_7^+$	39	34	5	3	4
3,3-Dimethylbutan-2-ol						
101	$C_6H_{13}O^+$	14	6	4	23	5
87	$C_5H_{11}O^+$	60	35	15	7	5
85	$C_6H_{13}^+$	100	100	100	100	100
83	$C_6H_{11}^+$	9	4	1	2	1
69	$C_5H_9^+$	9	4	1	2	1
57	$C_4H_9^+$	29	16	5	3	3
56	$C_4H_8^+$	6	4	3	2	1
45	$C_2H_5O^+$	14	8	R[a]	R[a]	1
43	$C_3H_7^+$	37	22	2	2	1
2-Methylpentan-3-ol						
101	$C_6H_{13}O^+$	14	6	3	20	4
87	$C_5H_{11}O^+$	8	6	4	1	1
85	$C_6H_{13}^+$	100	100	100	100	100
83	$C_6H_{11}^+$	8	2	1	1	1
73	$C_4H_9O^+$	14	9	4	1	3
69	$C_5H_9^+$	11	9	3	1	1
59	$C_3H_7O^+$	25	13	7	3	1
57	$C_4H_9^+$	17	13	3	1	1
55	$C_4H_7^+$	6	2	3	—	—
43	$C_3H_7^+$	50	36	7	1	3

Can. J. Chem. Downloaded from www.nrcresearchpress.com by 210.87.254.6 on 09/06/12
For personal use only.

TABLE 2. (*Concluded*)

m/z	Ion	H_2 CI	N_2/H_2 CI	CO_2/H_2 CI	N_2O/H_2 CI	CO/H_2 CI
2-Methylpentan-2-ol						
101	$C_6H_{13}O^+$	4	2	1	1	1
87	$C_5H_{11}O^+$	22	20	11	4	4
85	$C_6H_{13}^+$	100	100	100	100	100
83	$C_6H_{11}^+$	6	4	3	4	3
69	$C_5H_9^+$	4	6	3	1	1
59	$C_3H_7O^+$	28	29	13	7	6
57	$C_4H_9^+$	8	6	1	1	1
43	$C_3H_7^+$	12	9	1	1	1
3-Methylpentan-3-ol						
101	$C_6H_{13}O^+$	4	2	1	1	1
87	$C_5H_{11}O^+$	14	10	6	4	3
85	$C_6H_{13}^+$	100	100	100	100	100
83	$C_5H_{11}^+$	6	2	1	1	1
73	$C_4H_9O^+$	22	16	11	7	8
69	$C_5H_9^+$	6	3	1	1	1
57	$C_4H_9^+$	8	5	1	1	—
55	$C_4H_7^+$	4	3	1	1	1
43	$C_3H_7^+$	18	12	3	1	1
2,3-Dimethylbutan-2-ol						
101	$C_6H_{13}O^+$	9	3	1	1	1
87	$C_5H_{11}O^+$	44	28	15	6	7
85	$C_6H_{13}^+$	100	100	100	100	100
83	$C_6H_{11}^+$	9	2	1	1	1
69	$C_5H_9^+$	9	3	1	1	1
59	$C_3H_7O^+$	18	12	7	4	5
57	$C_4H_9^+$	7	3	1	1	1
43	$C_3H_7^+$	18	8	1	1	1

[a]Fragment ion masked by reagent ion peak.

The dependence of the reaction competition between propylene loss and ethylene loss on the nominal $C_6H_{13}^+$ ion structure is examined in Table 3 which records the intensity ratio $C_3H_7^+/C_4H_9^+$ observed in the N_2/H_2 CI mass spectra. The results clearly show that the carbonium ion derived from 3,3-dimethylbutan-1-ol preferentially eliminates ethylene. This is the reaction mode predicted (Fig. 3) for the 3,3-dimethyl-1-butyl cation. On the other hand the $C_6H_{13}^+$ ion derived from 4-methylpentan-2-ol, which, in the absence of rearrangement, should have the 4-methyl-2-pentyl structure, does not show an enhanced elimination of propylene as one would predict it should if it is in fact the reacting configuration for propylene elimination. It is not clear whether in this case there has been a rearrangement of the carbonium ion or whether, as is more likely, propylene elimination is a more complex reaction which cannot be attributed to this specific reacting structure. The results of Table 3 show that for all $C_6H_{13}^+$ ions, except that derived from 3,3-dimethylbutan-1-ol, elimination of propylene is favoured over elimination of ethylene. This is in agreement with the metastable ion studies. The ratio shows considerable variation for the $C_6H_{13}^+$ ions derived from different alcohols; the significance of this variation is not clear.

TABLE 3. $C_3H_7^+/C_4H_9^+$ ratio in N_2/H_2 CI of C_6 alkanols

Alkanol	Ratio	Alkanol	Ratio
	4.5	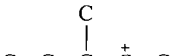	2.3
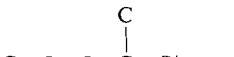	5.1	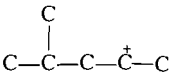	1.9
	2.1	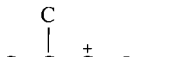	1.4
	4.0		2.8
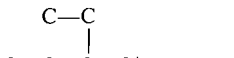	3.3	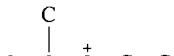	1.5
	0.5		2.4
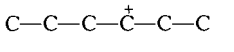	1.4	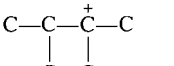	2.7

TABLE 4. Heats of formation of C_5 alkyl ions and protonated alcohols[a]

R	$\Delta H^0_f(R^+)$	$\Delta H^0_f(ROH)^b$	$\Delta H^0_f(ROH_2^+)^c$
1-Pentyl	194[d]	−70.7	105
2-Methyl-1-butyl	193[e]	−72.2	104
3-Methyl-1-butyl	196[e]	−72.0	104
3,3-Dimethyl-1-propyl	188[d]	−75.5	101
2-Pentyl	179[d]	−75.2	101
3-Pentyl	175[e]	−75.2	101
3-Methyl-2-butyl	175[e]	−75.4	101
2-Methyl-2-butyl	161[d]	−79.1	97

[a]Data in kcal mol^{-1}.
[b]From ref. 10.
[c]Calculated taking PA(alcohol) = 190 kcal mol^{-1} (3).
[d]From ref. 9.
[e]Estimated as outlined by Bowen and Williams (6).

Obviously for both the $C_5H_{11}^+$ and $C_6H_{13}^+$ ions additional studies involving isotopic labelling, metastable ion characteristics, and collisional activation spectra are desirable. The present results show only that the extent of rearrangement in forming the alkyl ions by chemical ionization is minimal but provide no information on the facility with which rearrangements occur after the carbonium ions are formed. The further studies

suggested should provide information on this aspect.

Acknowledgements

The authors are indebted to the Natural Sciences and Engineering Research Council of Canada for financial support and to Professor D. K. Bohme for communication of results prior to publication.

1. F. H. Field. J. Am. Chem. Soc. **92**, 2672 (1970).
2. D. K. Bohme, G. I. Mackay, and H. I. Schiff. J. Chem. Phys. **73**, 4976 (1980).
3. F. M. Benoit and A. G. Harrison. J. Am. Chem. Soc. **99**, 3980 (1977).
4. R. D. Bowen and A. G. Harrison. Org. Mass Spectrom. In press.
5. A. Fiaux, B. Wirz, and T. Gäumann. Helv. Chim. Acta, **57**, 708 (1974).
6. R. D. Bowen and D. H. Williams. J. Chem. Soc. Perkin Trans. II, 1479 (1976).
7. D. F. Hunt and J. F. Ryan. J. Chem. Soc. Chem. Commun. 620 (1972).
8. J. A. Herman and A. G. Harrison. Can. J. Chem. **59**, 2133 (1981).
9. F. P. Lossing and A. Maccoll. Can. J. Chem. **54**, 990 (1976).
10. J. D. Cox and G. Pilcher. Thermochemistry of organic and organometallic compounds. Academic Press, New York. 1970.
11. H. M. Rosenstock, K. Draxl, B. W. Steiner, and J. T. Herron. Energetics of gaseous ions. J. Phys. Chem. Ref. Data, **6**, Suppl. 1 (1977).
12. H. M. Rosenstock, V. H. Dibeler, and F. N. Harlee. J. Chem. Phys. **40**, 591 (1964).
13. F. P. Lossing. Can. J. Chem. **50**, 3973 (1972).

Appendix

The heats of formation of the C_5 alkyl ions, C_5 alkanols, and C_5 protonated alkanols are summarized in Table 4. Other relevant heats of formation (in kcal mol^{-1}) are: i-$C_3H_7^+$, 192 (12); $C_4H_7^+$, 204 (13); $C_5H_9^+$, 184 (6); C_2H_4, 12.5 (10); CH_4, −17.9 (10).

Can. J. Chem. Downloaded from www.nrcresearchpress.com by 210.87.254.6 on 09/06/12
For personal use only.

Energetics and structural effects in the fragmentation of protonated esters in the gas phase

JAN A. HERMAN[1] AND ALEX. G. HARRISON

Department of Chemistry, University of Toronto, Toronto, Ont., Canada M5S 1A1

Received November 20, 1980

Can. J. Chem. Downloaded from www.nrcresearchpress.com by 210.87.254.6 on 09/06/12
For personal use only.

JAN A. HERMAN and ALEX. G. HARRISON. Can. J. Chem. **59**, 2133 (1981).

A series of formate (methyl through butyl) and acetate (methyl through pentyl) esters have been protonated in the gas phase by the Brønsted acids H_3^+, N_2H^+, CO_2H^+, N_2OH^+, and HCO^+. Carbonyl oxygen protonation is 87–97 kcal mol^{-1} exothermic for H_3^+ and 47–57 kcal mol^{-1} exothermic for the weakest acid HCO^+, permitting a study of the effect of protonation exothermicity on the decomposition modes of the protonated esters. With the exception of protonated methyl formate, three decomposition modes, (a) to (c) are observed.

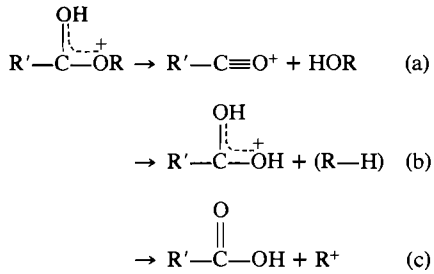

Reaction (a) is unimportant for formates; for acetates it is the sole decomposition channel for the methyl ester, but is less important for higher acetates. The dependence of the relative importance of this reaction mode on the protonation exothermicity indicates an activation energy considerably in excess of ΔH^0, presumably because the reaction involves a symmetry-forbidden 1,3-H shift for the carbonyl protonated ester. For the higher acetates where the difference in the proton affinities of the carbonyl and ether oxygens is less, acyl ion formation results, in part, from protonation at the ether oxygen. For protonated methyl formate the major fragmentation reaction yields $CH_3OH_2^+ + CO$; this reaction also appears to have an activation energy considerably in excess of the ΔH_0. For the remaining esters either reaction (b) or (c) is the major decomposition mode. The competition between these two channels depends strongly on the protonation exothermicity and the relative activation energies. From the reaction competition we conclude that 1,2-H shifts occur in the case of primary alkyl esters yielding more stable secondary or tertiary alkyl ions. This rearrangement appears to occur after the excess energy has been partitioned between the alkyl ion and the neutral acid since the extent of further fragmentation of the alkyl ion reflects the original structure of the alkyl group.

JAN A. HERMAN et ALEX. G. HARRISON. Can. J. Chem. **59**, 2133 (1981).

Les acides de Brønsted H_3^+, N_2H^+, CO_2H^+, N_2OH^+ et HCO^+ ont servi à l'étude de la protonation en phase gazeuse des deux séries d'esters: formiates (de méthyle à butyle) et acétates (de méthyle à pentyle). L'exothermicité de la réaction de protonation du groupement carbonyle varie de 87–97 kcal mol^{-1} pour H_3^+ à 47–57 kcal mol^{-1} pour l'acide le plus faible, HCO^+, ce qui permet d'étudier l'effet de la chaleur de la réaction de protonation sur les modes de décomposition des esters protonés. Sauf dans le cas du formiate de méthyle protoné, on observe trois modes de décomposition, (a) à (c).

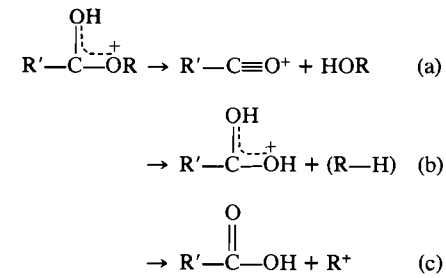

Alors qu'elle n'intervient guère dans le cas des formiates, la réaction (a) est l'unique voie de décomposition de l'acétate de méthyle et perd ensuite de l'importance pour les acétates supérieurs. La dépendance de l'importance relative de ce mode de réaction vis-à-vis l'exothermicité de la protonation indique une énergie d'activation excédant considérablement ΔH^0, probablement en raison du transfert d'H-1,3 symétriquement interdit impliqué dans la réaction de l'ester protoné. La différence des affinités protoniques des oxygènes du carbonyle et de l'éther étant moindres pour les acétates supérieurs, la formation de l'ion acylium provient en partie de la

---

[1]Visiting Professor 1979–1980. Permanent address: Département de Chimie, Université Laval, Québec (Qué.).

0008-4042/81/142133-13$01.00/0

©1981 National Research Council of Canada/Conseil national de recherches du Canada

protonation de l'oxygène de l'éther. Dans le cas du formiate de méthyle protoné, la principale réaction de fragmentation produit $CH_3OH_2^+ + CO$; cette réaction semble elle aussi avoir une énergie d'activation beaucoup plus grande que le ΔH^0. Le principal mode de décomposition des autres esters est l'une des deux dernières réactions (b) ou (c). La compétition entre ces deux voies est fortement influencée par l'exothermicité de la protonation et les énergies d'activation relatives. Cette compétition permet de voir que les transferts d'hydrogène-1,2 se produisent dans le cas des esters d'alkyle primaire pour conduire aux ions alkyles secondaires ou tertiaires plus stables. Ce réarrangement s'effectue apparemment après répartition de l'excès d'énergie entre l'ion alkyle et l'acide neutre puisque le degré de fragmentation ultérieure de l'ion alkyle reflète la structure originale du groupement alkyle.

Can. J. Chem. Downloaded from www.nrcresearchpress.com by 210.87.254.6 on 09/06/12
For personal use only.

Introduction

Since the original survey (1) of the chemical ionization (CI) mass spectra of esters, there have been numerous investigations (2–7) designed to elucidate details of the dissociation reactions occurring following proton transfer to esters in the gas phase. It has been established clearly that there are three main fragmentation modes, reactions [1] to [3].

[1] $R'CO_2R \cdot H^+ \rightarrow R'C{\equiv}O^+ + ROH$

[2] $\rightarrow R'CO_2H + R^+$

[3] $\rightarrow R'CO_2H_2^+ + (R{-}H)$

Reaction [1], involving formation of the acylium ion by acyl carbon–oxygen bond cleavage, and reaction [2], involving formation of the alkyl carbonium ion by alkyl carbon–oxygen bond cleavage, are analogous to the $A_{Ac}I$ and $A_{Al}I$ mechanisms for fragmentation of esters in concentrated acid solutions (8). Reaction [3] has no direct solution analogue.

The factors which determine the competition between these three channels in the gas phase have not been established clearly. In general, reaction [1] appears to be of lesser importance in the gas phase than in solution, possibly (6, 7) because it requires formation of the energetically less favourable ether oxygen-protonated ester. Alternatively, it has been suggested (7) that the ether oxygen-protonated species may fragment in the gas phase preferentially to form the protonated acid (reaction [3]) through formation of a six-membered cyclic transition state (reaction [4]).

[4] 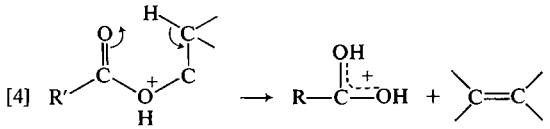

However, for propyl esters at least, it has been shown (6) that the hydrogen transferred from the alkyl group is not specifically the β-hydrogen as required by the proposed mechanism.

From a detailed study of the H_2 and CH_4 CI mass spectra of a series of formate esters, Harrison and Tsang (5) concluded that the relative importance of the fragmentation reactions of protonated formates was not determined by the relative enthalpies of decomposition of ground state $HCO_2R \cdot H^+$ but rather was determined by the relative fragmentation rate coefficients averaged over the appropriate internal energy distribution of the excited $HCO_2R \cdot H^+$ ions formed in the protonation reaction.

In electron impact studies a valuable approach in elucidating the factors controlling the competition between decomposition channels has been that of varying the average internal energy of the fragmenting species (9–11); it appeared that a similar approach should prove equally fruitful in chemical ionization systems. Recent work in this laboratory (12, 13) has shown that the protonation exothermicity and, thus, the average internal energy of the protonated species, can be varied over a significant and useful range by using the family of protonating agents XH^+, where X = H_2 (101), N_2 (117), CO_2 (129), N_2O (137), and CO (141); the numbers in brackets give the proton affinities of X in kcal mol^{-1} (14) and show that the protonation exothermicity can be varied by ~40 kcal mol^{-1}. The present work reports a detailed study of the effect of reaction exothermicity on the CI mass spectra of formate and acetate esters using this family of protonating agents. A similar study of a few selected esters using the flowing afterglow method has been reported recently (7).

Experimental

The chemical ionization mass spectra were obtained using a DuPont 21-490 mass spectrometer equipped with a high pressure chemical ionization source. The source temperature was ~60°C and the ionizing electron energy 70 eV, with the repellers at cage potential. The liquid samples were introduced through a heated inlet system held below 100°C. Reagent gas pressures were not measured directly but were estimated to be 0.2–0.3 Torr. The mass resolution of the instrument is sufficient to resolve the $C_2H_3O^+$–$C_3H_7^+$ doublet at m/z 43.

The H_3^+ reactant ion (X = H_2) was produced in pure H_2. As described elsewhere (12, 13) the N_2H^+, CO_2H^+, N_2OH^+, and HCO^+ reactant ions were prepared by electron impact ionization of the appropriate gas X (~10%) in H_2. Except for the N_2O/H_2 mixture the relevant XH^+ ion was the only significant ion in the reagent gas mass spectrum; in the N_2O/H_2 system ~10–15% of the total ionization was found as NO^+. As is evident from the results presented in the following section the NO^+ ion reacts with the esters primarily by addition to give the $M \cdot NO^+$ complex.

Reagent gases were of highest possible purity (Matheson and Co.) while the esters were either commercial samples of high purity or were prepared by standard procedures. Ethyl-d_5 formate was obtained from Merck, Sharp, and Dohme, Montreal.

Can. J. Chem. Downloaded from www.nrcresearchpress.com by 210.87.254.6 on 09/06/12
For personal use only.

Results and Discussion

Some general observations are in order to set the stage for the discussion of the chemical ionization results. The proton affinities reported (15) for formate and acetate esters range from 188 kcal mol^{-1} for methyl formate to 198 kcal mol^{-1} for *n*-propyl acetate; both refer to protonation at the carbonyl oxygen, the proton affinity of the ether oxygen being 11 to 22 kcal mol^{-1} lower depending on the ester (16). Thus carbonyl oxygen protonation of the esters by ground state H_3^+ is 87 to 97 kcal mol^{-1} exothermic, while protonation by ground state HCO^+ is 47 to 57 kcal mol^{-1} exothermic. In addition it is likely that the reagent ions in our system are not completely thermalized, making the protonation exothermicity even larger. The fraction of this reaction exothermicity which remains with the protonated molecule is not known, although arguments have been presented (12) from a detailed study of the protonation of C_3H_6O isomers, that, on average, a large fraction, approaching unity, of the exothermicity is retained by the product ions.

As discussed previously (12), the fragmentation of these excited ions (reaction [5]) is in competition with collisional stabilization (reaction [6]). At the

$$[5] \quad RH^{+*} \xrightarrow{k_5} \text{Fragments}$$

$$[6] \quad \xrightarrow[k_6[M]]{} RH^+$$

total pressures applicable in the present study, and assuming that a single collision with M is sufficient to stabilize RH^{+*} to below the decomposition threshold, $k_6[M] \simeq 1 \times 10^7 s^{-1}$. Thus the fragmentation reactions observed as reaction [5] correspond to those with rate coefficients, k_5, equal to or greater than $\sim 10^7 s^{-1}$. This is significantly higher than the threshold rate coefficients observed in electron impact mass spectrometry, particularly those observed as metastable ions ($k \simeq 10^4$–$10^6 s^{-1}$). This has important implications for the fragmentation reactions observed in chemical ionization mass spectrometry compared to those observed in electron impact mass spectrometry. The rate coefficient for the unimolecular decomposition of a gas-phase ion can be expressed in its simplest form (9–11) as

$$[7] \quad k(E) = \nu\left(\frac{E - \varepsilon_0}{E}\right)^S$$

where ν is an energy independent term or frequency factor, E is the internal energy, S is the effective number of oscillators, and ε_0 is the activation energy (referred to the ground state of the ion) for the reaction. It is well established (9–11) in electron impact studies that, at low internal energies, the relative rates of competing fragmentation reactions are determined largely by the relative activation energies, while at high internal energies the relative rates are strongly influenced by the energy independent term or frequency factor. In general, simple bond cleavage reactions have high frequency factors compared to those reactions which involve molecular rearrangement. Consequently, rearrangement fragmentation reactions cannot compete effectively with simple bond cleavage reactions at high internal energies and, normally, are observed following electron impact ionization because they have lower activation energies and, therefore, are dominant at lower internal energies. Similar considerations should apply in chemical ionization systems. Because, as discussed above, the average internal energy of fragmenting ions in CI systems is higher than in electron impact systems (especially for EI metastable ion studies), simple bond cleavage reactions should be favoured over rearrangement reactions. Further, as the average internal energy is increased by increasing the protonation exothermicity, the simple bond cleavage reactions should become increasingly favoured. These effects are observed in the results presented below.

The discussion which follows relies heavily on thermochemical arguments. The heats of formation of the carbonyl protonated esters and acids were derived from the reported proton affinities (15) or proton affinities estimated from these data, while the heats of formation of the ether oxygen-protonated species were derived from the estimates (16) of the proton affinities of these species. The heats of formation of alkyl ions were taken from the work of Lossing and Maccoll (17) or estimated from these data by the method outlined by Bowen and Williams (18). The remaining thermochemical data were taken from standard sources (19, 20). The data used are summarized in the Appendix.

Chemical Ionization Mass Spectra of Formate Esters

The chemical ionization mass spectra of the formate esters studied are summarized in Table 1. The H_2 CI mass spectra are in satisfactory agreement with those reported earlier (5).

The major fragmentation reaction of protonated methyl formate involves formation of protonated methanol (reaction [8]), a reaction which has a ΔH^0

$$[8] \quad \begin{matrix} & & OH \\ & & | \\ H- & C & -OCH_3 \end{matrix} \rightarrow CO + CH_3OH_2^+ \quad \Delta H^\circ = 15 \text{ kcal mol}^{-1}$$

Can. J. Chem. Downloaded from www.nrcresearchpress.com by 210.87.254.6 on 09/06/12
For personal use only.

of 15 kcal mol^{-1} for the carbonyl protonated ester but would be ~5 kcal mol^{-1} exothermic for the ester protonated at the ether oxygen. Despite these low ΔH^0 values, the extent of fragmentation decreases rapidly with decreasing protonation exothermicity, with the $CH_3OH_2^+$ ion signal representing less than 20% of the total ionization in the N_2/H_2 CI system and less than 10% in the CO_2/H_2 CI system, where the protonation exothermicity is still >60 kcal mol^{-1}. This rapid decrease in the extent of fragmentation with decreasing exothermicity of protonation implies either that the fraction of the exothermicity retained by HCO_2-$CH_3 \cdot H^+$ is small or that the activation energy for fragmentation is considerably larger than the ΔH^0. The former explanation appears unlikely in view of the results obtained for the remaining esters and for other compounds (12, 13) and we conclude that the latter explanation holds. The overall reaction forming $CH_3OH_2^+$ probably is best represented by [8*a*] involving hydrogen migration from the carbonyl to the ether oxygen followed by bond cleavage accompanied by synchronous or near-synchronous proton transfer from the carbon to the developing methanol molecule (7, 21).

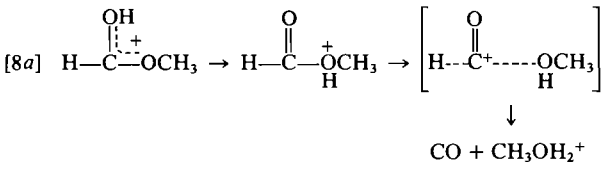

The initial step in this reaction has a ΔH^0 of 20 kcal mol^{-1} but probably has a considerably higher activation energy since the H transfer reaction is a [1,3]-symmetry-forbidden shift and such migrations have been shown to have an activation energy considerably in excess of the ΔH^0 (22). The ether oxygen-protonated form of the ester should have a much lower activation energy for fragmentation and it is possible that the small extent of fragmentation observed with weaker protonating agents represents fragmentation of this species.

In the CI of ethyl-d_5 formate, formation of $C_2D_5OH_2^+$ (*m*/*z* 52) is only a minor process even though this is the thermochemically favoured mode of fragmentation ($\Delta H^0 \simeq$ 12 kcal mol^{-1}); this supports the contention that the activation energy for this rearrangement is considerably higher than the ΔH^0. As observed previously (15), the major fragmentation reaction is [9] to form HCO_2HD^+; this fragmentation channel remains important (forming the base peak) even following protonation by HCO^+. The alternative fragmentation [10], forming $C_2D_5^+$ by simple bond fission, has a much higher ΔH_0 (and presumably, activation energy) and consequently competes ineffectively with the rearrangement reaction of lower activation energy. However, it should be noted that the simple bond fission reaction becomes more important at higher average internal energies (cf. H_2 CI), where the relative rates are more strongly influenced by frequency factors.

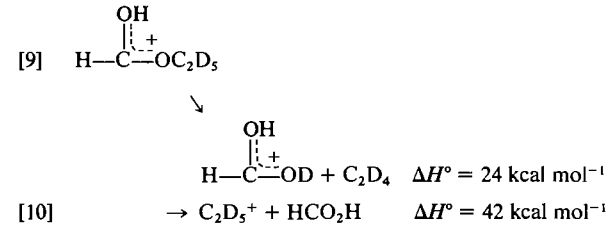

The CI mass spectra of both *n*-propyl and *i*-propyl formate are dominated, for all protonating agents, by the $C_3H_7^+$ alkyl ion, with $HCO_2H_2^+$ being only 10–20% of the alkyl ion intensity. For *i*-propyl formate the ΔH^0's, and, presumably, the activation energies, of the two reaction channels [11] and [12] are very similar consequently, it is not

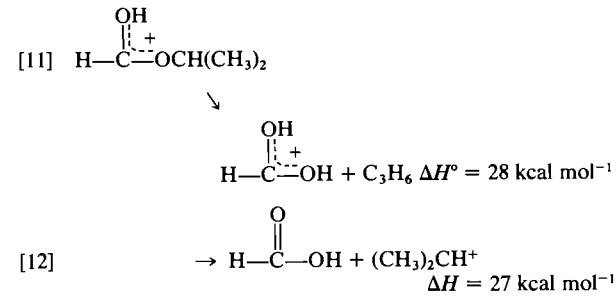

surprising that the simple bond cleavage reaction [12] should dominate. The relative importance of the rearrangement reaction [11] increases slightly as the average internal energy is decreased by using weaker protonating agents. For protonated *n*-propyl formate, cleavage to form the *n*-propyl cation has a ΔH^0 of ~38 kcal mol^{-1}, considerably higher than that for formation of $HCO_2H_2^+$ ($\Delta H^0 \simeq$ 28 kcal mol^{-1}) yet $C_3H_7^+$ is the dominant fragment ion. It is probable that the bond fission is accompanied by a [1,2]-H shift to form the *i*-$C_3H_7^+$ ion. As Hopkinson *et al.* (7) have noted, *ab initio* MO calculations (23, 24) have shown that *n*-$C_3H_7^+$ collapses into *i*-$C_3H_7^+$ without an energy barrier. The alternative mechanism proposed by Hopkinson *et al.* (7) (reaction [13]), involving hydrogen transfer to the carbonyl oxygen followed by proton transfer from protonated formic acid to propene as the products separate, appears unlikely. First, it involves the thermochemically disfavoured ether

Can. J. Chem. Downloaded from www.nrcresearchpress.com by 210.87.254.6 on 09/06/12
For personal use only.

TABLE 1. Chemical ionization mass spectra of formate esters[a]

m/z	Ion	H_2 CI	N_2/H_2 CI	CO_2/H_2 CI	N_2O/H_2 CI	CO/H_2 CI
Methyl formate						
90	$HCO_2CH_3 \cdot NO^+$				4	
61	$HCO_2CH_3 \cdot H^+$	21	100	100	100	100
33	$CH_3OH_2^+$	100	27	10	3	12
31	CH_2OH^+	8	3	2	1	5
15	CH_3^+	6	—	—	—	—
Ethyl-d_5-formate						
109	$HCO_2C_2D_5 \cdot NO^+$				26	
80	$HCO_2C_2D_5 \cdot H^+$	15	25	48	97	71
52	$C_2D_5OH_2^+$	4	1	2	3	4
48	HCO_2HD^+	100	100	100	100	100
34	$C_2D_5^+$	22	11	4	6	7
n-Propyl formate						
118	$HCO_2C_3H_7 \cdot NO^+$				16	
89	$HCO_2C_3H_7 \cdot H^+$	5	15	37	44	27
59	C_3H_7O	8	3	2	6	2
47	$HCO_2H_2^+$	13	12	15	16	18
43	$C_3H_7^+$	100	100	100	100	100
41	$C_3H_5^+$	8	5	2	2	2
31	CH_2OH^+	9	6	3	6	3
i-Propyl formate						
118	$HCO_2C_3H_7 \cdot NO^+$				12	
89	$HCO_2C_3H_7 \cdot H^+$	6	16	47	45	37
59	$C_3H_7O^+$	6	3	2	8	2
47	$HCO_2H_2^+$	11	14	16	16	21
45	CH_3CHOH^+	12	11	R[b]	R[b]	17
43	$C_3H_7^+$	100	100	100	100	100
41	$C_3H_5^+$	5	3	2	2	2
n-Butyl formate						
132	$HCO_2C_4H_9 \cdot NO^+$				15	
103	$HCO_2C_4H_9 \cdot H^+$	9	12	17	25	16
57	$C_4H_9^+$	100	100	100	100	100
55	$C_4H_7^+$	14	4	1	2	1
47	$HCO_2H_2^+$	4	4	7	7	7
41	$C_3H_5^+$	21	7	3	3	3
i-Butyl formate						
132	$HCO_2C_4H_9 \cdot NO^+$				9	
103	$HCO_2C_4H_9 \cdot H^+$	6	8	12	16	8
73	$C_4H_9O^+$	8	3	1	3	1
59	$C_3H_7O^+$, $HCO_2CH_2^+$	6	4	3	1	1
57	$C_4H_9^+$	100	100	100	100	100
55	$C_4H_7^+$	5	1	—	—	—
47	$HCO_2H_2^+$	3	3	5	5	8
41	$C_3H_5^+$	12	5	3	3	1
sec-Butyl formate						
132	$HCO_2C_4H_9 \cdot NO^+$				16	
103	$HCO_2C_4H_9 \cdot H^+$	8	22	29	20	25
73	$C_4H_9O^+$	9	3	1	2	3
59	$C_3H_7O^+$, $HCO_2CH_2^+$	6	3	3	2	2
57	$C_4H_9^+$	100	100	100	100	100
55	$C_4H_7^+$	3	3	1	2	2
47	$HCO_2H_2^+$	3	3	7	10	8
45	$C_2H_5O^+$	6	4	R[b]	R[b]	6
41	$C_3H_5^+$	8	3	3	3	2

[a]Intensities as % of base peak arising from additive.
[b]R indicates fragment ion obscured by reagent ion peak.

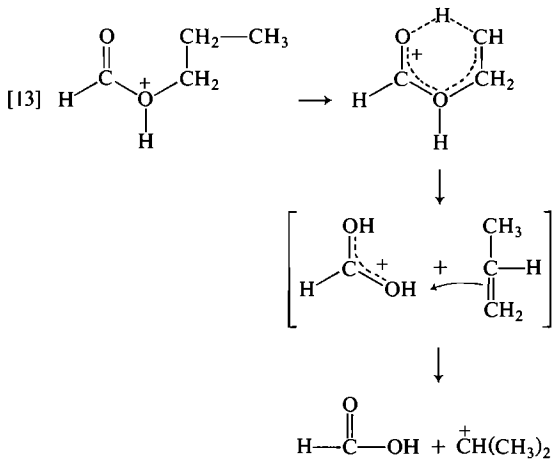

oxygen-protonated species. More importantly, it would suggest that with deuterated reagent gases, which form $HCO_2C_3H_7{\cdot}D^+$ originally, the isopropyl cation produced should contain significant deuterium; earlier studies (5) of the D_2 CI mass spectra of formates show that there is practically no deuterium incorporation in the $C_3H_7^+$ product from either *n*-propyl or *i*-propyl formate. Finally, reaction [13] is a rearrangement at least as complex as that resulting in formation of $HCO_2H_2^+$ and consequently one would not anticipate the observed increase in importance of $HCO_2H_2^+$ formation with decreasing internal energy in such a situation.

The butyl formates examined all show extensive fragmentation, with $C_4H_9^+$ the dominant fragment ion with all reagent gases. For protonated *sec*-butyl formate, formation of $s\text{-}C_4H_9^+$ (ΔH^0 = 24 kcal mol^{-1}) is favoured over formation of $HCO_2H_2^+$ (ΔH^0 = 26 kcal mol^{-1}); consequently, dominant fragmentation by simple bond cleavage is to be expected. However, for the *n*-butyl formate and *i*-butyl formate, formation of the primary butyl cations ($\Delta H^0 \simeq$ 40 kcal mol^{-1}) is thermochemically unfavourable compared to formation of $HCO_2H_2^+$ (ΔH^0 = 25 kcal mol^{-1}). It appears that in these two cases fragmentation must be accompanied by [1,2]-H shifts to form the more stable *sec*-butyl and *tert*-butyl structures respectively.

Chemical Ionization Mass Spectra of Acetates

The chemical ionization mass spectra of the methyl through butyl acetates are presented in Table 2, while the CI mass spectra of some isomeric pentyl acetates are presented in Table 3.

The only significant fragmentation channel for protonated methyl acetate involves methanol elimination to form the acetyl ion (*m*/*z* 43). The intensity of this fragment drops off markedly with decreasing protonation exothermicity, accounting for only ~20% of the total ionization in the CO_2/H_2 CI system. Pescheck and Butrill (3) have proposed that this fragment arises as a result of protonation at the ether oxygen followed by simple bond cleavage (reaction [14]), the analogue of the $A_{Ac}l$ solution

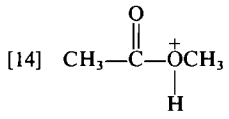

reaction. This simple bond cleavage reaction should not have an activation energy significantly greater than the endothermicity; consequently, assuming this mechanism, it is surprising that the acetyl ion is not more abundant in the CO_2/H_2 CI system where the protonation exothermicity to form the ether oxygen-protonated species is 53 kcal mol^{-1}. A likely explanation is that the major part of the acetyl ion arises by the route

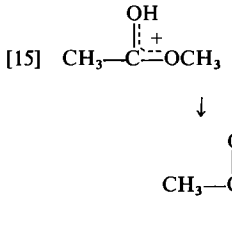

This route, involving initial formation of the thermodynamically favoured carbonyl protonated species, requires a symmetry-forbidden [1,3]-H shift prior to fragmentation. The activation energy barrier for this step is undoubtedly much higher than the ΔH^0 of ~15 kcal mol^{-1} or the overall ΔH^0 of ~37 kcal mol^{-1}; such a high activation energy barrier would explain the strong dependence of the extent of fragmentation on the protonation exothermicity. The persistent $CH_3{-}C{\equiv}O^+$ ion signal with the weaker protonating agents may represent a contribution from reaction [14].

In the CI mass spectra of ethyl acetate the dominant fragmentation reaction involves formation of protonated acetic acid (reaction [16]), with minor formation of the acetyl ion (reaction [17]); formation of $C_2H_5^+$, the product of the $A_{Al}l$ fragmentation (reaction [18]), is observed with very low abundance in the H_2 CI spectrum

Can. J. Chem. Downloaded from www.nrcresearchpress.com by 210.87.254.6 on 09/06/12
For personal use only.

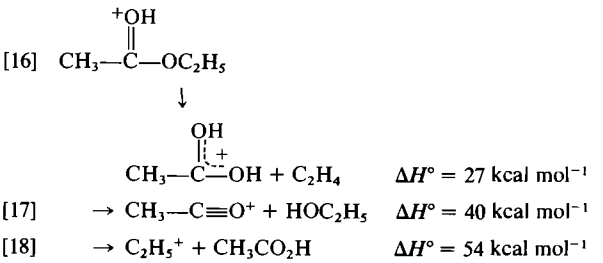

[16] $CH_3—\overset{+}{C}(OH)—OC_2H_5$

$\downarrow$

$CH_3—C(OH)=\overset{+}{O}H + C_2H_4$ $\Delta H° = 27$ kcal mol^{-1}

[17] $\rightarrow CH_3—C\equiv O^+ + HOC_2H_5$ $\Delta H° = 40$ kcal mol^{-1}

[18] $\rightarrow C_2H_5^+ + CH_3CO_2H$ $\Delta H° = 54$ kcal mol^{-1}

The relative fragment ion abundances are in agreement with the relative reaction endothermicities. The acetyl ion may arise, in part, by formation of the ether oxygen-protonated species and simple bond cleavage; this fragmentation reaction would have a ΔH^0 of $\sim$22 kcal mol^{-1} and, if it were a major route, should be more competitive with that leading to formation of protonated acetic acid. Thus it appears likely that the major route to acetyl ion formation is by fragmentation of the carbonyl protonated species, as discussed in detail for protonated methyl acetate.

Three fragmentation modes, reactions [19] to [21], are observed for protonated *i*-propyl acetate and protonated *n*-propyl acetate. Reaction [19],

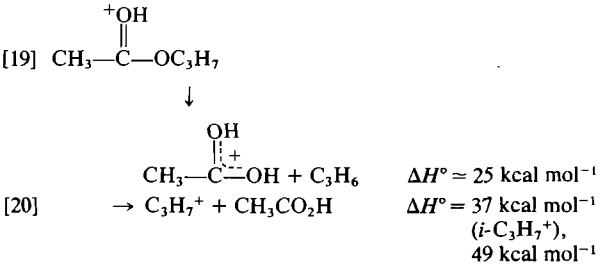

[19] $CH_3—\overset{+}{C}(OH)—OC_3H_7$

$\downarrow$

$CH_3—C(OH)=\overset{+}{O}H + C_3H_6$ $\Delta H° \simeq 25$ kcal mol^{-1}

[20] $\rightarrow C_3H_7^+ + CH_3CO_2H$ $\Delta H° = 37$ kcal mol^{-1} (*i*-$C_3H_7^+$), 49 kcal mol^{-1} (*n*-$C_3H_7^+$)

[21] $\rightarrow CH_3—C\equiv O^+ + C_3H_7OH$ $\Delta H° \simeq 40$ kcal mol^{-1}

forming protonated acetic acid, has a considerably lower ΔH^0 and, presumably, activation energy, than the other fragmentation reactions and the protonated acetic acid ion froms the base peak in all CI mass spectra. The $C_3H_7^+$ and $CH_3—C\equiv O^+$ fragment ions are of approximately equal intensity in all CI spectra and decrease in abundance relative to the rearrangement product $CH_3CO_2H_2^+$ with decreasing protonation exothermicity. Reaction [21], as written, involves a symmetry-forbidden [1,3]-shift and, as discussed above, the activation energy should be considerably higher than the ΔH^0 and one would not anticipate that this reaction should be competitive with the other two reactions. However, the ether oxygen proton affinity of *n*-propyl acetate is only $\sim$12 kcal mol^{-1} less than the carbonyl oxygen proton affinity (16) and it may be that an appreciable fraction of the $CH_3—C\equiv O^+$ ion signals arises by the fragmentation

[22] $CH_3—\overset{O}{\overset{\|}{C}}—\overset{+}{O}(H)—C_3H_7$

$\downarrow$

$CH_3—C\equiv O^+ + C_3H_7OH$ $\Delta H° = 28$ kcal mol^{-1}

which would not be expected to have an activation energy significantly greater than the ΔH^0. The formation of $C_3H_7^+$ in the CI mass spectra of *n*-propyl acetate has a ΔH^0 of $\sim$49 kcal mol^{-1} (assuming *n*-$C_3H_7^+$ formation) and should not be competitive with the alternative fragmentations. It is probable that, here also, rearrangement to the *i*-propyl structure occurs. In addition, formation of alkyl ions by the $A_{Al}1$ mechanism from the ether oxygen-protonated species is possible and would have $\Delta H°$'s $\sim$12 kcal mol^{-1} lower than those quoted for reaction [20].

The CI mass spectra of the four butyl acetates show an interesting dependence of the relative importance of the three fragmentation reactions [23] to [25] on the identity of the butyl group.

[23] $CH_3—\overset{+}{C}(OH)—OC_4H_9 \rightarrow CH_3—C(OH)=\overset{+}{O}H + C_4H_8$

[24] $\rightarrow C_4H_9^+ + CH_3CO_2H$

[25] $\rightarrow CH_3—C\equiv O^+ + C_4H_9OH$

For *tert*-butyl acetate, formation of *t*-$C_4H_9^+$ is favoured thermochemically ($\Delta H^0 \simeq 21$ kcal mol^{-1}) over formation of protonated acetic acid ($\Delta H^0 \simeq 29$ kcal mol^{-1}) or formation of $CH_3—C\equiv O^+$ ($\Delta H^0 \simeq 40$ kcal mol^{-1}) and $C_4H_9^+$ is the dominant fragment ion in all CI mass spectra. For protonated *sec*-butyl acetate, fragmentation to form *s*-$C_4H_9^+$ has a ΔH^0 ($\sim$33 kcal mol^{-1}) higher than that for formation of protonated acetic acid ($\Delta H^0 \simeq 25$ kcal mol^{-1}); as a consequence, $CH_3CO_2H_2^+$ is the base peak in all CI mass spectra. The $C_4H_9^+$ ion is of appreciable intensity and increases in relative abundance with increasing protonation exothermicity, as expected for a simple bond cleavage reaction compared to a rearrangement fragmentation.

For both the *n*-butyl and *i*-butyl acetate systems fragmentation of the protonated ester to form the primary *n*-butyl or *i*-butyl cations would be much less favourable thermochemically ($\Delta H^0 \simeq 47$ kcal mol^{-1}) than formation of protonated acetic acid ($\Delta H^0 \simeq 25$ kcal mol^{-1}); nevertheless, $C_4H_9^+$ is the base peak in all CI mass spectra of *i*-butyl acetate

Can. J. Chem. Downloaded from www.nrcresearchpress.com by 210.87.254.6 on 09/06/12
For personal use only.

Can. J. Chem. Downloaded from www.nrcresearchpress.com by 210.87.254.6 on 09/06/12
For personal use only.

TABLE 2. Chemical ionization mass spectra of methyl through butyl acetates[a]

m/z	Ion	H_2 CI	N_2/H_2 CI	CO_2/H_2 CI	N_2O/H_2 CI	CO/H_2 CI
Methyl acetate						
104	$CH_3CO_2CH_3 \cdot NO^+$				16	
75	$CH_3CO_2CH_3 \cdot H^+$	31	100	100	100	100
59	$CO_2CH_3^+$	4	4	1	1	1
43	$CH_3C{\equiv}O^+$	100	91	27	22	16
15	CH_3^+	1	1	—	—	—
Ethyl acetate						
118	$CH_3CO_2C_2H_5 \cdot NO^+$				31	
89	$CH_3CO_2C_2H_5 \cdot H^+$	45	60	64	100	100
61	$CH_3CO_2H_2^+$	100	100	100	76	70
43	$CH_3C{\equiv}O^+$	31	17	12	10	9
n-Propyl acetate						
132	$CH_3CO_2C_3H_7 \cdot NO^+$				34	
103	$CH_3CO_2C_3H_7 \cdot H^+$	44	68	45	79	52
61	$CH_3CO_2H_2^+$	100	100	100	100	100
43	$C_3H_7^+$	84	55	39	32	30
43	$CH_3C{\equiv}O^+$	82	56	39	32	30
41	$C_3H_5^+$	6	—	—	—	—
i-Propyl acetate						
132	$CH_3CO_2C_3H_7 \cdot NO^+$				19	
103	$CH_3CO_2C_3H_7 \cdot H^+$	30	48	34	46	65
61	$CH_3CO_2H_2^+$	100	100	100	100	100
43	$C_3H_7^+$	43	27	19	12	16
43	$CH_3C{\equiv}O^+$	43	27	19	12	16
41	$C_3H_5^+$	3	2	—	—	—
n-Butyl acetate						
146	$CH_3CO_2C_4H_9 \cdot NO^+$				36	
117	$CH_3CO_2C_4H_9 \cdot H^+$	42	66	41	62	35
115	$C_6H_{11}O_2^+$	6	3	1	5	—
73	$C_3H_5O_2^+$	6	5	4	2	4
61	$CH_3CO_2H_2^+$	100	100	100	100	100
57	$C_4H_9^+$	76	55	31	21	20
55	$C_4H_7^+$	15	5	2	1	2
43	$CH_3C{\equiv}O^+$	42	21	12	10	11
41	$C_3H_5^+$	9	2	—	—	—
i-Butyl acetate						
146	$CH_3CO_2C_4H_9 \cdot NO^+$				54	
117	$CH_3CO_2C_4H_9 \cdot H^+$	38	54	37	86	87
115	$C_6H_{11}O_2^+$	8	3	1	6	3
73	$C_3H_5O_2^+$	3	—	5	3	6
61	$CH_3CO_2H_2^+$	57	73	89	86	67
57	$C_4H_9^+$	100	100	100	100	100
55	$C_4H_7^+$	4	5	—	—	—
43	$CH_3{-}C{\equiv}O^+$	46	27	24	14	40
41	$C_3H_5^+$	6	5	—	—	—
sec-Butyl acetate						
146	$CH_3CO_2C_4H_9 \cdot NO^+$				19	
117	$CH_3CO_2C_4H_9 \cdot H^+$	35	47	26	49	40
115	$C_6H_{11}O_2^+$	3	—	2	5	—
87	$C_4H_7O_2^+$	5	2	5	3	8
73	$C_3H_5O_2^+$	14	2	4	2	5
61	$CH_3CO_2H_2^+$	100	100	100	100	100
57	$C_4H_9^+$	62	40	22	13	13
55	$C_4H_7^+$	2	2	—	—	—
43	$CH_3C{\equiv}O^+$	32	16	13	6	38
41	$C_3H_5^+$	5	2	—	—	—

TABLE 2. (*Concluded*)

m/z	Ion	H_2 CI	N_2/H_2 CI	CO_2/H_2 CI	N_2O/H_2 CI	CO/H_2 CI
tert-Butyl acetate						
146	$CH_3CO_2C_4H_9 \cdot NO^+$				10	
117	$CH_3CO_2C_4H_9 \cdot H^+$	6	29	18	37	30
101	$CH_3CO_2C(CH_3)_2^+$	3	3	4	2	7
61	$CH_3CO_2H_2^+$	4	5	9	8	4
57	$C_4H_9^+$	100	100	100	100	100
55	$C_4H_7^+$	1	2	—	—	—
43	$CH_3—C\equiv O^+$	15	8	6	4	14
41	C_3H_5	3	2	—	—	—

[a]Intensities expressed as % of base peak.

and is of appreciable abundance in the CI mass spectra of *n*-butyl acetate. It appears likely that there is significant rearrangement to the *tert*-butyl and *sec*-butyl structures, respectively, during fragmentation of these protonated esters. These rearrangements can occur by relatively simple [1,2]-H shifts in the developing cation. For all the butyl acetates there is significant formation of the $CH_3—C\equiv O^+$ ion; this may represent fragmentation of the ether oxygen protonated species. The proton affinity difference between the carbonyl oxygen and the ether oxygen of esters decreases as the size of the ester increases (16) and one might expect more protonation at the ether oxygen as a result.

The CI mass spectra of the six pentyl acetates examined are summarized in Table 3. The usual fragmentation reactions, [26] to [28], are observed.

[26] $CH_3—\overset{OH^+}{C}—OC_5H_{11} \rightarrow CH_3—\overset{OH^+}{C}—OH + C_5H_{10}$

[27] $\rightarrow C_5H_{11}^+ + CH_3CO_2H$

[28] $\rightarrow CH_3—C\equiv O^+ + C_5H_{11}OH$

In addition, in several cases extensive fragmentation of $C_5H_{11}^+$ is observed by the reaction channels, [29, [30], and [31], established previously (13).

[29] $C_5H_{11}^+ \rightarrow C_5H_9^+ + H_2$

[30] $\rightarrow C_4H_7^+ + CH_2$

[31] $\rightarrow C_3H_7^+ + C_2H_4$

The fragmentation of $C_5H_{11}^+$ ions produced by dissociative proton transfer to isomeric pentyl alcohols has been studied in detail (13). It was observed that the extent of fragmentation was greatest for $C_5H_{11}^+$ ions derived from primary alcohols, less for $C_5H_{11}^+$ derived from secondary alcohols, and very slight for the $C_5H_{11}^+$ ion derived from *tert*-pentanol. As expected, the extent of fragmentation decreased as the protonation exothermicity decreased. These results were interpreted as indicating that there was negligible rearrangement to more stable alkyl structures prior to achievement of the critical reacting configuration which determined the energy partitioning between R^+ and H_2O in the decomposition of ROH_2^+. In terms of the extent of further fragmentation of the $C_5H_{11}^+$ ions the present results for protonated pentyl acetates are in essential agreement with the results for the protonated pentyl alcohols. However, in terms of the competition between reactions [26] and [27] there is substantial evidence for alkyl ion rearrangement. This is illustrated most clearly in terms of the relative intensities for the $CH_3CO_2H_2^+$ and $C_5H_{11}^+$ ions observed in the CO_2/H_2 CI spectra summarized in Table 4, along with the ΔH^0 for formation of these ions from the ground state protonated ester. The ΔH^0 values for $C_5H_{11}^+$ formation have been calculated assuming an alkyl ion structure identical to the neutral alkyl moiety. For 2-pentyl acetate and 3-pentyl acetate the ΔH^0 for formation of $C_5H_{11}^+$ is slightly larger than that for formation of $CH_3CO_2H_2^+$ and we observe that the alkyl ion intensity is lower than that of the protonated acetic acid ion. For the secondary acetate, 3-methyl-2-pentyl acetate, the ΔH^0 values are very similar, yet the $C_5H_{11}^+$ ion is the dominant ion in the mass spectra. This strongly indicates a [1,2]-H shift to yield the more stable *tert*-pentyl ion. Collin and Herman (25) have reported an activation energy of $\sim$2 kcal mol^{-1} for this isomerization from studies of the protonation of 3-methyl-1-pentene in radiolysis experiments. Indeed, their results for the extent of fragmentation of $C_5H_{11}^+$ as a function of protonation exothermicity are in agreement with the present data. For the primary acetates the ΔH^0's for formation of the respective primary alkyl ions are much larger than the ΔH^0 for formation of $CH_3CO_2H_2^+$, yet the alkyl ion intensities are as great as, or greater than, the $CH_3CO_2H_2^+$ ion intensities. Clearly this unexpected result can only be accommodated by assum-

Can. J. Chem. Downloaded from www.nrcresearchpress.com by 210.87.254.6 on 09/06/12
For personal use only.

Can. J. Chem. Downloaded from www.nrcresearchpress.com by 210.87.254.6 on 09/06/12
For personal use only.

TABLE 3. Chemical ionization mass spectra of pentyl acetates[a]

m/z	Ion	H_2 CI	N_2/H_2 CI	CO_2/H_2 CI	N_2O/H_2 CI	CO/H_2 CI
n-Pentyl acetate						
160	$CH_3CO_2C_5H_{11}\cdot NO^+$				23	
131	$CH_3CO_2C_5H_{11}\cdot H^+$	34	58	72	21	29
129	$C_7H_{13}O_2^+$	4	2	—	4	—
71	$C_5H_{11}^+$	51	65	71	45	43
69	$C_5H_9^+$	37	23	7	4	6
61	$CH_3CO_2H_2^+$	86	100	100	100	100
55	$C_4H_7^+$	15	19	10	4	2
43	$C_3H_7^+$	100	85	18	9	16
43	$CH_3—C\equiv O^+$	66	35	20	17	21
3-Methyl-1-butyl acetate						
160	$CH_3CO_2C_5H_{11}\cdot NO^+$				17	
131	$CH_3CO_2C_5H_{11}\cdot H^+$	40	68	56	13	37
129	$C_7H_{13}O_2^+$	4	2	1	4	—
71	$C_5H_{11}^+$	100	100	100	100	100
69	$C_5H_9^+$	35	9	4	2	2
61	$CH_3CO_2H_2^+$	56	35	42	57	47
55	$C_4H_7^+$	19	12	7	4	2
43	$C_3H_7^+$	97	50	12	9	16
43	$CH_3—C\equiv O^+$	62	30	15	12	22
2-Methyl-1-butyl acetate						
160	$CH_3CO_2C_5H_{11}\cdot NO^+$				36	
131	$CH_3CO_2C_5H_{11}\cdot H^+$	39	6	77	87	48
129	$C_7H_{13}O_2^+$	4	—	2	8	2
71	$C_5H_{11}^+$	100	100	100	100	100
69	$C_5H_9^+$	35	9	3	3	2
61	$CH_3CO_2H_2^+$	62	62	51	52	26
55	$C_4H_7^+$	19	15	5	3	2
43	$C_3H_7^+$	96	71	15	13	11
43	$CH_3—C\equiv O^+$	50	31	12	8	12
3-Pentyl acetate						
160	$CH_3CO_2C_5H_{11}\cdot NO^+$				11	
131	$CH_3CO_2C_5H_{11}\cdot H^+$	30	34	39	39	51
129	$C_7H_{13}O_2^+$	—	—	—	4	—
101	$C_5H_9O_2^+$	13	10	8	3	5
87	$C_4H_7O_2^+$	30	7	3	11	5
71	$C_5H_{11}^+$	81	90	74	58	68
69	$C_5H_9^+$	13	7	3	5	3
61	$CH_3CO_2H_2^+$	100	100	100	100	100
55	$C_4H_7^+$	11	10	3	—	3
45	$C_2H_5O^+$	6	4	R[b]	R[b]	—
43	$C_3H_7^+$	80	62	13	8	15
43	$CH_3C\equiv O^+$	72	40	20	15	28
2-Pentyl acetate						
160	$CH_3CO_2C_5H_{11}\cdot NO^+$				14	
131	$CH_3CO_2C_5H_{11}\cdot H^+$	41	15	65	33	42
129	$C_7H_{13}O_2^+$	3	—	—	6	—
87	$C_4H_7O_2^+$	36	15	12	7	5
71	$C_5H_{11}^+$	84	85	76	44	62
69	$C_5H_9^+$	18	9	3	5	2
61	$CH_3CO_2H_2^+$	100	100	100	100	100
55	$C_4H_7^+$	8	9	3	2	2
45	$C_2H_5O^+$	9	6	R[b]	R[b]	—
43	$C_3H_7^+$	70	58	11	7	15
43	$CH_3C\equiv O^+$	52	25	18	14	27
3-Methyl-2-butyl acetate						
160	$CH_3CO_2C_5H_{11}\cdot NO^+$				19	
131	$CH_3CO_2C_5H_{11}\cdot H^+$	14	11	27	51	43
87	$C_4H_7O_2^+$	16	3	5	2	4

TABLE 3. (*Concluded*)

m/z	Ion	H_2 CI	N_2/H_2 CI	CO_2/H_2 CI	N_2O/H_2 CI	CO/H_2 CI
71	$C_5H_{11}^+$	100	100	100	100	100
69	$C_5H_9^+$	4	2	2	—	—
61	$CH_3CO_2H_2^+$	6	6	8	7	7
55	$C_4H_7^+$	4	2	—	—	—
43	$C_3H_7^+$	33	19	10	7	11
43	$CH_3—C\equiv O^+$	30	20	12	8	14

[a]Intensities as % of base peak.
[b]R denotes ion signal obscured by reagent ion signal.

TABLE 4. Relative $C_5H_{11}^+$ and $CH_3CO_2H_2^+$ intensities in CO_2/H_2 CI of pentyl acetates

R of $ROCOCH_3$	$C_5H_{11}^+$	ΔH^{0a}	$CH_3CO_2H_2^+$	ΔH^{0a}
$CH_3CH_2CH_2CH_2CH_2—$	45	45	100	27
$CH_3—\underset{\displaystyle CH_3}{\underset{\vert}{CH}}—CH_2CH_2—$	100	47	57	26
$CH_3CH_2\underset{\displaystyle CH_3}{\underset{\vert}{CH}}—CH_2—$	100	45	52	26
$CH_3CH_2—\underset{\displaystyle \vert}{CH}—CH_2—CH_3$	48	34	100	26
$CH_3CH_2CH_2\underset{\displaystyle \vert}{CH}—CH_3$	44	34	100	26
$CH_3—\underset{\displaystyle CH_3}{\underset{\vert}{CH}}—\underset{\displaystyle \vert}{CH}—CH_3$	100	29	7	26

[a]ΔH^0 (kcal mol^{-1}) for formation of fragment ion from carbonyl protonated ester.

ing that rearrangement to a more stable secondary or tertiary alkyl ion occurs during fragmentation. The extent of formation of $CH_3—C\equiv O^+$ is higher than one would anticipate for fragmentation of the carbonyl protonated species and formation of this fragment may represent an increased importance of protonation at the ether oxygen.

Thus, we are left with the apparent paradox that the energy partitioning between neutral and ionic fragments, as reflected in the extent of further fragmentation of the alkyl ions, supports a reaction model in which no significant rearrangement in the alkyl moiety occurs, while the competition between fragmentation channels indicates that rearrangement has occurred in the alkyl moiety. A possible resolution of this paradox is given by the detailed reaction model proposed in Scheme 1 for a primary alkyl acetate. As the alkyl carbon–oxygen bond lengthens, a critical state (or transition state) *a* is reached corresponding to an unrearranged alkyl ion bonded to neutral acetic acid largely by ion–dipole interactions (21). The partitioning of the excess energy between the neutral acetic acid and alkyl ion appears to be determined at this stage. A simple [1,2]-H shift in the alkyl ion leads to the secondary ion interacting with acetic acid by ion–dipole forces; this structure *b*, which will be more stable than *a*, may then undergo simple fission of the weak bond to acetic acid yielding the alkyl ion or may transfer a proton to acetic acid yielding the protonated acid and an appropriate olefin. Isotopic labelling studies (6) in *n*-propyl acetate show that the H transferred from the propyl group does not originate from a specific position of the alkyl group but may come from any position. It is possible that this proton shift may go through the intermediacy of *c*, a proton solvated by both the olefin and acetic acid (21), which might be considered as an alterna-

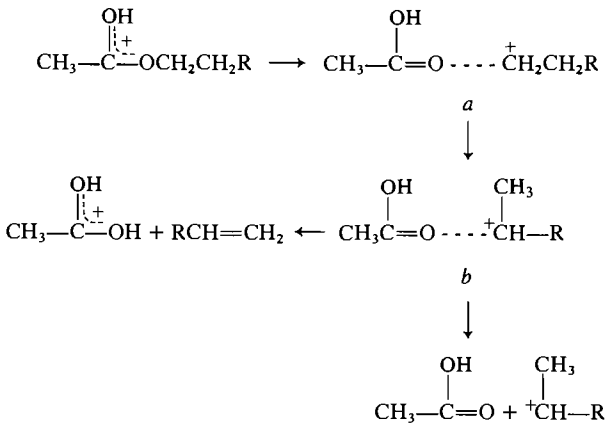

SCHEME 1

Can. J. Chem. Downloaded from www.nrcresearchpress.com by 210.87.254.6 on 09/06/12
For personal use only.

TABLE 5. Thermochemistry of carboxylic acids and protonated carboxylic acids[a]

R—COOR'	ΔH_f (RCOOR')[b]	PA[c] C=O	OR'[d]	ΔH^0_f(R—C(OH)=OR'$^+$)	ΔH^0_f(R—C(=O$^+$)—OHR')
HCOOH	−90.6	178	152	97	123
$HCOOCH_3$	−83.7	188	167	94	115
$HCOOC_2H_5$	−88.7	191	168	86	109
HCOO*n*-C_3H_7	−95	192	171	79	100
HCOO*i*-C_3H_7	−99	192	171	75	96
HCOO*n*-C_4H_9	−100	191	171	75	95
HCOO*i*-C_4H_9	−102	192	171	72	93
HCOO*s*-C_4H_9	−104	192	171	70	91
HCOO*t*-C_4H_9	−109	192	171	65	86
CH_3COOH	−103.3	189	161	74	102
CH_3COOCH_3	−97.9	195	180	73	88
$CH_3COOC_2H_5$	−105.9	198	180	62	80
CH_3COO*n*-C_3H_7	−111	199	187	56	68
CH_3COO*i*-C_3H_7	−115	199	183	52	68
CH_3COO*n*-C_4H_9	−116	199	183	51	67
CH_3COO*i*-C_4H_9	−118	199	183	49	65
CH_3COO*s*-C_4H_9	−120	199	183	47	63
CH_3COO*t*-C_4H_9	−124	199	183	43	59

[a]All data in kcal mol^{-1}.
[b]Taken from refs. 19 and 20 or estimated by group equivalent methods (27).
[c]Taken from ref. 15 or, for higher members, estimated.
[d]Taken from estimates given in ref. 16 or estimated from that data.

tive structure to *b*; in principle *c* could fragment to either the protonated acid or the appropriate stable alkyl ion. However, if such were the case, the rate constant expressions for formation of both the alkyl ion and protonated acetic acid should have similar frequency factors. As discussed above, the internal energy dependence of the relative fragment ion yields suggests that the reaction forming protonated acetic acid has a lower frequency

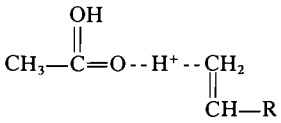

c

factor, indicating a more complex rearrangement. This is most readily interpreted on the basis that the alkyl ion originates by simple dissociation of the loosely-bound complex *b* of Scheme 1.

Acknowledgements

The authors are indebted to the Natural Sciences and Engineering Research Council of Canada for financial support, to Dr. R. K. M. R. Kallury for assistance in synthesis of some of the esters, and to Dr. D. K. Bohme for communication of results prior to publication.

1. M. S. B. MUNSON and F. H. FIELD. J. Am. Chem. Soc. **88**, 4337 (1966).
2. B. L. JELUS, J. MICHNOWICZ, and B. MUNSON. J. Org. Chem. **39**, 2130 (1974).
3. C. V. PESCHECK and S. E. BUTRILL. J. Am. Chem. Soc. **96**, 6027 (1974).
4. C. W. TSANG and A. G. HARRISON. J. Chem. Soc. Perkin Trans. II. 1718 (1975).
5. A. G. HARRISON and C. W. TSANG. Can. J. Chem. **54**, 2029 (1975).
6. F. M. BENOIT and A. G. HARRISON. Org. Mass Spectrom. **13**, 128 (1978).
7. A. C. HOPKINSON, G. I. MACKAY, and D. K. BOHME. Can. J. Chem. **57**, 2996 (1979).
8. K. YATES. Acc. Chem. Res. **4**, 136 (1971).
9. D. H. WILLIAMS and I. HOWE. Principles of organic mass spectrometry. McGraw-Hill, New York. 1972.
10. C. W. TSANG and A. G. HARRISON. *In* Biochemical applications of mass spectrometry. *Edited by* G. R. Waller, Wiley, New York. 1972.
11. K. LEVSEN. Fundamental aspects of organic mass spectrometry. Verlag Chemie, New York. 1978.
12. R. D. BOWEN and A. G. HARRISON. Org. Mass Spectrom. In press.
13. J. A. HERMAN and A. G. HARRISON. Can. J. Chem. **59**, 2125 (1981).
14. D. K. BOHME, G. I. MACKAY, and H. I. SCHIFF. J. Chem. Phys. **73**, 4976 (1980).
15. P. KEBARLE. Ann. Rev. Phys. Chem. **28**, 445 (1977).
16. F. M. BENOIT and A. G. HARRISON. J. Am. Chem. Soc. **99**, 3980 (1977).
17. F. P. LOSSING and A. MACCOLL. Can. J. Chem. **54**, 990 (1976).
18. R. D. BOWEN and D. H. WILLIAMS. J. Chem. Soc. Perkin Trans. II, 1479 (1976).
19. J. D. COX and G. PILCHER. Thermochemistry of organic and organometallic compounds. Academic Press, New York. 1970.
20. H. M. ROSENSTOCK, K. DRAXL, B. W. STEINER, and J. T. HERRON. Energetics of gaseous ions. J. Phys. Chem. Ref. Data, **6**, Suppl. 1 (1977).
21. R. D. BOWEN and D. H. WILLIAMS. J. Am. Chem. Soc. **102**, 2752 (1980).
22. N. E. MIDDLEMISS and A. G. HARRISON. Can. J. Chem. **57**, 2827 (1979).

Can. J. Chem. Downloaded from www.nrcresearchpress.com by 210.87.254.6 on 09/06/12
For personal use only.

23. L. RADOM, J. A. POPLE, V. BUSS, and P. VON R. SCHLEYER. J. Am. Chem. Soc. **94**, 311 (1972).
24. P. C. HARIHARAN, L. RADOM, J. A. POPLE, and P. VON R. SCHLEYER. J. Am. Chem. Soc. **96**, 599 1974).
25. G. J. COLLIN and J. A. HERMAN. J. Chem. Soc. Faraday Trans. I, **74**, 1939 (1978).
26. R. H. STALEY. R. D. WIETING, and J. L. BEAUCHAMP. J. Am. Chem. Soc. **99**, 5964 (1977).
27. S. W. BENSON. Thermochemical kinetics. Wiley-Interscience, New York. 1976.

Appendix

The thermochemical data relevant to the heats of formation of protonated carboxylic acids and esters are summarized in Table 5. In view of the estimates made the uncertainty is probably at least ± 3 kcal mol^{-1} in the heats of formation.

Other relevant ion heats of formation (all in kcal mol^{-1}) are: $C_2H_5^+$, 219; n-$C_3H_7^+$, 208; i-$C_3H_7^+$, 192; n-$C_4H_9^+$, 201; i-$C_4H_9^+$, 199; s-$C_4H_9^+$, 183; t-$C_4H_9^+$, 167; all from ref. 17. A value of ΔH^0_f (CH_3—$C{\equiv}O^+$) = 158 kcal mol^{-1} was used (26). ΔH_{0f} ($CH_3OH_2^+$) = 136 kcal mol^{-1} was derived from the reported proton affinity of 182 kcal mol^{-1} (15).

Neutral heats of formation, from refs. 19 and 20, all in kcal mol^{-1}, are: CH_3OH, −48.1; C_2H_5OH, −56.1; n-C_3H_7OH, −61.2; i-C_3H_7OH, −65.1; n-C_4H_9OH, −65.8; i-C_4H_9OH, −67.8; s-C_4H_9OH, −70.0; t-C_4H_9OH, −74.7; C_2H_4, 12.5; C_3H_6, 5.0; 1-C_4H_8, −0.2; 2-C_4H_8, −1.9; i-C_4H_8, −4.3.

Can. J. Chem. Downloaded from www.nrcresearchpress.com by 210.87.254.6 on 09/06/12
For personal use only.

Oxidation of hydrocarbons. X. Concerning the formation of ketols and diones during the oxidation of alkenes by permanganate ion

DONALD G. LEE AND N. S. SRINIVASAN
Department of Chemistry, University of Regina, Regina, Sask., Canada S4S 0A2

Received September 26, 1980

DONALD G. LEE and N. S. SRINIVASAN. Can. J. Chem. **59**, 2146 (1981).

The oxidation of *E*-5-decene by potassium permanganate in slightly acidic aqueous acetone solutions has been studied. An analysis of the reaction mixture at various time intervals indicates that the ketol, 5-hydroxy-6-decanone, is the initially formed product under these conditions. The other major product, 5,6-decanedione, is formed sequentially from oxidation of the ketol rather than directly from the alkene.

DONALD G. LEE et N. S. SRINIVASAN. Can. J. Chem. **59**, 2146 (1981).

On a étudié l'oxydation du décène-5 (*E*) par le permanganate de potassium dans des solutions aqueuses d'acétone légèrement acides. Une analyse du mélange réactionnel après divers temps de réaction indique que, dans ces conditions, le premier produit à se former est le cétol hydroxy-5 décanone-6. L'autre produit principal, la décanedione-5,6 provient de l'oxydation subséquente du cétol plutôt que d'une oxydation directe de l'alcène.

[Traduit par le journal]

Introduction

Although the products obtained from the oxidation of alkenes by permanganate ion are largely determined by the reaction conditions, it is generally accepted that they are all formed from a single intermediate cyclic manganate(V) diester, **1** (1, 2, 3*a*). For example, Ogino and Mochizuki (4) have presented evidence which indicates that treatment of such an intermediate with aqueous base results in hydrolysis and yields a diol (eq. [2]). This observation provides concrete evidence in support of the widely accepted explanation for the formation of diols during the oxidation of alkenes by basic permanganate (3*a*).

[1] 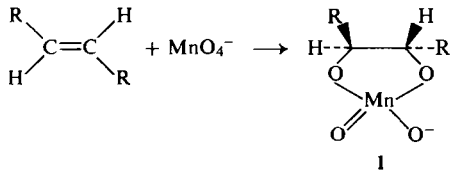

1

[2] 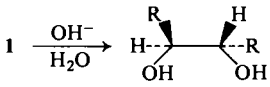

On the other hand, treatment of **1** with aqueous acid leads to cleavage products (4). Protonation of the intermediate presumably increases the oxidation potential of manganate(V) (3*b*) and promotes a cyclic decomposition (eq. [3]).

[3] 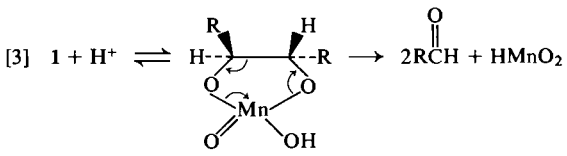

Under approximately neutral conditions two products have been obtained; in aqueous solutions ketols are the major products (5), while under nonaqueous conditions diones are often obtained (6). Previous studies (1, 7) have suggested that ketols are formed in neutral aqueous solutions because the intermediate manganate(V) ester, **1**, is oxidized to a manganate(VI) ester, **2**, before hydrolysis to the diol can occur; i.e. hydrolysis of **1** gives a diol, but oxidation of **1** to **2** followed by hydrolysis and oxidative decomposition gives a ketol.

[4] 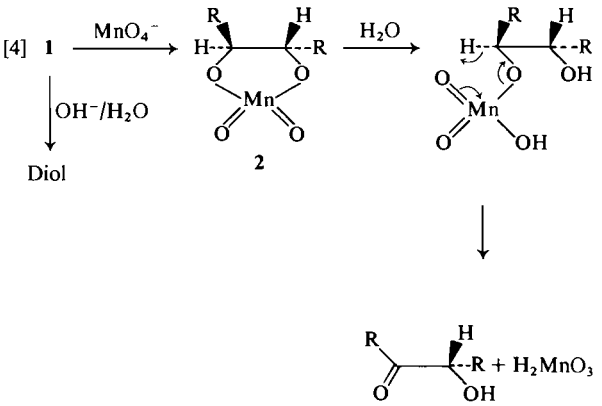

Wiberg and Saegebarth (7) have shown clearly that the ratio of ketol to diol formed is the result of a competition between oxidant and base for reaction with **1** as depicted in reaction [4].

In nonaqueous solvents it is conceivable that the products (diones) could be formed directly from **1** as in reaction [5] or from the sequential oxidation of the initial products (ketols) as in reaction [6].

0008-4042/81/142146-04$01.00/0

©1981 National Research Council of Canada/Conseil national de recherches du Canada

Can. J. Chem. Downloaded from www.nrcresearchpress.com by 210.87.254.105 on 09/06/12
For personal use only.

Can. J. Chem. Downloaded from www.nrcresearchpress.com by 210.87.254.105 on 09/06/12
For personal use only.

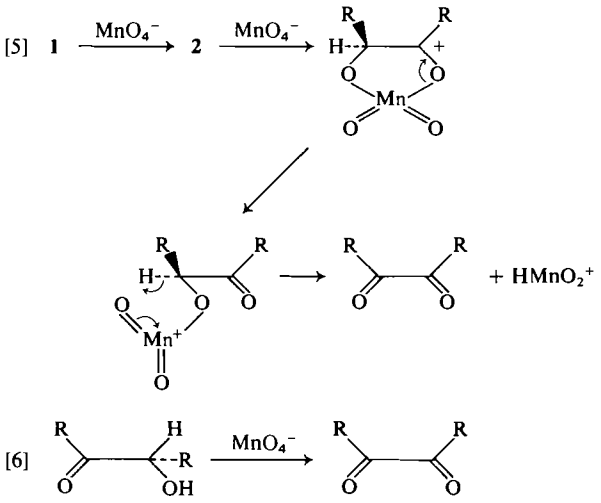

It is not likely that diols could be precursors to the diones because the oxidation of diols by permanganate is known to lead to cleavage products (8).

The purpose of the experiments described in this paper was to determine if the diones are formed directly (reaction [5]) or sequentially (reaction [6]). The approach taken was to withdraw, quench, and analyze aliquots while *E*-5-decene was being oxidized by potassium permanganate in slightly acidic aqueous acetone solutions. The analysis was done by injection of a portion of the quenched solution into a gas chromatograph under conditions where the various possible products were separable.

Experimental

Reagents and Solvents

E-5-Decene (99+%), *n*-decane (99+%), and acetone (99+%) were obtained from the Aldrich Chemical Company and used without further purification. Reagent grade acetic acid was purified by refluxing with sodium dichromate and distilling under reduced pressure (9). Distilled water, obtained from an all-glass still, was redistilled from alkaline permanganate before use. Allyl alcohol, anhydrous sodium sulfate, and molecular sieves type 4A, all of certified grade, were obtained from the Fisher Scientific Company. Pentanoic and butanoic acid were purified by distillation using a microstill equipped with a thirty plate Teflon spinning band fractionation column. Authentic samples of 5-hydroxy-6-decanone (10) and 5,6-decanedione (11) were prepared and identified by use of nmr and ir spectroscopy. Potassium permanganate in a very finely powdered form (Cairox M) was obtained from the Carus Chemical Company.

The Rate of Oxidation of E*-5-Decene*

A 250 mL Erlenmeyer flask was charged with potassium permanganate (1.21 g, 0.00766 mol), acetone (25 mL), acetic acid 1.5 mL), and water (1.5 mL). It was placed in a thermostated bath (25.0 ± 0.1°C) and the solution was stirred magnetically. After 20 min *n*-decane (0.5 mL), which was used as an internal standard, and *E*-5-decene (1.00 mL, 0.00529 mol) were injected into the flask. A timer was started and approximately 0.75 mL aliquots were withdrawn at intervals and quenched by addition to an excess of cold allyl alcohol.

The quenched aliquot was dried over anhydrous sodium sulfate and the solids (sodium sulfate and manganese dioxide) were removed by centrifugation. The clear solution was pipetted into a test tube containing molecular sieves, stoppered, and refrigerated.

The aliquots were analyzed by injecting a portion (3 μL) into a dual column Hewlett-Packard Research Chromatograph 7620 A fitted with an 8 ft column containing 20% Carbowax 20 M and terephthalic acid on Chrom W DMCS 60/80 mesh. Peak areas were determined using a disc integrator and compared to those of the internal standard, *n*-decane. Calibration curves, correlating the ratios of the peak areas to the concentrations of *E*-5-decene and all detectable products, were prepared and used to calculate the amount of each product present. These were then plotted against the time at which each aliquot had been obtained (see Fig. 1).

The internal standard, *n*-decane, was stable to permanganate over the reaction time. The quenching agent, allyl alcohol, and the products of its oxidation did not interfere with the glc analysis. Similar procedures were used to determine the rates of oxidation of 5-hydroxy-6-decanone and 5,6-decanedione.

The Oxidation of 5-Hydroxy-6-decanone

A 250 mL Erlenmeyer flask, immersed in a water bath at room temperature, was charged with 5-hydroxy-6-decanone (2.50 g, 0.0147 mol), reagent grade acetone (50 mL), acetic acid (3 mL), and water (3 mL). To this was added potassium permanganate (3.0 g, 0.019 mol), and the solution was stirred magnetically for 40 min. It was then quenched by addition of a few drops of allyl alcohol and the precipitated manganese dioxide was removed by filtration. The precipitate was washed with ether (4 × 50 mL) and the combined organic solutions were dried (anhydrous magnesium sulfate) and concentrated using a rotary evaporator. The residue was analyzed by glc. The yield of 5,6-decanedione, based on the amount of ketol which had reacted, was 83%.

Rate Constants

Approximate second order rate constants were obtained from plots of ln ($[MnO_4^-]$/[substrate]) against time (12). The concentrations of the organic substrates were calculated using the glc

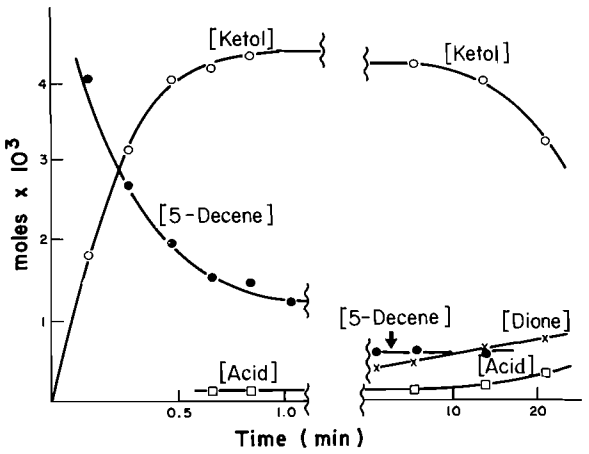

FIG. 1. Composition of the reaction mixture during the oxidation of *E*-5-decene by permanganate ion in acetone containing 5% water and 5% acetic acid.

Can. J. Chem. Downloaded from www.nrcresearchpress.com by 210.87.254.105 on 09/06/12
For personal use only.

analytical procedure described above and the permanganate concentrations were obtained from a knowledge of the initial concentration and the amount of organic product that had been produced.

Some typical rate plots have been reproduced in Figs. 2 and 3.

Results and Discussion

The results obtained from an analysis of the composition of the reaction mixture at various time intervals have been summarized in Fig. 1. This figure clearly indicates that the first detectable product formed is the ketol and that the dione is likely formed in a subsequent reaction. (This is also consistent with the fact that dione could be obtained in 83% yield from the oxidation of the ketol under these same conditions.) Furthermore, an examination of the reaction rates indicates that the second order rate constant of oxidation of the alkene ($0.414\,M^{-1}\ s^{-1}$) is almost twice that for oxidation of the ketol ($0.234\,M^{-1}\ s^{-1}$).

Oxidation of the dione would produce carboxylic acids (13). However, it is of interest to note that pentanoic acid began to accumulate before any dione could be detected in the product. This may simply reflect the fact that carboxylic acids are stable products and not susceptible to further degradation, whereas the diones can be oxidized.

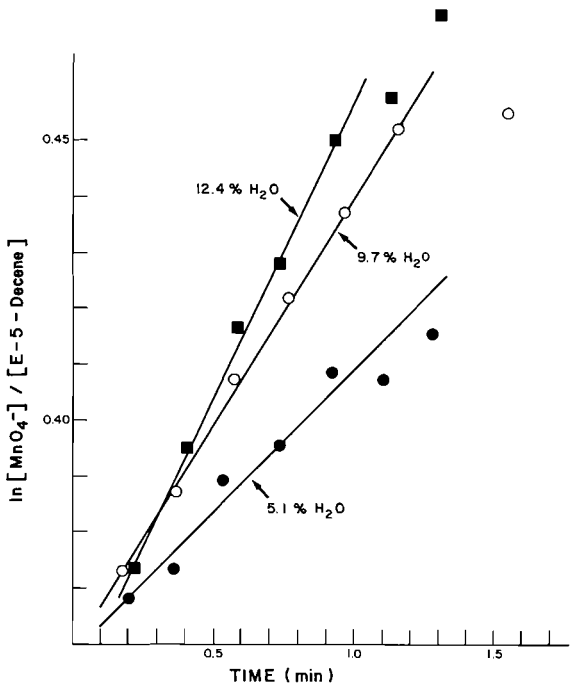

FIG. 2. Second order rate plots for the oxidation of *E*-5-decene by permanganate ion in aqueous acetone solutions containing 5% acetic acid.

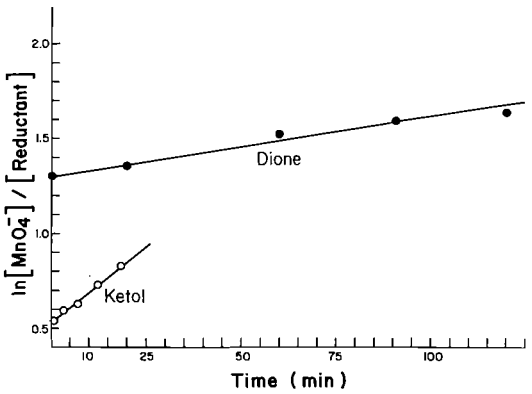

FIG. 3. Second order rate plots for the oxidation of 5-hydroxy-6-decanone and 5,6-decanedione by permanganate ion in acetone solutions containing 5% water and 5% acetic acid.

However, the rate constant for dione oxidation is very small ($0.00986\,M^{-1}\ s^{-1}$) compared to the reaction time scale and it seems more likely that some of the carboxylic acid is formed directly from the intermediate cyclic manganate(V) ester as in eq. [3]. The product of such a cleavage, pentanal, was not detected, probably because of the ease with which it would be oxidized to pentanoic acid.

It may also be noted that the rate of formation of ketol is accelerated by increasing the amount of water present in the solvent (Fig. 2). Since increasing the amount of water also increases the polarity of the solvent this result suggests that the transition state for reaction [1] must be more polar than the ground state. If it is assumed that the reaction involves a transfer of electrons from the HOMO of the alkene to the LUMO of the permanganate ion (14), a possible transition state may be visualized as follows:

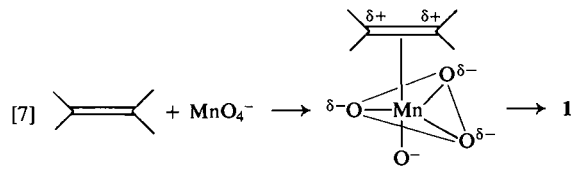

A transition state of this type is also consistent with the evidence Sharpless *et al.* (15) have recently presented, which indicates that reactions between alkenes and transition metal oxides are initiated by an interaction between the π orbitals of the double bond and the *d* orbitals of the metal.

Finally, one may attempt, on the basis of these results, to understand why ketols are obtained as the products of permanganate oxidations in neutral aqueous media while diones are obtained in approximately neutral nonaqueous solvents. The

answer lies in a consideration of the relative rate constants. Although the rate constant for formation of ketol increased from 0.414 M^{-1} s^{-1} in a solvent mixture containing 5.1% H_2O to 0.819 M^{-1} s^{-1} for one containing 12.4% H_2O, the corresponding rate constants for oxidation of the ketol to the dione actually decreased slightly (from 0.234 M^{-1} s^{-1} to 0.205 M^{-1} s^{-1}). Hence in an aqueous solution it appears that the ketol would be formed much faster than the dione. Therefore in aqueous solutions the product would be a ketol unless excess oxidant was used. Furthermore, it is known that α-diones are rather easily cleaved by permanganate in aqueous solution (10) and a use of excess oxidant would tend to give carboxylic acids rather than diones. Under anhydrous conditions the rates of oxidation of the alkene and the ketol are more comparable and the dione less susceptible to cleavage. Hence the dione is more likely to accumulate when nonaqueous solvents are used.

Acknowledgments

The authors are grateful for financial support from the Natural Sciences and Engineering Research Council of Canada and the Carus Chemical Company.

1. K. B. WIBERG, C. J. DEUTSCH, and J. ROČEK. J. Am. Chem. Soc. **95**, 3034 (1973); D. G. LEE and J. R. BROWNRIDGE. J. Am. Chem. Soc. **96**, 5517 (1974).
2. L. I. SIMÁNDI and M. JÁKY. J. Am. Chem. Soc. **98**, 1995 (1976).
3. R. STEWART. *In* Oxidation in organic chemistry. Part A. *Edited by* K. B. Wiberg. Academic Press, New York. 1965. (*a*) p. 42; (*b*) p. 35.
4. T. OGINO and K. MOCHIZUKI. Chem. Lett. 443 (1979).
5. J. E. COLEMAN, C. RICCIUTI, and D. SWERN. J. Am. Chem. Soc. **78**, 5342 (1956); G. KING. J. Chem. Soc. 1788 (1936).
6. K. G. SHARPLESS, R. F. LAUER, O. REPIČ, A. Y. TERANISHI, and D. R. WILLIAMS. J. Am. Chem. Soc. **93**, 3303 (1971); H. P. JENSEN and K. B. SHARPLESS. J. Org. Chem. **39**, 2314 (1974); D. G. LEE and V. S. CHANG. J. Org. Chem. **43**, 1532 (1978).
7. K. B. WIBERG and K. A. SAEGEBARTH. J. Am. Chem. Soc. **79**, 2822 (1957).
8. W. L. EVANS. J. Am. Chem. Soc. **45**, 171 (1923).
9. K. B. WIBERG and T. MILL. J. Am. Chem. Soc. **80**, 3022 (1958).
10. N. S. SRINIVASAN and D. G. LEE. Synthesis, 520 (1979).
11. N. S. SRINIVASAN and D. G. LEE. J. Org. Chem. **44**, 1574 (1979).
12. K. J. LAIDLER. Chemical kinetics. McGraw-Hill, Toronto. 1950. pp. 8–10.
13. D. G. LEE and V. S. CHANG. J. Org. Chem. **44**, 2726 (1979).
14. K. TOYOSHIMA, T. OKUYAMA, and T. FUENO. J. Org. Chem. **45**, 1600 (1980).
15. K. B. SHARPLESS, A. Y. TERANISHI, and J. E. BACKVALL. J. Am. Chem. Soc. **99**, 3120 (1977).

Can. J. Chem. Downloaded from www.nrcresearchpress.com by 210.87.254.105 on 09/06/12
For personal use only.

The cybrodins, a new class of sesquiterpenes[1,2]

WILLIAM A. AYER AND ROBERT H. MCCASKILL
Department of Chemistry, University of Alberta, Edmonton, Alta., Canada T6G 2G2

Received February 3, 1981

WILLIAM A. AYER and ROBERT H. MCCASKILL. Can. J. Chem. **59**, 2150 (1981).

The isolation and structure determination of the "cybrodins", a new group of sesquiterpenoids produced by a new strain of the bird's nest fungus *Cyathus bulleri*, is reported. Cybrodol (**3**), isocybrodol (**4**), cybrodal (**5**), trisnorcybrodolide (**6**), and cybrodic acid (**7**) may be classified as *seco*-illudalane sesquiterpenes. The evidence leading to the structural assignments is presented, along with chemical correlations among the cybrodins. The possible mode of biogenesis is discussed. Pterosin-C (**13**), a known norsesquiterpene, and 3-methyllumichrome (**17**) were also isolated. Small quantities of a new sesquiterpenoid, broderol, believed to possess structure **21**, were obtained on two occasions.

WILLIAM A. AYER and ROBERT H. MCCASKILL. Can. J. Chem. **59**, 2150 (1981).

On rapporte la séparation et la détermination de la structure des "cybrodines", un nouveau groupe de sesquiterpènes produits par une nouvelle déformation du champignon des nids d'oiseaux: le *Cyathus bulleri*. On peut classifier le cybrodole (**3**), l'isocybrodole (**4**), le cybrodale (**5**), le trisnorcybrodolide (**6**) et l'acide cybrodique (**7**) comme des sesquiterpènes du type *seco*-illudalane. On présente des données qui permettent d'attribuer des structures ainsi que les corrélations chimiques entre les cybrodines. On discute du mode possible de biogénèse. On a également isolé la ptérosine-C (**13**) un norsesquiterpènes connu ainsi que la méthyl-3 lumichrome (**17**). On a obtenu à deux reprises des petites quantités de brodérol, un nouveau sesquiterpène qui possèderait la structure **21**.

[Traduit par le journal]

Some time ago we reported the isolation and structure determination of the degraded eudesmane-type sesquiterpene cybullol (**1**) from *Cyathus bulleri* Brodie (Brodie strain 6620, ATCC 38347) (3). At that time we also reported the isolation and characterization of small amounts of a $C_{15}H_{28}O_3$ triol which had properties consistent with it being a biogenetic precursor of cybullol such as **2** (3, 4). In pursuit of further quantities of this triol we examined the metabolites of a different strain[3] of *C. bulleri* (Brodie strain 6680a, ATCC 38351) which we find does not produce cybullol (**1**) or the triol $C_{15}H_{28}O_3$ but which instead produces a series of new sesquiterpenes which we have called the cybrodins.[4] In this paper we discuss the isolation and structure determination of the cybrodins and other minor metabolites, and in the following paper we describe the total syntheses of the cybrodins.

Liquid cultures of *C. bulleri* were grown on an aerated yeast–malt extract medium in a fermentation apparatus. After a growth period of two weeks, the mycelial cells were removed by filtration, and the culture broth was extracted with ethyl acetate.

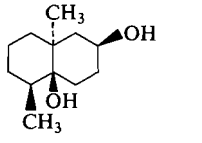

1

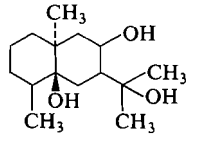

2

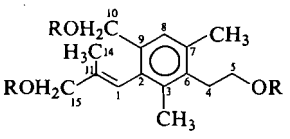

3 R = H
3*a* R = Ac

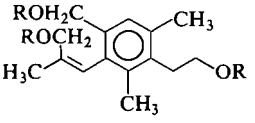

4 R = H
4*a* R = Ac

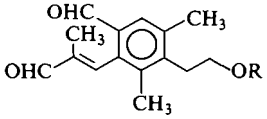

5 R = H
5*a* R = Ac

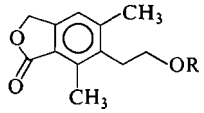

6 R = H
6*a* R = Ac

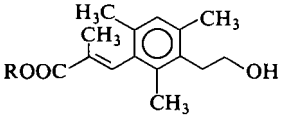

7 R = H
7*a* R = CH_3

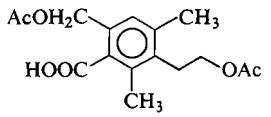

8

The ethyl acetate soluble metabolites were divided into neutral and acidic components by extraction with aqueous sodium bicarbonate. The metabolites were further separated by chromatography over Sephadex LH-20 (this separates the metabolites

[1]Part 15 in the series Metabolites of Bird's Nest Fungi. For part 14, see ref. 1.

[2]A preliminary report on a portion of this work is contained in ref. 2.

[3]Stock cultures of the strain used previously no longer produced **1** or the triol.

[4]The compounds are named in honor of Harold J. Brodie, Professor Emeritus, University of Alberta, the discoverer of this species of *Cyathus*.

0008-4042/81/142150-09$01.00/0
©1981 National Research Council of Canada/Conseil national de recherches du Canada

Can. J. Chem. Downloaded from www.nrcresearchpress.com by 210.87.254.5 on 09/06/12
For personal use only.

Can. J. Chem. Downloaded from www.nrcresearchpress.com by 210.87.254.5 on 09/06/12
For personal use only.

from the polypropylene glycol antifoaming agent necessary in the fermentation apparatus and also affords a useful preliminary separation of the metabolites) and then silica gel. The major metabolites isolated from the neutral fraction are two isomeric compounds $C_{15}H_{22}O_3$ (named cybrodol (**3**) and isocybrodol (**4**)), a compound $C_{15}H_{18}O_3$ (cybrodal (**5**)), and a compound $C_{12}H_{14}O_3$ (trisnorcybrodolide (**6**)). From the acid fraction, cybrodic acid ($C_{15}H_{20}O_3$ (**7**)) was the only compound isolated.

Inspection of the ^1H and ^{13}C nuclear magnetic resonance (nmr), infrared (ir), and ultraviolet (uv) spectra of cybrodol (**3**) and *O,O,O*-triacetylcybrodol (**3***a*) reveals that cybrodol is a pentasubstituted benzene derivative and that the substituents are two methyl groups, an hydroxymethyl group, a β-hydroxyethyl group, and a four-carbon unit containing a double bond, a methyl group, and an hydroxymethyl group. Thus the ^{13}C nmr spectrum has eight signals in the region δ 120–140 where sp^2 carbons not bonded to heteroatoms normally appear. Off-resonance decoupling reveals that six of these signals are due to fully substituted carbons, the remaining two bear single hydrogen atoms. The ^1H nmr spectrum of cybrodol has one proton signal at δ 7.10 and δ 6.45 corresponding to aromatic and olefinic hydrogens respectively. The ^{13}C nmr spectrum also has three methylene signals in the region δ 60–70 typical of oxygenated sp^3 carbons (5). That these represent the carbons of three primary alcohols is indicated by the presence of three two proton signals (δ 4.50, 4.23, and 3.76) in the ^1H nmr spectrum of cybrodol, all of which are shifted downfield by about 0.5 ppm in the spectrum of *O,O,O*-triacetylcybrodol. The signal at δ 4.50 is characteristic of a benzylic alcohol. Irradiation of the olefinic proton of cybrodol sharpens the signal at δ 4.23, indicating the presence of an allylic alcohol function. The signal at δ 3.76 is one half of an A_2X_2 system (J_{AX} = 7 Hz) the second half of which appears at δ 2.99. These shifts are consistent with the presence of the β-phenethyl alcohol grouping.[5] Mass spectral evidence supports this assignment, since the mass spectrum of cybrodol shows a strong peak (95%) at *m/e* 219 ($M^+ - CH_2OH$) for the resulting benzylic carbonium ion.

The ^1H nmr spectrum of cybrodol shows aromatic *C*-methyl signals at δ 2.36 and 2.18 and an olefinic methyl at δ 1.44. The latter signal is a doublet (J = 1 Hz) which collapses to a singlet when the olefinic proton at δ 6.45 is simultaneously irradiated. This latter finding establishes the structure of the four carbon side chain, except for stereochemistry, since the small splitting indicates that the olefinic hydrogen is not on the same carbon as the methyl group or the hydroxymethyl group. It now remains to determine the arrangement of the substituents on the aromatic ring.

Comparison of the aryl methyl group signals shows that the signal at δ 2.18 is noticeably sharper than the signal at δ 2.36, and a nuclear Overhauser experiment demonstrated that the latter methyl group is *ortho* to the aromatic proton. Ozonolysis of *O,O,O*-triacetylcybrodol (**3***a*) followed by oxidative work-up gave the acid **8**. This confirmed the structure of the olefinic sidechain and also provided evidence as to its environment. In going from a styrene type system to a benzoic acid it is expected that the groups *ortho* to the carboxyl group will experience substantial downfield shifts (7, 8). Only two of the groups in **8** are significantly shifted relative to their positions in **3***a*. The benzylic acetate methylene group is deshielded by 0.17 ppm, and the methyl group which is not *ortho* to the aromatic hydrogen is deshielded by 0.46 ppm. Thus the olefinic side chain in cybrodol is flanked by these two groups. In agreement with this the acid **8**, when treated with 10-camphorsulfonic acid in benzene–methanol, undergoes transesterification and lactonization to provide the phthalide **6**. This phthalide is identical with trisnorcybrodolide (**6**), one of the naturally occurring compounds mentioned above. Trisnorcybrodolide (**6**) has a uv spectrum very similar to that of phthalide itself (9), and the ir (1730 cm^{-1}) is consistent with the formulation. The methylene group in the five-membered ring resonates at δ 5.15 (phthalide itself δ 5.35), and the A_2X_2 system of the β-hydroxyethyl group appears at δ 3.06 and 3.79. This latter system displays the appropriate acetylation shift in the spectrum of *O*-acetyltrisnorcybrodolide (**6***a*). Thus the carboxyl group in the acid **8** is located *ortho* to the benzylic alcohol.

The fact that the β-hydroxyethyl group is located between the two aromatic methyl groups was demonstrated in the following way. Dehydration of trisnorcybrodolide (**6**) to the olefin **9** was effected, albeit in low yield, in two different ways. Firstly the alcohol was converted to the selenide **10** by treatment with 4-nitrophenylselenocyanate and tri-*n*-butylphosphine (10). Oxidative elimination then provided the olefin **9** in 15% overall yield. Secondly, mesylation of **6** followed by treatment of the mesylate with 1,5-diazabicycloundecene (DBU)

[5]β-Phenethyl alcohol itself shows shifts of δ 3.85 and δ 2.82 for these methylene groups (6).

Can. J. Chem. Downloaded from www.nrcresearchpress.com by 210.87.254.5 on 09/06/12
For personal use only.

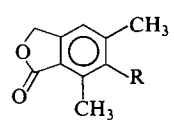

9 R = $-CH_2{=}CH_2$
10 R = $-CH_2CH_2SePh$
11 R = $-CHO$

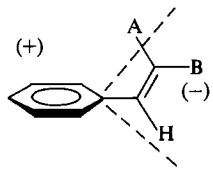

12

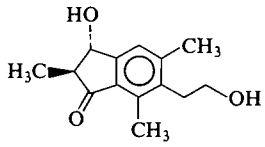

13

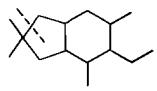

14

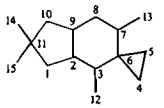

15

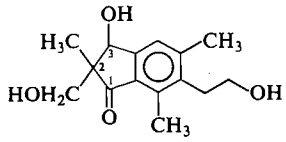

16

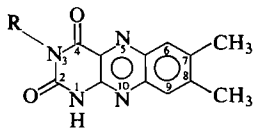

17 R = CH_3
18 R = H

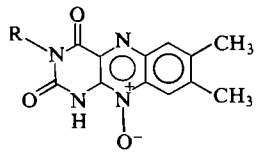

19 R = H
20 R = CH_3

gave **9** in about 20% yield. Ozonolysis of **9** followed by reductive work-up furnished the aldehyde **11** in 40% yield. Both methyl groups experience downfield shifts in **11** (C-5 CH_3 δ 2.69, C-7 CH_3 δ 2.98) relative to **6** (δ 2.48 and 2.73 respectively), now falling within the deshielding cone of the aldehyde carbonyl (7). The aromatic hydrogen of **11** is only slightly deshielded (δ 7.18, δ 7.11 in **6**). The synthesis of trisnorcybrodolide reported in the following paper provides confirmation of structure **6**.

The determination of the double bond geometry of cybrodol (**3**) was greatly facilitated by the isolation of three closely related metabolites: isocybrodol (**4**), cybrodal (**5**), and cybrodic acid (**7**). Comparison of the ^1H nmr spectra of cybrodol (**3**) and isocybrodol (**4**) reveals that the two compounds have the same aromatic substituents and differ only in the stereochemistry of the olefinic sidechain. This is confirmed by the fact that ozonolysis of *O,O,O*-triacetylisocybrodol (**4***a*) followed by methanolysis and lactonization provided trisnorcybrodolide (**6**). The olefinic hydrogen (δ 6.27) and allylic alcohol methylene group (δ 3.69) are both upfield relative to the analogous protons of cybrodol. The olefinic methyl group (δ 2.02) of isocybrodol resonates at lower field than that of cybrodol. Neither cybrodol nor isocybrodol shows a styrene-like chromophore in the uv, both display unconjugated benzenoid absorption. Inspection of space-filling models shows that the isobutenyl side chain is twisted out of the plane of the benzene ring. Some degree of restricted rotation also explains why in the case of isocybrodol (**4**) the protons of the benzyl alcohol methylene group show nonequivalence (AB quartet centered at δ 3.69, J = 12 Hz). This feature is precedented in biphenyl chemistry (ref. 8, p. 378). The high field position of the olefinic methyl group (δ 1.44) in cybrodol and its rather low field position (δ 2.02) in isocybrodol can be explained if in the former the methyl is in the shielding region of the aromatic ring (i.e., A in **12**) and in the latter it is in the deshielding region (i.e., B in **12**). The hydroxymethyl signals show the same trend (δ 4.20 in **3**, δ 3.69 in **4**). On this basis cybrodol was assigned the *E* configuration, isocybrodol the *Z* configuration.

Cybrodal (**5**) has two conjugated aldehyde groups (ir 1688 cm^{-1}, ^1H nmr δ 9.75 and 9.92). Reduction of *O*-acetylcybrodal (**5***a*) with lithium aluminum hydride (LAH) gave cybrodol (**3**). Oxidation of cybrodol (**3**) with manganese dioxide gave cybrodal (**5**). Relative to cybrodol the vinyl and the aromatic hydrogens of cybrodal are deshielded by 1.16 ppm and 0.51 ppm, respectively, in the ^1H nmr spectrum. The former perturbation reflects the β-position and *cis*-relationship of the olefinic hydrogen to a formyl group. The latter deshielding is consistent with an *ortho* relationship of a formyl group to the aromatic hydrogen in **5**.

Cybrodic acid (**7**) readily forms a methyl ester (**7***a*) on treatment with diazomethane. The chemical shifts (^1H nmr) of the aromatic substituents do not differ significantly from those of cybrodol. The allylic alcohol methylene group is not evident, however, and the vinylic proton is shifted significantly downfield (δ 7.65) relative to **3**. The vinyl methyl appears at δ 1.60 and is coupled to the vinylic hydrogen, thereby unambiguously identifying the two signals. Comparison of the vinyl hydrogen shift (δ 7.65) with that of *E*-α-methylcinnamic acid (δ 7.80) (11) and *Z*-α-methylcinnamic acid (δ 6.73) (11) provides compelling evidence for the *E*-geometry in cybrodic acid (**7**). Reduction of methyl cybrodate (**7***a*) with LAH gives cybrodol (**3**). The uv spectrum of methyl cybrodate (λ_{max} 215 (ε 18 000), 258 nm (ε 4300)) reveals that the benzene and acrylate chromophores, as expected, are twisted out of conjugation (*trans*-cinnamates normally absorb at ca. 275 nm (ε ~ 20 000) (ref. 8, p. 119)).

Can. J. Chem. Downloaded from www.nrcresearchpress.com by 210.87.254.5 on 09/06/12
For personal use only.

Final proof of the structures of cybrodol (**3**), isocybrodol (**4**), cybrodal (**5**), and cybrodic acid (**7**) is provided by the syntheses described in the following paper.

Several of the fractions (see Experimental) from the initial Sephadex chromatography deposited a crystalline compound when allowed to evaporate slowly. This compound, mp 160–162°C, has a molecular formula $C_{14}H_{18}O_3$ and was identified as (2*R*,3*R*)-pterosin C (**13**), a known norsesquiterpene isolated from *Pteridium* ferns, by comparison of spectroscopic (ir, ^{1}H nmr) and physical (mp, rotation) data with published values (12–14). Roughly two dozen 1-indanone sesquiterpenoids and norsesquiterpenoids with the skeleton of **13** and collectively known as the pterosins have been isolated from ferns (14, 15). The pterosins belong to the so-called illudalane class of sesquiterpenes, compounds which have the carbon skeleton **14** (16). The cybrodins possess the same carbon skeleton except that the five-membered ring is cleaved as indicated in **14**, and thus they may be classified as *seco*-illudalanes. The illudalanes are in turn *seco*-illudanes, the illudanes possessing the carbon skeleton **15** (16). It is tempting to speculate that the biosynthesis of the cybrodins proceeds from farnesyl pyrophosphate via humulene, a protoilludane, an illudane, and an illudalane (**14**) intermediate.[6] Pterosin L (**16**), or a derivative thereof, by retroaldolization involving the C-3 hydroxyl (indanone numbering) and the C-1 carbonyl (or a suitable leaving group) could give rise to the cybrodin skeleton. Retroaldol cleavage involving the hydroxymethyl group at C-2 leads to pterosin C (**13**), also formed by *C. bulleri*. The numbering scheme used for the cybrodins (as shown in **3** and **15**) is derived for the numbering of the presumed biosynthetic precursor, farnesyl pyrophosphate.

During the final chromatographic purification of the natural trisnorcybrodolide (**6**) a highly uv active (λ_{max} 250, 337, 383 nm) yellow substance $C_{13}H_{12}N_4O_2$ was isolated. This compound was identified as 3-methyllumichrome (**17**), a known (19, 20) riboflavin derivative which has not previously been reported as a natural product. Identity was indicated by comparison with literature data (20) and established by comparison with a synthetic sample. Lumichrome (**18**) was synthesized by the method of Berezovskii and Tul'chinskaya (21), and transformed to the *N*-oxide **19** by treatment with hydrogen peroxide in formic acid (22). Methylation of **19** provided the 3-*N*-methyl, 10-*N*-oxide **20**. The *N*-oxide oxygen was removed by treatment with triphenylphosphine in refluxing 1-propanol to give 3-methyllumichrome (**17**), identical with that isolated from *C. bulleri*.

Two of the early liquid cultures of *C. bulleri*, grown on Brodie's medium (23), provided a small amount of a crystalline compound which could not be isolated from later growths (either on Brodie's medium or on yeast–malt extract medium). This compound, for which we suggest the name broderol, has the molecular formula $C_{15}H_{24}O_2$ and shows hydroxyl absorption but no carbonyl absorption in the ir. The nmr (^{13}C and ^{1}H) spectra reveal the presence of a trisubstituted double bond, one of the substituents being a methyl group. The ^{13}C nmr spectrum reveals the presence of 3 sp^3 oxygenated carbon atoms, one a methylene group and the other two fully substituted carbons, which indicates that the oxygen atoms are present as an hydroxyl group and an ether function. A pair of double doublets at δ 3.25 (J = 10.8, 2.5 Hz) and δ 3.52 (J = 10.8, 1 Hz) in the ^{1}H nmr also indicates the presence of an oxygenated methylene group. Broderol is resistant to acetylation, but was derivatized in an nmr tube by treatment with trichloroacetyl isocyanate (24). A single carbamate NH signal is seen in the derivative, confirming the presence of a single hydroxyl group. Furthermore, since the protons *geminal* to oxygen have virtually the same chemical shift in broderol and in its carbamate derivative, the oxygenated methylene group is associated with the ether function. Broderol thus has a tertiary alcohol and a primary–tertiary ether.

The most striking feature of the ^{13}C nmr spectrum of broderol is the presence of two methylene group signals at unusually high field (δ 6.3, 8.7), indicative of cyclopropyl methylenes (25). The ^{1}H nmr spectrum of broderol has four complex one proton multiplets (δ 0.54, 0.68, 0.82, 0.95) in the region where cyclopropyl protons commonly resonate.

Given the demonstrated proclivity of *C. bulleri* to produce metabolites derived from the illudane–illudalane pathway, it is not unreasonable to assume that broderol possesses an illudane (**15**) skeleton. Of the several possible ways to arrange the known functionality of broderol in skeleton **15** we prefer that shown in **21** on the following grounds. A comparison of the chemical shifts of the vinyl hydrogen in broderol (**21**) (δ 5.70) and its trichloroacetylcarbamate (δ 6.11) reveals that the vinyl hydrogen is β to the hydroxyl group (26). In agreement with this the vinyl hydrogen also shows a pronounced (−0.32 ppm) pyridine shift in the ^{1}H nmr spectrum (27). The tertiary ether oxygen must

[6]For discussions of this biosynthetic pathway see refs. 17 and 18.

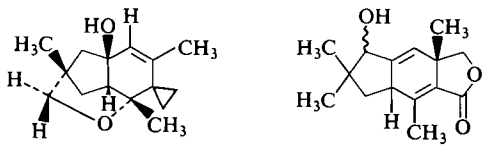

21

22

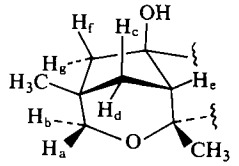

21*a*

then be located at C-2 or C-3 (see **15**) and since the remaining methyl signals are singlets, C-3 is indicated. Chemical shift data and coupling constants rule out the possibility that the ether is an epoxide, so the primary terminus of the ether must be at C-14 or C-15. Steric constraints then dictate a *cis*-fused hydrindane system with the cyclic ether on the concave side as shown in **21** (no absolute configuration implied). The protons of the oxabicyclo-[3.2.1]octane ring system present in broderol are all visible in the 400 MHz ^{1}H nmr spectrum determined in pyridine-d_5 and may be analyzed in terms of part structure **21***a*. H_e (δ 2.11), the ring junction proton has *ax–eq* (4.8 Hz) and *eq–eq* (2.0 Hz) couplings to H_c (δ 2.27) and H_d (δ 1.72) respectively. These latter two are *geminally* coupled (10.8 Hz) and H_c has an additional four bond *W* coupling (2.8 Hz) (ref. 8, pp. 334–344) to H_b (δ 3.28) which in turn is *geminally* coupled to H_a (δ 3.54). H_a has a four bond *W* coupling (1.2 Hz) to H_f (δ 2.10) which is *geminally* coupled (12.4 Hz) to H_g (δ 1.90). H_f and H_c are both *syn* to the hydroxyl group and are therefore deshielded (in pyridine) relative to their *geminal* partners (27).[7]

Small quantities of the alcohol nidulol (**22**) and the corresponding ketone, nidulone, also obtained from *Cyathus pygmaeus*,[8] were isolated from the neutral metabolites of *C. bulleri*.

The total synthesis of each of the cybrodins (cybrodol (**3**), isocybrodol (**4**), trisnorcybrodolide (**6**), and cybrodic acid (**7**)) is described in the following paper (28). To the best of our knowledge, these compounds represent the first *seco*-illudalanes to be reported.

Experimental

Fermentations were carried out in a New Brunswick Scientific MF-214 microferm laboratory fermentor. Water used at all stages of the fungal culturing process was distilled in an all glass apparatus.

All solvents were distilled prior to use. Skellysolve B refers to Skelly Oil Company light petroleum, bp 62–70°C. A Hitachi CLC-3 centrifugal liquid chromatograph packed with Baker TLC Silica Gel 7 (< 40 μm) was used for centrifugal liquid chromatography. Macherey Nagel silica gel (< 80 μm) was used for column chromatography. Whatman LPS-2 Chromedia (37–53 μm) was used for flash chromatography (29). Analytical thin layer chromatography (tlc) was carried out on glass plates (75 × 25 or 75 × 50 mm) coated (~0.3 mm) with silica gel G (W. Merck, Darmstadt) containing 1% electronic phosphor (General Electric, Cleveland). Preparative thin layer chromatography (ptlc) was carried out on glass plates (20 × 20, 10 × 20, or 5 × 20 cm) coated (0.5 mm) with the same adsorbent. Materials were detected by visualization under an ultraviolet lamp (254 or 350 nm). The plate (only a thin vertical band in the case of ptlc) was then sprayed with a solution of vanillin (1%) in concentrated sulfuric acid and charred using a heat gun.

Mass spectra (ms) were recorded on an A.E.I. MS-50 mass spectrometer coupled to a DS 50 computer or an A.E.I. MS-9) mass spectrometer (chemical ionization). Data is reported as *m/e* (relative intensity). Unless diagnostically significant, peaks with intensities less than 20% of the base peak are omitted. Infrared spectra were recorded on a Nicolet 7199 FT interferometer, ultraviolet spectra on a Unicam SP 1700 ultraviolet spectrophotometer, and optical rotations on a Perkin Elmer Model 141 polarimeter. Optical rotatory dispersion and circular dichroism measurements were made with a Durrum Jasco ORD/UV-5 (SS-20 modification) recording spectropolarimeter. The ^{1}H nmr spectra were measured on a Bruker WP-60 spectrometer interfaced to a Nicolet 1080 computer, a Varian HA-100 spectrometer interfaced to a Digilab FTS/NMR-3 data system, a Bruker WH-200 spectrometer, or a Bruker WH-400 spectrometer. The ^{13}C nmr spectra were measured on the aforementioned Bruker WP-60 instrument or a Bruker HFX-90 spectrometer interfaced to a Nicolet 1085 computer. The numbering used in reporting nmr spectral data is that used in the systematic (IUPAC) name. All nuclear magnetic resonance measurements employed tetramethylsilane as an internal standard. Melting points were recorded on a Fisher-Johns melting point apparatus and are uncorrected. All compounds for which spectral data are reported showed single spots on tlc using at least two solvent systems.

Growth of C. bulleri *Cultures and Extraction of Metabolites*

Stock cultures of *C. bulleri* 6680a (ATCC 38351), obtained from Dr. J. H. Ginns, Biosystematics Research Institute, Agriculture Canada, Ottawa, were maintained in slant tubes on agar impregnated with Brodie's medium (23). To initiate large scale cultures petri dishes (9 cm × 1 cm) containing Brodie's agar were inoculated from stock cultures. These were allowed to mature for two weeks at which time the mycelial growth covered nearly the entire surface of the plate. The agar discs were blended (Waring blender) along with sterile yeast–malt extract medium (500 mL, containing the following nutrients per liter: dextrose, 4 g; yeast extract (Difco), 4 g; malt extract (Difco), 10 g). This inoculum was gently agitated in an Erlenmeyer flask (2 L) for a two week period, then transferred to a fermentation apparatus charged with 10 L of sterile culture medium and approximately 1 mL of the antifoaming agent polypropylene glycol. Fermentation proceeded for two weeks under the following standard conditions: 25°C, 200 rpm agitation rate, 3 L/min air flow.

The metabolites were isolated in the following manner. The mycelium was removed by vacuum filtration through coarse filter paper (Grade 230). The culture broth was then extracted with ethyl acetate (4 × 1/3 volumes). The ethyl acetate extracts

[7]Verification of structure **21**, which is contingent on the biogenetic argument presented, by X-ray crystallography will be attempted.

[8]W. A. Ayer, R. H. McCaskill, and T. Reffstrup, manuscript in preparation.

Can. J. Chem. Downloaded from www.nrcresearchpress.com by 210.87.254.5 on 09/06/12
For personal use only.

Can. J. Chem. Downloaded from www.nrcresearchpress.com by 210.87.254.5 on 09/06/12
For personal use only.

were heavily emulsified and filtration through Celite facilitated the separation of the organic and aqueous phases. The extracts were then concentrated *in vacuo* to 150 mL. Acidic components were removed by extraction with saturated aqueous sodium bicarbonate (3 × 50 mL). The bicarbonate extracts were then back-extracted with ethyl acetate (2 × 50 mL). The combined ethyl acetate solutions were washed with water (50 mL) and brine (50 mL). After drying over magnesium sulfate, filtration and concentration gave the neutral extract as a yellow oil. The bicarbonate extracts were acidified (~pH 1) with concentrated hydrochloric acid and then extracted with ethyl acetate (4 × 50 mL). These combined ethyl acetate extracts were washed with water (50 mL) and brine (40 mL) and then dried over magnesium sulfate. Filtration and concentration gave the acidic extract as a dark brown oil. From 20 L of fermentation broth a typical yield was: neutral extract, 1.6 g; acidic extract, 0.6 g; total metabolite yield, 2.2 g.

Preliminary Fractionation of the Crude Metabolites

The neutral extract (1.6 g) was dissolved in methanol (5 mL) and filtered through a cotton wool plug. The filtrate was applied to a column of LH-20 Sephadex (100 g, 65 cm × 2.8 cm). The column was eluted with methanol at a flow rate of 30 mL/h. Fractions (400 drops, ~7 mL) were collected with the aid of an automatic fraction collector equipped with a drop counter. The antifoaming agent, polypropylene glycol (mol. wt. >2000), eluted in tubes 18–25 (480 mg). The metabolites eluted in tubes 30–60 (1.14 g). The acidic extract (0.6 g) was handled in exactly the same fashion. No antifoaming agent was present in this extract. The acidic metabolites also eluted in tubes 30–60.

The next step in the fractionation of the neutral extract involved silica gel chromatography of selected Sephadex fractions. During the early phases of this work, a Centrifugal Liquid Chromatograph (CLC) was used for this purpose; however, ordinary column chromatography was found to be more reliable and convenient. Thus column chromatography (50 g of silica gel) of Sephadex fractions 38–41 (450 mg) gave some virtually pure metabolites as well as several semi-pure compounds. The preliminary column was eluted with the following solvent mixtures: Skellysolve B – chloroform (1:1, 500 mL), chloroform (500 mL), chloroform–methanol (100:1, 500 mL), chloroform–methanol (50:1, 500 mL), chloroform–methanol (20:1, 500 mL), and chloroform–methanol (10:1, 500 mL).

*Isolation of Cybrodol (**3**, 3-((3-(2-Hydroxyethyl)-6-hydroxymethyl-2,4-dimethyl)phenyl)-2-methyl-(E)-2-propenol)*

Cybrodol (**3**) eluted in Sephadex fractions 40–41 of the neutral extract. It was obtained in pure form as a colourless oil (62 mg) when the preliminary silica gel column of Sephadex fractions 38–41 was eluted with chloroform–methanol (20:1); uv (CH_3OH) λ_{max}: 210 (ε 6200), 270 nm (sh, ε ~320); ir ($CHCl_3$ cast): 3300, 1670 (w), 1440, 1380, 1030, 1010, 890, 760 cm^{-1}; ^1H nmr ($CDCl_3$) δ: 1.46 (3H, d (1 Hz), vinyl CH_3), 1.8 (3H, bs, 3 × OH), 2.18 (3H, s, C-2 CH_3), 2.36 (3H, s, C-4 CH_3), 2.99 (2H, t (7 Hz), CH_2CH_2O), 3.76 (2H, t (7 Hz), CH_2CH_2O), 4.23 (2H, bs, $W_{1/2}$ = 2 Hz, CH_2O), 4.50 (2H, s, $ArCH_2O$), 6.45 (1H, bs, $W_{1/2}$ = 4 Hz, vinyl H), 7.10 (1H, s, ArH); ^{13}C nmr (CD_3OD) δ: 14.9, 16.5, 20.3, (CH_3); 34.3, 61.8, 63.3, 67.9, (CH_2); 123.9, 127.8, (CH); 134.9, 135.0, 135.8, 136.1, 137.9, 140.0, (C); ms *m/e* calcd. for $C_{15}H_{22}O_3$ (M^+): 250.1569; found: 250.1562 (5), 232 (35), 219 (95), 217 (90), 201 (100), 199 (35), 191 (68), 187 (42), 183 (20), 173 (29), 171 (38), 159 (20), 157 (32), 156 (20), 143 (24), 128 (20). Chemical ionization (NH_3) ms shows an M +18 (*m/e* 268) peak.

*Isolation of Trisnorcybrodolide (**6**, 6-(2-Hydroxyethyl)-5,7-dimethylphthalide)*

Trisnorcybrodolide (**6**) eluted in Sephadex fractions 43–48 (66 mg) of the neutral extract. Silica gel chromatography (chloroform–methanol, 50:1; 20 g of silica gel) of these combined fractions gave pure trisnorcybrodolide (**6**, 13 mg) as a tan powder. Crystallization (methanol) afforded white prisms, mp 188–190°C; uv (CH_3OH) λ_{max}: 242 (ε 6400), 282 (ε 1100), 289 nm (ε 1300); ir ($CHCl_3$ cast): 3450, 1730, 1610, 1590, 1460, 1380, 1350, 1260, 1040, 1030, 1010, 860, 800 cm^{-1}; ^1H nmr ($CDCl_3/CD_3OD$) δ: 2.48 (3H, s, C-5 CH_3), 2.73 (3H, s, C-7 CH_3), 3.06 (2H, t (7 Hz), CH_2CH_2O), 3.79 (2H, t (7 Hz), CH_2CH_2O), 5.15 (2H, s, CH_2O), 7.11 (1H, s, ArH); ^{13}C nmr (DMSO-d_6) δ: 12.7, 20.7, (CH_3); 32.1, 59.8, 67.9, (CH_2); 121.3, (CH); 120.5, 137.1, 137.4, 143.9, 145.6, (C); 171.1, (C=O); ms *m/3* calcd. for $C_{12}H_{14}O_3$ (M^+): 206.0944; found: 206.0944 (78), 191 (66), 175 (100), 163 (16), 147 (43), 119 (20). Chemical ionization (NH_3) ms shows a peak at *m/e* 224 (M +18).

*Isolation of Isocybrodol (**4**, 3-((3-(2-Hydroxyethyl)-6-hydroxymethyl-2,4-dimethyl)phenyl)-2-methyl-(Z)-2-propenol)*

Isocybrodol (**4**) eluted in Sephadex fractions 40–41 of the neutral extract. It was obtained in very crude form (75 mg) when the preliminary silica gel column of Sephadex fractions 38–41 was eluted with chloroform–methanol (20:1). The crude fractions of isocybrodol along with pyridine (0.1 mL) and acetic anhydride (1 mL) were refluxed overnight in methylene chloride (10 mL). Evaporation to dryness *in vacuo* gave a brown oil (123 mg) which was chromatographed (chloroform–ether, 97:3, 10 g of silica gel) affording crude triacetylisocybrodol (**4***a*, 65 mg). This material was stirred overnight in methanol (10 mL) along with potassium carbonate (1 g). The volatiles were removed *in vacuo* and the residue was partitioned between ethyl acetate (50 mL) and water (10 mL). The organic solution was dried over magnesium sulfate, filtered, and evaporated to dryness, leaving crude isocybrodol (**4**, 45 mg). Chromatography (chloroform–methanol, 50:1; 10 g of silica gel) gave pure isocybrodol (**4**, 39 mg). Crystallization (chloroform–methanol) gave white prisms, mp 102–103°C; uv (CH_3OH) λ_{max}: 210 (ε 6200), 270 nm (sh, ε ~350); ir ($CHCl_3$ cast): 3290, 1660 (w), 1440, 1380, 1035, 1030, 1005, 880, 750 cm^{-1}; ^1H nmr ($CDCl_3$) δ: 2.02 (3H, d (1 Hz), vinyl CH_3), 2.16 (3H, s, C-2 CH_3), 2.36 (3H, s, C-4 CH_3), 2.97 (2H, t (7 Hz), CH_2CH_2O), 3.60 (1H, d)12 Hz), CH_2O), 3.70 (2H, t (7 Hz), CH_2CH_2O), 3.78 (1H, d (12 Hz), CH_2O), 4.35 (1H, d (11 Hz), $ArCH_2O$), 4.54 (1H, d (11 Hz), $ArCH_2O$), 6.27 (1H, bs, vinyl H), 7.05 (1H, s, ArH); ^{13}C nmr ($CDCl_3$) δ: 16.9, 20.3, 20.4, (CH_3); 34.3, 61.9, 62.4, 63.5, (CH_2); 126.3, 128.7, (CH); 134.3, 135.2, 136.0, 136.5, 138.0, 139.9, (C); ms *m/e* calcd. for $C_{15}H_{22}O_3$ (M^+): 250.1569; found: 250.1578 (3), 232 (52), 219 (92), 217 (85), 201 (100), 199 (37), 191 (62), 187 (46), 183 (21), 173 (34), 171 (34), 159 (22), 158 (22), 157 (38), 156 (21), 143 (27), 142 (22), 141 (21), 129 (21), 128 (23).

*Isolation of Cybrodal (**5**, 3-((2-Formyl-5-(2-hydroxyethyl)-4,6-dimethyl)phenyl)-2-methyl-(E)-2-propenal)*

Cybrodal (**5**) eluted in Sephadex fractions 40–41 of the neutral extract. It was obtained in crude form (26 mg) when the preliminary silica gel column of Sephadex fractions 38–41 was eluted with chloroform–methanol, 100:1. The crude material was chromatographed (Skellysolve B – ether, 3:1; 10 g of silica gel) affording pure cybrodal (**5**) as a yellow oil (12 mg); ir ($CHCl_3$ cast): 3450, 2740, 1688, 1630, 1040, 1010, 890, 860, 830 cm^{-1}; ^1H nmr ($CDCl_3$) δ: 1.57 (3H, d (1 Hz), vinyl CH_3), 2.26 (3H, s, C-6 CH_3), 2.46 (3H, s, C-4 CH_3), 3.10 (2H, t (7 Hz), CH_2CH_2O), 3.80 (2H, t (7 Hz), CH_2CH_2O), 7.61 (2H, bs, ArH + vinyl H), 9.75 (1H, s, CHO), 9.92 (1H, s, CHO); ms *m/e* calcd. for $C_{15}H_{18}O_3$ (M^+): 246.1256; found; 246.1254 (1), 217 (100), 186 (24). Chemical ionization (NH_3) ms shows a peak at *m/e* 264 (M +18).

*Isolation of Cybrodic Acid (**7**, 3-((3-(2-Hydroxyethyl)-6-hydroxymethyl-2,4-dimethyl)phenyl)-2-methyl-(E)-2-propenoic Acid)*

Cybrodic acid eluted in Sephadex fractions 39–41 (96 mg) of the acidic extract. In early work, fractions similar to these

Can. J. Chem. Downloaded from www.nrcresearchpress.com by 210.87.254.5 on 09/06/12
For personal use only.

(40 mg) were subjected to ptlc (toluene–acetone – acetic acid, 75:25:1) affording pure acid **7** as a yellow solid (5 mg). Crystallization (ethyl acetate – Skellysolve B) gave white plates, mp 176–178°C; ir (CH_3OH cast): 3320, 2600, 1693, 1640, 1440, 1400, 1380, 1340, 1260, 1130, 1040, 1030, 980, 870, 810, 750 cm^{-1}; ^1H nmr (CD_3OD) δ: 1.60 (3H, d (1 Hz), vinyl CH_3), 2.19 (3H, s, C-2 CH_3), 2.38 (3H, s, C-4 CH_3), 2.96 (2H, t (7 Hz), CH_2CH_2O), 3.61 (2H, t (7 Hz), CH_2CH_2O), 4.38 (2H, bs, CH_2O), 7.15 (1H, s, ArH), 7.65 (1H, bs, vinyl H); ^{13}C nmr (DMSO-d_6) δ: 16.2, 17.4, 19.9, (CH_3); 33.3, 60.0, 61.9, (CH_2); 126.4, 134.1, (CH); 130.8, 131.5, 133.0, 135.3, 136.6, 137.9, (C); 168.6, (C=O); ms *m/e* calcd. for $C_{15}H_{20}O_4$ (M^+): 264.1361; found: 264.1365 (4), 246 (47), 233 (64), 215 (100), 201 (24), 187 (48), 173 (32), 171 (54), 159 (23), 129 (21), 128 (23).

Isolation of Methyl Cybrodate (7a, Methyl 3-((3-(2-Hydroxyethyl)-6-hydroxymethyl-2,4-dimethyl) phenyl)-2-methyl-(E)-2-propenoate)

The acid was more conveniently isolated as its methyl ester, methyl cybrodate (**7a**). Thus Sephadex fractions 39–41 (96 mg) in methanol (5 mL) were treated with an excess of diazomethane in methylene chloride at 0°C. Evaporation to dryness gave crude methyl cybrodate (**7a**, 99 mg). Silica gel chromatography (chloroform–methanol, 50:1; 20 g of silica gel) gave pure methyl cybrodate (**7a**) as an oil (75 mg); uv (CH_3OH) λ_{max}:215 (ε 18 000), 258 nm (ε 4300); ir ($CHCl_3$ cast): 3400, 1715, 1640, 1430, 1380, 1340, 1260, 1210, 1190, 1120, 1080, 1040, 1000, 750 cm^{-1}; ^1H nmr ($CDCl_3$) δ: 1.65 (3H, d (1 Hz), vinyl CH_3), 2.18 (3H, s, C-2 CH_3), 2.39 (3H, s, C-4 CH_3), 3.00 (2H, t (7 Hz), CH_2CH_2O), 3.75 (2H, t (7 Hz), CH_2CH_2O), 3.82 (3H, s, CO_2CH_3), 4.48 (2H, bs, CH_2O), 7.14 (1H, s, ArH), 7.66 (1H, bs, vinyl H): ^{13}C nmr (CD_3OD) δ: 13.9, 16.6, 20.2, 52.4, (CH_3); 34.0, 61.7, 63.0, (CH_2); 128.1, 140.2, (CH); 131.7, 133.1, 134.6, 135.4, 137.0, 137.3, (C); 169.5, (C=O); ms *m/e* calcd. for $C_{16}H_{22}O_4$ (M^+): 278.1518; found: 278.1522 (4), 260 (38), 247 (42), 233 (36), 229 (100), 218 (24), 203 (21), 201 (41), 188 (20), 187 (52), 173 (31), 171 (41), 170 (22), 128 (20).

O,O,O-*Triacetylcybrodol (3a, 3-((3-(2-Acetoxyethyl)-6-acetoxymethyl-2,4-dimethyl)phenyl)-2-methyl-(E)-2-propenyl Acetate)*

A mixture of cybrodol (**3**, 109 mg, 0.44 mmol), pyridine (0.1 mL), acetic anhydride (1 mL), and chloroform (10 mL) was refluxed for 6 h and then evaporated to dryness *in vacuo*. This gave, after chromatography, triacetylcybrodol (**3a**, 156 mg, 95%) as an oil; ir ($CHCl_3$ cast): 1745 cm^{-1}; ^1H nmr ($CDCl_3$) δ: 1.44 (3H, d (1 Hz), vinyl CH_3), 2.05 (3H, s, OAc), 2.06 (3H, s, OAc), 2.12 (3H, s, OAc), 2.20 (3H, s, C-2 CH_3), 2.37 (3H, s, C-4 CH_3), 3.00 (2H, t (7 Hz), CH_2CH_2O), 4.14 (2H, t (7 Hz), CH_2CH_2O), 4.65 (2H, bs, CH_2O), 4.91 (2H, s, $ArCH_2O$), 6.39 (1H, bs, vinyl H), 7.05 (1H, s, ArH); ms *m/e* calcd. for $C_{21}H_{28}O_6$ (M^+): 376.1886; found: 376.1890 (1), 196 (100).

Ozonolysis of Triacetylcybrodol (3a).

A stirred solution of triacetylcybrodol (**3a**, 78 mg, 0.21 mmol) in methanol was cooled to −78°C. Ozone in oxygen was bubbled through the solution for 45 min (0.03 mL/min). After a further 45 min at −78°C, the solution was purged with nitrogen and then warmed to room temperature. Aqueous hydrogen peroxide (30%, 1 mL) was added and the mixture was refluxed for one hour. Most of the volatiles were removed *in vacuo*, the residue was taken up in ethyl acetate (100 mL) and then washed with water (10 mL) and brine (10 mL). After drying over magnesium sulfate, filtration and concentration gave crude 3-(2-acetoxyethyl)-6-(acetoxymethyl)-2,4-dimethylbenzoic acid (**8**, 73 mg); ^1H nmr ($CDCl_3$) δ: 1.98 (6H, s, 2 × OAc), 2.42 (3H, s, C-4 CH_3), 2.66 (3H, s, C-2 CH_3), 3.01 (2H, t (7 Hz), CH_2CH_2O), 4.10 (2H, t (7 Hz), CH_2CH_2O), 5.08 (2H, s, CH_2O), 7.04 (1H, s, ArH); ms *m/e* calcd. for $C_{16}H_{18}O_5$ (P − H_2O, parent ion not seen): 290.1154, found: 290.1154 (5), 248 (26), 188 (100), 187 (54), 175 (26), 160 (23), 159 (21), 147 (24), 115 (20), 91 (26).

The crude acid (**8**, 73 mg) and 10-camphorsulfonic acid (100 mg) in benzene–methanol (10:1, 30 mL) were refluxed for one day. Evaporation to dryness and column chromatography (methylene chloride – methanol, 50:1; 10 g of silica gel) of the residue afforded a white powder (29 mg, 69%) judged to be identical with natural trisnorcybrodolide (**6**) by comparison of tlc, ir, ^1H nmr, and ms data.

O-*Acetyltrisnorcybrodolide (6a, 6-(2-Acetoxyethyl)-5,7-dimethylphthalide)*

A mixture of trisnorcybrodolide (**6**, 20 mg, 0.097 mmol), pyridine (10 mL), and acetic anhydride (1 mL) was stirred overnight at room temperature. Evaporation to dryness *in vacuo* gave acetyltrisnorcybrodolide (**6a**, 23 mg, 96%) as a white powder. Crystallization (acetone) gave long clear needles, mp 117–118°C; ir ($CHCl_3$ cast): 1741 cm^{-1}; ^1H nmr ($CDCl_3$) δ: 2.04 (3H, s, OAc), 2.48 (3H, s, C-5 CH_3), 2.73 (3H, s, C-7 CH_3), 3.08 (2H, t (7 Hz), CH_2CH_2O), 4.17 (2H, t (7 Hz), CH_2CH_2O), 5.14 (2H, s, CH_2O), 7.10 (1H, s, ArH); ms *m/e* calcd. for $C_{14}H_{16}O_4$ (M^+): 248.1048; found: 248.1050 (14), 188 (100), 176 (20), 159 (28), 147 (36), 129 (24).

6-(2-(4-Nitrophenylseleno)ethyl)-5,7-dimethylphthalide (10)

Freshly distilled tri-*n*-butylphosphine (45 μL, 36.5 mg, 0.18 mmol) and 4-nitrophenylselenocyanate (40 mg, 0.18 mmol) in dry tetrahydrofuran (500 μL) were added to a stirred solution of trisnorcybrodolide (**6**, 16.7 mg, 0.081 mmol) in dry tetrahydrofuran (500 μL) under a nitrogen atmosphere. The deep-red mixture was stirred for 30 min at room temperature and then evaporated to dryness *in vacuo*. The residue was chromatographed (10 g of silica gel). Nonpolar side products eluted with Skellysolve B and then chloroform eluted selenide **10** (15 mg, 43%) as a yellow foam. Continued elution with chloroform gave recovered starting material (6 mg); ^1H nmr ($CDCl_3$) δ: 2.23 (3H, s, C-5 CH_3), 2.70 (3H, s, C-7 CH_3), 3.10 (2H, t (7 Hz), $ArCH_2CH_2$), 4.28 (2H, t (7 Hz), $ArCH_2CH_2$), 7.11 (1H, s, ArH), 7.59 (2H, d (9 Hz), 2 × ArH), 8.10 (2H, d (9 Hz), 2 × ArH); ms *m/e* calcd. for $C_{18}H_{17}NO_4Se$ (M^+): 391.0323; found: 391.0318 (5), 189 (100).

6-Vinyl-5,7-dimethylphthalide (9)

Aqueous hydrogen peroxide (30%, 0.1 mL) was added to a solution of selenide **10** (15 mg, 0.038 mmol) in tetrahydrofuran (2 mL). The mixture was stirred at room temperature for one day and then evaporated to dryness *in vacuo*. The residue was dissolved in ether (50 mL) and washed with saturated aqueous sodium bicarbonate (10 mL), water (10 mL), and brine (10 mL). After drying over magnesium sulfate, filtration and concentration gave crude **9** (7.4 mg) as a yellow oil; ptlc purification (Skellysolve B – ether, 3:1 triple elution) gave pure **9** (2.3 mg, 32%) as a white powder. Crystallization (methylene chloride) gave clear needles, mp 93–95°C; ir ($CHCl_3$ cast): 1740, 1610, 1000, 910 cm^{-1}; ^1H nmr ($CDCl_3$) δ: 2.38 (3H, s, C-5 CH_3), 2.65 (3H, s, C-7 CH_3), 5.16 (2H, s, CH_2O), 5.24 (1H, dd (2, 18 Hz), vinyl H), 5.65 (1H, dd (2, 11 Hz), vinyl H), 6.65 (1H, dd (11, 18 Hz), vinyl H), 7.10 (1H, s, ArH); ms *m/e* calcd. for $C_{12}H_{12}O_2$ (M^+): 188.0837; found: 188.0836 (100), 187 (22), 159 (26), 143 (38), 129 (43), 128 (25), 115 (20).

6-Formyl-5,7-dimethylphthalide (11)

Ozone in oxygen was bubbled through a stirred solution of olefin **9** (4 mg, 0.021 mmol) in methanol (5 mL) at −78°C for 30 min. The ozone was then purged with nitrogen and the solution was warmed to room temperature. Sodium iodide (150 mg, 1 mmol) and acetic acid (75 μL) were added and the

Can. J. Chem. Downloaded from www.nrcresearchpress.com by 210.87.254.5 on 09/06/12
For personal use only.

solution was stirred for two days at room temperature. The volatiles were removed *in vacuo*, the residue was dissolved in ether (50 mL) and washed with water (10 mL), 10% aqueous sodium thiosulfate (10 mL), saturated aqueous sodium bicarbonate (10 mL), water (10 mL), and brine (10 mL). After drying over sodium sulfate, filtration and concentration gave crude aldehyde **11** (3 mg) which was purified by ptlc (benzene–ether, 1:1) affording pure **11** (1.6 mg, 40%) as a white powder. Crystallization (methylene chloride) gave white prisms, mp 159–160°C; ir ($CHCl_3$ cast): 1746, 1683 cm^{-1}; ^1H nmr ($CDCl_3$) δ: 2.69 (3H, s, C-5 CH_3), 2.98 (3H, s, C-7 CH_3), 5.21 (2H, s, CH_2O), 7.18 (1H, s, ArH), 10.70 (1H, s, CHO); ms *m/e* calcd. for $C_{11}H_{10}O_3$ (M^{++}): 190.0629; found: 190.0629 (100), 162 (37), 161 (27), 149 (23), 133 (31), 103 (21).

O,O,O-*Triacetylisocybrodol (**4**a, 3-((3-(2-Acetoxyethyl)-6-acetoxymethyl-2,4-dimethyl)phenyl)-2-methyl-(Z)-2-propenyl Acetate)*

A mixture of isocybrodol (**4**, 40 mg, 0.16 mmol), pyridine (0.1 mL), acetic anhydride (0.5 mL), and methylene chloride (10 mL) was refluxed for 6 h and then evaporated to dryness *in vacuo*. After filtering through silica gel this gave triacetylisocybrodol (**4**, 59 mg, 98%) as an oil; ir ($CHCl_3$ cast): 1745 cm^{-1}; ^1H nmr ($CDCl_3$) δ: 1.93 (3H, d (1 Hz), vinyl CH_3), 1.98 (3H, s, OAc), 2.06 (3H, s, OAc), 2.08 (3H, s, OAc), 2.21 (3H, s, C-2 CH_3), 2.36 (3H, s, C-4 CH_3), 3.00 (2H, t (7 Hz), CH_2CH_2O), 4.13 (2H, t (7 Hz), CH_2CH_2O), 4.26 (2H, bs, CH_2O), 4.84 (1H, d (12 Hz), $ArCH_2O$), 4.98 (1H, d (12 Hz), $ArCH_2O$), 6.30 (1H, bs, vinyl H), 7.02 (1H, s, ArH); ms *m/e* calcd. for $C_{21}H_{28}O_6$ (M^+): 376.1886; found: 376.1903 (3), 256 (24), 248 (28), 106 (100), 103 (20).

*Ozonolysis of Triacetylisocybrodol (**4**a)*

Ozone was bubbled through a stirred solution of triacetylisocybrodol (**4***a*, 14.6 mg) in methanol (5 mL) at −78°C for 45 min. The solution was stirred at −78°C for a further 45 min, purged with nitrogen, and then warmed to room temperature. Aqueous hydrogen peroxide (30%, 0.2 mL) was added and the mixture was refluxed for one hour. Benzene–methanol (10:1, 30 mL) and 10-camphorsulfonic acid (100 mg) were added and reflux was continued overnight. Evaporation to dryness and column chromatography (methylene chloride – methanol, 50:1; 10 g of silica gel) gave a white powder (7 mg, 70%) judged to be identical with natural trisnorcybrodolide (**6**) by comparison of tlc, ir, ^1H nmr, and ms data.

O-*Acetylcybrodal (**5**a, 3-((2-Formyl-5-(2-acetoxyethyl)-4,6-dimethyl)phenyl)-2-methyl-(E)-2-propenal)*

A mixture of cybrodal (**5**, 6 mg, 0.024 mmol), pyridine (0.5 mL), acetic anhydride (1 mL), and methylene chloride (8 mL) was refluxed overnight and then evaporated to dryness. Purification by ptlc (Skellysolve B – acetone, 7:3) gave pure acetylcybrodal (**5***a*, 5 mg) as a clear oil; ir ($CHCl_3$ cast): 2730, 1740, 1689, 1639 cm^{-1}; ^1H nmr ($CDCl_3$) δ: 1.58 (3H, d (1 Hz), vinyl CH_3), 2.07 (3H, s, OAc), 2.27 (3H, s, C-2 CH_3), 2.47 (3H, s, C-4 CH_3), 3.12 (2H, t (7 Hz), CH_2CH_2O), 4.19 (2H, t (7 Hz), CH_2CH_2O), 7.63 (2H, bs, vinyl H + ArH), 9.77 (1H, s, CHO), 9.95 (1H, s, CHO); ms *m/e* calcd. for $C_{16}H_{19}O_3$ (M − CHO, parent peak not seen): 259.1334; found: 259.1337 (100), 199 (73). Chemical ionization (NH_3) ms shows a peak at *m/e* 306 (M + 18).

*Manganese Dioxide Oxidation of Cybrodol (**3**)*

Cybrodol (**3**, 9.7 mg, 0.039 mmol) and activated manganese dioxide (30) (150 mg, 1.7 mmol) in benzene (2 mL) were stirred for one day at room temperature. The mixture was filtered through Celite, the filter cake was washed with chloroform (5 × 10 mL), and the combined washings were concentrated to a syrup (8 mg). Purification by ptlc (methylene chloride – methanol, 10:1) gave a clear oil (6.7 mg) with physical properties (tlc, ^1H nmr, ms) identical with those of natural cybrodal (**5**).

Lithium Aluminum Hydride Reduction of Acetylcybrodal (5a)

Lithium aluminum hydride (20 mg, 0.53 mmol) was added to a stirred solution of acetylcybrodal (**5***a*, 5 mg, 0.017 mmol) in dry ether (2 mL). After two and one-half hours at room temperature, water (10 mL) was added and the mixture was extracted with ether (5 × 10 mL). The combined ether extracts were washed with brine (10 mL) and dried over magnesium sulfate. Filtration and concentration followed by ptlc purification (methylene chloride – methanol, 10:1) gave a clear oil (3 mg) judged to be identical with natural cybrodal (**3**) by comparison of tlc, ir, and ^1H nmr data.

*Lithium Aluminum Hydride Reduction of Methyl Cybrodate (**7**a)*

Lithium aluminum hydride (15 mg, 0.39 mmol) was carefully added to a stirred solution of methyl cybrodate (**7***a*, 5 mg, 0.018 mmol) in dry tetrahydrofuran (5 mL). The mixture was stirred for 6 h at room temperature. Water (15 mL) was added and the solution was extracted with chloroform (3 × 30 mL). The chloroform extracts were washed with water (10 mL) and brine (10 mL). After drying over magnesium sulfate, filtration and concentration gave a light yellow oil (4 mg) judged to be identical with natural cybrodol (**3**) by comparison of tlc, ^1H nmr, and ms data.

*Isolation of (2R,3R)-Pterosin C (**13**)*

(2*R*,3*R*)-Pterosin C (**13**) eluted in Sephadex fractions 43–46 (50 mg) of the neutral extract. Slow evaporation of these fractions usually caused this compound to crystallize as clear needles. Alternatively, it could be isolated by silica gel column chromatography (20 g of silica gel). Compound **13** (18 mg) eluted with chloroform–methanol, 50:1. Crystallization (ethyl acetate – Skellysolve B) afforded clear needles, mp 160–162°C (lit. (14) 162–164°C); $[\alpha]_D^{25}$ −61° (*c* 0.36, CH_3OH); ir ($CHCl_3$ cast): 3360, 1681, 1600, 1060, 1040, 1020, 1010 cm^{-1}; ^1H nmr (CD_3OD) δ: 1.30 (3H, d (7 Hz), C-2 CH_3), 2.48 (3H, s, C-5 CH_3), 2.5 (1H, dq (J_d = 4 Hz, J_q = 7 Hz), C-2 H), 2.65 (3H, s, C-7 CH_3), 2.99 (2H, t (7 Hz), CH_2CH_2O), 3.62 (2H, t (7 Hz), CH_2CH_2O), 4.67 (1H, d (4 Hz), C-3 H), 7.34 (1H, s, ArH); ^{13}C nmr (DMSO-d_6) δ: 12.7, 13.3, 20.8 (CH_3); 32.0, 59.8, (CH_2); 53.1, 73.7, 124.3, (CH); 130.7, 135.5, 136.9, 144.0, 153.6, (C); 205.1, (C=O); ms *m/e* calcd. for $C_{14}H_{18}O_3$ (M^+): 234.1256; found: 234.1254 (55), 203 (100), 185 (21).

*Isolation of 3-Methyllumichrome (**17**)*

3-Methyllumichrome (**17**) eluted in Sephadex fractions 43–46 (50 mg). Silica gel column chromatography (chloroform–methanol, 50:1; 20 g of silica gel) of fractions 43–48 (66 mg) gave 3-methyllumichrome (**17**, 8 mg) as a yellow powder. This compound eluted prior to trisnorcybrodolide (**6**). Crystallization (acetone – Skellysolve B) gave fine yellow needles, mp >300°C (lit. (20) >300°C); uv (CH_3OH) λ_{max}: 250 (ε 9000), 337 (ε 2400), 383 nm (ε 2400); ir ($CHCl_3$ cast): 3170, 3060, 1680, 757, 678 cm^{-1}; ^1H nmr ($CDCl_3$) δ: 2.49 (3H, s, $ArCH_3$), 2.52 (3H, s, $ArCH_3$), 3.56 (3H, s, CH_3N), 7.76 (1H, bs, ArH), 8.06 (1H, bs, ArH), 8.7 (1H, bs, NH); ms *m/e* calcd. for $C_{13}H_{12}N_4O_2$ (M^+): 256.0959; found: 256.0959 (100), 199 (33), 171 (50), 156 (28).

*Preparation of 3-Methyllumichrome-N-oxide (**20**)*

Lumichrome (**18**, 2.5 g (21)) and 30% hydrogen peroxide (30 mL) in 99% formic acid (100 mL) were heated under reflux for 2 h. After cooling, the reactive mixture was made alkaline (saturated $NaHCO_3$) and the precipitate, lumichrome-10-*N*-oxide (**19**), was filtered off, washed with ethanol, water and acetone, and dried. The yield of crude product was 2.2 g (83%). Crude **19** (500 mg) and freshly distilled methyl iodide (20 mL) in

Can. J. Chem. Downloaded from www.nrcresearchpress.com by 210.87.254.5 on 09/06/12
For personal use only.

0.1 *N* aqueous sodium hydroxide (400 mL) were stirred for 4 days at room temperature. The organic layer was then removed and the aqueous layer acidified with glacial acetic acid. The yellow precipitate was filtered and recrystallized from dimethylformamide–water (3:7) to give 3-methyllumichrome-*N*-oxide (**20**, 300 mg), suitable for use in the next step.

Preparation of 3-Methyllumichrome (17)

3-Methyllumichrome-10-*N*-oxide (**20**, 100 mg, 0.37 mmol) and triphenylphosphine (200 mg, 0.76 mmol) in 1-propanol (100 mL) were heated at reflux for two days. The solvent was removed *in vacuo* and the residue was chromatographed over silica gel (chloroform, 130 g of silica gel) affording 3-methyllumichrome (**17**, 75 mg, 80%). Crystallization (acetone – Skellysolve B) gave fine yellow needles, mp >300°C, the physical properties of which were identical with those of the natural product (tlc, ir, ^{1}H nmr, ms).

Isolation of Broderol (21)

Broderol (**21**) eluted in Sephadex fractions 42 and 43 of the neutral extract. It was obtained in pure form as white flakes (17 mg) when these fractions were subjected to column chromatography (chloroform, 10 g of silica gel). Broderol (**21**) was only obtained in two early growths using Brodie's medium. The first isolation afforded 17 mg from 10 L of broth, the next harvest gave 2.5 mg from 20 L of broth. Broderol (**21**) was crystallized (carbon tetrachloride) affording white plates, mp 113–115°C; $[\alpha]_D^{25}$ −99 (*c* 0.09, CH_3OH); ir ($CHCl_3$ cast): 3400, 3360, 1660 (w), 1460, 1400, 1380, 1090, 1070, 1060, 1020, 800 cm^{-1}; ^{1}H nmr ($CDCl_3$) δ: 0.54 (1H, m), 0.68 (1H, m), 0.82 (1H, m), 0.88 (3H, s), 0.95 (1H, m), 0.97 (3H, s), 1.49 (3H, d (1 Hz)), 1.5–2.0 (5H, m), 3.25 (1H, dd (10.8, 2.5 Hz)), 3.52 (1H, dd (10.8, 1 Hz)), 5.70 (1H, bs); ^{1}H nmr (C_5D_5N) δ: 0.40 (1H, ddd (4.8, 6.4, 9.2 Hz)), 0.58 (1H, ddd (4.8, 6.4, 9.2 Hz)), 0.84 (3H, s), 0.92 (3H, s), 0.9 (2H, m), 1.40 (3H, d (1 Hz)), 1.72 (1H, dd (2.0, 10.8 Hz)), 1.90 (1H, d (12.4 Hz)), 2.10 (1H, dd (1.2, 12.4 Hz)), 2.11 (1H, dd (2.0, 4.8 Hz)), 2.27 (1H, ddd (2.8, 4.8, 10.8 Hz)), 3.28 (1H, dd (2.8, 10.0 Hz)), 3.54 (1H, dd (1.2, 10.0 Hz)), 6.02 (1H, q (1 Hz)); ^{13}C nmr ($CDCl_3$) δ: 14.5, 18.8, 21.3 (CH_3); 6.3, 8.7, 36.8, 50.6, 74.0, (CH_2); 53.5, 127.5, (CH); 27.9, 41.2, 76.1, 79.4, 133.7, (C); ms *m/e* calcd. for $C_{15}H_{22}O_2$ (M^+): 234.1620; found: 234.1615 (48), 205 (22), 161 (23), 159 (27), 151 (70), 149 (36), 137 (100), 135 (48), 134 (20), 124 (29), 123 (50), 122 (37), 121 (20), 119 (34), 109 (46), 107 (28), 105 (38), 97 (49), 96 (20), 93 (31), 91 (41), 79 (26), 77 (31), 69 (24), 55 (35).

Derivatization of Broderol (21) with Trichloroacetyl Isocyanate

A few drops of trichloroacetyl isocyanate were added to a chloroform-*d* solution of broderol (**21**, 1 mg) in an nmr tube; ^{1}H nmr ($CDCl_3$) δ: 0.90 (3H, s), 0.98 (3H, s), 1.49 (3H, d (1 Hz)), 3.26 (1H, d (10.8 Hz)), 3.55 (1H, d (10.8 Hz)), 6.11 (1H, bs), 8.25 (1H, s).

Acknowledgements

We wish to thank Dr. T. T. Nakashima and his associates for their help and advice in determining the nmr measurements, Dr. Alan Hogg and associates for the mass spectral measurements, and Drs. P. P. Singer and T. Reffstrup for their help and interest. We gratefully acknowledge the financial support of the Natural Sciences and Engineering Research Council of Canada in the form of operating grants (W.A.A.) and scholarships (R.H.M.).

1. W. A. Ayer and P. P. Singer. Phytochemistry. In press.
2. W. A. Ayer and R. H. McCaskill. Tetrahedron Lett. **21**, 1917 (1980).
3. W. A. Ayer and M. G. Paice. Can. J. Chem. **54**, 910 (1976).
4. M. G. Paice. M.Sc. Thesis, University of Alberta, Edmonton. 1975. pp. 83–97.
5. F. W. Wehrli and T. Wirthlin. Interpretation of carbon-13 nmr spectra. Heyden and Son. Ltd., New York. 1976. p. 311.
6. C. J. Pouchert and J. R. Campbell. The Aldrich library of nmr spectra. Vol. 5. Aldrich Chemical Co., Milwaukee, WI. 1974. p. 20.
7. G. Häfelinger, F. Hack, and G. Westermayer. Chem. Ber. **109**, 833 (1976).
8. L. M. Jackman and S. Sternhell. Applications of nuclear magnetic resonance spectroscopy in organic chemistry, 2nd ed. Pergamon Press, Oxford. 1969.
9. A. I. Scott. Interpretation of the ultraviolet spectra of natural products. Pergamon Press, Oxford. 1974. p. 119.
10. P. A. Grieco, S. Gilman, and M. Nishizawa. J. Org. Chem. **41**, 1485 (1976).
11. L. A. Singer and N. P. Kong. J. Am. Chem. Soc. **88**, 5213 (1966).
12. (*a*) H. Hikino, T. Takahashi, and T. Takemoto. Chem. Pharm. Bull. **20**, 212 (1972); (*b*) K. Yoshihina, M. Fukuoka, and M. Kuroyanagi. Chem. Pharm. Bull. **20**, 426 (1972).
13. M. Wij and S. Rangaswami. Indian J. Chem. **15B**, 16 (1977).
14. M. Kuroyanagi, M. Fukuoka, K. Yoshihira, and S. Natori. Chem. Pharm. Bull. **27**, 592 (1979).
15. M. Fukuoka, M. Kuroyanagi, K. Yoshira, and S. Natori. Chem. Pharm. Bull. **26**, 2365 (1978).
16. T. Money. Terpenoids and steroids (Specialist periodical reports). Vol. 4. *Edited by* K. H. Overton. The Chemical Society, London. 1974. p. 80.
17. D. V. Banthorpe and B. V. Charlwood. Terpenoids and steroids (Specialist periodical reports). Vol. 7. *Edited by* J. R. Hanson. The Chemical Society, London. 1977. pp. 192–193.
18. D. E. Cane and R. B. Nachbar. Tetrahedron Lett. **21**, 437 (1980).
19. F. Yoneda, Y. Sakuma, T. Nagamatsu, and S. Migumoto. J. Chem. Soc. Perkin Trans. I, 2398 (1976).
20. F. Müller and K. H. Dudley. Helv. Chim. Acta, **54**, 1487 (1971).
21. V. M. Berezovskii and L. S. Tul'chinskaya. J. Gen. Chem. USSR, (Engl. Transl.) **31**, 2592 (1961).
22. V. M. Berezovskii and Zh. I. Aksel'rod. Dokl. Chem. (Engl. Transl.) **168**, 506 (1966).
23. H. J. Brodie. The bird's nest fungi. University of Toronto Press, Toronto, Ont. 1975. p. 156.
24. I. R. Trehan, C. Monder, and A. K. Bose. Tetrahedron Lett. 67 (1968).
25. J. B. Stothers. Carbon-13 nmr spectroscopy. Academic Press, New York. 1972. pp. 161–163.
26. D. R. Taylor. Can. J. Chem. **54**, 189 (1976).
27. D. V. Demarco, E. Farkas, D. Doddrell, B. L. Mylari, and E. Wenkert. J. Am. Chem. Soc. **90**, 5480 (1968).
28. W. A. Ayer and R. H. McCaskill. Can. J. Chem. **59**, 2159 (1981).
29. W. C. Still, M. Kahn, and A. Mitra. J. Org. Chem. **43**, 2923 (1978).
30. J. Attenburrow, A. F. B. Cameron, J. H. Chapman, R. M. Evans, B. A. Hems, A. B. A. Jansen, and T. Walker. J. Chem. Soc. 1094 (1952).

The total synthesis of the cybrodins[1,2]

WILLIAM A. AYER AND ROBERT H. MCCASKILL
Department of Chemistry, University of Alberta, Edmonton, Alta., Canada T6G 2G2

Received February 3, 1981

WILLIAM A. AYER and ROBERT H. MCCASKILL. Can. J. Chem. **59**, 2159 (1981).

The total syntheses of cybrodol (**1**), isocybrodol (**2**), cybrodal (**3**), cybrodic acid (**4**), and trisnorcybrodolide (**5**), starting from 2-bromomesitylene (**6**) are described. The route involves oxidation of the 5-methyl group of **6** by means of chromyl acetate, addition of the β-hydroxyethyl chain by aryllithiation and reaction with ethylene oxide, and addition of the fifth carbon substituent by aryllithiation and treatment with ethyl chloroformate to give the key intermediate, methyl 3-(2-hydroxyethyl)-6-methoxymethyl-2,4-dimethylbenzoate (**18***d*). The latter was transformed into trisnorcybrodolide (**5**), and further elaborated via the corresponding aldehyde **21** into the remaining cybrodins.

WILLIAM A. AYER et ROBERT H. MCCASKILL. Can. J. Chem. **59**, 2159 (1981).

On décrit les synthèse totales du cybrodol (**1**), de l'isocybrodol (**2**), du cybrodal (**3**), de l'acide cybrodique (**4**) et du trisnorcybrodolide (**5**) à partir du bromo-2 mésitylène (**6**). Le cheminement implique l'oxydation du groupe méthyle en position 5 du composé **6** par l'acétate de chromyle, l'addition de la chaîne β-hydroxyéthyle par lithiation arylique et réaction avec l'oxyde d'éthylène et finalement l'addition du cinquième carbone substituant par une lithiation arylique suivie de l'action du chloroformate d'éthyle qui conduit à l'intermédiaire principal le (hydroxy-2 éthyl)-3 méthoxyméthyl-6 diméthyl-2,4 benzoate de méthyle (**18***d*). Ce composé peut être transformé en trisnorcybrodolide (**5**) et on peut aussi l'utiliser pour obtenir les autres cybrodines par l'intermédiaire de l'aldéhyde correspondant **21**.

[Traduit par le journal]

In the preceding paper we described the isolation and structure determination of cybrodol (**1**), isocybrodol (**2**), cybrodal (**3**), cybrodic acid (**4**), and trisnorcybrodolide (**5**), metabolites of the bird's nest fungus *Cyathus bulleri* Brodie (2). In this paper we report the synthesis of each of the compounds (collectively called the cybrodins), providing confirmation of the assigned structures.

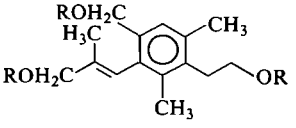

1 R = H
1*a* R = Ac

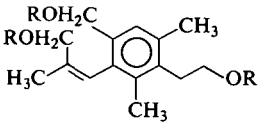

2 R = H
2*a* R = Ac

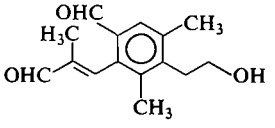

3

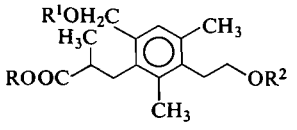

4 R = R¹ = R² = H
4*a* R = R¹ = CH₃, R²=H
4*b* R = CH₃, R¹ = R² = Ac

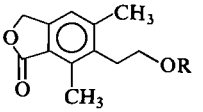

5 R = H
5*a* R = Ac

The approach to the synthesis of the cybrodins (Scheme 1) involves elaboration of a symmetrical diether A followed by addition of a one carbon unit at either of the equivalent unsubstituted centers to give B. This allows easy access to trisnorcybrodolide (**5**). Addition of a three carbon unit then provides the fifteen carbon cybrodin skeleton C.

The starting material for the preparation of the diether of type A (Scheme 1) was the readily available 2-bromomesitylene (**6**) (3). Chromyl acetate oxidation of toluenes is often a convenient route to benzylidene diacetates (4). Since 4-nitrotoluene is more readily oxidized than 2-nitrotoluene by chromyl acetate (5), we felt that **6** might

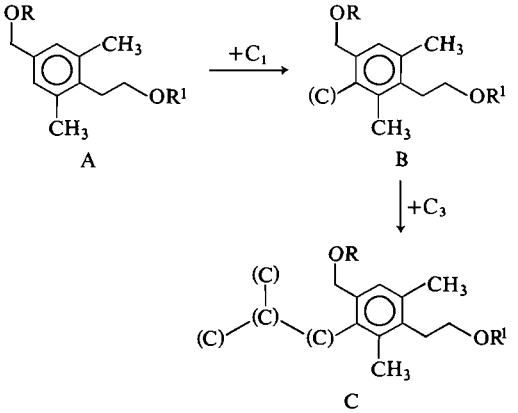

SCHEME 1

[1]Part 16 in the series Metabolites of Bird's Nest Fungi. For part 15 see preceding paper.

[2]A preliminary report on a portion of this work is contained in ref. 1.

0008-4042/81/142159-11$01.00/0

©1981 National Research Council of Canada/Conseil national de recherches du Canada

Can. J. Chem. Downloaded from www.nrcresearchpress.com by 210.87.254.105 on 09/06/12
For personal use only.

Can. J. Chem. Downloaded from www.nrcresearchpress.com by 210.87.254.105 on 09/06/12
For personal use only.

preferentially oxidize at the C-4 methyl group. Indeed, oxidation of **6** under controlled conditions (6) on a small (7 g) scale gave a 41% yield of crystalline diacetate **7**, the structure of which was apparent from the equivalence displayed in the ^1H and ^{13}C nmr spectra. When the reaction was carried out on a larger scale (100 g) a crystalline product was not obtained and ^1H nmr evidence indicated a mixture of **7** and the isomer **8** in a ratio of ca. 9:1. This mixture was normally used in the subsequent steps. Reduction of the mixture of **7** and **8** with lithium aluminum hydride (LAH) gave the corresponding alcohols **9** and **10** which were immediately transformed into the methyl ethers **11** and **12** by treatment with methyl iodide – sodium hydride. The methyl ethers **11** and **12** are separable by careful chromatography, but normally the mixture was carried forward into the next step. Nuclear magnetic resonance examination of the separated ethers **11** and **12** clearly demonstrates that the major product is the symmetrical bromoether **11**. One signal is seen for the aromatic methyl groups (^1H nmr δ 2.42, ^{13}C nmr δ 23.7) in **11**. The ^{13}C nmr has only four signals attributable to aromatic carbons. In contrast, the aromatic methyls of **12** are nonequivalent (^1H nmr δ 2.26, 2.35, ^{13}C nmr δ 20.8, 23.2) and six distinct aromatic carbon signals appear in the ^{13}C nmr spectrum.

A mixture of **11** and **12** (9:1) was lithiated (*n*-butyllithium) in tetrahydrofuran (THF)–hexane at room temperature and ethylene oxide was added. The major product, isolated by chromatography of the complex product mixture, was the alcohol **13**, resulting from Wittig rearrangement and protonolysis of the lithiated species. When this reaction was carried out at −78°C, however, the desired alcohol **14** was obtained in 66% yield after complexation with calcium chloride followed by distillation. The isomeric alcohol **15**, derived from bromoether **12**, did not contaminate this product. An authentic sample of **15** was prepared in low yield by lithiation of pure **12** and treatment with ethylene oxide overnight at −5°C. Presumably the aryllithium **16** reacts sluggishly due to intramolecular complexation with the ethereal oxygen, and at −78°C no reaction occurs with the ethylene oxide. In agreement with the assigned structure, alcohol **14** shows only one aromatic methyl signal (6H) and one sharp aromatic proton peak (2H).

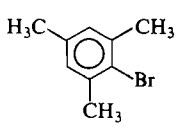

6

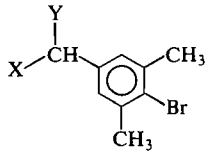

7 X = Y = OAc
9 X = OH, Y = H
11 X = OCH_3, Y = H

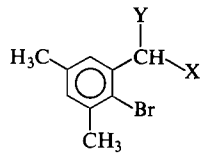

8 X = Y = OAc
10 X = OH, Y = H
12 X = OCH_3, Y = H

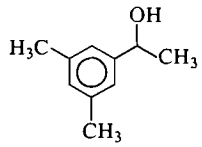

13

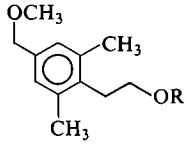

14 R = H
14*a* R = Ac

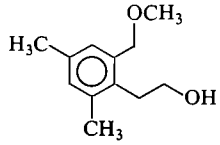

15

We now turned our attention to the introduction of the fifth substituent on to the aromatic ring. Attempted Rieche formylation of the acetyl derivative (**14***a*) of alcohol **14** with α,α-dichloromethyl methyl ether and titanium tetrachloride (7) gave the benzylic chloride as the only product. When stannic chloride was used as the catalyst an intractable mixture of highly polar products was formed. Because of the known liability of benzyl methyl ethers to Wittig rearrangement (8) direct lithiation of **14***a* was not attempted, instead bromination followed by metal exchange was utilized. Treatment of **14** with bromine in nitromethane at 0°C gave bromoalcohol **18** in 94% yield. The alcohol function of **18** was then protected as the tetrahydropyranyl (THP) ether (**18***a*). Treatment of the bromide **18***a* with *n*-butyllithium gave the aryllithium **18***b* which was caused to react with methyl chloroformate (0°C) to give the ester **18***c* in 62% yield.

Olah *et al.* have reported that iodotrimethylsilane, generated *in situ* from chlorotrimethylsilane and sodium iodide in acetonitrile, will convert methyl esters to silyl esters, cleave methyl ethers to alcohols, and transform benzylic alcohols to iodides (9). We reasoned that exposure of **18***c* to this reagent might afford intermediate **19**, a species which should be well suited to lactonization and thus formation of trisnorcybrodolide (**5**) or a derivative thereof. The fate of the THP ether was unclear from Olah's results.

Treatment of **18***c* with the Olah reagent (9) gave a mixture of products from which trisnorcybrodolide (**5**) was isolated in 11% yield. The major product (60%) was the primary iodide **20**, likely formed from **5** by the action of excess reagent. In order to

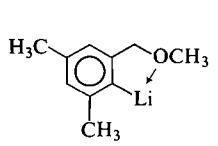
16

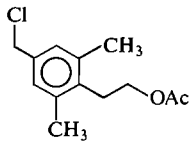
17

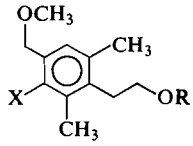
18 R = H, X = Br
18*a* R = THP, X = Br
18*b* R = THP, X = Li
18*c* R = THP, X = CO_2CH_3
18*d* R = H, X = CO_2CH_3
18*e* R = Ac, X = CO_2CH_3

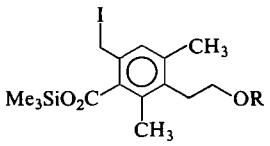
19

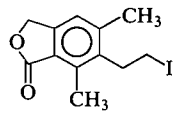
20

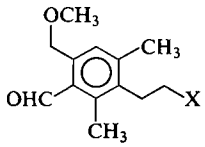
21 X = OTHP

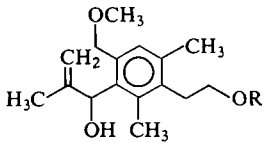
22 R = THP
22*a* R = H

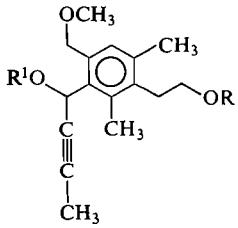
23 R = THP, R^1 = H
23*a* R = H, R^1 = CH_3

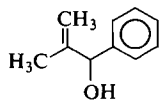
24

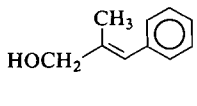
25

avoid this side reaction, the THP protecting group was replaced by an acetyl group (methanolysis of **18***c* to **18***d* and acetylation to give **18***e*). Exposure of **18***e* to Olah's reagent in refluxing acetonitrile gave *O*-acetyltrisnorcybrodolide (**5***a*) which was hydrolyzed (K_2CO_3–CH_3OH) directly to trisnorcybrodol (**5**), identical with the natural product, in an overall yield of 75%.

In order to introduce the three carbons necessary for the elaboration of the side chain of the remaining cybrodins, the ester **18***c* was transformed (LAH reduction, pyridinium chlorochromate oxidation) to the aldehyde **21** in 76% overall yield. The first attempt at introducing the functionalized side chain involved treatment of **21** with isopropenyllithium prepared from 2-bromopropene (10). The product, isolated in low (15%) yield, was not the expected allylic alcohol **22** but the propargylic alcohol **23**. Removal of the THP group of **23** (pyridinium tosylate – methanol) was accompanied by solvolysis of the propargylic alcohol to give the hydroxy diether **23***a*. Neither **23** nor **23***a* show acetylenic triple bond stretching in the ir, but this is not too unusual for internal acetylenes (11). The presence of the triple bond in **23** was indicated by the ^{13}C nmr spectrum, which shows fully substituted carbons at δ 83.0 and δ 108.4, and most indicatively, a methyl signal at δ 3.8 (12). The alkyne methyl group is seen in the ^1H nmr spectrum of **23***a* as a doublet (δ 1.83, J = 3 Hz) coupled to the propargyl ether proton at δ 5.38 (J = 3 Hz). This is typical of acetylenic systems where protons on the α and α′ carbons usually couple by ~3 Hz (13). Presumably **23** arises by condensation with 1-lithiopropyne, formed from 1-propyne, which in turn results from dehydrohalogenation of 2-bromopropene by initially formed isopropenyllithium.

The desired allylic alcohol **22** was obtained in 80% yield by addition of isopropenylmagnesium bromide to aldehyde **21**. Mild acid hydrolysis (pyridinium tosylate – aqueous THF) gave the diol **22***a* with analytical and spectral properties in full

Can. J. Chem. Downloaded from www.nrcresearchpress.com by 210.87.254.105 on 09/06/12
For personal use only.

Can. J. Chem. Downloaded from www.nrcresearchpress.com by 210.87.254.105 on 09/06/12
For personal use only.

accord with the assigned structure. The alcohol **22** was also prepared directly by the addition of the lithiated intermediate **18***b* to methacrolein, although the yield in this case was only twenty-five percent.

We now turned our attention to the allylic rearrangement of alcohol **22** which should lead directly to cybrodol and/or isocybrodol. Braude and Evans have reported that alcohol **24** is rearranged in ca. 50% yield to the alcohol **25**, which probably possesses the *E* stereochemistry shown (10). Accordingly, alcohol **22** was exposed to dilute sulfuric acid in refluxing 60% aqueous acetone. The THP ether was cleaved in short order as tlc examination revealed that diol **22***a* was formed within minutes. Over a period of several hours, the monitoring indicated the disappearance of diol **22***a* while two new products, **26** and **27**, were formed in an overall yield of 67%. Assignment of structure **26** followed readily from comparison of the ^{1}H nmr spectrum with that of cybrodol (1). Except for the presence of the *O*-methyl signal (δ 3.34) in the synthetic sample, the spectra are virtually superimposable. The second product was initially assigned structure **27***a*. However, when **27** was acetylated, it was the *benzylic alcohol rather than the allylic alcohol* which showed the typical acetylation shift. The assignment was verified by MnO_2 oxidation of **27** to the benzaldehyde, in which the aromatic proton, not the olefinic proton, undergoes a downfield shift (δ 7.11 → δ 7.60). The uv spectrum of **28** (λ_{max} 266, 310 nm) is very similar to that of mesitaldehyde (λ_{max} 264, 300 nm) (14). The formation of the rearranged ether **27** can be rationalized by the intermediacy of the cation **29** formed from an initially produced allylic carbonium ion.

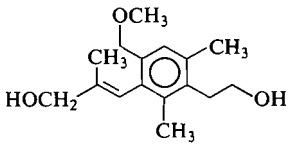

26

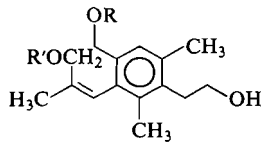

27 R = H, R′ = CH_3
27*a* R = CH_3, R′ = H

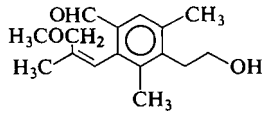

28

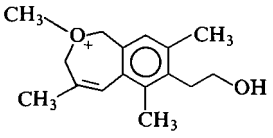

29

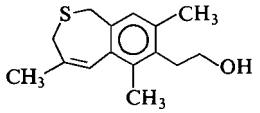

30

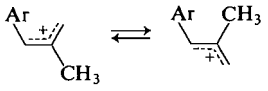

31*a* **31***b*

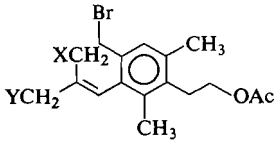

31 X = Br, Y = H
31*a* X = H, Y = Br

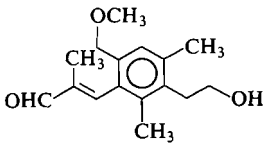

32

It now remained to cleave the methyl ethers in **26** and **27** to generate cybrodol (**1**) and isocybrodol (**2**), respectively. Treatment of isocybrodol methyl ether (**27**) with pyridine hydrochloride – acetic anhydride (15) gave only the diacetyl derivative. Use of Fujita's method (BF_3–ethanedithiol) (16) led to the interesting, although undesired, formation of a compound $C_{15}H_{20}OS$, assigned the cyclic sulfide structure **30** on the basis of its spectral characteristics.[3] Success in the ether cleavage was achieved using the method reported by Ganem and Small (18). When an acetic anhydride solution of **27** and ferric chloride was stirred overnight at room temperature the product (78% yield after chromatography) was a 4:1 mixture (as judged by nmr) of triacetylcybrodol (**1***a*) and triacetylisocybrodol (**2***a*). When cybrodol methyl ether (**26**) was treated in like fashion, the same product mixture resulted. Compounds **1***a* and **2***a* were difficult to separate and the crude product mixture was hydrolyzed (CH_3OH–K_2CO_3) and the resulting cybrodol (**1**) and isocybrodol (**2**) were separated by chromatography. The synthetic compounds were identical (tlc, ir, ^{1}H nmr, ms) with natural materials.[4] Since cybrobol (**1**) has previously been transformed to cybrodal (**3**), the above synthesis also represents a total synthesis of cybrodal.

The results of the $FeCl_3$ – acetic anhydride cleavage, and those from the earlier cited acid catalyzed isomerization of **22** to **26** and **27** imply the intermediacy of interconverting carbonium ions (**31***a*, **31***b*) in these reactions. In the present case the bulky acetoxyl groups (or lack of H-bonding) appear to bias the product distribution in favor of the *E* olefin geometry. Based on these results, we felt that a more direct route to cybrodol (**1**) might result from direct treatment of **22***a* with $FeCl_3$ – acetic anhydride. In the event, diol **22***a* afforded, after deacetylation, a 51% overall yield of **1** and **2** (ratio 7:3), providing a somewhat shorter but not more efficient (in terms of yield) sequence.

[3]For a discussion of the possible mechanism of this reaction, see ref. 17.

[4]Natural cybrodol was obtained as a clear oil which had resisted all attempts at crystallization. The synthetic material crystallized readily from $CHCl_3$–CH_3OH, mp 101–102°C. The natural material, which is optically inactive, crystallized when seeded with synthetic **1**.

Can. J. Chem. Downloaded from www.nrcresearchpress.com by 210.87.254.105 on 09/06/12
For personal use only.

Since isocybrodol (**2**) is the minor product in the above deprotection sequence, we desired a synthesis of **2** which avoids the substantial isomerization to the *E* geometry that occurs when isocybrodol methyl ether (**27**) is exposed to Ganem's conditions. When the diacetyl derivative of **27** was treated with boron tribromide in methylene chloride at −20°C the product mixture (86% total yield) consisted of a mixture of **31** and **31***a*, the desired isomer **31** representing >95% of the mixture as judged by ^{1}H nmr. Treatment of the mixture of **31** and **31***a* with tetraethylammonium acetate in acetone afforded triacetylisocybrodol (**2***a*) in greater than 90% yield. Since **2***a* is readily hydrolyzed to isocybrodol (**2**), this route offers the most economical synthesis of the latter.

Cybrodic acid (**4**) was prepared from cybrodol methyl ether (**26**) in the following manner. Activated manganese dioxide oxidation of **26** gave aldehyde **32** in quantitative yield. Treatment of **32** with sodium cyanide, acetic acid, and manganese dioxide in methanol (19) gave a 95% yield of the ester **4***a*, which when treated with Ganem's ferric chloride reagent (18) gave methyl diacetylcybrodate (**4***b*) in 77% yield. Saponification of **4***b* (KOH, CH_3OH, reflux) gave cybrodic acid (**4**, 97% yield), identical with the natural product.

The syntheses of cybrodol (**1**), isocybrodol (**2**), cybrodal (**3**), cybrodic acid (**4**), and trisnorcybrodolide (**5**) described herein serve to confirm the structures proposed (2) for these metabolites of *C. bulleri*.

Experimental

The general experimental details are described in the preceding paper (2). Elemental analyses were carried out by the microanalytical laboratory of this department or by Schwarzkopf Microanalytical Laboratory, New York.

4-Bromo-3,5-dimethylbenzylidene Diacetate (7)

2-Bromomesitylene (99.5 g, 0.5 mol), acetic acid (770 mL), and acetic anhydride (770 mL) were cooled to 0°C in an ice–salt bath. Concentrated sulfuric acid (115 mL) was added dropwise over a ten minute period to the mechanically stirred solution. After the solution temperature reached 5°C, chromium trioxide (135 g, 1.35 mol) was added in small portions over a period of one hour. During the addition period the solution temperature was maintained between 5 and 10°C. The mixture was stirred at 5°C for a further 30 min and then poured onto crushed ice (3 L). Water was added to bring the total volume to six litres. When the reaction was conducted on a smaller scale (7.16 g) a crude, semi-crystalline product (5.20 g) could be filtered off at this point. This material was used to obtain spectral data. On a larger scale the product was quite oily and could not be effectively isolated by filtration. Instead, the product was isolated by ether extraction (3 × 2 L). The extract was taken to dryness leaving a green semi-solid which was dissolved in ether (500 mL). This solution was washed with water (100 mL) and brine (100 mL). After drying over magnesium sulfate, filtration and evaporation to dryness gave a yellow semi-solid (147 g) which was used without purification in the next step.

The crude product from 7.16 g of 2-bromomesitylene was recrystallized (95% ethanol) affording pure **7** (4.65 g, 41%) as white prisms, mp 91–93°C. Sublimation of this material (80°C, 1 Torr) gave an analytically pure sample, mp 94–95°C (clear prisms); ir ($CHCl_3$ cast): 1751, 1240, 1205 cm^{-1}; ^{1}H nmr ($CDCl_3$) δ: 2.10 (6H, s, 2 × OAc), 2.43 (6H, s, 2 × $ArCH_3$), 7.20 (2H, s, 2 × ArH), 7.55 (1H, s, CH); ^{13}C nmr ($CDCl_3$) δ: 20.8 (2C), 23.9 (2C), (CH_3); 89.4, 126.3 (2C), (CH); 129.0, 134.0, 138.8 (2C)(C); 168.7 (2C), (C=O); ms *m/e* calcd. for $C_{13}H_{15}O_4{}^{81}Br$ (M + 2): 316.0133; found: 316.0140 (60); calcd. for $C_{13}H_{15}O_4{}^{79}Br$ (M^+): 314.0154; found: 314.0152 (64), 106 (100), 105 (48), 104 (77), 103 (56), 91 (28), 78 (33), 77 (65), 51 (21). *Anal.* calcd. for $C_{13}H_{15}O_4Br$: C 49.54, H 4.80, Br 25.35; found: C 49.52, H 4.78, Br 25.57.

4-Bromo-3,5-dimethylbenzyl Alcohol (9)

A solution of crude **7** (147 g) in anhydrous ether (750 mL) was added over a two hour period to a mechanically stirred slurry of lithium aluminum hydride (31 g, 0.82 mol) in anhydrous ether (1.2 L). The mixture was stirred for a further 90 min and then quenched by sequential dropwise addition of water (31 mL), 15% aqueous sodium hydroxide (31 mL), and water (93 mL). The solids, after removal by filtration, were washed with anhydrous ether (10 × 50 mL). The combined ether solutions were concentrated *in vacuo* leaving crude **9** (100 g) as a semi-solid which was used without purification in the next step.

Compound **9** has the following physical properties: ir ($CHCl_3$): 3600 cm^{-1}; ^{1}H nmr ($CDCl_3$) δ: 2.42 (6H, s, 2 × $ArCH_3$), 4.55 (2H, s, CH_2O), 7.03 (2H, s, 2 × ArH); ms *m/e* calcd. for $C_9H_{11}O^{81}Br$ (M + 2): 215.9973; found: 215.9973 (73); calcd. for $C_9H_{11}O^{79}Br$ (M^+): 213.9993; found: 213.9988 (77), 135 (73), 107 (100), 106 (60), 105 (32).

4-Methoxymethyl-2,6-dimethylbromobenzene (11)

To a magnetically stirred solution of crude **9** (100 g) and methyl iodide (100 g, 0.70 mol) in dry dimethoxyethane (200 mL), sodium hydride (57% in oil, washed with Skellysolve B; 17 g, 0.71 mol) was added in small portions over a 30 min period. The mixture was stirred for a further two hours at room temperature. The solution volume was reduced to 50 mL by distillation at atmospheric pressure, ether (200 mL) was added, and the salts were removed by filtration. The filter cake was extracted with ether (5 × 50 mL) and the combined ethereal solutions were concentrated leaving a brown oil (62.5 g). Polar impurities were removed by rapid passage of a Skellysolve B solution of this material through a short column of acidic alumina (200 g). The washings were concentrated to a yellow oil (57.3 g) which on distillation (100–105°C, 0.8 Torr) gave an 89:11 mixture (as judged by ^{1}H nmr) of 4-methoxymethyl-2,6-dimethylbromobenzene (**11**) and 2-methoxymethyl-4,6-dimethylbromobenzene (**12**) (50.5 g, 44% from 2-bromomesitylene). These isomers could be separated by flash chromatography (Skellysolve B – ether, 9:1; 1 g of sample/5 cm column), however, for synthetic purposes the mixture was used as such in the next step. A small sample of pure **11** was evaporatively distilled (80°C, 0.03 Torr) for microanalysis.

Compound **11** has the following physical properties: ir ($CHCl_3$ cast): 1105, 1030, 860 cm^{-1}; ^{1}H nmr ($CDCl_3$) δ: 2.42 (6H, s, 2 × $ArCH_3$), 3.38 (3H, s, CH_3O), 4.35 (2H, s, CH_2O), 7.04 (2H, s, 2 × ArH); ^{13}C nmr ($CDCl_3$) δ: 23.7 (2C), 58.0 (CH_3); 73.9 (CH_2); 127.4 (2C) (CH); 126.4, 136.9, 138.1 (2C) (C); ms *m/e* calcd. for $C_{10}H_{13}O^{81}Br$ (M + 2): 230.0129; found: 230.0113 (40); calcd. for $C_{10}H_{13}O^{79}Br$ (M^+): 228.0150; found: 228.0143 (40), 149 (100), 119 (24). *Anal.* calcd. for $C_{10}H_{13}OBr$: C 52.42, H 5.72, Br 34.88; found: C 52.40, H 5.67, Br 34.61.

Compound **12** has the following physical properties: ir (film): 1100 cm,$^{-1}$; ^{1}H nmr ($CDCl_3$) δ: 2.26 (3H, s, $ArCH_3$), 2.35 (3H, s, $ArCH_3$), 3.46 (3H, s, CH_3O), 4.48 (2H, s, CH_2O), 6.97 (1H, s, ArH), 7.08 (1H, s, ArH); ^{13}C nmr ($CDCl_3$) δ: 20.8, 23.2, 58.5

Can. J. Chem. Downloaded from www.nrcresearchpress.com by 210.87.254.105 on 09/06/12
For personal use only.

(CH_3); 74.5 (CH_2); 127.0, 130.6 (CH), 121.8, 136.6, 137.6, 137.9 (C); ms *m/e* calcd. for $C_{10}H_{13}O^{81}Br$ (M + 2): 230.0129; found: 230.0132 (30); calcd. for $C_{10}H_{13}O^{79}Br$ (M^+): 228.0150; found: 228.0156 (29), 149 (100), 119 (21), 104 (22).

*Attempted Preparation of **14** using* n*-Butyllithium at Room Temperature*

n-Butyllithium (8.8 *M* in hexane, 2.5 mL, 22 mmol) was added to a mixture of bromides **11** and **12** (4.35 g, 19 mmol) in dry tetrahydrofuran (20 mL) at room temperature under a nitrogen atmosphere. The mixture was stirred for one hour during which time a purple colour developed. Ethylene oxide (5 g, 0.11 mol) was distilled through a drying tube and condensed into the reaction vessel by means of a dry-ice condenser. The mixture was stirred at room temperature for one hour and then saturated aqueous ammonium chloride (10 mL) was added. The products were isolated by ether extraction (3 × 10 mL). The combined ether extracts were dried over magnesium sulfate, filtered, and concentrated to a brown oil (3.73 g). Thin-layer chromatographic examination of the reaction mixture revealed that compound **14** (*vide infra*) was not present. The major product, isolated as a clear oil by column chromatography (chloroform, 150 g of silica gel) was 1-(3,5-dimethylphenyl)ethanol (**13**, 1.06 g, 37%): ir (film): 3450 cm^{-1}; ^1H nmr ($CDCl_3$) δ: 1.49 (3H, d (7 Hz), CH_3CH), 2.32 (6H, s, 2 × $ArCH_3$), 4.82 (1H, q (7 Hz), $CHCH_3$), 6.90 (1H, s, ArH), 6.97 (2H, s, 2 × ArH); ms *m/e* calcd. for $C_{10}H_{14}O$ (M^+): 150.1045; found: 150.1047 (55), 135 (53), 107 (100), 91 (28).

*2-(4-Methoxymethyl-2,6-dimethylphenyl)ethanol (**14**)*

A magnetically stirred solution of *n*-butyllithium (1.6 *M* in hexane, 75 mL, 0.12 mol) in dry tetrahydrofuran (80 mL) was cooled to −78°C under a nitrogen atmosphere. A mixture of bromides **11** and **12** (25.0 g, 0.109 mol) in dry tetrahydrofuran (30 mL) was added over a period of 15 min causing a creamy white precipitate to form. The solution was stirred at −78°C for a further hour. Ethylene oxide (25 g, 0.57 mol), purified by passage through a drying tube (2 × 30 cm) containing potassium hydroxide and anhydrous calcium sulfate, was condensed in the reaction flask by means of a dry-ice condenser. Introduction of the ethylene oxide required one hour. The reaction mixture was stirred for an additional four hours. Saturated aqueous ammonium chloride (50 mL) was added and the mixture was allowed to warm to room temperature. Water (200 mL) was added to dissolve the salts and the organic layer was removed. The aqueous phase was extracted with ether (5 × 100 mL), the combined organic extracts were dried over magnesium sulfate, filtered, and concentrated. On a smaller scale (5 g of starting material) purification was conveniently achieved by column chromatography (chloroform, 100 g of silica gel) which afforded pure **14** (2.16 g, 51%). On the present scale, however, the above crude product (24.6 g) was dissolved in Skellysolve B (250 mL). Finely powdered anhydrous (dried overnight at 120°C) calcium chloride (50 g) was added and the mixture was cooled to −70°C for two hours. The solids were filtered off and washed with cold (0°C) Skellysovle B (3 × 30 mL). The filtrate was set aside and water (200 mL) was added to the filter cake. After 30 min, the aqueous solution was extracted with ether (3 × 200 mL). The ether extracts were dried over magnesium sulfate, filtered, and evaporated to dryness leaving crude alcohol **14** (15.2 g) as a viscous yellow oil. Distillation (120–130°C, 0.12 Torr) gave pure **14** (14.0 g, 66%): ir ($CHCl_3$ cast): 3400 cm^{-1}; ^1H nmr ($CDCl_3$) δ: 2.33 (6H, s, 2 × $ArCH_3$), 2.91 (2H, t (7 Hz), CH_2CH_2O), 3.37 (3H, s, CH_3O), 3.67 (2H, t (7 Hz), CH_2CH_2O), 4.35 (2H, s, CH_2OCH_3), 6.99 (2H, s, 2 × ArH); ^{13}C nmr ($CDCl_3$) δ: 20.0 (2C), 58.2 (CH_3); 32.8, 61.6, 74.7 (CH_2); 127.9 (2C), (CH); 134.3, 136.0, 137.1 (2C), (C); ms *m/e* calcd. for $C_{12}H_{18}O_2$ (M^+): 194.1307; found: 194.1310 (44), 163 (100), 132 (24). *Anal.* calcd. for $C_{12}H_{18}O_2$: C 74.19, H 9.34; found: C 74.03, H 9.36.

*2-(2-Methoxymethyl-4,6-dimethylphenyl)ethanol (**15**)*

n-Butyllithium (1.6 *M* in hexane, 0.63 mL, 1 mmol) was added to a solution of bromide **12** (200 mg, 0.87 mmol) in dry tetrahydrofuran (1 mL) at −78°C under a nitrogen atmosphere. The mixture was stirred at −78°C for one hour. Ethylene oxide (2 mL, 40 mmol) was added (cooled syringe) in one portion. The mixture was stirred at −78°C for 5 h and then left overnight at −5°C. The reaction mixture was diluted with water (20 mL) and extracted with ether (4 × 20 mL). The combined ether extracts were dried over sodium sulfate, filtered, and concentrated. Flash chromatography (methylene chloride – methanol, 100:1; 2 cm column) gave **15** as a clear oil (33 mg, 19%); ir (film): 3400 cm^{-1}; ^1H nmr ($CDCl_3$) δ: 2.26 (3H, s, $ArCH_3$), 2.29 (3H, s, $ArCH_3$), 2.92 (2H, t (7 Hz), CH_2CH_2O), 3.38 (3H, s, CH_3O), 3.76 (2H, t (7 Hz), CH_2CH_2O), 4.40 (2H, s, CH_2O), 6.95 (2H, s, 2 × ArH); ^{13}C nmr ($CDCl_3$) δ: 19.8, 20.7, 58.0 (CH_3); 32.1, 61.7, 73.7 (CH_2); 128.8, 131.6 (CH); 133.2, 135.6, 136.1, 137.3 (C); ms *m/e* calcd. for $C_{12}H_{18}O_2$ (M^+): 194.1306; found: 194.1313 (17), 149 (34), 133 (68), 132 (100).

*2-(4-Methoxymethyl-2,6-dimethylphenyl)ethyl Acetate (**14**a)*

Alcohol **14** (750 mg, 3.87 mmol), acetic anhydride (1 mL), and pyridine (1 mL) in methylene chloride (10 mL) were stirred overnight at room temperature. Evaporation to dryness gave **42** as a clear oil (863 mg): ir (film): 1740 cm^{-1}; ^1H nmr ($CDCl_3$) δ: 2.05 (3H, s, OAc), 2.36 (6H, s, 2 × $ArCH_3$), 2.98 (2H, t (7 Hz), CH_2CH_2O), 3.37 (3H, s, CH_3O), 4.15 (2H, t (7 Hz), CH_2CH_2O), 4.35 (2H, s, CH_2O), 6.98 (2H, s, 2 × ArH); ms *m/e* calcd. for $C_{14}H_{20}O_3$ (M^+): 236.1412; found: 236.1420 (35), 176 (100), 163 (43), 161 (59), 149 (20), 145 (36), 144 (21), 131 (20).

*2-(3-Bromo-4-methoxymethyl-2,6-dimethylphenyl)ethanol (**18**)*

A stirred solution of arene **14** (10.0 g, 51.5 mmol) in nitromethane (50 mL) was cooled to 0°C. Bromine (4.0 mL, 12.4 g, 78 mmol) in nitromethane (50 mL) was added dropwise over a 30 min period. The reaction mixture was stirred at 0°C for a further 30 min and then saturated aqueous sodium carbonate (50 mL) was added. Most of the nitromethane was removed *in vacuo* and the residue was extracted with ether (5 × 50 mL). The combined ether extracts were washed with water (50 mL) and brine (50 mL). After drying over magnesium sulfate, filtration and concentration gave bromide **18** (13.3 g, 94%) as a viscous orange oil. Attempted bulb to bulb distillation (150°C, 0.1 Torr) caused extensive decomposition. A small sample of crude **18** was crystallized from Skellysolve B – methylene chloride (1:1) affording buff coloured crystals, mp 101–106°C, which were sublimed (100°C, 0.023 Torr) giving analytically pure **18** (mp 104–106°C); ^1H nmr ($CDCl_3$) δ: 2.29 (3H, s, $ArCH_3$), 2.42 (3H, s, $ArCH_3$), 2.95 (2H, t (7 Hz), CH_2CH_2O), 3.42 (3H, s, CH_3O), 3.65 (2H, t (7 Hz), CH_2CH_2O), 4.44 (2H, s, CH_2OCH_3), 7.09 (1H, s, ArH); ms *m/e* calcd. for $C_{12}H_{17}O_2{}^{81}Br$ (M + 2): 274.0392; found: 274.0395 (1); calcd. for $C_{12}H_{17}O_2{}^{79}Br$ (M^+): 272.0411; found: 272.0403 (1), 243 (100), 241 (94), 213 (44), 211 (45), 132 (35), 131 (21), 115 (24), 91 (21). *Anal.* calcd. for $C_{12}H_{17}O_2Br$: C 52.76, H 6.27, Br 29.25; found: C 52.87, H 6.12, Br 29.13.

*1-Bromo-3-(2-(tetrahydro-2H-pyran-2-yl)oxyethyl)-6-methoxymethyl-2,4-dimethylbenzene (**18**a)*

A solution of alcohol **18** (18.05 g, 66.1 mmol), dihydropyran (17 mL, 15.7 g, 0.186 mol), and pyridinium tosylate (700 mg, 2.8 mmol) in methylene chloride (70 mL) was stirred at room temperature for one hour. The solution was washed with water (10 mL) and dried over magnesium sulfate. Filtration and evaporation to dryness gave crude ether **18***a* as a brown oil. Flash chromatography (Skellysolve B – ethyl acetate, 20:1) gave pure **18***a* (22.5 g, 95%) as a light yellow oil; ^1H nmr ($CDCl_3$) δ: 1.4–1.8 (6H, m, 3 × CH_2), 2.32 (3H, s, $ArCH_3$), 2.45 (3H, s, $ArCH_3$), 3.00 (2H, t (7 Hz), $ArCH_2CH_2$), 3.42 (3H, s, CH_3O), 3.5

Can. J. Chem. Downloaded from www.nrcresearchpress.com by 210.87.254.105 on 09/06/12
For personal use only.

(2H, m, CH_2O), 3.70 (2H, t (7 Hz), $ArCH_2CH_2$), 4.44 (2H, s, CH_2OCH_3), 4.56 (1H, bs, CH), 7.09 (1H, s, ArH); ms *m/e* calcd. for $C_{17}H_{25}O_3{}^{81}Br$ (M + 2): 358.0965; found: 358.0968 (2); calcd. for $C_{17}H_{25}O_3{}^{79}Br$ (M^+): 356.0965; found: 356.0988 (2), 274 (1), 272 (1), 85 (100).

*Methyl 3-(2-(Tetrahydro-2*H*-pyran-2-yl)oxyethyl)-6-methoxymethyl-2,4-dimethylbenzoate (**18***c*)

A solution of *n*-butyllithium (1.6 *M* in hexane, 44 mL, 70 mmol) in dry tetrahydrofuran (100 mL) was cooled to −78°C under a nitrogen atmosphere. Bromide **18***a* (22.5 g, 63.0 mmol) in dry tetrahydrofuran (20 mL) was added over a 10 min period, the mixture was then stirred at −78°C for a further 50 min. Freshly distilled methyl chloroformate (36 mL, 44 g, 0.47 mol) was rapidly injected (syringe) into the reaction pot. The solution was warmed to 0°C and kept at this temperature for 16 h. The reaction was quenched by addition of saturated aqueous sodium carbonate (50 mL) followed by water (100 mL). The organic phase was removed and the aqueous residue extracted with ether (3 × 50 mL). The combined organic extracts were dried over magnesium sulfate, filtered, and concentrated *in vacuo*. Flash chromatography (Skellysolve B – ethyl acetate, 3 : 1; 5 cm column; 5 runs) provided pure ester **18***c* (13.2 g, 62%) as a clear oil; ir ($CHCl_3$ cast): 1730 cm^{-1}; ^1H nmr ($CDCl_3$) δ: 1.4–1.8 (6H, m, 3 × CH_2), 2.31 (3H, s, $ArCH_3$), 2.37 (3H, s, $ArCH_3$), 2.98 (2H, t (7 Hz), $ArCH_2CH_2$), 3.30 (3H, s, CH_3OCH_2), 3.5 (2H, m, CH_2O), 3.75 (2H, t (7 Hz), $ArCH_2CH_2$), 3.87 (3H, s, CO_2CH_3), 4.38 (2H, s, CH_2OCH_3), 4.56 (1H, bs, CH), 7.00 (1H, s, ArH); ms *m/e* calcd. for $C_{19}H_{28}O_5$ (M^+): 336.1936; found: 336.1939 (1), 305 (6), 190 (28) 85 (100).

*Trisnorcybrodolide (5, 6-(2-Hydroxyethyl)-5,7-dimethylphthalide, Direct Route from **18**c)*

Chlorotrimethylsilane (140 μL, 120 mg, 1.1 mmol) was added to a solution of ester **18***c* (52 mg, 0.15 mmol) and sodium iodide (165 mg, 1.1 mmol) in dry acetonitrile (5 mL). The mixture was refluxed for one day under nitrogen, extra chlorotrimethylsilane (140 μL) was added, and reflux was continued for a further 24 h. The reaction mixture was cooled and then diluted with ether (100 mL). The ether solution was washed with water (3 × 10 mL), 10% aqueous sodium thiosulfate (10 mL), and saturated aqueous sodium bicarbonate (3 × 10 mL). After drying over sodium sulfate, filtration and concentration gave a crude product mixture (53 mg) which was subjected to ptlc (Skellysolve B – ethyl acetate, 3 : 1) affording two major components: R_f 0.33 (28 mg, 60%) and R_f 0.09 (3.4 mg, 11%).

The R_f 0.33 component (mp 182–184°C, Skellysolve B) was identified as 6-(2-iodoethyl)-5,7-dimethylphthalide (**20**) on the basis of the following spectral properties; ir ($CHCl_3$ cast): 1750 cm^{-1}; ^1H nmr ($CDCl_3$) δ: 2.43 (3H, s, $ArCH_3$), 2.67 (3H, s, $ArCH_3$), 3.2 (4H, m (A_2B_2), CH_2CH_2), 5.11 (2H, s, CH_2O), 7.08 (1H, s, ArH); ms *m/e* calcd. for $C_{12}H_{13}O_2I$ (M^+): 315.9960; found: 315.9949 (3), 189 (100).

The R_f 0.09 component was identical (tlc, ir, ^1H nmr, ms) with natural trisnorcybrodolide (**5**).

*Methyl 3-(2-Hydroxyethyl)-6-methoxymethyl-2,4-dimethylbenzoate (**18**d)*

A solution of tetrahydropyranyl ether **18***c* (303 mg, 0.902 mmol) and pyridinium tosylate (100 mg, 0.4 mmol) in methanol (5 mL) was stirred overnight at room temperature. The solvent was removed *in vacuo* and the residue was taken up in ether (100 mL) and then washed with water (10 mL) and brine (10 mL). After drying over sodium sulfate, filtration and concentration gave compound **18***d* (220 mg, 97%), a clear oil sufficiently pure for further work (*vide infra*). For the purpose of characterization, a small sample (500 mg) from a parallel run was chromatographed (Skellysolve B – ethyl acetate, 1 : 1; 20 g silica gel) affording pure **18***d* (450 mg). Evaporative distillation (110°C, 0.017 Torr) of a portion of this material provided an analytically pure sample; ir ($CHCl_3$ cast): 3440, 1727 cm^{-1}; ^1H nmr ($CDCl_3$) δ: 2.26 (3H, s, $ArCH_3$), 2.32 (3H, s, $ArCH_3$), 2.50 (1H, s, OH), 2.90 (2H, t (7 Hz), CH_2CH_2O), 3.28 (3H, s, CH_3OCH_2), 3.60 (2H, t (7 Hz), CH_2CH_2O), 3.85 (3H, s, CO_2CH_3), 4.36 (2H, s, CH_2OCH_3), 7.00 (1H, s, ArH); ms *m/e* calcd. for $C_{14}H_{20}O_4$ (M^+): 252.1362; found: 252.1363 (29), 221 (25), 207 (21), 205 (100), 189 (32). *Anal.* calcd. for $C_{14}H_{20}O_4$: C 66.65, H 7.99; found: C 66.75, H 7.87.

*Methyl 3-(2-Acetoxyethyl)-6-methoxymethyl-2,4-dimethylbenzoate (**18**e)*

A solution of alcohol **18***d* (*vide supra*, 330 mg) in acetic anhydride (4 mL) and pyridine (10 mL) was stirred at room temperature for three hours. Evaporation to dryness under high vacuum gave crude **18***e* (241 mg) as a brown oil which was purified by chromatography; ir (film): 1750, 1745 cm^{-1}; ^1H nmr ($CDCl_3$) δ: 2.01 (3H, s, OAc), 2.29 (3H, s, $ArCH_3$), 2.35 (3H, s, $ArCH_3$), 2.98 (2H, t (7 Hz), CH_2CH_2O), 3.30 (3H, s, CH_3OCH_2), 3.85 (3H, s, CO_2CH_3), 4.10 (2H, t (7 Hz), CH_2CH_2O), 4.36 (2H, s, CH_2OCH_3), 7.02 (1H, s, ArH); ms *m/e* calcd. for $C_{16}H_{22}O_5$ (M^+): 294.1468; found: 294.1472 (7), 263 (42), 262 (92), 247 (20), 234 (38), 219 (100), 207 (72), 203 (21), 189 (21), 187 (55).

*Trisnorcybrodolide (5) via Compounds **18**e and **5**a*

A mixture of crude **18***e* (241 mg), sodium iodide (1.2 g, 8 mmol), and chlorotrimethylsilane (1.0 mL, 856 mg, 7.9 mmol) in dry acetonitrile (20 mL) was refluxed under nitrogen for 24 h. Water (100 mL) was added and the product was extracted into ether (5 × 20 mL). The combined ether extracts were washed successively with water (20 mL), 10% aqueous sodium thiosulfate (20 mL), water (20 mL), and brine (20 mL). After drying over magnesium sulfate, filtration and concentration gave a brown powder. The major component of this crude product mixture was shown to be identical with the acetyl derivative (**5***a*) of natural trisnorcybrodolide (**5**) by tlc examination. Crude **5***a* and potassium carbonate (1.0 g) were taken up in methanol (10 mL) and stirred overnight at room temperature. The methanol was removed *in vacuo* and the residue was partitioned between ethyl acetate (100 mL) and water (10 mL). Nonpolar impurities were removed from the residue by trituration with methylene chloride (3 × 1 mL) leaving virtually pure trisnorcybrodolide (**5**, 139 mg, 74% overall from **18***c*). Recrystallization (methanol) gave colourless prisms, mp 189–191°C, which were sublimed (120°C, 0.015 Torr) providing an analytical sample. *Anal.* calcd. for $C_{12}H_{14}O_3$: C 69.89, H 6.84; found: C 69.87, H 7.05.

*3-(2-(Tetrahydro-2*H*-pyran-2-yl)oxyethyl)-6-methoxymethyl-2,4-dimethylbenzyl Alcohol*

Methyl ester **18***c* (7.07 g, 21.0 mmol) in dry ether (50 mL) was added over a 30 min period to a stirred slurry of lithium aluminum hydride (1.00 g, 26.3 mmol) in dry ether (100 mL). The mixture was stirred at room temperature for two hours and then quenched by dropwise addition of water (1 mL), 15% aqueous sodium hydroxide (1 mL), and water (3 mL). The granular precipitate was filtered off and washed with ether (5 × 50 mL). The combined ether solutions were concentrated leaving the crude title alcohol (6.5 g). Flash chromatography (Skellysolve B – ethyl acetate, 1 : 1; 5 cm column) afforded the pure alcohol (5.00 g, 77%) as a clear oil; ir ($CHCl_3$ cast): 3440 cm^{-1}; ^1H nmr ($CDCl_3$) δ: 1.4–1.8 (6H, m, 3 × CH_2), 2.36 (3H, s, $ArCH_3$), 2.46 (3H, s, $ArCH_3$), 2.70 (1H, t (7 Hz), OH), 3.03 (2H, t (7 Hz), $ArCH_2CH_2$), 3.42 (3H, s, CH_3O), 3.5 (2H, m, CH_2O), 3.75 (2H, t (7 Hz), $ArCH_2CH_2$), 4.48 (2H, s, CH_2OCH_3), 4.58 (1H, bs, CH), 4.66 (2H, d (7 Hz), CH_2OH), 6.95 (1H, s, ArH); ms *m/e* calcd. for $C_{18}H_{28}O_4$ (M^+): 308.1988; found: 308.1984 (1), 174 (21), 162 (34), 146 (32), 85 (100).

Can. J. Chem. Downloaded from www.nrcresearchpress.com by 210.87.254.105 on 09/06/12
For personal use only.

*3-(2-Tetrahydro-2*H*-pyran-2-yl)oxyethyl)-6-methoxymethyl-2,4-dimethylbenzaldehyde (**21**)*

A solution of the above alcohol (5.00 g, 16.2 mmol) in methylene chloride (10 mL) was added in one portion to a solution of pyridinium chlorochromate (5.40 g, 25 mmol) and sodium acetate (400 mg, 4.88 mmol) in methylene chloride (20 mL). The mixture was stirred at room temperature for one hour, diluted with ether (100 mL), and then filtered through Celite. The filter cake was washed with additional ether (5 × 30 mL). The combined filtrates were rapidly passed through a Florisil column (50 g). An extra portion of ether (200 mL) completely eluted the product. Concentration provided aldehyde **21** (4.85 g, 98%) sufficiently pure for further work; ir ($CHCl_3$ cast): 1690 cm^{-1}; ^1H nmr ($CDCl_3$) δ: 1.4–1.8 (6H, m, 3 × CH_2), 2.43 (3H, s, $ArCH_3$), 2.61 (3H, s, $ArCH_3$), 3.04 (2H, t (7 Hz), $ArCH_2CH_2$), 3.42 (3H, s, CH_3O), 3.5 (2H, m, CH_2O), 3.77 (2H, t (7 Hz), $ArCH_2CH_2$), 4.57 (1H, bs, CH), 4.69 (2H, s, CH_2OCH_3), 7.21 (1H, s, ArH), 10.54 (1H, s, CHO); ms *m/e* calcd. for $C_{18}H_{26}O_4$ (M^+): 306.1831; found: 306.1832 (15), 204 (37), 189 (24), 85 (100).

*1-((3-(2-(Tetrahydro-2*H*-pyran-2-yl)oxyethyl)-6-methoxymethyl-2,4-dimethyl)phenyl)-2-butyn-1-ol (**23**)*

2-Bromopropene (3.0 mL, 4.1 g, 34 mmol) was added to a suspension of finely divided lithium (1% sodium, 270 mg, 38.9 mmol) in dry ether (50 mL). The mixture was refluxed for three hours under nitrogen at which time little reaction (as indicated by dissolution of lithium) was evident. Extra lithium (200 mg, 28.8 mmol) was added and the mixture was stirred overnight. Aldehyde **21** (2.28 g, 7.45 mmol) in dry ether (10 mL) was added in one portion and the mixture was stirred for one hour. Saturated ammonium chloride (50 mL) was added and the products were extracted into ether (2 × 100 mL). After drying over magnesium sulfate, filtration, and concentration, the crude product was chromatographed (Skellysolve B – ether, 1 : 1; 150 g of silica gel) affording recovered starting material **21** (210 mg) and product **23** (391 mg, 15%) as a yellow oil; ir ($CHCl_3$ cast): 3400 cm^{-1}; ^1H nmr ($CDCl_3$) δ: 1.4–1.8 (6H, m, 3 × CH_2), 1.84 (3H, d (3 Hz), $CH_3C{\equiv}C$), 2.34 (3H, s, $ArCH_3$), 2.48 (3H, s, $ArCH_3$), 3.02 (2H, t (7 Hz), $ArCH_2CH_2$), 3.40 (3H, s, CH_3O), 3.5 (2H, m, CH_2O), 3.77 (2H, t (7 Hz), $ArCH_2CH_2$), 4.32 (1H, d (11 Hz), CH_2OCH_3), 4.60 (1H, bs, CH), 5.26 (1H, d (11 Hz), CH_2OCH_3), 5.85 (1H, bs, CHOH), 6.98 (1H, s, ArH); ms *m/e* calcd. for $C_{21}H_{30}O_4$ (M^+): 346.2144; found: 346.2142 (1), 85 (100).

*1-((3-(2-Hydroxyethyl)-6-methoxymethyl-2,4-dimethyl)phenyl)-1-methoxy-2-butyne (**23**a)*

A solution of compound **23** (106 mg, 0.306 mmol) and pyridinium tosylate (50 mg, 0.199 mmol) in methanol (5 mL) was stirred overnight at room temperature. Methanol was removed *in vacuo*, the residue was dissolved in chloroform (100 mL) and washed with water (10 mL). After drying over magnesium sulfate, filtration and concentration gave **23***a* (82 mg, 97%) as an oil; ir (film): 3400 cm^{-1}; ^1H nmr ($CDCl_3$) δ: 1.83 (3H, d (3 Hz), $CH_3C{\equiv}C$), 2.32 (3H, s, $ArCH_3$), 2.50 (3H, s, $ArCH_3$), 2.95 (2H, t (7 Hz), CH_2CH_2O), 3.33 (3H, s, CH_3O), 3.36 (3H, s, CH_3O), 3.67 (2H, t (7 Hz), CH_2CH_2O), 4.44 (1H, d (11 Hz), CH_2OCH_3), 4.60 (1H, d (11 Hz), CH_2OCH_3), 5.38 (1H, q (3 Hz), HCO), 7.00 (1H, s, ArH); ^{13}C nmr ($CDCl_3$) δ: 3.8, 16.2, 20.3, 56.2, 57.9 (CH_3); 33.2, 61.3, 73.1 (CH_2); 69.2, 129.5 (CH); 83.0, 108.4, 134.1, 134.2, 136.0, 136.7, 136.9 (C); ms *m/e* calcd. for $C_{17}H_{24}O_3$ (M^+): 276.1725; found: 276.1734 (2), 229 (100), 214 (32), 213 (22), 201 (33), 183 (21).

*1-((3-(2-(Tetrahydro-2*H*-pyran-2-yl)oxyethyl)-6-methoxymethyl-2,4-dimethyl)phenyl)-2-methyl-2-propen-1-ol (**22**)*

A solution of freshly distilled 2-bromopropene (7.1 mL, 9.67 g, 79.9 mmol) and 1,2-dibromoethane (0.9 mL, 1.96 g, 10.4 mmol) in dry tetrahydrofuran (30 mL) was added dropwise over a 30 min period to a magnetically stirred suspension of magnesium powder (2.20 g, 90.5 mmol) in dry tetrahydrofuran (10 mL) under a nitrogen atmosphere. The addition of the bromide solution caused vigorous boiling. Reflux was maintained for two hours after the addition was complete. The mixture was cooled to 0°C and then a solution of aldehyde **21** (5.00 g, 16.4 mmol) in dry tetrahydrofuran (30 mL) was added in one portion. The mixture was warmed to room temperature and then refluxed for two hours. The mixture was carefully poured over crushed ice (~500 g) and the products were isolated by ether extraction (5 × 100 mL). After drying over magnesium sulfate, filtration and concentration gave a brown oil (7.6 g). Flash chromatography (Skellysolve B – ethyl acetate, 5 : 1) afforded pure carbinol **22** (4.56 g, 80%) as a clear oil; ir ($CHCl_3$ cast): 3420, 1650, 900 cm^{-1}; ^1H nmr ($CDCl_3$) δ: 1.4–1.8 (6H, m, 3 × CH_2), 1.56 (3H, bs, vinyl CH_3), 2.30 (3H, s, $ArCH_3$), 2.36 (3H, s, $ArCH_3$), 2.98 (2H, t (7 Hz), $ArCH_2CH_2$), 3.26 (3H, s, CH_3O), 3.5 (2H, m, CH_2O), 3.72 (2H, t (7 Hz), $ArCH_2CH_2$), 4.11 (1H, d (11 Hz), CH_2OCH_3), 4.56 (1H, bs, CH), 4.75 (1H, d (11 Hz), CH_2OCH_3), 4.93 (1H, bs, vinyl H), 5.08 (1H, bs, vinyl H), 5.47 (1H, bs, HCOH), 6.91 (1H, s, ArH); ms *m/e* calcd. for $C_{21}H_{34}O_4$ (M^+): 348.2301; found: 348.2295 (2), 214 (46), 199 (57), 85 (100).

*1-((3-(2-Hydroxyethyl)-6-methoxymethyl-2,4-dimethyl)phenyl)-2-methyl-2-propen-1-ol (**22**a)*

A solution of tetrahydropyranyl ether **22** (890 mg, 2.56 mmol) and pyridinium tosylate (500 mg, 2 mmol) in water–tetrahydrofuran (1 : 2, 30 mL) was refluxed overnight. Most of the tetrahydrofuran was removed *in vacuo*, water (15 mL) was added, and the product was isolated by chloroform extraction (5 × 20 mL). After drying over magnesium sulfate, filtration and concentration gave diol **22***a* (657 mg, 97%). Evaporative distillation (100–120°C, 0.017 Torr) of a small sample (80 mg) afforded analytically pure material; ir ($CHCl_3$ cast): 3380, 1650, 900 cm^{-1}; ^1H nmr ($CDCl_3$) δ: 1.56 (3H, bs, vinyl CH_3), 2.26 (3H, s, $ArCH_3$), 2.32 (3H, s, $ArCH_3$), 2.90 (2H, t (7 Hz), CH_2CH_2O), 3.29 (3H, s, CH_3O), 3.63 (2H, t (7 Hz), CH_2CH_2O), 4.12 (1H, d (11 Hz), CH_2O), 4.73 (1H, d (11 Hz), CH_2O), 4.93 (1H, bs, vinyl H), 5.08 (1H, bs, vinyl H), 5.46 (1H, bs, HCOH), 6.91 (1H, s, ArH); ms *m/e* calcd. for $C_{16}H_{24}O_3$ (M^+): 264.1725; found: 264.1735 (4), 232 (100), 217 (85), 201 (67), 199 (25), 191 (66). *Anal.* calcd. for $C_{16}H_{24}O_3$: C 72.69, H 9.15; found: C 72.75, H 8.97.

*Direct Conversion of Bromide **18**a to Alcohol **22***

A solution of *n*-butyllithium (1.6 *M* in hexane, 10.6 mL, 17 mmol) in dry tetrahydrofuran (20 mL) was cooled to −78°C under nitrogen. A solution of bromide **18***a* (5.71 g, 16 mmol) in dry tetrahydrofuran (20 mL) was added and the mixture was stirred at −78°C for one hour. Freshly distilled methacrolein (6.6 mL, 5.6 g, 80 mmol) was added in one portion and the cooling bath was removed. The mixture was stirred at room temperature for five hours whereupon water (100 mL) was added. The organic layer was removed and the aqueous phase was extracted with ether (5 × 40 mL). The combined organic solutions were washed with brine (20 mL) and dried over sodium sulfate. Filtration and concentration gave a yellow oil (8.8 g) which was purified by flash chromatography (Skellysolve B – ethyl acetate, 5 : 1) affording alcohol **22** (1.38 g, 25%).

*Cybrodol Methyl Ether (**26**, 3-((3-(2-Hydroxyethyl)-6-methoxymethyl-2,4-dimethyl)phenyl)-2-methyl-(E)-2-propen-1-ol) and Isocybrodol Methyl Ether (**27**, 4-(2-Hydroxyethyl)-2-(3-methoxy-2-methyl-(Z)-1-propenyl)-3,5-dimethylbenzyl Alcohol)*

A mixture of alcohol **22** (610 mg, 1.75 mmol), 0.3 *M* aqueous sulfuric acid (16 mL), and acetone (24 mL) was heated at reflux for 7 h and then diluted with saturated aqueous sodium carbon-

Can. J. Chem. Downloaded from www.nrcresearchpress.com by 210.87.254.105 on 09/06/12
For personal use only.

ate (50 mL). The products were extracted into methylene chloride (5 × 25 mL), the organic extracts were dried over sodium sulfate, filtered, and evaporated to dryness. Flash chromatography of the residue (methylene chloride – methanol, 50:1; 3 cm column) gave isocybrodol methyl ether (**27**, 152 mg) and cybrodol methyl ether (**26**, 158 mg) as yellow oils (67% combined yield). An analytically pure sample of **26** was obtained by evaporative distillation (130–140°C, 0.027 Torr). Compound **27** has the following physical properties: ir ($CHCl_3$ cast): 3350, 1680 (2), 880 cm^{-1}; ^1H nmr ($CDCl_3$) δ: 2.00 (3H, d (1 Hz), vinyl CH_3), 2.19 (3H, s, $ArCH_3$), 2.38 (3H, s, $ArCH_3$), 2.99 (2H, t (7 Hz), CH_2CH_2O), 3.21 (3H, s, CH_3O), 3.48 (1H, d (11 Hz), CH_2OCH_3), 3.68 (1H, d (11 Hz), CH_2OCH_3), 3.76 (2H, t (7 Hz), CH_2CH_2O), 4.34 (1H, d (12 Hz), $ArCH_2OH$), 4.56 (1H, d (12 Hz), $ArCH_2OH$), 6.37 (1H, bs, vinyl H), 7.11 (1H, s, ArH); ms *m/e* calcd. for $C_{16}H_{24}O_3$ (M^+): 264.1725; found: 264.1723 (5), 232 (26), 219 (100), 217 (42), 202 (21), 201 (53), 197 (30), 191 (35), 187 (28), 183 (21), 171 (27), 157 (23).

Compound **26** has the following physical properties: ir ($CHCl_3$ cast): 3350, 1680 (2), 870 cm^{-1}; ^1H nmr ($CDCl_3$) δ: 1.44 (3H, d (1 Hz), vinyl CH_3), 2.20 (3H, s, $ArCH_3$), 2.37 (3H, s, $ArCH_3$), 2.99 (2H, t (7 Hz), CH_2CH_2O), 3.34 (3H, s, CH_3O), 3.74 (2H, t (7 Hz), CH_2CH_2O), 4.3 (4H, bs, 2 × CH_2O), 6.38 (1H, bs, vinyl H), 7.08 (1H, s, ArH); ms *m/e* calcd. for $C_{16}H_{24}O_3$ (M^+): 264.1725; found: 264.1730 (5), 233 (33), 232 (74), 217 (60), 201 (100), 199 (29), 187 (36), 183 (22), 171 (35), 157 (27). *Anal.* calcd. for $C_{16}H_{24}O_3$: C 72.69, H 9.15; found: C 72.35, H 9.39.

4-(2-Acetoxyethyl)-2-(3-methoxy-2-methyl-(Z)-1-propenyl)-3,5-dimethylbenzyl Acetate (27a)

Alcohol **27** (222 mg, 0.84 mmol), acetic anhydride (10 mL), and pyridine (10 mL) were stirred overnight at room temperature. Concentration under high vacuum gave compound **27a** (287 mg, 98%) as a yellow oil; ir ($CHCl_3$ cast): 1740 cm^{-1}; ^1H nmr ($CDCl_3$) δ: 1.95 (3H, d (1 Hz), vinyl CH_3), 2.06 (3H, s, OAc), 2.08 (3H, s, OAc), 2.21 (3H, s, $ArCH_3$), 2.37 (3H, s, $ArCH_3$), 3.01 (2H, t (7 Hz), CH_2CH_2O), 3.15 (3H, s, CH_3O), 3.59 (2H, s, CH_2O), 4.14 (2H, t (7 Hz), CH_2CH_2O), 4.85 (1H, d (12 Hz), $ArCH_2O$), 5.01 (1H, d (12 Hz), $ArCH_2O$), 6.25 (1H, bs, vinyl H), 7.02 (1H, s, ArH); ms *m/e* calcd. for $C_{20}H_{28}O_5$ (M^+): 348.1937; found: 348.1944 (1), 288 (49), 273 (23), 213 (41), 201 (22), 199 (22), 197 (100), 196 (87), 185 (21), 183 (43), 181 (21).

4-(2-Hydroxyethyl)-2-(3-methoxy-2-methyl-(Z)-1-propenyl)-3,5-dimethylbenzaldehyde (28)

Isocybrodol methyl ether (**27**, 27 mg, 0.10 mmol) and activated manganese dioxide (500 mg, 5.7 mmol) in methylene chloride (10 mL) were stirred for two hours at room temperature. The mixture was filtered through Celite and the filter cake was washed with ether (5 × 50 mL). The combined filtrates were concentrated and the residue was purified by flash chromatography (methylene chloride – methanol, 100:1; 1 cm column) affording **28** as a clear oil (25 mg, 93%); uv (CH_3OH) λ_{max}: 208, 266, 310 nm; ir ($CHCl_3$ cast): 3440, 1684 cm^{-1}; ^1H nmr ($CDCl_3$) δ: 2.01 (3H, d (1 Hz), vinyl CH_3), 2.25 (3H, s, $ArCH_3$), 2.40 (3H, s, $ArCH_3$), 3.04 (2H, t (7 Hz), CH_2CH_2O), 3.10 (3H, s, CH_3O), 3.58 (2H, bs, CH_2OCH_3), 3.76 (2H, t (7 Hz), CH_2CH_2O), 6.47 (1H, bs, vinyl H), 7.60 (1H, s, ArH), 9.38 (1H, s, CHO); ms *m/e* calcd. for $C_{16}H_{22}O_3$ (M^+): 262.1569; found: 262.1568 (3), 217 (100).

Attempted Demethylation of 27 with Ethanedithiol

Isocybrodol methyl ether (**27**, 16.8 mg, 0.064 mmol) and boron trifluoride etherate (30 μL, 34 mg, 0.24 mmol) in ethanedithiol (0.5 mL) were stirred at room temperature for four days. The solution was diluted with brine (10 mL) and extracted with methylene chloride (3 × 10 mL). The combined organic solutions were washed with 20% aqueous sodium hydroxide (2 × 10 mL), brine (10 mL), and dried over sodium sulfate. Filtration and concentration gave a foul smelling oil which was subjected to ptlc (benzene–ether, 1:3) affording 5-(2-hydroxyethyl)-4,6,10-trimethyl-2*H*-benzothiapin (**30**) as a clear oil (10 mg, 63%); ir ($CHCl_3$ cast): 3360 cm^{-1}; ^1H nmr ($CDCl_3$) δ: 2.06 (3H, d (1 Hz), vinyl CH_3), 2.20 (3H, s, $ArCH_3$), 2.34 (3H, s, $ArCH_3$), 2.81 (2H, s, CH_2S), 2.96 (2H, t (7 Hz), CH_2CH_2O), 3.43 (2H, s, $ArCH_2S$), 3.74 (2H, t (7 Hz), CH_2CH_2O), 6.34 (1H, s vinyl H), 6.93 (1H, s, ArH); ms *m/e* calcd. for $C_{15}H_{20}OS$ (M^+): 248.1235; found: 248.1232 (78), 233 (22), 217 (13), 207 (100). Chemical ionization (NH_3) ms shows a peak at *m/e* 266 (M + 18).

Cybrodol (1, 3-((3-(2-Hydroxyethyl)-6-hydroxymethyl-2,4-dimethyl)phenyl)-2-methyl-(E)-2-propen-1-ol) and Isocybrodol (2, 3-((3-(2-Hydroxyethyl)-6-hydroxymethyl-2,4-dimethyl)phenyl)-2-methyl-(Z)-2-propen-1-ol)

A solution of alcohol **27**[5] (201 mg, 0.76 mmol) and ferric chloride (100 mg, 0.62 mmol) in acetic anhydride (5 mL) was stirred for 18 h at room temperature. The mixture was diluted with water (50 mL) and then extracted with methylene chloride (5 × 20 mL). In a preliminary experiment (88 mg of **26**) the methylene chloride extracts were dried over sodium sulfate, filtered, and concentrated. Flash chromatography (Skellysolve B – acetone, 8:1; 1 cm column) gave an inseparable mixture of triacetylcybrodol (**1a**) and triacetylisocybrodol (**2a**, 98 mg total, 78%). The relative proportions were 78:22 in favor of the *E* isomer **1a** as determined by ^1H nmr. Normally, however, the wet methylene chloride extracts were taken to dryness under high vacuum and then dissolved in methanol (10 mL). Potassium carbonate (1 g) was added and the mixture was stirred at room temperature overnight. The volatiles were removed *in vacuo* and the residue was partitioned between ethyl acetate (50 mL) and water (10 mL). The organic phase was dried over sodium sulfate, filtered, and concentrated. Flash chromatography (methylene chloride – methanol, 20:1; 2 cm column) gave isocybrodol (**2**, 32 mg) and cybrodol (**1**, 111 mg, 75% combined overall yield) as oils. These materials were identical in all respects (tlc, ir, ^1H nmr, ms) with the natural products. Synthetic cybrodol (**1**) was crystallized (chloroform–methanol, 50:1) affording white prisms, mp 109–110°C. Synthetic isocybrodol (**2**) was crystallized (acetone – Skellysolve B) affording white prisms, mp 101–102°C. Analytically pure samples of both compounds were prepared by evaporative distillation (140–160°C, 0.025 Torr). Cybrodol (**1**), *Anal.* calcd. for $C_{15}H_{22}O_3$: C 71.97, H 8.86; found: C 72.27, H 9.08. Isocybrodol (**2**), *Anal.* calcd. for $C_{15}H_{22}O_3$: C 71.97, H 8.86; found: C 72.21, H 9.09.

Allylic Rearrangement of 22 with Ferric Chloride in Acetic Anhydride

A solution of alcohol **22** (103 mg, 0.39 mmol) and ferric chloride (50 mg, 0.31 mmol) in acetic anhydride (5 mL) was stirred for 18 h at room temperature. This reaction mixture was treated in exactly the same fashion as the previous one. In this instance, after deacetylation and flash chromatography, isocybrodol (**2**, 15.3 mg) and cybrodol (**1**, 34.3 mg, combined overall yield of 51%) were obtained as oils.

3-((3-(2-Acetoxyethyl)-6-bromomethyl-2,4-dimethyl)phenyl)-2-methyl-(Z)-2-propenyl Bromide (31) and 3-((3-(2-Acetoxyethyl)-6-bromomethyl-2,4-dimethyl)phenyl)-2-methyl-(E)-2-propenyl Bromide (31a)

A solution of boron tribromide (200 mg, 0.80 mmol) in dry methylene chloride (1 mL) was added to a solution of diacetyl methyl ether **27** (105 mg, 0.30 mmol) in dry methylene chloride (12 mL) at −20°C. The mixture was stirred under nitrogen at −20°C for one hour and then diluted with saturated aqueous

[5]Compound **26** or mixtures of compounds **26** and **27** may be used with the same results.

Can. J. Chem. Downloaded from www.nrcresearchpress.com by 210.87.254.105 on 09/06/12
For personal use only.

sodium carbonate (20 mL). The organic layer was removed and the aqueous residue was extracted with methylene chloride (3 × 20 mL). The combined extracts were dried over sodium sulfate, filtered, and concentrated leaving dibromide **31** as an orange oil (114 mg, 86%). This material contained a small amount (< 5%) of isomer **31***a* as judged by ^{1}H nmr. In a preliminary experiment, the reaction was conducted at 0°C resulting in the production of **31** and **31***a* in a 3 : 1 ratio as determined by ^{1}H nmr. Compounds **31** and **31***a* have practically identical tlc characteristics, however, careful ptlc (Skellysolve B – acetone, 20 : 1; double elution) of this 3 : 1 mixture did allow isolation of sufficient quantities for spectral analysis of each compound (brownish oils). Compound **31** has the following physical properties: ir ($CHCl_3$ cast): 1740, 1240, 605 cm^{-1}; ^{1}H nmr ($CDCl_3$) δ: 2.05 (3H, s, OAc), 2.10 (3H, d (1 Hz), vinyl CH_3), 2.23 (3H, s, $ArCH_3$), 2.35 (3H, s, $ArCH_3$), 3.00 (2H, t (7 Hz), CH_2CH_2O), 3.70 (2H, s, CH_2Br), 4.14 (2H, t (7 Hz), CH_2CH_2O), 4.29 (1H, d (11 Hz), $ArCH_2Br$), 4.46 (1H, d (11 Hz), $ArCH_2Br$), 6.35 (1H, bs, vinyl H), 7.07 (1H, s, ArH); ms *m/e* calcd. for $C_{17}H_{22}O_2{}^{81}Br$ (M − Br, parent ion not seen): 339.0783; found: 339.0802 (1); calcd. for $C_{17}H_{22}O_2{}^{79}Br$ (M − Br): 337.0803; found: 337.0799 (1), 217 (100). Compound **31***a* has the following physical properties: ir ($CHCl_3$ cast): 1740, 1240, 605 cm^{-1}; ^{1}H nmr ($CDCl_3$) δ: 1.60 (3H, d (1 Hz), vinyl CH_3), 2.05 (3H, s, OAc), 2.20 (3H, s, $ArCH_3$), 2.36 (3H, s, $ArCH_3$), 3.00 (2H, t (7 Hz), CH_2CH_2O), 4.14 (2H, t (7 Hz), CH_2CH_2O), 4.17 (2H, s, CH_2Br), 4.35 (2H, s, $ArCH_2Br$), 6.60 (1H, bs, vinyl H), 7.07 (1H, s, ArH); ms *m/e* calcd. for $C_{17}H_{22}O_2{}^{81}Br$ (M − Br, parent ion not seen): 339.0783; found: 339.0786 (77); calcd. for $C_{17}H_{22}O_2{}^{79}Br$ (M − Br): 337.0803; found: 337.0806 (79), 279 (99), 277 (100), 257 (38), 215 (27), 198 (92), 197 (76), 185 (63), 184 (42), 183 (53), 171 (47), 170 (34), 169 (38), 156 (31), 155 (45), 153 (20), 141 (23), 128 (20), 87 (30).

*Conversion of Dibromide **31** to Triacetylisocybrodol (**1**a)*

A solution of dibromide **31** (109 mg, 0.25 mmol) and tetraethylammonium acetate (500 mg, 2.7 mmol) in acetone (10 mL) was refluxed for one hour and then taken to dryness. The residue was dissolved in ether (50 mL), washed with water (10 mL) and brine (10 mL), and then dried over magnesium sulfate. Filtration and concentration gave triacetylisocybrodol (**2***a*, 91 mg, 97%). This material was deacetylated in the usual fashion and the product was purified by flash chromatography. In this way, isocybrodol (**2**, 55 mg) plus a small amount of cybrodol (**1**, 3 mg) were obtained.

*3-((3-(2-Hydroxyethyl)-6-methoxymethyl-2,4-dimethyl)phenyl)-2-methyl-(E)-2-propenal (**32**)*

Cybrodol methyl ether (**26**, 104 mg, 0.39 mmol) and activated manganese dioxide (622 mg, 7.1 mmol) in methylene chloride (10 mL) were stirred overnight at room temperature. The mixture was filtered through Celite, the filter cake was washed with methylene chloride (5 × 10 mL), and the combined filtrates were concentrated, leaving aldehyde **32** (103 mg, 100%) as a clear oil; ir ($CHCl_3$ cast): 3460, 2850, 1687, 1640 cm^{-1}; ^{1}H nmr ($CDCl_3$) δ: 1.57 (3H, d (1 Hz), vinyl CH_3), 2.18 (3H, s, $ArCH_3$), 2.38 (3H, s, $ArCH_3$), 3.00 (2H, t (7 Hz), CH_2CH_2O), 3.33 (3H, s, CH_3O), 3.74 (2H, t (7 Hz), CH_2CH_2O), 4.20 (2H, s, CH_2O), 7.12 (1H, s, ArH), 7.46 (1H, bs, vinyl H), 9.79 (1H, s, CHO); ms *m/e* calcd. for $C_{16}H_{22}O_3$ (M^+): 262.1571; found: 262.1597 (0.3), 217 (100).

*Methyl 3-((3-(2-Hydroxyethyl)-6-methoxymethyl-2,4-dimethyl)phenyl)-2-methyl-(E)-2-propenoate **4**a*

A mixture of aldehyde **32** (98 mg, 0.37 mmol), acetic acid (50 μL, 52 mg, 0.87 mmol), sodium cyanide (50 mg, 1 mmol), and activated manganese dioxide (1.4 g, 16 mmol) in methanol (10 mL) was stirred at room temperature for two days. The mixture was filtered through Celite and the filter cake was washed with ether (5 × 50 mL). The combined filtrates were washed with saturated aqueous sodium carbonate (20 mL), water (20 mL), and brine (20 mL). After drying over sodium sulfate, filtration and concentration gave methyl ester **4***a* (103 mg, 95%) as a clear oil; ir ($CHCl_3$ cast): 3400, 1720, 1640 cm^{-1}; ^{1}H nmr ($CDCl_3$) δ: 1.65 (3H, d (1 Hz), vinyl CH_3), 2.18 (3H, s, $ArCH_3$), 2.38 (3H, s, $ArCH_3$), 2.98 (2H, t (7 Hz), CH_2CH_2O), 3.35 (3H, s, CH_3O), 3.74 (2H, t (7 Hz), CH_2CH_2O), 3.82 (3H, s, CO_2CH_3), 4.22 (2H, s, CH_2O), 7.11 (1H, s, ArH), 7.64 (1H, bs, vinyl H); ms *m/e* calcd. for $C_{17}H_{24}O_4$ (M^+): 292.1674; found: 292.1670 (1), 260 (56), 247 (32), 229 (100), 201 (29), 171 (25).

*Methyl 3-((3-(2-Acetoxyethyl)-6-acetoxymethyl-2,4-dimethyl)phenyl)-2-methyl-(E)-2-propenoate (**4**b)*

A solution of ester **4***a* (50 mg, 0.17 mmol) and ferric chloride (50 mg, 0.31 mmol) in acetic anhydride (5 mL) was stirred for two hours at room temperature. The reaction mixture was diluted with water (20 mL) and the product was extracted into methylene chloride (5 × 10 mL). After the solution was washed and dried over sodium sulfate, filtration and concentration gave crude **4***b* (65 mg) as a brown oil. Flash chromatography (Skellysolve B – ethyl acetate, 3 : 1; 1 cm column) gave pure **4***b* as a clear oil (48 mg, 77%); ir ($CHCl_3$ cast): 1740, 1720 cm^{-1}; ^{1}H nmr ($CDCl_3$) δ: 1.65 (3H, d (1 Hz), vinyl CH_3), 2.05 (3H, s, OAc), 2.06 (3H, s, OAc), 2.20 (3H, s, $ArCH_3$), 2.39 (3H, s, $ArCH_3$), 3.03 (2H, t (7 Hz), CH_2CH_2O), 3.82 (3H, s, CO_2CH_3), 4.15 (2H, t (7 Hz), CH_2CH_2O), 4.90 (2H, bs, CH_2O), 7.07 (1H, s, ArH), 7.63 (1H, bs, vinyl H); ms *m/e* calcd. for $C_{20}H_{26}O_6$ (M^+): 362. 1729; found: 362.1719 (13), 302 (48), 289 (37), 288 (23), 259 (26), 243 (38), 242 (61), 229 (43), 228 (36), 227 (22), 215 (26), 201 (23), 200 (23), 199 (62), 183 (100), 171 (22), 151 (23).

*Cybrodic Acid (**4**, 3-((3-(2-Hydroxyethyl)-6-hydroxymethyl-2,4-dimethyl)phenyl)-2-methyl-(E)-2-propenoic Acid)*

A mixture of ester **4***b* (88 mg, 0.24 mmol), potassium hydroxide (1.2 g, 21 mmol), water (4 mL), and methanol (8 mL) was heated at reflux for 90 min. The solution was cooled to 0°C and acidified (~pH 1) with concentrated sulfuric acid. Brine (100 mL) was added and the product was isolated by ethyl acetate extraction (5 × 30 mL). The combined extracts were dried over sodium sulfate, filtered, and concentrated, leaving crude acid **4** (63 mg, 97%) as a brown oil which on prolonged refrigeration in acetone (2 mL) gave crystalline cybrodic acid (**4**, mp 179–180°C). This material was identical with the natural acid by the following criteria: mp, tlc, ir, ^{1}H nmr, and ms. Sublimation (160°C, 0.025 Torr) of the crystalline synthetic acid afforded an analytically pure sample. *Anal.* calcd. for $C_{15}H_{20}O_4$: C 68.16, H 7.63; found: C 68.18, H 7.62.

Acknowledgements

We wish to thank the Natural Sciences and Engineering Research Council of Canada for financial support in the form of research grants (W.A.A.) and scholarships (R.H.M.).

1. W. A. Ayer and R. H. McCaskill. Tetrahedron Lett. **21**, 1921 (1980).
2. W. A. Ayer and R. H. McCaskill. Can. J. Chem. **59**, 2150 (1981).
3. L. I. Smith. Org. Synth. Coll. Vol. 2. Wiley, New York. 1943. pp. 713–715.
4. K. B. Wiberg. *In* Oxidation in organic chemistry. Part A. *Edited by* K. B. Wiberg. Academic Press, New York. 1965. pp. 92–94.
5. T. Nishimura. Org. Synth. Coll. Vol. 4. Wiley, New York. 1963. pp. 713–715.

6. S. V. LIEBERMAN and R. CONNOR. Org. Synth. Coll. Vol. 2. Wiley, New York. 1943. pp. 441–443.
7. A. RIECHE, H. GROSS, and E. HÖFT. Org. Synth. Coll. Vol. 5. Wiley, New York. 1973. pp. 49–51.
8. H. W. GSCHWEND and H. R. RODRIGUEZ. *In* Organic reactions. Vol. 26. *Edited by* W. G. Dauben. Wiley, New York. 1979. pp. 1–360, especially pp. 43–77.
9. G. A. OLAH, S. C. NARANG, B. G. B. GUPTA, and R. MALHOTRA. J. Org. Chem. **44**, 1247 (1979).
10. E. A. BRAUDE and E. A. EVANS. J. Chem. Soc. 3333 (1956).
11. R. M. SILVERSTEIN, G. C. BASSLER, and T. C. MORRILL. Spectrometric identification of organic compounds. 3rd ed. John Wiley, New York. 1974. p. 89.
12. J. B. STOTHERS. Carbon-13 nmr spectroscopy. Academic Press, New York. 1972. pp. 86–90.
13. L. M. JACKMAN and S. STERNHELL. Applications of nuclear magnetic resonance spectroscopy in organic chemistry. Pergamon Press, Oxford. 1969. pp. 328–330.
14. A. I. SCOTT. Interpretation of the ultraviolet spectra of natural products. Pergamon Press, Oxford. 1964. p. 106.
15. N. P. PEET and R. CARGILL. J. Org. Chem. **38**, 1215 (1973).
16. M. NODE, H. HORI, and E. FUJITA. J. Chem. Soc. Perkin Trans. I. 2237 (1976).
17. R. H. MCCASKILL. Ph.D. Thesis, University of Alberta, Edmonton. 1980. p. 176.
18. B. GANEM and V. R. SMALL, JR. J. Org. Chem. **39**, 3728 (1974).
19. E. J. COREY, N. W. GILMAN, and B. E. GANEM. J. Am. Chem. Soc. **90**, 5616 (1968).

Can. J. Chem. Downloaded from www.nrcresearchpress.com by 210.87.254.105 on 09/06/12
For personal use only.

Activation parameters for transport and thermal expansion

ROBERT A. STAIRS

Department of Chemistry, Trent University, Peterborough, Ont., Canada K9J 7B8

Received November 11, 1980

ROBERT A. STAIRS. Can. J. Chem. **59**, 2170 (1981).

A correlation is proposed between the ratios: $Y = \pi\Delta V^{\ddagger}/E_{(p)}{}^{\ddagger}$ (where π is the internal pressure of a liquid, $\Delta V^{\ddagger}$ the volume of activation $RT(\partial \ln \eta/\partial p)_T$, and $E_{(p)}{}^{\ddagger}$ the activation energy at constant pressure for viscous flow, or the corresponding quantities for diffusion) and $X = E_{(p)}{}^{\ddagger}/E_\rho$ (where E_ρ is the "energy of thermal expansion", defined by: $-R[\partial \ln(\rho^{-1} - \rho_0{}^{-1})/\partial T^{-1}]_p$). The first, Y, involves quantities measured at high pressures, while X requires only measurements at ordinary pressure. The correlation will permit estimation of viscosities and diffusion coefficients at high pressures from low-pressure measurements.

ROBERT A. STAIRS. Can. J. Chem. **59**, 2170 (1981).

On propose une corrélation entre les raisons: $Y = \pi\Delta V^{\ddagger}/E_{(p)}{}^{\ddagger}$ (où π est la pression intèrnelle d'une liquide, $\Delta V^{\ddagger}$ est la volume d'activation, $RT(\partial \ln \eta/\partial p)_T$, et $E_{(p)}{}^{\ddagger}$ l'énergie d'activation à pression constante pour l'écoulement visqueux, ou les quantités correspondantes pour la diffusion) et $X = E_{(p)}{}^{\ddagger}/E_\rho$ (où E_ρ est "l'énergie d'expansion thermique", défini par: $-R[\partial \ln(\rho^{-1} - \rho_0{}^{-1})/\partial T^{-1}]_p$). La première, Y, comprend des propriétés qu'il faut mesurer à haute pression, mais X demande les mesures à la pression ordinaire seulement. La corrélation permettera l'estimation des viscosités et des coefficients de diffusion à haute pression à partir des mesures prises à basse pression.

Experiments conducted at high pressures are notoriously difficult and, therefore, expensive. It is highly desirable to be able to predict the results of high-pressure measurements using data obtained at low pressures only, using a reliable method of extrapolation. It would be better still if measurements at a single pressure, specifically at 1 atm, could be used for such predictions. For instance, knowledge of the dependence of viscosity of a liquid on pressure, especially at high pressures, is required in the study of convection in the Earth's mantle, of the movement of deep groundwater and of deep ocean currents. The measurement of viscosity as a function of temperature over moderate ranges at ordinary pressure is easy, but measurement of viscosity at extreme pressures is particularly difficult. High-pressure diffusion measurements are only a little easier.

Isobaric viscosity has in the past been considered from the points of view of the transition-state theory (1, 2) and of the free-volume theory (3, 4). Each has proponents claiming good fits of the data by their favoured equations, viz.

$$[1] \quad \ln \eta = \ln \eta^* + E_{(p)}{}^{\ddagger}/RT$$

and

$$[2a] \quad \eta^{-1} = B(V - V_0)/V_0$$

$$[2b] \quad = b(\rho^{-1} - \rho_0{}^{-1})$$

(In these equations η is viscosity, η^* a constant, $E_{(p)}{}^{\ddagger}$ is the energy of activation at constant pressure, R and T have their usual significance, B and b are empirical constants, V is the molar volume measured at the same temperature as η, V_0 is a constant, the intrinsic volume, and ρ and ρ_0 are the corresponding densities.)

For most non-associated liquids, not too close either to their critical temperatures or their freezing points, both equations are in fact very good, though Davies and Matheson (5) point out that with non-spherical molecules departures from both equations occur as rotation becomes restricted near the freezing point. Cleaver (6) and Macedo and Litovitz (7) have drawn attention to the role played by the volume of activation in viscosity and other transport properties of liquids of different types and suggest that, at low pressures,

$$E_{(p)}{}^{\ddagger} = E_{(v)}{}^{\ddagger} + (\alpha T/\beta)\Delta V^{\ddagger}$$
$$= E_{(v)}{}^{\ddagger} + \pi\Delta V^{\ddagger}$$

where $E_{(p)}{}^{\ddagger}$ and $E_{(v)}{}^{\ddagger}$ are the energies of activation at constant pressure and constant volume, α is the thermal coefficient of expansion, β the compressibility, π the internal pressure and $\Delta V^{\ddagger}$ the volume of activation, $RT[\partial \ln \eta/\partial p]_T$. That is to say, the empirical activation energy as usually measured at constant pressure consists of an energy apparently needed to create volume in order to permit flow, and another energy term, the origin of which Cleaver prudently leaves unspecified, "until an adequate theory of the liquid state is available". For most molecular liquids, the term $\pi\Delta V^{\ddagger}$ is a large fraction of $E_{(p)}{}^{\ddagger}$, i.e. $\pi\Delta V^{\ddagger} > E_{(v)}{}^{\ddagger}$. Flow in such liquids is described (6) as "volume restrained".

For some of these liquids, e.g. CCl_4, the term $E_{(v)}{}^{\ddagger}$ is very small. In these cases, one may make a connection between eqs. [1] and [2] by assuming a van't Hoff type dependence of free volume on temperature:

$$[3a] \quad \ln\left(\frac{V - V_0}{V_0}\right) = A - E_\rho/RT$$

0008-4042/81/142170-03$01.00/0

©1981 National Research Council of Canada/Conseil national de recherches du Canada

Can. J. Chem. Downloaded from www.nrcresearchpress.com by 210.87.254.42 on 09/06/12
For personal use only.

Can. J. Chem. Downloaded from www.nrcresearchpress.com by 210.87.254.42 on 09/06/12
For personal use only.

TABLE 1. Fit of the equation: $\ln(1/\rho - 1/\rho_0) = a - E_\rho/RT$ to data from the literature for the density of a number of liquids

Liquid	ρ_0 (g cm^{-3})	a	E_ρ (kJ)	s_ρ (g cm^{-3})	mp (K)	Range (K)	References
CCl_4*	1.77503	0.6784	8.36	0.0002	250	293 to 353	9, 10
$CHCl_3$	1.7335	0.2862	6.44	0.0005	210	233 to 313	11
c-C_6H_{12}	0.8681	1.3749	8.29	0.0001	280	273 to 333	11, 12
n-C_6H_{14}	0.78125	1.1906	6.51	0.0004	178	223 to 323	12
C_6H_6	0.97455	1.3542	8.65	0.0002	279	283 to 353	12, 13
C_6H_5Cl	1.2290	0.4807	7.04	0.0003	228	273 to 353	11, 13
Hg	13.830	−3.9709	6.14	0.0013	233	273 to 473	9, 11, 15
Ga	6.10	−3.010	10.6	0.02	303	323 to 1273	14, 15
Cl_2	1.696	1.6543	9.19	0.0003	172	238 to 303	11

*Inclusion of data for CCl_4 down to 233 K gives E_ρ = 6.5 kJ and moves the point for this liquid onto the plotted line, at the expense of much poorer fit of the density data: s_ρ = 0.0016 g cm^{-3}.

TABLE 2. Transport and expansion energy parameters compared. Data from the literature

Liquid	T (K)	π (GPa)	$\Delta V^\ddagger$ (10^{-6} m^3)	$\pi\Delta V^\ddagger$ (kJ)	$E_{(p)}{}^\ddagger$ (kJ)	E_ρ (kJ)	References
CCl_4	293	0.397	25.0	9.93	10.44	8.36*	9, 11
$CHCl_3$	293	0.400	13.5	5.40	7.32	6.44	9, 11
c-C_6H_{12}	303	0.316	34.5	10.90	12.14	8.29	9, 12, 13
n-C_6H_{14}	293	0.255	24.1	6.14	7.35	6.51	9, 12
C_6H_6	293	0.397	18.1	7.34	10.36	8.65	9, 13
C_6H_5Cl	293	0.406	16.5	6.70	8.86	7.04	9, 16
Hg	293	1.33	0.57	0.76	2.96	6.14	9, 15, 17, 18
Ga†	303	0.91	(0.65)‡	0.59	4.7	10.6	14, 15

*See footnote to Table 1.
†I have followed Cleaver (6) in using one set of data, for gallium, based on diffusion, since mercury is the only liquid in the "energy restrained" class for which data for viscosity as a function of pressure seem to be available.
‡Inferred from ref. 14.

or

$$[3b] \quad \ln(\rho^{-1} - \rho_0{}^{-1}) = a - E_\rho/RT$$

The "expansion energy" E_ρ represents work done against the internal pressure π, or if the external pressure is not small, against $\pi + P$, to create the volume needed for flow. (This terminology is loose (6, 8) but useful.) At low pressure it should be at least approximately equal to $\pi\Delta V^\ddagger$.

If one converts eq. [2a] into logarithmic form, and replaces $\ln[(V - V_0)/V_0]$ by the appropriate expression from eq. [3a], the result is of the form of eq. [1], with E_ρ in the place of $E_{(p)}{}^\ddagger$. Thus, it is suggested that for a "normal", molecular liquid, $E_{(p)}{}^\ddagger$, $\pi\Delta V^\ddagger$ and E_ρ should all be about equal.

For the other class of liquids, exemplified here by mercury and gallium, $\pi\Delta V^\ddagger$ is a small fraction of $E_{(p)}{}^\ddagger$. For these a mechanism must exist that does not require creation of free volume, but is more directly dependent on the availability of energy $E_{(v)}{}^\ddagger$. These liquids are termed "energy restrained" (6). For them the above analysis will fail.

The "expansion energy" E_ρ should be derived from fit of eqs. [3a], [3b] to molar volume or density data. Unfortunately it is not in a form convenient for least-squares fitting. Sets of three points, however, may be used to find values for ρ_0, by the requirement that the slope of the graph of $\ln(\rho^{-1} - \rho_0{}^{-1})$ vs. T^{-1} be constant. An average value may then be calculated. The other constants may then be found in a straightforward manner. Table 1 contains the results of applying this procedure to a number of liquids, chosen from Cleaver's "volume restrained" and "energy restrained" groups (see second footnote to Table 2). As the values of s_ρ, the standard error of estimate of density, indicate, the fit of eq. [3b] to the data is within or close to the claimed experimental error (judging by the number of significant figures in the sources) in all cases. For the "volume restrained" liquids, E_ρ is approximately equal to $\pi\Delta V^\ddagger$, and is only a little less than $E_{(p)}{}^\ddagger$ as may be seen in Table 2 and Fig. 1. (Omitting cyclohexane, the average ratios are $\pi\Delta V^\ddagger/E_\rho = 0.93 \pm 0.09$ and $E_\rho/E_{(p)}{}^\ddagger = 0.84 \pm 0.04$.). For these liquids, therefore, it is no surprise that they follow both the Arrhenius and the Batschinski–Hildebrand equations for viscosity. The other liquids, however, show another aspect. Each value of E_ρ, rather than being similar to $\pi\Delta V^\ddagger$ and smaller than $E_{(p)}{}^\ddagger$ is larger even than the latter quantity. The mechanistic implications of these facts seem to be that, on one hand, if creation of holes in the liquid of near-molecular size is relatively easy, then molecules can slip into these holes with little additional energy being required. On the other hand, if there exists a mode of flow that avoids the creation of

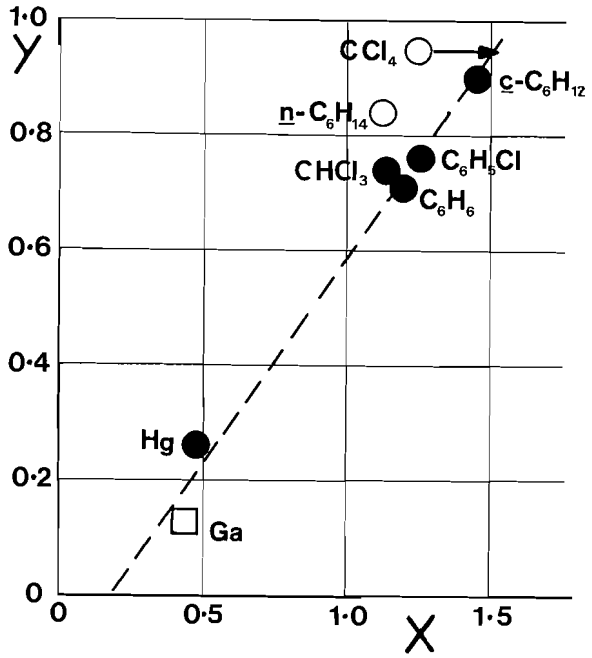

FIG. 1. Comparison of transport and expansion parameters. The ratios $Y = \pi\Delta V^{\ddagger}/E_{(p)}^{\ddagger}$ and $X = E_{(p)}^{\ddagger}/E_{\rho}$ as ordinate and abscissa. The square represents the self-diffusion of gallium, the circles viscosity data. The dashed line was drawn omitting the two open circles: the point for *n*-hexane because it was the only non-globular molecule, and the point for carbon tetrachloride because it was too uncertain (see footnote to Table 1).

large holes, flow will occur with a small volume of activation, but the energy of activation will arise from other sources. With the metals, it seems clear that the reason for this behaviour lies in the difference between the size of the ion, which is probably the entity for which free volume must be found, and the "atom", i.e. the ion plus its share of the common cloud of electrons. For the molecular liquids, $\Delta V^{\ddagger}$ is between one sixth and one third of the molar volume. For the metals it is less than one twentieth.

A consequence of the discrepancy between E_{ρ} and $E_{(p)}^{\ddagger}$ for the "energy restrained" liquids is that they cannot obey both viscosity equations. Mercury obeys eq. [1] and eq. [3*b*] better than it does eq. [2*b*]. Elimination of T between eqs. [1] and [3*b*] with $E_{\rho} \neq E_{(p)}^{\ddagger}$ leads to

$$\eta^{-r} = c(\rho^{-1} - \rho_0^{-1})$$

where c is a constant and $r = E_{\rho}/E_{(p)}^{\ddagger}$. For mercury, r is about 2. The graph of η^{-2} vs. ρ^{-1} is a somewhat better straight line than η^{-1} vs. ρ^{-1}, though η^{-3} vs. ρ^{-1} is better still: $s_{-1} = 0.030$, $s_{-2} = 0.026$, $s_{-3} = 0.008$ (s_{-r} is the standard error of estimate for η^{-r} vs. ρ^{-1} from 0 to 300°C).

A curious feature of the values of E_{ρ} obtained is that they are all rather similar, in spite of great differences in other properties between the various liquids. The mean and standard deviation of these nine values are 7.9 ± 1.6; compared to $\overline{E_{(p)}^{\ddagger}} = 8.0 \pm 3.5$ kJ mol^{-1} and $\overline{\pi\Delta V^{\ddagger}} = 6.0 \pm 4.2$ kJ mol^{-1}.

There appears to be potential utility in the correlation of $\pi\Delta V^{\ddagger}/E_{(p)}^{\ddagger}$ with $E_{(p)}^{\ddagger}/E_{\rho}$. The latter ratio contains only quantities measurable at ordinary pressure. The former ratio contains the constant-pressure quantity $E_{(p)}^{\ddagger}$ and two quantities that are pressure-related, the internal pressure π and $\Delta V^{\ddagger}$. The calculation of π requires the compressibility β, which is, however, known for a great many substances. The correlation described here permits, therefore, the estimation of the hard-to-obtain quantity $\Delta V^{\ddagger}$, and through it the prediction of the high-pressure viscosity and diffusion behaviour. That is to say, the high-pressure transport properties are now accessible by means of low-pressure measurements plus the state properties of the liquid.

Acknowledgements

This work was done in part while the author was a guest of the Department of Chemistry, University of Southampton, and supported in part by funds allotted from an institutional grant to Trent University from the Natural Sciences and Engineering Research Council of Canada. The manuscript was typed by Winnie Janzen.

1. H. EYRING. J. Chem. Phys. **4**, 283 (1936).
2. L. D. EICHER and B. J. ZWOLINSKI. Science, **177**, 369 (1972).
3. A. J. BATSCHINSKI. Z. Phys. Chem. **84**, 643 (1913).
4. J. H. HILDEBRAND. Science, **174**, 490 (1971); **178**, 1120 (1972).
5. D. B. DAVIES and A. J. MATHESON. J. Chem. Phys. **45**, 1000 (1966).
6. B. CLEAVER. Discuss. Faraday Soc. **43**, 241 (1967).
7. P. B. MACEDO and T. A. LITOVITZ. J. Chem. Phys. **42**, 245 (1965).
8. D. LAZARUS and N. H. NACHTRIEB. Solids under pressure. McGraw Hill, New York. 1963. p. 47.
9. International Critical Tables. McGraw-Hill, New York. 1927.
10. R. M. WAXLER and C. E. WEIR. J. Res. Natl. Bur. Std. **67A** (2), 163 (1963).
11. Landolt-Bornstein, 6th ed. Springer-Verlag, Berlin. 1969.
12. F. D. ROSSINI, K. S. PITZER, R. L. ARNETT, R. M. BAUM, and G. C. PIMENTEL. Selected values of physical and thermodynamic properties of hydrocarbons and related compounds. A.P.I., Carnegie Press, Pittsburgh. 1953.
13. J. TIMMERMANS. Physico-chemical constants of pure organic compounds. Elsevier, New York. 1950.
14. M. K. NAGARAJAN and J. O'M. BOCKRIS. J. Phys. Chem. **70**, 1854 (1966).
15. C. J. SMITHELLS. Metals reference book. Vol. 3. 4th ed. Butterworths, London. 1967.
16. J. MEYER and B. MYLIUS. Z. Phys. Chem. **95**, 355 (1920).
17. P. W. BRIDGMAN. Physics of high pressure. Bell, London. 1949.
18. G. V. SAMSONOV (*Editor*). Handbook of the physicochemical properties of the elements. I.F.I./Plenum, New York. 1968.

Can. J. Chem. Downloaded from www.nrcresearchpress.com by 210.87.254.42 on 09/06/12
For personal use only.

Ring size and positional constraints for μ-hydrido-bridging in dimethylcycloalkyl cations (n = 6–9)

R. P. KIRCHEN, K. RANGANAYAKULU, B. P. SINGH, AND T. S. SORENSEN[1]

The Department of Chemistry, University of Calgary, Calgary, Alta., Canada T2N 1N4

Received November 26, 1980

R. P. KIRCHEN, K. RANGANAYAKULU, B. P. SINGH, and T. S. SORENSEN. Can. J. Chem. **59**, 2173 (1981).

The *in situ* preparation and nmr characterization of a series of selected 1,*n*-dimethylcycloalkyl cations is reported. Both the 1,5-dimethylcyclononyl and the 1,5-dimethylcyclooctyl cations are assigned a μ-hydrido-bridged structure. However, the corresponding 1,4-dimethylcycloоctyl, 1,4-dimethylcycloheptyl, and 1,4-dimethylcyclohexyl cations are normal unbridged tertiary cations. The μ-hydrido-bridged cyclononyl cation rearranges in part to the 1-methyl-5-ethylcyclooctyl cation which is also μ-hydrido-bridged and this rearrangement can be followed by noting the disappearance of the δ −5.8 μ-H peak of the former and the appearance of a δ −6.4 μ-H peak for the latter. The 1,5-dimethylcyclooctyl cation is the most thermally stable μ-hydrido-bridged cation yet prepared and possesses a chair – twist boat (*TB*) conformation which is "frozen-out" in the nmr spectrum at −120°C. At higher temperatures one gets a chair–*TB* ⇌ *TB*–chair equilibration, $\Delta G^{\ddagger} = 30$ kJ mol^{-1} from nmr line-broadening observations.

R. P. KIRCHEN, K. RANGANAYAKULU, B. P. SINGH et T. S. SORENSEN. Can. J. Chem. **59**, 2173 (1981).

On rapporte la préparation *in situ* et l'identification à l'aide de la rmn d'une série choisie de cations diméthyl-1,*n* cycloalkyles. On attribue aux deux cations diméthyl-1,5 cyclononlye et diméthyl-1,5 cyclooctyle une structure contenant un pont μ-hydrido. Cependant les cations diméthyl-1,4 correspondants en séries cyclooctyle, cycloheptyle et cyclohexyle sont des cations tertiaires normaux n'impliquant pas de pont. Le cation cyclononyle μ-hydrido impliquant un pont se transpose en partie en cation méthyl-1 éthyl-5 cyclooctyle qui contient aussi un pont μ-hydrido; on peut suivre l'évolution de cette transposition en se basant sur la disparition à δ −5.8 du pic dû au μ-H du réactif et sur l'apparition à δ −6.4 du pic dû au μ-H du produit. Le cation diméthyl-1,5 cyclooctyle est le cation contenant un pont μ-hydrido le plus stable thermiquement à être préparé jusqu'à maintenant et il existe sous une conformation chaise bateau-croisé (*BC*) qui apparait comme figée dans le spectre rmn à − 120°C. A des températures plus élevées, on obtient un équilibre chaise–*BC* ⇌ *BC*–chaise pour lequel on a évalué le $\Delta G\ddagger$ à 30 kJ mol^{-1} à partir de l'observation de l'étalement des pics en rmn.

[Traduit par le journal]

A recent study in this laboratory involved the preparation of a series of secondary cycloalkyl cations (n = 7–11), which showed that the members from n = 8–11 could be directly observed by nmr spectroscopy and that they possess a μ-hydrido-bridged structure **1** (1, 2). However,

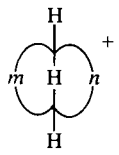

1

Cyclooctyl $n = m = 3$
Cyclononyl $n = 3$, $m = 4$
Cyclodecyl $n = 3$, $m = 5$
Cycloundecyl $n = 4$, $m = 5$ or $n = 3$, $m = 6$

these ions are not thermally very stable, the cyclononyl and cyclooctyl members, for example, collapsing very readily to the tertiary 1-methylcyclooctyl and 1-methylcycloheptyl cations, respectively (2). Attempts to prepare the secondary cycloheptyl cation were unsuccessful and only the ring-contracted 1-methylcyclohexyl cation was observed. Thus, one cannot ascertain whether or not the cycloheptyl cation is also bridged.

It is also possible to observe di-tertiary μ-hydrido-bridged cations and the 1,5- and 1,6-dimethylcyclodecyl cations **2** and **3** have been reported (3, 4). Note that even though the secondary cyclodecyl cation itself appears to favor a 1,5-bridge, it is possible by specific methyl substitution to create an "unnatural bridge", in this case between the 1- and 6-carbon positions in **3**. These di-tertiary cations are also, in general, much more stable than their secondary counterparts.

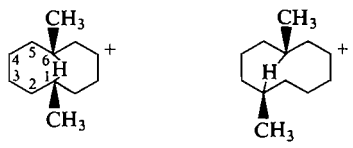

3 **2**

As part of a general characterization of these unique structures, it would be interesting to obtain crystalline salts for X-ray or neutron diffraction study and also to prepare cations which are relatively stable with respect to internal exchange of the μ-H with other hydrogens (for ir–Raman studies where one wishes to fix a μ-D atom in the cation). The previously prepared di-tertiary cyclodecyl systems **2** and **3** suffer in the above regard since these isomers readily interconvert at −100°C

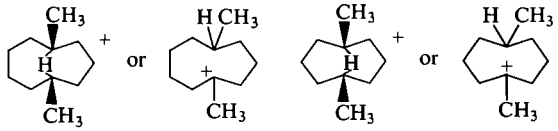

4 **5**

[1]Author to whom correspondence may be addressed.

0008-4042/81/142173-06$01.00/0

©1981 National Research Council of Canada/Conseil national de recherches du Canada

Can. J. Chem. Downloaded from www.nrcresearchpress.com by 210.87.254.6 on 09/06/12
For personal use only.

Can. J. Chem. Downloaded from www.nrcresearchpress.com by 210.87.254.6 on 09/06/12
For personal use only.

and a μ-D is even more rapidly scrambled with ring protons (these have a common origin).

The corresponding 1,5-dimethylcyclononyl **4** and 1,5-dimethylcyclooctyl **5** cations, as yet unknown, appeared to be attractive alternatives for the above purposes since, besides the 1,5-μ-H bridge, the only bridged positional isomers which seemed remotely possible were the 1,4-dimethyl isomers **6** and **7**, and indeed these seemed unlikely.

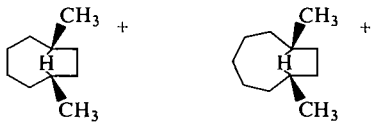

7 **6**

In chemical reactions performed on various medium ring compounds, there are scattered reports of transannular 1,4-hydride shifts; nevertheless, ring conformational considerations certainly dictate against the possibility of an actual bridged intermediate (5).

In order to settle these questions, we set out to prepare and characterize the 1,5-dimethyl cations **4** and **5**, which we hoped would be bridged (and also relatively stable) and we have also investigated in this paper three 1,4-dimethylcycloalkyl cations, the 1,4-dimethylcyclooctyl cation **7**, the 1,4-dimethylcycloheptyl cation **8**, and the 1,4-dimethylcyclohexyl cation **9**, which are

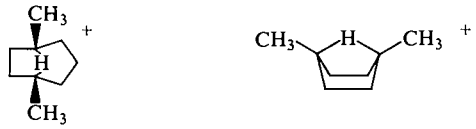

8 **9**

each shown in their possible, though seemingly improbable, μ-hydrido-bridged structures.

Results

The cations were prepared either from the tertiary alcohols, or in the case of **5** and **7**, by protonation of the alkenes **10** and **11**. Each case will be discussed separately.

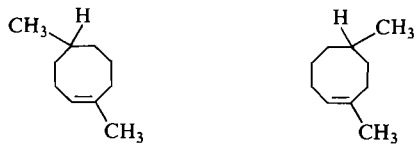

10 **11**

1,5-Dimethylcyclononyl Cation

Although the nmr spectra appear at first sight to be consistent with either a normal tertiary carbocation undergoing a very rapid 1,5-hydride shift *or* a bridged structure, i.e. there are only six ^{13}C peaks, there are three crucial features which are consistent only with a μ-hydrido-bridged structure **4***a*. These criteria have been thoroughly discussed recently in connection with cyclodecyl cation systems (4) and are: (*1*) a very high field μ-hydrogen found in **4** at δ 5.8 ppm; (*2*) an abnormally small $^1H—^{13}C$ coupling constant for this μ-hydrogen, $J = 38$ Hz; and (*3*) a Saunders δ separation of only 1.5 ppm due to the isotopic perturbation caused by substitution of a single CD_3 group (structure **4***b*) (6). Pertinent nmr feature of **4***a* and **4***b* are noted with the structures. The ^1H spectrum shows the two equivalent methyls at δ 2.05, with the remaining ring protons in the range δ 1.69–2.74. The μ-hydrogen is coupled to a small extent with the methyl protons since mutual decoupling sharpens both peaks.

The assignment of peaks to the α and α′ carbons of the five- and six-membered sides in **4***a* is based on analogies with the 1,5-dimethylcyclooctyl cation (next section).

The ring conformation in **4***a* is unknown. It is not unexpected that both α′ carbons of the five-membered side are equivalent, but this is also found for the six-ring side, in contrast to the bridged 1,6-dimethylcyclodecyl cation, where a *cis*-decalin type geometry results in the nonequivalence of the two α carbons in each six-membered ring. There is a noticeable temperature dependence of the δ 33.1 ^{13}C peak assigned to the α carbons of the six-ring side in **4***a*, e.g. δ 33.1 at −110°C, but 34.4 at −92°C, with intermediate values in between, and this may indicate a shifting population consisting of several rapidly equilibrating conformers.

Cation **4** was not as stable as had been hoped for. At about −90°C, the ion begins to rearrange to produce a very complex nmr spectrum (^1H and ^{13}C), $k_{\text{loss of 4}} = 1.5 \times 10^{-3}\ s^{-1}$ at −90°C, $\Delta G^{\ddagger} = 54\ kJ\ mol^{-1}$. On the basis of work with the cyclooctyl system, one of the rearrangement products is easily identified as yet another μ-hydrido-bridged species, the 1-methyl-5-ethylcyclooctyl cation **12** and this is discussed in the following section.

1,5-Dimethylcyclooctyl Cation

This cation clearly has the μ-hydrido-bridged structure **5***a*, based on the same three criteria noted for the cyclononyl analog: (*1*) a μ-hydrogen found at δ −6.3; (*2*) an $^1H—^{13}C$ coupling constant for this μ-hydrogen of 40 Hz; and (**3**) a δ separation of 1.4–2.7 ppm on isotopic perturbation by substitution of a CD_3 group, structure **5***b* (6). Interestingly, this δ separation is temperature dependent but in the opposite sense compared to that observed for equilibrating systems. Thus, δ is 1.43 at −127°C, 1.57 at −115°C, 2.0 at −100°C, 2.35 at −85°C, and 2.7 at −75°C. Pertinent ^1H and ^{13}C nmr features of

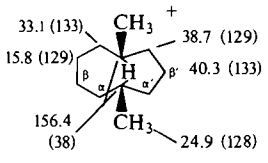

4a

^{13}C assignments (δ)
^{1}H—^{13}C coupling constants in brackets (Hz)

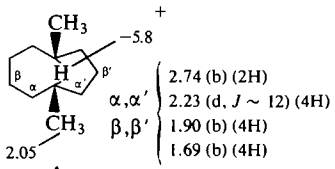

4a

^{1}H assignments (δ)

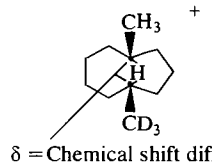

δ = Chemical shift difference between the indicated carbons = 1.5 ppm

4b

5*a* are noted with the structures. In this cation one sees the coupling between the μ-H proton and the methyl groups, J = 2.4 Hz, confirmed by decoupling experiments.

The conformation of **5***a* can be deduced because both the ^{1}H and ^{13}C nmr spectra show a very specific reversible line-broadening as the cation solution is warmed. In the ^{13}C spectrum, the only peaks affected are those assigned to the α- and β-CH_2 carbons. In the ^{1}H spectrum, these same CH_2 protons are involved but not the CH_3 signal. The ^{1}H and ^{13}C results undoubtedly have a common origin but the ^{13}C spectra are much simpler to evaluate and two extreme spectra are shown in Fig. 1. The two single intensity peaks at −120°C (frozen-out spectrum) must be from two different β-carbons. Previously, we have assigned a boat–chair conformation to the 1-methylcyclooctyl cation (7) and the present bridged ion fits this same pattern, i.e. as shown in structure **5***a*. The lower field of the two β-CH_2 carbons is assigned to the chair side on the basis of the previous work. The two sets of α-CH_2 carbons are nearly accidentally equivalent and are not resolvable into two separate peaks, although some broadening is evident.

The nmr line-broadening must be due to a conformational process which mutually interchanges these nonequivalent carbons, i.e. β = β′ and α = α′. This could involve either a *BC* (boat-chair) ⇌ [*CC*] or a BC ⇌ [*BB*] equilibrium, as shown below, with the former probably the more likely. From the coalescence temperature, $\Delta G^{\ddagger}$ for the process was determined as 30 kJ mol^{-1}.

Cation **5** is the most thermally stable μ-hydrido-bridged cation which has yet been prepared and is not rearranged/decomposed until about −60°C.

1-Methyl-5-ethylcyclooctyl Cation

As mentioned, rearrangement of **4** yields about 30% of a cation having nmr properties similar to those found for the 1,5-dimethylcyclooctyl cation **5** and this can be assigned a 1-methyl-5-ethyl-μ-hydrido-bridged cyclooctyl cation structure **12**. There is already precedent for the collapse of simple tertiary cyclononyl cations to cyclooctyl and smaller ring cations (8). The partial nmr parameters of **12** are shown with the structure (only those very diagnostic of the bridged ion can be unequivocally located). The kinetics for **4** → **12** can be conveniently followed by noting the decrease of the δ −5.8 signal of **4** and the appearance of the δ −6.4 signal of **12**.

1,4-Dimethylcyclooctyl Cation

This cation does not have a μ-hydrido-bridged structure, i.e. there is no very high-field μ-hydrogen. Moreover, there is no indication for even a conventional 1,4-hydride shift, at least on the nmr time scale. This is most clearly seen in the fact that the $>C^{+} - CH_3$ methyl signal remains sharp in both the ^{1}H and ^{13}C nmr spectra up to the temperature where rearrangements occur (~ −80°C). The ^{1}H and ^{13}C nmr assignments, taken from "averaged" spectra at −85°C, are given below (structure **13**), along with the probable chair–boat conformations of this cation (**13***a* and **13***b*). At low temperatures, four isomers are possible and there are indications from both the low

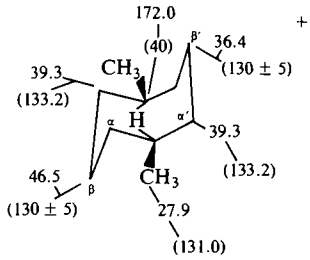

5a

^{13}C assignments (δ), −120°C, ^{1}H—^{13}C coupling constants in brackets (Hz)

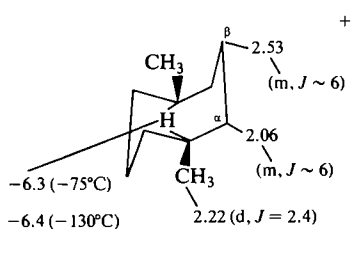

5a

^{1}H assignments (δ) (under conformational averaging conditions, −75°C).

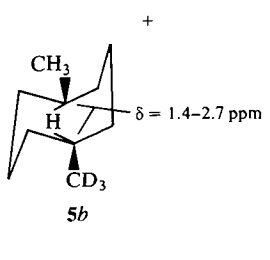

5b

Can. J. Chem. Downloaded from www.nrcresearchpress.com by 210.87.254.6 on 09/06/12
For personal use only.

Can. J. Chem. Downloaded from www.nrcresearchpress.com by 210.87.254.6 on 09/06/12
For personal use only.

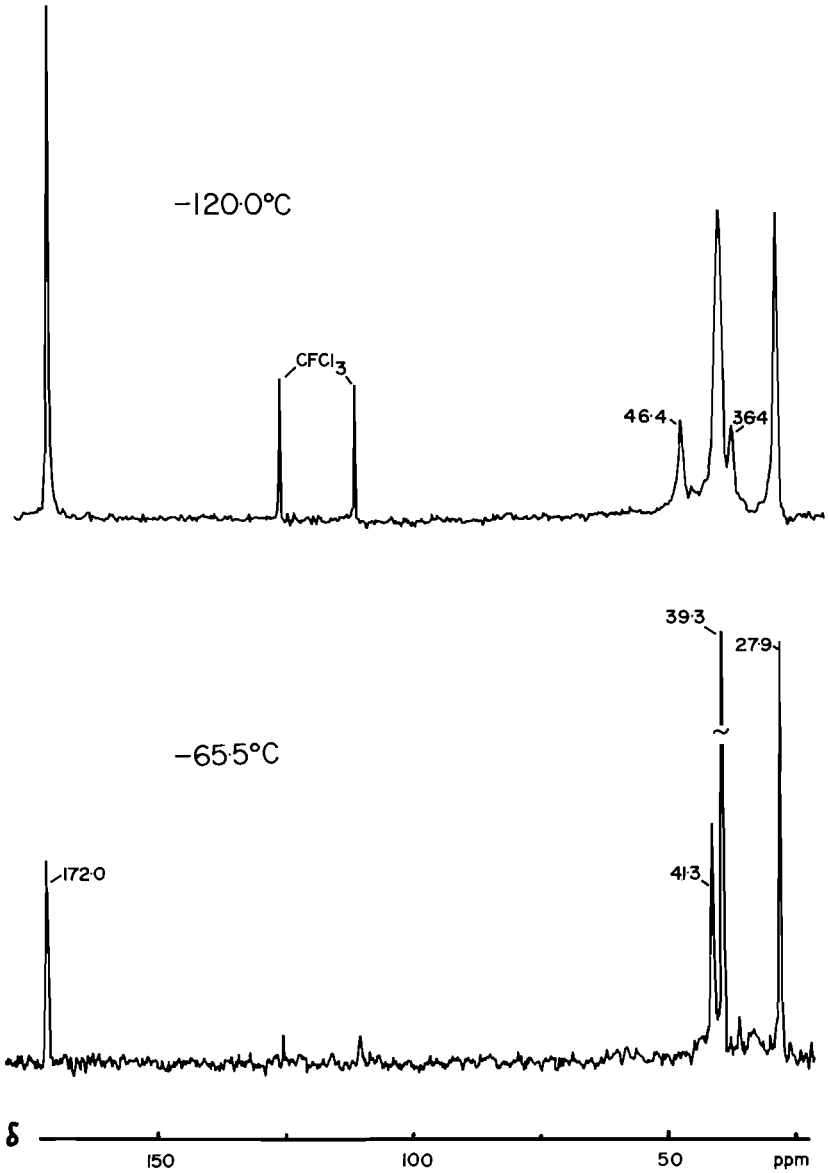

FIG. 1. ^{13}C nmr spectrum of the 1,5-dimethyl-1,5-μ-hydridocyclooctyl cation, broadband decoupled (assignments are given in the text). The upper spectrum at −120°C corresponds to "frozen-out" conditions for the conformational interchange process depicted in the text. The −65.5°C spectrum shows the same ion under conditions of rapid conformational interchange.

temperature ^1H and ^{13}C spectra that there is more than one populated species, probably the chair equatorial methyl ⇌ boat equatorial methyl pair **13***a* and **13***b* in about equal amounts.

The chair–boat conformations **13***a* and **13***b* are clearly not conducive to 1,4-μ-hydrido-bridging or even to 1,4-hydride transfer involving a transition state of less than about 35 kJ mol^{-1} (based on the lack of nmr line-broadening).

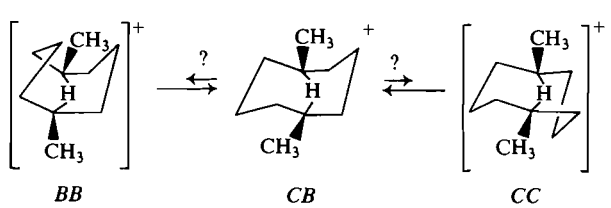

BB *CB* *CC*

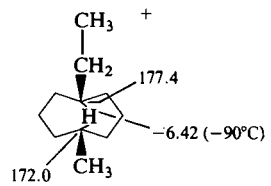

12

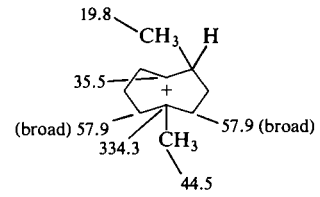

13
^{13}C assignments (δ), remainder broad or not assignable

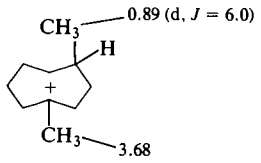

13
^{1}H assignments (δ), remainder broad and overlapping

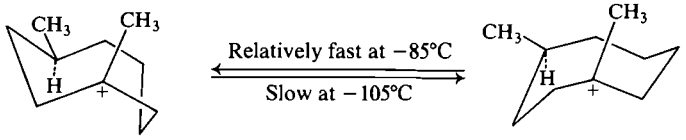

13*a* **13***b*

1,4-Dimethylcycloheptyl Cation

This cation **14** is also not a μ-hydrido structure for the same experimental reasons as for **13**, e.g. the potential μ-hydrido proton is found at the "normal" value of δ ~1.72. Likewise, there is no evidence for the occurrence of a conventional 1,4-hydride shift on the nmr time scale up to the decomposition temperature (~−90°C), therefore

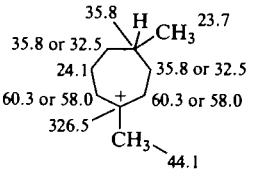

14
^{13}C assignments (δ)

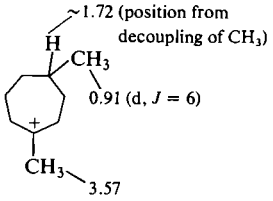

14
^{1}H assignments (δ), remainder are broad and overlapping

$\Delta G^{\ddagger}$ for this process must be >30 kJ mol^{-1}. Unlike the eight ring analog, there is no conformationally derived nmr line-broadening on cooling and like the parent 1-methylcycloheptyl cation (7), this implies low pseudo-rotation type barriers between conformers of similar energy. The pertinent nmr parameters for **14** are given with the structures.

Since **14** shows no sign of μ-hydrido-bridging or even hydride shifts, it is almost certain that the secondary cycloheptyl cation would also not have a μ-H-bridged structure. This same conclusion was tentatively reached on the basis of reactivity differences between cycloheptyl and cyclooctyl systems.

1,4-Dimethylcyclohexyl Cation

Based on the results from **13** and **14**, it comes as no surprise to find that the cyclohexyl member is also not μ-hydrido-bridged. Proton and ^{13}C nmr results are shown with the structure **15** and resemble those of other tertiary cyclohexyl cations. At higher temperatures, the 1,4-dimethyl isomer equilibrates with the 1,3-dimethyl isomer but even up to −40°C, there is no ^{13}C line-broadening evidence for a conventional 1,4-hydride shift.

In conclusion, we have found two new μ-hydrido-bridged systems **4** and **5**, one of which (**5**) is stable for short periods at temperatures as high as −60°C. We have also shown that 1,4-μ-hydrido bridges are not formed, even in a medium ring milieu.

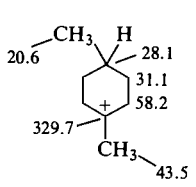

15
^{13}C assignments (δ)

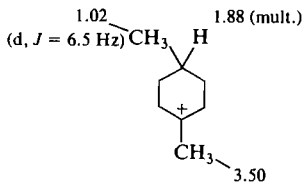

15
^{1}H assignments (δ), remainder are not easily assigned

Experimental

The tertiary alcohols, 1,5-dimethylcyclononan-1-ol (9), 1,4-dimethylcycloheptan-1-ol (10), and 1,4-dimethylcyclohexan-1-ol (11) were prepared as described in the literature, starting from the corresponding ketones. All are mixtures of *cis* and *trans* isomers by ^{13}C nmr spectroscopy but this is immaterial considering our intended use. The starting ketones were carefully purified and the purity checked by ^{13}C nmr spectroscopy. 5-Methylcyclononanone had ^{13}C peaks: δ 218.1, 43.9, 42.5, 34.3, 32.0, 30.4 (CH), 24.6 (2C, CH_3 + CH_2), 22.7 (2C). 5-Methylcyclooctanone (12) had ^{13}C peaks: δ 217.3, 42.5 (2C), 36.3 (2C), 31.4 (CH), 25.5 (2C), 25.2 (CH_3). 1,5-Dimethylcyclooct-1-ene and 1,4-dimethylcyclooct-2-ene, as a mixture, were a gift from Koninklijke/Shell Laboratorium, Amsterdam, Holland. They were separated by preparative glc on Carbowax 20 M. The 1,5-isomer had ^{13}C peaks: δ 137.0 (Cq), 124.8 (=CH_2), 39.6, 35.7, 33.4, 31.2, 27.5, 26.8, 26.2, 24.2. The 1,4-isomer had: δ 137.4 (q), 123.4 (=CH_2), 35.9, 35.1, 33.6, 30.0, 28.8, 24.7, 23.9, 22.4. The deuterated alcohols 1-methyl-d_3-5-methylcyclononan-1-ol and 1-methyl-d_3-5-methylcyclooctan-1-ol, as a *cis*–

Can. J. Chem. Downloaded from www.nrcresearchpress.com by 210.87.254.6 on 09/06/12
For personal use only.

trans mixture, were prepared from the corresponding ketone and methyl-d_3-magnesium iodide. The cations were prepared *in situ* in a similar manner to that described previously (7). The acid system used for preparing the carbocations was 1:1 FSO_3H–SbF_5 diluted 1:4 with SO_2ClF solvent, or for very low temperatures, a mixture of SO_2ClF and SO_2F_2 (ca. 3:1) was used as solvent. The ^{13}C nmr spectra were referenced to internal $CFCl_3$, taken as δ 117.9 ppm relative to TMS, and the probe temperatures were calibrated as previously described (7). For the dynamic conformational interchange of **5**, a series of spectra were run at different temperatures (two of which are shown in Fig. 1). The coalescence temperature was found to be −103°C and a $\Delta G^{\ddagger}$ value determined from this by the standard procedure.

Acknowledgments

We wish to thank the Natural Sciences and Engineering Research Council of Canada for generous financial assistance and Shell Amsterdam for the gift of the dimethylcyclooctenes.

1. R. P. KIRCHEN, T. S. SORENSEN, and K. WAGSTAFF. J. Am. Chem. Soc. **100**, 6761 (1978).
2. R. P. KIRCHEN and T. S. SORENSEN. J. Am. Chem. Soc. **101**, 3240 (1979).
3. R. P. KIRCHEN and T. S. SORENSEN. J. Chem. Soc. Chem. Commun. 769 (1978).
4. R. P. KIRCHEN, K. RANGANAYAKULU, A. RAUK, B. P. SINGH, and T. S. SORENSEN. J. Am. Chem. Soc. **103**, 588 (1981).
5. (*a*) V. PRELOG and J. G. TRAYNHAM. *In* Molecular rearrangements. Vol. 1. *Edited by* P. de Mayo. Interscience, New York. 1963. p. 593; (*b*) A. C. COPE, M. M. MARTIN, and M. A. MCKERVEY. Q. Rev. Chem. Soc. **20**, 119 (1960).
6. M. SAUNDERS, L. TELKOWSKI, and M. R. KATES. J. Am. Chem. Soc. **99**, 8070 (1977).
7. R. P. KIRCHEN and T. S. SORENSEN. J. Am. Chem. Soc. **100**, 1487 (1978).
8. R. P. KIRCHEN, T. S. SORENSEN, and K. E. WAGSTAFF. J. Am. Chem. Soc. **100**, 5134 (1978).
9. A. T. BLOMQUIST and Y. C. MEINWALD. J. Am. Chem. Soc. **80**, 630 (1958).
10. C. S. DEAN, D. A. JONES, S. H. GRAHAM, and D. O. LEWIS. J. Chem. Soc. C, 3045 (1968).
11. H. KOCH and W. HAAF. Ann. **618**, 251 (1958).
12. A. C. COPE and G. L. WOO. J. Am. Chem. Soc. **85**, 3601 (1963).

Can. J. Chem. Downloaded from www.nrcresearchpress.com by 210.87.254.6 on 09/06/12
For personal use only.

Ionic strength effect on liquid chromatographic retention of benzenesulfonates on nonpolar adsorbents

TERRY D. ROTSCH, W. R. CAHILL, JR., AND DONALD J. PIETRZYK[1]

Department of Chemistry, University of Iowa, Iowa City, IA 52242, U.S.A.

AND

FREDERICK F. CANTWELL

Department of Chemistry, University of Alberta, Edmonton, Alta., Canada T6G 2G2

Received November 13, 1980

TERRY D. ROTSCH, W. R. CAHILL, JR., DONALD J. PIETRZYK, and FREDERICK F. CANTWELL. Can. J. Chem. **59**, 2179 (1981).

Chromatographic retention of substituted benzenesulfonate ions is studied on two nonpolar styrene–divinylbenzene adsorbents as a function of mobile phase ionic strength. On both Amberlite XAD-2 and Hamilton PRP-1, a plot of reciprocal of the capacity factor for each benzenesulfonate versus reciprocal of the square root of ionic strength is linear as predicted by Stern–Gouy–Chapman electrical double layer theory. Chromatographic resolution is improved by using an electrolyte-containing mobile phase.

TERRY D. ROTSCH, W. R. CAHILL, JR., DONALD J. PIETRZYK et FREDERICK F. CANTWELL. Can. J. Chem. **59**, 2179 (1981).

On étudie la retention chromatographique d'ions benzènesulfonates substitués sur deux adsorbants styrène–divinylbenzène non polaires en fonction de la force ionique de la phase mobile. Dans les cas de l'Amberlite XAD-2 ainsi que de l'Hamilton PRP-1, on obtient une corrélation linéaire entre l'inverse du facteur de capacité de chaque benzènesulfonate et l'inverse de la racine carrée de la force ionique; ce résultat est en accord avec la théorie électrique de la couche double de Stern–Gouy–Chapman. On améliore la résolution chromatographique en utilisant une phase mobile contenant un électrolyte.

[Traduit par le journal]

Amberlite XAD-2 is a macroporous nonionic copolymer of styrene and divinylbenzene that acts as a nonpolar (reversed phase) adsorbent and exhibits retention not only for organic nonelectrolytes but also for the charged forms of organic acids, bases, and ampholytes. It has several advantages as a stationary phase in liquid chromatography such as low cost, pH stability in the range of 0–14, compatibility with aqueous, organic, and mixed solvents, high linear sample capacity, and strong adsorbent properties. XAD-2 and related macroporous copolymers have been used as stationary phases for liquid chromatographic separations of many different organic analytes using eluting variables such as pH, type of organic solvent, solvent–water ratio, and type and concentration of inorganic or organic electrolytes (1–7). Also, it was recently shown that columns containing microparticulate XAD-2 exhibit efficiencies comparable to those obtained with columns containing microparticulate reversed bonded phases of the alkyl-modified silica type (8).

Recently a spherical, highly cross-linked, macroporous styrene–divinylbenzene copolymer of 10 μm particle diameter has appeared on the market as a liquid chromatography column packing (9). This packing, PRP-1, has been shown to closely resemble Amberlite XAD-2 and can be used interchangeably with it. Its commercial availability as both a loose packing and in the form of pre-packed columns makes PRP-1 an attractive alternative to silica-based reversed phase alkyl-bonded phases, which cannot be used at mobile phase pH above about 8.

Several workers have shown that the retention of organic ions, such as sulfonates, benzoates, phthalates, and protonated amines, increases on XAD-2 as the concentration of an inert electrolyte in the mobile phase increases (1, 2, 4, 10–12). The nature of the electrolyte was also shown to be a significant parameter (1, 2). In a study of this electrolyte effect on XAD-2, Cantwell and Puon (13) demonstrated that the retention of ions such as diphenylguanidinium and benzylammonium could be quantitatively described by the Stern–Gouy–Chapman (SGC) electrical double layer theory. In these systems the analyte cation is absorbed onto the XAD-2 surface and small inorganic counterions, such as chloride ion, occupy the diffuse part of the electrical double layer.

In this report the adsorption of substituted benzenesulfonate anions is studied on XAD-2 and PRP-1 as a function of concentration of inorganic electrolyte in the mobile phase. According to the SGC model the sulfonate analyte is adsorbed onto the adsorbent surface while the diffuse layer is made up of small inorganic cations, such as sodium ion. The fact that the retention data described here are consistent with the SGC theory is additional evidence in support of the postulate that this

[1]Author to whom inquiries should be directed.

0008-4042/81/142179-05$01.00/0

©1981 National Research Council of Canada/Conseil national de recherches du Canada

Can. J. Chem. Downloaded from www.nrcresearchpress.com by 210.87.254.105 on 09/06/12
For personal use only.

Can. J. Chem. Downloaded from www.nrcresearchpress.com by 210.87.254.105 on 09/06/12
For personal use only.

sorption model is a general one and satisfactorily accounts for the retention of organic cations and anions on nonpolar adsorbents in the presence of small counterions.

Experimental

Reagents

Benzenesulfonic acids and their sodium salts were obtained from Eastman Organic Chemicals; Matheson, Coleman and Bell; and Pfister Chemical. The compounds used and their abbreviations are benzenesulfonic acid (BSA), *p*-aminobenzenesulfonic acid (*p*-NH_2BSA), *p*-methylbenzenesulfonic acid (*p*-CH_3BSA), sodium *m*-nitrobenzenesulfonate (*m*-NO_2BSNa), *p*-nitrobenzenesulfonic acid (*p*-NO_2BSA), sodium *p*-chlorobenzenesulfonate (*p*-ClBSNa), 2,5-dimethylbenzenesulfonic acid (2,5-diCH_3BSA), 2,4-dinitrobenzenesulfonic acid (2,4-diNO_2BSA), and 2,5-dichlorobenzenesulfonic acid (2,5-diClBSA). Inorganic salts were analytical reagent grade. Liquid chromatography quality acetonitrile (Matheson, Coleman, and Bell) and 95% ethanol were used in preparing aqueous – organic solvent mobile phase mixtures. Water was treated by passing distilled water through a Bantam Demineralizer Model BD-1 (mixed bed ion exchanger), a column of activated charcoal, and a series of 0.2 μm stainless steel filter discs.

Amberlite XAD-2 was purchased from Rohm and Haas or Mallinckrodt Chemical Works as 20–60 mesh average particles. The copolymer was washed with ethanol in a Soxhlet extractor for at least one week prior to crushing.

Procedures

The XAD-2 column was prepared as follows. A water–ethanol slurry of the XAD particles was ground in a Waring blender and those particles that passed through an 80 mesh screen were air dried. The portion of this dried material passing through a 200 mesh sieve was slurried with ethanol and placed in an ultrasonic bath for 20 min to break up aggregrates. Subsequently, this slurry was passed through a combination of 400 and 500 mesh screens (Cistron Corp., Elmsford, NY) and the particles retained on the 500 mesh screen (25–38 μm) were kept and washed with EtOH and water. This latter process was monitored with a microscope to ensure that fines were not present. Although the XAD-2 particles were nonspherical they were uniform in particle size. A stainless steel column with 5 μm end frits, that was 30 cm long and had an id of 0.236 cm, was slurry packed with the resin. A quantity of 0.5 to 1 g of the 25–38 μm resin was slurred in 20 mL of 20% ethanol – 80% water and pumped from a small stirred pressurized chamber into the column at an initial flow rate of 9.9 mL/min. As the pressure drop on the column increased the flow rate was decreased. Following this, the column was conditioned for several hours with 95% ethanol – 5% water as the mobile phase.

The PRP-1 column, 0.41 cm × 15 cm, was obtained prepacked from the manufacturer (Hamilton Co., Reno, NV).

Chromatograms were obtained with a Waters Model 202 chromatograph equipped with a Model 6000 pump, and a Model U6K injector (Waters Associates, Milford, MA). A Tracor Model 970 detector was used at 208 nm (Tracor Instruments, Austin, TX). Samples were prepared by dissolving 1 to 5 mg of sample per mL of water and stored in 6 mL Hypovials fitted with Hycar Septa and sealed with aluminum caps (Pierce Chemical Co., Rockford, IL). Pressure Lock Series B-110 μL syringes (Precision Sampling Corporation, Rockford, IL) were used to inject 5 μL of sample (1 to 16 μg of analyte). Flow rates were controlled at about 1 mL/min.

Water – organic solvent mixtures are expressed as percent by volume. The benzenesulfonic acid samples were used as the free acid, except where noted (Table 1); in these cases they were used as the sodium salt. The different ionic strength solutions of sodium chloride were prepared by dissolving a known weight in the solvent mixture. In calculating the weight required for a specific ionic strength it was assumed that the NaCl was 100% ionized.

Capacity factors were calculated by:

$$[1] \quad k' = (V_R - V_M)/V_M$$

where V_R is the retention volume for the sulfonate chromatographic peak and V_M is the retention volume for the unretained peak (sodium nitrate). Experiments were run in duplicate at a temperature of 24°C.

Results and Discussion

Benzenesulfonic acids are strong acids with pK_a values smaller than 1. Since they are highly ionized in aqueous solution, it is possible to study the retention of the sulfonate anion, free of the neutral sulfonic acid species, without having to add buffers to convert the sulfonic acid into its anionic form. This eliminates the effect of added buffer components on the retention.

The relationship between the capacity factor (k') of a sample ion such as a substituted benzenesulfonate and the ionic strength (μ) of the mobile phase is given by the SGC theory of double layer adsorption (13) as:

$$[2] \quad 1/k' = 1/C_1 + C_2/\mu^{1/2}$$

where C_1 and C_2 are constants. It is implicitly assumed in this expression that the concentration of sample ion in the mobile phase is small enough

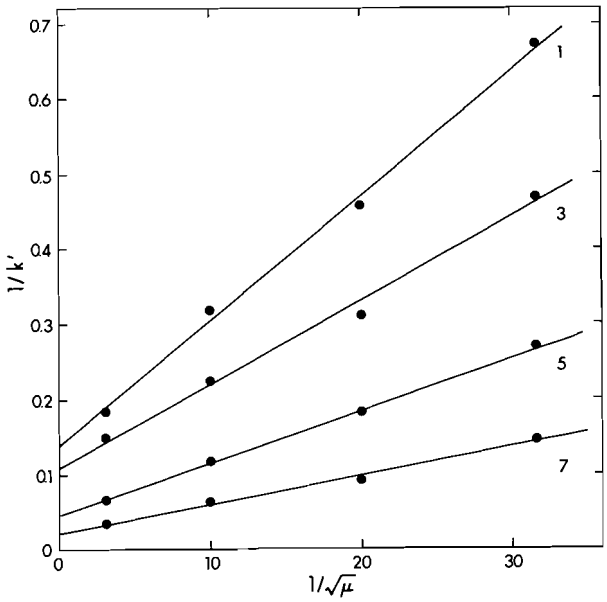

FIG. 1. Plot of $(k')^{-1}$ vs. $\mu^{-1/2}$ for substituted benzenesulfonates on XAD-2 using 1% ethanol containing sodium chloride. Compounds identified in Table 1.

TABLE 1. Linear least-squares parameters for regression of $(k')^{-1}$ on $\mu^{-1/2}$ for benzenesulfonate ions

No.	Compound[a]	XAD-2[b] Slope	XAD-2[b] Intercept	XAD-2[b] r	PRP-1[b] Slope	PRP-1[b] Intercept	PRP-1[b] r
1	p-CH_3BSA	1.66×10^{-2}	0.139	0.9984	1.64×10^{-2}	0.138	0.9972
2	m-NO_2BSNa	1.29×10^{-2}	0.131	0.9962	1.32×10^{-2}	0.128	0.9950
3	p-NO_2BSA	1.11×10^{-2}	0.110	0.9957	9.4×10^{-3}	0.118	0.9965
4	p-ClBSNa	9.3×10^{-3}	0.048	0.9958	7.7×10^{-3}	0.053	0.9911
5	2,5-DiCH_3BSA	6.4×10^{-3}	0.043	0.9938	6.3×10^{-3}	0.046	0.9955
6	2,4-DiNO_2BSA	6.9×10^{-3}	0.047	0.9995	6.1×10^{-3}	0.053	0.9992
7	2,5-DiClBSA	3.78×10^{-3}	0.023	0.9960	—[c]	—	—

[a]BSA is benzenesulfonic acid and BSNa is sodium benzenesulfonate.
[b]r is the correlation coefficient.
[c]Compound 7 not run on PRP-1.

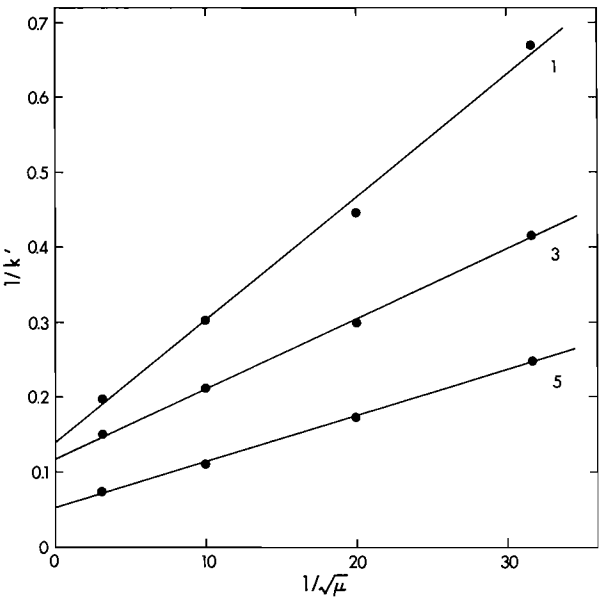

FIG. 2. Plot of $(k')^{-1}$ vs. $\mu^{-1/2}$ for substituted benzenesulfonates on PRP-1 using 5% ethanol containing sodium chloride. Compounds identified in Table 1.

that the surface potential of the resin (ψ_o) is independent of sample concentration (13). Since the quantity of sample injected was on the order of 10^{-7} equivalents this assumption is reasonable.

Equation [2] predicts a linear relationship between $(k')^{-1}$ and $\mu^{-1/2}$. This relationship was tested for six or seven substituted benzenesulfonate sample ions on both Amberlite XAD-2 and PRP-1 columns using sodium chloride to adjust the ionic strength of the mobile phase to values between 10^{-3} and 10^{-1}. The data for several of the compounds are plotted according to eq. [2] in Figs. 1 and 2 where the straight lines shown were calculated by the method of linear least-squares. Presented in Table 1 are the capacity factors obtained for all of the compounds along with the slopes, intercepts, and correlation coefficients obtained in the least-squares calculations for the linear regression of $(k')^{-1}$ on $\mu^{-1/2}$. Compounds with smaller k' values such as p-NH_2BSA and BSA are not included because of the relatively large uncertainties in measuring $(V_R - V_M)$ for use in eq. [1].

Considering all of the compounds and both nonpolar adsorbents, correlation coefficients vary from 0.9911 to 0.9995. The observed linearity of the relationship between $(k')^{-1}$ and $\mu^{-1/2}$ over a range of two orders of magnitude in ionic strength lends support to the view that the SGC theory describes the adsorption of organic *anions* from solutions of inorganic electrolyte into nonpolar adsorbents, just as it does for organic cations (13). From the chromatographic point of view, a knowledge of this reciprocal square root relationship makes the process of selecting a mobile phase composition less empirical.

A comment is in order about the choice of NO_3^- ion as the unretained component, since the values obtained for k' depend upon having an accurate value for V_M. The following values were obtained for V_M at the several ionic strengths (given in parentheses): 0.94 (0.001), 0.96 (0.0025), 1.00 (0.01), and 1.00 (0.1) on the XAD-2 column; and 1.36 (0.001), 1.39 (0.0025), 1.49 (0.01), and 1.49 (0.1) on the PRP-1 column. The slight increase in V_M with increasing μ is predictable from the SGC theory at the low surface potentials which are involved (13). Assuming a negative surface potential, the theory predicts a decrease in expulsion of the co-ion NO_3^- from the diffuse part of the electrical double layer as the NaCl concentration is increased. The effect is analogous to that of "Donnan exclusion" (14, 15) in gel type ion exchangers through, of course, the effect occurs to a much less extent in the double layer case. As expected, a maximum limiting value of V_M is obtained at higher μ (i.e. $\mu \gtrsim 0.01$) and this value of V_M is the same as that which would be found for the retention volume

Can. J. Chem. Downloaded from www.nrcresearchpress.com by 210.87.254.105 on 09/06/12
For personal use only.

Can. J. Chem. Downloaded from www.nrcresearchpress.com by 210.87.254.105 on 09/06/12
For personal use only.

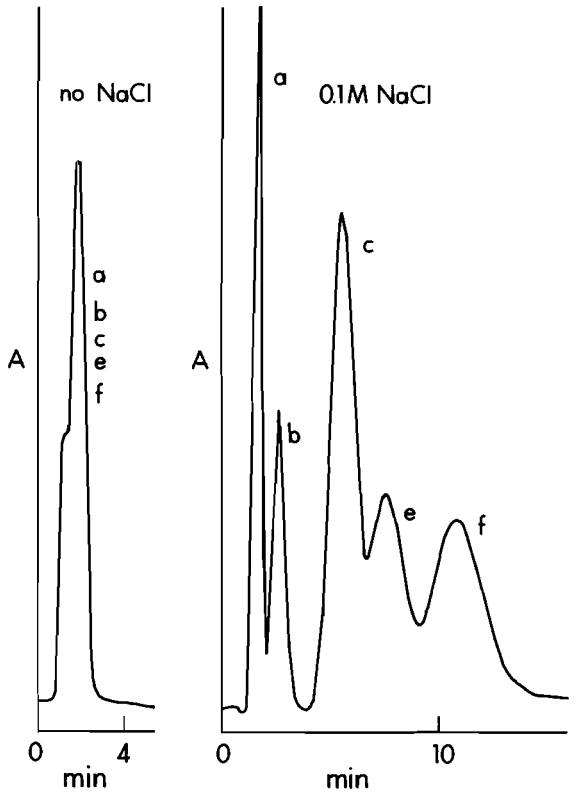

FIG 3. Chromatograms of (a) p-NH_2BSA, (b) BSA, (c) p-CH_3BSA, (e) p-NO_2BSA, (f) p-ClBSNa, on XAD-2 using 3% acetonitrile containing either no electrolyte or 0.1 M sodium chloride.

of an unretained neutral compound under the same conditions.

The use of a univalent anion as unretained component, rather than a neutral compound, is necessary to compensate for this slight electrolyte exclusion effect. To a first approximation, electrolyte exclusion, whether Donnan (15) or double layer (16), depends only on the sign and magnitude of the charge on the ion involved. For example, Waki and Tokunaga (14) working with an ion exchanger have shown that the retention volumes are the same for all univalent anions studied under conditions of Donnan exclusion.

As a consequence of this exclusion behavior, the slight decrease in retention of NO_3^- at lower μ is expected to be reflected in a corresponding decrease in the retention of the univalent sulfonate sample anions. In other words, the sulfonate ions are excluded from the same fraction of the intraparticle pore volume as is NO_3^- ion at the same μ. Consequently, V_M should be identified with the retention volume of NO_3^- obtained at the ionic strength in question.

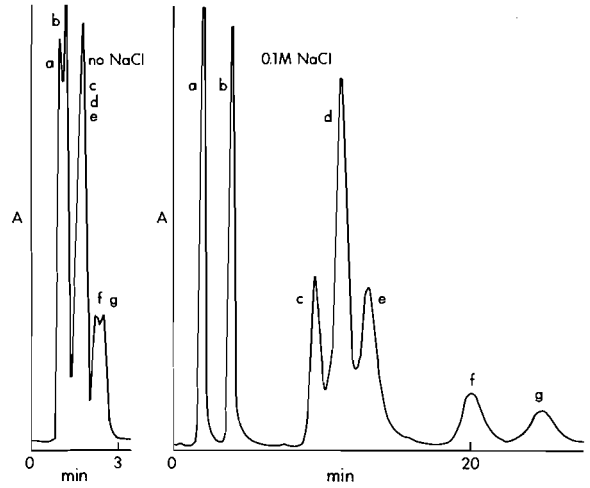

FIG. 4. Chromatograms of (a) p-NH_2BSA, (b) BSA, (c) p-CH_3BSA, (d) m-NO_2BSNa, (e) p-NO_2BSA, (f) p-ClBSNa, (g) unidentified impurity, on PRP-1 using 2.8% acetonitrile containing either no electrolyte or 0.1 M sodium chloride.

The linearity of the plots in Figs. 1 and 2 would not be expected to persist if the number of moles of sulfonate injected is made very much larger. At much higher concentrations the sulfonate ion would make a significant contribution to the surface potential which would then not be constant as μ is varied. To prevent this it would be possible to control the surface potential by the addition to the mobile phase of a relatively high and constant concentration of another potential-determining ion, as was done for the chromatography of cations on XAD-2 (13). The plots in Figs. 1 and 2 might also be expected to deviate from linearity if a very much lower number of moles of sulfonate sample is injected. In this case one would expect to see a perturbation of SGC behavior because of such phenomena as ion exchange involving the very small number of ionic impurity groups present even on nominally nonionic adsorbents (4).

Enhancement of chromatographic retention in the presence of electrolyte greatly improves the chromatographic resolution of ionic sample species. Figure 3 shows the chromatographic separation of a mixture of five substituted benzenesulfonates in a moderately efficient column of Amberlite XAD-2 using two mobile phases which differ only in their ionic strength. With 0.1 M NaCl, capacity factors are greatly increased over those in the electrolyte-free mobile phase and this leads to improved resolution. Compound d was omitted because of its severe overlap with compounds c and e. Figure 4 shows six of the compounds chromatographed on the high efficiency PRP-1 column in the presence and absence of 0.1 M NaCl.

Here too, increased ionic strength leads to enhanced retentions and resolutions. On the high efficiency column *compounds c, d, and e are resolved from one another*. Comparing the chromatograms in Fig. 4 with those in Fig. 3, it is evident that the use of a microparticle packing yields greatly enhanced column efficiency and resolution. Presumably the use of microparticle XAD-2 (8) would also yield high efficiency separations like those in Fig. 4, but the packing was not employed in the present study.

It is evident from the data in Table 1 that the retention *sequence* of benzenesulfonates on PRP-1 adsorbent is the same as that on XAD-2. Chromatography of a variety of other types of compounds on both XAD-2 and PRP-1 shows that this conclusion is a general one (17). This is a reflection of the very similar chemical nature of the two adsorbents. The nearly identical values of slope and intercept for a few of the compounds (e.g. p-CH_3BSA) on the two adsorbent columns is somewhat coincidental. It results probably from a cancelling of the effect of the larger specific surface area of PRP-1 (415 m^2/g vs. 330 m^2/g for XAD-2) by the use of a somewhat stronger solvent for PRP-1 (5% ethanol vs. 1% ethanol for XAD-2). The larger specific surface area leads to increased capacity factors, while the greater mobile phase strength has the opposite effect. Ethanol content of the mobile phases was chosen initially to give similar capacity factors for the same compound in both columns.

Acknowledgements

This work was supported by the National Science Foundation, the National Cancer Institute, the Department of Health, Education, and Welfare (U.S.A.), the Natural Sciences and Engineering Research Council of Canada, and the University of Alberta.

1. D. J. Pietrzyk and C.-H. Chu. Anal. Chem. **49**, 860 (1977).
2. H. Y. Mohammed and F. F. Cantwell. Anal. Chem. **50**, 419 (1978).
3. E. P. Kroeff and D. J. Pietrzyk. Anal. Chem. **50**, 502 (1978).
4. S. Puon and F. F. Cantwell. Anal. Chem. **49**, 2156 (1977).
5. T. D. Rotsch, R. J. Sydor, and D. J. Pietrzyk. J. Chromatogr. Sci. **17**, 339 (1979).
6. T. D. Rotsch and D. J. Pietrzyk. Anal. Chem. **52**, 1323 (1980).
7. T. D. Rotsch and D. J. Pietrzyk. J. Chromatogr. Sci. **18**, 88 (1981).
8. R. G. Baum, R. Saetre, and F. F. Cantwell. Anal. Chem. **52**, 15 (1980).
9. D. P. Lee and J. H. Kindsvater. Anal. Chem. **52**, 2425 (1980).
10. R. L. Gustafson, R. L. Albright, J. Heisler, J. A. Lirio, and O. T. Reid, Jr. Ind. Eng. Chem. Prod. Res. Dev. **7**, 107 (1968).
11. M. W. Scoggins and J. W. Miller. Anal. Chem. **40**, 1155 (1968).
12. M. W. Scoggins. Anal. Chem. **44**, 1285 (1972).
13. F. F. Cantwell and S. Puon. Anal. Chem. **51**, 623 (1979).
14. H. Waki and Y. Tokunaga. J. Chromatogr. **201**, 259 (1980).
15. F. Helfferich. Ion exchange. McGraw-Hill, New York. 1962. Chapt. 5.
16. J. Th. Overbeek. *In* Colloid science. Vol. 1. *Edited by* H. R. Kruyt. Elsevier, New York. 1952. Chapt. 4.
17. Z. Iskandarani and D. J. Pietrzyk. Anal. Chem. **53**, 489 (1981).

Can. J. Chem. Downloaded from www.nrcresearchpress.com by 210.87.254.105 on 09/06/12
For personal use only.

A kinetic electron spin resonance study of the reaction of some oxy radicals with vanadyl acetylacetonate[1]

J. A. HOWARD,[2] J. C. TAIT,[3] T. YAMADA,[4] AND J. H. B. CHENIER
Division of Chemistry, National Research Council of Canada, Ottawa, Ont., Canada K1A 0R9

Received October 14, 1980

J. A. HOWARD, J. C. TAIT, T. YAMADA, and J. H. B. CHENIER. Can. J. Chem. **59**, 2184 (1981).

Reactions of phenoxyl, iminoxyl, nitroxyl, peroxyl, and alkoxyl radicals with $VO(acac)_2$ in solution have been studied by kinetic esr spectroscopy. Rates of reaction are first-order with respect to each reactant and radical reactivity increases in the order galvinoxyl < 2,4,6-tri-*tert*-butylphenoxyl < di(1-adamantyl)methylene-iminoxyl < *tert*-butylperoxyl. Rates of reaction are retarded by pyridine and accelerated by methanol and there is an isotope effect on the rate when the hydroxyl proton of CH_3OH is replaced by deuterium. Vanadium-51 nmr spectroscopy has demonstrated that several vanadium(V) products are formed while conventional product studies have indicated that, in the case of phenoxyl and alkoxyl, the radical is reduced almost exclusively to the parent phenol and alcohol and that $VO(acac)_2$ is eventually regenerated in substantial yields. The net reaction is, therefore, catalytic reduction of the radical. Variable temperature esr studies have shown that phenoxyl and iminoxyl radicals and $VO(acac)_2$ exist in equilibrium with diamagnetic reaction products.

J. A. HOWARD, J. C. TAIT, T. YAMADA et J. H. B. CHENIER. Can. J. Chem. **59**, 2184 (1981).

Utilisant la spectroscopie de rpe cinétique, on a étudié les réactions des radicaux phénoxyle, iminoxyle, nitroxyle, péroxyle et alkoxyle avec le $VO(acac)_2$ en solution. Les vitesses de réaction sont du premier ordre par rapport à chaque réactif et la réactivité des radicaux augmente dans l'ordre suivant: galvinoxyle < tri-*tert*-butyl-2,4,6 phénoxyle < di(adamantyl-1) méthylène iminoxyle < *tert*-butylperoxyle. Les vitesses de réaction sont ralenties par la pyridine et accélérées par le méthanol et le remplacement du proton hydroxylique du CH_3OH par un deutérium provoque un effet isotopique cinétique. La spectroscopie de rmn du vanadium-51 a démontré qu'il se forme plusieurs produits du vanadium(V) tandis que des études conventionnelles des produits indiquent que, dans le cas du phénoxyle et de l'alkoxyle, le radical est presqu'exclusivement réduit en phénol apparenté et en alcool alors que le composé $VO(acac)_2$ est régénéré avec des rendements qui sont éventuellement substantiels. La réaction globale est cependant une réduction catalytique du radical. Des études de rpe à température variable révèlent que les radicaux phénoxyle et iminoxyle et le $VO(acac)_2$ existent en équilibre avec des produits de réaction diamagnétiques.

[Traduit par le journal]

Introduction

It is well known that oxidation of olefins, sulphides, sulphoxides, and amines by alkyl hydroperoxides (ROOH) is catalyzed by vanadyl acetylacetonate, $VO(acac)_2$ (1).

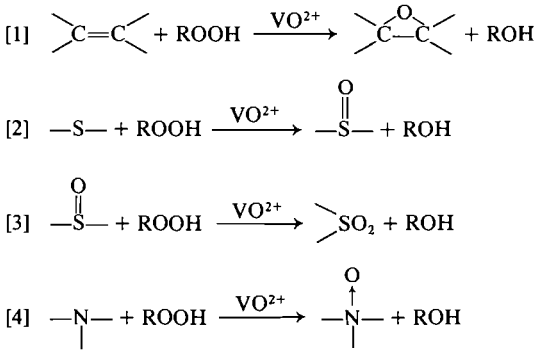

Furthermore there appears to be general agreement that the reaction mechanism involves association of the hydroperoxide with $VO(acac)_2$ to give a vanadium(V)–ROOH complex which is followed by nucleophilic attack at the "activated" —O—O— bond of the hydroperoxide by the nucleophile.

Although these oxidations are heterolytic there is some evidence that free-radicals are produced by reaction of $VO(acac)_2$ with ROOH. Thus Brandon and Elliott (2) detected *tert*-butylperoxy radicals by electron spin resonance spectroscopy during reaction of *tert*-BuOOH with $VO(acac)_2$ in ethanol at room temperature while Symons (3) suggested that this reaction also gives a vanadium(V) peroxy radical of the form $L_nVO_2^{\cdot}$ where L_n represents unspecified ligands.

The kinetics and mechanisms of VO^{2+} catalyzed nonradical oxidations have been thoroughly studied whereas free-radical reactions of these chelates have received little attention. In order to redress this imbalance we have investigated the reaction of $VO(acac)_2$ with several oxy radicals and the results of this work are reported here.

Experimental

Reagents

Commercial vanadyl acetylacetonate was purified either by recrystallization from methanol or sublimation and standard solutions were freshly prepared before use.

[1]Issued as NRCC No. 19269.

[2]Author to whom all correspondence should be addressed.

[3]NRCC Research Associate 1975–1977. Present address: A.E.C.L., Pinawa, Manitoba.

[4]NRCC Research Associate 1979–1981.

0008-4042/81/142184-07$01.00/0

©1981 National Research Council of Canada/Conseil national de recherches du Canada

Can. J. Chem. Downloaded from www.nrcresearchpress.com by 210.87.254.42 on 09/06/12
For personal use only.

Can. J. Chem. Downloaded from www.nrcresearchpress.com by 210.87.254.42 on 09/06/12
For personal use only.

2,4,6-Tri-*tert*-butylphenol (Aldrich) was recrystallized from hexane to a purity of >99.9%.

Standard solutions of 2,4,6-tri-*tert*-butylphenoxyl, **1**, were prepared by passing solutions of 2,4,6-tri-*tert*-butylphenol down a column of PbO_2–Celite (4:1) (4). If oxygen was rigorously excluded during this procedure, conversion of the phenol to the radical was quantitative. Solutions of the radical could be kept for several hours with no loss in radical concentration. The concentration of **1** was determined either by uv spectroscopy at 630 nm (ε = 410) or by esr spectroscopy relative to a standard solution of DPPH.

tert-Butylperoxy radicals were produced either by photolysis of azoisobutane (Merck, Sharpe, and Dohme, Canada Ltd.) or 2,2,4,4-tetramethyl-3-pentanone (Chemical Samples Co.) in an air-saturated solvent. Cumylperoxy radicals were obtained by thermolysis of azocumene (5) in oxygen saturated chlorobenzene at 323 K. Cumyloxy radicals were generated by thermolysis of di-α-cumyl hyponitrite (6). Galvinoxyl was obtained from Aldrich and di(1-adamantyl) methylene-iminoxyl was a gift from Dr. K. U. Ingold. Hydrogalvinoxyl was prepared by the method described by Adam and Chiu (7).

Kinetic Procedures

Reactions of tri-*tert*-butylphenoxyl, galvinoxyl, and di(1-adamantyl)methylene-iminoxyl with $VO(acac)_2$ were studied in Pyrex tubes (5 mm od) directly in the cavity of a Varian E-4 EPR spectrometer. In a typical *dark* experiment 50 μL of a strong standard solution of $VO(acac)_2$ were added to 250 μL of a weaker standard solution of **1** as the solution was being agitated with a fine stream of argon to ensure rapid mixing. The decay of the minor component was then followed by monitoring the decrease in the intensity of its esr spectrum with respect to time. Faster reactions were studied by generating the radical photochemically in the presence of excess $VO(acac)_2$ directly in the cavity of the EPR spectrometer and following the change in the radical concentration with time after the initiating light was masked.

Stoichiometric factors n, i.e., the number of radicals destroyed by each molecule of $VO(acac)_2$, were determined by the esr titration method described previously (8).

Product Analysis

Volatile reaction products were identified and their yields determined by gas chromatography using a Varian model 2800 chromatograph equipped with an OV-101 column and flame ionization detector. Reaction products were also examined by infrared spectroscopy and high performance liquid chromatography before distillation. The volatile fraction was obtained by pumping the reaction mixture at room temperature into a trap maintained at 77 K. Vanadium-51 nuclear magnetic resonance spectra were obtained before pumping on a Bruker CXP 180 pulsed NMR spectrometer at 47.3 MHz.

Results and Discussion

*2,4,6-Tri-*tert*-butylphenoxyl, 1*

In nonpolar aromatic solvents, such as toluene, *tert*-butylbenzene, and *o*-dichlorobenzene, **1** disappeared completely upon addition of a large excess of $VO(acac)_2$ at 294 K. Decays of **1** were accurately exponential and pseudo-first-order rate constants were linearly dependent on the concentration of $VO(acac)_2$.

Similarly $VO(acac)_2$ disappeared completely upon addition of a large excess of **1**. Decays of $VO(acac)_2$ followed first-order kinetics and pseudo-first-order rate constants were linearly dependent on the concentration of **1**. These results suggest that the *initial* reaction is a straight-forward combination as shown in [5].

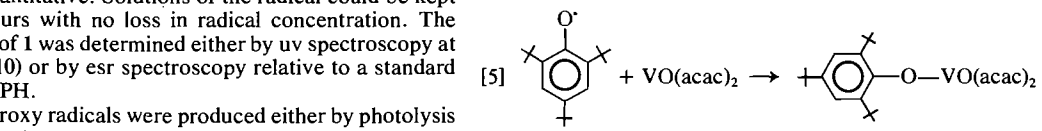

Bimolecular rate constants for reaction [5] were determined from decays of both **1** and $VO(acac)_2$ in several solvents and the results are summarized in Table 1. Somewhat surprisingly, rate constants obtained from decays of $VO(acac)_2$ were consistently smaller than rate constants obtained from decays of **1**. Furthermore, the nature of the solvent had an appreciable effect on the magnitude of k_5.

Attempts to measure the stoichiometric factor in nonpolar solvents suggested that $VO(acac)_2$ reacted with between 1 and 2 equivalents of **1** (Table 2). It did, however, become apparent that soon after the *minimum* concentration of $VO(acac)_2$ was reached the concentration of this reactant began to increase *slowly* with time until most of it had been regenerated. Clearly the diamagnetic product of reaction [5] is thermally unstable and decomposes irreversibly back to $VO(acac)_2$. The smaller values of k_5 obtained from decays of $VO(acac)_2$ are, therefore, almost certainly associated with regeneration of this reactant during reaction and values of k_5 determined from decays of **1** are probably the more reliable rate constants for reaction [5].

Values of k_5 determined from decays of **1** were measured from 223 to 303 K in toluene and approximately fit the Arrhenius equation

$$\log(k_5/M^{-1}\,s^{-1}) = (3.7 \pm 0.5) - (4 \pm 0.5)/\theta$$

where $\theta = 2.303RT$ kcal mol^{-1}. Clearly reaction [5] has a low activation energy and an extremely low pre-exponential factor.

Rapid changes in the temperature between 303 and 363 K when the minimum concentrations of

TABLE 1. Rate constants for reaction of 2,4,6-tri-*tert*-butylphenoxyl with $VO(acac)_2$ at 294 K

Solvent	$\frac{k_\psi}{[VO(acac)_2]}$ (M^{-1} s^{-1})	$\frac{k_\psi'}{[1]}$ (M^{-1} s^{-1})
$C_6H_5C(CH_3)_3$	12.25±4.2	0.84±0.04
o-$C_6H_4Cl_2$	7.0 ±1.5	0.7 ±0.1
$C_6H_5CH_3$	4.9 ±1.5	0.68±0.1

TABLE 2. Stoichiometric factors for reaction of 2,4,6-tri-*tert*-butylphenoxyl with $VO(acac)_2$ at 294 K

	Initial reactant concentration (M)		Final reactant concentration (M)		$\Delta[1]$
Solvent[a]	$10^3[1]$	$10^3[VO(acac)_2]$	$10^3[1]$	$10^3[VO(acac)_2]$	$\Delta[VO(acac)_2]$
A	2.25	0.55	1.16	0.085	2.3
A	1.9	3.7	0	1.85	1.0
A	3.0	1.2	1.04	0	1.6
A	2.3	1.2	1.2	0	1.0
B	1.06	1.42	0.0003	0.345	1.0
B	0.85	0.65	0.185	0	1.0

[a]A: toluene; B: toluene–methanol 9.5: 0.5, v/v.

$VO(acac)_2$ and **1** had been reached, after reaction of equimolar reactant concentrations, revealed the presence of reversible equilibria. Thus the concentration of both $VO(acac)_2$ and **1** could be increased and decreased by raising and lowering the temperature.

Analysis of the final products of reaction [5] by infrared spectroscopy and gas–liquid chromatography indicated that **1** was reduced almost quantitatively to 2,4,6-tri-*tert*-butylphenol. In most experiments a trace of 2,6-di-*tert*-butyl-*p*-benzoquinone was also formed. The most likely source of this product is oxidation of the phenol by a vanadium(V) species during work-up.

Examination of reaction mixtures by ^{51}V nmr spectroscopy revealed the presence of at least ten vanadium(V) products with δ_V between −466 and −614.5 ppm relative to external $VOCl_3$.

Attempts to prepare

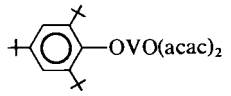

from 2,4,6-tri-*tert*-butylphenol and $VO(acac)_2Cl$ have so far failed. In fact the reaction mixture did not give a ^{51}V nmr spectrum and appeared to contain mainly $VO(acac)_2$.

Rates of reaction [5] were much faster in toluene containing 5–20% methanol and were in fact so fast that radical decays could not be studied by the dark method. Instead **1** was produced by photolysis of a solution of 2,4,6-tri-*tert*-butylphenol in mixtures of toluene–methanol containing $VO(acac)_2$ and radical decays were monitored after the initiating light was masked. Using this method **1** was found to decay exponentially with k_5 (CH_3OH) = 120 M^{-1} s^{-1}. Interestingly a significant isotope effect was observed when the hydroxylic hydrogen of methanol was replaced by deuterium and k_5 (CH_3OD) = 30 M^{-1} s^{-1}, i.e., $k_5(H)/k_5(D) \sim 4$.

The stoichiometric factor, n, was exactly 1 in mixtures of toluene and methanol when *minimum* residual concentrations of reactants were determined after initial rapid reaction (Table 2).

Final reaction mixtures after reaction of equimolar concentrations of **1** and $VO(acac)_2$ were ruby red, indicative of the presence of vanadium(V) species. The ^{51}V nmr spectrum of the reaction products was much simpler in the presence of 5% methanol and two major vanadium(V) species were observed with chemical shifts of −488.6 and −586.6 ppm in the ratio of ~2:1. At higher concentrations of methanol the quantity of the species with δ_V = −586.6 ppm increased dramatically. In addition these two vanadium(V) products appeared to be in thermal equilibrium.

An esr spectroscopic study sometime after the reaction of almost equal concentrations of **1** (10 mM) and $VO(acac)_2$ (7.6 mM) in toluene–methanol indicated the presence of residual concentrations of $VO(acac)_2$ (2.6 mM) and **1** (0.022 mM). More interestingly, the concentration of both $VO(acac)_2$ and **1** could be increased and decreased reversibly by raising and lowering the temperature between 293 and 343 K. Both reactants were, therefore, in equilibrium with diamagnetic dimer(s). There was, however, a slow irreversible reaction because $[VO(acac)_2]$ increased slowly and [**1**] decreased slowly with time.

The difference in the residual concentrations of $VO(acac)_2$ and **1** appears to preclude a simple reversal of reaction [5]

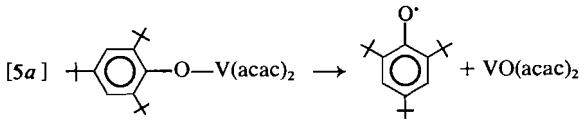

If, however, we make the reasonable assumption that **1** was in reversible equilibrium with **1**-$VO(acac)_2$ we can calculate that ΔH_5^0 is ~ −10 kcal mol.

Unfortunately we were unable to measure [**1**-$VO(acac)_2$] and consequently values of K_5 and ΔS_5^0 could not be determined.

A product of reaction [5] prepared in the presence of MeOH was found to be photochemically unstable and photolysis gave $VO(acac)_2$. Furthermore, photolysis in the presence of phenyl *tert*-

Can. J. Chem. Downloaded from www.nrcresearchpress.com by 210.87.254.42 on 09/06/12
For personal use only.

Can. J. Chem. Downloaded from www.nrcresearchpress.com by 210.87.254.42 on 09/06/12
For personal use only.

butylnitrone produced a nitroxide with the esr parameters $g = 2.0064$, $a_N = 13.33$ G, $a_H = 1.52$ G; values which are similar to the parameters for the nitroxyls obtained by adding alkoxy radicals to PBN (9). We also found that regeneration of $VO(acac)_2$ was significantly faster in the presence of oxygen than it was in degassed solution.

It is apparent from these results that one product of reaction [5], in methanol, behaves exactly like methoxo-oxobis(8-quinolyloxo)vanadium(V) (10) and we tentatively conclude that it is methoxo-oxobis(acetylacetonato)vanadium(V), $CH_3OVO(acac)_2$, and is probably the product with $\delta_V = -466$ ppm in the ^{51}V nmr spectrum. This assignment was made of the basis of the fact that a rather impure sample of methoxo-oxobis(8-quinolyloxo)-vanadium(V) gave strong ^{51}V nmr transitions with $\delta_V = -477$ and -467 ppm and the product from reaction of $VO(acac)_2Cl$ with methanol gave a strong peak at $\delta_V = -465$ ppm. The second transition in the ^{51}V nmr spectrum at $\delta_V = -586.6$ ppm had a chemical shift about 10 ppm upfield from $VO(OC_2H_5)_3$. It should be noted that $CH_3OVO(acac)_2$ is quite unstable and has a half-life of ~5.5 h in toluene at 295 K.

The observation of an isotope effect when CH_3OD was used instead of CH_3OH implies that the hydroxylic proton is abstracted in the rate controlling step, perhaps by reaction of **1** with coordinated methanol.

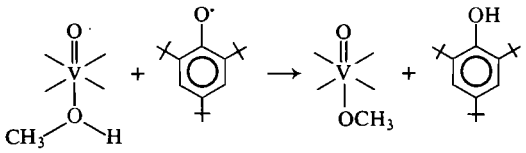

The reaction of **1** with $VO(acac)_2$ in aprotic solvents was retarded by low concentrations of pyridine, probably because pyridine coordinates at the reactive vacant coordination site of the complex and prevents inner sphere electron transfer.

Galvinoxyl 2

Galvinoxyl also reacted with $VO(acac)_2$ to destroy the paramagnetism of both reactants and rates of radical decay obeyed the rate law

$$-d[\mathbf{2}]/dt = k_6[\mathbf{2}][VO(acac)_2]$$

Values of k_6 were calculated from rates of radical decay because $-d[\mathbf{2}]/dt > -d[VO(acac)_2]/dt$ and the results are summarized in Table 3. It is apparent from this data that **2** is about 10 times less reactive than **1**, that CH_3OH accelerates the rate of reaction [6] by a factor of about 35 whereas CH_3OD only accelerates the rate by a factor of about 8, and that pyridine completely inhibits the reaction.

[6] 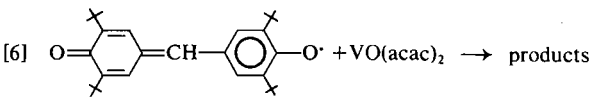 products

The vanadium-51 nmr spectrum obtained after reaction of **2** (38 m*M*) with $VO(acac)_2$ (38 m*M*) in toluene–methanol (5:1, v/v) showed three peaks at $\delta_V = -498$, -504, and -574 ppm in approximately equal yields. This solution contained a residual galvinoxyl concentration of 10 m*M* and a residual $VO(acac)_2$ concentration of 1 m*M*. This residual $[VO(acac)_2]$ was in thermal equilibrium with a vanadium(V) species. There was, however, only a small change in $[VO(acac)_2]$ over the temperature range studied, indicating a small enthalpy of activation, ΔH^0 (~2 kcal mol^{-1}). On the other hand, the concentration of galvinoxyl did not increase when the temperature was raised from 296 to 315 K, probably because the change in concentration was too small to measure.

Over a long period of time (several weeks) the original $VO(acac)_2$ concentration (38 m*M*) was regenerated and the galvinoxyl was completely destroyed. High pressure liquid chromatographic analysis of the final reaction mixture indicated the formation of hydrogalvinoxyl (**2**-H), a trace of 2,6-di-*tert*-butyl-*p*-benzoquinone and products indicative of methoxy radical attack on galvinoxyl and/or hydrogalvinoxyl.

Di(1-adamantyl)methylene-iminoxyl 3

In *tert*-butylbenzene at 294 K **3** (0.05 m*M*) decayed rapidly with first-order kinetics in the presence of a ten-fold excess of $VO(acac)_2$ and $VO(acac)_2$ (0.1 m*M*) decayed with first-order kinetics in the presence of a 100-fold excess of **3**. The half-life of **3** ($\tau_{1/2} = 4.2$ ms) was, however, about 3 times shorter than the half-life of $VO(acac)_2$ ($\tau_{1/2} = 12.5$ ms). Absolute values of the rate constants for reaction of **3** with $VO(acac)_2$ (k_7) determined from radical decays in different solvents are given in Table 4 and it is apparent that the overall rate of reaction [7] depends on the nature of the solvent and that the rate is enhanced by low concentrations of methanol and retarded by low concentrations of pyridine.

The stoichiometric factor estimated from *minimum* reactant concentrations was close to one for this radical. The concentrations of each reactant did not, however, reach zero when equal concentrations were mixed. The residual reactant concentrations, which were about 2% of the initial concentrations, were approximately equal in this case and there was a slow regeneration of $VO(acac)_2$ and a slow disappearance of **3**. A variable temperature study on this system demonstrated that the resi-

Can. J. Chem. Downloaded from www.nrcresearchpress.com by 210.87.254.42 on 09/06/12
For personal use only.

TABLE 3. Rate constants for reaction of galvinoxyl with $VO(acac)_2$ at 294 K[a]

Solvent	k_6/M^{-1} s^{-1}
Toluene	0.6
Toluene–CH_3OH	22±1.7
Toluene–CH_3OD	4.6±0.4
Toluene–pyridine	No reaction

[a]Determined from radical disappearances.

TABLE 4. Rate constants for reaction of di(1-adamantyl)methylene-iminoxyl with $VO(acac)_2$ at 294 K

Solvent	k_7/M^{-1} s^{-1}
Toluene	66±10
tert-Butylbenzene	250
o-Dichlorobenzene	358
Toluene–methanol[a]	>300
Toluene–pyridine[b]	3

[a]9.5: 0.5, v/v
[b]9.75: 0.25, v/v

dual concentrations of both reactants could be increased and decreased reversibly by raising and lowering the temperature between 294 and 333 K. We can therefore conclude that **3** reacts reversibly with $VO(acac)_2$ to give di(1-adamantyl)methylene-imino-oxobis(acetylacetonato) vanadium(V) and that there is a slow irreversible decay of this compound to give reaction products.

[7] $(1\text{-Ad})_2C{=}NO^{\cdot} + VO(acac)_2 \rightleftharpoons (1\text{-Ad})_2C{=}NOVO(acac)_2 \rightarrow$ reaction products

The concentrations of **3** and $VO(acac)_2$ at the different temperatures allowed us to calculate an approximate value of -15.5 kcal mol^{-1} for the enthalpy change (ΔH_7^0) for reaction [7].

Vanadium-51 nmr spectra of reactions performed in toluene–methanol revealed the formation of three major vanadium products at -493, -503, and -578 ppm which can probably be assigned to **3**-$VO(acac)_2$, $CH_3OVO(acac)_2$, and a third vanadium species which could have been regenerated $VO(acac)_2$.

tert-*Butylperoxyl* ***4***

This radical reacts rapidly with $VO(acac)_2$ at 183 K and one radical is destroyed by each molecule of complex. Rates of decay of **4** were found to obey the rate expression

$$-d[\mathbf{4}]/dt = k_8[\mathbf{4}][VO(acac)_2]$$

where k_8 is the rate constant for reaction [8].

[8] $t\text{-}BuO_2^{\cdot} + VO(acac)_2 \rightarrow$ products.

Absolute values of k_8 from 173–233 K are given in Table 5. This data can be represented by the

TABLE 5. Rate constants for reaction of $(CH_3)_3COO^{\cdot}$ with $VO(acac)_2$ in toluene.

Temperature (K)	$10^5[VO(acac)_2]$ (M)	k_ψ (s^{-1})	$10^{-4}k_\psi/[VO(acac)_2]$ (M^{-1} s^{-1})
208	1.7	0.63	3.7
	2.5	0.82	3.3
198	1.7	0.58	3.4
	8.6	2.3	2.7
188	1.7	0.44	2.6
	8.6	2.1	2.5
178	1.7	0.34	2.0
	8.6	1.7	2.0

Arrhenius equation

$$\log(k_8/M^{-1}\text{ s}^{-1}) = (6.0 \pm 0.2) - (1.4 \pm 0.2)/\theta$$

indicating that reaction [8] has a normal A-factor and is fast because of a low activation energy.

A solution of azocumene (25 mM) and $VO(acac)_2$ (50 mM) in chlorobenzene absorbed oxygen at an initial rate of 2.7×10^{-6} M s^{-1} at 323 K, slightly faster than the rate in the absence of $VO(acac)_2$ (1.6×10^{-6} M s^{-1}). Oxygen (50 mM) was absorbed and acetophenone (13.3 mM), α-methylstyrene (10 mM), and α-cumyl alcohol (6 mM) were produced. If it is assumed that α-methylstyrene was formed by dehydration of α-cumyl alcohol, the alcohol to ketone ratio, A/K, was 1.2 which is about twice as large as the ratio in the absence of metal complex (A/K = 0.54) and is very similar to the ratio obtained from reaction of $PhCMe_2O_2^{\cdot}$ with $Co(acac)_2$ (11).

Cumyloxyl

No attempt was made to measure rate constants for reaction of cumyloxyl with $VO(acac)_2$ because of the expected high rate of this reaction. We did, however, investigate the products of this reaction and found that thermolysis of α-cumyl hyponitrite (22 mM) in chlorobenzene containing $VO(acac)_2$ (40 mM) at 303 K for 4 days gave α-cumyl alcohol (25 mM), acetophenone (2 mM), α-methylstyrene (3.2 mM), and chlorotoluene (2 mM); acetylacetone was not formed although there was a significant yield of 4-hydroxypentan-2-one. The ratio A/K was ~14 which is considerably higher than the ratio obtained from reaction of cumylperoxyl with $VO(acac)_2$ and is very similar to the ratio obtained from reaction of $PhCMe_2O^{\cdot}$ with $Co(acac)_2$ (11). The residue which remained after removing the solvent and volatile reaction products was dissolved in chlorobenzene and the esr spectrum showed that $VO(acac)_2$ (~20 mM) had been regenerated.

Can. J. Chem. Downloaded from www.nrcresearchpress.com by 210.87.254.42 on 09/06/12
For personal use only.

The vanadium-51 nmr spectrum of the reaction mixture before distillation showed the presence of two major vanadium(V) species ($\delta_V = -522.3$ and -564.8 ppm) in almost equal yields and one minor vanadium component ($\delta_V = -656.8$ ppm). The product with $\delta_V = -522.3$ ppm increased in concentration at the expense of the product with $\delta_V = -564.8$ ppm upon standing at room temperature.

Nitroxyls

Reactions of nitroxides with $VO(acac)_2$ were not studied in any detail. We did, however, find that di-*tert*-butyl nitroxide and 2,2,6,6-tetramethyl-4-oxo-piperidine-1-oxyl react slowly with $VO(acac)_2$ in toluene, e.g., the rate constant for $(Me_3C)_2NO^\cdot$ is $\sim 0.7\ M^{-1}\ s^{-1}$ at 296 K.

Conclusions

The results of the kinetic and product study of the reaction of oxy radicals ($RO^\cdot$) with $VO(acac)_2$ presented in this paper can best be rationalized on the basis of a mechanism which involves an initial reversible reaction between the complex and the radical to give a vanadium(V) species followed by the slow irreversible decomposition of this species to give the final reaction products.

$$RO^\cdot + VO(acac)_2 \underset{-a}{\overset{a}{\rightleftharpoons}} ROVO(acac)_2$$

$$ROVO(acac)_2 \xrightarrow{b} \text{reaction products}$$

This means that the rate of radical disappearance should be given by

$$\frac{-d[RO^\cdot]}{dt} = \frac{k_b K_a [RO^\cdot][VO(acac)_2]}{1 + K_a[VO(acac)_2}$$

and the rate of disappearance of $VO(acac)_2$ by

$$\frac{-d[VO(acac)_2]}{dt} = \frac{k_b K_a [RO^\cdot][VO(acac)_2]}{1 + K_a[RO^\cdot]}$$

Rates of disappearance of $RO^\cdot$ and $VO(acac)_2$ under pseudo-first-order conditions are linearly dependent on the concentration of the reactant in excess suggesting that $K_a[RO^\cdot]$ and $K_a[VO(acac)_2]$ are both < 1. The measured rate constants k_5, k_6, k_7, and k_8 are, therefore, composite rate constants made of k_b and K_a and differences in these rate constants almost certainly reflect differences in the stability of $ROVO(acac)_2$, i.e., stability increases in the order galvinoxyl < tri-*tert*-butylphenoxo < di(1-adamantyl)methylene-iminoxo < *tert*-butylperoxo.

All the radicals except *tert*-butylperoxyl, for which the appropriate experiments were impossible to carry out, gave $-d[RO^\cdot]/dt > -d(VO(acac)_2]/dt$ suggesting that $VO(acac)_2$ was being regenerated during reaction.

Variable temperature studies on residual concentrations of phenoxy and iminoxy radicals, $VO(acac)_2$, and diamagnetic reaction products, very tentatively indicate that enthalpy changes, ΔH_a^0, increase in the order galvinoxy < 2,4,6-tri-*tert*-butylphenoxy < di-(1-adamantyl)methylene-iminoxy, in agreement with the order surmised from reactant decays.

Rates of reaction of oxy radicals with $VO(acac)_2$ are accelerated by methanol, an effect which may be accounted for by solvolysis of $ROVO(acac)_2$ to give the more stable $VO(OCH_3)_3$. The formation of a vanadium(V) species with a chemical shift similar to the shift for $VO(OC_2H_5)_3$ and quantitative reduction to ROH are, of course, consistent with this mechanism. We could, however, find no evidence for the formation of acetylacetone, a product of such a ligand exchange process.

The influence of the O—H bond strength in methanol on rates of reaction suggests that abstraction of the hydroxylic hydrogen from coordinated methanol as shown in [9] is rate controlling.

[9] 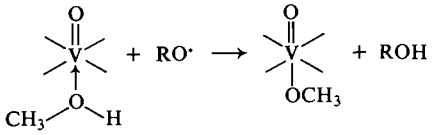

Interestingly, Nishinaga *et al.* (12) have reported an isotope effect of 1.6 for the reductive cleavage of 3,5-di-*tert*-butyl-4-oxo-1-alkylcyclohexa-1, 4-dienyl-1-peroxo(bis-3-salicylidene aminopropyl) amino cobalt(III) by CH_3OH and CH_3OD. These workers suggested that reduction involves the concerted hydrogen transfer mechanism

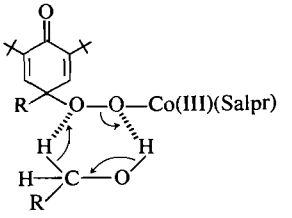

An analogous mechanism is, of course, improbable for vanadium(V) species of the form $ROVO(acac)_2$.

Reactions of cumylperoxy and cumyloxy radicals with $VO(acac)_2$ gave the same ratios of cumyl alcohol to acetophenone as reactions of these radicals with $Co(acac)_2$ (11), suggesting a common reaction mechanism.

Final reaction products in some cases were quite

complex. It should, however, be realized that glc, hplc, and nmr studies were performed sometimes after minimum radical and $VO(acac)_2$ concentrations were reached. Secondary reactions could, therefore, have been quite significant.

Acknowledgement

The authors are indebted to Dr. J. Ripmeester for measurement of the ^{51}V nmr spectra.

1. (*a*) R. HIATT. Organic peroxides. Vol. 2. *Edited by* D. Swern. J. Wiley and Sons, Inc., New York. 1971. Chapt. 1; (*b*) E. S. GOULD, R. R. HIATT, and K. C. IRWIN. J. Am. Chem. Soc. **90**, 4573 (1968); (*c*) C.-C. SU, J. W. REED, and E. S. GOULD. Inorg. Chem. **12**, 337 (1973); (*d*) R. CURCI, F. DI FURIA, R. TESTI, and G. MODENA. J. Chem. Soc. Perkin Trans. II, 752 (1974); (*e*) A. O. CHONG and K. B. SHARPLESS. J. Org. Chem. **42**, 1587 (1977); (*f*) R. CURCI, F. DI FURIA, and G. MODENA. J. Chem. Soc. Perkin Trans. II, 576 (1977); (*g*) S. CENCIA, F. DI FURIA, G. MODENA, R. CURCI, and J. O. EDWARDS. J. Chem. Soc. Perkin Trans. II, 979 (1978).
2. R. W. BRANDON and C. S. ELLIOTT. Tetrahedron Lett. 4375 (1967).
3. M. C. R. SYMONS. J. Chem. Soc. A, 1889 (1970).
4. M. A. DAROOGE and L. R. MAHONEY. J. Org. Chem. **32**, 1 (1967).
5. S. F. NELSEN and P. D. BARTLETT. J. Am. Chem. Soc. **88**, 137 (1966).
6. J. A. HOWARD and J. H. B. CHENIER. Can. J. Chem. **54**, 382 (1976).
7. W. ADAM and W. T. CHIU. J. Am. Chem. Soc. **93**, 3687 (1971).
8. J.H. B. CHENIER, E. FURIMSKY, and J. A. HOWARD. Can. J. Chem. **52**, 3682 (1974).
9. A. FORRESTER. Landholt–Börnstein, New Series, Vol. 9. Part B. *Edited by* H. Fischer and K.-H. Kellwege, Springer Verlag, Berlin, Heidelberg. 1979.
10. S. M. ALIWI and C. H. BAMFORD. J. Chem. Soc. Faraday Trans. I, 1733 (1975).
11. J. A. HOWARD and S. B. TONG. Can. J. Chem. **58**, 1962 (1980).
12. A. NISHINAGA, H. TOMITA, and T. MATSUURA. Tetrahedron Lett. **21**, 1261 (1980).

Can. J. Chem. Downloaded from www.nrcresearchpress.com by 210.87.254.42 on 09/06/12
For personal use only.

Studies on the products resulting from the conversion of aspen poplar to an oil[1]

RICHARD L. EAGER, JOSEPH F. MATHEWS, JAMES M. PEPPER,[2] AND HUSSEIN ZOHDI

Department of Chemistry and Chemical Engineering, University of Saskatchewan, Saskatoon, Sask., Canada S7N 0W0

Received February 13, 1981

RICHARD L. EAGER, JOSEPH F. MATHEWS, JAMES M. PEPPER, and HUSSEIN ZOHDI. Can. J. Chem. **59**, 2191 (1981).

Some observations are made on the nature of the reactions involved in the conversion of aspen poplar into a variety of chemical products as a result of its interaction with carbon monoxide and water in the presence of sodium carbonate at elevated temperatures and pressures. The original carbon content of the wood is distributed between an oil phase, a complex mixture of highly oxygenated water-soluble products many of which have been identified as low molecular weight aliphatic alcohols, ketones, and acids, and a gaseous phase consisting of mainly hydrogen and carbon dioxide. Using model substances (cellulose, cellobiose, D-glucose, D-fructose, D-xylose, D-sorbitol, glycerol, and an isolated lignin) information was obtained on the origin of the oil and of the water-soluble products. Studies at temperatures from 160° to 360°C revealed a marked exothermic reaction occurring in the 200–240°C range for wood and cellulose and which was reflected in the nature of the resulting product. With increasing temperature there is an increase in the yields of the water-soluble derivatives and also a change in their relative abundance.

RICHARD L. EAGER, JOSEPH F. MATHEWS, JAMES M. PEPPER et HUSSEIN ZOHDI. Can. J. Chem. **59**, 2191 (1981).

On a fait quelques observations sur la nature des réactions impliquées dans la transformation du peuplier en un certain nombre de produits sous l'action du monoxyde de carbone et de l'eau en présence du carbonate de sodium à des températures et à des pressions élevées. Le carbone contenu dans le bois avant la réaction est distribué entre une phase huileuse formée d'un mélange complexe de produits fortement oxygénés solubles dans l'eau parmi lesquels on retrouve plusieurs alcools aliphatiques, les cétones et acides de faibles masses moléculaires et une phase gazeuse constituée principalement d'oxygène et de bioxyde de carbone. En utilisant des substances modèles (cellulose, cellobiose, D-glucose, D-fructose, D-xylose, D-sorbitol, glycérol et une lignine isolée), on a obtenu des informations sur l'origine de l'huile et des produits solubles dans l'eau. Des études à des températures allant de 160 à 360°C ont révélé que, dans le cas du bois et de la cellulose, il se produit une réaction fortement exothermique dans l'intervalle de 200–240°C et que cette réaction se réflète dans la nature des produits obtenus. Une augmentation de la température provoque une augmentation des rendements en dérivés solubles dans l'eau ainsi qu'une évolution dans leur abondance.

[Traduit par le journal]

Introduction

The conversion of lignocellulosic materials into oils with potential use as fuels has been the subject of increasing interest. Several recent studies (1–6) have dealt with the variables affecting the yield and properties of the oil that is produced. In general the process involves the high temperature – high pressure reaction of carbon monoxide and/or hydrogen with the lignocellulosic material in the presence of water and a suitable catalyst. Similar studies are being conducted in these laboratories (6) using aspen wood (*Populus tremuloides*, Michx) to determine optimum conditions of reaction for oil production. The total conversion of the holocellulose (carbohydrate) and lignin (aromatic) components of the wood into markedly changed products must involve very complex chemical changes. It is best thought of as essentially a reductive process whereby oxygen is removed from the original lignocellulosic substrate to produce the oil with a greatly increased carbon content. The nature of this reducing action is not clear and may involve any or all of several pathways resulting from attack by the carbon monoxide, or by hydrogen (added or formed as a result of the water–gas shift reaction), or by other transient reducing species such as formate ion that may be generated under the conditions of the reaction.

By this process the lignocellulosic material is converted to products which are found to be distributed among the oil phase, the residual gaseous phase, and the aqueous phase which may be readily decanted from the oil phase. Since a significant amount (approximately one-third by weight) of the original mass of the wood was to be found in the aqueous phase, and since it was thought that such water-soluble compounds may be of relatively low molecular weight and thus more amenable to isolation and identification, this fraction was chosen for an initial more detailed study. It was believed that identification of these compounds could contribute to a clearer picture of the overall chemistry of the process. This paper reports mainly on the chemical nature of the compounds found in the aqueous layer, and, to a lesser extent, by means of a study of model substances, on the mechanism of formation of the oil, and of the water-soluble and gaseous products.

General Experimental Procedures

The reaction conditions chosen for this study were those

[1]Presented, in part, at the 63rd Canadian Chemical Conference, Ottawa, Ontario, June 1980.

[2]Author to whom correspondence should be addressed.

0008-4042/81/142191-08$01.00/0

©1981 National Research Council of Canada/Conseil national de recherches du Canada

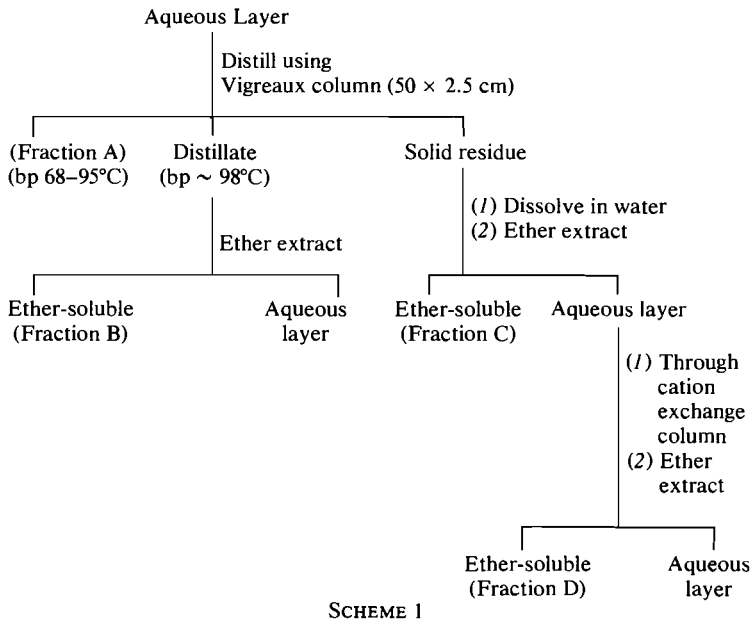

SCHEME 1

found earlier (6) to produce an oil in approximately 35% yield (based on wood meal) and whose fuel value was sufficiently attractive to warrant further study and to examine the mechanism of the reaction. The following standard conditions were adopted. The air-dried wood meal (5.4% moisture, 30 mesh) 100 g) from local aspen (*Populus tremuloides*, Michx) (18.8% lignin) was placed in the reaction vessel (1410 mL capacity) of a model 406-010A Aminco high pressure hydrogenator. To this was added a solution of water (500 mL) containing sodium carbonate (10 g), and carbon monoxide was admitted to an initial pressure of 3.4 MPa after twice flushing out the reactor. While being rocked the reactor was heated with continuous monitoring to 360°C (ca. 2.5 h required), held at this temperature (± 5°C) for one hour, and allowed to cool overnight. After sampling, the excess gases were released and the aqueous phase decanted from the oil phase. In a similar fashion cellulose (ashless powder for chromatographic use), cellobiose, D-glucose, D-fructose, D-xylose, an isolated lignin,[3] D-sorbitol, and glycerol were subjected separately to the same reaction conditions.

Gas Analysis

Chromatographic analysis of the gaseous phase was made using a copper column (1/8 in. × 15 ft) packed with silica gel (60–100 mesh), with argon as the carrier gas at a flow rate of 18 mL/min. Peak areas for individual gases were measured and their abundance determined from a previously prepared calibration curve.

Treatment of Aqueous Phase

From each run the aqueous phase (pH 6–7), which was initially colorless but rapidly darkened on exposure to air,[4] was treated as illustrated in Scheme 1.

Gas chromatographic analyses of fractions A, B, C, and D were made with a Model 5760 F & M Chromatograph with dual flame ionization detectors using stainless steel columns (1/8 in. od × 6 ft. Injections were made using 0.5 μL samples at an attenuation of $10^2 \times 16$ with nitrogen as carrier gas at a flow rate of 40 mL/min for fractions A, B, and C and 20 mL/min for fraction D. The amount of the cation exchange resin (REXYN 101; 220 mL) used was more than required to exchange the sodium ions.

Fraction A

The pale yellow liquid was chromatographed using a 1/8 in. od × 6 ft stainless steel column packed with Porapak Q (80/100 mesh), temperature programmed from 60 to 240°C at 6°/min and then held at 240°C. Typical chromatograms, with the main peaks identified, of this fraction from the runs using aspen wood, cellulose, and the isolated aspen lignin are shown in Figures 1, 2, and 3.

Fraction B

This small fraction was chromatographed using a 6 ft × 1/8 in. od column packed with 10% Carbowax 20 M on Chromosorb G (AW-DMCS treated) (60–80 mesh). The temperature was programmed from 40°C to 180°C at 6°/min and then held at 180°C. Several compounds were shown to be present differing from those found in fraction A but which have not been studied further.

Fraction C

The brown viscous liquid was chromatographed using the same column described for fraction B. The temperature was held at 30°C for six minutes, then programmed from 30°C to 180°C at 10°/min, and finally held at 180°C for two hours. Several peaks appeared representing higher boiling compounds than those found in fraction A. Their identification is under study but initial observations indicated the presence of low molecular weight phenolic compounds.

Fraction D

This fraction containing acidic compounds was chromatographed using a 6 ft × 1/8 in. od column packed with 10% SP-1200/1% H_3PO_4 on Chromosorb W (80–100 mesh, AW), programmed from 80°C to 180°C at 10°/min, and held at 180°C. Typical chromatograms with the main peaks identified from the runs using aspen wood and cellulose are shown in Figs. 4 and 5.

[3]Isolated according to the procedure of Pepper *et al.* (7, 8).

[4]For one run, emf measurements, relative to a standard calomel electrode, were made and showed an initial decrease from −0.0324 V to −0.496 V if done under nitrogen. Subsequent exposure to air resulted in a rapid increase of potential to around −0.12 V with simultaneous progressive darkening in color.

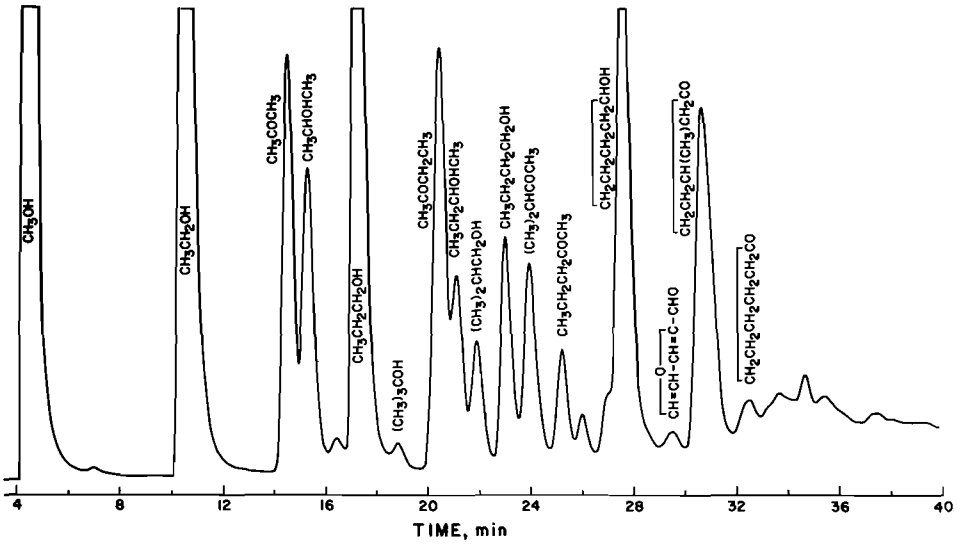

FIG. 1. Gas chromatogram of fraction A from aspen poplar.

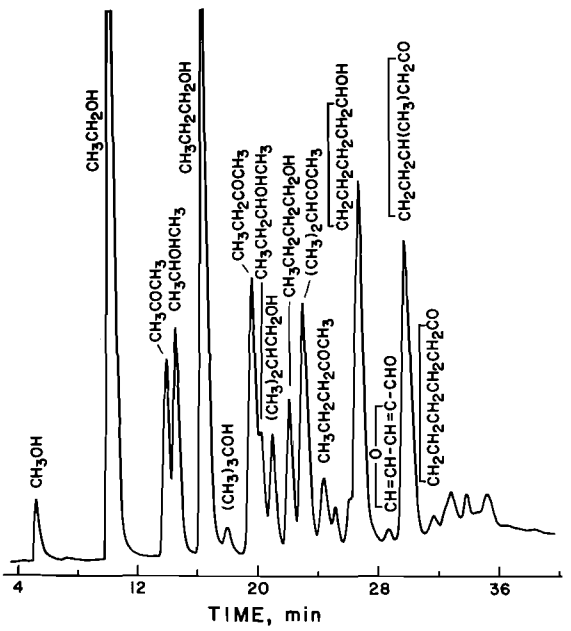

FIG. 2. Gas chromatogram of fraction A from cellulose.

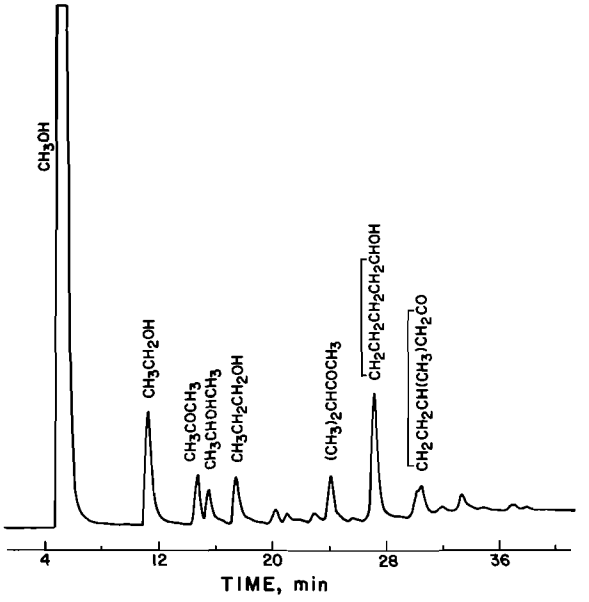

FIG. 3. Gas chromatogram of fraction A from aspen lignin.

Discussion of Results

Any consideration of the overall mechanism of this reaction must involve an understanding of the changes undergone by the wood (or its component parts) in its conversion to the oil, gases, and water-soluble products. The magnitude and complexity of these changes is illustrated by the analytical data given in Table 1 and in Figs. 1 and 4.

A few general observations about the mechanism may now be made. It is significant that from the polymeric cellulose as well as from the smaller units of cellobiose, glucose, and xylose an oil is produced very similar to that obtained from the whole wood. This would suggest that all the wood components (cellulose, hemicelluloses, and lignin) are converted to a closely related product. If the oil were being produced from the cellulose only, then the yields using pure cellulose should have been correspondingly greater. However, using the isolated lignin there is a significant difference, the proportional yield of product is greater and is of a charry nature rather than an oil. It is suggested that

TABLE 1. Analysis of starting materials and products

	Initially		Oil fraction			Fraction A	Residual gases[b]		
	C (%)	H (%)	Weight,[a] g	C (%)	H (%)	weight, g	CO_2	CO	H_2
Aspen wood	47.8	6.1	33	72.8	7.0	6.5	63	4	33
Cellulose	43.3	6.47	32	74.9	8.14	5.0	65	2	33
Lignin	58.3	5.4	27[c, d]	66.0 (tar)	6.55				
				60.2 (char)	5.85	2.5			
Cellobiose	42.1	6.43	37	71.1	7.62	4.7	60	1	39
Glucose	40	6.66	30	73.2	7.13	4.4			
Fructose	40	6.66	29.1[d]	73.2	6.7	4.5	67	2	31
Xylose	40	6.66	36.3	72.4	6.5	4.2			
Sorbitol	39.6	7.7	4.5	71.5	7.3	11.1	66	0	34
Glycerol	39.1	8.7	3.0	72.4	8.7	12.0	54	0	46
Blank[e]							53	3	44

[a] Per 100 g starting material.
[b] Calculated as mole percentages.
[c] Per 50 g lignin.
[d] Mostly char.
[e] Only water, sodium carbonate, and carbon monoxide.

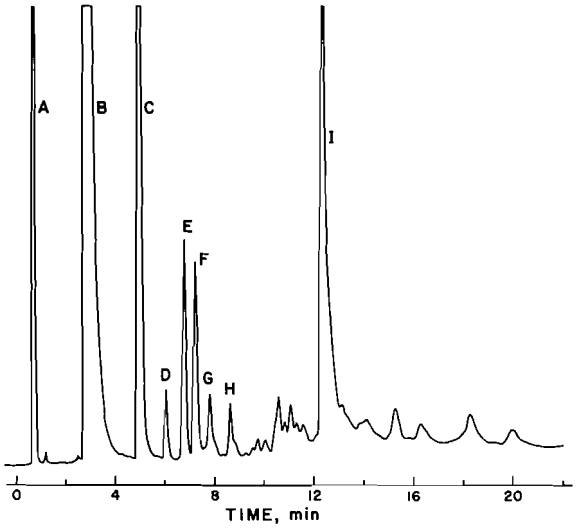

FIG. 4. Gas chromatogram of fraction D from aspen poplar. Compounds are: A, formic acid; B, acetic acid; C, propionic acid; D, isobutyric acid; E, butyric acid; F, γ-butyrolactone; G, 2- and/or 3-methylbutyric acid; H, valeric acid; I, γ-hydroxybutyric acid.

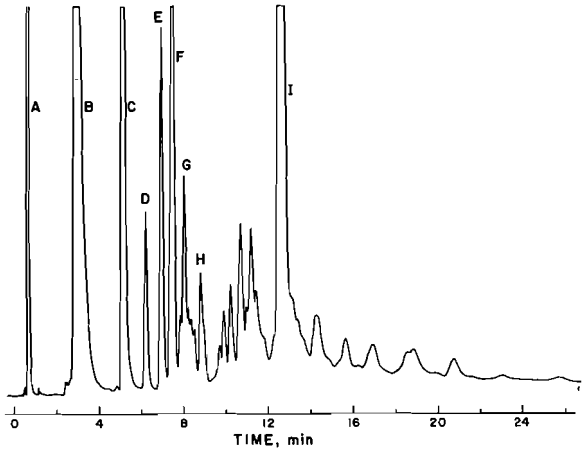

FIG. 5. Gas chromatogram of fraction D from cellulose. For compound identity see Fig. 4.

this may also occur if whole wood is used but that the char from the lesser lignin component is dissolved in the major oil fraction from the carbohydrates. Indeed this is borne out since the fluidity of wood oil is less than that from the carbohydrate model substances.

Of some mechanistic significance is that only from the potentially available aldoses was a fluid oil produced. Fructose (a ketose) gave rise to a char whereas sorbitol and glycerol gave minimal amounts of an oil product. A depolymerization of the cellulose (and likely the hemicelluloses) to smaller units more closely related to the dimer and the monomer is suggested, followed by conversion to the oil product. To check if the aqueous layer may contain such units, a recycling of this layer under the original conditions of temperature and pressure was made but no further oil was produced. Indeed this run also showed that the low molecular weight alcohols, ketones, and acids that were later found to be present in the aqueous layer did not contribute to the formation of the oil. The reduction (loss of oxygen content) of the starting materials to the oil product may result from a combination of dehydration and deoxygenation reactions with the oxygen reappearing in the highly complex mixture of highly oxygenated products (alcohols, ketones, and acids) found in the aqueous phase (Figs. 1 and 4) and in the components of the gaseous phase. The

TABLE 2. Role of sodium carbonate and/or carbon monoxide

Run	Reactant	Initial pressure psi CO	Initial pressure psi N_2	Na_2CO_3 g	Nonaqueous product Nature	Weight g	C %	H %	Aqueous phase pH[a]	Fraction A[b] g
1	Wood	500	0	0	Fine black powder	35.5	66.2	5.3	3	3.0
2	Wood	0	500	10	Tarry lump	28	70.3	6.8	6	4.5
3	Wood	0	500	0	Fine black powder	36.2	72.7	4.6	3	3.2
4	Wood	0	~20	0	Black powder	36	65.9	4.3	3	1.3
5	Cellulose	0	500	0	Fine black powder	42.5	68.6	4.3	3	0.65
6	Wood	500	0	10	Oil	33	72.8	7.0	7	6.5
7	Cellulose	500	0	10	Oil	32	74.9	8.1		5.0

[a] As determined using color pHast pH indicator sticks.
[b] All fractions A were pale yellow in color.

specific mode of production of these low molecular weight products is not yet understood. A blank run with only water, sodium carbonate, and carbon monoxide did not give rise to any of these compounds with the exception of a small amount of methanol, which may be expected from the reduction of the carbon dioxide formed as a result of the shift reaction at 360°C.

It is significant that the gas chromatograms of fraction A obtained from aspen wood (Fig. 1), cellulose (Fig. 2), cellobiose, glucose, fructose, or xylose are, with one exception, essentially identical in terms of the types and relative abundance of the oxygenated compounds. This exception is the significant production of methanol from the wood only and presumably is derived from the lignin (see below). These same fractions from sorbitol and glycerol show the presence of the same oxygenated compounds but in different relative abundance. In the case of the isolated lignin (Fig. 3), the interesting feature is the large methanol peak, which may have arisen from the methoxyl groups of the lignin. The much lesser amounts of the alcohols and ketones from the lignin sample are thought to have originated from the small amount of carbohydrate still associated with the lignin as a result of the procedure used for the isolation.[5] Analysis of the various fractions A obtained from the aqueous layers of fourteen similar experiments carried out in these laboratories (6) using wood meal and combinations of temperatures of 320°, 340°, and 360°C, sodium carbonate concentrations of 7.5, 10, and 12.5% (relative to dry wood meal), and initial pressures of carbon monoxide of 1.7, 3.4, and 5.1 MPa revealed no significant differences. Whatever the reactions are that produce the multiplicity of compounds obtained, they were not affected significantly by the variations of these parameters that were studied.

No mechanistic significance can be attached to the composition of the residual gases of runs carried out at 360° (Table 1). Indeed it would appear that the final relative abundance is largely a result of the shift reaction involving carbon monoxide. The role of the necessary carbon monoxide is not clear: it may function in part as a direct oxygen abstractor or be involved in the production of formate as proposed by Appell *et al.* (2).

The observations from the use of wood and model compounds suggested that the water-soluble products may arise from the high temperature and high pressure decomposition of carbohydrates, unrelated to the process of the oil production and independent of the presence of sodium carbonate and/or carbon monoxide. Some further information was obtained from a set of experiments, the details of which are given in Table 2. There is ample evidence for the need of both sodium carbonate and carbon monoxide if an oily fraction is to be produced. Carbonization of carbohydrates is believed to occur after the decomposition of the polysaccharides into monosaccharides. The carbohydrate fragments are then converted to intermediates by elimination of oxygen as carbon dioxide and water. This elimination is in agreement with the data obtained from Run 2, which resulted in the production of ~12 g of carbon as carbon dioxide, only ~1.1 g of which would have arisen from the added sodium carbonate. It is also of interest to note that the water-insoluble product is produced in each case in similar yields (35 ± 7%). This suggests

[5] An attempt was made by Dr. Ian Reid, Prairie Regional Laboratory, NRC, Saskatoon, to remove any residual carbohydrate by microbial degradation. However, neither the use of ONEZUKA R-10 Cellulase enzyme or Driselase Enzyme effected any change in the percentage carbon.

TABLE 3. Observations on the effect of reaction temperature

Temperature °C	Solid products: Nature	Weight g	Analysis % C	H	Aqueous phase: pH	Fraction A g	Gas phase (Mole percentage) H_2	CO	CO_2
160	"Unchanged" meal	82.5	47.4	6.27	7	0.40	—	90	10
190	Modified Meal	73.5	49.1	5.93	6	0.50	—	85	15
220	Powdery solid	66.0	51.6	6.30	4	1.2	—	80	20
245	Fluffy powder[a]	11.7	54.9	6.53	4	2.4	—	62	37
	Char[b]	36.9	64.0	6.00					
280	Tarry char	41.7	66.5	6.50	4	3.5	13	40	47
320	Tar	38.5	68.8	7.24	6	5.1	30	20	50
360	Oil	30.0	72.0	7.00	7	7.2	34	3	63

[a] From three replicate runs a total of ~45 g was recovered and recycled in an aqueous phase (no sodium carbonate added) and treated under standard conditions. A tarry material was produced weighing 12.5 g and analyzed: C 72.4%, H 7.4%.

[b] In a duplicate run when ~35 g were recycled in the aqueous phase (no sodium carbonate added) and treated under standard conditions, an oil was produced which weighed 28.6 g and analyzed: C 73.5%, H 7.4%.

that the overall conversion may be a two-stage process, an initial one to produce the significantly deoxygenated fraction, which is then subsequently converted (by reduction?) to the oily material.

Analysis of fraction A in each case showed essentially the same pattern of low-boiling monomeric compounds to be present (as per Fig. 1) but with a distinct variation in relative abundance. With the exception that from Run 5 there was negligible methanol produced, the products from Runs 3, 4, and 5 (without CO and Na_2CO_3) were similar, but the predominant compounds were the ketones with a much reduced relative abundance of the alcohols. If either carbon monoxide (Run 1) or sodium carbonate (Run 2) were present the relative abundance of the alcoholic components increased, suggesting a reducing role for each of these substances. The higher the initial applied pressure, be it from carbon monoxide or nitrogen (refer Runs 1, 2, 4), there is a marked increase in the yield of fraction A suggesting an enhanced penetration into the pores of the wood with a resulting increase in the overall reaction.

In monitoring the temperature of the reaction involving wood meal during the heating-up period, it had been noted that there always occurred a sudden rise in temperature indicative of a significant exothermic reaction. This happened in the 200–280°C range, depending on the initial reaction conditions. Such a temperature inflection appeared to a lesser degree with cellulose and not at all with the other model substances. To study this observation further a series of experiments, using wood meal, was carried out under the standard conditions used in this investigation but at several temperatures ranging from 160–360°C. The results are given in Table 3.

In this study of the liquefaction process of wood meal over the temperature range of 160–360°C, it is clear that a marked physical and chemical change of the wood substance occurs, which in turn appears to be associated in part with the observed exothermic reaction that occurs between 220°C and 240°C. It has been suggested (9) that such an exothermic reaction may be related to aromatization of carbohydrate substances. Before the inflection temperature (220°C) a powdery solid was left, representing 66% of the original wood mass, while after the inflection temperature (245°C) a light fluffy powder (11.7%) together with a charry material (~37%) was obtained. The carbon analysis of these products indicated that over the temperature range of the exothermic reaction, major chemical changes had also occurred and the overall conversion process had begun. The subsequent conversion, upon recycling, of the char and the fluffy powder (separately) into oil with an analysis similar to oil produced by a one-step treatment showed that these materials are the precursors of the oil in a standard run.

Another observation was made which may be of mechanistic significance. Recycling of the charry product (obtained at 245°C) resulted in the formation of 28.6 g of oil, while recycling of the fluffy powder (obtained from three runs at 245°C) produced 12.5 g of oil, or ~4 g of oil from one run. Combining the amount of oil obtained from recycling both the char and the fluffy powder (obtained from initially 100 g wood at 245°C) gives ~32.5 g of oil which is the average amount of oil obtained from a standard run. This observation suggests that each of the char and the fluffy powder is responsible for the production of a certain component of the oil. These products may differ in chemical composition and a further investigation of the nature of these oils will be required.

From the gas phase analyses it may be concluded that, as the temperature of the reaction increases,

TABLE 4. Gas chromatographic analysis of fractions A from runs at different temperatures[a]

Compound	Temperature (°C)						
	160	190	220	245	280	320	360
Methanol	8.2	22.1	22.8	16.5	31.3	47.2	30.8
Acetaldehyde	0.36	2.0	2.9	0.93	—	—	—
Ethanol	—	0.34	1.0	3.5	6.2	9.1	14.4
Acetone	1.2	3.6	7.7	8.1	6.4	5.1	4.7
2-Propanol	—	—	0.2	0.90	3.3	4.1	3.8
1-Propanol	—	—	0.12	1.0	4.8	7.8	10.3
2-Me-2-propanol	—	—	—	0.07	0.54	—	0.19
2-Butanone	0.36	2.7	7.2	5.4	7.2	6.1	5.9
2-Butanol	—	—	—	—	1.1	1.7	2.3
2-Me-1-propanol	—	—	—	0.05	0.46	1.4	1.5
1-Butanol	—	—	—	—	—	1.3	3.0
3-Me-2-butanone	—	—	0.24	2.4	7.1	4.6	2.8
2-Pentanone	—	0.24	1.06	1.07	1.4	1.7	1.7
Cyclopentanol	0.12	0.17	0.75	4.6	14.4	13.2	8.9
Furfural	0.20	5.1	2.8	1.9	0.76	0.8	0.23
3-Me-cyclopentanone	—	—	—	1.7	8.1	8.6	6.5
Cyclohexanone	0.37	1.1	2.2	4.3	3.7	0.79	1.1

[a] Data given are the abundances calculated relative to the yields from the run carried out at 360°C, and for which the sum of the peak areas identified and unidentified was assigned a value of 100.

carbon dioxide is being produced as a result of conversion of carbon monoxide by removal of oxygen from the wood components. Starting with the run at 220°C, the total number of moles of gases steadily increases. This may be seen from the data in Table 3 and as revealed by initial and final pressures measured at room temperature. It can be shown that for these runs the amount of carbon dioxide produced is greater than the corresponding loss of carbon monoxide, which suggests a removal of carbon from the wood and its conversion to carbon dioxide. At the higher temperatures further increases in the number of moles of gaseous products indicated that the shift reaction is becoming important. The relatively greater increase in carbon dioxide over hydrogen, however, may be the result of either more wood carbon being converted to carbon dioxide or the concurrent utilization of the hydrogen by some reduction process.

Although there is ample evidence (1) that water is necessary for oil production, its role is not clear. It should be noted that, as the temperature increases, the pH of the produced aqueous phase decreases from pH 12 (at 25°C; original sodium carbonate solution) to a minimum of pH 4 at 220–280°C and then increases again to pH 7 at 360°C. This suggests that as the temperature increases, acidic compounds are formed, and at higher temperatures (above 280°C), they are removed either by reduction or by decarboxylation.

It may be seen from Table 3, that as the temperature increases so does the yield of fraction A (low-boiling alcohols and ketones). From a gas chromatographic analysis of fraction A from each separate run, the relative abundances of the low-boiling compounds were calculated and are reported in Table 4. The relative abundance data are calculated relative to the yields of the run carried out at 360°C, and for which the sum of the peak areas (identified and unidentified) was assigned a value of 100. The peak area representing any compound (from any of the described runs) is reported as a percentage of the total area of the peaks in the chromatogram obtained from the run carried out at 360°C. It may be seen that at temperatures below the inflection point, the low-boiling distillate was composed, apart from methanol, mainly of ketonic compounds. As the temperature increases above the inflection temperature, the concentration of the alcoholic compounds increases while that of most of the ketonic compounds decreases. This suggests that the alcoholic compounds are formed by the reduction of ketonic compounds and/or formed directly from carbohydrate precursors.

Under the conditions used in this study the recovery of carbon and hydrogen in the oil represents approximately only half that originally present in the wood. Even though it has been shown (6) that the yield of the oil may be increased such that nearly two-thirds of the original carbon and hydrogen are recoverable in the oil, any successful commercialization of this type of process may depend on the utilization of all the products. In this study using aspen poplar wood, the recovery from 100 g of wood gave average yields of 33 g of an oil and a total of 19.5 g of water-soluble products (fraction A, 6.5 g; B, 0.7 g; C, 1.8 g; and D, 10.5 g).

These products represent a significant part of the wood in the form of recoverable chemicals of potential commercial value. Therefore an understanding of the chemical nature of water-soluble products is important and further research is needed to continue this study as well as to identify the chemical constituents of the oil. The approximately twenty percent oxygen content of the oil may mean that a secondary upgrading step would be required to produce a more useable higher quality fuel. In the long run it may be that this method of utilization of biomass be best adapted as a source of chemicals and, as such, as a viable alternative to the current use of fossil fuels for this purpose.

Acknowledgements

The authors gratefully acknowledge financial assistance from the Saskatchewan Research Council and the Canadian Forestry Service, Department of Environment (ENFOR Programme), and for the award (to H.Z.) of a University of Saskatchewan Graduate Scholarship.

1. H. R. APPELL. The production of oil from wood waste. Fuels from waste. Academic Press, Inc., New York. 1977. Chapt. VIII.
2. H. R. APPELL, Y. C. FU, S. FRIEDMAN, P. M. YAVORSKY, and I. WENDER. Converting organic wastes to oil. U.S. Bureau of Mines Report of Investigation No. 7560. 1971.
3. J. C. CAVALIER and E. CHORNET. Fuel, **56**, 57 (1977).
4. D. G. B. BOOCOCK, D. MACKAY, M. MCPHERSON, S. NADEAU, and R. THURIER. Can. J. Chem. Eng. **57**, 98 (1979).
5. D. G. B. BOOCOCK, D. MACKAY, H. FRANCO, and P. LEE. Can. J. Chem. Eng. **58**, 466 (1980).
6. R. L. EAGER, J. F. MATHEWS, and J. M. PEPPER. To be published.
7. J. M. PEPPER, P. E. T. BAYLIS, and E. ADLER. Can. J. Chem. **37**, 1241 (1959).
8. J. M. PEPPER and M. SIDDIQUEULLAH. Can. J. Chem. **39**, 390 (1961).
9. F. SHAFIZADEH. Adv. Carbohydr. Chem. **23**, 419 (1968).

Diastéréosélectivité de la réduction des alkyl-2 alkylidène-3 cyclopropyl alkyl cétones. Addition de RLi sur les aldéhydes α-cyclopropylidéniques

DOMINIQUE AUDO, MAURICE VINCENS, CLAUDE DUMONT ET MICHEL VIDAL[1]

Laboratoire de Chimie Organique, Université Scientifique et Médicale de Grenoble, B.P. 53 X, 38041 Grenoble Cedex, France

Reçu le 23 juin 1980[2]

DOMINIQUE AUDO, MAURICE VINCENS, CLAUDE DUMONT et MICHEL VIDAL. Can. J. Chem. **59**, 2199 (1981).

L'addition de RLi sur les alkyl-2 méthylène-3 cyclopropane carboxaldéhydes dans lesquels le groupement fonctionnel et le groupe alkyle présentent une relation *trans*, n'est pas diastéréosélective alors que la réduction des (alkyl-2 alkylidène-3 cyclopropyl) alkyl cétones présente pour certains termes une diastéréosélectivité élevée qui peut atteindre la stéréospécificité à basse température. Cette sélectivité dépend non seulement du degré de substitution du groupe fixé sur le carbonyle mais également du radical fixé en position 2 sur le cycle même s'il présente une relation *trans* par rapport au groupement fonctionnel. Les configurations relatives des alcools secondaires α-cyclopropylidéniques sont déterminées à partir de leurs données en ir et rmn; ces attributions de structures s'appuient, par ailleurs, sur une filiation chimique établie antérieurement.

DOMINIQUE AUDO, MAURICE VINCENS, CLAUDE DUMONT, and MICHEL VIDAL. Can. J. Chem. **59**, 2199 (1981).

The addition of RLi on *trans* 2-alkyl-3-methylene cyclopropane carboxaldehydes is not diastereoselective, while the reduction of *trans* (2-alkyl-3-alkylidene cyclopropyl) alkyl ketones shows for some compounds a high diastereoselectivity which may reach stereospecificity at low temperatures. This selectivity depends not only on the degree of substitution of the group fixed on the carbonyl but on the radical fixed in position 2 on the ring even though it shows a *trans* relation with the functional group.

The relative configurations of secondary α-cyclopropylidene alcohols are determined from their ir and nmr data.

Introduction

Un travail, actuellement en cours, sur la réactivité en milieu acide et à basse température des alcools secondaires α-cyclopropylidéniques nous a conduits à envisager l'étude de la réduction des (alkyl-2 alkylidène-3 cyclopropyl) alkyl cétones et de l'alkylation des alkyl-2 méthylène-3 cyclopropane carboxaldéhydes. Les alcools diastéréoisomères obtenus au cours de ces réactions, traités à basse température par un superacide (1), conduisent, en effet, au cation α-cyclopropylidénique. Ces dérivés peuvent donc apporter d'utiles informations pour la description de ce cation et pour l'étude de ses réactions de réarrangement.

L'induction asymétrique au cours de la réduction des cétones α-cyclopropaniques saturées ou vinyliques qui possèdent en α du carbonyle un carbone asymétrique, a motivé ces dernières années de nombreuses études (2 à 8). La diastéréosélection observée est généralement interprétée par le modèle stéréochimique de Karabatsos (9): le réactif nucléophile attaque la face du carbonyle la moins encombrée dans la conformation privilégiée du composé carbonylé. Ce type d'induction qui se situe dans le cadre plus général de l'induction asymétrique 1,2 (27, 28) et 1,3 (28, 29) a fait l'objet de nombreuses études.

La réduction des cétones α-cyclopropylidéniques qui possèdent, de même, un carbone asymétrique en α du groupement fonctionnel, n'a par contre pas été abordée. Cette étude pose le problème de l'identification des alcools diastéréoisomères qui résultent de cette réduction; à notre connaissance, seuls Bertrand et coll. ont proposé des attributions de configurations relatives dans le cas des (alkylidène-2 cyclopropyl) alkyl carbinols (10). On peut noter, par ailleurs, qu'en série cyclopropanique, il n'existe pas de méthode d'identification chimique simple permettant de distinguer les deux configurations relatives des alcools secondaires. Leur identification est généralement fondée sur des modèles stéréochimiques appliqués aux réactions de synthèse diastéréosélectives de ces alcools.

Dans ce mémoire, nous envisagerons successivement: (*1*) les résultats observés, quant à la diastéréosélection, au cours de la réduction des (alkyl-2 alkylidène-3 cyclopropyl) alkyl cétones dans lesquels le groupement fonctionnel et le groupe alkyle présentent une relation *trans* et de l'alkylation des aldéhydes homologues; (*2*) l'identification des configurations relatives des alcools secondaires α-cyclopropylidéniques. Cette identification est fondée sur les données ir et rmn de ces dérivés; les critères de configuration étant contrôlés sur un couple d'alcools diastéréoisomères, identifiés antérieurement par voie chimique (11); (*3*) le modèle stéréochimique permettant de prévoir la diastéréosélection observée. Nous envisagerons

[1]Auteur à qui correspondance doit être adressée.

[2]Révision reçue le 6 janvier 1981.

0008-4042/81/142199-11$01.00/0

©1981 National Research Council of Canada/Conseil national de recherches du Canada

Can. J. Chem. Downloaded from www.nrcresearchpress.com by 210.87.254.105 on 09/06/12
For personal use only.

Can. J. Chem. Downloaded from www.nrcresearchpress.com by 210.87.254.105 on 09/06/12
For personal use only.

essentiellement le cas de la réduction des cétones qui dans certaines conditions expérimentales peut être diastéréospécifique.

Partie expérimentale

(Alkyl-2 alkylidène-3 cyclopropyl) méthyl cétones 1, 7, 8, 9

A 0,2 mol d'acide cyclopropylidénique en solution dans 200 mL d'éther anhydre, on ajoute 0,4 mol de méthyllithium (1 *M* dans l'éther) en 30 min. Le mélange réactionnel est maintenu au reflux pendant une heure après la fin de l'addition. Après hydrolyse à 0°C en milieu acide (pH ≃ 3) et extraction à l'éther, la cétone est isolée par distillation sous pression réduite, puis purifiée par cpv (colonne Carbowax 20% de 6 m Chromosorb WAW 60/80, gaz vecteur H_2, θ = 140°C). Le rendement varie selon les termes de 70 à 80%.

Cétone 1: Composé **9** de la réf. 11.

Cétone 7: n_D^{20} 1,460$_5$; *E* 72°C/5 Torr; ir (film): ν(C=O) = 1700 cm^{-1}, ν(C=C) = 1740 cm^{-1}, ν(=C—H) = 3080 cm^{-1}, δ′(=CH_2) = 890 cm^{-1}; rmn (CCl_4/TMS): δH_1 = 2,18 ppm (1H, m), δH_2 = 2,00 ppm (1H, m), δ(=CH_2) = 5,38 ppm (2H, m), δ(CH_3—CO) = 1.98 ppm (3H, s), δ((CH_3)$_3$C) = 0,92 ppm (9H, s). Couplages: $^3J_{(H_1,H_2)}$ = 4,3 Hz, $^4J_{(H_2,H_{3b})}$ = 2,2 Hz, $^4J_{(H_1,H_{3b})}$ = 2,7 Hz, $^4J_{(H_1,H_{3a})}$ = 2.1 Hz, $^4J_{(H_2,H_{3a})}$ = 3,0 Hz.

Cétone 8: n_D^{20} 1,455$_0$; *E* 69°C/10 Torr; ir (film): ν(C=O) = 1696 cm^{-1}, ν(C=C) = 1750 cm^{-1}, ν(=C—H) = 3070 cm^{-1}, δ′(=CH_2) = 890 cm^{-1}; rmn (CCl_4/TMS): δH_1 = 2,10 ppm (1H, m), δ(=CH_2) = 5,32 et 5.37 ppm (2H, m), δ(*H_2*, CH_3CO) = de *1,80 à 2,00* (m), 1,96 ppm (s), (4H), δ(*CH_3*—CH_2) = 1,01 ppm (3H, t), δ(CH_3—*CH_2*) = 1,42 ppm (2H, m). Couplages: $^4J_{(H_2,H_{3b})} \simeq {}^4J_{(H_1,H_{3b})} \simeq {}^4J_{(H_1,H_{3a})} \simeq {}^4J_{(H_2,H_{3a})} \simeq$ 2,3 Hz. *Anal.* calc.: C 77,38, H 9,74, O 12,88; trouvé: C 77,48, H 9,52, O 12,85%.

Cétone 9: n_D^{20} 1,456$_0$: *E* 66°C/12 Torr; ir (film): ν(C=O) = 1695 cm^{-1}, ν(C=C) = 1750 cm^{-1}, ν(=C—H) = 3065 cm^{-1}, δ′(=CH_2) = 890 cm^{-1}; rmn (CCl_4/TMS): δH_1 = 2,06 ppm (1H, m), δ(=CH_2) = 5,36 et 5,41 ppm (2H, m), δ(*H_2*,CH_3CO) = de *1,80 à 2,00* ppm (m), 1,96 ppm (s), (4H), δCH_3 = 1,22 ppm (3H, d). Couplages: $^4J_{(H_2,H_{3b})} \simeq {}^4J_{(H_1,H_{3b})} \simeq$ 2,4 Hz, $^4J_{(H_1,H_{3a})}$ = 2,1 Hz, $^4J_{(H_2,H_{3a})}$ = 2,3 Hz. *Anal.* calc.: C 76,33, H 9,15, O 14,52; trouvé: C 76,47, H 9,11, O 14,46%.

(Alkyl-2 méthylène-3 cyclopropyl) alkyl cétones 2, 3, 4. Réaction d'alkylation

A une solution–suspension de 4 × 10^{-2} mol de $NaNH_2$ dans 50 mL de benzène, on ajoute 2 × 10^{-3} mol de cétone méthylée; le mélange réactionnel est maintenu à 40°C pendant 30 min. En maintenant la température constante, on ajoute alors 14 × 10^{-3} mol de MeI. L'agitation est poursuivie pendant deux heures. Après hydrolyse et extraction à l'éther la cétone est distillée puis purifiée dans les conditions précédentes. Le rendement est de l'ordre de 70 à 80%.

Cétone 2: *E* 75°C/8 Torr; ir (film): ν(C=O) = 1690 cm^{-1}, ν(C=C) = 1740 cm^{-1}, ν(=C—H) = 3075 cm^{-1}, δ′(=CH_2) = 885 cm^{-1}; rmn (CCl_4/TMS): δ(H_1,H_2) = 2 à 2,27 ppm (2H, m), δ(=CH_2) = 5,13 et 5,40 ppm (2H, m), δCH_3 = 1,02 (3H, d), δ((CH_3)$_3$C) = 1,14 ppm (9H, s).

Cétone 3: n_D^{20} 1,455$_6$; *E* 73°C/5 Torr; ir (film): ν(C=O) = 1690 cm^{-1}, ν(C=C) 1745 cm^{-1}, ν(=C—H) = 3067 cm^{-1}, δ′(=CH_2) = 882 cm^{-1}; rmn (CCl_4/TMS): δH_1 = 2,35 ppm (1H, m), δH_2 = 2,20 ppm (1H, m), δ(=CH_2) = 5,23 et 5,39 ppm (2H, m), δCH_3 = 1,01 (3H, t), δCH_2 = 1,42 (2H, m), δ(CH_3)$_3$C = 1,18 (9H, s). Couplages: $^3J_{(H_1,H_2)}$ = 4,4 Hz, $^4J_{(H_2,H_{3b})} = {}^4J_{(H_1,H_{3b})} \simeq$ 2,3 Hz, $^4J_{(H_1,H_{3a})}$ = 1,9 Hz, $^4J_{(H_2,H_{3a})}$ = 2,9 Hz.

Cétone 4: n_D^{20} 1,452$_5$; *E* 73°C/3 Torr; ir (film); ν(C=O) = 1695 cm^{-1}, ν(C=C) = 1745 cm^{-1}, ν(=C—H) = 3068 cm^{-1}, δ′(=CH_2) = 885 cm^{-1}; rmn (CCl_4/TMS): δH_1 = 2,46 ppm (1H, m), δH_2 = 2,13 ppm (1H, m), δ(=CH_2) = 5,20 et 5,30 ppm (2H, m), δ(CH_3)$_3$C = 0,93 ppm (9H, s), δ((CH_3)$_3$C—CO) = 1,18 ppm (9H, s).

(Tertiobutyl-2 méthylène-3 cyclopropyl) alkyl cétones 5, 6

Ces composés ont été préparés par alkylation partielle de la cétone méthylée **7** (26). A une solution–suspension de 7 × 10^{-2} mol de $NaNH_2$ dans 150 mL de benzène, on ajoute 4 × 10^{-2} mol de cétone méthylée; le mélange réactionnel est chauffé à 40°C pendant 30 min. En maintenant la température constante, on ajoute alors 4 × 10^{-2} mol de MeI; l'agitation est poursuivie pendant deux heures. Après hydrolyse, extraction à l'éther, la distillation du mélange brut (68 à 78°C/5 Torr) fournit 5 g de produits volatils dans lesquels on retrouve 50% de cétone **7** qui n'a pas réagi, 10% de cétone **6**, 25% de cétone **5** et 15% de cétone **4**. Ces quatre produits ont été séparés en chromatographie en phase gazeuse (dans les mêmes conditions que précédemment).

Cétone 6: ir (film): ν(C=O) = 1697 cm^{-1}, ν(C=C) = 1742 cm^{-1}, ν(=C—H) = 3070 cm^{-1}, δ′(=CH_2) = 885 cm^{-1}; rmn ^{1}H (CCl_4/TMS): δ$_1$(H_1,H_2) = 1,90 à 2,30 ppm (2H, m), δ(=CH_2) = 5,33 ppm (2H, m), δ(C*H_3*—CH_2) = 1,02 ppm (3H, t), $^3J_{(CH_2-CH_3)}$ = 7,2 Hz, δ(C*H_2*—CH_3) = 2,38 ppm (2H, q), δ(CH_3)$_3$C = 0,92 ppm (9H, s).

Cétone 5: n_D^{20} 1,450$_5$; ir (film): ν(C=O) = 1695 cm^{-1}, ν(C=C) = 1745 cm^{-1}, ν(=C—H) = 3068 cm^{-1}, δ′(=CH_2) = 885 cm^{-1}; rmn ^{1}H (CCl_4/TMS): δH_1 = 2,21 ppm (1H, m), δH_2 = 2,08 ppm (1H, m), δ(=CH_2) = 5,28 ppm (2H, m), δ$\left(CH(CH_3)_2\right)$ = 2,46 ppm (1H, h), δ$\left(CH(CH_3)_2\right)$ = 1,08 ppm (6H, d), $^3J\left(CH(CH_3)_2\right)$ = 8 Hz, δ(CH_3)$_3$C = 0,92 ppm (9H, s).

(Diméthyl-2,2 méthylène-3 cyclopropyl) méthyl cétone 10

En présence de cuivre en poudre (1 g) on ajoute lentement, en maintenant la température à 80°C, 0,35 mol de diazoacétate d'éthyle à 0,44 mol de bromo-2 méthyl-3 butène-2. Après décantation et distillation on obtient 0,046 mol de bromo-2 triméthyl-2,3,3 cyclopropanecarboxylate d'éthyle (rendement 13%). Les deux isomères n'ont pas été séparés; *E* 70 à 75°C/8 Torr; ir (film): ν(C=O) = 1725 cm^{-1}; rmn ^{1}H (CCl_4/TMS) du mélange des deux isomères: δ$\left(CH_3-C(Br)\right)$ = 1,99 et 1,50 ppm, δ(H—◁) = 1,92 et 1,87 ppm, δ$\left(C(CH_3)_2\right)$ = 1,29 ppm, δ(CH_2—CH_3) = 4,23 et 4,11 ppm, δ(CH_2—CH_3) = 1,29 et 1,25 ppm.

0,04 Mol de bromo-2 triméthyl-2,3,3 cyclopropanecarboxylate d'éthyle sont ajoutés à 100 mL d'une solution de potasse 3 *M* dans le butanol-1; le contact est maintenu pendant 12 h à 120°C. Après évaporation de l'alcool butylique sous pression réduite, le résidu est dissous dans l'eau et l'acide cyclopropylidénique précipité par addition d'acide chlorhydrique *N*.

Après extraction de la phase aqueuse à l'éther, la distillation fournit 4,3 g d'acide diméthyl-2,2 méthylène-3 cyclopropanecarboxylique (rendement: 80%); *E* 67°C/0,3 Torr; ir (film): ν(C=O) 1695 cm^{-1}, δ′(CH_2) = 895 cm^{-1}; rmn ^{1}H (CCl_4/TMS): δ$\left(H-\triangledown\right)$ = 1,85 ppm (1H, m), δ$\left(C(CH_3)_2\right)$ = 1,29 et 1,32 ppm (6H, 2 singulets), δ(=CH_2) = 5,37 ppm (2H, m), δ(OH) = 8,27 ppm (1H, s).

Le mode opératoire de la réduction de l'acide diméthyl-2,2 méthylène-3 cyclopropanecarboxylique par MeLi est identique à celui décrit pour la synthèse de **1**, **7**, **8**, **9**. La distillation (*E* 69°C/11 Torr) permet d'obtenir la cétone **10** avec un rendement de 46%.

Can. J. Chem. Downloaded from www.nrcresearchpress.com by 210.87.254.105 on 09/06/12
For personal use only.

Cétone 10: ir (film): ν(C=O) = 1700 cm^{-1}, ν(C=C) = 1745 cm^{-1}, ν(=C—H) = 3055 cm^{-1}, δ′(=CH_2) = 883 cm^{-1}; rmn ^1H (CCl_4/TMS): δ(H_1) = 2,11 ppm (1H, m), δ(H_{3a}) = 5,18 ppm (1H, d), δ(H_{3b}) = 5,26 (1H, d), $^4J_{H_1-H_{3a}} \simeq 2{,}0$ Hz, $^4J_{H_1-H_{3b}} \simeq 2{,}5$ Hz, δ(CH_3—C=O) = 2,05 ppm (3H, s), δ($(CH_3)_2$C) = 1,13 ppm et 1,24 ppm (6H, 2 singulets).

Réduction des cétones 1à 10

A une solution de 0,1 mol de cétone dans l'éther anhydre, on ajoute 0,1 mol de $AlLiH_4$ en solution–suspension dans l'éther. Après la fin de l'addition, le mélange réactionnel est maintenu au reflux pendant 30 min puis hydrolysé à 0°C, neutralisé par HCl (1 *N*) et extrait à l'éther. Le mélange d'alcools est distillé sous pression réduite; le rendement de réduction (diastéréoisomères I + II) varie de 80 à 95%. L'étude en cpv analytique du mélange réactionnel brut ne permet de détecter que les isomères I et II qui sont isolés en cpv préparative sur colonne Carbowax (20%) de 4 m (Chromosorb P, NAW 60/80, gaz vecteur H_2).

Les masses molaires déterminées par spectrométrie de masse correspondent aux composés décrits et les formules brutes sont en accord avec leur analyse élémentaire; quelques-unes de celles-ci seront détaillées. Les indices de réfraction n_D^{20} n'ont pas été déterminés pour les alcools **17**, **18**, **19**, **21** et **22** longs à obtenir à l'état pur. La rmn ^1H a été réalisée à 60 MHz.

Couple d'isomères 11 et 12: voir réf. 11.

Couple d'isomères 13 et 14: *E* (du mélange) ≃ 42 à 47°C/1,9 Torr. Alcool **13**: n_D^{20} $1{,}454_0$; ir (film): ν(=C—H) = 3055 cm^{-1}, ν(C=C) = 1750 cm^{-1}, δ′(=C—H) = 890 cm^{-1}, ν(OH) voir tableau 1; rmn ^1H (CCl_4/TMS): δR′ = 1,15 ppm (3H, pic large), δR = 0,92 ppm (9H, s), δH_4 = 2,70 ppm (1H, d), δH_{3a} et H_{3b} = 5,20 ppm (2H, pic large), δH_1 et H_2 massif entre 1,0 et 1,2 ppm (2H), $^3J_{H_1-H_4}$ = 7,4 Hz. Alcool **14**: n_D^{20} $1{,}454_7$; ir (film): ν(=C—H) = 3058 cm^{-1}, ν(C=C) = 1760 cm^{-1}, δ′(=C—H) = 885 cm^{-1}, ν(OH) voir tableau 1; rmn ^1H (CCl_4/TMS): δR′ = 1,20 ppm (3H, pic large), δR = 0,92 (9H, s), δH_4 = 2,64 ppm (1H, d), δH_{3a} et H_{3b} = 5,02 et 5.17 ppm (1H × 2), δH_1 et H_2 massif entre 1,2 et 1,4 ppm (2H), $^3J_{H_1-H_4}$ = 8,4 Hz. *Anal.* calc.: C 77,87, H 11,76, O 10,37; trouvée (**13**): C 77,60, H 11,82, O 10,75; (**14**): C 78,05, H 11,46, O 10,20%.

Couple d'isomères 15 et 16: *E* (du mélange) ≃ 44 à 49°C/1,5 Torr. Alcool **15** n_D^{20} $1{,}455_7$; ir (film): ν(=C—H) = 3060 cm^{-1}, ν(C=C) = 1755 cm^{-1}, δ′(=C—H) = 883 cm^{-1}, ν(OH) voir tableau 1; rmn ^1H (CCl_4/TMS): δR′, H_1 et H_2 massif entre 1,0 et 1,4 ppm (7H), δR = 0,97 ppm (9H, s), δH_4 = 2,77 ppm (1H, d), δH_{3a} et H_{3b} = 5,36 ppm (2H, pics larges), $^3J_{H_1-H_4}$ = 6.9 Hz. Alcool **16** n_D^{20} $1{,}454_8$; ir (film): ν(=C—H) = 3058 cm^{-1}, ν(C=C) = 1755 cm^{-1}, δ′(=C—H) = 888 cm^{-1}, ν(OH) voir tableau 1; rmn ^1H (CCl_4/TMS): δR′, H_1 et H_2 massif entre 1,0 et 1,4 ppm (7H), δR = 0,95 ppm (9H, s), δH_4 = 2,65 ppm (1H, d), δH_{3a} et H_{3b} = 5,20 et 5,32 ppm (1H × 2), $^3J_{H_1-H_4}$ = 8,5 Hz.

Couple d'isomères 17 et 18: *E* (du mélange) ≃ 50 à 55°C/0,8 Torr. Alcool **17**: ir (film): ν(=C—H) = 3055 cm^{-1}, ν(C=C) = 1750 cm^{-1}, δ′(=C—H) = 890 cm^{-1}, ν(OH) voir tableau 1; rmn ^1H (CCl_4/TMS): δR′ = 0.88 ppm (9H, s), δR = 0,92 ppm (9H, s), δH_4 = 2,81 ppm (1H, d), δH_{3a} et H_{3b} = 5,20 et 5,40 ppm (1H × 2), δH_1 et H_2 massif vers 1,1 ppm (2H), $^3J_{H_1-H_4}$ = 5,7 Hz. Alcool **18**: ir (film): ν(=C—H) = 3060 cm^{-1}, ν(C=C) = 1755 cm^{-1}, δ′(=C—H) = 890 cm^{-2}, ν(OH) voir tableau 1; rmn ^1H (CCl_4/TMS): δR′ = 0,87 ppm (9H, s), δR = 0,92 ppm (9H, s), δH_4 = 2,60 ppm (1H, d), δH_{3a} et H_{3b} = 5,25 ppm (2H, pic large), δH_1 et H_2 massif vers 1,4 ppm (2H), $^3J_{H_1-H_4}$ = 8,6 Hz. Remarque: les composés **17** et **18** dont les temps de rétentions sont voisins ont été purifiés par passages répétés en cpv sur colonne Carbowax. Le composé **18** a été isolé à partir du mélange de réduction de la cétone **4**, le composé **17** à partir du mélange de réduction de l'aldéhyde **38** par *t*BuLi.

Couple d'isomères 19 et 20; non distillé: la cétone **5** étant difficile à obtenir en quantité suffisante, **19** et **20** ont été isolés en cpv à partir du mélange brut de réduction. Alcool **19**: ir (film): ν(=C—H) = 3057 cm^{-1}, ν(C=C) = 1757 cm^{-1}, δ′(=C—H) = 887 cm^{-1}, ν(OH) voir tableau 1; rmn ^1H (CCl_4/TMS): δR′ = 0,90 ppm (9H, s), δR = 0,95 ppm (6H, d) et 1,55 ppm (1H, m), δH_4 = 2,90 ppm (1H, m), δH_{3a} et H_{3b} = 5,38 et 5,50 ppm (1H × 2), δH_1 et H_2 = 1,2 et 1,4 ppm (2H, m), $^3J_{(H_1-H_4)}$: mal lisible, $^3J((CH_3)_2$–C*H*) = 6,8 Hz, $^3J_{H_4-R} \simeq 7$ Hz. Alcool **20**: n_D^{20} $1{,}456_0$; ir (film): ν(=C—H) = 3062 cm^{-1}, ν(C=C) = 1752 cm^{-1}, δ′(=C—H) = 892 cm^{-1}; ν(OH) voir tableau 1; rmn ^1H (CCl_4/TMS): δR′ = 0,90 ppm (9H, s), δR = 0,95 ppm (6H, d), δH_4 = 2,80 ppm (1H, m), δH_{3a} et H_{3b} = 5,35 ppm (2H, pic large), δCH(R) et δH_1 et H_2: massif entre 1,2 et 1,5 ppm (3H), $^3J_{H_1-H_4}$ = 5,8 Hz, $^3J((CH_3)_2$–C*H*) = 6,8 Hz, $^3J_{H_4-R}$ = 7,0 Hz.

Couple d'isomères 21 et 22; non distillé: la cétone **6** étant difficile à obtenir en quantité suffisante, **21** et **22** ont été isolés en cpv à partir du mélange brut de réduction. Alcool **21**: ir (film): ν(=C—H) ≃ 3060 cm^{-1}, δ′(=C—H) ≃ 890 cm^{-1}, ν(OH) voir tableau 1; rmn ^1H: δR′ = 0,90 ppm (9H, s), δCH_3(R) = 0,95 ppm (3H, t), δH_4 = 3,00 ppm (1H, m), δH_{3a} et H_{3b}: massif entre 5,4 et 5,5 ppm (2H), δCH_2(R) et δH_1 et H_2: massif entre 1,2 et 1,5 ppm (3H), $^3J_{H_1-H_4}$ et $^3J_{H_4-CH_2}$ mal lisibles, $^3J(CH_2-CH_3) \simeq 6{,}8$ Hz. Alcool **22**: ir (film): ν(=C—H) ≃ 3060 cm^{-1}, δ′(=C—H) ≃ 890 cm^{-1}, ν(OH) voir tableau 1: rmn ^1H: δR′ = 0,89 ppm (9H, s), δCH_3(R) = 0,95 ppm (3H, t), δH_4 = 3,03 ppm (1H, m), δH_{3a} et H_{3b} = 5,35 ppm (2H, pic large), δCH_2(R) et δH_1 et H_2: massif entre 1,2 et 1,5 ppm (3H), $^3J_{H_1-H_4}$ = 6,2 Hz, $^3J_{H_4-CH_2}$ = 6,4 Hz, $^3J(CH_2-CH_3) \simeq 6{,}8 \pm 0{,}2$ Hz.

Couple d'isomères 23 et 24: *E* du mélange ≃ 47 à 55°C/2,6 Torr. Alcool **23**: n_D^{16} $1{,}454_8$; ir (film): ν(=C—H) = 3050 cm^{-1}, ν(C=C) = 1740 cm^{-1}, δ′(=C—H) = 882 cm^{-1}, ν(OH) voir tableau 1; rmn ^1H (CCl_4/TMS): δR′ = 0,81 ppm (9H, s), δR = 1,13 ppm (3H, d), δH_4 = 3,24 ppm (1H, m), δH_{3a} et H_{3b} = 5,25 et 5,38 ppm (1H × 2), δH_1 et H_2 = 1,25 et 1,11 ppm (1H × 2, m), δH_1-H_4 = 7,3 Hz, $^3J(CH_3-H_4)$ = 6,5 Hz. Alcool **24**: n_D^{16} $1{,}455_5$; ir (film): ν(=C—H) = 3055 cm^{-1}, ν(C=C) = 1745 cm^{-1}, δ′(=C—H) = 884 cm^{-1}, ν(OH) voir tableau 1; rmn ^1H (CCl_4/TMS): δR′ = 0,87 ppm (9H, s), δR = 1,15 ppm (3H, d), δH_4 = 3,28 ppm (1H, m), δH_{3a} et H_{3b} = 5,28 ppm (2H, pic large), δH_1 et H_2: massif entre 1,21 et 1.26 (2H, m), $^3J_{H_1-H_4}$ = 6,8 Hz, $^3J(CH_3-H_4)$ = 6,6 Hz. *Anal.* calc.: C 77,87, H 11,76, O 10,37; trouvé (**23**): C 77,43, H 11,82, O 10,60; (**24**): C 77,36, H 11,95, O 10,72%.

Couple d'isomères 26 et 27: *E* du mélange ≃ 41 à 50°C/5 Torr. Alcool **26**: n_D^{20} $1{,}451_2$; ir (film): ν(=C—H) = 3052 cm^{-1}, δ′(=C—H) = 885 cm^{-1}, ν(OH) voir tableau 1; rmn ^1H: δR′ = 1,15 ppm (3H, d), δR,H_1,H_2: massif vers 1,20 ppm (5H), δH_4 = 3,40 ppm (1H, m), δH_{3a} et H_{3b} = 5,30 et 5,40 ppm (1H × 2), $^3J_{H_1-H_4}$ = 6,9 ± 0,2 Hz, $^3J_{H_4-CH_3} \simeq 6{,}4$ Hz. Alcool **27**: n_D^{20} $1{,}451_7$; ir (film): ν(=C—H) = 3055 cm^{-1}, δ′(=C—H) = 885 cm^{-1}, ν(OH) voir tableau 1; rmn ^1H: δR′ = 1,15 ppm (3H, d), δR,H_1,H_2: massif vers 1,15 à 1,20 ppm (5H), δH_4 = 3,25 ppm (1H, m), δH_{3a} et H_{3b} = 5,27 ppm (2H, pic large), $^3J_{H_1-H_4}$ = 7,2 Hz, $^3J_{H_4-CH_3}$ = 6,4 Hz. *Anal.* calc.: C 74,95, H 10,78, O 14,26; trouvée (**26**): C 74,70, H 10,95, O 14,67; (**27**): C 74,61, H 10,80, O 14,45%.

Couple d'isomères 28 et 29: *E* du mélange ≃ 43 à 52°C/1,5 Torr. Alcool **28**: ir (film): ν(=C—H) = 3060 cm^{-1}, δ′(=C—H) = 883 cm^{-1}, ν(OH) voir tableau 1; rmn ^1H (CCl_4/TMS): δR′ = 1,07 et 1,12 ppm (6H, 2 singulets), δR = 1,22 ppm (3H, d), δH_4 = 3,40 ppm (1H, m), δH_{3a} et H_{3b} = 5,28 et 5,42 ppm (1H × 2, pics larges), δH_1 vers 1,30 ppm (1H), $^3J_{(H_1-H_4)}$ = 8,6 Hz, $^3J_{(H_4-CH_3)}$ = 6,4 Hz. Alcool **29**: ir (film): ν(=C—H) = 3055 cm^{-1}, ν(=C—H) = 885 cm^{-1}, ν(OH) voir tableau 1; rmn ^1H (CCl_4/TMS): δR′ = 1,20 ppm (6H, s), δR = 1,25 ppm (3H, pic large), δH_4 = 3,42 ppm (1H, m), δH_{3a} et H_{3b} = 5,15 et 5,21 ppm (1H × 2), δH_1 entre 1,25 et 1,30 ppm (1H), $^3J_{H_1-H_4}$ = 9,1 Hz, $^3J_{H_4-CH_3}$ = 6,3 Hz. *Anal.*

Can. J. Chem. Downloaded from www.nrcresearchpress.com by 210.87.254.105 on 09/06/12
For personal use only.

calc.: C 76,14, H 11,18, O 12,68; trouvée (**28**): C 76,02, H 11,20, O 12,75; (**29**): C 76,00, H 11,25, O 12,80%.

Synthèse des alcools α-cyclopropylidéniques primaires 33 à 35

Les alcools α-cyclopropéniques **30** à **32** sont préparés selon réf. 14. On additionne les alcools ainsi obtenus (0,006 mol) à une solution–suspension de 0,03 mol de tertiobutylate de potassium dans 10 mL de diméthylsulfoxyde anhydre. Après une heure de réaction à 20°C, on hydrolyse à froid avec 80 mL d'eau. La phase organique, extraite à l'éther, lavée à l'eau, est séchée sur sulfate de sodium. La distillation conduit aux alcools cyclopropylidéniques **33** à **35** avec un rendement moyen de 70%.

Alcool 33: *E* 37°C/7 Torr; ir (film): ν(=CH) = 3065 cm^{-1}, ν(C=C) = 1758 cm^{-1}, δ′(=CH) = 880 cm^{-1}; rmn de H_1, 60 MHz (CCl_4/TMS): δ(CH_3) = 1,20 ppm (3H, d), δ(=CH_2) = 5,35 ppm (2H, m), δ(CH_2OH) = 3,40 ppm (2H, m). H_1 et H_2 résonnent entre 1,20 et 1,50 ppm et ne sont pas analysables; $J_{(H_2, CH_3)}$ = 6,4 Hz.

Alcool 34: *E* (**34**) 40°C/6 Torr; *E* (**35**) 42°C/3,4 Torr; ir (film): ν(=CH) = 3065 cm^{-1}, ν(C=C) = 1755 cm^{-1}, δ′(=CH) = 875 cm^{-1}; rmn de ^1H (CCl_4/TMS): δ(CH_2—CH_3) = 1,0 ppm (3H, t), δ(=CH_2) = 5,33 ppm (2H, m), δ(CH_2OH) = 3,43 ppm. H_1, H_2 et CH_2—CH_3 résonnent entre 1,20 et 1,70 ppm et ne sont pas analysables à 60 MHz; $J_{(H_2-CH_2CH_3)}$ = 6,4 Hz et $J(CH_2-CH_3)$ = 6,5 Hz, ont été déterminés à 250 MHz. L'alcool **35** présente en ir et rmn des caractéristiques analogues à celles de **33** et **34**.

Oxydation des alcools 33 à 35 en aldéhydes 36 à 38

Elle a été réalisée selon la méthode de Sarett et coll. (15); 4,5 g d'anhydride chromique sont introduits par petites portions dans 50 mL de pyridine anhydre maintenue à 15°C. On ajoute 0,01 mol d'alcool **33** à **35** et on poursuit l'agitation pendant 15 h. Le mélange réactionnel est versé dans de l'eau glacée et extrait à l'éther. La phase organique est acidifiée à pH ≃ 2 par une solution acide 3 *N*. Après sèchage, évaporation du solvant, la distillation fournit les aldéhydes **36** à **38**; rendement moyen: 45%.

Aldéhyde 36: *E* 45°C/2,5 Torr; ir (film): ν(=CH_2) = 3080 cm^{-1}, ν(CHO) = 2730 cm^{-1}, ν(C=O) = 1720 cm^{-1}, δ′(C=C) = 895 cm^{-1}; rmn de ^1H, 60 MHz (CCl_4/TMS): δ(CH_3) = 1,25 ppm (3H, d), δ(H_1 et H_2) ≃ 2,05 ppm, δ(CHO) = 8,70 ppm (1H, d), δ(=CH_2) = 5,55 ppm (2H, m); $^3J_{(H_1,CHO)}$ = 5,5 Hz, $^3J_{(H_2,CH_2)}$ = 6,0 Hz.

Aldéhyde 37: *E* 51°C/1,7 Torr; ir (film): ν(=CH_2) = 3080 cm^{-1}, ν(CHO) = 2730 cm^{-1}, ν(C=O) = 1715 cm^{-1}, δ′(C=C) = 890 cm^{-1}; rmn de ^1H, 60 MHz (CCl_4/TMS): δ(CH_2,CH_3) = 0,95 ppm (3H, t), δ(H_1,H_2,CH_2) vers 2 ppm, δ(CHO) = 8,70 ppm (1H, d), δ(=CH_2) = 5,40 ppm (2H, m), $^3J_{(H_1,CHO)}$ = 5,4 Hz.

Aldéhyde 38: *E* 55°C/1,9 Torr; ir (film): ν(=CH_2) = 3075 cm^{-1}, ν(CHO) = 2720 cm^{-1}, ν(C=O) = 1710 cm^{-1}, δ′(C=C) = 895 cm^{-1}; rmn de ^1H, 60 MHz (CCl_4/TMS): δ(*t*Bu) = 0,96 ppm (9H, s), δ(H_1,H_2) vers 2,10 ppm, δ(CHO) = 8,78 ppm (1H, d), δ(=CH_2) = 5,60 ppm, $^3J_{(H_1,CHO)}$ = 5,5 Hz.

Alkylation des aldéhydes 36 à 38 par RLi

Les alkyllithiums commerciaux utilisés sont en solution dans le pentane. La réaction est réalisée sous azote à −70°C, et l'alkyllithium est introduit à la seringue au travers d'une membrane dans les proportions suivantes: 0,016 mol de RLi dans une solution de 0,004 mol d'aldéhyde dans 50 mL d'éther. L'agitation est maintenue pendant 2 h, la température du mélange réactionnel demeurant inférieure à −60°C. Après hydrolyse sur un mélange eau–glace et extraction à l'éther, les alcools diastéréoisomères (**13** à **20**) sont séparés en cpv sur colonne Carbowax NAW, 4,30 m; rendement moyen: 50 à 60%.

Equilibration des alcools 23 et 24 en présence de Al(OiPr)$_3$

Une solution contenant 180 mg d'alcool **23** (ou **24**), 240 mg d'isopropylate d'aluminium, 50 μL d'acétone et 3 mL d'isopropanol est maintenue à ébullition pendant 5 jours. Après hydrolyse et neutralisation, le mélange est analysé en cpv sur colonne Carbowax (20%) de 4 m (Chromosorb P NAW 60/80, gaz vecteur: H_2; θ = 150°C).

Techniques analytiques

Les spectres rmn de ^1H ont été tracés sur appareils Perkin-Elmer R.10 (60 MHz) et Cameca (250 MHz). Les constantes de couplages allyliques et homoallyliques ont été déterminées à 250 MHz.

Les spectres ir ont été tracés sur un appareil Perkin-Elmer 521 à réseaux (vitesse 3 cm min^{-1}). Une dilution progressive dans CCl_4 séché, jusqu'à 10^{-3} mol L^{-1}, a permis d'éliminer les associations intermoléculaires. Les solutions ont été préparées sous atmosphère d'azote anhydre (KOH; P_2O_5) et les cuves maintenues dans une enceinte sèche pendant le tracé des spectres; ces conditions sont nécessaires pour éliminer les bandes d'absorption de l'eau.

Résultats et discussion

1. *Réduction des (alkyl-2 alkylidène-3 cyclopropyl) alkyl cétones (1 à 10)*

L'isomérisation en milieu basique des esters α-cyclopropéniques, dont la synthèse est maintenant bien connue (12), conduit aux acides α-cyclopropylidéniques dans lesquels le groupe alkyle et le groupement fonctionnel présentent une relation *trans* par rapport au cycle (13). La réduction du groupement carboxylique par le méthyllithium fournit les cétones α-cyclopropylidéniques méthylées **1**, **7**, **8**, **9**,**10**. L'alkylation de certains de ces termes, en solution dans le benzène et en présence d'amidure de sodium, par l'iodure de méthyle, permet d'accéder aux dérivés **2**, **3**, **4**, **5**, **6**.

La réduction à 39°C (par une solution–suspension dans l'éther d'aluminohydrure de lithium) des cétones α-cyclopropylidéniques **1** à **10**, dont les faces du carbonyle sont diastéréotopiques, conduit au couple d'alcools diastéréoisomères I et II (**11** à **29**). Les diastéréoisomères II sont ceux dans lesquels R et C_3 d'une part et H_4 et C_2 d'autre part peuvent être simultanément quasi-éclipsés.

Les alcools ont été isolés par cpv préparative à l'exception de **25***a* et **25***b* qui ont cependant été détectés et dosés en cpv analytique et en rmn de ^1H.

2. *Réduction des alkyl-2 méthylène-3 cyclopropane carboxaldéhydes (36 à 38)*

La réduction des esters cyclopropylidéniques par $AlLiH_4$ en solution dans l'éther conduit facilement aux alcools cyclopropéniques (14) qui, traités en milieu basique, subissent la migration exocyclique de la double liaison. L'oxydation ménagée (15) des alcools cyclopropylidéniques ainsi obtenus permet d'accéder aux aldéhydes **36** à **38**.

La transformation des aldéhydes **36** à **38** par les alkyllithium (EtLi, *i*PrLi, *t*BuLi), en solution dans l'éther à 0°C, présente une diastéréosélection négli-

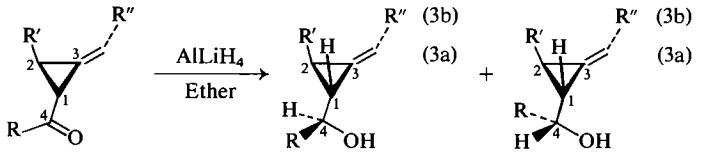

R	R′	R″		Diastéréoisomère[a] (II)	Diastéréoisomère (I)
Me	Et	Me	**1** 1*R**, 2*R**	**11** 4*S** (43%)	**12** 4*R** (57%)
*t*Bu	Me	H	**2** 1*R**, 2*R**	**13** 4*R** (42%)	**14** 4*S** (58%)
*t*Bu	Et	H	**3** 1*R**, 2*R**	**15** 4*R** (36%)	**16** 4*S** (64%)
*t*Bu	*t*Bu	H	**4** 1*R**, 2*S**	**17** 4*R** (10%)	**18** 4*S** (90%)
*i*Pr	*t*Bu	H	**5** 1*R**, 2*S**	**19** 4*S** (20%)	**20** 4*R** (80%)
Et	*t*Bu	H	**6** 1*R**, 2*S**	**21** 4*S** (28%)	**22** 4*R** (72%)
Me	*t*Bu	H	**7** 1*R**, 2*S**	**23** 4*S** (35%)	**24** 4*R** (65%)
Me	Et	H	**8** 1*R**, 2*R**	**25***a* 4*S** (40%)	**25***b* 4*R** (60%)
Me	Me	H	**9** 1*R**, 2*R**	**26** 4*S** (48%)	**27** 4*R** (52%)
Me[b]	$(Me)_2$	H	**10** 1*R**	**28** 4*S** (3%)	**29** 4*R** (97%)

[a]La réduction des cétones **1** à **10** ne modifie pas les configurations relatives des carbones 1 et 2.
[b]Le carbone 2 de la cétone **10** porte deux groupes méthyles.

SCHÉMA 1

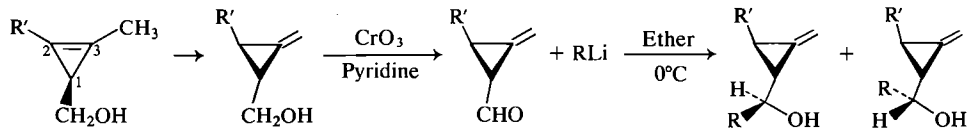

R′ =				
Me **30**	**33**	**36** + *t*BuLi	**13** (53%)	**14** (47%)
Et **31**	**34**	**37** + *t*BuLi	**15** (54%)	**16** (46%)
*t*Bu **32**	**35**	**38** + *i*PrLi	**19** (50%)	**20** (50%)
		38 + *t*BuLi	**17** (55%)	**18** (45%)
			II	I

SCHÉMA 2

geable. Cette méthode est cependant intéressante car elle permet d'avoir accès aux diastéréoisomères II qui sont obtenus avec des rendements souvent très faibles au cours de la réduction des cétones α-cyclopropylidéniques (ex: **17** et **19**).

3. *Attribution des configurations relatives aux alcools secondaires α-cyclopropylidéniques 11 à 29*

Les configurations relatives des alcools secondaires **11** et **12** ont été établies antérieurement par voie chimique (11).

Dans une première phase, l'identification des [éthyl-2 vinyl-3 cyclopropyl (1*R**,2*S**,3*S**)]-1 éthanol 4*S** (**39**) et 4*R** (**40**) est réalisée par l'étude en résonance magnétique nucléaire de ^1H et de ^{13}C des oxa-3 bicyclo[3.1.0] hexanes obtenus par oxymercuration cyclisante de ces alcools.

Dans une seconde phase, une filiation chimique est établie entre les alcools vinylcyclopropaniques **39** et **40** d'une part et les alcools cyclopropylidéniques **11** et **12** d'autre part.

Cette méthode d'identification chimique, si elle a permis d'affecter les configurations relatives 1*R**, 2*R**,4*S**(**11**) et 1*R**,2*R**,4*R** (**12**) aux (éthyl-2 éthylidène-3 cyclopropyl)-1 éthanols E, reste difficile à mettre en œuvre; par ailleurs, elle n'est pas applicable aux alcools méthylènecyclopropaniques. Nous avons donc recherché des corrélations en spectrophotométrie infrarouge et en résonance magnétique nucléaire qui permettent de généraliser facilement ce type d'attribution.

Spectrophotométrie infrarouge

L'ensemble des données infrarouge est en accord avec la structure cyclopropylidénique; on note en particulier les vibrations ν(=C—H), ν(C=C) et δ′(=C—H) localisées respectivement vers 3050, 1750 et 880 cm^{-1}.

L'étude des vibrations ν(OH libre) et ν(OH ché-

Can. J. Chem. Downloaded from www.nrcresearchpress.com by 210.87.254.105 on 09/06/12
For personal use only.

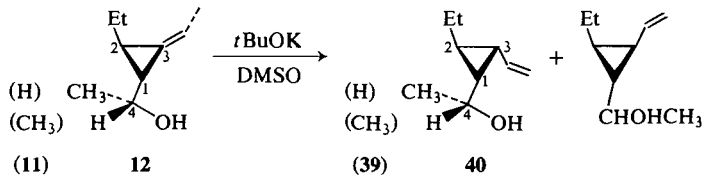

SCHÉMA 3

laté) réalisée par dilution des alcools dans CCl_4 est résumée dans le tableau 1. Ces données permettent de classer l'ensemble des alcools cyclopropylidéniques en deux catégories.

Composés I. Le spectre de ces alcools présente une bande d'absorption ν(OH libre), très intense, localisée vers 3617–3621 cm^{-1}. Cependant, dans tous les cas étudiés, on note la présence sur cette bande d'absorption d'un épaulement de faible intensité vers 3585–3595 cm^{-1} qui subsiste à dilution élevée. Cette bande ne peut donc être attribuée qu'à une vibration ν(OH chélaté).

Composés II. Le spectre de ces composés présente, pour une dilution élevée, deux bandes d'absorption, très nettement individualisées, localisées vers 3618–3620 cm^{-1} (ν(OH libre)) et vers 3570–3580 cm^{-1}. Cette dernière bande, d'intensité moyenne, a été attribuée comme précédemment à une vibration ν(OH chélaté).

Il est important de signaler, par ailleurs, l'homogénéité de ces deux catégories de composés. En effet, quelque soit le couple de diastéréoisomères considéré, l'intensité de la bande d'absorption attribuée à la vibration ν(OH chélaté) des composés I, est très inférieure à celle des composés II (tableau 1).

Les vibrations ν(OH chélaté) observées ne peuvent correspondre qu'à deux types d'interaction: l'interaction OH – double liaison cyclopropylidénique (16) qui se traduit généralement par une vibration ν(OH chélaté) localisée vers 3580 cm^{-1}; l'interaction OH – liaison σ du cycle propanique visualisée par une bande d'absorption localisée vers 3595 cm^{-1} (16, 17). Compte tenu de ces valeurs nous devons conclure que les composés I présentent une très faible chélation OH – liaison σ alors que pour les composés II la chélation est du type OH – double liaison.

Si l'on admet que les conformères privilégiés autour de la liaison C_1—COH sont décalés, seuls les conformères a et a′ peuvent permettre une liaison intramoléculaire OH... π. Dans cette conformation, en effet, l'hydrogène du groupement fonctionnel, lorsqu'il est au-dessus du plan du cycle, est situé à 2 Å environ de la double liaison cyclopropanique. Dans les conformères c et c′, l'hydrogène qui reste relativement éloigné du système $\pi(d \geq 3$ Å) tend à se rapprocher au contraire du plan du cycle ce qui défavorise l'interaction OH – double liaison.

Les conformères b, b′, c et c′, dans lesquels l'hydrogène du groupement OH peut se rapprocher du plan du cycle en C_3, favoriseront par contre la chélation OH – liaison σ du cycle.

Il est a priori difficile d'établir une relation entre les données infrarouges des alcools α-cyclopropylidéniques I et II et leur configuration relative. La libre rotation du groupement fonctionnel autour de la liaison C_1—COH combinée à celle de l'hydrogène autour de la liaison C—OH conduit, en effet, à neuf conformères dont les populations dépendent de cette configuration. Cependant, si nous faisons l'hypothèse que la nature de la liaison hydrogène observée dépend au premier ordre des populations conformationnelles autour de la liaison C_1—COH, on peut prévoir que les diastéréoisomères (II) présenteront une liaison hydrogène OH – double liaison alors que dans le cas des configurations (I) on doit éventuellement observer une chélation OH – liaison σ. En effet, en raison de l'interaction stérique $R–H_{(2)}$, le conformère a, qui permet seul la chélation, OH – double liaison, sera nettement favorisé dans II par rapport à I.

L'étude des [éthyl-2 éthylidène-3 cyclopropyl ($1R^*$, $2R^*$)]-1 éthanol $4S^*$ (**11**) et $4R^*$ (**12**), dont les configurations ont été déterminées par voie chimique, confirme cette hypothèse; seul l'isomère **11** présente en effet une liaison hydrogène OH – π

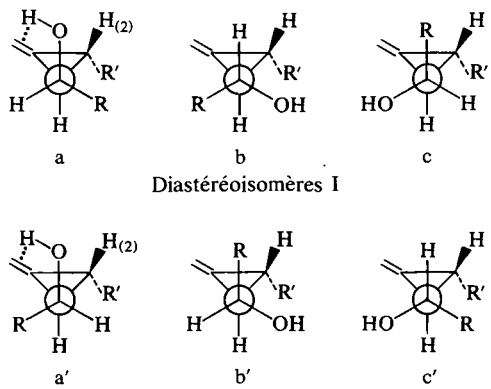

SCHÉMA 4

Can. J. Chem. Downloaded from www.nrcresearchpress.com by 210.87.254.105 on 09/06/12
For personal use only.

Can. J. Chem. Downloaded from www.nrcresearchpress.com by 210.87.254.105 on 09/06/12
For personal use only.

TABLEAU 1. Données ir et rmn permettant de différencier les alcools secondaires α-cyclopropylidéniques diastéréoisomères

			ir solution/CCl_4 C = 3 × 10^{-3} mol L^{-1}		rmn ^1H (CCl_4)	
R′	R	no.	ν(OH) (cm^{-1}) libre	ν(OH) (cm^{-1}) lié*	δH_{3a} et δH_{3b} (ppm, TMS)	$^3J_{H_1-H_4}$ (Hz)
Me	*t*Bu	**13**	3620	3570	5,20	7,4
		14	3615	e 3588	5,02 et 5,17	8,4
Et	*t*Bu	**15**	3620	3572	5,36	6,9
		16	3623	e 3590	5,20 et 5,32	8,5
*t*Bu	*t*Bu	**17**	3619	3572	5,20 et 5,40	5,7
		18	3619	e 3594	5,25	8,6
*t*Bu	*i*Pr	**19**	3619	3575	5,38 et 5,50	—
		20	3620	e	5,35	7,2
*t*Bu	Et	**21**	3621	3577	Massif entre 5,40 et 5,50	—
		22	3620	e	5,35	6,2
*t*Bu	Me	**23**	3619	3580	5,25 et 5,38	7,3
		24	3617	e 3595	5,28	6,8
Me	Me	**26**	3617	3580	5,30 et 5,40	6,7 à 7,1
		27	3618	e 3590	5,27	7,2
$(Me)_2$	Me	**28**	3618	3577	5,28 et 5,42	8,6
		29	3618	e	5,15 et 5,21	9,1
Et	Me	**11**	3618	3574		
		12	3619	e 3585		

*Epaulement.

(νOH = 3574 cm^{-1}) alors que dans le cas de l'alcool **12** on note uniquement la présence d'un épaulement (ν ≃ 3588 cm^{-1}) sur la bande OH libre. Ces résultats permettent d'attribuer à l'ensemble des composés I la configuration dans laquelle R et C_3 ainsi que H_4 et C_2 peuvent être quasi-éclipsés et à l'ensemble des composés II la deuxième configuration relative. Ils constituent, par ailleurs, une confirmation des attributions de structures proposées par Bertrand et coll. pour quelques couples de méthylènecyclopropylcarbinols (10).

Résonance magnétique nucléaire de ^1H

L'ensemble des données rmn est en accord avec une structure cyclopropylidénique dans laquelle les deux groupes substitués sur le cycle présentent une relation *trans*. La valeur de la constante de couplage $^3J_{H_1-H_2}$, qui a pu être déterminée pour quelques termes en utilisant un appareil fonctionnant à 250 MHz, est en effet de l'ordre de 5 Hz (18).

Les valeurs des constantes de couplage $^3J_{H_1-H_4}$ (tableau 1) permettent de confirmer, pour certains couples de diastéréoisomères, les attributions de configuration relative. La valeur de cette constante est en effet reliée aux populations conformationnelles par l'équation des équilibres rapides (19):

$$^3J_{H_1-H_4} = \Sigma\, n_i J_i$$

pour les composés I:

$$^3J_{H_1-H_4} = {}^3J_{60}\,(n_a + n_c) + {}^3J_{180} n_b$$

pour les composés II:

$$^3J_{H_1-H_4} = {}^3J_{60}\,(n_{a'} + n_{b'}) + {}^3J_{180} n_{c'}$$

Comparaison des valeurs des constantes $^3J_{H_1-H_4}$ pour les termes I et II d'un même couple de diastéréoisomères

Lorsque la taille du substituant R est très supérieure à celle de l'hydroxyle (R = *t*Bu), les populations conformationnelles autour de C_1—COH sont essentiellement déterminées par les interactions stériques R, H_2 et R, C_2—C_3. Dans une première approximation on peut admettre que les populations c et b′, très défavorisées par ce type d'interaction, sont négligeables.

$$n_c \simeq n_{b'} \simeq 0$$

On peut de même prévoir:

$$n_a < n_{a'}$$

$$n_b > n_{c'}$$

Ce qui conduit à la relation:

$$^3J_{H_1-H_4}\,(I) > {}^3J_{H_1-H_4}\,(II)$$

C'est effectivement ce que l'on observe pour les couples de diastéréoisomères **13–14, 15–16, 17–18.** Ce résultat confirme les attributions de configura-

Can. J. Chem. Downloaded from www.nrcresearchpress.com by 210.87.254.105 on 09/06/12
For personal use only.

tion relative réalisées sur la base des données infrarouges.

Lorsque la taille de R est du même ordre de grandeur que celle du groupement fonctionnel (R = CH_3), il est difficile de prévoir l'influence de la configuration sur la valeur de la constante $^3J_{H_1-H_4}$ car, dans ce cas, on ne peut plus négliger l'un des conformères. Les données expérimentales démontrent, en effet, que les valeurs de cette constante pour les deux diastéréoisomères **23–24** ou **26–27** sont très voisines.

Evolution de la valeur de la constante de couplage $^3J_{H_1-H_4}$ avec la nature du substituant R'

Bien que le groupement fonctionnel et le groupe R' présentent une relation *trans* par rapport au cycle propylidénique, la valeur de la constante $^3J_{H_1-H_4}$ dépend du degré de substitution du groupe R'. L'influence de ce groupe sur les populations conformationnelles a ... c', qui est particulièrement sensible lorsque la taille de R est très importante (R = *t*Bu), ne peut être due qu'à une modification des interactions stériques entre R et R' ou R et H_2. Compte tenu de la relation *trans* de R et R' par rapport au cycle il est possible que, lorsque l'on parcourt les séries **13**, **15**, **17** et **14**, **16**, **18**, seules les variations d'interaction stérique R—H_2 soient à l'origine des modifications de populations conformationnelles: le pouvoir électrodonneur de R', qui augmente avec son degré de substitution, provoquerait alors une diminution de la longueur de la liaison C_1—C_2 ce qui accroitrait l'interaction R—H_2.

Dans cette hypothèse, si comme précédemment on admet dans une première approximation que lorsque R = *t*Bu, les populations n_c et n_b sont négligeables, lorsque le degré de substitution de R' augmente, on peut prévoir:

pour les diastéréoisomères I $n_b \nearrow$; $n_a \searrow$; $^3J_{H_1-H_4} \nearrow$

pour les diastéréoisomères II $n_{a'} \nearrow$; $n_{c'} \searrow$; $^3J_{H_1-H_4} \searrow$

Bien que la variation de ^3J reste faible pour les configurations (I), c'est effectivement ce que l'on observe pour l'ensemble des termes **13** à **18**.

*Analyse conformationnelle des alcools **13**, **14**, **17**, **18** et **23**, **24***

L'étude de la variation de la valeur de la constante de couplage $^3J_{H_1-H_4}$ avec la température a été réalisée pour les couples d'alcools diastéréoisomères **17**, **18** et **23**, **24** (tableau 2). Les populations conformationnelles obtenues sont en accord avec les hypothèses précédentes et confirment donc les attributions de structure.

Pour **23** et **24**, la valeur de cette constante n'évolue plus à partir de 120°C; à cette température on a donc égalité des populations conformationnelles:

$$n_a = n_b = n_c = 0{,}33$$
$$n_{a'} = n_{b'} = n_{c'} = 0{,}33$$

soit:

$$J_{H_1-H_2} = 6{,}3 = \tfrac{1}{3}(^3J_{180} + 2\,^3J_{60})$$

A l'aide des courbes de Karplus, cette valeur de J permet d'évaluer les deux constantes de couplage; nous avons retenu les valeurs suivantes:

$$^3J_{60} \simeq 3 \text{ Hz et } ^3J_{180} \simeq 13 \text{ Hz}$$

Ces paramètres permettent de déterminer les populations conformationnelles pour les autres couples d'alcools (tableau 2). Si pour R = Me, (**23** et **24**) les populations n_b et $n_{c'}$ sont très voisines, lorsque R = *t*Bu (**17**, **18** et **13**, **14**), on observe bien l'inégalité $n_b > n_{c'}$. De même, lorsque R = *t*Bu, et que le degré de substitution de R' augmente, on observe une légère augmentation de n_b alors que pour les diastéréoisomères II $n_{c'}$ décroît de manière très sensible.

Corrélation par chromatographie en phase gazeuse

Devant les difficultés d'attribution des configurations relatives aux alcools secondaires α-cyclopropylidéniques, certains auteurs utilisent la différence de temps de rétention des diastéréoisomères II et I sur colonne polaire (10*a*). Les composés II, qui présentent une liaison OH–π plus forte qu'une liaison OH – liaison σ, doivent avoir un temps de rétention plus faible que les composés I. Le tableau 3 montre clairement que selon la nature de R' le rapport des temps de rétention t_R(II)/t_R(I) peut être inférieur ou supérieur à 1; ce rapport ne constitue donc pas un critère de configuration. Cependant sa variation continue, en fonction des substituants R et R' confirme l'homogénéité des séries I et II, quant aux attributions de configurations relatives.

En conclusion, les configurations relatives des alcools secondaires α-cyclopropylidéniques peuvent être attribuées sans ambiguïté sur la base des données infrarouges de ces composés. En rmn de ^{1}H, les valeurs de la constante de couplage $^3J_{H_1-H_4}$ permettent également dans un certain nombre de cas des attributions de structure qui sont dans tous les cas en accord avec les attributions précédentes.

4. *Stéréosélection dans la réduction des cétones α-cyclopropylidéniques par $AlLiH_4$*

Signalons tout d'abord que nous avons vérifié

Can. J. Chem. Downloaded from www.nrcresearchpress.com by 210.87.254.105 on 09/06/12
For personal use only.

TABLEAU 2. Populations conformationnelles (n) des alcools secondaires α-cyclopropylidéniques

Composés	θ°C	$^3J_{H_1-H_4}$ (Hz)	Composé I		Composé II	
			n_b,	$(n_a + n_c)$	$n_{c'}$,	$(n_{a'} + n_{b'})$
23	−50	8,0	—	—	0,50	0,60
	−10	7,7	—	—	0,47	0,53
	+40	7,3	—	—	0,43	0,57
	+90	6,4	—	—	0,34	0,66
	+120	6,3	—	—	0,33	0,67
24	−50	8,5	0,55	0,45	—	—
	−10	7,3	0,43	0,57	—	—
	+40	6,8	0,38	0,62	—	—
	+90	6,5	0,35	0,65	—	—
	+120	6,3	0,33	0,67	—	—
	+150	6,3	0,33	0,67	—	—
17	−10	5,6	—	—	0,26	0,74
	+40	5,6	—	—	0,26	0,74
	+90	5,7	—	—	0,27	0,73
	+150	5,7	—	—	0,27	0,73
18	−10	8,9	0,59	0,41	—	—
	+40	8,6	0,56	0,44	—	—
	+90	8,0	0,50	0,50	—	—
	+150	7,6	0,46	0,54	—	—
13	+40	7,4	—	—	0,44	0,56
14	+40	8,4	0,54	0,46	—	—

TABLEAU 3. Rapports des temps de rétention des diastéréoisomères sur colonne Carbowax (20%) de 4 m (Chromosorb P NAW 60/80, gaz vecteur: H_2, θ = 150°C)

R	*t*Bu	*t*Bu	*t*Bu	*i*Pr	Et	Me
R'	Me	Et	*t*Bu	*t*Bu	*t*Bu	*t*Bu
No.	**13/14**	**15/16**	**17/18**	**19/20**	**21/22**	**23/24**
$\Delta = t_R(II)/t_R(I)$	0,73	0,89	1,02	1,06	1,07	1,1

que l'utilisation d'une solution–suspension d'hydrure dans l'éther provoque une induction asymétrique comparable à celle que l'on observe avec une solution de $AlLiH_4$ dans ce même solvant (1,5 *M*); les différences d'induction observées sont en effet de 2 à 5% alors que la précision des mesures est, au maximum, de 2 à 3%.

La réduction des (alkyl-2 alkylidène-3 cyclopropyl) alkyl cétone par $AlLiH_4$ est sous contrôle cinétique

Un test classique de l'évaluation des proportions correspondant à l'équilibre thermodynamique entre alcools diastéréoisomères consiste à équilibrer dans les conditions de la réaction et en présence d'isopropylate d'aluminium l'un des alcools diastéréoisomères et la cétone homologue. Cette équilibration a été réalisée avec les deux alcools isomères **23** et **24**; dans les deux cas, nous avons obtenu, à l'équilibre, des proportions identiques: 47% de **23** (1*R**,2*S**,4*S**) et 53% de **24** (1*R**,2*S**,4*R**) ce qui correspond à une différence d'enthalpie libre négligeable entre les deux épimères.

Ces proportions sont nettement différentes de celles obtenues lors de la réduction de la (tertiobutyl-2 méthylène-3 cyclopropyl) méthyl cétone (**7**) par $AlLiH_4$ dans l'éther au reflux: 35% d'isomère **23** et 65% d'isomère **24**. Ces résultats démontrent que la réduction des cétones α-cyclopropylidéniques se fait essentiellement sous contrôle cinétique.

Cette conclusion est confirmée par l'étude de la réduction de la cétone **4** par $AlLiH_4$, en solution dans l'éther, à différentes températures. La variation du rapport des alcools diastéréoisomères obtenus **18/17** est indiquée ci-dessous.

θ (°C):	39	−10	−70
18/17:	9	20	>100

La diminution du pourcentage d'isomère minoritaire à basse température, constitue un argument complémentaire en faveur d'un contrôle cinétique de la réaction. Notons, par ailleurs, que dans ce cas l'abaissement de la température permet d'atteindre la stéréospécificité: à −70°C, l'alcool **17** n'est pas détecté dans le mélange réactionnel brut par rmn ou par cpv.

Modèle stéréochimique

La réduction étudiée présente une induction

Can. J. Chem. Downloaded from www.nrcresearchpress.com by 210.87.254.105 on 09/06/12
For personal use only.

asymétrique 1,3 due à un effet de substitution à longue distance. L'interprétation de l'induction observée au cours de la réduction des composés carbonylés a progressé récemment grâce à la contribution de travaux théoriques (19, 20). Dans notre série, cependant, l'existence en α du carbonyle du carbone cyclopropylidénique C_1 permet difficilement de transposer les conclusions de Nguyen Trong Anh et coll. En particulier la spécificité du cycle propylidénique avec ses "orbitales moléculaires de Walsh" combinées aux orbitales π du système éthylénique, rend aléatoire l'examen d'un recouvrement optimal des orbitales de C_1 avec les orbitales π du carbonyle. En conséquence, il nous a semblé intéressant de discuter nos résultats expérimentaux en les confrontant aux modèles stéréochimiques de Cram (21), de Karabatsos (9) et de Felkin et coll. (25) comme cela a été fait dans d'autres séries (27 à 29).

Dans le modèle de Cram (21), l'oxygène du groupement fonctionnel qui complexe le réactif, est le groupe le plus volumineux de la molécule; il se placera de préférence entre les groupes M (▷═) et P (▷—H).

Le réactif attaquera, pour des raisons stériques, du côté du petit substituant P. L'attaque *a* conduit, selon Cram, à l'état de transition le plus stable donc au diastéréoisomère principal. C'est effectivement ce que l'on observe expérimentalement; cependant, ce modèle ne permet pas d'interpréter la variation d'induction observée lorsque la grosseur de R augmente. Dans ce cas, en effet, on devrait favoriser l'attaque *b* donc assister à une diminution de la stéréosélection et non l'inverse comme nous l'observons. Par ailleurs, la position quasi-éclipsée de $H_{(2)}$ et R dans l'état de transition nous semble très défavorisée en série cyclopropylidénique, en particulier lorsque R = *t*Bu.

Le modèle de Karabatsos (9) postule que les populations conformationnelles des états de transition et du réactant sont approximativement dans le même rapport, l'attaque du réactif nucléophile se faisant toujours du côté du groupe P. Pour que ce modèle soit prévisionnel et puisse donner lieu à un traitement semi-quantitatif, il est nécessaire de connaître les différentes populations conformationnelles des composés carbonylés. Si les cétones α-cyclopropaniques saturées ont suscité de nombreuses études qui ont démontré la conformation préférentielle *s-cis* de ces composés (22, 23), la stéréochimie des composés carbonylés α-cyclopropylidénique n'a, par contre, pas été abordée.

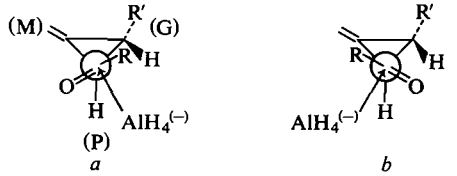

Diastéréoisomère I majoritaire Diastéréoisomère II minoritaire

SCHÉMA 5

L'effet de solvant ASIS permet, en appliquant la règle empirique de Connolly et MacCrindle (24), de prévoir quelle est la conformation préférentielle des cétones. Pour les conformations *s-cis* et *s-trans*, on peut s'attendre aux effets Δ ($\Delta = \delta CCl_4 - \delta C_6D_6$) qui suivent:

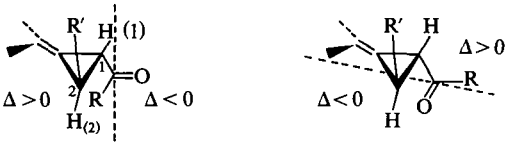

Tous les Δ sont positifs

$\Delta R > 0$
$\Delta H_1 > 0$
$\Delta R' > 0$
$\Delta(= -H) > 0$
$\Delta H_2 < 0$

SCHÉMA 6

Les valeurs expérimentales (tableau 4), obtenues pour les composés **4**, **7** et **8**, démontrent clairement que l'ensemble de ces dérivés n'est pas homogène quant aux populations conformationnelles d'une part et que d'autre part les effets de solvant ne peuvent s'interpréter à partir d'un équilibre conformationnel *s-cis* ⇄ *s-trans*. Compte tenu de ces résultats, le modèle de Karabatsos nous semble difficilement applicable dans cette série.

Dans le modèle de Felkin (25), la stéréosélection est déterminée par les contraintes de Pitzer et les interactions stériques. Les trois états de transition favorisés seront:

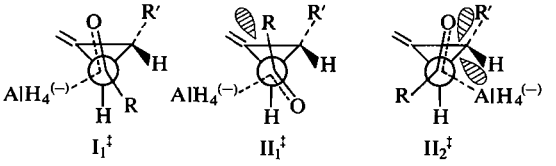

SCHÉMA 7

Ce modèle permet d'interpréter l'ensemble des résultats expérimentaux obtenus dans le cas de la réduction des cétones.

L'état de transition $I_1^{\ddagger}$, qui se forme préférentiellement et qui correspond par ailleurs à l'attaque du réactif sur la face diastéréotopique du carbonyle la moins encombrée dans la conformation *s-cis* du composé carbonylé, conduira à la configuration relative majoritaire (I), $II_1^{\ddagger}$ et $II_2^{\ddagger}$ conduiront au contraire au produit minoritaire (II).

TABLEAU 4. Cétones α-cyclopropylidéniques, effet de solvant $\Delta = \delta CCl_4 - \delta C_6H_6$ (Hz)

Composé	ΔH_1	ΔH_2	$\Delta = -H$	$\Delta R'$	ΔR
4	+3	−12	−2 +2	+6	+7
7	−2	−4	+9 +9	+12	+9
8	+4		+3 +4	+13 +12	+12

Lorsque la grosseur du groupe R′ augmente (série **2**, **3**, **4** ou **9**, **8**, **7**), $II_2^{\ddagger}$ est nettement défavorisé, la stéréosélectivité augmente. La présence d'un méthyle *cis* du carbonyle dans **10** accentue cet effet puisque la stéréosélectivité de la réduction de cette cétone atteint 97%; il est probable que dans ce cas l'intermédiaire $II_1^{\ddagger}$ est comme $II_2^{\ddagger}$ négligeable.

De même, lorsque l'encombrement de R augmente, $II_1^{\ddagger}$ est très nettement défavorisé en raison de l'interaction M ↔ R, le pourcentage du diastéréoisomère principal (I) sera plus élevé (série **7**, **6**, **5**, **4**).

Conclusion

Les attributions de configuration relative aux alcools secondaires α-cyclopropylidéniques ne font pas appel a un modèle stéréochimique de la réduction des précurseurs carbonylés. Ces attributions sont fondées sur les propriétés en ir et en rmn de ^1H des alcools diastéréoisomères et sont par ailleurs confirmées (pour un couple d'alcools) par identification chimique. Il est possible d'étendre ces déterminations de structure aux alcools α-cyclopropéniques, α-cyclopropaniques et α-spiropentaniques en réalisant des filiations chimiques entre ces alcools α-cycliques et les dérivés cyclopropylidéniques à l'aide de réactions dont la stéréochimie est bien connue (migration exocyclique de la double liaison cyclopropénique en milieu basique, réduction de la double liaison cyclopropylidénique, transfert de carbènes).

L'étude de la diastéréosélection au cours de la réduction par $AlLiH_4$ des (alkyl-2 alkylidène-3 cyclopropyl) alkyl cétones démontre que l'induction dépend de la taille du groupe R′ qui présente pourtant une relation *trans* par rapport au carbonyle. Par ailleurs, le modèle de Felkin dont une étude théorique récente a démontré qu'il représentait approximativement les états de transition de moindre énergie, permet d'interpréter et de prévoir la stéréosélectivité au cours de la réduction des cétones α-cyclopropylidéniques.

1. G. A. OLAH, J. S. STARAL, R. J. SPEAR et G. LIANG. J. Am. Chem. Soc. **97**, 5489 (1975).
2. E. TOROMANOFF. Bull. Soc. Chim. Fr. 2457 (1968), et références citées.
3. F. ROCQUET, A. SEVIN et W. CHODKIEWICZ. C.R. Acad. Sci. Ser. C, **272**, 417 (1971).
4. F. ROCQUET et A. SEVIN. Bull. Soc. Chim. Fr. 895 (1974).
5. G. DESCOTES, A. MENET et F. COLLONGES. Tetrahedron, **29**, 2931 (1973).
6. F. ROCQUET, A. SEVIN et W. CHODKIEWICZ. Tetrahedron Lett. 1249 (1971).
7. F. ROCQUET, A. SEVIN et W. CHODKIEWICZ. C.R. Acad. Sci. Ser. C, **270**, 848 (1970).
8. P. CHAUTEMPS et J. L. PIERRE. C.R. Acad. Sci. Ser. C, **282**, 349 (1976).
9. G. J. KARABATSOS. J. Am. Chem. Soc. **89**, 1367 (1967).
10. (*a*) R. MAURIN et M. BERTRAND. Bull. Soc. Chim. Fr. 2261 (1970); (*b*) G. LEANDRI, H. MONTI et M. BERTRAND. C.R. Acad. Sci. Ser. C, **271**, 560 (1970); (*c*) G. LEANDRI et H. MONTI. C.R. Acad. Sci. Ser. C, **277**, 1474 (1970).
11. M. VINCENS, C. DUMONT et M. VIDAL. Can. J. Chem. **57**, 2314 (1979).
12. M. VIDAL, M. VINCENS et P. ARNAUD. Bull. Soc. Chim. Fr. **2**, 657 (1972).
13. M. VIDAL, M. VINCENS et P. ARNAUD. Bull. Soc. Chim. Fr. **2**, 665 (1972).
14. M. VIDAL et P. ARNAUD. Bull. Soc. Chim. Fr. **2**, 675 (1972).
15. G. I. POOS, G. E. HARTH, R. E. BEYLER, et L. H. SARETT. J. Am. Chem. Soc. **75**, 422 (1953).
16. L. JORIS, P. VON R. SCHLEYER et R. GLEITER. J. Am. Chem. Soc. **90**, 327 (1968).
17. S. E. WIBERLEY et S. C. BUNCE. Anal. Chem. **24**, 623 (1952).
18. R. BARLET et M. VINCENS. Tetrahedron, **33**, 1291 (1977).
19. NGUYEN TRONG ANH et O. EISENSTEIN. Nouv. J. Chim. **1**, 61 (1976), et références citées.
20. NGUYEN TRONG ANH et O. EISENSTEIN. Tetrahedron Lett. 155 (1976).
21. (*a*) D. J. CRAM et F. A. ABD ELHAFEZ. J. Am. Chem. Soc. **74**, 5828 (1952); (*b*) D. J. CRAM et F. D. GREENE. J. Am. Chem. Soc. **75**, 6005 (1953); (*c*) D. J. CRAM et D. R. WILSON. J. Am. Chem. Soc. **85**, 1245 (1963).
22. M. PELISSIER, A. SERAFINI, J. DEVANNEAUX, J. F. LABARRE et J. F. TOCANNE. Tetrahedron, **27**, 3271 (1971), et références citées.
23. J. F. TOCANNE. Tetrahedron, **28**, 389 (1972).
24. J. D. CONNOLLY et R. MACCRINDLE. Chem. Ind. 379 (1965).
25. M. CHEREST, H. FELKIN et N. PRUDENT. Tetrahedron Lett. 2199 (1968).
26. S. C. BUNCE. J. Am. Chem. Soc. **77**, 6616 (1955).
27. S. YAMADA et K. KOGA. Selective organic transformations. Vol. 1. *Edité par* B. S. Thyagarajan. Wiley-Interscience, New York. 1970. p. 1.
28. J. D. MORRISON et H. S. MOSHER. Asymmetric organic reactions. Prentice-Hall. 1971. p. 87.
29. M. J. BRIENNE, C. OUANNES et J. JACQUES. Bull. Soc. Chim. Fr. 1036 (1968).

Can. J. Chem. Downloaded from www.nrcresearchpress.com by 210.87.254.105 on 09/06/12
For personal use only.

Excess volumes of an alcohol + 1,2-dichloroethane

NETTEM V. CHOUDARY AND PULIGUNDLA R. NAIDU

Department of Chemistry, College of Engineering, Sri Venkateswara University, Tirupati 517 502, India

Received December 9, 1980

NETTEM V. CHOUDARY and PULIGUNDLA R. NAIDU. Can. J. Chem. **59**, 2210 (1981).

Excess volumes for binary mixtures of 1,2-dichloroethane with *n*-propanol, *n*-butanol, *n*-pentanol, *n*-hexanol, *n*-heptanol, and *n*-octanol have been determined at 303.15 K. V^E is positive over the whole range of composition in all the mixtures. However, it is noticed that the positive values of V^E of mixtures of 1,2-dichloroethane with *n*-hexanol, *n*-heptanol, and *n*-octanol differ from those for the mixtures of 1,2-dichloroethane with corresponding alkanes. The difference has been explained in terms of the break up of hydrogen bonds, interstitial accommodation of 1,2-dichloroethane in alcohol aggregates, and possible hydrogen bond interaction of the type Cl...H—O between unlike molecules.

NETTEM V. CHOUDARY et PULIGUNDLA R. NAIDU. Can. J. Chem. **59**, 2210 (1981).

On a déterminé à 303,15 K les volumes en excès des mélanges binaires formés de dichloro-1,2 éthane avec les alcools suivants: *n*-propanol, *n*-butanol, *n*-pentanol, *n*-hexanol, *n*-heptanol et *n*-octanol. Sur toute l'étendue de composition de tous les mélanges, V^E est positif. Cependant on note que les valeurs positives de V^E dans les mélanges de dichloro-1,2 éthane avec le *n*-hexanol, le *n*-heptanol et le *n*-octanol diffèrent de celles des mélanges du dichloro-1,2 éthane avec les alcanes correspondants. On explique la différence en fonction d'une rupture des liaisons hydrogènes, de l'adaptation intersticielle du dichloro-1,2 éthane dans les agrégats d'alcools et d'une interaction possible de la liaison hydrogène du type Cl ... H—O entre les molécules dissemblables.

[Traduit par le journal]

Introduction

Excess volumes for binary mixtures of 1,2-dichloroethane with *n*-hexane, *n*-heptane, *n*-octane, and *n*-nonane, have been reported by Krishnaiah and Naidu (1). V^E is positive over the whole range of composition in the four mixtures. Since the unlike molecules are non-polar in character, the positive excess volumes may be ascribed to differences in sizes and shapes of molecules. If 1,2-dichloroethane is mixed with alcohols, derivatives of *n*-alkanes, new factors begin to influence excess volume. The factors include: (*a*) break up of hydrogen bonds, (*b*) interstitial accommodation of 1,2-dichloroethane molecules in self-associated alcohol, and (*c*) the possible hydrogen bond interaction between unlike molecules. With a view to study the effect of these factors on excess volume, V^E data for binary mixtures of 1,2-dichloroethane with *n*-propanol, *n*-butanol, *n*-pentanol, *n*-hexanol, *n*-heptanol, and *n*-octanol have been determined.

Experimental

The dilatometer used for measuring excess volumes was similar to that described by Rao and Naidu (2). The mixing cell contained two bulbs of different capacities that were connected through a U-tube having mercury to separate the two compartments. One end of the first bulb was fitted with a capillary outlet and the opposite end of the second bulb was closed with a ground glass stopper. Four dilatometers of this type were used to cover the whole range of composition. Composition of each mixture was determined directly by weighing. All weights were corrected for buoyancy. Measurements were made using a thermostatic bath controlled to within ±0.01 K. The excess volumes were reproducible to ±0.003 cm^3 mol^{-1}.

Purification of Materials

All materials were purified by the methods described by Reddick and Bunger (3). 1,2-Dichloroethane (BDH) was washed with dilute potassium hydroxide solution and water, dried over anhydrous calcium chloride, and fractionally distilled. 1-Propanol (J. T. Baker) and 1-butanol (BDH) were refluxed over freshly ignited calcium oxide for 6 h and distilled using a fractionating column. 1-Pentanol (J. T. Baker) was dried over Drierite and fractionally distilled. 1-Hexanol (B.D.H., England), 1-heptanol (Koch-Light Laboratories Ltd., England), and 1-octanol (B.D.H., England) were fractionally distilled. A fractionating column that contained 30 theoretical plates was used in all cases. The purity of the samples was checked by comparing the measured densities of the compounds with those reported in the literature (4). Densities were determined using a bicapillary type pycnometer which offered an accuracy of 2 parts in 10^5. The measured density data are reported in Table 1 along with those reported in the literature.

Results

The experimental excess volumes of the six binary mixtures are graphically presented in Fig. 1 along with those for mixtures of 1,2-dichloroethane with *n*-hexane, *n*-heptane, and *n*-octane. The dependence of V^E on composition may be expressed

TABLE 1. Densities, ρ, of liquids at 303.15 K

Component	Density ρ/(g cm^{-3})	
	Present work	Literature
1,2-Dichloroethane	1.23829	1.23831
1-Propanol	0.78767	0.78764
1-Butanol	0.80203	0.80206
1-Pentanol	0.80762	0.80764
1-Hexanol	0.81205	0.81201
1-Heptanol	0.81572	—
1-Octanol	0.82188	0.82192

0008-4042/81/142210-02$01.00/0

©1981 National Research Council of Canada/Conseil national de recherches du Canada

Can. J. Chem. Downloaded from www.nrcresearchpress.com by 210.87.254.5 on 09/06/12
For personal use only.

TABLE 2. Standard deviation $\sigma(V^E)$ and values of the constants in eq. [1] at 303.15 K

System	a_0	a_1	a_2	$\sigma(V^E)$ / cm^3 mol^{-1}
1,2-Dichloroethane + *n*-propanol	0.937	0.581	0.296	0.004
1,2-Dichloroethane + *n*-butanol	1.130	0.574	0.154	0.006
1,2-Dichloroethane + *n*-pentanol	1.733	0.526	0.243	0.004
1,2-Dichloroethane + *n*-hexanol	2.071	0.769	0.599	0.006
1,2-Dichloroethane + *n*-heptanol	2.458	0.898	0.454	0.006
1,2-Dichloroethane + *n*-octanol	2.770	1.092	0.348	0.005

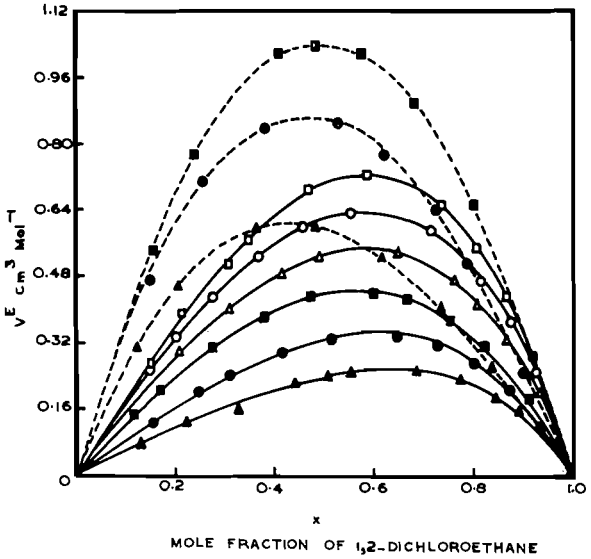

FIG. 1. Excess volumes V^E plotted against mole fraction of 1,2-dichloroethane at 303.15 K for the mixtures of 1,2-dichloroethane with alcohols (—) and alkanes (---); ▲, 1-propanol; ●, 1-butanol; ■, 1-pentanol; △, 1-hexanol; ○, 1-heptanol; □, 1-octanol; ⧋, 1-hexane, ⊙, 1-heptane; ⊡, 1-octane.

by an empirical equation of the form

$$[1]\quad V^E/(\text{cm}^3\ \text{mol}^{-1}) = x(1-x) \times \{a_0+a_1(2x-1)+a_2(2x-1)^2\}$$

where a_0, a_1, and a_2 are adjustable parameters and x is the mole fraction of 1,2-dichloroethane. The values of the parameters obtained by the least-square method, are included in Table 2 along with the standard deviation, $\sigma(V^E)$.

Discussion

The curves included in Fig. 1 show that V^E is positive over the whole range of composition in the six mixtures. The excess volumes for the six mixtures fall in the order: *n*-octanol > *n*-heptanol > *n*-hexanol > *n*-pentanol > *n*-butanol > *n*-propanol. This order is similar to that observed for mixtures of 1,2-dichloroethane with *n*-hexane, *n*-heptane, *n*-octane, and *n*-nonane. However, the values of V^E for the mixtures of 1,2-dichloroethane with *n*-hexanol and *n*-heptanol are smaller than those obtained for 1,2-dichloroethane with corresponding alkanes up to mole fractions 0.6 and 0.8 respectively of the halogenated hydrocarbon. V^E values of the two mixtures become more positive over the remaining mole fraction ranges. V^E values for mixtures of 1,2-dichloroethane with *n*-octanol are smaller than those for mixtures containing *n*-octane over the whole range of composition. These suggest that excess volumes of mixtures containing alcohols are influenced by break up of hydrogen bonds present in self-associated alcohols, interstitial accommodation of 1,2-dichloroethane in hydrogen bonded aggregates of alcohols, and possible hydrogen bond interactions of the type C1...H—O between unlike molecules. While the first factor contributes to the expansion of volume, the remaining two factors may lead to contraction in volume. The actual value of V^E would depend upon the balance between the two opposing contributions. The experimental values for mixtures of alcohols indicate that the factors responsible for opposing contributions counteract each other to different degrees in *n*-hexanol and *n*-heptanol mixtures. Further, the two factors that contribute to contraction in volume dominate over the whole range of composition in the system containing *n*-octanol.

Finally the maxima in V^E curves for the alcohol mixtures occur around 0.6 mole fraction of 1,2-dichloroethane while the maxima in mixtures containing corresponding alkanes occur below 0.5 mole fraction. This may be attributed to the effect of interstitial accommodation of 1,2-dichloroethane in alcohol aggregates which decreases with increase in concentration of the former.

Acknowledgement

One of the authors (N.V.C.) thanks the Council of Scientific and Industrial Research, New Delhi, India for the award of Junior Research Fellowship.

1. A. KRISHNAIAH and P. R. NAIDU. J. Chem. Eng. Data, **25**(1), 135 (1980).
2. M. V. P. RAO and P. R. NAIDU. Can. J. Chem. **52**, 788 (1974).
3. J. A. REDDICK and W. S. BUNGER. Techniques of chemistry. Vol. II. 3rd ed. Wiley-Interscience, New York. 1970.
4. J. TIMMERMANS. Physico-chemical constants of pure organic compounds. Elsevier Publishing Co., Amsterdam. 1950.

Can. J. Chem. Downloaded from www.nrcresearchpress.com by 210.87.254.5 on 09/06/12
For personal use only.

Isentropic compressibilities of electrolytes in acetonitrile at 25°C

ISOBEL DAVIDSON,[1] GÉRALD PERRON, and JACQUES E. DESNOYERS[2]

Department of Chemistry, Université de Sherbrooke, Sherbrooke, P.Q., Canada J1K 2R1

Received October 15, 1980

ISOBEL DAVIDSON, GÉRALD PERRON, and JACQUES E. DESNOYERS. Can. J. Chem. **59**, 2212 (1981).

The sound velocities of some 1:1 electrolytes in acetonitrile were measured by the "sing around" method. Apparent molal isentropic compressibilities $\phi_{K,S}$ of the electrolytes were derived from these data and from previously determined densities. Infinite dilution partial molal compressibilities $\bar{K}_S^0$ were obtained by extrapolation from the plot $\phi_{K,S}$ against the square-root of the molality. Approximate ionic values are obtained on the assumption that $\bar{K}_S^0(\phi_4B^-) \simeq 0$. In general, $\bar{K}_S^0$ of inorganic ions are much more negative in acetonitrile than in water and, except for Li^+, show little dependence on ionic size. On the other hand, $\bar{K}_S^0$ of tetraalkylammonium bromides become increasingly positive as the size of the cations increases. This is again in contrast with $\bar{K}_S^0$ of these electrolytes in water which remain negative. These large positive values arise from the free space between the ions and the solvent molecules, which is large in acetonitrile solutions.

ISOBEL DAVIDSON, GÉRALD PERRON, et JACQUES E. DESNOYERS. Can. J. Chem. **59**, 2212 (1981).

Les vitesses ultrasonores de certains électrolytes 1:1 ont été mesurées dans l'acétonitrile à 25°C par la méthode "sing around". Les compressibilités molaires apparentes à entropie constante $\phi_{K,S}$ des électrolytes ont été dérivées de ces données et des masses volumiques déjà publiées. Les compressibilités isentropiques molaires partielles à dilution infinie $\bar{K}_S^0$ ont été obtenues par extrapolation de $\phi_{K,S}$ portés en fonction de la racine carrée de la molalité. Des valeurs ioniques approximatives ont été calculées à partir de l'hypothèse que $\bar{K}_S^0(\phi_4B^-) \simeq 0$. En général, les $\bar{K}_S^0$ des ions inorganiques dans l'acétonitrile sont beaucoup plus négatifs que les valeurs dans l'eau et, à part Li^+, montrent peu de dépendance sur la taille de l'ion. Par contre, $\bar{K}_S^0$ des sels quaternaires d'ammonium R_4NX deviennent très positifs pour les sels de gros cations, ce qui est contraire au système aqueux où ils demeurent négatifs. Ces grandes valeurs de $\bar{K}_S^0$ réflectent la grande quantité d'espace libre entre les ions et les molécules de solvant qui est présent dans les solutions d'acétonitrile.

Introduction

Recently, in an overview on the solvation of ions (1), a comparison was made of the main thermodynamic and transport properties of alkali and tetraalkylammonium halides in water, heavy water, urea–water mixtures and in typical protic and aprotic solvents. In the preparation of this manuscript, it was surprising to find very few precise compressibility data on electrolytes in nonaqueous solvents. Compressibilities are necessary for predicting the pressure dependence of various equilibrium properties, and, like other properties related to the second derivatives of the chemical potential (i.e. heat capacities and expansibilities), they should be highly sensitive to structural effects in ion–solvent interactions. Thus, a comparison of the compressibilities of ions in non-aqueous and in aqueous solvents should be very helpful in evaluating the relative importance of structural and coulombic interactions to this property, since no structural effects should be present in most non-aqueous systems.

The solubility of electrolytes is in general not very high in most non-aqueous solvents. However, with modern compressibility techniques based on sound velocities, e.g. "sing-around" method, it is possible to measure differences in compressibilities of fairly dilute solutions, thus allowing a study in many non-aqueous systems with solvents such as methanol, propylene carbonate, acetonitrile, dimethylsulfoxide.

The solvent chosen to initiate this study is acetonitrile (AN). It is a fairly typical aprotic solvent, and volumes and heat capacities of alkali and tetraalkylammonium halides in this solvent have already been measured in this laboratory (2).

II. Experimental

The electrolytes used in this study are the same as those of a previous study (2); their origin and purification procedures were given therein.

The sound velocities were obtained by the "sing around" method which has been described by various authors in the literature (3–5). The ultrasonic pulse repetition rate (frequency) was determined with a Nusonic Model 6105 solution monitor (Mapco Inc). The transducer area of stainless steel probe was coated with Teflon by the manufacturer.

The cell was thermoregulated to ±0.001 K with a Sodev circulating thermostat. The temperature of the bath was measured with a Hewlett-Packard quartz thermometer. It was kept at 25.00°C throughout this study. The cell and its thermostated jacket were covered with styro foam to minimize heat losses. The monitor was fitted inside the cylindrical cell with a rubber O-ring. The monitor could then be displaced like a piston, thus enabling further addition of one of the components while keeping the dead space to a minimum. It was found however that AN attacks the O-ring, and no Teflon O-rings of the proper size could be found. The situation was remedied by covering the O-ring with Teflon tape.

[1]Present address: Department of Chemistry, McMaster University, Hamilton, Ont., Canada L8S 4M1.

[2]To whom all correspondence should be addressed.

0008-4042/81/142212-06$01.00/0

©1981 National Research Council of Canada/Conseil national de recherches du Canada

Can. J. Chem. Downloaded from www.nrcresearchpress.com by 210.87.254.105 on 09/06/12
For personal use only.

TABLE 1. Isentropic compressibilities of some electrolytes in water at 25°C: parameters $\bar{K}_S^0$ and A_K of eq. [3] for $\phi_{K,S}$ in $cm^3\ bar^{-1}\ mol^{-1}$[a]

	$-10^4\ \bar{K}_S^0$	$10^4\ A_K$	$m^{1/2}$
NaCl	51.0, 50.45 (10), 50.5(4), 50.4(5), 52.88 (11)	5.9	0.09–0.34
KCl	43.4, 43.6 (10), 43.5(4), 44.1(5), 46.34 (11)	4.9	0.09–0.34
KBr	35.0, 35.8 (10), 36.0(4), 35.0(5)	4.0	0.1 –0.34

[a]Reference numbers in parentheses.

Depending on the solubility of the salts, two different methods of making measurements were employed. For the more soluble salts, i.e. Bu_4NBr and Pr_4NBr, the cell was initially filled with solvent and the concentration was increased by the addition of aliquots of concentrated solutions. For the less-soluble salts, the salt wad added directly to the solvent in the cell and the concentration was decreased by the addition of solvent aliquots. All concentrations were prepared by weight. NaI and *n*-Pen_4NBr were done by both the dilution method and by the addition of stock solutions, and the results of the two methods were in good agreement.

The solvent was of M.C.B. spectroquality and was found to contain approximately 600 μg H_2O per cm^3 by the Karl-Fischer method. On very humid days it was found that the water content of the solution in the cell increased by as much as 380 μg H_2O per cm^3 over the time required to complete a series of measurements. With most systems this overall quantity of water did not appear to affect the results significantly. On the other hand, for LiBr, sodium tetraphenyl boride ($Na\phi_4B$) and tetraphenylphosphonium bromide (ϕ_4PBr), water had a significant effect on the results. In these cases, the AN was dried as much as possible by storing it over 3 Å molecular sieves prior to use.

III. Results

The isentropic compressibilities β_S in bar^{-1} were calculated from the ultrasonic pulse frequency with the relation (6)

$$[1]\quad \beta_S = \frac{10^2}{dc^2} = \left(\frac{7/f - B10^{-6}}{A(1+\alpha t)}\right)^2 \frac{10^2}{d}$$

where A is the sound path length, B is the electronic delay time, f is the ultrasonic pulse repetition rate in Hz, α is the coefficient of thermal expansion for the ultrasonic probe, c is the sound velocity in $m\ s^{-1}$, and d is the solution density in $g\ cm^{-3}$. The values of A and B obtained by calibration with water at various temperatures (7) are essentially those predetermined by the manufacturer. The densities were obtained by linear interpolation of the data of Zana *et al* (2).

The isentropic compressibility of AN, $\beta_{S0} = 78.95 \times 10^{-6}\ bar^{-1}$, compares reasonably well with those of Blandamer *et al*. (8), $76.0 \times 10^{-6}\ bar^{-1}$, considering the presence of traces of water. On the other hand, the agreement is less satisfactory with the value of $98 \times 10^{-6}\ bar^{-1}$ calculated from isothermal compressibility data of Dack *et al*. (9). The sound velocity in pure AN is $1277.03 \pm 0.13\ m\ s^{-1}$.

The apparent molal isentropic compressibilities were calculated from the difference between β_S and that of the pure solvent β_{S0},

$$[2]\quad \phi_{K,S} = \beta_S\phi_V + 1000\,(\beta_S - \beta_{S0})/md_0$$

where ϕ_V is the apparent molal volume given by Zana *et al*., d_0 is the density of AN containing 600 μg of H_2O per cm^3 (0.77668 $g\ cm^{-1}$), and m is the molality.

The accuracy of the technique was checked through measurements of the standard partial molal isentropic compressibilities of NaCl, KCl, and KBr in water at 25°C. The results obtained can be compared with reliable literature values in Table 1. This technique is therefore capable of measuring $\phi_{K,S}$ to $\pm 10^{-5}\ cm^3\ mol^{-1}\ bar^{-1}$.

The original data and derived apparent molal isentropic compressibilities are given in Table 2. Sound velocities can be calculated from β_S and d using eq. [1]. It would be possible to calculate isothermal compressibilities if precise heat capacities and expansibilities were known (12). Reliable heat capacities are available (2) but unfortunately not expansibilities.

Some typical results are plotted against the square-root of the molality in Fig. 1. In the case of NaI runs were repeated under different conditions (see Experimental section) and quite reasonable agreement was observed. The Debye–Hückel limiting slopes are not known for electrolytes in AN. Therefore, the standard values $\phi_{K,S}^0$ ($= \bar{K}_S^0$) have to be obtained by extrapolation of $\phi_{K,S}$ against $m^{1/2}$. Despite the increased uncertainty with this type of extrapolation, reasonably good values were obtained with most electrolytes. However, LiBr is a typical case where extrapolation is very difficult since this pair of ions forms a complex with the traces of water; as in the case of heat capacities (2), $\phi_{K,S}$ probably goes through a maximum or hump at low concentration. Therefore it is not possible to obtain a reliable $\bar{K}_S^0$ from LiBr data and the value for Li^+ was calculated from $LiClO_4$. Similar extrapolation difficulties were also encountered with RbI, ϕ_4PBr, and $Na\phi_4B$.

The best values of $\bar{K}_S^0$ that could be extracted

Can. J. Chem. Downloaded from www.nrcresearchpress.com by 210.87.254.105 on 09/06/12
For personal use only.

Can. J. Chem. Downloaded from www.nrcresearchpress.com by 210.87.254.105 on 09/06/12
For personal use only.

Table 2. Isentropic compressibilites of some electrolytes in acetonitrile at 25°C, the headings are: solute, m, $10^6(\beta_S-\beta_{So})$, $10^4\phi_{K,S}$, $10^3\Delta d$

NaI	.01062	- 0.160	- 188.7	1.193	$LiClO_4$	.06677	- 0.893	- 136.0	5.507	n-Pen_4NBr	.12174	- 1.661	99.4	9.342
	.01721	- 0.256	- 186.2	1.933		.06362	- 0.858	- 137.4	5.250		.11581	- 1.588	98.6	8.911
	.02421	- 0.356	- 183.8	2.716		.04115	- 0.825	- 137.5	5.048		.11086	- 1.515	98.2	8.592
	.03632	- 0.527	- 180.8	4.060		.05803	- 0.792	- 139.6	4.794		.10612	- 1.447	97.4	8.306
	.04431	- 0.643	- 177.3	5.160		.05316	- 0.751	- 139.6	4.559		.10116	- 1.402	97.1	7.936
	.05621	- 0.795	- 175.6	6.251		.05222	- 0.706	- 138.2	4.327		.09757	- 1.357	96.6	7.569
	.06726	- 0.944	- 173.8	7.465		.04961	- 0.663	- 136.9	4.093		.09276	- 1.295	96.1	7.210
	.07832	- 1.087	- 171.3	8.665		.04760	- 0.638	- 137.4	3.930		.08867	- 1.244	95.3	6.903
	.08715	- 1.206	- 170.7	9.631		.04543	- 0.618	- 139.0	3.784		.08490	- 1.193	95.1	6.623
	.09759	- 1.344	- 169.8	10.774		.04380	- 0.599	- 140.5	3.637		.08175	- 1.153	95.1	6.388
	.10751	- 1.474	- 168.9	11.866		.04242	- 0.581	- 140.8	3.524		.07855	- 1.110	94.5	6.147
	.11583	- 1.581	- 167.9	12.763		.04088	- 0.553	- 138.7	3.397		.07708	- 1.092	93.8	6.036
	.12828	- 1.741	- 166.7	14.113							.07555	- 1.074	93.2	5.919
	.13786	- 1.861	- 165.9	15.156		.11053	- 1.132	- 136.3	7.786					
	.14362	- 1.936	- 165.6	15.778		.10596	- 1.087	- 136.6	7.468		.00965	- 0.143	82.1	0.773
	.15072	- 2.025	- 164.7	16.543		.10057	- 1.033	- 136.7	7.093		.02245	- 0.338	83.7	1.808
						.09663	- 0.996	- 137.3	6.820		.03133	- 0.467	85.5	2.509
	.00920	- 0.140	- 190.5	1.033		.09165	- 0.954	- 137.5	6.475		.04516	- 0.662	88.5	3.591
	.01930	- 0.289	- 187.5	2.168		.08729	- 0.901	- 137.6	6.173		.05460	- 0.791	90.3	4.319
	.02845	- 0.421	- 184.8	3.186		.08266	- 0.855	- 138.0	5.852		.06610	- 0.949	91.7	5.202
	.04045	- 0.590	- 181.6	4.516		.07918	- 0.821	- 138.4	5.611		.07703	- 1.094	93.6	6.031
	.05416	- 0.778	- 178.3	6.025		.07555	- 0.781	- 138.4	5.359		.08538	- 1.202	94.2	6.659
	.06242	- 0.892	- 177.2	6.937		.07235	- 0.750	- 138.5	5.138		.09617	- 1.342	96.0	7.684
	.07157	- 1.015	- 175.1	7.933		.06827	- 0.719	- 138.8	4.925		.10521	- 1.458	97.0	8.139
	.08309	- 1.167	- 173.4	9.186		.06276	- 0.662	- 121.2	4.675		.11218	- 1.544	98.0	8.648
	.09386	- 1.307	- 171.7	10.366		.05944	- 0.629	- 121.2	4.243		.11977	- 1.638	99.0	9.199
	.10163	- 1.407	- 171.0	11.196		.05636	- 0.600	- 122.6	4.027		.12448	- 1.699	99.2	9.541
	.11089	- 1.530	- 169.9	12.229		.05321	- 0.568	- 123.1	3.806		.13095	- 1.779	99.8	10.010
	.11872	- 1.631	- 168.9	13.075		.05052	- 0.539	- 123.3	3.617					
	.12708	- 1.737	- 168.0	13.983		.04808	- 0.515	- 123.7	3.447	i-Pen_4NBr	.11859	- 1.584	103.4	9.099
	.13401	- 1.828	- 167.4	14.737		.04601	- 0.494	- 124.1	3.301		.11319	- 1.518	102.9	8.699
	.14125	- 1.918	- 166.7	15.524		.04395	- 0.472	- 124.3	3.156		.10695	- 1.439	102.6	8.237
	.14788	- 2.002	- 166.0	16.237		.04188	- 0.449	- 124.1	3.009		.10183	- 1.377	101.9	7.858
											.09683	- 1.310	102.0	7.487
	.01261	- 0.192	- 190.7	1.618	Et_4NClO_4	.19315	- 2.912	- 63.0	14.000		.09270	- 1.261	101.1	7.182
	.02210	- 0.329	- 186.3	2.682		.18609	- 2.814	- 63.4	13.508		.08809	- 1.203	100.5	6.841
	.03620	- 0.529	- 182.2	4.067		.17659	- 2.681	- 64.2	12.868		.08498	- 1.165	99.9	6.610
	.05043	- 0.723	- 178.0	5.613		.16834	- 2.567	- 65.8	12.272		.08140	- 1.118	99.7	6.342
	.05981	- 0.853	- 176.9	6.648		.16134	- 2.466	- 65.2	11.779		.07833	- 1.081	98.9	6.109
	.06936	- 0.983	- 175.6	7.694		.15465	- 2.372	- 65.7	11.307		.07551	- 1.046	98.3	5.896
	.07947	- 1.105	- 173.8	8.790		.14912	- 2.293	- 66.2	10.917					
	.08851	- 1.234	- 173.9	9.778		.14558	- 2.244	- 66.6	10.667	ϕ_4PBr	.04104	- 1.070	-116.9	6.291
	.09846	- 1.365	- 170.9	10.870		.14169	- 2.190	- 67.1	10.393		.03877	- 1.012	-115.2	5.948
	.10576	- 1.458	- 169.8	11.672		.13654	- 2.115	- 67.6	10.029		.03651	- 0.953	-114.4	5.606
	.11520	- 1.581	- 168.1	12.749		.13152	- 2.044	- 68.1	9.674		.03459	- 0.900	-114.9	5.300
	.12318	- 1.682	- 167.8	13.558		.12770	- 1.985	- 68.1	9.404		.03278	- 0.853	-114.0	5.041
											.03113	- 0.810	-114.1	4.788
	.15053	- 2.022	- 164.6	16.522		.09731	- 1.364	- 72.1	7.229		.02944	- 0.766	-113.7	4.532
	.14081	- 1.895	- 166.0	15.400		.09402	- 1.498	- 72.3	6.987		.02809	- 0.731	-113.7	4.326
	.13178	- 1.790	- 166.7	14.493		.08991	- 1.432	- 72.5	6.688		.02699	- 0.702	-113.5	4.158
	.12415	- 1.692	- 167.4	13.664		.08633	- 1.369	- 71.6	6.429		.02581	- 0.670	-112.7	3.977
	.11927	- 1.629	- 167.9	13.135		.08224	- 1.312	- 72.8	6.132					
	.11470	- 1.567	- 168.1	12.641		.07907	- 1.265	- 73.5	5.898					
	.10984	- 1.506	- 168.7	12.126		.07580	- 1.217	- 74.1	5.663					
	.10522	- 1.441	- 168.7	11.613		.07262	- 1.166	- 74.0	5.430	ϕ_4AsCl	.05918	- 1.486	- 101.2	8.898
	.10220	- 1.405	- 169.1	11.281							.05628	- 1.409	- 100.1	8.468
	.09887	- 1.361	- 169.6	10.915	$LiBr$	.06465	- 0.647	- 134.0	4.417		.05301	- 1.333	- 101.3	7.984
						.06172	- 0.617	- 134.0	4.219		.04986	- 1.252	- 100.8	7.514
	.14101	- 1.917	- 166.8	15.502		.05902	- 0.588	- 134.0	3.970		.04715	- 1.187	- 101.6	7.113
	.13341	- 1.846	- 167.4	14.890		.05670	- 0.566	- 134.1	3.746		.04466	- 1.125	- 101.6	6.747
	.12876	- 1.798	- 167.7	14.469		.05177	- 0.532	- 133.7	3.549		.04269	- 1.072	- 102.1	6.427
	.12340	- 1.688	- 167.7	13.982		.04895	- 0.503	- 133.8	3.359		.04056	- 1.024	- 102.4	6.138
	.11708	- 1.614	- 169.6	13.897		.04656	- 0.481	- 134.7	3.197		.03863	- 0.977	- 102.8	5.855
	.11195	- 1.566	- 170.0	12.344		.04417	- 0.455	- 134.3	3.036		.03699	- 0.935	- 102.5	5.608
	.10719	- 1.476	- 169.7	11.820		.04224	- 0.432	- 133.6	2.906					
	.10352	- 1.437	- 171.1	11.426		.04076	- 0.416	- 133.2	2.806	ϕ_4BNa	.02240	- 0.494	- 82.1	2.467
	.09944	- 1.375	- 170.3	10.977							.02167	- 0.474	- 82.3	2.364
	.09632	- 1.344	- 172.1	10.636		.11328	- 1.145	- 133.0	7.553		.02017	- 0.447	- 83.3	2.222
						.10635	- 1.076	- 133.2	7.092		.01904	- 0.424	- 84.6	2.097
KI	.06754	- 0.999	- 174.5	7.864		.09883	- 1.016	- 133.0	6.720		.01809	- 0.402	- 83.9	1.992
	.06360	- 0.944	- 175.2	7.410		.09257	- 0.956	- 133.4	6.299		.01731	- 0.388	- 86.4	1.907
	.06037	- 0.899	- 175.9	7.037		.08756	- 0.900	- 133.1	5.961		.01652	- 0.369	- 85.3	1.820
	.05775	- 0.863	- 176.5	6.734		.08325	- 0.856	- 133.2	5.670		.01574	- 0.352	- 85.7	1.735
	.05541	- 0.832	- 177.5	6.464		.07943	- 0.818	- 133.5	5.413		.01510	- 0.337	- 85.0	1.664
	.05320	- 0.798	- 177.4	6.209		.07532	- 0.777	- 133.8	5.136		.01450	- 0.329	- 89.7	1.597
	.05091	- 0.767	- 178.2	5.943		.07228	- 0.747	- 134.0	4.933					
	.04887	- 0.735	- 178.0	5.709		.07015	- 0.726	- 134.3	4.787					
	.04704	- 0.711	- 179.1	5.498										
	.04579	- 0.686	- 179.2	5.309	Et_4NBr	.09458	- 1.508	- 92.8	7.059					
	.04372	- 0.663	- 179.9	5.117		.09088	- 1.455	- 93.6	6.792					
						.08812	- 1.381	- 93.7	6.643					
RbI	.07101	- 1.075	- 176.2	10.671		.08093	- 1.300	- 96.0	6.084					
	.06800	- 1.032	- 176.7	10.221		.07769	- 1.250	- 96.4	5.827					
	.06497	- 0.987	- 176.9	9.767		.07417	- 1.198	- 95.2	5.570					
	.06222	- 0.945	- 177.4	9.336		.07106	- 1.168	- 95.2	5.343					
	.05929	- 0.905	- 178.0	8.918		.06813	- 1.102	- 95.5	5.128					
	.05637	- 0.863	- 178.5	8.480		.06544	- 1.061	- 96.0	4.932					
	.05439	- 0.833	- 178.8	8.178		.06304	- 1.022	- 96.0	4.756					
	.05241	- 0.803	- 178.8	7.886		.06071	- 0.986	- 96.4	4.588					
	.05125	- 0.787	- 179.2	7.715										
	.04958	- 0.764	- 179.9	7.468		.05696	- 0.929	- 97.4	4.306					
	.04846	- 0.747	- 180.1	7.301		.05438	- 0.895	- 98.2	4.115					
	.04748	- 0.733	- 180.5	7.155		.05159	- 0.843	- 97.7	3.908					
	.04615	- 0.713	- 180.6	6.956		.04889	- 0.798	- 97.7	3.707					
	.03945	- 0.617	- 183.3	5.956		.04653	- 0.765	- 99.0	3.531					
	.03760	- 0.598	- 186.8	5.678		.04405	- 0.722	- 98.5	3.348					
	.03572	- 0.568	- 186.9	5.397		.04224	- 0.697	- 99.6	3.213					
	.03406	- 0.543	- 187.4	5.147		.04085	- 0.671	- 98.9	3.109					
	.03255	- 0.520	- 188.0	4.916		.03919	- 0.647	- 100.0	2.986					
	.03120	- 0.502	- 189.4	4.717		.03764	- 0.621	- 99.9	2.869					
	.02994	- 0.482	- 189.6	4.528		.03615	- 0.597	- 100.1	2.757					
Et_4NI	.07909	- 1.261	- 80.8	8.072	Pr_4NBr	.01351	- 0.214	- 35.4	1.047					
	.07652	- 1.192	- 81.5	7.616		.02438	- 0.382	- 32.9	1.874					
	.07082	- 1.139	- 82.6	7.246		.03784	- 0.582	- 29.0	2.885					
	.06716	- 1.081	- 82.7	6.876		.04833	- 0.737	- 26.0	3.669					
	.06399	- 1.035	- 83.7	6.557		.05706	- 0.858	- 24.7	4.314					
	.06153	- 0.996	- 83.8	6.309		.06500	- 0.972	- 23.6	4.896					
	.05897	- 0.957	- 84.4	6.051		.07241	- 1.069	- 22.3	5.394					
	.05650	- 0.917	- 84.5	5.801		.08871	- 1.276	- 20.9	6.483					
	.05420	- 0.883	- 85.3	5.570		.09448	- 1.382	- 19.8	7.042					
	.05202	- 0.848	- 85.3	5.349		.10127	- 1.475	- 19.1	7.530					
	.05008	- 0.822	- 86.7	5.152		.10966	- 1.590	- 18.3	8.132					
						.11868	- 1.681	- 17.3	8.637					
Et_4NCl	.15639	- 2.202	- 72.5	6.641		.12400	- 1.727	- 16.4	9.153					
	.14969	- 2.120	- 73.5	6.366		.13003	- 1.840	- 16.1	9.579					
	.14207	- 2.023	- 74.4	6.053		.13634	- 1.940	- 15.2	10.025					
	.13543	- 1.940	- 75.1	5.780										
	.12869	- 1.849	- 75.9	5.503		.01325	- 0.211	- 17.5	1.056					
	.12234	- 1.765	- 76.3	5.251	n-Bu_4NBr	.02414	- 0.376	- 22.1	1.909					
	.11726	- 1.698	- 77.1	5.034		.03689	- 0.584	- 25.5	2.900					
	.11341	- 1.645	- 77.6	4.876		.04571	- 0.689	- 28.3	3.573					
	.10826	- 1.574	- 78.0	4.664		.05400	- 0.808	- 29.6	4.204					
	.10331	- 1.511	- 80.1	4.469		.06284	- 0.932	- 31.3	4.831					
	.09448	- 1.366	- 80.7	4.074		.06963	- 1.027	- 32.2	5.381					
	.08028	- 1.187	- 81.1	3.497		.08172	- 1.195	- 33.6	6.283					
	.07619	- 1.129	- 81.5	3.323		.09082	- 1.318	- 34.8	6.959					
	.07260	- 1.076	- 81.8	3.164		.10166	- 1.443	- 36.1	7.760					
	.06909	- 1.027	- 82.1	3.025		.11256	- 1.564	- 37.4	8.554					
	.06623	- 0.986	- 82.4	2.904		.12151	- 1.724	- 38.2	9.211					
	.06364	- 0.947	- 82.4	2.795		.12750	- 1.802	- 38.8	9.644					
	.06092	- 0.907	- 82.5	2.680		.13814	- 1.938	- 39.8	10.418					
	.05870	- 0.877	- 83.2	2.586		.14343	- 2.011	- 40.0	10.814					
						.15170	- 2.114	- 40.7	11.384					
$NaClO_4$	.10345	- 1.384	- 151.6	8.431										
	.10144	- 1.331	- 152.0	8.293		.02067	- 0.324	- 20.5	1.640					
	.09376	- 1.260	- 152.8	7.840		.03220	- 0.500	- 22.6	2.534					
	.09066	- 1.197	- 153.3	7.631		.04749	- 0.721	- 25.7	3.726					
	.08626	- 1.140	- 153.5	7.060		.06359	- 0.970	- 31.8	5.076					
	.08181	- 1.084	- 154.1	6.724		.07237	- 1.065	- 32.3	5.587					
	.07796	- 1.034	- 154.6	6.413		.07986	- 1.168	- 33.6	6.146					
	.07471	- 0.992	- 155.6	6.155		.09150	- 1.325	- 35.2	7.010					
	.07167	- 0.953	- 155.0	5.907		.10147	- 1.457	- 36.7	7.753					
	.06911	- 0.924	- 155.9	5.698		.10961	- 1.551	- 37.4	8.270					
						.11549	- 1.663	- 38.2	8.788					
						.12503	- 1.767	- 38.8	9.467					
						.13910	- 1.929	- 39.7	9.835					
						.13894	- 1.959	- 39.8	10.476					
						.14472	- 2.030	- 40.4	10.891					
						.15474	- 2.157	- 41.0	11.601					

m: molality in mol kg^{-1}

β_S: isentropic compressibilities of the solution in bar^{-1}

β_{SO}: isentropic compressibility of acetonitrile

$\phi_{K,S}$: apparent molal isentropic compressibility in cm^3 bar^{-1} mol^{-1}

Δd: difference in density between the solution and the solvent in g cm^{-3}

Can. J. Chem. Downloaded from www.nrcresearchpress.com by 210.87.254.105 on 09/06/12
For personal use only.

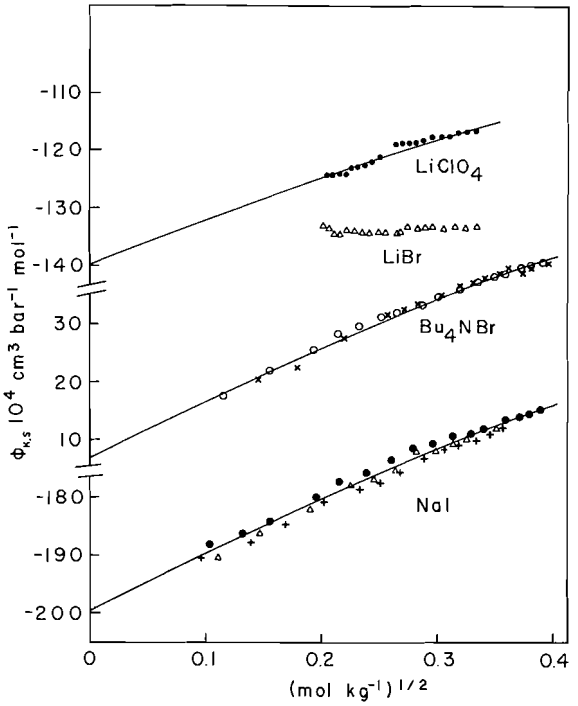

FIG. 1. Some typical plots of $\phi_{K,S}$ against the square root of the molality. With Bu_4NBr two sets of measurements were made. With NaI some runs were carried by the dilution method and others by the concentration one. With systems like $LiClO_4$, the extrapolation is difficult in view of the short working zone available. Cases like LiBr are extreme in that only estimates of infinite dilution values are possible assuming an average slope.

from our data and the slope A_K of the relation

[3] $\phi_{K,S} = \phi_{K,S}^0 + A_K m^{1/2}$

are given in Table 2. Ionic additivity can usually give some idea of the reliability of results. Unfortunately, very few pairs of electrolytes can be used for this purpose in the present case because of their limited solubility in AN. The differences between NaI and $NaClO_4$ and between Et_4NI and Et_4NClO_4 are respectively -21.9 and -12.5×10^{-4} cm^3 bar^{-1} mol^{-1}, which is not very satisfactory since the ultrasonic technique is capable of measuring $\phi_{K,S}$ to 10^{-5} cm^3 bar^{-1} mol^{-1}. Therefore, in view of the limited solubility range of most electrolytes, the method of extrapolation, the effect of association, and the influence of traces of H_2O in the solvent with some systems, the present $\bar{K}_S^0$ can probably be considered reliable to $\pm 5 \times 10^{-4}$ cm^3 bar^{-1} mol^{-1} only.

IV. Discussion

The best way of comparing and interpreting the values of $\bar{K}_S^0$ is to plot them against some function of the size of the ions. For this purpose, values of $\bar{K}_S^0$ were calculated for electrolytes with a common cation or anion by the additivity rule and plotted against the cationic radii for the series MBr and against the anionic radii for the series NaX (Fig. 2). For comparison, the same function is shown for the corresponding aqueous systems (1).

The most striking observation in Fig. 2 is the large negative values of $\bar{K}_S^0$ of alkali halides and the large positive values for the $\bar{K}_S^0$ of the larger R_4NBr in AN in comparison with the aqueous system. Most of the interpretations of $\bar{K}_S^0$ in terms of solvation effects (4, 5, 13–15) assume that $\bar{K}_S^0$ of unsolvated ions is negligible, although Conway and Verrall (15) recognized that large organic ions could have some intrinsic compressibility due to the intramolecular free space. This contribution to the compressibility should be much smaller than the observed 72×10^{-4} cm^3 bar^{-1} mol^{-1} for n-Pen_4NBr. Volumes and heat capacities of these ions in AN suggest very little solvation of the higher homologs (2). A plausible explanation for these high values comes from the compressibility studies of ionic surfactants (16, 17). For example, in the postmicellar region, $\bar{K}_S$ of nonyl and decyltrimethylammonium bromides (16) have constant values of about 85 and 95×10^{-4} cm^3 bar^{-1} mol^{-1}, corresponding to the values of the hypothetical liquid hydrocarbons. The values of $\bar{K}_S^0$ of alcohols in propylene carbonate are also all large and positive (18). Therefore, the high compressibility of the larger R_4NBr results from the compression of

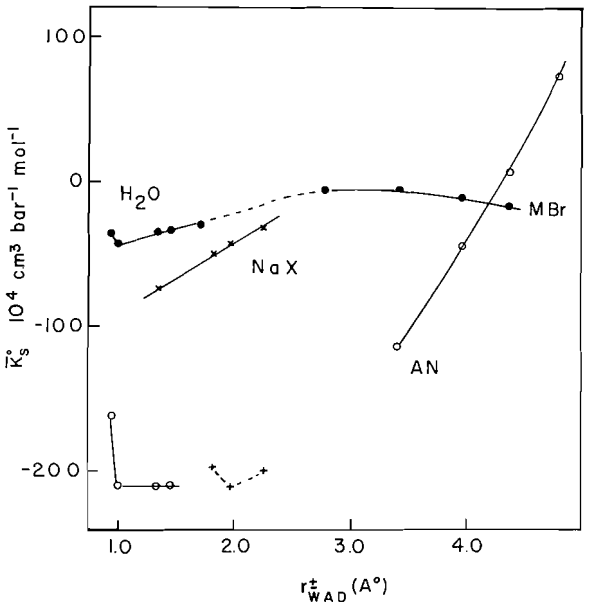

FIG. 2. The dependence of $\bar{K}_S^0$ on the Waddington ionic radii at 25°C: MBr, ● (water), ○ (AN); NaX, × (water), + (AN).

Can. J. Chem. Downloaded from www.nrcresearchpress.com by 210.87.254.105 on 09/06/12
For personal use only.

TABLE 3. Apparent molal isentropic compressibilities of some electrolytes in acetonitrile at 25°C: parameters of eq. [3] for $\phi_{K,S}$ in $cm^3\ bar^{-1}\ mol^{-1}$

Electrolyte	$10^4\ \bar{K}_S^0$	A_K	$m^{1/2}$
LiBr	−135.5[a]	7.2	0.2–0.34
$LiClO_4$	−138.6	70.1	0.2–0.34
NaI	−198.1	86.6	0.1–0.4
$NaClO_4$	−176.2	76.6	0.2–0.33
$Na\phi_4B$	−103.1	138.9	0.06–0.075
KI	−200.9	101.5	0.21–0.28
RbI	−198	100	0.17–0.27
Et_4NCl	−99.4	65.8	0.24–0.40
Et_4NBr	−112.4	64.0	0.19–0.32
Et_4NI	−104.9	85.2	0.22–0.28
Et_4NClO_4	−92.4	67.2	0.27–0.44
Pr_4NBr	−44.4	79.6	0.12–0.37
Bu_4NBr	9.4	82.9	0.11–0.40
n-Pen_4NBr	71.8	78.6	0.1–0.36
i-Pen_4NBr	79.1	71.4	0.27–0.35
ϕ_4AsCl	−110.7	41.9	0.19–0.24
ϕ_4PBr	−105.2	−49.3	0.16–0.20

[a] Actual fit of experimental data. This value was not used for the determination of $\bar{K}_S^0$ (Li^+) (see text).

the free space between the large unsolvated cation and AN. It is consequently incorrect to assume that the compressibility of "unsolvated" ions in solution is negligible. Even with small solutes some free space is present and a positive contribution to $\bar{K}_S^0$ would be observed. The only exceptions to this rule are the hydrophobic solutes in water. If, as it is usually believed (1), the hydrophobic co-sphere resembles to some extent that of a clathrate hydrate, very little free space is present between the solute and the solvent co-sphere, and this accounts to a large extent for the lower compressibilities of R_4NBr in water.

The values of $\bar{K}_S^0$ of alkali halides and other inorganic electrolytes are all much more negative than in water. To appreciate the significance of these values, it is convenient to consider the interpretations given in terms of solvation numbers. Although we recognize that solvation numbers have no absolute meaning (1), this concept is useful in comparing different solvents or different ions. Since the early work of Passynsky (19), many authors have tried to extract hydration numbers from compressibility data, e.g. Padova (13), Tamura and Sasaki (14), Allan and Lee (20), Bockris and Saluja (21). Their approaches vary to some extent, but they all essentially assume that the unsolvated ions and the water molecules in the hydration co-sphere are incompressible. Although these assumptions are obviously oversimplified, especially in non-aqueous solvents (e.g. the intrinsic $\bar{K}_2$ is not zero), they lead to a very simple relation between the isothermal $\bar{K}_2^0$ and the solvation number h;

$$[4]\quad \bar{K}_2^0 = -hv_0\beta_0$$

Neglecting the difference between isentropic and isothermal compressibilities, and taking the molar volume of AN, $v_0 = 53\ cm^3\ mol^{-1}$, and the compressibility of AN, $\beta_0 = 7.90 \times 10^{-5}\ bar^{-1}$ (isentropic value), the solvation numbers of LiBr, NaBr, and KBr are respectively 3.7, 5, and 5. These numbers are of the same magnitude as those obtained in water (22) and in methanol (20). Therefore, despite the crudeness of this approach, we can conclude that the number of solvent molecules affected by the ions are comparable in AN and in H_2O, and the large negative $\bar{K}_S^0$ observed in AN is a direct consequence of the larger volume and compressibility of AN.

The relative independence of $\bar{K}_S^0$ on the size of the alkali halides in AN in contrast with aqueous systems is harder to explain. The Born equation predicts that the coulombic solvation should vary inversely with the ionic radii. We would therefore expect that $\bar{K}_S^0$ in AN would increase with both the radii of the cations and anions with a more positive slope than in H_2O. The uncertainty of the data in AN is much larger than in water but it cannot be *much more than* $5 \times 10^{-4}\ cm^3\ K^{-1}\ mol^{-1}$. Even by allowing for maximum uncertainty, the slope in Fig. 2 would not be large. The trend therefore is real. Further systematic studies in other non-aqueous solvents would be required before we can venture an explanation. On the other hand, the less negative $\bar{K}_S^0$ of the salts made up of small cations or anions (Li^+, Cl^-) is a more general phenomenon and is usually explained through the smaller coordination number of these ions (2). The solvent molecules are held more tightly by these ions but few solvent molecules can fit in the first coordination shell of the ion.

There are no reliable methods of dividing $\bar{K}_S^0$ into its ionic components. However, some extrathermodynamic approach can be used to estimate these values. Millero (23) has suggested dividing $\bar{V}^0$ of $\phi_4As^+\phi_4B^-$ into ionic components assuming $\bar{V}^0$ (ϕ_4As^+)/$\bar{V}^0$ (ϕ_4B^-) is equal to the ratio of their van der Waals volumes. Such a method cannot be used since we do not know the ratio of the compressibilities of the pure (solid or gaseous) ions. However, if this pair of ions is split into two, the value of ϕ_4B^- is $-11 \times 10^{-4}\ cm^3\ bar^{-1}\ mol^{-1}$. A better assumption (2) seems to be the splitting into two of the pair $\phi_4P^+\phi_4B^-$. This gives a value for ϕ_4B^- near 0. The extrapolation method suggested by Conway *et al.* (24) for volumes cannot really be used for $\bar{K}_S^0$ in

TABLE 4. Ionic standard partial molal isentropic compressibilities in acetonitrile at 25°C based on the assumption $\bar{K}_S^0(\phi_4B^-) = 0$

Ion	$10^4\ \bar{K}_S^0$/(cm³ bar⁻¹ mol⁻¹)	Ion	$10^4\ \bar{K}_S^0$/(cm³ bar⁻¹ mol⁻¹)
Li^+	−56	Cl^-	−90
Na^+	−103	Br^-	−103
K^+	−106	I^-	−95
Rb^+	−103	ClO_4^-	−83
Et_4N^+	−9	ϕ_4B^-	0
Pr_4N^+	+59	ϕ_4As^+	−21
Bu_4N^+	+112	ϕ_4P^+	−2
n-Pen_4N^+	+175		
i-Pen_4N^+	+182		

view of the large contribution of the intrinsic compressibility which does not seem to be a simple function of the size of the ions. Therefore, taking the value of $\phi_4B^- \simeq 0$ seems to be about the best we can do at the moment. Ionic $\bar{K}_S^0$ based on this assumption are given in Table 4. From this table $\bar{K}_S^0(Na^+) \simeq \bar{K}_S^0(Br^-)$. This is probably of the right magnitude since these two ions correspond to minimum values of $\bar{K}_S^0$ of cations and anions in Fig. 2.

A final remark can be made on the difference between n-Pen_4NBr and i-Pen_4NBr. In previous work with AN, it was observed that no significant difference in $\bar{V}^0$ and $\bar{C}_p^0$ could be observed with these isomers (2). The same seems to be true of $\bar{K}_S^0$ since they differ by only 7×10^{-4} cm³ bar⁻¹ mol⁻¹ and the uncertainty on each is of the order of 5×10^{-4} cm³ bar⁻¹ mol⁻¹. Therefore this confirms the unimportance of the compactness of the solute molecule on the thermodynamic properties in AN.

Acknowledgements

The authors are grateful to the Natural Sciences and Engineering Research Council of Canada and to the Quebec Ministry of Education for financial support.

1. J. E. DESNOYERS and C. JOLICOEUR. *In* Treatise of electrochemistry. *Edited by* J. O'M. Bockris, B. E. Conway, and E. Yeager. Plenum Press. In press.
2. R. ZANA, G. PERRON, and J. E. DESNOYERS. J. Solution Chem. **9**, 59 (1980).
3. R. GARNSEY, R. J. BOE, R. MAHONEY, and T. A. LITOVITZ. J. Chem. Phys. **50**, 5222 (1969).
4. J. G. MATHIESON and B. E. CONWAY. J. Solution Chem. **3**, 455 (1973); see also J. Chem. Soc. Faraday I, **70**, 752 (1974).
5. F. J. MILLERO and T. KUBINSKI. J. Acoust. Soc. Am. **57**, 312 (1975) see also: F. J. Millero, G. K. Ward, and P. V. Chetirkin. J. Acoust. Soc. Am. **61**, 1492 (1977).
6. Instruction manual for sonic solution monitor Model 6105.
7. V. A. DEL GROSSO and C. W. MADER. J. Acoust. Soc. Am. **52**, 1442 (1972).
8. M. J. BLANDAMER, M. J. FOSTER, and D. WADDINGTON. J. Chem. Soc. Faraday I, **66**, 1369 (1970).
9. M. R. J. DACK, K. S. BIRD, and A. J. PARKER. Aust. J. Chem. **28**, 955 (1975).
10. M. SAKURAI, T. NAKAJIMA, T. KOMATSU, and T. NAKAGAMA. Chem. Lett. 971 (1975).
11. F. T. GUCKER, D. STUBLEY, and D. J. HILL. J. Chem. Thermodyn. **7**, 865 (1975).
12. J. E. DESNOYERS and P. R. PHILIP. Can. J. Chem. **50**, 1094 (1972).
13. J. PADOVA. Bull. Res. Council Israel A**10**, 63 (1961).
14. K. TAMURA and T. SASAKI. Bull. Chem. Soc. Jpn. **36**, 975 (1963).
15. B. E. CONWAY and R. E. VERRALL. J. Phys. Chem. **70**, 3952 (1966).
16. T. S. BRUN, H. HØILAND, and B. VIKINGSTAD. J. Coll. I. Sci. **63**, 89 (1978).
17. R. DELISI, C. OSTIGUY, G. PERRON, and J. E. DESNOYERS. J. Coll. Interface Sci. **71**, 147 (1979).
18. H. HØILAND. J. Solution Chem. **6**, 291 (1977).
19. A. G. PASSINSKY. Acta Physicochem. **8**, 835 (1938).
20. D. S. ALLAN and W. H. LEE. J. Chem. Soc. A, **6** (1966).
21. J. O'M. BOCKRIS and P. S. S. SALUJA. J. Phys. Chem. **76**, 2140 (1972).
22. J. E. DESNOYERS and C. JOLICOEUR. *In* Modern aspects of electrochemistry. *Edited by* J. O'M. Bockris and B. E. Conway. Plenum Press, New York. 1969. Chapt. 1.
23. F. MILLERO. J. Phys. Chem. **75**, 280 (1971).
24. B. E. CONWAY, R. E. VERRALL, and J. E. DESNOYERS, Trans. Faraday Soc. **62**, 2738 (1966).

Can. J. Chem. Downloaded from www.nrcresearchpress.com by 210.87.254.105 on 09/06/12
For personal use only.

Field desorption mass spectrometry of sodium carboxylates. Intermolecular exchange of hydrogens and alkyl groups as shown by labelling

GORDON WALTER WOOD[1] AND WING FUNG SUN

Department of Chemistry, University of Windsor, Windsor, Ont., Canada N9B 3P4

Received December 23, 1980

GORDON WALTER WOOD and WING FUNG SUN. Can. J. Chem. **59**, 2218 (1981).

Field desorption mass spectra of sodium acetate and sodium propionate, labelled analogs, and mixtures were used to investigate hydrogen and alkyl group exchange accompanying the desorption process. At low anode temperatures, decomposition products are minimized and formation of homologous carboxylates by alkyl transfer is significant. The complexity of these intermolecular reactions precludes a simple mechanistic scheme. Reproducibility of minor ions is much improved by the addition of pentaerythritol to these samples.

GORDON WALTER WOOD et WING FUNG SUN. Can. J. Chem. **59**, 2218 (1981).

On a fait appel aux spectres de masse par désorption de champ de l'acétate et du propionate de sodium ainsi que de leurs analogues marqués et de leurs mélanges pour étudier les échanges entre l'hydrogène et le groupe alkyle qui accompagnent le phénomène de désorption. Lorsque les températures de l'anode sont faibles, les produits de décomposition sont nettement défavorisés et la formation des carboxylate analogues par transfert d'alkyles devient plus importante. La complexité de ces réactions intermoléculaires exclut un mécanisme simple. L'addition du pentaérythritol à ces échantillons permet d'améliorer grandement la reproducibilité des ions minoritaires.

[Traduit par le journal]

Introduction

Although sodium acetate has become the prototypical organic salt for field desorption mass spectrometry (FDMS) studies (1–5), a number of questions about its behavior remain unanswered. The first reported spectrum (1) showed m/z 23 (Na^+) as base peak at 25, 30, and 32 mA, with no other ions at the lowest anode temperature, some ions of structural significance at 30 mA (chiefly m/z 105), and decomposition products at 32 mA. In a later description of this work it was pointed out (4) that m/z 105 is only the first member of a series of cluster ions $[Na_xOAc_{x-1}]$ where $x = 2$ and that ions are found corresponding to higher values of x to the limit of the mass scale. In this later review, among other ions listed as characteristic were: $[Na\cdot HOAc]^+$, referred to as $(M + H)^+$, and fragments thereof, $[HOAc]^{+\cdot}$, and products of "thermally field-induced decomposition reactions", such as CH_2CONa^+, $HCO_2Na_2^+ + x$NaOAc, $CH_3CH_2CO_2Na_2^+ + x$NaOAc, where $x = 1, 2$. In subsequent presentation (3) and publication (2) the Bonn group showed a high resolution FD mass spectrum of sodium acetate obtained by photoplate. This full-mass range (to m/z 570) spectrum presented for the first time examples of the various types of ions derived from sodium acetate.

Ambiguities within these reports (1–4), and between them and concurrent work in our laboratory wherein we found some, but not all, of the reported ions led us to question (5) the purity of the sodium acetate as well as part of the interpretation offered in the earlier work. We now report that the purity of the samples has been verified, and that therefore the apparent formate and propionate entities found in sodium acetate spectra (2–5) must arise as part of the FD process. We have also extended the analysis of minor ions formed in addition to the fundamental m/z 105, 187, 269 ... series through use of labelled samples. Thoughout this work we have relied on matrix materials, such as earlier reported for fructose (5), to improve the desorption characteristics of the salt samples. As will be discussed in more detail later (6), pentaerythritol (PE) is a compound which greatly increases the detectable ion yield from sodium carboxylates without itself contributing to the spectrum. In several of the spectra presented here, addition of 0.5 mol of PE per mol of salt allows one to accumulate 5–7 scans (12 s each) to give a spectrum with a usable dynamic range of 10^3, about one order of magnitude greater than the pure salt. At the same time, the abundance of Na^+ is greatly reduced.

Results and Discussion

Field desorption of an equimolar mixture of NaOAc/NaOAc-d_3 gave spectra as summarized in Table 1. This sample was deposited on the field anode from a solution containing 0.5 mol of pentaerythritol per mol of salt. Species differing only in deuterium content are combined so that the most abundant cluster, Na_4OAc_3 containing 0–9 deuteriums, is reported as m/z 269–278. As expected, the major species correspond to clusters of this type,

[1]To whom all correspondence should be addressed.

0008-4042/81/142218-05$01.00/0

©1981 National Research Council of Canada/Conseil national de recherches du Canada

Can. J. Chem. Downloaded from www.nrcresearchpress.com by 210.87.254.42 on 09/06/12
For personal use only.

TABLE 1. Field desorption mass spectrum of equimolar mixture of NaOAc/NaOAc-d_3 plus pentaerythritol.[a,b,c]

m/z	%	Assignment[d]	D content	m/z	%	Assignment	D content
23	1.4	Na		302–304	0.1	Na_4OAc_2OBu	5–7
91–92	1.0	Na_2OFor	0–1	324–325	0.1		
105–108	59	Na_2OAc	0–3	337–344	0.7	Na_5OAc_3OFor	0–7
120–123	0.4	Na_2OPr	1–4	352–362	8.1	Na_5OAc_4	1–11
173–177	2.8	$Na_3OAcOFor$	0–4	369–373	0.2	Na_5OAc_3OPr	4–8
187–193	69	Na_3OAc_2	0–6	421–427	0.5	Na_6OAc_4OFor	2–8
202–207	0.7	$Na_3OAcOPr$	2–7	436–446	4.8	Na_6OAc_5	3–13
255–262	5.2	Na_4OAc_2OFor	0–7	507–510	0.1	Na_7OAc_5OFor	6–9
269–278	100	Na_4OAc_3	0–9	520–529	1.9	Na_7OAc_6	5–14
284–292	1.7	Na_4OAc_2OPr	1–9	606–610	0.3	Na_8OAc_7	9–13
294–300	0.6			693	0.03	Na_9OAc_8	14

[a] Peaks shown represent 99.7% of ionization above threshold of 0.25% of most abundant peak, m/z 274. The latter constitutes about one-quarter of the m/z 269–278 manifold (see Table 2). Most of the remaining 0.3% of ionization is accounted for by: m/z 44, 45(CO_2, HCO_2), m/z 84–85, 171–172 (NaHOAc-d_{1-2} and its dimer-d_{5-6}), m/z 129 (Na_3CO_3, see ref. 2).
[b] No ions related to pentaerythritol are found.
[c] Anode heating current 21.1–21.5 mA.
[d] Formate = OFor, acetate = OAc, propionate = OPr, butyrate = OBu.

with lesser amounts of clusters in which one of the acetates has been replaced by formate or proprionate.[2] With the Na_4 clusters these peaks are found at m/z 255–262 and 284–292 respectively. Further detail on several of these clusters, along with justification for the assignments made, is provided in Table 2 where single m/z values are normalized to m/z 274 = 100. The cluster which contains this peak shows a distribution of deuterium which corresponds to randomization of the equal numbers of H/D atoms over the 9 sites available in Na_4OAc_3. Similar results are found throughout, from the single site in formate (m/z 91, 92) to the 11 sites in Na_4OAc_2OPr and all the other species through m/z 606–610. In these latter examples the statistics are less precise because of reduced ion abundance.

Only two minor peaks in Table 1 have not been assigned. The m/z 324, 325 group doesn't fit with any expected composition, but the series m/z 294–300 is a good fit for Na_5OAc_3 where $d_0 = 292$ and the ions recorded would then correspond to d_2–d_8. This assignment is tentative, however, since that ion might be expected to be doubly-charged and the appropriate peaks, 147.5, 148.5, 149.5 are found in only one scan.

These results confirm the importance of some form of carbon exchange among the acetate moieties and demonstrate a concurrent complete exchange of hydrogen (deuterium). Altogether formate and propionate containing species account for more than 5% of the total ionization in this spectrum. Other species reported previously are either absent or negligible. Since we have achieved the same result within a lowered detection limit by omitting the pentaerythritol, the latter does not appear to explain the "clean" spectrum. Our anode temperature was maintained at a considerably lower value than in the previous work, 19–22 mA vs. 30–32 mA, which suggests that some of the previously observed low mass species may have been decomposition products.

The apparent presence of butyrate (m/z 302–304 in Table 1) and other higher carboxylates in trace amounts prompted the experiment with a mixture of sodium propionate (NaOPr) and labelled sodium acetate (NaOAc-d_3) summarized in Tables 3 and 4. When allowance is made for the "deficiency" of deuterium in this experiment (5H and only 3D for 8 sites), the results are the same as for sodium acetate. Thus, the most abundant cluster, Na_2OAc, is distributed among d_0, d_1, d_2, and d_3 in the expected fashion and m/z 91, 92 is now 57% d_0, close to the ratio 5/8 expected in the absence of isotope effects.

A much richer complement of intermolecular exchange products is found when proprionate is involved. There is evidence for mixed carboxylates containing caproate (C_6, m/z 162–168), valerate (C_5, m/z 147–155, 243–251), and butyrate (C_4, m/z 133–140, 230–237, 328–336) in addition to the previously observed formate. These various clusters represent most of the ionization from m/z 91

[2]Species which are apparent homologs of acetate will be referred to as carboxylate anions throughout. Although there is no proof of this structure, atomic composition is fixed by the earlier high resolution study (2) and we find this structural assumption more attractive than the alternative whereby $C_3H_5O_2$ and higher members would become esters: $CH_3COOCH_2^-$ or $^-CH_2COOCH_3$, for example.

Can. J. Chem. Downloaded from www.nrcresearchpress.com by 210.87.254.42 on 09/06/12
For personal use only.

Can. J. Chem. Downloaded from www.nrcresearchpress.com by 210.87.254.42 on 09/06/12
For personal use only.

TABLE 2. Isotope composition of selected peaks from field desorption mass spectrum of NaOAc/NaOAc-d_3[a]

m/z	%	d_x[b]	m/z	%	d_x	m/z	%	d_x
	Na_2OFor			Na_3OAc_2			Na_4OAc_3	
91	2.1	d_0	187	5.7	d_0	269	1.2	d_0
92	2.0	d_1	188	28		270	7.4	
			189	65		271	28	
	Na_2OAc		190	79		272	65	
105	31	d_0	191	66		273	93	
106	88		192	28		274	100	
107	88		193	6.6	d_6	275	66	
108	32	d_3				276	32	
						277	11	
	$Na_3OAcOFor$			Na_4OAc_2OFor		278	2.6	d_9
173	1.0	d_0	255	0.6	d_0			
174	2.7		256	1.7			Na_4OAc_2OPr	
175	3.9		257	3.5		283	—	d_0
176	2.7		258	5.3		284	0.3	
177	1.0	d_4	259	5.2		285	0.7	
			260	3.0		286	1.2	
			261	1.4		287	1.0	
			262	0.3	d_7	288	1.0	
						289	1.2	
						290	0.7	
						291	0.5	
						292	0.2	
						293	—	
						294	—	d_{11}

[a] These peaks are reported in summary form in Table 1. Ion abundances are normalized to m/z 274 = 100.
[b] Apparent deuterium content from d_0 to perdeuteration of all species in cluster.

TABLE 3. Field desorption mass spectrum of equimolar mixture of NaOPr/NaOAc-d_3 plus pentaerythritol[a,b,c]

m/z	%	Assignment[d]	D content	m/z	%	Assignment	D content
23	23	Na		297–310	11	$Na_4OAcOPr_2$	0–13
39	0.02	NaO		311–323	3.0	Na_4OPr_3	0–12
65	0.07	CH_2CONa		328–336	0.5	Na_4OPr_2OBu	3–11
91–92	5.3	Na_2OFor	0–1	339–347	0.3	Na_5OAc_3OFor	2–10
105–108	100	Na_2OAc	0–3	352–361	1.6	Na_5OAc_4	1–10
113–115	0.2			367–376	2.8	Na_5OAc_3OPr	2–11
119–124	75	Na_2OPr	0–5	382–391	2.7	$Na_5OAc_2OPr_2$	3–12
129	0.3	Na_3CO_3		397–406	1.3	$Na_5OAcOPr_3$	4–13
133–140	1.5	Na_2OBu	0–7	412–419	0.3	Na_5OPr_4	5–12
147–155	1.2	Na_2OVal	0–8	424–426	0.1	$Na_6OAcOFor_5$	2–4
				436–444	0.6	$Na_6OAc_2OFor_4$	0–8
162–168	0.2	Na_2OCap	1–7	450–459	1.4	$Na_6OAc_3OFor_3$	0–9
173–177	2.6	$Na_3OAcOFor$	0–4	465–475	1.5	$Na_6OAc_4OFor_2$	1–11
187–193	29	Na_3OAc_2	0–6	480–489	1.0	Na_6OAc_5OFor	2–11
201–209	29	$Na_3OAcOPr$	0–8	496–502	0.3	Na_6OAc_6	4–10
215–224	7.2	Na_3OPr_2	0–9	522–526	0.1	Na_7OAc_6	7–11
230–237	0.6	$Na_3OPrOBu$	1–8	535–542	0.3	Na_7OAc_5OPr	6–13
243–251	0.3	$Na_3OPrOVal$	0–8	550–557	0.5	$Na_7OAc_4OPr_2$	7–14
255–262	2.4	Na_4OAc_2OFor	0–7	564–571	0.4	$Na_7OAc_3OPr_3$	7–14
269–278	13	Na_4OAc_3	0–9	580–585	0.2	$Na_7OAc_2OPr_4$	9–14
283–294	20	Na_4OAc_2OPr	0–11				

[a] Peaks shown represent 99.7% of ionization above threshold for single isotopic species of 0.04% of m/z 106.
[b] No ions related to pentaerythritol are found.
[c] Anode heating current 20.7–21.1 mA.
[d] formate = OFor, acetate = OAc, propionate = OPr, butyrate = OBu, Valerate = OVal, caproate = OCap.

TABLE 4. Isotopic composition of selected peaks from field desorption mass spectrum of NaOPr/NaOAc-d_3[a]

m/z	%	d_x[b]	m/z	%	d_x	m/z	%	d_x
	Na_2OFor			Na_2OBu			$Na_3OAcOFor$	
91	6.9	d_0	133	0.2	d_0	173	0.6	d_0
92	5.2	d_1	134	0.4		174	1.7	
			135	0.7		175	2.0	
	Na_2OAc		136	0.8		176	1.1	
105	33	d_0	137	0.7		177	0.4	d_4
106	100		138	0.4				
107	72		139	0.2			$Na_3OAcOPr$	
108	22	d_3	140	0.04	d_7	201	0.7	d_0
						202	3.3	
	Na_2OPr			Na_2OVal		203	11	
119	11	d_0	147	0.1	d_0	204	18	
120	44		148	0.3		205	17	
121	55		149	0.5		206	10	
122	40		150	0.6		207	3.9	
123	17		151	0.6		208	1.2	
124	3.8	d_5	152	0.3		209	0.2	d_8
			153	0.2				
			154	0.1				
			155	0.1				
			156	—	d_9			

[a] These peaks are reported in summary form in Table 3. Ion abundances are normalized to m/z 106 = 100.
[b] Apparent deuterium content from d_0 to perdeuteration of all species in cluster.

through 419. Among the low mass ions previously reported only m/z 39, 65, and 129 were detected, two of these at very low levels.

A significant set of species shown in Table 3 are the *molecular ions* corresponding to hexameric sodium acetate (m/z 496–502) and the various formate containing analogs (m/z 424–426 through 480–489). Together these species amount to 5% of the most abundant cluster. The individual peaks are close to the detection limit which may explain the failure to detect the usually less intense propionate homologs. The apparent dominance of hexamers may reflect some facet of structure in the solid state, or of the vapor above it.

Sodium propionate and its 2-^{13}C- and 3-^{13}C-labelled analogs gave FD results typified by Table 5. Cluster ions containing carboxylates from C_1 through C_5 are detected throughout the complete mass range (to m/z 800). This spectrum shows remarkably low Na^+ abundance in spite of the presence of Na_2Cl^+ clusters amounting to 2% of total ionization. The m/z 39 peak, which we would ordinarily assign to K^+, has previously been identified as NaO^+ (2). Likewise, the series m/z 136, 233, 330 ... may perhaps contain NaO^+ instead of K^+. Trace levels of doubly-charged ions are included mainly to indicate that the complexity of this FD spectrum is no doubt a function of the level of minimum detectable signal (ca. 0.01% of total ionization).

Comparison of the spectra from sodium propionate and its labelled analogs yields some information on the origin of the carbons transferred in the formation of homologs. Since formate from labelled substrate contains no excess ^{13}C, it appears to arise completely from C-1 of propionate. Acetate gets excess ^{13}C from C-2, but not from C-3, and thus is composed of C-1 and C-2. Propionate contains the original level of ^{13}C and, therefore, these carbons are not scrambled. Butyrate from C-3 labelled substrate contains 2 × ^{13}C and therefore the "extra" carbon must come by transfer of C-3. Valerate contains 2 × ^{13}C from both labelled substrates, suggesting transfer of CH_3CH_2— to propionate in intact form. While these generalizations are fairly straightforward, we have been unable to construct any simple mechanism consistent with these results as well as those reported for acetate and mixed carboxylates.

In summary, we have shown that sodium acetate and sodium propionate may be field desorbed from conditioned 10 μ wires at heating currents of 19–22 mA. Desorption in the presence of pentaerythritol has little effect on the temperature or the composition of cluster ions detected. This additive does, however, reduce the abundance of free sodium ion and increase the total ionization per unit time so that minor ions may be recorded reliably. Perhaps most importantly, the desorption process is much smoother, short-time fluctuations of ion current are greatly reduced, and ion production from a given sample extends over a longer time.

Can. J. Chem. Downloaded from www.nrcresearchpress.com by 210.87.254.42 on 09/06/12
For personal use only.

TABLE 5. Field desorption mass spectrum of NaOPr-2-^{13}C plus pentaerythritol[a,b]

Anion	$(Na^+)_2$ anion$^-\cdot x$ NaOPr					
	Σ20–800[c]	$x = 0$	$x = 1$	$x = 2$	$x = 3$	$x = 4$
Formate	3	1.0	0.7	0.9	0.3	0.2
Acetate	2	0.4	0.5	0.7	0.3	0.2
Propionate	86	29	23	20	8	4
Butyrate	2	0.2	0.5	0.5	0.2	0.1
Valerate	4	0.5	1.1	1.3	0.6	0.4
Chloride	2	0.5	0.3	0.6	0.4	0.2

Other ions

m/z 23 0.8 Na^+
m/z 39 0.2 NaO^+ or K^+
m/z 136, 233, 330, 427 $\cdots$, Σ_{20-800}0.3, $Na^+K^+OPr^-\cdot x$ NaOPr, $x = 0$–3
m/z 119.6, 120.5, 168.5, 265.7, 362.6 $\cdots$, trace, $Na_4OPr_2^{2+}$, $Na_5OPr_3^{3+}\cdots$

[a] No ions related to pentaerythritol are found.
[b] Anode heating current 19.5–20.8 mA.
[c] Sum of ionization between m/z 20 and 800.

Several of the ions previously reported from sodium acetate probably arise from thermal decomposition at an overheated anode. However, formation of apparent homologs by alkyl transfers between carboxylate substrates is shown to be a significant process even at the lowest desorption temperatures. This alkyl transfer is accompanied by scrambling of all hydrogen sites. Our mechanistic speculations have not proven fruitful, and considering the complications inherent in the condensed phase where these reactions occur, further effort in this direction may not be justified. Finally, the demonstrated complexity of intermolecular reactions accompanying FD of sodium carboxylates at moderate temperatures strikes a cautionary note on interpretation of other FD spectra.

Experimental

Mass spectra were recorded on a Varian MAT CH5 DF spectrometer operating under the control of an INCOS 2000 data system as previously described (7), except that the mass range 900-10 was scanned in 12 s.

Sodium acetate (Fisher), pentaerythritol (Aldrich), and the deuterium and carbon-13 labelled compounds (Merck Sharp and Dohme) were used as received. Sodium propionate was prepared from an equimolar mixture of propionic acid and sodium hydroxide. The product was then recrystallized twice from a chloroform/methanol mixture. Purity of this and the other carboxylates was checked by nmr. A standard qualitative method was used to demonstrate the absence of formate in the acetate used (8).

Samples were prepared for analysis by dissolving 10–20 mg in 1 mL of deionized H_2O, and loaded on the activated anodes by dipping.

Acknowledgements

Support of this work by the Natural Sciences and Engineering Research Council of Canada is gratefully acknowledged.

1. H.-R. SCHULTEN and H. D. BECKEY. Org. Mass Spectrom. **6**, 885 (1972).
2. H.-R. SCHULTEN and F. W. RÖLLGEN. Org. Mass Spectrom. **10**, 649 (1975).
3. H.-R. SCHULTEN and H. D. BECKEY. 22nd Annual Conf. Mass Spectrom. and Allied Topics, Philadelphia, May 19–24, 1974, Paper 07.
4. H. D. BECKEY. Principles of field ionization and field desorption mass spectrometry. Pergamon, Oxford. 1977. pp 286*ff*.
5. G. W. WOOD, E. J. OLDENBURG, and P.-Y. LAU. Can. J. Chem. **56**, 2750 (1978).
6. G. W. WOOD and W. F. SUN. To be published.
7. G. W. WOOD, E. J. OLDENBURG, P.-Y. LAU, and D. L. WADE. Can. J. Chem. **56**, 1372 (1978).
8. W. W. SCOTT. Standard methods of chemical analysis. Vol. 2. 5th ed. *Edited by* N. H. Furman, Van Nostrand, New York. 1925. p. 2249.

Can. J. Chem. Downloaded from www.nrcresearchpress.com by 210.87.254.42 on 09/06/12
For personal use only.

Synthesis of some new tetracyclic heteroaromatic chromans via quinone methide intermediates

MOHINDER S. CHAUHAN AND DAVID M. MCKINNON
Department of Chemistry, University of Manitoba, Winnipeg, Man., Canada R3T 2N2
Received January 19, 1981

MOHINDER S. CHAUHAN and DAVID M. MCKINNON. Can. J. Chem. **59**, 2223 (1981).

Synthesis of several new tetracyclic heteroaromatic chromans has been achieved through the reaction of various uracil and 1,3-thiazine derivatives with 1,2-naphthoquinone-1-methide. The spirodimer **4** is a better source of naphthoquinone methide than the naphthol derivatives which provide chromans in low yield due to side reactions. The structure and mechanisms of the various products formed are discussed.

MOHINDER S. CHAUHAN et DAVID M. MCKINNON. Can. J. Chem. **59**, 2223 (1981).

On a réalisé la synthèse de plusieurs chromanes tétracycliques hétéroaromatiques en faisant appel à la réaction de divers dérivés de l'uracile ou de la thiazine-1,3 avec le méthide-1 de la naphtoquinone-1,2. Le spiro-dimère **4** est une meilleure source de méthide-1 de la naphtoquinone-1,2 que les dérivés du naphtol qui ne fournissent les chromanes qu'avec de faibles rendements par suite des réactions secondaires. On discute de la structure et du mécanisme de formation des divers produits.

[Traduit par le journal]

Introduction

As a suitable model approach to the preparation of some potentially biologically active chroman derivatives, especially those fused to other heterocyclic nuclei, we have examined the reactions of 1,2-naphthoquinone-1-methide, (**1**), with uracil and 1,3-thiazine derivatives. In addition these reactions permit a suitable variation of the nature of groups attached to the 5–6 carbon to carbon bond in the uracil and 1,3-thiazine derivatives respectively, which is expected to be one substrate for the quinone methide in these reactions. However, in such studies it is known (1) that the *o*-quinone methide may react in either a dipolar form, **2**, or a diradical form, **3**. Thus although **1** may add stereo- and regiospecifically to *cis* or *trans* stilbene via a (4 + 2) cycloaddition (2*a*), the reaction of **1** with ethyl maleate or fumarate proceeds nonstereospecifically and thus gives the same products (2*a*, *b*). Also its addition to dihydropyran, vinyl ethers, and unsaturated esters occurs via a polar mechanism, while the formation of the *o*-quinone methide spiro dimer, **4**, and a benzofuran adduct indicates a diradical mechanism. The reactivity has been rationalized in terms of ready polarizability of *o*-quinone methide by the substrate (2*c*).

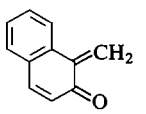

1

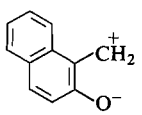

2

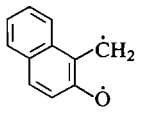

3

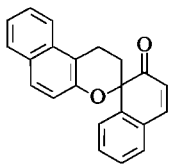

4

Results

In these studies, *o*-quinone methides were made by *in situ* thermal decomposition of the spirodimer (**4**) in refluxing mesitylene, which provides a better source than other methods, such as thermal elimination of water, methanol, or dimethylamine from 2-naphthol derivatives (2*b*). These methods are unsuitable because of side reactions, especially those induced by the above eliminated species (3–11). Some of the various uracil (**5***a–d*) and 1,3-thiazine-2-thione derivatives (**6**) were prepared by literature methods (12–15) or were commercially available. The preparation of one other (**5***e*) is described.

The reaction with 1,3-dimethyluracil (**5***a*) gave two products. One of these appears to be a chroman, assigned the structure **7***a*. This compound is likely formed by a (4 + 2) cycloaddition reaction. A *cis* geometry is indicated since the coupling constant of the protons on the bridgehead carbon atoms ($J_{2,3}$) is 2.5 Hz. This value is too small to indicate a *trans* fused ring system. It is known that dihydropyran, coumarin, 1,4-napthoquinone, and other unsaturated substrates also give adducts with *cis* geometry with *o*-quinone methides (2*a*), and with similar *J* values. The other product appears to be a phenol, assigned the structure **8***a*, indicated by an ir absorption at 3300 cm^{-1} and a peak in the nmr spectrum at δ 6.68, assigned to the olefinic proton

0008-4042/81/142223-05$01.00/0
©1981 National Research Council of Canada/Conseil national de recherches du Canada

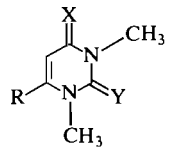

5

a X = Y = O, R = H
b X = S, Y = O, R = H
c X = Y = S, R = H
d X = Y = O, R = CH_3
e X = S, Y = O, R = CH_3

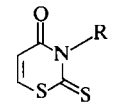

6

a R = H
b R = CH_3

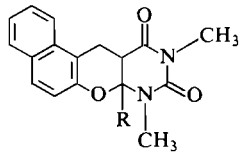

7

a R = H
b R = CH_3

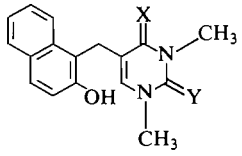

8

a X = Y = O
b X = S, Y = O
c X = Y = S

on the uracil nucleus. The peak appears to be slightly broadened, possibly by *cis* allylic coupling to the two methylene protons. This phenol probably arises from the fission of the chroman ring in **7***a* by a mechanism similar to that proposed for an *o*-quinone methide – indole adduct (2*b*), involving electron release from the nitrogen atom. The adduct **7***a* was not converted to **8***a* by chromatography on silica gel, a possible acidic catalyst, indicating that it is not an artifact of the work-up procedure. This mechanism also seems more likely in view of the results obtained with other uracils, which will be discussed later.

The possible formation of phenol **7***a* from the thermal rearrangement of chroman **8***a* was also investigated by heating pure chroman **8***a* in refluxing mesitylene. No phenol was observed and a careful chromatographic analysis of the reaction mixture gave a small amount of the starting spirodimer, 1,3-dimethyluracil, and 1,1-ethylenedi-2-naphthol, along with resinous material and some unidentified products. Similar retro additions have been reported (2*a*).

1,3-Dimethyl-4-thiouracil (**5***b*) and 1,3-dimethyl-2,4-dithiouracil (**5***c*) gave only the phenols **8***b* and **8***c* respectively. No chroman products were isolated. These structures were confirmed by ir and nmr data. It may be that ring opening of the chroman ring, with regeneration of the conjugated uracil structure, is more favored by the presence of thione sulfur in the uracil ring.

In contrast, the reaction of 1,3,6-trimethyluracil (**5***d*) gave two isomeric chromans. One of these exhibited a multiplet at δ 2.85 to 3.68, consistent with the protons at positions 3 and 4 of the chroman ring in **7***b*. The other compound exhibited two singlets at δ 3.20 and 4.13 assigned to the methylene and methine protons of the isomeric structure **9**, the chroman C-4 and C-2 positions, respectively. No ir absorptions characteristic of phenols were evident. Interestingly, when *o*-quinone methide was treated with 1,3,6-trimethyl-4-thiouracil (**5***e*), it produced, in high yield, an entirely different product. This was a very insoluble material whose analysis showed a loss of a sulfur and a nitrogen atom. Its insolubility has prevented much further investigation of its structure. The reactions of the two 1,3-thiazine-2-thiones (**6***a*, *b*) with the *o*-quinone methide gave in each case a 1:1 cyclic adduct, assigned the structures **10***a*, *b* respectively, and the 2-methyl derivative **11** afforded the adduct **12**. No phenolic products were detected in these reactions. If the fission of the chroman ring occurs by electron release from a heteroatom, N or S in the uracil and thiazine rings respectively, then these results are consistent with the electron releasing effects of these atoms. The formation of π bonds, as would be required by the mechanism of fission, would be less favored for sulfur than nitrogen.

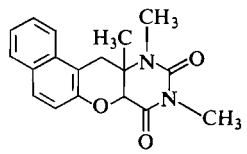

9

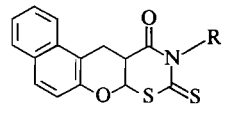

10

a R = H
b R = CH_3

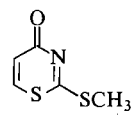

11

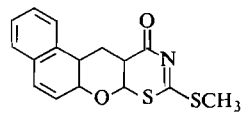

12

Discussion

In view of the similarity of the double bond substrate in the uracils and thiazines to those in unsaturated esters (2*b*), we favor the ionic mechanism (Scheme 1a) for the formation of all of the above products, except the product **9** (Schemes 1b, 2). Nevertheless a discrete dipolar initial addition product (Scheme 1a) could conceivably cyclize in a *cis* or *trans* fashion. Fortunately, examination of a molecular model and application of ring closure rules (6-*endo* trig, when appropriate resonance structures are considered), also indicates that the *cis* fusion is favored. The formation of product **9** appears to be consistent with a radical mechanism. An ionic mechanism in this case would involve an intermediate which would possess a carbonium ion

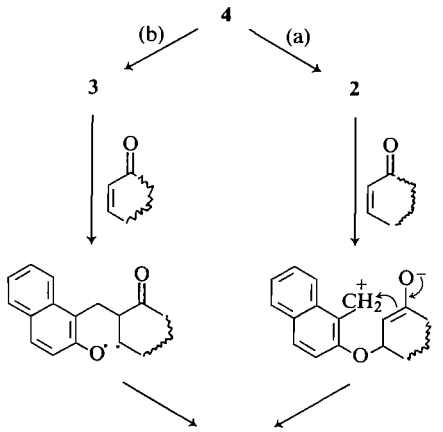

SCHEME 1

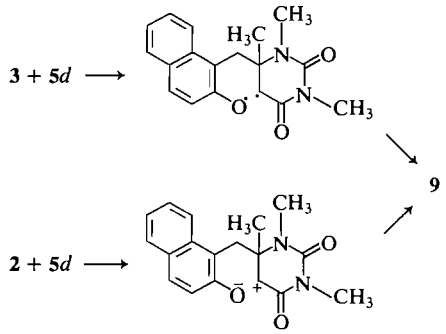

SCHEME 2

adjacent to a carbonyl group. This mechanism could be in agreement with that proposed for benzofuran reactions (2*a*).

The formation of this chroman **9** by a different mechanism only in the case of reaction of **5***d* suggests that the methyl substituent at position 6 has some special bearing on the course of the reaction. It possibly may provide extra stability at some reaction intermediate, and/or interfere sterically, allowing an alternate reaction mode. In all of these reactions the products isolated arise by reaction of the quinone methide with the 5–6 double bond of the substrate. No products were isolated by reaction of the quinone methide with either a thione function, or the imine function in compound **11**. This is surprising in view of the known reactivity (16) of the thione function to electrophilic and nucleophilic reagents, but it may be that steric effects are very important. In the one case studied, **5***e*, where the uracil has a *C*-methyl substituent and the 4-thione function, the reaction takes an entirely different course.

Experimental

Chromatography was performed on 1 mm thick "Camag" silica gel type D.S.F. 5 supplied by Terochem Laboratories. The ir spectra were obtained on a Perkin-Elmer model 337 spectrophotometer and nmr spectra on a Varian model 56/60 A spectrometer using tetramethylsilane as internal standard. Mass spectra were obtained on a Finnegan 1015 quadruple mass spectrometer and melting points obtained on a precalibrated "Thermopan" apparatus. Microanalyses were performed by Micro-Tech Laboratories, Inc. and are given in Table 1.

Preparation of the Spirodimer (4)

1-Dimethylaminomethyl-2-naphthol (5.0 g) was refluxed with xylene (150 mL) under nitrogen until there was no further evolution of dimethylamine. The solvent was removed under reduced pressure on a rotary evaporator and the residue chromatographed on a silica gel column. Elution with benzene followed by a mixture of benzene/chloroform (1 : 1, v/v) gave the spirodimer (4.0 g) in 51.5% yield. It was crystallized from a mixture of methanol/ether, mp 142–143°C identical with an authentic specimen (2*b*).

Preparation of 1,3,6-Trimethyl-4-thiouracil (5e)

1,3,6-Trimethyluracil (15) (2 g) was refluxed with phosphorus pentasulfide (2 g) in dry toluene for 7 h. Toluene was removed under reduced pressure and the residue was treated with 10% sodium carbonate solution. The basic solution was extracted with chloroform (25 mL × 4) and the combined organic extract was dried over anhydrous magnesium sulfate. The organic solvent was removed and the residue (2.1 g) crystallized from benzene, mp 172–173°C. The nmr spectrum in $CDCl_3$, δ: 6.57 (s, 1H, olefinic proton), 3.4 (s, 3H, N—CH_3), 3.75 (s, 3H, N—CH_3), 2.18 (s, 3H, C—CH_3). The infrared spectrum: 1685 cm^{-1}, C=O stretch. Mass spectrum, calcd.: 170; found: M^+ 170. *Anal.* calcd. for $C_7H_{10}N_2OS$: C 49.41, H 5.88, N 16.47, S 18.82; found: C 49.14, H 5.99, N 16.25, S 19.10.

General Method for Chroman Synthesis

The uracil or thiazine derivative under study (2 mmol) was treated with an excess of the spirodimer **4** (4 mmol) in refluxing pure, dry mesitylene (25 mL) for 7–8 h under nitrogen. Stirring was maintained throughout the course of reaction and, after the stated reaction time, the organic solvent was removed under reduced pressure. The residue was chromatographed over silica gel to separate the desired adduct from the starting material and other minor by-products. The adducts were then crystallized from chloroform or a mixture of chloroform and benzene for further purification. The results are summarized in Table 1.

Reaction of 1,3-Dimethyluracil (5a) with Spirodimer 4

The reaction was performed as above, and chromatography using chloroform as an eluant gave chroman **7***a* (332 mg) and the phenol **8***a* (156 mg). They were further purified by crystallization from a mixture of chloroform and benzene. The nmr spectrum of chroman **7***a* in $CDCl_3$, δ: 3.17 (s, 3H, *N*-methyl), 3.27 (s, 3H, *N*-methyl), 3.29 (d, 2H, methylene protons), 3.8–4.3 (m, 1H, methine proton), 5.15 (d, J = 2.5 Hz, 1H, methine proton), 6.88–7.98 (m, 6H, aromatic protons). The infrared spectrum: 1685 and 1720 (shoulder) cm^{-1}, C=O stretch. Mass spectrum, calcd.: 296; found: M^+ 296. The nmr spectrum of the phenol **8***a* in $CDCl_3$ and CD_3OD, δ: 3.06 (s, 3H, *N*-methyl), 3.25 (s, 3H, *N*-methyl), 3.92 (d, J = 1.8 Hz, 2H, methylene protons), 6.68 (d, J = 1.8 Hz, olefinic proton), 6.8–8.0 (m, 6H, aromatic protons). The infrared spectrum: 3300 cm^{-1}, OH; 1665 and 1712 cm^{-1}, C=O; 1625 cm^{-1}, C=C stretch. Mass spectrum, calcd.: 296; found: M^+ 296.

Thermolysis of Chroman (7a) with Mesitylene

Chroman (100 mg) was refluxed with pure, dry mesitylene

TABLE 1. Reactions of *o*-quinone methides with uracils and thiazines

Compound	Reference	Product	Yield(%)	Melting point (°C)	Formula	Analysis (%) Calculated C	H	N	S	Found C	H	N	S
5*a*	14	**7***a*	56	208–209	$C_{17}H_{16}N_2O_3$	68.91	5.40	9.46	—	68.79	5.37	9.45	—
5*a*	14	**8***a*	26	254–255	$C_{17}H_{16}N_2O_3$	68.91	5.40	9.46	—	68.92	5.54	9.35	—
5*b*	12	**7***b*	73.9	235–236	$C_{17}H_{16}N_2O_2S$	65.38	5.12	8.97	10.25	65.30	5.21	8.97	10.19
5*c*	12	**7***c*	79.8	222–223	$C_{17}H_{16}N_2O_2S$	62.19	4.87	8.53	19.51	62.14	4.96	8.52	18.81
5*d*	15	**7***b*	56	206–207	$C_{18}H_{18}O_3N_2$	69.67	5.80	9.03	—	69.57	5.87	8.95	—
5*d*	15	**9**	14	203–204	$C_{18}H_{18}O_3N_2$	69.67	5.80	9.03	—	69.83	5.90	9.06	—
6*a*	13	**10***a*	71.9	228–229	$C_{15}H_{11}NO_2S_2$	59.80	3.65	4.65	21.26	59.52	3.71	4.73	21.04
6*b*	13	**10***b*	75	212–213	$C_{16}H_{13}NO_2S_2$	60.95	4.12	4.44	20.31	61.20	4.18	4.73	20.36
11	13	**7***e*	60	186–187	$C_{16}H_{13}NO_2S_2$	60.95	4.12	4.44	20.31	61.17	4.14	4.32	20.27

(10 mL) under nitrogen for 14 h. Mesitylene was removed under reduced pressure and the residue chromatographed over a silica gel plate. Elution of the plate with a mixture of chloroform/benzene (9:1) gave starting spirodimer (1.5 mg), 1,3-dimethyluracil (3 mg), and 1,1-ethylenedi-2-naphthol (1 mg), mp 252°C (lit. (17) mp 252°C), along with a large amount of resinous material and some minor unidentified products.

*Reaction of 1,3-Dimethyl-4-thiouracil (5*b*) with Spirodimer 4*

Chromatography of the reaction mixture using chloroform containing 0.5% methanol gave the phenol **8***b* (461 mg). The phenol was crystallized from chloroform for further purification. The nmr spectrum in acetone-d_6, δ:3.17 (s, 3H, *N*-methyl), 3.8 (s, 3H, *N*-methyl), 4.37 (d, J = 1.8 Hz, 2H, methylene protons), 6.62 (d, J = 1.8 Hz, 1H, olefinic proton), 7.0–8.0 (m, 6H, aromatic protons). The infrared spectrum: 3300 cm^{-1}, OH; 1710 cm^{-1}, C=O stretch. Mass spectrum, calcd.: 312; found: M^+ 312.

*Reaction of 1,3-Dimethyl-2,4-dithiouracil (5*c*) with Spirodimer 4*

Chromatography of the reaction mixture with chloroform gave the phenol **8***c* (524 mg). It was crystallized from a mixture of chloroform and benzene for further purification. The nmr spectrum in acetone-d_6, δ:3.6 (s, 3H, *N*-methyl), 4.38 (s, 3H, *N*-methyl), 4.44 (d, J = 1.8 Hz, 2H, methylene protons), 6.90 (d, J = 1.8 Hz, 1H, olefinic proton), 7.18–8.00 (m, 6H, aromatic protons). The infrared spectrum: 3300 cm^{-1}, OH; 1630 cm^{-1}, C=O stretch. Mass spectrum, calcd.: 328; found: M^+ 328.

*Reaction of 1,3,6-Trimethyluracil (5*d*) with Spirodimer 4*

Chromatography of the reaction mixture in chloroform gave the chromans **7***b* (348 mg) and **9** (87 mg). These were crystallized from a mixture of chloroform and benzene for further purification. The nmr spectrum of chroman **7***b* in $CDCl_3$, δ:1.73 (s, 3H, *C*-methyl), 3.1 (s, 3H, *N*-methyl), 3.2 (s, 3H, *N*-methyl), 2.8–3.68 (m, 3H, methylene and methine protons), 7.0–8.0 (m, 6H, aromatic protons). The infrared spectrum: 1722 and 1670 cm^{-1}, C=O stretch. Mass spectrum, calcd.: 310; found: M^+ 310. The nmr spectrum of the isomeric chroman **9** in $CDCl_3$, δ:2.3 (s, 3H, *C*-methyl), 3.23 (s, 2H, methylene protons), 3.33 (s, 3H, *N*-methyl), 3.40 (s, 3H, *N*-methyl), 4.13 (s, 1H, methine proton), 6.9–8.0 (m, 6H, aromatic protons). The infrared spectrum: 1705 cm^{-1}, C=O stretch. Mass spectrum, calcd.: 310; found: M^+ 310.

*Reaction of 1,3,6-Trimethyl-4-thiouracil (5*e*) with Spirodimer 4*

The reaction mixture formed an insoluble product in mesitylene. It was removed by filtration (550 mg). It is insoluble in most organic solvents. Its structure is under investigation.

Chromatography of the filtrate in chloroform gave only the starting materials in small amounts.

*Reaction of 1,3-Thiazine-2-thione (6*a*) with Spirodimer 4*

Chromatography of the reaction mixture in chloroform gave the chroman **10***a* (433 mg). It was crystallized from a mixture of benzene and chloroform for further purification. The nmr spectrum in DMSO-d_6 and $CDCl_3$, δ:5.75 (d, J = 2.5 Hz, 1H, methine proton), 6.9–8.1 (m, 6H, aromatic protons). Since the signals due to the methylene and other methine protons (δ 3.75–3.0) were overlapped by the DMSO and water, their assignments could not be made. The infrared spectrum: 1700 cm^{-1}, C=O stretch. Mass spectrum, calcd.: 301; found: M^+ 301.

Reaction of N*-Methyl-1,3-thiazine-2-thione (6*b*) with Spirodimer 4*

Chromatography of the reaction mixture in benzene gave the chroman **10***b* (473 mg). It was crystallized from benzene for further purification. The nmr spectrum in $CDCl_3$, δ:3.7 (s, 3H,

N-methyl), 3.0–4.24 (m, 3H, methylene and methine proton), 5.33 (d, J = 2.5 Hz, 1H, methine proton), 6.9–8.1 (m, 6H, aromatic protons). The infrared spectrum: 1710 cm^{-1}, C=O stretch. Mass spectrum, calcd.: 315; found: M^+ 315.

Reaction of 2-Methylthio-1,4-dihydro-1,3-thiazine-4-one (11) with Spirodimer 4

Chromatography of the reaction mixture in chloroform yielded the chroman **12** (378 mg). It was crystallized from benzene for further purification. The nmr spectrum in $CDCl_3$, δ: 2.60 (s, 3H, *S*-methyl), 3.15–3.76 (m, 3H, methine and methylene protons), 5.85 (d, J = 2.5 Hz, 1H, methine proton), 6.9–8.0 (m, 6H, aromatic protons). The infrared spectrum: 1705 cm^{-1}, C=O stretch. Mass spectrum, calcd.: 315; found: M^+ 315.

Acknowledgments

We are grateful to the Natural Sciences and Engineering Research Council of Canada for financial support. We also wish to thank Mr. W. Buchannon and Mr. K. Marat for prepartion of spectra.

1. S. PATAI (*Editor*). The chemistry of the quinonoid compounds. Vol. 2. John Wiley, New York. 1974. p. 1145.
2. (*a*) M. S. CHAUHAN, F. M. DEAN, S. McDONALD, and M. L. ROBINSON. J. Chem. Soc. Perkin Trans. I, 359 (1973); (*b*) M. S. CHAUHAN, F. M. DEAN, D. MATKIN, and M. L. ROBINSON. J. Chem. Soc. Perkin Trans. I, 120 (1973); (*c*) N. D. EPIOTIS. J. Am. Chem. Soc. **94**, 1924 (1972); **94**, 1935 (1972).
3. S. B. CAVITT, H. SARRAFIZADEH, and P. D. GARDNER. J. Org. Chem. **27**, 1211 (1962).
4. K. JULTZSCH. J. Prakt. Chem. **158**, 275 (1941); **159**, 180 (1941); Angew. Chem. **60**, 170 (1948); H. EULER, E. ADLER, and J. O. CEDWALL. Arkiv Kemi, **14A**, 1 (1941).
5. J. BRUDIGOU and H. CHRISTOL. C. R. Acad. Sci. **256**, 3149 (1963); **256**, 3323 (1963).
6. A. H. COOK, J. DOWNER, and B. HORNUNG. J. Chem. Soc. 502 (1941).
7. D. SHIRLEY and W. C. SHEEHAN. J. Am. Chem. Soc. **77**, 4606 (1955).
8. P. W. CLUTTERBUCK and J. B. COHEN. J. Chem. Soc. **123**, 2507 (1923).
9. R. N. SEN and N. N. SARKAR. J. Am. Chem. Soc. **47**, 1079 (1925).
10. R. FOSSE, P. DE GRAEVE, and P. E. THOMAS. C. R. Acad. Sci. **200**, 1450 (1935); **201**, 105 (1935).
11. D. A. SULTANOVA. Mater. Nauchn. Konf. Aspirantov, Azerb. Gos. Univ. 83 (1964); Chem. Abstr. **64**, 17,505d (1966).
12. D. J. BROWN and J. S. HARPER. J. Chem. Soc. 1298 (1961).
13. E. N. CAIN and R. N. WARRENER. Aust. J. Chem. **23**, 51 (1970); R. N. WARRENER and E. N. CAIN. Chem. Ind. 1989 (1964).
14. D. DAVIDSON and O. BAUDISCH. J. Am. Chem. Soc. **48**, 2379 (1926).
15. R. BEHREND and R. THURM. Ann. **323**, 165 (1902).
16. R. MAYER. Synthesis and properties of thiocarbonyl compounds. *In* Organosulfur chemistry. *Edited by* M. J. Janssen. Interscience, New York. 1967.
17. R. PUMMERER and E. CHERBULIEZ. Ber. **52**, 1392 (1919).

Gas phase heats of formation of alkyl immonium ions[1]

F. P. LOSSING[2]

Division of Chemistry, National Research Council of Canada, Ottawa, Ont., Canada K1A 0R9

AND

YAI-TAI LAM AND ALLAN MACCOLL

Christopher Ingold Laboratory, University College, 20 Gordon Street, London, England, WC1H 0AJ

Received February 6, 1981

F. P. LOSSING, YAI-TAI LAM, and ALLAN MACCOLL. Can. J. Chem. **59**, 2228 (1981).

Using an energy-resolved electron beam, the gas-phase heats of formation of $[CH_2NH_2]^+$, $[CH_3CHNH_2]^+$, $[CH_3NHCH_2]^+$, $[(CH_3)_2CNH_2]^+$, $[(CH_3)_2NCH_2]^+$, $[CH_3CHNHCH_3]^+$, $[CH_3CH_2NHCH_2]^+$, and $[CH_3CH_2CHNH_2]^+$ ions have been measured from their appearance energies in ionic dissociations. All of these ions can have a quaternary immonium structure as one of the canonical forms and are consequently more stable than other isomers. Introduction of the $—NH_2$ group into a CH_3^+ ion brings about a decrease of over 4 eV in the heterolytic bond dissociation energy $D(R^+—H^-)$, with slightly larger decreases for —NHR and $—NR_2$ groups.

F. P. LOSSING, YAI-TAI LAM et ALLAN MACCOLL. Can. J. Chem. **59**, 2228 (1981).

En utilisant un faisceau d'électron à énergie résolue, on a mesuré les chaleurs de formation en phase gazeuse des ions $[CH_2NH_2]^+$, $[CH_3CHNH_2]^+$, $[CH_3NHCH_2]^+$, $[(CH_3)_2CNH_2]^+$, $[(CH_3)_2NCH_2]^+$, $[CH_3CHNHCH_3]^+$, $[CH_3CH_2NHCH_2]^+$ et $[CH_3CH_2CHNH_2]^+$ à partir de leurs potentiels d'apparition lors de dissociations ioniques. Tous ces ions peuvent avoir une structure immonium quaternaire comme forme canonique et ils sont par conséquent plus stables que les autres isomères. L'introduction du groupe $—NH_2$ dans l'ion CH_3^+ provoque une diminution (plus de 4 eV) de l'énergie de dissociation hétérolytique de la liaison $D(R^+—H^-)$; cette diminution est légèrement plus grande dans les cas des groupes —NHR et $—NR_2$.

[Traduit par le journal]

Introduction

Studies of the structure and reactivity of the gaseous ions $[C_2H_6N]^+$ and $[C_3H_8N]^+$, using metastable ion dissociation patterns (1) and collisional activation (CA) (2) techniques, have shown that two $[C_2H_6N]^+$ isomers and five $[C_3H_8N]^+$ isomers (2) are non-interconverting under mass spectrometric conditions. These ions are the following:

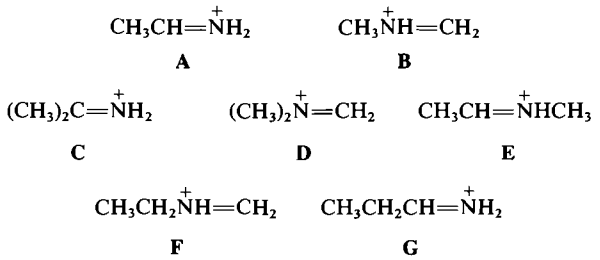

A B C D E F G

As pointed out by Levsen and McLafferty, these structures are formally immonium ions, and would consequently be expected to be considerably more stable than other isomeric structures such as $\overset{+}{C}H_2CH_2NH_2$, $CH_3\overset{+}{N}HCH_3$, and $CH_3CH_2\overset{+}{N}H$. These ions were found not to retain their identity, but to isomerize to one of the immonium ion structures (2). These results indicate that the appearance energies (AE) for production of these immonium ions in the ionic dissociations of suitable precursors can be used to derive their gas-phase heats of formation without interference from rearrangements. A similar study of $[C_2H_5O]^+$, $[C_3H_7O]^+$, and $[C_4H_9O]^+$ isomeric ions has been published recently (3).

Experimental

As in the earlier work (3), the ionic dissociations used in this study were carefully chosen to be the minimum-energy single-bond rupture processes in order to minimize interference from kinetic shift and reverse activation energy (4). The appearance energies were measured as described previously (3), using an electrostatic electron monochromator coupled to a quadrupole mass spectrometer (5). The initial portions of the ionization efficiency curves were scanned repeatedly over a range of 0.8 eV, and analyzed using a minicomputer data system (6). The electron beam from the monochromator was of the order of 2×10^{-8} Å, with an energy dispersion (FWHM) of about 0.07 eV.

For many of these dissociations, the onsets were unusually gradual; extreme care was therefore taken to avoid interference at the threshold from ions of neighboring mass. Because of these experimental difficulties, measurements were made in two similar, but not identical, instruments; one at University College London, and the other at the National Research Council of Canada in Ottawa. The agreement between the appearance energies measured in the two laboratories was in all cases better than 0.1 eV.

[1]NRCC No. 19382.

[2]Present address: Department of Chemistry, University of Ottawa, Ottawa, Ont., Canada K1N 6N5.

0008-4042/81/142228-04$01.00/0

©1981 National Research Council of Canada/Conseil national de recherches du Canada

Can. J. Chem. Downloaded from www.nrcresearchpress.com by 210.87.254.6 on 09/06/12
For personal use only.

Can. J. Chem. Downloaded from www.nrcresearchpress.com by 210.87.254.6 on 09/06/12
For personal use only.

TABLE 1. Heats of formation of $[CH_2NH_2]^+$

Precursor	ΔH_f(precursor) (kcal mol^{-1})	Neutral fragment	AE (eV)	$\Delta H_f(CH_2NH_2^+)$
CH_3NH_2	−5.5[a]	H	10.18	177
$CH_3CH_2NH_2$	−11.4[a]	CH_3	9.69 9.71[b]	178
$CH_3CH_2CH_2NH_2$	−16.8[a]	C_2H_5	9.56 9.54[b]	178
$H_2NCH_2CH_2OH$	−48.2[c]	CH_2OH[d]	9.49	177

[a]Reference 9.
[b]Photoionization value, ref. 4.
[c]Calculated, ref. 10.
[d]$\Delta H_f(CH_2OH) = -6.2$ kcal mol^{-1}, ref. 11.

TABLE 2. Heats of formation of $[C_2H_6N]^+$ isomers

Precursor	ΔH_f(precursor) (kcal mol^{-1})	Neutral fragment	AE (eV)	$\Delta H_f(C_2H_6N^+)$
(*a*) $[CH_3CHNH_2]^+$				
$CH_3CH_2NH_2$	−11.4[a]	H	9.55(9.61[d])	157
$(CH_3)_2CHNH_2$	−20.0[a]	CH_3	9.12(8.86[d])	156
$CH_3CH_2CH(CH_3)NH_2$	−25.1[b]	C_2H_5	9.03	157
$CH_3CH(NH_2)CH_2OH$	−56.9[c]	CH_2OH	9.00	157
(*b*) $[CH_3NHCH_2]^+$				
CH_3NHCH_3	− 4.4[a]	H	9.65(9.41[d])	166
$CH_3NHCH_2CH_3$	−11.4[c]	CH_3	9.15(8.49[d])	166
$CH_3NHCH_2CH_2OH$	−47.7[c]	CH_2OH	8.99	166

[a]Reference 9.
[b]Reference 12.
[c]Calculated, ref. 10.
[d]Reference 7.

Results and Discussion

$[H_2NCH_2]^+$ *Ion*

The heat of formation of this ion has been established by photoionization studies (4) as 178 kcal mol^{-1}. Further measurements made in this work, shown in Table 1, are in excellent agreement with this value.

$[CH_3NHCH_2]^+$ *and* $[CH_3CHNH_2]^+$

The appearance energies and derived heats of formation for these two isomeric species are given in Table 2, together with the heats of formation for the parent molecules. For both ions, the internal agreement of the results is good, fortuitously better than the thermochemical data would warrant. The overall uncertainty in the ΔH_f(ion) values is estimated to be ±2 kcal mol^{-1}. It has been assumed that the neutral products C_2H_5 and CH_2OH are not dissociated; to assume C_2H_4 + H and CH_2O + H as the neutral products leads to impossibly low values for the ionic heats of formation.

Also given in Table 2 are four AE-values from an earlier study of $[C_2H_6N]^+$ ions (7), using the Retarding Potential Difference (RPD) method for obtaining a quasi-monoenergetic electron beam. Although the two H-loss values agree reasonably well with the present results, those for the CH_3 loss reactions are in poor agreement. The reason for the discrepancy is not known. It is clear from the present result that ions A and B retain their identity during the dissociation process, in agreement with earlier conclusions (1, 2).

$[C_3H_8N]^+$ *Ions*

The appearance energies and the derived heats of formation for the five isomeric $[C_3H_8N]^+$ ions are given in Table 3, together with heats of formation of the parent molecules. The internal agreement is reasonably good, with the exception of the loss of CH_2OH from $(CH_3)_2C(NH_2)CH_2OH$, which appears to be about 6 kcal mol^{-1} too high. For ion **E** there is only one value. The H-loss reaction from the precursor $CH_3CH_2NHCH_3$ could form either ion **E** or ion **F**:

$$CH_3CH_2NHCH_3 \rightarrow H + [CH_3CHNHCH_3]^+ \quad \mathbf{E}$$

$$CH_3CH_2NHCH_3 \rightarrow H + [CH_3CH_2NHCH_2]^+ \quad \mathbf{F}$$

Can. J. Chem. Downloaded from www.nrcresearchpress.com by 210.87.254.6 on 09/06/12
For personal use only.

TABLE 3. Heats of formation of $[C_3H_8N]^+$ isomers

Precursor	ΔH_f(precursor) (kcal mol^{-1})	Neutral fragment	AE (eV)	$\Delta H_f(C_3H_8N^+)$
(*c*) $[(CH_3)_2CNH_2]^+$				
$(CH_3)_2CHNH_2$	−20.0[a]	H	9.20	140
$(CH_3)_3CNH_2$	−28.9[a]	CH_3	8.89	142
$(CH_3)_2C(NH_2)CH_2OH$	−64.9[b]	CH_2OH	8.92	(147)
(*d*) $[(CH_3)_2NCH_2]^+$				
$(CH_3)_3N$	− 5.7[a]	H	9.38	159
$(CH_3)_2NCH_2CH_3$	−12.4[b]	CH_3	8.80	157
$(CH_3)_2NCH_2CH_2OH$	−48.7[b]	CH_2OH	8.68	158
(*e*) $[CH_3CHNHCH_3]^+$				
$(CH_3)_2CHNHCH_3$	−20.0[b]	CH_3	8.71	147
(*f*) $[CH_3CH_2NHCH_2]^+$				
$(CH_3CH_2)_2NH$	−17.2[a]	CH_3	8.92	155
$CH_3CH_2NHCH_2CH_2OH$	−54.3[b]	CH_2OH	8.89	157
(*g*) $[CH_3CH_2CHNH_2]^+$				
$CH_3CH_2CH(CH_3)NH_2$	−25.4[a]	CH_3	9.12	151
$CH_3CH_2CH(NH_2)CH_2OH$	−61.8[b]	CH_2OH	9.06	153

[a] Reference 9.
[b] Calculated, ref. 10.

TABLE 4. Heterolytic bond dissociation energies (HBDE, kcal mol^{-1}) and relative stabilization ΔHBDE

Bond	ΔH_f(parent molecule)	ΔH_f(ion)	HBDE[a]	ΔHBDE[b]
HCH_2^+—H^-	−17.89[c]	259[d]	312	0
$HOCH_2^+$—H^-	−48.07[c]	169[c]	252	60
$H_2NCH_2^+$—H^-	−5.5[c]	178	218	94
$[CH_3CHNH_2]^+$—H^-	−11.4[c]	157	203	109
$[CH_3NHCH_2]^+$—H^-	−4.4[c]	166	205	107
$[(CH_3)_2CNH_2]^+$—H^-	−20.0[c]	141	196	116
$[(CH_3)_2NCH_2]^+$—H^-	−5.7[c]	158	198	114
$[CH_3CH_2CHNH_2]^+$—H^-	−16.8[c]	152	204	108
$[CH_3CH_2NHCH_2]^+$—H^-	−11.4[f]	156	202	110
$[CH_3CHNHCH_3]^+$—H^-	−11.4[f]	147	193	119

[a] Using $\Delta H_f(H^-) = 34.7$ kcal mol^{-1}.
[b] $D(CH_3^+—H^-) - D(R^+—H^-)$.
[c] Reference 9.
[d] Reference 13.
[e] Reference 3.
[f] Calculated, ref. 10.

Because of this ambiguity, the AE for this reaction was not considered sufficiently reliable for inclusion.

It seems evident that dissociation processes leading to an isomeric ion other than an immonium ion cannot interfere at the observed thresholds. For example, the dissociation

$$(CH_3)_2NCH_2CH_3 \rightarrow CH_3 + CH_3\overset{+}{N}CH_2CH_3$$

will have a much higher AE than that given in Table 3.

Stabilization in Alkyl Immonium Ions

The stabilizing effects of substitution of —NH_2, —NHR, and —NR_2 groups in alkyl ions can best be evaluated in terms of the heterolytic bond dissociation energy (8) (hydride ion affinity):

$$\begin{aligned} \text{HBDE} &= D(R^+—H^-) \\ &= \Delta H_f(R^+) + \Delta H_f(H^-) - \Delta H_f(RH) \end{aligned}$$

Table 4 gives the values of HBDE for the eight immonium ions, together with those for CH_3^+ and $\overset{+}{C}H_2OH$ for comparison. It can be seen that substitution by the —NH_2 group has a much larger stabilizing effect than that caused by substitution by the —OH group into CH_3^+ ion. The stabilization (ΔHBDE) brought about by substitution by —NH_2, —$N(H)CH_3$, and —$N(CH_3)_2$ groups are respectively 94, 107, and 114 kcal mol^{-1}.

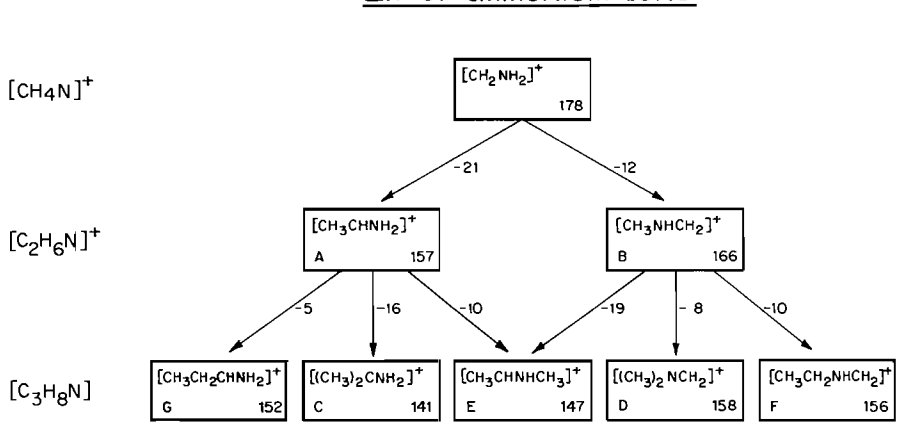

FIG. 1. Schematic illustration of the relationships in ionic heats of formation of alkyl immonium ions.

It is of interest to note that, using $D(R^+—H^-)$ as the criterion, the most stable $[C_3H_8N]^+$ isomer is $[CH_3CHNHCH_3]^+$, although it is not the isomer with the lowest heat of formation. This reversal arises from the heats of formation of the neutral parent molecules: $(CH_3)_2CHNH_2$ is 8.6 kcal mol^{-1} more stable than $CH_3CH_2NHCH_3$.

The effect of substitution on the heats of formation of $[C_2H_6N]^+$ and $[C_3H_8N]^+$ isomeric ions is shown schematically in Fig. 1. It can be seen that the stabilization brought about by CH_3 substitution is significantly greater when the substitution is on a C atom rather than on an N atom. The situation is similar to that found recently (3) for substitution on C and O atoms in $[CH_2OH]^+$, although the differences for the C and N positions are less marked. Of the canonical forms

$$^+CH_2NH_2 \leftrightarrow CH_2{=}\overset{+}{N}H_2$$

the quaternary immonium structure may well play a greater role in stabilization than does the oxonium structure $CH_2{=}\overset{+}{O}H$ in oxycarbonium ions.

Acknowledgements

The authors wish to thank Dr. D. H. Williams for the gift of purified amines, and Dr. L. Lompa-Krzymien for preparing methylamine and methylethylamine from the hydrochlorides.

1. N. A. UCELLA, I. HOWE, and D. H. WILLIAMS. J. Chem. Soc. B, 1933 (1971).
2. K. LEVSEN and F. W. MCLAFFERTY. J. Am. Chem. Soc. **96**, 139 (1974).
3. F. P. LOSSING. J. Am. Chem. Soc. **99**, 7526 (1977).
4. W. A. CHUPKA. J. Chem. Phys. **30**, 191 (1959).
5. K. MAEDA, G. P. SEMELUK, and F. P. LOSSING. Int. J. Mass Spectrom. Ion Phys. **1**, 395 (1968).
6. F. P. LOSSING and J. C. TRAEGER. Int. J. Mass Spectrom. Ion Phys. **19**, 9 (1976).
7. B. H. SOLKA and M. E. RUSSELL. J. Phys. Chem. **78**, 1268 (1974).
8. A. MACCOLL. The transition state. Special publication, No. 16, The Chemical Society, London. 1962.
9. J. D. COX and G. PILCHER. Thermochemistry of organic and organometallic compounds. Academic Press, New York. 1970.
10. S. W. BENSON, F. R. CRUIKSHANK, D. M. GOLDEN, G. R. HAUGEN, H. E. O'NEAL, A. S. RODGERS, R. SHAW, and R. WALSH. Chem. Rev. **69**, 279 (1969).
11. D. M. GOLDEN and S. W. BENSON. Chem. Rev. **69**, 125 (1969).
12. J. B. PEDLEY and J. RYLANCE. Sussex-NPL computer analysed thermochemical data: organic and organometallic compounds. University of Sussex. 1977.
13. H. M. ROSENSTOCK, K. DRAXL, B. W. STEINER, and J. T. HERRON. J. Phys. Chem. Ref. Data, Suppl. 1, **6** (1977).

Can. J. Chem. Downloaded from www.nrcresearchpress.com by 210.87.254.6 on 09/06/12
For personal use only.

Kinetics of the oxidation of ethane by nitric oxide over manganese(III) oxide

R. A. Ross[1] and C. Fairbridge

Department of Chemistry, Lakehead University, Thunder Bay, Ont., Canada P7B 5E1

Received October 29, 1980

R. A. Ross and C. Fairbridge. Can. J. Chem. **59**, 2232 (1981).

The catalytic reaction between ethane and nitric oxide over manganese(III) oxide has been investigated in a continuous flow system from 673 to 573 K at atmospheric pressure. The products of catalysis were nitrogen, carbon dioxide, nitrous oxide, and water. The rate of nitrous oxide formation was constant over this temperature region, while the apparent activation energies for nitrogen and carbon dioxide formation increased from 32 ± 4 and 22 ± 4 kJ mol^{-1}, respectively, at 573 to 613 K, to 78 ± 4 and 63 ± 4 kJ mol^{-1} between 613 and 673 K. The kinetic results were best described by the rate equation:

$$r = \frac{kap_{C_2H_6}bp_{NO}}{(1 + ap_{C_2H_6} + bp_{NO})^2}(p_{C_2H_6}p_{NO})$$

The surface mechanism appears to be complex and has been interpreted by a scheme involving interaction of the reactants in an absorbed layer. Both nitric oxide and ethane are believed to be involved further in subsequent steps. Infrared evidence indicates the possibility of a surface nitrate intermediate consistent with the mechanistic proposal. Scanning electron microscopy and X-ray powder diffraction techniques were used to assess the catalyst structure.

R. A. Ross et C. Fairbridge. Can. J. Chem. **59**, 2232 (1981).

Opérant dans un système à écoulement continu à pression atmosphérique entre 673 et 573 K, on a étudié la réaction catalytique entre l'éthane et l'oxyde nitrique déposé sur l'oxyde de manganèse(III). Les produits de la catalyse sont l'azote, le bioxyde de carbone, l'oxyde nitreux et l'eau. La vitesse de formation de l'oxyde nitreux est constante dans cet intervalle de température, tandis que les énergies apparentes d'activation pour la formation de l'azote et du bioxyde de carbone augmentent respectivement de 32 ± 4 et 22 ± 4 kJ mol^{-1} entre 573 et 613 K à 78 ± 4 et 63 ± 4 kJ mol^{-1} entre 613 et 673. On peut convenablement décrire les résultats cinétiques par l'équation de vitesse

$$r = \frac{kap_{C_2H_6}bp_{NO}}{(1 + ap_{C_2H_6} + bp_{NO})^2}(p_{C_2H_6}p_{NO})$$

Le mécanisme de surface semble être complexe et on l'a interprété selon un schéma impliquant une interaction des réactifs dans la couche absorbée. On croit que l'oxyde nitrique ainsi que l'éthane sont aussi impliqués dans les étapes suivantes. Les données infrarouges suggèrent la possibilité d'un intermédiaire nitrate à la surface qui est en accord avec le mécanisme proposé. Pour déterminer la structure du catalyseur, on a utilisé les techniques de la microscopie par balayage électronique et la diffraction des poudres par rayons-X.

[Traduit par le journal]

Introduction

The activities and surface chemical properties of manganese oxides have been observed for a number of heterogeneous catalytic reactions including the decomposition of 2-propanol (1), the water–gas shift reaction (2), the decomposition of formic acid (3) and, more recently, the reaction of nitrous oxide with carbon monoxide (4). The present work was designed to expand the redox reaction studies to include the evaluation of the catalytic activity of manganese(III) oxide in hydrocarbon oxidation. In the first instance, ethane has been used as the hydrocarbon and nitric oxide as the oxidizing species.

It is important also to note that the technological development of catalysts suitable for the control of the emission of nitrogen oxides from both mobile and stationary sources has received and continues to receive considerable attention. Much of the published work has focused on reactions of nitric oxide and especially the NO/CO reaction (5). Previously, it has been postulated that nitrous oxide may be an important intermediate in the mechanism of such reactions (6, 7).

Experimental

Apparatus and Procedure

The all-glass flow system and quartz reactor were described previously (8). High-purity helium, passed through a molecular sieve drying column (Davison, Grade 564), was used as the carrier gas in both the flow system and the Hewlett-Packard Research Chromatograph, Model 5754B. Nitrogen, nitric oxide, carbon dioxide, nitrous oxide, ethane, and water were analysed by a thermal conductivity bridge using stainless steel columns 305 × 0.32 cm o.d. packed with Poropak Q and run at 293 K. A Beckman Model 951 NO/NO_x Analyser was used in series with the gas chromatograph for calibration purposes as well as to monitor the atmosphere in the laboratory.

To establish the experimental conditions for which the reaction rates were not influenced by external or internal diffusion, the influences of space velocity, catalyst mass, and particle size were studied in the usual manner (9). As a result,

[1]Present address: Alcan International Limited, Kingston Laboratories, P.O. Box 8400, Kingston, Ont., Canada K7L 4Z4.

0008-4042/81/142232-07$01.00/0

©1981 National Research Council of Canada/Conseil national de recherches du Canada

Can. J. Chem. Downloaded from www.nrcresearchpress.com by 210.87.254.40 on 09/06/12
For personal use only.

Can. J. Chem. Downloaded from www.nrcresearchpress.com by 210.87.254.40 on 09/06/12
For personal use only.

kinetic measurements were conducted at a total gas flow rate of 350 mL min^{-1} (NTP) on 1 g catalyst samples of particle size $<37\,\mu m$ with surface area 15.5 $m^2\ g^{-1}$ as measured by low temperature krypton adsorption (BET; 77 K; $\sigma = 19.5\ A^2$).

All reaction rate measurements were recorded after steady catalyst activity had been obtained and at less than 15% total conversion. Exposure of black manganese(III) oxide to nitric oxide and ethane (approximately 2.66 kPa of each) produced a brownish surface colouration on the samples but no significant change of structure was found after catalysis from XRD, chemical analysis, and surface area measurements. Infrared spectra were obtained with a Beckman IR-12 Spectrophotometer using 0.5% w/w samples in KBr pellets.

Materials

Manganese(III) oxide was prepared and analysed as described previously (1). Analysis by XRD confirmed the α-Mn_2O_3 structure (10) and chemical analysis (11) indicated 69.73% w/w manganese (theory 69.59%).

Ethane (99.0%), carbon dioxide (99.5%), nitrogen (99.99%), and helium (99.995%) were obtained from Canadian Liquid Air Ltd. Nitric oxide (99.0%) was supplied by Matheson of Canada Ltd. and nitrous oxide (99.9%) by Liquid Carbonic Ltd. The nitric oxide contained approximately 2.5% nitrous oxide impurity as determined by gas chromatography. A simple cold trap of liquid nitrogen and technical pentane (150 K) was demonstrated to be sufficient to remove this impurity to within limits of detection < 0.002 kPa.

Results

Reaction Rate Order Measurements

Rate orders for the NO/C_2H_6 reaction were measured at 623 K for nitrogen (r_1), carbon dioxide (r_2), and nitrous oxide (r_3) formation.

Ethane

The dependence of reaction rates on variations in the ethane partial pressure from 0.73 to 6.59 kPa was examined with nitric oxide maintained constant at 3.0 kPa. Plots of ln (rate) versus ln (partial pressure of ethane) exhibited linear relationships over the range studied, Fig. 1, and the reaction rate orders with respect to the ethane partial pressure were given by $r_1 \propto p_{C_2H_6}{}^{0.5}$; $r_2 \propto p_{C_2H_6}{}^{0.7}$, and $r_3 \propto p_{C_2H_6}{}^{0.5}$.

Nitric Oxide

With the partial pressure of ethane held constant at 2.71 kPa, the effect of nitric oxide on reaction rates was observed by varying its partial pressure from 0.83 to 11.75 kPa. Again, linear relationships were observed, as shown in Fig. 1, and rate orders with respect to the nitric oxide partial pressure were described by $r_1 \propto p_{NO}{}^{0.5}$; $r_2 \propto p_{NO}{}^{0.3}$; and $r_3 \propto p_{NO}{}^{1.2}$.

Nitrogen

The effect of nitrogen on the reaction rates r_2 and r_3 was observed by maintaining the partial pressures of ethane and nitric oxide constant at 2.52 and 2.61 kPa, respectively, and altering the partial pressure of nitrogen from 0.09 to 9.21 kPa. The rate orders with respect to nitrogen were zero throughout the range investigated.

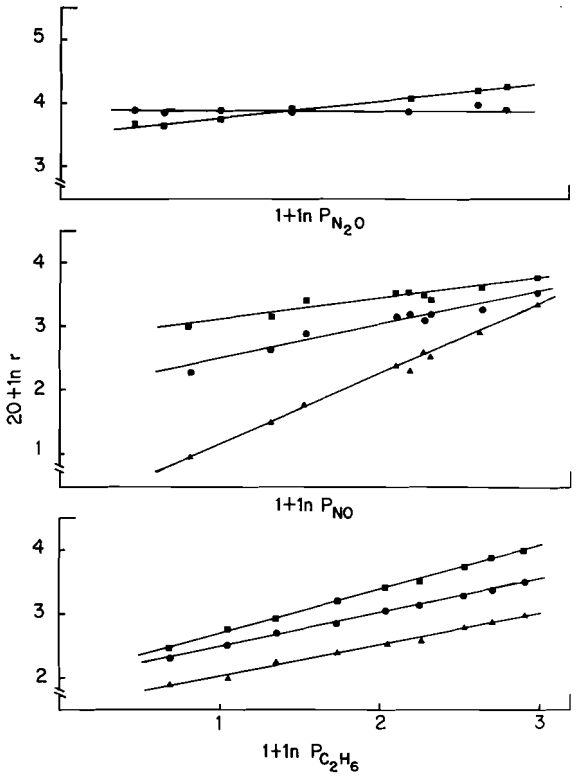

FIG. 1. The effects of component partial pressures on the rates of formation of nitrogen (●), carbon dioxide (■), and nitrous oxide (▲).

Carbon Dioxide

Carbon dioxide partial pressure was altered from 0.15 to 5.87 kPa with the partial pressures of ethane, 2.57 kPa, and nitric oxide, 2.93 kPa, held constant in order to observe the effects of carbon dioxide on reaction rates. The relationships were: r_1 and $r_3 \propto p_{CO_2}{}^0$).

Water Vapour

With the partial pressures of ethane and nitric oxide maintained at 2.47 and 2.88 kPa, respectively, from 0.04 to 1.4 kPa of water vapour was added to the system and shown to have no effect on the reaction rates.

Nitrous Oxide

The partial pressure of nitric oxide was maintained at 2.82 kPa and ethane at 2.41 kPa while the partial pressure of nitrous oxide was varied from 0.23 to 6.06 kPa. Over the range studied, nitrous oxide had no effect upon the rate of nitrogen

Can. J. Chem. Downloaded from www.nrcresearchpress.com by 210.87.254.40 on 09/06/12
For personal use only.

formation ($r^1 \propto p_{N_2O}{}^0$) and a linear relationship was observed for the rate of carbon dioxide formation, $r_2 \propto p_{N_2O}{}^{0.3}$, as shown in Fig. 1.

On the basis of these studies, the rate of reaction of nitric oxide with ethane over the manganese(III) oxide catalyst at 623 K can be expressed as:

[1] $r_1 = k_1 p_{NO}{}^{0.5} p_{C_2H_6}{}^{0.5}$ mol m^{-2} s^{-1}

[2] $r_2 = k_2 p_{NO}{}^{0.3} p_{C_2H_6}{}^{0.7} p_{N_2O}{}^{0.3}$ mol m^{-2} s^{-1}

[3] $r_3 = k_3 p_{NO}{}^{1.2} p_{C_2H_6}{}^{0.5}$ mol m^{-2} s^{-1}

The Effect of Temperature

The catalytic reaction rates were determined from 673 to 573 K in decreasing 10 K intervals after catalyst pretreatment at 673 K for 2 h with nitric oxide and ethane at 2.74 and 2.71 kPa, respectively. Rate constants were calculated by integration of eqs. [1], [2], or [3] as a function of concentration and the values obtained were plotted in the Arrhenius fashion, Fig. 2. The rate of nitrous oxide formation was constant over this temperature range and hence the specific rate constant did not change with temperature. Two distinct temperature regions were observed in the linear plots obtained for both nitrogen and carbon dioxide formation, namely, from 673 to 613 K and from 613 to 573 K as shown in Table 1.

Infrared Spectra

The infrared spectrum of unreacted Mn_2O_3, Fig. 3 *A*, consisted of peaks at 670 (m), 600 (sh), 570 (s), 525 (s), 495 (sh), 450 (sh), and 400 (w) cm^{-1}. The spectrum of pure Mn_2O_3 (Alfa Inorganics, Ventron) was similar with the single exception that no peak was apparent at 400 cm^{-1}. This may be ascribed to a very small amount of MnO_2 (Alfa Inorganics, Ventron), 615, 400, and 335 cm^{-1}.

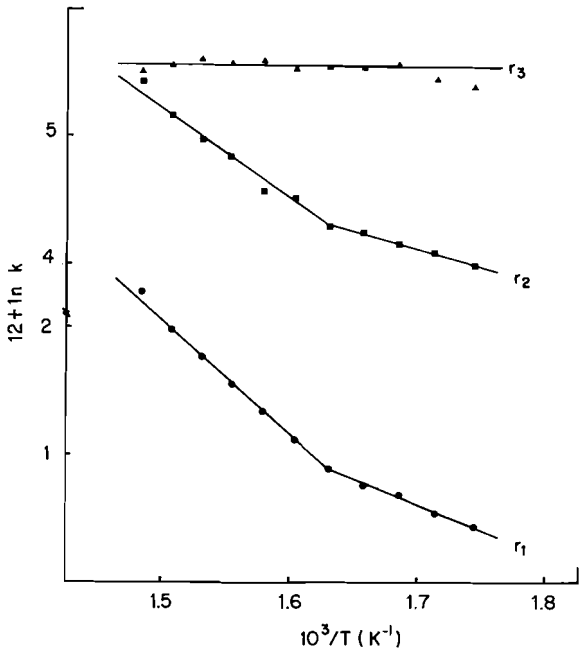

FIG. 2. Arrhenius plots for the reaction of nitric oxide (2.74 kPa) and ethane (2.71 kPa) on manganese(III) oxide. Symbols correspond to Fig. 1.

TABLE 1. Kinetic parameters for the ethane/nitric oxide reaction over manganese(III) oxide

T (K)	E_a (from [1]) (kJ mol^{-1})	A	E_a (from [1]) (kJ mol^{-1})	A
673–613	7.48±4	1.10×10^7	63 ± 4	1.59×10^7
613–573	32 ±4	1.28×10^3	22 ± 4	6.08×10^3

After catalysis of the NO/C_2H_6 reaction, the sample spectrum was altered to yield peaks at 1630 (m), 1390 (s), and 845 (w) cm^{-1}, which, along with the peak at 350 (m) cm^{-1}, Fig. 3 *C*, is consistent with the spectrum of manganese(II) nitrate, Fig. 3 *B*. Other peaks appeared at 615 (s), 490 (s), and 425 (m) cm^{-1} and these may indicate the presence of an Mn_3O_4 phase. The spectrum observed for pure MnO (Alfa Inorganics, Ventron) also indicated a single peak at 340 cm^{-1}. Thus, the catalyst may contain a trace of MnO after reaction but chemical analysis and XRD indicated no significant difference from the starting material.

Scanning Electron Micrographs

The scanning electron micrographs, Fig. 4, appear to show a separate crystalline phase on the oxide surface after catalysis at 673 K. The observation resembles that made previously in studies of the surface formation of manganese(II) formate from the dehydration and dehydrogenation of formic acid on manganese(II) oxide (3). The presence of smaller, more ordered particles may be observed in Fig. 4 *A* and *B*, while the condition of the remainder of the surface of the particles, Fig. 4 *C*, indicates rounded edges and a high degree of surface roughness. This surface appears identical to that noted for manganese(III) oxide prior to catalysis. Samples which were further heated under reaction conditions to 873 K exhibited surface sintering and crack formations, Fig. 4 *D*.

Discussion

The kinetic results were analysed by computer tests of standard gas/solid reaction rate expressions based mainly on the Langmuir–Hinshelwood model (12, 13). On the basis of statistical criteria (14–16), eq. [4] described the data best and was thus adopted as a general guide to the nature of the surface reaction:

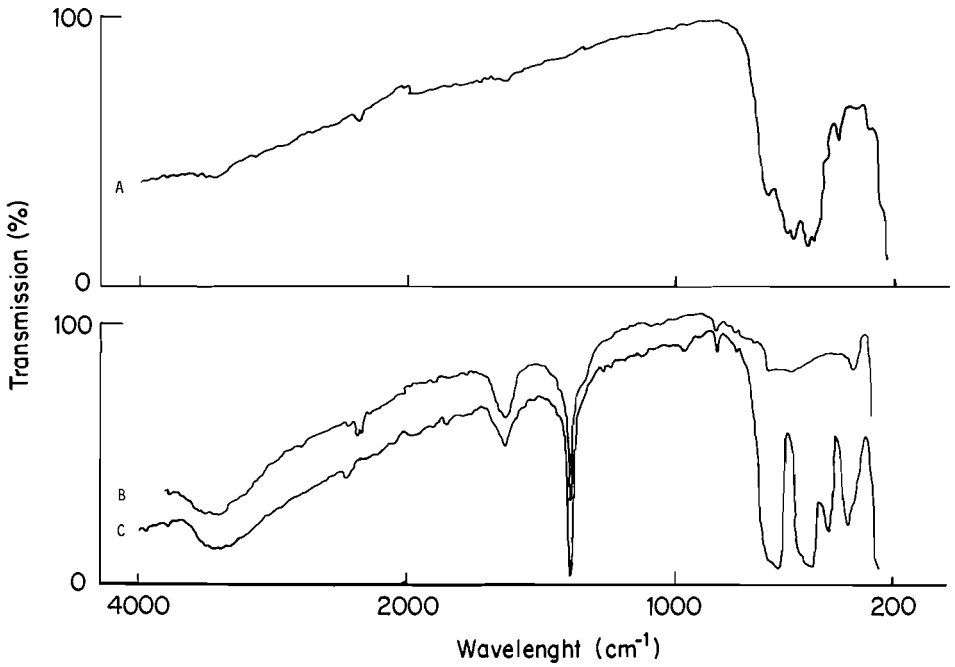

FIG. 3. The infrared spectra of unreacted manganese(III) oxide, *A*; manganese(II) nitrate, *B*; and catalyst after reaction, *C*.

$$[4] \quad r = \frac{kap_{C_2H_6}bp_{NO}}{(1 + ap_{C_2H_6} + bp_{NO})^2}\,(p_{C_2H_6}p_{NO})$$

where a and b represent adsorption coefficients. Plots of $p/r^{0.5}$ versus p were linear as shown in Fig. 5. The form of the equation is consistent with that for an irreversible bimolecular reaction between reactive species adsorbed on the same type of site (17). The reaction rate is proportional to the probability that the reactants are adsorbed on neighbouring sites and, in turn, proportional to the product of the fractions of surface covered by the reactants, $\theta_{C_2H_6}$ and θ_{NO}. Thus:

$$[5] \quad r = k\theta_{C_2H_6}\theta_{NO}$$

where

$$[6] \quad \theta_{C_2H_6} = \frac{K_{C_2H_6}p_{C_2H_6}}{(1 + K_{C_2H_6}p_{C_2H_6} + K_{NO}p_{NO})}$$

and

$$[7] \quad \theta_{NO} = \frac{K_{NO}p_{NO}}{(1 + K_{C_2H_6}p_{C_2H_6} + K_{NO}p_{NO})}$$

The additional $(p_{C_2H_6}p_{NO})$ multiplier term in [4] indicates that, at the steady-state, catalysis includes additional interactions involving nitric oxide with ethane molecules either from the gaseous state or as weakly chemisorbed species. Previously, a mechanism for the oxidation of hydrocarbons has been postulated to occur through the initial interaction of chemisorbed hydrocarbon species with either gaseous or chemisorbed oxygen followed by a complex sequence of steps which invokes surface radical reactions (18). The chemisorption of ethane on iron(III) and nickel(II) oxides has been shown to involve C—H bond rupture (19) while studies on ethane oxidation (20) on nickel(II) oxide indicated that the hydrocarbon was adsorbed prior to any surface reaction with preadsorbed oxygen.

A plausible scheme consistent with eq. [4] for the nitric oxide/ethane surface reaction is:

$$[8] \quad C_2H_{6(g)} \rightleftharpoons C_2H_{6(ads)}$$

$$[9] \quad NO_{(g)} \rightleftharpoons NO_{(ads)}$$

$$[10] \quad C_2H_{6(ads)} + NO_{(ads)} \rightarrow C_2H_{5(ads)} + HNO_{(ads)}$$

$$[11] \quad 2HNO_{(ads)} \rightarrow N_2O_{(ads)} + H_2O_{(ads)}$$

The formation of $C_2H_{5\,(ads)}$ in [10] is a step similar to that in the proposal (20) regarding the oxygen/ethane reaction on nickel(II) oxide. The formation of N_2O and H_2O from adsorbed HNO species in [11] has been described in observations of the reduction of nitric oxide by both hydrazine (21) and ammonia (22).

In a current review of nitric oxide surface reactions (23), evidence obtained from ir, epr, and oxygen-exchange experiments is cited in favour of the proposal that adsorption of nitric oxide on transition metal oxides occurs through partial coordination to a surface oxygen ion, O^{2-}. An intermediate surface nitrite or nitro complex was invoked

Can. J. Chem. Downloaded from www.nrcresearchpress.com by 210.87.254.40 on 09/06/12
For personal use only.

Can. J. Chem. Downloaded from www.nrcresearchpress.com by 210.87.254.40 on 09/06/12
For personal use only.

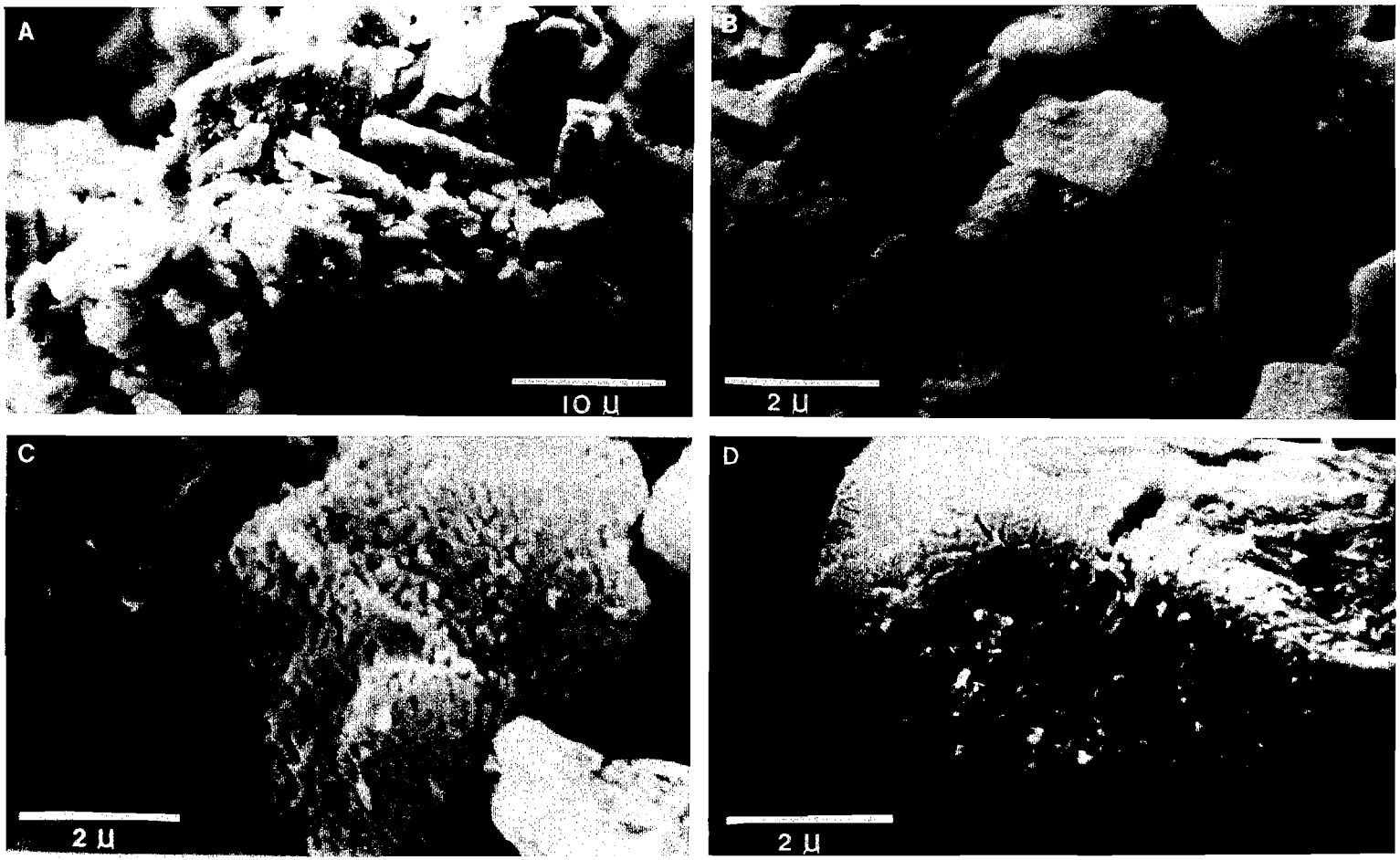

FIG. 4. Scanning electron micrographs of manganese(III) oxide after catalysis with nitric oxide and ethane at 673 K, *A*, *B*, and *C*; and after further heat treatment at 873 K, *D*.

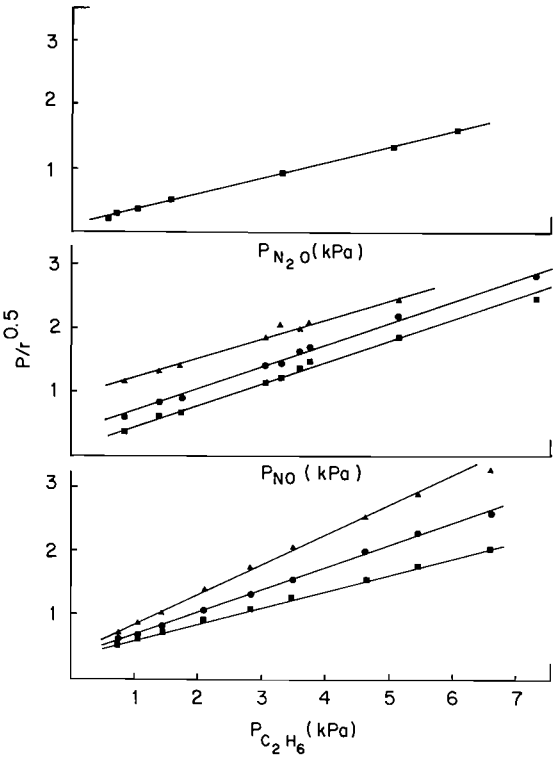

FIG. 5. Reduced plots for the rate order results according to expression [7]. Symbols correspond to Fig. 1.

and such a species has been identified from infrared evidence in this work.

Nitric oxide has been shown to oxidize MnO to Mn_2O_3 with subsequent chemisorption of nitrous oxide (24), thus:

[12] $2NO_{(ads)} + \square + Mn^{2+} \rightarrow N_2O_{(ads)} + [O^-] + Mn^{3+}$

where $\square$ represents a surface anion vacancy. The nitrous oxide produced from [11] or [12] could subsequently react with the $C_2H_{5(ads)}$ species to form carbon dioxide, water vapour, and nitrogen.

The values of the apparent activation energies for both carbon dioxide and nitrogen formation were similar to those obtained for the water–gas shift reaction on manganese(II) oxide (2) which was believed to involve an active [Mn^{3+}—O^-] surface species. A two-step Arrhenius plot was also observed from 623 to 673 K and from 573 to 613 K with activation energies 67 and 46 kJ mol^{-1}, respectively. This effect may be related to the presence of two forms of chemisorbed oxygen which have not been distinguished (25) or to a change in surface oxygen mobility at the Curie transition temperature which lies around 610 K.

The mechanism of the decomposition of nitrous oxide on manganese oxides (25) has been explained by a redox scheme which shows that oxidation should be enhanced by conditions that tend to preserve the 3+ oxidation state. And, although the proposed chemisorbed oxygen species were not identified (25), it was suggested that a weak form such as O_2^- or O_2^{2-} could be sustained during catalysis. Oxygen desorption studies from MnO_2 have also indicated the presence of two surface states which have apparent activation energies for desorption of 67 and 126 kJ mol^{-1} (26).

In the present study, the rate of formation of nitrous oxide appears to be constant from 573 to 673 K. Nitrous oxide has been observed as a gaseous intermediate (7) in the NO/CO reaction on various supported oxides and mixed oxide catalysts, but not when the reaction took place over supported MnO. In most cases, nitrous oxide was observed to reach a maximum concentration at various temperatures from a low of 453 K for $CuCr_2O_4$ to a high of 623 K for Co_3O_4.

Studies of the NO/CO reaction on platinum indicate that the dissociation of nitric oxide may be rate-limiting (27, 28):

[16] $NO(ads) \rightarrow N(ads) + O(ads)$

followed by nitrogen formation:

[17] $N(ads) + N(ads) \rightarrow N_2(ads)$

The adsorbed oxygen species could act as a hydrocarbon oxidation source. However, the reaction of nitric oxide with ethane is quite complex since it does not appear to occur by a simple two-step process involving first the formation of nitrous oxide followed by ethane reduction. This is evidenced by the rates of product formation. In the direct reaction of nitrous oxide with ethane over manganese(III) oxide (29), the rates of formation of carbon dioxide and nitrogen coincide with that expected for complete oxidation in excellent accord with an overall stoichiometry:

[18] $C_2H_6 + 7N_2O \rightarrow 2CO_2 + 3H_2O + 7N_2$

The rates of product formation in the nitric oxide/ethane reaction, however, do not lend themselves to such a facile interpretation; indeed, the low apparent activation energy value for the low temperature region may imply that the boundary between diffusion rate control and chemical reaction rate control is at hand.

Acknowledgement

We thank Imperial Oil Ltd., Toronto, for financial support.

Can. J. Chem. Downloaded from www.nrcresearchpress.com by 210.87.254.40 on 09/06/12
For personal use only.

1. E. F. McCaffrey, D. G. Klissurski, and R. A. Ross. J. Catal. **26**, 380 (1972); Can. J. Chem. **49**, 3778 (1971).
2. B. W. Krupay and R. A. Ross. Can. J. Chem. **51**, 3520 (1973).
3. B. W. Krupay and R. A. Ross. J. Catal. **39**, 369 (1975).
4. B. W. Krupay and R. A. Ross. Can. J. Chem. **56**, 10 (1978).
5. M. Shelef. Catal. Rev. Sci. Eng. **11**, 1 (1975).
6. R. Schleppy and Y. T. Shah. Ind. Eng. Chem., Prod. Res. Devel. **16**, 47 (1977).
7. M. Shelef and K. Otto. J. Catal. **10**, 408 (1968).
8. D. V. Fikis, W. J. Murphy, and R. A. Ross. Can. J. Chem. **56**, 2530 (1978).
9. C. N. Satterfield. Mass transfer in heterogeneous catalysis. M. I. T. Press. 1970.
10. American Society for Testing and Materials. Card Index (1967).
11. A. I. Vogel. A textbook of inorganic analysis. 3rd ed. Longman's, Green and Company Limited, London. 1962. p. 434.
12. K. H. Yang and O. A. Hougen. Chem. Eng. Prog. **46**, 146 (1950).
13. O. A. Hougen and K. M. Watson. Chemical process principles. Part III. Wiley, New York and London. 1966.
14. M. Boudart. A.I.Ch.E.J. **2**, 62 (1956).
15. S. W. Weller. Chemical reaction engineering reviews. *Edited by* H. M. Hulbert. Am. Chem. Soc., Washington, DC. 1975.
16. L. Beránek. Catal. Rev. Sci. Eng. **16**, 1 (1977).
17. P. H. Emmett (*Editor*). Catalysis. Vol. V. Reinhold, New York. 1954.
18. G. D. Lyubarskii. Dokl. Akad. Nauk SSSR Otd. khim. Nauk, 1173 (1958).
19. W. J. Thomas. Trans. Faraday Soc. **53**, 1124 (1957).
20. W. J. Thomas. Trans. Faraday Soc. **55**, 624 (1959).
21. K. Otto and M. Shelef. Proceedings of the Fifth International Congress on Catalysis. *Edited by* J. W. Hightower. North Holland, Amsterdam. 1973. Paper No. 16.
22. K. Otto and M. Shelef. J. Phys. Chem. **74**, 2690 (1970); **75**, 875 (1971); **76**, 37 (1972).
23. M. Shelef. Catal. Rev. Sci. Eng. **11**, 1 (1975).
24. H. C. Yao and M. Shelef. J. Catal. **31**, 377 (1973).
25. A. Cimino and V. Indovina. J. Catal. **17**, 54 (1970).
26. B. Halpern and J. E. Germain. J. Catal. **37**, 49 (1975).
27. D. Lorimer and A. T. Bell. J. Catal. **59**, 223 (1979).
28. R. M. Lambert and C. M. Comrie. Surf. Sci. **46**, 61 (1974).
29. C. Fairbridge, R. A. Ross, and J. R. MacCallum. To be published.

Can. J. Chem. Downloaded from www.nrcresearchpress.com by 210.87.254.40 on 09/06/12
For personal use only.

Can. J. Chem. Downloaded from www.nrcresearchpress.com by 210.87.254.6 on 09/06/12
For personal use only.

COMMUNICATION

Electrophilic cyclization of an olefinic β-keto ester

MARGOT ALDERDICE AND LARRY WEILER[1]

Department of Chemistry, University of British Columbia, Vancouver, B.C., Canada V6T 1Y6

Received January 20, 1981

MARGOT ALDERDICE and LARRY WEILER. Can. J. Chem. **59**, 2239 (1981).

Benzeneselenenyl chloride and aluminum chloride or benzenesulphenyl chloride and silica gel initiate an electrophilic cyclization of methyl 7-methyl-3-oxo-7-octenoate to cyclohexyl derivatives. These products of the cyclization reaction have been converted into intermediates of potential use in the synthesis of unusual carotenoids.

MARGOT ALDERDICE et LARRY WEILER. Can. J. Chem. **59**, 2239 (1981).

Le chlorure de benzènesélényle en présence de chlorure d'aluminium ou le chlorure de benzènesulfényle en présence de gel de silice induisent la cyclisation électrophile du méthyl-7 oxo-3 octène-2 oate de méthyle en dérivés cyclohexaniques. On a transformé les produits de cyclisation en des intermédiaires ayant une utilité potentielle dans la synthèse de caroténoides particuliers.

[Traduit par le journal

Following the initial suggestion that the biosynthesis of several steroids and other terpenoid compounds may involve an electrophilic cyclization of a polyolefin (1), there has been a continuing interest in this type of reaction from a mechanistic, biosynthetic, and synthetic viewpoint (2). A number of these polyolefin cyclizations are initiated by protons and frequently these cyclizations do not allow for the introduction of functional groups at the electrophilic terminus of the cyclization. In an effort to overcome this limitation a variety of electrophiles have been utilized to initiate cyclizations related to eq. [1] (3). However, in most of

[1] 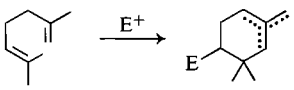

these cyclizations there are serious drawbacks due to low yields and/or generation of isomeric mixtures. Although the synthesis of heterocyclic systems by electrophilic cyclization of a substituted olefin is frequently used in synthetic chemistry, there are very few examples of C—C bond formation in nonproton initiated electrophilic cyclizations proceeding in useful yields. Usually the successful examples of C—C bond formation involve transannular cyclizations (3*d*, 4).

We would like to present some preliminary studies on the cyclization of an olefinic β-keto ester initiated by electrophiles other than protons.[2] In our studies, we have concentrated on selenium and sulfur electrophiles because of the potential to convert seleno- or thioethers into other functional groups (6). We chose β-keto ester **1** (5*b*) for this study because of the potential utility of this cyclization in the synthesis of C-2 substituted carotenoid end groups (7).

Treatment of the olefin **1** with benzeneselenenyl chloride in acetonitrile or dichloromethane gave a mixture of products containing predominantly the product **2***a* as a result of addition to the double bond.[3] Earlier we had found that benzeneselenenyl chloride added cleanly to the alkene of methyl 3-oxo-6-heptenoate without any cyclization (5*c*) and Kametani *et al.* have reported that treatment of

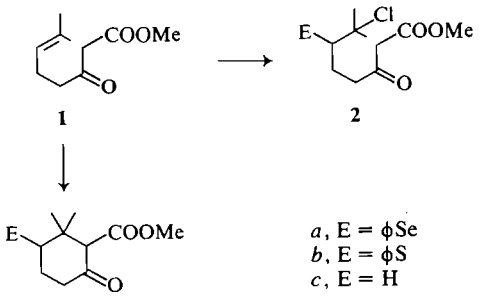

geranyl acetate with benzeneselenenyl chloride in acetic acid gave only an addition product (4*b*). However, when benzeneselenenyl chloride was added to a vigorously stirred suspension of aluminum chloride in dichloromethane containing **1**, a smooth (84%) and facile (30 min at room tempera-

[1]Author to whom correspondence should be addressed.

[2]There are several examples of proton initiated cyclizations of olefinic β-keto esters, see ref. 5, and a single example of cyclization of an olefinic β-keto ester enol phosphate, see ref. 4*e*. However, we are unaware of any cyclizations initiated by a nonprotonic electrophile and trapped at the nucleophilic terminus by a β-keto ester.

[3]Although the regiochemistry of the adduct **2***a* is not known unambiguously the ^{1}H nmr data on the crude material suggest the structure of the adduct is **2***a*.

0008-4042/81/142239-03$01.00/0

©1981 National Research Council of Canada/Conseil national de recherches du Canada

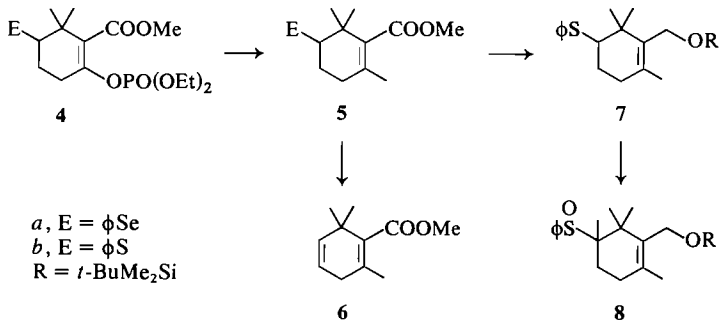

ture) cyclization to **3***a* occurred. No addition product could be detected in the crude reaction mixture. Although the cyclic product **3***a* is a mixture of two diastereomers as determined from its ^{1}H nmr and chromatographic properties, its structure was consistent with the observed spectral data and with the reductive cleavage (4*a*) of **3***a* to **3***c* (5*b*).

A similar addition of benzenesulphenyl chloride to a suspension of aluminum chloride and **1** in dichloromethane did not lead to significant amounts of cyclic product **3***b*. However, the synthesis of **3***b* from **1** could be carried out in the following fashion. Benzenesulphenyl chloride added cleanly to the olefin of **1** in dichloromethane to give a single addition product **2***b* in quantitative yield of crude material. Refluxing a suspension of silica gel (8) and adduct **2***b* in dichloromethane gave the cyclic product **3***b*. Eventually the reaction was carried out on a preparative scale by adding the benzenesulphenyl chloride to a suspension of silica gel and **1** in dichloromethane. After the addition was complete (30 min) the reaction mixture was refluxed for three hours and worked up to give **3***b* in 90–95% crude yield. Again the spectral data was consistent with the assigned structure of **3***b*, but the ^{1}H nmr data and chromatographic properties of **3***b* indicated that it was a mixture of diastereomers. Thus we have been able to cyclize an olefinic β-keto ester using either a sulphenyl or selenenyl electrophile to initiate the cyclization and a β-keto ester as the nucleophilic terminus. Both of these functional groups have the potential to introduce additional groups at either side of the molecule. Some of our preliminary results from manipulating these groups are outlined below.

The crude diastereomers of **3** were easily converted into their corresponding enol phosphates **4** (9). Usually it was more efficient to purify at this stage because **4** no longer exists as a pair of diastereomers. The enol phosphates **4** react with lithium dimethylcuprate (9) to give the ester **5** in yields of 75–80% from **1**. The selenide **5***a* was oxidized (10) to the corresponding selenoxide which was not isolated, but on refluxing in dichloromethane solution gave the diene **6** in approximately quantitative yield. The sulphide **5***b* has been reduced with excess diisobutylaluminum hydride to the alcohol and protected (11) as the *tert*-butyldimethylsilyl ether **7** in 60% yield. The sulphoxide from **7** can be alkylated in 60–80% yield (3 equiv. *n*-butyllithium and iodomethane) to give **8**. Both **6** and **8** should serve as useful precursors in the synthesis of ring A substituted carotenoids. The crucial step in this sequence was the successful introduction of E in **3**.[4]

Acknowledgements

We are grateful to the Natural Sciences and Engineering Research Council of Canada and the University of British Columbia for support of this work.

1. (*a*) G. Stork and A. W. Burgstahler. J. Am. Chem. Soc. **77**, 5068 (1955); (*b*) A. Eschenmoser, L. Ruzicka, O. Jeger, and D. Arigoni. Helv. Chim. Acta, **38**, 1890 (1955).
2. (*a*) E. E. van Tamelen. Acc. Chem. Res. **8**, 152 (1975); (*b*) W. S. Johnson. Angew. Chem., Int. Ed. Engl. **15**, 9 (1976).
3. (*a*) Y. Kitahara, T. Kato, and I. Ichinose. Chem. Lett. 283 (1976); (*b*) D. J. Faulkner. Pure Appl. Chem. **78**, 25 (1976); (*c*) A. G. Gonzalez, J. D. Martin, C. Perez, and M. A. Ramirez. Tetrahedron Lett. 137 (1976); (*d*) W. A. Smit, A. V. Semenovsky, V. F. Kucherov, T. N. Chernova, M. Z. Krimer, and D. V. Lubinskaya. Tetrahedron Lett. 3101 (1971); (*e*) S. Kumazawa, Y. Nakano, T. Kato, and Y. Kitahara. Tetrahedron Lett. 1757 (1974).
4. (*a*) D. L. J. Clive, G. Chittattu, and C. K. Wong. J. Chem. Soc. Chem. Commun. 441 (1978); (*b*) T. Kametani, K. Suzuki, H. Kurabe, and H. Nemoto. J. Chem. Soc. Chem. Commun. 1128 (1979); (*c*) N. S. Zefirov, A. S. Koz'min, V. V. Zhdankins, V. W. Kirin, B. B. Sedov, and V. G. Rau. Tetrahedron Lett. 3533 (1979); (*d*) D. Heissler and J. J. Riehl. Tetrahedron Lett. 3957 (1979);

[4]After submission of this paper we received the reports of Jackson *et al.* (12) on selenium initiated cyclizations of other olefinic β-keto esters.

Can. J. Chem. Downloaded from www.nrcresearchpress.com by 210.87.254.6 on 09/06/12
For personal use only.

(*e*) E. J. COREY, M. A. TIUS, and J. DAS. J. Am. Chem. Soc. **102**, 1742 (1980).
5. (*a*) R. W. SKEEAN, G. L. TRAMMELL, and J. D. WHITE. Tetrahedron Lett. 525 (1976); (*b*) F. W. SUM and L. WEILER. Tetrahedron Lett. 707 (1979); (*c*) F. W. SUM. Ph.D. Thesis, University of British Columbia, Vancouver, B.C. 1979.
6. (*a*) D. L. J. CLIVE. Tetrahedon. **34**, 1049 (1978); (*b*) H. J. REICH. Acc. Chem. Res. **12**, 22 (1979).
7. B. C. L. WEEDON. Carotenoids. Vol. 4 (Berne, 1975). *Edited by* B. C. L. Weedon. Pergamon Press, Oxford. 1977. pp. 161–171.
8. D. L. J. CLIVE, C. G. RUSSELL, G. CHITTATTU, and A. SINGH. Tetrahedron, **36**, 1399 (1980).
9. F. W. SUM and L. WEILER. Can. J. Chem. **57**, 1431 (1979).
10. H. J. REICH, J. M. RENGA, and I. L. REICH. J. Am. Chem. Soc. **97**, 5434 (1975).
11. E. J. COREY and A. VENKATESWARLU. J. Am. Chem. Soc. **94**, 6190 (1972).
12. W. P. JACKSON, S. V. LEY, and J. A. MORTON. J. Chem. Soc. Chem. Commun. 1028 (1980); 1173 (1980).

Can. J. Chem. Downloaded from www.nrcresearchpress.com by 210.87.254.6 on 09/06/12
For personal use only.

Correlation between thermodynamic parameters (GLC) and structure of esters

F. SAURA CALIXTO AND P. M. DEYÁ

Organic Chemistry Department, Faculty of Science, University of Palma de Mallorca, Balearic Islands, Spain

Received December 18, 1980

F. SAURA CALIXTO and P. M. DEYÁ. Can. J. Chem. **59**, 2243 (1981).

The ΔH_s and $\Delta G_s - \Delta G_{s_0}$ (ΔG_{s_0} = value of *n*-decane) values of some one hundred esters belonging to twenty different homologous series are determined experimentally in the polar stationary phase (Carbowax 1540) by gas–liquid chromatography.

Correlations between thermodynamic values and the molecular structure of esters are studied. The influence of the number of carbon atoms in the acid and alcohol chains and the position of the carboxylic group and branching chains on the ΔH_s and $\Delta G_s - \Delta G_{s_0}$ values is considered.

F. SAURA CALIXTO et P. M. DEYÁ. Can. J. Chem. **59**, 2243 (1981).

Faisant appel à la chromatographie en phase gazeuse impliquant du Carbowax 1540 comme phase stationnaire on a déterminé expérimentalement les valeurs de ΔH_s et de $\Delta G_s - \Delta G_{s_0}$ (ΔG_{s_0} = valeur du *n*-décane) d'une centaine d'esters appartenant à 20 séries homologues différentes.

On a étudié les corrélations entre les valeurs thermodynamiques et la structure moléculaire des esters. On a considéré l'influence du nombre d'atomes de carbone dans les chaînes d'acides et d'alcool, la position du groupe acide carboxylique et les chaînes latérales sur les valeurs de ΔH_s et de $\Delta G_s - \Delta G_{s_0}$.

[Traduit par le journal]

Introduction

As is well known since the inception of gas chromatography, its application to the determination of thermodynamic parameters has experienced a progressive development, becoming one of the most precise and rapid methods for this purpose.

Since the publication of the work of Greene and Pust (1) concerning the determination of heats of adsorption of some light hydrocarbons on alumina and silica gel, many papers have been published on the determination of ΔH_{ads} (heat of adsorption) by gas–solid chromatography. Other papers deal with the calculations of several parameters concerning solution phenomena by gas–liquid chromatography. Some of the more significant are referred to in the bibliography (2–7). Some authors also employ thermodynamic values for quantitative determinations of polarity of stationary phases in gas chromatography (8, 9).

Several different procedures are available for calculating ΔH_s (heat of solution) and ΔG_s (free enthalpy of solution) by gas–liquid chromatography. Oberholtzer and Rogers (7) calculate ΔH_s from the following eq. [1]:

$$[1] \quad \ln \frac{V_R^0 - V_M}{V_M} = -\frac{\Delta H_s}{RT} + C$$

where V_R^0 is the corrected retention volume, V_M is the dead volume, R is the gas constant, T is the absolute temperature, and C is a constant of integration.

Golovnya and Arsenyev (10, 11) compare the ΔH_s values found from ln V_g^0 (specific retention volume) versus $1/T$ plots with the values calculated by means of eq. [2]:

$$[2] \quad \Delta H_{s_x} = -\Delta H_{v_n} + \Delta H_{s_n} + \frac{4.6 \cdot 10^{-5} T_1 T_2}{T_2 - T_1} \times [b_{T_1} \Delta I + \Delta b (I_{T_1} - 100n)]$$

where T_1 and T_2 are temperatures, ΔH_{s_x} is the partial molar enthalpy of solution of the unknown substance, ΔH_{v_n} is the partial molar enthalpy of evaporation of the *n*-alkane with "*n*" number of carbons, ΔH_{s_n} is the partial molar enthalpy of solution of the *n*-alkane, b is the slope of the straight line of ln V_g^0 versus "*n*" plot, I_T is the retention index at T temperature and V_g^0 is the specific retention volume. Significant differences between the two methods have not been found.

These authors also determined ΔG_s values using the classical expression [3]:

$$[3] \quad \Delta G_s = 2.3RT \log K_H$$

where K_H is the Henry's law constant.

In our laboratories, the heats of adsorption of some alkyl-aromatic hydrocarbons on several porous solids have been estimated (12) by the above mentioned methods.

In this paper an attempt has been made to correlate the ΔH_s and ΔG_s values with the molecular structure of esters. In this way we have determined experimentally the retention chromatographic parameters of some one hundred esters in Carbowax 1540 stationary phase at different temperatures. We can group these esters in twenty

0008-4042/81/152243-04$01.00/0

©1981 National Research Council of Canada/Conseil national de recherches du Canada

Can. J. Chem. Downloaded from www.nrcresearchpress.com by 210.87.254.105 on 09/06/12
For personal use only.

Can. J. Chem. Downloaded from www.nrcresearchpress.com by 210.87.254.105 on 09/06/12
For personal use only.

different homologous series. As the purpose of this work has been to study the relationship between thermodynamic parameters and molecular structure in order to deduce the general behaviour of esters, and since the quantitative differences between the values obtained by using different methods were not significant, we have chosen the more general method described by eq. [4]:

$$[4] \quad \ln V_g^0 = -\Delta H_s/RT + C$$

The values of ΔH_s can be calculated from the values of the slopes obtained by plotting V_g^0 versus $1/T$ or by plotting V_R^0/T versus $1/T$, where V_R^0 is the corrected retention volume. In this study we have used the latter, thereby avoiding any discussion of their theoretical precision.

In order to study the relationship between free energy and ester structure, we have compared values of this magnitude to a standard linear hydrocarbon, *n*-decane. In this way, the magnitude used ($\Delta G_s - \Delta G_{s_0}$) is easily calculated from the retention data by means of eq. [5]:

$$[5] \quad \Delta G_s - \Delta G_{s_0} = -RT \ln (V_R^0/V_{R_0}^0)$$

This expression can be deduced from eq. [3], taking into account the corresponding expressions of Henry's constant [6] and the specific retention volume [7]:

$$[6] \quad K_H = V_g \cdot T \cdot \rho/273.16$$

$$[7] \quad V_g^0 = \frac{V_R^0}{w_L} \cdot \frac{p_0 - p_w}{p_0} \cdot j \cdot \frac{273.16}{T}$$

where:

w_L = weight of the stationary phase

$\frac{p_0 - p_w}{p_0}$ = correction for partial pressure of water vapor at T temperature

j = compressibility factor, $\frac{3}{2} \cdot \frac{(p_i/p_0)^2 - 1}{(p_i/p_0)^3 - 1}$

p_i = inlet pressure

ρ = density of stationary phase at the column temperature.

Experimental

Determinations of V_R^0 were carried out with a Perkin Elmer chromatograph, Model 900, equipped with a SIP-1 digital integrator and a counter, model 56. The detection system was flame ionization. One capillary column of Carbowax 1540 + KOH (99:1) made of stainless steel with dimensions of 150 ft × 0.02 in. was used.

Most of the esters used came from the firm Merck and Fluka. In some cases they were synthesized and purified using standard laboratory methods.

The assays were carried out at three different temperatures, 70, 81, and 90°C, and the gas flow rate at these temperatures was 2.8, 2.7, and 2.6 mL min^{-1} respectively. The other experimental conditions were: inlet pressure, 930.9 Torr; outlet pressure, 760.0 Torr; detector temperature, 200°C; injector temperature, 200°C, and splitter 44:1. The vapor pressure of water at ambient temperature (20°C) was 17.5 Torr.

The sample size was 0.04 μL which proved ideal to obtain symmetrical chromatographic peaks, a necessary condition for the correct calculation of retention data. These conditions produce reproducible retention data with a standard deviation of 0.02% which was stated in an earlier work (13).

Dead volume (V_M) was determined by injection of methane by the Peterson and Hirsch method (14) using measurements on a homologous series of *n*-paraffins (nonane, decane, undecane, dodecane, and tridecane).

Some one hundred esters were used which can conveniently be grouped in the following homologous series: formates, acetates, propionates, butyrates, pentanoates, hexanoates, heptanoates, octanoates, nonanoates, isobutyrates and isopentanoates; methyl, ethyl, propyl, butyl, pentyl, hexyl, isopropyl, isobutyl, and isopentyl esters.

Results and Discussion

Figure 1 shows $\ln V_R^0/T$ versus $1/T$ plots for a few compounds. In all cases, however, the correlation coefficients of the straight lines are equal to or greater than 0.999.

The ΔH_s values obtained from the slopes of the above straight lines are shown in Table 1 which refers to homologous series with linear chains. The values for different series can be seen by reference to the horizontal rows and vertical columns. By

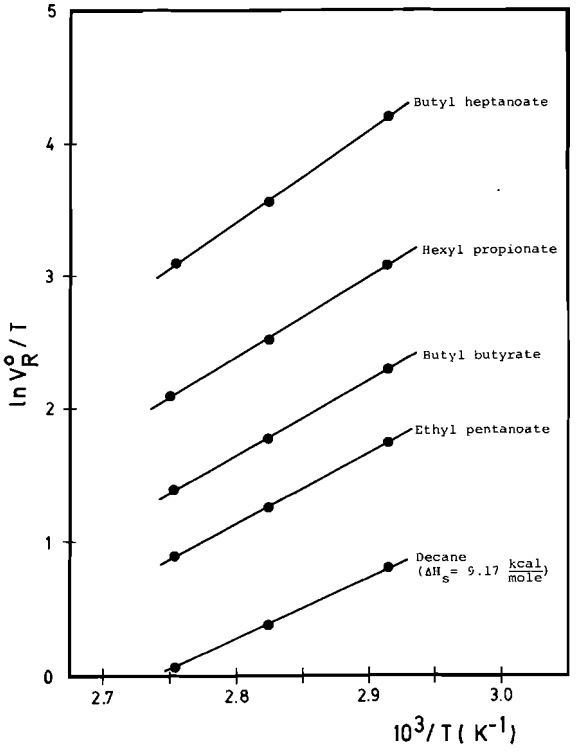

FIG. 1. Plot of $\ln V_R^0/T$ vs reciprocal temperature.

TABLE 1. Heats of solution ($-\Delta H_s$) of the esters with linear chains (kcal mol^{-1})

	Methyl	Ethyl	Propyl	Butyl	Pentyl	Hexyl	Heptyl	Octyl	$\overline{\Delta(\Delta H_s)}$	s^a
Formate	—	—	—	9.52	10.34	11.24	12.24	13.22	0.93	0.08
Acetate	—	—	8.52	9.74	10.78	11.70	12.84	13.88	1.04	0.09
Propionate	—	8.65	9.65	10.44	11.42	12.30	13.19	14.07	0.90	0.08
Butyrate	9.02	9.61	10.40	11.20	12.06	12.93	13.78	—	0.83	0.04
Pentanoate	10.04	10.54	11.19	12.04	12.91	13.75	14.55	15.34	0.80	0.08
Hexanoate	10.85	11.45	12.11	12.90	13.73	14.51	15.25	16.04	0.77	0.06
Heptanoate	11.74	12.26	12.97	13.76	—	—	—	—	—	—
Octanoate	12.69	13.15	13.86	14.60	—	—	—	—	—	—
$\overline{\Delta(\Delta H_s)}$	0.90	0.90	0.89	0.81	0.74	0.70	—	—		
s^a	0.09	0.06	0.13	0.07	0.11	0.10	—	—	—	

[a]Standard deviation.

reading diagonally, it can be observed that the ΔH_s values of esters which have the same total number of carbon atoms ($n_t = n_{ac} + n_{al}$) always show minimum ΔH_s values when the charge center and the mass center are as close as possible.

We were able to find very few values for ΔH_s relating to esters in the literature. We can cite the work of Golovnya and Arsenyev (11) which determines ΔH_s of several substances, among which the following esters are found: pentyl acetate, hexyl acetate, and butyl propionate. These ΔH_s values were determined in polar stationary phases of PEG-20.000 and XF-1153. They are of the same order as those referred to in this paper. Thus, the ΔH_s values expressed in kcal mol^{-1} for butyl propionate are −9.55 (PEG-20.000) and −9.83 (XF-1153) while the calculated value in this work is −10.44 (Carbowax 1540). The polarities of these stationary phases according to the Tarján *et al.* (15) scale are 70.75 for PEG-20.000, 75.43 for XF-1153, and 86.24 for Carbowax 1540.

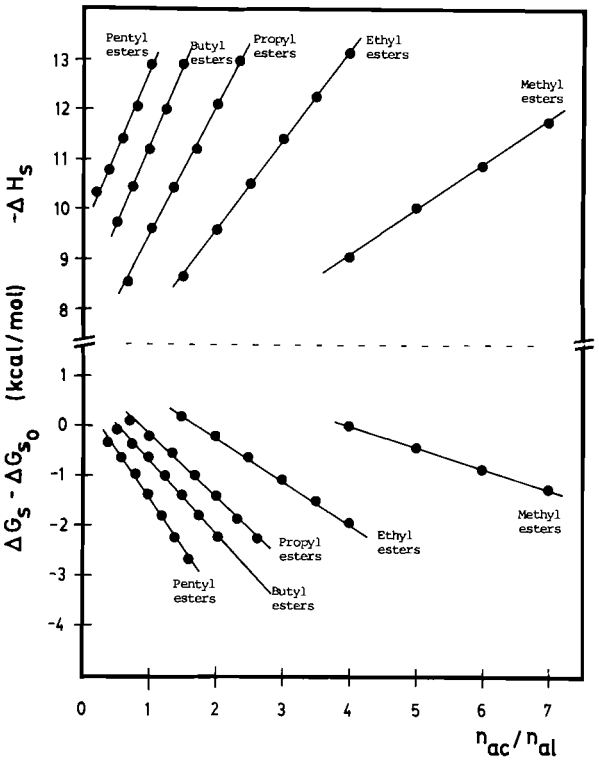

FIG. 2. Variation of ΔH_s and $\Delta G_s - \Delta G_{s_0}$ with n_{ac}/n_{al}. (For an ester R-COOR,' n_{ac} = number of carbon atoms in the R-COO group; and n_{al} = number of carbon atoms in the R' group.)

The graphs in Fig. 2, taken from the data in Table 1, show that like $\overline{\Delta(\Delta H_s)}$ values corresponding to step-by-step numerical increase in the number of —CH_2— groups in the acid chain are nearly constant for each series, although a slight decrease of the values can be seen as we progress from methyl, to ethyl, to propyl esters, and so on.

By comparing the ΔH_s of esters of complementary chain-lengths of acid and alcohol groups, it can be deduced that the values increase from the acetate, propionate, butyrate series and so on, which shows that the successive addition of —CH_2— groups in the alcohol chains is a greater contributing factor than a similar addition in the acid chains (Table 1).

The length of the alcohol chain has a greater influence on ΔH_s than the length of the acid group. This can be shown taking into account the values from Table 1 corresponding to esters of comple-

TABLE 2. ΔH_s of isoesters

Compound	ΔH_s (kcal mol^{-1})
Propyl pentanoate	−11.19
Propyl isopentanoate	−10.87
Isopropyl pentanoate	−10.33
Isopropyl isopentanoate	−10.30
Pentyl butyrate	−12.06
Pentyl isobutyrate	−11.65
Isopentyl butyrate	−11.57
Propyl octanoate	−13.86
Isopropyl octanoate	−13.62

Can. J. Chem. Downloaded from www.nrcresearchpress.com by 210.87.254.105 on 09/06/12
For personal use only.

TABLE 3. $\overline{\Delta(\Delta G_s - \Delta G_{s_0})}$ of the esters with linear chains (kcal mol^{-1}) at 81°C

	Methyl	Ethyl	Propyl	Butyl	Pentyl	Hexyl	Heptyl	Octyl	$\overline{\Delta(\Delta G_s - \Delta G_{s_0})}$	s[a]
Formate	—	—	—	−0.13	−0.57	−1.01	−1.45	−1.86	−0.43	0.02
Acetate	—	—	0.07	−0.36	−0.80	−1.32	−1.67	−2.10	−0.43	0.01
Propionate	—	0.16	−0.22	−0.65	−1.08	−1.51	−1.95	−2.38	−0.42	0.02
Butyrate	0.02	−0.20	−0.58	−0.99	−1.42	−1.84	—	—	−0.41	0.02
Pentanoate	−0.43	−0.63	−1.01	−1.41	−1.83	−2.25	−2.66	−3.07	−0.41	0.02
Hexanoate	−0.86	−1.05	−1.42	−1.83	−2.25	−2.66	−3.07	−3.49	−0.41	0.02
Heptanoate	−1.29	−1.49	−1.85	−2.25	—	—	—	—	—	—
Octanoate	−1.73	−1.92	−2.28	−2.68	—	—	—	—	—	—
$\overline{\Delta(\Delta G_s - \Delta G_{s_0})}$	−0.44	−0.42	−0.39	−0.36	−0.36	−0.36	—	—		
s[a]	0.01	0.03	0.06	0.06	0.07	0.06	—	—		

[a]Standard deviation.

mentary acid and alcohol chain lengths, for example: hexyl formate ($\Delta H_s = -11.24$ kcal mol^{-1}) and methyl hexanoate ($\Delta H_s = -10.84$ kcal mol^{-1}).

The branching of the alcohol or acid chains in esters produces a lowering of ΔH_s, an effect more pronounced in the alcohol group. In Table 2 some examples of this type are included. Logically, when both types of branching occur in the same ester, lowest values are obtained.

Table 3 shows the values obtained using the value obtained for *n*-decane as "zero" (ΔG_{s_0}). In this case, it can be observed that $\Delta G_s - \Delta G_{s_0}$ presents maximum values when the ratio n_{ac}/n_{al} is nearly one. It can be observed from Fig. 2 that the linear plots for methyl esters, ethyl esters, and so on have slopes of opposite sign to those obtained for ΔH_s. The effect of varying the —CH_2— group on values of $\Delta G_s - \Delta G_{s_0}$ is analogous to that for values of ΔH_s.

Conclusion

From the experimental data previously stated it can be concluded that in the values of ΔH_s and $\Delta G_s - \Delta G_{s_0}$ for esters, aside from the total number of carbon atoms, the ratio between the number of carbon atoms of the acid group (n_{ac}) and the alcohol group (n_{al}), the branching of these chains, and the position of the carboxylic group in the molecule are also influencing factors.

The methylene groups in the alcohol chain have a greater influence than those in the acid chain on the value of these thermodynamic quantities. The branching of the chains produces a diminution of these values, which is the more pronounced in the alcohol group. For esters with the same number of carbon atoms, the ΔH_s value is smaller the nearer the carboxylic group is to the center of the carbon chain.

1. S. A. GREENE and H. PUST. J. Phys. Chem. **62**, 55 (1958).
2. K. ARITA, Y. KUGE, and Y. YOSHIKAWA. Bull. Chem. Soc. Jpn. **38**, 632 (1965).
3. YI HUA HA and C. MANCEL. Molecular sieves. Adv. Chem. Ser. Monogr. 121. A.C.S. Washington. 1973. p. 392.
4. D. ATKINSON and G. CURTHOYS. J. Chem. Educ. **55**, 564 (1978).
5. C. L. YOUNG. Chromatogr. Rev. **10**, 129 (1968).
6. R. KOBAYASHI, P. S. CHAPPELEAR, and H. A. DEANS. Ind. Eng. Chem. **59**, 63 (1967).
7. J. E. OBERHOLTZER and L. B. ROGERS. Anal. Chem. **41**, 1234 (1969).
8. E. KOVATS. Chimia, **22**, 459 (1968).
9. J. NOVAK, J. RUZICKOVA, S. WICAR, and J. JANAK. Anal. Chem. **45**, 1365 (1973).
10. R. V. GOLOVNYA and Y. N. ARSENYEV. Chromatographia, **3**, 455 (1970).
11. R. V. GOLOVNYA and Y. N. ARSENYEV. Chromatographia, **4**, 250 (1971).
12. P. M. DEYÁ, A. COSTA, J. V. SINISTERRA, and J. M. MARINAS. Proc. VIIth Iber. Symp. Catal. 1980. p. 44.
13. F. S. CALIXTO and A. G. RASO. Chromatographia, **14**, 143 (1981).
14. M. L. PETERSON and J. HIRSCH. J. Lipid Res. **1**, 132 (1959).
15. G. TARJAN, A. KISS, G. KOCSIS, S. MESZAROS, and J. M. TAKACS. J. Chromatogr. **119**, 327 (1976).

Can. J. Chem. Downloaded from www.nrcresearchpress.com by 210.87.254.105 on 09/06/12
For personal use only.

The synthesis of uridine diphosphate *N*-acetylhexosamines and uridine 5′-(2-acetamido-2-deoxy-α-D-mannopyranosyluronic acid diphosphate)[1]

TATSUMI YAMAZAKI, CHRISTOPHER D. WARREN, ANNETTE HERSCOVICS, AND ROGER W. JEANLOZ

Laboratory for Carbohydrate Research, Departments of Biological Chemistry and Medicine, Harvard Medical School and Massachusetts General Hospital, Boston, MA 02114, U.S.A.

Received December 15, 1980

This paper is dedicated to Prof. Raymond U. Lemieux on the occasion of his 60th birthday

TATSUMI YAMAZAKI, CHRISTOPHER D. WARREN, ANNETTE HERSCOVICS, and ROGER W. JEANLOZ. Can. J. Chem. **59**, 2247 (1981).

2-Methyl-(2-acetamido-3,4,6-tri-*O*-acetyl-1,2-dideoxy-β-D-mannopyrano)-[2,1-*d*]-2-oxazoline was efficiently converted into 2-acetamido-3,4,6-tri-*O*-acetyl-2-deoxy-α-D-mannopyranosyl phosphate, by treatment with dibenzyl phosphate, followed by catalytic hydrogenolysis of the benzyl groups. Similarly, 2-acetamido-3,4,6-tri-*O*-acetyl-2-deoxy-α-D-glucopyranosyl phosphate and -galactopyranosyl phosphate were synthesized from the respective peracetyl oxazolines. In each case, the procedures for preparing the oxazoline, and conversion into the glycosyl phosphate, were modified to give high yields of pure products. 2-Acetamido-3,4,6-tri-*O*-acetyl-2-deoxy-α-D-mannopyranosyl phosphate was coupled with 2′,3′-di-*O*-acetyluridine 5′-monophosphate by a modification of the mixed anhydride procedure, to give 2′,3′-di-*O*-acetyluridine 5′-(2-acetamido-3,4,6-tri-*O*-acetyl-2-deoxy-α-D-mannopyranosyl diphosphate), which was readily purified by preparative tlc and *O*-deacetylated to give "uridine diphosphate *N*-acetylmannosamine" in high yield. Similarly, uridine 5′-(2-acetamido-2-deoxy-α-D-glucopyranosyl- and -galactopyranosyl diphosphates) were synthesized by rapid, efficient procedures, not involving ion-exchange chromatography. Uridine 5′-(2-acetamido-2-deoxy-α-D-mannopyranosyl diphosphate) was converted into uridine 5′-(2-acetamido-2-deoxy-α-D-mannopyranosyluronic acid diphosphate), required for biosynthetic studies, without the preparation of a special platinum catalyst. All the synthetic uridine diphosphate sugars were characterized by optical rotation, ^{1}H nmr spectrum, and elemental analysis.

TATSUMI YAMAZAKI, CHRISTOPHER D. WARREN, ANNETTE HERSCOVICS et ROGER W. JEANLOZ. Can. J. Chem. **59**, 2247 (1981).

La 2-méthyl-(2-acétamido-3,4,6-tri-*O*-acétyl-1,2-didésoxy-β-D-mannopyrano)-[2,1-*d*]-2-oxazoline a été convertie avec un bon rendement en phosphate de 2-acétamido-3,4,6-tri-*O*-acétyl-2-désoxy-α-D-mannopyranosyle par traitement avec le phosphate de dibenzyle suivi par l'hydrogénolyse catalytique des groupes benzyles. D'une manière semblable, les phosphates de 2-acétamido-3,4,6-tri-*O*-acétyl-2-désoxy-α-D-glucopyranosyle et -galactopyranosyle ont été synthétisés à partir des oxazolines peracétylées respectives. Dans chaque cas, la méthode de préparation de l'oxazoline et la conversion en phosphate de glycosyle ont été modifiées pour donner d'excellent rendements en produit pur. Le phosphate de 2-acétamido-3,4,6-tri-*O*-acétyl-2-désoxy-α-D-mannopyranosyle a été condensé avec le 5′-monophosphate de 2,3-di-*O*-acétyluridine par une modification de la méthode à l'anhydride mixte, pour donner la 2′,3′-di-*O*-acétyluridine (5′-diphosphate de 2-acétamido-3,4,6-tri-*O*-acétyl-2-désoxy-α-D-mannopyranosyle). Celle-ci a été purifiée par ccm préparative et *O*-désacétylée pour donner l'"uridine diphosphate de *N*-acétylmannosamine" avec un excellent rendement. D'une manière semblable, les uridine 5′-(diphosphate de 2-acétamido-2-désoxy-α-D-glucopyranosyle et -galactopyranosyle) ont été synthétisées par des méthodes rapides et efficaces qui ne demandent pas une purification par chromatographie sur résines échangeuses d'ions. L'uridine 5′-(diphosphate de 2-acétamido-2-désoxy-α-D-mannopyranosyle) a été convertie en uridine 5′-(diphosphate de l'acide 2-acétamido-2-désoxy-α-D-mannopyranosyluronique) (produit nécessaire pour des études de biosynthèse) sans préparation d'un catalyste de platine spécial. Tous les uridine diphosphates de sucre ont été caractérisés par leurs pouvoirs rotatoires, spectre de rmn ^{1}H et analyse élémentaire.

Introduction

Nucleoside diphosphate sugars are uniquely important as glycosyl donors in a wide variety of biosynthetic processes (1), including the formation, via lipid intermediates, of antigenic polysaccharides in bacteria (2). These compounds are therefore frequently required for biosynthetic investigations, and good methods of synthesis, both chemical and enzymic, are essential.

The chemical methods available for preparing nucleoside diphosphate sugars, especially the hexosamine derivatives (3), are often inconvenient and time-consuming, especially in the purification stages, and yields are variable. This is particularly true for uridine 5′-(2-acetamido-2-deoxy-α-D-mannopyranosyluronic acid diphosphate) (**20**) (4) which was required by us for the study of the biosynthesis of the antigenic polysaccharide in the cell wall of *Micrococcus lysodeikticus* (5, 6). Furthermore, when compound **20** was prepared previously (4), it was characterized indirectly, and its properties were not recorded. We have, therefore, developed a rapid and efficient synthesis of **20**, utilizing an improved method for the coupling of

[1]Amino Sugars 127. This is publication No. 866 of the Robert W. Lovett Memorial Group for the Study of Diseases Causing Deformities, Harvard Medical School and Massachusetts General Hospital. This work was supported by research grant No. AI-06692 from the National Institute of Allergy and Immunology, National Institutes of Health, U.S. Public Health Service.

0008-4042/81/152247-06$01.00/0

©1981 National Research Council of Canada/Conseil national de recherches du Canada

Can. J. Chem. Downloaded from www.nrcresearchpress.com by 210.87.254.40 on 09/06/12
For personal use only.

Can. J. Chem. Downloaded from www.nrcresearchpress.com by 210.87.254.40 on 09/06/12
For personal use only.

the glycosyl phosphate residue (as the peracetyl derivative) with uridine 5′-monophosphate, and show that this method is generally applicable to the synthesis of nucleoside diphosphate hexosamine derivatives. All the synthetic compounds were characterized by recording optical rotation, ^{1}H nmr spectrum, and elemental analysis. A preliminary account of part of this work has previously appeared (7).

Results and Discussion

For the synthesis of uridine 5′-(2-acetamido-2-deoxy-α-D-mannopyranosyl diphosphate) (**15**), a procedure similar to that of Salo and Fletcher (8) was followed. Thus, the oxazoline derivative **1** of 2-acetamido-2-deoxy-D-mannose was phosphorylated before being coupled with an activated derivative of uridine 5′-monophosphate. Repetition of the preparation of Khorlin *et al.* (9) of the oxazoline **1** gave, in our hands, only average yields (40–60%), and an alternative procedure was developed. Thus, 2-acetamido-3,4,6-tri-*O*-acetyl-2-deoxy-α-D-mannopyranosyl chloride (**2**), prepared by treatment of 2-acetamido-2-deoxy-D-mannose monohydrate with acetyl chloride for 8 h, was smoothly converted (74% yield) into 2-methyl-(3,4,6-tri-*O*-acetyl-1,2-dideoxy-β-D-mannopyrano)-[2,1-*d*]-2-oxazoline (**1**) by treatment with an excess of potassium carbonate in acetonitrile. Treatment of **1** with dibenzylphosphate, followed by catalytic hydrogenolysis of the resulting dibenzyl derivative, gave, in 61% yield, 2-acetamido-3,4,6-tri-*O*-acetyl-2-deoxy-α-D-mannopyranosyl phosphate (**5**), which was suitable for synthetic purposes, and was *O*-deacetylated, in quantitative yield, to give 2-acetamido-2-deoxy-α-D-mannopyranosyl phosphate (**6**).

2-Methyl-(2-acetamido-3,4,6-tri-*O*-acetyl-1,2-dideoxy-α-D-glucopyrano)-[2,1-*d*]-2-oxazoline (**3**) was prepared in quantitative yield by a method similar to that of Lemieux and Driguez (10), and then condensed with dibenzyl phosphate, followed by the same hydrogenolysis procedure as that employed for the preparation of **5** to give, in 63% yield, 2-acetamido-3,4,6-tri-*O*-acetyl-2-deoxy-α-D-glucopyranosyl phosphate (**7**), which was characterized further as the *O*-deacetylated compound **8**. It has been shown by Khorlin *et al.* (11), and Warren *et al.* (12), that oxazolines derived from 2-acetamido-2-deoxy-D-glucose and di-*N*-acetylchitobiose yield α-D-glycosyl phosphates by this procedure, rather than the kinetic product, the β-D anomer.

The yield in the synthesis (62% yield) of 2-methyl-(3,4,6-tri-*O*-acetyl-1,2-dideoxy-α-D-galactopyrano)-[2,1-*d*]-2-oxazoline (**4**) by treatment of 2-acetamido-1,3,4,6-tetra-*O*-acetyl-2-deoxy-β-D-galactopyranose with anhydrous ferric chloride in dichloromethane according to Matta *et al.* (13) was improved to 84%. Phosphorylation performed by the same procedure as that described for **5** and **7** gave 2-acetamido-3,4,6-tri-*O*-acetyl-2-deoxy-α-D-galactopyranosyl phosphate (**9**) in 70% yield. *O*-Deacetylation with sodium methoxide in methanol gave 2-acetamido-2-deoxy-α-D-galactopyranosyl phosphate (**10**) in 92% yield.

The mixed anhydride method developed by Michelson (14) was selected among the methods for the synthesis of uridine diphosphate sugars (for a review, see ref. 3), as it has been successfully applied to uronic acid (15) and deoxy sugar (16) derivatives, and has been adapted in this laboratory to the synthesis of "lipid intermediates" (12). Treatment of the tributylammonium salt of uridine 5′-monophosphate with diphenyl phosphorochloridate in a mixture of 1,4-dioxane and *N*,*N*-dimethylformamide gave a precipitate of uridine 5′-(diphenyl diphosphate) (**13**), which was immediately treated with two equivalent amounts of the tribu-

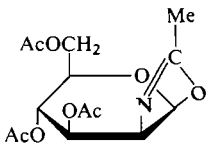

1

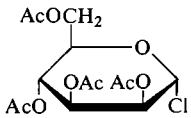

2

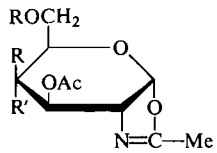

3 R = H, R′ = OAc
4 R = OAc, R′ = H

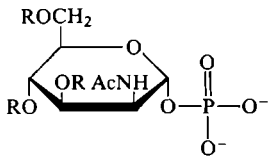

5 R = Ac
6 R = H

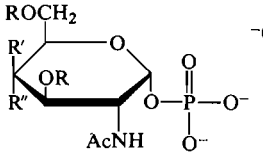

7 R = Ac, R′ = H, R″ = OAc
8 R = R′ = H, R″ = OH
9 R = Ac, R′ = OAc, R″ = H
10 R′ = OH, R = R″ = H

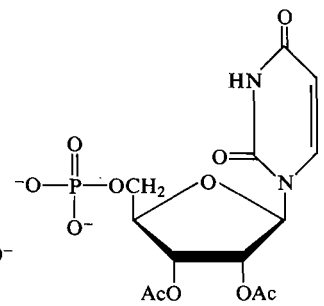

11

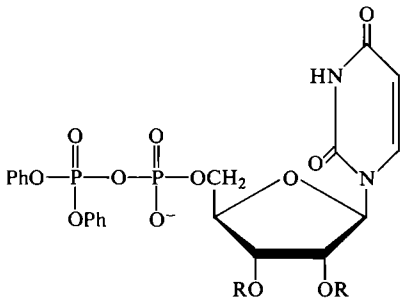

12 R = Ac
13 R = H

tylammonium salt of a sugar phosphate (**6** or **8**) in a mixture of 1,4-dioxane and pyridine for 15 h at room temperature. After purification by ion-exchange column chromatography, the desired uridine 5′-(2-acetamido-2-deoxy-α-D-mannopyranosyl diphosphate) (**15**) and uridine 5′-(2-acetamido-2-deoxy-α-D-glucopyranosyl diphosphate) (**17**) were obtained in 39 and 47% yield, respectively.

In order to obtain these moderate yields, extreme care had to be taken in drying the starting materials, solvents, and apparatus. Moreover, complete drying of the uridine 5′-monophosphate and glycosyl phosphate was difficult because of the presence of traces of water tightly bound to the hydroxyl groups. Therefore, a modified procedure, in which these groups were protected by *O*-acetylation, was introduced. Per-*O*-acetylglycosyl phosphates have already been extensively used in this laboratory in the synthesis of glycosyl polyprenyl mono- and di-phosphates (12, 17). Thus, 2′,3′-di-*O*-acetyluridine 5′-monophosphate (**11**) was prepared in 72% yield from uridine 5′-(disodium monophosphate) by acetylation with acetic anhydride in a mixture of pyridine and *N*,*N*-dimethylformamide. As expected, a product containing both acetylated hydroxyl and phosphate groups was obtained. Further treatment with pyridine and methanol and subsequent evaporation gave the desired compound **11**. Condensation (14) of the tributylammonium salt **11** with diphenyl phosphorochloridate in dry 1,4-dioxane for 2 h at room temperature under nitrogen, and subsequent evaporation of the reaction mixture gave syrupy 2′,3′-di-*O*-acetyluridine 5′-(diphenyl diphosphate) (**12**), which was immediately treated with a slight excess of the tributylammonium salt of the acetylated hexosamine phosphate (**5**, **7**, or **9**) in dry pyridine for 8 to 10 h at room temperature. Evaporation of the reaction mixture, and purification by preparative tlc (eluting solvent: chloroform–methanol–water 10:10:3) gave the corresponding peracetylated uridine 2-amino-2-deoxy sugar diphosphates (**14**, **16**, and **18**), in 86, 82, and 80% yield, respectively. Each compound was converted easily by treatment with aqueous sodium hydroxide into the *O*-deacetylated uridine diphosphate derivative **15**, **17**, and **19**, in 94, 86, and 82% yield, respectively.

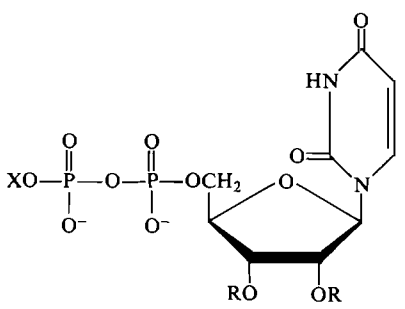

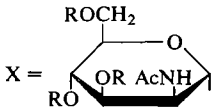

14 R = Ac **15** R = H

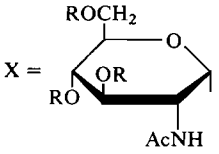

16 R = Ac **17** R = H

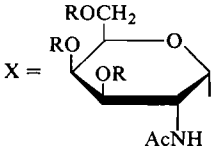

18 R = Ac **19** R = H

Anderson *et al.* (4) have described the selective oxidation at C-6 of the 2-acetamido-2-deoxy-D-mannosyl group of **15**, in 12% yield, by use of a platinum catalyst prepared by the procedure of Dutton and Slessor (18). The preparation of the catalyst is time-consuming and did not give a catalyst of consistent quality. Therefore, compound **15** was selectively oxidized, in the presence of commercially available 10% platinum-on-carbon

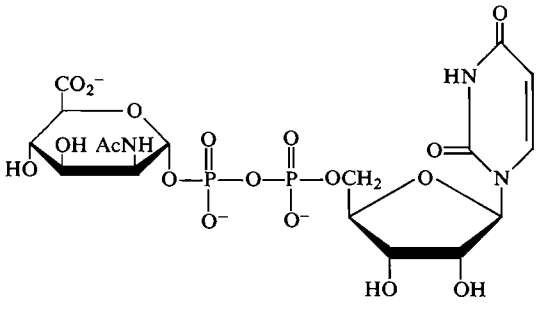

20

Can. J. Chem. Downloaded from www.nrcresearchpress.com by 210.87.254.40 on 09/06/12
For personal use only.

Can. J. Chem. Downloaded from www.nrcresearchpress.com by 210.87.254.40 on 09/06/12
For personal use only.

(Fluka-Tridom), by bubbling oxygen into a mixture of **15** in aqueous sodium hydrogen carbonate solution for 7 h at 75°C, to give uridine 5′-(2-acetamido-2-deoxy-α-D-mannopyranosyluronic acid diphosphate) (**20**) in 20% yield.

Experimental

Melting points were determined with a Mettler FP-2 apparatus and optical rotations on solutions in a 1 dm, semimicro tube with a Perkin–Elmer polarimeter, Model 141. The ir spectra were recorded with a Perkin–Elmer spectrophotometer, Model 237. Thin-layer chromatography was performed on precoated plates of Silica Gel F245 (Merck), and the spots were detected by (*a*) a spray of 5% phosphomolybdic acid in ethanol, (*b*) the spray reagent of Dittmer and Lester (19) for phosphate groups, and (*c*) uv visualization. Preparative tlc was conducted on precoated plates of Silica Gel F254 (Merck, 0.5 and 2 mm thickness). When the compound did not quench uv fluorescence, it was detected by spraying a narrow band (1–2 mm) with one or both of the spray reagents used for the analytical tlc.

The ^{1}H nmr spectra were recorded at 60 MHz with a Varian T-60 spectrometer, at 80 MHz with a Varian FT-80 spectrometer, or at 270 MHz with a Bruker WP-270 instrument. The high-field nmr experiments were performed at the NMR Facility for Biomolecular Research located at the F. Bitter National Magnet Laboratory, Massachusetts Institute of Technology, Cambridge, MA 02139. Acetonitrile was dried by distillation from phosphorus pentoxide and storage over 3 Å molecular sieves (Sigma). The microanalyses were performed by Galbraith Laboratories, Inc., Knoxville, TN 37921. The criteria for inclusion of occluded solvent molecules in the analyses are (*1*) the spectral data are consistent with their presence; (*2*) these solvents have been employed in the final purification step; (*3*) the calculated and found figures fit closely; and (*4*) the identity of the compound is unambiguously established by other data.

*2-Methyl-(2-acetamido-3,4,6-tri-*O*-acetyl-1,2-dideoxy-*β*-D-mannopyrano)-[2,1-d]-2-oxazoline (1)*

A suspension of 2-acetamido-2-deoxy-D-mannose monohydrate (500 mg, 2.1 mmol) in acetyl chloride (6 mL) was saturated with dry hydrogen chloride gas at −10°C. The reaction flask was sealed and stored at room temperature for 10 h. The dark-red solution was evaporated to dryness, and the remaining traces of solvent co-evaporated with benzene. The residue was dissolved in chloroform, and the solution was washed rapidly with aqueous potassium hydrogen carbonate, dried ($MgSO_4$), and evaporated to give a colored syrup (930 mg), which was dissolved in dry acetonitrile (6 mL). Anhydrous powdered potassium carbonate (1 g) was added, and the mixture was stirred vigorously for 2 h at room temperature under nitrogen, filtered, and evaporated to a syrup, which was applied to a short column (2 cm × 5 cm) of alumina (neutral, Sigma). Washing of the column with chloroform containing 1% of pyridine (70 mL) and evaporation gave a crystalline residue. Recrystallization from ether afforded needles (514 mg, 74%), mp 132–133°C; $[\alpha]_D^{20}$ −30° (*c* 1.0, $CHCl_3$) (lit. (9), mp 133–134°C, $[\alpha]_D^{17}$ −31 ± 2° (*c* 1.02, $CHCl_3$)); ^{1}H nmr ($CDCl_3$) δ: 5.85 (d, $J_{1,2}$ = 6 Hz, H-1).

*2-Methyl-(2-acetamido-3,4,6-tri-*O*-acetyl-1,2-dideoxy-*α*-D-glucopyrano)-[2,1-d]-2-oxazoline (3)*

2-Acetamido-3,4,6-tri-*O*-acetyl-2-deoxy-α-D-glucopyranosyl chloride (20) (**2**, 10.0 g, 22.4 mmol) was dissolved in dry acetonitrile (30 mL) containing tetraethylammonium chloride (4.0 g, 24 mmol) and anhydrous sodium hydrogen carbonate (4.0 g, 48 mmol). The mixture was kept at 55°C for 20 min, the solvent was removed *in vacuo*, and the residue was dissolved in dichloromethane (50 mL). The solution was washed three times with water (100 mL), dried (Na_2SO_4), and evaporated to give a syrup (8.9 g, 99%) that was suitable for phosphorylation without purification, and gave a single spot in tlc (R_f 0.55, ether–methanol 19:1). Purification by column chromatography on Florisil (100–200 mesh) with ethyl acetate – hexane (4:1) as eluent gave pure **3**, $[\alpha]_D^{20}$ +12° (*c* 1.0, $CHCl_3$) (lit. (9) $[\alpha]_D^{17}$ +10 ± 2° (*c* 0.97, $CHCl_3$); lit. (10) $[\alpha]_D$ +10° (*c* 1, $CHCl_3$)); ^{1}H nmr ($CDCl_3$) δ: 5.96 (d, $J_{1,2}$ = 7.8 Hz, H-1).

*2-Methyl-(2-acetamido-3,4,6-tri-*O*-acetyl-1,2-dideoxy-*α*-D-galactopyrano)-[2,1-d]-2-oxazoline (4)*

To a solution of 2-acetamido-1,3,4,6-tetra-*O*-acetyl-2-deoxy-β-D-galactopyranose (21) (100 mg) in dichloromethane (25 mL) was added anhydrous ferric chloride (100 mg). The reaction mixture was stirred for 1 h at room temperature, and then poured into cold water (100 mL). The organic layer was washed with saturated aqueous sodium hydrogen carbonate, and then with water, dried (Na_2SO_4), and evaporated to give syrupy **4**, pure according to tlc (R_f 0.57, ether–methanol 19:1) (71 mg, 84%), $[\alpha]_D^{20}$ +26° (*c* 1.0, $CHCl_3$) (lit. (13) $[\alpha]_D^{23}$ +25.8° (*c* 1.0, $CHCl_3$)); ^{1}H nmr ($CDCl_3$) δ: 5.95 (d, $J_{1,2}$ = 6.5 Hz, H-1), 5.45 (bt, $J_{2,3}$ = $J_{3,4}$ = 3.5 Hz, H-3), 4.95 (dd, $J_{1,2}$ = 6.5, $J_{2,3}$ = 3.5 Hz, H-2), 4.3–3.6 (m), 2.15 (s, N=C—Me), and 2.05 (OAc).

Dipotassium Salt of 2-Acetamido-2-deoxy-α-D-mannopyranosyl Phosphate (6)

The oxazoline **1** (700 mg, 2.12 mmol) and dibenzyl phosphate (800 mg, 2.88 mmol) were dissolved in dry benzene (50 mL). The solution was stored overnight at room temperature under nitrogen, and then diluted with methanol (60 mL) and hydrogenated at 1 atm in the presence of 10% palladium-on-charcoal (700 mg, Fluka-Tridom), for 1 h at room temperature. After filtration, the solution was concentrated to 3 mL and directly applied to four plates of silica gel (20 × 20 cm, 2 mm thickness). The band (R_f 0.75, chloroform–methanol–water 10:10:3) was scraped and eluted with the same solvent, followed by filtration, and evaporation to a syrup. A small amount of methanol was added to the residue and the undissolved material was filtered off. Ether was added dropwise to give a solid of 2-acetamido-3,4,6-tri-*O*-acetyl-2-deoxy-α-D-mannopyranosyl phosphate (**5**) (550 mg, 61%), $[\alpha]_D^{20}$ +25° (*c* 1.0, methanol). This product was used for coupling reactions without further purification.

Compound **5** (100 mg) was *O*-deacetylated by treatment with 1 *M* sodium methoxide in methanol (5 mL) at 0°C for 1 h. After neutralization with Dowex 50 (H+) the mixture was filtered and evaporated to a small volume of solution, which was applied to three plates (0.5 mm thickness). The band (R_f 0.15, chloroform–methanol– water 10:10:3) was scraped and extracted with the same solvent. Evaporation of the solution to dryness afforded a syrup that dissolved in water, and the solution was passed through a short column of cation-exchange resin AG 50W-X8 (pyridinium form, Bio-Rad Labs.). The pH was adjusted to 7.5–8 with a 1 *M* potassium hydroxide solution and, after evaporation to a small volume, ethanol–acetone 5:1 was added to the residual solution to give a white hygroscopic solid (83 mg, 94%), $[\alpha]_D^{20}$ +23° (*c* 1.0, H_2O) (lit. (8) $[\alpha]_D^{20}$ +21.3° (*c* 0.93, H_2O), for dicyclohexylammonium salt); ^{1}H nmr (D_2O) δ: 5.24 (bd, 1H, $J_{1,P}$ = 8.0 Hz, H-1), 4.33 (bd, 1H, $J_{2,3}$ = 4.5 Hz, H-2), 4.10 (dd, 1H, $J_{2,3}$ = 4.5, $J_{3,4}$ = 10.0 Hz, H-3), 3.85 (s, 2H, H-6a, -6b), 2.04 (s, 3H, NAc). *Anal.* calcd. for $C_8H_{14}K_2NO_9P{\cdot}0.5\ EtOH{\cdot}2H_2O$: C 24.77, H 4.85, N 3.21; found: C 24.31, H 4.64, N 3.08.

Dipotassium Salt of 2-Acetamido-2-deoxy-α-D-glucopyranosyl Phosphate (8)

This compound (459 mg) was prepared in 57% yield from the oxazoline **3** (500 mg) by the same procedure as described for **6**, $[\alpha]_D^{20}$ +61° (*c* 1.0, H_2O) (lit. (22) $[\alpha]_D^{25}$ +76.1° (*c* 3.44, H_2O)); ^{1}H

Can. J. Chem. Downloaded from www.nrcresearchpress.com by 210.87.254.40 on 09/06/12
For personal use only.

nmr (D_2O) δ: 5.30 (dd, 1H, $J_{1,2}$ = 3.0, $J_{1,P}$ = 7.5 Hz, H-1), 4.25–3.25 (m, 4H), 3.80 (s, 2H, H-6a, -6b), 2.05 (s, 3H, NAc). *Anal.* calcd. for $C_8H_{14}K_2NO_9P \cdot 3H_2O$: C 22.27, H 4.67, N 3.24; found: C 22.42, H 4.52, N 3.14.

Dipotassium Salt of 2-Acetamido-2-deoxy-α-D-galactopyranosyl Phosphate (10)

The same procedures as those employed for the preparation of **6** and **8** were used for converting the oxazoline **4** (200 mg) into **10** (yield 206 mg, 64%), $[\alpha]_D^{20}$ +107° (*c* 1.0, H_2O) (lit. (23) $[\alpha]_D^{25}$ +112.4° (*c* 2.9, H_2O)); ^1H nmr (D_2O) δ: 5.45 (dd, 1H, $J_{1,2}$ = 3.0, $J_{1,P}$ = 7.35 Hz, H-1), 4.18 (m, 2H, H-2, -4), 4.03 (bm, 1H, H-5), 3.94 (dd, 1H, $J_{2,3}$ = 10.8, $J_{3,4}$ = 3.2 Hz, H-3), 3.80 (m, 2H, H-6a, -6b), 2.03 (s, 3H, NAc). *Anal.* calcd. for $C_8H_{14}K_2NO_9P \cdot H_2O$: C 24.30, H 4.08, N 3.54; found: C 24.34, H 4.12, N 3.39.

Dilithium Salt of 2',3'-Di-O-acetyluridine 5'-Monophosphate (11)

Commercially available disodium uridine 5'-monophosphate (500 mg, Aldrich) was suspended in a mixture of pyridine (6 mL) and *N*,*N*-dimethylformamide (6 mL) containing acetic anhydride (1 mL). The mixture was stirred at room temperature for 24 h, when tlc (chloroform–methanol–water 10:10:3) indicated the formation of a major compound, R_f 0.85. The mixture was evaporated to dryness, the residue dissolved in methanol, and the solution applied to three plates of silica gel (2 mm thickness), which were developed in the same solvent as that used for the analytical tlc. The band detected by uv visualization was scraped off and eluted with the same solvent, followed by evaporation to give a syrup. Nuclear magnetic resonance analysis showed that this compound had three acetyl groups. The syrup was dissolved in aqueous methanol–pyridine 1:9 (2 mL), and the mixture was stored at room temperature for 1–2 days. Thin-layer chromatographic analysis (same solvent as just described) indicated that a compound having R_f 0.6 was formed with the disappearance of the spot having R_f 0.85. The preparative tlc as just described gave syrupy **11**, which was dissolved in a small amount of methanol and precipitated by addition of acetone–ether 3:1 (72% yield). This material was suitable for synthetic purposes without further purification. To obtain an analytically pure sample of **11**, the product was dissolved in methanol and AG 50W-X8 cation-exchange resin (300 mg, pyridinium form) was added. The mixture was stirred for 2 h at room temperature, the resin filtered off and washed with methanol, and the combined filtrate and washings evaporated. The residue was dissolved in water, the pH adjusted to 7.5 by addition of 1 *M* lithium hydroxide solution, and the resulting solution concentrated to a small volume. Addition of ether–acetone (1:1) gave a precipitate of **11** as the solid dilithium salt, $[\alpha]_D^{20}$ +6.1° (*c* 0.14, CH_3OH). *Anal.* calcd. for $C_{13}H_{15}Li_2N_2O_{11}P \cdot CH_3OH \cdot 2H_2O$: C 34.44, H 3.92, N 5.74; found: C 34.93, H 3.93, N 6.20.

General Procedure for the Preparation of Dilithium Salts of Uridine 5'-(2-Acetamido-2-deoxy-α-D-hexopyranosyl Diphosphates)

2',3'-Di-*O*-acetyluridine 5'-monophosphate (**11**) and 2-acetamido-per-*O*-acetyl-2-deoxyhexopyranosyl phosphate were each converted into the tributylammonium salts by the procedure reported earlier (24).

The tributylammonium salt of **11** (52 mg, 0.13 mmol) was dissolved in 1,4-dioxane (2 mL) containing ca. 20 mg of tributylamine. To this solution was added dropwise diphenyl phosphorochloridate (38 mg, 0.145 mmol; 0.24 mL of a solution containing 140 mg in 1 mL of 1,4-dioxane) at room temperature under nitrogen. The mixture was stirred under the same conditions for 2 h, dry methanol (1 mL) added, and stirring continued for 5 min, followed by evaporation and co-evaporation of the residual solvent with toluene to give the syrupy diphosphate **12**. A solution of this compound in dry pyridine (1 mL) was introduced dropwise into a solution of the tributylammonium salt of the peracetylglycosyl phosphate (**5**, **7**, or **9**, 64 mg, 0.14 mmol) in dry pyridine (2 mL) under nitrogen. The mixture was stirred at room temperature for 8–10 h under nitrogen, followed by evaporation. Preparative tlc (chloroform–methanol–water 10:10:3, R_f ca. 0.4), and evaporation of the eluted material gave a syrup that solidified on addition of ether, to yield the 2',3'-di-*O*-acetyluridine 5'-(2-acetamido-3,4,6-tri-*O*-acetyl-2-deoxy-α-D-hexopyranosyl diphosphates **14**, **16**, and **18**), in yields of 86, 82, and 80%, respectively.

O-Deacetylation of **14**, **16**, and **18** was performed by treatment with aqueous sodium hydroxide as follows. Compound **14**, **16**, or **18** (50 mg) was treated with a mixture of 1 *M* sodium hydroxide (0.55 mL) and water (2.5 mL) at room temperature for 1 h. The base was neutralized with AG 50W-X8 (pyridinium form, Bio-Rad) cation-exchange resin and the suspension filtered. The resin was washed with water and the combined filtrates were evaporated to a small volume that was applied to four 0.25 mm thick plates of silica gel. These were developed in chloroform–methanol–water (10:10:3). The band detected by uv light ($R_f \sim$ 0.2) was scraped off and eluted with the same solvent. In some cases, the product was not completely pure in tlc and it was necessary to perform a paper chromatography (Whatman No. 3 MM, ethanol – 1 *M* ammonium acetate 5:2). The compound eluted from the tlc plate or paper chromatogram was passed through a short column of Sephadex LH-20 or Bio-gel P-6 to remove traces of silica gel or cellulose. Evaporation to a small volume, adjustment of the pH to 7.5–8 with lithium hydroxide, and addition of methanol–acetone 1:4 afforded a precipitate of the desired compounds, **15** (94%), **17** (86%), or **19** (82%), respectively.

Dilithium Salt of Uridine 5'-(2-Acetamido-2-deoxy-α-D-mannopyranosyl Diphosphate) (15)

This compound showed $[\alpha]_D^{20}$ +16° (*c* 1.0, H_2O); ^1H nmr (D_2O) δ: 7.88 (d, 1H, $J_{5,6}$ = 8.0 Hz, H-6 of uracil), 5.90 (d, 1H, $J_{1',2'}$ = 4.0 Hz, H-1 of D-ribofuranosyl), 5.88 (d, 1H, $J_{5,6}$ = 8.0 Hz, H-5 of uracil), 5.37 (bd, 1H, $J_{1,P}$ = 8.0 Hz, H-1 of 2-acetamido-2-deoxy-D-mannopyranosyl), 5.0–3.8 (m, 9H), 3.83 (s, 2H, H-6a, -6b of 2-acetamido-2-deoxy-D-mannopyranosyl), and 2.00 (s, 3H, NAc). *Anal.* calcd. for $C_{17}H_{25}Li_2N_3O_{17}P_2 \cdot CH_3OH \cdot 3H_2O$: C 30.65, H 5.00, N 5.96; found: C 30.95, H 4.44, N 5.56.

This compound was previously reported (8) as the hygroscopic dipotassium salt, and no optical rotation was recorded.

Dilithium Salt of Uridine 5'-(2-Acetamido-2-deoxy-α-D-glucopyranosyl Diphosphate) (17)

This compound showed $[\alpha]_D^{20}$ +58° (*c* 1.0, H_2O) (lit. (25) $[\alpha]_D^{25}$ +54.6° (*c* 1.0, H_2O)); ^1H nmr (D_2O) δ: 7.83 (d, 1H, $J_{5,6}$ = 8.0 Hz, H-6 of uracil), 5.86 (d, 1H, $J_{5,6}$ = 8.0 Hz, H-5 of uracil), 5.84 (d, 1H, $J_{1',2'}$ = 4.0 Hz, H-1 of D-ribofuranosyl), 5.40 (dd, 1H, $J_{1',2'}$ = 3.2, $J_{1,P}$ = 7.2 Hz, H-1 of 2-acetamido-2-deoxy-D-glucopyranosyl), and 2.05 (s, 3H, NAc). *Anal.* calcd. for $C_{17}H_{25}Li_2N_3O_{17}P_2 \cdot 4H_2O$: C 29.54, H 4.81, N 6.08; found: C 29.80, H 4.34, N 5.58.

Dilithium Salt of Uridine 5'-(2-Acetamido-2-deoxy-α-D-galactopyranosyl Diphosphate) (19)

This compound showed $[\alpha]_D^{20}$ +81° (*c* 1.0, H_2O) (lit. (23) $[\alpha]_D^{25}$ +81.7° (*c* 0.8, H_2O)); ^1H nmr (D_2O) δ: 7.86 (d, 1H, $J_{5,6}$ = 8.0 Hz, H-6 of uracil), 5.93 (d, 1H, $J_{1',2'}$ = 3.8 Hz, H-1 of ribofuranosyl), 5.90 (d, 1H, $J_{5,6}$ = 8.0 Hz, H-5 of uracil), 5.60 (dd, 1H, $J_{1,2}$ = 3.0, $J_{1,P}$ = 7.8 Hz, H-1 of 2-acetamido-2-deoxy-D-galactopyranosyl), 4.4–4.1 (m), 4.05 (d), 3.95 (q, 1H, $J_{2,3}$ = 10.5, $J_{3,4}$ = 3.4 Hz, H-3 of 2-acetamido-2-deoxy-D-galacto-

pyranosyl), 3.80 (m, 2H), and 2.00 (s, 3H, NAc). *Anal.* calcd. for $C_{17}H_{25}Li_2N_3O_{17}P_2 \cdot 4H_2O$: C 29.54, H 4.81, N 6.08; found: C 29.89, H 4.37, N 5.52.

*Trilithium Salt of Uridine 5'-(2-Acetamido-2-deoxy-α-D-mannopyranosyluronate Diphosphate) (**20**)*

10% Platinum-on-charcoal (Fluka–Tridom, 300 mg) was added to a solution of **15** (32 mg) in a mixture of 4.2% aqueous sodium hydrogen carbonate (1.65 mL) and water (4.8 mL), and oxygen was bubbled into the suspension at 75°C for 7 h. After filtration, the mixture was concentrated to a small volume, and applied to a paper chromatogram (Whatman No 3 MM), which was developed in ethanol – 1 *M* ammonium acetate 5:2 (pH 7.5). Usually, three bands were detected by uv light (R_{UDP} 1.0, 2.43, and 4.52). The compound having R_{UDP} of 4.52 was unreacted starting material **15**. The band having R_{UDP} 2.43 was eluted with water and applied to a 0.25 mm thick tlc plate of silica gel, which was developed in chloroform–methanol–water 10:10:3. The band having R_f 0.2 was scraped off and eluted with the same solvent. Evaporation gave a syrup that was further purified on a Bio-Gel P-6 column (1 cm × 100 cm) with 0.5 *M* pyridinium acetate, pH 7.0. The pooled eluant was evaporated to a small volume, and 1 *M* lithium hydroxide solution was added to give a pH of 7.5–8. Addition of methanol–acetone 1:4 precipitated **20**, $[\alpha]_D^{20}$ +19° (*c* 0.2, CH_3OH); ^1H nmr (D_2O) δ: 7.90 (d, 1H, $J_{5,6}$ = 8.0 Hz, H-6 of uracil), 5.95 (d, 1H, $J_{1',2'}$ = 4.0 Hz, H-1 of ribofuranosyl), 5.92 (d, 1H, $J_{5,6}$ = 8.0 Hz, H-5 of uracil), 5.42 (bd, 1H, $J_{1,P}$ = 8.0 Hz, H-1 of 2-acetamido-2-deoxy-D-mannopyranosyluronic acid), 5.0–3.5 (m, 9H), and 2.05 (s, 3H, NAc). *Anal.* calcd. for $C_{17}H_{22}Li_3N_3O_{18}P_2 \cdot CH_3OH \cdot 3H_2O$: C 29.81, H 4.45, N 5.79; found: C 29.69, H 4.10, N 5.40.

1. H. Nikaido and W. Z. Hassid. Adv. Carbohydr. Chem. Biochem. **26**, 351 (1971).
2. W. J. Lennarz and M. G. Scher. Biochim. Biophys. Acta, **265**, 417 (1972).
3. N. K. Kochetkov and V. N. Shibaev. Adv. Carbohydr. Chem. Biochem. **28**, 307 (1973).
4. J. S. Anderson, R. L. Page, and W. L. Salo. J. Biol. Chem. **247**, 2480 (1972).
5. H. R. Perkins. Biochem. J. **86**, 475 (1963).
6. S. Hase and Y. Matsushima. J. Biochem. **81**, 1181 (1977).
7. T. Yamazaki, C. D. Warren, A. Herscovics, and R. W. Jeanloz. Carbohydr. Res. **79**, C9 (1980).
8. W. L. Salo and H. G. Fletcher, Jr. Biochemistry, **9**, 878 (1970).
9. A. Ya. Khorlin, M. L. Shul'man, S. E. Zurabyan, I. M. Privalova, and Yu. L. Kopaevich. Izv. Akad. Nauk SSSR, Ser. Khim. **9**, 2094 (1968).
10. R. U. Lemieux and H. Driguez. J. Am. Chem. Soc. **97**, 4063 (1975).
11. A. Ya. Khorlin, S. E. Zurabyan, and T. S. Antonenko. Tetrahedron Lett. 4803 (1970).
12. C. D. Warren, A. Herscovics, and R. W. Jeanloz. Carbohydr. Res. **61**, 181 (1978).
13. K. L. Matta, E. A. Johnson, and J. J. Barlow. Carbohydr. Res. **26**, 215 (1973).
14. A. M. Michelson. Biochim. Biophys. Acta, **91**, 1 (1964).
15. A. M. Michelson and F. Wold. Biochemistry, **1**, 1171 (1962).
16. G. A. Barber. Biochemistry, **8**, 3692 (1969).
17. C. D. Warren and R. W. Jeanloz. Methods Enzymol. **50**, Part C, 122 (1978).
18. G. G. S. Dutton and K. N. Slessor. Can. J. Chem. **42**, 1110 (1964).
19. J. C. Dittmer and R. L. Lester. J. Lipid Res. **5**, 126 (1969).
20. D. Horton and M. L. Wolfrom. J. Org. Chem. **27**, 1794 (1962).
21. Z. Tarasiejska and R. W. Jeanloz. J. Am. Chem. Soc. **80**, 6325 (1958).
22. P. J. O'Brien. Biochim. Biophys. Acta, **86**, 628 (1964).
23. D. M. Carlson, A. L. Swanson, and S. Roseman. Biochemistry, **3**, 402 (1964).
24. C. D. Warren and R. W. Jeanloz. Biochemistry, **14**, 412 (1975).
25. S. Roseman, J. J. Distler, J. G. Moffatt, and H. G. Khorana. J. Am. Chem. Soc. **83**, 659 (1961).

Can. J. Chem. Downloaded from www.nrcresearchpress.com by 210.87.254.40 on 09/06/12
For personal use only.

Absolute rate constants for hydrocarbon autoxidation. 30. On the self-reaction of the α-cumylperoxy radical in solution[1]

J. A. HOWARD

Division of Chemistry, National Research Council of Canada, Ottawa, Ont., Canada K1A 0R9

AND

J. E. BENNETT AND G. BRUNTON

Shell Research Ltd., Thornton Research Centre, P.O. Box 1, Chester, CH1 3SH, England

Received February 2, 1981

J. A. HOWARD, J. E. BENNETT, and G. BRUNTON. Can. J. Chem. **59**, 2253 (1981).

Although it is generally accepted that the self-reaction of cumylperoxy radicals is a second-order process, recent reports have cast doubt on the overall validity of this assumption. Therefore we have reinvestigated some aspects of the self-reaction to clarify the kinetic and mechanistic features.

Our product studies are entirely consistent with the accepted mechanism for the self-reaction of cumylperoxy radicals and no evidence was obtained for competing reactions. Results obtained with $^{36}O_2$ labelled materials confirm the previous conclusion that reversible scission of cumylperoxy radicals to give oxygen and cumyl radicals does not compete significantly with the self-reaction at ambient temperatures. Kinetic studies, under both steady-state and transient conditions, establish clearly that the self-reaction of cumylperoxy radicals is a second order process. A possible explanation is proposed to account for the previous observations which indicated that the self-reaction was a first order process. Further, we show that the changes observed in the esr spectrum of the cumylperoxy radicals, which were attributed to the formation of a complex with cumyl hydroperoxide, are caused by changes in the viscosity of the solution.

J. A. HOWARD, J. E. BENNETT, et G. BRUNTON. Can. J. Chem. **59**, 2253 (1981).

De récentes publications ont mis en doute la validité de l'hypothèse généralement acceptée à l'effet que l'autoréaction des radicaux cumylpéroxy est une réaction d'ordre 2. Nous avons donc réexaminé quelques aspects de cette réaction afin d'en clarifier les caractéristiques cinétiques et mécanistiques.

Nos études sont entièrement en accord avec le mécanisme accepté pour l'auto-réaction des radicaux cumylpéroxy et nous n'avons pas trouvé de données permettant de croire qu'il existe des réactions en compétition. Les résultats obtenus avec des produits marqués au $^{36}O_2$ confirment ce qui a été trouvé antérieurement à savoir que, à la température ambiante la scission réversible des radicaux cumylpéroxy qui donne de l'oxygène et des racidaux cumyles n'entre pas en compétition de façon significative avec l'auto-réaction. Des études cinétiques tant dans des conditions d'état stationnaire que transitoire établissent clairement que l'auto-réaction des radicaux cumylpéroxy est d'ordre 2. On propose une explication possible des observations antérieures qui indiquent une réaction du premier ordre. De plus, nous montrons que les variations observées dans les spectres rpe des radicaux cumylpéroxy, qui ont été attribuées à la formation d'un complexe avec l'hydropéroxyde de cumyle, sont provoquées par des variations dans la viscosité de la solution.

[Traduit par le journal]

Introduction

It is generally accepted (1) that the self-reaction of cumylperoxy radicals ($PhCMe_2O_2^{\cdot}$) in solution, produced either by autoxidation of cumene ($PhCMe_2H$), induced decomposition of α-cumene hydroperoxide ($PhCMe_2OOH$), or photolysis of azocumene in an oxygenated-solvent can be described by reactions [1]–[3].

The existence of the equilibrium [1] has been demonstrated by electron spin resonance spectroscopy (2) and di-α-cumyl tetroxide is a reaction intermediate with an appreciable lifetime. Irreversible decomposition of $PhCMe_2O_4CMe_2Ph$ gives α-cumyloxy radicals and a fraction, f, of these radicals escape the solvent cage while a fraction $1 - f$ combine in the cage to give di-α-cumyl peroxide. The cumyloxy radicals produced by reaction [3b] either abstract a hydrogen atom from cumene, the solvent, or a reaction product such as cumene hydroperoxide, reactions [4] and [5], or they undergo β-scission to give acetophenone and a methyl radical, reaction [6]. Methyl radicals produced by this reaction combine rapidly with molecular oxy-

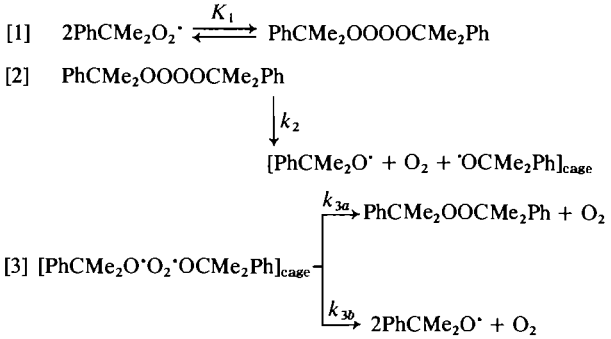

SCHEME 1

[1]NRCC No. 19261.

0008-4042/81/152253-08$01.00/0

©1981 National Research Council of Canada/Conseil national de recherches du Canada

Can. J. Chem. Downloaded from www.nrcresearchpress.com by 210.87.254.5 on 09/06/12
For personal use only.

Can. J. Chem. Downloaded from www.nrcresearchpress.com by 210.87.254.5 on 09/06/12
For personal use only.

[4] $PhCMe_2O^{\cdot} + PhCMe_2H \xrightarrow{k_4} PhCMe_2OH + PhCMe_2^{\cdot}$

[5] $PhCMe_2O^{\cdot} + PhCMe_2OOH \xrightarrow{k_5} PhCMe_2OH + PhCMe_2O_2^{\cdot}$

[6] $PhCMe_2O^{\cdot} \xrightarrow{k_6} PhC(O)Me + Me^{\cdot}$

[7] $Me^{\cdot} + O_2 \longrightarrow MeO_2^{\cdot}$

[8] $MeO_2^{\cdot} + PhCMe_2H \longrightarrow MeOOH + PhCMe_2^{\cdot}$

[9] $MeO_2^{\cdot} + PhCMe_2OOH \longrightarrow MeOOH + PhCMe_2O_2^{\cdot}$

[10] $MeO_2^{\cdot} + PhCMe_2O_2^{\cdot} \xrightarrow{k_{10}} CH_2O + O_2 + PhCMe_2OH$

gen to give methylperoxy radicals which either abstract a hydrogen atom, reactions [8] and [9], or react with cumylperoxy by cross-termination reaction [10].

The overall termination rate constant ($2k_t$) for autoxidation of cumene is, therefore, given by the complex expression [11].

$$[11]\quad 2k_t = 2(1-f)k_2K_1 + 2fk_2K_1\frac{k_6}{k_6 + k_4[PhCMe_2H]} \times \frac{4k_{10}[PhCMe_2O_2^{\cdot}]}{4k_{10}[PhCMe_2O_2^{\cdot}] + k_8[PhCMe_2H]}$$

where $f = k_{3b}/(k_{3a} + k_{3b})$

Consequently the magnitude of $2k_t$ depends on k_2, K_1, f, the fraction of cumyloxy radicals which undergo β-scission, and the fraction of methylperoxy radicals which are consumed in the cross-termination reaction [10] (3, 4).

Over ten years ago, Thomas (5) made the important discovery that addition of *pure* $PhCMe_2OOH$ to $PhCMe_2H$ at 57.2°C increased the rate of autoxidation. This rate increase was not due to an increase in the rate of chain initiation, as might have been expected, but to a decrease in the overall termination rate constant ($2k_t$) because cumyloxy and methylperoxy radicals undergo the chain transfer reactions [5] and [9] rather than the cross-termination reaction [10].

The termination rate constant, $2k_t'$, when all the secondary-radicals undergo reactions [5] and [9], is equal to $2(1-f)k_2K_1$, which is the rate constant for reaction of two $PhCMe_2O_2^{\cdot}$ to give di-α-cumyl peroxide.

Kinetic and product studies of the autoxidation of $PhCMe_2O_2^{\cdot}$ have usually supported this mechanism (2–10). There have, however, been several recent reports which have cast considerable doubt on the overall validity of this mechanism.

First, Fukuzumi and Ono (11, 12) reported that $PhCMe_2O_2^{\cdot}$, prepared by oxidation of $PhCMe_2OOH$ using heterogeneous catalysts like manganese dioxide and cobalt oxide supported on silica, decay with *first*-order kinetics in the cavity of an esr spectrometer at 301 K. This result prompted these workers to propose a reaction mechanism which involves a slow unimolecular decomposition of $PhCMe_2O_2^{\cdot}$ to give acetophenone and methoxy followed by a fast reaction of methoxy with $PhCMe_2O_2^{\cdot}$ to give stable products.

[12] $PhCMe_2O_2^{\cdot} \longrightarrow PhC(O)Me + MeO^{\cdot}$

[13] $MeO^{\cdot} + PhCMe_2O_2^{\cdot} \longrightarrow$ stable products

These workers also invoked the formation of a 2:1 complex between cumene hydroperoxide and the cumylperoxy radical to explain the observed effect of concentration on the initial rate of oxygen evolution during the decomposition of cumene hydroperoxide by lead dioxide (13). In their treatment they assumed that the complexed cumylperoxy radical did not undergo self-termination. To support these postulates they showed that the observed variations in the line width and g-value of the cumylperoxy radical as a function of the concentration of cumene hydroperoxide were consistent with the formation of the complex.

Secondly, Belyakov, Vasil'ev, and Fedorova (14) have argued that the general features of the chemiluminescence emitted during autoxidation of $PhCMe_2H$ are not consistent with the energetics and products of reaction [10]. They concluded that a cross-termination reaction between 2-phenyl-1-propylperoxy radicals (produced by abstraction of a primary hydrogen atom from $PhCMe_2H$) and $PhCMe_2O_2^{\cdot}$ plays an important role in termination.

According to this mechanism, $2k_t$ is larger than $2k_t'$ because of the influence of reaction [15] on termination.

[14] $PhCMe_2O^{\cdot} + PhCMe_2H \xrightarrow{O_2} PhCMe_2OH + PhCH(Me)CH_2O_2^{\cdot}$

[15] $PhCH(Me)CH_2O_2^{\cdot} + PhCMe_2O_2^{\cdot} \longrightarrow PhCH(Me)CHO + PhCMe_2OH + O_2$

Thirdly, Nangia and Benson (15) have suggested that the value of $2k_t'$ at 303 K for $PhCMe_2O_2^{\cdot}$ ($6 \times 10^3\ M^{-1}\ s^{-1}$) is 5 times larger than $2k_t'$ for t-$BuO_2^{\cdot}$ ($1.2 \times 10^3\ M^{-1}\ s^{-1}$) because k_{3b}/k_{3a} for $PhCMe_2O_2^{\cdot}$ is less than k_{3b}/k_{3a} for t-$BuO_2^{\cdot}$. In other words, the

Can. J. Chem. Downloaded from www.nrcresearchpress.com by 210.87.254.5 on 09/06/12
For personal use only.

efficiency of cage escape for $PhCMe_2O^{\cdot}$ produced by decomposition of $PhCMe_2O_4CMe_2Ph$ is less than the efficiency for production of t-$BuO^{\cdot}$ by decomposition of t-BuO_4Bu-t. They have also concluded from thermochemical calculations that β-scission of $PhCMe_2O_2^{\cdot}$ [16] at ambient temperatures and normal oxygen pressures is not fast enough to produce a significant steady-state concentration of cumyl radicals. Thus $2k_t$ for autoxidation of cumene should not contain a contribution from the rate constant for reaction of cumyl with cumylperoxy radicals [17].

[16] $PhCMe_2O_2^{\cdot} \longrightarrow PhCMe_2^{\cdot} + O_2$

[17] $PhCMe_2^{\cdot} + PhCMe_2O_2^{\cdot} \longrightarrow PhCMe_2OOCMe_2Ph$

In the present paper we present a thorough product study of the autoxidation of $PhCMe_2H$ at 303 K and at oxygen pressures from 0.5 to 100 atm with particular emphasis on the products of the self-reaction of $PhCMe_2O_2^{\cdot}$ and of the induced decomposition of $PhCMe_2OOH$ under an atmosphere of $^{36}O_2$. In addition, we report some new kinetic data for autoxidation of $PhCMe_2H$ and the self-reaction of $PhCMe_2O_2^{\cdot}$. The results of all this work are discussed in terms of the mechanisms for the self-reaction of tertiary aralkylperoxy radicals.

Experimental

Materials

Cumene, α-cumene hydroperoxide, chlorobenzene, α,α'-azo-bis-isobutyronitrile, α-cumyl alcohol, acetophenone, α-methylstyrene, and di-α-cumyl peroxide were obtained from commercial sources and were purified by standard procedures. Di-*tert*-butyl hyponitrite (16), azocumene (17), and di-α-cumyl hyponitrite (18) had been prepared previously in our laboratory. 2,2,3,3,-Tetraphenylbutane (19, 20) was a gift from Dr. L. R. Mahoney (Ford Motor Co., Dearborn). $^{36}O_2$ (99.1 at.%) was obtained from Merck, Sharp and Dohme Canada Ltd. 1-Methyl-1-phenyloxirane was prepared from α-methylstyrene and *m*-chloroperbenzoic acid (Aldrich) by the method of Bissing and Speziale (21).

Initiators

The initiators, In_2, used for thermally initiated autoxidations were di-*tert*-butyl hyponitrite, DTBH ($e = 0.9$, $k_d = 2.92 \times 10^{-6}$ s^{-1}), and 2,2,3,3,-tetraphenylbutane, TPB ($e = 1.0$, $k_d = 2.1 \times 10^{-6}$ s^{-1}), where e is the efficiency of radical production and k_d is the rate constant for unimolecular decomposition at 303 K. DTBH was also used as the thermal source of *tert*-butoxy radicals for product studies of induced decomposition of cumene hydroperoxide and measurement of steady-state cumylperoxy radical concentrations by esr spectroscopy.

Procedures

Rates of autoxidation at oxygen pressures from 0.1 to 1 atm were measured as described previously (22).

Radical Production

Cumylperoxy radicals were formed in the cavity of a Varian E-4 EPR spectrometer by photolysis of oxygen-saturated solutions of di-*tert*-butyl peroxide in cumene; cumene hydroperoxide in toluene, cumene, and *n*-hexane; azocumene in 2,2-dimethylbutane; and by thermolysis of di-*tert*-butyl hyponitrite in cumene. Steady-state radical concentrations were measured at different concentrations of the thermal initiator and at different light intensities for photochemically initiated reactions. Radical decays after the initiating light was masked were followed by standard procedures (23) and absolute radical concentrations were measured relative to a standard solution of DPPH.

Product Studies

Cumene, containing a thermal initiator in a Pyrex reactor, was either shaken rapidly with oxygen at 0.4 and 1 atm or allowed to react with O_2 at 10 and 100 atm in a high pressure stainless steel device to 5–10% conversion. The products were analysed by hplc before reduction and by glc and glc–ms after quantitative reduction of accumulated hydroperoxide with triphenylphosphine.

Cumene hydroperoxide in chlorobenzene (1 mL) was allowed to react with thermally generated *tert*-butoxy radicals from DTBH in a closed Pyrex vessel (130 mL) at 303 K under an atmosphere of $^{36}O_2$ for ten half-lives of the initiator (24). Products were identified and yields determined by standard hplc and glc procedures. Oxygen containing products, with the exception of hydroperoxides and peroxides, were analysed for ^{18}O content by mass spectrometry. The percentage of $PhCMe_2$-^{18}OH in cumyl alcohol was estimated from the ratio of peaks at m/e = 123 and 121 corresponding to m/e = parent minus 15, after correction for natural abundance ^{18}O. The percentage of $PhC(^{18}O)Me$ in PhC(O)Me was obtained from the relative intensities of the peaks at m/e = 122, 120, 107, and 105.

The production of trace amounts of 1-methyl-1-phenyl oxirane from the induced decomposition of $PhCMe_2OOH$ was deduced from the presence in the mass spectrum of a parent peak at m/e = 134.

Viscosity measurements were made with a suspended level viscometer and using standard experimental procedures (25).

Instruments

The high performance liquid chromatograph was a Waters ALC 201 model fitted with a UV detector and reverse phase column (Waters 0.65 cm id × 27 cm, μBondapak C_{18}). The initial eluting solvent was a mixture of acetonitrile and water (25:75 v/v) and the percentage of CH_3CN was gradually increased to 75% by solvent programming. A Varian 2800 gas chromatograph equipped with FC 431, FFAP, and OV-101 columns was used for glc analyses. The gc–ms analyses utilized the same columns with a Finnigan 4000 automated gas chromatograph/EI-CI mass spectrometer system, operated in the electron impact mode.

Results

Products of Autoxidation of Cumene

Analysis of cumene which had been autoxidized at 303 K and oxygen pressures from 0.4 to 100 atm for 25–35 h by hplc revealed that α-cumene hydroperoxide, α-cumyl alcohol, acetophenone, and di-cumyl peroxide were the major reactions products and that they were formed in the yields given in Table 1. Yields of $PhCMe_2OOH$ were confirmed by iodometric titration and by glc analyses for $PhCMe_2OH$ after reduction with Ph_3P. Gas–liquid chromatography also revealed the formation of a trace of α-methylstyrene.

The total concentration of oxygen absorbed by

TABLE 1. Products from thermally initiated autoxidation of cumene at 303 K

Run no.	Initiator (*M*)	P_{O_2} (atm)	Reaction time (h)	$PhCMe_2OOH$ (*M*)	$PhCMe_2OH$ (*M*)	PhC(O)Me (*M*)	$(PhCMe_2O)_2$ (*M*)	$Ph_2CMeOOH$[a] (*M*)
1	TPB	0.4	48	0.36	0.035	0.0014	0.0015	0.0062
2	TPB	1	14	0.19	0.011	0.0009	0.0013	0.0047
3	TPB	10	48	0.36	0.034	0.002	—	0.0088
4	TPB	100	48	0.33	0.046	0.0024	0.0013	0.0044
5	DTBH	0.4	65.5	0.61	0.062	0.0015	0.0035	—
6	DTBH	5	65.5	0.54	0.054	0.0012	0.0038	—

[a] From the initiator tetraphenylbutane.

$PhCMe_2H$ was determined for the run at 1 atm of O_2 and it was approximately equal to the final concentration of $PhCMe_2OOH$, indicating a long kinetic chain length. All the other runs gave final hydroperoxide concentrations consistent with the oxidizability of $PhCMe_2H$, $k_p/(2k_t)^{\frac{1}{2}} = 1.5 \times 10^{-3}\ M^{-\frac{1}{2}}\ s^{-\frac{1}{2}}$ (26), the average calculated rate of chain initiation, R_i, and the total reaction time, t, i.e., $[PhCMe_2OOH]_f = k_p[PhCMe_2H]R_i^{\frac{1}{2}}t/(2k_t)^{\frac{1}{2}}$.

1,1-Diphenylethyl hydroperoxide was well separated from $PhCMe_2OOH$ by hplc and yields of this product from 2,2,3,3-tetraphenylbutane (TPB) initiated reactions were of the order of 85–100%, based on the total quantity of 1,1-diphenylethylperoxy radicals generated by thermolysis of tetraphenylbutane.

Di-cumyl peroxide was produced in the yields given in the penultimate column in Table 1 and these yields were compatible with yields calculated from

$$[18]\quad [PhCMe_2OOCMe_2Ph] = k_t'\,[PhCMe_2O_2\cdot]^2_{qs}t$$

and

$$[19]\quad [PhCMe_2O_2\cdot]_{qs} = (R_i/2k_t)^{\frac{1}{2}}$$

where $[PhCMe_2O_2\cdot]_{qs}$ is the quasi steady-state concentration of cumylperoxy radicals and $2k_t' = 6 \times 10^3\ M^{-1}\ s^{-1}$ and $2k_t = 1.5 \times 10^4\ M^{-1}\ s^{-1}$ (26).

Total concentrations of $PhCMe_2OH$ and PhC(O)Me were 10 to 40 times larger than concentrations of $PhCMe_2OOCMe_2Ph$, giving a rate constant ratio, $k_{3b}/k_{3a} = 5$ to 20 which can be compared with our previous estimate of 6.3 from the induced decomposition of cumene hydroperoxide (27). These results suggest that cumyloxy radicals are produced with an efficiency of 83–94% by decomposition of di-cumyl tetroxide which is similar to the efficiency with which alkoxy radicals are produced by thermolysis of di-*tert*-alkyl hyponitrites (17, 28).

Final ratios of $PhCMe_2OH$ to PhC(O)Me were quite high and were dependent on the final concentration of $PhCMe_2OOH$. This is because $PhCMe_2OOH$ is ~30 times more reactive than cumene to $PhCMe_2O\cdot$. Thus decomposition of di-α-cumyl hyponitrite in $PhCMe_2H$ (7.1 *M*) containing $PhCMe_2OOH$ (0.1 *M*) gave $[PhCMe_2OH]/[PhC(O)Me] = 30.5$, whereas in the absence of the hydroperoxide this ratio was 21.3.

Induced Decomposition of Cumene Hydroperoxide under an Atmosphere of $^{36}O_2$

$PhCMe_2OOH$ (0.62 *M*) in chlorobenzene was completely decomposed by thermally generated *t*-BuO· (0.1 *M*) in 30 days at 303 K under $^{36}O_2$ to acetophenone, α-cumyl alcohol, and di-α-cumyl peroxide in the yields given in Table 2. α-Methylstyrene was produced in low yields while 1-methyl-1-phenyloxirane was formed in trace amounts. In this experiment the total yield of $PhCMe_2OH$ and PhC(O)Me was about 20 times larger than the yield of $PhCMe_2OOCMe_2Ph$ and the final ratio of $PhCMe_2OH$ to PhC(O)Me was 6.

Under these conditions the final atmosphere contained 25% $^{32}O_2$ and both PhC(O)Me and $PhCMe_2OH$ were enriched in ^{18}O. Somewhat surprisingly, however, the percentage enrichment of PhC(O)Me (7.6%) was larger than the percentage enrichment of $PhCMe_2OH$ (1.25%), a difference that was confirmed by repeated analyses using different gas chromatography columns for product separation and preparative hplc to separate the alcohol and ketone from the rest of the reaction mixture.

TABLE 2. Product yields from induced decomposition of $PhCMe_2OOH$ (0.62 *M*) under an atmosphere of $^{36}O_2$ at 303 K

Product	Yield (*M*)
$PhCMe_2OH$	0.48
$PhCMe_2{}^{18}OH$	0.006
PhC(O)Me	0.070
$PhC(^{18}O)Me$	0.0058
$PhC(Me)=CH_2$	0.014
$PhCMe_2OOCMe_2Ph$	0.03
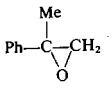	Trace

Can. J. Chem. Downloaded from www.nrcresearchpress.com by 210.87.254.5 on 09/06/12
For personal use only.

Can. J. Chem. Downloaded from www.nrcresearchpress.com by 210.87.254.5 on 09/06/12
For personal use only.

The formation of $PhCMe_2{}^{18}OH$ from cumylperoxy radicals generated in the presence of $^{36}O_2$ means that these radicals must exist in equilibrium with cumyl radicals and oxygen at 303 K. It is clear from reactions [1] to [6] that there should have been no difference in the percentage enrichment of α-cumyl alcohol and acetophenone. The difference that we observed must have resulted from enrichment of the acetophenone by a nonradical process involving reaction of acetophenone with $H_2{}^{18}O$ formed in the autoxidation.

$$[20]\quad PhC(=O)Me + H_2{}^{18}O \rightleftharpoons PhC(OH)(^{18}OH)Me \rightleftharpoons PhC(=\,^{18}O)Me + H_2O$$

Reaction of the methyl radicals formed in reaction [7] with $^{36}O_2$ is an obvious route to $H_2{}^{18}O$ and the acid (formic) necessary to catalyse this exchange.

$$[21]\quad Me^{\cdot} + {}^{36}O_2 \longrightarrow Me^{36}O_2{}^{\cdot}$$

$$[22]\quad Me^{36}O_2{}^{\cdot} + PhCMe_2OOH \longrightarrow Me^{36}O_2H + PhCMe_2O_2{}^{\cdot}$$

$$[23]\quad Me^{36}O_2H \longrightarrow Me^{18}O^{\cdot} + {}^{18}OH \longrightarrow H_2{}^{18}O$$

$$[24]\quad Me^{36}O_2{}^{\cdot} + RO_2{}^{\cdot} \longrightarrow CH_2{}^{18}O + O_2 + ROH$$

$$[25]\quad CH_2{}^{18}O + O_2 \longrightarrow CH(^{18}O)OH$$

Kinetics of the Autoxidation of Cumene

Steady-state Studies

Rates of autoxidation of cumene initiated by thermolysis of α,α′-azobisisobutyronitrile and by photolysis of α,α′-azobiscyclohexane carbonitrile have been shown previously to be proportional to the square root of the initiator concentration and the light intensity, respectively (3, 5, 6, 8). Our present results show that steady-state concentrations of $PhCMe_2O_2{}^{\cdot}$ (generated by thermolysis of di-*tert*-butyl hyponitrite in oxygenated cumene) are *exactly* proportional to the square root of the thermal initiator concentration (Fig. 1). The overall rate of termination (R_t) is, therefore, given by

$$R_t = 2k_t\,[PhCMe_2O_2{}^{\cdot}]^2_{ss}$$

There is, therefore, no steady-state kinetic evidence for a termination reaction that is first-order with respect to $[PhCMe_2O_2{}^{\cdot}]$, analogous to the one that occurs during autoxidation of styrene (29).

In addition, rates of autoxidation of cumene or cumene containing cumene hydroperoxide, at a constant rate of chain initiation, do not depend on the pressure of oxygen above the liquid at oxygen pressures in the range 50–700 Torr. This indicates that the termination reaction [17] is not kinetically important.

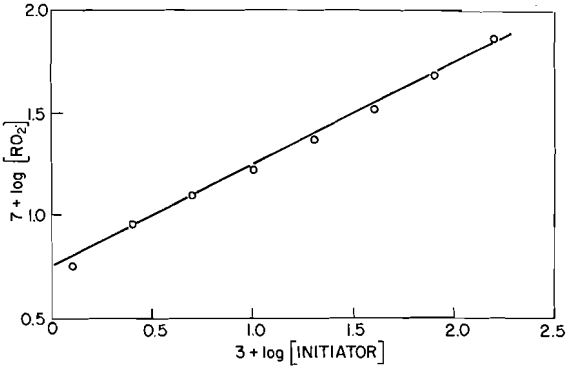

FIG. 1. A plot of log $[RO_2{}^{\cdot}]_{ss}$ against log[initiator] for the *tert*-butyl hyponitrite initiated autoxidation of cumene at 303 K.

Non-steady-state Studies

Plots of $[PhCMe_2O_2{}^{\cdot}]^{-1}$ against time for the disappearance of $PhCMe_2O_2{}^{\cdot}$ (prepared by photolysis of azocumene in oxygen-saturated 2,2-dimethylbutane for ~3 s at 303 K) were accurately linear indicating second-order radical decay with a rate constant $k_{esr} = (6.3 \pm 0.5) \times 10^4\ M^{-1}\ s^{-1}$. This rate constant is not equal to $2k_t$ or $2k_t'$ because it contains contributions from rate constants for the cross-termination of $PhCMe_2O_2{}^{\cdot}$ with peroxy radicals formed by reaction of $PhCMe_2O^{\cdot}$ (from reaction [3b]) with the solvent. The important point is, however, that the radical decays followed *second*-order kinetics.

Cumylperoxy radicals which were generated by longer periods of continuous photolysis still decayed with second-order kinetics. However, the steady-state radical concentrations were lower and values of k_{esr} were up to a factor of 3 times larger.

When toluene was used as the solvent instead of 2,2-dimethylbutane the plot of $[PhCMe_2O_2{}^{\cdot}]^{-1}$ against time for radicals produced after 3 s photolysis showed pronounced upward curvature. In fact, plots of ln $[PhCMe_2O_2{}^{\cdot}]$ against time were linear, indicating first-order radical decay, almost certainly because reaction of $PhCMe_2O_2{}^{\cdot}$ with the solvent was rate controlling.

Decays of $PhCMe_2O_2{}^{\cdot}$ prepared by photolysis of $PhCMe_2OOH$ in $PhCMe_2H$ and n-C_6H_{14} could not be analysed in terms of either second or first-order kinetics. Plots of $[PhCMe_2O_2{}^{\cdot}]^{-1}$ against time exhibited marked upward curvature even for radicals prepared after only 3 s photolysis of a freshly prepared solution. Furthermore, initial rates of radical decay increased as the length of continuous photolysis was increased.

SEE ERRATA
V60#6.19.82...P.812...
or attached slip.

TABLE 3. Viscosities of solutions of cumene hydroperoxide in carbon tetrachloride at 298 K

$PhCMe_2OOH$ (M)	Viscosity (cP)
0.5	1.12
1	1.24
2	1.74
4	3.42
5	4.79

Viscosity Measurements

Measured values for the viscosity of solutions of different concentrations of cumene hydroperoxide in carbon tetrachloride are summarized in Table 3. Over the concentration range studied (which is comparable to that used by Fukuzumi and Ono (11–13) for their esr studies) the viscosity varies, markedly, increasing four-fold between 0.5 and 5.0 M. We conclude, therefore, that in this concentration range, viscosity effects are likely to play a significant role in determining solution properties. As discussed below, they can provide an explanation for the concentration dependence of the line width and g-value of the esr spectrum of the cumylperoxy radical.

ERRATA

Discussion

Page 2253. In the discussion section of the paper the corrected ratio of $[PhCMe_2{}^{36}O_2{}^{\cdot}]/[PhCMe_2O_2{}^{\cdot}]$ should have been 0.015 and not 0.05 and Nangia and Benson's estimated of $\Delta H_{16}{}^0$ was −20.2 kcal mol^{-1} and not −10.2 kcal mol^{-1}.

ERRATA

reactions [1] to [16]. We could find no evidence for the formation of products from termination reactions of 2-phenyl-1-propylperoxy radicals, indicating that the involvement of these radicals in the rate-controlling termination reactions is not important at ambient temperatures. Thus we are unable to concur with the conclusions reached by Belyakov *et al.* (14), on the basis of chemiluminescence studies, that these radicals play an important role during the autoxidation of cumene.

It is possible to calculate a value for the rate constant for β-scission of $PhCMe_2O_2{}^{\cdot}$ radicals, k_{16}, from our product yields in the presence of $^{36}O_2$ and $PhCMe_2OOH$. Under these conditions:

$$+\frac{d[PhCMe_2{}^{36}O_2{}^{\cdot}]}{dt} = k_{16}[PhCMe_2O_2{}^{\cdot}] - k_{dis}[PhCMe_2{}^{36}O_2{}^{\cdot}][PhCMe_2OOH]$$

and in steady-state,

$$k_{16} = \frac{k_{dis}(PhCMe_2{}^{36}O_2{}^{\cdot}][PhCMe_2OOH]}{[PhCMe_2O_2{}^{\cdot}]}$$

where k_{dis} is the rate constant for reaction of $RO_2{}^{\cdot}$ with ROOH and can be assumed to be ca. 570 M^{-1} s^{-1} at 303 K (30). The ratio of $PhCMe_2{}^{18}OH$ to $PhCMe_2OH$ of 0.0125 (Table 2) gives $[PhCMe_2{}^{36}O_2{}^{\cdot}]/[PhCMe_2O_2{}^{\cdot}] = 0.05$ (after correction for $^{32}O_2$ evolved in the reaction). At an average hydroperoxide concentration of 0.31 M, the rate constant k_{16} is ca. 2 s^{-1}. Therefore, assuming $k_{-16} = 10^{9.5}\ M^{-1}$ s^{-1} (31), the equilibrium constant, K_{16}, is estimated to be $1.6 \times 10^9\ M^{-1}$, which is in good agreement with the value of $10^9\ M^{-1}$ estimated by Nangia and Benson from $\Delta S^0{}_{16} = -25.8$ gibbs mol^{-1} and $\Delta H^0{}_{16} = -10.2$ kcal mol^{-1} (15).

The steady-state concentration of $PhCMe_2{}^{\cdot}$ at 1 atm of O_2 ($10^{-2}\ M$) is, therefore, ca. 6×10^{-8} $[PhCMe_2O_2{}^{\cdot}]\ M$, and if k_{17} is $10^8\ M^{-1}$ s^{-1} (32), the rate reaction [17] can be calculated to be ca. 6 $[PhCMe_2O_2{}^{\cdot}]^2\ M$ s^{-1} which is insignificant compared to the rate of self-reaction of $PhCMe_2O_2{}^{\cdot}$ to give $PhCMe_2OOCMe_2Ph$. The results of our product studies are consistent with the conclusion of Nangia and Benson (15) that, at ambient temperatures and normal oxygen pressures, the β-scission of cumylperoxy radicals is not fast enough to produce a significant steady-state concentration of cumyl radicals and that $2k_t$ for autoxidation of cumene does not contain a contribution from the rate constant for reaction of cumyl with cumylperoxy radicals.

The yields of di-cumyl peroxide reported in Table 1 are consistent with a value for $2k_t' = 6 \times 10^3\ M^{-1}$ s^{-1} and yields of acetophenone plus cumyl alcohol relative to di-cumyl peroxide are consistent with k_{3b}/k_{3a} in the range 5–20. This is comparable with a previous estimate of 6.3 (27) and with the analogous ratio for the *tert*-butylperoxy radical, for which k_{3b}/k_{3a} is estimated to be in the range 6–10 (27, 33). The ratio k_{3b}/k_{3a} is thus comparable for the two alkylperoxy radicals within experimental error, and differences in the ratio cannot account for the factor of 5 difference between $2k_t'$ for the two radicals. For the five-fold difference to be accounted for solely in terms of different k_{3b}/k_{3a} ratios (i.e. different values of f, the efficiency of cage escape) the value of k_{3b}/k_{3a} for $PhCMe_2O_2{}^{\cdot}$ would have to be at least a factor of ten less than the lower limit of the experimental data. We propose that the difference in the values of $2k_t'$ for cumylperoxy and *tert*-butylperoxy radicals is due to a difference in k_2, the rate constant for unimolecular decomposition of the tertiary alkyl and aralkyl tetroxides. A difference in the stability of these two tetroxides is not unreasonable in view of Kiefer and Traylor's findings (28) that di-α-cumyl hyponitrite decomposes 10 times faster than di-*tert*-butyl hyponitrite.

Steady-state rates of termination for autoxida-

Can. J. Chem. Downloaded from www.nrcresearchpress.com by 210.87.254.5 on 09/06/12
For personal use only.

Can. J. Chem. Downloaded from www.nrcresearchpress.com by 210.87.254.5 on 09/06/12
For personal use only.

tion of cumene are accurately second-order with respect to the concentration of alkylperoxy radicals. Non-steady-state decays of cumylperoxy radicals are dependent on the initiator and solvent systems. In an alkane solvent, cumylperoxy radicals generated by photolysis of azocumene decay by clean second-order kinetics. In toluene, the decay at 294 K is first-order due to the dominance of reaction with the solvent:

[26] $PhCMe_2O_2^{\cdot} + PhCH_3 \longrightarrow PhCMe_2OOH + PhCH_2^{\cdot}$

A similar solvent effect has been observed for the decay of *tert*-butylperoxy radicals.[2]

Cumene hydroperoxide is a much less satisfactory radical source, the decay of cumylperoxy radicals produced by photolysis of the hydroperoxide obeyed neither first-order nor second-order kinetics. It should be noted that a great deal of care and patience has to be exercised to obtain cumene hydroperoxide free of phenol. The presence of even a trace of this decomposition product is likely to have a significant effect on the kinetic observations, because of the rapid rate of reaction between phenol and a tertiary alkylperoxy radical (34). Our observation that initial rates of radical decay increased as the length of continuous photolysis was increased is also consistent with the formation of a reactive decomposition product.

We believe, therefore, that first-order decays observed by time resolved esr spectroscopy for $PhCMe_2O_2^{\cdot}$ prepared by heterogenous decomposition of the hydroperoxide are fortuitous and are a result of reaction with either the solvent or adventitious impurity. This impurity could be a phenol or a transition metal ion, either of which would react with $PhCMe_2O_2^{\cdot}$ by a pseudo-first-order process. The inability to detect an esr spectrum from the transition metal ion initiator does not necessarily mean that it is insoluble, because the spectrum may be broad and the sensitivity correspondingly low. Concentrations of initiator below the limit detectable by esr could still be sufficient to markedly influence the radical kinetics (35).

At the high cumene hydroperoxide concentrations used by previous workers, viscosity effects will play an important role. The line width arising from the spin–rotation interaction is given by

$$\Delta H \propto \Delta g\ ^2T/a^3\ \eta$$

where Δg is the mean shift in g-value from the free spin value, T is the absolute temperature, a the mean diameter of the radical, and η is the solvent viscosity.

[2]J. E. Bennett and G. Brunton, unpublished results.

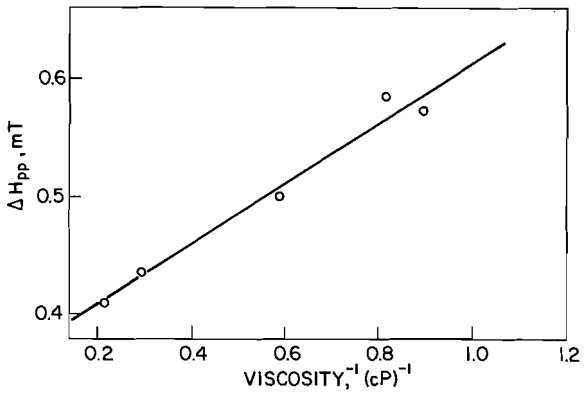

FIG. 2. Plot of peak-to-peak line width of cumylperoxy radical against viscosity of solution of cumene hydroperoxide in carbon tetrachloride.

Our results show that for a range of solutions of cumene hydroperoxide the plot of the reciprocal of the viscosity versus the line width of the cumylperoxy radical is linear (Fig. 2), which is in agreement with the above relationship. Thus the variations of line width with concentration observed by Fukuzumi and Ono (13) can be explained adequately by viscosity effects, and do not provide unambiguous evidence for a complex between cumylperoxy radicals and the hydroperoxide.

Similarly, the small g-value variations observed by these workers (13) can be explained by viscosity effects. An increase in the viscosity of the solution will cause a reduction in the degree of rotational averaging of the anisotropic components of the g-tensor. This effect will produce an apparent shift in the measured g-value as the anisotropic terms become more important.

Overall our studies show that cumene hydroperoxide is not a very satisfactory source of cumylperoxy radicals for esr investigations, and spectra and kinetic results obtained using this source should be interpreted with extreme caution.

Acknowledgements

We thank Mr. J. H. B. Chenier for performing much of the experimental work and Mr. M. Bednas for measurement of the mass spectra. We also thank a referee for comments regarding the mechanism of ^{18}O exchange into acetophenone.

1. J. A. HOWARD. A.C.S. Symp. Ser. **69**, 413 (1978).
2. K. ADAMIC, J. A. HOWARD, and K. U. INGOLD. Can. J. Chem. **47**, 3803 (1969).
3. D. G. HENDRY. J. Am. Chem. Soc. **89**, 5433 (1967).
4. J. A. HOWARD and K. U. INGOLD. Adv. Chem. Ser. **75**, 6 (1968).
5. J. R. THOMAS. J. Am. Chem. Soc. **89**, 4872 (1967).
6. H. W. MELVILLE and S. RICHARDS. J. Chem. Soc. 944 (1954).

7. H. S. BLANCHARD. J. Am. Chem. Soc. **81**, 4548 (1959).
8. J. A. HOWARD and J. C. ROBB. Trans. Faraday Soc. **59**, 1590 (1963).
9. P. D. BARTLETT and T. G. TRAYLOR. J. Am. Chem. Soc. **85**, 2407 (1963).
10. T. G. TRAYLOR and C. A. RUSSELL. J. Am. Chem. Soc. **87**, 3698 (1965).
11. S. FUKUZUMI and Y. ONO. J. Chem. Soc. Perkin Trans. II, 622 (1977).
12. S. FUKUZUMI and Y. ONO. J. Chem. Soc. Perkin Trans. II, 784 (1977).
13. S. FUKUZUMI and Y. ONO. J. Chem. Soc. Perkin Trans. II, 625 (1977).
14. V. A. BELYAKOV, R. F. VASIL'EV, and G. F. FEDOROVA. Dokl. Akad. Nauk SSSR, **239**, 344 (1978).
15. D. S. NANGIA and S. W. BENSON. Int. J. Chem. Kinet. **12**, 29 (1980).
16. H. KIEFER and T. G. TRAYLOR. Tetrahedron Lett. 6163 (1966).
17. S. F. NELSON and P. D. BARTLETT. J. Am. Chem. Soc. **88**, 137 (1966).
18. J. A. HOWARD and J. H. B. CHENIER. Can. J. Chem. **54**, 382 (1976).
19. K. ZEIGLER, A. SEIB, K. KROEVENAGEL, P. HERTE, and F. ANDREAS. Justus Liebigs Ann. Chem. **551**, 150 (1942).
20. L. R. MAHONEY. J. Am. Chem. Soc. **88**, 3035 (1966).
21. D. E. BISSING and A. J. SPEZIALE. J. Am. Chem. Soc. **87**, 2683 (1965).
22. J. A. HOWARD and K. U. INGOLD. Can. J. Chem. **47**, 3809 (1969).
23. E. FURIMSKY and J. A. HOWARD. J. Am. Chem. Soc. **95**, 369 (1973).
24. T. A. B. M. BOLSMAN and D. M. BROUWER. Recl. Trav. Chim. Pays-Bas, **97**, 320 (1978).
25. I. P. Standards for Petroleum and its Products. Part 1. The Institute of Petroleum. 1971. p. 290.
26. J. A. HOWARD. Adv. Free Radical Chem. **4**, 49 (1972).
27. J. A. HOWARD and K. U. INGOLD. Can. J. Chem. **47**, 3797 (1969).
28. H. KIEFER and T. G. TRAYLOR. Abstract of paper presented to the International Symposium on the Chemistry of Organic Peroxides. Berlin–Adlershof. September, 1967.
29. J. A. HOWARD and K. U. INGOLD. Can. J. Chem. **43**, 2729 (1965).
30. J. H. B. CHENIER and J. A. HOWARD. Can. J. Chem. **53**, 623 (1975).
31. J. A. HOWARD. Free Radicals. Vol II. *Edited by* J. K. Kochi. Wiley, New York. 1973. Chapt. 12.
32. J. A. HOWARD and K. U. INGOLD. Can. J. Chem. **46**, 2655 (1968).
33. R. HIATT, J. CLIPSHAM, and T. VISSER. Can. J. Chem. **42**, 2754 (1964).
34. J. H. B. CHENIER, E. FURIMSKY, and J. A. HOWARD. Can. J. Chem. **52**, 3682 (1974).
35. K. U. INGOLD. J. Phys. Chem. **76**, 1385 (1972).

Can. J. Chem. Downloaded from www.nrcresearchpress.com by 210.87.254.5 on 09/06/12
For personal use only.

Glycosides from *Muscari comosum*. 1. Eucosterol glycoside and structure of its methanolysis products[1]

MICHELANGELO PARRILLI,[2] ROSA LANZETTA, VINCENZO DOVINOLA,[3] MATTEO ADINOLFI, AND LORENZO MANGONI

Istituto di Chimica Organica e Biologica, Universita' di Napoli, Via Mezzocannone 16, 80134 Napoli, Italy

Received October 24, 1980

MICHELANGELO PARRILLI, ROSA LANZETTA, VINCENZO DOVINOLA, MATTEO ADINOLFI, and LORENZO MANGONI. Can. J. Chem. **59**, 2261 (1981).

A mixture of at least four glycosides has been isolated from bulbs of *Muscari comosum*. Acidic methanolysis of this mixture afforded a crystalline fraction consisting of four diols **1***a* differing in the configuration at the epimerizable C-20 and/or C-24 centers. Benzoylation of this diol fraction allowed the isolation of one pure dibenzoate, mp 175–176°C, to which structure **1***b* was assigned on the basis of chemical and spectral evidence. This allowed the deduction that one of the aglycone moieties was 27-norlanostane triterpene eucosterol **4***a*. This conclusion has been confirmed by identification of **4***a* as the major product of the enzymatic hydrolysis of the glycoside mixture.

MICHELANGELO PARRILLI, ROSA LANZETTA, VINCENZO DOVINOLA, MATTEO ADINOLFI et LORENZO MANGONI. Can. J. Chem. **59**, 2261 (1981).

A partir des bulbes de *Muscari comosum*, on a isolé un mélange contenant au moins 4 glycosides. La méthanolyse acide de ce mélange permet d'obtenir une fraction cristalline consituée de 4 diols (**1***a*) qui diffèrent par la configuration au niveau des centres épimérisables C-20 ou C-24 ou les deux à la fois. La benzoylation de ces diols permet d'isoler un dibenzoate à l'état pur de pf 175–176°C auquel on attribue la structure **1***b* en se basant sur des preuves chimiques et spectroscopiques. Ceci permet de conclure que l'une des portions aglycone est l'eucostérol **4***a* un terpène de la famille du nor-27 lanostane. On a confirmé cette conclusion en identifiant le composé **4***a* comme produit principal de l'hydrolyse enzymatique du mélange de glycosides.

[Traduit par le journal]

The bulbs of *Muscari comosum* Mill. (Liliaceae) are a rather popular food in the Mediterranean area and are well known for their bitter taste. The aqueous extract from the plant has been reported (2) to display antitumoral activity. Following a preliminary communication (1), in this paper we present details of the structural elucidation of the products obtained by methanolysis of a glycoside mixture extracted from the bulbs and of the isolation of the authentic aglycones obtained by enzymatic hydrolysis.

Fresh sliced bulbs were extracted with boiling acetone and the resulting crude extract was washed with various solvents and fractionated by column chromatography (cellulose). Elution with water-saturated *n*-butanol gave a fraction glycosidic in nature according to the ^{1}H nmr signals in the δ 3.0–3.8 zone and the ^{13}C nmr signals in the δ 97–110 zone (3). Although tlc (cellulose) showed it to consist of at least four main compounds all migrating in a narrow range of R_f, any attempt to isolate pure glycosides yielded very poor results. Also on account of the possibility, then rejected, that they differed only in their sugar moieties, we decided to submit the whole glycoside mixture to acidic methanolysis in refluxing hydrochloric methanol.

Chromatography of the chloroform fraction of the crude product afforded a main crystalline fraction which ran as one spot on thin layers of silica gel but melted over a wide temperature range (142–155°C) in spite of repeated crystallizations. The ir and uv spectra showed the presence of hydroxyl and conjugated (and possibly unconjugated) keto groups. Spectral and chemical investigation of some readily accessible derivatives showed that the fraction consisted of four dihydroxy compounds with structure **1***a* and differing in the configuration at C-20 and/or C-24.

Benzoylation (BzCl/Py) followed by plc gave two main fractions. Their mass spectra displayed the same molecular ion peak (694 *m/e*) and, most important, an identical fragmentation pattern. On crystallization from ethanol, the less polar fraction gave finally a pure compound (mp 175–176°) having a formula of $C_{44}H_{54}O_7$ (hrms), to which was attributed structure **1***b* (the C-20 and C-24 configuration remaining unestablished) on the basis of the following evidence.

The ir spectrum of the compound melting at 175–176°C displayed ester and keto group bands, but no hydroxyl band. The ^{1}H nmr spectrum (see

[1]Work supported by Consiglio Nazionale delle Richerche (CNR).

[2]Author to whom correspondence should be addressed.

[3]Present address: Istituto di Chimica dell'Università, Salerno, Italy.

0008-4042/81/152261-05$01.00/0

©1981 National Research Council of Canada/Conseil national de recherches du Canada

Can. J. Chem. Downloaded from www.nrcresearchpress.com by 210.87.254.105 on 09/06/12
For personal use only.

Can. J. Chem. Downloaded from www.nrcresearchpress.com by 210.87.254.105 on 09/06/12
For personal use only.

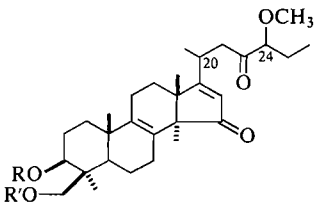

1*a* R = R′ = H
1*b* R = R′ = COC_6H_5
1*c* R = R′ = Ac
1*d* R, R′ = $>C(CH_3)_2$

Fig. 1) clearly indicated the presence of four tertiary methyl groups, one secondary methyl, one primary methyl, and one methoxyl group and of one olefinic proton. It was also evident that benzoylation had occurred at a primary and at an equatorial secondary hydroxyl group (AB q at δ 4.58 and δ 4.78, J_{AB} = 12.5 Hz; dd at δ 4.92, $W_{1/2}$ = 21 Hz). The ^{13}C nmr spectra (proton decoupled, noise off resonance decoupled and single frequency off resonance decoupled) allowed detection of the signals (see Table 1) due to the carbons of a keto group (δ 211.0), of a >C=CH—CO— system (δ 185.8, 123.4, 209.5, respectively), besides two ester carbonyl groups (δ 166.4 and 167.2). The signals due to the carbons implied by one tetrasubstituted double bond (δ 132.9 s and 135.3 s) were also present in the sp^2 carbon zone. The signals of six methyl, one methoxyl, eight methylene, one oxymethylene, two methine, and two oxymethine groups and of four quaternary carbons were also observed.

TABLE 1. ^{13}C nmr (67.88 MHz) chemical shifts of dibenzoate melting at 175–176°C in $CDCl_3$ and tentative assignments of the signals[a]

δ	Carbon	δ	Carbon
9.4 q	C-26	88.6 d	C-3
18.7 q	C-19	123.4 d	C-16
20.4 q	C-21		
22.6 q	C-30	37.6 s	C-10
28.1 q	C-18[b]	41.9 s	C-4
29.4 q	C-32[b]	51.4 s	C-13
58.2 q	24-OCH_3	57.5 s	C-14
		132.9 s	C-8
19.4 t	C-6[c]	135.3 s	C-9
20.4 t	C-11[c]	185.8[c] s	C-17
23.4 t	C-12	209.5[c] s	C-15
24.3 t	C-7[d]	211.0 s	C-23
24.8 t	C-25[d]		
27.8 t	C-2	128.3 d	Phenyl carbons
35.4 t	C-1	128.5 d	
43.4 t	C-22	129.6 d	
65.9 t	C-31	132.7 s	
29.3[c] d	C-29		
51.7 d	C-5	166.4 s	Benzoate carbonyl carbons
80.8 d	C-24	167.2 s	

[a]In ppm relative to TMS. Assignments are based on data from refs. 3, 4, and 5.
[b,d]Those assignments could be reversed.
[c]Corrected value (1).

With all the unsaturated functional groups thus established, a tetracyclic structure was to be assumed for the compound to account for the whole number of unsaturations implied by the molecular formula.

The structure of the side chain was deduced essentially from the ^1H nmr spectrum. Decoupling experiments showed that the primary methyl at δ 0.91 and the proton appearing at δ 3.53 are both coupled by the same constant value with the —CH_2— group appearing as a quintuplet at δ 1.66. These data accorded with the fragment —CO—$CH(OCH_3)$—CH_2—CH_3. On the other hand, irradiation of the sextet centered at δ 3.09 (1H) caused the further coupling of the AB q at δ 2.75 to disappear, the olefinic signal at δ 5.54 to sharpen, and the methyl doublet at δ 1.13 to coalesce into a singlet. This was rationalized by assigning the signal at δ 3.09 to the 20-proton and the double AB q at δ 2.75 to the 22-protons. The chemical shift of these latter was consistent with their adjacency to the (23)CO. Accordingly, a loss of 115 mass units due to fragmentation at the (20)C—(22)C bond was measured in the mass spectrum.

The structure of the side chain being so established (the stereochemistry at C-20 and C-24 excepted), the sharpening of the signal at δ 5.54 upon irradiation of the 20-H signal indicated that the olefinic proton was located at C-16. In an expanded spectrum the signal at δ 5.54 was observed actually to be a doublet with J = 0.6 Hz, this value according with an allylic 16,20 coupling. On the other hand, the chemical shift value suggested that this proton was located at the α-position of an α,β-unsaturated carbonyl system. Thus the conjugated keto group responsible for the cyclopentenone absorption (6) at 238 nm in diols **1***a* had to be at C-15.

The 8,9-location for the tetrasubstituted double bond discerned in the ^{13}C nmr spectrum was deduced from the obtaining of enedione **2** upon oxidation of the dibenzoate having mp 175–176°C with CrO_3 in glacial AcOH. In fact, the uv spectrum of **2** displayed a band at 273 nm (ε = 8000) which is diagnostic of an all-*trans* O=C—C=C—C=O

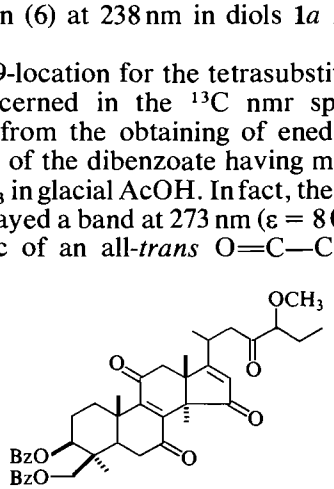

2

Can. J. Chem. Downloaded from www.nrcresearchpress.com by 210.87.254.105 on 09/06/12
For personal use only.

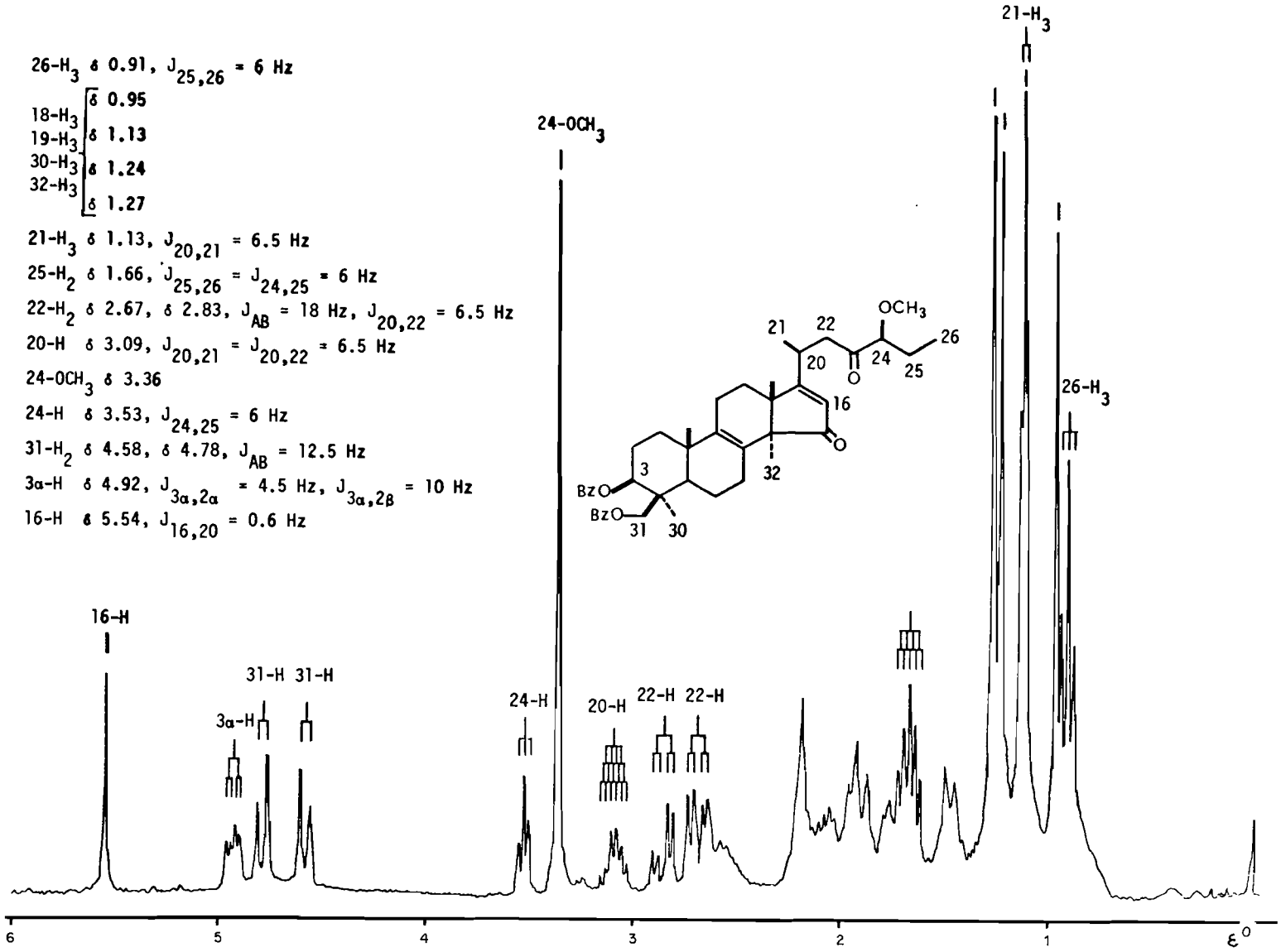

FIG. 1. ^{1}H nmr (270 MHz) spectrum (δ 0–6) of dibenzoate, mp 175–176°C in $CDCl_3$. All reported couplings have been inferred from pertinent decoupling experiments.

Can. J. Chem. Downloaded from www.nrcresearchpress.com by 210.87.254.105 on 09/06/12
For personal use only.

chromophore of a 7,11-diketo-$\Delta^{8,9}$-tetracyclic triterpene (7).

The diastereoisomeric relationship among diols **1***a* was shown by ^{1}H nmr examination of the remaining dibenzoate fractions. The signals of the spectrum of the solid left from evaporation of the mother liquors allowed the presence of a second diastereoisomeric dibenzoate to be inferred. On the other hand, the signals of the spectrum of the more polar fraction indicated that this latter was a mixture of two more diastereoisomers. Conclusive evidence that the four dibenzoates differ in the configuration at the epimerizable C-20 and C-24 centers came from hydrolysis both under acidic and alkaline conditions of the pure **1***b* melting at 175–176°C, which did not give a pure diol in any case but did lead to a mixture identical (^{1}H nmr) with that resulting from methanolysis of the glycosides.

Acetylation (Ac_2O/Py) of the diol mixture from the methanolysis yielded an unseparable mixture of diacetates **1***c* whose relevant ^{1}H nmr signals at δ 4.27 (AB q, —C*H*$_2$—OAc) and δ 4.59 (m, $W_{1/2}$ = 21 Hz, >C*H*OAc) could be regarded as the signals generally detected for the 4β-C*H*$_2$OAc and (3)C*H*$_\alpha$OAc protons, respectively, in the A-ring of a triterpene diol acetate (8). On the other hand, reaction of the diol mixture with dry acetone/$CuSO_4$ gave an unseparable mixture of acetonides **4***d*, showing that the arrangement of the two hydroxyl groups was suitable for the closure of a di-*O*-isopropylidene ring.

All above data accorded with the structure **1***b* (or its euphanic counterpart) for the dibenzoate melting at 175–176°C and its accompanying stereoisomers. However, lanostane structure **1***a* turned out to be closely related to that of the compound **3**,

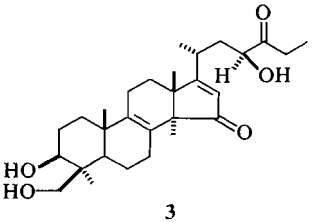

3

a product of alkali-catalyzed retroaddition from eucosterol **4***a*, a biogenetically interesting norlanostane triterpenoid missing the side-chain 27-carbon and carrying a spirofused tetrahydrofuran ring, previously found as a free compound in some *Eucomis* species (9). Therefore we suspected stereoisomeric diols might be not the authentic aglycones but artefacts from eucosterol. In fact, retroaddition from **4***a* to **3** may also be promoted by acid and more than one path leading from **3** to **1***a*

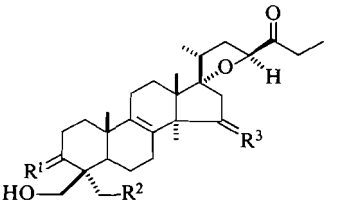

4*a* R^1 = β-OH, α-H; R^2 = H; R^3 = O
4*b* R^1 = R^3 = O; R^2 = H
4*c* R^1 = β-OH, α-H; R^2 = OH; R^3 = H_2
4*d* R^1 = O; R^2 = OH; R^3 = H_2

might be easily imagined. For instance, **3** might have been converted into its methyl hemiketal at C-24 and this latter dehydrated to the enol form of **1***a*. Confirmatory evidence came from the results of the enzymatic hydrolysis of the glycoside mixture obtained from *M. comosum* bulbs which was finally achieved by the use of digestive juice of *Helix pomatia* (10) after several pure glycolitic enzymes were found to be ineffective. Chromatography of the aglycone fraction yielded four pure compounds. The major one (mp 232–233°C) was identical (ir, ms, nmr, uv) with eucosterol **4***a*. Treatment of **4***a* with boiling hydrochloric methanol afforded a diol mixture which was found identical (ir, mp) both with the crystalline diol fraction (mp 142–155°C) obtained by acidic methanolysis of the glycosides and with the diol mixture obtained by hydrolysis of the pure dibenzoate, mp 175–176°C. This allowed us to definitively assign lanostane structure **1***a* to the diastereoisomeric diols.

Structural elucidation of the minor authentic aglycones **4***b*, **4***c*, and **4***d* has been reported elsewhere (11).

Experimental[4]

General

Melting points were determined on a Kofler block. The ir spectra were measured in chloroform solutions on a Perkin Elmer model 399 spectrophotometer. Rotations were determined with chloroform solutions on a Perkin Elmer model 141 polarimeter. Mass spectra were measured on an AEI model 902 instrument. The ^{1}H nmr (270 MHz) and ^{13}C nmr (67.88 MHz) spectra were recorded on a Fourier transform Bruker WH270 spectrometer with $CDCl_3$ as solvent and TMS as internal reference. The uv spectra were taken on a Perkin Elmer model 402 spectrophotometer with ethanol solutions. Silica gel 0.05–0.20 mm (Merck) and cellulose powder (Whatman, CF11) were used for column chromatography; tlc and plc were performed on silica gel F_{254} layers (Merck) of thickness 0.25 and 2 mm, respectively, and on cellulose layers (Merck) of thickness 0.1 mm.

Extraction of the Glycosides from Bulbs of Muscari comosum

Sliced fresh bulbs (1 kg) of the plant (collected in autumn in Puglia, Italy) were boiled in acetone (4 L) for 8 h. The acetone extract was evaporated *in vacuo*. The residue (50 g) was washed with water (500 mL) and then with acetone (500 mL) at room

[4]With the assistance of Italo Giudicianni.

Can. J. Chem. Downloaded from www.nrcresearchpress.com by 210.87.254.105 on 09/06/12
For personal use only.

temperature. The solid residue (17 g) was dissolved in 1:2 water–methanol (1 L) and the solution was washed with carbon tetrachloride (5 × 100 mL). The hydromethanolic phase was evaporated *in vacuo* to give a brown powder (13 g) which was chromatographed on a cellulose (390 g) column. Elution with water-saturated *n*-butanol (2 L) gave a highly bitter yellow-brown powder (9 g). Thin-layer chromatography (cellulose, 5:1:4 *n*-butanol – methanol–water) showed that this fraction consisted of four main compounds all migrating in a narrow range of R_f; ^{1}H nmr (DMSO-d_6): relevant signals in the δ 3–3.8 zone; ^{13}C nmr (CD_3OD): relevant signals in the δ 97–110 zone.

Methanolysis of the Glycoside Mixture

A solution of the above glycoside fraction (5 g) in dry methanol (100 mL) containing HCl (2.5% w/v) was refluxed for 4 h. To the cooled solution solid Na_2CO_3 (600 mg) was added. The residue from evaporation of the solvent *in vacuo* was dissolved in chloroform and washed with saturated Na_2CO_3 and water. Evaporation of chloroform afforded a solid (1.5 g) which was chromatographed on silica gel (65 g). Elution with 3:2 benzene–ether gave a white solid (300 mg) which was crystallized from benzene–hexane to give the mixture of diols **1***a* as white crystals (260 mg), mp 142–155°C; ir: 3350, 1710–1690 cm^{-1}; uv: λ_{max} 238, $E_{1\,cm}^{1\%}$ = 94.

Diols **1***a* (150 mg) were benzoylated with BzCl/Py (room temperature, 24 h). After usual work-up, plc on silica gel (4:1 hexane – ethyl acetate, 4 runs) afforded two fractions. Their mass spectra displayed the same molecular ion peak (694 *m/e*) and an identical fragmentation pattern.

The less-polar fraction (75 mg) was crystallized from ethanol to give pure dibenzoate **1***b* (45 mg) as white needles, mp 175–176°C; $[\alpha]_D$ +211° (*c* 0.5); ir: 1740–1690 cm^{-1}, uv: λ_{max} 230 nm, ε = 31 000; ^{1}H nmr: see Fig 1; ^{13}C nmr: see Table 1. The solid left from evaporation of mother liquors displayed an ^{1}H nmr spectrum where the signals of a second diastereoisomeric dibenzoate were almost overlapping those of the dibenzoate of mp 175–176°C, whereas additional singlets at δ 3.37 and δ 5.60 were observed. Mass spectrum *m/e*: 694.38714 (M^+; calcd. for $C_{44}H_{54}O_7$: 694.38703), 614, 579.31112 ($M - C_6H_{11}O_2$; calcd. for $C_{38}H_{43}O_5$: 579.31102), 502, 464, 435, 264, 219.

The more polar fraction (85 mg) also displayed an ^{1}H nmr spectrum very similar to that of the dibenzoate of mp 175–176°C, the main differences being the presence of two singlets (1H in all) at δ 5.58 and δ 5.64 and two triplets (3H in all) at δ 0.91 and δ 0.93.

Another sample (50 mg) of diols **1***a* was acetylated with Ac_2O/Py (room temperature, 24 h). The acetate **1***c* mixture (40 mg) obtained by usual work-up and purified by filtration on silica gel (4:1 benzene–ether as eluent) was a crystalline solid; uv: λ_{max} 245 nm, ε = 6 500; ^{1}H nmr: ABq at δ 4.27 (—C*H*$_2$OAc); m at δ 4.59, $W_{1/2}$ = 21 Hz (>C*H*OAc); singlets at δ 2.04 (3H) and 2.06 (3H) (2 × OCOC*H*$_3$); ms, *m/e*: 570, M^+.

A sample of diols **1***a* (30 mg) was dissolved in acetone (10 mL) and shaken with anhydrous $CuSO_4$ (200 mg) for 12 h at room temperature. Filtration and evaporation of the solvent *in vacuo* afforded an acetonide **1***d* mixture as a solid (22 mg); ^{1}H nmr:s at δ 1.38 (3H), s at δ 1.45 (3H), ABq (2H) at δ 3.29 and 4.09 and m (1H) at δ 3.60 (—C*H*$_2$—O—C(C*H*$_3$)$_2$—O—C*H*<); ms, *m/e*: 526, M^+.

Enedione 2

Pure dibenzoate (mp 175–176°C) (20 mg) was dissolved in glacial AcOH (2 mL) and treated with 0.4 mL of a solution of CrO_3 (25 mg) in glacial AcOH (1 mL). After 2 h at 40°C, methanol (a few drops) was added to the cooled solution. Evaporation of the solvent *in vacuo* afforded a yellow solid which was dissolved in ethyl acetate and washed with water. The organic layer was evaporated to give a yellow crystalline solid (18 mg). Filtration on silica gel (1:1 hexane – ethyl acetate as eluent) and crystallization from methanol afforded pure **2** as yellow needles, mp 176.5–177.5°C; $[\alpha]_D$ +325° (*c* 0.4); uv: λ_{max} 273 nm, ε = 8000; ^{1}H nmr, δ: 0.92 (3H, t, *J* = 7 Hz, —CH$_2$—C*H*$_3$), 1.13 (3H, s, C*H*$_3$), 1.14 (3H, d, *J* = 6 Hz, >CH—C*H*$_3$), 1.28 (3H, s, C*H*$_3$), 1.32 (3H, s, C*H*$_3$), 1.37 (3H, s, C*H*$_3$), 3.36 (3H, s, —OC*H*$_3$), 3.53 (1H, t, *J* = 6 Hz, —OC—C*H*(OCH$_3$)—CH$_2$—), 4.77 (2H, AB q, —C*H*$_2$OBz), 5.00 (1H, m, >C*H*OBz), 5.70 (1H, s, >C=C*H*—CO—); ms, *m/e*: 722.34558 (M^+; calcd. for $C_{44}H_{50}O_9$: 722.34545).

Hydrolysis of Dibenzoate Melting at 175–176°C

Two samples (10 mg each) were separately treated with 10% KOH methanol and 10% concentrated HCl methanol at boiling temperature for 3 h. In both cases a diol mixture was obtained identical (^{1}H nmr, tlc) to that obtained from the methanolysis of the glycoside mixture.

Enzymatic Hydrolysis of Glycoside Mixture

To a solution of the glycoside mixture (1 g) in water (300 mL) digestive juice of *Helix pomatia* (1 mL; Industrie Biologique Francaise) was added. The solution was stirred for 40 days at room temperature. After concentration *in vacuo*, the solution was extracted with chloroform. Evaporation of the chloroform extract gave a solid (110 mg); plc on silica gel (4:1 chloroform – ethyl acetate, 4 runs) afforded four fractions: A (25 mg), B (35 mg), C (5 mg), and D (20 mg), in order of increasing polarity. Fraction B was found to consist of eucosterol **4**, mp 232–233°C (from ethanol; lit. (9) mp 235–236°C); $[\alpha]_D$ +21° (*c* 0.7; lit. (9) α_D +20.4°); ^{1}H nmr δ: 0.94 (3H, s, 18-*H*$_3$), 0.96 (3H, s, 19-*H*$_3$), 1.08 (3H, t, $J_{25,26}$ = 7.35 Hz, 26-*H*$_3$), 1.13 (3H, d, $J_{20,21}$ = 6.7 Hz, 21-*H*$_3$), 1.23 (3H, s, 30-*H*$_3$), 1.36 (3H, s, 32-*H*$_3$), 1.95 (2H, dd, $J_{22,23}$ = 9.46 Hz, $J_{20,22}$ = 3.1 Hz, 22-*H*$_2$), 2.22 and 2.72 (2H, AB q, J_{AB} = 19.4 Hz, 16-*H*$_2$), 2.35 (m, 20-*H*), 2.51 (2H, q, $J_{25,26}$ = 7.35 Hz, 25-*H*$_2$), 3.36 and 4.23 (2H, AB q, J_{AB} = 11.27 Hz, 31-*H*$_2$), 3.48 (1H, dd, $J_{3\alpha,2\beta}$ = 11.1 Hz, $J_{3\alpha,2\alpha}$ = 4.1 Hz, 3α-*H*), 4.71 (1H, t, $J_{22,23}$ = 9.46 Hz, 23-*H*) (cf. ref. 9); ^{13}C nmr and ms spectra as in ref. 9.

A sample of **4***a* (5 mg) in dry methanol (1 mL) containing HCl (2.5% w/v) was refluxed for 4 h. Work-up as above afforded a solid (5 mg) which was found identical (mp, ir, uv) to the crystalline diol fraction (mp 142–155°C) obtained by acidic methanolysis of the glycoside mixture.

1. M. Parrilli, M. Adinolfi, V. Dovinola, and L. Mangoni. Gazz. Chim. Ital. **109**, 391 (1979).
2. B. Prescott and G. Caldes. Proc. Soc. Exp. Biol. Med. **129**, 190 (1969); Chem. Abstr. **70**, 14359f (1969).
3. J. B. Stothers. Carbon-13 nmr spectroscopy. Academic Press, New York. 1972.
4. G. Lukacs, F. K. Huong-Hun, G. R. Bennett, B. L. Buckwalter, and E. Wenkert. Tetrahedron Lett. 3515 (1972).
5. J. Polonsky, Z. Baskevitch, N. Cagnoli, P. Ceccherelli, B. L. Buckwalter, and E. Wenkert. J. Am. Chem. Soc. **94**, 4369 (1972).
6. A. I. Scott. Interpretation of the uv spectra of natural products. Pergamon Press, London. 1964. p. 55.
7. E. R. H. Jones and T. G. Halsall. Fortschr. Chem. Org. Naturst. **12**, 44 (1955).
8. A. Gaudemer, J. Polonsky, and E. Wenkert. Bull. Soc. Chim. Fr. 407 (1964).
9. R. Ziegler and C. Tamm. Helv. Chim. Acta, **59**, 1997 (1976).
10. H. Huber, F. Blindenbacher, K. Mohr, P. Speiser, and T. Reichstein. Helv. Chim. Acta, **34**, 46 (1951).
11. M. Parrilli, M. Adinolfi, and L. Mangoni. Gazz. Chim. Ital. **109**, 611 (1979); M. Parrilli, R. Lanzetta, M. Adinolfi, and L. Mangoni. Tetrahedron, **36**, 3591 (1980).

Carbon-13 nmr shifts and C—H coupling constants of deoxybenzoins and related acetophenones

HEM CHANDRA JHA AND FRITZ ZILLIKEN

Institute of Physiological Chemistry, The University of Bonn, Nussallee 11, D-5300 Bonn 1, Federal Republic of Germany

AND

WERNER OFFERMANN AND EBERHARD BREITMAIER

Institute of Organic Chemistry and Biochemistry, The University of Bonn, Gerhard-Domagk-Str. 1, D-5300 Bonn 1, Federal Republic of Germany

Received November 4, 1980

HEM CHANDRA JHA, FRITZ ZILLIKEN, WERNER OFFERMANN, and EBERHARD BREITMAIER. Can. J. Chem. **59**, 2266 (1981).

^{13}C Chemical shifts and resolved carbon–proton couplings of 39 deoxybenzoins and 11 acetophenones, most of which have naturally occurring substitution patterns, are assigned. Individual benzene rings turned out to have typical parameters not affected by structural variations in the rest of the molecule. Due to substitutional saturation, however, these benzenoid carbon shifts markedly deviate from increment additivity. A few trends of these deviations are described. Phenolic hydrogens, fixed between hydroxyl and carbonyl oxygen due to internal hydrogen bonding, are shown to give rise to additional carbon-splittings.

HEM CHANDRA JHA, FRITZ ZILLIKEN, WERNER OFFERMANN et EBERHARD BREITMAIER. Can. J. Chem. **59**, 2266 (1981).

On a identifié les déplacements chimiques du ^{13}C et les couplages carbone–proton résolus de 39 déoxybenzoïnes et de 11 acétophénones qui présentent pour la plupart des schémas de substitution que l'on retrouve dans les produits naturels. On note que les cycles benzéniques individuels ont des paramètres typiques qui ne sont pas affectés par les variations structurales dans le reste de la molécule. Toutefois à cause de la saturation par substitution, les déplacements chimiques des carbones benzénoïdes dévient fortement des valeurs prédites par l'additivité des incréments. On décrit quelques tendances dans ces variations. On montre que les hydrogènes phénoliques fixés entre les oxygènes de l'hydroxyle et du carbonyle par des liaisons hydrogènes intramoléculaires provoquent une augmentation du dédoublement des carbones.

[Traduit par le journal]

Introduction

Deoxybenzoins are the synthetic precursors as well as the alkaline degradation products of isoflavones. This fact bestows a considerable importance to this class of substances in the structural elucidation of natural isoflavones (1, 2). Deoxybenzoins, obtained by degradation of isoflavones, can be used again for the resynthesis of the corresponding isoflavones with suitable reagents to confirm their structure. They are also valuable as intermediates for other isoflavonoids such as isoflavanones, isoflavans, and pterocarpans. As one of the degradation products, they assume significance in the catabolic studies of the isoflavones with intestinal microflora (3).

We therefore performed a comprehensive carbon-13 nuclear magnetic resonance investigation of deoxybenzoins with naturally occurring substitution pattern. The present study involves 39 deoxybenzoins (dob) **1** to **39**, and eleven acetophenones (ap) **40** to **50**. Chemical shifts and one-, two-, three-, and four-bond C—H couplings have been assigned as far as possible. The structures are listed in Table 1, including a few synthetic compounds which were useful in spectral analyses.

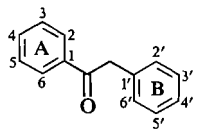

Deoxybenzoin structures **1** to **39**

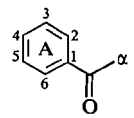

Acetophenone structures **40** to **50**

Experimental

Synthesis of the Deoxybenzoins and Ketones

The compounds have been prepared by using the Friedel–Crafts reaction, Fries rearrangement, or Houben–Hoesch condensation with suitable phenols. The known compounds have been checked for their authenticity by comparison of the mp's and bp's, and the new compounds have been verified by elemental analyses and spectroscopic methods (4).

Carbon-13 Nuclear Magnetic Resonance Spectra

The spectra were recorded on a Bruker WP 80-FT instrument operating at 20.115 MHz in the ^{13}C observation channel, 80 MHz in the proton decoupling channel, and 11.56 MHz in the deuterium lock channel. The experimental conditions were identical to those reported previously (1), but resulting in 0.6 Hz or 0.03 ppm digital resolution. Proton-coupled spectra were recorded by the gated-decoupling technique, with a 60° pulse

0008-4042/81/152266-17$01.00/0

©1981 National Research Council of Canada/Conseil national de recherches du Canada

Can. J. Chem. Downloaded from www.nrcresearchpress.com by 210.87.254.40 on 09/06/12
For personal use only.

Can. J. Chem. Downloaded from www.nrcresearchpress.com by 210.87.254.40 on 09/06/12
For personal use only.

TABLE 1. List of compounds. Each compound is identified by its CA name, substituents, and a running number.

No.	Z2	Z3	Z4	Z5	Z6	Z2′	Z3′	Z4′	Z5′	
1										1,2-Diphenylethanone
2	OH							OCH_3		1-(2-Hydroxyphenyl)-2-(4-methoxyphenyl)ethanone
3	OH		OH					OH		1-(2,4-Dihydroxyphenyl)-2-(4-hydroxyphenyl)ethanone
4	OH		OH					OCH_3		1-(2,4-Dihydroxyphenyl)-2-(4-methoxyphenyl)ethanone
5	OH		OCH_3					OH		1-(2-Hydroxy-4-methoxyphenyl)-2-(4-hydroxyphenyl)ethanone
6	OH		OCH_3					OCH_3		1-(2-Hydroxy-4-methoxyphenyl)-2-(4-methoxyphenyl)ethanone
7	OH		OCH_3					Cl		1-(2-Hydroxy-4-methoxyphenyl)-2-(4-chlorophenyl)ethanone
8	OH	OH	OH					OCH_3		1-(2,3,4-Trihydroxyphenyl)-2-(4-methoxyphenyl)ethanone
9	OH	OCH_3	OCH_3							1-(2-Hydroxy-3,4-dimethoxyphenyl)-2-phenylethanone
10	OH	OCH_3	OCH_3					OCH_3		1-(2-Hydroxy-3,4-dimethoxyphenyl)-2-(4-methoxyphenyl)ethanone
11	OH		OH	OH						1-(2,4,5-Trihydroxyphenyl)-2-phenylethanone
12	OH		OH	OH		OCH_3				1-(2,4,5-Trihydroxyphenyl)-2-(2-methoxyphenyl)ethanone
13	OH		OH	OH				OH		1-(2,4,5-Trihydroxyphenyl)-2-(4-hydroxyphenyl)ethanone
14	OH		OH	OH				OCH_3		1-(2,4,5-Trihydroxyphenyl)-2-(4-methoxyphenyl)ethanone
15	OH		OH	OH				OCH_2CH_3		1-(2,4,5-Trihydroxyphenyl)-2-(4-ethoxyphenyl)ethanone
16	OH		OH	OH				$OCH_2CH_2CH_3$		1-(2,4,5-Trihydroxyphenyl)-2-(4-propoxyphenyl)ethanone
17	OH		OH	OH				$OCH(CH_3)_2$		1-(2,4,5-Trihydroxyphenyl)-2-[4-(1-methyl)ethoxyphenyl]ethanone
18	OH		OH	OH				$OCH_2CH_2CH_2CH_3$		1-(2,4,5-Trihydroxyphenyl)-2-(4-butoxyphenyl)ethanone
19	OH		OH	OH			OCH_3	OCH_3		1-(2,4,5-Trihydroxyphenyl)-2-(3,4-dimethoxyphenyl)ethanone
20	OH		OCH_3	OH						1-(2,5-Dihydroxy-4-methoxyphenyl)-2-phenylethanone
21	OH		OCH_3	OH				OH		1-(2,5-Dihydroxy-4-methoxyphenyl)-2-(4-hydroxyphenyl)ethanone
22	OH		OCH_3	OH				OCH_3		1-(2,5-Dihydroxy-4-methoxyphenyl)-2-(4-methoxyphenyl)ethanone
23	OH		OCH_3	OH			OH	OH		1-(2,5-Dihydroxy-4-methoxyphenyl)-2-(3,4-dihydroxyphenyl)ethanone
24	OH		OCH_3	OH			OCH_3	OCH_3		1-(2,5-Dihydroxy-4-methoxyphenyl)-2-(3,4-dimethoxyphenyl)ethanone
25	OH		OH	OCH_3						1-(2,4-Dihydroxy-5-methoxyphenyl)-2-phenylethanone
26	OH		OH	OCH_3				OH		1-(2,4-Dihydroxy-5-methoxyphenyl)-2-(4-hydroxyphenyl)ethanone
27	OH		OH	OCH_3				OCH_3		1-(2,4-Dihydroxy-5-methoxyphenyl)-2-(4-methoxyphenyl)ethanone
28	OH		OCH_3	OCH_3						1-(2-Hydroxy-4,5-dimethoxyphenyl)-2-phenylethanone
29	OH		OCH_3	OCH_3				NO_2		1-(2-Hydroxy-4,5-dimethoxyphenyl)-2-(4-nitrophenyl)ethanone
30	OH		OCH_3	OCH_3				OH		1-(2-Hydroxy-4,5-dimethoxyphenyl)-2-(4-hydroxyphenyl)ethanone
31	OH		OCH_3	OCH_3				OCH_3		1-(2-Hydroxy-4,5-dimethoxyphenyl)-2-(4-methoxyphenyl)ethanone
32	OH		OCH_3	OCH_3			OCH_3	OCH_3		1-(2-Hydroxy-4,5-dimethoxyphenyl)-2-(3,4-dimethoxyphenyl)ethanone
33	OH		O—CH_2—O					OCH_3		1-(2-Hydroxy-4,5-methylenedioxyphenyl)-2-(4-methoxyphenyl)ethanone
34	OH		OH		OH			OH		1-(2,4,6-Trihydroxyphenyl)-2-(4-hydroxyphenyl)ethanone
35	OH		OH		OH			OCH_3		1-(2,4,6-Trihydroxyphenyl)-2-(4-methoxyphenyl)ethanone
36	OH		OH		OH		OCH_3	OH		1-(2,4,6-Trihydroxyphenyl)-2-(4-hydroxy-3-methoxyphenyl)ethanone
37	OH		OH		OH		OCH_3	OCH_3		1-(2,4,6-Trihydroxyphenyl)-2-(3,4-dimethoxyphenyl)ethanone
38	OH		OH		OH		O—CH_2—O			1-(2,4,5-Trihydroxyphenyl)-2-(3,4-methylendioxyphenyl)ethanone
39	OH		OH		OH		OCH_3	OCH_3	OCH_3	1-(2,4,6-Trihydroxyphenyl)-2-(3,4,5-trimethoxyphenyl)ethanone

Can. J. Chem. Downloaded from www.nrcresearchpress.com by 210.87.254.40 on 09/06/12
For personal use only.

TABLE 1 (*Concluded*)

No.	Z2	Z4	Z5	CH_2	
40					1-Phenylethanone
41	OH				1-(2-Hydroxyphenyl)ethanone
42	OH	OH		CH_2CH_3	1-(2,4-Dihydroxyphenyl)butanone
43	OH	OH	OH		1-(2,4,5-Trihydroxyphenyl)ethanone
44	OH	OH	OH	CH_3	1-(2,4,5-Trihydroxyphenyl)propanone
45	OH	OH	OH	CH_2CH_3	1-(2,4,5-Trihydroxyphenyl)butanone
46	OH	OH	OH	$CH(CH_3)_2$	1-(2,4,5-Trihydroxyphenyl)-3-methylbutanone
47	OH	OH	OH	$CH_2CH_2CH_3$	
48	OH	OH	OCH_3	CH_3	1-(2,4-Dihydroxy-5-methoxyphenyl)propanone
49	OH	OCH_3	OCH_3		1-(2-Hydroxy-4,5-dimethoxyphenyl)ethanone
50	OH	O—$C(Ph)_2$—O			1-[2-Hydroxy-4,5-(diphenylmethylenedioxy)phenyl]ethanone

and 2.5 s decoupling time. Deuterium exchange of the internally chelated proton was achieved by addition of 0.2 mL CD_3OD. The spectra of **1** and **40** in H_2SO_4 ($d = 1.84$) were referenced to external TMS.

Results and Discussion

The shifts are assigned in Tables 2 to 5, which are divided into sections containing the shifts of substructures with identical substitutional pattern. This arrangement reflects the fact that A-ring, B-ring, and -CO—CH_2- can be treated as subsystems with spectral properties independent of structural changes in different parts of the molecule. For identical substructures, the average shift δ of equal carbons is given. The standard deviation from the average shift never exceeds 0.6 ppm and is, in 55% of compounds examined, equal to or smaller than 0.1 ppm. Even identical A-ring substructures in dob and ap (cf. Tables 2 and 5) agree very well.

Following the guideline of subsystem constancy, the coupling constants are grouped like the shift values. For a single carbon, the constants are given in the order of decreasing magnitude. For identical A- and B-ring substructures, the multiplicity is given, average values $\bar{J}$ and the standard deviations (sd) are calculated, and the coupling protons are identified. Again, the values within a given substructure agree well.

Chemical Shifts

Signals were assigned on the basis of signal intensities, chemical shift ranges (5, 6), comparison with shieldings calculated from substituent-induced chemical shifts (scs) (5, 7), and matching to identical substructures, multiplicities of one-bond and three-bond C—H coupling, and matching against the fine-splitting pattern of assigned signals. These familiar directives left only two ambiguities in the dob and none in the ap series. Less trivial cases are discussed in the comments on the tables (*vide infra*).

In the A- and B-substructures with more than two substituents the experimental shifts differ grossly from the values obtained by simple summation of appropriate scs, even if the internal chelation between 1- and 2-substituent is accounted for (*vide infra*). This is expected, as *para*-substitution is always involved (8). The deviation affects all ring carbons in the subsystem and ranges from 8.9 ppm downfield to 5.7 ppm upfield. For the 2,4,5-trisubstituted A- and the 3′,4′-disubstituted B-subsystems the effect can be expressed qualitatively: oxygen-carrying carbons are shifted downfield, the other carbons upfield.

The 4′-substituted B-substructure also escapes additivity, although less significantly. The experi-

Can. J. Chem. Downloaded from www.nrcresearchpress.com by 210.87.254.40 on 09/06/12
For personal use only.

TABLE 2. Chemical shifts of deoxybenzoin A-ring carbons and carbons in adhering substituents, including scs calculated and mean experimental values.

	C-1	C-2	C-3	C-4	C-5	C-6	3-OCH_3	4-OCH_3	5-OCH_3
1	136.54	128.41	128.41	133.14	128.41	128.41			
calc	137.8	128.7	128.7	132.7	128.7	128.7			
1-δ_{PhH}	8.0	−0.1	−0.1	4.6	−0.1	−0.1			
2	119.45	161.88	117.97	136.24	119.10	131.02			
calc	123.9	155.3	115.8	134.7	120.8	130.0			
2-calc	−4.5	6.6	2.2	1.5	−1.7	1.0			
3	112.09	165.31	102.80	165.16	108.29	133.11			
4	112.15	165.31	102.83	165.25	108.39	133.16			
$\bar{\delta}$	112.12	165.31	102.82	165.21	108.34	133.14			
sd	0.04	0	0.02	0.06	0.07	0.04			
calc	111.9	163.5	105.4	163.1	106.5	132.6			
$\bar{\delta}$-calc	0.2	1.8	−2.6	2.1	1.8	0.5			
5	112.97	165.28	100.98	165.95	107.32	132.72		55.50	
6	113.03	165.28	101.01	166.01	107.38	132.69		55.53	
7	113.12	165.25	101.04	166.16	107.54	132.51		55.56	
$\bar{\delta}$	113.04	165.27	101.01	166.04	107.41	132.64		55.53	
sd	0.08	0.02	0.03	0.11	0.11	0.07		0.03	
calc	111.4	162.8	103.3	166.4	104.4	131.9			
$\bar{\delta}$-calc	1.6	2.5	−2.3	−0.4	3.0	0.7			
8	112.48	152.72	132.54	152.87	107.96	122.77			
calc	108.5	150.9	132.3	150.5	108.1	125.0			
8-calc	4.0	1.8	0.2	2.4	−0.1	−2.2			
9	114.73	156.90	136.38	158.63	103.83	127.44	60.02	56.16	
10	114.39	156.87	136.15	158.48	103.53	127.47	59.96	56.01	
$\bar{\delta}$	115.56	156.89	136.27	158.56	103.68	127.46	59.99	56.09	
sd	0.24	0.02	0.16	0.11	0.21	0.02	0.04	0.11	
calc	112.3	148.1	133.5	151.7	105.3	123.8			
$\bar{\delta}$-calc	2.3	8.8	2.8	6.9	−1.6	3.7			
11	110.84	159.12	103.49	154.99	138.36	115.45			
12	110.96	158.36	103.20	154.75	138.30	115.33			
13	110.66	158.82	103.23	154.84	138.30	115.61			
14	110.72	158.94	103.35	154.99	138.43	115.55			
15	110.66	158.88	103.26	154.93	138.36	115.52			
16	110.72	158.91	103.32	154.96	138.39	115.58			
17	110.75	158.91	103.32	154.93	138.39	115.58			
18	110.69	158.82	103.26	154.93	138.39	115.58			
19	110.78	158.94	103.35	154.93	138.36	115.55			
$\bar{\delta}$	110.75	158.86	103.31	154.92	138.36	115.53			
sd	0.10	0.21	0.09	0.08	0.04	0.09			
calc	113.5	155.9	107.0	150.5	133.4	120.0			
$\bar{\delta}$-calc	−2.8	3.0	−3.6	4.4	5.0	−4.5			
20	111.3	158.79	100.16	155.87	139.21	114.88		55.83	
21	111.15	158.63	100.16	155.75	139.09	115.03		55.80	
22	111.21	158.63	100.19	155.78	139.12	114.94		55.83	
23	111.21	158.91	100.10	155.72	139.03	115.09		55.83	
24	111.21	158.72	100.13	155.78	139.12	114.88		55.83	
$\bar{\delta}$	111.22	158.74	100.15	155.78	139.11	114.96		55.82	
sd	0.05	0.12	0.03	0.06	0.07	0.09		0.01	
calc	113.0	155.2	104.9	153.8	131.3	119.3			
$\bar{\delta}$-calc	−1.8	3.5	−4.8	2.0	7.8	−4.3			
25	110.51	160.21	103.68	155.93	141.22	112.97			56.50
26	110.39	160.03	103.56	155.72	141.10	113.21			56.44
27	110.45	160.03	103.62	155.84	141.19	113.27			56.53
$\bar{\delta}$	110.45	160.00	103.62	155.83	141.17	113.15			56.49
sd	0.06	0.10	0.06	0.11	0.06	0.16			0.05
calc	112.8	155.4	106.3	148.4	136.7	117.9			
$\bar{\delta}$-calc	−2.4	4.7	−2.7	7.4	4.5	−4.8			

TABLE 2 (*Concluded*)

	C-1	C-2	C-3	C-4	C-5	C-6	3-OCH_3	4-OCH_3	5-OCH_3		
28	110.93	159.97	100.53	156.84	141.88	112.42		55.95	56.44		
29	111.15	159.79	100.59	151.00	142.13	112.18		56.01	56.53		
30	110.78	160.03	100.53	156.72	141.79	112.48		55.92	56.41		
31	110.84	159.97	100.53	156.78	141.76	112.45		55.92	56.41		
32	110.87	159.97	100.53	156.78	141.85	112.45		55.92	56.44		
$\bar{\delta}$	110.91	159.98	100.54	156.84	141.88	112.40		55.94	56.45		
sd	0.14	0.03	0.03	0.14	0.15	0.12		0.04	0.05		
calc	112.3	154.7	104.2	151.7	134.6	117.2					
$\bar{\delta}$-calc	−1.4	5.3	−3.7	5.1	7.3	−4.8					
							O—CH_2—O	C-1″	C-2″	C-3″	C-4″
33	111.41	161.39	98.25	153.35	139.79	108.39	117.79	139.27	125.95	128.47	129.47
34	103.97	164.58	95.00	165.01	95.00	164.58					
35	103.96	164.55	95.00	165.04	95.00	164.55					
36	103.68	164.58	94.97	165.01	94.97	164.58					
37	103.96	164.58	95.00	165.04	95.00	164.58					
38	103.80	164.49	94.94	165.07	94.94	164.49					
39	103.96	164.55	95.00	165.10	95.00	164.55					
$\bar{\delta}$	103.89	164.56	94.99	165.05	94.99	164.56					
sd	0.12	0.04	0.03	0.04	0.03	0.04					
calc*	103.7	158.9	95.6	163.6							
calc†	99.3	165.1	97.8	164.7	93.9	159.5					
$\bar{\delta}$-calc†	4.6	−0.6	−2.8	0.4	1.1	5.1					
$\bar{\delta}$-calc*	0.2	5.7	−0.6	1.5							

*Based upon δ_2 and scs.
†Based upon δ_1 and scs.

mental shifts conform to a single parameter relationship (8)

[1] $\delta_{1'} = 135.0 + 1.15\ scs_p$ ($r^2 = 0.98$)

where scs_p is the *para*-scs of the 4′-substituent. The amplification factor (1.15) fits into the general trend found by Lynch (8).

Long range effects cause small deviations in the -CH_2—CO- subsystem. The carbonyl signals cover a range of ca. 4.6 ppm (neglecting **1**), and the methylene signals span more than 10 ppm (neglecting the ap). Table 4 arranges these shifts as A- and B-groups. A few relations are obvious although, once more, no general description can be presented.

The 2,4,6-trihydroxy-A-ring deshields the methylene signals by ca. 4.5 ppm. This polarization extends to the Cl′ carbon, which resonates ca. 1 ppm downfield from the respective average value $\delta_{Cl'}$, clearly beyond the standard deviation. The 2′-methoxy group in **12** shifts the methylene signal upfield to 38.8 ppm. Apparently, both effects are transmitted sterically. The remaining dob methylene carbons appear between 43.4 and 44.9 ppm, with no eye-catching correlation.

The series **5**, **6**, **7** and **30**, **31**, **28**, **29**, respectively, in which in a given structure only the 4′-substituent is altered, are examples of the now well documented scs via methylene insulators (9). The carbonyl shifts may be correlated to the σ_p-constants (10) of the 4′-substituents[1]

[2] **5**,**6**,**7**: $\delta_{C=O} = 202.14 - 2.005\ \sigma_p$ ($r^2 = 0.999$)

[3] **30**, **31**, **28**, **29**: $\delta_{C=O} = 201.84 - 1.961\ \sigma_p$ ($r^2 = 0.997$)

In contrast, the methylene shifts respond irregularly to 4′-substitution, similar to results of Cook and co-workers (9).

C—H Coupling Constants

The proton-coupled spectra of all compounds could be analysed by first order rules, with very few exceptions (see Tables 6 to 8). Again, less trivial splittings are referred to in the footnotes of the tables (*vide infra*).

The one-bond coupling constants ^1J follow the known trend, decreasing on electron-releasing substitution and vice versa. Exceptions are C-3,6 in **33** and **50** and C-2′,5′ in **38**, all of which are located

[1]The correlation coefficients r^2 are given for illustrative reasons only; of course, the correlations lack statistical significance because of the low number of data points. On the other hand, the close resemblance of slopes and intercepts gives some weight to the approach.

Can. J. Chem. Downloaded from www.nrcresearchpress.com by 210.87.254.40 on 09/06/12
For personal use only.

TABLE 3. Chemical shifts of deoxybenzoin B-ring carbons and carbons in adhering substituents, including scs calculated and mean experimental values.

	C-1′	C-2′	C-3′	C-4′	C-5′	C-6′	2′-OCH_3	3′-OCH_3	4′-OCH_3
1	135.00	129.69	128.60	126.59					
9	134.97	129.53	118.50	126.78					
11	135.12	129.38	128.50	126.71					
20	135.00	129.47	128.47	126.71					
25	135.18	129.44	128.47	126.68					
28	135.12	129.53	128.47	126.71					
$\bar{\delta}$	135.07	129.51	128.52	126.70					
sd	0.09	0.11	0.09	0.06					
calc	137.8	129.1	128.5	125.4					
$\bar{\delta}$-calc	−2.7	0.4	0.0	1.3					
12	123.71	157.18	110.66	128.20	120.31	130.96	55.35		
calc	120.4	159.7	113.8	127.6	120.4	130.4			
12-calc	3.3	−2.5	−3.1	0.6	−0.1	0.6			
3	125.10	130.23	115.42	156.33					
5	124.83	130.00	115.49	156.42					
13	125.26	130.20	115.43	156.27					
21	125.04	130.26	115.49	156.39					
26	125.29	130.26	115.46	156.30					
30	125.01	130.29	115.49	156.42					
34	126.29	130.57	115.15	156.07					
$\bar{\delta}$	125.27	130.26	115.42	156.3					
sd	0.48	0.17	0.12	0.12					
calc	127.5	131.1	115.9	153.6					
$\bar{\delta}$-calc	−2.2	−0.8	−0.5	2.7					
29	142.13	131.08	123.31	146.74					54.98
calc	141.1	130.3	123.2	146.3					
29-calc	1.0	0.8	0.1	0.4					
2	126.32	130.63	113.94	158.37					54.98
4	126.93	130.45	113.94	158.36					54.98
6	126.65	130.45	158.42						54.98
8	126.99	130.45	131.91	158.30					54.98
10	126.62	130.48	113.97	158.39					54.98
14	127.08	130.41	113.97	158.36					55.01
22	126.83	130.45	113.94	158.33					55.01
27	127.11	130.45	113.94	158.33					54.98
31	126.92	130.54	113.97	158.36					54.98
33	126.68	130.45	113.97	158.39					54.98
35	128.02	130.69	113.54	158.09					54.95
$\bar{\delta}$	126.92	130.50	113.91	158.34					54.98
sd	0.43	0.09	0.13	0.09					0.02
calc	127.0	130.4	113.8	156.9					
$\bar{\delta}$-calc	0.1	0.1	−0.1	1.4					
7	132.24	131.26	128.44	133.54*					
calc	133.1	130.5	128.7	133.1					
7-calc	−0.9*	0.8	−0.7	0.4*					

					C-α	C-β	C-γ	C-δ
15	126.89	130.32	114.42	157.56	63.02	14.69		
16	126.89	130.35	114.51	157.84	69.12	22.27	10.41	
17	126.83	130.4	115.76*	156.60*	69.39	21.94		
18	126.89	130.35	114.48	157.81	67.27	30.98	18.87	13.68
$\bar{\delta}$	126.88	130.36	114.47*	157.74*				
sd	0.03	0.04	0.05	0.15				

Can. J. Chem. Downloaded from www.nrcresearchpress.com by 210.87.254.40 on 09/06/12
For personal use only.

TABLE 3 (*Concluded*)

	C-1′	C-2′	C-3′	C-4′	C-5′	C-6′	O—CH_2—O	3′-OCH_3	4′-OCH_3
23	125.80	116.55	145.31	144.25	115.76	120.22			
calc	129.1	118.5	142.8	141.0	117.5	123.5			
23-calc	−3.3	−1.9	2.5	3.3	−1.7	−3.3			
36	128.84	117.12	146.38	146.38	111.84	120.37		55.77	
calc	128.4	116.4	146.1	138.9	116.8	123.2			
36-calc	0.4	0.7	0.3	7.5	−5.0	−2.6			
19	127.59	113.30	148.89	147.89	111.84	121.58		55.68	55.68
24	127.38	113.30	148.92	147.92	111.84	121.65		55.68	55.68
32	127.47	113.42	148.98	147.98	111.97	121.71		55.62	55.62
37	128.69	113.82	148.62	147.62	111.60	121.80		55.68*	55.62*
$\bar{\delta}$	127.78	113.46	148.85	147.85	111.82	121.71		55.67*	55.65*
sd	0.61	0.25	0.16	0.16	0.15	0.13		0.03*	0.03*
calc	127.9	115.7	144.0	142.2	114.7	122.3			
$\bar{\delta}$-calc	−0.1	−2.2	4.9	5.7	−2.9	−0.6			
38	129.63	110.21	147.26	145.95	107.84	122.59	100.68		
39	131.69	107.26	152.75	136.42				55.86	60.11
calc	128.8	107.6	144.9	127.5					
39-calc	2.9	−0.3	7.9	8.9					

*Assignments may be reversed.

next to a five-ring acetal. Their ^1J constants are distinctly larger than those of corresponding hydroxy- and methoxy-substituted compounds (differences up to 7.9 Hz, see Table 9). Similar effects were reported for strained benzocycloalkanes relative to benzocyclohexene (11). Of the methoxy carbons, not only the chemical shift is typical of the substitutional position, but also the one-bond coupling. Both parameters are helpful in signal assignment.

As usual (12), three-bond constants ^3J are the largest observed long-range couplings. Oxy-substituents slightly affect the ^3J values. Generally, $^3J_A \geqq {}^3J_B$ (differences up to 2.6 Hz), and $^3J_C \leqq {}^3J_D$ (differences up to 2.2 Hz). Three-bond coupling exceeds the arene rings and involves more remote substituent atoms: C=O/2,6-H; C-1/2-OH; C-3/2-OH; C-2′,6′/CH_2-; C/OCH_3. The latter coupling usually makes the respective carbon appear as a broad unresolved signal. An oxy-substituent on a carbon magnifies its ^2J constants into the resolution range of the spectrometer, up to values as large as 4.9 Hz. We observe these couplings for C-2/3-H; C-2/2-OH; C-4/5-H; C-6/5-H; C-4′/3′,5′-H.

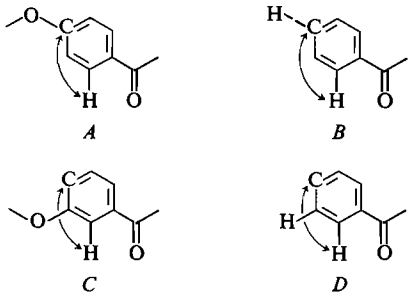

Internal Chelation

In **2** to **39** and **41** to **50**, the 2-OH proton is chelated by the carbonyl oxygen in an internal hydrogen-bond, which is reflected both in the coupled and decoupled spectra. It destroys the scs-additivity expected for the A-ring shifts of **2** and **41** (8). The experimental shifts δ_{exp} are linear combinations of the calculated values δ_0 and $\delta_\pm$ for the hypothetical structures *E* and *F*, with a slight excess of *E*.

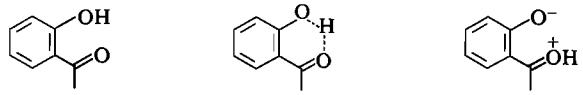

2: $\delta_{exp} = 8.18 + 0.494\,\delta_0 + 0.442\,\delta_\pm$ ($R = 0.005$)[2]

41: $\delta_{exp} = 9.08 + 0.505\,\delta_0 + 0.424\,\delta_\pm$ ($R = 0.005$)

In order to obtain the scs of the protonated carbonyl substituents, we determined the shifts of C-1 to C-6 of H_2SO_4 solutions of **1** and **40**:

	C-1	C-2,6	C-3,5	C-4
1	128.81	135.18	130.54	144.55
40	129.78	135.43	131.12	145.08

[2] $R = \Sigma(y\text{-}y)^2/\Sigma(y\text{-}\bar{y})^2$. In contrast to r^2, $R = 0$ means ideal, $R = 1$ no correlation.

Can. J. Chem. Downloaded from www.nrcresearchpress.com by 210.87.254.40 on 09/06/12
For personal use only.

Can. J. Chem. Downloaded from www.nrcresearchpress.com by 210.87.254.40 on 09/06/12
For personal use only.

TABLE 4. Chemical shifts of deoxybenzoin carbonyl and methylene carbons, following (a) the sequences in Table 2, and (b) in Table 3.

(a)			(b)		
	C=O	CH_2		C=O	CH_2
1	197.38	44.94	**1**	197.38	44.94
2	204.39	44.21	**9**	203.00	44.76
3	202.48	43.48	**11**	201.30	44.51
4	202.24	43.36	**20**	201.84	44.60
5	202.90	43.66	**25**	201.39	44.78
6	202.66	43.57	**28**	201.93	44.85
7	201.69	43.66	**12**	201.45	38.81
8	202.97	44.33	**29**	200.29	44.45
9	203.00	44.76	**3**	202.48	43.48
10	203.39	43.75	**5**	202.90	43.66
11	201.30	44.51	**13**	201.96	43.63
12	201.45	38.81	**21**	202.48	43.82
13	201.96	43.63	**26**	202.12	43.85
14	201.66	43.63	**30**	202.54	44.06
15	201.63	43.57	**34**	203.09	48.31
16	201.69	43.60	**2**	204.39	44.21
17	201.72	43.51	**4**	202.24	43.36
18	201.69	43.51	**6**	202.66	43.51
19	201.60	44.06	**8**	202.97	43.33
20	201.84	44.60	**10**	203.39	43.75
21	202.48	43.82	**14**	201.66	43.63
22	202.21	43.72	**22**	202.21	43.72
23	202.54	44.18	**27**	201.84	43.79
24	202.05	44.21	**31**	202.33	43.94
25	201.39	44.78	**33**	202.27	43.72
26	202.12	43.85	**35**	202.78	48.28
27	201.84	43.79	**15**	201.63	43.51
28	201.93	44.85	**16**	201.69	43.60
29	200.29	44.45	**17**	201.72	43.51
30	202.54	44.06	**18**	201.69	43.51
31	202.33	43.94	**7**	201.69	43.66
32	201.21	44.36	**23**	202.54	44.18
33	202.27	43.72	**36**	202.42	48.64
34	203.09	48.31	**19**	201.60	44.06
35	202.78	48.28	**24**	202.05	44.21
36	202.42	48.64	**32**	202.21	44.36
37	202.66	48.70	**37**	202.66	48.70
38	202.42	48.64	**38**	202.42	48.70
39	202.30	49.34	**39**	202.30	49.34

	C=O	C-α	C-β	C-γ	C-δ
40	204.94	26.64			
41	204.57	39.36	18.02	13.75	
42	201.84	26.16			
43	204.72	30.83	8.47		
44	204.03	39.45	17.93	13.75	
45	203.88	46.58	25.55	22.64	
46	204.24	37.32	26.76	22.12	13.81
47	204.51	30.86	8.34		
48	202.39	26.52			
49	202.48	26.61			

To our knowledge, the *para*-scs are the largest downfield shifts reported so far. The shift calculations for **3** to **39** and for **42** to **50** are based on δ_{exp} of **2** and **41**, respectively.

In contrast to ordinary hydroxy protons, the internally chelated 2-hydroxy group gives rise to carbon splittings (13, 14). ^3J coupling with C-1 and C-3 and ^2J coupling with C-2 are observed (see Tables 6 and 8). These splittings could be eliminated by deuterium exchange (13). Remarkably, the 2,4,6-trihydroxy compounds **34** to **39** lack these splittings, most probably because the 6-OH group sterically interacts with methylene (*vide supra*) and cannot be chelated as a result. Only very few ^4J constants are resolved. We observe, in **35** and **37**, C-2/5-H and C-6/3-H (^4J = 1.2, 1.5 Hz); in **33**, C-3/6-H (^4J = 1.2 Hz).

Comments on the Assignments in the Tables

C-1/C-1', C-2,6/C-3,5, C-2',6'/C-3',5' in 1 (Tables 2 and 3) A rough assessment of the arene shifts using scs values for -$COCH_3$ and -CH_3 (see Table 2) does not sufficiently discriminate the named carbons. C-1' and C-2',6'/C-3',5' are identified by matching against the spectra of **9**, **11**, **20**, **25**, and **28**, with identical B-rings; C-2',6' show more long range splitting (two *meta* couplings) than C-3',5' (one *meta*-coupling) and hence lower and broader signals (Table 8).

C-3/C-5 in 2 (Table 2) and 40 (Table 5) C-3 is recognized by its additional three-bond coupling to 2-OH found in all spectra of **2** to **33** (Table 7) and **40** to **49** (Table 9). Also, the C-5 signal shifts only slightly upon oxy-substitution (**8**, **9**, **10**, Table 2) in the 3-position.

C-2/C-4 in 11 to 19 and 25 to 27 (Table 2) The C-2 signal is dt (6-H, 3-H, 2-OH), C-4 is dd (C-6, 3-H). Also, the relative signal sequence is predicted by the calculation. Finally, the C-2 shifts agree well with those in **20** to **24**.

C-2,6/C-4 in 34 to 39 The carbons are identified by their relative signal intensities in the nOe suppressed gated-decoupling spectrum of **35** as well as in the broad-band decoupled spectra.

C-1'/C-4' in 7 (Table 3) From eq. [1] (*vide supra*), $\delta_{C\text{-}1'}$ = 132.70 ppm. This value is closer to 132.24 ppm than to 133.54 ppm.

C-3'/C-4' in 23 (Table 3) In the coupled spectrum, C-3' appears as dd (5'-H, 2'-H), C-4' as td (2'-H, 6'-H, 5'-H).

C-2'/C-5' in 23, 36, 19, 24, 32, 37 (Table 3) C-2' is identified by its long range splittings (6'-H, CH_2), whereas C-5' only couples to 5'-H (Table 7).

C-1'/C-4' in 39 (Table 3) C-4' is a long range t,

TABLE 5. Chemical shifts of acetophenones, including scs calculated and mean experimental values.

	C-1	C-2	C-3	C-4	C-5	C-6	4-OCH_3	5-OCH_3			
40	120.04	162.24	118.16	136.48	119.16	131.32					
calc	125.2	155.6	116.1	134.3	121.1	130.3					
40-calc	−5.0	6.6	2.1	2.2	−1.9	1.0					
41	112.63	165.06	102.89	165.06	108.23	132.45					
calc	112.4	163.8	105.6	163.4	106.6	132.9					
41-calc	0.2	1.3	−2.7	1.7	1.6	−0.4					
42	111.48	158.15	103.11	154.75	138.27	115.73					
43	111.09	158.42	103.38	154.33	138.15	114.94					
44	111.06	158.33	103.23	154.54	138.24	115.03					
45	111.45	158.69	103.32	154.63	138.21	115.24					
46	111.09	158.48	103.29	154.54	138.21	115.06					
$\bar{\delta}$	111.23	158.41	103.27	154.56	138.22	115.20					
sd	0.21	0.20	0.10	0.15	0.04	0.32					
calc	114.0	156.2	107.2	150.8	133.5	120.3					
$\bar{\delta}$-calc	−2.8	2.2	−3.9	3.8	4.7	−5.1					
47	110.72	159.60	103.69	155.51	141.16	124.8		56.59			
calc	113.3	155.7	106.5	148.7	136.8	118.2					
47-calc	−2.6	3.9	−2.8	6–9	4.3	−5.7					
48	111.63	159.48	100.31	156.81	141.82	112.69	55.92	56.47			
calc	112.8	155.0	104.4	152.0	134.7	117.5					
48-calc	−1.2	4.5	−4.0	4.8	7.1	−4.8					
							O—CH_2—O	C-1″	C-2″	C-3″	C-4″
49	112.54	161.39	98.25	153.35	139.79	108.39	117.79	139.27	125.95	128.47	129.47

Can. J. Chem. Downloaded from www.nrcresearchpress.com by 210.87.254.40 on 09/06/12
For personal use only.

with a constant (5.8 Hz) typical of three-bond coupling.

Methoxy Carbons

From the methoxy carbon signals, δ and ^1J values are obtained. Obviously, these data have constant values, typical for any given substitution position (Tables 2, 3, 5–8). Thus, 4-OCH_3 (δ = 55.5 to 56.1 ppm; ^1J = 145.3 to 145.9 Hz), 5-OCH_3 (55.0 to 55.7 ppm; 143.9 to 144.0) are easily assigned by matching against the respective subsystem spectra. Only 3′-OCH_3 and 4′-OCH_3 cannot be discriminated in the single case where their resonances are resolved (**37**). In the spectrum of **39**, where steric crowding breaks up these rules, 3′-OCH_3 and 4′-OCH_3 are recognized from their relative signal intensities.

C—H Coupling

C-2′, C-5′, C-6′ in 1, 9, 11, 20, 25, 28 (Table 7) Low and high field parts of the ^1J-doublets are not identical. We ascribe this to spin state mixing.

C-2′,6′ in 1, 9, 11, 20, 25, 28 (Table 7) These signals appear as odd long-range multiplets. They are less intense and broader than those of C-3′,5′.

C-3′,5′ in 1, 9, 11, 20, 25, 28 (Table 7) The high field part of the ^1J-doublet is a doublet, at low field the X-part of an ABX system appears.

C-4′ in 1, 9, 11, 20, 25, 28 (Table 7) The high field part has a quintet- or septet-like shape, the low field part is more complicated.

C-1′ in 12, 3, 5, 13, 21, 26, 30, 2, 4, 6, 8, 10, 14, 22, 27, 31, 35, 16, 17, 18 (Table 7) The signals have quintet-shape, ascribed to ^3J coupling with 3,5-H and, tentatively, to ^2J coupling of similar magnitude to either 2,6-H or to the methylene protons.

C-1′ in 23, 26, 32 (Table 7) The signals are quartets, from ^3J coupling to 5-H and one pair of the above mentioned protons.

Can. J. Chem. Downloaded from www.nrcresearchpress.com by 210.87.254.40 on 09/06/12
For personal use only.

TABLE 6. C—H coupling constants in deoxybenzoin A-rings and adhering substituents, including mean experimental values.

	C-1	C-2	C-3	C-4	C-5	C-6	C=O	3-OCH_3	4-OCH_3
1	t 6.3 (3,5-H)	d —	d —	d 162.0 (4-H) t 7.5 (2,6-H)	d —	d —	t 6.0 (2,6-H) t 2.5 (CH_2)		
1·H^+	t 8.3 (3,5-H)	d 167.3 (2-H)	d 170.0 (3-H)	d 168.0 (4-H)	See C-3	See C-2	m		
2	d 6.0 (2-OH) t 5.0 (3,5-H)	qa 6.0 (4,6-H)	d 162.2 (3-H) t 7.1 (5-H, 2-OH)	d 161.4 (4-H) d 8.8 (6-H)	d 163.3 (5-H) m*	d —	qa ~5.6 (6-H, CH_2)		
3	—	d ~11.5 —	d 161.1 b	d ~11.1 —	d 162.6 d 4.9	d 158.1	qa ~4.9		
4	—	d ~11.5 d ~3.0 (3-H)	d 161.7 b	d ~11.5 t ~3.1 (3,5-H)	d 163.3 d 5.2	d 158.1	qa 4.3		
$\bar{J}\pm$sd		d 11.5 (6-H)	d 161.2±0.4 (3-H)	d 11.1 (6-H)	d 163.0±0.5 (5-H) d 5.1±0.2(3-H)	d 158.1 (6-H)	qa 4.6±0.4 (6-H, CH_2)		
5	t ~5.7 (3,5-H)	d ~8.4 d ~4.8	d 161.1 d ~6.0 d ~4.8	b	d 164.2 d 4.9	d 158.7	t ~5.7		qa 145.3
6	qa ~6.0 (3,5-H, 2-OH)	d ~9.0 d ~4.8	d 161.2 d ~6.6 d ~4.5	d	d 164.2 d 4.9	d 159.3	qa 4.5 (6-H, CH_2)		qa 145.3
7	t ~6.2 (3,5-H)	d 8.5 d 4.3	d 161.1 d 4.3 (5-H)	b	d 163.9 d 5.2	d 158.7	qa 5.1 (6-H, CH_2)		qa 145.3
$\bar{J}\pm$sd		d 8.6±0.3 (6-H) d 4.6±0.3 (3-H)	d 161.1±0.1 (3-H) d 6.3±0.4 (2-OH) d 4.5±0.3 (5-H)		d 164.1±0.2 (5-H) d 5.0±0.2 (3-H)	d 158.9±0.4 (6-H)			qa 145.3±0
8	d 7.9 (5-H)	d 9.2 (6-H)	d 5.8 d 0.9 (5-H, 2-OH)	d 11.0 (6-H) d 2.4 (5-H)	d 161.7 (5-H)	d 158.7 (6-H)	qa 5.8 (6-H, CH_2)		
10	d 8.5 (5-H)	d 9.8 (6-H)	d 8.7 d 5.1 (5-H, 2-OH)	—	d 163.0 (5-H)	d 159.9 (6-H)	qa 6.1 (6-H, CH_2)	qa 144.6	qa 145.9
11	t ~5.2	d ~8.8 t ~4.0	d 159.5 d 6.7	d 8.5 d 3.7	d 7.3 d 4.9	d 156.3	qa 5.5		

Can. J. Chem. Downloaded from www.nrcresearchpress.com by 210.87.254.40 on 09/06/12
For personal use only.

TABLE 6 (*Continued*)

	C-1	C-2	C-3	C-4	C-5	C-6	C=O	4-OCH_3	5-OCH_3
12	t 4.9	d 9.8 t 4.9	d 158.1 d 7.3	d 8.0 b	d 7.0 d 4.6	d 151.5	qa 4.4		
13	t ~4.2	d ~9.6 t ~4.8	d 160.2 d 6.4	d 8.2 d 3.4	d 7.3 d 4.9	d 158.1	qa 4.3		
14	b	b	d ~160.0 d ~4.8	d 8.2 d 3.4	d 7.3 d 4.9	d 156.9	qa ~4.8		
15	t ~7.2	m	d ~159.7 d ~5.9	d 6.5 m	d ~7.2 b	d 156.9	qa ~4.8		
16	—	d ~7.2 b	d ~160.0 b	d 7.9 d 3.7	d 7.3 d 4.9	d 151.5	qa 5.5		
17	t 5.2	d 8.8 t 4.9	d 159.3 d 7.3	d 7.2 b	d 7.3 d 4.9	d 158.7	qa ~5.1		
18	—	d m	d ~159.4 b	d 8.6 d 3.7	d 7.0 d 4.9	d 156.9	qa 5.2		
19	t 4.5	d 9.2 t 3.4	d 160.2 d 5.9	d 8.1 d 3.4	d 7.0 d 4.9	d 157.2	qa 5.4		
$\bar{J}\pm$sd	t 5.2±1.1 (3-H, 2-OH)	d 8.9±0.9 (6-H) t 4.4±0.7 (3-H, 2-OH)	d 159.6±0.7 (3-H) d 6.3±0.9 (2-OH)	d 7.9±0.7 (6-H) d 3.6±0.2 (3-H)	d 7.2±0.2 (3-H) d 4.9±0.1 (6-H)	d 157.3±0.7 (6-H)	qa 5.0±0.5 (6-H, CH_2)		
20	t 5.5	d 9.4 t 4.7	d 159.9 d 7.3	b	d 7.3 d 4.9	d 156.3	qa 5.5	qa 145.3	
21	—	d 9.4 t 4.6	d 159.9 d 7.3	—	d 7.6 d 4.8 d 2.4	d 158.1 d 4.2	qa 5.2	qa 145.7	
22	t 5.5	d 9.4 t 4.6	d 159.9 d 7.3	b	d 7.3 d 4.9	d 175.5	qa 4.6	qa 145.7	
23	—	d 9.6 t 4.0	d 160.3 d 6.6	m	d 7.4 d 4.8	d 157.5	qa 5.6	qa 145.3	
24	t ~5.0	d 9.0 t 4.0	d 159.9 d 6.0	d ~9.0 b	d 7.3 d 4.9	d 158.1	qa 5.2	qa 145.6	
$\bar{J}\pm$sd	t 5.3±0.3 (3-H, 2-OH)	d 9.4±0.2 (6-H) t 4.4±0.4 (3-H, 2-OH)	d 160.0±0.2 (3-H) d 6.9±0.6 (2-OH)		d 7.4±0.1 (3-H) d 4.9±0.1 (6-H)	d 157.5±0.7 (6-H)	qa 5.2±0.4 (6-H, CH_2)	qa 145.5±0.2	
25	t 4.5	d 8.6 t 3.9	d 159.8 d 6.1	d 8.5 d 3.4	qi 7.5 qi 4.3	d 156.9	qa 5.2		qa 144.0
26	t 5.2	d 9.0 d 5.0 d 3.8	d 160.5 d 7.3	—	qi ~7.5 qi ~3.8	d 157.5	qa 5.5		qa 144.0
27	t 5.5	d 9.1 t 4.3	d 160.2 d 7.6	d ~7.7 d	m	d 156.9	qa 4.3		qa 144.3
$\bar{J}\pm$sd	t 5.1±0.5 (3-H, 2-OH)	d 8.9±0.3 (6-H) d 4.4±0.6 d 4.0±0.3 (3-H, 2-OH)	d 160.2±0.4 (3-H) d 7.0±0.8 (2-OH)	d 8.1±0.6 (6-H) d 3.4	d 7.5 (3-H)	d 157.1±0.4 (6-H)	qa 5.0±0.6 (6-H, CH_2)		qa 144.1±0.2

Can. J. Chem. Downloaded from www.nrcresearchpress.com by 210.87.254.40 on 09/06/12
For personal use only.

TABLE 6 (*Concluded*)

	C-1	C-2	C-3	C-4	C-5	C-6	C=O	4-OCH_3	5-OCH_3
28	t 4.8	d ~8.3 t ~4.2	d 160.5 d 6.1	b	d 7.4 t 3.7	d 157.5	qa ~5.8	qa 145.7	qa 144.3
29	t 5.2	d 9.0 t 4.6	d 160.8 d 7.0	b	d 7.4 qi 4.0	d 158.1	qa ~5.8	qa 145.9	qa 144.3
30	t 5.5	d 8.5 t 4.3	d 160.2 d 7.6	—	d ~7.8 qi ~3.9		~		
31	t 4.5	d 8.9 t 4.5	d 161.0 d 6.0	d 8.0 qi 4.0	d 8.0 qi 4.0	d 157.5	qa 4.9	qa 145.7	qa 144.3
32	t 5.5	d 9.2 t 4.6	d 161.1 d 7.3	d ~9.0 qi ~4.5	d 8.1 qi 4.1	d 158.1	qa 5.2	qa 145.7	qa 144.0
$\bar{J}\pm$sd	t 1.5±0.4 (3-H, 2-OH)	d 8.8±0.4 (6-H) t 4.4±0.2 (3-H, 2-OH)	d 160.7±0.4 (3-H) d 6.7±0.7 (2-OH)	d 8.5±0.7 (6-H) qi 4.3±0.4 (3-H, 4-OCH_3)	d 7.9±0.3 (3-H) qi 3.9±0.2 (6-H, 5-OCH_3)	d 157.7±0.4 (6-H)	qa 5.5±0.4 (6-H, CH_2)	qa 145.7±0.1	qa 144.2±0.1
33	t ~5.7 (3-H, 2-OH)	d ~7.9 (6-H) d ~4.0 (2-OH) d ~3.3 (3-H)	d ~167.2 (3-H) d ~7.3 (2-OH) d ~1.2	d ~6.6 b	m	d 164.2 (6-H)	qa ~5.2 (6-H, CH_2)	t 176.4	(OCH_2O)
34	—	b	d 161.4 d ~4.8	t ~3.0	See C-3	See C-2	b		
35	t 4.9	t 1.2	d 161.4 d 4.6	t 3.1	See C-3	See C-2	t 6.1		
36	t ~5.2	b	d ~161.0 b	b	See C-3	See C-2	t 5.6		
37	t ~5.2	t 1.5	d 161.4 d 4.6	t 3.1	See C-3	See C-2	t 6.2		
38	t ~7.2	b	d ~162.8 b	b	See C-3	See C-2	t 6.5		
39	t ~4.0	b	d 161.4 d 4.6	t 3.1	See C-3	See C-2	t 6.1		
$\bar{J}\pm$sd	t 4.8±0.6 (3,5-H)	t 1.4±0.2 (3-H)	d 161.3±0.2 (3-H) d 4.7±0.1 (5-H)	t 3.1±0.1 (3,5-H)	d 161.3±0.2 (5-H) d 4.7±0.1 (3-H)	t 1.4±0.2 (3-H)	t 6.1±0.3 (CH_2)		

Can. J. Chem. Downloaded from www.nrcresearchpress.com by 210.87.254.40 on 09/06/12
For personal use only.

TABLE 7. C—H coupling constants in deoxybenzoin B-rings and adhering substituents, including mean experimental values.

	CH_2	C-1′	C-2′	C-3′	C-4′	C-5′	C-6′	2′-OCH_3
1		5.7 d 2.2 m[x]	158.0 d	162.8 d ~6.0‡ m*	160.8 d	See C-3′	See C-2′	See text
11	t 128.8 t 1.5	m	157.9 d m[x]	158.7 d 4.9‡ m*	160.5 d	See C-3′	See C-2′	
20	t 129.0 b	m	156.5 d m[x]	158.9 d 4.9‡ m*	159.4 d	See C-3′	See C-2′	
25	t 128.8 b	b	158.4 d b[x]	159.9 d 4.9‡ m*	159.4 d	See C-3′	See C-2′	
28	t ~128.5 b	m	157.6 d m[x]	158.7 d 5.5‡ m*	161.2 d	See C-3′	See C-2′	
$\bar{J}$+sd	t 128.8±0.2 (CH_2)		157.7±0.7 d (2′-H)	159.8±1.8 d (3′-H) 5.2±0.5 d (5′-H)	160.3±0.8 d (4′-H)	159.8±1.8 d (5′-H) 5.2±0.5 d (3′-H)	157.7±0.7 d (6′-H)	
12	t ~127.2 (CH_2) b	qi ~6.0 (3′,5′-H)	m	158.7 d (3′-H) 7.9 d (5′-H)	158.7 d (4′-H) 8.6 d (6′-H)	161.4 d (5′-H) 7.6 d (3′-H)	~158.9 d (6′-H) ~8.2 d (4′-H) ~5.2 t (CH_2)	141.0 qa (2′-OCH_3)
29	t 128.8 (CH_2) t 3.7 (2′,6′-H)	t 7.6 (3′-5′-H)	164.8 d (2′-H) 6.7 d (6′-H) 4.6 t (CH_2)	169.1 d (3′-H) 4.8 d (5′-H)	t	See C-3′	See C-2′	
3	t	qi 8.9	156.9 d 7.3 d 4.9 t	158.4 d 5.2 d	8.9 t 2.4 t	See C-3′	See C-2′	
5	t ~129.6 qa 4.3	qi 7.3	157.5 d 6.7 d 4.9 t	~159.4 d b	~7.8 t b	See C-3′	See C-2′	
13	t 128.2 3.7	qi 7.6	157.7 d 7.0 d	158.7 d 5.2 d	8.9 t 2.4 t	See C-3′	See C-2′	
21	t 127.8 3.7	qi 7.4	157.5 d 7.2 d	159.3 d 4.6 t	9.0 t 2.2 qa	See C-3′	See C-2′	
26	t 128.2 t 3.7	qi 6.7	157.5 d 7.3 d 4.9 t	159.3 d 4.3 t	~9.0 t b	See C-3′	See C-2′	
30	t 128.2 t 4.3	qi 7.0	157.5 d 7.3 d 4.4 t	158.7 d ~4.7 d	~9.0 t b	See C-3′	See C-2′	
34	t ~127.5 t	—	d m	158.7 d ~4.6 d	~8.3 t b	See C-3′	See C-2′	
$\bar{J}$±sd	t 128.3±0.2 (CH_2) t 3.9±0.3 (2′,6′-H)	qi 7.5±0.8 (3′,5′-H)	157.4±0.3 d (2′-H) 7.1±0.2 d (6′-H) 4.9±0.3 d (CH_2)	158.0±0.4 d (3′-H) 4.8±0.4 d (5′-H)	8.7±0.5 t (2′,6′-H) 2.3±0.1 t (3′,5′-H)	158.8±0.4 d (5′-H) 4.8±0.4 d (3′-H)	157.4±0.3 d (6′-H) 7.1±0.2 d (2′-H) 4.9±0.3 t (CH_2)	

Can. J. Chem. Downloaded from www.nrcresearchpress.com by 210.87.254.40 on 09/06/12
For personal use only.

TABLE 7 (*Continued*)

	CH_2	C-1′	C-2′	C-3′	C-4′	C-5′	C-6′	Others
2	t 128.5 t 4.1	qi 6.8	d 157.2 d t	d 159.9 d 4.9	b	See C-3′	See C-2′	qa 144.0
4	t 128.8 t 4.3	qi 7.3	d 158.5 d 6.9 t 4.9	d 159.3 d 4.9	m	See C-3′	See C-2′	qa 143.8
6	t 128.8 t 4.3	qi 6.1	d 158.7 d 7.3 t 4.9	d 159.9 d 4.9	t 9.2 (2′,6′-H) b	See C-3′	See C-2′	qa 144.0
8	t ~126.9 b	qi ~7.8	d ~159.3 d ~6.9 t ~5.2	d 159.6 d 4.6	m	See C-3′	See C-2′	qa 144.0
10	t 128.8 t 5.5	qi 7.3	d 158.7 d 7.3 t 4.3	d 159.9 d 4.9	—	See C-3′	See C-2′	qa 144.0
14	t 128.2 t 4.3	qi 7.3	d 158.1 d 7.3 t 4.9	d 159.6 d 4.6	b	See C-3′	See C-2′	qa 143.8
22	t 128.2 t 3.7	qi 7.3	d 158.7 d 7.3 t 4.3	d 159.6 d 5.2	—	See C-3′	See C-2′	qa 143.8
27	t 128.8 t 3.7	qi 7.3	d 158.7 d 7.3 t 4.7	d 160.2 d 4.6	b	See C-3′	See C-2′	qa 144.0
31	t 128.2 t 4.5	qi 7.3	d 158.1 d 7.3 t 4.9	d 159.9 d 4.9	b	See C-3′	See C-2′	qa 144.0
33	t 128.6 t 3.8	—	d 158.7 d 7.3 t 5.1	d 160.2 d 4.6	b	See C-3′	See C-2′	qa 144.0
35	t 129.4 t 3.7	qi 6.7	d 158.1 d 7.3 t 4.9	d 159.5 d 4.9	b	See C-3′	See C-2′	qa 143.6
$\bar{J}\pm$sd	t 128.5±0.6 (CH_2) t 4.2±0.6 (2′,6′-H)	qi 7.1±0.4 (3′,5′-H)	d 158.4±0.5 (2′-H) d 7.2±0.2 (6′-H) t 4.8±0.3 (CH_2)	d 159.8±0.3 (3′-H) d 4.8±0.2 (5′-H)		d 159.8±0.3 (5′-H) d 4.8±0.2 (3′-H)	d 158.4±0.5 (6′-H) d 7.2±0.2 (2′-H) t 4.8±0.3 (CH_2)	qa 143.9±0.1 (4′-OCH_3)
15	t ~27.5 b	t ~5.9 b	d ~155.6 d ~6.5 t ~5.3	d 159.9 d 4.9	t ~8.3 b	See C-3′	See C-2′	t ~144.0 (OCH_2) qa 4.3 (CH_3) qa ~26.5 (CH_3) t 2.4 (OCH_2)
16	t 128.2 t 3.7 (2′,6′-H)	qi 7.9 qi 7.9	d 158.1 d 7.3 t 4.9	d 159.9 d 4.9	t 9.1 t 2.1	See C-3′	See C-2′	t 142.8 (OCH_2) qa 5.2 (OCH_2) t 126.0 (CHMe) m qa 126.5 (CH_3) m
17	t ~129.0 t 3.7 (2′,6′-H)	qi 7.3	d ~159.6 d 6.7 t 4.9	d 159.0 d 5.2	t ~7.5 qa ~1.8 (3′,5′-H) ($OCHMe_2$)	See C-3′	See C-2′	d 142.8 (OCH_2) sp 4.3 ($(CH_3)_2$) qa 126.7 (CH_3) qa 5.1 (CH_3)
18	t ~129.0 m	qi 7.3 qi	d 158.7 d 7.3 t 4.9	d ~159.9 d 4.9	t b	See C-3′	See C-2′	t 142.8 (OCH_2) t 3.7 (CH_2Et) t 127 (m) (CH_2Et) t 127.0 (m) (CH_2Me) qa 126.0 (m) (CH_3)

Can. J. Chem. Downloaded from www.nrcresearchpress.com by 210.87.254.40 on 09/06/12
For personal use only.

TABLE 7 (*Concluded*)

	CH_2	C-1′	C-2′	C-3′	C-4′	C-5′	C-6′	Others			
$\bar{J}\pm$sd	t 128.4±0.7 (CH_2)	qi 7.1±0.9 (3′,5′-H)	d 158.0±1.7 (2′-H) d 7.0±0.4 (6′-H) t 5.0±0.2 (CH_2)	d 159.7±0.5 (3′-H) d 5.0±0.2 (5′-H)	t 8.3±0.8 (2′,6′-H)	d 159.7±0.5 (5′-H) d 5.0±0.2 (3′-H)	d 158.0±1.7 (6′-H) d 7.0±0.4 (2′-H) t 5.0±0.2 (CH_2)				
7	t 129.4 (CH_2) b	b	d 160.9 (2′-H) d 5.1 (6′-H) t 4.9 (CH_2)	d 166.0 (3′-H) d 2.4 (5′-H)	b	d 166.0 (5′-H) d 2.4 (3′-H)	d 160.9 (6′-H) d 5.1 (2′-H) t 4.9 (CH_2)				
23	t 130.0 (CH_2) b	qa 6.7 (5′-H) b	d 156.0 (2′-H) d 6.7 (6′-H) t 5.4 (CH_2)	d 6.1 (5′-H) d 3.7 (2′-H)	t 7.1 (2′,6′-H) d 1.7 (5′-H)	d 157.5 (5′-H)	d 159.3 (6′-H) d 7.6 (2′-H) t 5.0 (CH_2)				
36	t ~132.5 (CH_2) b	qa ~6.5 (5′-H)	d ~156.5 (2′-H) d t			d 157.5 (5′-H)	d ~160.5 (6′-H) d t	qa 143.7 (3′-OCH_3)			
19	t 129.4 b	m	d ~156.0 d 5.0 b	qa 4.0 b	m	d 158.7	d ~157.8 d 7.0 t ~4.8	qa 144.0	qa 144.0		
24	t ~126.3	d 6.5 b	d ~156.0 d 5.2 t ~4.5	m	m	d 158.7	d ~159.0 d 6.0 t ~4.2	qa 144.0	qa 144.0		
32	t 127.6 b	qa ~6.0 d ~4.2	d ~156.0 qa ~5.0 b	m	b	d 158.7	d ~158.7 d 7.3 t 4.9	qa 144.3	qa 144.3		
37	t 130.0 b	d 6.0 b	d ~156.0 qa 5.0			d 158.1	d ~161.4 d 6.5 t ~5.0	qa 143.8	qa 143.8		
$\bar{J}\pm$sd	t 128.3±1.7 (CH_2)	d 6.2±0.3 (5′-H)	d 156.0±0 (2′-H) d 5.1±0.1 (6′-H) t 4.8±0.3 (CH_2)			d 158.6±0.3 (5′-H)	d 159.2±1.5 (6′-H) d 6.7±0.6 (2′-H) t 4.7±0.4 (CH_2)	qa 144.0±0.2 (3′-OCH_3)	qa 144.0±0.2 (4′-OCH_3)	qa ~126.5 (CH_3) m	
38	t ~128.8 (CH_2) b	m	d ~162.8 qa ~5.0	—	—	d 164.3	d ~160.5 qa ~5.5 (CH_2)	t ~175.0 (OCH_2O)		t ~127.0 (CH_2Me) m	qa ~126.0 (CH_3) m
39	t ~130.0 (CH_2) t ~4.3 (2′,6′-H)	m	d 159.3 (2′-H) d 7.3 (6′-H) t 5.2 (CH_2)	1.8	t 5.8 (2′,6′-H) b	1.8	d 159.3 (6′-H) d 7.3 (2′-H) t 5.2 (CH_2)	qa 144.3 (3′-OCH_3)	qa 144.0 (4′-OCH_3)	qa 144.3 (5′-OCH_3)	

Can. J. Chem. Downloaded from www.nrcresearchpress.com by 210.87.254.40 on 09/06/12
For personal use only.

TABLE 8. C—H coupling constants in acetophenones, including mean experimental values.

	C-1	C-2	C-3	C-4	C-5	C-6	C=O	C-α	C-β	C-γ
Acetophenone	—	d 160.2 (2-H) t 7.0 (4,6-H)	d 163.0 (3-H) d 5.3 (5-H) d 3.0 (2-H)	d 161.3 (4-H) t 7.5 (2,6-H)	See C-3	See C-2	m	qa 127.3 (α-H)		
Acetophenone H^+	t 7.9 (3,5-H)	d 166.3 (2-H) t 6.3 (4,6-H)	d 169.1 (3-H) d 7.1 (5-H)	d 165.4 (4-H) t 7.2 (2,6-H)	See C-3	See C-2	qa 4.1 (α-H)	qa 132.0 (α-H)		
40	b	b	d 166.6 (3-H) t 7.0 (5-H, 2-OH)	d 161.1 (4-H) d 9.1 (6-H)	d 165.4 (5-H) d 7.9 (3-H)	d 160.8 (6-H) d 8.0 (4-H)	qi 5.5 (6,α-H)	qa 128.1 (α-H)		
41	m	—	d 159.9 (3-H) d ~6.8 (2-OH) d ~4.4 (5-H)	—	d 162.4 (5-H) d 4.9 (3-H)	d 158.1 (6-H)	b	t m	t m	qa m
42	t ~6.5	d 9.3 t 4.3	d 159.6 d 7.0	d 8.0 d 3.1	d 7.0 d 4.6	d 157.5	qi 5.8 (6,α-H)	qa 128.2 (α-H)		
43	t 5.0	d 9.2 t 4.5	d 159.9 d 6.7	d 8.2 d 3.4	d 7.0 d 4.6	d 156.3	m	t 126.2 (α-H) qa 4.3 (β-H)	qa 128.0 (β-H) t 4.3 (α-H)	
44	t 5.5	d 9.8 t 4.7	d 159.0 d 7.0	d 8.5 d 3.5 d 0.8	d 6.7 d 4.9	d 156.9	qa 4.9 (6,α-H)	t ~126.3 (α-H) b	t ~128.5 (β-H) qa	
45	—	d 8.6 t 4.2	d 159.3 d 6.7	d 7.5 d 3.0	d 6.7 d 4.9	d 156.9	m	t ~127.5 (α-H) m	d ~127.5 (β-H) b	
46	t 5.5	d 9.5 t 4.5	d 159.6 d 7.6	d 8.0 d 3.5	d 6.2 d 5.0	d 156.9	b	t	t	
$\bar{J}\pm$sd	t 5.6±0.6 (3-H, 2-OH)	d 9.3±0.4 (6-H) t 4.4±0.2 (3-H, 2-OH)	d 159.5±0.3 (3-H) d 7.0±0.4 (2-OH)	d 8.0±0.4 (6-H) d 3.3±0.2 (3-H)	d 6.7±0.3 (3-H) d 4.8±0.2 (6-H)	d 156.9±0.4 (6-H)				
47	t ~4.0 (3-H, 2-OH)	m (6-H)	d 159.9 (3-H) d 7.3 (2-OH)	d ~8.5 (6-H) d ~4.0 (3-H)	m (3-H)	d 156.5 (6-H)	m	t 126.3 (α-H) qa 4.3 (β-H)	qa 127.6 (α-H) t (β-H)	

Can. J. Chem. Downloaded from www.nrcresearchpress.com by 210.87.254.40 on 09/06/12
For personal use only.

TABLE 8 (*Concluded*)

	C-1	C-2	C-3	C-4	C-5	C-6	C=O	C-α	C-β	C-γ
48	t ~4.3 (3-H,2-OH)	d 9.2 (6-H)	d 160.5 (3-H)	m	d 7.8 (3-H)	d 157.5 (6-H)	qa ~6.0 (α-H)	qa 128.2 (α-H)	qa 145.9 ($4\text{-}OCH_3$)	
		t 4.6 (3-H, 2-OH)	d 6.7 (2-OH)		d 4.2 (6-H)					
49	b	d 7.9 (6-H)	d 166.9 (3-H)	d 8.2 (6-H)	d 7.4 (3-H)	d 164.8 (6-H)	qi ~6.0 (6,α-H)	qa 128.0 (α-H)	m	
		d 4.6 }	d 7.6	d 3.7	d 4.4					
		d 3.5 } (3-H, 2-OH)	(2-OH)	(3-H)	(6-H)					
				d 1.9						

TABLE 9. $^1J_{C\text{-}H}$ constants of carbons next to a five-ring acetal.

	$^1J_{C\text{-}3/H}$(Hz)	$^1J_{C\text{-}6/H}$(Hz)
33	167.2	164.2
28 to **32** (di-OMe)	160.7	157.7
difference to **33**	6.5	6.5
11 to **19** (di-OH)	159.6	157.3
difference to **33**	7.6	6.9
50	166.9	164.8
49 (di-OMe)	160.5	157.5
difference to **50**	6.4	7.3
43 to **47** (di-OH)	159.5	156.9
difference to **50**	7.4	7.9

	$^1J_{C\text{-}2'/H}$	$^1J_{C\text{-}5'/H}$	$^1J_{C\text{-}6'/H}$
38	162.8	164.3	160.5
19, 24, 32, 37 (di-OMe)	156.0	158.6	159.2
difference to **38**	6.8	5.7	1.3
23 (di-OH)	156.0	157.5	159.3
difference to **38**	6.8	6.8	1.2

1. H. C. JHA, F. ZILLIKEN, and E. BREITMAIER. Can. J. Chem. **58**, 1211 (1980).
2. M. SHAMMA and L. D. STIVA. Tetrahedron, **25**, 3887 (1969).
3. G. TANG and R. H. COMMON. Biochim. Biophys. Acta, **158**, 402 (1968).
4. H. C. JHA and F. ZILLIKEN. In press.
5. J. B. STOTHERS. Carbon-13 nmr spectroscopy. Academic Press, New York. 1972.
6. E. BREITMAIER and W. VOELTER. ^{13}C nmr spectroscopy. 2nd ed. Verlag Chemie, Weinheim. 1978.
7. E. BREITMAIER and G. BAUER. ^{13}C-NMR-Spektroskopie. Georg Thieme Verlag, Stuttgart. 1977.
8. B. M. LYNCH. Can. J. Chem. **55**, 541 (1977).
9. J. A. ARROWSMITH, J. COOK, and D. J. HARDSTONE. Org. Magn. Reson. **11**, 160 (1978).
10. D. H. MCDANIEL and H. C. BROWN. J. Org. Chem. **23**, 420 (1958).
11. H. GÜNTHER, G. JIKELI, H. SCHMICKLER, and J. PRESTIEN. Angew. Chem. **85**, 826 (1973).
12. F. VON MASSOW and M. A. R. SMITH. J. Chem. Soc. Perkin Trans. II, 977 (1976).
13. F. W. WEHRLI. J. Chem. Soc. Chem. Commun. 663 (1975).
14. A. PELTER, R. S. WARD, and R. J. BASS. J. Chem. Soc. Perkin Trans. I, 666 (1978).

The conformational properties of seven-membered heterocycles: 1,3-dioxacyclohept-5-ene and its 2-substituted derivatives

R. ST-AMOUR AND M. ST-JACQUES[1]

Département de Chimie, Université de Montréal, C.P. 6210, Succ. A, Montréal (Qué.), Canada H3C 3V1

Received November 27, 1980

R. ST-AMOUR and M. ST-JACQUES. Can. J. Chem. **59**, 2283 (1981).

1,3-Dioxacycloheptene and its 2-CH_3, 2-OCH_3, 2-*t*-Bu, and 2,2-dimethyl derivatives were studied by ^1H and ^{13}C dnmr methods. Substituent effects and the interpretation of spectral changes in ^{13}C nmr at low temperature allow the determination of the most stable conformation of these compounds (TB for **1**–**4***b* and C for **5***b*) and the characterization of the dynamic processes observed for **2***b*, **4***b*, and **5***b*. The differences between the conformational and dynamic properties of the above compounds and their benzo analogs are rationalized in terms of different torsional interactions in the two series.

R. ST-AMOUR et M. ST-JACQUES. Can. J. Chem. **59**, 2283 (1981).

La dioxa-1,3 cycloheptene (dioxépine-1,3) et ses dérivés substitués en position 2 par les groupements -CH_3, -OCH_3, *t*-Bu et $(CH_3)_2$ ont fait l'objet d'une étude de rmn dynamique ^1H et ^{13}C. Les effets de substituants en rmn ^{13}C et la compréhension des changements spectraux à basse température ont permis de déterminer les conformations adoptées préférentiellement par tous les composés étudiés (bateau-croisé pour **1**–**4***b* et chaise pour **5***b*) ainsi que de caractériser la nature et les énergies des processus dynamiques observés pour les dérivés **2***b*, **4***b* et **5***b*. La différence des comportements conformationnels et dynamiques entre les composés dérivés de la dioxépine-1,3 et ceux de la série analogue dérivés de la benzodioxépine-1,3 est expliquée par la différence des interactions torsionnelles présentes dans les deux séries.

The conformational analysis of 1,3-dioxacycloalkanes has received considerable attention over the years and, among this group of molecules, 1,3-dioxanes have been most studied (1). As it turns out, six-membered heterocyclic conformations other than the chair form assume relatively little importance (2) (except possibly for some substituted derivatives exhibiting strong *syn*-1,3-diaxial interactions in the chair form (**2***b*)) and consequently the effects of substituents on C-2 can be explained in terms of an axial–equatorial conformer equilibrium. On the other hand, substituted derivatives of 1,3-dioxacyclopentanes (3), 1,3-dioxacycloheptanes (4), and 1,3-dioxacyclooctanes (5) potentially exhibit a more complex behaviour because of the possible existence of several low-energy ring conformations which can interconvert by low-energy (pseudorotational or other) processes.

Previous nmr studies on derivatives of cycloheptene and benzocycloheptene have provided unique information regarding the conformational changes produced in the seven-membered ring (6–10) by certain functional groups. Significant stabilization of the twist-boat conformation was observed in some cases. 1,3-Dioxabenzocycloheptene (**1***a*) and its derivatives (**2***a* to **4***a*) revealed a most interesting behaviour (7) whereby signals of molecules existing in the chair and/or the twist-boat forms were detected. Enhanced amounts of the twist-boat form were explained in terms of effects associated with steric and electronic interactions of the 2-substituents. Because previously unsuspected insight was derived from those dnmr experiments (7), it was decided to investigate the analogous series of molecules in which the benzo group is replaced by a double bond, namely 1,3-dioxacycloheptene (**1***b*) and several of its derivatives (**2***b* to **5***b*). Thus we wished to characterize the conformational effect of 2-substituents for this series of fundamental molecules and through comparison with compounds **1***a*–**5***a* determine the conformational effect brought about by the small structural change.

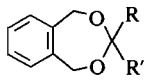

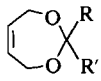

R = R′ = H	**1***a*	**1***b*
R = R′ = CH_3	**2***a*	**2***b*
R = CH_3, R′ = H	**3***a*	**3***b*
R = OCH_3, R′ = H	**4***a*	**4***b*
R = $C(CH_3)_3$, R′ = H	**5***a*	**5***b*

Published work aimed at defining the geometry of the stable conformations of some of these compounds is not conclusive. A previous ^1H dnmr report (8) on **1***b* and **2***b* proved to be negative while a recent ^{13}C nmr study (9) at ambient temperature indicated that the conformation of **1***b* is most elusive (9, 10) while that of **2***b* could not be determined with confidence (9). The results reported herein will show clearly that **1***b* exists predominantly in the twist-boat form (unlike **1***a*) and will

[1]Author to whom correspondence may be addressed.

0008-4042/81/152283-07$01.00/0

©1981 National Research Council of Canada/Conseil national de recherches du Canada

Can. J. Chem. Downloaded from www.nrcresearchpress.com by 210.87.254.6 on 09/06/12
For personal use only.

provide new information concerning the conformational changes brought about by the 2-substituents.

Results

Compounds **1***b* to **5***b* were studied by variable temperature ^1H and ^{13}C nmr and spectral changes were observed for **2***b*, **4***b*, and **5***b*.

The 80 MHz ^1H nmr spectrum of **2***b* in $CDCl_3$ at room temperature contains three signals of which the allylic methylene protons (H-4,7) doublet at δ 4.25 (separation = 1.8 Hz) undergoes a spectral change. For a solution in CHF_2Cl, as illustrated in Fig. 1, this signal consists of a slightly broadened line at −105°C which splits below −130°C (the coalescence temperature, T_c) into four broad lines which have the general appearance of an AB pattern at −149°C. Unresolved coupling with the olefinic protons appears responsible in part for the above line broadening. Analysis of the low temperature spectrum as an AB yielded a chemical shift difference of 40.5 Hz and a coupling constant of −16.0 ± 1 Hz. From the rate constant obtained at T_c, a free energy of activation of 6.8 kcal/mol was calculated at −130°C using the Eyring equation with a transmission coefficient of one (11). The 20.15 MHz ^{13}C nmr spectrum of **2***b* did not exhibit a spectral change at low temperatures. Table 1 contains the ^{13}C chemical shifts measured at room and low temperatures for compounds **1***b* to **5***b*.

The 20.15 MHz ^{13}C nmr spectra of **4***b* in CHF_2Cl, shown partially in Fig. 2 for several temperatures, reveal a spectral change whereby only the C-4,7 signal splits into a doublet below −160°C. At −163°C, the separation between the equally intense components is 77 Hz and the true chemical shift difference could be slightly larger because of the nearness to T_c. Other pertinent chemical shifts are given in Table 1. The rate constant for the averaging process underlying the spectral change was calculated (12) at coalescence from which a free energy of activation of 5.2 kcal/mol was obtained at −160°C using a transmission of one in the Eyring equation.

The 80 MHz ^1H nmr spectrum of **4***b* also showed a spectral change. The approximate AB pattern observed for H-4,7 below −100°C broadens quite significantly below −155°C to become a complex unresolved broadened pattern below −160°C. In spite of the poor resolution resulting in large part from coupling with the olefinic protons, the above behaviour is compatible with the existence of two broad and overlapping AB patterns similar to those reported (7) for **4***a* at −150°C. Thus both ^1H and ^{13}C nmr spectra point to nonequivalent allylic methylene groups.

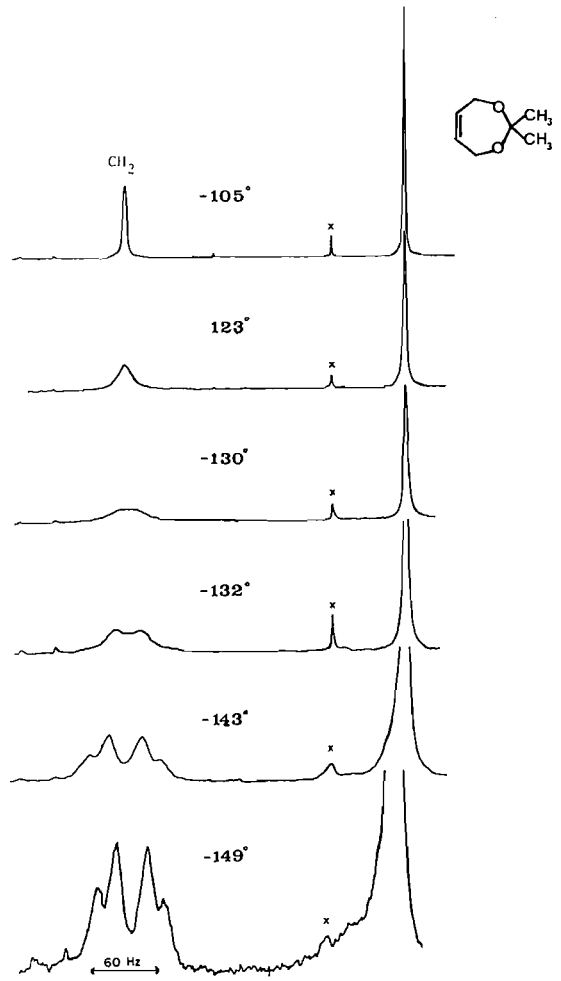

FIG. 1. Partial 80 MHz ^1H nmr spectra (CH_2 and CH_3) of **2***b* in CHF_2Cl at several temperatures (X denotes an impurity).

A spectral change was also observed for the methyl ^1H and ^{13}C signals of **5***b* which undergo a splitting from singlet to doublet with component intensities in the ratio 2:1, the more intense line appearing at low field. All pertinent ^{13}C chemical shifts are reported in Table 1. Using the two-site approximation (12), a free energy of activation of 6.1 kcal/mol was calculated at −136°C (T_c).

Discussion

Conformations of the Seven-Membered Ring

Previous work (7) has shown that only three conformations need to be considered for the seven-membered ring of cycloheptene and its derivatives: the chair (C), the boat (B), and the twist-boat (TB) forms. Furthermore, the substituent in 2-monosubstituted derivatives of 1,3-dioxepins can either be axially or equatorially oriented in the C and B forms thus giving rise to the C-a, B-a, C-e, and B-e forms.

Can. J. Chem. Downloaded from www.nrcresearchpress.com by 210.87.254.6 on 09/06/12
For personal use only.

TABLE 1. ^{13}C chemical shifts for compounds in series *b* at room and low temperature[a]

Compound	Temperature (°C)	C-5,6	C-2	C-4,7	Other ^{13}C atoms (substituted on C-2)
1*b*	25	131.78	98.05	68.49	
	−148	131.45	96.93	67.22	
2*b*	25	131.12	103.46	62.63	24.59 (CH_3)
	−148	130.58	103.21	61.97	23.94 (CH_3)
3*b*	25	131.56	103.17	66.07	20.63 (CH_3)
	−148	130.94	102.40	65.54	20.22 (CH_3)
4*b*	25	130.83	115.90	62.78	54.00 (OCH_3)
	−163	130.21	114.23	64.08	54.23 (OCH_3)
				60.29	
5*b*	25	130.65	113.44	69.92	37.37 (C) 25.38 (CH_3)
	−148	129.29	112.92	70.02	36.89 (C) 26.96 (CH_3)
					20.79

[a] In ppm downfield from TMS for solutions in CHF_2Cl containing TMS and CD_2Cl_2 (~15%) as lock signal.

Nuclear magnetic resonance parameters, obtained from spectra recorded at a temperature below coalescence, normally give direct information on the nature of the most stable conformation(s) of a given molecule provided further averaging does not take place through conformational processes involving low activation barriers. Of the five compounds in series *b* only **2***b* and **4***b* fall into this category. The spectral change observed for **5***b* is due to slowing down of the rotation of the *tert*-butyl group (13) and will not be considered further.

The broadened AB pattern observed for H-4,7 in the ^1H nmr spectrum of **2***b* at −149°C (Fig. 1) indicates that the nonaveraging stable conformation contains only two nonequivalent methylene proton environments and together with the ^{13}C nmr spectrum show that the two allylic carbons are equivalent. Furthermore the ^1H and ^{13}C spectra indicate that both methyl groups have the same environment. Consequently the conformation of **2***b* must be the TB form as was also determined (7) for the analogous compound **2***a*.

Similarly, ^1H and ^{13}C nmr data obtained for **4***b* below coalescence show that it exists in the TB form as was also found (7) for compound **4***a*. The nonequivalence of the allylic carbons, clearly revealed from the splitting in the ^{13}C nmr spectrum (Fig. 2 and Table 1), rules out the C-a, B-a, C-e, and B-e forms which all contain equivalent allylic carbon atoms. The absence of splitting in signals of other carbons and a comparison of the ^{13}C shift parameters for **4***a* and **4***b* rule out an equimolar mixture of two of the above conformations for **4***b*.

Unfortunately, direct evidence of this kind is not available for the identification of the stable conformation(s) of the parent compound **1***b* and of the two monoalkyl derivatives **3***b* and **5***b* because for these molecules neither ring protons nor ring carbons gave rise to a spectral change. Consequently, one of the following situations must apply to these molecules: (*1*) the existence of a single nonaveraging ring conformation, (*2*) the existence of a single but rapidly averaging (i.e. through ring inversion) conformation, or (*3*) the existence of a mixture of different but rapidly interconverting conformations. ^{13}C nuclear magnetic resonance was found to be most useful to unravel a similar conformational problem (7). The arguments are based on the C-4,7 chemical shifts measured at low temperatures which are summarized in Table 1.

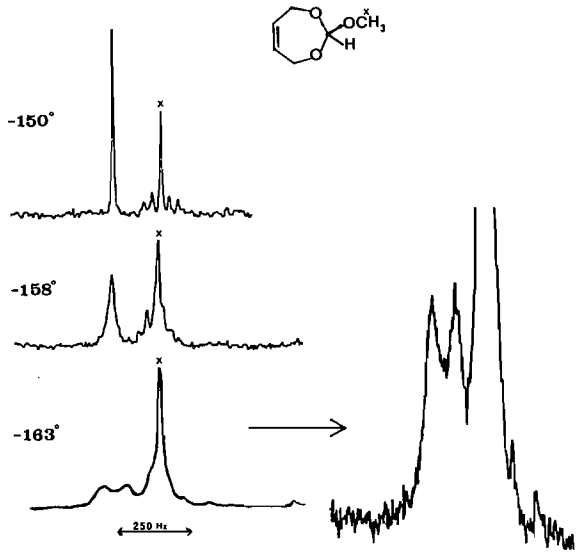

FIG. 2. Partial 20.15 MHz ^{13}C nmr spectra of the allylic carbons (signal on the left) and methyl carbon (denoted by X) of **4***b* in CHF_2Cl at several temperatures.

Can. J. Chem. Downloaded from www.nrcresearchpress.com by 210.87.254.6 on 09/06/12
For personal use only.

Can. J. Chem. Downloaded from www.nrcresearchpress.com by 210.87.254.6 on 09/06/12
For personal use only.

Our first objective is to determine the nature of the most stable conformation of **1***b* through analysis of the relationship between its C-4,7 chemical shift with those of **2***b* and **4***b* whose conformations are known to be TB. We must accordingly determine whether the 5.25 ppm difference between the signals of **1***b* and **2***b* as well as the 5.03 ppm difference for **1***b* and the mean of the two signals of **4***b* point to a specific form for **1***b*. Because compound **1***a* was found (7) to exist as a mixture of C (79%) and TB (21%) while both **2***a* and **4***a* exist as TB forms, data obtained from series *a* can in principle be used as reference. Thus the chemical shift difference between the benzylic C-4,7 signals of **1***a* (TB) and **2***a* is 4.87 ppm while the difference between the C-4,7 of **1***a* (TB) and the mean of the two C-4,7 signals of **4***a* is 5.18 ppm. The remarkable closeness of the shift differences in both series, which must arise from the same substituent effects, strongly indicates that **1***b* exists predominantly in the TB form at −148°C. The upfield shift of the C-4,7 signal of **2***b* relative to **1***b* therefore represents the γ-effect of the 2,2-dimethylsubstitution in the TB conformation while the upfield shifts of 3.14 and 6.93 ppm of the two TB C-4,7 signals of **4***b* relative to **1***b* are compatible with the *anti* relationship to the OCH_3 group of one of the allylic carbons (namely C-4 in structure **6**) and a *gauche* allylic carbon (namely C-7 in structure **6**). These upfield shifts, characterizing the effect of the methoxy group substitution on the TB conformation of **1***b*, are very similar to those determined previously (7) for the benzylic carbons of **4***a* which are 2.54 and 7.81 ppm. The small difference between the two series of molecules could arise in part (*a*) from imprecision in the δ_c of **4***b* because these were measured only a few degrees below T_c, and/or (*b*) from slight temperature differences, and/or (*c*) from small differences in TB ring geometries brought about by the small structural difference, and/or (*d*) from the existence of a small amount of the C form in equilibrium with TB for **1***b*, which would shift the reference used to determine the substituent parameters for **4***b*. The above reasoning in terms of γ-shifts is not quantitative enough to allow a choice to be made between these possible rationales and we are therefore not able to estimate an upper limit for the amount of the minor C form that could be present in the solution of **1***b* at low temperatures.

Let us now turn our attention to the conformations of **3***b* and **5***b*. Table 1 reveals that the C-4,7 signals have very different chemical shifts relative to that of **1***b*. In fact the 2-methyl substitution produces an upfield shift of 1.68 ppm while the *tert*-butyl substitution produces a downfield shift of 2.80 ppm. Thus the chemical shift difference between the C-4,7 signals of **3***b* and **5***b* is 4.48 ppm. By contrast, the C-4,7 chemical shifts of **3***a* and **5***a* are very similar[2] because they both exist in the C-e form.

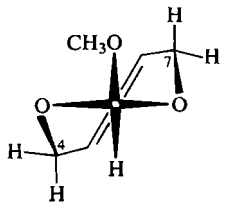

6

Now the data for **3***b* and **5***b* shown in Table 1 indicate that the most stable conformation of these two molecules must be different and because both **3***a* and **5***a*, which exist in the same C-e conformation, have larger C-4,7 chemical shifts than **1***a* (TB) (7), it then follows that **5***b* must exist in the C-e form, as does **5***a*, but that **3***b* must exist predominantly in the TB form, contrary to **3***a* which exists predominantly in the C-e form (7).

It is also interesting to point out that, even though both monosubstituted derivatives **3***b* and **4***b* exist predominantly in the TB form, the activation barrier for pseudorotation (*vide infra*) is lower for **3***b* so that rapid conformational averaging still takes place at −160°C as indicated from the absence of a spectral change for this compound. Furthermore, if **3***b* existed solely in the TB form, the 1.7 ppm upfield shift of the C-4,7 signal relative to **1***b* would represent the average of a γ-*anti* and a γ-*gauche* methyl effect. Unfortunately, reference values for these substituent parameters are not known for the seven-membered cyclic conformations so that a quantitative interpretation of the averaged γ-effect of the methyl group in **3***b* is not possible in order to determine the upper limit for the amount of the minor C form that could be present in the solution at low temperature.

Conformational Averaging Processes

The accepted conformational interconversion pathways characterizing the cycloheptene ring are illustrated in Scheme 1 where the * indicates inverted (or mirror image) conformations.

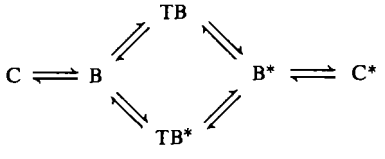

SCHEME 1

[2]R. St-Amour and M. St-Jacques, unpublished results, which gave δ = 75.40 for C-4,7 of **5***a* in CHF_2Cl at low temperature, whereas that of **3***a* is 74.67 ppm (7).

TABLE 2. Free energy barriers characterizing the conformational processes of several seven-membered cyclic molecules

Compound	Stable conformation(s)	ΔG^* C ⇌ C* (kcal/mol)	ΔG^* TB ⇌ TB* (kcal/mol)	Reference
Benzocycloheptene	C	10.9	—	16
Cycloheptene	C	5.0	—	15
1*a*	C (79%)[a]	8.0		7
	TB (21%)		<5	See footnote 3
1*b*	TB	—	<5	This work
2*a*	TB	—	10.0	7
2*b*	TB	—	6.8	This work
4*a*	TB	—	6.7	7
4*b*	TB	—	5.2	This work
8	C (50%)[b]	8.9		18
	TB (50%)[b]		6.6	
9	TB	—	5.3	18

[a] In CHF_2Cl at −130°C.
[b] In CHF_2Cl at −100°C.

It is well known that, in the chair inversion process of cycloheptene and benzocycloheptene (6, 14), the C → B transformation is the rate-determining step for which free energy values of 5.0 and 10.9 kcal/mol were determined respectively (15, 16). The corresponding energy barrier for **1***a* was recently (7) reported to be 8.0 kcal/mol. Unfortunately, the dnmr method did not provide data allowing the determination of the free energy barrier for the pseudorotation process (i.e. TB ⇌ B ⇌ TB*) for these three fundamental molecules. Furthermore, it is interesting to point out that the 300 MHz ^{1}H nmr investigation[3] of a dideuterated derivative of **1***a* (**7**) at temperatures as low as −155°C and the 100 MHz spectrum at −170°C did not reveal a spectral change for the signals of the TB conformation. It therefore appears that the pseudorotation of **1***a* is characterized by an energy barrier of less than 5 kcal/mol.

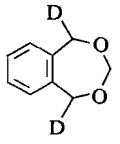

7

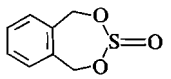

8

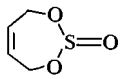

9

The failure to detect a spectral change for **1***b* unfortunately prevents the determination of any kinetic parameter. Nevertheless, the conclusion that the TB form is very predominant for **1***b* suggests that the only process that might have been characterized by the dnmr method is the TB inversion (or pseudorotation) for which the absence of a spectral change suggests that the free energy barrier is less than 5.0 kcal/mol.

Dimethyl substitution on C-2 raises the pseudorotation barrier to 6.8 kcal/mol for **2***b*. A similar increase was observed for **2***a* ($\Delta G^* = 10.0$ kcal/mol) and interpreted in terms of increased steric interactions in the transition state for pseudorotation (7). It would then appear that a similar effect is responsible for the energy barrier difference between **1***b* and **2***b*.

The difference in dynamic behaviour for **3***b* (2-CH_3 derivative) and **4***b* (2-OCH_3) is most interesting since both compounds are found to exist predominantly in the TB form and yet only **4***b* gives rise to a spectral change at the low temperatures reached. Because the methyl group is expected to exert greater steric compression than the methoxy group, it appears reasonable to think that the observed barrier differences might arise from electronic effects either through the same pathway or through a different one.

Furthermore, data given in Table 2 for **4***a*, **4***b*, **8**, and **9** suggest that electronic effects contribute significantly to the similarity of the pseudorotation free energy barriers of the TB form of each molecule. Anet and Yavari (17) have shown that the generalized anomeric effect raises the rotational barrier of chloromethylmethyl ether and it therefore appears highly probable that stereoelectronic interactions could be responsible for the increased magnitude of the pseudorotation barrier of these four compounds.

Two pathways are available for the TB inversion of **3***b* and **4***b* as illustrated in Scheme 2 where a_1 and a_2 represent forms of intermediate geometries with five coplanar ring atoms (14) differing only by the position of the substituent. The choice between these two pathways (i.e. either through B-a or B-e) for **4***b* requires the assessment of the relative importance of steric and electronic interactions in the ground state TB conformation and along each

[3] R. St-Amour and M. St-Jacques, unpublished results, courtesy of Bruker, USA.

Can. J. Chem. Downloaded from www.nrcresearchpress.com by 210.87.254.6 on 09/06/12
For personal use only.

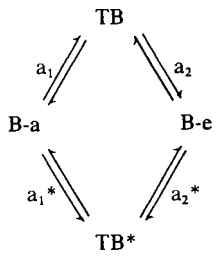

SCHEME 2

pathway. A quantitative approach to this question is beyond the scope of our present work.

Nevertheless, a qualitative assessment of the effect of steric interactions of methyl groups on the pseudorotation of TB proves to be useful for **3***b*. The fact that **2***b* must possess a methyl group at both axial and equatorial positions of the B form suggests that it is an acceptable model for estimating the energy demand of the pathway through B-a in Scheme 2. A model for the pathway through B-e is provided by **1***b*. Consequently, the failure to observe a spectral change for **3***b* indicates that its TB form inverts through a pathway closer to that of **1***b* (i.e. B-e) rather than that of **2***b*, which gave rise to a spectral change in accord with a higher pseudorotation barrier expected for passage through B-a.

The Conformational Effect of the Benzo Group

The increased stability of the TB form of the dioxepin rings of **1***a* and **1***b* relative to the corresponding hydrocarbon rings is largely a consequence of electronic interactions associated with the anomeric effect in the acetal moiety of the heterocycles (7). In addition, the results obtained for the pairs of molecules **1***a*,**1***b* and **3***a*,**3***b* provide information on the magnitude of the conformational change produced by the replacement of the double bond by a benzo group in the seven-membered ring. Together with recent results (18) for the sulfites **8** and **9**, they show that a general trend exists whereby the replacement of a benzo group by a double bond significantly stabilizes the TB conformation relative to the C form.

The explanation for the observed trend can be derived from ideas first advanced by Allinger and Sprague (14) who pointed out that differences in torsional interactions at the allylic bonds (H/H eclipsing similar to that in propene whose rotational barrier is 1.98 kcal/mol) and benzylic bonds (H/C_{sp^2} eclipsing as in toluene whose rotational barrier is about 0.5 kcal/mol) play an important role in determining the conformational properties. Thus the replacement of a benzo group by a double bond stabilizes the TB form relative to C because the higher torsional strain about the allylic bonds found in C is relieved significantly by the conformational change to TB in which torsional angles lead to reduced torsional energy.

Furthermore, results published for molecules **10** and **11** fall in line with the above conclusion, for it had been reported that **10** exists uniquely in the C form whereas **11** exists as a mixture of C and TB forms (8).

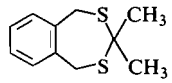

10

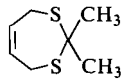

11

The structural change under consideration also affects the dynamic properties of the members of each pair of molecules (Table 2) by perturbing both the energy barriers of the C → B step of the C inversion as well as of the pseudorotation motion of the TB inversion. The effect of benzo substitution on the $\Delta G^{\ddagger}$ barrier for C inversion is an increase of about 6 kcal/mol for the cycloheptene–benzocycloheptene pair and about 4 kcal/mol for the **10**–**11** pair and for which free energies of 12.2 and 8.2 kcal/mol were reported (8). Relief of torsional strain about the allylic bonds in reaching the transition state for the C → B transformation was claimed to be largely responsible for the above differences (14).

Table 2 also reveals that molecules **2***a*, **4***a*, and **8** all possess slightly larger pseudorotation barriers than their counterparts **2***b*, **4***b*, and **9**. It would appear that differential changes in allylic and benzylic torsional strain during the pseudorotation cycle are responsible at least in part for this effect, although the difference in $\Delta G^{\ddagger}$ for the 2,2-dimethyl derivatives **2***a* and **2***b* suggests that other factors, possibly of electronic or solvation origin, might come into play.

Experimental

High-resolution mass spectra at 70 eV were recorded using an Associated Electrical Industries spectrometer model MS-902.

Both ^1H and ^{13}C variable temperature nmr spectra were recorded in the FT mode on a Bruker WP-80 spectrometer equipped with the standard variable temperature accessory (B-VT-1000) and operating at 80 and 20.15 MHz respectively.

All ^{13}C nmr spectra were recorded with proton decoupling for solutions in CHF_2Cl (200–270 mg in 2.5 mL of solution) containing Me_4Si and about 15–20% of CD_2Cl_2 (for locking purpose) in standard 10 mm tubes which had been degassed and sealed. The ^1H nmr spectra were also recorded in 5 mm tubes as degassed solutions in $CDCl_3$ and/or CHF_2Cl containing CD_2Cl_2 and Me_4Si; about 20–30 mg in 0.50 mL of solution were used.

The following instrumental conditions were used; ^{13}C nmr: flip angle = 35–40°, except for **4***b* below −150°C for which 90° pulses were used, SW = 6,000 Hz, data size = 8K; ^1H nmr: flip angle ≈ 10°, SW = 1,200 Hz, data size = 8K.

Can. J. Chem. Downloaded from www.nrcresearchpress.com by 210.87.254.6 on 09/06/12
For personal use only.

Can. J. Chem. Downloaded from www.nrcresearchpress.com by 210.87.254.6 on 09/06/12
For personal use only.

Temperatures were measured accurately with a calibrated copper–constantan thermocouple placed inside a solvent-containing dummy nmr tube. A precision of ± 1° is expected.

Preparation of 1b, 3b *and* 5b

These three compounds were prepared according to a published general procedure (19) from 2-butene-1,4-diol (Aldrich, 91% *cis*, distilled before use). The benzene solvent was removed by distillation at atmospheric pressures and each compound was obtained pure by reduced pressure distillation (20). The yields were 60%, 16%, and 54% respectively. The ^{1}H nmr spectra of each compound were found to be identical to those reported earlier for **1***b* (9, 21), **3***b* (21), and **5***b* (9). The ^{13}C nmr chemical shifts reported in Table 1 confirm the identity of each compound.

*2,2-Dimethyl-1,3-dioxa-5,6-cycloheptene (***2***b)*

Compound **2***b* was prepared from 2-butene-1,4-diol, dimethoxypropane, and acetone by the procedure (7) used for **2***a*. The ^{1}H nmr spectrum was found to be identical to that published (9, 21) while the ^{13}C nmr data reported in Table 1 confirm the structure.

*2-Methoxy-1,3-dioxa-5,6-cycloheptene (***4***b)*

Compound **4***b* was prepared by the procedure (7) used previously for **4***a*. After distillation of the benzene at atmospheric pressures, the product was purified by reduced pressure distillation (30°C/0.5 Torr); its yield was 20%. The ^{1}H nmr spectrum in $CDCl_3$ showed the following signals δ: 3.41 (s, OCH_3), 4.14 and 4.49 (AB pattern, CH_2), 5.40 (s, CH), and 5.72 (m, olefinic H). The ^{13}C nmr parameters, summarized in Table 1, are also compatible with structure **4***b*.

Mol. Wt. calcd. for $C_5H_7O_2$ ($M^+ - OCH_3$): 99.0446; found (mass spectrum at 70 eV): 99.0448.

Acknowledgements

We wish to acknowledge the technical assistance of Mr. R. Mayer and financial assistance from the Natural Sciences and Engineering Research Council of Canada.

1. (*a*) F. G. RIDDELL. The conformational analysis of heterocyclic compounds. Academic Press, Toronto. 1980; (*b*) W. L. F. ARMAREGO. Stereochemistry of heterocyclic compounds. Part II. John Wiley and Sons, Toronto. 1977.
2. (*a*) F. W. NADER and E. L. ELIEL. J. Am. Chem. Soc. **92**, 3050 (1970); (*b*) G. M. KELLIE and F. G. RIDDELL. J. Chem. Soc. B, 1030 (1971).
3. (*a*) W. E. WILLY, G. BINSCH, and E. L. ELIEL. J. Am. Chem. Soc. **92**, 5394 (1970); (*b*) M. ANTEUNIS, R. VAN CAUWENBERGHE, and C. BECU. Bull. Soc. Chim. Belg. **82**, 591 (1973).
4. (*a*) D. F. BOCIAN and H. L. STRAUSS. J. Am. Chem. Soc. **99**, 2876 (1977); (*b*) M. H. GIANNI, J. SAAVEDRA, and J. SAVOY. J. Org. Chem. **38**, 3971 (1973); (*c*) I. YAVARI. Org. Magn. Reson. **14**, 511 (1980).
5. F. A. L. ANET, P. J. DEGEN, and J. KRANE. J. Am. Chem. Soc. **98**, 2059 (1976).
6. (*a*) M. ST-JACQUES and C. VAZIRI. Org. Magn. Reson. **4**, 77 (1972); (*b*) M. ST-JACQUES and C. VAZIRI. Can. J. Chem. **51**, 1192 (1973); (*c*) G. BODENNEC and M. ST-JACQUES. Can. J. Chem. **55**, 1199 (1977).
7. A. BLANCHETTE, F. SAURIOL-LORD, and M. ST-JACQUES. J. Am. Chem. Soc. **100**, 4055 (1978).
8. H. FRIEBOLIN, R. MECKE, S. KABUSS, and A. LUTTRINGHAUS. Tetrahedron Lett. 1929 (1964).
9. M. H. GIANNI, M. ADAMS, H. G. KUIVILA, and K. WURSTHORN. J. Org. Chem. **40**, 450 (1975).
10. M. H. GIANNI, R. CODY, M. R. ASTHANA, K. WURSTHORN, P. PATANODE, and H. G. KUIVILA. J. Org. Chem. **42**, 365 (1977).
11. D. KOST, E. H. CARLSON, and M. RABAN. Chem. Commun. 656 (1971), and references cited therein.
12. F. A. L. ANET and R. ANET. Dynamic nuclear magnetic resonance spectroscopy. *Edited by* F. A. Cotton and L. M. Jackman. Academic Press, New York, NY. 1975. p. 543.
13. F. A. L. ANET, M. ST-JACQUES, and G. N. CHMURNY. J. Am. Chem. Soc. **90**, 5243 (1968).
14. N. L. ALLINGER and J. T. SPRAGUE. J. Am. Chem. Soc. **94**, 5734 (1972).
15. M. ST-JACQUES and C. VAZIRI. Can. J. Chem. **49**, 1256 (1971).
16. S. KABUSS, H. FRIEBOLIN, and H. SCHMID. Tetrahedron Lett. 469 (1965).
17. F. A. L. ANET and I. YAVARI. J. Am. Chem. Soc. **99**, 6752 (1977).
18. H. FAUCHER, A. C. GUIMARAES, J. B. ROBERT, F. SAURIOL, and M. ST-JACQUES. Tetrahedron, **37**, 689 (1981).
19. K. C. BRANNOCK and G. R. LAPPIN. J. Org. Chem. **21**, 1366 (1956).
20. C. E. PAWLOSKI. *In* Heterocyclic compounds; 7-membered heterocyclic compounds containing oxygen and sulfur. Vol. 26. *Edited by* A. Rosowsky. Wiley-Interscience, New York, NY. 1972. Chapt. 5.
21. J. SOULIER, M. FARINES, A. LAGUERRE, and A. BONAFOS-BASTOVILL. Bull. Soc. Chim. Fr. 307 (1976).

Complexes of methylmercury(II) with 1-methylcytosine and crystal structure of μ-(1-methylcytosinato-N3,N4)bis(methylmercury(II)) nitrate

LEONARDO PRIZANT, ROLAND RIVEST, AND ANDRÉ L. BEAUCHAMP[1]

Département de Chimie, Université de Montréal, C.P. 6210, Succ. A, Montréal, (Qué.), Canada H3C 3V1

Received October 9, 1980

LEONARDO PRIZANT, ROLAND RIVEST, and ANDRÉ L. BEAUCHAMP. Can. J. Chem. **59**, 2290 (1981).

Two types of solid complexes are isolated by reaction of CH_3HgX (X = NO_3 and ClO_4) with 1-methylcytosine (MCy). The CH_3Hg^+ ion is probably bonded to N(3) in the $[CH_3Hg(MCy)]X$ compounds. Mercury binding to N(3) and the deprotonated amino group in $[(CH_3Hg)_2(MCy—H)]X$ is confirmed by X-ray work on the nitrate salt. The crystals are orthorhombic, space group *Pbca*, with $a = 12.014$, $b = 13.573$, $c = 16.353$ Å, and $Z = 8$. The structure was refined on 962 independent reflections to an R factor of 0.038. The CH_3Hg^+ groups are arranged in a *syn* configuration and the angles around the mercury-bonded nitrogen atoms are severely distorted to prevent short Hg...Hg contacts. N(3)-coordination in the 1:1 complexes introduces minor changes in the infrared spectra, but the substitution of an amino proton in the 1:2 compounds produces important modifications. ^1H nmr data in DMSO-d^6 are reported for both types of compounds. This work emphasizes the important acidity enhancement experienced by the amino protons upon initial coordination to N(3), which facilitates further reaction of CH_3Hg^+ by proton displacement even in acidic media.

LEONARDO PRIZANT, ROLAND RIVEST et ANDRÉ L. BEAUCHAMP. Can. J. Chem. **59**, 2290 (1981).

Deux catégories de complexes ont été isolées par réaction de CH_3HgX (X = NO_3 and ClO_4) avec la méthyl-1 cytosine (MCy). L'ion CH_3Hg^+ est probablement lié à N(3) dans les composés $[CH_3Hg(MCy)]X$. Dans le cas de $[(CH_3Hg)_2(MCy—H)]X$, le mercure se lie à N(3) et au groupe amino déprotoné, comme l'indique la structure cristalline du nitrate. Ce composé appartient au groupe orthorhombique *Pbca* et ses constantes réticulaires sont $a = 12{,}014$, $b = 13{,}573$, $c = 16{,}353$ Å et $Z = 8$. La structure a été affinée au moyen de 962 réflexions indépendantes jusqu'à un facteur R de 0,038. Les deux groupes CH_3Hg^+ se trouvent dans une configuration *syn* et des déformations importantes des angles touchant les atomes d'azote coordinés permettent d'éviter des contacts courts Hg...Hg. Les spectres infrarouges sont peu modifiés par coordination à N(3) dans les complexes 1:1, mais des changements majeurs se produisent lors de la substitution d'un atome d'hydrogène du groupe amino dans les composés 1:2. Les mesures de rmn ^1H sont présentées pour les composés dissous dans DMSO-d^6. Ce travail met en évidence l'accroissement considérable de l'acidité de la fonction amine par coordination initiale du mercure en N(3), ce qui rend possible le déplacement de proton par un autre groupe CH_3Hg^+ même en milieu acide.

Introduction

Spectroscopic studies have shown that amino hydrogens of adenosine and cytidine can be displaced by CH_3Hg^+ in aqueous solutions (1–3). In earlier reports (4, 5), we have presented crystallographic evidence that substitution takes place with 9-methyladenine even in moderately acidic solutions, provided another CH_3Hg^+ group is simultaneously bonded to N(1). This prompted us to examine the behavior of 1-methylcytosine (MCy), a ligand containing a similar arrangement of nitrogen atoms.

Cytosine is a versatile ligand. Most metal ions react predominantly at N(3) with a varying degree of participation of the adjacent carbonyl O(2) atom (6,7). Coordination with O(2) only has been observed so far in one crystal structure (8), but a recent nmr study indicates that in DMSO, unidentate binding through O(2) is more common than anticipated (9). Selective reaction of CH_3Hg^+ with the deprotonated amino group has been reported to take place at high pH (1, 3) and this mode of bonding has also been observed for ruthenium compounds (10, 11). Very recently, MCy has been found to be bridging via N(3) and the deprotonated amino group in dimeric platinum complexes (12).

In the present work, we have investigated the reactions of CH_3Hg^+ with MCy in aqueous media, in order to obtain solid compounds on which detailed structural analyses could be carried out. Complexes of two types have been isolated and the crystal structure of one of those is reported.

Experimental Section

Preparations

1-Methylcytosine (Vega) was used after recrystallization from 95% ethanol. CH_3HgI (Alfa) was the starting material to make solutions of methylmercury salts.

Aqueous ~1 *M* solutions of CH_3HgNO_3 were prepared by refluxing CH_3HgI (5% excess) suspended in 1 *M* $AgNO_3$ for 1 h. AgI and excess CH_3HgI were filtered and the filtrate was treated again with a small amount of CH_3HgI to remove any remaining silver. The ~1 *M* CH_3HgClO_4 solutions were similarly obtained from $AgClO_4$ solutions.

$[CH_3Hg(MCy)]NO_3$. MCy (2 mmol) was dissolved in hot water (20–30 mL) and the CH_3HgNO_3 solution (2 mmol) was added while stirring. After 24 h at room temperature, the colorless solid was filtered and dried under vacuum. Recrystallization from 95% ethanol yielded a crystalline material. *Anal.* calcd. for $C_6H_{10}N_4O_4Hg$: C 17.89, H 2.50, N 13.91, Hg 49.80; found: C 17.99, H 2.57, N 14.21, Hg 49.75.

[1]To whom all correspondence should be addressed.

0008-4042/81/152290-08$01.00/0

©1981 National Research Council of Canada/Conseil national de recherches du Canada

Can. J. Chem. Downloaded from www.nrcresearchpress.com by 210.87.254.105 on 09/06/12
For personal use only.

Can. J. Chem. Downloaded from www.nrcresearchpress.com by 210.87.254.105 on 09/06/12
For personal use only.

[$CH_3Hg(MCy)$]ClO_4. Same method as above, using CH_3HgClO_4. Recrystallized from 95% ethanol as a flaky solid. *Anal.* calcd. for $C_6H_{10}N_3O_5ClHg$: C 16.37, H 2.29, N 9.55, Hg 45.57; found: C 16.09, H 2.29, N, 9.63, Hg, 45.48.

[$(CH_3Hg)_2(MCy—H)$]NO_3. MCy (2 mmol) was dissolved in water as above and 4 mmol of CH_3HgNO_3 were added while stirring. NaOH (1 mmol) was then added as a ~1 *M* solution. After 24 h, a colorless material deposited. Colorless crystals were isolated by recrystallization from 95% ethanol. *Anal.* calcd. for $C_7H_{12}N_4O_4Hg_2$: C 13.62, H 1.96, N 9.07, Hg 64.98; found: C 13.41, H 1.99, N 9.19, Hg 64.79.

[$(CH_3Hg)_2(MCy—H)$]ClO_4. Same method as the previous compound, using CH_3HgClO_4. Recrystallization from 95% ethanol yielded a flaky colorless solid. *Anal.* calcd. for $C_7H_{12}N_3O_5ClHg_2$: C 12.84, H 1.85, N 6.42, Cl 5.41, Hg 61.26; found: C 12.61, H 1.85, N 6.43, Cl 5.36, Hg 60.97.

The analyses were carried out by Schwarzkopf Laboratories, New York.

The infrared spectra (4000–300 cm^{-1}) were recorded as KBr pellets and Nujol mulls (CsI windows) using a Beckman IR4250 spectrophotometer.

The ^1H nmr spectra were taken at room temperature using a Bruker WH-90 (90 MHz) apparatus. The compounds were dissolved in DMSO-d_6 (SILANOR, Merck, Sharp & Dohme) and tetramethylsilane was used as an internal standard.

Crystal data

$C_7H_{12}Hg_2N_4O_4$ f.w. = 617.38

Orthorhombic, *Pbca*, a = 12.014(3), b = 13.573(4), c = 16.353(2) Å, V = 2667 Å^3, Z = 8, D_c = 3.075 g cm^{-3}, μ(MoKα) = 230.3 cm^{-1}, λ(MoK$\bar{\alpha}$) = 0.71069 Å (graphite monochromator), t = 23°C.

Crystallographic Measurements

A fragment of dimensions 0.27 × 0.17 × 0.33 mm^3 was cut from one of the large crystals obtained by recrystallization in 95% ethanol. Precession photographs clearly revealed *mmm* Laue symmetry and the space group was unambiguously determined from the systematic absences: $0kl$, $k \neq 2n$, $h0l$, $l \neq 2n$ and $hk0$, $h \neq 2n$.

The crystal was mounted on an Enraf-Nonius CAD4 diffractometer and the cell parameters were accurately determined by least-squares fit of the setting angles for 25 reflections centered in the counter aperture. Intensity data were collected by using the $\omega/2\theta$ scan technique. A fixed slit of 3.0 mm was used and the scan range (ω) was $(1.00 + 0.35 \tan\theta)°$ extended 25% on either side for backgrounds. Prescans at 6.7° min^{-1} were made and all reflections having $I/\sigma(I) < 1$ were labeled "weak" and not remeasured. Scan speed S between 6.7 and 0.67° min^{-1} was automatically selected to make the $I/\sigma(I) = 100$, but the scan time was limited to 135 s. Three standard reflections used as a check on instrument and crystal stability showed random fluctuations of < ±3%. Crystal orientation was checked every 100 measurements by centering three reflections. No crystal recentering was needed during data collection.

A total of 1733 independent *hkl* reflections ($2\theta \leq 45°$) were measured using Enraf-Nonius option FLAT, a procedure to measure intensity at the ψ position where absorption is minimum. Net intensity I was calculated from $I = (P - 2B)S$, where P is the peak count and B is the total background counted during one half of the scan time. Standard deviations were obtained from $\sigma^2(I) = (P + 4B)S^2 + (0.04I)^2$. A set of 962 reflections with $I < 3.0\ \sigma(I)$ was retained for structure determination. An absorption correction was applied (Gaussian integration, grid 8 × 8 × 8); the transmission factor ranged from 0.030 to 0.080. The data were finally corrected for Lp effects.

Structure Determination

The structure was solved by the heavy-atom method and refined by full-matrix least-squares. Both independent Hg atoms were positioned from a Patterson synthesis and the remaining nonhydrogen atoms were located in a subsequent difference Fourier map. Isotropic refinement using unit weights converged to $R = \Sigma||F_o| - |F_c||/\Sigma|F_o| = 0.108$. The nonhydrogen atoms were then refined anisotropically. Hydrogens on C(5), C(6), and N(4) were fixed at their calculated positions (assuming sp^2 hybridization and C(N)—H = 0.95 Å) with isotropic temperature factors B of 4.0 Å^2; their coordinates were recalculated after each cycle of refinement. Individual weights based on counting statistics $w = 1/\sigma^2(F_o)$ were applied in the last least-squares cycles. Anisotropic refinement converged to R = 0.038 and $R_w = \Sigma[w(|F_o| - |F_c|)^2/\Sigma w|F_o|^2]^{1/2} = 0.050$. The goodness-of-fit ratio was 1.63. The hydrogens of the methyl groups could not be unambiguously recognized in the final difference Fourier map. The map had a general background < ±0.7 e/Å^3, except for a few peaks of ±1.1–1.2 e/Å^3 close to Hg.

The form factors used were those of Cromer and Waber (13), except for hydrogen (14). Anomalous dispersion terms f' and f'' were used for Hg (15). The refined coordinates are listed in Table 1. The anisotropic temperature factors, and the list of observed and calculated structure factors are part of the unpublished material.[2] The computer programs used are listed elsewhere (16).

Results

Two pairs of compounds have been isolated by reacting CH_3HgX (where X = NO_3 and ClO_4) with MCy: complexes of 1:1 stoichiometry without proton substitution and 2:1 compounds in which one proton per ligand has been displaced. The ^1H nmr and ir spectra (except for bands of the anions) of corresponding compounds are very similar, indicating that both salts contain the same complex cation. In the 1:1 compounds, CH_3Hg^+ is probably bonded to N(3) as commonly observed, especially for soft metals (6, 7, 9). The crystal structure of the nitrate of 2:1 stoichiometry shows that mercury coordination takes place with N(3) and the deprotonated amino group N(4).

Description of the Crystal Structure of [$(CH_3Hg)_2(MCy—H)$]NO_3

Unexpectedly, the CH_3Hg^+ groups are in the *syn* arrangement (Fig. 1), instead of the presumably less constrained *anti* configuration already found in [(9-methyladeninato)$(CH_3Hg)_2$]ClO_4 (4). The *syn* configuration has been observed in two dimeric N(3),N(4)-bonded platinum complexes (12), but in that case the *syn* arrangement can be stabilized by the stacking of square planes commonly found with platinum (with or without Pt—Pt bonding). In the

[2]The supplementary material includes a table of temperature factors, a list of structure factors, and details of least-squares plane calculations. Complete set of data is available, at a nominal charge, from the Depository of Unpublished Data, CISTI, National Research Council of Canada, Ottawa, Ont., Canada K1A 0S2.

Can. J. Chem. Downloaded from www.nrcresearchpress.com by 210.87.254.105 on 09/06/12
For personal use only.

TABLE 1. Refined atomic coordinates ($\times 10^3$, Hg $\times 10^5$)

Atom	X	Y	Z
Hg(3)	8581(10)	17111(9)	4057(8)
Hg(4)	11233(9)	39298(9)	−1251(8)
N(1)	290(2)	164(2)	246(2)
C(1)	328(3)	80(2)	302(2)
C(2)	215(2)	152(2)	187(2)
O(2)	174(2)	66(2)	176(1)
N(3)	181(2)	228(2)	133(1)
C(4)	227(2)	317(2)	147(2)
N(4)	198(2)	389(2)	97(2)
C(5)	299(3)	335(2)	214(2)
C(6)	332(3)	261(2)	261(2)
N(10)	339(3)	352(2)	445(2)
O(10)	424(2)	364(3)	406(2)
O(11)	284(2)	273(2)	441(2)
O(12)	291(2)	417(2)	491(2)
C(13)	−14(3)	122(3)	−60(3)
C(14)	25(3)	386(3)	−124(2)
H(4)*	222	452	116
H(5)*	323	400	226
H(6)*	384	273	304

*Parameters not refined.

present structure, the preference for the *syn* orientation is hard to explain and ^{1}H nmr results (see below) suggest that the structure may be different in solution. Even though the distortions are severe, they are not unprecedented. For instance, the Hg(4)—N(4)—C(4) angle (133(2)°) is only slightly greater than those observed in [Ru(NH_3)$_5$(MCy—H)] (PF_6)$_2$, 129.2(7)° (11) and in [(NH_3)$_4$$Pt_2$(MCy—H)$_2$]($NO_3$)$_2$.2$H_2O$, 131(2)° (12), although the value of ~124° obtained in the 9-methyladenine complex (4) and in (H_5O_2)-[(Pt_2(NO_2)$_2$(NH_3)$_4$(MCy—H)$_2$](NO_3)$_2$ (12) appears to be more normal. On the other hand, there is a large difference of 24° between Hg(3)—N(3)—C(4) and Hg(3)—N(3)—C(2), which is not found in the platinum complexes (12). However, a similar difference has been observed in Hg_2Cl_4-(MCy)$_2$ (16) and still larger values have been reported (17). As a result of that distortion, Hg(3) lies at 2.84(2) Å from carbonyl oxygen O(2) and the angular deformation at N(3) is possibly balanced by some Hg...O bonding interaction. The resulting Hg...Hg contact (3.150(2) Å) is greater than twice the short van der Waals radius proposed by Grdenic (1.50 Å) (18), but it is shorter than the intramolecular non-bonded Hg...Hg contacts (3.27–3.31 Å) found in similar complexes (19). If severe repulsion remained between the Hg atoms, the CH_3Hg groups would be expected to slip out of the molecular plane, in *opposite* directions. They are found at large distances from the plane of the ring (Hg(3), 0.214(1) Å; C(13), 0.45(4) Å; Hg(4), 0.393(1) Å; C(14), 0.74(3) Å), but on the *same* side. Consequently, in spite of an obvious departure for

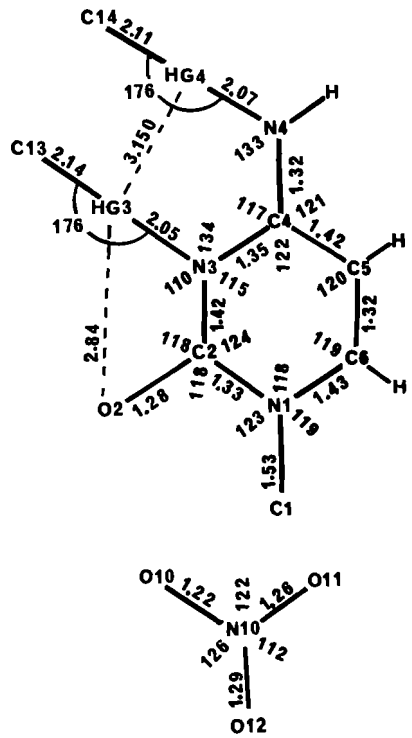

FIG. 1. Interatomic distances and bond angles in [(CH_3Hg)$_2$-(MCy—H)]NO_3. The standard deviations on distances are 0.04–0.05 Å, except for Hg—Hg, 0.002 Å, Hg—N(O), 0.02 Å, and Hg—C, 0.03–0.04 Å. On bond angles, they are 2–3°, except for N—Hg—C, 1° and O—N—O, 4°.

ideality, this molecule is probably not extremely strained.

The Hg—N and Hg—C bond lengths (ave. 2.06(2) and 2.12(3) Å, respectively) are normal and there is no appreciable departure from the usual linear coordination of mercury (C—Hg—N = 176(1)°).

Because of the large esd's, the distances and angles in the coordinated ligand show no significant differences from either neutral or protonated MCy (20), so that no effects of coordination can be detected. The six-membered ring of the ligand is planar within 1.3σ (0.04 Å) and the distances from the exocyclic groups to the plane are small: N(4), 0.08(2) Å; O(2), −0.06(2) Å; C(1), 0.03(3) Å.

The NO_3^- ion is planar within 0.5σ (0.02 Å). The bond lengths (ave. 1.26(4) Å) and angles 120(4)° are as expected.

A stereo view of the molecular packing is shown in Fig. 2. There is no long-range stacking of the bases, which is rather unusual for CH_3Hg^+ complexes with free or methylated bases. The only hydrogen bond is established between N(4)—H(4) and carbonyl group O(2) at $\frac{1}{2}-x, \frac{1}{2}+y, z$. It is rather weak (N(4)...O(2) = 3.13(3) Å) and the geometry is

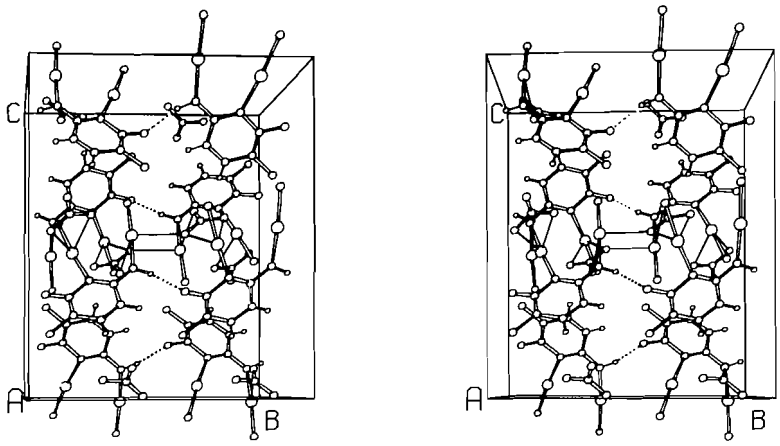

FIG. 2. ORTEP drawing of the unit cell of $[(CH_3Hg)_2(MCy—H)]NO_3$. The ring atoms can be identified by reference to Fig. 1. The larger and smaller spheres correspond to Hg and H, respectively. The secondary Hg...O bonds are shown as thin continuous lines and H-bonds, as dashed lines.

TABLE 2. Secondary bonds to mercury

Atoms	Distance (Å)	Atoms	Distance (Å)
Hg(3)—O(11)[a]	2.98(3)	Hg(4)—O(10)[b]	2.88(3)
Hg(3)—O(12)[a]	2.86(2)	Hg(4)—O(12)[c]	2.83(3)
Bonds	**Angle (deg)**	**Bonds**	**Angle (deg)**
C(13)—Hg(3)—O(11)[a]	96.1(12)	C(14)—Hg(4)—O(10)[b]	97.2(11)
C(13)—Hg(3)—O(12)[a]	97.8(12)	C(14)—Hg(4)—O(12)[c]	105.3(11)
N(3)—Hg(3)—O(11)[a]	82.0(8)	N(4)—Hg(4)—O(10)[b]	82.2(10)
N(3)—Hg(3)—O(12)[a]	83.4(8)	N(4)—Hg(4)—O(12)[c]	78.6(9)
O(11)[a]—Hg(3)—O(12)[a]	42.5(7)	O(10)[b]—Hg(4)—O(12)[c]	115.7(8)

$a = x, \frac{1}{2} - y, -\frac{1}{2} + z$; $b = -\frac{1}{2} + x, y, \frac{1}{2} - z$; $c = \frac{1}{2} - x, 1 - y, -\frac{1}{2} + z$.

not particularly favorable (C(4)—N(4)—O(2) = 101(2)°, C(2)—O(2)—N(4) = 125(2)°). Each Hg atom forms secondary bonds with two nitrate oxygens close to the equatorial plane (Table 2). Hg...O contacts in the range 2.83–2.98 Å are common with nitrate ions and definitely shorter than observed with the less basic ClO_4^- ion (19). The NO_3^- ion acts as a three-way link between complex cations: it is chelating bidentate by O(11) and O(12) toward Hg(3), while O(10) interacts with one Hg(4) atom and O(12), already bonded to Hg(3), also interacts with a different Hg(4) atom.

Infrared Spectroscopy

The spectra of MCy and both types of complexes are represented in Fig. 3. Our results for MCy are in good agreement with those published by Lord and Thomas (21). Pairs of salts of the same stoichiometry have very similar spectra, except for the bands originating from the anions. The ir-active ν_3 and ν_4 modes of ClO_4^- are easily related to the very strong bands at $\sim$1080 cm^{-1} and the medium band at $\sim$625 cm^{-1}, respectively (22). Weak bands at $\sim$928 cm^{-1} probably correspond to the ir-inactive ν_1 mode gaining some intensity by reduced site symmetry. The NO_3^- ion is identified from its very strong and broad ν_3 band at $\sim$1360 cm^{-1} and weaker absorption ν_2 at $\sim$823 cm^{-1}. Some of the weak features around 710 and 1040 cm^{-1} could correspond to ν_4 and ν_1 respectively, the latter mode being normally ir-inactive.

The ir spectra of a number of CH_3Hg^+ compounds have been discussed (23). The vibrations due to the CH_3 group are not easily identified, because the ligand shows N(1)—CH_3 or other bands in the same regions. The sharp peak at 2925 cm^{-1} is due to the superimposed ν_s modes of both methyl groups. The ν_a, δ_a, and δ_s modes expected to produce weak bands around 3000, 1410, and 1200 cm^{-1}, respectively, could not be unambiguously assigned. Comparisons with the spectra obtained for similar Ag^+—MCy compounds (24) reveals

Can. J. Chem. Downloaded from www.nrcresearchpress.com by 210.87.254.105 on 09/06/12
For personal use only.

Can. J. Chem. Downloaded from www.nrcresearchpress.com by 210.87.254.105 on 09/06/12
For personal use only.

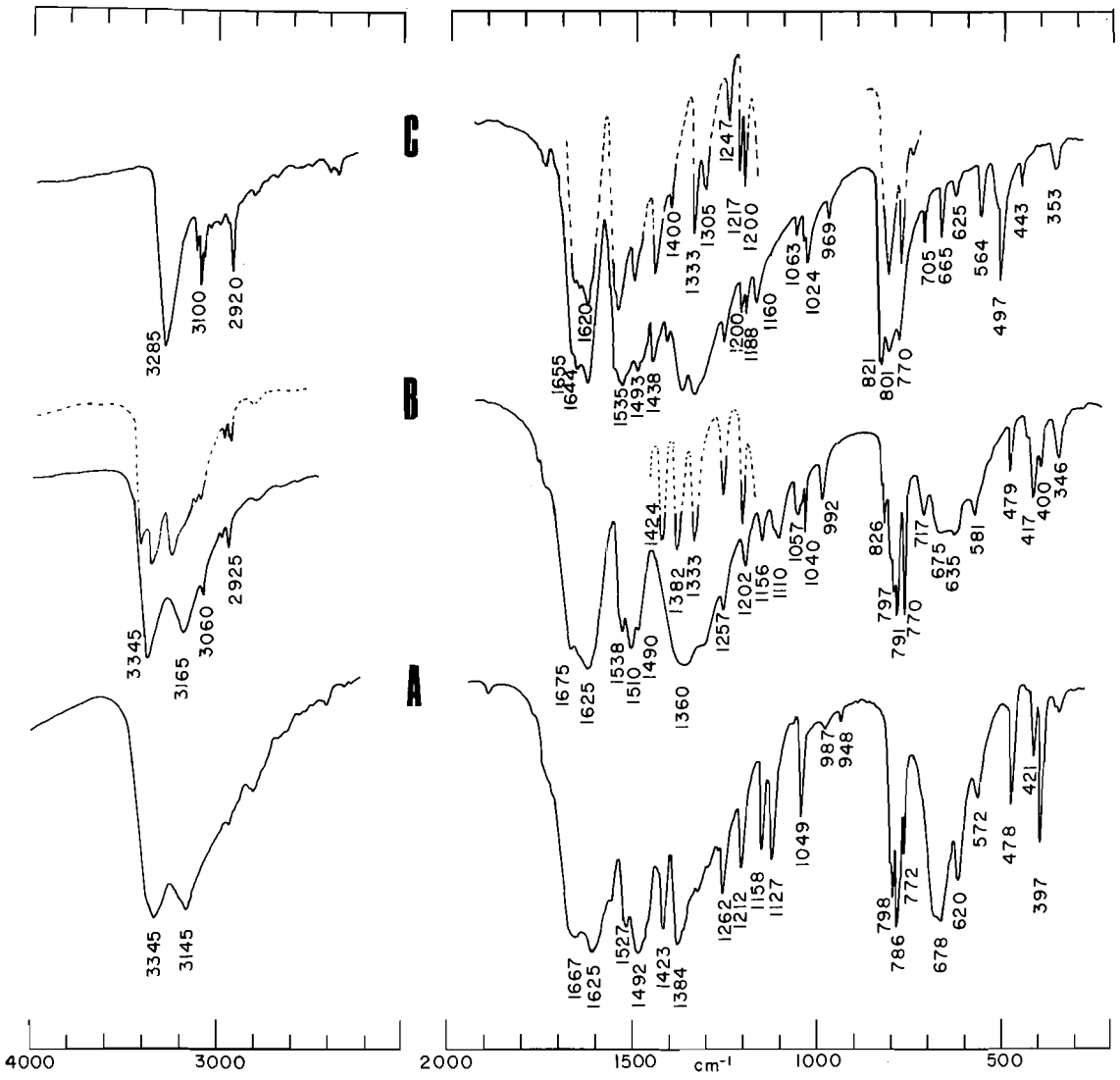

FIG. 3. Infrared spectra. A = MCy, B = $[CH_3Hg(MCy)]NO_3$, C = $[(CH_3Hg)_2(MCy\text{-}H)]NO_3$. Portions of spectra in dotted lines correspond to the perchlorate analog.

extra strong bands at 801 cm^{-1} in $[(CH_3Hg)_2$-(MCy—H)]X and ~790 cm^{-1} in $[CH_3Hg(MCy)]X$, which probably correspond to $\rho(CH_3)$. The Hg—C stretching vibration can be identified only in the N(3),N(4)-bonded complexes as a weak band at 564 cm^{-1}. In the 1:1 compounds, that absorption is masked by the very broad $w(NH_2)$ vibration found at ~680 cm^{-1} in the ligand (21, 25) and displaced to lower wavenumbers in the complexes.

N(3)-binding

The most obvious spectral changes in the N(3)-bonded compounds are associated with the NH_2 group. The N—H stretching bands at 3345 and 3145 cm^{-1} (21, 25) are not displaced appreciably, but they become sharper (and split in the case of the perchlorate) (Fig. 3). As a result, the weak C—H stretching bands of the ring and methyl groups (2900–3100 cm^{-1}) are better defined. Two ligand bands at 1127 and 1049 cm^{-1} are shifted by −17 and +8 cm^{-1} respectively in the complexes. They are believed to involve a large amount of NH_2 rocking motion (25). Those changes are likely to simply reflect different hydrogen-bonding patterns.

The most interesting spectral change is the appearance in the perchlorate salt of a well-defined band at 1333 cm^{-1}, where free MCy does not absorb appreciably. According to Tsuboi *et al.*

Can. J. Chem. Downloaded from www.nrcresearchpress.com by 210.87.254.105 on 09/06/12
For personal use only.

(25), this vibration should be located in the N(1)—C(6)—C(5) side of the ring. The utility of this band for predicting N(3)-binding could not be checked with the nitrate, which strongly absorbs at that position.

Other regions (~1500, ~800, and ~635 cm^{-1}) have been reported to be sensitive to N(3)-coordination (2, 12), but they could not be used in this case because of insufficient resolution or interference from the CH_3Hg groups.

N(3),N(4)-bridging

This type of bonding leads to major changes in the ligand spectrum. Only one sharp ν(N—H) band at 3285 cm^{-1} is observed for the deprotonated amino group. The weak C—H stretching modes are now clearly observed. The absence of an amino group can be detected by the much sharper absorptions between 1620 and 1650 cm^{-1}, where the scissoring motion of the amino group absorbed, and by the complete disappearance of the w(NH_2) band at 680 cm^{-1}. The band at 1127 cm^{-1} involving the rocking NH_2 motion (25) is no longer present. It has apparently been replaced by a medium band at 1305 cm^{-1}, which might involve in-plane N—H bending of the substituted amino group.

A number of other modifications in positions and intensities are observed throughout the spectrum. For instance, the bands at 1024, 1200, and 1247 cm^{-1} have all been shifted with respect to the free ligand. Those wavenumbers, together with 1305 cm^{-1}, seem to correspond to characteristic values reported by Mansy *et al.* (3) for the CH_3Hg^+ species formed in basic solutions with deprotonated cytidine. The "ring breathing" region (~780 cm^{-1}) is also affected in a similar manner as in the 1:1 complexes. It is noteworthy that the band at 1333 cm^{-1}, suggested as a characteristic for N(3)-coordination, is still present in these compounds. Finally, there is a sharp absorption of medium intensity at ~497 cm^{-1}, which is found neither in the free ligand, nor in the 1:1 complexes. A similar band at ~480 cm^{-1} was assigned to the Hg—N(amino) stretching mode in 9-methyladenine complexes (26).

^1H Nuclear Magnetic Resonance Spectroscopy

The spectrum for MCy (Table 3) is in good agreement with the results of other workers (12, 27, 28). The doublets at 5.60 and 7.55 ppm are due to H(5) and H(6), coupled by 7 Hz (27). The sharp signal at 3.19 ppm originates from the N(1)—methyl group. The amino protons give a broad singlet at 6.92 ppm.

The H(5) and H(6) doublets are shifted downfield by 0.49 and 0.35 ppm, respectively, in the N(3)-bonded 1:1 complexes (Table 3). These shifts are of the same magnitude as those observed when MCy is protonated by $HClO_4$, an acid devoid of extra effects due to anion–ligand H-bonding (28). Similar shifts have been noted for other N(3)-bonded complexes with Pt (12, 29) and when $ZnCl_2$ (30) or $HgCl_2$ (31) are reacted with cytidine in DMSO. The NH_2 signal is shifted from 6.92 to 8.73 ppm and appears as two very close ($\Delta\delta = 0.08$ ppm) but resolved components of equal intensities. Signal splitting has been reported for protonation (28) and complexation with Pt (12) and Hg (31), but the separation is much greater. Splitting results from hindered rotation about the C(4)—N(4) bond, making the amino protons inequivalent. Since the NO_3^- and ClO_4^- ions used in this work have been shown not to interfere with the ligand signals through H-bonding (28), we conclude that introducing CH_3Hg^+ at N(3) led to a small, but detectable, inequivalence of the amino protons.

The spectra of the N(3),N(4)-bonded complexes show only one resonance at ~0.78 ppm for the protons of the two rapidly exchanging CH_3Hg groups. Proton substitution on the 4-NH_2 group by the electropositive Hg atom produces, as expected, an upfield shift from 8.73 ppm (1:1 complex) to 7.49 ppm. However, it is noteworthy that the remaining amino proton appears to be more acidic than it was in free MCy (6.92 ppm). In this respect, $[(CH_3Hg)_2(MCy—H)]X$ differs markedly from $[(NH_3)_4Pt_2(MCy—H)_2](NO_3)_2$, for which the same proton has a chemical shift of 6.16 ppm (12). The Pt complex was shown by X-ray diffraction to have a similar *syn* arrangement of metal atoms in the solid and the structure is likely to be retained by this non-labile system in solution. A similar spectrum was reported for a silver-cytidine species in which Ag is bonded to the deprotonated amino group and probably interacts with N(3) as well, although the exact structure is not known (32). Differences are also found for the H(5) and H(6) resonances. With Pt and Ag, both doublets shift upfield in going from the N(3)-bonded to the N(3),N(4)-bonded compounds. For $[(CH_3Hg)_2(MCy—H)]X$, the shifts are downfield for H(5) and upfield for H(6).

The above chemical shifts suggest that the CH_3Hg compounds might undergo some rearrangement in DMSO. However, the ^1H–^{199}Hg coupling constants are not inconsistent with a structure in which both CH_3Hg groups would remain coordinated.[3] With rapid exchange, the observed J value

[3]The following discussion concerning the coupling constants is largely based on suggestions of one of the referees, who also kindly provided relevant references.

TABLE 3. ^1H nmr data[a]

Molecule	δ N(1)—CH_3	H(5)	H(6)	H(41)—H(42)	Hg—CH_3	$^2J_{H5—H6}$	$^2J_{H—^{199}Hg}$
MCy	3.19s	5.60d	7.55d	6.92s		7	—
$[CH_3Hg(MCy)]NO_3$	3.34s	6.09d	7.90d	8.76b 8.71b	0.80s	7	227
$[CH_3Hg(MCy)]ClO_4$	3.34s	6.09d	7.89d	8.73b 8.64b	0.85s	7	226
$[(CH_3Hg)_2(MCy—H)]NO_3$	3.28s	6.24d	7.69d	7.48s, b	0.77s	—	207
$[(CH_3Hg)_2(MCy—H)]ClO_4$	3.28s	6.23d	7.68d	7.50s, b	0.78s	7	205

[a] In DMSO-d^6, chemical shifts (ppm) from internal tetramethylsilane. Coupling constants in Hz. s = singlet, d = doublet, b = broad.

(206 Hz) should be the average for the groups bonded to N(3) and N(4), respectively. The value for the 1:1 complex (226 Hz), which is close to the one obtained for the N(7)-bonded compound with guanosine (33), may be used as an estimate for the contribution of the N(3)-bonded group. Then, J for the other CH_3Hg ion should be ~186 Hz. There are no data in the literature for CH_3Hg compounds with RNH^- species, of which the $C_6H_5NH^-$ ion derived from aniline would be a simple example. However, the related compound $[CH_3Hg(OC_6H_5)]$ with phenol has been studied and the J value is 206 Hz (34). Comparisons of oxygen and nitrogen donors in analogous molecules reveal that the J values are lower for nitrogen: 252 Hz for $[CH_3Hg(CH_3OH)]^+$ (35) and 212 Hz for $[CH_3Hg(CH_3NH_2)]^+$ (36). Thus J should be substantially lower than 206 Hz for the complexation to the deprotonated amino group of aniline or MCy, and the above estimate (186 Hz) would be reasonable. On the other hand, there are extra possibilities if the difference of 40 Hz between the CH_3OH and CH_3NH_2 compounds would also apply to the phenolate/anilinate pair. In that case, the J value for the N(4)-coordinated CH_3Hg group in $[(CH_3Hg)_2(MCy—H)]X$ should be ~166 Hz, and the other CH_3Hg group, originally bonded to N(3) in the solid, should have a J value of 246 Hz in order to obtain an average value of 206 Hz. This would be consistent with partial dissociation of the latter CH_3Hg group (J for CH_3HgNO_3 in DMSO = 260 Hz (37)) or migration to the adjacent carbonyl group. It appears that data on a 1:1 complex of the type $[CH_3Hg(MCy—H)]$ are required to determine the nature of the 2:1 species in solution, but we have been unable to prepare this compound so far.

Discussion

Although the fixation of the first CH_3Hg^+ ion on N(3) was anticipated, its ability to acidify the amino protons was not expected to be so important. Increased acidic character is evidenced from the large downfield shift (1.8 ppm) of the ^1H nmr signal (Table 3) of the amino protons between MCy and its 1:1 complex, on the one hand, and from the possibility of preparing the $[(CH_3Hg)_2(MCy—H)]X$ compounds even under slightly acidic conditions, on the other hand. In this respect, the cytosine ring compares well with N(9)-substituted adenine, in which initial coordination to N(1) induces a similar effect on the 6-amino group (4, 5).

The availability of the 4-amino protons of cytosine for substitution suggests new possibilities for inserting ions like Ag^+ and Hg^{2+} between pairs of complementary bases in nucleic acids. Indeed, such linear two-coordinated cations are known to replace some of the hydrogen atoms normally involved in the base-pairing hydrogen bonds (38). Models in which one or two hydrogens per base pair are replaced by silver have been proposed (39). The present work supports the assumption that two metal ions can be inserted between the same pair of bases, since the positions occupied by the metal atoms would be approximately as found in the *syn* configuration revealed by the crystal structure of $[(CH_3Hg)_2(MCy—H)]NO_3$. In addition, if two metal atoms cross-link a G–C pair, the 4-NH_2 group of cytosine could be involved. Substitution of H(1) of guanine with concomitant formation of N(3C)—M—N(1G) bonds (**1**) is expected to facilitate the insertion of a second metal atom between N(4C) and O(6G), because the acidity of the amino group of cytosine would be enhanced by initial coordination with N(3C) and the basicity of O(6G) would be increased by substitution of H(1G).

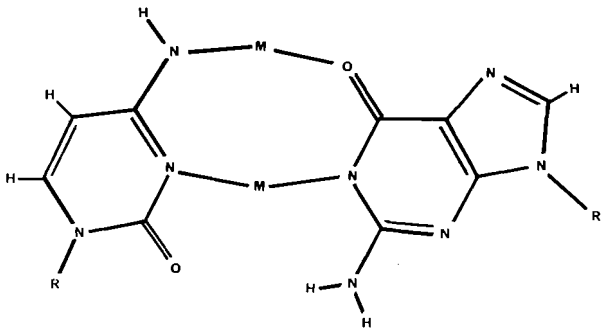

Can. J. Chem. Downloaded from www.nrcresearchpress.com by 210.87.254.105 on 09/06/12
For personal use only.

Can. J. Chem. Downloaded from www.nrcresearchpress.com by 210.87.254.105 on 09/06/12
For personal use only.

The ^1H nmr results for the $[(CH_3Hg)_2(MCy—H)]X$ compounds are puzzling. In spite of a similar mode of bonding in the solid state $[(NH_3)_4Pt_2(MCy—H)_2](NO_3)_2$ (12) and the CH_3Hg complexes show strikingly different spectra in DMSO, suggesting structural reorganization in the latter case. Besides simple dissociation of a CH_3Hg group, two structural changes might take place. First, rotation about the C4—N4 bond could lead to an *anti* orientation of the CH_3Hg groups. Second, the bulkiness of the amino-bonded CH_3Hg group could promote a transfer of the other CH_3Hg group from N(3) to O(2). It has been shown that $HgCl_2$ binds to O(2) rather than N(3) in N^4,N^4-dimethyl-N^1-methylcytosine, owing to the steric hindrance of the dimethylamino group (9). From our present data, the species present in DMSO cannot be clearly identified but this problem is currently being examined.

Acknowledgements

We are grateful to Prof. C. J. L. Lock and B. Lippert for providing copy of their paper (ref. 12) prior to publication and to a referee for his constructive comments. We wish to thank R. Mayer for recording the nmr spectra. We acknowledge financial support from the National Research Council of Canada and the Ministère de l'Education du Québec.

1. R. B. Simpson. J. Am. Chem. Soc. **86**, 2059 (1964).
2. S. Mansy, T. E. Wood, J. C. Sprowles, and R. S. Tobias. J. Am. Chem. Soc. **96**, 1762 (1974).
3. S. Mansy, J. P. Frick, and R. S. Tobias. Biochim. Biophys. Acta, **378**, 319 (1975).
4. L. Prizant, M. J. Olivier, R. Rivest, and A. L. Beauchamp. J. Am. Chem. Soc. **101**, 2765 (1979).
5. M. J. Olivier and A. L. Beauchamp. Inorg. Chem. **19**, 1064 (1980).
6. L. G. Marzilli. Prog. Inorg. Chem. **23**, 255 (1977).
7. D. J. Hodgson. Prog. Inorg. Chem. **23**, 211 (1977); V. Swaminathan and M. Sundaralingam. CRC Crit. Rev. Biochem. **6**, 245 (1979). H. Sigel (*Editor*). Metal ions in biological systems. Vol. 8. Marcel Dekker, New York. 1979. pp. 57.
8. K. Aoki. J. Chem. Soc. Chem. Commun. 748 (1976).
9. L. G. Marzilli, B. de Castro, J. P. Caradonna, R. C. Stewart, and C. P. Van Vuuren. J. Am. Chem. Soc. **102**, 916 (1980).
10. M. J. Clarke. J. Am. Chem. Soc. **100**, 5068 (1978).
11. B. J. Graves and D. J. Hodgson. J. Am. Chem. Soc. **101**, 5608 (1979).
12. R. Faggiani, B. Lippert, C. J. L. Lock, and R. A. Speranzini. J. Am. Chem. Soc. **103**, 1111 (1981).
13. D. T. Cromer and J. T. Waber. Acta Crystallogr. **18**, 104 (1965).
14. R. F. Stewart, E. R. Davidson, and W. T. Simpson. J. Chem. Phys. **42**, 3175 (1965).
15. D. T. Cromer. Acta Crystallogr. **18**, 17 (1965).
16. M. Authier-Martin and A. L. Beauchamp. Can. J. Chem. **55**, 1213 (1977).
17. C. Gagnon, A. L. Beauchamp, and D. Tranqui. Can. J. Chem. **57**, 1372 (1979).
18. D. Grdenic. Q. Rev. **19**, 303 (1965).
19. J. Hubert and A. L. Beauchamp. Can. J. Chem. **58**, 1439 (1980); Acta Crystallogr. B**36**, 2613 (1980).
20. T. J. Kistenmacher, M. Rossi, J. P. Caradonna, and L. G. Marzilli. Adv. Mol. Relaxation Interact. Processes, **15**, 119 (1979).
21. R. C. Lord and G. J. Thomas. Spectrochim. Acta, **23A**, 2551 (1967).
22. K. Nakamoto. Infrared spectra of inorganic and coordination compounds. 2nd ed. Interscience. 1970. pp. 98, 111.
23. J. H. S. Green. Spectrochim. Acta, **24A**, 863 (1968); R. P. J. Cooney and J. R. Hall. Austr. J. Chem. **22**, 2117 (1969).
24. M. Simard and A. L. Beauchamp. To be published.
25. M. Tsuboi, T. Takahashi, and I. Marada. Physicochemical properties of nucleic acids. Vol. 2. *Edited by* J. Duchesne. Academic Press, London. 1973. Chapt. 11.
26. R. Savoie, D. Poirier, L. Prizant, and A. L. Beauchamp. J. Raman Spectrosc. In press.
27. E. D. Becker, H. T. Miles, and R. B. Bradley. J. Am. Chem. Soc. **87**, 5575 (1965).
28. L. G. Marzilli, C. H. Chang, J. P. Caradonna, and T. J. Kistenmacher. Adv. Mol. Relaxation Interact. Processes, **15**, 85 (1979).
29. P. C. Kong and T. Theophanides. Inorg. Chem. **13**, 1981 (1974); Bioinorg. Chem. **5**, 51 (1975).
30. S. M. Wang and N. C. Li. J. Am. Chem. Soc. **88**, 4592 (1966); **90**, 5069 (1968).
31. L. S. Kan and N. C. Li. J. Am. Chem. Soc. **92**, 4823 (1970).
32. R. Cini, P. Colamarino, and P. L. Orioli. Bioinorg. Chem. **7**, 345 (1977).
33. A. J. Canty and R. S. Tobias. Inorg. Chem. **18**, 413 (1979).
34. L. F. Sytsma and R. J. Kline. J. Organomet. Chem. **54**, 15 (1973).
35. A. J. Canty and A. Marker. Inorg. Chem. **15**, 425 (1976).
36. D. L. Rabenstein, R. Ozubko, S. Libich, C. A. Evans, M. T. Fairhurst, and C. Suvanprakorn. J. Coord. Chem. **3**, 263 (1974).
37. Y. Kawasaki, M. Aritomi, and J. Iyoda. Bull. Chem. Soc. Jpn. **49**, 3478 (1976).
38. G. L. Eichhorn. Inorganic biochemistry. Elsevier, Amsterdam. 1973. Chapt. 34.
39. T. J. Kistenmacher, M. Rossi, and L. G. Marzilli. Inorg. Chem. **18**, 240 (1979).

Synthesis of α-thiohemiaminal derivatives of deoxynupharidine

ROBERT T. LALONDE AND TIMOTHY S. ECKERT

Department of Chemistry, State University of New York, College of Environmental Science and Forestry, Syracuse, NY 13210, U.S.A.

Received October 24, 1980

ROBERT T. LALONDE and TIMOTHY S. ECKERT. Can. J. Chem. **59**, 2298 (1981).

Disulfides, sulfenyl chlorides, thiosulfonates, and sulfensuccinimides were evaluated as electrophilic thiating agents for converting the enamine 6-dehydrodeoxynupharidine to α-thiohemiaminal derivatives of the alkaloid deoxynupharidine. Sulfensuccinimides were generally the most useful but other types of agents produced better yields in some individual cases.

ROBERT T. LALONDE et TIMOTHY S. ECKERT. Can. J. Chem. **59**, 2298 (1981).

On utilise les disulfures, les chlorures de sulfényles, les thiosulfonates et les sulfènesuccinimides comme agents de sulfuration électrophile pour transformer l'ènamine, déhydro-6 déoxynupharidine, en dérivés α-thiohémiaminal de l'alcaloide déoxynupharidine. Les sulfènesuccinimides sont généralement les agents les plus utiles, mais dans quelques cas individuels d'autres types de réactifs peuvent conduire à de meilleurs rendements.

[Traduit par le journal]

We have examined various electrophilic thiating agents (ArSX) for use in the conversion of 6-dehydrodeoxynupharidine, **1**, to diastereomeric α-arylthiohemiaminals **2** and **3**. Previous work had shown that **2***a* and **3***a* (1) were active against human pathogenic fungi. The α-thiohemiaminals also have pH dependent chiroptical properties (2) whose occurrence was attributed to the stabilizing intramolecular association of iminium ion with divalent sulfur (3). Here we treat the synthetic aspects of α-arylthiohemiaminal formation as it relates to the choice of the electrophilic thiating agent and the characterization of the products.

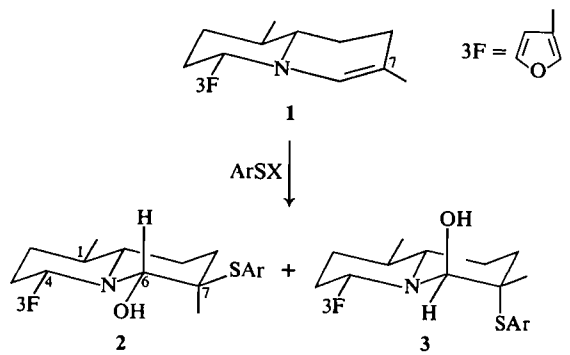

1 **2** **3**

Ar
a, C_6H_5–
b, 4-$H_3CC_6H_4$–
c, 4-$O_2NC_6H_4$–
d, 4-ClC_6H_4–
e, 4-$H_3COC_6H_4$–
f, 4-$F_3CC_6H_4$–
g, 4-HOC_6H_4–
h, 4-$H_2NC_6H_4$–

Electrophilic Thiating Agents

Enamines of cyclohexanone have been thiated by nitrophenyldisulfide (4), sulfenyl chlorides (4), and sulfensuccinimides (5). The reactive C-7 position of the enamine **1** has been thiated intentionally by phenyl benzenethiosulfonate (1) and unintentionally by *p*-toluenesulfonyl chloride (6).

As indicated by the results summarized in Table 1, *p*-nitrophenyldisulfide was the only disulfide of five which reacted with **1**. This result indicates that the nitro groups are required to make the sulfur atoms electrophilic and stabilize the leaving thiolate anion. Noteworthy, however, is the observation that even with the activating *p*-nitro groups, the *p*-nitrophenyl disulfide required a longer reaction time than any of the other nondisulfide thiating agents.

Of the other thiating agents, the sulfensuccinimides were the most dependable generally. The latter were prepared by heating a disulfide with *N*-bromosuccinimide according to a standard procedure (7). An exception was *p*-tosyloxyphenylsulfensuccinimide which could not be prepared in this manner nor by an alternative procedure whereby the corresponding sulfenyl chloride was added to succinimide in the presence of a *tert*-amine (8). However, in every case where the sulfenimide could be prepared, α-arylthiohemiaminal products were obtained in amounts adequate for the separation of C-7 epimers and the characterization of each. Sulfensuccinimides also offered the advantage that the crude thiating agent was sufficiently pure to be used directly without any purification.

The sulfenyl chlorides were judged to be of limited utility as a class because the attempted syntheses of the *p*-nitro and *p*-chloro derivatives was unsuccessful. *p*-Nitrophenyl disulfide and *p*-

0008-4042/81/152298-05$01.00/0
©1981 National Research Council of Canada/Conseil national de recherches du Canada

Can. J. Chem. Downloaded from www.nrcresearchpress.com by 210.87.254.105 on 09/06/12
For personal use only.

Can. J. Chem. Downloaded from www.nrcresearchpress.com by 210.87.254.105 on 09/06/12
For personal use only.

chlorophenylthiol did not react reliably with chlorine under the standard conditions (9). However, *p*-tosyloxyphenylsulfenyl chloride, required for the preparation of the *p*-hydroxyphenylthiohemiaminals, was prepared from *p*-tosyloxyphenyl disulfide in this manner.

Although the sulfensuccinimides quickly found favor as the most dependable general thiating agents, representatives of all four classes were used as preferred reagents to synthesize particular α-arylthiohemiaminals. Thus the *p*-chlorophenylthiohemiaminals were prepared from the thiosulfonate, which was obtained reliably in high yield and purity by standard procedures (10, 11). The mixture of *p*-nitrophenylthiohemiaminals was prepared preferentially from the disulfide, the tosyloxy compounds from the sulfenyl chloride, and the remaining five from the sulfenimides.

Formation of α-Arylthiohemiaminals

Sulfensuccinimides in methylene chloride solution produced equal amounts of epimeric α-arylthiohemiaminals **2** and **3** as determined by integrating the axial and equatorial C-6 ^{1}H nmr signals observed in the spectra of the crude reaction products. However, phenylsulfenyl chloride in methylene chloride or phenyl benzenethiosulfonate in benzene gave mixtures rich in **2***a*.

α-Arylthiohemiaminals **2***a–f* and **3***a–f* were obtained directly from the reaction of the appropriate agent with **1**. However, to prepare **2***g–h* and **3***g–h* it was necessary to employ thiating agents wherein hydroxyl and amino groups were protected. In the case of phenolic **2***g* and **3***g*, whose formation is traced below, an arenesulfonyl protecting group was favored over an alkyl group because the 3-furyl was considered vulnerable to the anticipated vigorous acidic conditions required for alkyl removal. Since alumina column chromatography of a small portion of the hemiaminal reaction mixture resulted in a proliferation of tlc spots, presumably because of tosyloxy hydrolysis, the remaining crude mixture was heated with aqueous base to effect the direct hydrolysis of the protecting tosyl group.

Proceeding in a manner similar to the above 4-hydroxyphenyl case, the amino groups of bis-4-aminophenyl disulfide were protected by treating the latter with hot 88% formic acid. The resulting bis-4-formamido derivative was treated with NBS. The sulfensuccinimide reacted with **1** and gave the thiohemiaminal whose amino protecting group was removed directly through acyl exchange with hydrazine. Noteworthy is the unusual care required for the formation of the sulfensuccinimide from NBS. This step was achieved only when the reaction mixture was warmed two hours at 55°C, a temperature 20° below the normal. Longer reaction times or higher temperatures resulted in the rapid deterioration of the sulfensuccinimide.

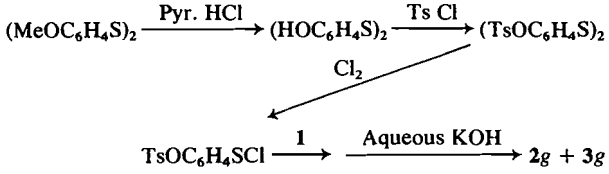

Characterization and Stereochemistry of the α-Thiohemiaminals

Earlier work in this laboratory with pairs of α-thiohemiaminals (**2***a* and **3***a* (1), **2***b* and **3***b* (6), and the 7-methylthio pair (12)) showed that α-thiohemiaminals were not highly stable compounds but the **2**-series diastereomers were more stable than those of the **3**-series. Therefore in the subsequent work, reported here, elemental composition was determined by combustion analysis or high resolution mass spectrometry on a mixture of the two diastereomers, the more stable diastereomer, or a stable derivative.

Spectra were determined on samples containing only a mixture of the two diastereomers. The ir indicated the presence of the 3-furyl and 1,4-disubstituted aryl groups respectively in the appearance of 11.5 and 12 μm absorption bands. The mass spectra revealed *m/e* 248, 231, 192, 176, 107, and 94, peaks characteristic of a C-6 hemiaminal incorporated in a deoxynupharidine skeleton (13).

The ^{1}H nmr of the α-arylthiohemiaminals were in all cases consistent with the compounds of earlier work (1, 6, 12). Of particular interest were the resonance signals from the β-proton of the furan ring, the C-6 proton, and the C-7 methyl group, since stereochemically dependent chemical shifts were observed. In each case, the **2**-series diastereomer had higher field signals for β-furyl and C-6 protons and a lower field signal for the C-7 methyl protons than the **3**-series counterpart. This interpretation of the spectra was based on previous observations for the individual **2** and **3** series diastereomers and made possible the estimation of relative amounts of the two diastereomers.

All **2**-series diastereomers were isolated from the mixture of two diastereomers for the acidic solution (pH 4) cd which showed positive bands in the 270–310 nm region and as a consequence could be assigned the C-7 configuration indicated in the

Can. J. Chem. Downloaded from www.nrcresearchpress.com by 210.87.254.105 on 09/06/12
For personal use only.

TABLE 1. Thiating agent employed and percentage yield of α-arylthiohemiaminals 2 and 3 obtained from 6-dehydrodeoxynupharidine, 1

ArSX		% Yield[a] of α-arylthiohemiaminal	
X	Ar	2	3
SAr[b]	C_6H_5	0	0
	4-$CH_3C_6H_4$	0	0
	4-ClC_6H_4	0	0
	4-$CF_3C_6H_4$	0	0
	4-$NO_2C_6H_4$	20	20
SO_2Ar[c]	C_6H_5	28	5
	4-ClC_6H_4	38	[d]
Cl[b]	C_6H_5	75	15
	4-$TsOC_6H_4$	33[e]	16[e]
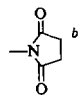	C_6H_5	42	42
	4-$CH_3C_6H_4$	18	18
	4-ClC_6H_4	39	39
	4-$CF_3C_6H_4$	5	2
	4-$NO_2C_6H_4$	[f]	[f]
	4-$MeOC_6H_4$	10	10
	4-$HCONHC_6H_4$	20[g]	20[g]

[a] Isolated.
[b] CH_2Cl_2 solvent.
[c] C_6H_6 solvent.
[d] The diastereomer was produced according to tlc but the amount could not be estimated from ^1H nmr.
[e] Values are obtained from the amount of the 7-(4-hydroxyphenylthio)deoxynupharidin-6-ols produced upon hydrolysis of the tosylate.
[f] Diastereomers were produced in nearly equal amounts but the yield was not determined.
[g] Values are obtained from the amount of the 7-(4-aminophenylthio)deoxynupharidin-6-ols produced upon hydrazinolysis.

structures (2). Two **3**-series diastereomers could be isolated for cd comparison with their **2**-series counterparts. In acidic solutions **3***c* and **3***g* gave negative cd bands in the 270–310 region which were the approximate inverted images of those observed for **2***c* and **2***g*.

Experimental

Spectra were obtained as follows: infrared (ir) in dichloromethane, unless otherwise indicated, on a Perkin–Elmer 137 spectrometer (symbols s, m, w refer to strong, medium, weak, respectively; wavelength in microns); proton magnetic resonance (^1H nmr) in deuterated chloroform with 1% TMS, unless otherwise noted, on a Varian A60 A spectrometer or, if noted as 100 MHz, on a Varian XL100 spectrometer operating in the pulsed Fourier mode (symbols s, d, m, br, eq refer to singlet, doublet, multiplet, broad, equatorial, respectively; absorption δ in ppm); low resolution mass spectra (ms), *m/e* (relative intensity), on a Hitachi–Perkin–Elmer RMU6E spectrometer using a direct inlet at 70 eV, chamber temperature 200°C unless otherwise noted; high resolution mass spectra (hrms) on an AEI MS-902 spectrometer using a direct inlet at 70 eV and performed at the Cornell Mass Spectrometry Facility, Ithaca, NY; circular dichroism (cd) in 70% MeOH – water at the concentration indicated, in a cell of 0.1 dm length, using a Jasco Model 5 spectropolarimeter; ultraviolet (uv) in 95% EtOH on a Cary 15 and a Beckman Acta MVI spectrophotometer. Uncorrected melting points were determined on a Mel-Temp apparatus. Elemental analyses were performed by Galbraith Laboratories, Knoxville, TN and by Micro-analysis, Inc., Wilmington, DE. Thin-layer chromatography (tlc) was visualized with Dragendorff–Munier reagent and performed on microscope slides uniformly coated with: A, alumina, GF-254 (0.25 mm thickness); or B, silica gel, GF-254 (0.50 mm thickness) (symbols DA, UVA refer to Dragendorff-active and uv-active spots, respectively). Column chromatography was done with neutral activity 2 alumina and by eluting with 25 mL fractions, unless otherwise noted. All solvents were distilled before use. Organic solutions from work-ups were dried with sodium sulfate. Acidifications were done with 4 *N* HCl and basifications with 4 *N* NaOH unless otherwise noted.

Disulfides

4-Nitrophenyl disulfide was used as obtained from the Aldrich Chemical Co. 4-Methoxyphenyl, 4-chlorophenyl, 4-tolyl, and phenyl disulfide were prepared as follows. A solution of 1 volume of thiol in 4 volumes of acetone was heated to reflux with 1 molar equivalent of $FeCl_3$ in 12 volumes of water. The acetone was evaporated and the residue was basified to pH 10 and extracted twice with CH_2Cl_2. The organic layers were washed with water and then brine, dried, concentrated to an oil, and recrystallized from MeOH or EtOH. 4-Trifluoromethylphenyl disulfide was prepared from 4-bromobenzotrifluoride according to a literature procedure (14) and purified by elution with hexane from a column of alumina.

4-Tosyloxyphenyl disulfide was prepared as follows. A solution of 1.96 mL of C_5H_5N (24.5 mmol) was treated with 2.17 mL of 12 *M* HCl (26 mmol) until the temperature rose to 220°C. The solution was cooled under N_2, then heated under N_2 with 680 mg of 4-methoxyphenyl disulfide (2.4 mmol) at 220°C for 10 min. The solution was cooled, diluted with water, and extracted with ether (4×). The ether solution was washed with water, brine, dried, and concentrated at reduced pressure. Crystallization of the concentrate gave 170 mg of 4-hydroxyphenyldisulfide (28%): tlc (B, 40% $Et_2O - C_6H_{14}$) R_f 0.2 (UVA); mp 113–115°C; ir: 2.80 (w), 6.26 (m), 8.60 (s), 12.09 (s), but no band at 8.03 μm. A

Can. J. Chem. Downloaded from www.nrcresearchpress.com by 210.87.254.105 on 09/06/12
For personal use only.

680 mg sample of 4-hydroxyphenyl disulfide (2.7 mmol) and 2.07 g of freshly recrystallized tosylchloride (10.9 mmol) slowly dissolved in 30 mL of C_5H_5N freshly distilled from KOH. The solution was kept at −4°C for 19 h and thereafter treated with water and extracted with CH_2Cl_2 (3×). The CH_2Cl_2 solution was washed with cold 4 *N* HCl, water, brine, then dried and finally concentrated at reduced pressure to give 1.15 g of crude brown oily 4-tosyloxyphenyl disulfide (76%): tlc (B, C_6H_6) R_f 0.6 (UVA); ir (neat): 6.25 (s), 8.35 (s), 11.61 (s), but no OH at 2.80 μm.

N-formyl-3-aminophenyl disulfide was prepared from 4-aminophenyl disulfide (purchased from the Aldrich Chemical Co.) as follows. The starting disulfide (2.0 mmol) was heated to reflux with 0.69 mL at 88% formic acid (16 mmol) in 10 mL of toluene in a Dean–Stark apparatus. After 0.5 h a grey solid formed; after 1.5 h water evolution ceased; after 2 h the mixture was cooled and the grey solid was collected by filtration and recrystallized from EtOH–water to obtain 460 mg (76%) of grey *N*-formyl-4-aminophenyl disulfide: tlc (A, Et_2O) R_f 0.5 (UVA); mp 160° C; ir (Nujol): 5.90 (s), 6.25 (m), 7.68 (s), 7.75 (s), 12.13 (s) μm.

Sulfensuccinimides

All the arylsulfensuccinimides, except the 4-tosyloxyphenylsuccinimide, were prepared by the following general method. The disulfide and 2 equivalents of recrystallized *N*-bromosuccinimide were heated to reflux in benzene (distilled from LAH) under N_2 for 15 min after the orange or red color no longer deepened in color (total time 0.5–1.0 h). The solvent was removed at reduced pressure to obtain an orange solid which in most cases was used in thiation without further purification. However, purification by recrystallization was performed on: 4-nitrophenylsulfensuccinimide (20% from chloroform), mp 160–171°C (lit. (7) mp 169.5°C); ir: 5.85 (s), 6.33 (w), 7.51 (s), 11.75 (m) μm; phenylsulfensuccinimide (48% from MeOH), mp 114–115°C (lit. (15) mp 116°C); ir: 5.82 μm; 4-tolylsulfensuccinimide (24% from MeOH), mp 99–106°C (lit. (7) mp 113.5°C); ir (KBr): 5.82 (s), 12.30 (s) μm.

Thiosulfonates

Phenyl benzenethiosulfonate and 4-chlorobenzenethiosulfonate were prepared from the appropriate arylthiol and sulfuryl chloride in the presence of acetic acid and water at 0–5°C according to a literature procedure (10, 11).

Sulfenylchlorides

Phenyl- and 4-tosyloxyphenylsulfenyl chlorides were prepared from the disulfides and chlorine or sulfuryl chloride according to published procedures (9). Thus in the case of 4-tosyloxyphenylsulfenyl chloride, chlorine (dried by passing through concentrated H_2SO_4) was bubbled through a solution of 870 mg of 4-tosyloxyphenyl disulfide (1.56 mmol) and a crystal of I_2 in 25 mL of $CHCl_3$ previously washed with water and distilled from $CaCl_2$. The solvent was removed at reduced pressure to obtain the crude red-orange oily 4-tosyloxyphenylsulfenyl chloride; tlc (B, benzene) R_f 0.7 UVA. This was employed in thiation without purification.

General Procedure for the Thiation of 6-Dehydrodeoxynupharidine

Thiosulfonates were used in benzene, but all other thiating agents were used in CH_2Cl_2. A CH_2Cl_2 solution of 6-dehydrodeoxynupharidine (**1**), freshly prepared from nupharidine (16), and an equal mole or one mole excess of thiating agent was flushed with N_2, sealed, and kept in the dark at 25°C until tlc showed no further increase in the relative amount of α-arylthiohemiaminal to starting amine. Unconverted enamine, **3**, and **2** ascended the plate in every case in the order just given. When sulfensuccinimides were employed, the CH_2Cl_2 solution was washed with water, brine, and then dried. The solvent was evaporated at reduced pressure and the residue was chromatographed on a column of alumina to obtain a mixture of the diastereomeric α-arylthiohemiaminals. When other thiating agents were used, the solvent was evaporated directly and the residue was chromatographed. These general work-up procedures were employed except where otherwise noted.

7β- and 7α-Phenylthiodeoxynupharidin-6-ol, **2**a *and* **3**a

The residue from a 22 h reaction of 0.3 mmol of sulfensuccinimide and 0.3 mmol of **1** gave, after chromatography, 90 mg of a mixture of **2***a* and **3***a* (84%): tlc, (A, 10% Et_2O – hexane) double spot, R_f 0.2–0.5 (DA, UVA); ^{1}H nmr: 7.28 (m, 7H, ArH, furyl α H), 6.56 (m, 0.5H, furyl β H with axial ArS), 6.15 (m, 0.5H, furyl α H with eq ArS), 4.12 (br s, 0.5H, C-6 H with axial ArS), 4.00 (br s, 0.5H, C-6 H with eq ArS), 3.70 (m, 1H, C-4 H), 3.13 (br s, 1H, OH), 1.16 (s, 1.5H, axial C-7 Me), 0.95 (m, 4.5H, eq C-7 Me). Re-chromatography gave **2***a* identical with authentic sample (1).

7β-(4-Tolylthio)-deoxynupharidin-6-ol, **2**b

The residue from a 20 h reaction of 0.3 mmol of sulfensuccinimide and 0.3 mmol of **1** gave, after chromatography, 20 mg of **2***b* (18%): tlc (A, C_6H_6 × 2) R_f 0.3 (DA, UVA); ir, ^{1}H nmr, and ms were identical with spectra of authentic sample (6); cd (70% MeOH – water, pH 4) 283 nm, [θ] 37 000°.

7β-(4-Nitrophenylthio)-deoxynupharidine-6-ol, **2**c

The residue from a 2 day reaction of 0.6 mmol of disulfide and 0.61 mmol of **1** gave, after chromatography, 100 mg of a mixture of **2***c* and **3***c* (41%): tlc (10% Et_2O – hexane) double spot, R_f 0.1 (DA, UVA); ^{1}H nmr: 7.83 (m, 6H, furyl α H, ArH), 6.55 (m, 0.5H, furyl β H with axial ArS), 6.37 (m, 0.5H, furyl β H with eq ArS), 4.36 (br s, 0.5H, C-6 H with axial ArS), 4.10 (br s, 0.5H, C-6 H with eq ArS), 3.60 (m, 1H, C-4 H), 1.17 (s, axial C-7 Me), 0.98 (m, eq C-7 Me, C-1 Me). A portion of the mixture of **2***c* and **3***c* was dissolved in dry MeOH and the solvent was evaporated at reduced pressure to obtain a yellow solid mixture of the methyl ethers of **2***c* and **3***c*: ms (130°C): 416 (3) M^+, 385 (3), 294 (8), 262 (5), 231 (100), 176 (16), 155 (9), 107 (23), 94 (50); hrms (200°C) calcd. for $C_{22}H_{28}O_4S$: M^+ 416.1770; found: M^+ 416.1803.

Another portion of the mixture of **2***c* and **3***c* was applied to a preparative layer chromatography plate (alumina, 0.5 mm thickness) which was developed twice with 25% C_6H_6 – CH_2Cl_2. From the band at R_f 0.5 (DA) was isolated **2***c*: cd (in 70% MeOH – water, pH 4) 273 nm, [θ] 10 000°. From the band at R_f 0.4 (DA) was isolated **3***c*: cd (in 70% MeOH – water, pH 4) 250 nm, [θ] −7400°; 334 nm, [θ] −7700°; cd (in 70% MeOH – water, neutral) 276 nm, [θ] −50°; 332 nm, [θ] +2300°.

7β-(4-Chlorophenylthio)-deoxynupharidin-6-ol, **2**d

The residue from a 1-day reaction of 1.7 mmol of 4-chlorophenylthio-4-chlorobenzenesulfonate and 1.6 mmol of **1** gave, after extensive chromatography of the mixture of diastereomers, 240 mg of white crystalline **2***d* (38%): mp 78–81°C; tlc (A, 20% Et_2O – hexane) R_f 0.5 (DA, UVA); ir (CCl_4): 2.85 (w), 9.24 (s), 11.45 (s) μm; uv (acidic 95% EtOH): 270 nm (ε 5300); ^{1}H nmr: 7.33 (m, 6H, ArH, furyl α H), 6.25 (m, 1H, furyl β H), 4.03 (br s, 1H, C-6 H), 3.76 (m, 1H, C-4 H), 3.05 (br s, 1H, OH), 1.15 (s, 3H, C-7 Me), 0.93 (m, 3H, C-1 Me); ms (110°C): 393 (9) M^+, 391 (24), 374 (5), 248 (100), 231 (47), 192 (27), 176 (9), 146 (10), 144 (26), 107 (45), 94 (34); cd (in 70% MeOH – water, pH 4) 284 nm, [θ] 20 000°. *Anal.* calcd. for $C_{21}H_{26}NO_2SCl$: C 64.34, H 6.69, N 3.57; found: C 64.14, H 6.78, N 3.48.

7β-(4-Methoxyphenylthio)-nupharidin-6-ol, **2**e

The residue from a 3.5 h reaction of 1.5 mmol of sulfensuccinimide and 0.74 mmol of **1** gave, after extensive chromatography of the mixture of diastereomers, 30 mg of **2***e* (10%): tlc (A, CH_2Cl_2) R_f 0.2 (DA, UVA); ir: 2.89 (w), 8.09 (s), 9.74 (s), 11.50 (s), 12.09 (s) μm; ^{1}H nmr: 7.00 (m, 6H, furyl α H, ArH), 6.20 (m,

Can. J. Chem. Downloaded from www.nrcresearchpress.com by 210.87.254.105 on 09/06/12
For personal use only.

1H, furyl β H), 3.97 (s, 1H, C-6 H), 3.78 (s, 3H, MeO), 3.14 (br s, 1H, OH), 1.12 (s, 3H, axial C-7 Me), 0.93 (m, 3H, C-1 Me); ms (110°C): 387 (69) M^+, 370 (25), 248 (80), 231 (100), 192 (13), 176 (15), 140 (64), 107 (29), 94 (41); cd (70% MeOH – water, pH 4) 294 nm, [θ] 21 000°.

A portion of **2***e* was dissolved in EtOH and treated with sodium borohydride overnight. The solvent was evaporated and the residue was eluted from alumina with 10% Et_2O – hexane. Fraction 1 contained colorless and oily 7-β-(4-methoxyphenylthio)-deoxynupharidine: tlc (A, 10% Et_2O – hexane) R_f 0.9 (DA); ir: 3.60 (m), 8.17 (m), 9.70 (s), 11.45 (s), 12.02 (s) μm; ^{1}H nmr: 7.10 (m, 6H, furyl α H, ArH), 6.30 (m, 1H, furyl β H), 3.80 (s, 3H, OMe), 1.23 (s, 3H, C-7 Me), 0.93 (br s, 3H, C-1 Me). *Anal.* calcd. for $C_{22}H_{29}NO_2S$: C 71.12, H 7.87, N 3.77, S 8.63; found: C 71.35, H 8.02, N 3.89, S 8.81.

7β-(4-Trifluoromethylphenylthio)-deoxynupharidin-6-ol, 2f

The residue from a 5 h reaction of 1.4 mmol of sulfensuccinimide and 0.69 mmol of **1** gave, after chromatography, 20 mg of oil **2***f* and **3***f* (7%): tlc double spot, R_f 0.2 (DA); ir: 7.61 (s), 8.59 (s), 8.90 (s), 11.47 (m), 11.90 (m) μm; ^{1}H nmr: 7.45 (m, 6H, ArH, furyl), 6.41 (m, 0.3H, furyl β H with axial ArS), 6.21 (m, 0.7H, furyl β H with eq ArS), 4.42 (br s, 0.3H, C-6 H with axial ArS), 4.03 (br s, 0.7H, C-6 H with eq ArS), 3.70 (m, 1H, C-4 H), 1.19 (s, 1H, axial C-7 Me), 0.97 (m, 5H, eq C-7 Me and C-1 Me); ms (100°C): 425 (25) M^+, 408 (5), 248 (89), 231 (38), 218 (100), 192 (31), 178 (29), 176 (9), 107 (65), 94 (57). The mixture was chromatographed on alumina and thereby was obtained 7.5 mg of **2***f* (2.4%): cd (70% MeOH – water, pH 4) 250 nm, [θ] 22 000°.

A 170 mg sample of **2***f* and **3***f* in EtOH was reduced with $NaBH_4$ and the product was chromatographed to obtain 36 mg of a mixture of 7α- and 7β-(4-trifluoromethylphenylthio)-deoxynupharidine: tlc (A, 5% Et_2O – hexane) R_f 0.9 (DA) and R_f 0.8 (DA); ir: 3.60 (w), 7.60 (s), 8.58 (s), 8.88 (s), 11.46 (s) 11.90 (s) μm. *Anal.* calcd. for $C_{22}H_{26}F_3NO_2S$: C 64.52, H 6.40, N 3.42, S 7.83; found: C 64.51, H 6.50, N 3.40, S 8.02.

7β-(4-Hydroxyphenylthio)-deoxynupharidin-6-ol, 2g

The residue from a 3.5 h reaction of 3.1 mmol of 4-tosyloxyphenylsulfenyl chloride and 1.6 mmol of **1** was washed with aqueous base, water, and brine, dried and concentrated to 1.16 g of an orange foam, impure 7-(4-tosyloxyphenylthio)-deoxynupharidine-6-ol. This was combined with 10 mL of MeOH and 2 mL of 20% aqueous KOH and stirred at 55°C under N_2. After 6 h practically no insolubles remained. The solution was concentrated at reduced pressure, neutralized, treated with 2 mL of saturated aqueous $NaHCO_3$, and extracted three times with CH_2Cl_2. The solution was washed with brine, dried, and concentrated to 670 mg of a yellow foam of which a 59 mg portion was applied to a preparative layer chromatography plate (0.5 mm-thick silica gel) which was developed with 70% Et_2O – hexane to obtain 5 uv-active bands. The third band from the base yielded 17.3 mg of white, solid **2***g* (33% based on the proportion of the original 670 mg of yellow foam purified): tlc (B, 50% Et_2O-hexane) R_f 0.4 (DA, UVA); ir (KBr): 2.90 (s, br), 6.09 (w), 8.58 (m), 11.46 (s), 11.97 (m) μm, no tosylate; cd (70% MeOH – water, pH 4): 298 nm, [θ] 26 400°.

The iminium perchlorate salt was prepared from **2***g* and was recrystallized from MeOH–water, mp 216–220°C (dec.). *Anal.* calcd. for $C_{21}H_{26}ClNO_6S$: C 55.32, H 5.75, N 3.07, S 7.03; found: C 55.56, H 6.00, N 2.87, S 6.84.

The second band from the base of the preparative layer chromatography plate yielded 8.3 mg of a white solid **3***g* (16%): tlc (B, 50% Et_2O – hexane) R_f 0.3 (DA, UVA); ir (KBr): identical with **2***f*; ^{1}H nmr (DMSO-d_6): 7.69 (br s, 2H, furyl α H), 6.96 (m, 4H, ArH), 6.55 (m, 1H, furyl β H), 4.12 (br s, 1H, C-6 H), 0.95 (m, 3H, C-1 Me), 0.83 (s, 3H, C-7 Me); cd (2.0 mg/mL EtOH, pH 4): 295 nm, [θ] −17 500°: 270 nm (sh, [θ] −5600°; ms (130°C): 372 (< 1), 355 (1), 231 (100), 192 (1) 176 (19), 125 (56) ArS, 107 (26), 94 (100), 192 (1).

7β-(4-Aminophenylthio)-deoxynupharidin-6-ol, 2h

The residue from a 10 h reaction of 0.72 mmol of sulfensuccinimide and 0.69 mmol of **1** was heated at 55°C for 10 h under N_2 with 0.73 mL of hydrazine hydrate (15 mmol) in CH_2Cl_2–EtOH. The volatiles were removed at reduced pressure. The residue was treated with water and CH_2Cl_2 (3×). The CH_2Cl_2 solution was washed with water and brine, dried, and concentrated to 210 mg of yellow oil which was chromatographed on alumina to afford a 100 mg mixture (40%) of **2***h* and **3***h*: tlc (A, 50% ether – hexane) two spots of equal size and intensity of R_f 0.7 (DA, UVA); ir: 2.85 (w), 2.93 (w), 6.27 (m), 11.46 (s), 12.14 (m, br), no absorption at 5.90 (*N*-formyl) μm; ^{1}H nmr: 7.30 (m, 4H, furyl α H, ArH *ortho* to S), 6.50 (m, 3H, furyl β H, ArH *ortho* to N), 3.45 (br, s, 2H, amino H), 1.23 (s, C-7 axial Me), 0.93 (m, C-1 Me, C-7 eq Me). A portion of the mixture of diastereomers was applied to a preparative layer chromatography plate (0.5 mm alumina) and developed with CH_2Cl_2 to obtain three UVA bands. The first band from the base yielded **17**: tlc (A, CH_2Cl_2) R_f 0.1 (DA, UVA); cd (70% MeOH – water, pH 4) 310 nm, [θ] 11 000°.

A 38 mg portion of **2***h* and **3***h* was dissolved in CH_2Cl_2, diluted with EtOH, and treated with 20 mg of NaBH initially and then with 10 mg more of NaBH at 1 h intervals. After 4 h the mixture was concentrated to dryness, dissolved in CH_2Cl_2, washed with aqueous base, water, and brine, then dried and concentrated to 28 mg of a yellow-brown gum. This was chromatographed on alumina to obtain 10 mg of a yellow gummy, 7-(4-aminophenylthio)-deoxynupharidine: tlc (A, benzene) one spot, R_f 0.5 (DA, UVA); ir: 2.95 (w), 3.60 (m) 6.20 (s), 11.49 (s), 12.10 (s) μm; ^{1}H nmr (100 MHz): 7.22 (m, furyl α H, ArH *ortho* to S), 6.55 (m, furyl β H with axial ArS, ArH *ortho* to N), 6.29 (br s, furyl β H with eq ArS), 3.56 (m, amino H), 1.22 (s, C-7 axial Me), 0.84 (d, 5 Hz, C-1 Me); ms (110°C): 356 (2) M^+, 232 (100), 178 (3), 124 (75), 107 (15), 94 (28); hrms (125°C) calcd. for $C_{21}H_{28}N_2OS$: M^+ 356.1920; found: M 356.1893.

1. R. T. LaLonde, A. I-M. Tsai, C. J. Wang, C. F. Wong, and G. Lee. J. Med. Chem. **19**, 214 (1976).
2. R. T. LaLonde and C. F. Wong. J. Org. Chem. **38**, 3225 (1973).
3. R. T. LaLonde. Acc. Chem. Res. **13**, 39 (1980).
4. M. Kuehne. J. Org. Chem. **28**, 2124 (1963).
5. M. Furukawa, Y. Kosima, Y. Okahara, and S. Hayashi. Chem. Pharm. Bull. **22**, 262 (1974).
6. R. T. LaLonde, A. I-M. Tsai, and C. F. Wong. J. Org. Chem. **41**, 2514 (1976).
7. M. Furukawa, Y. Fujino, Y. Kojima, M. Ono, and S. Hayashi. Chem. Pharm. Bull. **20**, 2024 (1972).
8. M. Behforoutz and J. E. Kerwood. J. Org. Chem. **34**, 51 (1969).
9. F. Kurzer and J. R. Powell. Org. Synth. Coll. Vol. 4. *Edited by* N. Rabjohn. John Wiley and Sons, Inc., New York. 1963. p. 934.
10. L. Field and T. F. Parsons. J. Org. Chem. **30**, 657 (1965).
11. D. Buckman, M. Bellas, H. K. Kim, and L. Field. J. Org. Chem. **32**, 1626 (1967).
12. R. T. Lalonde, C. F. Wong, and K. C. Das. J. Am. Chem. Soc. **95**, 6342 (1973).
13. R. T. LaLonde, C. F. Wong, and A. I-M. Tsai. Org. Mass Spectrom. **11**, 183 (1976).
14. U.S. Patent No. 3,397,188 (1968); Chem. Abstr. **69**, P77976e (1968).
15. K. H. Buchel and A. Conte. Chem. Ber. **100**, 1248 (1967).
16. R. T. LaLonde, E. Auer, C. F. Wong, and V. P. Muralidharan. J. Am. Chem. Soc. **93**, 2501 (1971).

Capsidiol and 1-epicapsidiol: absolute configuration, nmr, and optical spectra of the dibenzoates[1]

M. J. STILLMAN[2] AND J. B. STOTHERS

Department of Chemistry, University of Western Ontario, London, Ont., Canada N6A 5B7

AND

A. STOESSL

Agriculture Canada, London Research Centre, University Sub Post Office, London, Ont., Canada N6A 5B7

Received February 24, 1981

M. J. STILLMAN, J. B. STOTHERS, and A. STOESSL. Can. J. Chem. **59**, 2303 (1981).

Application of the exciton chirality method has confirmed that capsidiol, a unique eremophilane, has the absolute stereochemistry depicted in **1**. The ^{1}H and ^{13}Cmr, circular dichroism, and magnetic circular dichroism spectra of capsidiol and 1-epicapsidiol dibenzoates are discussed.

M. J. STILLMAN, J. B. STOTHERS et A. STOESSL. Can. J. Chem. **59**, 2303 (1981).

La méthode de la chiralité de l'exciton a confirmé que le capsidiol, une eremophilane spéciale, a la stéréochimie absolue décrite en **1**. On discute des spectres de rmn du ^{1}H et du ^{13}C, des spectres de dichroisme circulaire et de dichroisme circulaire magnétique des dibenzoates et de l'épi-1 capsidiol.

[Traduit par le journal]

Capsidiol, an antifungal stress compound ("phytoalexin") produced by *Capsicum frutescens, Datura stramonium,* and *Nicotiana* spp. (1, 2), is almost unique as a 4,5-*trans*-eremophilane.[3] Its structure **1** and relative stereochemistry have been established by chemical and nmr studies (4, 5) and by single crystal X-ray analysis (5) but assignment of the absolute configuration, as shown in **1**, was based on transparent biogenetic relationships to other bicyclic, sesquiterpenoidal stress metabolites of the Solanaceae (1, 2). A recent preparation, in another context, of capsidiol dibenzoate (**2**) gave the opportunity to confirm this assignment by Nakanishi's exciton chirality method (6). The method has been used previously for the determination of the absolute configurations of the dibenzoates of rishitin (**3**) (7) and 3-hydroxylubimin (**4**) (8) but it should be noted that these compounds are vicinal diols.

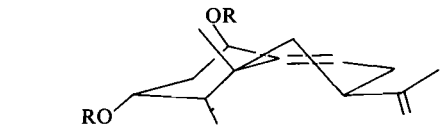

1 R = H
2 R = COPh

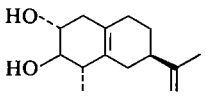

3

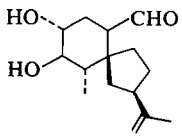

4

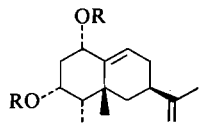

5 R = COPh
6 R = H

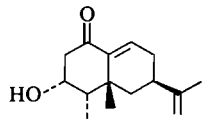

7

Except for the anticipated acylation shifts, all relevant parameters in the ^{1}H and ^{13}Cmr spectra of **2** are very similar to those of **1** (see Table 1). It follows that the relative stereochemistry and conformation of **2** are correctly depicted by the structural drawing. If this also corresponds to the absolute configuration, then Fieser molecular models indicate an angle of about 110° between the BzO-C-3—C-1-OBz bonds, with a clockwise (right-handed) sense of rotation as in Fig. 1. According to the dibenzoate rule (6), the cd curve should therefore exhibit a positive Cotton effect, of predictably small amplitude, near 233 nm, whereas a negative Cotton effect would be observed if the assignment needed reversal.

The optical absorption, cd, and magnetic circular dichroism (mcd) spectra of a solution of capsidiol dibenzoate (**2**) in EtOH are shown in Fig. 2A. As expected (6), the most intense natural cd bands arise from exciton mixing of the charge transfer

[1]Part 95 in the series ^{13}Cmr Studies; for Part 94 see ref. 11; for Part 93 see ref. 12. Part XXXIX of the series "Postinfectional inhibitors from plants"; for part XXXVIII, ref. 10.

[2]Member of the Centre for Interdisciplinary Studies in Chemical Physics at the University of Western Ontario.

[3]Apart from derivatives of capsidiol which have been found in sweet pepper, the only other known member of the class was reported, during the final stages of the preparation of this paper, as a metabolite of *Senecio amplexicaulis* (3).

0008-4042/81/152303-03$01.00/0

©1981 National Research Council of Canada/Conseil national de recherches du Canada

Can. J. Chem. Downloaded from www.nrcresearchpress.com by 210.87.254.40 on 09/06/12
For personal use only.

Can. J. Chem. Downloaded from www.nrcresearchpress.com by 210.87.254.40 on 09/06/12
For personal use only.

TABLE 1. ^{13}C and ^{1}H data for **1**, **2**, **5**, and **6**[a]

Carbon	1	2	5	6
1	75.0	76.3	67.2	70.6
2	36.3	31.4	39.8	33.0
3	65.3	70.1	67.0	69.3
4	47.7	44.3	47.1	44.2
5	39.1	39.2	38.7	39.0
6	44.9	44.5	44.3	44.0
7	40.2	39.9	39.4	39.3
8	30.4	30.4	29.9	29.9
9	128.8	132.9	118.9	120.2
10	140.3	135.3	140.6	135.8
11	149.1	148.9	149.4	149.2
12	108.7	109.0	108.6	109.0
13	21.0	21.0	21.0	21.0
14	8.9	10.3	9.4	10.7
15	32.1	31.3	30.1	29.8
Proton				
H-1	4.35 [2.5, 3.7]	5.78	4.34 [1.9, 5.2, 11.4]	5.85
H-3	4.59 [4.8, 4.8, 12.0]	5.98	4.24 [4.6, 4.6, 12.4]	5.62
H-9	5.91 [2.4, 6.3]	6.30	5.94 [1.9, 1.9, 6.3]	5.90
H-12	4.70, 4.73 [2]	4.74	4.69, 4.72 [2]	4.68
H-13	1.74	1.76	1.73	1.74
H-14	0.88 [7]	1.04	0.93 [7]	1.04
H-15	1.37	1.50	1.12	1.34
Benzoate signals: δ_C 165.4 (CO), 130.6 (C-1), 129.6 (C-2,6), 128.4 (C-3,5), 133.0 (C-4) δ_H 7.5 (m), 8.0 (m)				

[a]For $CDCl_3$ solutions ~10% (w/v). Shieldings in ppm from internal TMS. Values in square brackets are the ^{1}H–^{1}H coupling constants in Hz.

bands located on the two benzoate chromophores. There is little absorption or cd intensity for the $^{1}A_{1g} \rightarrow {}^{1}B_{2u}$ transition in the 280 nm region. The positive sign of the 239 nm cd band confirmed the right-handedness of the orientation of the two benzoate groups. The rather reduced intensities of $+7.5 \times 10^3$ deg dL dm^{-1} mol^{-1} at 239 nm and -1.6×10^4 deg dL dm^{-1} mol^{-1} at 220 nm, compared with bands observed for compounds with adjacent benzoates (6), presumably arises from the increased separation of the two chromophores in capsidiol dibenzoate. The cd spectrum thus confirms that the stereochemistry of the dibenzoate **2**, and hence also that of **1**, is correctly represented in Fig. 1.

To obtain further confirmation of the stereochemistry of **1**, we also prepared the dibenzoate **5** of the readily accessible 1-epicapsidiol (**6**). The ^{1}H and ^{13}C spectral data for **5** and **6** are listed in Table 1. As noted above, the expected shifts produced by benzoylation are apparent, with upfield shifts exhibited by C-2, -4, and -10 which flank the carbinyl carbons, while the latter (C-1, -3) and their protons shift downfield. The nuclei of the 14-methyl group also show downfield shifts. It is interesting that C-9 and its proton are both significantly deshielded by benzoylation of the axial 1-hydroxyl in capsidiol, whereas much smaller shifts accompany benzoylation of its equatorial epimer **6**.

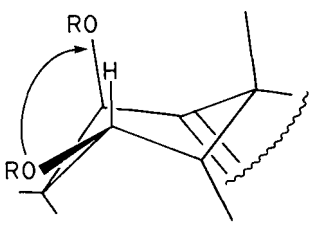

FIG. 1. A stereo representation of capsidiol dibenzoate (**2**).

Molecular models for the 1-epi case indicated that the angles between the benzoate groups would be very small or even close to zero, which would result in an almost zero exciton splitting (6) and hence negligible cd intensity. Both the absorption spectrum and, especially, the mcd spectrum of **6** confirm the close similarity between the electronic states of **6** and **2** (Fig. 2B). However, the cd band envelope of **6**, unlike that of **2**, was extremely weak and almost completely buried in noise. This implies that the two benzoate chromophores are indeed eclipsed.

Can. J. Chem. Downloaded from www.nrcresearchpress.com by 210.87.254.40 on 09/06/12
For personal use only.

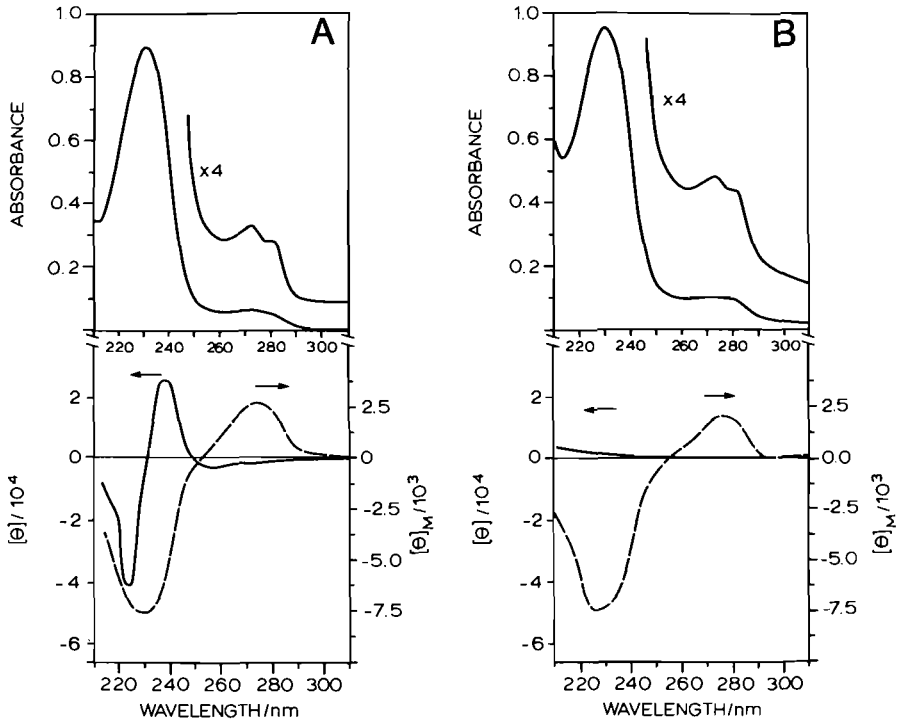

FIG. 2. Absorption (upper), cd (lower, solid line) and mcd (lower, broken line) spectra of 3.55×10^{-5} *M* capsidiol dibenzoate (A) and 3.96×10^{-5} *M* epicapsidiol dibenzoate (B) in 95% ethanol solutions.

Experimental

The ^{1}H and ^{13}Cmr spectra were determined on deuteriochloroform solutions, with TMS as internal reference, using a Varian XL-100 system operating in the Fourier transform mode. Optical absorption, cd, and mcd spectra were measured at room temperature on ca. 3.5×10^{-5} *M* solutions in 96% EtOH, using a Cary 219 for the absorption spectra, a Jasco J5-ORD/CD spectrometer modified to Sproul SS-20 specifications for cd spectra, and an Oxford Instruments SM2 superconducting magnet operating at 5.5 T in the Jasco for mcd measurements; 1 cm path length cells were used in all experiments. The cd and mcd spectra were calibrated conventionally and as previously described (9). The natural cd spectra have been subtracted from the mcd spectra recorded in Fig. 2. The cd intensities are reported as molar ellipticities, $[\theta]$, with units of deg dL dm^{-1} mol^{-1}, while the mcd intensities, $[\theta]_M$, have units deg dL dm^{-1} mol^{-1} T^{-1}; conversion to scales with $\Delta\varepsilon$ and $\Delta\varepsilon_M$ units is accomplished by multiplying each of the present scales by 1/3300.

Capsidiol (**1**) and capsenone (**7**) were available from earlier studies. 1-Epicapsidiol was prepared from **7** as previously described (5). Benzoylations were done at room temperature, by adding benzoyl chloride (0.2 mL) to the substrate (20 mg) in pyridine (0.5 mL) containing a few small crystals of 4-dimethylaminopyridine. The crude products, isolated after 2 days by dropwise addition to ice (10 mL) and extraction into ether, were purified by repeated chromatography over silica gel (BDH, 60–120 mesh, 20 g) with increasing concentrations of ether (0–10%) in light petrol. Both compounds, **2** and **6**, were obtained as syrups homogeneous by tlc.

Acknowledgements

We thank H. Schroeder for obtaining the ^{1}Hmr spectra, and the Natural Sciences and Engineering Research Council of Canada for financial support in the form of operating grants to J.B.S. and M.J.S.

1. A. STOESSL, J. B. STOTHERS, and E. W. B. WARD. Phytochemistry, **15**, 855 (1976).
2. A. STOESSL, E. W. B. WARD, and J. B. STOTHERS. *In* Host plant resistance to pests. ACS Symposium Series, No. 62. *Edited by* P. A. Hedin. American Chem. Soc., Washington, DC. 1977. p. 61–77.
3. F. BOHLMANN and J. ZIESCHE. Phytochemistry, **19**, 2681 (1980).
4. M. GORDON, A. STOESSL, and J. B. STOTHERS. Can. J. Chem. **51**, 748 (1973).
5. G. I. BIRNBAUM, A. STOESSL, S. H. GROVER, and J. B. STOTHERS. Can. J. Chem. **52**, 993 (1974).
6. N. HARADA and K. NAKANISHI. Acc. Chem. Res. **5**, 257 (1972); S. L. CHEN, N. HARADA, and K. NAKANISHI. J. Am. Chem. Soc. **96**, 7352 (1974).
7. N. HARADA and K. NAKANISHI. J. Am. Chem. Soc. **91**, 3989 (1969).
8. N. KATSUI, H. KITAHARA, F. YAGIHASHI, A. MATSUNAGA, and T. MASAMUNE. Chem. Lett. 861 (1976).
9. W. R. BROWETT and M. J. STILLMAN. Biochim. Biophys. Acta, **623**, 21 (1980).
10. A. STOESSL, G. L. ROCK, and S. K. GAYED. Z. Pflanzenkr. Pflanzensch. In press.
11. P. DEMAYO, J. MIRANDA, and J. B. STOTHERS. Tetrahedron Lett. 509 (1981).
12. A. STOESSL and J. B. STOTHERS. Can. J. Bot. In press.

Pyrolysis of bacterial polyalkanoates

HIROMICHI MORIKAWA[1] AND ROBERT H. MARCHESSAULT[2]

Département de Chimie, Université de Montréal, Montréal (Qué.), Canada H3C 3V1

Received August 7, 1980[3]

HIROMICHI MORIKAWA and ROBERT H. MARCHESSAULT. Can. J. Chem. **59**, 2306 (1981).

Pyrolysis products from bacterial polyesters, poly-β-hydroxybutyrate (PHB), and from a heteropolyester (β-hydroxyvalerate and β-hydroxybutyrate) were identified. Different physical forms of PHB were studied: PHB purified by dissolution in chloroform, native granules of PHB, and PHB in bacterial cells. The products were characterized by gc, ms, and nmr analysis. The yield of crotonic acid obtained by the pyrolysis of purified PHB was 60 to 65%. Pyrolysis of PHB native granules yielded crotonic acid as well as oligomers of PHB with a terminal crotonate. Upon direct pyrolysis of dry bacterial cells, the yield of crotonic acid was 20 to 25% of the PHB in the cells. From the heteropolymer, 2-pentenoic acid and terminally unsaturated oligomers of polyhydroxyvalerate were obtained. The usefulness of the pyrolysis method for obtaining vinyl compounds from bacterial cultures containing polyalkanoates is discussed.

HIROMICHI MORIKAWA et ROBERT H. MARCHESSAULT. Can. J. Chem. **59**, 2306 (1981).

On a identifié les produits provenant de la pyrolyse des polyesters bactériens poly-β-hydroxybutyrate (PHB) et du polyester hétérogène (β-hydroxyvalérate et β-hydroxybutyrate). On a étudié les différentes formes physiques du PHB: le PHB purifié par dissolution dans le chloroforme, les granules naturels de PHB et le PHB des cellules bactériennes. On a caractérisé les produits par chromatographie en phase gazeuse, par spectrométrie de masse et par la rmn. Le rendement en acide crotonique provenant de la pyrolyse du PHB purifié est de 60 à 65%. La pyrolyse des granules naturels de PHB conduit aussi bien à l'acide crotonique qu'à des oligomères du PHB avec un crotonate terminal. La pyrolyse directe des cellules bactériennes sèches conduit à un rendement en acide crotonique qui représente 20 à 25% du PHB contenu dans les cellules. On a obtenu du polymère hétérogène l'acide penten-2 oique et des oligomères du polyhydroxyvalérate insaturé en position terminale. On discute de l'utilité de la méthode de pyrolyse en vue d'obtenir des composés vinyliques à partir des cultures bactériennes contenant des polyalcanoates.

[Traduit par le journal]

Introduction

Because of the increasing cost of petroleum, the need for new types of chemical feedstocks has focussed attention on renewable resources (1, 2). Obviously, bacterial fermentation is an established way for obtaining useful products from biomass or industrial wastes. Aside from ethanol and other small molecules (3), important polysaccharides (4) and proteins (3) are obtained as products of fermentation.

Poly-β-hydroxybutyrate (PHB) is an example of a microbial polyester. This chiral polymer occurs as spherical hydrophobic granules in the cells of a wide variety of bacteria (5) and is easily harvested by a simple cell rupture (6, 7). The solid state structure of this polymer has been studied intensively (8–11). Because of its β-hydroxyalkanoate structure, PHB and its related family of poly-β-hydroxyalkanoates (PHA) are thermally unstable (12) and have potential as a source of small molecule organic chemicals rather than as thermoplastics (cf. Fig. 1). It is well known (12–14) that, on heating, PHB produces crotonic acid. Treatment of PHB with methanolic BF_3 produces β-hydroxybutyrate oligomers with ester endgroups (15, 16).

A bacterial polyester heteropolymer, composed primarily of β-hydroxyvalerate and β-hydroxybutyrate (HV-HB heteropolymer), has been isolated from activated sludges by Wallen and co-workers (17, 18). Usefulness of this polymer as a raw material has not been explored. Wallen and Rohwedder (18) have reported that, upon thermal degradation, this polymer produces crotonic acid and 2-pentenoic acid. This material, along with PHB, were the substrates for this pyrolytic study.

The pyrolysis method in combination with other physical methods has been extensively used for identification and characterization of various synthetic and biological polymers (19–23). The utility of the pyrolysis method for production of important chemicals such as levoglucosan and dextrins from cellulose (24) and starch (25) is well known. Recently Soltes and co-workers (26) have reported characterization of various phenolic compounds obtained from pine waste in a pyrolysis pilot plant.

DeJongh and co-workers have developed a controlled pyrolysis method (27–29) and applied it to polyesters (30, 31). In the present study we employed this same method and identified vinyl compounds derived from the pyrolysis of PHB before and after isolation from bacterial cells.

[1]On leave from: Department of Agricultural Chemistry, Kyoto University, Kyoto 606, Japan.

[2]Author to whom correspondence should be sent at present address: Xerox Research Centre of Canada, 2480 Dunwin Drive, Mississauga, Ont., Canada L5L 1J9.

[3]Revision received April 2, 1981.

0008-4042/81/152306-08$01.00/0

©1981 National Research Council of Canada/Conseil national de recherches du Canada

Can. J. Chem. Downloaded from www.nrcresearchpress.com by 210.87.254.40 on 09/06/12
For personal use only.

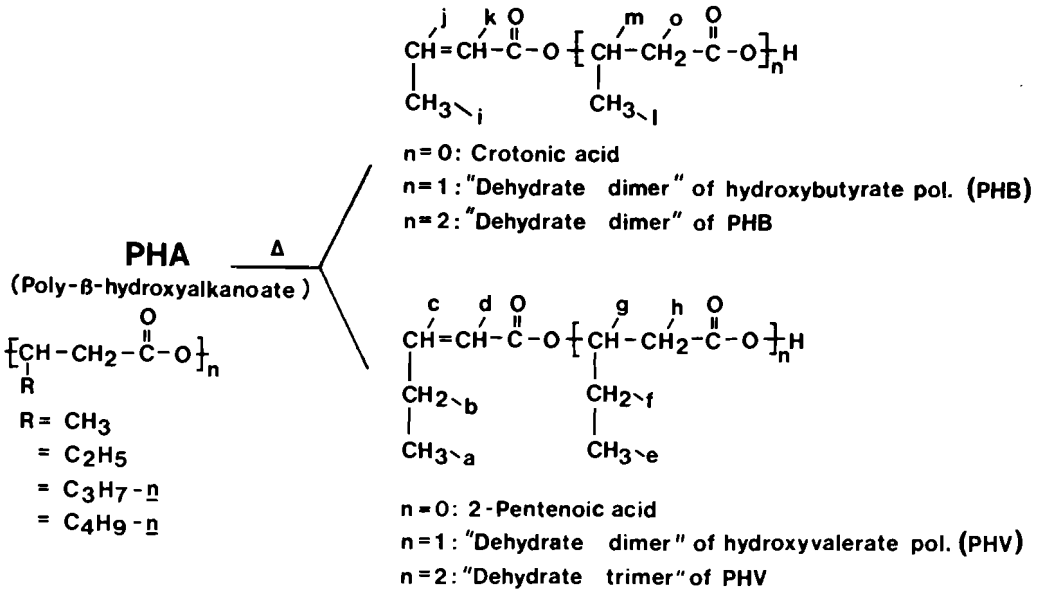

FIG. 1. Monomers and oligomers obtained by pyrolysis of bacterial poly-β-hydroxyalkanoates (PHA). The reaction scheme is shown for only two different R substituents (18). The oligomers with a vinylic endgroup are referred to as "dehydrates".

Experimental

Cultivation of Bacillus cereus *Cells*

Bacillus cereus TATCC14579 was grown in "1.5% Tryptic Soy Broth" (Difco) in a 25-liter carboy at 37°C under agitation with bubbling air. Preliminary experiments showed that the best yield of PHB was obtained 9 h after the inoculation under the present culture condition, after which the cells were harvested by centrifugation in a Sharples Continuous Centrifuge. The cell paste thus obtained was suspended in cold distilled water and washed twice by centrifugation. The washed cells were then suspended in acetone, filtered, and again suspended in a fresh portion of acetone to stand for 15 h at room temperature. After another filtration, the bacterial cells were air-dried at room conditions until the odor of acetone disappeared.

Preparation of PHB Samples

The isolation of PHB from the dry cells was made according to the method of Williamson and Wilkinson (6). About one gram of dry cells was suspended in 5% of hypochlorite (Baker) and stirred at 37°C for 2 h. The suspension was then centrifuged and a white granular PHB preparation was obtained and washed with distilled water, ethanol, and acetone. The washed PHB preparation was dissolved in chloroform and the solution was filtered. The filtrate was evaporated to dryness under reduced pressure at room temperature yielding a translucent film (purified PHB). The yield of PHB was 10.0% of the initial dry cells.

The PHB "native" granules isolated from *Bacillus megaterium* according to the method of Merrick and Doudoroff (7) were kindly supplied by Dr. J. M. Merrick, Department of Bacteriology, State University of New York, Buffalo, NY. The HV-HB heteropolymer sample, as a purified powder, was kindly supplied by Dr. L. L. Wallen, Northern Regional Research Laboratory, Peoria, IL. This material and PHB were the compounds used for this pyrolytic study.

Pyrolysis

The pyrolysis was made in accord with the method of Messier and DeJongh (30) and Messier (31). Briefly, a sample of 10 to 100 mg in a platinum boat was pyrolyzed in a quartz tube under a constant flow of dried nitrogen gas. The pyrolysis was conducted at atmospheric pressure and controlled temperature between 250 and 600°C. The sample was usually placed near the exit of the heated zone although pyrolysis with the sample near the entrance of the heated zone was also studied. The travel distances for volatile product through the heated zone were about 5 and 20 cm respectively. The pyrolysate was collected in cold traps connected to the end of the pyrolysis tube. Usually the sample was kept at a specified temperature for 30 min though the pyrolysis was observed to be complete within 5 to 10 min. The pyrolysate collected in the traps was recovered by dissolving in chloroform followed by evaporation to dryness at room temperature under reduced pressure.

Gas Chromatography and Mass Spectrometry

The pyrolysate was dissolved in chloroform, derivatized into *O*-trimethylsilyl (O-TMS) esters with *N,O*-bis(trimethylsilyl)trifluoroacetamide (BSTFA) and analysed by gas chromatography in combination with mass spectrometry. The gas chromatographic analysis was carried out with a Tracor Model 550 instrument equipped with a flame ionization detector (FID). The column (6 ft × 4 mm id) had Silicone OV-17 as the liquid phase on a solid support of 60–80 mesh Chromosorb W/AW DMCS. Helium carrier gas flowed at the rate of 60 mL/min. The detector block temperature was 330°C and the injection port temperature was 240°C. Runs were usually initiated at a column temperature of 50°C and programmed at 15°C/min to a maximum operating temperature of 270°C. The mass spectrum was obtained with a Hitachi Model RMU-6D GC/MS instrument operated at 70 eV, ion source temperature and gas chromatography conditions are same as above.

Proton-nmr Spectrometry.

Proton-nmr spectra were recorded on a Bruker Model WH-90 pulsed spectrometer using deuterated chloroform as solvent and tetramethylsilane as an internal standard.

Chemicals

BSTFA was purchased from Chromatographic Specialties

Can. J. Chem. Downloaded from www.nrcresearchpress.com by 210.87.254.40 on 09/06/12
For personal use only.

Can. J. Chem. Downloaded from www.nrcresearchpress.com by 210.87.254.40 on 09/06/12
For personal use only.

Ltd., London, Ont., crotonic acid was obtained from ICN Pharmaceuticals, Inc., Plainview, NY, and *trans*-2-pentenoic acid was obtained from Fluka AG, Chemische Fab., Buchs SG. All other chemicals were reagent grade.

Results and Discussion

Pyrolysis of Purified PHB

A typical gas chromatogram of the O-TMS derivative of the pyrolysate of purified PHB is shown in Fig. 2 (top), where the polymer was pyrolyzed at 400°C. In the chromatogram, after the peaks due to the solvent and by-products of BSTFA, one major peak (A) was observed. The retention time of this peak was identical with that of the derivative of authentic crotonic acid. The mass spectrum corresponding to this peak and the interpretation of the spectrum are shown in Scheme 1. The molecular ion was not detected in the mass spectrum but the fragment-ion at *m/z* 143 was detected corresponding to the loss of the $\cdot CH_3$ group from the molecular ion. The ion at *m/z* 99 is due to the loss of CO_2 from the ion at *m/z* 143. This type of fragmentation is known in the case of bis-TMS derivatives of *p*-aminobenzoic acid (32). The ion at *m/z* 69 corresponds to the fragment $C_4H_5O^+$.

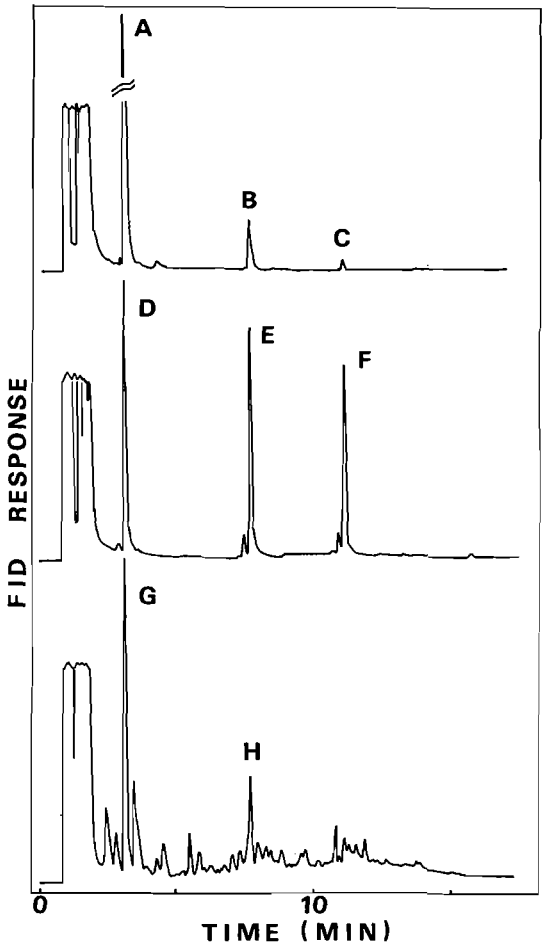

FIG. 2. Gas chromatograms of O-TMS derivatives of pyrolysate of purified PHB (top), that of PHB native granules (middle), and that formed by direct pyrolysis of PHB in *Bacillus cereus* cells (bottom). Pyrolyses were made at 400°C with the sample near the exit of the heated zone.

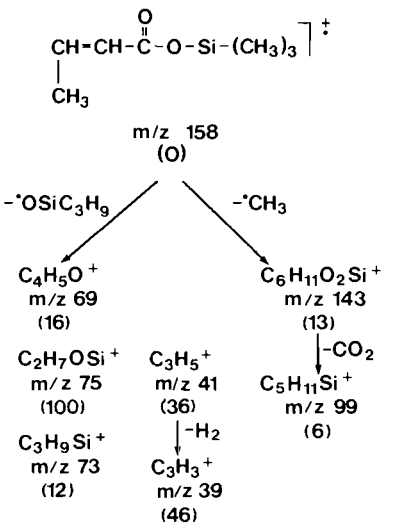

Note:
Relative abundances to 70 eV are shown in parentheses

SCHEME 1

In a pyrolysate of PHB, Messier (31) isolated and identified the "dehydrate dimer" of PHB, which is composed of the crotonate and β-hydroxybutyrate moieties (see Fig. 1). The retention time of peak B in Fig. 2 was the same as found by Messier (31) for the derivative of the dimer. Peak C in Fig. 2 can be attributed to the "dehydrate trimer" of PHB (see Fig. 3). The presence of crotonic acid monomer and "dehydrate oligomers" of PHB in the pyrolysate was confirmed by the proton nmr spectra.

Figure 3 (upper curve) shows the proton nmr spectrum of the pyrolysate of purified PHB. In the spectrum the signals at 1.9, at 5.8, and at 7.1 ppm are assignable to the protons of the CH_3, CH (bonded to C=O), and CH (bonded to CH_3) groups, respectively, of crotonic acid and the crotonate moiety of the "dehydrate oligomers" in the pyrolysate. Less intense but distinct signals were also observed at 1.3, 2.6, and 5.6 ppm for PHB native granule pyrolysate (Fig. 3). Since the same nmr peaks were observed in the spectra of PHB oligomers (Fig. 4), these signals were assigned to the protons of the CH_3, CH_2, and CH groups, respectively, of the β-hydroxybutyrate

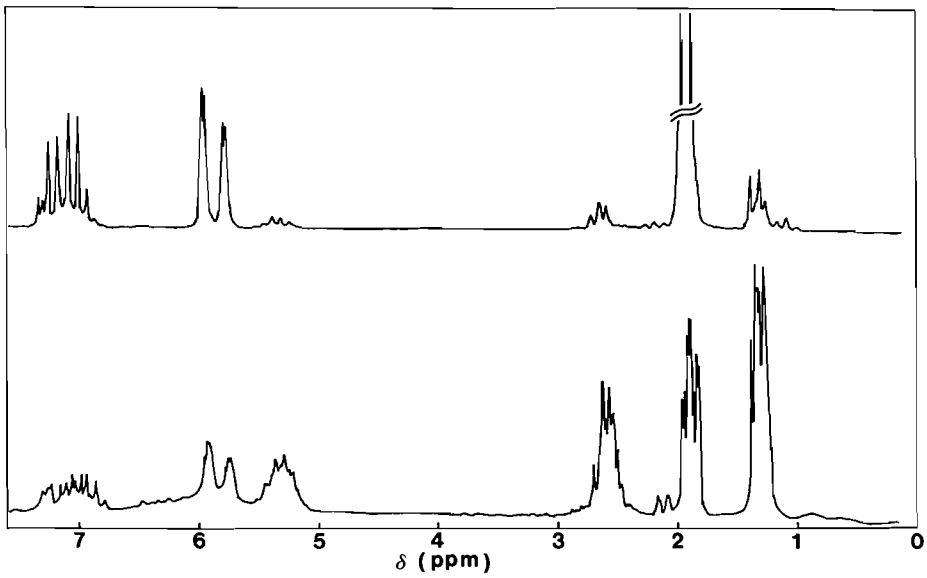

FIG. 3. Proton nmr spectra of pyrolysates: purified PHB (upper curve), PHB native granules (lower curve). Pyrolysis conditions as in Fig. 2.

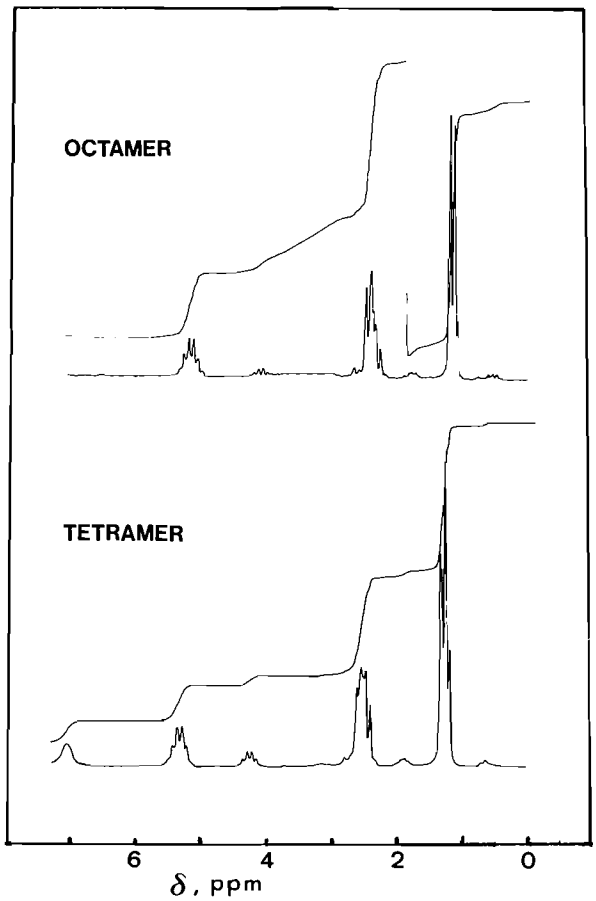

FIG. 4. Proton nmr spectra of PHB oligomers (tetramer and octamer).

moiety in the "dehydrate oligomers" of PHB in the pyrolysate.

The results of the pyrolysis of purified PHB at three different temperatures are listed in Table 1. The pyrolysis results were not significantly changed by temperature. The major product was crotonic acid and the yield was 60 to 65% of the initial amount of PHB. The results are in good agreement with those obtained by Messier (31) using a different preparation of PHB.

Pyrolysis of Native Granules of PHB

The gas chromatogram of the O-TMS derivative of the native granule pyrolysate is shown in Fig. 2 (middle). Three major peaks were observed (peaks D, E, and F). Based on a comparison of the retention times, the peaks in this figure can be attributed to the derivatives of crotonic acid (D), "dehydrate dimer" of PHB (E), and "dehydrate trimer" of PHB (F). This conclusion was confirmed by the proton nmr analysis on the pyrolysate (Fig. 3; lower curve). In the spectrum the signals attributable to the crotonate were observed near 1.9, 5.8, and 7.1 ppm. In these regions of the spectrum some unidentified signals were also observed (see below). Significant signals were observed at 1.3, 2.6, and 5.3 ppm which are attributable to the β-hydroxybutyrate moiety in the oligomers as discussed above. Note that these oligomer signals are much more intense than in the case of the pyrolysate of purified PHB (see Fig. 3).

Coulombe (15) has shown that in the proton nmr spectra of β-hydroxybutyrate oligomers (tetramer

Can. J. Chem. Downloaded from www.nrcresearchpress.com by 210.87.254.40 on 09/06/12
For personal use only.

TABLE 1. Summary of results of pyrolysis of different PHB samples[a]

Sample	Temperature °C	Pyrolysis residue %	Crude product %	Crotonic acid %	"Dehydrate dimer" of PHB %	"Dehydrate trimer" of PHB %
Purified (exit)[b]	250	9.1	83.1	64.4	7.2	1.2
	400	5.9	88.9	65.4	8.2	2.1
	600	3.4	86.1	58.3	9.0	2.7
Native granules (exit)[b]	400	10.4	82.3	25.0	18.0	15.3
	500	6.5	83.7	12.1	20.2	15.2
Bact. cells (exit)[b]	400	31.8	28.1	2.1	0.5	—
	500	22.2	30.9	2.1	0.5	—
	600	26.1	31.3	1.6	0.6	—
Bact. cells (entrance)[b]	400	34.7	27.4	2.5	—	—
	500	26.9	30.1	1.9	—	—
	600	21.4	23.7	1.3	—	—

[a]The values are expressed in per cent of the initial materials. The yield of crotonic acid was determined by comparison of the area under the peak with the area under the peak of a standard solution of O-TMS derivative of crotonic acid. (The same degree of the FID response was assumed for the derivative of the "oligomers" as for the derivative of crotonic acid).
[b]Exit, pyrolyzed near the exit of the heated zone; entrance, pyrolyzed near the entrance of the heated zone.

to octamer) a quartet is observed at 4.23 ppm (Fig. 4). This quartet arises from the proton of the CH group bonded to the terminal OH group in oligomers prepared by ester interchange. The same nmr signals were also observed in the spectrum of β-hydroxybutyric acid. Since no signals were observed at this position in the spectra of the pyrolysates (Fig. 3), the absence of β-hydroxybutyric acid and hydroxyl terminated oligomers in the pyrolysates is clearly demonstrated.

The results of the pyrolysis of PHB native granules at two temperatures are listed in Table 1. The yield of crotonic acid was decreased by half with the increase in the temperature while no appreciable changes in the yield of "dehydrate dimer" and "dehydrate trimer" of PHB were observed. Clearly, in the pyrolysate of the native granules the major products were these oligomers, which is in contrast to the case of purified PHB. It should be noted that the total yield of crotonates (the sum of the yield of crotonic acid and the oligomers) was relatively low (47.5 to58.3%) in the pyrolysis of the native granules while in the case of the purified PHB the total recovery was high (70.0 to 75.7%). With the former pyrolysate, nmr signals and gc peaks which were not identified were observed (see Figs. 2 and 3). These results suggest the presence of significant amounts of "non-crotonate" compounds in the pyrolysate of the native granules.

No complete explanation is available at present for the difference in the crotonate products between the pyrolyses of the native granules (oligomer-rich product) and of the purified PHB (monomer-rich product). Chemical impurities in these polymer preparations perhaps affect the pyrolysis products of the polymer (24). PHB native granule preparations usually contain (33) a few percent of "non-lipid" materials (mostly protein) while the purified PHB preparation used here was chemically pure based on the proton nmr and infrared analysis. The degree of polymerization (DP) of the polymer in the purified PHB is probably lower than in the native granules since the former had undergone an alkaline treatment (see the Experimental) (34). However, differences in the pyrolysis results are unlikely to be due solely to differences in DP which is known (24) to be rapidly lowered by this type of treatment. Textural differences are more likely to be the reason (8, 11, 34, 35).

Direct Pyrolysis of PHB in the Cells

The dried *Bacillus cereus* cells were pyrolyzed directly. Preliminary experiments indicated that in the direct pyrolysis at a temperature lower than 400°C the bulk of the products remained in the residue; for example, the residues amounted to 80 and 50% for the pyrolysis at 200°C and 300°C, respectively. Thus the direct pyrolysis was carried out at 400, 500, and 600°C. Also, the samples were pyrolyzed at both the exit and the entrance of the heated zone.

Fig. 2 (bottom) shows the gas chromatogram of the O-TMS derivative of the product of the direct pyrolysis of PHB in *Bacillus cereus* cells, where the cells were pyrolyzed at 400°C near the exit of the heated zone. In the chromatogram one major peak (G) was observed. This peak was attributed to the derivative of crotonic acid while peak H was attributed to the derivative of "dehydrate dimer" of PHB. The latter peak was always observed for pyrolysis near the exit of the heated zone but was

Can. J. Chem. Downloaded from www.nrcresearchpress.com by 210.87.254.40 on 09/06/12
For personal use only.

Can. J. Chem. Downloaded from www.nrcresearchpress.com by 210.87.254.40 on 09/06/12
For personal use only.

not observed when the pyrolysis was at the entrance of the heated zone. No distinct peak was observed corresponding to the "dehydrate trimer" of PHB. It should be noted that with the pyrolysate of the cells from which PHB had been extracted with a boiling mixture of chloroform and ethanol (36), no appreciable peaks corresponding to crotonic acid or the "oligomers" of PHB were observed.

Pyrolysis of HV-HB Heteropolymer

The gas chromatograms of the O-TMS derivatives of the pyrolysates of this heteropolymer produced at 250°C (lower curve) and at 400°C (upper curve) are shown in Fig. 5. Peak A in Fig. 5 was identified as the derivative of crotonic acid by the peak enrichment method; this peak is derived from the β-hydroxybutyrate moiety of the heteropolymer. Based on peak enrichment and mass spectrometry, peak B was identified as the derivative of 2-pentenoic acid which is derived from the β-hydroxyvalerate moiety of the polymer (18). The mass spectrum corresponding to this peak and the interpretation of the spectrum are summarized in Scheme 2. In the mass spectrum the molecular ion was not detected but the ions at *m/z* 157 and 143 were detected corresponding to the loss of the $\cdot CH_3$ and $\cdot C_2H_5$ groups, respectively, from the molecular ion. The ion at *m/z* 113 is due to the loss of CO_2 from the ion at *m/z* 157 (see Discussion). The ions at *m/z* 83 and 55 correspond to the ions $C_5H_7O^+$ and $C_4H_7^+$, respectively.

The retention time of peak C in Fig. 5 was much greater than that of the derivative of 2-pentenoic acid and distinctly different from that of the derivative of the "dehydrate dimer" of PHB (arrow in Fig. 5). In the light of these facts and considering

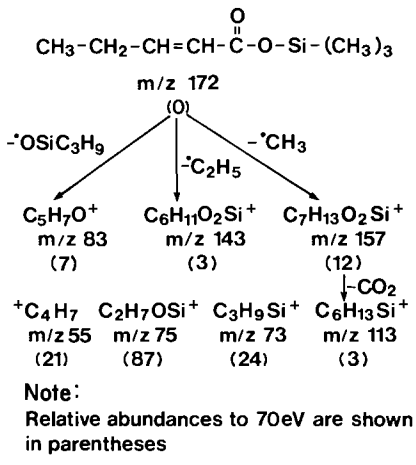

SCHEME 2

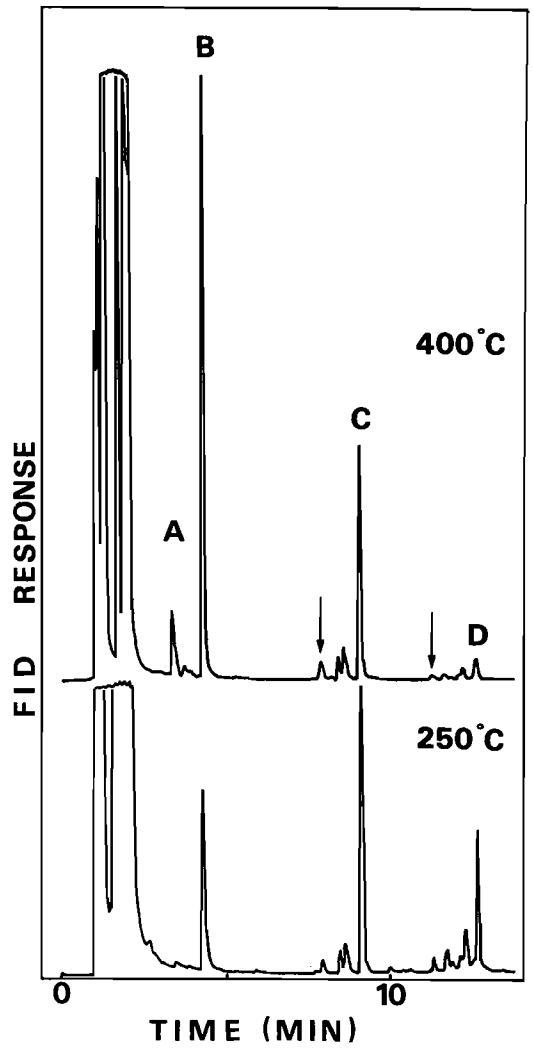

FIG. 5. Gas chromatograms of O-TMS derivatives of pyrolysate of HV-HB heteropolymer. Pyrolysis was done at 250°C (lower curve) and at 400°C (upper curve) with the sample near the exit of the heated zone. The arrows indicate the peak positions corresponding to the "dehydrate dimer" and "dehydrate trimer" of PHB.

that the major product in the pyrolysate is 2-pentenoic acid, it is reasonable to conclude that peaks C and D are due to the "dehydrate dimer" and "dehydrate trimer" of polyhydroxyvalerate (PHV) (Fig. 1). With the increase of the pyrolysis temperature, the peaks due to crotonic acid and 2-pentenoic acid were much intensified (see also Table 3). The presence of these oligomers was confirmed by proton nmr analysis on the pyrolysate.

Table 2 summarizes the proton nmr results on the pyrolysate of the HV-HB heteropolymer produced at 400°C. In the spectrum of the pyrolysate the signal characteristic of the α-proton in *trans*-2-

Can. J. Chem. Downloaded from www.nrcresearchpress.com by 210.87.254.40 on 09/06/12
For personal use only.

TABLE 2. Tentative assignment of proton nmr spectrum of pyrolysate[a] of HV-HB heteropolymer

δ (ppm)	Relative intensity	Assignment[b]
0.9	27	e
1.1	100	a
1.3	16	l
1.7	29	f
1.9	20	i
2.2	58	b
2.6	21	h
2.7	19	o, b
5.2	19	g, m
5.8	46	c (*cis* and *trans*), j
6.3	5	d (*cis*)
7.1	41	d (*trans*), k

[a]Pyrolysis was made at 400°C with the sample near the exit of the heated zone.
[b]See Fig. 1.

pentenoic acid was observed at 7.1 ppm, and the signal characteristic of the α-proton in *cis*-2-pentenoic acid (37) was observed at 6.3 ppm. Thus one can conclude that *cis* and *trans* isomers of 2-pentenoic acid are present in the pyrolysate. These isomers can be present either as monomer or as the terminal unit of "dehydrate oligomers" of PHV in the pyrolysate. The presence of crotonic acid is shown by the characteristic allylic proton signals at 1.9 ppm. A relatively intense signal for the butyrate oligomers was observed at 1.3 ppm indicating that the "dehydrate oligomers" of PHB are present in the pyrolysate (see Table 3). The presence of the "dehydrate oligomers" of PHV in the pyrolysate was confirmed by the presence of the signals at 0.9, 1.7, and 2.6 ppm in the spectrum, assignable to the protons of the CH_3, CH_2 (bonded to CH_3), and CH_2 (bonded to CH) groups, respectively, of the hydroxyvalerate moiety in the oligomers (18).[4]

Table 3 summarizes the results of the pyrolysis of the HV-HB polymer at two temperatures. At 250°C the bulk of the polymer weight remained in the residue and the pyrolysate yield was very low. At 400°C the pyrolysis yield was much enhanced and high yields of 2-pentenoic acid (53.3% of the initial polymer) and the "dehydrate dimer" of PHV (18.7%) were obtained. The high yield of 2-pentenoates is an indication that this heteropolymer is composed mainly of β-hydroxyvalerate (18).

Pyrolysis Mechanisms

The family of aliphatic polyesters including PHB (31), poly-β-propiolactone (38), and poly-α-methyl-β-propiolactone (31) and the aromatic polyesters such as poly(ethylene terephthalate) (39) demonstrate a typical ester-pyrolysis mechanism (or intramolecular *cis*-elimination) (40) in which a cyclic transition state (I) is involved followed by synchronous breakage of the C(α)—O and C(β)—H bonds. Because of the similarity in chemical structures between PHB and HV-HB heteropolymer one can expect that this heteropolymer undergoes the same pyrolysis mechanism as proposed for these polyesters. However, a marked temperature effect was observed on the pyrolysis of the heteropolymer while no appreciable temperature effect was observed in the case of PHB. This suggests that the "small" difference in chemical structures of these two polymers can affect the pyrolysis mechanism.

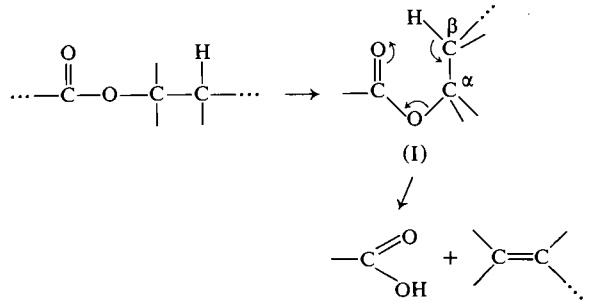

Conclusions

Crotonic acid is a 1,2-disubstituted ethylene and is known not to homopolymerize as readily as its isomer, methacrylic acid (41). However, copolymers with vinyl acetate have been fabricated in the 1 to 30 mol% range of crotonic acid (41). These copolymers are used commercially as adhesives and sizing agents. The usefulness of 2-pentenoic acid has not been explored but a reactivity similar to that of crotonic acid can be expected. The vinyl "oligomers" of PHB and PHV are also interesting raw materials since they retain the optical activity of their parent polymers in the side chain.

In the bacterial cells used in this study the PHB content was relatively low. Nevertheless the formation of crotonic acid upon direct pyrolysis of the dry cells is interesting. Under optimum growth conditions, PHB is accumulated to as much as 70 to 80% of the weight of dry cells (42) whereupon the direct pyrolysis yield should be considerably enhanced. Wallen and Rohwedder (18) have suggested the presence of a homologous series of bacterial polyesters, including poly-β-hydroxyhexanoate and poly-β-hydroxyheptanoate (see Fig. 1), in activated sludges which leads to still further expectations in terms of potential pyrolysis products.

The results of this study demonstrate that the

[4]H. Morikawa and R. H. Marchessault, unpublished results.

TABLE 3. Pyrolysis results for HV-HB heteropolymer[a]

Temperature (°C)	Residue of pyrolysis (%)	Crude product (%)	Crotonic acid (%)	2-Pentenoic acid (%)	"Dehydrate dimer" of PHV (%)	"Dehydrate trimer" of PHV (%)
250	77.0	14.0	0.3	4.6	6.2	2.9
400	1.6	95.9	5.8	53.3	18.7	2.1

[a]Pyrolyzed near the exit of the heated zone. Values are expressed in per cent of the initial polymer. Determination of the yield of crotonic acid and 2-pentenoic acid (using *trans*-2-pentenoic acid as standard) was made as specified in the footnote in Table 1. (The same degree of the FID response was assumed for the derivatives of the "oligomers" as for the derivative of 2-pentenoic acid.)

pyrolysis products of the HB moiety in the HV-HB heteropolymer are derived from macromolecular segments and not just from isolated hydroxybutyrate comonomers. In the latter case only crotonic acid would have been found. The significant yield of "dehydrate oligomers" of PHB in Fig. 5 argues for the presence of at least blocks of PHB in the HV-HB heteropolymer. X-ray studies have confirmed this conclusion.[4]

Acknowledgements

We are grateful to Prof. Don DeJongh as well as Drs. F. Messier and A. Martineau for their valuable discussions and their help in performing this study. Professors L. G. Mathieu, J. De Repentigny, and G. R. Drapeau of the Department of Microbiology, Université de Montréal, kindly provided facilities for microbial culture. We wish to thank Mr. Robert Mayer for his help in nmr analyses. Our thanks are extended to Miss Suzanne Coulombe for providing nmr data for PHB oligomers. The financial support of the Natural Sciences and Engineering Research Council of Canada and of the Ministère de l'Education du Québec is also acknowledged.

1. R. H. MARCHESSAULT and J. ST-PIERRE. Proceedings of CHEMRAWN Conference. Pergamon Press, New York. 1980. pp. 613–625.
2. R. H. MARCHESSAULT, S. COULOMBE, T. HANAI, and H. MORIKAWA. Pulp Pap. Mag. Can. **6**, TR 52 (1980).
3. M. J. PELCZAR, JR., R. D. REID, and E. C. S. CHAN. Microbiology. McGraw-Hill, New York. 1977. p. 845.
4. T. HARADA. Process Biochem. **9**, 21 (1974).
5. M. DOUDOROFF and R. Y. STANIER. Nature, **183**, 1440 (1959).
6. D. H. WILLIAMSON and J. F. WILKINSON. J. Gen. Microbiol. **19**, 198 (1958).
7. J. MERRICK and M. DOUDOROFF. J. Bacteriol. **88**, 60 (1964).
8. K. OKAMURA. Ph.D. Thesis, State Univ. N.Y. College of Forestry. 1967.
9. J. CORNIBERT and R. H. MARCHESSAULT. J. Mol. Biol. **71**, 735 (1972).
10. M. YOKOUCHI, Y. CHATANI, H. TADOKORO, K. TERANISHI, and H. TANI. Polymer, **14**, 267 (1973).
11. R. H. MARCHESSAULT, S. COULOMBE, H. MORIKAWA, K. OKAMURA, and J. F. REVOL. Can. J. Chem. **59**, 38 (1981).
12. J. N. BAPTIST and F. X. WERBER. Soc. Plast. Eng. Trans. **4**, 245 (1964).
13. M. LEMOIGNE. Ann. Inst. Pasteur, **39**, 144 (1925).
14. R. M. MACRAE and J. F. WILKINSON. J. Gen. Microbiol. **19**, 210 (1958).
15. S. COULOMBE. M.Sc. Thesis, Chem. Dept., Univ. de Montréal. 1977.
16. B. HAUTTECOEUR, M. JOLIVET, and R. GAVARD. C. R. Acad. Sci. Paris, Ser. D, **274**, 2729 (1972).
17. L. L. WALLEN and E. N. DAVIS. Environ. Sci. Technol. **6**, 161 (1972).
18. L. L. WALLEN and W. K. ROHWEDDER. Environ. Sci. Technol. **8**, 576 (1974).
19. H.-R. SCHULTEN and W. GORTZ. Anal. Chem. **50**, 428 (1978).
20. A. ZEMAN. Angew. Makromol. Chem. **31**, 1 (1973).
21. H.-R. SCHULTEN and H. D. BECKEY. Adv. Mass Spectrom. **6**, 499 (1974).
22. P. D. ZEMANY. Anal. Chem. **24**, 1709 (1952).
23. E. REINER. Nature, **206**, 1272 (1965).
24. F. SHAFIZADEH. Adv. Carbohyd. Chem. **23**, 419 (1968).
25. C. T. GREENWOOD. Adv. Carbohyd. Chem. **22**, 483 (1967).
26. T. J. ELDER and E. J. SOLTES. Abstracts, 178th ACS National Meeting, Washington, DC. Sept. 9–14, 1979.
27. D. C. DEJONGH, D. C. K. LIN, and M. L. THOMSON. Adv. Mass Spectrom. **6**, 99 (1974).
28. D. C. K. LIN, M. L. THOMSON, and D. C. DEJONGH. Can. J. Chem. **53**, 2293 (1975).
29. A. MARTINEAU and D. C. DEJONGH. Can. J. Chem. **55**, 34 (1977).
30. F. MESSIER and D. C. DEJONGH. Can. J. Chem. **55**, 2732 (1977).
31. F. MESSIER. Ph.D. Thesis, Chem. Dept., Univ. de Montréal. 1979.
32. W. H. ELLIOT and G. R. WALLER. *In* Biochemical applications of mass spectrometry. *Edited by* G. R. Waller. Wiley-Interscience, New York. 1972. p. 530.
33. R. GRIEBEL, Z. SMITH, and J. M. MERRICK. Biochemistry, **7**, 3676 (1968).
34. D. ELLAR, D. G. LUNDGREN, K. OKAMURA, and R. H. MARCHESSAULT. J. Mol. Biol. **35**, 489 (1968).
35. D. G. LUNDGREN, R. M. PFISTER, and J. M. MERRICK. J. Gen. Microbiol. **34**, 441 (1964).
36. J. N. BAPTIST. U.S. Pat. No. 3,044,942 (1962).
37. J. F. NORMANT, G. CAHIEZ, C. CHUIT, and J. VILLIERAS. J. Org. Chem. **54**, C53 (1973).
38. S. IWABUCHI, V. JAACKS, and W. KERN. Makromol. Chem. **177**, 2675 (1976).
39. J. DEVAUX, P. GODARD, and J.-P. MERCIER. Makromol. Chem. **179**, 2201 (1978).
40. G. S. GOULD. Mechanism and structure in organic chemistry. Holt, Rinehart and Winston, New York. 1959. p. 502.
41. C. J. KNUTH and A. M. SCHILLER. *In* Encyclopedia of polymer science and technology. Vol. 1. *Edited by* H. F. Mark, N. G. Gaylord, and N. M. Bikales. Interscience Pub., N.Y. 1964. p. 131.
42. H. G. SCHLEGEL and G. GOTTSCHALK. Angew. Chem. **74**, 342 (1962).

Can. J. Chem. Downloaded from www.nrcresearchpress.com by 210.87.254.40 on 09/06/12
For personal use only.

ipso Nitration. XXIII.[1] Reactions of cyclohexadiene adducts from nitration of 4-ethyltoluene in acetic anhydride

ALFRED FISCHER AND GEORGE N. HENDERSON

Department of Chemistry, University of Victoria, Victoria, B.C., Canada V8W 2Y2

Received January 27, 1981

Can. J. Chem. Downloaded from www.nrcresearchpress.com by 210.87.254.6 on 09/06/12
For personal use only.

ALFRED FISCHER and GEORGE N. HENDERSON. Can. J. Chem. **59**, 2314 (1981).

The diastereoisomers of 4-ethyl-1-methyl-4-nitrocyclohexa-2,5-dienyl acetate (**1**) and 1-ethyl-4-methyl-4-nitrocyclohexa-2,5-dienyl acetate (**2**) are stereospecifically reduced to the corresponding nitrocyclohexadienols with aluminum hydride. Each dienol is stereospecifically methylated to the corresponding methyl ether with methyl iodide, silver oxide, and potassium hydroxide. Acid-catalysed solvolysis of the acetates **1** and **2** results in the substitution of the acetate moiety by other nucleophiles and these reactions are not stereospecific. The products of rearomatization of dienyl acetates, dienols, and dienyl methyl ethers depend on the acidity and ionizing power of the solvents and are readily explained in terms of reactions involving a nitrocyclohexadienyl cation or acetoxy- (hydroxy-, methoxy-)cyclohexadienyl cation as key intermediates. In the 4-acetoxy-4-alkylcyclohexadienyl cation 1,2-migration of the acetoxyl group is more rapid than alkyl migration, but 1,2-alkyl migration is faster than migration of the hydroxyl or methoxyl groups in the corresponding cations. 1-Ethyl-4-methoxy-4-methylcyclohexa-2,5-dien-1-ol and 4-ethyl-3-nitrotoluene are significant minor products in the solvolysis of 1-ethyl-4-methyl-4-nitrocyclohexa-2,5-dien-1-ol in aqueous methanol. Nitration of *p*-ethyltoluene in the presence of sulfuric acid or in trifluoroacetic anhydride gives a mixture of 4-ethyl-2-nitro- and 4-ethyl-3-nitrotoluene in a 2:1 ratio.

ALFRED FISCHER et GEORGE N. HENDERSON. Can. J. Chem. **59**, 2314 (1981).

L'hydrure d'aluminium permet de réduire stéréospécifiquement les diastéréoisomères de l'acétate de l'éthyl-4 méthyl-1 nitro-4 cyclohexadiène-2,5 yle (**1**) de l'acétate de l'éthyl-1 méthyl-4 nitro-4 cyclohexadiène-2,5 yle (**2**) en nitrocyclohexadiènols correspondants. Sous l'influence de l'iodure de méthyle en présence d'oxyde d'argent et d'hydroxyde de potassium, chaque diénol peut être transformé stéréospécifiquement en éther méthylique correspondant. La solvolyse des acétates **1** et **2**, catalysée par un acide, provoque la substitution des acétates par d'autres nucléophiles; ces réactions ne sont pas stéréospécifiques. La nature des produits de réaromatisation des diénylacétates, des dièenols et des méthoxydiényles dépend de l'acidité et du pouvoir ionisant des solvants; on peut facilement expliquer la formation de divers produits sur la base de réactions impliquant, comme intermédiaire clé, soit un cation nitrocyclohexadiényle ou un cation acétoxy (hydroxy ou méthoxy) cyclohexadiényle. Dans le cation acétoxy-4 alkyl-4 cyclohexadiényle, la migration-1,2 du groupe acétoxy est plus rapide que la migration alkyle, mais la migration-1,2 des groupes alkyles est plus rapide que la migration correspondante des groupes hydroxyle ou méthoxyle. L'éthyl-1 méthoxy-4 méthyl-4 cyclohexadiène-2,5 ol-1 et l'éthyl-4 nitro-3 toluène sont des produits secondaires importants de la solvolyse de l'éthyl-1 méthyl-4 nitro-4 cyclohexadiène-2,5 ol-1 dans le méthanol aqueux. La nitration du *p*-éthyltoluène en présence d'acide sulfurique ou dans l'anhydride trifluoroacétique donne un mélange d'éthyl-4 nitro-2 et d'éthyl-4 nitro-3 toluène dans un rapport 2:1.

[Traduit par le journal]

In an earlier report we described the nitration of *p*-ethyltoluene in acetic anhydride which gave as the main products a mixture of the diene adducts 4-ethyl-1-methyl-4-nitrocyclohexa-2,5-dienyl acetate (**1**) and 1-ethyl-4-methyl-4-nitrocyclohexa-2,5-dienyl acetate (**2**). Each of the structurally isomeric adducts was obtained as a pair of diastereoisomers and the isomers were separated by chromatography on alumina (1). In each case the lower melting diastereoisomer (**1***a*, **2***a*) was eluted before the high melting diastereoisomer (**1***b*, **2***b*). The (*E*)-configuration has been assigned to the *a* diastereomers and the (*Z*)-configuration to the *b* diastereomers (2). In the series of *p*-alkyltoluenes (R = Me, Et, *i*-Pr, *t*-Bu) *p*-ethyltoluene is the only member which gives structurally isomeric 1,4-adducts as a consequence of nitration *ipso* to both alkyl groups (3–5).[2] Such structurally isomeric 1,4-adducts are particularly useful for the study of adduct reactions since they allow the elucidation of the regiospecificity of the reactions. In the earlier paper examples of two such reactions were reported (1). Reaction of both **1***a* and **1***b* in trifluoroacetic acid – trifluoroacetic anhydride gave exclusively 4-ethyl-3-nitrotoluene whereas **2***a* and **2***b* gave 4-ethyl-2-nitrotoluene. The observations are in accord with the mechanism (1, 7, 8) in which the acetate is first protonated and then expelled as acetic acid to generate the *ipso*-nitrocyclohexadienyl cation (**3***i* from **1** and **4***i* from **2**). A 1,2 shift of the nitro group followed by deprotonation then gives the observed products. Solvolysis of both **1***a*

[1]For Part XXII, see ref. 2.

[2]*p*-Xylene is nitrated at both *ipso* positions but the same products are formed in each case. *p*-Cymene is also nitrated at both *ipso* positions but nitration at the isopropyl position results in de-isopropylation (4, 6).

0008-4042/81/152314-14$01.00/0

©1981 National Research Council of Canada/Conseil national de recherches du Canada

Can. J. Chem. Downloaded from www.nrcresearchpress.com by 210.87.254.6 on 09/06/12
For personal use only.

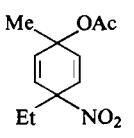

1

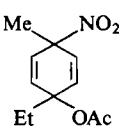

2

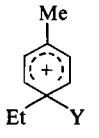

3

i Y = NO_2
j Y = OAc
k Y = OMe
l Y = OCHO
m Y = OH

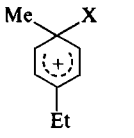

4

i X = NO_2
j X = OAc

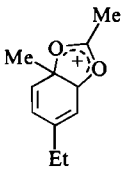

5

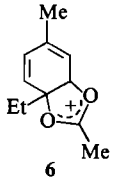

6

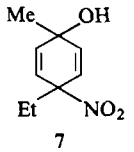

7

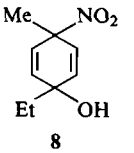

8

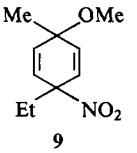

9

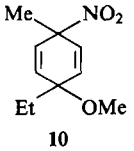

10

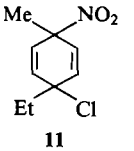

11

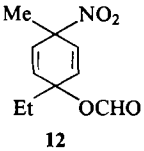

12

and **1***b* in 50% (v/v) aqueous methanol gave 5-ethyl-2-methylphenyl acetate whereas solvolysis of **2***a* and **2***b* gave 2-ethyl-5-methylphenyl acetate. According to the proposed mechanism (1, 8) initial ionization of the nitro group as nitrite anion gives the *ipso*-acetoxycyclohexadienyl cation (**4***j* from **1** and **3***j* from **2**). A 1,2 shift of the acetate, presumably through the bicyclic ions **5** and **6**, followed by deprotonation, gives the observed acetates with the appropriate regiospecificity. The present paper reports other reactions of the adducts **1** and **2**.

Studies of the solvolysis of nitronium acetate adducts have been carried out by Myhre and his co-workers[3] and by Moodie and co-workers (9). Both groups have studied the solvolysis of the *p*-xylene adduct in conditions of varied acidity. The products obtained in these and in our previous studies of rearomatization of tertiary acetate adducts can be explained in terms of the formation of cyclohexadienyl cations and their subsequent reactions. The set of five reactions 2–6 and the analogous set 2′–6′ shown in Scheme 1 are sufficient to account for essentially all of the products they observed or those observed in the present work.[4,5]

Results and Discussion

Formation of Nitrodienols, Nitrodienyl Methyl Ethers, and Related Diene Derivatives

Reaction of the nitrodienyl acetates **1***a*, **1***b*, **2***a*, and **2***b* with excess aluminum hydride in tetrahydrofuran gave, in each case, an essentially quantitative yield of the corresponding nitrodienol **7***a*, **7***b*, **8***a*, and **8***b*, respectively. The reaction involves acyl–oxygen cleavage in the acetate group and thus the stereochemistry at C-1 of the cyclohexadiene ring is not disturbed. Thus **1***a* and **7***a* have the same stereochemistry (*E*) as do **1***b* and **7***b* (*Z*), **2***a* and **8***a* (*E*), and **2***b* and **8***b* (*Z*). Reaction of the nitrodienols **7***a*, **7***b*, **8***a*, and **8***b* with methyl iodide in the presence of silver oxide and potassium hydroxide gave, in close to quantitative yield, the corresponding ethers **9***a*, **9***b*, **10***a*, and **10***b*, respectively. As in the reaction of acetates with aluminum hydride, the alkyl–oxygen bond is not broken and the stereochemistry at C-1 is undisturbed. Thus **1***a*, **7***a*, and **9***a* all have the same stereochemistry (*E*) as do **1***b*, **7***b*, and **9***b* (*Z*). Similarly, **2***a*, **8***a*, and **10***a* have the (*E*)-configuration and **2***b*, **8***b*, and **10***b*, the (*Z*)-configuration.

The acetates **1** and **2** are both tertiary and di-allylic: they each give a cyclohexadienyl cation (**3***i* and **4***i*, respectively) on heterolysis of the acetate group. Not surprisingly, the acid-catalysed loss of acetate is very facile. Thus, on treatment with acidified aqueous acetone, acetate **1***b* gave both diastereoisomers **7***a* and **7***b* of the dienol, and, on reaction with acidified methanol, both diastereoisomers **9***a* and **9***b* of the ether. Similarly, acetate **2***a* gave dienols **8***a* and **8***b* and ethers **10***a* and **10***b* and acetate **2***b* likewise gave both diastereomers of the dienol (**8***a* and **8***b*) and ether (**10***a* and **10***b*). These reactions are examples of $A_{AL}1$ ester hydrolysis or methanolysis. From the perspective of the cyclohexadienyl groups they are S_N1 reactions. Other examples of such reactions are: the reaction of acetate **2***b* with trifluoroacetic acid (3% v/v) in acetic anhydride, where initial isomerization to a mixture of the diastereoisomers **2***a* and **2***b* occurred; with acetic anhydride in acetic acid initial partial isomerization to **2***a* occurred; the reaction of

[3]P. C. Myhre. Personal communication.

[4]Note that the set of reactions 2′–6′ can be generated from the set 2–6 by (*i*) replacing X by Y and (*ii*) interchanging the methyl and ethyl groups.

[5]The ethyl group would of course be replaced by methyl in the *p*-xylene series. Note also the isomeric series in which the positions of the methyl and ethyl groups are interchanged.

Can. J. Chem. Downloaded from www.nrcresearchpress.com by 210.87.254.6 on 09/06/12
For personal use only.

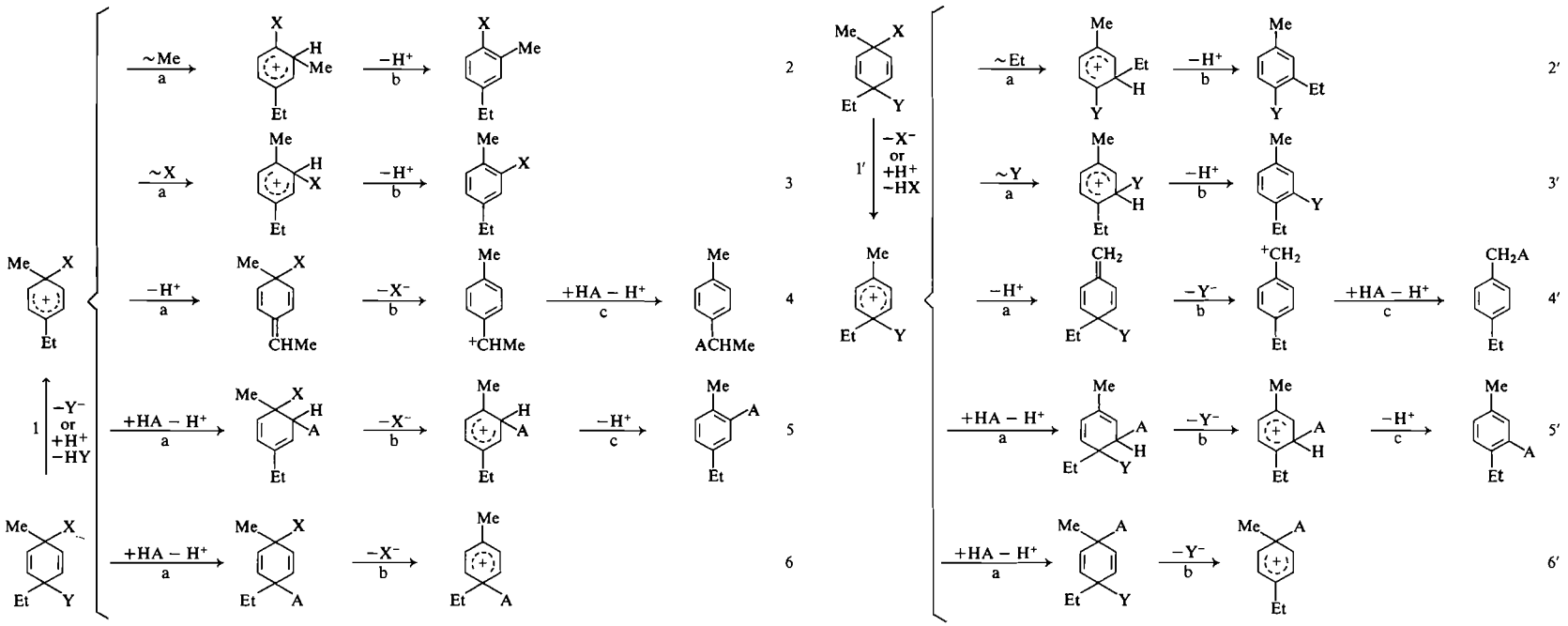

SCHEME 1. Reactions of dienes.

Can. J. Chem. Downloaded from www.nrcresearchpress.com by 210.87.254.6 on 09/06/12
For personal use only.

2*a* with hydrogen chloride in ether, which gave the nitrochlorodienes **11***a* and **11***b*; and the reactions of acetate **2***b* with formic acid in deuteriochloroform, which gave (as initial products) the nitrodienyl formates **12***a* and **12***b*. Most of these acid-catalyzed S_N1 reactions[6] were accompanied by simultaneous or subsequent rearomatization reactions. Study of the results (see Experimental) shows that conditions most conducive to the observation of the S_N1 reactions uncomplicated by rearomatization reactions are increased acidity (which speeds up the acid-catalysed loss of acetate relative to the competing uncatalysed solvolysis of the nitro group), low temperature (which suppresses the solvolytic reaction), and weakly ionizing solvents (good ionizing solvents aid the solvolysis of the nitro group (8)). However, if conditions are too acidic, the immediate product of the S_N1 reaction, e.g., the dienol, will reform the cyclohexadienyl cation and this will eventually give aromatic products (see below). This unfavourable consequence of increased acidity can be mitigated by working at low temperature (−30 to −40°C). This slows the acid-catalysed rearomatization reactions and thus allows the acidity to be raised to levels which would lead to rearomatization at ambient temperature. There is no reason to doubt that in those acid-catalysed reactions carried out at 35°C, in which only rearomatization products were observed, S_N1 type reactions did occur but on too short a time scale for detection.

Dienol **8***a* predominated (67–82%) in the mixture of **8***a* and **8***b* obtained on acid-catalysed hydrolysis of both **2***a* and **2***b*. This presumably reflects a kinetically controlled situation since under the reaction conditions the product dienols were not observed to equilibrate (nor expected to do so: hydroxyl is a poorer leaving group than acetate). In the single acid-catalysed hydrolysis experiment carried out in the **1** series **1***b* gave marginally more of **7***a* than **7***b*. The acid catalysed methanolysis results were more ambiguous. Acetate **2***a* gave more of **10***b* than **10***a* in acidified methanol and, to a lesser extent, in 50% trifluoroacetic acid in methanol. However, **2***b* gave more of **10***a* in acidified methanol and also in neutral methanol, but approximately equal amounts of **10***a* and **10***b* in acidified methanolic acetone. In the **1** series only the isomer **1***b* was investigated and it gave more of **9***b* than **9***a* when reacted in both acidified methanol and acidified methanolic acetone.

When both **2***a* and **2***b* were treated with nitric acid in acetic anhydride at −40°C, less than 5% isomerisation and less than 5% rearomatization occurred in each case. This indicates that the dienes are not equilibrated under the conditions under which they are formed in nitration. The experiment also illustrates the particular advantage of acetic anhydride as a solvent for nitration studies involving adduct formation. The acidity of the system is greatly reduced by the formation of acetyl nitrate and the complication of reversible formation of the *ipso*-nitrocyclohexadienyl cation from the adduct is thereby removed. Such reformation of the cation would eventually lead to aromatic products (Scheme 1).

All of the above S_N1, $A_{AL}1$, or "exchange" reactions are encompassed by reactions 1 and 6a (X = NO_2, Y = OAc) of Scheme 1 for the acetates **2** or reactions 1′ and 6′a (X = OAc, Y = NO_2) for the acetates **1**, and in which HA = H_2O, HOMe, HOAc, HCl, or HOCHO.

Rearomatization Reactions

As indicated above, observation of reactions in which the diene system is retained requires carefully chosen and controlled conditions to prevent the too successful competition by rearomatization. Rearomatization also involves the initial formation of the cyclohexadienyl cation as depicted in Scheme 1; the stabilization energy of this cation makes it the preferred intermediate for reaction paths to both dienyl and aromatic products.

Scheme 1 shows that starting from one diene it is possible in principle to generate all of the isomeric A-1-ethyl-4-methylcyclohexadienyl cations by a series of ionizations and S_N1 substitutions, and S_N1' substitutions with rearrangement. If the group A is not present in the original diene it can be introduced at either tertiary position by the exchange process (reaction 1 followed by 6a, or their counterparts 1′ and 6′a). Reaction 1 followed by 5a, or 1′ followed by 5′a will introduce the group A at the 2- or 3-position. Reactions 3a and 3′a provide for A to rearrange from a tertiary position to the adjacent secondary position and since A can be introduced at both tertiary positions it can appear through rearrangement at both secondary positions. Furthermore, the 1-A-4-ethyl-2-methyl and 1-A-2-ethyl-4-methyl cations can be generated by migration of the methyl or ethyl group (reactions 2a or 2′a) in the appropriate precursor cation. Thus, in principle it is possible to obtain (after deprotonation) any of the isomeric benzene derivatives containing 2-A-1-ethyl-4-methyl, 3-A-1-ethyl-4-methyl, 2-A-1-ethyl-5-methyl, or 2-A-5-ethyl-1-methyl substitution patterns, from a single diene. The only restriction on the group A is that it be present in the solvent as a nucleophile (or that it

[6]In an earlier paper these reactions were described as "exchange reactions" (3).

TABLE 1. Aromatic products from reaction of diene **2** in methanol solutions (mol%)

Conditions[a]	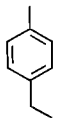	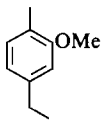	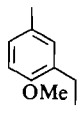	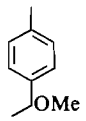	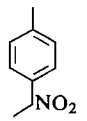	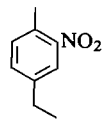	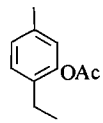	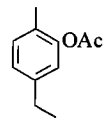
90% TFA	—	—	—	—	—	100	—	—
80% TFA	—	—	—	—	—	100	—	—
65% TFA	—	—	—	—	20	80	—	—
90% Acetone-1% H_2SO_4	—	—	18[b]	82	—	—	—	—
50% TFA	—	23	73	4	—	—	—	—
10% TFA	—	38	59	3	—	—	—	—
100% MeOH	0.3	14	31[c]	10	—	—	42	3
10% Aqueous	4	7	10[c]	9	—	—	66	4
50% Aqueous	—	—	—	—	—	—	100	—

[a]Methanol solvent in all cases, other components are listed: TFA = trifluoroacetic acid.
[b]Not distinguishable from 4-ethyl-2-methoxytoluene in this experiment.
[c]Not distinguishable from 4-ethyl-3-methoxytoluene in this experiment but 3-ethyl-4-methoxytoluene is the more likely product.

must have been present in the original adduct). In practice, the number of products is limited by the normal preferential formation of one or the other of the X- or Y-substituted cations and by both reaction conditions and the nature of the substituent (X, Y, A) which result in a particular reaction or reactions in the sets 1–6 and 1′–6′ being favoured; e.g., we have described the reaction of **2** in strongly acidic conditions which involves preferential formation of cation **4*i*** followed by 1,2-nitro group migration and deprotonation to 4-ethyl-2-nitrotoluene, formed exclusively. Three points with respect to Scheme 1 are to be noted here: (*i*) formation of one cation (reaction 1: X = NO_2, Y = OAc) is favoured; (*ii*) reaction of this cation with solvent nucleophile (which must be weak in the strongly acidic conditions) to give either a new diene (reactions 5a or 6a) or, through deprotonation, a triene (reaction 4a), is not competitive with rearrangement (reaction 3a), or is rapidly reversible; in the latter case ionization of the nitro group as shown in reactions 5b and 6b is not competitive with the reverse reaction of 5a or 6a: (*iii*) migration of the nitro group (reaction 3a) is preferred to migration of the methyl group (reaction 2a). We have also described the reaction of **2** in 50% aqueous methanol involving preferential formation of cation **3*j*** followed by a 1,2 shift of the acetate group and formation of 2-ethyl-5-methylphenyl acetate. Here we may note (*i*) formation of one cation Y = OAc (reaction 1′) is favoured under these conditions; (*ii*) reaction of this cation with solvent nucleophile (reactions 5′a and 6′a) or with solvent base (reaction 4′a) is not competitive with rearrangement (reaction 3′a): the cyclic acetoxonium cation **6** presumably provides a particularly favourable pathway for 1,2 migration of the acetate function; (*iii*) migration of acetate (reaction 3′a) is preferred to migration of the ethyl group (reaction 2′a), again a reflection of the favoured cyclic acetoxonium ion pathway.

It is possible to gradually change reaction conditions from strongly acidic, favouring formation of the nitrocyclohexadienyl cation (**3*i*** or **4*i*** in the present study), to neutral ionizing, favouring formation of the acetoxycyclohexadienyl cation (**4*j*** or **3*j***). In some intermediate conditions both cations should be formed. Also in some intermediate conditions there exists the possibility of reactions other than the 1,2 shift of the hetero group. Such other reactions would lead to a greater variety of aromatic products than the regiospecifically formed 2,5-dialkylnitrobenzene and 2,5-dialkylphenyl acetate. We have made studies of this type in other systems and as mentioned both Moodie and co-workers (9) and Myhre and co-workers have also made investigations of product distribution as a function of acidity with the *p*-xylene adducts and some other substrates (ref. 8 and footnote 3).

Aromatic products obtained on the reaction of dienes **2*a*** and **2*b*** in acidified methanol, methanol, and aqueous methanol are shown in Table 1. Reaction of dienes **2*a*** and **2*b*** with acidified methanol resulted in the initial formation of the methoxy dienes **10*a*** and **10*b*** (Scheme 1, X = NO_2, HA = HOMe, reaction 1, 6a) which then rearomatized. At high acidities (80–100% trifluoroacetic acid), 4-ethyl-2-nitrotoluene was the only aromatic product. Protonation and loss of the methoxyl group as methanol results in the reformation of cation **4*i*** (reverse of reaction 6a) which eventually rearranges by the 1,2-nitro shift to (after deprotonation) the nitroarene (reaction 3). At lower acidities deprotonation of the ethyl group at the α-position in

Can. J. Chem. Downloaded from www.nrcresearchpress.com by 210.87.254.6 on 09/06/12
For personal use only.

Can. J. Chem. Downloaded from www.nrcresearchpress.com by 210.87.254.6 on 09/06/12
For personal use only.

4*i* to form a triene (reaction 4a) is competitive with the rearrangement (reaction 3a). Thus in 65% trifluoroacetic acid the side-chain nitro derivative was formed (reaction 4b,c, A = NO_2). At still lower acidities (0.1 mol dm^{-3} H_2SO_4) formation of the nitroarene was completely suppressed and formation of the side-chain derivative (1-methoxy-1-(*p*-tolyl)ethane, 82%) was the dominant reaction (reaction 4, HA = HOMe). At still lower acidities and/or more strongly ionizing conditions (10–50% trifluoroacetic acid) ionization of the nitro group to form the cation **3*k*** (reaction 6b, HA = HOMe) becomes competitive with the reversion of the methoxydiene **10** to the cation **4*i*** (reverse of 6a). Consequently, the yield of the side-chain derivative (by reaction 4, for which **4*i*** is an essential precursor) was suppressed, only a minor amount being formed, and the rearranged ether 3-ethyl-4-methoxytoluene was the major product. Here we may note that under these conditions the acid-catalysed loss of the acetate group of **2** (reaction 1, X = NO_2, Y = OAc) is apparently faster than ionization of the nitro group (reaction 1′), hence, the initial rapid formation of **10**. However, the ionization of the nitro group of **10** (reaction 6b, X = NO_2, A = OMe) and subsequent reaction of the methoxy-cation **3*k*** (reaction 2′, Y = OMe) is faster than the acid-catalysed loss of the methoxyl group (reverse of reaction 6a) and subsequent reaction (reaction 4) of the nitro-cation **4*i***. Furthermore, it is to be noted that whereas migration of the hetero group is preferred to migration of the alkyl group in cations **4*i*** and **3*j***, migration of the methyl group is preferred to migration of the methoxyl group in **3*k***. The sequence OAc > Me > OMe is the same as the sequence of relative migration tendencies in the acid-catalysed dienone–phenol rearrangement, a reaction involving a similar transition state (10, 11). A substantial amount of 4-ethyl-2-methoxytoluene was also obtained in the reactions carried out in 10% and 50% trifluoroacetic acid. The pathway here is presumably that involving the conjugated diene (reaction 5, HA = HOMe). As in the case of the 1,4-diene **10** in the 1,3-diene isomer the loss of the nitro group (reaction 5b, A = OMe) and subsequent reaction (here, deprotonation, reaction 5c) of the resulting methoxycyclohexadienyl cation is faster than the reprotonation and loss of methanol (reverse of reaction 5a) followed by reaction 4 of the nitro-cation **4*i***. The reverse reactions of reactions 5a and 6a may themselves be fast, such that **10** and its 1,3-diene isomer are in equilibrium through **4*i***. However, provided that the stationary state concentration of **4*i*** is sufficiently low, its reactions, other than the forward reactions to **10** and its isomer (reactions 5a and 6a: we know that 6a is faster than all other reactions of **4*i***), cannot compete with the alternative reactions of **10** (reaction 6b, A = OMe and 2′, Y = OMe) and its isomer (reactions 5b,c). Such an equilibrium, with the conjugated diene present to a minor extent, coupled with a higher rate constant for reaction of the conjugated diene than of **10**, could account for the facts that, although a substantial amount of the product from the conjugated diene is formed in 10% and in 50% trifluoroacetic acid, the conjugated diene is not present at such a level as to be clearly evident by nmr in these experiments. Indeed, to account for the observations it is not even necessary that **10** and its isomer be in equilibrium, only that **10** be in equilibrium with **4*i*** and that the rate of the reaction sequence 5 be comparable to the rate of the sequence 6b (A = OMe), 2′(Y = OMe). It should be noted that the foregoing arguments are not dependent on the assumption expressed in Scheme 1 that the elimination of methanol from the conjugated diene follows an E1 pathway. The two-step elimination pathway was postulated by analogy with the known E1 mechanism for elimination of nitrous acid in nitrocyclohexa-1,4-dienyl secondary acetates (8).

As the acidity is reduced still further, the ionization of the nitro group in the nitrodienyl acetate to form cation **3*j*** (reaction 1′, X = NO_2, Y = OAc) becomes competitive with the protonation and loss of acetate to form cation **4*i*** (reaction 1). Correspondingly, in neutral methanol and in neutral 10% aqueous methanol the amount of methoxydiene **10** formed and of the aromatic ethers derived from this declined and 2-ethyl-5-methylphenyl acetate became an increasingly important product (reaction 3′). The aryl acetate was the only product in neutral 50% aqueous methanol (1). In the experiments carried out in methanol and 10% aqueous methanol, some of the methoxy-aromatics could have arisen from thermolysis of methoxynitrocyclohexadienes **10** in the glc inlet. Although we could not distinguish between 3-ethyl-4-methoxytoluene and 4-ethyl-3-methoxytoluene in these experiments (by glc), the former is the expected solvolytic product since the latter is not found in other experiments in which the distinction is possible and this accords with the expected preferential migration of ethyl rather than methoxyl in the ion **3*k***.

Solvolysis of the nitrodienyl acetates **1** was investigated much less extensively than that of the isomer **2**. In acidified methanol the dienyl ethers **9*a*** and **9*b*** were formed (reactions 1′ and 6′a, X = OAc, Y = NO_2, A = OMe) and subsequent aromatization gave 4-ethyl-3-methoxytoluene as

Can. J. Chem. Downloaded from www.nrcresearchpress.com by 210.87.254.6 on 09/06/12
For personal use only.

the major product (86%). Presumably, this was formed through the conjugated diene by reversion of **9** to cation **3*i*** (reverse of reaction 6′a followed by 5′, HA = HOMe). Although the corresponding reaction for **2** was not observed to be the major reaction, it was significant in 10% and 50% trifluoroacetic acid as noted above and it may well be that it would be the dominant reaction under correctly chosen conditions of acidity. In 10% aqueous methanol, ionization of the nitro group of **1** was able to compete effectively with loss of the acetate. As a consequence, the yield of aryl ethers was reduced and 5-ethyl-2-methylphenyl acetate became the major product, and the only product in 50% aqueous methanol (reactions 1 and 3, X = OAc, Y = NO_2).

Reactions of **2** in acetic anhydride, acetic acid, and formic acid solutions followed similar pathways to those described for methanol (Scheme 1). As already discussed, the S_N1 exchange of the acetate for solvent nucleophile to form a new or isomeric diene occurred (reactions 1 and 6a) and this reaction was most cleanly observed in the more acidic mixtures. Further reaction led to aromatic products derived from the cation **4*i***, 4-ethyl-2-nitrotoluene predominating under the most strongly acidic conditions (reaction 3, X = NO_2) and 1-(*p*-tolyl)ethyl derivatives predominating under somewhat less acidic conditions (reaction 4). Under the most mildly acidic conditions formation and reaction of cation **3*j*** from the dienyl acetate **2** (reactions 1′ and 3′, X = NO_2, Y = OAc), is competitive with formation and reaction of cation **4*i*** and 2-ethyl-5-methylphenyl acetate predominates. Thus 4-ethyl-2-nitrotoluene (40%) was the major aromatic product recognised when **2*b*** was reacted with trifluoroacetic acid (3% v/v) in acetic anhydride. The nitro compound became a minor product (7%) when the reaction was carried out in acetic acid containing 0.2% sulfuric acid and 10% acetic anhydride. In this case, 1-(*p*-tolyl)ethane derivatives derived from cation **4*i*** by reaction 4 were the dominant products: *p*-methylacetophenone (24%), 1-(*p*-tolyl)ethyl acetate (20%), and 1-nitro-(*p*-tolyl)-ethane (31%). The *p*-methylacetophenone was presumably formed from 1-(*p*-tolyl)ethyl nitrite (cf. 3, 12, 13) or equivalent species such as the alcohol and nitrous acid. *p*-Ethyltoluene (10%) was also formed in this reaction and is likely to originate by loss of the nitronium ion from cation **4*i***. *p*-Ethyltoluene was also detected in other reactions but in those few cases some dienes were present in the mixture subjected to glc analysis and the arene could have arisen by thermolysis of the dienes. Side-chain product 1-(*p*-tolyl)ethyl acetate was also the major product on reaction of diene **2*b*** with 0.1% sulfuric acid in acetone containing 10% acetic anhydride. At lower acidity, on reaction in acetic acid containing 10% acetic anhydride, the side-chain products were still formed: 1-(*p*-tolyl)ethyl acetate (24%), 1-(*p*-tolyl)ethanol (11%), and 1-nitro-(*p*-tolyl)-ethane (9%). However, the major product was 2-ethyl-5-methylphenyl acetate, indicating the solvolysis of the nitro group (reaction 1′, X = NO_2, Y = OAc) was competitive with formation of cation **4*i*** (reaction 1) and its subsequent reaction. The fact that the acetate group was exchanged with the solvent ([$^2H_4$]acetic acid was used) indicates that under these conditions formation of cation **4*i*** is faster than formation of cation **3*j***, i.e., loss of the acetate group (reaction 1) is faster than solvolysis of the nitro group (reaction 1′), but the rearrangement of cation **3*j*** by reaction 3′ is faster than the further reaction (deprotonation) of cation **4*i*** (reaction 4a). Thus cation **4*i*** recombines with acetic acid to regenerate diene **2** (reverse of reaction 1), accounting for both the isomerization (epimerization) of the original diene **2*a*** and the presence of the labelled acetate in the aryl acetate ultimately obtained. 2-Ethyl-5-methylphenyl acetate (51%) was again the major product on solvolysis of diene **2*b*** in aqueous acetic acid. Only a small amount of side-chain products (4%) was formed under these conditions and the other significant products were two ethylmethylnitrophenols, presumably formed via the dienol **8** whose presence was noticed in the course of the reaction. Although the structures of these nitrophenols were not elucidated, it seems likely that the major one was 2-ethyl-4-methyl-6-nitrophenol (29%) formed by nitration (nitrosation and oxidation) of 2-ethyl-4-methylphenol, itself determined to be the major solvolysis product of diene **8** (see below). The minor nitrophenol was probably 3-ethyl-6-methyl-2-nitrophenol, obtained on nitration of 5-ethyl-2-methylphenol, the expected minor product of solvolysis of **8**. The solvolysis reaction generates nitrous acid which reacts rapidly with phenols.

Reaction of diene **2*b*** with formic acid in chloroform resulted as previously mentioned in initial exchange to form the formyloxydiene **12** (reactions 1 and 6a, X = NO_2, Y = OAc, A = OCHO). Subsequent aromatization gave 2-ethyl-5-methylphenyl formate (44%) as the major product and presumably formed like the corresponding acetate through ionization of the nitro group (reaction 6b) and migration of the formate group (reaction 3′, Y = OCHO) through a bicyclic cation analogous to **6**. The other significant product was 4-ethyl-2-nitrotoluene (30%). Formic acid is a significantly

Can. J. Chem. Downloaded from www.nrcresearchpress.com by 210.87.254.6 on 09/06/12
For personal use only.

stronger acid than acetic acid and it appears to be sufficiently strong to allow the concentration of cation **4*i*** to rise to such a level that its reactions competed with the rearrangement of cation **3*l***. Moreover, the formic acid is less likely to accept a proton from cation **4*i*** than acetic acid, hence although the side-chain product 1-(*p*-tolyl)ethyl formate (7%) is formed by reaction 4 (X = NO_2, A = OCHO), the competing nitro group rearrangement product is dominant (reaction 3, X = NO_2).

Solvolysis of Dienol **8**a *and Dienyl Ether* **10**a

Solvolysis of the dienol **8*a*** in aqueous methanol gave 2-ethyl-4-methylphenol as the major aromatic product. The pathway here involves reaction 1′ (X = NO_2, Y = OH) to form cation **3*m*** which undergoes ethyl group migration: reaction 2′. In dienone–phenol rearrangement hydroxyl, like methoxyl, migrates less readily than alkyl (14). Both we and Myhre and co-workers have noted similar behaviour in the dienes obtained from *p*-xylene.[3,7] When the solvolysis was repeated in aqueous methanol in the presence of *N*,*N*-diisopropylethylamine (to neutralize acid formed which would catalyse aromatization of diene) the cation **3*m*** was partially trapped and the diastereoisomers of 1-ethyl-4-methoxy-4-methylcyclohexa-2,5-dien-1-ol (19%) obtained, together with the expected 2-ethyl-4-methylphenol (65%) and 4-ethyl-3-nitrotoluene (16%). The formation of the last product can be accounted for by reaction of cation **3*m*** with nitrite ion released on ionization, most likely while the ions are still closely associated as an ion pair, followed by subsequent elimination of water (reaction 5′, Y = OH, A = NO_2).[8] Minor amounts of 4-ethyl-3-nitrotoluene were observed in some of the solvolytic reactions described above and a similar pathway is likely in those cases.

Solvolysis of the methoxydiene **10*a*** in aqueous [$^2H_4$]methanol (20:80 v/v) gave 3-ethyl-4-methoxytoluene (71%) and 4-ethyl-2-methoxytoluene (24%) as the major products. The product ethers contained 75% [$^2H_3$]methoxyl, indicative of the formation of **4*i*** (reaction 1, X = NO_2, Y = OMe), which allowed exchange (reaction 6a, A = OCD_3). The major product was obtained via reaction 1′ (X = NO_2, Y = OMe) or reaction 6b (A = OCD_3), followed in either case by reaction 2′ (Y = OMe or OCD_3). The 4-ethyl-2-methoxytoluene presumably was formed by reaction 1 to give cation **4*i*** followed by reaction 5 (A = OCD_3).

The rearranged phenols were obtained in essentially quantitative yield when the dienyl acetates were reacted with sodium methoxide in methanol. Thus **2*b*** gave 2-ethyl-4-methylphenol, **1*b*** gave 4-ethyl-2-methylphenol, and 1,4-dimethyl-4-nitrocyclohexa-2,5-dienyl acetate gave 2,4-dimethylphenol. The analogous reaction of 1-isopropyl-4-methyl-4-nitrocyclohexa-2,5-dienyl acetate to give 2-isopropyl-4-methylphenol has been reported previously and a mechanism involving concerted migration of alkyl group and loss of nitrite in the diene alkoxide ion obtained on $B_{AC}2$ hydrolysis proposed (4).

Nitration of p-*Ethyltoluene with Mixed Acid and with Nitric Acid in Trifluoroacetic Anhydride*

Nitration of *p*-ethyltoluene in trifluoroacetic anhydride gave a small amount (5%) of dienes, probably the trifluoroacetate analogues of **1** and **2**. The major products were the 4-ethyl-2-nitro- and 4-ethyl-3-nitrotoluenes formed in a 3:2 ratio. Indubitably a major portion of the two nitroarenes was formed by *ipso* attack by the nitronium ions to form the cations **3*i*** and **4*i*** which then rearranged by reactions 3′ (Y = NO_2) and 3 (X = NO_2), respectively. The nitration of *p*-ethyltoluene with nitric acid and sulfuric acid in acetic acid likewise gave a similar mixture of the ethylnitrotoluenes.

Shift Reagent Studies

Shift reagent effects with tris(1,1,1,2,2,3,3-heptafluoro-7,7,-[$^2H_6$]dimethyl-4,6-[$^2H_3$]octanedionato)-europiumIII (Eu([$^2H_9$]fod)$_3$) on the ^{13}C nmr spectra of the acetates **2*a*** and **2*b*** and on the ^1H nmr spectra of the acetates **1*a***, **1*b***, **2*a***, and **2*b*** have been reported previously (1, 2). Table 2 shows the effect of the reagent on the ^1H nmr spectra of the nitrodienols **7*a***, **7*b***, **8*a***, and **8*b***. As expected, relative shift gradients decline with increasing distance of the proton from the site of complexation: the hydroxyl group. The differences between the relative gradients of the 4-CH_3 or 4-CH_2 groups in the pairs of diastereoisomers is too small to be of any value in assigning the configurations. In fact, the differences are in the wrong direction with the (*E*)-isomer (the *a* isomers) having the smaller relative gradients. A seemingly significant difference between the members of each pair of diastereoisomers is in the overall sensitivity to the shift reagent. The gradient of a plot of the chemical shift of the 1-CH_3 or 1-CH_2 group vs. Eu/mg is ca. 50% greater in the *a* isomers than in the *b*. For **7*a*** and **7*b*** the measurements were made simultaneously by addition of shift reagent to a mixture of the pair

[7]A. Fischer, G. N. Henderson, and T. A. Smyth. Unpublished work.

[8]The elimination of water could follow an E2 or E1cb pathway.

TABLE 2. Relative gradients (gradient 1-CH_2 or 1-CH_3 = 1.00) of proton chemical shifts for diene adducts from addition of Eu([$^2H_9$]fod)$_3$

Compound	1-CH_2CH_3	1-OH	2-H	3-H	4-CH_3 or 4-CH_2CH_3	4-CH_2CH_3	1-CH_2/Eu[a]
7*a*	—	—	0.96	0.38	0.24	0.22	0.08
7*b*	—	—	1.07	0.46	0.28	0.25	0.53
8*a*	0.40	5.22	0.88	0.35	0.21	—	0.73
8*b*	0.37	5.06	0.89	0.38	0.24	—	0.44

[a]Gradient of shift of 1-CH_2CH_3 or 1-CH_3 vs.Eu/mg.

of diastereoisomers. Thus although the absolute values of shift sensitivity will depend on the concentrations, the relative shift sensitivities for the two isomers will not. The diastereoisomers **8***a* and **8***b* were investigated separately. However, solutions of identical concentrations were used and again the relative shift sensitivities for the two isomers should be concentration independent. The results suggest that the (*E*)-isomers are complexed to a greater extent by the reagent than are the (*Z*)-isomers.

Experimental

General experimental methods have been described previously (1, 15). The preparation of the acetates **1***a*, **1***b*, **2***a*, and **2***b* has been described (1). The C-2 and C-3 carbon atoms of the acetates were incorrectly assigned in the ^{13}C nmr spectra reported in the earlier paper. The correct (interchanged) assignments are reported in ref. 2. Shift reagent studies on the dienols **7***a*, **7***b*, **8***a*, and **8***b* were carried out as described for the acetates (1). Reaction mixtures containing product dienes were worked up by first quenching at low temperature with liquid ammonia and extracting the products with ether after evaporation of excess ammonia. Aromatization reactions were worked up by first neutralizing with liquid ammonia at low temperature or with aqueous bicarbonate at 0°C followed by ether extraction. In appropriate cases where both solvent and reagent (if any) were volatile (e.g., neutral methanol), these were simply pumped off at reduced pressure.

1-Ethyl-4-methyl-4-nitrocyclohexa-2,5-dienols (8)

Acetate **2***a* (1 g, 4.4 mmol) in dry tetrahydrofuran (5 cm^3) was added dropwise with stirring to a solution of aluminum hydride (37 mmol) in tetrahydrofuran (100 cm^3) at −20°C, under an argon atmosphere, and the resulting solution stirred for 15 min. The solution was cooled to −40°C and excess aluminum hydride decomposed by the careful addition of water. Cold work-up gave colourless crystals (0.73 g, 90%) of 1-ethyl-4-methyl-4-nitrocyclohexa-2,5-dienol (**8***a*), mp 97–98°C; ir (Nujol): 3270 (OH), 1540, and 1335 (NO_2) cm^{-1}; ^1H nmr ($CDCl_3$) δ: 0.77 (t, 3, *J* = 7.2 Hz, CH_2CH_3), 1.65 (q, 2, *J* = 7.2 Hz, CH_2CH_3), 1.73 (s, 3, 4-CH_3), 2.12 (broad s, 1, O*H*), 6.00 (d, 2, *J* = 10.4 Hz, 2-*H* and 6-*H*), 6.08 (d, 2, *J* = 10.4 Hz, 3-*H* and 5-*H*) ppm; ^1H nmr (CD_3COCD_3) δ: 0.73 (t), 1.61 (q), 1.69 (s), 4.10 (s, O*H*), 6.02 (s, 2-*H*, 3-*H*, 5-*H* and 6-*H*) ppm; ^{13}C nmr ($CDCl_3$) δ_c: 8.3 (CH_2CH_3), 27.1 (4-CH_3), 33.2 (CH_2CH_3), 68.8 (*C*-1), 83.7 (C-4), 126.5 (*C*-3 and *C*-5), 136.0 (*C*-2 and *C*-6) ppm.

Similar reduction of acetate **2***b* (0.70 g) gave a 96% yield of the other diastereoisomer of 1-ethyl-4-methyl-4-nitrocyclohexa-2,5-dienol (**8***b*), mp (needles from ether–pentane at −20°C) 56°C; ir (film): 3400 (OH), 1545 and 1337 (NO_2) cm^{-1}; ^1H nmr ($CDCl_3$) δ: 0.75 (t, 3, *J* = 7.2 Hz, CH_2CH_3), 1.64 (q, 2, *J* = 7.2 Hz, CH_2CH_3), 1.67 (s, 3, 4-CH_3), 3.06 (s, 1, O*H*), 5.97 (d, 2, *J* = 10.4 Hz, 2-*H* and 6-*H*), 6.07 (d, 2, *J* = 10.4 Hz, 3-*H* and 5-*H*) ppm; ^1H nmr (CD_3COCD_3) δ: 0.75 (t), 1.59 (q), 1.64 (s), 3.6 (broad s, O*H*), 5.95 (d), 6.07 (d) ppm; ^{13}C nmr ($CDCl_3$) δ_c: 8.4 (CH_2CH_3), 27.2 (4-CH_3), 32.7 (CH_2CH_3), 68.4 (*C*-1), 83.9 (C-4), 126.6 (*C*-3 and *C*-5), 135.3 (*C*-2 and *C*-6) ppm.

4-Ethyl-1-methyl-4-nitrocyclohexa-2,5-dienols (7)

Reduction of acetate **1***a* (0.30 g) gave a 98% yield of 4-ethyl-1-methyl-4-nitrocyclohexa-2,5-dienol (**7***a*) as colourless needles, mp 82–84°C; ir (Nujol): 3300 and 1080 (OH), 1557 and 1360 (NO_2) cm^{-1}; ^1H nmr ($CDCl_3$) δ: 0.86 (t, 3, *J* = 7 Hz, CH_2CH_3), 1.33 (s, 3, 1-CH_3), 2.10 (q, 2, *J* = 7 Hz, CH_2CH_3), 2.29 (broad s, 1, O*H*), 5.97 (d, 2, *J* = 10 Hz, 3-*H* and 5-*H*), 6.16 (d, 2, *J* = 10 Hz, 2-*H* and 6-*H*) ppm; ^{13}C nmr ($CDCl_3$) δ_c: 8.5 (CH_2CH_3), 27.8, (1-CH_3), 32.5 (CH_2CH_3), 65.4 (*C*-1), 87.6 (*C*-4), 123.6 (*C*-3 and *C*-5), 138.6 (*C*-2 and *C*-6) ppm.

Reduction of acetate **1***b* (0.30 g) gave a 95% yield of 4-ethyl-1-methyl-4-nitrocyclohexa-2,5-dienol (**7***b*) as colourless needles, mp 56–58°C; ir (Nujol): 3310 and 1080 (OH), 1555 and 1360 (NO_2) cm^{-1}; ^1H nmr ($CDCl_3$) δ: 0.80 (t, 3, *J* = 7 Hz, CH_2CH_3), 1.28 (s, 3, 1-CH_3), 2.05 (q, 2, *J* = 7 Hz, CH_2CH_3), 2.74 (broad s, 1, O*H*), 5.97 (d, 2, *J* = 10 Hz, 3-*H* and 5-*H*), 6.12 (d, 2, *J* = 10 Hz, 2-*H* and 6-*H*) ppm; ^{13}C nmr ($CDCl_3$) δ_c: 8.3 (CH_2CH_3), 27.8 (1-CH_3), 32.9 (CH_2CH_3), 65.0 (*C*-1), 87.6 (*C*-4), 123.4 (*C*-3 and *C*-5), 137.8 (*C*-2 and *C*-6) ppm.

1-Ethyl-4-methyl-4-nitrocyclohexa-2,5-dienyl Methyl Ether (10)

A mixture of 1-ethyl-4-methyl-4-nitrocyclohexa-2,5-dien-1-ol, (**8***a*, 250 mg), freshly precipitated silver oxide (920 mg), potassium hydroxide (23 mg), and methyl iodide (2.5 cm^3) was stirred for 6 h at ambient temperature in a closed vessel. Ether (10 cm^3) and magnesium sulfate were added, the mixture filtered, and the residue washed with ether. Evaporation of the combined filtrate and ether washings gave, as an oil, 1-ethyl-4-methyl-4-nitrocyclohexa-2,5-dienyl methyl ether (**10***a*, 260 mg); ir (film): 2855 (OCH_3), 1565 and 1352 (NO_2), 1060 (COC) cm^{-1}; ^1H nmr ($CDCl_3$) δ: 0.76 (t, 3, *J* = 7 Hz, CH_2CH_3), 1.64 (q, 2, *J* = 7 Hz, CH_2CH_3), 1.74 (s, 3, 4-CH_3), 3.04 (s, 3, OCH_3), 5.83 (d, 2, *J* = 10 Hz, 2-*H* and 6-*H*), 6.27 (d, 2, *J* = 10 Hz, 3-*H* and 5-*H*) ppm; ^{13}C nmr ($CDCl_3$) δ_c: 8.1 (CH_2CH_3), 27.2 (4-CH_3), 32.6 (CH_2CH_3), 51.9 (OCH_3), 74.6 (*C*-1), 84.0 (*C*-4), 129.8 (*C*-3 and *C*-5), 134.6 (*C*-2 and *C*-6) ppm.

Similar methylation of the dienol **8***b* gave the corresponding diastereoisomer of the methyl ether **10***b* (229 mg); ir (film): 2822 (OCH_3), 1547 and 1342 (NO_2), 1072 (COC) cm^{-1}; ^1H nmr ($CDCl_3$) δ: 0.73 (t, 3, *J* = 7 Hz, CH_2CH_3), 1.60 (q, 2, *J* = 7 Hz, CH_2CH_3), 1.69 (s, 3, 4-CH_3), 3.08 (s, 3, OCH_3), 5.79 (d, 2, *J* = 10 Hz, 2-*H* and 6-*H*), 6.25 (d, 2, *J* = 10 Hz, 3-*H* and 5-*H*) ppm; ^{13}C nmr ($CDCl_3$) δ_c: 8.3 (CH_2CH_3), 27.4 (4-CH_3), 32.6 (CH_2CH_3), 52.3 (OCH_3), 74.3 (*C*-1), 83.6 (*C*-4), 127.9 (*C*-3 and *C*-5), 133.9 (*C*-2 and *C*-6) ppm.

4-Ethyl-1-methyl-4-nitrocyclohexa-2,5-dienyl Methyl Ether (9)

Methylation of the dienol **7***a* following the procedure for the methylation of **8***a* gave the methyl ether **9***a* (225 mg); ir (film):

Can. J. Chem. Downloaded from www.nrcresearchpress.com by 210.87.254.6 on 09/06/12
For personal use only.

Can. J. Chem. Downloaded from www.nrcresearchpress.com by 210.87.254.6 on 09/06/12
For personal use only.

2820 (OCH_3), 1547 and 1347 (NO_2), 1102 (COC) cm^{-1}; ^1H nmr ($CDCl_3$) δ: 0.91 (t, 3, J = 7 Hz, CH_2CH_3), 1.28 (s, 3, 1-CH_3), 2.14 (q, 2, J = 7 Hz, CH_2CH_3), 3.03 (s, 3, OCH_3), 6.00 (d, 2, J = 10 Hz, 2-*H* and 6-*H*), 6.12 (d, 2, J = 10 Hz, 3-*H* and 5-*H*) ppm; ^{13}C nmr ($CDCl_3$) δ_c: 8.6 (CH_2CH_3), 27.3 (1-CH_3), 32.9 (CH_2CH_3), 52.5 (OCH_3), 70.9 (*C*-1), 87.6 (*C*-4), 126.9 (*C*-3 and *C*-5), 137.6 (*C*-2 and *C*-6) ppm.

Similar methylation of the dienol **7***b* (240 mg) gave the methyl ether **9***b* (220 mg); ir (film): 2820 (OCH_3), 1547 and 1347 (NO_2), 1100 (COC) cm^{-1}; ^1H nmr ($CDCl_3$) δ: 0.83 (t, 3, J = 7 Hz, CH_2CH_3), 1.26 (s, 3, 1-CH_3), 2.08 (q, 2, J = 7 Hz, CH_2CH_3), 3.03 (s, 3, OCH_3), 5.94 (d, 2, J = 10 Hz, 2-*H* and 6-*H*), 6.16 (d, 2, J = 10 Hz, 3-*H* and 5-*H*) ppm; ^{13}C nmr ($CDCl_3$) δ_c: 8.3 (CH_2CH_3), 27.8 (1-CH_3), 32.9 (CH_2CH_3), 52.3 (OCH_3), 70.4 (*C*-1), 87.4 (*C*-4), 126.9 (*C*-3 and *C*-5), 136.2 (*C*-2 and *C*-6) ppm.

Hydrolysis of the Dienyl Acetates 1 and 2 in Acidified Aqueous Acetone

A solution of acetate **2***a* (35 mg) in aqueous [$^2H_6$]acetone (350 mm^3; 10:90, v/v) containing sulfuric acid (0.05 mol dm^{-3}), at 35°C was observed by ^1H nmr. A mixture of the dienols **8***a* and **8***b* was slowly formed ($t_{1/2}$ = 2 h). After hydrolysis was complete the reaction mixture was worked up. The presence of the diastereoisomeric dienols was confirmed by ^1H nmr in $CDCl_3$ and the ratio **8***a*:**8***b* = 67:33 was determined after addition of Eu([$^2H_9$]fod)$_3$, which increases the separation of the signals.

The hydrolysis of acetate **2***b* in aqueous [$^2H_6$]acetone containing sulfuric acid (0.05 mol dm^{-3}) had $t_{1/2} \approx$ 2 h and gave **8***a*:**8***b* = 70:30. When the hydrolysis was carried out with more dilute acid (0.01 mol dm^{-3}) the half-life was increased (~ 6 h) and the product ratio was **8***a*:**8***b* = 82:18.

Reaction of acetate **1***b* under the same conditions as **2***a* gave the diastereoisomeric dienols **7***a* and **7***b*, with $t_{1/2}$ = 1.3 h. The ratio **7***a*:**7***b* = 55:45 was determined after work-up and addition of shift reagent.

Reaction of Dienes 2a *and* 2b *with Acidified Methanol*

A solution of diene **2***b* (35 mg) in [$^2H_4$]methanol containing sulfuric acid (0.01 mol dm^{-3}), at 35°C, was observed by nmr. The conversion of the acetoxydiene **2***b* into a mixture of the diastereoisomers of 1-ethyl-4-methyl-4-nitrocyclohexa-2,5-dienyl [$^2H_3$]methyl ether (**10***a* and **10***b*) was complete in 30 min. After work-up **10***a* (62%) had nmr ($CDCl_3$) δ: 0.75 (t, J = 7.6 Hz, CH_2CH_3), 1.64 (q, J = 7.6 Hz, CH_2CH_3), 1.74 (s, 4-CH_3), 5.84 (d, J = 9.9 Hz, 2-*H* and 6-*H*), and 6.31 (d, J = 9.9 Hz, 3-*H* and 5-*H*) ppm; and **10***b* (38%) had nmr ($CDCl_3$) δ: 0.75, 1.60, 1.70, 5.82, and 6.31 ppm.

The reaction was repeated with less acid (0.005 mol dm^{-3}) when aromatic compounds were formed as well as the dienyl methyl ether. When the reaction was carried out in the absence of acid it required 72 h for completion and 65% of aromatic products and 35% of [$^2H_3$]methoxydienes (**10***a*:**10***b* = 60:40) were formed. Analysis by glc and glc–ms showed that the products were, in order of retention time on FFAP, *p*-ethyltoluene (0.3%), 1-[$^2H_3$]methoxy-1-*p*-tolylethane (10%), 3-ethyl-4-[$^2H_3$]methoxytoluene[9] (31%), 4-ethyl-2-[$^2H_3$]methoxytoluene (14%), 2-ethyl-5-methylphenyl acetate (42%), and 5-ethyl-2-methylphenyl acetate (3%). At 35°C in methanol-[$^2H_6$]acetone (10:90 v/v) containing sulfuric acid (0.01 mol dm^{-3}) the acetoxy diene **2***b* was completely converted into approximately equal amounts of the methoxydienes **10***a* and **10***b* in 20 min. When the reaction was repeated with more sulfuric acid (0.1 mol dm^{-3}) formation of the methoxydienes was complete in less than 5 min and subsequently the latter slowly aromatized ($t_{1/2}$ ~ 4 h) to a mixture of 1-methoxy-1-(*p*-tolyl)ethane (82%) and 3-ethyl-4-methoxytoluene and/or 4-ethyl-2-methoxytoluene (18%).

Reaction of diene **2***b* in aqueous [$^2H_4$]methanol (10:90 v/v), at 35°C, gave methoxydienes (10%) and aromatic compounds (90%) within 24 h; glc and glc–ms analysis gave, in order of retention time, *p*-ethyltoluene (4%), 1-[$^2H_3$]methoxy-1-(*p*-tolyl)-ethane (9%), 3-ethyl-4-[$^2H_3$]methoxytoluene[9] (10%), 4-ethyl-2-[$^2H_3$]methoxytoluene (7%), 2-ethyl-5-methylphenyl acetate (66%), 5-ethyl-2-methylphenyl acetate (4%). Each of the identified components had a retention time identical to that of a co-injected authentic sample.

Diene **2***a* with sulfuric acid (0.01 mol dm^{-3}) in methanol at 35°C gave the methoxydienes **10***a* (36%) and **10***b* (64%) in 30 min. Trifluoroacetic acid (315 mm^3) was added to a solution of diene **2***a* (35 mg) in [$^2H_4$]methanol (35 mm^3) at −78°C and the mixture warmed to 0°C. The nmr taken at 0°C within 2 min of mixing showed only 4-ethyl-2-nitrotoluene, confirmed by glc after work-up. In similar experiments in 80% trifluoroacetic acid – 20% [$^2H_4$]methanol the acetoxydiene **2***a* was completely converted into a mixture of the methoxydienes **10***a* and **10***b* (70%) and 4-ethyl-2-nitrotoluene (30%) in 1 min; in 5 min 90% of the methoxydienes had been converted into the nitroarene and in 10 min 4-ethyl-2-nitrotoluene was the only product, confirmed by glc after work-up. In 65% trifluoroacetic acid the [$^2H_3$]methoxydienes **10***a* and **10***b* formed within 4 min and then rearomatized over 2 h to a mixture of 4-ethyl-2-nitrotoluene (80%) and 1-nitro-(*p*-tolyl)ethane (20%). In 50% trifluoroacetic acid the [$^2H_3$]methoxydienes **10***a* and **10***b* were formed in 11 min with **10***b* being present in slightly greater amount than **10***a*. Subsequently rearomatization occurred to the extent of 35% in seven days (0°C). After a further twelve days at ambient temperature rearomatization was complete. After work-up, analysis by ^1H nmr and glc identified the products as 1-[$^2H_3$]methoxy-1-(*p*-tolyl)ethane (4%), 3-ethyl-4-[$^2H_3$]methoxytoluene (73%), and 4-ethyl-2-[$^2H_3$]methoxytoluene (23%). In 10% trifluoroacetic acid (1.4 mol dm^{-3}), approximately equal amounts of the [$^2H_3$]-methoxydienes **10***a* and **10***b* were formed with a half-life of 11 h (0°C). The methoxydienes subsequently rearomatized with a half-life of ca. 20 days at ambient temperature. After completion of the reaction ^1H nmr and glc identified the products as 1-[$^2H_3$]methoxy-1-(*p*-tolyl)ethane (3%), 3-ethyl-4-[$^2H_3$]methoxytoluene (59%), and 4-ethyl-2-[$^2H_3$]methoxytoluene (38%).[10]

Diene **1***b* in [$^2H_4$]methanol containing sulfuric acid (0.01 mol dm^{-3}), at 35°C, was completely converted into the diastereoisomers of 4-ethyl-1-methyl-4-nitrocyclohexa-2,5-dienyl [$^2H_3$]-methyl ether (**9***a* (44%) and **9***b* (56%)) in 9 min. Subsequent aromatization of the [$^2H_3$]methoxydienes ($t_{1/2}$ = 27 h) gave, after work-up and analysis by ^1H nmr and glc, 1-[$^2H_3$]methoxy-1-(*p*-tolyl)ethane (3%), 4-ethyl-3-[$^2H_3$]methoxytoluene (86%), 4-ethyl-2-[$^2H_3$]methoxytoluene (5%), and 5-ethyl-2-[$^2H_3$]methoxytoluene (6%).

In methanol – [$^2H_6$]acetone (10:90 v/v) containing sulfuric acid (0.01 mol dm^{-3}), at 35°C, the conversion of **1***b* to the methoxydienes was complete in 11 min. After work-up and addition of Eu([$^2H_9$]fod)$_3$ the methoxyl peaks could be separately integrated and showed **9***a*:**9***b* = 42:58.

Diene **1***b* rearomatized ($t_{1/2}$ = 12 h) in aqueous [$^2H_4$]methanol

[9]Not distinguishable from the 4-ethyl-3-[$^2H_3$]methoxy isomer by glc.

[10]The ^1H nmr showed three aromatic methyl peaks at δ 2.27 (5%, 1-methoxy-1-*p*-tolylethane and/or 4-ethyl-3-methoxytoluene), 2.24 (60%, 3-ethyl-4-methoxytoluene), and 2.15 ppm (35%, 4-ethyl-2-methoxytoluene). Co-injection of authentic samples identified the three glc peaks, in order of retention time, as 1-methoxy-1-*p*-tolylethane (3%), 3-ethyl-4-methoxytoluene and/or 4-ethyl-3-methoxytoluene (59%), and 4-ethyl-2-methoxytoluene (38%). The combined analysis allowed the unambiguous assignment of the product.

Can. J. Chem. Downloaded from www.nrcresearchpress.com by 210.87.254.6 on 09/06/12
For personal use only.

(10:90 v/v) and gave after work-up: 1-[$^2H_3$]methoxy-1-(*p*-tolyl)ethane (1%), 4-ethyl-3-[$^2H_3$]methoxytoluene (29%), 4-ethyl-2-[$^2H_3$]methoxytoluene (5%), 5-ethyl-2-[$^2H_3$]methoxytoluene or 4-ethyl-1-[$^2H_3$]methoxymethylbenzene (4%), 2-ethyl-5-methylphenyl acetate (7%), and 5-ethyl-2-methylphenyl acetate (54%).

Reaction of Diene 2 in Acetic Anhydride, Acetic Acid, and Formic Acid Solutions

A solution of **2***b* in acetic anhydride containing trifluoroacetic acid (3% v/v) was observed by nmr at −30°C. Isomerization of **2***b* to a 1:1 mixture of **2***a* and **2***b* occurred over 30 min and the dienes subsequently slowly aromatized ($t_{1/2}$ = 30 h). 4-Ethyl-2-nitrotoluene (~40%) was present in the aromatic products.

Reaction of diene **2***b* in acetic anhydride – [$^2H_6$]acetone (10:90, v/v) containing sulfuric acid (0.01 mol dm^{-3}), at 35°C, resulted in complete rearomatization in 7 min. The major product was 1-(*p*-tolyl)ethyl acetate.

Reaction of diene **2***b* in acetic anhydride – [$^2H_4$]acetic acid (10:90, v/v) containing sulfuric acid (0.02 mol dm^{-3}), at 35°C, resulted in complete rearomatization in < 2 min. The distinctive signals of 1-nitro-(*p*-tolyl)ethane were evident in the nmr of the mixture (δ 1.46 (d), 2.26 (s), 5.83 (q)). Work-up and analysis by glc and glc–ms (FFAP column) indicated the following composition (relative retention time, *m/e* of the characteristic ion in the chemical ionization ms, % composition): *p*-ethyltoluene (0.25, 121 (*M* + 1), 10); unknown (0.53, —, 2); *p*-methylacetophenone (0.83, —, 24); 1-(*p*-tolyl)ethyl acetate (0.89, 119 (*M* − OCOCH$_3$), 20); 2-ethyl-5-methylphenyl acetate (1.00, —, 2); 5-ethyl-2-methylphenyl acetate (1.05, —, 2); 4-ethyl-3-nitrotoluene (1.43, 166(*M* + 1), 1); 4-ethyl-2-nitrotoluene (1.60, 166 (*M* + 1), 7); 1-nitro-(*p*-tolyl)ethane (2.38, 119 (*M* − NO$_2$), 31). With the exception of the last compound, which partially decomposed on glc, each of the identified compounds had a retention time identical to that of a co-injected authentic sample.

Reaction of diene **2***b* in acetic anhydride – [$^2H_4$]acetic acid (10:90, v/v) at 35°C led to partial isomerization to **2***a* and rearomatization ($t_{1/2}$ = 20 h); glc and glc–ms analysis of the worked-up product gave: 1-(*p*-tolyl)ethyl acetate (0.90, 119 (*M* − OCOCH$_3$), 24); 2-ethyl-5-methylphenyl acetate (1.00, 179 (*M* + 1, 25%) and 182 ([$^2H_3$]*M* + 1, 75%), 53); 1-(*p*-tolyl)ethanol (1.19, 119 (*M* − OH), 11); 4-ethyl-3-nitrotoluene (1.42, 166 (*M* + 1), 3); 4-ethyl-2-nitrotoluene (1.56, 166 (*M* + 1), 1); 1-nitro-1-(*p*-tolyl)ethane (2.16, 119 (*M* − NO$_2$), 9). With the exception of the 1-nitro-1-(*p*-tolyl)ethane, which partially decomposed on the column, the components had retention times identical to those of co-injected authentic samples.

Reaction of diene **2***b* in [$^2H_2$]water – [$^2H_4$]acetic acid (10:90, v/v), at 35°C, resulted in partial hydrolysis to form hydroxydiene **8** (45% after 1 h) and concurrent rearomatization and aromatization of the hydroxydiene, which was completed in 16 h. The glc and glc–ms analyses of the worked-up product gave 1-(*p*-tolyl)ethyl acetate (0.86, 119 (*M* − OAc), 2); 2-ethyl-5-methylphenyl acetate (1.00, 179 (*M* + 1, 66%) and 182 ([$^2H_3$]*M* + 1, 34%), 51); 5-ethyl-2-methylphenyl acetate (1.03, —, 8); 1-(*p*-tolyl)ethanol (1.22, 119 (*M* − OH), 2); 2-ethyl-4-methyl-6-nitrophenol (1.85, 182 (*M* + 1) and 164 (*M* − OH), 29); and 3-ethyl-6-methyl-2-nitrophenol (1.93, 182 (*M* + 1) and 164 (*M* − OH), 8). The substitution pattern of the nitrophenols was not determined and the assignment is based on the structures of the expected phenol solvolysis products and the most likely position of nitration of these phenols (see Discussion).

A solution of acetyl nitrate in acetic anhydride was prepared by adding acetic anhydride (5 cm^3) to nitric acid (1.89 g), each at −70°C. The mixture was warmed to 0°C and cooled again to −70°C. The acetyl nitrate solution (250 mm^3) was added to a solution of diene **2***a* (112 mg) in acetic anhydride (250 mm^3) at −78°C and the mixture warmed to −40°C and maintained at that temperature for 30 min with occasional shaking. After work-up analysis by nmr indicated that < 5% of the diastereomer **2***b* and < 5% of aromatic compounds had been formed. A similar experiment starting with diene **2***b* showed a similar small amount of isomerization and rearomatization.

Reaction of **2***b* in formic acid – [$^2H_3$]chloroform (33:67) at 0°C resulted in the formation of the formyloxydienes and subsequent aromatization. After work-up, glc and glc–ms gave 2-ethyl-5-methylphenyl formate (0.78, 165 (*M* + 1) 44); 1-(*p*-tolyl)-ethyl formate (0.90, 119 (*M* − OCHO), 7); 2-ethyl-5-methylphenyl acetate (1.00, —, 5); 4-ethyl-3-nitrotoluene (1.34, 166 (*M* + 1), 8); 4-ethyl-2-nitrotoluene (1.50, 166 (*M* + 1), 30); and 2-ethyl-4-methyl-6-nitrophenol (1.96, 182 (*M* + 1) and 164 (*M* − OH), 6). The aryl acetate and nitroarenes had retention times identical to those of authentic samples. The side-chain formate and acetate have similar retention times. However, the protons of the ethylidene group were shifted to distinctly lower field (δ 1.56 and 5.99) compared with those of 1-(*p*-tolyl)ethyl acetate (δ 1.45 and 5.83) and on this basis the formate structure was assigned.

Reaction of Diene 2a with Hydrogen Chloride

Hydrogen chloride was passed through a solution of diene **2***a* (100 mg) in anhydrous ether (10 cm^3) at −78°C, for 10 min. After work-up, ^{1}H nmr showed that the acetoxydiene had been converted into another diene (presumably the chlorodiene **11**) and 30% rearomatization had occurred. The chlorodiene was formed as the expected pair of diastereoisomers since, although there was only a single vinyl peak at δ 6.14 ppm, there were two singlet methyl peaks at δ 1.72 and 1.76 ppm in the ratio 65:35.

Solvolysis of Dienol 8a

Dienol **8***a* in aqueous [$^2H_4$]methanol (20:80, v/v), at 35–45°C over 12 h, gave as the major product 2-ethyl-4-methylphenol, with nmr and glc retention time identical to that of an authentic sample and chemical ionization ms *m/e* 137 (*M* + 1).

Solvolysis in $^2H_4$[methanol] containing *N*,*N*-diisopropylethylamine (10% v/v) at 60°C gave, with a half-life at 44 min (by ^{1}H nmr) 4-ethyl-3-nitrotoluene (16%), 2-ethyl-4-methylphenol (65%), and the diastereoisomers of 1-ethyl-4-[$^2H_3$]methoxy-4-methylcyclohexa-2,5-dien-1-ol (19%); glc of the product confirmed the presence of 4-ethyl-3-nitrotoluene (and the absence of its 2-nitro isomer) and of 2-ethyl-4-methylphenol.

Solvolysis of Methoxydiene 10a

The ether **10***a* in D_2O–CD_3OD (20:80 v/v) at 35°C rearomatized with a half-life of 11.5 h. After complete rearomatization had occurred, ^{1}H nmr indicated that 75% of the methoxyl function had exchanged with the solvent. The ^{1}H nmr and glc of the worked-up product showed that it was composed of 3-ethyl-4-methoxytoluene (71%) and 4-ethyl-2-methoxytoluene (24%) (containing 75% of the [$^2H_3$]methoxy compounds) with minor amounts of 2-ethyl-4-methylphenol[11] (3%) and 5-ethyl-2-methylphenol (2%).

Reaction of Tertiary 1,4-Dialkylnitrocyclohexadienyl Acetates with Sodium Methoxide

A solution of sodium methoxide (0.31 mmol) in methanol (200 mm^3) was added to a solution of diene **2***b* (35 mg, 0.16 mmol) in methanol. The diene rearomatized over 30 min at 35°C to give 2-ethyl-4-methylphenol with identical ^{1}H nmr and retention time on glc to that of an authentic sample. In a similar experiment diene **1***b* was converted, in 3 h at 35°C, into 4-ethyl-2-methylphenol, identified by ^{1}H nmr and glc retention time comparison with an authentic sample. Similarly 1,4-dimethyl-4-

[11]Not distinguishable from 2-ethyl-5-methylphenol in this experiment. The 2-ethyl-4-methylphenol is the more likely product (see Discussion).

Can. J. Chem. Downloaded from www.nrcresearchpress.com by 210.87.254.6 on 09/06/12
For personal use only.

nitrocyclohexa-2,5-dienyl acetate gave 2,4-dimethylphenol with ^{1}H nmr and glc retention time identical to an authentic sample (Aldrich).

Nitration of p-*Ethyltoluene with Mixed Acid*

A mixture of nitric acid (14.8 g) and sulfuric acid (22 cm^3) at −5°C – 0°C was added, with stirring, over 45 min to a solution of *p*-ethyltoluene (20 g, 0.17 mol) in sulfuric acid (22 cm^3) and acetic acid (12 cm^3) at −15°C – −10°C (cf. ref. 16). Stirring was continued for 15 min and the mixture was then poured onto crushed ice. After neutralization with solid sodium carbonate, extraction with ether gave a mixture of unreacted *p*-ethyltoluene, 4-ethyl-2-nitrotoluene, and 4-ethyl-3-nitrotoluene. The *p*-ethyltoluene was removed by distillation under reduced pressure and a mixture of the pure 4-ethyl-nitrotoluenes (19 g, 0.12 mol) was obtained, confirmed by ir 1530 and 1350 cm^{-1} (NO_2), ^{1}H nmr (1), and glc and glc–ms: 4-ethyl-3-nitrotoluene (*m/e* 166 (*M* + 1), 39%) and 4-ethyl-2-nitrotoluene (*m/e* 166 (*M* + 1), 61%).

Nitration of p-*Ethyltoluene with Nitric Acid in Trifluoroacetic Anhydride*

A solution of nitric acid in trifluoroacetic anhydride (25 cm^3) was prepared at −70°C, warmed to 0°C and recooled to −65°C, and added, with stirring, to a solution of *p*-ethyltoluene (6.1 g, 0.05 mol) in trifluoroacetic anhydride (25 cm^3), at −70°C. The mixture was warmed to −40°C, maintained at −40°C for 30 min, then warmed to ambient temperature and allowed to stand for 30 min. Nuclear magnetic resonance data indicated that 75% of 4-ethyl-nitrotoluenes and 5% of dienes had been formed. After work-up, the product was absorbed on alumina and the *p*-ethyltoluene eluted with petroleum ether. The nitrotoluenes were eluted with ether and the presence of 4-ethyl-2-nitrotoluene and 4-ethyl-3-nitrotoluene confirmed by ^{1}H nmr (1), ^{13}C nmr (1), and glc: 4-ethyl-3-nitrotoluene (36%), 4-ethyl-2-nitrotoluene (64%).

*Preparation of 1-(*p*-Tolyl)ethane Derivatives*[12]

1-(*p*-Tolyl)ethanol, pure by glc, was obtained in quantitative yield on reduction of 4-methylacetophenone (40 g) with excess lithium aluminum hydride (10 g) and had ^{1}H nmr ($CDCl_3$) δ: 1.34 (d, 3, *J* = 6 Hz, CH(OH)C*H*$_3$), 2.24 (s, 3, *p*-C*H*$_3$), 3.42 (d, 1, *J* = 2.5 Hz, O*H*), 4.66 (octet, 1, *J* = 6 Hz and 2.5 Hz, C*H*(OH)CH$_3$), 7.03 (d, 2, *J* = 8 Hz, *m-H*), 7.13 (d, 2, *J* = 8 Hz, *o-H*) ppm, on addition of D_2O the OH doublet disappeared and the methine octet was converted into a quartet; ^{13}C nmr ($CDCl_3$) δ$_c$: 21.0 ($C_6H_4CH_3$), 25.1 (CH*C*H$_3$), 69.7 (*C*HCH$_3$), 125.4 (*C*-2′ and *C*-6′), 128.9 (*C*-3′ and *C*-5′), 136.4 (*C*-4′) and 143.1 (C-1′) ppm.

1-(*p*-Tolyl)ethyl acetate, pure by glc, was obtained in 80% yield by acetylation of the alcohol (2.5 g) with acetic anhydride (25 cm^3) in the presence of pyridine (10 cm^3) and had ir (film): 1740 and 1245 (OCOC*H*$_3$) cm^{-1}; ^{1}H nmr ($CDCl_3$), δ: 1.45 (d, 3, *J* = 6.5 Hz, CHC*H*$_3$), 1.94 (s, 3, OCOC*H*$_3$), 2.25 (s, 3, $C_6H_4C\mathit{H}_3$), 5.83 (q, 1, *J* = 6.5 Hz, C*H*CH$_3$), 7.08 (d, 2, *J* = 8 Hz, *m-H*), 7.19 (d, 2, *J* = 8 Hz, *o-H*) ppm; ^{13}C nmr ($CDCl_3$) δ$_c$: 21.1 (OCOCH$_3$ and $C_6H_4C\mathit{H}_3$), 22.1 (CH*C*H$_3$), 72.1 (*C*HCH$_3$), 126.1 (*C*-2′ and *C*-6′), 129.1 (*C*-3′ and *C*-5′), 137.4 (*C*-4′), 138.8 (*C*-1′), and 169.9 (O*C*OCH$_3$) ppm; ms (70 eV), *m/e* (relative intensity) 178.098 (42, M_r ($^{12}C_{11}$ $^1H_{14}$ $^{16}O_2$) 178.099), 136 (46, *M* − CH_2CO), 121 (48), 119 (60), 118 (100, *M* − CH_3CO_2H), 117 (60), 91 (32), 77 (12).

Methyl 1-(*p*-tolyl)ethyl ether was obtained in 87% yield by refluxing the alcohol (0.02 mol) with sodium (0.024 mol) in toluene (25 cm^3) for five days to form the alkoxide which was then reacted with excess methyl iodide (5 cm^3). It had ir (film): 2830 (OCH$_3$) and 1105 (COC) cm^{-1}; ^{1}H nmr ($CDCl_3$) δ: 1.38 (d, 3, *J* = 6.5 Hz, CHC*H*$_3$), 2.27 (s, 3, $C_6H_4C\mathit{H}_3$), 3.12 (s, 3, OC*H*$_3$), 4.19 (q, 1, *J* = 6.5 Hz, C*H*CH$_3$), 7.12 (s, 4, $C_6\mathit{H}_4$) ppm; ^{13}C nmr δ$_c$: 21.1 ($C_6H_4CH_3$), 23.9 (CH*C*H$_3$), 56.2 (O*C*H$_3$), 79.5 (*C*HCH$_3$), 126.2 (*C*-2′), 129.1 (*C*-3′), 136.9 (*C*-4′), 140.6 (*C*-1′) ppm; ms (70 ev), *m/e* (relative intensity) 150.098 (14, M_r ($^{12}C_{10}$ $^1H_{14}$ ^{16}O), 150.104), 135 (100, *M* − CH_3), 118 (55, *M* − CH_4O), 105 (10), 91 (34).

1-Bromo-1-(*p*-tolyl)ethane was obtained from 1-(*p*-tolyl)-ethanol by reaction with a saturated solution of hydrogen bromide in ether for two days and had ^{1}H nmr ($CDCl_3$) δ: 1.98 (d, 3, *J* = 7 Hz, CHBrC*H*$_3$), 2.28 (s, 3, *p*-C*H*$_3$), 5.12 (q, 1, *J* = 7 Hz, C*H*BrCH$_3$), 7.06 (d, 2, *J* = 8.5 Hz, *m-H*), 7.25 (d, 2, *J* = 8.5 Hz, *o-H*) ppm. A solution of the bromide in ether was stirred with silver nitrite for 24 h in the dark and gave, as the major product (65%), 1-nitro-1-(*p*-tolyl)ethane, ir (film): 1570 and 1370 (NO_2) cm^{-1}; ^{1}H nmr δ: 1.54 (d, *J* = 7 Hz, CH(NO$_2$)C*H*$_3$), 2.28 (s, *p*-C*H*$_3$), 6.32 (q, *J* = 7 Hz, C*H*(NO$_2$)CH$_3$), 7.11 (s, $C_6\mathit{H}_4$) ppm. Attempts to purify the nitroethane by extraction into base and re-precipitation were unsuccessful.

Preparation of p-*Ethylbenzyl Derivatives*

p-Ethylbenzyl alcohol was obtained in 92% yield by reduction of p-ethylbenzoic acid with excess lithium aluminum hydride and had ir (film): 3280 (OH), 1005 (C—O) cm^{-1}; ^{1}H nmr ($CDCl_3$) δ: 1.17 (t, 3, *J* = 7.5 Hz, $CH_2C\mathit{H}_3$), 2.57 (q, 2, *J* = 7.5 Hz, C*H*$_2$CH$_3$), 2.96 (t, 1, *J* = 5 Hz, O*H*), 4.46 (d, 2, *J* = 5 Hz, C*H*$_2$OH), 7.11 (s, 4, $C_6\mathit{H}_4$) ppm; ^{13}C nmr ($CDCl_3$) δ$_c$: 15.7 (CH_2CH_3), 28.6 (*C*H$_2$CH$_3$), 64.3 (*C*H$_2$OH), 127.2 and 127.8 (*C*-2, *C*-3, and *C*-5, *C*-6), 138.4 (*C*-1), 143.1 (*C*-4) ppm; ms *m/e* 136.097 (M_r ($^{12}C_9$$^1H_{12}$$^{16}O$) 136.089).

p-Ethylbenzyl acetate, pure by glc, was obtained in 93% yield by acetylation of the alcohol (1.5 g) with acetic anhydride (15 cm^3) in the presence of pyridine (6 cm^3), ir: 1745 and 1225 (OCOCH$_3$) cm^{-1}; ^{1}H nmr ($CDCl_3$) δ: 1.15 (t, 3, *J* = 7.5 Hz, $CH_2C\mathit{H}_3$) 1.96 (s, 3, OCOC*H*$_3$), 2.55 (q, 2, *J* = 7.5 Hz, C*H*$_2$CH$_3$), 4.99 (s, 2, C*H*$_2$OCOCH$_3$), 7.09 (d, 2, *J* = 9 Hz, 3-*H* and 5-*H*), 7.18 (d, 2, *J* = 9 Hz, 2-*H* and 6-*H*) ppm; ^{13}C nmr ($CDCl_3$) δ$_c$: 15.6 (CH_2CH_3), 20.8 (OCOCH$_3$), 28.7 (*C*H$_2$CH$_3$), 66.2 (*C*H$_2$OCOCH$_3$), 128.0 and 128.6 (*C*-2, *C*-6 and C-3, *C*-5), 133.4 (*C*-1), 144.3 (*C*-4), 170.8 (OCOCH$_3$) ppm; ms, *m/e* 178.100 (M_r ($^{12}C_{11}$ $^1H_{14}$$^{16}O_2$) 178.099).

p-Ethylbenzyl methyl ether, pure by glc, was obtained in 81% yield from the alcohol as described for methyl 1-(*p*-tolyl)ethyl ether, ir: 1095 (C—O—C) cm^{-1}; ^{1}H nmr ($CDCl_3$) δ: 1.19 (t, 3, *J* = 7 Hz, $CH_2C\mathit{H}_3$), 2.57 (q, 2, *J* = 7 Hz, C*H*$_2$CH$_3$), 3.28 (s, 3, OC*H*$_3$), 4.33 (s, 2, C*H*$_2$OCH$_3$), 7.10 (d, 2, *J* = 8.5 Hz, 2-*H* and 6-*H*), 7.19 (d, 2, *J* = 8.5 Hz, 3-*H* and 5-*H*) ppm; ^{13}C nmr ($CDCl_3$) δ$_c$: 15.7 (CH_2CH_3), 28.6 (*C*H$_2$CH$_3$), 57.8 (O*C*H$_3$), 74.6 (*C*H$_2$OCH$_3$), 127.9 (*C*-2, *C*-3, *C*-5, *C*-6), 135.4 (*C*-1), 143.7 (*C*-4) ppm; ms, *m/e* 150.100 (M_r ($^{12}C_{10}$$^1H_{14}$$^{16}O$) = 150.104).

p-Ethylbenzyl chloride, pure by glc, was obtained in 73% yield after distillation by reaction of the alcohol (7.1 g) with thionyl chloride in benzene (cf. ref. 17), ^{1}H nmr ($CDCl_3$) δ: 1.17 (t, 3, *J* = 8 Hz, $CH_2C\mathit{H}_3$), 2.57 (q, 2, *J* = 8 Hz, C*H*$_2$CH$_3$), 4.45 (s, 2, C*H*$_2$Cl), 7.13 (d, 2, *J* = 9 Hz, 3-*H* and 5-*H*), 7.21 (d, 2, *J* = 9 Hz, 2-*H* and 6-*H*) ppm. A mixture of the chloride (1.54 g, 0.01 mol) and silver nitrite (3.05 g, 0.02 mol) in anhydrous ether (15 cm^3) was stirred for nine days in the dark, in a closed vessel at ambient temperature. Analysis by ^{1}H nmr indicated that 36% of the chloride was still present and more silver nitrite (3 g) and ether (10 cm^3) were added and stirring continued for a further nine days, when ^{1}H nmr analysis indicated complete reaction. On work-up a mixture (1.47 g) of *p*-ethylbenzyl alcohol (8%, δ 4.46 ppm), *p*-ethylbenzyl nitrite (28%, δ 5.60 ppm), and *p*-ethylbenzyl nitrate plus *p*-ethylphenylnitromethane (64%, δ

[12]Enumeration of the 1-(*p*-tolyl)ethane derivatives starts at the carbon *ipso* to the substituent ethyl group as 1′. This is different from the enumeration used previously for 1-(*p*-tolyl)ethyl nitrate in which the carbon *ipso* to the methyl group was 1 (1).

Can. J. Chem. Downloaded from www.nrcresearchpress.com by 210.87.254.6 on 09/06/12
For personal use only.

5.30 ppm) was obtained. Analysis by ^{13}C nmr indicated that approximately equal amounts of nitrate (δ_c 75.1 ppm) and nitromethane (δ_c 79.7 ppm) with a smaller amount of nitrite (δ_c 70.1 ppm). A portion of the crude product (0.8 g) was reacted with sodium methoxide (1.3 g) in methanol (12 cm^3). After 10 min the methanol was evaporated at ambient temperature, water added, and the mixture extracted (×3) with ether. The aqueous layer was cooled to 5°C and neutralized with solid hydroxylamine hydrochloride (2 g). After 30 min the mixture was extracted with ether. Evaporation of the ethereal extract gave *p*-ethylphenylnitromethane (0.22 g, 25% from the chloride), ir (film): 1580 and 1390 (NO_2) cm^{-1}; ^1H nmr ($CDCl_3$) δ: 1.17 (t, 3, J = 7.5 Hz, CH_2CH_3), 2.59 (q, 2, J = 7.5 Hz, CH_2CH_3), 5.27 (s, 2, CH_2NO_2), 7.17 (d, 2, J = 9 Hz, 3-*H* and 5-*H*), 7.27 (d, 2, J = 9 Hz, 2-*H* and 6-*H*) ppm; ^{13}C nmr ($CDCl_3$) δ_c: 15.3 (CH_2CH_3), 28.6 (CH_2CH_3), 79.8 (CH_2NO_2), 127.1 (*C*-1), 128.5 (*C*-3 and *C*-5), 130.0 (*C*-2 and *C*-6), 146.3 (*C*-4) ppm.

Preparation of Ethylmethylphenols and Methyl Ethers

2-Ethyl-5-methylphenyl methyl ether, pure by glc, was obtained in 78% yield by methylation of the phenol (1) with dimethyl sulfate, ir: 1262 and 1042 (C—O—Ar) cm^{-1}; ^1H nmr ($CDCl_3$) δ: 1.14 (t, 3, J = 7 Hz, CH_2CH_3), 2.27 (s, 3, 5-CH_3), 2.57 (q, 2, J = 7 Hz, CH_2CH_3), 3.72 (s, 3, OCH_3), 6.61 (s, 1, 6-*H*), 6.65 (d, 1, J = 8 Hz, 4-*H*), 6.98 (d, 1, J = 8 Hz, 3-*H*) ppm; ^{13}C nmr ($CDCl_3$) δ_c: 14.4 (CH_2CH_3), 21.4 (5-CH_3), 22.9 (CH_2CH_3), 55.2 (OCH_3), 111.2 (*C*-6), 120.9 (*C*-4), 128.7 (*C*-3), 129.6 (*C*-2), 136.5 (*C*-5), 157.2 (*C*-1) ppm; ms (70 ev), *m/e* (relative intensity): 150.097 (50, M_r ($^{12}C_{10}{}^1H_{14}{}^{16}O$) 150.104), 135 (100, $M - CH_3$), 105 (49), 91 (18).

2-Hydroxy-5-methylacetophenone was obtained by treatment of *p*-cresol with acetyl chloride in the presence of titanium tetrachloride. After crystallization from pentane it was pure by glc; ^1H nmr ($CDCl_3$) δ: 2.26 (s, 3, 5-CH_3), 2.54 (s, 3, $COCH_3$), 6.84 (d, 1, J = 8.1 Hz, 3-*H*), 7.25 (d of d, 1, J = 8.1 Hz, J = 2 Hz, 4-*H*), 7.46 (d, 1, J = 2 Hz, 6-*H*), 11.97 (s, 1, O*H*) ppm. Reduction of the 2-hydroxy-5-methylacetophenone with amalgamated zinc and hydrochloric acid gave 2-ethyl-4-methylphenol, pure by glc, ir (film): 3400 (OH), 1225 (C—OH) cm^{-1}; ^1H nmr ($CDCl_3$) δ: 1.15 (t, 3, J = 7 Hz, CH_2CH_3), 2.18 (s, 3, 4-CH_3), 2.53 (q, 2, J = 7 Hz, CH_2CH_3), 5.15 (s, 1, O*H*), 6.53 (d, 1, J = 8 Hz, 6-*H*), 6.78 (d of d, 1, J = 8 Hz, J = 2 Hz, 5-*H*), 6.86 (d, 1, J = 2 Hz, 3-*H*) ppm; ^{13}C nmr ($CDCl_3$) δ_c: 14.1 (CH_2CH_3), 20.5 (4-CH_3), 23.0 (CH_2CH_3), 115.3 (*C*-6), 127.3 (*C*-5), 130.0 (*C*-2, *C*-3, *C*-4), 151.1 (*C*-1) ppm; mass spectrum (70 eV), *m/e* (relative intensity): 136.090 (48 M_r ($^{12}C_9{}^1H_{12}{}^{16}O$) = 136.089), 122 (12), 121 (100, $M - CH_3$), 107 (10), 91 (19), 77 (19). Methylation of the phenol with dimethyl sulfate gave 2-ethyl-4-methylphenyl methyl ether, pure by glc, ir (film): 2865 ($ArOCH_3$), 1260 and 1045 (C—O—Ar) cm^{-1}; ^1H nmr ($CDCl_3$) δ: 1.16 (t, 3, J = 7 Hz, CH_2CH_3), 2.24 (s, 3, 4-CH_3), 2.58 (q, 2, J = 7 Hz, CH_2CH_3), 3.74 (s, 3, OCH_3), 6.70 (d, 1, J = 8 Hz, 6-*H*), 6.92 (m, 2, 3-*H* and 5-*H*) ppm; ^{13}C nmr ($CDCl_3$) δ_c: 14.3 (CH_2CH_3), 20.5 (4-CH_3), 23.2 (CH_2CH_3), 55.4 (OCH_3), 110.2 (*C*-6), 126.9 (*C*-5), 129.5 (*C*-4 or *C*-2), 129.8 (*C*-3), 132.4 (*C*-2 or *C*-4), 155.3 (*C*-1) ppm; ms *m/e* (relative intensity): 150.093 (70, M_r ($^{12}C_{10}{}^1H_{14}{}^{16}O$) 150.104), 135 (100, $M - CH_3$), 113 (30), 105 (55), 91 (25), 85 (20), 77 (15).

3-Hydroxy-4-methylacetophenone was obtained by reaction of the dilithium salt of 3-hydroxy-4-methylbenzoic acid (Aldrich) with methyllithium (18) and had ^1H nmr ($CDCl_3$) δ: 2.25 (s, 3, 4-CH_3), 2.49 (s, 3, $COCH_3$), 7.09 (d, 1, J = 8 Hz, 5-*H*), 7.33 (d of d, 1, J = 8 Hz, J = 1.5 Hz, 6-*H*), 7.41 (d, 1, J = 1.5 Hz, 2-*H*) ppm. Clemmensen reduction of the acetophenone gave 5-ethyl-2-methylphenol with identical ^1H nmr, ^{13}C nmr, and glc retention time to that prepared from 4-ethyl-2-nitrotoluene (1) and mass spectrum (70 ev) *m/e* (relative intensity): 136.086 (42, M_r ($^{12}C_9{}^1H_{12}$-QYO) = 136.089), 121 (100, $M - CH_3$), 103 (60), 91 (15), 77 (13).

Methylation of 3-hydroxy-4-methylbenzoic acid with dimethyl sulfate gave methyl 3-methoxy-4-methylbenzoate, ^1H nmr ($CDCl_3$) δ: 2.22 (s, 3, 4-CH_3), 3.84 (s, 3, OCH_3 or CO_2CH_3), 3.86 (s, 3, CO_2CH_3 or OCH_3), 7.14 (d, 1, J = 8 Hz, 5-*H*), 7.47 (d, 1, J = 1.5 Hz, 2-*H*), 7.53 (d of d, 1, J = 1.5 and 8 Hz, 6-*H*) ppm. Hydrolysis of methyl 3-methoxy-4-methylbenzoate with aqueous sodium hydroxide gave 3-methoxy-4-methylbenzoic acid, ^1H nmr ($CDCl_3$) δ: 2.25 (s, 3, 4-CH_3), 3.85 (s, 3, OCH_3), 7.18 (d, 1, J = 8 Hz, 5-*H*), 7.52 (d, 1, J = 1.5 Hz, 2-*H*), 7.64 (d of d, 1, J = 1.5 and 8 Hz, 6-*H*) ppm. Reaction of the lithium salt of the acid with methyllithium gave 3-methoxy-4-methylacetophenone, needles from pentane, mp 132–134°C; ir (film): 1705 (C═O), 1285 and 1045 (C—O—Ar) cm^{-1}; ^1H nmr ($CDCl_3$) δ: 2.23 (s, 3, 4-CH_3), 2.53 (s, 3, $COCH_3$), 3.84 (s, 3, OCH_3), 7.16 (d, 1, J = 8 Hz, 5-*H*), 7.41 (d, 1, J = 1.5 Hz, 2-*H*), 7.42 (d of d, 1, J = 1.5 and 8 Hz, 6-*H*) ppm; ^{13}C nmr ($CDCl_3$) δ_c: 16.5 (4-CH_3), 26.4 ($COCH_3$), 55.3 (OCH_3), 108.4 (*C*-2), 121.5 (*C*-6), 130.4 (*C*-5), 133.0 (*C*-4), 136.3 (*C*-1), 157.9 (*C*-3), 197.7 ($COCH_3$) ppm; mass spectrum (70 eV), *m/e* (relative intensity): 164.083 (62, M_r ($^{12}C_{10}{}^1H_{12}{}^{16}O_2$) = 164.084), 149 (100, $M - CH_3$), 121 (20), 91 (33), 83 (20), 77 (15). Clemmensen reduction of the ketone gave 5-ethyl-2-methylphenyl methyl ether, distilled at 30–70°C/1 kPa, as a colourless oil, ir (film): 1270 and 1050 (C—O—Ar) cm^{-1}; ^1H nmr ($CDCl_3$) δ: 1.20 (t, 3, J = 7 Hz, CH_2CH_3), 2.15 (s, 3, 2-CH_3), 2.57 (q, 2, J = 7 Hz, CH_2CH_3), 3.77 (s, 3, OCH_3), 6.64 (d, 1, J = 1 Hz, 6-*H*), 6.67 (d of d, 1, J = 1 and 8 Hz, 4-*H*), 7.00 (d, 1, J = 8 Hz, 3-*H*) ppm; ^{13}C nmr ($CDCl_3$) δ_c: 15.8 (2-$CH_3CH_2CH_3$), 29.0 (CH_2CH_3), 55.1 (OCH_3), 109.8 (*C*-6), 119.5 (*C*-4), 123.7 (*C*-2), 130.5 (*C*-3), 143.1 (*C*-5), 157.7 (C-6) ppm; mass spectrum (70 eV), *m/e* (relative intensity): 150.102 (65, M_r ($^{12}C_{10}{}^1H_{14}{}^{16}O$) = 150.104), 135 (100, $M - CH_3$), 121 (19), 105 (12), 91 (31), 77 (16).

4-Hydroxy-3-methylacetophenone was obtained by titanium tetrachloride catalysed acetylation of *o*-cresol and was recrystallized from ether at −20°C, ^1H nmr ($CDCl_3$) δ: 2.25 (s, 3, 3-CH_3), 2.51 (s, 3, $COCH_3$), 6.87 (d, 1, J = 8 Hz, 5-*H*), 7.68 (d of d, 1, J = 2 Hz, J = 8 Hz, 6-*H*), 7.74 (d, 1, J = 2 Hz, 2-*H*), 7.95 (s, 1, O*H*) ppm. Clemmensen reduction of the 4-hydroxy-3-methylacetophenone gave 4-ethyl-2-methylphenol, ir (film): 3390 (OH) and 1260 (C—O) cm^{-1}; ^1H nmr ($CDCl_3$) δ: 1.14 (t, 3, J = 7 Hz, CH_2CH_3), 2.15 (s, 3, 2-CH_3), 2.48 (q, 2, CH_2CH_3), 5.66 (s, 1, O*H*), 6.62 (d, 1, J = 8 Hz, 6-*H*), 6.82 (d of d, 1, J = 8 Hz, J = 2 Hz, 5-*H*), 6.88 (d, 1, J = 2 Hz, 3-*H*) ppm; ^{13}C nmr ($CDCl_3$) δ_c: 15.9 (2-CH_3,CH_2CH_3), 27.9 (CH_2CH_3), 115.0 (*C*-6), 124.1 (*C*-2), 126.1 (*C*-5), 130.5 (*C*-3), 136.5 (*C*-4), 151.6 (C-1) ppm, ms (70 eV), *m/e* (relative intensity): 136.091 (43, M_r ($^{12}C_9{}^1H_{12}{}^{16}O$) = 136.089), 121 (100, $M - CH_3$), 91 (12), 77 (12). Methylation of the phenol with dimethyl sulfate gave 4-ethyl-2-methylphenyl methyl ether, obtained on molecular distillation as a colourless oil, ir (film): 1257 and 1042 (C—O—Ar) cm^{-1}; ^1H nmr ($CDCl_3$) δ: 1.18 (t, 3, J = 7 Hz, CH_2CH_3), 2.17 (s, 3, 2-CH_3), 2.52 (q, 2, J = 7 Hz, CH_2CH_3), 3.75 (s, 3, OCH_3), 6.71 (d, 1, J = 8 Hz, 6-*H*), 6.93 (m, 2, 3-*H* and 5-*H*) ppm; ^{13}C nmr ($CDCl_3$) δ_c: 16.0 (CH_2CH_3 or 2-CH_3), 16.2 (2-CH_3 or CH_2CH_3), 28.0 (CH_2CH_3), 55.3 (OCH_3), 109.9 (*C*-6), 126.4 (*C*-2), 127.7 (*C*-5), 130.3 (*C*-3), 136.0 (*C*-4), 155.9 (*C*-1) ppm; ms (70 eV), *m/e* (relative intensity): 150.098 (55, M_r ($^{12}C_{10}{}^1H_{14}{}^{16}O$) = 150.104), 135 (100, $M - CH_3$), 91 (26), 77 (18).

1. A. Fischer, G. N. Henderson, and R. J. Thompson. Aust. J. Chem. **31**, 1241 (1978).
2. A. Fischer, G. N. Henderson, T. A. Smyth, F. W. B. Einstein, and R. E. Cobbledick. Can. J. Chem. **59**, 584 (1981).
3. A. Fischer and J. N. Ramsay. Can. J. Chem. **52**, 3960 (1974).
4. A. Fischer and R. Röderer. Can. J. Chem. **54**, 423 (1976).

5. A. FISCHER and R. RÖDERER. Can. J. Chem. **54**, 3978 (1976).
6. G. A. OLAH and S. J. KUHN. J. Am. Chem. Soc. **86**, 1067 (1964).
7. P. C. MYHRE. J. Am. Chem. Soc. **94**, 7921 (1972).
8. T. BANWELL, C. S. MORSE, P. C. MYHRE, and A. VOLLMAR. J. Am. Chem. Soc. **99**, 3042 (1977).
9. H. W. GIBBS, R. B. MOODIE, and K. SCHOFIELD. J. Chem. Soc. Perkin Trans. II, 1145 (1978).
10. S. GOODWIN and B. WITKOP. J. Am. Chem. Soc. **79**, 179 (1957).
11. V. P. VITULLO and E. A. LOGUE. J. Org. Chem. **37**, 3339 (1972).
12. R. G. GILLIS. J. Org. Chem. **21**, 805 (1956).
13. A. FISCHER and K. C. TEO. Can. J. Chem. **56**, 1758 (1978).
14. E. BAMBERGER. Chem. Ber. **33**, 3600 (1901); Justus Liebigs Ann. Chem. **390**, 164 (1912).
15. A. FISCHER and K. C. TEO. Can. J. Chem. **56**, 258 (1978).
16. K. A. KOBE and T. F. DOUMANI. Org. Synth. Coll. Vol. 3, 653 (1955).
17. M. S. NEWMAN. J. Am. Chem. Soc. **62**, 2295 (1940).
18. T. M. BARE and H. O. HOUSE. Org. Synth. Coll. Vol. 5, 775 (1973).

Can. J. Chem. Downloaded from www.nrcresearchpress.com by 210.87.254.6 on 09/06/12
For personal use only.

Observation of two oxa-azabicyclo[2.2.0]hexenone intermediates along the reaction pathway of the photochemical isomerization of 1,3-oxazin-6-ones[1]

PAUL DE MAYO, ALAN C. WEEDON, AND RALPH W. ZABEL
Photochemistry Unit, Department of Chemistry, University of Western Ontario, London, Ont., Canada N6A 5B7

Received February 25, 1981

PAUL DE MAYO, ALAN C. WEEDON, and RALPH W. ZABEL. Can. J. Chem. **59**, 2328 (1981).

Irradiation of 4-methyl-2-phenyl-1,3-oxazin-6-one, **1**, yields a photochemical equilibrium between **1** and 2-methyl-4-phenyl-1,3-oxazin-6-one, **2**. The isomerization proceeds through two intermediates, the oxa-azabicyclo[2.2.0]hexenones **3** and **4**, both of which can be observed spectroscopically (ir, uv, ^{1}H nmr) at low temperature.

PAUL DE MAYO, ALAN C. WEEDON et RALPH W. ZABEL. Can. J. Chem. **59**, 2328 (1981).

L'irradiation de la méthyl-4 phényl-2 oxazine-1,3 one-6 (**1**) conduit à un équilibre photochimique entre le composé **1** et la méthyl-2 phényl-4 oxazin-1,3 one-6 (**2**). L'isomérisation implique deux intermédiaires, les oxa-azabicyclo[2.2.0] hexenones **3** et **4**, que l'on peut observer par spectroscopie (i.r., uv, rmn du ^{1}H) à basse température.

[Traduit par le journal]

Introduction

The irradiation of α-pyrones is known to result in the formation of a mixture of isomeric dimers, which on heating extrude carbon dioxide to yield cyclooctatetraenes (1) (Scheme 1). By analogy we considered that photochemical dimerization of oxazinones could yield dimers which on thermolysis might give the diazocine ring system (2) (Scheme 2). However, we have found that direct irradiation of the 1,3-oxazin-6-one **1** results in a novel photochemical isomerization, the details of which we describe here (3).

Results and Discussion

Thermolysis of ethyl 3-benzamidocrotonate (4) at 300°C is reported to give the oxazinone **1** in poor yield (5). In our hands the thermolysis gave a mixture of the desired oxazinone **1**, 2,6-diphenyl-4-methylpyrimidine, 4,6-dimethyl-2-phenylpyridine, ethyl benzoate, and benzamide along with unconverted ethyl 3-benzamidocrotonate. The pyrimidine and pyridine derivatives are presumably derived

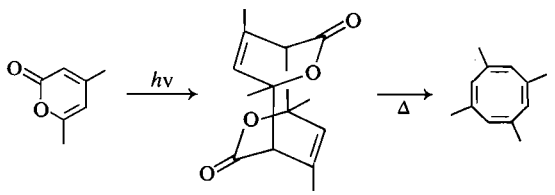

+ isomers

SCHEME 1

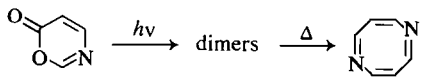

+ isomers

SCHEME 2

from Diels–Alder dimerization of the oxazinone **1** followed by extrusion of propyne or benzonitrile from the intermediate adducts (5). Ethyl benzoate and benzamide are most probably derived from ethanolysis of the ethyl 3-benzamidocrotonate by ethanol released in the formation of **1**. Isolation of **1** from the product mixture proved to be difficult; it was found, however, that heating ethyl 3-benzamidocrotonate in dilute diphenyl ether solution reduced the rate of bimolecular side reactions considerably (6). Furthermore, purging the reaction solution with nitrogen gas removed ethanol being formed and avoided undesirable ethanolysis of the starting material. With these modifications the isolated yield of the oxazinone **1** was raised from 37% (5) to 85%.

Irradiation through Pyrex of the oxazinone **1** in chloroform or benzene resulted in the appearance of a single discrete product as judged by ir and nmr although it was indistinguishable from starting material by tlc. At extended irradiation times the ratio of **1** to product became static (2:3) suggesting that a photostationary state had been attained. That a photostationary state had indeed been formed, rather than inhibition of the reaction owing to light absorption by the product, was suggested by the fact that the absorption spectrum of the product was subsequently found to be less intense than that of **1** at the irradiating wavelengths.

The single product of the reaction was separated

[1]Contribution number 260 from the Photochemistry Unit, University of Western Ontario.

0008-4042/81/152328-06$01.00/0

©1981 National Research Council of Canada/Conseil national de recherches du Canada

Can. J. Chem. Downloaded from www.nrcresearchpress.com by 210.87.254.105 on 09/06/12
For personal use only.

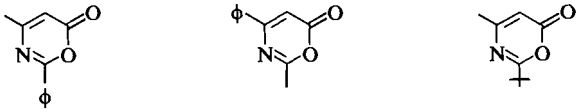

1 2 8

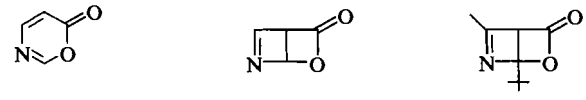

6 7 9

from the starting material **1** by fractional crystallization from ethanol in 45% yield. The ir and mass spectra of the product suggested it to be an isomeric oxazinone, and in the ^{1}H nmr spectrum recorded in chloroform-*d* the methyl and methine protons present in **1** at 2.30 and 6.05 ppm had shifted to 2.47 and 6.52 ppm respectively. Furthermore, in **1** these protons showed allylic coupling ($J \approx 0.5$) which was absent in the product and this is consistent with a number of oxazinone structures in which the methyl and methine groups have become separated. Subsequent observations, described below, suggested structure **2** for the product and this was confirmed by its synthesis from thermolysis of ethyl 3-acetamidocinnamate (7) in diphenyl ether. No evidence was observed for dimer formation during direct irradiation of **1**.

The formation of **2** represents an example of a previously unobserved photochemical ring scrambling reaction. A reasonable mechanism for the isomerization is shown in Scheme 3, and is suggested by two previous reports concerning the photochemistry of oxazinones. The parent oxazinone **6** when irradiated in an argon matrix at 8 K gives, initially, a substance tentatively assigned the oxa-azabicyclo[2.2.0]hexenone structure **7**, ν_{max} 1840 cm^{-1}, along with other species. Further irradiation gave carbon dioxide, hydrogen cyanide, and acetylene (8). More recently, Maier and Schafer (9) have shown that the oxazinone **8**, when irradiated in tetrahydrofuran-d_8 at −70°C, gives the oxa-azabicyclo[2.2.0]hexenone **9** which reverts thermally to **8**, or breaks down photochemically to give acetonitrile, 3,3-dimethyl-1-butyne, carbon dioxide, 2,2-dimethylpropionitrile, and propyne via the presumed intermediate, 2-methyl-4-*tert*-butylazacyclobutadiene. Also, an intermediate zwitterion similar to **5** has been proposed to account for the products obtained from the irradiation of pyrone (10).

In order to test the mechanism outlined in Scheme 3, the irradiation of oxazinones **1** and **2** was carried out at low temperatures in the hope of detecting the intermediates **3** and **4**. This was successful, and evidence was also obtained for the intermediacy of the zwitterion **5**.

Irradiation of the oxazinone **1** through Pyrex in toluene-d_8 at −78°C and monitoring of the ^{1}H nmr spectrum allowed the observation of clean conversion to a new species, identified as **3**. At high conversion extra peaks consonant with the formation of secondary products were seen. These are assumed to arise from secondary irradiation of **3**. Both Krantz and Hoppe (8) and Maier and Schafer (9) observed photochemical extrusion of carbon dioxide from oxa-azabicyclo[2.2.0]hexenones, and subsequent thermal fragmentation of the azacyclobutadienes presumed to be produced gave a mixture of acetylenes and nitriles.

The oxa-azabicyclo[2.2.0]hexenone **3** appeared to be stable at −78°C, but warming to −40°C resulted in clean rearrangement to a second intermediate, identified as the isomeric oxa-azabicyclo-[2.2.0]hexenone **4**. The conversion of **3** to **4** was quantitative, as indicated by ^{1}H nmr, and a typical experiment is shown in Fig. 1 where the transformation was monitored at −55°C. In toluene-d_8 the intermediate **4** was stable at 0°C and at room temperature was converted quantitatively into a mixture of oxazinones **1** and **2**, as judged by ^{1}H nmr spectroscopy. The ratio of **1** to **2** produced by the thermal opening of **4** was approximately 1:1. The conversion of **3** to **4** at −55°C along with the production of *both* **1** and **2** on warming **4** to room temperature suggests that an equilibrium exists between **3** and **4** in which **4** is thermodynamically the more stable. This stability may be attributed to conjugation of the phenyl and imine functions of **4**.

The apparent formation of a photostationary state between **1** and **2** when **1** was irradiated at room temperature in benzene and chloroform-*d* was further confirmed by irradiation of **2** in toluene-d_8 at −78°C. Clean conversion to **4** was observed by ^{1}H

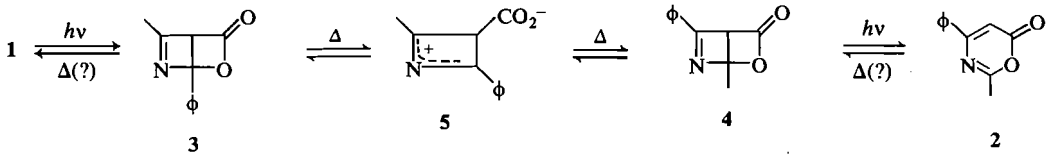

3 5 4 2

SCHEME 3

Can. J. Chem. Downloaded from www.nrcresearchpress.com by 210.87.254.105 on 09/06/12
For personal use only.

Can. J. Chem. Downloaded from www.nrcresearchpress.com by 210.87.254.105 on 09/06/12
For personal use only.

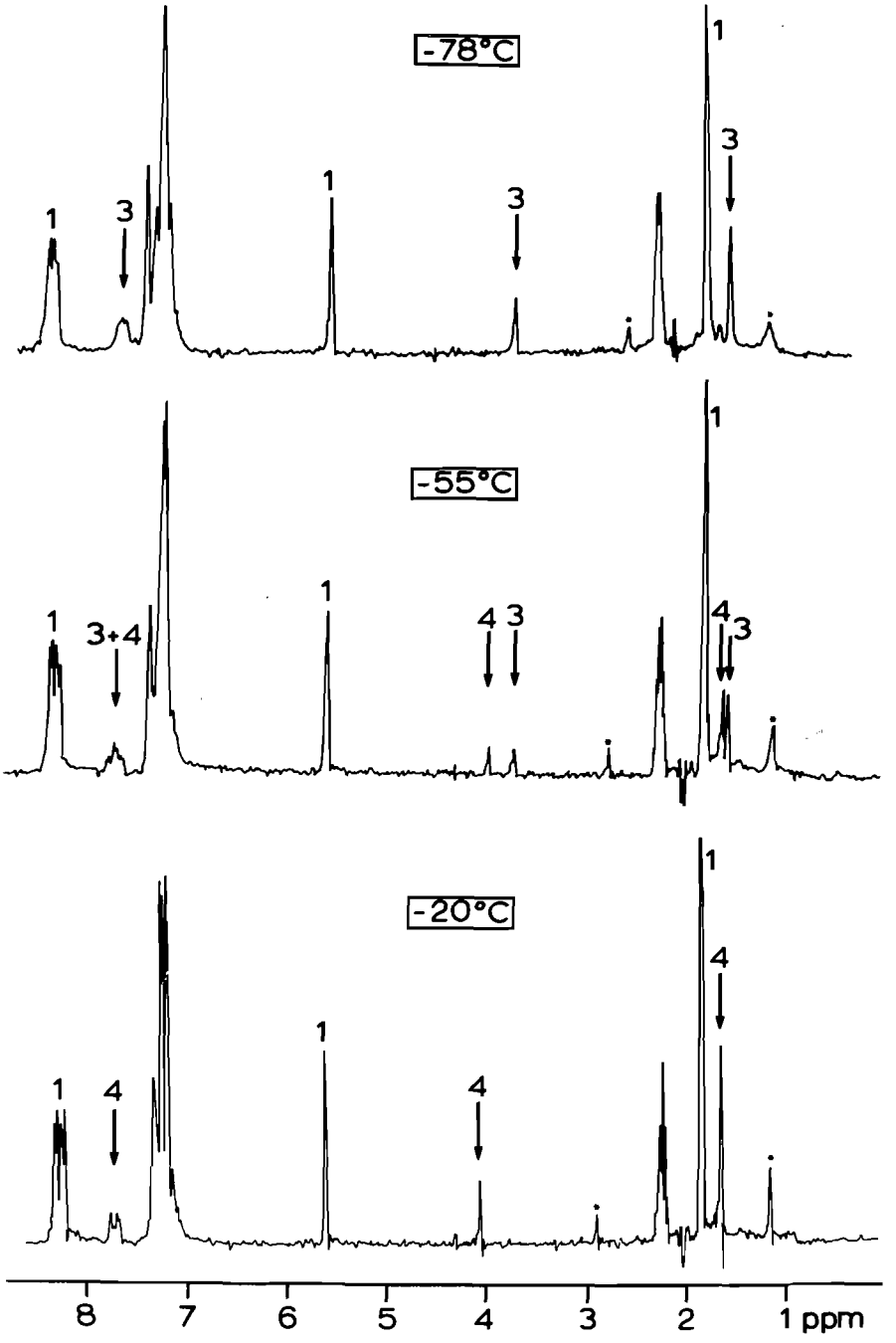

FIG. 1. The ^{1}H nmr spectra of oxa-azabicyclo[2.2.0]hexenone intermediates **3** and **4** in toluene-d_8. The top spectrum is of the intermediate **3** at −78°C, following partial conversion of oxazinone **1** by irradiation through Pyrex. The bottom spectrum is that of the same solution after warming to −20°C and shows the second intermediate **4**. The middle spectrum was recorded at −55°C whilst intermediate **3** was rearranging to **4**. The peak at ca. 2.2 ppm corresponds to toluene containing some protium. The peaks marked by asterisks correspond to photodecomposition products of **3**.

nmr. Warming the solution of **4** resulted in no change until room temperature was reached, when a mixture of **1** and **2** in the ratio approximately 1:1 was again produced, quantitatively.

When the oxazinone **1** was irradiated in methylene chloride-d_2 at −78°C, the intermediate **2** was not detected by ^{1}H nmr. Instead the oxa-azabicyclo[2.2.0]hexenone **4** was apparently formed

Can. J. Chem. Downloaded from www.nrcresearchpress.com by 210.87.254.105 on 09/06/12
For personal use only.

directly. This is consistent with the intermediacy of zwitterion **5** in the reversible transformation between **3** and **4**; thus in methylene chloride-d_2 the zwitterion is sufficiently stabilized that **3** has the necessary activation energy at −78°C to open to **5** and hence be transformed into **4**, whereas in the less polar solvent toluene-d_8 **3** must be warmed to −55°C before opening to **5** can occur.

In Table 1 are given the chemical shifts of the methyl and methine protons in oxa-azabicyclo-[2.2.0]hexenones **3** and **4** along with those of the previously reported analogous compounds (9). As can be seen, the chemical shifts are extremely susceptible to solvent effects, and it was also observed that they varied considerably with temperature.

The oxa-azabicyclo[2.2.0]hexenones were also generated under conditions such that their ir and uv absorption spectra could be observed. Oxazinone **1** was irradiated in methylene chloride and toluene at −78°C and the ir spectra were monitored between 2000 and 1700 cm^{-1}. The formation of a band at 1830 cm^{-1} was observed in both cases and is assigned to the β-lactone function of **3**. No change was observed on warming until room temperature was reached, when the band disappeared. A similar result was obtained when oxazinone **2** was used indicating that both **3** and **4** have ν_{max} at ~1830 cm^{-1}.

Irradiation of oxazinone **1** in anhydrous ether or hexanes (10^{-1} *M*) resulted in the disappearance of the electronic absorption spectrum and appearance of a weak band (ε approximately 250, assuming complete conversion of **1** to **2**) centred around 260 nm, which possessed vibrational structure. This band was very similar to that obtained when the uv spectrum of toluene was recorded under identical conditions, and is assigned to the isolated phenyl group of **3**. Warming to −40°C caused a stronger absorption to emerge with its maximum at 255 nm (ε ca. 6000 assuming complete conversion of **1**) tailing to long wavelengths, and assigned to the conjugated phenyl group of **4**. Further warming resulted in the disappearance of the chromophore responsible for the 255 nm band and the appearance of bands consistent with a mixture of **1** and **2**. As could be expected for a transformation of a single component to two different products, no isobestic points were observed. When the isomeric oxazinone **2** was irradiated in hexanes at −78°C, or the oxazinone **1** was irradiated in methylene chloride at −78°C, only the absorption at 255 nm was observed following disappearance of the spectra of **1** and **2**, as expected for the formation of **4** directly. Warming to room temperature again gave a spectrum consistent with a mixture of **1** and **2**, and no isobestic point was observed. Some of these spectral changes are shown in Fig. 2.

In Fig. 3 is shown a potential energy surface diagram for the reversible photochemical transformation between **1** and **2**. Excitation of **1** onto the excited surface followed by a crossing onto the ground state surface gives **3** which in the nonpolar solvents at −78°C is stable. In polar solvents at −78°C, or on warming nonpolar solvents to −40°C, **3** equilibrates with the more stable isomer **4**, via the

TABLE 1. Chemical shifts of methyl and methine protons in oxa-azabicyclo[2.2.0]hexenones

Structure	δ (Me)	δ(H)	Temperature °C	Solvent
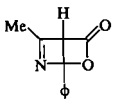	1.29	3.31	−78	Toluene-d_8
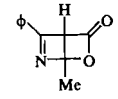	1.45	3.79	−20	Toluene-d_8
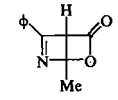	2.04	5.00	−20	CH_2Cl_2-d_2
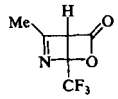	2.38	5.49	−70	THF-d_8[a]
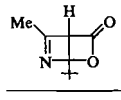	2.26	4.74	−70	THF-d_8[a]

[a]From ref. 9.

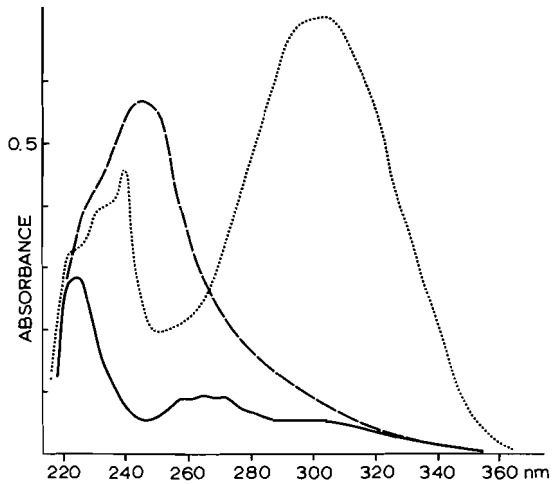

FIG. 2. Electronic absorption spectra of **1**, **3** and **4**; ----- oxazinone **1** (10^{-4} *M*) in diethyl ether at −78°C; — oxa-azabicyclohexenone **3** at −78°C following irradiation of **1**; – – – oxa-azabicyclohexenone **4** at −20°C formed from **3**.

Can. J. Chem. Downloaded from www.nrcresearchpress.com by 210.87.254.105 on 09/06/12
For personal use only.

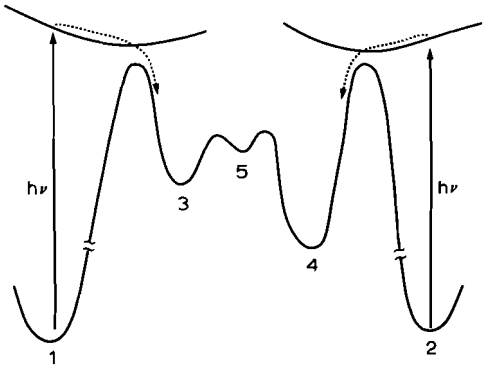

FIG. 3. Potential energy diagram for part of the ground state and excited state surfaces relating oxazinones **1** and **2**.

presumed zwitterionic intermediate **5**. Similarly, excitation of **2** gives **4** directly.

The opening of **3** and **4** to give **1** and **2** is analogous to the case of Dewar benzenes. Disrotatory opening to give the product is forbidden, whilst conrotatory opening also involves a high energy transition state as it leads to a *trans* double bond in a six membered ring. The fact that approximately equal amounts of **1** and **2** are obtained when **4** is heated suggests that the barriers leading to the products are of similar magnitude or possibly that an alternative route through a common intermediate exists. Such a route is shown in Scheme 4 where the zwitterion **5** is identified as the common intermediate. This scheme may have some relevance for the transformation of bicyclo[2.2.0]pyrones to benzvalene structures (11) and is supported by the observation of thermal equilibria between azetines and azabutadienes (12).

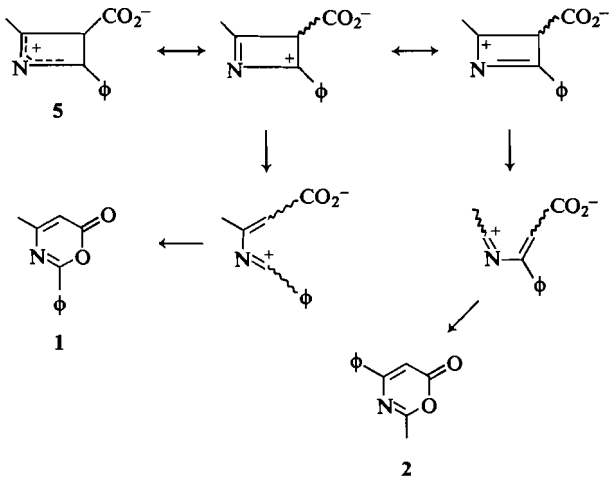

SCHEME 4

Experimental

Room temperature irradiations were performed using medium and high pressure mercury sources, and a high pressure xenon source. Low temperature irradiations for ^{1}H nmr experiments were carried out in 5 mm od nmr tubes submerged in transparent Dewars containing Dry Ice and methanol as coolant. Low temperature ^{1}H nmr measurements were made on a Varian XL 100 machine, irradiated samples being rapidly transferred from the irradiation Dewar to the precooled probe. Low temperature uv experiments were performed in quartz cells mounted in a cryostat capable of being cooled to temperatures down to 77 K and designed to allow periodic monitoring of the electronic absorption spectrum of the sample undergoing irradiation. Low temperature ir experiments were performed in a similar apparatus in sodium chloride cells. Solutions for uv and ^{1}H nmr experiments were degassed by three freeze–pump–thaw cycles to a residual pressure of 5×10^{-5} Torr and were sealed into their cells and tubes respectively.

Preparation of 4-Methyl-2-phenyl-1,3-oxazin-6-one

Ethyl acetoacetate was converted to ethyl 3-aminocrotonate by the method of Collie (13) and had δ ($CDCl_3$): 6.60 (b, 2H), 3.74 (q, 2H, J = 7 Hz), 1.60 (s, 3H), 0.90 (t, 3H, J = 7 Hz). Ethyl 3-aminocrotonate was converted to the benzoyl derivative by the method of Benary (4) as follows.

Benzoyl chloride (22 g) was dropped into an ice-cooled solution of pyridine (13.5 g), anhydrous ether (75 mL), and ethyl 3-aminocrotonate (21 g). At completion of addition the mixture was given an aqueous work-up and the crude product was crystallized from ether to give *E* ethyl 3-benzamidocrotonate; evaporation of the mother liquors and crystallization from ethanol gave *Z* ethyl 3-benzamidocrotonate. The combined yield was 81%. The *E*-isomer had mp 94–95°C (lit. (4) mp 95°C) and δ ($CDCl_3$): 11.94 (b, 1H), 8.13–7.90 (m, 2H), 7.70–7.35 (m, 3H), 5.09 (q, 1H, J = 1 Hz), 4.26 (q, 2H, J = 7.5 Hz), 2.58 (d, 3H, J = 1 Hz), 1.32 (t, 3H, J = 7.5 Hz). The *Z*-isomer had mp 44–46°C (lit. (4) mp 44–48°C) and δ ($CDCl_3$): 8.2–7.2 (b, 1H), 7.78–7.19 (m, 5H), 6.79 (q, 1H, J = 1 Hz), 4.09 (q, 2H, J = 7 Hz), 2.42 (d, 3H, J = 1 Hz), 1.21 (t, 3H, J = 7 Hz).

Condensation of ethyl 3-benzamidocrotonate was initially attempted by the method of Steglich (5). A mixture of *E*- and *Z*-isomers of ethyl 3-benzamidocrotonate was heated under nitrogen at 300°C in a Woods metal bath (the isomers interconvert at 200°C) for 3 h. Bulb to bulb distillation of the product gave an oil (44–54°C, 0.2 Torr) which on the basis of nmr, ir, and mass spectra contained ethyl benzoate and benzonitrile. A second fraction (100–105°C, 0.2 Torr) was a solid identified as benzamide (mixture mp). The nondistilled residue was separated by preparative tlc to give 2,4-diphenyl-6-methyl pyrimidine, δ ($CDCl_3$): 8.54–8.27 (m, 2H), 8.14–7.94 (m, 2H), 7.53–7.25 (m, 6H), 7.03 (s, 1H), 2.61 (s, 3H); *m/e*: 246 (39%), 160 (29), 105 (100), 77 (38), and 4,6-dimethyl-2-phenyl pyridine, δ ($CDCl_3$): 7.86–7.64 (m, 2H), 7.41–7.03 (m, 4H), 6.72 (s, 1H), 2.54 (s, 3H), 2.30 (s, 3H); *m/e*: 183 (100%) 167 (25), 105 (19), 77 (24), along with ethyl 3-benzamidocrotonate and 4-methyl-2-phenyl-1,3-oxazin-6-one, **1**.

The yield of **1** was greatly improved by performing the condensation in diphenylether solution. This method has also been reported elsewhere (6). A mixture of the *E*- and *Z*-isomers of ethyl 3-benzamidocrotonate (1.0 g) in diphenyl ether (20 mL) was heated at 255°C for 1.5 h whilst nitrogen gas was bubbled through the solution. The diphenyl ether was distilled off under vacuum to yield crude oxazinone in 94% yield. Crystallization from ethanol gave pure oxazinone (0.67 g, 85%), mp 89–90°C (lit. (5) mp 93°C). Oxazinone **1** had λ_{max} (EtOH) (ε): 301 (14 200),

238 (10900), 222 nm (6400); ν_{max} (Nujol): 1770, 1622 cm^{-1}; δ (toluene-d_8): 8.08 (m, 2H), 7.08 (m, 3H), 5.45 (q, 1H, J = 1 Hz), 1.72 (d, 3H, J = 1 Hz); *m/e* 187 (14%), 159 (23) 105 (100%) 77 (96); $C_{10}H_9NO_2$ requires 187.0633; found, 187.0631.

Preparation of 2-Methyl-4-phenyl-1,3-oxazin-6-one, 2

(a) *By Irradiation of 1*

The oxazinone **1** (0.830 g) in benzene (3.5 mL) was irradiated under a nitrogen blanket and at room temperature using a Pyrex filtered medium pressure mercury lamp until no further change occurred, as judged by ^1H nmr (191 h). The benzene was removed and the residue was passed through a short column of silica gel with chloroform to remove polymeric material. Removal of solvent gave a yellowish solid (0.752 g) which from its ^1H nmr spectrum consisted of a mixture of oxazinones **1** and **2** in the ratio 38:60 with ~2% minor products. Fractional crystallization from ethanol gave **2** (0.374 g, 45%).

(b) *By Condensation of Ethyl 3-Acetamidocinnamate*

Ethyl 3-aminocinnamate was prepared by the method of Lukes and Kloubek (14), by addition of phenyl magnesium bromide to ethyl cyanoacetate, and had ν_{max}: 3460, 3350, 1670, 1660 cm^{-1}; δ ($CDCl_3$): 7.30 (m, 5H), 6.47 (b, 2H), 4.06 (q, 2H, J = 7 Hz), 1.26 (t, 3H, J = 7 Hz). The product was acetylated by the method of Kato *et al.* (7) to give ethyl 3-acetamidocinnamate as a mixture of *E*- and *Z*-isomers in the ratio 3:2 (nmr). The mixture had λ_{max} (hexanes) (ε): 291 (13300), 221 nm (7100); ν_{max}: 3290, 1720, 1672 cm^{-1}. For the *E*-isomer, δ ($CDCl_3$): 10.48 (s, 3H), 7.26 (bs, 5H), 5.20 (s, 1H), 4.16 (q, 2H, J = 7 Hz), 2.14 (s, 3H), 1.27 (t, 3H, J = 7 Hz). For the *Z*-isomer, δ ($CDCl_3$): 7.28 (bs, 5H), 7.14 (s, 1H), 5.42 (b, 1H), 3.67 (q, 2H, J = 7 Hz), 2.28 (s, 3H), 0.67 (t, 3H, J = 7 Hz). The ^1H nmr spectra were recorded on a mixture of the isomers and were assigned by identification of the intramolecularly hydrogen-bonded N—H group of the *E*-isomer.

The acetamidoester was condensed to give **2** as follows: ethyl 3-acetamidocinnamate (0.80 g, mixture of isomers) in diphenyl ether (18 mL) was heated at 255°C whilst nitrogen gas bubbled through the solution to remove ethanol. The progress of the reaction was followed by examination of the ^1H nmr spectra of removed aliquots; after 5 min, all of the *Z*-isomer had converted to the *E*-isomer. After 3 h no starting material remained and a single product was observed. The solvent was removed under vacuum and the residue was chromatographed on silica gel with chloroform to give 2-methyl-4-phenyl-1,3-oxazin-6-one, **2** (0.46 g, 72%), mp (EtOH) 109–110°C. The oxazine had λ_{max} (EtOH), (ε): 296 (7900), 254 (6100), 226 nm (10400); ν_{max} (Nujol): 1766, 1627 cm^{-1}; δ (toluene-d_8): 7.69 (m, 2H), 7.08 (m, 3H), 6.12 (s, 1H), 1.76 (s, 3H); *m/e*: 187 (35%), 172 (10), 159 (48), 105 (100%), 77 (89); $C_{10}H_9NO_2$ requires 187.0633, found 187.0633.

1. P. DE MAYO and R. W. YIP. Proc. Chem. Soc. 84 (1964); P. DE MAYO, C. L. MCINTOSH, and R. W. YIP. Organic photochemical syntheses. Vol. 1. *Edited by* R. Srinivasan. Wiley-Interscience, New York. 1971. p. 99.
2. B. M. TROST, P. H. SCUDDER, R. M. CORY, N. J. TURRO, V. RAMAMURTHY, and T. J. KATZ. J. Org. Chem. **44**, 1264 (1979).
3. P. DE MAYO, A. C. WEEDON, and R. W. ZABEL. Chem. Commun. 881 (1980).
4. F. BENARY. Chem. Ber. **42**, 3921 (1898).
5. S. GOTZE and W. STEGLICH. Chem. Ber. **109**, 2327 (1976); E. BUSCHMANN and W. STEGLICH. Angew. Chem. Int. Ed. Engl. **13**, 484 (1974).
6. F. EIDEN and B. S. NAGAR. Naturwissenschaften, **50**, 403 (1963).
7. T. KATO, H. YAMANAKA, and T. HOZUMI. Yakugaku Zasshi, **91**, 740 (1971).
8. A. KRANTZ and B. HOPPE. J. Am. Chem. Soc. **97**, 6590 (1975).
9. G. MAIER and U. SCHAFER. Tetrahedron Lett. 1053 (1977).
10. J. P. GUTHRIE, C. L. MCINTOSH, and P. DE MAYO. Can. J. Chem. **48**, 237 (1970).
11. W. H. PIRKLE and L. H. MCKENDRY. J. Am. Chem. Soc. **91**, 1179 (1969); E. J. COREY and W. H. PIRKLE. Tetrahedron Lett. 5255 (1967).
12. T. S. CANTRELL. J. Org. Chem. **42**, 4238 (1977).
13. D. COLLIE. Ann. Chem. **226**, 301 (1884).
14. R. LUKES and J. KLOUBEK. Collect. Czech. Chem. Commun. **25**, 607 (1960).

Can. J. Chem. Downloaded from www.nrcresearchpress.com by 210.87.254.105 on 09/06/12
For personal use only.

Studies related to biological detoxification of kraft pulp mill effluent. I. The biodegradation of dehydroabietic acid with *Mortierella isabellina*

JAMES P. KUTNEY,[1] MAHATAM SINGH, GARY HEWITT, PHILLIP J. SALISBURY, AND BRIAN R. WORTH
Department of Chemistry, University of British Columbia, 2036 Main Mall, University Campus, Vancouver, B.C., Canada V6T 1Y6
AND
JAMES A. SERVIZI, DENNIS W. MARTENS, AND ROBERT W. GORDON
Sweltzer Creek Salmon Research Laboratory, International Pacific Salmon Fisheries Commission, Cultus Lake, B.C., Canada

Received February 13, 1981

JAMES P. KUTNEY, MAHATAM SINGH, GARY HEWITT, PHILLIP J. SALISBURY, BRIAN R. WORTH, JAMES A. SERVIZI, DENNIS W. MARTENS, and ROBERT W. GORDON. Can. J. Chem. **59**, 2334 (1981).

A study related to biological detoxification of kraft pulp mill effluent is presented. A series of fungal and bacterial preparations were evaluated for their action on dehydroabietic acid (DHA), one of the effluent constituents toxic to fish. *Mortierella isabellina* was the organism selected for the biodegradation of DHA and subsequent chemical studies established the structures of four novel diterpenoid substances with very much lower acute toxicity to *Daphnia pulex*.

JAMES P. KUTNEY, MAHATAM SINGH, GARY HEWITT, PHILLIP J. SALISBURY, BRIAN R. WORTH, JAMES A. SERVIZI, DENNIS W. MARTENS et ROBERT W. GORDON. Can. J. Chem. **59**, 2334 (1981).

On présente une étude portant sur la désintoxication du résidu du moulin à pâte de kraft. On a évalué l'action d'une série de préparations fongiques et bactériennes sur l'acide déhydroabiétique (DHA), l'un des constituants, toxiques pour les poissons, présents dans le résidu. On a choisi l'organisme *Mortierella isabellina* pour la biodégradation du DHA et les études chimiques subséquentes établissent la structure de 4 nouvelles substances diterpéniques avec une toxicité beaucoup plus faible envers le *Daphnia pulex*.

[Traduit par le journal]

Introduction

It is generally conceded that microbiological treatment is one of the best available methods for detoxifying kraft pulp mill effluents (KME). Although the activated sludge process and aerated lagoons have found extensive use, they have not proved reliable in every case and their effects have not been readily quantified (1).

The major toxicity from KME has been shown to arise from the significant resin acid content, in particular: dehydroabietic (DHA) (**1**), abietic (**2**), isopimaric acids (**3**) (2).

Biodetoxification of KME from B.C. mills by aerated lagoons and activated sludges has been studied and in fact shown to be partially successful (1, 3). However, treatment times up to 14 days were necessary for detoxification and statistics from operating lagoons reveal that the method is not always dependable (1). Furthermore, no detailed studies have been made of the actual biodegradation products or the environmental consequences of the discharge of these metabolites to waters associated with fisheries resources.

Work in these laboratories has been directed towards four strategic goals: (*i*) determination and quantitation of the specific biodegradation products from the major resin acid toxicants; (*ii*) elucidation of the sequential pathway(s) of metabolism; (*iii*) measurement of the toxicity of the metabolites; (*iv*) identification of a readily available stable organism which might be used as a supplement to existing biological treatment basins to enhance the efficiency of detoxification.

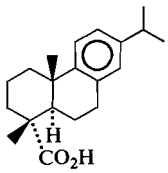

1(DHA)

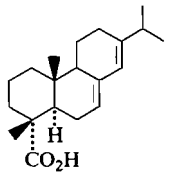

2

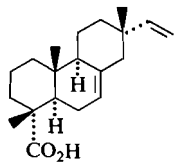

3

The information from (*i*)–(*iii*) is needed to fill an important gap in our knowledge concerning the environmental consequences of currently widely used waste treatment practices in the Canadian pulp and paper industry. Achievement of the fourth goal is expected to significantly enhance performance control over bio-basins and perhaps allow

[1]Author to whom correspondence should be addressed.

0008-4042/81/152334-08$01.00/0
©1981 National Research Council of Canada/Conseil national de recherches du Canada

Can. J. Chem. Downloaded from www.nrcresearchpress.com by 210.87.254.105 on 09/06/12
For personal use only.

TABLE 1. Microorganisms screened for ability to degrade dehydroabietic acid

Fungi	Bacteria
Ascochyta pinodella	*Bacillus mycoides* (1, 4)
Aureobasidium pullulans ATCC 9348	*Pseudomonas acidovorans* ATCC 9355
Cephalosporium sp. (1, 2)	*Pseudomonas aeruginosa* ATCC 1066
Fusarium culmorum CBS 171.28	9 bacterial isolates (2)
Lentinus lepideus WFPL #44B	
Lenzites trabea WFPL #47D	
Mortierella isabellina UBC #129	
Mucor globosus (1, 5)	
Nodulisporium sp. (1, 5)	
Polyporus hirsutus WFPL #89B	
Polysporus versicolor WFPL #105E	
Stereum purpureum WFPL #148A	
Trichoderma viride I (1, 2)	
Trichoderma viride II (1, 3)	
Three fungal isolates (2)	

Legend: UBC, the University of British Columbia culture collection in botany; WFPL, Western Forest Products Laboratory (now called Forintek Canada Corporation); ATCC, American Type Culture Collection; CBS, Centraalbureau voor Shimmelcultures; (1), provisional identification based on morphological characteristics; (2), isolated from kraft pulp mill effluent; (3), obtained from British Columbia Research Council laboratory fermentation sludge courtesy of Dr. J. C. Mueller, British Columbia Research Council; (4), isolated as a laboratory contaminant; (5), isolated from lichen.

the practice of secondary treatment at mills where there is a limited amount of available land.

Although a large number of fungal and bacterial preparations (Table 1) were tested for their action on DHA (**1**), greatest success was attained with *Mortierella isabellina*, an organism we had already shown effective in the biodegradation of other complex organic molecules (4). The present work deals mainly with the biodegradation of DHA (**1**) by *M. isabellina*.

Methods and Results

Growth and Microbial Activity of Various Organisms

Preliminary screening of numerous microorganisms (Table 1) for the ability to degrade DHA revealed that 12 fungi and 9 bacteria possessed this capability. Quantification of the degree of degradation by these organisms (Table 2) showed that *M. isabellina* (5) was the most effective over short incubation periods. The incubation times shown in Table 2 reflect the relative growth rates of the different microbes since cultures were harvested only after good growth, as assessed visually. *M. isabellina* has a further advantage of being a prolific spore former that allows for heavy spore inocula which result in rapid growth and reduced mycelial balling in liquid culture.

A typical growth curve for *M. isabellina* grown in dextrose–yeast extract broth (DYE) at 27°C and 200 rpm is presented in Fig. 1. After a lag phase of approximately 12 h, the culture grew quickly to reach a maximum dry weight of about 2.8 mg/mL by 24 to 30 h. There was a growth-associated decrease in pH from 6.8 to 2.8. Inclusion of 250 mg/L of DHA resulted in retardation of growth rate and a slightly higher final pH. Cultures were inhibited to a lesser degree if only 80 mg/L DHA was added.

TABLE 2. Microbial degradation of dehydroabietic acid with various microorganisms. Dehydroabietic acid analysis performed using hplc

Microorganism	Incubation time (h)	Percentage DHA degradation
(A) Fungi		
Mortierella isabellina	24	94
	48	98
Stereum purpureum	96	90
Nodulisporium sp.	96	90
Ascochyta pinodella	96	89
Trichoderma viride I	48	62
Trichoderma viride II	96	61
Cephalosporium sp.	24	60
Pink yeast isolate	48	58
Aureobasidium pullulans	96	57
Fusarium culmorum	48	26
Yellow fungal isolate	48	17
Black fungal isolate	96	16
(B) Bacteria		
Isolate–T4	24	60
Isolate–T3	24	54
Bacillus mycoides	24	15
	96	30
Five *Pseudomonas* species	24	10 to 20
	96	Less than 30
Isolate–T2	64	24

Quantitative Analysis

In order to evaluate the course and efficiency of

Can. J. Chem. Downloaded from www.nrcresearchpress.com by 210.87.254.105 on 09/06/12
For personal use only.

Can. J. Chem. Downloaded from www.nrcresearchpress.com by 210.87.254.105 on 09/06/12
For personal use only.

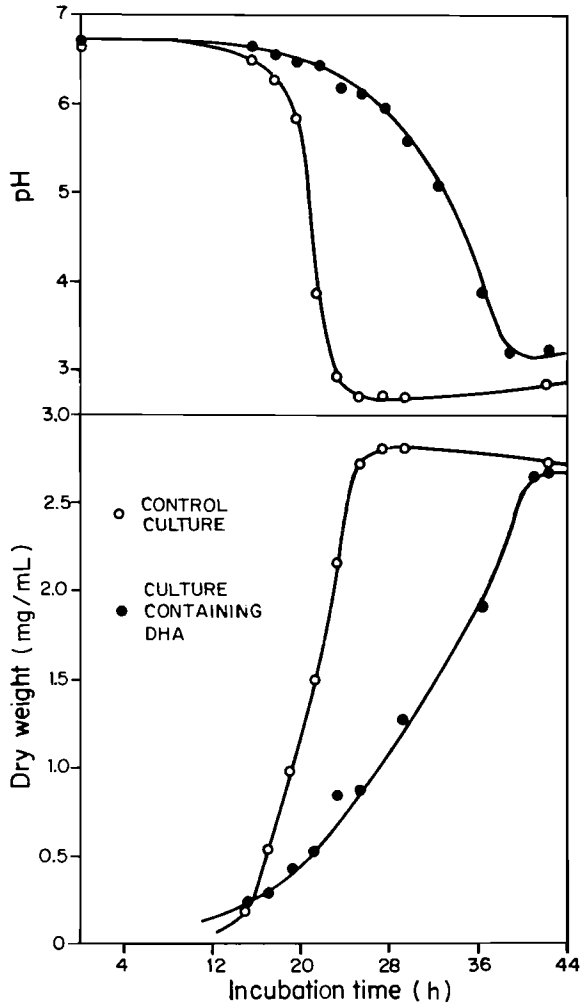

FIG. 1. Growth of *M. isabellina* in DYE and DYE plus DHA (250 mg/L).

biodegradation, it was essential to develop analytical methods for the quantitative determination of DHA.

(*i*) Radiotracing: DHA, tritium labelled in the aromatic ring, was prepared by catalysed exchange with CF_3CO_2T (see Experimental). Repeated purification gave Ar-^{3}[H]-DHA with activity of 1.0471 $\times$ 10^9 dpm/mmol. Labelled material was fed to *M. isabellina* (and other organisms) for various time periods, the culture extracted, and the organics separated by chromatography (usually preparative tlc). Scintillation counting of the various fractions then gave values for residual DHA and an indication of the location and concentration of different biodegradation products.

(*ii*) High pressure liquid chromatography: a quantitative analysis of DHA was developed using Waters Associates hplc equipment standardized as shown in Fig. 2.

The screening results shown in Table 2 indicate the utility of this hplc analysis.

Biodegradations of DHA

Results from the preliminary screen (Table 2) clearly showed *M. isabellina* to be the most efficient microorganism for our purposes and it was used in all subsequent experiments.

In a typical experiment, ca. 0.5 g of DHA was converted to its sodium salt and incubated with *M. isabellina* for 24 h. The harvested mixture was acidified and extracted to give the crude mixture of metabolites; hplc examination of the crude metabolites (e.g. see Fig. 4) indicated four major products (**4**–**7**). These were isolated by preparative layer chromatography and each acid identified after purification of its corresponding methyl ester (viz. **8**–**11**, Fig. 3).

The methyl ester **8** of the major component **4** had molecular formula $C_{21}H_{30}O_3$ indicating the introduction of one additional oxygen to the skeleton. The uv spectrum was very similar to that of DHA (**1**) strongly suggesting no change in ring C. The ir spectrum did, however, indicate hydroxyl stretching at ν 3700–3400 cm^{-1}. The ^{1}H nmr spectrum revealed a nine line, one proton absorbance at δ 4.1 for a ring proton geminal to the hydroxyl group. The splitting pattern (tt, J_{aa} = 12 Hz, J_{ae} = 4 Hz) was consistent with an axial proton split by two adjacent methylenes. Thus the hydroxyl group was situated at $C_{2\alpha}$, confirmed by a downfield shift of 1.12 ppm for H-2β in the corresponding acetate (**12**, mp 74–75°C). Further proof of this structure was obtained by formation of the lactone **13** by treatment of **4** with *p*-toluenesulphonic acid (PTS) in refluxing benzene. Absorption at 1768 cm^{-1} confirmed the γ-lactone function. Furthermore, oxidation of **8** with pyridinium chlorochromate gave the ketone **14** in high yield. The spectral data for **14** were dissimilar to those reported for the corresponding 6-ketone (6).

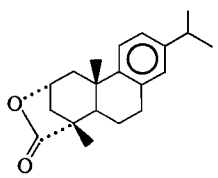

13

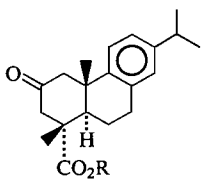

14 R = CH_3

One of the other metabolites (as the methyl ester) also had molecular formula $C_{21}H_{30}O_3$ and its spectral data suggested a secondary alcohol (**9**) isomeric with **8**. This assignment was supported by data from the acetate **15** and confirmed by pyridinium chlorochromate oxidation of **15** to give the ketone **14**, identical with that obtained from **8**.

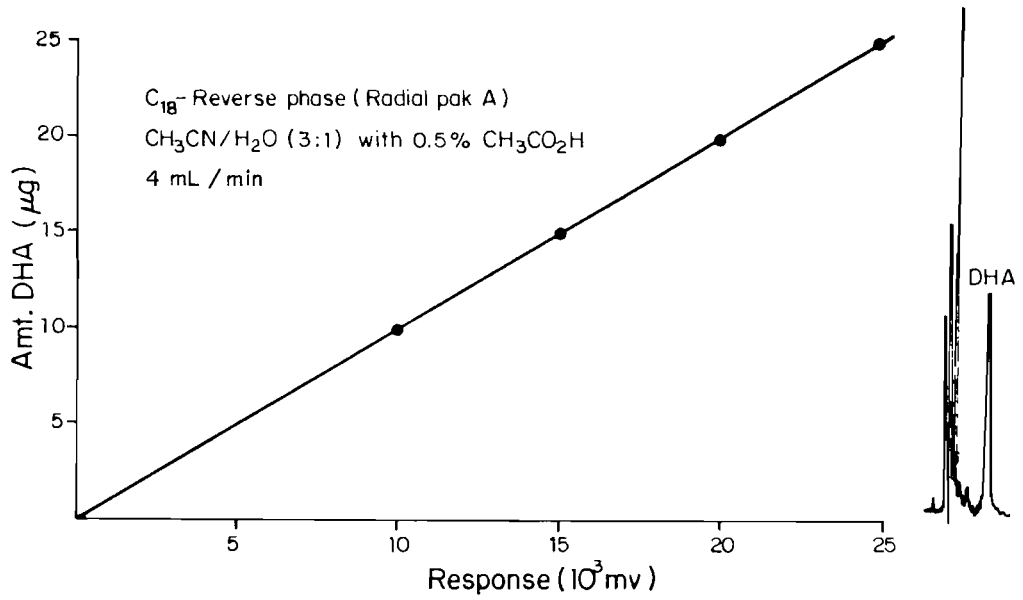

FIG. 2. The hplc quantitation of DHA. Response as measured on a Shimadzu Chromatopac-E1A integrator and Waters Associates Model 440 detector (at 280 nm and sensitivity 0.1).

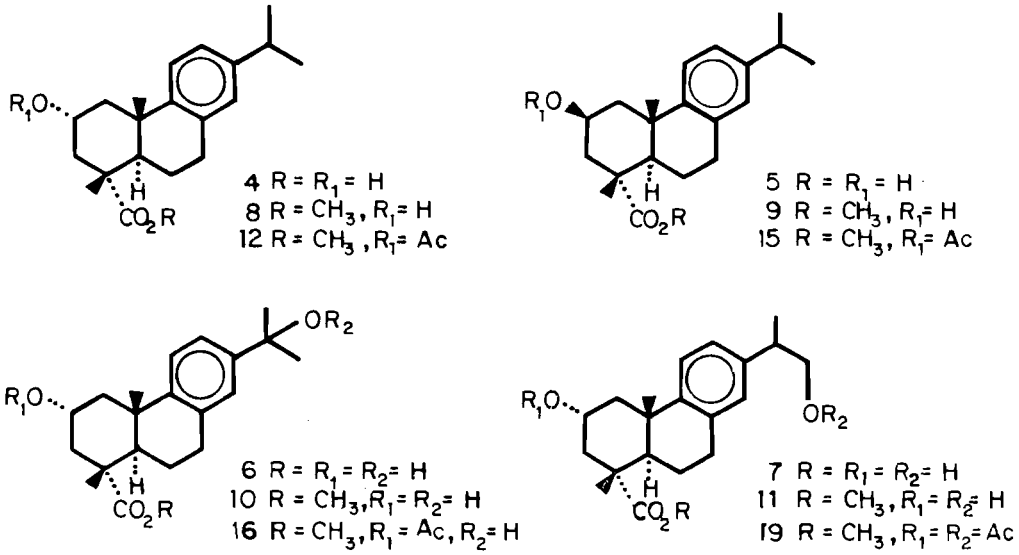

FIG. 3.

The methyl ester (**10**) of the second most predominant product (**6**) had molecular formula $C_{21}H_{30}O_4$. The ^1H nmr spectra of **10** and the corresponding acetate (**16**) showed the characteristic splitting pattern for H-2β as found in the 2α-oxygenated derivatives **8** and **12**. The six proton doublet for the isopropyl methyls of DHA was replaced by a six proton singlet at δ 1.56 suggesting a C_{15}-hydroxyl as shown. These assignments were confirmed by several chemical transformations (Fig. 5). Lactonization of **6** gave the olefin lactone **17** in 88% yield. The spectral data for this product were consistent with structure **17**: M^+ *m/e* 296; λ_{max} 248 (14000) nm, ν_{max} 1768 cm^{-1}; ^1H nmr signals at δ 5.0 and 5.28 (vinylic H) and δ 2.1 ppm (vinyl methyl). Similar treatment (PTS in C_6H_6) of the acetate **16** gave the isopropenyl derivative **18** which on hydrogenation over Adams catalyst gave **12**, identical with that obtained from the major biodegradation product (**4**).

The methyl ester (**11**) of the fourth product (**7**) of the biodegradation of DHA was also a dihydroxy

Can. J. Chem. Downloaded from www.nrcresearchpress.com by 210.87.254.105 on 09/06/12
For personal use only.

Can. J. Chem. Downloaded from www.nrcresearchpress.com by 210.87.254.105 on 09/06/12
For personal use only.

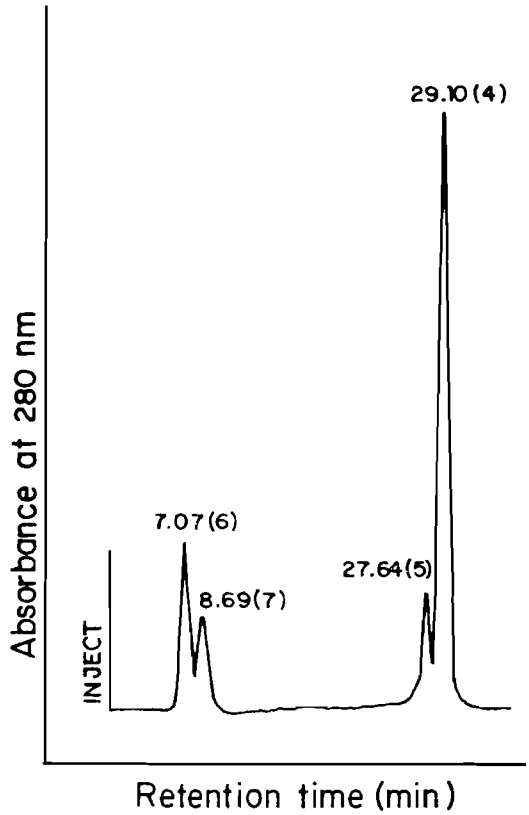

FIG. 4. Chromatogram. Column: reverse phase C_{18}; radial pak A. Solvent: 75% H_2O + 25% CH_3CN for 10 min followed by linear gradient to 55% H_2O + 45% CH_3CN over 20 min. Flow: 4 mL/min. Detector: Waters Associates Model 440 uv (at 280 nm).

compound; $C_{21}H_{30}O_4$. The ^1H nmr spectrum of **11** again indicated 2α-hydroxylation but also showed one of the isopropyl methyl groups to be missing, suggesting primary hydroxylation. This was supported by the appearance of a two proton doublet at δ 3.68 which suffered a 0.5 ppm downfield shift on formation of the diacetate (**19**). Once again, reaction of the hydroxy acid (**7**) with PTS in refluxing benzene gave the corresponding lactone (**20**) in high yield.

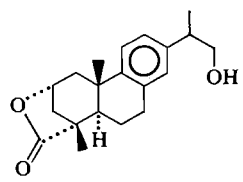

20

Discussion

The experiments outlined above clearly indicate the tendency for *M. isabellina* to oxygenate the DHA molecule at C_2 (α and β), C_{15}, and C_{16}. That C_2 oxygenation was the first step in the biodegradation was confirmed by separate degradation of the major catabolite (**4**) to give both **6** and **7**, identified as their corresponding methyl esters **10** and **11**. Thus the sequence of reactions may be described as:

$$\begin{array}{l} \mathbf{1} \rightarrow \mathbf{4} + \mathbf{5} \\ \quad\quad\downarrow \\ \quad\quad\mathbf{6} + \mathbf{7} \end{array}$$

Preliminary toxicity measurements on the crude degradation mixture and on the specific major products indicate very efficient detoxification of DHA by *M. isabellina*. Quantitative evaluation is presently underway.

Recent investigations by Biellmann *et al.* (7) revealed that DHA is attacked by two bacterial strains, *Flavobacterium resinovorum* and *Pseudomonas resinovorum*, to provide products oxygenated at positions 3, 7, 11, or 12, in some cases with concomitant decarboxylation. Similar results have been obtained by other workers (8, 9). *M. isabellina*, however, offers a uniquely different mode of microbial transformation, efficiently, to what appear to be nontoxic products. Investigations with other resin acids (e.g. **2** and **3**) are continuing.

Experimental

Ultraviolet spectra were recorded on a Cary 15 spectrophotometer. Low resolution mass spectra were recorded on either an Atlas CH-4B or an AEI MS-902 spectrometer. High resolution mass measurements were made on an AEI MS-50 spectrometer. The ^1H nmr spectra were recorded on Varian XL-100 and Nicolet Oxford H-270 instruments. Chemical shifts are reported as ppm from tetramethylsilane, used as internal standard. Microanalyses were carried out by Mr. P. Borda, Microanalytical Laboratory, University of British Columbia.

Screening of Microorganisms for the Ability to Degrade DHA

To media containing 40 mg/L of DHA were added either one mL of a cell suspension resulting from washing of a slant culture with some sterile water or a loopful of culture picked from a slant culture. Cultures were incubated at room temperature and 120 rpm on a rotary shaker until visual examination revealed good growth. Harvested cultures were tested for the presence of DHA using hplc. Bacterial slant cultures were prepared on nutrient agar (Difco) and tested against DHA in nutrient broth (Difco). Fungal slant cultures were prepared on potato–dextrose agar (PDA; Difco) and tested against DHA in dextrose–yeast extract broth (DYE) (5.0 g dextrose, 0.5 g yeast extract, 1.0 g KH_2PO_4, 1.0 g $(NH_4)_2HPO_4$, 1.0 g NaCl, and 0.5 g $MgSO_4 \cdot 7\ H_2O$, in a liter of distilled water).

Maintenance and Growth of Mortierella isabellina

M. isabellina stock culture (5) was maintained in PDA and grown in DYE. Cultures to be used as inocula were grown on 100 mL PDA in Roux bottles at room temperature. Inocula were prepared by washing the surface of a confluent mature culture with 50 mL of sterile distilled water or 50 mL of sterile detergent solution (450 μL Aerosol OT (Fisher Scientific) per liter distilled water). One mL of the spore suspension containing 4.4×10^5 to 3.7×10^7 spores per mL (as determined using a Howard mold counting chamber) was used to inoculate each 50 mL of liquid medium. Cultures of 50 or 100 mL were grown in 250 or 500 mL

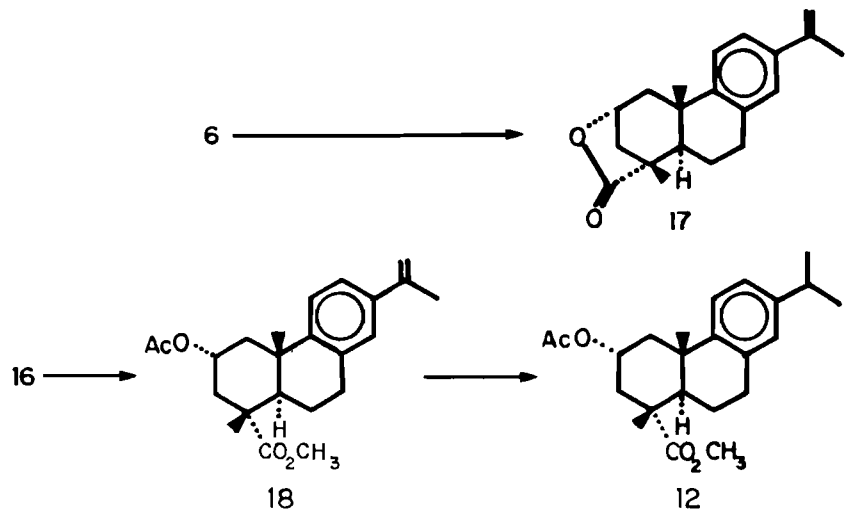

FIG. 5.

Erlenmeyer flasks, respectively. Cultures were incubated at room temperature (ca. 21 to 25°C) or at 27°C on a rotary shaker at 120 or 200 rpm.

Culture dry weight (mg/mL) was determined by suction filtering a whole culture through a cellulose acetate membrane filter (0.45 μm pores, Millipore Corporation), washing twice with about 10 mL distilled water, freezing the cell mat, and freeze drying to constant weight.

Biodegradation of DHA by M. isabellina

In a typical large-scale experiment designed to obtain large amounts of the degradation products, DYE broth was prepared at double concentration and dispensed at half the normal culture volume into a series of flasks. To each flask an equivalent volume of DHA solution (500 mg/L) was added. The DHA solution was prepared by dissolving 500 mg of DHA in a mixture of 1 *N* NaOH (2.20 mL) and EtOH (1.25 mL) and making up to volume with H_2O. The media was then autoclaved at 121°C for 15 min. In order to recover residual DHA and its breakdown products, harvested cultures were acidified (pH ca. 2) with 6 *N* HCl and extracted with EtOAc (3×). The extracts were washed with water (3×) and brine, dried (Na_2SO_4), and concentrated to give the crude metabolite mixture. The mixtures were chromatographed (on silica gel preparative plates using $CHCl_3$–MeOH (9:1) containing 0.5% HOAc) to give several products which were converted to their methyl esters by treatment with diazomethane.

Quantitative Analysis for DHA

DHA (56 mg) was dissolved in acetonitrile, and the solution made up to 50 mL. Aliquots of this solution were injected into an hplc instrument comprised of the following: Waters Associates U6K injection loop, M-6000A delivery systems, RCM module with C_{18}-radial pak-A column, Model 440 UV detector (280 nm at sensitivity 0.1). Electrical response was measured using a Shimadzu Chromatopak-E1A integrator. A solvent system of CH_3CN–H_2O (3:1), each containing 0.5% HOAc, was used at a flow rate of 4 mL/min. The standard curve generated is shown in Fig. 2, and was used for the determination of DHA in culture extracts.

Ar-[^{3}H]-DHA

Trifluoroacetic anhydride (3.2 mL) was distilled (bulb to bulb under high vacuum) into T_2O (0.4 mL, 400 mCi) maintained at −78°C. The system was allowed to attain atmospheric pressure with N_2 and brought to ambient temperature. The CF_3COOT thus formed was then distilled (bulb to bulb under high vacuum) into a mixture of DHA (90 mg), CCl_4 (5 mL), and Pt/C/CCl_4 suspension (0.4 mL) maintained at −78°C. The system was filled with N_2 and the mixture stirred at ambient temperature for 40 h. The mixture was filtered, the residue washed (2 × 5 mL) with CH_2Cl_2 and the combined organics extracted with H_2O (6 × 10 mL), dried (Na_2SO_4), and concentrated *in vacuo*. Five recrystallizations from EtOH–H_2O gave labelled DHA (30 mg) with constant activity of 1.047×10^9 dpm/mmol.

Methyl-2α-hydroxyabieta-8,11,13-trien-18-oate (8)

This compound was obtained as a white solid (335 mg, 57%), mp 155–157°C (ether – petroleum ether 30–60°C); uv (EtOH) λ_{max}: 272 (690), 265 (632) nm; ir ($CHCl_3$) ν_{max}: 3700–3400, 1720 cm^{-1}; ^{1}H nmr ($CDCl_3$) δ: 1.22 (6H, d, *J* = 7 Hz, C16 and C17-methyls), 1.30 (3H, s, C20-methyl), 1.35 (3H, s, C19-methyl), 3.70 (3H, s, $-CO_2CH_3$), 4.1 (1H, tt, *J* = 12, 4 Hz, C2β-*H*), 6.87 (1H, brs, C14-*H*), 7.07 (1H, brd, *J* = 8 Hz, C12-*H*), 7.17 (1H, d, *J* = 8 Hz, C11-*H*); ms *m/e*: 330 (M^+), 315, 312, 297, 283, 255, 253, 237, 195. *Anal.* calcd. for $C_{21}H_{30}O_3$: C 76.36, H 9.09; found: C 76.13, H 9.34. High resolution molecular weight determination, calcd. 330.2195; found 330.2185.

Methyl 2α-Acetoxyabieta-8,11,13-trien-18-oate (12)

A mixture of the hydroxy ester **8** (33 mg), pyridine (2 mL), and acetic anhydride (1.0 mL) was stirred overnight at ambient temperature, diluted with anhydrous toluene (10 mL), and concentrated under reduced pressure to give the acetate **12** (100%) as a thick liquid which solidified after standing; mp 74–75°C (petroleum ether 30–60°C): uv (EtOH) λ_{max}: 273 (685), 265 (631) nm; ir ($CHCl_3$) ν_{max}: 1720 cm^{-1}; ^{1}H nmr ($CDCl_3$) δ: 1.22 (6H, d, *J* = 7 Hz, C16- and C17-methyls), 1.3 (3H, s, C20-methyl), 1.35 (3H, s, C19-methyl), 2.07 (3H, s, $-OCOCH_3$), 2.23 (1H, dd, *J* = 8 Hz and 3 Hz, C5α-*H*), 2.81 (1H, septet, *J* = 6 Hz, C15-*H*), 2.88 (2H, dd, *J* = 8, 4 Hz, C7-*H*), 3.68 (3H, s, CO_2CH_3), 5.22 (1H, tt, *J* = 12, 4 Hz, C2β-*H*), 6.87 (1H, bs, C14-*H*), 7.07 (1H, bd, *J* = 8 Hz, C11-H); ms *m/e*: 372 (M^+), 253, 237, 195. *Anal.* calcd. for $C_{23}H_{32}O_4$: C 74.19, H 8.60; found: C 73.51 H 9.08. High resolution molecular weight determination, calcd. 372.2301; found 372.2312.

Methyl 2β-Hydroxyabieta-8,11,13-trien-18-oate (9)

This compound was obtained as a white solid (15 mg, 2.5%), mp 126–129°C (ether – petroleum ether 30–60°C); uv (EtOH) λ_{max}: 272 (688), 265 (632) nm; ir ($CHCl_3$): ν_{max}: 3700–3400, 1720 cm^{-1}; ^{1}H nmr ($CDCl_3$) δ: 1.23 (6H, d, *J* = 7 Hz, C16- and

Can. J. Chem. Downloaded from www.nrcresearchpress.com by 210.87.254.105 on 09/06/12
For personal use only.

Can. J. Chem. Downloaded from www.nrcresearchpress.com by 210.87.254.105 on 09/06/12
For personal use only.

C17-methyls), 1.25 (3H, s, C20-methyl), 1.32 (3H, s, C19-methyl), 3.7 (3H, s, CO_2CH_3), 4.1 (1H, m, C2α-*H*), 6.87 (1H, bs, C14-*H*), 7.07 (1H, bd, J = 8 Hz, C12-*H*), 7.17 (1H, d, J = 8 Hz, C11-*H*); ms *m/e*: 330 (M^+), 315, 297, 253, 237, 195. *Anal.* calcd. for $C_{21}H_{30}O_3$: C 76.36, H 9.09; found: C 75.82 H 9.62. High resolution molecular weight determination, calcd. 330.2195; found 330.2195.

Methyl 2β-Acetoxyabieta-8,11,13-trien-18-oate (15)

The acetate derivative was obtained in 95% yield from **9** by the procedure described earlier; uv (EtOH) λ_{max}: 272 (683), 265 (632) nm; ir ($CHCl_3$) ν_{max}: 1720 cm^{-1}; ^1H nmr ($CDCl_3$) δ: 1.22 (6H, d, J = 7 Hz, C16- and C17-methyls), 1.3 (3H, C20-methyl), 1.35 (3H, s, C19-methyl), 2.07 (3H, s, C2β-OCOC*H*$_3$), 2.23 (1H, dd, J = 8, 3 Hz, C5α-*H*), 2.81 (1H, septet, J = 6 Hz, C15-*H*), 2.88 (2H, dd, J = 8, 4 Hz, C7-*H*), 3.68 (3H, s, CO_2CH_3), 5.22 (1H, m, C2d-*H*), 6.87 (1H, bs, C14-*H*), 7.07 (1H, bd, J = 8 Hz, C12-*H*), 7.17 (1H, d, J = 8 Hz, C11-*H*); ms *m/e*: 372 (M^+), 253, 237. *Anal.* calcd. for $C_{23}H_{32}O_4$: C 74.19, H 8.60; found: C 73.63 H 8.23. High resolution molecular weight determination, calcd. 372.2300; found 372.2309.

Methyl 2α,15-Dihydroxyabieta-8,11,13-trien-18-oate (10)

This compound was obtained as a white solid (60 mg, 10%), mp 128–130°C (ether – petroleum ether 30–60°C); uv (EtOH) λ_{max}: 273 (685), 265 (630) nm; ir ($CHCl_3$) ν_{max}: 3700–3400, 1725 cm^{-1}; ^1H nmr ($CDCl_3$) δ: 1.26 (3H, s, C20-methyl), 1.32 (3H, s, C19-methyl), 1.56 (6H, s, C16- and C17-methyls), 2.26 (1H, dd, J = 9, 4 Hz, C5-H), 3.7 (3H, s, CO_2CH_3), 4.14 (1H, tt, J = 12, 4 Hz, C2β-H), 7.25 (3H, m, aromatic); ms *m/e*: 346 (M^+), 331, 328, 253, 236, 235, 195. *Anal.* calcd. for $C_{21}H_{30}O_4$: C 72.83, H 8.67; found: C 72.51, H 8.26. High resolution molecular weight determination, calcd. 346.2143; found 346.2143.

Methyl 2α-Acetoxy-15-hydroxyabieta-8,11,13-trien-18-oate (16)

Compound **10** was acetylated in the manner described previously to furnish a solid (93%), which after crystallization from petroleum ether (30–60°C) containing traces of ether had mp 137–139°C; uv (EtOH) λ_{max}: 273 (690), 265 (623) nm; ir ($CHCl_3$) ν_{max}: 3700–3400, 1725 cm^{-1}; ^1H nmr ($CDCl_3$) δ: 1.3 (3H, s, C20-methyl), 1.35 (3H, s, C19-methyl), 1.56 (6H, s, C16- and C17-methyls), 2.07 (3H, s, OCOC*H*$_3$), 2.27 (1H, dd, J = 8 and 3 Hz, C5-*H*), 2.93 (2H, dd, J = 8 and 4 Hz, C7-*H*), 3.68 (3H, s, $-CO_2CH_3$), 5.22 (1H, tt, J = 12 and 4 Hz, C2-H), 7.2 (3H, m, aromatic): ms *m/e*: 388 (M^+), 370, 313, 253, 235, 195. *Anal.* calcd. for $C_{23}H_{32}O_5$: C 71.13, H 8.24; found: C 70.86, H 8.45. High resolution molecular weight determination, calcd. 388.2249; found 388.2248.

Methyl 2α,16-Dihydroxyabieta-8,11,13-trien-18-oate (11)

This compound was obtained as a white solid (25 mg, 4%); crystals from ether – petroleum ether (30–60°C), mp 140–143°C; uv (EtOH) λ_{max}: 273 (682), 266 (638) nm; ir ($CHCl_3$) ν_{max}: 3700–3400, 1725 cm^{-1}; ^1H nmr ($CDCl_3$) δ: 1.25 (3H, d, J = 7 Hz, C17-methyl), 1.24 (3H, s, C20-methyl), 1.32 (3H, s, C19-methyl), 3.68 (2H, d, J = 7 Hz, C16-methylene), 3.7 (3H, s, CO_2CH_3), 4.12 (1H, tt, J = 12, 4 Hz, C2β-H), 6.9–7.26 (3H, m, aromatic); ms *m/e*: 346 (M^+) 331, 315, 253, 235, 131. *Anal.* calcd. for $C_{21}H_{30}O_4$: C 72.83, H 8.67; found: C 72.43, H 8.49. High resolution molecular weight determination, calcd. 346.2143; found 346.2139.

Methyl 2α,16-Diacetoxyabieta-8,11,13-trien-18-oate (19)

The diacetyl derivative **19** was prepared in 90% yield from the dihydroxy compound **11** by following the procedure described above; uv (EtOH) λ_{max}: 274 (692), 266 (628) nm; ir ($CHCl_3$) ν_{max}: 1720 cm^{-1}; ^1H nmr ($CDCl_3$) δ: 1.24 (3H, d, J = 7 Hz, C17-methyl), 1.25 (3H, s, C20-methyl), 1.32 (3H, s, C19-methyl), 2.04 (3H, s, C16-OCOC*H*$_3$), 2.07 (3H, s, C2α-OCOC*H*$_3$), 2.25 (1H, dd, J = 8, 3 Hz, C5α-*H*), 2.92 (2H, dd, J = 8, 4 Hz, C7-*H*), 3.03 (1H, sextet, J = 6 Hz, C15-*H*), 3.7 (3H, s, CO_2CH_3), 4.15 (1H, d, J = 7 Hz, C16-methylene), 4.16 (1H, d, J = 7 Hz, C16-methylene), 5.24 (1H, tt, J = 12, 4 Hz, C2β-*H*), 6.94 (1H, bs, C14-*H*), 7.1 (1H, bd, J = 8 Hz, C12-*H*), 7.20 (1H, d, J = 8 Hz, C11-*H*); ms *m/e*: 430 (M^+), 388, 370, 357, 295, 269. *Anal.* calcd. for $C_{25}H_{34}O_6$: C 67.76, H 7.90; found: C 69.50, H 8.12. High resolution molecular weight determination, calcd. 430.2355; found 430.2354.

Methyl 2-Oxoabieta-8,11,13-trien-18-oate (14)

Pyridinium chlorochromate (20 mg, 0.09 mmol) was suspended in methylene chloride (1.5 mL), and the alcohol **8** (13 mg, 0.039 mmol) in 1.0 mL of CH_2Cl_2 was rapidly added at room temperature. The solution became briefly homogeneous before depositing the black insoluble reduced agent. After stirring the reaction mixture for 1.5 h it was diluted with 20 mL of anhydrous ether, the solvent was decanted, and the black solid was washed twice with ether. The combined extract was dried ($MgSO_4$) and the solvent removed *in vacuo*. Chromatography on silica gel furnished the ketone (**14**) (11.5 mg, 89%); uv (EtOH) λ_{max}: 298 (60), 273 (688), 264 (634), 258 (464) nm; cd (molecular ellipticity σ): −3734.41; ir ($CHCl_3$) ν_{max}: 1710, 1725 cm^{-1}; ^1H nmr ($CDCl_3$) δ: 1.25 (6H, d, J = 7 Hz, C16- and C17-methyls), 1.28 (3H, s, C20-methyl), 1.31 (3H, s, C19-methyl), 3.75 (3H, s, CO_2CH_3), 7.0 (2H, bd, J = 8 Hz, C11-*H* and C12-*H*), 7.07 (1H, bs, C14-H); ms *m/e*: 328 (M^+), 313, 269, 253, 204. *Anal.* calcd. for $C_{21}H_{28}O_3$: C 76.82, H 8.53; found: C 76.53, H 8.72. High resolution molecular weight determination, calcd. 328.2038; found 328.2038.

The Lactone 13

To hydroxy acid **4** (22.12 mg, 0.07 mmol), taken up in 20 mL of benzene, was added 15 mg of *p*-toluenesulphonic acid and the reaction mixture was refluxed for 20 min, cooled, washed with water, and dried ($MgSO_4$). Solvent removal followed by chromatography on silica gel afforded the lactone **13** (17.73 mg, 85%); uv (EtOH) λ_{max}: 272 (694), 266 (624) nm; ir ($CHCl_3$) ν_{max}: 1768 cm^{-1}; ^1H nmr ($CDCl_3$) δ: 1.22 (6H, d, J = 7 Hz, C16- and C17-methyls), 1.28 (3H, s, C20-methyl), 1.38 (3H, s, C19-methyl), 4.8–5.0 (1H, m, $W/2$ = 12 Hz, C2β-*H*), 6.85–7.1 (3H, m, aromatic); ms *m/e*: 298 (M^+), 283, 239, 197, 159. *Anal.* calcd. for $C_{20}H_{26}O_2$: C 80.53, H 8.72; found: C 80.16, H 8.91. High resolution molecular weight determination, calcd. 298.1932; found 298.1936.

The Lactone 20

The dihydroxy acid **7** (20.12 mg, 0.06 mmol) was lactonized to the compound **20** in 80% yield by the procedure described above; uv (EtOH) λ_{max}: 274 (696), 265 (631) nm; ir ($CHCl_3$) ν_{max}: 3700–3550, 1768 cm^{-1}; ^1H nmr ($CDCl_3$) δ: 1.23 (3H, d, J = 7 Hz, C17-methyl), 1.28 (3H, s, C20-methyl), 1.37 (3H, s, C19-methyl), 3.69 (2H, d, J = 7 Hz, C16-OC*H*$_2$), 4.8–5.0 (1H, m, $W/2$ = 12 Hz, C2β-H), 6.85–7.1 (3H, m, aromatic); ms *m/e*: 314 (M^+), 296, 283, 253, 235. *Anal.* calcd. for $C_{20}H_{26}O_3$: C 76.43, H 8.28; found: C 76.01, H 8.37. High resolution molecular weight determination, calcd. 314.1881; found 314.1882.

The Lactone 17

The dihydroxy carboxylic acid **6** (20.12 mg, 0.06 mmol) was refluxed in benzene containing a catalytic amount of *p*-toluenesulphonic acid and worked up in the manner mentioned earlier to give **17** (15.7 mg, 88%); uv(EtOH) λ_{max}: 248 (14 000) nm; ir ($CHCl_3$) ν_{max}: 1768 cm^{-1}; ^1H nmr ($CDCl_3$) δ: 1.27 (3H, s, C20-methyl), 1.35 (3H, s, C19-methyl), 2.1 (3H, bs, vinyl methyl at C15), 4.75–4.95 (1H, m, $W/2$ = 12 Hz, C2β-*H*), 5.0 (1H, m, C16-*H*), 5.28 (1H, m, C16-*H*), 6.82–7.22 (3H, m, aromatic); ms *m/e*: 296 (M^+). *Anal.* calcd. for $C_{20}H_{24}O_2$: C 81.08, H 8.10;

found: C 80.73, H 8.67. High resolution molecular weight determination, calcd. 296.1776; found 296.1781.

Methyl 2α-Acetoxyabieta-8,11,13,15-tetraen-18-oate **18**

To a suspension of calcium chloride (20 mg) in benzene (20 mL) was added the hydroxy acetate **16** (19.4 mg, 0.05 mmol) and *p*-toluenesulphonic acid (5 mg) and the mixture was refluxed for 20 min. The cooled mixture was filtered, washed with water, and dried ($MgSO_4$). Concentration under vacuum furnished the product **18** (17.52 mg, 94%) as a thick oil, sufficiently pure for spectral purposes; uv (EtOH) λ_{max}: 248 (14 200) nm; ir ($CHCl_3$) ν_{max}: 1720 cm^{-1}; ^1H nmr δ: 1.3 (3H, s, C20-methyl), 1.36 (3H, s, C19-methyl), 2.07 (3H, s, C2α-OCOCH_3), 2.14 (3H, bs, vinyl methyl at C15), 3.7 (3H, s, CO_2CH_3), 5.06 (1H, m, C16-*H*), 5.24 (1H, m, C2β-H), 5.34 (1H, bs, C16-*H*), 7.1–7.28 (3H, m, aromatic); ms *m/e*: 370 (M^+). High resolution molecular weight determination, calcd. for $C_{23}H_{30}O_4$: 370.2143; found: 370.2140.

Catalytic Reduction of Methyl 2α-Acetoxyabieta-8,11,13,15-tetraen-18-oate

The acetate **18** (8 mg, 0.021 mmol) in anhydrous methanol (5 mL) was hydrogenated over platinum–charcoal (10 mg, 10%) at room temperature and atmospheric pressure. After the reaction was complete, as monitored by tlc, the mixture was filtered through Celite, the Celite cake washed with anhydrous methanol (3 × 5 mL), and the combined extracts evaporated under reduced pressure. The residue (8 mg), after purification over silica gel, was identical with a sample of **12** obtained earlier.

Acknowledgements

Financial aid from the Natural Sciences and Engineering Research Council of Canada is gratefully acknowledged. We also wish to thank Drs. J. W. Rowe and D. F. Zinkel, U.S. Department of Agriculture, Forest Products Laboratory, Madison, WI, and Dr. I. H. Rogers, Pacific Environment Institute, West Vancouver, B.C., for generous gifts of dehydroabietic acid.

1. J. M. Leach, J. C. Mueller, and C. C. Walden. Canadian Pulp and Paper Association, Technical Section Transactions, **3**, 126 (1977), and references therein.
2. G. M. Kruzynski. Ph.D. Thesis, University of British Columbia, Vancouver, B.C. 1979.
3. J. A. Servizi and R. W. Gordon. Pulp Pap. Mag. Can. **74**, T295, (1973).
4. J. P. Kutney, W. H. Baarschers, O. Chin, Y. Ebizuka, L. Harley, J. D. Lehman, P. J. Salisbury, I. H. Sanchez, and T. Yee. Can. J. Chem. **55**, 2930 (1977).
5. R. J. Bandoni and G. H. N. Towers. Can. J. Biochem. **45**, 1197 (1967).
6. R. C. Cambie and R. A. Franich. Aust. J. Chem. **24**, 571 (1971).
7. J. F. Biellmann, G. Branlant, M. Gero-Robert, and M. Poiret. Tetrahedron, **29**, 1227 (1973).
8. R. Ekman and R. Sjoholm. Acta Chem. Scand. Ser. B, **33**, 76 (1979).
9. I. H. Rogers and H. W. Mahood. Abstracts of papers presented in Environmental Chemistry Division, Second Chemical Congress of the North American Continent, Las Vegas, NV. August 25–29, 1980.

Can. J. Chem. Downloaded from www.nrcresearchpress.com by 210.87.254.105 on 09/06/12
For personal use only.

Rearrangement studies with ^{14}C. XLVI. Isotopic scrambling studies on the acetolysis of trianisylvinyl bromide labeled with ^{13}C and with ^{14}C[1]

CHOI CHUCK LEE, CRAIG A. OBAFEMI, AND J. WILSON QUAIL
Department of Chemistry and Chemical Engineering, University of Saskatchewan, Saskatoon, Sask., Canada S7N 0W0
AND
ZVI RAPPOPORT
Department of Organic Chemistry, The Hebrew University of Jerusalem, Jerusalem, Israel
Received January 29, 1981

CHOI CHUCK LEE, CRAIG A. OBAFEMI, J. WILSON QUAIL, and ZVI RAPPOPORT. Can. J. Chem. **59**, 2342 (1981).

Acetolyses of a 15 m*M* solution of a doubly labeled trianisylvinyl substrate, 1,2-dianisyl-2-*p*-[^{14}C]methoxyphenyl[2-^{13}C]vinyl bromide (1-Br-2-^{13}C-2-methoxy-^{14}C), were carried out in the presence of different amounts of added NaOAc (30–450 m*M*) or NaOAc (30 or 300 m*M*) and Et_4NBr (75–1000 m*M*). Isotopic scramblings of the ^{13}C or ^{14}C label from C-2 to C-1 were observed in both the reaction product and the recovered unconsumed reactant, indicating the occurrence of cycles of ionization, 1,2-anisyl shift, and return. The extent of scrambling was found to decrease with increasing concentrations of NaOAc, and a further decrease in scrambling was noted with the additional presence of Et_4NBr. These findings are attributable to a competition between the 1,2-shift process and capture of the cation by the added nucleophiles. Analysis of the experimental data suggests that the nucleophilic species chiefly involved in the product-forming capture reaction is the acetate ion rather than HOAc or the Na^+OAc^- ion-pair. Comparisons of the scrambling data, expressed as "% rearrangement", with the assumption that 100% rearrangement corresponds to 33.3% and 50.0% scramblings of the ^{14}C ring label and the ^{13}C chain label, respectively, led to the conclusion that complete equilibration of the labels is achieved in that portion of the molecules that have undergone rearrangement only when the acetolyses are carried out in the presence of high concentrations of added salts. Mechanistic implications of these observations are discussed.

CHOI CHUCK LEE, CRAIG A. OBAFEMI, J. WILSON QUAIL et ZVI RAPPOPORT. Can. J. Chem. **59**, 2342 (1981).

On a réalisé l'acétolyse d'une solution 15 m*M* du substrat trianisylvinyle doublement marqué, le bromure de dianisyl-1,2-*p*-[^{14}C] méthoxy-2 phényle[^{13}C-2] vinyle (Br-1-^{13}C-2 méthoxy-2 ^{14}C) en présence de différentes quantités de AcONa (30–450 m*M*) ou de AcONa (30 ou 300 m*M*) et de Et_4NBr (75–450 m*M*). On a observé des mélanges isotopiques des marqueurs ^{13}C ou ^{14}C de C-2 à C-1 dans les deux produits de réaction et dans le réactif résiduel indiquant ainsi l'existence de cycles d'ionisation, glissement anisyle-1,2 puis retour à l'état initial. On a trouvé que le taux de mélange diminue quand les concentrations en AcONa augmentent et on a noté que le mélange diminue encore d'avantage lorsque Et_4NBr est également présent. Ces observations sont attribuables à une compétition entre le glissement-1,2 et la capture d'un cation par les nucléophiles ajoutés. L'analyse des données expérimentales suggère que l'ion acétate plutôt que AcOH ou la paire d'ions Na^+AcO^- est le nucléophile impliqué principalement dans le composé provenant de la réaction de capture. En comparant les données de mélange exprimés en "% de transposition" en partant du fait qu'une transposition à 100% correspond à des mélanges respectifs de 33,3% et de 50,0% du ^{14}C du cycle et du ^{13}C de la chaîne conduit à conclure qu'il s'établit un équilibre complet entre les marqueurs dans cette position des molécules qui se transposent uniquement lors de l'acétolyse en présence de fortes concentrations de sels. On discute également des implications mécanistiques de ces observations.

[Traduit par le journal]

The first kinetic study on the solvolysis of trianisylvinyl substrates was reported in 1969 by Rappoport and Gal (1). The data led to the conclusion that the reaction proceeded via the trianisylvinyl cation without anchimeric assistance by β-anisyl participation. Additional studies on the trianisylvinyl and related systems by Rappoport and co-workers (2–4) all provided further kinetic evidence in support of the dissociated trianisylvinyl cation as reaction intermediate. The first degenerate rearrangement arising from 1,2-anisyl shifts in the trianisylvinyl cation to give scrambling of the isotopic label was observed in 1975 by Oka and Lee (5) in the reaction of trianisyl[2-^{13}C]vinyl bromide (1-Br-2-^{13}C) with HOAc–AgOAc or with CF_3COOH–CF_3COOAg. Subsequently, similar degenerate rearrangements from 1,2-shifts were reported for the solvolyses of 1,2-dianisyl-2-*p*-[$^2H_3$]methoxyphenylvinyl bromide (1-Br-2-methoxy-d_3) (6) and for the decomposition of trianisyl[2-^{14}C]vinylphenyltriazene (1-NNNHPh-2-^{14}C) (7). Recently, Lee *et al.* (8) studied the acetolysis (9:1 HOAc–Ac_2O) of trianisyl[2-^{14}C]vinyl bromide (1-Br-2-^{14}C) in the presence of various amounts of added NaOAc or NaOAc and LiBr. The results were interpreted by a mechanism involving formation of the dissociated trianisylvinyl cation which could competitively undergo 1,2-anisyl shifts to give scrambling, be captured by Br^- ion to return to scrambled reactant, and be captured by solvent or by OAc^- ion to give

[1]Vinylic cations from solvolysis, part 34, from the Hebrew University of Jerusalem.

0008-4042/81/152342-08$01.00/0
©1981 National Research Council of Canada/Conseil national de recherches du Canada

Can. J. Chem. Downloaded from www.nrcresearchpress.com by 210.87.254.105 on 09/06/12
For personal use only.

Can. J. Chem. Downloaded from www.nrcresearchpress.com by 210.87.254.105 on 09/06/12
For personal use only.

scrambled product. Since many cycles of ionization, return, and 1,2-shift could influence the overall extent of scrambling in the product and in the unconsumed reactant, the use of double labeling may be capable of providing information on such repeated cycles of processes. The present paper reports on the results from a study using both ^{14}C and ^{13}C as labels in the acetolysis of trianisylvinyl bromide.

Results and Discussions

The preparation of the labeled substrate was carried out using procedures similar to those employed in the synthesis of *cis*- and *trans*-1,2-dianisyl-2-phenyl[2-^{13}C]vinyl bromides (9). 1,2-Dianisyl[1-^{13}C]ethanone was prepared as described previously (9). Instead of reaction with C_6H_5MgBr (9), this ^{13}C-labeled ketone was treated with *p*-[^{14}C]methoxyphenylmagnesium bromide to give the tertiary alcohol, 1,1,2-trianisylethanol, with the ^{13}C-label at C-1 and with the *p*-CH_3O group of one of the C-1 anisyl groups labeled with ^{14}C. Treatment of this tertiary alcohol with Br_2 in HOAc (5, 9) gave the desired trianisylvinyl bromide with the ^{13}C label at C-2 and with the *p*-CH_3O group of one of the C-2 anisyl groups labeled with ^{14}C, namely, 1,2-dianisyl-2-*p*-[^{14}C]methoxyphenyl[2-^{13}C]vinyl bromide (**1**-Br-2-^{13}C-2-methoxy-^{14}C).

The solvolytic experiments with **1**-Br-2-^{13}C-2-methoxy-^{14}C were carried out in glacial acetic acid containing different amounts of NaOAc or NaOAc and Et_4NBr. These conditions differed slightly from those used in the earlier study with **1**-Br-2-^{14}C (8) since no acetic anhydride was added to the reaction medium and Et_4NBr was employed instead of LiBr. Besides the experiments with the doubly labeled **1**-Br-2-^{13}C-2-methoxy-^{14}C, control experiments were also carried out using singly labeled **1**-Br-2-^{13}C or **1**-Br-2-methoxy-^{14}C as well as an intermolecular mixture of these two singly labeled substrates.

Scramblings of both the ^{13}C and ^{14}C labels from C-2 to C-1 were determined in the reaction product, and in the unconsumed reactant when the reaction was not carried to completion and a recoverable amount of reactant was obtained. The degradation procedures were the same as those used in the earlier study with **1**-Br-2-^{14}C (8). Upon two successive treatments with $LiAlH_4$ (5, 8), the reaction product, trianisylvinyl acetate, with the ^{13}C and ^{14}C labels scrambled (**1**-OAc-1,2-^{13}C-1,2-methoxy-^{14}C), was converted to the scrambled 1,2,2-trianisylethanol (**2**-1,2-^{13}C-1,2-methoxy-^{14}C) and, at the same time, any unconsumed reactant, **1**-Br-1,2-^{13}C-1,2-methoxy-^{14}C, would be converted to the scrambled trianisylethene (**3**-1,2-^{13}C-1,2-methoxy-^{14}C) (10). The alcohol, **2**-1,2-^{13}C-1,2-methoxy-^{14}C, and the olefin, **3**-1,2-^{13}C-1,2-methoxy-^{14}C, were then separated by passage through an alumina column (8). To determine the scrambling of the ^{14}C label, after the addition of an appropriate amount of inactive carrier, $KMnO_4$ oxidation of the alcohol **2** and ozonolysis of the olefin **3** both gave dianisyl [^{14}C]ketone and the scrambling of the [^{14}C]-methoxy-labeled anisyl group from C-2 to C-1 in the reaction product and in the unconsumed reactant, respectively (8).

To determine the scrambling of the ^{13}C-label in the reaction product, the alcohol **2**-1,2-^{13}C-1,2-methoxy-^{14}C, derived from the product, was analyzed by ^{13}C nmr as described by Oka and Lee (5). The ^{13}C contents at C-1 and C-2, and hence the scramblings from C-2 and C-1, were measured quantitatively using the relative intensities of the C-1 and C-2 absorptions with the CH_3O absorption containing ^{13}C in its natural abundance as an internal standard (5). To determine the scrambling of the ^{13}C label in the unconsumed reactant, the olefin **3**-1,2-^{13}C-1,2-methoxy-^{14}C, derived from the unconsumed reactant, was hydrogenated to give the corresponding 1,1,2-trianisylethane (**4**-1,2-^{13}C-1,2-methoxy-^{14}C). It is to be noted that C-1 and C-2 of hydrocarbon **4** would correspond to C-2 and C-1, respectively, of the reactant **1**-Br. Again by means of the relative intensity method (5), and using the ^{13}C absorptions of CH_3O, C-1, and C-2 of **4**-1,2-^{13}C-1,2-methoxy-^{14}C at 53.6, 50.6, and 40.3 ppm, respectively, the ^{13}C contents at C-1 and C-2, and hence the scrambling of the ^{13}C label from C-2 to C-1 in the unconsumed reactant, were measured.

Table 1 shows the isotopic scrambling data from the acetolyses of various singly or doubly labeled trianisylvinyl bromides under comparable experimental conditions. Comparisons of the extents of scrambling, both in the reaction product and in the recovered reactant, from the sets of experiments A, B, C, and D indicate that the doubly labeled substrate, **1**-Br-2-^{13}C-2-methoxy-^{14}C, gave the same scrambling results, within the usually observed precision of about $\pm 1\%$ scrambling, as the 1:1 intermolecular mixture of the singly labeled **1**-Br-2-^{13}C and **1**-Br-2-methoxy-^{14}C. These findings are not unreasonable since the scrambling of the ^{14}C label was measured by its radioactivity while the ^{13}C scrambling was determined by ^{13}C nmr, the two methods being independent of and not affecting each other. Thus with the presently employed doubly labeled **1**-Br-2-^{13}C-2-methoxy-^{14}C as sub-

TABLE 1. Data from duplicate solvolyses of 15 m*M* labeled trianisylvinyl bromide (**1**-Br) in glacial acetic acid containing 30 m*M* NaOAc at 120 ± 2°C

Expt.	Substrate	Reaction time (h)	% Reaction[c]	Scrambling of [^{14}C]CH_3O-labeled anisyl from C-2 to C-1 (%)		Scrambling of ^{13}C- or ^{14}C-labeled carbon from C-2 to C-1 (%)	
				Product	Recovered reactant	Product	Recovered reactant
A-1	**1**-Br-2-^{13}C-2-methoxy-^{14}C[a]	5	21 —	9.3; —	1.1; —	10.1 —	1.7 —
A-2		9.5	36; 36	10.0; 10.1	3.1 —	10.9; 10.9	4.2 —
A-3		70	84; 84	22.0; 20.1	22.7; 21.6	22.1; 23.2	27.8; 27.8
A-4		102	91; 91	23.3; 22.5	25.6; 24.8	25.3; 25.3	— —
A-5		336	97; 97	26.7; 27.1	33.6; 33.4	29.6 —	— —
B-1	**1**-Br-2-^{13}C +	5	24; 23	8.1; 8.3	1.0 —	10.1; 10.0	1.3 —
B-2	**1**-Br-2-methoxy-^{14}C[b]	10	46; 46	9.6; 9.8	3.9; 3.9	12.3; 12.6	5.1 —
B-3		70	83; 84	20.1; 20.1	21.1; 22.3	21.7; 22.0	27.2; 27.2
B-4		336	96; 96	25.5; 26.0	32.7; 32.8	28.9; 29.1	— —
C-1	**1**-Br-2-methoxy-^{14}C	5	24; 24	8.0; 8.1	0.8; 0.8		
C-2		10	45; 46	9.3; 9.4	3.8; 3.8		
C-3		70	84; 85	19.2; 20.0	22.3; 21.0		
C-4		336	96; 97	25.4; 26.1	32.6; 32.4		
D-1	**1**-Br-2-^{13}C	5	23; 23			10.1; 10.1	1.2; 1.2
D-2		10	46; 45			11.9; 11.9	4.7; 5.3
D-3		70	85; 84			22.1; 22.1	27.2; 27.2
D-4		336	97; 97			27.5; 29.1	— —
E-1	**1**-Br-2-^{14}C	5	23; 24			9.2; 9.2	1.2; 1.1
E-2		10	48; 46			10.3; 10.5	5.1; 5.2
E-3		70	84; 84			21.1; 21.2	26.1; 26.3
E-4		336	97; 97			28.6; 28.0	48.2; 48.0

[a]Doubly labeled substrate.
[b]Mixture (1:1) of singly labeled substrates.
[c]From titration of the liberated Br^- ion.

strate, any scrambling results may be treated as if they were obtained from simultaneous experiments with two singly labeled substrates.

Previously, we have reported that the use of ^{13}C as label coupled with analysis by ^{13}C nmr and the use of the ^{14}C tracer technique gave essentially the same extent of scrambling in the reaction of triphenyl[2-^{13}C]vinyl or triphenyl[2-^{14}C]vinyl bromide with HOAc–AgOAc (11). A comparison of the data from the sets of experiments D and E in Table 1, with **1**-Br-2-^{13}C or **1**-Br-2-^{14}C as substrate, again showed that the two methods of determining scrambling gave results that were within the expected precision of ±1% scrambling. It may also be of interest to note that recently Oka and co-workers (12, 13) have reported on the use of the ^{13}C nmr technique in their studies of acid catalyzed rearrangements in a number of aliphatic ketones.

Given in Tables 2 and 3 are the scrambling data from the acetolyses of **1**-Br-2-^{13}C-2-methoxy-^{14}C carried out in the presence of different amounts of NaOAc or NaOAc and Et_4NBr, the results from Expt. A-1 to A-5 in Table 1 being included in Table 2 for completeness. It can be seen from Tables 2 and 3 that in all cases, the % scrambling of the chain labeled C-2 is greater than that of the corresponding ring labeled anisyl group. This finding is not unreasonable since the maximum extents of scrambling for the chain and ring labels are 50.0% and 33.3%, respectively. The observed extents of scrambling of both the chain and ring labels also confirm our previous finding from the acetolysis of **1**-Br-2-^{14}C (8) that repeated cycles of ionization, 1,2-shift, and return could occur, giving rise to isotopic scramblings in both the reaction product and recovered unconsumed reactant. A simple mechanism depicting these processes is given in Scheme 1, where I and I′ are the isotopically unrearranged and rearranged trianisylvinyl cations or ion-pairs, RX and R′X are the unrearranged and rearranged reactants, and RY and R′Y are the unrearranged and rearranged products.

It is clearly seen from Table 2 that increasing amounts of added NaOAc resulted in lower extents of isotopic scrambling. Similarly, from Table 3, the presence of Et_4NBr in addition to NaOAc gave rise to a further decrease in scrambling (compare, for example, Expt. A-1 with A-20 and Expt. A-21 with

Can. J. Chem. Downloaded from www.nrcresearchpress.com by 210.87.254.105 on 09/06/12
For personal use only.

Can. J. Chem. Downloaded from www.nrcresearchpress.com by 210.87.254.105 on 09/06/12
For personal use only.

TABLE 2. Data from duplicated solvolyses of 15 m*M* doubly labeled trianisylvinyl bromide, 1-Br-2-^{13}C-2-methoxy-^{14}C, in glacial acetic acid in the presence of NaOAc at 120 ± 2°C

Expt.	[NaOAc] (m*M*)	Reaction time (h)	% Reaction[a]	Scrambling of [^{14}C]CH_3O-labeled anisyl from C-2 to C-1 (%) Product	Scrambling of [^{14}C]CH_3O-labeled anisyl from C-2 to C-1 (%) Recovered reactant	Scrambling of ^{13}C-labeled carbon from C-2 to C-1 (%) Product	Scrambling of ^{13}C-labeled carbon from C-2 to C-1 (%) Recovered reactant
A-1	30	5	21 —	9.3 —	1.1 —	10.1 —	1.7 —
A-2	30	9.5	36; 36	10.0; 10.1	3.1 —	10.9; 10.9	4.2 —
A-3	30	70	84; 84	22.0; 20.1	22.7; 21.6	22.1; 23.2	27.8; 27.9
A-4	30	102	91; 91	23.3; 22.5	25.6; 24.8	25.3; 25.3	— —
A-5	30	336	97; 97	26.7; 27.1(29)[b]	33.6; 33.4	29.6 — (33)[b]	— —
A-6	60	3	20; 24	5.8; 6.1	0.4; 0.4	7.9; 8.2	— —
A-7	60	8	50; 50	6.5; 6.5	2.6; 2.7	8.4; 9.0	4.1; 3.9
A-8	60	16	70; 72	10.2; 10.3	14.9; 15.1	13.9; 14.4	20.9; 19.5
A-9	60	217	93; 95	18.2; 18.0(24)[b]	19.2; 19.5	26.3; 26.5(31)[b]	29.3; 29.6
A-10	150	1.75	29; 27	5.0; 4.9	0 ; 0	7.0; 7.0	0 ; 0
A-11	150	4	51; 51	6.0; 5.9	1.0; 1.0	8.3; 8.3	1.4; 1.5
A-12	150	8	70; 68	8.4; 8.4	4.0; 4.0	12.0; 12.6	7.4; 7.5
A-13	150	195	95; 94	16.7; 16.7(20)[b]	11.6; 11.8	23.0; 23.4(27)[b]	17.5; 17.6
A-14	300	2.75	50; 49	5.3; 5.4	0.4; 0.4	7.9; 7.9	0.7; 0.7
A-15	300	6	74; 72	6.5; 6.4	2.0; 2.2	9.2; 8.9	3.2; 3.5
A-16	450	192	98; 98	12.2; 12.1(13)[b]	8.4; 8.5	18.0; 18.1(19)[b]	12.0; 12.4
A-17	450	1.75	50; 50	4.0; 3.8	0.2; 0.2	5.4; 6.1	Trace
A-18	450	4	70; 72	5.5; 5.4	0.8; 0.8	8.1; 8.2	1.2; 1.2
A-19	450	196	98 —	10.6; — (11)[b]	6.9; —	15.8; — (17)[b]	— —

[a]From titration of the liberated Br^- ion.
[b]Extrapolated value for 100% reaction.

TABLE 3. Data from duplicate solvolyses of 15 m*M* doubly labeled trianisylvinyl bromide, 1-Br-2-^{13}C-2-methoxy-^{14}C, in glacial acetic acid in the presence of NaOAc and Et_4NBr at 120 ± 2°C

Expt.	[NaOAc] (m*M*)	[Et_4NBr] (m*M*)	Reaction time (h)	% Reaction[a]	Scrambling of [^{14}C]CH_3O-labeled anisyl from C-2 to C-1 (%) Product	Scrambling of [^{14}C]CH_3O-labeled anisyl from C-2 to C-1 (%) Recovered reactant	Scrambling of ^{13}C-labeled carbon from C-2 to C-1 (%) Product	Scrambling of ^{13}C-labeled carbon from C-2 to C-1 (%) Recovered reactant
A-20	30	75	12	24; 24	6.2; 5.9	0.3; 0.3	7.7; 7.6	0.5; 0.4
A-21	30	75	30	52; 53	8.8; 8.8	4.7; 4.6	10.9; 11.2	6.9; 6.4
A-22	30	75	99	80; 87	16.2; 16.4	17.3; 17.5	20.6; 20.9	24.0; 24.5
A-23	30	75	336	91; 91	22.1; 22.4	31.2; 32.0	32.9; 33.0	— —
A-24	30	300	52	50; 51	6.0; 5.8	2.6; 2.8	7.7; 7.9	4.0; 4.1
A-25	30	300	336	85; 85	20.1; 20.2	29.7; 30.0	30.1; 29.7	43.8; 44.4
A-26	30	750	340	70; 68	15.0; 15.0	26.0; 26.0	22.4; 21.8	36.2; 36.1
A-27	30	1000	336	60 —	11.2 —	20.8 —	16.9 —	31.2 —
A-28	300	300	5.5	50; 50	3.6; 3.7	1.4; 1.3	5.3; 5.4	2.1; 2.0
A-29	300	300	336	96; 96	17.0; 16.9	15.2; —	25.9; 25.2	— —

[a]From titration of the liberated Br^- ion.

A-24). These findings can be attributed to the competitive occurrence of scrambling arising from 1,2-anisyl shifts (the k_r process in Scheme 1) and capture reactions of the trianisylvinyl cation with the nucleophiles (the k_p and k_{-1} processes in Scheme 1). An increase in the concentration of the more nucleophilic acetate ion will enhance the product-forming capture of the unrearranged trianisylvinyl cation, thereby decreasing the relative extent of scrambling from the 1,2-shift process. Similarly, in the presence of added bromide ions, a further decrease in 1,2-shifts will occur because of the additional capture reaction between the unrearranged trianisylvinyl cation and the added bromide ion.

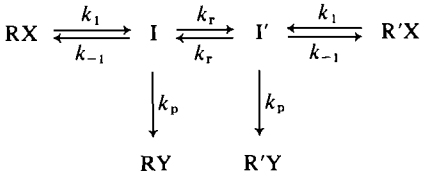

SCHEME 1

Can. J. Chem. Downloaded from www.nrcresearchpress.com by 210.87.254.105 on 09/06/12
For personal use only.

In a review on ions and ion-pairs in solvolysis reactions, Raber *et al.* (14) have pointed out that since inorganic salts are known to be largely undissociated in glacial acetic acid (15–17), the free ions are in equilibrium with ion-pairs. Consequently, for salts with univalent cations and anions such as NaOAc, the concentration of the free ions would be proportional to the square root of the concentration of the added salt. When the % scramblings in the reaction products from various sets of experiments with different amounts of added NaOAc were extrapolated to 100% reaction, the values obtained are given in parentheses in Table 2. Plotting of these values vs. the square roots of the concentrations of added NaOAc gave reasonably good linear correlations as shown in Fig. 1. Such linear behavior thus suggests that the free acetate ion may be chiefly responsible for the observed decrease in scrambling with increasing added NaOAc concentration; that is, under the conditions employed in the present work, the nucleophile involved in the product-forming capture reaction may chiefly be the acetate ion rather than HOAc or the Na^+OAc^- ion-pair. This finding thus constitutes a further confirmation of previous conclusions that in the solvolysis of certain vinylic substrates including **1**-Br in HOAc–NaOAc, the capturing nucleophile is the acetate ion, as discussed recently by Rappoport and co-workers (18).

It is also of interest to note from Tables 2 and 3 that under any given set of experimental conditions, at the early stages of reaction, the scrambling in the recovered reactant is less than the scrambling in the corresponding reaction product. This is to be expected since there would be a relatively large amount of unchanged reactant remaining in the reaction mixture. In the later stages of reaction and with added NaOAc concentrations of 30 or 60 m*M*, the scrambling in the recovered reactant becomes higher than that found in the corresponding product (e.g. Expts. A-3 to A-5 and A-25 to A-27). This can be explained by the occurrence of cycles of ionization, 1,2-shift, and return, leading to the accumulation of a greater amount of scrambling in the relatively small amount of unconsumed reactant (8). When the concentration of added NaOAc is higher at 150, 300, or 450 m*M*, even after prolonged reaction times as in Expts. A-13, A-16, A-19, and A-29, the scrambling in the recovered reactant is still lower than that found in the product. It appears that with such high concentrations of added NaOAc, the return process competes less effectively with the second order product-forming capture reaction by the acetate ion, resulting in a lesser accumulation of scrambling in the recovered reactant.

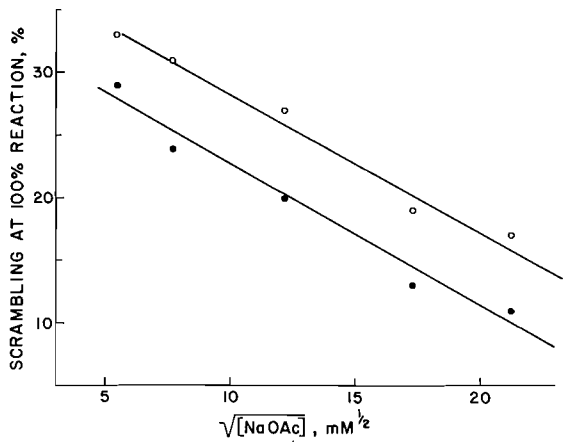

FIG. 1. Plot of % scrambling in the acetolysis product from **1**-Br-2-^{13}C-2-methoxy-^{14}C at complete reaction vs. the square root of the concentration of added NaOAc; open circles, scrambling of ^{13}C-labeled C-2, closed circles, scrambling of [^{14}C]-CH_3O-labeled anisyl.

Previously, Rappoport and co-workers (6) had expressed the scrambling data in triarylvinyl systems in terms of % rearrangement, with the assumption that 100% rearrangement corresponds to 33.3% and 50.0% scrambling, respectively, for **1**-Br-2-methoxy-^{14}C and **1**-Br-2-^{13}C. The data in Tables 2 and 3 may be converted to "% rearrangements" by multiplying the % scramblings for the ring and chain labels by factors of 3 and 2, respectively, and these values are summarized in Table 4. It is of interest to note from Table 4 that, on comparison of the % rearrangements for the ring and chain labels, two types of behavior appear. In most of the experiments, the % rearrangement found for the ring label is greater than that observed for the corresponding chain label. In some cases, however, such as Expts. A-17 to A-19 and A-27 to A-29, the % rearrangements found for both the ring and chain labels are about equal, and these cases generally involve the presence of large amounts of added salts as can be seen from the reaction conditions given in Tables 2 and 3. At high salt concentrations, apparently complete statistical equilibration of the labels has been achieved in that portion of the molecules which has undergone isotopic rearrangement. Thus in Expt. A-27, for example, the % scrambling for the ring label is 11.2% (Table 3). For the fraction of molecules that have rearranged, complete equilibration would correspond to

$$\underset{22.4\%}{An^*AnC{=}\overset{+}{C}An} \underset{2k_r}{\overset{k_r}{\rightleftharpoons}} \underset{11.2\%}{{}^*An\overset{+}{C}{=}CAn_2}$$

Can. J. Chem. Downloaded from www.nrcresearchpress.com by 210.87.254.105 on 09/06/12
For personal use only.

TABLE 4. Scrambling data from the acetolysis of 1-Br-2-^{13}C-2-methoxy-^{14}C expressed as % rearrangement

	% Rearrangement[a]			
	[^{14}C]CH_3O-labeled anisyl		^{13}C-labeled C-2	
Expt.	Product	Recovered reactant	Product	Recovered reactant
A-1	27.9 —	3.3 —	20.2 —	3.4 —
A-2	30.0; 30.3	9.3 —	21.8; 21.8	8.4 —
A-3	66.0; 60.3	68.1; 64.8	44.2; 46.4	55.6; 55.6
A-4	69.9; 67.5	76.8; 74.4	50.6; 50.6	— —
A-5	80.1; 81.3	100.8; 100.2	59.2 —	— —
A-6	17.4; 18.3	1.2; 1.2	15.8; 16.4	— —
A-7	19.5; 19.5	7.8; 8.1	16.8; 18.0	8.2; 7.8
A-8	30.6; 30.9	44.7; 45.3	27.8; 28.8	41.8; 39.0
A-9	54.6; 54.0	57.6; 58.5	52.6; 53.0	58.6; 59.2
A-10	15.0; 14.7	0 ; 0	14.0; 14.0	0 ; 0
A-11	18.0; 17.7	3.0; 3.0	16.6; 16.6	2.8; 3.0
A-12	25.3; 25.2	12.0; 12.0	24.0; 25.2	14.8; 15.0
A-13	50.1; 50.1	34.8; 35.4	46.0; 46.8	35.0; 35.2
A-14	15.9; 16.2	1.2; 1.2	15.8; 15.8	1.4; 1.4
A-15	19.5; 19.2	6.0; 6.6	18.4; 17.8	6.4; 7.0
A-16	36.6; 36.3	25.2; 25.5	36.0; 36.2	24.0; 24.8
A-17	12.0; 11.4	0.6; 0.6	10.8; 12.2	— —
A-18	16.5; 16.2	2.4; 2.4	16.2; 16.4	2.4; 2.4
A-19	31.8 —	20.7 —	31.6 —	— —
A-20	18.6; 17.7	0.9; 0.9	15.4; 15.2	1.0; 0.8
A-21	26.4; 26.4	14.1; 13.8	21.8; 22.4	13.8; 12.8
A-22	48.6; 49.2	51.9; 52.5	41.2; 41.8	48.0; 49.0
A-23	66.3; 67.2	93.6; 96.0	65.8; 66.0	— —
A-24	18.0; 17.4	7.8; 8.4	15.4; 15.8	8.0; 8.2
A-25	60.3; 60.6	89.1; 90.0	60.2; 59.4	87.6; 88.8
A-26	45.0; 45.0	78.0; 78.0	44.8; 43.6	72.4; 72.2
A-27	33.6 —	62.4 —	33.8 —	62.4 —
A-28	10.8; 11.1	4.2; 3.9	10.6; 10.8	4.2; 4.0
A-29	51.0; 50.7	45.6 —	51.8; 50.4	— —

[a]Complete. 100% rearrangement for 1-Br-2-methoxy-^{14}C and for 1-Br-2-^{13}C corresponds to 33.3% and 50.0% scramblings, respectively; thus the % rearrangement was obtained by multiplying the % scrambling of the [^{14}C]CH_3O-labeled anisyl group and the % scrambling of the ^{13}C-labeled C-2 (Tables 2 and 3) by factors of 3 and 2, respectively.

The chain label in the same experiment gave 16.9% scrambling (Table 3). Again for the fraction of molecules that have rearranged, complete equilibration would correspond to

$$\underset{16.9\%}{An_2{}^*C{=}\overset{+}{C}An} \underset{2k_r}{\overset{2k_r}{\rightleftharpoons}} \underset{16.9\%}{An{}^*\overset{+}{C}{=}CAn_2}$$

Thus the "% rearrangement", 3 × 11.2 = 33.6% and 2 × 16.9 = 33.8% (Table 4) are about equal.

When the equilibration is not complete, the conversion of % scrambling by multiplication with a factor of 3 or 2 would not give equal % rearrangements. In the extreme case when there is an irreversible 1,2-shift with no equilibrating at all, suppose a 1% An shift occurs, the following situation would result:

$$An{}^*AnC{=}\overset{+}{C}An \longrightarrow \underset{1\%}{{}^*An\overset{+}{C}{=}CAn_2}$$

$$An_2{}^*C{=}\overset{+}{C}An \longrightarrow \underset{1\%}{An{}^*\overset{+}{C}{=}CAn_2}$$

If the factors of 3 and 2 were applied, one would get 3% rearrangement for the ring label and 2% rearrangement for the chain label; i.e., the % rearrangement of the ring label would be greater than the % rearrangement for the chain label. It may be pointed out that the data in Table 4 show that in the experiments where the % rearrangement of the ring label is greater than that of the corresponding chain label, the difference is never greater than the ratio of 3:2. Thus under the conditions employed in the present study, some equilibration from reversible 1,2-anisyl shifts took place in all cases.

Can. J. Chem. Downloaded from www.nrcresearchpress.com by 210.87.254.105 on 09/06/12
For personal use only.

The question arises as to why, in the experiments with high salt concentrations, for the molecules that have rearranged, the equilibration of the labels is complete, while with low salt concentrations, the equilibration is not complete. As a working hypothesis, it may be suggested that in glacial HOAc, under conditions which did not give complete equilibration, some of the 1,2-shifts might have occurred in the ion-pair stage. The presence of the counterion would give rise to a frontside hindrance by the leaving group, resulting in an incomplete equilibration of the labels. When the dissociation proceeds further, the 1,2-shifts are unhindered by any counterion and complete equilibration of the labels is attained. As suggested in Ingold's qualitative explanation of the normal salt effect (14, 19), an increase in salt concentration increases the polarity of the medium, which would give rise to a greater stabilization of the ionic transition state and hence promote the formation of the dissociated trianisylvinyl cation. Thus with high salt concentrations, complete equilibration was observed in those molecules that have undergone rearrangement. It is worth noting that these findings were obtained as a result of the use of double labeling or the simultaneous use of two singly labeled substrates. It would not have been detected if only singly labeled **1**-Br were employed as substrate.

Very recently, Rappoport and co-workers (18) reported the simultaneous studies on the kinetics of solvolysis and ^{82}Br exchange for a number of vinyl substrates including **1**-Br. The reactions were carried out mostly in the presence of 87 m*M* NaOAc and 71 m*M* Et_4Br. These conditions are similar to, though not identical with, those employed in the present work to obtain the data given in Table 3. Over the range of NaOAc concentrations of 87 to 175 m*M*, it was noted that the rate of solvolysis of **1**-Br in HOAc–NaOAc–Et_4NBr showed a first order dependence on NaOAc concentration. Thus the S_N1 process becomes the rarely observed $S_N2(C^+)$ process with the cation–nucleophile reaction becoming rate determining. This finding, while demonstrating the importance of added nucleophiles such as OAc^-, does not affect the present discussion which deals qualitatively with the observed isotopic scrambling behavior that arose from 1,2-shifts in the cationic species.

It has been pointed out that while ion-pairs from the acetolysis of triarylvinyl substrates may be involved in the return process, their reactions are intramolecular and they are unreactive toward external nucleophiles (18, 20). It has also been suggested that while the presence of added NaOAc can decrease the extent of scrambling that takes place in the dissociated triarylvinyl cation, the scrambling that occurs in the ion-pair stage may be insensitive to added NaOAc (7, 21, 22). In many of the present experiments which did not give rise to an equal amount of "% rearrangement" for the ring and chain labels (Table 4), ion-pairs possibly may have played at least a minor role. Thus the observed decrease in the extent of scrambling with increasing amounts of added NaOAc may be due only to the effect of NaOAc on the scrambling that occurred in the dissociated ion, the scrambling that took place in the ion-pair stage being unaffected by NaOAc. The deviations in Fig. 1 from a perfectly linear correlation might be due at least in part to perturbations by minor amounts of scrambling in the ion-pair stage which were insensitive to the presence of added NaOAc.

Experimental

*1,2-Dianisyl-2-*p*-[^{14}C]methoxyphenyl[2-^{13}C]vinyl Bromide (**1**-Br-2-^{13}C-2-methoxy-^{14}C)*

1,2-Dianisyl[1-^{13}C]ethanone (carbonyl-labeled desoxyanisoin) was prepared as described by Lee and Oka (9). *p*-[^{14}C]-methoxybromobenzene was obtained by methylation of *p*-bromophenol with [^{14}C]methyl iodide supplied by New England Nuclear Canada.

A solution of 10.0 g (30 mmol) of 1,2-dianisyl[1-^{13}C]ethanone in 150 mL of tetrahydrofuran (THF) was added dropwise over a period of 45 min to a Grignard solution prepared from 15.0 g (80 mmol) of *p*-[^{14}C]methoxybromobenzene and 2.4 g (100 mmol) of Mg in 150 mL of THF. The mixture was refluxed for 4.5 h and the resulting material was concentrated by the removal of most of the THF by distillation. The residual material was then poured into 600 mL of a 5% solution of NH_4Cl containing 7.5 mL of 25% NH_4OH. After cooling, the solid product was collected by filtration, washed with H_2O, and then recrystallized from methanol–acetone to give 11.4 g (80%) of 1,2-dianisyl-1-*p*-[^{14}C]methoxyphenyl[1-^{13}C]ethanol, mp 129–131°C (lit. (23) mp 130–131°C). This doubly labeled tertiary alcohol was then converted to 1,2-dianisyl-2-*p*-[^{14}C]-methoxyphenyl[2-^{13}C]vinyl bromide (**1**-Br-2-^{13}C-2-methoxy-^{14}C) by treatment with Br_2 in HOAc as described previously by Oka and Lee (5).

Acetolysis Reactions

A solution of 640 mg (1.5 mmol) of **1**-Br-2-^{13}C-2-methoxy-^{14}C in 100 mL of HOAc, containing various amounts of NaOAc or NaOAc and Et_4NBr as given in Tables 2 and 3, was placed in a sealed tube and heated at 120 ± 2°C for the desired length of time. After cooling in an ice-bath, the tube was opened and its content was poured into 200 mL of ether. The ether solution was extracted three times with 50-mL portions of H_2O. The combined aqueous extract was titrated potentiometrically with 0.1 *M* $AgNO_3$ to give the amount of liberated Br^- ion and hence the extent of reaction. The ether solution was dried over $MgSO_4$ and the solvent was removed under reduced pressure to give a residual oil containing the scrambled reaction product, **1**-OAc-1,2-^{13}C-1,2-methoxy-^{14}C, and any scrambled unconsumed reactant, **1**-Br-1,2-^{13}C-1,2-methoxy-^{14}C.

Analyses for Isotopic Scrambling

The residual oil containing the reaction product and the unconsumed reactant from each acetolysis experiment was treated twice successively with $LiAlH_4$ as previously described

Can. J. Chem. Downloaded from www.nrcresearchpress.com by 210.87.254.105 on 09/06/12
For personal use only.

(8) to give the scrambled 1,2,2-trianisylethanol, **2**-1,2-^{13}C-1,2-methoxy-^{14}C, derived from the acetate product, and the scrambled trianisylethene, **3**-1,2-^{13}C-1,2-methoxy-^{14}C, derived from the unconsumed reactant. Separation of the alcohol from the olefin was effected by passage through an alumina column again as previously described (8). The olefin, **3**-1,2-^{13}C-1,2-methoxy-^{14}C, was eluted first with a 9:1 mixture of petroleum ether and diethyl ether, and then the alcohol, **2**-1,2-^{13}C-1,2-methoxy-^{14}C, was recovered after the eluant was changed to $CHCl_3$.

The ^{13}C nmr spectrum of the alcohol **2**-1,2-^{13}C-1,2-methoxy-^{14}C was then obtained and it was used for the analysis of the ^{13}C contents at C-1 and C-2, the method employed for the analysis being the same as was described by Oka and Lee (5). The ^{13}C contents at C-1 and C-2 of the alcohol **2**-1,2-^{13}C-1,2-methoxy-^{14}C thus gave the % scrambling of the ^{13}C-label from C-2 to C-1 in the reaction product. After the ^{13}C nmr spectrum was obtained, the entire sample of **2**-1,2-^{13}C-1,2-methoxy-^{14}Cwas diluted with inactive carrier (about 500 mg) and then oxidized with $KMnO_4$ to give dianisyl ketone (8), whose ^{14}C activity, when compared with that of the alcohol **2**, gave the % scrambling of the [^{14}C]CH_3O-labeled anisyl group from C-2 to C-1 in the reaction product (8).

The scrambled trianisylethene, **3**-1,2-^{13}C-1,2-methoxy-^{14}C, eluted from the alumina columns, was divided into two portions. One portion (about 50 mg), without dilution by any carrier, was catalytically hydrogenated (H_2–PtO_2) in ethyl acetate to give 1,1,2-trianisylethane (**4**-1,2-^{13}C-1,2-methoxy-^{14}C), mp 88–89°C (lit. (23) mp 86–87°C). Control experiments show that this hydrogenation gave yields of about 90%. The ^{13}C nmr spectrum of hydrocarbon **4** showed C-2, C-1, and CH_3O absorptions at 40.3, 50.6, and 53.6 ppm, respectively, and these absorptions were utilized for the analysis of the ^{13}C contents at C-1 and C-2 by the intensity ratio method as described by Oka and Lee (5), thus giving the % scrambling of the ^{13}C-label from C-2 to C-1 in the recovered unconsumed reactant. The second portion of the olefin **3**-1,2-^{13}C-1,2-methoxy-^{14}C was diluted with inactive carrier (about 300 mg) and then it was degraded by ozonolysis to give dianisyl ketone (8), whose ^{14}C activity when compared with that of olefin **3** gave the % scrambling of the [^{14}C]CH_3O-labeled anisyl group from C-2 to C-1 in the recovered unconsumed reactant.

Acknowledgments

Valuable comments generously given by C. J. Collins of the Oak Ridge National Laboratory and I. D. Spenser of McMaster University, and the financial support given by the Natural Sciences and Engineering Research Council of Canada are gratefully acknowledged.

1. Z. Rappoport and A. Gal. J. Am. Chem. Soc. **91**, 5246 (1969).
2. Z. Rappoport and Y. Apeloig. Tetrahedron Lett. 1817 (1970).
3. Z. Rappoport and A. Gal. Tetrahedron Lett. 3233 (1970).
4. Z. Rappoport and J. Kaspi. J. Am. Chem. Soc. **92**, 3220 (1970).
5. M. Oka and C. C. Lee. Can. J. Chem. **53**, 320 (1975).
6. Y. Houminer, E. Noy, and Z. Rappoport. J. Am. Chem. Soc. **98**, 5632 (1976).
7. C. C. Lee and E. C. F. Ko. Can. J. Chem. **54**, 3041 (1976).
8. C. C. Lee, U. Weber, and C. A. Obafemi. Can. J. Chem. **57**, 1384 (1979).
9. C. C. Lee and M. Oka. Can. J. Chem. **54**, 604 (1976).
10. C. C. Lee and U. Weber. J. Org. Chem. **43**, 2721 (1978).
11. F. H. A. Rummens, R. D. Green, A. J. Cessna, M. Oka, and C. C. Lee. Can. J. Chem. **53**, 314 (1975).
12. M. Oka, J. Hinton, A. Fry, and T. W. Whaley. J. Org. Chem. **44**, 3545 (1979).
13. A. Fry and M. Oka. J. Am. Chem. Soc. **101**, 6353 (1979).
14. D. J. Raber, J. M. Harris, and P. v. R. Schleyer. *In* Ions and ion-pairs in organic reactions. Vol. 2. *Edited by* M. Szwarc. John Wiley and Sons, New York. 1974. Chapt. 3.
15. M. M. Jones and E. Griswold. J. Am. Chem. Soc. **76**, 3247 (1954).
16. S. Bruckenstein and I. M. Kolthoff. J. Am. Chem. Soc. **78**, 2974 (1956).
17. S. Winstein, P. E. Klinedinst, Jr., and G. C. Robinson. J. Am. Chem. Soc. **83**, 885 (1961).
18. F. I. M. van Ginkel, E. R. Hartman, G. Lodder, J. Greenblatt, and Z. Rappoport. J. Am. Chem. Soc. **102**, 7514 (1980).
19. L. C. Bateman, M. G. Church, E. D. Hughes, C. K. Ingold, and N. A. Taher. J. Chem. Soc. 979 (1940).
20. Z. Rappoport and Y. Apeloig. J. Am. Chem. Soc. **97**, 821 (1975).
21. C. C. Lee, A. J. Cessna, B. A. Davis, and M. Oka. Can. J. Chem. **52**, 2679 (1979).
22. C. C. Lee, E. C. F. Ko, and Z. Rappoport. Can. J. Chem. **58**, 2369 (1980).
23. R. S. Shelton, M. G. V. Campen, Jr., D. F. Meisner, S. M. Parmerter, E. R. Andrews, R. E. Allen, and K. K. Wykoff. J. Am. Chem. Soc. **75**, 5491 (1953).

Multivariate analysis of data for the ionization of weak acids in water – dimethyl sulfoxide solvent mixtures

JOHN T. EDWARD,[1] MICHAEL SJÖSTRÖM, AND SVANTE WOLD

Research Group for Chemometrics, Department of Chemistry, Umeå University, S-901 87 Umeå, Sweden

Received January 5, 1981

JOHN T. EDWARD, MICHAEL SJÖSTRÖM, and SVANTE WOLD. Can. J. Chem. **59**, 2350 (1981).

The ionization constants $p({}_sK_a)$ reported for 41 weak acids of varying chemical type in ten water–DMSO solvent mixtures have been analysed by the SIMCA version of principal components analysis. This shows the data to fit a two-component model. The significance of the results for acidity function theory is discussed.

JOHN T. EDWARD, MICHAEL SJÖSTRÖM et SVANTE WOLD. Can. J. Chem. **59**, 2350 (1981).

On a analysé, par la version SIMCA de l'analyse des composants principaux, les constantes d'ionization $p({}_sK_a)$ de 41 acides faibles en dix solvants mixtes eau–DMSO. Les résultats indiquent un modèle à deux composants. On démontre la pertinence des résultats pour la théorie de la fonction d'acidité.

Can. J. Chem. Downloaded from www.nrcresearchpress.com by 210.87.254.42 on 09/06/12
For personal use only.

Introduction

The basicity of a solution of tetramethylammonium hydroxide in water – dimethyl sulfoxide (DMSO) solvent mixtures, as measured by the ionization of weak acids AH, becomes enormously greater as the water is progressively replaced by DMSO (1–4). Dolman and Stewart (4) constructed a H_- scale for 0.11 *M* tetramethylammonium hydroxide at 25°C in water–DMSO mixtures containing up to 99.6 mol% DMSO, and used this scale to determine the ionization constants $p({}_wK_a)$ at 25°C (referred to infinite dilution in water as the standard state) of very weak acids.

Schaal, Hallé, and their colleagues (5–10) also studied the ionization (but at 20°C) of weak acids in water–DMSO mixtures; however, their ionization constants $p({}_sK_a)$ are referred to infinite dilution in the mixed solvent as the standard state. They used a variety of procedures. In some determinations (7) they used an electrochemical cell containing a hydrogen electrode to measure the activity $\{S^+\}$ of the solvated proton S^+ in a series of colourless buffers in different water–DMSO solvent mixtures. The variation of the standard potential of this cell with $\{S^+\}$ had been determined previously using dilute solutions of hydrochloric acid (assumed to be completely ionized) in the same water–DMSO mixtures. The buffer could then be used to regulate pS^+ ($\equiv -\log\{S^+\}$) in any given water–DMSO mixture. When ionization of AH took place in this pS^+ range, and could be followed spectrophotometrically at concentrations of AH too low to affect pS^+, the ionization constant was given by:

[1] $$p({}_sK_a) = pS^+ - \log[A^-]/[AH] - \log {}_s\gamma_{A^-}$$

where ${}_s\gamma_{A^-}$ is the molar activity coefficient of the anion A^-. Measurements were made at different ionic strengths, and the apparent pK_a values thus obtained extrapolated to zero ionic strength, when $\log {}_s\gamma_{A^-}$ should become zero.

For weaker acids a small amount *b* of a strong base (sodium hydroxide) was added to the dilute solution of AH in water–DMSO. The equilibrium constant ${}_sK_b$ for the reaction

$$AH + S^- \rightleftarrows A^- + SH$$

was given by

[2] $${}_sK_b = \frac{[A^-]}{[AH][S^-]}\,\frac{{}_s\gamma_{A^-}}{({}_s\gamma_{AH})({}_s\gamma_{S^-})}$$

For a weak acid in low concentration, $[S^-] \approx b$, and rearrangement of [2] gives

[3] $$\frac{1}{[A^-]} = \frac{1}{([A^-]+[AH])} \times \left[1 + \frac{{}_s\gamma_{A^-}}{{}_sK_b b({}_s\gamma_{AH})({}_s\gamma_{S^-})}\right]$$

At low ionic strengths ${}_s\gamma_{A^-} \approx {}_s\gamma_{S^-}$ and $\gamma_{AH} \approx 1$, so that plots of $1/[A^-]$ against *b* should be linear. This in fact was found, and from the slopes of the plots ${}_sK_b$ could be obtained, and thence ${}_sK_a$:

[4] $$p({}_sK_a) = pK_s + p({}_sK_b)$$

This required a knowledge for each solvent mixture of the autoprotolysis constant K_s defined by:

[5] $$K_s = \{S^+\}\{S^-\} = [S^+][S^-]({}_s\gamma_\pm)^2$$

where $[S^+]$ designates the molar concentration of

[1]Permanent address: Department of Chemistry, McGill University, Montreal (Que.), Canada H3A 2K6.

0008-4042/81/152350-08$01.00/0

©1981 National Research Council of Canada/Conseil national de recherches du Canada

Can. J. Chem. Downloaded from www.nrcresearchpress.com by 210.87.254.42 on 09/06/12
For personal use only.

the solvated proton in its diverse forms, $[S^-]$ the molar concentration of anions formed by removal of a proton from one or other of the solvent species, and ${}_s\gamma_\pm$ the mean ion activity coefficient. The pK_s ($\equiv -\log K_s$) values had been determined, and changed progressively from 14.32 in 10.8 (w/w)% DMSO to 24.0 in 95.5 (w/w)% DMSO (5) at 20.0°C. For 100% DMSO at 25°C a pK_D of 31.3 has been reported (11).

For reasonably strong acids (carboxylic acids, ammonium ions), $p({}_sK_a)$ can be determined by potentiometric titration in water–DMSO (12).

Hallé, Schaal, *et al.* (8–10, 12) showed that $p({}_sK_a)$ varies with solvent composition, and that different classes of compounds behave differently. In the present paper we apply the methods of principal components (pc) analysis (13–16) to the $p({}_sK_a)$ values reported by them for 41 weak acids, listed in Table 1, in ten water–DMSO solvent mixtures, listed in Table 2.

Methods

To apply pc analysis, the data were set up in a matrix containing the elements $y_{is} = p({}_sK_{a(i)})$ values for M compounds (the variables) in N solvents (the objects). Index i is used for the compounds and index s for the solvents. This data matrix can then be approximated by the statistical model:

$$[6] \qquad y_{is} = p({}_sK_{a(i)}) = \alpha_i + \sum_{a=1}^{A} \beta_{ia}\theta_{as} + \varepsilon_{is}$$

In this model θ are parameters varying with solvent composition, α and β are parameters characteristic of the acidic compound, and ε are residuals not explained by the α, β, and θ parameters. If the correct number of terms A is used, the parameters α, β, and θ describe the systematic part of the data and the residuals ε contain only "noise", which consists both of model errors and errors of measurement.

Hence one crucial objective of the data analysis is to find out whether [6] with $A = 1$ is sufficient to model the data. If a second term is required, its magnitude relative to the first is also of great interest. The appropriate number of terms can be determined for a matrix without missing data by the cross-validation (cv) technique (17).

For our calculations we used the statistical package SIMCA (16, 18). This package includes pc analysis, cv, and has proved successful in application to other chemical problems (16, 19).

The principal components model [6] has the same form as an A-term linear free energy relationship (LFER). Thus the data analysis conforms to the LFER treatments of acidity function by Bunnett and Olsen (20) and others (21). A single term model (i.e. $A = 1$) would correspond to the ordinary acidity function concept where shift in equilibria of all compounds undergoing protonation is modelled by a linear function.[2]

It must be understood that a data analysis of this type only gives parameters θ_{as} which best approximate the systematic information in the data. These parameters are such that θ_{1s} describes as much as possible of the linear correlations between the indicators, θ_{2s} as much as possible of the linear deviations from the first correlation structure, i.e. quadratic terms, θ_{3s} (if significant) as much of the linear deviation from the first two correlations, and so on.

The chemical interpretation of these parameters is more difficult, in particular since any rotations, θ_{as}' are also adequate chemical descriptors. In case more fundamental variables are thought to be involved, such rotations can be tried. See, further, the footnote to Table 2.

Results

Twelve different data analyses were made of different submatrices of the Schaal–Hallé data. In order to allow a cv choice of A, only complete submatrices with data for all i and s were analysed. Table 3 summarizes the results.

Set 1

Data set 1 ($N = 9$, $M = 9$) contains three compounds of the set used by Stewart and Dolman (4) to establish their H_- scale. In all, three types of compounds (diphenylamines, anilines, and aminopyridines) are included. The published data give $p({}_sK_a)$ values for these compounds in nine solvent compositions from 31.7 to 95.5 (w/w)% DMSO. Data sets of this range of solvent compositions are henceforth called "long" matrices.

The data analysis shows convincingly that a linear model ($A = 1$) is *not* sufficient to describe the data. Cross-validation shows that $A = 2$, and it is seen from S_1 and S_2 in Table 3 that the second component is highly significant. Thus, the RSD after one component (S_1) is 0.155 and after two components (S_2) is 0.038. The precision of the data is estimated to be about 0.03. Hence with $A = 1$ the unexplained variation of 0.12 (=0.155 − 0.038) is

[2]The function need not, of course, be linear in terms of solvent composition. Linearity in this context means that if the protonation data for one compound are plotted against the data for another, the plot is linear.

Can. J. Chem. Downloaded from www.nrcresearchpress.com by 210.87.254.42 on 09/06/12
For personal use only.

TABLE 1. Parameters for compounds from set no. 4

i	Acid (ref.)	α	β_1	β_2
Diphenylamines				
1	3′-Chloro-2,4,6-trinitro (8)	7.998	0.1844	0.3406
2	4′-Chloro-2,4,6-trinitro (8)	8.190	0.1895	0.3569
3	2,4,6-Trinitro (8)	8.739	0.1776	0.2789
4	3′-Chloro-2,4-dinitro (8)	—	—	—
5	4′-Chloro-2,4-dinitro (8)	12.550	0.1110	0.2508
6	2,4-Dinitro (8)	13.051	0.0807	0.2423
7	4,4-Dinitro (8)	13.789	−0.0298	0.2423
8	4-Nitro (8)	—	—	—
Anilines				
9	6-Bromo-2,4-dinitro (8)	13.013	0.0852	0.2962
10	2,4-Dinitro (8)	—	—	—
11	2,6-Dichloro-4-nitro (8)	—	—	—
12	4,6-Dichloro-2-nitro (8)	—	—	—
13	2-Chloro-4-nitro (8)	—	—	—
14	4-Chloro-2-nitro (8)	—	—	—
Aminopyridines				
15	4-Anilino-3,5-dinitro (8)	10.217	0.0729	0.2050
16	2-Anilino-5-nitro (8)	14.393	−0.1308	0.1325
17	2-Anilino-3-nitro (8)	—	—	—
18	2-Amino-5-nitro (8)	—	—	—
19	2-Amino-3-nitro (8)	—	—	—
2,4-Dinitrodiphenylamine carboxylates				
20	2,4-Dinitro 4′-carboxylate (10)	13.158	0.0238	0.1483
21	3′-Chloro-2,4-dinitro 4′-carboxylate (10)	12.842	0.0228	0.1791
22	2,4-Dinitro 3′-carboxylate (10)	13.588	0.0129	0.1287
23	4′-Chloro-2,4-dinitro 3′-carboxylate (10)	13.168	0.0215	0.1696
24	2,4-Dinitro 3′-carboxylate (10)	—	—	—
25	5′-Chloro-2,4-dinitro 2′-carboxylate (10)	—	—	—
26	4′-Chloro-2,4-dinitro 2′-carboxylate (10)	—	—	—
Azadiphenylamine carboxylates				
27	2-Aza-4-nitro 4′-carboxylate (10)	14.710	−0.1954	0.0963
28	2-Aza-4-nitro 3′-carboxylate (10)	14.917	−0.2051	0.1175
29	2-Aza-4′-chloro-4-nitro 3′-carboxylate (10)	14.526	−0.1936	0.1456
30	2-Aza-5′-chloro-4-nitro 2′-carboxylate (10)	—	—	—
31	2-Aza-4′-chloro-4-nitro 2′-carboxylate (10)	—	—	—
32	2-Aza-6-nitro 4′-carboxylate (10)	—	—	—
Nitrodiphenylamine carboxylates				
33	4-Nitro 4′-carboxylate (10)	—	—	—
34	3′-Chloro-4-nitro 4′-carboxylate (10)	—	—	—
35	4′-Chloro-4-nitro 3′-carboxylate (10)	—	—	—
Cyclohexylammonium Ions				
36	(Parent) (12)	10.412	−0.0513	0.2382
37	4-*trans-tert*-Butyl (12)	10.379	−0.0604	0.2471
38	4-*cis-tert*-Butyl (12)	10.282	−0.0583	0.2177
Cyclohexanecarboxylic Acids				
39	(Parent) (12)	7.953	−0.4937	0.0682
40	4-*trans-tert*-Butyl (12)	7.928	−0.4971	0.1325
41	4-*cis-tert*-Butyl (12)	8.287	−0.4788	0.1028

Can. J. Chem. Downloaded from www.nrcresearchpress.com by 210.87.254.42 on 09/06/12
For personal use only.

TABLE 2. Parameters for water–DMSO solvent mixtures[a]

S	% (w/w) DMSO	θ_1	θ_2
1	21.3	5.506	1.552
2	31.7	4.954	1.123
3	41.4	4.335	0.530
4	51.2	3.502	−0.004
5	61.2	2.250	−0.638
6	70.5	0.705	−0.922
7	80.4	−1.42	−0.874
8	86.4	−3.17	−0.610
9	91.0	−4.59	0.109
10	95.5	−6.56	1.285

[a] The $\beta_{i\alpha}$ and $\theta_{\alpha k}$ parameters are not uniquely defined in [6] and they can be arbitrarily rotated Φ degrees to $\beta_{i\alpha}'$ and $\theta_{\alpha s}'$. With two components as in the present case:

$$y_{is} - \alpha_i - \varepsilon_{is} = \beta_{i1}\theta_{1s} + \beta_{i2}\theta_{2s} = \beta_{i1}\theta_{1s}' + \beta_{i2}\theta_{2s}'$$
$$= (\beta_{i1}\cos\Phi + \beta_{i2}\sin\Phi)(\theta_{1s}\cos\Phi + \theta_{2s}\sin\Phi)$$
$$+ (\beta_{i1}\sin\Phi - \beta_{i2}\cos\Phi)(\Phi_{1s}\sin\Phi - \theta_{2s}\cos\Phi)$$
$$= [(\beta_{i1}b_1 + \beta_{i2}b_2)(\theta_{1s}b_1 + \theta_{2s}b_2) + (\beta_{i1}b_2 - \beta_{i2}b_1)(\theta_{1s}b_2 - \theta_{2s}b_1)]/(b_1^2 + b_2^2)$$

Thus, the θ_{sk} values can be rotated in such a way that θ_{1s}' will correlate to an external variable vector. As suggested by a referee, such a rotation can be done against pK_s, the autoprotolysis of water (5). This is accomplished by determining b_1 and b_2 by fitting pK_s by multiple regression to θ_{1s} and θ_{2s}. Thus $pK_s = a + b_1\theta_{1s} + b_2\theta_{2s} + e$, (SD(e) = 0.063, r = 0.9998, n = 10, a = 18.5178, b_1 = −0.7766, b_2 = 0.2468). Rotated $\theta_{\alpha s}'$ can now be calculated as:

$$\theta_{1s}' = (b_1\theta_{1s} + b_2\theta_{2s})/(b_1^2 + b_2^2)^{1/2}$$
$$\theta_{2s}' = (b_2\theta_{1s} - b_1\theta_{2s})/(b_1^2 + b_2^2)^{1/2}$$
$$\beta_{i1}' = (b_1\beta_{i1} + b_2\beta_{i2})/(b_1^2 + b_2^2)^{1/2}$$
$$\beta_{i2}' = (b_2\beta_{i1} - b_1\beta_{i2})/(b_1^2 + b_2^2)^{1/2}$$

Notice, however, that the $\theta_{\alpha s}$ and $\theta_{\alpha s}'$ scales will give identical models from the statistical point of view.

From the good description of pK_s of water by the two $\theta_{\alpha s}$ scales, our conclusion is that water (that can also be considered as an indicator) is behaving in a similar way to the other indicators.

significant compared with the original data variability (S_0 = 0.583) and the estimated error of 0.03.

We conclude that two components are needed to get an adequate modelling of the data in set 1.

Set 2

Set 2 includes more compounds of the three types found in set 1 but to keep the matrix complete a restriction to six solvents was necessary (short, fat matrix).

The results are precisely the same as those of the previous analysis.

Sets 3, 4

To investigate the generality of the two-component model, the data set was expanded to include more types of compounds: five types in set 3, seven types in set 4. Cross-validation (cv) analysis of these "long" matrices shows A = 2, with no indication of a third component. It is interesting to note that the RSD after two components remains very stable at around 0.040.

To get θ-values for the first solvent composition (21.3 (w/w)%DMSO), a solvent vector corresponding to this composition was fitted to the pc model obtained in the analyses of set 4. We note that such fitting can be made even when the fitted vector is incomplete (17). The compounds having values defined for this solvent composition were 1, 2, 3, 5, 15, 20, 21, and 23.

Sets 5, 8

Subanalyses of data set 4 were then performed to investigate the possibility that one-component models might describe sets which are more homogeneous with respect to compound types (sets 6, 8) or solvents (set 5). This was not the case; A = 2 was required (but sufficient) for these subsets also.

Sets 9, 10

Further restrictions in the diversity of compounds were then introduced: set 9 contains only diphenylamines, set 10 only anilines. Even for these matrices (one long; one short, fat) it was found necessary to include second components.

Sets 11, 12

Data set 11 was confined to aminopyridines and data set 12 to dinitrodiphenylamine carboxylates. Here we finally find one-component models adequate, but the RSD's are rather large. This result is explained by the very small number of compounds (M = 4) included in each set. In this case the size of the data matrices is too small to carry statistically the second components, even if they are required from the chemical point of view (to reproduce the precision of the measurements).

Discussion

The analysis above show convincingly that two solvent parameters, θ_1 and θ_2, are required to describe the acidity (basicity) of water–DMSO mixtures, and hence the tendency of weak acids to dissociate in these solvent mixtures, and that one parameter is not sufficient.

Plots of θ_1 and θ_2 against solvent composition are shown in Fig. 1. Extrapolation of the curves gives θ_1 = 6.60 and θ_2 = 1.87 for 100% water, and θ_1 = −8.75 and θ_2 = 3.50 for 100% DMSO; however, the extrapolations are rather lengthy, and these values should be regarded as provisional until more experimental data are available.

Using these values and [6] it becomes possible to calculate for those examples of compounds 1–41 for which β_1 and β_2 values are listed the ionization constants in water, $p({}_wK_a)$, and in DMSO, $p({}_DK_a)$. This has been done for six compounds in Table 4.

Agreement between values thus calculated and values obtained by other routes is reasonable, although only in the case of compound 3 (and, to a lesser extent, of compounds 36 and 39) are these other routes free from objection. For the remaining

Can. J. Chem. Downloaded from www.nrcresearchpress.com by 210.87.254.42 on 09/06/12
For personal use only.

TABLE 3. Summary of 12 data analyses

Set no.	Solvent[a]	Compound[b]	Comments	Results A^c	$S_0{}^c$	$S_1{}^c$	$S_2{}^c$
1	2–10	1–3, 5–7, 9, 15, 16	Long matrix, 3 types of compounds	2	0.583	0.155	0.038
2	5–10	1–12, 15, 16, 18	Short, fat, 3 types	2	0.394	0.154	0.035
3	2–10	1–3, 5–7, 9, 15, 16, 20–23, 27–29	Long, 5 types	2	0.571	0.190	0.035
4	2–10	1–3, 5–7, 9, 15, 16, 20–23, 27–29, 36–41	Long, 7 types	2	0.488	0.121	0.040
5	5–10	1–12, 15, 16, 18, 20–29, 33–35	Shorter, fatter, 7 types	2	0.488	0.121	0.037
6	2–10	20–23, 27–29	Long, 2 types	2	0.638	0.128	0.031
7	4–10	20–23, 25, 26	Med. long	2	0.373	0.094	0.031
8	1–10	36–41	Long, 2 types	2	1.488	0.175	0.025
9	3–10	1–7	Long, 1 type	2	0.554	0.114	0.030
10	6–10	9–14	Very short, 1 type	2	0.375	0.068	0.029
11	6–10	15–18	Very short, 1 type	1	0.479	0.043	—
12	2–10	20–23	1 Type	1	0.373	0.094	—

[a]Numbering according to Table 2.
[b]Numbering according to Table 1.
[c]Number of significant terms (A) in [6]. S_0, S_1, and S_2 are the RSD's of the data for $A = 0$ (each compound in data series described by its α_i) $A = 1$ (linear model), and $A = 2$ (nonlinear model) respectively. Thus

$$S_A = \sum_i \sum_s [\varepsilon_{is}{}^2/(N - A - 1)(M - A)]^{1/2}$$

TABLE 4. Ionization constants in water $p({}_WK_a)$ and in dimethyl sulfoxide $p({}_DK_a)$

i	Acid	$p({}_WK_a)$ From [6]	$p({}_WK_a)$ Other routes	$p({}_DK_a)$ From [6]	$p({}_DK_a)$ Other routes
3	2,4,5-Trinitrodiphenylamine	10.47	10.38(2)[a]	8.16	—
6	2,4-Dinitrodiphenylamine	14.04	13.83(2)[b], 14.06(22)[c]	13.19	—
20	2,4-Dinitrodiphenylamine-4′-carboxylate	13.59	13.31(3)[d], 14.28(6)[e]	13.46	—
22	2,4-Dinitrodiphenylamine-3′-carboxylate	13.91	13.65(3)[d], 14.57(6)[e]	13.92	—
36	Cyclohexylammonium	10.52	10.70(12)[f]	11.64	11.70(12)[g]
39	Cyclohexanecarboxylic	4.82	4.91(12)[f]	12.51	12.75(12)[g]

[a]Determined in aqueous buffers.
[b]Determined using H_- values in pyridine–water.
[c]Determined using M.C.P. approach in DMSO–water.
[d]Determined using H_- values in DMSO–water.
[e]Determined using H_- values of concentrated aqueous NaOH or KOH.
[f]By extrapolation to 100% water.
[g]By extrapolation to 100% DMSO.

three compounds $p({}_WK_a)$ values were obtained by the H_- route. We show below that in principal this method is defective. However, its results are least erroneous when solvent systems as close as possible to 100% water are used; this is the case for compounds 6, 20, and 22 of Table 4. Values of $p({}_WK_a)$ determined by the H_- method can be expected to diverge increasingly from values calculated from [6] as the solvent mixture becomes richer in DMSO.

Can. J. Chem. Downloaded from www.nrcresearchpress.com by 210.87.254.42 on 09/06/12
For personal use only.

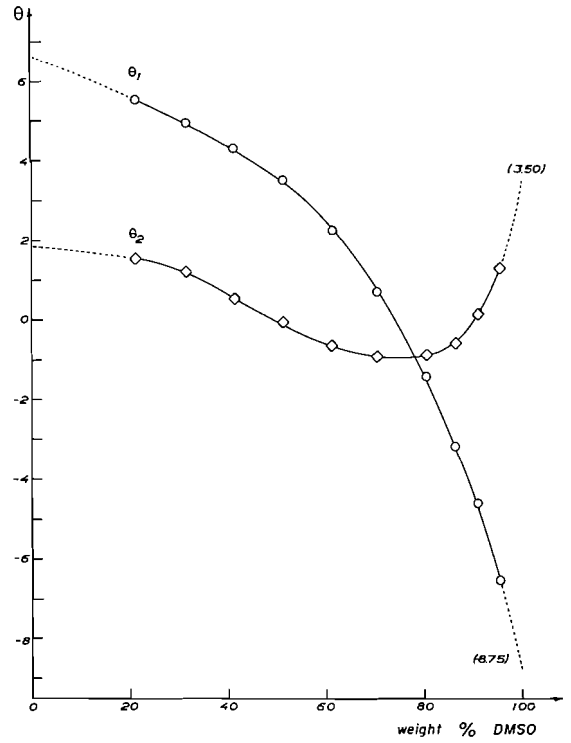

FIG. 1. Variation of θ_1 and θ_2 with DMSO content of water–DMSO solvent mixtures.

Equation [6] provides a bridge linking pK_a values in the two important solvents, water and DMSO. Unfortunately, no $p({}_DK_a)$ values are yet available from the researches of Bordwell and his collaborators (23, 24) for any of the compounds 1–41 of Table 1.

Thermodynamic Interpretation of the Results

The change in pK_a with solvent composition is a manifestation of the "medium effect" (25):

$$[7] \quad \Delta pK_a = p({}_sK_a) - p({}_wK_a) = \log ({}_m\gamma_{H^+})({}_m\gamma_{A^-}) - \log ({}_m\gamma_{AH})$$

where ${}_m\gamma_i = {}_w\gamma_i/{}_s\gamma_i$ measures the change in activity coefficient of solute i with change of solvent from water to water–DMSO. The effect of changing solvent on the activity coefficient of ions and molecules (referred to infinite dilution in water) has been discussed by King (25), Buncel and Wilson (26), Parker (27) and others, and so it becomes tempting to try to relate [7] to our empirical [6*a*]:

$$[6a] \quad p({}_sK_a) = \alpha_1 + \beta_1\theta_1 + \beta_2\theta_2$$

It is admitted that any such attempt can only be speculative, but the exercise may be useful in giving an intuitive appreciation of the terms of [6*a*].

In general, ion–solvent interactions are stronger than molecule–solvent interactions, and so it is possible to assume that $\beta_1\theta_1$ is affected chiefly by such interactions. The increase in $\beta_1\theta_1$ for carboxylic acids (compounds 39–41 of Table 1) with increase in DMSO content of solvent can then be ascribed to an increase in both ${}_m\gamma_{H^+}$ and ${}_m\gamma_{A^-}$: these small ions of localized charge are solvated and stabilized well by H_2O, less well by DMSO (26, 27), and this first term is proportional to the free energy of transfer of the ions from infinite dilution in water to infinite dilution in water–DMSO. Thus for cyclohexane – carboxylic acid (compound 39) we note a monotonic increase in $\beta_1\theta_1$ from −2.72 in 5.9 mol% DMSO to +3.24 in 83.1% DMSO.

On the other hand, for 3′-chloro-2,4,6-trinitrodiphenylamine (compound 1) over this solvent range $\beta_1\theta_1$ changes monotonically from +1.02 to −1.21. The anion A^- derived from compound 1 has an extensively delocalized charge; such ions are found to be well solvated and stabilized by DMSO (27), and hence ${}_m\gamma_{A^-}$ can be expected to decrease with increasing DMSO content.

The term $\beta_2\theta_2$ may reflect chiefly the solvent activity coefficient ${}_m\gamma_{AH}$ of AH with increasing concentration of DMSO in the solvent. It has been found that ${}_m\gamma_i$ of nonelectrolytes such as diethylacetal and ethyl acetate first increase and then decrease with increase in DMSO content of solvent (27). Similar data are not available for any of the compounds 1–41 of Table 1, but would be most useful to have in the present connection.

Extrathermodynamic Interpretation of the Results

In the present case we study the process of ionization of a weak acid. This process is modified in two ways, (*i*) by substitution in the acid (change of indicator) and (*ii*) by changing the solvent composition. The output of the process, y, (here $y = p({}_sK_a)$) can be described as a continuous function in terms of vector variables relating to the two modes of change. If this function is differentiated with respect to these vector variables and if the modes of change are sufficiently small, one can derive a model from the output as eq. [8], see (13, 14).

$$[8] \quad y = \alpha + \sum_{a=1}^{A} \beta_a\theta_a + R(g)$$

Here the parameters α and β relate only to the first mode of change and θ only to the second mode, respectively. The remainder $R(g)$ contains terms of a Taylor expansion of gth degree and higher. $R(g)$ can be made arbitrarily small by making the two modes of change sufficiently small.

Can. J. Chem. Downloaded from www.nrcresearchpress.com by 210.87.254.42 on 09/06/12
For personal use only.

The two simplest models corresponding to the least pertubation of the system, i.e. the most minute amounts of change, are

$$[9a] \quad y = \alpha + \beta\theta + R(g)$$

and

$$[9b] \quad y = \alpha + \beta_1\theta + \beta_2\theta^2 + R(g)$$

The first of these two models [9*a*] corresponds to the single one-term LFER and is valid for any process provided that its pertubation is sufficiently small. When the pertubation is larger, however, the data are not well approximated by [9*a*] but one must use first eq. [9*b*] and then more complicated models like eq. [8] with $A \geq 2$. In the present case we note that eq. [9*b*] turns out to be adequate. Figure 2, displaying a plot of θ_1 against θ_2, clearly shows that θ_2 is quadratically related to θ_1. The extrathermodynamic interpretation of this result is that the change of solvent composition corresponds to the change in a single "effect" in the process. This effect shows a quadratic behaviour over larger intervals of solvent composition. This interpretation is consistent with the thermodynamical interpretation above, where the "activity coefficient" is included to describe the quadratic change of the main effect, "the solvent interaction."

Consequence of Two Terms for Validity of Acidity Functions

The various acidity function treatments (Bunnett–Olsen (20), Marziano–Cimino–Passerini (28), Cox–Yates (29)) require the term log ($\gamma_A\gamma_{H^+}/\gamma_{HA}$) to be a linear function of the term log ($\gamma_P\gamma_{H^+}/\gamma_{HP}$) in a series of solutions of varying acidity (PH being a set of acids which obey an acidity function H_P), or alternatively the term log ($\gamma_A/\gamma_{HA}\gamma_{OH^-}$) to be a linear function of the term log ($\gamma_P/\gamma_{HP}\gamma_{OH^-}$) in a series of solutions of varying basicity. In such a case a single solvent term θ_1 should describe the change in acidity or basicity of the solvent. We see that in the case of water–DMSO solutions such a treatment is inadequate.

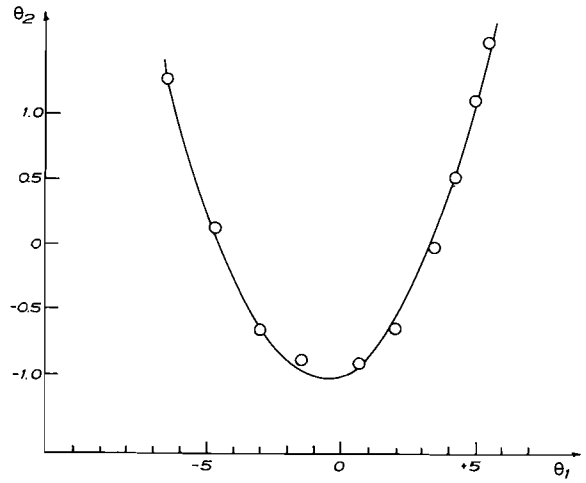

FIG. 2. θ_2 can be approximated by a function of θ_1:$\theta_2 = a + b\theta_1 + c\theta_1^2$.

However, for very short intervals of solvent composition, θ_1 and θ_2 are approximately linear to each other, see Fig. 2. Thus one might be misled to believe that a linear model ($A = 1$) is applicable for larger variations of solvent composition as assumed in the stepwise construction of acidity scales.

Further, it is seen from data set analyses 11 and 12 that by limiting the number of compounds to four or less, a second component is masked. This has nothing to do with limiting the diversity of compounds (see results for data analyses 6–10) but is just a consequence of having too few data to allow a statistical calculation of the second component. We note that in the Hammett "overlap procedure" generally used to establish acidity scales both for the basic and acidic regions, one compares only two compounds at a time, thereby ensuring that a second component is not seen.

Acknowledgments

Support from the Swedish Natural Science Research Council (to S.W. and M.S.) and from the Natural Sciences and Engineering Research Council of Canada (to J.T.E.) is gratefully acknowledged. Additionally, one of us (J.T.E.) wishes to acknowledge his gratitude to Prof. R. Schaal for his hospitality during a sabbatical leave in 1979–1980, and to the National Research Council – Le Centre de la Recherche Scientifique de France Scientific Cooperation program for financial support.

1. R. STEWART and J. P. O'DONNELL. J. Am. Chem. Soc. **84**, 493 (1962).
2. R. STEWART and J. P. O'DONNELL. Can. J. Chem. **42**, 1681 (1964); **42**, 1694 (1964).
3. K. BOWDEN, A. BUCKLEY, and R. STEWART. J. Am. Chem. Soc. **88**, 947 (1966).
4. D. DOLMAN and R. STEWART. Can. J. Chem. **45**, 911 (1967).
5. J. C HALLE, R. GABORIAUD, and R. SCHAAL. Bull. Soc. Chim. Fr. 1851 (1969).
6. J. C. HALLE, F. TERRIER, and R. SCHAAL. Bull. Soc. Chim. Fr. 4569 (1969).
7. J. C. HALLE, R. GABORIAUD, and R. SCHAAL. Bull. Soc. Chim. Fr. 2047 (1970).
8. J. C. HALLE, F. TERRIER, and R. GABORIAUD. Bull. Soc. Chim. Fr. 1225 (1973).
9. J. C. HALLE, F. TERRIER, and R. GABORIAUD. Bull. Soc. Chim. Fr. 1231 (1973).

10. J. C. HALLE. Bull. Soc. Chim. Fr. 1553 (1973).
11. E. C. STEINER and J. M. GILBERT. J. Am. Chem. Soc. **87**, 382 (1965).
12. J. T. EDWARD, P. G. FARRELL, J. KIRCHNEROVA, J. C. HALLE, and R. SCHAAL. Can. J. Chem. **54**, 1899 (1976).
13. S. WOLD and M. SJÖSTRÖM. Correlation analysis in chemistry: recent advances. *Edited by* J. Shorter and N. B. Chapman. Plenum Press, London. 1978. p. 1.
14. S. WOLD. Chem. Scr. **6**, 97 (1973).
15. S. WOLD and M. SJÖSTRÖM. Chem. Scr. **2**, 49 (1972).
16. S. WOLD and M. SJÖSTRÖM. Chemometrics, theory and practice. ACS Symposium Series No. 52, *Edited by* R. B. Kowalski. Am. Chem. Soc., Washington, DC. 1977.
17. S. WOLD. Tetrometrics, **20**, 397 (1978).
18. S. WOLD. SIMCA-27 manual, available from S. Wold.
19. S. WOLD. Pattern Recognition, **8**, 127 (1976).
20. J. F. BUNNETT and F. P. OLSEN. Can. J. Chem. **44**, 1899 (1966); **44**, 1917 (1966).
21. J. W. BARNETT and C. J. O'CONNOR. Aust. J. Chem. **26**, 2083 (1973); G. SCORRANO. Acc. Chem. Res. **6**, 132 (1973).
22. R. A. COX and R. STEWART. J. Am. Chem. Soc. **98**, 488 (1976).
23. W. S. MATTHEWS, J. E. BARES, J. E. BARTMESS, F. G. BORDWELL, F. J. CORNFORTH, G. E. DRUCKER, Z. MARGOLIN, R. J. MCCALLUM, G. J. MCCOLLUM, and N. R. VANIER. J. Am. Chem. Soc. **97**, 7006 (1975).
24. F. G. BORDWELL and J. A. HAUTALA. J. Org. Chem. **43**, 3116 (1978), and earlier papers.
25. E. J. KING. Acid-base equilibria. MacMillan, New York. 1965. Chapts. 10–12.
26. E. BUNCEL and H. WILSON. Acc. Chem. Res. **12**, 42 (1979).
27. A. J. PARKER. Chem. Rev. **69**, 1 (1969).
28. N. C. MARZIANO, G. M. CIMINO, and R. C. PASSERINI. J. Chem. Soc. Perkin Trans. II, 1915 (1973).
29. R. A. COX and K. YATES. J. Am. Chem. Soc. **100**, 3861 (1978).

Can. J. Chem. Downloaded from www.nrcresearchpress.com by 210.87.254.42 on 09/06/12
For personal use only.

A reinvestigation of the rate of reaction of *N*-decylimidazole with *p*-nitrophenyl decanoate

J. PETER GUTHRIE AND STELLA O'LEARY

Department of Chemistry, University of Western Ontario, London, Ont., Canada N6A 5B7

Received January 28, 1981

J. PETER GUTHRIE and STELLA O'LEARY. Can. J. Chem. **59**, 2358 (1981).

Reinvestigation of the reaction of *p*-nitrophenyl decanoate with *N*-decylimidazole shows that the rate enhancement attributable to 1 : 1 complex formation between reactants is small (12-fold), consistent with what we have found in related systems, and much less than values reported by other workers. Kinetics were carried out at very low concentrations to avoid problems of aggregation, and at pH 8.0 to minimize the contribution from solvolysis. Numerous difficulties were encountered with reactive degradation products from Tris buffers. At pH 8.0 the apparent second order rate constant was $2.25 \pm 0.64\ M^{-1}\ s^{-1}$.

J. PETER GUTHRIE et STELLA O'LEARY. Can. J. Chem. **59**, 2358 (1981).

Une nouvelle étude de la réaction du décanoate de *p*-nitrophényle avec le *N*-décylimidazole montre que l'augmentation de vitesse attribuable à la formation de complexe 1:1 entre les réactifs est faible (12 fois) en accord avec nos résultats relatifs à des systèmes apparentés et elle est de beaucoup inférieure aux valeurs rapportées par d'autres chercheurs. Pour éviter les problèmes d'association on a réalisé l'étude cinétique à de très faibles concentrations, et à un pH de 8,0 pour minimiser la contribution de solvolyse. On a rencontré plusieurs difficultés avec des produits de dégradation réactifs provenant du tampon de Tris. A un pH de 8,0 la constante de vitesse apparente d'ordre 2 est de $2{,}25 \pm 0{,}64\ M^{-1}\ s^{-1}$.

[Traduit par le journal]

Introduction

Numerous studies have been reported (1–6) of systems which might show rate enhancements due to stabilization of the transition state as a result of hydrophobic interactions involving two (or more) alkyl chains. Large rate effects have been claimed in several of these systems, (1–3, 5, 6), and the effects have been attributed to what has been assumed (implicitly or explicitly) to be a 1:1 interaction. We have had occasion to cast doubt upon the validity of this interpretation of the rate phenomena which were observed (7, 8, 10). In the first place, some of the early work was done at concentrations of substrate such that most of the substrate was aggregated (7–9). In the second place, the steroidal imidazole **1**[1] which should be similar to an alkyl imidazole in its hydrophobic binding properties, though it is much more soluble and does not form micelles (both effects resulting from the presence and location of the two ammonium groups) (11–13), showed *small* (1.6-fold) rate enhancements for *p*-nitrophenyl alkanoates relative to the acetate, although the rate enhancements which were observed increased in a regular fashion with increasing chain length (10).

Oakenful and Fenwick have recently reinvestigated the reaction of *N*-decyl imidazole with *p*-nitrophenyl alkanoates (2). They have confirmed our observation that, e.g., *p*-nitrophenyl decanoate can only be used at concentrations less than $2 \times 10^{-6}\ M$ if aggregation is to be avoided (7, 8). However, they report even larger rate constants than were reported by Blyth and Knowles (1), with similarly large rate enhancements (228-fold) for the reaction with *p*-nitrophenyl decanoate. The obvious discrepancy between our claim that alkyl groups can only give *small* rate enhancements and Oakenful's claim that they can give *large* rate enhancements has prompted us to study the reaction of *p*-nitrophenyl decanoate with *N*-decyl imidazole. We now report that at *low* concentrations of *N*-decyl imidazole the limiting second order rate constant corresponds to a *small* (12-fold) rate enhancement, which is consistent with the results we have reported for the reaction of **1** with *p*-nitrophenyl decanoate.

[1]Compound **1** is 17β-(4-imidazolyl)-5α-androstane-3β,11β-diamine (11–13).

Results

The reaction was studied both at pH 10 (carbonate buffer) and at pH 8 (Tris buffer). The studies at pH 10 were intended to reproduce the conditions employed by Knowles and Oakenful; however, these experiments suffered from the anticipated problem of a major contribution from hydroxide catalyzed reaction. At pH 8 this background rate was much smaller: unfortunately, major experimental difficulties were encountered as a result of decomposition of the Tris buffer. These buffer solutions were made up from either primary standard grade Tris (Fisher) (which had been recrystallized prior to use) or else from Sigma "Trizma Base" using glass distilled water in every case. With either sample of Tris, within about a week some reactive impurity was generated, which led to

0008-4042/81/152358-06$01.00/0

©1981 National Research Council of Canada/Conseil national de recherches du Canada

Can. J. Chem. Downloaded from www.nrcresearchpress.com by 210.87.254.6 on 09/06/12
For personal use only.

Can. J. Chem. Downloaded from www.nrcresearchpress.com by 210.87.254.6 on 09/06/12
For personal use only.

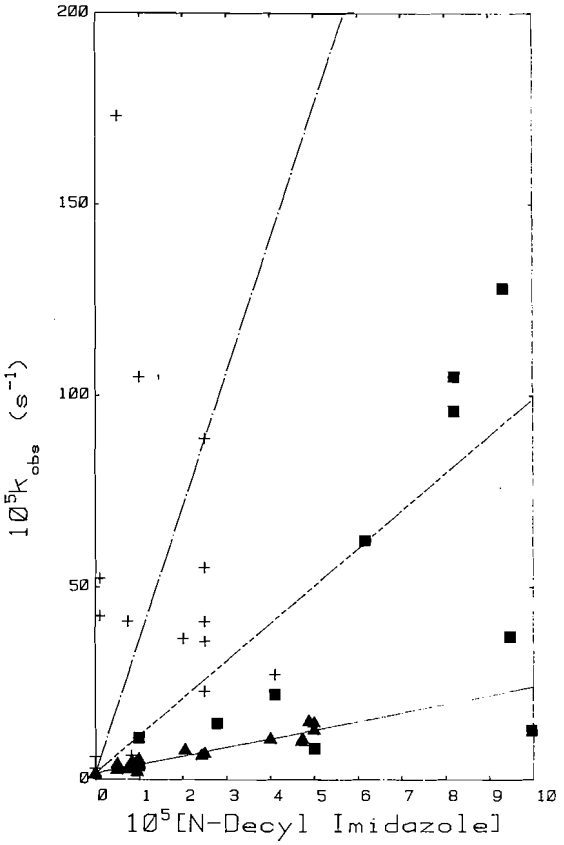

FIG. 1. Observed rate constants for *N*-decylimidazole catalyzed hydrolysis of *p*-nitrophenyl decanoate at pH 8.0, 25°C. (+) Reactions in aged Tris buffer (more than a week old). (■) Runs which were not included in the least squares fit. (●) Runs which were used in the least squares fit. (—) Best line by least squares. (-·-) Line calculated using the second order rate constant from ref. 2. (— - - —) Line calculated using the second order rate constant from ref. 1.

anomalously fast reactions. In an attempt to compensate for this problem, we have run replicate reactions, always using fresh buffer solutions, using two sources of Tris, and two different preparations of *N*-decylimidazole. Runs which did not give linear pseudo-first order plots were discarded as were runs leading to anomalously high rates. Since decomposition of the buffer leads to spuriously *fast* reactions, we should at least be able to put an *upper* limit on the true rate constants.

The rate constants which we obtained are found in the Supplementary Table,[2] and are compared with the predicted values based upon the published second order rate constants of Blyth and Knowles (1) and Oakenful and Fenwick (2) in Figs. 1 and 2. Qualitatively it is clear, particularly at pH 8, that our pseudo-first order rate constants correspond to a *much* smaller second order rate constant than those reported by Knowles (1) and Oakenful (2) and co-workers. At pH 10 the discrepancy between our results and those of Knowles is much less marked. Under either set of conditions the discrepancy between our results and those of Oakenful is enormous and inexplicable. Our kinetics were done with substrate concentrations of 1×10^{-6} *M* or 5×10^{-7} *M* which we and Oakenful agree is below the critical concentration for this ester. We have employed 10 cm cells, and a Gilford model 240 spectrophotometer, following a total absorbance change of ≥0.080, so that with an instrumental

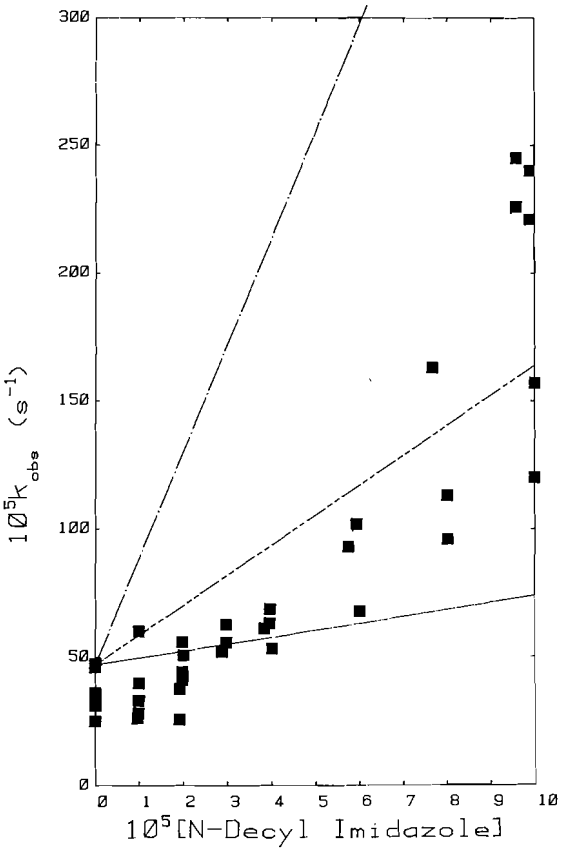

FIG. 2. Observed rate constants for *N*-decylimidazole catalyzed hydrolysis of *p*-nitrophenyl decanoate, pH 9.9, 25°C. (—) Line drawn using the second order rate constant determined at pH 8.0, with the intercept chosen to give the best fit to the observed data. (-·-) Line calculated using the same intercept and the second order rate constant from ref. 2. (— - - —) Line calculated using the same intercept and the second order rate constant from ref. 1.

[2]Copies of the Supplementary Table may be obtained, at a nominal charge, from the Depository of Unpublished Data, CISTI, National Research Council of Canada, Ottawa, Ont., Canada, K1A 0S2.

Can. J. Chem. Downloaded from www.nrcresearchpress.com by 210.87.254.6 on 09/06/12
For personal use only.

error of ca. 0.002 in absorbance we anticipate that the maximum uncertainty in pseudo-first order rate constants attributable to the uncertainty in absorbance change should be ca. 20%, and in fact this is approximately the scatter which is observed.

For the data at pH 8 we endeavored to determine the best second order rate constant by fitting the data to $k_{obs} = k_0 + k_2$ [catalyst]. In order to do this it was necessary to discard various points which deviated drastically from the best line. First, all runs carried out using old Tris solutions were discarded. Then all runs for decyl imidazole concentrations greater than 5×10^{-5} M were discarded, because most of these points (but not all, see Fig. 1) were drastically faster than predicted by the best line. Then points deviating by more than two standard deviations from the best line by least squares were discarded and the least squares calculation was repeated to give $k_0 = 1.65 \pm 1.63$ s^{-1} and $k_2 = 2.25 \pm 0.64$ M^{-1} s^{-1}. An extreme, but defensible, position regarding these experiments would be that systematic errors are going to be in the sense of anomalously fast reaction rates; in general this is illustrated by Fig. 1. A line fitted to the lowest values at each concentration of *N*-decylimidazole would have a significantly lower slope. We must regard our least squares line as an upper limit to the true value, which may be smaller.

The data at pH 10 do not permit evaluation of a line: the scatter is greater, the background rate is higher, and there is a clear upward curvature to the plot of k_{obs} vs. [catalyst]. We did not attempt to determine a second order rate constant from these data: Fig. 2 shows that a line corresponding to the second order rate constant determined at pH 8 can give a plausible fit to the data for catalyst concentrations below 5×10^{-5} M. The second order rate constant was corrected for partial protonation of the imidazole at pH 8, using an estimated pK_a for *N*-decylimidazole of 7.30 (the value for *N*-ethylimidazole (19)). The line corresponding to the second order rate constant reported by Blyth and Knowles (1) is also consistent with the data (and would pass through our data at all concentrations of *N*-decylimidazole if a lower intercept were used). Once again, the line corresponding to the second order rate constant reported by Oakenful and Fenwick (2) is not consistent with our data.

Discussion

The use of linear alkyl groups as hydrophobic binding regions in enzyme models has had a considerable appeal, since very simple syntheses lead to incorporation of these groups. Although it has generally been recognized that micellization will be a problem, attempts have been made to circumvent this difficulty and numerous claims of large rate enhancements are to be found in the literature (1–3, 5). A summary of the results of these studies is to be found in Table 1. The most striking feature of this table is the remarkable inconsistency in rate enhancements from one experiment to the next. If the simplest interpretation of the data in this table, namely that they all represent the consequences of 1:1 association, were true, one would expect that the rate enhancements in part (a) of this table would be similar for each of the three systems for constant n, and that there would be a regular increase in rate enhancement with increasing n, as is found. Furthermore, one would expect, in the absence of extraneous factors such as strain in the transition state, that the systems in part (b) of the table would show larger rate enhancements than the analogous systems in part (a). In general this is not what is seen, but on careful examination some pattern can be discerned. Two of the systems in part (b) are probably artefactural; these are the $n = 10$ case of system (*v*), for which the substrate was apparently used at a concentration greater than its solubility limit; and system (*viii*), for which the catalyst is a very large hydrophobic molecule with very few hydrophilic residues to draw it into solution, and the substrates, *p*-nitrophenyl decanoate, dodecanoate, and hexadecanoate were used at concentrations above their solubility limits. The remaining systems in parts (b) and (c) of the table can be taken as giving reliable data, with two perturbing features which lead to apparent inconsistencies. The binding sites differ in the degree to which they can remove the alkyl chain of the substrate from solution. Systems (*v*) (*vi*), and (*viii*) are the ones expected to give the most complete removal, and for (*v*) and (*vi*), plots of log (rate enhancement) vs. π (14, 15) have slopes of 1.04 and 1.06 respectively. For systems (*iv*) and (*vii*), part of the alkyl chain may not be in contact with the binding site, and there may be some strain introduced in achieving a conformation which permits binding. Both of these effects will lead to lower rate enhancements than would otherwise be expected. The large slope (0.94) observed for the dependence of log (rate enhancement) upon n for system (*iv*) is surprising and a source of some concern. System (*viii*) used large hydrophobic compounds, and one must suspect that the components were not in true solution.

After all of these caveats have been considered, there remains the general picture that where the rate enhancements in part (b) might have been expected to be significantly larger than the analogous

Can. J. Chem. Downloaded from www.nrcresearchpress.com by 210.87.254.6 on 09/06/12
For personal use only.

TABLE 1. Rate enhancements attributed to hydrophobic interactions of alkyl chains

System	n^b =	Rate enhancements[a] 4	5	6	7	8	9	10	11	Ref.
(a) Single chain – single chain interactions										
(*i*) R—COOAr + R—N⟨N[c]		10		60		550				[d]
(*ii*) R—COOAr + R—N⟨N[e]		6		66		372				[f]
(*iii*) R—$^+$N$(CH_3)_2$—$(CH_3)_2$OCOOAr Br$^-$ + RCONH—CH(CH$_2$—⟨N)—COO$^-$	[g]								2300	[h]
(b) Single chain – complex binding site interactions										
(*iv*) R—NH_2 + ⟨N (RCO—O)[i]					1.3[j] 1.5[k]		11.5[j] 12.4[k]			[l]
(*v*) RCOOAr + Z—N⟨$(CH_2)_{12}$⟩N—Z[m] Z = CH_2—CO—$N(CH_3)$OH		8.8		97				4470		[n]
(*vi*) RCOOAr + chymotrypsin[o]		13.1	45.4							[p]
(*vii*) RCOOAr + 17β-(4(5)-imidazolyl)-5α-androstane-3β,11β-diamine[q]		1.11		1.28		1.82				[r]
(*viii*) RCOOAr + 10-hydroxy-11-hydroximino-[20]-paracyclophane[s]							300		1014	[t]
(c) Double chain – complex binding site interactions										
(*ix*) R—NH + ⟨C(=O)—O—C(=O) (R)[u]		14.7	26.1	38.7						[v]

[a] Unless otherwise stated, rate enhancements are expressed as ratios of k_{rel} values for a substrate (catalyst relative to a reference catalyst) relative to a reference substrate.
[b] Number of extra methylenes able to interact compared to the reference reaction.
[c] Reference catalyst is *N*-ethyl imidazole; reference substrate is *p*-nitrophenyl acetate.
[d] Reference 1.
[e] Reference compounds as in footnote *c*; k_{rel} values for *N*-ethylimidazole taken from ref. 1.
[f] Reference 2.
[g] Rate enhancement is k_{rel} for *N*-stearoyl histidine relative to *N*-acetylhistidine with *p*-nitrophenyl *N*-dodecyl-*N*,*N*-dimethylammonioethyl carbonate.
[h] Reference 3.
[i] Reference catalyst is ethylamine; reference substrate is the acetate ester.
[j] 8-Hydroxyquinoline esters.
[k] 6-Hydroxyquinoline esters.
[l] Reference 4.
[m] Reference catalyst is $((CH_3)_2CHCH_2)_2NCH_2CON(CH_3)OH$; reference substrate is *p*-nitrophenyl acetate.
[n] Reference 5.
[o] Reference catalyst is OH^-; reference substrate is *p*-nitrophenyl acetate.
[p] Reference 16.
[q] Reference catalyst is imidazole; reference substrate is *p*-nitrophenyl acetate.
[r] Reference 10.
[s] Reference catalyst is 2-hydroxycyclodecanone oxime; reference substrate is *p*-nitrophenyl acetate.
[t] Reference 6.
[u] Rate enhancements are k_{rel} values relative to diethylamine as standard nucleophile.
[v] Reference 17.

rate enhancements in part (a), they are in fact either similar or even smaller. The three systems in part (a) of the table appear to be out of line, and it is this feature which led us to reinvestigate the *N*-decylimidazole – *p*-nitrophenyl decanoate reaction. For system (*iii*), although the authors (3) clearly state that they interpret their rate enhancements in terms of 1:1 complex formation, it seems highly probable that mixed micelles are present. For systems (*i*) and (*ii*), three factors seem

Can. J. Chem. Downloaded from www.nrcresearchpress.com by 210.87.254.6 on 09/06/12
For personal use only.

to be involved. First, some of the experiments in system (*i*) were carried out at concentrations of ester greater than the solubility limit (8, 9). Second (and related), the relative rate constant for *p*-nitrophenyl decanoate (with the acetate as standard) reacting with *N*-ethylimidazole is ten times smaller than expected, i.e. than the relative rate constant for the analogous reaction with imidazole, and adequately low concentrations of ester (8). Since the rate constant for *N*-ethylimidazole with *p*-nitrophenyl decanoate is spuriously low the apparent rate enhancement for *N*-decylimidazole is spuriously high. Thirdly, it appears on the basis of the work reported in this paper that the second order rate constant for the reaction of *N*-decylimidazole with *p*-nitrophenyl decanoate is too high, in part because the earlier studies were not done at low enough concentrations. Our rate enhancement was calculated using the value for the rate constant for the reaction of *N*-decylimidazole with *p*-nitrophenyl acetate reported by Blyth and Knowles (1), and our rate constants for the reactions of imidazole with *p*-nitrophenyl acetate and decanoate (8), as well as the rate constant for the reaction of *N*-decylimidazole with *p*-nitrophenyl decanoate determined in the present work; the value so obtained is 12-fold. This rate enhancement appears more reasonable than the larger values previously claimed for an association process which involves partial removal of alkyl chains from water. There should be only modest strain involved in achieving the transition state with hydrophobic contact between alkyl chains, so that most of the potential rate enhancement should be manifested.

Why is a linear alkyl chain so poor as a binding site for hydrophobic stabilization of a transition state? In part this reflects the fact that in a 1:1 complex, only about a quarter of the surface area will be removed from contact with water, unless the alkyl chain binds to a cavity. Rather more serious is the problem of loss of conformational flexibility imposed by the requirement that the chain be in contact with another molecule along its entire length. Only a small fraction of the available conformations will satisfy this constraint, so that there is a serious loss in conformational entropy if binding occurs. As a consequence, the binding is weak unless the binding site is a cavity. This entropic constraint does not apply so seriously to binding to a micelle, since the interior of the micelle is liquid-like in nature and most conformations of the alkyl chain are accessible.

Why has it proven so difficult to obtain reproducible and reliable rate constants in the experiments reported here? We believe that the problem is, in part, the extreme sensitivity to traces of catalytic agents, of whatever nature such as appeared in aged Tris solutions. Using fresh solutions and glass distilled water was a workable solution. Nitrophenyl esters are very sensitive to nucleophilic impurities in solvents: we have always purified our acetonitrile by passage through active alumina. It seems very probable that results are sensitive to the technique of reaction initiation, since a relatively concentrated solution of a very water insoluble compound is being added to an aqueous reaction medium. Minor delays in mixing can lead to formation of slowly dissolving microdroplets, which could conceivably serve as nuclei for some sort of micellar aggregation which would lead to enhanced reaction rates at concentrations where micelles are thermodynamically unstable. Although we can speculate about the reasons for the observed erratic behavior, we wish to stress the severe problems which were encountered in this work, and caution anyone planning to investigate related systems to be suitably cautious.

Conclusions

1. In accord with our earlier statements, 1:1 binding of alkyl chains produces *small*, up to 12-fold, rate enhancements.

2. Because of the extreme experimental difficulties which may be encountered in obtaining reliable rate constants, and the many artefacts which can arise, we recommend that chains longer than eight carbons not be used except when micellar catalysis is desired, and that even for eight-carbon chains, low concentrations should be employed, with long path length cells for spectrophotometric studies.

3. We suggest that plots of log (rate enhancement) vs. π be constructed whenever hydrophobic rate enhancements are reported, and that the magnitude of the slope be used as a criterion of reasonableness: the slope should be similar to the fraction of total hydrophobic surface removed from contact with water. In the present case the slope (based on decanoate and acetate) is 0.24, which appears reasonable.

Experimental

Materials

Trishydroxymethylaminomethane was obtained from two sources, Fisher Chemical Co. (recrystallized before use) and Sigma Chemical Co., "Trizma Base," used without further purification.

KCl, $NaHCO_3$ and Na_2CO_3 were reagent grade chemicals used without further purification.

N-Decylimidazole was prepared according to the method of Haring (18). Acetonitrile (Fisher Scientific Co.) was passed through a column of grade I neutral alumina (Woelm) to remove nucleophilic impurities.

Kinetic Procedures

Reactions were initiated by adding a small portion of a solution of substrate in purified acetonitrile to temperature-equilibrated buffer in a 10 cm spectrophotometer. All solutions of *N*-decylimidazole at pH 8, buffered with trishydroxymethylaminomethane, were made up freshly every 3–4 days. Solutions at pH 9.8, buffered with carbonate, were made up freshly every 5 days. The solutions were made up by weighing out the *N*-decylimidazole in an aluminium foil boat, which was then transferred to a volumetric flask. The solutions were stirred overnight before use, to ensure complete solution of the *N*-decylimidazole in the water. Changes in absorbance were followed using a Gilford Model 240 spectrophotometer. pH values were measured at the end of the reaction using a Radiometer pH Meter 25 SE with a GK 2301C combined electrode. Reactions were followed for at least three half-lives.

1. C. A. BLYTH and J. R. KNOWLES. J. Am. Chem. Soc. **93**, 3017 (1971).
2. D. G. OAKENFUL and D. E. FENWICK. Aust. J. Chem. **27**, 2149 (1974).
3. R. G. SHORENSTEIN, C. S. PRATT, C. J. HSU, and T. E. WAGNER. J. Am. Chem. Soc. **90**, 6199 (1968).
4. T. MAUGH and T. C. BRUICE. J. Am. Chem. Soc. **93**, 6584 (1971).
5. R. HERSHFIELD and M. L. BENDER. J. Am. Chem. Soc. **94**, 1376 (1972).
6. Y. MURAMAKI, J. SUNAMOTO, H. OKAMOTO, and K. KAWANAMI. Bull. Chem. Soc. Jpn. **48**, 1537 (1975).
7. J. P. GUTHRIE. Chem. Commun. 897 (1972).
8. J. P. GUTHRIE. Can. J. Chem. **51**, 3494 (1973).
9. Y. MURAMAKI, Y. AOYAMA, and M. KIDO. J. Chem. Soc. Perkin Trans. II, 1947 (1977).
10. J. P. GUTHRIE and Y. UEDA. Chem. Commun. 991 (1974).
11. J. P. GUTHRIE. Can. J. Chem. **50**, 3993 (1972).
12. J. P. GUTHRIE and Y. UEDA. Chem. Commun. 898 (1973).
13. J. P. GUTHRIE and Y. UEDA. Can. J. Chem. **54**, 2745 (1976).
14. T. FUJITA, J. IWASA, and C. HANSCH. J. Am. Chem. Soc. **86**, 5175 (1964).
15. M. S. TUTE. Adv. Drug Res. **6**, 1 (1971).
16. T. H. MARSHALL and A. AKGUN. J. Biol. Chem. **246**, 6019 (1971).
17. I. H. PETMAN, K. UEKAMA, T. HIGUCHI, and W. E. HALL. J. Am. Chem. Soc. **94**, 8147 (1972).
18. M. HARING. Helv. Chim. Acta, **42**, 1845 (1959).
19. W. P. JENCKS and J. REGENSTEIN. *In* Handbook of biochemistry. 1st ed. Chemical Rubber Publishing Co., Cleveland, OH. 1968.

Can. J. Chem. Downloaded from www.nrcresearchpress.com by 210.87.254.6 on 09/06/12
For personal use only.

The crystal and molecular structure of 2,2-dimethyl-4,4,6,6-tetrafluorocyclotriphosphazene

A. WALLACE CORDES AND PAUL N. SWEPSTON

Department of Chemistry, The University of Arkansas, Fayetteville, AR 72701, U.S.A.

AND

RICHARD T. OAKLEY, NORMAN L. PADDOCK, AND T. N. RANGANATHAN

Department of Chemistry, The University of British Columbia, 2036 Main Mall, University Campus, Vancouver, B.C., Canada V6T 1Y6

Received October 13, 1980

A. WALLACE CORDES, PAUL N. SWEPSTON, RICHARD T. OAKLEY, NORMAN L. PADDOCK, and T. N. RANGANATHAN. Can. J. Chem. **59**, 2364 (1981).

Crystals of the title compound are orthorhombic, $a = 7.387(1)$, $b = 8.502(2)$, $c = 14.662(2)$ Å, $Z = 4$, space group *Pnma*. The structure was solved by direct methods and refined by least-squares procedures to a final R of 0.058, $R_w = 0.097$ for the 530 reflections with $I > 3\sigma(I)$. The P_3N_3 ring is slightly but significantly non-planar with a crystallographically-imposed mirror plane normal to the ring, and the PN bond lengths in order from the PMe_2 group are 1.601(7), 1.552(7), and 1.560(6) Å. The ring angles are 114.0(4)°, (PMe_2); 120.0(4)°, PF_2; 123.2(5)°, N(3); 119.6(5)°, N(4). The mean exocyclic bond lengths are P—C, 1.77(1), P—F, 1.522(6), and the exoangles are 107.4(4)° (PMe_2) and 97.2(3)°, (PF_2). The bond lengths within the ring are well described in terms of simple perturbation theory, but comparison with the structures of other molecules shows the importance of factors other than π-electron distribution.

A. WALLACE CORDES, PAUL N. SWEPSTON, RICHARD T. OAKLEY, NORMAN L. PADDOCK et T. N. RANGANATHAN. Can. J. Chem. **59**, 2364 (1981).

Les cristaux du composé mentionné dans le titre sont orthorhombiques avec $a = 7,387(1)$, $b = 8,502(2)$, $c = 14,662(2)$ Å, $Z = 4$, groupe d'espace *Pnma*. On a résolu la structure par les méthodes directes et on l'a affinée par la méthode des moindres carrés jusqu'à des valeurs de $R = 0,058$ et de $R_w = 0,097$ pour 530 réflexions avec $I > 3\sigma(I)$. Le cycle P_3N_3 dévie légèrement, mais d'une façon significative, du plan et il comporte un plan miroir imposé cristallographiquement qui est normal au cycle; les longueurs de la liaison PN, à partir du groupe PMe_2, sont: 1,601(7), 1,552(7) et 1,560(6) Å. Les angles du cycle sont: 114,0(4)°, (PMe_2); 120,0(4)°, PF_2; 123,2(5)°, N(3); 119,6(5)°, N(4). Les longueurs moyennes des liaisons exocycliques sont P—C, 1,77(1), P—F, 1,522(6) et les angles *exo* sont de 107,4(4)° (PMe_2) et de 97,2(3)° (PF_2). Les longueurs des liaisons à l'intérieur du cycle sont bien décrites par la théorie de perturbation simple; toutefois la comparaison avec des structures d'autres molécules révèle l'importance de facteurs autres que la distribution des électrons π.

[Traduit par le journal]

Introduction

An interesting feature of the geometry of inhomogeneously substituted cyclophosphazenes is that the lengths of the bonds within the ring are often significantly unequal. One example is $N_4P_4F_6Me_2$ (1) (the 1,1-dimethyl isomer), in which it is supposed (2) that electron release by the methyl groups reduces the electronegativity of the phosphorus atom to which they are attached, so altering the π-electron distribution within the ring. The large bond length inequalities found experimentally (1) parallel the changes in bond order estimated by a perturbation treatment (2).

Another important source of information has been the study of the effect of the number of PN units in the ring on chemical and physical properties. Such studies have been used, through photoelectron spectroscopy, to identify the π-systems (3), and through nmr spectroscopy (4), to assess the separate inductive and conjugative interactions between phenyl and phosphazenyl rings.

In the simplest case, approximated by methyl substitution, the interaction is purely inductive. The preparation of *gem*-$N_3P_3F_4Me_2$ (5) allows us to examine the comparative effects of inductive interactions in 6- and 8-membered rings, and to see whether simple perturbation theory adequately describes the effect of ring size on the bond length inequalities.

Experimental

A mixture of methylfluorocyclotriphosphazenes was prepared by the addition of a two-fold excess of methyllithium in ether to hexafluorocyclotriphosphazene $N_3P_3F_6$ in ether at −20°C. The principal product was the monomethyl derivative $N_3P_3F_5Me$ (bp 105.7/752, lit. (6) 65/280). It was accompanied by a small amount of a volatile crystalline solid, which was recrystallised from $CHCl_3/CCl_4$ as $N_3P_3F_4Me_2$, mp 127.5–128°C. *Anal.* calcd for $C_2H_6F_4N_3P_3$: C 9.93, H 2.30, N 17.17; found C 10.19, H 2.48, N 17.40. High resolution mass measured 240.970; calcd for $N_3P_3F_4Me_2$, 240.971. The nmr spectra show that methyl substitution is geminal. Details are given in Table 1.

The crystal of $N_3P_3F_4Me_2$ used for all X-ray data collection was bounded by five pairs of parallel faces, parallel to the (010), (100), (001), (102), and ($\bar{1}02$) planes, at face-to-center distances of 0.16, 0.10, 0.10, 0.10, and 0.10 mm (all ±0.02 mm). The crystal was mounted on a fiber with the b axis parallel to the φ axis of the diffractometer. A least-squares refinement of 18 values of 2 sin θ/λ gave cell constants for $P_3N_3F_4C_2H_6$ (fw =

0008-4042/81/152364-04$01.00/0

©1981 National Research Council of Canada/Conseil national de recherches du Canada

Can. J. Chem. Downloaded from www.nrcresearchpress.com by 210.87.254.4 on 09/06/12
For personal use only.

Can. J. Chem. Downloaded from www.nrcresearchpress.com by 210.87.254.4 on 09/06/12
For personal use only.

TABLE 1. Nuclear magnetic resonance parameters[a]

	PMe_2			PF_2		
Compound	δ_P	δ_H	J_{PH}	δ_P	δ_F	J_{PF}
$N_3P_3F_4Me_2$[b]	−71.0	1.65	14.6	−104.3	−68.8	(927)
$N_4P_4F_6Me_2$[c]	−93.0	1.64	14.6	−126.5[d]	−69.2[d]	870
				−126.5	−68.5	845(846)

[a]Shifts (ppm) relative to internal TMS, $CFCl_3$, external P_4O_6. Downfield shifts positive. Coupling constants in Hz; those in parentheses from F spectrum.
[b]In solution in $CDCl_3$; $^4J_{PH}$ = 1.90 Hz, $^3J_{PP}$ = 45.0 Hz.
[c]Neat liquid. $^4J_{PH}$ = 1.4 Hz.
[d]PF_2 group remote from PMe_2.

241.01) of $a = 7.387(1)$, $b = 8.502(2)$, $c = 14.662(2)$ Å, $V = 920.9$ Å^3; and ρ_{calcd} (for $Z = 4$) = 1.74 g cm^{-3}. The Laue symmetry and the systematic absences of the orthorhombic crystal indicated space group *Pnma*; four molecules per unit cell in this space group imposes either a mirror plane (the case here) or an inversion center on the molecules.

A Datex-automated General Electric XRD 6 diffractometer was used with Ni-filtered CuKα (λ = 1.5418 Å) radiation. For the intensity data a θ–2θ scan over a range of (1.80 + 0.86 tan θ)° in 2θ was made at a speed of 4° min^{-1}; stationary crystal – stationary counter background readings were taken for 10 s at each end of the scans. All reflections (732) with $2\theta < 120°$ were scanned. Of these, 530 had $I > 3\sigma(I)$ and were used for the solution and refinement of the structure. A check reflection measured every 50 reflections during data collection indicated an 18% decay during the last half of data collection, due to crystal decomposition, for which a simple linear correction was made. The extent of decay, which was also found to occur in a second crystal, precluded the collection of data beyond $2\theta = 120°$. The crystal has a value of 55.6 cm^{-1}; an absorption correction with summation points every 0.004 cm gave a range of correction factors (for I) of 0.34 to 0.44.

The structure was solved by direct methods and refined by full-matrix least-squares procedures. One P atom, one N atom, two C atoms, and two H atoms are located on the mirror at $y = 0.25$. Neutral atom scattering factors were used (7) and real and imaginary anomalous dispersion corrections were made for P (8). Least-squares weights of $w = 1/(2|F_{min}| + |F_{obs}| + 2|F_{obs}|^2/|F_{max}|)$ for the 530 observed reflection, 71 parameter, refinement gave a final $R = 0.068$, $R_w = 0.097$, a standard deviation of observation of unit weight of 0.46, and no dependence of $\Delta F/\sigma(F)$ on either F or sin θ. The final least-squares cycle included refinement of the positional parameters of the methyl hydrogen atoms, with constrained isotropic temperature factors of $B = 5.0$. No parameter shifted by more than 0.3σ in the final cycle, and a final difference Fourier showed no peaks above 0.3 e/Å^3. Final positional parameters are listed in Table 2. Observed and calculated structure factors and thermal parameters have been placed in the Depository of Unpublished Data.[1] Bond lengths and angles are shown in Fig. 1.

Results and Discussion

All the intermolecular distances exceed the normal Van der Waals distances, so that the molecular geometry is unlikely to be affected significantly by intermolecular interaction. Figure 1 shows a general view of the molecule, with the crystallographic numbering scheme and the principal molecular dimensions. The six ring atoms are coplanar within 0.02(1) Å ($\chi^2 = 20.0$); N(3) and N(3′) are 0.019(6) Å above the P_3 plane, and N(4) is 0.022(10) Å below (details deposited).[1] The PF_2 plane makes a dihedral angle of 88.9(2)° with the best plane of the ring. The deviations from the ideal symmetry of C_{2v} are small enough to allow averaging of related lengths and angles.

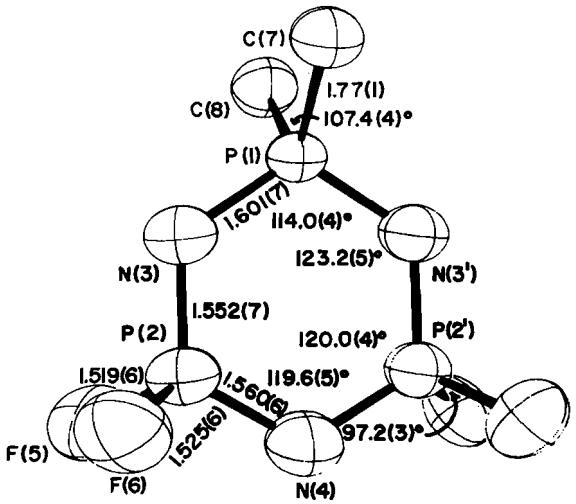

FIG. 1. Molecular diagram of $N_3P_3F_4Me_2$, showing bond lengths (Å) and angles (deg).

To some extent, the mean geometry of the ring can be correlated with ligand electronegativity. The ring angle at phosphorus decreases in the series $N_3P_3F_6$, 119.6° (9), $N_3P_3Cl_6$, 118.4 (10), $N_3P_3Me_6$, 116.8 (11), as the π-electron density moves from phosphorus towards nitrogen. Correspondingly, the P—N bond lengths increase; 1.570, 1.581, 1.605 Å. In $N_3P_3Ph_6$, P—N = 1.597 Å, $\hat{P}$ = 117.8° (12), so that, from this point of view, the phenyl group is slightly more electronegative than the methyl group. The implication is corroborated by the PPh_2 and PF_2 chemical shifts in $N_3P_3F_4Ph_2$, which are −82.1, −101.1 ppm respectively (13),

[1]The structure factor table and the table of thermal parameters are available, at a nominal charge, from the Depository of Unpublished Data, CISTI, National Research Council of Canada, Ottawa, Ont., Canada K1A 0S2.

TABLE 2. Final fractional positional parameters with esd's in parentheses

Atom	x	y	z
P(1)	0.4084 (4)	0.25	0.5401 (2)
P(2)	0.1636 (3)	0.0914 (3)	0.6502 (1)
N(3)	0.3220 (8)	0.0921 (8)	0.5807 (4)
N(4)	0.082 (1)	0.25	0.6848 (7)
F(5)	0.0094 (7)	−0.0099 (6)	0.6150 (4)
F(6)	0.2105 (8)	−0.0087 (7)	0.7332 (3)
C(7)	0.644 (1)	0.25	0.5625 (9)
C(8)	0.381 (2)	0.25	0.4200 (8)
H(C7)	0.68 (2)	0.25	0.62 (1)
H(C8)	0.26 (2)	0.25	0.407 (9)
H'(C7)	0.69 (1)	0.37 (1)	0.548 (7)
H'(C8)	0.43 (1)	0.35 (1)	0.399 (7)

and indicate a greater polarisation of charge in the methyl derivative. The small variations of P—N bond lengths within the structure of $N_3P_3Ph_4Me_2$ (14) show that the electronegativity difference in this sense is small. It is not surprising, therefore, that the mean PN bond lengths in $N_3P_3F_4Me_2$ and $N_3P_3F_4Ph_2$ (15) should be so nearly equal (1.571, 1.572 Å), but the bonds are unexpectedly short; simple averaging of the bond lengths in $N_3P_3F_6$, $N_3P_3Me_6$ would suggest 1.582 Å as a likely value. Such a shortening is found in other compounds — in $N_3P_3F_4(NH_2)_2$ (16) the mean P—N bond length is 1.562 Å, shorter than in $N_3P_3F_6$ itself — but it is at present unexplained.

Perhaps the greatest interest in the structures of inhomogeneously substituted phosphazenes is in the inequality of ring bond lengths induced by the substituents, here the pair of methyl groups. They reduce the electronegativity of the phosphorus atom to which they are attached, so weakening the π-interaction in the immediate P—N bonds. The weakening, indicated by a slightly greater bond length of 1.601 Å, is accompanied by a decrease of angle at P(1) to 114.0°, which is even less than in $N_3P_3Me_6$ (116.8°). The corresponding exo-angle increases from 102.6° to 107.4° in $N_3P_3F_4Me_2$, a greater change than the 2° increase expected from the change in σ-hybridisation. The increased localisation of π-bonding in the second and third bonds is accompanied by an increase of 0.4° in the ring angle at P(2) compared to that at N(4).

The application of HMO theory shows that if $\alpha_N = \alpha_p + 2\beta$, an assumption which is not critical, the deviations of the successive π-bond orders from the mean should be in the ratio −1:0.7:0.3. The deviations from the mean bond length are in the ratio 1, −0.63, −0.37, as good an agreement as can be expected, since the difference between the lengths of the second and third bonds is not crystallographically significant. In $N_3P_3F_4Ph_2$ the agreement is even closer. The structure of $N_4P_4F_6Me_2$ makes an interesting comparison. As pointed out earlier (2), the variation of bond lengths away from the perturbing centre is paralleled by the calculated bond-atom polarisabilities, which is good evidence that the bond length changes are well described in terms of the π-inductive effect of the methyl substituents. However, the deviations of the π-bond orders from the mean, calculated as just described for those of the trimeric derivatives, are in the ratios −1:0.57:0.16:0.27. The deviations of the bond lengths from the mean are in the ratios 1:−0.73:0.21:−0.47. Both sets of numbers oscillate, but the bond lengths have greater variation. In $N_3P_3F_4Me_2$, the mean deviation from the calculated mean bond order is 0.042, and the mean deviation from the mean bond length is 0.020 Å. In the tetrameric derivative, a calculated smaller bond order deviation (0.036) is associated with a larger mean bond length deviation (0.039 Å); localisation of the double bonds is more pronounced.

These comparisons show that, although the qualitative variations in bond length in inhomogeneously substituted phosphazenes are well described in terms of the perturbation of a π-electron system, bond order calculations by themselves are not enough for a quantitative treatment. The problem is related to that of bond alteration in annulenes (17), with the difference that the bonds are highly polar, and it may be that, in so far as the π-systems involved are homomorphic, the π-electron energy (per electron) to be set against σ-bond compression energy (18) is smaller in the 8-membered than in the 6-membered ring. At present, too little is known of the ring force constants. It is likely that a full discussion would require both these and the use of the theoretical concepts developed earlier (19).

Acknowledgements

We are grateful to the National Research Council of Canada for a Post-Doctoral Fellowship (to R.T.O) and for financial support, to the University of British Columbia for a University Graduate Fellowship (to T.N.R.) and to the University of Arkansas Research Council for a computing grant.

1. W. C. MARSH and J. TROTTER. J. Chem. Soc. A, 573 (1971).
2. T. N. RANGANATHAN, S. M. TODD, and N. L. PADDOCK. Inorg. Chem. **12**, 316 (1973).
3. G. R. BRANTON, C. E. BRION, D. C. FROST, K. A. R. MITCHELL, and N. L. PADDOCK. J. Chem. Soc. A, 151 (1970).
4. T. CHIVERS and N. L. PADDOCK. Inorg. Chem. **11**, 848 (1972).
5. T. N. RANGANATHAN. Thesis. University of British Columbia. 1971.

Can. J. Chem. Downloaded from www.nrcresearchpress.com by 210.87.254.4 on 09/06/12
For personal use only.

6. E. NIECKE, H. THAMM, and O. GLEMSER, Z. Naturforsch. **26**b, 366 (1971).
7. D. T. CROMER and J. T. WABER. International tables for X-ray crystallography. Kynoch Press. 1974.
8. D. T. CROMER. International tables for X-ray crystallography. Kynoch Press. 1974.
9. M. W. DOUGILL. J. Chem. Soc. 3211 (1963).
10. G. J. BULLEN. J. Chem. Soc. A, 1450 (1971).
11. R. T. OAKLEY, N. L. PADDOCK, S. J. RETTIG, and J. TROTTER. Can. J. Chem. **55**, 4206 (1977).
12. F. R. AHMED, P. SINGH, and W. H. BARNES. Acta Crystallogr. Sect. B, **25**, 316 (1969).
13. C. W. ALLEN, F. Y. TSANG, and T. MOELLER. Inorg. Chem. **7**, 2183 (1968).
14. M. W. DOUGILL, N. L. PADDOCK, and B. SHELDRICK. Acta Crystallogr. In press.
15. C. W. ALLEN, J. B. FAUGHT, T. MOELLER, and I. C. PAUL. Inorg. Chem. **8**, 1719 (1969).
16. S. POHL and B. KREBS. Chem. Ber. **109**, 2622 (1976).
17. D. P. CRAIG and N. L. PADDOCK. *In* Non-benzenoid aromatics. *Edited by* J. P. Snyder, Vol. II. Academic Press, New York. 1971. pp. 273, 300.
18. C. A. COULSON. Valence. 2nd ed. Oxford University Press, Oxford. 1961. p. 250.
19. C. W. HAIGH and L. SALEM. Nature, **196**, 1307 (1962); D. W. DAVIES. Nature. **196**, 1309 (1962).

Can. J. Chem. Downloaded from www.nrcresearchpress.com by 210.87.254.4 on 09/06/12
For personal use only.

Dynamic aspects of the behavior of aromatic ketone triplets in anionic micelles. A laser flash photolysis study[1]

J. C. SCAIANO AND J. C. SELWYN[2]

Division of Chemistry, National Research Council, Ottawa, Ont., Canada K1A 0R6

Received January 20, 1981

J. C. SCAIANO and J. C. SELWYN. Can. J. Chem. **59**, 2368 (1981).

The behavior of several aromatic ketone triplets has been examined in sodium dodecyl sulfate micelles using laser flash photolysis techniques. The molecules examined, acetophenone, propiophenone, isobutyrophenone, *p*-methoxyacetophenone, benzophenone, and xanthone are mainly resident in the micellar phase. Phenyl alkyl ketones show considerable self-quenching, a process that is rather sensitive to steric factors. All the molecules examined seem to reside near the Stern layer. Typical rate constants for triplet state entry into the micelle are around $1.8 \times 10^{10}\ M^{-1}\ s^{-1}$.

J. C. SCAIANO et J. C. SELWYN. Can. J. Chem. **59**, 2368 (1981).

Faisant appel à la technique de photolyse flash au laser, on a étudié le comportement de diverses cétones aromatiques à l'état triplet dans des micelles de dodécylsulfate de sodium. Les molécules étudiées, l'acétophénone, la propiophénone, l'isobutyrophénone, la *p*-méthoxyacétophénone, la benzophénone et la xanthone, résident principalement dans la phase micellaire. Les phénylalkylcétones présentent beaucoup d'autopiégeage, un processus sensible aux facteurs stériques. Toutes les molécules étudiés semblent demeurer près de la couche de Stern. La constante typique de vitesse d'entrée de l'état triplet dans la micelle est d'envirion $1{,}8 \times 10^{10}\ M^{-1}\ s^{-1}$.

[Traduit par le journal]

Introduction

Carbonyl triplets, and in particular the triplet state of aromatic ketones, have been the subject of considerable attention (1–4). While their behavior in homogeneous solution is relatively well understood, their behavior in organized assemblies, such as micelles, is not. A few aspects have received some attention, for example, benzophenone probes have been used to examine the conformation of hydrocarbon chains in micelles (5); de Mayo and co-workers have studied the effect of the micellar environment upon the dimerization of 3-*n*-butylcyclopentenone (6) and its photocycloaddition to alkenes (7); the Norrish Type II process of carbonyl compounds has been examined by Whitten and co-workers (8, 9), Turro *et al.* (10), and ourselves (11). Among other aspects of the behavior of carbonyl compounds in micelles which have also been examined are: the Norrish Type I cleavage (12–16), energy migration (11), the decay of benzophenone ketyls (17), and the initiation of emulsion polymerization (18, 19).

Most of the studies mentioned above have been published during the last two or three years, a fact that emphasizes the current interest in using organized assemblies to change the course of photochemical reactions. Despite these studies, many fundamental questions, such as the triplet lifetimes in micellar solution, the location of the excited chromophores in the system, the rates of exit and entry, and the possible role of intramicellar self-quenching frequently remain unanswered. In this study we use nanosecond laser flash photolysis techniques in an attempt to answer some of these questions.

Results

All our experiments were carried out under oxygen-free conditions using the pulses (337.1 nm, ~8 ns, up to 10 mJ) from a nitrogen laser for excitation and a computerized system with nanosecond response to monitor the transient signals (20).

The decay of the triplet state was monitored following the decrease of the absorption due to T–T transitions with time. We find that the lifetimes of phenyl alkyl ketones depend upon the bulk ketone concentration. Acetophenone, which is known to undergo self-quenching in homogeneous solution (21), shows the highest sensitivity.

Concentration effects were not examined in the case of xanthone because all experiments (see below) could be carried out under conditions where the occupancy levels were substantially lower than one; self-quenching could be expected to be of importance at higher concentrations (20, 21). Benzophenone triplet lifetimes were quite insensitive to the ketone bulk concentration, even when the average occupancy was well over two.

Table 1 summarizes the triplet lifetimes measured in 0.23 *M* sodium dodecyl sulfate (SDS) solution. All values have been extrapolated to zero ketone concentration (not just to single occupancy)

[1]NRCC No. 19217.
[2]NRCC Summer Student, 1980.

0008-4042/81/152368-05$01.00/0
©1981 National Research Council of Canada/Conseil national de recherches du Canada

Can. J. Chem. Downloaded from www.nrcresearchpress.com by 210.87.254.42 on 09/06/12
For personal use only.

TABLE 1. Kinetics of triplet decay in SDS 0.23 *M* at 26°C

Ketone	N_{occ}[a]	τ_T^0[b]	k_{app}[c]	λ_{mon}[d]
Acetophenone	0.25– 9	3850	6.16×10^7	365
Propiophenone	0.3 –10	3800	3.44×10^7	365
Isobutyrophenone	0.2 –11.5	(17000)	2.91×10^7	365
p-Methoxyacetophenone	~1	19000	—	400
Benzophenone	0.3 – 2.9	360	$<3 \times 10^6$	540/590
Xanthone	0.2	7650	—	610

[a]Occupancy level range.
[b]In nanoseconds.
[c]In units of M^{-1} s^{-1}.
[d]Wavelength used to monitor T–T absorptions (in nm).

using a plot of τ_T^{-1} vs. the ketone concentration; the corresponding slopes (k_{app}) are also given in Table 1, and representative plots shown in Fig. 1. The values of k_{app} are formally rate constants for the self-quenching process, and are a function of the surfactant concentration. Typical occupancy levels in our experiments were in the 0.2 to 10.0 range for the phenyl alkyl ketones and lower for the others. Micellar occupancies were calculated using CMC = 0.0082 *M* and an aggregation number of 62 (22). Experiments at lower surfactant concentrations (but over CMC) showed similar effects and led to τ_T^0 values consistent with those in Table 1.

It is interesting to note that even in cases where the triplet lifetimes were short enough to suggest chemical decay, the yield of detectable ketyl radicals was quite low. For example, in the case of benzophenone the triplet lifetime in SDS micelles was 360 ns at 26°C. This value compares well with the 330 ns obtained in decane solution (23); however, the yield of ketyl radicals in SDS is only ca. 7% of that in decane. We have also observed that the yield of the so-called "light absorbing transients" (24–26) is much higher in micelles than in homogeneous solution. It is not clear at this point if these two phenomena are related. This aspect of the problem will be discussed in detail elsewhere.

The triplet state of aromatic ketones in micellar solution can also be quenched by water soluble quenchers. We chose nitrite ions for these experiments because the negative charge is expected to prevent any significant association with the micelles (27). Plots of τ_T^{-1} vs. the nitrite concentration were expected and confirmed to be nonlinear, approaching, at the high limit the sum of rates of triplet decay in the micelle and of triplet exit from the micelle.

The experimentally observed rate of triplet decay ($k_{expt} = \tau_T^{-1}$) is given by eq. [1].

$$[1] \quad k_{expt} = k_0 + \frac{k_- k_q[Q]}{k_q[Q] + k_+[M]}$$

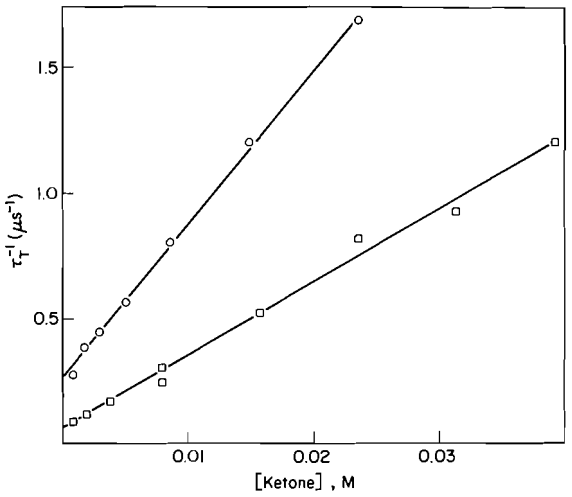

FIG. 1. Dependence of the triplet lifetimes on the ketone bulk concentration for SDS 0.23 *M* at 26°C, for acetophenone (○) and isobutyrophenone (□).

where k_0 is the rate of triplet decay in the absence of quencher Q, k_- and k_+ are the rate constants for exit and entry into the micelle, respectively, [M] is the concentration of micelles, and k_q is the rate constant for triplet quenching in the aqueous phase. Equation [1] assumes that the ketone is largely solubilized in the micellar phase, that its triplet state does not decay in the water phase by any process other than quenching by Q, and that Q is insoluble in the micellar phase. When $[Q] \rightarrow \infty$ the experimental rate constant is given by eq. [2].

$$[2] \quad k_{expt} = k_0 + k_-$$

In the intermediate concentration range eq. [3] provides an adequate type of linear representation (27).

$$[3] \quad \frac{1}{k_{expt} - k_0} = \frac{1}{k_-} + \frac{k_+[M]}{k_- k_q[Q]}$$

Figure 2 shows representative plots according to

Can. J. Chem. Downloaded from www.nrcresearchpress.com by 210.87.254.42 on 09/06/12
For personal use only.

TABLE 2. Kinetic and equilibrium data for the exit and entry of aromatic ketones in sodium dodecyl sulfate micelles

Ketone	$k_+[M]/k_-k_q$[a]	k_+/k_-[b]	k_-[c]
Acetophenone	1.13×10^{-9}	2040	7.8×10^6[d]
Propiophenone	2.63×10^{-9}	4700	3.0×10^6[d]
Isobutyrophenone	4.14×10^{-9}	7500	1.6×10^6[d]
p-Methoxyacetophenone	1.66×10^{-9}	3000	(9.2×10^6)[e]
Benzophenone	(1.5×10^{-8})	(26000)	(2×10^6)[f]
Xanthone	3.52×10^{-9}	6300	2.7×10^6

[a]In units of M s at 26°C for [SDS] = 0.23 M.
[b]In units M^{-1}.
[c]In units of s^{-1}.
[d]From energy transfer studies, see ref. 11.
[e]Intercept poorly defined.
[f]All values for benzophenone are subject to considerable error (approx. a factor of two) because its short triplet lifetime and the possible overlap of ketyl signals (at 540 nm) or very weak absorptions (at 590 nm) make the measurements quite difficult.

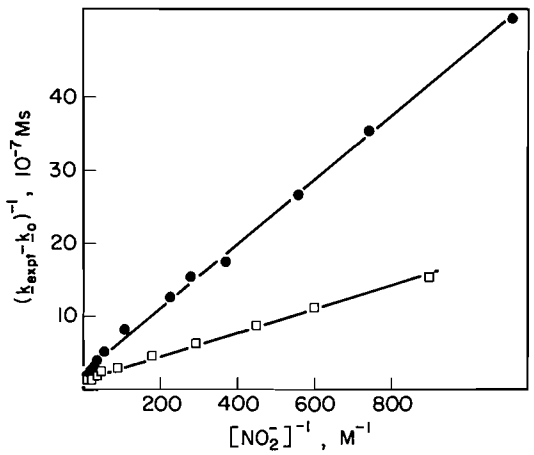

FIG. 2. Plot according to eq. [3] for isobutyrophenone (●) and *p*-methoxyacetophenone (□) in SDS 0.23 M using sodium nitrite as quencher.

eq. [3] for [SDS] = 0.23 M (corresponding to [M] = 0.0036 M) at 26°C.

In order to determine the k_+/k_- ratio it is necessary to have some knowledge of the value of k_q. In order to obtain this value we carried out experiments with xanthone, which has a large extinction coefficient at the excitation wavelength (337 nm) so that measurements are viable using the saturated solution in water. From a study at 26°C in which xanthone triplets were monitored at 600 nm we obtained $k_q = 6.5 \times 10^9\ M^{-1}\ s^{-1}$. The value of k_q may be slightly dependent upon the ketone used; however, we expect this dependence to be quite small, since all sensitizers used are in a relatively narrow triplet energy range, i.e. ~69 to 73 kcal/mol (28), and nitrite anions are reported to have a triplet energy of 53 kcal/mol (27, 29). The same value of k_q was used for all the systems examined. Table 2 summarizes the data obtained. It should be noted that according to eq. [3] one can obtain the separate values of k_- and k_+, if k_q is known. In some cases the intercept from plots such as those in Fig. 2 is not very well defined. In a few cases the values of k_- had been obtained before from energy migration studies; whenever available (11) we have preferred these values of k_- rather than those derived from eq. [3] (see Table 2). The average value of k_+ that can be obtained from the data in Table 2 is $1.8 \times 10^{10}\ M^{-1}\ s^{-1}$. In principle, all values of k_- could have been accurately determined by working at very high nitrite concentration; in practice this would lead to a new problem, i.e. the change in micellar properties due to excessive changes in the ionic strength.

Discussion

It is important to emphasize that all the kinetic parameters obtained in this study correspond to the triplet state; rates of exit and entry could be somewhat different for the ground state.

Triplet ketones are far from being static probes. For example, in the case of acetophenone, if we combine the data obtained here with rates of exit determined from energy transfer studies (11), we conclude that in dilute solution every acetophenone triplet will on average visit ca. 30 micelles before decay occurs.

Self-quenching plays an important role in the decay of acetophenone triplets. For example the lifetime of 3.8 μs for C → O is reduced to ca 1.45 μs when the occupancy level is two. The literature gives no indication whether the rate constant for self-quenching (k_{SQ}) reported for acetophenone (21) can be regarded as a representative value for other phenyl alkyl ketones. Our results indicate that self-quenching in acetophenone is considerably faster than in other phenyl alkyl ketones. The increased efficiency of self-quenching in micellar solution seems to somewhat exceed the concentration effect expected in the micelles. For example, for SDS 0.23 M a plot of τ_T^{-1} vs. $[\text{acetophenone}]_{bulk}$

Can. J. Chem. Downloaded from www.nrcresearchpress.com by 210.87.254.42 on 09/06/12
For personal use only.

Can. J. Chem. Downloaded from www.nrcresearchpress.com by 210.87.254.42 on 09/06/12
For personal use only.

gives an apparent rate constant $k_{app} = 6.2 \times 10^7 M^{-1}$ s^{-1}, and the reported (21) value of k_{SQ} in carbon tetrachloride is $1.1 \times 10^6 M^{-1}$ s^{-1}. That is, the effect on the rates is around a factor of sixty while the effect of reagent concentration due to micellization for SDS 0.23 M is only ca. one order of magnitude. The enhanced rates of self-quenching may be partially reflecting the anchoring of the ketone *and* the ketone triplet near the micellar surface, with the quenching occurring in this area and with the reaction partners in adequate orientation for interaction. The dependence of product ratios in the photochemistry of 3-*n*-butylcyclopentenone upon micellization (6, 7) has been explained using similar arguments.

We carried out a few exploratory experiments using benzaldehyde; we found that triplet lifetimes are much shorter than in the case of acetophenone, and it becomes virtually impossible to work at the very dilute limit and still have enough light absorbed at the excitation wavelength (337.1 nm).

In the case of benzophenone, no significant self-quenching was observed; this agrees with the data in homogeneous solution, which also showed relatively inefficient quenching (21). The highest occupancy level in these experiments was 2.9.

No attempt was made to measure self-quenching in the case of xanthone; the process is extremely fast in homogeneous solution (20, 21) and one should probably expect self-quenching to manifest itself as a static process.

The lifetime of xanthone triplets has been shown to be very sensitive to the polarity of the media (20, 30), being as long as 17.2 μs in 1:1 water–acetonitrile and only 22 ns in cyclohexane. The sensitivity of xanthone triplet lifetimes to the media is the result of an inversion of the triplet n,π^* and π,π^* states and the changes in reactivity which frequently accompany such an inversion of states. It is interesting to note that the lifetime measured in SDS compares well with those measured in methanol and in acetonitrile (20); we take this result to mean that the ketone triplet resides in a very polar environment, probably with the carbonyl group in the Stern layer, as proposed by de Mayo and co-workers (6, 7). It is interesting to note that earlier results, showing that the Norrish Type II process occurs with high quantum yields (10) and that the biradical has a relatively long lifetime (11), can only provide information on the location of the biradical, not the triplet state.

The relatively long lifetimes of triplet phenyl alkyl ketones (at zero concentration) are consistent with the decrease in hydrogen abstraction ability frequently observed in polar media (31). *p*-Methoxyacetophenone was quite unreactive, as expected (32, 33).

Benzophenone, which is known to remain with predominant n,π^* character even in polar media (1, 31), where it is highly reactive, showed triplet lifetimes similar to those obtained in hydrocarbons with abundant secondary C—H bonds, such as decane. Much to our surprise, ketyl radicals seem to be produced very inefficiently. Whether the explanation for this effect is that ketyls are not formed, that the radical-pair loses its triplet character quite rapidly, or that new decay paths become of importance in micellar solution, remains to be resolved. Preliminary results indicate that the so called "light absorbing transients" (24–26) are formed more efficiently than in homogeneous solution.

In conclusion, our results show that aromatic ketones, particularly phenyl alkyl ketones, are very mobile probes; further, self-quenching is in many cases an important phenomena, which in some cases (e.g. acetophenone) can become the predominant triplet decay mode. Micellization produces a substantial enhancement of the self-quenching process, which under these conditions reveals its sensitivity to substitution at the carbonyl centre. All the ketones examined are largely resident in the micellar phase, but their exit and entry rates are quite large, thus making them very dynamic probes.

Lifetimes, reactivities, and self-quenching effects all are consistent with the assumption that ketones reside in a highly polar environment.

Experimental

Materials

Xanthone was a Fluka product, acetophenone was from BDH, and all other ketones were from Aldrich; they were distilled or recrystallized before use. A sample of acetophenone purified by preparative vpc gave the same results as the distilled material. Sodium dodecyl sulfate (BDH, specially purified) was used as received. Sodium nitrite was a Fisher product.

Sample Preparation

The samples were contained in Suprasil cells made of 3 × 7 mm rectangular tubing (Vitro Dynamics). All experiments were carried out under oxygen-free conditions. Other details are similar to those reported previously (34).

Laser Flash Photolysis

The samples were excited with the pulses from a Molectron UV-24 nitrogen laser. Our facility has been fully interfaced with a PDP11-03L computer which controls the experiment and processes the data initially acquired by an R-7912 Textronik transient digitizer. Further details have been given elsewhere (20).

Acknowledgement

The authors are grateful to Mr. S. E. Sugamori for his technical assistance.

1. J. C. SCAIANO. J. Photochem. **2**, 81 (1973/74).
2. P. J. WAGNER. Acc. Chem. Res. **4**, 168 (1971).
3. N. J. TURRO. Modern molecular photochemistry. Benjamin-Cummings, Menlo Park, CA. 1978.
4. J. C. SCAIANO, E. A. LISSI, and M. V. ENCINA. Rev. Chem. Intermed. **2**, 139 (1978).
5. R. BRESLOW, S. KITABATAKE, and J. ROTHBARD. J. Am. Chem. Soc. **100**, 8156 (1978).
6. K. H. LEE and P. DE MAYO. Photochem. Photobiol. **31**, 311 (1980).
7. P. DE MAYO and L. K. SIDNES. J. Chem. Soc. Chem. Commun. 994 (1980).
8. P. R. WORSHAM, D. W. EAKER, and D. G. WHITTEN. J. Am. Chem. Soc. **100**, 7091 (1978).
9. D. G. WHITTEN. Angew. Chem. Int. Ed. Engl. **18**, 440 (1979).
10. N. J. TURRO, K.-C. LIU, and M. F. CHOW. Photochem. Photobiol. **26**, 413 (1977).
11. J. C. SCAIANO and J. C. SELWYN. Photochem. Photobiol. In press.
12. N. J. TURRO and W. R. CHERRY. J. Am. Chem. Soc. **100**, 7431 (1978).
13. B. KRAEUTLER and N. J. TURRO. Chem. Phys. Lett. **70**, 266 (1980); **70**, 270 (1980).
14. N. J. TURRO, B. KRAEUTLER, and D. R. ANDERSON. J. Am. Chem. Soc. **101**, 7435 (1979).
15. N. J. TURRO and B. KRAEUTLER. J. Am. Chem. Soc. **100**, 7432 (1978).
16. H. HAYASHI, Y. SAKAGUCHI, and S. NAGAKURA. Chem. Lett. 1149 (1980).
17. Y. SAKAGUCHI, S. NAGAKURA, and H. HAYASHI. Chem. Phys. Lett. **72**, 420 (1980).
18. A. MERLIN and J.-P. FOUASSIER. Polymer, **21**, 1363 (1980).
19. N. J. TURRO, M.-F. CHOW, C.-J. CHUNG, and C.-H. TUNG. J. Am. Chem. Soc. **102**, 7391 (1980).
20. J. C. SCAIANO. J. Am. Chem. Soc. **102**, 7747 (1980).
21. J.-P. JEANDRAU, J.-C. GRAMAIN, and J. LAMAIRE. J. Chem. Res. (S), 186 (1979).
22. K. J. MYSELS and L. H. PRINCEN. J. Phys. Chem. **63**, 1696 (1959).
23. J. C. SCAIANO and E. B. ABUIN. Chem. Phys. Lett. In press.
24. J. CHILTON, L. GIERING, and C. STEEL. J. Am. Chem. Soc. **98**, 1865 (1976).
25. N. FILIPESCU and F. L. MINN. J. Am. Chem. Soc. **90**, 1544 (1968).
26. P. J. WAGNER. Mol. Photochem. **1**, 71 (1969).
27. M. ALMGREN, F. GRIESER, and J. K. THOMAS. J. Am. Chem. Soc. **101**, 279 (1979).
28. S. L. MUROV. Handbook of photochemistry. Dekker, New York. 1973, Section 2.
29. A. TREININ and E. HAYON. J. Am. Chem. Soc. **98**, 3884 (1976).
30. A. GARNER and F. WILKINSON. J. Chem. Soc. Faraday Trans. II, **72**, 1010 (1976).
31. H. LUTZ, M.-C. DUVAL, E. BRÉHÉRET, and L. LINDQVIST. J. Phys. Chem. **76**, 821 (1972).
32. P. J. WAGNER, A. E. KEMPPAINEN, and H. N., SCHOTT. J. Am. Chem. Soc. **95**, 5604 (1973).
33. J. C. SELWYN and J. C. SCAIANO. Polymer, **21**, 1365 (1980).
34. J. C. SELWYN and J. C. SCAIANO. Can. J. Chem. **59**, 663 (1981).

Can. J. Chem. Downloaded from www.nrcresearchpress.com by 210.87.254.42 on 09/06/12
For personal use only.

Lactonisation par ouverture, en milieu acide, de cyclopropanes γ-carboxyliques

LAURENT CHICHE, HENRI CHRISTOL, JACQUES COSTE ET FRANÇOISE PLÉNAT[1]

ERA No 610, Laboratoire de Chimie Organique, E.N.S. Chimie, 8, rue de l'Ecole Normale, 34075 Montpellier Cédex. France

Reçu le 25 avril 1980[2]

LAURENT CHICHE, HENRI CHRISTOL, JACQUES COSTE et FRANÇOISE PLÉNAT. Can. J. Chem. **59**, 2373 (1981).

L'ouverture dans l'acide formique de composés cyclopropaniques porteurs d'une fonction carboxyle conduit à des mélanges complexes contenant moins de 30% de lactones, dues à l'intervention du nucléophile interne au cours de la réaction. On montre que la stéréochimie relative de la fonction carboxyle vis-à-vis du cycle à trois carbones n'est pas déterminante quant à la proportion de lactonisation obtenue. En revanche, lorsque l'ouverture est réalisée par un acide de Lewis (BF_3–OEt_2), la lactonisation devient très prépondérante (84%); bien que le mécanisme de la cyclisation intramoléculaire n'ait pu être clairement établi dans ce cas, la réaction constitute une bonne voie d'accès aux lactones.

LAURENT CHICHE, HENRI CHRISTOL, JACQUES COSTE, and FRANÇOISE PLÉNAT. Can. J. Chem. **59**, 2373 (1981).

The opening of cyclopropanes, bearing a carboxyl group, in formic acid leads to complex mixtures containing less than 30% lactones formed by an intramolecular nucleophilic process during the reaction. We show that the relative stereochemistry of the carboxyl group and the cyclopropyl group does not determine the proportion of lactone formed. On the other hand, when the opening is performed by a Lewis acid (BF_3–etherate), lactonisation is the major route (84%) and although the mechanism of intramolecular cyclisation is not yet clear, this reaction provides a good route to lactones.

[Journal translation]

Can. J. Chem. Downloaded from www.nrcresearchpress.com by 210.87.254.105 on 09/06/12
For personal use only.

La participation de nucléophiles internes à l'ouverture de cyclopropanes activés ou lors de la solvolyse de cyclopropyl-carbinols s'est révélée utile en synthèse organique (1). Nous avons pour notre part envisagé de faire intervenir un tel processus dans l'ouverture acidocatalysée de cyclopropanes non activés; cet objectif n'a en effet suscité que peu de travaux qui montrent toutefois qu'il est formellement réalisable (2, 3). Nous avons donc entrepris d'observer les possibilités de lactonisation d'acides γ-cyclopropyliques en milieu acide, qui n'ont pas encore été étudiées à notre connaissance. Nous avons choisi les composés tricycliques **1** et **2**. En effet, ceux-ci sont après protonation, formellement comparables à certains composés d'addition électrophile sur des norbornènes analogues, pour lesquels la γ-lactonisation est un processus souvent exclusif (4). Le groupement carboxylique en position 6-*exo* est destiné à éviter, par son caractère attracteur d'électrons, la transposition de Wagner–Meerwein de la simple liaison (C-5)—(C-6), processus qui a été observé (3) lors de l'ouverture acidocatalysée de l'*exo*-tricyclo[3.2.1.$0^{2,4}$]octane.

Synthèse des composés 1 et 2

Le composé **1***a* a pu être obtenu par transfert de méthylène, selon la méthode de Simmons–Smith modifiée par Rawson et Harrison (5), sur le diméthoxycarbonyl-2 *endo*-3 *exo* bicyclo[2.2.1]heptène-5 (6). Pour que la réaction procède à une vitesse suffisante, nous avons dû utiliser un large excès de

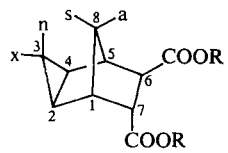

1*a* R = Me
b R = H

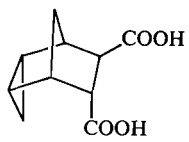

2

FIG. 1

réactif; il est probable que les deux substituants carboxyliques, en appauvrissant la double liaison en électrons, la rendent peu réactive (7).

La formation exclusive d'*exo*-tricyclo[3.2.1.$0^{2,4}$]-octane **1***a* est attendue; en effet, sur les composés norbornéniques, les additions *cis*, se font de façon très préférentielle en *exo* (7*b*, 8–11). La structure proposée pour les composés **1** est confirmée par leur spectre de rmn.[3] On observe pour **1***a*, à δ = 0,03 ppm, un signal de quatre raies correspondant à H-3x ($J_{3x-2} = J_{3x-4} \simeq 7$ Hz; $J_{3x-3n} = 6{,}5$ Hz); H-3n résonne à δ = 0,44 ppm sous la forme de cinq raies ($J_{3n-3x} = 6{,}5$ Hz; $J_{3n-2} = J_{3n-4} \simeq 3$ Hz). Ces deux signaux sont en parfait accord avec les données de la littérature pour la structure *exo*-tricyclo-[3.2.1.$0^{2,4}$]octane (11*b*, 12), notamment du point de vue de la différence de déplacement chimique entre H-3x et H-3n qui se trouve déblindé.

Le composé **2** a été préparé à partir de l'oléfine **3**. On sait en effet qu'en série norbornadiénique, la cyclopropanation se fait en *exo* et en *endo* (7*b*, 11*a*, 13). En outre, étant donné la présence de deux

[1]Auteur à qui toute correspondance doit être adressée.
[2]Révision reçue le 2 avril 1981.

[3]L'abréviation "rmn" sans autre précision, est afférante à la résonance magnétique nucléaire du proton.

0008-4042/81/152373-09$01.00/0
©1981 National Research Council of Canada/Conseil national de recherches du Canada

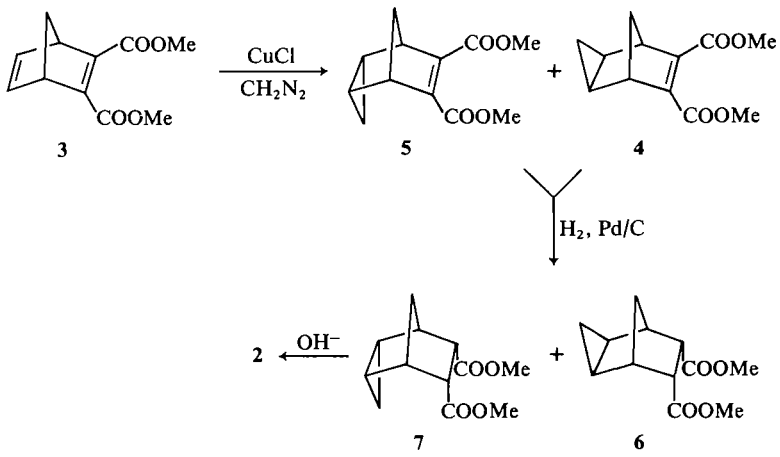

SCHÉMA 1

doubles liaisons différentes dans le composé **3**, nous avons généré le carbène par le diazométhane en présence de chlorure cuivreux (14), méthode connue pour ne pas donner d'adduit sur des doubles liaisons appauvries en électrons (15); nous avons ainsi obtenu un mélange dont les caractéristiques spectrographiques correspondent aux composés **4** et **5** attendus; on note en particuler la disparition des protons vinyliques.

Lors de l'hydrogénation catalytique du mélange précédent, l'approche du catalyseur favorisée en *exo* (16) conduit aux composés **6** et **7** possédant les deux groupes esters méthyliques en *endo*. Le composé **6** est connu (7*b*). En ce qui concerne le composé **7** inconnu, la simplicité du spectre de rmn montre clairement que le produit est symétrique. En outre, on observe un signal (δ = 3,03 ppm, 2H, signal large, $W_{\frac{1}{2}}$ = 5 Hz) très similaire au signal obtenu pour les protons H-6 et H-7 du composé **6** (δ = 2,92 ppm, 2H, signal large, $W_{\frac{1}{2}}$ = 4,7 Hz), ce qui dénote l'identité de stéréochimie des fonctions méthoxycarbonyles entre les produits **6** et **7**. La stéréochimie *endo* du cyclopropane du composé **7** a été attribuée sur la base des arguments suivants: (*a*) il n'apparait pas de signal vers 0 ppm présent dans les spectres de **1***a* et **6** et dû au proton H-3x d'un pont méthylénique *exo*; (*b*) d'autre part, il est connu que, pour la structure tricyclo[3.2.1.$0^{2,4}$]octanique, les protons H-2 et H-4 *endo* (au pied d'un cyclopropane *exo*) sont très faiblement couplés avec les protons têtes de pont H-1 et H-5 (17), alors que ce couplage est d'environ 4 Hz pour des protons H-2 et H-4 *exo* (au pied d'un cyclopropane *endo*) (18); on observe effectivement une largeur à mi-hauteur du pic correspondant à H-1 et H-5, nettement plus importante pour le composé **7** que pour le composé **6** *exo* (9,0 Hz au lieu de 5,4 Hz).

L'hydrolyse basique du diester **7** s'accompagne de l'épimérisation de l'un des carboxyles et conduit au diacide recherché **2**. La perte de symétrie est évidente à la vue du spectre de rmn; le proton H-6, blindé par rapport au même proton du composé **7** (2,43 ppm au lieu de 3,03 ppm) résonne maintenant sous forme d'un doublet (couplé avec H-7, J = 4,5 Hz) alors que H-7, inchangé quant au déplacement chimique, résonne sous la forme d'un triplet (couplé de façon équivalente avec H-6 et H-1); les couplages ainsi observés sont semblables à ceux relevés sur le spectre de rmn du composé **1***a*, ce qui confirme la stéréochimie *trans* des deux substituants en position −6 et −7. Par ailleurs, l'absence de signal vers 0 ppm traduit le maintien de la stéréochimie *endo* du cyclopropane.

Ouverture en milieu acide du noyau cyclopropanique des composés 1 et 2; détermination des structures

Les ouvertures ont été réalisées dans l'acide formique pur utilisé comme solvant; nous l'avons choisi pour son caractère suffisamment polaire et peu nucléophile, mais aussi parce que c'est ce réactif qui a été utilisé dans l'ouverture de noyaux cyclopropaniques lors de la mise en évidence de la participation de l'oxygène d'un éther (2*e*).

Par chauffage à 80°C pendant 6 h dans l'acide formique, le composé **1***b* conduit à un mélange complexe (schéma 2) ne présentant plus, en rmn, les caractéristiques du noyau cyclopropanique. Une séparation partielle a été réalisée par chromatographie au niveau des acides ou de leurs dérivés; nous n'avons cependant pas pu isoler tous les isomères.[4]

Composé **8**b

Il s'agit d'une γ-lactone acide; en effet le spectre ir de l'ester correspondant **8***a* montre deux vibrations

[4]Dans tout les cas, produits purs ou mélanges, l'analyse élémentaire concorde avec la structure proposée.

Can. J. Chem. Downloaded from www.nrcresearchpress.com by 210.87.254.105 on 09/06/12
For personal use only.

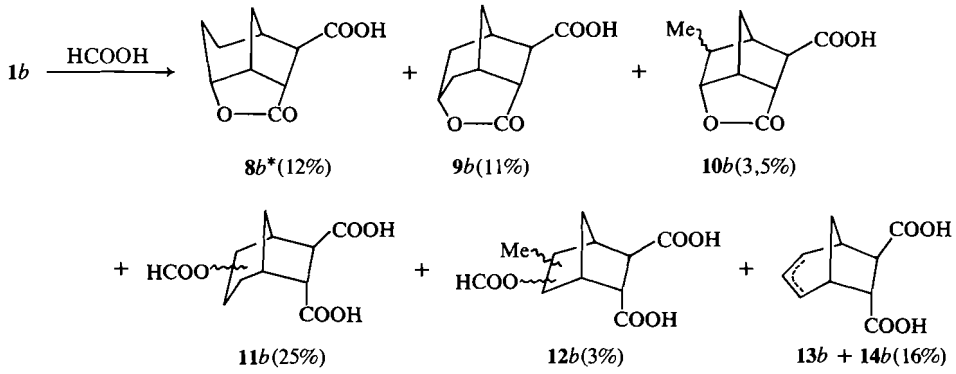

*Les esters méthyliques dérivés des acides portent le même numéro suivi de la lettre *a*

SCHÉMA 2

$\nu_{C=O}$ à 1762 cm^{-1} (γ-lactone) et 1730 cm^{-1} (ester méthylique). En outre, l'allure et l'intégration du spectre de rmn de **8***b* correspondent bien à une telle structure; en particulier, nous avons vérifié, par double résonance, que le proton au pied de l'oxygène lactonique est bien couplé avec le proton tête de pont H-1 (J = 9 Hz).

Composé **9**b

Le spectre de rmn de l'ester correspondant **9***a* montre la présence d'un seul groupement ester méthylique ainsi qu'un signal (δ = 4,65 ppm) pouvant correspondre au proton situé au pied de l'oxygène lactonique. Ce composé montre en ir une seule vibration $\nu_{C=O}$ à 1738 cm^{-1} qui peut traduire la présence d'une δ-lactone ou d'une lactone à cycle plus grand, simultanément à celle de l'ester méthylique. La valeur faible du couplage observé pour le proton au pied de l'oxygène lactonique permet d'éliminer la structure de la figure 2 pour laquelle les modèles moléculaires indiquent un angle dièdre (H-4)–(C-4)–(C-5)–(H-5) voisin de 0°. Par ailleurs les caractéristiques spectrographiques de la lactone **9***a* sont similaires à celles de la lactone de l'acide hydroxy-3 *endo* bicyclo[3.2.1]octane carboxylique-6 *endo* décrite récemment par Moriarty *et al.* (19).

Fraction ***10***b

La troisième fraction lactonique issue de **1***b*, de même formule brute que les précédentes, est con-

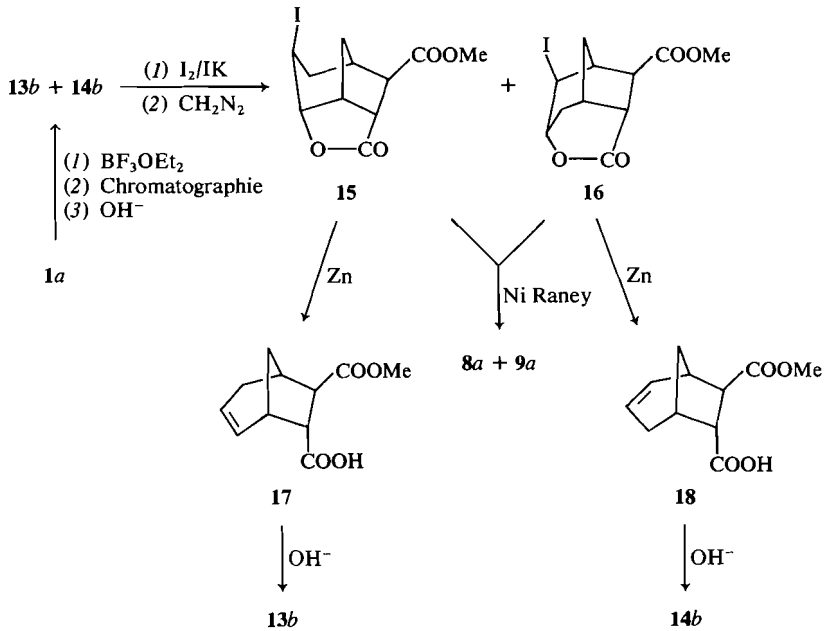

SCHÉMA 3

Can. J. Chem. Downloaded from www.nrcresearchpress.com by 210.87.254.105 on 09/06/12
For personal use only.

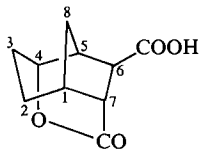

FIG. 2

stituée d'un mélange. Sur la base des spectres ir et de rmn des esters méthyliques dérivés **10***a*, et par comparaison avec des produits du même type (20), il est vraisemblable qu'il s'agit du mélange des deux isomères indiqués, à méthyles *exo* et *endo*. La présence inattendue d'un produit à méthyle *endo* pourrait résulter d'une isomérisation préalable du diacide **1***b* en composés méthyl-bicyclo[2.2.1]-hepténiques.

*Fraction 11*b

Il s'agit d'un mélange complexe constitué de formiates diacides de structure bicyclo[3.2.1]octanique comme l'indiquent les spectres ir et rmn des alcools-esters dérivés (deux isomères ont été isolés aprés acétylation: cf. Partie expérimentale).

*Fraction 12*b

Le spectre de rmn montre, outre des fonctions formiates, la présence de deux méthyles secondaires. Nous proposons donc qu'il s'agit d'un mélange de deux composés de structure méthyl-bicyclo[2.2.1]-heptanique indiqués.

*Fraction 13*b + *14*b

Le spectre de rmn dénote qu'il s'agit d'oléfines. Nous avons pu préparer un mélange des mêmes oléfines, en quantités plus importantes, par isomérisation du composé **1***a* en présence de BF_3–OEt_2, puis hydrolyse basique. La séparation des deux isomères s'est révélée possible au niveau des deux iodolactones (produits γ et δ lactoniques) formées intermédiairement (Schéma 3). Les identifications s'appuient sur les corrélations chimiques renforcées par les propriétés spectrographiques des composés.

Dans les mêmes conditions que pour le composé à cyclopropane *exo* **1***b*, l'isomère *endo* **2** s'ouvre en 0,5 heure et conduit à un mélange plus simple:

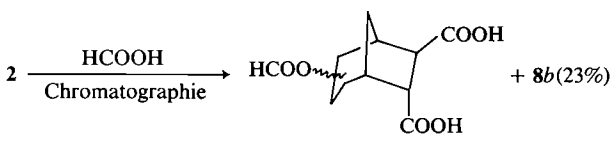

SCHÉMA 4

Le composé lactonique obtenu ici est absolument identique (ir, rmn) à la lactone **8***b* résultant de l'ouverture du composé **1***b*. On obtient également un mélange de formiates diacides en quantité importante (48%) dont nous n'avons pas jugé indispensable de séparer et identifier avec précision les composantes.

Discussion

Chacun des produits **8***b* et **9***b* ainsi que le mélange de **10***b*, **11***b* et **12***b* restent inchangés dans les conditions de la réaction. Le mélange **13***b* + **14***b* évolue peu mais conduit cependant à 2% des composés **10***b*, **11***b*, **12***b*, 2,5% de lactone **8***b* et 7,3% de lactone **9***b*; étant donné le pourcentage réduit d'oléfines **13***b* + **14***b* obtenu dans la réaction, on peut considérer, en première approximation, que les produits obtenus par formolyse proviennent directement de l'ouverture de **1***b* et **2**.

Le composé **1***b* a donc conduit en milieu acide à: (*a*) 16% d'oléfines résultant d'une isomérisation du noyau cyclopropanique; (*b*) 28% de formiates provenant de l'entrée du solvant (HCOOH) en tant que nucléophile; (*c*) 26,5% de lactones résultant de l'intervention de l'acide carboxylique interne. Notons que la formation de la lactone **9***b* implique une migration d'hydrure, phénomène déjà demontré dans certaines ouvertures de cyclopropanes en milieu acide (21).

On observe donc un taux de lactonisation réduit. Pour comparaison, l'ouverture en milieu acide de l'*exo*-tricyclo[3.2.1.$0^{2,4}$]octane avait donné lieu à 20% de transposition de Wagner–Meerwein (3). On peut s'étonner alors que la fonction carboxylique en position-7 dans le composé **1***b* n'ait pas participé de façon plus importante; en effet, il avait été constaté au cours de travaux sur l'ouverture d'époxy-bicyclo[2.2.1]heptanes (4*a*, 22) que la participation d'une fonction carboxyle est généralement beaucoup plus importante que celle d'une simple liaison par transposition de Wagner–Meerwein.

Il était cependant possible que l'attaque du nucléophile interne de **1***b*, qui doit prendre place en position-2 *endo* pour conduire à la lactone **8***b*, soit défavorisée par une exigence stéréoélectronique d'entrée en *exo* du nucléophile: en effet l'acétoxy-2 *exo* bicyclo[3.2.1] octane est le composé majoritaire formé lors de l'ouverture de l'*exo*-tricyclo[3.2.1.$0^{2,4}$]-octane (3), conformément à l'inversion de configuration souvent observée pour l'attaque nucléophile sur un cyclopropane protoné (23).

Il devenait alors interessant d'observer le comportement du composé **2**, à cyclopropane *endo*, pour lequel l'entrée du nucléophile interne en position-2 *endo* devrait être favorisée pour les mêmes raisons stéréoélectroniques que précédemment. On constate qu'en effet la proportion de lactone **8***b* augmente (23% contre 12% précédemment). Toutefois le pourcentage global de lactonisation reste sensiblement inchangé. Il est clair que la participation d'acides carboxyliques à l'ouverture acidocatalysée de cyclopropanes n'est pas aussi facile que celle qui avait été constatée lors de la solvolyse de cyclopropyl-carbinols (1*d*), ou encore au cours d'additions électro-

Can. J. Chem. Downloaded from www.nrcresearchpress.com by 210.87.254.105 on 09/06/12
For personal use only.

Can. J. Chem. Downloaded from www.nrcresearchpress.com by 210.87.254.105 on 09/06/12
For personal use only.

philes sur des norbornènes porteurs d'une fonction carboxylique (4).[5] Nous pensons que la différence réside dans la complexité du mécanisme d'ouverture acidocatalysée des cyclopropanes due à la présence de plusieurs sites et modes de protonations possibles (23*a*).

Puisque la participation du nucléophile interne n'est pas ici favorisée vis-à-vis de l'entrée du nucléophile externe, un procédé éventuel pour favoriser la lactonisation consistait à éliminer le nucléophile externe. En catalyse par le PTS dans le benzène, nous n'avons pas obtenu de résultats exploitables. En revanche, l'utilisation d'un acide de Lewis (BF_3–OEt_2), à la fois comme catalyseur et comme solvant, a permis l'obtention d'une forte proportion de lactones à partir du composé **1***b*:[6]

$$\mathbf{1}b \xrightarrow[(2)\quad OH^-]{(1)\ BF_3\text{–}OEt_2} \mathbf{8}b(56\%) + \mathbf{9}b(14{,}7\%) + \mathbf{10}b(13{,}3\%) + \mathbf{13}b \text{ et } \mathbf{14}b(10{,}9\%)$$

La γ-lactone **8***b* est maintenant le composé majoritaire avec 56% de rendement, le pourcentage global de lactone s'élevant à 84%. On peut cependant envisager ici que le processus de lactonisation soit consécutif, au moins en partie, à une isomérisation du cycle à trois carbones en oléfines **13***b* et **14***b*: en effet, placés dans des conditons parfaitement identiques, ces composés évoluent pour donner 47% de lactone **8***b* et 13,9% de lactone **9***b*, 26,1% des composés **13***b* et **14***b* restant inchangés. En effectuant, par rmn, une analyse à différents temps de réaction, de l'ouverture du noyau cyclopropanique, et de la lactonisation des composés éthyléniques, il nous est apparu difficile de trancher en faveur de l'une ou l'autre possibilité mécanistique. Ce travail nous a cependant permis de montrer que les acides γ-cyclopropyliques constituent une source valable de lactones.

Partie expérimentale

Indications générales

Les points de fusion, non corrigés, ont été déterminés en capillaires à l'aide de l'appareil du Dr. Tottoli. Les points d'ébullition sont indiqués par le sigle Eb_x où x représente la pression en Torr. Les chromatographies en phase vapeur (cpv) ont été réalisées dans l'une des conditions suivantes précisées pour chaque cas; condition A: appareil Carlo Erba Fractovap GT série 200 à ionisation de flamme, équipé d'une colonne de 2 m × 2 mm et de remplissage 5% SE 30 sur CGLA 80/100 mesh; condition B: appareil Intersmat IGC 120 DFL à ionisation de flamme, équipé d'une colonne de 1,5 m × 3,2 mm et de remplissage 10% SE 30 sur PAW 80/100 mesh; on indiquera le temps de rétention (t_r), la température de colonne (T_c) et la pression de gaz vecteur (P). Les spectres de résonance magnétique nucléaire du proton (rmn) ont été enregistrés à 60 MHz et température ambiente sur appareil Varian modèle EM-360 ou A-60; pour les spectres enregistrés à 90 et 100 MHz (précisé dans chaque cas), nous avons utilisé les modèles EM-390 et HA-100; les valeurs des déplacements chimiques sont données en ppm (référence interne TMS); les lettres s, d, t, q et m signifient respectivement singulet, doublet, triplet, quadruplet et multiplet. Les spectres d'infrarouge (ir) ont été enregistrés sur spectrophotomètre Perkin Elmer 221 ou 377, en solution 0,2 *M* sauf indication contraire; on indiquera pour les bandes principales les valeurs de ν_{max} en cm^{-1}. L'éther de pétrole utilisé pour les chromatographies et recristallisations a un point d'ébullition de 45°C à 60°C sous 760 Torr. Les analyses centésimales ont été effectuées au laboratoire de Microanalyse du C.N.R.S. à l'E.N.S.C. de Montpellier.

Diméthoxycarbonyl-6 exo, *7*-endo *H-2* endo *H-4* endo *tricyclo[3,2,1,0^{2,4}]octane*, ***I***a

On utilise en la modifiant légérement la méthode de Rawson et Harrison (5), le traitement du produit réactionnel étant effectué selon Shank et Shechter (25). On porte au reflux pendant 0,5 h, sous agitation et courant d'azote sec, un mélange constitué de 120 g de Zn en poudre, 18 g de CuCl, et 100 cm^3 d'éther anhydre (un barbotteur à H_2SO_4 est disposé en fin de montage). On laisse ensuite évaporer l'éther; lorsque le mélange est à sec, on ajoute 150 cm^3 d'éther anhydre, 15 g de diméthoxycarbonyl-2 *endo*, 3 *exo* bicyclo[2.2.1]heptène-5, puis goutte à goutte 75 cm^3 de CH_2I_2. On porte au reflux et suit l'avancement par cpv. Après 9 h le produit de départ a disparu.[7] Le mélange réactionnel est étendu à l'éther, filtré, acidifié (HCl 5%) et lavé ($NaHCO_3$ 10% puis H_2O/NaCl). On sèche (Na_2SO_4), concentre et distille. On obtient 12 g (75%) du composé **1***a*: $Eb_{0,05}$ 100–105°C; cpv (condition A, T_c 195°C, P 0,5 bar): 11 min 31 s; ir (CCl_4): 3075 et 3017 (CH cyclopropyliques), 1739 (C=O) cm^{-1}; rmn (CCl_4, 100 MHz) δ: 3,62 (s, 3H, COOMe), 3,59 (s, 3H, COOMe), 3,10 (t, 1H, J = 4,5 Hz, H-7), 2,82 (d, 1H, J = 4,5 Hz, H-6), 2,6 (m, 1H, $W_{\frac{1}{2}}$ = 7 Hz, H-1), 2,52 (1H, $W_{\frac{1}{2}}$ = 4 Hz, H-5), 0,93 (1H, $W_{\frac{1}{2}}$ = 4 Hz, H-8), 0,6 à 0,9 (8 raies; d'autres raies se trouvent sous le signal dû aux H-8, H-2 et H-4), 0,04 (5 raies, ddd, 1H, $J \simeq$ 6,5 Hz, 3 Hz et 3 Hz, H-3n), 0,03 (4 raies, ddd, 1H, $J \simeq$ 6,5 Hz, 7 Hz et 7 Hz, H-3x). *Anal.* calc. pour $C_{12}H_{16}O_4$: C 64,28, H 7,14; trouvée: C 64,0, H 7,1%.

Acide H-2 endo *H-4* endo *tricyclo[3.2.1.0^{2,4}]octane dicarboxylique-6* exo, *7* endo ***I***b

On agite 15 h un mélange de 12 g du diester **1***a* et 250 cm^3 d'une solution de soude 2,17 *M*. On lave à l'éther, acidifie à froid (HCl 50%) et extrait à AcOEt; la phase organique, séchée (Na_2SO_4) et concentrée, laisse 9,5 g (90%) du diacide **1***b* pratiquement homogène en ccm: *F* 187–188°C (AcOEt); ir (KBr): 2400 à 3600 large (OH acide), 1730 et 1710 (C=O) cm^{-1}; rmn (DMSO-d_6) δ: 11,6 (signal large, 2H, COOH), 3,01 (dd ≃ t, 1H, J = 4,5 et 4 Hz, H-7), 2,69 (d, 1H, J = 4,5 Hz, H-6), 2,4 à 2,6 (m, 2H, H-1 et H-5), 0,6 à 1,0 (m, 4H), 0,35 à 0,65 (m, 1H, H-3n), 0,06 (quatre raies, ddd, 1H, J = 6,5 Hz, H-3x). *Anal.* calc. pour $C_{10}H_{12}O_4$: C 61,22, H 6,17; trouvée: C 61,1, H 6,1%.

Mélange des diméthoxycarbonyl-6,7 tricyclo[3.2.1.0^{2,4}]-octénes-6 ***4*** *et* ***5***

On utilise le mode opératoire de Pincock et Wells (26); pour

[5]Afin d'éliminer l'influence d'éventuels caractères spécifiques des substrats utilisés, nous avons également étudié, dans les mêmes conditions, l'ouverture des acides *cis* et *trans* (bicyclo[3.1.0]hexyl)-2 acétiques. Nous avons obtenu un résultat semblable, soit 35% de lactonisation. Ce travail est décrit par ailleurs (24).

[6]Dans ces conditions, les fonctions carboxyliques libres ont conduit en partie à des esters éthyliques dûs à l'action de l'éthérate de trifluorure de bore.

[7]Le temps de réaction peut varier de 8 à 24 h selon les essais.

Can. J. Chem. Downloaded from www.nrcresearchpress.com by 210.87.254.105 on 09/06/12
For personal use only.

4,16 g d'oléfine **3** (27), on utilise 4,95 g de CuCl et 3 cm³ d'éther et fait barbotter huit équivalents de CH_2N_2 générés au fur et à mesure (à partir de 25 g de *N*-nitrosométhylurée). Après 48 h, on filtre, concentre et distille. On obtient 3,3 g des composés **4** et **5** contenant également 7% d'oléfine **3** (rmn): *Eb* 115–125°C; ir (CCl_4): 3075 (CH cyclopropyliques), 1720 (C=O) et 1613 (C=C) cm^{-1}; rmn (CCl_4) on note en particulier δ: 3,68 (s, COOMe), 3,12 (signal large, 2H, $W_{\frac{1}{2}}$ = 4 Hz, H-1 et H-5), 0,65 à 1,65 (m, 6H).

Diméthoxycarbonyl-6,7 diendo *tricyclo[3.2.1.0^{2,4}]octanes* ***6*** et ***7***

On hydrogène, sous pression atmosphérique à température ambiante, 6,6 g de mélange ci-dessus dans 100 cm³ d'éthanol en présence de 666 mg de Pd/C 10%. Après 5 h, on filtre, concentre et chromatographie sur colonne de silice avec éther – éther de pétrole (25:75). On isole: (*a*) 4,73 g d'isomère **6** (liquide); cpv (condition B, T_c 170°C, *P* 1,3 bar): 14 min 18 s; rmn (CCl_4) δ: 3,6 (s, 6H, COOMe), 2,92 (signal large, 2H, $W_{\frac{1}{2}}$ = 4,7 Hz, H-6 et H-7), 2,52 (signal large, 2H, $W_{\frac{1}{2}}$ = 5,4 Hz, H-1 et H-5), 1,0 à 1,4 (m, 3H, H-2, H-4 et H-8), 0,75 (Partie A de AB à composantes élargies, *J* = 11,0 Hz, $W_{\frac{1}{2}}$ = 4 Hz, H-8), 0,42 (cinq raies: ddd, 1H, *J* = 6,5, 3 et 3 Hz, H-3n), 0,01 (quatre raies: ddd, 1H, *J* = 6,5, 7 et 7 Hz), spectre en accord avec celui décrit dans la littérature (*7b*); (*b*) 1,47 g de mélange **6** + **7**; (*c*) 0,42 g d'isomère **7**, souillé d'environ 10% de l'isomère *exo* **6** (rmn), *F* 62°C; cpv (condition B, T_c 170°C, *P* 1,3 bar): 14 min 18 s; caractéristiques rmn du composé **7** (CCl_4) δ: 3,75 (s, 6H, COOMe), 3,03 (signal large, 2H, $W_{\frac{1}{2}}$ = 5 Hz, H-6 et H-7), 2,73 (signal large, 2H, $W_{\frac{1}{2}}$ = 9,0 Hz, H-1 et H-5), 2,22 (dt, 1H, *J* = 8,5 et 2 Hz), 0,8 à 1,9 (m, 5H).

Acide H-2 exo *H-4* exo *tricyclo[3.2.1.0^{2,4}]octane dicarboxylique-6* exo, *7* endo, ***2***

On agite 0,448 g du diester **7** dans une solution aqueuse contenant 0,4 g de NaOH et quelques gouttes de méthanol pendant 15 h à température ambiante. On lave (Et_2O), acidifie à froid (HCl 50%), extrait à l'acétate d'éthyle; la phase organique est séchée (Na_2SO_4) et concentrée. On obtient 0,356 g (90%) d'acide **2** pratiquement homogène en ccm: *F* 230°C (AcOEt–Et_2O); ir (KBr): 2400 à 3600 large (O—H), 1690 avec épaulement à 1705 (C=O) cm^{-1}; rmn (DMSO-d_6, 90 MHz) δ: 11,2 à 11,8 (2H, COOH), 3,06 (t, 1H, *J* = 4,5 Hz, H-7), 2,35 à 2,75 (m, 2H, H-1 et H-5), 2,43 (d, 1H, *J* = 4,5 Hz, H-6n), 1,87 (Partie A de AB, 1H, *J* = 9 Hz, H-8s), 1,65 (Partie B de AB, 1H, *J* = 9 Hz, H-8a), 1,3 à 1,7 (m, 2H, H-2 et H-4), 0,60 à 1,15 (m, 2H, H-3); l'irradiation du massif dû à H-2 et H-4 affine le massif dû à H-1 et H-5 et modifie fortement le multiplet dû à H-3; l'irradiation de H-6n transforme H-7x en d et affine les signaux de H-8s de 1 Hz environ; l'irradiation de H-1 et H-5 transforme H-7x en singulet large, améliore le découplage du massif dû à H-2 et H-4 et affine le système AB dû aux H-8. *Anal.* calc. pour $C_{10}H_{12}O_4$: C 61,22, H 6,17; trouvée: C 60,8, H 6,1%.

Ouverture du diacide ***1***b

On porte à 80°C, 1,9 g de diacide **1***b* dissous dans 10 cm³ d'acide formique pur. L'avancement est suivi par rmn. Après 6 h, on élimine l'acide formique sous pression réduite et récupère un produit brut présentant quatre taches en ccm (silice, éther – éther de pétrole – acide formique 49,5:49,5:1). Par chromatographie sur colonne (mêmes conditions), on isole quatre fractions: (*a*) 235 mg (12%) de lactone **8***b*; (*b*) 200 mg (11%) de lactone **9***b*; (*c*) 1,04 g de mélange **10***b* + **11***b* + **12***b*; (*d*) 310 mg (16%) de mélange **13***b* + **14***b*.

Lactone de l'acide hydroxy-2 endo *bicyclo[3.2.1]octane dicarboxylique-6* exo, *7* endo, ***8***b

F 149–150°C (Ether–acétone); ir ($CHCl_3$): 2500 à 3500 large (OH), 1760 (C=O lactone), 1710 (C=O acide) cm^{-1}; rmn ($CDCl_3$, 100 MHz) δ: 10,86, (s, 1H, COOH), 4,96 (d, 1H, *J* = 9 Hz, $W_{\frac{1}{2}}$ = 13,5 Hz, H-2), 3,38 (dd, 1H, *J* = 8 et 1,8 Hz, H-7), 3,13 (six raies: ddd, 1H, *J* = 3,5, 9 et 9 Hz, H-1), 2,85 (signal large, 1H, $W_{\frac{1}{2}}$ = 4 Hz, H-6), 2,71 (dd, 1H, *J* = 10,0 et 3,5 Hz, H-5), 1,2 à 2,4 (m, 6H); l'irradiation de H-1 transforme H-2 en singulet large ($W_{\frac{1}{2}}$ = 8 Hz) et H-7 en massif ($W_{\frac{1}{2}}$ = 7 Hz); l'irradiation de H-2 transforme H-1 en massif ($W_{\frac{1}{2}}$ = 15 Hz). *Anal.* calc. pour $C_{10}H_{12}O_4$: C 61,22, H 6,17; trouvée: C 61,0, H 6,1%.

L'action d'un excès de diazométhane en solution éthérée sur 220 mg de **8***b* conduit à 210 mg (90%) de l'ester correspondant **8***a* pratiquement homogène en ccm (silice, éther – éther de pétrole 60:40), que l'on purifie par filtration sur colonne (mêmes conditions); ir ($CHCl_3$): 1762 (C=O lactone), 1730 (C=O ester) cm^{-1}; rmn ($CDCl_3$) δ: 4,95 (d, 1H, *J* = 8,2 Hz, $W_{\frac{1}{2}}$ = 12 Hz, H-2), 3,70 (s, 3H, COOMe), 2,9 à 3,5 (m, 2H), 2,4 à 2,9 (m, 2H), 1,1 à 2,4 (m, 6H).

Lactone de l'acide hydroxy-3 endo *bicyclo[3.2.1]octane dicarboxylique-6* exo, *7* endo, ***9***b

F 159–160°C (Ether–acétone); ir (KBr): 2500 à 3600 large (OH), 1720 (C=O) cm^{-1}; rmn (DMSO-d_6, 100 MHz) δ: 12,48 (signal large, COOH), 4,53 (signal large, 1H, $W_{\frac{1}{2}}$ = 8 Hz, H-3), 3,26 (d, 1H, *J* = 8 Hz, H-7), 2,90 (signal large, 1H, $W_{\frac{1}{2}}$ = 3,4 Hz, H-6), 2,45 à 2,75 (m, 2H, H-1 et H-5), 1,5 à 2,0 (m, 6H); l'irradiation de H-1 et H-5 transforme H-3 en multiplet ($W_{\frac{1}{2}}$ = 7 Hz) et H-7 en singulet. *Anal.* calc. pour $C_{10}H_{12}O_4$: C 61,22, H 6,17; trouvée: C 61,1, H 6,1%.

L'action d'un excès de diazométhane en solution éthérée sur 0,8 g de **9***b* dissous dans quelques cm³ de diméthoxy-1,2 éthane conduit, après dilution à AcOEt, lavage (Na_2Co_3 10%, puis à l'eau), séchage (Na_2SO_4) et concentration à 0,8 g (90%) de l'ester correspondant **9***a*: *F* 113°C (éther–acétone); ir ($CHCl_3$): 1738 (C=O ester et lactone) cm^{-1}; rmn ($CDCl_3$) δ: 4,65 (signal large, 1H, $W_{\frac{1}{2}}$ = 9 Hz, H-3), 3,72 (s, 3H, COOMe), 3,52 (d, 1H, *J* = 7, 7 Hz, H-7), 3,05 (signal large, 1H, $W_{\frac{1}{2}}$ = 3,5 Hz, H-6), 2,77 (signal large, 2H, $W_{\frac{1}{2}}$ = 11 Hz, H-1 et H-5), 1,45 à 2,25 (m, 6H). *Anal.* calc. pour $C_{11}H_{14}O_4$: C 62,85, H 6,71; trouvée: C 62,9, H 6,6%.

Analyse du mélange des composés ***10***b + ***11***b + ***12***b

On agite 3,8 g du mélange considéré pendant 15 h à température ambiante dans 50 cm³ de NaOH à 8%. On dilue (H_2O), lave (Et_2O), acidifie à froid (HCl 50%) et extrait à AcOEt. La phase organique est séchée (Na_2SO_4) et concentrée sous vide (1 Torr). On obtient 3,1 g de produit brut que l'on estérifie par un excès de diazométhane dans du diméthoxy-1,2 éthane. Après traitement, on récupère 5,3 g de produit brut que l'on chromatographie sur colonne de silice avec éther – éther de pétrole (50:50). On obtient: (*a*) 293 mg (3,5% par rapport à **1***b*) de **10***a*; (*b*) 250 mg (3% par rapport à **1***b*) de **12***a*-OH; (*c*) 2,16 g (25% par rapport à **1***b*) de **11***a*-OH.

Fraction ***10***a: ir ($CHCl_3$): 1772 (C=O lactone), 1732 (C=O ester) cm^{-1}; rmn ($CDCl_3$) δ: 4,92 (signal large, 0,3H, $W_{\frac{1}{2}}$ = 15 Hz, H-2), 4,35 (d, 0,7H, *J* = 4,7 Hz, $W_{\frac{1}{2}}$ = 8 Hz, H-2), 3,73 (s, 3H, COOMe), 2,9 à 3,4 (m, 2H), 2,74 (signal large, 1H, $W_{\frac{1}{2}}$ = 4,5 Hz), 2,51 (signal large, 1H, $W_{\frac{1}{2}}$ = 5 Hz), 1,2 à 2,4 (m, 3H), 1,01 (d, 2,1 H, *J* = 6,5 Hz, CH—*Me*), 0,96 (d, 0,9H, *J* = 6,5 Hz, CH—*Me*). *Anal.* calc. pour $C_{11}H_{14}O_4$: C 62,85, H 6,71; trouvée: C 62,8, H 6,8%.

Fraction ***12***a-*OH*: rmn ($CDCl_3$) δ: 3,6 à 4,0 (m, 1H, *CH*—OH), 3,71 (s, 6H, COOMe), 3,14 (dd, 1H, *J* = 6 et 4 Hz), 2,6 à 2,9 (m, 2H avec signal se déplaçant par dilution), 2,47 (signal large, 1H), 2,15 à 2,55 (m, 1H), 1,2 à 1,1 (m, 3H), 1,14 (d, 0,9H, *J* = 7,2 Hz, CH—*Me*), 0,93 (d, 2,1H, *J* = 7,5 Hz, CH—*Me*); ce mélange d'alcools est acétylé: à 0,168 g de ces derniers on ajoute à 0°C, 0.2 cm³ d'Ac_2O et 2 cm³ de pyridine,

Can. J. Chem. Downloaded from www.nrcresearchpress.com by 210.87.254.105 on 09/06/12
For personal use only.

puis abandonne 15 h. On ajoute de la glace, puis extrait à AcOEt. On élimine la pyridine (lavage par $CuSO_4$ en solution aqueuse saturée), lave (H_2O, Na_2CO_3 10% puis H_2O/NaCl), sèche (Na_2SO_4), concentre et filtre sur colonne de silice avec éther – éther de pétrole (80:20). On obtient 143 mg (78%) de mélange d'acétates **12***a*-OAc; ir ($CHCl_3$): 1730 (C=O), 1200 large (C—O—C) cm^{-1}; rmn ($CDCl_3$) δ: 4,5 à 5,0 (signal large, 1H, avec d à 4,86, J = 7, 4 Hz, CH—OAc), 3,70 (s, 6H, COOMe), 3,05 à 3,35 (m, 1H), 1,2 à 3,0 (m, 7H), 2,05 et 2,02 (deux s, 3H, O—CO—CH_3), 1,07 (d, 0,9H, J = 7, 3 Hz, CH—*Me*), 0,86 (d, 2,1H, J = 7,3 Hz, CH—*Me*). *Anal.* calc. pour $C_{14}H_{20}O_6$: C 59,14, H 7,09; trouvée: C 59,8, H 7,1%.

Fraction **11***a*-*OH*: celle-ci se compose de deux sous fractions séparées par chromatographie sur colonne de silice avec éther – éther de pétrole (60:40). La 1ère sous-fraction (48%): rmn (DMSO-d_6) on note en particulier à δ: 4,3 à 4,6 (six raies qui disparaissent par addition de CF_3–COOH, 1H, OH), 3,67, 3,64 et 3,62 (trois s, 6H, COOMe). 0,29 g de ce mélange est acétylé selon la technique utilisée pour les alcools **12***a*-OH. Après filtration sur colonne de silice avec éther – éther de pétrole (80:20), on obtient 262 mg d'acétates (77%); ir ($CHCl_3$): 1729 (C=O), 1200 large (C—O—C) cm^{-1}. *Anal.* calc. pour $C_{14}H_{20}O_6$: C 59,14, H 7,09; trouvée: C 59,1, H 7,0%. La 2ème sous-fraction (52%): rmn (DMSO-d_6) on note en particulier à δ: 4,70 (d, 0,7H, J = 3,5 Hz, OH disparaît par addition de CF_3-COOH), 4,61 (d, 0,3H, J = 3,5 Hz, OH, disparait par addition de CF_3–COOH), 3,65 et 3,62 (deux s, 6H, COOMe); 1,2 g de ce mélange est acétylé comme précédemment. On obtient 1,2 g (91%) d'acétates; ir ($CHCl_3$): 1730 (C=O), 1250 et 1202 (C—O—C) cm^{-1}. *Anal.* calc. pour $C_{14}H_{20}O_6$: C 59,14, H 7,09; trouvée: C 59,2, H 7,1%. Par cpv préparative (colonne 200 × 1 cm de SE 30 15% sur CPLA 30/60 mesh, T_c 200°C, P 0,8 bar), on parvient à isoler le diméthoxycarbonyl-6 *exo*, 7 *endo* acétoxy-4 *exo* bicyclo-[3.2.1]octane; rmn ($CDCl_3$, 100 MHz) δ: 4,94 (signal large, 1H, $W_{\frac{1}{2}}$ = 11 Hz, H-4), 3,73 (s, 3H, COOMe), 3,46 (t, 1H, J = 6 Hz, H-7), 3,16 (d, 1H, J = 6 Hz, H-6), 2,65 (m, 2H, $W_{\frac{1}{2}}$ = 11 Hz, H-1 et H-5), 2,06 (s, 3H, O—CO—CH_3), 1,4 à 2 (m, 6H, H-3, H-4 et H-8); et le diméthoxycarbonyl-6 *exo*, 7 *endo* acétoxy-2 *exo* bicyclo[3.2.1]octane; rmn ($CDCl_3$, 100 MHz) δ: 4,86 (signal large, 1H, $W_{\frac{1}{2}}$ = 9 Hz, H-2), 3,74 (s, 3H, COOMe), 3,70 (s, 3H, COOMe), 3,51 (t, 1H, J = 6,5 Hz, H-7), 3,19 (d, 1H, J = 6,5 Hz, H-6), 2,75 (signal large, 1H, $W_{\frac{1}{2}}$ = 18 Hz, H-1), 2,49 (signal large, 1H, $W_{\frac{1}{2}}$ = 11 Hz, H-5), 2,05 (s, 3H, O—CO—CH_3), 1,45 à 2 (m, 6H).

Analyse du mélange des composés **13**b *et* **14**b

Ce mélange présente le spectre de rmn suivant (DMSO-d_6, 100 MHz) δ: 5,2 à 6,2 (m, 2H, H éthyléniques), 3,1 à 3,45 (m, 1,57H), 2,86 (d, large, 0,43H, J = 7 Hz), 1,5 à 2,8 (6H). La présence d'un signal d'intégration inférieure à 1H montre qu'il s'agit d'un mélange; l'obtention des produits purs exposée ci-dessous a permis d'en établir la composition par rmn, soit 43% de **13***b* et 57% de **14***b*.

Isomérisation du composé **1**a

On place 5,1 g du composé tricyclique **1***a* dans 11 cm^3 de BF_3–OEt_2 préalablement distillé sur CaH_2. On porte à 90°C et suit l'avancement par rmn. Après 2 h 50 min on étend à l'éther, neutralise (K_2CO_3 10%), décante et extrait la phase aqueuse à l'éther. Les phases organiques jointes sont séchées (K_2CO_3) puis concentrées et chromatographiées sur colonne de silice avec éther – éther de pétrole (20:80). On obtient: (*a*) 3,7 g de mélange des esters méthyliques et éthyliques des composés **13** et **14**. Ce mélange est agité 15 h avec une solution de soude à 8%. On acidifie à froid (HCl 50%) et extrait à AcOEt. La phase organique est séchée (Na_2SO_4) et concentrée, puis estérifiée par un excès de diazométhane en solution éthérée. On obtient 3,2 g (63% global) d'un mélange contenant 64% de **13***a* et 36% de **14***a*; rmn ($CDCl_3$) δ: 5,2 à 6,2 (m, 2H), 3,7 (s, 6H, COOMe), 3,3 à 3,7 (m, 1,36H), 3,15 (d, 0,64H, J = 7 Hz, H-6 de **13***a*), 1,5 à 3,0 (m, 6H); (*b*) 113 mg (2,2%) de l'ester éthylique du mélange **10***b*, structure attribuée par comparaison du spectre de rmn avec celui de **10***a*: rmn ($CDCl_3$): 4,90 (signal à allure de t, 0,4H, J = 6 Hz), 4,19 (q, 2,6H, J = 7 Hz se superpose à un autre signal), 2,9 à 3,3 (m, 2H), 2,74 (signal large, 1H, $W_{\frac{1}{2}}$ = 4,5 Hz), 2,50 (signal large, 1H, $W_{\frac{1}{2}}$ = 5 Hz), 1,9 à 2,4 (m, 1H), 1,5 à 1,9 (m, 2H), 1,28 (t, 3H, J = 7 Hz), 1,02 et 0,96 (deux doublets, 3H, J = 7 Hz, CH_3), contient également des esters méthyliques à 3,73 (COOMe); (*c*) 430 mg (9%) du mélange **10***a*.

Iodolactonisation du mélange des composés **13**b *et* **14**b

On opère selon la référence 28 à partir de 7,3 g de mélange d'olefines **13***b* et **14***b* (dans le rapport 64:36), 28,5 cm^3 de MeOH, 12,5 cm^3 de soude à 20% et 118 cm^3 de bicarbonate de soude à 5%. Après traitement, on sèche (Na_2SO_4), concentre et estérifie par un excès de diazométhane en solution éthérée. On obtient 11,7 g de produit brut présentant deux taches en ccm (silice, benzène–éther 97:3) dans les proportions 57:43 (rmn). Par recristallisation on isole 470 mg (3,7%) de l'iodolactone minoritaire, soit la lactone de l'acide hydroxy-3 *endo* iodo-4 méthoxycarbonyl-6 *exo* bicyclo[3.2.1]octane carboxylique-7 *endo*, **16**; F 120–121°C (benzène–éther); ir ($CHCl_3$): 1740 (C=O δ-lactone et ester) cm^{-1}; rmn ($CDCl_3$) δ: 4,76 (signal large, 1H, $W_{\frac{1}{2}}$ = 7,5 Hz), 4,63 (m, 1H, $W_{\frac{1}{2}}$ = 7,5 Hz), 3,72 (s, 3H, COOMe), 3,54 (d, 1H, J = 8 Hz, H-7x), 3,13 (signal large, 2H, $W_{\frac{1}{2}}$ = 5 Hz), 2,5 à 3,0 (m, 1H), 2,2 à 2,5 (m, 1H), 1,5 à 2,2 (m, 3H). *Anal.* calc. pour $C_{11}H_{13}O_4I$: C 39,28, H 3,86, I 37,79; trouvée: C 39,0, H 4,0, I 37.8%.

Une chromatographie, sur colonne de silice avec benzène–éther (97:3), des eaux-mères de la recristallisation ci-dessus permet d'isoler 1,23 g (9,8%) de la lactone de l'acide hydroxy-2 *endo* iodo-3 méthoxycarbonyl-6 *exo* bicyclo[3.2.1]octane carboxylique-7 *endo*, **15**; ir ($CHCl_3$): 1778 (C=O γ-lactone), 1735 (C=O ester) cm^{-1}; rmn ($CDCl_3$) δ: 5,28 (d, 1H, J = 7,4 Hz, CH—OCO), 4,36 (d, 1H, J = 7 Hz, CH—I), 3,73 (s, 3H, COOMe), 1,5 à 3,6 (8H). *Anal.* calc. pour $C_{11}H_{13}O_4I$: C 39,28, H 3,86, I 37,79; trouvée: C 39,3, H 4,1, I 36,9%.

Deshalogénation des composés **15** *et* **16**

On opère selon la référence 29: on porte au reflux 45 min, 336 mg de mélange de **15** et **16** (59:41, rmn), 2,8 g de Ni Raney et 18 cm^3 d'EtOH. On étend à l'eau, extrait à l'acétate d'éthyle. La phase organique est séchée (Na_2SO_4), concentrée et chromatographiée sur colonne de silice avec éther – éther de pétrole (30:70). On obtient 51 mg (26%) de **8***a* et 35 mg (18%) de **11***a* (ccm, ir).

Acide méthoxycarbonyl-6 exo *bicyclo[3.2.1]octène-2 carboxylique-7* endo, ***17***

On opère selon la référence 30. On porte au reflux 1 h, 560 mg de l'iodolactone **15**, 250 mg de Zn en poudre et 10 cm^3 de pyridine anhydre; on étend à l'eau, acidifie à froid (HCl 20%) et extrait (AcOEt). La phase organique est lavée (H_2O), séchée (Na_2SO_4), concentrée et chromatographiée sur colonne de silice avec éther – éther de pétrole – acide formique (14,5:84,5:1). On obtient 179 mg (55%) du composé **17**; F 120–121°C (éther – éther de pétrole); ir ($CHCl_3$): 2400 à 3600 large (OH acide), 1730 (C=O ester), 1710 (C=O acide) cm^{-1}; rmn ($CDCl_3$) δ: 11,2 (s large, 1H, COOH), 5,3 à 6,1 (m, 2H, H éthyléniques), 3,71 (s, 3H, COOMe), 3,51 (dd, 1H, J = 5,5 et 7 Hz, H-7), 3,10 (dd, 1H, J = 7 et 1 Hz, H-6), 2,45 à 3,0 (2H), 2,0 à 2,45 (2H), 1,5 à 2,0 (2H). *Anal.* calc. pour $C_{11}H_{14}O_4$: C 62,85, H 6,71; trouvée: C 62,9, H 6,5%.

Can. J. Chem. Downloaded from www.nrcresearchpress.com by 210.87.254.105 on 09/06/12
For personal use only.

Acide bicyclo[3.2.1]octène-2 dicarboxylique-6 exo, *7* endo, ***13***b

On agite 200 mg du composé précédent, 15 h dans 4 cm³ de NaOH 8% et 5 cm³ de MeOH. On lave (Et_2O), acidifie à froid (HCl 50%) et extrait (AcOEt). La phase organique est lavée (H_2O), séchée (Na_2SO_4) et concentrée. On obtient 150 mg (81%) de **13***b* purifié par filtration sur silice; *F* 195–197°C; ir (KBr): 2300 à 3600 large (OH acide), 1710 et 1692 (C=O) cm^{-1}; rmn (DMSO-d_6, 100 MHz) δ: 10,9 (2H, COOH), 5,77 (dd large, 1H, J = 6,0 et 10 Hz, $W_{\frac{1}{2}}$ = 18 Hz, H-2), 5,46 (d large, J = 10 Hz, $W_{\frac{1}{2}}$ = 16 Hz, H-3), 3,23 (dd, 1H, J = 5 et 6,5 Hz, H-7), 2,86 (d, 1H, J = 6,5 Hz, H-6), 2,6 à 2,8 (1H), 2,25 à 2,6 (2H), 1,8 à 2,15 (1H), 1,45 à 1,80 (2H). *Anal.* calc. pour $C_{10}H_{12}O_4$: C 61,22, H 6,17; trouvée: C 60,9, H 6,1%.

Acide méthoxycarbonyl-7 exo *bicyclo[3.2.1]octène-2 carboxylique-6* endo, ***18***

Comme précédemment, mais à partir de 337 mg d'iodolactone **16**, on obtient 139 mg (66%) du composé attendu; *F* 99–100°C; ir ($CHCl_3$): 2400 à 3600 large (OH acide), 1725 (C=O ester), 1710 (C=O acide) cm^{-1}; rmn ($CDCl_3$) δ: 11,3 (s, 1H, COOH), 6,0 (dd, 1H, J = 9,5 et 7 Hz, H-2), 5,44 (dt, 1H, J = 9,5 et 3 Hz, H-3), 3,70 (s, 3H, COOMe), 3,3 à 3,7 (m, 2H, H-6 et H-7), 2,5 à 3,1 (2H), 2,0 à 2,4 (2H), 1,7 à 2,0 (2H). *Anal.* calc. pour $C_{11}H_{14}O_4$: C 62,85, H 6,71; trouvée: C 62,8, H 6,7%

Acide bicyclo[3.2.1]octène-2 dicarboxylique-6 endo, *7* exo, ***14***b

On hydrolyse 100 mg du composé précédent selon la méthode utilisée pour l'obtention de **13***b*. On obtient 77 mg (82%) de diacide **14***b*; *F* 215–217°C; ir (KBr): 2300 à 2600 large (OH acide), 1700 (C=O) cm^{-1}; rmn (DMSO-d_6, 100 MHz) δ: 10,7 (large, 2H, COOH), 5,95 (dd, 1H, J = 9,5 et 7 Hz, H-2), 5,37 (dt, 1H, J = 9,5 et 3 Hz, H-3), 3,34 (Partie A de AB, J_{AB} = 5 Hz, dédoublée, J = 7 Hz, H-6x), 3,18 (Partie B de AB, J_{AB} = 5 Hz, H-7n), 1,5 à 2,8 (6H). *Anal.* calc. pour $C_{10}H_{12}O_4$: C 61,22, H 6,17; trouvée: C 60,9, H 6,1%.

Ouverture du diacide ***2***

On porte à 80°C, 150 mg de diacide **2** dans 1 cm³ d'acide formique et suit l'avancement en rmn. Après 0,5 h on concentre et chromatographie sur colonne de silice avec éther – éther de pétrole – acide formique (64,5:34,5:1). On obtient (*a*) 15 mg (10%) du composé de départ; (*b*) 90 mg (48%) des composés **19** qui présentent deux taches en ccm (éther – éther de pétrole – acide formique: 79,5:19,5:1); ir ($CHCl_3$): 2400 à 3600 large (OH acide), 1712 (C=O) cm^{-1}; rmn ($CDCl_3$) δ: 10,7 (large, 2H, COOH), 8,12 (s, 0,68H, O—COH), 7,00 (s, 0,32H, O—COH), 5,07 (signal large, 2H, $W_{\frac{1}{2}}$ = 14 Hz, *CH*—OCOH), 3,2 à 3,7 (2H), 2,72 (signal large, 2H, $W_{\frac{1}{2}}$ = 14 Hz), 1,2 à 2,2 (6H); (*c*) 34 mg (23%) de lactone **8***b* (ir, rmn).

Stabilité des produits dans les conditions réactionnelles

Chacun des produits ou mélanges est porté 6 h à 80°C dans l'acide formique. La lactone **8***b*, la lactone **9***b*, le mélange **10***b* + **11***b* + **12***b* restent inchangés (CCM, rmn); 440 mg d'un mélange **13***b* + **14***b* (80:20, rmn) conduisent, après chromatographie sur colonne de silice avec éther – éther de pétrole – acide formique (49,5:49,5:1) à: (*a*) 385 mg (88%) de mélange **13***b* + **14***b* (80:20) (ccm, rmn); (*b*) 8 mg (2%) de mélange de **10***b* + **11***b* + **12***b* (ccm, rmn); (*c*) 11 mg (2,5%) de lactone **8***b* (CCM); (*d*) 32 mg (7,3%) de lactone **9***b* (ccm, ir).

Ouverture du diacide ***1***b *par* BF_3–OEt_2

On porte à 90°C, 1,4 g de diacide **1***b* dans 5 cm³ de BF_3–OEt_2 préalablement distillé sur CaH_2. La disparition du noyau cyclopropanique est suivie par rmn. Après 2 h, on étend à l'éther, neutralise à froid (K_2CO_3 10%) puis acidifie toujours à froid (HCl 50%). On décante et extrait à AcOEt. La phase organique, lavée (H_2O), séchée (Na_2SO_4) puis concentrée, laisse 1,46 g de produit brut. Après hydrolyse (NaOH 8%, 15 h), les composantes, séparées par chromatographie sur gel de silice, sont reconnues par rmn et ir pour les lactones **8***b* et **9***b*, et rmn pour les autres fractions. Le rendement global après chromatographie est de 95%, les proportions relatives étant indiquées dans la discussion.

Action de BF_3–OEt_2 *sur les oléfines diacides* ***13***b *et* ***14***b

Dans les mêmes conditions que ci-dessus, 490 mg de mélange **13***b* + **14***b* (73:27, rmn) conduisent à 26,1% de mélange **13***b* + **14***b* (80:20, rmn) qui n'a pas réagi, 47% de lactone **8***b* et 13,9% de lactone **9***b*.

1. (*a*) S. Danishefsky. Acc. Chem. Res. 66 (1979); (*b*) G. Stork et M. Marx. J. Am. Chem. Soc. **91**, 2371 (1969); G. Stork et P. A. Grieco. Tetrahedron Lett. 1807 (1971); P. A. Grieco et R. S. Finkeldor. Tetrahedron Lett. 527 (1974); (*c*) H. Sekisaki, M. Ito et S. Inoue. Bull. Chem. Soc. Jpn. **52**, 3113 (1979); (*d*) J. A. Marshall et R. H. Ellison. J. Org. Chem. **40**, 2070 (1975); J. Am. Chem. Soc. **98**, 4312 (1976).
2. (*a*) N. C. Deno, W. E. Billups, D. La Vietes, P. C. Scholl et S. Schneider. J. Am. Chem. Soc. **92**, 3700 (1970); (*b*) R. R. Sauers et P. E. Sonnet. Tetrahedron, **20**, 1029 (1964); (*c*) P. E. Peterson et G. Thompson. J. Org. Chem. **33**, 968 (1968); (*d*) T. Hasselstrom. J. Am. Chem. Soc. **53**, 1097 (1931); (*e*) L. A. Paquette et M. K. Scott. J. Am. Chem. Soc. **94**, 6451 (1972); (*f*) M. H. Battiste, J. M. Coxon et R. Edelman. Tetrahedron Lett. 4577 (1972); (*g*) S. J. Cristol et A. L. Noreen. J. Org. Chem. **41**, 4016 (1976); cf. également la référence 3.
3. R. T. Lalonde et J. J. Batelka. Tetrahedron Lett. 445 (1964); R. T. Lalonde, J. Ding et M. H. Tobias. J. Am. Chem. Soc. **89**, 6651 (1967).
4. (*a*) H. B. Henbest et B. Nicchols. J. Chem. Soc. 221 (1969); H. Christol, J. Coste et F. Plénat. Bull. Soc. Chim. Fr. 3934 (1969); **II**, 1064 (1973); H. Christol, J. Coste, F. Plénat et G. Renard. Bull. Soc. Chim. Fr. **II**, 421 (1979); (*b*) B. Giese. Chem. Ber. **108**, 2998 (1975); (*c*) K. C. Nicolaou et Z. Lysenko. J. Chem. Soc. Chem. Commun. 293 (1973).
5. R. J. Rawson et I. T. Harrison. J. Org. Chem. **35**, 2057 (1970).
6. H. Koch. Monatsh. **93**, 1943 (1962).
7. (*a*) H. E. Simmons, T. L. Cairns, S. A. Vladuchick et C. M. Hoiness. Organic reactions. Vol. 20. *Edité par* W. E. Dauben. J. Wiley, New York. 1973. p. 41; (*b*) X. Creary. J. Org. Chem. **40**, 3326 (1975).
8. H. C. Brown, J. H. Kawakami et K. T. Liu. J. Am. Chem. Soc. **95**, 2209 (1973).
9. S. Inagaki, H. Fujimoto et K. Fukui. J. Am. Chem. Soc. **98**, 4054 (1976).
10. P. von R. Schleyer. J. Am. Chem. Soc. **89**, 701 (1967).
11. (*a*) R. A. Moss. Selective organic transformations. Vol. 1. *Edité par* B. S. Thyagarajan. J. Wiley, New York. 1970. p. 35; (*b*) J. Haywood-Farmer, H. Malkus et M. A. Battiste. J. Am. Chem. Soc. **94**, 2209 (1972).
12. (*a*) J. S. Haywood-Farmer et R. E. Pincock. J. Am. Chem. Soc. **91**, 3020 (1969); (*b*) P. K. Freeman, T. D. Ziebarth et R. S. Raghavan. J. Am. Chem. Soc. **97**, 1875 (1975); (*c*) S. C. Clarke, K. J. Frayne et B. L. Johnson. Tetrahedron, **25**, 1265 (1969).
13. (*a*) J. W. Wilt et D. R. Sullivan. J. Org. Chem. **40**, 1036 (1975); (*b*) J. Haywood-Farmer, R. E. Pincock et J. I. Wells. Tetrahedron, **22**, 2007 (1966).
14. J. P. Chesick. J. Am. Chem. Soc. **84**, 3250 (1962).

15. P. G. GASSMAN et K. T. MANSFIELD. J. Org. Chem. **32**, 915 (1967).
16. F. VAN RANTWŸK, A. VAN VLIET et H. VAN DEKKUM. J. Chem. Soc. Chem. Commun. 234 (1973).
17. (*a*) J. W. WILT, T. P. MALLOY, P. K. MOOKERJEE et D. R. SULLIVAN. J. Org. Chem. **39**, 1327 (1974); (*b*) N. FILIPESCU et J. R. DEMEMBER. Tetrahedron, **24**, 5181 (1968).
18. V. V. PLEMENKOV, V. A. BREUS, A. W. GRECHKIN et L. K. NOVIKOVA. J. Org. Chem. USSR, **12**, 787 (1976).
19. R. M. MORIARTY, C. C. CHIEN et T. B. ADAMS. J. Org. Chem. **44**, 2210 (1979).
20. F. R. JENSEN et J. J. MILLER. Tetrahedron Lett. 4861 (1966).
21. R. T. LALONDE et J. DING. J. Org. Chem. **37**, 2555 (1972).
22. H. M. WALBORSKY et D. F. LONCRINI. J. Am. Chem. Soc. **76**, 5396 (1954); J. K. CRANDALL. J. Org. Chem. **29**, 2830 (1964); H. CHRISTOL, J. COSTE et F. PLÉNAT. Bull. Soc. Chim. Fr. 2005 (1970).
23. (*a*) C. H. DE PUY. Top. Curr. Chem. **40**, 74 (1973); (*b*) C. H. DE PUY, P. C. FUNFSCHILLING et A. H. ANDRIST. J. Am. Chem. Soc. **96**, 948 (1974); C. H. DE PUY, P. C. FUNFSCHILLING, A. H. ANDRIST et J. M. OLSON. J. Am. Chem. Soc. **99**, 6297 (1977); (*c*) R. T. LALONDE et A. D. DEBOLLI JR. J. Org. Chem. **35**, 2657 (1970).
24. L. CHICHE. Thèse d'Etat, Montpellier, 1978.
25. R. S. SHANK et H. SHECHTER. J. Org. Chem. **24**, 1825 (1959).
26. R. E. PINCOCK et J. I. WELLS. J. Org. Chem. **29**, 965 (1964).
27. O. DIELS et K. ALDER. Ann. **490**, 236 (1931).
28. C. D. VER NOY et C. S. RONDESTVEDT. J. Am. Chem. Soc. **77**, 4878 (1955).
29. A. DONCHE. Thèse d'Etat, Montpellier, 1965.
30. H. HOGEVEN, G. MACCAGNANI et F. MONTANARI. J. Chem. Soc. C, 1585 (1966).

Can. J. Chem. Downloaded from www.nrcresearchpress.com by 210.87.254.105 on 09/06/12
For personal use only.

Synthesis and bromination of 3-alkyl-5α-cholestan-2-one

C. AKIRA HORIUCHI AND J. YASUO SATOH

Department of Chemistry, Rikkyo (St. Paul's) University, Nishi-Ikebukuro, Toshima-ku, Tokyo, Japan

Received January 27, 1981

C. AKIRA HORIUCHI and J. YASUO SATOH. Can. J. Chem. **59**, 2382 (1981).

3β-Alkyl-5α-cholestan-2-ones (R = CH_3, C_2H_5, and $CH_3CH_2CH_2$) were prepared by the direct alkylation of 5α-cholestan-2-one with alkyl iodide and potassium *tert*-butoxide in a reflux of *tert*-butyl alcohol – benzene. The bromination of these 3β-alkyl ketones gave 3α-bromo-3β-alkyl-5α-cholestan-2-one.

C. AKIRA HORIUCHI et J. YASUO SATOH. Can. J. Chem. **59**, 2382 (1981).

On a préparé les alkyl-3β cholestan-5α ones-2 (R = CH_3, C_2H_5 et $CH_3CH_2CH_2$) en alkylant directement la cholestan-5α one-2 avec un iodure d'alkyle en présence du *tert*-butylate de potassium dans un mélange d'alcool *tert*-butylique – benzène au reflux. La bromation des cétones alkylées en position 3β conduit à la bromo-3α alkyl-3β cholestan-5α one-2.

[Traduit par le journal]

The methylation of steroids which have an oxo group in ring A has been investigated (1–4), and the preparation of methyl ketones using hydroxymethylene derivatives of 5β-stigmast-22-en-3-one (5) and of pregn-4-ene-3,20-dione (6) has also been described. More recently, the present authors reported (7) the direct alkylation of 5β-cholestan-2-one and the bromination of these alkyl ketones. In the present paper, the direct alkylation of 5α-cholestan-2-one with alkyl iodide (RI; R = CH_3, C_2H_5, or $CH_3CH_2CH_2$) and potassium *tert*-butoxide is described, together with the bromination of these alkyl derivatives.

Results and Discussion

The reaction of 5α-cholestan-2-one (**1**) with alkyl iodide (RI; R = CH_3, C_2H_5, and $CH_3CH_2CH_2$) and potassium *tert*-butoxide yielded the corresponding alkylated ketones (**2***a* (8, 9), **2***b*, and **2***c*). Each alkylated ketone showed a weak positive Cotton effect in the cd spectrum compared with that of 5α-cholestan-2-one (**1**). By comparison with the cd spectra of the 3β-methyl ketone (**2***a*), the alkyl ketones (**2***b* and **2***c*) were presumed to be 3β-ethyl- (**2***b*) and 3β-propyl-5α-cholestan-2-one (**2***c*). Spencer *et al.* (10) had reported that the methylation of the α-bromo ketone with zinc powder – methyl iodide in benzene – dimethyl sulfoxide (10:1) in a nitrogen atmosphere gave the α-methyl ketone. The reaction of 3α-bromo-5α-cholestan-2-one (**4**) with methyl iodide in the presence of zinc powder according to the procedures described by Spencer afforded compound **5***a* in 80% yield. This product **5***a* was isomerized by treatment with concentrated sulfuric acid in ethanol to give the stable compound **2***a*. On the synthesis of 3α-methyl-5α-cholestan-2-one, Jones and Grayshan (8) reported that a 2β-hydroxy-3α-methyl derivative was obtained from 2β,3β-epoxy-5α-cholestane through the epoxy ring opening with 2-lithio-1,3-dithian and desulfurization. The method used in the present work, which was that described by Spencer *et al.*, gave a better yield than Jones and Grayshan's method.

The bromination of the alkylated ketones (**2***a*, **2***b*, and **2***c*) gave the bromo derivative (**3***a*, **3***b*, or **3***c*). On the basis of the cd, ir, and nmr spectral data for **3***a*, **3***b*, and **3***c*, these bromo derivatives were determined to be 3α-bromo-3β-alkyl-5α-cholestan-2-ones. This finding was supported by the fact that the bromo derivatives (**3***a*, **3***b*, and **3***c*) were reduced with sodium borohydride to give the bromohydrins (**6***a*, **6***b*, and **6***c*). The nmr spectra of these bromohydrins showed a quartet at δ 2.94 ppm (J = 4.5 and 11.25 Hz) for **6***b*, and a multiplet at δ 3.00 ppm ($W/2$ = 33 Hz) for **6***c* assignable to the 2β-H of an axial character. Compound **6***a* was converted to the bromohydrin acetate (**7***a*). The nmr spectrum of this bromohydrin acetate showed a quartet at δ 4.21 ppm (J = 5.0 and 11.0 Hz) assignable to the 2β-H of an axial character. Therefore, **6***a*, **6***b*, and **6***c* were presumed to be 2α-hydroxy-3α-bromo-3β-alkyl-5α-cholestane. By treating these bromohydrins with potassium hydroxide, the corresponding 3β-alkyl ketone (**2***a*, **2***b*, or **2***c*) was obtained. These results showed that a hydroxyl group and a bromine atom of the bromohydrins (**6***a*, **6***b*, and **6***c*) were *cis*, and this led to 3α-bromo-3β-alkyl-2α-hydroxy-5α-cholestane structures for these bromohydrins.

It was found that the enolisation of the methyl ketone (**2***a*) with 60% perchloric acid – acetic anhydride occurred in the direction of a carbon atom possessing a methyl group, as shown by the nmr spectra. The bromination of the enolisation product (**8***a*) of the methyl ketone yielded the 3α-bromo-3β-methyl ketone (**3***a*).

0008-4042/81/152382-04$01.00/0

©1981 National Research Council of Canada/Conseil national de recherches du Canada

Can. J. Chem. Downloaded from www.nrcresearchpress.com by 210.87.254.40 on 09/06/12
For personal use only.

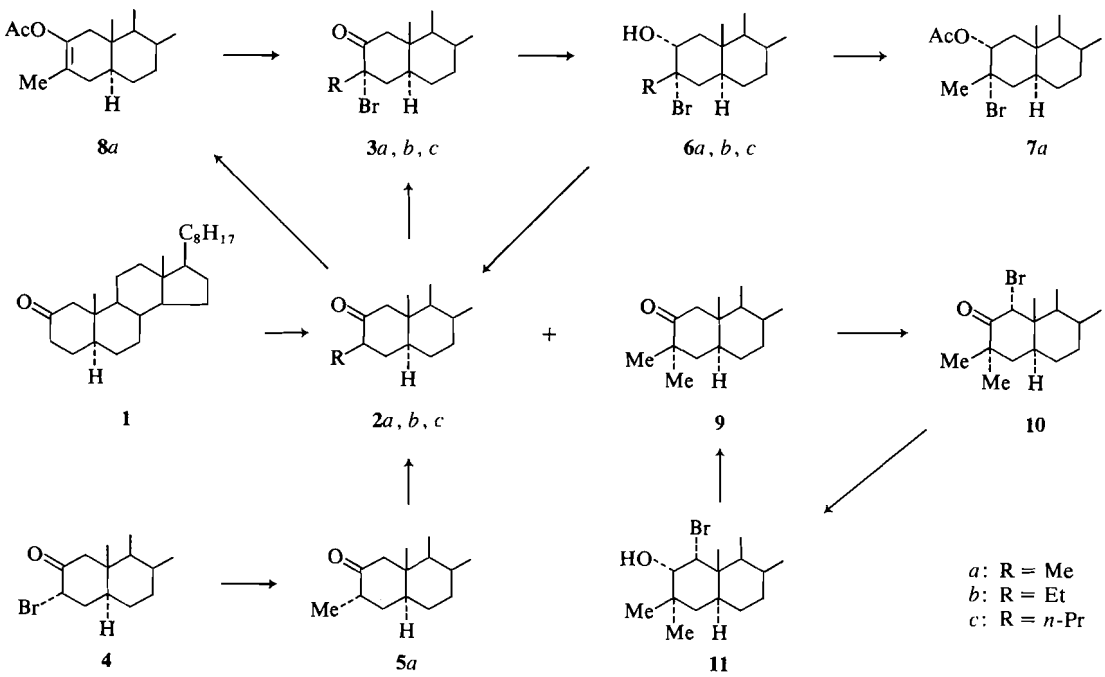

SCHEME 1

These results show that the enolisation of the alkylated ketone occurs at the C(2)—C(3) position. The bromination of the 3β-alkyl ketone occurs at a carbon atom having an alkyl group, namely, the C(3)α-bond, as has been reported for the bromination of the alkylated ketone (2).

The reaction of 5α-cholestan-2-one (**1**) with excess methyl iodide yielded the dimethylated ketone (**9**) and 3β-methyl ketone (**2***a*). The bromination product of the former was presumed to be 1α-bromo-3,3-dimethyl ketone (**10**) from the sign of the Cotton effect, and Δ[θ]- and $\Delta\lambda_1$-values (+15 600 and +30 nm, as compared with the corresponding values for the dimethylated ketone (**9**)) in the cd spectrum, the shift of the C=O stretching band (1700 cm^{-1}) in the ir spectrum, and from the signal (δ 4.04 ppm, singlet) due to the C(1)HBr in the nmr spectrum. From these spectral data, it can be considered that the conformation in the A-ring of **10** is a little distorted due to the 1:3-interaction between the C(1)α—Br bond and the C(3)α—Me bond.

The bromo ketone (**10**) was then converted to the dimethylated bromohydrin (**11**) by reduction with sodium borohydride, as described above. By treatment of **11** with potassium hydroxide in ethanol under refluxing conditions, the dimethylated ketone (**9**) was obtained. From these results, the dimethylated bromohydrin (**11**) was identified as 1α-bromo-2α-hydroxy-3,3-dimethyl-5α-cholestane.

Thus, on the basis of all of the foregoing results, it was concluded that the α-alkylation of 5α-cholestan-2-one (**1**) occurred at the C(3) position, as has been reported for the case of the condensation (9) of 5α-cholestan-2-one (**1**) with ethyl formate. It was further concluded that the enolisation of the alkylated ketone occurred in the direction of C(3), and that the bromination of these alkylated ketones gives the 3α-bromo-3β-alkyl ketones. These results are also in agreement with the facts that the alkylation of 5β-cholestan-2-one occurs at the C(3) position, and the enolisation and the bromination of the alkylated ketone occur in the direction of C(3).

Experimental

All the melting points are uncorrected. The ir and cd spectra were measured using a Hitachi model 215 grating infrared spectrophotometer and a model J-20 spectropolarimeter. The nmr spectra were measured in carbon tetrachloride, with TMS as the internal standard, using a nuclear magnetic resonance spectrometer, Hitachi-Perkin Elmer R-20A. The high-resolution mass spectra were recorded on JMS-O1SG-2 (JEOL) instrument with direct inlet at 75 eV.

*3β-Methyl-5α-cholestan-2-one (***2a***)*

A mixture of **1** (1.0 g), methyl iodide (9.5 mL), and potassium *tert*-butoxide (400 mg) in *tert*-butyl alcohol – dry benzene (1:1) (20 mL) was refluxed under stirring in a nitrogen atmosphere for

Can. J. Chem. Downloaded from www.nrcresearchpress.com by 210.87.254.40 on 09/06/12
For personal use only.

Can. J. Chem. Downloaded from www.nrcresearchpress.com by 210.87.254.40 on 09/06/12
For personal use only.

4 h. The solvent was then removed under reduced pressure; the residue was poured into water and extracted with ether. The ethereal solution was washed with water, dried, and evaporated under reduced pressure. Crystallization of the residue from ethanol–acetone gave needles of **2***a* (383 mg), mp 149–151°C (lit. (8) mp 151–153°C); ir (KBr): 1708 cm^{-1}; cd (*c* 0.0806, Di) at 24.5°C: $[\theta]_{302}$ +6517 (peak), $[\theta]_{298}$ +6268 (trough), and $[\theta]_{293}$ +6566 (peak).

The mother liquor was evaporated under reduced pressure and the resultant oil was chromatographed on silica gel. Elution with benzene gave needles of **1** (490 mg), mp 127–129°C.

*3β-Ethyl-5α-cholestan-2-one (***2b***)*

A mixture of **1** (1.69 g), potassium *tert*-butoxide (680 mg), and ethyl iodide in *tert*-butyl alcohol – benzene was treated according to the procedure described for the methylation of **1**. After the usual work-up, the resultant oil was chromatographed on silica gel. Elution with hexane–benzene (1:1) gave needles of **2***b* (357 mg) from ethanol, mp 110–113°C; ir (KBr): 1705 cm^{-1}; cd (*c* 0.427, Di) at 20°C: $[\theta]_{312}$ +2912 (shoulder), $[\theta]_{302}$ +4707 (peak), $[\theta]_{298}$ +4561 (trough), and $[\theta]_{295}$ +4658 (peak). *Anal.* calcd. for $C_{29}H_{50}O$: C 83.99, H 12.15; found: C 84.22, H 11.94.

*3β-Propyl-5α-cholestan-2-one (***2c***)*

A mixture of **1** (1.69 g), potassium *tert*-butoxide (680 mg), and propyl iodide (6.3 mL) in *tert*-butyl alcohol – benzene (1:1) was treated according to the procedure described for the methylation of **1**. After the usual work-up, the resultant oil (1.99 g), on crystallization from ethanol, gave needles of **2***c* (835 mg), mp 118–120°C; ir (KBr): 1707 cm^{-1}; cd (*c* 0.360, Di) at 23°C: $[\theta]_{363}$ +5740 (peak), $[\theta]_{299}$ +5574 (trough), and $[\theta]_{295}$ +5693 (peak). *Anal.* calcd. for $C_{30}H_{52}O$: C 84.04, H 12.23; found: C 84.35, H 12.40.

*3α-Methyl-5α-cholestan-2-one (***5a***)*

The bromo ketone (**4**) (1.0 g) in benzene – dimethyl sulfoxide (10:1) (55 mL) was stirred with zinc powder (2.5 g) and methyl iodide (12.5 mL) in a nitrogen atmosphere at 40–45°C for 3 h. After the usual work-up, crystallization from methanol afforded plates of **5***a* (690 mg), mp 124–125°C (lit. (8) mp 127–128°C); ir (KBr): 1705 cm^{-1}; cd (*c* 0.199, Di) at 23°C: $[\theta]_{304}$ +8256 (peak), $[\theta]_{301}$ +8175 (trough), and $[\theta]_{296}$ +8578 (peak).

*Isomerization of 3α-Methyl-5α-cholestan-2-one (***5a***)*

3α-Methyl ketone (**5***a*) (15 mg) in ethanol (10 mL) was treated with a few drops of concentrated sulfuric acid under reflux for 2 h. After the usual work-up, crystallization from methanol afforded needles of **2***a* (10 mg) (mp 150–152°C).

*3α-Bromo-3β-methyl-5α-cholestan-2-one (***3a***)*

The methylated ketone (**2***a*) (260 mg) in acetic acid (16 mL) was treated with bromine (114 mg) in acetic acid (3.2 mL) containing a few drops of 48% hydrobromic acid at room temperature for 20 min. The reaction mixture was taken up in ether, and the ethereal extracts were washed with a sodium hydrogen carbonate solution and water, then dried and evaporated. Crystallization of the residue from methanol gave needles of **3***a* (213 mg), mp 192–195°C; ir (KBr): 1708 cm^{-1}; cd (*c* 0.102, Di) at 24.5°C: $[\theta]_{314}$ +25797 (peak). *Anal.* calcd. for $C_{28}H_{47}OBr$: C 70.11, H 9.88; found: C 70.09, H 9.86.

*3α-Bromo-3β-ethyl-5α-cholestan-2-one (***3b***)*

The bromination of **2***b* (250 mg) was carried out using the technique described for the synthesis of 3α-bromo-3β-methyl-5α-cholestan-2-one. After the usual work-up, the resultant oil, on crystallization from methanol–ether, gave plates of **3***b* (213 mg), mp 154–156°C; ir (KBr): 1705 cm^{-1}; cd (*c* 0.367, Di) at 20°C: $[\theta]_{315}$ +18846 (peak). *Anal.* calcd. for $C_{29}H_{49}OBr$: C 70.57, H 10.01; found: C 70.64, H 10.19.

*3α-Bromo-3β-propyl-5α-cholestan-2-one (***3c***)*

The bromination of **2***c* (400 mg) was carried out using the technique described for the synthesis of 3α-bromo-3β-methyl-5α-cholestan-2-one. After the usual work-up, the resultant oil, on crystallization from ethanol, gave needles of **3***c* (278 mg), mp 100–102°C; ir (KBr): 1707 cm^{-1}; cd (*c* 0.470, Di) at 23°C: $[\theta]_{317}$ +12529 (peak). *Anal.* calcd. for $C_{30}H_{51}OBr$: C 70.98, H 10.13; found: C 70.85, H 9.80.

*3,3-Dimethyl-5α-cholestan-2-one (***9***)*

The ketone (**1**) (1.0 g) in *tert*-butyl alcohol – dry benzene (1:1) (25 mL) was treated with methyl iodide (4.0 mL) and potassium *tert*-butoxide (3.0 g) under refluxing in a nitrogen atmosphere for 5 h. After the usual work-up, the resultant oil (1.06 g) was chromatographed on silica gel (100 g). Elution with benzene (300 mL) gave plates of **9** (317 mg) from acetone, mp 156–157.5°C; ir (KBr): 1700 cm^{-1}; cd (*c* 0.293, Di) at 26°C: $[\theta]_{304}$ +12791 (peak), $[\theta]_{300}$ +12225 (trough), and $[\theta]_{296}$ +12791 (peak). *Anal.* calcd. for $C_{29}H_{50}O$: C 83.99, H 12.15; found: C 84.04, H 12.16.

Eluted with the same solvent (200 mL), the next fraction, on crystallization from ethanol–acetone, gave 3β-methyl-5α-cholestan-2-one (**2***a*) (130 mg), mp 149–150°C.

*1α-Bromo-3,3-dimethyl-5α-cholestan-2-one (***10***)*

The bromination of **9** (667 mg) was carried out using the technique described for the synthesis of **3***a*. After the usual work-up, the resultant oil, on crystallization from acetone, gave plates of **10** (534 mg), mp 134–134.5°C; ir (KBr): 1700 cm^{-1}; nmr (CCl_4) δ: 4.04 (1H, s); cd (*c* 0.253, Di) at 26°C: $[\theta]_{324}$ −2807 (trough). *Anal.* calcd. for $C_{29}H_{49}OBr$: C 70.57, H 10.01; found: C 70.34, H 9.95.

*The Enolisation of 3β-Methyl-5α-cholestan-2-one (***2a***)*

This enolisation was carried out according to the method described for 5β-cholestan-2-one (11). The reaction product gave plates of 2-acetoxy-3-methyl-5α-cholest-2-ene (**8***a*) from ethanol, mp 69–71°C; ir (KBr): 1754 and 1712 cm^{-1}; nmr (CCl_4) δ: 2.05 (3H, s). *Mol. Wt.* calcd. for $C_{30}H_{50}O_2$: 442.3808; found (ms): 442.3814. A mixture of **8***a* (20 mg), bromine (7.9 mg) in tetrachloromethane, and tetrachloromethane (10 mL) containing a few drops of epichlorohydrin was prepared in accordance with the directions described for 2-acetoxy-5β-cholest-1-ene (11). After the usual work-up, the resultant oil, on crystallization from ethanol, gave needles of **3***a* (16 mg), mp 192–195°C.

*Confirmation of the Configuration of 3α-Bromo-3β-alkyl-5α-cholestan-2-one (***3a***, 3b, or 3c) by Chemical Reactions*

The bromo derivative (**3***a*) (30 mg) in methanol–ether (1:2) (10 mL) was treated with sodium borohydride (10 mg) at room temperature. After 10 min, water was added and the mixture was extracted with ether. The ethereal solution was washed with water, dried, and evaporated under reduced pressure. Attempts to crystallize the resultant oil (**6***a*) were unsuccessful, and the product was used for the next step without purification (ir (NaCl): 3550 cm^{-1}). In the case of **3***b* (100 mg) and **3***c* (100 mg), crystallization from ethanol afforded plates of **6***b* (23 mg), mp 133–134°C; ir (KBr): 3410 cm^{-1}; nmr (CCl_4) δ: 2.94 (1H, dd, J = 4.5 and 11.5 Hz); *Mol. Wt.* calcd. for $C_{29}H_{51}OBr$: 494.3121; found (ms): 494.3061; and **6***c* (52 mg), mp 133–135°C; ir (KBr): 3550 cm^{-1}; nmr (CCl_4) δ: 3.00 (1H, m, $W/2$ = 33 Hz). *Mol. Wt.* calcd. for $C_{30}H_{53}OBr$: 508.3278; found (ms): 508.3286. A mixture of the methyl bromohydrin (**6***a*) (30 mg), acetic anhydride (5 mL), and pyridine (5 mL) was allowed to stand at room temperature overnight. After the usual work-up, the resultant oil, on crystallization from ethanol, afforded needles of **7***a*, mp 123–125°C; ir (KBr): 1735 and 1240 cm^{-1}; nmr (CCl_4) δ:

4.21 (1H, dd, J = 5 and 11 Hz). *Mol. Wt.* calcd. for $C_{30}H_{51}O_2Br$: 522.3070; found (ms): 522.3085. The alkylated bromohydrin (**6***a*, **6***b*, or **6***c*) (15 mg) in ethanol (5 mL) was treated with a solution of potassium hydroxide (9 mg) in the same solvent (3 mL) and the mixture was refluxed for 2 h. Ethanol was then removed under reduced pressure, and the residue was diluted with water and extracted with ether. The ethereal solution was washed with water, dried, and evaporated under reduced pressure. Crystallization of the residue from ethanol gave needles of **2***a* (10 mg), mp 149–151°C, **2***b* (11 mg), mp 109–112°C, and **2***c* (8 mg), mp 108–113°C, respectively.

*Confirmation of the Configuration of 1α-Bromo-3,3-dimethyl-5α-cholestan-2-one (**10**) by Chemical Reactions*

The dimethylated bromo ketone (**10**) (134 mg) in methanol–ether (26 mL) was treated with sodium borohydride (45 mg) at room temperature. After the usual work-up, the resultant oil, on crystallization from ethanol–ether, gave needles of dimethylated bromohydrin (**11**) (74 mg), mp 125.5–127°C; ir (KBr): 3550 cm^{-1}; nmr (CCl_4) δ: 4.48 (1H, d, J = 3.0 Hz) and 3.51 (1H, d, J = 3.0 Hz). *Mol. Wt.* calcd. for $C_{29}H_{51}OBr$: 494.3121; found (ms): 494.3088. A mixture of **11** (300 mg) and potassium hydroxide (24 mg) in ethanol (10 mL) was allowed to react according to the procedure described for the synthesis of 3β-methyl ketone (**2***a*) from 3-methyl bromohydrin (**6***a*). After the usual work-up, the resultant oil, on crystallization from ethanol, gave needles of **9** (17 mg), mp 153–155°C.

Acknowledgments

The authors are indebted to Nippon Kayaku Co., Ltd., Pharmaceutical Division Research Laboratory, for elementary analyses and to Messrs. Koichi Hattori and Noburo Sakata for collaboration in the experimental work. Thanks are also due to Associate Professor Sukekatsu Nozaki, Josai University, for his measurement of the high resolution mass spectra. This research was supported in part by a Matsunaga Research Grant from the Matsunaga Science Foundation.

1. R. B. Woodward, A. A. Patchett, D. H. R. Barton, D. A. J. Ives, and R. B. Kelly. J. Am. Chem. Soc. **76**, 2852 (1954).
2. Y. Mazur and F. Sondheimer. J. Am. Chem. Soc. **80**, 5220 (1958).
3. P. Morand, J. M. Lyall, and H. Stollar. J. Chem. Soc. 2117 (1970).
4. F. Sondheimer, Y. Klinbansky, Y. M. Y. Haddad, G. H. Summer, and W. Klyne. J. Chem. Soc. 767 (1961).
5. R. O. Clinton, R. L. Clarke, F. W. Stonner, A. J. Manson, K. F. Jennings, and D. K. Phillips. J. Org. Chem. **27**, 2800 (1962).
6. K. Tsuda and S. Nozoe. Chem. Pharm. Bull. **7**, 232 (1959).
7. J. Y. Satoh, C. A. Horiuchi, and A. Hagitani. Bull. Chem. Soc. Jpn. **51**, 192 (1978).
8. J. B. Jones and R. Grayshan. J. Chem. Soc. Chem. Commun. 141 (1970).
9. A. Nickon, J. B. Digiorgio, and P. J. L. Daniels. J. Org. Chem. **38**, 533 (1973).
10. T. A. Spencer, R. W. Britton, and D. S. Watt. J. Am. Chem. Soc. **89**, 5727 (1967).
11. J. Y. Satoh, C. A. Horiuchi, and A. Hagitani. Bull. Chem. Soc. Jpn. **43**, 491 (1970).

Can. J. Chem. Downloaded from www.nrcresearchpress.com by 210.87.254.40 on 09/06/12
For personal use only.

Deuterium isotope exchange between molecular hydrogen and cyclopentylamine[1]

E. ALLAN SYMONS[2] AND MICHEL J. CLERMONT

Physical Chemistry Branch, Atomic Energy of Canada Limited, Research Company, Chalk River Nuclear Laboratories, Chalk River, Ont., Canada K0J 1J0

Received February 9, 1981

E. ALLAN SYMONS and MICHEL J. CLERMONT. Can. J. Chem. **59**, 2386 (1981).

Over the temperature range −68 to −10°C the ability of the alkali metal cyclopentylamide salts to catalyze deuterium exchange between D_2 and cyclopentylamine (CPA) is in the order CsCPA ≥ KCPA > NaCPA ≫ LiCPA. The rate constant ratio at −68°C for CsCPA/LiCPA is $> 10^3$. The measured Arrhenius activation parameters and kinetic isotope effect data are only slightly different for the Li and Na salts. The in-solution exchange reaction is so fast for the KCPA and CsCPA catalysts that rate constants independent of mass transfer could not be measured for them in the stirred gas/liquid reactor even at −68°C.

The gas solubility isotope effect, sie = $[D_2]/[H_2]$, has been determined in CPA over the range −50 to +25°C. From the values obtained (e.g. 1.08 at 25°C, 1.10 at −25°C) and the limited literature data available it appears that the sie for hydrogen gas may be greater for polar than for nonpolar solvents.

E. ALLAN SYMONS et MICHEL J. CLERMONT. Can. J. Chem. **59**, 2386 (1981).

Dans l'intervalle de température allant de −68 à −10°C la tendance des sels de cyclopentylamide de métal alcalin à catalyser l'échange de deutérium entre le D_2 et la cyclopentylamine (CPA) est dans l'ordre suivant: CsCPA ≥ KCPA > NaCPA ≫ LiCPA. Le rapport des constantes de vitesse à −68°C est $> 10^3$ pour le CsCPA/LiCPA. Les paramètres d'activation d'Arrhénius mesurés et les données d'effet isotopique cinétique sont légèrement différentes pour les sels de Li et de Na. La réaction d'échange en solution est si rapide avec les catalyseurs KCPA et CsCPA qu'on ne peut pas mesurer leurs constantes de vitesse indépendantes du transfert de masse dans un réacteur gaz/liquide sous agitation même à −68°C.

On a déterminé l'effet isotopique de la solubilité du gaz eis $[D_2]/[H_2]$ dans le CPA dans l'intervalle de −50 à 25°C. A partir des valeurs obtenues (par exemple 1,08 à 25°C, 1,10 à −25°C) et à partir des données limitées disponibles il apparait que le eis de l'hydrogène à l'état gazeux peut être plus grand dans les solvants polaires que dans les solvants non polaires.

[Traduit par le journal]

Introduction

Hydrogen isotope exchange between molecular hydrogen and organic amines is of interest for possible development of more efficient deuterium extraction processes. We have previously reported the results for a study of catalysis of exchange between D_2 and cyclohexylamine (CHA) by alkali metal cyclohexylamides (1). Two particular problems were encountered in trying to determine kinetic isotope effects in that system: (*a*) for the cesium and potassium salts the exchange reaction was so fast even at −15°C that rate constants independent of stirring rate in the gas/liquid reactor could not be obtained, and (*b*) for the sodium and lithium salts, although chemically-limited rate constants were measured, it was difficult to derive completely reliable k_{HD} values by computer analysis of the experimental data (eq. [1]). It was suggested that a change to the similar cyclopentylamine (CPA) as solvent, with its much lower freezing point (−85.7°C vs. −17.8°C for CHA), would permit kinetic measurements at lower temperature where mass transfer effects in the apparatus should be reduced (1).

$$[1]\quad D_2 \xrightarrow{k_{D_2}} HD \xrightarrow{k_{HD}} H_2$$

Several series of kinetic runs have been carried out using various CPA salts as catalysts, and with D_2 and HD gases, at temperatures as low as −68°C. The solubilities of both H_2 and D_2 in CPA have been measured over the temperature range +25 to −70°C.

Experimental

Reagents

The H_2, D_2, methylamine, alkali metals, and alkali metal hydrides were obtained and used as previously described (1). Cyclopentylamine was purchased from both Aldrich Chemical Co. and Tokyo Kasei Kogyo Co. Ltd., Japan (through CTC Organics, Atlanta, GA). It was first purified by fractional distillation (main fraction 107.4–108.4°C at 100.4 kPa; lit. (2) 108.5°C, and (3) 108.0°C at 101.3 kPa). Drying was done under vacuum over fresh potassium metal, ultimately with the solvent temperature raised above 64°C to provide molten K spheres.

A lecture bottle of compressed HD (30 L at STP) was purchased from Merck, Sharp & Dohme Canada Ltd. Mass spectral analysis indicated a purity of 98.4 mol% HD, with most of the balance being D_2. *CAUTION*. We originally attempted to synthesize a large batch of HD by scaling up a literature procedure for controlled reaction between $LiAlH_4$ and D_2O (4). A one litre stainless steel tank system had been pressure-tested to the equilibrium pressure expected for 2.6 moles of HD. The tank (containing $LiAlH_4$, distilled dimethoxydiethyl ether as a powder-dispersing agent, and D_2O added at liquid nitrogen

[1]Issued as AECL No. 7321.

[2]Author to whom correspondence should be addressed.

0008-4042/81/152386-05$01.00/0

©1981 National Research Council of Canada/Conseil national de recherches du Canada

Can. J. Chem. Downloaded from www.nrcresearchpress.com by 210.87.254.105 on 09/06/12
For personal use only.

TABLE 1. Cyclopentylamine vapour pressure*

Temperature† °C	Vapour pressure kPa	Vapour pressure mm‡	Temperature† °C	Vapour pressure kPa	Vapour pressure mm‡
25.1	3.47	26.0	5.1	1.07	8.0
19.4	2.47	18.5	0.5	0.80	6.0
16.9	2.13	16.0	−4.4	0.60	4.5
13.2	1.73	13.0	−7.9	0.47	3.5
10.0	1.47	11.0	−12.4	0.33	2.5
9.7	1.40	10.5	−17.1	0.27	2.0
5.8	1.13	8.5	−23.0	0.17	1.3

*Measured by the isoteniscope method (6); estimated error ± 0.07 kPa.
†Stolab electronic thermometer, ±0.05°C.
‡Heise gauge, ±0.5 mm.

temperature) was being "warmed" in an ice/water bath when a poorly connected metal fitting failed. Considerable damage was done to a fumehood in the chemical explosion that followed blowout of the contents. Although failure of the fitting was important it is possible that the accident was precipitated by a rapid pressure rise (i.e. a thermal runaway process (5)) caused by poor heat transfer through the steel tank wall.

CPA Vapour Pressure

The vp of purified CPA was determined using the isoteniscope method (6) over the temperature range −23 to +25°C. The bulb volume was 25 mL. The pressure was measured with a Heise gauge. The experimental data are given in Table 1. Agreement with values calculated using the equation of Good *et al.* (7) is within ± 0.04 kPa (0.3 mm) over most of the temperature range.

Hydrogen Solubility in CPA

Solubilities were determined by a gas chromatographic procedure as before (1). The instrument response was calibrated with H_2 and D_2 gas as appropriate. A net hydrogen pressure of 101 kPa was maintained in the gas/liquid equilibration flask; the solvent vapour pressure was interpolated from the data in Table 1.

Catalyst Solutions and Kinetic Runs

The LiCPA, NaCPA, KCPA, and CsCPA catalyst solutions were prepared and analyzed as described for the corresponding CHA solutions (1). As with CHA, only Cs metal reacts directly with the cyclic amine; the methylamide salts were used as the intermediates for the others. KH does react with CPA, but only slowly at 90°C, while LiH is unreactive.

Most isotope exchange runs were carried out in the modified gas/liquid reactor (1). Analysis of the $D_2/HD/H_2$ gas mixtures was by mass spectrometry; the calibration problems encountered in the earlier work were only partly alleviated by incorporating D^+ corrections of 1–2% for the equilibrated standard mixtures and kinetic samples.

For the LiCPA and NaCPA catalysts, rate constants independent of stirring rate were obtained above 8000 r min^{-1}. However, for the KCPA and CsCPA catalysts, rate constants independent of mass transfer effects could not be determined even at −68°C and 20 000 r min^{-1}.

The vapour/solution conversion factors used to calculate the in-solution rate constants for exchange ranged between 200 and 400 depending on reaction vessel volume and temperature; k_{obs}(solution) = factor × k_{obs}(vapour) (1).

A calibration curve relating the solution temperature in the stirred reactor to the bath temperature (Neslab LT9 unit) was prepared by using a thermocouple inserted in the solution compartment of the reactor. The differential between the solution and bath temperatures increased with decreasing bath temperature and increasing stirring rate (10 000 to 20 000 r min^{-1}). The correction to the solution temperature varied from +0.2 at −10°C to +1.0–1.8 at −50°C and +2.2–3.8 at −70°C. The time to reach "operating" solution temperature from stirrer startup increased from < 5 min at −10°C to 10 min at −50°C and 30 min at −70°C; kinetic samples were not usually taken during this period.

Results

H_2 and D_2 Solubility in CPA

The data are plotted in Fig. 1. Computer analysis of each set, via a linear least squares program, produced the following second order fit equations, where the concentrations are expressed as mole fraction and T is the solution temperature in °C:

$$10^4\,[H_2] = 2.041 + 0.0178\,T + 0.0000452\,T^2$$

$$10^4\,[D_2] = 2.235 + 0.0188\,T + 0.0000339\,T^2$$

The standard deviations for H_2 and D_2 were ± 0.040 × 10^{-4} and ± 0.056 × 10^{-4} respectively.

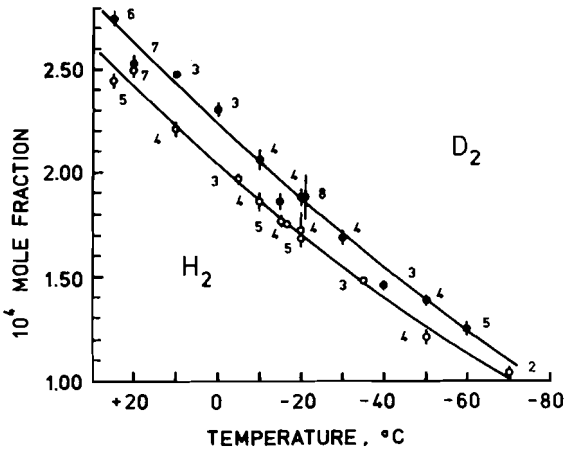

FIG. 1. The solubility of H_2 and D_2 in cyclopentylamine at 101 kPa gas pressure. The figures beside the points refer to the number of experimental measurements averaged for each point, while the range is indicated by the vertical bars.

Can. J. Chem. Downloaded from www.nrcresearchpress.com by 210.87.254.105 on 09/06/12
For personal use only.

Can. J. Chem. Downloaded from www.nrcresearchpress.com by 210.87.254.105 on 09/06/12
For personal use only.

Where solubility data were required as mol L^{-1} (e.g. for calculation of the vapour/solution conversion factors (1)), the mole fraction values were converted using solvent density. The limited data available for CPA density at 0 to 30°C (2) were extrapolated linearly down to −70°C. The resulting error should be less than one percent; for example, the density of liquid methylamine is known to be very nearly a linear function of temperature over the same temperature range (8).

The measured enthalpies of solution for H_2 and D_2 are 5.4 ± 0.5 and 5.2 ± 0.5 kJ mol^{-1} at 0°C; the ln (mol fraction) versus $1/T$ plots (9) are slightly curved, with ΔH being larger at higher T. The entropies of solution, obtained from plots of ln (mol fraction) versus ln T (9), are 19.7 ± 2.0 and 19.4 ± 2.0 J mol^{-1} K^{-1} for H_2 and D_2 over the range −50 to +25°C (standard state 101 kPa gas pressure). The corresponding enthalpy and entropy values for H_2 in CHA were 6.6 ± 0.4 kJ mol^{-1} and 24.4 ± 2.0 J mol^{-1} K^{-1} at 0°C (1).

D_2 and HD Exchange with CPA

Activation energies, E_a, determined from the temperature dependence of the k_{obs} (solution) rate constants for exchange of D_2 and HD with CPA, catalyzed by LiCPA (0.23 mol L^{-1}, −10 to −50°C, 3–4 points) and NaCPA (0.07–0.10 mol L^{-1}, −20 to −50°C, 3–4 points), are given in Table 2. The Arrhenius plots were all quite linear ($R = 0.998 - 1.000$). These results were obtained with different batches of catalyst solution over a period of more than a year; the reproducibility is clearly better in the case of LiCPA.

The averaged values of E_a for these two catalysts (Table 2) were used with kinetic rate constant data at −50°C (k_2(solution) = k_{obs}(solution) ÷ [catalyst]$_{stoich}$) to calculate the entropies of activation. The results were: for LiCPA, −158 J mol^{-1} K^{-1}; for NaCPA, −143 J mol^{-1} K^{-1}.

Even at −70°C the KCPA (0.048 mol L^{-1}) and CsCPA (0.15 mol L^{-1}) catalyzed reactions were not independent of stirring rate up to 20 000 r min^{-1}, the limit available. The following are, therefore, only the minimum k_2(solution) rate constants for these two very effective catalysts for D_2 exchange: for KCPA at −67°C, 10 L mol^{-1} s^{-1}; for CsCPA at −67°C, 10 L mol^{-1} s^{-1}.

The kinetic isotope effect values, $2k_{HD}/k_{D_2}$, presented in Table 3, were obtained in one of three ways from the "vapour phase" (1) rate constant data. For separate kinetic runs involving D_2 and HD with the same catalyst solution, the independent rate constants were used. For individual D_2 runs carried out under conditions of no interference from mass transfer effects, a "best fit" k_{HD} can be calculated from the D_2/HD/H_2 distribution as a function of time (1). Also, for the HD runs the decreasing D_2 concentration, initially ca. 2 mol%, could be employed to obtain k_{D_2}. As can be seen in Table 3, the magnitude of the isotope effect was somewhat dependent on the method of calculation.

TABLE 2. Activation energies for LiCPA and NaCPA catalyzed deuterium exchange between D_2, HD, and CPA at −10 to −50°C

LiCPA(0.23 mol L^{-1})		NaCPA(0.07–0.10 mol L^{-1})	
Gas	E_a, kJ mol^{-1}	Gas	E_a, kJ mol^{-1}
D_2	28.9	D_2	29.9
D_2	29.5	D_2	21.1†
D_2	27.9*	HD	23.7†
HD	32.4*		

*Same catalyst solution stock.
†Same catalyst solution stock.
Averaged values: for LiCPA, 30 ± 2 kJ mol^{-1}; for NaCPA, 25 ± 4 kJ mol^{-1}.

TABLE 3. Kinetic isotope effects for exchange between D_2/HD and CPA*

Catalyst	$2k_{HD}/k_{D_2}$	Temperature °C	Method†
LiCPA	2.7	−10	A
(0.23 mol L^{-1})	2.2	−30	A
	1.8	−30	A
	2.4	−30	B
	1.5	−10	C
	1.2	−30	C
NaCPA	2.4	−20	A
(0.07–0.10 mol L^{-1})	2.4	−30	A
	2.0	−50	A
	2.9	−20	B
	3.8	−20	B
	2.9	−30	B
	3.0	−50	B
	1.6	−20	C
	1.6	−30	C
	1.4	−50	C
KCPA	2.2‡	−58	A
(0.048 mol L^{-1})	2.0‡	−58	A
	1.2‡	−69	A

*Values are based on "vapour phase" (1) rate constants. Since HD is probably about 5% less soluble than D_2 (cf. D_2 and H_2 solubility data, Fig. 1 and text), the pn-solution kie figures will be about 5% greater than shown.
†Method A: independent D_2 and HD runs; B: computer fit of data for D_2 runs; C: D_2 decrease during HD runs (see text for details).
‡k_{obs} data *not* independent of mass transfer interference.

Discussion

H_2 and D_2 Solubility in CPA

Over the temperature range −60 to +25°C the curve for H_2 solubility in CPA falls between those for H_2 in methylamine (lower) and ethylamine (10). Also, H_2 is about 15% less soluble in CPA than in CHA above the latter's freezing point (1).

Can. J. Chem. Downloaded from www.nrcresearchpress.com by 210.87.254.105 on 09/06/12
For personal use only.

H_2 and D_2 concentrations obtained from the equations given above were used to calculate the following values of the $[D_2]/[H_2]$ ratio as a function of temperature: 1.08 at 25°C, 1.09 at 0°C, 1.10 at −25°C, and 1.09 at −50°C. The estimated error ranges from ± 0.03 to ± 0.05. There is very little data in the literature pertaining to the solubility isotope effect for hydrogen gas in polar liquids. In water, D_2 is reported to be more soluble than H_2, with the ratio being 1.065 at 30°C and 1.086 at 5°C (11). More recent data for water are the following (12): 1.055 at 60°C, 1.066 at 30°C, and 1.074 at 5°C. In dimethyl sulfoxide $[D_2]/[H_2] = 1.050$ at 25°C (17).

Cook *et al.* (13) had earlier found that D_2 was 2–4 percent more soluble than H_2 in a series of eight nonpolar solvents (including benzene, carbon tetrachloride, and octane) over the temperature range −35 to +35°C. Thus the solubility isotope effect for D_2/H_2 would appear to be significantly larger for polar than nonpolar solvents, judging from the information available to date.

It is usual for the heavier isotopic species of a pair to have the higher solubility. The difference in zero point energy of the isotopic gas molecules oscillating in solvent cages is considered to be a major contributor to the observed effect (11).

D_2 and HD Exchange with CPA

The catalytic reactivity of the CPA salts is in the order CsCPA ≥ KCPA > NaCPA ≫ LiCPA, the same as observed for the CHA salts in cyclohexylamine (1). Although a literature value for the dielectric constant of CPA was not found, it is likely to be quite low, comparable to that for CHA (4.5 at 20°C). As a result, the catalyst solutions will contain ion pairs and larger ion aggregates but few free cyclopentylamide ions (14).

It is not possible to compare directly the kinetic reactivity of all the alkali metal salts in the CHA and CPA systems for D_2 exchange catalysis, since the temperature regions examined do not overlap significantly (−15 to +15°C for CHA (1) versus −67 to −9°C for CPA). However, in-solution rate constants for the Li salts are similar at −9°C: 2.0×10^{-2} s^{-1} for 0.23 mol L^{-1} LiCPA and 0.9×10^{-2} s^{-1} for 0.08 mol L^{-1} LiCHA.

The measured Arrhenius activation energies are higher in CPA than CHA, e.g. 25 versus 11 kJ mol^{-1} for the sodium salt, while $\Delta S^{\ddagger}$ values average −150 cal mol^{-1} K^{-1} for CPA and −200 cal mol^{-1} K^{-1} for CHA (1). For both CHA and CPA solvents E_a is ca. 5 kJ mol^{-1} lower for the sodium than the lithium salt. It is probable that differences in the extent of ion aggregation are responsible for these effects.

The available kinetic isotope effect (kie) data for the Li, Na, and K salts of CPA, recorded in Table 3, show a significant dependence on the method of calculation. However, two trends are clear: the kie values generally decrease with decreasing temperature for a given method; and the values are comparable for the three catalyst salts, within an experimental error of ±0.2, for a given temperature and method. The reason for the dependence on method of determination is not known. Method B (Table 3) should be valid for experimental conditions where the measured rate constants are independent of mass transfer (1).

The kie values appear fairly small, in the approximate range 2 to 3, but this is still quite consistent with rate-determining proton transfer from molecular hydrogen (15). The mechanism for the exchange reaction involving CPA should parallel that for the CHA system; detailed discussion for the latter is available (1).

It was originally hoped that the various kinetic parameters associated with the D_2/CPA exchange reaction could be determined for the full range of alkali metal cations (Li^+ to Cs^+), in order to identify the role of the cation–cyclopentylamide anion interaction in the reaction. However, it has proved to be impossible to obtain kinetically usable rate constant data for the very active potassium and cesium salts, using the stirred gas/liquid reactor. A thin liquid film type of apparatus, such as the single sphere absorber system of Kalra and Otto (16), would be more suitable.

Acknowledgements

The authors wish to thank J. B. Schnittker for assistance with some of the H_2/CPA solubility measurements. Comments on the manuscript by Dr. J. H. Rolston were much appreciated.

1. E. A. Symons, M. F. Powell, J. B. Schnittker, and M. J. Clermont. J. Am. Chem. Soc. **101**, 6704 (1979).
2. M. J. Timmermans and Mme. Roland. J. Chim. Phys. **52**, 223 (1955).
3. J. D. Roberts and V. C. Chambers. J. Am. Chem. Soc. **73**, 5030 (1951).
4. A. Fookson, P. Pomerantz, and E. H. Rich. Science, **112**, 748 (1950); I. Wender, R. A. Friedel, and M. Orchin. J. Am. Chem. Soc. **71**, 1140 (1949).
5. D. I. Townsend and J. C. Tou. Thermochim. Acta, **37**, 1 (1980); D. W. Smith, M. C. Taylor, R. Young, and T. Stephens. Am. Lab. 51, June 1980.
6. S. Glasstone and D. Lewis. Elements of physical chemistry. D. Van Nostrand. Princeton, NJ. 1960. p. 131.
7. W. D. Good, J. F. Messerly, A. G. Osborn, and D. R. Douslin. J. Chem. Thermodyn. **7**, 285 (1975).

8. J. TIMMERMANS. Physico-chemical constants of pure organic compounds. Elsevier, New York. 1950; Matheson Gas Data Book. 4th ed. Matheson Co. 1966.
9. R. BATTINO and H. L. CLEVER. Chem. Rev. **66**, 395 (1966).
10. R. G. MOORE and F. D. OTTO. Can. J. Chem. Eng. **50**, 355 (1972).
11. J. MUCCITELLI and W.-Y. WEN. J. Solution Chem. **7**, 257 (1978).
12. B. B. BENSON and D. KRAUSE, JR. Report COO-5031-1 prepared for the U.S. Dept. of Energy, October 1979.
13. M. W. COOK, D. N. HANSON, and B. J. ALDER. J. Chem. Phys. **26**, 748 (1957).
14. A. STREITWIESER, JR. and R. A. CALDWELL. J. Am. Chem. Soc. **87**, 5394 (1965).
15. E. BUNCEL, E. A. SYMONS, and R. A. MORE O'FERRALL. J. Am. Chem. Soc. **100**, 1084 (1978).
16. H. KALRA and F. D. OTTO. Can. J. Chem. Eng. **52**, 258 (1974).
17. J. H. DYMOND. J. Phys. Chem. **71**, 1829 (1967).

Can. J. Chem. Downloaded from www.nrcresearchpress.com by 210.87.254.105 on 09/06/12
For personal use only.

Crystal and molecular structures of three transition metal complexes incorporating the anionic tridentate chelating ligands $[Me_2Ga(N_2C_5H_7)OCH_2CH_2SR]^-$ where R = Et or Ph

STEVEN J. RETTIG, ALAN STORR, AND JAMES TROTTER

Department of Chemistry, University of British Columbia, 2036 Main Mall, Vancouver, B.C., Canada V6T 1Y6

Received January 23, 1981

STEVEN J. RETTIG, ALAN STORR, and JAMES TROTTER. Can. J. Chem. **59**, 2391 (1981).

X-ray crystallographic studies of three transition metal complexes incorporating the novel anionic tridentate chelating ligand $[Me_2Ga(N_2C_5H_7)OCH_2CH_2SR]^-$ (R = Et or Ph) show that the ligand is facially coordinated in each case. Crystals of [dimethyl(3,5-dimethyl-1-pyrazolyl) (2-thioethoxyethoxy)gallato(*N*(2), *O*,*S*)]nitrosylnickel(I) are monoclinic, a = 8.8313(4), b = 7.2402(2), c = 26.539(1) Å, β = 94.390(3)°, Z = 4, space group $P2_1/c$, R = 0.040 and R_w = 0.050 for 2489 reflections. The Ni atom is in a distorted tetrahedral environment with bond angles about Ni ranging from 87.90(7) to 127.9(1)°. The nitrosyl coordination is slightly non-linear with Ni—N—O = 170.1(4)°. Important bond lengths (corrected for libration) are: Ni—S, 2.326(1), Ni—O, 2.019(2), Ni—N(pyrazolyl), 1.980(3), Ni—N(O), 1.633(3) and N—O, 1.156(4) Å. Crystals of [dimethyl(3,5-dimethyl-1-pyrazolyl) (2-thiophenoxyethoxy)gallato(*N*(2),*O*,*S*)]tricarbonylmanganese(I) are triclinic, a = 9.4911(5), b = 10.4323(6), c = 11.7618(7) Å, α = 86.17(1), β = 69.547(5), γ = 81.402(4)°, Z = 2, space group $P\bar{1}$, R = 0.029 and R_w = 0.035 for 2496 reflections. The Mn atom is coordinated to the *fac*-tridentate gallate ligand and to three carbonyl ligands resulting in a slightly distorted octahedral geometry. Important corrected bond lengths are: Mn—S, 2.397(1), Mn—O, 2.055(2), Mn—N, 2.082(3), and Mn—C, 1.794(4), 1.807(4), and 1.807(4) Å. Crystals of [dimethyl(3,5-dimethyl-1-pyrazolyl) (2-thioethoxyethoxy)gallato(*N*(2),*O*,*S*)][η^3-cycloheptatrienyl)dicarbonylmolybdenum are monoclinic, a = 17.030(3), b = 19.097(2), c = 15.908(3) Å, β = 115.99(1)°, Z = 8, space group $P2_1/n$, R = 0.036 and R_w = 0.043 for 4477 reflections. The two crystallographically independent molecules differ primarily in the orientation of the *S*-ethyl moiety and each contains an η^3-C_7H_7 ligand which occupies one coordination site of a distorted octahedron as a π-donating ligand. Important corrected bond distances are: Mo—S, 2.527(2) and 2.541(2), Mo—O, 2.241(5) and 2.237(4), Mo—N, 2.277(5) and 2.254(5), Mo—C(O), 1.940(7)–1.960(7), and Mo—C(C_7H_7), 2.198(6)–2.391(7) Å.

STEVEN J. RETTIG, ALAN STORR et JAMES TROTTER. Can. J. Chem. **59**, 2391 (1981).

Des études par diffraction des rayons-X des complexes métalliques tridimensionnels incorporant le nouveau ligand chélatant tridentate anionique $[Me_2Ga(N_2C_5H_7)OCH_2CH_2SR]^-$ (R = Et ou Ph) révèlent que le ligand est coordonné dans chaque cas d'une manière faciale. Les cristaux de [diméthyl(diméthyl-3,5 pyrazolyl-1) (thioéthoxy-2 éthoxy) gallato (*N*(2),*O*,*S*)] nitrosylnickel(I) sont monocliniques avec a = 8,8313(4), b = 7,2402(2), c = 26,539(1) Å, β = 94,390(3)°, Z = 4, groupe d'espace $P2_1/c$, R = 0,040 et R_w = 0,050 pour 2489 réflexions. L'atome de Ni se situe dans un environnement tétraédrique déformé avec des angles de liaison autour du Ni que se situent entre 87,90(7) et 127,9(1)°. La coordination du nitrosyle dévie légèrement de la linéarité avec Ni—N—O=170,1(4)°. Les longueurs importantes de liaison (corrigées pour la libration) sont: Ni—S, 2,326(1), Ni—O, 2,019(2), Ni—N(pyrazolyl), 1,980(3), Ni—N(O), 1,633(3) et N—O, 1,156(4) Å. Les cristaux de [diméthyl(diméthyl-3,5 pyrazolyl-1)-(thiophénoxy-2 éthoxy)gallato(*N*(2),*O*,*S*]tricarbonylmanganèse(I) sont tricliniques avec a = 9,4911(5), b = 10,4323(6), c = 11,7618(7) Å, α = 86,17(1), β = 69,547(5), γ = 81,402(4)°, Z = 2, groupe d'espace $P\bar{1}$, R = 0,029 et R_w = 0,035 pour 2496 réflexions. L'atome de Mn est coordonné au ligand gallate *fac* tridentate et à trois ligands carbonyles; sa géométrie est octaédrique et légèrement déformé. Les longueurs importantes de liaison corrigées sont: Ms—S, 2,397(1), Mn—O, 2,055(2), Mn—N, 2,082(3) et Mn—C, 1,794(4), 1,807(4) et 1,807(4) Å. Les cristaux de [diméthyl(diméthyl-3,5 pyrazolyl-1) (thioéthoxy-2 éthoxy) gallato (*N*(2),*O*,*S*] (η^3-cycloheptatriényl) dicarbonylmolybdène sont monocliniques avec a = 17,030(3), b = 19,097(2), c = 15,908(3) Å, β = 115,99(1)°, Z = 8, groupe d'espace $P2_1/n$, R = 0,036 et R_w = 0,043 pour 4477 réflexions. Les deux molécules cristallographiquement indépendantes diffèrent principalement par l'orientation de la portion *S*-éthyl et contiennent chacune un ligand η^3-C_7H_7 lié sous forme de ligand donneur π à un site de coordination d'un octaèdre déformé. Les distances importantes de liaison sont Mo—S, 2,527(2) et 2,541(2), Mo—O, 2,241(5) et 2,237(4), Mo—N, 2,277(5) et 2,254(5), Mo—C(O), 1,940(7)–1,960(7) et Mo—C(C_7H_7) 2,198(6)–2,391(7) Å.

[Traduit par le journal]

Introduction

Numerous crystal structures of transition metal complexes incorporating the $[Me_2Ga(N_2C_3H_3)OCH_2CH_2NH_2]^-$ ligand, or its methyl-substituted derivatives, have been reported (1–9). The present paper describes the structures of three transitional metal complexes which incorporate the new ligand systems **1**.

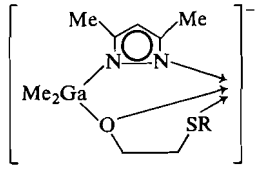

R = Et or Ph

1

The synthesis and characterization of these complexes are detailed in a recent publication (10), and the X-ray structural data reported herein provide conclusive evidence for some of the arguments based on nmr, ir, and mass spectral results.

0008-4042/81/152391-11$01.00/0

©1981 National Research Council of Canada/Conseil national de recherches du Canada

Can. J. Chem. Downloaded from www.nrcresearchpress.com by 210.87.254.5 on 09/06/12
For personal use only.

Can. J. Chem. Downloaded from www.nrcresearchpress.com by 210.87.254.5 on 09/06/12
For personal use only.

Experimental

[Dimethyl(3,5-dimethyl-1-pyrazolyl)(2-thioethoxyethoxy)-gallato(N(2),O,S)]nitrosylnickel(I), 2

A crystal ca. 0.22 × 0.56 × 0.12 mm in size was mounted in a general orientation. Unit-cell parameters were refined by least-squares on 2 sin θ/λ values for 25 reflections measured on a diffractometer with Cu K_α radiation (λ = 1.54184 Å). Crystal data at 22°C are:

$C_{11}H_{22}GaN_3NiO_2S$ f.w. = 388.81
Monoclinic, a = 8.8313(4), b = 7.2402(2), c = 26.539(1) Å, β = 94.390(3)°, V = 1691.9(1) Å^3, Z = 4, ρ_c = 1.526 g cm^{-3}, $F(000)$ = 800, μ(Cu K_α) = 42.4 cm^{-1}. Absent reflections: $h0l$, $l \neq 2n$ and $0k0$, $k \neq 2n$ uniquely indicate the space group $P2_1/c$ (C_{2h}^5, No. 14).

Intensities were measured with graphite-monochromatized Cu K_α radiation on an Enraf-Nonius CAD4-F diffractometer. An ω–2θ scan at 1.18–10.06° min^{-1} over a range of (0.80 + 0.14 tan θ) degrees in ω (extended by 25% on both sides for background measurement) was employed. Data were measured to 2θ = 150°. The intensities of 3 check reflections, measured every 3600 s throughout the data collection, remained constant to within 1%. After data reduction, an absorption correction was applied using the Gaussian integration method (11, 12). Transmission factors ranged from 0.249 to 0.650 for 336 sampling points. Of the 3449 independent reflections measured, 2489(72%) had intensities greater than 3σ(I) above background where $\sigma^2(I) = S + 2B + (0.04(S - B))^2$ with S = scan count and B = background count.

The coordinates of the gallium, nickel, and sulfur atoms were determined from the three-dimensional Patterson function and those of the remaining non-hydrogen atoms from a subsequent Fourier map. Full-matrix least-squares refinement of the non-hydrogen atoms with anisotropic thermal parameters gave R = 0.055. A difference map at this point gave positions for all 22 hydrogen atoms which were included in subsequent cycles of refinement with isotropic thermal parameters. The scattering factors of ref. 13 were used for non-hydrogen atoms and those of ref. 14 for hydrogen atoms. Anomalous scattering factors from ref. 15 were used for the Ga, Ni, and S atoms. The weighting scheme, $w = 1/\sigma^2(F)$ where $\sigma^2(F)$ is derived from the previously defined $\sigma^2(I)$ gave uniform average values of $w(|F_o| - |F_c|)^2$ over ranges of $|F_o|$ and was employed in the final stages of refinement. An isotropic Type I extinction correction (Thornley–Nelmes definition of mosaic anisotropy with a Lorentzian distribution) was applied (16–18). The final value of g was 0.124(9) × 10^4. Convergence was reached at R = 0.040 and R_w = 0.050 for 2489 reflections with $I \geq 3\sigma(I)$. For all 3449 reflections R = 0.055 and R_w = 0.053. The function minimized was $\Sigma w(|F_o| - |F_c|)^2$, $R = \Sigma||F_o| - |F_c||/\Sigma|F_o|$ and $R_w = (\Sigma w(|F_o| - |F_c|)^2/\Sigma w|F_o|^2)^{1/2}$.

On the final cycle of refinement the mean and maximum parameter shifts corresponded to 0.08 and 0.77σ respectively. The mean error in an observation of unit weight was 1.918. A final difference map showed no unusual features. The final positional and thermal parameters appear in Tables 1 and 2[1] respectively. Measured and calculated structure factors have been placed in the Depository of Unpublished Data.[1]

[Dimethyl(3,5-dimethyl-1-pyrazolyl)(2-thiophenoxyethoxy)-gallato(N(2),O,S)]tricarbonylmanganese(I), 3

Experimental details for **3** and **4** are as for **2** except where noted. The crystal used for data collection had dimensions of ca. 0.32 × 0.44 × 0.23 mm and graphite-monochromatized Mo K_α radiation (λ = 0.71073 Å) was used for both **3** and **4**. Crystal data are:

$C_{18}H_{22}GaMnN_2O_4S$ f.w. = 487.11
Triclinic, a = 9.4911(5), b = 10.4323(6), c = 11.7618(7) Å, α = 86.17(1), β = 69.547(5), γ = 81.402(4)°, V = 1079.5(1) Å^3, Z = 2, ρ_c = 1.499 g cm^{-3}, $F(000)$ = 496, μ(Mo K_α) = 18.68 cm^{-1}. Absent reflections: none, space group $P\bar{1}$ (C_i^1, No. 2) from structure analysis.

An ω–2θ scan at 0.91–10.06° min^{-1} over a range of (0.60 + 0.35 tan θ)° in ω was employed. Of 3774 reflections measured (to 2θ = 50°), 2496(66.1%) had intensities greater than 3σ(I) above background. An absorption correction was applied, transmission factors ranging from 0.516 to 0.686 for 202 sampling points.

Analysis was initiated in the centrosymmetric space group $P\bar{1}$ on the basis of the E-statistics. The coordinates of the Ga, Ni, and S atoms were determined from the Patterson function and those of the remaining non-hydrogen atoms from a subsequent Fourier map. Refinement of the non-hydrogen atoms with anisotropic thermal parameters gave R = 0.044. The hydrogen atoms were all located from a difference map at this point and were included in the final stages of refinement with isotropic thermal parameters; no extinction correction was applied. Convergence was reached at R = 0.029 and R_w = 0.035 for 2496 reflections with $I \geq 3\sigma(I)$, R = 0.066 and R_w = 0.038 for all 3774 reflections. The mean and maximum parameter shifts on the final cycle of refinement corresponded to 0.13 and 2.8σ respectively. The mean error in an observation of unit weight was 1.192. A final difference map showed no unusual features.

[Dimethyl(3,5-dimethyl-1-pyrazolyl)(2-thioethoxyethoxy)-gallato(N(2),O,S)](η^3-cycloheptatrienyl)dicarbonyl-molybdenum, 4

Crystal dimensions were ca. 0.25 × 0.35 × 0.46 mm. Crystal data are:

$C_{20}H_{29}GaMoN_2O_3S$ f.w. = 543.19
Monoclinic, a = 17.030(3), b = 19.097(2), c = 15.908(3) Å, β = 115.99(1)°, V = 4651(1) Å^3, Z = 8, ρ_c = 1.552 g cm^{-3}, $F(000)$ = 2208, μ(Mo K_α) = 17.9 cm^{-1}. Absent reflections: $h0l$, $h + l \neq 2n$ and $0k0$, $k \neq 2n$ uniquely indicate the space group $P2_1/n$ (non-standard setting of $P2_1/c$; C_{2h}^5, No. 14).

An ω–2θ scan at 1.06–10.06° min^{-1} over a range of (0.65 + 0.35 tan θ)° in ω was employed. Of 8159 reflections measured, 4477(54.9%) had intensities greater than 3σ(I) above background. An absorption correction was applied, transmission factors ranging from 0.492 to 0.668 for 160 sampling points.

The structure was solved by direct methods, the coordinates of the metal and sulfur atoms of each of the two crystallographically independent molecules being determined from an E-map and those of the remaining non-hydrogen atoms from a subsequent difference map. After refinement of all non-hydrogen atoms with anisotropic thermal parameters to R = 0.047, a difference map gave the positions of 50 of the 58 hydrogen atoms. In subsequent cycles of refinement only the protons associated with the coordinated cycloheptatrienyl carbons were refined, the remaining hydrogen positions were calculated and included as fixed atoms. Convergence was reached at R = 0.036 and R_w = 0.043 for 4477 reflections with $I \geq 3\sigma(I)$, R = 0.106 and R_w = 0.050 for all 8159 reflections. The mean and maximum parameter shifts on the final cycle of refinement were 0.12 and 1.2σ respectively and the mean error in an observation of unit weight was 1.275. A final difference map showed maximum fluctuations of ±1.1 e Å^{-3} near the molybdenum atoms and ±0.25 e Å^{-3} away from the heavier atoms. The thermal parameters indicate probable disordering of the S-ethyl group of molecule A (which contains Mo(1)). Since no such problem is evident for the second independent molecule, no attempt to resolve this

[1]The structure factor table and Table 2 (thermal parameters) are available, at a nominal charge, from the Depository of Unpublished Data, CISTI, National Research Council of Canada, Ottawa, Ont., Canada K1A 0S2.

Can. J. Chem. Downloaded from www.nrcresearchpress.com by 210.87.254.5 on 09/06/12
For personal use only.

disorder was made. The thermal parameters for molecule A were found to be generally larger than those for molecule B.

Analysis of Thermal Motion

The thermal motion in each of the molecules (shown in Figs. 1 and 2) has been analysed in terms of the rigid-body modes of translation, libration, and screw motion (19). The rms errors in the U_{ij} (derived from the least-squares analyses) are 0.0022, 0.0025, and 0.0047 Å^2 respectively for **2**, **3**, and **4**. Two successful analyses were carried out for **2**; one rigid group included all non-hydrogen atoms except the nitrosyl oxygen and the second consisted of the gallium and the four atoms bonded to it (rms ΔU_{ij} = 0.0059 and 0.0023 Å^2, respectively). For molecule **3** two analyses were again performed, one including the entire molecule and the other the gallium coordination group (rms ΔU_{ij} = 0.0099 and 0.0022 Å^2 respectively; the first value being somewhat higher than desired, independent motion being indicated for carbonyl oxygen atoms and phenyl carbons. Separate analysis of the phenyl group failed). Each of the two independent molecules of **4** was analysed; for molecule A all non-hydrogen atoms excluding carbonyl oxygens, the *S*-ethyl carbons and all methyl carbons gave rms ΔU_{ij} = 0.0080 Å^2. Molecule B was treated in the same way except that the *S*-ethyl α-carbon was included in the rigid body and resulted in rms ΔU_{ij} = 0.0047 Å^2. All of the above analyses yielded physically reasonable rigid body parameters. The appropriate bond distances have been corrected for libration (20), using shape parameters q^2 of 0.08 for all atoms involved. Corrected bond lengths appear along with the uncorrected values in Table 3 and corrected bond angles are all within one standard deviation of the uncorrected values listed in Table 4. Intra-annular torsion angles defining chelate (and C_7H_7 for **4**) ring conformations are given in Table 5.

Results and Discussion

The X-ray crystallographic analyses of **2–4** have shown that the ligands **1** are tridentate chelating ligands, displaying "facial" coordination in each case and being stereochemically equivalent to *fac*-coordinated ligands of the type $[Me_2Ga(N_2C_3HR_2)OCH_2CH_2NR_2']^-$ (R, R′ = H or Me) (2–4, 6, 8, 9). Although there are several significant differences between the geometry of the ligand **1** in the tetrahedral complex **2** and that observed in the octahedral complexes **3** and **4**, the overall arrangement is quite similar. Chelation of a transition metal ion by the ligand **1** results in a system of three fused five-membered rings with the central GaOMNN ring being approximately coplanar with the pyrazolyl ring and perpendicular to the MOCCS ring. The pyrazolyl rings are planar within experimental error (χ^2 = 3.3, 1.0, 0.4, and 0.8 for N_2C_3 in **2**, **3** and the two molecules of **4** respectively) with the metal atoms considerably displaced from the pyrazolyl mean planes (for **2**, Ga 0.0489(4), Ni 0.2100(5), for **3**, Ga 0.3329(4), Mn −0.3338(5), and for **4**, Ga 0.3141(9) and −0.2471(8), Mo −0.2911(5) and 0.1767(5) Å). The MOCCS rings in **2–4** are very similar, each having an envelope conformation with the carbon atom bonded to oxygen displaced from the approximate plane defined by the four other atoms (see torsion angles in Table 5). In each case the trivalent S and O atoms have distinctly pyramidal coordination.

The intraligand bond distances and angles in **2**, **3**, and **4** all assume normal values. The gallium atoms in all three molecules have distorted tetrahedral coordination geometry with bond angles ranging from 90.4(1)–92.6(1)° for O—Ga—N to 117.2(3)–124.7(3)° for C—Ga—C. The Ga—O and Ga—N distances in **2** (1.921(2) and 2.001(3) Å respectively) differ slightly but significantly from those in **3** and **4** (mean values: 1.931(3) and 1.985(3) Å).[2] The Ga—C bonds in all three molecules are equal within experimental error, mean Ga—C = 1.975(6) Å.

$[Me_2Ga(N_2C_5H_7)OCH_2CH_2SC_2H_5]Ni(NO)$, 2

The crystal structure of **2** consists of discrete molecules separated by normal van der Waals distances. The geometry of **2** is very similar to that of the closely related complex $[Me_2Ga(N_2C_5H_7)OCH_2CH_2NMe_2]Ni(NO)$, **5** (4). The coordination geometry about the Ni atom is distorted tetrahedral, bond angles ranging from 87.90(7)° for S—Ni—O(1) to 127.9(1)° for O(1)—Ni—N(3). The magnitude of the distortion from ideal tetrahedral geometry in **2** is not as great as in **5** where bond angles range from 84.4(1) to 133.5(1)°, likely a result of the larger radius of the sulfur atom. The rt ^{1}H nmr spectrum of **2** is explicable in terms of a square-planar coordination geometry about Ni but low-temperature studies confirm a tetrahedral geometry and suggest that the complex is fluxional in solution at ambient temperature (10).

The nitrosyl coordination is slightly non-linear with Ni—N—O = 170.1(4)°, Ni—N = 1.633(3) and N—O = 1.156(4) Å, compared to corresponding values of 162.3(4)°, 1.632(4), and 1.147(4) Å in **5**. It has been shown that as the coordination geometry of a $\{MNO\}^{10}$ complex changes from tetrahedral towards square-planar, the M—N—O angle decreases from 180° towards the square-planar limit of ~120° with a corresponding increase in the M—NO distance (21–23). On the basis of this argument, the Ni—NO bond in **5** is presumably stronger than that in **2** even though the two bond lengths are essentially equal. The Ni—O and Ni—N(pyrazolyl) distances in **2** (2.019(2) and 1.980(3) Å) are shorter than those in **5** (2.045(2) and 1.989(3) Å) while the Ga—O and Ga—N distances in the two molecules are equal within experimental error. Based on the difference between the covalent radii of nitrogen and sulfur, the Ni—S bond in **2**

[2]Here and elsewhere in this report mean values refer to weighted means with rms deviations from the mean in parentheses.

TABLE 1. Final positional parameters (fractional; O, N, and C × 10^4, metal and S × 10^5, H × 10^3) with estimated standard deviations in parentheses

Atom	x	y	z
	2		
Ga	19662(5)	24469(6)	13029(2)
Ni	53817(6)	25591(7)	8827(2)
S	63711(11)	54050(13)	11379(3)
O(1)	3299(3)	3691(3)	879(1)
O(2)	6907(5)	993(5)	113(1)
N(1)	3686(3)	1239(4)	1707(1)
N(2)	5114(3)	1375(4)	1540(1)
N(3)	6162(4)	1577(4)	415(1)
C(1)	969(7)	4219(10)	1729(2)
C(2)	912(6)	522(8)	894(2)
C(3)	3758(4)	199(5)	2129(1)
C(4)	5242(4)	−326(5)	2239(1)
C(5)	6057(4)	418(4)	1864(1)
C(6)	3319(5)	5643(5)	849(2)
C(7)	4537(6)	6434(7)	1215(2)
C(8)	6920(6)	6564(7)	575(2)
C(9)	8464(7)	5956(11)	440(3)
C(10)	2381(6)	−224(9)	2394(2)
C(11)	7704(5)	251(8)	1782(2)
H(1a)	154(7)	510(10)	179(2)
H(1b)	31(9)	497(11)	155(3)
H(1c)	60(8)	355(11)	198(3)
H(2a)	13(7)	107(9)	73(2)
H(2b)	148(7)	37(9)	64(2)
H(2c)	57(8)	−9(11)	116(3)
H(4)	549(4)	−106(6)	249(1)
H(6a)	357(5)	603(7)	49(2)
H(6b)	241(5)	612(6)	98(1)
H(7a)	432(6)	624(8)	153(2)
H(7b)	467(6)	770(7)	122(2)
H(8a)	623(6)	615(8)	27(2)
H(8b)	668(6)	793(8)	63(2)
H(9a)	849(7)	453(11)	32(2)
H(9b)	891(9)	667(13)	13(3)
H(9c)	918(7)	624(9)	73(2)
H(10a)	174(10)	90(13)	242(3)
H(10b)	148(7)	−56(9)	217(2)
H(10c)	253(6)	−88(9)	264(2)
H(11a)	792(8)	−62(11)	163(3)
H(11b)	809(5)	141(8)	162(2)
H(11c)	825(8)	27(10)	208(3)
	3		
Ga	29275(4)	32736(4)	33723(3)
Mn	65668(6)	22169(5)	17325(5)
S	65655(9)	31220(8)	−1869(8)
O(1)	6475(4)	1170(3)	4137(3)
O(2)	9857(3)	2162(3)	1114(3)
O(3)	7217(3)	−513(3)	986(3)
O(4)	4305(2)	2204(2)	2062(2)
N(1)	5921(3)	4121(2)	2313(2)
N(2)	4499(3)	4401(3)	3172(2)
C(1)	6460(5)	1615(4)	3230(4)
C(2)	8559(5)	2228(4)	1367(4)
C(3)	6962(4)	557(4)	1248(3)
C(4)	2514(10)	2309(7)	4919(5)
C(5)	1271(6)	4232(8)	2878(7)
C(6)	6640(4)	5166(3)	2231(3)
C(7)	5675(5)	6098(4)	3024(4)
C(8)	4361(5)	5588(3)	3593(3)
C(9)	3942(4)	2103(4)	1005(3)
C(10)	4553(4)	3176(4)	113(3)
C(11)	7458(4)	1953(3)	−1348(3)
C(12)	6728(6)	1334(4)	−1910(4)
C(13)	7548(7)	468(5)	−2828(4)
C(14)	9083(8)	214(5)	−3168(5)
C(15)	9805(7)	830(6)	−2596(5)
C(16)	9025(5)	1708(5)	−1699(4)
C(17)	8199(5)	5257(5)	1359(6)
C(18)	2916(9)	6152(7)	4542(6)
H(4a)	336(8)	179(7)	498(6)
H(4b)	197(6)	289(6)	547(5)
H(4c)	191(7)	168(6)	485(5)
H(5a)	78(6)	353(5)	286(4)
H(5b)	82(6)	474(5)	340(5)
H(5c)	148(8)	455(7)	220(6)
H(7)	594(4)	696(4)	313(3)
H(9a)	433(3)	126(3)	66(2)
H(9b)	282(4)	218(3)	124(3)
H(10a)	412(4)	409(3)	52(3)
H(10b)	436(4)	311(3)	−62(3)
H(12)	589(4)	147(3)	−173(3)
H(13)	697(4)	8(4)	−313(3)
H(14)	968(5)	−37(5)	−380(5)
H(15)	1086(6)	58(5)	−284(4)
H(16)	945(5)	210(4)	−129(4)
H(17a)	835(5)	618(5)	124(4)
H(17b)	842(5)	485(4)	56(4)
H(17c)	892(7)	484(5)	165(5)
H(18a)	258(8)	703(8)	454(7)
H(18b)	217(9)	563(7)	478(7)
H(18c)	306(7)	634(6)	520(6)
4, equivalent positions: $\pm(x, y, z; 1/2 - x, 1/2 + y, 1/2 - z)$			
Mo(1)	38540(3)	33946(3)	26303(4)
Mo(2)	34981(3)	19643(3)	66596(3)
Ga(1)	37946(5)	15801(5)	21169(6)
Ga(2)	32102(5)	37510(4)	70950(5)
S(1)	25184(11)	35731(14)	11039(12)
S(2)	48318(9)	19351(9)	82308(10)
O(1)	4146(4)	4990(3)	2607(4)
O(2)	2925(3)	4010(3)	3762(3)
O(3)	3217(2)	2344(2)	2406(3)
O(4)	3456(3)	352(3)	6774(4)
O(5)	4605(3)	1471(3)	5650(3)
O(6)	3917(2)	3083(2)	6832(2)
N(1)	4293(3)	2924(3)	1596(3)
N(2)	4372(3)	2213(4)	1577(4)
N(3)	2949(3)	2322(3)	7640(3)
N(4)	2772(3)	3024(3)	7671(3)
C(1)	4062(4)	4397(5)	2613(5)
C(2)	3278(4)	3765(4)	3360(5)
C(3)	2929(6)	992(5)	1118(7)
C(4)	4631(5)	1141(4)	3285(5)
C(5)	4624(5)	2939(4)	4173(5)
C(6)	5114(4)	2977(5)	3668(5)
C(7)	5377(4)	3613(5)	3458(5)
C(8)	5718(4)	4207(4)	4092(6)
C(9)	5674(5)	4328(4)	4907(6)
C(10)	5225(5)	3922(5)	5320(5)
C(11)	4760(4)	3355(5)	4990(5)
C(12)	2016(5)	2730(6)	972(5)
C(13)	2285(4)	2379(5)	1912(5)
C(14)	1733(6)	4164(9)	1267(6)
C(15)	1340(10)	4626(7)	626(12)

Can. J. Chem. Downloaded from www.nrcresearchpress.com by 210.87.254.5 on 09/06/12
For personal use only.

TABLE 1 (*Concluded*)

Atom	*x*	*y*	*z*	Atom	*x*	*y*	*z*
C(16)	4618(4)	3201(5)	1041(5)	H(12b)	219	243	58
C(17)	4910(5)	2670(6)	672(5)	H(13a)	205	190	182
C(18)	4753(5)	2064(5)	1013(5)	H(13b)	206	265	228
C(19)	4621(6)	3971(5)	879(6)	H(14a)	128	387	132
C(20)	4932(7)	1304(6)	861(7)	H(14b)	205	442	185
C(21)	3438(4)	955(4)	6732(4)	H(15a)	177	491	52
C(22)	4180(4)	1673(4)	6000(4)	H(15b)	96	438	4
C(23)	3936(5)	4435(4)	8056(6)	H(15c)	98	493	81
C(24)	2311(5)	4129(4)	5909(5)	H(17)	517	272	26
C(25)	2733(4)	2347(4)	5095(5)	H(19a)	490	421	148
C(26)	2215(4)	2268(4)	5562(4)	H(19b)	495	407	52
C(27)	2025(4)	1618(4)	5804(5)	H(19c)	402	414	53
C(28)	1777(4)	994(4)	5211(5)	H(20a)	440	103	70
C(29)	1859(4)	880(4)	4422(5)	H(20b)	511	128	35
C(30)	2270(4)	1310(4)	4015(4)	H(20c)	540	112	144
C(31)	2677(4)	1923(4)	4308(4)	H(23a)	447	420	850
C(32)	5131(4)	2847(3)	8324(4)	H(23b)	409	482	775
C(33)	4843(4)	3163(3)	7371(4)	H(23c)	361	461	838
C(34)	5771(4)	1538(4)	8169(5)	H(24a)	193	445	604
C(35)	5706(5)	752(5)	8142(6)	H(24b)	260	438	558
C(36)	2667(4)	1988(4)	8201(4)	H(24c)	196	374	552
C(37)	2310(4)	2442(5)	8592(5)	H(28)	153	62	541
C(38)	2385(4)	3101(4)	8234(5)	H(29)	161	46	410
C(39)	2754(5)	1209(4)	8330(5)	H(30)	225	114	345
C(40)	2101(6)	3807(5)	8424(6)	H(31)	297	210	396
H(5)	440(3)	256(3)	417(4)	H(32a)	485	310	866
H(6)	521(4)	259(3)	344(4)	H(32b)	577	289	867
H(7)	555(3)	367(3)	302(4)	H(33a)	515	293	705
H(25)	291(3)	278(3)	505(3)	H(33b)	499	366	744
H(26)	208(4)	263(3)	572(4)	H(34a)	581	170	760
H(27)	182(3)	165(3)	617(3)	H(34b)	630	168	872
H(3a)	235	120	91	H(35a)	548	60	858
H(3b)	308	96	59	H(35b)	531	60	751
H(3c)	293	52	136	H(35c)	629	55	832
H(4a)	438	114	374	H(37)	191	268	877
H(4b)	474	66	316	H(39a)	261	107	884
H(4c)	518	141	354	H(39b)	235	98	775
H(8)	601	456	391	H(39c)	336	107	848
H(9)	598	473	525	H(40a)	256	400	900
H(10)	527	408	590	H(40b)	201	412	790
H(11)	447	319	534	H(40c)	155	376	848
H(12a)	138	279	67				

should be longer than the Ni—N(amino) bond in **5** by 0.33 Å. The actual difference is 0.255 Å (2.326(1) vs. 2.071(3) Å) and indicates a relatively stronger bond in the present structure, due in part to lower strain in chelated ligands **1** than in their ethanolamine counterparts.

[$Me_2Ga(N_2C_5H_7)OCH_2CH_2SPh$]$Mn(CO)_3$, 3

The crystal structure of **3** consists of discrete molecules, joined across an inversion centre by weak C—H···S interactions (C(10)—H(10a)···S(1 − *x*, 1 − *y*, 1 − *z*), C···S = 3.847(4), H···S = 2.91(4) Å, C—H···S = 148(2)°) to form weakly associated dimeric units. All other intermolecular interactions correspond to normal van der Waals contacts.

This manganese tricarbonyl derivative is the only $LM(CO)_3$ complex (where L = **1** or [$Me_2Ga(N_2C_3HR_2)OCH_2CH_2NR_2'$]$^-$; R, R′ = H or Me) structurally characterized to date and is also the only fully characterized compound of the ligand **1** with R = Ph (10). It was postulated that the steric requirements of the ligand **1** (R = Ph) do not allow more bulky groups to coordinate to the transition metal and are responsible for the failure of the *S*-phenyl ligand to form complexes easily prepared with the *S*-ethyl analog. The crystal structure of **3**, however, shows no close contacts of the *S*-phenyl group with any other part of the molecule. Although the possibility of steric interference in solution cannot be ruled out, the differing donor properties of the aryl- relative to the alkyl-substituted sulfur may be partially responsible for the differences in reactivity of the ligands **1** where R = Et or Ph.

Can. J. Chem. Downloaded from www.nrcresearchpress.com by 210.87.254.5 on 09/06/12
For personal use only.

Can. J. Chem. Downloaded from www.nrcresearchpress.com by 210.87.254.5 on 09/06/12
For personal use only.

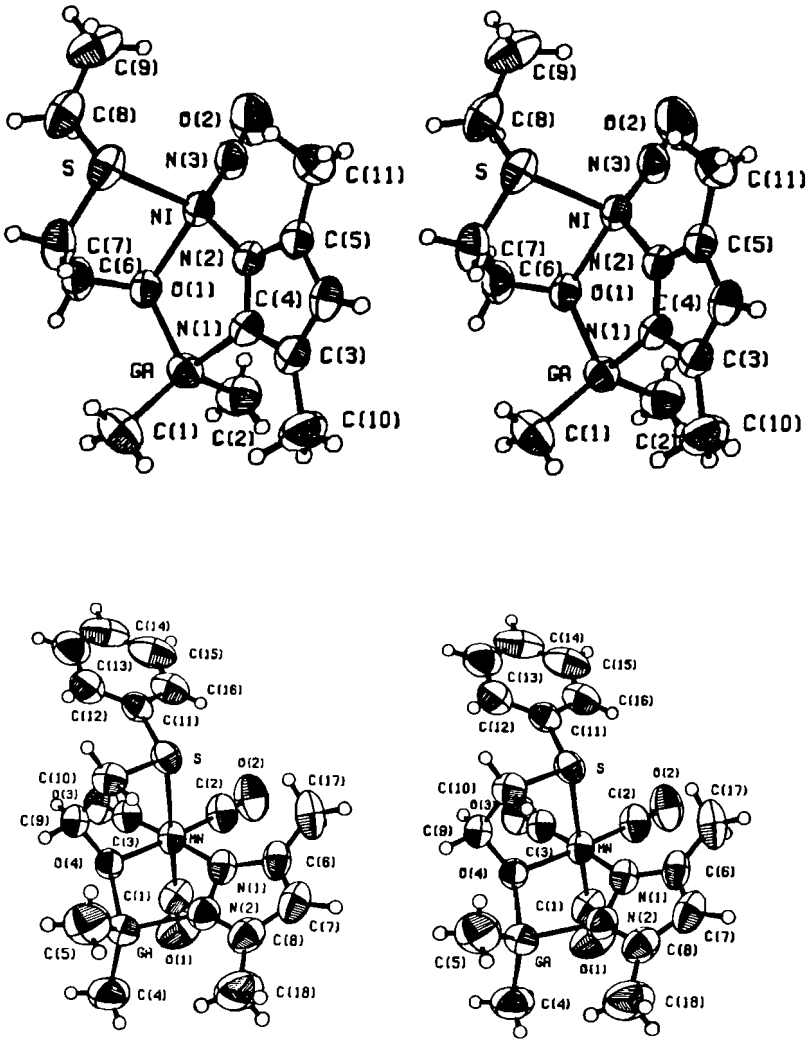

FIG. 1. Stereo views of **2** (top) and **3** (bottom). 50% probability thermal ellipsoids are shown for non-hydrogen atoms, hydrogen atoms assigned artificially small spheres for clarity.

The Mn atom in **3** is in a trigonally distorted octahedral environment, mean bond angles at Mn being: L—M—L, 84.4(6), OC—Mn—CO, 88.6(4), *cis* and *trans* L—Mn—CO, 93.3(20) and 176.2(10)° respectively (L = S, O, or N). Bond distances involving Mn all lie within the ranges normally observed for such bonds. The carbonyl groups are all slightly, but significantly, non-linear with Mn—C—O angles ranging from 175.2(4) to 177.2(3)°. The Mn—CO bond *trans* to O is marginally shorter than the other two Mn—CO bonds (1.794(4) vs. 1.807(4) Å) and a corresponding difference in the C—O distances is also noted (1.156(4) *trans* to O, mean of 1.143(4) Å for the others). These small differences between the carbonyl groups are probably the result of structural *trans* effects (3, 6, 9).

Comparison of the ligand geometries in **2** and **3** illustrates the general structural differences between the "facially" coordinated ligand of the types **1** and $[Me_2Ga(N_2C_3HR_2)OCH_2CH_2NR_2']^-$ (R, R' = H or Me) in octahedral transition metal complexes compared to tetrahedral complexes. The intraligand bond angles at the metal (in particular the *S*/*N*(amino)—M—N(pyrazolyl) angle) are greater and vary over a wider range in tetrahedral complexes (4, 8) than in octahedral (2) or pseudo-octahedral complexes (3, 6, 7, 9). The M—O distance is significantly longer than the M—N(pyrazolyl) distance in the tetrahedral complexes, whereas the converse is true for octahedral complexes. These differences arise from a combination of sterically induced hybridization and electronic effects.

The phenyl ring is planar within experimental

TABLE 3. Bond lengths (Å) with estimated standard deviations in parentheses

Bond	Length Uncorr.	Length Corr.	Bond	Length Uncorr.	Length Corr.
			2		
Ga —O(1)	1.914(2)	1.921	O(2) —N(3)	1.156(4)	1.156
Ga —N(1)	1.993(3)	2.001	N(1) —N(2)	1.371(3)	1.376
Ga —C(1)	1.963(5)	1.972	N(1) —C(3)	1.347(4)	1.349
Ga —C(2)	1.957(5)	1.967	N(2) —C(5)	1.342(4)	1.344
Ni —S	2.319(1)	2.326	C(3) —C(4)	1.374(5)	1.377
Ni —O(1)	2.013(2)	2.019	C(3) —C(10)	1.483(5)	1.484
Ni —N(2)	1.975(3)	1.980	C(4) —C(5)	1.382(5)	1.384
Ni —N(3)	1.629(3)	1.633	C(5) —C(11)	1.492(5)	1.494
S —C(7)	1.809(5)	1.813	C(6) —C(7)	1.507(7)	1.510
S —C(8)	1.813(5)	1.814	C(8) —C(9)	1.502(8)	1.503
O(1) —C(6)	1.416(4)	1.419			
			3		
Ga —O(4)	1.928(2)	1.935	O(4) —C(9)	1.415(4)	1.419
Ga —N(2)	1.977(3)	1.988	N(1) —N(2)	1.377(4)	1.381
Ga —C(4)	1.963(5)	1.973	N(1) —C(6)	1.351(4)	1.354
Ga —C(5)	1.976(6)	1.985	N(2) —C(8)	1.336(4)	1.337
Mn —S	2.389(1)	2.397	C(6) —C(7)	1.383(5)	1.384
Mn —O(4)	2.047(2)	2.055	C(6) —C(17)	1.491(6)	1.493
Mn —N(1)	2.077(3)	2.082	C(7) —C(8)	1.362(5)	1.367
Mn —C(1)	1.804(4)	1.807	C(8) —C(18)	1.501(7)	1.503
Mn —C(2)	1.789(4)	1.794	C(9) —C(10)	1.517(5)	1.521
Mn —C(3)	1.803(4)	1.807	C(11) —C(12)	1.358(6)	1.361
S —C(10)	1.811(3)	1.817	C(11) —C(16)	1.387(5)	1.390
S —C(11)	1.782(4)	1.785	C(12) —C(13)	1.386(6)	1.386
O(1) —C(1)	1.138(4)	1.139	C(13) —C(14)	1.359(8)	1.361
O(2) —C(2)	1.155(4)	1.156	C(14) —C(15)	1.360(8)	1.361
O(3) —C(3)	1.146(4)	1.147	C(15) —C(16)	1.372(7)	1.372
			4		
Mo(1)—S(1)	2.519(2)	2.527	Mo(2)—S(2)	2.537(2)	2.541
Mo(1)—O(3)	2.233(5)	2.241	Mo(2)—O(6)	2.231(4)	2.237
Mo(1)—N(1)	2.270(5)	2.277	Mo(2)—N(3)	2.248(5)	2.254
Mo(1)—C(1)	1.950(9)	1.954	Mo(2)—C(21)	1.936(7)	1.940
Mo(1)—C(2)	1.952(7)	1.956	Mo(2)—C(22)	1.957(7)	1.960
Ga(1) —O(3)	1.925(5)	1.931	Ga(2) —O(6)	1.923(4)	1.927
Mo(1)—C(5)	2.383(7)	2.391	Mo(2)—C(25)	2.363(6)	2.367
Mo(1)—C(6)	2.205(6)	2.214	Mo(2)—C(26)	2.194(6)	2.198
Mo(1)—C(7)	2.375(7)	2.384	Mo(2)—C(27)	2.364(6)	2.369
Ga(1) —N(2)	1.976(6)	1.983	Ga(2) —N(4)	1.981(5)	1.985
Ga(1) —C(3)	1.976(8)	1.976	Ga(2) —C(23)	1.980(7)	1.980
Ga(1) —C(4)	1.966(8)	1.968	Ga(2) —C(24)	1.974(7)	1.975
S(1) —C(12)	1.792(10)	1.797	S(2) —C(32)	1.802(7)	1.806
S(1) —C(14)	1.853(11)	1.853	S(2) —C(34)	1.811(7)	1.813
O(3) —C(13)	1.431(7)	1.434	O(6) —C(33)	1.435(6)	1.437
N(1) —N(2)	1.365(8)	1.370	N(3) —N(4)	1.379(6)	1.381
N(1) —C(16)	1.341(8)	1.344	N(3) —C(36)	1.344(7)	1.346
N(2) —C(18)	1.348(9)	1.351	N(4) —C(38)	1.333(8)	1.334
C(1) —O(1)	1.142(8)	1.147	C(21) —O(4)	1.153(7)	1.154
C(2) —O(2)	1.151(7)	1.152	C(22) —O(5)	1.156(7)	1.156
C(5) —C(6)	1.391(10)	1.395	C(25) —C(26)	1.389(9)	1.392
C(5) —C(11)	1.452(10)	1.454	C(25) —C(31)	1.458(9)	1.461
C(6) —C(7)	1.384(10)	1.390	C(26) —C(27)	1.379(10)	1.383
C(7) —C(8)	1.459(11)	1.461	C(27) —C(28)	1.463(9)	1.465
C(8) —C(9)	1.349(11)	1.351	C(28) —C(29)	1.340(9)	1.342
C(9) —C(10)	1.434(11)	1.437	C(29) —C(30)	1.407(10)	1.410
C(10) —C(11)	1.308(10)	1.312	C(30) —C(31)	1.336(9)	1.338
C(10) —C(11)	1.308(10)	1.312	C(30) —C(31)	1.336(9)	1.503
C(14) —C(15)	1.291(14)	1.291	C(34) —C(35)	1.505(10)	1.507
C(16) —C(17)	1.371(11)	1.373	C(36) —C(37)	1.357(9)	1.358
C(16) —C(19)	1.492(11)	1.495	C(36) —C(39)	1.501(10)	1.503
C(17) —C(18)	1.353(11)	1.357	C(37) —C(38)	1.410(10)	1.413
C(18) —C(20)	1.524(12)	1.525	C(38) —C(40)	1.507(11)	1.508

Can. J. Chem. Downloaded from www.nrcresearchpress.com by 210.87.254.5 on 09/06/12
For personal use only.

Can. J. Chem. Downloaded from www.nrcresearchpress.com by 210.87.254.5 on 09/06/12
For personal use only.

TABLE 4. Bond angles (deg) with estimated standard deviations in parentheses, non-hydrogen atoms

Bonds	Angle (deg)	Bonds	Angle (deg)
2			
O(1) —Ga —N(1)	92.6(1)	Ga —N(1) —N(2)	118.4(2)
O(1) —Ga —C(1)	110.7(2)	Ga —N(1) —C(3)	132.7(2)
O(1) —Ga —C(2)	107.3(2)	N(2) —N(1) —C(3)	108.8(3)
N(1) —Ga —C(1)	109.5(2)	Ni —N(2) —N(1)	119.4(2)
N(1) —Ga —C(2)	107.2(2)	Ni —N(2) —C(5)	132.7(2)
C(1) —Ga —C(2)	124.7(3)	N(1) —N(2) —C(5)	107.3(2)
S —Ni —O(1)	87.90(7)	Ni —N(3) —O(2)	170.1(4)
S —Ni —N(2)	101.28(8)	N(1) —C(3) —C(4)	108.3(3)
S —Ni —N(3)	116.0(1)	N(1) —C(3) —C(10)	121.4(4)
O(1) —Ni —N(2)	90.5(1)	C(4) —C(3) —C(10)	130.2(4)
O(1) —Ni —N(3)	127.9(1)	C(3) —C(4) —C(5)	106.3(3)
N(2) —Ni —N(3)	124.8(1)	N(2) —C(5) —C(4)	109.2(3)
Ni —S —C(7)	94.5(2)	N(2) —C(5) —C(11)	120.9(3)
Ni —S —C(8)	106.8(2)	C(4) —C(5) —C(11)	129.8(3)
C(7) —S —C(8)	101.6(3)	O(1) —C(6) —C(7)	110.7(3)
Ga —O(1) —Ni	114.1(1)	S —C(7) —C(6)	111.8(3)
Ga —O(1) —C(6)	120.9(3)	S —C(8) —C(9)	111.4(4)
Ni —O(1) —C(6)	113.0(2)		
3			
O(4) —Ga —N(2)	90.4(1)	Mn —N(1) —N(2)	116.6(2)
O(4) —Ga —C(4)	110.3(2)	Mn —N(1) —C(6)	135.6(3)
O(4) —Ga —C(5)	109.9(2)	N(2) —N(1) —C(6)	106.7(3)
N(2) —Ga —C(4)	110.4(2)	Ga —N(2) —N(1)	120.2(2)
N(2) —Ga —C(5)	109.8(2)	Ga —N(2) —C(8)	129.7(3)
C(4) —Ga —C(5)	121.5(3)	N(1) —N(2) —C(8)	108.9(3)
S —Mn —O(4)	83.74(6)	Mn —C(1) —O(1)	175.2(4)
S —Mn —N(1)	84.51(8)	Mn —C(2) —O(2)	176.1(3)
S —Mn —C(1)	176.1(1)	Mn —C(3) —O(3)	177.2(3)
S —Mn —C(2)	93.7(1)	N(1) —C(6) —C(7)	109.0(3)
S —Mn —C(3)	94.9(1)	N(1) —C(6) —C(17)	122.9(4)
O(4) —Mn —N(1)	84.95(9)	C(7) —C(6) —C(17)	128.0(4)
O(4) —Mn —C(1)	93.8(1)	C(6) —C(7) —C(8)	106.4(3)
O(4) —Mn —C(2)	177.2(1)	N(2) —C(8) —C(7)	109.0(3)
O(4) —Mn —C(3)	90.2(1)	N(2) —C(8) —C(18)	120.6(4)
N(1) —Mn —C(1)	92.3(1)	C(7) —C(8) —C(18)	130.4(4)
N(1) —Mn —C(2)	95.9(1)	O(4) —C(9) —C(10)	109.3(3)
N(1) —Mn —C(3)	175.2(1)	S —C(10) —C(9)	109.9(2)
C(1) —Mn —C(2)	88.8(2)	S —C(11) —C(12)	125.2(3)
C(1) —Mn —C(3)	88.1(2)	S —C(11) —C(16)	115.3(3)
C(2) —Mn —C(3)	88.9(2)	C(12) —C(11) —C(16)	119.5(4)
Mn —S —C(10)	96.8(1)	C(11) —C(12) —C(13)	120.1(5)
Mn —S —C(11)	110.4(1)	C(12) —C(13) —C(14)	120.8(5)
C(10) —S —C(11)	105.0(2)	C(13) —C(14) —C(15)	118.8(5)
Ga —O(4) —Mn	116.0(1)	C(14) —C(15) —C(16)	121.7(5)
Ga —O(4) —C(9)	119.5(2)	C(15) —C(16) —C(11)	119.2(5)
Mn —O(4) —C(9)	114.0(2)		
4			
S(1) —Mo(1)—O(3)	78.3(1)	S(2) —Mo(2)—O(6)	78.5(1)
S(1) —Mo(1)—N(1)	78.5(1)	S(2) —Mo(2)—N(3)	77.8(1)
S(1) —Mo(1)—C(1)	86.9(2)	S(2) —Mo(2)—C(21)	88.1(2)
S(1) —Mo(1)—C(2)	92.7(2)	S(2) —Mo(2)—C(22)	92.1(2)
S(1) —Mo(1)—C(5)	154.0(2)	S(2) —Mo(2)—C(25)	152.5(2)
S(1) —Mo(1)—C(6)	160.4(2)	S(2) —Mo(2)—C(26)	159.9(2)
S(1) —Mo(1)—C(7)	144.7(2)	S(2) —Mo(2)—C(27)	145.8(2)
O(3) —Mo(1)—N(1)	79.6(2)	O(6) —Mo(2)—N(3)	80.3(2)
O(3) —Mo(1)—C(1)	163.4(2)	O(6) —Mo(2)—C(21)	165.5(2)
O(3) —Mo(1)—C(2)	94.9(2)	O(6) —Mo(2)—C(22)	96.0(2)

Can. J. Chem. Downloaded from www.nrcresearchpress.com by 210.87.254.5 on 09/06/12
For personal use only.

TABLE 4 (*Concluded*)

Bonds	Angle (deg)	Bonds	Angle (deg)
O(3) —Mo(1)—C(5)	81.2(2)	O(6) —Mo(2)—C(25)	80.3(2)
O(3) —Mo(1)—C(6)	92.3(2)	O(6) —Mo(2)—C(26)	89.9(2)
O(3) —Mo(1)—C(7)	125.6(2)	O(6) —Mo(2)—C(27)	122.7(2)
N(1) —Mo(1)—C(1)	105.0(3)	N(3) —Mo(2)—C(21)	102.3(2)
N(1) —Mo(1)—C(2)	170.3(2)	N(3) —Mo(2)—C(22)	169.7(2)
N(1) —Mo(1)—C(5)	113.2(2)	N(3) —Mo(2)—C(25)	115.6(2)
N(1) —Mo(1)—C(6)	83.0(2)	N(3) —Mo(2)—C(26)	84.2(2)
N(1) —Mo(1)—C(7)	81.1(2)	N(3) —Mo(2)—C(27)	79.9(2)
C(1) —Mo(1)—C(2)	78.1(3)	C(21) —Mo(2)—C(22)	78.9(3)
C(1) —Mo(1)—C(5)	110.6(3)	C(21) —Mo(2)—C(25)	110.5(3)
C(1) —Mo(1)—C(6)	104.0(3)	C(21) —Mo(2)—C(26)	104.5(3)
C(1) —Mo(1)—C(7)	71.0(3)	C(21) —Mo(2)—C(27)	71.7(2)
C(2) —Mo(1)—C(5)	73.3(2)	C(22) —Mo(2)—C(25)	72.9(2)
C(2) —Mo(1)—C(6)	105.3(3)	C(22) —Mo(2)—C(26)	105.5(3)
C(2) —Mo(1)—C(7)	108.5(3)	C(22) —Mo(2)—C(27)	110.0(3)
C(5) —Mo(1)—C(7)	61.2(3)	C(25) —Mo(2)—C(27)	61.6(2)
O(3) —Ga(1) —N(2)	92.5(2)	O(6) —Ga(2) —N(4)	92.0(2)
O(3) —Ga(1) —C(3)	110.1(3)	O(6) —Ga(2) —C(23)	111.6(3)
O(3) —Ga(1) —C(4)	109.4(3)	O(6) —Ga(2) —C(24)	109.4(3)
N(2) —Ga(1) —C(3)	109.7(4)	N(4) —Ga(2) —C(23)	109.9(3)
N(2) —Ga(1) —C(4)	112.3(3)	N(4) —Ga(2) —C(24)	114.1(3)
C(3) —Ga(1) —C(4)	119.6(4)	C(23) —Ga(2) —C(24)	117.2(3)
Mo(1)—S(1) —C(12)	100.1(2)	Mo(2)—S(2) —C(32)	99.1(2)
Mo(1)—S(1) —C(14)	110.5(3)	Mo(2)—S(2) —C(34)	112.8(2)
C(12) —S(1) —C(14)	103.1(6)	C(32) —S(2) —C(34)	100.6(3)
Mo(1)—O(3) —Ga(1)	117.1(2)	Mo(2)—O(6) —Ga(2)	117.7(2)
Mo(1)—O(3) —C(13)	113.0(5)	Mo(2)—O(6) —C(33)	112.6(3)
Ga(1) —O(3) —C(13)	117.6(5)	Ga(2) —O(6) —C(33)	115.3(3)
Mo(1)—N(1) —N(2)	118.5(4)	Mo(2)—N(3) —N(4)	118.9(4)
Mo(1)—N(1) —C(16)	133.1(6)	Mo(2)—N(3) —C(36)	133.9(4)
N(2) —N(1) —C(16)	107.8(6)	N(4) —N(3) —C(36)	106.9(5)
Ga(1) —N(2) —N(1)	121.7(4)	Ga(2) —N(4) —N(3)	122.2(4)
Ga(1) —N(2) —C(18)	129.5(6)	Ga(2) —N(4) —C(38)	129.1(5)
N(1) —N(2) —C(18)	107.8(7)	N(3) —N(4) —C(38)	108.2(6)
Mo(1)—C(1) —O(1)	176.6(7)	Mo(2)—C(21) —O(4)	175.5(6)
Mo(1)—C(2) —O(2)	176.8(6)	Mo(2)—C(22) —O(5)	176.0(6)
Mo(1)—C(5) —C(6)	65.5(4)	Mo(2)—C(25) —C(26)	65.7(4)
Mo(1)—C(5) —C(11)	121.5(6)	Mo(2)—C(25) —C(31)	122.1(5)
C(6) —C(5) —C(11)	126.0(7)	C(26) —C(25) —C(31)	125.5(7)
Mo(1)—C(6) —C(5)	79.5(4)	Mo(2)—C(26) —C(25)	79.1(4)
Mo(1)—C(6) —C(7)	79.3(4)	Mo(2)—C(26) —C(27)	79.3(4)
C(5) —C(6) —C(7)	121.6(8)	C(25) —C(26) —C(27)	121.9(7)
Mo(1)—C(7) —C(6)	65.8(4)	Mo(2)—C(27) —C(26)	65.7(3)
Mo(1)—C(7) —C(8)	121.8(5)	Mo(2)—C(27) —C(28)	122.2(5)
C(6) —C(7) —C(8)	126.1(8)	C(26) —C(27) —C(28)	126.1(7)
C(7) —C(8) —C(9)	128.5(8)	C(27) —C(28) —C(29)	128.2(7)
C(8) —C(9) —C(10)	127.8(7)	C(28) —C(29) —C(30)	127.8(6)
C(9) —C(10) —C(11)	127.9(7)	C(29) —C(30) —C(31)	129.6(6)
C(10) —C(11) —C(5)	129.9(8)	C(30) —C(31) —C(25)	127.9(6)
S(1) —C(12) —C(13)	111.1(6)	S(2) —C(32) —C(33)	110.5(4)
O(3) —C(13) —C(12)	110.2(6)	O(6) —C(33) —C(32)	110.4(5)
S(1) —C(14) —C(15)	117.5(9)	S(2) —C(34) —C(35)	111.3(5)
N(1) —C(16) —C(17)	108.7(8)	N(3) —C(36) —C(37)	111.3(7)
N(1) —C(16) —C(19)	122.5(7)	N(3) —C(36) —C(39)	121.3(6)
C(17) —C(16) —C(19)	128.8(8)	C(37) —C(36) —C(39)	127.5(7)
C(16) —C(17) —C(18)	106.8(7)	C(36) —C(37) —C(38)	104.3(7)
N(2) —C(18) —C(17)	108.9(8)	N(4) —C(38) —C(37)	109.3(6)
N(2) —C(18) —C(20)	119.7(9)	N(4) —C(38) —C(40)	122.1(7)
C(17) —C(18) —C(20)	131.4(9)	C(37) —C(38) —C(40)	128.6(7)

Can. J. Chem. Downloaded from www.nrcresearchpress.com by 210.87.254.5 on 09/06/12
For personal use only.

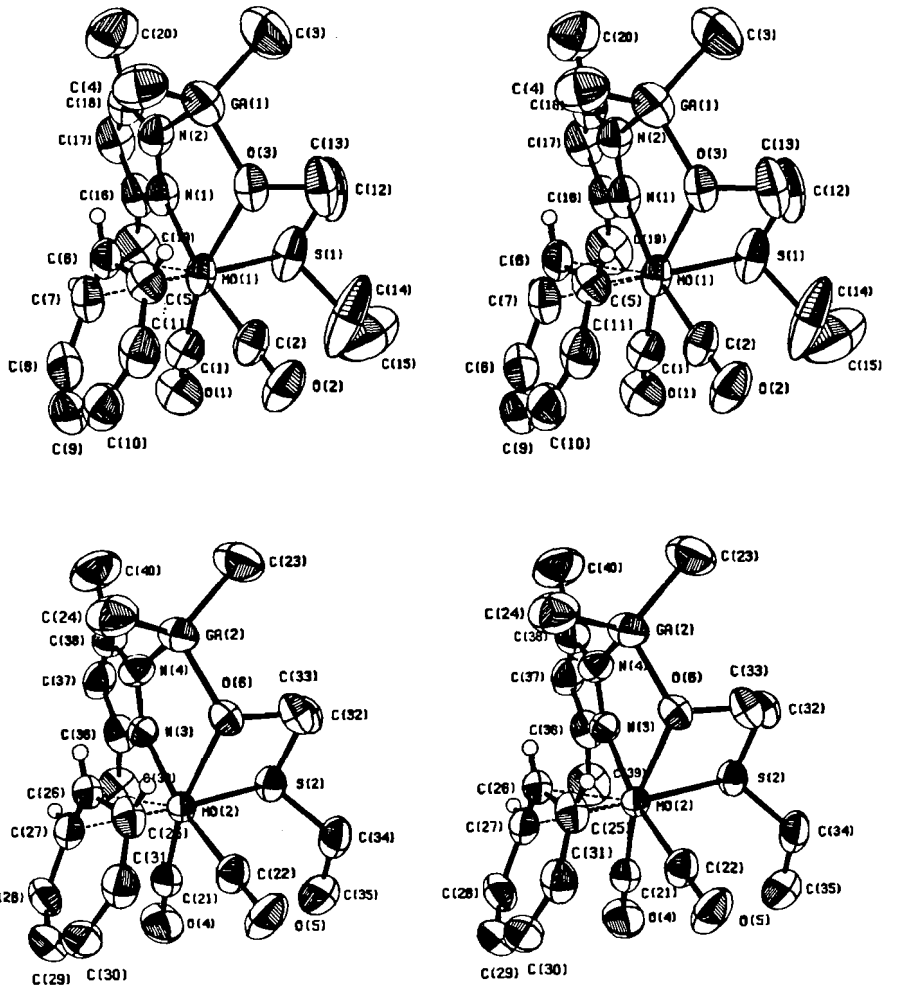

FIG. 2. Stereo views of the two independent molecules of **4**: molecule A (top) and molecule B (bottom). 50% probability thermal ellipsoids are shown for the non-hydrogen atoms, all H atoms except those bonded to the coordinated C_7H_7 atoms have been omitted for clarity.

error (χ^2 = 5.8 for C_6), the sulfur atom being significantly displaced from the phenyl mean plane (by 0.0354(8) Å).

$[Me_2Ga(N_2C_5H_7)OCH_2CH_2SC_2H_5]Mo(CO)_2(\eta^3\text{-}C_7H_7)$, 4

The crystal structure of **4** consists of discrete molecules separated by normal van der Waals distances. The asymmetric unit contains two crystallographically independent molecules (shown in Fig. 2), the most obvious differences between them being the orientation of the *S*-ethyl group and the generally larger thermal motion observed for molecule A (which contains Mo(1)). There are a number of small but statistically significant differences between corresponding geometrical parameters for the two molecules of **4**, presented side by side in Tables 3–5 for ease of comparison.

In each of the two independent molecules of **4** the coordination about the Mo atom may be regarded as distorted pseudo-octahedral with an η^3-C_7H_7 ligand occupying one coordination site as a π-donor. The η^3-C_7H_7 ligand is situated *trans* to the sulfur, thus the complex is stereochemically equivalent to the related molecule $[Me_2Ga(N_2C_5H_7)OCH_2CH_2NH_2]Mo(CO)_2(\eta^3\text{-}C_7H_7)$, **6** (9), in which the substitution occurs *trans* to the amino nitrogen. As noted earlier (3, 10), in η^3-C_3H_5 and η^3-C_4H_7 analogs of **4** and **6** the allylic ligand is situated *trans* to the pyrazolyl nitrogen. The Mo coordination spheres of **4** and **6** are so similar that the differences between the two crystallographically independent molecules of **4** are roughly the same as those between the two different compounds.

The significant differences between the Mo coordination groups of the two molecules of **4** involve

Can. J. Chem. Downloaded from www.nrcresearchpress.com by 210.87.254.5 on 09/06/12
For personal use only.

TABLE 5. Intra-annular torsion angles (deg) chelate rings

Bond	Obs.	Bond	Obs.
	2		
Ga —O(1)	19.8(1)	Ni —S	6.4(2)
O(1) —Ni	−21.7(1)	S —C(7)	−31.5(3)
Ni —N(2)	16.2(2)	C(7) —C(6)	53.1(4)
N(2) —N(1)	−5.3(2)	C(6) —O(1)	−46.4(3)
N(1) —Ga	−9.3(2)	O(1) —Ni	20.4(2)
	3		
Ga —O(4)	24.9(1)	Mn —S	2.1(1)
O(4) —Mn	−32.0(1)	S —C(10)	−29.0(2)
Mn —N(1)	31.1(2)	C(10) —C(9)	58.9(3)
N(1) —N(2)	−21.8(2)	C(9) —O(4)	−54.7(3)
N(2) —Ga	−1.8(2)	O(4) —Mn	27.7(2)
	4* (molecule A on left, B on right)		
Mo(1)—S(1)	1.6(3)	Mo(2)—S(2)	−0.1(2)
S(1) —C(12)	25.5(5)	S(2) —C(32)	28.1(4)
C(12) —C(13)	−54.7(6)	C(32) —C(33)	−57.4(5)
C(13) —O(3)	57.9(6)	C(33) —O(6)	58.6(4)
O(3) —Mo(1)	−31.1(4)	O(6) —Mo(2)	−29.8(3)
Mo(1)—O(3)	30.3(2)	Mo(2)—O(6)	28.7(2)
O(3) —Ga(1)	−26.0(2)	O(6) —Ga(2)	−25.9(2)
Ga(1) —N(2)	4.3(4)	Ga(2) —N(4)	7.7(3)
N(2) —N(1)	18.8(4)	N(4) —N(3)	13.3(4)
N(1) —Mo(1)	−27.9(4)	N(3) —Mo(2)	−23.6(3)
	Cycloheptratrienyl rings		
C(5) —C(6)	−41.9(9)	C(25) —C(26)	−43.3(8)
C(6) —C(7)	42.3(9)	C(26) —C(27)	43.5(8)
C(7) —C(8)	−15.8(10)	C(27) —C(28)	−15.3(9)
C(8) —C(9)	−4.9(10)	C(28) —C(29)	−5.7(9)
C(9) —C(10)	−0.5(11)	C(29) —C(30)	−0.5(9)
C(10) —C(11)	6.1(10)	C(30) —C(31)	6.4(9)
C(11) —C(5)	14.5(10)	C(31) —C(25)	15.0(8)

*Coordinates for molecule B have been inverted through the centre of symmetry for direct comparison with molecule A.

the Mo—S and Mo—N distances, the former being shorter and the latter longer in molecule A than in molecule B. The mean Mo—C(C_7H_7) distance in molecule A is longer than that in molecule B by 0.018(11) Å, not significant, but consistent with the observed Mo—S distances. On the basis of the same argument invoked above for **2**, the Mo—S bonds in **4** are relatively stronger than the Mo—N(amino) bond in **6**. As a result of the stronger bond *trans* to the η^3-C_7H_7 ligand in **4** the Mo—C(C_7H_7) distances are slightly longer than in **6**. The distances from the metal to the centre of mass of the three coordinated C_7H_7 carbon atoms are 2.077 and 2.062 Å for molecules A and B of **4** respectively compared to 2.051 Å for **6**. The Mo—N(pyrazolyl), Mo—O, and Mo—CO distances in **4** and **6** are not significantly different although the Mo—N and Mo—O distances are marginally shorter and the Mo—CO distances marginally longer in **4**.

The carbonyl groups are slightly, but significantly, non-linear and the mean C—O distance of 1.152 Å is somewhat shorter than the corresponding value of 1.171 Å observed in **6**. This difference must be attributed to solid-state effects since the ν_{CO} values for **4** and **6** in cyclohexane solutions differ by no more than 2 cm^{-1} (3, 10). The conformations of the C_7H_7 rings in **4** and **6** are also very similar and have six atoms roughly coplanar with the central coordinated carbon displaced from this plane.

Acknowledgments

We thank the Natural Sciences and Engineering Research Council of Canada for financial support and the University of British Columbia Computing Centre for assistance.

1. K. S. CHONG, S. J. RETTIG, A. STORR, and J. TROTTER. Can. J. Chem. **55**, 4166 (1977).
2. K. S. CHONG, S. J. RETTIG, A. STORR, and J. TROTTER. Can. J. Chem. **56**, 1212 (1978).
3. K. S. CHONG, S. J. RETTIG, A. STORR, and J. TROTTER. Can. J. Chem. **57**, 1335 (1979).
4. K. S. CHONG, S. J. RETTIG, A. STORR, and J. TROTTER. Can. J. Chem. **57**, 3107 (1979).
5. K. S. CHONG, S. J. RETTIG, A. STORR, and J. TROTTER. Can. J. Chem. **57**, 3113 (1979).
6. K. S. CHONG, S. J. RETTIG, A. STORR, and J. TROTTER. Can. J. Chem. **58**, 1080 (1980).
7. K. S. CHONG, S. J. RETTIG, A. STORR, and J. TROTTER. Can. J. Chem. **58**, 1091 (1980).
8. K. S. CHONG, S. J. RETTIG, A. STORR, and J. TROTTER. Can. J. Chem. **59**, 518 (1981).
9. K. S. CHONG, S. J. RETTIG, A. STORR, and J. TROTTER. Can. J. Chem. **59**, 1665 (1981).
10. K. S. CHONG and A. STORR. Can. J. Chem. **59**, 1331 (1981).
11. P. COPPENS, L. LEISEROWITZ, and D. RABINOVICH. Acta Crystallogr. **18**, 1035 (1965).
12. W. R. BUSING and H. A. LEVY. Acta Crystallogr. **22**, 457 (1967).
13. D. T. CROMER and J. B. MANN. Acta Crystallogr. Sect. A, **24**, 321 (1968).
14. R. F. STEWART, E. R. DAVIDSON, and W. T. SIMPSON. J. Chem. Phys. **42**, 3175 (1965).
15. D. T. CROMER and D. LIBERMAN. J. Chem. Phys. **53**, 1891 (1970).
16. P. J. BECKER and P. COPPENS. Acta Crystallogr. Sect. A, **30**, 129 (1974); **30**, 148 (1974); **31**, 417 (1975).
17. P. COPPENS and W. C. HAMILTON. Acta Crystallogr. Sect. A, **26**, 71 (1970).
18. F. R. THORNLEY and R. J. NELMES. Acta Crystallogr. Sect. A, **30**, 748 (1974).
19. V. SCHOMAKER and K. N. TRUEBLOOD. Acta Crystallogr. Sect. B, **24**, 63 (1969).
20. D. W. J. CRUICKSHANK. Acta Crystallogr. **9**, 747 (1956); **9**, 754 (1956); **14**, 896 (1961).
21. J. H. ENEMARK and R. D. FELTHAM. Coord. Chem. Rev. **13**, 339 (1974).
22. K. J. HALLER and J. H. ENEMARK. Inorg. Chem. **17**, 3552 (1978).
23. J. H. ENEMARK. Private communication.

Effect of pollutant gases on chlorophyll *a* multilayer

CAMILLE CHAPADOS, DENIS GERMAIN, AND ROGER M. LEBLANC

Groupe de Recherche en Biophysique, Département de Chimie-Biologie, Université du Québec à Trois-Rivières, Trois-Rivières, Qué., Canada G9A 5H7

Received December 22, 1980

CAMILLE CHAPADOS, DENIS GERMAIN, and ROGER M. LEBLANC. Can. J. Chem. **59**, 2402 (1981).

The aim of this paper is to examine the direct effect of polluting gases on chlorophyll *a* (chl *a*) multilayer arrays. The pollutants studied are CO, CO_2, SO_2, H_2S, NO, and NO_2. Electronic and infrared spectroscopies were used to monitor the time effect of the polluting gases on chl *a* molecules. TLC, atomic absorption, and electronic spectroscopies were used to characterise the reaction products. The results show that neither CO nor CO_2 affect the chl *a* molecules in the multilayer arrays. Upon exposure to SO_2, we notice many modifications on the electronic and ir spectra. All the evidence confirms that one of the reaction products is pheophytin *a*. A mechanism is presented to explain the reaction of SO_2 with chl *a*. The effect of H_2S on chl *a* is less pronounced than that of SO_2, but the end products are the same. NO and NO_2 have exactly the same effect on the chl *a* multilayer. The reaction is much more drastic than the reaction of chl *a* with either SO_2 or H_2S. There is opening of the cycle and nitration of the chl *a* molecule.

CAMILLE CHAPADOS, DENIS GERMAIN et ROGER M. LEBLANC. Can. J. Chem. **59**, 2402 (1981).

On a étudié l'effet de polluants gazeux (CO, CO_2, SO_2, H_2S, NO et NO_2) sur les molécules de chlorophylle *a* (chl *a*) dans un arrangement multicouche. Les spectroscopies électronique et infrarouge ont été utilisées pour déterminer l'effet de ces polluants sur la chl *a*. La chromatographie sur couche mince ainsi que les spectroscopies d'absorption atomique et électronique ont été employées pour caractériser les produits de réaction. Les résultats montrent que le CO_2 et le CO n'ont pas d'effet sur la multicouche de chl *a*. En présence de SO_2, on note des modifications importantes sur les spectres électroniques et les spectres infrarouges de la chl *a*. Toutes les évidences expérimentales indiquent qu'un des produits de la réaction est la phéophytine *a*. Un mécanisme réactionnel est présenté pour expliquer l'interaction du SO_2 avec la chl *a*. L'effet du H_2S sur la chl *a* est moins prononcé que dans le cas du SO_2 bien que les produits de la réaction soient les mêmes. Avec le NO et le NO_2, qui se comportent d'une façon identique avec la chl *a*, l'effet est plus drastique que dans le cas du SO_2 et H_2S. Il se produit une ouverture du cycle avec nitration de la chl *a*.

Introduction

Vegetation is affected to various degrees by atmospheric pollution. In addition to killing plants when the air pollution is high, the atmospheric pollutants adversely affect plants in various ways (1–3).

Pollution injuries are usually classified as (*i*) acute, when the tissue of the plant is killed (necrosis); (*ii*) chronic or chlorotic, when there is yellowing of the leaves, progressing slowly to a whiter color as the chlorophyll (chl) and the carotenoid in the plant are destroyed; or (*iii*) hidden when the growth of the plant is inhibited without visible marks on the leaves of the plant (1). Although the mechanisms of pollution injury to plants are complex, necrosis and chlorosis of the leaves in vascular plants indicate damage to chlorophyll by the polluting gases. In lichens, especially the epiphetic ones, no such injury can be seen but the scarcity of these species in polluted areas where other factors are favorable suggests the destruction of the chlorophyll molecules by the atmospheric pollutants (4).

Among the gaseous pollutants, SO_2 is the most important in any major agglomeration and it is the resultant of smelting mineral ore and of burning fossil fuels. This pollutant is responsible for the partial destruction of crops and the defoliation of forests near the sources of this gas (1–6). In most cases, it results in discoloration of the plant, suggesting a partial destruction of the chlorophyll molecules which are responsible for the green color in plants. With more resistant plants or at lower dosages of SO_2, the pollutant is either absorbed by the plant without visible effects or reduced to H_2S and given off as such (6). In lichens exposed to SO_2, the chl molecules are transformed to pheophytin; in dry lichens, this process is reduced (4). H_2S is a natural pollutant (3 to 30 $\mu g\ m^{-3}$), and it may sometimes be a man-made pollutant near D_2O generation plants and Kraft paper mills. It is not usually considered a pollution problem except in topical places and at low concentration it may serve as a source of sulfur to the plant (6). NO and NO_2 are major pollutants in urban areas resulting from combustion processes by heat-induced combination of atmospheric N_2 and O_2 (1). NO and NO_2 (50 parts $\times$ 10^{-8}) reduce net photosynthesis before there is any externally visible effect (7–10). Higher concentrations of the pollutant and longer exposures will produce symptoms of plant injury similar to those caused by sulfur dioxide (11). Although CO and CO_2 are not considered pollutants for the plants, they are gases which result from the combustion of fossil fuel that may affect the chl molecules in various ways.

The studies of the air pollution on chlorophyll usually start with the study of the plant (1, 2, 4, 5).

0008-4042/81/152402-10$01.00/0

©1981 National Research Council of Canada/Conseil national de recherches du Canada

Can. J. Chem. Downloaded from www.nrcresearchpress.com by 210.87.254.6 on 09/06/12
For personal use only.

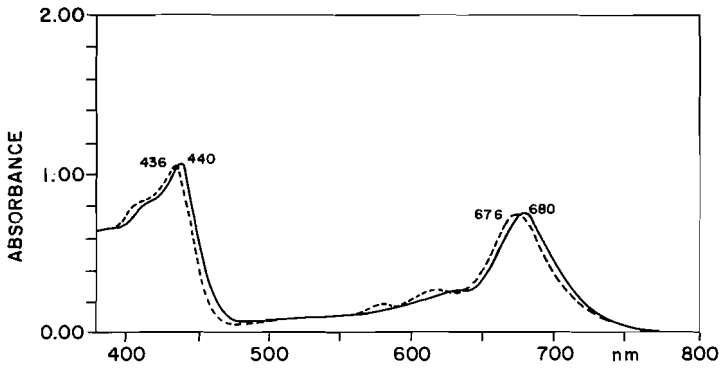

FIG. 1. CO_2 effect (29 kPa) on the absorption spectra of chl *a* multilayer (2 × 40 layers): initial spectrum (—); in CO_2 vapors for 2 days (---).

There is little study on the direct effect of the polluting gases on chlorophyll. Having been involved in several studies on the aggregation of chlorophyll in mono- and multilayer arrays (12–14), we pursued the study on the effect of gaseous pollutants on chlorophyll *a* in a multilayer state.

To simulate the *in vivo* system, we used a chlorophyll *a* multilayer. The main reasons for using this model are the following: (*i*) uniform deposition of the pigment at the air–solid interfaces; (*ii*) high concentration of the pigment (number of molecules per unit area); (*iii*) orientation of the pigment at an angle similar to the one *in vivo*.

The pollutants we studied are the following: CO, CO_2, SO_2, H_2S, NO, and NO_2. Since we were concerned with the overall effect of the pollutant molecules on chl *a* molecules, we have used much higher concentrations than the ones usually present in a highly polluted environment.

Experimental

The extraction and purification of chl *a* was done from spinach leaves by the standard method of Strain and Svec (15). Chlorophyll obtained from Sigma Chemical Company, St. Louis, MO gave the same results.

The materials, the preparation of slides, the deposition of monolayers and the Langmuir film balance apparatus have previously been described in detail (16).

Electronic Spectra

Thirty-two to forty layers of chl *a* were deposited, at a surface pressure of 20 mN m^{-1}, on both sides of a quartz slide. The slide was enclosed in a vacuum tight brass cell having quartz windows. The mean deposition ratio was 1.00 ± 0.01; the deposition ratio is defined as A_w/A_s where A_w is the decrease of area occupied by the monolayer at the air–water interface and A_s is the area coated by the monolayer at the air–solid interface.

The absorption measurements were carried out on a Unicam SP1800 spectrophotometer.

A vacuum of 0.1 Pa was maintained on the sample for 10 min, then the dry gas was introduced. Spectra were obtained at different time intervals.

Infrared Spectra

Thirty-two to forty layers of chl *a* were deposited at a surface pressure of 20 mN m^{-1} on each side of a germanium multiple internal reflexion (MIR) plate using the Langmuir film balance to monitor the deposition. The mean deposition ratio was 1.00 ± 0.01.

When the multilayer of chl *a* has reached equilibrium (14), the ir spectrum is taken, and the chl *a* multilayer is placed in a desiccator where a vacuum of 0.1 Pa is obtained. The dry gas is introduced and made to react with chl *a*. After a certain period of time, the ir spectrum is obtained. If there is reaction, the sample is washed with hot water to get rid of any inorganic water soluble substances, and the ir spectrum taken. Another sample of chl *a* having reacted with the gas is washed with diethyl ether to get rid of any organic substances, and the ir spectrum taken.

The ir spectra were recorded on a Perkin Elmer model 180 spectrometer using a FMIR accessory to increase the signal of the absorbing bands. The resolution was around 2 cm^{-1} in the carbonyl region and around 4 cm^{-1} in the C—H and O—H regions.

Thin layer chromatography, atomic absorption spectroscopy, and electronic spectroscopy were used to characterise the washing products.

Results and Discussion

The Effect of CO and CO_2 on Chlorophyll a Multilayer

As the two gases behave the same way after exposure to the chlorophyll *a* multilayer, we present only the results on CO_2 gas.

The electronic spectrum of 40 layers of chl *a* deposited on each side of a quartz slide is shown in Fig. 1. The spectrum is similar to that used in ref. 14. Following the exposure of the multilayer to CO_2 vapors (P = 29 kPa) for 2 days, we observed a 4 nm blue shift of the band maxima. Since the hypsochromic shift is identical to the one for a multilayer kept in the same conditions but without exposure to the gas, the results show that the CO_2 has no effect on the chl *a* multilayer. The hypsochromic shift is explained by a reorganisation of the chl *a* molecules in the array with time (14). To confirm the

Can. J. Chem. Downloaded from www.nrcresearchpress.com by 210.87.254.6 on 09/06/12
For personal use only.

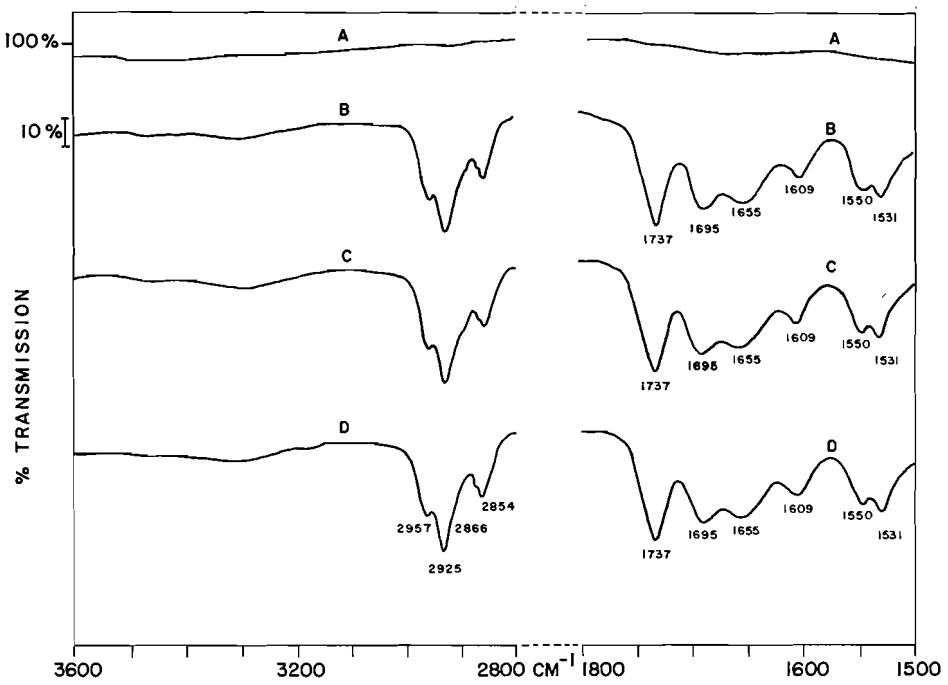

FIG. 2. CO_2 effect (28 kPa) on the infrared spectra of chl *a* multilayer (2 × 40 layers). *A*, background spectrum; *B*, multilayer after reorganisation; *C*, 24 h in CO_2 vapors; *D*, 48 h in CO_2 vapors.

absence of an effect, we have exposed 40 layers of chl *a* deposited on each side of a Ge MIR plate to CO_2. There is no modification in the ir spectrum as seen in Fig. 2 between spectrum *B* taken after the chl *a* multilayer has reorganised and spectrum *C* taken after the chl *a* molecules have been in contact with the gas for 24 h. After 2 days of exposure to the gas there was no change in the ir spectrum (Fig. 2*D*). The assignment of the bands is given in Table 1. Similar results have been obtained for CO. From our results, we conclude that neither CO nor CO_2 affect the chl *a* molecules in the multilayer arrays. Our conclusions confirm the observation made on the fluorescence intensity showing that CO_2 does not affect the chlorophyll-containing monolayers at the vapor–liquid interface (17).

The Effect of SO_2 on chl a *Multilayer*

The electronic spectra of 32 layers of chl *a* deposited on each side of a quartz slide and exposed to SO_2 vapors (P = 37 kPa) are presented in Fig. 3. Spectra at time intervals up to 12 h are given. Upon exposure to SO_2, we notice a rapid decrease of the band intensities and a displacement of the band maxima. There are two isobestic points situated at 572 nm and 465 nm indicating a one-to-one conversion. To determine the nature of these modifications, we have taken some ir spectra of the multilayer of chl *a* (2 × 36 layers) in contact with SO_2 vapors (P = 37 kPa) for 24 h and 36 h. These are presented in Fig. 4 *C* and *D*, respectively. In the OH region, a strong broad band has appeared at 3395 cm^{-1} with a shoulder at 3280 cm^{-1}. In the carbonyl region, the C=O ester group situated at 1737 cm^{-1} in the spectrum of chl *a* multilayer (Fig. 4*B*) is broadened and displaced to 1740 cm^{-1}. The free carbonyl band at 1692 cm^{-1} increases in intensity and is displaced to 1700 cm^{-1} upon fumigation. The coordinated C=O ketone is modified to a sharper band at 1655 cm^{-1} and has a shoulder at 1622 cm^{-1}. The 1609 band has almost disappeared and a new weaker band has appeared at ~1580 cm^{-1}. The doublet at 1550–1535 is modified, leaving a small structureless band at 1550 cm^{-1}. When the SO_2 exposed chl *a* sample is washed with hot water to remove all the water soluble substances in the multilayer, we are left with the sample that gives the spectrum presented in Fig. 4*E*. In the 3400 cm^{-1} region, the broad band has disappeared, leaving a small band that can be assigned to a N—H stretch vibration. In the carbonyl region, the band situated at 1655 cm^{-1} has disappeared, and the shoulder at 1622 cm^{-1} has become a weak band. The weaker band at 1580 cm^{-1}, not modified after the hot water treatment, can be assigned to a N—H deformation vibration. The spectrum in Fig. 4*E* can be compared with the spectrum of pheophytin *a* (18); the positions of the bands of both species are

Can. J. Chem. Downloaded from www.nrcresearchpress.com by 210.87.254.6 on 09/06/12
For personal use only.

Can. J. Chem. Downloaded from www.nrcresearchpress.com by 210.87.254.6 on 09/06/12
For personal use only.

TABLE 1. Wavenumber positions (cm^{-1}) of the infrared spectra of chlorophyll and pheophytin in the solid state

Description	N—H strech	C—H strech	Ester C=O	Free keto C=O	Coordinate keto C=O---Mg	Skeletal C=C C=N	N—H def.	Skeletal	References
Anhydrous chl *a* solid film	—		1736	1695	1655	1610	—	1550, 1530	18
Multilayer 15 min after deposition	—	2957, 2925 2866, 2854	1737	1692	1658	1609	—	1550, 1535	14
Multilayer 6 h after deposition	—	2957,2925 2866, 2854	1737	1695	1655	1610	—	1550, 1531	14
Monolayer	—		1738	1698	—	1620	—		13
Pheophytin *a*	~3385*		1740	1700	—	1622	1582	1555, 1540	18
SO_2 exposed chl *a* washed with hot water	3380	2956, 2925 2866, 2855	1742, 1735	1700	—	1622	1580	1555,1538 sh	This work (Fig. *4E*)

*This position has been measured on the spectra given in ref. 18, although the authors give a value of 3400 cm^{-1} in the text.

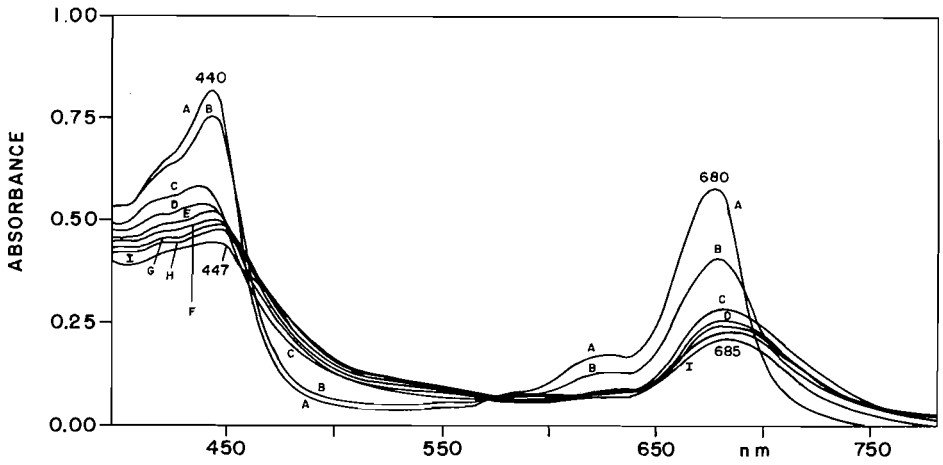

FIG. 3. SO_2 effect (37 kPa) on the absorption spectra of chl *a* multilayer (2 × 32 layers). *A*, initial spectrum; *B*, after the introduction of SO_2 vapors; in contact with SO_2 vapors: *C*, 8 min, *D*, 16 min, *E*, 24 min, *F*, 32 min, *G*, 45 min, *H*, 60 min, *I*, 12 h.

tabulated in Table 1. An atomic absorption spectrum of the water washings has revealed the presence of Mg. From this evidence, we conclude that one of the reaction products of the SO_2-treated chl *a* is pheophytin *a*. The determination of the other reaction products has been done in the following way: a multilayer of chl *a* was treated with SO_2 in a fashion similar to that previously described so that its spectrum was similar to the one given in Fig. 4*D*; the sample was then washed with diethyl ether and the remaining substance gave a spectrum presented in Fig. 4*F*. The broad bands in this spectrum can be assigned to water molecules where 3395 cm^{-1} is the O—H stretch vibration and 1655 cm^{-1} is the O—H deformation vibration. Since this water is not volatile, it must be bounded to an inorganic sulfur containing magnesium salt. The reaction of SO_2 with chl *a* would then proceed in the following way:

[1] chl $a \cdot H_2O + SO_2 \rightleftharpoons$ chl $a + SO_2 \cdot H_2O$
[2] chl $a \cdot H_2O + SO_2 \cdot H_2O \rightleftharpoons$ chl $a + HSO_3^- + H_3O^+$
[3] chl $a \cdot H_2O + HSO_3^- \rightleftharpoons$ chl $a + SO_3^{2-} + H_3O^+$
[4] chl $a + 2H_3O^+ \rightleftharpoons$ Pheophytin $a + 2H_2O + Mg^{2+}$
[5] $H_2O + SO_2 \rightleftharpoons SO_2 \cdot H_2O$

In reaction [1], the water molecule is tightly bound to chl *a* by a coordination bond with magnesium (14). SO_2 will react with H_2O to give the species $SO_2 \cdot H_2O$ which will then react with another chl $a \cdot H_2O$ to generate HSO_3^- and H_3O^+ species. The bisulfite ion will react further with chl $a \cdot H_2O$ to give SO_3^{2-} and another hydronium ion. These hydronium ions will react with the liberated chl *a* to produce pheophytin *a*, magnesium ion, and two water molecules. The latter molecules will associate with SO_2 to give $SO_2 \cdot H_2O$ species which will then proceed as in reaction [2]. The magnesium

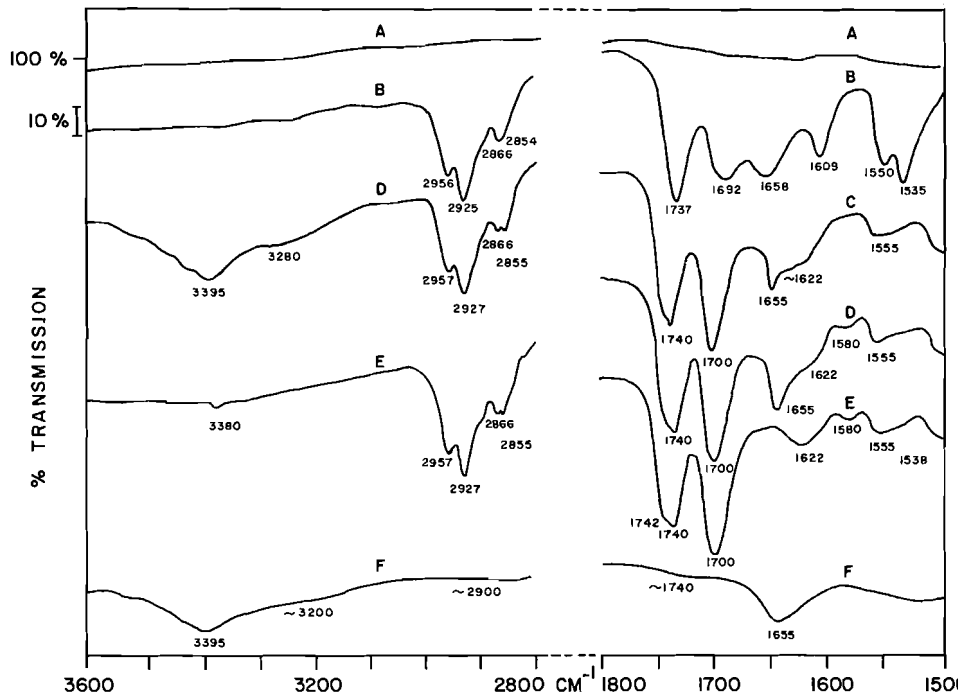

FIG. 4. SO_2 effect (37 kPa) on the infrared spectra of chl *a* multilayer (2 × 36 layers). *A*, background spectrum; *B*, multilayer after reorganisation; *C*, 24 h in SO_2 vapors; *D*, 36 h in SO_2 vapors; *E*, sample washed with hot water; *F*, another sample treated with SO_2 vapors for 18 h, and then washed with diethyl ether (taken from ref. 14).

TABLE 2. Wavenumber positions (cm^{-1}) of the infrared spectra of water

Description/mode	ν_3,ν_1	$2\nu_2$			$\nu_L+\nu_2$		ν_2	Reference
Liquid water at 30°C	3420	~3280 sh						24
Liquid water at 25°C	~3450	~3225 sh			2150		1645	25
8.5% H_2SO_4 in H_2O	3400				2150	1750 sh	1655	20
25.5% H_2SO_4 in H_2O	3400					1750	1650	20
46% H_2SO_4 in H_2O	3400		~2910	2450		1750	1655	20
78.5% H_2SO_4 in H_2O	3400 sh		~2950	2450	2250	1740	~1650	20
SO_2-exposed chl *a* washed with diethyl ether	3395	~3200	~2900			~1740	1655	This work (Fig. 4*F*)
H_2S-exposed chl *a* washed with diethyl ether	3395	~3280	~2900			~1740	1655	This work (Fig. 7*E*)
NO_2-exposed chl *a* washed with diethyl ether	3395	~3270	~2950			~1730	1655	This work (Fig. 10*E*)

produced in reaction [4] will form with the sulfite ion in reaction [3], a sulfite salt which can be hydrated with up to six water molecules (19). If SO_2 is oxidised to SO_3 by the catalytic action of the chl *a* molecules, a sulfate salt would then be formed which can also be hydrated.

Figure 4*F* is mainly the spectrum of water, and the association of water with either SO_3^{2-} or SO_4^{2-}. These species will not be spectroscopically very different. Nevertheless since Mg^{2+} cation does not influence the association of water molecules with the anion to a great degree, we can compare the spectrum of this species (Fig. 4*F*) with the spectrum of different mixtures of water in sulfuric acid (20). The position of the bands of different mixtures of H_2O and H_2SO_4 is given in Table 2. From this table, we gather that the species most comparable with ours is the one containing 46% SO_4^{2-} in H_2O. This value is, of course, only approximate and will vary from experiment to experiment depending on the water available and is given only to show that the association of the water molecules with an anion will displace slightly the position of H_2O vibration bands. Some examples of such a dis-

Can. J. Chem. Downloaded from www.nrcresearchpress.com by 210.87.254.6 on 09/06/12
For personal use only.

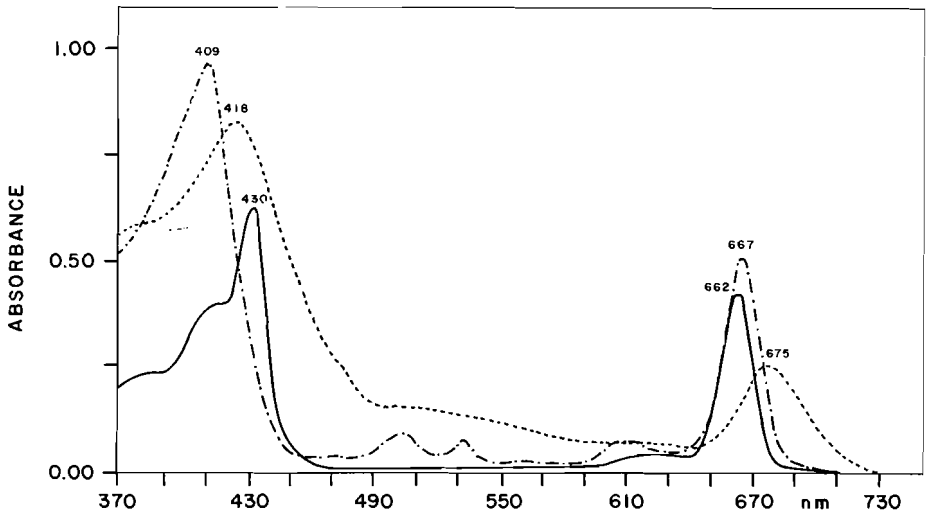

FIG. 5. Absorption spectra in diethyl ether of the reaction products of chl *a* with different pollutants: pure chl *a* (—); with SO_2 or H_2S vapors (-·--); with NO or NO_2 (---).

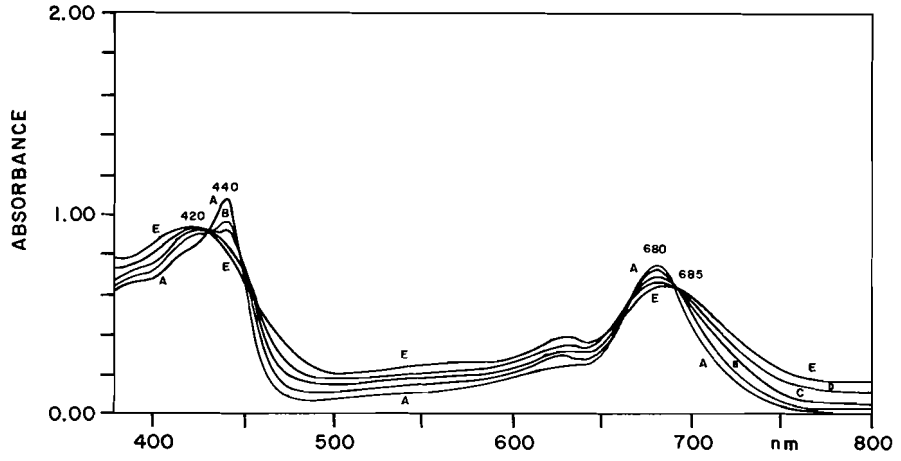

FIG. 6. H_2S effect (37 kPa) on the absorption spectra of chl *a* multilayers (2 × 40 layers). *A*, initial spectrum; in contact with H_2S vapors: *B*, 30 min, *C*, 60 min, *D*, 90 min, *E*, 120 min.

placement are given in the work of Miller and Wilkins (21).

The electronic spectrum of the diethyl ether washing of the reaction product of chl *a* with SO_2 (Fig. 5) is identical to the spectrum of pheophytin *a*. A thin layer chromatography of this solution has revealed that the reaction product is mainly pheophytin *a* with traces of chl *a*.

This evidence confirms that one of the products of chl *a* hydrate reacting with SO_2 is pheophytin *a*. The reaction can only proceed in the presence of water. In the absence of water, chl *a* molecules do not react with SO_2 molecules even after an exposure of 48 h (14). The other reaction product is a hydrate of a magnesium salt: a sulfite, a sulfate, or a combination of the two.

The Effect of H_2S on chl a *Multilayer*

The electronic spectra of 40 layers of chl *a* deposited on each side of a quartz slide and exposed to the vapors of H_2S (P = 37 kPa) are shown in Fig. 6. Spectra at time intervals up to 2 h are presented. With contact with H_2S, there is a decrease of the band intensities and a shift of the maxima. There are four isobestic points situated at 689, 664, 465, and 430 nm indicating a one-to-one conversion of chl *a* to a new species. The decrease of the band intensities is less rapid and is less pronounced than with the SO_2 reaction, but the red bands are situated at the same position in the two cases. In the blue region, the bands are broad and structureless in reactions with either SO_2 or H_2S, so that it is not possible to account for the differ-

Can. J. Chem. Downloaded from www.nrcresearchpress.com by 210.87.254.6 on 09/06/12
For personal use only.

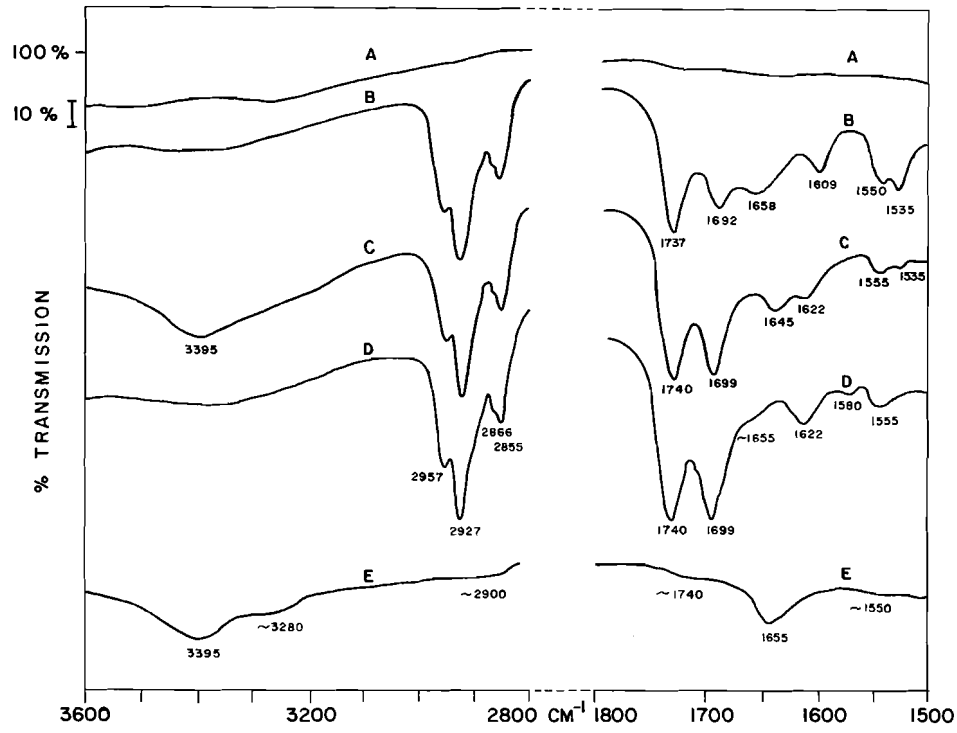

FIG. 7. H_2S effect (36 kPa) on the infrared spectra of chl *a* multilayer (2 × 36 layers). *A*, background spectrum; *B*, multilayer after reorganisation; *C*, 36 h in H_2S vapors; *D*, sample washed with hot water; *E*, another sample treated with H_2S vapors for 38 h, and then washed with diethyl ether.

ence in λ_{max} of the two reactions. To determine the nature of the end product of the reaction of H_2S with chl *a*, a stable multilayer (2 × 36 layers) of chl *a* (Fig. 7*B*) has been put in contact with H_2S ($P = 36$ kPa) for 36 h and the ir spectrum taken (Fig. 7*C*), then washed with hot water (Fig. 7*D*). The procedure is repeated using a similar multilayer and after it has been exposed to H_2S, it is washed with diethyl ether. This spectrum is presented in Fig. 7*E*. The ir spectra of the H_2S exposed chl *a* multilayer are similar to the ones exposed to SO_2, indicating that the end products are the same. In the case of the multilayer washed with hot water (Fig. 7*D*) this product is pheophytin *a*, and when the multilayer is washed with diethyl ether (Fig. 7*E*), the product is water bound to a magnesium salt. There are some small differences between the spectra of Fig. 4 and those of Fig. 7; these can be explained in the following way: first, in the stable multilayer of chl *a* in Fig. 7*B*, there is a weak broad band appearing at $\sim 3400\,cm^{-1}$ which persists after H_2S fumigation (Fig. 7*C*) followed by the hot water treatment (Fig. 7*D*). On the other hand the water band that appeared in Fig. 7*C* disappeared in Fig. 7*D*. The weak broad band can hardly be assigned to water, in good agreement with previous work (18), but it can not be assigned to an overtone either, as was speculated in that work, since this band is not always present as in Fig. 4*B*. The origin of this band is not known. Secondly, the small N—H strech band at $\sim 3400\,cm^{-1}$ has not appeared in Fig. 7*D* (it is probably smeared out) but the N—H deformation band is present at $1580\,cm^{-1}$ confirming the formation of pheophytin *a*. Thirdly, the weak shoulder at $\sim 1655\,cm^{-1}$ can be assigned to unreacted chl *a*. All these small differences can be attributed to the fact that the samples vary somewhat from experiment to experiment. H_2S-exposed chl *a* multilayer washed with diethyl ether (Fig. 7*E*) is similar to the SO_2-exposed one (Fig. 4*F*), confirming that this product is water bound to a magnesium salt. The position of the bands and even the shoulder bands appearing at ~3280, ~2900, ~1740, and $\sim 1550\,cm^{-1}$ are coincident with the ones of Fig. 4*F*. This indicates that the inorganic matrix has the same properties for the H_2S- and the SO_2-exposed chl *a* multilayer.

The electronic spectrum of the diethyl ether washing (Fig. 5) indicates that the end product of the reaction between H_2S and a multilayer of chl *a* is pheophytin *a*. Thin layer chromatography revealed the presence of mostly pheophytin *a* with

Can. J. Chem. Downloaded from www.nrcresearchpress.com by 210.87.254.6 on 09/06/12
For personal use only.

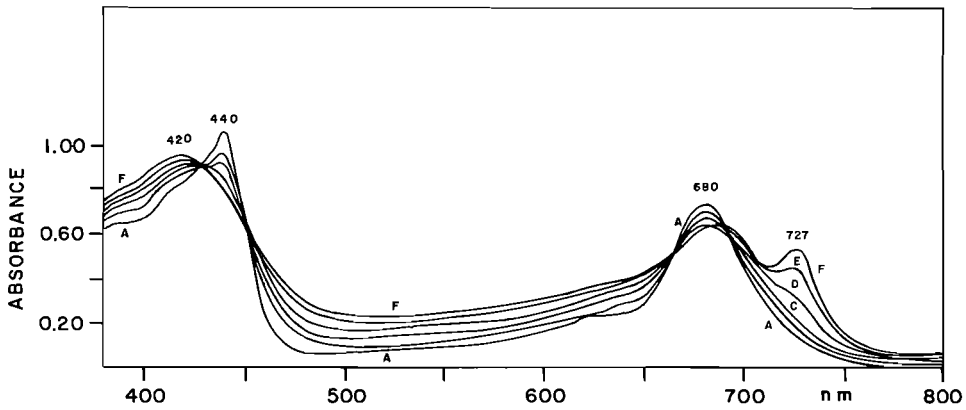

FIG. 8. H_2S effect (36 kPa) on the absorption spectra of chlorophyll *a* multilayer (2 × 40 layers) saturated with water. *A*, initial spectrum; in contact with H_2S vapors: *B*, 1 min, *C*, 8 min, *D*, 16 min, *E*, 24 min, *F*, 32 min.

traces of chl *a*. The reaction between chl *a* and H_2S would proceed in the following way:

[6] chl $a \cdot H_2O + H_2S \rightleftharpoons$ chl $a + H_2S \cdot H_2O$
[7] chl $a + H_2S \cdot H_2O \rightleftharpoons$ chl $a + HS^- + H_3O^+$
[8] chl $a \cdot H_2O + HS^- \rightleftharpoons$ chl $a + S^{2-} + H_3O^+$
[9] chl $a + 2H_3O^+ \rightleftharpoons$ Pheophytin $a + 2H_2O + Mg^{2+}$
[10] $H_2O + H_2S \rightleftharpoons H_2S \cdot H_2O$

Based on the pK_a values for reactions [7] and [8], only the former is favored (22). The HS^- will be oxidised before reacting with Mg^{2+}. The magnesium salt formed will interact with the available water to form a stable hydrate.

The Effect of H_2S on a chl a *Multilayer Saturated with Water*

Eighty layers (2 × 40) of chl *a* freshly prepared and still containing the characteristic water mist was put in an H_2S atmosphere (P = 36 kPa). The electronic spectra are presented in Fig. 8. Spectra at time intervals up to 32 min are presented. The end products have major bands situated at 727, 685, and 420 nm and isobestic points at 696, 662, 450, and 430 nm. The major bands have been displaced from the position of chl *a* (680 and 440 nm) and two are at the same position as pheophytin *a* (685 and 420 nm), but there is a new band situated at 727 nm which can be assigned to a complex containing chl *a*, pheophytin *a*, and water. Such a complex has been postulated (23) where a maximum at 720 nm was observed in a non-polar solvent. In our case, we obtain a maximum at 727 nm; the difference is explainable by the fact that the band is broad and a multilayer arrangement was used. The complex protects the Mg of chl *a* from being leached away by the anion formed from H_2S as was done in the previous case. Water plays an ambiguous role in the reaction of H_2S with chl *a*; if there is too little, there is no reaction, if there is too much, the reaction is stopped by the formation of a complex.

The Effect of NO and NO_2 on a chl a *Multilayer*

These two gases have exactly the same effect on the chl *a* multilayer. Therefore we will only present the results of NO_2 on chl *a*.

The electronic spectra of 2 × 34 layers of chl *a* in contact with NO_2 vapors (P = 26 kPa) are presented in Fig. 9. After 3 min of contact, the reaction is complete and the main bands of chl *a* have disappeared, leaving two weak bands situated at 688 and 457 nm. The overall absorption is due to NO_2 and to scattering. The reaction products dissolved in diethyl ether gave the spectrum presented in Fig. 5. A TLC of this solution has shown that there is no migration of the reaction products.

To determine the end products, a stable multilayer (2 × 32 layers) of chl *a* has been put in contact with NO_2 vapors (P = 29 kPa) for 15 h. The ir spectra are presented respectively in Fig. 10*B* and *C*. After washing the sample with hot water, ir spectrum is taken (Fig. 10*D*). In this spectrum, we notice that there is not much modification from the previous spectrum, except for a decrease in the overall intensity, and for the fact that the small water band noticed in spectrum *C* at ~1650 cm^{-1} has disappeared in spectrum *D*. Repeating the experiment, but washing the reaction product with diethyl ether instead, gave the spectrum in Fig. 10*E*. In this figure, the bands can be identified with water bands but the intensity is smaller than what has been obtained for the reaction between chl *a* and SO_2 or H_2S. The positions of the main bands are the same as the previous ones, but the secondary features are different indicating that the inorganic matrices are different. Following the reaction

Can. J. Chem. Downloaded from www.nrcresearchpress.com by 210.87.254.6 on 09/06/12
For personal use only.

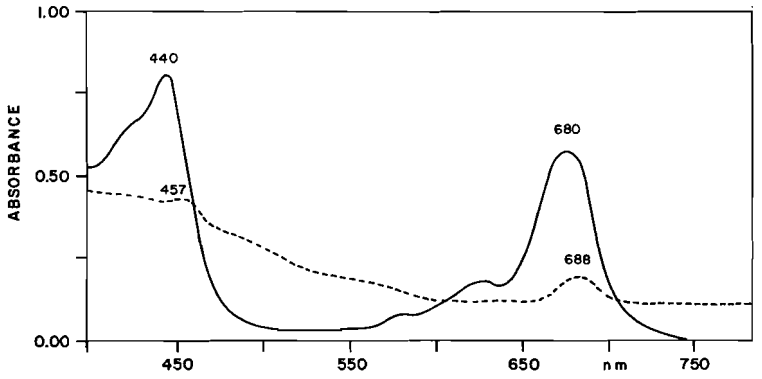

FIG. 9. NO_2 effect (29 kPa) on the absorption spectra of chlorophyll *a* multilayer (2 × 34 layers): initial spectrum (—); in NO_2 vapors for 3 min (---).

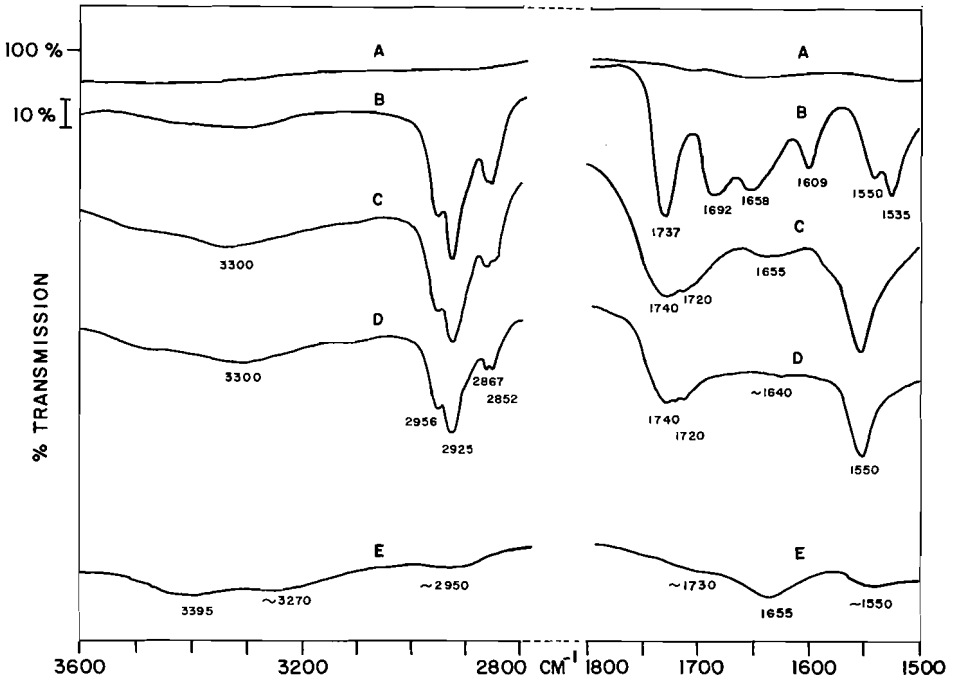

FIG. 10. NO_2 effect (29 kPa) on the infrared spectra of chl *a* multilayer (2 × 32 layers). *A*, background spectrum; *B*, multilayer after reorganisation; *C*, 15 h in NO_2 vapors; *D*, sample washed with hot water; *E*, another sample treated with NO_2 vapors for 16 h, and then washed with diethyl ether.

of NO_2 on the chl *a* multilayer (Fig. 10*C*), there is a formation of a strong band centered at ~3300 cm^{-1} which does not completely disappear upon washing with hot water. The C=O ester band at 1737 cm^{-1} is broadened to a 1740 cm^{-1} band with a shoulder at 1720 cm^{-1}, the C=O ketone bands at 1692 and 1658 cm^{-1} have disappeared, the C=C, C=N band at 1609 cm^{-1} and the skeletal doublet at 1550, 1535 cm^{-1} are modified leaving a strong structureless band which can be identified with a nitro group at 1550 cm^{-1}. This nitro group will render the molecule partly soluble, and this is the reason for the decrease of the intensity of the bands after the hot water washing. Although it is difficult to propose a mechanism for the reaction of NO_2 on chl *a*, the following observations can be made: first, the reaction is much more drastic than the reaction of chl *a* with either SO_2 or H_2S; secondly, there seems to be opening of the cycle; and thirdly, there is nitration of the chlorophyll *a* molecule.

Acknowledgements

This work was supported by the Ministère de l'Education du Québec (FCAC) and the Natural

Can. J. Chem. Downloaded from www.nrcresearchpress.com by 210.87.254.6 on 09/06/12
For personal use only.

Sciences and Engineering Research Council of Canada.

1. T. T. KOZLOWSKI and J. B. MUDD. *In* Responses of plants to air pollution. *Edited by* J. B. Mudd and T. T. Kozlowski. Academic Press, New York. 1975. Chapt. I.
2. J. S. JACOBSON and A. C. HILL (*Editors*). Recognition of air pollution injury to vegetation: A pictorial atlas. Air Pollution Control Association, Pittsburgh, PA. 1970.
3. R. C. LOOMIS and W. H. PADGETT. United States Department of Agriculture Forest Service. Atlanta, GA. 1975.
4. D. N. RAO and F. LEBLANC. Bryologist, **69**, 69 (1965); F. LEBLANC and D. N. RAO. *In* Responses of plants to air pollution. *Edited by* J. B. Mudd and T. T. Kozlowski. Academic Press, New York. 1975. Chapt. 11.
5. G. COMEAU and F. LEBLANC. Nat. Can. **98**, 347 (1971).
6. AD HOC PANEL OF EXPERTS. *In* Sulfur and its inorganic derivatives in the Canadian environment. *Edited by* Publications, NRCC, Ottawa, Canada. Publication No. NRCC 15015.
7. T. M. CAPRON and T. A. MANSFIELD. J. Exp. Bot. **27**, 1181 (1976).
8. O. C. TAYLOR and F. M. EATON. Plant Physiol. **41**, 132 (1966).
9. A. C. HILL and J. H. BENNETT. Atm. Environ. **4**, 341 (1970).
10. J. H. BENNETT and A. C. HILL. J. Environ. Qual. **2**, 526 (1973).
11. SUBCOMMITTEE ON AIR. *In* Photochemical air pollution: formation, transport and effects. *Edited by* Publications, NRCC, Ottawa, Canada. Publication no. NRCC 14096.
12. R. M. LEBLANC and C. CHAPADOS. Biophys. Chem. **6**, 77 (1977).
13. C. CHAPADOS and R. M. LEBLANC. Chem. Phys. Lett. **49**, 180 (1977).
14. C. CHAPADOS, D. GERMAIN, and R. M. LEBLANC. Biophys. Chem. **12**, 189 (1980).
15. H. H. STRAIN and W. A. SVEC. *In* The chlorophylls. *Edited by* L. P. Vernon and G. R. Seely. Academic Press, New York. 1966. Chapt. 2.
16. R. M. LEBLANC, G. GALINIER, A. TESSIER, and L. LEMIEUX. Can. J. Chem. **52**, 3723 (1974).
17. A. G. TWEET, G. L. GAINES JR., and W. D. BELLAMY. J. Chem. Phys. **40**, 2596 (1964).
18. K. BALLSCHMITER and J. J. KATZ. Biochim. Biophys. Acta, **256**, 307 (1972).
19. R. C. WEAST (*Editor*). Handbook of chemistry and physics. CRC Press, Cleveland, OH. 57th ed. 1976–1977. p. B-129.
20. P. A. GIGUÈRE and R. SAVOIE. Can. J. Chem. **38**, 2467 (1960).
21. F. A. MILLER and C. H. WILKINS. Anal. Chem. **24**, 1253 (1952).
22. S. J. BRODERIUS and L. L. SMITH. Anal. Chem. **49**, 424 (1977).
23. J. M. NORRIS, H. SCHEER and J. J. KATZ. Ann. N.Y. Acad. Sci. **244**, 260 (1975).
24. A. CABANA and C. JOLICOEUR. Can. Spectrosc. **3**, 1 (1967).
25. G. E. WALRAFEN. J. Chem. Phys. **36**, 1035 (1962).

Can. J. Chem. Downloaded from www.nrcresearchpress.com by 210.87.254.6 on 09/06/12
For personal use only.

The gas phase reactivity of the dimethylchloronium ion with alkylbenzenes

JOHN A. STONE, MARGARET S. LIN, AND JEFFREY VARAH
Department of Chemistry, Queen's University, Kingston, Ont., Canada K7L 3N6

Received July 29, 1980

JOHN A. STONE, MARGARET S. LIN, and JEFFREY VARAH. Can. J. Chem. **59**, 2412 (1981).

The reactivity of the dimethylchloronium ion with a series of aromatic hydrocarbons has been studied in a high pressure mass spectrometer ion source using the technique of reactant ion monitoring. Benzene is unreactive but all others, from toluene to mesitylene, react by CH_3^+ transfer to yield σ-bonded complexes. The relative rate of reaction increases with increasing exothermicity in line with current theories of nucleophilic displacement reactions.

JOHN A. STONE, MARGARET S. LIN et JEFFREY VARAH. Can. J. Chem. **59**, 2412 (1981).

Faisant appel à la technique de l'enregistrement de l'ion réactif dans un spectromètre de masse à haute pression on a étudié la réactivité de l'ion diméthylchloronium avec une série d'hydrocarbures aromatiques. Le benzène ne réagit pas mais tous les autres à partir du toluène jusqu'au mésitylène réagissent par transfert de CH_3^+ en donnant des complexes liés par des liaisons σ. La vitesse relative de la réaction augmente avec le caractère exothermique en accord avec les théories courantes sur les réactions de déplacements nucléophile.

[Traduit par le journal]

Introduction

Dialkylhalogenonium cations (RXR^+, X = Cl, Br, I) have been formed in strong acid solution by the reaction of RX with SbF_5–SO_2, HF–SbF_5 or anhydrous silver hexafluoroantimonate in SO_2 (1). The ions are good alkylating agents in the condensed phase for aromatic compounds, for example $C_2H_5XC_2H_5^+$, yields ethylbenzene by reaction with benzene and $CH_3XCH_3^+$ forms *o*-, *m*-, and *p*-xylene with toluene (2).

Dialkylfluoronium cations cannot be formed in strong acid solution but their presence as intermediates in γ-irradiated gaseous CH_3F has been postulated (3). When a small amount of aromatic (~0.1%) was present in CH_3F at 760 Torr the methyl addition product, toluene, was observed in good yield ($G \approx 1$, i.e. one molecule per 100 eV of absorbed energy). The relative rates of methylation as determined by competition studies were about the same for benzene, toluene, the xylenes, and mesitylene. When, however, a small amount of benzene was irradiated in either gaseous CH_3Cl or CH_3Br the yield of toluene was small ($G < 0.01$). This lack of alkylating ability of $CH_3ClCH_3^+$ towards benzene was confirmed by icr double resonance experiments at much lower pressures. Whereas $CH_3FCH_3^+$ was a precursor of $C_7H_9^+$ in CH_3F–C_6H_6 mixtures, $CH_3ClCH_3^+$ was not a precursor of $C_7H_9^+$ in CH_3Cl–C_6H_6 mixtures. This different behaviour was ascribed to the different geometries of the methyl group in $CH_3XCH_3^+$. It was suggested that $CH_3FCH_3^+$ possesses the higher degree of charge delocalization, i.e. the carbon atoms have the greater sp^2 character. This more planar —CH_3 group aids attack by the aromatic base. Conversely the much lower reactivity of $CH_3ClCH_3^+$ is due to a higher activation barrier engendered by the greater sp^3 character of the —CH_3 group. In this argument, the nature of the nucleophilic substrate is not considered.

We have therefore studied the reaction of $CH_3ClCH_3^+$ with an extended series of alkylbenzenes in a high pressure mass spectrometer in order to examine the influence, if any, of the structure of the nucleophile on the reaction rate. We have measured relative rates of reaction using the technique of reactant ion monitoring (RIM) (4, 5).

Experimental

The equipment used and the technique of reactant ion monitoring have been previously described in detail (5). The field-free photoionization source was operated at 300 K. Argon resonance radiation (11.7 eV) was used for ionization of CH_3Cl (~0.25 Torr) in helium (0.6–0.7 Torr). The signal due to $CH_3{}^{35}ClCH_3^+$ was monitored as small amounts of aromatic compounds entered the ion source from a chromatograph. From the relative decreases in signal for the different compounds, relative rate constants are obtained (4, 5). The 1 μL samples injected into the chromatograph contained ~0.1% of each of four aromatics in *n*-hexane as solvent. The amount of sample injected was such that the maximum decrease in monitored ion current was always less than 10% of the steady state value and under these conditions the relative rate constants obtained are independent of sample size.

Results and Discussion

The molecular ion (CH_3Cl^+) is the only ion formed when CH_3Cl is ionized by 11.7 eV photons. At pressures greater than 50 mTorr this ion disappears completely, being replaced by the halonium ion (6, 7)

0008-4042/81/152412-05$01.00/0
©1981 National Research Council of Canada/Conseil national de recherches du Canada

Can. J. Chem. Downloaded from www.nrcresearchpress.com by 210.87.254.42 on 09/06/12
For personal use only.

Can. J. Chem. Downloaded from www.nrcresearchpress.com by 210.87.254.42 on 09/06/12
For personal use only.

[1] $CH_3Cl^+ + CH_3Cl \rightarrow CH_3ClH^+ + CH_2Cl$

[2] $CH_3ClH^+ + CH_3Cl \rightarrow CH_3ClCH_3^+ + HCl$

Figure 1 shows both a gc trace and the monitored $CH_3{}^{35}ClCH_3^+$ ion signal for a sample containing fluorobenzene, toluene, ethylbenzene, and mesitylene in roughly equal concentrations. The same relative decreases in ion signal were observed when $CH_3{}^{37}ClCH_3^+$ was monitored. Obviously mesitylene is much more reactive than the other aromatics and although the *n*-hexane solvent also causes a decrease in the monitored ion current, the magnitude of the decrease is not very different from that due to mesitylene. The *n*-hexane, present at much higher concentration than the aromatics as shown by the gc trace, could be reacting either with $CH_3ClCH_3^+$ or with its precursor CH_3ClH^+ since the reaction product is $C_6H_{13}^+$, presumably formed by hydride transfer

[3] $CH_3ClCH_3^+ + n\text{-}C_6H_{14} \rightarrow CH_3Cl + CH_4 + C_6H_{13}^+$

[4] $CH_3ClH^+ + n\text{-}C_6H_{14} \rightarrow CH_3Cl + H_2 + C_6H_{13}^+$

When the *n*-hexane is present at a concentration comparable with that of the aromatics shown in Fig. 1, it has no observable effect on the monitored ion current.

Figure 2 shows the relative rates of reaction of a series of alkylaromatics and of aniline and nitrobenzene. In all cases the only observable product of reaction when the decrease in monitored ion current is less than 10% of the steady state value, is the methyl cation adduct, MCH_3^+, of the neutral M.

[5] $M + CH_3ClCH_3^+ \rightarrow MCH_3^+ + CH_3Cl$

Neither benzene nor fluorobenzene is found to react (rate of reaction < 10% that of ethylbenzene). This confirms the icr observation of Speranza and Pepe (3) and also substantiates our method. Both compounds would react exothermically with the precursors of $CH_3ClCH_3^+$, with CH_3ClH^+ by proton transfer and with CH_3Cl^+ by charge transfer. We are therefore studying the reaction of the $CH_3ClCH_3^+$ ion under the stated experimental conditions.

The nature of reaction [5] is of interest. It may be regarded as a nucleophilic displacement reaction, the nucleophile M displacing CH_3Cl from $CH_3ClCH_3^+$. If this is a direct displacement then either a σ complex is formed directly

[6] $CH_3ClCH_3^+ +$ 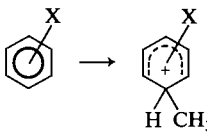 $+ CH_3Cl$

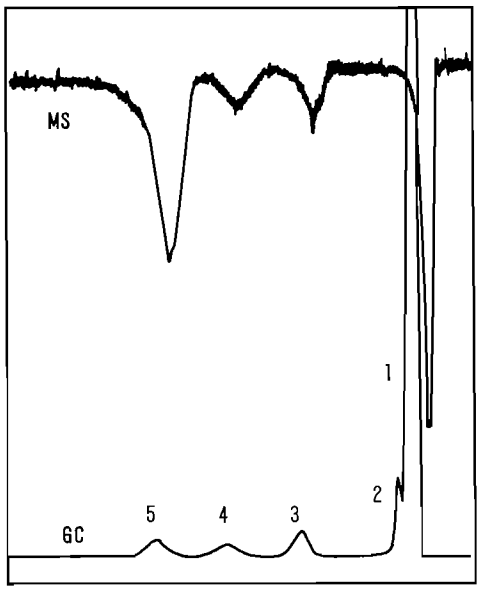

FIG. 1. Lower curve, flame ionization detector trace; upper curve, $CH_3{}^{35}ClCH_3^+$ signal. *1*, *n*-Hexane (solvent); *2*, fluorobenzene; *3*, toluene; *4*, ethylbenzene; *5*, mesitylene. The traces are offset by the dual pen strip-chart recorder.

or a π complex is formed which might or might not pass over into the more stable σ form. The relative rates of reaction provide no details of the reaction mechanism but the trend shown is more consistent with that for liquid phase S_N2 reactions which are presumed to proceed via a σ complex formation (8).

The participation of π complexes in condensed phase displacement reactions has been strongly advocated (9) but the concept has not received widespread support (10). A similar situation prevails for the gas phase. Arguments have been advanced for prior π complex formation in gas-phase aromatic methylenation by $C_2H_5O^+$ (11) and for acetylation of anisoles by $CH_3COCO(COCH_3)$-CH_3^+ (12). In each case anomalous substituent effects on reaction rate was cited as evidence. In neither case was the character of the product ion probed, it being presumed to be the final, more stable σ complex.

Direct evidence for the formation of a stable π complex in the gas phase nitrosation of benzene by CH_2ONO^+ was obtained using icr by Reents and Freiser (13). The $C_6H_6NO^+$ formed was found to transfer only NO^+ to toluene, a stronger NO^+ acceptor than benzene, whereas there was no proton transfer to pyridine as should occur for a σ-bonded complex. We confirmed this finding under different conditions. In a 60/40/0.01 He/NO/C_6D_6 mixture,

Can. J. Chem. Downloaded from www.nrcresearchpress.com by 210.87.254.42 on 09/06/12
For personal use only.

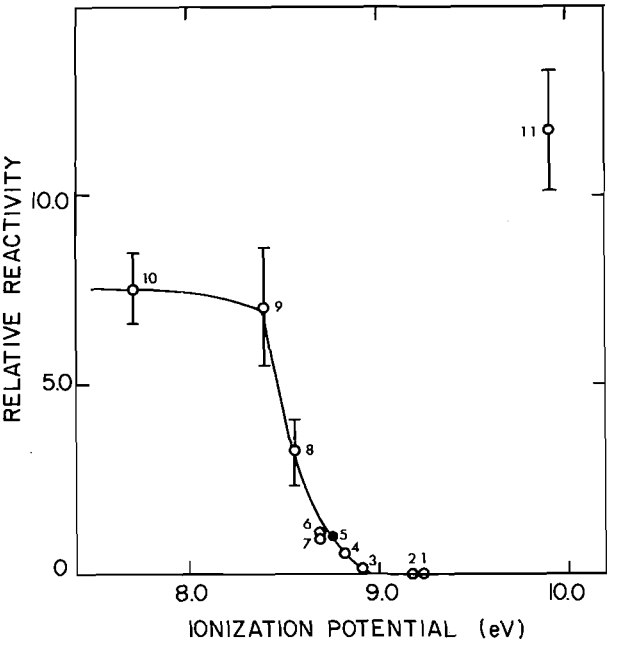

FIG. 2. The dependence of the relative reactivity of neutral molecules towards $CH_3ClCH_3^+$. *1*, Benzene; *2*, fluorobenzene; *3*, *m*-fluorotoluene; *4*, toluene; *5*, *n*-butylbenzene; *6*, ethylbenzene (standard); *7*, isopropylbenzene; *8*, *o*-xylene; *9*, mesitylene; *10*, aniline; *11*, nitrobenzene. The error bars show the precision obtained from four experiments.

the $C_6D_6NO^+$ formed transfers NO^+ but not D^+ to pyridine. The same behaviour is found for the toluene-d_8 NO^+ complex.

We have examined the MCH_3^+ ions formed by the aromatic hydrocarbons in a similar manner but find no evidence for the formation of a stable π complex. These experiments were performed in a field-free, electron impact, chemical ionization source (14) which has a greater sensitivity for product detection than the photoionization source but operates at a slightly higher temperature (60°C) and also generates other ions from CH_3Cl in addition to the molecular ion.

The CH_3^+ adduct of nitrobenzene-d_5 formed in a 60/40/0.02 $He/CH_3Cl/C_6D_5NO_2$ mixture at a total pressure of 0.9 Torr transfers only CH_3^+ to pyridine whereas when ring deuterated mesitylene-d_3 or *o*-xylene is substituted for the nitrobenzene, CH_3^+ is not transferable but $D^+(H^+)$ is. Therefore CH_3^+ is on oxygen in the nitrobenzene complex and a σ complex is formed with the hydrocarbons.

This conclusion is supported by observation of the further reaction of MCH_3^+. A 60/40/0.04 He/CH_3Cl/mesitylene mixture was examined at different pressures from 0.7 to 1.5 Torr (Fig. 3). At high pressure the predominant peaks are MH^+ and MCH_3^+ with the former growing at the expense of the latter. The ion arrival time distribution obtained by pulsing the electron beam, confirms that MCH_3^+ is the precursor of MH^+ (Fig. 4). The reaction is proton transfer from the product of reaction [6], i.e. ipso-protonated 1,2,3,5-tetramethylbenzene, to mesitylene and the rate of reaction, estimated from the normalized curves of Fig. 4, is $\sim 6 \times 10^{11}$ cm^3 molecule^{-1} s^{-1}.

[7]

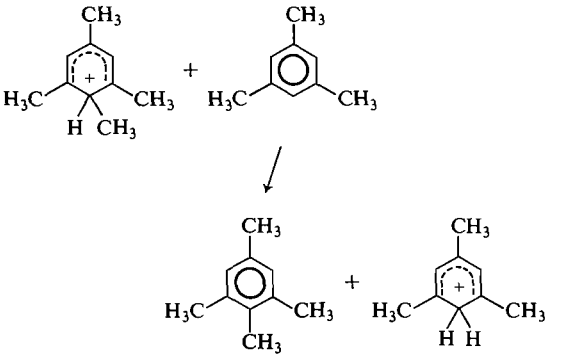

Such a low rate constant implies that the ipso-proton affinity of the tetramethylbenzene must be very close to that of mesitylene and hence a little lower than the proton affinity for a non-substituent site. Although the latter value is not available, proton affinity for the methylbenzenes appears to increase monotonically with the number of methyl groups (15). Calculation suggests that ipso-protonated toluene is $\sim$6 kcal mol^{-1} less stable than the *para*-protonated form but that such differences decrease with increasing alkyl substitution on the ring (16). The energy difference between ipso and non-ipso-protonation is obviously still significant for tetramethylbenzene.

The calculated exothermicities for reaction [5], i.e. formation of a σ complex are large for benzene through mesitylene (20–35 kcal mol^{-1}), increasing with increasing alkyl substitution, i.e., with decreasing ionization potential of M.[1] On this basis it is surprising that benzene shows no reaction but this is in keeping with the present theory of nucleophilic displacement reactions. Olmstead and Brauman (17) have shown that many other gas phase nucleophilic displacement reactions, although also highly exothermic, may be very slow. Their explanation of such behaviour is given in terms of a potential energy surface which has a double minimum corresponding to the formation of two intermediate complexes. For CH_3Cl displacement from $CH_3ClCH_3^+$ this corresponds to a

[1]The CH_3Cl—CH_3^+ dissociation energy is 64 kcal mol^{-1} (P. Kerbarle, private communication) so that $\Delta H_f^\circ(CH_3ClCH_3^+) = 177$ kcal mol^{-1}).

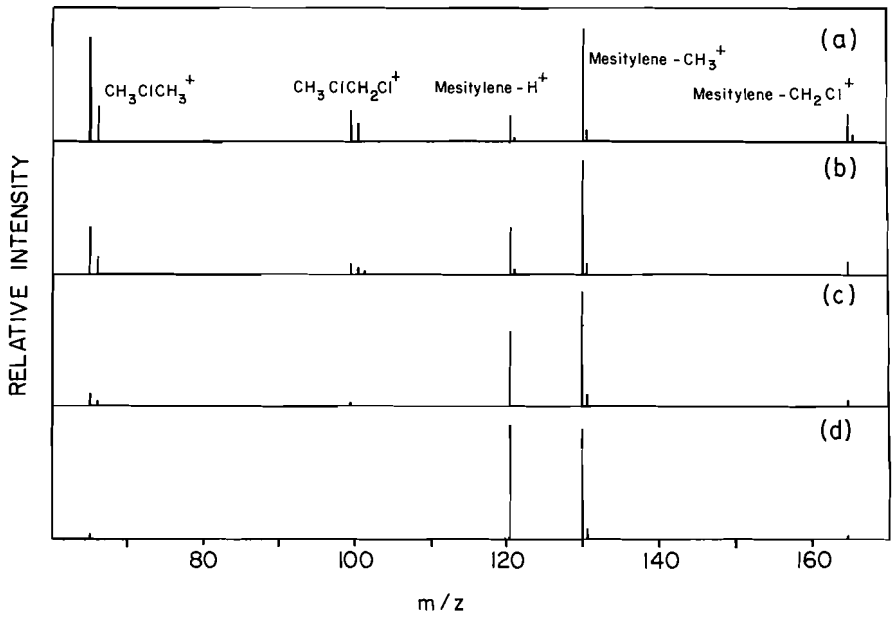

FIG. 3. The mass spectrum of a He (60%), CH_3Cl (40%), mesitylene (0.04%) mixture at 60°C as a function of total pressure. (*a*) 0.87 Torr, (*b*) 1.0 Torr, (*c*) 1.2 Torr, (*d*) 1.7 Torr.

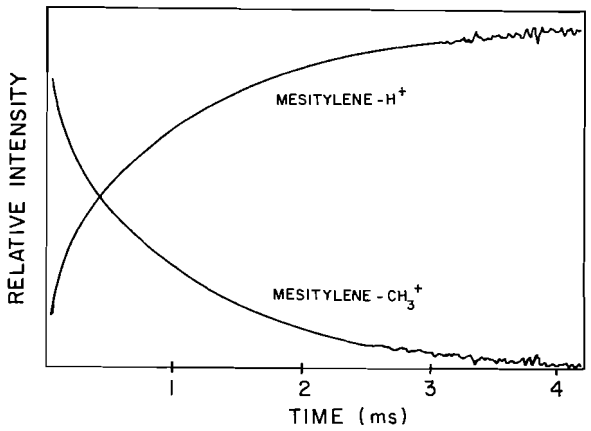

FIG. 4. Time dependence of the relative intensities of ions observed at 1.5 Torr and 60°C in a mixture containing He (60%), CH_3Cl (40%), mesitylene (0.04%). Duration of electron pulse 30 μs.

scheme for reaction [3] of the form

$$M + CH_3ClCH_3^+ \rightarrow (M \cdots CH_3ClCH_3)^+ \rightarrow$$

A

$$(MCH_3 \cdots ClCH_3)^+ \rightarrow MCH_3^+ + CH_3Cl$$

B

In order to pass from **A** to **B** the CH_3 group must invert, i.e. pass through a tight transition state complex whereas for the reaction to regenerate products the transition state is very loose. The latter has much more closely spaced energy levels and so although the overall reaction is exothermic, entropy considerations favour product regeneration. As the potential energy difference between reactants and products increases with increasing methyl substitution, presumably the level of the central potential energy maximum decreases relative to that of the reactants. Thus with increasing exothermicity, energetic factors overcome entropic factors and the relative rate of reaction increases. If this mechanism is correct the reaction rate constants should exhibit negative temperature coefficients. Unfortunately the necessary temperature studies cannot be performed with the present photoionization source due to the decrease in intensity of an already weak signal when the ion source temperature is raised above 298 K.

There is a similarity between the shape of the curve in Fig. 2 and similar plots for the reactions of NO_2^+ and $C_2H_5ONO_2NO_2^+$ with a series of aromatics (18). The threshold for reaction by these ions is attributed to an initial step which is thermoneutral electron transfer from the aromatic to the attacking electrophile. The major product under these conditions is the NO_2^+ adduct. With increasing exothermicity, i.e. decreasing ionization potential of the aromatic, charge transfer soon predominates to yield the aromatic ion as the major product. This does not appear to be the mechanism for $CH_3ClCH_3^+$ since (*a*) the relative rate constant for nitrobenzene is large, even though its ionization potential (9.9 eV (19)) is well above threshold and

Can. J. Chem. Downloaded from www.nrcresearchpress.com by 210.87.254.42 on 09/06/12
For personal use only.

(*b*) we see no evidence for the formation of aromatic molecular ions even with mesitylene and aniline for which charge transfer would be exothermic by ≥ 0.5 eV.

The slope of the curve in Fig. 2 is, as noted, similar to those for the reactions of NO_2^+ and $C_2H_5ONO_2NO_2^+$ (19). The measured absolute rate constants for these ions become equal to the rate constants for collision at an ionization potential of the neutral about 0.5 eV below the threshold for reaction. By analogy we propose that the plateau drawn in Fig. 2 also signifies reaction at every collision for mesitylene and aniline (and therefore also for nitrobenzene). In support of this suggestion, the relative rates of reaction and collision (calculated using the average dipole orientation theory (20), values in parentheses)) are mesitylene 1.0 (1.0), aniline 1.1 (1.0), and nitrobenzene 1.7 (1.7). The generalization of Speranza and Pepe (3) that $CH_3ClCH_3^+$ is a poor alkylating agent for aromatics in general is therefore not borne out, although the lack of significant reaction with benzene is confirmed. The dimethylchloronium ion is a selective methylating agent.

Acknowledgements

The authors thank D. E. Splinter for technical assistance. Financial support for this work was provided by the Natural Sciences and Engineering Research Council of Canada and by the Advisory Research Committee of Queen's University.

1. G. A. Olah. Halonium ions. Wiley Interscience, New York. 1975.
2. G. A. Olah, J. R. DeMember, Y. K. Mo, J. J. Svoboda, P. Schilling, and J. A. Olah. J. Am. Chem. Soc. **96**, 884 (1974).
3. M. Speranza and N. Pepe. J. Chem. Soc. Perkin II, 1179 (1979).
4. F. Hatch and M. S. B. Munson. J. Phys. Chem. **82**, 2362 (1978).
5. J. A. Stone and M. S. Lin. Can. J. Chem. **58**, 1666 (1980).
6. J. L. Beauchamp, D. Holtz, S. D. Woodgate, and S. L. Patt. J. Am. Chem. Soc. **94**, 2798 (1972).
7. L. W. Sieck and R. Gorden Jr. Int. J. Chem. Kinet. V, 445 (1973).
8. J. March. Advanced organic chemistry. 2nd ed. McGraw-Hill. 1977.
9. G. A. Olah. Acc. Chem. Res. **4**, 240, 1971.
10. D. V. Banthorpe. Chem. Rev. **70**, 295 (1970).
11. R. C. Dunbar, J. Shen, E. Melby, and G. A. Olah. J. Am. Chem. Soc. **95**, 7200 (1973).
12. D. A. Chatfield and M. M. Bursey. J. Am. Chem. Soc. **98**, 6492 (1976).
13. W. D. Reents and B. S. Freiser. J. Am. Chem. Soc. **102**, 271 (1980).
14. J. A. Stone and W. M. Splinter. To be published.
15. K. N. Hartman, S. Lias, P. Ausloos, H. M. Rosenstock, S. S. Schroyer, C. Schmidt, D. Martinsen, and G. W. A. Milne. Natl. Bur. Stand., Washington NBSIR-1777.
16. J. L. Devlin, J. F. Wolf, R. W. Taft, and W. J. Hehre. J. Am. Chem. Soc. **98**, 1990 (1976).
17. W. N. Olmstead and J. I. Brauman. J. Am. Chem. Soc. **99**, 4219 (1977).
18. P. Ausloos and S. G. Lias. Int. J. Chem. Kinet. **10**, 657 (1978).
19. H. M. Rosenstock, K. Draxl, B. Steiner, and J. Herron. J. Phys. Chem. Ref. Data, 6, Suppl. 1, 1977.
20. T. Su and M. T. Bowers. *In* Gas phase ion chemistry. Vol. 2. *Edited by* M. T. Bowers. Academic Press, New York. 1979.

Can. J. Chem. Downloaded from www.nrcresearchpress.com by 210.87.254.42 on 09/06/12
For personal use only.

A spectroscopic investigation of trimethyl- and triphenyl-arsine adducts of boron trihalides

JOHN E. DRAKE, LAYLA N. KHASROU, AND ABDUL MAJID

Department of Chemistry, University of Windsor, Windsor, Ont., Canada N9B 3P4

Received January 6, 1981

JOHN E. DRAKE, LAYLA N. KHASROU, and ABDUL MAJID. Can. J. Chem. **59**, 2417 (1981).

Trimethyl- and triphenyl-arsine adducts of the type $(CH_3)_3AsBX_3$ and $(C_6H_5)_3AsBX_3$, X = Cl, Br, I, have been prepared and characterised by infrared, Raman, ^1H and ^{13}C nmr spectroscopy. The vibrational assignments based on normal coordinate analysis are presented for the series $(CH_3)_3AsBX_3$. Potential energy distributions and modified Urey–Bradley potential parameters are reported.

JOHN E. DRAKE, LAYLA N. KHASROU et ABDUL MAJID. Can. J. Chem. **59**, 2417 (1981).

On a préparé les adduits triméthyl- et triphénylarsine du type $(CH_3)_3AsBX_3$ et $(C_6H_5)_3AsBx_3$ (X = Cl, Br, I) et on les a caractérisés par la spectroscopie infrarouge, Raman et rmn du ^1H et du ^{13}C. Dans le cas des séries $(CH_3)_3AsBX_3$, on a identifié les mouvements de vibration en se basant sur une analyse normale de coordonnées. On rapporte les distributions d'énergie potentielle et les paramètres de potentiel modifiés de Urey–Bradley.

[Traduit par le journal]

Introduction

Although numerous studies have been undertaken of amines as Lewis bases and the properties of phosphine–boranes have been investigated with the use of nmr spectroscopy (1–4), relatively little has been reported on the simple adducts of trimethylarsine and triphenylarsine with boron halides. A thorough vibrational analysis of $(CH_3)_3AsBH_3$ and $(CH_3)_3AsBD_3$ has been reported (5) as has the preparation of $(CH_3)_3AsBCl_3$ (6, 7) and the ^1H and ^{11}B nmr spectra of $(CH_3)_3AsBBr_3$ and $(CH_3)_3AsBI_3$ (8). There have also been gas phase calorimetric studies of tertiary phosphines, arsines, and stibines with boron trihalides (9) and a brief report on infrared and Raman spectra (10). We describe the ^1H and ^{13}C nmr, spectra of $(CH_3)_3AsBX_3$ and $(C_6H_5)_3AsBX_3$, X = Cl, Br, I as well as carrying out an analysis of their vibrational spectra. As this manuscript was being prepared, a vibrational analysis of the $(CH_3)_3AsBX_3$ series appeared in the literature (11). This work emphasized the assignments and calculations of the As—B stretch and related force constants. While in general their conclusions are in agreement, our assignments of the modes in the region below 800 cm^{-1} do differ in detail and as a result so do the values of the force constants.

Experimental

The adducts $(CH_3)_3AsBX_3$ were prepared under vacuum line conditions by the same method of molecular addition outlined previously (12). The formation of the $(C_6H_5)_3AsBX_3$ adducts was achieved under moisture-free conditions in a standard nitrogen glove box.

Trimethylarsine (Strem Chemicals), triphenylarsine (ROC/RIC), and the boron trihalides (ROC/RIC) were all commercially available.

The ^1H nmr spectra were recorded, using a high resolution JEOL C60-HL nmr, spectrometer operating at 60 MHz. The ^{13}C nmr spectra were recorded on a Bruker CXP 100 multinuclear pulsed Fourier transform spectrometer operating at 22.64 MHz at a probe temperature of 35°C, under ^1H noise decoupling conditions. Chemical shifts were calculated as parts per million from TMS as internal standard in CH_2Cl_2 and in the case of the ^{13}C nmr, CD_2Cl_2 was used as internal lock. The adducts are at best only slightly soluble in all solvents tried. Thus, for example the ^1H nmr peaks of the methyl groups in $(CH_3)_3AsBCl_3$ are not very much more intense than those of the proton impurity in the CD_2CL_2 solvent, and we could not possibly identify the positions of $\delta(C_x)$ in two cases, for $(C_6H_5)_3AsBX_3$ compounds.

Mid ir spectra were recorded on a Beckman IR-12 instrument and the far ir spectra were recorded, for solid compounds, as Nujol mulls between two polyethylene plates on a Perkin-Elmer 180 spectrometer operating in conjunction with an Interdata model 6/16 computer. Difference routines were used to subtract the Nujol and CH_2Cl_2 peaks. Raman spectra of the solid and of solutions in CH_2Cl_2 and CH_3I were recorded on a Spectra-Physics 700 spectrometer, using the argon line at 488.0 nm.

The normal coordinate analysis was performed using an IBM S/360-50 series computer with a program written by Dr. J. L. Hencher of this Department. The assignments of the fundamental vibrations were made assuming that the $(CH_3)_3AsBX_3$ molecules have C_{3v} symmetry.

All angles at carbon and boron were assumed to be tetrahedral. The other dimensions (C—H 109, C—As 195, As—B 203, B—Cl 184, B—Br 202, B—I 226 pm, and ∠CAsC 105.5, ∠AsBX 109.5 deg) were based on related molecules (13) such as $(CH_3)_3As$ (14) and $(CH_3)_3AsBH_3$ (5). A cross section of adducts was analyzed to confirm that they were 1:1 adducts.

Anal. calcd. for $(CH_3)_3AsBCl_3$: C 15.19, H 3.83, Cl 44.84; found C 15.15, H 3.57, Cl 40.01; calcd. for $(CH_3)_3AsBBr_3$: C 9.73, H 2.45, Br 64.70; found C 9.90, H 2.45, Br 64.83; calcd. for $(CH_3)_3AsBI_3$: C 7.04, H 1.77, I 74.43, found C 7.32, H 1.89, I 74.01; calcd. for $(C_6H_5)_3AsBCl_3$: C 51.06, H 3.57, Cl 25.12, found C 51.62, H 3.66, Cl 25.20.

All compounds are white or off-white and are moisture-sensitive solids.

0008-4042/81/152417-12$01.00/0

©1981 National Research Council of Canada/Conseil national de recherches du Canada

Can. J. Chem. Downloaded from www.nrcresearchpress.com by 210.87.254.105 on 09/06/12
For personal use only.

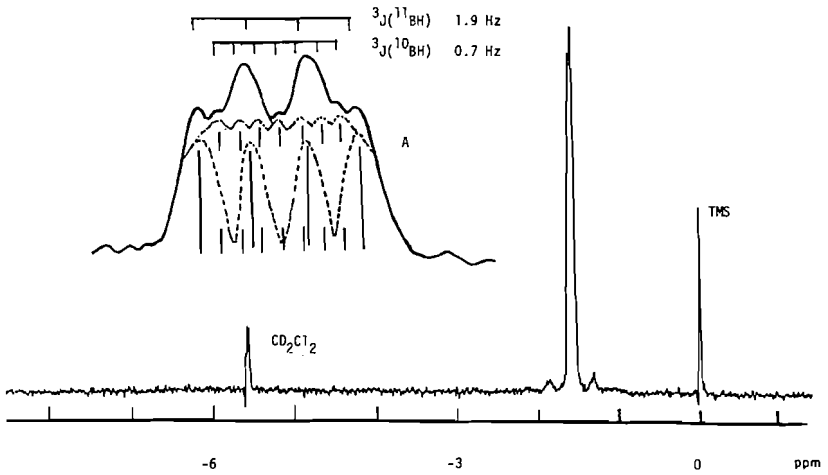

FIG. 1. ^1H nmr spectrum of $(CH_3)_3AsBCl_3$ in CD_2Cl_2 solution, referenced to TMS (A = high resolution and ^1H nmr schematic spectrum of $(CH_3)_3AsBCl_3$).

TABLE 1. ^1H and ^{13}C nmr chemical shifts[a] for $(CH_3)_3AsBX_3$ and $(C_6H_5)_3AsBX_3$, X = Cl, Br, I

Compound	$\delta^b(^1H)$	$\delta(^{13}C)$	$\delta(C_x)$	$\delta(C_m)$	$\delta(C_o)$	$\delta(C_p)$	$\sigma_R{}^{oc}$
$(CH_3)_3As$	0.94	10.56	—	—	—	—	—
$(CH_3)_3AsBCl_3$	1.51	4.42	—	—	—	—	—
$(CH_3)_3AsBBr_3$	1.60	4.78	—	—	—	—	—
$(CH_3)_3AsBI_3$	1.68	5.33	—	—	—	—	—
$(C_6H_5)_3As$	7.10	—	140.25	128.95	134.02	128.75	−0.090
$(C_6H_5)_3AsBCl_3$	7.65	—	135.90	129.34	134.02	130.0	0.029
$(C_6H_5)_3AsBBr_3$	7.70	—	n.o.	130.12	134.47	132.46	0.106
$(C_6H_5)_3AsBI_3$	7.75	—	n.o.	129.92	134.54	132.52	0.117

[a]All nmr spectra recorded in CD_2Cl_2 solution.
[b]δ in ppm downfield relative to internal TMS.
[c]δ_R" obtained from the relationship $\delta(C_p) - \delta(C_m) = -22.06$.

Results and Discussion

The ^1H Nuclear Magnetic Resonance Spectrum of $(CH_3)_3AsBCl_3$ is displayed in Fig. 1 and the ^1H and ^{13}C nmr chemical shifts for $(CH_3)_3AsBX_3$ and $(C_6H_5)_3AsBX_3$, X = Cl, Br, I, are listed in Table 1. The ^1H nmr signal of the methyl group in $(CH_3)_3As$ is broadened considerably on adduct formation as had been noted previously (10). However, under higher resolution these broad singlets appear as distorted quartets. These can be assigned as arising from the overlapping of a 1:1:1:1 quartet from coupling with the ^{11}B nucleus ($I = 3/2$; 81.2%) with a 1:1:1:1:1:1:1:1 septet from coupling with the ^{10}B nucleus ($I = 3$; 18.8%). If the value of $^3J(^{11}BH)$ is estimated as ca. 1.9 Hz from the positions of the two outermost peaks and then the value of $^3J(^{10}BH)$ is assumed to be ca. 0.7 Hz from the gyromagnetic ratios ^{11}B and ^{10}B, then a theoretical schematic spectrum can be sketched. Considering the broadening effect of the boron quadrupole, this fits the observed spectrum reasonably well (see Fig. 1). Similar long range BH coupling has been observed in amine adducts (4, 15). The values of the ^1H chemical shifts for these $(CH_3)_3AsBX_3$ species are very close to those in the corresponding $(CH_3)_3PBX_3$ (16).

By contrast the ^{13}C chemical shifts are closer to TMS for the $(CH_3)_3AsBX_3$ than the corresponding values in $(CH_3)_3PBX_3$ ($\delta(^{13}C$ for $(CH_3)_3PBCl_3$ 6.30, $(CH_3)_3PBBr_3$ 6.72, and $(CH_3)_3PBI_3$ 7.12 ppm). In fact, the shifts are very close to those of the methyl carbons in $(CH_3)_3GeCl$ (17). However, as with the ^1H shifts, there is a steady increase along the series $BCl_3 < BBr_3 < BI_3$ which is consistent with the concept of an increasing deshielding as the acidity of the boron halide increases. The same trend, to a slightly lesser degree, is seen for the $(C_6H_5)_3AsBX_3$ series.

In $(C_6H_5)_3As$, the ^{13}C chemical shifts are observed as four distinct signals for the *ortho* $\delta(C_o)$, *para* $\delta(C_p)$, *meta* $\delta(C_m)$ and substituted carbon atom $\delta(C_x)$. The latter signal is often not readily detected (18) and indeed is only identified for the BCl_3 adduct. The assignment of our ^{13}C spectrum of triphenylarsine is based largely on the previous results for the diphenylarsine (19). It has been

Can. J. Chem. Downloaded from www.nrcresearchpress.com by 210.87.254.105 on 09/06/12
For personal use only.

Can. J. Chem. Downloaded from www.nrcresearchpress.com by 210.87.254.105 on 09/06/12
For personal use only.

reported that substituent effects on the π-electron distribution in benzene derivatives can be related to the Hammett–Taft constants σ_R^0 (20) which can be calculated from $\delta_p(^{13}C) - \delta_m(^{13}C) = 22.06\ \sigma_R^0$ (18). The σ_R^0 value for Ph_2As was found to be −0.0099 while for Ph_3As it is −0.0090. This implies that the phenylarsenic π interactions are negligible and if occurring at all, indicate an electron release from arsenic towards the phenyl ring. By contrast, the significant positive values obtained for the adducts indicate that delocalization of π charge has occurred from the phenyl group to the vacant, low energy $3d_\pi$ orbitals of arsenic. The values obtained for Ph_3AsBX_3 are relatively similar to values obtained for $^+As(C_6H_5)_3I^-$ 0.149 (18). On formation of the adducts, arsenic would indeed be expected to become relatively more electropositive, thus allowing for the ($\pi \rightarrow d$) transitions to occur. The trend of increasing values of σ_R^0 along the series $BCl_3 < BBr_3 < BI_3$ is also consistent with their increase in Lewis acidity.

The infrared and Raman spectra of the $(CH_3)_3AsBX_3$ adducts are displayed in Figs. 2–4 to show features of the solid Raman, mid-infrared, and solution Raman spectra. Complete spectroscopic information, along with the calculated frequencies and assigned frequencies and potential energy distributions are given for $(CH_3)_3AsBCl_3$, $(CH_3)_3AsBBr_3$ and $(CH_3)_3AsBI_3$ in Tables 2–4 respectively. The conventional descriptions of the fundamental vibrations are presented in Table 5 and the derived force constants in Table 6. The methyl group stretching vibrations are observed in the same region as the free Lewis base (21). The three asymmetric CH_3 stretches, ν_1, ν_{16}, ν_{17}, are contained in a single envelope in the region 3000–2980 cm^{-1} in all three adducts. Both of the symmetric CH_3 stretches, ν_2 and ν_{18}, are assigned to the more intense, polarised Raman band at 2931, 2920, and 2923 cm^{-1} in the chloride, bromide, and iodide respectively. The intensity of these bands in the Raman is apparently greater than that reported by previous workers (11) (see Fig. 2) possibly because of a different excitation source (22). These CH_3 stretches are essentially pure modes, well described by fCH^2 which has a marginally higher value than in the free base, while the interaction constant fCH/CH, has a slightly lower value. The CH_3 asymmetric deformations, ν_3, ν_{19}, ν_{20}, lead to broad features in both effects and show minimal changes in frequency in all adducts, compared with free methylarsines such as $(CH_3)_3As$ (21), $(CH_3)_2AsH$ (23), and CH_3AsH_2 (24). The symmetric CH_3 deformations, ν_{21} and ν_4, show up as two peaks in all adducts, the splitting of the e and a_1 modes

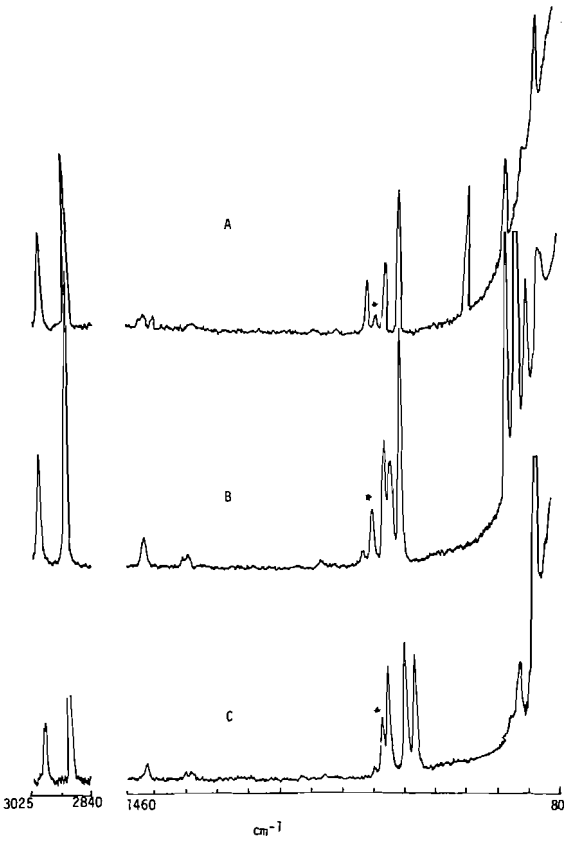

FIG. 2. The solid Raman spectrum of *A*, $(CH_3)_3AsBCl_3$; *B*, $(CH_3)_3AsBBr_3$; *C*, $(CH_3)_3AsBI_3$.

being also demonstrated in the calculations. Once again, the distribution of force constants $fHCH^2$, $fHCAs^2$, and $fHCAs/HCAs$ are virtually the same in all adducts, with slightly changing values for the latter two along the series. The values of fCH^2, fCH/CH and $fHCH^2$ are very similar to those used in the treatment of the $(CH_3)_3PBX_3$ adducts (25), those of $fHCAs^2$ are slightly lower, as might be expected, than those of $fHCP^2$, and the interaction constants $fHCAs/HCAs$ are again negative. The CH_3-rocking modes ν_{22}, ν_5, ν_{23} are assigned to the next three features, close to ca. 920, 850, and 800 cm^{-1} in all three adducts. The two stronger peaks in the infrared spectra, at ca. 920 and 800 cm^{-1}, which have corresponding weak depolarised Raman bands, are assigned to ν_{22} and ν_{23}, leaving ν_5 to be assigned to ca. 850 cm^{-1} (as can be seen in Figs. 2 and 3). Once again, the distribution of the force constants is essentially unchanged for all three adducts. The interaction term, *fcis*-HCAs/HCAs, which allows for the interaction of an HCAs angle on one methyl group with an HCAs angle on another methyl in the *cis*-position, is

Can. J. Chem. Downloaded from www.nrcresearchpress.com by 210.87.254.105 on 09/06/12
For personal use only.

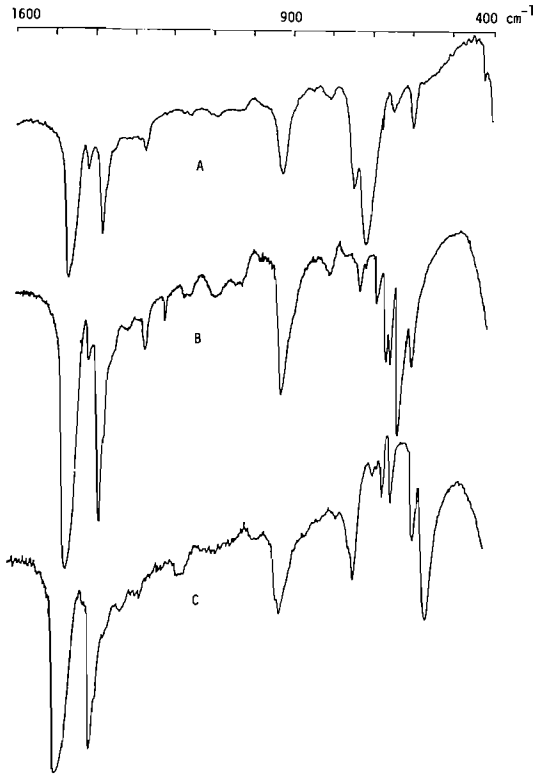

FIG. 3. Selected region of the infrared (Nujol mull) spectra of *A*, $(CH_3)_3AsBCl_3$; *B*, $(CH_3)_3AsBBr_3$; *C*, $(CH_3)_3AsBI_3$.

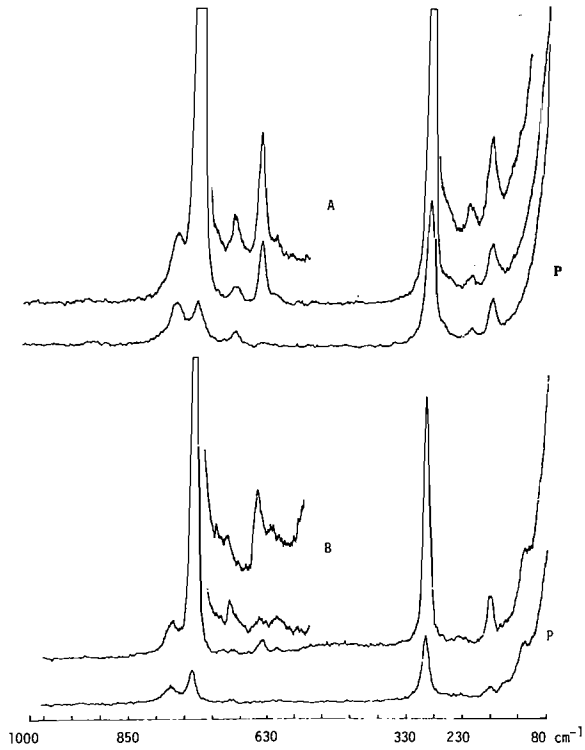

FIG. 4. Selected region of the solution Raman spectra of *A*, $(CH_3)_3AsBBr_3$; *B*, $(CH_3)_3AsBI_3$ in CH_2Cl_2.

needed to reproduce the splitting of these rocking modes. Thus, it is clear that the $(CH_3)_3As$ entity behaves very much as an isolated group being little effected by the change of halogen on boron. The AsC_3 stretching vibrations, ν_{24} and ν_7, are therefore expected to behave in a similar manner and indeed in all three adducts can be identified as depolarised, ν_{24}, and polarised, ν_7, bands in the regions 630–642 cm^{-1} and 578–598 cm^{-1} respectively, with corresponding bands in the infrared spectra (Fig. 3). These bands and their relative intensities are typical of the bands noted for $(CH_3)_3AsBH_3$ and $(CH_3)_3AsBD_3$ (5, 22) and by the previous workers (11). The shift to higher wavenumber is to be expected for a shortening of the As—C bond as was demonstrated for $(CH_3)_3AsBH_3$ (1.945 ± 0.01 Å) (5) relative to $(CH_3)_3As$ (1.959 ± 0.01 Å) (14). A high frequency shift was also observed for the quaternarization of $(CH_3)_3As$ to $(CH_3)_4As^+$ (26). The values in the latter case are very close to those observed for these $(CH_3)_3AsBX_3$ adducts, suggesting that the formation of the strong adducts with BX_3 has a similar effect on the As—C bond as does the quaternary salt. This is a clear indication that the re-arrangement of the CAsC angles is approaching tetrahedral as was illustrated for $(CH_3)_3AsBH_3$ (5). Our calculations, in contrast to those reported in the recently published paper (11) suggest that the value of $fCAs^2$ progressively increases from the free base to the chloride, then bromide, than iodide in accord with the expected increase in base strength. The AsC_3 asymmetric, ν_{26}, and symmetric, ν_9, deformation modes are assigned at ca. 225 cm^{-1} and 210 cm^{-1} in all adducts (Fig. 4) with the former, being weak and depolarised in the Raman effect and the latter stronger and polarised. The corresponding lines in the far-infrared spectra show up as medium intensity bands for the asymmetric mode with weak shoulders assignable as the symmetric AsC_3 deformations. Surprisingly, in view of the opening-up of the C—As—C angle, the value of $fCAsC^2$ is much lower than in the free arsine. Finally, for modes involving the $(CH_3)_3As$ group, the AsC_3 rocking mode, ν_{27}, is assigned to a weak, broad, depolarised band in the Raman at 170 cm^{-1} with a corresponding broad band in the far-infrared at ca. 172 cm^{-1}, in $(CH_3)_3AsBCl_3$. The band is slightly split, probably reflecting a loss of degeneracy. (The previous workers assigned this band as the symmetric, a_1, BCl_3 deformation mode but this is

Can. J. Chem. Downloaded from www.nrcresearchpress.com by 210.87.254.105 on 09/06/12
For personal use only.

TABLE 2. Observed ir and Raman frequencies (cm^{-1}), $\pm 3\,cm^{-1}$, for $(CH_3)_3AsBCl_3$, with potential energy distributions

Assignment		Infrared[a]	Raman[b]	Calcd.	P.E.D.[c]
$\nu_1, \nu_{16}, \nu_{17}$	CH_3 as. str.	(2980 w)	(2989 m)	2999	$100fCH^2 - 1fCH/CH$
ν_2, ν_{18}	CH_3 s. str.	(2925 w)	2930 m, p	2930	$98fCH^2 + 2fCH/CH$
$\nu_3, \nu_{19}, \nu_{20}$	CH_3 as. def.	1417 m	(1421 w)	1416	$79fHCH^2 + 13fHCAs/HCAs$
ν_{21}	CH_3 s. def.	(1290 m)	(1298 w, br)	1298	$43fHCH^2 + 63fHCAs^2 - 14fHCAs/HCAs$
ν_4		(1275 m)	(1270 vw)	1282	
ν_{22}	CH_3 rocks	923 m	923 w, dp	917	$85fHCAs^2 + 6fHCH^2$
ν_5		850 vw	(858 w)	866	
ν_{23}		800 w	(800 w)	798	$93fHCAs^2 + 5fHCH^2 - 10fC—HCAs/HCAs$
ν_{25} (^{10}B)	BCl_3 as. str.	(740 w)	745 w, dp	740	$60K_{BX} + 10H_{AsBX} + 7H_{XBX} - 1fCAs/CAs - 3fT—BX/C - As$
ν_{25}		(701 vs)	(700 m)	700	
ν_6	As—B str.	669 m, sh	670 w, p	672	$55K_{AsB} + 12K_{BX} + 10H_{AsBX}$
ν_{24}	C—As as. str.	641 ms	640 w, dp	632	$81fCAs^2 - 7fCAs/CAs + 4fT - BX/CAs$
ν_7	C—As s. str.	595 s	591 m, p	592	$62fCAs^2 + 11fCAs/CAs + 2fT—BX/CAs$
ν_8	BCl_3 s. str.	370 m	373 s, p	372	$34K_{BX} + 33F_{XX} + 10F_{AsX} + 2fT—BX/CAs$
ν_{28}	BCl_3 as. def.	255 m	256 w, dp	255	$23F_{XX} + 19fCAsC^2 + 16K_{BX} + 12H_{AsBX}$
ν_{26}	AsC_3 as. def.	229 m	225 w, dp	221	$58fCAsC^2 + 10H_{XBX} + 20F_{XX}$
ν_9	AsC_3 s. def.	210 w, sh	205 w, p	205	$22fCAsC^2 + 20fCAsB^2 + 13H_{AsBX} + 19F_{XX} + 10F_{AsX} - 5fCAsB/CAsB$
ν_{27}	AsC_3 rock	172 ms	170 m, dp	171	$25fCAsB^2 + 16fCAsC^2 + 10H_{AsBX} + 13H_{XBX} + 20F_{XX}$
ν_{10}	BCl_3 s. def.	160 vw	160 w	160	$28H_{AsBX} + 30fCAsC^2 + 11K_{AsB} + 15F_{AsX} - 6fAsBX/AsBX$
ν_{29}	BCl_3 rock	132 w	140 sh	140	$30H_{AsBX} + 17F_{AsX} + 40f_{CAsB^2} + 5fCAsB/CAsB$

[a]Spectrum recorded in Nujol; CsI spectra indicated in parentheses for regions masked or unclear in Nujol.
[b]Spectrum recorded in CH_2Cl_2 and CH_3I; solid spectra indicated in parentheses for regions masked by solvent peaks.
[c]Contribution greater than 10% except for significant interaction.

Can. J. Chem. Downloaded from www.nrcresearchpress.com by 210.87.254.105 on 09/06/12
For personal use only.

TABLE 3. Observed ir and Raman frequencies (cm^{-1}) for $(CH_3)_3AsBBr_3$[a] with potential energy distributions

Assignment		Infrared	Raman	Calcd.	P.E.D.
$\nu_1, \nu_{16}, \nu_{17}$	CH_3 as. str.	(2980 w)	(2987 m)	2994	$100fCH^2 - 1fCH/CH$
ν_2, ν_{18}	CH_3 s. str.	(2920 w)	2920 w, p	2923	$98fCH^2 + 2fCH/CH$
$\nu_3, \nu_{19}, \nu_{20}$	CH_3 as. def.	1409 m	(1411 m)	1409	$79fHCH^2 + 13fHCAs/HCAs$
ν_{21}	CH_3 s. def.	(1300 w)	(1287 m)	1290	$42fHCH^2 + 62fHCAs^2 - 13fHCAs/HCAs$
ν_4		(1265 m)	(1271 m)	1280	
ν_{22}	CH_3 rocks	915 s	920 w, dp	915	$85fHCAs^2 + 6fHCH^2$
ν_5		860 sh	(843 w)	859	
ν_{23}		800 m	(800 w)	790	$93fHCAs^2 + 5fHCH^2 - 10fC—HCAs/HCAs$
				782	
$\nu_{6(^{10}B)}$		680 mw, sh	(700 w)	678	$52K_{AsB} + 13fAsC^2 + 7fHCAs^2$
ν_6	As—B str.	655 m	660 w, p	659	
ν_{24}	C—As as. str.	636 m	636 m, dp	630	$72fCAs^2 + 10fCAsC^2 - 8fCAs/CAs$
ν_{25}	BBr_3 as. str.	618 vs	610 w, dp	618	$45K_{BX} + 18fCAsB^2 + 18fCAs^2 + 5F_{XX} - 2fCAs/CAs + 2fCAsB/CAsB$
ν_7	C—As s. str.	587 m	583 s, p	585	$54fCAs^2 + 13K_{AsB} + 11fCAs/CAs$
ν_8	BBr_3 s. st.	245 s	245 m, p	245	$25K_{BX} + 10fCAsB^2 + 45F_{XX} + 7K_{AsB} - 5fCAsB/CAsB$
ν_{26}	AsC_3 as. def.	(227 w)	(225 w, sh)	220	$85fCAsC^2 + 5fCAs^2$
ν_9	AsC_3 s. def.	209 mw	214 mw, p	210	$30fCAsC^2 + 31fCAsB^2 + 12K_{BX} + 17F_{AsX} - 14fCAsB/CAsB$
ν_{28}	BBr_3 as. def.	183 m	178 m, dp	180	$66F_{XX} + 22H_{XBX}$
ν_{27}	AsC_3 rock	145 m	139 w, dp	145	$45fCAsB^2 + 22K_{BX} + 12fCAsB/CAsB$
ν_{10}	BBr_3 s. def.	130 w	124 w, sh	122	$24fCAsB^2 + 23fCAsC^2 + 12K_{AsB} + 13F_{XX} + 17F_{AsX} - 12fCAsB/CAsB$
ν_{29}	BBr_3 rock	94 m	(90 w)	90	$40K_{AsBX} + 39F_{AsX}$

[a]See footnotes to Table 2.

Can. J. Chem. Downloaded from www.nrcresearchpress.com by 210.87.254.105 on 09/06/12
For personal use only.

unlikely in view of the depolarisation (Fig. 4). Similar comments apply to their assignments in the other adducts.) The AsC_3 rock is seen, with similar features in the two effects, at around 140 cm^{-1} in the bromide and 110 cm^{-1} in the iodide. The AsC_3 rock involves a number of force constants, as might be expected, principally fCAsB^2. In other words, it might be better considered as arising from CAsB angle bending.

The BX_3 asymmetric mode, ν_{25}, is typically a strong, distinctive band in the infrared spectrum with a corresponding medium intensity, depolarised band in the Raman spectrum. It can be identified at 700 cm^{-1} in the chloride, 615 cm^{-1} in the bromide, and 548 cm^{-1} in the iodide. The values of K_{BX} are similar in value to those in the $(CH_3)_3PBX_3$ series (25) as is to be expected, because the peaks are actually seen at 712, 621, and 556 cm^{-1} within that series. Thus, the same trend of a weakening of the BX bond as the boron adopts an "sp^3" rather than "sp^2" configuration is observed. We had previously noted, in the spectra of the $(CH_3)_3PBX_3$ series, that this mode was one of two for which the calculations predicted and the spectra showed a weaker feature to higher wave-numbers corresponding to the $^{10}BX_3$ asymmetric stretch. In the chloride this is seen as a depolarised band at 745 cm^{-1} but in the bromide it is masked by the AsC_3 asymmetric stretch and in the iodide by the AsC_3 symmetric stretch. The assignment of the BX_3 symmetric stretch, ν_8, is probably one of the easiest because this appears as an intense polarised band in the Raman at 373, 245, and 172 cm^{-1} in the three adducts as expected at the slightly lower wave-number than that observed in $(CH_3)_3PBX_3$ (25). It is interesting to note the increasing dependence of this motion on the force constant F_{XX}, the Urey–Bradley nonbonded repulsion constants (27) along the series Cl < Br < I. The BX_3 deformations, ν_{28} and ν_{10} show the usual general trend in their frequencies with decreasing values along the adduct series, as indicated in the far-infrared spectra of the trichloride, tribromide, and triiodide adducts with 255, 160; 180, 130 and 117, 95 cm^{-1} respectively. The corresponding peaks in the Raman for the asymmetric mode are depolarised but the peaks corresponding to the symmetric mode are weak and too close to the exciting line to give clear polarisation data. However, once again there is an obvious increasing dependence on F_{XX}, particularly for the asymmetric mode, from Cl< Br < I, while for the symmetric mode, H_{AsBX} makes a significant contribution. Finally, for the BX_3 group, the BX_3 rock is assigned in all adducts to the lowest frequency fundamental at 132, 94, and 80 cm^{-1}

TABLE 4. Observed ir and Raman frequencies (cm^{-1}) ± 3 cm^{-1}, for $(CH_3)_3AsBI_3$, with potential energy distribution[a]

Assignment		Infrared	Raman	Calcd.	P.E.D.
$\nu_1, \nu_{16}, \nu_{17}$	CH_3 as. str.	(3000 m)	(2987 m)	2990	$100fCH^2 - 1fCH/CH$
ν_2, ν_{18}	CH_3 s. str.	(2910 w)	2923 s, p	2915	$98fCH^2 + 2fCH/CH$
$\nu_3, \nu_{19}, \nu_{20}$	CH_3 as. def.		(1403 m)	1405	$79fHCH^2 + 12fHCAs/HCAs$
ν_{21}		(1285 sh)	1270 w	1285	$42fHCH^2 + 61fHCAs^2 - 13fHCAs/HCAs$
ν_4	CH_3 s. def.	(1270 m)	1260 m	1279	
ν_{22}		910 s	920 w, dp	914	$85fHCAs^2 + 6fHCH^2$
ν_5	CH_3 rocks	850 w	(842 w)	850	
ν_{23}		780 w	(767 w)	790	$93fHCAs^2 + 6fHCH^2 - 11fC—HCAS/HCAs$
ν_6 (^{10}B)	As—B str.	(683 sh)	(695 w, sh)	682	$49K_{AsB} + 22fAsC^2 + 10fHCAs$
ν_6		656 m	651 m, p	651	
ν_{24}	C—As as. st.	632 m	630 m, dp	629	$79fCAs^2 + 13fHCAs^2 - 8fCAs/CAs$
ν_7	C—As. s. st.	580 s	578 m, p	580	$46fCAs^2 + 30K_{AsB} + 9fCAs/CAs$
ν_{25}	BI_3 as. st.	542 vs	548 m, dp	546	$49K_{BX} + 20fCAsB^2 + 10fCAs^2 + 5fAsBX/AsBX$
ν_{26}	AsC_3 as. def.	220 m	(220 sh)	220	$89fCAsC^2$
ν_9	AsC_3 s. def.	—	209m, p	208	$39fCAsC^2 + 50fCAsB^2 - 15fCAsB/CAsB$
ν_8	BI_3 s. st.	170 s	172 m, p	172	$26K_{BX} + 60F_{XX} - 2fCAsB/CAsB$
ν_{28}	BI_3 as. def.	117 m	108 w, dp	118	$82F_{XX} + 11H_{XBX}$
ν_{27}	AsC_3 rock	110 w	100 w, sh, dp	110	$48fCAsB^2 + 30K_{BX} + 7fCAsB/CAsB$
ν_{10}	BI_3 s. def.	95 vw	95 w	95	$13H_{AsBX} + 13H_{XBX} + 42F_{XX} + 35F_{AsX} - 17fAsBx/AsBX$
ν_{29}	BI_3 rock	80 m	80 vw	80	$24H_{AsBX} + 40F_{AsX} + 16fAsBX/AsBX$

[a]See footnotes to Table 2.

Can. J. Chem. Downloaded from www.nrcresearchpress.com by 210.87.254.105 on 09/06/12
For personal use only.

TABLE 5. Approximate descriptions and symmetry species of the fundamental vibrations of $(CH_3)_3AsBX_3$ (X = Cl, Br, I)[a]

A_1	A_2	E	Description
ν_1	ν_{11}	ν_{16}, ν_{17}	CH_3 stretch (asym)
ν_2		ν_{18}	CH_3 stretch (sym)
ν_3	ν_{12}	ν_{19}, ν_{20}	CH_3 def. (asym)
ν_4		ν_{21}	CH_3 def. (sym)
ν_5	ν_{13}	ν_{22}, ν_{23}	CH_3 rock
ν_7		ν_{24}	C—As stretch
ν_9		ν_{26}	AsC_3 def.
ν_6			As—B stretch
ν_8		ν_{25}	BX_3 stretch
		ν_{27}	AsC_3 rock
ν_{10}		ν_{28}	BX_3 def.
		ν_{29}	BX_3 rock
	ν_{14}	ν_{30}	CH_3 torsion
	ν_{15}		Frame torsion

[a]The 45 fundamentals are distributed, in C_{3v} symmetry, as $10A_1 + 5A_2 + 15E$; the A_1 and E modes being active in both ir and Raman and the A_2 modes inactive.

where once again their positions are very close to those observed in $(CH_3)_3PBX_3$.

The only fundamental remaining to be assigned is thus the As—B stretch, ν_6. As is typical of many boron adducts, this is not only the mode of most interest but also the hardest to assign with reasonable certainty. However, in all three adducts, there is indeed one feature remaining, which is polarised in the Raman effect and which is seen with reasonable clarity in the infrared. Because of its central importance this mode is marked with an asterisk in Fig. 2. Thus, the assignment to the As—^{11}B stretch, ν_6, is at 670, 660, and 651 cm^{-1} respectively in the chloride, bromide, and iodide, In the spectrum of $(CH_3)_3AsBCl_3$, previous workers (11) placed ν_6 as coincident with the BCl_3 asymmetric stretch at ca. 701 cm^{-1}, but the relative intensity of the band at 670 cm^{-1} and the fact that it is polarised make our assignment acceptable. As we had noted in the case of the $(CH_3)_3PBX_3$ adducts (25), this mode is one in which the calculations predict and one can normally detect a sufficient difference between the As—^{10}B and As—^{11}B stretches and the additional low-intensity peak can be seen clearly in the bromide and iodide and is presumably masked by ν_{25} in the chloride. This splitting has subsequently been confirmed (11). The same trend of slightly decreasing wave-number along the series $BCl_3 > BBr_3 > BI_3$ was also seen in the phospine adducts. However, as can be seen from the calculations, this does not indicate a weakening of the As—B bond. On the contrary, the value of K_{AsB} increases steadily in accord with the increasing acidity of the BX_3 group with $BCl_3 < BBr_3 < BI_3$. The values are about 15% lower than that found for K_{PB} in each case and change by some 18% from the chloride to iodide. This seems a more reasonable degree of change than the 40% claimed by others (11).

The infrared and Raman spectra of the $(C_6H_5)_3AsBX_3$ adducts in the region below 1600 cm^{-1} are summarized in Table 7, together with the suggested assignments. The investigation of the spectra of the trimethylarsine adducts provided a general background to the assignment and comparisons were also made with the reported assignments of some substituted benzenes (28–31), phenylarsines (26, 32), and phenylphosphine (33). The vibrations associated with the phenyl ring can be classified in accord with Hertzberg's notation (34). The high frequency region of the spectra (above 1600 cm^{-1}) can be satisfactorily correlated with the corresponding benzene vibrations (35, 36). These vibrations are expected to be substituent-insensitive ν(C—H) vibrations, while the six substituent-sensitive modes, Whiffen's (29) q, r, t, y, u, and x (X-sensitive, see Table 7) are all expected to be below 1600 cm^{-1}.

The l, k, ν(C—C) stretches are known to appear near 1600 cm^{-1} and are seen as one strong Raman line at 1573 cm^{-1} in $(C_6H_5)_3As$. This band is virtually unchanged in the adducts appearing at 1575, 1570, and 1575 cm^{-1} in the chloride, bromide, and iodide respectively. The other ν(C—C) bands, m, n, o, are present as a strong infrared absorption in the region just below the l, k frequencies, again essentially unchanged in the free arsine and the adducts. The in-plane C—H deformations (B) are almost unchanged from those of monohalosubstituted benzenes (29). The extremely strong polarised Raman band at 997 in $(C_6H_5)_3As$ and 999, 991, and 995 cm^{-1} in the BCl_3, BBr_3, and BI_3 adducts respectively, arises from ring breathing modes in which a substituent is not involved. The lowest of the out-of-plane C—H deformations f, γ(C—H) at 738 cm^{-1} in $(C_6H_5)_3As$ and at 735, 732, and 750 cm^{-1} in the adduct series are known to give very strong infrared absorptions, while the g, i, h, j, γ(C—H) deformations are indicated by medium or weak intensity bands in both the ir and Raman effects. This corresponds to what was found in $(C_6H_5)_2AsX_2$, X = Cl, Br (32). The out-of-plane ring deformation ϕ(C—C) is seen as a very strong infrared absorption 695, 685, and 700 cm^{-1} in the adducts, in agreement with the observed and calculated values of 698 cm^{-1} for benzene and deuterated benzene (35). The in-plane ring deformation, α(C—C—C), is seen in the Raman spectra at 617, 618, and 610 cm^{-1} in the $(C_6H_5)_3AsBX_3$ adducts in agreement with all substituted benzenes and $(C_6H_5)_3As$. Thus, for halosubstituted benzenes there is a clear trend to lower wave-number

TABLE 6. Modified Urey–Bradley force fields for $(CH_3)_3AsBX_3$

	Force constant[c]	Value			
		X = Cl	X = Br	X = I	$(CH_3)_3As$[a]
1	fCH[2b]	4.800	4.790	4.790	4.77
2	fHCH[2]	0.437	0.435	0.435	0.53
3	fHCAs[2]	0.590	0.584	0.573	0.51
4	fCAsC[2]	0.665	0.676	0.68	0.99
5	fCAsB[2]	0.654	0.694	0.714	
6	fCAs[2]	2.692	2.733	2.855	2.56
7	K_{BX}	1.330	1.102	0.789	
8	K_{AsB}	1.523	1.652	1.855	
9	H_{AsBX}	0.655	0.411	0.278[d]	
10	H_{XBX}	0.338[d]	0.399[d]	0.256[d]	
11	F_{XX}	0.53	0.55	0.58	
12	F_{AsX}	0.25	0.23	0.18	
13	fCH/CH	0.045	0.045	0.045	0.05
14	fCAs/CAs	0.266	0.285	0.300	—
15	fBX/BX	0.01	0.01	0.00	
16	fT—BX/CAs[c]	−0.10[d]	—	—	
17	fHCAs/HCAs	−0.157	−0.127	−0.106	−0.05
18	fCAsB/CAsB	−0.055	−0.079	−0.045	
19	fAsBX/AsBX	−0.748	−0.123	−0.193	
20	fCAsC/CAsC	0.038	0.076	0.152	0.18
21	fC—HCAs/HCAs[c]	0.040	0.045	0.050	—

[a]Reference 5, the bending force constant are divided by 1 Å.
[b]General valence force constant f_{ij}; Urey–Bradley force constants K (stretch); H (bend); F (repulsions).
[c]This interaction is between CAs and BX trans to each other. While fC—HCAs/HCAs is the interaction of HCAs *cis* to HCAs angle on other carbon atom.
[d]Given fixed value in the least-squares analysis.
[e]Stretching constant in mdyn Å^{-1} (10^2 N m^{-1}), bending in mdyn Å rad^{-2} (10^2 N m rad^{-2}); and stretch/bend interaction constant in mdyn rad^{-1}.

for these frequencies along the series F > Cl > Br > I. The values do not change from $(C_6H_5)_3As$ to the various adducts, but in all cases (X-sensitive) are close to the values found for bromo substitution (29). The X-sensitive bands in phenylphosphine (33) are similarly close to those in chloro-substituted benzene (29). Thus, the relationship of the position of the X-sensitive bands to the mass of the atom joined to the ring is reinforced.

In the region of the C—As stretching frequencies coupling is to be expected between the C—As vibration and the mass sensitive vibrations of the phenyl group. Thus, the q, r, and t, X-sensitive modes are normally assumed to be those most closely corresponding to C—X stretches (29). In a study of phenylarsenic(III) halides, it was suggested that the strongest coupling occurs with the t vibrations (37). Similar conclusions have been reached for other arsenic compounds (38) and have been shown to be valid for a variety of phenylsilanes (19) and germanes (39), which are supported by calculation (40). The C—As stretches in trimethylarsine adducts with BX_3 are assigned in the regions of ca. 635 and 585 cm^{-1}, while the polarised q, r, and t lines in $(C_6H_5)_3AsBX_3$ (where X = Cl, Br, I) adducts are placed at 1082, 1088, 1080 cm^{-1}; 660, 655, 650? cm^{-1}; and 300, 292, 305 cm^{-1}. The skeletal region also contains low frequency ring modes and it is the most difficult region in the spectrum to assign.

Modes involving compression or bending of the C_3As bonds and the low lying X-sensitive ring vibrations are expected to be mixed with the BX_3 vibrations, especially the BCl_3 vibrational activity. By selecting the BX_3 mode by comparison with the corresponding modes in $(CH_3)_3AsBX_3$ and other related adducts (25) we are able to distinguish tentatively the low-lying X-sensitive vibrations in the skeletal region from those of the BX_3 groups.

The selection is rather difficult because the BX_3 modes are always associated with phenyl vibrations. Thus, for example, the out-of-plane α(C—C—C) deformation is expected to occur close to the asymmetric, ν_{as}(B—Br) vibration in $(C_6H_5)_3AsBBr_3$ so that a broad feature would not be surprising and is indeed seen. The ν_{as}(B—Cl) stretching mode is, however, one which can be seen clearly and is assigned to the band of medium intensity in the infrared at 722 cm^{-1}. This is consistent with the assignment of ν_{as}(B—Cl) to 720 cm^{-1} in $(CH_3)_3AsBCl_3$. Accordingly, the frequency at 370 cm^{-1} in the Raman spectrum of the triphenylarsine chloride adduct is assigned to the ν_s(B—Cl) stretching mode, while ν_s(B—Br), ν_s(B—I) are assigned to 228 and 153 cm^{-1} where a very strong Raman band is seen in the solid spectrum of

Can. J. Chem. Downloaded from www.nrcresearchpress.com by 210.87.254.105 on 09/06/12
For personal use only.

Can. J. Chem. Downloaded from www.nrcresearchpress.com by 210.87.254.105 on 09/06/12
For personal use only.

TABLE 7. The vibration spectra below[c] 1600 cm^{-1} of the triphenylarsine adducts $(C_6H_5)_3AsBX_3$, X = Cl, Br, I

$(C_6H_5)_3AsBCl_3$		$(C_6H_5)_3AsBBr_3$		$(C_6H_5)_3AsBI_3$		
Infrared[a]	Raman[b]	Infrared[a]	Raman[b]	Infrared[d]	Raman[b]	Assignment
1580 mw	1575 s, dp	1575 w	1570 s, dp	1585, 1570 ms	1575 s, dp	*l*, *k*, ν(C—C)
1480 m, sh	1473 w, p	1475 sh	1472 vw	1470 s	1470 vw	*m*, ν(C—C)
1430 m, sh	1430 vw?	1430 sh	1429 w, dp	1450 mw, sh; 1435 m	1430 w, sh?	*n*, ν(C—C)
1380 sh	1375 vw	1380 vw	—	1381 mw	1380 vw	*w* + *i*
1335, 1310 w	1330 w	1330 mw 1305 mw	1328 mw 1300 vw	1335 m 1308 s	1330 mw 1278 mw	*o*, ν(C—C)
1265 mw, br	1260 w	1255 m	1250 w	1275 m 1262 m	1250 mw	*e*, β(C—H)
1220 vw				1200 vw, sh	—	
1180 m 1158 mw	1170 mw 1155 mw dp	1179 mw 1155 w	1164 1154 dp	1181 s 1157 ms	1165 1152 dp	*a*, β(C—H) *c*, β(C—H)
1080 m	1082 mw, p	1080 sh 1075 ms	1094 sh 1088 m, p	1072 vs	1080 mw, p	*q*, X-sens.
1075 w, sh 1065 m	1060 w, sh, p	1065 w	1056 w, sh	1065 sh	1050 w, p	*d*, β(C—H)
1023 s	1020 m, p	1018 ms	1017 m, p	1022 s	1015 mw, p	*b*, β(C—H)
999 s	999 s, p	991 m	994 vs, p	999 s	995 ms, p	*p*, ring
978 w	975 w, sh	970 vw	970 w, sh	971 mw	970 w, sh	*j*, γ(C—H)
950 vw	945 w, sh	950 vw	944 w, sh	950 mw	951 w, sh	*h*, γ(C—H)
925 vw	924 vw?	920 vw	923 vw, dp	920 m	920 w, dp	*i*, γ(C—H)
849 w	830 w	842 vw	852 mw	839 m	—	*g*, γ(C—H)
805 w	806 sh	810, 800 m, br	822 mw 804 sh	802 m, br	—	
790 vw	—	795 vw	—	—	790 vw	*x* + *s*
765, 735 m, sh; ms	730 w, p	732 m	753, 729 vw, p	750 vs, br	750 w, p	*f*, γ(C—H)
722 m	719 w, dp	—	—	—	—	ν_{as}(B—Cl)
695 ms	678 m	685 ms	674 m	700 vs, br	678 mw	*v*, ϕ(C—C)
675, 665 m	660 w, sh 640 m?	655 m 625 m	651 w 639, 623 mw	670 w, sh 640 w, sh	650 mw 630 mw	*r*, X-sens. + ν(As—B)
642 615 vw	614 m, dp	612, 600 sh	618 m, dp	611, 587 m, sh; s	610 mw, dp	*s*, α(C—C—C)
545 s[d]	—	—	543 vw	560 s	—	+ν_{as}(B—Br)
—	—	—	—	550 s	550 vw	ν_{as}(B—I)
462 s	460 w	463 ms[c]	468 w	455 ms	—	*y*, X-sens.
415 w[d]	412 vw	410 vw[c]	409 vw	405 m	—	*w*, ϕ(C—C)
395 vw	—	390 vw[c]	391 vw	390 vw, br	—	
374 m[c] 350 mw, sh	370 m	—	—	—	—	ν_s(B—Cl)

Can. J. Chem. Downloaded from www.nrcresearchpress.com by 210.87.254.105 on 09/06/12
For personal use only.

TABLE 7. (*Concluded*)

$(C_6H_5)_3AsBCl_3$		$(C_6H_5)_3AsBBr_3$		$(C_6H_5)_3AsBI_3$		Assignment
Infrared[a]	Raman[b]	Infrared[a]	Raman[b]	Infrared[d]	Raman[b]	
—	—	343 m[c]	356 m	332 m		
325 ms[c]	320 w, dp	311 m[c]	292 vw, dp	309 m	305 w, dp	*t*, X-sens.
270 mw	260 vw	250 vw[c]	266 vw	270 vw	270 w	
245 w[c]	250 w, dp	265 vw	253 m, sh, dp	250 vw	—	*u*, X-sens. + (BCl_3 def.)
	—	230 vw	228 vs	—	—	ν_s(B—Br)
225 w	218 w, sh?	208 mw	210 m, sh, dp	210 m	212 m, sh, dp	*x*, X-sens.
180 w	180 w	180 w	183 m, p	200 vw[c]	—	
170 vw	170 w	160	153 ms, p	160[c]	160 m	ν_s(B—I) + (BBr_3, BI_3 def.)
		150 m, br		132 mw	146 w, sh	
		140		—	123 w	
			132 w		100 vw, sh	BX_3 rock.
			125 w	111 w		
135 w	140 w, sh	100 w	100	90[c]	90	

[a] Nujol ir.
[b] Spectra taken from both Raman solid and solution in CH_2Cl_2 or CH_3I.
[c] far infrared spectra.
[d] CsI pellet.
[e] Other substituent-insensitive phenyl modes are observed above 1600 cm^{-1}, *z*, ν(C—H), 3070 ms, *p*; 3050 s, p in the infrared and Raman.

$(C_6H_5)_3AsBBr_3$ and $(C_6H_5)_3AsBI_3$ respectively. The region below 300 cm^{-1} also contains absorptions due to vibrations arising from skeletal $(C_6H_5)_3As$ deformations, in particular the *u* and *x* species. Tentative assignments of the BX_3 deformation modes are shown in Table 7. That the assignments can be made on the assumption that the BX_3 bands are essentially in the same positions in the triphenyl series as in the trimethyl suggests a similarity in the B—X bond strengths. However, given the uncertainty inherent in these assignments, this is perhaps a circular argument.

No features that could be definitely assigned to an isolated As—B frequency are observed in the $(C_6H_5)_3AsBX_3$ adducts, but a medium broad band in the Raman with a maximum at 640 cm^{-1} in $(C_6H_5)_3AsBCl_3$, 639 cm^{-1} in $(C_6H_5)_3AsBBr_3$ and 630 cm^{-1} in $(C_6H_5)_3AsBI_3$ can be reasonably assigned to the As—B stretching frequency. Because of the uncertainty in the polarisation data and broad nature of these bands, the assignment cannot be more than tentative. The presence of *r*, X-sensitive $(C_6H_5)_3As$ vibrations in this region further complicates the spectra and decreases the certainty of assignment. If correct, however, they do imply only a slight decrease from the assignment in the $(CH_3)_3AsBX_3$ adducts.

Acknowledgement

We wish to thank the Natural Sciences and Engineering Research Council of Canada for financial support.

1. A. H. COWLEY and M. C. DAMASCO. J. Am. Chem. Soc. **93**, 6815 (1971).
2. R. W. RUDOLPH and C. W. SHULTZ. J. Am. Chem. Soc. **93**, 6821 (1971).
3. D. E. YOUNG, G. E. MCACHRAN, and S. G. SHORE. J. Am. Chem. Soc. **88**, 4390 (1966).
4. C. W. HEITSCH. Inorg. Chem. **4**, 1019 (1965).
5. J. R. DURIG, B. A. HUDGENS, and J. D. ODOM. Inorg. Chem. **13**, 2306 (1974).
6. F. HEWITT and A. K. HOLLIDAY. J. Chem. Soc. 530 (1953).
7. G. M. PHILLIPS, J. S. HUNTER, and L. E. SUTTON. J. Chem. Soc. 146 (1945).
8. M. L. DENNISTON and D. R. MARTIN. J. Inorg. Nucl. Chem. **36**, 2175 (1974).
9. D. C. MENTE, J. L. MILLS, and R. E. MITCHELL. Inorg. Chem. **14**, 123 (1975).
10. D. C. MENTE and J. L. MILLS. Inorg. Chem. **14**, 1862 (1975).
11. Y. GUSHIKEM and F. WATARI. J. Chem. Soc. Dalton, **10**, 2016 (1980).
12. J. E. DRAKE, J. L. HENCHER and B. RAPP. J. Chem. Soc. Dalton, 595 (1974).
13. Tables of interatomic distances and configuration in molecules and ions. Special Publications II, and 18. The Chemical Society, London, 1958 and 1965.

14. D. R. LIDE. Spectrochim. Acta, **15**, 473 (1959).
15. O. OHASHI, Y. KURITA, T. TOTANI, H. WATANABE, T. NAKAGAWA, and M. KUBO. Bull. Chem. Soc. Jpn. **35**, 1317 (1962).
16. M. L. DENNISTON and D. R. MARTIN. J. Inorg. Nucl. Chem. **36**, 1461 (1974).
17. J. E. DRAKE, B. M. GLAVINČEVSKI, R. E. HUMPHRIES, and A. MAJID. Can. J. Chem. **57**, 1426 (1979).
18. L. F. WUYTS, D. F. VEN DE VONDEL, and G. P. VAN DER KELEN. J. Organomet. Chem. **129**, 163 (1977).
19. A. L. SMITH. Spectrochim. Acta, **24**A, 695 (1968).
20. R. W. TAFT, JR., S. EHRENSON, I. C. LEWIS, and R. E. GLICK. J. Am. Chem. Soc. **81**, 5352 (1959).
21. G. BOUQUET and M. BIGORGNE. Spectrochim. Acta, **23**A, 1231 (1967); E. G. CLAEYS and G. P. VAN DER KELEN. Spectrochim. Acta, **22**A, 2095 (1966); P. J. D. PARK and P. J. HENDRA. Spectrochim. Acta, **24**A, 2081 (1968).
22. F. WATARI. Bull. Chem. Soc. Jpn. **50**, 1287 (1977).
23. A. J. F. CLARK, J. E. DRAKE, and Q. SHEN. Spectrochim. Acta, **34**A, 311 (1978).
24. A. B. HARVEY and M. K. WILSON. J. Chem. Phys. **44**, 3535 (1966).
25. J. E. DRAKE, J. L. HENCHER, and B. RAPP. Inorg. Chem. **16**, 2289 (1977).
26. W. R. CULLEN, G. B. DEACON, and J. H. S. GREEN. Can. J. Chem. **43**, 3193 (1965); W. R. CULLEN, G. B. DEACON, and J. H. S. GREEN. Can. J. Chem. **44**, 717 (1966).
27. T. SHIMANOUCHI. Physical chemistry, an advanced treatise. Vol. IV. *Edited by* D. Henderson. Academic Press, New York. NY. 1970. p. 233.
28. A. M. NORTH, R. A. PETHRICK, and A. D. WILSON. Spectrochim. Acta, **30**A, 1317 (1974).
29. D. H. WHIFFEN. J. Chem. Soc. 1350 (1956).
30. S. HIGUCHI, H. TSUYAMA, S. TANAKA, and H. KAMADA. Spectrochim. Acta, **30**A, 463 (1974).
31. C. V. STEPHENSON, W. C. COBURN, JR., and W. S. WILCOX. Spectrochim. Acta, **17**, 933 (1961).
32. D. M. REVITT and D. B. SOWERBY. Spectrochim. Acta, **26**A, 1581 (1970).
33. J. H. S. GREEN and W. KYNASTON. Spectrochim. Acta, **25**A, 1677 (1969).
34. G. HERZBERG. Molecular spectra and molecular structure. Vol. II. Van Nostrand, Princeton, NJ. 1968. pp. 118, 491.
35. N. HERZFIELD, C. K. INGOLD, and H. G. POOLE. J. Chem. Soc. 222 (1946); 235 (1946); 239 (1946); 244 (1946); 252 (1946); 272 (1946); 288 (1946); 299 (1946); 316 (1946); R. D. MUIR and D. F. HORNIG. J. Chem. Phys. **17**, 1236 (1949).
36. P. C. PAINTER and J. L. KOENIG. Spectrochim. Acta, **33**A, 1019 (1977).
37. K. M. MACKAY, D. B. SOWERBY, and W. C. YOUNG. Spectrochim. Acta, **24**A, 611 (1968).
38. J. H. S. GREEN, W. KYNASTON, and G. A. RODLEY. Spectrochim. Acta, **24**A, 853 (1968).
39. J. R. DURIG, C. W. SINK, and J. B. TURNER. J. Chem. Phys. **49**, 3422 (1968); J. R. DURIG and J. B. TURNER. J. Chem. Phys. **79**, 1558 (1972).
40. F. HÖFLER. Monat. Chem. **107**, 705 (1976).

Can. J. Chem. Downloaded from www.nrcresearchpress.com by 210.87.254.105 on 09/06/12
For personal use only.

Complexes of dodecamethylcyclohexaphosphazene with palladium(II) chloride and platinum(II) chloride. Crystal and molecular structure of *cis*-dichloro[η^2-dodecamethylcyclohexaphosphazene (*N*,*N'*)] palladium(II) sesquihydrate

NORMAN L. PADDOCK, T. N. RANGANATHAN, STEVEN J. RETTIG, RAJENDRA D. SHARMA, AND JAMES TROTTER

Department of Chemistry, University of British Columbia, 2036 Main Mall, Vancouver, B.C., Canada V6T 1Y6

Received December 15, 1980

NORMAN L. PADDOCK, T. N. RANGANATHAN, STEVEN J. RETTIG, RAJENDRA D. SHARMA, and JAMES TROTTER. Can. J. Chem. **59**, 2429 (1981).

Dodecamethylcyclohexaphosphazene $N_6P_6Me_{12}$, **1**, forms 1:1 complexes with palladium(II) chloride, **2**, and platinum(II) chloride, **3**. Their ^{31}P, ^1H, and ^{13}C nmr spectra show them to be rigid molecules in solution, with an approximate plane of symmetry. Crystals of **2** are orthorhombic, $a = 17.4030(3)$, $b = 15.4897(5)$, $c = 10.7417(2)$ Å, $Z = 4$, space group $P2_12_12$. The structure was determined from diffractometer X-ray data and refined by full-matrix least-squares methods to $R = 0.031$ for 3545 reflections with $I \geq 3\sigma(I)$. The metal atom has square planar coordination, and forms 6- and 10-membered chelate rings with the phosphazene ligand. The mean P—N bond length is 1.609 Å; the variation of bond lengths within the ring is consistent with model calculations of changes in bond order arising from the localization of bonding electrons.

NORMAN L. PADDOCK, T. N. RANGANATHAN, STEVEN J. RETTIG, RAJENDRA D. SHARMA et JAMES TROTTER. Can. J. Chem. **59**, 2429 (1981).

La dodécaméthylcyclohexaphosphazène $N_6P_6Me_{12}$, **1**, forme les complexes 1:1 avec le chlorure du palladium(II), **2**, et du platine(II), **3**. Leurs spectres rmn ^{31}P, ^1H et ^{13}C indiquent que les molécules sont rigides en solution, et elles ont approximativement un plan de symétrie. Les cristaux de **2** sont orthorhombiques, $a = 17.4030(3)$, $b = 15.4897(5)$, $c = 10.7417(2)$ Å, $Z = 4$, groupe d'espace $P2_12_12$. On a résolu la structure au moyens de données diffractométriques des rayons X et on l'a raffinée par la méthode des moindres carrés (matrice complète) jusqu'à une valeur finale de $R = 0.031$ pour 3545 réflexions avec $I \geq 3\sigma(I)$. L'atome du métal a la coordination d'un plan carré, et forme les cycles chélatés de six et dix membres avec le ligand phosphazène. La longeur moyenne des liaisons P—N est de 1.609 Å; la variation des longeurs de liaisons au dedans la cycle est en accord avec des calculations modèles de variation de l'ordre des liaisons, qui résultent des localizations des électrons liants.

Introduction

An earlier study (1) described the donor properties of the cyclic dimethylphosphazenes $(NPMe_2)_{3-5}$. The larger ring compounds $(NPMe_2)_{6-10}$ which are now available (2) have a greater number of donor sites, and can coordinate with metals in various ways. In this paper we describe the complexes of palladous and platinous chloride with dodecamethylcyclohexaphosphazene $(NPMe_2)_6$, **1**, and the crystal and molecular structure of its palladium complex.

Experimental

The ligand **1** was prepared from the fluoride by a Grignard reaction (2). Solvents were dried over lithium aluminum hydride or phosphorus pentoxide. Nuclear magnetic resonance spectra were obtained on a Varian XL-100FT instrument with heteronuclear decoupling, a Nicolet-Oxford H-270 instrument (270 MHz), and a Bruker WH400 (400 MHz).

Palladium Complex

A filtered solution of dichlorodibenzonitrilepalladium(II) (3) (0.138 g; 0.36 mmol) in 40 mL benzene was added dropwise over 30 min to **1** (0.171 g; 0.38 mmol) in 30 mL benzene under nitrogen, a yellow solid being precipitated. The solution was filtered under nitrogen, and the solid $(N_6P_6Me_{12})PdCl_2$, **2**, was washed with and recrystallized from benzene (0.206 g, 90%); dec. 250°C. *Anal.* calcd. for $C_{12}H_{36}Cl_2N_6P_6Pd$: C 23.0, H 5.8, Cl 11.3, N 13.4; found: C 23.1, H 5.7, Cl 11.2, N 13.2. The complex was a non-conductor in nitrobenzene.

Platinum Complex

A similar reaction with dichlorodibenzonitrileplatinum(II) occurred less rapidly, and required heating under reflux for 72 h. The 1:1 complex was obtained as a yellow powder, which was recrystallized from dichloromethane as $(N_6P_6Me_{12})PtCl_2$, **3**, dec. 250°C. *Anal.* calcd. for $C_{12}H_{36}Cl_2N_6P_6Pt$: C 20.1, H 5.1, Cl 9.9, N 11.7; found: C 20.5, H 5.1, Cl 9.8, N 11.4. The nmr parameters for both complexes are given in Table 1.

X-ray Analysis

Crystals of the sesquihydrate of **2** were obtained by recrystallization from aqueous nitromethane. A crystal ca. 0.30 × 0.20 × 0.50 mm in size was mounted in a general orientation. Unit-cell parameters were refined by least-squares on 2 sin θ/λ values for 25 reflections measured on a diffractometer with Cu K_α radiation (λ = 1.54184 (Cu) and 0.71073 (Mo) Å). Crystal data at 22°C are:

$C_{12}H_{36}Cl_2N_6P_6Pd \cdot 1.5\ H_2O$ fw = 654.64

Orthorhombic, $a = 17.4030(3)$, $b = 15.4897(5)$, $c = 10.7417(2)$ Å, $V = 2895.6(1)$ Å^3, $\rho_m = 1.50(1)$ (flotation in aqueous KI), $Z = 4$, $\rho_c = 1.502$ g cm^{-3}, $F(000) = 1340$, μ(Mo K_α) = 11.6 cm^{-1}. Absent reflections: $h00$, $h \neq 2n$ and $0k0$, $k \neq 2n$ uniquely indicate the space group $P2_12_12$ (D_2^3, No. 18).

Intensities were measured with graphite-monochromatized Mo K_α radiation on an Enraf-Nonius CAD4-F diffractometer. An ω–1.33θ scan at 0.91–6.71° min^{-1} over a range of (0.70 + 0.35

0008-4042/81/162429-06$01.00/0

©1981 National Research Council of Canada/Conseil national de recherches du Canada

Can. J. Chem. Downloaded from www.nrcresearchpress.com by 210.87.254.40 on 09/06/12
For personal use only.

TABLE 1. Nuclear magnetic resonance parameters of palladium and platinum complexes[a]

Complex	Group A[b]		Group B[b]		Group C[b]	
	δ_P	δ_H[d]	δ_P	δ_H[d]	δ_P	δ_H[d]
2[c]	(1)-83.24	(2)2.78(13.9)	(2)-86.06	(2)2.21(12.2)	(1)-105.27	(2)1.61(13.0)
	(1)-83.61	(2)1.72(14.0)		(2)1.85(10.8)	(1)-105.56	(2)1.59(12.7)
3	(1)-83.32	(2)2.64(13.9)	(2)-85.16[e]	(2)2.23(13.0)	(1)-104.72	(1)1.56(12.5)[f]
	(1)-82.76	(1)1.75(13.8)		(2)1.86(10.3)	(1)-105.16	(1)1.56(11.9)[f]
		(1)1.74(13.9)				(2)1.52(13.0)

[a]All in $CDCl_3$, relative to internal tetramethylsilane (^1H, ^{13}C) or external P_4O_6 (^{31}P). Positive shifts to low field of reference. Shifts in ppm, preceded by the number of Me or P groups, and followed by J_{PH} (Hz), both in parentheses.
[b]See Fig. 1.
[c]^{13}C frequencies at 100.60 MHz: 1982.898, 2066.263, 2071.474, 2169.725, 2265.744, 2272.443, 2286.585, 2374.416 (×2), 2398.235, 2459.270, 2496.487 Hz. Parameters tentatively assigned as: $C_{A'}$, $C_{A''}$, −24.21 (122.1), −23.59 (172.7); $B_{B'}$, $C_{B''}$, −23.21 (125.8), −23.06 (108.7); $C_{C'}$, $C_{C''}$, −21.05 (103.5), −20.15 (88.6). For **1**, δ_C, (J_{CP}) = −22.53 (95.2).
[d]Detailed configuration of methyl groups unknown; those in a particular Group are associated jointly with the one or two phosphorus environments observed.
[e]J_{P-N-Pt}: 99.0 Hz.
[f]Chemical shift difference 0.002 ppm.

tan θ) degrees in ω (extended by 25% on both sides for background measurement) was employed. Data were measured to $2\theta = 60°$. The intensities of 3 check reflections, measured every 3600 s throughout the data collection, remained constant to within ±3.5%. After data reduction, an absorption correction was applied using the Gaussian integration method (4, 5). Transmission factors ranged from 0.745 to 0.823 for 216 sampling points. Of the 4660 independent reflections measured, 3545 (76%) had intensities greater than $3\sigma(I)$ above background where $\sigma^2(I) = S + 2B + (0.04(S - B))^2$ with S = scan count and B = background count.

The positions of the Pd, Cl, and two of the P atoms were determined from the Patterson function and those of the remaining non-hydrogen atoms from a subsequent difference map. After full-matrix least-squares refinement of all non-hydrogen atoms except O(2) with anisotropic thermal parameters (O(2) having an isotropic temperature factor[1]) to $R = 0.048$, a difference map gave positions for most of the methyl hydrogen atoms. The hydrogen atoms associated with the solvent molecules were not located. Ideal positions were calculated for all methyl hydrogen atoms (C—H = 0.98 Å, $U_H = 1.2 \times U_c$) which were included as fixed atoms in subsequent cycles of refinement. The scattering factors of ref. 6 were used for non-hydrogen atoms and those of ref. 7 for hydrogen atoms. Anomalous scattering factors from ref. 8 were used for the Pd, Cl, and P atoms. The weighting scheme, $w = 1/\sigma^2(F)$ where $\sigma^2(F)$ is derived from the previously defined $\sigma^2(I)$ gave uniform average values of $w(|F_o| - |F_c|)^2$ over ranges of $|F_o|$ and was employed in the final stages of refinement. An isotropic Type I extinction correction (Thornley–Nelmes definition of mosaic anisotropy with a Lorentzian distribution) was applied (9–11). The final value of g was $1.0(3) \times 10^4$. Convergence was reached at $R = 0.031$ and $R_w = 0.037$ for 3545 reflections with $I \geq 3\sigma(I)$. For all 4660 reflections $R = 0.051$ and $R_w = 0.039$.

The absolute configuration of the structure has been determined through the anomalous scattering of the heavier atoms. Parallel refinements of the structure represented by the coordinates in Table 2 and its mirror image were undertaken resulting in R and R_w ratios of 1.56 and 1.22 respectively, clearly indicating the correct structure. The function minimized was $\Sigma w(|F_o| - |F_c|)^2$, $R = \Sigma||F_o| - |F_c||/\Sigma|F_o|$ and $R_w = (\Sigma w(|F_o| - |F_c|)^2/\Sigma w|F_o|^2)^{1/2}$.

On the final cycle of refinement the mean and maximum parameter shifts corresponded to 0.14 and 1.0 σ respectively. The mean error in an observation of unit weight was 1.207. A final difference map showed maximum fluctuations of ±0.8 e Å^{-3} near the palladium atom and was essentially featureless elsewhere. The final positional and thermal parameters appear in Tables 2, 3 and 4.[2] Measured and calculated structure factors have been placed in the Depository of Unpublished Data.[2]

The ellipsoids of thermal motion for the non-hydrogen atoms are shown in Fig. 1. The thermal motion has been analysed in terms of the rigid-body modes of translation, libration, and screw motion (12) using the computer program MGTLS. The rms standard error in the temperature factors σU_{ij} (derived from the least-squares analysis) is 0.0040 Å^2. Analyses of each of the six phosphorus tetrahedra and the nine-atom group consisting of the coordination group of Pd and the four attached P atoms all gave physically reasonable rigid-body parameters and rms ΔU_{ij} values of 11, 13, 6, 19, 8, 19, and 22 (all × 10^4) Å^2. The appropriate bond distances have been corrected for libration (13), using shape parameters q^2 of 0.08 for all atoms involved. Corrected bond lengths appear along with the uncorrected distances in Table 5 and corrected bond angles do not differ by more than 1 standard deviation from the uncorrected values listed in Table 6. Intra-annular torsion angles defining the conformations of the phosphazene and chelate rings are given in Table 7.

Results and Discussion

The nmr results for both **2** and **3** (Table 1) are uniquely consistent with the qualitative coordination scheme of Fig. 2 in which the dotted line denotes an approximate plane of symmetry relating such atoms as A′, A″. The ^{31}P shifts are assigned to atoms P_A, P_B, P_C on the basis of charge densities obtained from an HMO calculation. As expected, the shift of P_C is closest to that of the uncomplexed ligand (−109.3 ppm (14)). The resonances of P_A and

[1]Refinement of O(2) with anisotropic thermal parameters resulted in a non-positive-definite thermal parameter, possibly due to a minor disordering of the water molecule about the twofold axis. The high temperature factor observed for this atom probably results from the fact that this water molecule is well separated from the rest of the structure.

[2]The structure factor table, Table 3 (calculated hydrogen coordinates and thermal parameters) and Table 4 (anisotropic thermal parameters) are available, at a nominal charge, from the Depository of Unpublished Data, CISTI, National Research Council of Canada, Ottawa, Ont., Canada K1A 0S2.

Can. J. Chem. Downloaded from www.nrcresearchpress.com by 210.87.254.40 on 09/06/12
For personal use only.

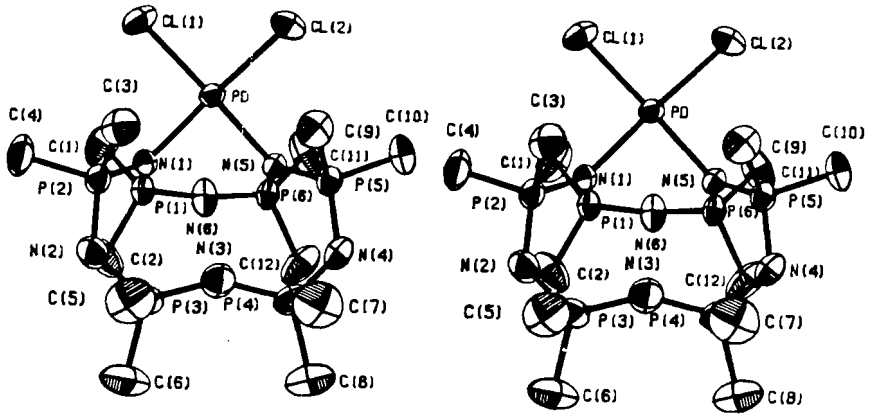

FIG. 1. Stereoscopic view of **2**, 50% probability thermal ellipsoids are shown. Hydrogen atoms are omitted for clarity.

TABLE 2. Final positional (fractional × 10^4, Pd, Cl, and P × 10^5) and isotropic thermal parameters ($U \times 10^3$ Å^2) with estimated standard deviations in parentheses

Atom	x	y	z	U_{eq}/U_{iso}
Pd	67812(2)	75414(3)	53609(3)	31
Cl(1)	77609(9)	75454(15)	39178(15)	62
Cl(2)	60963(11)	65585(13)	41974(16)	60
P(1)	69005(8)	93939(9)	62092(15)	37
P(2)	81195(8)	83043(11)	72396(15)	39
P(3)	76445(10)	81786(12)	98008(15)	49
P(4)	61362(11)	72694(11)	99906(15)	48
P(5)	56447(8)	67991(9)	75441(14)	35
P(6)	54520(8)	85256(9)	64663(16)	36
N(1)	7337(2)	8477(3)	6422(5)	34
N(2)	8102(3)	8594(4)	8653(5)	51
N(3)	6844(3)	7780(4)	9443(5)	59
N(4)	5509(3)	7026(4)	8966(5)	46
N(5)	5899(2)	7609(3)	6654(4)	31
N(6)	5999(3)	9299(3)	6134(6)	48
C(1)	7224(5)	9875(5)	4807(9)	77
C(2)	7161(5)	10158(5)	7370(10)	76
C(3)	8344(4)	7179(5)	7061(7)	56
C(4)	8917(4)	8863(6)	6537(9)	68
C(5)	8262(5)	7388(6)	10520(7)	76
C(6)	7563(7)	9011(6)	10944(8)	83
C(7)	6437(6)	6317(5)	10796(8)	80
C(8)	5631(6)	7864(7)	11162(8)	81
C(9)	6353(4)	5961(4)	7337(7)	54
C(10)	4766(4)	6337(4)	6988(7)	55
C(11)	4768(4)	8444(5)	5257(10)	78
C(12)	4895(5)	8790(5)	7812(9)	80
O(1)	9463(6)	9341(8)	9964(15)	204
O(2)	10000	5000	8714(37)	330(15)

P_C are each split into two close lines, so illustrating the imperfection of the mirror symmetry. The proton spectrum of **2** shows six distinct environments (Fig. 3), all downfield of **1** (1.50 ppm, J = 12.3 Hz (14)). Selective decoupling identified methyl groups 1 and 4 as belonging to P_A, 2 and 3 to P_B and 5 and 6 to P_C. The two methyl groups attached to a particular phosphorus atom are strongly differentiated, especially those which are near the metal atom, whereas methyl groups which are symmetrically related by the "plane" of Fig. 2 are not differentiated. The molecule is evidently made rigid in solution, with the approximate symmetry indicated, by coordination of the phosphazene to the metal. In this respect, its behavior contrasts with the flexibility of the parent ligand, whose ^{1}H spectrum consists of a simple doublet, even though the methyl groups are not symmetrically related in the crystal (15). The rigidity of **2** in solution (unusual among phosphazenes) is confirmed by its ^{13}C spectrum. Eleven lines are seen (one of double intensity), as expected, but the doublet structure is not obvious, and, since decoupling from phosphorus was not available, the parameters derived from the frequencies given in Table 1 are tentative. The ^{1}H nmr spectrum of **3** is almost identical to that of **2**, the principal qualitative difference being a small further splitting of doublets 4 and 5, implying a small but significant inequivalence in those methyl groups at P_A and P_C which correspond in the sense of Fig. 2. The ^{1}H spectrum of **3** also showed it to contain a minor but persistent impurity, which could not be removed chromatographically. It was possibly an ionic complex, which would account for the small electrical conductivity of **3** observed in nitrobenzene.

The crystal structure of **2** consists of discrete molecules which are linked by N···H—O hydrogen bonds to water molecules of crystallization to form helices of alternating molecules of water and **2** extending along a about the twofold screw axes (O(1)···N(2) = 2.99(1) Å and O(1)···N(4) ($1/2 + x$, $3/2 - y$, $2 - z$) = 3.02(1) Å). The second water of crystallization, located on the twofold axis, is not involved in hydrogen-bonding, the shortest nonbonded distance involving O(2) (O(2)···H(8b) = 2.62 Å) corresponding to a normal van der Waals

Can. J. Chem. Downloaded from www.nrcresearchpress.com by 210.87.254.40 on 09/06/12
For personal use only.

Can. J. Chem. Downloaded from www.nrcresearchpress.com by 210.87.254.40 on 09/06/12
For personal use only.

TABLE 5. Bond lengths (Å) with estimated standard deviations in parentheses

Bond	Length		Bond	Length	
	Uncorr.	Corr.		Uncorr.	Corr.
Pd —Cl(1)	2.304(2)	2.309	P(6)—N(5)	1.631(4)	1.636
Pd —Cl(2)	2.302(2)	2.308	P(6)—N(6)	1.572(5)	1.584
Pd —N(1)	2.082(5)	2.088	P(1)—C(1)	1.772(8)	1.788
Pd —N(5)	2.073(4)	2.079	P(1)—C(2)	1.778(8)	1.793
P(1)—N(6)	1.577(5)	1.589	P(2)—C(3)	1.796(8)	1.803
P(1)—N(1)	1.628(5)	1.633	P(2)—C(4)	1.801(7)	1.811
P(2)—N(1)	1.642(4)	1.650	P(3)—C(5)	1.803(8)	1.818
P(2)—N(2)	1.584(6)	1.591	P(3)—C(6)	1.787(9)	1.802
P(3)—N(2)	1.603(6)	1.611	P(4)—C(7)	1.788(8)	1.801
P(3)—N(3)	1.572(6)	1.584	P(4)—C(8)	1.790(9)	1.804
P(4)—N(3)	1.578(6)	1.590	P(5)—C(9)	1.803(7)	1.811
P(4)—N(4)	1.595(6)	1.602	P(5)—C(10)	1.791(7)	1.799
P(5)—N(4)	1.585(6)	1.592	P(6)—C(11)	1.766(8)	1.783
P(5)—N(5)	1.638(5)	1.645	P(6)—C(12)	1.788(8)	1.805

TABLE 6. Bond angles (deg) with estimated standard deviations in parentheses, non-hydrogen atoms

Bonds	Angle (deg)	Bonds	Angle (deg)
Cl(1)—Pd —Cl(2)	91.12(7)	N(1) —Pd —N(5)	86.7(2)
Cl(1)—Pd —N(1)	91.3(1)	Cl(2) —Pd —N(5)	90.8(1)
Cl(1)—Pd —N(5)	177.0(1)	Cl(2) —Pd —N(1)	176.4(1)
N(1) —P(1) —N(6)	113.0(2)	N(5) —P(6) —N(6)	113.8(2)
N(1) —P(1) —C(1)	109.7(3)	N(5) —P(6) —C(11)	110.4(3)
N(1) —P(1) —C(2)	111.3(3)	N(5) —P(6) —C(12)	111.0(3)
N(6) —P(1) —C(1)	108.2(4)	N(6) —P(6) —C(11)	107.2(4)
N(6) —P(1) —C(2)	110.6(4)	N(6) —P(6) —C(12)	109.7(4)
C(1) —P(1) —C(2)	103.6(5)	C(11)—P(6) —C(12)	104.3(5)
N(1) —P(2) —N(2)	116.8(3)	N(5) —P(5) —N(4)	115.6(3)
N(1) —P(2) —C(3)	106.3(3)	N(5) —P(5) —C(9)	107.1(3)
N(1) —P(2) —C(4)	109.7(3)	N(5) —P(5) —C(10)	110.0(3)
N(2) —P(2) —C(3)	112.4(3)	N(4) —P(5) —C(9)	112.4(3)
N(2) —P(2) —C(4)	106.3(4)	N(4) —P(5) —C(10)	106.4(3)
C(3) —P(2) —C(4)	104.7(4)	C(9) —P(5) —C(10)	104.7(3)
N(2) —P(3) —N(3)	114.2(3)	N(4) —P(4) —N(3)	113.3(3)
N(2) —P(3) —C(5)	107.8(3)	N(4) —P(4) —C(7)	109.8(4)
N(2) —P(3) —C(6)	106.1(4)	N(4) —P(4) —C(8)	105.7(4)
N(3) —P(3) —C(5)	111.5(4)	N(3) —P(4) —C(7)	111.4(4)
N(3) —P(3) —C(6)	112.4(4)	N(3) —P(4) —C(8)	112.9(4)
C(5) —P(3) —C(6)	104.1(4)	C(7) —P(4) —C(8)	103.2(5)
Pd —N(1)—P(1)	108.3(2)	Pd —N(5)—P(6)	108.3(2)
Pd —N(1)—P(2)	124.4(3)	Pd —N(5)—P(5)	123.5(2)
P(1) —N(1)—P(2)	127.2(3)	P(6) —N(5)—P(5)	127.6(3)
P(2) —N(2)—P(3)	129.3(4)	P(5) —N(4)—P(4)	128.0(3)
P(3) —N(3)—P(4)	142.9(4)	P(1) —N(6)—P(6)	131.5(3)

TABLE 7. Intra-annular torsion angles (deg) phosphazene and chelate rings

Atoms	Angle	Atoms	Angle
P(6) —N(6)—P(1) —N(1)	12.8(3)	N(5)—P(6) —N(6)—P(1)	−13.9(3)
N(6)—P(1) —N(1)—P(2)	−145.0(2)	P(5) —N(5)—P(6) —N(6)	151.0(2)
P(1) —N(1)—P(2) —N(2)	56.3(3)	N(4)—P(5) —N(5)—P(6)	−55.0(3)
N(1)—P(2) —N(2)—P(3)	71.4(3)	P(4) —N(4)—P(5) —N(5)	−71.2(3)
P(2) —N(2)—P(3) —N(3)	−33.5(4)	N(3)—P(4) —N(4)—P(5)	32.9(4)
N(2)—P(3) —N(3)—P(4)	176.9(2)	P(3) —N(3)—P(4) —N(4)	−176.5(2)
N(5)—Pd —N(1)—P(1)	−72.9(2)	P(6) —N(5)—Pd —N(1)	71.6(2)
Pd —N(1)—P(1) —N(6)	39.2(3)	N(6)—P(6) —N(5)—Pd	−37.5(3)
N(1)—P(1) —N(6)—P(6)	12.8(3)	P(1) —N(6)—P(6) —N(5)	−13.9(3)

Can. J. Chem. Downloaded from www.nrcresearchpress.com by 210.87.254.40 on 09/06/12
For personal use only.

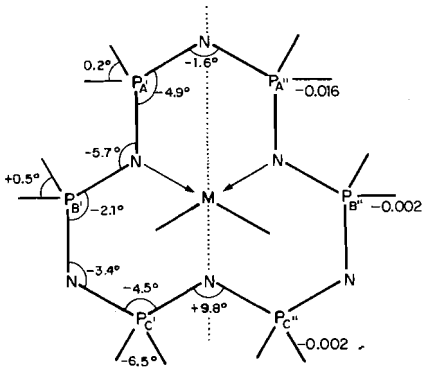

FIG. 2. Coordination diagram of **2** and **3**, the dashed line representing an approximate plane of symmetry. The diagram also shows (for **2**) the mean deviations (4 P—C bonds at each of P_A, P_B, P_C) from the geometry of the free ligand.

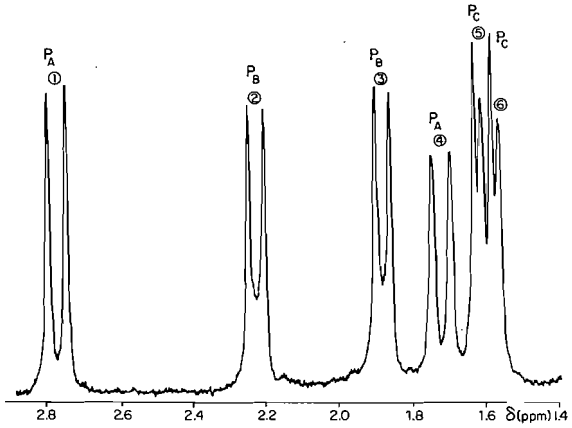

FIG. 3. The ^1H nmr spectrum of **2** (270 MHz).

contact. There are two weak intramolecular C—H···Cl hydrogen bonds present (C(3)—H(3b)···Cl(1), C···Cl = 3.571(8), H···Cl = 2.74 Å, C—H···Cl = 144° and C(9)—H(9b)···Cl(2), C···Cl = 3.525(8), H···Cl = 2.77 Å, C—H···Cl = 136°).

The molecular structure of **2** confirms the coordination scheme of Fig. 2 and adds important numerical detail. A stereoscopic view of the molecule is shown in Fig. 1, and another view in Fig. 4. The palladium atom is coordinated at N(1) and N(5), and the molecule is clearly almost symmetrical across the plane N(6)PdN(3). Corresponding P—N bond lengths are in fact very nearly equal (mean and maximum differences 0.004 and 0.009 Å); there are small differences between corresponding bond angles and torsion angles. In contrast, the lengths of successive bonds differ significantly in a pattern which will be discussed below.

The metal has the expected planar coordination, and the individual bond angles differ little from 90°: the Pd—Cl and Pd—N bond lengths are normal.

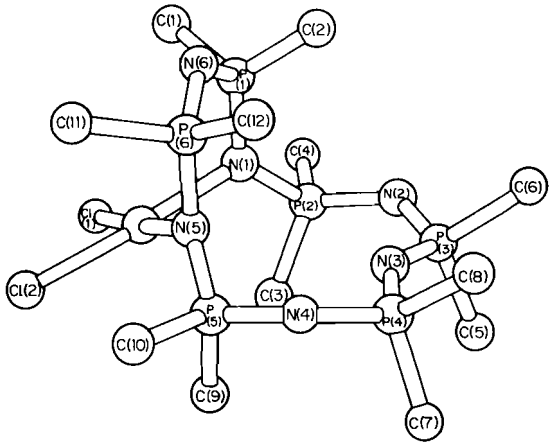

FIG. 4. General view of **2**.

The Pd—N vectors are almost coplanar with the local PNP planes (deviations: Pd—N(1), 4.0°; Pd—N(5), 8.0°), but the coordination directions at nitrogen are not quite those expected from idealized lone pairs at nitrogen, since the (mean) angles there are Pd—N—P = 124.0, 108.3°. The molecule is evidently slightly strained at these points. The pairs of methyl groups on P(6), P(1), and on P(3), P(4) are related by the approximate mirror plane through N(3)PdN(6), and are hence nearly eclipsed. Some steric strain is relieved by the large angles at N(3), N(6).

The structure can be understood in terms of the localization of electrons at N(1) and N(5), and the angular constraints imposed by the coordination at these positions. The mean P—N bond length is 1.609 Å, compared with 1.593 Å in the free ligand (15). The small increase on complexing can be attributed partly to the localization of bonding electrons, and partly to changes in σ-hybridization. The effect of coordination is to reduce most of the angles, as shown in Fig. 2. It is surprising that there is no significant compensatory increase of the exocyclic angles, and except at P_A, the P—C bond lengths are hardly changed; the effect of coordination largely confined to the P_6N_6 ring. The geometrical effects differ in the complexes of $N_6P_6(NMe_2)_{12}$ (16). In $[N_6P_6(NMe_2)_{12}](CoCl_2)_2$, for instance (17), in which the metal is bound to four nitrogen atoms, the mean length of the ring bonds is greatly increased, and the decrease in the ring angles is accompanied both by an increase in exocyclic angle and a decrease in exocyclic bond length; the ligand differs from **1** in being a stronger donor with extensive conjugative release from the exocyclic nitrogen atoms.

The localization of electrons in **2** at N(1) and N(5)

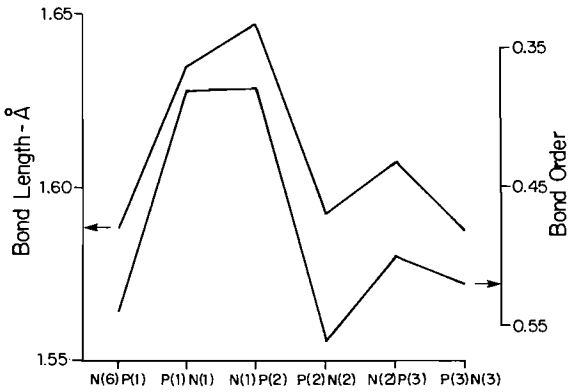

FIG. 5. Comparison of lengths of successsive bonds in **2** with bond order calculations (HMO, $\alpha_N = -1$, $\alpha_P = +1$, all β's $= -1$. For atoms coordinated at N(1), N(5), $\alpha = -0.3$).

by complex formation has a significant effect on the lengths of symmetrically related bonds, which is illustrated in Fig. 5 in comparison with calculated bond orders. The qualitative correspondence confirms that the metal withdraws bonding electrons from the ring, thereby changing the bond lengths, but there is no evidence for any more specific interaction between the metal and the ring.

It does not appear that the detailed electronic structure of the ligand has any important bearing on the coordination. Model calculations on an N_6P_6 ring in which electrons are supposedly localized at N(1) show that the charge density is highest and the second localization energy lowest at the antipodal position N(4), and, from this point of view, the metal might be expected to bridge the ligand so as to form two eight-membered rings. The reason it does not do so may be that, once the metal is coordinated at N(1), it interacts most easily with the nearest nitrogen atom with which it can form a stable ring, i.e., N(5). As the reported results show, the molecule is then rigid, and any further interaction is likely to be with the near atoms N(2) and N(4), as found in the complexes of $N_6P_6(NMe_2)_{12}$ (16). Coordination of $PtCl_2$ to $N_4P_4(NHCH_3)_8$ (18) and to $N_4P_4Me_8$ (19) occurs similarly, antipodal substitution giving two six-membered rings, with similarly pronounced inequalities in the lengths of the ring bonds. If the six-membered chelate ring retains its stability in complexes of the larger phosphazenes, so that the metal remains near one end of the molecule, it may be possible to include two or more atoms within the same ligand, as in the crown ethers (20).

Acknowledgments

We thank the Natural Sciences and Engineering Research Council of Canada for financial support and the University of British Columbia Computing Centre for assistance.

1. H. T. SEARLE, J. DYSON, N. L. PADDOCK, and T. N. RANGANATHAN. J. Chem. Soc. Dalton Trans. 203 (1975).
2. K. D. GALLICANO, R. T. OAKLEY, N. L. PADDOCK, S. J. RETTIG, and J. TROTTER. Can. J. Chem. **55**, 304 (1977).
3. J. R. DOYLE, P. E. SLADE, and H. B. JONASSEN. Inorg. Synth. **6**, 218 (1960).
4. P. COPPENS, L. LEISEROWITZ, and D. RABINOVICH. Acta Crystallogr. **18**, 1035 (1965).
5. W. R. BUSING and H. A. LEVY. Acta Crystallogr. **22**, 457 (1967).
6. D. T. CROMER and J. B. MANN. Acta Crystallogr. Sect. A, **24**, 321 (1968).
7. R. F. STEWART, E. R. DAVIDSON, and W. T. SIMPSON. J. Chem. Phys. **42**, 3175 (1965).
8. D. T. CROMER and D. LIBERMAN. J. Chem. Phys. **53**, 1891 (1970).
9. P. J. BECKER and P. COPPENS. Acta Crystallogr. Sect. A, **30**, 129 (1974); **30**, 148 (1974); **31**, 417 (1975).
10. P. COPPENS and W. C. HAMILTON. Acta Crystallogr. Sect. A, **26**, 71 (1970).
11. F. R. THORNLEY and R. J. NELMES. Acta Crystallogr. Sect. A, **30**, 748 (1974).
12. V. SCHOMAKER and K. N. TRUEBLOOD. Acta Crystallogr. Sect. B, **24**, 63 (1969).
13. D. W. J. CRUICKSHANK. Acta Crystallogr. **9**, 747 (1956); **9**, 754 (1956); **14**, 896 (1961).
14. R. T. OAKLEY. PhD Thesis. University of British Columbia, Vancouver, B.C. 1976.
15. R. T. OAKLEY, N. L. PADDOCK, S. J. RETTIG, and J. TROTTER. Can. J. Chem. **55**, 3118 (1977).
16. H. P. CALHOUN, N. L. PADDOCK, and J. N. WINGFIELD. Can. J. Chem. **53**, 1765 (1975).
17. W. HARRISON and J. TROTTER. J. Chem. Soc. Dalton Trans. 61 (1973).
18. R. W. ALLEN, J. P. O'BRIEN, and H. R. ALLCOCK. J. Am. Chem. Soc. **99**, 3987 (1977).
19. J. P. O'BRIEN, R. W. ALLEN, and H. R. ALLCOCK. Inorg. Chem. **18**, 2230 (1979).
20. M. MERCER and M. R. TRUTER. J. Chem. Soc. Dalton Trans. 2469 (1973).

Can. J. Chem. Downloaded from www.nrcresearchpress.com by 210.87.254.40 on 09/06/12
For personal use only.

The preparation and crystal structure of η^2-nitrato(η^4-hexadecamethylcyclooctaphosphazene (N^1,N^2,N^4,N^5))cobalt(II) nitrate

KEITH D. GALLICANO, NORMAN L. PADDOCK, STEVEN J. RETTIG, AND JAMES TROTTER

Department of Chemistry, University of British Columbia, 2036 Main Mall, Vancouver, B.C., Canada V6T 1Y6

Received January 8, 1981

KEITH D. GALLICANO, NORMAN L. PADDOCK, STEVEN J. RETTIG, and JAMESTROTTER. Can. J. Chem. **59**, 2435 (1981).

Hexadecamethylcyclooctaphosphazene $N_8P_8Me_{16}$, **1**, forms a 1:1 complex, **2**, with cobalt(II) nitrate. Crystals of **2** are triclinic, $a = 10.891(2)$, $b = 11.201(2)$, $c = 14.944(2)$ Å, $\alpha = 93.21(1)$, $\beta = 95.66(1)$, $\gamma = 104.69(1)°$, $Z = 2$, space group $P\bar{1}$. The crystal structure was solved by direct methods and was refined by full-matrix least-squares procedures to $R = 0.037$ and $R_w = 0.047$ for 5165 reflections with $I \geq 3\sigma(I)$. All the hydrogen atoms were found. The structure consists of a cation $[N_8P_8Me_{16}\ CoNO_3]^+$ and a free nitrate anion. The cobalt atom is coordinated by an unsymmetrical bidentate nitrate ion and by four nitrogen atoms of the phosphazene ring. The metal is attached near one end of the ring, forming six-, ten-, and two four-membered chelate rings, and induces bond length variations which are independent of local conformation and which arise from the localization of bonding electrons.

KEITH D. GALLICANO, NORMAN L. PADDOCK, STEVEN J. RETTIG et JAMES TROTTER. Can. J. Chem. **59**, 2435 (1981).

Hexadécaméthylcyclooctaphosphazène $N_8P_8Me_{16}$, **1**, forme un complexe 1:1, **2**, avec le nitrate du cobalt(II). Les cristaux de **2** sont tricliniques, $a = 10.891(2)$, $b = 11.201(2)$, $c = 14.944(2)$ Å, $\alpha = 93.21(1)$, $\beta = 95.66(1)$, $\gamma = 104.69(1)°$, $Z = 2$, groupe d'espace $P\bar{1}$. On a résolu la structure au moyens de méthodes directes et on l'a affinée par la méthode des moindres carrés (matrice complète) jusqu'à une valeur finale de $R = 0.037$ et de $R_w = 0.047$ pour 5165 refléxions avec $I \geq 3\sigma(I)$. La structure se compose d'un cation $[N_8P_8Me_{16}\ CoNO_3]^+$ et d'un anion libre du nitrate. L'atome de cobalt est coordiné par un anion du nitrate asymétrique et bidenté, et par quatre atomes d'azote du cycle phosphazène. Le métal est lié presqu'une extrémité du cycle, en formant les cycles chelatés de six, dix, et deux de quatre membres, et il amène aux variations des longeurs des liaisons qui sont indépendantes de la conformation locale et qui résultent des localizations des électrons de liaisons.

Introduction

In previous papers, we have described the donor properties of $(NPMe_2)_{3-5}$ (1), and complex formation by $(NPMe_2)_6$ (2). Even in a 12-membered ring, however, the possible range of coordination types is restricted, and we have therefore studied complex formation by the 16-membered ring compound $(NPMe_2)_8$, **1**. The preparation of this compound has been outlined (3) and its crystal structure determined (4). Part of the interest in its coordination behavior lies in its high symmetry (C_4) in the crystal, four nitrogen atoms being well adapted to square planar or tetrahedral geometry. The present paper describes the preparation and crystal structure of $(NPMe_2)_8 \cdot Co(NO_3)_2$, **2**.

Experimental

A solution of $Co(NO_3)_2$ (0.252 mmol) in 15 mL dry acetonitrile was added under a stream of nitrogen to a solution of **1** (0.151 g, 0.252 mmol) in 15 mL acetonitrile. The purple solution was heated under reflux for 24 h. After removal of the solvent, the residual purple solid was washed with light petroleum to remove unchanged **1**. The complex **2** (75%) was recrystallized from acetonitrile/toluene as purple air-stable crystals, mp 223–224°C. *Anal.* calcd for $C_{16}H_{48}CoN_{10}O_6P_8$: C 24.5, H 6.2, N 17.9; found: C 24.8, H 6.4, N 17.7. The infrared spectrum (Nujol) showed a band at 1345 cm^{-1} (br), attributed to the E' asymmetric NO_3 stretching mode of a free nitrate ion (5). The asymmetric NO_2 stretching frequency (B_1) of a coordinated nitrate ion can be seen at 1483 cm^{-1}; the symmetric NO_2 stretching frequency (A_1) near 1280 cm^{-1} is easily confused with ligand vibrations and is not assigned. The numerical values resemble those found for the bound bidentate nitrate ion (1280 (s) and 1490 cm^{-1} (s)) and the free nitrate ion (1375 cm^{-1} (s, br)) in a complex of a cyclic tetramine $[Ni(tet\ b)NO_3]NO_3$ (6), and those (~1470, ~1300 cm^{-1}) in an unsymmetrical bidentate nitrato complex $(Ph_4As)_2[Co(NO_3)_4]$ (7).

X-ray Analysis

Crystals suitable for X-ray analysis were obtained by recrystallization from acetonitrile/toluene. A crystal ca. 0.06 × 0.27 × 0.30 mm in size was mounted in a general orientation. Unit-cell parameters were refined by least-squares on 2 sin θ/λ values for 25 reflections measured on a diffractometer with Mo K_α radiation (λ = 0.71073 Å). Crystal data at 22°C are:

$C_{16}H_{48}CoN_{10}O_6P_8$ f.w. = 783.35

Triclinic, $a = 10.891(2)$, $b = 11.201(2)$, $c = 14.944(2)$ Å, $\alpha = 93.21(1)$, $\beta = 95.66(1)$, $\gamma = 104.69(1)°$, $V = 1748.6(5)$ Å^3, $Z = 2$, $\rho_c = 1.488$ g cm^{-3}, $F(000) = 818$, μ(Mo K_α) = 8.32 cm^{-1}. Absent reflections: none, space group $P\bar{1}$ (C_i^1, No. 2) from structure analysis. Cell constants refer to the Delaunay reduced cell.

Intensities were measured with graphite-monochromatized Mo K_α radiation on an Enraf-Nonius CAD4-F diffractometer. An ω–2θ scan at 0.65–6.71° min^{-1} over a range of (0.60 + 0.35 tan θ) degrees in ω (extended by 25% on both sides for background measurement) was employed. Data were measured to 2θ = 57.5°. The intensities of 3 check reflections, measured every 3600 s throughout the data collection, remained constant to within ±4%. After data reduction, an absorption correction was applied using the Gaussian integration method (8, 9). Transmission factors ranged from 0.790 to 0.948 for 120 sampling points. Of the 9034 independent reflections measured, 5165 (57%) had intensities greater than $3\sigma(I)$ above background where $\sigma^2(I) = S + 2B + (0.04(S - B))^2$ with S = scan count and B = background count.

Analysis was initiated in the centrosymmetric space group $P\bar{1}$

0008-4042/81/162435-06$01.00/0

©1981 National Research Council of Canada/Conseil national de recherches du Canada

Can. J. Chem. Downloaded from www.nrcresearchpress.com by 210.87.254.42 on 09/06/12
For personal use only.

Can. J. Chem. Downloaded from www.nrcresearchpress.com by 210.87.254.42 on 09/06/12
For personal use only.

on the basis of the *E*-statistics. The structure was solved by direct methods, the coordinates of the Co and P atoms being determined from an *E*-map and those of the remaining non-hydrogen atoms from a subsequent difference map. After full-matrix least-squares refinement of the non-hydrogen atoms with anisotropic thermal parameters to $R = 0.082$, disordering of the free nitrate anion was apparent from anomalously large thermal parameters and the appearance on a difference map of several large peaks in the vicinity of the free anion. This nitrate group was then left out of the calculations and the remainder of the structure refined to $R = 0.086$. A difference map was calculated and a three-dimensional contour map of the free nitrate region was constructed. Careful examination of the difference map indicated threefold disorder with near coincidence of the nitrogen atoms. The disorder was accounted for by three rigid groups with idealized geometry (N—O = 1.25 Å), only group parameters and group temperature factors being varied. Occupancy factors were initially estimated from peak heights of non-superimposed oxygen atoms and later adjusted to give nearly equal group temperature factors.

All 48 hydrogen atoms were located and refined with isotropic thermal parameters. The scattering factors of ref. 10 were used for non-hydrogen atoms and those of ref. 11 for hydrogen atoms. Anomalous scattering factors from ref. 12 were used for the Co and P atoms. The weighting scheme, $w = 1/\sigma^2(F)$ where $\sigma^2(F)$ is derived from the previously defined $\sigma^2(I)$ gave uniform average values of $w(|F_o| - |F_c|)^2$ over ranges of $|F_o|$ and was employed in the final stages of refinement. Convergence was reached at $R = 0.037$ and $R_w = 0.047$ for 5165 reflections with $I \geq 3\sigma(I)$. For all 9034 reflections $R = 0.095$ and $R_w = 0.047$. The function minimized was $\Sigma w(|F_o| - |F_c|)^2$, $R = \Sigma||F_o| - |F_c||/\Sigma|F_o|$ and $R_w = (\Sigma w(|F_o| - |F_c|)^2/\Sigma w|F_o|^2)^{1/2}$.

On the final cycle of refinement the mean and maximum parameter shifts corresponded to 0.26 and 1.54σ respectively. The mean error in an observation of unit weight was 1.439. A final difference map showed maximum fluctuations of −2.3 to 0.75 e Å^{-3} in the vicinity of the disordered nitrate group and ±0.25 e Å^{-3} elsewhere. The final positional and thermal parameters appear in Tables 1 and 2[1] respectively. Measured and calculated structure factors have been placed in the Depository of Unpublished Data.[1] Rigid group parameters are given in Table 3.[1]

The thermal motion has been analysed in terms of the rigid-body modes of translation, libration, and screw motion (13) using the computer program MGTLS (described in ref. 13). The rms standard error in the temperature factors U_{ij} (derived from the least-squares analysis) is 0.0021 Å^2. Analysis of the entire cation gave rms $\Delta U_{ij} = 0.0075$ Å^2 and indicated some independent motion of the methyl and nitrate groups. Each of the eight phosphorus tetrahedra was separately analysed giving rms ΔU_{ij} values of 12, 15, 11, 14, 10, 15, 12, and 10 (all × 10^{-4}) Å^2 respectively for P(1)—P(8). The Co coordination group gave a non-positive-definite libration tensor thus corrections to bonds involving the Co atom were based on the analysis of the cation as a whole. The appropriate bond distances have been corrected for libration (14), using shape parameters q^2 of 0.08 for all atoms involved. Corrected bond lengths appear in Table 4 along with the uncorrected values and corrected bond angles do not differ by more than 1σ from the uncorrected values given in Table 5[1]. Intra-annular torsion angles defining the conformations of chelate and phosphazene rings are listed in Table 6. Details of the weak C—H···O interactions are given in Table 7.[1]

[1]The structure factor table, Tables 2 (thermal parameters), 3 (rigid group parameters), 5 (bond angles) and 7 (C—H···O interactions) and Fig. 2 (stereo view of the cation) are available, at a nominal charge, from the Depository of Unpublished Data, CISTI, National Research Council of Canada, Ottawa, Canada K1A 0S2.

Results and Discussion

The crystal structure of **2** consists of discrete $N_8P_8Me_{16}\cdot CoNO_3^+$ cations and NO_3^- anions which are linked by an extensive network of weak C—H···O interactions (details in Table 7). These weak interactions are probably responsible for the observed disordering of the free nitrate anion since for each of the three orientations there is at least one O···H contact of less than 2.4 Å. There are also two weak intramolecular C—H···O interactions of possible significance, also included in Table 7.

A general view of the cation is shown in Fig. 1, and stereoscopic view in Fig. 2.[1] Contrary to what might have been expected from the structure of the free ligand (4), coordination of the metal atom does not preserve fourfold symmetry. The cobalt atom is coordinated by a bidentate nitrate group and by the ring nitrogen atoms N(1), N(2), N(4), and N(5), so forming, within the PN ring, one six-membered and two four-membered rings. This coordination scheme is the same as that found in complexes of $N_6P_6(NMe_2)_{12}$ (15, 16), and presumably arises from the same cause. It seems likely that the second coordination takes place at the nitrogen atom with which it can form a stable ring, which is a six-membered ring for a cyclic phosphazene. This is what is found in the complex (η^2-$N_6P_6Me_{12}$)$PdCl_2$ (2) and in (η^2-$N_4P_4Me_8$)$PtCl_2$ (17). Subsequent coordination then takes place at the nearest donor sites, to form four-membered rings, rather than at the remote site, which is the most nucleophilic, or at the intermediate sites, which would allow the formation of four stable six-membered rings. In complexes of larger phosphazenes, we can expect the metal atom to occupy one corner of the ligand, so allowing the possible incorporation of additional metal atoms.

The irregular coordination scheme of the metal is shown in Fig. 3. Because of the small angular "bite" of the ligands (which are temporarily regarded as chemically identical), the stereochemistry cannot be regular octahedral, but moves towards trigonal prismatic configuration. The distortion is such that N(1)CoN(4) are nearly colinear (164.7(1)°), and form the axis of a nearly trigonal bipyramidal arrangement, the equatorial sites being occupied by N(2), N(5), and the η^2-nitrato ligand. The significant variation in the Co—N distances (2.113(3)–2.197(3) Å) reflects the trigonal bipyramidal character of the complex **2**, the "equatorial" bond lengths being significantly shorter than the "axial" distances with the exception of the pair Co–N(1)/N(2).

Can. J. Chem. Downloaded from www.nrcresearchpress.com by 210.87.254.42 on 09/06/12
For personal use only.

TABLE 1. Final positional parameters (fractional: O, N, and C × 10^4; Co and P × 10^5; H × 10^3) with estimated standard deviations in parentheses

Atom	x	y	z
Co	59105(4)	80329(4)	18779(3)
P(1)	80569(9)	72898(9)	4815(6)
P(2)	82081(9)	95964(8)	15908(7)
P(3)	72049(10)	108606(9)	30757(7)
P(4)	45109(10)	97914(9)	30023(7)
P(5)	47040(9)	72968(9)	33739(6)
P(6)	62005(9)	54897(8)	29246(6)
P(7)	89808(9)	64455(9)	31599(6)
P(8)	101019(9)	64853(9)	14718(6)
O(1)	5023(3)	8737(3)	609(2)
O(2)	4571(3)	6857(3)	873(2)
O(3)	3836(4)	7360(4)	−406(2)
N(1)	7584(3)	8175(3)	1210(2)
N(2)	7265(3)	9750(3)	2339(2)
N(3)	5854(3)	10642(3)	3458(2)
N(4)	4491(3)	8366(3)	2740(2)
N(5)	5716(3)	6758(3)	2875(2)
N(6)	7604(3)	5661(3)	2676(2)
N(7)	10022(3)	6908(3)	2495(2)
N(8)	9447(3)	7134(3)	702(2)
N(9)	4480(3)	7665(3)	335(2)
C(1)	6875(4)	5848(4)	335(3)
C(2)	7993(6)	7891(6)	−602(3)
C(3)	9848(4)	9908(5)	2035(4)
C(4)	8150(6)	10641(5)	728(4)
C(5)	8381(5)	11004(6)	4029(4)
C(6)	7637(7)	12310(5)	2593(5)
C(7)	3965(6)	10375(5)	1996(4)
C(8)	3341(6)	9862(6)	3752(4)
C(9)	5333(6)	7869(6)	4514(3)
C(10)	3221(5)	6175(5)	3442(5)
C(11)	5990(5)	4904(5)	4016(4)
C(12)	5149(5)	4322(5)	2145(4)
C(13)	8855(5)	7772(4)	3847(3)
C(14)	9592(5)	5531(5)	3949(4)
C(15)	9587(6)	4822(4)	1282(4)
C(16)	11742(5)	6883(7)	1277(4)
H(1a)	610(5)	594(4)	13(3)
H(1b)	695(4)	549(4)	86(3)
H(1c)	709(5)	537(5)	−6(4)
H(2a)	869(5)	863(5)	−54(3)
H(2b)	716(5)	806(5)	−75(4)
H(2c)	812(6)	724(6)	−99(4)
H(3a)	1015(4)	1071(5)	226(3)
H(3b)	1030(5)	972(5)	152(4)
H(3c)	998(5)	941(5)	243(4)
H(4a)	733(5)	1065(5)	47(3)
H(4b)	876(5)	1053(5)	35(4)
H(4c)	860(5)	1142(6)	100(4)
H(5a)	919(5)	1114(5)	384(4)
H(5b)	818(5)	1021(5)	429(4)
H(5c)	831(5)	1165(5)	442(4)
H(6a)	701(5)	1229(5)	211(4)
H(6b)	848(7)	1242(6)	241(5)
H(6c)	760(6)	1279(6)	294(4)
H(7a)	314(6)	991(6)	181(4)
H(7b)	388(5)	1120(5)	214(3)
H(7c)	453(6)	1036(5)	161(4)
H(8a)	322(5)	1067(5)	382(4)
H(8b)	274(6)	938(6)	357(4)
G(8c)	365(5)	957(4)	439(4)

TABLE 1 (*Concluded*)

Atom	x	y	z
H(9a)	552(5)	728(5)	474(4)
H(9b)	474(5)	809(5)	480(3)
H(9c)	609(6)	855(5)	449(4)
H(10a)	293(5)	574(5)	287(4)
H(10b)	335(5)	568(5)	392(4)
H(10c)	268(5)	658(5)	359(3)
H(11a)	624(5)	422(5)	401(3)
H(11b)	644(4)	551(4)	449(3)
H(11c)	512(5)	475(4)	407(3)
H(12a)	437(4)	411(4)	236(3)
H(12b)	550(6)	372(5)	210(4)
H(12c)	503(6)	462(6)	168(4)
H(13a)	964(5)	829(4)	406(3)
H(13b)	841(5)	746(4)	438(4)
H(13c)	842(5)	822(4)	356(3)
H(14a)	1043(4)	603(4)	429(3)
H(14b)	962(5)	475(5)	363(3)
H(14c)	904(5)	534(5)	435(4)
H(15a)	859(6)	457(5)	128(4)
H(15b)	963(5)	452(5)	69(4)
H(15c)	1006(6)	449(5)	174(4)
H(16a)	1212(5)	769(5)	151(4)
H(16b)	1211(6)	654(6)	157(5)
H(16c)	1184(7)	665(7)	68(5)

All of the Co—N distances in **2** are intermediate between the mean[2] equatorial and axial Co—N distances of 2.058(8) and 2.248(15) Å in the unambiguously five-coordinate complex cation $[\eta^4\text{-}N_6P_6(NMe_2)_{12}]CoCl^+$ (15) and in spite of the wide variation in the individual values the average Co—N distance is the same (2.15 Å) in both structures. In **2**, the non-spherical electron distribution of the d^7 Co(II) ion shows up in a different way. The metal is truly six-coordinate, and perhaps the most striking feature of the local geometry is the unsymmetrical coordination of the nitrate group, the Co—O distances differing by 0.193(5) Å. Other examples of unsymmetrical bidentate coordination by a nitrate group are known, especially with transition metal ions, like Co(II) and Cu(II), which are not spherically symmetrical (18).

The geometry of the phosphazene ring shows several interesting features. The lengthening of the mean P—N bond distance, to 1.613(20) Å from 1.590(13) Å in the ligand, corresponds to the withdrawal of bonding electrons by the cobalt. It should be noted that in both the free ligand **1** (4) and in **2** there is considerable variation in the P—N distances, ranging from 1.575(2) to 1.606(2) Å in **1** and from 1.579(3) to 1.645(3) Å in **2**. In both molecules hybridization effects are an important

[2]Here and elsewhere in this report mean values refer to weighted means with rms deviations from the mean in parentheses.

Can. J. Chem. Downloaded from www.nrcresearchpress.com by 210.87.254.42 on 09/06/12
For personal use only.

TABLE 4. Bond lengths (Å) with estimated standard deviations in parentheses*

	Length			Length	
Bond	Uncorr.	Corr.	Bond	Uncorr.	Corr.
Co —O(1)	2.312(4)	2.314	P(8)—N(8)	1.599(3)	1.608
Co —O(2)	2.119(3)	2.121	P(1)—C(1)	1.779(4)	1.786
Co —N(1)	2.139(3)	2.142	P(1)—C(2)	1.789(4)	1.798
Co —N(2)	2.136(3)	2.139	P(2)—C(3)	1.782(5)	1.788
Co —N(4)	2.195(3)	2.197	P(2)—C(4)	1.797(5)	1.803
Co —N(5)	2.110(3)	2.113	P(3)—C(5)	1.791(5)	1.800
P(1)—N(1)	1.637(3)	1.642	P(3)—C(6)	1.786(6)	1.795
P(1)—N(8)	1.572(3)	1.579	P(4)—C(7)	1.782(5)	1.792
P(2)—N(1)	1.611(3)	1.617	P(4)—C(8)	1.790(5)	1.798
P(2)—N(2)	1.621(3)	1.625	P(5)—C(9)	1.792(5)	1.801
P(3)—N(2)	1.633(3)	1.639	P(5)—C(10)	1.794(5)	1.803
P(3)—N(3)	1.596(4)	1.602	P(6)—C(11)	1.806(5)	1.813
P(4)—N(3)	1.593(3)	1.599	P(6)—C(12)	1.786(5)	1.793
P(4)—N(4)	1.617(3)	1.623	P(7)—C(13)	1.800(5)	1.807
P(5)—N(4)	1.615(3)	1.619	P(7)—C(14)	1.792(5)	1.801
P(5)—N(5)	1.608(3)	1.616	P(8)—C(15)	1.802(5)	1.812
P(6)—N(5)	1.639(3)	1.645	P(8)—C(16)	1.785(5)	1.796
P(6)—N(6)	1.575(3)	1.580	O(1)—N(9)	1.224(4)	1.225
P(7)—N(6)	1.610(3)	1.615	O(2)—N(9)	1.260(4)	1.262
P(7)—N(7)	1.588(3)	1.594	O(3)—N(9)	1.232(4)	1.232
P(8)—N(7)	1.593(3)	1.599			

*Corrected distances are employed throughout the discussion, esd's assumed equal to those of the uncorrected values.

TABLE 6. Intra-annular torsion angles (deg) phosphazene and chelate rings

Atoms	Value	Atoms	Value
P(8)—N(8)—P(1)—N(1)	67.4(2)	P(4)—N(4)—P(5)—N(5)	−131.7(1)
N(8)—P(1)—N(1)—P(2)	56.1(2)	N(4)—P(5)—N(5)—P(6)	−163.8(1)
P(1)—N(1)—P(2)—N(2)	−175.0(1)	P(5)—N(5)—P(6)—N(6)	−152.6(1)
N(1)—P(2)—N(2)—P(3)	177.3(1)	N(5)—P(6)—N(6)—P(7)	67.4(2)
P(2)—N(2)—P(3)—N(3)	164.1(1)	P(6)—N(6)—P(7)—N(7)	−150.1(1)
N(2)—P(3)—N(3)—P(4)	−22.0(2)	N(6)—P(7)—N(7)—P(8)	−17.7(2)
P(3)—N(3)—P(4)—N(4)	54.6(2)	P(7)—N(7)—P(8)—N(8)	87.8(2)
N(3)—P(4)—N(4)—P(5)	64.2(2)	N(7)—P(8)—N(8)—P(1)	−55.4(2)
N(1)—Co —N(5)—P(6)	−30.1(2)	N(2)—Co —N(1)—P(2)	−8.8(1)
Co —N(5)—P(6)—N(6)	44.5(2)	Co —N(1)—P(2)—N(2)	11.1(2)
N(5)—P(6)—N(6)—P(7)	67.4(2)	N(1)—P(2)—N(2)—Co	−11.1(2)
P(6)—N(6)—P(7)—N(7)	−150.1(1)	P(2)—N(2)—Co—N(1)	8.7(1)
N(6)—P(7)—N(7)—P(8)	−17.7(2)		
P(7)—N(7)—P(8)—N(8)	87.8(2)	N(5)—Co —N(4)—P(5)	2.3(1)
N(7)—P(8)—N(8)—P(1)	−55.4(2)	Co —N(4)—P(5)—N(5)	−2.9(1)
P(8)—N(8)—P(1)—N(1)	67.4(2)	N(4)—P(5)—N(5)—Co	3.0(2)
N(8)—P(1)—N(1)—Co	−132.7(1)	P(5)—N(5)—Co —N(4)	−2.3(1)
P(1)—N(1)—Co —N(5)	71.3(1)		
		O(2)—Co —O(1)—N(9)	−4.3(2)
N(4)—Co —N(2)—P(3)	0.4(1)	Co —O(1)—N(9)—O(2)	6.8(2)
Co —N(2)—P(3)—N(3)	−4.7(2)	O(1)—N(9)—O(2)—Co	−7.5(3)
N(2)—P(3)—N(3)—P(4)	−22.0(2)	N(9)—O(2)—Co —O(1)	4.2(2)
P(3)—N(3)—P(4)—N(4)	54.6(2)		
N(3)—P(4)—N(4)—Co	−54.6(2)		
P(4)—N(4)—Co —N(2)	28.1(1)		

factor in the P—N length variation while in **2** perturbations which result from coordination to the Co are also important (see below). The P—C bond lengths do not vary greatly within the molecule, P—C = 1.786(4)–1.813(5), mean 1.799(7) Å, somewhat shorter than in the ligand (1.811(2) Å). Since coordination draws the molecule together, the ring angles decrease, especially near the coordination centres, and resemble those in the ligand at P(7) and P(8). In **1** the mean N—P—N angle (117.2(10)°) is

Can. J. Chem. Downloaded from www.nrcresearchpress.com by 210.87.254.42 on 09/06/12
For personal use only.

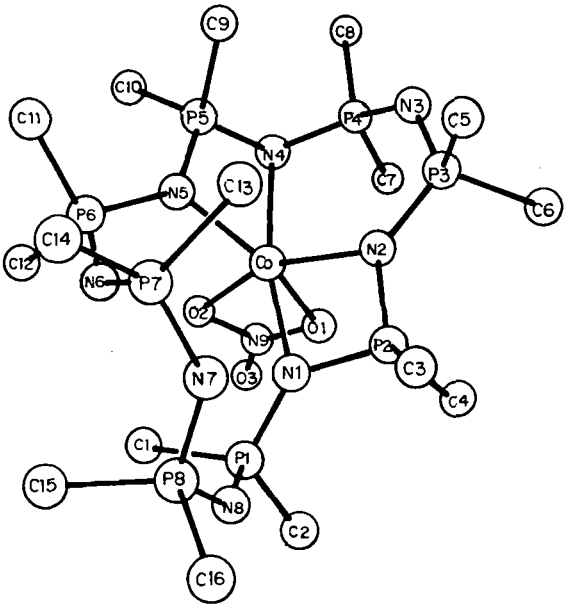

FIG. 1. General view of the $N_8P_8Me_{16}\cdot CoNO_3^+$ cation.

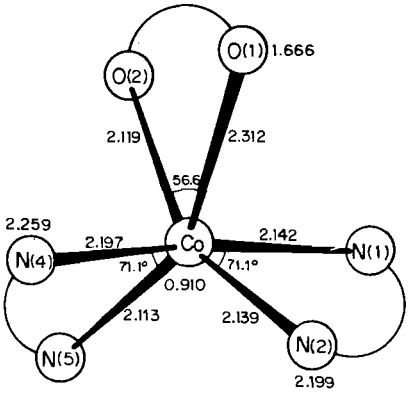

FIG. 3. Coordination scheme of Co, viewed perpendicular to the N(1)O(2)N(5) plane, showing heights (Å) above this plane, bond lengths (Å, σ = 0.003–0.004) and bond angles (deg, σ = 0.1°).

associated with a mean C—P—C angle of 103.5(10)°; *s*–*p* hybridization[3] would require 103.2°. In the complex **2**, the decreased ring angles at phosphorus (100.5(2)–117.8(2), mean 112(7)°) are associated with slightly increased C—P—C angles, but the effect is not large, and even at P(2) and P(5), the exocyclic angle is only 105.8(3)°; from *s*–*p* hybridization, 120.5° would be expected. Electronic effects within the ring have little effect on the geometry of the exocyclic groups.

[3]Given the N—P—N angle, the opposite C—P—C angle may be calculated assuming that the bonding orbitals are hybrids of *s* and *p* orbitals only by the formula: $\theta' = 2\ \mathrm{csc}^{-1}\ [3 - \mathrm{csc}^2(\theta/2)]^{1/2}$, where θ' = C—P—C and θ = N—P—N.

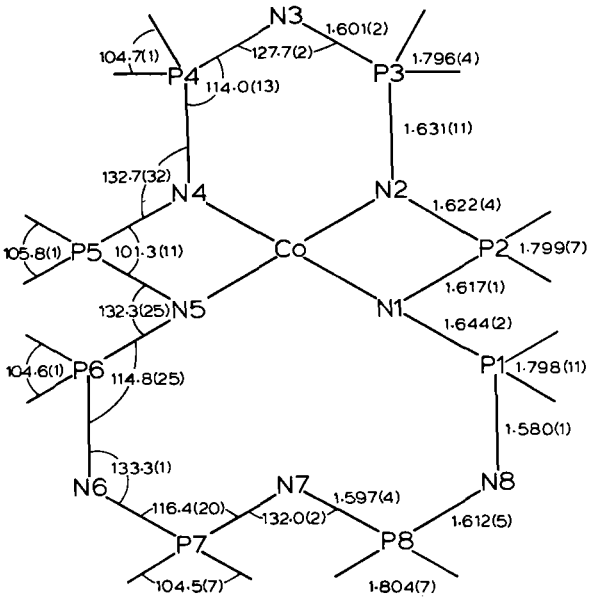

FIG. 4. Averaged geometry of **2** (rms deviations from the mean in parentheses). The P—C bond lengths are averaged in sets of four, other parameters in corresponding pairs.

Although the mean P—N bond length does not differ greatly from that in the ligand, coordination causes the systematic variations in bond length which are illustrated in Fig. 4. Except for P(3)–N(2) and P(4)–N(4), which differ by 0.016(4) Å, all pairs of bonds which are symmetrically related in Fig. 4 differ by 0.007(4) Å or less, and are averaged. This closeness to equality is interesting, in view of the total lack of symmetry in the ten-membered ring CoN(5)···N(1)Co; the systematic inequalities of bond length seen in Fig. 4 are independent of conformation. Qualitatively, the bond length varia-

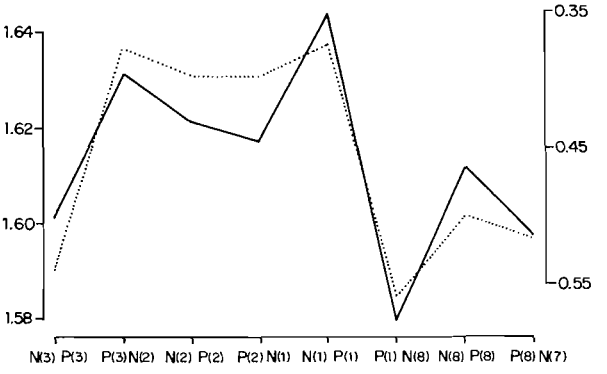

FIG. 5. Comparison of averaged P—N bond lengths (full line, l.h. scale) with calculated bond orders (dashed line, r.h. scale) (HMO, $\alpha_N = -1$, $\alpha_P = +1$, $\alpha_{pert.} = -0.3$, all β's = -1).

tion follows the trend of bond orders calculated for electron withdrawal by four acceptor atoms from the ring through the coordinated nitrogen atoms (Fig. 5). The major geometrical change occurs in the region N(1)—P(1)—N(8), where there is a marked disporportionation in bond length. In the region most remote from the coordination sites, both the bond lengths and the calculated π-bond order resemble those of the free ligand (1.590(13) Å, 0.517). It is also interesting that if the four donor sites, and hence the remainder of the molecule, are allowed to interact by conjugation through the acceptor atom, a different pattern of bond orders is found, P(3)–N(2) and P(1)–N(1) being greatly strengthened. It is clear that conjugative interactions between the metal and the ring are quite insignificant. As concluded earlier (16), phosphazenes resemble simple amines in their donor properties.

Acknowledgements

We are grateful to NSERC for financial support through operating grants (J.T, N.L.P.) and for an NSERC Scholarship (K.D.G.) and to the University of British Columbia Computing Centre for assistance.

1. H. T., SEARLE, J. DYSON, N. L. PADDOCK, and T. N. RANGANATHAN. J. Chem. Soc. Dalton Trans. 203 (1975).
2. N. L. PADDOCK, T. N. RANGANATHAN, S. J. RETTIG, R. D. SHARMA, and J. TROTTER. Can. J. Chem. **59**, 2429 (1981).
3. K. D. GALLICANO, R. T. OAKLEY, N. L. PADDOCK, S. J. RETTIG, and J. TROTTER. Can. J. Chem. **55**, 304 (1977).
4. R. T. OAKLEY, N. L. PADDOCK, S. J. RETTIG, and J. TROTTER. Can. J. Chem. **55**, 2530 (1977).
5. C. C. ADDISON and B. M. GATEHOUSE. J. Chem. Soc. 613 (1960).
6. N. F. CURTIS and T. M. CURTIS. Inorg. Chem. **4**, 804 (1965).
7. R. J. FEREDAY and D. SUTTON. J. C. S. Chem. Commun. 510 (1966).
8. P. COPPENS, L. LEISEROWITZ, and D. RABINOVICH. Acta Crystallogr. **18**, 1035 (1965).
9. W. R. BUSING and H. A. LEVY. Acta Crystallogr. **22**, 457 (1967).
10. D. T. CROMER and J. B. MANN. Acta Crystallogr. Sect. A, **24**, 321 (1968).
11. R. F. STEWART, E. R. DAVIDSON, and W. T. SIMPSON. J. Chem. Phys. **42**, 3175 (1965).
12. D. T. CROMER and D. LIBERMAN. J. Chem. Phys. **53**, 1891 (1970).
13. V. SCHOMAKER and K. N. TRUEBLOOD. Acta Crystallogr. Sect. B, **24**, 63 (1969).
14. D. W. J. CRUICKSHANK. Acta Crystallogr. **9**, 747 (1956); **9**, 754 (1956); **14**, 896 (1961).
15. W. HARRISON and J. TROTTER. J. Chem. Soc. Dalton Trans. 61 (1973).
16. H. P. CALHOUN, N. L. PADDOCK, and J. N. WINGFIELD. Can. J. Chem. **53**, 1765 (1975).
17. J. P. O'BRIEN, R. W. ALLEN, and H. R. ALLCOCK. Inorg. Chem. **18**, 2230 (1979).
18. C. C. ADDISON, N. LOGAN, and S. C. WALLWORK. Q. Rev. Chem. Soc. **25**, 289 (1971); F. A. COTTON and J. G. BERGMAN. J. Am. Chem. Soc. **86**, 2941 (1964).

Can. J. Chem. Downloaded from www.nrcresearchpress.com by 210.87.254.42 on 09/06/12
For personal use only.

Site selective fluorescence and purity of a rare earth garnet crystal[1]

L. V. HALEY, B. JACQUIER,[2] AND J. A. KONINGSTEIN
Department of Chemistry, Carleton University, Ottawa, Ont., Canada K1S 5B6
Received December 16, 1980

L. V. HALEY, B. JACQUIER, and J. A. KONINGSTEIN. Can. J. Chem. **59**, 2441 (1981).

Site selective fluorescence spectroscopy of a crystal of europium gallium garnet containing Cr^{3+} as an impurity has been carried out. An analysis of the experimental results reveals that the strongest fluorescence spectrum between 590.0 nm and 620.0 nm is due to emission from an Eu^{3+}–Cr^{3+} pair. Fluorescences of farther removed pairs and that of Eu^{3+} occupying the 8-coordinated *d* site and 6-coordinated Ga^{3+} site are also assigned. Energy transfer between the various sites occurs while the excitation spectra for the R lines of Cr^{3+} show that extremely fast transfer takes place between the R_2 and R_1 levels.

L. V. HALEY, B. JACQUIER et J. A. KONINGSTEIN. Can. J. Chem. **59**, 2441 (1981).

On a étudié la spectroscopie de fluorescence par sélection d'un cristal de grenat d'europium gallium contenant du Cr^{3+} comme impureté. Une analyse des résultats expérimentaux révèle que le spectre de fluorescence le plus intense entre 590,0 nm et 620,0 nm est dû à l'émission par la paire Eu^{3+}–Cr^{3+}. On a également identifié les fluorescences des paires éloignées et celles du Eu^{3+} occupant 8 sites *d* coordonnés et 6 sites Ga^{3+} coordonnés. L'énergie de transfert entre les différents sites qui apparait, lors du spectre d'excitation, des lignes R du Cr^{3+}, montre que ce transfert extrêmement rapide à lieu entre les niveaux R_2 et R_1.

[Traduit par le journal]

I. Introduction

Rare earth garnets have in the past been studied in great detail; in particular, the refinement of the energy level diagram for the trivalent lanthanide ions (1–4). This diagram is composed of the crystal field levels of the split *LSJ* manifolds arising from the ($4f$) configuration of the trivalent lanthanides, and is normally arrived at from a comparison of spectroscopic results which include absorption, fluorescence, and light scattering studies in various parts of the electromagnetic spectrum. The assignment of the spectra is not always straightforward in that the identification of pure electronic transitions is made difficult as a result of the appearance of vibronic transitions. These vibronic effects, for instance, dominate the absorption and fluorescence spectrum of the ytterbium aluminum and gallium garnet to such a degree (5) that the assignment of the 0–0 transitions could only be made after elaborate studies.

Apart from such spectral complications as vibronic coupling effects, information has recently become available (6–8) that not all rare earth ions replace the 8-coordinated yttrium ions which occupy the orthorhombic *d* sites in the unit cell of the cubic garnet crystals (space group O_h^{10}). Some of the trivalent lanthanide ions are thought (7) to be substituted for the 6-coordinated Al^{3+} (or Ga^{3+}) ions in the *a* sites. Also, nearly all these garnet crystals could contain Cr^{3+} as an impurity and transitions of europium gallium garnet (EuGaG) have already been observed (9) which are assigned to Eu^{3+}–Cr^{3+} pairs. The energy level diagram of rare earth ions being part of a pair is of course different if compared to that of the lanthanide ions in the orthorhombic *d* sites and hence the appearance of another type of spectral interference. The latter, however, are more easily assigned (8) than the vibronic features because the method of site selective spectroscopy may be applied to distinguish transitions from one site to those from others. In the present article, we discuss site selective spectroscopy of a single crystal of EuGaG which contains a small amount (50 ppm) of Cr^{3+}. The europium compound is ideally suited for site selective spectroscopy with cw lasers in that the position of the $^5D_0$ excited state (which is some 17 200 cm^{-1} above the $^7F_0$ ground state) can be probed with the radiation from the rhodamine 6G dye laser, and both states are not split by crystal field effects. The laser radiation can be used to (*i*) induce the $^5D_0$–^7F_J (J = 0, 1, 2, ..., 6) fluorescence transitions, and because the crystal field levels of $^7F_1$ are some 200–450 cm^{-1} above $^7F_0$, we can (*ii*) also probe absorptions of $^5D_0 \leftarrow {}^7F_{0,1}$ with the tunable laser source.

Our results show that for EuGaG containing Cr^{3+} as an impurity, we have besides transitions of Eu^{3+} occupying the orthorhombic sites also those of Eu^{3+}–Cr^{3+} pairs and Eu^{3+} replacing the Ga^{3+} ions. In particular, we demonstrate that the excitation spectrum of the Cr^{3+} R_1 line contains important

[1]Research supported by the Natural Sciences and Engineering Research Council of Canada.

[2]Permanent address: Physico-Chimie des Matériaux Luminescents, Université de Lyon I, France.

0008-4042/81/162441-08$01.00/0
©1981 National Research Council of Canada/Conseil national de recherches du Canada

Can. J. Chem. Downloaded from www.nrcresearchpress.com by 210.87.254.5 on 09/06/12
For personal use only.

Can. J. Chem. Downloaded from www.nrcresearchpress.com by 210.87.254.5 on 09/06/12
For personal use only.

information on the type of sites which are present in this and perhaps other rare earth garnet crystals. We also present evidence that the strongest among the fluorescence transitions is not due to europium ions of the orthorhombic sites but that of nearest neighbour Cr^{3+}–Eu^{3+} pairs.

II. Specific Fluorescence and Absorptions

The absorption and fluorescence spectrum of a single crystal of EuGaG containing Cr^{3+} as an impurity has been discussed by van der Ziel and Van Uitert (9). These authors found, apart from the well known $^5D_0$–^7F_J fluorescence which occurs between 590–850 nm, evidence of fluorescence of Eu^{3+}–Cr^{3+} pairs. The spectrum assigned to transitions of the pair is in the region of 710–1100 nm and can be interpreted as originating in the components of the ^2E_g state of a Cr^{3+}–Eu^{3+} pair and terminating on those of the pair ^7F_J states. The Eu^{3+} ions of EuGaG-space group O_h^{10} occupy 8-coordinated *d* sites with D_2 symmetry, and the Cr^{3+} ions substitute (10) for Ga^{3+}, occupy 6-coordinated *a* sites having C_{3i} symmetry. The Eu^{3+}–Cr^{3+} pair is bridged (11) via an O^{2-} ion, and the overall situation resembles that of the Cr^{3+} pairs in ruby (12). Neither the number of components nor the position of the ^7F_J and ^2E_g states of the pair equals that of the crystal field levels of the non-paired Eu^{3+} ions. If for instance spin–spin exchange interaction of the type $^7F_J(Eu^{3+})$–$^4A(Cr^{3+})$ is introduced, then a doubling of the number of crystal field levels of the ^7F_J series is computed (for a total of 98 components). The position of these levels depends on the value of the coupling parameter, and a rather complex energy level diagram is anticipated if apart from nearest neighbours next to nearest neighbours pairs etc. are taken into consideration. The situation with regard to the Cr^{3+} ion is different in that contrary for Eu^{3+} — assuming all Eu^{3+} occupies the *d* sites — all these transitions metal ions are part of a pair. Because the position of the ^5D_J manifolds of Eu^{3+} is closest in energy to that of ^2E_g of Cr^{3+} in the 6-coordinated C_{3i} sites, one finds that to a first approximation the E_g levels can split into two main components each one being composed of five Kramers pairs. On the other hand, the $^5D_0$ state of Eu^{3+} is nearly isoenergetic with $^2T_{1g}$ of Cr^{3+}, and as a result, we expect six levels for the pair as compared to only one crystal field level for the non-paired ion.

Van der Ziel and Van Uitert indeed found a rather complicated pair fluorescence spectrum (9) of an EuGaG crystal containing Cr^{3+} as the impurity, but the absorption spectrum from 590–600 nm which is due to $^5D_0 \leftarrow {}^7F_1$ is rather simple in that it consists of three lines. These lines have their counterpart in the emission spectrum and are thought to be due to europium ions experiencing a site of lower than tetragonal symmetry. Furthermore, it appears from the number of absorptions due to $^5D_0 \leftarrow {}^7F_1$ transitions that the majority of Eu^{3+} occupies this site which must be the 8-coordinated *d* sites. Of relevance here is a recent study of Eu doped yttrium aluminum garnet where arguments (8) were presented that the strongest fluorescence lines of the $^5D_0 \rightarrow {}^7F_1$ series is not due to Eu^{3+} ions replacing the Y^{3+} of the *d* sites. The same apparently also holds for EuGaG because van der Ziel and Van Uitert found that if excited with blue light, those $^5D_0 \rightarrow {}^7F_1$ fluorescence lines which have their counterpart with the $^5D_0 \leftarrow {}^7F_1$ absorption spectrum are weaker than other features due to europium ions experiencing a different environment than those in the *d* sites.

Figure 1 shows part of the absorption spectrum of our EuGaG single crystal in the region of 579.0–600.0 nm. These spectra are difference spectra and were recorded with a tunable cw dye laser having a band width of ~0.025 nm. The laser beam was chopped and, after passing through a beam splitter, entered the crystal. Reference and sample beams were directed towards two diodes and their signals were processed by a boxcar integrator. We find a rather pronounced decrease in the line width of the $^5D_0 \leftarrow {}^7F_1$ transitions upon a decrease of the temperature of the sample. The relevant part of the energy level diagram of Eu^{3+} of EuGaG is also shown in Fig. 1, and the $^7F_1$ intermanifold electronic Raman spectrum (3) at 77 K is shown in Fig. 2. Note that if the FWHM of the bands of the fluorescence spectrum ($^5D_0 \rightarrow {}^7F_1$) is taken as the actual width of the $^7F_1$ crystal field levels, the FWHM of the electronic Raman transitions is much smaller. The phenomenon is similar to experimental features recently (13) recorded for Cr^{3+} in αAl_2O_3 and YAlG, and the seeming decrease in line width has its origin in the dynamical nature of the homogeneous broadening processes (14) which govern the linewidths at ambient and lower temperatures.

The absorption band of EuGaG at ~580.67 nm (see Fig. 1) is due to the $^5D_0 \leftarrow {}^7F_0$ transitions. This transition is highly forbidden, and only a weak band is recorded. This band, however, appears to have a shoulder towards lower wavelength.

III. Site Selection Fluorescence and their Excitation Spectrum

A. The Europium System

Five distinct sets of fluorescence spectra of EuGaG containing Cr^{3+} are excited and recorded if the cw laser is tuned from 579.0–581.0 nm. These

Can. J. Chem. Downloaded from www.nrcresearchpress.com by 210.87.254.5 on 09/06/12
For personal use only.

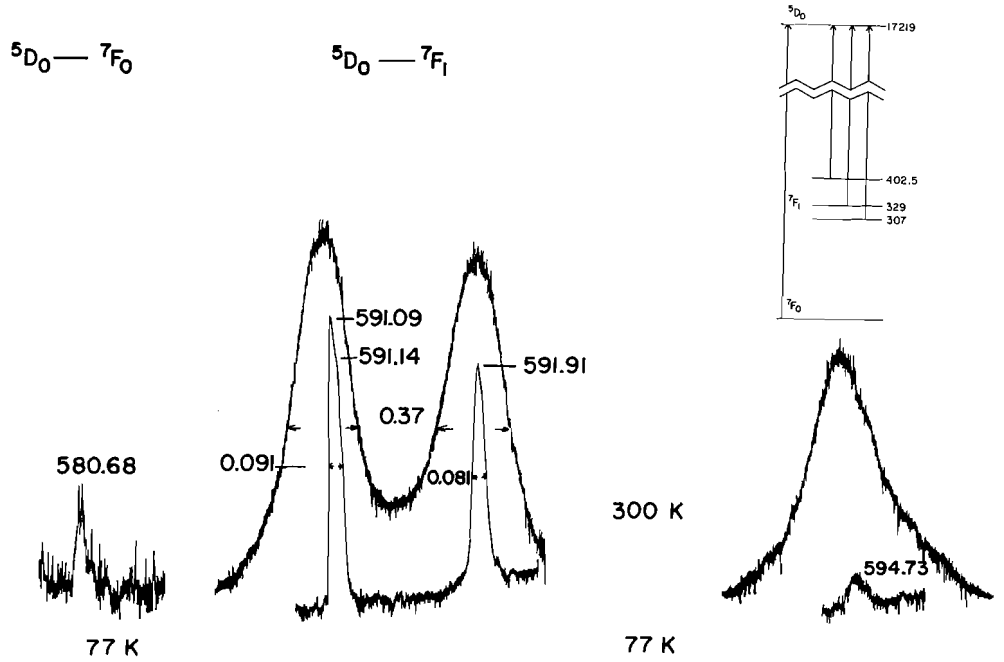

FIG. 1. The $^5D_0 \rightarrow {}^7F_0$ absorptions due to Eu^{3+} occupying the 8-coordinated orthorhombic *d* sites of EuGaG. All wavelengths are in nm and part of the relevant energy level diagram is indicated.

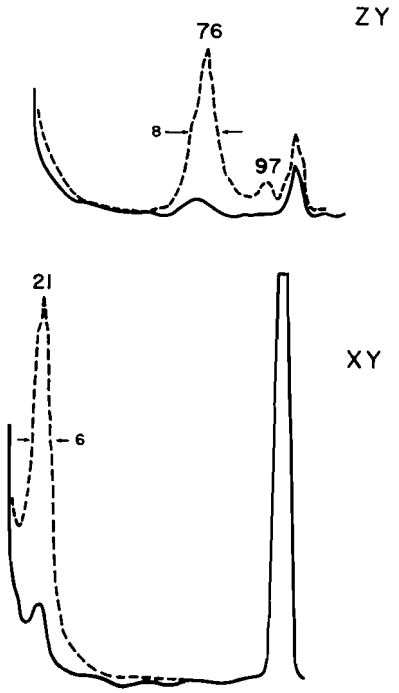

FIG. 2. Part of the Raman spectrum at 300 K (---) and 77 K (—) of EuGaG excited with $\lambda_l = 488.0$ nm showing the $^7F_1$ intramanifold transitions of Eu^{3+} in the *d* sites of EuGaG. The shift at $\sim 21\ cm^{-1}$ is due to transitions between the $^7F_1$ levels at 307 and $329\ cm^{-1}$ (see Fig. 1). The width of these levels as determined from the $^5D_0 \rightarrow {}^7F_1$ absorption spectrum is $\sim 11\ cm^{-1}$ while the width of the electronic Raman transition is $6\ cm^{-1}$.

fluorescence spectra are weak, and the intensity of the transition is comparable to those of the stronger Raman phonon bands of this crystal. The intensity of these phonons have been used as a standard which permits a comparison of the intensity of the fluorescence line of the five sites. Some representative spectra are shown in Fig. 3, and all data are collected and presented as stick spectra in Fig. 4. Two of the spectra, those of sites I and II, are unique in that the region where $^5D_0 \rightarrow {}^7F_1$ transitions of Eu^{3+} are expected, three lines are recorded and fluorescence due from other sites are not present. On the other hand, the spectra of sites III, IV, and V always contain fluorescence lines from site II. Also, while tuning the wavelength λ_l of the tunable dye laser from one specific excitation value to another, we find that the intensity of the fluorescence spectra goes through a minimum (zero intensity). The spectrum of site II is important from another point of view in that the position of the $^5D_0 \rightarrow {}^7F_1$ lines, contrary to those of the other sites, is within experimental error equal to those of the absorption transitions $^5D_0 \leftarrow {}^7F_1$ shown in Fig. 1 (see also Table 1). We assign the spectrum of site II to that of the majority of Eu^{3+} ions of EuGaG which occupy the orthorhombic *d* sites and note in passing that (compared to the phonon at $346.5\ cm^{-1}$) the fluorescence spectrum of site V and not that of site II is the most intense. Excitation spectra of the fluorescence lines at 591.95 nm (site II) and 592.14 nm

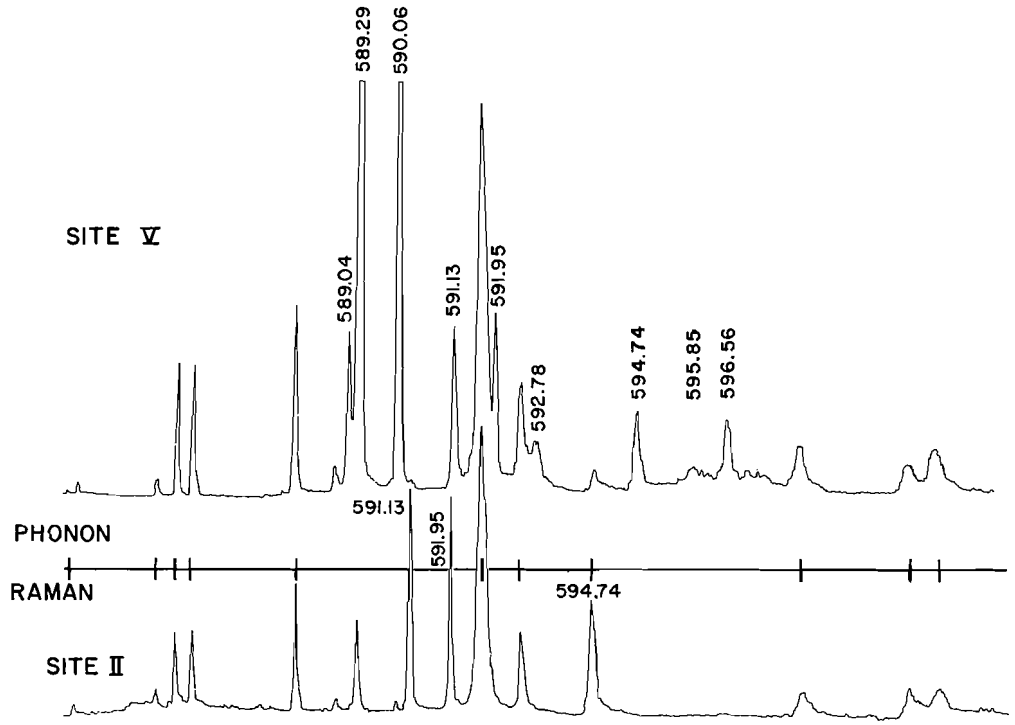

FIG. 3. $^5D_0 \rightarrow {}^7F_1$ fluorescence at 77 K due to site V representing the nearest neighbour Eu^{3+}–Cr^{3+} pair of EuGaG containing Cr^{3+}. This fluorescence is excited with $\lambda_l = 579.34$ nm. Also indicated is fluorescence due to site II (Eu^{3+} in the orthorhombic *d* sites) which is excited with $\lambda_l = 580.72$ nm. The position of the bands for site II is equal to that of the $^5D_0 \leftarrow {}^7F_1$ absorptions at 77 K (see Fig. 1). The Raman spectrum of EuGaG is also excited and the corresponding phonon Raman shifts are marked.

(site I) are displayed in Fig. 5. These spectra reveal, apart from the six relatively sharp maxima, two rather broad features. They are not part of the excitation spectrum but represent Raman scattering from phonons at 346 cm^{-1} and 366 cm^{-1} which occurs at the wavelength 591.95 nm (and 592.14 nm) to which the monochromator is tuned when the wavelength of the tunable laser is at 580.08 nm and 579.40 nm. The wavelength for which the sharp maxima occurs for fluorescence from site II are within experimental error equal to the wavelength for λ_l which yields the spectra of sites II–V of Fig. 4 (see also Table 1). A close examination of the data reveals that there exists another site, but the fluorescence spectrum of this site II*a* is so close to that of site II that its fluorescence cannot be separately recorded.

The excitation spectrum of that of site I, on the other hand, is rather simple (one maximum) and the fluorescence due to this site is the weakest among the series.

B. The Chromium System

Van der Ziel and Van Uitert found fluorescence (9) for a crystal of EuGaG containing Cr^{3+} as an impurity which is due to transitions of the type $^2E_g(\text{pair}) \rightarrow {}^7F_J(\text{pair})$, where ^2E_g and ^7F_J pair states are those discussed in section II. The $^2E_g \rightarrow {}^7F_0$ pair transitions are recorded at 698.8 nm (R_2) and 695.6 nm (R_1) and in Fig. 6 we show the excitation profiles for these lines in the range of 579.0–581.0 nm.

We note that the profile of the R_1 line is similar to that of the fluorescence from site II but different from that for site I. As a consequence of these observations, we conclude that while pumping in the $^5D_0$ state of sites II–V, energy is transferred into the ^2E_g pair level which in turn suggests that spectra of sites III–V are due to Eu^{3+}–Cr^{3+} pairs. Apparently, the position of the ^2E_g states of nearest neighbour (first), second and third pairs, etc. is not shifted significantly from each other, and emission to the ground state occurs in one band (the R_1 line). Of relevance here is the fact that for Cr^{3+}:EuGaG all Cr^{3+} are part of an Eu^{3+}–Cr^{3+} pair but not vice versa. The Eu^{3+} ions giving rise to the spectral features of sites III–V are associated with such pairs. Energy, however, is also transferred among these pairs because (see Table 1) the emission spectrum of site V contains the features of sites III and IV. Also at 77 K, energy transfer takes place from the excited non-paired Eu^{3+} ions (occupying to 8-coordinated *d* site II) to the various pairs (sites

Can. J. Chem. Downloaded from www.nrcresearchpress.com by 210.87.254.5 on 09/06/12
For personal use only.

TABLE 1

(*a*) Positions (nm) and assignments of absorptions of EuGaG:Cr^{3+}

Absorption	Excitation profile (maxima)	Transition	Assignment
	579.75	$^5D_0 \leftarrow {}^7F_0$	First (nearest neighbour) Eu^{3+}–Cr^{3+} pair
	580.36		Second
	580.47		Third
580.67	580.68		Eu^{3+} in 8-coordinated *d* sites
	580.77		Fourth
580.80 (sh)	580.83		Eu^{3+} in 6-coordinated *a* sites
591.09		$^5D_0 \leftarrow {}^7F_1$	Eu^{3+} in *d* sites
591.14			Fourth Eu^{3+}–Cr^{3+} pair
591.91			Eu^{3+} in *d* sites
594.73			Eu^{3+} in *d* sites

(*b*) Fluorescence data of EuGaG containing Cr^{3+} impurity

	Site				
Eu^{3+} in:	I 6-coordinated *a* sites	II 8-coordinated *d* sites	III 3rd EuCr pair	IV 2nd pair	V 1st pair
Optical pump at: ($^5D_0 \leftarrow {}^7F_0$)	580.80	580.72	580.48	580.35	579.34
Fluorescence	580.80	580.72	580.48	580.35	579.84
				589.08	(589.04)
					589.29
			590.28		(590.06)
		591.13	(591.13)	(591.13)	(591.13)
	591.29		591.47		
$^5D_0 \rightarrow {}^7F_1$		591.95	(591.95)	(591.95)	(591.95)
	592.14				
			592.67	592.66	
			592.76	592.77	(592.78)
		594.74	(594.74)	(594.74)	(594.74)
	594.93				
			595.76	(595.79)	595.86
					596.56
$^5D_0 \rightarrow {}^7F_2$			(609.95)		
			610.20	(610.19)	
					610.45

III, IV, and V) and vice versa. The appearance of fluorescence of site II in the spectra of sites III, IV, and V (see Fig. 3) demonstrates energy transfer from Eu^{3+} in the *d* sites to the pairs, while the excitation profile of Fig. 4 suggest energy transfer from the pairs to the non-paired europium ions. The excitation profile for the R_1 line, however, shows that energy is not transferred from site I to the pairs, and we assign (6) the fluorescence spectrum of site I to Eu^{3+} ions which substitute for the gallium ions in the *a* sites. The actual site symmetry for these sites is C_{3i} but replacement of Ga^{3+} by Eu^{3+} causes a distortion towards lower symmetry and hence the complete removal of the threefold degeneracy of the $J = 1$ manifold. From a comparison of the fluorescence and absorption spectra, we estimate that not more than 10% of all europium ions are occupying these *a* sites. This concentration is small, and the ions of that site may be looked upon as being another impurity. Consequently, the probability of forming pairs with the Cr^{3+} impurity is small (compared to that for the pairs involving Eu^{3+} of the *d* site) and this explains the absence of a maximum of 580.80 nm in the excitation profile of the R_1 line. The profile for the R_2 line (see Fig. 5) does not exhibit maxima, which presently is interpreted as being due to extreme fast energy relaxation from R_2 to R_1. It appears that the excitation profiles of these R lines yield important information on the formation of pairs in garnets.

The fluorescence spectrum of site V is assigned to that of the nearest neighbour pair because its intensity and frequency spectrum differs more from that of site II (if compared to those of III and

Can. J. Chem. Downloaded from www.nrcresearchpress.com by 210.87.254.5 on 09/06/12
For personal use only.

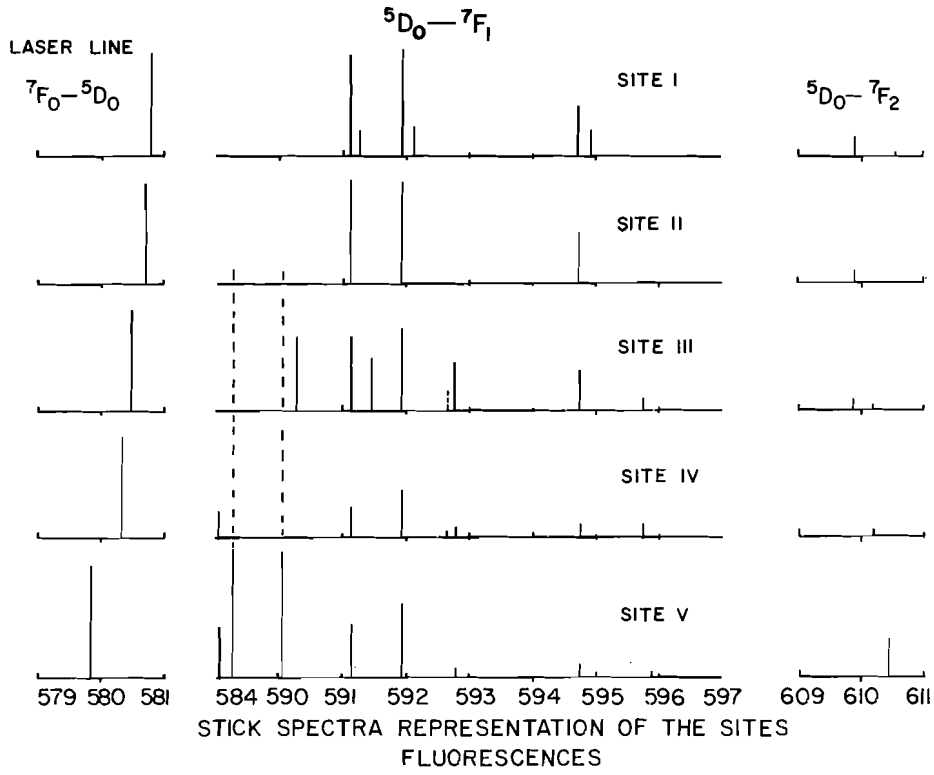

FIG. 4. Stick spectra of the (fluorescence) transitions of all five sites of EuGaG containing Cr^{3+}.

IV). The Cr^{3+} ion of this nearest neighbour pair interacts also with europium ions in other and more removed *d* sites and gives rise to the spectra of sites IV, III, and II*a* respectively. Finally for even larger distances, the interactions become smaller and smaller, and the fluorescence spectra due to such loosely bound pairs approaches that of the unpaired ion of site II. Shown in Fig. 7 is a comparison of spectra excited with $\lambda = 580.75$ nm of cw and pulsed dye lasers. Whereas the fluorescence features associated with sites I and II are recorded for the former, we did not record their features with the pulsed laser and as a result were not in a position to determine the lifetime of the various excited states of europium ions and Eu^{3+}–Cr^{3+} pairs. The absence of the fluorescence is presumably due to the population of $^5D_0$ and the subsequent absorption of another photon with $\lambda = 580.70$ nm to an even higher lying excited state. Thus, the energy reaches $^5D_0$ via a path which does not involve $^5D_0 \rightarrow {}^7F_1$ emission.

IV. Concluding Remarks

The results discussed in the preceding section suggest that the excitation profile of the R lines of a Cr^{3+} in the rare earth garnet crystal may be used to determine the presence of Eu^{3+}–Cr^{3+} pairs. The $^5D_0$–^7F_J fluorescence spectrum of a single crystal of $Eu_{0.03}Y_{2.97}Al_5O_{12}$ was recently investigated (8), but contrary to EuGaG we found evidence of two, rather than five centres. Relevant information on the position of some of the ^7F_J and $^5D_0$ states of Eu:YAlG are given in Table 2. This crystal also contains Cr^{3+} as an impurity, and part of the emission spectrum due to $^2E_g \rightarrow {}^4A$ transitions is shown in Fig. 8. The four transitions are at 686.2 nm, 687.1 nm, 688.2 nm, and 689.3 nm and the position of these lines may be compared with those of the R lines at 686.7 nm and 687.6 nm of YAlG containing Cr^{3+}. Because the intensity of the R_1 line of non-paired Cr^{3+} is larger than that of the R_2 line we assign the R lines of non-paired Cr^{3+} of Eu:YAlG so that $R_1 = 686.2$ nm and $R_2 = 687.6$ nm. The lines at 688.2 nm and 689.3 nm are assigned to those belonging to the nearest neighbour Eu^{3+}–Cr^{3+} pair in the crystal. Following the discussion of the results obtained for EuGaG, we assign the strongest of the fluorescence $^5D_0 \rightarrow {}^7F_1$ to that originating from the pair, see Table 2. This assignment is consistent with a crystal field analysis of the splitting pattern of the ^7F_J manifolds to Eu^{3+} ions in Eu:YAlG.

Can. J. Chem. Downloaded from www.nrcresearchpress.com by 210.87.254.5 on 09/06/12
For personal use only.

Can. J. Chem. Downloaded from www.nrcresearchpress.com by 210.87.254.5 on 09/06/12
For personal use only.

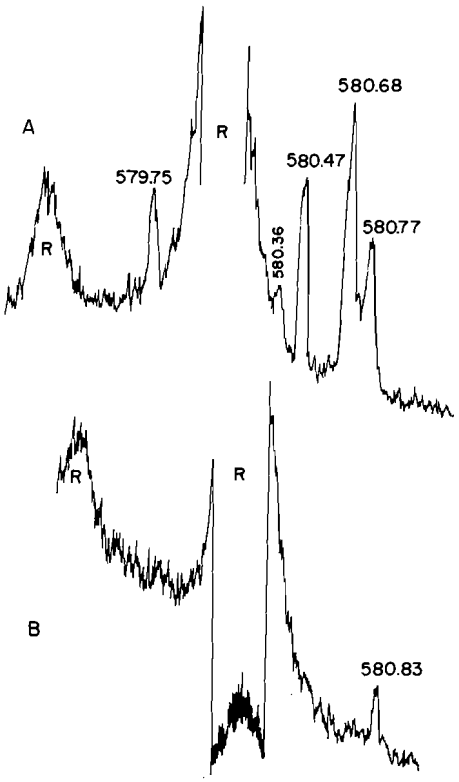

FIG. 5. The excitation profile at 77 K of the $^5D_0 \rightarrow {}^7F_1$ transitions at 591.13 nm for Eu^{3+} of site II, upper curve *A*, and that of the $^5D_0 \rightarrow {}^7F_1$ transition at 591.29 nm of Eu^{3+} occupying the 6-coordinated Ga^{3+} ions (site I), lower curve *B*.

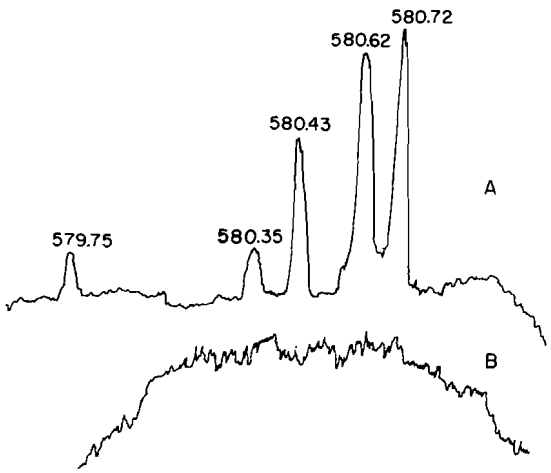

FIG. 6. Excitation profiles at 77 K for (*A*) the R_1 and (*B*) the R_2 chromium fluorescences of EuGaG containing Cr^{3+} (50 ppm). The R lines are at 695.6 nm and 698.8 nm, respectively.

The excitation profiles for all fluorescence lines of Fig. 8 are identical, and maxima are recorded at 580.31 nm and 580.92 nm. These wavelengths are identical to those yielding a maximum intensity of

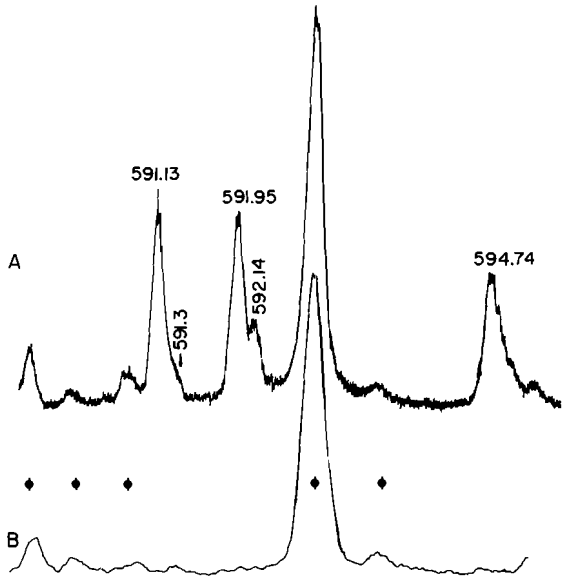

FIG. 7. Part of the fluorescence and Raman spectrum of the EuGaG crystal excited with a cw laser at 580.75 nm (upper curve *A*) and a pulsed laser (curve *B*) also operating at 580.75 nm. The upper spectrum is due to transitions $^5D_0 \rightarrow {}^7F_1$ of sites I and II.

TABLE 2. Fluorescence data of Eu:YAlG containing Cr^{3+} impurity[a]

	Site	
Eu^{3+} in:	I 8-coordinated *d* sites	II Eu^{3+}–Cr^{+} pair
Optical pump at: ($^5D_0 \leftarrow {}^7F_0$)	580.32	580.92
Fluorescence	590.11	
	(590.56)	590.56
	(591.40)	591.40
$^5D_0 \rightarrow {}^7F_1$	593.21	
	594.10	
	(596.69)	596.69

[a] The values in parentheses indicate the occurrence of fluorescence of site II in that of the spectrum of site I but not vice versa.

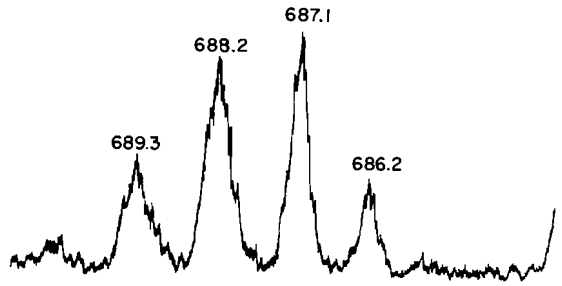

FIG. 8. Part of the spectrum of Eu:YAlG containing Cr^{3+} showing R line fluorescences.

the $^5D_0 \rightarrow {}^7F_J$ fluorescence of sites I and II. The excitation profiles are all equal because contrary to EuGaG the europium fluorescence of Eu:YAlG is much stronger. Thus by pumping into $^5D_0$ of sites I and II, the sample emits strongly in the spectral range of 590 nm–850 nm and the radiation between 590 nm–670 nm is reabsorbed by Cr^{3+} and Eu^{3+}–Cr^{3+} of the sample, hence the similarity of the excitation profiles.

V. Acknowledgements

The authors wish to thank Dr. L. G. Van Uitert for providing them with a crystal of EuGaG. They also wish to thank Mr. M. Kilpatrick for recording the fluorescence spectra.

This research was carried out under the exchange program between Canada and France.

1. M. T. Hutchings and W. P. Wolt. J. Chem. Phys. **41**, 617 (1964).
2. R. H. Wadsack, J. L. Lewis, B. E. Argyle, and R. K. Chang. Phys. Rev. B**3**, 4342 (1971).
3. I. Dabrowski, P. Grunberg, and J. A. Koningstein. J. Chem. Phys. **56**, 1264 (1972).
4. C. A. Morrison, P. E. Wortman, and N. Karayiamis. J. Phys. C, Solid State Phys. **9**, 419 (1976).
5. R. A. Buchanan. Phys. Rev. **159**, 245 (1967).
6. M. Kh. Ashurov, Yu. K. Voronko, V. V. Osiko, A. A. Sobol, and M. I. Timoshechkin. Phys. Stat. Sol. **42**, 101 (1977).
7. R. C. Powell. Bulletin A.P.S. **24**, 894 (1979).
8. M. Asano and J. A. Koningstein. Chem. Phys. **42**, 369 (1979).
9. J. P. van der Ziel and L. G. Van Uitert. Phys. Rev. **106**, 332 (1969).
10. D. L. Wood, J. Ferguson, K. Knox, and J. F. Dillon Jr. J. Chem. Phys. **39**, 890 (1963).
11. G. Z. Menner. Kristallografica **69**, 300 (1929).
12. M. J. Berggren, G. F. Imbusch, and P. L. Scott. Phys. Rev. **108**, 675 (1968).
13. B. Halperin, D. Nicollin, and J. A. Koningstein. Chem. Phys. **42**, 277 (1979).
14. B. D. Bartolo. Optical interactions in solids. Wiley, New York. 1968.

Can. J. Chem. Downloaded from www.nrcresearchpress.com by 210.87.254.5 on 09/06/12
For personal use only.

Spectrophotometric investigation on the interaction of acridine orange with methylene blue, phenosafranine, and disulphine blue in aqueous medium

SUHASCHANDRA GHOSH AND SATYA P. MOULIK[1]
Department of Chemistry, Jadavpur University, Calcutta 700032, India
AND
AKHIL R. DAS
Department of Physical Chemistry, Indian Association for the Cultivation of Science, Calcutta 700032, India
Received April 15, 1980[2]

SUHASCHANDRA GHOSH, SATYA P. MOULIK, and AKHIL R. DAS. Can. J. Chem. **59**, 2449 (1981).

The results of dye–dye interactions for the pairs, acridine orange – methylene blue, acridine orange – phenosafranine, and acridine orange – disulphine blue have been presented. It has been found that at comparable concentrations the interaction is rather weak, and the formation of mixed entities is only possible at relatively high proportions of one of the components. However, the evidence of mixed dimers in the form of a new absorption band is lacking. Phenosafranine remarkably promotes dimerization of acridine orange. An experimental demonstration of the dimer spectra of acridine orange has thus been possible. The interaction of the anionic dye disulphine blue with cationic acridine orange has been observed to be the weakest of all the pairs, indicating the vital role of the structural parity for interaction. At comparable low concentrations, none of the dye-pairs studied have revealed compound metachromasy in the presence of a polyelectrolyte, suggesting unfavorable mixed dye aggregation under ordinary conditions.

SUHASCHANDRA GHOSH, SATYA P. MOULIK et AKHIL R. DAS. Can. J. Chem. **59**, 2449 (1981).

On présente les résultats relatifs aux interactions colorant – colorant dans les paires de colorants suivants: acridine orange – bleu de méthylène, acridine orange – phénosafranine et acridine orange – bleu de disulfine. L'interaction est plutôt faible si les colorants ont des concentrations comparables et la formation d'entités mixtes est possible uniquement si l'un des constituants est dans une proportion relativement élevée. Cependant, on constate l'absence d'une nouvelle bande d'absorption qui indiquerait la présence de dimères mixtes. La phénosafranine favorise remarquablement la dimérisation de l'acridine orange. Il est alors possible de démontrer expérimentalement le spectre du dimère de l'acridine orange. L'interaction du colorant anionique, bleu de disulfine, avec le colorant cationique, acridine orange, est la plus faible de toutes les paires étudiées, ceci constitue une indication du rôle vital de la parité structurale lors de l'interaction. A de faibles concentrations aucune des paires de colorants étudiées ne révèlent la métachromasie composée en présence d'un polyélectrolique, suggérant ainsi une association défavorable du colorant mixte dans les conditions ordinaires.

[Traduit par le journal]

Introduction

Interactions of large charged organic molecules in aqueous medium in the presence of salts, co-solvents, and other additives have been considered important over the last decade in view of their relevance to biology (1). Dyes may serve as models for such organic molecules and have been used in many instances of physico-chemical investigations (2). The self association (mainly dimerization) has been the focus of such studies. Investigations on the mixtures of dyes have been rarely done. Only a few reports of mixed dimer formation (3–7) and compound metachromasy (8, 9) in the presence of polymers appear in the literature.

In the present work, we have described the interactions of acridine orange (AO) dye cation with two other cationic dyes, methylene blue (MB) and phenosafranine (PSAF), and an anionic dye disulphine blue (DSB) from spectrophotometric studies.

Of the four dyes, AO and MB are structurally comparable; PSAF is also not very different except for the bulky phenyl ring attached to one of the central ring nitrogens. Apart from it being anionic, DSB has a completely different structure. According to our knowledge, the present elaborate spectrophotometric report dealing with different types of dyes, studied at relatively excess concentrations of one of the components, is the first of its kind.

Experimental

The specification of AO was the same as reported earlier (10). Both MB and PSAF were BDH Analar products. MB showed a shoulder at 610 nm and a main band at 660 nm. PSAF had only a broad band at 525 nm without any discernible shoulder. All these corresponded well with literature reports (11, 12). The DSB was the same sample as that used by Mandal *et al.* (13).

Other chemicals used were either BDH Analar or E. Merck pro-analysis grades. Double distilled water was used as the solvent. The non-aqueous solvents used were purified by following standard procedures.

All measurements were taken in a Hilger-Watts digital spec-

[1]To whom all correspondence should be addressed. Present address: Department of Chemistry, Georgia State University, Atlanta, GA 30303, U.S.A.

[2]Revision received April 2, 1981.

0008-4042/81/162449-08$01.00/0
©1981 National Research Council of Canada/Conseil national de recherches du Canada

Can. J. Chem. Downloaded from www.nrcresearchpress.com by 210.87.254.40 on 09/06/12
For personal use only.

Can. J. Chem. Downloaded from www.nrcresearchpress.com by 210.87.254.40 on 09/06/12
For personal use only.

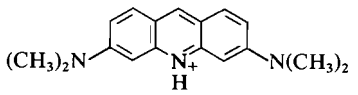

Acridine orange
λ_{max} = 490 nm
$\varepsilon = 9.0 \times 10^4$ L mol^{-1} cm^{-1}

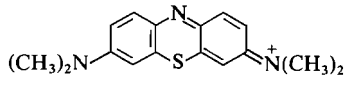

Methylene blue
λ_{max} = 660 nm
$\varepsilon = 9.6 \times 10^4$ L mol^{-1} cm^{-1}

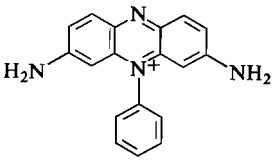

Phenosafranine
λ_{max} = 525 nm
$\varepsilon = 1.8 \times 10^4$ L mol^{-1} cm^{-1}

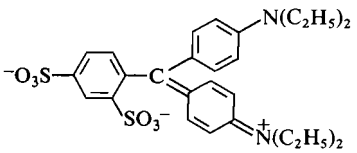

Disulphine blue
(basic form)
λ_{max} = 640 nm
$\varepsilon = 5.7 \times 10^4$ L mol^{-1} cm^{-1}

trophotometer using 1 cm and 0.5 cm cuvettes at a constant temperature of 25 ± 0.1°C.

In general, each set of experiments was done keeping the concentration of one of the components constant and varying that of the other. Each experimental set was repeated to check the reproducibility of the systems. For other details of spectrophotometric measurements we refer to our earlier publication (10).

Results

(1) AO–MB pair

MB has a small absorption peak at 490 nm, the wave length of the maximum absorption of the AO monomers. At lower MB:AO ratios, the spectrum of a low concentration of AO (2.5 μ*M*) is not affected, and the absorbances are all additive. Higher proportions of MB helped increasing the monomer absorption peak of AO at 490 nm. At a relatively high concentration of AO (20 μ*M*), increased proportion of MB perceptibly increased the monomer peak of AO at this wave length. The calculated absorbances (the sum of the absorbances of the individual dyes) of the mixtures were significantly different than the experimental values. The departure from additivity is the evidence for AO and MB interaction. The reverse set of experiments, i.e., the effect of increasing proportions of AO on MB (20 μ*M*) studied at its long wavelength monomer band revealed a remarkable difference (Fig. 1). At lower AO:MB ratios, the absorbance at 660 nm increased a little and the usual dimer shoulder was there at 610 nm. At ratios of 4 or greater, the absorbance at the same wavelength decreased with increasing AO:MB ratio and the band was slightly red-shifted. At larger proportions (ratios 50 and 75) of AO, the band shifted further to 673 nm along with significant lowering of absorbance. In this process of red shift and concomitant lowering of intensity, the family of curves passed through an isosbestic point at 680 nm. The results suggest an interaction of AO with MB at higher proportions of the latter.

The interactions of AO and MB were also studied in the presence of KCl and ethanol. MB also influenced the effect of both the salt and the

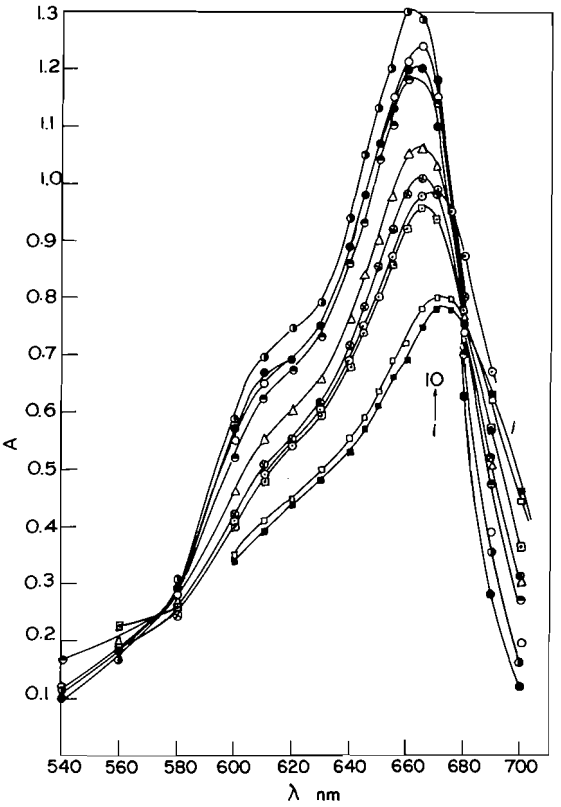

FIG. 1. The spectra of AO and MB mixtures containing a constant concentration of MB. Curve *8*, 20 μ*M* MB in water vs. a water blank. Curves *1–7*, *9* and *10*, AO–MB mixtures, each with 20 μ*M* MB and AO:MB ratios of 75, 50, 25, 15, 10, 7.5, 4, 2, and 1, respectively, each recorded vs. a solution containing 20 μ*M* MB as blank.

Can. J. Chem. Downloaded from www.nrcresearchpress.com by 210.87.254.40 on 09/06/12
For personal use only.

alcohol on the monomer–dimer equilibrium of AO prevalent at the concentration used. On the other hand, the AO induced depression of MB spectra (Fig. 1) was considerably influenced by both the salt and the alcohol. The salt induced dimer peak at 610 nm of MB was considerably lowered and practically disappeared in the presence of high proportions of AO and AO plus salt. A product of the $(AO)_n$–$(MB)_m$ type is suggested.

(2) AO–PSAF Pair

The spectra of AO and PSAF were affected by each other. With increasing proportions of PSAF, the 465 nm dimer shoulder of AO became prominent along with a corresponding decrease of the monomer peak at 490 nm. The 465 nm shoulder ultimately became a well shaped symmetric peak and in the presence of a large excess of PSAF, the band suffered a gradual blue shift. Figures 2 and 3 illustrate these results.

In the presence of 200 μM PSAF (sufficient to produce a distinct 465 nm band symmetric on both sides), the spectra of AO at different concentrations along with Beer's law plots at 465 nm and 490 nm are shown in Fig. 4. The dimer extinction coefficients at 25°C were calculated to be 4.65×10^4 (465 nm) and 2.76×10^4 (490 nm) L mol^{-1} cm^{-1}.

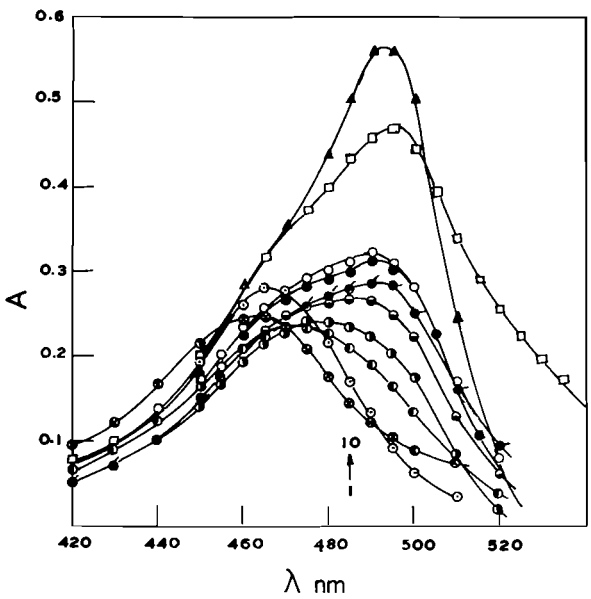

FIG. 2. The spectra of AO and PSAF mixtures containing a constant concentration of AO. Curve *7*, 20 μM AO in water vs. a water blank. Curves *1–6* and *8*, AO–PSAF mixtures, each with 20 μM AO and PSAF:AO ratios of 10, 8, 5, 4, 3, and 2 respectively, each recorded vs. a solution containing an equal concentration of PSAF as blank. Curves *9* and *10*, 1:1 AO–PSAF mixture and AO in 80% v/v alcohol respectively, each recorded vs. a water blank.

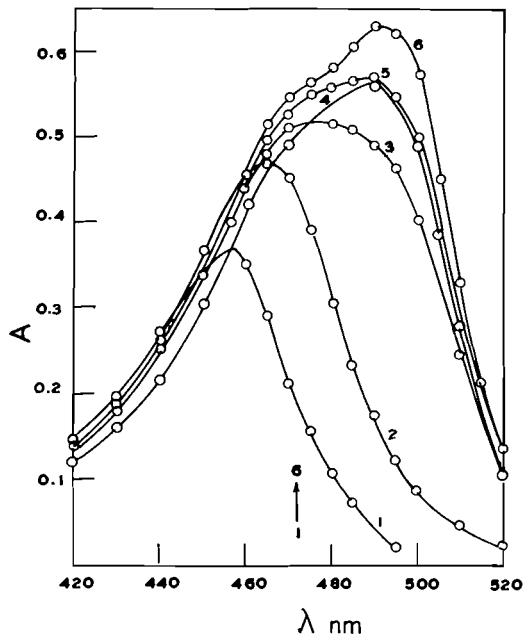

FIG. 3. The spectra of AO and PSAF mixtures containing a constant concentration of AO. Curve *6*, 40 μM AO in water vs. a water blank. Curves *1–5*, AO–PSAF mixtures, each with 40 μM AO and PSAF:AO ratios of 8, 5, 2, 0.5, and 1 respectively, each recorded vs. a solution containing an equal concentration of PSAF as blank.

The results of the reverse experiments, i.e., the effect of increasing the AO:PSAF ratio are presented in Fig. 5. The 525 nm PSAF band slightly improved at lower AO:PSAF ratios, but was depressed subsequently. At lower ratios a shoulder appeared at 485 nm but became flat at higher ratios. All these facts indicate a strong AO–PSAF interaction. The effects of salts and alcohol on the spectra of PSAF are also shown in the figure for a comparison.

(3) AO–DSB Pair

Shown in Fig. 6*a* are the effects of AO on the spectrum of DSB. In the region where DSB absorbs most, AO has little absorbance. In excess AO, a weak band at 500 nm appeared. The reverse, that is the effect of DSB on the spectrum of AO (Fig. 6*b*), was also not appreciable. Excess DSB could, however, slightly affect the spectra of AO by an initial increase in the 490 nm band of AO followed by a decrease; at still higher DSB:AO ratios, it started rising again. In this process, the spectral shape did not alter. AO–DSB interactions were thus seen to be weak indeed.

(4) The Effects of a Surfactant and a Polyelectrolyte

The effects of sodium dodecyl sulfate (SDS), an

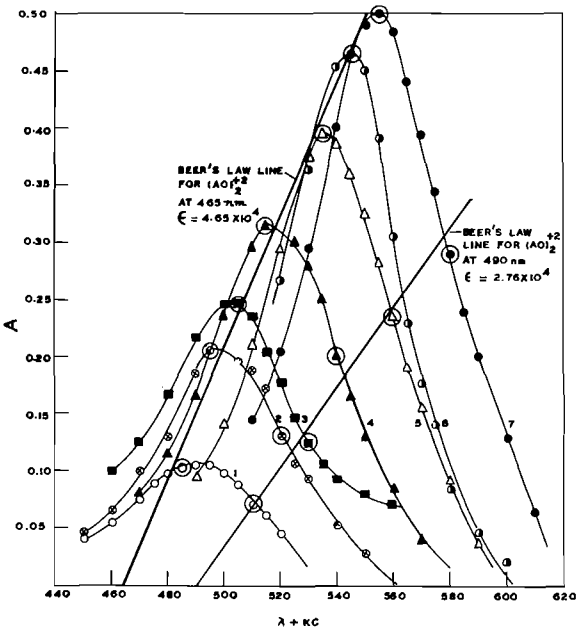

FIG. 4. The PSAF induced dimer spectra of AO. Also shown are Beer's law plots for the dimer at 465 nm and 490 nm. Curves *1*, *2*, *4–7*, AO–PSAF mixtures each with 200 μ*M* PSAF and AO concentrations of 10, 15, 25, 35, 40 and 45 μ*M* respectively, each recorded vs. a solution of 200 μ*M* PSAF as blank. Curve *3*, AO–PSAF mixture of 320 μ*M* PSAF and 20 μ*M* AO recorded vs. a solution of 320 μ*M* PSAF as blank. The value of the constant *K* (on the *X*-axis) is 20×10^{-5}.

anionic surfactant, and the Na-salt of carboxymethyl cellulose, a polyelectrolyte, on the spectra of the dyes, singly and in pairs, are presented in Fig. 7. While the presence of the polyelectrolyte revealed normal metachromasy, SDS, at a concentration below the critical micelle concentration (cmc), only depressed the bands. DSB was not affected by the polyelectrolyte or SDS. The effect of SDS on PSAF, though not insignificant, was much less than that on AO. The spectra of the three pairs of the dyes used in presence of the polyelectrolyte were conspicuous by the absence of any new metachromatic band to be assigned to any mixed dimer formation.

Discussion

Binary mixtures of dyes such as AO–MB, MB–PSAF, MB–pyronine G, crystal violet – rohdamine 6G, etc. have been reported to form mixed dimers in solution (4, 5, 7). This was anticipated not because of the appearance of a new absorption band in each case but mainly due to the nonadditivity of the absorbance. Pal and Schubert (8) reported compound metachromasy in the presence of certain polyanions. In the present binary dye systems using AO as one of the components, we have observed interactions of different types. For the AO–MB system, the absorbance of AO increased in the presence of MB resulting in an upward displacement of the spectra as a whole. No new absorption band or shoulder appeared to indicate the formation of a new entity in solution by interaction. Addition of more and more MB increased the probability of the electronic transition of AO leading to increased absorbance. When we explored the effect of AO on the spectra of MB, we noticed that the 660 nm monomer absorption peak of MB got depressed after an initial rise and was red shifted to 673 nm. The spectrum shifted towards the red as a whole (Fig. 1). Pal and Schubert (8) missed this observation in their work with AO–MB system since they did not use one of the components in large excess. Such spectral perturbations of MB in the presence of large excess of AO are unlikely to be due to mixed dimers since AO existed in highly aggregated state at such high concentrations. We anticipated that MB cations (both monomeric and dimeric) are incorporated in the stacks of oligomers and their transition dipoles are perturbed in the new environment.

PSAF influenced AO much more markedly than AO did PSAF. A clear monomer–dimer conversion of AO took place in the presence of a suitable excess of PSAF. At sufficiently high proportions of PSAF, AO showed typical metachromatic behavior (Figs. 2 and 3). Dimerization of a dye in the presence of another dye, particularly one which does not differ radically in structural pattern, has not been reported in the past. Neglecting other effects, the extinction coefficient of the AO dimer has been evaluated and compared with the earlier reports.

Extinction coefficient of the AO dimer at 25°C (ε_d^{490} L mol^{-1} cm^{-1})	Authors
1.55×10^4	Lamm and Neville (14)
1.60×10^4	Ballard and Parks (15)
1.30×10^4	Robinson *et al.* (2)
2.70×10^4	Present work

While our value resulted from an experimental demonstration of the dimer spectra, the other previously reported values were obtained by indirect methods.

The influence of AO on PSAF was not as remarkable as the reverse; but the spectra showed considerable variation. A shoulder appeared at some AO:PSAF ratios (2:1 and 0.5:1) around 485 nm (Fig. 5). At higher ratios, it disappeared and the absorbance remained significantly constant over a considerable region of wavelength up to 495 nm,

Can. J. Chem. Downloaded from www.nrcresearchpress.com by 210.87.254.40 on 09/06/12
For personal use only.

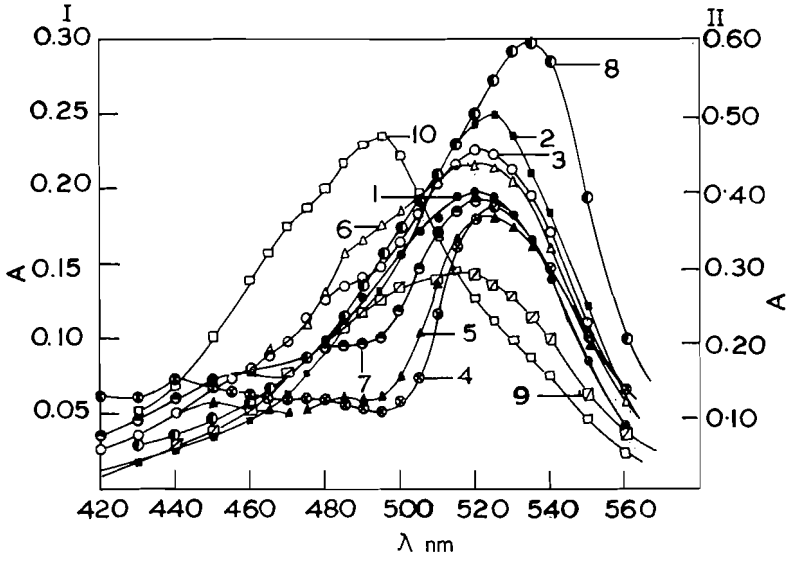

FIG. 5. The spectra of AO–PSAF mixtures containing a constant concentration of PSAF. Curves *1*, *8*, and *9*, 20 μ*M* PSAF in water, 80% v/v ethanol/water and 2 *M* aqueous KCl respectively, each recorded vs. a water blank (Scale I). Curves *2–7*, AO–PSAF mixtures each with 20 μ*M* PSAF and AO:PSAF ratios of 1, 2, 10, 6, 0.5, and 4 respectively, each recorded vs. a solution containing an equal concentration of AO as blank (Scale I). Curve *10*, same mixture as in *2* recorded vs. a water blank (Scale II).

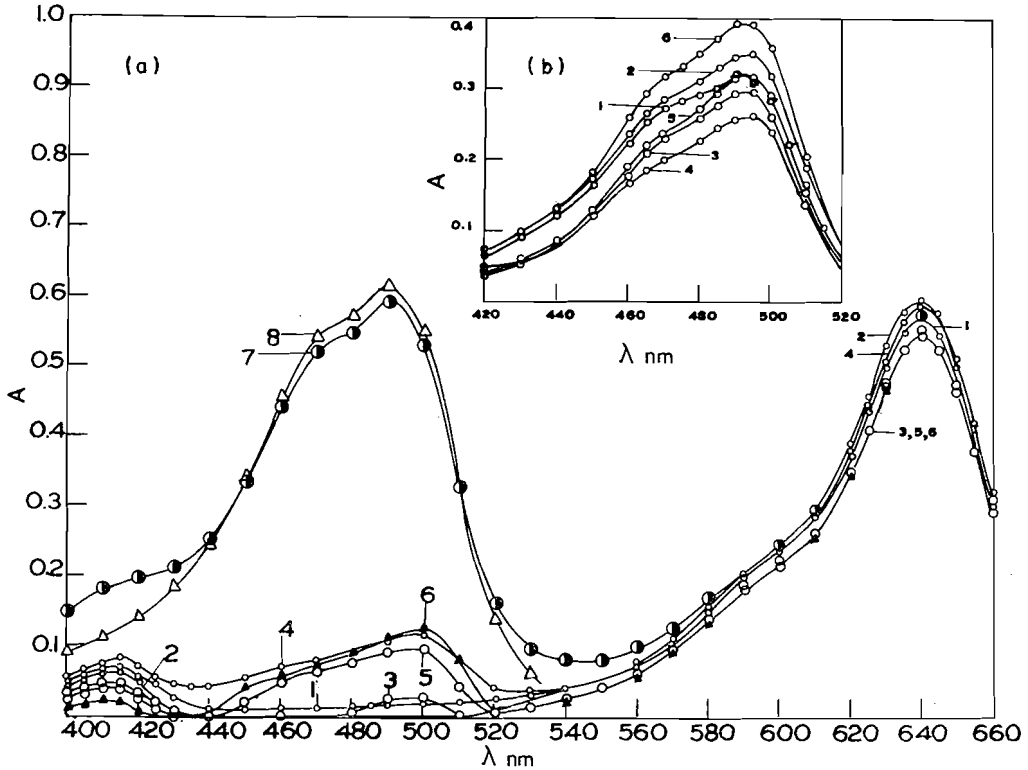

FIG. 6. (*a*) The spectra of AO–DSB mitures containing a constant concentration of DSB. Curves *1*, *7*, and *8*, 20 μ*M* DSB, 20 μ*M* DSB plus 40 μ*M* AO, and 40 μ*M* AO respectively, each recorded vs. a water blank. Curves *2–6*, AO–DSB mixtures each with 20 μ*M* DSB and AO:DSB ratios of 1, 5, 8, 10, and 15 respectively, each recorded vs. a solution containing 20 μ*M* DSB as blank. (*b*) The spectra of AO–DSB mixtures containing a constant concentration of AO. Curve *1*, 20 μ*M* AO vs. a water blank. Curves *2–6*, AO–DSB mixtures each with 20 μ*M* AO and DSB:AO ratios of 0.5, 1, 2, 4, and 10 respectively, each recorded vs. a solution containing 20 μ*M* AO as blank.

Can. J. Chem. Downloaded from www.nrcresearchpress.com by 210.87.254.40 on 09/06/12
For personal use only.

Can. J. Chem. Downloaded from www.nrcresearchpress.com by 210.87.254.40 on 09/06/12
For personal use only.

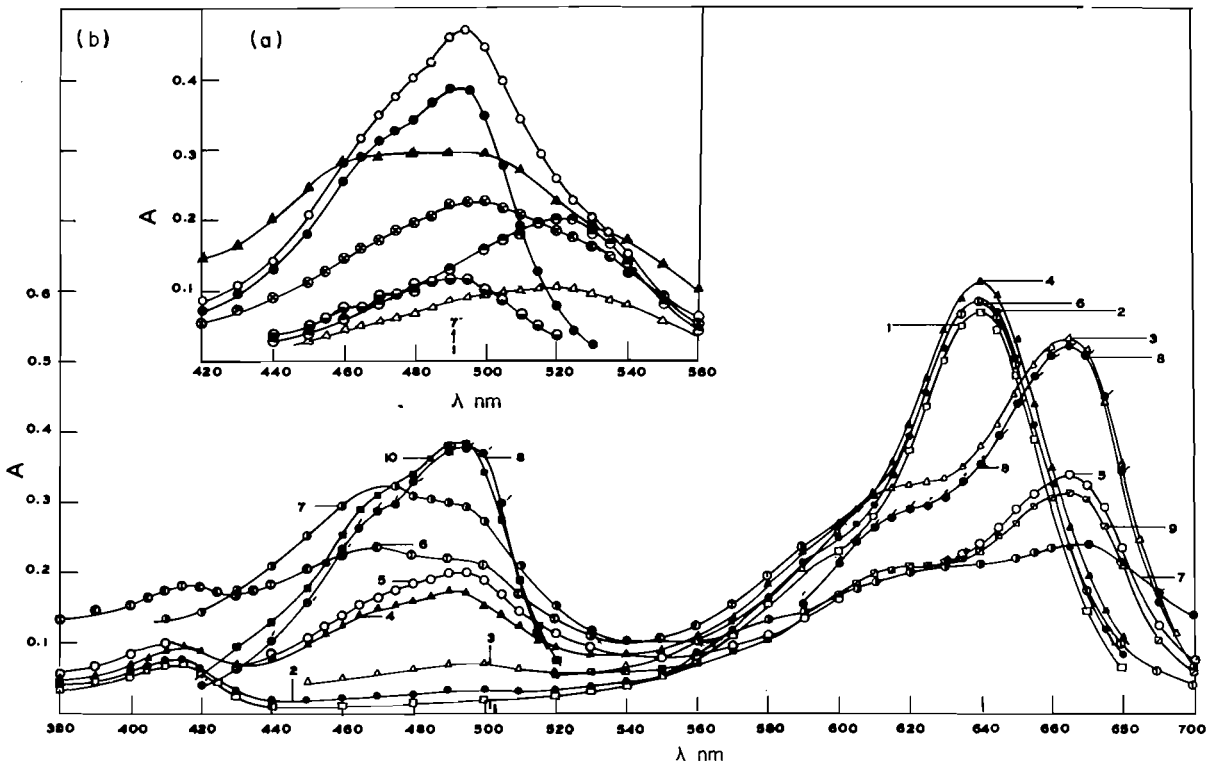

FIG. 7. (*a*) The spectra of AO, PSAF, and their 1:1 mixture in water, SDS, and CMC (Na salt) solutions. Curves *1* and *3*, 20 μ*M* PSAF in 60 μ*M* aqueous SDS and in water respectively. Curves *4*, *5*, and *7*, 20 μ*M* AO plus 20 μ*M* PSAF in 60 μ*M* aqueous SDS, in 0.35% aqueous CMC and in water respectively. Water, 60 μ*M* aqueous SDS, and 0.35% aqueous CMC were used as the respective blanks. (*b*) The spectra of AO and 1:1 mixtures of AO–MB and AO–DSB containing a constant concentration (20 μ*M*) of AO in water, aqueous SDS and aqueous CMC media. Curves *1*, *3*, *8*, and *10*, that of DSB, MB, AO plus MB, and AO respectively in water. Curves *2*, *4*, *5*, and *9*, that of DSB, DSB plus AO, AO plus MB, and MB in 60 μ*M* aqueous SDS respectively. Curves *6* and *7*, that of AO plus DSB and AO plus MB in 0.35% aqueous CMC respectively. Water, 60 μ*M* aqueous DSB, and 0.35% aqueous CMC were used as the respective blanks.

which was indicative of the formation of a new entity.

In spite of the opposite charge, DSB revealed little interaction with AO. The spectral pattern of DSB remained almost unaffected in the presence of AO; no new band appeared on the higher wavelength side of DSB absorption peak but a weak band appeared at 500 nm (Fig. 6*a*).

The above discussed results have shown significant effects of PSAF on AO and AO on MB. The effect of MB on AO is moderate. PSAF has helped dimerizing the AO while MB reduced the extent of dimerization. When present in large excess, AO complexes with MB monomers. A quantitative approach of the above phenomena has been attempted in the following.

The monomer–dimer equilibrium has been considered to calculate the percent of AO monomer and the dimerization constant, K_d, under the influences of PSAF and MB.

$$[1] \quad 2\,AO \overset{K_d}{\rightleftharpoons} (AO)_2$$

Also,

$$[2] \quad A = \varepsilon_m C_m + \varepsilon_d C_d$$

where, A, ε_m, C_m, ε_d, and C_d are the absorbance, the extinction coefficient of the monomer, the concentration of the monomer, the extinction coefficient of the dimer and the concentration of the dimer respectively.

The estimated ε_m used earlier (10) and the ε_d evaluated under the influence of excess PSAF and reported herewith have been used in the calculation. Thus, C_m and C_d are obtained from the relations,

$$[3] \quad C_m = (A - \tfrac{1}{2}\varepsilon_d C_t)/(\varepsilon_m - \tfrac{1}{2}\varepsilon_d)$$

and

$$[4] \quad C_d = \tfrac{1}{2}(C_t - C_m)$$

where the new term C_t denotes the total AO concentration.

The dimerization constant has been calculated from the relation,

Can. J. Chem. Downloaded from www.nrcresearchpress.com by 210.87.254.40 on 09/06/12
For personal use only.

[5] $K_d = C_d/(C_m)^2$

Since activity is uncorrected, the K_d values are not truly thermodynamic but they are not far from this as the solutions employed were dilute and the arguments given earlier (16) in this regard favor low significance of such a correction. The calculated parameters are given in Tables 1 and 2.

The following model has been chosen for MB–AO complexation to calculate the uncomplexed (free) MB in solution in AO environment.

[6] $MB + nAO \rightleftharpoons MB(AO)_n$

where n is greater than one but the value is at present unknown. Without known values of n, the system cannot be fully characterized.

The free MB has been considered to be monomers because of rapid loss of dimer shoulder in the spectra with AO addition. Besides, calculations have been made on mixtures that did not register dimer shoulders. The limiting absorbance of the solutions containing constant MB and increased AO has been considered to be the absorbance of the complex. The concentration of MB thus equals the concentration of the complex (according to eq. [6]) and the extinction coefficient of the complex ($\varepsilon_{comp} = A/C_{MB}$) has been calculated to be 4.98×10^4 L mol^{-1} cm^{-1}.

The absorbance of the mixed dye solution is given by

[7] $A = A_{MB} + A_{comp} + A_{AO}$

TABLE. 1. Dimerization of AO by PSAF*

PSAF:AO	% AO(monomer)	$K_d \times 10^{-5}$ (L mol^{-1})
0	23.31	3.57
1	25.09	3.17
2	23.21	3.57
3	19.64	5.53
4	17.49	6.74
6	12.59	13.79
8	8.08	35.20
10	7.32	43.24
12	3.27	226.15

*$\varepsilon^{480}_{AO(monomer)} = 9.0 \times 10^4$ L mol^{-1} cm^{-1}; $\varepsilon^{480}_{AO(dimer)} = 2.7 \times 10^4$ L mol^{-1} cm^{-1}; $C_{AO} = 2.0 \times 10^{-5}$ M; $T = 25$°C.

TABLE 2. Monomerization of AO by MB*

MB:AO	% AO(monomer)	$K_d \times 10^{-5}$ L mol^{-1}
0	23.21	3.57
1	33.01	1.54
2	32.88	1.55
4	47.72	0.57
8	55.9	0.35
10	53.4	0.41

*$\varepsilon^{480}_{AO(monomer)} = 9.0 \times 10^4$ L mol^{-1} cm^{-1}; $\varepsilon^{480}_{AO(dimer)} = 2.7 \times 10^4$ L mol^{-1} cm^{-1}; $C_{AO} = 2.0 \times 10^{-5}$ M; $T = 25$°C.

Since at the experimental wave length (660 nm) AO hardly absorbs, eq. [7] becomes

[8] $A = A_{MB} + A_{comp} = \varepsilon_{MB}C_{MB} + \varepsilon_{comp}(C_t - C_{MB})$

Therefore,

[9] $C_{MB} = (A - C_t\varepsilon_{comp})/(\varepsilon_{MB} - \varepsilon_{comp})$

In Table 3, the concentration of the MB monomer and its percentages are shown. Lack of exact knowledge of the composition of the complex has restricted calculation of the equilibrium constant.

The results given in the tables offer some quantitative aspects of the interactions of the dye pairs. Powerful effect of PSAF on the dimerization of AO is revealed through very large K_d values at PSAF:AO ratios >12. Complexation of MB monomers with AO is prominent at ratios 16 and above.

In the presence of the polyelectrolyte, carboxymethylcellulose (Na salt), no compound metachromasy was observed in the binary mixtures of AO and MB. Only the normal metachromatic behavior of the individual dyes was evident. Compound metachromasy was also not observed in the AO–PSAF and the AO–DSB systems (Fig. 7 *a* and *b*). Such behaviors were not unexpected as interactions in all the cases were apparent only at higher proportions of one of the components. The polyelectrolyte effect was studied at a comparable dye concentration of 20 μM for all the combinations. The carbohydrate origin polymer γ-carrageenan, however, induced compound metachromasy in the AO–MB pair at 1:1 composition (12.5 μM) as reported by Pal and Shubert (8). The present observations revealed that even a polymer chain with suitable binding sites was not good enough to induce dye–dye interaction; only normal metachromasy of the individual dyes was observed. Once a given dye cation is bound to a site, for nearest neighbor interaction there is an equal choice (considering the comparable dye concentration) between a dye cation of its own type and a different type. The results indicated that for the

TABLE 3. Percentage of uncomplexed MB in excess AO*

AO:MB	$C_{MB} \times 10^5$ M	% MB
4	0.464	23.2
6	0.335	16.8
8	0.260	13.0
10	0.118	5.9
16	0.012	0.6

*$\varepsilon^{660}_{MB} = 9.6 \times 10^4$ L mol^{-1} cm^{-1}; $\varepsilon^{660}_{comp} = 4.98 \times 10^4$ L mol^{-1} cm^{-1}; $C_t = 2.0 \times 10^{-5}$ M; $T = 25$°C.

pairs of the dye studied, mixed dimer formation is less favorable.

Since SDS was used at a concentration below cmc, it depressed the spectra of both MB and AO as a whole without much altering the monomer–dimer ratios of the dyes, a behavior that may be noticed in individual dyes in the presence of SDS (17). Similar behaviors were obtained for the AO–PSAF pair. For the AO–DSB pair, the AO part of the spectrum underwent similar changes as with pure AO and the DSB part remained unaltered (Fig. 7). These results suggested that the anionic surfactant, SDS, could not induce interactions of AO with MB, PSAF, and DSB in their binary mixtures.

The following general conclusions can be made from the present results on the dye systems studied. (*1*) To get an appreciable spectral change one of the two dyes must be in significant excess. (*2*) The effect of the added dye on AO and vice-versa can become noteworthy if it is not structurally much different from AO. (*3*) If the structure of the added dye is significantly different from AO (AO–DSB pair), the interaction is minimum even though the dyes are oppositely charged. (*4*) An anionic polyelectrolyte or an anionic surfactant cannot bring about in solution any altered metachromasy other than that exhibited by the individual dyes.

Acknowledgements

Sincere thanks are due to Professor E. M. Eyring, University of Utah, U.S.A., for his keen interest and helpful discussions during his tenure in our laboratory as a Visiting Scientist under Indo-US exchange program. We would also like to thank the co-operation of Dr. S. N. Ganguli, Bose Research Institute, Calcutta, in recording the spectra. One of us (A.R.D.) thanks the authorities of C.S.I.R., Government of India for a pool officership.

1. G. I. Mukhayer and S. S. Davis. J. Colloid Interface Sci. **56**, 350 (1976).
2. B. H. Robinson, A. Loffler, and G. Schwarz. J. Chem. Soc. Faraday I. **69**, 56 (1973).
3. W. West and S. Pearce. J. Phys. Chem. **69**, 1894 (1965).
4. H. Ecker. Kolloid Z. **92**, 35 (1940).
5. D. R. Lemin and T. Vickerstaff. Trans. Faraday Soc. **43**, 491 (1947).
6. L. V. Levshin and V. S. Suvorov. Opt. spectrosc. **4**, 678 (1958).
7. Kh. L. Arvan. Dokl. Akad. Nauk SSSR. **121**, 485 (1959); Chem. Abstr. **54**, 285835e (1960).
8. M. K. Pal and M. Shubert. J. Phys. Chem. **67**, 1821 (1963).
9. M. Shirai, T. Nagatuska, and M. Tanaka. Makromol. Chem. **179**, 173 (1978).
10. S. P. Moulik, S. Ghosh, and A. R. Das. Indian J. Chem. **14A**, 302 (1976).
11. P. Mukherjee and A. K. Ghosh. J. Phys. Chem. **67**, 193 (1963).
12. L. Michelis and S. Garnick. J. Am. Chem. Soc. **67**, 1212 (1945).
13. H. K. Biswas and B. M. Mandal. Anal. Chem. **44**, 1636 (1972).
14. M. E. Lamm and D. M. Neville. J. Phys. Chem. **69**, 3872 (1965).
15. R. E. Ballard and C. H. Park. J. Chem. Soc. A, 1340 (1970).
16. P. Mukherjee and A. K. Ghosh. J. Am. Chem. Soc. **92**, 6403 (1970).
17. S. P. Moulik, S. Ghosh, and A. R. Das. J. Colloid Poly. Sci. **257**, 645 (1979).

Can. J. Chem. Downloaded from www.nrcresearchpress.com by 210.87.254.40 on 09/06/12
For personal use only.

Theoretical study of regioselectivity in nucleophilic addition to unsymmetrical cyclic anhydrides. Intrinsic reactivity and influence of the cation

MARGARET M. KAYSER
Department of Chemistry, University of Ottawa, Ottawa, Ont., Canada K1N 9B4
AND
ODILE EISENSTEIN
Laboratoire de Chimie Theorique, Batiment 490 Centre de Paris-Sud, 91405 Orsay, France
Received January 19, 1981

MARGARET M. KAYSER and ODILE EISENSTEIN. Can. J. Chem. **59**, 2457 (1981).

Ab initio molecular orbital calculations have been carried out for the series of succinic, maleic, and phthalic anhydrides unsymmetrically substituted with CH_3, CH_3O, Cl, F, and CN. The size of the LUMO coefficient on the carbon atom of the carbonyl group provides a reliable guide to the relative reactivities of the two carbonyl functions. The predictions based on the intrinsic reactivities are in good agreement with the regioselectivities observed in metal hydride reductions of succinic anhydrides. In the series of maleic and phthalic anhydrides the above considerations are applicable only to methyl derivatives. The compounds substituted with lone pairs-bearing groups (OCH_3, Cl, F) form stable chelates with the cations present in the reaction media. Since the chelated carbonyl group is strongly activated toward the nucleophilic addition, the "bridging" effect is the dominant factor controlling orientation of hydride addition. The optimum position for the nucleophilic attack in cyclic anhydrides was calculated. The results confirm the generality of the nonperpendicular, restricted path of nucleophilic attack on the carbonyl group in succinic anhydride.

MARGARET M. KAYSER et ODILE EISENSTEIN. Can. J. Chem. **59**, 2457 (1981).

Une série d'anhydrides succiniques, maleiques et phtaleiques substitués de façon non symétrique ont été calculés par une méthode *ab initio*, base minimale. La réactivité intrinsèque des deux fonctions carbonyles en présence des substituants est donnée par la valeur du coéfficient du carbone dans la LUMO. Les résultats théoriques et expérimentaux sont en bon accord pour la série des anhydrides succiniques réduits par $LiAlH_4$ et $NaBH_4$. Dans la série des anhydrides maleiques et phtaleiques, l'indice de réactivité ainsi défini ne permet d'expliquer que la réduction des dérivés méthylés. Lorsque les anhydrides en question portent des substituants possédant des paires libres, des chélates sont formés avec le cation présent dans le milieu réactionnel. Comme le carbonyle chélate est fortement activé par le cation, il sera sélectivement réduit par le nucléophile. La direction optimum d'attaque par le nucléophile sur les anhydrides cycliques a également été examinée. Les résultats confirment la généralité de l'approche non perpendiculaire.

Introduction

Cyclic anhydrides may be converted directly to the corresponding lactones by reduction with metal hydrides (1). Unsymmetrically substituted anhydrides such as, for example, 2,2-dimethylsuccinic anhydride **1** can potentially yield isomeric lactones **2** and **3**. In fact, lactone **2** is the major product obtained in a large excess (the ratio **2**:**3** = 19:1) (2). A similar regioselectivity has been observed in metal hydride reductions of a variety of unsymmetrical cyclic anhydrides belonging to vastly different classes of compounds (3). At present only a few exceptions (i.e., cases of selective reduction at the less hindered carbonyl group or reduction without preference for either group) are known (2, 4).

The marked preference for nucleophilic attack to occur at the sterically more hindered site has provoked some speculation (3, 5), particularly as such regioselectivity is not restricted to cyclic anhydrides. Unsymmetrically substituted succinimides (6*a*), diesters, and diacids (6*b*) are also reduced by metal hydrides selectively at the more sterically encumbered carbonyl group.

Why metal hydrides attack the more hindered carbonyl function is still not clear.[1] This "unusual" regioselectivity has been considered in terms of steric and stereoelectronic effects and several mechanisms were proposed, each explaining some but not all of the results obtained experimentally (2, 3, 5). The anhydrides most exhaustively studied can be divided, on the basis of their geometry, into two groups: (*1*) unsymmetrically substituted succinic anhydrides with substituents projected above and below the plane of the ring **4**, and (*2*) planar, conjugated maleic and phthalic anhydrides **5** and **6**.

1 **2** **3**

[1]In contrast, Grignard reagents add preferentially in a "normal" manner to the less hindered carbonyl group in substituted succinic anhydrides (P. Canonne, private communication).

0008-4042/81/162457-06$01.00/0
©1981 National Research Council of Canada/Conseil national de recherches du Canada

Can. J. Chem. Downloaded from www.nrcresearchpress.com by 210.87.254.42 on 09/06/12
For personal use only.

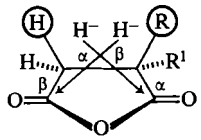

4

R = CH_3	R^1 = CH_3	**4***a*
R = CH_3	R^1 = H	**4***b*
R = Cl	R^1 = Cl	**4***c*
R = Cl	R^1 = H	**4***d*
R = F	R^1 = F	**4***e*
R = F	R^1 = H	**4***f*
R = CN	R^1 = H	**4***g*

Preferential reduction of the carbonyl group α, adjacent to the most fully substituted carbon atom in succinic anhydrides, has been described in terms of the most favourable path for the nucleophilic attack on the carbon atom of the carbonyl group (7). Since at a moderate distance to the molecular plane the best angle for nucleophilic approach is about 110° to the C=O double bond (8, 9), the carbonyl function α next to the substituents is effectively less hampered than the carbonyl group β, viewed from the position of approaching nucleophile **4**. This argument explains preferential reduction of the α-carbonyl group in succinic anhydrides but fails to account for the selectivities observed in reductions of planar maleic and phthalic anhydrides where both carbonyl functions are equally accessible to the nonperpendicular attack (10). Obviously in the latter case factors other than "the most favourable path of nucleophilic approach" must be responsible for the regioselectivities observed.

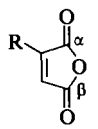

5

R = CH_3	**5***a*
R = OCH_3	**5***b*
R = Cl	**5***c*
R = F	**5***d*

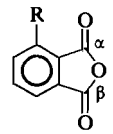

6

R = CH_3	**6***a*
R = OCH_3	**6***b*
R = Cl	**6***c*
R = F	**6***d*

We have suggested previously (2) that a preferential attack by metal hydrides on the carbonyl group adjacent to the most highly substituted carbon atom is linked to the discrete characteristics of the two groups. This study was undertaken for the following specific purposes: (*1*) to probe the intrinsic differences in reactivity of the carbonyl functions in unsymmetrical cyclic anhydrides; (*2*) to examine the effect of the counterion on the regioselectivity of metal hydride reductions; (*3*) to compute the optimum geometry for the nucleophilic (H^-) attack on the surface of succinic anhydride, in order to confirm generality of the nonperpendicular approach.

Discussion

Ab initio molecular orbital calculations using the Gaussian 70 programme (11) with the minimal STO-3G basis set were performed for a number of substituted succinic, maleic, and phthalic anhydrides. The geometries for the parent succinic and maleic anhydrides were obtained from the crystallographic data (12). For the substituted compounds standard bond lengths and bond angles were used (13).

Intrinsic Differences Between the Two Carbonyl Groups in "Naked" (i.e., Not Associated with a Cation) Unsymmetrical Cyclic Anhydrides

From the perturbational viewpoint (14), the electrophilic reactivity of a molecule resides fundamentally in the energy and localization of its low lying vacant orbitals. Thus in terms of the perturbational theory a nucleophile should add preferentially to the atom bearing the largest coefficient on the lowest unoccupied molecular orbital (LUMO).

The *ab initio* calculations performed on the series of "naked" succinic, maleic, and phthalic anhydrides show in most cases a small but significant difference in the magnitude of the LUMO coefficients on the carbon atoms of the two carbonyl functions (Table 1). This suggests that there is an intrinsic difference in reactivity between the two carbonyl groups in unsymmetrical cyclic anhydrides. How do theoretical predictions compare with the available experimental data?

In succinic anhydrides, the LUMO coefficient on the carbon atom of the α-carbonyl group is consistently larger than the coefficient on the β-carbonyl function (Table 1). As a result the orbital interaction with a nucleophile's highest occupied molecular orbital (HOMO) is more favourable at the α-carbon atom. According to theory, preferential attack should be directed at the α-carbonyl function. The experimental results show that, despite intrinsic difference in electronic nature between chloro and methyl groups, compounds **4***a*, **4***b*, and **4***d* are all reduced selectively at the carbonyl group adjacent to the substituent(s).

If our argument, suggesting that the localization of the LUMO coefficients is an important factor in orienting regioselectivity of metal hydride reductions, is correct, we may also predict preferential reduction of the α-carbonyl function in fluoro and cyanosuccinic anhydrides **4***e*, **4***f*, and **4***g* (Table 1).

Can. J. Chem. Downloaded from www.nrcresearchpress.com by 210.87.254.42 on 09/06/12
For personal use only.

TABLE 1. Comparison between theoretical results (LUMO coefficients) and experimental data (ratio of lactonic products obtained)

Succinic anhydrides	R	R¹	No.	ε_L	LUMO coefficients C_α	LUMO coefficients C_β	Experimental ratio, reduction at: C_α	C_β	Ref.
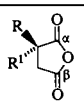 Maleic anhydrides	CH_3	CH_3	4*a*	0.275	0.599	−0.591	19	1	2
	CH_3	H	4*b*	0.274	0.601	−0.588	2.2	1	3*a*
	Cl	Cl	4*c*	0.216	0.658	−0.204			
	Cl	H	4*d*	0.243	0.684	−0.343	100[a]	—	
	F	F	4*e*	0.244	0.676	−0.452			
	F	H	4*f*	0.258	0.655	−0.506			
	CN	H	4*g*	0.246	0.677	−0.466			
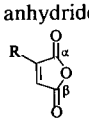 Phthalic anhydrides	CH_3		5*a*	0.1640	0.356	−0.348	9	1	10
	CH_3O—		5*b*	0.1682	0.386	−0.342	100	—	3*d*
	Cl		5*c*	0.1381	0.338	−0.338	9	1	10
	F		5*d*	0.1537	0.374	−0.342			
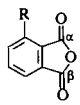	CH_3		6*a*	0.1737	0.329	−0.328	1.1	1	3*e*
	CH_3O[b]		6*b*	—	—	—	87	13	3*e*
	Cl		6*c*	0.1578	0.309	−0.314	—	—	3*e*
	F		6*d*	0.1645	0.309	−0.324	5.6	1	10

[a] $NaBH_4$ reduction of chloromaleic anhydride occurs in 1,2 and 1,4 fashion. Under the reaction conditions the competitive 1,4 addition yields chlorosuccinic anhydride which is further reduced to give β-chloro-γ-butyrolactone.
[b] For computational reasons methoxy and nitro substituted phthalic anhydrides could not be calculated.

We should point out that similar regioselectivity was forecast on the basis of the nonperpendicular approach (7). The computations of the optimal geometry for the nucleophilic attack on the unsubstituted succinic anhydride show that at the distance of 2 Å the optimal location for the hydride ion is at 110° to the carbon–oxygen double bond (Fig. 1).

In planar, conjugated anhydrides, the localization of LUMO cannot serve as a guide in forecasting the reaction site since there is no systematic correspondence between the calculated LUMO coefficients and the experimental facts (Table 1). Thus the difference between coefficients C_α and C_β is moderately large in favour of C_α in methoxymaleic anhydride **5***b*, smaller in methylmaleic anhydride **5***a*, and negligible in chloromaleic and 3-methylphthalic anhydrides **5***c* and **6***a*. In fluoro and chloro substituted phthalic anhydrides **6***d* and **6***c* the largest LUMO coefficients are on the carbon atom of the β-carbonyl group. As a result our qualitative analysis should predict an excess of the α reduction for methoxy and methylmaleic anhydrides, an equal mixture of the two lactones for the chloromaleic and methylphthalic anhydrides, and a preferential reduction at the β site for the remaining compounds. In contrast, $NaBH_4$ and $LiAlH_4$ reductions occur consistently at the α-carbonyl function (Table 1). Apparently factors other than those mentioned above make one of the two carbonyl groups a better target for the nucleophilic attack.

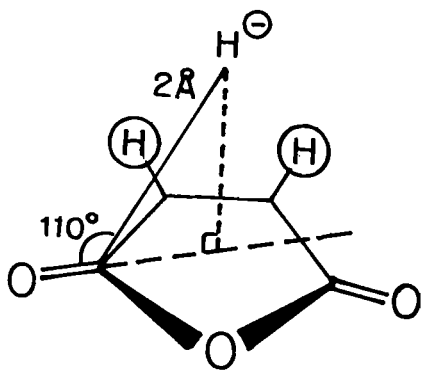

FIG. 1. The optimal position for hydride attack in the H^--succinic anhydride "super-molecule".

Influence of a Cation and Chelating Effects

We would like to point out that our discussion so far was limited to the consideration of "naked molecules" and did not allow for the intervention of a cation. Nevertheless, it is well documented that the association of a cation with the carbonyl function increases the reactivity (15) of the latter by lowering the LUMO π* of the substrate to the level of the nucleophile's HOMO, hence permitting a better interaction (16).

The cyclic anhydrides are not different in this respect. Indeed, the presence of an appropriate crown ether prevents reduction of 2,2-dimethylsuccinic anhydride by $LiAlH_4$.[2] In principle a

[2] M. M. Kayser, unpublished results.

Can. J. Chem. Downloaded from www.nrcresearchpress.com by 210.87.254.42 on 09/06/12
For personal use only.

Can. J. Chem. Downloaded from www.nrcresearchpress.com by 210.87.254.42 on 09/06/12
For personal use only.

cation can interact with any of the three negatively charged centres of the cyclic anhydride: the oxygen atoms of the two carbonyl groups and the oxygen atom of the ring.[3] However, the study of protonation of formic acid by the *ab initio* method (17) predicts that the carbonyl protonated formic acid is considerably more stable than the hydroxy protonated isomer. The nmr results confirm the theoretically obtained relative stabilities (17*b*). We may anticipate similar selectivity in anhydrides, i.e., preferential association of a proton or a cation with the oxygen atom of a carbonyl group. However, in unsymmetrically substituted anhydrides, a proton (or a cation) has an additional choice between the two carbonyl groups.

The calculations show that in unsymmetrically substituted succinic anhydrides both carbonyl groups have similar affinity for a cation.[4] Thus it is not a cation which determines the preferred site for the reduction but the intrinsic reactivity of each carbonyl group. Here, the cation's role is essentially to speed up the reaction. The situation is quite different in maleic and phthalic anhydrides. Due to the planar geometry of these compounds, the cation may form a bridge between the oxygen atom of the α-carbonyl group and the substituent, in those cases where the latter has lone pairs capable of interacting with a cation (OCH_3, Cl, F). It has been shown (19) that in protonated α-haloacetaldehydes **7** the proton preferred the *syn* position

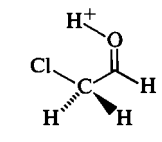

7 *syn*

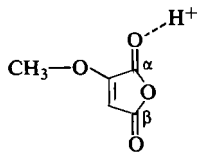

8 *anti*

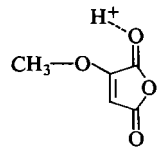

9 *syn*

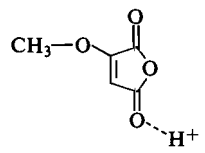

10

between the substituent and the oxygen atom by 5 kcal when the carbon–halogen bond was eclipsing the carbonyl group. A similar but weaker effect was observed in methoxymaleic anhydride. The *syn* isomer **9** was favoured over the *anti* isomer **8** by 3 kcal, suggesting the existence of intramolecular hydrogen bonding and the possibility of a proton being simultaneously bound to both oxygen atoms. However, to our dismay the ultimately preferred site for the protonation proved to be the β-carbonyl group, **10**. Actually, this situation could have been anticipated since the total and π electron density is higher on the oxygen of the β-carbonyl group (Table 2) and a proton used in our calculations is too small to be able to chelate effectively the two oxygen atoms. We expected that the larger cation such as Li^+ or Na^+ should prefer the "bridging" position between the oxygen atom and π-electron donating substituent to any other site in the molecule.

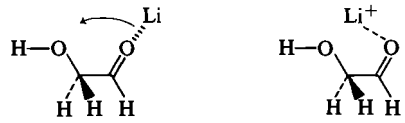

11

In order to determine if the chelating effect is in fact involved we have explored association of Li^+ with the model compound **11**. The optimum distances for Li^+—O in carbonyl and Li^+—O in ether have been reported to be 1.76 Å and 1.81 Å respectively (20). When Li^+ is placed simultaneously at approximately those distances from the two oxygen atoms in a model compound the situation should correspond to an important chelating effect. The optimization of Li^+ position in fact gives energy which is considerably lower (48.8 kcal) than the energy of the usual complex in which Li^+ is aligned with the carbonyl group (Fig. 2).

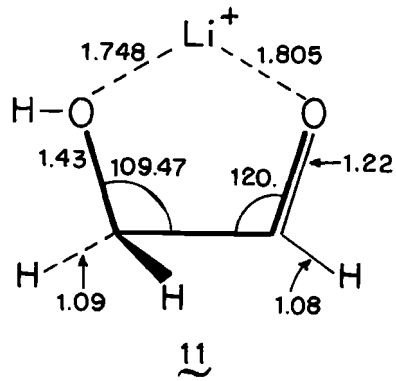

11

FIG. 2. Optimum geometry for Li^+ chelated in α-hydroxy ketone. The standard geometry was assumed for the compound **11** (13).

[3]We are neglecting in this discussion the possibility of a cation being associated with a substituent.

[4]Since the order of Li^+ and H^+ affinities for carbonyl functions was found to be similar (18) we have represented a cation by a proton in a study of cationic effects on succinic anhydrides. The optimum geometry for the protonated formaldehyde has been calculated (16). The distance O—H was found to be 0.96 Å and the angle C—O—H^+ 120°. We have used the same geometry for the succinic anhydride – proton complexes.

TABLE 2. Methoxymaleic anhydride: electron density on the carbonyl oxygen atoms and the relative energy of protonated methoxymaleic anhydride

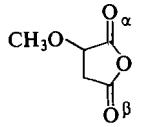	Density on oxygen atom	π Density on oxygen atom	Relative energy of the protonated molecule, kcal/mol
α Oxgen	8.215	1.186	*anti* Structure **8** 0 *syn* Structure **9** −3.2
β Oxygen	8.232	1.203	Structure **10** −11.8

Using optimized binding distances we have calculated the energy of the methoxymaleic anhydride – Li^+ chelate **12**. The chelated structure **12** was compared with the alternative isomeric forms **13** and **14**. It was gratifying to see that in contrast with

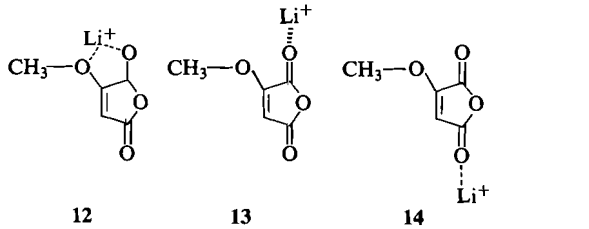

12 $E = -10$ **13** $E = 0$ **14** $E = -4 \rightarrow$ (kcal/mol)

the proton, Li^+ cation does prefer to complex the α-carbonyl group when there is a possibility of simultaneous binding with the substituent. Since the cation activates the carbonyl function to which it is attached toward the nucleophilic addition, the regioselective reduction of the α-carbonyl group in methoxy and chloromaleic anhydrides is principally due to the chelating effect. It is worthwhile to note that 1-methoxy-2-methylmaleic anhydride **15** and 1-methoxy-1-phenylmaleic anhydride **16** are

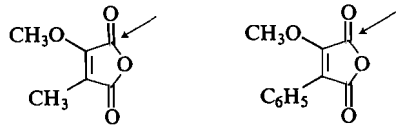

15 **16**

specifically reduced by $LiAlH_4$ at the carbonyl group neighbouring the methoxy substituent (3*d*). Consequently, electronic influences of alkyl and aryl groups apparent in monosubstituted methyl and phenylmaleic anhydrides, are unable to reverse directional effects resulting from the formation of chelates.

The cation binding the "bridged" position should also determine regioselectivity of nucleophilic addition in phthalic anhydrides substituted with lone pairs-bearing groups (CH_3O, Cl, F). The geometry of the molecule is particularly suitable for the formation of six centre chelates, **17**. Such an arrangement corresponds to the strong overlap between the cation and the lone pairs on the oxygen and the substituent atoms. This prediction is in agreement with the experimental results.

In 3-methylphthalic anhydride **6***a* the chelating effect is absent. Moreover, the LUMO coefficients on the carbon atoms of the two carbonyl groups are nearly identical (α:β = 0.329:0.328), therefore we should expect no selectivity. This prediction is confirmed experimentally as the ratio of the two lactones obtained is found to be 53:47.

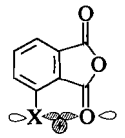

17

Conclusion

In this study we have demonstrated that in order to predict regioselectivity of nucleophilic addition to the unsymmetrically substituted cyclic anhydrides the following factors must be taken into consideration: (*1*) intrinsic reactivity of the two carbonyl functions represented by the size of the LUMO coefficient, (*2*) direction of the nucleophilic approach, (*3*) the preferred binding sites for the cation, as the energy-favoured formation of chelates may override any effects due to the intrinsic reactivities of the carbonyl groups involved.

We believe that the chelating effect (*3*), where applicable, is a determining factor controlling regioselectivities of metal hydride reductions. When chelation cannot occur other influences become more evident. Here, we should point out that the intrinsic reactivities of the two carbonyl functions

Can. J. Chem. Downloaded from www.nrcresearchpress.com by 210.87.254.42 on 09/06/12
For personal use only.

represented by the sizes of the LUMO coefficients (*1*) may be modified, i.e., amplified or diminished by the effects whose relative importance is difficult to estimate: for example, the direction of nucleophilic attack (*2*) which itself is dependent on the geometry of the substrate molecule and the coordination of the carbonyl function with a cation or a protic solvent.

Acknowledgements

The authors gratefully acknowledge financial support from the NATO Research Grant, No. 8G 026.80. M.M.K. would like to thank the Department of Chemistry, University of Ottawa, for making the computing facilities available. We are also in debt to Dr. Bernd Schweizer at the E.T.H. for a search in the Cambridge file and to Dr. Yves Jean for stimulating discussions.

1. B. Belleau and H. Puranen. Can. J. Chem. **43**, 2551 (1965); R. Granger and H. Techer. R. Acad. Sci. Sec. C, **250**, 142 (1960).
2. M. M. Kayser and P. Morand. Can. J. Chem. **56**, 1524 (1978).
3. (*a*) J. J. Bloomfield and S. L. Lee. J. Org. Chem. **32**, 3919 (1967); (*b*) D. M. Baily and R. E. Johnson. J. Org. Chem. **35**, 3575 (1970); (*c*) E. Burke and P. H. Le Quesne. J. Org. Chem. **36**, 2397 (1971); (*d*) D. W. Knight and G. Pattenden. J. Chem. Soc. Perkin Trans. I, 62 (1979); (*e*) A. J. McAlees, R. McCrindle, and D. W. Sheddon. J. Chem. Soc. Perkin Trans I, 2037 (1977).
4. F. Weygand, K. G. Kinkel, and D. Tietjen. Chem. Ber. **83**, 394 (1950); B. E. Cross and J. C. Stewart. Tetrahedron Lett. 3589 (1968).
5. H. O. House. Modern synthetic reactions. 2nd ed. W. A. Benjamin, Inc., Reading, MA. 1972. pp. 88 and 89.
6. (*a*) J. B. Wynberg, W. N. Speckamp, and H. E. Schoemaker. Tetrahedron Lett. 4073 (1974); J. C. Hubert, J. B. Wynberg, and W. N. Speckamp. Tetrahedron, **31**, 137 (1975); (*b*) M. M. Kayser and P. Morand. J. Org. Chem. **44**, 1338 (1979).
7. (*a*) M. M. Kayser and P. Morand. Tetrahedron Lett. 695 (1979); (*b*) R. E. Rosenfield, Jr. and J. D. Dunitz. Helv. Chim. Acta, **61**, 2176 (1978).
8. H. B. Bürgi, J. D. Dunitz, and E. Shafter. J. Am. Chem. Soc. **95**, 5065 (1973); Acta Crystallogr. Sec. B, **30**, 1517 (1974).
9. H. B. Bürgi, J. M. Lehn, and G. Wipff. J. Am. Chem. Soc. **96**, 1956 (1974); H. B. Bürgi, J. D. Dunitz, J. M. Lehn, and G. Wipff. Tetrahedron, **30**, 1563 (1974).
10. M. M. Kayser and P. Morand. Can. J. Chem. **58**, 2484 (1980).
11. W. J. Hehre, W. A. Lathan, R. Ditchfield, M. D. Newton, and J. A. Pople. Gaussian 70, Q.C.P.E. No. 236. Bloomington, IN.
12. (*a*) R. Destro, G. Filippini, C. M. Gramaccioli, and M. Simonetta. Acta. Crystallogr. Sect. B, **27**, 2023 (1971); (*b*) R. E. Marsh, E. Ubell, and H. E. Wilcox. Acta. Crystallogr. **15**, 35 (1962).
13. J. A. Pople and D. L. Beveridge. Approximate molecular orbital theory. McGraw-Hill, New York. 1970. p. 111; W. J. Hehre, R. Ditchfield, R. F. Stewart, and J. A. Pople. J. Chem. Phys. **52**, 2769 (1970).
14. E. Heilbronner and H. Bock. Das HMO Modell und seine Anwendung. Verlag Chemie, Weinheim Gergstr, Germany. 1968; R. Hoffmann. Acc. Chem. Res. **4**, 1 (1971); Nguyen Trong Anh. L'actualité Chimique, 9 (1974); I. Fleming. Frontier orbitals and organic chemical reactions. J. Wiley, London. 1976.
15. E. C. Ashby, J. R. Boone, and J. P. Oliver. J. Am. Chem. Soc. **95**, 5437 (1973); J. L. Pierre and H. Handel. Tetrahedron Lett. 2317 (1974); E. C. Ashby and J. R. Boone. J. Org. Chem. **41**, 2890 (1976).
16. Nguyen Trong Anh and O. Eisenstein. Nouv. J. Chem. **1**, 61 (1977); O. Eisenstein, J. M. Lefour, and C. Minot. Tetrahedron Lett. 1681 (1976).
17. (*a*) A. C. Hopkinson, K. Yates, and I. G. Csizmadia. J. Chem. Phys. **52**, 1784 (1970); (*b*) G. A. Olah, A. R. White, and D. H. O'Brien. Chem. Rev. **70**, 561 (1970).
18. J. E. Del Bene. Chem. Phys. **40**, 329 (1979).
19. R. Jost, J. Sommer, and G. Wipff. Nouv. J. Chim. **2**, 63 (1978).
20. P. Kollman and S. Rothenberg. J. Am. Chem. Soc. **99**, 1333 (1977).

Can. J. Chem. Downloaded from www.nrcresearchpress.com by 210.87.254.42 on 09/06/12
For personal use only.

Etude théorique et vibrationnelle du biphényldicarboximide-2,2', $C_{14}H_9NO_2$. Conjugaison et délocalisation électronique

ALAIN BOTREL

Laboratoire de Chimie Théorique, Laboratoire associé au C.N.R.S. no. 254, Chimie du Solide et Inorganique Moléculaire, Université de Rennes, Campus de Beaulieu, 35042 Rennes-Cedex, France

ET

PAUL CAILLET

Laboratoire de Chimie Minérale B, Laboratoire associé au C.N.R.S. no. 254, Chimie du Solide et Inorganique Moléculaire, Université de Rennes, Campus de Beaulieu, 35042 Rennes-Cedex, France

Reçu le 13 février 1981

ALAIN BOTREL et PAUL CAILLET. Can. J. Chem. **59**, 2463 (1981).

Les spectres de vibration du biphényldicarboximide-2,2' ont été déterminés et ont permis le calcul d'un champ de forces de valence. Les ordres de liaison issus de ce calcul ont été confrontés à l'analyse de population et aux énergies électroniques bicentriques déterminées par l'intermédiaire d'un calcul CNDO/2, permettant ainsi une double approche de la délocalisation électronique sur la molécule de biphényldicarboximide-2,2'.

ALAIN BOTREL and PAUL CAILLET. Can. J. Chem. **59**, 2463 (1981).

Vibrational spectra for 2,2'-diphenyldicarboximide have been determined and allow for a valence force field calculation. Bond orders obtained in this way have been compared with a population analysis and to the bicentric electronic energies determined by a CNDO/2 calculation, thus providing a twofold approach to the electron delocalization in 2,2'-diphehyldicarboxamide.

[Journal translation]

Introduction

La molécule du biphényldicarboximide-2,2' (ou B.P.I.) a déjà fait l'objet d'une étude expérimentale et théorique (1). Les calculs, effectués dans le cadre de la méthode EHT, avaient permis de proposer une structure pour ce composé en procédant, en particulier, à une étude systématique du cycle imidique grâce à un calcul de minimisation de tensions associé aux résultats énergétiques fournis par la méthode EHT.

Plus récemment, Caillet et Le Marouille (2) ont déterminé la structure de la molécule de B.P.I. à l'état solide.

La géométrie issue des calculs et la géométrie expérimentale diffèrent principalement par la position relative des deux cycles benzéniques, qui avaient été choisis coplanaires dans le premier cas, alors qu'ils sont caractérisés par une torsion d'environ 30° autour de la liaison C(1)—C(7) (cf. Fig. 1).

Il nous a alors paru intéressant de reprendre les calculs théoriques sur la molécule non substituée en utilisant, cette fois, la géométrie expérimentale, afin de pouvoir, en particulier, comparer les résultats obtenus pour l'analyse de population avec les ordres de liaison calculés selon la formule de Siebert (3) après le calcul d'un champ de forces de valence effectué à partir des spectres de vibration.

Après la partie expérimentale, nous discuterons brièvement de l'analyse vibrationnelle puis les résultats du calcul du champ de force seront confrontés aux conclusions de l'étude théorique pour permettre la discussion des liaisons chimiques.

Partie expérimentale et méthodologie

Le B.P.I. monodeutérié $(C_6H_4CO)_2ND$ est préparé par recristallisation du composé hydrogéné dans de l'alcool éthylique C_2H_5OD à 95% dans D_2O. Après 5 recristallisations, le spectre de masse montre que le composé est monodeutérié à plus de 95%.

Les spectres d'absorption infrarouge, entre 4000 et 200 cm^{-1}, ont été réalisés au Laboratoire de Chimie Minérale B de l'Université de Rennes sur un spectrophotomètre Beckmann IR 12. Le solide est finement broyé puis mis en suspension dans le Nujol entre deux lames d'iodure de césium.

Les spectres de diffusion Raman, entre 4000 et 10 cm^{-1}, ont été effectués au Laboratoire de Spectroscopie Infrarouge de l'Université de Bordeaux I sur un spectrophotomètre Coderg T800.

Quel que soit l'appareil utilisé, la précision est de ± 1 cm^{-1} sur les bandes les plus fines.

Les calculs ont été effectués au C.I.C.B. de Rennes, à l'aide des programmes de l'Université de Bordeaux I pour la partie vibrationnelle, et suivant la méthode CNDO/2 (4) pour la partie théorique.

Nous nous sommes plus spécialement intéressés dans le cadre de cette dernière à l'analyse de population entre les atomes et pour ce faire nous avons déterminé l'indice de liaison[1]:

$$[1] \quad p_{AB} = \sum_{\mu}^{A} \sum_{\nu}^{B} \rho_{\mu\nu} S_{\mu\nu}$$

[1]Voir la ref. 12.

0008-4042/81/162463-07$01.00/0

©1981 National Research Council of Canada/Conseil national de recherches du Canada

Can. J. Chem. Downloaded from www.nrcresearchpress.com by 210.87.254.5 on 09/06/12
For personal use only.

TABLEAU 1. Paramètres géométriques de la molécule de B.P.I.

Liaison	Distances (Å)	Angles de liaisons	Degrés	Angles de torsion	Degrés
C—C (benzénique)	1,395	C—C—C (cycle benzénique)	120,0	Entre les deux cycles benzèniques	30,0
C(1)—C(7)	1,487	C(6)—C(1)—C(7)	124,5	C(15)—C(13)—C(6)—C(1)	−42,078
C(6)—C(13)	1,494	C(1)—C(6)—C(13)	127,0		
C(13)—N(15)	1,382	C(6)—C(13)—N(15)	121,0		
C(13)—CO(16)	1,223	C(13)—N(15)—C(14)	129,64		

où $\rho_{\mu\nu}$ et $S_{\mu\nu}$ représentent respectivement un élément de la matrice densité et une intégrale de recouvrement; l'indice de liaison calculé selon Wiberg (5)

$$[2] \quad p_{AB}{}^{W} = \sum_{\mu}^{A} \sum_{\nu}^{B} \rho_{\mu\nu}{}^{2}$$

et l'énergie électronique bicentrique E_{AB} que l'on peut décomposer en trois parties (6):

$$[3] \quad E_{AB} = E_{AB}{}^{(1)} + E_{AB}{}^{(2)} + E_{AB}{}^{(3)}$$

avec

$$[4]^{2} \quad E_{AB}{}^{(1)} = 2 \sum_{\mu}^{A} \sum_{\nu}^{B} \rho_{\mu\nu} S_{\mu\nu} \beta_{AB}{}^{0}$$

$$[5]^{2} \quad E_{AB}{}^{(2)} = -\frac{1}{2} \sum_{\mu}^{A} \sum_{\nu}^{B} \rho_{\mu\nu}{}^{2} \gamma_{AB}$$

$$[6] \quad E_{AB}{}^{(3)} = q_{A} q_{B} \gamma_{AB} + Z_{A} Z_{B} \left(\frac{1}{R_{AB}} - \gamma_{AB} \right)$$

Géométrie et notation

Nous avons, tout en conservant les caractéristiques géométriques principales de l'analyse cristalline, effectué tous les calculs sur une molécule admettant un axe de symétrie C_2 (cf. Fig. 1). Nous avons, en particulier, utilisé pour les cycles benzéniques une géométrie régulière (distances C—C de 1,395 Å et angles de liaison de 120°).

Les principaux paramètres géométriques ainsi adoptés sont réunis dans le tableau 1 (cf. Fig. 1 pour la numérotation).

Dans le but d'obtenir une meilleure comparaison des résultats, tous les calculs ont été effectués en considérant une molécule isolée possèdant la géométrie indiquée dans le tableau 1; celle-ci n'a donc pas été optimisée dans le calcul CNDO/2.

Etude vibrationnelle

Interprétation des spectres et détermination du champ de force

Une molécule isolée de B.P.I. de symétrie C_2 possède 72 vibrations (36A + 36B), toutes actives en infrarouge et en Raman. A l'état solide, la molécule est placée dans un site de symétrie C_1 et la présence de deux molécules dans la maille primitive amène, dans le groupe facteur C_{2h}, à la représentation $\Gamma = 78\,Ag + 78\,Bg + 77\,Au + 76\,Bu$. En réalité, même à l'état solide, la molécule est très voisine de la symétrie C_2 (2), l'effet du "champ cristallin" consistera donc essentiellement en l'éclatement de chaque vibration de type A (ou B) en deux composantes Ag et Au (ou Bg et Bu) l'une active en Raman et l'autre en infrarouge.

Les fréquences observées ainsi que les attributions sont données dans le tableau 2. Ces dernières tiennent compte des intensités relatives des bandes ir et des raies Raman et sont effectuées par comparaison avec les résultats que nous avons obtenus pour le maléimide (7) et le benzène (8), ainsi qu'avec les résultats de Zerbi et Sandroni concernant le biphényle (9). Les vibrations qui font intervenir les cycles benzéniques sont désignées suivant la numérotation classique (8, 10).

Précisons que les fréquences à 1362 et 1361 cm^{-1} pour le dérivé hydrogéne sont attribuées à la fois à νCN et δNH, tandis que δND apparait dans le composé deutérié à 1031 cm^{-1}.

Les coordonnées utilisées sont les coordonnées internes "de groupe" déjà précisées lors de précédents calculs (7, 8). Le champ de force de départ a été construit à partir des valeurs obtenues pour le mésitylène (11) pour les cycles aromatiques, et de celles du maléimide (7) pour la fonction imide; il comprenait, en outre, toutes les constantes d'interaction entre des coordonnées possèdant au moins 1 atome commun. Un premier calcul montre qu'un certain nombre de ces dernières sont pratiquement sans influence sur les valeurs des fréquences calculées, elles ont été fixées à zéro pour la suite. Le champ de force utilisé comporte finalement 21 constantes de forces principales et 69 d'interactions, 45 d'entre elles sont transférées du mésitylène, 39 du maléimide, les 6 dernières sont des interactions qui sont nouvelles.

Dès le premier calcul, les fréquences attribuées aux cycles benzéniques sont toutes voisines des valeurs observées et, en l'absence de dérivés isotopiques sur les cycles benzèniques, nous n'avons pas cherché à améliorer cet accord et avons conservé dans la suite du calcul les valeurs des 52 constantes de forces correspondantes.

Par contre, il apparaît que les fréquences calculées pour δNH et γNH sont trop basses et que les fréquences attribuées au cycle imidique sont mal ajustées par suite de la différence de géométrie, sensible surtout au niveau des angles, entre le maléimide et le B.P.I. Nous avons donc augmenté

[2] γ_{AB} et $\beta_{AB}{}^{0}$ sont l'intégrale coulombienne bicentrique et le paramètre de liaison habituels de la méthode CNDO/2 (4).

Can. J. Chem. Downloaded from www.nrcresearchpress.com by 210.87.254.5 on 09/06/12
For personal use only.

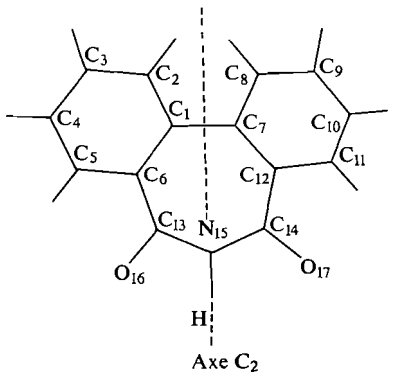

FIG. 1. Numérotation utilisée pour la molécule de B.P.I.

les valeurs des constantes de force δNH et γNH et modifié les valeurs de celles relatives aux angles intérieurs du cycle. En ce qui concerne les fréquences νCN, c'est à la fois ν_aCN et ν_sCN qui sont mal ajustées et la simple modification de la constante de force principale ne permettrait, au mieux, que d'ajuster l'une d'entre elles. Nous avons donc modifié les constantes d'interaction, entre νCN, νCO et νCC en particulier, pour obtenir à la fois un meilleur accord de fréquence et des effets isotopiques corrects. Au total 6 constantes de forces principales et 14 interactions ont été modifiées dans cette étape du calcul.

Pour conclure, nous avons soumis les 38 constantes de force non fixées à un affinement qui n'a pratiquement pas modifié les valeurs précédemment obtenues, l'écart absolu moyen entre fréquences calculées et observées est inférieur à 6 cm^{-1}. Les valeurs des constantes de force les plus significatives sont données dans le tableau 3.

Modes de vibrations

La distribution de l'énergie potentielle (tableau 2) et l'analyse de la matrice L des vecteurs propres montrent que les attributions qui ont été faites par comparaison des spectres ne sont qu'une grossière approximation. En effet, en ce qui concerne les cycles benzéniques, les vibrations 8a et 8b donnent ensemble les quatre modes situés vers 1600 cm^{-1}, de même 5 et 17b conduisent, également ensemble, aux quatre modes situés entre 950 et 1000 cm^{-1}. Les modes faisant intervenir le groupement imide résultent également de couplages, et on observe même de nombreux modes dans lesquels interviennent à la fois les cycles benzéniques et le groupement imide; c'est le cas, par exemple, des vibrations "νCO", ou encore de celles situées à 1247, 1200, 1150 ou encore 616 cm^{-1}. Enfin, du fait des torsions entre les cycles, on observe également des modes dans lesquels interviennent à la fois des torsions ou des mouvements "hors du plan" (γCH,γCO) et des mouvements "dans le plan" en particulier pour les modes situés aux basses fréquences.

En conclusion, on peut dire qu'à l'exception des modes situés au-dessus de 2000 cm^{-1} et qui sont bien décrits par les mouvements νCH et νNH tous les autres modes de vibration sont complexes et font intervenir de nombreuses coordonnées.

Liaisons chimiques: résultats et discussion

Les constantes de forces caractéristiques du B.P.I. sont données dans le tableau 3, où elles sont comparées aux valeurs obtenues pour le triméthylbenzène (T.M.B.) d'une part, et pour le maléimide d'autre part.[3]

Nous avons regroupé dans le tableau 4 l'ensemble des résultats obtenus (p_{AB}, p_{AB}^{W} et énergies électroniques bicentriques) sur les molécules de B.P.I. et de maléimide en CNDO/2, ainsi que les ordres de liaison déterminés à partir du champ de forces (p_{AB}^{S}) par la formule de Siebert (3).

Enfin, nous donnons dans le tableau 5 les valeurs des charges nettes CNDO des atomes principaux de la molécule de B.P.I.

Précisons que la valeur calculée du moment dipolaire de la molécule de B.P.I. (3,38 D) est en bon accord avec la valeur expérimentale 3,34 D (1).

Comparaison "Théorie–Expériences"

Les comparaisons entre ordres de liaisons calculés à partir des constantes de forces d'une part, et les résultats CNDO/2 d'autre part sont illustrés par des corrélations du type:

$$p_{AB}^{S} = aX_{AB}^{CNDO} + b$$

où X_{AB}^{CNDO} représente les indices ou les énergies électroniques fournis par la méthode CNDO sur la molécule de B.P.I.

Les valeurs des constantes a, b et du coefficient de régression linéaire r, déterminées par une méthode de moindres carrés, sont regroupés dans le tableau 6.

Précisons que les calculs du tableau 6 ont été effectués en prenant pour les liaisons C—C des cycles benzéniques des valeurs moyennes (déterminées à partir des résultats du tableau 4) des X_{AB}^{CNDO}.

Les résultats de l'analyse expérimentale (p_{AB}^{S}) et de l'analyse théorique (p_{AB}, p_{AB}^{W} et E_{AB}^{T}) sont dans l'ensemble cohérents.

Toutefois, les valeurs relativement médiocres obtenues pour les coefficients r des deux premières

[3]Le tableau complet des constantes de forces utilisées peut être demandé à P. Caillet.

Can. J. Chem. Downloaded from www.nrcresearchpress.com by 210.87.254.5 on 09/06/12
For personal use only.

Can. J. Chem. Downloaded from www.nrcresearchpress.com by 210.87.254.5 on 09/06/12
For personal use only.

TABLEAU 2. Fréquences de vibration et distribution de l'énergie potentielle (D.E.P.)

Biphényldicarboxamide-2,2′ d_0					Biphényldicarboxamide-2,2′ d_1			
Infrarouge	Raman	Calc.	D.E.P.		Infrarouge	Raman	Calc.	D.E.P.
3180 m		3174	99νNH	νNH				
3110 f		3103	98νCH	νCH	3110 f		3103	98νCH
		3103	98νCH				3103	98νCH
		3095	99νCH				3095	99νCH
		3095	99νCH				3095	99νCH
		3093	99νCH				3093	99νCH
		3093	99νCH				3093	99νCH
	3082 f	3092	99νCH			3084 f	3092	99νCH
		3092	99νCH				3092	99νCH
				νND	2330 m		2345	96νND
1694 TF	1692 F	1686	57νCO + 12νCC(ϕ)	ν_sCO	1686 TF	1679 F	1685	57νCO + 13νCC(ϕ)
1674 TF		1683	34νCO + 27νCC(ϕ)	ν_{as}CO	1657 TF		1672	49νCC(ϕ) + 15νCO
	1659 TF	1652	41νCC(ϕ) + 25νCO			1640 F	1642	49νCO + 22νCC(ϕ)
1599 m	1599 TF	1611	62νCC(ϕ) + 23δCH + 12α(ϕ)	8a et 8b	1599 m	1599 TF	1611	62νCC(ϕ) + 23δCH + 12α(ϕ)
1581 m		1606	63νCC(ϕ) + 21δCH + 14α(ϕ)		1581 m		1605	60νCC(ϕ) + 20δCH + 13α(ϕ)
	1566 m	1605	56νCC(ϕ) + 16α(ϕ) + 13νCO			1566 m	1605	55νCC(ϕ) + 15α(ϕ) + 13νCO
	1501 m	1497	44νCC(ϕ) + 41δCH	19a		1500 m	1496	44νCC(ϕ) + 42δCH
1484 tf		1483	41δCH + 41νCC(ϕ) + 13νC_1C_7		1484 f		1483	42δCH + 42νCC(ϕ) + 13νC_1C_7
1449 f		1437	52δCH + 40νCC(ϕ)	19b	1448 m		1436	51δCH + 40νCC(ϕ)
		1433	49δCH + 37νCC(ϕ)				1433	50δCH + 38νCC(ϕ)
	1361 f	1373	41νCN + 18νCC + 21δCO	ν_sCN	1367 m	1364 f	1355	38νCN + 21νCC + 21δCO
1362 m		1366	61δNH + 13νCN + 13νCO	δNH				
1321 F		1323	73δCH + 19νCC(ϕ)		1342 F		1324	75δCH + 22νCC(ϕ)
	1330 m	1307	137νCC(ϕ)	3 et 14		1330 m	1307	137νCC(ϕ)
1273 f	1273 ep	1282	127νCC(ϕ)		1274 tf		1284	123νCC(ϕ)
1261 m	1259 F	1276	61δCH + 21νCC(ϕ)		1262 m	1260 F	1274	60δCH + 21νCC(ϕ)
1247 f	1248 f	1244	30δCH + 27νCC(ϕ) + 26νC_1C_7	νC_1C_7	1247 f	1247 f	1241	29δCH + 27νCC(ϕ) + 26νC_1C_7
1171 f		1182	37δCH + 26νCC + 22νCN + 16νCC(ϕ)	ν_aCN	1208 f		1205	42νCN + 38νCC + 19νCC(ϕ)
	1168 m	1165	91δCH + 16νCC(ϕ)	9 et 15		1168 m	1165	93δCH + 16νCC(ϕ)
1171 f		1163	77δCH + 23νCC(ϕ)		1172 f		1165	93δCH + 18νCC(ϕ)
1163 f		1161	43δCH + 21νCC(ϕ) + 12α(ϕ)		1163 tf		1159	41δCH + 22νCC(ϕ) + 12α(ϕ)
1151 F		1144	47δCH + 22νCN + 21νCC(ϕ)	ν_aCC et 18	1151 tf		1145	50δCH + 22νCC(ϕ) + 16νCN
1131 tf	1130 m	1132	59νCN + 12νCC(ϕ) + 12δCH		1131 F	1126 m	1132	59νCN + 12νCC(ϕ) + 12δCH
1123 tf		1106	47α(ϕ) + 19α + 14δCH	12			1106	48α(ϕ) + 19α + 14δCH
1086 f		1075	45α(ϕ) + 20νCC(ϕ) + 16α		1088 tf		1076	38α(ϕ) + 23νCC(ϕ) + 17δCH
	1055 TF	1050	55νCC(ϕ) + 18δCH	1		1055 TF	1050	55νCC(ϕ) + 18δCH
1054 f		1042	50νCC(ϕ) + 19α(ϕ)				1050	27α(ϕ) + 24νCC(ϕ) + 22δND
				δND	1031 F		1019	51δND + 31νCC(ϕ)

Can. J. Chem. Downloaded from www.nrcresearchpress.com by 210.87.254.5 on 09/06/12
For personal use only.

TABLEAU 2. (*Concluded*)

Biphényldicarboximide-2,2′ d_0					Biphényldicarboximide-2,2′ d_1			
Infrarouge	Raman	Calc.	D.E.P.		Infrarouge	Raman	Calc.	D.E.P.
999 tf	999 tf	990	100γCH + 25τ(ϕ)	}5{			990	100γCH + 25τ(ϕ)
991 tf		989	100γCH + 25τ(ϕ)		992 tf		989	100γCH + 25τ(ϕ)
967 tf	967 tf	964	91γCH + 18τ(ϕ)	}17b{	968 tf		964	91γCH + 18τ(ϕ)
955 f		960	92γCH + 19τ(ϕ)		956 f		960	92γCH + 19τ(ϕ)
900 f		905	78γCH	}17a{	901 f		905	78γCH
890 f		899	82γCH + 10τ(ϕ)		891 f		899	82γCH + 10τ(ϕ)
875 f		873	41γCO + 10νCC(ϕ) + 10α	γ_aCO	876 f		870	42γCO
837 m		837	57γNH + 25γCO	γNH				
800 m	801 f	822	35α(ϕ) + 28νCC(ϕ) + 18νCC		800 f	801 f	821	34α + 29νCC(ϕ) + 18νCC
				γ_sCO	792 m		793	57γCO + 21γND
774 m	770 f	777	42νCC + 23νCC(ϕ) + 12α(ϕ)					
747 f	743 f	748	98γCH	}11{			749	47γCH + 18νCC + 11νCC(ϕ)
726 F		747	93γCH		726 F		747	98γCH
							741	53γCH + 14γCO + 12νCC
726 F		725	62γCO	γ_sCO				
		702	38νCC(ϕ) + 35α(ϕ)				701	41νCC(ϕ) + 38α(ϕ)
	676 m	670	34α + 19γCO + 11νCO	}α{		675 m	666	35α + 19γCO + 11νCO
656 m	651 f	662	49α(ϕ) + 39νCC(ϕ)		653 m		662	48α(ϕ) + 38νCC(ϕ)
648 m	647 tf	645	25τ(ϕ) + 22γCH	}4{	650 m	645 f	645	25τ(ϕ) + 22γCH
617 f		627	28τ(ϕ) + 24γCH		618 f		626	27τ(ϕ) + 24γCH
	617 f	616	64δCO + 30α(ϕ) + 20νCC(ϕ)	δCO		617 f	619	27δCO + 18νCC(ϕ) + 14γND
				γND	576 m		573	57δCO + 20γND
566 m	561 f	561	26δCO + 21νCC(ϕ) + 19δC_1C_7		560 f	561 f	548	17νCC(ϕ) + 13γND + 13δC_1C_7
488 m	489 f	494	25νCC + 17νCC(ϕ)	} 6	486 m	488 f	491	25νCC + 17νCC(ϕ)
436 f	435 F	419	31α + 22δC_1C_7	et } δCO {	438 tf	436 F	416	30α + 21δC_1C_7
411 m	407 tf	404	39δCO + 16νCN		411 m	407 tf	404	39δCO + 16νCN
		372	20δCC + 15νC_1C_7 + 15νCC(ϕ)				372	20δCC + 15νC_1C_7 + 15νCC(ϕ)
344 m		372	37τ(ϕ) + 13γCH	}16{	344 m		370	36τ(ϕ) + 13γCH
335 m	337 m	360	46τ(ϕ) + 17γCH		334 m	335 m	360	46τ(ϕ) + 17γCH
298 m	298 m	315	26δCO + 15α + 13νCC(ϕ)		299 m	299 f	310	26δCO + 14α
		258	45δC_1C_7 + 22α(ϕ)	δC_1C_7			258	45δC_1C_7 + 22α(ϕ) + 13νCC(ϕ)
226 tf	229 f	236	23τ(ϕ) + 20δCC + 11τ		228 tf	224 f	235	24τ(ϕ) + 20δCC + 11τ
		202	37τ(ϕ) + 16τCN + 11γNH				200	36τ(ϕ) + 18τCN + 10γNH
	185 f	180	52τ(ϕ) + 25α			182 f	180	52τ(ϕ) + 23α
	170 f	159	29τC_1C_7 + 28τ + 11δCC			169 f	159	29τC_1C_7 + 28τ + 11δCC
		123	50τ(ϕ) + 43δCC + 20τ				123	50τ(ϕ) + 43δCC + 19τ
	85 m	88	63τ + 39τC_1C_7			84 m	87	63τ + 39τC_1C_7
	48 f	42	99τ + 40τ(ϕ)			48 f	42	99τ + 40τ(ϕ)
	26 f	28	140τ			27 f	28	140τ

Can. J. Chem. Downloaded from www.nrcresearchpress.com by 210.87.254.5 on 09/06/12
For personal use only.

TABLEAU 3. Comparaison des constantes de forces caractéristiques

Constantes de forces	T.M.B.[a]	B.P.I.[b]	Maléimide
νC—C(φ)	6,031	6,031	
$\nu C_1—C_7$	4,710	4,711	
$\nu C_6—C_{13}$	4,710	4,789	4,790
νC—N		6,225	6,224
νC—O		9,013	9,015
νN—H		5,54	5,685
νCC(φ),νCC(φ)	0,848	0,848	
$\nu CC(\varphi),\nu C_1—C_7$	0,120	0,151	
$\nu CC(\varphi),\nu C_6—C_{13}$	0,120	0,067	
$\nu C_6—C_{13},\nu CN$		0,553	0,457
$\nu C_6—C_{13},\nu CO$		0,479	0,011
νCO,νCN		0,537	0,548
νCN,νCN		0,904	0,314
δCO		1,04	0,999
δNH		0,543	0,418
νCN,δNH		0,362	0,279
γCO		0,662	0,759
γNH		0,185	0,116

[a]T.M.B. = triméthylbenzène.
[b]B.P.I. = biphénylidicarboximide-2,2'.

corrélations (0,919 et 0,901) sont dues, de façon générale, au petit nombre de points utilisés (6 compte tenu des valeurs moyennées pour les liaisons C—C des cycles benzéniques) et à leur dispersion insuffisante. Elles proviennent également: (*1*) pour la corrélation $p_{AB}^S - p_{AB}$ des valeurs certainement trop faibles obtenues pour le p_{AB} des liaisons C—O et C—N (inférieures au p_{AB} moyen d'une liaison C—C benzénique). L'indice p_{AB}, qui peut être considéré comme étant une mesure de la force d'une liaison covalente (12), ne semble pas donner une bonne image de la liaison quand celle-ci est assez fortement polarisée (cas de CO et CN; voir tableau 5) et présente donc un caractère ionique non négligeable; et (*2*) pour la corrélation $p_{AB}^S - p_{AB}^W$: d'une part, de l'inversion observée pour les indices p_{AB}^W des liaisons C(1)—C(7) et C(6)—C(13) par rapport aux valeurs correspondantes des p_{AB}^S, inversion dont il est difficile, cependant, de tenir compte de façon sérieuse compte tenu des valeurs très voisines des indices; d'autre part, des valeurs relatives des indices p_{AB}^W et p_{AB}^S de la liaison C(13)—O(16), le premier mettant en évidence un caractère marqué de double-liaison, le second, caractérisant (en accord avec l'indice p_{AB}^S de la liaison C(13)—N(15)) une délocalisation sensiblement plus importante sur l'ensemble du groupement imidique.

La troisième corrélation (indice p_{AB}^S – énergie électronique bicentrique E_{AB}^T) apparaît ici comme la plus représentative de la comparaison expérience–théorie, sans doute parce que l'énergie E_{AB}^T rend compte pour une grande part de toutes les caractéristiques d'une liaison donnée (cf. les expressions [3] à [6]); cette analyse se trouve confirmée par l'étude des corrélations entre l'indice p_{AB}^S et les différents termes de l'énergie E_{AB}^T (cf. tableau 6): si l'énergie $E_{AB}^{(1)}$, ou terme d'énergie covalente, apparaît la mieux corrélée à p_{AB}^S, il est clair que les énergies $E_{AB}^{(2)}$ (terme d'échange) et $E_{AB}^{(3)}$ (terme d'interaction électrostatique) apportent une contribution non négligeable à l'énergie électronique bicentrique totale.

Conjugaison et délocalisation

Signalons tout d'abord que, dans le cas des cycles benzéniques, les valeurs moyennes $\bar{E}_{AB}^T$ et

TABLEAU 4. Résultats des calculs CNDO/2 et indices de Siebert pour les molécules de B.P.I. et de maléimide

Liaisons	p_{AB}	p_{AB}^W	$E_{AB}^{(1)}$ (eV)	$E_{AB}^{(2)}$ (eV)	$E_{AB}^{(3)}$ (eV)	E_{AB}^T (eV)	p_{AB}^S
Biphényldicarboximide-2,2'							
C(1) —C(2)	0,939	1,401	−39,443	−6,825	9,220	−37,048	1,48
C(2) —C(3)	0,957	1,456	−40,187	−7,094	9,221	−38,060	1,48
C(3) —C(4)	0,954	1,435	−40,052	−6,989	9,223	−37,818	1,48
C(4) —C(5)	0,956	1,453	−40,173	−7,078	9,223	−38,028	1,48
C(5) —C(6)	0,936	1,399	−39,296	−6,814	9,211	−36,899	1,48
C(6) —C(1)	0,932	1,366	−39,159	−6,653	9,209	−36,603	1,48
C(1) —C(7)	0,760	1,030	−31,926	−4,776	6,544	−30,158	1,16
C(6) —C(13)	0,762	1,019	−32,013	−4,709	6,233	−30,489	1,18
C(13)—N(15)	0,751	1,066	−34,551	−5,331	7,591	−32,291	1,32
C(13)—O(16)	0,903	1,790	−46,940	−9,966	13,944	−42,962	1,52
N(15)—H	0,606	0,941	−20,607	−6,003	6,340	−20,270	1,06
Maléimide							
C(3) —C(4)	1,110	1,876	−46,620	−9,608	13,014	−43,214	1,86
C(2) —C(3)	0,767	1,014	−32,213	−4,742	6,814	−30,141	1,18
C(2) —N(1)	0,861	1,129	−39,595	−6,040	12,862	−32,773	1,32
C(2) —O(6)	0,858	1,719	−44,604	−9,416	12,259	−41,761	1,52
N(1) —H	0,621	0,939	−21,127	−6,073	6,980	−20,220	0,90

TABLEAU 5. Charges nettes CNDO de la molécule de B.P.I.

	C1	C2	C3	C4	C5	C6	C13	N15	O16
q	0,035	−0,007	0,017	−0,001	0,027	−0,040	0,344	−0,238	−0,326

TABLEAU 6. Régressions linéaires. Résultats

	X_{AB}^{CNDO}					
	p_{AB}	p_{AB}^{W}	$E_{AB}^{(1)}$	$E_{AB}^{(2)}$	$E_{AB}^{(3)}$	E_{AB}^{T}
a	1,399	0,507	−0,020	−0,070	0,053	−0,023
b	0,184	0,672	0,609	0,849	0,845	0,551
r	0,919	0,901	0,938	0,745	0,854	0,941

$\bar{p}_{AB}^{W}$ par exemple sont très proches de celles obtenues dans le cas de la molécule de benzéne isolée (−37,4 eV pour −37,9 eV et 1,42 pour 1,45).

De façon plus générale, les valeurs obtenues pour p_{AB}^{W}, E_{AB}^{T}, p_{AB}^{S} et pour les constantes de forces d'interaction montrent que la molécule de B.P.I. peut se décomposer en trois fragments principaux si on considère la délocalisation électronique: chacun des deux cycles benzéniques et le groupement imidique. On constate, en effet, une très sensible diminution des différents indices et une nette déstabilisation des énergies électroniques bicentriques pour les liaisons C(1)—C(7), C(6)—C(13) et C(12)—C(14).

Ceci rappelle des résultats que nous avions déjà obtenus dans le cas du maléimide pour lequel on constatait (cf. tableaux 3 et 4 et Fig. 2) une coupure très semblable au niveau des atomes C(2) et C(3) (ou C(4) et C(5)), bien que la molécule plane du maléimide ne présentât pas les torsions observées dans le B.P.I.

En ce qui concerne le groupement imidique les valeurs de p_{AB}^{W}, E_{AB}^{T} et p_{AB}^{S} obtenues pour le maléimide et le B.P.I. sont très proches, ou même identiques, et ne permettent que difficilement une comparaison des délocalisations sur la chaîne O—C—N—C—O. Par contre, la comparaison des constantes de forces d'interactions montre que la délocalisation électronique est plus élevée pour le B.P.I. puisque la constante νCN, νCN passe de

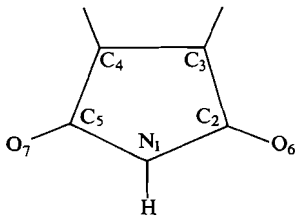

FIG. 2. Numérotation utilisée pour la molécule de maléimide.

0,314 pour le maléimide à 0,904 pour le B.P.I.; cette dernière valeur est même supérieure à celle observée au niveau du cycle benzénique (0,848). Les valeurs élevées trouvées pour les autres interactions (cf. tableau 3) confirment les conjugaisons des différentes liaisons de la fonction imide.

Enfin, les valeurs trouvées pour la liaison C(1)—C(7) montrent que cette liaison est proche d'une simple liaison C—C et constitue une coupure à la délocalisation électronique entre les deux cycles. Ce résultat, qui est en accord avec les conclusions de Zerbi et Sandroni (9*b*) sur le biphényle, et la coupure constituée par les liaisons C(6)—C(13) et C(12)—C(14), ne doivent pas être attribués aux torsions entre les cycles ou entre cycle et groupement imide puisque les mêmes conclusions sont obtenues pour le biphényle (9) et le maléimide (7) qui sont plans.

Conclusion

Nous avons déterminé et interprété les spectres de vibration du biphényldicarboximide-2,2'. La détermination d'un champ de force de valence, jointe aux résultats d'un calcul théorique par la méthode CNDO/2, permet la discussion des liaisons de cette molécule. Nous montrons qu'il existe trois fragments pour lesquels la délocalisation électronique est très élevée ce sont: les deux cycles benzéniques et le groupement imide. Chacun de ces groupements est bien isolé des autres par de simples liaisons C—C qui constituent autant de coupures des conjugaisons.

1. A. BOTREL et C. R. GUERILLOT. J. Chim. Phys. **71**, 1293 (1974).
2. P. CAILLET et J. Y. LE MAROUILLE. Acta Crystallogr. Sect. B, **34**, 175 (1978).
3. H. SIEBERT. Z. Anorg. Allgem. Chem. **275**, 225 (1954).
4. J. A. POPLE et G. A. SEGAL. J. Chem. Phys. (*a*) **43**, 5136 (1965); (*b*) **44**, 3289 (1966).
5. K. B. WIBERG. Tetrahedron, **24**, 1083 (1968).
6. M. S. GORDON. J. Am. Chem. Soc. **91**, 3122 (1969).
7. L. LE GALL, P. CAILLET et M. T. FOREL. J. Chim. Phys. **75**, 444 (1978).
8. J. FAVROT, P. CAILLET et M. T. FOREL. J. Chim. Phys. **71**, 2337 (1974).
9. G. ZERBI et S. SANDRONI. Spectrochim. Acta, Part A, (*a*) **24**, 483 (1968); (*b*) **24**, 511 (1968); (*c*) **26**, 1951 (1970).
10. G. VARSANYI. Vibrational spectra of benzene derivatives. Academic Press, New York and London. 1969.
11. J. FAVROT et M. T. FOREL. Can. J. Spectrosc. **21**, 144 (1976).
12. F. CORRE. J. Mol. Struct. In press.

Can. J. Chem. Downloaded from www.nrcresearchpress.com by 210.87.254.5 on 09/06/12
For personal use only.

Nucleophilic addition and displacement in the reaction of 2,4,6-trimethylphenoxide ion with 1,3,5-trinitrobenzene. An oxygen-bonded aryloxide σ-complex

ERWIN BUNCEL, ROBERT Y. MOIR, AND ALBERT R. NORRIS
Department of Chemistry, Queen's University, Kingston, Ont., Canada K7L 3N6
AND
ALAIN-PIERRE CHATROUSSE
Laboratoire de Physicochimie des Solutions, E.N.S.C.P., Université Pierre et Marie Curie, F-75231 Paris, France

Received July 24, 1980[1]

ERWIN BUNCEL, ROBERT Y. MOIR, ALBERT R. NORRIS, and ALAIN-PIERRE CHATROUSSE. Can. J. Chem. **59**, 2470 (1981).

Reaction of 1,3,5-trinitrobenzene with potassium 2,4,6-trimethylphenoxide in dimethyl sulfoxide solution leads to σ-complex formation concurrently with displacement of a nitro group. The results provide definitive evidence for σ-complex formation via the oxygen of aryloxide ion in this system, and contrast with the situation that obtains with phenoxide ion itself, which under corresponding conditions yields the carbon-bonded σ-complex as the product of thermodynamic control. Stereoelectronic factors in σ-complex formation and in the diaryl ether resulting from nitro displacement are also discussed.

ERWIN BUNCEL, ROBERT Y. MOIR, ALBERT R. NORRIS et ALAIN-PIERRE CHATROUSSE. Can. J. Chem. **59**, 2470 (1981).

La réaction du trinitro-1,3,5 benzène avec le triméthyl-2,4,6 phénolate de potassium, en solution dans le diméthylsulfoxyde, conduit à la formation de complexes σ en même temps qu'au déplacement du groupe nitro. Les résultats confirment définitivement la formation des complexes σ par l'intermédiaire de l'oxygène de l'ion arylate de ce système et ils sont contraires à ceux obtenus avec l'ion phénolate lui-même, qui dans les mêmes conditions conduit à un complexe σ lié par le carbone en tant que produit de contrôle thermodynamique. On discute également des facteurs stéréoélectroniques lors de la formation des complexes σ et de l'éther diarylique provenant du déplacement du groupe nitro.

[Traduit par le journal]

Investigation of the anionic covalent adducts (Meisenheimer or σ-complexes) resulting from nucleophilic attack on aromatic systems has been of considerable interest recently (1–7). Such a process is shown in eq. [1] with EWG representing two or more electron withdrawing groups, e.g. NO_2, CN etc., as a general condition for the adduct **2** to be a spectrally detectable species. In cases where X is a displaceable group, these adducts are believed to be formed as reaction intermediates in the overall nucleophilic aromatic substitution (SNAr) process (8–10).

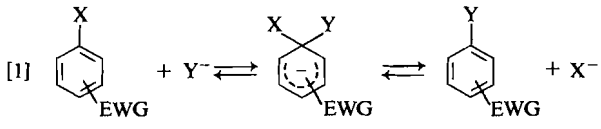

1 **2** **3**

The σ-complexes **4** and **5** formed from the reaction of methoxide ion with 1,3,5-trinitrobenzene (TNB) and 2,4,6-trinitroanisole (TNA), respectively, have been formulated structurally since ca. 1900 (11) while **6** was detected by nmr in 1965 as the kinetically preferred species (12). Many other σ-complexes of these types have been characterized in recent years (1–7, 13).

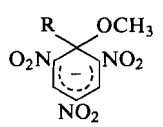

4 (R = H)
5 (R = OCH_3)

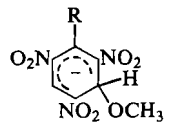

6 (R = OCH_3)

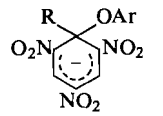

7 (R = H)
8 (R = OCH_3)

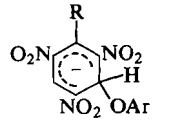

9 (R = OCH_3)

Surprisingly, though, aryloxide σ-complexes have received attention only relatively recently and have been the subject of considerable controversy. In fact, a stable aryloxide σ-complex of the type **7–9**, corresponding to **4–6**, has not yet been observed, though such species have been reported to be formed as transient intermediates.

The reason for this anomaly is that phenoxide ion can act in an ambident manner, either as an oxygen or as a carbon nucleophile, as shown in Scheme 1 (14, 15). It is also apparent from Scheme 1 that whereas oxygen attack will occur reversibly, carbon attack can become effectively irreversible on loss of a proton from the initially formed adduct **11**. Thus, whereas **7** may be formed initially as the

[1]Revision received March 30, 1981.

0008-4042/81/162470-05$01.00/0
©1981 National Research Council of Canada/Conseil national de recherches du Canada

Can. J. Chem. Downloaded from www.nrcresearchpress.com by 210.87.254.6 on 09/06/12
For personal use only.

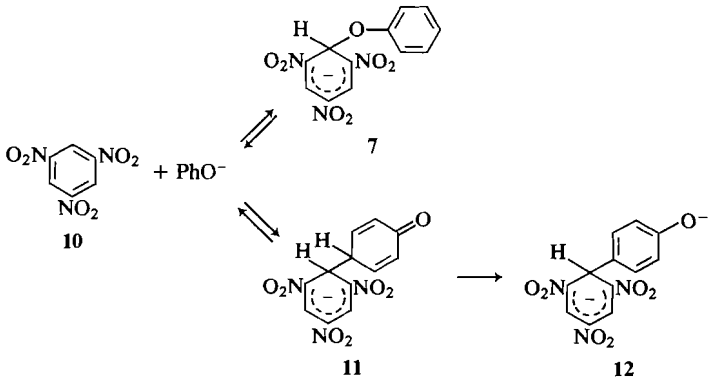

SCHEME 1

product of kinetic control, **12** will be obtained eventually as the product of thermodynamic control.

Shein and Byval'kevich (16) had initially reported that only the oxygen-bonded species **7** is formed in the reaction between TNB and phenoxide ion in dimethyl sulfoxide (DMSO), while Buncel *et al.* (15) observed only the carbon-bonded adduct **12** under apparently similar conditions. However, in DMSO–methanol (80:20 vol/vol) solution, it was found that the TNB–OMe^- σ-complex **4** was formed first as the kinetically preferred species and was followed by the formation of the carbon-bonded adduct **12** as the eventual reaction product (15). Subsequently, Shein *et al.* (17) reported also the obtention of **12** but claimed that **7** was formed as a transient species, observable through its transient nmr spectrum. Sterba and co-workers (18) investigated the reaction of TNB with 2-naphthoxide ion and reported results analogous to those observed by Buncel *et al.* (15). However, in this system (18), a 2:1 ArO^-–TNB carbon-bonded adduct, as well as the 1:1 adduct, was obtained. Bernasconi and Muller (19), using fast reaction techniques, observed the formation of **8** (rather than **7**) as the initially formed species in the interaction of phenoxide ion with TNA but did not examine the products at long reaction times. Relles *et al.* (20) proposed the formation of the oxygen-bonded adduct **13** in the interaction of 4-methylphenoxide ion with diisobutyl 3-nitrophthalate. Interestingly, they suggested that **13** could lose an electron by reaction with diisobutyl 3-nitrophthalate to yield the corresponding radical and the radical anion.

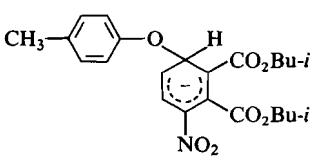

13

In view of the variance in these results and the hypotheses regarding aryloxide σ-complexes, it was desirable to investigate a system which would lead definitively to the formation of an oxygen-bonded aryloxide σ-complex and that such species should preferably be characterized by nmr. The present work was undertaken with that end in view, and while this objective could not be reached totally, this work has contributed to it in large measure. Our choice of 2,4,6-trimethylphenoxide ion was based on the assumption that this would react only as an oxygen nucleophile towards TNB (1–5).

Results and Discussion

The Reaction Pathways

The reaction of TNB (0.40 *M*) with potassium 2,4,6-trimethylphenoxide (**14**, 0.35 *M*) in DMSO solution at room temperature was followed by nuclear magnetic resonance and uv–visible absorption spectroscopy. An nmr spectrum of the dark red solution 2 min after mixing of the reagents showed the absence of the absorptions due to TNB (δ 9.20) or **14** (δ 6.38 (H-3,5), 1.97 (4-CH_3), 1.85 (2,6-$(CH_3)_2$)) but exhibited instead resonances at 8.48 (t, J = 2 Hz), 8.35 (d, J = 1 Hz), 7.88 (d, J = 2 Hz), 7.06 (s), 6.67 (s), 6.20 (t, J = 1 Hz), 2.31 (s), 2.10 (s), and 2.06 (s). On further scanning of the solution at ambient temperature, the signals at δ 8.35, 6.67, 6.20, and 2.10 decreased in intensity while those at δ 8.48, 7.88, 7.06, and 2.31 increased relative to the common signal at δ 2.06. After 48 h only the second set remained.

The uv–visible spectrum of the reaction solution 2 min after preparation was taken on appropriate dilution and showed absorptions at 432 and 500 nm, with a ratio of the absorbance values at λ_{max} being 1.5:1. On further sampling and scanning of the

Can. J. Chem. Downloaded from www.nrcresearchpress.com by 210.87.254.6 on 09/06/12
For personal use only.

Can. J. Chem. Downloaded from www.nrcresearchpress.com by 210.87.254.6 on 09/06/12
For personal use only.

solution at various intervals these absorptions steadily decreased in intensity, becoming negligibly small after 48 h. Acidification of the solution at any given time led to the destruction of the 432/500 nm absorptions.

The electronic absorption spectra of σ-complexes have been found to be characteristic of their structures (1–7). Thus the TNB–OMe^- σ-complex **4** in DMSO solution exhibits absorption maxima at 428 and 505 nm, the molar extinction coefficients at λ_{max} being in the ratio 1.5:1 (1–4). The oxygen-bonded TNA–phenoxide σ-complex **8** has been reported to have an electronic absorption spectrum very similar to that of the corresponding TNA–methoxide complex **5** (19). On the other hand, the carbon-bonded TNB–phenoxide complex **12** exhibits absorption maxima at 468 and 570 nm (15). Moreover, the spectral absorption due to this σ-complex is found to be stable in dilute acid media (15), whereas oxygen-bonded σ-complexes such as **4** do not survive acidification. These results concerning the uv–visible spectral characteristics of σ-complexes provide strong evidence that the interaction between TNB and **14** leads to the formation of the oxygen-bonded σ-complex **15**.

The proton nmr spectra also agreed fully with the initial formation and slow decomposition of the σ-complex **15**, represented by signals at δ 8.35, 6.67, 6.20, 2.10, and 2.06. Comparison with the TNB–OMe^- σ-complex **4**, for which the signals due to the aromatic protons occur at δ 8.48 while the sp^3 proton resonance is found at δ 6.17, reveals a close similarity between the two sets of data. On this basis, it is concluded that the δ 8.35 and 6.20 signals arising in the interaction of TNB with **14** are assignable, respectively, to the aromatic protons and the sp^3 proton of the σ-complex **15**.

The nmr signals which are observed to be increasing with time can be attributed to the diaryl ether **16**. Thus work-up of the reaction mixture, when there were no longer any changes observed in the nmr spectra, yielded a pale yellow solid with characteristics completely in accord with the structure **16** (δ 8.48, 7.88, 7.06, 2.31, and 2.06).

Our observations are in accord with the reaction pathways indicated in Scheme 2. Thus interaction of TNB with **14** acting as an oxygen nucleophile can occur by two concurrent pathways: reversible formation of σ-complex **15** through nucleophilic addition at an unsubstituted carbon, and substitution of NO_2 to yield the diphenyl ether **16** in an irreversible SNAr process. Displacement of NO_2 in SNAr processes has been observed previously (8, 21*a*).

It is interesting to note that there was no evidence in the nmr spectra for the formation of the σ-complex **17**, the intermediate in displacement of NO_2^- from TNB. Such species can hence be present in only very small concentration.

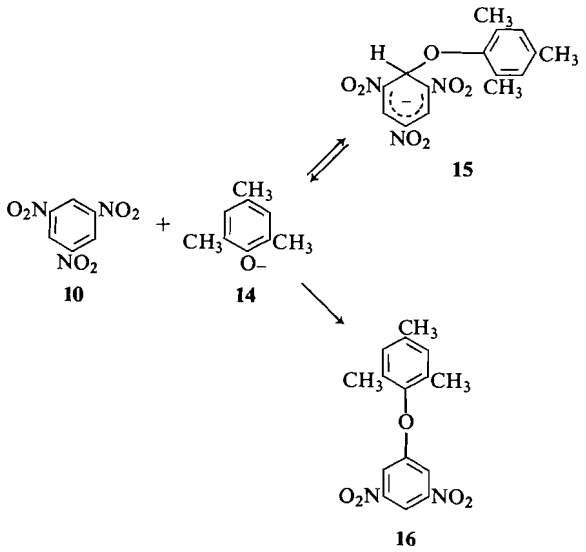

SCHEME 2

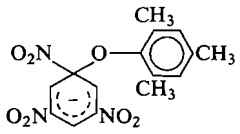

Stereoelectronic Factors in σ-Complex and Aryl Ether Formation

Complementary evidence concerning the structure of **15** was obtained from detailed analysis of its nmr spectrum in comparison with related σ-complexes (14, 15, 21). This study also brought to light a most interesting contrast between the principal conformation of **15** and the related diaryl ether **16**, especially in the light of previous studies of conformations of diphenyl ethers (22–24).

The nmr parameters of **15** and **16** are given below, and those of the TNB–OMe^- σ-complex **2** and 2,4,6-trimethylphenol, **18**, are shown for comparison. A striking feature of these parameters is that in **15** the chemical shifts of the protons in the 2,4,6-trinitrohexadienate moiety are changed only slightly with respect to σ-complex **2**, while those of the 2,4,6-trimethylphenoxy moiety resemble the phenol **18**. On the other hand, in the diphenyl ether **16**, the chemical shifts of protons in the 2,4,6-trimethylphenoxy moiety differ appreciably from **18**.

Two possible conformational structures of **15** are given below; namely **15***a* which can be termed a "butterfly" conformation, and **15***b* which is termed

Can. J. Chem. Downloaded from www.nrcresearchpress.com by 210.87.254.6 on 09/06/12
For personal use only.

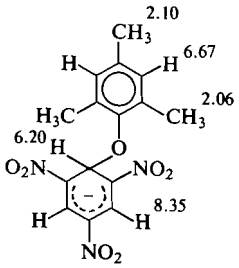

15

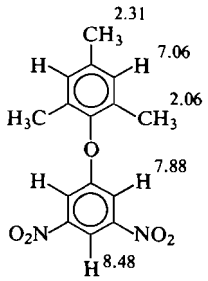

16

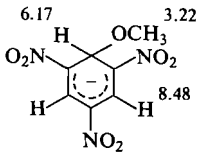

4

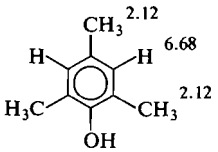

18

the "NO_2 inside" conformation. A structure corresponding to **15***b* (not shown) would be the "CH_3 inside" conformation. The latter is disregarded since models show that this conformation would entail severe steric interaction between the "inside methyl" and the cyclohexadienate aromatic ring, which would not be relieved by even large oscillations of the rings. The "butterfly" conformation **15***a* is also considered improbable owing to the large interactions between the *ortho* methyl and nitro groups of the two rings.

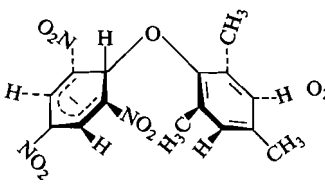

15*a* ("butterfly")

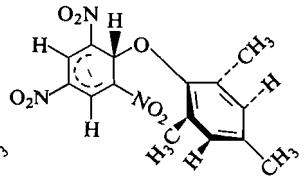

15*b* ("NO_2 inside")

Since the "butterfly" and the "CH_3 inside" conformations have been shown to be improbable, this would leave the "NO_2 inside" conformation **15***b* as the most likely candidate. This conformation allows large oscillations about the aromatic rings, making it both energetically and entropically favorable. The 2(6)-CH_3 groups in such a conformation would be expected to be shielded by the ring current of the cyclohexadienate moiety, as the results indicate, but this effect would be opposed by its electron withdrawing effect (14, 25). The resultant of these two effects is not readily predictable and further progress must await the preparation of other phenoxy complexes.

Considering next the diphenyl ether **16**, analogous reasoning shows that this could exist in the "butterfly" conformation **16***a*, the "H-inside" conformation **16***b*, as well as a "CH_3 inside" conformation (not shown). The latter is expected to be sterically much less favored in comparison with **16***b*. The "butterfly" conformation, though less crowded than **15***a*, is nevertheless considered unlikely by analogy with numerous diphenyl ethers which have been found *not* to exist in such a conformation (22–24). A possible factor contributing to this result is that the butterfly conformation does not permit overlap between the *p* orbital on the ether oxygen and either of the aromatic ring π systems.

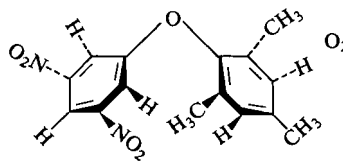

16*a* ("butterfly")

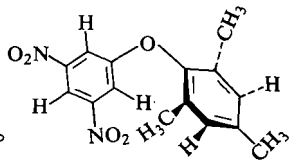

16*b* ("H inside")

Good overlap between the oxygen *p* orbitals and the aromatic π system occurs in the "H-inside" conformation **16***b*. However, optimum overlap need not occur at the exact rotational position represented by the "pure" conformation, in which the left hand ring is coplanar with the oxygen bonds and the right hand ring is perpendicular to them. In agreement with this, large angular distortions have frequently been observed in the crystal structures of diphenyl ethers (26).

Other major factors are also operative in compound **16**. Interaction between the *ortho* methyls and *ortho* hydrogens would be minimized by large (45°) *concerted* rotations of both rings away from the pure conformation **16***b*. However, this optimum rotation is much reduced by the interaction between the *ortho* methyls and the neighbouring vertices and edges of the other ring.[2] Confirmation of the existence of this distortion is most clearly shown by the observed shielding of the *ortho* methyl protons. Calculations show that in the pure conformation **16***b* the ring current of the left hand ring has little effect upon the methyls; concerted rotation of both rings leads to shielding (as observed) while antisymmetrical rotations lead to deshielding.

Our conclusions are strongly supported by comparison of the chemical shift of the *ortho* hydrogens in **16** with the corresponding value for 3,5-dinitroanisole (δ $H_{2,6}$ 8.14, H_4 8.43). As expected for the H-inside conformation, the *ortho* hydrogens in **16** are notably shielded, but calculation again shows the presence of considerable concerted rotation from "pure" **16***b*.

The method of calculation is an extension of that

[2]Diagrams summarizing the van der Waals interactions of various *ortho* substituents for a large number of rotational positions are given in ref. 27.

used previously (23). A description, together with tabulated data obtained from the present system, is available as Supplementary Material.[3]

Experimental

Potassium 2,4,6-trimethylphenoxide (**14**) was prepared from the phenol **18** (Aldrich, recrystallized twice from petroleum ether, mp 72°C) by a procedure based on the method given by Kornblum and Laurie (28). The treatment of a methanolic solution of **18** with KOH in MeOH–H_2O (85 : 15 v/v) and removal of solvent under *vacuum* yielded a violet liquid. Repeated extraction of this liquid with petroleum ether yielded as residue an off-pink powdery material which was dried *in vacuo* to yield a faint brown solid. This substance was kept under nitrogen and handled in the dry-box. Nuclear magnetic resonance (DMSO-d_6, relative to tetramethylsilane): δ 6.38 (2H, s), 1.97 (3H, s), 1.85 (6H, s).

The course of the reaction between TNB (0.40 *M*) and **14** (0.35 *M*) in DMSO-d_6 solution was followed at ambient temperature on a Varian EM 360 nmr spectrometer, spectra being taken at various intervals of time. For observation of the electronic absorption spectrum, 20 μL aliquots of the reaction solution were withdrawn periodically, diluted to 10 mL with DMSO, and the spectrum recorded in a 1 mm cell on a Unicam SP800B spectrophotometer. The uv–visible spectrum was recorded again following acidification with 2 μL of trifluoroacetic acid. A small but constant residual absorption in the visible region was noted for all the acidified solutions, presumably as a result of formation of a minor side product. At the completion of the reaction, when there were no further changes seen in the nmr spectra, the DMSO was removed under vacuum and the dark solid residue was extracted with ether. Evaporation of the ether and recrystallization from methanol yielded a yellow crystalline material, mp 128–130°C. After several more recrystallizations the pale yellow solid had mp 131.0°C; nmr (DMSO-d_6, Brucker 60 MHz HFX-60) δ: 8.48 (1H, t, J = 2.0 Hz), 7.88 (2H, d, J = 2.0 Hz), 7.06 (2H, s), 2.31 (3H, s), 2.06 (6H, s). *Anal.* calcd. for $C_{15}H_{14}N_2O_5$: C 59.60, H 4.64, N 9.27%; found: C 59.78, H 4.72, N 9.21%.

The nmr spectrum of 3,5-dinitroanisole, previously reported for dioxane as solvent (29), was recorded in DMSO-d_6, δ: 8.43 (1H, t, J = 2.0 Hz), 8.14 (2H, d, J = 2.0 Hz), 3.33 (3H, s).

Acknowledgments

A.P.C. thanks NATO for a grant under which most of this research was conducted at Queen's University. The authors also thank the Natural Sciences and Engineering Research Council of Canada for operating grants. Professor F. Terrier is thanked for the gift of a sample of 3,5-dinitroanisole and for valuable discussions.

1. R. Foster and C. A. Fyfe. Rev. Pure Appl. Chem. **16**, 61 (1966).
2. E. Buncel, A. R. Norris, and K. E. Russell. Q. Rev. Chem. Soc. **22**, 123 (1968).
3. M. R. Crampton. Adv. Phys. Org. Chem. **7**, 211 (1969).
4. M. J. Strauss. Chem. Rev. **70**, 667 (1970).
5. C. F. Bernasconi. MTP. Int. Rev. Sci. Org. Chem. Ser. One, **3**, 33 (1973).
6. J. H. Fendler, W. L. Hinze, and L. J. Liu. J. Chem. Soc. Perkin Trans. II, 1768 (1975).
7. F. Terrier, A. P. Chatrousse, C. Paulmier, and R. Schaal. J. Org. Chem. **40**, 2911 (1975).
8. J. Miller. Nucleophilic aromatic substitution. Elsevier, Amsterdam. 1968. Chapt. 5.
9. F. Pietra. Q. Rev. Chem. Soc. **23**, 504 (1969).
10. J. A. Orvik and J. F. Bunnett. J. Am. Chem. Soc. **92**, 2417 (1970).
11. (*a*) C. L. Jackson and W. F. Boos. Am. Chem. J. **20**, 444 (1898); (*b*) J. Meisenheimer. Ann. **323**, 205 (1902).
12. K. L. Servis. J. Am. Chem. Soc. **87**, 5495 (1965).
13. (*a*) L. H. Gan and A. R. Norris. Can. J. Chem. **52**, 1 (1974); **52**, 18 (1974); (*b*) C. A. Fyfe, C. D. Malkiewich, S. W. H. Damji, and A. R. Norris. J. Am. Chem. Soc. **98**, 6983 (1976); (*c*) E. Buncel and W. Eggimann. J. Am. Chem. Soc. **99**, 5958 (1977); (*d*) E. Buncel, J. G. K. Webb, and W. F. Wiltshire. J. Am. Chem. Soc. **99**, 4429 (1977); (*e*) E. Buncel and H. Wilson. Adv. Phys. Org. Chem. **14**, 133 (1977); (*f*) M. J. Strauss. Acc. Chem. Res. **7**, 181 (1974); (*g*) C. F. Bernasconi. Acc. Chem. Res. **11**, 147 (1978); (*h*) M. R. Crampton and M. J. Willison. J. Chem. Soc. Perkin Trans. II, 901 (1976); (*i*) R. H. DeRossi and R. A. Rossi. J. Org. Chem. **24**, 3486 (1974); (*j*) F. Terrier and A. P. Chatrousse. J. Chem. Res. M, 2413 (1977); (*k*) F. Terrier, J. Morel, M. J. Pouet, and M. P. Simonnin. Can. J. Chem. **58**, 65 (1980); (*l*) L. DiNunno, S. Florio, and P. E. Todesco. J. Chem. Soc. Perkin Trans. II, 1469 (1975); (*m*) G. Doddi, G. Illuminati, and F. Stegel. J. Org. Chem. **36**, 1918 (1971).
14. E. Buncel and J. G. K. Webb. Can. J. Chem. **52**, 630 (1974).
15. E. Buncel, A. Jonczyk, and J. G. K. Webb. Can. J. Chem. **53**, 3761 (1975).
16. S. M. Shein and O. G. Byval'kevich. Zh. Org. Khim. **8**, 328 (1972).
17. S. M. Shein, O. G. Byval'kevich, and A. D. Khmelinskaya. Zh. Org. Khim. **12**, 134 (1976).
18. V. Mahacek, V. Sterba, and A. Sterbova. Collect. Czech. Chem. Commun. **41**, 2556 (1976).
19. C. F. Bernasconi and M. C. Muller. J. Am. Chem. Soc. **100**, 5530 (1978).
20. H. M. Relles, D. S. Johnson, and J. S. Manello. J. Am. Chem. Soc. **99**, 6677 (1977).
21. (*a*) E. Buncel, M. Hamaguchi, and A. R. Norris. J. Chem. Soc. Perkin Trans. I, 2205 (1980); (*b*) E. Buncel, N. Chuaqui-Offermanns, R. Y. Moir, and A. R. Norris. Can. J. Chem. **57**, 494 (1979); (*c*) E. Buncel, N. Chuaqui-Offermanns, and A. R. Norris. J. Chem. Soc. Perkin Trans. I, 415 (1977).
22. W. D. Chandler, W. MacF. Smith, and R. Y. Moir. Can. J. Chem. **42**, 2549 (1964).
23. J. J. Bergman, W. D. Chandler, and R. Y. Moir. Can. J. Chem. **49**, 225 (1971).
24. G. A. Neville and R. Y. Moir. Can. J. Chem. **47**, 2787 (1969).
25. M. R. Crampton. J. Chem. Soc. B, 2112 (1971).
26. J. Toussaint. Bull. Soc. Chim. Belg. **54**, 319 (1945).
27. J. B. Rowbotham. Ph.D. Thesis, Queen's University, Kingston, Ont. 1970.
28. N. Kornblum and A. P. Laurie. J. Am. Chem. Soc. **81**, 2705 (1959).
29. E. J. Fendler, J. H. Fendler, N. L. Arthur, and C. E. Griffin. J. Org. Chem. **37**, 819 (1972).

[3]Copies of the Supplementary Material are available, at a nominal charge, from the Depository of Unpublished Data, CISTI, National Research Council of Canada, Ottawa, Canada, K1A 0S2.

Can. J. Chem. Downloaded from www.nrcresearchpress.com by 210.87.254.6 on 09/06/12
For personal use only.

Effect of bis(acetylacetonato) copper(II) catalyst on the reaction of benzoylphenyldiazomethane with primary amines. A novel example of insertion of benzoylphenylcarbene into N—H bonds of amines

S. B. SINGH AND K. N. MEHROTRA

Department of Chemistry, Banaras Hindu University, Varanasi-221005, India

Received December 29, 1980

S. B. SINGH and K. N. MEHROTRA. Can. J. Chem. **59**, 2475 (1981).

Bis(acetylacetonato) copper(II) catalysed thermal decomposition of benzoylphenyldiazomethane (**1**) leads to the insertion of benzoylphenylcarbene into the N—H bond of amines; the insertion products undergo facile air oxidation giving rise to ketoimines. The uncatalysed thermal decomposition of benzoylphenyldiazomethane yields the corresponding diphenylacetamide derivatives of amines.

S. B. SINGH et K. N. MEHROTRA. Can. J. Chem. **59**, 2475 (1981).

La décomposition thermique du benzoyldiphénylméthane (**1**) catalysée par le bis(acétylacétonato) cuivre II conduit à l'insertion du benzoylphenylcarbène dans la liaison N—H des amines; le produit d'insertion s'oxyde facilement à l'air en cétoimines. La décomposition thermique non catalysée du benzoylphényldiazométhane conduit aux dérivés diphénylacétamide des amines correspondantes.

[Traduit par le journal]

Can. J. Chem. Downloaded from www.nrcresearchpress.com by 210.87.254.5 on 09/06/12
For personal use only.

The thermal decomposition of benzoylphenyldiazomethane in the presence of substituted anilines yields diphenylacetamides and 1,2-diphenyl-2(arylamino)ethanones (1). Wolff rearrangement of α-diazoketones has been prevented in the presence of copper powder (2), cupric chloride (3), or bis(acetylacetonato) copper (II) (4). Modified carbenes, having enhanced electrophilic character, are produced in the decomposition of diazocompounds catalysed by copper or its salts (5). Similar reaction of diaryldiazomethanes in the presence of 1,1-diphenylmethyleneimine has been shown to lead to an unusual insertion of diarylcarbenes into the N—H bond of imine (6). We now report the thermal decomposition of benzoylphenyldiazomethane (**1**) in the presence of amines **2***a–c* which produces *N*-substituted diphenylacetamides **4***a–c* in excellent yields. The bis(acetylacetonato) copper(II) (**3**) catalysed thermal decomposition of **1** in the presence of amines **2***a–c* may lead to the insertion of benzoylphenylcarbene into the N—H bond of the amines **2***a–c*. Subsequent air oxidation of the insertion products yields ketoimines.

Results and Discussion

The reaction between benzoylphenyldiazomethane (**1**) and benzhydrylamine (**2***a*) afforded a white crystalline solid, identified as *N*-benzhydryldiphenylacetamide (**4***a*) by the analytical and spectral (ir, uv, and nmr) data. Similar treatment of **1** with amines **2***b*, *c* gave *N*-substituted diphenylacetamides **4***b*, *c* characterized on the basis of the analytical and spectral data (Tables 1 and 2). The product **4***b* has been identified as *N*-(α-phenylethyl)diphenylacetamide.

The reaction mixture obtained with benzhydrylamine (**2***a*) from the bis(acetylacetonato) copper (II) (**3**) catalysed decomposition of **1** was separated by elution chromatography and crystallisation from ethanol to give a yellow solid characterized as benzilmonobenzhydrylimine (**5***a*) by analytical and spectral data (Tables 3 and 4). Similar treatment with amines **2***b*, *c* gave benzilmonoimines **5***b*, *c* characterized by analytical and spectral data (Tables 3 and 4). Authentic samples of ketoimines **5***a–c* were prepared according to the reported methods (7, 8) and were identical to the products (ir, nmr, and mmp). The product **5***b* has been identified as benzilmono-α-phenylethylimine.

Since the amine **2***b* is racemic, the products derived from it, **4***b* and **5***b*, are also racemic. The probable reaction sequence for the formation of *N*-substituted diphenylacetamides (**4***a–c*) and benzilmonoimines (**5***a–c*) can be shown in Scheme 1.

The thermal decomposition of benzoylphenyldiazomethane (**1**) may lead to the formation of benzoylphenylcarbene, which on Wolff rearrangement may give diphenylketene (9). The reaction of diphenylketene with amines **2***a–c* leads to the formation of *N*-substituted diphenylacetamides **4***a–c*. The catalysed thermal decomposition of **1** may lead to the formation of a complex of benzoylphenyldiazomethane (**1**) and bis(acetylacetonato) copper (**3**) which on elimination of nitrogen may give rise to carbene complex. Similar complexes of bis(acetylacetonato) copper(II) with benzoyldiazo-

0008-4042/81/162475-04$01.00/0

©1981 National Research Council of Canada/Conseil national de recherches du Canada

TABLE 1. Conversion of amines **2** to *N*-substituted diphenylacetamides **4**

Amines **2**	R	Product **4** Yield (%)	Melting point (°C)	Molecular formula	Elemental analysis (%) Found C	H	N	Calculated C	H	N
a	$CHPh_2$	88	201–202	$C_{27}H_{23}NO$	85.71	6.22	3.92	85.94	6.10	3.71
b	$CH(CH_3)Ph$	91	120–121	$C_{22}H_{21}NO$	84.05	6.33	4.64	83.81	6.66	4.44
c	Ph	80	178–179	$C_{20}H_{17}NO$	83.33	6.07	4.73	83.62	5.92	4.84

TABLE 2. Spectral data of *N*-substituted diphenylacetamides **4**

Compound	Ultraviolet (EtOH) λ_{max} (nm)	Infrared (Nujol) (cm^{-1}) ν_{N-H}	$\nu_{C=O}$	Nuclear magnetic resonance ($CDCl_3$) δ (ppm)
4*a*	248, 253, 259, 265	3285	1645	5.06 (s, 1H, >CH—CO-), 6.38 (s, 1H, NH, D_2O exchangeable), 6.38 (s, 1H, N−CH<, 7.10–7.53 (m, 20H, aromatic)
4*b*	255, 260, 265	3270	1640	1.65 (d, 3H, CH_3, J = 7 Hz), 5.03 (s, 1H, >CH—CO), 5.30 (q, 1H, CHMePh, J = 7 Hz), 6.17 (b, 1H, NH, D_2O exchangeable), 7.17–7.67 (m, 15H, aromatic)
4*c*	245	3300	1650	5.10 (s, 1H, >CH—CO-), 7.07–7.90 (m, 15H, aromatic and 1H, NH, exchangeable on deuteration)

TABLE 3. Conversion of amines **2** to benzilmonoimines **5**

Amines **2**	R	Product **5** Yield (%)	Melting point (°C)	Molecular formula	Elemental Analysis (%) Found C	H	N	Calculated C	H	N
a	$CHPh_2$	43	129–130 (lit. (7) 130)	$C_{27}H_{21}NO$	85.90	5.38	3.39	86.40	5.60	3.73
b	$CH(CH_3)Ph$	28	93–94 (lit. (7) 95)	$C_{22}H_{19}NO$	84.33	6.36	4.60	84.34	6.07	4.47
c	Ph	53	105–106 (lit. (8) 105–106)	$C_{20}H_{15}NO$	83.98	5.42	4.88	84.21	5.26	4.41

methane (4) or diphenyldiazomethane (5) leading to the formation of esters and cyclopropane derivatives, respectively, have been proposed earlier. The benzoylphenylcarbene, from the carbene complex, may insert into N—H bonds of amines **2***a–c* to form ketoamines **6***a–c* which on facile air oxidation during purification (column chromatography or crystallization) may lead to the benzilmonoimines **5***a–c*. Absence of products **4***a–c* in the catalysed decomposition of **1** in the presence of **3** indicates that the carbene complex does not form diphenylketene.

Experimental

Melting points were determined on a Büchi apparatus (capillary method) and have been uncorrected. Ultraviolet spectra were obtained in 95% ethanol on a Cary-14 spectrophotometer. Infrared spectra were recorded in Nujol mull on a Perkin-Elmer 720 spectrophotometer. Proton nuclear magnetic resonance

Can. J. Chem. Downloaded from www.nrcresearchpress.com by 210.87.254.5 on 09/06/12
For personal use only.

TABLE 4. Spectral data of benzilmonoimines **5**

Compound	Ultraviolet (EtOH) λ_{max} (nm)	Infrared (Nujol) (cm^{-1}) $\nu_{C=O}$	$\nu_{C=N}$	Nuclear magnetic resonance (CCl_4) δ (ppm)
5a	253	1660	1620	5.68 (s, 1H, CH), 7.18 (m, 16H, aromatic), 7.75 (m, 4H, aromatic).
5b	250	1660	1620	1.48 (d, 3H, CH_3, J = 6 Hz), 4.61 (q, 1H, CH, J = 6 Hz), 7.05–8.13 (m, 15H, aromatic).
5c	250	1660	1620	6.67–8.20 (m, H, aromatic).

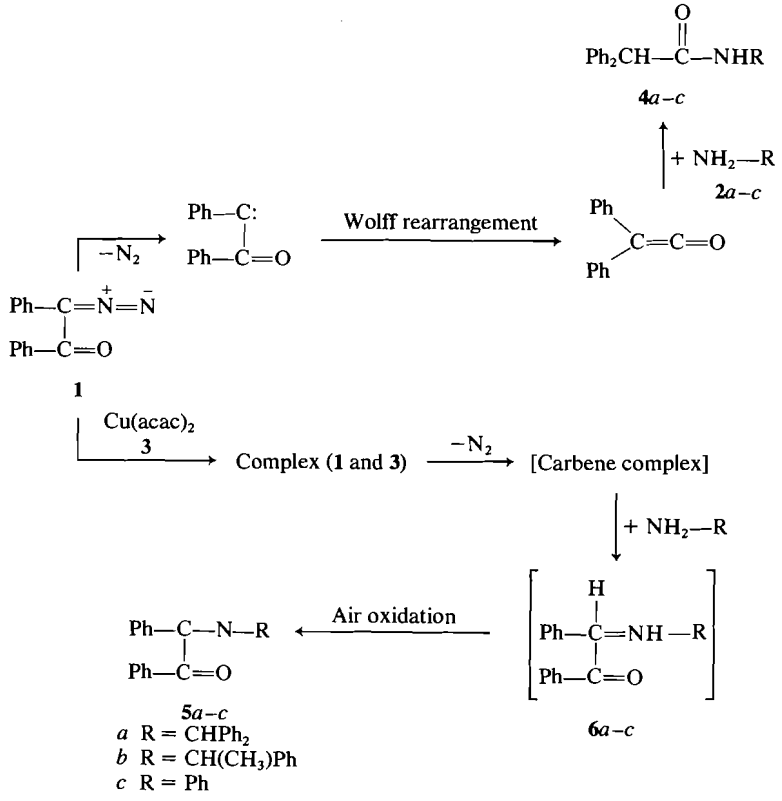

SCHEME 1

data were obtained on a Varian A-60D spectrometer in CCl_4 or $CDCl_3$ using TMS as an internal standard.

Materials

Benzophenone and aniline were obtained from BDH India, benzil and bis(acetylacetonato) copper(II) from EGA Chemicals, West Germany, and benzoylphenyldiazomethane (10), benzhydrylamine (11), and (±) α-phenylethylamine (12) were prepared according to the reported methods.

General Procedure for Preparation of N-*Substituted Diphenylacetamides* 4a–c

A mixture containing benzoylphenyldiazomethane (0.01 mol) and amine (0.01 mol) in 80 mL of dry benzene (thiophene free), in a 250 mL three-necked round bottom flask equipped with condenser and a mercury trap, was heated under reflux for 6 h under a nitrogen atmosphere. The reaction mixture was kept overnight at room temperature. The solvent was removed on a rotatory evaporator and the residual material was triturated with ethanol. The solid obtained was crystallized from ethanol to afford the products. The analytical results are given in Table 1 and the spectral data of the products in Table 2.

General Procedure for Bis(acetylacetonato) Copper(II) (3) Catalysed Thermal Decomposition of Benzoylphenyldiazomethane (1) in Presence of Amines 2a–c

To a suspension containing 2 mmol of bis(acetylacetonato) copper(II) in 30 mL of dry benzene (thiophene free) heated under reflux with stirring, a solution containing benzoylphenyldiazomethane (10 mmol) and amine (10 mmol) in 80 mL of dry benzene (thiophene free) was slowly added over 3 h from a pressure-equalizing funnel under a nitrogen atmosphere. The contents were heated under reflux for 5 h and kept overnight at room temperature. The reaction mixture was passed through a neutral alumina (10 g, 1.2 × 10 cm) column and the products were eluted with benzene to remove the copper salt. The solvent was removed on a rotatory evaporator and the residual material was triturated with ethanol.

Can. J. Chem. Downloaded from www.nrcresearchpress.com by 210.87.254.5 on 09/06/12
For personal use only.

The solid obtained was crystallized from ethanol to afford the products. The analytical results are given in Table 3 and spectral data of the products in Table 4. The authentic samples of **5***a*–*c* were prepared for comparison (mixture melting point, ir, and nmr spectra) by the condensation of benzil and appropriate amine according to the reported methods (7, 8).

Acknowledgements

We thank Professor B. M. Shukla for providing facilities and the Council of Scientific and Industrial Research, New Delhi, for grant of a fellowship to S.B.S.

1. W. JUGELT and D. SCHMIDT. Tetrahedron, **25**, 969 (1969).
2. P. YATES. J. Am. Chem. Soc. **74**, 5376 (1952).
3. J. L. E. ERICKSON, J. M. DECHARY, and M. R. KESLING. J. Am. Chem. Soc. **73**, 5301 (1951).
4. M. TAKEBAYASHI, T. IBATA, H. KOHARA, and B. H. KIM. Bull. Chem. Soc. Jpn. **40**, 2392 (1967).
5. H. NOZAKI, H. TAKAYA, S. MORIUTI, and R. NOYORI. Tetrahedron, **24**, 3655 (1968).
6. K. N. MEHROTRA and G. PRASAD. Tetrahedron Lett. 4179 (1978).
7. R. HARO-RAMOS, A. JIMENEZ-TEBAR, R. PEREZ-OSSORIO, and J. PLUMET. Tetrahedron Lett. 1355 (1979).
8. A. PADWA. J. Am. Chem. Soc. **87**, 4365 (1965).
9. V. FRANZEN. Justus Liebigs Ann. Chem. **87**, 4365 (1965).
10. C. D. NENITSESCU and E. SOLOMONICA. Org. Synth. Coll. Vol. **II**, 496 (1950).
11. A. MICHAELIS. Chem. Ber. **26**, 2169 (1893).
12. A. W. INGERSOLL. Org. Synth. Coll. Vol. **II**, 503 (1950).

Can. J. Chem. Downloaded from www.nrcresearchpress.com by 210.87.254.5 on 09/06/12
For personal use only.

The total synthesis of (±)-N_α-methyl-N_β-acetylphlegmarine

ANDRZEJ LENIEWSKI,[1] JERZY SZYCHOWSKI,[1] AND DAVID B. MACLEAN
Department of Chemistry, McMaster University, Hamilton, Ont., Canada, L8S 4M1

Received February 23, 1981

ANDRZEJ LENIEWSKI, JERZY SZYCHOWSKI, and DAVID B. MACLEAN. Can. J. Chem. **59**, 2479 (1981).

(±)-N_α-Methyl-N_β-acetylphlegmarine has been synthesized in a manner that defines the relative configuration at four of the five chiral centres of the molecule. Five isomers of the title compound have also been prepared and characterized.

ANDRZEJ LENIEWSKI, JERZY SZYCHOWSKI et DAVID B. MACLEAN. Can. J. Chem. **59**, 2479 (1981).

On a synthétisé la (±)-N_α-méthyl-N_β acétylphlégmarine selon une méthode qui permet de définir la configuration relative de quatre des cinq centres chiraux de la molécule. On a également synthétisé et caractérisé cinq isomères du composé mentionné dans le titre.

[Traduit par le journal]

Can. J. Chem. Downloaded from www.nrcresearchpress.com by 210.87.254.40 on 09/06/12
For personal use only.

The phlegmarines **1** are a group of Lycopodium alkaloids that were described by Nyembo *et al.* (1) in 1978. The basic carbon skeleton of phlegmarine itself and its *N*-substituted derivatives was established by spectroscopic studies. A synthesis of a mixture of stereoisomers of the naturally occurring bases was also achieved and the spectroscopic properties of the natural and synthetic materials compared. These studies, particularly the mass spectrometric work, left no doubt that the natural and synthetic materials had the same carbon skeleton but they shed no light on the stereochemistry of the phlegmarines. Here we report a synthesis of N_α-methylphlegmarine and its N_β-acetyl derivative that has defined the stereochemistry of four of the five chiral centres in the molecule.

When we began this synthesis we set out to prepare a phlegmarine with the relative stereochemistry shown in Scheme 1. This arrangement was chosen for two reasons. Firstly, the configuration shown at C-5, C-7, and C-10 is the same as that found in the majority of Lycopodium alkaloids (2, 3) at corresponding centres. One would expect the same relative configuration if the phlegmarines are biosynthetic intermediates on the pathway to other alkaloids as suggested by Nyembo *et al.* (1). Secondly there is a close structural and seemingly biosynthetic relationship between the phlegmarines **1** and luciduline **2** (4) and the recently described lycolucine **3** (5). Both **1** and **2** may be derived from a common biosynthetic precursor such as **4** or the corresponding amino acid as already suggested (1). Luciduline contains all the carbon atoms of **4** and its formation from **4** is easily envisaged and has been effected chemically (6). The phlegmarines in turn have been postulated (1) to arise by combination of piperideine **5** and the

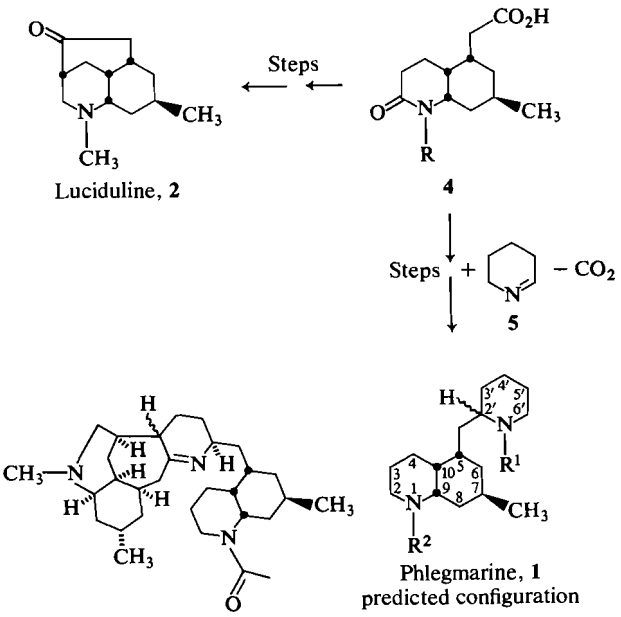

SCHEME 1

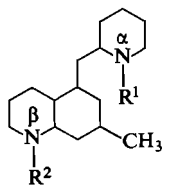

a $R^1 = H; R^2 = H$
b $R^1 = CH_3; R^2 = H$
c $R^1 = H; R^2 = CH_3$
d $R^1 = COCH_3; R^2 = CH_3$

The phlegmarines, **1**

[1]Present address: Institute of Fundamental Problems of Chemistry, University, Pasteura 1, 02-093 Warsaw, Poland.

0008-4042/81/162479-12$01.00/0
©1981 National Research Council of Canada/Conseil national de recherches du Canada

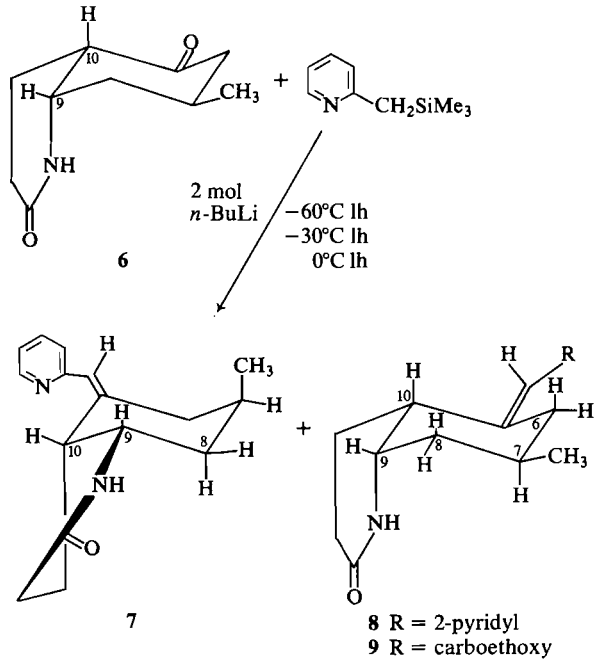

SCHEME 2

amino acid related to **4**, accompanied by loss of CO_2. Examination of the structure of lycolucine **3** shows that it contains within its structure both a phlegmarine unit and a unit related to **4** minus CO_2 (**1** and **4** may be combined in two different ways). Alternatively, **3** may be considered to be derived from two units of **4** minus two moles of CO_2 and one unit of **5** as pointed out by Ayer *et al.* (5). It seemed reasonable therefore that phlegmarine would have incorported into its structure the stereochemical features present in the related systems shown in Scheme 1. We made no attempt, however, to predict the stereochemistry at C-2′. We therefore set about to synthesize the phlegmarines in a manner that would define the stereochemistry in the tetrahydroquinoline portion of the molecule. As it turned out, our predicted configuration was not correct.

The approach used to prepare the phlegmarine skeleton (Scheme 2) was similar to that used in the early stages of the synthesis of luciduline (6). Lactam **6** (prepared as before (6)) was treated in the presence of a strong base with 2-trimethylsilylmethylpyridine, prepared, with some modifications, according to the procedure of Musker and Scholl (7). Two products were isolated from this reaction that are assigned structures **7** and **8** on the basis of spectroscopic examination. As in the previous study on luciduline (6), the signal at H-9 proved to be the key to the assignment of the conformation of the hydroquinoline ring system. Not only is this signal normally well separated from others but it also sharpens on D_2O exchange because of removal of NH coupling. In isomer **7**, the major component of the reaction, the signal at H-9 appears (after D_2O exchange) at 3.60 δ as a quintet (from superposition of a doublet of triplets) and this is compatible with the conformation shown for **7**. Another lower field signal at 4.14 δ also appears as a near quintet, also from superposition of a doublet of triplets, and has been assigned to H-10. By decoupling experiments it was shown that these two protons are coupled, $J = 6$ Hz. Both H-9 and H-10 must be coupled to two other protons with coupling constants of ca. 6 Hz each and to one other proton with coupling constants of 12 Hz and 10 Hz, respectively. In the case of H-9 the 6 Hz couplings are to H-10 and H-8e and the 12 Hz coupling to H-8a, while for H-10 the 6 Hz couplings are to H-9 and H-4e and the 10 Hz coupling to H-4a. The low field position of H-10 is compatible with the *Z* configuration about the bond bearing the pyridyl group. H-10 is allylic to the double bond and is also deshielded by the pyridine ring in the conformation shown.

Isomer **8**, the minor component of the reaction (ratio **7** to **8** = 4:1), shows a pattern for H-9 similar to that of ketolactam **6**. The signal at H-9 appears at 3.83 δ as a near quartet from superposition of a doublet of triplets, $J = 4.5$, 4.5, and 6 Hz. A signal at 2.83 δ has been assigned to H-6e which shows one large and one small coupling, $J_{6e,7a} = 4$ and $J_{6e,6a} = 14$ Hz. This behaviour is very similar to that of **9** which was the main product of reaction of $(Me_3SiCHCO_2Et)^-Li^+$ with **6** as discussed in a previous paper (6). For similar reasons we assign **8** the *E* configuration about the double bond and the conformation shown.

The hydrogenation of **7** was brought about with H_2 over Adams' catalyst. This reaction was highly stereoselective giving a single product, assigned structure **10**, in which the methyl and the pyridylmethyl groups occupy equatorial positions on the carbocyclic ring. The *E* isomer **8** on similar treatment yielded a mixture of two isomers, the minor component was identical with **10** on tlc while the major component was assigned structure **11**. (The ratio **10**:**11** = 1:4.) The configurational assignments to **10** and **11** are based upon ^1H nmr examination of the two isomers and in particular on the signals associated with H-9 and the *C*-methyl group. In **10** the signal for H-9 appears as a near quartet at 3.71 δ with couplings of ca. 3 Hz with each of H-10, H-8a, and H-8e. The *C*-methyl signal of **10** appears at 0.83 δ. On the other hand the signal of H-9 in **11** appears at 3.55 δ as a broad multiplet

Can. J. Chem. Downloaded from www.nrcresearchpress.com by 210.87.254.40 on 09/06/12
For personal use only.

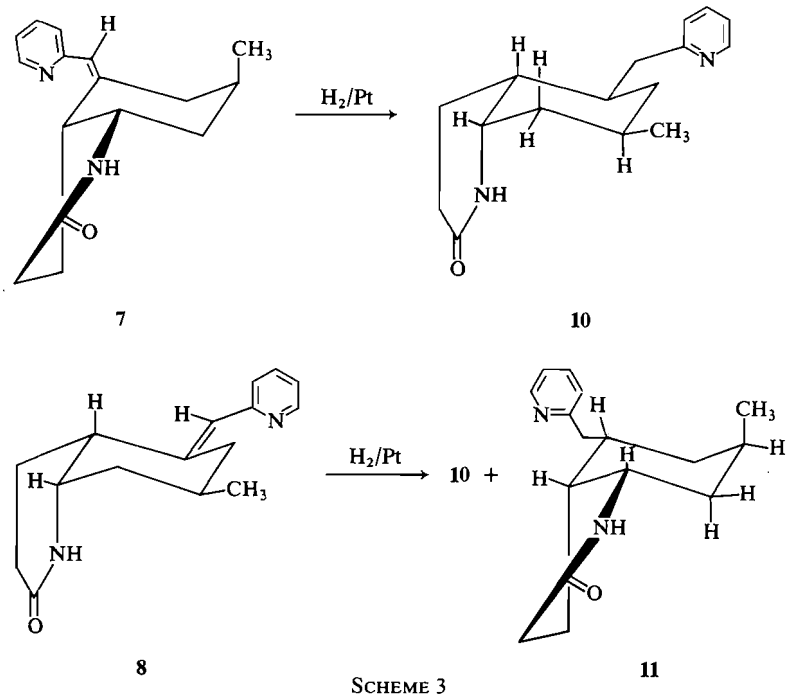

SCHEME 3

overlapping with another signal, probably that of H-11. The *C*-methyl group of **11** appears at 0.96 ppm considerably shifted from that of **10**, reflecting its axial character. Compound **11** was, however, not obtained free of its isomer **10** and the spectral data cited are extracted from the spectrum of the mixture (see Scheme 3).

Compound **10** was converted next to the quaternary salt, **12**. The ^{1}H nmr examination of **12** revealed that there was no change in conformation on quaternization.

The pyridine ring of **12** was now reduced (H_2/Pt) yielding a substance that appeared from its behaviour to be a single component but which on the basis of its subsequent reaction must have been a mixture of epimers at C-2′. In any event the reaction product was treated with lithium aluminum hydride to reduce the lactam function. The product derived from this reaction showed no amide absorption in the infrared and showed two spots on tlc. An nmr examination of the reaction mixture showed two *N*-methyl signals of almost equal intensity indicating for the first time that both epimers at C-2′ had formed in the catalytic reduction. Hydride reduction would not be expected to bring about isomerization at any centre in the transformation of the amide to the secondary amine. The two components of the mixture were separated by column chromatography on alumina yielding **14***a* and **14***b* but there was no way to differentiate between the two although they did show slightly different ^{1}H nmr spectra.

In the final stage of this synthesis both **14***a* and **14***b* were converted separately to their acetyl derivatives, **15***a* and **15***b*, respectively, by treatment with acetyl chloride – pyridine. The ^{1}H nmr spectra of both isomers showed very broad signals for the protons adjacent to the acylated nitrogen atom, which are attributed to the presence of two rotamers caused by restricted rotation about the amide linkage. The presence of rotamers was confirmed by a variable temperature study. At −61°C it was possible to observe signals for both rotamers but unfortunately the solubility at this temperature was low and the resolution poor. However there were two N—$COCH_3$ signals differing by 0.03 to 0.06 ppm, and two *N*-methyl signals differing by ca. 0.10 ppm and two pairs of multiplets associated with the protons vicinal to the *N*-acetyl group differing by 0.9 to 0.8 ppm. The situation was the same for both **15***a* and **15***b* and consequently there was no basis to differentiate between them in a stereochemical sense. The *C*-methyl absorption at 1.05 δ and 1.06 δ in **15***a* and **15***b*, respectively, suggests that on *N*-acylation the conformations of the molecules change (the *C*-methyl in both **14***a* and **14***b* appears at 0.85). Similar conformational changes were observed on *N*-methylation in the luciduline synthesis (6). This change would now place the *C*-methyl and the

Can. J. Chem. Downloaded from www.nrcresearchpress.com by 210.87.254.40 on 09/06/12
For personal use only.

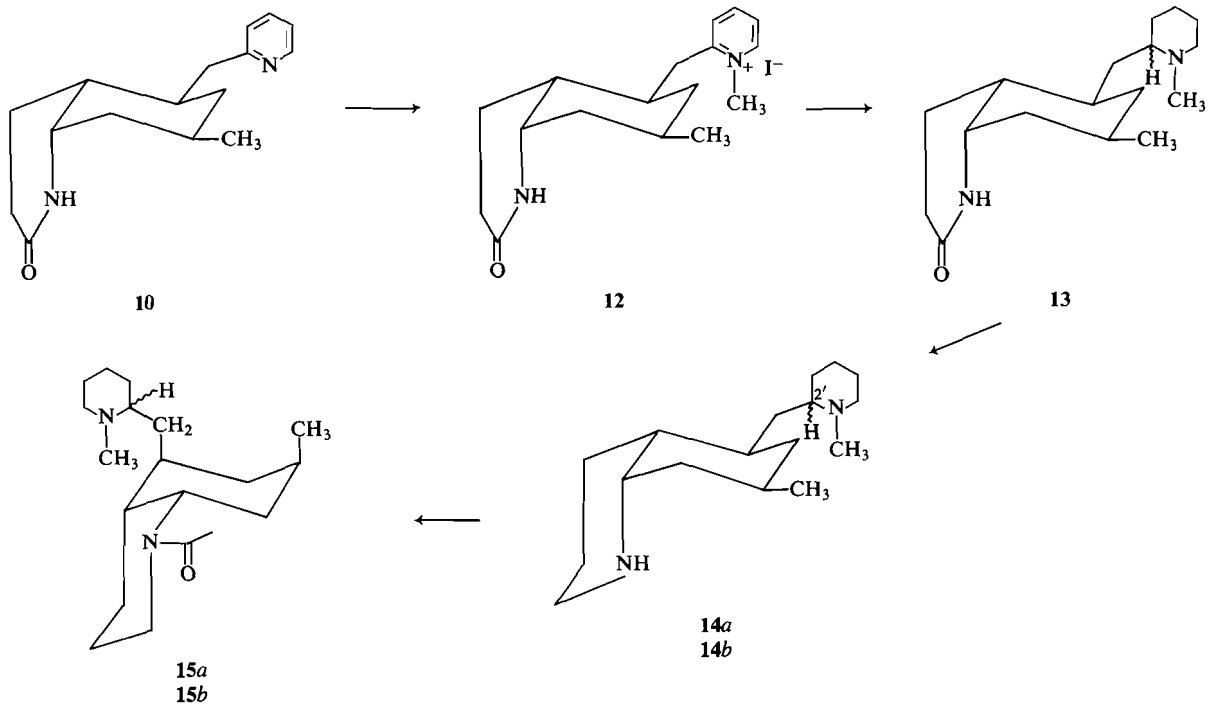

SCHEME 4

piperidyl groups in an axial orientation as shown but the steric crowding of the *N*-acetyl group that would exist in a conformation similar to **14***a* and **14***b* is relieved (see Scheme 4).

When the ^{1}H nmr spectra of **15***a* and **15***b* were compared with the reported ^{1}H nmr spectrum of the compound derived from nature there were distinct differences (1). Thus neither **15***a* nor **15***b* represents the stereochemistry of N_β-acetyl-N_α-methylphlegmarine.

The conversion of **11** to compounds of structure **16** (Scheme 5) was not pursued. It has been shown that the methyl group of **11** must be in the axial orientation because of the conformation of the molecule. In **16** this conformation would be even more favoured because of the acetyl group on nitrogen. In the light of previous results discussed in this paper the CHCH_3 resonance in **16** in the conformation shown would be predicted to be considerably greater than 0.90 δ, the value recorded for N_β-acetyl-N_α-methylphelgmarine (1). Therefore it seemed pointless to pursue further studies in the *cis*-series. Accordingly we turned our attention to the preparation of compounds with a *trans* ring fusion.

The most likely alternative configuration of the phlegmarines has the epimeric configuration at C-9. Their synthesis would require as starting material *trans*-ketolactam **17**, a compound reported to form along with isomer **6** (6) but in low yield and difficult to separate from the *cis* compound. We therefore investigated other routes to its preparation based upon reduction of **18**, a compound that is available in high yield by treatment of 2-(2-cyanoethyl)-5-

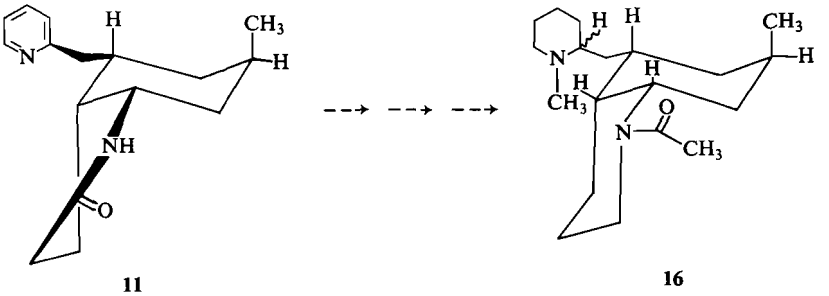

SCHEME 5

Can. J. Chem. Downloaded from www.nrcresearchpress.com by 210.87.254.40 on 09/06/12
For personal use only.

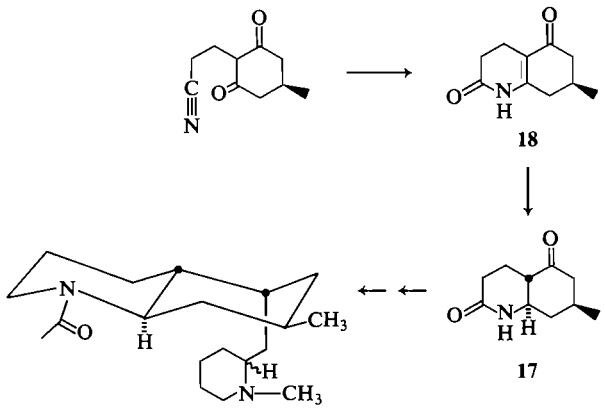

SCHEME 6

methyl-1,3-cyclohexanedione with 50% acetic acid according to the general method described by Vill *et al.* (8). A number of reducing agents were therefore investigated to effect the conversion of **18** to **17**. Among the reagents investigated were the following: $NaCNBH_3$, $TiCl_3/H_2O$ (9), Zn/AcOH, Mg/MeOH (10), $NaBH_4$/EtOH, H_2/Pd, and Li/NH_3. Only the last three showed promise and the results are reported in the Experimental. The most effective proved to be treatment with Li in liquid ammonia, a reaction that proceeded in 30% yield. The reaction is instantaneous and on work-up gave **17** but none of its isomer **6** nor starting material **18**. The bulk of the product was comprised of highly polar substances from which **17** was easily separated by crystallization from methanol or water (see Scheme 6).

The *trans*-ketolactam **17** was now subjected to the same series of reactions as its isomer **6**. Reaction with 2-trimethylsilylmethylpyridine in the presence of *n*-butyllithium gave compounds **19** and **20** in a ratio of ca. 50:1. Molecular models show that there is strong interaction between the pyridyl substituent and the lactam ring in the case of the *Z* isomer, **19**. This is reflected in the ultraviolet spectrum of **19** in which the absorption maxima are shifted to shorter wavelengths and the extinction coefficients are smaller that those observed for **20** (see Scheme 7).

In the ^1H nmr spectrum of **19** the signal at H-9 is observed at 3.30 δ as a triplet split into doublets (J = 13 and 3 Hz) corresponding to the pattern observed for H-9 in **17** (6). In the spectrum of **20** there is a two-proton multiplet in the 3.4 δ region probably formed by the overlap of signals from H-9 and H-6e.

Hydrogenation of **19** over Pt was not selective. It gave, besides some starting material, the isomers **21** and **22** in nearly equal amount (*vide infra*) and also products formed by partial reduction of the pyridine ring. To ensure that **19** was completely consumed (it was difficult to separate from the reduction products) the reaction was allowed to continue until a 10–15% excess of H_2 was consumed. We were unable to separate the epimers **21** and **22** by tlc or by column chromatography. However their *N*-oxides, **23** and **24**, formed by oxidation with *m*-chloroperbenzoic acid, were separable on an alumina column. The faster moving epimer has the pyridylmethyl group at C-5 in the equatorial position (see Scheme 8).

The configuration at C-5 was resolved by examination of the 360 MHz ^1H nmr spectra of **23** and **24**. In the case of **23** the chemical shift of every proton

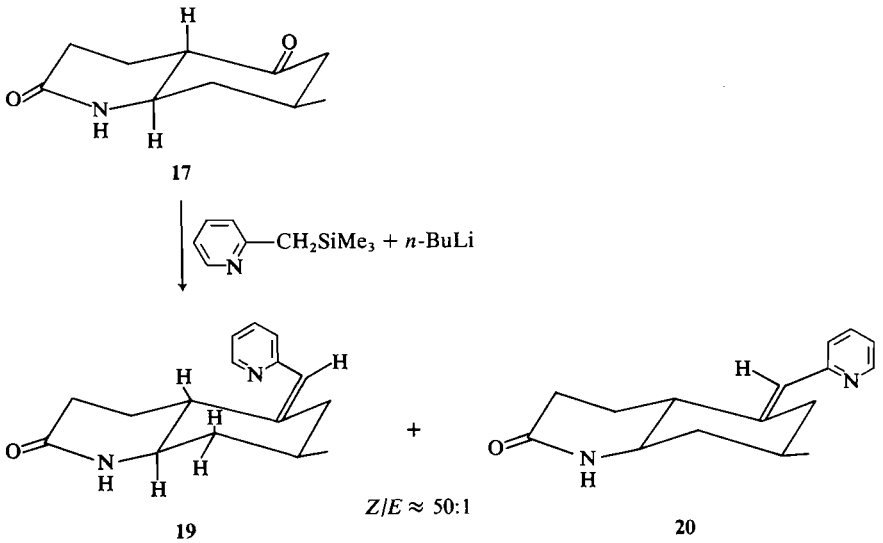

SCHEME 7

Can. J. Chem. Downloaded from www.nrcresearchpress.com by 210.87.254.40 on 09/06/12
For personal use only.

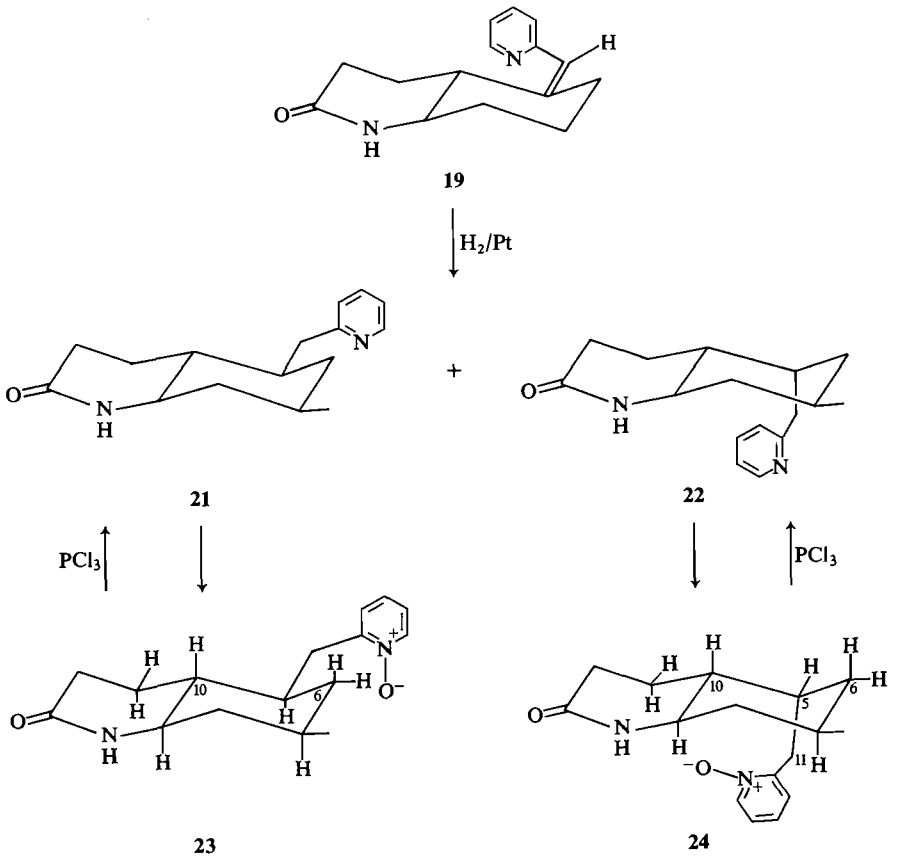

SCHEME 8

and nearly all coupling constants with adjacent protons could be assigned. In the case of **24**, however, the signals of four protons overlapped in a complex multiplet but the rest were clearly differentiated. In both cases the assignments were made by double irradiation using the signals for H-9 and the $CHCH_3$ group as points of reference. The signals at H-10 and H-6a provide the clue to the configuration at C-5. Thus in **24**, H-10 appears at 1.63 δ as a triplet split into triplets (i.e. flanked by two axial and two equatorial hydrogens) and in **23** this signal appears at 1.18 δ as a quartet split into doublets (i.e. flanked by three axial hydrogens and one equatorial hydrogen). Thus in **24** the substituent at C-5 is axial, in **23** it is equatorial.

A high field signal at 0.79 δ in **23**, a quartet, showing three identical coupling constants, J = 10 Hz, has been assigned to H-6a. The same proton in **24** appears at 1.12 δ as an almost regular triplet split into doublets showing two large couplings (J_1 = 13.8 and J_2 = 13.0 Hz) and one small coupling (4.5 Hz). The 13.8 Hz coupling is attributed to geminal coupling to H-6e, the 13.0 Hz coupling to vicinal coupling to H-7a. The small coupling to H-5e indicates that the pyridylmethyl group is axial in **24**.

The presence of a doublet split into doublets at 3.53 δ in the spectrum of **23** has been assigned to one of the "benzylic" protons at C-11. This signal is part of an AMX spin system involving H-11′, H-11″, and H-5a appearing at 3.53, 2.53, and 1.96 ppm, respectively. These observations imply that substitution at the nitrogen atom of the pyridine ring strongly restricts rotation of the pyridylmethyl substituent about the C-5—C-11 bond. Similar behaviour is observed in the case of **24** and in the methiodides, **25** and **26** (*vide infra*).

These stereochemical assignments at C-5 were confirmed by examination of the ^{13}C nmr spectra of **23** and **24**. In **24**, with an axial group at C-5, the signals at C-7, C-9, and C-11 should be shielded by 4–7 ppm relative to the same signals in **23** (12). The actual shieldings observed were −4.4, −5.0, and −6.5 ppm for C-7, C-9, and C-11, respectively. The pyridines **21** and **22** derived from the *N*-oxides through treatment with PCl_3 showed almost identical behaviour in their ^{13}C spectra.

The pure pyridines **21** and **22** were transformed

Can. J. Chem. Downloaded from www.nrcresearchpress.com by 210.87.254.40 on 09/06/12
For personal use only.

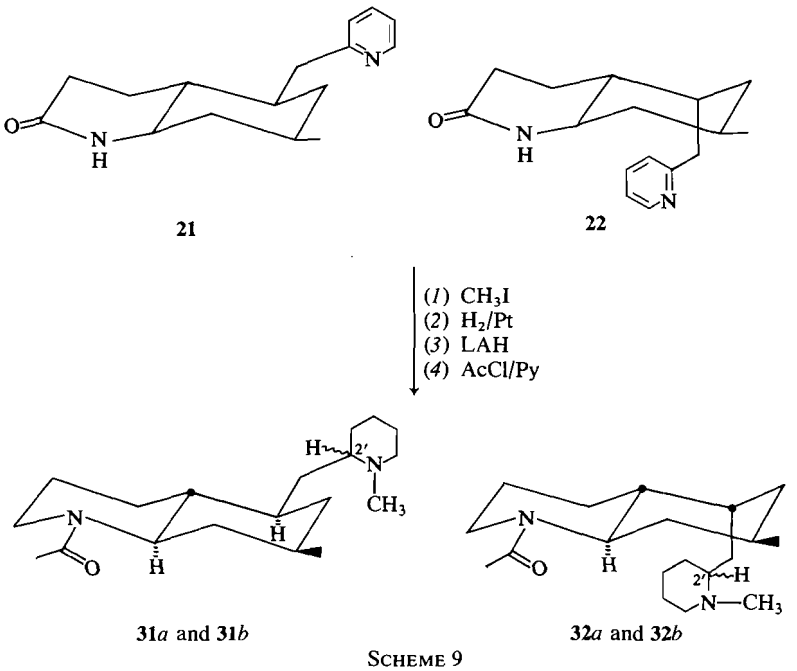

SCHEME 9

into their methiodides **25** and **26**, respectively, whose spectra are in accord with the assigned structures. Reduction of the methiodides (H_2/Pt) gave mixtures of piperidines **27** and **28**, epimeric at C-2′, but we were unable to effect their separation. The mixtures were therefore reduced with lithium aluminum hydride to mixtures of diamines, **29***a*, and **29***b* and **30***a* and **30***b*, and again separation was not effected. The mixtures were therefore acylated with acetyl chloride in pyridine to mixtures of *N*-acyl compounds, **31***a* and **31***b* and **32***a* and **32***b*. Each pair of epimers was separable by chromatography over basic alumina (activity 3) yielding four pure isomers as colorless oils. Isomer **32***b*, the more polar of the pair with the axial group at C-5, proved to be identical in its tlc behaviour in several solvent systems with a sample supplied to us by J.-C. Braekman. Unfortunately we did not have sufficient amounts of the natural material to make direct spectroscopic comparison with our synthetic material. It is of interest that the four *N*-acyl compounds give distinct spots on tlc and that **31***a* and **31***b* have higher R_f values than **32***a* and **32***b* (see Scheme 9). The four compounds all gave distinct ^{13}C nmr spectra which will be discussed in a forthcoming publication.

In summary this work has resulted in a total synthesis of N_α-acetylphlegmarine and has established the relative configuration of four of its five chiral centres. As it stands the synthesis suffers from a lack of stereoselectivity in the reduction of **19** but studies to improve this aspect of the work will be undertaken.

Experimental

Apparatus, Methods, and Materials

The infrared spectra were determined on a Perkin Elmer 383 spectrophotometer in chloroform solution. The nmr spectra were run at 90 MHz on a Varian EM 390 spectrometer or Bruker WP80 or Bruker WH 90 spectrometer. The 360 MHz proton spectra were recorded at the University of Toronto through the courtesy of Dr. A. A.Grey. Chemical shifts are reported in ppm (δ) from tetramethylsilane unless otherwise specified. The symbols s (singlet), d (doublet), t (triplet), q (quartet), and m (multiplet) are used to report the multiplicity of signals. Coupling constants are accurate within ± 0.5 Hz. Mass spectra were recorded on a CEC 21-110B mass spectrometer at an ionizing voltage of 80 eV and a source temperature of 150–200°C or on a VG 7070F mass spectrometer under similar source conditions and are reported as *m/e* values with relative intensities in brackets. High resolution measurements were performed by the method already described (11). Natural abundance ^{13}C nuclear magnetic resonance spectra were recorded on a Bruker WP80 Fourier transform spectrometer at 20.115 MHz and a probe temperature of +35.0°C. Samples were 0.08–0.15 *M* in $CDCl_3$; TMS was used as an internal reference.

Melting points and boiling points are uncorrected.

The purity of all samples was checked by thin-layer chromatography in several solvent systems. Silica gel 60F-254 (Merck) was used for tlc and for column chromatography. Aluminum oxide GF-254 (type 60/E, Merck) was used for tlc and Fischer neutral and basic alumina for column chromatography.

2-Trimethylsilylmethylpyridine

The compound was prepared using the method of Musker and Scholl (7) with some modifications. *n*-Butyllithium (80 mL, 2.47 *M* in hexane, ca. 0.2 mol) was added with stirring to solution of α-picoline (0.2 mol) in ether (250 mL) at −40 to

Can. J. Chem. Downloaded from www.nrcresearchpress.com by 210.87.254.40 on 09/06/12
For personal use only.

Can. J. Chem. Downloaded from www.nrcresearchpress.com by 210.87.254.40 on 09/06/12
For personal use only.

−30°C, under an argon atmosphere. The reaction mixture was stirred for 0.5 h and then allowed to come slowly to room temperature (some orange precipitate appeared). The solution was cooled to −30°C and trimethylchlorosilane (0.1 mol) was added dropwise. The suspension was allowed to warm to room temperature and stirred for a further 1 h. Water (1.8 g, 0.1 mol) was added and stirring was continued for an additional 0.5 h whereupon the solution was filtered and then distilled through a Vigreux column. 2-Trimethylsilylmethylpyridine (10 g) was obtained as a colorless oil, bp 114–116°C at 67 Torr; yield 60%, based on trimethylchlorosilane. Musker and Scholl (7) report a bp of 113–116°C at 63 Torr, and a yield of 40%. ^{1}H nmr (90 MHz), δ: 0.02 (9H, s, $(CH_3)_3Si$), 2.30 (2H, s, CH_2), and overlapping aromatic protons centred at 6.89 (1H, m, $J_{3,4}$ = 7.7 Hz, $J_{3,5}$ = 1.0 Hz and $J_{3,6}$ = 0.7 Hz, H-3), 6.92 (1H, m, $J_{4,5}$ = 7.6 Hz, $J_{5,6}$ = 4.3 Hz, H-5), 7.43 (1H, m, $J_{4,6}$ = 1.8 Hz, H-4), 8.38 (1H, m, H-6) ppm.

Reaction 2-Trimethylsilylmethylpyridine with Lactam 6

2-Trimethylsilylmethylpyridine (1.32 g, 8 mmol) in THF (25 mL) was treated with 2.47 *M* *n*-butyllithium (3.2 mL, ca. 8 mmol) at −65°C with stirring under an argon atmosphere. The solution was allowed to warm to room temperature and kept there for 0.25 h. It was then cooled to −65°C and lactam **6** (6) (0.652 g, 3.6 mmol) was added. The mixture was maintained at −65°C for 0.5 h, next at 1.0 h at −30°C, and finally at 0°C for an additional hour before treatment with 1 mL of 50% acetic acid. The solution was decanted from a small amount of precipitate and the latter washed with ether (5 mL) and benzene (5 mL). The combined organic phase was evaported and the residue (0.9 g) showed two products as well as starting material on tlc (silica; ether–methanol, 8:1). The products were separated from one another and from starting material by column chromatography on silica (100 g, SiO_2 for tlc; ether–methanol, 8:1). The first compound eluted, **7** (0.35 g, 38%), was followed by starting lactam (0.32 g, with traces of **7**), and this in turn by the second product, **8** (0.09 g, ca. 10%).

Compound **7**, the *Z* isomer, melted at 181–182°C after recrystallization from acetone and had the following properties. Infrared (ir) ν_{max}: 3400 (NH), 1655 (lactam), 1590, 1560 (pyridine) cm^{-1}; ^{1}H nmr (90 MHz), δ: 0.98 (3H, d, J = 7 Hz, CHCH_3), 3.60 (1H, br sextet, changes to sharp quintet after D_2O exchange, superposition of a doublet of triplets, J = 6 and 12 Hz, H-9), 4.14 (1H, near quintet from superposition of two triplets, J = 6 and 10 Hz, H-10), 6.30 (1H, d, J < 1 Hz, =C*H*), 6.65 (1H, br s, disappears on D_2O exchange, NH), 7.10 (2H, m, pyridine protons in β-positions), 7.63 (1H, m, pyridine proton in γ-position), 8.60 (1H, m, pyridine proton in α-position) ppm. *Exact Mass* calcd. for $C_{16}H_{20}N_2O$: 256.157; found (hrms): 256.156.

Compound **8**, the *E* isomer, melted at 211–212°C, with sublimation, after recrystallization from acetone, and had the following properties; ir ν_{max}: 3400 (NH), 1655 (lactam), 1590, 1560 (pyridine) cm^{-1}; ^{1}H nmr (90 MHz), δ: 0.90 (3H, d, J = 6 Hz, CHCH_3), 283 (1H, d of d, J = 4 and 14 Hz, partly superimposed on another proton, probably H-6e), 3.83 (1H, near quartet that is better defined after D_2O exchange, superposition of a doublet of triplets, J = 4.5 and 6 Hz, H-9), 6.53 (1H, s, =C*H*), 6.63 (1H, s, disappears on D_2O exchange, NH), 7.15 (2H, m, pyridine protons in β-positions), 7.66 (1H, m, pyridine proton in γ-position), 8.60 (1H, m, pyridine proton in α-position). *Exact Mass* calcd. for $C_{16}H_{20}N_2O$: 256.157; found (hrms): 256.156.

Hydrogenation of the Z *Isomer, 7*

A solution of **7** (0.3 g) in ethanol (10 mL) and acetic acid (0.5 mL) was treated with hydrogen over Adams' catalyst (60 mg) at atmospheric pressure. The reaction was terminated after 1.1 mole equivalent of hydrogen was consumed (ca. 3 h) whereupon the solution was decanted from the catalyst. The residue remaining after removal of solvent was homogeneous on tlc and melted at 179–181°C, after recrystallization from ether–THF. The product **10**, obtained in greater than 90% yield, had the following physical properties. Infrared ν_{max}: 3400 (NH), 1650 (lactam), 1590, 1570 (pyridine) cm^{-1}; ^{1}H nmr (90 MHz), δ: 0.83 (3H, d, J = 6 Hz, CHCH_3), 3.10 (1H, d of d, J = 4 and 14 Hz, probably H-11), 3.71 (1H, near quartet, J = 3 Hz, H-9), 6.00 (1H, s, disappears on D_2O exchange, NH), 7.16 (2H, m, pyridine protons at the β-positions), 7.66 (1H, m, pyridine proton at the γ-position), 8.56 (1H, m, pyridine proton at the α-position) ppm. *Exact Mass* calcd for $C_{16}H_{22}N_2O$: 258.173; found (hrms): 258.175.

Preparation of Methiodide 12

Compound **10** (0.166 g) was dissolved in acetone (10 mL) and treated with an excess of methyl iodide (0.5 g). The solution was set away and over a period of 72 h at room temperature the product **12** slowly crystallized from solution. The quaternary salt so obtained (0.135 g, 75%) melted at 272–273°C and had the following physical properties. Nuclear magnetic resonance ^{1}H nmr (90 MHz, CD_3OD), δ: 0.85 (3H, d, J = 6 Hz, CHCH_3), 3.60 (1H, d of d, J = 4 and 15 Hz, probably H-11), 3.80 (1H, near quartet, J = 3 Hz, H-9), 4.42 (3H, s, N—CH_3), 7.96 and 8.06 (2H, overlapping multiplets, pyridine protons at the β-positions), 8.50 (1H, m, pyridine proton at γ-position), 8.90 (1H, br d, J = 7 Hz, pyridine proton at α-position) ppm.

Hydrogenation of 12

A solution of **12** (0.2 g, 0.5 mmol) in water (10 mL) was hydrogenated over Adams' catalyst (60 mg) at atmospheric pressure for 6 h during which time 34.6 mL hydrogen (theoretical = 33.6 mL) were consumed. The solution was decanted from the catalyst, the solution made basic with ammonia, and the aqueous solution extracted with chloroform (3 × 5 mL). Evaporation yielded 140 mg (100% yield) of a crystalline solid, **13***a* and **13***b*, that melted at 169–170°C after recrystallization from acetone and had the physical properties listed below. This product gave a single spot on tlc and otherwise appeared to be a single compound. Subsequent reduction of the lactam function (*vide infra*) gave, however, two isomers indicating that this product must have been a mixture.

Infrared ν_{max}: 3400 (NH), 1655 (lactam), 2790 (N—CH_3) cm^{-1}; ^{1}H nmr (90 MHz), δ: 0.90 (3H, d, J = 6 Hz, CHCH_3), 2.24 (3H, s, N—CH_3), 2.80 (1H, br d, J = 14 Hz, probably H-11), 3.70 (1H, br s, $W_{1/2}$ = 7 Hz, probably H-9), 5.77 (1H, br s, disappears after D_2O exchange, NH) ppm. *Exact Mass* calcd. for $C_{17}H_{30}N_2O$: 278.236; found (hrms): 278.236.

*Reduction of 13*a *and 13*b *with Lithium Aluminium Hydride*

The epimeric amides (130 mg) in THF (5 mL) were added to a suspension of lithium aluminum hydride (100 mg) in ether (30 mL) and the mixture boiled for 1.5 h. The excess of LAH was decomposed with wet ether, the ether solution separated from the suspended solid, and the precipitate washed with ether (2 × 5 mL). The combined extract was dried over $MgSO_4$ and evaporated, yielding a colorless oily residue (118 mg, 95% yield). Examination of the residue by tlc on alumina showed two spots and an nmr spectrum of the crude showed two *N*-methyl resonances at 2.29 and 2.27 ppm of almost equal intensity. The two components of the mixture were separated by column chromatography on alumina (15 g, activity 3). Isomer **14***a* (40 mg) was eluted with benzene–chloroform 1:1 and isomer **14***b* (54 mg) with chloroform; both isomers were obtained as oils and had the following physical properties.

Isomer **14***a*: ir ν_{max}: 3150 (br) NH, 2790 (N—CH_3) cm^{-1}; ^{1}H nmr (90 MHz), δ: 0.85 (3H, d, J = 6 Hz, CHCH_3), 2.27 (3H, s, N—CH_3), 2.5–3.2 (4H, m, N—C*H* protons) ppm.

Can. J. Chem. Downloaded from www.nrcresearchpress.com by 210.87.254.40 on 09/06/12
For personal use only.

Isomer **14***b*: ir ν_{max}: 3150 br (NH), 2790 (N—CH_3) cm^{-1}; ^1H nmr (90 MHz), δ: 0.85 (3H, d, J = 6 Hz, CHCH_3), 2.29 (3H, s, N—CH_3), 2.5–3.2 (4H, m, N—C*H* protons) ppm.

Acylation of the Isomeric Amines ***14****a and* ***14****b*

The procedure was identical for each isomer and is reported here for amine **14***a* only. Amine **14***a* (30 mg) in pyridine (1 mL) was treated with a few drops of acetyl chloride. The solution was held at room temperature for 0.5 h, then quenched with water (10 mL), and extracted with chloroform (2 × 5 mL). The residue from the chloroform extract was a colorless oil which was purified by filtration through alumina in a chloroform solution. There was obtained 20 mg of **15***a* as a colorless oil with the following properties. Infrared ν_{max}: 2800 (N—CH_3), 1625 (amide) cm^{-1}; ^1H nmr (90 MHz), δ: 1.05 (3H, d, J = 7 Hz, CHCH_3), 2.06 (3H, s, CH_3CO), 2.29 (3H, s, N—CH_3), 2.90 (2H, m, N—C*H* protons from piperidine ring), 3.8–5.0 (3H, very br m, N—C*H* protons adjacent to CH_3(CO)N) ppm. *Exact Mass* calcd. for $C_{19}H_{34}N_2O$: 306.267; found (hrms): 306.265.

Compound **15***b* was also obtained as a colorless oil in comparable yield from **14***b*; ir ν_{max}: 2800 (N—CH_3), 1625 (amide) cm^{-1}; ^1H nmr (90 MHz), δ: 1.06 (3H, d, J = 7 Hz, CHCH_3), 2.07 (3H, s, CH_3CO), 2.29 (3H, s, N—CH_3), 2.90 (2H, m, N—*CH* protons of piperidine ring), 3.6–5.0 (3H, m, protons adjacent to CH_3(CO)N). *Exact Mass* calcd. for $C_{19}H_{34}N_2O$: 306.267; found (hrms): 306.265.

Hydrogenation of the E *Isomer* ***8***

The procedure followed was identical with that used for the *Z* isomer **7** but the reaction was carried out on 53 mg of **8** and 10 mg of PtO_2. The tlc showed a spot of the same R_f as **10**, another new major component, and a trace of starting compound. An nmr spectrum showed that the reduction product was a mixture of **10** and **11** in a ratio of ca. 1:4. The nmr of **11**, extracted from the spectrum of the mixture, was as follows; ^1H nmr (90 MHz), δ: 0.96 (3H, d, J = 7 Hz, CHCH_3), 3.55 (2H, br m, H-9 and probably H-11), 9.3 (1H, br s, disappears on D_2O exchange, NH), 7.2 (2H, m, pyridine protons in β-positions), 7.7 (1H, m, pyridine proton in γ-position), 8.6 (1H, m, pyridine proton in α-position).

5-Keto-7-methyl-1,2,3,4,5,6,7,8-octahydro-2-quinolone ***18***

The ketoenamide was prepared using the method of Vill *et al.* (8). A mixture of 2-(2′-cyanoethyl)-5-methyl-1,3-cyclohexanedione (35.8 g, 0.2 mol) and 50% aqueous acetic acid (2 mL) was heated in a sealed tube for 4 h at 200°C. The yellow solid that separated on cooling was dissolved in boiling chloroform (100 mL) and precipitated by addition of petroleum ether (30–60°C, 450 mL). The product so obtained (a light yellow powder, 34.4 g, 96% yield) melted at 197–199°C. An analytical sample was recrystallized from water (methanol or ethanol) with activated charcoal, colorless crystals, mp 199°C (lit. (8) mp 198–199°C). Infrared ν_{max} ($CHCl_3$): 3400 (NH), 1706 (unsaturated C=O), 1634 (C=O lactam) cm^{-1}; ^1H nmr (90 MHz), δ: 1.12 (3H, d, J = 4.5 Hz), 8.9 (1H, br s, NH), 2.0–3.0 (10H, m) ppm; ms: 179 (M^+, 100), 178 (31), 151 (23), 150 (66), 109 (37), 108 (21), 81 (76), 55 (25), 41 (34%).

Reduction of ***18***

Hydrogenation in the Presence of Palladium on Charcoal

A solution of ketoenamide **18** (145 mg, 0.81 mmol) in ethanol (10 mL) was treated with hydrogen at room temperature and atmospheric pressure over 10% Pd/C (100 mg). The reduction was complete in 2.5 h and the volume of hydrogen consumed was 42.3 mL. The catalyst was filtered off and washed with ethanol. To the oily residue remaining after removal of ethanol, benzene (10 mL) was added and the solution evaporated to dryness yielding a colorless solid (133 mg) which contained four products (tlc on silica, diethyl ether – methanol 3:1 as the solvent system). Three of the products were obtained pure by column chromatography on silica (15 g) using ether–methanol (10:1) as the developing system.

The first compound, assumed to be 7-methyl-3,4,5,6,7,8,9,10-octahydro-2-quinolone (42 mg), melted at 129–130°C; ir ν_{max}: 3385 (NH), 1644 (C=O) cm^{-1}; ^1H nmr, δ: 0.90 (3H, d, J = 6 Hz, CH—CH_3), 3.64 (1H, q, J = 3 Hz, H-9), 6.9 (1H, br s, NH); ms: 167 (M^+, 82), 110 (82), 97 (32), 96 (29), 82 (65), 69 (52), 55 (100%).

The second compound was the *trans*-ketolactam **17** (17 mg, mp 225–227°C with sublimation). It had the same spectral properties (ir, ^1H mnr, ms) as described (6) and the same R_f value on silica when compared with an authentic sample. The third product, *cis*-ketolactam **6** (61 mg), after recrystallization from benzene, had the same spectral and physical properties as described (6). The fourth compound has not been isolated in a pure state.

Sodium Borohydride Reduction

A solution of ketoenamide **18** (670 mg, 3.7 mmol) and sodium borohydride (400 mg, 10.5 mmol) in absolute ethanol (25 mL) was strirred at room temperature for 22 h. Then glacial acetic acid (0.6 mL) was added and stirring continued for another 40 min. The reaction mixture was evaporated to dryness, water (10 mL) was added, and the mixture extracted with chloroform (2 × 10 mL). The combined extracts were washed with water and dried over anhydrous sodium sulfate. After removal of the solvent a pale yellow, partly solidified, oil was obtained (282 mg). The main product of reduction, possessing an R_f value identical with **6** on silica (but different on alumina) was purified by column chromatography on alumina (13 g, activity 3). The fractions eluted with chloroform – 0.5–1% methanol contained 227 mg of colorless solid, mp 125–128°C, assumed to be 5-hydroxy-7-methyl-3,4,5,6,7,8-hexahydro-2-quinolone. After crystallization from chloroform it melted at 128–129°C. Infrared ν_{max}: 3580 (OH), 3403 (NH), 1701 (shoulder), and 1674 (C=O), 1452, 1374, 997 cm^{-1}; ^1H nmr (80 MHz), δ: 1.03 (3H, d, J = 5.9 Hz, CH—CH_3), 1.8 (OH), disappears in D_2O, 4.28 (1H, m, H-5), 7.61 (1H, br s, NH) ppm, disappears in D_2O; ms: 181 (M^+, 65), 180 (49), 164 (76), 163 (50), 148 (100), 139 (78), 138 (38), 120 (23), 111 (22), 110 (37), 93 (22), 83 (20), 55 (74).

Reduction with Lithium in Liquid Ammonia

To liquid ammonia (700 mL, distilled from sodium), lithium (2.3 g, 0.33 g atom) was added and the mixture stirred for 0.5 h. Solid ketoenamide **18** (17.9 g, 0.1 mol) was then added at −33°C. After 1 min the deep-blue solution was quenched with ammonium chloride (16 g, 0.3 mol) and the ammonia allowed to evaporate overnight. Water and chloroform (50 mL of each) were added to the residue. The aqueous layer was extracted with an additional two portions of chloroform. The combined extracts were washed with water and dried over anhydrous magnesium sulfate. After removal of the solvent under reduced pressure the colorless solid residue (14.4 g) was dissolved in boiling methanol (50 mL), filtered from a small amount of white powdered substance, diethyl ether (200 mL) added, and the solution set aside to crystallize in the refrigerator. The *trans*-ketolactam **17** (5.8 g, 32%) melted at 224–227°C with sublimation (lit. (6) mp 225–227°C). The pure compound may be obtained by continuous extraction of the crude (crystallized) material with anhydrous ether or by sublimation at 120–140°C/0.25 Torr followed by recrystallization from water or methanol. Melting point 229°C (with sublimation).

Reaction of 2-Trimethylsilylmethylpyridine with Lactam ***17***

The reaction of *trans*-ketoamide **17** (2.715 g, 15 mmol), trimethylsilylmethylpyridine (5.95 g, 36 mmol), and 1.60 *M* solution of *n*-butyllithium – hexane (22.5 mL, 36 mmol) in THF (150 mL) yielded a mixture from which *Z*-isomer **19** separated as

Can. J. Chem. Downloaded from www.nrcresearchpress.com by 210.87.254.40 on 09/06/12
For personal use only.

a solid after quenching the reaction mixture with 50% aqueous acetic acid (4.0 mL). The THF solution was decanted from the white precipitate, and the latter washed with benzene (20 mL) and dissolved in chloroform (45 mL) and water (15 mL). The aqueous layer was removed and the organic extract was shaken with water and dried over anhydrous magnesium sulphate. After removal of the solvent, chromatographically pure **19** was obtained (2.30 g), mp 210–212°C (tlc on silica in $CHCl_3$–MeOH 10:1). Evaporation of the tetrahydrofuran solution gave a partly solidified residue (5.66 g). Petroleum ether (40 mL) was added to the residue and the crystals (0.56 g) that separated were recrystallized from methanol (6 mL) and ether (20 mL) yielding 0.40 g of pure **19**. The mother liquor and petroleum ether residues were collected and chromatographed on a Lobar Si 60 column (size B) using chloroform–methanol (100:3, v/v) as the developing system. Another portion of the *Z*-isomer **19** (0.29 g, overall yield 2.99 g or 77.9%) and 51 mg of the *E*-isomer **20** (yield 1.3%, mp 200–202°C) were obtained.

Compound **19**, the *Z*-isomer, melted at 213–214°C after recrystallization from methanol–ether; uv λ_{max} (MeOH) (ε): 223 (4800), 262 (4200) nm; ir ν_{max}: 3400 (NH), 1662 and 1648 (lactam), 3070, 1590 and 1568 (pyridine) cm^{-1}; ^1H nmr (80 MHz), δ: 1.02 (3H, d, J = 5.6 Hz, $CHCH_3$), 3.30 (1H, td, J = 12.7 and 3.2 Hz, H-9), 6.12 (1H, br s, disappears on D_2O exchange, NH), 6.53 (1H, s, =C*H*), 7.19 (2H, m, pyridine protons in β-positions), 7.60 (1H, td, J = 7.6 and 1.7 Hz, pyridine proton in γ-position), 8.55 (1H, m, pyridine proton in α-position) ppm; ms: 256 (M^+, 65), 255 (47), 241 (13), 224 (12), 214 (100), 198 (34), 184 (39), 170 (26), 144 (17), 143 (18%). *Exact Mass* calcd. for $C_{16}H_{20}N_2O$: 256.158; found (hrms): 256.156.

Compound **20**, the *E*-isomer, melted at 202°C after recrystallization from acetone; uv λ_{max} (MeOH) (ε): 240 (16500), 274 (10400) nm; ir ν_{max}: 3393 (NH), 1662 and 1650 (lactam), 3084, 1588 and 1564 (pyridine) cm^{-1}; ^1H nmr (80 MHz), δ: 0.98 (3H, d, J = 4.2 Hz, $CHCH_3$), 3.45 (2H, m, H-9 and H-6e), 6.48 (1H, s, =C*H*), 6.93 (1H, br s, disappears on D_2O exchange, NH), 7.19 (2H, m, pyridine protons in β-positions), 7.63 (1H, td, J = 7.8 and 2.0 Hz, pyridine proton in λ-position), 8.58 (1H, m, pyridine proton in α-position) ppm; ms: 256 (M^+, 56), 255 (41), 241 (53), 224 (14), 214 (100), 198 (69), 197 (59), 184 (86), 170 (54), 169 (54), 168 (68), 167 (40), 165 (54), 144 (50), 143 (54), 130 (64%). *Exact Mass* calcd. for $C_{16}H_{20}N_2O$: 256.158; found (hrms): 256.155.

Treatment of Z-Isomer 19 with H_2

Hydrogenation of the *Z*-isomer **19** (1.53 g, 6.0 mmol) in ethanol was performed in the presence of Adams' catalyst (200 mg) without acetic acid. After absorption of 160 mL of hydrogen (4.5 h) the reaction was stopped. The usual work-up gave 1.52 g of partly solidified product. Thin-layer chromatography on silica (developed three times in ether–methanol 4:1) showed three spots: traces of the starting material, the inseparable epimers **21** and **22**, and a spot (R_f = 0), inactive in uv light but developable in the presence of iodine vapour. The mixture of **21** and **22** was separated by column chromatography on silica using ether–methanol (6:1) as the developing system. From 530 mg of the crude product (50 g SiO_2), the starting material (34 mg) and the epimeric products **21** and **22** (393 mg of a solid melting at 148–186°C) were obtained; ir ν_{max}: 3390 (NH), 1655 (lactam C=O), 1594 and 1572 (pyridine) cm^{-1}; ^1H nmr (90 MHz), δ: 0.89 and 0.88 (doublets, J = 6.3 and 6.0 Hz, respectively, $CHCH_3$), 6.87 (1H, br s, disappears on D_2O exchange, NH), 7.01 (2H, m, pyridine protons in β-positions), 7.52 (1H, td, pyridine proton in γ-position), 8.50 (1H, m, pyridine proton in α-position) ppm. ms: 258 (M^+, 12), 93 (100%).

Pure epimers **21** and **22** were obtained by transformation of the mixture to their pyridine *N*-oxides, separation by column chromatography on alumina, and regeneration of the pyridines using phosphorus trichloride (see below).

Conversion of 21 and 22 to Their N*-Oxides*

The mixtures of epimers **21** and **22** (ca. 1:1, 760 mg) was dissolved in chloroform (15 mL) and 85% *m*-chloroperbenzoic acid (630 mg) was added. The oxidation was monitored by tlc on alumina (chloroform–methanol 50:1). The reaction was complete after 8 to 10 h at 25°C. The oily residue obtained after removal of the solvent was chromatographed on an alumina column (activity 1, 120 g) using progressively increasing concentrations of ethanol in chloroform. *N*-oxide **23** (338 mg) was obtained as colorless crystals, after crystallization from methanol – ethyl acetate, that melted at 259–261°C (with sublimation). The second fraction, *N*-oxide **24** (180 mg), melted at 274–277°C.

N-oxide **23**: ir ν_{max}: 3400 (NH), 1660 (lactam) cm^{-1}; ^1H nmr (80 MHz), δ: 0.87 (3H, d, J = 6.5 Hz, $CHCH_3$), 3.11 (1H, td, J = 10.0 and 3.0 Hz, H-9), 3.52 (1H, dd, J = 12.5 and 2.7 Hz), 6.31 (1H, br s, disappears on D_2O exchange, NH), 7.21 (3H, m, pyridine protons in β- and γ-positions), 8.24 (1H, m, pyridine proton in α-position) ppm; ^1H nmr (360 MHz), δ: 2.40 (H-3a, $J_{3a,3e}$ = 18.8, $J_{3a,4a}$ = 7.3 Hz), 2.55 (H-3e, $J_{3e,3a}$ = 18.8, $J_{3e,4a}$ = 6.3, $J_{3e,4e}$ = 1.3 Hz), 1.58 (H-4a, $J_{4a,4e}$ = 10, $J_{4a,3a}$ = 7.3, $J_{4a,3e}$ = 6.3, $J_{4a,10a}$ = 12.0 Hz), 2.30 (H-4e, overlapped with high field signal H-11″ at δ 2.35 ppm), 1.96 (H-5, $J_{5,10a}$ = $J_{5,6a}$ = 10, $J_{5,11'}$ = $J_{5,6e}$ = 3 Hz), 0.79 (H-6a, $J_{6a,6e}$ = $J_{6a,5}$ = $J_{6a,7}$ = 10 Hz), 1.50 (H-6e and H-7, $J_{6e,5}$ = 3, $J_{6e,6a}$ = $J_{7,6a}$ = $J_{7,8a}$ = 10), $J_{7,CH3}$ = 6.5, $J_{7,8e}$ = 2 Hz), 1.04 (H-8a, $J_{8a,7}$ = 10, $J_{8a,8e}$ = 12.5, $J_{8a,9}$ = 12.0 Hz), 1.77 (H-8e, $J_{8e,8a}$ = 12.5, $J_{8e,7}$ = 2.0, $J_{8e,9}$ = 3.8 Hz), 3.11 (H-9, $J_{9,10}$ = 12.5, $J_{9,8a}$ = 12.0, $J_{9,8e}$ = 3.8 Hz), 1.18 (H-10, $J_{4a,10}$ = 12.0, $J_{4e,10}$ = 3.0; $J_{5,10}$ = 10, $J_{9,10}$ = 12.5 Hz), 2.35 (H-11″), 3.53 (H-11′, $J_{11',11''}$ = 13.8, $J_{11',5}$ = 3.0 Hz), 0.86 (CH_3, $J_{CH_3,7}$ = 6.5 Hz), 5.99 (NH), 7.21 (pyridine protons in β- and γ-positions), 8.24 (pyridine proton in α-position) ppm. ms: 274 (M^+, 1) 258 (18), 257 (62), 166 (16), 164 (100), 120 (21), 109 (65), 94 (43), 93 (72), 92 (18), 55 (13%). *Exact Mass* calcd. for $C_{16}H_{22}N_2O_2$: 274.168; found (hrms): 274.165.

N-oxide **24**, mp 276–277°C (methanol–acetone); uv λ_{max} (MeOH) (ε): 262 (8100) nm; ir ν_{max}: 3400 (NH), 1658 (lactam) cm^{-1}; ^1H nmr (80 MHz), δ: 0.91 (3H, d, J = 6.1 Hz, $CHCH_3$), 3.19 (1H, dd, J = 11.4 and 1.9 Hz), 3.42 (1H, m, H-9), 6.26 (1H, br s, disappears on D_2O exchange, NH), 7.20 (3H, m, pyridine protons in β- and γ-positions), 8.24 (1H, m, pyridine proton in α-position) ppm; ^1H nmr (360 MHz), δ: 2.40 (H-3a, $J_{3a,3e}$ = 17.5, $J_{3a,4a}$ = 11.3, $J_{3a,4e}$ = 7.5 Hz), 2.53 (H-3e, $J_{3e,3a}$ = 17.5, $J_{3e,4a}$ = 5.5, $J_{3e,4e}$ = 2.5 Hz), 1.9 (4H, m, H-4e, H-4a, H-7, and H-8e), 2.56 (H-5, $J_{5,11''}$ = 11, $J_{5,10}$ = 3 Hz, and three couplings of order 1–2 Hz with H-11′, H-6a, and H-6e), 1.12 (H-6a, $J_{6a,6e}$ = 13.8, $J_{6a,7}$ = 13, $J_{6a,5}$ = ca. 1 Hz), 1.50 (H-6e, $J_{6e,6a}$ = 13.8, $J_{6e,7}$ = 3 Hz), 1.02 (H-8a, $J_{8a,8e}$ = 13, $J_{8a,7}$ = 12, $J_{8a,9}$ = 11.3 Hz), 3.39 (H-9, $J_{9,10}$ = 10.5, $J_{9,8a}$ = 11.3, $J_{9,8e}$ = 4 Hz), 1.63 (H-10, $J_{10,9}$ = 10.5, $J_{10,4a}$ = 10.5, $J_{10,4e}$ = $J_{10,5}$ = 3 Hz), 2.73 (H-11″, $J_{11'',11'}$ = 13.8, $J_{11'',5}$ = 11 Hz), 3.18 (H-11′, $J_{11',11''}$ = 13.8, $J_{11',5}$ ≈ 2; and J ≤ 1 Hz, possibly long range "*W*" coupling with H_{6e}), 0.92 (CH_3, $J_{CH_3,7}$ = 6.5 Hz), 5.90 (br s, NH), 7.20 (3H, m, pyridine protons in β- and γ-positions), 8.24 (1H, m, pyridine proton in α-position) ppm; ms: 274 (M^+, 1.2), 258 (17), 257 (32), 166 (18), 164 (96), 120 (30), 109 (59), 94 (39), 93 (100), 92 (17%) *m/e*. *Exact Mass* calcd. for $C_{16}H_{22}N_2O_2$: 274.168; found (hrms): 274.169.

Conversion of N*-oxides 23 and 24 to Pyridines 21 and 22, Respectively*

The reaction was performed in the same manner in both cases. To a solution of *N*-oxide (1.0 mmol) in chloroform (10 mL) freshly distilled phosphorus trichloride (0.3 mL) was

TABLE 1. R_f values of the isomeric N_α-methyl-N_β-acetylphlegmarines on alumina (plate length: 20 cm)

Compound	R_f value			
	Chloroform	Chloroform–5% Et_2NH/MeOH 50:1	Acetone–methanol 25:1	Ethyl acetate – ethanol 40:1
31*a*	0.25	0.58	0.35	0.40
31*b*	0.23	0.55	0.32	0.38
32*a*	0.19	0.47	0.25	0.32
32*b*	0.16	0.39	0.19	0.28
Natural compound	0.16	0.39	0.19	0.28

added at 0°C and the mixture kept at room temperature for 17 h. After removal of volatile substances at reduced pressure dilute aqueous sodium carbonate solution was added and the mixture was extracted with chloroform. Almost quantitative yields of pyridines **21** and **22** were obtained.

Epimer **21**, colorless crystals, melted at 170°C after recrystallization from ethyl acetate; ir ν_{max}: 3400 (NH), 1659 (lactam), 1596 and 1572 (pyridine) cm^{-1}; ^1H nmr (80 MHz), δ: 0.86 (3H, d, J = 5.9 Hz, CHCH_3), 3.09 (2H, d, $J_{11,5}$ = 3.9 Hz, H-11), 3.11 (1H, td, J = 11.7 and 3.4 Hz, H-9), 6.17 (1H, br s, NH), 7.10 (2H, m, pyridine protons in β-positions), 7.59 (1H, td, J = 7.9 and 1.7 Hz, pyridine proton in γ-position), 8.54 (1H, m, pyridine proton in α-position) ppm; ms: 258 (M^+, 40), 257 (28), 241 (4), 240 (4), 146 (8), 144 (5), 132 (5), 130 (6), 120 (16), 118 (8), 93 (100%).

Epimer **22**, colorless crystals, mp 180.5–182°C; ir ν_{max}: 3400 (NH), 1660 (lactam), 1598 and 1577 (pyridine) cm^{-1}; ^1H nmr (80 MHz), δ: 0.88 (3H, d, J = 6.1 Hz, CHCH_3), 3.38 (1H, td, J = 11.2 and 4 Hz, H-9), 5.85 (1H, br s, NH), 7.10 (2H, m, pyridine protons in β-positions), 7.60 (1H, td, J = 8.0 and 1.9 Hz, pyridine proton in γ-position), 8.54 (1H, m, pyridine proton in α-position) ppm; ms: 258 (M^+, 10), 120 (26), 106 (9), 93 (100%). *Exact Mass* calcd. for $C_{16}H_{22}N_2O$: 258.173; found (hrms): 258.175.

Preparation of Quaternary Salts 25 and 26

Quaternization of **21** and **22** under similar conditions to those described before gave methiodides **25** and **26** in yields of 92 and 93%, respectively.

Methiodide **25**, mp 257–258°C (methanol–acetone); ir ν_{max} (KBr): 3200 (NH), 1655 and 1635 (lactam), 1579 and 1517 (pyridine) cm^{-1}; ^1H nmr (80 MHz, D_2O), (sodium β-trimethylsilypropionate-d_4 (TSP) as the internal standard): 0.88 (3H, d, J = 6 Hz, CHCH_3), 2.97 (1H, dd, J = 16 and 4.4 Hz, H-3e), 3.24 (1H, m, H-9), 3.59 (1H, dd, J = 14 and 3.2 Hz, H-11′), 4.33 (3H, s, $\overset{+}{N}$—CH_3), 7.96 (2H, m, pyridine protons in β-positions), 8.43 (1H, m, pyridine proton in γ-position), 8.71 (1H, m, pyridine proton in α-position) ppm.

Methiodide **26**, mp 177–178°C (methanol–acetone); ir ν_{max} (KBr): 3480, 3400, and 3220 (NH), 1645 and 1636 (lactam), 3080, 3050, 1577 and 1512 (pyridine) cm^{-1}; nmr (80 MHz, D_2O), (TSP) δ: 0.93 (3H, d, J = 6.1 Hz, CHCH_3), 3.17 (2H, m), 3.52 (1H, td, J = 11 and 3.5 Hz, H-9), 4.33 (3H, s, $\overset{+}{N}$—CH_3), 7.92 (2H, m, pyridine protons in β-positions), 8.41 (1H, m, pyridine proton in γ-position), 8.72 (1H, m, pyridine proton in α-position) ppm.

Reduction of Methiodides 25 and 26

The methiodides were reduced catalytically as previously described. From methiodide **25** (170 mg) a mixture of *N*-methylpiperidines **27***a* and **27***b* was obtained (116 mg, 96% yield) as a colorless solid (120–176°C). This product gave also a single spot in tlc; ir ν_{max}: 3400 (NH), 2795 (NCH_3), 1661 and 1655 (C=O) cm^{-1}; ^1H nmr (90 MHz) δ: 0.94 (3H, d, J = 6 Hz, CHCH_3), 2.23 (3H, s, N—CH_3), 2.3–3.3 (m, 5H, N—CH protons), 6.80 (1H, br s, NH) ppm; ms: 278 (M^+, 3), 277 (5), 263 (1), 223 (2), 166 (2), 164 (3), 98 (100), 93 (16), 84 (13), 70 (12).

From methiodide **26** (309 mg) an inseparable mixture of **28***a* and **28***b* was obtained (194 mg, 88% yield); mp 98–170°C; ir ν_{max}: 3400 (NH), 2780 (NCH_3), 1659 (C=O) cm^{-1}; ^1H nmr (90 MHz), δ: 0.92 and 0.93 (3H, two doublets, J = 6 Hz, CHCH_3), 2.27 (3H, s, NCH_3), 2.3–2.6 (3H, m), 2.83 (1H, m), 3.23 (1H, m), 6.40 (1H, br s, NH); ms: 278 (M^+, 8), 277 (12), 223 (2), 166 (2), 164 (2), 98 (100%). *Exact Mass* calcd. for $C_{17}H_{30}N_2O$: 278.236; found (hrms): 278.235.

*Reduction of the Mixture (27*a *and 27*b*) with Lithium Aluminum Hydride*

The lactams were reduced as previously described. The epimeric amides (**30***a* and **30***b*, 110 mg) gave 84 mg of a mixture of **29***a* and **29***b* (yield 80%) as a partly solidified colorless oil; ir ν_{max}: 3170 (br, NH), 2800 (N—CH_3) cm^{-1}; ^1H nmr (90 MHz), δ: 0.83 (1H, br s, NH), 0.92 (3H, d, J = 6 Hz, CHCH_3), 2.25 (3H, s, NCH_3), 2.3–3.2 (5H, m) ppm; ms: 264 (M^+, 2) 263 (6), 152 (20), 150 (20), 99 (97), 98 (100), 96 (34), 83 (30), 70 (97), 55 (48%).

*Reduction of the Mixture 28*a *and 28*b *with Lithium Aluminum Hydride*

The epimeric amides (**28***a* and **28***b*, 190 mg) gave 141 mg of a mixture of **30***a* and **30***b* (yield 78%) as a partly crystalline colorless oil; ir ν_{max}: 3160 (br, NH), 2798 (N—CH_3) cm^{-1}; ^1H nmr (90 MHz), δ: 0.88 and 0.89 (3H, two doublets, J = 6 Hz, CHCH_3), 1.6 (NH), 2.25 and 2.26 (3H, two s, N—CH_3), 2.3–3.2 (5H, m) ppm; ms: 264 (M^+, 3), 263 (8), 152 (22), 150 (21), 98 (100%).

*Acetylation of Amine Mixtures (29*a *and 29*b*) and (30*a *and 30*b*)*

Mixtures of the epimeric diamines **29***a*, **29***b* and **30***a*, **30***b* gave after acetylation by the previously described procedure the two pairs of epimeric acetamides **31***a*, **31***b* and **32***a*, **32***b*, respectively. Each of the four compounds showed a separate spot on tlc on alumina (chloroform – 5% diethylamine in methanol, 50:1). Components **31***a* and **31***b* possess higher R_f values than **32***a* and **32***b*. Isomer **32***b* had identical tlc behaviour with an authentic sample of N_β-acetyl-N_α-methylphlegmarine derived from natural sources in several solvent systems as shown in Table 1.

The crude yellow oils obtained from the acetylation reaction (96 mg of **31***a*, **31***b* from 80 mg of diamines **29***a*, **29***b*, and 160 mg **32***a*, **32***b* from 138 mg of **30***a*, **30***b*) were separated on basic alumina (activity 3) yielding four pure isomers as colourless oils: **31***a* (29 mg), **31***b* (16 mg), **32***a* (26 mg), and **32***b* (45 mg). *Exact Mass* calcd. for $C_{19}H_{34}N_2O$: 306.267; found: 306.266, 306.263,

Can. J. Chem. Downloaded from www.nrcresearchpress.com by 210.87.254.40 on 09/06/12
For personal use only.

TABLE 2. Selected spectroscopic data on isomeric N_α-methyl-N_β-acetylphlegmarines

Compound	^{1}H nmr data (90 MHz), ppm (δ in Hz)				Ir data ν_{max} ($CHCl_3$), cm^{-1}	
	$CHCH_3$[a]	$COCH_3$[b]	NCH_3[b]	Others[c]	N—CH_3	C=O amide
31*a*	0.93(6.5)[d]	2.08[e]	2.27[f]	2.4–3.9	2800	1624
31*b*	0.92(6.5)[d]	2.06[e]	2.24[f]	2.5–3.9	2800	1623
32*a*	0.90(6.0)	2.07[g]	2.26	2.4–3.9	2804	1624
32*b*	0.90(6.0)	2.06[g]	2.26	2.5–3.9	2800	1622

[a]Doublet.
[b]Singlet.
[c]5H, m.
[d, e, f, g]It is possible to observe these differences in the nmr spectra of the respective mixtures.

306.271, 306.263, respectively for **31***a*, **31***b*, **32***a*, and **32***b*. All four synthetic compounds and the natural compound gave similar mass spectra.[2] Selected nmr and ir data of **31** and **32** are given in Table 2.

Acknowledgements

We are grateful to the Natural Sciences and Engineering Research Council of Canada for financial support of this work. We thank Mr. B. Sayer for recording the ^{13}C nmr spectra and Dr. A. A. Grey for the 360 MHz spectra of the epimeric *N*-oxides. We are particularly indebted to Dr. J.-C. Braekman for a sample of N_α-methyl-N_β-acetylphlegmarine derived from a natural source and for copies of mass spectra and nmr spectra of this compound.

1. L. NYEMBO, A. GOFFIN, C. HOOTELÉ, and J.-C. BRAEKMAN. Can. J. Chem. **56**, 851 (1978).

[2]Mass spectral data given for **32***b* in the original paper (1) correspond to that of an isomer and are apparently in error.

2. D. B. MACLEAN. *In* The alkaloids. Vol. X. *Edited by* R. H. F. Manske. Academic Press, New York, London. 1968. p. 305.
3. D. B. MACLEAN. *In* The alkaloids. Vol. XIV. *Edited by* R. H. F. Manske. Academic Press, New York, London. 1973. p. 437.
4. W. A. AYER, N. MASAKI, and D. S. NKUNIKA. Can. J. Chem. **46**, 3631 (1968).
5. W. A. AYER, L. M. BROWNE, Y. NAKAHARA, M. TORI, and L. T. J. DELBAERE. Can. J. Chem. **57**, 1105 (1979).
6. J. SZYCHOWSKI and D. B. MACLEAN. Can. J. Chem. **57**, 1631 (1979).
7. W. K. MUSKER and R. L. SCHOLL. J. Organomet. Chem. **27**, 37 (1971).
8. J. J. VILL, T. P. STEADMAN, and J. J. GODFREY. J. Org. Chem. **29**, 2780 (1964).
9. L. C. BLASZCZAK and J. E. MCMURRY. J. Org. Chem. **39**, 258 (1974).
10. R. BRETTLE and S. M. SHIBIB. Tetrahedron Lett. 2915 (1980).
11. C. K. YU and D. B. MACLEAN. Can. J. Chem. **49**, 3025 (1971).
12. R. J. ABRAHAM and P. LOFTUS. Proton and carbon-13 nmr spectroscopy. Heyden and Son, Ltd., London. 1978. p. 29.

Can. J. Chem. Downloaded from www.nrcresearchpress.com by 210.87.254.40 on 09/06/12
For personal use only.

Acidité dans les mélanges H_2O–ODPN. I. Etude de l'acidité dans l'oxydipropionitrile pur

M. PERSIN ET J. Y. GAL

Laboratoire de Chimie Analytique de l'Université des Sciences et Techniques du Languedoc, Place E. Bataillon, 34060 Montpellier Cedex, France

Reçu le 19 janvier 1981

M. PERSIN et J. Y. GAL. Can. J. Chem. **59**, 2491 (1981).

L'étude des réactions acide–base dans l'oxydipropionitrile à l'aide des électrodes de verre et à hydrogène nous a permis de déterminer les pK_A de quelques couples acide–base. L'utilisation de l'hypothèse de Strehlow permet de corréler les échelles d'acidité dans l'eau, l'acétonitrile et l'oxydipropionitrile. Par suite de la dégradation du solvant en milieu trop alcalin il n'a pas été possible de déterminer le produit ionique du milieu et par conséquent les pK_B des divers couples. La faible basicité de la molécule d'ODPN permet de titrer facilement des bases très faibles dans l'eau comme l'urée, le DMSO, le HMPT. Dans le cas des acides faibles HA il a été clairement mis en évidence l'importance des phénomènes d'homoconjugaison qui résultent à la fois de la faible aptitude du milieu à solvater les anions et le proton. Quelques constantes d'homoconjugaison ont pu être déterminées à partir de l'analyse des courbes de titrage potentiométrique. Enfin l'étude sommaire du couple quinone–hydroquinone montre qu'il est également indicateur du pH dans l'oxydipropionitrile. En l'état actuel de nos travaux nous disposons d'une échelle de pK d'environ 20 unités utilisable pratiquement.

M. PERSIN and J. Y. GAL. Can. J. Chem. **59**, 2491 (1981).

The study of acid–base reactions in oxydipropionitrile (ODPN) by means of glass and hydrogen electrodes allows us to determine the pK_A's of several acid–base pairs. Use of Strehlow's hypothesis leads to a correlation of acidity scales in water, acetonitrile and oxydipropionitrile. Because of solvent degradation in highly alkaline solution it proved impossible to determine the ionic product of the medium and consequently the pK_B's of several acid–base pairs. The weak basicity of ODPN allows for the easy titration of very weak bases such as urea, DMSO, and HMPT in water. For weak acid the importance of homoconjugation is clearly shown leading to the weak ability of the medium to solvate both anions and protons. Some homoconjugation constants have been determined by the analysis of the potentiometric titration curves. Finally a study of the quinone–hydroquinone couple shows that this is also a pH indicator in ODPN. At the present time our studies provide a pK scale of practical use over 20 units.

[Journal translation]

Can. J. Chem. Downloaded from www.nrcresearchpress.com by 210.87.254.42 on 09/06/12
For personal use only.

Introduction

L'oxydipropionitrile est un solvant très polaire $\mu = 4{,}91$ D[1] et de forte constante diélectrique $\varepsilon = 66{,}6$ (1), il constitue un milieu fortement dissociant et nous avons pu montrer au cours de nos travaux antérieurs que de nombreux électrolytes y sont totalement dissociés (2). A l'heure actuelle, l'oxydipropionitrile sert principalement de phase stationnaire en chromatographie, certains auteurs l'ont également mentionné pour effectuer la séparation des paraffines et des carbures aromatiques (3–6). Depuis quelque temps nous étudions les possibilités d'emploi de ce solvant en extraction liquide–liquide du fait de l'existence d'une importante zone de démixtion avec l'eau. Des séparations peuvent être mises au point et la connaissance des propriétés solvatantes des deux milieux qui se séparent permet de définir les conditions optimales (7).

De manière à accroître les possibilités d'utilisation en extraction, il est intéressant de pouvoir disposer de quelques couples acide–base pouvant servir de tampons permettant de fixer le pH dans les deux phases.

Aucune étude relative à l'acido-basicité dans le solvant pur n'ayant été entreprise, il nous a paru nécessaire de préciser nos connaissances dans ce milieu et de définir une échelle d'acidité. Celle-ci a été établie au moyen de titrages potentiométriques à l'électrode de verre et les résultats comparés avec ceux obtenus en utilisant l'électrode à hydrogène. Notre étude montre que les phénomènes observés dans l'oxydipropionitrile sont complexes par suite de l'intervention d'équilibres d'homoconjugaison dont il faut tenir compte pour interpréter correctement les courbes de titrage, les résultats présentent alors beaucoup d'analogie avec ceux obtenus par Kolthoff dans l'acétronitrile. L'échelle d'acidité obtenue peut être corrélée à celle de l'eau par l'utilisation d'hypothèses extrathermodynamiques simples, nous nous sommes volontairement limités à celle de Strehlow pour comparer nos résultats à ceux obtenus dans l'eau et l'acétonitrile.

Partie Expérimentale

Synthèse et purification du solvant

L'établissement d'une échelle d'acidité dans l'oxydipropionitrile nécessite l'utilisation d'un solvant particulièrement propre difficile à obtenir. Le solvant est synthétisé au laboratoire suivant la méthode proposée par Selcer et de Barde (8) qui consiste à faire réagir l'acrylonitrile sur l'eau selon la réaction:

[1]J. C. Bollinger et M. Persin, travaux non publiés.

0008-4042/81/162491-12$01.00/0

©1981 National Research Council of Canada/Conseil national de recherches du Canada

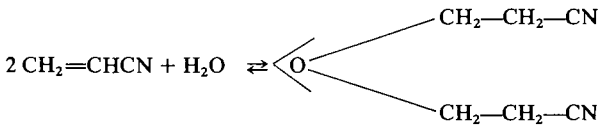

Celle-ci s'effectue en présence de soude, la réaction est arrêtée par neutralisation à l'acide sulfurique concentré. Après filtration du sulfate de sodium formé et élimination de l'excès d'acrylonitrile le résidu est distillé sous vide de gaz inerte; on obtient un produit incolore dont les spectres infrarouge et rmn correspondent à l'oxydipropionitrile.

L'usage d'un tel solvant ne s'est pas avéré correct pour établir une échelle d'acidité, le milieu contenant alors une impureté acido-basique à concentration voisine de 10^{-3} *M* (1) qui peut être mise en évidence par titrage acide–base en milieu aqueux. Cette impureté d'ailleurs également présente dans le produit commercial peut être totalement éliminée après passage du solvant sur colonne d'alumine neutre. Dans ces conditions on obtient un solvant "propre" de conductivité spécifique inférieure à 10^{-7} Ω^{-1} cm^{-1}. Le solvant est alors conservé sur tamis moléculaire 4A.

Réactifs

Les acides et bases utilisés sont des produits pour analyse Prolabo. Le perchlorate de tetrabutylammonium provient des établissements K et K. L'alumine utilisée pour purifier le solvant est de l'alumine neutre Merck activée contenant 0,1% d'eau.

Réalisation des mesures

Pour titrer les bases nous avons utilisé l'acide perchlorique commercial dilué dans le solvant, dans le cas du titrage des acides la butylamine sert de titrant. La force ionique est généralement maintenue constante à 0,1 *M* par le perchlorate de tetrabutylammonium. L'électrode de verre utilisée est une électrode Tacussel pour milieux aqueux; dans le cas de l'utilisation de l'électrode à hydrogène celle-ci est constituée d'un carré de platine platiné de 0,5 cm de côté. Les potentiels sont mesurés par rapport à l'électrode de référence $Ag\downarrow/Ag^+$ 10^{-2} *M* déjà décrite (9).

Les titrages conductimétriques ont été réalisés à l'aide d'un conductimètre CD7 Tacussel et d'une cellule de conductimétrie, la température étant régulée à 25°C ± 0,1°C (constante de la cellule: 0,7).

Le traitement mathématique des courbes de titrages obtenues a été effectué à l'aide d'un calculateur miniature Hewlett Packard HP 25.

Résultats

Recherche d'un acide fort dans l'oxydipropionitrile

L'obtention d'un acide fort dans le solvant permet de fixer l'origine de l'échelle d'acidité, la position de celle-ci étant conditionnée par la basicité du solvant.

La solvolyse d'un acide fort dans un solvant S peut se traduire par la réaction:

$$HA + S \rightarrow SH^+ + A^-$$

Dans ces conditions la réponse de l'électrode de verre ou de l'électrode à hydrogène en milieu acide fort dans l'ODPN doit être Nernstienne à courant nul.

$$E = A + 0{,}06 \log C_{SH^+}$$

Des acides minéraux usuels seul l'acide perchlorique est totalement dissocié dans l'oxydipropionitrile, ceci est conforme à sa position sur l'échelle générale d'acidité ($pK_{H_2O} = -8{,}6$) et à la relative solvatation de l'anion perchlorate dans ce milieu (7).

De manière à pouvoir mesurer l'influence de l'eau nous avons utilisé successivement de l'acide perchlorique préparé dans l'acide acétique anhydre et la solution commerciale à 70% en poids, les résultats sont identiques. Pour des raisons de commodités nous avons utilisé dans la suite de notre travail l'acide perchlorique commercial dilué dans l'oxydipropionitrile.

On peut noter que les résultats concernant l'acétonitrile sont tout à fait similaires, Desbarres y décrit également l'acide perchlorique comme totalement dissocié en solution diluée (10).

Comme nous le verrons par la suite l'oxydipropionitrile est moins basique que l'eau; cette dernière étant toujours présente dans le milieu [10^{-2} *M*], il est probable que le proton solvaté SH^+ puisse exister sous deux formes: $ODPNH^+$ et H_3O^+. Dans ces conditions la réaction de solvolyse d'un acide fort HA précédemment écrite constitue une simple commodité d'écriture. Par ailleurs le fait d'obtenir une réponse correcte de l'électrode de verre pour milieux aqueux laisserait même supposer que l'on soit uniquement en présence d'ions H_3O^+ dans nos conditions expérimentales. Les résultats présentés sont cependant intéressants puisqu'ils peuvent être obtenus dans des conditions opératoires usuelles qui correspondent à l'utilisation d'un mélange H_2O–ODPN de fraction molaire 0,998 en ODPN. Nous reviendrons sur cette question au cours du paragraphe concernant la corrélation des échelles d'acidité entre les divers solvants.

Etude des couples HA/A⁻

Si l'on admet la dissociation simple des acides HA selon l'équilibre:

$$HA \rightleftarrows H^+ + A^-$$

de constante K_{HA}. Au cours du titrage avant le point équivalent le pH doit varier selon:

$$pH = pK_{HA} + \log \frac{[A^-]}{[HA]}$$

L'analyse des courbes de titrages potentiométri-

Can. J. Chem. Downloaded from www.nrcresearchpress.com by 210.87.254.42 on 09/06/12
For personal use only.

Can. J. Chem. Downloaded from www.nrcresearchpress.com by 210.87.254.42 on 09/06/12
For personal use only.

ques peut nous renseigner sur le mode de dissociation de ces acides. Dans le tableau 1 nous avons reporté les résultats observés dans le cas du titrage de différents acides. On peut remarquer que pratiquement pour tous les acides étudiés, la pente de la courbe $E = f\{\log[A^-]/[AH]\}$ est différente de 59 mV excepté pour l'acide picrique. Ces acides ne se dissocient donc pas selon le mode simple proposé, de tels résultats sont souvent observés dans les solvants aprotiques où l'on doit tenir compte des phénomènes d'homoconjugaison par suite du caractère peu solvatant du solvant vis à vis des anions. Ainsi dans l'acétonitrile, pratiquement tous les acides sont dissociés selon l'équilibre:

$$K_{2HA} = \frac{[HA_2^-]\,H^+]}{[HA]^2}$$

$$2\,HA \rightleftarrows HA_2^- + H^+$$

Dans ces conditions si $K_{HA_2^-}$ est la constante d'homoconjugaison relative à l'équilibre

$$K_{HA_2^-} = \frac{[HA_2^-]}{[HA][A^-]}$$

$$HA + A^- \rightleftarrows HA_2^-$$

il vient:

$$K_{2HA} = \frac{[HA_2^-]\,H^+]}{[HA]^2} = K_{HA}K_{HA_2^-}$$

Kolthoff et Chantooni (11) ont alors montré que selon les valeurs du produit $K_{HA_2^-}\,C_a$ (où C_a est la concentration initiale d'acide), la courbe de titrage par une base peut présenter deux points équivalents correspondant aux deux réactions successives:

$$2\,HA + B \rightleftarrows BH^+ + HA_2^-$$

$$BH^+ + HA_2^- + B \rightleftarrows 2\,BH^+ + 2\,A^-$$

Lorsque $K_{HA_2^-}$ est voisin de zéro la courbe retrouve son allure habituelle observée dans l'eau; si $K_{HA_2^-} \cdot C_a$ n'est pas trop grand on observe une déformation de la courbe sans apparition du point équivalent pour $x = 0{,}5$.

Récemment Courtot-Coupez et collaborateurs ont montré également l'intervention des équilibres d'homoconjugaison sur les réactions acide–base dans le carbonate de propylène (12), ces résultats permettent de mieux comprendre leurs travaux antérieurs (13).

L'oxydipropionitrile étant comme nous l'avons déjà montré (7) un milieu peu solvatant vis à vis des anions, il est normal d'y retrouver ce type d'association dont nous avons pu confirmer l'existence par l'étude des courbes de titrages conductimétriques. Ainsi dans le cas des acides chlorhydrique, nitrique, salicylique, benzoïque, acétique, les courbes de titrages conductimétriques par une base faible présentent deux points singuliers pour $x = 0{,}5$ et $x = 1$ (figures 1 et 2). Selon Kolthoff et Chantooni l'allure de ces courbes s'explique par les mobilités différentes des espèces HA_2^- et A^- et par la non totale dissociation du sel HB^+A^- aux fortes concentrations (14). Le titrage conductimétrique de l'acide picrique ne met pas en évidence la formation de l'espèce homoconjuguée $H(Pi)_2^-$ confirmant ainsi l'allure normale de la courbe de titrage potentiométrique. Comme dans d'autres solvants où des phénomènes de conjugaison sont observés l'acide picrique possède un comportement singulier s'expliquant par la relative solvatation de l'anion picrate volumineux et polarisable.

L'analyse des courbes de titrage conductimétrique et la connaissance des conductivités équivalentes limites des deux ions présents permettent théoriquement de déterminer les constantes d'homoconjugaison $K_{HA_2^-}$; Kolthoff *et al.* ont ainsi pu calculer les constantes de dissociation K_{HA} de nombreux acides faibles dans l'acétonitrile (15). Plus récemment ils ont pu étudier par cette méthode la dissociation d'acides faibles dans le carbonate de propylène (16). Si cette méthode donne de bons résultats elle présente l'inconvénient de faire appel à un solvant rigoureusement exempt de traces d'acides ou de bases qui modifient les conductivités mesurées, étant donné la difficulté de purification de l'oxydipropionitrile nous avons renoncé à son utilisation pour déterminer le pK_{HA} des acides étudiés.

L'analyse des courbes de titrage potentiométrique d'un acide par une base permet de déterminer le pK_{HA} de l'acide si l'on tient compte de toutes les espèces présentes en solution, en particulier HA_2^-.

Si C_a est la concentration d'acide initiale en solution et C_s la concentration du sel on peut écrire les bilans suivants si l'on suppose les sels $BH^+\,HA_2^-$ et BH^+A^- totalement dissociés:

$$C_a = [HA] + [HA_2^-]$$

$$C_s = [HA_2^-] + [A^-]$$

Connaissant la constante d'acidité K_{HA} et la constante d'homoconjugaison $K_{HA_2^-}$ on obtient finalement la relation de Kolthoff qui relie H^+, C_s, C_a, K_{HA}, $K_{HA_2^-}$ (11)

$$C_s[H^+]^2 - K_{HA}[H^+]\{(C_a + C_s) + K_{HA_2^-}(C_s - C_a)^2\} + K_{HA}^2 C_a = 0$$

TABLEAU 1. Caractéristiques des courbes de titrage des différents acides étudiés (référence électrode Ag/Ag^+ 10^{-2} M)

Acides	$E_{1/2}$ verre	Pente $E = f\{\log [A^-]/[HA]\}$	pK_{ODPN} ±0,1	pK_{H_2O}	pK_{ACN}* (a)	pK_{ACN}* (b)	$pK_{ODPN} - pK_{H_2O}$
Salicylique	−244	82	13,7	3	12,2	16,7	10,7
Sulfurique I	+274	84	5,1	−4	4,6	7,2	9,1
Sulfurique II	−116		11,5	1,9	15,8		9,6
Monochloracétique	−290	90	14,5	2,9	13,5	18,8·	11,6
Trichloracétique	~+30	Attaque du solvant	9,1	0,7			8,4
Nitrique	+128	71	7,5	−1,8		8,9	9,3
Chlorhydrique	+120	90	7,6	−3,7	6,2	8,9	11,3
Oxalique I	−90	68	11,1	1,3		14,5·	9,8
Oxalique II	−280		14,3	4,3			10
Picrique	+70	60	8,5	0,4	8,2	11,1	8,1
Benzoïque	−404	85	16,4	4,2	16,1	20,7	12,2
Acétique			Intitrable	4,7	17,3	22,3	
Aminosalicylique	−324	85	15,0				

*pK_{ACN} (a) résultats calculés à partir des potentiels de 1/2 neutralisation d'après Desbarres (10); (b) résultats d'après Kolthoff (23, 24); ·résultats d'après Kolthoff et Chantooni (20).

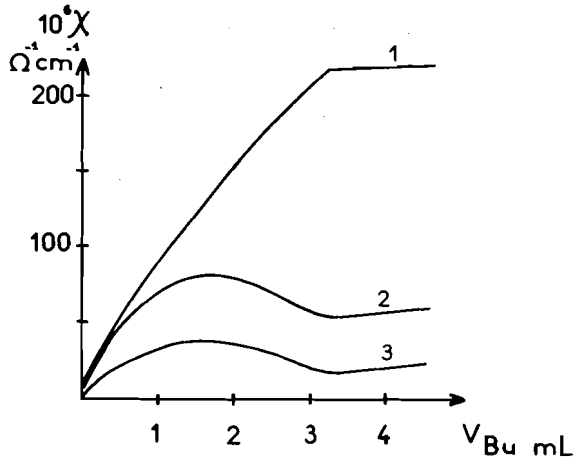

FIG. 1. Titrage conductométrique de quelques acides HA par la butylamine. (1) Acide picrique 0,05 M; (2) acide salicylique 0,05 M; (3) acid benzoïque 0,05 M.

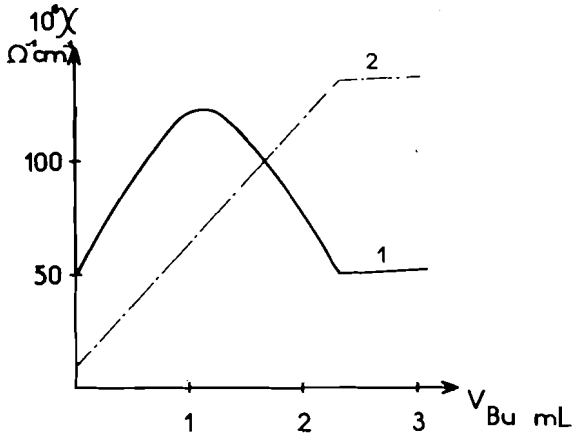

FIG. 2. Titrage conductométrique de l'acide chlorhydrique par la butylamine dans l'ODPN. (1) Dans l'ODPN [HCl] = 0,05 M; (2) courbe de titrage théorique d'un acide faible HA selon la dissociation classique.

La résolution de cette équation permet de calculer le pH en tout point de la courbe de titrage. Lorsque $C_s = C_a$, c'est-à-dire à la demi-neutralisation, l'équation précédente devient:

$$C_s[H^+]^2 - 2K_{HA}C_s[H^+] + K_{HA}^2C_a = 0$$

dont la solution est:

$$[H^+] = K_{HA}$$

Aussi quelle que soit la valeur de la constante d'homoconjugaison $K_{HA_2^-}$, le pH de demi-neutralisation est égal au pK_{HA} de dissociation classique de l'acide HA et la première partie de la courbe de titrage admet ce point comme centre de symétrie.

Dans le tableau récapitulatif 1 nous avons classé tous les acides selon leur pK déterminé par cette méthode. L'examen des résultats montre que les acides HA sont considérablement affaiblis dans l'oxydipropionitrile, seul l'acide perchlorique est un acide fort. L'ordre de force observé est conservé par rapport à l'échelle générale d'acidité rapportée à l'eau. L'écart de pK_{HA} mesuré par rapport à l'eau est de l'ordre de 8,5 unités ce qui est considérable; cet écart ne peut s'expliquer que par une très faible solvatation des anions A^-. Dans ce tableau nous avons reporté les valeurs de pK_{HA} des acides dans l'acétonitrile, on peut remarquer qu'elles sont très voisines de celles observées dans l'oxydipropionitrile.

D'après l'équation de Kolthoff on peut connaissant le pH et K_{HA} déterminé précédemment, calculer la constante $K_{HA_2^-}$ pour chacun des acides étudiés. Nous donnons dans le tableau 2 les constantes $K_{HA_2^-}$ pour quelques acides faibles.

A partir des constantes ainsi déterminées il est possible de prévoir la répartition de toutes les

Can. J. Chem. Downloaded from www.nrcresearchpress.com by 210.87.254.42 on 09/06/12
For personal use only.

TABLEAU 2. Constantes d'homoconjugaison de quelques acides HA

Acide chlorhydrique

x	E mV	[H⁺] M L⁻¹	$K_{HA_2^-}$
0,1	222	$10^{-5,91}$	$10^{3,08}$
0,2	200	$10^{-6,28}$	$10^{3,24}$
0,3	176	$10^{-6,68}$	$10^{3,25}$
0,4	152	$10^{-7,08}$	$10^{3,28}$
0,5	128	$10^{-7,51}$	
0,6	106	$10^{-7,85}$	$10^{2,98}$
0,7	82	$10^{-8,25}$	$10^{3,09}$
0,8	60	$10^{-8,61}$	$10^{3,05}$
0,9	20	$10^{-9,28}$	$10^{3,29}$

$K_{HA} = 10^{-7,6}$; $pK_{HA_2^-} = -3,2 \pm 0,2$

Acide nitrique

x	E mV	[H⁺] M L⁻¹	$K_{HA_2^-}$
0,1	188	$10^{-6,48}$	$10^{1,55}$
0,2	172	$10^{-6,75}$	$10^{2,20}$
0,3	156	$10^{-7,01}$	$10^{2,29}$
0,4	140	$10^{-7,28}$	$10^{2,90}$
0,5	128	$10^{-7,48}$	
0,6	114	$10^{-7,71}$	$10^{2,32}$
0,7	100	$10^{-7,95}$	$10^{2,29}$
0,8	80	$10^{-8,28}$	$10^{2,43}$
0,9	58	$10^{-8,65}$	$10^{2,33}$

$K_{HA} = 10^{-7,5}$; $pK_{HA_2^-} = -2,2 \pm 0,2$

Acide sulfurique (I)

x	E mV	[H⁺] M L⁻¹	$K_{HA_2^-}$
0,1	336	$10^{-4,01}$	$10^{2,20}$
0,2	320	$10^{-4,28}$	$10^{2,64}$
0,3	304	$10^{-4,55}$	$10^{2,73}$
0,4	290	$10^{-4,78}$	$10^{2,93}$
0,5	274	$10^{-5,05}$	
0,6	260	$10^{-5,28}$	$10^{2,62}$
0,7	244	$10^{-6,55}$	$10^{2,73}$
0,8	224	$10^{-5,88}$	$10^{2,82}$
0,9	200	$10^{-6,28}$	$10^{2,77}$

$K_{HA} = 10^{-5,1}$; $pK_{HA_2^-} = -2,7 \pm 0,2$

Acide benzoique

x	E mV	[H⁺] M L⁻¹	$M_{HA_2^-}$
0,1	−330	$10^{-15,11}$	$10^{1,70}$
0,2	−354	$10^{-15,51}$	$10^{1,75}$
0,3	−372	$10^{-15,81}$	$10^{1,78}$
0,4	−288	$10^{-16,08}$	$10^{1,83}$
0,5	−404	$10^{-16,35}$	
0,6	−416	$10^{-16,55}$	*
0,7	−429	$10^{-16,76}$	*
0,8	−440	$10^{-16,95}$	*
0,9			*

$K_{HA} \simeq 10^{-16,4}$; $pK_{HA_2^-} = -1,7$

Acide salicylique

x	E mV	[H⁺] M L⁻¹	$K_{HA_2^-}$
0,1	−174	$10^{-12,51}$	$10^{2,33}$
0,2	−196	$10^{-12,88}$	$10^{2,44}$
0,3	−212	$10^{-13,15}$	$10^{2,55}$
0,4	−230	$10^{-13,45}$	$10^{2,32}$
0,5	−244	$10^{-13,68}$	
0,6	−260	$10^{-13,95}$	$10^{2,63}$
0,7	−276	$10^{-14,21}$	$10^{2,55}$
0,8	−294	$10^{-14,51}$	$10^{2,52}$
0,9	−324	$10^{-15,01}$	$10^{2,60}$

$K_{HA} = 10^{-13,7}$; $pK_{HA_2^-} = -2,5 \pm 0,2$

*La constante n'a pu être déterminée par suite du caractère trop faible de cet acide.

espèces en solution compte tenu des divers équilibres:

$$K_{HA} = \frac{[H^+][A^-]}{[HA]}$$

$HA \rightleftarrows H^+ + A^-$

$$K_{HA_2^-} = \frac{[HA_2]}{[HA][A^-]}$$

$HA_2^- \rightleftarrows HA + A^-$

En considérant les sels totalement dissociés on peut écrire les bilans suivants:

$$C_a = [HA] + 2[HA_2^-] + [A^-]$$

$$[H^+] = [A^-] + [HA_2^-]$$

Il vient en remplaçant A^- et HA_2^- par leur expression en fonction de HA:

Can. J. Chem. Downloaded from www.nrcresearchpress.com by 210.87.254.42 on 09/06/12
For personal use only.

$$[H^+]^2 = K_{HA}[HA] + K_{HA_2^-}K_{HA}[HA]^2$$

$$C_a = [HA] + K_{HA}\frac{[HA]}{[H^+]} + \frac{2K_{HA}K_{HA_2^-}[HA]^2}{[H^+]}$$

Si l'acide est suffisamment faible et la concentration initiale suffisamment forte, il est logique de supposer:

$$[HA] \# C_a$$

Dans ces conditions l'expression de K_{HA} permet de déterminer aisément la concentration en protons libres, la concentration en ions A^- et en espèces conjuguées HA_2^- sont obtenues par les relations:

$$[A^-] = K_{HA}\frac{[HA]}{[H^+]}$$

$$[HA_2^-] = K_{HA_2^-}[HA][A^-]$$

Sur les figures 3 et 4 nous avons reporté les variations des concentrations des différentes espèces en fonction de la concentration analytique initiale dans le cas des acide chlorhydrique et nitrique; l'intérêt de ces graphiques est de montrer de façon claire l'influence de la concentration sur le mode de dissociation de l'acide envisagé. Dans le cas de l'acide HCl la variation du pH s'effectue en 1/2 log C_a pour des concentrations d'acide inférieures à 10^{-4} M, c'est-à-dire pour les solutions les plus diluées, l'acide se dissocie ici comme dans l'eau selon l'équilibre simple:

$$HCl \rightleftarrows H^+ + Cl^-$$

Le pH est donné par la formule:

$$pH = \tfrac{1}{2}\,pK_{HA} - \tfrac{1}{2}\log C_a$$

Au contraire pour des concentrations supérieures à 10^{-2} M la variation du pH s'effectue en log C_a, l'acide se dissocie alors principalement selon l'équilibre:

$$2\,HCl \rightleftarrows H^+ + HCl_2^-$$

Le pH est donné par la formule:

$$pH = \tfrac{1}{2}\,pK_{2HA} - \log C_a$$

La figure 4 montre qu'il y a exaltation de l'acidité lorsque ce mode de dissociation prédomine. Lorsque la concentration d'acide évolue entre 10^{-2} M et 10^{-4} M, c'est-à-dire aux concentrations analytiques courantes il y a superposition des deux équilibres. Les résultats sont tout à fait analogues dans le cas de l'acide nitrique et des autres acides étudiés.

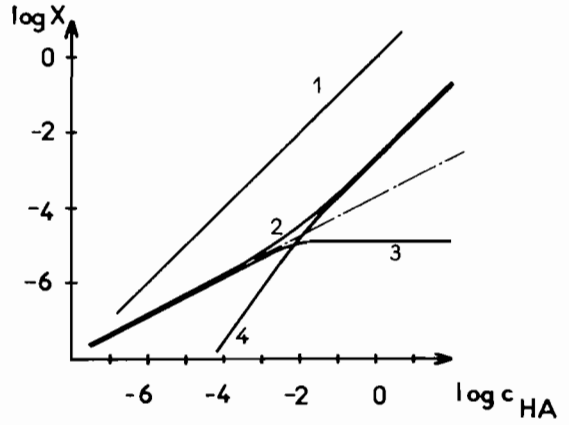

FIG. 3. Concentration des différentes espèces X en fonction du log de la concentration d'acide nitrique. (1) HNO_3; (2) H^+; (3) NO_3^-; (4) $H(NO_3)_2^-$.

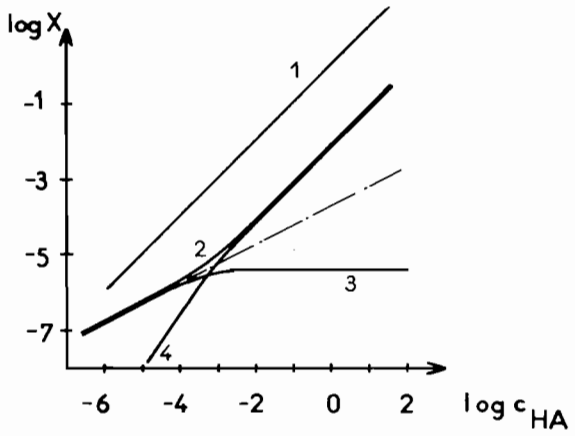

FIG. 4. Concentration des différentes espèces X en fonction du log de la concentration d'acide chlorhydrique. (1) HCl; (2) H^+; (3) Cl^-; (4) $H(Cl)_2^-$.

Sur les figures 5 et 6 relatives à l'acide chlorhydrique nous avons également représenté le pourcentage des différentes espèces en fonction du logarithme de la concentration d'acide C_0 et du pH. Cette dernière représentation est intéressante car elle matérialise l'évolution des concentrations au cours du titrage de l'acide. Le calcul a été effectué pour deux concentrations, on y voit en particulier que le pourcentage d'espèces HA_2^- formé passe par un maximum pour pH = pK_{HA} et qu'il est d'autant plus important que la concentration initiale est grande ainsi que la constante $K_{HA_2^-}$. Dans le cas de l'acide chlorhydrique à la concentration 0,004 M le pourcentage d'espèces HCl_2^- formé à la demi-équivalence n'excède pas 30% alors que la formation quantitative correspondrait à 50% de la concentration initiale d'acide.

Can. J. Chem. Downloaded from www.nrcresearchpress.com by 210.87.254.42 on 09/06/12
For personal use only.

Can. J. Chem. Downloaded from www.nrcresearchpress.com by 210.87.254.42 on 09/06/12
For personal use only.

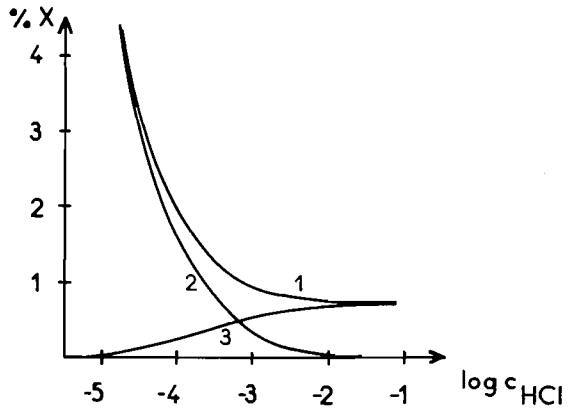

FIG. 5. Pourcentage des espèces X dans des solutions d'acide chlorhydrique de diverses concentrations. (1) H^+; (2) Cl^-; (3) $H(Cl)_2^-$.

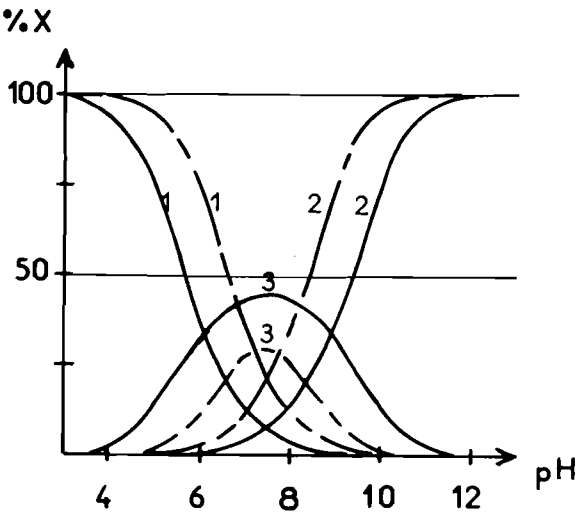

FIG. 6. Répartition des différentes espèces au cours du titrage d'une solution d'acide chlorhydrique en fonction du pH. $[HCl]_0 = 0{,}05\ M$ (—); $[HCl]_0 = 0{,}004\ M$ (---); (1) HCl; (2) Cl^-; (3) $H(Cl)_2^-$.

Etude des couples B/BH⁺

Nous avons étudié la neutralisation de nombreuses bases faibles B dans l'oxydipropionitrile, contrairement au cas des acides les courbes de titrages potentiométriques à l'électrode de verre ou à hydrogène sont facilement interprétables dans la plupart des cas.

L'analyse mathématique de la courbe de titrage avant le point équivalent montre que le potentiel adopté par l'électrode répond à l'équation:

$$E = A + 0{,}06 \log \frac{[B]}{[HB^+]}$$

L'équilibre de dissociation de l'acide HB^+ est donc de la forme:

$$K_{HB^+} = \frac{[B][H^+]}{[HB^+]}$$

$$HB^+ \rightleftarrows B + H^+$$

Dans ce cas, l'absence de phénomène d'homoconjugaison du type:

$$B + HB^+ \rightarrow B_2H^+$$

peut s'expliquer par la possibilité pour l'ion HB^+ d'être solvaté par échange de liaison hydrogène avec une molécule d'oxydipropionitrile. Dans le tableau 3 sont reportés les pK_{HB^+} pour un certain nombre de couples B/HB^+. L'examen des résultats montre que les acides HB^+ sont très affaiblis par rapport à l'eau, cependant la force des bases B ne peut être déterminée étant donné l'inconnue concernant le produit ionique de l'oxydipropionitrile probablement non accessible.

Néanmoins la connaissance du pK_{HB^+} des couples B/HB^+ permet d'apprécier l'importance du saut de pH lors du titrage d'une base B par un acide.

L'écart ΔpK_{HB^+} mesuré dans l'eau et l'oxydipropionitrile pour les couples B/HB^+ permet grossièrement de les répartir en deux groupes. Le premier groupe comprend les bases ayant une structure d'aniline pour lequel ΔpK_{HB^+} est voisin de 3,5 unités; le second groupe comprend les autres bases étudiées pour lesquelles ΔpK_{HB^+} est de l'ordre de 6,5 unités (tableau 3).

Dans l'oxydipropionitrile des bases aussi faibles que l'urée, la *méta*-nitroaniline, la *para*-nitroaniline, le DMSO, le HMPT peuvent être dosées; nous verrons que le décalage de l'échelle d'acidité vers les milieux acides permet d'expliquer ce comportement.

Remarque: l'analyse des courbes de titrage conductimétriques de bases faibles B par des acides très faibles HA dans l'oxydipropionitrile (benzoïque, salicylique) montre que ces courbes n'ont pas même allure que dans l'eau (fig. 7). La première partie est semblable et correspond à la formation de l'espèce HB^+A^-, au-delà du point équivalent on constate que la conductivité continue de croître, ceci est dû à la formation de l'espèce homoconjuguée $HB^+HA_2^-$. Lors du titrage par l'acide picrique l'allure de la courbe est identique à celle observée dans l'eau, ceci confirme le comportement différent de cet acide dans l'oxydipropionitrile.

Corrélation des échelles d'acidité; discussion des résultats

La connaissance du paramètre de solvatation du proton $\gamma_{t(H^+)E\rightarrow S}$ permet de situer l'échelle d'acidité dans l'oxydipropionitrile par rapport à celle de l'eau par exemple, il est alors nécessaire d'évaluer

Can. J. Chem. Downloaded from www.nrcresearchpress.com by 210.87.254.42 on 09/06/12
For personal use only.

TABLEAU 3. Caractéristiques des courbes de titrage des différentes bases étudiées

Bases	$E_{1/2}$ verre	Pente $E = f\{\log [B]/[HB^+]\}$	pK_{ODPN} ±0,1	pK_{ACN}*	pK_{H_2O}†	$pK_{ODPN} - pK_{H_2O}$
Butylamine	−432	60	16,8	18,3	10,6	6,2
Dibutylamine	−466	60	17,4	18,3	11,3	6,1
Tributylamine	−440	60	16,9	18,1	10,9	6,0
Ethanolamine	−384	60	16,0	17,5	9,5	6,5
Diethanolamine	−394	60	16,2		9,0	7,2
Triethanolamine	−320	60	14,9		7,8	7,1
Triethylamine	−470	60	17,4	18,4	10,7	6,7
Propylamine	−472	60	17,5	18,2	10,6	6,9
Methoxy-4-nitro-2-aniline	+332	60	4,1		0,7	3,3
p-Nitroaniline	+320	60	4,3		1,0	3,3
m-Nitroaniline	+218	60	6,0		2,5	3,5
Aniline	+40	60	8,9	10,6	4,6	4,3
N,*N*-Diethylaniline	−86	60	11,0		6,5	4,5
Pyridine	−80	60	10,9	12,3	5,2	5,7
Morpholine	−320	60	14,9	16,6	8,7	6,2
Diphenylguanidine	−400	60	16,3	17,9	10	6,3
Piperidine	−486	60	17,7	18,9	11,1	6,6
1-10 Phénanthroline	−132	60	11,8		4,9	6,9
Dipyridyle	−86	60	11,0		4,4	6,6
Oxine	−8	60	9,7		4,9	4,8
4,7-Diphenyl 1-10-phenanthroline	−152	60	12,1			
Ammoniaque	−324	60	15,0	16,5	9,2	5,8
Aminopropanol	−420	60	16,6			
HMPT		≫60	7,0			
DMSO		60	4,2	5,8		
Urée		≫60	6,6	7,7	0,3	6,3

*D'après Coetzee et Padmanabhan (21).
†D'après Charlot (22).

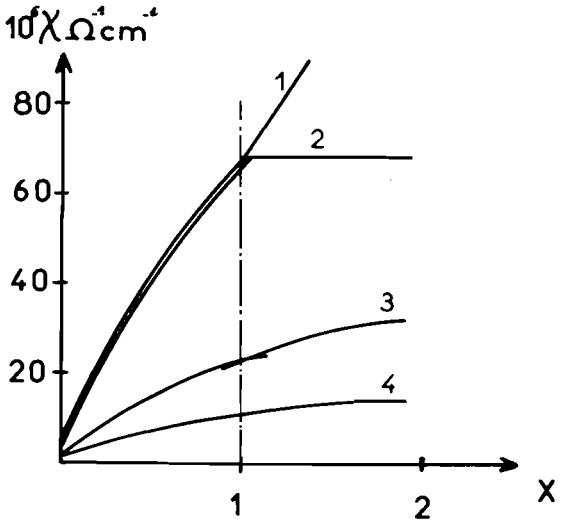

FIG. 7. Titrage conductométrique de la butylamine 0,01 *M* par différents acides. (1) Par acide perchlorique; (2) par acide picrique; (3) par acide salicylique; (4) par acide benzoïque.

le potentiel normal de l'électrode à hydrogène par rapport à une référence de potentiel commune à tous les milieux. Pour des raisons de commodité, nous utiliserons l'hypothèse de Strehlow malgré ses inconvénients déjà cités (17, 18).

Le potentiel normal du système H^+/H_2 a été déterminé au moyen de l'électrode à hydrogène en étudiant la partie située au-delà du point équivalent du titrage d'une base par un acide fort. Les électrodes de verre et à hydrogène ayant un fonctionnement correct dans l'oxydipropionitrile comme le montre la courbe $(E_{1/2})_{H_2} = f(E_{1/2})_{verre}$[2] qui est une droite de pente 1; on peut facilement connaissant le potentiel mesuré à l'électrode de verre pour une solution 1 *M* en déduire le potentiel normal apparent du couple H_2/H_S^+, les résultats sont équivalents. La mesure ayant été effectuée par rapport à l'électrode de référence Ag/Ag^+ 10^{-2} *M*, il suffit d'effectuer le décalage correspondant:

$$E^0_{H^+/H_2(Fc/Fc^+)} = E^0_{H^+/H_2(Ref)} - E^0_{Ref(Fc/Fc^+)}$$

Dans ces conditions Strehlow définit la fonction Redox $R_0{}^0(H^+)$ qui s'identifie à $\log \gamma_{t(H^+)}$ au signe près:

$$R_0{}^0(H^+) = \frac{{}^E E^0_{H^+/H_2} - {}^S E^0_{H^+/H_2}}{0{,}06}$$

$$= \frac{-0{,}390 + 0{,}143}{0{,}06} = -3{,}95$$

[2]$E_{1/2}$ = potentiel de demi-neutralisation d'une base ou d'un acide.

Can. J. Chem. Downloaded from www.nrcresearchpress.com by 210.87.254.42 on 09/06/12
For personal use only.

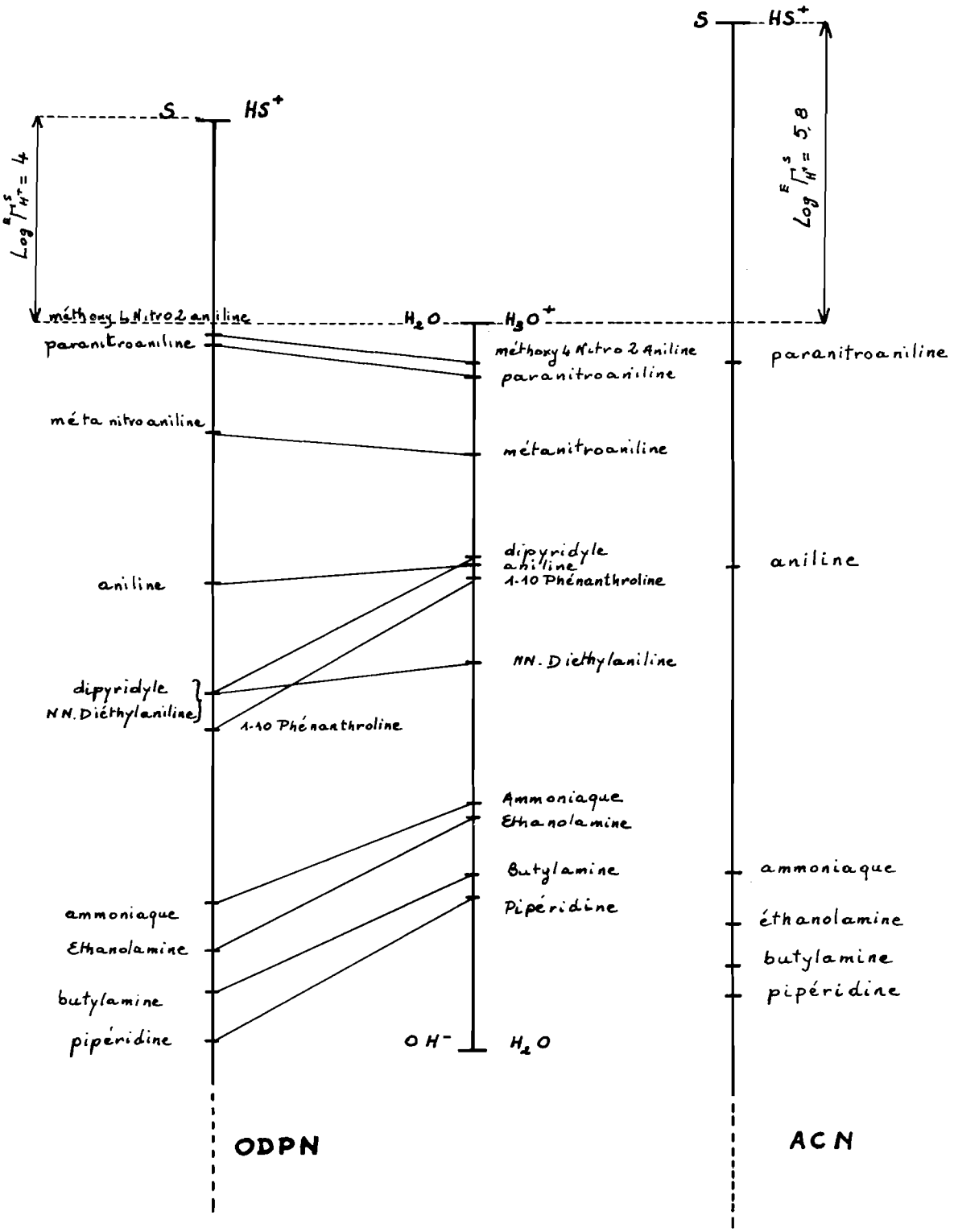

FIG. 8. Echelles d'acidité comparées dans l'ODPN, l'eau et l'acétonitrile (couple B/HB$^+$ référence ferrocène–ferricinium).

Can. J. Chem. Downloaded from www.nrcresearchpress.com by 210.87.254.42 on 09/06/12
For personal use only.

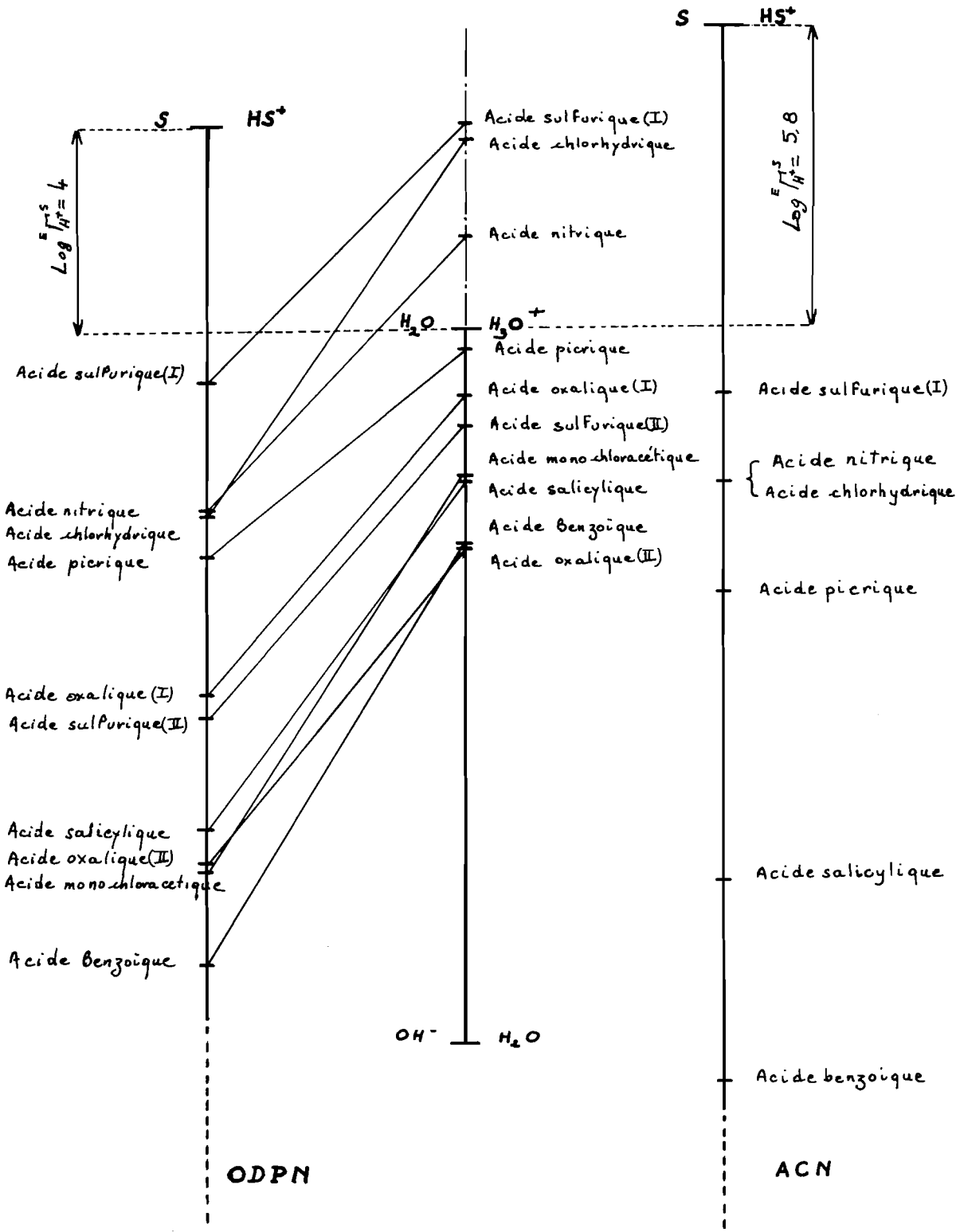

FIG. 9. Echelle d'acidité comparées dans l'ODPN, l'eau et l'acétonitrile (couple A^-/HA référence ferrocène–ferricinium).

Can. J. Chem. Downloaded from www.nrcresearchpress.com by 210.87.254.42 on 09/06/12
For personal use only.

Le proton est donc beaucoup moins solvaté dans l'oxydipropionitrile (en réalité le mélange ODPN + H_2O = 0,01 *M*) que dans l'eau et l'échelle est décalée de 4 unités vers les milieux acides. La comparaison avec l'acétonitrile où log $\gamma_{t(H^+)}$ = +5,95 (19) montre que le proton est légèrement plus solvaté dans l'oxydipropionitrile (figures 8 et 9). L'obtention de la véritable valeur de log $\gamma_{t(H^+)}$ en milieu rigoureusement anhydre se heurterait aux mêmes difficultés que dans d'autres solvants peu basiques.

Force des acides HB^+

Connaissant ${}^{E}pK_{HB^+}$, ${}^{S}pK_{HB^+}$ et log $\gamma_{t(H^+)}$ on calcule aisément le terme log $\gamma_{t(B)}/\gamma_{t(HB^+)}$ qui est voisin de −0,2 dans le cas des différentes anilines étudiées. Dans ces conditions l'augmentation du pK_{HB^+} de cette catégorie d'acide n'est due qu'à la plus faible solvatation du proton et les pK_{HB^+} de ces couples dans l'eau, l'acétonitrile et l'ODPN se situent approximativement sur des horizontales (fig. 8). Ceci permet de vérifier approximativement l'hypothèse de Hammett puisque log $\gamma_{t(B)}$ # log $\gamma_{t(HB^+)}$.

Dans le cas des autres acides HB^+ l'affaiblissement de la force est dû à la faible solvatation du proton et à l'augmentation du terme log $\gamma_{t(B)}/\gamma_{t(HB^+)}$ qui varie d'ailleurs selon l'acide.

Force des acides HA

L'affaiblissement des acides HA est dû à la faible solvatation du proton et à la très faible solvatation de l'anion A^- qui se traduit par l'importance du terme log $\gamma_{t(A^-)}/\gamma_{t(HA)}$ voisin de 6 unités. Ces résultats sont tout à fait en accord avec l'existence des phénomènes d'homoconjugaison précédemment démontrés pour la plupart des acides HA. On peut observer que l'ODPN permet de différencier les acides forts dans l'eau, il n'y a pas d'effet nivelant du milieu.

Mesure du pH par utilisation du couple quinone–hydroquinone

Dans l'eau le système quinone–hydroquinone est un indicateur de pH utilisable pratiquement entre 0 et 8 de façon commode. L'acide H_2Q étant un acide HA, on peut prévoir d'après les résultats précédents un affaiblissement de cet acide permettant d'envisager une utilisation dans un domaine de pH plus important dans l'ODPN.

Nous avons représenté sur la figure 10 la courbe de titrage d'un mélange de pyridine et de triéthanolamine par l'acide perchlorique. Le traitement mathématique de chaque partie de la courbe de titrage montre que le potentiel de l'électrode à quinhydrone varie linéairement avec une pente de 60 mV en fonction de log [B]/[HB^+], l'hydroquinone se trouve donc sous forme H_2Q dans ce domaine de pH.

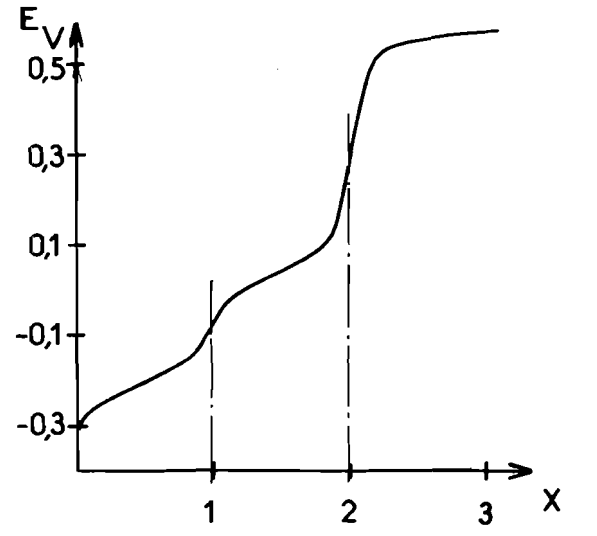

FIG. 10. Titrage potentiométrique d'un mélange pyridine–triéthanolamine par l'acide perchlorique (électrode indicatrice à quinhydrone).

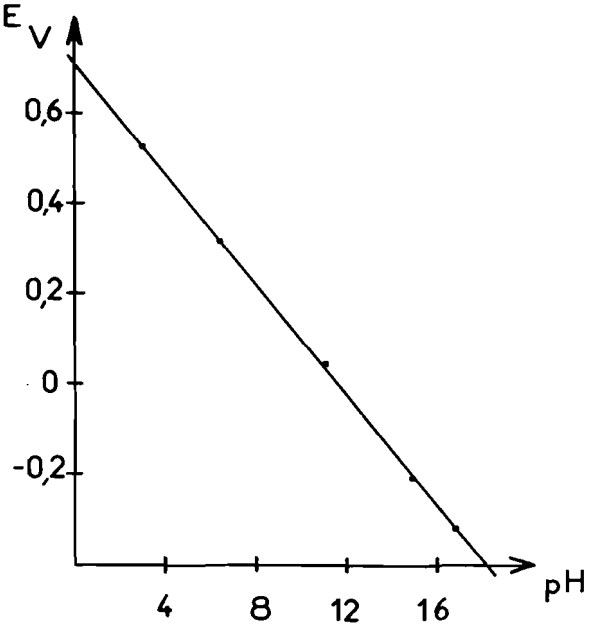

FIG. 11. Diagramme potentiel pH du système quinone hydroquinone.

L'équation de réponse de l'électrode est donnée par:

$$E = E_0 - 0{,}06\ pK_{HB^+} - 0{,}06 \log \frac{[B]}{[HB^+]}$$

Sur la figure 11 sont reportées les variations du potentiel de l'électrode H_2Q/Q en fonction du pH

de demi-neutralisation de quelques amines, on observe une variation linéaire permettant de déterminer le potentiel normal apparent du couple H_2Q/Q.

E^0 = 0,720 V par rapport à la référence Ag/Ag^+ $10^{-2}M$

Le résultat est identique à celui obtenu en étudiant la réponse de l'électrode en milieu acide fort.

Conclusion

Cette étude nous a permis de montrer que les électrodes de verre et à hydrogène sont indicatrices de l'activité du proton dans l'oxydipropionitrile. Malgré la forte constante diélectrique de ce milieu les acides HA sont très peu dissociés par suite de la faible solvatation des anions, l'allure des courbes de titrage montre qu'il faut tenir compte des phénomènes d'homoconjugaison. Par suite du décalage de l'échelle d'acidité dans les milieux acides, on peut titrer des bases très faibles dans l'eau avec une meilleure précision, de même il est possible de différencier facilement les acides forts dans l'eau. L'ensemble de ces propriétés laisse apparaître un comportement de l'oxydipropionitrile voisin de l'acétonitrile vis à vis des acides et des bases. Si l'origine de l'échelle d'acidité a pu être déterminée il n'est pas de même du pK_i de l'oxydipropionitrile, le solvant apparaît comme non limitant vers les milieux basiques, néanmoins il paraît exclu d'y trouver une base forte ne le décomposant pas.

Enfin l'utilisation du couple oxydoréducteur H_2Q/Q faisant intervenir le pH permet de couvrir en partie l'échelle d'acidité déterminée; l'étude plus approfondie d'autres systèmes quinoniques indicateurs du pH semblerait pouvoir être envisagée.

Actuellement notre travail porte plus spécialement sur la définition d'une échelle d'acidité dans les mélanges eau–oxydipropionitrile se séparant lors de la démixtion il fera l'objet d'un prochain mémoire rassemblant les résultats concernant l'acidité dans les mélanges H_2O–ODPN.

1. M. Persin. Thèse d'Etat, Montpellier. 1979.
2. J. Y. Gal et M. Persin. C. R. Acad. Sci. Ser. C, **280**, 1259 (1975).
3. J. Durandet.Rev. Inst. Fr. Pet. Ann. Combust. Liq. **12**, 1161 (1957).
4. D. A. Skinner. Ind. Eng. Chem. **47**, 222 (1975).
5. K. W. Saunders. Ind. Eng. Chem. **43**, 121 (1951).
6. D. Ripa, A. de Angelis et V. Berti. Riv. Combust. **10**, 809 (1956).
7. D. de Barros, J. Y. Gal, M. Persin et F. Persin. J. Electroanal. Chem. **99**, 347 (1979).
8. W. H. Selcer et D. de Barde. U.S. Patent No. 2, 816, 130 (1957).
9. J. Y. Gal et M. Persin. J. Electroanal. Chem. **77**, 361 (1977).
10. J. Desbarres. Bull. Soc. Chim. Fr. 2103 (1962).
11. I. M. Kolthoff et M. K. Chantooni. J. Am. Chem. Soc. **87**, 4428 (1965).
12. J. Talarmin, M. L'Her et J. Courtot-coupez. J. Chem. Res. (M), 327 (1977).
13. M. L'Her et J. Courtot-Coupez. J. Electroanal. Chem. **48**, 265 (1973).
14. I. M. Kolthoff et M. K. Chantooni. J. Am. Chem. Soc. **87**, 1004 (1965).
15. I. M. Kolthoff, M. K. Chantooni et S. Bhowmik. J. Am. Chem. Soc. **88**, 5430 (1966).
16. K. Isutsu, I. M. Kolthoff, T. Fuginaga, M. Hattori et M. K. Chantooni. Anal. Chem. **49**, 503 (1977).
17. J. Lelievre, C. Lefeuvre et R. Gaboriaud. C. R. Acad. Sci. Ser. C, **257**, 1455 (1972).
18. R. Alexander, A. J. Parker, J. H. Sharp et W. E. Waghorne. J. Am. Chem. Soc. **94**, 1148 (1972).
19. D. Bauer et A. Foucault. J. Electroanal. Chem. **67**, 19 (1976).
20. I. M. Kolthoff et M. K. Chantooni. J. Phys. Chem. **79**, 1177 (1975).
21. J. F. Coetzee et G. R. Padmanabhan. J. Am. Chem. Soc. **87**, 5005 (1965).
22. G. Charlot. Chimie analytique générale. Tome I. Masson, Paris. 1967.
23. I. M. Kolthoff, S. Bruckenstein et M. K. Chantooni. J. Am. Chem. Soc. **83**, 3927 (1961).
24. I. M. Kolthoff et M. K. Chantooni. J. Phys. Chem. **70**, 856 (1966).

Can. J. Chem. Downloaded from www.nrcresearchpress.com by 210.87.254.42 on 09/06/12
For personal use only.

Thermal fragmentation of 3-alkyl-2-phenyloxetanes, 3,3-dimethyl-2-aryloxetanes, and related compounds. A case study of 2-aryl-substituted oxetanes

TOSHIRO IMAI AND SHINYA NISHIDA[1]

Department of Chemistry, Faculty of Science, Hokkaido University, Sapporo, Hokkaido 060, Japan

Received August 19, 1980[2]

TOSHIRO IMAI and SHINYA NISHIDA. Can. J. Chem. **59**, 2503 (1981).

Thermolyses of epimeric 3-alkyl-2-phenyloxetanes (**1***c*, **1***t*, **2***c*, **2***t*, **3***c*, and **3***t*), 3,3-dimethyl-2-aryloxetanes (**4**, **5**, **6**, **7**, and **8**), 3,3,4,4-tetramethyl-2,2-diphenyloxetane (**9**), and 3,3-dimethyl-2,2-diphenyloxetane (**10**) were studied in degassed *N,N,N',N'*-tetramethylethylenediamine at 270–350°C. Although the fragmentation of **9** and **10** can be understandable on the basis of a diradical mechanism, there were several observations, in the reaction of certain other oxetanes, which could hardly be explained simply in terms of such a mechanism. Namely, (*1*) less strained **1***t* reacted faster than more strained **1***c*; (*2*) a major mode of the fragmentation for **1***c*, **2***c*, and **3***c* was "B" (forming an alkene and benzaldehyde), whereas that for **1***t*, **2***t*, and **3***t* was "A" (forming an alkenylbenzene and formaldehyde); (*3*) the apparent energy of activation for the "B" process seemed to be larger than that for the "A"; (*4*) a dramatic change of the major fragmentation mode from "B" to "A" was brought about by a substituent on the phenyl group, as was observed in **4**–**8**. These results may be explained reasonably by assuming that the fragmentation proceeds, at least, in dual reaction courses. In competition with an anticipated diradical pathway, there will be another process, which is energetically little more favorable than the diradical fragmentation, rather specific to the "A" mode of fragmentation, and important particularly in the reaction of the *trans* isomers. Probable candidates for the second process are discussed.

TOSHIRO IMAI et SHINYA NISHIDA. Can. J. Chem. **59**, 2503 (1981).

Dans la *N,N,N',N'*-tétraméthyléthylènediamine dégazée à 270–350°C on a étudié la thermolyse des alkyl-3 phényl-2 oxetannes (**1***c*, **1***t*, **2***c*, **2***t*, **3***c* et **3***t*), des diméthyl-3,3 aryl-2 oxetannes (**4**, **5**, **6**, **7** et **8**) épimères, du tétraméthyl-3,3,4,4 diphényl-2,2 oxetanne (**9**) et de la diméthyl-3,3 diphényl-2,2 oxetanne (**10**). On peut comprendre la fragmentation des composés **9** et **10** en fonction d'un mécanisme biradicalaire, mais certains faits observés dans la réaction de certains autres oxétannes, ne peuvent être interprétés selon ce mécanisme. En particulier (*1*) le composé le moins encombré **1***t* réagit plus rapidement que le composé **1***c* plus encombré; (*2*) la voie principale de fragmentation de **1***c*, **2***c* et **3***c* est la voie "B" (conduisant à un alcène et à la benzaldéhyde) tandis que les composés **1***t*, **2***t* et **3***t* se fragmentent suivant la voie "A" (conduisant à un alcénylbenzène et à la formaldéhyde); (*3*) l'énergie apparente d'activation de la voie "B" semble être plus élevée que celle de la voie "A"; (*4*) dans le cas des composés **4**–**8** la présence d'un substituant sur le groupe phényle provoque un changement radical dans la fragmentation qui passe de la voie "B" à la voie "A". On peut raisonablement expliquer ces résultats en admettant que la fragmentation se fait au moins des deux façons au cours de la réaction. Il existe un autre processus énergiquement plus favorisé qui entre en compétition avec la fragmentation biradicalaire et qui est plus spécifique à la voie de fragmentation "A". Ce processus est particulièrement plus important dans la réaction des isomères *trans*. On discute des substances qui éventuellement se fragmenteront selon ce second processus.

[Traduit par le journal]

Introduction

The thermal fragmentation of oxetanes has most frequently been discussed in terms of a stepwise diradical mechanism (1) although several workers have stated that a concerted pathway cannot be rigorously ruled out (1*d*,*f*,*g*). We noted some time ago that the thermal behavior of isomeric 3-propyl-2-phenyloxetanes in decane seems to indicate an intervention of a nonradical pathway, particularly in the reaction of the *trans* isomer (2). Shortly after our communication, however, Jones and Kleinman (3) demonstrated that both rates and modes of the oxetane fragmentation are influenced by impurities, probably acidic contaminants, in the reaction system. Several other workers also noted high sensitivity of the cleavage modes to wall effects in the vapor phase thermolysis (1*h*, *j*, *k*). These observations suggest that the oxetanes are quite sensitive to the acidic sites in the reaction system. It turns out that our previous results may possibly be an outcome of the thermal process intermingled with acid-catalyzed decomposition. Accordingly, we re-examined the thermolyses of several representative 2-aryloxetanes (**1**–**10**) under conditions which may guarantee us the reaction free from the stain of the acid-catalyzed process. The solvent we chose is *N,N,N',N'*-tetramethylethylenediamine (TMEDA), which has been used to investigate the thermal behavior of extremely acid-sensitive compounds, such as bicyclobutane (4). In TMEDA, it was demonstrated that the acid-catalyzed process was absent, but the products were not stable enough to allow us to carry out the kinetic studies. The thermolysis was, therefore, examined only qualitatively.

Results and Discussion

Preparation of Oxetanes

cis and *trans*-3-Methyl-2-phenyloxetanes (**1***c* and **1***t*) and *cis*-3-*tert*-butyl-2-phenyloxetane (**3***c*) were synthesized from corresponding *erythro*- and

[1]Author to whom all correspondence should be addressed.
[2]Revision received April 3, 1981.

0008-4042/81/162503-07$01.00/0
©1981 National Research Council of Canada/Conseil national de recherches du Canada

Can. J. Chem. Downloaded from www.nrcresearchpress.com by 210.87.254.40 on 09/06/12
For personal use only.

Can. J. Chem. Downloaded from www.nrcresearchpress.com by 210.87.254.40 on 09/06/12
For personal use only.

threo-2-alkyl-1-phenyl-1,3-propanediols according to the procedures described by Balsamo *et al.* (5). The other oxetanes, including *cis*- and *trans*-3-isopropyl-2-phenyloxetanes (**2***c* and **2***t*), *trans*-3-*tert*-butyl-2-phenyloxetane (**3***t*), 3,3-dimethyl-2-*p*-methoxyphenyloxetane (**4**), 3,3-dimethyl-2-*p*-methylphenyloxetane (**5**), 3,3-dimethyl-2-phenyloxetane (**6**), 3,3-dimethyl-2-*p*-chlorophenyloxetane (**7**), 3,3-dimethyl-2-*m*-chlorophenyloxetane (**8**), 3,3,4,4-tetramethyl-2,2-diphenyloxetane (**9**), and 3,3-dimethyl-2,2-diphenyloxetane (**10**), were prepared by the Paterno–Büchi reaction (6). Compounds **2***t* and **2***c* were separated and purified by vpc. Compound **4** was readily decomposed under the vpc conditions, but its purification was accomplished successfully by medium-pressure liquid chromatography followed by repeated vacuum distillations. The stereochemical assignment of **1***c*, **1***t*, and **3***c* based on the ^{1}H nmr data was in accordance with that deduced from the consequence of the ring closure process (5). The configurations of **2***c*, **2***t*, and **3***t* were assigned from the characteristics observed in the ^{1}H nmr spectra: $J_{2,3}(cis) > J_{2,3}(trans)$, $\delta_{C2\text{-}H}(cis) > \delta_{C2\text{-}H}(trans)$, and $\delta_{C3\text{-}H}(cis) > \delta_{C3\text{-}H}(trans)$.

Thermolysis of 9 and 10; Examination of Reaction Conditions

As reported by Jones and Kleinman (3), the fragmentation of **9** was indeed sensitive to the reaction conditions. Base treatments of solvent and/or the reaction vessel resulted in an increase in the amount of benzophenone and 2,3-dimethyl-2-butene ("B" mode product)[3] at the expense of the amount of 1,1-diphenyl-2-methylpropene and acetone ("A" mode products).[3] For example, at 310°C, the A/B ratio was 4:96 in simply dried and distilled decane, but it was 2:98 in repeatedly base-washed, dried, and distilled decane. Similarly, varing degrees (1–4%) of the "A" mode fragmentation were observed in diphenylmethane, diphenyl ether, and *N*,*N*-dimethylformamide. Finally, we found that the "A" products (A/B = 0.4:99.6) were produced in least amount in organic bases, such as TMEDA and *N*,*N*-dimethylaniline.

In order to see whether the extreme A/B ratio observed in the amines was meaningful or not, we evaluated the relative importance of the two modes in the diradical fission of **9**. Among four possible diradicals expected from **9** in the first step of the homolytic ring cleavage, **11** and **12** may be worthy

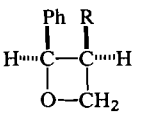

1*c* R = Me
2*c* R = *iso*-Pr
3*c* R = *tert*-Bu

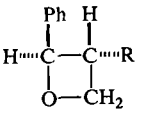

1*t* R = Me
2*t* R = *iso*-Pr
3*t* R = *tert*-Bu

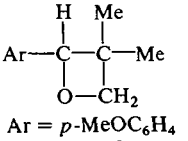

4 Ar = *p*-MeOC$_6$H$_4$
5 Ar = *p*-MeC$_6$H$_4$
6 Ar = Ph
7 Ar = *p*-ClC$_6$H$_4$
8 Ar = *m*-ClC$_6$H$_4$

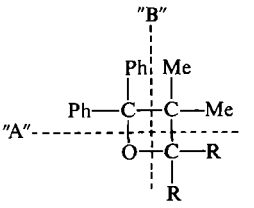

9 R = Me
10 R = H

$Ph_2C{=}CMe_2 + R_2C{=}O$ ("A" mode products)

$R_2C{=}CMe_2 + Ph_2C{=}O$ ("B" mode products)

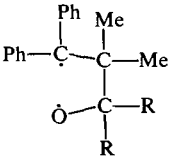

11

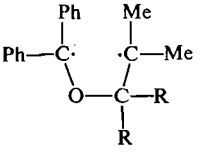

12

of consideration, since only these two held a benzhydryl radical portion. We, therefore, assume that the relative rates of producing **11** and **12** will be reflected in the A/B ratio. As mentioned in the following section, the geometrical isomerization of the starting oxetane is slower than its fragmentation. Therefore, the first bond fission will practically be a product controlling step, as has been concluded in the thermolysis of 2,3-dimethyloxetanes (**1***c*).

Now, the evaluation of the heat of formation of **11** and **12** meets with difficulties, because two key values, namely $\dot{C}\text{-}(C_B)_2(O)$ and $\dot{C}\text{-}(C)(C_B)_2$, are not available in the literature (7). We, therefore, used kinetic data in the following estimation. At first, we assume that the cleavage of the 1–2 (C—O) bond and the 2–3 (C—C) bond will occur with nearly equal ease provided that the substituent effects are common to both cleavages. This assumption is based on the fact that the precise thermochemical calculations have shown that all four bonds in parent oxetane are approximately equally easily broken (**1***f*, *g*). Experimental verification of this assumption is found in the thermolysis of 2-ethyloxetane (**1***h*), which produces the "A" and "B" products in nearly the same amounts (A/B = 53:47). A similar result has been obtained in the photolysis of 2,2-dimethyloxetane (A/B = 54:46) (**1***l*). The second assumption we made is that the substituent effects exerted by the groups at C3 and

[3]For convenience, the terms "A" and "B" are used in the present paper. The "A" mode refers to a cleavage of 1–2 and 3–4 bonds to produce a styrene derivative, which is a preferred mode observed in the acid-catalyzed decomposition.

Can. J. Chem. Downloaded from www.nrcresearchpress.com by 210.87.254.40 on 09/06/12
For personal use only.

C4 in the remote 1–2 bond cleavage will be small enough to neglect, compared to those in the 2–3 cleavage. If these assumptions are accepted, the difference in the activation barriers leading to **11** and **12** may be estimated simply from two factors operating in the 2–3 bond fission. Namely, (*a*) the electronic effect of the substituents at C3, and (*b*) the steric effect caused by the interactions between the groups at C2 and C3. For (*a*), it has been reported that 3,3-dialkyloxetanes have E_a lower than the parent compound by ca. 3 kcal/mol (1*g*). It suggests that the two methyl groups at C3 in **9** will lower the energy barrier of the 2–3 fission by ca. 3 kcal/mol relative to that of the 1–2 cleavage. As to (*b*), the steric repulsion between the methyls at C3 and phenyls at C2 may be estimated from the "*cis* correction terms" (7*a*), which suggests that the strain release of ca. 3 kcal/mol will be anticipated in going from **9** to **12**. As a total, the process producing **12** will be energetically more favorable than that yielding **11** by ca. 6 kcal/mol. Although the energy difference thus estimated will be valid only in round numbers, it may safely be concluded that the "B" fragmentation will be favorable over the "A" process by several kcal/mol. It turns out that the A/B ratio at 310°C will be ca. 0.6:99.4.

Experimentally, the A/B ratio observed in the thermolysis of **9** was 0.4:99.6. Compound **10** also gave a close A/B ratio, 0.3:99.7, although **10** lacked the two methyl groups at C4. This result, therefore, supports the previous assumption that the 3–4 and 1–4 cleavages are of negligible importance as the first step of the homolytic decomposition of **9**. Since the observed ratio is close to that estimated, it may safely be said that the reaction in the amine is totally the homolytic process free from the stain of the acid-catalyzed fragmentation. In addition, the exclusion of oxygen was necessary to obtain reproducible results. Thus, the thermolyses described hereafter were carried out in degassed TMEDA.

Regioselectively in the Thermolysis of 3-Alkyl-2-phenyloxetanes

In degassed TMEDA, **1***c*, **1***t*, **2***c*, **2***t*, **3***c*, and **3***t* were pyrolyzed. Unfortunately, benzaldehyde (one of the "B" mode products) was unstable under the reaction conditions. The resultant alkenyl benzene (the "A" mode product) isomerized slowly to the geometrical isomer in hot TMEDA, as well. Accordingly, kinetic studies could not adequately be carried out. We therefore examined the reaction qualitatively and paid special attention to the A/B ratio. The reaction was interrupted at relatively early stages and the figures were calibrated for the decreased amount of benzaldehyde under the given reaction conditions.

From the results summarized in Table 1, we can note several characteristic points of the present thermolyses. (*1*) The extent of the decomposition of **1***t* was apparently greater than that of **1***c* after the same reaction period at 270°C or 310°C. This was further confirmed in the competitive thermolysis. Thus, after heating a 1:1 mixture of **1***t* and **1***c* at 310°C for 3.5 h, the consumption of **1***t* was 37% whereas that of **1***c* was 28%. In contrast, **2***c* and **3***c* were more reactive than **2***t* and **3***t*, respectively. (*2*) The major mode of the fragmentation was different in the epimeric pair of these oxetanes. In the reaction of the *cis* isomers, the "B" mode was major (79–97%), whereas it was minor (ca. 30%) in the thermolysis of *trans* isomers. (*3*) The proportion of the "B" process in a given oxetane increased at the higher temperature, suggesting that the "B" fragmentation will have a greater apparent energy of activation than the "A" process has.

Epimerization of Oxetanes during the Thermolysis

3-Alkyl-2-phenyloxetanes isomerized in hot TMEDA, but the extent of the epimerization remained small, as has been reported for the thermolyses of 2,3-dimethyloxetanes and 1,2-dimethylcyclobutanes (1*c*, 8*a*). After 3 h at 310°C, the amount of the epimer present in the recovered oxetane was 2.2% for **1***c* (21% conversion), 1.4% for **1***t* (29%), 2.7% for **2***c* (25%), 0.7% for **2***t* (14%), 15% for **3***c* (62%), and none for **3***t* (14%). Except for the *tert*-butyl derivatives, the extent of the isomerization after 50% conversion may be calculated as ca. 5% for the *cis* isomers and ca. 2.5% for the *trans* isomers, if both the fragmentation and epimerization are assumed to be the unimolecular process. The decomposition is clearly faster than the *cis*–*trans* isomerization of the reactant. Even in the case of **3***c*, the epimerization will occur to the extent of only 12.5% after 50% conversion. Therefore, the epimerization of the starting oxetanes is neglected in the following discussion.

Mechanistic Consideration

In the homolytic decomposition of 3-alkyl-2-phenyloxetanes, four diradicals, **13** and **14** from C—C fission and **15** and **16** from C—O fission, are possibly produced. Among them, **13** and **15** will play the major role in determining the preferential mode of the fragmentation, because they place an electron at the benzylic carbon atom whereas the other two do not. Now, certain results may be explained simply by the diradical mechanism. Namely; the most highly strained **3***c* exhibits the highest reactivity, **3***c* gives overwhelmingly the

TABLE. 1. Regioselectivity in the thermal fragmentation of oxetanes in degassed TMEDA*

	270°C, 16 h		310°C, 3 h		350°C, 0.5 h	
	Conversion		Conversion		Conversion	
Oxetane	(%)	A : B†	(%)	A : B†	(%)	A : B†
1*c*	7.5	36 : 64	21	21 : 79	44	12 : 88
2*c*			25	21 : 79		
3*c*			62	3 : 97		
1*t*	25	91 : 9	29	72 : 28	43	55 : 45
2*t*			14	71 : 29		
3*t*			14	70 : 30		
4	50	91 : 9‡	54	60 : 40‡		
5	16	37 : 63	44	14 : 86		
6	13	7 : 93	41	3 : 97	85	2 : 98
7	13	3 : 97‡	46	1 : 99‡		
8	15	< 1 : > 99‡	46	< 1 : > 99‡		
9			72	0.4 : 99.6		
10			> 99	0.3 : 99.7		

*All figures are a mean value of 2–4 runs.
†After correction for the consumption of benzaldehyde under the reaction conditions, except for **4**, **7**, **8**, **9**, and **10**.
‡Based on the amounts of a styrene derivative and isobutene.

"B" products (97%),[4] **2***c* and **3***c* react faster than **2***t* and **3***t*, respectively, and the *cis* isomer produces a larger amount of the "B" fragments than the corresponding *trans* isomer does. Partial isomerization of the reactant will also be compatible with such a mechanism, although a possibility that the epimerization takes place not in the ring cleavage–reclosure process but via a benzylic carbanion produced by the deprotonation with hot TMEDA may not be ruled out.

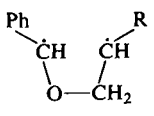

13

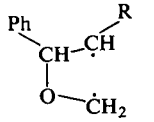

14

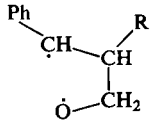

15

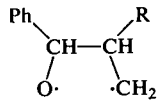

16

On the other hand, the features (*1*)–(*3*) summarized in the previous section may not adequately be explained by the diradical mechanism alone. In the thermolytic studies of *cis*- and *trans*-2,3-dimethyloxetanes, Holbrook and Scott (1*c*) have shown that *the* cis *isomer exhibits a higher reactivity than the* trans *isomer* and *that propene formation ("B" process) is favoured over 2-butene production ("A" process) in both isomers*; the [propene]/[butene] ratio is 1.7 for *cis* and 1.3 for *trans*. Similar results ([propene]/[butene] = 2.1 for *cis* and 1.2 for *trans*) have also reported by Carless (1*e*). These results are qualitatively the same as those observed in the thermolysis of 1,2-dimethylcyclobutane (8*a*), although the more pronounced preference for propene formation has been noted. A higher reactivity and a larger [propene]/[butene] ratio for the *cis* isomer is attributed to the *cis* effect, which has been considered as an important factor in the cyclobutane fragmentation (8). The fact that the propene formation is the major course even in the reaction of the *trans* isomer sounds reasonable, because a large portion of propene may be produced from a more stable secondary–secondary diradical. In the oxetane fragmentation, as discussed in the previous section, we need practically no discrimination for the intrinsic ease of C—C and C—O fissions. Therefore, the secondary–secondary carbon–carbon diradical will be produced more favorably, at least to a small extent, than other diradicals including a secondary carbon–oxygen diradical. The experimental results have been in accordance with these arguments (1*c*, *e*).

After this discussion, it may be found that the feature (*2*) in the previous section seems to be unexpected. Diradical **13** will be slightly more stable than, or as stable as, **15** and hence the "B" process should occur to an extent at least similar to that of the "A" process, if the reaction proceeds totally via the diradical intermediates. The temperature dependency of the A/B ratio also seems to contradict the presumed relative stability of **13** and **15**. Finally, the most peculiar result was (*3*); the less strained **1***t* reacted faster than the more

[4]Since a considerable extent of epimerization was observed in **3***c*, the "B" process in genuine **3***c* should be larger than 97%.

Can. J. Chem. Downloaded from www.nrcresearchpress.com by 210.87.254.40 on 09/06/12
For personal use only.

Can. J. Chem. Downloaded from www.nrcresearchpress.com by 210.87.254.40 on 09/06/12
For personal use only.

strained **1***c*. All these contradictions seem to suggest that there could be a second reaction pathway, which is in narrow competition with the diradical process. The second pathway should be energetically more favorable than the diradical fission, rather specific to the "A" cleavage, and important especially in the reaction of the *trans* isomer. A possible candidate for such a process will be either a stepwise process via a zwitterionic intermediate or a concerted cycloreversion (1*d*, *f*, *g*, 9).

Interposition of the stepwise ionic process may satisfy the above requirements in the following way. The ionic cleavage wil be energetically more favorable than the diradical fission in TMEDA and specific to the "A" fragmentation, since a benzylic cation and an oxy-anion should be preferentially produced. A reason for the unimportance of the ionic process in the reaction of *cis* isomer will be the steric effect. As suggested by Mulzer *et al.* (10) in the thermolytic studies of 2-oxetanones, the phenyl group may not rotate in the plane of the developing sp^2 carbon atom in the transition state of the *cis* isomer.

Alternatively, intervention of the concerted fragmentation may fulfill the requirements in the following manner. The concerted process may be the pathway of lower energy barrier. The preferred "A" mode in the cycloreversion will be due to the more favorable HOMO–LUMO interaction for the "A" fragmentation than for the "B" (11). In the "A" fission, the HOMO–LUMO pair should be styrene and formaldehyde, whereas it should be ethylene and benzaldehyde in the "B" process. From the ionization potential data (12) and n–π^* transition energies (13), we can estimate that the HOMO–LUMO gap of the "A" cleavage will be 1.7 eV, which is substantially smaller than that of the "B" fission, 4.8 eV. Unimportance of the concerted cycloreversion in the *cis* isomers, as well as in **9** and **10**, may be due to the steric destabilization of the transition state. In the thermolytic studies of 2-oxetanones, we[5] have demonstrated that the *cis* isomer reacts more slowly than the corresponding *trans* isomer and proposed that the important factor is the steric destabilization of the concerted transition state (14).

Among these alternatives, we prefer to take the concerted fragmentation as a possibility for the second reaction pathway. This is because we could find no anomaly in the thermal behavior of **9** and **10**; the results were consistent with the diradical mechanism. The aforementioned steric destabilization of the ionic process will be most important in the *cis-tert*-butyl derivative, but only moderately in the *cis*-methyl derivative (10). In **9** and **10**, the substituent at C3 *cis* to the phenyl group at C2 is a methyl group. Therefore, a certain degree of stabilization of the incipient cation will be provided by the phenyl groups in the reaction of **9** and **10**. In such a case, the ionic process should take a part in the reaction and the results may not simply be analyzed by the diradical mechanism alone.

A possibility that the concerted fragmentation may be feasible in the fragmentation of oxetanes has been pointed out by several workers (1*c*, *d*, *f*, *g*), but the experimental verification of such a process has not yet been carried out successfully. The present results suggest that, if our conclusion is valid, the concerted process will be favored over the diradical process only to a small magnitude. The 2-aryloxetanes will indeed be decomposed in the competing dual reaction courses. Small steric destabilization of the transition state will easily make an intervention of the second reaction pathway obscure. The reactivity reversal was in fact observed only in the 3-methyl derivatives, **1***c* and **1***t*. In the literature, somewhat unusual behavior of 2-phenyloxetane has occasionally been described (1*j*, *k*, *l*). The HOMO–LUMO gap may be sufficiently small in 2-aryloxetanes but may not be so in other oxetanes, including 2-alkyl derivatives. After all, it will be concluded that the diradical fission is, in general, the preferred mode of the oxetane fragmentation. 2-Aryloxetanes seem to be exceptional.

Thermolysis of 3,3-Dimethyl-4-aryloxetanes; the Substituent Effect on the A/B Ratio

Parent oxetane **6** gave an A/B ratio of 7:93 at 270°C. The fragmentation will proceed primarily via the diradical intermediates. In contrast, the oxetanes substituted by an electron-donating group at the benzene ring showed dramatic changes in the A/B ratio: A/B = 37:63 for **5** and 91:9 for **4**. Introduction of an electron-withdrawing chlorine to the aromatic ring yielded a small, opposite effect on the A/B ratio (Table 1). Again, the results may be explained by the dual mechanism, with intervention of either the stepwise ionic process or the concerted cycloreversion in addition to the diradical fission in the reaction of **4** and **5**. In terms of the concerted process, it can be anticipated that the

[5]We have thermolyzed 4-aryl-2-oxetanones in decane and found that $\rho = -1.52$ (14). Together with the clean stereospecificity of the reaction, we have proposed a concerted mechanism. Recently, however, Mulzer *et al.* (10) have examined the reaction in 1,2-dichlorobenzene. They have observed $\rho = -3.4$ and proposed an ionic process. The usage of a relatively polar solvent ($\varepsilon = 9.93$) seems to result in more pronounced charge development at the transition state.

Can. J. Chem. Downloaded from www.nrcresearchpress.com by 210.87.254.40 on 09/06/12
For personal use only.

TABLE 2. Stereochemical results of the "A" mode fragmentation in degassed TMEDA at 310 °C for 3 h

2-Phenyloxetane	Percent retention of configuration		
	Methyl (**1**)	Isopropyl (**2**)	*tert*-Butyl (**3**)
cis-3-Alkyl	69 (83)*	83 (87)*	42
trans-3-Alkyl	96	99	99.9

*Only after 1.5 h.

electron-releasing substituent wil lower the HOMO level of the styrene moiety and hence reduce the HOMO–LUMO gap for the "A" fragmentation. At present, however, we cannot rule out a possibility that the second process for **4** and **5** is the stepwise ionic pathway.[6]

Stereochemical Results of the "A" Fragmentation

If the concerted process intervenes in the "A" fragmentation to a significant extent, the alkenylbenzene produced should retain the configuration of the starting oxetane to a considerable degree. Unfortunately, however, alkenylbenzenes were found to isomerize significantly to the geometrical isomer under the reaction conditions. For example, 1-propenylbenzene produced in the thermolysis of **1***c* at 310°C was a mixture of *cis* and *trans* isomers in a ratio of 83 : 17 after 1.5 h, but in a ratio of 69 : 31 after 3 h (Table 2). The epimerization of the starting oxetane also took place to a certain extent in hot TMEDA, as mentioned in the previous section. Moreover, the "A" process will not totally be the concerted cycloreversion. It is, therefore, meaningless to draw any conclusion regarding the stereochemical consequence of the present fragmentation. Qualitatively, we can point out that the degree of the retention of configuration observed in the present study is higher than that observed in the thermolysis of 2-alkyl substituted oxetanes (1*c*, *d*, *e*).

Experimental

Infrared spectra were recorded on a Hitachi 215 grating spectrophotometer. The ^{1}H nmr spectra were obtained with a JEOL PS-100 spectrometer; the chemical shifts are given in parts per million from tetramethylsilane. Vapor phase chromatography work was done on a Hitachi 063 gas chromatograph. For the analysis of oxetanes, the Pyrex vpc column and solid supports (Celite 545) were pretreated with a 5% solution of chlorotrimethylsilane in toluene. Liquid phases used were Apiezon grease L (15%), polyethyleneglycol 20M (20%), and polyethyleneglycol succinate (15%). High-pressure liquid chromatography was carried out with a Hitachi 635 liquid chromatograph. Microanalyses were performed by the Center for Instrumental Analysis of Hokkaido University. Melting points and boiling points are uncorrected.

Oxetanes

Most of the oxetanes were prepared by the Paterno–Büchi reaction (6). Since the separation and purification of **1***c* and **1***t* obtained in the photoreaction were troublesome, they were synthesized from *erythro*- and *threo*-2-methyl-1-phenyl-3-(*p*-toluenesulfonyloxy)-1-propanols by following the reported procedures (5). The photoreaction of benzaldehyde with 3,3-dimethyl-1-butene gave a mixture rich in **3***t*. Compound **3***c* was prepared by the cyclization reaction.

The known oxetanes were identified by comparing their spectral data with those described in the literature: **1***c*, bp 60°C/3 Torr, n_D^{25} 1.5195 (5); **1***t*, bp 68–72°C/3 Torr, n_D^{25} 1.5145 (5); **6**, n_D^{25} 1.5073 (lit. (15) n_D^{20} 1.5118); **9**, mp 124–125°C (lit. (16) mp 123–125°C); **10**, mp 87–89°C (lit. (16) mp 88.5–90°C).

3-Isopropyl-2-phenyloxetanes (2c and 2t)

A benzene (100 mL) solution of benzaldehyde (2.9 g, 27 mmol) and 3-methyl-1-butene (7.8 g, 111 mmol) was irradiated with a high-pressure mercury lamp in a Pyrex reaction vessel under an argon atmosphere. After all benzaldehyde was consumed, the solvent was removed and the residue (4.5 g) was distilled under vacuum. A fraction, bp 59–69°C/1 Torr (1.6 g), was collected, which contained **2***c* and **2***t* in a 43 : 57 ratio as the major components (69%); **2***c* and **2***t* were isolated in a pure form by vpc. Compound **2***c*, ir (thin film) ν: 985 cm^{-1}; ^{1}H nmr (CCl_4) δ: 0.40 (d, J = 7 Hz, 3H), 0.65 (d, J = 7 Hz, 3H), 1.60 (m, 1H), 2.81 (m, 1H), 4.36 (t, J = 6.5 Hz, 1H), 4.67 (d of d, J = 8 and 6 Hz, 1H), 5.69 (d, J = 8 Hz, 1H), 7.28 (m, 5H); n_D^{25} 1.5106. *Anal.* calcd. for $C_{12}H_{16}O$: C 81.77, H 9.15; found: C 81.58, H 9.10. Compound **2***t*, ir (thin film) ν: 980 cm^{-1}; ^{1}H nmr (CCl_4) δ: 0.90 (t, J = 7 Hz, 6H), 2.1 (m, 1H), 2.4 (m, 1H), 4.32 (t, J = 6 Hz, 1H), 4.60 (d of d, J = 8 and 6 Hz, 1H), 5.28 (d, J = 6 Hz, 1H), 7.28 (m, 5H); n_D^{25} 1.5066. *Anal.* calcd. for $C_{12}H_{16}O$: C 81. 77, H 9.15; found: C 81. 87, H 9.12.

trans-*3-tert-Butyl-2-phenyloxetane (3t)*

From 8.9 g of benzaldehyde (84 mmol) and 7.4 g of 3,3-dimethyl-1-butene (88 mmol), a colorless liquid, bp 70–90°C/1 Torr (5.2 g), was obtained as above. The fraction contained 43% of **3***c* and **3***t* in a 25:75 ratio, from which **3***t* was isolated by vpc. Compound **3***t*, ir (thin film) ν: 985 cm^{-1}; ^{1}H nmr (CCl_4) δ: 0.95 (s, 9H), 2.57 (d of t, J = 8.7 and 6.8 Hz, 1H), 4.30–4.66 (m, 2H), 5.34 (d, J = 6.5 Hz, 1H), 7.28 (m, 5H); n_D^{25} 1.5048. *Anal.* calcd. for $C_{13}H_{18}O$: C 82.06, H 9.54; found: C 81.96, H 9.53.

3,3-Dimethyl-2-aryloxetanes (4, 5, 7, and 8)

The Paterno–Büchi reaction of *p*-methoxybenzaldehyde, *p*-methylbenzaldehyde, *p*-chlorobenzaldehyde, and *m*-chlorobenzaldehyde with 2-methylpropene proceeded without trouble to give **4**, **5**, **7**, and **8**. In all cases, a regioisomer was also produced but the desired oxetane was the major product (in a ratio of 8:2). Isolation and purification of **5**, **7**, and **8** were carried out as above, but **4** was unstable under the vpc conditions. Accordingly, **4** was isolated with a medium-pressure liquid chromatograph (Merck Lichroprep Si 60, hexane–ether 9:1 as an eluant) followed by vacuum distillation. Compound **4**, bp 60–65°C (bath temperature)/10^{-4} Torr; ir (thin film) ν: 980 cm^{-1}; ^{1}H nmr (CCl_4) δ: 0.75 (s, 3H), 1.33 (s, 3H), 3.76 (s, 3H), 4.10 (d, J = 5.2 Hz, 1H), 4.37 (d, J = 5.2 Hz, 1H), 5.29 (s, 1H), 6.79 (d, J = 8.5 Hz, 2H), 7.08 (d, J = 8.5 Hz, 2H); n_D^{25} 1.5177. *Anal.* calcd. for $C_{12}H_{16}O_2$: C 74.97, H 8.39; found: C 74.67, H 8.43. Compound **5**, ir (thin film) ν: 980 cm^{-1}; ^{1}H nmr (CCl_4) δ: 0.79 (s, 3H), 1.35 (s, 3H), 2.33 (s, 3H), 4.11 (d, J = 5.3 Hz, 1H), 4.37 (d, J = 5.3 Hz, 1H), 5.31 (s, 1H), 6.9–7.3 (m, 4H); n_D^{25} 1.5072. *Anal.* calcd. for $C_{12}H_{16}O$: C 81.77, H 9.15; found: C 81.92, H 9.12. Compound **7**, ir (thin film) ν: 980 cm^{-1}; ^{1}H nmr (CCl_4) δ: 0.77 (s, 3H), 1.37 (s, 3H), 4.12 (d, J = 5.3 Hz, 1H), 4.41 (d, J = 5.3 Hz, 1H), 5.33 (s, 1H), 7.0–7.4 (m, 4H); n_D^{25} 1.5227. *Anal.* calcd. for $C_{11}H_{13}OCl$: C 67.17, H 6.68, Cl 18.02; found: C 66.94, H 6.69, Cl 17.88. Compound **8**, ir (thin film) ν: 985 cm^{-1}; ^{1}H nmr (CCl_4) δ: 0.80 (s, 3H), 1.38 (s, 3H), 4.14 (d, J = 5.3 Hz, 1H), 4.40 (d, J =

[6]Suggested by a referee.

Can. J. Chem. Downloaded from www.nrcresearchpress.com by 210.87.254.40 on 09/06/12
For personal use only.

5.3 Hz, 1H), 5.33 (s, 1H), 6.9–7.4 (m, 4H); n_D^{25} 1.5224. *Anal.* calcd. for $C_{11}H_{13}OCl$: C 67.17, H 6.68, Cl 18.02; found: C 67.15, H 6.64, Cl 18.02.

cis-*3*-tert-*Butyl-2-phenyloxetane (3c)*

erythro-2-*tert*-Butyl-1-phenyl-3-(*p*-toluenesulfonyloxy)-1-propanol was prepared from the corresponding diol (5): mp 115–116°C; ir (KBr disk) ν: 3530, 1355, and 1175 cm^{-1}; ^1H nmr (acetone-d_6) δ: 1.06 (s, 9H), 1.7–2.0 (m, 1H), 2.47 (s, 3H), 3.63 (d of d, J = 10 and 3.3 Hz, 1H), 4.17 (d of d, J = 10 and 3.3 Hz, 1H), 4.25 (d, J = 4.1 Hz, 1H, disappeared by the addition of D_2O), 4.87 (d of d, J = 8.0 and 4.1 Hz, 1H, became d, J = 8.0 Hz, by the addition of D_2O), 7.21 (m, 5H), 7.44 (d, J = 8.0 Hz, 2H), 7.68 (d, J = 8.0 Hz, 2H). *Anal.* calcd. for $C_{20}H_{26}O_4S$: C 66.27, H 7.23, S 8.84; found: C 66.28, H 7.30, S 8.78. The treatment of this hydroxytosylate with potassium *tert*-butoxide gave **3***c* (16%) and benzaldehyde. Compound **3***c* was purified by vpc: ir (thin film) ν: 985 and 965 cm^{-1}; ^1H nmr (CCl_4) δ: 0.66 (s, 9H), 3.16 (nearly d of t, J = 7.3 and 8.7 Hz, 1H), 4.50 (d of d, J = 7.4 and 6.0 Hz, 1H), 4.67 (d of d, J = 8.8 and 6.0 Hz, 1H), 5.83 (d, J = 8.6 Hz, 1H), 7.1–7.5 (m, 5H); n_D^{25} 1.5109. *Anal.* calcd. for $C_{13}H_{18}O$: C 82.06, H 9.54; found: C 81. 98, H 9.50.

Thermolysis of Oxetanes

In general, a TMEDA solution of an oxetane (0.1–0.4 *M*) and diethylaniline (an internal standard for the vpc analysis) was introduced into a freshly base-treated Pyrex tube, degassed by several freeze–thaw cycles, sealed, and heated in an oven controlled at the desired temperature (± 0.5°C). TMEDA and diethylaniline were freshly distilled over potassium hydroxide pellets just before use. The product analyses were carried out by vpc for styrene derivatives, the aromatic carbonyl compounds, and/or alkene. All products are known compounds and hence they were characterized by comparing the spectral data of the isolated sample with those reported in the literature (14).

Since the amount of the aromatic aldehyde decreased gradually in TMEDA at 270–350°C, control experiments were carried out for the calibration of the results. After 16 h at 270°C, 3 h at 310°C, and 0.5 h at 350°C, benzaldehyde decreased to 51%, 73%, and 71% of the starting quantity. The amount of *p*-methylbenzaldehyde decreased to 46% after 16 h at 270°C and to 77% after 3 h at 310°C. Corrections for the amount of these aldehydes were made by assuming that the extent of the aldehyde consumption should be half of that observed in the control experiments. Since *p*-methoxybenzaldehyde, *p*-chlorobenzaldehyde, and *m*-chlorobenzaldehyde were much more unstable than benzaldehyde in hot TMEDA, the proportion of the "B" process in the reaction of **4**, **7**, and **8** was determined from the amount of isobutene produced. The figures obtained as an average of two to four runs are summarized in Table 1.

In an experiment, a 1:1 mixture of **1***c* and **1***t* was heated at 310°C in TMEDA. After 3.5 h, the consumption of **1***t* was 37% whereas that of **1***c* was 28%.

As described in the text, the produced alkenylbenzenes isomerized slowly to the corresponding geometrical isomer under reaction conditions. In the control experiments, authentic alkenylbenzenes were found to isomerize in hot TMEDA, but the extent of the isomerization was far less than that observed during the pyrolysis. For example, after heating at 310°C for 3 h in TMEDA, authentic *cis*-1-propenylbenzene isomerized to the *trans* isomer to an extent of only 4.2%. Similar results were obtained in other alkenylbenzenes: *trans*-1-propenylbenzene 1%, (*cis*-3-methyl-1-butenyl)benzene 2.3%, its *trans* isomer 0.2%, (*cis*-3,3-dimethyl-1-butenyl)benzene 6.5%, its *trans* isomer none. Some catalytic isomerization took place in the pyrolysis mixture. The results summarized in Table 2 are the compositions of the resultant mixtures without any corrections.

1. (*a*) D. A. Bittker and W. D. Walters. J. Am. Chem. Soc. 77, 1429 (1955); (*b*) G. F. Cohoe and W. D. Walters. J. Phys. Chem. **71**, 2326 (1967), and references cited therein; (*c*) K. A. Holbrook and R. A. Scott. J. Chem. Soc. Faraday Trans. I, **70**, 43 (1974); (*d*) G. Jones, II, and J. C. Staires. Tetrahedron Lett. 2099 (1974); (*e*) H. A. J. Carless. Tetrahedron Lett. 3425 (1974); (*f*) K. A. Holbrook and R. A. Scott. J. Chem. Soc. Faraday Trans. I, **71**, 1849 (1975); (*g*) A. D. Clements, H. M. Frey, and J. G. Frey. J. Chem. Soc. Faraday Trans. I, **71**, 2485 (1975); (*h*) M. J. Clarke and K. A. Holbrook. J. Chem. Soc. Faraday Trans. I, **73**, 890 (1977); (*i*) S. Braslavsky and J. Heicklen. Chem. Rev. **77**, 473 (1977); (*j*) E. A. S. Cavell, R. E. Parker, and A. W. Scaplehorn. J. Chem. Soc. C, 389 (1966); (*k*) M. Bartok. Kem. Kozlem. **28**, 79 (1967); Acta Chim. Acad. Sci. Hung. **51**, 403 (1967); (*l*) J. D. Margerum, J. N. Pitts, Jr., J. G. Rutgers, and S. Searles. J. Am. Chem. Soc. **81**, 1549 (1959).
2. N. Shimizu and S. Nishida. J. Chem. Soc. Chem. Commun. 734 (1974).
3. G. Jones II and H. H. Kleinman. Tetrahedron Lett. 2103 (1974); G. Jones II, S. B. Schwartz, and M. T. Marton. J. Chem. Soc. Chem. Commun. 374 (1973); G. Jones II, M. A. Acquadro, and M. A. Carmody. J. Chem. Soc. Chem. Commun. 206 (1975).
4. M. Cristl, U. Heinman, and W. Kristof. J. Am. Chem. Soc. **97**, 2299 (1975).
5. A. Balsamo, C. Ceccarelli, R. Crotti, and F. Macchia. J. Org. Chem. **40**, 473 (1975).
6. D. R. Arnold. Adv. Photochem. **6**, 301 (1968).
7. (*a*) S. W. Benson, F. R. Cruickshank, D. M. Golden, G. R. Hangen, H. E. O'Neal, A. S. Roders, R. Shaw, and R. Walsh. Chem. Rev. **69**, 279 (1969); (*b*) H. K. Eigenmann, D. M. Golden, and S. W. Benson. J. Phys. Chem. **77**, 1687 (1973); (*c*) H. E. O'Neal and S. W. Benson. *In* Free radicals. Vol. II. *Edited by* J. K. Kochi. Wiley-Interscience, New York, NY. 1973. p. 275; (*d*) S. W. Benson. Thermochemical kinetics. Wiley, New York, NY. 1968; (*e*) H. E. O'Neal and S. W. Benson. J. Phys. Chem. **72**, 1866 (1968).
8. (*a*) H. R. Gerberich and W. D. Walters. J. Am. Chem. Soc. **83**, 3935 (1961); **83**, 4884 (1961); (*b*) R. Willcott, R. L. Cargill, and B. Sears. Prog. Phys. Org. Chem. **9**, 25 (1972); (*c*) H. M. Frey and R. Walsh. Chem. Rev. **69**, 103 (1969); (*d*) G. Kaupp. Angew. Chem. Int. Ed. Engl. **13**, 817 (1974); (*e*) G. Kaupp and W. H. Laarhoven. Tetrahedron Lett. 941 (1976); (*f*) G. Kaupp and M. Stark. Chem. Ber. **110**, 3084 (1977); (*g*) G. Kaupp, M. Stark, and H. Frits. Chem. Ber. **111**, 3624 (1978).
9. R. B. Woodward and R. Hoffmann. The conservation of orbital symmetry. Academic Press, New York, NY. 1970.
10. J. Mulzer, M. Zippel, and G. Brüntrup. Angew. Chem. Int. Ed. Engl. **19**, 465 (1980).
11. K. Fukui. Acc. Chem. Res. **4**, 57 (1971); N. D. Epiotis. Angew. Chem. Int. Ed. Engl. **13**, 751 (1974).
12. A. Streitwieser, Jr. Prog. Phys. Org. Chem. **1**, 1 (1963); K. Watanabe, T. Nakayama, and J. Mottl. J. Quant. Spectrosc. Radiat. Transfer, **2**, 369 (1962); M. I. Al-Joboury and D. W. Turner. J. Chem. Soc. 4434 (1964).
13. J. G. Calvert and J. N. Pitts, Jr. Photochemistry. Wiley, New York, NY. 1967.
14. T. Imai and S. Nishida. J. Org. Chem. **44**, 3574 (1979); J. Org. Chem. **45**, 2354 (1980); and references cited therein.
15. F. Nerdel, H.Kaminski, and P. Weyerstahl. Chem. Ber. **102**, 3679 (1969).
16. D. R. Arnold, R. L. Hinman, and A. H. Glick. Tetrahedron Lett. 1425 (1964).

The stereochemistry and regiochemistry of the Diels–Alder reactions of 6-acetoxy-2,6-dimethyl-2,4-cyclohexadienone

HILLAR AUKSI[1] AND PETER YATES

Lash Miller Chemical Laboratories, University of Toronto, Toronto, Ont., Canada M5S 1A1

Received February 13, 1981

HILLAR AUKSI and PETER YATES. Can. J. Chem. **59**, 2510 (1981).

6-Acetoxy-2,6-dimethyl-2,4-cyclohexadienone (**1**) and maleic anhydride in boiling benzene give a single adduct, *exo*-5-acetoxy-1,5-dimethyl-6-oxobicyclo[2.2.2]oct-7-ene-*endo*-2,3-dicarboxylic acid anhydride (**2**). With propiolic acid **1** gives *exo*-5-hydroxy-1,5-dimethyl-6-oxobicyclo[2.2.2]octa-2,7-diene-2-carboxylic acid (**15**). The high stereoselectivity and regioselectivity of these reactions is interpretable in terms of orbital overlap, closed-shell repulsion, steric, and van der Waals – London effects.

HILLAR AUKSI et PETER YATES. Can. J. Chem. **59**, 2510 (1981).

L'acétoxy-6 diméthyl-2,6 cyclohexadiénone-2,4 (**1**) et l'anhydride maléique dans le benzène au reflux donnent un adduit unique l'anhydride de l'acide acétoxy-5-*exo* diméthyl-1,5 oxo-6 bicyclo[2.2.2] octène-7 dicarboxylique-2,3-*endo* (**2**). Le composé **1** en présence de l'acide propiolique conduit à l'acide hydroxy-5-*exo* diméthyl-1,5 oxo-6 bicyclo[2.2.2] octadiène-2,7 carboxylique-2 (**15**). On peut interpréter la stéréosélectivité et la régiosélectivité élevées de ces réactions en fonction d'un recouvrement d'orbitales, de la répulsion des couches électroniques complètes, des effects stériques et des effets de van der Waals – London.

[Traduit par le journal]

In the course of our studies on the intramolecular Diels–Alder reactions of 6-acryloxy-2,6-dimethyl-2,4-cyclohexadienone derivatives formed by "modified" Wessely oxidation (1), we had occasion to investigate two intermolecular Diels–Alder reactions of 6-acetoxy-2,6-dimethyl-2,4-cyclohexadienone (**1**) formed by conventional Wessely oxidation. We report now on the elucidation of the stereochemical and regiochemical courses of these reactions.[2]

Reaction of Maleic Anhydride with 6-Acetoxy-2,6-dimethyl-2,4-cyclohexadienone

Reaction of maleic anhydride with 6-acetoxy-2,6-dimethyl-2,4-cyclohexadienone (2,6-dimethyl-*o*-quinol acetate; **1**) in boiling benzene gave a single adduct, whose structure has been established as **2**. Its ir and ^{1}H nmr spectra are given in Table 1;[3] these confirm its gross structure, but do not distinguish unambiguously between structure **2** and the stereoisomeric structures **3**–**5**.

Catalytic hydrogenation of **2** proceeded rapidly and cleanly with the uptake of one molar equivalent of hydrogen to give the dihydro product **6** (Scheme 1). Comparison of its ^{1}H nmr spectrum (Table 1) with that of **2** shows that the H.2 and H.3 signals of **2** undergo an upfield shift of ca. 0.1 ppm on saturation of the ethylenic bond. This indicates that the adduct has the 2,3-*endo* configuration as in **2** (or **4**) rather than the 2,3-*exo* configuration as in **3** (or **5**), since in the latter cases the H.2 and H.3 protons are expected to be shielded by the ethylenic bond and thus show a downfield shift of their signals upon hydrogenation (4).

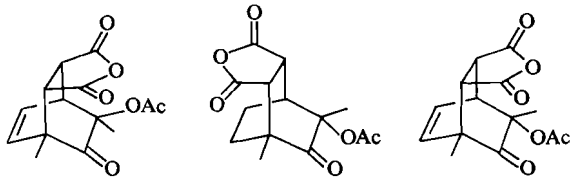

3 **4** **5**

Hydrolysis of **2** with 0.2 *N* aqueous sodium hydroxide at room temperature followed by acidification and sublimation gave the hydroxy anhydride **7**, which on hydrogenation as before gave the corresponding dihydro compounds **8** (Scheme 1). The ir and ^{1}H nmr spectra of these compounds (Table 1) show that reclosure of the anhydride ring has occurred. Comparison of the latter spectra with the ^{1}H nmr spectra of compounds **2** and **6** shows that while the H.2 and H.3 signals of **2** and **6** have very similar chemical shifts, those of **7** and **8** are significantly different ($\Delta\delta$ 0.7–0.9 ppm), largely owing to a downfield shift of the H.3 signal ($\Delta\delta$ 0.5–0.6 ppm). This effect can be interpreted in

[1]Present address: Raylo Chemicals Ltd., 8045 Argyll Road, Edmonton, Alta., Canada T6C 4A9.

[2]For earlier work that established the gross structure, but not the stereochemistry, of the adduct of maleic anhydride with **1**, see ref. 2.

[3]The ^{13}C nmr spectra of **2** and related compounds have been discussed elsewhere (3).

[4]This conclusion is more rigorously based in the case of **2** and **7** than that of **6** and **8**, since the spectrum of **8** was recorded in a mixture of $CDCl_3$ and DMSO-d_6 rather than in $CDCl_3$.

0008-4042/81/162510-08$01.00/0

©1981 National Research Council of Canada/Conseil national de recherches du Canada

Can. J. Chem. Downloaded from www.nrcresearchpress.com by 210.87.254.5 on 09/06/12
For personal use only.

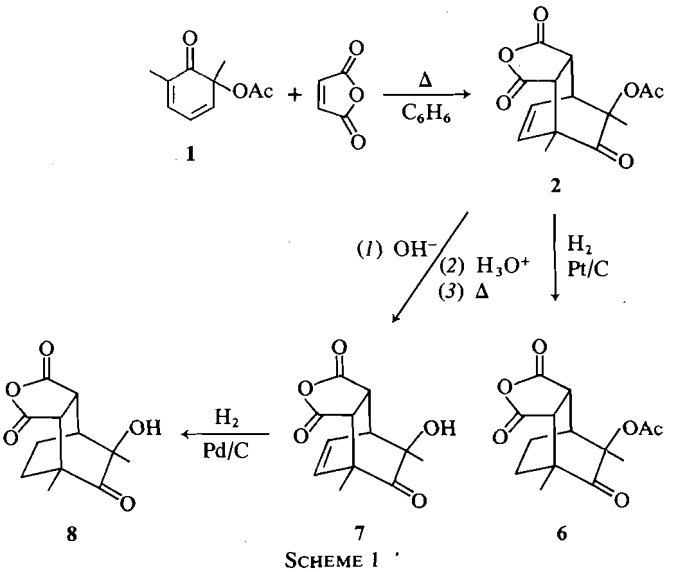

SCHEME 1

terms of shielding of H.3 by the acetyl group in **2** and **6**, which is absent in **7** and **8**.[4] Shielding of this magnitude requires that H.3 be spatially proximate to the acetyl group and again shows that the adduct has the 2,3-*endo* stereochemistry as in **2** or **4**, and indicates further that cycloaddition has occurred on the acetoxy face of **1** to give **2** rather than on the methyl face to give **4**.

Corroboration of these stereochemical assignments was sought by the utilization of a technique that has been introduced by Verma *et al.* (5–7) for determining the *exo* or *endo* stereochemistry of Diels–Alder adducts of maleic anhydride. In one variant of this method (6) the anhydride is converted to the corresponding *N'*,*N'*-diacetyl-*N*-aminosuccinimide and the difference between the

TABLE. 1. Infrared and ^1H nmr spectra of compounds **2** and **6–8**[a]

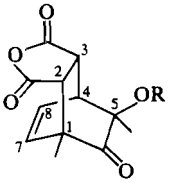

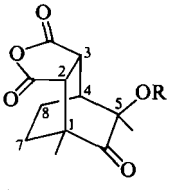

		2 (R = Ac)	**7** (R = H)	**6** (R = Ac)	**8** (R = H)
$\lambda_{max}^{CHCl_3}$, μm		5.34 (w), 5.60, 5.73	2.95 (w), 5.35 (w), 5.62, 5.74	5.35 (w), 5.62, 5.75	3.07 (w), 5.48 (w) 5.62, 5.76
$^H\delta$[b]	H.2	3.47	3.13 (*d*, *J* 9 Hz)	3.37 (m)	3.13 (m)[c]
	H.3		4.06 (dd, *J* 9, 3 Hz)		3.83 (dd, *J* 10, 3 Hz)
	H.4	4.04 (dt, *J* 7, 2 Hz)	3.53 (ddd, *J* 7, 3, 2Hz)	2.97 (br s)	3.13 (m)[c]
	H.7	6.03 (dd, *J* 8, 2 Hz)	6.04 (dd, *J* 8, 2 Hz)	1.75 (m)	1.67 (br s)
	H.8	6.48 (dd, *J* 8, 7 Hz)	6.53 (dd, *J* 7, 8 Hz)		
	CH_3(1)	1.53 (s)	1.38 (s)	1.37 (s)	1.18 (s)
	CH_3(5)	1.61 (s)	1.61 (s)	1.57 (s)	1.33 (s)
	CH_3CO	2.09 (s)	—	2.08 (s)	—
	OH	—	2.63 (br s)[d]	—	5.67 (s)[e]

[a] The signal intensities in the ^1H nmr spectra are in accord with the assignments.
[b] In $CDCl_3$, except for **8**, which was in $CDCl_3$–DMSO-d_6.
[c] H.2 and H.4 signals overlap.
[d] Absent after D_2O treatment.
[e] Concentration dependent.

Can. J. Chem. Downloaded from www.nrcresearchpress.com by 210.87.254.5 on 09/06/12
For personal use only.

Can. J. Chem. Downloaded from www.nrcresearchpress.com by 210.87.254.5 on 09/06/12
For personal use only.

chemical shifts of the two acetyl signals is used as a probe of the stereochemistry of the adduct. Thus in the case of **9**, the imide formed from the *endo* adduct of cyclopentadiene and maleic anhydride, the acetyl chemical shift difference, although small (Δδ 0.33 ppm) (5), is identical with that (Δδ 0.33 ppm) in a related case that has been interpreted in terms of shielding by the olefinic bond of the acetyl group *syn* to that bond (6). However, we have found that the difference in the case of the *exo* adduct **10** (Δδ 0.28 ppm) is very similar and clearly this method cannot be used in cases of this kind. Verma and Singh have reached a similar conclusion (8).

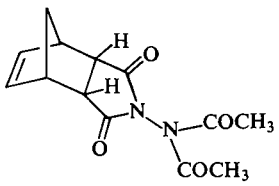

9

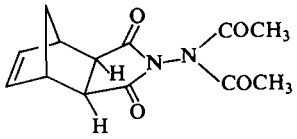

10

The second variant involves conversion of the adduct to the corresponding *N'*-acetyl-*N'*-benzoyl-*N*-aminosuccinimide (5, 7) and comparison of the chemical shifts of the olefinic protons in the resulting pair of conformational isomers. In the case of the imide **11** from the *endo* adduct of maleic anhydride and cyclopentadiene a large chemical shift difference (Δδ 1.0 ppm) was observed between the two sets of olefinic signals arising from the two conformational isomers. This was interpreted as resulting from shielding of the vinyl protons by the benzene ring in the isomer in which the benzoyl group is *syn* to the olefinic bond. We have prepared the imide **12** from the adduct **2** and find that one rotational isomer has vinyl proton signals (δ 5.93 and 6.35 ppm) at similar positions to those of **2** itself (δ 6.03 and 6.48 ppm), while the other has these signals shifted greatly upfield (δ 4.93 and 5.53 ppm); the differences in the chemical shifts for the two isomers (Δδ 1.00 and 0.82 ppm) are similar to those in the case of **11** (Δδ 0.97 ppm) (5). Since shift differences of these magnitudes appear to be impossible in the case of a 2,3-*exo* isomer, we conclude that the original adduct must have the

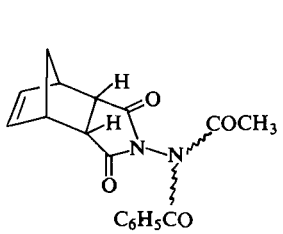

11

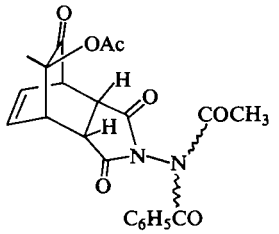

12

2,3-*endo* stereochemistry as in **2** (or **4**). It is noteworthy that in these terms the preponderant rotational isomer of both **11** and **12** is that with the *N*-benzoyl group *syn* to the olefinic bond (cf. ref. 7).

The assignment of structure **2** rather than **4** to the original adduct was confirmed by the transformations shown in Scheme 2. Methanolysis of **2** gave a mixture of two acid esters, which was converted to the diester **13** with diazomethane. Treatment of this with methanolic sodium methoxide at room temperature gave the lactone **14**, which was shown to be identical with the product obtained by "modified" Wessely oxidation of 2,6-dimethylphenol in the presence of methyl hydrogen fumarate (1). Formation of **14** from **13** must involve epimerization at C.3 prior to lactonization. The latter process can occur only if the acetoxyl group in **13** has the *exo* orientation, thus confirming that the structure of the original adduct is **2** rather than **4**.

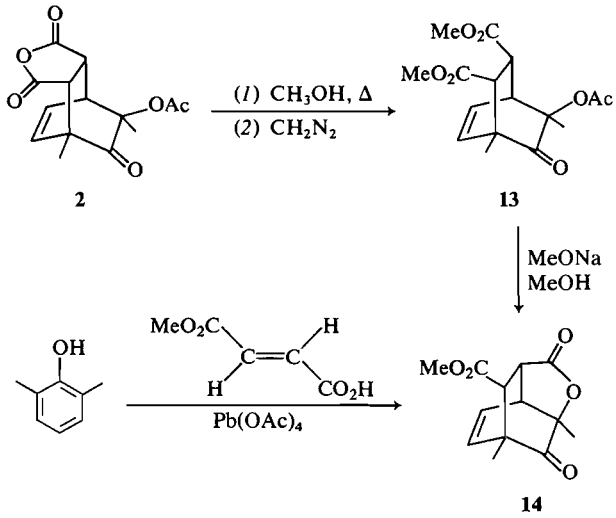

SCHEME 2

Reaction of Propiolic Acid with 6-Acetoxy-2,6-dimethyl-2,4-cyclohexadienone

Reaction of **1** with propiolic acid in boiling benzene for 25 days gave a product in 46% yield that is assigned structure **15**: the only other compounds detected in the reaction mixture were the dimer of **1** (9) (*vide infra*) and unconsumed starting material. The ir and ^{1}H nmr spectra of **15** (Table 2) establish its gross structure and the latter spectrum permits the assignment of the regiochemistry of the product as in **15** or **16** rather than as in **17** or **18**. This follows from the fact that the signal at δ 7.47 ppm, which from its chemical shift can be unambiguously assigned to the vinylic proton in the β relationship to the carboxylic acid (i.e., H.3), is a

TABLE 2. Infrared and ^1H nmr spectra of compounds **15** and **19–21**[a]

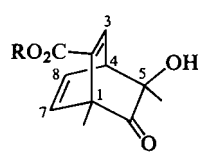

15 (R = H)

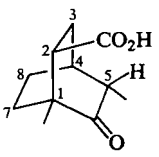

19 (R = Me)

20

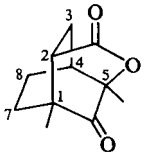

21

λ_{max}, μm[b]		3.20 (m), 3.0–3.9 (m), 5.76	3.03 (w), 5.76	3.12 (w), 3.0–4.9 (m) 5.79, 5.87 (m)	5.60, 5.68
$^H\delta$[c]	H.2	—	—	2.80 (dd, *J* 11, 6.5 Hz)	2.6–2.9 (m)
	H.3	7.47 (d, *J* 6.5 Hz)	7.39 (d, *J* 6 Hz)	1.62–2.5 (m)	1.6–2.2 (m)[d]
	H.4	3.83 (dt, *J* 2, 6.5 Hz)	3.83 (dt, *J* 2, 6 Hz)		2.2–2.5 (m)
	H.7	6.10 (dd, *J* 7.5, 2 Hz)	6.05 (dd, *J* 7, 2 Hz)		1.6–2.2 (m)[d]
	H.8	6.51 (t, *J* 7 Hz)	6.40 (t, *J* 6.5 Hz)		
	CH_3(1)	1.33 (s)	1.30 (s)	1.03 (s)	1.15 (s)
	CH_3(5)	1.68 (s)	1.70 (s)	1.35 (s)	1.44 (s)
	OH (5)	4.95 (br s)[e]	2.57 (s)[e]	6.4 (br s)[e]	—
	CO_2H		—		—
	OCH_3	—	3.70 (s)	—	—

[a] The signal intensities in the ^1H nmr spectra are in accord with the assignments.
[b] **15** in KBr; **19** and **20** in $CHCl_3$; **21** in CCl_4.
[c] In $CDCl_3$ except for **15**, which was in CD_3OD.
[d] H.3, H.7, and H.8 signals overlap.
[e] Concentration dependent.

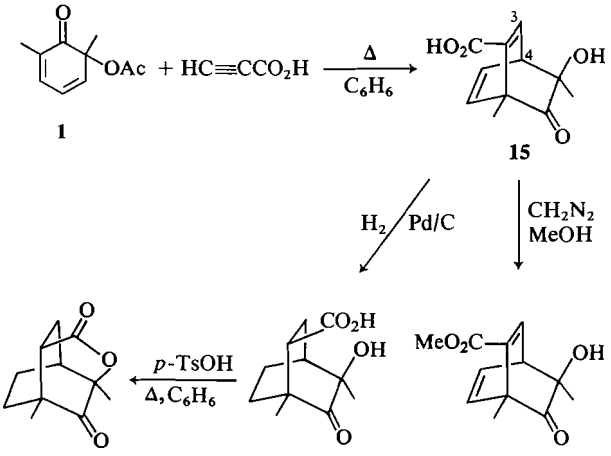

SCHEME 3

doublet with J = 6.5 Hz. The magnitude of this coupling constant clearly shows that the coupling is vicinal rather than allylic, requiring the presence of a hydrogen atom at C.4 as in **15** or **16**. Esterification of **15** with diazomethane gave **19** (Scheme 3), whose ^1H nmr spectrum (Table 2) shows an analogous doublet (J = 6 Hz) at δ 7.39 ppm. In this case the validity of the basis of the assignment of regiochemistry could be tested directly by comparison with the spectrum of the ester **23**, formed on treatment of **22** with methanol and *N*,*N*-dimethylhydrazine (Scheme 4) (1), which corresponds to the acid **17**. This spectrum shows a doublet at δ 6.98 ppm that can be assigned unambiguously to H.3; the coupling constant is 2 Hz, showing allylic rather than vicinal coupling with the bridgehead proton H.1. Further, the signal of the bridgehead proton in **23** (δ 4.35 ppm) is at considerably lower field than that in **15** (δ 3.83 ppm) in accord with the expectation that the ester group will exert a strong anisotropic deshielding effect in the case of the former but not the latter compound.

Distinction between the stereoisomeric structures **15** and **16** was made on the following basis. Hydrogenation of **15** gave the tetrahydro compound **20**, which on dehydration gave the lactone **21** (Scheme 3). This lactone underwent very facile hydrolysis to return **20**. The ir and ^1H nmr spectra of the hydrogenated product (Table 2) are in accord with the gross structure of **20** and its stereochemistry can be assigned on the basis of its reversible lactonization, establishing that the original adduct has the stereochemistry of **15** and not **16**. The

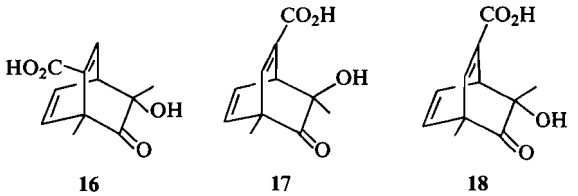

16 **17** **18**

Can. J. Chem. Downloaded from www.nrcresearchpress.com by 210.87.254.5 on 09/06/12
For personal use only.

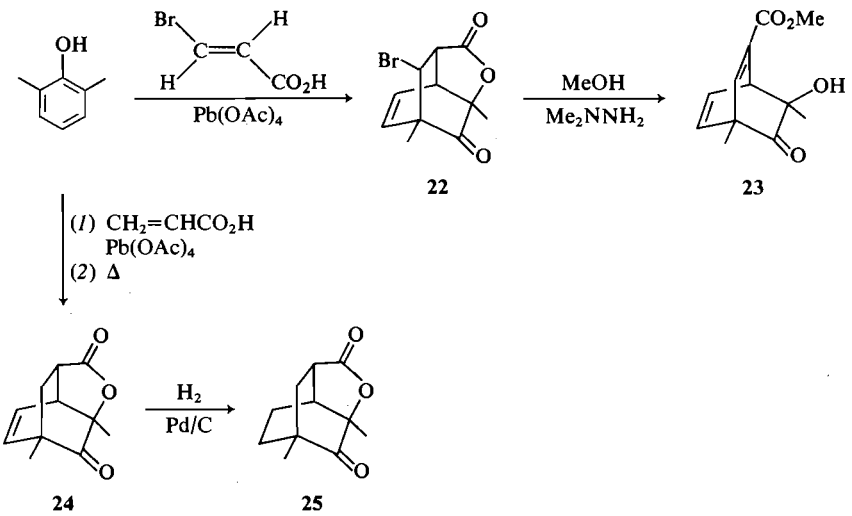

SCHEME 4

formation of the lactone **21**, which is different from the lactone **25** obtained on hydrogenation of **24** (Scheme 4) (1), also confirms that the adduct has the regiochemistry of **15** and not **17**. The ir spectrum of **21** shows it to be highly strained, as also indicated by its very ready hydrolysis.

Discussion

The reaction of the 6-acetoxy-2,4-cyclohexadienone **1** is highly stereoselective in that no adduct other than **2** could be detected in the reaction mixture. Since the reaction occurs under mild conditions it is most probable that **2** is formed under kinetic control. Such high stereoselectivity has also been observed in the addition of 6-hydroxy-2,4-cyclohexadienones to *p*-benzoquinones under conditions of kinetic control (10). For example, reaction of 6-hydroxy-2,4-cyclohexadienone (**26**), formed by treatment of 2,6-dimethylphenol with sodium metaperiodate, with *p*-benzoquinone in aqueous ethanolic solution at room temperature gives a single adduct, which has been assigned structure **27**, together with **28**, a dimer of **26**. Formation of the Diels–Alder dimer is also highly stereoselective (and in addition highly chemoselective and regioselective) for only a single such product is observed. A number of analogous dimers of 6-hydroxy- and 6-acetoxy-2,4-cyclohexadienones have been prepared, and in several cases their structures have been demonstrated by X-ray crystallography to be analogous to **28** (8, 11). In the case of **29**, the dimer of **1**, it has been shown that this is formed under kinetic control at 120°C since at this temperature it is the only dimer formed, while at 160–190°C it is converted to a mixture of **29** and its epimer **30** (9).

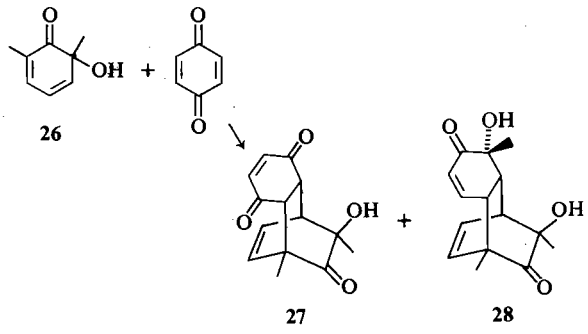

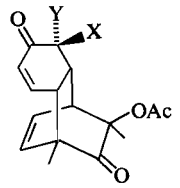

29 X = CH_3, Y = OAc
30 X = OAc, Y = CH_3

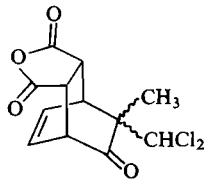

31

In all of these cases, like that of **2**, the Diels–Alder reaction gives the *endo* product.[5] This, of course, is frequently observed with dienophiles such as maleic anhydride and *p*-benzoquinone and has been interpreted in terms of secondary orbital overlap and closed-shell repulsion (13–15). A less frequently encountered aspect of the stereochemistry of these products concerns the relative configuration at the carbon atoms that were originally C.6 in the 2,4-cyclohexadienone. This is determined by which face of the dienone undergoes bonding with the dienophile (and, in the case of the

[5]This has also been shown to be the case for the adduct **31** from 6-dichloromethyl-6-methyl-2,4-cyclohexadienone (12).

Can. J. Chem. Downloaded from www.nrcresearchpress.com by 210.87.254.5 on 09/06/12
For personal use only.

Can. J. Chem. Downloaded from www.nrcresearchpress.com by 210.87.254.5 on 09/06/12
For personal use only.

dimers, by which face of the dienophile undergoes attack by the diene). Compound **2**, like compounds of type **27–29**, is formed with high stereoselectivity by attack on the acetoxyl- (or hydroxyl-) bearing face of the dienone. This can be interpreted in terms of a combination of steric, van der Waals – London, and secondary orbital overlap factors (16). It can be compared with the exclusive formation of **32** from 5-acetoxycyclopentadiene and ethylene (17) and contrasted with the exclusive formation of **33** from 1-methoxy-6-methyl-1,3-cyclohexadiene and maleic anhydride (18) and the formation of a ca. 1:1 mixture of **34** and **35** from 5-methylcyclopentadiene and *N*-phenylmaleimide and a 1:12 mixture of **36** and **37** from 5-methylcyclopentadiene and maleic anhydride (19). In this connection it may be suggested that the very much greater rate of dimerization of 6-hydroxy-2,4-cyclohexadienones of type **26** relative to that of their acetoxy analogues of type **1** reflects both a reduced steric effect and enhanced secondary orbital overlap with the unshared electron pairs on the oxygen atom.

The reaction of **1** with propiolic acid to give **15** is highly regioselective. Although the extended reaction time (25 days) might have resulted in thermodynamic rather than kinetic control there was no evidence for the presence of the other regioisomer at intermediate reaction times. The sense of the regioselectivity, which is analogous to that in the dimerization of **1** and **26**, is in accord with expectation based on consideration of terminal and secondary orbital overlap (14, 20). The reaction is also highly stereoselective and the relative configuration at the carbon atom that was originally C.6 in the 2,4-cyclohexadienone again shows that attack occurs on the acetoxyl-bearing face of the dienone.

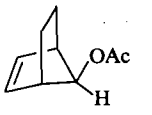

32

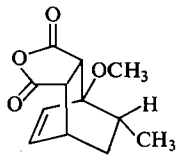

33

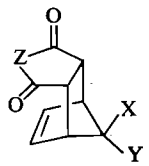

34 X = CH_3, Y = H, Z = NC_6H_5
35 X = H, Y = CH_3, Z = NC_6H_5
36 X = CH_3, Y = H, Z = O
37 X = H, Y = CH_3, Z = O

The formation of the hydroxy compound **15** is thought to involve hydrolysis of the corresponding acetoxy compound by adventitious water during the lengthy reaction period. It is considered to be unlikely that it arises by hydrolysis of **1** and **26** followed by addition of propiolic acid to the latter since none of **27**, the dimer of **26**, was observed to be present in the reaction mixture nor was any formed on treatment of **1** with propiolic acid in boiling benzene in the presence of water for 24 h.

Experimental

Melting points are uncorrected. Unless otherwise specified, ir spectra were recorded in chloroform, uv spectra in methanol, and ^1H and ^{13}C nmr spectra in deuteriochloroform. Solutions in organic solvents were dried over anhydrous $MgSO_4$.

6-Acetoxy-2,6-dimethyl-2,4-cyclohexadienone (2,6-Dimethyl-o-quinol Acetate; 1)

A solution of 2,6-dimethylphenol (9.00 g, 73.7 mmol) in dry dichloromethane (50 mL) was added dropwise over a 10 min period with stirring to a solution of lead tetraacetate (36.40 g, 82.2 mmol) in dry dichloromethane (700 mL), and stirring was continued at room temperature for 1 h. Ethylene glycol (1 mL) was added to destroy excess Pb(IV). Filtration followed by evaporation gave a reddish amber oil, which was taken up in benzene (250 mL). The solution was washed with water (2 × 250 mL) and aqueous 1% sodium carbonate (250 mL), dried, and evaporated to give a red oil (11.4 g). Distillation (60°C/0.005 Torr) gave **1** as a pale yellow liquid (9.04 g, 68%), which solidified on standing. Recrystallization from ether at −78°C gave **1** as a pale yellow solid, mp 34–35°C (lit. (21) mp 35°C).

exo-*5-Acetoxy-1,5-dimethyl-6-oxobicyclo[2.2.2]oct-7-ene*-endo-*2,3-dicarboxylic Acid Anhydride (2)*[6]

A solution of 2,6-dimethyl-*o*-quinol acetate (**1**) (freshly distilled; 5.45 g, 30.2 mmol) and maleic anhydride (2.97 g, 30.3 mmol) in benzene (100 mL) was boiled under reflux for 26 h. Evaporation gave a bright yellow oil, which crystallized on standing. The solid material was dissolved in benzene (25 mL), cyclohexane was added (50 mL), and the solution was heated on a steam bath until material began to precipitate. After the solution had cooled to room temperature, filtration gave a white crystalline solid (4.74 g). Recrystallization from chloroform/cyclohexane gave **2** as a white crystalline solid (4.44 g, 53%). Sublimation (80°C/0.005 Torr) gave **2**, mp 159.5–160.5°C; $\lambda_{max}(\varepsilon)$: 301 (70) nm; C nmr δ: 201.4 (s), 171.4 (s), 170.0 (s), 169.4 (s), 134.9 (d), 134.0 (d), 77.0 (s), 50.4 (s), 47.0 (d), 43.2 (d), 42.5 (d), 23.4 (q), 21.2 (q), 14.7 (q); ms *m/e* (M^+): 278. *Anal.* calcd. for $C_{14}H_{14}O_6$: C 60.43, H 5.07; found: C 60.20, H 5.02.

exo-*5-Acetoxy-1,5-dimethyl-6-oxobicyclo[2.2.2]octane*-endo-*2,3-dicarboxylic Acid Anhydride (6)*

exo-5-Acetoxy-1,5-dimethyl-6-oxobicyclo[2.2.2]oct-7-ene-*endo*-2,3-dicarboxylic acid anhydride (**2**) (500 mg, 1.80 mmol) was hydrogenated in acetic acid (20 mL) over 5% Pd/C (50 mg) at room temperature and atmospheric pressure until uptake of hydrogen ceased. Filtration followed by evaporation gave a

[6]The following convention has been used to describe the stereochemistry of bicyclo[2.2.2]octanone derivatives: substituents are designated as being *exo* or *endo* with respect to the unsaturated bridge of lowest priority, and in saturated compounds to the bridge of lowest priority.

Can. J. Chem. Downloaded from www.nrcresearchpress.com by 210.87.254.5 on 09/06/12
For personal use only.

clear, colorless oil which was taken up in dichloromethane (30 mL). The solution was extracted with aqueous 1% sodium bicarbonate (30 mL). The organic layer was dried and evaporated to give a clear, colorless oil (0.43 g), which crystallized on standing. Sublimation (85°C/0.005 Torr) gave **6** as a white crystalline solid (0.40 g, 80%), mp 187–188°C; $\lambda_{max}(\varepsilon)$: 305 (30) nm; C nmr δ: 206 (s), 172.3 (s), 170.3 (s), 170.1 (s), 80.2 (s), 46.2 (d), 44.9 (d), 44.9 (s), 41.8 (d), 39.0 (d), 26.1 (t), 21.8 (q), 21.1 (q), 18.7 (t), 17.2 (q); ms *m/e* (M^+): 280. *Anal.* calcd. for $C_{14}H_{16}O_6$: C 59.99, H 5.75; found: C 59.88, H 5.75.

exo-*5-Hydroxy-1,5-dimethyl-6-oxobicyclo[2.2.2]oct-7-ene*-endo-*2,3-dicarboxylic Acid Anhydride (7)*

exo-5-Acetoxy-1,5-dimethyl-6-oxobicyclo[2.2.2]oct-7-ene-*endo*-2,3-dicarboxylic acid anhydride (**2**) (0.59 g, 2.12 mmol) and sodium hydroxide (0.5 *N*; 15 mL, 7.50 mmol) were dissolved in water (30 mL) and the solution was stirred at room temperature for 48 h. Acidification with dilute hydrochloric acid to pH 5 followed by evaporation gave a white solid. The solid was extracted repeatedly with ether and the extract was evaporated to give a white crystalline material (0.48 g). Sublimation (135°C/0.005 Torr) gave **7** as a white crystalline solid (0.43 g, 86%), mp 158.0–160°C; $\lambda_{max}(\varepsilon)$: 310 (70) nm; C nmr δ: 208.7 (s), 172.0 (s), 169.3 (s), 134.5 (d), 133.7 (d), 70.7 (s), 49.9 (s), 46.5 (d), 44.8 (d), 42.0 (d), 25.4 (q), 14.5 (q); ms *m/e* (M^+): 236. *Anal.* calcd. for $C_{12}H_{12}O_5$: C 61.01, H 5.12; found: C 60.85, H 5.13.

exo-*5-Hydroxy-1,5-dimethyl-6-oxobicyclo[2.2.2]octane*-endo-*2,3-dicarboxylic Acid Anhydride (8)*

exo-5-Hydroxy-1,5-dimethyl-6-oxobicyclo[2.2.2]oct-7-ene-*endo*-2,3-dicarboxylic acid anhydride (**7**) (223 mg, 0.94 mmol) was hydrogenated in ethyl acetate (15 mL) over 5% Pd/C (20 mg) at room temperature and atmospheric pressure until uptake of hydrogen ceased. Filtration followed by evaporation gave a white solid. Sublimation (82°C/0.005 Torr) gave **8** as a white crystalline solid (221 mg, 99%), mp 179–180°C; $\lambda_{max}(\varepsilon)$: 305 (30) nm; C nmr δ: 214.3, 172.5, 170.1, 73.7, 46.0, 43.9, 40.8, 40.0, 25.1, 23.1, 17.9, 16.9; ms *m/e* (M^+): 238. *Anal.* calcd. for $C_{12}H_{14}O_5$: C 60.50, H 5.92; found: C 60.63, H 5.90.

N′,N′-*Diacetyl*-N-*aminobicyclo[2.2.1]hept-5-ene*-exo-*2,3-dicarboximide (10)*

Bicyclo[2.2.1]hept-5-ene-*exo*-2,3-dicarboxylic acid anhydride (0.705 g, 4.29 mmol) and hydrazine hydrate (0.162 g, 4.30 mmol) were dissolved in 95% ethanol (70 mL) and the solution was boiled at reflux for 1 h. Evaporation gave *N*-aminobicyclo[2.2.1]hept-5-ene-*exo*-2,3-dicarboximide (0.76 g). The *N*-amino dicarboximide (0.215 g, 1.21 mmol) was dissolved in acetic anhydride (25 mL) and the solution was heated on a steam bath for 1 h. Evaporation gave a gummy material (0.341 g) which was chromatographed on a silica gel plate (0.5 mm) with 20% ethyl acetate in benzene to give two major bands (R_f = 0.1 and 0.4). The leading band (R_f = 0.4) gave an oil (0.200 g) which crystallized on standing. The crystalline material was chromatographed on a silica gel plate (0.25 mm) with ether to give two bands (R_f = 0.3 and 0.6). The leading band (R_f = 0.6) gave **10** (0.163 g, 51% based on the anhydride) as an oil which slowly crystallized on standing. Sublimation (60°C/0.005 Torr) gave **10**, mp 107–108°C; λ_{max}: 5.55 (w), 5.75, 6.20 (w) μm; H nmr δ: 1.4–2.1 (m, 2H), 2.22 (s, 3H), 2.50 (s, 3H), 2.7–2.8 (m, 2H), 3.3–3.5 (m, 2H), 6.3–6.5 (m, 2H); C nmr δ: 179.5 (s), 169.3 (s), 168.3 (s), 137.9 (d), 46.0 (d), 45.5 (d), 43.3 (t), 25.3 (q), 23.6 (q); ms *m/e* (M^+): 262. *Anal.* calcd. for $C_{13}H_{14}O_4N_2$: C 59.53, H 5.38, N 10.68; found: C 59.54, H 5.45, N 10.53.

N′-*Acetyl*-N′-*benzoyl*-N-*amino*-exo-*5-acetoxy-1,5-dimethyl-6-oxobicyclo[2.2.2]oct-7-ene*-endo-*2,3-dicarboximide (12)*

A solution of *exo*-5-acetoxy-1,5-dimethyl-5-oxobicyclo[2.2.2]oct-7-ene-*endo*-2,3-dicarboxylic acid anhydride (2.50 g, 8.98 mmol) and hydrazine hydrate (0.49 g, 8.32 mmol) in 95% ethanol (125 mL) was boiled at reflux for 1.25 h. Evaporation gave a white solid, which was dissolved in hot benzene (40 mL), ether (190 mL) was added, and the resulting solution was cooled to −70°C. Filtration gave a white crystalline solid (1.76 g). The filtrate was evaporated and the residue was taken up in hot benzene (15 mL), ether (90 mL) was added, and the resulting solution was cooled to −78°C. Filtration gave additional white crystalline material (0.18 g). The two crops were combined to give *N*-amino-*exo*-5-acetoxy-1,5-dimethyl-6-oxobicyclo-[2.2.2]oct-7-ene-*endo*-2,3-dicarboximide (1.94 g, 74%), mp 171–172°C; λ_{max}: 5.57 (w), 5.72 μm; λ_{max} (ε): 300 (55) nm; H nmr δ: 1.51 (s, 3H), 1.61 (s, 3H), 2.08 (s, 3H), 3.12 (m, 2H), 4.03 (ddd, J = 6.5, 2.5, 2 Hz, 1H), 4.37 (bs, 2H, variable), 5.88 (dd, J = 8, 2 Hz, 1H), 6.30 (dd, J = 8, 6.5 Hz, 1H); C nmr δ: 202.7 (s), 173.9 (s), 172.5 (s), 169.8 (s), 134.0 (d), 134.4 (d), 77.6 (s), 50.7 (s), 44.1 (d), 42.5 (d), 39.8 (d), 23.1 (q), 21.4 (q), 15.0 (q); ms *m/e* (M^+): 292. *Anal.* calcd. for $C_{14}H_{16}O_5N_2$: C 57.53, H 5.52, N 9.95; found: C 57.57, H 5.50, N 9.57.

N-Amino-5-acetoxy-1,5-dimethyl-6-oxobicyclo[2.2.2]oct-7-ene-*endo*-2,3-dicarboximide (2.43 g, 8.31 mmol), pyridine (1.40 g, 17.70 mmol), and benzoyl chloride (1.17 g, 8.32 mmol) were dissolved in benzene (150 mL), and the solution was allowed to stand for 1.5 h. Acetyl chloride (0.65 g, 8.28 mmol) was added to the reaction mixture, and the solution was allowed to stand for 5 h. The reaction mixture was filtered, the solid residue was extracted with boiling benzene (50 mL), and the extract was filtered. The benzene solutions were combined and extracted with water (100 mL), aqueous 1% sodium bicarbonate (100 mL), and aqueous 1% hydrochloric acid. The organic phase was dried, filtered, and evaporated to give a pale yellow oil (2.87 g), which crystallized on standing. The crude product was chromatographed on a silica gel column (300 g) with ether. The fractions that contained both a benzoyl group and an acetyl group, as indicated by ^{1}H nmr spectroscopy, were combined and evaporated to give a white crystalline solid. This was chromatographed on a silica gel column (40 g) with ether. The fractions that contained both a benzoyl and an acetyl group were combined and evaporated to give a white crystalline solid (1.09 g). Two recrystallizations from ether at −30°C gave **12** (0.18 g), mp 149–180°C; λ_{max}: 5.57 (w), 5.74 μm; H nmr δ: 2.03, 2.06 (2 s, 3H), 2.43 (s, 0.9H), 2.60 (s, 2.1H), 4.93 (dd, J = 8, 2 Hz, 0.7H), 5.53 (dd, J = 8, 7 Hz, 0.7H), 5.93 (dd, J = 8, 2 Hz, 0.3H), 6.35 (dd, J = 8, 7 Hz, 0.3H); ms *m/e* (M^+): 438. *Anal.* calcd. for $C_{23}H_{22}O_7N_2$: C 63.01, H 5.06, N 6.39; found: C 63.02, H 5.18, N 6.63.

Dimethyl exo-*5-Acetoxy-1,5-dimethyl-6-oxobicyclo[2.2.2]oct-7-ene*-endo-2-endo-*3-dicarboxylate (13)*

exo-5-Acetoxy-1,5-dimethyl-6-oxobicyclo[2.2.2]oct-7-ene-*endo*-2,3-dicarboxylic acid anhydride (**2**) (1.10 g, 3.95 mmol) was dissolved in methanol (50 mL), and the solution was boiled at reflux for 21 h. Evaporation gave a clear, colorless oil, which was taken up in ether (100 mL). The solution was titrated with ethereal diazomethane until the yellow color persisted. Evaporaion gave a clear, colorless oil, which crystallized on standing. Recrystallization from methanol at −20°C gave **13** as a white crystalline solid (1.15 g, 90% from **2**). Recrystallization from methanol gave **13**, mp 137.5–138°C; λ_{max}: 5.76 μm; λ_{max} (ε): 302 (90) nm; H nmr δ: 1.27 (s, 3H), 1.55 (s, 3H), 2.06 (s, 3H), 3.31 (s, 2H), 3.62 (s, 3H), 3.66 (s, 3H), 4.08 (br d, J = 7 Hz, 1H), 5.87 (dd, J = 8, 2 Hz, 1H), 6.61 (dd, J = 8, 7 Hz, 1H); C nmr δ: 203.0 (s), 171.7 (s), 171.2 (s), 169.8 (s), 134.9 (d), 131.5 (d), 79.4 (s), 52.0 (q), 51.9 (q), 50.3 (s), 49.5 (d), 44.4 (d), 42.6 (d), 21.7 (q), 15.6 (q); ms *m/e* (M^+): 324. *Anal.* calcd. for $C_{16}H_{20}O_7$: C 59.25, H 6.22; found: C 59.24, H 6.15.

exo-*5-Hydroxy-1,5-dimethyl-6-oxobicyclo[2.2.2]octa-2,7-diene-2-carboxylic Acid (15)*

2,6-Dimethyl-*o*-quinol acetate (**1**) (3.00 g, 16.65 mmol) and propiolic acid (1.16 g, 16.56 mmol) were dissolved in benzene (100 mL) and the solution was boiled at reflux for 600 h. The reaction mixture was extracted with aqueous sodium hydroxide (0.666 g, 16.65 mmol) in 80 mL of water. The aqueous phase was acidified with concentrated hydrochloric acid to pH 5 and extracted with ether (5 × 5 mL). The ethereal extracts were combined, dried, filtered, and evaporated to give a brown oil (2.06 g), which slowly crystallized on standing. Sublimation (170°C/0.005 Torr) followed by a second sublimation (100°C/0.005 Torr) gave a pale amber solid. Two recrystallizations from ether/benzene gave **15** (1.57 g, 46%) as a white crystalline solid. Recrystallization from ether/benzene gave **15**, mp 196–196.5°C; λ_{max} (ε): 237 (2200), 306 (90) nm; C nmr δ: 205.7 (s), 167.6 (s), 147.5 (d), 137.4 (d), 136.3 (s), 136.0 (d), 68.8 (s), 50.5 (d), 57.8 (s), 27.3 (q), 14.9 (q); ms *m/e* (M^+): 208. *Anal.* calcd. for $C_{11}H_{12}O_4$: C 63.45, H 5.81; found: C 63.31, H 5.86.

exo-*5-Hydroxy-1,5-dimethyl-6-oxobicyclo[2.2.2]octane-exo-2-carboxylic Acid (20)*

exo-5-Hydroxy-1,5-dimethyl-6-oxobicyclo[2.2.2]octa-2,7-diene-2-carboxylic acid **15** (81.6 mg, 0.392 mmol) was hydrogenated in methanol (50 mL) over 5% Pd/C (52 mg) at room temperature and atmospheric pressure until uptake of hydrogen ceased. Filtration followed by evaporation gave a clear, colorless oil, which solidified slowly on standing. Sublimation (140°C/0.005 Torr) gave **20** (81.5 mg, 98%) as a white crystalline solid, mp 158–158.5°C; λ_{max} (ε): 292 (41), 303 (39) nm; C nmr δ: 216.3 (s), 180.1 (s), 74.9 (s), 48.6 (d), 44.5 (s), 37.9 (d), 30.4 (t), 25.8 (t), 23.1 (q), 22.0 (t), 18.0 (q); ms *m/e* (M^+): 212. *Anal.* calcd. for $C_{11}H_{16}O_4$: C 62.25, H 7.60; found: C 62.29, H 7.58.

exo-*5-Hydroxy-1,5-dimethyl-6-oxobicyclo[2.2.2]octane-exo-2-carboxylic Acid Lactone (21)*

exo-5-Hydroxy-1,5-dimethyl-6-oxobicyclo[2.2.2]octane-*exo*-2-carboxylic acid (**20**) (58 mg, 0.27 mmol) and *p*-toluenesulfonic acid (4 mg) were dissolved in dry benzene (100 mL). The solution was boiled under reflux in a Soxhlet apparatus containing calcium hydride in the extraction thimble for 18 h. Evaporation gave a white solid which was sublimed (35°C/0.001 Torr) to give **21** (49 mg, 92%) as a white crystalline solid. Addition of calcium hydride to a benzene solution of **21**, followed by evaporation after evolution of hydrogen ceased, and then sublimation (35°C/0.001 Torr) gave **21**, mp 42–47°C; C nmr δ: 208.1 (s), 173.0 (s), 85.5 (s), 46.4 (d), 41.4 (s), 36.4 (d), 31.7 (t), 26.8 (t), 23.0 (t), 17.2 (q), 14.7 (q). On exposure to the atmosphere **21** was rapidly hydrolyzed to **20**, and a satisfactory elemental analysis could not be obtained.

Acknowledgement

We thank the Natural Sciences and Engineering Research Council of Canada for support of this work.

1. P. YATES and H. AUKSI. Can. J. Chem. **57**, 2853 (1979); Chem. Commun. 1016 (1976).
2. W. METLESICS, F. WESSELY, and H. BUDZIKIEWICZ. Monatsh. Chem. **89**, 102 (1958).
3. G. E. LANGFORD, H. AUKSI, J. A. GOSBEE, F. N. MACLACHLAN, and P. YATES. Tetrahedron, **37**, 1091 (1981).
4. K. TORI, Y. TAKANO, and K. KITAHONOKI. Chem. Ber. **97**, 2798 (1964).
5. S. M. VERMA and C. K. RAO. Tetrahedron, **28**, 5029 (1972).
6. S. M. VERMA, O. S. RAO, and C. K. RAO. Tetrahedron Lett. 1639 (1973).
7. S. M. VERMA and O. S. RAO. Tetrahedron, **30**, 2371 (1974).
8. S. M. VERMA and A. K. SINGH. Indian J. Chem. **15B**, 700 (1977).
9. K. HOLMBERG. Acta Chem. Scand. Ser. B, **28**, 857 (1974).
10. K. HOLMBERG, H. KIRUDD, and G. WESTIN. Acta Chem. Scand. Ser. B, **28**, 913 (1974).
11. N. G. VANNENBERG and S. BRASEN. Acta Chem. Scand. **24**, 1894 (1970); E. ADLER, S. BRASEN, and H. MIYAKE. Acta Chem. Scand. **25**, 2055 (1971); E. ADLER and K. HOLMBERG. Acta Chem. Scand. **25**, 2775 (1971); Acta Chem. Scand. Ser. B, **28**, 465 (1974); **28**, 549 (1974); B. KARLSSON, P. KIERKEGAARD, A.-M. PILOTTI, A.-C. WIEHAGER, and B. O. LINDGREN. Acta Chem. Scand. **27**, 1428 (1973); B. KARLSSON, A.-M. PILOTTI, and A.-C. WIEHAGER. Acta Chem. Scand. **27**, 2945 (1973); **27**, 2955 (1973); H.-D. BECKER. Justus Liebigs Ann. Chem. 1675 (1973).
12. R. C. COOKSON and N. S. WARIYAR. J. Chem. Soc. 2302 (1956).
13. R. B. WOODWARD and R. HOFFMANN. The conservation of orbital symmetry. Academic Press, New York. 1970. pp. 145–146.
14. I. FLEMING. Frontier orbitals and organic chemical reactions. Wiley, New York. 1976. Chapt. 4.
15. M. KAKUSHIMA. Can. J. Chem. **57**, 2564 (1979).
16. K. L. WILLIAMSON, Y.-F. L. HSU, R. LACKO, and C. H. YOUN. J. Am. Chem. Soc. **91**, 6129 (1969); K. L. WILLIAMSON and Y.-F. L. HSU. J. Am. Chem. Soc. **92**, 7385 (1970); N. T. ANH. Tetrahedron, **29**, 3227 (1973).
17. S. WINSTEIN, M. SHATAVSKY, C. NORTON, and R. B. WOODWARD. J. Am. Chem. Soc. **77**, 4183 (1955).
18. P. YATES and G. E. LANGFORD. Can. J. Chem. **59**, 344 (1981).
19. S. MCLEAN and P. HAYNES. Tetrahedron, **21**, 2313 (1965); V. A. MIRONOV, T. M. FADEEVA, and A. A. ARKHEM. Dokl. Chem. **174**, 519 (1967).
20. K. N. HOUK. Acc. Chem. Res. **8**, 361 (1975); O. EISENSTEIN, J. M. LEFOUR, N. T. ANH, and R. F. HUDSON. Tetrahedron, **33**, 523 (1977); P. V. ALSTON, R. M. OTTENBRITE, and T. COHEN. J. Org. Chem. **43**, 1864 (1978); I. FLEMING, J. P. MICHAEL, L. E. OVERMAN, and G. F. TAYLOR. Tetrahedron Lett. 1313 (1978).
21. G. W. K. CAVILL, E. R. COLE, P. T. GILHAM, and D. J. MCHUGH. J. Chem. Soc. 2785 (1954).

Can. J. Chem. Downloaded from www.nrcresearchpress.com by 210.87.254.5 on 09/06/12
For personal use only.

Some regularities in the behavior of salting constants for polar molecules in aqueous electrolyte solutions

CLAUDE TREINER

Laboratoire d'Electrochimie, Université P. et M. Curie, 4, place Jussieu, 75230 Paris, France

Received December 19, 1980

CLAUDE TREINER. Can. J. Chem. **59**, 2518 (1981).

The salting effect of polar molecules in aqueous electrolyte solutions has been examined in the case of 22 solute molecules. It is observed that the salting constants of polar and nonpolar molecules of the same size in a given salt solution are close to each other and are generally greater than a critical diameter of the solute molecules. Using the available data from the literature, the salting constants k_s of neutral polar molecules by univalent cation electrolytes has been classified in three groups: (*1*) Organic molecules and inorganic salts: for a given electrolyte k_s is a monotonous function of the solute size and the nonelectrolyte dipole moment plays no role. (*2*) Organic molecules and organic salts: again a smooth variation of k_s with size is observed whatever the polar mono-functional molecule. (*3*) Inorganic molecules and inorganic salts: a correlation is exhibited between k_s and the solute dipole moment. These observations may be interpreted by assuming that both ends of a dipole are to be available to solute + solvent interactions for a dipole effect to be observed.

Furthermore it is shown that in case *1*, the scaled-particle theory with incorporation of a preferential solvation phenomenon may be useful for predicting salting out effects of polar molecules in inorganic salt solutions. In case *2* an approach based on microscopic surface tension and molecular surface area is also considered.

CLAUDE TREINER. Can. J. Chem. **59**, 2518 (1981).

L'effet de sel de molécules polaires dans des solutions aqueuses électrolytiques a été considéré dans le cas de 22 molécules de soluté. On a observé que les constantes de relarguage de molécules polaires et non polaires de même taille dans une solution électrolytique donnée sont proches les unes des autres et généralement égales au dessus d'un diamètre critique des molécules de soluté. En utilisant les données de la littérature concernant les constantes de relarguages k_s de molécules polaires neutres dans des solutions électrolytiques de cations monovalents, trois types de comportement ont été analysés. (*1*) Molécules organiques et sels inorganiques: pour un sel donné, k_s est une fonction monotone croissante de la taille du soluté et son moment dipole permanent ne joue aucun rôle. (*2*) Molécules organiques et sels organiques: à nouveau k_s varie de manière linéaire avec la taille du soluté polaire mono fonctionnel. (*3*) Molécules inorganiques et sels inorganiques: une corrélation est observée entre k_s et le moment dipolaire du soluté. Ces observations peuvent être interprétées en admettant que les deux extrémités d'un dipole doivent être disponibles à une interaction soluté + solvant pour observer un effet dipolaire.

De plus, on a montré que dans le cas *1*, la théorie des sphères rigides avec incorporation d'un phénomène de solvatation préférentielle peut être utile pour prédire l'effet de sel de molécules polaires par des sels inorganiques. Dans le cas *2*, une approche basée sur la tension interfaciale microscopique et sur la surface moléculaire de contact est également considérée.

Introduction

The salting effect of a nonpolar molecule in an electrolyte aqueous media has been the subject of a number of developments in recent years (1–6). Electrostatic, thermodynamic, and mixed models have been able to characterize the essential features of the salting phenomenon (7); thus the salting constant of a nonpolar molecule in an aqueous electrolyte solution may be predicted with reasonable success using, for example, the scaled-particle theory (3–5, 8) (SPT). The case of polar solutes is much less documented although some attempts of generalization have been made in the reviews by McDevit and Long (9) and by Sergeeva (10).

The usual way of investigating ion + solvent interactions in solution is to use a polar component as a cosolvent to water for example, the electrolytes being used as solutes. There is a very large literature on such systems because mixed solvents are useful media for a number of chemical reactions (11). However, mixed solvents are very difficult media to deal with from a theoretical point of view, in particular because structural effects are responsible for many of the essential phenomena which occur in these mixtures; moreover, there are some reasons to believe that the investigations of solute + solvent interactions using solutes standard thermodynamic quantities as obtained by extrapolation procedures at constant solvent composition may lead to difficulties in their interpretation (12). Some attempts have been made to apply the SPT to large ions considered as nonpolar solutes (13–16) in mixtures of polar solvents, the influence of the charge being neglected, an approach which cannot be generalized.

Several investigations have also applied the SPT approach to the salting effect of polar molecules by organic and inorganic electrolytes in water (17–21) but the reasons of the semi-success of these at-

0008-4042/81/162518-09$01.00/0

©1981 National Research Council of Canada/Conseil national de recherches du Canada

Can. J. Chem. Downloaded from www.nrcresearchpress.com by 210.87.254.40 on 09/06/12
For personal use only.

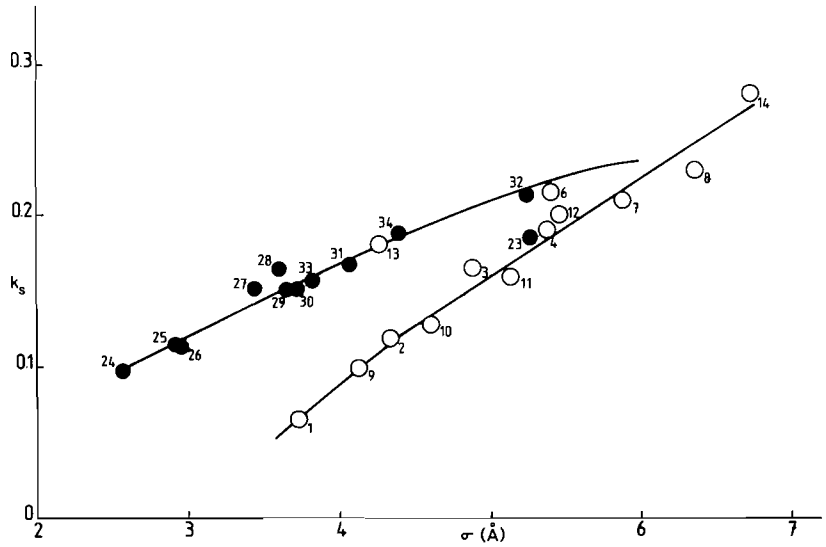

FIG. 1. Salting constant versus hard-sphere diameter for polar ○ and nonpolar ● solutes in aqueous NaCl solutions (chart for polar, see Table 3; for nonpolar: He = 24, Ne = 25, H_2 = 26, Ar = 27, Kr = 28, O_2 = 29, N_2 = 30, Xe = 31, SF_6 = 32, CH_4 = 33, C_2H_6 = 34).

tempts has not been discussed. This is surprising since the permanent dipole of the solute molecules was ignored in these developments (5).

In this article we shall try to consider the different types of behavior of polar molecules with respect to electrolytes in aqueous media by comparing the experimental data available for a large number of molecules in a given electrolyte solution; we shall also show under which conditions the SPT might be useful as a predictive tool in the case of polar solutes in inorganic salt solutions, and suggest some directions for future research in the field of ion–molecule interactions.

Presentation of Data

There are several formal definitions of the salting constant k_s of a molecule in a given medium. The following definition may be preferred (22):

$$k_s = -\left(\frac{\partial \ln m_{NE}}{\partial m_E}\right)\mu_{NE}$$

This equation represents the variation of m_{NE}, the molal solubility of a nonelectrolyte (NE), with electrolyte molality m_E at constant NE chemical potential in a given solvent. k_s is the Setchenov constant. In the case of a soluble volatile solute, m_{NE} may be replaced by applying Henry's law.

All data are presented on the molarity scale as advocated by Ben-Naim (23). Before any discussion on the behavior of polar molecules as such, it may be instructive to compare the Setchenov constant of polar and nonpolar molecules in a given electrolyte solution. We have chosen firstly NaCl as the electrolyte because the most extensive and accurate set of data are available for NaCl aqueous solutions. Figure 1 presents these data as a function of the hard sphere diameter of the solute molecule. We shall return to this parameter in the following section. We have avoided some nonpolar molecules such as CO_2 which presents some complications with water (24) and polar molecules such as acids or bases with specific properties in aqueous solutions. The solutes of Figs. 1 to 3 should be considered as neutral molecules as defined by Long and McDevit (9).

The essential characteristic of the curves of Fig. 1 is their amazing regularity. k_s increases with increasing size of the solute for nonpolar and for polar solutes and the two lines seem to join each other for a solute molecule with $\sigma \sim 6$ Å: thus benzene is on the polar line and *tert*-butanol on the nonpolar one. Clearly the salting effect is not very different for both classes of solutes for a given size, and the dipole moment of the polar molecules plays no role (μ ranges from 1.6 to 3.4 D); no correlation can be found between k_s and the dipole moment of these organic molecules.

There are two exceptions among the monofunctional organic molecules for which data were available from the literature: one is nitromethane which seems to behave as a nonpolar molecule although its dipole moment is μ = 3.37 D and the other (not

Can. J. Chem. Downloaded from www.nrcresearchpress.com by 210.87.254.40 on 09/06/12
For personal use only.

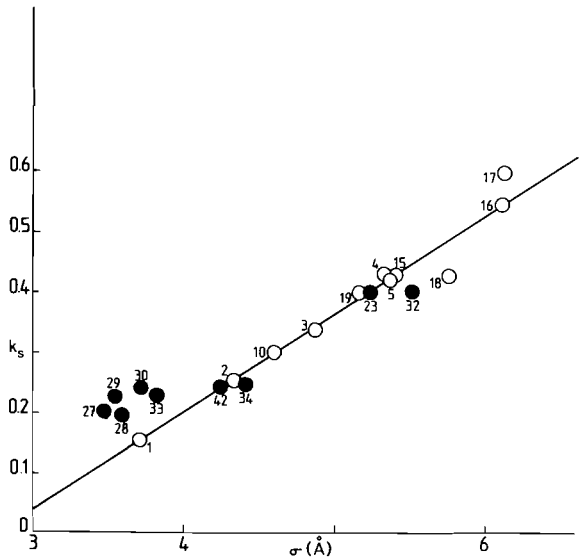

FIG. 2. Salting constants versus hard-sphere diameters for polar ○ and nonpolar ● solutes in aqueous $(NH_4)_2SO_4$ solutions. (C_2H_4 = 42 otherwise as Fig. 2).

shown here) is the *n*-alkylacetate series of Cross and McTigue (25) which is essentially below the polar line and joins it only for the tetrapropylacetate. Whether this is the result of a specific behavior or is related to some experimental difficulty cannot be identified at the present time.

Figure 2 presents another series of salting constants of polar molecules with ammonium sulfate as the electrolyte, taken from the Deno and Spink compilation (26). We observe a smooth variation of k_s with solute size. The aldehyde series is an exception just like the alkylacetate was for sodium chloride with only butyraldehyde on the polar line. The solutes represent a large variety in monofunctional group molecules and dipole moments; the figure again stresses the importance of the volume effect. Data for nonpolar solutes were not available for a valuable comparison of polar and nonpolar molecules in this case; however, as the SPT theory has been shown to be able to predict the salting constant of nonpolar molecules by aqueous inorganic salt solutions (3–5), we have calculated theoretical values for a number of nonpolar molecules of Fig. 1 using Masterton and Lee (3) equations (see Appendix) and the physical parameters quoted therein. The difference between the nonpolar and the polar molecules is even smaller than in the case of NaCl. There may be a certain degree of coincidence in this case but for other less well documented cases such as sodium sulfate, the difference between nonpolar and polar salting effects is also small and decreases with increasing size of the solute molecule.

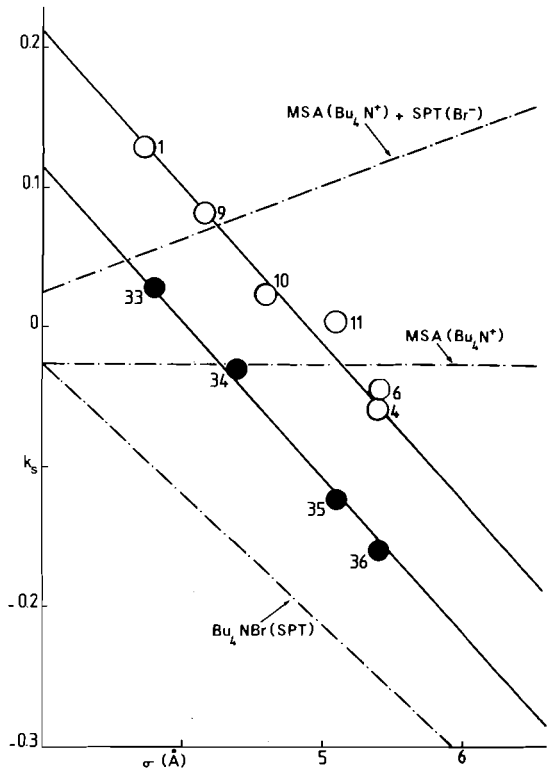

FIG. 3. Salting constants versus hard-sphere diameters for polar ○ and nonpolar ● solutes in aqueous $n Bu_4NBr$ solutions. Full curves (experimental), dotted curves (calculated); SPT = scaled-particle theory, MSA (molecular surface area concept, eq. [7]).

This rule seems general enough at least in the case of inorganic electrolytes with monovalent cations to be used as a criterion for testing the accuracy of salting constants in a given electrolyte solution.

Salting constant values of polar molecules by salts with multivalent cations such as transition metal ions are unfortunately scarce. The available data (20, 21, 27) suggest that the situation is more complex than in the case of monovalent cations; this might be true even for nonpolar molecules with hardly any data at all.

Figure 3 presents an apparently different situation of a salting effect of polar molecules by a classical organic electrolyte: tetrabutylammonium bromide. We also observe a smooth variation of k_s with solute size and the passage of a salting-out to a salting-in effect with increasing size of the solutes. The hydrocarbon gases are more salted-in than the polar molecules; the difference observed is relatively small (the same order of magnitude as for the preceding cases) but the two lines run parallel to each other. A known exception among the nonpolar molecules is benzene which is much more

Can. J. Chem. Downloaded from www.nrcresearchpress.com by 210.87.254.40 on 09/06/12
For personal use only.

Can. J. Chem. Downloaded from www.nrcresearchpress.com by 210.87.254.40 on 09/06/12
For personal use only.

salted-in than the other solutes in Fig. 3. However, for aromatic molecules as a class of compounds, the salting-in effect is also a quasi-linear function of the size of the substituents. Again the dipole moment plays no role and benzene with a dipole moment of zero and nitrobenzene with a dipole moment of $\mu = 3.99$ D have nearly the same k_s value in aqueous NaCl solutions. Other examples of that sort may be found in Long and McDevit (9) review or in Aveyard and Heselden paper (18).

Interpretation of Salting Constants

(A) The Scaled-particle Theory

We have observed that the salting effect of polar organic molecules by electrolytes in water is essentially a size- or volume-effect. The scaled-particle theory approach is then the most obvious model to be used in the complex situation we are dealing with.

Formally the SPT model (28, 29) as used by most authors (3) in the case of the salting effect may be described by the following relationship:

$$[2] \quad k_s = \frac{1}{2.303RT}\left(\frac{\partial G(\mathrm{CAV})}{\partial m_E}\right)_{m_E \to 0} + \frac{1}{2.303RT} \times \left(\frac{\partial G(\mathrm{INT})}{\partial m_E}\right)_{m_E \to 0} + \left(\frac{\partial \log \rho_i}{\partial m_E}\right)_{m_E \to 0}$$

where G(CAV) is the free energy of cavity formation, G(INT) the free energy interaction term between the solute and all solvent molecules, and ρ_i the density of each particular species. G(CAV) may be calculated from a knowledge of the hard sphere diameter of the solute and solvent molecules and the partial molar volume at infinite dilution of the ions.

The free energy interaction term that is proposed by Shoor and Gubbins or by Lucas (4, 5) is an enthalpy term (the entropy of interaction is assumed negligible). In the present formulation (see Appendix) the only forces taken into account are the dispersion forces between solute and all solvent particles (Lennard–Jones potential), and induction forces between solute and water dipoles; in particular no induction forces are introduced between the ion and the solute molecules. This is a simplification even for a nonpolar molecule (5) as it assumes that the radial distribution function $g_{1j}(r) = 1$ for the solute molecule in the interaction term:

$$[3] \quad G(\mathrm{INT}) \approx \sum_{j=1}^{m} \int_{r=a_{1j}}^{\infty} u_{1j}(r) g_{1j}(r) \rho_j 4\pi r^2 \, dr$$

where u_{1j} is the pair potential, ρ_{1j} the particle density, 1 stands for the solute and j for all solvent molecules (2 for water, 3 and 4 for the ions). In other words, the distribution of the ions is supposed to be uniform around the solute molecule (5). This assumption is certainly wrong for a polar solute. We have shown recently (21) that a reasonable agreement may be found between theory and experiment if we assume that polar molecules, unlike nonpolar ones, induce a preferential solvation phenomenon. Numerous investigations on the behavior of electrolytes in mixed aqueous solvents using extrathermodynamic approaches have shown that the standard free energy of transfer of cations or anions from water to mixed solvents is of opposite sign; this empirical finding has been widely interpreted as a consequence of a preferential solvation of cations by the organic component of the mixture and of anions by water (30). This conclusion may be introduced into eq. [3] by assuming that $g_{13}(r) = 0$ for anions and $g_{14}(r) = 1$ for cations. Of course the real situation is not as clear-cut but there is no way of calculating the distribution of ions around a solute and with these assumptions we avoid the introduction of an adjustable parameter. Finally, the interactions between water molecules and ions are taken into account through the cavity term by making use of the partial molar volume of the ions at infinite dilution in water.

The physical parameters used in the calculations were chosen as follows:

(*1*) The hard-sphere diameters: they were deduced, in the case of the polar solutes, from de Ligny's empirical formula (24) in order to get a consistent set of data.

$$[4] \quad \tfrac{1}{6}\pi N \sigma_1^3 = -10 + 1.13 V_W$$

where V_W is Bondi's van der Waals volumes (31). These values (Table 1) are close to those derived by Kim (32) from an empirical correlation between hard sphere diameters and solvent molar volumes. It is noteworthy that in the case of a salting-out phenomenon G(CAV) and G(INT) are of opposite sign so that relatively small errors on σ mostly cancel out. The hard-sphere diameters for the ions (Table 2) were deduced from SPT calculations for the case of nonpolar solutes using appropriate combination of salts (case of ammonium sulfate) and the set of eqs. [8] to [10] (see Appendix). Crystallographic radii were used for Na^+ and Cl^-. Finally Hirschfelder values (33) were adopted for the nonpolar molecules of Figs. 1 to 3.

(*2*) The energy parameter ε/k: the energy parameters of the Lennard–Jones potential for the ions were calculated using Mavroyannis–Stephen theory as recommended by Shoor and Gubbins (5); the recommended values of Mauritz and Rummens

Can. J. Chem. Downloaded from www.nrcresearchpress.com by 210.87.254.40 on 09/06/12
For personal use only.

were used for the polar molecules (34). The same value was used for a series of compounds (e.g. alkylethers) as the dependence of ε/k on size is small in a polar series (34).

(*3*) The polarizability of the molecules was calculated using the refraction index additivity principle with

$$[5] \quad \alpha = 3R/4\pi N$$

where N is Avogadro's number.

Before presenting the results of these calculations it is interesting to note that ε/k averages a value of 417 ± 60 for all polar solutes of Table 1. As for the nonpolar molecules, ε/k varies from 10 for the smallest molecule of the nonpolar series of Fig. 1 (helium) to 200 for hexafluorosulfide (33). Thus, the G(INT) term being negative it is clear that k_s will be less for a polar molecule than for a nonpolar one of equal size simply because the interaction parameter ε/k is larger in the former case than in the latter. The relative position of the two lines of Fig. 1 is therefore a consequence of the value of a parameter which concerns only the nonpolar part of the molecules.

Table 2 presents the results of our calculations in the case of the inorganic salts, assuming preferential solvation of the anions by water; note that as an average $k_{s(calc)}$ is off by $0.04k_s$ unit with a systematic deviation towards high values; this is a remarkable result as no adjustable parameter was introduced and that precision of the order of ± 0.02 is common

TABLE 1. Some physical properties of polar molecules

Solutes	σ_1 (Å)	(ε/k) (K)	$\alpha_1\ 10^{-24}$ ($cm^3\ mol^{-1}$)	μ (D)
Methanol	3.71	385	3.27	1.66
Ethanol	4.34	450	5.11	1.66
1-Propanol	4.88	480	6.96	1.66
1-Butanol	5.38	480	8.81	1.66
2-Butanol	5.39	480	8.81	1.66
tert-Butanol	5.39	480	8.65	1.66
1-Pentanol	5.77	480	10.66	1.8
1-Hexanol	6.12	480	12.55	1.8
Acetonitrile	4.12	491	4.41	3.37
Acetone	4.60	458	6.37	2.72
Tetrahydrofuran	5.11	484	7.79	1.85
Ethylacetate	5.65	372	10.99	1.86
Nitromethane	4.26	527	4.95	3.17
Benzoyltrifluoroacetone	6.73	460	13.94	2.7
Diethylether	5.41	348	8.89	1.22
Dipropylether	6.14	348	12.52	1.22
Diisopropylether	6.14	348	12.52	1.22
Cyclohexanone	5.78	395	11.08	2.8
Butyraldehyde	5.18	414	8.27	2.57
Propionaldehyde	4.68	414	6.41	2.57
Acetaldehyde	4.04	414	4.55	2.49
Formaldehyde	3.44	414	2.68	2.49
Benzene	5.21	401	9.89	0

in the case of the salting parameter of polar molecules due to the experimental conditions. The reason for the presentation of data for NaCl and $(NH_4)_2SO_4$ is not only that a relatively large amount of experimental values were available for these salts but also because they present the extreme cases of most common inorganic salts from the simpler ones to more complicated structures. We believe therefore that the SPT model can be used to predict within a few percent the salting constant of a polar molecule by an inorganic salt solution. This procedure may be useful when no data are available; it can also be used to estimate the precision of a series of solutes in a given electrolyte solution as the dispersion of experimental values around a single line should be minimum.

The above procedure is not feasible in the case of organic electrolytes. The dotted line in Fig. 3 shows the importance of the cavity term alone for a round value of the hard-sphere diameters of Bu_4NBr ($\sigma = 8.0$ Å). The result is known, i.e. the SPT alone can predict a salting-in effect and, as shown in Fig. 3, also the rate of change of k_s with solute size. This means that the free energy of interaction is also size dependent. However, we know that the interaction of organic compounds in water is essentially an entropic phenomenon. Thus it is unjustified to use Shoor and Gubbins' purely enthalpic term for G(INT), an approach which is acceptable for inorganic ions; moreover there is a great deal of compensation between enthalpy and entropy in aqueous media so that the error on evaluation of k_s is less by assuming only a cavity term than by adding an oversimplified interaction term. One of the consequences of this situation is that the use of the SPT approach to obtain the size of organic ions using nonpolar solutes such as the hydrocarbon series (35) may not be valid: a value of 7.81 Å is found for the hard sphere diameter of n-Bu_4NBr.

(B) Model Based on Molecular Surface Area and Surface Tensions

The difficulties related to the choice of the size of the organic ions and especially with the interaction term may lead to an alternative path such as that proposed by Herman (36) and extensively used by Yalkowsky *et al.* (37, 38) in the case of the solubility of scarcely soluble compounds in water and in mixed solvents. As k_s is a standard thermodynamic quantity it can be divided into a cationic contribution and an ionic contribution; we thought it would be interesting to apply this approach to the large organic cation in the present situation of the salt effect, the case of the bromide ion being treated by the SPT as shown in the preceding section.

TABLE 2. Experimental and calculated salting constants for polar molecules in aqueous electrolyte solutions at 25°C

Solutes	NaCl		$(NH_4)_2SO_4$		nBu$_4$NBr
	k_s(th)	k_s(exp)	k_s(th)	k_s(exp)[h]	k_s(exp)
1, Methanol	0.124	0.066[a]	0.245	0.154	0.130[i]
2, Ethanol	0.162	0.118[a]	0.305	0.249	
3, 1-Propanol	0.193	0.165[a]	0.363	0.336	
4, 1-Butanol	0.23	0.19[m]	0.426	0.417	−0.056[j]
5, 2-Butanol			0.42	0.40	
6, *tert*-Butanol	0.23	0.22[b]			−0.045[b]
7, 1-Pentanol	0.25	0.22[m]			
8, 1-Hexanol	0.28	0.24[m]			
9, Acetonitrile	0.17	0.10[c]	0.33	0.30	0.080[k]
10, Acetone	0.177	0.131[c]			0.025[k]
11, Tetrahydrofuran	0.217	0.161[d]			0.011[k]
12, Ethylacetate	0.26	0.20[e]			
13, Nitromethane	0.157	0.181[f]			
14, Benzoyltrifluoroacetone	0.338	0.282[g]			
15, Diethylether			0.47	0.42	
16, Dipropylether			0.58	0.62	
17, Diisopropylether			0.58	0.54	
18, Cyclohexanone			0.46	0.42	
19, Butyraldehyde			0.43	0.42	
20, Propionaldehyde			0.36	0.26	
21, Acetaldehyde			0.31	0.14	
22, Formaldehyde			0.23	−0.02	
23, Benzene		0.178[h]			−0.532[l]

[a] Reference 17.
[b] Reference 51.
[c] Reference 21.
[d] Reference 20.
[e] Reference 52.
[f] Reference 53.
[g] Reference 54.
[h] Reference 55.
[i] Reference 56.
[j] Reference 19.
[k] Reference 42.
[l] Reference 57.
[m] Reference 18.

The solubility of nonpolar compounds in water and in mixed aqueous solvents has been described by the classical relationship (37):

$$[6] \quad \log X/X_0 = k_s x$$

This is the equivalent of the Setchenov equation which can be deduced as eq. [6] from the regular solution theory (39); x is the mole fraction of co-solvent which can be, under ideal or dilute conditions, any of the three components of the solution. Thus k_s may characterize the solute or the co-solvent. It has been shown experimentally that k_s is the same for both components in the present case of a dilute ternary solution (40). Herman (36) and Yalkowsky and co-workers (37) have shown that k_s may be considered a function of the molecular surface area (MSA) of the nonpolar molecule and of the microscopic surface tension of that molecule with each solvent in the case of a ternary solution.

One gets the following relation in the mole fraction scale:

$$[7] \quad k_s = \frac{C\Delta\gamma^0(\mathrm{MSA})M_1}{2.303kT\ 1000}$$

$C = 0.55$ represents a curvature factor, $\Delta\gamma^0$ is the difference of macroscopic surface tensions between the nonpolar component (the tetrabutylammonium ion surface will be assumed to be similar to that of a hydrocarbon solvent such as tetradecane) and water and with the polar component, M_1 is the water molecular weight, k the Boltzmann constant. We have applied eq. [7] to some of the solutes of Table 3. The MSA for Bu_4N^+ is estimated from group values assuming minimum areas (38) to be about 280 Å^2. $\Delta\gamma^0$ was obtained from a plot of surface tension against interfacial tension values obtained with tetradecane (37). The surface tensions of the polar solvents were taken from the literature (41); they are close to each other. As a result the $k_s^{(+)}$ values obtained from eq. [7] are nearly identical: $k_s^{(+)} = -0.026 \pm 0.003$ mol^{-1} in the molarity scale. The contribution of the bromide ion may be calculated using the SPT theory and the

Can. J. Chem. Downloaded from www.nrcresearchpress.com by 210.87.254.40 on 09/06/12
For personal use only.

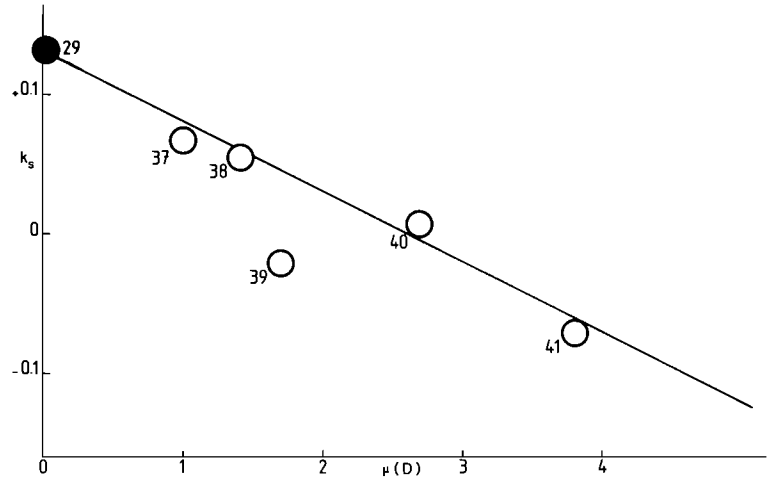

FIG. 4. Salting constant versus dipole moment for polar molecules in aqueous KCl solutions; H_2S = 37, NH_3 = 38, SO_2 = 39, HCN = 40, $N_2H_2NO_2$ = 41.

data of Table 3. The results of these calculations are shown in Fig. 3. The order of magnitude is correct but the bromide ion contribution, being highly size dependent, determines the wrong trend of the variation of k_s with size. It should be pointed out that in deriving eq. [7] it is assumed that the microscopic interfacial tension is an additive combination of its constituent values (37). Figure 3 shows that this assumption is not valid. Again a preferential solvation phenomenon occurs which cannot be taken care of by simple models (additive effects).

Exceptions to the Predominant Volume Effect

There are at least three types of exceptions to the above observations.

The first one is obviously the case of specific interactions, e.g. complexation; they are difficult to predict. Examples are the specific interaction of the silver ion with acetonitrile (21) or that of benzene with tetraalkylammonium ions: k_s for benzene (in aqueous Bu_4NBr solution) is -0.53 and only -0.16 for butane. Specific interactions of aromatic molecules such as naphthalene with a cationic surfactant such as cetyltrimethylammonium bromide has been proposed in order to interpret a high solubility of the solute molecule in these surfactant solutions (43).

The second type of exception is that of polar molecules with polyfunctional groups. It had been already noted by Long and McDevit that when two or more functional groups are attached to the same molecule the resultant effect is not an average value of the effect of each group alone. This is also true for two identical groups: *p*-dioxane for example is situated much below the line corresponding to the regular curve of Fig. 3 with $(NH_4)_2SO_4$. Another characteristic example may be given with the salting constants of compounds with alcohol groups in aqueous *n*-hexylaminobenzoate solutions (38).

TABLE 3. Physical parameters of ions

Ion	σ (Å)	α × 10^{24}	$V_0^{a,b}$
NH_4^+	2.86	1.43	12.46
SO_4^{2-}	4.51	5.83	24.8
Na^+	1.90	0.21	−6.6
Cl^-	3.62	3.02	23.2
Bu_4N^+	8.0	31.2	270.26
Br^-	3.90	4.17	30.1

[a] References 49, 50.
[b] $V_0(H^+) = -5.4\ cm^3\ mol^{-1}$.

We observe the following decreasing order:

ethanol > ethylene glycol > glycerol

Evidently the reverse order would be found from the relative size of each molecule.

In these cases it seems that the prediction of salting constants can only be deduced from some group additivity approach such as that of Savage and Wood (44) specialized to three component systems (45). This approach, however, necessitates a very large number of data which are not available for the moment.

A third type of exception is the most obvious one: the case for which the dipole moment of the solute plays the major role. This case has been noted by Long and McDevit for aqueous KCl with a number of inorganic polar solutes (9). Figure 4 presents the salting constant of such molecules as a function of the dipole moment of the molecule. There is indeed a good correlation which could not be found were the size of the molecules taken as the variable parameter. Thus this observation is in

Can. J. Chem. Downloaded from www.nrcresearchpress.com by 210.87.254.40 on 09/06/12
For personal use only.

Can. J. Chem. Downloaded from www.nrcresearchpress.com by 210.87.254.40 on 09/06/12
For personal use only.

direct contrast to that of Figs. 1 to 3 as it implies that the permanent dipole moment of the molecule should be taken into account for the prediction of salting constants of these polar molecules.

The following arguments may reconcile these apparently conflicting observations. It has been pointed out before that for all aprotic organic polar molecules the negative end of the dipole is much more accessible than the positive end (46). This is also the case for alcohols and indeed all the molecules of Figs. 1 and 2. The first consequence of this situation is that most organic molecules solvate preferentially cations but a second consequence might be that the positive charge of the dipole is shielded in such a way that the molecule does not behave as a permanent dipole. This would be due to the presence of the methyl group in small molecules which usually bears the positive charge of the dipole. In the case of the inorganic molecules of Fig. 5 both ends of each dipolar molecule are equally accessible and thus the molecules do behave as effective dipoles.

Furthermore there are indications that dipole–dipole and ion–dipole interactions in the gas phase are stronger than in the liquid phase. It can be shown that a Setchenov constant is proportional to the free energy of pair wise interactions in solution and that it is equivalent to a second virial coefficient in the liquid phase (22): Rossky and Friedman (47) have shown that the second virial coefficient B_{12} of benzene in aqueous solution is about half its value in the gas phase. The same general conclusion has been noted by Wood (48); the solvent mediates the dispersion forces and the structural effects and this may diminish the dipole–dipole interactions in the liquid phase. The same reasoning may be applied to ion–molecule interactions. Kebarle and co-workers (46) have indeed convincingly proven the importance of the change of solvation free energy in the gas phase when several solvent molecules compete to build the solvation shell of the ion and its relation to structural effects. Thus a single acetonitrile molecule is a better ion solvating agent than a water molecule but the opposite is true when several molecules participate to form the solvation shell.

Finally one cannot rule out completely the possibility of partial cancellation of opposite effects although the cancellation would be almost perfect in the cases of Figs. 1 and 2 especially. For example, permanent dipole–dipole forces between the polar components would contribute to increase k_s whereas the permanent dipole–ion interactions would decrease the salting constant. We have also noted that the entropic interaction term has been ignored. Thus the set of eqs. [9] to [11] may be considered (in the case of polar molecules) as a useful predicative instrument of partly empirical origin.

Conclusions

The previous discussion has shown that the salting constant of neutral mono-functional polar molecules in aqueous electrolyte with univalent cationic solutions may be classified in several groups: (*1*) Organic molecules in aqueous inorganic salt solutions are systematically salted out, the k_s values present an almost linear dependence upon the solute size for a given electrolyte; as a result of the absence of specific interactions the SPT model may be used together with an interaction term between the polar molecule and the cation in order to predict the salting-out effect with a surprisingly good agreement with experiment. The theoretical reasons for such an agreement may only be guessed at the present time. (*2*) Organic molecules in aqueous organic salt solutions may be salted-in or -out according to the respective size of the molecules. A linear dependence upon size is also noted. However, the interaction term between the organic ions and the organic molecules cannot be calculated using simple classical models; an empirical approach based on molecular surface areas reveals the same shortcomings due to the difficulties to incorporate the preferential solvation phenomenon. (*3*) Inorganic molecules in inorganic salt solutions show a salting dependence upon the dipole moment of the molecules which might be related to the availability of both ends of the dipole to interactions with the ions. (*4*) The interaction of inorganic molecules with organic ions is not experimentally known at all and experiments in this area may be found very useful.

1. B. E. Conway, J. E. Desnoyers, and A. C. Smith. Phil. Trans. R. Soc. London, A**256**, 389 (1964).
2. B. E. Conway, D. M. Novak, and L. Laliberte. J. Solution Chem. **3**, 683 (1974).
3. W. L. Masterton and T. P. Lee. J. Phys. Chem. **74**, 1776 (1970).
4. M. Lucas. Bull. Soc. Chim. Fr. 2994 (1969).
5. S. K. Shoor and K. E. Gubbins. J. Phys. Chem. **73**, 498 (1969).
6. C. V. Krishnan and H. L. Friedman. J. Solution Chem. **3**, 727 (1974).
7. B. E. Conway and D. M. Novak. *In* Chemistry and physics of aqueous gas solutions. *Edited by* W. A. Adams. The Electrochemical Society. 1975. p. 115.
8. C. L. de Ligny and N. G. Van der Veen. Rec. Trav. Chim. **90**, 984 (1971).
9. F. Long and W. McDevit. Chem. Rev. **51**, 119 (1952).
10. V. F. Sergeeva. Russian Chem. Rev. **34**, 309 (1965).
11. J. B. F. N. Engberts. *In* Water. Vol. VI. *Edited by* F. Franks. Plenum Press. 1979.

12. E. GRUNWALD and A. EFFIO. J. Am. Chem. Soc. **96**, 423 (1974).
13. M. LUCAS and A. FEILLOLAY. Bull. Soc. Chim. Fr. 1267 (1970).
14. C. TREINER, P. TZIAS, M. CHEMLA, and G. N. POLTORATSKI. J. Chem. Soc. Faraday Trans. I, **72**, 2007 (1976).
15. G. PERRON, N. DESROSIERS, and J. E. DESNOYERS. Can. J. Chem. **54**, 2163 (1976).
16. C. TREINER. Can. J. Chem. **55**, 682 (1977).
17. F. L. WILCOX and E. E. SCHRIER. J. Phys. Chem. **75**, 3757 (1971).
18. R. AVEYARD and R. HESELDEN. J. Chem. Soc. Faraday Trans. I, **70**, 312 (1975).
19. R. AVEYARD and R. HESELDEN. J. Chem. Soc. Faraday Trans. I, **69**, 1953 (1974).
20. M. FROMON and C. TREINER. J. Chem. Soc. Faraday Trans. I, **75**, 1837 (1979).
21. C. TREINER and M. FROMON. J. Chem. Soc. Faraday Trans. I, **76**, 1062 (1980).
22. H. L. FRIEDMAN. J. Phys. Chem. **59**, 161 (1955).
23. A. BEN-NAIM. J. Phys. Chem. **82**, 792 (1978).
24. C. L. DE LIGNY and N. G. VAN DER VEEN. Chem. Eng. Sci. **27**, 391 (1972).
25. R. F. CROSS and P. T. MCTIGUE. Aust. J. Chem. **30**, 2597 (1977).
26. N. C. DENO and C. H. SPINK. J. Phys. Chem. **67**, 1347 (1963).
27. C. JOLICOEUR and P. BERNIER. *In* Chemistry and physics of aqueous gas solutions. *Edited by* W. A. Adams. The Electrochemical Society. 1975. p. 135.
28. H. REISS, H. L. FRISCH, and J. L. LEBOWITZ. J. Chem. Phys. **31**, 369 (1959).
29. R. A. PIEROTTI. J. Phys. Chem. **67**, 1840 (1963).
30. O. POPOVYCH. Crit. Rev. Anal. Chem. **1**, 73 (1970).
31. A. BONDI. J. Phys. Chem. **68**, 441 (1964).
32. J. I. KIM. Z. Phys. Chem. Neue Folge, **113**, 129 (1978).
33. J. O. HIRSCHFELDER, C. F. CURTISS, and R. B. BIRD. *In* Molecular theory of gases and liquids. J. Wiley and Sons. New York. 1954.
34. F. M. MAURITZ and F. H. A. RUMMENS. Can. J. Chem. **55**, 3007 (1977).
35. W. L. MASTERTON, D. BOLOCOFSKY, and T. P. LEE. J. Phys. Chem. **75**, 2809 (1971).
36. H. B. HERMANN. J. Phys. Chem. **76**, 2574 (1972).
37. S. H. YALKOWSKY, S. C. VALVANI, and G. L. AMIDON. J. Pharm. Sci. **65**, 1488 (1976).
38. S. C. VALVANI, S. H. YALKOWSKY, and G. L. AMIDON. J. Phys. Chem. **80**, 829 (1976).
39. J. H. HILDEBRAND, J. M. PRAUSNITZ, and R. L. SCOTT. *In* Regular and related solutions. Van Nostrand Rheinhold Co. 1970. p. 131.
40. J. E. DESNOYERS, G. PERRON, J. P. MOREL, and L. AVEDIKIAN. *In* Chemistry and physics of aqueous gas solutions. *Edited by* W. A. Adams. The Electrochemical Society. 1975. p. 172.
41. A. WEISSBERGER and S. PROSKAUER. Organic solvents. Vol. VII. Interscience Publishers, New York. 1955.
42. C. TREINER, P. TZIAS, and M. CHEMLA. Can. J. Chem. **56**, 844 (1978).
43. M. ALMGREN, F. GRIESER, and J. K. THOMAS. J. Am. Chem. Soc. **101**, 279 (1979).
44. J. J. SAVAGE and R. H. WOOD. J. Solution Chem. **5**, 33 (1976).
45. C. DE VISSER, W. J. M. HEUVESLAND, and G. SOMSEN. J. Solution Chem. **7**, 193 (1978).
46. R. YAMDAGNI and P. KEBARLE. J. Am. Chem. Soc. **94**, 2940 (1972).
47. P. J. ROSSKY and H. L. FRIEDMAN. J. Phys. Chem. **84**, 587 (1980).
48. R. H. WOOD. Private communication.
49. F. J. MILLERO. Chem. Rev. **71**, 147 (1971).
50. H. L. FRIEDMAN and C. V. KRISHNAN. *In* Water. Vol. 3. *Edited by* F. Franks. Plenum Press. 1973.
51. G. PERRON, D. JOLY, J. E. DESNOYERS, L. AVEDIKIAN, and J. P. MOREL. Can. J. Chem. **56**, 552 (1978).
52. A. P. ALTSHULLER and H. E. EVERSON. J. Am. Chem. Soc. **75**, 4823 (1953).
53. G. R. HANGEN and H. L. FRIEDMAN. J. Phys. Chem. **59**, 161 (1955).
54. Y. YOSHIMURA and N. SUZUKI. Talanta, **25**, 489 (1978).
55. N. C. DENO and C. H. SPINK. J. Phys. Chem. **67**, 1347 (1963).
56. C. TREINER. Unpublished data.
57. J. E. DESNOYERS, G. E. PELLETIER, and C. JOLICOEUR. Can. J. Chem. **43**, 3232 (1965).

Appendix

The three terms of eq. [2] as obtained by Masterton and Lee (3) may be put under the form:

[8] $k_s = k_\alpha + k_\beta + k_\gamma$

with

[9] $$k_\alpha = 2.15 \times 10^{20}(\sigma_3^3 + \sigma_4^3) - 2.47 \times 10^{-4}V_0 + \sigma_1[6.45 \times 10^{20}(\sigma_3^2 + \sigma_4^2) + 1.34 \times 10^{28}(\sigma_3^3 + \sigma_4^3) - 4.23 \times 10^4 V_0] + \sigma_1^2[6.45 \times 10^{20}(\sigma_3 + \sigma_4) + 4.01 \times 10^{28}(\sigma_3^2 + \sigma_4^2) + 1.32 \times 10^{36}(\sigma_3^3 + \sigma_4^3) - 4.17 \times 10^{12}V_0]$$

[10] $$k_\beta = -1.85 \times 10^{14}\left(\frac{\varepsilon_1}{k}\right)^{1/2}\left[\alpha_3^{3/4}Z_3^{1/4}\left(\frac{\sigma_1+\sigma_3}{\sigma_3^3}\right)^3 + \alpha_4^{3/4}Z_4^{1/4}\left(\frac{\sigma_1+\sigma_4}{\sigma_4^3}\right)^3 + 6.26 \times 10^{17}V_0\left(\frac{\varepsilon_1}{k}\right)^{1/2}(\sigma_1+\sigma_2)^3 + 4.00 \times 10^{-2}\frac{(V_0\alpha_1)}{(\sigma_1+\sigma_2)^3}\right.$$

[11] $$k_\gamma = 0.016 - 4.34 \times 10^{-4}V_0$$

Indices 1 to 4 refer respectively to solute, water, and ions. (See Tables 1 and 3.) In order to simulate preferential solvation of anions by water molecules α_4 (for example) is put equal to zero, and $V_0 = V_0(+)$ in eq. [10]. Z is the total number of electrons on an ion. The physical constants for water have been already introduced in the calculations of the terms of eqs. [9] to [11] (3).

Can. J. Chem. Downloaded from www.nrcresearchpress.com by 210.87.254.40 on 09/06/12
For personal use only.

Nuclear magnetic resonance studies of proton exchange in imidate esters and amides in strong acid

CHARLES L. PERRIN AND ERIC R. JOHNSTON

Department of Chemistry, D-006, University of California at San Diego, La Jolla, CA 92093, U.S.A.

Received January 6, 1981

CHARLES L. PERRIN and ERIC R. JOHNSTON. Can. J. Chem. **59**, 2527 (1981).

Saturation-transfer or lineshape measurements of kinetics of proton exchange show that H_Z of ethyl acetimidate in 46% H_2SO_4 or ethyl *N*-methylformimidate in 40% H_2SO_4 exchanges faster than H_E, and H_E of protonated 2-iminotetrahydrofuran exchanges faster than H_Z, as expected on the basis of the stabilities of the stereoisomeric imidate esters. In contrast, amide exchange is too fast to measure in aqueous H_2SO_4, but can be measured in 100% H_2SO_4, where H_E and H_Z exchange at equal rates. Also, there is intramolecular exchange occurring at this same rate. These results are interpreted as evidence for exchange in amides via the *N*-protonated intermediate, whose lifetime in H_2SO_4 is sufficiently long to permit the protons on nitrogen to become equivalent. By comparing OH exchange with NH exchange, it is concluded that *N*-protonation is the rate-limiting step. Even though this is a thermodynamically favorable proton transfer in H_2SO_4, its rate constant is significantly lower than the diffusion-controlled limit. The contrasts between imidate esters and amides and between dilute solutions and H_2SO_4 are discussed.

CHARLES L. PERRIN et ERIC R. JOHNSTON. Can. J. Chem. **59**, 2527 (1981).

Le transfert de saturation ou les mesures de la forme des lignes de la cinétique d'échange du proton montre que le H_z de l'acétimidate d'éthyle dans du H_2SO_4 à 46% ou du *N*-méthylformimidate d'éthyle dans du H_2SO_4 à 40% s'échange plus rapidement que H_E, tandis que le H_E de l'imino-2 tétrahydrofuranne protoné s'échange plus rapidement que le H_z tel qu'attendu en se basant sur les stabilités des stéréoisomères des esters imidates. L'échange d'amide, au contraire, est trop rapide pour être mesuré dans du H_2SO_4 aqueux mais il peut être mesuré dans du H_2SO_4 à 100%, où les vitesses d'échange du H_E et du H_z sont égales il y a également un échange intramoléculaire qui s'effectue à cette même vitesse. Les résultats prouvent que l'échange dans les amides se fait via un intermédiaire *N* protoné dont le temps de vie dans le H_2SO_4 est suffisamment long pour permettre aux protons sur l'azote de devenir équivalents. En comparant l'échange de OH à celui du NH ou conclut que la protonation de l'azote est l'étape déterminante. Bien que le transfert de proton dans le H_2SO_4 soit thermodynamiquement favorisé, sa constante de vitesse est significativement plus faible que la limite contrôlée de diffusion. On discute des différences entre les esters imidates et les amides et entre les solutions diluées et de H_2SO_4.

[Traduit par le journal]

Introduction

Two mechanisms have been proposed for acid-catalyzed proton exchange in amides, one involving *N*-protonation (k_p in Scheme 1) (1) and the other a more circuitous one involving the imidic acid (k_o and k_{-i}) (2). We originally sought to distinguish between these by comparing rates of exchange of H_E and H_Z in primary amides (**1**) (3). We observed that H_E exchanges faster, whereas analogy to imidate esters (4) would require H_Z to exchange faster if exchange proceeded via the imidic acid. We therefore concluded (3) that exchange proceeds via *N*-protonation. However, to account for the greater reactivity of H_E, we proposed the additional feature that $RCONH_3^+$ is so strong an acid that its lifetime is too short to permit rotational equilibration about the C—N single bond. Additional evidence for this mechanism has recently been obtained by lineshape (5) and saturation-transfer methods (6–8), as well as evidence for the imidic-acid mechanism for amides with electron-withdrawing substituents (6, 8). In this paper we present our results for exchange in imidate esters, and we compare them with amides.

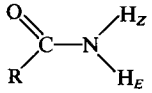

I

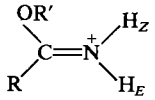

2

$$\begin{array}{lll} RCONHR' + H^+ \underset{k_d}{\overset{k_p}{\rightleftharpoons}} RCONH_2{}^+R' & & K_a{}^N = k_d/k_p \\ k_o \Big\| \; k_{-o} & & K_a{}^O = k_{-o}/k_o \\ RC(OH){=}NHR'^+ \underset{k_i}{\overset{k_{-i}}{\rightleftharpoons}} RC(OH){=}NR' + H^+ & \text{imidic acid} & K_a{}^I = k_{-i}/k_i \end{array}$$

SCHEME 1. *N*-protonation and imidic-acid mechanisms for acid-catalyzed proton exchange in amides.

Exchange in protonated imidate esters (**2**) is a good model for exchange via the imidic acid. (Protonated imidate esters have often been used as models of protonated amides, for study of hydrolysis kinetics (9).) Deprotonation of **2** ought to be comparable to k_{-i} of Scheme 1, so that a determination of the relative reactivities of H_E and H_Z can test whether the imidic-acid mechanism really requires H_Z to exchange faster. Also, a comparison of the

0008-4042/81/162527-09$01.00/0

©1981 National Research Council of Canada/Conseil national de recherches du Canada

Can. J. Chem. Downloaded from www.nrcresearchpress.com by 210.87.254.5 on 09/06/12
For personal use only.

Can. J. Chem. Downloaded from www.nrcresearchpress.com by 210.87.254.5 on 09/06/12
For personal use only.

relative reactivities of amides and imidate esters might permit assessment of the significance of the imidic-acid route.

A definitive distinction between the *N*-protonation and imidic-acid mechanisms is that only the former involves intramolecular exchange. Specifically, it can be derived (8) that for the *N*-protonation mechanism in primary amides

$$[1] \quad k_{ZS} = k_{ZE} = k_{EZ}$$

where k_{ij} is the pseudo-first-order rate constant for exchange of protons from site i (H_E, H_Z, $H_{Solvent}$) to site j. In contrast, the imidic-acid mechanism requires that

$$[2] \quad k_{EZ} = 0 = k_{ZE}$$

Intramolecular exchange cannot occur, since the lifetime of the imidic acid before reprotonation is far too short to permit rotation or inversion (10). Thus the two mechanisms may be distinguished by comparing the rates of intramolecular and intermolecular exchange. Moreover, intramolecular exchange is again impossible for imidate esters, so that these can serve as a check on the experimental methods.

With secondary amides, eqs. [1] and [2] hold only qualitatively. The counterpart of intramolecular exchange is *E*/*Z* isomerization accompanying proton exchange. Such isomerization can occur only in the *N*-protonation mechanism, and not in the imidic-acid mechanism, nor in imidate esters.

It is not easy experimentally to distinguish intramolecular exchange or isomerization from intermolecular proton exchange. The familiar line-broadening or lineshape methods (11) do not measure individual rate constants, but rather the lifetime of a nucleus in each site, whose reciprocal is the sum of all the rate constants for exchange from that site. These methods are adequate for qualitative conclusions regarding secondary amides, but totally inadequate for primary amides. Fortunately, the saturation-transfer method (12, 13) is capable of measuring each individual rate constant. Thus we can test for intramolecular exchange or isomerization.

Experimental

Ethyl acetimidate hydrochloride was prepared according to MacKenzie *et al.* (14); nmr (DMSO-d_6) δ: 1.32 (t, 3H), 2.45 (s, 3H), 4.50 (q, 2H), 11.25 (br s, 1H), 12.20 (br s, 1H). Ethyl *N*-methylformimidate·HBF_4 was prepared according to Kohn and Olofson (15) and extracted from CH_2Cl_2 into aqueous H_2SO_4; nmr (54 wt.% H_2SO_4) δ: 9.7 (v br), 8.32 (d, under solvent peak, visible in 40% H_2SO_4), 4.66 (q, J = 7 Hz, 2H), 3.04 (dd, J = 5.4, 1.2 Hz, 3H), 1.42 (t, J = 7 Hz, 3H); there is also a minor doublet (J = 5 Hz) at δ 3.16, present to the extent of 8%. 2-Iminotetrahydrofuran hydrochloride was prepared from 4-hydroxybutyronitrile (16) according to Nohira *et al.* (17); nmr (DMSO-d_6) δ: 2.30 (m, 2H), 3.20 (t, 2H), 4.80 (t, 2H), 11.49 (br s, 1H), 11.75 (br s, 1H). Other imidates and amides (Aldrich, Fluka, Eastman) and sulfuric acid (Mallinckrodt AR or fuming, standardized vs. NaOH) were commercially available and used without further purification. Samples for nmr studies were quite concentrated, up to 2.5 *M* in amide or 4.5 *M* in imidate. The ratio of solvent protons to NH protons was determined from the weights of the components used to prepare the solutions, or by integrating the nmr spectrum.

The nmr measurements were performed on a Varian HR-220 FT spectrometer at 23°C, except for ethyl *N*-methylformimidate, which was studied on a Varian EM-390 spectrometer at 34°C. Simulation was by Nicolet's ITRCAL program. Details of the methods, including saturation transfer and the advantages of viscous solvents, have been described (13, 18, 19). Specifically, we measure six values of $t_i(j)$, the transfer of saturation (18) from each site j (H_E, H_Z, $H_{Solvent}$) to each other site, i, or the fractional loss of intensity at site i, I_i, on saturating site j:

$$[3] \quad t_i(j) = \frac{I_i^0 - I_i(j)}{I_i^0}$$

and we also measure $M_S(E, Z)$, the apparent spin–lattice relaxation rate constant ($=1/T_{1S}^{app}$) of solvent protons, under conditions that both H_E and H_Z are saturated, as well as $M_E(S)$ and $M_Z(S)$, apparent spin–lattice relaxation rate constants of H_E and H_Z under conditions of solvent saturation. Rate constants were then calculated from equations adapted from Perrin and Johnston (13). In particular,

$$[4] \quad k_{ES} = M_S(E, Z)\frac{t_S(E) - t_S(Z)t_Z(E)}{1 - t_E(S)t_S(E)}\frac{p_S}{p_E}$$

where p_i is the relative population of site i. Also,

$$[5] \quad k_{SE} = M_E(S)\frac{t_E(S) - t_E(Z)t_Z(S)}{1 - t_E(Z) + t_S(Z)[t_E(S) - t_Z(S)]}\frac{p_E}{p_S}$$

$$[6] \quad k_{ZE} = M_E(S)\frac{t_E(Z) - t_E(S)t_S(Z)}{1 - t_E(Z) + t_S(Z)[t_E(S) - t_Z(S)]}\frac{p_E}{p_Z}$$

The equations for k_{ZS}, k_{SZ}, and k_{EZ} are analogous.

Results

Signal Assignments

The downfield substituent of various *N*,*N*-disubstituted imidates and protonated amides has been assigned (20–22) as *E*, just as in amides (23). The only assignment (22) for a protonated primary amide was by analogy of $^1J_{^{15}NH}$ in amides, and this is opposite to the assignment based on long-range couplings. We therefore sought unambiguous assignments.

Figure 1 shows the nmr spectrum of formamide in 100% H_2SO_4(**2**, R = H = R′), along with two simulated spectra. In Fig. 1b the coupling constants of the CH to the downfield and upfield NH are taken as 7 and 15 Hz, respectively (cf. 5 and 14 Hz observed (24) in protonated ethyl formimidate); in Fig. 1c they are reversed. The observed spectrum (both the CH regions and the broadened NH regions) is in better agreement with Fig. 1b. Since $^3J_{trans} > {}^3J_{cis}$, we conclude that H_E is downfield. Figure 2 shows results of an nOe (25) experiment on

Can. J. Chem. Downloaded from www.nrcresearchpress.com by 210.87.254.5 on 09/06/12
For personal use only.

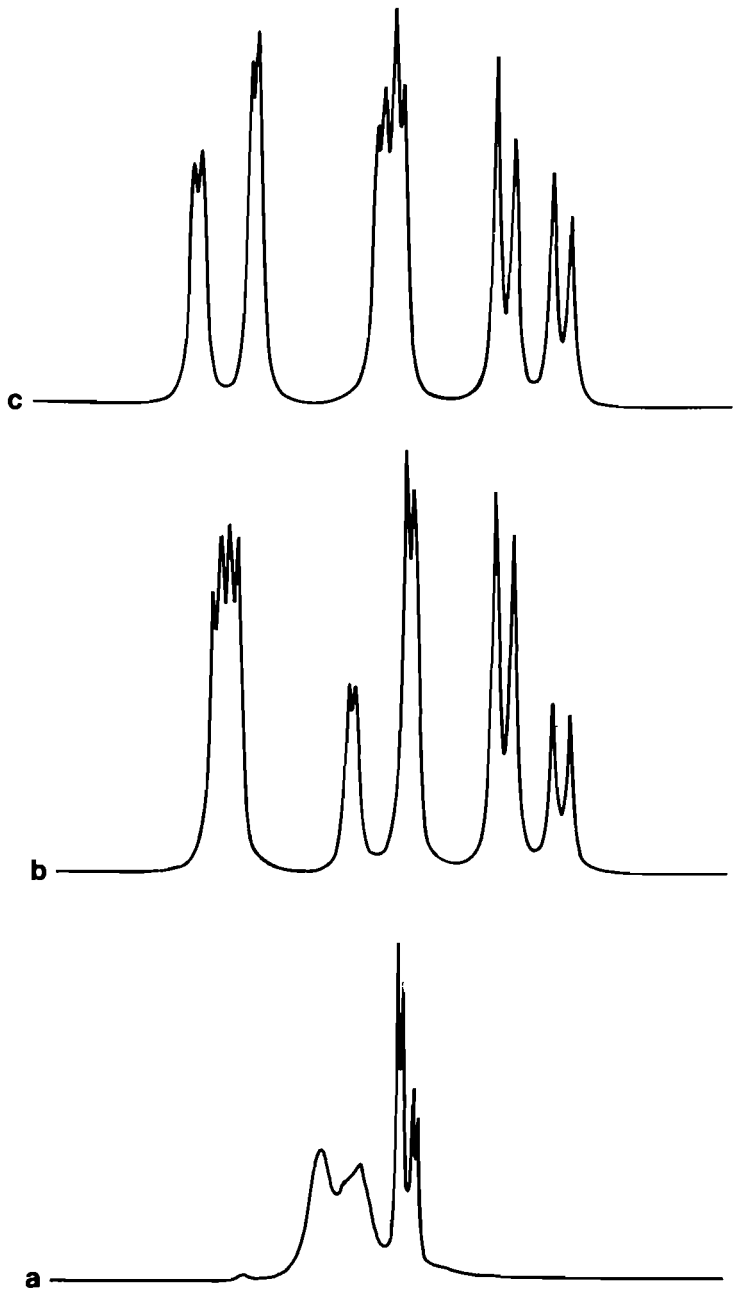

FIG. 1. (a) The nmr spectrum of *O*-protonated formamide. Plot width 600 Hz at 220 MHz. (b,c) Simulated spectra, expanded (see text).

methyl trichloroacetimidate (**2**, R = Cl_3C, R′ = CH_3) in 95% H_2SO_4: $f_{OCH_3}(NH_{upfield})$ = 3.7%, also (not shown) $f_{NH_{downfield}}(OCH_3)$ = 3.8% and $f_{OCH_3}(NH_{downfield})$ = 1.2% (from "spillover"). Therefore we conclude that H_E is again downfield. Since there are no known exceptions, we assume that this assignment also holds for all the other protonated amides and imidates under study.

Exchange Rates

Figure 3 shows a saturation-transfer spectrum of ethyl acetimidate (**2**, R = CH_3, R′ = C_2H_5); the greater transfer of saturation to H_Z shows clearly that this proton exchanges faster. Saturation-transfer data for various imidates and amides are summarized in Table 1, and the kinetic results are in Table 2. The rate constants for intramolecular

Can. J. Chem. Downloaded from www.nrcresearchpress.com by 210.87.254.5 on 09/06/12
For personal use only.

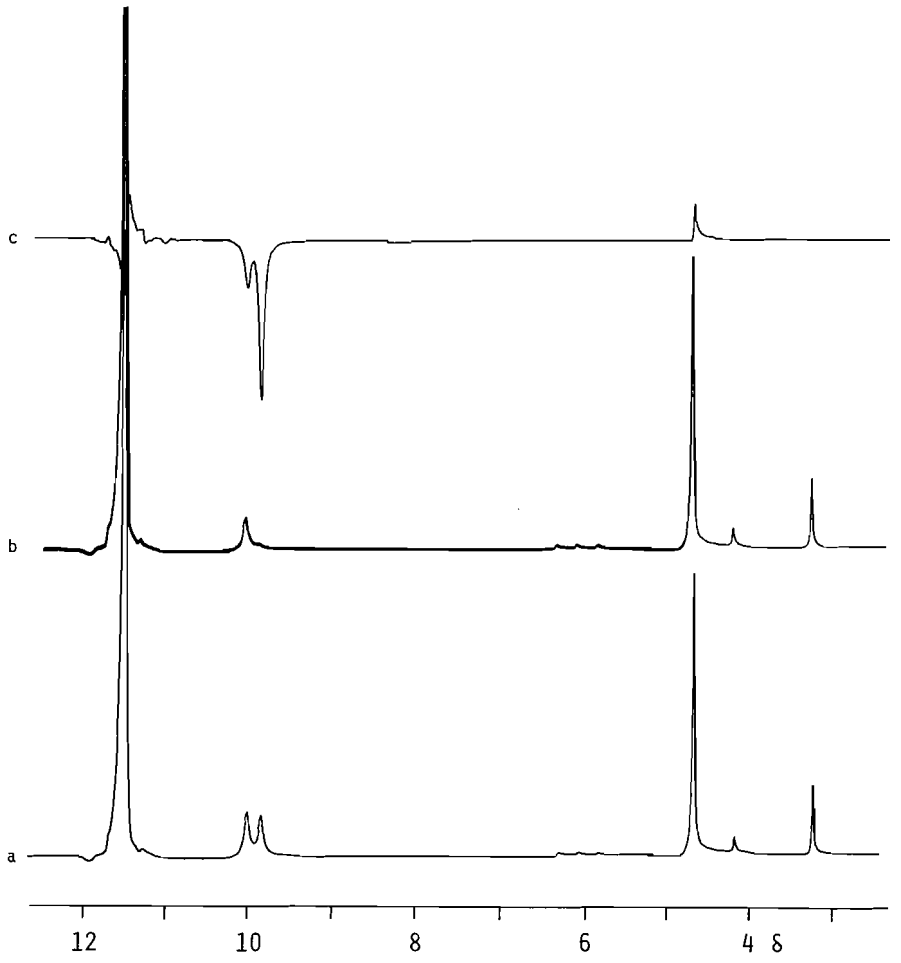

FIG. 2. 220 MHz nOe experiment on methyl trichloroacetimidate in 95% H_2SO_4. (a) Off-resonance-saturation spectrum showing peaks, from left to right: OH, NH_E, NH_Z, OCH_3, impurity, Me_4N^+ (internal standard). (b) Spectrum with upfield NH saturated. (c) Difference spectrum, (b) − (a), X4, showing nOe of OCH_3.

exchange in ethyl acetimidate and acetamide have been corrected for dipole–dipole cross-relaxation (25), determined in 57% H_2SO_4 and fuming H_2SO_4, respectively, where exchange is slow. This correction is small, less than 1.0 s^{-1}, and has been neglected in 3,5-dinitrobenzamide. Figure 4 shows the nmr spectrum of *N*-methylformamide exchanging in ca. 100% H_2SO_4.

Exchange of imidate esters in dilute solutions is too fast to measure. Since the pK_a of a protonated imidate ester is ca. 7.6 (ethyl acetimidate (26)), and since reprotonation of an imidate by H_3O^+ would be diffusion-controlled (27), the lifetime of a protonated imidate in aqueous solution must be ca. 10^{-3} s, far too short for our nmr methods. To reduce the exchange rate, it is necessary to reduce the activity of water. Thus we find that exchange in ethyl acetimidate is slow in 57% H_2SO_4 and measurable by saturation transfer in 46% H_2SO_4. Similarly, exchange in ethyl *N*-methylformimidate, $HC(OC_2H_5)=NHCH_3^+$, is slow in 54% H_2SO_4 and measurable by lineshape analysis in 40% H_2SO_4. Therefore we are definitely dealing with a base-catalyzed exchange, with water as base, quite analogous to k_{-i} in the imidic-acid mechanism for amides. (Hydroxide concentration in these solutions is too low to contribute even at a diffusion-controlled rate.)

Kinetics of amide exchange are quite different, both in dilute acid and in H_2SO_4. Although imidate esters exchange too fast to measure in aqueous solutions, amide exchange is readily measurable (1, 2, 5–8). Of course this difference arises merely because amide exchange requires protonation, whereas the imidate ester is already *O*-alkylated.

The contrast in H_2SO_4 is of greater interest. In stronger acid the amide is converted to its *O*-protonated conjugate acid, so that it is quite

Can. J. Chem. Downloaded from www.nrcresearchpress.com by 210.87.254.5 on 09/06/12
For personal use only.

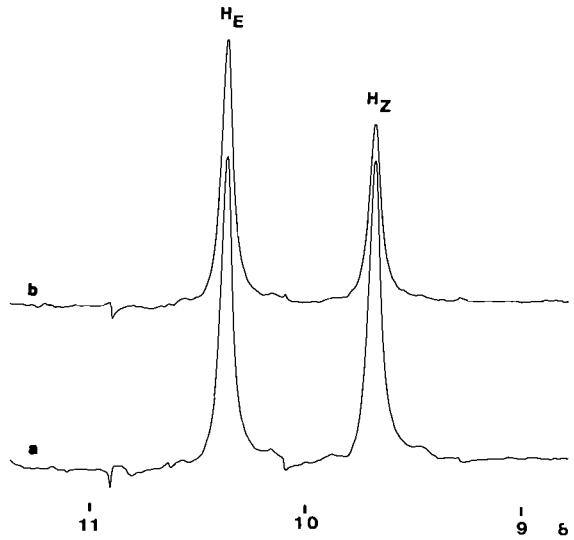

FIG. 3. Saturation-transfer experiment on ethyl acetimidate in 46% H_2SO_4. (a) Off-resonance spectrum. (b) Spectrum with solvent peak (offscale to right) saturated.

comparable to a protonated imidate ester. Then, if the imidic-acid pathway contributes to amide exchange, the two types of substrates should exchange at comparable rates. Nevertheless in 40–50% H_2SO_4, where imidate-ester exchange is readily measurable, amide exchange is too fast to measure. To measure exchange in amides, it is necessary to retard the exchange by going to concentrated H_2SO_4. The reaction is still a base-catalyzed exchange, with HSO_4^- as base (28), since less basic amides exchange faster (29) and since we find that the exchange is stopped in fuming H_2SO_4, where HSO_4^- is converted to the less basic $HS_2O_7^-$. The marked contrast between imidate esters and amides might suggest that different mechanisms are operative. This is discussed below.

Discussion

Exchange in Imidate Esters

The data of Table 2 show that there is no intramolecular proton exchange in ethyl acetimidate; within experimental error k_{EZ} and k_{ZE} are zero. Of course, none is expected, since the lifetime of the imidate before reprotonation by solvent is ca. 10^{-11} s (30), far too short to permit rotation or inversion (10, 22). Thus this result shows that the saturation–transfer method is valid for quantitatively distinguishing intramolecular exchange from intermolecular.

Similarly, there is no *E*/*Z* isomerization accompanying proton exchange of ethyl *N*-methylformimidate. Even in 29% H_2SO_4, where proton exchange is quite fast, the methyl doublets of the *E*

TABLE 1. Saturation-transfer data for proton exchange of imidate esters and amides

	$p_S/p_{E,Z}$	$t_Z(Z)$	$t_Z(E)$	$t_S(E)$	$t_S(Z)$	$t_E(S)$	$t_Z(S)$	$M_E(S)$, s^{-1}	$M_Z(S)$, s^{-1}	$M_S(E, Z)$, s^{-1}
Ethyl Acetimidate	10.65	-0.137 ± 0.01 [a]	-0.119 ± 0.007 [a]	0.025 ± 0.001	0.062 ± 0.004	0.105 ± 0.009	0.03 ± 0.02	6.6 ± 0.3	10.3 ± 0.4	4.08 ± 0.16
2-Iminotetra-hydrofuran·HCl				0	0	0.485	0.450			
Acetamide	12.03	0.202 ± 0.012	0.261 ± 0.015	0.054 ± 0.003	0.052 ± 0.003	0.36 ± 0.02	0.35 ± 0.02	7.8 ± 0.3	7.8 ± 0.3	6.1 ± 0.24
3,5-Dinitro-benzamide	28.1	0.56	0.51	0.26	0.24	0.84	0.76	28 [b]	28	4.1

[a] A negative saturation transfer represents a nuclear Overhauser enhancement.
[b] Taken equal to $M_Z(S)$.

TABLE 2. Kinetic results for proton exchange of imidate esters and amides

	Solvent	k_{ES}, s^{-1}	k_{ZS}, s^{-1}	k_{ZE}, s^{-1}	k_{EZ}, s^{-1}	k_{SE}, s^{-1}	k_{SZ}, s^{-1}
Ethyl Acetimidate	46 wt.% H_2SO_4	1.43 ± 0.09	2.9 ± 0.2	-0.01 ± 0.08[a]	-0.13 ± 0.12[a]	0.083 ± 0.005	0.29 ± 0.02
Ethyl *N*-Methyl-formimidate	40 wt.% H_2SO_4	ca. 4[b]	ca. 70[b]	0[c]	0[c]		
2-Iminotetra-hydrofuran · HCl	Wet DMSO-d_6					Ratio $\cong$ 1.15	
Acetamide	ca. 100% H_2SO_4	3.1 ± 0.3	3.2 ± 0.3	2.3 ± 0.2[a]	3.1 ± 0.3[a]	0.23 ± 0.02	0.23 ± 0.03
3,5-Dinitro-benzamide[d]	ca. 100% H_2SO_4	22	15	22	19	0.9	0.70
Trichloro-acetamide	ca. 100% H_2SO_4	13[b]	13[b]				

[a]Corrected for *E–Z* cross-relaxation.
[b]$k_{ES} + k_{EZ}$ or $k_{ZS} + k_{ZE}$, by line broadening.
[c]From the separate coalescence in 29% H_2SO_4. See text.
[d]Overlap of peaks prevented error analysis. Comparison of $p_i k_{ij}$ with $p_j k_{ji}$ indicates errors of $\pm 15\%$.

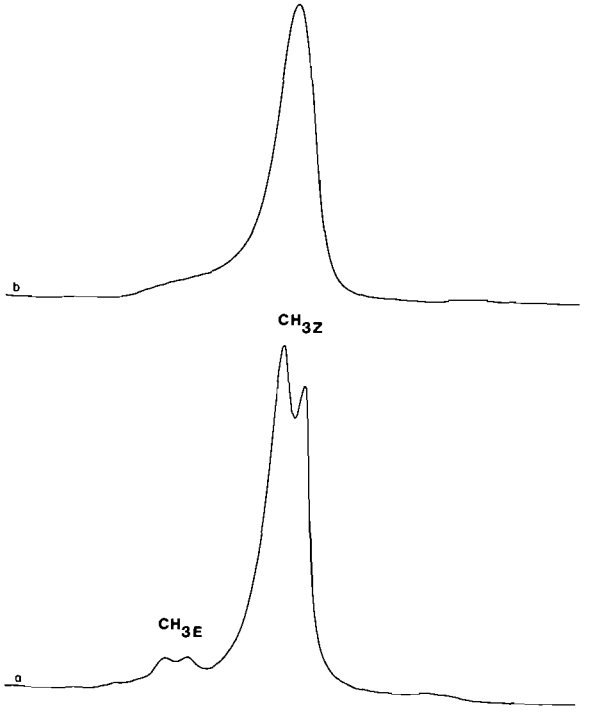

FIG. 4. *N*-Methyl region of *N*-methyl formamide in (a) fuming H_2SO_4. (b) ca. 100% H_2SO_4. Plot width 125 Hz at 220 MHz.

and *Z* forms are seen to coalesce to separate signals. Of course, this is exactly as expected for imidate esters, and gives us confidence that we can distinguish isomerization from proton exchange in secondary amides.

The data also show that in all three imidate esters the more acidic proton exchanges faster. In protonated ethyl acetimidate (**2**, R = CH_3, R′ = C_2H_5) H_Z exchanges significantly faster than H_E, as expected on the basis of the greater stability of the *E* configuration of imidate esters (4). Likewise, H_Z of the *E* isomer of protonated ethyl *N*-methylformimidate, $HC(OC_2H_5)$=$NHCH_3^+$, exchanges much faster than H_E of the *Z* isomer. (This is an intermolecular comparison, and the disparity in rates precluded accurate measurement.) The greater reactivity of H_Z in both these imidate esters is a partial justification for having excluded (3) the imidic-acid mechanism for amide exchange on the basis of the observation that H_E is more reactive. In contrast to the other two imidate esters, in protonated 2-iminotetrahydrofuran (**2**, RR′ = $CH_2CH_2CH_2$), it is H_E that exchanges faster (by 15%, assuming equal T_1's for the two protons). This result is also expected, since 2-(phenylimino)-tetrahydrofuran is predominantly *Z* (31), and since MO calculations (32) on the parent HC(OH)=NH suggest that if the C—O bond is fixed in the less stable *syn*-periplanar conformation, as required by the ring structure, then the *Z* configuration is the more stable.

Exchange in Amides

In contrast to imidate esters, amides show substantial intramolecular exchange accompanying intermolecular. Within experimental error (apparently underestimated for k_{ZE} of acetamide), rate constants for intramolecular exchange, k_{EZ} and k_{ZE}, in acetamide and 3,5-dinitrobenzamide are the same as the rate constant k_{ZS}. This is the requisite condition, eq. [1], and constitutes strong evidence against the imidic-acid mechanism (k_{-i} of Scheme 1) and for the *N*-protonation mechanism (k_{-o} and k_p), not only for acetamide, which exchanges via

Can. J. Chem. Downloaded from www.nrcresearchpress.com by 210.87.254.5 on 09/06/12
For personal use only.

Can. J. Chem. Downloaded from www.nrcresearchpress.com by 210.87.254.5 on 09/06/12
For personal use only.

this mechanism in dilute acid (8), but also for 3,5-dinitrobenzamide, which presumably exchanges via the imidic acid in dilute acid. Similarly, Fig. 4 shows that the doublets of the two stereoisomers of *N*-methylformamide coalesce and coalesce with each other. In less concentrated acid (not shown) only one singlet is seen; k_{ZE} is definitely nonzero, although the spectrum is not of sufficient quality to permit a quantitative comparison of isomerization and proton exchange. Since the imidic-acid mechanism does not permit isomerization, this result is evidence that the *N*-protonation mechanism (k_{-o} and k_p of Scheme 1) is also operative for secondary amides in concentrated H_2SO_4.

In contrast to imidate esters, where H_E and H_Z exchange at different rates, and in contrast to the behavior of amides in dilute acid, where H_E exchanges up to 70% faster than H_Z (for benzamide in ethylene glycol (8)), in strong acid H_E and H_Z exchange at the same rate, within experimental error, for all three primary amides, by two different nmr methods, saturation transfer and line broadening. Of course, the equal reactivityof H_E and H_Z is just what would be expected naively for the *N*-protonation mechanism. In $RCONH_3^+$ the protons become equivalent and must exchange at equal rates. The unusual feature of exchange in dilute acid is that $RCONH_3^+$ is so acidic ($pK_a \cong -9$ (33)) that deprotonation is diffusion-controlled and occurs faster than the protons can become equivalent through rotation about the C—N bond. But relative to 100% H_2SO_4 ($H_o = -12.2$ (34)) $RCONH_3^+$ is *not* a strong acid, so its lifetime becomes long enough that the protons become equivalent and do exchange at the same rate. This change, from unequal rates in dilute acid to equal rates in concentrated H_2SO_4, is strong evidence for competition in dilute solution between deprotonation and rotation.

Comparison of Dilute Solutions with H_2SO_4

The contrast in reactivity between ethyl acetimidate and acetamide or between ethyl *N*-methylformimidate and *N*-methylformamide is due to the availability of the *N*-protonation mechanism for amides, in both dilute solution and H_2SO_4. Yet trichloroacetamide (and presumably 3,5-dinitrobenzamide) exchanges via the imidic acid in dilute solution (8) but via *N*-protonation in H_2SO_4, since eq. [1] is obeyed. This change of mechanism may be understood by steady-state analysis of Scheme 1, plus microscopic reversibility, so as to express rates in terms of the equilibrium constants and the rate constants for the diffusion-controlled proton transfers. The rates of exchange via *N*-protonation and imidic acid are

$$[7] \quad v_N = \frac{k_d}{K_a^N} \frac{K_a^O[H^+]}{K_a^O + [H^+]} C_A$$

$$[8] \quad v_I = k_i \frac{K_a^I[H^+]}{K_a^O + [H^+]} C_A$$

where C_A is the stoichiometric concentration of amide. This readily leads to eq. [8] of ref. 8, and the conclusion that electron-withdrawing substituents favor the imidic-acid mechanism. In strong acid we must replace each $[H^+]$ by an appropriate acidity function. For *O*-protonation of amides (35) or *N*-protonation of imidate esters this is $h_A = 10^{-H_A}$, but the acidity function governing *N*-protonation of amides is unknown. According to rates of acid-catalyzed isomerization of tertiary amides (36), this acidity function might increase slightly less rapidly than h_A. However, for simplicity we use h_A. Then, in sufficiently strong acid we may neglect K_a^O relative to h_A, to obtain

$$[9] \quad v_N = k_d \frac{K_a^O}{K_a^N} C_A$$

$$[10] \quad v_I = (k_i h_A) \frac{K_a^I}{h_A} C_A$$

We have written v_I so as to emphasize the feature that reprotonation of the imidic acid is a diffusion-controlled process whose rate constant, $k_i h_A$, approaches a limiting value when the solvent becomes the proton donor. Despite sulfuric acid's high viscosity, proton mobility (37) is nearly as large as in water, so we take (18) 10^{11} s^{-1} for this limiting value of $k_i h_A$. Thus under these conditions v_I is inhibited by acid, as observed for imidate esters, but v_N becomes nearly acidity-independent (36), so that the mechanism changes, as observed for 3,5-dinitrobenzamide and trichloroacetamide.

Qualitative considerations of the transition-state structures lead to the same conclusion. Since both mechanisms involve diffusion-controlled proton transfer (38), the transition states resemble $RCONH_3^+$ and RC(OH)=NH. Therefore exchange via *N*-protonation involves only tautomerism, so it is nearly acidity-independent. In contrast, exchange via the imidic acid requires deprotonation, so that this mechanism is retarded by strong acid, and becomes negligible compared to the *N*-protonation mechanism.

In very strong acid, the *N*-protonation mechanism changes in that $RCONH_2R'^+$ becomes a weaker acid than solvent, so that its deprotonation is no longer diffusion-controlled. Also we must

adapt Scheme 1 so that HSO_4^- is the base that removes the proton (28). Then steady-state analysis leads to

$$[11] \quad v_N = (k_o[H_2SO_4]) \frac{K_a^{o}}{K_a^{H_2SO_4}} \frac{[HSO_4^-]}{[H_2SO_4]} \times \frac{k_p}{k_o + k_p} C_A$$

where $k_o[H_2SO_4]$ cannot exceed the first-order limit of 10^{11} s^{-1}. As evidence for the change from diffusion-controlled deprotonation of $RCONH_3^+$ (eq. [9]) to diffusion-controlled protonation (eq. [11]), we do observe that in 100% H_2SO_4 the exchange rate increases with $[HSO_4^-]$.

For generality eq. [11] does not distinguish which step is rate-limiting. Exchange requires initial deprotonation, by HSO_4^-, to form the amide, which then partitions between *O*-protonation, with probability $k_o/(k_o + k_p)$, and *N*-protonation, with probability $k_p/(k_o + k_p)$. In sufficiently strong acid both *O*-protonation and *N*-protonation of an amide are exergonic, and therefore diffusion-controlled (38). We might then expect both k_o and k_p to equal 10^{11} s^{-1}, so that neither step alone would be rate-limiting.

However, it is possible to demonstrate that *N*-protonation is the rate-limiting step. To do so we must compare the observed rate of exchange with the rate of formation of the intermediate amide, estimated from its steady-state concentration and an assumed diffusion-controlled lifetime of 10^{-11} s. For acetamide $pK_a^{o} = -0.90$ (39) and H_A in 100% H_2SO_4 is -7.24 (40), so the rate constant for amide formation may be estimated as ca. $10^{11} K_a^{o}/h_A$, or 5×10^4 s^{-1}, far greater than the observed 3.1 ± 0.3 s^{-1}. Admittedly our solution was only approximately 100% H_2SO_4, but it is quite unlikely that this estimate is vastly too high. Furthermore a high rate of deprotonation is consistent with the absence of an OH peak for the protonated amide, which appears only at low temperature in FSO_3H (20, 29, 41). Since the observed rate is much less than the rate of OH exchange, we conclude that *N*-protonation must be rate-limiting, with k_p/k_o only ca. 10^{-4}. Thus the rate constant for *N*-protonation is only ca. 10^7 s^{-1}, considerably lower than that of other thermodynamically favored proton transfers involving *N* and *O* (27, 38). We suggest that the slowness of this "diffusion-controlled" protonation is a manifestation of a solvent structure that is strongly hydrogen-bonded to the oxygen but not to the nitrogen line pair.

Comparison of Amides with Imidate Esters

The contrast between the reactivities of imidate esters and amides strongly suggests that there is an additional pathway available for exchange in amides, namely *N*-protonation. This contrast is so extreme (a $>10^8$-fold difference in water activity (42) between 50 and 100% H_2SO_4) as to suggest that the *N*-protonation mechanism is tremendously faster than the imidic-acid mechanism, and that the latter cannot possibly compete. This conclusion is correct in H_2SO_4, but not in dilute solution (8). The error in extrapolating from H_2SO_4 to dilute solution is revealed through eqs. [9] and [10], which show that only the imidic-acid mechanism is strongly inhibited by acid, so that although it does not contribute in strong acid, it can do so in aqueous solution. Moreover, the observation that amides with electron-withdrawing substituents show a changeover in behavior (from $k_{ES} \neq k_{ZS}$, without extensive intramolecular exchange, in dilute solution (8) to $k_{ES} = k_{ZS} = k_{ZE} = k_{EZ}$ in H_2SO_4) is evidence for a changeover in mechanism, and difficult to rationalize by exclusive *N*-protonation, as has been proposed (7).

Acknowledgements

This research was supported by National Science Foundation Grants CHE76-02408 and CHE78-12256. We thank Dr. John Wright for assistance with nmr spectrometers, which were supported by National Institutes of Health Grant RR-708.

1. A. BERGER, A. LOEWENSTEIN, and S. MEIBOOM. J. Am. Chem. Soc. **81**, 62 (1959).
2. R. S. MOLDAY and R. G. KALLEN. J. Am. Chem. Soc. **94**, 6739 (1972); R. B. MARTIN. Chem. Commun. 793, (1972); R. B. MARTIN and W. C. HUTTON. J. Am. Chem. Soc. **95**, 4752 (1973).
3. C. L. PERRIN. J. Am. Chem. Soc. **96**, 5628 (1974).
4. C. O. MEESE, W. WALTER, and M. BERGER. J. Am. Chem. Soc. **96**, 2259 (1974); A. C. SATTERTHWAIT and W. P. JENCKS. J. Am. Chem. Soc. **96**, 7045 (1974).
5. R. A. MCCLELLAND and W. F. REYNOLDS. Can. J. Chem. **57**, 2896 (1979).
6. C. L. PERRIN and E. R. JOHNSTON. J. Am. Chem. Soc. **101**, 4753 (1979).
7. A. G. REDFIELD and S. WAELDER. J. Am. Chem. Soc. **101**, 6151 (1979).
8. C. L. PERRIN and E. R. JOHNSTON. J. Am. Chem. Soc. In press.
9. C. R. SMITH and K. YATES. J. Am. Chem. Soc. **94**, 8811 (1972); M. CASWELL and G. L. SCHMIR. J. Am. Chem. Soc. **101**, 7323 (1979), and references cited.
10. W. WALTER and C. O. MEESE. Chem. Ber. **110**, 2463 (1977), and references cited.
11. C. S. JOHNSON, JR. Adv. Magn. Reson. **1**, 33 (1965).
12. R. A. HOFFMAN and S. FORSÉN. Prog. Nucl. Magn. Reson. Spectrosc. **1**, 15 (1964).

Can. J. Chem. Downloaded from www.nrcresearchpress.com by 210.87.254.5 on 09/06/12
For personal use only.

13. C. L. PERRIN and E. R. JOHNSTON. J. Magn. Reson. **33**, 619 (1979).
14. C. A. MACKENZIE, G. A. SCHMIDT, and L. R. WEBB. J. Am. Chem. Soc. **73**, 4990 (1951).
15. H. KOHN and R. A. OLOFSON. J. Org. Chem. **37**, 3504 (1972).
16. G. AKSNES and J. E. PRUE. J. Chem. Soc. 103 (1959).
17. H. NOHIRA, Y. NISHIKAWA, Y. FURUYA, and T. MUKAIYAMA. Bull. Chem. Soc. Jpn. **38**, 897 (1965).
18. C. L. PERRIN, E. R. JOHNSTON, and J. L. RAMÍREZ. J. Am. Chem. Soc. **102**, 6299 (1980).
19. C. L. PERRIN, E. R. JOHNSTON, P. A. KOBRIN, and C. P. LOLLO. J. Am. Chem. Soc. In press; E. R. JOHNSTON. Ph.D. Thesis, University of California, San Diego. 1980.
20. G. FRAENKEL and C. FRANCONI. J. Am. Chem. Soc. **82**, 4478 (1960); R. J. GILLESPIE and T. BIRCHALL. Can. J. Chem. **41**, 148 (1963).
21. C. RABILLER, J. P. RENOU, and G. J. MARTIN. J. Chem. Soc. Perkin Trans. II, 536 (1977).
22. M. LILER. J. Chem. Soc. Perkin Trans. II 816 (1972).
23. W. E. STEWART and T. H. SIDDALL, III. Chem. Rev. **70**, 517 (1970).
24. J. NEMATOLLAHI and L. D. TUCK. J. Pharm. Sci. **56**, 684 (1967).
25. J. NOGGLE and R. SCHIRMER. The nuclear Overhauser effect. Academic Press, New York. 1972.
26. C. A. STREULI. Anal. Chem. **31**, 1652 (1959).
27. M. EIGEN. Angew. Chem. Intl. Ed. Engl. **3**, 1 (1964).
28. R. A. COX. J. Am. Chem. Soc. **96**, 1059 (1974).
29. M. LILER. J. Chem. Soc. Perkin Trans. II, 71 (1974).
30. H. F. GILBERT and W. P. JENCKS. J. Am. Chem. Soc. **101**, 5774 (1979).
31. H. SAITO and K. NUKADA. Tetrahedron, **22**, 3313 (1966).
32. L. RADOM, W. J. HEHRE, and J. A. POPLE. J. Am. Chem. Soc. **93**, 289 (1971).
33. A. R. FERSHT. J. Am. Chem. Soc. **93**, 3504 (1971).
34. M. J. JORGENSON and D. R. HARTTER. J. Am. Chem. Soc. **85**, 878 (1963).
35. K. YATES, J. B. STEVENS, and A. R. KATRITZKY. Can. J. Chem. **42**, 1957 (1964).
36. C. A. BUNTON, B. F. FIGGIS, and B. NAYAK. Adv. Mol. Spectrosc. **3**, 1209 (1962); B. G. COX. J. Chem. Soc. B, 1780 (1970).
37. R. J. GILLESPIE and S. WASIF. J. Chem. Soc. 209 (1953).
38. A. J. KRESGE and G. L. CAPEN. J. Am. Chem. Soc. **97**, 1795 (1975); A. J. KRESGE. Acc. Chem. Res. **8**, 354 (1975).
39. M. LILER. J. Chem. Soc. B, 385 (1969).
40. G. D. FREDERICK and C. D. POULTER. J. Am. Chem. Soc. **97**, 1797 (1975).
41. J. L. SUDMEIER and K. E. SCHWARTZ. Chem. Commun. 1646 (1968).
42. W. F. GIAUQUE, E. W. HORNUNG, J. E. KUNZLER, and T. R. RUBIN. J. Am. Chem. Soc. **82**, 62 (1960).

Can. J. Chem. Downloaded from www.nrcresearchpress.com by 210.87.254.5 on 09/06/12
For personal use only.

1-Sterpurene-3,12,14-triol and 1-sterpurene, metabolites of silver-leaf disease fungus *Stereum purpureum*

WILLIAM A. AYER AND M. HOSSEIN SAEEDI-GHOMI
Department of Chemistry, University of Alberta, Edmonton, Alta., Canada T6G 2G2

Received March 30, 1981

WILLIAM A. AYER and M. HOSSEIN SAEEDI-GHOMI. Can. J. Chem. **59**, 2536 (1981).

Two new sterpurane-type sesquiterpenes, sterpurene-3,12,14-triol (**4**) and 1-sterpurene (**5**), 2,6,10,10-tetramethyltricyclo-[6.3.0.$0^{3,6}$]undec-1-ene, have been isolated from among the neutral metabolites of the fungus *Stereum purpureum*. The structures were determined mainly on the basis of mass and nuclear magnetic resonance spectrometry.

WILLIAM A. AYER et M. HOSSEIN SAEEDI-GHOMI. Can. J. Chem. **59**, 2536 (1981).

A partir des métabolites neutres du champignon *Stereum purpureum*, on a isolé deux nouveaux sesquiterpènes du type sterpurane, le sterpurenetriol-3,12,14 (**4**) et le sterpurene-1 (**5**) (tétraméthyl-2,6,10,10 tricyclo[6.3.0.$0^{3,6}$]undecène-1). On a déterminé les structures en se basant principalement sur la spectrométrie de masse et sur la rmn.

[Traduit par le journal]

Recently we reported the isolation and structure determination of sterpuric acid (**1**) and hydroxysterpuric acid (**2**), metabolites of the fungus *Stereum purpureum* (Pers. ex Fr.) Fr., the causative agent of the so-called "silver-leaf disease" of a variety of trees and scrubs (1). The sterpuric acids represent a type of sesquiterpenoid not previously found in nature. We have also reported on the sterepolides (e.g., sterepolide (**3**)), new isolactarane-type sesquiterpenes produced by *S. purpureum* (2). We now wish to report on the isolation and structure determination of sterpurene-3,12,14-triol (**4**) and 1-sterpurene (**5**) from the neutral metabolites of this fungus.

Sterpurene-3,12,14-triol, $C_{15}H_{24}O_3$, mp 146–148°C, was isolated by flash chromatography (3) of the neutral fraction of the *S. purpureum* culture broth extracts (1). The mass spectrum of the triol shows an intense peak at $M^+ - 28$ due to the loss of ethylene from the cyclobutane ring, a characteristic feature of compounds with the sterpurane (**6**) skeleton (1). The infrared spectrum shows hydroxyl but no carbonyl absorption. The ^{1}H nmr spectrum displays AB quartets at δ 4.22 (J = 12 Hz) and 3.39 (J = 2 Hz), indicative of the presence of two hydroxymethyl groups, one of which is allylic (C-12, see **6** for numbering system). As is the case with sterpuric acid, the allylic proton at C-8 appears as a broad multiplet at δ 2.62. The highest field signal, a double doublet at δ 0.91 (J's 11 and 13 Hz), is also reminiscent of the sterpuric acids where this high field signal is attributed to one of the hydrogens on C-7 (1)[1].

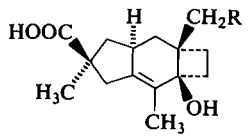

1 R = H
2 R = OH

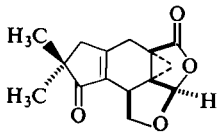

3

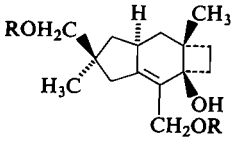

4 R = H
4*a* R = Ac

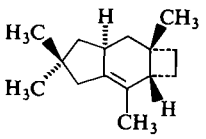

5

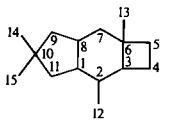

6

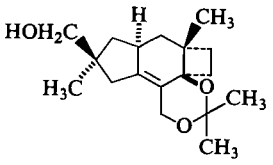

7

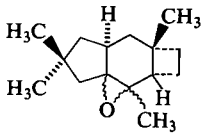

8

Acetylation of triol **4** provides the diacetyl derivative **4***a*, which shows hydroxyl as well as acetoxyl absorption in the ir. The 400 MHz ^{1}H nmr spectrum of **4***a* is extremely informative in that almost all of the protons may be distinguished and assigned. The signals for the C-12 protons appear at δ 4.72 (AB q, J = 12 Hz) and those for the C-14 protons at δ 3.90 (AB q, J = 12 Hz). The C-12 protons show a

[1]A detailed analysis of the ^{1}H nmr spectrum of the compound is provided in the Experimental.

0008-4042/81/162536-03$01.00/0
©1981 National Research Council of Canada/Conseil national de recherches du Canada

Can. J. Chem. Downloaded from www.nrcresearchpress.com by 210.87.254.40 on 09/06/12
For personal use only.

Can. J. Chem. Downloaded from www.nrcresearchpress.com by 210.87.254.40 on 09/06/12
For personal use only.

large pyridine shift ($\delta_{CDCl_3} - \delta_{py} = -0.46$ ppm) in agreement with their proximity to the C-3 hydroxyl function (4). The methyl group at C-6 also shows an appreciable (−0.2 ppm) pyridine shift. The proton at C-8 appears as a broad multiplet and is coupled to the C-7 methylene protons and the C-9 methylene protons. The allylic methylene group at C-11 gives rise to an AB quartet at δ 2.33 (J = 17 Hz). As expected, the C-4 and C-5 protons give rise to complete multiplets.[1] The ^{13}C nmr spectrum shows the presence of two olefinic carbons (δ 147.6, 127.2) and three carbons attached to oxygen (δ 72.9, 72.4, 62.1) and is otherwise in accord with the structure formulated.

The 1,3-relationship of the C-3 and C-12 hydroxyl groups in **4** was confirmed by acid-catalyzed treatment with 2,2-dimethoxypropane which provided the acetonide **7**. The assignment of the stereochemistry of the hydroxymethyl group on C-10 is tentative and is made on the assumption that the oxygenation pattern is the same on that carbon as for sterpuric acid (**1**). The similarity of the ^1H nmr coupling constants observed for the protons on C-7, C-8, and C-9 to those observed for the same spin system in **1** and **2** (1) is the basis for the stereochemical assignment at C-8.

Chloroform extraction of the mycelium obtained from liquid cultures of *S. purpureum* provided a dark brown oil which was partially dissolved in Skellysolve B. Chromatography of the hydrocarbon soluble portion provided a volatile, colorless oil[2] which we believe to be the "parent" hydrocarbon of this series of compounds, 1-sterpurene (**5**).[3] High resolution mass spectrometry indicates the molecular formula $C_{15}H_{24}$ and shows the prominent $M^+ - C_2H_4$ peak, characteristic of this ring system. The ^1H nmr spectrum shows three quaternary methyl signals (δ 1.23, 1.10, 1.08) and a vinylic methyl signal (δ 1.53). The allylic proton at C-8 appears as a broad multiplet at δ 2.65, coupled to the methylene groups at C-9 and C-7. Again one of the protons of the C-7 methylene group is at abnormally high field (δ 0.69). The allylic methine proton at C-3 appears as a double doublet (J's 10.5 and 13.5 Hz) at δ 2.39.[1] Treatment of 1-sterpurene with *m*-chloroperbenzoic acid gives the epoxide **8** as a single isomer. The ^1H nmr spectrum of **8** does not show a vinylic methyl. The four quaternary methyls give rise to singlets at δ 1.19, 1.18, 1.15, and 1.12 which cannot be individually assigned. Attempts to bring about acid-catalyzed rearrangement (or ring-opening) of the epoxide led to an intractable mixture of compounds. Lack of material prevented us from carrying out further studies on this hydrocarbon, but we feel that the structural asignment, although based on limited evidence, is both chemically and biogenetically sound.

[2]Since only 12 mg of the oil was isolated, its boiling point has not been determined.

[3]The systematic name for **5** is 2,6,10,10-tetramethyltricyclo-[6.3.0.0^{3,6}]undec-1-ene.

Experimental

General

Mass spectra were recorded on an AEI model MS-50 mass spectrometer. The formulas of all peaks reported were determined by high resolution measurements. Infrared spectra were recorded on a Nicolet 7199 FT interferometer. Optical rotations were measured on a Perkin-Elmer model 141 automatic polarimeter. The ^1H nmr spectra were determined on a Bruker WH 400 spectrometer with TMS as internal standard. The ^{13}C nmr spectra were measured on a Bruker HFX-90 spectrometer interfaced to a Nicolet 1085 computer. Melting points were recorded on a Fisher-Johns melting point apparatus and are uncorrected. Skellysolve B refers to Skelly Oil Company light petroleum, bp 62–70°C. Column chromatography was carried out using Macherey Nagel Kieselgel 60 (100 g/g substrate). Preparative layer chromatography (plc) was carried out on silica gel G (E. Merck, 0.75 mm layers) containing 1% electronic phosphor (General Electric, Cleveland). All solvents were distilled prior to use. All compounds for which spectral data are reported showed single spots on tlc using at least two different solvent systems.

Isolation of Sterpurene-3,12,14-triol (4)

The crude neutral metabolites of *S. purpureum* (0.52 g) (1) were subjected to flash chromatography (eluent chloroform–methanol (19:1)) (3) to give the crude triol **4** (75 mg). Further purification by column chromatography (eluent benzene–acetone (3:1)) provided a crystalline sample of **4** (42 mg) which was recrystallized from ether to give pure sterpurene-3,12-14-triol (**4**, 30 mg) as white needles, mp 146–148°C, $[\alpha]_D^{25}$ +64° (*c* 0.1, CH_3OH); ir (film): 3315, 1436, 1420, 1368, 1207, 1170, 1138, 1072, 1027, 998 cm^{-1}; ^1H nmr ($CDCl_3$) δ: 4.22 (2H on C-12, AB quartet, J = 12 Hz), 3.39 (2H on C-14, AB quartet, J = 12 Hz), 2.86 (3H (OH), br, exchangeable), 2.62 (1H on C-8, br mult), 2.57 (1H on C-11, d, J = 18 Hz), 2.24 (1H on C-9, dd, J's 11 and 19 Hz), 2.10 (1H on C-11, d, J = 18 Hz), 2.04 (1H, complex mult), 1.68 (1H, m), 1.48 (1H on C-9, dd, J's 9.5 and 19 Hz), 1.22 (2H, complex mult), 1.21 (3H, s), 1.10 (3H, s), 0.91 (1H on C-7, dd, $J_{7,8}$ = 11 Hz, J_{gem} = 13 Hz); ms (probe, 150°C): *m/e* calcd. for $C_{15}H_{24}O_3$: 252.1725; found: 252.1730 (3), 234 (46), 224 (49), 216 (20), 204 (24), 203 (67), 188 (94), 175 (100), 173 (36), 159 (54), 145 (25), 131 (22), 119 (27), 107 (20), 105 (44), 91 (40).

Acetylation of Sterpurenetriol (4)

Acetic anhydride (0.25 mL) was added to a solution of triol **4** (5 mg) in pyridine (0.5 mL). The reaction mixture was stirred at room temperature for 0.5 h, then toluene (5 mL) was added and the solvents were evaporated under reduced pressure. Column chromatography (eluent benzene–ether (9:1)) provided the diacetate **4*a*** as a colorless oil (5 mg); ir (film): 3455, 1737, 1450, 1422, 1365, 1929, 1130, 1021 cm^{-1}; ^1H nmr ($CDCl_3$) δ: 4.74 (2H on C-12, AB quartet, J = 12 Hz), 3.90 (2H on C-14, AB quartet, J = 12 Hz), 2.68 (1H on C-8, br mult), 2.42 (1H on C-11, d, J_{gem} = 17 Hz), 2.25 (1H on C-11, d, J_{gem} = 17 Hz), 2.20 (1H on C-4 or 5, m), 2.08 (3H, acetyl methyl, s), 2.07 (1H on C-4 or 5, m), 2.06

Can. J. Chem. Downloaded from www.nrcresearchpress.com by 210.87.254.40 on 09/06/12
For personal use only.

(3H, acetyl methyl, s), 1.71 (1H on C-9, dd, $J_{8,9}$ = 12 Hz, J_{gem} = 12.5 Hz), 1.63 (1H on C-7, dd, $J_{7,8}$ = 6 Hz, J_{gem} = 13 Hz), 1.55 (1H on C-5 or 4, m), 1.30 (1H on C-5 or 4, m), 1.26 (1H on C-9, $J_{8,9}$ = 6 Hz, J_{gem} = 12.5 Hz), 1.24 (3H on C-13, s), 1.14 (3H on C-15, s), 0.88 (1H on C-7, dd, $J_{7,8}$ = 11 Hz, J_{gem} = 13 Hz). The assignments of the coupling partners were confirmed by double irradiation experiments; ^{1}H nmr (Py-d_5) δ:5.20 (2H on C-12, AB quartet, J = 12 Hz), 4.03 (2H, AB quartet, J = 12 Hz), 2.71 (1H, br mult), 2.06 (3H, s), 1.55 (1H, m), 1.42 (3H on C-13, s), 1.32 (1H, m), 1.12 (3H, s), 0.84 (1H, dd, J's 11 and 13 Hz); ^{13}C nmr ($CDCl_3$ δ: 20.9, 21.0, 23.9, 24.9 (CH_3); 22.1, 35.2, 35.3, 40.0, 42.9, 62.1, 72.4 (CH_2); 37.1 (CH); 40.6, 44.6, 72.9, 127.2, 147.6 (C); 171.2 (2 × C=O); ms (probe, 150°C): the highest peak corresponded to $M^+ - H_2O$); *m/e* calcd. for $C_{19}H_{26}O_4$ ($M^+ - H_2O$): 318.1831; found: 318.1851 (0.5), 308 (14), 276 (20), 247 (21), 216 (41), 203 (33), 188 (100), 175 (55), 173 (44), 105 (21), 91 (20). Chemical ionization (NH_3) ms shows an $M^+ + 18$ (*m/e*) 354 peak.

Sterpurene-3,12,14-triol Acetonide (7)

Sterpurene-3,12,14-triol (7 mg) was dissolved in 2,2-dimethoxypropane (0.5 mL) and a catalytic amount of *p*-toluenesulfonic acid added. After two hours stirring at room temperature, ether (50 mL) was added and the solution was washed successively with saturated sodium bicarbonate, water (three times), and brine. The solution was dried (Na_2SO_4) and evaporated to give the crude product which was purified by chromatography (eluent benzene–ether (19:1)) to provide acetonide **7** as a colorless oil (7 mg); ir (film): 3385, 1453, 1378, 1240, 1192, 1087, 1030 cm^{-1}; ^{1}H nmr ($CDCl_3$) δ: 4.33 (2H on C-12, AB quartet, J = 12 Hz), 3.47 (2H on C-14, s), 2.64 (1H, br mult), 2.38 (1H, d, J_{gem} = 17 Hz), 2.17 (1H, m), 1.92 (1H, d, J_{gem} = 17 Hz), 1.44 (3H, s), 1.25 (3H, s), 1.18 (3H, s), 1.10 (3H, s), 0.92 (1H on C-7, dd, $J_{7,8}$ = 11 Hz, J_{gem} = 13 Hz); ms (probe, 25°C): *m/e* calcd. for $C_{18}H_{28}O_3$: 292.2039; found: 292.2034 (0.7), 235 (27), 234 (100), 216 (29), 206 (38), 204 (39), 203 (89), 189 (21), 188 (78), 187 (33), 175 (41), 159 (27), 119 (23), 105 (35), 91 (41), 79 (20), 77 (20), 55 (23).

Extraction of the Mycelium of S. purpureum *and the Isolation of 1-Sterpurene (5)*

The mycelium from a 10 L growth of *S. purpureum* (1) was kept at −12°C for three months. It was then extracted with chloroform for 2 days in a Soxhlet apparatus. The chloroform extract was washed with water and brine, dried (Na_2SO_4), and concentrated under reduced pressure to provide the crude mycelium extract as a dark brown oil (0.62 g). Skellysolve B (10 mL) was added to the crude extract and the mixture was heated at 60°C for 5 min. After cooling to room temperature, the Skellysolve B soluble portion was evaporated to give a yellow oil (0.35 g). The latter was subjected to column chromatography (eluent Skellysolve B) to provide 1-sterpurene as a colorless oil (12 mg); ir (film): 1457, 1445, 1433, 1372, 1361, 1355 cm^{-1}; ^{1}H nmr ($CDCl_3$) δ: 2.65 (1H on C-8, br mult), 2.39 (1H on C-3, dd, J's 10.5 and 13.5 Hz), 2.16 (1H, m), 2.10 (2H on C-11), 1.94 (1H, m), 1.68 (1H on C-9, dd, $J_{8,9}$ = 7.5 Hz, J_{gem} = 12 Hz), 1.58 (1H on C-7, m), 1.53 (3H on C-12, s), 1.48 (1H, m), 1.44 (1H, m), 1.23 (3H, s), 1.10 (3H, s), 1.08 (3H, s), 0.94 (1H, m), 0.69 (1H on C-7, dd, $J_{7,8}$ = 11 Hz, J_{gem} = 13 Hz); ms (probe, 100°C): *m/e* calcd. for $C_{15}H_{24}$: 204.1878; found: 204.1878 (34), 176 (100), 175 (82), 161 (81), 149 (24), 121 (37), 120 (41), 119 (43), 111 (26), 107 (42), 105 (54), 97 (32), 95 (29), 93 (32), 91 (32), 85 (28), 83 (30), 81 (29), 79 (22), 71 (35).

Epoxidation of 1-Sterpurene (5)

m-Chloroperbenzoic acid (10 mg of 85%) was added to an ice cold solution of 1-sterpurene (**5**, 7 mg), in methylene chloride (0.8 mL). The reaction mixture was kept in the fridge for 1 h, then for an additional 0.5 h at room temperature. Ether (25 mL) was added and the resultant solution was washed successively with saturated sodium bicarbonate, water (two times), and brine. Drying (Na_2SO_4) and evaporation of the solvents gave the crude product (7 mg) which was purified by chromatography (eluent Skellysolve B) to provide epoxide **8** as a colorless oil (4 mg); ir (film): 1600, 1455, 1445, 1432, 1363, 1355, 1280, 1188 cm^{-1}; ^{1}H nmr ($CDCl_3$) δ: 2.45 (1H, br mult), 2.14 (2H, m), 1.95 (1H, d, J = 15 Hz), 1.85 (1H, br mult), 1.67 (1H, dd, J's 7 and 12 Hz), 1.60–1.30 (6H, complex), 1.19 (3H, s), 1.18 (3H, s), 1.15 (3H, s), 1.12 (3H, s); ms (probe, 100°C): *m/e* calcd. for $C_{15}H_{24}O$: 220.1827; found: 220.1819 (24), 129 (22), 163 (21), 149 (91), 95 (100), 57 (65), 55 (33).

Acknowledgements

We wish to thank the Natural Sciences and Engineering Research Council of Canada for financial support and Dr. Y. Hiratsuka for the cultures of *S. purpureum*. We wish to thank Dr. T. T. Nakashima for his assistance in determining the nmr spectra.

1. W. A. Ayer, M. H. Saeedi-Ghomi, D. van Eggen, B. Tagle, and J. Clardy. Tetrahedron, **37**, Suppl. No. 1, 379 (1981).
2. W. A. Ayer and M. H. Saeedi-Ghomi. Tetrahedron Lett. **22**, 2071 (1981).
3. W. C. Still, M. Kahr, and A. Mitra. J. Org. Chem. **43**, 2923 (1978).
4. D. V. Demarco, E. Farkas, D. Doddrell, B. L. Mylari, and E. Wenkert. J. Am. Chem. Soc. **90**, 5480 (1968).

Purification and characterization of the indicator calmagite

BYRON KRATOCHVIL,[1] JAMES NOLAN, AND FREDERICK F. CANTWELL

Department of Chemistry, University of Alberta, Edmonton, Alta., Canada T6G 2G2

AND

ROBERT B. FULTON

Department of Chemistry, St. John's University, Collegeville, MN 56321, U.S.A.

Received March 18, 1981

BYRON KRATOCHVIL, JAMES NOLAN, FREDERICK F. CANTWELL, and ROBERT B. FULTON. Can. J. Chem. **59**, 2539 (1981).

A scheme for the purification of the azo dye calmagite is described which involves solvent extraction, column partition chromatography, and adsorption chromatography on a nonpolar adsorbent. The final product, analyzed by thin-layer chromatography and by acid–base and ion-pair titrations, is of >99% purity. Molar absorptivities and acid ionization constants are reported for the conjugate species.

BYRON KRATOCHVIL, JAMES NOLAN, FREDERICK F. CANTWELL et ROBERT B. FULTON. Can. J. Chem. **59**, 2539 (1981).

On décrit un procédé de purification du colorant azoté, la calmagite, qui fait intervenir une extraction à l'aide de solvants, une chromatographie de partage sur colonne et une chromatographie d'adsorption sur un adsorbant non polaire. Le produit final, analysé par chromatographie sur couches minces et par des titrages acide–base et de paire d'ions, a une pureté >99%. On rapporte les capacités molaires d'absorption et les constantes d'ionisation de ces espèces conjuguées.

[Traduit par le journal]

The dihydroxyazo dye calmagite, 3-hydroxy-4-[(2-hydroxy-5-methylphenyl)azo]-1-napthalene sulfonic acid, was introduced by Lindstrom and Diehl in 1960 as an indicator for the EDTA titration of calcium and magnesium (1). The indicator properties of calmagite are similar to those of Eriochrome Black T, the first dye used for this purpose, but solutions of Eriochrome Black T are not stable, whereas those of calmagite are stable indefinitely. Both indicators form red complexes with both calcium and magnesium; however, the formation constant between calmagite and magnesium is approximately one hundred times greater than that with calcium. Because of this selectivity, calmagite has also been used for the spectrophotometric determination of free or ionic magnesium in biological materials which contain calcium (2, 3). This application is of particular interest because an ion selective electrode for the determination of ionic magnesium in the presence of calcium is not yet commercially available.

A recent paper proposed a modified spectrophotometric method for the determination of free metal ion concentrations which extends the range and applicability of previous methods but which requires indicators of high purity (4). Most commercially available calmagite has a purity of less than 60 percent, the major impurities being inorganic salts. A number of organic impurities are also present, the kind and amount depending on the purity of the starting materials and the care taken in synthesis.

Lindstrom and co-workers studied in detail the properties of calmagite, and outlined procedures for preparation of pure dye (5, 6). The procedure described by Lindstrom and Isaac (5) involves washing the synthesized material repeatedly to remove KCl, extracting for several hours with petroleum ether, and then extracting for several more hours with dry chloroform. The air-dried material is then dissolved in a mixture of 200 mL of 95% ethanol and 150 mL of dilute HCl (1:50), and the alcohol is evaporated gently over a warm steam bath. Upon slow cooling, microscopic crystals of pure calmagite form.

We found the last stage of the above procedure to be difficult to control, and the purity of the final product to be variable. Accordingly, we turned to purification of commercial material. The procedure of Lindstrom and Isaac is not suitable for commercial calmagite, probably because the starting materials are less pure. Kendrick (7) has described a procedure for purification of Arsenazo III, a dye similar in structure to calmagite, in which the dye is first passed through a column of Chelex-100 chelating ion exchange resin to remove calcium contamination, and then through a column of DEAE cellulose using *n*-butanol – pyridine – acetic acid – water, 15:10:3:12, as mobile phase. However, the procedure is tedious; about five days are required for the purified dye to be eluted from the second column alone.

[1]Author to whom correspondence should be directed.

0008-4042/81/162539-04$01.00/0

©1981 National Research Council of Canada/Conseil national de recherches du Canada

Can. J. Chem. Downloaded from www.nrcresearchpress.com by 210.87.254.42 on 09/06/12
For personal use only.

Can. J. Chem. Downloaded from www.nrcresearchpress.com by 210.87.254.42 on 09/06/12
For personal use only.

Because of its excessive length, Kendrick's procedure was not considered for calmagite. Instead, a faster method involving both solvent extraction and column chromatography was developed. This procedure takes less than two days and yields calmagite of high purity as shown by thin-layer chromatography, and by acid–base and ion-pair extraction titrations.

Experimental

Apparatus

Spectrophotometric measurements were made with a Cary 118 spectrophotometer (Varian Associates, Palo Alto, CA) using either a standard 1 cm cuvette or a 1 cm flow cell (Hellma Co., Toronto). An Accumet Model 520 pH meter with separate glass and calomel electrodes (Fisher Scientific Co.) was used for pH measurements. The meter was standardized with standard buffers prepared according to Bates (8).

Reagents and Materials

Calmagite was obtained from Aldrich Chemical Co. Inc. (Lot No. 060647), Eastman Kodak Co. (Lot No. A6D), and G. Frederick Smith Chemical Co. (Lot No. 278). Precoated silica gel tlc plates (0.25 mm coating with fluorescent indicator and organic binder) were purchased from Brinkmann Instruments Inc. Dextromethorphan hydrobromide, used as a titrant, was obtained from Endo Laboratories, Inc. (Garden City, NY) and assayed by nonaqueous, Fajan's, and both acid–base and ion-pair two-phase titrations as 95.4% (9), the remainder being water. The support in the liquid–liquid chromatography work, Whatman CC-41 cellulose powder, was used as supplied. All solvents and inorganic chemicals were ACS Reagent Grade or better. Demineralized water was used throughout.

Thin-Layer Chromatography Techniques

Purity of the commercial material and of that isolated at each stage of the purification procedure was monitored by thin-layer chromatography on silica gel plates using as developer a mixture of butanol, ethanol, 1.5 *M* aqueous ammonia, and pyridine (BEAP) in the volume ratio 4:1:3:2. For reproducible results the plates, once spotted, were equilibrated with the solvent atmosphere in a developing chamber (Gelman Instruments Co., Model 51325-1) for at least 10 min prior to development. Under these conditions calmagite migrates as a purple spot with $R_f = 0.4$. To prevent interference from calcium, plates with $CaSO_4$ binder were not used.

Procedure for Solvent Extraction

A preliminary solvent extraction sequence was used to reduce the level of impurities to the point where a much larger loading of calmagite could be applied to the liquid–liquid partition chromatography column in the next step. The solvent extraction procedure is as follows.

Dissolve 2.0 g of the crude commercial calmagite in 80 mL of 0.10 *M* sodium acetate. Adjust the pH of the solution to 4.5 with glacial acetic acid and extract four times with 40 mL portions of 1-butanol, readjusting the pH of the aqueous layer to 4.5 with glacial acetic acid after each extraction. Pool the butanol fractions, which contain most of the calmagite, and back-extract the dye four times with 50 mL portions of 0.01 *M* NaOH. Because some acetic acid is extracted from the aqueous phase into the butanol phase during the first set of extractions, and is back-extracted in the second set, it is necessary to neutralize this acid during the first NaOH back-extraction by dropwise addition of 2.5 *M* NaOH until both the aqueous and organic phases remain blue after shaking. Subsequent back-extractions with 0.01 *M* NaOH do not require this pH adjustment. After the last extraction discard the butanol layer and combine the four aqueous NaOH extracts.

Precipitate the dye from the combined extracts by slowly adding with stirring a volume of concentrated HCl equal to 10% of the volume of the combined extracts. This produces a solution 1.2 *M* in HCl and precipitates the neutral sulfonic acid form of calmagite. Recover the gel-like precipitate by vacuum filtration on a 10–20 μm sintered-glass funnel and dry it overnight in a vacuum desiccator over $Mg(ClO_4)_2$.

Column Chromatography

Purification of the solvent-extracted dye is achieved using liquid–liquid partition chromatography followed by adsorption chromatography. The procedure is as follows.

For the partition chromatography, prepare the stationary aqueous phase by adjusting the pH of a 0.10 *M* solution of EDTA to 11.0 with 2.5 *M* NaOH solution. As the mobile phase use 1-butanol presaturated with the stationary phase. Add dropwise, with vigorous mixing, 100 mL of the stationary aqueous phase to 250 g of Whatman CC-41 cellulose powder (used as received). Next add 800 mL of mobile phase to form a slurry, pack it into a 4 × 60 cm glass chromatography column, and continue to pass mobile phase through the column until the volume of the bed no longer shrinks; this will require on the order of 4 h and 250 mL of mobile phase. The final bed should be about 50 cm long.

Dissolve 1 g of the solvent-extracted dye in a minimum volume of presaturated butanol mobile phase (about 15 mL) and load it onto the column. Elute with the mobile phase at a flow rate of 50 mL/h. The calmagite elutes as a purple-blue band after about 400 mL of eluent has passed. It is preceded by a brown band and followed by several bands of various colors. As soon as the calmagite begins to elute, collect the eluate in 5 mL fractions, subjecting the early and late fractions to thin-layer chromatography in order to locate the middle cut which is free of colored impurities. Pool the fractions in this middle cut and remove the solvent in a rotary evaporator. The cellulose powder can be reused after clean-up and drying.

For the adsorption chromatography, pack a 2 × 20 cm column with 60–80 mesh Amberlite XAD-2 resin (Rohm and Haas Co., Philadelphia, PA) in 40% MeOH/60% 1:10 HCl (v/v). Prepare a saturated solution of the product from the liquid–liquid partition column by dissolving about 1 g in 75 mL of methanol and adding 1:10 HCl until the first appearance of a precipitate, then adding sufficient methanol to just clear the solution. Load this solution onto the column and pass 250 mL of 40% MeOH/60% 1:10 HCl mobile phase through the column at a flow rate of 1 mL per min. Under these conditions calmagite is completely retained on the resin as the neutral sulfonic acid form while salt impurities are eluted. (Care should be taken that the dye does not precipitate during loading owing to evaporation of methanol.) Elute the purified calmagite with 95% ethanol and precipitate it as the sulfonic acid as follows.

Add to the ethanol eluate an equal volume of 1:10 HCl followed by sufficient ethanol to just dissolve the resulting precipitate. Warm the solution gently to remove the ethanol, thereby allowing the calmagite to precipitate slowly. Filter the precipitate and store it in a vacuum desiccator over $Mg(ClO_4)_2$ to prevent the uptake of atmospheric moisture by this highly hygroscopic material.

Spectral Properties and Acid Dissociation Constants

The spectral properties of the various protonated forms of purified calmagite were measured as a test of the purity of the material. The second and third acid dissociation constants were measured by the spectrophotometric procedure described in Albert and Serjeant (10) at 25°C and an ionic strength of 0.1. The

TABLE 1. Molar absorptivities (ε) and pK_a^M values of the conjugate species of calmagite at ionic strength of 0.1.

	ε and (λ_{max})		pk_a^M	
Species	Present study	Previous study[a]	Present study	Previous study[a]
H_2In^-	2.02×10^4 (530 nm)[b]	1.95×10^4 (525 nm)[c]	7.91±0.02[d]	8.14
HIn^{2-}	2.04×10^4 (615 nm)	2.03×10^4 (610 nm)	12.34±0.02[d]	12.35

[a]Reference 1.
[b]Dilute solution value obtained in the present study. See text.
[c]Interpolated from Fig. 1 in ref. 1.
[d]Mixed ionization constants (10) obtained at 25°C and 0.1 ionic strength. Total calmagite concentration 2×10^{-5} *M*.

following buffers were used for the determination of pK_{a2}^M (for H_2In^-): acetic acid – acetate from pH 4.2 to 5.3, THAM from 7.3 to 8.8, and ethanolamine from 9.1 to 10.1. For the determination of pK_{a3}^M (for HIn^-) the pH was adjusted with 0.1 *M* sodium hydroxide. Values of the constants are reported in Table 1 as "mixed ionization constants" (10).

Titrimetric Assay of Calmagite

Due to the hygroscopic nature of calmagite, samples were first dried overnight in a vacuum oven at 80°C and then weighed out, taking care to minimize exposure to the atmosphere. In the potentiometric acid–base titration 50 mg portions of purified calmagite were titrated with 0.05 *M* NaOH, using a glass and saturated calomel electrode pair to monitor pH.

For the two-phase photometric titration a porous Teflon membrane "filter-probe" phase separator was employed to facilitate monitoring the absorbance of the chloroform phase at 520 nm. The titration was performed in an apparatus previously described (11) with 70.0 mL of chloroform and 30.0 mL of aqueous 0.059 *M* phosphate buffer of pH 3.0 containing 2.20 mg of calmagite sample. Because of a slight amount of interfacial adsorption of the ion-pair, the magnetic stirrer was turned off during the absorbance measurement (11). The titrant was an aqueous solution of dextromethorphan hydrobromide.

Results and Discussion

Thin-layer chromatographic analysis of the three lots of commercial calmagite as received revealed the presence of two major types of organic impurities, colored impurities visible to the naked eye and fluorescent impurities appearing under 365 nm radiation. All lots tested contained significant quantities of impurities from each class. No attempt was made to isolate or characterize the impurities.

Further tlc analysis using the BEAP – silica gel system showed a considerable increase in purity of the calmagite after the initial liquid–liquid extraction. Significant amounts of colored impurities were shown by tlc to be retained in the original aqueous phase, while the butanol layer was found to contain the major proportion of the fluorescent impurities originally present. Only small amounts of calmagite were detected in the discarded layers; much of the weight loss during the extraction procedure was the result of removal of inorganic salts, which constitute the major impurity in commercial calmagite.

Product yields for the extraction step varied between 51 and 55% for the three batches of commercial calmagite studied. The yield from the combined partition and adsorption chromatographic steps varied from 60 to 80%, giving an overall yield of 30 to 40% purified calmagite.

The tlc analysis of the partition chromatographic fractions containing colored material showed that all of the fractions containing significant amounts of calmagite were free of colored impurities. A trace fluorescent impurity was still detectable just ahead of the calmagite spot. The same impurity was also detected in the final product.

Titrimetric assay of the purified product with sodium hydroxide gave a value of 99.4% ± 0.1% rsd, and the ion-pair titration gave 98.9% ± 0.3% rsd. The H_3In (sulfonic acid) form of calmagite is very hygroscopic and the product likely contains several tenths of a percent water.

Spectral properties and acid dissociation constants obtained for the purified product in the present study are shown in Table 1 along with the corresponding values reported by Lindstrom and Diehl (1). The spectrum of the species H_2In^- is concentration dependent with both the molar absorptivity (ε) and wavelength of maximum absorbance (λ_{max}) of this species decreasing with increasing concentration. Below about 2×10^{-5} *M* calmagite the concentration dependence is negligible and Beer's law is observed. The value of ε and λ_{max} for H_2In^- reported by Lindstrom and Diehl was measured at 9.1×10^{-5} *M*. When this concentration was used with the purified material obtained in the present study ε was found to be 1.96×10^4, and λ_{max} was 525 nm; both values are in good agreement with the earlier reported values (Table 1). The difference between the values of λ_{max} obtained for the HIn^{2-} species in the present and the previous studies may be largely caused by uncertainty in reading the broad absorption band.

No accurate values of ε and λ_{max} could be obtained for the In^{3-} species of calmagite because of the large value of pK_{a3}^M and the instability of calmagite at high pH.

The value obtained here for pK_{a2}^M at an ionic strength of 0.1 was 7.91 which is lower than the

Can. J. Chem. Downloaded from www.nrcresearchpress.com by 210.87.254.42 on 09/06/12
For personal use only.

earlier reported value of 8.14 (Table 1). This is because the spectrophotometric measurements in the present study were performed at a sample concentration ($2 \times 10^{-5} M$) sufficiently low that Beer's law is observed for the H_2In^- species, as discussed above. The earlier value of 8.14 was obtained at a sample concentration of $9 \times 10^{-5} M$ (1), while a value of 8.00 ± 0.02 was obtained at an intermediate concentration of $4.4 \times 10^{-5} M$.[2]

The values of pK_{a3}^M from both studies agree well. The proton on the sulfonic acid group in the H_3In species is almost completely dissociated, so no attempt was made to measure a pK_{a1}^M value.

Conclusion

In summary, a convenient method for the purification of commercially available calmagite has been developed and the product has been shown to conform on the basis of chromatographic, chemical, and optical properties to pure calmagite obtained by others through careful synthesis and exhaustive recrystallization. The partition chromatography column and procedure described here should be applicable to other indicators, particularly those of the *o,o'*-dihydroxyazo class. By varying the pH of the stationary phase buffer it is possible to optimize separation of the desired component. In a future communication we shall describe the application of purified calmagite to the determination of free magnesium ion concentration using the sample ion increment method (4).

[2]J. Polta and R. B. Fulton, St. John's University, unpublished data (1980).

Acknowledgements

The authors thank Joe McRaith and John Polta for assistance with portions of the experimental work while on a Macpherson Fellowship Award from St. John's University, and Hussain Mohammed for performing the two-phase titrations. Research support by the Natural Sciences and Engineering Research Council of Canada and the University of Alberta is also gratefully acknowledged.

1. F. LINDSTROM and H. DIEHL. Anal. Chem. **32**, 1123 (1960).
2. A. SCARPA. Biochemistry, **13**, 2789 (1974).
3. U. P. S. CHAUHAN and B. C. RAY SARKAR. Anal. Biochem. **32**, 70 (1969).
4. R. B. FULTON and B. KRATOCHVIL. Anal. Chem. **52**, 546 (1980).
5. F. LINDSTROM and R. ISAAC. Talanta, **13**, 1003 (1966).
6. F. LINDSTROM and A. E. WOMBLE. Talanta, **20**, 589 (1973).
7. N. C. KENDRICK. Anal. Biochem. **74**, 487 (1976).
8. R. G. BATES. Determination of pH. John Wiley, Toronto. 1973. Chapt. 4.
9. H. Y. MOHAMMED and F. F. CANTWELL. Anal. Chem. **51**, 1006 (1979).
10. A. ALBERT and E. P. SERJEANT. The determination of ionization constants. 2nd ed. Chapman and Hall, London. 1971. Chapt. 4.
11. H. Y. MOHAMMED and F. F. CANTWELL. Anal. Chem. **52**, 553 (1980).

Can. J. Chem. Downloaded from www.nrcresearchpress.com by 210.87.254.42 on 09/06/12
For personal use only.

The thermotropic phase behavior of ascorbyl palmitate: an infrared spectroscopic study[1]

HELMUT SAPPER,[2] DAVID G. CAMERON, AND HENRY H. MANTSCH

Division of Chemistry, National Research Council of Canada, Ottawa, Ont., Canada K1A 0R6

Received March 27, 1981

HELMUT SAPPER, DAVID G. CAMERON, and HENRY H. MANTSCH. Can. J. Chem. **59**, 2543 (1981).

The infrared spectra of aqueous potassium ascorbyl palmitate were studied as a function of temperature using Fourier transform infrared techniques. From a light scattering experiment the Krafft point of 0.1 *M* potassium ascorbyl palmitate was determined to be 48°C. The temperature-induced changes in infrared spectral parameters such as frequency and bandwidth characterize this Krafft point as a phase transition from a conformationally ordered, poorly hydrated solid phase, to an isotropic micellar phase. The phase transition of this "pseudosoap" occurs over a temperature range of about 10°C, reflecting the progressive hydration of the solid upon micellization, a behavior typical of surfactants such as soaps.

HELMUT SAPPER, DAVID G. CAMERON et HENRY H. MANTSCH. Can. J. Chem. **59**, 2543 (1981).

En utilisant les techniques infrarouges de la transformation de Fourier, on a étudié les spectres infrarouges des solutions aqueuses de palmitateascorbyle de potassium en fonction de la température. A partir d'un expérience de dispersion de la lumière, on a déterminé que le point Krafft pour une solution 0,1 *M* de palmitateascorbyle de potassium est de 48°C. La température provoque des changements dans les paramètres spectraux tels la fréquence et la largeur des bandes qui caractérisent ce point Krafft en tant que transition de phase à partir d'une conformation ordonnée, mal hydratée dans la phase solide, jusqu'à une phase micellaire isotropique. La transition de phase de ce "pseudo" savon se produit au dessus d'un intervalle de température de 10°C environ réflétant ainsi l'hydratation progressive du solide lors de la formation des micelles, c'est un comportement typique des savons.

[Traduit par le journal]

Introduction

Ascorbyl palmitate, the C-6 monoester of vitamin C with palmitic acid, was first synthesized by Swern *et al.* in 1943 (1) with the intention in mind to combine the reductive properties of ascorbic acid with the lipid solubility of a fatty acid. This derivative of ascorbic acid is actually a lipophilic vitamin C and has been shown to be as biologically active as its original hydrophilic counterpart (2, 3). Since both vitamin C and palmitate esters are natural food ingredients, ascorbyl palmitate is now widely used in the food industry as a natural preserver of oils and fats (4, 5).

The effectiveness of ascorbyl palmitate in protecting against oxidation is similar to that of other commercial lipid antioxidants, such as α-tocopherol (vitamin E). In fact, it has been shown that tocopherols become more powerful antioxidants when used in combination with ascorbyl palmitate (5, 6) and this effect can be further enhanced by addition of lecithin (3, 6). The synergism between vitamin C and vitamin E when used as antioxidants in biomembranes has been recently confirmed by pulse radiolysis measurements (7). Thus, the chemical behavior of ascorbyl palmitate as a lipophilic analogue of vitamin C is of interest not only in view of its value as a food additive, but also with respect to its possible biological role as a lipophilic vehicle of vitamin C.

Despite its importance to the food industry, there are few data in the literature regarding the structure and physicochemical properties of ascorbyl palmitate or its salts. In principle, one would expect these properties to reflect both those of vitamin C and those of a fatty acid ester. In addition, the salts of ascorbyl palmitate (at neutral pH ascorbyl palmitate is always a salt) are amphiphilic molecules and structurally similar to soaps such as the *n*-alkanoates or the *n*-alkyl sulphates. A common property of such surfactants is that above a certain temperature, referred to as the Krafft point (8–14), the solubility of the surfactant in water increases dramatically. The salts of ascorbyl palmitate exhibit the same behavior. Using a light scattering technique and Fourier transform infrared spectroscopy we have studied the Krafft point transition, and report on the data herein.

Experimental

Materials and Sample Preparation

Ethyl palmitate was from Sigma, St. Louis, MO and sodium ascorbate from Merck, Darmstadt, Germany. Ascorbyl palmitate (O^6-palmitoyl-L-ascorbic acid) was a commercial product from the U.S. Biochemical Corporation, Cleveland, OH. The potassium (or sodium) salts were prepared from equimolar amounts of ascorbyl palmitate and KOH (or NaOH), each dissolved in the minimal amount of absolute ethanol. The salts which precipitated upon mixing the two ethanolic solutions were filtered off, washed with absolute ethanol, and dried under vacuum.

[1]NRCC No. 19405.

[2]NRCC Visiting Scientist. On leave of absence from the Institute of Biophysics, Justus Liebig Universität, D-6300 Giessen, West Germany.

0008-4042/81/162543-07$01.00/0

©1981 National Research Council of Canada/Conseil national de recherches du Canada

Can. J. Chem. Downloaded from www.nrcresearchpress.com by 210.87.254.105 on 09/06/12
For personal use only.

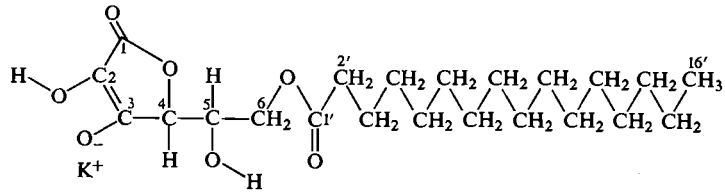

Samples of aqueous 0.1 *M* (4.5 wt.%) potassium or sodium ascorbyl palmitate were obtained by warming the solid salt in the corresponding amount of D_2O to about 50°C in a closed flask; above 40°C the opaque suspension becomes a clear solution which upon cooling turns into a uniform curd at room temperature. The pD (meter reading) of the clear solution was 8.1. Thin samples (15 μm thick in CaF_2 cells) of the curd were prepared for infrared spectroscopy according to the detailed methods reported elsewhere (15, 16).

Spectra and Data Processing

Infrared spectra were recorded with a Digilab FTS-11 Fourier transform infrared spectrometer equipped with a mercury cadmium telluride detector (Infrared Associates, New Brunswick, NJ). Typically, six hundred scans were accumulated and co-added using a maximal optical retardation of 0.5 cm and a moving mirror velocity of 0.6 cm/s. The resultant interferograms were triangularly apodized and Fourier transformed with one level of zero filling to yield a resolution of $\sim 2\,cm^{-1}$. The spectra of solid samples were recorded as KBr pellets (1 mg sample in 100 mg KBr) of 1 cm^2 surface area. Temperature control was achieved by using a hollow cell mount thermostated by a flow of ethanol–water which gives a temperature stability of better than ±0.1°C (17). The temperature was monitored with a thermocouple located against the cell window, and temperatures were continuously recorded by a Newport digital pyrometer equipped with a printer. The spectrometer computer controlled the complete operation of recording a spectrum, printing and incrementing the temperature, waiting for temperature equilibration, and then repeating the sequence (18). Frequencies were measured by determining the center of area of the top five data points of a peak. Bandwidths were obtained by digitally subtracting a linearly interpolated baseline extending from 3000 to 2800 cm^{-1} and computing the widths at ¾ of the peak height. The precision (and reproducibility) of measuring temperature-induced changes in frequency and bandwidth is better than ±0.05 cm^{-1} (19).

The light scattering experiment was performed by measuring the light transmitted at 580 nm through a 1 mm quartz cell containing the system under study. A Cary 219 uv–vis spectrophotometer equipped with the automated temperature reactant accessory and a coupled chart drive was employed.

Results and Discussion

General Thermal Properties

At room temperature potassium ascorbyl palmitate (APK) and sodium ascorbyl palmitate (APNa) are insoluble in water except at extremely low concentrations. However, on heating a water–APK (or water–APNa) mixture, the solubility increases rapidly above a certain temperature, and a clear solution is formed. If the solution is then cooled it solidifies as an opaque curd.

This behavior is well known in ionic surfactant–water systems (8–15). The curd is a semicrystalline mesophase in which the surfactant molecules form lamellar structures. According to the degree of hydration and three dimensional ordering it may be referred to as a gel (well hydrated and unilamellar) or a coagel (poorly hydrated and multilamellar) (20). While X-ray measurements are required to unequivocally determine if at a given temperature a system forms a gel or a coagel, the extreme opacity observed in the aqueous ascorbyl palmitate salts is indicative of a coagel system.

The temperature at which the transition occurs from the coagel (or gel) to the micellar phase is generally referred to as the Krafft point or as the "melting" point of the hydrated solid surfactant. However, the physical meaning of the solubility curve is different from that of ordinary solid–solute equilibrium curves and a stricter definition of the Krafft point is that of the concentration at which the coagel, monomers, and micelles are in equilibrium (10).

The Krafft point is dependent on the concentration and the type of counterion. In the case of 0.1 *M* potassium and sodium palmitate soaps, Krafft points of 30°C and 60°C respectively have been reported (21). Using light scattering techniques we find Krafft points of 48°C and 44°C for 0.1 *M* APK and APNa respectively. That is, the influence of the counterion is much smaller and, contrary to the behavior of the corresponding palmitate soaps, that of sodium ascorbyl palmitate is lower than that of potassium ascorbyl palmitate.

Infrared Spectra

The thermotropic properties of potassium ascorbyl palmitate were investigated in detail by infrared spectroscopy. The 1800–1300 cm^{-1} region of the spectra of the anhydrous solid, the ordered coagel, and the isotropic micellar phase of APK are shown in the bottom segment of Fig. 1. The top segments show spectra of sodium ascorbate and ethyl palmitate, accurate frequencies are given in Table 1. It can be seen that, in general, the spectrum of APK is comprised of the summation of the palmitate and ascorbate spectra, particularly in the micellar phase.

Of more significance to this study are the differences between the spectra of the solid, the coagel, and the micellar phases of APK. Considering first the spectra of the solid and the coagel (Fig. 1, C and B respectively), it can be seen that the C=O stretching bands at 1744 and 1735 cm^{-1} are broad-

Can. J. Chem. Downloaded from www.nrcresearchpress.com by 210.87.254.105 on 09/06/12
For personal use only.

Can. J. Chem. Downloaded from www.nrcresearchpress.com by 210.87.254.105 on 09/06/12
For personal use only.

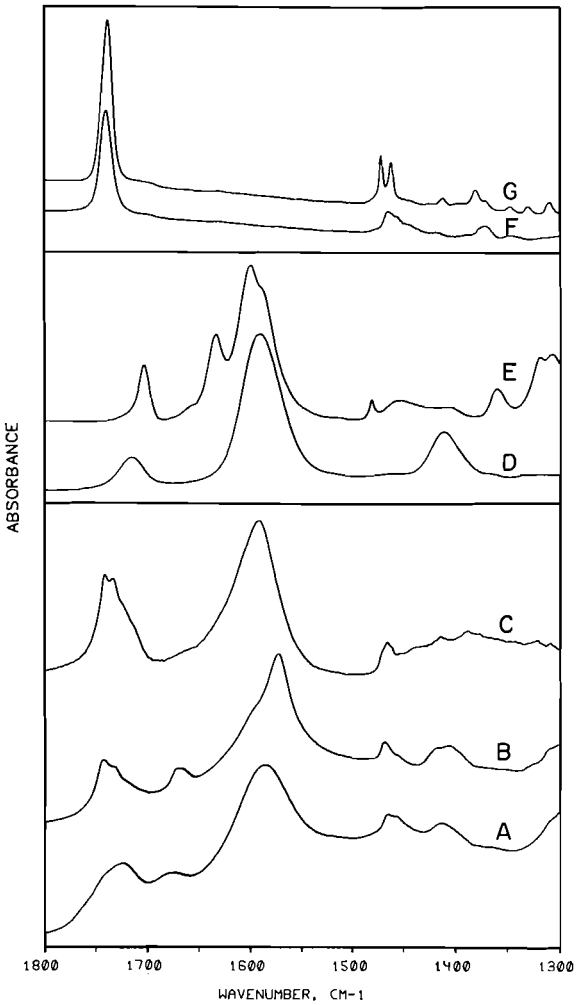

FIG. 1. Infrared spectra in the 1800–1300 cm^{-1} region of 0.1 *M* potassium ascorbyl palmitate in D_2O at 56°C (A) and at 20°C (B), polycrystalline APK at 20°C (C), sodium ascorbate in D_2O (D) and as polycrystalline solid (E), and ethyl palmitate in KBr at 30°C (F) and at 8°C (G).

ened on formation of the coagel, suggesting some degree of hydrogen bond formation with water of hydration. Rather more dramatic changes are evident in the C=C stretching bands. The weak broad band at ~1660 cm^{-1} in the spectrum of the solid gains intensity and has two components in the coagel (see Table 1). Even greater changes are observed in the strong C=C stretching band near 1600 cm^{-1}. Formation of the coagel results in a strong narrow band at 1574 cm^{-1}, while a weak band near 1600 cm^{-1} is retained. The shift to lower frequency of the main C=C stretching band suggests a reduction of the double bond character of the C(2)=C(3) bond. The sensitivity of this bond to the state of the ascorbate moiety has already been demonstrated. Formation of the sodium salt shifts the C=O stretching band from 1753 to 1702 cm^{-1}, and the C(2)=C(3) stretching band from 1670 to 1593 cm^{-1} (23), and increases the C=O and C(2)=C(3) double bond lengths by 0.017 Å and 0.035 Å respectively (24).

The interaction resulting in the shift of the C(2)=C(3) stretching band to 1574 cm^{-1} is specific to the coagel and must result from a particular intra- or intermolecular interaction, possibly involving partial hydration. At this point, we are unable to assign the individual C=C stretching bands, other than to give them the general classification of double bond stretching vibrations associated with the ascorbyl moiety.

The spectrum of the micellar phase is somewhat simpler than that of the coagel. The broad bands in this region are typical of those encountered in solution spectra of materials capable of engaging in extensive hydrogen bond formation, while the bandshapes indicate an enhanced mobility of the particular functional groups. Nonetheless, discrete absorptions are still present, as suggested by the asymmetry of the C=O stretching band contour, and demonstrated by the distinct frequency maxima found after Fourier self-deconvolution (see Table 1).

Another vibrational mode of interest is the CH_2 scissoring band around 1468 cm^{-1}, which is used extensively for the characterization of the packing of acyl chains in solid hydrocarbons, lipids, and surfactants (25, 26). Its observation at 1471.5 cm^{-1} in the coagel is indicative of a triclinic packing of

TABLE 1. Characteristic group frequencies (in cm^{-1}) of potassium ascorbyl palmitate and of selected model compounds[a]

	Acyl chain vibrations		Head group vibrations						
	$\nu_{as}(CH_2)$	$\nu_s(CH_2)$	ν(C(1)=O)		ν(C(1')=O)		ν(C=C)		
APK, solid (KBr)	2917.8	2850.3	1744*	1735*	1725*		~1660	1609*	1594*
APK, coagel (D_2O)	2917.8	2850.3	1745*	1733*	1723*	1673*	1663*	1599*	1574*
APK, micellar (D_2O)	2923.6	2853.2	1744*	—	1724*	1678			1590
ANa, solid (KBr)			—	—	1702		~1660	1602*	1593*
ANa, solution (D_2O)			—	—	1717				1591
EP solid (KBr)	2917.0	2849.0	1744*	1738*	—				
EP melt (KBr)	2924.9	2854.1	1742*	1738*	—				

[a] Abbreviations: APK, potassium ascorbyl palmitate; ANa, sodium ascorbate; EP, ethyl palmitate. The asterisks indicate frequencies obtained by Fourier self-deconvolution (22), a technique which reduces the spectral linewidth of component bands at the expense of the line shape and the signal-to-noise ratio.

Can. J. Chem. Downloaded from www.nrcresearchpress.com by 210.87.254.105 on 09/06/12
For personal use only.

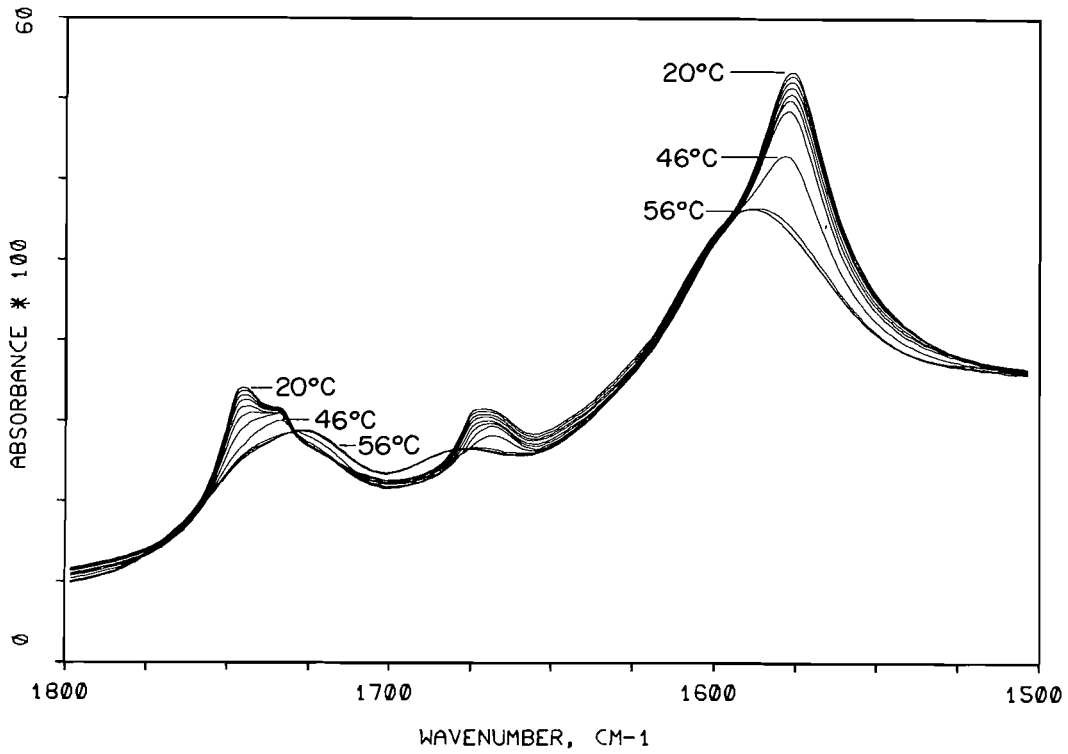

FIG. 2. Infrared spectra in the 1800–1500 cm^{-1} region of 0.1 *M* APK in D_2O as a function of temperature. There are 11 individual spectra taken in 3.6°C intervals; the top spectrum (with the largest peak height) is at 20°C, and the bottom spectrum (with the smallest peak height) at 56°C.

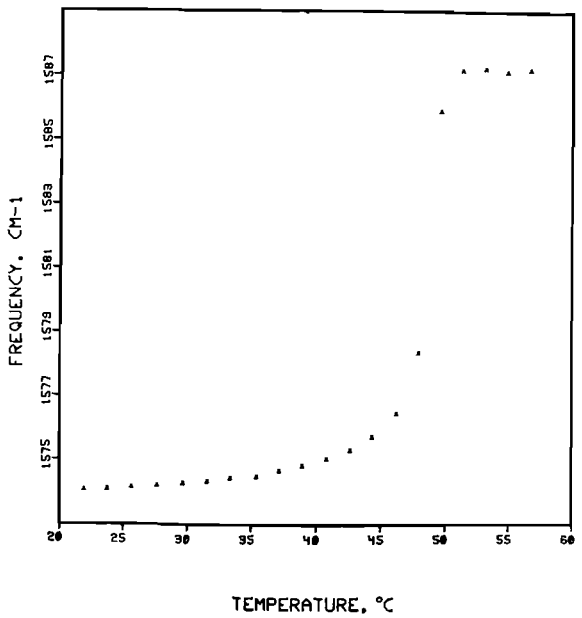

FIG. 3. Temperature-dependence of the frequency (band maximum) of the C=C stretching vibration of APK in D_2O.

this surfactant below the Krafft point. Such packing has previously been observed in solid *n*-alkanoates (27).

The temperature dependence of the 1800–1500 cm^{-1} region of the infrared spectrum of 0.1 *M* APK is shown in Fig. 2. The abrupt changes on transition from the coagel to the micellar phase are clearly evident. Also demonstrated are continuous spectral changes prior to micellization. As the temperature is raised from 20°C to ~40°C these changes are evident as reductions in the heights of the bands at 1745, 1673, and 1574 cm^{-1}. Other bands characteristic of the coagel (1733 and 1663 cm^{-1}) do not change as rapidly. Although there will be a slight increase in the monomer concentration in this range, these spectral changes are too large to be simply accounted for in terms of a decrease in the coagel concentration. Therefore we believe that these changes result from progressive hydration of the palmitate C=O group and of the ascorbate moiety prior to micellication.

In the range 40 to 51°C, the rate of change is much greater. This is illustrated in Fig. 3, which shows a

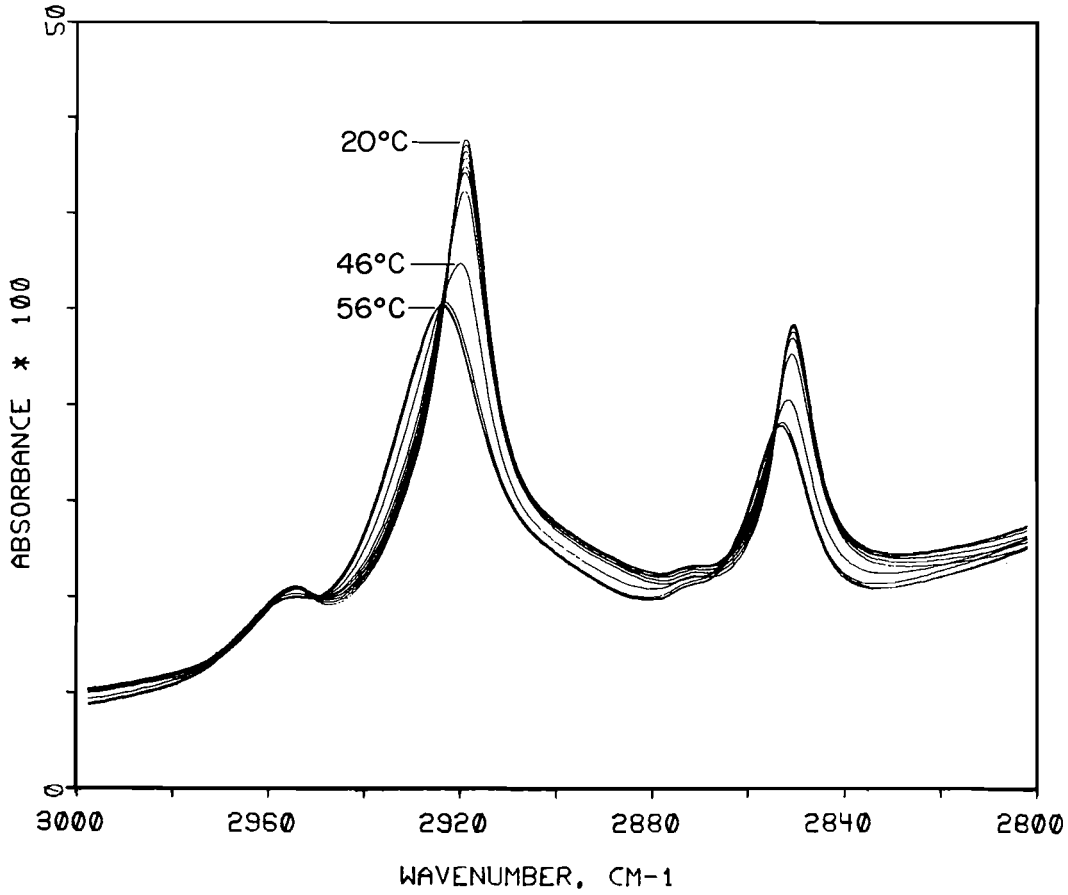

FIG. 4. Infrared spectra in the C—H stretching region of 0.1 *M* APK in D_2O. For further details, see caption to Fig. 2.

plot of the temperature dependence of the position of the maximum of the C=C stretching band contour at 1574 cm^{-1}. Although the parameter reflects the sum of the changes in the two component bands, it does provide an excellent monitor of the rate of change of the bands. It can be seen that the frequency varies throughout the entire temperature range with a maximal rate of change (>90% of the entire change) between 45 and 51°C (48 ± 3°C). Within this range the changes can be attributed to the continuously changing concentrations of the coagel and micellar phases.

The C—H stretching region of the infrared spectrum is shown in Fig. 4. There are four distinct groups of absorption bands in this region, the strong antisymmetric and symmetric CH_2 stretching bands around 2920 and 2850 cm^{-1}, respectively, and the weaker asymmetric and symmetric CH_3 stretching bands at 2955 and 2873 cm^{-1}, respectively. Also evident is a weak Fermi resonance band near 2900 cm^{-1}. These bands exhibit a thermotropic behavior similar to that of the vibrational modes originating in the head group.

Two distinct types of spectra are observed in Fig. 4. The spectra at temperatures below 40°C are narrow, indicating relatively low acyl chain mobility and the absolute frequencies are characteristic of fully extended all-*trans* acyl chains. As the temperature is raised, continuous changes are observed prior to the transition to the micellar phase. These changes were monitored by plotting the temperature dependence of the frequency and bandwidth of the symmetric CH_2 stretching band, and are shown in Fig. 5. Identical plots (not shown here) were obtained from the temperature-dependence of the antisymmetric CH_2 stretching mode.

Below 40°C the frequency indicating all-*trans* acyl chains in the ordered coagel is almost invariant, whereas the bandwidth shows continuous changes between 20 and 40°C. This demonstrates an increase in the acyl chain mobility within this

Can. J. Chem. Downloaded from www.nrcresearchpress.com by 210.87.254.105 on 09/06/12
For personal use only.

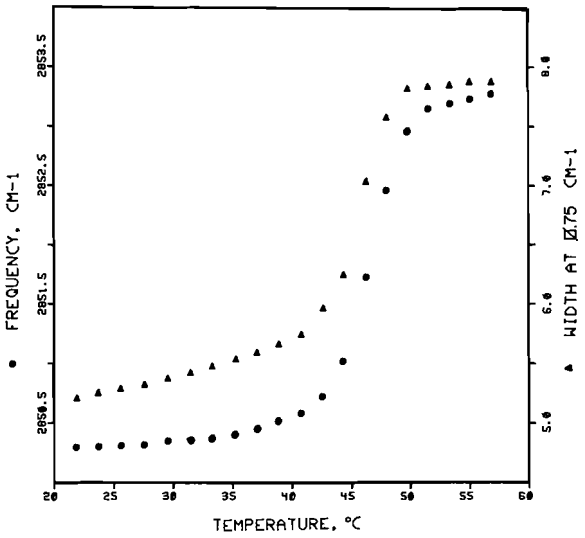

FIG. 5. Temperature-dependence of the frequency (●) and the width at ¾ height (▲) of the symmetric CH_2 stretching band of APK in D_2O.

temperature range, behavior which has also been observed prior to the melting transition of phospholipids (19, 28).

As the temperature is raised above 40°C progressive changes in both frequency and bandwidth are evident, the maximum rate of change being observed between 45 and 51°C. As with the head group absorptions this reflects the continuously changing concentrations of the coagel and micellar species. Confirmation that this is indeed the case comes from two sources. Firstly, the changes in frequency and bandwidth are not concerted. Rather, the maximum rates of change of frequency are observed at higher temperatures than those of the bandwidth. This is particularly evident in the plots in Fig. 5 in which the bandwidth is constant in the temperature range 49 to 51°C while the frequency is still changing. This behavior is typical of that resulting from the overlap of similar bands from two different species and has previously been observed in studies of the critical micelle concentration of *n*-alkanoates (29). Secondly, the contours of the CH_2 stretching bands at 46°C (Fig. 4) show flattened peak tops and are highly asymmetric compared to the spectra recorded at either higher or lower temperatures, indicating that at this temperature the two component spectra have roughly equal intensities.

The frequencies and bandwidths of the symmetric and antisymmetric CH_2 stretching vibration of an aqueous suspension of potassium ascorbyl palmitate increase dramatically between 45 and 51°C. The shift to higher frequencies is due to the appearance of a large number of *gauche* conformers in the all-*trans* acyl chains, whereas the increased bandwidth is the consequence of an increase in the mobility of the palmitate chains. Both phenomena are typical of acyl chain melting phase transitions (19, 28, 29) and were also observed at the melting point of solid ethyl palmitate (Table 1).

Conclusions

Aqueous suspensions of potassium and sodium ascorbyl palmitate show thermotropic behavior typical of dilute ionic surfactant systems. In 0.1 *M* suspensions of potassium ascorbyl palmitate in D_2O abrupt increases in the solubility are observed at 48 ± 3°C, as are spectral changes typifying a transition from a conformationally ordered, poorly hydrated, solid state to an isotropic micellar state. The transition generally occupies about 10°C, and within this range continuously changing concentrations of both species are present. This behavior is typical of that observed in aqueous *n*-alkyl carboxylate ions (soaps). However, unlike in soaps, due to the different nature of the head group, the transition temperature of the sodium salt of ascorbyl palmitate is lower than that of the corresponding potassium salt.

1. D. SWERN, A. J. STIRTON, J. TURNER, and P. A. WELLS. Oil Soap, **20**, 224 (1943).
2. A. M. ABROSE and F. DeEDS. Arch. Biochem. **12**, 375 (1947).
3. J. DELGA and R. BOULU. Ann. Pharm. Fr. **15**, 691 (1957).
4. W. M. CORT. J. Am. Oil Chem. Soc. **51**, 321 (1974).
5. H. KLAUI. Int. Flavour Food Addit. **7**, 165 (1976).
6. G. PONGRACZ. Int. J. Vit. Nut. Res. **43**, 517 (1973).
7. J. E. PACKER, T. F. SLATER, and R. L. WILLSON. Nature, **278**, 737 (1979).
8. F. KRAFFT and H. WIGLOW. Ber. **28**, 2566 (1895).
9. N. K. ADAM and K. G. A. PANKHURST. Trans. Faraday Soc. **42**, 523 (1946).
10. K. OGINO and Y. ICHIKAWA. Bull. Chem. Soc. Jpn. **49**, 2683 (1976).
11. K. SHINODA, Y. MINEGISHI, and H. ARAI. J. Phys. Chem. **80**, 1987 (1976).
12. J. DANIELSSON, J. B. ROSENHOLM, P. STENIUS, and S. BACKLUND. Prog. Colloid Polym. Sci. **61**, 1 (1976).
13. H. WENNERSTROM and B. LINDMAN. Phys. Rep. **52**, 1 (1979).
14. K. SHINODA. Pure Appl. Chem. **52**, 1195 (1980).
15. D. G. CAMERON, H. L. CASAL, and H. H. MANTSCH. J. Biochem. Biophys. Meth. **1**, 21 (1979).
16. J. UMEMURA, D. G. CAMERON, and H. H. MANTSCH. J. Phys. Chem. **84**, 2272 (1980).
17. D. G. CAMERON and R. N. JONES. Appl. Spectrosc. In press.
18. D. G. CAMERON and G. M. CHARETTE. Appl. Spectrosc. **35**, 224 (1981).
19. D. G. CAMERON, H. L. CASAL, H. H. MANTSCH, Y. BOULANGER, and I. C. P. SMITH. Biophys. J. **35**, 1 (1981).

Can. J. Chem. Downloaded from www.nrcresearchpress.com by 210.87.254.105 on 09/06/12
For personal use only.

20. J. M. VINCENT and A. SKOULIOS. Acta Crystallogr. **20**, 441 (1966).
21. J. W. MCBAIN. J. Am. Oil Chem. Soc. **25**, 221 (1948).
22. J. K. KAUPPINEN, D. J. MOFFATT, H. H. MANTSCH, and D. G. CAMERON. Appl. Spectrosc. **35**, 271 (1981).
23. J. HVOSLEF and P. KLAEBOE. Acta Chem. **25**, 3043 (1971).
24. J. HVOSLEF. Acta Crystallogr. Sect. B, **25**, 2214 (1969).
25. Y. KOYAMA, M. YANAGISHITA, S. TODA, and T. MATSUO. J. Colloid Interface Sci. **61**, 438 (1977).
26. D. G. CAMERON, H. L. CASAL, F. E. GUDGIN, and H. H. MANTSCH. Biochim. Biophys. Acta, **596**, 463 (1980).
27. J. H. DUMBLETON and T. R. LOMER. Acta Crystallogr. **19**, 301 (1965).
28. D. G. CAMERON, H. L. CASAL, and H. H. MANTSCH. Biochemistry, **19**, 3665 (1980).
29. D. G. CAMERON, J. UMEMURA, and H. H. MANTSCH. J. Colloid Interface Sci. In press.

Can. J. Chem. Downloaded from www.nrcresearchpress.com by 210.87.254.105 on 09/06/12
For personal use only.

Bis(triethylammonium) hexachlorostannate (IV): crystal structure and hydrogen bonding[1]

OSVALD KNOP, T. STANLEY CAMERON, AND MARGARET ANN JAMES
Department of Chemistry, Dalhousie University, Halifax, N.S., Canada B3H 4J3
AND
MICHAEL FALK
Atlantic Research Laboratory, National Research Council of Canada, Halifax, N.S., Canada B3H 3Z1
Received March 3, 1981

OSVALD KNOP, T. STANLEY CAMERON, MARGARET ANN JAMES, and MICHAEL FALK. Can. J. Chem. **59**, 2550 (1981).

The crystal structure of $(Et_3NH)_2SnCl_6$ at room temperature consists of a monoclinically distorted antifluorite packing of Et_3NH^+ and $SnCl_6^{2-}$ ions. Each anion has two cations centrosymmetrically associated with it through bifurcated hydrogen bonds to four of the Cl atoms, leaving two of the six chlorines unengaged. The bifurcation is nearly symmetric and the N—H···2Cl group is nearly planar. Infrared spectra of undeuterated and partially deuterated polycrystalline $(Et_3NH)_2SnCl_6$ show that the NH stretching vibration is essentially uncoupled while the corresonding ND vibration undergoes a complex Fermi resonance resulting in a multiplet in the spectrum of even weakly deuterated material. The hydrogen bonding in $(Et_3NH)_2SnCl_6$ is stronger than in the corresponding ammonium compound. A negative temperature coefficient of the NH and ND stretching frequencies is consistent with the bifurcation of the hydrogen bond. If a low-temperature transition exists, it was not evident in the NH and ND stretching absorptions.

OSVALD KNOP, T. STANLEY CAMERON, MARGARET ANN JAMES et MICHAEL FALK. Can. J. Chem. **59**, 2550 (1981).

La structure cristalline du $(Et_3NH)_2SnCl_6$ comporte, à la température ambiante, un assemblage de type antifluorine déformée des ions Et_3NH^+ et $SnCl_6^{2-}$. Chaque anion est associé, d'une façon centrosymétrique, à deux cations par des liaisons hydrogène bifurquées; ces liaisons engagent quatre des six atomes chlore de l'anion, laissant libres les deux autres. La bifurcation est presque symétrique et le groupement N—H···2Cl est presque plan. Les spectres infrarouges du $(Et_3NH)_2SnCl_6$ polycristallin non-deutéré ainsi que partiellement deutéré montrent que la vibration NH de valence est essentiellement découplée, tandis que la vibration ND correspondante subit une résonance Fermi complexe, ce qui donne lieu à un multiplet dans le spectre du composé même légèrement deutéré. La liaison hydrogène dans le $(Et_3NH)_2SnCl_6$ est plus forte que celle dans le composé ammonium correspondent. Le coefficient de la variation thermique des fréquences NH et ND de valence est négatif, ce qui s'accorde bien avec la bifurcation de la liaison hydrogène. Si une transition à basse température existe dans le $(Et_3NH)_2SnCl_6$, elle n'est pas évidente dans les absorptions dues aux vibrations NH et ND de valence.

Study of the spectroscopic manifestations of hydrogen bonding in crystals is complicated by a number of factors. One of them, vibrational coupling of XH groups in neighbouring X—H···Y bonds, may modify the frequency, shape, and breadth of ir absorptions involving XH to such an extent that it precludes extraction of numerical parameters required in comparisons of the strength and type of hydrogen bonding in different classes of compounds. Detailed analysis of the ir spectrum should, of course, determine the nature and magnitude of the coupling and thus remove the difficulty, but in practice this is possible only in relatively simple cases and even then not without a considerable effort. In general it is preferable to secure the desired information by the use of the isotopic isolation technique (1, 2), which yields decoupled XH (or XD) absorption bands. This approach is workable provided the pertinent decoupled absorptions can be resolved and identified. Occasionally, however, situations are encountered where the XH absorptions are sufficiently free from complications to yield the information without further analysis or sample manipulation, viz. where the coupling is minimal owing mostly to wide separation of the XH groups in the crystal. Apart from the simplicity of the XH spectra such situations are of interest in their own right in that they permit the conditions to be investigated beyond which effective coupling can no longer be expected to exist. Because of this they seemed to us to merit a closer look in the context of our continuing study of hydrogen bonding in crystals.

In searching for suitable compounds trialkylammonium salts appeared promising for several reasons, among them the possibility of comparison with the corresponding ammonium salts that had been studied previously. Exploratory trials with several such salts led to the selection of the title compound as the first to be examined in some detail. The crystal is ionic, which indicated that the structure would be determined primarily by Coulombic interactions and thus likely to be related to one of the simple AB_2 types of packing of cations

[1]NRCC No. 19385.

0008-4042/81/162550-06$01.00/0
©1981 National Research Council of Canada/Conseil national de recherches du Canada

Can. J. Chem. Downloaded from www.nrcresearchpress.com by 210.87.254.6 on 09/06/12
For personal use only.

Can. J. Chem. Downloaded from www.nrcresearchpress.com by 210.87.254.6 on 09/06/12
For personal use only.

and anions. This and the low NH/Cl ratio in turn implied that the N—H···Cl bonds would not share Cl atoms or form continuous networks, thereby minimizing the opportunity for effective coupling; coupling across $SnCl_6^{2-}$ octahedra would involve appreciable H···H distances and heavy intervening atomic masses and therefore be weak. Thus each crystallographically nonequivalent cation would be expected to give rise to *one* NH stretching vibration. Barring fortuitous complications arising from Fermi resonance, the number of observed NH stretching bands would (except for accidental overlap) then correspond to the actual number of crystallographically distinct sets of cations in the crystal, analogous to what is observed for ND stretching absorptions in spectra of isotopically isolated NH_3D^+ species (2). In the following we describe the room-temperature crystal structure of $(Et_3NH)_2SnCl_6$ and the conclusions, from the ir spectra of undeuterated and partially deuterated polycrystalline material, relevant to hydrogen bonding.

Experimental

Preparation and Infrared Spectra

$(Et_3NH)_2SnCl_6$ was prepared by combining a solution of Et_3N in 95% EtOH with an equivalent amount of an aqueous solution of H_2SnCl_6. The large, colourless crystals which appeared on slow evaporation at room temperature were recrystallized from EtOH. Low-level deuteration (1–5% replacement of the amino H) was achieved by recrystallization from weakly deuterated EtOH.

Spectra were recorded on a Perkin-Elmer model 180 spectrophotometer fitted with a closed-cycle He refrigerator (Displex model 202, Air Products and Chemicals Co.). Suitable samples were obtained by mulling finely ground crystals with fluorocarbon (4000–1330 cm^{-1}) or hydrocarbon (1330–400 cm^{-1}) oil. The mulls were sandwiched between KBr or CaF_2 plates.

Crystal Data

$C_{12}H_{32}Cl_6N_2Sn$ f.w. = 535.8

Monoclinic, $P2_1/n$ (systematic absences: $h0l$, $h + l = 2n + 1$; $0k0$, $k = 2n + 1$); $a = 9.950(2)$ Å, $b = 10.698(2)$ Å, $c = 10.767(3)$ Å, $\beta = 100.22(2)°$, $V = 1127.9$ Å^3, $Z = 2$, $\rho_0 = 1.585$ g/cm^3, $\rho_c = 1.577$ g/cm^3 (20 ± 2°C); Mo $K\alpha_1$, $\lambda = 0.70926$ Å (graphite monochromator), $\mu_{Mo} = 17.05$ cm^{-1}, $F(000) = 540$ e.

Structure Determination

A CAD-4 four-circle diffractometer was used to determine the unit-cell dimensions from 25 general reflections with $12 < \theta < 15°$. 1976 unique reflections in the range $1 < \theta < 25°$ were measured, of which 1301 had $I > 3\sigma(I)$. The intensities were reduced by routine procedures which are described in ref. 3. Lorentz and polarization corrections were applied but no absorption or extinction corrections. The scattering factors for neutral atoms were taken from ref. 4. The structure was solved using the SHELX system (5).

The Sn atoms were located from the *E*-map and all other nonhydrogen atoms were found on a subsequent Fourier map. Full-matrix least-squares ($w\Delta F^2$ = min.) refinement was carried out with isotropic temperature factors on heavy atoms until $R = 0.081$. The hydrogens were located from a difference Fourier map calculated at this stage. Refinement was continued with anisotropic temperature factors on the nonhydrogen atoms and isotropic factors on the hydrogens until $R = 0.022$, based on 1297 reflections; the reflections 110, $\bar{1}01$, 101, and 011 were omitted because of extinction effects. The least-squares weights[2] were calculated from $w^{-1} = \sigma^2|F_0| + 0.000553|F_0|^2$, where σ is the weight for an individual reflection derived from the diffractometer counting statistics. The atomic and thermal parameters are given in Tables 1 and 2, interactomic distances and bond angles in Table 4.[3].

Results and Discussion

Description of the Structure

The structure (Figs. 1 and 2) is a distorted version of the *fcc* antifluorite-type packing represented by $(NH_4)_2PtCl_6$. The centrosymmetric $SnCl_6$ octahedra, which are close to regular, are rotated by significant amounts from the edges of the cuboid cells defined by the Sn sublattice. The Et_3NH^+ ion in each of these cells is hydrogen-bonded to two Cl atoms of an $SnCl_6$ octahedron. This bifurcated N—H···2Cl bond is nearly symmetric; the H atom is only about 0.16 Å away from the respective N—Cl(1)—Cl(2) plane, and the N—H—Cl angle is 138(3)° for Cl(1) and 136(3)° for Cl(2). The hydrogen bonding results in centrosymmetric $Et_3NH···SnCl_6···HNEt_3$ units which are arranged in layers approximately coincident with the 200 planes. The C—H bond lengths are unexceptionable.

The shortest interatomic distances between NH groups are ca 6.2 Å for N···N and ca 6.7 Å for H···H. The NH groups are thus well separated. Considering that the H···H separation in an $Et_3NH···SnCl_6···HNEt_3$ unit is 7.3 Å, vibrational coupling of the NH groups across the bulky, heavy $SnCl_6$ anion would be expected to be weak.

The H···Cl distances in the bifurcated hydrogen bonds, 2.50(5) and 2.67(5) Å, are somewhat shorter than the H···Cl distance in the cubic $(NH_4)_2SnCl_6$, 2.79 Å (assuming symmetric trifurcation N—H···3Cl). Unlike in the latter crystal, the N—H vectors in $(Et_3NH)_2SnCl_6$ point in the direction of the Sn atoms; the N, H, and Sn atoms are almost collinear and in a direction that corresponds to a cube diagonal in $(NH_4)_2SnCl_6$.

In its general organization the structure resembles that of $(Et_3NH)_2CuCl_4$ (6) (Fig. 3). Both structures contain discrete $Et_3NH···anion···HNEt_3$

[2]A table of σ will be provided by the authors on request.

[3]Tables 2 and 3 (structure factors) have been deposited. Copies are available, at a nominal charge, from the Depository of Unpublished Data, CISTI, National Research Council of Canada, Ottawa, Ont., Canada K1A 0S2.

Can. J. Chem. Downloaded from www.nrcresearchpress.com by 210.87.254.6 on 09/06/12
For personal use only.

TABLE 1. Positional parameters and temperature factors of atoms in $(Et_3NH)_2SnCl_6$ at room temperature*

Atom	x	y	z	Temperature factor
Sn(1)	0	0	1	328(1)
Cl(1)	2040(1)	951(1)	9398(1)	459(4)
Cl(2)	1261(1)	−1893(1)	10686(1)	613(5)
Cl(3)	623(1)	865(1)	12086(1)	689(6)
N(1)	4048(3)	−1526(3)	7265(3)	395(16)
C(11)	5325(4)	−737(4)	7479(4)	457(22)
C(12)	5170(5)	527(5)	8053(5)	639(31)
C(21)	3655(5)	−2016(4)	8469(4)	494(23)
C(22)	4675(5)	−2909(5)	9168(5)	635(25)
C(31)	2832(4)	−907(4)	6476(4)	458(21)
C(32)	3103(5)	−493(5)	5216(5)	619(29)
H(1)	425(6)	−231(4)	684(5)	98(20)
H(111)	563(4)	−70(4)	664(2)	42(10)
H(112)	601(3)	−122(3)	808(3)	38(10)
H(121)	432(4)	104(6)	781(7)	140(32)
H(122)	488(6)	45(6)	889(8)	104(21)
H(123)	490(7)	100(6)	726(4)	144(33)
H(211)	344(5)	−125(3)	893(4)	55(12)
H(212)	274(3)	−241(4)	818(4)	55(13)
H(221)	427(5)	−328(5)	985(4)	80(17)
H(222)	554(4)	−245(5)	951(6)	93(19)
H(223)	477(5)	−366(3)	864(4)	75(16)
H(311)	260(4)	−17(3)	696(3)	50(11)
H(312)	214(3)	−159(3)	640(4)	44(11)
H(321)	368(4)	25(3)	522(5)	72(15)
H(322)	353(5)	−118(4)	478(4)	69(15)
H(323)	224(3)	−22(5)	466(4)	82(17)

*The parameters have been multiplied by 10^4; those of hydrogen, by 10^3. The temperature factor values represent mod(U) for the nonhydrogen atoms and the isotropic temperature factor U for the hydrogens. Thermal parameters U_{ij} are listed in Table 2.

TABLE 4. Bond distances (Å) and angles (deg) in $(Et_3NH)_2SnCl_6$

Bond	Distance	Bonds	Angle
Sn(1)—Cl(1)	2.458(1)	Cl(1)—Sn(1)—Cl(2)	91.07(4)
Sn(1)—Cl(2)	2.427(1)	Cl(1)—Sn(1)—Cl(3)	89.94(4)
Sn(1)—Cl(3)	2.407(1)	Cl(2)—Sn(1)—Cl(3)	90.20(4)
N(1)—C(11)	1.509(5)	C(11)—N(1) —C(21)	113.7(3)
N(1)—C(21)	1.513(5)	C(11)—N(1) —C(31)	114.3(3)
N(1)—C(31)	1.504(5)	C(21)—N(1) —C(31)	109.4(3)
C(11)—C(12)	1.505(7)	N(1)—C(11)—C(12)	114.9(4)
C(21)—C(22)	1.496(7)	N(1)—C(21)—C(22)	113.4(4)
C(31)—C(32)	1.497(7)	N(1)—C(31)—C(32)	112.7(4)

units held together by bifurcated hydrogen bonds[4] but the tetrachlorocuprate structure is less symmetric, as evidenced by the existence of two nonequivalent sets of Et_3NH ions and the dissimilarity of the two shortest N(2)···Cl distances, 3.17 and 3.59 Å respectively (the H positions were not determined). In neither case was there evidence of significant disorder in the structure. This is in contrast to Et_3NHCl, where the ethyl groups are statically disordered with respect to planes of reflection through the N atoms (7); the N—H···Cl bonds in this structure ($P6_3mc$) are in threefold axes and hence constrained by symmetry to be normal (N···Cl, 3.11 Å).

Infrared Spectra: NH Stretching

The NH stretching band in the room-temperature spectrum of undeuterated $(Et_3NH)_2SnCl_6$ is

[4]This similarity is not obvious in the description of the tetrachlorocuprate structure in ref. 6.

Can. J. Chem. Downloaded from www.nrcresearchpress.com by 210.87.254.6 on 09/06/12
For personal use only.

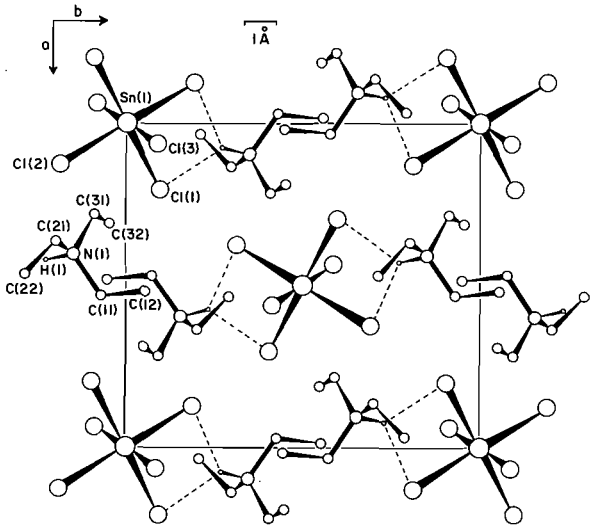

FIG. 1. Projection of the $(Et_3NH)_2SnCl_6$ structure along *c*. *Dashed lines represent H···Cl bonds.*

simpler in shape and much narrower than the corresponding band of $(NH_4)_2SnCl_6$, $\Delta\nu_{1/2} \sim 25\,cm^{-1}$ as against $>100\,cm^{-1}$ (Figs. 4 and 5). On deuterating the crystal to a varying degree the frequency of the band was practically unaffected and its halfwidth was reduced by no more than $5\,cm^{-1}$, while in the ammonium compound a drastic narrowing occurred. From this we concluded that in the triethylammonium compound, unlike in the ammonium salt, the NH stretching vibrations are essentially uncoupled, thus confirming the expectation from the geometry of the structure.

Cooling the crystal caused the ν(NH) band to sharpen, $\Delta\nu_{1/2}(10\,K) \sim 10\,cm^{-1}$ (Fig. 5). The frequency *increased* on cooling, by about $8\,cm^{-1}$ between 293 and 10 K (Fig. 6), consistent with the criterion formulated previously for highly-bent hydrogen bonds (8). The changes in the frequency, halfwidth, and shape of the ν(NH) band were gradual and gave no indication of a low-temperature transition.

The room-temperature frequency of ν(NH) in the triethylammonium compound is about $130\,cm^{-1}$ lower than in $(NH_4)_2SnCl_6$. The N···Cl (3.33 and 3.46 Å) and H···Cl (2.50 and 2.67 Å) distances in $(Et_3NH)_2SnCl_6$ are shorter than the corresponding distances in the ammonium compound (3.55 and 2.79 Å respectively), hence the hydrogen bonding in the alkyl compound is stronger. To what extent this strengthening reflects the effects of the shorter H···Cl distances, the alkyl substitution, and the change from trifurcation (in the ammonium compound) to bifurcation can only be answered when more information on compounds of this type has accumulated. However, the effect of structure expansion on ν(NH), important in the $(NH_4)_2MX_6$ compounds (8, 9), is probably absent in $(Et_3NH)_2SnCl_6$, owing to the lower connectivity of the hydrogen-bond system in the latter structure. A discussion of this point is reserved for another occasion.

Infrared Spectra: ND Stretching

Instead of the expected replication of the simple

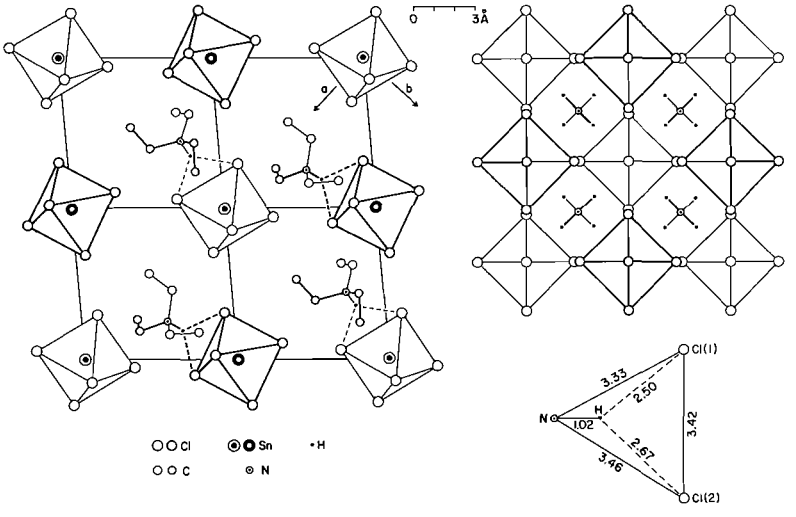

FIG. 2. (*Left*) Projection of a slab (parallel to 001) of the $(Et_3NH)_2SnCl_6$ structure along *c* displaying the face-centred antifluorite packing of cations and anions. (*Top right*) A similar projection of the cubic $(NH_4)_2SnCl_6$ structure. (*Bottom right*) The hydrogen-bonding geometry in $(Et_3NH)_2SnCl_6$. The H atom is only about 0.16 Å out of the N—Cl(1)—Cl(2) plane.

Can. J. Chem. Downloaded from www.nrcresearchpress.com by 210.87.254.6 on 09/06/12
For personal use only.

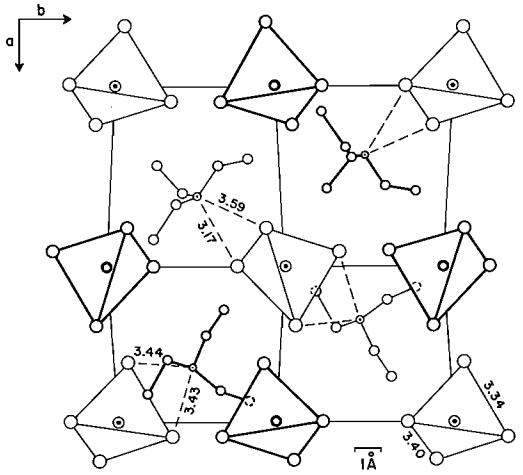

FIG. 3. A slab (parallel to 001) of the $(Et_3NH)_2CuCl_4$ structure (after ref. 6) projected along c so as to display the similarity with $(Et_3NH)_2SnCl_6$; compare with Fig. 2. For legend, see caption of Fig. 2, substituting Cu for Sn. Hydrogen positions have not been determined.

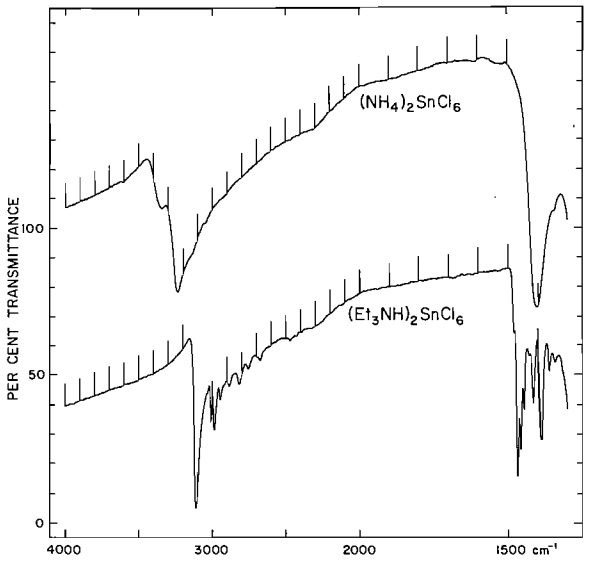

FIG. 4. Survey spectra of undeuterated $(Et_3NH)_2SnCl_6$ and $(NH_4)_2SnCl_6$ in the 4000–1330 cm^{-1} region (fluorocarbon mulls, room temperature).

NH band a complex absorption was observed in the ND stretching region of a weakly deuterated sample (Fig. 7). This absorption at first sight appeared to be a doublet, but comparison with spectra of the undeuterated compound showed it to contain additional minor components. The entire group of peaks between 2350 and 2270 cm^{-1} increased in intensity roughly in proportion to the D content of the sample. The structure of the absorp-

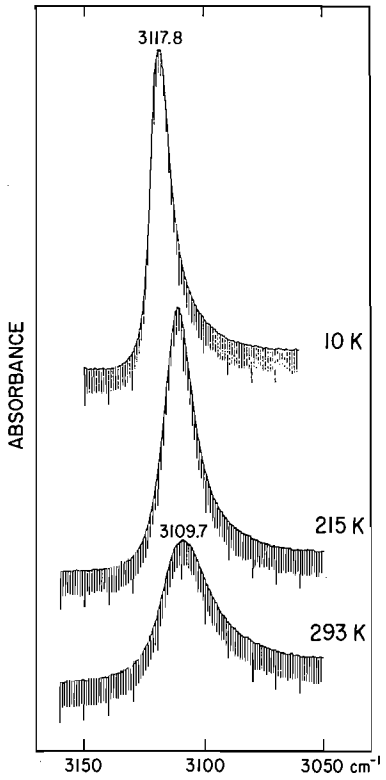

FIG. 5. The NH stretching region of the spectrum of undeuterated $(Et_3NH)_2SnCl_6$ at different temperatures.

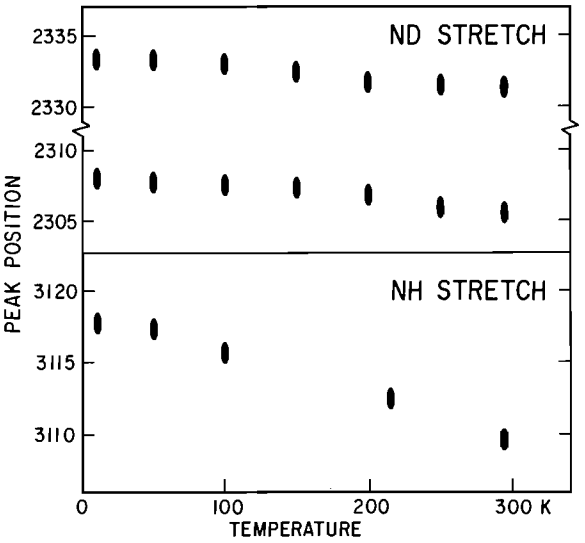

FIG. 6. Temperature variation of the peak position (cm^{-1}) of the NH and ND stretching absorptions of $(Et_3NH)_2SnCl_6$ (6% D). For ND the peak positions of the two most intense components are plotted.

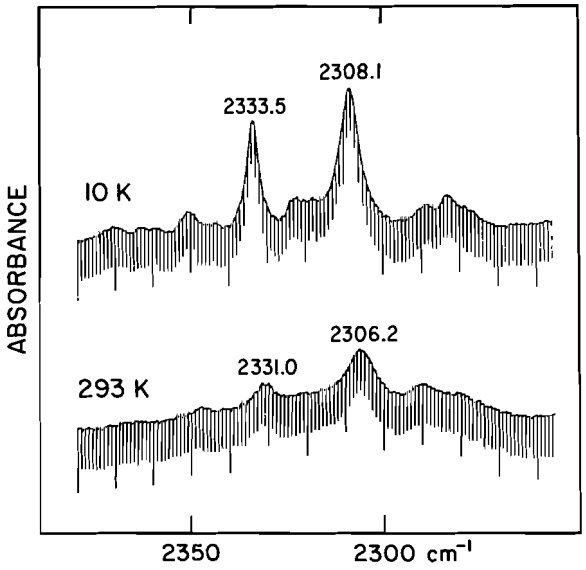

FIG. 7. The ND stretching region of $(Et_3NH)_2SnCl_6$ (6% D). The two most prominent features of the complex of bands corresponding to ND stretching are identified.

tion no doubt arises from a complex Fermi resonance between the ND fundamental and overtones and combinations of the vibrations of the Et_3N part of the cation. The frequency variation of the ND stretching vibration would be expected to parallel that of the NH stretching vibration and thus to increase by about $5\,cm^{-1}$ on cooling from 293 to 10 K (the observed increase in $(NH_4)_2SnCl_6$ is about $6\,cm^{-1}$, cf. ref. 10). However, the increase is only about $2\,cm^{-1}$ for the most intense component of the multiplet and the frequencies of the other components shift in the same direction by similar amounts (Fig. 6). This means that the increase in ν(ND) which would be expected to occur in the absence of Fermi resonance is counteracted by the resonance and reduced to a fraction of the estimate based on the ν(NH) shift. Fermi resonances involving ν(ND) are known to occur in other trialkylammonium salts (results to be published), but the present case is unusual in that the resonance gives rise to an absorption sufficiently complex to preclude the use of the ND stretching for structural deductions.

The estimated mean of the ν(ND) frequencies of the two most intense components of the multiplet is $2321\,cm^{-1}$ at 100 K. This is $54\,cm^{-1}$ lower than the ν(ND) frequency in $(NH_4)_2SnCl_6$, which is consistent in direction and magnitude with the corresponding lowering observed for ν(NH).

Acknowledgment

This investigation was supported by grants from the Natural Sciences and Engineering Research Council of Canada to the two first-named authors.

1. V. SEIDL, O. KNOP, and M. FALK. Can. J. Chem. **47**, 1361 (1969).
2. I. A. OXTON, O. KNOP, and M. FALK. J. Phys. Chem. **80**, 1212 (1976).
3. T. S. CAMERON and R. E. CORDES. Acta Crystallogr. B, **35**, 748 (1979).
4. International Tables for X-Ray Crystallography. Vol. IV. Kynoch Press, Birmingham, Eng. 1974.
5. G. SHELDRICK. X-Ray System Report. University Chemical Laboratory, Lensfield Road. Cambridge, England. 1976.
6. J. LAMOTTE-BRASSEUR, L. DUPONT, and O. DIDEBERG. Acta Crystallogr. B, **29**, 241 (1973).
7. F. GENET. Bull. Soc. Fr. Miner. Crist. **88**, 463 (1965).
8. O. KNOP, W. J. WESTERHAUS, and M. FALK. Can. J. Chem. **58**, 867 (1980).
9. O. KNOP, I. A. OXTON, and M. FALK. Can. J. Chem. **57**, 404, 2003 (1979).
10. O. KNOP, I. A. OXTON, W. J. WESTERHAUS, and M. FALK. J. Chem. Soc. Faraday 2, **77**, 811 (1981).

Can. J. Chem. Downloaded from www.nrcresearchpress.com by 210.87.254.6 on 09/06/12
For personal use only.

Secondary deuterium isotope effects on both rate and product determining steps in the thermolysis of 4-methylene-1-pyrazoline

MOON HO CHANG AND ROBERT J. CRAWFORD

Department of Chemistry, The University of Alberta, Edmonton, Alta., Canada T6G 2G2

Received October 16, 1980

MOON HO CHANG and ROBERT J. CRAWFORD. Can. J. Chem. **59**, 2556 (1981).

The secondary deuterium kinetic isotope effect in the thermolysis of 4-methylene-1-pyrazoline and four of its deuterated isomers has been studied. The value of $\delta\Delta G^{\ddagger}/n$ is 142 cal mol^{-1} if it is a single C—N cleavage process or 71 cal mol^{-1} if it is a concerted rupture of two C—N bonds. The product distributions can only be rationalized in terms of a mechanism involving a rate determining C—N bond rupture to form a diazenyl diradical intermediate which then can close to methylenecyclopropanes by three possible modes. This requires a secondary isotope effect in the product determining step of 1.33 ± 0.05, for the rotation of CH_2 (CD_2) out of the plane of the allylic radical in the intermediate.

MOON HO CHANG et ROBERT J. CRAWFORD. Can. J. Chem. **59**, 2556 (1981).

On a étudié l'effet isotopique cinétique secondaire du deutérium lors de la thermolyse de la méthylène-4 pyrazoline-1 et de 4 de ses isomères deutérés. La valeur de $\delta\Delta G^{\ddagger}/n$ est de 142 cal mol^{-1} s'il s'agit d'un processus de rupture de la liaison simple C—N ou de 71 cal mol^{-1} dans le cas d'une rupture concertée de deux liaisons C—N. On peut rationaliser la distribution des produits uniquement en fonction d'un mécanisme impliquant dans l'étape déterminante la rupture de la liaison C—N pour former un intermédiaire diazényle biradicalaire qui peut alors s'approcher des méthylènecyclopropanes de trois façons possibles. Ceci exige un effet isotopique secondaire dans l'étape déterminante de 1,33 ± 0,05 pour la rotation de CH_2 (CD_2) hors du plan du radical allylique de l'intermédiaire.

[Traduit par le journal]

Introduction

Unsymmetrical azoalkanes (**1**) have been shown to undergo thermolysis by a step-wise sequence of carbon–nitrogen bond cleavages (1) and evidence for diazenyl radicals has been provided by several research groups (2). The case for the step-wise cleavage of symmetrical azoalkanes (**1**, R = R′) is not so clear (1, 3). With cyclic azo compounds there is strong evidence to indicate that compounds such as **2** and **3** undergo cleavage of both C—N bonds in the rate determining step (3) and that the diazenyl radical is not implicated.

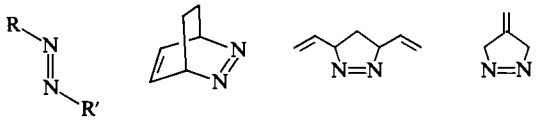

1 **2** **3** **4**

To date the information pertaining to the mechanism of thermolysis of 4-methylene-1-pyrazolines (**4**) has been inconclusive (5). Berson *et al.* (6) have provided convincing data that diyl-species are present in the photolysis and thermolysis of **5**, but as yet we do not know whether the C—N bond cleavages are sequential or concerted. The rearrangement of **5** to **6** is readily explained in terms of a diazenyl radical (7).

The 4-methylene-1-pyrazoline system is unique in that if it undergoes concerted cleavage of both C—N bonds the diradical produced would be the trimethylenemethane (TMM) species, which can exist in the all-planar configuration **7**, or the orthogonal form **8**.

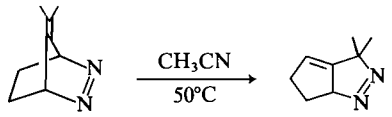

5 **6**

The planar TMM has been the subject of much theoretical and experimental work since it has a triplet ground state which is significantly below the singlet state (9). The singlet would be expected from the thermolysis of **4** on the basis of conservation of spin. Indeed Dowd *et al.* (8) have demonstrated that the triplet is the ground state for **7** and that it can be generated photochemically from **4**. While our first efforts to define the mechanism of thermolysis of **4** suggested that, on the basis of secondary deuterium kinetic isotope effects, both C—N bonds are cleaving in the rate determining step, our later work with methylated derivatives suggests that the system is very sensitive to steric factors, and that the mechanism changes on going from **4** to 3,3,5,5-tetramethyl-4-methylene-1-pyrazoline (**9**); the activation energy increases from 32 kcal mol^{-1} for **4** (10) to 40 kcal mol^{-1} for **9** (11). Consequently we have undertaken a detailed study of the secondary deuterium

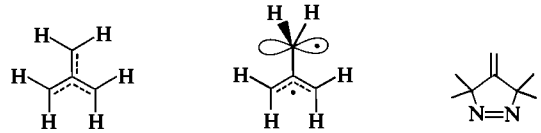

7 **8** **9**

0008-4042/81/162556-12$01.00/0

©1981 National Research Council of Canada/Conseil national de recherches du Canada

Can. J. Chem. Downloaded from www.nrcresearchpress.com by 210.87.254.105 on 09/06/12
For personal use only.

Can. J. Chem. Downloaded from www.nrcresearchpress.com by 210.87.254.105 on 09/06/12
For personal use only.

isotope effects on **10–14**, both of the kinetics and of the product distributions. Compounds **10–12** have been examined earlier (5). In our earlier experiments with these compounds we did not have access to ^{2}Hmr and we have significantly improved our temperature control on the reaction vessel, thus increasing the precision with which we can measure secondary deuterium kinetic isotope effects. Compounds **13** and **14** are new and provide an interesting set of data as to product ratios and tests for common intermediates with **11** and **10** respectively.

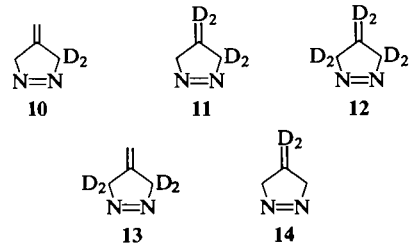

Results

Synthesis

The deuterated 4-methylene-1-pyrazolines, **10**, **11**, and **12** were prepared by methods described earlier (10) and their deuterium content assessed by (*a*) low ionization potential mass spectrometry, (*b*) ^{1}Hmr, and (*c*) ^{2}Hmr. The tetradeuterio compound **13** was prepared by the methods outlined in Scheme 1. The synthesis of **14** was achieved from the acetal (**22**) as outlined in Scheme 2. The ketone (**23**) in Scheme 2 was produced in a substantially improved yield over that reported earlier (11) by periodate oxidation under carefully buffered conditions.

The isotopic purity for samples **10–15** is given in Table 1. In each case ^{1}Hmr and ^{2}Hmr indicated that no scrambling of the label had occurred during synthesis.

TABLE 1. Percentage deuterium substitution of **10–14** by low ionization potential mass spectrometry

	Compound				
	10	**11**	**12**	**13**	**14**
% D-incorporation	97.0±0.1	95.0	97.1	95.4	96.8

Kinetics

The gas phase thermolyses of the 4-methylene-1-pyrazolines were carried out in a 250 mL stainless steel reaction vessel contained in a well-thermostatted air bath; the details of the injection and pressure monitoring equipment are described in the Experimental. The reaction was always accompanied by the isomerization of the 1-pyrazolines to the more stable 2-pyrazoline tautomers, however, the observed thermolysis rate constants were found to be independent of the percent conversion. The kinetic results were obtained by following the increase of pressure with time. The pressure inside the reaction vessel would be expected to double upon completion. The pressure was measured as an emf by a pressure transducer connected to a voltmeter and digital printer. The transducer emf was calibrated and was found to be directly proportional to the pressure used (0–200 Torr). The long term stability of the transducer emf was found to be better than ±0.002 V throughout the reaction and an emf of 1 V was equivalent to 75 Torr. Reproducible first-order kinetics were observed only after repeated thermolyses in the stainless steel reaction vessel. The percent conversion increased dramatically from 37 to 92% after 10 samples had been run at 175°C, and the rate constants were reproducible to ±1%. The introduction of air into the reaction vessel caused the surface to be destroyed, and reconditioning to be required. The kinetic data used to calculate the activation energy and log A values are given in Table 2 along with the probable error at the 90% confidence limit.

The activation parameters calculated from these data are E_a = 33.6 ± 0.7 kcal mol^{-1} and log A =

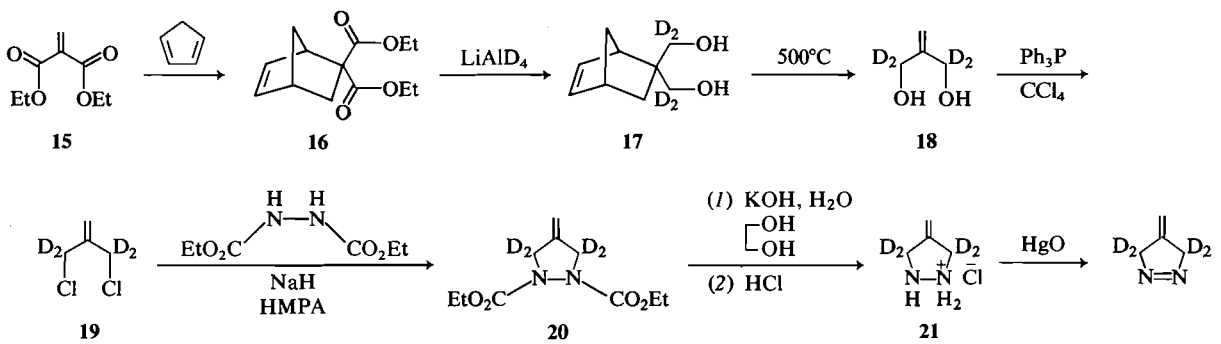

SCHEME 1

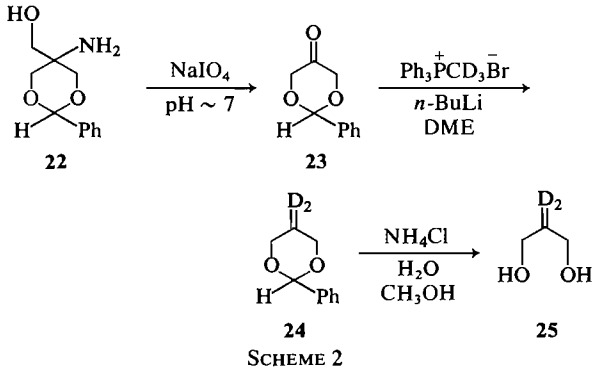

SCHEME 2

13.75 ± 0.35, which gives $\Delta S_{443}^{\ddagger}$ of +1.3 ± 1.6 eu, and are comparable to our earlier results of E_a = 32.8 ± 0.2 and log A = 13.31 ± 0.10 (5).

Table 3 gives the observed and corrected rate constants, at 170°C, for the deuterated 4-methylene-1-pyrazolines. The correction applied is to accommodate the incomplete incorporation of deuterium into the indicated position. The percentage deuterium incorporation was determined by low ionization potential mass spectrometry on the methylenecyclopropane produced and the rate constant corrections were made using the equation $k_D = (k - f_H k_H)/f_D$, where f_H and f_D are the mole fractions of **4** and the deuterated compound. This approximation gives the same result, within experimental error, as the more lengthy equation used for correcting at each level of deuterium incorporation.

TABLE 2. Rate constants for the thermolysis of 4-methylene-1-pyrazoline and probable error at the 90% confidence limit (cl)

Temperature (°C)	Run	10^3k (s^{-1})	10^3k (s^{-1}) (ave.)	Error (90% cl)
165.0	1	0.926		
	2	0.942	0.937	±0.006
	3	0.934		
170.0	4	1.450		
	5	1.458		
	6	1.450	1.450	±0.005
	7	1.443		
	8	1.451		
175	9	2.222		
	10	2.230	2.218	±0.019
	11	2.203		

TABLE 3. Secondary deuterium kinetic isotope effects for the thermolysis of the deuterated 4-methylene-1-pyrazolines (170.0°C)

Compound	Deuterium[a] isotopic purity (%)	$10^3\,k_{obs}$	$10^3\,k_{(corr)}$[b]	k_H/k_D
4		1.45±0.01[c]		
10	97.0±0.1	1.27±0.01	1.26±0.01	1.15±0.02
11	97.1	1.23±0.01	1.22±0.01	1.19±0.02
12	96.8	1.03±0.01	1.02±0.01	1.42±0.02
13	95.4	1.07±0.01	1.05±0.01	1.38±0.02
14	95.0	1.41±0.01	1.41±0.01	1.03±0.02

[a]Determined by mass spectral analysis.
[b]Corrected for incomplete deuteration by the equation $k_D = (k_{obs} - k_H f_H)/f_D$ where f_H and f_D are the mole fractions of H and D.
[c]The errors quoted are the 90% confidence limits.

Product Studies

Samples of deuterated 4-methylene-1-pyrazolines (ca. 60 Torr) were heated in the thermostatted bath at 175°C for 20 min (93% completion). Control runs indicated that the interconversion of deuterated methylenecyclopropanes is negligible at this temperature. The thermolysis products were condensed in a liquid nitrogen cooled tube and upon warming to 0°C the methylenecyclopropanes were transferred to an nmr tube and any tautomeric pyrazolines stayed behind. Chloroform-d_1 or carbon tetrachloride was then added and the 100 MHz ^{1}Hmr or 13.8 MHz ^{2}Hmr spectra were obtained. It should be noted that the isomer proportions were calculated directly without concern for the isotopic purity when ^{2}Hmr data were used. Each value of the percentage distribution in Table 4 is the average from three analyses carried out on each of three independently obtained samples, and the error quoted is the 90% confidence limit. The isomer proportions obtained from **10** and

TABLE 4. Deuterium distribution in methylenecyclopropanes from the thermolysis of deuterated 4-methylene-1-pyrazolines (175.0°C)

		Distribution[a] (%)			
Reactant	Method of analysis	**32**	**31**	**35**	**34**
14	^{1}Hmr[b]	66±1	34±1		
	^{2}Hmr	66±1	34±1		
10	^{1}Hmr[b]	59±1	41±1		
	^{2}Hmr	60±1	40±1		
11	^{1}Hmr[b]			72±1	28±1
	^{2}Hmr			71±1	29±1
13	^{1}Hmr[b]			77±1	23±1
	^{2}Hmr			76±1	24±1

[a]The errors quoted are the 90% confidence limits from three samples.
[b]Corrected for the percent isotopic purity.

Can. J. Chem. Downloaded from www.nrcresearchpress.com by 210.87.254.105 on 09/06/12
For personal use only.

Can. J. Chem. Downloaded from www.nrcresearchpress.com by 210.87.254.105 on 09/06/12
For personal use only.

11 are the same, within experimental error, as those reported earlier (10).

Discussion

The activation energy for the thermolysis of 4-methylene-1-pyrazoline (**4**) is 33.6 ± 0.7 kcal mol^{-1} which is 8.9 kcal mol^{-1} less than the value of 42.5 kcal mol^{-1} ascribed to the parent 1-pyrazoline (12). It is attractive to rationalize such a decrease in activation energy as being due to the allylic resonance in the putative diazenyl radical, **26**. Our earlier work

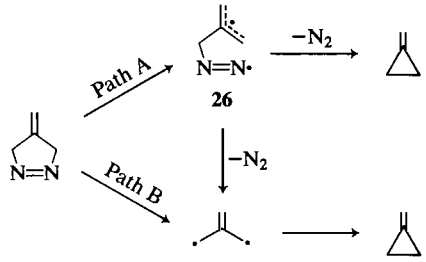

(5) indicated that on the basis of the generally accepted value of $\delta\Delta G^{\ddagger}$ of 90–120 cal mol^{-1} per deuterium (13), the secondary deuterium isotope effects of **10–12** were larger than expected for path A and smaller than anticipated for path B. Two possible reasons come to mind, firstly that the rigid ring system of the 4-methylene-1-pyrazolines may distort the value of the kinetic isotope effect, or secondly that possible pivoting of the *exo*-methylene deuteriums in the thermolysis of **11** and **12** had been underestimated in our earlier work (10), an aspect which has recently been brought to our attention by the work of Gajewski and Chou (14) and that of Roth and Wegener (15). In both of these latter cases evidence suggests that a remote methylene group rotates, possibly giving rise to a torsional isotope effect, so as to avoid an all-planar TMM configuration. To this end we have examined by FT–ir the gas phase spectrum of **10–14** and the principal assignments are made in Table 5. Using the data in Table 5 and assuming the C–N stretch to be the reaction coordinate we have evaluated the change in zero point energy for the series **10–14**. As our model for the transition state we considered the change of the sp^3 α-methylene group to the sp^2 methylene of the diazenyl radical **26** using the methylenecyclopentane (**27**) and **28** assignments of Malloy *et al.* (16). The predicted changes in zero point energies are summarized in Tables 6 and 7 for both the one-bond cleavage, path A, and the two-bond cleavage, Path B.

27 **28**

Using the model that the secondary kinetic isotope effects are the result of the creation, or deletion, of isotopically sensitive vibrational frequencies on going from the reactant to the transition state (17) and eq. [1] we obtain the predicted values in Table 7. It

$$[1] \quad \delta\Delta\omega = [\sum\omega(\mathbf{4}) - \sum\omega(\mathbf{13})] - [\sum\omega(\mathbf{27}) - \sum\omega(\mathbf{28})]$$

TABLE 5. Assignment of major frequencies from the FT–ir spectra of 4-methylene-1-pyrazolines and their deuterated isomers

	Frequencies, cm^{-1}					
						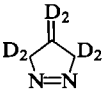
Approximate description of modes[a]	**4**	**10**	**14**	**11**	**13**	**12**
=CH_2 asym str	3092	3094	2330	2331	3090	2325
=CH_2 sym str	3005	3005	2224	2230	3000	2227
α-CH_2 asym str (ip)	2947	2942	2949	2940	2217	2214
α-CH_2 asym str (op)	2940	2218	2938	2214	2154	2154
α-CH_2 sym str (ip)	2860	2860	2858	2858	2142	2138
α-CH_2 sym str (op)	2849	2142	2846	2140	2068	2065
C=C str	1685	1683	1652	1652	1682	1654
N=N str	1552	1550	1543	1538	1532	1531
α-CH_2 deformation (ip)	1432	1422	1433	1420	1040	1037
α-CH_2 deformation (op)	1418	1051	1417	1045	1027	1025
=CH_2 wagging	892	892	712	709	876	709
H_2C-N str (op)	[b]	[b]	912	900	[b]	872
H_2C-N str (ip)	[b]	[b]	895	876	[b]	854

[a]Abbreviations used: sym str, symmetric stretch; asym str, antisymmetric stretch; ip, in-phase, and op, out-of-phase.
[b]Screened by large band of =CH_2 wagging mode.

Can. J. Chem. Downloaded from www.nrcresearchpress.com by 210.87.254.105 on 09/06/12
For personal use only.

TABLE 6. Infrared frequencies used to calculate the secondary deuterium isotope effect in the thermolysis of **13**

Mode	Frequencies[a] (cm^{-1}) **4**	**13**	Mode	Frequencies[b] (cm^{-1}) **27**	**28**
α-CH_2 asym str	2947 2940	2217 2154	=CH_2 asym str	3084	2314
α-CH_2 sym str	2860 2849	2142 2068	=CH_2 sym str	3005	2209
α-CH_2 def	1432 1418	1037 1025	=CH_2 def	1405	1103
α-CH_2 wag[b]	1288 1261	1020 1005	=CH_2 twist	977	745
α-CH_2 twist[b]	1241 1149	973 923	=CH_2 rock	927	706
α-CH_2 rock[b]	892 789	656 612	=CH_2 wag	880	700
C—N str	912 895	872 854			
$\sum\omega$	22873	17558	$\sum\omega$	10278	7777
$\Delta\omega_1$	5315		$\Delta\omega_2$	2501	

[a]Data from Table 5.
[b]Data from ir spectra of 133 and 134 (ref. 16).

TABLE 7. Predicted and observed values of $\delta\Delta G^{\ddagger}$ per deuterium, and k_H/k_D at 170.0°C, for one-bond (A) and two-bond (B) cleavage pathways in the thermolysis of **13**

	One-bond cleavage		Two-bond cleavage	
	$\delta\Delta G^{\ddagger}/_n$ (cal mol^{-1})	k_H/k_D	$\delta\Delta G^{\ddagger}/_n$ (cal mol^{-1})	k_H/k_D
Predicted	112[a]	1.29	112[a]	1.66
Observed	142	1.38[b]	71	1.38[b]

[a]Using data from Table 6 and eq. [1].
[b]Using data from Table 3 and the equation $\delta\Delta G^{\ddagger}/n = (RT/n) \ln k_H/k_D$.

should be noted that the values $\Delta\omega_1$ and $\Delta\omega_2$ in Table 6 represent the values for four deuteriums in **13** and the value for two deuteriums in **28** respectively. Therefore, for the two-bond cleavage pathway, $\delta\Delta\omega = \Delta\omega_1 - 2(\Delta\omega_2) = 313\ cm^{-1}$. Since $E_0 = hc\omega/2$, this is an energy difference ($\delta\Delta G^{\ddagger}$) of 448 cal mol^{-1} for four α-deuteriums. For the one-bond cleavage process, $\delta\Delta\omega = \frac{1}{2}\Delta\omega_1 - \Delta\omega_2 = 156\ cm^{-1}$ which gives $\delta\Delta G^{\ddagger}$ of 224 cal mol^{-1} for two α-deuteriums. By using these data, the values of $\delta\Delta G^{\ddagger}$ per deuterium, the kinetic isotope effects for the two pathways are calculated and presented in Table 7.

The calculated $\delta\Delta G^{\ddagger}/n$ value of 112 cal mol^{-1} in Table 7 is within the range of the frequently observed values of 90–120 cal mol^{-1} (13, 17). These results are suggestive of a one-bond cleavage mechanism, but the observed value is not compelling in that the free energy is large for the implication of two deuteriums, but not large enough to clearly implicate four.

Product Studies

Lacking a clear cut decision from the kinetic data we then examined the product proportions, as in Table 4, in search of a rational explanation for the nonstatistical product distributions.

It is clear from the data in Table 4 that a fully concerted pathway, wherein the sp^3 carbons of the reactant become the ring carbons of the product, can be rejected. Similarly a concerted or sequential rupture of both carbon–nitrogen bonds to form a planar TMM intermediate can be ruled out since the distribution of products from **10** and **14**, and from **11** and **13**, wherein a common intermediate is expected, is different. For the same reasons the data in Table 4 rule out the possibility of a rapidly equilibrating set of orthogonal-TMM intermediates. The orthogonal-TMM is an attractive possibility in that it is the ground state geometry for singlet TMM (**8**) and has been implicated by Chesick (18) and others in the isomerization of methylenecyclopropanes (14).

The work of Roth and Wegener (15) and that of Gajewski and Chou (14) leads us to examine the possibility of the *exo*-methylene group rotating to form an orthogonal-TMM, and then closure of the diradical by rotation of one of the allylic methylenes e.g.

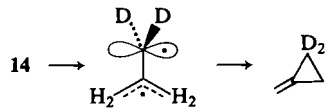

Such a mechanism can be ruled out on the basis that only one isomer would be expected from **13**, and one from **14**.

An attractive mechanism is that represented by Scheme 3 wherein the orthogonal-TMM intermediate is generated by simply rotating one of the nitrogen-bearing methylenes of the reactant. The thermolysis of **14** produces one such intermediate **29** whereas the thermolysis of **10** gives **30** as well as **29**. If k_1 and k_2 are the first order rate constants for the formation of **29** and **30** from **10**, and k_3 and k_4 are the rate constants for the product-determining steps, then using the steady state approximation for **29** and **30** we can calculate the ratio k_1/k_2 by using the product data in Table 4. Using the steady state approximation for **29** and **30** in Scheme 3, the ratio of **31**:**32** produced from **10** is given by eq. [2], provided none of the reactions is reversible, and control reactions indicate no interconversion of **10** and **14**, nor of **31** and **32**

$$[2]\quad \frac{[31]}{[32]} = \frac{k_3k_1}{k_4k_1 + k_2(k_3 + k_4)} = \frac{k_3/k_4}{1 + (k_2/k_1)(k_3/k_4 + 1)}$$

under the reaction conditions. The value k_3/k_4 is the ratio of [**31**]/[**32**] obtained from **14** and is 0.52 ± 0.02, a value difficult to justify in terms of the process involved as it would require the CD_2 group of **29** to be essentially twice as facile as the CH_2 group in rotating out of the allylic plane into the ring methylene position. Scheme 3 would predict that a larger proportion of **32** should be produced from **10** than from **14**, since **30** gives rise to only **32**. Using the aforementioned ratio of 0.52 in eq. [2] and the product proportions from **10**, the value of $k_1/k_2 = -0.17$ is the unique solution and is not possible. An analogous treatment of the product proportions for the isomeric pair **11** and **13** similarly gives an irrational result. It is thus apparent that none of the reasonably possible two-bond cleavage processes can explain the product distribution in Table 4.

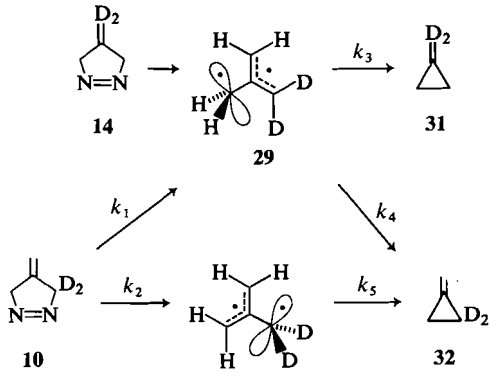

SCHEME 3

Stepwise One C—N-bond Cleavage

Allylic resonance may be effective in bringing about one-bond cleavage in the rate-determining step and as a result an α-methylene group of **13** will have to rotate into the plane to give the allylic diazenyl species **33**. In order to examine the product

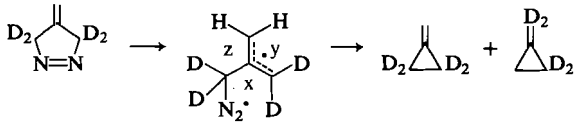

13 **33** **34** **35**

forming step, we define the displacement of nitrogen by the allylic terminus which was originally the α-methylene as x-closure, the displacement of nitrogen by the allylic terminus which was the *exo*-methylene as z-closure, and the electrocyclic closure of the two allylic termini as y-closure. Any mechanism that uses only one mode of closure (x, y, or z) for the intermediate diazenyl species can be rejected since such a scheme would predict a single product from each of the deuterated pyrazolines. The formation of **31** from **14**, and of **34** from **13** requires that x-closure be included in the product-forming process but other processes (y and/or z) must be involved to account for the isomeric products **32** from **14**, and **35** from **13**. Thus we must, at a minimum, consider three possibilities, i.e. (x + y)-closure, (x + z)-, or (x + y + z)-closure, as possible mechanisms. It is convenient to examine the (x + y + z)-closure initially as the most general case, and then the other two closures can be treated as extreme cases wherein y = 0 and z = 0.

Information about the relative proportions of the three modes of closure for the diazenyl species from 4-methylene-1-pyrazoline is required. We chose the product distribution from 4-methylene-1-pyrazoline-3-^{13}C (**36**) as the best model for **4**.

If k_x, k_y, and k_z represent the partial relative rate factors (i.e. $k_x + k_y + k_z = 1.0$) for x-, y-, and z-closure from each diazenyl species produced from the reactant then the isotopic substitution (^{13}C for ^{12}C) should give rise to a minimal difference on going from **4** to **36**. Defining k_α and k_β as the partial relative rate factors (i.e. $k_\alpha + k_\beta = 1.0$) for the faster and the

Can. J. Chem. Downloaded from www.nrcresearchpress.com by 210.87.254.105 on 09/06/12
For personal use only.

slower steps for the C—N bond-breaking process and using the normal ^{13}C isotope effect of 1.03 (61),[1] we obtain the ratio k_α/k_β as 0.505:0.495. Substituting this ratio and the product ratio of 64:36 for **39**:**40** into eq. [3] the ratio $k_x(\mathbf{36})/k_y(\mathbf{36})/k_z(\mathbf{36})$ can be calculated by adding the relationship that

$$[3]\quad \frac{[\mathbf{39}]}{[\mathbf{40}]} = \frac{0.64}{0.36} = \frac{0.505[k_x(\mathbf{36}) + k_z(\mathbf{36})] + 0.495[k_x(\mathbf{36}) + k_y(\mathbf{36})]}{0.505k_y(\mathbf{36}) + 0.495k_z(\mathbf{36})}$$

$k_x(\mathbf{36}) = k_z(\mathbf{36})$. This gives the ratio 0.28:0.44:0.28. Chemically such would be the case if the diazenyl radical were an intermediate of sufficient lifetime

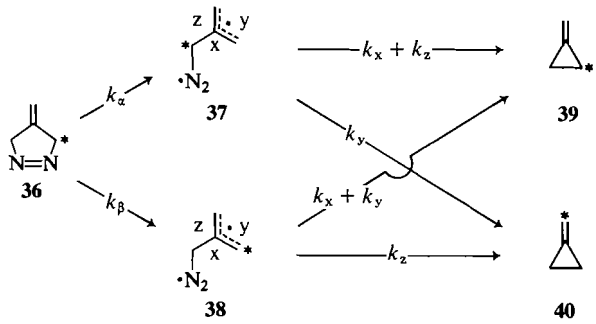

SCHEME 4

that the rotamer equilibrium **41** ⇌ **42** could be achieved (or if frontside and rearside attack in the initially produced rotamer were of equal importance in the closure step).

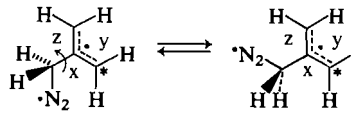

In generalizing this mechanism to the other deuterated compounds (**10**–**13**) to see whether or not the product proportions in Table 4 can be accounted for, we must first decide which modes of closure are isotopically sensitive for the diazenyl radical going to product, and then attempt to evaluate them. If **14** generated the diazenyl radical as in Scheme 5 and there were no deuterium isotope effect, we would expect the product proportions from x-, y-, and z-closure to give **32**:**31** in the ratio 72:28. Because $k_y(\mathbf{14})$ and $k_z(\mathbf{14})$ involve a rotation of the allylic CD_2 bond, and $k_x(\mathbf{14})$ has minimal change at the isotopically substituted position, we have assumed that the isotope effect R is associated with the former two modes. Using eq. [4] the value of R is found to be

$$[4]\quad \frac{[\mathbf{32}]}{[\mathbf{31}]} = \frac{66}{34} = \frac{k_y(\mathbf{14}) + k_z(\mathbf{14})}{k_x(\mathbf{14})} = \frac{k_y(\mathbf{36})/R + k_z(\mathbf{36})/R}{k_y(\mathbf{36})}$$

[1]The ratios calculated are quite insensitive to this isotope effect, a value of 1.1 giving essentially the same result.

1.33 ± 0.05 (using the ^{2}Hmr data from Table 4). If we use this value for **13** and assume that the secondary deuterium kinetic isotope value for the closures x, y, and z from the diazenyl intermediate are unaffected by the deuteriums on the diazenyl methylene group[2] then eq. [5] can be used to predict the product proportions for **35** and **34**. The value obtained

$$[5]\quad \frac{[\mathbf{35}]}{[\mathbf{34}]} = \frac{k_y(\mathbf{13}) + k_z(\mathbf{13})}{k_x(\mathbf{13})} = \frac{k_y(\mathbf{36}) + k_z(\mathbf{36})\cdot R}{k_x(\mathbf{36})}$$

75 ± 2:25 ± 2 compares favourably with that found in Table 4.

Carrying out the same analysis for **10** and **11** as outlined in Scheme 6 requires the use of two diazenyl species for each. We have used the kinetic data from Table 3 and have assumed that the rate constant for the faster bond, k_α in Scheme 6, is one half the value of the rate constant for **10**, and that the value for the

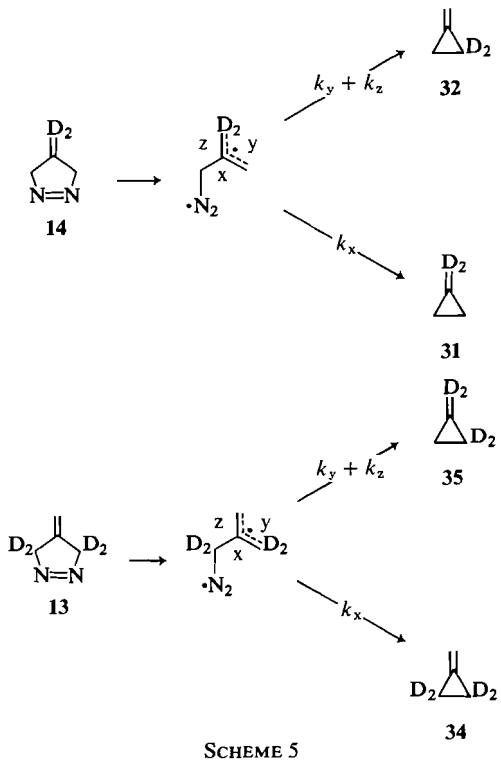

SCHEME 5

[2]This assumption is made on the basis of the generally small value of the isotope effect for S_N2 type processes (19).

Can. J. Chem. Downloaded from www.nrcresearchpress.com by 210.87.254.105 on 09/06/12
For personal use only.

slower rate, k_β, is one half the value of the rate constant for **13**. Thus the intermediates **43** and **44** (and similarly **45** and **46**) occur in the proportions 0.58:0.42.

Equations [6]–[9] are used to predict the product proportions by inserting the value $R = 1.33$ wherever

$$[6]\quad k_x(\mathbf{10}):k_y(\mathbf{10}):k_z(\mathbf{10}) = k_x(\mathbf{36}):k_y(\mathbf{36}):k_z(\mathbf{36}) = 0.28:0.44:0.28$$

$$[7]\quad k_x'(\mathbf{10}) : k_y'(\mathbf{10}) : k_z'(\mathbf{10}) = \frac{k_x(\mathbf{36})}{R} : \frac{k_y(\mathbf{36})}{R} : k_z(\mathbf{36}) = 0.26 : 0.40 : 0.34$$

$$[8]\quad k_x(\mathbf{11}) : k_y(\mathbf{11}) : k_z(\mathbf{11}) = k_x(\mathbf{36}) : \frac{k_y(\mathbf{36})}{R} : \frac{k_z(\mathbf{36})}{R} = 0.34 : 0.40 : 0.26$$

$$[9]\quad k_x'(\mathbf{11}) : k_y'(\mathbf{11}) : k_z'(\mathbf{11}) = \frac{k_x(\mathbf{36})}{R} : \frac{k_y(\mathbf{36})}{R} : \frac{k_z(\mathbf{36})}{R} = 0.31 : 0.37 : 0.31$$

applicable (i.e. whenever CD_2 rotation competes with CH_2, effectively $k_H/k_D = 1.33 \pm 0.05$). The values given have been normalized to satisfy $k_x + k_y + k_z = 1.0$ (for the major intermediate) and $k_x' + k_y' + k_z' = 1.0$ (for the minor intermediate). The product ratios for **10** and **11** can be calculated using eqs. [10] and [11].

$$[10]\quad \frac{[\mathbf{32}]}{[\mathbf{31}]} = \frac{k_\alpha[k_x(\mathbf{10}) + k_z(\mathbf{10})] + k_\beta[k_x'(\mathbf{10}) + k_y'(\mathbf{10})]}{k_\alpha k_y(\mathbf{10}) + k_\beta k_z'(\mathbf{10})} = \frac{0.60}{0.40}$$

$$[11]\quad \frac{[\mathbf{35}]}{[\mathbf{34}]} = \frac{k_\alpha[k_x(\mathbf{11}) + k_y(\mathbf{11})] + k_\beta[k_x'(\mathbf{11}) + k_z'(\mathbf{11})]}{k_\alpha k_z(\mathbf{11}) + k_\beta k_y'(\mathbf{11})} = \frac{0.70}{0.30}$$

The calculated product ratios obtained above are summarized in Table 8 along with data for a mechanism having no z-closure (z = 0), and for when there is no y-closure (y = 0). These latter two modes do not predict the correct product proportions for **10**, **11**, and **13**. It should be noted that the case for (x + y + z)-closure in Table 8 is that wherein $k_x = k_z$. Attempts to fit $k_x = 0.8\,k_z$ and $k_x = 1.25\,k_z$ caused one or more of the predicted values to move away from the observed by greater than ±2%.

TABLE 8. Predicted and observed product ratios for the thermolysis of deuterated 4-methylene-1-pyrazolines using (x + y + z)-closure from diazenyl intermediates

		Product ratio			
		Predicted[b]			Observed[a]
Reactant	Products	(x + y + z)[d]	(x + y)	(x + z)	^{2}Hmr
10	**32/31**	1.50±0.06	2.70±0.15	2.45±0.12	1.50±0.06
11	**35/34**	2.33±0.12	2.85±0.16	1.63±0.07	2.45±0.12
13	**35/34**	3.00±0.17	2.45±0.12	2.45±0.12	3.17±0.18
14	**32/31**	1.94[e]	1.94	1.94	1.94±0.09
	R[c]	1.33±0.05	1.39±0.05	1.26±0.05	

[a]Data from Table 4.
[b]Error calculated from ± 1% error in ^{2}Hmr analysis to give R value from **14**.
[c]Effectively the k_H/k_D value for the closure step from the diazenyl radical **45**.
[d]Closure wherein $k_x = k_z$.
[e]The value used to calculate the isotope effect as a model for **10**, **11**, and **13**.

Can. J. Chem. Downloaded from www.nrcresearchpress.com by 210.87.254.105 on 09/06/12
For personal use only.

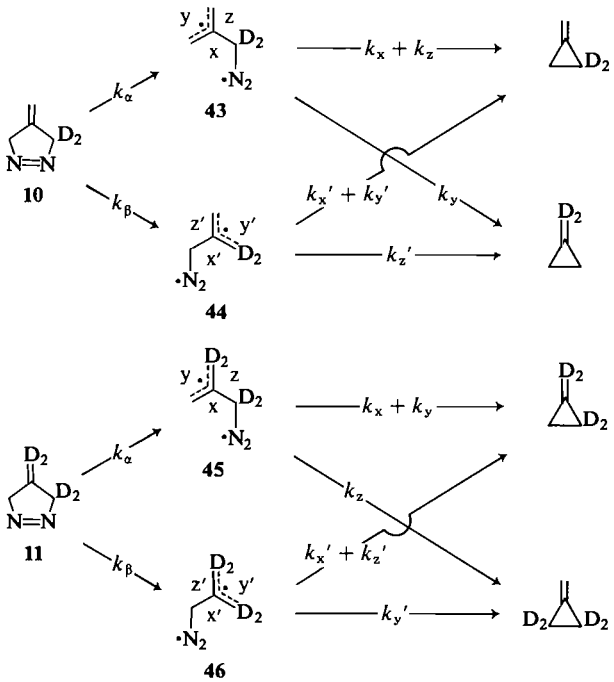

SCHEME 6

The secondary deuterium kinetic isotope effect value of 1.33 ± 0.05 is at first glance larger than one might have expected, but Gajewski and Chou (14) have observed a value of 1.31 ± 0.04 for the thermal isomerization of the methylenecyclopropane (**47**) to the ethylidenecyclopropane (**48**) and have explained the result in terms of the torsional vibrational mode of the vinylic hydrogens (deuteriums) (20).

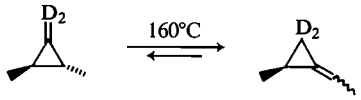

We conclude that the secondary deuterium kinetic isotope effects and product isotope effects can be explained by a mechanism involving diazenyl intermediates such as **43–46**. These intermediates appear to have a sufficient stability that if backside displacement is the principle mode (2*d*) then the energy barrier for rotation about the C—CH_2N_2• bond is smaller than the energy for ring closure. Baird and Kathpol (21) have carried out *ab initio* MO calculations using the STO-3G basis set and suggest that species of the type R—N = N• are discrete intermediates requiring an energy barrier for conversion to R• and N_2.

Experimental

All boiling points are uncorrected.

Gas chromatographic separations on a preparative scale were achieved on a Nester Faust Model 850 "Prepkromat" connected to an Elecktronik 18 strip chart recorder.

The proton nuclear magnetic resonance spectra were obtained using a Varian A-60 spectrometer, a Varian HA-100 spectrometer, and a Bruker WH-400 high field cryospectrometer. The deuterium nuclear magnetic resonance analyses were carried out on a Bruker HFX 90 spectrometer in the Fourier transform mode, and a Bruker WH-400 high field cryospectrometer.

Exact masses were determined on an A.E.I. MS9 mass spectrometer. The mass spectra analyses at low ionization potential were performed on an A.E.I. MS2 instrument.

The Fourier transform infrared spectra were obtained using a Nicolet 7199 Transform Interferometer.

Microanalyses were performed by the Microanalytical Laboratory of the Department of Chemistry, University of Alberta.

Kinetic Measurements

The kinetic experiments in the thermolysis of the 4-alkylidene-1-pyrazolines were conducted in a static vacuum system. Transducer emf was shown to be directly proportional to the pressure used (0–200 Torr) by plotting emf against the pressure as recorded on a mercury manometer. The system was equipped with Hoke stainless steel diaphragm and bellow valves. A 250 mL cylindrical type stainless steel reaction vessel (6.5 cm × 7.0 cm id) was situated in a well-insulated air bath (10) with fast air circulation provided by a high-speed fan located at the bottom of the bath. The main heater, controlled by a Variac variable resistance, was used to bring the temperature to about 20° below the desired operating temperature, and a secondary heater controlled by a Melabs Model CTCIA proportional temperature controller was used to maintain the desired temperature.

The temperature was measured by a Hewlett-Packard (HP) Model 2802A thermometer system calibrated against an ice-point reference. The temperature of the system was monitored by an HP Model 3470A digital display system, and the long term stability of the temperature was better than ±0.1°.

The measurement of the transducer emf was performed using an HP Model 34701A DC voltmeter coupled to an HP Model 34721B BCD module which was connected to a National Semiconductor LX 1702A transducer functional in the pressure range of 0–1 atm. The emf was monitored by an HP Model 3470A digital display system and was then recorded as a function of time by an HP Model 5150A thermal printer. The stability of the emf was better than ±0.002 volt during the measurements.

4-Methylene-1-pyrazoline (4), 4-Methylene-1-pyrazoline-3,3-d_2 (10), and 4-Methylene-d_2-1-pyrazoline-3,3-d_2 (11)

These compounds were prepared as described earlier (4). Each was checked for isotopic purity by mass spectrometry and for positional purity by both ^{1}Hmr and ^{2}Hmr.

5-Oxo-2-phenyl-1,3-dioxan (23)

The method of synthesis by Marei and Raphael (11) was modified to improve the yield considerably and to achieve a one-step synthesis of the product without the intermediate formation of 5,5-dihydroxy-2-phenyl-1,3-dioxan. A mixture of 5-amino-5-(hydroxymethyl)-2-phenyl-1,3-dioxan (70.6 g, 0.338 mol) (**22**) and pH 6 buffer solution (2.0 L) in a 3-L round-bottomed flask was stirred mechanically at room temperature. The reaction mixture initially became homogeneous when sodium metaperiodate (72.3 g, 0.338 mol) was added all at once with vigorous stirring. Later a white solid appeared. After 15 min of stirring, the product was extracted with dry dichloromethane (3 × 2.0 L), the extract was dried over

Can. J. Chem. Downloaded from www.nrcresearchpress.com by 210.87.254.105 on 09/06/12
For personal use only.

Can. J. Chem. Downloaded from www.nrcresearchpress.com by 210.87.254.105 on 09/06/12
For personal use only.

anhydrous sodium sulfate, and the solvent was evaporated using a rotatory evaporator at less than 20°C. A slightly yellow solid (55.7 g) was produced. The solid was dissolved in boiling dry pentane (6.0 L). Decantation of the clear solution, followed by cooling and evaporation of the solvent using a rotatory evaporator at less than 20°C, gave a white solid (50.7 g, 0.285 mol, 84.3% yield) which was pure, judging from the ^{1}Hmr spectrum, and mp 68–69°C (lit. (11) mp 69–71°C). The product should be stored in a freezer below −20°C to prevent it from decomposing slowly into a yellow oil. The 100 MHz ^{1}Hmr spectrum TMS ($CDCl_3$) showed δ: 4.47 singlet, 4H), 5.87 (singlet, 1H), and 7.42 (complex multiplet, 5H).

5-Methylene-2-phenyl-1,3-dioxan-7,7-d_2 *(**24**)*

The procedure was a modification of that of Malloy *et al.* (22). A 3-L three-necked round-bottomed flask was fitted with a reflux condenser, a dropping funnel, a mechanical stirrer, and a gas inlet tube. A gentle flow of dry argon through the apparatus was maintained throughout the reaction. Dry 1,2-dimethoxyethane (0.8 L, freshly distilled three times from lithium aluminum hydride) and methyl-d_3-triphenylphosphonium bromide (151 g, 0.423 mol) were added to the flask which was cooled in an ice–water bath. While stirring vigorously, a hexane solution (111 mL) of 2.29 *M* *n*-butyllithium was added through a dropping funnel. The temperature of the reaction mixture was then raised to 65°C over a period of 2 h and maintained at this temperature for 3 h to give a yellow to brown solution of methylenetriphenylphosphorane. This solution was cooled in an ice–water bath and 5-oxo-2-phenyl-1,3-dioxan (40.6 g, 0.228 mol; freshly purified from *n*-pentane before use) in dry 1,2-dimethoxyethane (0.4 L) was added through a dropping funnel while stirring vigorously. The temperature of the reaction mixture was then gradually increased over 3 h until the solvent began to reflux. After refluxing for a day, the reaction mixture was cooled to room temperature. Acetone (50 mL) was added and the mixture was stirred for 30 min. This was followed by the addition of ether (1 L) and stirring was continued for a further 30 min. Solids were removed by filtration and the solvents including benzene and 1,2-dimethoxyethane were almost completely evaporated using a rotatory evaporator. The residual solution was extracted with *n*-pentane (3 × 500 mL). After evaporating the *n*-pentane from the combined extracts, the residual solution distilled at reduced pressure to give the product (32.5 g, 0.183 mol, 80.2% yield), bp 68–69°C/0.15 Torr (lit. (23) bp 76–78°C/3 Torr for nondeuterated material).

The 100 MHz ^{1}Hmr spectrum TMS ($CDCl_3$) showed δ: 4.47 (singlet, 4H), 5.57 (singlet, 1H), and 7.37 (complex multiplet, 5H). The mass spectrum indicated 95 ± 1% isotopic purity (D_0 = 0.9, D_1 = 7.9, D_2 = 91.2). The 13.6 MHz ^{2}Hmr spectrum (CCl_4) indicated >99.8% of total deuterium at the *exo*-methylene position.

2-(Methylene-d_2*)-1,3-propanediol (**25**)*

5-Methylene-2-phenyl-1,3-dioxan-7,7-d_2 (31.1 g, 0.175 mol) in methanol (1.0 L) was added to ammonium chloride (165 g) in distilled water (400 mL) in a 3-L three-necked round-bottomed flask fitted with a reflux condenser and a mechanical stirrer. The mixture was vigorously stirred at 40°C for three days and then neutralized with 5% sodium bicarbonate solution. After evaporation of solvents using a rotatory evaporator, acetone (600 mL) was added to the residue. The solid was filtered and the solvents were again evaporated. The residue was extracted with acetone (400 mL) and the solvent was evaporated completely under reduced pressure (1 Torr) at room temperature. The residue was then extracted with ether (3 × 250 mL) and the extracts were dried over anhydrous magnesium sulfate. The ether was evaporated to give yellow crude product. Distillation of the remaining solution gave a colorless liquid (13.0 g, 0.145 mol, 83% yield), bp 96.5–97.5°C/3.5 Torr (lit. (24) bp 127–129°C/32 Torr). The 100 MHz ^{1}Hmr spectrum TMS (DMSO-d_6) showed δ: 3.91 (doublet, J = 5.5 Hz, 4H) and 4.66 (triplet, J = 5.5 Hz, 2H), and indicated 95 ± 1% isotopic purity.

3-Chloro-2-(chloromethyl)propene-1,1-d_2

The procedure was a modification of that of Hooz and Gilani (25). Freshly prepared dry triphenylphosphine (dried at room temperature at 0.2 Torr overnight; 95.5 g, 0.365 mol) was added to a mechanically stirred solution of glycol **25** (12.6 g, 0.140 mol) in dry tetrahydrofuran (110 mL; distilled twice from lithium aluminum hydride) and carbon tetrachloride (255 mL; distilled from phosphorous pentoxide) in a 2-L three-necked round-bottomed flask fitted with a mechanical stirrer, a reflux condenser, and a gas inlet tube. A gentle flow of dry argon through the apparatus was maintained throughout the reaction. After refluxing for 2 h a light reddish solution formed and a large quantity of white solid appeared. *n*-Pentane (700 mL) was added, and the reaction mixture was stirred for 10 min. The solid was filtered and washed with *n*-pentane (250 mL). The solvents were removed by distillation below 37°C. Distillation of the residue yielded the product (9.3 g, 73.2 mmol, 52% yield), bp 57.0–58.0°C/40 Torr (lit. (26) bp 137–138°C/756 Torr).

The 100 MHz ^{1}Hmr spectrum TMS ($CDCl_3$) showed δ: 4.19 (singlet), and indicated 95 ± 1% isotopic purity. The mass spectrum indicated 94 ± 1% isotopic purity (D_0 = 1.8, D_1 = 9.0, D_2 = 89.2). The 13.6 MHz ^{2}Hmr spectrum (CCl_4) indicated >99.8% of total deuterium at the *exo*-methylene position.

1,2-Dicarbethoxy-4-methylenepyrazolidine-6,6-d_2

The procedure was adapted from that used by Rubottom and Chabala (27). A solution of *sym*-dicarbethoxyhydrazine (12.1 g, 68.4 mmol; purified by recrystallization from 95% ethanol and drying under high vacuum (28) in hexamethylphosphoramide 100 mL; dried over Molecular Sieves 4A) was placed in a 500-mL three-necked round-bottomed flask fitted with a reflux condenser, a mechanical stirrer, and a gas inlet tube. A gentle flow of dry argon was maintained in the apparatus during the reaction. The reaction mixture was cooled in an ice–salt bath. Sodium hydride (57% dispersion, 2.88 g, 68.4 mmol) which had been washed three times to remove protective oil, was added to the reaction mixture in small portions with the aid of *n*-pentane. The mixture was allowed to warm to room temperature, and stirred mechanically for 6 h. After cooling in an ice–salt bath, 3-chloro-2-(chloromethyl)propene-1,1-d_2 (8.5 g, 66.9 mmol) was added dropwise. The mixture was then allowed to warm to room temperature and kept at this temperature for 3 days. After cooling in an ice-salt bath, sodium hydride (57% dispersion; 2.88 g, 68.4 mmol; washed with *n*-pentane) was slowly added in small portions with the aid of *n*-pentane. Once more, the reaction mixture was allowed to warm to room temperature and kept at this temperature for a day. After cooling in an ice–water bath, distilled water (150 mL) was slowly added, and the mixture was stirred vigorously for 30 min. Extraction of the product with absolute ether (5 × 200 mL), and evaporation of the solvent using a rotatory evaporator followed by distillation of the residue yielded the liquid product (10.9 g, 47.4 mmol, 71% yield), bp 88–89°C/0.08 Torr.

The 100 MHz ^{1}Hmr spectrum TMS ($CDCl_3$) showed δ: 1.20 (triplet, J = 7.3 Hz, 6H) and 4.16 (quartet + broad peak, J = 7.3 Hz, 8H; ester CH_2 + ring methylene) and indicated 94 ± 1% isotopic purity. The mass spectrum indicated

Can. J. Chem. Downloaded from www.nrcresearchpress.com by 210.87.254.105 on 09/06/12
For personal use only.

94.8 ± 0.1% isotopic purity ($D_0 = 0.7$, $D_1 = 9.1$, $D_2 = 90.2$) based on the molecular ion peak. The 13.6 MHz ^{2}Hmr spectrum (CCl_4) indicated >99.8% of total deuterium at the *exo*-methylene position.

4-Methylenepyrazolidine-6,6-d_2 *Hydrochloride*

The procedure was that described previously for the synthesis of 4-methylenepyrazolidine hydrochloride from 1,2-dicarbethoxy-4-methylenepyrazolidine (10). Ethylene glycol (70 mL), distilled water (17 mL), potassium hydroxide (16.4 g, 295 mmol), 1,2-dicarbethoxy-4-methylenepyrazolidine-6,6-d_2 (10.0 g, 43.5 mmol), and concentrated hydrochloric acid (4.3 mL, 51.8 mmol) reacted to give the product (4.8 g, 39.2 mmol, 90.1% yield).

The 60 MHz ^{1}Hmr spectrum, external TMS (D_2O) showed δ: 4.04 (singlet, 4H) and 4.88 (singlet, 3H), and indicated 94 ± 1% isotopic purity.

4-Methylene-1-pyrazoline-6,6-d_2 *(14)*

The procedure was that described previously for the synthesis of 4-methylene-1-pyrazoline from 4-methylenepyrazolidine hydrochloride (10). 4-Methylenepyrazolidine-6,6-d_2 hydrochloride (4.4 g, 36.7 mmol), red mercuric oxide (50 g), and anhydrous sodium sulfate (50 g) in absolute ether (100 mL) reacted to give the product (1.4 g, 16.7 mmol, 45.5% yield).

The 100 MHz ^{1}Hmr spectrum TMS (benzene-d_6) showed δ: 4.47 (singlet), and indicated 95 ± 1% isotopic purity. The mass spectrum indicated 95.0 ± 1% isotopic purity ($D_0 = 0.4$, $D_1 = 9.2$, $D_2 = 90.4$). The 13.6 MHz ^{2}Hmr spectrum (CCl_4) indicated >99.8% of total deuterium at the *exo*-methylene position.

5,5-Dicarbethoxy-2-norbornene (16)

Freshly prepared cyclopentadiene (60.0 g, 0.910 mol) was added slowly to diethyl methylenemalonate (**15**) (110.0 g, 0.640 mol) (29) which had been cooled in an ice–water bath. The reaction mixture was warmed to room temperature and kept at this temperature for an hour. It was then heated to 100°C over a period of 1 h and kept at this temperature for 3 h. Distillation of the mixture gave a colorless liquid (122.6 g, 0.516 mol, 80.6%), bp 107–108.5°C/2.5 Torr. The ir spectrum ν_{max}: 1733 (C=O) cm^{-1}. The 100 MHz ^{1}Hmr spectrum TMS ($CDCl_3$) showed δ: 1.21 (triplet, J = 7.3 Hz, 3H), 1.23 (triplet, J = 7.3 Hz, 3H), 1.57 (multiplet, 2H), 2.04 (multiplet, 2H), 2.89 (singlet, 1H), 3.37 (singlet, 1H), 4.10 (quartet, J = 7.3 Hz, 2H), 4.17 (quartet, J = 7.3 Hz, 2H), 5.95 (multiplet, 1H) and 6.24 (multiplet, 1H). *Exact Mass* calcd. for $C_{13}H_{18}O_4$: 238.2828; found: 238.2806. *Anal.* calcd. for $C_{13}H_{18}O_4$: C 65.53, H 7.61, O 26.86; found: C 65.34, H 7.75, O 26.91.

5,5-Bis(hydroxymethyl-d_2*)-2-norobornene (17)*

The procedure was an adaptation of that of Moffet (30). In a 2-L three-necked round-bottomed flask fitted with a reflux condenser, a dropping funnel, a gas inlet tube, and a mechanical stirrer, pulverized lithium aluminum deuteride (13.5 g, 0.321 mol) in absolute ether (600 mL) was refluxed overnight in an oil bath under a gentle flow of dry argon. After the oil bath had been removed, 5,5-dicarbethoxy-2-norbornene (63.0 g, 0.264 mol) in dry ether (100 mL) was added with vigorous stirring at such a rate that the solvent refluxed gently. The reaction mixture was refluxed for 4 h and then cooled. Distilled water (12 mL), 15% sodium hydroxide solution (12 mL), and distilled water (36 mL) were added successively to destroy the excess lithium aluminum hydride, and the mixture was stirred for 5 h. Dry ether (500 mL) was added, and the solution was warmed almost to boiling, since the product is quite soluble in hot ether but not in cold. After filtration by vacuum, the residue was extracted with hot ether (2 × 0.5 L) and the combined ethereal solutions were evaporated to dryness on a rotatory evaporator under reduced pressure (0.1 Torr) overnight. Recrystallization from hot benzene (ca. 300 mL) and washing with cold Skelly B gave the product (34.3 g, 0.216 mol, 82% yield) in needles, mp 112–112.5°C (23).

The 100 MHz ^{1}Hmr spectrum TMS (DMSO-d_6) showed δ: 0.46–1.60 (multiplet, 4H), 2.59 (1H), 2.61 (1H), 4.16 (singlet, 1H), 4.40 (singlet, 1H), and 6.08 (2H).

2-Methylene-1,3-propanediol-1,1,3,3-d_4 *(18)*

The procedure used was an adaptation of that of Corey and Suggs (31). A 22 cm quartz column (2.54 cm id) was packed with Pyrex beads which were heated to 480–520°C by a heating tape wrapped around the column. To the column was added neat 5,5-bis(hydroxymethyl-d_2)-2-norbornene (**17**) (32.9 g, 0.208 mol) in small portions. Argon was passed through the apparatus so that the contact time of the vaporized reagent with the column was 7–10 s. The crude product was collected, in two successive traps cooled to −78°C, under slightly reduced pressure (500 Torr). Water was added to the crude product, and the aqueous solution was washed once with *n*-pentane. After concentration of the aqueous extract using a rotatory evaporator, distillation gave the colorless liquid (14.0 g, 0.152 mol, 73% yield).

The 100 MHz ^{1}Hmr spectrum TMS (DMSO-d_6) showed δ: 4.64 (singlet, 2H) and 4.97 (singlet, 2H), and indicated 96 ± 1% isotopic purity.

3-Chloro-2-(chloromethyl-d_2*)-propene-3,3-*d_2 *(19)*

The procedure was that described previously for the synthesis of 3-chloro-2-(chloromethyl)propene from 2-methylene-1,3-propanediol.

The 100 MHz ^{1}Hmr spectrum TMS ($CDCl_3$) showed δ: 4.19 (triplet, J = 0.6 Hz, 4H) and 5.32 (pentet, J = 0.6 Hz 2H).

4-Methylene-1-pyrazoline-3,3,5,5-d_4 *(13)*

The procedure was that described previously for the synthesis of 4-methylene-1-pyrazoline from 4-methylenepyrazolidine hydrochloride. 4-Methylenepyrazolidine-3,3,5,5-d_4 hydrochloride (4.7 g, 37.8 mmol), red mercuric oxide (52 g), and anhydrous sodium sulfate (52 g) in absolute ether (100 mL) were reacted to give the product (1.4 g, 16.3 mmol, 43.1% yield).

The 100 MHz ^{1}Hmr spectrum TMS (benzene-d_6) showed δ: 4.70 (singlet), and indicated 95 ± 1% isotopic purity. The mass spectrum indicated 95.4 ± 0.1% isotopic purity ($D_0 = 0.6$, $D_1 = 0.0$, $D_2 = 7.0$, $D_3 = 2.0$, $D_4 = 90.4$). The 13.6 MHz ^{2}Hmr spectrum (CCl_4) indicated >99.8% of total deuterium at the 3- and 5-methylene (ring methylene) positions.

Conclusion

Secondary deuterium kinetic isotope effects do not allow a decision between one-bond and concerted two-bond cleavage for 4-methylene-1-pyrazoline. The product proportions from the various deuterated substrates cannot be rationalized in terms of a trimethylenemethane intermediate. The kinetic data and product proportions can be readily rationalized in terms of a diazenyl radical which is long enough lived that the allylic termini become equivalent, and for which the rotation of the methylene group out of

the allylic plane has an isotope effect k_H/k_D of 1.33 ± 0.05.

Acknowledgements

We wish to acknowledge the assistance of Dr. H. Tokunaga in many aspects of this work, and the help of Dr. A. Hogg in terms of the mass spectrometry. The efforts of Dr. T. Nakashima in obtaining the ^{2}Hmr spectra are most appreciated and finally the authors wish to acknowledge the financial support of the Natural Sciences and Engineering Research Council of Canada and of the University of Alberta.

1. R. T. Crawford and K. Takagi. J. Am. Chem. Soc. **94**, 7406 (1972).
2. (*a*) N. A. Porter and L. J. Marnett. J. Am. Chem. Soc. **95**, 938 (1973); (*b*) J. G. Green, G. R. Dubay, and N. A. Porter. J. Am. Chem. Soc. **99**, 1264 (1977); (*c*) A. Tsolis, S. G. Mylonakis, M. T. Nieh, and S. Seltzer. J. Am. Chem. Soc. **94**, 829 (1972); (*d*) K. R. Kopecky, P. Pope, and J. M. Lopez-Sastre. Can. J. Chem. **54**, 2639 (1976).
3. A. W. Garner, J. W. Timberlake, P. S. Engel, and R. A. Melaugh. J. Am. Chem. Soc. **97**, 7377 (1975).
4. N. Rieber, J. Alberts, J. A. Lipsley, and D. M. Lemal. J. Am. Chem. Soc. **91**, 5668 (1969); R. J. Crawford and M. Ohno. Can. J. Chem. **52**, 3134 (1974).
5. R. J. Crawford and D. N. Cameron. J. Am. Chem. Soc. **45**, 691 (1967).
6. (*a*) J. A. Berson, C. D. Duncan, and L. R. Corwin. J. Am. Chem. Soc. **96**, 6175 (1974); (*b*) J. A. Berson, R. J. Rushby, J. M. McBride, and M. Trembling. J. Am. Chem. Soc. **93**, 1544 (1971); (*c*) J. A. Berson, C. D. Duncan, G. C. O'Connell, and M. S. Platz. J. Am. Chem. Soc. **98**, 2538 (1976); (*d*) J. A. Berson, L. R. Corwin, and J. H. Davis. J. Am. Chem. Soc. **96**, 6177 (1974).
7. (*a*) D. Cichra, M. S. Platz, and J. A. Berson. J. Am. Chem. Soc. **99**, 8507 (1977); (*b*) J. A. Berson. Acc. Chem. Res. **11**, 446 (1978).
8. (*a*) P. Dowd and M. Chow. J. Am. Chem. Soc. **99**, 6438 (1972); (*b*) P. Dowd. Acc. Chem. Res. **5**, 242 (1972); (*c*) P. Dowd, G. Sengupta, and K. Sachdev. J. Am. Chem. Soc. **92**, 5726 (1970); (*d*) P. Dowd and K. Sachdev. J. Am. Chem. Soc. **89**, 715 (1967); (*e*) P. Dowd. J. Am. Chem. Soc. **88**, 2587 (1966); (*f*) J. J. Gajewski, A. Yeshurun, and E. J. Bair. J. Am. Chem. Soc. **94**, 2138 (1972); (*g*) M. J. S. Dewar and J. S. Wasson. J. Am. Chem. Soc. **93**, 3081 (1971); (*h*) J. H. Davis and W. A. Godard, III. J. Am. Chem. Soc. **98**, 303 (1976); (*i*) W. J. Hehre, L. Salem, and M. R. Willcott, III. J. Am. Chem. Soc. **96**, 4328 (1974); (*j*) W. T. Borden. J. Am. Chem. Soc. **98**, 2695 (1976); (*k*) D. A. Dixon, R. Foster, T. A. Halgren, and W. N. Lipscomb. J. Am. Chem. Soc. **100**, 1359 (1978).
9. D. R. Yarkony and H. F. Schaeffer, II. J. Am. Chem. Soc. **96**, 3754 (1974).
10. R. J. Crawford, D. M. Cameron, and H. Tokunaga. Can. J. Chem. **52**, 4025 (1974).
11. A. A. Marei and R. A. Raphael. J. Chem. Soc. 886 (1960).
12. R. J. Crawford and A. Mishra. J. Am. Chem. Soc. **88**, 3963 (1966).
13. (*a*) S. Seltzer and F. T. Dunne. J. Am. Chem. Soc. **87**, 2628 (1965); (*b*) E. A. Halevi. Progress in physical organic chemistry. Vol. 1. Interscience Publishers, Inc., New York, NY. 1963. p 109.
14. J. J. Gajewski and S. K. Chou. J. Am. Chem. Soc. **99**, 5696 (1977).
15. W. R. Roth and G. Wegener. Agnew. Chem. Int. Ed. Engl. **14**, 758 (1975).
16. T. B. Malloy, Jr., F. Fisher, J. Laane, and R. M. Hedges. J. Mol. Spectrosc. **40**, 239 (1971).
17. (*a*) K. B. Wiberg. Physical organic chemistry. John Wiley and Sons, Inc., New York. 1964. p 377; (*b*) I. Safarik and O. P. Strausz. J. Phys. Chem. **76**, 3613 (1972).
18. J. P. Chesick. J. Am. Chem. Soc. **85**, 2720 (1963).
19. D. E. Sunko and S. Borcic. Isotope effects in chemical reactions. van Nostrand Reinhold Co., New York. 1970. p 172.
20. J. E. Bertie and M. G. Norton. Can. J. Chem. **49**, 2229 (1971).
21. N. C. Baird and H. B. Kathpal. Can. J. Chem. **55**, 863 (1977).
22. T. B. Malloy, Jr., R. M. Hedges, and F. Fisher. J. Org. Chem. **35**, 4256 (1970).
23. F. Weiss, A. Isard, and R. Bensa. Bull. Soc. Chim. Fr. 1355 (1965).
24. F. Mutterer, J.-M. Morgen, J.-M. Biedermann, J.-P. Fleury, and F. Weiss. Bull. Soc. Chim. Fr. 4478 (1969).
25. J. Hooz and S. S. H. Gilani. Can. J. Chem. **46**, 86 (1968).
26. (*a*) A. Moordian and J. B. Cloke. J. Am. Chem. Soc. **67**, 942 (1945); (*b*) C. H. Issidorides and A. I. Matar. J. Am. Chem. Soc. **77**, 6382 (1955).
27. M. Rubottom and J. C. Chabala. Org. Synth. **54**, 60 (1974).
28. N. Rabjohn. Org. Synth. Coll. Vol. **III**, 375 (1955).
29. G. B. Bachman and H. A. Tanner. J. Org. Chem. **4**, 493 (1939).
30. R. B. Moffet. Org. Synth. Coll. Vol. **IV**, 834 (1963).
31. E. J. Corey and J. W. Suggs. Tetrahedron Lett. **44**, 3775 (1975).

Can. J. Chem. Downloaded from www.nrcresearchpress.com by 210.87.254.105 on 09/06/12
For personal use only.

Analytic solution of relaxation and dissociation of ozone and sulphur dioxide at low pressures

WENDELL FORST

Centre de Recherches sur les Atomes et les Molécules (CRAM) and Department of Chemistry, Université Laval, Québec (Qué.), Canada G1K 7P4

Received December 15, 1980

WENDELL FORST. Can. J. Chem. **59**, 2569 (1981).

The analytic solution of vibrational relaxation in a low-pressure gas is applied to the thermal dissociation of O_3 in helium and of SO_2 in argon. Use is made of experimental relaxation times to obtain average energy lost per collision. Calculated weak-collision rate constants are in very good agreement with experiment in the case of SO_2, but only in fair agreement in the case of ozone. Several curious aspects of the ozone system, both experimental and theoretical, are discussed.

WENDELL FORST. Can. J. Chem. **59**, 2569 (1981).

On se sert d'une solution analytique de la relaxation vibrationnelle dans un gaz à basse pression pour l'appliquer à la dissociation thermique de O_3 dans l'hélium et du SO_2 dans l'argon. On fait usage des temps de relaxation expérimentaux pour calculer l'énergie moyenne perdue par collision. Les constantes de vitesse calculées pour des collisions faibles s'accordent très bien avec l'expérience dans le cas du SO_2, mais seulement assez bien dans le cas de l'ozone. On discute, du point de vue expérimental et théorique, plusieurs aspects curieux du système ozone.

Can. J. Chem. Downloaded from www.nrcresearchpress.com by 210.87.254.42 on 09/06/12
For personal use only.

1. Introduction

The general relaxation problem in a gas at low pressure can be solved analytically for the case of exponential transition probabilities, as we have shown in recent publications (1–4). The calculations were tested, with good results, on the (spin-forbidden) dissociation and relaxation of two triatomics, N_2O and CO_2, both of which are linear. Since relaxation data in O_3 and SO_2 have recently become available (5, 6), we now propose to do the same kind of calculations for the relaxation and the (spin-allowed) dissociation of O_3 and SO_2, which are both non-linear. This should allow a further test of the theory, in that the number of rotational degrees of freedom is now increased to three, relative to two in the linear triatomics. Also, the relaxation data have some unusual features, which should give some idea of the sensitivity of the theory to the relaxation data input.

2. Theory

Since the theory has been adequately described before (1, 2), we give only those equations that are necessary for the comprehension of the text. For a transition from an initial state of energy y to final state of energy x, the exponential transition probability (per collision and per unit energy), which we call Model B, is given by

$$[1] \quad q(x,y) = \begin{cases} C(x)\exp[-(y-x)\gamma] & x < y \text{ (down)} \\ C(y)\exp[-(x-y)\gamma'] & x > y \text{ (up)} \end{cases}$$

where the constant γ is to a very good approximation the average energy transferred in a down-collision (i.e. lost), and $\gamma' = 1/\gamma + 1/kT$. The explicit form of the factors $C(x)$ and $C(y)$ is known (ref. 2, eq. [3]). The $q(x,y)$ of eq. [1] is normalized in $(0, \infty)$ and satisfies detailed balance in the form

$$q(x,y)\exp(-y/kT) = q(y,x)\exp(-x/kT)$$

The time-dependent population density is written in the form of an eigenfunction expansion (ref. 2, eq. [26]) which makes use of two parameters, S and R_j. The first is the solution of

$$[2] \quad \frac{2S}{2+(\gamma/kT)(1-S^2)} = \tanh\left(\frac{SE_0^*}{2kT}\right)$$

and the R_j's are the solutions of

$$[3] \quad \frac{2R}{2+(\gamma/kT)(1+R^2)} = \tan\left(\frac{RE_0^*}{2kT}\right)$$

where E_0^* is the effective threshold to reaction. Once S and the R_j's are known, all steady-state and pre-steady-state properties of the system can be calculated. Given the nature of the available experimental data for O_3 and SO_2, we shall need only the steady-state rate constant for dissociation $k_0\dagger$ (cm^3 $molecule^{-1}$ s^{-1}) which is given by

$$[4] \quad k_0\dagger = \frac{Z(\gamma/kT)^2(1-S^2)}{(\gamma/kT)^2(1-S^2)+4(1+\gamma/kT)}$$

where Z is the collision number, and the first relaxation time τ_1 which is given, in dimensionless form, by

$$[5] \quad \omega\tau_1 = 1 + \frac{4}{1+R_1}\left[\left(\frac{kT}{\gamma}\right)^2 + \frac{kT}{\gamma}\right]$$

0008-4042/81/172569-06$01.00/0

©1981 National Research Council of Canada/Conseil national de recherches du Canada

where R_1 is the first solution of eq. [3] and ω is the collision frequency. The effective threshold E_0^* is defined as (ref. 2, eq. [69])

$$[6] \quad E_0^* = E_0 - kT \ln \left\{ Q_{vr}^{-1} \int_0^\infty N_{vr}(x + E_0) \times [\exp(-x/kT)]\, dx \right\}$$

where E_0 is the (0 K) bond dissociation energy of the bond undergoing rupture, Q_{vr} is the molecular vibrational–rotational partition function, and $N_{vr}(x)$ is the vibrational–rotational density of states at energy x. It can be shown that for a threshold that is not too small ($E_0^* > kT$), eqs. [2], [4], and [6] yield

$$[7] \quad k_0\dagger = \frac{Z \int_{E_0}^\infty N_{vr}(x)[\exp(-x/kT)]\, dx}{Q_{vr}(1 + kT/\gamma)^2}$$

which is the analytic approximation to the "exact" weak-collision rate constant.

The only parameter that remains to be specified is γ, and it is obtained from experiment. The experimentally measured relaxation time τ_{expt} is identified with τ_1, and eq. [5] is then solved for γ; the γ so obtained is called γ_{exptl}.

The integral in eq. [6] is calculated using a 15-point Gauss–Laguerre integration (7), and the densities of states by the method of steepest descents (8) for a collection of (in the present case) three harmonic oscillators and three rigid rotors. Equations [2] and [3] are solved by the usual Newton–Raphson method. For the sake of consistency, Q_{vr} is calculated by the same 15-point Gauss–Laguerre integration as

$$Q_{vr} = \int_0^\infty N_{vr}(x)[\exp(-x/kT)]\, dx$$

3. Results

(a) *The Low-pressure Dissociation $O_3 + He \rightarrow O + O_2 + He$*

Relaxation times in O_3 have been measured several times in the past (9–11), but only recently Moy, Mao, and Gordon (5) have measured them over a range of temperatures in the presence of helium. They used a pulsed CO_2 laser to excite the stretching mode (001) in O_3 in the presence of NO and the relaxing gas, and from the decay of the laser-enhanced chemiluminescence of NO_2^* they obtained the thermally averaged relaxation rate for the bending mode (010) of O_3. A least-squares fit of their data (ref. 5, Table II) over the range 164 to 444 K yields for the dimensionless relaxation time $\omega\tau_{exptl}$ (which is equal to the inverse of the transition probability)

$$[8] \quad \omega\tau_{exptl} \equiv \omega\tau_1 = 4.2925 \exp(46.603/T^{1/3})$$

based on the hard-sphere collision frequency ω (using the collision diameter $\sigma = 3.42$ Å for ozone–He collisions (9)). Owing to the uncertainty in the Lennard–Jones (LJ) well-depth parameter ε for O_3, it is not useful to calculate collision numbers under LJ potential (Z_{LJ}), which would probably be more appropriate.

Vibrational frequencies of ozone necessary for calculating $N_{vr}(x)$, and the O_2—O bond energy in O_3 used for E_0 in eq. [6] were all taken from Johnston (12) ($E_0 = 24.25$ kcal mol^{-1}).

The results are shown in Table 1, where γ_{exptl} is the solution of eqs. [5] and [8], while $k_0\dagger$ and $\omega\tau_1$ are calculated from eqs. [4] and [5], respectively, the latter merely as a check that numerical values of the relaxation times given by eq. [8] are in fact recovered. Least-squares fit of $k_0\dagger$ in Table 1 gives

$$k_0\dagger = 1.70 \times 10^{-9} \times [\exp(-12752/T)] \text{ cm}^3 \text{ molecule}^{-1} \text{ s}^{-1}$$

Although there are numerous determinations of the dissociation rates of ozone at high temperature, and of the reverse association $O_2 + O + M$ at low temperature, few have been done for helium as third body. However, recently Endo, Glänzer, and Troe (EGT) (13) have determined relative efficiencies of various M at 300 and 800 K. Using their $k_{exptl}(He)/k_{exptl}(Ar) = 2.8$ at 800 K, the "best" rate constant for O_3 dissociation in argon $k_{exptl}(Ar)$ given by Baulch (14) can be converted into dissociation rate in helium, with the result $k_{exptl}(He) = 7.26 \times 10^{-16}$ cm^3 molecule^{-1} s^{-1} at 800 K. EGT's direct determination gives $k_{exptl}(He) = 7.47 \times 10^{-16}$ cm^3 molecule^{-1} s^{-1} at the same temperature. The rate constant expression for $k_{exptl}(O_3)$ given by Heimerl and Coffee (15) cannot be usefully converted in $k_{exptl}(He)$ because it is based mainly on data for M = Kr and M = Ar that have been converted into $k_{exptl}(O_3)$ using temperature-independent relative efficiencies that are probably inappropriate in this case.

At room temperature, it can be calculated from EGT's data that at 300 K $k_{exptl}(He)/k_{exptl}(Ar) = 1.82$, $k_{exptl}(He)/k_{exptl}(N_2) = 0.90$, the latter of which agrees with Johnston's (12) 300 K value, but the former is about 40% higher. Based on the above relative rate constants of EGT, and using JANAF (16) values for the equilibrium constant, the more recent determinations (refs. 17, 18 for M = N_2; refs. 19, 20 for M = Ar) of the association rate all yield

Can. J. Chem. Downloaded from www.nrcresearchpress.com by 210.87.254.42 on 09/06/12
For personal use only.

Can. J. Chem. Downloaded from www.nrcresearchpress.com by 210.87.254.42 on 09/06/12
For personal use only.

TABLE 1. Calculated results* for low-pressure dissociation of O_3 and SO_2

T (K)	γ_{exptl} (cm^{-1})	$k_0\dagger$ (cm^3 molecule^{-1} s^{-1})	$\omega\tau_{inc}$	$\omega\tau_1$	k_{exptl} (cm^3 molecule^{-1} s^{-1})
		O_3 + He			See text
200	2.5	3.34 (−37)	1.6 (5)	1.24 (4)	
300	6.2	5.8 (−28)	3.7 (4)	4.5 (3)	~2 (−26)
400	11.1	2.58 (−23)	1.4 (4)	2.4 (3)	
600	23.4	1.06 (−18)	3.9 (3)	1.1 (3)	
800	35.5	1.77 (−16)	1.8 (3)	6.5 (2)	~7.3 (−16)
		SO_2 + Ar			Ref. 33
2000	110.8	1.57 (−22)	3.6 (3)	6.3 (2)	2.0 (−21)
3000	226.1	6.12 (−18)	1.1 (3)	3.0 (2)	1.34 (−17)
4000	339.6	8.80 (−16)	4.8 (2)	1.8 (2)	1.1 (−15)
5000	423.7	1.33 (−14)	2.9 (2)	1.3 (2)	1.53 (−14)
6000	473.2	6.76 (−14)	2.0 (2)	9.4 (1)	8.9 (−14)

*Powers of ten in parentheses.

the remarkably consistent value for the dissociation rate $k_{exptl}(He) \sim 2 \times 10^{-26}$ cm^3 molecule^{-1} s^{-1} at 300 K, which is substantially the same result that can be obtained by extrapolating Baulch's (14) expression for $k_{exptl}(Ar)$ to 300 K and multiplying by 1.82, the helium rate relative to argon.

Alternatively, we can make use of data for relaxation of ozone in presence of argon which are known only at one temperature. Gordon and Liu (11) report that the ratio of transition probabilities for He and Ar is ~3.5 at room temperature, which agrees fairly well with the results of Rosen and Cool (9) and Kaldor and co-workers (10). Thus $\omega\tau_1$ (Ar) $\sim 1.5 \times 10^4$ at 298 K. Calculation then gives for argon as heat bath gas $\gamma_{exptl} \sim 3.5\,cm^{-1}$, $k_0\dagger \sim 10^{-28}$ cm^3 molecule^{-1} s^{-1}, so that $r = k_0\dagger(Ar)/k_0\dagger(He) \sim 0.25$, which is the calculated argon rate relative to He. This is based on hard-sphere collisions; for collisions under LJ potential, the relative rate is 1.5 times larger, owing to the small LJ well depth ε for He (note that in taking the ratio of rate constants, the unknown ε for O_3 drops out). Thus $r \sim 0.4$, which compares reasonably well with EGT's $k_{exptl}(Ar)/k_{exptl}(He) = 0.55$ at 300 K.

The results in Table 1 show a considerable discrepancy between experiment and theory at room temperature. Quite obviously relaxation data give a γ_{exptl} that is about right in relative terms (γ_{He} vs. γ_{Ar}), but too small in absolute value.

(b) The Low-pressure Dissociation $SO_2 + Ar \rightarrow SO + O + Ar$

Relaxation times in SO_2–Ar mixtures have been measured behind incident shock waves by Kishore, Babu, and Rao (6) between 700 and 2100 K who obtained

$$p\tau_{exptl} = 9.562 \times 10^{-3} \exp(40.32/T^{1/3}) \text{ atm-}\mu s$$

which leads to

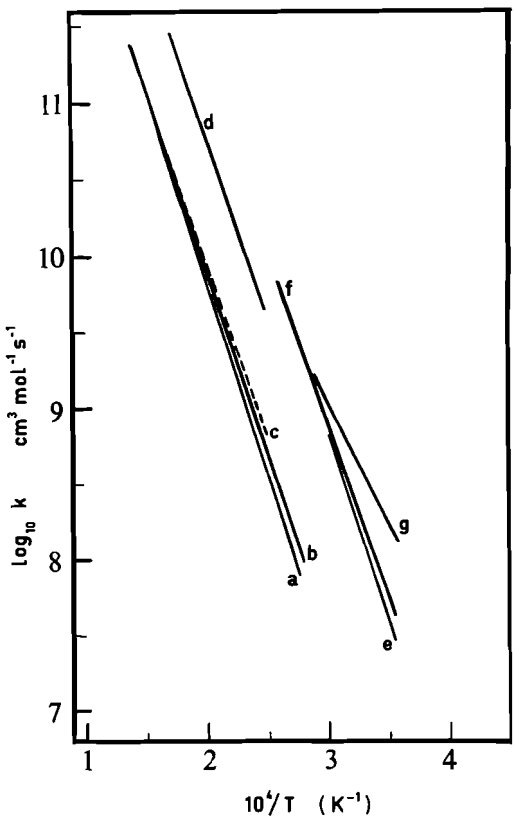

FIG. 1. Comparison of calculated and experimental Arrhenius plots for the decomposition of SO_2 in argon at low pressure. (*a*) is calculated, the rest are experimental. (*a*), this work; (*b*), ref. 28; (*c*), ref. 33; (*d*), ref. 31; (*e*), ref. 27; (*f*), ref. 29; (*g*), ref. 25.

$$[9] \quad \omega\tau_{exptl} \equiv \omega\tau_1 = \frac{1.445 \times 10^4}{T^{1/6}} \exp(40.32/T^{1/3})$$

based on Z_{LJ}. LJ parameters for SO_2 were taken from Monchick and Mason (21) ($\varepsilon/k = 363°$, $\sigma = 4.026$ Å), vibrational frequencies from Shimanouchi

Can. J. Chem. Downloaded from www.nrcresearchpress.com by 210.87.254.42 on 09/06/12
For personal use only.

(22), and the SO—O bond energy from Darwent (23) (E_0 = 130.8 kcal mol^{-1}).

The results are shown in Table 1; least-squares fit gives

$$k_0\dagger = 8.82 \times 10^{14} \times \exp(-117.3 \text{ kcal mol}^{-1}/RT) \quad \text{cm}^3 \text{ mol}^{-1} \text{ s}^{-1}$$

There are numerous experimental investigations of this reaction (24–33), the more recent of which are compared in Fig. 1 with the present results. There appears to be agreement now that the decomposition of SO_2 is complex in mixtures (33) containing more than about 0.1% SO_2, but that at lower concentrations the elementary reaction of decomposition into SO + O can be measured. Thus the two measurements (28, 33) done at very low concentrations are now in substantial agreement, the most recent result being (33)

$$k_{\text{exptl}} = 3.55 \times 10^{14} \times \exp(-104.92 \text{ kcal mol}^{-1}/RT) \quad \text{cm}^3 \text{ mol}^{-1} \text{ s}^{-1}$$

It can be seen that the calculated results agree quite well with the experimental rate constant for the elementary step.

It should be noted nevertheless that agreement between theory and experiment would look much worse if we were to take the group of experimental measurements that give much higher values for the rate constant (cf. Fig. 1), of which one (curve *e*, ref. 27) was also done at very low (~ppm) concentrations of SO_2. It now appears, however, that there was an experimental problem associated with the measurement of ref. 27 (cf. footnote 12 in ref. 33).

4. Discussion

Equation [60] in ref. 2 makes it clear that τ_1 refers to bulk relaxation of average internal energy. At first sight, this may appear not to be what has been measured in either the O_3–He or SO_2–Ar relaxation measurements.

While in the O_3–He case ozone was pumped by a nonthermal process, there is good reason to believe (34) that the cited relaxation measurements nevertheless represent bulk relaxation at the temperature of the experiment via the slowest V–T mode. Thus even if the present calculations at 600 and 800 K make use of relaxation data extrapolated beyond the temperature range actually covered by experiment, it is clear from Table 1 that in the case of ozone the theory has not been successful in fitting simultaneously the rate constant and the relaxation time. Part of the problem may be that the calculated rate constants $k_0\dagger$ are based on hard-sphere collision numbers. If we take Troe's (35) value ε/k = 162.2° for the LJ well depth in O_3–Ar collisions, one gets ε/k = 47.0° for O_3–He collisions, which means that in order to correct for collisions under the more appropriate LJ potential, the calculated $k_0\dagger$ in Table 1 should be multiplied by 1.46 at 300 K, and by 1.05 at 800 K. This does not significantly improve agreement with experiment.

Alternatively, we may compare with other information the values of γ_{exptl} in Table 1, which is the average energy loss in a collision as calculated from the measured relaxation time. In terms of EGT's (13) measured collision efficiency β_c,

$$\gamma = \beta_c^{1/2} kT/(1 - \beta_c^{1/2})$$

(Note that EGT give their results in terms of $\langle \Delta E \rangle$, the average energy transferred in *all* collisions, up *and* down; thus $\langle \Delta E \rangle = -\gamma\beta_c^{1/2}$). From their data on O_3 + He, one gets γ = 146.3 cm^{-1} at 300 K, γ = 106.9 cm^{-1} at 800 K, which, if used in the present calculations, would yield $k_0\dagger = 9.3 \times 10^{-26}$ at 300 K, $k_0\dagger = 1.3 \times 10^{-15}$ at 800 K in units of cm^3 molecule^{-1} s^{-1}. Compared with experiment, the rate constants are now too large, but the discrepancy is much smaller in absolute terms, especially at low temperature. The most striking is the difference in the temperature dependence of γ: when calculated from relaxation times, it *increases* with temperature, as a result of the $T^{-1/3}$ temperature dependence of the usual Landau–Teller plot, whereas γ calculated from β_c *decreases* with temperature.

Stace and Murrell (36) have done a trajectory study of collisional energy transfer in ozone, and their calculations also give a γ that invariably *increases* with temperature. At the temperatures of interest here, they only give data for the O_3 + Ar system at 500 and 1000 K, from which one obtains by interpolation γ = 244 cm^{-1} at 800 K, and, by extrapolation, $\gamma \sim 7$ cm^{-1} at 300 K. EGT (3) give β_c = 0.019 (800 K) and 0.19 (300 K), i.e. γ = 88.9 cm^{-1} (800 K) and 161.1 cm^{-1} (300 K) for M = Ar. Thus the trajectory study also gives a γ that disagrees with that obtained from β_c with respect to both magnitude and temperature coefficient.

The dissociation of ozone consequently represents a real difficulty for theory, especially at low temperature. The problem could be that the present theory gives an incorrect relation between γ and the relaxation time. One would then have to ask why ozone is the only case so far where such difficulty has come up, and why apparently the trajectory study calculation suffers from the same disability. Or it could be that the cited relation

Can. J. Chem. Downloaded from www.nrcresearchpress.com by 210.87.254.42 on 09/06/12
For personal use only.

between γ and β_c is not correct, or that there is some difficulty with the experimental rate measurements. At room temperature, this means the reverse association

$$O(^3P) + O_2(^3\Sigma_g^-) + M \rightarrow O_3(^1A_1) + M$$

It has been reported recently (37, 38) that more than half the ozone is first formed in the $^3B_2$ state which subsequently relaxes to $^1A_1$, so that presumably the experimental rates refer to this two-stage process rather than to the direct formation of $O_3(^1A_1)$ supposedly represented (via the equilibrium constant) by k_{exptl} in Table 1. It is not clear at present how large the correction (if any) of the 300 K value of k_{exptl} would have to be in order to account for the two-stage process. Until this problem is resolved, the exact nature of the disagreement at room temperature between theory and experiment is in doubt. The choice is clearly this: either k_{exptl} is too large, or γ based on relaxation data is too small. Conceivably kinetic decomposition (or association) experiments do not measure the same γ as do relaxation experiments, in view of the different temperature dependence of γ that the two methods produce.

In the SO_2–Ar case, the problem is of a different nature. Here the cited relaxation measurements in shock waves represent bulk relaxation of average energy, but eq. [5] assumes that there is just one (principal) relaxation time, and this is usually the case. However, SO_2 is a well-known (39) example where there is more than one relaxation time because of a large gap between the two lowest vibrational modes (518 and 1151 cm^{-1}, respectively). The shorter relaxation time (which could not be measured in the experiments of Kishore *et al.*) corresponds to relaxation of the lowest bending mode, while the slower relaxation, measured in the experiments on which eq. [9] is based, corresponds to relaxation of the two higher stretching modes. It can be argued that this is not a very serious handicap since the dissociation of SO_2 proceeds by excitation of the antisymmetric stretch at 1362 cm^{-1}, and therefore it is the relaxation of the stretching modes that is most important for the process of dissociation. As a result, the rate constant, though calculated by means of a theory that recognizes only one relaxation time for average energy, nevertheless agrees quite well with experimental result. The agreement in fact supports the interpretation of the low-concentration measurements in terms of the elementary step $SO_2 \rightarrow SO + O$.

The values of γ_{exptl} obtained in the SO_2 case fit in with the results of calculations for the other triatomics. For example, at 2000 K, we have (2) γ_{exptl} = 42 cm^{-1} for CO_2 + Ar, 59 cm^{-1} for N_2O + Ar, and 111 cm^{-1} for SO_2 + Ar. The higher value for SO_2 dissociation is what one would expect for energy transfer involving a highly polar molecule like SO_2, relative to the weakly polar N_2O and non-polar CO_2.

Table 1 includes also values of the dimensionless incubation time $\omega\tau_{inc}$ calculated from the large-threshold expression (ref. 2, eq. [39])

$$[10] \quad \omega\tau_{inc} = \frac{(E_0^*/kT)(1 + \gamma_{exptl}/kT) - (3 + 2\gamma_{exptl}/kT)}{(\gamma_{exptl}/kT)^2}$$

Although this incubation time has not yet been measured in either of the systems discussed here, it is useful as an indication of the number of collisions the system must undergo before reaching steady state.

In common with previous work, experimental relaxation data, in particular in the SO_2 case, had to be extrapolated to temperatures higher than those at which they were measured, in order to calculate the rate constants. This of course introduces an additional uncertainty. However, the present work shows that useful, and fairly accurate, results can be obtained for the rate constants even if the relaxation data, in addition to the extrapolation, are not exactly of the kind required by the theory. This is another example of the well-known fact that thermal systems can be successfully described on the basis of very limited information.

Acknowledgments

Financial support from the Natural Sciences and Engineering Research Council of Canada is gratefully acknowledged. The author is indebted to Joe Michael for discussion and to Huw Pritchard for correspondence.

1. A. P. Penner and W. Forst. J. Chem. Phys. **67**, 5296 (1977).
2. W. Forst and A. P. Penner. J. Chem. Phys. **72**, 1435 (1980).
3. W. Forst. J. Phys. Chem. **84**, 3050 (1980).
4. W. Forst. Int. J. Chem. Kinet. In press.
5. J. Moy, C. R. Mao, and R. J. Gordon. J. Chem. Phys. **72**, 4216 (1980); **73**, 4713 (1980).
6. V. V. N. Kishore, S. V. Babu, and V. S. Rao. Chem. Phys. **46**, 297 (1980).
7. M. Abramowitz and I. A. Stegun. Handbook of mathematical functions. AMS 55, Washington 1965. p. 923.
8. W. Forst. Theory of unimolecular reactions. Academic Press, New York. 1973. Appendix.
9. D. I. Rosen and T. A. Cool. J. Chem. Phys. **59**, 6097 (1973); **62**, 466 (1975).
10. M. J. Kurylo, W. Braun, and A. Kaldor. Chem. Phys. Lett. **27**, 249 (1974).
11. R. J. Gordon and M. C. Liu. J. Chem. Phys. **64**, 1058 (1976).

12. H. S. JOHNSTON. Gas phase reaction kinetics of neutral oxygen species. NSRDS-NBS 20, Washington. 1968.
13. H. ENDO, K. GLÄNZER, and J. TROE. J. Phys. Chem. **83**, 2083 (1979).
14. D. L. BAULCH, D. D. DRYSDALE, J. DUXBURY, and S. J. GRANT. Evaluated kinetic data for high temperature reactions. Vol. 3. Butterworths, London, 1976. p. 65.
15. J. M. HEIMERL and T. P. COFFEE. Comb. Flame, **35**, 117 (1979).
16. JANAF thermochemical tables. 2nd ed. NSRDS-NBS Washington. 1971.
17. R. D. HUDSON and E. I. REED (*Editors*). NASA RP 1049. 1979.
18. Recommendation of CODATA Task Group on Chemical Kinetics.
19. O. KLAIS, P. C. ANDERSON, and M. J. KURYLO. Int. J. Chem. Kinet. **12**, 469 (1980).
20. I. ARNOLD and F. J. COMES. Chem. Phys. **42**, 231 (1979).
21. L. MONCHICK and E. A. MASON. J. Chem. Phys. **35**, 1676 (1961).
22. T. SHIMANOUCHI. Tables of molecular vibrational frequencies. NSRDS-NBS 39, Vol. 1, Washington. 1972.
23. B. DE B. DARWENT. Bond dissociation energies in simple molecules. NSRDS-NBS 31, Washington. 1970.
24. H. A. OLSCHEWSKI, J. TROE, and H. GG. WAGNER. Z. Physik. Chem. NF **44**, 173 (1965).
25. B. P. LEVITT and D. B. SHEEN. Trans. Faraday Soc. **63**, 2955 (1967).
26. J. H. KIEFER. J. Chem. Phys. **62**, 1354 (1975).
27. T. JUST and G. RIMPEL. Proceedings of 11th International Symposium on Shock Tubes and Shock Waves. Seattle, WA. 1978. p. 226.
28. D. C. ASTHOLZ, K. GLÄNZER, and J. TROE. Proceedings of 11th International Symposium on Shock Tubes and Shock Waves. Seattle, WA. 1978. p. 232.
29. A. GRILLO, R. REED, and M. W. SLACK. J. Chem. Phys. **70**, 1634 (1979); 12th International Symposium on Shock Tubes and Shock Waves. Israel. 1979.
30. K. SAITO, T. YOKUBO, T. FUSE, H. TAHARA, O. KONDO, T. HIGASHIHARA, and I. MURAKAMI. Bull. Chem. Soc. Jpn. **52**, 3507 (1979).
31. M. T. RAJU, S. V. BABU, and S. V. RAO. Chem. Phys. **48**, 411 (1980).
32. K. SAITO, T. YOKUBO, T. HIGASHIHARA, and I. MURAKAMI. Bull. Chem. Soc. Jpn. **53**, 1439 (1980).
33. K. SAITO, T. YOKUBO, and I. MURAKAMI. J. Chem. Phys. **73**, 3017 (1980).
34. H. O. PRITCHARD. Can. J. Chem. **54**, 2372 (1976).
35. J. TROE. J. Chem. Phys. **66**, 4758 (1977).
36. A. J. STACE and J. N. MURRELL. J. Chem. Phys. **68**, 3028 (1978).
37. T. KLEINDIENST, J. B. BURKHOLDER, and E. J. BAIR. Chem. Phys. Lett. **70**, 117 (1980).
38. T. KLEINDIENST, J. R. LOCKER, and E. J. BAIR. J. Photochem. **12**, 67 (1980).
39. J. D. LAMBERT. Vibrational and rotational relaxation in gases. Clarendon Press. Oxford. 1977. p. 89*ff*.

Can. J. Chem. Downloaded from www.nrcresearchpress.com by 210.87.254.42 on 09/06/12
For personal use only.

Internal energy randomisation in weak-collision unimolecular reaction systems

H. O. PRITCHARD AND S. R. VATSYA

Centre for Research in Experimental Space Science, York University, Downsview, Ont., Canada M3J 1P3

Received January 20, 1981

H. O. PRITCHARD and S. R. VATSYA. Can. J. Chem. **59**, 2575 (1981).

We examine the conjecture that the principal difference between weak-collision and strong-collision behaviour in thermal unimolecular reaction systems arises from a difference in internal energy randomisation rates. To do this, we solve analytically the strong-collision master equation for a thermal unimolecular reaction including explicit allowance for the randomisation processes, and we show that all weak-collision effects so far observed in thermal systems can be accommodated within this framework.

In an appendix, we give the extension of this analytic solution for reactions yielding two (or more) distinct sets of products.

H. O. PRITCHARD et S. R. VATSYA. Can. J. Chem. **59**, 2575 (1981).

Nous examinons l'hypothèse relative au fait que la différence principale de comportement entre une collision faible et collision forte, dans les systèmes de réactions thermique unimoléculaire, provient de la différence entre les vitesses de distribution au hasard de l'énergie interne. Pour ce faire nous résolvons analytiquement l'équation principale de collision forte pour une réaction thermique unimoléculaire incluant une correction explicite pour le processus de distribution au hasard, et nous montrons que tous les effets de collision faible observés dans les systèmes thermiques peuvent s'intégrer dans ce cadre.

En appendice nous donnons le développement de cette solution analytique pour les réactions conduisant à deux (ou plus) ensembles distincts de produits.

[Traduit par le journal]

Can. J. Chem. Downloaded from www.nrcresearchpress.com by 210.87.254.6 on 09/06/12
For personal use only.

Introduction

The concept of a strong collision has been bound intimately with the development of the theory of unimolecular reactions ever since its inception in the 1920's (1–5). The usual manner in which a strong collision was described was an intuitive one, generally adequate within the framework of a steady-state treatment of the reaction process, but not always consistent with the principle of detailed balancing. Recently, however, Nordholm (6) has given precision to the definition of a strong collision, although his statement is recognisably the same as the qualitative one given by Bunker (2, 5). At about the same time, Yau and Pritchard (7) showed that it was possible to derive an analytic solution to the master equation for a thermal unimolecular reaction by using a particular set of collisional transition probabilities for the activation–deactivation processes; it was realised subsequently that this set of transition probabilities was identical with the definition given by Nordholm for strong collisions (8). The beauty of Nordholm's definition is that it can be extended unambiguously to describe collision processes which take place more slowly than "on every collision", and this extended definition is in fact the one used by Yau and Pritchard. By this definition, it is perfectly legitimate therefore to say (provided that one does not need to know the actual *pathways* by which the relaxation took place) that a certain non-equilibrium distribution was reduced to a Boltzmann distribution on a time scale of 10 collisions, or 1000 collisions, — or for that matter, one-thousandth of the period between collisions — and describe all processes with the same form of *strong-collision* relaxation matrix.

This realisation presents us with a dilemma when we come to discuss weak-collision systems. No such precise definition has ever, to our knowledge, been given for a weak collision; the definition, if there is one, is one of the exception — in other words, if it is not a strong collision, then it is a weak collision. But how can we draw a distinction between a weak collision as we normally imagine it, and an inefficient strong collision having the same relaxation rate? Theoretically it is quite straightforward, for any relaxation matrix which has more than one non-zero eigenvalue describes a weak collision process; from a practical point of view, a more useful concept would be that there are some very fast processes and also some rather slow ones, and hence that the eigenvalues are well spaced out — perhaps over two orders of magnitude or more. The determination of such eigenvalues experimentally is rather difficult, and in general we have found ourselves in the position of trying to draw qualitative inferences by making observations on bulk reaction rates. The observation of the rate of formation of some reaction product gives us the integral of the product of the $k(E)$ function with the steady-state distribution — and since the $k(E)$ function is usually taken to be fixed, changes in reaction rate reflect changes in the steady-state distribution. However, by using the result of Lemma 2 from another paper (9), we can conclude that in the weak-collision case, the prin-

0008-4042/81/172575-12$01.00/0

©1981 National Research Council of Canada/Conseil national de recherches du Canada

Can. J. Chem. Downloaded from www.nrcresearchpress.com by 210.87.254.6 on 09/06/12
For personal use only.

cipal determinant of the steady-state distribution is the perturbation of the Boltzmann distribution by the $k(E)$ function, and that contributions to the perturbation from the detailed forms of the relaxation processes are of only secondary importance.[1] Thus, unless we are fortunate in our choice of initial distribution, we cannot hope to discriminate decisively between various transition probability models, and in fact this is precisely what we have come to expect from a long series of chemical activation studies (3, 13); gross insensitivity of computed reaction rates to the assumed transition probability models has been commonplace for a decade now in another closely related problem, that of the dissociation of a diatomic gas (14).

If we specialise the argument to the study of thermal unimolecular reactions, the situation is even more clear cut. Typically, the time scale (t) on which the reaction rate is measured is several orders of magnitude greater than the internal relaxation time (τ); values of $t/\tau > 10^6$ are not uncommon. At these long times, the choice of initial distribution is quite irrelevant and the only information in the steady-state distribution comes from the perturbed eigenvector ψ_0 itself.[2] Consequently, there is little scope for deducing information about weak-collision effects from bulk measurements on thermal reactions. During the incubation period, however, this is not the case,[2] but as yet, no such measurements appear to have been made. Knowledge of the *length* of the incubation period provides no further information, because this is determined solely by ψ_0 and $\eta(0)$, the initial distribution (15). Here again, this conclusion is reinforced by the complete insensitivity of computed values for the ratio of the relaxation time to the incubation time for widely differing sets of transition probabilities (15, 16) (note also that there is a marked divergence between the calculated ratios and the experimental ones for N_2O (17) — perhaps indicating that the theoretical approach may be deficient). We conclude therefore that as far as *current* experimental data on thermal unimolecular reactions are concerned, it cannot matter much what kind of transition probability model we use, step-ladder, Poisson, Gaussian, exponential — or strong, but rendered inefficient by the inclusion of a scale factor in the manner of Nordholm (6) or of Yau and Pritchard (7).

Consequently, we have to re-examine the distinction we usually make between strong collisions and weak collisions to see if there is, in fact, a distinction to be made. In one case, we know already that there is not: we have shown recently (18) that a strong-collision treatment of chemical activation gives rise to a "low-pressure turn-up". In other words, low-pressure turn-up in chemical activation is a result of inefficient collisions, not weak collisions.[3]

On the other hand, we know that there are certain properties of unimolecular reactions which cannot be accommodated within the usual strong-collision formalism, even with the scaling to allow for inefficient energy transfer. Most obvious is the shape of the fall-off curves in so-called weak-collision reactions. For example, if we were to perform a standard strong-collision calculation (7) for the thermal dissociation of CO_2, then the fall-off curve would be far too broad, and would not fit the experimental data in the way such a calculation would fit for a larger molecule; clearly the strong-collision assumption is defective in some way in this case. In his dis-

[1]The key equation here is that the perturbed eigenvector Ψ_0 (which determines the steady state) is given by

$$\Psi_0 = S_0 - \sum_{j=1}^{n-1} \frac{p_j}{\lambda_j - \gamma_0} \mathbf{D}^{1/2} \left[\mathbf{1} + \mathbf{D}^{1/2} \sum_{j=1}^{n-1} \frac{p_j}{\lambda_j - \gamma_0} \mathbf{D}^{1/2} \right]^{-1} \mathbf{D}^{1/2} S_0$$

where S_0 is the unperturbed eigenvector, $\mathbf{D}$ is a diagonal matrix representing the $k(E)$ function in discrete form, λ_j and p_j are the eigenvalues and eigenprojections respectively for the unperturbed matrix, and γ_0 is the rate constant. Given that for weak collisions the λ_j are well spaced, the dominant contribution in the perturbation term will come from λ_1 and p_1, the vibrational relaxation, and a series of numerical experiments (10–12) on H_2 suggests that the form of *this* relaxation is generally determined by the energy-level spectrum rather than by the detailed forms of the transition probabilities.

[2]The important equation here is that the population evolution is given by (7)

$$\eta_i(t) = \tilde{n}_i^{1/2} \sum_j \exp(-\gamma_j t)(\Psi_j)_i \sum_k (\Psi_j)_k \eta_k(0) \tilde{n}_k^{-1/2} \xrightarrow[t \to \infty]{} \tilde{n}_i^{1/2} \exp(-\gamma_0 t)(\Psi_0)_i \sum_k (\Psi_0)_k \eta_k(0) \tilde{n}_k^{-1/2}$$

From the equation given in footnote 1, the dominant term in Ψ_0 is S_0, so that the steady state, to a first approximation, is the equilibrium distribution, independent of the starting distribution $\eta(0)$, depreciated by the factor $\exp(-\gamma_0 t)$. Modification of this Boltzmann distribution to give the actual steady state arises from the perturbation term, which we have already argued in footnote 1, is dominated by the contribution from $k(E)$. This perturbation also introduces into the steady state a memory of the initial distribution $\eta(0)$, which we normally regard as being irrelevant when we discuss thermal reactions. Finally, a still smaller contribution to the determination of the steady state comes from the nature of the normal modes of relaxation themselves, viz. the p_j, λ_j of footnote 1, and are clearly irrelevant if the memory effects are ignorable.

The only way in which the initial distribution and the detailed forms of the relaxation processes can enter is if we consider times $t \sim \gamma_1^{-1}, \gamma_2^{-1}, \ldots$ etc.

[3]We note, however, that there has yet to be a modelling of a real chemical activation process using the inefficient-strong-collision formalism, to see whether the shape of the turn-up is reproduced as well by this method as it is by others, or not.

Can. J. Chem. Downloaded from www.nrcresearchpress.com by 210.87.254.6 on 09/06/12
For personal use only.

course on the theory of unimolecular reactions, Bunker (2) discussed two possible (assumedly complementary) reasons for such a failure; the breakdown of the strong-collision assumption, or the breakdown of the randomisation hypothesis. We have already ruled out, in the arguments just presented, the transition probability model as the cause of the failure, and we will now assert that it is due, in fact, to an inability to achieve full randomisation of the internal energy in these small molecules.

Existing discussions of the problem of internal energy randomisation in thermal unimolecular reactions range over a wide spectrum, from those which partition the molecule into two oscillator pools with an appropriate time delay for transfer of energy between them, all the way to those which try to account for the multiplicity of the quantum states within the system and recognise detailed mechanisms for interchange between the states (1, 19–28). From this range, the treatments of Gelbart, Rice, and Freed (23), Wilson (26), and Nordholm (27) have the most in common with the present approach. Both Wilson and Nordholm wrote down a total master equation which may be represented as follows

$$[1] \qquad d\boldsymbol{\eta}(t)/dt = (\mathscr{A} + \mathscr{V} - \mathbf{D})\boldsymbol{\eta}(t)$$

where $\boldsymbol{\eta}(t)$ is a vector having $\eta_i(t)$ as the fractional population of the quantum state i at time t. $\mathscr{A}$ is a matrix which contains the collisional activation and deactivation rate constants, $\mathscr{V}$ is a matrix constructed from the rate constants for the randomisation processes, and $\mathbf{D}$ is a (diagonal) matrix containing elements d_i, ... which are the specific rate constants for decay of states, i, ... to products. The matrix $\mathscr{A}$ has dimensions equal to the number of states considered to be important in the molecule, but $\mathscr{V}$ is a band matrix of rather limited bandwidth, coupling only states whose energies are rather close together. Nordholm showed (27) that we can only consider the collisional activation–deactivation processes and the randomisation processes independently of each other if the matrix $\mathscr{A}$ commutes with the matrix $(\mathscr{V} - \mathbf{D})$; this is an impossibly stringent condition, but Nordholm goes on to discuss the conditions under which it is plausible to make this separation. Along rather similar lines, Pritchard (28) assumed a specific form for the matrix $(\mathscr{V} - \mathbf{D})$, and accepting separability on the reasonable grounds that the time constant for the relaxation described by $\mathscr{V}$ was always orders of magnitude faster than that of the relaxation described by $\mathscr{A}$, went on to perform a practical calculation on the methyl isocyanide reaction.

In what follows, we do not have to make the assumption of separability. Instead, we choose a form for the matrix elements in eq. [1] which leads to an analytic solution for the unimolecular rate: this form of eq. [1] is very similar to that proposed in ref. 28, but not quite equivalent; however, the arguments upon which the choice of the elements of $\mathscr{V}$ and $\mathbf{D}$ was made remain essentially unchanged.

An Exactly Solvable Model for Unimolecular Reaction with Internal Randomisation Processes

We index the individual rotation–vibration states of the molecule in order of increasing energy, with $\tilde{n}_i$ being the equilibrium population of state i, and with the $\tilde{n}_i$ normalised so that $\sum_i \tilde{n}_i = 1$. We then subdivide this energy-level spectrum into "grains", designated by the index r. It is assumed that all the states within one grain are capable of being transformed into each other by the randomising mechanism (whatever that may be) with a rate constant μ_r; according to our previous arguments (28), μ_r will probably have both first-order and second-order components, i.e.

$$[2] \qquad \mu_r = \mu_1 + \mu_2 p$$

where p is the pressure, and μ_r can vary from grain to grain. The equilibrium population in each grain is designated by

$$\beta_r = \sum_i \tilde{n}_{i,r}$$

For the matrix $\mathscr{A}$, describing the collisional relaxation among the various states of the molecule, we choose as before the scaled strong-collision form

$$[3a] \qquad a_{ij} = \mu\{(1 - \delta_{ij})\tilde{n}_i - \delta_{ij}(1 - \tilde{n}_i)\}$$

where μ is the collisional relaxation rate constant in s^{-1} (μ is implicitly proportional to the pressure, p). In view of the arguments presented in the preceding paragraphs, there can now no longer be any doubts about the validity of using this form to describe all thermal unimolecular reactions in the long-time regime.

For the matrix $\mathscr{V}$, describing the randomisation processes, we assume that it can be broken down into small components $\mathscr{V}_r$, each describing the relaxation only within the grain r. We will assume likewise that the elements of $\mathscr{V}_r$ are given by

$$[3b] \qquad v_{ij,r} = \mu_r\{(1 - \delta_{ij})\tilde{n}_{i,r}/\beta_r - \delta_{ij}(1 - \tilde{n}_{i,r}/\beta_r)\}$$

where μ_r is the randomisation rate constant, again in s^{-1}; μ_r is generally expected to be very much greater than μ. For the first-order randomisation processes, the use of [3b] is equivalent to the assumption of exponential decay within the grain, which is reasonably acceptable within the framework of con-

temporary discussions of radiationless transitions; for the second-order randomisation processes, we have already given arguments (28) for representing them by [3*b*]. The total $\mathscr{V}$ matrix, which is the sum of the individual $\mathscr{V}_r$ components, is therefore block-diagonal, and as such it excludes the possibility of transfer of population *between* grains by the randomisation processes; in view of the infinitesimal breadth of the grains when compared with the dimensions of the whole matrix, we regard this as a relatively minor flaw in the model, and one whose effects can be delineated by numerical calculation using different grain sizes.

The matrix **D** is a diagonal matrix of rate constants for decay to products, and following the concept of Polanyi and Wigner (29) as we have reinterpreted it (28, 30), the elements of **D** are either zero or

[4*a*] $d = 2cv \quad s^{-1}$

where c is the velocity of light and v is the vibration frequency in wavenumber units of that vibration which, if sufficiently excited, leads to the products in question. Remembering that the specific rate constant $k(E)$ can be deduced with good accuracy as the inverse Laplace transform of the infinite-pressure rate law (7, 31), we have that for each grain

[4*b*] $k_r(E) = dg_{r1}/g_r \simeq d\beta_{r1}/\beta_r = 2cv\beta_{r1}/\beta_r$

where β_{r1} is the sum of the equilibrium populations of the *reactive* states within the grain (28, 30), i.e. those for which d is non-zero. Thus, despite the puzzles that still exist in using the Polanyi–Wigner concept to make *a priori* estimates of $k(E)$, we know that given $k(E)$ from experiment, choice of the frequency v for the local mode which leads to reaction tells us the fraction of the states g_{r1}/g_r at any energy E having more than the required number of quanta for reaction to occur.

Having defined all the elements of the total matrix $(\mathscr{A} + \mathscr{V} - \mathbf{D})$, it can be symmetrised as before (18, 32) to give an equivalent matrix $(\mathbf{A} + \mathbf{V} + \mathbf{D})$. It is then a straightforward matter to derive an exact solution for the rate constant (i.e. the smallest eigenvalue) by using the results already derived in our earlier paper on the strong-collision problem (18).

Spectral Structure of (V + D)

Let $\mathbf{I}_r$ be the projection on the subspace corresponding to the rth grain, and let

$$\rho_{r0} = I_r S_0 (I_r S_0, \quad)/(S_0, I_r S_0)$$

where S_0 is the vector whose elements are $\tilde{n}_i^{1/2}$ (9, 18, 32) and the notation (,) represents the scalar product of two vectors. By definition,

$$\mathbf{V} = \sum_{r=1}^{M} \mathbf{V}_r$$

where

$$\mathbf{V}_r = \mu_r(I_r - \rho_{r0}) = \mathbf{V}I_r = I_r\mathbf{V}$$

and M is the number of grains. Since **D** is a diagonal matrix, we also have that

$$\mathbf{D} = \sum_{r=1}^{M} \mathbf{D}_r$$

where

$$\mathbf{D}_r = \mathbf{D}I_r = I_r\mathbf{D};$$

hence

$$(\mathbf{V} + \mathbf{D}) = \sum_{r=1}^{M} (\mathbf{V}_r + \mathbf{D}_r)$$

such that for each r, $(\mathbf{V}_r + \mathbf{D}_r)$ commutes with I_r. It is now clear that the set of eigenvalues of $(\mathbf{V} + \mathbf{D})$ is the collection, for all r, of the eigenvalues of $(\mathbf{V}_r + \mathbf{D}_r)$, with corresponding eigenprojections satisfying

$$\bar{\rho}_{rj} = I_r\bar{\rho}_{rj} = \bar{\rho}_{rj}I_r$$

Can. J. Chem. Downloaded from www.nrcresearchpress.com by 210.87.254.6 on 09/06/12
For personal use only.

Can. J. Chem. Downloaded from www.nrcresearchpress.com by 210.87.254.6 on 09/06/12
For personal use only.

The required results on the spectral structure of $(\mathbf{V}_r + \mathbf{D}_r)$, which we have derived previously (18), are now collected here.

Let I_r^0 be the projection defined by $I_r^0\mathbf{D}_r = 0$. Since $\mathbf{D}_r$ is a diagonal matrix with only one numerical value d for the non-zero elements, and since $\mathbf{V}_r = \mu_r(I_r - \rho_{r0})$, $(\mathbf{V}_r + \mathbf{D}_r)$ has four eigenvalues with corresponding eigenspaces within the range of I_r as follows:

$$\kappa_{r0} < \kappa_{r2} = \mu_r < \kappa_{r1} < \kappa_{r3} = \mu_r + d$$

The multiplicities of κ_{r2}, κ_{r3} are $[\dim(I_r^0) - 1]$, $[\dim(I_r - I_r^0) - 1]$ respectively, where dim( ) denotes the dimension (of the range). The simple eigenvalues (18) κ_{r0}, κ_{r1} are the solutions of

$$[5] \qquad \mu_r(\boldsymbol{S}_0, [\mu_r - \kappa + \mathbf{D}_r]^{-1} I_r \boldsymbol{S}_0) = (\boldsymbol{S}_0, I_r \boldsymbol{S}_0)$$

and are easily seen to be

$$[6] \qquad \kappa_{r0,1} = \frac{\mu_r + d}{2} \mp \left[\frac{(\mu_r + d)^2}{4} - \frac{\mu_r d \beta_{r1}}{\beta_r}\right]^{1/2}$$

where

$$\beta_{r1} = (\boldsymbol{S}_0, [I_r - I_r^0]\boldsymbol{S}_0)$$

and

$$\beta_r = (\boldsymbol{S}_0, I_r \boldsymbol{S}_0)$$

Thus, all the eigenvalues of $(\mathbf{V}_r + \mathbf{D}_r)$ are known exactly. The eigenspaces corresponding to κ_{rj} $(j = 0, 1)$ are spanned by $[\mu_r - \kappa_{rj} + \mathbf{D}_r]^{-1} I_r \boldsymbol{S}_0$ and thus

$$[7] \qquad (\boldsymbol{S}_0, \bar{\rho}_{rj}\boldsymbol{S}_0) = \frac{(\boldsymbol{S}_0, [\mu_r - \kappa_{rj} + \mathbf{D}_r]^{-1} I_r \boldsymbol{S}_0)^2}{(\boldsymbol{S}_0, [\mu_r - \kappa_{rj} + \mathbf{D}_r]^{-2} I_r \boldsymbol{S}_0)} = \frac{(\boldsymbol{S}_0, I_r \boldsymbol{S}_0)^2}{\mu_r^2 (\boldsymbol{S}_0, [\mu_r - \kappa_{rj} + \mathbf{D}_r]^{-2} I_r \boldsymbol{S}_0)}$$

from [5]. The eigenprojections corresponding to κ_{r2}, κ_{r3} are uniquely determined by

$$\bar{\rho}_{r2} = I_r^0 \bar{\rho}_{r2} = \bar{\rho}_{r2} I_r^0; \qquad \bar{\rho}_{r2} I_r^0 \boldsymbol{S}_0 = 0$$
$$\bar{\rho}_{r3} = (I_r - I_r^0)\bar{\rho}_{r3} = \bar{\rho}_{r3}(I_r - I_r^0); \qquad \bar{\rho}_{r3}(I_r - I_r^0)\boldsymbol{S}_0 = 0$$

Consequently,

$$\bar{\rho}_{rj}\boldsymbol{S}_0 = 0, \quad j = 2, 3$$

Exact Solution for the Rate Constant γ_0

Let ρ_0 be the eigenprojection corresponding to the smallest eigenvalue γ_0 of $[\mu(1 - p_0) + \mathbf{V} + \mathbf{D}]$, where p_0 is defined as usual (18) to be $\boldsymbol{S}_0(\boldsymbol{S}_0,)$. Since $\mathbf{D}_r = 0$ for at least one r (i.e. for each of the unreactive grains below threshold) and $(\mathbf{V} + \mathbf{D}) \geq 0$, the smallest eigenvalue of $(\mathbf{V} + \mathbf{D})$ is zero. Further, since $\mu p_0 \geq 0$, $\gamma_0 \leq \mu$.

Consider

$$\bar{\phi}(x) = \mu(\boldsymbol{S}_0, [\mu + \mathbf{V} + \mathbf{D} - x]^{-1}\boldsymbol{S}_0)$$

for x in $(-\infty, \mu)$. We have

$$\lim_{x \to -\infty} \bar{\phi}(x) = 0, \qquad \lim_{x \uparrow \mu} \bar{\phi}(x) = \infty, \qquad \text{and} \quad \frac{d\bar{\phi}(x)}{dx} \geq 0.$$

In fact, $d\bar{\phi}(x)/dx > 0$ for x in $(-\infty, \mu)$, for the equality implies that $[\mu + \mathbf{V} + \mathbf{D} - x]^{-1}\boldsymbol{S}_0 = 0$ and hence $\boldsymbol{S}_0 = 0$. Thus, $\bar{\phi}(x_0) = 1$ has a unique solution $x_0 < \mu$. It is easy to see that

$$\psi_0 = \mu[\mu + \mathbf{V} + \mathbf{D} - x_0]^{-1}\boldsymbol{S}_0$$

solves the eigenvalue equation

$$[8] \qquad [\mu + \mathbf{V} + \mathbf{D} - x_0]\psi_0 = \mu \boldsymbol{S}_0 = \mu p_0 \psi_0$$

and hence x_0 is an eigenvalue of $[\mu(1 - p_0) + \mathbf{V} + \mathbf{D}]$. It is also the smallest eigenvalue, for if $\gamma_0 < x_0$, then it is easy to see that $\bar{\phi}(\gamma_0) = 1, \gamma_0 < \mu$ and x_0 has been established to be the unique solution of $\bar{\phi}(x) = 1$ in $(-\infty, \mu)$. Since $\gamma_0 < \mu$, $[\mu + \mathbf{V} + \mathbf{D} - \gamma_0]$ is invertible. From [8], it follows that the range of ρ_0 is spanned by ψ_0 and hence γ_0 is a simple eigenvalue; also, from [8], we have that

$$[9] \quad \gamma_0 = (\boldsymbol{S}_0, [\mathbf{V} + \mathbf{D}]\psi_0) = \mu(\boldsymbol{S}_0, [\mu + \mathbf{V} + \mathbf{D} - \gamma_0]^{-1}[\mathbf{V} + \mathbf{D}]\boldsymbol{S}_0)$$
$$= \mu \sum_{\substack{r=1 \\ \mathbf{D}_r \neq 0}}^{M} \sum_{j=0}^{1} \frac{\kappa_{rj}}{\mu - \gamma_0 + \kappa_{rj}} \|\bar{\rho}_{rj}\boldsymbol{S}_0\|^2 = \phi(\gamma_0)$$

i.e. γ_0 is a fixed point of $\phi(x)$; in [9], $\| \ . \ \|$ denotes the norm and is given by [7] i.e. $\|\bar{\rho}_{rj}\boldsymbol{S}_0\|^2 = (\boldsymbol{S}_0, \bar{\rho}_{rj}\boldsymbol{S}_0)$. As before (9), if $\gamma_0 < \mu$, then it is easy to conclude that γ_0 is uniquely defined by [9]; also, it follows (9) that γ_0 is the unique fixed point of $\chi(x)$ in $(-\infty, \mu)$ where

$$[10] \quad \chi(x) = ([\mathbf{V} + \mathbf{D}]^{1/2}\boldsymbol{S}_0, [1 + (\mu - x)^{-1}(\mathbf{V} + \mathbf{D})^{1/2}(1 - p_0)(\mathbf{V} + \mathbf{D})^{1/2}]^{-1}[\mathbf{V} + \mathbf{D}]^{1/2}\boldsymbol{S}_0)$$
$$= \frac{\|J(x)\boldsymbol{S}_0\|^2}{1 - (\mu - x)^{-1}\|J(x)\boldsymbol{S}_0\|^2}$$

and

$$J(x) = [1 + (\mu - x)^{-1}(\mathbf{V} + \mathbf{D})]^{-1/2}[\mathbf{V} + \mathbf{D}]^{1/2}$$

i.e.

$$[11] \quad \|J(x)\boldsymbol{S}_0\|^2 = \sum_{\substack{r=1 \\ \mathbf{D}_r \neq 0}}^{M} \sum_{j=0}^{1} \frac{\kappa_{rj}}{1 + (\mu - x)^{-1}\kappa_{rj}} \|\bar{\rho}_{rj}\boldsymbol{S}_0\|^2$$

The convergence properties of the iterative sequences generated by $\phi(x)$ and $\chi(x)$ have already been given in detail before (9, 18).

Limiting Behaviour of γ_0 with μ and with μ_r

According to the conjecture which led to this formulation of the unimolecular reaction process, we should recover the usual strong-collision behaviour in the limit of $\mu_r \to \infty$, and as a corollary, the limiting weak-collision behaviour as $\mu_r \to 0$. Therefore, we now examine the four limits $\mu, \mu_r \to 0, \infty$.

$$\text{(i)} \quad \lim_{\mu \to \infty} \gamma_0 = (\boldsymbol{S}_0, \mathbf{D}\boldsymbol{S}_0) = d \sum_{\substack{r=1 \\ \mathbf{D}_r \neq 0}}^{M} (\boldsymbol{S}_0, [I_r - I_r^0]\boldsymbol{S}_0) = d \sum_{\substack{r=1 \\ \mathbf{D}_r \neq 0}}^{M} \beta_{r1}$$

Since (9)

$$\chi(0) \geq \gamma_0 > 0$$

and

$$\lim_{\mu \to \infty} \chi(0) = (\boldsymbol{S}_0, [\mathbf{V} + \mathbf{D}]\boldsymbol{S}_0) = (\boldsymbol{S}_0, \mathbf{D}\boldsymbol{S}_0),$$

γ_0 remains finite in the limit of $\mu \to \infty$; the result now follows from [10]. Remembering that

$$k_\infty = \sum_{\substack{r=1 \\ k_r(E) \neq 0}}^{M} k_r(E)\beta_r,$$

substitution for $k_r(E)$ from [4*b*] shows that this limit is the usual high-pressure limit.

$$\text{(ii)} \quad \lim_{\mu \to 0} (\gamma_0/\mu) = 1 - \sum_{\substack{r=1 \\ \mathbf{D}_r = 0}}^{M} (\boldsymbol{S}_0, I_r\boldsymbol{S}_0) = 1 - \sum_{\substack{r=1 \\ \mathbf{D}_r = 0}}^{M} \beta_r = \sum_{\substack{r=1 \\ \mathbf{D}_r \neq 0}}^{M} \beta_r$$

From [9] we have

Can. J. Chem. Downloaded from www.nrcresearchpress.com by 210.87.254.6 on 09/06/12
For personal use only.

$$\gamma_0/\mu = (\boldsymbol{S}_0, [\mu - \gamma_0 + \mathbf{V} + \mathbf{D}]^{-1}[\mathbf{V} + \mathbf{D}]\boldsymbol{S}_0)$$

and since $0 < \gamma_0 < \mu$

$$\lim_{\mu\to 0}(\gamma_0/\mu) = \lim_{\varepsilon\downarrow 0}(\boldsymbol{S}_0, [\varepsilon + \mathbf{V} + \mathbf{D}]^{-1}[\mathbf{V} + \mathbf{D}]\boldsymbol{S}_0) = \lim_{\varepsilon\downarrow 0}\sum_{r=1}^{M}\sum_{k=0}^{3}\frac{\kappa_{rk}}{\varepsilon + \kappa_{rk}}(\boldsymbol{S}_0, \bar{\rho}_{rk}\boldsymbol{S}_0)$$

$$= \sum_{\substack{r=1\\ \mathbf{D}_r\neq 0}}^{M}\sum_{k=0}^{3}(\boldsymbol{S}_0, \bar{\rho}_{rk}\boldsymbol{S}_0) = \sum_{\substack{r=1\\ \mathbf{D}_r\neq 0}}^{M}(\boldsymbol{S}_0, I_r\boldsymbol{S}_0)$$

Thus, provided that μ_r is finite, this is the same low-pressure limit as we proved for the strong-collision case previously (18).

(iii) $$\gamma_0^{\infty} = \lim_{\mu_r\to\infty}\gamma_0 = \mu d\sum_{\substack{r=1\\ \mathbf{D}_r\neq 0}}^{M}\frac{\beta_{r1}}{\mu - \gamma_0^{\infty} + d\beta_{r1}/\beta_r}$$

We have the following limits:

$$\lim_{\substack{\mu_r\to\infty\\ \mathbf{D}_r\neq 0}}\kappa_{r0};\ \|\bar{\rho}_{r0}\boldsymbol{S}_0\|^2;\ \|\bar{\rho}_{r1}\boldsymbol{S}_0\|^2;\ \kappa_{r1} = \frac{d\beta_{r1}}{\beta_r};\ \beta_r;\ 0;\ \infty \text{ respectively.}$$

Thus, since $\gamma_0 < \mu$, the result follows from [7], [10], and [11]. With the appropriate transcription of symbols, viz. $d_k \equiv d\beta_{k1}/\beta_k$ and $\bar{n}^k \equiv \beta_k$, this is the same expression as the standard strong-collision result, i.e. eq. [11] of ref. 18, or the analogous eq. [20] of ref. 6.

(iv) $$\lim_{\mu_r\to 0}\gamma_0 = \frac{\mu + d}{2} - \left[\left(\frac{\mu + d}{2}\right)^2 - \mu d\sum_{\substack{r=1\\ \mathbf{D}r\neq 0}}^{M}\beta_{r1}\right]^{1/2}$$

Since

$$\lim_{\substack{\mu_r\to 0\\ \mathbf{D}_r\neq 0}}\kappa_{r0};\ \kappa_{r1};\ \|\bar{\rho}_{r1}\boldsymbol{S}_0\|^2 = 0;\ d;\ \beta_{r1} \text{ respectively,}$$

we have that

$$\lim_{\mu_r\to 0}\|J(x)\boldsymbol{S}_0\|^2 = \frac{d}{1 + (\mu - x)^{-1}d\sum_{\substack{r=1\\ \mathbf{D}_r\neq 0}}^{M}\beta_{r1}} = \|J_0(x)\boldsymbol{S}_0\|^2$$

Now solving

$$x_0 = \frac{\|J_0(x_0)\boldsymbol{S}_0\|^2}{1 - (\mu - x_0)^{-1}\|J_0(x_0)\boldsymbol{S}_0\|^2}$$

and observing that $x_0 = \lim_{\mu_r\to 0}\gamma_0$ yields the desired result.

Note that this final limiting form is the *exact* solution for the case of a unimolecular reaction when $k(E)$ is constant — the particular case for which we have already deduced that an *approximate* solution, γ_{ap}, is strict Lindemann in form (9). Thus, all four limits behave in a perfectly acceptable fashion: when μ_r is finite, the limits for $\mu \to 0, \infty$ are the usual ones we have already established (18); when $\mu_r = 0$, the fall-off is very close to being strict Lindemann, and when $\mu_r = \infty$, we recover the standard strong-collision result.

Practical Calculations

The exact solution for the rate constant given either in [9] or in [10] and [11] is in an iterative form: a trial value of $x = x_0 < \mu$ is substituted in each denominator to give the first approximation to γ_0, viz. $\phi(x)$ or $\chi(x)$, and this new value is resubstituted until convergence is achieved; with this initial choice, the $\phi(x)$ series will converge from below, whereas the $\chi(x)$ series will converge in an alternating fashion (9, 18). However, for thermal reactions at ordinary temperatures where $\mu \gg \gamma_0$, an extremely good approximation

Can. J. Chem. Downloaded from www.nrcresearchpress.com by 210.87.254.6 on 09/06/12
For personal use only.

Can. J. Chem. Downloaded from www.nrcresearchpress.com by 210.87.254.6 on 09/06/12
For personal use only.

to γ_0 (which we have previously called γ_{ap}) is obtained without iteration simply by substituting $x = 0$ in [10] and [11]. Thus, we can perform a direct calculation for the rate constant at all pressures by evaluating

$$[12] \quad \gamma_{ap} = \frac{\|J(0)\boldsymbol{S}_0\|^2}{1 - \mu^{-1}\|J(0)\boldsymbol{S}_0\|^2}$$

where

$$[13] \quad \|J(0)\boldsymbol{S}_0\|^2 = \sum_{\substack{r=1 \\ D_r \neq 0}}^{M} \sum_{j=0}^{1} \frac{\left[\beta_{r0} + \beta_{r1}\left(1 + \frac{d}{\mu_r - \kappa_{rj}}\right)^{-1}\right]^2}{\left[\beta_{r0} + \beta_{r1}\left(1 + \frac{d}{\mu_r - \kappa_{rj}}\right)^{-2}\right]} \frac{\kappa_{rj}}{1 + \mu^{-1}\kappa_{rj}}$$

In [13], κ_{rj} ($j = 0, 1$) are the simple eigenvalues for grain r, given by eq. [6], d is the rate constant for decay of the reactive vibrational states to products, i.e. eq. [4], and β_r, β_{r0}, and β_{r1} are respectively the equilibrium populations of grain r, of the passive states in grain r, and of the reactive states in grain r. In both equations, μ is the rate constant for collisional relaxation at the pressure in question, in units of s^{-1}, and likewise, in [13], μ_r is the randomisation rate constant in grain r in the same units.

There are neater and more elegant ways of writing [13], by using [11] and [7], whereas we have used [11] and [5]. This is because the numerical calculation is susceptible to underflow and overflow difficulties at the extremes of μ, μ_r, and as written in [13], the expressions can easily be rearranged to avoid these problems should they arise (c.f. also Appendix 4 of ref. 7 where a similar procedure is used).

The behaviour of these rate constants is shown in Figs. 1 and 2 for a model simulating the thermal dissociation of carbon dioxide; the details of the model are not important.[4] For simplicity, μ_r was taken to be the same for all grains, although this is not a necessary restriction. In Fig. 1, μ_r is taken to be constant (i.e. a first-order randomisation process), and from top to bottom, the values of μ_r are ∞, 10^{11}, 10^{10}, ... 10^5, 10^4, 0 s^{-1} respectively; with $\mu_r = 10^{12}$ s^{-1}, the calculated fall-off curve is virtually coincident with the strong-collision ($\mu_r = \infty$) curve. In Fig. 2, μ_r is taken to be $\mu_2 p$ (i.e. second-order randomisation) and from top to bottom, the values of μ_2 are ∞, 10^8, 10^7, ... 10^5, 10^4, 0 $Torr^{-1}$ s^{-1} respectively.

The behaviour shown in Fig. 2 is very similar in form to that found by using the separable model

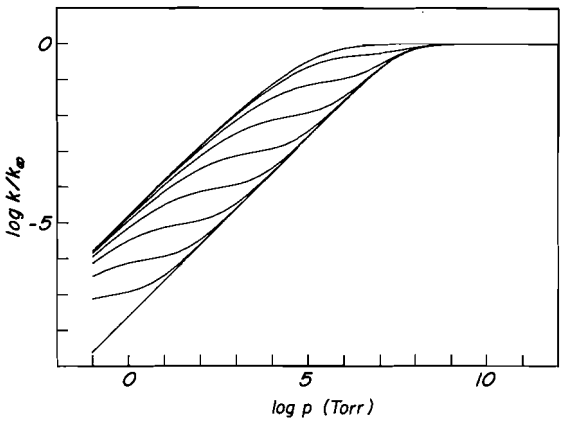

FIG. 1. Fall-off curves for the thermal dissociation of carbon dioxide, model calculation, at 4000 K, considering only first-order randomisation. In descending order, $\mu_1 = \infty$, 10^{11}, 10^{10}, 10^9, 10^8, 10^7, 10^6, 10^5, 10^4, 0 s^{-1} respectively.

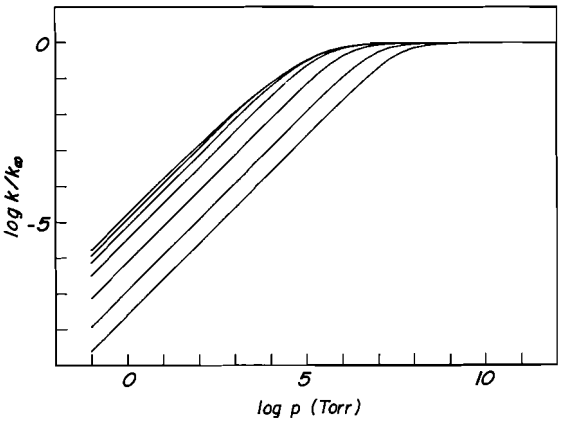

FIG. 2. Fall-off curves for the thermal dissociation of carbon dioxide, model calculation, at 4000 K, considering only second-order randomisation. In descending order, $\mu_2 = \infty$, 10^8, 10^7, 10^6, 10^5, 10^4, 0 $Torr^{-1}$ s^{-1} respectively.

previously (28). However, in the first-order randomisation case (Fig. 1) the high-pressure limits are all the same, unlike the behaviour found for the separable model. This is because the two models are

[4]The energy-level spectrum of the model CO_2 comprises 2.0401×10^{11} states spanning the first 200 kcal; no reactive states occur below 120 kcals. Above threshold, the grains are each taken to be 1 kcal wide, and reactive states each having the value $d = 10^{11}$ s^{-1} (c.f. ref. 30) are distributed in increasing numbers according to the relation $[(E - E_{threshold})/E]^s$, i.e. in RRK form with $s = 4$. The collisional relaxation rate constant μ is taken to be 2.5×10^3 $Torr^{-1}$ s^{-1} and $T = 4000$ K.

Can. J. Chem. Downloaded from www.nrcresearchpress.com by 210.87.254.6 on 09/06/12
For personal use only.

not quite equivalent in the high-pressure limits: the present model admits a relaxation process within each grain with relaxation rate constant μ, which is absent from the separable model;[5] in this respect, the present behaviour is consistent with earlier calculations showing false high-pressure limits (19–25).

Because of this difference between the two models, we have repeated the calculations for the isomerisations of CH_3NC and CD_3NC reported in the earlier paper (28), by using eqs. [12] and [13]. The new rate constants agree with the old ones to better than 4 decimal places over the whole range of pressures, so that our earlier conclusions remain unchanged. This was to be expected because our present analysis shows that the separable method will give the correct solution when $\mu_r \to \infty$, and the intuitive reasoning which led to the separable model depended on the fact that $\mu_r \gg \mu$.

Discussion

We have presented here a complete formulation and solution of the thermal unimolecular reaction problem including explicit consideration of the internal energy randomisation processes. This formulation rests upon our reinterpretation (30) of the Polanyi and Wigner concept (29) — that in the conventional strong-collision case, the $k(E)$ function is simply the fraction of the states of energy E having more than the critical energy in a chosen oscillator divided by half the vibrational period of that oscillator. There still remain, however, some points to be solved before practically useful correlations can be made between $k(E)$ functions and molecular vibrational properties; the majority of these are evident from our earlier discussion (30). Nevertheless, the use of the Polanyi–Wigner concept provides us with the opportunity to describe unimolecular reactions in purely molecular dynamic terms, and therefore seems preferable in the long run to existing procedures (3, 4).

We do not specify for the time being the precise mechanisms by which the internal energy randomisation processes occur but, based on our previous discussion (28), we accept that both first-order and second-order processes may be important. Nor have we yet specified the limits of the range of states which may be coupled by these processes: we have chosen so far to use a grain as the domain, and clearly the final result may be subject to errors in the same way as any numerical integration depends upon the step size; other choices are equally possible — for example the domains could be restricted not only by energy, but by vibrational symmetry type and/or rotational angular momentum as well.[6] Our equations will admit any kind of definition of the domain of the randomising processes and will also allow each individual domain to have its own randomisation rate constant μ_r.

We then argue that if the value of μ_r for any grain r is too small, the rate of decay from that grain will be limited by the randomisation rate, and the $k(E)$ will have a fallen-off value rather than its limiting value according to the Polanyi–Wigner concept. And it is at this juncture that the Polanyi–Wigner concept is crucial, for in its simplest form there is only one type of vibration leading to reaction, whence all the decay rate constants d are the same: this assumption simplifies the eigenvalue spectrum enormously for the grain r, and allows a completely analytic solution for γ_{ap}. The solution remains tractable, however, as we show in the Appendix, if any number of different decay constants occurs in **D**.

We have argued in the opening paragraphs that hitherto, there has been an insufficient distinction between inefficient collisions and weak collisions, and that experiments purporting to measure the effects of weak collisions cannot distinguish between weak collisions and inefficient collisions. We have already mentioned incubation times and "low-pressure turn-up", and should also include in this context the inefficiency of gas–gas collisions relative to gas–wall collisions found in many thermal reactions (33–37); likewise, neither measurement of relative collision efficiencies in the fall-off region (38–40) nor of absolute collision efficiencies, viz. $\bar{\lambda} = \mu/Z[M]$ (7), provides us with any discriminating power. Probably the only symptom of weak-collision effects that can be observed in thermal systems

[5]The original separable model is readily made consistent with the present treatment by redefining $\mu_r = \mu + \mu_1 + \mu_2 p$ instead of simply $\mu_1 + \mu_2 p$ as before. Re-examination of the series of model calculations carried out in ref. 28 reveals only one small difference with the new results, when μ_r is small and p is very high, viz. $\mu_1 = 10^{10}\ s^{-1}$ for $p > 10^3$ Torr.

[6]It may sometimes be possible to deduce information concerning the domains within which randomisation occurs by analysis of energy distribution among the products of a reaction. It is clear that if $\mu_r = \infty$, the internal degrees of freedom of the reaction products will be fully equilibrated. The corollary is not true, however, because the residual interaction between two product fragments as they recede may be sufficient to cause complete randomisation among the product states even though they were not initially formed in that way. It is true, however, that the observation of non-statistical distributions of internal energy in the product states presents clear evidence of the failure to achieve complete randomisation in the reactant molecule before fragmentation occurred. There is an analogous connection between the relaxation rate μ and the translational energy distribution of the fragments: thus, a non-Boltzmann translational distribution shows that μ is insufficiently large for the reaction to be at its high pressure limit, but again, the corollary is not necessarily true.

Can. J. Chem. Downloaded from www.nrcresearchpress.com by 210.87.254.6 on 09/06/12
For personal use only.

lies in the observation of a fall-off curve which is more severe than would be predicted by using strong-collision formulae. There are two possibilities here. One is the case of multi-channel reactions where the fall-off curves for upper channels are more severe than that for the dominant channel (41). However, there are too few reliably documented examples of this behaviour so far (41–43) and it is not yet clear whether such behaviour is adequately described by the formulae given in the Appendix of this paper.[7] Better documented is the almost Lindemann shape of the fall-off in many reactions of very simple molecules (45).[8] It is clear from the results shown in Figs. 1 and 2 that any shape of fall-off curve from the standard strong-collision one to strict Lindemann can be reproduced by appropriate choices for the randomisation rates μ_r; in fact, we can get a monotonic change from strict Lindemann to strong-collision behaviour simply by increasing μ_2 from zero to infinity in the absence of μ_1. Useful values for the two randomisation rate constants can only be deduced by detailed comparison of theoretical and experimental fall-off curves, as we showed before (28). The present calculation is only schematic, but comparison with the experimental fall-off curves for CO_2 (46) suggests that in this case, $\mu_1 < 10^9\ s^{-1}$ and $\mu_2 < 10^8\ Torr^{-1}\ s^{-1}$, *very* approximately.

1. N. B. SLATER. Theory of unimolecular reactions. Methuen, London 1959.
2. D. L. BUNKER. Theory of elementary gas reactions. Pergamon, London. 1966.
3. P. J. ROBINSON and K. A. HOLBROOK. Unimolecular reactions. Wiley-Interscience, London. 1972.
4. W. FORST. Theory of unimolecular reactions. Academic Press, New York. 1973.
5. D. C. TARDY and B. S. RABINOVITCH. Chem Rev. **77**, 369 (1977).
6. S. NORDHOLM. Chem. Phys. **29**, 55 (1978).

[7]An alternative so-called weak-collision treatment of this problem (44) falls into the category where the distinction between weak collisions and inefficient collisions is unclear: this study shows that the shape of the fall-off curve for the upper channel is quite sensitive to the form of the transition rate matrix. However, our conclusions in footnote 2 about the lack of connection between the steady-state distribution and the form of the relaxation matrix probably remain valid, whence randomisation failure is the more likely determinant of the shapes of the fall-off curves in such systems.

[8]Our original conjecture that fall-off curves for small molecules become more Lindemann with increasing temperature (45) because of a bottleneck in the activation process, together with our subsequent analysis (9), could perhaps provide a false clue in the light of the present discussion: we do not need bottleneck effects of this type to cause strict Lindemann behaviour. There are *small* differences in the shapes of Figs. 1 and 2 with varying temperature, but they should be examined using more realistic models before any conclusions are drawn concerning temperature effects.

7. A. W. YAU and H. O. PRITCHARD. Can. J. Chem. **56**, 1389 (1978); erratum, **58**, 626 (1980).
8. H. O. PRITCHARD and A. LAKSHMI. Can. J. Chem. **57**, 2793 (1979).
9. S. R. VATSYA and H. O. PRITCHARD. Proc. R. Soc. London. A**375**, 409 (1981).
10. H. O. PRITCHARD and N. I. LABIB. Can. J. Chem. **54**, 329 (1976).
11. H. O. PRITCHARD, N. I. LABIB, and A. LAKSHMI. Can. J. Chem. **57**, 1115 (1979).
12. A. MOISE and H. O. PRITCHARD. Can. J. Chem. **59**, 1277 (1981).
13. M. QUACK and J. TROE. Specialist Periodical Reports: Gas kinetics and energy transfer, **2**, 175 (1977).
14. H. O. PRITCHARD. Specialist Periodical Reports: Gas kinetics, **1**, 243 (1975).
15. A. W. YAU and H. O. PRITCHARD. Can. J. Chem. **57**, 1723 (1979).
16. W. FORST and A. P. PENNER. J. Chem. Phys. **72**, 1435 (1980).
17. J. E. DOVE, W. S. NIP, and H. TEITELBAUM. Fifteenth Symposium (International) on Combustion, Pittsburgh, PA. 1974. p. 903.
18. S. R. VATSYA and H. O. PRITCHARD. Can. J. Chem. **59**, 772 (1981).
19. O. K. RICE. Z. Phys. Chem. B, **7**, 226 (1930).
20. E. K. GILL and K. J. LAIDLER. Proc. R. Soc. London, A**250**, 121 (1959).
21. M. ŠOLC. Mol. Phys. **11**, 579 (1966); **12**, 101 (1967); Chem. Phys. Lett. **1**, 160 (1967).
22. N. B. SLATER. Mol. Phys. **12**, 107 (1967).
23. W. M. GELBART, S. A. RICE, and K. F. FREED. J. Chem. Phys. **52**, 5718 (1970).
24. D. L. BUNKER and W. L. HASE. J. Chem. Phys. **59**, 4621 (1973).
25. E. THIELE, M. F. GOODMAN, and J. STONE. Chem. Phys. Lett. **69**, 18 (1980).
26. D. J. WILSON. J. Phys. Chem. **64**, 323 (1960).
27. S. NORDHOLM. Chem. Phys. **15**, 59 (1976).
28. H. O. PRITCHARD. Can. J. Chem. **58**, 2236 (1980).
29. M. POLANYI and E. WIGNER. Z. Phys. Chem. **139**, 439 (1928).
30. H. O. PRITCHARD, G. M. DIKER, and A. W. YAU. Can. J. Chem. **58**, 1516 (1980).
31. A. W. YAU and H. O. PRITCHARD. Can. J. Chem. **57**, 2458 (1979).
32. S. R. SINGH and H. O. PRITCHARD. Chem. Phys. Lett. **73**, 191 (1980).
33. A. D. KENNEDY and H. O. PRITCHARD. J. Phys. Chem. **67**, 161 (1963).
34. P. C. BEADLE, D. M. GOLDEN, K. D. KING, and S. W. BENSON. J. Am. Chem. Soc. **94**, 2943 (1972).
35. D. M. GOLDEN, G. N. SPOKES, and S. W. BENSON. Angew. Chem. **12**, 534 (1973).
36. R. G. GILBERT and K. D. KING. Chem. Phys. **49**, 367 (1980).
37. B. D. BARTON, D. F. KELLEY, and B. S. RABINOVITCH. J. Phys. Chem. **84**, 1299 (1980).
38. H. O. PRITCHARD, R. G. SOWDEN, and A. F. TROTMAN-DICKENSON. Proc. R. Soc. London A**217**, 563 (1953).
39. S. C. CHAN, B. S. RABINOVITCH, J. T. BRYANT, L. D. SPICER, T. FUJIMOTO, Y. N. LIN, and S. P. PAVLOU. J. Phys. Chem. **74**, 3160 (1970).
40. H. O. PRITCHARD. Chem. Phys. Lett. **78**, 618 (1981).
41. M. H. B. VAYJOOEE, A. W. YAU, and H. O. PRITCHARD. Can. J. Chem. **55**, 1595 (1977).

42. M. C. FLOWERS. Can. J. Chem. **56**, 29 (1978).
43. K. D. KING, B. J. GAYNOR, and R. G. GILBERT. Int. J. Chem. Kinet. **11**, 11 (1979).
44. TH. JUST and J. TROE. J. Phys. Chem. **84**, 3068 (1980).
45. A. W. YAU and H. O. PRITCHARD. Chem. Phys. Lett. **60**, 140 (1978).
46. H. GG. WAGNER and F. ZABEL. Ber. Bunsenges. Phys. Chem. **78**, 705 (1974).

Appendix: Reaction by Two or More Pathways

Suppose that the molecule breaks up in two distinct ways by accumulating energy in either one or other of two types of vibration with decay constants d^1 and d^2 respectively. Suppose also that within any one grain, provided that the energy is above *both* thresholds, both manifolds of decaying states are coupled to the remaining unreactive states with the same randomisation rate constant μ_r. As before (18), we have

$$[A1] \quad \gamma_0 = \lim_{t\to\infty} \frac{1}{N(t)} \frac{dN(t)}{dt}$$

where

$$[A2] \quad N(t) = \sum_{i=0}^{n-1} \eta_i(t) \sim \exp(-\gamma_0 t)(\boldsymbol{S}_0, \boldsymbol{\Psi}_0)(\boldsymbol{\Psi}_0, \mathbf{E}^{-1/2}\boldsymbol{\eta}(0))$$

and

$$[A3] \quad \frac{dN(t)}{dt} = -\sum_{i=0}^{n-1} d_i\eta_i(t) \sim \exp(-\gamma_0 t)(\boldsymbol{S}_0, \mathbf{D}\boldsymbol{\Psi}_0)(\boldsymbol{\Psi}_0, \mathbf{E}^{-1/2}\boldsymbol{\eta}(0))$$

In these equations, $N(t)$ is the total population of molecules remaining at time t, $\eta_i(t)$ is the population remaining in the ith state, $\boldsymbol{\eta}(0)$ is the initial distribution at time $t = 0$, and $\mathbf{E}^{-1/2}$ arises from the original symmetrising transformation (18, 32). Thus

$$[A4] \quad \gamma_0 = (\boldsymbol{S}_0, \mathbf{D}\boldsymbol{\Psi}_0)/(\boldsymbol{S}_0, \boldsymbol{\Psi}_0) = (\boldsymbol{S}_0, [\mathbf{V} + \mathbf{D}]\boldsymbol{\Psi}_0)/(\boldsymbol{S}_0, \boldsymbol{\Psi}_0)$$

as expected. Now

$$\mathbf{D} = \sum_{r=1}^{M} \mathbf{D}_r$$

where $\mathbf{D}_r$ can have two non-zero elements d^1, d^2. The required decomposition is $\gamma_0 = \gamma_0{}^1 + \gamma_0{}^2$ where

$$[A5] \quad \gamma_0{}^{1,2} = \lim_{t\to\infty} \sum_{i=0}^{n-1} d_i{}^{1,2}\eta_i(t) \Big/ \sum_{i=0}^{n-1} \eta_i(t) = (\boldsymbol{S}_0, \mathbf{D}^{1,2}\boldsymbol{\Psi}_0)/(\boldsymbol{S}_0, \boldsymbol{\Psi}_0)$$

$$= \mu(\boldsymbol{S}_0, \mathbf{D}^{1,2}[\mu - \gamma_0 + \mathbf{V} + \mathbf{D}]^{-1}\boldsymbol{S}_0)$$

and

$$\mathbf{D}^{1,2} = \sum_{r=1}^{M} \mathbf{D}_r{}^{1,2}$$

with $\mathbf{D}_r{}^{1,2}$ being a diagonal matrix with only one non-zero element $d^{1,2}$ exactly where it appears in $\mathbf{D}$ while the other elements are zero.

$\mathbf{D}$ now has three distinct elements along the diagonal: 0, d^1, d^2 and hence

$$(\mathbf{V}_r + \mathbf{D}_r) = (\mathbf{V}_r + \mathbf{D}_r{}^1 + \mathbf{D}_r{}^2)$$

has *six* distinct eigenvalues:

$$\kappa_{r0} < \mu_r = \kappa_{r3} < \kappa_{r1} < \mu_r + d^1 = \kappa_{r4} < \kappa_{r2} < \kappa_{r5} = \mu_r + d^2$$

assuming that $d^1 < d^2$. Since $\bar{\rho}_{rj}\boldsymbol{S}_0 = 0$ for $j = 3, 4, 5$, we have

$$[A6] \quad \gamma_0{}^{1,2} = \mu \sum_{\substack{r=1 \\ \mathbf{D}_r \neq 0}}^{M} \sum_{j=0}^{2} \frac{1}{\mu - \gamma_0 + \kappa_{rj}} (\mathbf{D}^{1,2}\boldsymbol{S}_0, \bar{\rho}_{rj}\boldsymbol{S}_0) = \phi^{1,2}(\gamma_0)$$

Can. J. Chem. Downloaded from www.nrcresearchpress.com by 210.87.254.6 on 09/06/12
For personal use only.

where $\kappa_{rj}, j = 0, 1, 2$ are the solutions of eq. [5] which is now a polynomial of degree three, and

$$[A7] \quad (\mathbf{D}^{1,2}\boldsymbol{S}_0, \bar{\rho}_{rj}\boldsymbol{S}_0) = \frac{(\mathbf{D}^{1,2}\boldsymbol{S}_0, \boldsymbol{I}_r\boldsymbol{S}_0)^2}{\mu_r{}^2(\boldsymbol{S}_0, [\mu_r - \kappa_{rj} + \mathbf{D}_r]^{-2}\boldsymbol{I}_r\boldsymbol{S}_0)}$$

An alternative expression for $\gamma_0{}^{1,2}$ may be obtained by realising that

$$\boldsymbol{\Psi}_0 = \frac{[1 + (\mu - \gamma_0)^{-1}(\mathbf{V} + \mathbf{D})]^{-1}\boldsymbol{S}_0}{1 - (\mu - \gamma_0)^{-1}\|J(\gamma_0)\boldsymbol{S}_0\|^2}$$

Hence

$$[A8] \quad \gamma_0{}^{1,2} = (\mathbf{D}^{1,2}\boldsymbol{S}_0, [1 + (\mu - \gamma_0)^{-1}(\mathbf{V} + \mathbf{D})]^{-1}\boldsymbol{S}_0)/(\boldsymbol{S}_0, [1 + (\mu - \gamma_0)^{-1}(\mathbf{V} + \mathbf{D})]^{-1}\boldsymbol{S}_0)$$

$$= \sum_{\substack{r=1 \\ \mathbf{D}_r \neq 0}}^{M} \sum_{j=0}^{2} \frac{(\mathbf{D}^{1,2}\boldsymbol{S}_0, \bar{\rho}_{rj}\boldsymbol{S}_0)}{1 + (\mu - \gamma_0)^{-1}\kappa_{rj}} \Bigg/ \sum_{\substack{r=1 \\ \mathbf{D}_r \neq 0}}^{M} \sum_{j=0}^{2} \frac{(\boldsymbol{S}_0, \bar{\rho}_{rj}\boldsymbol{S}_0)}{1 + (\mu - \gamma_0)^{-1}\kappa_{rj}} = \chi^{1,2}(\gamma_0)$$

Extension to more pathways is now straightforward, although it will become necessary to solve eq. [5] numerically for the κ_{rj} if there are too many distinct values of d in $\mathbf{D}_r$.

Can. J. Chem. Downloaded from www.nrcresearchpress.com by 210.87.254.6 on 09/06/12
For personal use only.

The effect of methanol on the stability of clathrate hydrates[1]

D. W. DAVIDSON, S. R. GOUGH, AND J. A. RIPMEESTER
Division of Chemistry, National Research Council of Canada, Ottawa, Ont., Canada K1A 0R9
AND
HARUO NAKAYAMA
Department of Chemistry, Faculty of Engineering, Yokohama National University, Tokiwadai, Hodogaya-ku, Yokohama 240, Japan

Received April 6, 1981

D. W. DAVIDSON, S. R. GOUGH, J. A. RIPMEESTER, and HARUO NAKAYAMA. Can. J. Chem. **59**, 2587 (1981).

From the effect of added methanol on the decomposition temperatures of the clathrate hydrates of ethylene oxide and tetrahydrofuran, it was recently reported that methanol can be readily enclathrated in hydrates of both structure I and II. Dielectric and nmr studies of these two hydrates prepared in the presence of methanol do not support this conclusion. It is shown thermodynamically that the original measurements may be interpreted without the need for incorporation of methanol in the hydrates formed.

D. W. DAVIDSON, S. R. GOUGH, J. A. RIPMEESTER et HARUO NAKAYAMA. Can. J. Chem. **59**, 2587 (1981).

A partir de l'effet du méthanol sur les températures de décomposition des hydrates de clathrate d'oxyde d'éthylène, et de tétrahydrofuranne, on a rapporté récemment que le méthanol peut être facilement inséré dans les hydrates de structures I et II. Les études diélectriques et de rmn de ces deux hydrates préparés en présence de méthanol ne confirment pas cette conclusion. On a montré thermodynamiquement que les mesures initiales peuvent être interprètées sans incorporer le méthanol dans les hydrates obtenus.

[Traduit par le journal]

Nakayama and Hashimoto recently reported (1) that methanol has the ability to form both structure I and structure II gas hydrates. Since large quantities of MeOH are used each year to inhibit gas hydrate formation in natural gas distribution systems, this conclusion warrants careful examination.

The evidence for incorporation of MeOH in clathrate hydrates is based on the melting-point behaviour of the hydrates formed in the ethylene oxide (EO) – MeOH – H_2O and tetrahydrofuran (THF)–MeOH–H_2O systems (1). Hydrate decomposition temperatures were plotted against the total mole fraction $x = x_2 + x_3$ of the non-aqueous components, where x_2 is the EO or THF mole fraction and x_3 that of MeOH, for a constant mole ratio $C = x_3/x_2$ (Fig. 1 *b* and *c*). The value of x at the temperature maximum appeared to be independent of C and to correspond to $x_{max} = 1/(n + 1)$, where n is the number of moles of water per mole of EO or THF in the hydrate in the absence of MeOH.[2] Similar (but less unexpected) behaviour was found (1) when known hydrate forming species (1,3-dioxolane, acetone) were added to the THF–H_2O system (e.g., Fig. 1*a*).

We report here the results of nmr and dielectric studies of EO and THF hydrates prepared in the presence of MeOH. These show no sign of enclathration of MeOH. It is demonstrated by simple thermodynamic arguments that lack of dependence of x_{max} on the value of C does not require incorporation of the third component in the hydrate and is in fact predicted for ideal liquid-phase behaviour.

Experimental Methods

Proton nmr spectra were obtained with a Bruker CXP-180 spectrometer for samples prepared from EO, MeOH, and D_2O. Liquid-phase spectra (recorded without spinning) showed peaks arising from OH, CH_3, and C_2H_4O protons, respectively, in the direction of increasing magnetic field (cf. Fig. 2). Results are reported for a sample containing 0.057 and 0.079 mole fraction of EO and MeOH respectively. To provide information about the water content, sufficient H_2O was added to bring the H content of the water (mainly HDO) and the hydroxyl group of methanol to about 16%, complete exchange being assumed. Peaks due to the OH group in methanol and water were not resolved. The sealed sample was cooled to −20°C, allowed to equilibrate, and spectra were recorded at a number of temperatures until the hydrate decomposition temperature (10°C) was reached. The broad line from ice and solid hydrate was unstructured over this temperature range (cf. ref. 2) and the analysis is based on liquid spectra alone. These were recorded under conditions (a sweep width setting of 10 kHz) for which the solid line was not observed.

Dielectric measurements were made on a sample of composition 0.5THF·0.5MeOH·17H_2O at temperatures to as low as 7 K. Instrumentation was as described elsewhere (3), except for the use of a Hewlett-Packard 4275A meter for capacitance and conductance measurements between 10 kHz and 4 MHz. The particular interest was to define the dielectric absorption arising from the encaged species and to measure the methanol-rich eutectic temperature.

[1]NRCC No. 19453.

[2]Because of the flat tops of the melting point curves, x_{max} is not accurately defined.

0008-4042/81/172587-04$01.00/0
©1981 National Research Council of Canada/Conseil national de recherches du Canada

Can. J. Chem. Downloaded from www.nrcresearchpress.com by 210.87.254.5 on 09/06/12
For personal use only.

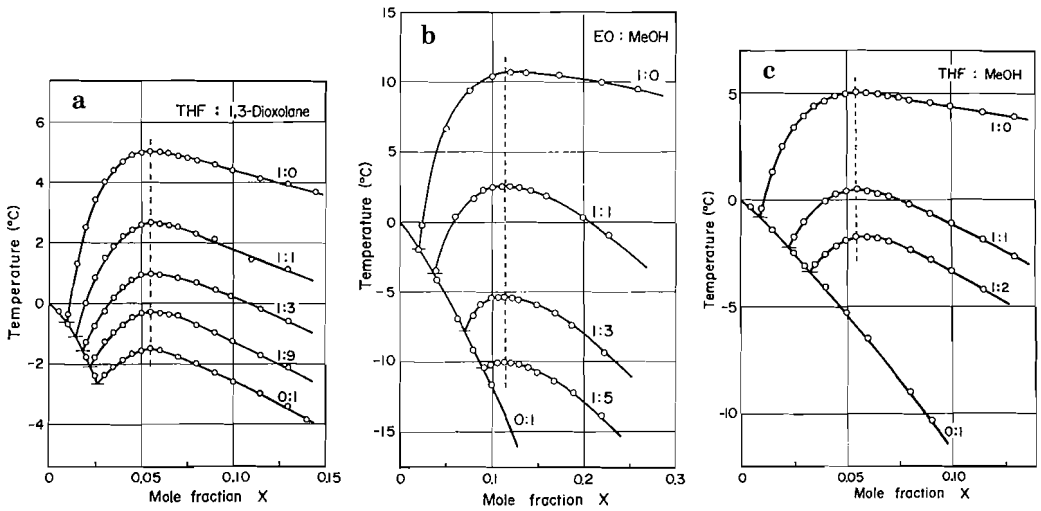

FIG. 1. Dependence of hydrate melting points on composition in (*a*) H_2O–THF–1,3-dioxolane, (*b*) H_2O–EO–MeOH, and (*c*) H_2O–THF–MeOH systems. The curves are drawn for constant mole ratios of the second to third component; x is the combined mole fraction of the non-aqueous components. Reproduced from ref. 1 by permission of the Editor of the Bulletin of the Chemical Society of Japan.

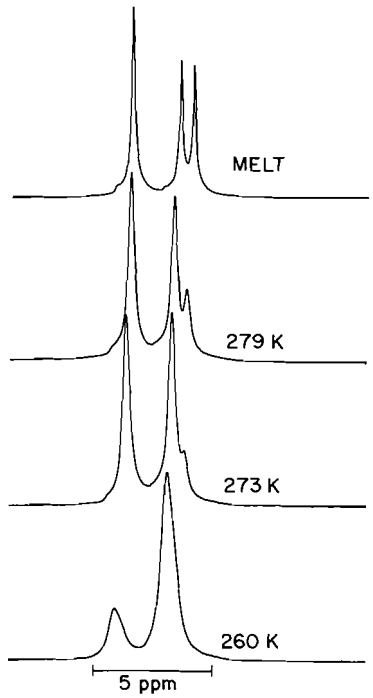

FIG. 2. Liquid-phase proton magnetic resonance spectra of an ethylene oxide – methanol – water sample in which the hydroxyl groups are 84% deuterated.

Results

Proton nmr spectra of the liquid phase in the EO–methanol–water system are shown for a number of temperatures in Fig. 2. The ratios of peak heights were used to estimate the liquid-phase mole ratios plotted in Fig. 3. The water/methanol ratio was obtained by assuming the same OH/OD ratio for methanol as for water.

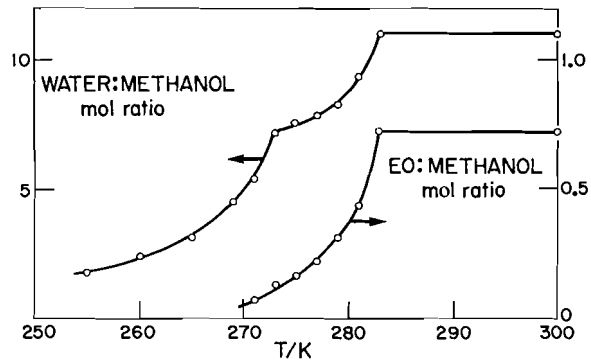

FIG. 3. Mole ratios of water to methanol and ethylene oxide to methanol in the liquid in equilibrium with solid hydrate.

Figure 3 clearly shows that the formation of the structure I hydrate removes both EO and water from the equilibrium liquid phase to a much greater extent than methanol. The hydrate can contain little or no methanol. Water is removed also as ice, the formation of which is marked in Fig. 3 by a rapid fall in liquid water content below 272 K. At 255 K the remaining liquid consists of water and methanol in about 2:1 mole ratio compared to the 11:1 ratio in the unfrozen sample.

The most relevant results of the dielectric studies of the THF–MeOH–H_2O system are contained in Figs. 4 and 5. The dielectric absorption at very low temperatures (Fig. 4) was identical to that shown by THF hydrate itself (3) except for an amplitude

Can. J. Chem. Downloaded from www.nrcresearchpress.com by 210.87.254.5 on 09/06/12
For personal use only.

Can. J. Chem. Downloaded from www.nrcresearchpress.com by 210.87.254.5 on 09/06/12
For personal use only.

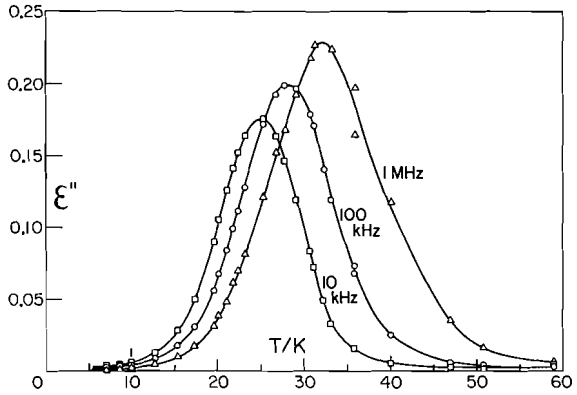

FIG. 4. Dielectric absorption at low temperatures in the 0.5THF·0.5MeOH·17H_2O sample.

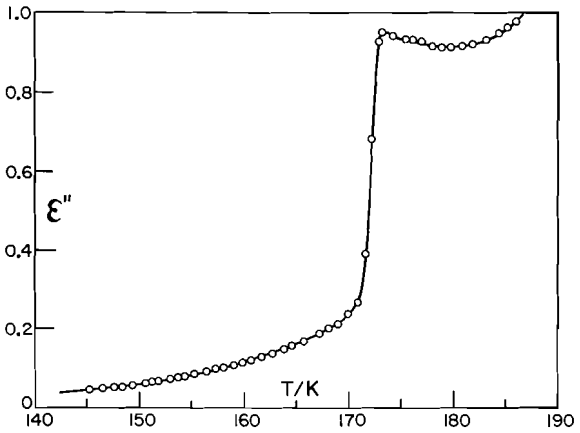

FIG. 5. Temperature dependence of the dielectric loss measured at 4 MHz for the THF–MeOH–H_2O sample.

only about 38% as large. This absorption arises from the reorientation of enclathrated THF molecules, the smaller amplitude reflecting the lower concentration of such molecules within the present sample. No additional absorption of the kind expected for an encaged molecule of the size of methanol was found over the temperature range between 7 and 150 K. The change in dielectric loss measured at 4 MHz as the sample was heated between 145 and 185 K at a rate of 0.44 K/min is shown in Fig. 5. Initial melting occurs sharply at $172\pm\frac{1}{3}$K. This is significantly higher than the eutectic temperature reported for the binary MeOH–H_2O system (156 K, eutectic liquid with ~82 mol% MeOH (4)) and is only a few degrees below the melting point of pure MeOH (175 K). Clearly the liquid present at very low temperatures in the three-component system consists largely of MeOH.

Two dielectric absorption-dispersion regions which occur at relatively high temperatures are ascribed

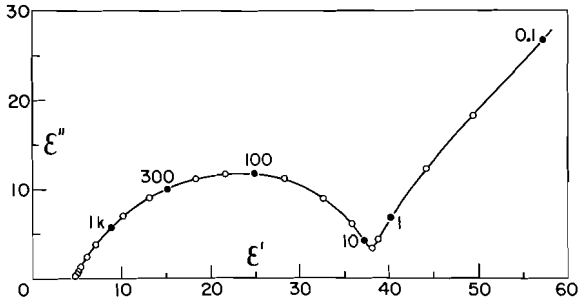

FIG. 6. Cole–Cole plot of the complex permittivity of the THF–MeOH–H_2O sample at 128.6 K. The numbers refer to frequencies in Hz.

to reorientation of the water molecules in THF hydrate and ice, respectively. The former (Fig. 6) is of about one-third the amplitude of that found in "pure" THF hydrate and, as expected from the sample heterogeneity and an increased concentration of "extrinsic" Bjerrum orientational defects (5), is shifted to somewhat higher frequencies. The ice dispersion region which occurs to the high-temperature (low-frequency) side of the hydrate dispersion is poorly defined mainly because of conductivity and space charge effects associated with the distribution of liquid within the sample.

The evidence is thus that no significant amounts of methanol are encaged in either structure I or structure II hydrates. It is possible that small quantities of methanol may participate as impurity in the hydrogen-bonded lattices but no indication of this is provided by the present results.

Discussion

It is possible to account for the effect of methanol on clathrate hydrate melting shown in Fig. 1 *b* and *c* by straightforward thermodynamic analysis without the need for incorporation of methanol in the hydrate.

Under equilibrium conditions, the Gibbs free energy of clathrate hydrate formation by a water-soluble species like EO or THF may be written

$$\Delta G(\mathrm{l} \rightarrow \mathrm{h}) = \mu^0(\mathrm{h}) - \mu_2(\mathrm{l}) - n\mu_1(\mathrm{l}) = 0$$
$$= \Delta H(\mathrm{l} \rightarrow \mathrm{h}) - T\Delta S(\mathrm{l} \rightarrow \mathrm{h})$$

where $\mu^0(\mathrm{h})$ is the chemical potential of the hydrate $\mathrm{M}\cdot n\mathrm{H_2O}$. The chemical potentials of the liquid components are

$$\mu_1(\mathrm{l}) = \mu_1^0(\mathrm{l}) + RT \ln x_1\gamma_1$$
$$\mu_2(\mathrm{l}) = \mu_2^0(\mathrm{l}) + RT \ln x_2\gamma_2$$

where the x's are mole fractions, the γ's are activity coefficients, and the standard states are those of the pure liquids.

The standard thermodynamic functions for hydrate formation from the separate liquids are then

$$\Delta G^0(l_1 + l_2 \rightarrow h) = \mu^0(h) - \mu_2{}^0(l) - n\mu_1{}^0(l)$$
$$= RT \ln x_2\gamma_2 + nRT \ln x_1\gamma_1$$
$$= \Delta H^0(l_1 + l_2 \rightarrow h) - T\Delta S^0(l_1 + l_2 \rightarrow h)$$

Thus,

$$[1] \quad \ln x_2 + n \ln x_1 + \ln \gamma_2 + n \ln \gamma_1 = \frac{\Delta H^0(l_1 + l_2 \rightarrow h)}{RT} - \frac{\Delta S^0(l_1 + l_2 \rightarrow h)}{R}$$

This equation describes the variation of the hydrate melting point with composition $x_2 = (1 - x_1)$ of the binary system in terms of the activity coefficients.

With the assumption of negligible dependence of ΔH^0 and ΔS^0 on temperature, the right-hand-side of eq. [1] is greatest (since ΔH^0 is negative) when T is greatest, that is, at the maximum of the hydrate melting curve. The value of x_2 at this temperature, by differentiation with respect to x_2, is given by

$$[2] \quad \frac{1}{x_2} - \frac{n}{1 - x_2} + \frac{d}{dx_2}(\ln \gamma_2 + n \ln \gamma_1) = 0$$

For the binary system the Gibbs–Duhem relationship

$$x_2 \, d \ln \gamma_2 + (1 - x_2) \, d \ln \gamma_1 = 0$$

ensures that the third term in eq. [2] is zero at the same concentration $x_2 = 1/(n + 1)$ that makes the sum of the first two terms zero. The maximum melting temperature thus corresponds to congruent melting of the hydrate in the binary system, even for a non-ideal solution.

It is now supposed that a third component (e.g., MeOH) is added to the binary system and that this component does not change the nature of the hydrate formed. Equation [1] is still valid, the effect of the third component being to change the activity coefficients and therefore the melting temperatures. It is convenient, as in ref. 1, to consider the case where $x_3 = Cx_2$ and the total solute mole fraction is $x = x_2 + x_3 = (C + 1)x_2$. With constant C, the condition at the maximum hydrate melting temperature is now

$$[3] \quad \frac{1}{x_2} - \frac{(C + 1)n}{1 - (C + 1)x_2} + \frac{d}{dx_2}(\ln \gamma_2 + n \ln \gamma_1) = 0$$

Under conditions (as in ideal solutions) where the derivative term is negligibly small, the maximum melting point occurs at $x_2 = 1/[(C + 1)(n + 1)]$ or $x = 1/(n + 1)$, just as for the binary system. Melting is of course no longer congruent.

The water activity coefficient in aqueous solutions of MeOH is not far from unity (6) and it is perhaps not surprising that the derivative term in eq. [3] varies little with C. The effect of large departures from ideality may be clearly seen, however, when the third component is diethylene glycol dimethyl ether. Nakayama and Hashimoto (1) show that in this case the maximum temperature of melting of THF hydrate moves increasingly to lower values of x as C increases, probably because of an increasingly large negative value of $d(n \ln \gamma_1)/dx_2$.

A maximum melting point, of course, may also occur at a value of x close to $1/(n + 1)$ when the third component forms a hydrate isostructural with that formed by the second component. The thermodynamics then become somewhat more complex. The mixed hydrate formed will not, in general, contain guest molecules in the same proportion as the solution in equilibrium with the hydrate because of the difference in the values of the Langmuir constant which relates cage occupancy to the activity of the corresponding species in solution (7). A larger value of the Langmuir constant for THF than for 1,3-dioxolane probably accounts for the relatively high values of the maximum melting points observed for the mixed hydrate (Fig. 1*a*) compared with those calculated from simple linearity between the melting points of the individual hydrates.

We conclude that hydrate melting point measurements alone are not sufficient to establish whether or not a third component can be enclathrated in a gas hydrate.

1. H. NAKAYAMA and M. HASHIMOTO. Bull. Chem. Soc. Jpn. **53**, 2427 (1980).
2. S. K. GARG, B. MORRIS, and D. W. DAVIDSON. J. Chem. Soc. Faraday Trans. II, **68**, 481 (1972).
3. S. R. GOUGH, R. E. HAWKINS, B. MORRIS, and D. W. DAVIDSON. J. Phys. Chem. **77**, 2969 (1973).
4. G. VUILLARD and M. SANCHEZ. Bull. Soc. Chim. Fr. 1877 (1961).
5. R. E. HAWKINS and D. W. DAVIDSON. J. Phys. Chem. **70**, 1889 (1966).
6. D. F. OTHMER and R. F. BENENATI. Ind. Eng. Chem. **37**, 299 (1945).
7. J. H. VAN DER WAALS and J. C. PLATTEEUW. Adv. Chem. Phys. **2**, 1 (1959).

Can. J. Chem. Downloaded from www.nrcresearchpress.com by 210.87.254.5 on 09/06/12
For personal use only.

Resolution of Raman spectra of aqueous sulfuric acid mixtures using principal factor analysis

ROBIN A. COX,[1] ÜLO L. HALDNA,[2] K. LORALEE IDLER, AND KEITH YATES

Department of Chemistry, University of Toronto, 80 St. George St., Toronto, Ont., Canada M5S 1A1

Received November 28, 1981

ROBIN A. COX, ÜLO L. HALDNA, K. LORALEE IDLER, and KEITH YATES. Can. J. Chem. **59**, 2591 (1981).

Principal factor analysis has been applied to Raman spectra of 26 sulfuric acid/water mixtures covering the 0–100% H_2SO_4 concentration range. The analysis greatly facilitates the identification of peaks due to different species. The results show that SO_4^{2-} ions and "free" HSO_4^- ions do not co-exist with undissociated H_2SO_4 molecules in solution and that two water molecules rather than one are required for the first ionization of H_2SO_4. A species with the composition $H_2SO_4 \cdot 2H_2O$, assigned a hydrated ion pair structure, reaches maximum concentration at the same medium composition at which SO_4^{2-}, free HSO_4^-, and H_2SO_4 are at concentration minima, about 75% w/w. The only species apparent in the more concentrated solutions are the ion pair and undissociated H_2SO_4, which could be taken to mean that H_2SO_4 is a weaker acid than H_3O^+, but a stronger one than $H_3O^+ \cdot H_2O$ (or $H_5O_2^+$, if this entity has a real existence). Separate peaks due to the postulated $H_3O^+ \cdot H_2SO_4$ (or $H_5SO_5^+$) were not observed.

ROBIN A. COX, ÜLO L. HALDNA, K. LORALEE IDLER et KEITH YATES. Can. J. Chem. **59**, 2591 (1981).

On a appliqué l'analyse du facteur principal aux spectres Raman de 26 mélanges d'acide sulfurique/eau ayant des concentrations en acide sulfurique allant de 0 à 100%. L'analyse facilite grandement l'identification des pics des différentes espèces. Les résultats indiquent que les ions SO_4^{2-} et les ions "libres" HSO_4^- ne coexistent pas avec les molécules de H_2SO_4 non dissociées en solution et que deux molécules d'eau plutôt qu'une sont nécessaires lors de la première ionisation du H_2SO_4. Une espèce ayant la composition $H_2SO_4 \cdot 2H_2O$ à laquelle on attribue une structure de paire d'ions, atteint la concentration maximum pour la même composition moyenne où SO_4^{2-}, HSO_4^- libre et H_2SO_4 sont à une concentration minimum, environ 75% w/w. Dans des solutions plus concentrées les seules espèces apparentes sont la paire d'ions et le H_2SO_4 non dissocié, qui peuvent signifier que H_2SO_4 est un acide plus faible que H_3O^+, mais plus fort que $H_3O^+ \cdot H_2O$ (ou $H_5O_2^+$ si cette entité existe réellement). On n'a pas observé de pics séparés provenant du $H_3O^+ \cdot H_2SO_4$ (ou $H_5SO_5^+$) proposé.

[Traduit par le journal]

Introduction

Factor analysis (1, 2) is an impartial mathematical technique, able to isolate individual variables from experimental data which are functions of two or more different variables. It is becoming quite widely used in chemistry, for instance in the study of solvent effects on proton chemical shifts (3), on thermodynamic data (4), and on equilibrium and rate constants (5), and in the analysis of ir (6, 7), Raman (8), and uv–visible (9) spectra. Simonds (10) has given a simple formulation for the first stage of factor analysis, principal factor analysis (PFA) (1); Simonds' method has been used to isolate medium effects from protonation effects in uv–visible spectra at different acidities by Edward and Wong (11) and others (12). In this paper PFA is used in the analysis of Raman spectra obtained at different acidities.

There have been several studies of the Raman spectra of aqueous sulfuric acid solutions (13–18). Of these, only the early study by Young's group (13) and a Russian study (17) cover the entire concentration range; most of the effort has involved the dilute acid region (14–16). However, the detailed interpretations of peak position, even the presence (14) or absence (15, 16) of certain peaks, sometimes differ considerably, as do the peak intensities or areas, from which species concentrations can be obtained. Accurate knowledge of the species present, and their concentrations, is necessary to the study of the kinetics and mechanisms of organic reactions in aqueous sulfuric acid media (19). For instance, undissociated sulfuric acid molecules are kinetically involved in the rearrangement of azoxybenzenes to hydroxyazobenzenes (20); bisulfate ions are involved in some azoxynaphthalene rearrangements (21) and in the enolization of acetone (22). Because of this, and as part of our continuing interest in this medium (19, 23, 24), we have applied PFA to Raman spectra obtained over the entire 0–100% H_2SO_4 concentration range.

Experimental

Sulfuric acid solutions were prepared and analyzed as before (24). Spectra were recorded at 25 ± 1°C on a Spex model 1401 Raman spectrophotometer, using the 488 nm exciting line from a Spectra Physics model 164 argon ion laser, at a slit width of 5 cm^{-1}. The *x*/*y* coordinates of 50–100 data points, taken from each spectral trace at about every 1 cm interval and including all peak maxima, were transferred to computer cards using a

[1]To whom all correspondence should be addressed.

[2]On academic leave from Tartu State University. Present address: Institute of Chemistry, Estonian Academy of Sciences, 15 Akadeemia tee, Tallinn 200026, Estonian S.S.R., Soviet Union.

0008-4042/81/172591-08$01.00/0

©1981 National Research Council of Canada/Conseil national de recherches du Canada

Can. J. Chem. Downloaded from www.nrcresearchpress.com by 210.87.254.42 on 09/06/12
For personal use only.

Can. J. Chem. Downloaded from www.nrcresearchpress.com by 210.87.254.42 on 09/06/12
For personal use only.

digitalizer. Baseline points were taken from "empty" spectral regions, and baseline values for each data point, obtained from these by polynomial interpolation (25*a*), were subtracted; the area under each spectrum was then computed (25*b*), for normalization purposes (6). PFA requires intensity data at the same frequency on each spectrum; 96 frequencies were chosen from the measured x-coordinates by an averaging process, and intensity values, normalized to equal area, were computed at these points on each spectrum by polynomial interpolation (25*a*). The resulting array of 96 points for each of 26 acid solutions was treated using a computer program incorporating Simonds' PFA algorithm (10). The average row and vectors obtained were curve-fitted as a sum of Voigt peaks using the approximation to the Voigt function given by Kielkopf (26), in combination with a curve-fitting routine adapted from Bevington (25*c*). The fourth-order polynomial curves in Fig. 2 were obtained using a standard multiple linear regression program (25*d*).

Results

The Raman spectra were of 26 sulfuric acid solutions, ranging in mole fraction sulfuric acid between 0.0087 (4.53% w/w) and 0.9723 (99.48%). Before analysis the spectra were corrected, as far as possible, for baseline variations, and the effects of changing acid concentration and changing signal amplification were removed by normalizing them all to the same total area (6). Intensity data, obtained at 96 reciprocal wavelength values from each of the 26 spectra, were then subjected to PFA according to Simonds (10). In this formulation the intensities (I) are first averaged, and the eigenvectors and coefficients result from analyzing the differences between each spectrum and the average; this is covariance about the mean (1, 27), eq. [1].

$$[1] \quad I(\nu) = \bar{I}(\nu) + c_1 v_1(\nu) + c_2 v_2(\nu) + \ldots$$

It was found that the average row ($\bar{I}$) and *two* eigenvectors (v_i) accounted for essentially all of the variation, any remaining being indistinguishable from random error (1). These are given as intensity (arbitrary units) vs. wavenumber graphs in Fig. 1 (experimental points). If the normalization to equal area is omitted, three vectors result; the first appears to concern the changing amplification and total acid concentration, and the second and third strongly resemble those given in Fig. 1. Thus normalizing to equal area is justified. The coefficients (c_i) of the first and second vectors, numbers characteristic of each acid solution, are plotted as a function of mole fraction sulfuric acid in Fig. 2, together with the best fourth-order polynomial curves drawn through them. To reconstitute the observed Raman spectrum at any acid strength, eq. [1] is applied to the curves in Figs. 1 and 2; the results of this strongly resemble the experimental spectra, both ours and those obtained by others (15, 16, 28).

The alternative factor analysis formulation, covariance about the origin (1, 27), in which the average row is omitted from eq. [1], was also tried; three vectors resulted, of which the first was very similar to the average row obtained before, and v_2 and v_3 corresponded to the v_1 and v_2 of Fig. 1. The coefficients of v_1 did not vary with acid concentration, and those of v_2 and v_3 resembled Fig. 2 closely. The residual errors indicated that no advantage was gained by this alternative procedure, and it was not pursued.

Figures 1 and 2 contain all of the information present in the original 26 Raman spectra. Accordingly Fig. 1 must consist of superpositions of individual Raman peaks (some positive and some negative), just as the original spectra do, and should be resolvable into individual peaks on this basis. To do this the Raman peak shape must be specified; opinions on this differ, with Irish and Chen (28) using one Gaussian–Lorentzian product function and Turner (16) another, and Ikawa and Kimura (15) a Voigt function, which is a Gaussian–Lorentzian convolution (29). Following Ikawa and Kimura we have used Kielkopf's approximation to the Voigt profile (26), with the additional assumption that the Gaussian part of the profile comes only from the finite slit width, 5 cm^{-1} in our case, i.e. that each peak has a Gaussian half-width of 3.00 cm^{-1} (29). This means that the Raman peaks can be specified by three parameters rather than four, since the ratio of Lorentzian to Gaussian half-widths (the Voigt parameter) (26, 29) is fixed for each peak. A subroutine to a standard least-squares curve-fitting program (25*c*) was written which obtains optimum values for peak position (ν_{max}), area and Lorentzian half-width, with their errors, these probably being the most useful parameters.[3]

The results of this curve-fitting procedure are given in Table 1. The resolved peaks are illustrated in Fig. 1, and the intensity profiles resulting from the combination of individual peaks are given as the theoretical curves in Fig. 1. As can be seen, agreement with experiment is very good; a slight baseline was still present in the average row, accounted for by a quadratic curve as shown. Column three of Table 1 shows that most of the peaks are almost entirely Lorentzian, being much broader than the 3 cm^{-1} Gaussian half-width. The

[3]Peak area is directly proportional to species concentration (14, 28); Lorentzian half-widths give information on the rates of proton transfer reactions in these systems (14, 15, 30).

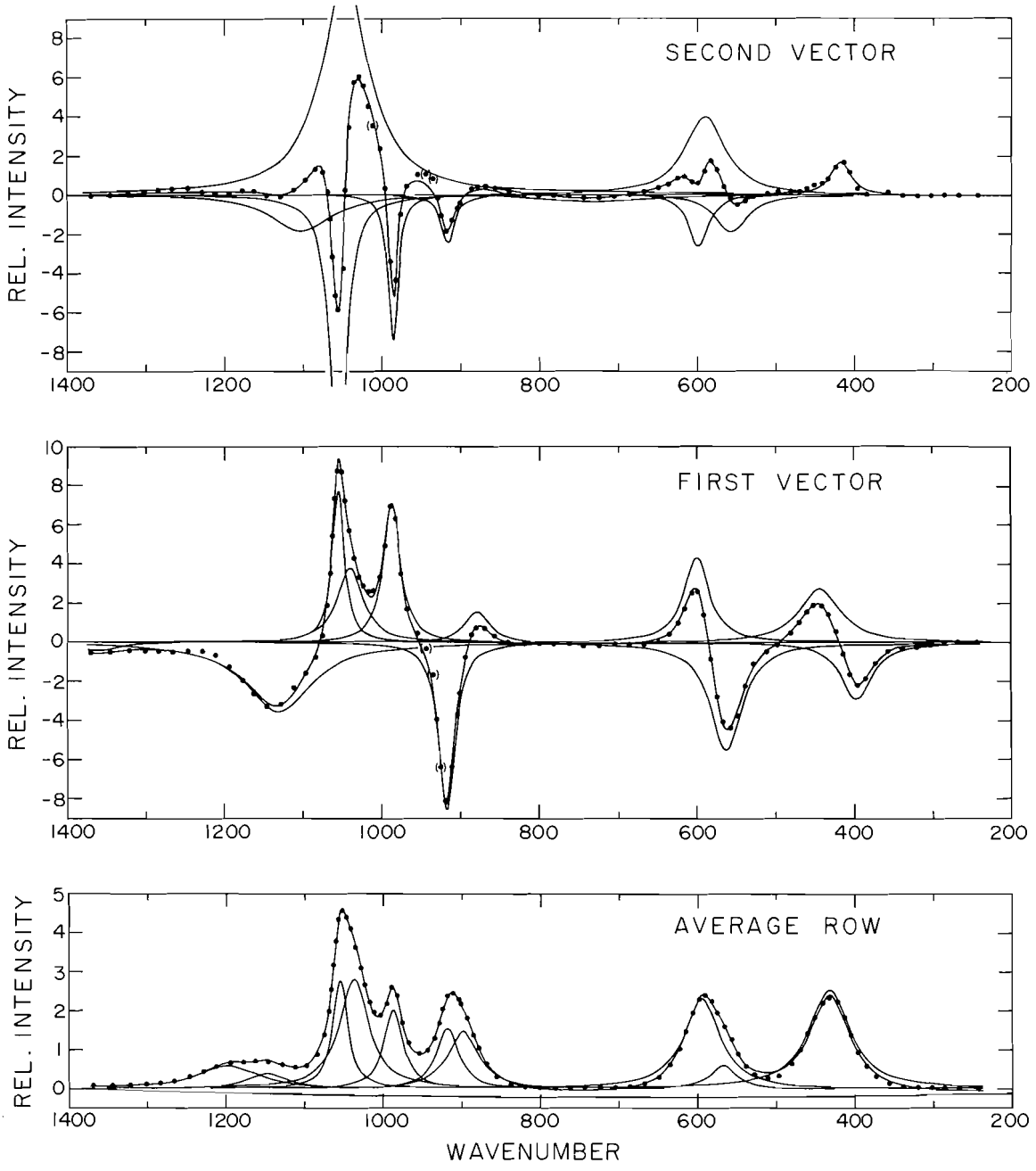

FIG. 1. Raman peaks of the sulfuric acid/water system, as given by principal factor analysis. Points are experimental; addition of the resolved peaks shown results in the theoretical curves drawn through the points.

criterion for the presence of a peak was that the standard deviation in its area should be smaller than the area itself (except in two cases, see below); this led to resolution of the average row into 10 peaks, and ν_1 and ν_2 into 11 each. Undoubtedly more data points would lead to the resolution of more peaks.[4] Overall 17, probably 18, individual peaks are involved; in Table 2 these are assigned by

[4]For instance, by using digital rather than analog recording of the spectra, unfortunately not available on the instrument used in this work.

Can. J. Chem. Downloaded from www.nrcresearchpress.com by 210.87.254.42 on 09/06/12
For personal use only.

Can. J. Chem. Downloaded from www.nrcresearchpress.com by 210.87.254.42 on 09/06/12
For personal use only.

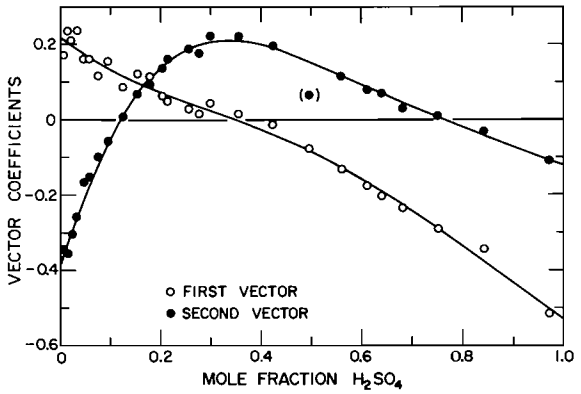

FIG. 2. Coefficients of the first and second vectors as a function of mole fraction H_2SO_4.

species, as far as possible, on the basis of previous assignments (28, 31–33).

The most evident observation from Table 2 is that two different types, or environmental variants, of bisulfate ion are present in these solutions. In every case two peaks rather than one are present, bracketing the expected frequencies (31). The sharp 1055 cm^{-1} peak, and the other peaks to higher wavenumber, are assigned to "free" aqueous HSO_4^- (HSO_4^-aq), and the broad 1040 cm^{-1} and other lower wavenumber peaks to HSO_4^- in the sulfuric acid medium, probably as an ion-pair (28) (HSO_4^-ip). Two bisulfate peaks in the 1025–1055 cm^{-1} region are generally acknowledged (15, 16, 28), but two peaks at the other frequencies have not, to the best of our knowledge, been reported before.

From Table 2 it is apparent that several peaks do not appear in all three of the average row (Av) and both vectors (ν_1 and ν_2). This does not mean that peaks are absent, but only that they could not be resolved out. For instance, an upward displacement at 1200 cm^{-1} in ν_1, and a downward one in ν_2, undoubtedly correspond to the 1200 cm^{-1} peak in Av, but when resolution was attempted the peaks which resulted had errors which were too large for the parameters to be meaningful. Of particular interest in this respect are experimental points at 935.0 and 943.5 cm^{-1} on both ν_1 and ν_2. The computer program used rejects points which fall too far away from the best regression curve,[5] and these two points are rejected as being too far above the curve for both vectors. An additional positive peak is inferred to be present at ~935 cm^{-1} on both ν_1 and ν_2, but, again, it could not be resolved out.

[5]Points which have a 95% or greater probability of not being part of the data set used to construct the regression curve, as determined by a test using t-statistics.

TABLE 1. Resolved positions, areas and half-widths of the Raman peaks of aqueous sulfuric acid mixtures[a]

ν_{max}' cm^{-1}	Area[b]	β_L' cm^{-1} [c]
Average row (Av)		
1198 ±12	85±44	48±15
1147.5± 7.3	33±30	27±13
1054.8± 0.5	99±25	11± 1
1037.0± 2.0	194±35	22± 2
987.1± 0.4	89± 6	14± 1
918.2± 1.9	79±34	16± 3
898.8± 4.1	105±39	23± 3
595.1± 2.1	197±29	27± 2
567.8± 4.1	36±25	19± 6
432.6± 0.4	250± 7	31± 1
First vector (ν_1)		
1361 ±25	−47±42	35±39
1131.4± 2.3	−569±42	51± 4
1055.4± 0.4	224±61	9± 1
1040.0± 4.1	232±88	19± 3
987.2± 0.3	284±14	12± 1
917.4± 0.3	−328±16	12± 1
878.7± 2.1	89±18	18± 4
599.8± 1.1	265±37	19± 2
562.8± 1.2	−420±43	24± 2
443.2± 2.9	261±51	30± 4
396.9± 1.9	−213±43	23± 3
Second vector (ν_2)		
1102 ±11	−259±137	44± 8
1055.8± 0.1	−550± 84	11± 1
1046.1± 3.1	1254±205	36± 2
985.6± 0.1	−167± 10	7± 1
916.7± 0.5	−76± 7	9± 1
871.8± 6.1	14± 12	13±12
729 ±33	−90± 76	82±62
598.4± 3.4	−119±332	14±11
590 ±22	380±171	30±23
556.9± 8.8	−142±241	24±13
417.4± 1.0	70± 8	13± 2

[a]Errors quoted are standard deviations.
[b]Peak areas in arbitrary units. Negative for negative peaks in Fig. 1.
[c]Lorentzian half-width.

Irish and Chen (28) reported a peak in this region, at 948 cm^{-1}, but its presence was not confirmed by Turner (16) or Ikawa and Kimura (15). On the basis of our results we are inclined to support Irish and Chen, but cannot do this rigorously.

Three peaks are clearly present in the 500–650 cm^{-1} region of ν_2. Resolution in terms of two positive and one negative gives better individual errors, but a worse overall error than the resolution as one positive and two negative peaks shown in Fig. 1. The latter is preferred, despite the worse individual errors, because of the better correspondence with peaks on ν_1 and Av which results. A similar situation should apply in the 350–450 cm^{-1} region of ν_2, but resolution better than one peak was not possible. In one case a weak H_2SO_4 peak at 976 cm^{-1} which should be visible (32) is not re-

Can. J. Chem. Downloaded from www.nrcresearchpress.com by 210.87.254.42 on 09/06/12
For personal use only.

TABLE 2. Species assignment of observed Raman peaks

Peak	ν_{max} observed[a] Av	ν_1	ν_2	Assignment[b,c]	ν_{max} expected[c] HSO_4^-	SO_4^{2-}	H_2SO_4
1	—	(−)1361	—	H_2SO_4			1368
2	1200	—	—	H_2SO_4, HSO_4^-ip, HSO_4^-aq[d]	1230		1195
3	1147	(−)1131	—	H_2SO_4			1137
4	—	—	(−)1102	SO_4^{2-}		1103	
5	1055	1055	(−)1056	HSO_4^-aq	[1050		
6	1037	1040	1046	HSO_4^-ip	1050]		
7	987	987	(−)986	SO_4^{2-}		982	976[e]
8	—	(935)[f]	(935)[f]	SO_4^{2-}ip[g]		948[g]	
9	918	(−)917	(−)917	H_2SO_4			910
10	—	877	872	HSO_4^-aq	[885		
11	899	—	—	HSO_4^-ip	885]		
12	—	—	(−)729	H_2SO_4			(741)[h]
13	595	600	(−)598	SO_4^{2-}, HSO_4^-aq	[593	617	
14	—	—	590	HSO_4^-ip	593]		
15	568	(−)563	(−)557	H_2SO_4			563
16	433	443	—	H_2SO_4, SO_4^{2-}, HSO_4^-aq	[420	452	422
17	—	—	417	HSO_4^-ip	420]		
18	—	(−)397	—	H_2SO_4			392

[a] From Table 1 and Fig. 1; negative peaks have minus signs.
[b] ip = ion pair, aq = aqueous, see text.
[c] HSO_4^- and SO_4^{2-}, ref. 31; H_2SO_4, ref. 32.
[d] A peak at 1200 cm^{-1} due to H_3O^+ is found in most acid solutions (38).
[e] Not observed in this work, see text.
[f] Inferred, see text.
[g] Assignment from ref. 28.
[h] From Leckie (33); not observed by Gillespie and Robinson (32).

solved anywhere; it appears to be "lost" as part of the excessively broad 1131 cm^{-1} H_2SO_4 feature on ν_1. This peak would undoubtedly be much sharper if better resolution of the weak peaks in the 1100–1400 cm^{-1} region on ν_1 had been possible.

The peaks in Fig. 1 are all explicable in terms of the species HSO_4^-aq, HSO_4^-ip, SO_4^{2-}, and undissociated H_2SO_4, with the possible addition of SO_4^{2-}ip (28), as indicated in Table 2. This work offers no evidence for the species $H_5SO_5^+$, or $H_3O^+ \cdot H_2SO_4$, postulated for the concentrated acid region (17*c*, 18, 34). If peaks due to HSO_4^-aq and HSO_4^-ip are resolvable, those due to H_2SO_4 and $H_2SO_4 \cdot H_3O^+$ should be resolvable also, but no extra or unexplained peaks are apparent in Fig. 1 or on the spectra themselves. We conclude that this species is absent.[6]

A comparison of Table 2 and Fig. 1 leads to the following general observations: (*a*) peaks attributable to SO_4^{2-} and HSO_4^-aq are positive on ν_1 and negative on ν_2; (*b*) H_2SO_4 peaks are negative on both ν_1 and ν_2; (*c*) peaks due to HSO_4^-ip (and SO_4^{2-}ip) are positive on ν_1 and, especially, on ν_2, the positive aspect of which is practically a Raman spectrum of this species in isolation.[7] The coefficients of the vectors, c_1 and c_2 in Fig. 2, therefore, reveal which species are predominant at a given stoichiometric H_2SO_4 concentration. At a mole fraction of 0.0 (i.e. infinite dilution in water), c_1 has its largest positive value, so the species with positive peaks on ν_1, SO_4^{2-} and HSO_4^-aq, reach their highest concentrations relative to HSO_4^-ip and H_2SO_4. The negative value of c_2 at this point reinforces this. Conversely, at mole fraction 1.0 c_1 is at its most negative, so that H_2SO_4, with negative peaks on ν_1, reaches its highest relative concentration here; c_2 makes a small but, again, reinforcing contribution. These reasonable conclusions lend confidence to the interpretation.

At a mole fraction of 0.35 (74.6% w/w) c_1 passes through zero and c_2 achieves its maximum positive value; SO_4^{2-}, H_2SO_4, and HSO_4^-aq are all at concentration minima and HSO_4^-ip is at a maximum. From this point HSO_4^-ip decreases; H_2SO_4 increases in the acid direction, and HSO_4^-aq and SO_4^{2-} increase in the aqueous direction. The experimental spectra bear this out: at 80.10% H_2SO_4 the HSO_4^-ip peaks at 1040, 900, 590, and 420 cm^{-1} are the only ones present; at 75.05% the 987 cm^{-1} SO_4^{2-} peak is just visible as a shoulder on the 1040 cm^{-1} peak; and at 84.26% the 916 cm^{-1}

[6] Professor G. E. Walrafen informs us that he abandoned the species $H_5SO_5^+$ (18) in 1964 in favour of a strong interaction between HSO_4^- and H_3O^+ where either the anion or the cation or both are hydrated, which is consistent with this work. The experimental Raman work leading to this conclusion was never published.

[7] Neglecting the small positive 872 cm^{-1} peak on ν_1 which may, in fact, be part of the postulated 935 cm^{-1} absorption of the SO_4^{2-} ion pair (28).

H_2SO_4 peak is becoming noticeable as an increase in intensity and a shift in ν_{max} of the broad 900 cm^{-1} peak. There is no "overlap" region where all four species are visible. The composition of the system at this point approximates $H_2SO_4 \cdot 2H_2O$, and can be further characterized as $HSO_4^- \cdot H_2O \cdot H_3O^+$ since the Raman spectrum is a bisulfate one. The conclusion seems inescapable that in the 0.3–0.4 mole fraction region practically all of the stoichiometric sulfuric acid is present in this form.

Discussion

Implicit in the above treatment is the assumption that the changing medium composition does not change the Raman peak positions. The raw spectra do show apparent shifts with increasing acidity, but most of this is due to increasing peak overlap, for instance, of the broad 1040 cm^{-1} HSO_4^-ip peak with the adjacent HSO_4^-aq and SO_4^{2-} peaks. If there is a slight residual medium effect, it would have to act in opposite directions on HSO_4^- and SO_4^{2-}, since the apparent medium shifts are to lower and higher frequencies, respectively (15), and this seems unlikely.

Another point to be considered is that the above analysis is only a PCA and not a full factor analysis with target testing (1). The first vector resulting from PCA accounts for the maximum possible data variation, the second, the maximum of the remaining variation, and so on; PCA is a mathematical process, with no chemical input, and the resulting vectors and coefficients may represent linear combinations of chemical parameters rather than the parameters themselves. This point can be decided in some cases by target testing (1). In our case this is difficult, (*a*) because the large 96 × 26 data matrix involved would make target testing costly and time-consuming, and (*b*) because the targets to be tested (presence of SO_4^{2-}, etc.) could only be specified after analysis of the PCA vectors, which presupposes the results of the tests. Accordingly we analyzed the PCA results only. There is one check that can be performed, and that is to see whether any relationship exists between v_1 and v_2, and between c_1 and c_2, by plotting them against one another; if there is a relationship, PCA has not produced fundamental chemical information. It was speedily concluded that v_1 and v_2 are unrelated; see Fig. 1. Plotting c_1 against c_2 produces two adequate straight lines, intersecting practically at right angles, so c_1 and c_2 are also unrelated over the whole composition range. The position of intersection in the latter plot corresponds almost exactly to a mole ratio H_2O:H_2SO_4 of 2:1, as would be anticipated from the appearance of Fig. 2.

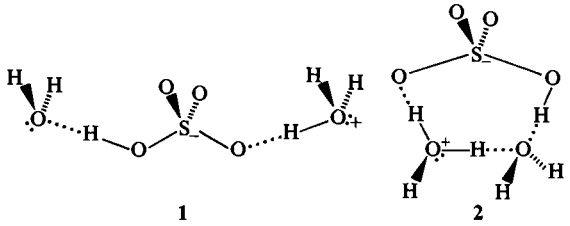

1 2

The major result of this work is the observation that only *two* principal factors are sufficient to explain the data. Since three equilibria appear to be involved, two acid dissociations and an ion-pairing process, reactions [2]–[4],

[2] $H_2SO_4 + 2H_2O \rightleftharpoons H_3O^+ \cdot H_2O \cdot HSO_4^-$

[3] $H_3O^+ \cdot H_2O \cdot HSO_4^- + \text{water} \rightleftharpoons H^+ \cdot aq + HSO_4^- \cdot aq$

[4] $HSO_4^- \cdot aq + \text{water} \rightleftharpoons H^+ \cdot aq + SO_4^{2-} \cdot aq$

this means that only two of them can be important at any given acid composition. The most likely possibility is that the first dissociation of H_2SO_4 to HSO_4^- is complete before dissociation of HSO_4^- to SO_4^{2-} begins, i.e. that there is no acid solution which contains all three of H_2SO_4, HSO_4^-, and SO_4^{2-}. Sufficient water to solvate SO_4^{2-} and "free" HSO_4^- is only present on the aqueous side of the 2:1 H_2O:H_2SO_4 composition. Thus sulfuric acid solutions more dilute than this contain SO_4^{2-}aq, HSO_4^-aq, H^+aq, and HSO_4^-ip only, and more concentrated ones HSO_4^-ip and H_2SO_4 only.

The changes in c_1 and c_2 which occur at the 2:1 H_2O:H_2SO_4 mole ratio point (see Fig. 2) lead to the second major conclusion of this work, which is that *two* water molecules rather than one are required for the first ionization of H_2SO_4, reaction [2] above. The HSO_4^-ip product of reaction [2] was assigned the structure **1** by Irish and Chen (28), and a likely alternative to this is the five-membered-ring structure (4 O's, 1 S; hydrogen bonds are collinear) of **2**. It is interesting that the volume contraction upon mixing H_2SO_4 with H_2O reaches a maximum at about the 2:1 composition (35*a*), and that melting-point studies reveal the presence of $H_2SO_4 \cdot 2H_2O$ as well as $H_2SO_4 \cdot H_2O$ and $H_2SO_4 \cdot 4H_2O$ as congruent-melting compounds (36). It seems unlikely that the two types of HSO_4^- observed simply represent different solvation environments for this ion, as Turner believes (16). The HSO_4^-ip peaks are visible in both quite dilute and quite concentrated acids, including the acid region containing no free H_2SO_4, so this cannot be a solvating species.

Without getting into the argument as to whether $H_5O_2^+$ exists in solution (37), or does not (38), if H_3O^+ is a stronger acid than H_2SO_4 in solution, as it

Can. J. Chem. Downloaded from www.nrcresearchpress.com by 210.87.254.42 on 09/06/12
For personal use only.

Can. J. Chem. Downloaded from www.nrcresearchpress.com by 210.87.254.42 on 09/06/12
For personal use only.

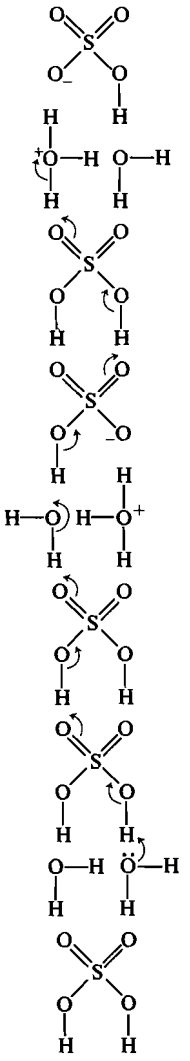

3

is in the gas phase (39), then H_2SO_4 may be able to protonate two water molecules, to $H_5O_2^+$ or $H_3O^+ \cdot H_2O$, but not one. It is a well-known fact that water does not behave as a strong base in sulfuric acid; melting-point depression studies show that fewer than two particles per molecule of added water are formed (40). This would be expected on the basis of reaction [2]. On the other hand, conductivity studies do show water acting as a strong base (41). This is not unreasonable either, since both HSO_4^- and $H_3O^+ \cdot H_2O$ can conduct charge through the hydrogen-bond network via a Grötthus chain mechanism (35*b*); two water molecules produce two highly conductive entities, and ion-pairing to structures like **2** will not affect this type of conductivity (41).

This chain-transfer conduction of $H_3O^+ \cdot H_2O$ through the solvent network is illustrated for the 0.5 mole fraction composition (84.482%) in **3**. The only equilibrium of consequence is reaction [2]; in reality only hydrogen-bond migrations are involved. It is likely that the two water molecules formed when $H_3O^+ \cdot H_2O$ deprotonates would not have sufficient time to diffuse apart, on average, since they are in a highly structured viscous solution; the lifetimes of individual entities in the system are very short, 10^{-11} to 10^{-13} s as determined from the Raman half-widths (14, 15). Obviously many possibilities for proton transfer exist; in **3** the arrows show $H_3O^+ \cdot H_2O$ moving from the $H_3O^+ \cdot H_2O \cdot HSO_4^-$ at the top to the $H_2SO_4 \cdot 2H_2O$ at the bottom, via three intermediate H_2SO_4 molecules and one intermediate $H_3O^+ \cdot H_2O \cdot HSO_4^-$ ion pair. (The hydrogen bonds are omitted for clarity.)

Raman spectroscopy facilitates the calculation of species concentrations, from the Raman peak areas, and offers insight into the kinetics of proton transfer, from the Lorentzian half-widths (30). We will report on any differences between our results and previous studies (14, 15) elsewhere. Preliminary work supports the Raman measurements of sulfate ion concentration given by Irish and Chen (14), and the values for undissociated sulfuric acid molecule concentrations measured by Maiorov and Librovich using attenuated total internal reflection ir spectroscopy (42). However, we cannot support all of the concentration estimates in Librovich and Maiorov's summary paper (43). It seems doubtful that HSO_4^-aq and HSO_4^-ip will differ appreciably in their kinetic behaviour as base and/or nucleophile in organic reactions, so the total HSO_4^- concentration, easily calculated by subtracting $C_{SO_4^{2-}}$ and $C_{H_2SO_4}$ from the stoichiometric sulfuric acid concentration, will probably prove most useful here; however, such reactions as have been observed (21, 22) occur in acidity regions where HSO_4^-ip is dominant. The predominant acid species would appear to be H_2SO_4 and $H_3O^+ \cdot H_2O$ in the concentrated region, and higher proton hydrates in the dilute region.

Acknowledgements

We would like to thank Professor E. A. Robinson for the use of the spectrophotometer, and R. M. Aroca for technical assistance. Financial support of this research is by the Natural Sciences and Engineering Research Council of Canada.

1. E. R. Malinowski and D. G. Howery. Factor analysis in chemistry. Wiley, Toronto. 1980.
2. P. H. Weiner. Chem. Tech. 321 (1977).
3. P. H. Weiner, E. R. Malinowski, and A. R. Levin-

STONE. J. Phys. Chem. **74**, 4537 (1970); P. H. WEINER and E. R. MALINOWSKI. J. Phys. Chem. **75**, 1207 (1971).
4. W. R. FAWCETT and T. M. KRYGOWSKI. Can. J. Chem. **54**, 3283 (1976).
5. G. H. E. NIEWDORP, C. L. DE LIGNY, and H. C. VAN HOUWELINGEN. J. Chem. Soc. Perkin Trans. II, 537 (1979).
6. J. T. BULMER and H. F. SHURVELL. J. Phys. Chem. **77**, 2085 (1973).
7. B. U. PETELENZ and H. F. SHURVELL. Can. J. Chem. **58**, 353 (1980); and earlier papers by Shurvell *et al.*
8. T. JARV, J. T. BULMER, and D. E. IRISH. J. Phys. Chem. **81**, 649 (1977); H. F. SHURVELL and A. DUNHAM. Can. J. Spectrosc. **23**, 160 (1978).
9. R. L. REEVES, M. S. MAGGIO, and S. A. HARKAWAY. J. Phys. Chem. **83**, 2359 (1979).
10. J. L. SIMONDS. J. Opt. Soc. Am. **53**, 968 (1963).
11. J. T. EDWARD and S. C. WONG. J. Am. Chem. Soc. **99**, 4229 (1977).
12. R. L. REEVES. J. Am. Chem. Soc. **88**, 2240 (1966); R. I. ZALEWSKI. J. Chem. Soc. Perkin Trans. II, 1637 (1979).
13. T. F. YOUNG, L. F. MARANVILLE, and H. M. SMITH. *In* The structure of electrolytic solutions. *Edited by* W. J. Hamer. Wiley, New York. 1959. p. 35.
14. H. CHEN and D. E. IRISH. J. Phys. Chem. **75**, 2672 (1971).
15. S. IKAWA and M. KIMURA. Bull. Chem. Soc. Jpn. **49**, 2051 (1976); S. IKAWA, M. YAMADA, and M. KIMURA. J. Raman Spectrosc. **6**, 89 (1977).
16. D. J. TURNER. J. Chem. Soc. Faraday Trans. II, **68**, 643 (1972); J. Chem. Soc. Faraday Trans. I, **70**, 1346 (1974).
17. (*a*) N. G. ZARAKHANI and M. I. VINNIK. Zh. Fiz Khim. **37**, 503 (1963); Engl. Transl. **37**, 260 (1963); (*b*) N. G. ZARAKHANI, N. B. LIBROVICH, and M. I. VINNIK. Zh. Fiz. Khim. **45**, 1733 (1971); Engl. Transl. **45**, 981 (1971); (*c*) N. G. ZARAKHANI. Zh. Fiz. Khim. **52**, 1954 (1978); Engl. Transl. **52**, 1129 (1978); (*d*) N. G. ZARAKHANI, V. S. MARKIN, and G. E. ZAIKOV. Zh. Fiz. Khim. **53**, 2289 (1979); **53**, 2294 (1979); Engl. Transl. **53**, 1304 (1979); **53**, 1306 (1979).
18. T. F. YOUNG and G. E. WALRAFEN. Trans. Faraday Soc. **57**, 34 (1961).
19. R. A. COX and K. YATES. Can. J. Chem. **57**, 2944 (1979).
20. R. A. COX. J. Am. Chem. Soc. **96**, 1059 (1974); R. A. COX and E. BUNCEL. J. Am. Chem. Soc. **97**, 1871 (1975).
21. R. A. COX, A. J. DOLENKO, and E. BUNCEL. J. Chem. Soc. Perkin Trans. II, 471 (1975).
22. R. A. COX, C. R. SMITH, and K. YATES. Can. J. Chem. **57**, 2952 (1979); Ü. HALDNA, H. KUURA, L. ERRELINE, and V. PALM. Reakts. Sposobn. Org. Soedin. **2**, 194 (1965); Chem. Abstr. **64**, 3304*c* (1966).
23. R. A. COX and K. YATES. J. Am. Chem. Soc. **100**, 3861 (1978); Ü. L. HALDNA, I. A. KOPPEL, and H. J. KUURA. Reakts. Sposobn. Org. Soedin. Engl. Edn. **14**, 235 (1977); Ü. L. HALDNA and H. J. KUUS. Reakts. Sposobn. Org. Soedin. Engl. Edn. **15**, 394 (1978).
24. U. HALDNA and R. M. AROCA. Reakts. Sposobn. Org. Soedin., Engl. Edn. **13**, 523 (1976).
25. P. R. BEVINGTON. Data reduction and error analysis for the physical sciences. McGraw-Hill, Toronto. 1969. (*a*) p. 266; (*b*) p. 272; (*c*) p. 237; (*d*) p. 171.
26. J. F. KIELKOPF. J. Opt. Soc. Am. **63**, 987 (1973).
27. R. W. ROZETT and E. M. PETERSEN. Anal. Chem. **47**, 1301 (1975).
28. D. E. IRISH and H. CHEN. J. Phys. Chem. **74**, 3796 (1970).
29. K. S. SESHADRI and R. N. JONES. Spectrochim. Acta, **19**, 1013 (1963).
30. M. M. KREEVOY and C. A. MEAD. J. Am. Chem. Soc. **84**, 4596 (1962).
31. J. H. R. CLARKE and L. A. WOODWARD. Trans. Faraday Soc. **64**, 1041 (1968).
32. R. J. GILLESPIE and E. A. ROBINSON. Can. J. Chem. **40**, 644 (1962).
33. A. H. LECKIE. Trans. Faraday Soc. **32**, 1700 (1936).
34. P. A. H. WYATT. Trans. Faraday Soc. **56**, 490 (1960).
35. M. LILER. Reaction mechanisms in sulfuric acid. Acdemic Press, London. 1971. (*a*) p. 4; (*b*) p. 72.
36. C. M. GABLE, H. F. BETZ, and S. H. MARON. J. Am. Chem. Soc. **72**, 1445 (1950).
37. G. ZUNDEL. *In* The hydrogen bond. Vol. II. *Edited by* P. Schuster, G. Zundel, and C. Sandorfy. North-Holland, Amsterdam. 1976. p. 683.
38. P. A. GIGUÈRE. J. Chem. Educ. **56**, 571 (1979).
39. M. FOURNIER, A. POTIER, and M. ALLAVENA. Theor. Chim. Acta, **42**, 213 (1976).
40. R. J. GILLESPIE. J. Chem. Soc. 2493 (1950).
41. R. H. FLOWERS, R. J. GILLESPIE, E. A. ROBINSON, and C. SOLOMONS. J. Chem. Soc. 4327 (1960).
42. V. D. MAIOROV and N. B. LIBROVICH. Zh. Fiz. Khim. **47**, 2298 (1973); Engl. Transl. **47**, 1295 (1973).
43. N. B. LIBROVICH and V. D. MAIOROV. Izv. Akad. Nauk SSSR, Ser. Khim. 684 (1977); Engl. Transl. 621 (1977).

Can. J. Chem. Downloaded from www.nrcresearchpress.com by 210.87.254.42 on 09/06/12
For personal use only.

Heat capacities and volumes of dilute aqueous solutions of 1,3-dioxane and trioxane

GÉRALD PERRON AND JACQUES E. DESNOYERS[1]

Department of Chemistry, Université de Sherbrooke, Sherbrooke, P.Q., Canada J1K 2R1

Received February 9, 1981

GÉRALD PERRON and JACQUES E. DESNOYERS. Can. J. Chem. **59**, 2599 (1981).

The densities and heat capacities per unit volume of 1,3-dioxane and trioxane were measured in water at 25°C in the concentration range 0.1 to 1 mol kg^{-1}. Apparent molal volumes ϕ_V and heat capacities ϕ_C were derived. The infinite dilution ϕ_V^0 shows excellent group additivity with other cyclic ethers in water but the additivity is less satisfactory for ϕ_C^0. No simple correlation can be made for the concentration dependence of these functions.

GÉRALD PERRON et JACQUES E. DESNOYERS. Can. J. Chem. **59**, 2599 (1981).

Les masses volumiques et capacités calorifiques du 1,3-dioxane et du trioxane ont été mesurées dans l'eau à 25°C pour des concentrations de 0.1 à 1 mol kg^{-1}. Les volumes et capacités calorifiques molaires apparents, ϕ_V et ϕ_C, ont été calculés. Les valeurs à dilution infinie ϕ_V^0 montrent une excellente additivité de groupe avec les autres valeurs d'éthers cycliques. Par contre l'addivité de groupe est beaucoup moins bonne dans le cas de ϕ_C^0. On ne peut pas établir de corrélation simple entre les variations de ces fonctions avec la concentration.

Can. J. Chem. Downloaded from www.nrcresearchpress.com by 210.87.254.42 on 09/06/12
For personal use only.

In a general study of Gibbs free energies and enthalpies of solute–solute interactions of cyclic ethers in water (1) it was necessary to know the heat capacities of the same systems. Tetrahydropyran (THP) and 1,4-dioxane (*p*-D) have already been investigated (2) but not 1,3-dioxane (*m*-D) and trioxane (T). The purpose of this article is to extend our heat capacity measurements to these two latter nonelectrolytes in water. Accurate densities are also required to calculate apparent molal heat capacities ϕ_C. Apparent molal volumes ϕ_V will therefore also be reported. These data, when combined with those of THP and *p*-D should be useful in discussing group additivity to the standard ϕ_V^0 and ϕ_C^0 and to the solute–solute interaction parameters.

As in previous studies (2), differences in the densities Δd of the solution and of the solvent and relative changes in the heat capacities per unit volume $\Delta\sigma/\sigma_0$ of the solution were determined with a flow densimeter and a flow microcalorimeter, both purchased from SODEV.

Reagents used in this study were obtained and purified as follows: *m*-D from Fluka (Purum) was dried over 3 Å molecular sieves; T from Matheson, Coleman and Bell was recrystallized from water and dried over $CaCl_2$. Solutions were prepared by weight with deionized distilled water. All measurements were made at 25°C.

Results of the measurements of apparent molal volumes and apparent molal heat capacities are given in Table 1. Apparent molal volumes and heat capacities were calculated in the usual method (2, 3). Results for ϕ_V were fitted as a function of concentration by the equation

$$[1] \quad \phi_V = \phi_V^0 + A_V m$$

Similarly, ϕ_C were fitted by the equation

$$[2] \quad \phi_C = \phi_C^0 + A_C m$$

Results of the least-squares fit for these and other compounds of interest from the literature are given in Table 2. Volumes of *m*-D and T were also measured by Lepori and Mollica (4) who obtained $\phi_V^0 = 80.82\,\text{cm}^3\,\text{mol}^{-1}$ and $69.51\,\text{cm}^3\,\text{mol}^{-1}$, respectively. These results agree very well with the present data.

The group additivity of ϕ_V^0 appears to be reasonably good since the average of the THP and T, $80.66\,\text{cm}^3\,\text{mol}^{-1}$, is very close to *m*-D. However, the additivity for ϕ_C^0 is less good since the average of THP and T is 287 J K^{-1} mol^{-1}, which is 44 J K^{-1} mol^{-1} larger than *m*-D. It also should be noted that ϕ_C^0 of the two isomers, *m*-D and *p*-D, differ significantly. (The experimental uncertainty in ϕ_C^0 should not be more than 5 J K^{-1} mol^{-1}). The average group contributions are

Group	ϕ_V^0 (cm^3 mol^{-1})	ϕ_C^0 (J K^{-1} mol^{-1})
CH_2	17.14±0.6	74±16
O	6.08±0.6	−16±16

These group contributions to ϕ_V^0 are in reasonably good agreement with straight chain ethers (5) but again the ϕ_C^0 are significantly different. For example, for straight chain ethers the O contribution to ϕ_C^0 is −57 J K^{-1} mol^{-1}.

The parameters A_V normally become more neg-

[1]To whom all correspondence should be addressed.

0008-4042/81/172599-02$01.00/0

©1981 National Research Council of Canada/Conseil national de recherches du Canada

TABLE 1. Volumes and heat capacities of some cyclic ethers in water at 25°C

Solute	m (mol kg^{-1})	$10^3\,\Delta d$ (g cm^{-3})	ϕ_V (cm^3 mol^{-1})	$10^3\,\Delta\sigma/\sigma_0$	ϕ_C (J K^{-1} mol^{-1})
m-D	0.10227	0.781	80.61		
	0.18977	1.440	80.62		
	0.28066	2.119	80.61	−6.45	237.7
	0.30479	2.305	80.58	−6.88	239.2
	0.34085	2.570	80.58	−7.79	237.7
	0.40646	3.054	80.57	−9.23	237.7
	0.50577	3.786	80.53	−11.5	236.5
	0.59950	4.468	80.51	−13.8	234.5
	0.81022	5.960	80.49	−18.6	233.3
	0.89871	6.571	80.49	−20.5	233.0
	0.99338	7.221	80.48	−22.8	231.8
T	0.10126	2.074	69.60	−2.54	184.4
	0.20494	4.166	69.61	−5.16	183.3
	0.28273	5.706	69.65	−7.16	182.3
	0.38315	7.679	69.65	−9.78	180.7
	0.45901	9.153	69.65	−11.8	179.4
	0.55055	10.903	69.66	−14.1	179.2
	0.73908	14.431	69.70	−18.9	178.1
	0.78508	15.273	69.71	−20.1	177.6
	0.86733	16.763	69.73	−22.2	177.2
	1.06454	20.276	69.77	−27.4	175.2

TABLE 2. Apparent molal volumes and heat capacities of cyclic ethers in water at 25°C[a]

Solute	ϕ_V^0 (cm^3 mol^{-1})	A_V (cm^3 mol^{-2} kg)	ϕ_C^0 (J K^{-1} mol^{-1})	A_C (J K^{-1} mol^{-2} kg)
THP	91.74[b]	−1.0	385[b]	0.6
m-D	80.64	−0.17(0.015)	241	−9.4(0.6)
p-D	80.94[b]	−0.11	220[b]	−10.5
T	69.58	0.17(0.01)	185	−9.2(0.6)

[a] Standard error of fit in parentheses.
[b] From Kiyohara *et al.* (2) corrected as indicated by Desnoyers *et al.* (3).

ative and A_C more positive as the hydrophobic character of the solute increases. This trend is followed by THP when compared with *m*-D and *p*-D. However, these parameters are not as expected for T since they are close to the values of the dioxanes. This is in contrast with enthalpic interaction parameters which showed a good additivity for all cyclic ethers.

Acknowledgement

We are grateful to the Natural Sciences and Engineering Research Council of Canada for financial support.

1. B. Y. OKAMOTO, R. H. WOOD, J. E. DESNOYERS, G. PERRON and L. DELORME. J. Solution Chem. In press.
2. O. KIYOHARA, G. PERRON, and J. E. DESNOYERS. Can. J. Chem. **53**, 2591 (1975).
3. J. E. DESNOYERS, C. de VISSER, G. PERRON, and P. PICKER. J. Solution Chem. **5**, 605 (1976).
4. L. LEPORI and V. MOLLICA. J. Chem. Eng. Data, **23**, 65 (1978).
5. G. PERRON and J. E. DESNOYERS. Fluid Phase Equil. **2**, 239 (1979).

Can. J. Chem. Downloaded from www.nrcresearchpress.com by 210.87.254.42 on 09/06/12
For personal use only.

Nucleic acid related compounds. 33. Conversions of adenosine and guanosine to 2,6-dichloro, 2-amino-6-chloro, and derived purine nucleosides[1]

MORRIS J. ROBINS and BOGDAN UZNAŃSKI[2]

Department of Chemistry, The University of Alberta, Edmonton, Alta., Canada T6G 2G2

Received March 2, 1981

MORRIS J. ROBINS and BOGDAN UZNAŃSKI. Can. J. Chem. **59**, 2601 (1981).

Enzymatic deamination of adenosine 1-*N*-oxide gave 1-hydroxyinosine (**2***a*) which was acetylated and then chlorinated to give 2,6-dichloro-9-(2,3,5-tri-*O*-acetyl-β-D-ribofuranosyl)purine (**3**). Ammonia in dry 1,2-dimethoxyethane converted **3** into 2-chloroadenosine triacetate (**4***a*). Treatment of **4***a* with trimethylamine at elevated temperatures in acetonitrile resulted in formation of 2-*N*,*N*-dimethylaminoadenosine triacetate (**4***b*). Guanosine (**5**) was acetylated smoothly by an improved procedure. The resulting triacetate (**6**) was chlorinated in ~85% yield to give 2-amino-6-chloro-9-(2,3,5-tri-*O*-acetyl-β-D-ribofuranosyl)purine (**7**). Treatment of **7** with trimethylamine at ambient temperature for 28 hours gave the 6-*N*,*N*-dimethylamino compound (**8***d*). However, potassium fluoride or sodium azide with catalytic quantities of trimethylamine in DMF or acetonitrile gave the 2-amino-6-fluoro (**8***a*) or 2-amino-6-azido (**8***b*) products in yields of greater than 90%.

MORRIS J. ROBINS et BOGDAN UZNAŃSKI. Can. J. Chem. **59**, 2601 (1981).

La désamination enzymatique du *N*-oxyde-1 d'adénosine conduit à l'hydroxy-1 inosine (**2***a*) qui par une acétylation, suivie d'une chloration donne la dichloro-2,6 (tri-*O*-acétyl-2,3,5 β-D-ribofurannosyl)-9 purine (**3**). Le composé **3** dans l'ammoniac avec le diméthoxy-1,2 éthane anhydre se transforme en triacétate de chloro-2 adénosine (**4***a*). Ce dernier, à haute température, réagit avec la triméthylamine dans l'acétonitrile pour donner le triacétate de *N*,*N*-diméthylamino-2 adénosine (**4***b*). Grâce à une méthode convenable on a acétylé facilement la guanosine (**5**). La chloration du triacétate (**6**) ainsi obtenu conduit avec un rendement de 85% à l'amino-2 chloro-6 (tri-*O*-acétyl-2,3,5 β-D-ribofurannosyl)-9 purine (**7**). Le composé **7** réagit avec la triméthylamine pendant 28 heures à la température de la pièce en donnant le composé *N*,*N*-diméthylamino-6 (**8***d*). Cependant le fluorure de potassium ou l'azoture de sodium en présence de quantités catalytiques de triméthylamine dans le DMF ou dans l'acétonitrile conduit aux composés fluoro-6 (**8***a*) ou amino-2 azido-6 (**8***b*) avec des rendements supérieurs à 90%.

[Traduit par le journal]

Potent effects on blood pressure and platelet aggregation are exerted by 2-chloroadenosine and related nucleoside derivatives (2). The cytotoxic 2-fluoroadenosine and modified sugar analogues have been studied as anticancer agents (3). Paterson and co-workers have observed recently that 6-*S*-(*p*-nitrobenzyl)thioinosine, a strong competitive inhibitor of nucleoside transport across cell membranes, exerts protection against toxic effects of certain nucleoside antibiotics and anticancer agents in animals (4). This observation stimulated our interest in evaluation of host protection against toxicity of 2-halopurine nucleosides. We have explored alternative routes to 2- and 6-chloro 2,6-disubstituted purine nucleosides from adenosine and guanosine. We now describe improved syntheses of acetyl-protected 6-amino-2-chloro- and 2-amino-6-chloropurine ribonucleosides. These have been converted to useful related 2 and 6 disubstituted compounds by nucleophilic replacements.

Syntheses of 2-halopurine nucleosides usually have employed classical methods of coupling a purine base with an activated carbohydrate derivative (5). The Fischer–Helferich condensation of the silver salt of 2,8-dichloroadenine with tetraacetylglucosyl bromide (6) was the original prototype for synthesis of the naturally occurring purine ribonucleosides (7). Nucleophilic replacements and hydrolytic diazotizations at C-2 and C-6 provided the natural amino and oxo substituents. Unwanted halo groups were removed reductively. More recent coupling methods have employed 2 and 6 disubstituted purines to give dihalo and aminohalo nucleosides (5,8). Montgomery and co-workers have used 2,6-dichloro- (**3***b*) and 2,6-diacetamidopurine (9) in coupling reactions followed by transformations to give fluoropurine nucleosides. Robins and co-workers have performed 6-chloro- to 6-fluoropurine conversions using silver fluoride in hot xylene (10). They also have utilized diazotization in aqueous acid for the introduction of chloro and fluoro groups (11). Kiburis and Lister have reported displacement of trimethylamine from 6-*N*-purinyltrimethylammonium chloride salts using potassium fluoride (12), a procedure applied successfully by ourselves for the synthesis of the 6-fluoropurine 2′-deoxyribonucleoside (13).

Owing to the high cost and limited availability of

[1]For the previous paper in this series see ref. 1.

[2]Postdoctoral Fellow 1979–1980. On leave from the Center of Molecular and Macromolecular Studies, Polish Academy of Sciences, 90–362 Łódź, Boczna 5, Poland.

0008-4042/81/172601-07$01.00/0

©1981 National Research Council of Canada/Conseil national de recherches du Canada

Can. J. Chem. Downloaded from www.nrcresearchpress.com by 210.87.254.40 on 09/06/12
For personal use only.

Can. J. Chem. Downloaded from www.nrcresearchpress.com by 210.87.254.40 on 09/06/12
For personal use only.

2,6-dichloropurine plus the yield and isomer considerations involved in base–sugar coupling methods (5,9), we opted for transformations of naturally occurring nucleosides (14). A sequence for conversion of adenosine (**1**) to 2,6-dichloro-9-(2,3,5-tri-*O*-acetyl-β-D-ribofuranosyl)purine (**3**) had been reported (15). Oxidation of **1** with *m*-chloroperoxybenzoic acid in aqueous acetic acid/dioxane gave adenosine 1-*N*-oxide in 96% yield.[3] Kawashima and Kumashiro used chemical deamination of this product to give 1-hydroxyinosine (**2***a*) in 56% crude yield (15). However, we employed adenosine deaminase to effect this conversion cleanly in 88% crystallized yield without formation of colored by-products. Acetylation of **2***a* to the tetraacetate (**2***b*) followed by treatment with aqueous pyridine gave 2′,3′,5′-tri-*O*-acetyl-1-hydroxyinosine (**2***c*). Phosphoryl chloride in hot 2-picoline converted **2***c* → **3** in 73% yield. With these improvements, the overall yield from **1** → **3** was 61%.[4]

Treatment of **3** with anhydrous ammonia in dry 1,2-dimethoxyethane (DME) effected nucleophilic replacement of the 6-chloro function without ammonolysis of the ester groups.[5] The resulting 2-chloroadenosine triacetate (**4***a*) was treated with trimethylamine in acetonitrile at elevated temperatures in a sealed pressure vessel. The sole nucleoside product isolated was 2-*N*,*N*-dimethylaminoadenosine triacetate (**4***b*). Carefully purified (dimethylamine-free) trimethylamine neat or in acetonitrile also converted **4***a* → **4***b*. The presumed intermediate 2-*N*-purinyltrimethylammonium chloride salt (**A**) was not observed. Temperatures required to effect displacement of the 2-chloro function from **4***a* apparently result in the facile displacement of amine nitrogen by attack of chloride on a methyl carbon of **A** to give **4***b*. Attempted *in situ* generation of **A** from **4***a* using excess potassium fluoride in the presence of trimethylamine again resulted in formation of **4***b*.[6] However, the *in situ* procedure functions smoothly at C-6 (*vide infra*).

A simple acetylation of guanosine (**5**) was reported in 1947 (19). However, this often quoted preparation employed inconvenient quantities of acetic anhydride and pyridine and can give rigid suspensions of incompletely acetylated products in larger scale work. An improved procedure that utilizes acetic anhydride and pyridine in *N*,*N*-dimethylformamide (DMF) to give clear solutions and yields of ~87% of 2′,3′,5′-tri-*O*-acetylguanosine (**6**) is described in the Experimental.

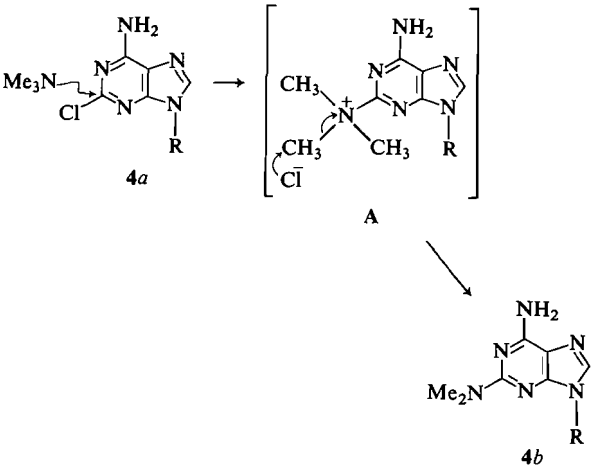

Chlorination of **6** has been studied previously (20) and improved procedures have been reported (21). However, the reaction conditions, especially heating, were difficult to duplicate with different sized preparations. Decomposition occurred in the heated mixtures and our yields of the crystalline 2-amino-6-chloro product (**7**) using those procedures seldom exceeded 50%.

We have examined this reaction utilizing ^{31}P nmr spectroscopy. A reference sample of $POCl_3$ in acetonitrile gave a broad ^{31}P singlet at 4.18 ppm from external H_3PO_4. Chlorination reaction conditions were simulated in an nmr tube containing phosphoryl chloride, *N*,*N*-dimethylaniline, and **6** in acetonitrile in a probe heated at 70°C. A second ^{31}P signal (sharp singlet) at −1.17 ppm (upfield from H_3PO_4) was observed immediately. A third singlet at −7.9 ppm increased steadily over a period of one hour. During this time, the peak at −1.17 ppm diminished to an insignificant intensity. Several aromatic phosphorodichloridates give ^{31}P singlets in the range of 1 to −2.5 ppm (22). A sample of dichlorophosphoric acid in acetonitrile gave a ^{31}P signal in the range of −2.96 to −8.85 depending on the amount of *N*,*N*-dimethylaniline present.

These data are compatible with phosphorylation of **6** to give the aromatic phosphorodichloridate intermediate (**B**) followed by attack of chloride at C-6 of **B** to give **7** plus dichlorophosphate (**C**). A higher concentration of external chloride anions should favor conversion of **B** → **7** before decompo-

[3]This modification of the procedures of Brown and MacCoss and their co-workers (16) will be published as part of an unrelated study with Dr. F. Hansske.

[4]An alternative synthesis was developed which requires only three steps from guanosine (**5**) and gives **3** in 64% overall yield (17).

[5]Ammonia in alcohol or liquid ammonia, used without drying, effects concomitant ammonolysis of the ester groups (18).

[6]An alternative approach employing nonaqueous diazotization has been developed for convenient fluorination at C-2 (17).

Can. J. Chem. Downloaded from www.nrcresearchpress.com by 210.87.254.40 on 09/06/12
For personal use only.

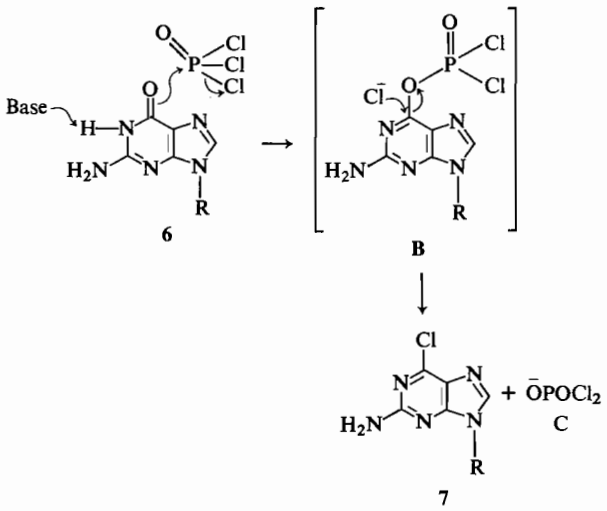

sition occurred. Indeed, addition of tetraethylammonium chloride to an identically prepared nmr experiment resulted in disappearance of the intermediate ^{31}P singlet at -1.49 ppm within 10 minutes. A singlet at -10.65 ppm increased steadily over the 10 minute period. Use of analogous carefully anhydrous reaction conditions described in the Experimental gave readily repeatable yields of ~85% of crystalline **7**.

Treatment of **7** with excess trimethylamine at room temperature for an extended time resulted in formation of the 6-*N*,*N*-dimethylamino derivative (**8***d*). A fluorescent salt-like product was formed with complete disappearance of **7** (tlc) within one hour at room temperature. Treatment of this hygroscopic solid with potassium fluoride in DMF at elevated temperature resulted in formation of a mixture of 2-amino-6-fluoro (**8***a*) and 2-amino-6-chloro (**7**) nucleosides. However, treatment of **7** with a catalytic quantity of trimethylamine and excess potassium fluoride in DMF at room temperature resulted in clean conversion to **8***a* in 93% yield.

Analogous conversion of **7** to **8***b* was effected quantitatively using sodium azide in acetonitrile with trimethylamine as catalyst. The nmr spectra of **8***b* were compatible with a 6-azido ⇄ cyclic tetrazole equilibrium (23). This phenomenon was not investigated further since smooth hydrogenolysis of **8***b* occurred to give 2-aminoadenosine triacetate (**8***c*) in 98% crude yield overall from **7**.

The present improved syntheses of **6** and **7** allow convenient and high yield preparation of the useful intermediates **7** and **8***a*–*c*. The solid-solution phase transfer catalysis employed in the conversions of **7** → **8***a* or **8***b* is a useful improvement over the stoichiometric quaternary salt procedure of Lister (12). The soluble nucleoside **7** reacts with trimethylamine to give the quaternary ammonium salt. Transfer of chloride to the solid phase as its less soluble sodium or potassium salt occurs concomitantly with anion exchange for azide or fluoride. Nucleophilic replacement at C-6 by the solubilized anion releases trimethylamine for the catalytic cycle. The ambient temperature allows selective displacement at C-6 without competing formation of the 6-*N*,*N*-dimethylamino by-product (**8***d*). However, this catalytic process did not function successfully at C-2. The reduced reactivity at the 2-position results in favored nucleophilic attack at the methyl carbon of the quaternary salt leading to formation of the 2-*N*,*N*-dimethylamino compound (**4***b*) as the exclusive product. Therefore, nonaqueous diazotization reactions have been developed to provide convenient access to the 2-halopurine nucleosides (17).

Experimental

General

Melting points were obtained on a Reichert microstage block and are uncorrected. Ultraviolet (uv) spectra were recorded using a Cary 15 spectrophotometer. The ^1H nmr spectra were determined using Bruker 90 or Varian 100-MHz spectrometers with Me_4Si as internal reference and $CDCl_3$ as solvent unless Me_2SO-d_6 is specified. Acetyl methyl singlets and base proton peaks are given. Sugar proton multiplets were as expected. The ^{19}F nmr spectra were determined in $CDCl_3$ unless Me_2SO-d_6 is specified. ^{19}F chemical shifts are expressed in δ ppm upfield (minus sign) from CCl_3F as internal reference. Mass spectra (ms) were measured at 70 eV with an AEI MS-50 instrument with coupled computer analysis using direct probe sample introduction at 150–230°C by the mass spectral laboratory of this department. The molecular ion (M^+), 2,3,5-tri-*O*-acetyl-D-ribofuranosyl ion ($M^+ - B = C_{11}H_{15}O_7 = 259.0818$), and the substituted purinyl ion (B) or a protonated species (BH or BH_2) are given with their % relative intensities if observed in the spectrum.

Trimethylamine was purified by heating with acetic anhydride, distillation *in vacuo*, and storage over CaH_2. Reagent grade acetonitrile and DMF were heated with and then distilled directly *in vacuo* from P_2O_5 into a flame-dried reaction flask assembly to provide rigorously anhydrous solvents. Chloroform, pyridine, 1,2-dimethoxyethane, 1,4-dioxane, dibromomethane, dichloromethane, 1,2-dichloroethane, and methanol were distilled and stored over drying agents. Silica refers to Mallinckrodt CC-7 silica gel for chromatography.

Evaporations were effected wtih a Buchler rotary evaporator equipped with a Dewar Dry-Ice condenser at mechanical oil pump (*in vacuo*) or water aspirator vacuum at room temperature.

1-Hydroxyinosine (2a)

Adenosine deaminase (100 mg, Sigma type II, crude from calf intestinal mucosa) was added to a solution of 1.0 g (3.5 mmol) of adenosine 1-*N*-oxide (16) in 200 mL of 0.05 *M* $NaH_2PO_4/Na_2HPO_4/H_2O$ buffer at pH 7.5. The solution was allowed to stand for 3 days at room temperature and was then evaporated to ~50 mL *in vacuo*. This concentrate was applied to a column of 120 mL of Amberlite IR-120 (H^+) resin and the column was developed with

Can. J. Chem. Downloaded from www.nrcresearchpress.com by 210.87.254.40 on 09/06/12
For personal use only.

Reaction Scheme

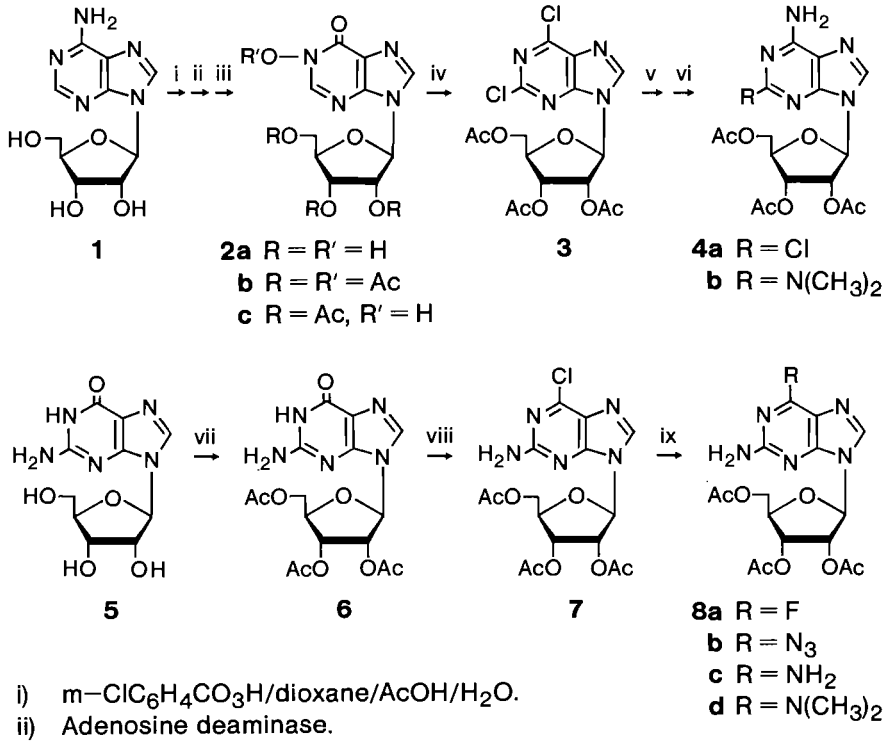

i) m−$ClC_6H_4CO_3H$/dioxane/AcOH/H_2O.
ii) Adenosine deaminase.
iii) Ac_2O/Pyridine, then H_2O.
iv) $POCl_3$ /2-picoline.
v) NH_3 / DME.
vi) $Me_3N/CH_3CN/\Delta$.
vii) Ac_2O/Pyridine/DMF.
viii) $POCl_3$ /$PhNMe_2$ /Et_4NCl/MeCN.
ix) a) KF/Me_3N/DMF.
b) NaN_3 /Me_3N/CH_3CN followed by
c) H_2 /Pd·C.
d) NMe_3 /CH_3CN.

SCHEME 1

H_2O. Appropriate fractions (~3L, uv detector) were pooled and evaporated *in vacuo*. The residue was crystallized from 95% EtOH to give 875 mg (88%) of colorless crystals of **2***a*, mp ~210°C dec.; uv (0.1 *N* HCl) max:251 nm (ε 9500); (0.1 *N* NaOH) max:294, 256, 228 nm (ε 4200, 6800, 29 700); ms *m*/*z*:284.0760 (3.5%, M^+ [$C_{10}H_{12}N_4O_6$] = 284.0756), 152.0331 (100%, BH = 152.0334). Literature mp > 200°C dec (15); > 400°C with decomposition above 170°C (24); lit. uv (pH 3) max:251 nm (ε 9100); (pH 9) max:294, 256, 229 nm (ε 4000, 6300, 30 000) (24).

2′,3′,5′-Tri-O-acetyl-1-hydroxyinosine (2c)

A 1 g sample of adenosine 1-*N*-oxide was deaminated by stirring with adenosine deaminase in 100 mL of pH 7.5 buffer for 35 h at room temperature. A 50 mL portion of 1-butanol was added and the mixture was evaporated *in vacuo*. The residue was dried for 15 h at 0.1 Torr and then 10 mL of pyridine and 20 mL of Ac_2O were added. The mixture was sonicated for 1 h and then stirred at room temperature for 9 h. The mixture was cooled and 50 mL of 1-butanol was added. The volume was reduced to ~30 mL and 3 successive portions of 50 mL of 1-butanol were added and evaporated *in vacuo*. Chloroform (50 mL) was added to the heavy suspension which was filtered using a membrane filter. This filtrate contained 2′,3′,5′-tri-*O*-acetyl-1-*N*-acetyloxyinosine (**2***b*) as indicated by four ^1H nmr acetyl methyl singlets at δ 2.10, 2.12, 2.14, and 2.45 in addition to the other expected proton signals. Compound **2***b* gave ms *m*/*z*:452 (3.6%, M^+ [$C_{18}H_{20}N_4O_{10}$] = 452), 259 (100%, M^+ − B) at low resolution at 200°C and 17 eV.

The filtrate was evaporated and the residual **2***b* was dissolved in 1,4-dioxane (40 mL), pyridine (5 mL), and water (2 mL). The resulting solution was stirred for 48 h at room temperature to ensure complete hydrolysis of the 1-*N*-acetyloxy function. Addition of 50 mL of 1-butanol was followed by slow evaporation of solvents to ~30 mL, during which crystallization of product occurred. The crystals were filtered, washed with 2-propanol, and dried *in vacuo* to give 1.12 g of **2***c*. The filtrate

Can. J. Chem. Downloaded from www.nrcresearchpress.com by 210.87.254.40 on 09/06/12
For personal use only.

was concentrated to ~1 mL and a further 138 mg of product was collected to give 1.26 g (88%) of **2***c*, mp 194–195°C (mp values of 203–205°C and 206–210°C also were observed depending on the rate of heating); lit. (15) mp 194.5–195.5°C; uv (0.1 *N* HCl/MeOH 9:1) max:251 nm (ε 9000); (0.1 *N* NaOH/MeOH 9:1) max:294, 256 nm (ε 4400, 6200); (MeOH) max:270 (sh), 251, 245 nm (ε 4100, 7600, 7600); ^{1}H nmr δ:2.08, 2.12, 2.14 (OAc's), 8.01 (s, 1, H-2), 8.40 (s, 1, H-8); ms *m/z*:410.1084 (2.3%, M^+ $[C_{16}H_{18}N_4O_9]$ = 410.1074, 259.0818 (100%, M^+–B), 153.0412 (14%, BH_2 = 153.0412).

*9-(2,3,5-Tri-*O*-acetyl-*β*-*D*-ribofuranosyl)-2,6-dichloropurine (**3**)*

A mixture of 0.9 g (2.2 mmol) of **2***c*, 3 mL of dried 2-picoline, and 10 mL of freshly distilled phosphoryl chloride was heated at reflux for 1 h. The red-brown solution was evaporated and the brown oily residue was dissolved in 10 mL of $CHCl_3$ and applied to a column of 30 mL of silica. The product was eluted with acetone/chloroform/cyclohexane 2:3:1. The orange eluate was evaporated and the residue again dissolved in 10 mL of $CHCl_3$ and applied to a layered column (1.5 cm dia) of 0.5 cm of silica, 5 cm of decolorizing carbon, and 1 cm of silica. The product was eluted with $CHCl_3$ and the 200 mL of eluate was evaporated. Addition of 3 mL of 1-butanol and partial evaporation resulted in separation of crystals which were filtered, washed with cold ether, and dried *in vacuo* to give 716 mg (73%) of **3**, mp 162–163°C; lit. (15) mp 160–161°C; uv (MeOH) max:273, 252 nm (ε 9100, 5100); ^{1}H nmr δ:2.04, 2.09, 2.12 (OAc's), 8.28 (s, 1, H-8); ms *m/z*:446.0392 (1.1%, M^+ $[C_{16}H_{16}Cl_2N_4O_7]$ = 446.0396), 259.0823 (100%, M^+–B).

*2',3',5'-Tri-*O*-acetyl-2-chloroadenosine (**4**a)*

Dry ammonia gas (passed through a drying tube packed with CaH_2) was bubbled slowly through a solution of 1.0 g (2.2 mmol) of **3** (dried at 60°C *in vacuo*) in 20 mL of dry 1,2-dimethoxyethane (distilled directly from NaH into the dried reaction flask) at room temperature for 8 h. The solution was evaporated and the colorless residue was treated with 10 mL of $CHCl_3$. This suspension was applied to a column of silica (50 g, 2 × 45 cm). Chloroform/acetone with an increasing gradient of acetone was used for elution. The appropriately pooled fractions were evaporated and the resulting colorless solid foam was dissolved in chloroform/2-propanol. The product crystallized upon slow evaporation of the solution. It was filtered, washed with ether, and dried to give 857 mg (91%) of **4***a*, mp 151–152°C; uv (MeOH) max:263 nm (ε 15 500); ^{1}H nmr δ:2.11, 2.17, 2.18 (OAc's) 7.97 (s, 1, H-8); ms *m/z*:427.0906 (6.1%, M^+ $[C_{16}H_{18}ClN_5O_7]$ = 427.0895), 259.0823 (100%, M^+–B). The corresponding deacylated nucleoside has a reported uv (pH 7) max:264 nm (ε 15 200) (8*e*).

*2',3,5'-Tri-*O*-acetyl-2-*N,N*-dimethylaminoadenosine (**4**b)*

A sealed ampule containing 130 mg (0.3 mmol) of **4***a* (dried *in vacuo* at 100°C for 2 h), 350 mg (6 mmol) of purified trimethylamine, and 1 mL of rigorously dried acetonitrile was heated at 100°C for 6 h inside a steel pressure bomb. After cooling to room temperature the ampule was opened and the mixture was filtered through a short column (1 × 1 cm) of silica. The column was washed with 50 mL of $CHCl_3$ and the combined eluate was evaporated to dryness. The residue was crystallized from 1-propanol, washed with ether, and dried to give 120 mg (92%) of **4***b*, mp 169–170°C; uv (MeOH) max:292, 264, 228 nm (ε 9000, 13 000, 22 400); (0.1 *N* HCl/MeOH 8:2) max:306, 260 nm (ε 9000, 16 400); (0.1 *N* NaOH/MeOH 8:2) max:294, 262 nm (ε 8400, 12 800); ^{1}H nmr δ:2.06, 2.12, 2.13 (OAc's), 3.16 (s, 6, NMe_2), 7.52 (s, 1, H-8); ms *m/z*:436.1711 (47%, M^+ $[C_{18}H_{24}N_6O_7]$ = 436.1706), 259.0817 (6.1%, M^+–B), 178.0964 (100%, BH = 178.0966). The corresponding deacylated nucleoside has reported uv (pH 1) max:305, 261 nm (ε 8760, 16 200); (pH 13) max:295, 262 nm (ε 8320, 12 500) (8*c*).

*2',3',5'-Tri-*O*-acetylguanosine (**6**)*

A mixture of 14.2 g (0.05 mol) of guanosine (**5**) (pre-dried *in vacuo* at 100°C for 2 days over P_2O_5), 30 mL of acetic anhydride, 15 mL of dry pyridine, and 40 mL of DMF was heated at 75°C with stirring for 3.75 h. The resulting clear solution was filtered while hot, cooled to room temperature, and evaporated *in vacuo* to a heavy crystalline suspension. The residue was treated with 50 mL of 2-propanol and filtered. The filter cake was washed with 2-propanol and dried to give 20.9 g (94%) of white crystals of **6** as the hemi-solvate (^{1}H nmr δ 2.82 (d, 3, 0.5 DMF)). This product was added to 750 mL of boiling 2-propanol with vigorous magnetic stirring. The partially dissolved suspension was stirred at reflux for 5 min and then was refrigerated at −5°C overnight. The product was filtered, washed with 2-propanol, and dried *in vacuo* at 80°C over P_2O_5 to give 17.88 g (87.4%) of tlc homogeneous **6**, mp ~230–233°C (softening from 195°C); lit. (19) mp 232°C; uv (MeOH) max:256 nm (ε 14 500); ^{1}H nmr (Me_2SO-d_6) δ:2.04 (s, 6, two OAc's), 2.10 (s, 3, OAc), 6.5 (s, 2, NH_2), 7.96 (s, 1, H-8).

*9-(2,3,5-Tri-*O*-acetyl-*β*-*D*-ribofuranosyl)-2-amino-6-chloropurine (**7**)*

Acetonitrile (50 mL) was distilled directly from P_2O_5 into a flask containing 10.23 g (0.025 mol) of pre-dried **6** and 8.3 g (0.05 mol) of Et_4NCl (pre-dried *in vacuo* at 85°C overnight over P_2O_5). *N,N*-Dimethylaniline (3.2 mL, 0.025 mol, dried over and distilled from CaH_2) and phosphoryl chloride (13.7 mL, 0.15 mol, freshly distilled) were added to the stirred solution at room temperature. The flask was placed in an oil bath preheated to 100°C and the solution was heated with stirring at reflux for 10 min. Volatile materials were flash evaporated immediately *in vacuo*. The resulting yellow foam was dissolved in 150 mL of $CHCl_3$ and stirred vigorously with crushed ice for 15 min. The layers were separated and the aqueous phase was extracted with 5 × 50 mL of $CHCl_3$. The combined organic phase was kept cold by addition of crushed ice. It was washed with 6 × 30 mL of cold water, 5% $NaHCO_3/H_2O$ to pH ~7, dried over $MgSO_4$ for 1 h, and filtered. A 60 mL portion of 2-propanol was added and the combined filtrate was slowly evaporated *in vacuo* to ~40 mL. The crystalline product that had separated was filtered, washed with 2-propanol (20 mL), and dried *in vacuo* overnight to give 9.31 g (87%) of crude **7**. This product was recrystallized from 90 mL of boiling 2-propanol to give 9.03 g (85%) of purified **7**, mp 152–153°C; lit. (20) mp 147.5–148.5°C; uv (MeOH) max:311, 249 nm (ε 7700, 7800); lit. (20) uv (EtOH) max:310, 249 nm (ε 7900, 8600); ^{1}H nmr δ:2.06, 2.08, 2.14 (OAc's), 5.70 (br, 2, NH_2), 7.94 (s, 1, H-8).

*9-(2,3,5-Tri-*O*-acetyl-*β*-*D*-ribofuranosyl)-2-amino-6-*N,N*-dimethylaminopurine (**8**d)*

A solution of 214 mg (0.5 mmol) of **7** (dried for 2 days over P_2O_5 in a desiccator) and 200 mg (3.4 mmol) of purified Me_3N in 4 mL of rigorously dried acetonitrile was allowed to stand at room temperature for 28 h in a sealed flask. The solution was evaporated to dryness. The residue was treated with 2 mL of $CHCl_3$ and applied to a silica column (1 × 5 cm) which was eluted with 100 mL of $CHCl_3$. The eluate was evaporated to a heavy syrup which crystallized upon exposure to ether overnight in a sealed desiccator (diffusion crystallization). The crystals were filtered, washed with ether, and dried to give 192 mg (88%) of **8***d*, mp 127–128°C; uv (MeOH) max:285, 267 (sh), 230 nm (ε 14 200, 10 600, 20 200); (0.1 *N* HCl/MeOH 8:2) max:300, 257 nm (ε 13 000, 12 000); (0.1 *N* NaOH/MeOH 8:2) max:284, 267 (sh) nm (ε 14 600, 10 400); ^{1}H nmr δ:2.05, 2.08, 2.10 (OAc's), 3.40 (s, 6, NMe_2), 4.67 (br s, 2, NH_2), 7.55 (s, 1, H-8); ms *m/z*:436.1710 (55%, M^+ $[C_{18}H_{24}N_6O_7]$ = 436.1706),259.0818 (5.7%, M^+–B), 178.0962 (100%, BH = 178.0966). The corres-

Can. J. Chem. Downloaded from www.nrcresearchpress.com by 210.87.254.40 on 09/06/12
For personal use only.

ponding deacylated nucleoside has reported uv (H_2O) max:284, 268 (sh), 228 nm (ε 15 600, 11 500, 19 100) (25).

9-(2,3,5-Tri-O-acetyl-β-D-ribofuranosyl)-2-amino-6-fluoropurine (8a)

A suspension of 4 g (69 mmol) of KF (dried *in vacuo* over a cold flame for 0.5 h) in a solution of 127 mg (2.1 mmol) of purified Me_3N (distilled directly into the flask *in vacuo* from CaH_2) and 2 g (4.7 mmol) of dried **7** in 45 mL of DMF (distilled directly into the flask *in vacuo* from CaH_2) was stirred vigorously at room temperature for 14 h. The mixture was evaporated to dryness *in vacuo*, the residue was treated with 50 mL of $CHCl_3$, and the suspension was filtered using a membrane filter. The filtrate was evaporated partially and 20 mL of 1-propanol was added. This was evaporated partially and a second 20 mL of 1-propanol was added. Evaporation was continued to ~10 mL. The separated crystalline product was filtered and washed with 1-propanol and then ether to give 1.78 g of **8a**. An additional 55 mg of product was recovered from the filtrate. The combined product was recrystallized from 14 mL of boiling 2-propanol to give 1.78 g (93%) of purified **8a**, mp 151–152°C; lit. (10) mp 144–146°C; uv (MeOH) max:289, 245 nm (ε 6800, 10 800); lit (10) uv (95% EtOH) max:289, 246 nm (ε 7000, 11 100); ^{1}H nmr δ:2.06, 2.07, 2.13 (OAc's), 5.30 (br s, 2, NH_2), 7.84 (d, $^5J_{H\text{-}8\text{-}F\text{-}6}$ = 0.45 Hz, 1, H-8); ^{19}F nmr (Me_2SO-d_6/$CDCl_3$) δ:−71.6 (s, 1, F-6); ms *m/z*:411.1190 (18%, M^+ [$C_{16}H_{18}FN_5O_7$] = 411.1190), 259.0822 (100%, M^+–B), 153.0457 (22%, BH = 153.0451).

9-(2,3,5,-Tri-O-acetyl-β-D-ribofuranosyl)-2-amino-6-azidopurine (8b)

A. A suspension of 0.5 g (7.7 mmol) of NaN_3 (dried *in vacuo* at room temperature for 3 days over P_2O_5) in a solution of 1 g (2.3 mmol) of dried **7** and 0.1 g (1.7 mmol) of purified Me_3N in 30 mL of rigorously dried acetonitrile was stirred at room temperature overnight. The mixture was evaporated *in vacuo*, the residue was treated with 30 mL of $CHCl_3$, and the suspension was applied to a column of silica (1 × 3 cm). The column was eluted with $CHCl_3$, the eluate was evaporated to dryness, and the residue was dissolved in 40 mL of 1,4-dioxane. This solution was frozen and lyophilized to give 1.09 g (quantitative) of a photosensitive white powder. The ^{1}H nmr spectrum of this powder indicated an equilibrium of two products (6-azido⇄ cyclic tetrazole) (23). Compound(s) **8b** had uv (MeOH) max: 299, 271, 238 nm; ^{1}H nmr δ:7.78 (s, 0.25, H-8), 7.95 (s, 0.75, H-8); ms *m/z*:434.1299 (13%, M^+ [$C_{16}H_{18}N_8O_7$] = 434.1299), 259.0814 (72%, M^+–B), 176.0532 (2.4%, BH = 176.0559). This material was hydrogenolyzed to a single product.

B. Alternatively, this reaction can be completed in 1.5 h at room temperature using 0.6 g (10.2 mmol) of Me_3N and 1.0 g (15.4 mmol) of NaN_3 with 0.5 g (1.2 mmol) of **7** in 30 mL of acetonitrile.

9-(2,3,5-Tri-O-acetyl-β-D-ribofuranosyl)-2,6-diaminopurine (8c)

A solution of 1.46 g (3.4 mmol) of **8b** in 50 mL of dry 1,4-dioxane was hydrogenolyzed at 30 psi with 0.5 g of 5% Pd/C catalyst at room temperature for 18 h in a Parr shaker. The mixture was filtered through a short silica column (2 × 1 cm) and the column was washed with acetone/$CHCl_3$ 1:1. The combined filtrate was evaporated to dryness and the tlc pure solid foam was dried *in vacuo* for 2 days to give 1.35 g (98%) of **8c**. A crystalline sample was obtained by diffusion of ether into a solution of **8c** in 1,4-dioxane. This sample had mp 105–106°C; uv (MeOH) max:282, 257 nm (ε 9400, 10 000); ^{1}H nmr δ:2.10 (s, 6, two OAc's), 2.14 (s, 3, OAc), 5.02 (br s, 2, 2-NH_2), 5.9 (br s overlapped by sugar protons, 2, 6-NH_2), 7.64 (s, 1, H-8); ms *m/z*:408.1385 (28%, M^+ [$C_{16}H_{20}N_6O_7$] = 408.1393), 259.0809 (M^+–B), 150.0647 (100%, BH = 150.0654). This compound has been reported previously as an amorphous intermediate (26). The corresponding deacylated nucleoside has reported uv (H_2O) max:280, 256 nm (ε 11 100, 10 700) (25).

Acknowledgements

We thank the Natural Sciences and Engineering Research Council of Canada (A5890), the National Cancer Institute of Canada, and the University of Alberta for generous financial support.

1. M. J. Robins and J. S. Wilson. J. Am. Chem. Soc. **103**, 932 (1981).
2. (*a*) G. V. R. Born, R. J. Haslam, M. Goldman, and R. D. Lowe. Nature, **205**, 678 (1965); (*b*) J. A. Angus, L. B. Cobbin, R. Einstein, and M. H. Maguire. Brit. J. Pharmacol. **41**, 592 (1971).
3. (*a*) J. A. Montgomery and K. Hewson. J. Am. Chem. Soc. **79**, 4559 (1957); (*b*) J. Med. Chem. **12**, 498 (1969); (*c*) R. W. Brockman, F. M. Schabel, Jr., and J. A. Montgomery. Biochem. Pharmacol. **26**, 2193 (1977).
4. (*a*) A. R. P. Paterson, S. Yang, E. Y. Lau, and C. E. Cass. Mol. Pharmacol. **16**, 900 (1979); (*b*) A. R. P. Paterson, J. H. Paran, S. Yang, and T. P. Lynch. Cancer Res. **39**, 3607 (1979).
5. L. Goodman. *In* Basic principles in nucleic acid chemistry. Vol. I. *Edited by* P. O. P. Ts'o. Academic Press, New York. 1974. pp. 93–208.
6. E. Fischer and B. Helferich. Chem. Ber. **47**, 210 (1914).
7. J. Davoll, B. Lythgoe, and A. R. Todd. J. Chem. Soc. 967 (1948); 1685 (1948).
8. (*a*) J. Davoll and B. A. Lowy. J. Am. Chem. Soc. **74**, 1563 (1952); (*b*) G. B. Brown and V. S. Weliky. J. Org. Chem. **23**, 125 (1958); (*c*) H. J. Schaeffer and H. J. Thomas. J. Am. Chem. Soc. **80**, 3738 (1958); (*d*) T. Sato, T. Shimadate, and Y. Ishido. Nippon Kagaku Zasshi, **81**, 1440 (1960); **81**, 1442 (1960); Chem. Abstr. **56**, 11692g (1962); (*e*) J. A., Montgomery and K. Hewson. J. Heterocycl. Chem. **1**, 213 (1964); (*f*) W. W. Lee, A. P. Martinez, L. Goodman, and D. W. Henry. J. Org. Chem. **37**, 2923 (1972); and references therein.
9. J. A. Montgomery, S. D. Clayton, and A. T. Shortnacy. J. Heterocycl. Chem. **16**, 157 (1979).
10. J. F. Gerster, A. G. Beaman, and R. K. Robins. J. Med. Chem. **6**, 340 (1963).
11. (*a*) J. F. Gerster and R. K. Robins. J. Am. Chem. Soc. **87**, 3752 (1965); (*b*) J. Org. Chem. **31**, 3258 (1966).
12. J. Kiburis and J. H. Lister. J. Chem. Soc. C, 3942 (1971).
13. M. J. Robins and G. L. Basom. Can. J. Chem. **51**, 3161 (1973).
14. M. J. Robins. *In* Bioorganic chemistry. Vol. III. Macro- and multimolecular systems. *Edited by* E. E. van Tamelen. Academic Press, New York. 1977. Chapt. 11.
15. H. Kawashima and I. Kumashiro. Bull. Chem. Soc. Jpn. **40**, 639 (1967).
16. (*a*) M. A. Stevens, D. I. Magrath, H. W. Smith, and G. B. Brown. J. Am. Chem. Soc. **80**, 2755 (1958); (*b*) M. MacCoss, E. K. Ryu, R. S. White, and R. L. Last. J. Org. Chem. **45**, 788 (1980).
17. M. J. Robins and B. Uznański. Can. J. Chem. **59**, 2608 (1981).
18. L. F. Christensen, A. D. Broom, M. J. Robins, and A. Bloch. J. Med. Chem. **15**, 735 (1972).
19. H. Bredereck and A. Martini. Chem. Ber. **80**, 401 (1947).
20. J. F. Gerster, J. W. Jones, and R. K. Robins. J. Org. Chem. **28**, 945 (1963).

21. (*a*) J. F. GERSTER, A. F. LEWIS, and R. K. ROBINS. *In* Synthetic procedures in nucleic acid chemistry. Vol. 1. *Edited by* W. W. Zorbach and R. S. Tipson. Wiley-Interscience, New York. 1968. pp. 242–243; (*b*) S. J. MANNING and L. B. TOWNSEND. *In* Nucleic acid chemistry: improved and new synthetic procedures, methods, and techniques. Part 2. *Edited by* L. B. Townsend and R. S. Tipson. Wiley-Interscience, New York. 1978. pp. 589–594.
22. M. M. CRUTCHFIELD, C. H. DUNGAN, J. H. LETCHER, V. MARK, and J. R. VAN WAZER. ^{31}P Nuclear magnetic resonance; topics in phosphorus chemistry. Vol. 5. Wiley-Interscience, New York. 1967. p. 287.
23. J. A. JOHNSON, JR., H. J. THOMAS, and H. J. SCHAEFFER. J. Am. Chem. Soc. **80**, 699. (1958).
24. J. C. PARHAM, J. FISSEKIS, and G. B. BROWN. J. Org. Chem. **31**, 966 (1966).
25. T. NAITO, K. UENO, and F. ISHIKAWA. Chem. Pharm. Bull. **12**, 951 (1964).
26. J. A. MONTGOMERY and K. HEWSON. J. Org. Chem. **33**, 432 (1968).

Can. J. Chem. Downloaded from www.nrcresearchpress.com by 210.87.254.40 on 09/06/12
For personal use only.

Nucleic acid related compounds. 34. Non-aqueous diazotization with *tert*-butyl nitrite. Introduction of fluorine, chlorine, and bromine at C-2 of purine nucleosides[1]

MORRIS J. ROBINS AND BOGDAN UZNAŃSKI[2]

Department of Chemistry, The University of Alberta, Edmonton, Alta., Canada T6G 2G2

Received March 2, 1981

MORRIS J. ROBINS and BOGDAN UZNAŃSKI. Can. J. Chem. **59**, 2608 (1981).

Treatment of 2,6-diamino-9-(2,3,5-tri-*O*-acetyl-β-D-ribofuranosyl)purine (**1***c*) with *tert*-butyl nitrite (TBN) in 60% anhydrous hydrogen fluoride/pyridine at −20°C gave 2-fluoroadenosine triacetate (**2**) in 48% yield. Analogous treatment of the acetylated 2-amino-6-fluoropurine nucleoside (**1***a*) gave the 2,6-difluoro compound (**3***a*) in 63% yield. Anhydrous ammonia in 1,2-dimethoxyethane converted **3***a* → **2** without ammonolysis of the acetate groups. The overall conversion of **1***a* → **3***a* → **2** without isolation of **3***a* proceeded in 80% yield. Similar diazotization of the 2-amino-6-chloro nucleoside (**1***b*) in HF/pyridine gave the 2-fluoro-6-chloro analogue (**3***b*) in 89% yield. Treatment of **1***b* with TBN and pyridine hydrochloride in dichloromethane (77%) or TBN and antimony trichloride in 1,2-dichloroethane (84%) gave the 2,6-dichloropurine nucleoside (**4***b*). The latter conditions converted **1***a* to the 2-chloro-6-fluoro product (**4***a*) in 77% yield. Conversions of **1***a* and **1***b* to the 2-bromo-6-fluoro (**5***a*, 67%) and 2-bromo-6-chloro (**5***b*, 78%) analogues were effected using TBN and antimony tribromide in dibromomethane.

MORRIS J. ROBINS et BOGDAN UZNAŃSKI. Can. J. Chem. **59**, 2608 (1981).

La diamino-2,6 (tri-*O*-acétyl-2,3,5 β-D-ribofurannosyl)-9 purine (**1***c*) réagit avec le nitrite de *tert*-butyle (NTB) dans un mélange de fluorure d'hydrogène anhydre/pyridine à 60% à −20°C en donnant le triacétate de fluoro-2 adénosine (**2**) avec un rendement de 48%. La réaction analogue du nucléoside amino-2 fluoro-6 purine acétylé (**1***a*) conduit au composé difluoro-2,6 (**3***a*) avec un rendement de 63%. L'ammoniac anhydre dans le diméthoxy-1,2 éthane permet de passer du composé **3***a* au composé 2 sans l'ammonolyse du groupe acétate. La transformation globale de **1***a* → **3***a* → **2** sans isoler le composé **3***a* se fait avec un rendement de 80%. Une diazotation analogue de l'amino-2 chloro-6 nucléoside (**1***b*) dans un mélange de HF/pyridine conduit au composé fluoro-2 chloro-6 apparenté (**3***b*) avec un rendement de 89%. Le composé **1***b* réagit avec NTB et le chlorhydrate de pyridine dans le dichlorométhane (77%) ou avec le NTB et le trichlorure d'antimoine dans le dichloro-1,2 éthane (84%) en donnant le nucléoside dichloro-2,6 purine (**4***b*). Dans les mêmes conditions le composé **1***a* se transforme en composé chloro-2 fluoro-6 (**4***a*) avec un rendement de 77%. On a réalisé la transformation des composés **1***a* et **1***b* en leurs analogues bromo-2 fluoro-6 (**5***a*, 67%) et en bromo-2 chloro-6 (**5***b*, 78%) en utilisant le NTB et le tribromure d'antimoine dans le dibromoéthane.

[Traduit par le journal]

Interest in 2-fluoroadenine nucleosides has been stimulated recently. The cytotoxic 2-fluoroadenosine and modified-sugar analogues are resistant toward deamination by the catabolic enzyme adenosine deaminase (2, 3*a*). Thus, their lifetimes in vivo are enhanced relative to their adenosine counterparts (3). It has been found that 2-fluoro-araA (9-β-D-arabinofuranosyl-2-fluoroadenine) is phosphorylated by deoxycytidine kinase. It therefore has a different mode of biochemical activation as well as different loci of action than 2-fluoroadenosine (3). It was noted recently that a protective effect against the toxicity of 5-fluorocytidine and certain other anticancer nucleosides in animals is exerted by 6-*S*-(*p*-nitrobenzyl)thioinosine, a potent inhibitor of nucleoside transport across cell membranes (4). We became interested in exploring improved routes to 2- and 6-fluoro 2,6-disubstituted purine nucleosides to make them available for examination of host toxicity protection.

Montgomery (5) and Robins (6) and their coworkers have utilized diazotization in aqueous acid media for introduction of fluorine and chlorine at C-2 of purine nucleosides. However, glycosyl and halo bond hydrolysis can occur during the heat-generating neutralization of the strong acid solutions. Direct hydrolytic dediazoniation also can give rise to the observed oxopurine base and nucleoside by-products. The low temperature limit for executing these diazotizations is defined by the freezing point of the aqueous solution.

Olah *et al.* reported conversion of aromatic amines to aryl fluorides using sodium nitrite in 70% poly(hydrogen fluoride)/30% pyridine solutions (7). A recent note described the use of *tert*-butyl nitrite and boron trifluoride etherate in methylene chloride or ether solutions to effect the conversion of aryl amines into their diazonium fluoroborate salts in high yields (8).

We began an investigation of nonaqueous diazotization of protected purine nucleosides based on these precedents. The 2,6-diamino- (**1***c*), 2-amino-6-chloro- (**1***b*), and 2-amino-6-fluoro-9-(2,3,5-tri-*O*-acetyl-β-D-ribofuranosyl)purine (**1***a*) precursors

[1]For the previous paper in this series see ref. 1.

[2]Postdoctoral Fellow 1979–1980. On leave from the Centre of Molecular and Macromolecular Studies, Polish Academy of Sciences, 90-362 Łódź, Boczna 5, Poland.

0008-4042/81/172608-04$01.00/0

©1981 National Research Council of Canada/Conseil national de recherches du Canada

Can. J. Chem. Downloaded from www.nrcresearchpress.com by 210.87.254.42 on 09/06/12
For personal use only.

Can. J. Chem. Downloaded from www.nrcresearchpress.com by 210.87.254.42 on 09/06/12
For personal use only.

were prepared by improved procedures in yields of ~70% overall from guanosine (1).

Treatment of **1***c* with *tert*-butyl nitrite (TBN) in 60% HF/pyridine at − 20°C for 10 minutes resulted in disappearance of starting material. The desired 2-fluoroadenosine triacetate (**2**) was obtained in 48% yield. A minor quantity of the 2,6-difluoro compound (**3***a*) was also formed (5*b*). However, attempts to improve the yield of **2** or to drive the reaction to give **3***a* were not promising. Analogous treatment of **1***a* at − 30°C resulted in rapid evolution of gas (N_2). The reaction was complete in less than 2 minutes. Crystalline **3***a* was isolated in 66% yield. Treatment of **3***a* with anhydrous ammonia in dry 1,2-dimethoxyethane for 15 minutes gave **2** in 85% yield. Ammonolysis of the protecting acetate esters did not occur under these carefully anhydrous conditions that effect smooth replacement of the 6-fluoro function. Alcoholic ammonia or liquid ammonia without drying convert **3***a* to the deprotected 2-fluoroadenosine (5*b*). When isolation of **3***a* was omitted, the conversion **1***a* → **3***a* → **2** proceeded to give 80% of **2**. This provides **2** in 58% overall yield from the readily available naturally occurring guanosine. Deacetylated **2** (2-fluoroadenosine) was prepared previously in 20% overall yield from **1***c* (5*b*). The 2-fluoro-6-chloro analogue (**3***b*) was prepared from **1***b* in 89% yield using identical conditions as for **1***a* → **3***a*. This transformation had been effected in 44% yield previously when aqueous fluoroboric acid conditions were employed (6*b*).

Several syntheses of the versatile intermediate 2,6-dichloropurine nucleoside (**4***b*) have been reported (see references quoted in ref. 1). These methods, again, usually involved base–sugar coupling. Treatment of **1***b* with TBN and pyridine hydrochloride in dichloromethane at − 10°C for 45 minutes gave **4***b* in 77% yield. This yield was elevated to 84% using TBN and antimony trichloride in 1,2-dichloroethane. Prior aqueous conditions were reported to effect this transformation in 43% yield (6*b*). Conversion of **1***a* into the 2-chloro-6-fluoro analogue (**4***a*) proceeded in 77% yield using our TBN/$SbCl_3$/$C_2H_4Cl_2$ conditions.

Treatment of **1***a* with TBN and antimony tribromide in dibromomethane gave the 2-bromo-6-fluoro product (**5***a*) in 69% yield. Analogous conversion of **1***b* to the 2-bromo-6-chloro compound (**5***b*) proceeded in 78% yield.

These diazotization–dediazoniation reactions (9) were monitored by tlc and in some cases by hplc. The structures of known products were confirmed by comparison of properties with literature values as well as by ^1H and ^{19}F nmr, uv, and mass spectral examination. Elemental analyses were obtained also as a check on purity and verification of the reliability of yields.

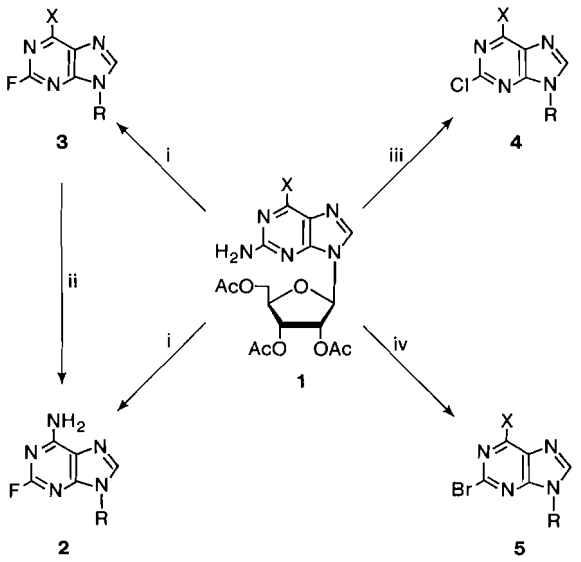

R = 2′, 3′, 5′ -tri-O-acetyl-β-D-ribofuranosyl

a series, X = F; **b** series, X = Cl; **1c**, X = NH_2

i) TBN/HF/pyridine. ii) NH_3 /DME. iii) TBN/$SbCl_3$/$C_2H_4Cl_2$

iv) TBN/$SbBr_3$ /CH_2Br_2.

SCHEME 1

These nonaqueous diazotization-replacements proceed readily at lowered temperatures. The reactions in HF/pyridine are exceptionally rapid. Complete disappearance of starting **1***a* or **1***b* occurred in less than 2 minutes at − 30°C. Montgomery had observed the formation of a hydroxybutylidene-substituted by-product nucleoside when tetrahydrofuran was used as a homogeneous cosolvent with 48% fluoroboric acid. He also had noted that 2-chloro as well as 2-fluoro substitution occurred when the 2-amino precursor was diazotized in a chloroform/48% fluoroboric acid two-phase system (5*c*).

We observed both 2-chloro and 2-fluoro products when BF_3 etherate (8) was employed with TBN in chloroform or dichloromethane solvents. Similarly, $SbBr_3$ and TBN in methylene chloride gave rise to a mixture of 2-bromo and 2-chloro compounds that were resolved by hplc and identified by mass spectrometry. Therefore, the halogen-compatible $SbBr_3$/CH_2Br_2 and $SbCl_3$/$C_2H_4Cl_2$ systems

Can. J. Chem. Downloaded from www.nrcresearchpress.com by 210.87.254.42 on 09/06/12
For personal use only.

were employed with TBN to give clean brominative and chlorinative diazotization–dediazoniations.

It was observed that the fluoro substitution process was inhibited by concentrations of HF/pyridine greater than ~65% HF. Use of a freshly prepared sample of 70% HF/30% pyridine resulted in the absence of gas evolution upon addition of TBN. After examination of several variables it was discovered that dilution of this reagent with anhydrous pyridine to concentrations of 45–65% HF provided reactive systems for the diazotization-replacement. We standardized our procedure using 60% HF/pyridine, but a 50% reagent functions equally well.

Nair and Richardson recently have reported some analogous nonaqueous diazotization reactions of 9-substituted adenines (10). They observed incorporation of halogen at C-6 of the purine ring upon treatment of their substrates with *n*-pentyl nitrite in halogenated solvents and interpreted their results in terms of a radical abstraction process.

Our present study provides convenient methods for the nonaqueous diazotization-replacement of the 2-amino group of protected purine nucleosides to give 2-fluoro, 2-chloro, and 2-bromo- compounds in good to high yields. These procedures are clearly superior in both convenience and yields to prior aqueous acid diazotizations. Purine nucleoside diazonium salts are presumptive unstable intermediates in these observed overall replacement reactions. Abstraction of halogen from solvent was observed. This problem was circumvented by the use of HF/pyridine and the compatible antimony trihalide/halo solvent for introduction of chloro and bromo substituents. Studies are in progress to investigate mechanistic considerations and further useful transformations of aminopurine nucleosides.

Experimental

General

General procedures and instrumentation used are given in ref. 1. Polyhydrogen fluoride/pyridine (70% HF by weight) was purchased from Aldrich Chemical Co. or was prepared by careful addition of HF to dry pyridine at − 78°C as described in ref. 7. It was diluted to 60% HF/pyridine by cautious addition of dry pyridine at − 50°C. Reactions performed in HF/pyridine were effected in polyethylene test tubes equipped with a small Teflon-coated magnetic stir bar. **CAUTIONS** in the use of HF/pyridine are noted in ref. 7. *tert*-Butyl nitrite (TBN) was prepared essentially as described in ref. 11. It was distilled at 0°C into a cold trap at − 78°C on a vacuum line. Elemental analyses were determined by the Microanalytical Laboratory of this department.

9-(2,3,5-Tri-O-acetyl-β-D-ribofuranosyl)-2,6-difluoropurine (3a)

A stirred solution of 500 mg (1.2 mmol) of **1***a* was prepared in 5.2 mL of 60% HF/pyridine at − 30°C in a Dry-Ice/acetone bath and 200 μL (1.7 mmol) of TBN was added. Vigorous evolution of gas (N_2) occurred for ~1 min. Stirring was continued for 1 min and the solution was poured into 100 g of crushed ice/H_2O. The aqueous mixture was extracted with 5 × 20 mL of $CHCl_3$. The combined organic phase was washed with 3 × 10 mL of H_2O, 5% $NaHCO_3/H_2O$ to pH~ 7, dried over $MgSO_4$ for 2 h, filtered, and 20 mL of 2-propanol was added to the filtrate. The combined filtrate was evaporated to ~2 mL and the resulting suspension was refrigerated at 5°C for 3 days. The crystalline product was filtered, washed with ether, and dried *in vacuo* to give 328 mg (66%) of **3***a*, mp 84–86°C; uv (MeOH) max: 254, 237 (sh) nm (ε 6700, 4000); lit. (5*b*) uv (pH 7) max: 253.5, 233 nm (ε 7300, 4000); ^{1}H nmr δ: 2.10, 2.18, 2.19 (OAc's), 8.26 (s, 1, H-8); ^{19}F nmr δ: − 65.8 (d, $^4J_{6-2}$ = 3.2 Hz, 1, F-6), −49.1 (d, $^4J_{2-6}$ = 3.2 Hz, 1, F-2); ms *m/z*: 414.0992 (0.3%, M^+ $[C_{16}H_{16}F_2N_4O_7]$ = 414.0987, 259.0815 (100%, M^+ −B). *Anal.* calcd. for $C_{16}H_{16}F_2N_4O_7$: C 46.39, H 3.89, N 13.52; found: C 46.15, H 3.91, N 13.51.

2′,3′,5′-Tri-O-acetyl-2-fluoroadenosine (2)

A. Dry ammonia was bubbled through a solution of 350 mg (0.85 mmol) of **3***a* in 5 mL of 1,2-dimethoxyethane (dried over NaH and distilled directly into the dried reaction flask) at room temperature for 15 min. The solution was evaporated to dryness and the residue was treated with 100 mL of hot $CHCl_3$ and filtered. A 50 mL portion of 2-propanol was added and the combined filtrate was evaporated to ~30 mL. The crystalline precipitate was filtered, washed with 2-propanol, and dried *in vacuo* to give 296 mg (85%) of **2**, mp 211–212°C; lit. (5*b*) mp 204°C; uv (MeOH) max: 261 nm (ε 15 900); lit. (5*b*) uv (pH 7) max: 261 nm (ε 14 900); ^{1}H nmr (Me_2SO-d_6) δ: 2.04, 2.06, 2.14 (OAc's), 8.34 (s, 1, H-8); ^{19}F nmr (Me_2SO-d_6) δ: −51.5 (s, 1, F-2); ms *m/z*: 411.1197 (15%, M^+ $[C_{16}H_{18}FN_5O_7]$ = 411.1190), 259.0815 (100%, M^+ −B), 153.0452 (34%, BH = 153.0451). *Anal.* calcd. for $C_{16}H_{18}FN_5O_7$: C 46.72, H 4.41, N 17.03; found: C 46.66, H 4.33, N 17.22.

B. A 500 mg (1.2 mmol) sample of **1***a* was treated with TBN/HF/pyridine as described. The resulting dried chloroform extract was filtered, 150 mL of toluene added, and evaporated to dryness. The resulting amorphous crude **3***a* was treated with dry ammonia/1,2-dimethoxyethane as described in method A to give 400 mg (80%) of **2**.

C. A stirred solution of 250 mg (0.61 mmol) of **1***c* in 1.5 mL of 60% HF/pyridine was treated at −30°C with 100 μL (0.85 mmol) of TBN. Stirring was continued at −30 to −20°C for 10 min and the reaction mixture was processed as in method A to give 120 mg (48%) of **2**.

The products from methods A, B, and C were identical by the usual direct comparisons.

9-(2,3,5-Tri-O-acetyl-β-D-ribofuranosyl)-6-chloro-2-fluoropurine (3b)

A 1.0 g (2.34 mmol) sample of **1***b* was added to 8.5 mL of 60% HF/pyridine at −50°C with stirring. The temperature was allowed to rise to −30°C and 400 μL (3.4 mmol) of TBN was added. Stirring was continued for 3 min (vigorous evolution of gas occurred for ~1 min) and the reaction was processed as in the conversion of **1***a* → **3***a*, method A. The dried $CHCl_3$ extract was treated with 5 mL of 1-propanol and evaporated to a small volume. The crystalline product that separated was filtered, washed with cold 1-propanol, and dried *in vacuo* to give 892 mg (89%) of pale yellow crystals. This product was recrystallized from 2-propanol to give 854 mg (85%) of pure **3***b*, mp 132.5–133.5°C; lit. (6*b*) mp 121–123°C; uv (MeOH) max: 269, 244 (sh)

Can. J. Chem. Downloaded from www.nrcresearchpress.com by 210.87.254.42 on 09/06/12
For personal use only.

nm (ε 9800, 3300); lit. (6*b*) uv (EtOH) max: 269 nm (ε 12 500); ^{1}H nmr δ: 2.10, 2.16, 2.17 (OAc's), 8.28 (s, 1, H-8); ^{19}F nmr δ: −50.9 (s, 1, F-2); ms *m/z*: 430.0685 (0.5%, M^+ [$C_{16}H_{16}{}^{35}ClFN_4O_7$] = 430.0691), 259.0764 (100%, M^+ −B), 173.0029 (13%, BH_2 = 173.0030). *Anal.* calcd. for $C_{16}H_{16}ClFN_4O_7$: C 44.62, H 3.74, N 13.01; found: C 44.48, H 3.74, N 12.93.

*9-(2,3,5-Tri-*O*-acetyl-*β*-*D*-ribofuranosyl)-2-chloro-6-fluoropurine (4a)*

Dry dichloroethane (15 mL) was added with stirring at 0°C to 500 mg (1.2 mmol) of **1***a* and 500 mg (2.2 mmol) of $SbCl_3$. The suspension was cooled to −10°C and 0.5 mL (4.3 mmol) of TBN was added. The mixture was stirred at −10 to −5°C for 3 h and was poured into a stirred mixture of 2 g of $NaHCO_3$ in 50 mL of crushed ice/water. The resulting mixture was filtered directly into a separatory funnel and the filtrate was extracted with 5 × 15 mL of $CHCl_3$. The combined organic phase was washed with H_2O, dried over $MgSO_4$ for 2 h, filtered, and evaporated to dryness. The pale yellow glassy residue was dissolved in 10 mL of $CHCl_3$ and filtered through a column (1 × 1.5 cm) of silica. The column was washed with $CHCl_3$ and 0.5 mL of 1-butanol was added to the combined eluate. This solution was evaporated slowly to remove most of the $CHCl_3$. The resulting suspension was refrigerated at 5°C overnight, filtered, and the crystals were washed with ether to give 403 mg (77%) of **4***a*, mp 167–168°C; uv (MeOH) max: 254, 245 nm (ε 6700, 6600); ^{1}H nmr δ: 2.13, 2.18, 2.21 (OAc's), 8.30 (s, 1, H-8); ^{19}F nmr δ: −66.3 (s, 1, F-6); ms *m/z*: 430.0681 (1.2%, M^+ [$C_{16}H_{16}{}^{35}ClFN_4O_7$] = 430.0691), 259.0683 (100%, M^+ − B), 173.0029 (23%, BH_2 = 173.0031). *Anal.* calcd. for $C_{16}H_{16}ClFN_4O_7$: C 44.62, H 3.74, N 13.01; found: C 44.40, H 3.69, N 13.03.

*9-(2,3,5-Tri-*O*-acetyl-*β*-*D*-ribofuranosyl)-2,6-dichloropurine (4b)*

A stirred solution of 2.14 g (5 mmol) of **1***b* in 80 mL of dry, 1,2-dichloroethane was cooled to −10°C and 1.6 g (7 mmol) of $SbCl_3$ in 10 mL of dry dichloroethane was added. After stirring for 5 min, 3 mL (26 mmol) of TBN was added and the suspension was stirred at −10°C for 2.5 h. Evolution of ~110 mL (~ quantitative) of N_2 was measured by displacement of water from a buret. The reaction mixture was poured over 30 g of crushed ice and stirred for 3 min. The mixture was filtered directly into a separatory funnel that contained crushed ice. The filtrate was extracted with 50 mL of $CHCl_3$. The combined organic phase was washed with 4 × 40 mL of ice and water, 5% $NaHCO_3/H_2O$ to pH ~7, dried over $MgSO_4$ for 1 h, filtered, and evaporated to ~20 mL. This yellow solution was filtered through a column (1 cm dia) of 3 cm of silica, 400 mg of decolorizing carbon, and 2 cm of silica. The column was washed with 150 mL of $CHCl_3$ and 60 mL of 2-propanol was added to the combined eluate. This solution was evaporated slowly to ~30 mL and the cream-colored crystals were filtered, washed with 2-propanol, and dried *in vacuo* to give 1.88 g (84%) of **4***b*, mp 167–168°C; uv (MeOH) max: 273, 252 nm (ε 9100, 5100); ^{1}H nmr δ: 2.08, 2.14, 2.16 (OAc's), 8.26 (s, 1, H-8); ms *m/z*: 446.0404 (1.3%, M^+ [$C_{16}H_{16}{}^{35}Cl_2N_4O_7$] = 446.0396), 259.0824 (100%, M^+ −B). This product was identical to that prepared in ref. 1.

*9-(2,3,5-Tri-*O*-acetyl-*β*-*D*-ribofuranosyl)-2-bromo-6-fluoropurine (5a)*

Dry dibromomethane (15 mL) was cooled to 0°C and added with stirring to a mixture of 500 mg (1.22 mmol) of **1***a* and 600 mg (1.66 mmol) of $SbBr_3$. The mixture was cooled to −10°C and treated with 0.5 mL (4.3 mmol) of TBN. Stirring was continued at −10° to −5°C for 3.5 h and the mixture was processed as in the conversion of **1***a* → **4***a* to give 422 mg (73%) of **5***a*, mp 186–187°C; uv (MeOH) max: 256 nm (ε 8800); ^{1}H nmr δ: 2.11, 2.16, 2.19 (OAc's), 8.24 (s, 1, H-8); ^{19}F nmr δ: −66.0 (s, 1, F-6); ms *m/z*: 474.0186 (0.5%, M^+ [$C_{16}H_{16}{}^{79}BrFN_4O_7$] = 474.0186), 259.0818 (100%, M^+ −B). *Anal.* calcd. for $C_{16}H_{16}BrFN_4O_7$: C 40.44, H 3.39, N 11.79; found: C 40.00, H 3.30, N 11.75.

*9-(2,3,5-Tri-*O*-acetyl-*β*-*D*-ribofuranosyl)-2-bromo-6-chloropurine (5b)*

A solution of 0.63 g (1.74 mmol) of $SbBr_3$ in 2 mL of CH_2Br_2 was added to a stirred solution of 0.5 g (1.17 mmol) of **1***b* in 20 mL of CH_2Br_2 at −10°C. TBN (0.75 mL, 6.4 mmol) was added, the mixture was stirred at −10°C for 2 h, and poured into a stirred mixture of 1 g of $NaHCO_3$ in 150 mL of crushed ice/H_2O. This mixture was filtered directly into a separatory funnel and extracted with 3 × 20 mL of $CHCl_3$. The combined organic phase was washed with 20 mL of H_2O, dried over $MgSO_4$ for 1 h, filtered, and evaporated to dryness. The heavy oil was dissolved in 5 mL of CH_2Cl_2 and 10 mL of MeOH and this solution was evaporated slowly to ~3 mL. The off-white crystals were filtered, washed with ether, and dried *in vacuo* to give 448 mg (78%) of **5***b*, mp 171–172°C; lit. (12) mp 153–154°C; uv (MeOH) max: 274, 253 nm (ε 9300, 5300); lit. (12) uv (MeOH) max: 274, 253 nm; ^{1}H nmr δ: 2.11, 2.15, 2.18 (OAc's), 8.28 (s, 1, H-8); ms *m/z*: 259.0826 (100%, M^+ −B), 232.9227 (11%, BH_2 = 232.9229), 231.9152 (3.6%, BH = 231.9151). *Anal.* calcd. for $C_{16}H_{16}BrClN_4O_7$: C 39.09, H 3.28, N 11.40; found: C 38.72, H 3.33, N 11.46.

Acknowledgements

We thank the National Cancer Institute of Canada, the Natural Sciences and Engineering Research Council of Canada (A5890), and the University of Alberta for generous financial support.

1. M. J. Robins and B. Uznański. Can. J. Chem. **59**, 2601 (1981).
2. H.-P. Baer, G. I. Drummond, and E. L. Duncan. Mol. Pharmacol. **2**, 67 (1966).
3. (*a*) R. W. Brockman, F. M. Schabel, Jr., and J. A. Montgomery. Biochem. Pharmacol. **26**, 2193 (1977); (*b*) R. W. Brockman, Y-C. Cheng, F. M. Schabel, Jr., and J. A. Montgomery. Cancer Res. **40**, 3610 (1980).
4. (*a*) A. R. P. Patterson, S. Yang, E. Y. Lau, and C. E. Cass. Mol. Pharmacol. **16**, 900 (1979); (*b*) A. R. P. Paterson, J. H. Paran, S. Yang, and T. P. Lynch. Cancer Res. **39**, 3607 (1979).
5. (*a*) J. A. Montgomery and K. Hewson. J. Am. Chem. Soc. **79**, 4559 (1957); (*b*) J. Org. Chem. **33**, 432 (1968); (*c*) J. A. Montgomery, S. D. Clayton, and A. T. Shortnacy. J. Heterocycl. Chem. **16**, 157 (1979).
6. (*a*) J. F. Gerster and R. K. Robins. J. Am. Chem. Soc. **87**, 3752 (1965); (*b*) J. Org. Chem. **31**, 3258 (1966).
7. G. A. Olah, J. T. Welch, Y. D. Vankar, M. Nojima, I. Kerekes, and J. A. Olah. J. Org. Chem. **44**, 3872 (1979).
8. M. P. Doyle and W. J. Bryker. J. Org. Chem. **44**, 1572 (1979).
9. H. Zollinger. Angew. Chem. Int. Ed. Engl. **17**, 141 (1978).
10. V. Nair and S. G. Richardson. J. Org. Chem. **45**, 3969 (1980).
11. W. A. Noyes. Org. Synth. Collect. Vol. 2. John Wiley & Sons, New York, 1943, pp. 108–109.
12. R. Marumoto, Y. Yoshioka, O. Miyashita, S. Shima, K. Imai, K. Kawazoe, and M. Honjo. Chem. Pharm. Bull. **23**, 759 (1975).

Thione photochemistry: on the formation of dipyranylidenes from pyranthiones[1,2]

NADER BERENJIAN AND PAUL DE MAYO

Photochemistry Unit, Department of Chemistry, University of Western Ontario, London, Ont., Canada N6A 5B7

Received March 19, 1981

NADER BERENJIAN and PAUL DE MAYO. Can. J. Chem. **59**, 2612 (1981).

The irradiation of the pyranthione **1** has been reinvestigated. The reaction proceeds through the (n,π^*) triplet and can be quenched with ferrocene. The reaction can be sensitized with Michler's ketone or triphenylene. The elimination of sulfur from two molecules of **1** to give the dipyranylidene **2** requires, surprisingly, a hydrogen donor solvent, and the quantum yield of product has been found to increase with greater dilution, presumably because of the well-known quenching of triplet thiones by the ground state thione. A mechanism for the formation of **2** is suggested.

NADER BERENJIAN et PAUL DE MAYO. Can. J. Chem. **59**, 2612 (1981).

On a repris l'étude de l'irradiation du pyranthione **1**. La réaction se fait par l'intermédiaire d'un triplet (n,π^*) et peut être bloquée par un ferrocène. Elle peut être sensibilisée par la cétone de Michler ou le triphénylène. L'élimination du soufre à partir de deux molécules de **1** qui conduit au dipyranilidène **2** nécessite, de façon étonnante, un solvant donneur de proton. On a trouvé qu'une plus grande dilution augmente le rendement quantique probablement à cause de la propriété bien connue, que possède le thione à l'état fondamental, de bloquer les thiones à l'état triplet. On propose un mécanisme qui explique la formation de **2**.

[Traduit par le journal]

Can. J. Chem. Downloaded from www.nrcresearchpress.com by 210.87.254.40 on 09/06/12
For personal use only.

The dimerization of thiones under thermolytic conditions, with the elimination of sulphur to give ethylenes, is a well-known reaction (see for instance, refs. 1–3); the induction of the same reaction under the action of light has been less frequently reported (4–6).

The photolysis of 2,6-diphenyl-4*H*-pyran-4-thione **1** to give **2** has been described (6) and the mechanism of this reaction has already been subject to some study. These earlier findings may be summarized as follows. (*a*) The reaction proceeded far better, i.e. in greater quantum yield, in solvents capable of hydrogen donation (isopropanol, dioxan, tetrahydrofuran) than in poor donors (benzene, acetonitrile). (*b*) The quantum yields of **2** increased with increasing thione concentration. (*c*) The formation of **2** was sensitized by Michler's ketone very efficiently ($\phi = 0.8$) and could be quenched (ca. 30%) by 3.2×10^{-2} *M* piperylene ($E_T \sim 57$ kcal/mol). Further, it was found (*d*) that the sulfur was not eliminated as elemental sulfur; and that two moles of hydrogen sulfide were detected for every mole of **2** formed. On this basis the possibilities indicated in Scheme 1 were proposed, the reaction deriving from the triplet of **1**.

Our attention was attracted by a number of disturbing features in the above proposals. First, the dimerization of the carbene **3** in an alcoholic solvent seemed improbable, in view of the ready addition of alcohols to carbenes (7), yet the reported yield of **2** found in isopropanol was high. In such good reducing solvents as tetrahydrofuran and dioxan, hydrogen abstraction by a carbene would also be expected.[3] Secondly, the formation of the carbene **3** itself appears to be without precedent (see, however, ref. 8). Finally, the formation of **2** via **4**, by whatever route, requires at least *two* photons, aside from any light concerned in the conversion of **4** → **3** or of **5** → **2**. The quantum yields for formation of **2** reported are very high and, on occasion, exceed the maximal possible, i.e., 0.5 (required since *two* molecules of **4** give one of **2**). For these reasons we were led to reinvestigate the reaction. Whilst the details have not been completely elucidated the general outline seems secure.

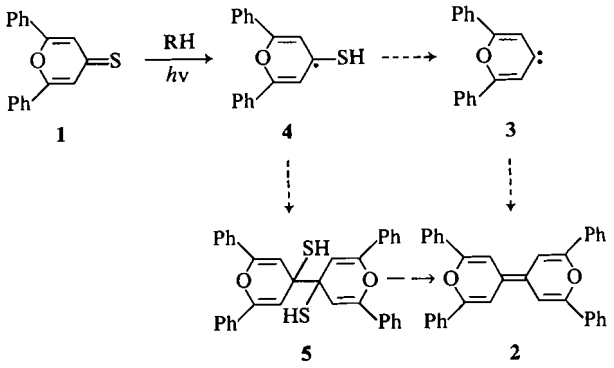

SCHEME 1

The thione **1** and 4-thioflavone **6** were prepared

[1]This paper is dedicated to the memory of the late Professor F. Šorm.

[2]Contribution number 264 from the Photochemistry Unit, University of Western Ontario.

[3]Reference 7, p. 209.

0008-4042/81/172612-05$01.00/0

©1981 National Research Council of Canada/Conseil national de recherches du Canada

Can. J. Chem. Downloaded from www.nrcresearchpress.com by 210.87.254.40 on 09/06/12
For personal use only.

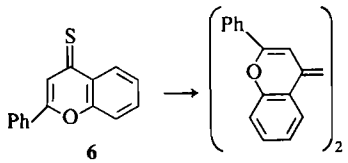

6 7

by a published procedure (2) and their properties were in accord with those in the literature (10–13).[4]

As previously described (6), **1** on irradiation through Pyrex in dioxan gave **2** in 70% yield. Irradiation of **6** gave the known **7** (2) in fair chemical yield, depending on the solvent.

We repeated the hydrogen sulfide estimation reported (6), but with an appropriate control, and we could find but 5–6% of the theoretical amount, as against the quantitative yield previously noted. This discrepancy in results may, perhaps, be attributed to iodine volatilization (see Experimental). The same low value for hydrogen sulfide formation was obtained by the precipitation and weighing of copper sulfide from acidified copper sulfate. It thus appeared that hydrogen sulfide was *not* the ultimate fate of the sulfur. It was confirmed that elemental sulfur was not present (6), and a search was, therefore, made in the solvent for sulfur-containing materials. An end-product was found in the form of 1,4-dioxan-2-thiol **8** which was present in substantial quantity: it was identified by comparison with a synthetic specimen. Unfortunately, our inability to isolate **8** in pure form precluded quantitative estimation.

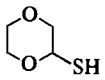

8

To confirm this identification **1** was irradiated in toluene solution; amongst the many products those identified were phenylmethanethiol, benzyl disulfide, and dibenzyl disulfide. The yield of the thiol was 11%; the other compounds were not accurately estimated, but were present in comparable amounts.

The multiplicity of the reactive state was further examined. The reaction was indeed, as reported, sensitized by Michler's ketone and, in addition, was sensitized by triphenylene where the possibility of carbonyl–thiocarbonyl interaction is excluded. Quenching by piperylene was previously reported as inefficient (6), possibly because of the relative energies of the quencher and thione. We determined the latter from the 0–0 band in the phosphorescence spectrum in EPA at 77 K (Fig. 1) and found a value of 48.8 kcal/mol (λ_{max} 586 nm). For this reason, and because of its relatively low absorbance at 360 nm, ferrocene ($E_T \sim 43$ kcal/mol) (14) was selected as a quencher. A Stern–Volmer plot (**1**; [6.8×10^{-4} *M*]) gave a good ($r = 0.999$) straight line with slope 1150 M^{-1} to 90% quenching (see Fig. 2). The value of k_{diff} calculated with the modified Debye equation was 7.8×10^9 M^{-1} s^{-1} from which a value of τ, the triplet lifetime under the condition of the experiment (dioxan solution), was found to be 1.3×10^{-7} s. This is somewhat shorter than that estimated, 3.0×10^{-7} s, for a comparable concentration of xanthione, the closest available model, in isopropanol (15). It is in general agreement with that expected for triplet thione decay (16).

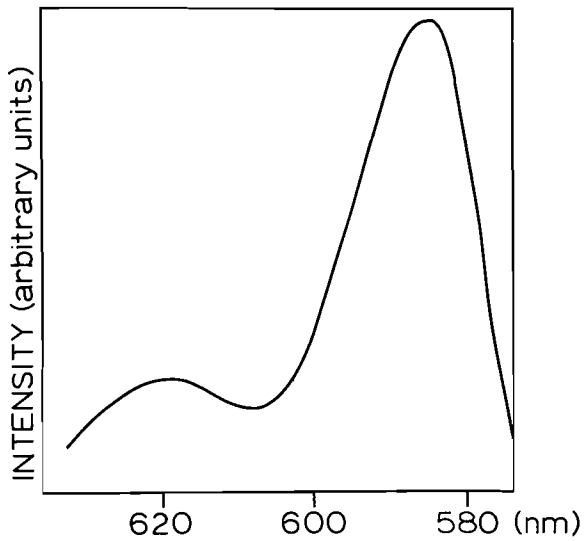

FIG. 1. Phosphorescence of **1** in EPA at 77 K.

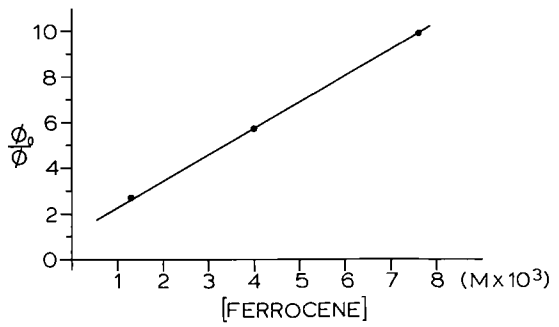

FIG. 2. Stern–Volmer plot for the quenching of **2** formation by ferrocene. The concentration of **1** was 6.8×10^{-4} *M* and the slope 1150 M^{-1} ($r = 0.999$).

[4]The data recorded for **1** in ref. 6 are not consistent with these.

Can. J. Chem. Downloaded from www.nrcresearchpress.com by 210.87.254.40 on 09/06/12
For personal use only.

TABLE 1. Quantum yields of formation of **2** in various solvents at 360 ± 5 nm

Solvent	Concentration of **1** ($M \times 10^{-4}$)	ϕ*†
Dioxan	2270‡	8.2×10^{-4}
	37	3.0×10^{-3}
	25	6.0×10^{-2}
	17	7.3×10^{-2}
	6.8	1.1×10^{-2}
Benzene	4.1	5.0×10^{-5}
Tetrahydrofuran	7.4	2.2×10^{-1}
Diethyl ether	4.5	8.0×10^{-2}
Acetonitrile	6.0	1.8×10^{-5}
Toluene	9.0	1.1×10^{-2}

*±10%.
†Irradiations were from 1–7% conversion.
‡Also irradiated at 458±9 nm; $\phi = 9.4 \times 10^{-4}$.

A common characteristic of all triplet thiones so far examined (16) is the quenching of the excited state by ground state thione. This process appears to be close to diffusion controlled (16–18). Hence, any chemical reaction proceeding from the triplet state would, unless its rate constant were comparable with that of ground state quenching, be expected to diminish in quantum yield with increasing thione concentration, and there is ample precedent to support this expectation (16). However, in the examination of **1** the reverse observation was originally reported (6). We, therefore, determined the effect of thione concentration on the quantum yield of **2** formation in dioxan solution. The results are tabulated in Table 1, and, indeed, the expected tendency was revealed.[5]

From the foregoing the following may be concluded. The reaction of **1** to give **2** proceeds from the triplet of the thione which, for spectral reasons, is designated as n,π^*. This assignment is consonant with its solution lifetime.

We have shown that the quantum yield is independent of exciting wavelength, by irradiating at 458±9 nm at the highest concentration of **1** used (Table 1). After correction for the small amount of light not absorbed, the quantum yield was identical with that obtained by excitation at 360 ± 5 nm.

As had been previously shown (6) the reaction requires the presence of a hydrogen donor. A process such as that indicated in eqs. [1]–[3], where

[1] $^3(\mathbf{1}) + \mathbf{1} \longrightarrow \mathbf{2.1}$

[2] $^3(\mathbf{1}) + \mathbf{1} \longrightarrow \mathbf{9} \xrightarrow{?} \mathbf{2}$

[3] $^3(\mathbf{1}) + \mathbf{1} \longrightarrow \mathbf{10} \xrightarrow{?} \mathbf{2}$

[5]We are unable to explain the fact that our quantum yields, under comparable conditions, differ by orders of magnitude, in some cases, from those previously reported (6).

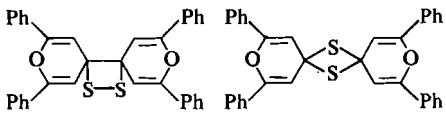

9 **10**

9 and **10** are the 1,2- and 1,3-dithietanes, respectively, must be discarded. 1,2-Dithietanes have not yet been prepared, whilst dimerization to 1,3-dithietanes has only been observed for aliphatic thiones. In its need for a hydrogen donor the present reaction differs from the only analogous process in the literature, the irradiation of **11**, in the absence of a solvent, to give **12** (4,5). In this case the ethyl group could act as donor, but the reported yield of **12** is too high for **11** to be its own hydrogen source, at least on an equivalent basis. The mechanism for the formation of **12** is unknown and 1,2-and 1,3-dithietanes have been suggested as intermediates.

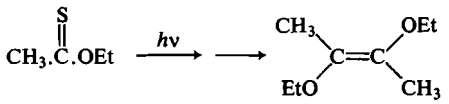

11 **12*a***

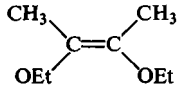

12*b*

The first step in the present reaction is most probably hydrogen abstraction by the excited **1**. Since this is the triplet (n,π^*) state the radical **4** should be the first intermediate formed, together with the radical R derived from the solvent. The following step, in view of the well-established radical scavenging abilities of thiones (19) should be reaction of **4** with **1**, in competition with disproportionation of R and **4** to regenerate starting material, **1** (15). If addition gave the radical **13** there appears no very plausible route from **13** to **2**; in particular, rearrangement to **14** would not be expected (20).

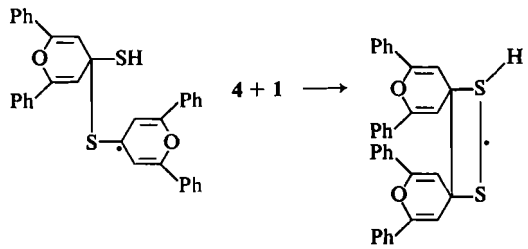

13 **14**

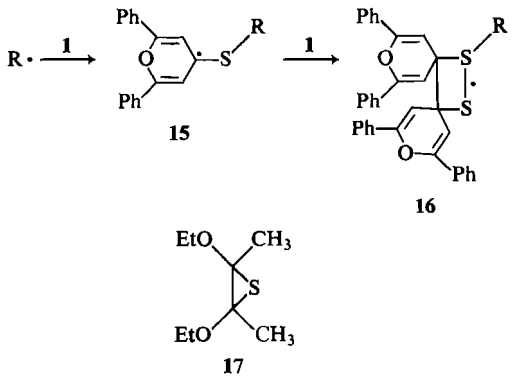

15 16 17

In view of the known comparative stability of radicals of the type $R_2\dot{S}SR$ (21) we suggest that cycloaddition of **4** to **1** does occur to give **14** where the extra electron is in a low-lying σ^* orbital of the S—S bond. Many possibilities are now open to **14**, including decomposition to **2** and HSS·. The latter may lead to the solvent insertion products observed. However, the situation is more complex since the solvent radical may also be trapped by thione to give **15**, itself reacting with a second molecule of **1** to give **16** which may also serve as a source of **2** (and RSS·).

The elimination of sulfur from **14** or **16** does not, howver, have to occur in one step: an episulfide may be an intermediate, and, in fact, the isolation of a small amount of **17** has already been reported in the irradiation of **11**. The elimination of sulfur from aromatic episulfides may occur easily thermolytically (see, for example, ref. 1) or by the action of alkyl radicals (9).

Experimental

General Procedure

The nmr spectra were recorded on Varian T-60 and XL 100 spectrometers with TMS as internal standard. Mass spectra were obtained on a MAT-311A spectrometer. The emission spectrum was measured in EPA at 77 K using a Jarrel-Ash model 82-020 spectrophotometer equipped with an EM1 9558QD Photomultiplier (S-20 response) which was cooled with solid carbon dioxide. This was connected to an Ortec (model 454) timing filter amplifier and fast discriminator (model 417). The signal was accumulated in a multichannel analyzer (Geos system model 7010) operating in the signal-averaging mode. The emission spectra were not corrected for photomultiplier response. The light source was a 150-W Xenon Hanovia lamp, the output of which was passed through a Bausch and Lomb 0.25-m monochromator. The spectrum is shown in Fig. 1.

Materials

2,6-Diphenyl-4*H*-pyran-4-thione **1** and 4-thioflavone **6** were prepared by a published procedure (2) and their melting points and spectra were as reported (10–12). The ultraviolet spectrum of **1** in pure dioxan showed the following bands: 256 (16 500), 233 (22 800), 378 (21 000), 538 (70) nm, unchanged on recrystallization. These data are not in accord with those recorded in ref. 6. Dioxan was purified by the method of Palyi (22). Tetrahydrofuran (Caledon Laboratories Ltd.) was purified by distillation over lithium aluminum hydride. Toluene and benzene were distilled prior to use. Diethyl ether (Fisher) and acetonitrile (Aldrich, Gold Label) were used as received.

Quantum Yield Determinations

Samples were degassed by at least three freeze–pump–thaw cycles to a residual pressure of 2×10^{-5} mm. The quantum yields were determined at 362 nm in a Spectroirradiator (Jasco). The light intensity was calibrated at 362 ± 8 nm using ferrioxalate actinometry; that at 548 nm was related to that at 362 nm using a thermopile. The results are given in Table 1. The yield of **2** was determined spectophotometrically at 458 and 480 nm on a Cary 118 spectrophotometer. At a thione **1** concentration of 6.8×10^{-4} *M* quantum yields were determined in the presence of ferrocene (Fig. 2). A plot of Φ_0/Φ versus the ferrocene concentration gave a straight line ($r = 0.999$) of slope 1150 M^{-1}. The quantum yield of **2** formation was also determined at 548 ± 9 nm (97% light absorbed) (Table 1).

Irradiations

As a control, 80 mL thione **1** solution in dioxane was irradiated under nitrogen through Pyrex with a 450 W medium pressure lamp for 6 h with almost complete consumption of starting material. The residue, after removal of solvent, was crystallized from xylene to give **2** in 70% yield.

The above irradiation was repeated, the hydrogen sulfide produced being entrained by nitrogen and passed through an acidified $CuSO_4$ solution (1 *M*). The sulfide precipitate was collected, washed, and dried (100°C) and was equivalent to a yield of hydrogen sulfide of 6%.

A similar solution was irradiated with the passage of nitrogen being directed into a standardized solution of iodine in aqueous potassium iodide. The excess iodine remaining was then estimated with sodium thiosulfate in the usual way (23). Although the vapour pressure of iodine over triiodide is less than over water it is, nonetheless, appreciable. To correct for the loss of iodine entrained by the passage of nitrogen an appropriate blank was carried out. With correction for the iodine loss the hydrogen sulfide estimated was 7%, but the correction was very large. If not made this could account for the large discrepancy between the earlier results (6) and those here reported.

Irradiation of Thioflavone 6

Thioflavone (85 mg) in diethyl ether (40 mL) was irradiated for 4.5 h through Pyrex with a 450 W medium pressure lamp. After evaporation of the solvent, crystallization (ethanol) of the residue gave 7 (9) in 33% yield, mass spectrum *m/e*: 412 (100, M^+) 413 (37), 307 (16), 206 (40), 169 (28). In other solvents, under similar conditions the following yields were obtained: dioxan (45%), cyclohexane (47%).

Analysis for Sulfur-containing Substances

(a) Irradiation with Toluene as Solvent

The thione **1** (99 mg) in toluene (40 mL) was irradiated through Pyrex with a 450 W medium pressure lamp for 13 h. The resulting solution was concentrated under reduced pressure at room temperature. The residue was analyzed by glc (5 ft. × ⅛ in., 3% SE 30 on Chromosorb P) and by glc–ms. Phenylmethanethiol, dibenzyl sulfide, and dibenzyl disulfide were identified. The yield of phenylmethanethiol (calibrating compound: diethyl succinate) was 11%.

(b) Irradiation with Dioxan as Solvent

The thione (48 mg) in dioxane (40 mL) was irradiated as described above until completion (5 h). Analysis of a portion by

Can. J. Chem. Downloaded from www.nrcresearchpress.com by 210.87.254.40 on 09/06/12
For personal use only.

tlc (hexane as eluent) did not reveal the presence of sulfur, nor was a positive indication given with the benzoin spot-test (24).

The remainder of the irradiated solution was concentrated under reduced pressure at room temperature. Gas–liquid chromatographic analysis revealed the presence of 1,4-dioxan-2-thiol in significant amount, mass spectrum *m/e*: 120 (23, M^+), 87 (100). The thiol itself was prepared by the method of Ketcham and co-workers (25) but was not obtained completely pure though sufficiently so to establish identity. *Exact Mass* calcd. for $C_4H_8O_2S$: 120.0245; found (ms): 120.0228.

Sensitization Experiments

(a) Michler's Ketone

The thione **1** (1.28×10^{-3} *M*) and the ketone (6.12×10^{-2} *M*) were irradiated in dioxane at 360 nm so that the ketone absorbed 90% of the light. Isolation of the product in the usual way afforded **2**.

(b) Triphenylene

The thione **1** (5.6×10^{-4} *M*; 3 mL) containing triphenylene (6.2×10^{-3} *M*) in tetrahydrofuran was irradiated at 280 ± 5 nm such that 97% of the light was absorbed by the hydrocarbon. Appearance of **2** was estimated at 458 nm with a quantum yield of 0.104 ± 0.01.

Acknowledgements

The authors thank the Natural Sciences and Engineering Research Council of Canada for support, and are indebted to Professors J. F. King and A. C. Weedon for helpful discussions.

1. A. Schonberg, K.-H. Brosowski, and E. Singer. Chem. Ber. **95**, 2144 (1962).
2. F. Arndt, E. Scholz, and P. Nachtwey. Ber. **57**, 1903 (1924).
3. R. Mayer, W. Broy, and R. Zahradnik. Adv. Heterocycl. Chem. **8**, 267 (1967).
4. U. Schmidt, K. H. Kabitzke, I. Boie, and C. Osterroht. Chem. Ber. **98**, 3819 (1965).
5. U. Schmidt and K. H. Kabitzke. Angew. Chem. Int. Ed. Engl. **3**, 641 (1964).
6. N. Ishibe, M. Sunami, and M. Odani. Tetrahedron, **29**, 2005 (1973).
7. W. Kirmse. Carbene chemistry. 2nd ed. Academic Press, New York. 1971. p. 423.
8. K. Muthuramu and V. Ramamurthy. J. Org. Chem. **45**, 4533 (1980).
9. E. Jakubowski, M. G. Ahmed, E. M. Lown, H. S. Sandhu, R. K. Gosavi, and O. P. Strausz. J. Am. Chem. Soc. **94**, 4094 (1972).
10. M. A.-F. El-Kuschef and M. H. Nosseir. J. Chem. Soc. 4643 (1963).
11. F. Arndt, P. Nachtwey, and J. Pusch. Chem. Ber. **58**, 1644 (1925).
12. P. Franzosini, G. Traverso, and M. Sanesi. Ann. Chim. Rome, **45**, 128 (1955); H. E. Ugnade. Organic Electronic Spectral Data, **2**, 518 (1960); **11**, 553, (1975).
13. I. El-Sayed El-Kholy and F. K. Rafla. J. Chem. Soc. C, 315 (1969).
14. M. Kikuchi, K. Kikuchi, and H. Kokubun. Bull. Chem. Soc. Jpn. **47**, 1331 (1974).
15. U. Bruhlmann and J. R. Huber. J. Photochem. **10**, 205 (1979).
16. P. de Mayo. Acc. Chem. Res. **9**, 52 (1976).
17. N. J. Turro and V. Ramamurthy. Tetrahedron Lett. **28**, 2423 (1976).
18. U. Bruhlmann and J. R. Huber. Chem. Phys. Lett. **54**, 606 (1978).
19. J. C. Scaiano and K. U. Ingold. J. Am. Chem. Soc. **98**, 4727 (1976).
20. J. S. Chapman, J. W. Cooper, and B. P. Roberts. J. Chem. Soc. Chem. Commun. 407 (1976).
21. R. L. Petersen, D. J. Nelson, and M. C. R. Symons. J. Chem. Soc. Perkin Trans. II, 226 (1978); M. C. R. Symons. J. Chem. Soc. Perkin Trans. II, 1618 (1974).
22. G. Palyi and F. Peter. Magy. Kem. Lapja, **17**, 354 (1962); Chem. Abstr. **58**, 6820 (1963).
23. A. I. Vogel. Textbook of quantitative inorganic analysis. 3rd ed. John Wiley Inc., New York. 1968.
24. F. Feigl and G. Stark. J. Anal. Chem. **27**, 1838 (1955).
25. M. G. Missakian, R. Ketcham, and A. R. Martin. J. Org. Chem. **39**, 2010 (1974).

Can. J. Chem. Downloaded from www.nrcresearchpress.com by 210.87.254.40 on 09/06/12
For personal use only.

A facile, versatile procedure for the preparation of fatty acid esters suitable for glc or hplc analyses

J. STUART GROSSERT,[1] W. M. NIMAL RATNAYAKE, AND TIW SWEE
Department of Chemistry, Dalhousie University, Halifax, N.S., Canada B3H 4J3
Received January 19, 1981

J. STUART GROSSERT, W. M. NIMAL RATNAYAKE, and TIW SWEE. Can. J. Chem. **59**, 2617 (1981).

The preparation of fatty acid methyl esters for glc analyses and of various aryl esters for hplc analyses has traditionally been carried out in totally unrelated operations. This paper draws attention to the use of fatty acid – trifluoroacetic acid mixed anhydrides which may be directly and efficiently converted into either type of ester. The utility of the method was demonstrated by the preparation of a series of methyl, 2-naphthyl, and vanillin fatty acid esters. The spectral characterization of some aryl fatty acid esters is recorded.

J. STUART GROSSERT, W. M. NIMAL RATNAYAKE et TIW SWEE. Can. J. Chem. **59**, 2617 (1981).

On a préparé des esters méthyliques d'acides gras en vue des analyses en cpg et différents esters aryliques en vue des analyses en clhp selon une méthode nouvelle qui utilise des réactions classiques. Cette publication attire l'attention sur l'utilisation d'anhydrides mixtes d'acides gras et d'acide trifluoroacétique qui peuvent être transformés directement et efficacement en n'importe quel type d'esters. On démontre l'utilité de la méthode en préparant une série d'esters méthyliques, naphtaliques-2 et vanilliques d'acides gras. On a enregistré les caractéristiques spectrales de quelques esters aryliques d'acides gras.

[Traduit par le journal]

The chromatographic separation and analysis of fatty acids from complex natural lipid mixtures is normally carried out on some suitable derivative of the acids (1–4). For example, gas chromatography (glc) is conveniently carried out on the reasonably volatile methyl esters (1,4). On the other hand, the best detectors available for modern liquid chromatography (hplc) work on spectrophotometric (generally at 254, 280, or 360 nm) or fluorimetric principles. Since very few naturally occurring fatty acids possess chromophores which absorb above 220 nm (5), it is necessary to derivatize the acids in order to achieve adequate sensitivity. Derivatives commonly used for this purpose, for example aryl esters, have chromophores that absorb at appropriate wavelengths (3).

There are many ways of converting carboxylic acids into esters, although in principle most reactions are of the general type set out in eq. [1], where X^+ is some electrophilic activator and YOR is some suitable oxygen nucleophile, usually an alcohol.

$$[1]\quad R\cdot CO\cdot OH + X^+ \rightarrow [RCO_2HX]^+ + YOR \rightarrow R\cdot CO\cdot OR + [HOXY]^+$$

Methyl esters are usually produced from free fatty acids by reaction with 1–2% sulfuric acid in methanol (6), with anhydrous hydrogen chloride in methanol (4), with boron trifluoride in anhydrous methanol (2), or with diazomethane (2, 7). Although the first three of these methods are popular, all suffer from the common problem of employing a strongly acidic medium which destroys acid-labile functionalities in such natural compounds as cyclopropane, cyclopropene, epoxy and phytenic acids (8–10). Other artefacts may be formed if reagents such as BF_3–MeOH are not used with caution (11). Even use of a reagent as well known as diazomethane is not without difficulties with complex naturally occurring mixtures where *rapid and quantitative reaction* is required (7); in addition, it is well known to be toxic and potentially explosive.

There are two generally used approaches to the preparation of fatty acid esters suitable for uv detection with hplc. The first approach utilizes carboxylate anions to attack reactive aralkyl halides, e.g. phenacyl bromide, to prepare phenacyl esters (2). The other major approach is to use aryldiazomethanes (2) or aryltriazenes (12) which react by loss of nitrogen. Difficulties that pertain to both the above approaches are that the reactions are not very facile and require heating, often with excesses of expensive reagents.

Carboxylic acids have also been esterified by heating with amide acetals (2), a method first developed by Meerwein *et al.* (13). This approach has been popularized commercially in that a range of acetals is readily available and carboxylic acids are heated with the acetal in pyridine to effect esterification. However, the reaction is not necessarily quantitative and relatively vigorous conditions are needed to provide a reasonable rate of reaction.

Our initial approach to facilitating ester formation was to explore activation of the carboxylic acid

[1]Author to whom correspondence may be addressed.

0008-4042/81/172617-04$01.00/0
©1981 National Research Council of Canada/Conseil national de recherches du Canada

Can. J. Chem. Downloaded from www.nrcresearchpress.com by 210.87.254.105 on 09/06/12
For personal use only.

Can. J. Chem. Downloaded from www.nrcresearchpress.com by 210.87.254.105 on 09/06/12
For personal use only.

TABLE 1. The yields of esters prepared by the mixed anhydride method in the presence of sodium fluoride*

Fatty acid	Oxygen nucleophile	Isolated yield of ester
Octadecanoic (**3**)	MeOH (1 mL)–pyridine (1 mL)	63
Octadecanoic (**3**)	MeOH (2 mL)–pyridine (1 mL)	62
cis-9-Octadecenoic (**4**)	MeOH (1 mL)–pyridine (1 mL)	59
Octadecanoic (**3**)	Vanillin (70 mg)–pyridine (1 mL)	72
Octadecanoic (**3**)	DMF–DMA (1 mL)†	73
dl-*cis*-9,10-Methyleneoctadecanoic (**5**)	DMF–DMA (1 mL)†	68
dl-*cis*-9,10-Epoxyoctadecanoic (**6**)	DMF–DMA (1 mL)†	‡
dl-*threo*-9,10-dihydroxyoctadecanoic (**7**)	DMF–DMA (1 mL)†	‡

*Other bases such as pyridine or sodium acetate gave much lower yields than did sodium fluoride.
†*N*,*N*-Dimethylformamide dimethyl acetal (2 mequiv./mL in pyridine; Pierce Chemical Co., Rockford, IL., U.S.A.).
‡Not isolated due to the complexity of the mixture, see Experimental.

with trifluoroacetic acid anhydride (TFAA) in the presence of sodium fluoride (to act as acid scavenger), followed by treatment with the dimethyl acetal of *N*,*N*-dimethylformamide ($Me_2NCH(OMe)_2$, **1**) (2). The reaction was rapid and facile since it would be carried out at room temperature. However, yields of methyl esters were no better than 75% (Table 1). It could well be that although the NaF would facilitate mixed anhydride formation (eq. [2]), it would suppress acylium ion formation, which is acid catalyzed (eq. [3]) (14). Presumably acylium ions are the active species that react with **1** to form the methyl esters. Furthermore the reaction was not useful for the esterification of acid-sensitive molecules such as **6** and **7** (Table 1).

[2] $RCOOH + (CF_3CO)_2O \rightleftharpoons RCOO{\cdot}COCF_3\,(\mathbf{2}) + CF_3COOH$

[3] $RCOO{\cdot}COCF_3 + H^+ \rightleftharpoons RCO^+ + CF_3COOH$

We then explored the utility of ester formation from fatty acids by a method first described by Bourne *et al.* (15), which does not appear to be widely known. The method is simple and versatile, since it involves only activation of a carboxylic acid with TFAA in an inert solvent to form **2**, which is rapidly susceptible to attack by a *wide range* of alcohols or phenols to form esters. It may be used on hindered acids (14). However, it does suffer from the drawback of being unsuited for acid-labile fatty acids. It is the purpose of this paper to draw attention to the versatility of this method of ester formation, and in particular to the fact that *both* methyl esters (for glc analyses) or aryl esters (for hplc analyses) are directly accessible from one common intermediate (eq. [4]). This is of special value for hplc analyses since a wide range of phenols and aryl-containing alcohols is readily available. Results are given in Table 2. Yields were very good, except in the cases of **6** and **7** which were obviously labile to the conditions of mixed anhydride formation (see also Table 1).

[4] $RCOOH \xrightarrow{TFAA} RCOO{\cdot}COCF_3 \xrightarrow{R'OH} RCOOR'$

In order to test the practical applicability of the method, the fatty acids from herring oil were converted into methyl esters by both the mixed anhydride method and by the commonly used BF_3–methanol method, a method recommended by the Association of Official Analytical Chemists (16). The methyl esters obtained by both methods were purified by preparative tlc and were analyzed in detail by capillary glc under identical conditions.[2] Twelve saturated, 13 monoenoic, 4 dienoic, 3 trienoic, 7 tetraenoic, 4 pentaenoic, and one hexaenoic fatty acid methyl esters were detected, quantitated, and identified by standard techniques (17). Detailed results on the analyses are presented elsewhere (18). In no case were there any significant differences between the results from the two methods, and with the small samples of acids used, conversion to esters was essentially quantitative.

The aryl esters prepared in this study were novel and their infrared, nmr, and mass spectra were studied. The infrared and nmr spectra of all esters were as expected for molecules containing their functional groups. It is worth noting that vanillin octadecanoate (4-carboxaldehydo-3-methoxyphenyl octadecanoate, **16**) has both aldehydic and methoxyl protons which are particularly characteristic in the ^1H nmr spectrum. The mass spectra of esters **13–16** were totally dominated by peaks attributable to phenol radical cations. This phenomenon is precedented for aryl esters (19), fatty acid benzyl esters (20), and for aryl carbamate esters (21), although we are not aware of any detailed studies on the mass spectrometry of fatty acid aryl esters. In contrast to the mass spectra of fatty acid methyl esters (22), the molecular ions of these aryl esters (**13–16**) were of very low intensity, as were the

[2]We thank Dr. R. G. Ackman for kindly providing the required facilities and advice to carry out these analyses.

TABLE 2. The yields of esters formed by reacting methanol or 2-naphthol with a fatty acid mixed anhydride

Fatty acid	Ester formed	Isolated yield of ester
Octadecanoic (**3**)	Methyl (**8**)	91
cis-9-Octadecenoic (**4**)	Methyl (**9**)	88
dl-*cis*-9,10-Methyleneoctadecanoic (**5**)	Methyl (**10**)	87
dl-*cis*-9,10-Epoxyoctadecanoic (**6**)	Methyl (**11**)	12
dl-*threo*-9,10-Dihydroxyoctadecanoic (**7**)	Methyl (**12**)	8
Octadecanoic (**3**)	2-Naphthyl (**13**)	93
cis-9-Octadecenoic (**4**)	2-Naphthyl (**14**)	96
dl-*cis*-9,10-Methyleneoctadecanoic (**5**)	2-Naphthyl (**15**)	88

classical McLafferty rearrangement ions, $RO{\cdot}C(OH){=}CH_2]^+$ (R = aryl). Only in the case of vanillin octadecanoate (**16**) was there a significant ion at higher mass, viz. *m/z* 267 which corresponds to the ion $C_{17}H_{35}CO]^+$. The only other major ions in all four spectra were low-mass ions, typical of aralkyl precursors.

Although we have only explored the preparation of 2-naphthyl and vanillin esters, the correct choice of derivative in practice will obviously depend on the hplc column and particular separation problem at hand. We conclude by emphasizing that this mixed anhydride method offers ready access to the formation of a wide range of fatty acid derivatives which may be suitable respectively for glc or hplc analyses. This should facilitate transfer of well-established glc methodology, built on methyl esters, to hplc techniques based on ultraviolet-absorbing or fluorescent esters.

Experimental

General

Chemicals used were ACS grade, solvents were distilled and dried according to standard techniques. Trifluoroacetic acid anhydride (TFAA) was used as obtained from the Aldrich Chemical Co. Silica gel for column and thin-layer chromatography was from E. Merck & Co. Silica gel for columns was prewashed with *n*-hexane; tlc plates were developed in ligroin (bp 40–60°C) – diethylether – acetic acid (90:10:1, v/v/v), and material from preparative tlc was removed by extracting three times with chloroform – *n*-hexane (1:1, v/v). Infrared spectra were recorded as liquid films, KBr pellets, or CCl_4 solutions as appropriate; nmr spectra were recorded at 60 MHz in $CDCl_3$ containing 1% TMS as internal standard and chemical shifts are reported in ppm as δ values. Mass spectra were recorded on a DuPont-CEC 21-104 mass spectrometer equipped with a heated glass probe at an ionizing voltage of 70 eV. Gas–liquid chromatography was carried out on a Hewlett-Packard 5750 instrument with an EGSS-X column (1.8 m × 3.2 mm ss column at 180–200°C, N_2 flow 20–30 mL/min, 10% EGSS-X on Chrom W, 80–100 mesh); alternatively, on Perkin-Elmer 900 and 990 instruments with wall-coated, open-tubular capillary columns (ss, 46 m × 0.25 mm) coated with either BDS or Silar-5CP liquid phases (Perkin-Elmer Corp., Norwalk, CT., U.S.A.), He pressure 60 psig, column temp. 170–180°, injection ports and split assemblies 270°, manifold assemblies 250°C.

*Preparation of dl-*cis*-9,10-Methyleneoctadecanoic Acid, 5*

The procedure of Simmons and Smith (23) gave pure **5** in 51% yield, mp 37–38°C (lit. (23) mp 36–38°C); ν_{max}(KBr): 3500–3400 (br), 1720 (s), 1020 (m), 866 (m) cm^{-1}; nmr ($CDCl_3$) δ: −0.3 (1H, m), 0.6 (3H, m), 0.9 (3H, m), 1.3 (26H, m), 2.2–2.3 (2H, m), 9.7–10.0 (1H, br s).

*Preparation of dl-*cis*-9,10-Epoxyoctadecanoic Acid, 6*

The procedure of Swern *et al.* (24) gave pure **6** in 70% yield, mp 58.0–59.0°C (lit. (24) mp 59.5–59.8°C); ν(KBr): 3500–3400 (br), 2950 (s), 2900 (s), 1715 (s), 850 (m) cm^{-1}; nmr ($CDCl_3$) δ: 0.91 (3H), 1.25 (20H), 2.2–2.3 (6H), 2.80 (2H), 9.6–10.0 (1H).

*Preparation of dl-*threo*-9,10-Dihydroxyoctadecanoic Acid, 7*

dl-*cis*-9,10-Epoxyoctadecanoic acid (**6**, 50 mg, 0.16 mmol) in glacial acetic acid (2 mL) was heated in a boiling water bath for 3 h, after which the excess acetic acid was evaporated under reduced pressure. To the residue, 5 *N* NaOH (10 mL) was added, the mixture was heated for 1 h on a boiling water bath, cooled, neutralized with 5 *N* HCl, and extracted with diethyl ether (3 × 50 mL). The extract was washed with water, dried, and evaporated under reduced pressure to give crude **7** as a white powder (45 mg). Recrystallization from methanol gave pure **7** (38 mg, 72%), mp 93–94°C (lit. (24) mp 92–93°C).

Esterification of Fatty Acids by the Mixed Anhydride Method in the Presence of Sodium Fluoride

Fatty acid (100 mg), anhydrous NaF (50 mg), and TFAA (1 mL, added dropwise) were stirred for 5 min at 25°C and then evaporated to dryness under reduced pressure. The above process was repeated with another portion of TFAA. The solution containing the oxygen nucleophile was added slowly and the mixture was stirred for 30 min at 25°C. Isolation of methyl esters was carried out by chromatography on silica gel (6% diethyl ether in ligroin (bp 40–60°C)). Isolation of vanillin octadecanoate (**16**) was achieved by partitioning the reaction mixture between water and ligroin (bp 40–60°C), followed by sequential base and acid washing, plus drying and evaporation of the ligroin solution to give crude **16** which was recrystallized from 95% ethanol. Results are given in Table 1. The identity of the methyl esters was confirmed by comparison with authentic samples. Vanillin octadecanoate had mp 65–66°C; ir (KBr): 1760, 1700, 1690, 1610, 1595, 1150, 800 cm^{-1}; nmr ($CDCl_3$) δ: 0.9 (3H, m), 1.2–2.6 (32H, m), 3.95 (3H, s), 7.1–7.5 (3H, m), and 9.80 (1H, s); mass spectrum *m/z*: 418 ($M^{+\cdot}$, 3) 283 (1), 267 (17), 152 (100), 149 (33), 123 (3), 97 (7), 85 (12), 71 (19), 69 (11), 57 (38), 55 (16), 43 (27), 41 (10).

Methylation of Fatty Acids with Trifluoroacetic Acid Anhydride and Methanol

Fatty acid (ca. 20 mg) was dissolved in benzene (1 mL). TFAA (1 mL) was added dropwise and the solution was stirred

Can. J. Chem. Downloaded from www.nrcresearchpress.com by 210.87.254.105 on 09/06/12
For personal use only.

Can. J. Chem. Downloaded from www.nrcresearchpress.com by 210.87.254.105 on 09/06/12
For personal use only.

for 10 min at 25°C. Anhydrous methanol (1 mL) was then added and the solution stirred for 30 min. The solution was diluted with ligroin (bp 40–60°C, 50 mL) which was washed with sodium hydroxide solution (10%, 3 × 20 mL) and water, dried (Na_2SO_4), and evaporated under reduced pressure, which permitted determination of the percentage yields of the methyl esters. Ester purity was checked by tlc and glc.

Esterification of Fatty Acids with Trifluoroacetic Acid Anhydride and 2-Naphthol

Fatty acid (100 mg, ca. 0.3 mmol), TFAA (1 mL, 7.2 mmol), and 2-naphthol (100 mg, 0.7 mmol) were combined and reacted in benzene as detailed above. Analytical tlc showed **13–15** as major components in the reactions of **3–5**, with minor spots due to **3–5** and 2-naphthol. Reaction of **6** and 7 showed at least 6 components. The esters **13–15** were isolated by dissolving the crude product in diethyl ether (50 mL). This ether solution was washed with sodium hydroxide (10%, 3 × 30 mL), with saturated sodium chloride solution (2 × 50 mL), and then dried and evaporated, as usual. Thin-layer chromatography of all three products showed only one spot. Esters **13** and **15** were recrystallized from 95% ethanol; **14** was a pale yellow oil.

2-Naphthyl octadecanoate, **13**, had mp 70–71°C; ir (KBr): 1750, 1600, 1500, 1280 cm^{-1}; nmr ($CDCl_3$) δ: 0.9 (3H, m), 1.2–1.6 (30H, m) 2.6 (—CO·CH_2—, m), 7.0–8.0 (7H, m); mass spectrum *m/z*: 410 ($M^{+\cdot}$, 4), 144 (100), 127 (1), 115 (7), 67 (7), 65 (9), 55 (12), 43 (16).

2-Naphthyl cis-*9-octadecenoate*, **14**, had ir ($CHCl_3$): 1750, 1600, 1510, 1250, 800 cm^{-1}; nmr ($CDCl_3$) δ: 0.9 (3H, m), 1.2–1.7 (26H, m), 1.8–2.2 (—CH_2·CH=CH·CH_2—, m), 2.60 (—CO·CH_2—, t), 5.40 (—CH=CH—, t), 7.0–8.0 (7H, m); mass spectrum *m/z*: 408 ($M^{+\cdot}$, 3), 379 (0.2), 145 (43), 144 (100), 115 (11), 97 (6), 95 (6), 83 (10), 69 (20), 67 (10), 55 (35), 43 (26).

2-Naphthyl dl-cis-*9,10-methyleneoctadecanoate*, **15**, had mp 66–67°C; ir (KBr): 1750, 1600, 1500, 1280, 1020 cm^{-1}; nmr ($CDCl_3$) δ: −0.73 (1H, m), 0.53–1.0 (6H, m), 1.2–2.1 (26H, m), 2.65 (—CO·CH_2—, t), 7.0–8.0 (7H, m); *m/z*: 422 ($M^{+\cdot}$, 0.2), 393 (3), 186 (0.2), 144 (100), 115 (6), 55 (8), 43 (12).

Preparation of Fatty Acid Methyl Esters from Herring Oil

Herring oil fatty acids were prepared by saponification of herring oil, with the use of a nitrogen atmosphere for all operations. A 10 mg sample of the fatty acids was dissolved in benzene (1 mL) in a 10 mL, screw-capped (Teflon-lined) centrifuge tube. TFAA (1 mL) was added slowly and the mixture was shaken vigorously in a vortex mixer. Anhydrous methanol (1 mL) was added and the mixture shaken for 20 min. Distilled water (4 mL) was added, the mixture again shaken thoroughly, and the methyl esters were extracted with benzene (3 × 2 mL). The benzene extract was concentrated by heating in a stream of nitrogen over a 50°C water bath. Preparative tlc gave 8.7 mg of methyl esters. *Alternatively*, herring oil fatty acids (10 mg) were dissolved in benzene as above, and heated with boron trifluoride – methanol reagent (14%, 1 mL) at 100°C for 10 min. Work-up and purification as above gave a comparable quantity of fatty acid methyl esters. The two methyl ester samples were analyzed under identical conditions by glc on a Silar-5CP capillary column (18).[2]

Acknowledgements

We thank the National Research Council of Canada and Dalhousie University for financial support, and the Canadian Commonwealth Scholarship Committee for a scholarship to W.M.N.R. Dr J.-H. Kim kindly ran the mass spectra.

1. A. Kuksis. *In* Handbook of lipid research. Vol. 1. *Edited by* A. Kuksis. Plenum, New York. 1978. p. 4.
2. A. Darbre. *In* Handbook of derivatives for chromatography. *Edited by* K. Blau and G. S. King. Heyden, London. 1977. p. 39.
3. J. F. Lawrence and R. W. Frei. Chemical derivatization in liquid chromatography. Elsevier, Amsterdam. 1976. p. 127.
4. W. W. Christie. Lipid analysis. Pergamon, Oxford. 1973. p. 85.
5. Hitoshi Aoshima. Anal. Biochem. **87**, 49 (1978).
6. Report of instrumental technique committee. A.O.C.S., (1962–1963). J. Am. Oil Chem. Soc. **41**, 618 (1964).
7. M. J. Levitt. Anal. Chem. **45**, 618 (1973).
8. W. W. Christie. Top. Lipid Chem. **3**, 171 (1972).
9. J. L. Gellerman, W. H. Anderson, and H. Schlenk. Lipids, **10**, 656 (1975).
10. D. E. Minnikin. Lipids, **7**, 398 (1972).
11. W. K. Fulk and M. S. Shorb. J. Lipid Res. **11**, 276 (1970).
12. I. R. Politzer, G. W. Griffin, B. J. Dowty, and J. L. Laseter. Anal. Lett. **6**, 539 (1973).
13. H. Meerwein, P. Borner, O. Fuchs, H. J. Sasse, H. Schrodt, and J. Spille. Chem. Ber. **89**, 2060 (1956).
14. R. C. Parish and L. M. Stock. J. Org. Chem. **30**, 927 (1965).
15. E. J. Bourne, M. Stacey, J. C. Tatlow, and J. M. Tedder. J. Chem. Soc. 2976 (1949).
16. L. D. Metcalfe and A. A. Schmitz. Anal. Chem. **33**, 363 (1961).
17. R. G. Ackman. Prog. Chem. Fats Other Lipids, **12**, 167 (1972).
18. W. N. Ratnayake. M.Sc. Thesis, Dalhousie University, 1978.
19. V. J. Feil and J. M. Sugihara. Org. Mass Spectrom. **6**, 265 (1972).
20. U. Hintze, H. Röper, and G. Gercken. J. Chromatogr. **87**, 481 (1973).
21. W. R. Benson and J. N. Damico. J. Assoc. Off. Anal. Chem. **51**, 347 (1968).
22. J. H. Beynon, R. A. Saunders, and A. E. Williams. The mass spectra of organic molecules. Elsevier, Amsterdam. 1968. pp. 215–250.
23. H. E. Simmons and R. D. Smith. J. Am. Chem. Soc. **81**, 4256 (1959).
24. D. Swern, T. W. Findley, and J. T. Scanlan. J. Am. Chem. Soc. **66**, 1925 (1944).

The *sec*-butyl cation; reaction with 2-butene[1]

PIERRE LACHANCE AND ARTHUR M. EASTHAM
Division of Chemistry, National Research Council of Canada, Ottawa, Ont., Canada K1A 0R9

Received December 12, 1980

PIERRE LACHANCE and ARTHUR M. EASTHAM. Can. J. Chem. **59**, 2621 (1981).

The products from the reaction of 2-butene with $BF_3.CH_3OH$ are olefins in the range C_8 to above C_{20}; about 60% of the product is the normal dimer–trimer–tetramer material but the remaining 40% is rearranged product. We have identified most of the skeletal structures up to C_{13} and suggest that the rearrangements are most easily interpreted by postulating that alkyl transfers can occur in the same way as proton transfers.

PIERRE LACHANCE et ARTHUR M. EASTHAM. Can. J. Chem. **59**, 2621 (1981).

La réaction entre le butène-2 et $BF_3.CH_3OH$ donne, comme produit de réaction, un mélange d'oléfines possédant entre huit et plus de vingt carbones. Les dimères, trimères, tétramères normaux forment 60% du produit, tandis que 40% sont des substances transposées. Nous avons identifié la plupart des structures carbonées contenant jusqu'à treize carbones. Aussi nous apparait-il qu'une des façons les plus faciles d'expliquer les transpositions observées, est de supposer un éventuel transfert de groupe alkyle semblable au transfert de proton.

Can. J. Chem. Downloaded from www.nrcresearchpress.com by 210.87.254.42 on 09/06/12
For personal use only.

With acidic catalysts of the type $BF_3.HX$, 2-butene can undergo oligomerization to a complex mixture of mono-olefins, generally in the molecular weight range 112 (C_8H_{16}) to somewhat beyond 224 ($C_{16}H_{32}$) (1). About half of the product is the expected dimers, trimers, and tetramers formed by the simple addition reaction but the remainder consists of rearranged products which must be of mechanistic importance if, as seems probable, the rearrangement occurs during the growth-limiting, transfer-termination step of the polymerization. We report here the characterization of most structures up to the tridecenes present in the product, with some suggestions as to how they might have been formed; identification of the remainder of the material, about 25% of the total and generally in the C_{14}–C_{20} range, will be a laborious task to be undertaken only if clearly necessary for interpretation of the results.

The product mixture of olefins, containing small amounts of alkanes and diolefins, can be separated by careful fractional distillation into groups of closely related olefins, usually of a single molecular weight. Each molecular weight group consists of a number of *cis–trans* pairs, usually with more than one carbon skeleton, which cannot be separated with available techniques, so identification of the components must be made within the mixture. Simplification can sometimes be achieved by hydrogenating the fraction in order to convert olefins of the same carbon skeleton to a single alkane but the improvement is often minimal because hydrogenation leads to new asymmetric centers and therefore to stereoisomers which may be clearly visible in the capillary chromatogram. The method used for identifying complex alkanes of this kind was discussed elsewhere (2), and is briefly as follows. The molecular weight and some idea of the structure of the olefin–alkane can be obtained for individual components of the mixture from the capillary chromatograph – mass spectrometer combination. An appropriate alkane is then synthesized by at least two reliable and independent methods and compared with the unknown by retention times and mass spectrum. We are aware that this comparison is not regarded as rigorous, and have in fact experienced the dangers in comparing two compounds on a single capillary column, but we are of the opinion that it is the best method available and is reasonably safe if one uses at least two appropriate capillary columns (e.g. squalane and OV-101). If the pure alkane gives a pattern of several stereoisomers, the comparison becomes very reliable and obviously, when unknown and known have different retention times, rejection of the structure is unequivocal.

The approximate composition of the olefin mixture is as follows:

C_8	10%	C_{14}	4%
C_9	5	C_{15}	3
C_{10}	10	C_{16}	18
C_{11}	8	C_{17}	3
C_{12}	17	C_{18}	5
C_{13}	3	C_{19} and higher	16

This composition is not strongly dependent on reaction variables such as conversion, concentration, etc. Lowering the temperature shifts the product to somewhat higher molecular weights, and prolonged reaction times produce secondary

[1]NRCC No. 19492.

0008-4042/81/172621-08$01.00/0
©1981 National Research Council of Canada/Conseil national de recherches du Canada

Can. J. Chem. Downloaded from www.nrcresearchpress.com by 210.87.254.42 on 09/06/12
For personal use only.

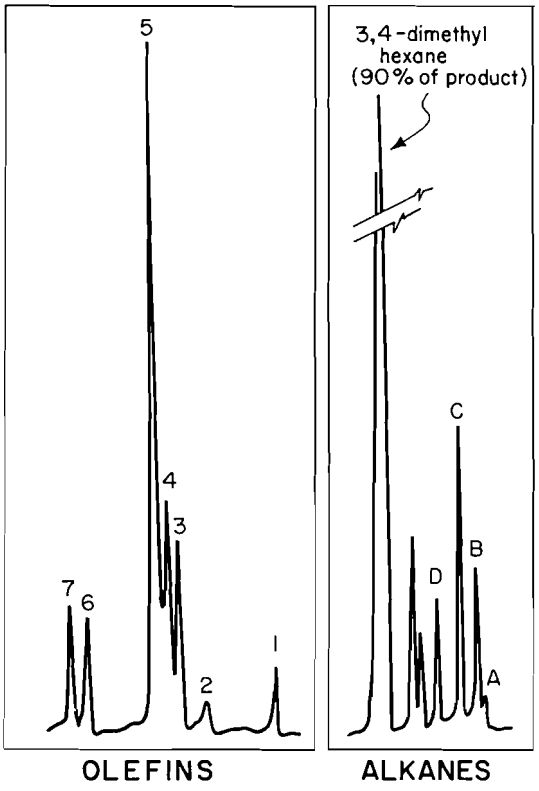

FIG. 1. Chromatograms for octenes and octanes; olefins on 150 ft × 0.01 in. WCOT OV-101 at 50°C, alkanes on 150 ft × 0.01 in. WCOT squalane at 40°C.

reaction products. We have not found products smaller than C_8 but introduction of small amounts of such materials into the reaction mixture indicates that they react with butene and disappear. Addition of small amounts of 2-butene to a nearly completed reaction mixture tends to reduce the relative amount of octenes present, presumably as a result of re-initiation of chain growth. The major peaks in the product chromatogram are, as might be expected, those corresponding to C_8, C_{12}, and C_{16} olefins, i.e. to dimer, trimer, and tetramer. Next largest is C_{10} which should perhaps be compared with $C_9 + C_{11}$, corresponding to symmetrical and unsymmetrical fission of the butene residue. Detailed description of the product follows.

Octenes

The octene fraction and its hydrogenation product are shown as capillary chromatograms in Fig. 1. Over 90% of the octene mixture has the skeletal structure of the expected butene dimer, 3,4-dimethylhexene, made up as follows. Peaks 3 and 5, *cis*- and *trans*-3,4-dimethylhexene-2; 6 and 7, *trans*- and *cis*-3,4-dimethylhexene-3, respectively; 4, 3,4-dimethylhexane. The minor peaks 1 and 2 have not been identified but 2 may be 2-ethyl-3-methyl-1-pentene. Hydrogenation gives rise to the expected large amount of 3,4-dimethylhexane but about 10% of the alkane is made up of half a dozen minor components (see Fig. 1), four of which have been tentatively identified as 2,4-dimethylhexane (A, trace only), 2,2,3-trimethylpentane (B), 3,3-dimethylhexane (C), and 2,3,4-trimethylpentane (D). Absent are 2,3- and 2,5-dimethylhexanes, 2,3,3- and 2,2,4-trimethylpentanes.

Nonenes

The nonenes on hydrogenation give exclusively 3,3,4- (**1**) and 2,3,4-trimethylhexanes (**2**) in the ratio of 2:7 respectively. The latter appears as a well-resolved doublet in both known and unknown materials.

Decenes

The C_{10} fraction consists of about a dozen olefins which on hydrogenation give rise to a very simple product chromatogram, a large singlet (90%) and a small triplet (Fig. 2). The major component was easily identified as 3,4,5-trimethylheptane (**3**) through comparison with a known sample by nmr, ir, etc; it is slightly resolved into the expected doublet by high resolution glc (very small samples, 300 ft WCOT squalane, ms detector) and shows a trace of a third component. The minor constituent alkanes have not been identified but are not 2,2,3,4-, 2,3,3,4-, or 2,3,4,4-tetramethylhexane, 2,4,5- or 3,5,5-trimethylheptane.

According to the mass spectra and retention times it seems probable that the original olefin mixture contains small amounts of two alkanes, one of which is 3,4,5-trimethylheptane.

Undecenes

The problem of identifying hydrocarbons is well illustrated by this C_{11} fraction. The mixture of several olefins, making up about 8% of the total product, upon hydrogenation gives a chromatogram showing a single large multiplet and a few very minor constituents. The multiplet was not well resolved even on 300 ft squalane, but showed identical retention times with the multiplet from an authentic sample of 3,4,5-trimethyl octane (**4**) synthesized for comparison (Fig. 3). We believe the two compounds to be identical except in their stereoisomer ratio. Scanning across the glc peaks with the ms revealed no obvious differences in cracking patterns either between or within the peaks (see ref. 2 for elaboration).

Can. J. Chem. Downloaded from www.nrcresearchpress.com by 210.87.254.42 on 09/06/12
For personal use only.

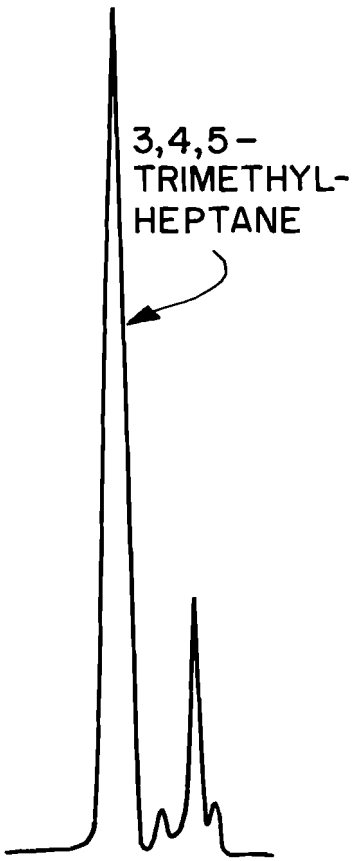

FIG. 2. C_{10} alkanes. Chromatogram on 150 ft × 0.01 in. WCOT squalane at 75°C.

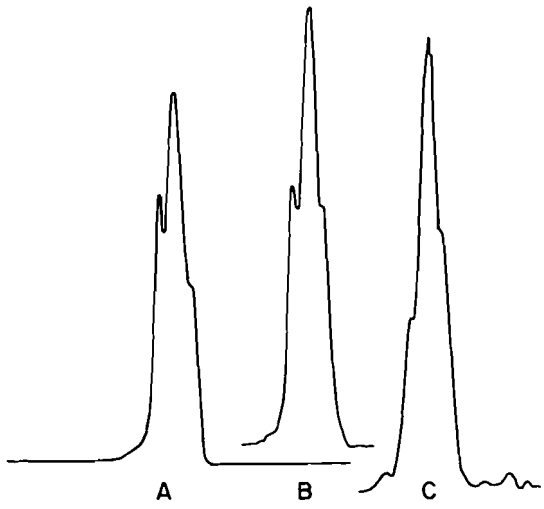

FIG. 3. C_{11} alkane. Chromatogram on 300 ft WCOT squalane at 110°C; A. synthetic 3,4,5-trimethyloctane; B. mixture of known and unknown; C. unknown.

Dodecenes

The C_{12} olefins, 15–20% of the product and therefore the major constituent, were separated from the C_{11} and C_{13} components by careful fractional distillation under reduced pressure and then examined in the glc–ms combination for molecular weight homogeneity. Most of these olefins, unlike the corresponding alkanes, give adequate parent-ion response. Both the C_{12} and C_{13} cuts showed excellent molecular weight purity and the intermediate fraction amounted to only 10–15% of the total C_{12}–C_{13} material.

The C_{12} fraction was hydrogenated to the dodecanes and then, according to glc, contained at least fifteen components, some of them undoubtedly stereoisomers. The major constituent was shown to be the expected butene trimer, 3,4,5,6-tetramethyloctane **5**, identified as described in detail elsewhere (2). In order to obtain some idea of the structure of the rest of the C_{12} constituents, distillation fractions were submitted to ozonization and the products examined by glc–ms. Fractions containing primarily olefins with the skeletal structure of **5** gave the expected C_8 and C_{10} ketones. The remaining C_{12} olefins gave rise to considerable amounts of C_7 ketones which on the basis of retention times on OV-17, OV-101, and UCON 550B were tentatively identified as 3,4- and 3,3-dimethyl-2-pentanone. The C_5 fraction was small and somewhat fleeting but reduction of the ozonide with H_2/Pd instead of low temperature Zn/HOAC gave fair yields and indicated the presence of 2-methylbutanal and 3-methyl-2-butanone. On the basis of these data it seemed probable that the C_{12} mixture contained structures analogous to 3,3,4,6-**7** and 2,3,4,6-tetramethyl octanes **6**.

The 2,3,4,6-tetramethyloctane **6** was synthesized and compared with hydrogenated fractions of the C_{12} olefins. On 150 ft of WCOT squalane the chromatogram of this compound shows a singlet and a poorly resolved multiplet which correspond exactly with an important pair of peaks in the chromatogram of the unknown (Fig. 4). On OV-101 the synthetic material shows a singlet and a nearly completely resolved doublet which match exactly the retention times of three peaks in the unknown, but the ratio of the two components of the doublet appears to be reversed in the two samples.

The 3,3,4,6-tetramethyloctane **7** was prepared by acid dehydration of 4-hydroxy-3,3,4,6-tetramethyloctane without noticeable rearrangement (see Experimental). This alkane appears, in the chromatogram, as a broad singlet which corresponds with a peak shown by the unknown.

Can. J. Chem. Downloaded from www.nrcresearchpress.com by 210.87.254.42 on 09/06/12
For personal use only.

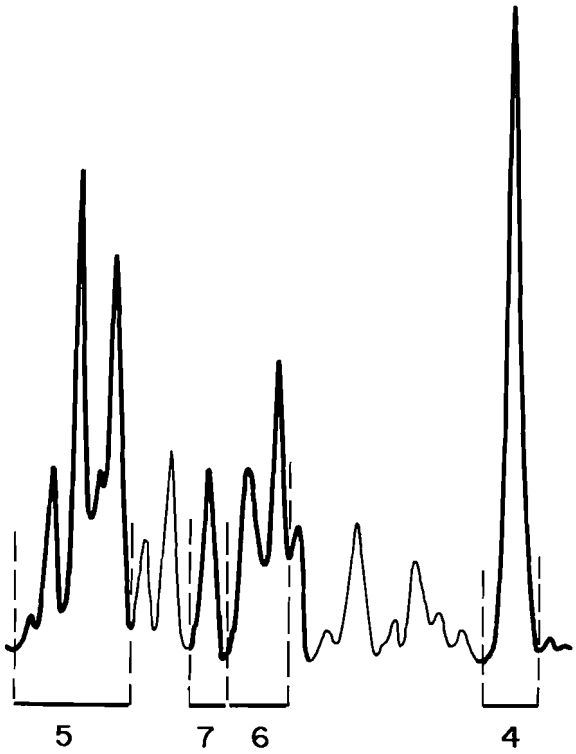

FIG. 4. C_{11} and C_{12} alkanes on 150 ft WCOT squalane at 100°C. Bold lines indicate identified sections; **4**, 3,4,5-trimethyloctane; **5**, 3,4,5,6-tetramethyloctane; **6**, 2,3,4,6-tetramethyloctane; **7**, 3,3,4,6-tetramethyloctane.

The 2,3,4,6- and 3,4,5,6-tetramethyloctanes **6**, **5**, and **7** together made up at least three-quarters of the C_{12} fraction (Fig. 4). The remainder does not include 4-ethyl-3,6-dimethyloctane, 2,3,4,5,5-pentamethylheptane, or 2,5,6,6-tetramethyloctane.

Tridecenes

The C_{13} fraction is rather small and, from analogy with the nonenes, was expected to consist primarily of olefins with skeletal structures corresponding to 2,3,4,5,6- and 3,3,4,5,6-pentamethyloctanes. Both of these were synthesized but only the first corresponded to the hydrogenated unknown. The 2,3,4,5,6-PMO shows one major and five minor peaks in its chromatogram on either squalane or OV-101 and these five peaks correspond exactly to a similar group in the unknown on the same column. The 3,3,4,5,6-isomer, if present at all, is in very small amounts compared to the 2,3,4,5,6-PMO.

The conventional view of a cationic olefin polymerization postulates initial protonation of the olefin (monomer) by the catalyst followed by rapid reaction of the resulting cation with further olefin to give either addition of monomer (chain growth), or transfer of a proton to monomer with initiation of a new polymer (chain transfer). Termination is usually regarded as transfer of the proton back to a catalyst anion but, as we have pointed out before (4), in the case of 2-butene the termination and proton transfer processes approach equivalence since the *sec*-butyl cation is more likely to lose a proton than to react with more butene.

In considering the formation of higher olefins from butene in the light of the above mechanism it is necessary to take account of the following points: (*a*) rearranged products make up over 40% of the total; (*b*) rearrangements are relatively simple; there is no indication of the mobility of groups observed by Deno (15) and others in H_2SO_4; (*c*) there is little alkane or diolefin formed; (*d*) product composition is largely independent of conversion although changes do occur on prolonged contact with catalyst.

We interpret these observations to mean that the olefins formed in the reaction are primary products and that the observed rearrangements occur in the transfer–termination step of the chain reaction. Re-activation of the chain reaction can occur by protonation of the olefin but its effect on the product mix is probably not great. We suggest that most of the observed products can be accounted for if we suppose that the transfer process is not restricted to protons but may include transfer of methyl or other group attached to the pertinent carbon. If we imagine that reaction between cation and olefin proceeds through an intermediate such as A then addition occurs upon completion of the

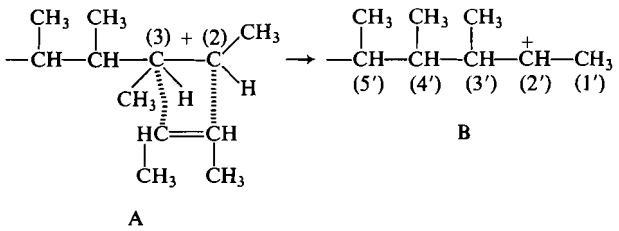

cation–monomer bond at carbon(2) while transfer occurs if the proton (or other group) at carbon(3) is transferred to butene. We think that these two reactions can occur separately or simultaneously and in either case will yield the "normal" addition products, viz. 3,4-dimethylhexene, 3,4,5,6-tetramethyloctene, etc., as predicted by classical concepts. The only difference in additions with or without proton transfer would be in the location of the regenerated charge at carbon(2′) or (5′) of the new ion B, and consequently either in the position of the resulting double bond, or in the structure of addition products of the new ion. These structural

Can. J. Chem. Downloaded from www.nrcresearchpress.com by 210.87.254.42 on 09/06/12
For personal use only.

effects would be observable only at the C_{16} levels or above since in the dimer ions carbons (2′) and (5′) are equivalent.

It would be very useful from a mechanistic point of view to know the position of the double bond in a newly-formed olefin. However, we know that the catalyst used here is excellent for olefin equilibration (3), and we have shown that the octene mixture produced in these reactions is very similar to that obtained by treating any one octene isomer with catalyst. On the other hand, ozonization of the dodecanes gave primarily a single product suggesting little migration of the double bonds, but we feel that the uncertainty is too great to permit conclusions.

Consider now the case where the methyl group rather than a proton is transferred to the incoming monomer. If the transfer is accompanied by addition, then in the case of dimer → trimer, the product will be 3,5,6,7-tetramethyloctene-3 (or -4), an important reaction product and one difficult to explain by more conventional mechanisms. If the transfer were to occur at the monomer → dimer stage the hydrogenated product would be a 2,3,4-trimethylpentane which in fact seems to be present though in very small amounts. We consider below the reason why transfers might become more important as the chain lengthens. If transfer occurs without addition, then in the case of the C_{12} cation, the product would be a new C_5 cation and an olefin hydrogenated to 3,4,5-trimethyloctane, again an important reaction product. The C_5 cation $[CH_3—CH(CH_3)—CH—CH_3]^+$ by adding monomer could yield the C_9 olefins giving on hydrogenation 2,3,4- and 3,3,4-trimethylhexane, both major reaction products. According to this scheme, the C_9 olefins should balance the C_{11} and to a rough approximation they do so. We can find no evidence for a C_7 olefin, a point considered in more detail later.

In order to account for the C_{10} olefins we may imagine the transfer of the "ethyl" group from carbon(3) to the monomer but this will require accompanying proton shifts from carbon(3) to (5)[2] and/or from carbon(3) to the leaving cation. If the transfer occurs from a C_{12} cation, then the products will be a C_{10} olefin and a C_6 cation and the latter, by adding monomer, could give rise to another molecule of C_{10} olefin; we can thus account for the large amount of decene formed in the reaction but note that it is somewhat less than the C_9 plus C_{11} formed by methyl transfer.

Perhaps a more satisfactory way of looking at ethyl transfer is to consider what happens if the secondary cation undergoes a hydride shift to give the energetically more favourable tertiary cation:

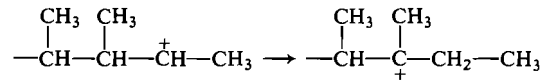

If this happens, then further addition may be very difficult because the tertiary ion is sterically hindered and because the resulting product would be secondary cation. The probable alternative reaction for the cation would then be to transfer a proton or alkyl group to monomer or catalyst. It should be noted that the difference between this view of ethyl transfer and the previous one is largely in the timing of the hydrogen shift.

The foregoing reaction scheme seems to account satisfactorily for most of the products so far identified but is less effective in dealing with compounds which are not present. Small molecules, in the C_5–C_7 range, are almost completely absent, perhaps because they undergo further reaction but their expected derivatives are also absent. For example if a dimer cation lost a methyl group by transfer one would expect to find the olefin 4-methyl-2-hexene or its derivatives, i.e.,

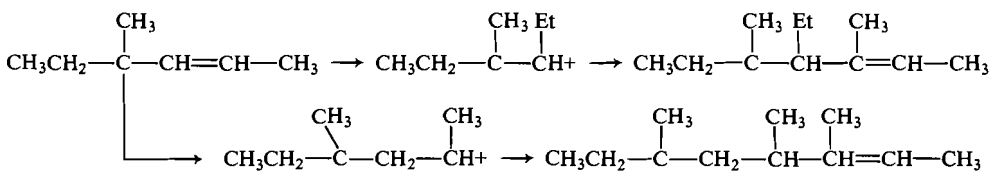

and these are not present. Another missing compound is the olefin giving 3,3,4,5,6-pentamethyloctane which is expected along with 2,3,4,5,6-pentamethyloctane from addition of two molecules of monomer to the postulated C_5 cation. We have synthesized both of these tridecanes but find only 2,3,4,5,6-PMO in the hydrogenated mixture; the other one is definitely absent.

We are of the opinion that small molecules are absent from the product because they are not formed rather than because they are consumed. It is clear from the formation of substantial amounts

[2]However, in the case of dimer → trimer, the new C_{12} cation, obtained by addition with proton transfer, would carry the charge on carbon(4) and therefore the proton would shift from carbon(3) to (4).

Can. J. Chem. Downloaded from www.nrcresearchpress.com by 210.87.254.42 on 09/06/12
For personal use only.

of normal dimer and trimer (and probably tetramer) that the *sec*-butyl cation and its lower homologues react rapidly with 2-butene, certainly more rapidly than the cation can isomerize. However, it is also clear from molecular models that as the polymer chain lengthens the methyl groups along the chain become increasingly compressed until, at about the pentamer stage, one can no longer add butene units as such. Admittedly models tend to exaggerate steric effects, but when the effects are this pronounced it seems safe to assume that the propagation rate will decline as the chain becomes longer. As this rate declines, the lifetime of an individual ion will increase and with it the probability of rearrangement and termination. The results of our experiments suggest that growth occurs readily to about the trimer stage after which the transfer and termination reactions start to dominate.

We have considered and abandoned the idea that the olefins described here might arise from fission of some longer chain, say a C_{20} or C_{24} oligomer, because we have been unable to devise a convincing scheme to account for the products observed.

It is useful to compare the polymerization of 2-butene and propylene. The latter has little steric restriction to growth and with some catalysts yields very high molecular weights, but under cationic conditions the chain length is limited to about 10–20 units depending somewhat on temperature (4). Kinetic studies (4) show that the molecular weight is independent of olefin concentration, an observation which is usually taken to mean that chain growth is limited by transfer to monomer, i.e. that both growth and transfer (and/or termination) are similarly dependent on monomer concentration as they would be in the present scheme. In comparing the transfer process for these two olefins we note that in the scheme described above a propylene oligomer will have no alkyl groups at carbon(3) and no easy route from a secondary to a tertiary cation, so we would expect little rearrangement. In fact there does seem to be a small amount in the initial stages of reaction (1) but not nearly to the same extent as with 2-butene, and it may cease after the first three or four additions. Proton transfer on the other hand is a common reaction, occurring apparently in about half of the reactions with monomer according to analysis of the molecular weight distribution curve for propylene oligomerization (3*b*). Actually there is some reason to believe that the ratio of addition to transfer increases during the initial stages and then levels off, since the most probable molecular weight appears at about the hexamer and there is little trimer. It is possible that the small amount of low molecular weight products (C_{12} and lower) results from scavenging of impurities but to explain the rapid rise to the maximum one requires a high addition/termination ratio.

In stressing the importance of transfer we are in obvious disagreement with the recent views of Puskas *et al.* (5). We also disagree with those authors in the importance we attach to the position of the olefinic groups. However, our conclusions are based on vastly different kinds of data so doubtless the differences will be resolved by further experiments.

Experimental

Boiling points are uncorrected, microanalyses were performed by H. Seguin of these laboratories. Identification of compounds was done by comparison with authentic samples by glc coinjection and ^{1}H nmr when possible. Capillary WCOT columns (150 ft) with squalane or OV-101 were used for the chromatographic analysis, the OV-101 column giving a better resolution of olefins. The ir spectra were recorded on a Beckman Acculab 4 and nmr spectra on a Varian XL-100. The glc–mass spectra analyses were obtained with a Finnigan 4000.

Polymerization reactions were carried out on a vacuum line using the usual techniques. The alkanes were prepared according to schemes similar to those already published (2). Reactions with organometallic reagents, including Grignards, were performed under argon atmosphere using at least 25% excess reagent. They were worked up by treating the reaction mixtures with NH_4Cl solution and extracting with ether. The dehydrations were performed by mixing β-naphthalene sulfonic acid with the alcohol and heating to boiling for a few minutes. This acid was used because rearrangements appeared to be minimal. The reaction mixtures were then poured into water and extracted with ether or pentane and distilled. Olefin hydrogenations were accomplished at atmospheric pressure over 5% palladium on charcoal as catalyst.

All the intermediates had ir, nmr, and mass spectra consistent with structures proposed for them.

2,4-Dimethylhexane

This compound was prepared by reacting 2-methylbutanal with isopropylmagnesium chloride in ether at −25°C. The octanol obtained (80% yield) was dehydrated and the olefins hydrogenated to 2,4-dimethylhexane; bp 106–107°C, lit. (6) bp 108.5°C; n: 1.3842, lit. (6) n: 1.3967; δ_{TMS} (CCl_4): 0.85 (d, J = 6.5, CH_3—$\underset{\underset{CH_3}{\|}}{C}$H), 0.86 (t, J = 6.5, CH_3—CH_2), 0.88 (d, J = 6.5, CH_3—CH), 1.2 (m, CH_2), 1.65 (m, CH).

2,2,3-Trimethylpentane

The reaction of 3,3-dimethyl-2-butanone with ethylmagnesium bromide in ether at −25°C gave an octanol which on dehydration gave a mixture of olefins hydrogenated to 2,2,3-trimethylpentane; bp 107–108°C, lit. (7) bp 109.8°C; n: 1.3951, lit. (7) n: 1.40285. The nmr spectrum shows a major peak at 0.8 ppm (*tert*-butyl) masking the other methyl groups.

2,2,4-Trimethylpentane

2,4,4-Trimethyl-1-pentene (Aldrich) was hydrogenated and the alkane purified by distillation; bp 96–97°C, lit. (8) bp 99.2°C; n: 1.3892, lit. (8) n: 1.3914; δ_{TMS} (CCl_4): 0.88 (s, *t*-butyl), 0.91

Can. J. Chem. Downloaded from www.nrcresearchpress.com by 210.87.254.42 on 09/06/12
For personal use only.

(d, $J = 7$, CH_3—$\underset{\|}{C}$H—CH_3), 1.64 (m, for CH_2 and the other proton).

2,2,3,4-Tetramethylhexane

(A) The addition of *sec*-butyllithium to 3,3-dimethyl-2-butanone in ether at 0°C gave an alcohol that was dehydrated, without purification, with $POCl_3$ in pyridine (14). The olefin obtained was hydrogenated to 2,2,3,4-tetramethylhexane; bp 155.5°C, lit. (9) bp 156.6°C; n: 1.4286, lit. (9) n: 1.4202; δ_{TMS} (CCl_4): 0.73 (d, $J = 7$, CH_3—CH), 0.77 (d, $J = 6$, CH_3—CH), 0.79 (t, $J = 6$, CH_3—CH_2), 0.87 (s, *t*-butyl), 1.19 (m, —CH_2—).

(B) 3-Methyl-3-penten-2-one was added to an ethereal solution of *tert*-butylmagnesium chloride in presence of CuCl at −30°C; 3,4,5,5-tetramethyl-2-hexanone was obtained in 63% yield; bp 82–84°C/13–15 Torr; n: 1.4385; ir ν_{max}: 1705 (carbonyl) cm^{-1}.

This ketone was reduced with $NaBH_4$ to an alcohol which on dehydration followed by hydrogenation of the olefins gave an alkane identical with the one described above.

2,4,5-Trimethylheptane

4-Methyl-2-pentanone was added to a solution of *sec*-butyllithium in hexane at 0°C to give, in 30% yield, 2,4,5-trimethyl-4-heptanol, bp 85°C/13–15 Torr. The alcohol was dehydrated with SO_2Cl_2 in pyridine and the olefin hydrogenated to 2,4,5-trimethylheptane; bp 154–155°C, lit. (10) bp 156°C; n: 1.4157, lit. (10) n: 1.4160.

3,3,5-Trimethylheptane

The 1,4-addition of ethylmagnesium bromide to 2-methyl-2-penten-4-one in ether at 35°C with CuCl gave 4,4-dimethyl-2-hexanone (yield 73%); bp 152°C, lit. (11) bp 154.4°C; n: 1.4172, lit. (10) n: 1.4185; ir ν_{max}: 1705 (carbonyl) cm^{-1}.

The ketone was then treated with an ethereal solution of ethylmagnesium bromide. The alcohol obtained was dehydrated without purification and the isolated olefins hydrogenated to 3,3,5-trimethylheptane; bp 154–155°C, lit. (12) bp 156.8°C, n: 1.4165, lit. (12) n: 1.4178. The nmr spectrum shows a great deal of overlapping, making the interpretation impossible.

2,3,3,4-Tetramethylhexane

(A) 2,3-Dimethyl-2-butene was acylated, in low yield with proprionyl chloride and $SnCl_4$, according to Colonge and Mostafavi (13), to give an unsaturated ketone which was then hydrogenated to 4,4,5-trimethyl-3-hexanone; bp 69–71°C; n: 1.4302; ir ν_{max}: 1703 (carbonyl) cm^{-1}. The ketone was allowed to react with an ethereal solution of CH_3Li at 0°C to give an alochol which was dehydrated. Hydrogenation of the resulting olefins gave 2,3,3,4-tetramethylhexane; bp 162.5°C; n: 1.4285; δ_{TMS} (CCl_4): 0.69 (d, $J = 1.5$, CH_3—$\underset{\|}{C}$—CH_3), 0.79 (d, $J = 7$, CH_3—$\underset{\|}{C}$H and CH_3—CH), 0.83 (t, $J = 7$, CH_3—CH_2—), 0.93 (m, —CH_2—), 1.68 (m, 2 CH). *Anal.* calcd. for $C_{10}H_{22}$: C 84.40, H 15.59; found: C 84.49, H 15:39.

(B) 3,4-Dimethyl-2-hexanone was brominated with Br_2 in $CHCl_3$ at 0°C. The crude bromoketone was dissolved in methanol and treated with sodium methoxide giving methyl 2,2,3-trimethylpentanoate in 39% yield; bp 67–69°C/13–17 Torr; ir ν_{max}: 1730 (ester) cm^{-1}. The ester was treated with two equivalents of CH_3Li in ether to give an alcohol. The alcohol was dehydrated and the resulting olefins hydrogenated to an alkane identical with the one described above.

2,3,4,4-Tetramethylhexane

3,4-Dimethyl-3-penten-2-one (prepared by reacting 3-methyl-2-butene with CH_3COCl and $SnCl_4$) was added to a solution of ethylmagnesium bromide in ether at −35°C with CuCl). 3,4,4-Trimethyl-2-hexanone was obtained (yield 43% in pure ketone); bp 70–75°C/13–15 Torr; n: 1.4310; ir ν_{max}: 1703 (carbonyl) cm^{-1}; ms (70 eV) m/e: 142 (M). The saturated ketone was added to CH_3Li in ether at −10°C. The alcohol obtained was dehydrated and the olefins hydrogenated to 2,3,4,4-tetramethylhexane; bp 159–160°C, lit. (11) bp 162.8°C; n: 1.4262, lit. (11) n: 1.4272; δ_{TMS} (CCl_4): 0.76 (t, $J = 7$, CH_3—CH_2), 0.79 (d, $J = 6.5$, CH_3—$\underset{\|}{C}$H—), 0.80 (s, CH_3—$\underset{|}{C}$—CH_3), 0.89 (d, $J = 6.8$, CH_3CH), 1.25 (m, CH_2), 1.91 (m, CH).

Ozonolysis

Careful distillation of polymerization products gave a fraction containing olefins having a molecular weight of 168 (C_{12}) only, of which 0.500 g were dissolved in 10 mL ethanol and the solution, kept at −78°C, was saturated with ozone (blue solution). After the solution had warmed up to room temperature, it was transferred to the hydrogenation flask and degassed. Palladium 5% on carbon was then added and the ozonides hydrogenated overnight. The mixture was poured into water and extracted with pentane. Identification of ketones and aldehydes was achieved by comparison of their retention times and their mass spectra with those of authentic material. The mixture was found to contain 3-methyl-2-butanone, 2-methylbutanal, 3,4-dimethyl-2-pentanone, 3,3-dimethyl-2-pentanone, 2-butanone, and 3-methyl-2-pentanone.

4-Ethyl-3,6-dimethyloctane

5-Methyl-3-hexanone was added to *sec*-butyllithium in hexane at −10°C. The alcohol (yield 60%) was dehydrated and the olefins hydrogenated to give 4-ethyl-3,6-dimethyloctane; bp 84°C/17 Torr; n: 1.4390. *Anal.* calcd. for $C_{12}H_{26}$: C 84.60, H 15.39; found: C 84.26, H 15.39.

2,3,4,6-Tetramethyloctane

3,4-Dimethyl-2-pentanone was treated at 0°C with a Grignard reagent prepared from 1-bromo-2-methylbutane and excess Mg. An alcohol was obtained (yield 30%); dehydration and hydrogenation of the olefins gave 2,3,4,6-tetramethyloctane; bp 86°C/17 Torr; n: 1.4320. *Anal.* calcd. for $C_{12}H_{26}$: C 84.60, H 15.39; found: C 84.53, H 15.18.

3,3,4,6-Tetramethyloctane

The 1,4-addition of *tert*-amylmagnesium chloride to 3-pentene-2-one in presence of CuCl at −25°C gave 4,5,5-trimethyl-2-heptanone (yield 38%); bp 85–86°C/17 Torr; n: 1.4381; ms (CI) m/e: 157 (M + 1). It was added at −100°C to an ethereal solution of ethylmagnesium bromide. The crude alcohol was divided into two parts. The first was dehydrated as usual and the olefins hydrogenated to an alkane. The second was added to a large excess of concentrated HCl to give the same mixture of olefins already obtained and another product (about 45% of the mixture) assumed to be the chloride, because of a positive Beilstein test. The chloride mixture was then treated with $LiAlH_4$ in THF to give the unchanged olefins and a product identified, by glc – mass spectrum analysis, as the alkane obtained from the first fraction. It seems unlikely that, under the experimental conditions, the HCl treatment gave a rearranged chloride (or olefins yielding the same chloride) which would be reduced to the isolated alkane. So this strongly suggests that no rearrangement occurs during the dehydration and that the isolated alkane is 3,3,4,6-tetramethylhexane; bp 86°C/17 Torr; n: 1.4327. *Anal.* calcd. for $C_{12}H_{26}$: C 84.60, H 15.39; found: C 84.32, H 15.10.

2,5,6,6-Tetramethyloctane

3,3-Dimethyl-2-pentanone was added at 0°C to a Grignard prepared from isoamylchloride and excess Mg. The reaction gave a mixture of products containing OH groups. The crude mixture was dehydrated and ir (peaks at 1615 and 1685 cm^{-1} for unsaturated ketone) showed that some aldol condensation had occurred. The mixture was fractionated and the fraction passing at 79°C/13–15 Torr was retained and identified by ir and nmr as a mixture of olefins with the desired structure. The mixture was then hydrogenated to 2,5,6,6-tetramethyloctane (overall yield 10%); bp 84°C/17 Torr; *n*: 1.4283. *Anal.* calcd. for $C_{12}H_{26}$: C 84.60, H 15.39; found: C 84.29, H 15.10.

2,3,4,5,5-Pentamethylheptane

The 1,4-addition of *tert*-amylmagnesium chloride to 3-methyl-3-penten-2-one with CuCl in ether at −35°C gave 3,4,5,5-tetramethyl-2-heptanone; bp 101°C/17 Torr; *n*: 1.4448. The saturated ketone was then treated with CH_3Li in ether at −10°C to give an alcohol dehydrated without purification and the olefins hydrogenated to 2,3,4,5,5-pentamethylheptane; bp 87°C/17 Torr; *n*: 1.4395. *Anal.* calcd. for $C_{12}H_{26}$: C 84.60, H 15.39; found: C 84.34, H 15.19.

Tridecanes

2,3,4,5,6-Pentamethyloctane

3,4,5-Trimethyl-2-hexanone (prepared by the addition of isopropylmagnesium chloride to 3-methyl-3-penten-2-one, bp 81–82°C/17 Torr; *n*: 1.4352 yield 70%), was treated at −10°C with a hexane solution of *sec*-butyllithium. The dehydration of the alcohol obtained and the hydrogenation of the olefins gave 2,3,4,5,6-pentamethylheptane; bp 98°C/17 Torr; *n*: 1.4382. *Anal.* calcd. for $C_{13}H_{28}$: C 84.67, H 15.32; found: C 84.85, H 15.10.

3,3,4,5,6-Pentamethyloctane

(A) 3,4,5,5-Tetramethyl-2-heptanone was added at −25°C to a 75% excess ethylmagnesium bromide in ether. The crude alcohol (yield 75%) was dehydrated and the olefins hydrogenated to 3,3,4,5,6-pentamethyloctane; bp 99°C/17 Torr; *n*: 1.4429. *Anal.* calcd. for $C_{13}H_{28}$: C 84.67, H 15.32; found: C 84.47, H 15.03.

(B) 3,4-Dimethyl-3-penten-2-one was added at 25°C to an ethereal solution of ethylmagnesium bromide and CuCl to give 3,3,4-trimethyl-2-hexanone.

The saturated ketone was treated with a solution of *sec*-butyllithium and the alcohol obtained dehydrated. The mixture of olefins was hydrogenated to give an alkane identical (glc. nmr) with the one described above.

1. (*a*) P. LACHANCE and A. M. EASTHAM. J. Polym. Sci. Polym. Chem. Ed. **13**, 1843 (1975); (*b*) H. R. ALLCOCK and A. M. EASTHAM. Can. J. Chem. **41**, 932 (1963).
2. P. LACHANCE, J. BROWNSTEIN, and A. M. EASTHAM. Can. J. Chem. **57**, 367 (1979).
3. (*a*) J. M. CLAYTON and A. M. EASTHAM. J. Chem. Soc. 1636 (1963); (*b*) P. LACHANCE and A. M. EASTHAM. J. Polym. Sci. Polym. Symp. No. 56, 203 (1976).
4. T. SZELL and A. M. EASTHAM. J. Chem. Soc. B, 30, (1966).
5. I. PUSKAS, E. M. BANAS, A. G. NERHEIM, and G. J. RAY. Macromolecules, **12**, 1024 (1979).
6. R. YA LEVINA, L. S. KLEIMENOVA, and N. P. SHUSHERINA. J. Gen. Chem. U.S.S.R. **17**, 117 (1947).
7. D. B. BROOKS, F. L. HOWARD, and H. C. CRAFTON, JR. J. Res. Natl. Bur. Stand. 637 (1939).
8. E. F. P. HARRIS and W. A. WATERS. J. Chem. Soc. 3108 (1952).
9. N. L. DRAKE and L. H. WELSH. J. Am. Chem. Soc. **60**, 488 (1938).
10. Z. RAPPOPORT (*Editor*). Handbook of Tables for Organic Compound Identification. 3rd ed. The Chemical Rubber Co. Cleveland. 1967. p. 5.
11. N. L. DRAKE, G. M. KINE, and W. G. ROSE. J. Am. Chem. Soc. **56**, 2076 (1934).
12. G. C. JOHNSON. J. Am. Chem. Soc. **69**, 146 (1947).
13. J. COLONGE and K. MOSTAFAVI. Bull. Soc. Chim. **6**, 335 (1939).
14. A. LARDON and T. REICHSTEIN. Helv. Chim. Acta, **41**, 904 (1958).
15. C. DENO. Surv. Prog. Chem. **2**, 155 (1964).

Can. J. Chem. Downloaded from www.nrcresearchpress.com by 210.87.254.42 on 09/06/12
For personal use only.

Preparation of a series of substituted fluoromethylnaphthalenes

ELISABETH A. DIXON,[1] ALFRED FISCHER, AND FRANK P. ROBINSON
Department of Chemistry, University of Victoria, Victoria, B.C., Canada V8W 2Y2

Received January 27, 1981

ELISABETH A. DIXON, ALFRED FISCHER, and FRANK P. ROBINSON. Can. J. Chem. **59**, 2629 (1981).

A series of 22 3- and 4-substituted 1-fluoromethylnaphthalenes have been synthesized. Details of practical procedures for the preparation of all intermediates are described, and physical properties for all of the substituted naphthalenes synthesized, and spectral parameters for 51 previously unknown compounds, are given.

ELISABETH A. DIXON, ALFRED FISCHER et FRANK P. ROBINSON. Can. J. Chem. **59**, 2629 (1981).

On a synthétisé une série de 22 fluoro-1 méthylnaphtalènes substitués en positions 3 et 4. On décrit en détail les méthodes utilisées pour préparer les intermédiaires et on rapporte les propriétés physiques de tous les naphtalènes substitués préparés, ainsi que les paramètres spectraux de 51 composés inconnus.

[Traduit par le journal]

Can. J. Chem. Downloaded from www.nrcresearchpress.com by 210.87.254.40 on 09/06/12
For personal use only.

The linear correlation analysis of ^{19}F substituent chemical shifts of a series of substituted benzyl fluorides led to a rather unexpected result for the sign of the response for the substituent chemical shift (1). We wished to carry out a similar study for a series of substituted fluoromethylnaphthalenes in order to ascertain whether or not this trend is paralleled in the naphthalene series. In this paper we report the preparation of the series of fluoromethylnaphthalenes. The shift study is reported in the following paper.

Fluoromethylnaphthalenes were not known at the beginning of our study, but the synthesis of five derivatives and the isolation of four of these were reported (2) soon after our study was completed (3). Their benzene analogues, the benzyl fluorides, were first synthesized by the Ingolds (4) in 1928. Benzyl fluorides have been reported in the literature several times since then (5–9) and have been studied both in a reactivity context by kinetic studies (5–7) and in the context of correlations between substituent effects and ^{19}F nmr chemical shifts (1).

The reaction sequences for the 22 fluoromethylnaphthalenes prepared are shown in Figs. 1–7. The 4-methyl-, 4-chloro-, 4-fluoro-, and 4-bromo-1-fluoromethylnaphthalenes were synthesized according to the transformations shown in Fig. 1. Friedel–Crafts acylation of the 1-substituted naphthalene was followed by hypochlorite oxidation of the resulting acetonaphthone to the naphthoic acid which was in turn reduced by lithium aluminum hydride to the carbinol. The final two steps were bromination and fluorination. For the unsubstituted fluoromethylnaphthalenes the corresponding carboxylic acids were commercially available and the preparations involved the last three steps of Fig. 1. Six of the substituted fluoromethylnaphthalenes, the 4-methoxymethyl, 4-fluoromethyl, 4-methoxycarbonyl, 4-ethoxycarbonyl, 4-acetyl, and 4-fluoroacetyl derivatives, were synthesized from 1-acetyl-4-methylnaphthalene as shown in Fig. 2. The replacement of bromide by fluoride always involved the same procedure and this step has been omitted for simplicity in Figs. 2–7. The bromide which was replaced to generate the corresponding fluoride is indicated by an asterisk thus: Br*.

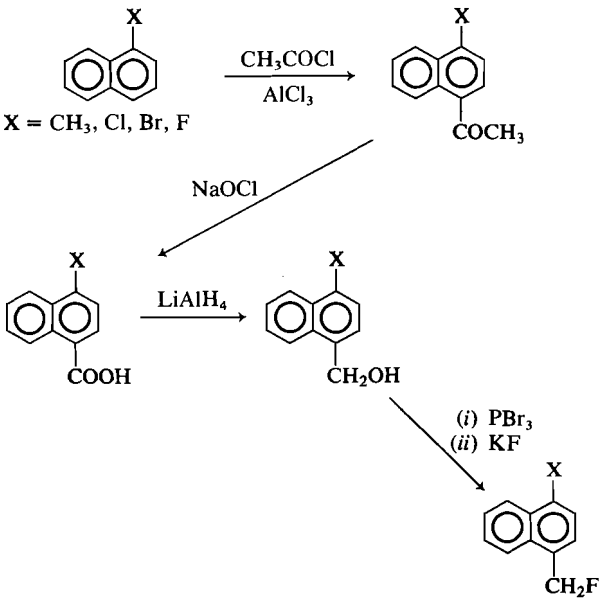

FIG. 1

Bromide–cyanide exchange of an aromatic bro-

[1]Current address: Department of Chemistry, University of Calgary, Calgary, Alberta.

0008-4042/81/172629-13$01.00/0
©1981 National Research Council of Canada/Conseil national de recherches du Canada

Can. J. Chem. Downloaded from www.nrcresearchpress.com by 210.87.254.40 on 09/06/12
For personal use only.

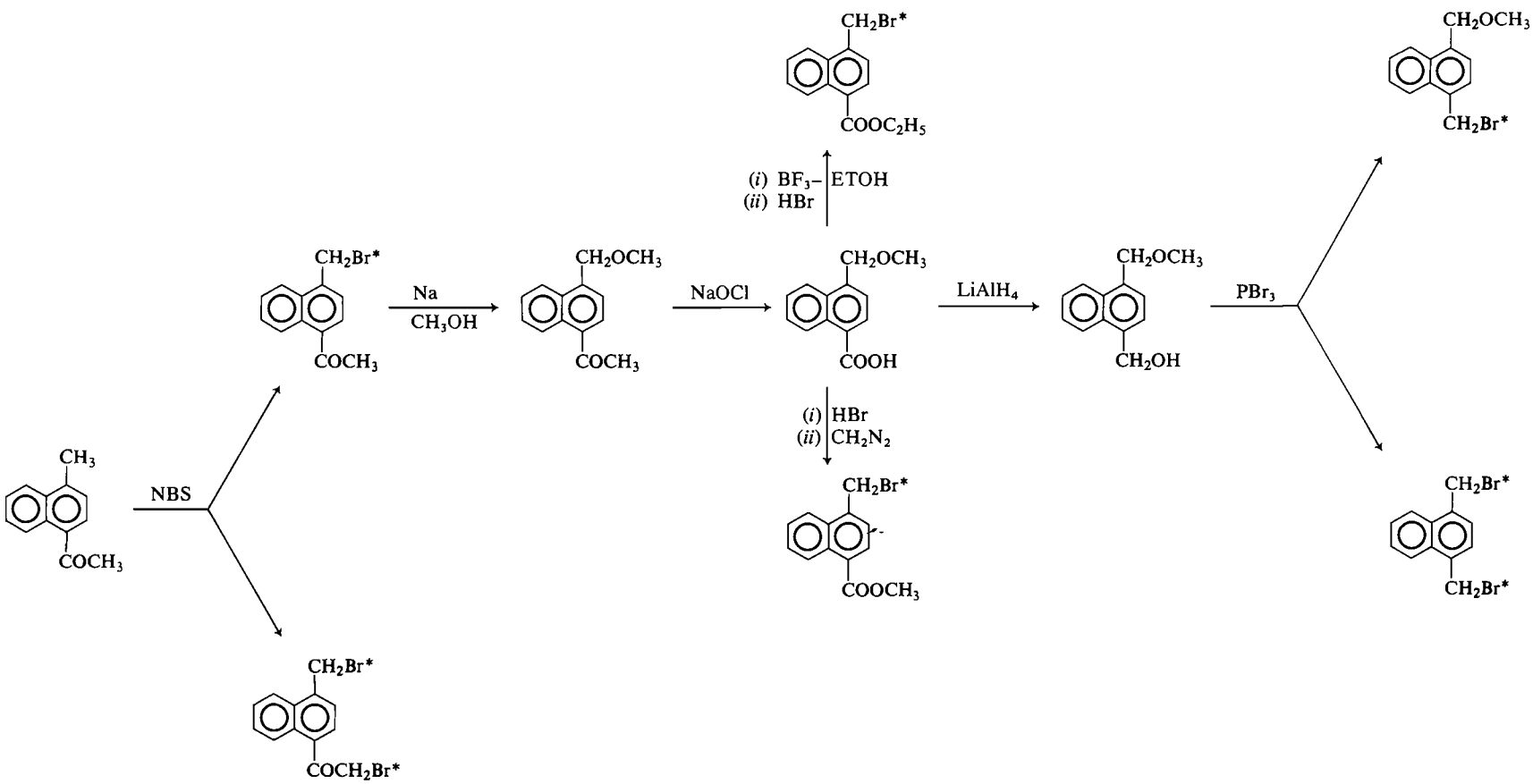

Note: Bromine atoms marked with an asterisk were replaced by fluorine by reaction with potassium fluoride in *N*-methylpyrrolidone (see text).

FIG. 2

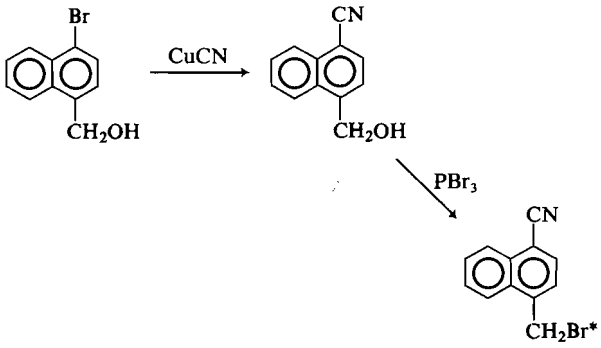

FIG. 3

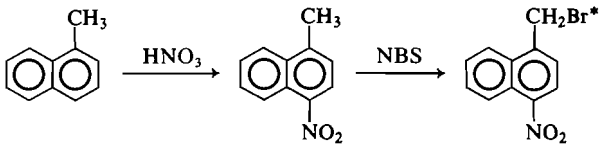

FIG. 4

mide provided access to both the 4-cyano derivative (Fig. 3) and the 3-cyano derivative (Fig. 5). The 3-cyano derivative proved to be very useful, itself giving rise to the 3-methoxycarbonyl, 3-ethoxycarbonyl, and 3-acetyl derivatives. 4-Nitro-1-fluoromethylnaphthalene was prepared from 1-methylnaphthalene according to the scheme shown in Fig. 4. 1,8-Naphthalic anhydride was the starting material for five of the 3-substituted fluoromethylnaphthalenes (Fig. 5), and 1,3-dimethylnaphthalene for two of the 3-substituted derivatives (Fig. 6). The 3-nitro compound was prepared from methyl 3-nitro-1-naphthoate (Fig. 7).

Synthetic intermediates, classified by functional group, were prepared as follows. Acetylnaphthalenes were prepared by the Friedel–Crafts acylation of the corresponding 1-substituted naphthalene (10), or by the reaction of the aromatic nitrile with methyl magnesium iodide (11). Details of yields and physical properties are shown in Table 1.

Naphthoic acids were prepared by the sodium hypochlorite oxidation of the methyl ketone, reaction of the appropriate Grignard reagent with carbon dioxide, alkaline hydrolysis of the nitrile, or by hydrolysis of the hydroxymercurinaphthoic acid with dilute hydrochloric acid. Preparative data for this group of compounds are listed in Table 2. Most of the 4-substituted-1-naphthoic acids were prepared by the sodium hypochlorite oxidation of the corresponding acetylnaphthalene. This reaction proved to be far more troublesome than was suggested by the brief accounts in the literature. After a long series of abortive attempts two factors emerged as being important. The method of preparation of the hypochlorite solution is critical; the solution must be maintained at 0–10°C and the amount of chlorine passed carefully controlled. The hypochlorite solution was eventually prepared according to the method of Newman and Holmes (12). Secondly, it is necessary to reflux the hypochlorite solution with the ketone until there is no residual ketone present as a separate phase. The period of reflux necessary to effect the oxidation was considerably longer, and the reaction temperature higher, than those recommended in the literature. 4-Methoxy-1-acetylnaphthalene underwent nuclear oxidation on treatment with hypochlorite solution and 4-methoxy-1-naphthoic acid was therefore prepared by Grignard synthesis (13). 4-Hydroxymethyl-2-naphthoic acid was prepared by alkaline hydrolysis of the corresponding nitrile; acid hydrolysis was ineffective. 3-Bromo-1-naphthoic acid was a key intermediate in the preparation of 3-substituted derivatives and was itself obtained from naphthalic anhydride by bromination, mercuridecarboxylation, and protodemercuration (14–16).

Naphthyl carbinols (Table 3) were, as indicated, prepared by reduction of the naphthoic acids with lithium aluminum hydride. However the preparation of 3-nitronaphthyl carbinol requires comment. Brown and Subba Rao have reported that the reagent sodium borohydride and anhydrous aluminum chloride in diglyme selectively reduce a nitro function in the presence of a carboxylic acid or its derivative (17). We were unable to effect the reduction of methyl 3-nitro-1-naphthoate by this reagent. Nystrom has described the selective reduction of *p*-nitrobenzaldehyde and the lack of reduction of *p*-nitrotoluene and nitrobenzene with lithium aluminum hydride and anhydrous aluminum chloride in anhydrous ether (18). We were able to selectively reduce the nitroester to the nitrocarbinol with this combination.

Bromomethylnaphthalenes (Table 4) were generally prepared from the corresponding carbinols by reaction with phosphorous tribromide (19). Bromination with *N*-bromosuccinimide (NBS) of the 1-methyl-4-nitronaphthalene gave 1-bromomethyl-4-nitronaphthalene. Similarly bromination of 1,3-dimethylnaphthalene gave 1,3-bisbromomethylnaphthalene, 3-bromomethyl-1-methylnaphthalene, and 1-bromomethyl-3-methylnaphthalene. Likewise bromination of 1-acetyl-4-methylnaphthalene gave 1-acetyl-4-bromomethylnaphthalene. Bromination of 4-methyl-1-naphthoic acid gave only 13% of 4-bromomethyl-1-naphthoic acid (a key intermediate) in a mixture of at least seven compounds, and this derivative was prepared from

Can. J. Chem. Downloaded from www.nrcresearchpress.com by 210.87.254.40 on 09/06/12
For personal use only.

Can. J. Chem. Downloaded from www.nrcresearchpress.com by 210.87.254.40 on 09/06/12
For personal use only.

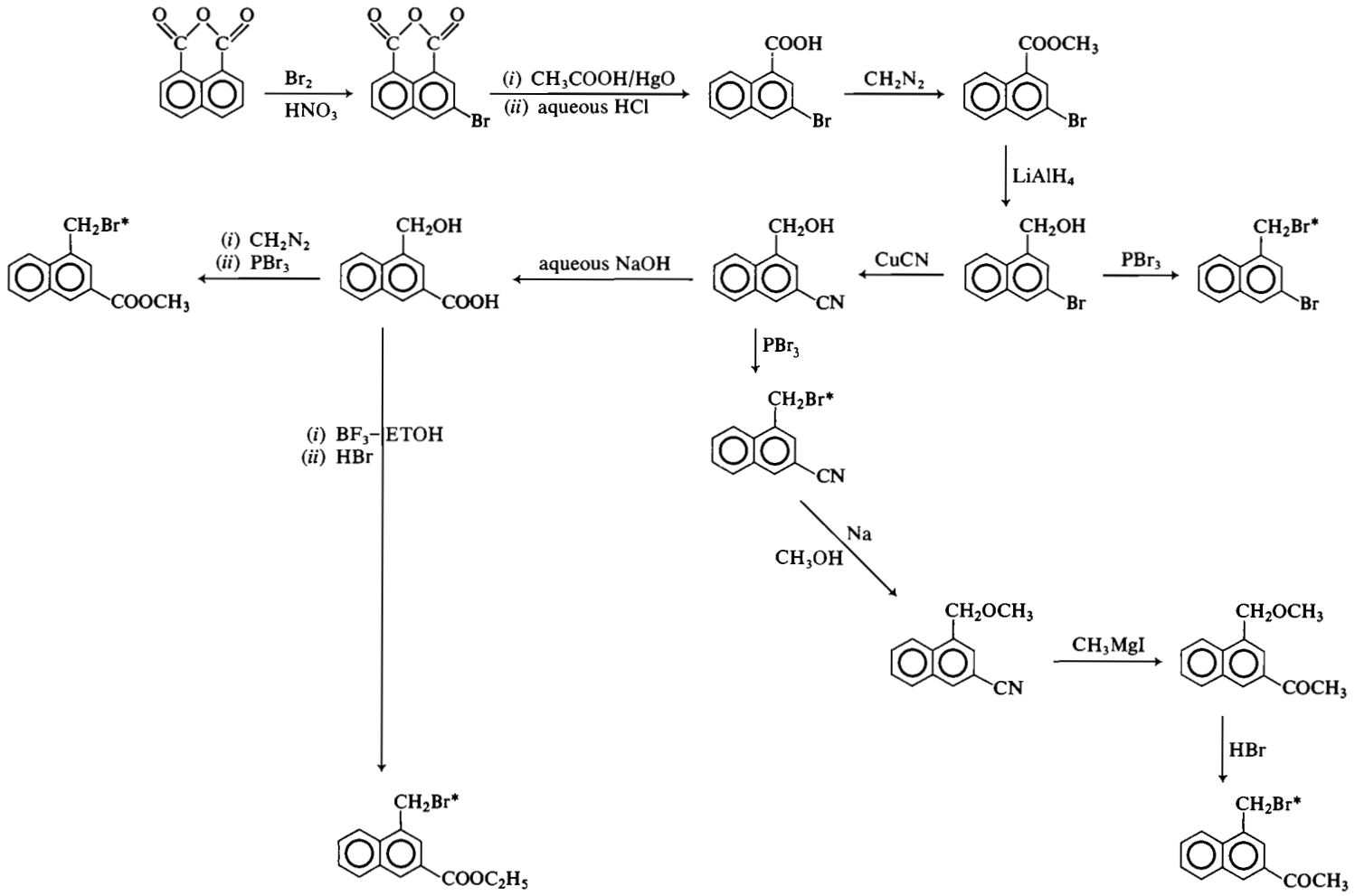

FIG. 5

Can. J. Chem. Downloaded from www.nrcresearchpress.com by 210.87.254.40 on 09/06/12
For personal use only.

TABLE 1. Acetylnaphthalenes

Substituents	Method[a]	Yield (%)	Melting point or boiling point/Torr (°C)	Literature value	Reference
1-$COCH_3$, 4-CH_3	a	71.4	115–120/0.2	175/15	21
1-$COCH_3$, 4-CH_2OCH_3	b	100			
1-$COCH_3$, 4-CH_2F	c	33			
1-$COCH_3$, 4-CH_2Br	d	24.5	83.0–84.0		
1-$COCH_3$, 4-F	a	100	110–115/0.01	138–140/4.5	10
1-$COCH_3$, 4-Cl	a	72	140–146/0.2	140–146/1.5	10
1-$COCH_3$, 4-Br	a	87	125–138/0.2–0.25	165–175/2.4	10
1-$COCH_3$, 4-OCH_3	a	85	72.0–74.0	72.0–73.0	29
2-$COCH_3$, 4-CH_2OCH_3	e	77			
2-$COCH_3$, 4-CH_2F	c	36			
2-$COCH_3$, 4-CH_2Br	f	100	109.0–110.5		

[a](a) Acetylation by Friedel–Crafts acylation with acetyl chloride and $AlCl_3$; (b) methyl ether formation by treatment of naphthyl bromide with NaOMe; (c) Br/F exchange by KF in *N*-methylpyrrolidone; (d) *N*-bromosuccinimide bromination of methylnaphthalene; (e) reaction of nitrile with methylmagnesium iodide; (f) cleavage of naphthyl methyl ether with HBr in benzene.

TABLE 2. Naphthoic acids

Substituents	Method[a]	Yield (%)	Melting point (°C)	Literature value	Reference
1-COOH, 4-CH_3	a	91	175.0–175.5	175.0	21
1-COOH, 4-CH_2OCH_3	a	62	136.0–137.0		
1-COOH, 4-CH_2Br	b	100	193.0–195.0		
1-COOH, 4-F	a	60	219.0–222.0	224.5–225.0	10
1-COOH, 4-Cl	a	38.5	222.0–224.0	223.0–224.0	10
1-COOH, 4-Br	a	94	217.5–220.0	217.0–219.0	10
1-COOH, 4-OCH_3	c	48	247.0–247.5	248.0	13
2-COOH, 4-CH_2OH	d	100	293.0–295.0		
1-COOH, 3-Br	e	50	230.5–232.0	231.0–232.0	14

[a](a) Sodium hypochlorite oxidation of methyl ketone; (b) cleavage of naphthyl methyl ether with HBr in benzene; (c) reaction of naphthyl Grignard reagent with CO_2; (d) alkaline hydrolysis of nitrile; (e) hydrolysis of hydroxymercuri-naphthoic acid with aqueous HCl.

TABLE 3. Naphthyl carbinols

Substituents	Method[a]	Yield (%)	Melting point (°C)	Literature value	Reference
1-CH_2OH	a	57	61.5–62.5	59.5–60.0	30
2-CH_2OH	a	65	79.5–80.5	80.0–80.5	31
1-CH_2OH, 4-CH_3	a	82.5	76.0–77.0	77.0	23
1-CH_2OH, 4-CH_2OCH_3	a	90	70.5–71.5		
1-CH_2OH, 4-F	a	55.5	74.0–75.0		
1-CH_2OH, 4-Cl	a	74	73.0–74.5		
1-CH_2OH, 4-Br	a	25	98.0–100.0		
4-CH_2OH, 1-CN	d	64	110.0–112.0		
4-CH_2OH, 1-$CONH_2$	e	100	146.0–147.0		
1-CH_2OH, 4-OCH_3	a	50	34.0–35.0	35.0	32
1-CH_2OH, 3-Br	a	100	106.0–107.0		
4-CH_2OH, 2-CN	d	51	87.0–89.0		
4-CH_2OH, 2-COOH	b	100	293.0–295.0		
4-CH_2OH, 2-$COOCH_3$	c	90	79.0–80.0		
4-CH_2OH, 2-$CONH_2$	e	50	155.0–156.0		
1-CH_2OH, 3-NO_2	f	84	131.5–133.5		

[a](a) $LiAlH_4$ reduction of naphthoic acid in anhydrous ether; (b) alkaline hydrolysis of nitrile; (c) diazomethane esterification of the naphthoic acid; (d) Br/CN exchange of bromo compound with CuCN; (e) alkaline peroxide oxidation of nitrile; (f) $LiAlH_4/AlCl_3$ reduction of ester.

Can. J. Chem. Downloaded from www.nrcresearchpress.com by 210.87.254.40 on 09/06/12
For personal use only.

TABLE 4. Bromomethyl naphthalenes

Substituents	Method[a]	Yield (%)	Melting point (°C)	Literature value	Reference
1-CH_2Br	a	91	54.5–56.0	56.0	33
2-CH_2Br	a	98	53.0–54.0	54.0	34
1-CH_2Br, 4-CH_3	a	84	77.0–79.0	80.0	
1-CH_2Br, 4-CH_2OCH_3	a	80	59.0–61.0		
1,4-bis CH_2Br	a	42	111.0–112.0		
1-CH_2Br, 4-F	a	100	68.5–69.5		
1-CH_2Br, 4-Cl	a	74.5	100.0–101.0		
1-CH_2Br, 4-Br	a	84.5	102.0–104.0	103.0–104.0	32
4-CH_2Br, 1-CN	a	77	131.0–132.5		
4-CH_2Br, 1-COOH	c	100	193.0–195.0		
4-CH_2Br, 1-$COOCH_3$	d	90	85.0–86.0		
4-CH_2Br, 1-$COOC_2H_5$	c	75	75.5–76.5		
4-CH_2Br, 1-$CONH_2$	a	100	198.5–199.0		
4-CH_2Br, 1-$COCH_3$	b	31.1	83.0–84.0		
4-CH_2Br, 1-$COCH_2Br$	b	28.5	118.5–119.5		
1-CH_2Br, 4-OCH_3	a	93	119.5–120.5 (dec.)	119.0–120.0 (dec.)	32
1-CH_2Br, 4-NO_2	b	20	93.0–94.5	87.5–89.5	2
1-CH_2Br, 3-CH_3	b	20.7	63.0–63.5		
2-CH_2Br, 4-CH_3	b	9.8	86.5–87.0		
1,3-bis CH_2Br	b	12.9	111.0–112.0	113–115	35
1-CH_2Br, 3-Br	a	85	94.0–96.0		
4-CH_2Br, 2-CN	a	90	151.5–153.0		
4-CH_2Br, 2-$COOCH_3$	a	80	125.0–126.5		
4-CH_2Br, 2-$COOC_2H_5$	c/e	98	114.0–115.0		
4-CH_2Br, 2-$CONH_2$	a	33	204.0–205.0		
4-CH_2Br, 2-$COCH_3$	c	100	109.0–110.5		
1-CH_2Br, 3-NO_2	a	87	149.0–151.0	149–151.5	2

[a](a)PBr_3 bromination of naphthyl carbinol; (b) *N*-bromosuccinimide bromination of methylnaphthalene; (c) cleavage of methylnaphthyl methyl ether with HBr in benzene; (d) diazomethane esterification of naphthoic acid; (e) HBr/benzene bromination of naphthyl carbinol.

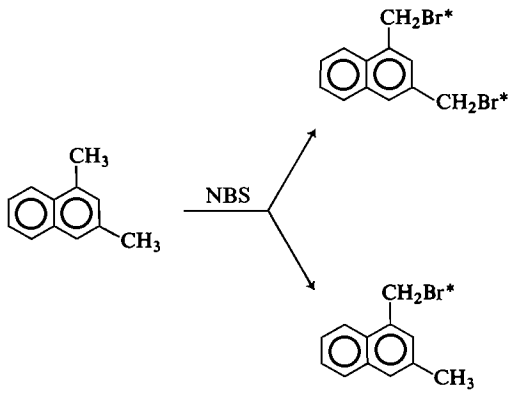

FIG. 6

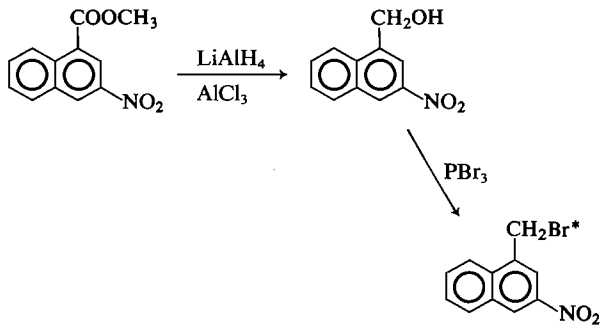

FIG. 7

the 1-acetyl-4-bromomethylnaphthalene. Oxidation of the last compound with sodium hypochlorite resulted in both functional groups being attacked. The bromomethyl group was therefore protected by conversion to the methyl ether before oxidation. After oxidation of the acetyl function, reaction of the methyl ether with hydrogen bromide regenerated the bromomethyl group.

Fluoromethylnaphthalenes (Table 5) were prepared by fluoride–bromide exchange of the corresponding bromomethylnaphthalene using anhydrous potassium fluoride in the dipolar aprotic solvent *N*-methylpyrrolidone (this provides a source of "strongly nucleophilic, weakly solvated and well dissociated fluoride ion" (20)). The fluoromethylnaphthalenes could not be characterized by their boiling points. Even on moderate warming these compounds showed a tendency towards polymerization. Polymerization of the benzyl fluorides was reported by Delpuech and Béguin (7), by the Ingolds (4), and by Bernstein *et al.* (5); it is an

Can. J. Chem. Downloaded from www.nrcresearchpress.com by 210.87.254.40 on 09/06/12
For personal use only.

TABLE 5. Fluoromethyl naphthalenes

Substituents	Yield (%) Converted[a]	Isolated[b]
1-CH_2F	63	56
2-CH_2F	85	41
1-CH_2F, 4-CH_3	90	54
1-CH_2F, 4-CH_2OCH_3	41	29
1,4-bis CH_2F	50	30
1-CH_2F, 4-F	85	71
1-CH_2F, 4-Cl	94	60
1-CH_2F, 4-Br	59	39
4-CH_2F, 1-CN	60	42
4-CH_2F, 1-$COOCH_3$	60	55
4-CH_2F, 1-$COOC_2H_5$	72	45
4-CH_2F, 1-$COCH_3$	50	33
4-CH_2F, 1-$COCH_2F$	30	27
1-CH_2F, 4-NO_2	50	32
1-CH_2F, 4-OCH_3	15	—
1-CH_2F, 3-CH_3	52	38
1,3-bis CH_2F	25	5
1-CH_2F, 3-Br	81	61
4-CH_2F, 2-CN	48	42
4-CH_2F, 2-$COOCH_3$	53	40
4-CH_2F, 2-$COOC_2H_5$	44	35
4-CH_2F, 2-$COCH_3$	52	36
1-CH_2F, 3-NO_2	28	13

[a]Detected by nmr spectroscopy (CH_2Br: CH_2F).
[b]Isolated as pure fractions by column chromatography on silica gel. Attempts were not made to maximize yields.

acid catalysed Friedel–Crafts type reaction. In the earlier preparations all the glassware was rinsed with an ethereal solution of quinoline and then dried. In later preparations one drop of *N,N*-diisopropylethylamine, a stronger but sterically hindered base, was added prior to the isolation of the fluoromethylnaphthalene to prevent the polymerization from occurring. This latter base is preferable as it does not interfere with the nmr spectra. All peaks in the spectrum of *N,N*-diisopropylethylamine appear at high field, viz. δ 1–2 ppm. Furthermore, it is considerably more volatile than quinoline and can be pumped off from the fluoromethylnaphthalenes.

In spite of the precaution of adding the base stabilizer, several samples did undergo the polymerization reaction. Addition of this trace amount of amine precluded elemental analysis and boiling point or melting point as a means of characterization. Accurate masses were determined, and the very characteristic ^1H and ^{19}F nmr spectra served to confirm the identity of the products.

Three separate attempts were made to prepare 4-methoxy-1-fluoromethylnaphthalene and in one instance a 15% yield was obtained. However, on chromatography on silica gel at −35°C to isolate the product, no fluoromethylnaphthalene was detected in any of the fractions collected. Appreciable quantities of a white solid melting at 149–150.5°C were obtained. Spectroscopic investigation of this solid indicated that it was a bis(4-methoxynaphthyl)methane.

We were unable to prepare 4-fluoromethyl-1-naphthamide from the corresponding bromide, and fluoride exchange was not attempted on 4-bromomethyl-2-naphthamide.

Experimental

The synthetic sequences used in the different preparations involve many of the same reactions carried out on the same functional group. For this reason the general synthetic method for one characteristic compound only is described and relevant data in tabular form are provided for similar transformations. Only in cases where difficulty was encountered which necessitated radical departure from the general method are details given for other compounds. Accurate mass data and C, H, N analytical data appear separately and are listed for each compound individually. Synthetic details are listed separately for compounds not included in the major groups. Spectral properties of previously unknown compounds are listed in Table 6. Infrared spectra were recorded on Perkin-Elmer model 337 spectrometer calibrated with polystyrene. Mass spectra were determined on a Hitachi Perkin-Elmer RMU-7 instrument. Nuclear magnetic resonance spectra were recorded on a Varian HA-60-IL spectrometer using tetramethylsilane as internal standard.

1-Acetyl-4-methylnaphthalene (21)

Acetyl chloride (38 cm^3; 39.3 g, 0.48 mol) was added over 45 min to a stirred mixture of 1-methylnaphthalene (Aldrich) (67.0 g, 0.48 mol), dry CH_2Cl_2 (340 cm^3), and finely ground anhydrous $AlCl_3$ (76 g, 0.57 mol) at 0°C. After the addition was complete the mixture was stirred at ambient temperature for 4 h and then heated under reflux for 2.5 h. Work-up followed by distillation under reduced pressure gave 1-acetyl-4-methylnaphthalene (71%), bp 115–120°C/0.2 Torr.

4-Methoxymethyl-2-acetylnaphthalene

4-Methoxymethyl-2-cyanonaphthalene (1.97 g, 0.01 mol) in benzene (10 cm^3) was added to a solution of methylmagnesium iodide in benzene, prepared from magnesium (0.05 mol) and methyl iodide (0.05 mol), and the solution stirred under reflux for 7 h. The solution was cooled and hydrochloric acid (0.6 mol in 100 cm^3) was added very cautiously. This solution was stirred under reflux for 36 h. The two layers were separated and the benzene layer washed with water, with 10% $NaHCO_3$ solution, and again with water (3 × 100 cm^3). The benzene solution was dried ($MgSO_4$) and evaporated. Chromatography on silica gel using a 10% benzene/petroleum ether (bp 35–45°C) mixture as the eluent gave 4-methoxymethyl-2-acetylnaphthalene in 77% yield.

4-Methyl-1-naphthoic acid

1-Acetyl-4-methylnaphthalene (40.66 g, 0.22 mol) was refluxed for 4.5 h with a hypochlorite solution prepared by dissolving NaOH (100 g, 2.5 mol) in water (135 cm^3) and ice (500 g), and bubbling Cl_2 into this solution until the increase in weight was 71 g (1 mol). The solution was allowed to cool and $NaHSO_3$ (60 g) added in order to destroy excess hypochlorite. Concentrated HCl (75 cm^3) was added to precipitate the 4-methyl-1-naphthoic acid. After recrystallization (95% EtOH)

TABLE 6. Spectral data for previously unknown compounds

Substituents	Infrared (cm^{-1})	Mass spectra *m/e* (relative abundance)	Nuclear magnetic resonance δ, (multiplicity), *J*, relative intensity
Acetylnaphthalenes			
1-$COCH_3$, 4-CH_2OCH_3	1680, 835, 760	214(91), 199(100), 171(60), 155(20), 141(15), 139(49)	δ1.2–2.8(m), 6H; δ4.7(s), 2H; δ3.31(s), 3H; δ2.55(s), 3H
1-$COCH_3$, 4-CH_2F	1680, 1058, 835, 765	202(55), 188(18), 187(100), 169(24), 159(65)	δ8.8–7.2(m), 6H; δ5.62(d), J = 48 Hz, 2H; δ2.55(s), 3H
1-$COCH_3$, 4-CH_2Br	1685, 830, 760, 552	264(24), 262(25), 184(29), 183(100), 168(24), 155(60)	δ8.75(m), 6H; δ4.8(s), 2H; δ2.55(s), 3H
2-$COCH_2$, 4-CH_2OCH_3	1680, 845, 735	214(75), 199(67), 183(35), 149(29), 139(46), 84(100)	δ8.2–7.15(m), 6H; δ4.58(s), 2H; δ3.21(s), 3H; δ2.44(s), 3H
2-$COCH_3$, 4-CH_2F	1680, 1060, 850, 735	202(90), 188(34), 187(100), 159(91), 157(24), 133(55)	δ8.33–7.38(m), 6H; δ5.55(d), J = 48 Hz, 2H; δ2.57(s), 3H
2-$COCH_3$, 4-CH_2Br	1680, 845, 730, 570	264(1), 262(1), 83(93), 141(13), 140(84), 139(100)	δ8.6–7.25(m), 6H; δ4.83(s), 2H; δ2.58(s), 3H
Naphthoic acids[b]			
1-COOH, 4-CH_2OCH_3	3200–2150, 1690, 840, 772	216(100), 186(30), 185(51), 171(80), 156(38), 128(50)	δ9.1–7.3(m), 6H; 4.9(s), 2H; δ3.4(s), 3H
2-COOH, 4-CH_2OH	3050, 1680, 860, 740	202(86), 173(52), 157(25), 155(42), 124(100), 123(52)	δ8.53–7.35(m), 6H; δ5.1(s), 2H; δ4.05(s), 1H
Naphthyl carbinols			
1-CH_2OH, 4-CH_2OCH_3	3475, 840, 760	202(76), 172(35), 171(100), 143(35), 141(54), 128(52)	δ7.95–7.0(m), 6H; δ4.62(s), 2H; δ4.55(s), 2H; δ3.55(s), 1H; δ3.2(s), 3H
1-CH_2OH, 4-F	3300, 825, 752	176(100), 175(25), 159(51), 146(12), 145(51)	δ8.2–6.6(m), 6H; δ4.79(s), 2H; δ2.99(s), 1H
1-CH_2OH, 4Cl	3300, 825, 755	194(26), 192(92), 177(6), 175(23), 163(52), 157(60), 128(100)	δ8.3–7.0(m), 6H; δ4.79(s), 2H; δ2.99(s), 1H
4-CH_2OH, 1-CN	3350, 2225, 835, 758	183(74), 182(18), 155(23), 154(100), 129(19), 128(28)	δ8.35–7.5(m), 6H; δ5.05(d), J = 6 Hz, 2H; δ2.12(t), J = 6 Hz, 1H[c]
4-CH_2OH, 1-$CONH_2$	3300, 3200, 1675, 835, 779	201(100), 185(27), 172(43), 155(23), 139(23), 129(90)	δ8.55–7.3(m), 6H; δ5.08(s), 3H; δ3.69(s), 3H[b]
1-CH_2OH, 3-Br	3350, 865, 745	238(39), 236(40), 157(18), 139(21), 129(91), 128(100)	δ8.05–7.2(m), 6H; δ4.97(s), 2H; δ1.49(s), 1H
4-CH_2OH, 2-CN	3425, 2220, 875, 740	183(48), 182(18), 165(11), 154(30), 153(100), 140(13)	δ8.05–7.3(m), 6H; δ5.05(d), J = 0.6 Hz, 2H; δ4.48(t), J = 0.6 Hz, 1H[c]
4-CH_2OH, 2-COOH	3050, 1680, 860, 740	202(86), 173(52), 157(25), 155(42), 141(13), 124(100)	δ8.53–7.35(m), 6H; δ5.1(s), 2H; δ4.05(s), 1H[b]
4-CH_2OH, 2-$COOCH_3$	3200, 1710, 850, 735	216(100), 187(61), 185(31), 157(29), 155(42), 141(9), 128(32)	δ8.7–7.3(m), 6H; δ5.0(s), 2H; δ3.85(s), 3H; δ3.35(s), 1H
4-CH_2OH, 2-$CONH_2$	3400, 3150, 1695, 850, 735	201(64), 185(15), 172(38), 155(20), 139(25), 129(100)	δ8.6–7.6(m), 6H; δ5.08(s), 2H; δ3.0(s), 1H[b]
1-CH_2OH, 3-NO_2	3200, 1349, 860, 755	203(100), 186(20), 188(25), 156(23), 139(36), 128(98), 127(50)	δ8.8–7.6(m), 6H; δ5.23(d), J = 6 Hz, 2H; δ4.6(t), J = 6 Hz, 1H[c]
Bromomethylnaphthalenes			
1-CH_2Br, 4-CH_2OCH_3	845, 780, 542	226(10), 264(11), 186(16), 185(100), 155(23), 154(38)	δ8.15–7.3(m), 6H; δ4.8(s), 2H; δ4.75(s), 2H; δ3.3(s), 3H
1,4-bis CH_2Br	843, 768, 522	316(4), 314(10), 235(57), 233(58), 154(100), 115(5)	δ8.15–7.4(m), 6H; δ4.9(s), 2H
1-CH_2Br, 4-F	1160, 840, 550	240(5), 238(5), 160(18), 159(100), 157(14), 141(2)	δ8.3–6.8(m), 6H; δ4.85(s), 2H[b]
1-CH_2Br, 4-Cl	830, 763, 550, 530	258(3), 256(9), 254(8), 177(35), 175(100), 141(25)	δ8.5–7.4(m), 6H; δ4.83(s), 2H
4-CH_2Br, 1-CN	2230, 840, 760, 560	247(9), 245(10), 167(46), 166(100), 140(53)	δ8.34–7.45(m), 6H; δ4.81(s), 2H[d]
4-CH_2Br, 1-COOH	3600–2400, 1700, 840, 775	266(6), 264(6), 185(100), 141(25), 140(36), 115(43)	δ9.15–7.5(m), 6H; δ5.11(s), 2H[b]
4-CH_2Br, 1-$COOCH_3$	1715, 850, 780, 550	280(8), 278(8), 200(16), 199(100), 171(43), 140(40)	δ9.0–7.5(m), 6H; δ5.05(s), 2H; δ3.9(s), 3H

Can. J. Chem. Downloaded from www.nrcresearchpress.com by 210.87.254.40 on 09/06/12
For personal use only.

TABLE 6 (*Concluded*)

Substituents	Infrared (cm^{-1})	Mass spectra *m/e* (relative abundance)	Nuclear magnetic resonance δ, (multiplicity), *J*, relative intensity
Bromomethylnaphthalenes			
4-CH_2Br, 1-$COOC_2H_5$	1725, 825, 770, 560	294(13), 292(13), 214(22), 213(100), 185(25), 157(13)	δ9.15–7.35(m), 6H; δ4.82(s), 2H; δ4.38(q), J = 7 Hz; δ1.45(t), 3H
4-CH_2Br, 1-$CONH_2$	3350, 1650, 835, 755, 742, 560	265(11), 263(12), 184(100), 156(50), 141(13), 140(38)	δ8.5–7.2(m), 6H; δ5.05(s), 2H[e]
4-CH_2Br, 1-$COCH_3$	1685, 830, 780, 760, 552	264(24), 262(25), 184(27), 183(100), 168(24), 155(60)	δ8.75–7.2(m), 6H; δ4.8(s), 2H; δ2.61(s), 3H
4-CH_2Br, 1-$COCH_2Br$	1795, 820, 760, 595, 555	344(6), 342(11), 340(6), 265(98), 263(100), 238(48)	δ8.7(m), 6H; δ4.85(s), 2H; δ4.45(s), 2H
1-CH_2Br, 3-NO_2	870, 885, 785, 770, 760, 545	267(10), 265(10), 202(8), 200(8), 187(13), 186(100)	δ9.2–7.2(m), 6H; δ5.2(s), 2H[b]
Fluoromethylnaphthalenes			
1-CH_2F	1060, 800, 785	160(100), 159(92), 141(9), 139(2), 133(39), 115(8)	δ8.1–7.0(m), 7H; δ5.6(d), J = 48 Hz, 2H
2-CH_2F	1065, 869, 750	160(100), 159(41), 141(8), 139(12), 133(28), 115(5)	δ7.8–7.2(m), 7H; δ5.35(d), J = 48 Hz, 2H
1-CH_2F, 4-CH_3	1060, 825, 758	174(14), 173(100), 172(25), 159(80), 141(36), 115(8)	δ8.15–7.0(m), 6H; δ5.68(d), J = 48 Hz, 2H; δ2.66(d), J = 2 Hz, 3H[f]
1-CH_2F, 4-CH_2OCH_3	1058, 840, 760	204(81), 173(71), 172(35), 171(100), 159(21), 141(30)	δ8.2–7.2(m), 6H; δ5.61(d), J = 48 Hz, 2H; δ4.7(s), 2H; δ3.3(s), 3H
1,4-bis CH_2F	1065, 840, 760	192(28), 159(100), 141(7), 133(20), 123(24), 115(5)	δ7.95–7.2(m), 6H; δ5.41(d), J = 48 Hz, 4H
1-CH_2F, 4-F	1170, 1058, 830, 770	178(100), 177(95), 159(35), 157(30), 151(35)	δ8.3–6.8(m), 6H; δ5.65(d), J = 48 Hz, 2H
1-CH_2F, 4-Cl	1060, 825, 750	146(22), 195(15), 194(67), 193(68), 159(100), 141(5)	δ8.5–7.0(m), 6H; δ5.62(d), J = 48 Hz, 2H
1-CH_2F, 4-Br	1063, 825, 755	240(8), 238(9), 159(24), 141(2), 115(5), 99(100), 98(75)	δ8.4–7.1(m), 6H; δ5.65(d), J = 48 Hz, 2H
4-CH_2F, 1-CN	1070, 850, 750	185(100), 184(81), 159(30), 158(16), 141(5), 133(5)	δ8.45–7.3(m), 6H; δ5.82(d), J = 48 Hz, 2H
4-CH_2F, 1-$COOCH_3$	1710, 1060, 835, 780	218(62), 200(11), 187(100), 186(21), 159(46), 141(16)	δ9.2–7.3(m), 6H; δ5.8(d), J = 48 Hz, 2H; δ4.0(s), 3H
4-CH_2F, 1-$COOC_2H_5$	1705, 1058, 835, 775	232(92), 214(15), 204(33), 188(20), 187(100), 159(75)	δ9.2–7.3(m), 6H; δ5.75(d), J = 48 Hz, 2H; δ4.38(q), J = 7 Hz, 2H; δ1.42(t), J = 7 Hz, 3H
4-CH_2F, 1-$COCH_3$	1680, 1058, 835, 765	202(55), 188(18), 187(100), 169(24), 159(65), 141(11), 115(10)	δ8.8–7.2(m), 6H; δ5.62(d), J = 48 Hz, 2H; δ2.55(s), 3H
4-CH_2F, 1-$COCH_2F$	1705, 1060, 1050, 835, 765	220(16), 203(21), 187(100), 169(28), 159(60), 141(18)	δ8.8–7.2(m), 6H; δ5.25(d), J = 48 Hz, 2H; δ5.75(d), J = 48 Hz, 2H
1-CH_2F, 4-NO_2	1062, 820, 770	205(100), 170(58), 159(50), 146(40), 141(3), 133(90)	δ9.0–7.15(m), 6H; δ5.83(d), J = 48 Hz, 2H
1-CH_2F, 3-CH_3	1065, 860, 730	174(100), 173(27), 159(90), 141(31), 133(9), 115(9)	δ8.0–7.05(m), 6H; δ5.55(d), J = 48 Hz, 2H; δ2.35(s), 3H
1,3-bis CH_2F	1060, 865, 730	192(97), 191(20), 170(13), 159(100), 141(6), 139(5)	δ8.0–7.1(m), 6H; δ5.55(d), J = 48 Hz, 2H; δ5.25(d), J = 48 Hz, 2H
1-CH_2F, 3-Br	1060, 1020, 830, 760	240(56), 239(15), 238(58), 160(17), 159(100), 158(13)	δ8.1–7.2(m), 6H; δ5.45(d), J = 48 Hz, 2H
4-CH_2F, 2-CN	2225, 1075, 835, 750	185(100), 184(86), 180(10), 166(9), 165(29), 164(10), 158(37)	δ9.3–7.3(m), 6H; δ5.9(d), J = 48 Hz, 2H[d]
4-CH_2F, 2-$COOCH_3$	1725, 1055, 865, 753	218(94), 200(9), 187(100), 159(71), 157(14), 141(7)	δ8.5–7.3(m), 6H; δ5.7(d), J = 48 Hz, 2H; δ3.85(s), 3H
4-CH_2F, 2-$COOC_2H_5$	1720, 1060, 800, 740	232(95), 214(67), 204(36), 188(25), 187(100), 186(27)	δ8.4–7.1(m), 6H; δ5.65(d), J = 48 Hz, 2H; δ4.3(q), J = 0.8 Hz, 2H; δ1.35(t), J = 0.8 Hz
4-CH_2F, 2-$COCH_3$	1680, 1060, 850, 735	202(90), 188(34), 187(100), 160(19), 159(91), 157(24)	δ8.33–7.38(m), 6H; δ5.55(d), J = 48 Hz, 2H; δ2.57(s), 3H
1-CH_2F, 3-NO_2	1060, 875, 775	205(100), 159(90), 157(30), 147(35), 141(8), 133(90)	δ8.8–7.3(m), 6H; δ5.75(d), J = 48 Hz, 2H

[a]The spectra recorded as a 10% solution in CCl_4 except where specified.
[b]The nmr recorded in $(CD_3)_2CO$.
[c]On D_2O exchange the triplet signal disappeared and the doublet collapsed to a singlet.
[d]Recorded in $CDCl_3$.
[e]Recorded in D_2O.
[f]Long-range coupling with fluorine.

Can. J. Chem. Downloaded from www.nrcresearchpress.com by 210.87.254.40 on 09/06/12
For personal use only.

Can. J. Chem. Downloaded from www.nrcresearchpress.com by 210.87.254.40 on 09/06/12
For personal use only.

TABLE 7. Accurate mass data and elemental analysis for previously unknown compounds

1-Acetyl-4-methoxymethylnaphthalene, *m/e*: 214.101; $M_r(^{12}C_{14}{}^1H_{14}{}^{16}O_2) = 214.099$

2-Acetyl-4-methoxymethylnaphthalene, *m/e*: 214.108; $M_r(^{12}C_{14}{}^1H_{14}{}^{16}O_2) = 214.099$

4-Methoxymethyl-1- naphthoic acid, *m/e*: 216.080; $M_r(^{12}C_{13}{}^1H_{12}{}^{16}O_3) = 216.078$. *Anal.* calcd. for $C_{13}H_{12}O_3$: C 72.20, H 5.59; found: C 72.04, H 5.33

4-Hydroxymethyl-2-naphthoic acid, *m/e*: 202.057; $M_r(^{12}C_{12}{}^1H_{10}{}^{16}O_3) = 202.063$. *Anal.* calcd. for $C_{12}H_{10}O_3$: C 71.30, H 4.47; found: C 71.60, H 4.69

4-Methoxymethyl-1-naphthylcarbinol, *m/e*: 202.101; $M_r(^{12}C_{13}{}^1H_{14}{}^{16}O_2) = 202.099$. *Anal.* calcd. for $C_{13}H_{14}O_2$: C 77.14, H 6.97; found: C 77.44, H 6.94

4-Fluoro-1-naphthylcarbinol, *m/e*: 176.056; $M_r(^{12}C_{11}{}^1H_9{}^{16}O_1{}^{19}F_1) = 176.065$. *Anal.* calcd. for $C_{11}H_9OF$: C 74.97, H 5.15; found: C 75.14, H 5.26

4-Chloro-1-naphthylcarbinol, *m/e*: 192.041; $M_r(^{12}C_{11}{}^1H_9{}^{16}O_1{}^{35}Cl_1) = 192.034$. *Anal.* calcd. for $C_{11}H_9OCl$: C 68.59, H 4.71; found: C 68.61, H 4.70

4-Hydroxymethyl-1-naphthonitrile, *m/e*: 183.068; $M_r(^{12}C_{12}{}^1H_9{}^{16}O_1{}^{14}N_1) = 183.068$. *Anal.* calcd. for $C_{12}H_{11}O_2N$: C 78.47, H 4.95, N 7.65; found: C 78.63, H 4.89, N 7.84

3-Bromo-1-naphthylcarbinol. *Anal.* calcd. for $C_{11}H_9OBr$: C 55.71, H 3.83; found: C 55.74, H 3.83

4-Hydroxymethyl-2-naphthonitrile, *m/e*: 183.072; $M_r(^{12}C_{12}{}^1H_9{}^{16}O_1{}^{14}N_1) = 183.068$. *Anal.* calcd. for $C_{12}H_9ON$: C 78.47, H 4.95, N 7.65; found: C 78.79, H 5.26, N 7.58

Methyl 4-hydroxymethyl-2-naphthoate, *m/e*: 216.076; $M_r(^{12}C_{13}{}^1H_{12}{}^{16}O_3) = 216.079$. *Anal.* calcd. for $C_{13}H_{12}O_3$: C 72.25, H 5.59; found: C 71.97, H 5.50

4-Hydroxymethyl-2-naphthamide, *m/e*: 201.088; $M_r(^{12}C_{12}{}^1H_{11}{}^{16}O_2{}^{14}N_1) = 201.079$. *Anal.* calcd. for $C_{12}H_{11}O_2N$: C 71.63, H 5.50, N 6.96; found: C 71.50, H 5.43, N 6.71

3-Nitro-1-naphthylcarbinol, *m/e*: 203.065; $M_r(^{12}C_{11}{}^1H_9{}^{16}O_3{}^{14}N_1) = 203.058$. *Anal.* calcd. for $C_{11}H_9O_3N$: C 65.01, H 4.47, N 6.85; found: C 64.87, H 4.48, N 6.99

1-Bromomethyl-4-methoxymethylnaphthalene, *m/e*: 266.012; $M_r(^{12}C_{13}{}^1H_{13}{}^{16}O_1{}^{81}Br_1) = 266.013$. *Anal.* calcd. for $C_{13}H_{13}OBr$: C 58.5, H 4.84; found: 58.23, H 4.72

1,4-Bisbromomethylnaphthalene, *m/e*: 315.916; $M_r(^{12}C_{12}{}^1H_{10}{}^{81}Br_2) = 315.911$. *Anal.* calcd. for $C_{12}H_{10}Br_2$: C 45.90, H 3.21; found: C 45.89, H 3.14

1-Bromomethyl-4-fluoronaphthalene, *m/e*: 239.978; $M_r(^{12}C_{11}{}^1H_8{}^{19}F_1{}^{81}Br_1) = 239.978$. *Anal.* calc. for $C_{11}H_8FBr$: C 55.21, H 3.37; found: C 55.51, H 3.32

1-Bromomethyl-4-chloronaphthalene, *m/e*: 257.953; $M_r(^{12}C_{11}{}^1H_8{}^{81}Br_1{}^{37}Cl_1) = 257.945$. *Anal.* calcd. for $C_{11}H_8BrCl$: C 51.70, H 3.17; found: C 51.44, H 3.08

4-Bromomethyl-1-naphthonitrile, *m/e*: 244.978; $M_r(^{12}C_{12}{}^1H_8{}^{14}N_1{}^{79}Br_1) = 244.984$. *Anal.* calcd. for $C_{12}H_8NBr$: C 58.55, H 3.28, N 5.69; found: C 58.51, H 3.24, N 5.65

4-Bromomethyl-1-naphthoic acid, *m/e*: 265.981; $M_r(^{12}C_{12}{}^1H_9{}^{16}O_2{}^{81}Br_1) = 265.977$. *Anal.* calcd. for $C_{12}H_9O_2Br$: C 54.36, H 3.42; found: C 54.11, H 3.59

Methyl 4-bromomethyl-1-naphthoate, *m/e*: 277.997; $M_r(^{12}C_{13}{}^1H_{11}{}^{16}O_2{}^{79}Br_1) = 277.994$. *Anal.* calcd. for $C_{13}H_{11}O_2Br$: C 55.95, H 3.97; found: C 56.06, H 3.85

Ethyl 4-bromomethyl-1-naphthoate, *m/e*: 292.003; $M_r(^{12}C_{14}{}^1H_{13}{}^{16}O_2{}^{79}Br_1) = 292.010$. *Anal.* calcd. for $C_{14}H_{13}O_2Br$: C 57.38, H 4.47; found: C 57.18, H 4.40

4-Bromomethyl-1-naphthamide, *m/e*: 262.990; $M_r(^{12}C_{12}{}^1H_{10}{}^{16}O_1{}^{14}N_1{}^{79}Br_1) = 262.994$. *Anal.* calcd. for $C_{12}H_{10}ONBr$: C 52.56, H 3.26, N 5.11; found: C 52.86, H 3.46, N 5.14

1-Acetyl-4-bromomethylnaphthalene, *m/e*: 263.998; $M_r(^{12}C_{13}{}^1H_{11}{}^{16}O_1{}^{81}Br_1) = 263.997$. *Anal.* calcd. for $C_{13}H_{11}OBr$: C 59.35, H 4.21; found: C 59.10, H 4.12

1-Bromoacetyl-4-bromomethylnaphthalene, *m/e*: 341.92; $M_r(^{12}C_{13}{}^1H_{10}{}^{16}O_1{}^{81}Br_1{}^{79}Br_1) = 341.910$. *Anal.* calcd. for $C_{13}H_{10}OBr_2$: C 45.64, H 3.15; found: C 45.85, H 2.99

1-Bromomethyl-4-nitronaphthalene, *m/e*: 264.983; $M_r(^{12}C_{11}{}^1H_8{}^{14}N_1{}^{16}O_2{}^{79}Br_1) = 264.982$. *Anal.* calcd. for $C_{11}H_8NO_2Br$: C 49.63, H 3.03, N 5.26; found: C 49.53, H 3.01, N 5.31

1-Bromomethyl-3-methylnaphthalene, *m/e*: 234.002; $M_r(^{12}C_{12}{}^1H_{11}{}^{79}Br_1) = 234.004$. *Anal.* calcd. for $C_{12}H_{11}Br$: C 61.53, H 4.73; found: C 61.52, H 4.78

2-Bromomethyl-4-methylnaphthalene, *m/e*: 233.994; $M_r(^{12}C_{12}{}^1H_{11}{}^{79}Br_1) = 234.004$. *Anal.* calcd. for $C_{12}H_{11}Br$: C 61.53, H 4.73; found: C 61.82, H 4.76

1,3-Bisbromomethylnaphthalene, *m/e*: 315.914; $M_r(^{12}C_{12}{}^1H_{10}{}^{81}Br_2) = 315.911$. *Anal.* calcd. for $C_{12}H_{10}Br_2$: C 45.9, H 3.21; found: C 45.92, H 3.19

3-Bromo-1-bromomethylnaphthalene, *m/e*: 301.897; $M_r(^{12}C_{11}{}^1H_8{}^{81}Br_2) = 301.896$. *Anal.* calcd. for $C_{11}H_8Br_2$: C 44.03, H 3.09; found: C 44.20, H 2.81

4-Bromomethyl-2-naphthonitrile, *m/e*: 244.978; $M_r(^{12}C_{12}{}^1H_8{}^{14}N_1{}^{79}Br_1) = 244.984$. *Anal.* calcd. for $C_{12}H_8NBr$: C 58.56, H 3.28, N 5.69; found: C 58.54, H 3.32, N 5.59

TABLE 7 (*Concluded*)

Methyl 4-bromomethyl-2-naphthoate, *m/e*: 277.997; $M_r(^{12}C_{13}{}^1H_{11}{}^{16}O_2{}^{79}Br_1)$ = 277.994. *Anal.* calcd. for $C_{13}H_{11}O_2Br$: C 55.95, H 3.97; found: C 56.60, H 4.05

Ethyl 4-bromomethyl-2-naphthoate, *m/e*: 292.010; $M_r(^{12}C_{14}{}^1H_{13}{}^{16}O_2{}^{79}Br_1)$ = 292.010. *Anal.* calcd. for $C_{14}H_{13}O_2Br$: C 57.35, H 4.47; found: C 57.28, H 4.43

4-Bromomethyl-2-naphthamide, *m/e*: 262.991; $M_r(^{12}C_{12}{}^1H_{10}{}^{16}O_1{}^{14}N_1{}^{79}Br_1)$ = 262.995. *Anal.* calcd. for $C_{12}H_{10}ONBr$: C 52.56, H 3.26, N 5.11; found: 52.69, H 3.48, N 5.05

2-Acetyl-4-bromomethylnaphthalene, *m/e*: 262.009; $M_r(^{12}C_{13}{}^1H_{11}{}^{16}O_1{}^{79}Br_1)$ = 261.999. *Anal.* calcd. for $C_{13}H_{11}OBr$: C 59.35, H 4.21; found: C 59.09, H 4.01

1-Bromomethyl-3-nitronaphthalene, *m/e*: 264.981; $M_r(^{12}C_{11}{}^1H_8{}^{16}O_2{}^{14}N_1{}^{79}Br_1)$ = 264.968. *Anal.* calcd. for $C_{11}H_8O_2NBr$: C 49.63, H 3.03, N 5.26; found: C 49.56, H 3.31, N 5.20

1-Fluoromethylnaphthalene, *m/e*: 160.069; $M_r(^{12}C_{11}{}^1H_9{}^{19}F_1)$ = 160.068

2-Fluoromethylnaphthalene, *m/e*: 160.069; $M_r(^{12}C_{11}{}^1H_9{}^{19}F_1)$ = 160.068

1-Fluoromethyl-4-methylnaphthalene, *m/e*: 174.074; $M_r(^{12}C_{12}{}^1H_{11}{}^{19}F_1)$ = 174.085

1-Fluoromethyl-4-methoxymethylnaphthalene, *m/e*: 204.096; $M_r(^{12}C_{13}{}^1H_{13}{}^{16}O_1{}^{19}F_1)$ = 204.095

4-Fluoro-1-fluoromethylnaphthalene, *m/e*: 178.052; $M_r(^{12}C_{11}{}^1H_8{}^{19}F_2)$ = 178.060

1,4-Bisfluoromethylnaphthalene, *m/e*: 159.056; $M_r(^{12}C_{11}{}^1H_8{}^{19}F_1)$ = 159.055

4-Chloro-1-fluoromethylnaphthalene, *m/e*: 196.023; $M_r(^{12}C_{11}{}^1H_8{}^{37}Cl_1{}^{19}F_1)$ = 196.028

4-Bromo-1-fluoromethylnaphthalene, *m/e*: 237.973; $M_r(^{12}C_{11}{}^1H_8{}^{19}F_1{}^{79}Br_1)$ = 237.973

4-Fluoromethyl-1-naphthonitrile, *m/e*: 185.0585; $M_r(^{12}C_{12}{}^1H_8{}^{14}N_1{}^{19}F_1)$ = 185.0581

Methyl 4-fluoromethyl-1-naphthoate, *m/e*: 218.072; $M_r(^{12}C_{13}{}^1H_{11}{}^{16}O_2{}^{19}F_1)$ = 218.074

Ethyl 4-fluoromethyl-1-naphthoate, *m/e*: 232.086; $M_r(^{12}C_{14}{}^1H_{13}{}^{16}O_2{}^{19}F_1)$ = 232.090

1-Acetyl-4-fluoromethylnaphthalene, *m/e*: 202.087; $M_r(^{12}C_{13}{}^1H_{11}{}^{16}O_1{}^{19}F_1)$ = 202.080

1-Fluoroacetyl-4-fluoromethylnaphthalene, *m/e*: 220.063; $M_r(^{12}C_{13}{}^1H_{10}{}^{16}O_1{}^{19}F_2)$ = 220.070

1-Fluoromethyl-4-nitronaphthalene, *m/e*: 205.058; $M_r{}^1(^{12}C_{11}{}^1H_8{}^{16}O_2{}^{14}N_1{}^{19}F_1)$ = 205.055

1-Fluoromethyl-3-methylnaphthalene, *m/e*: 174.081; $M_r(^{12}C_{12}{}^1H_{11}{}^{19}F_1)$ = 174.084

1,3-Bisfluoromethylnaphthalene, *m/e*: 192.073; $M_r(^{12}C_{12}{}^1H_{10}{}^{19}F_2)$ = 192.075

3-Bromo-1-fluoromethylnaphthalene, *m/e*: 237.973; $M_r(^{12}C_{11}{}^1H_8{}^{79}Br_1{}^{19}F_1)$ = 237.973

4-Fluoromethyl-2-naphthonitrile, *m/e*: 185.074; $M_r(^{12}C_{12}{}^1H_8{}^{14}N_1{}^{19}F_1)$ = 185.058

Methyl 4-fluoromethyl-2-naphthoate, *m/e*: 218.074; $M_r(^{12}C_{12}{}^1H_{11}{}^{16}O_2{}^{19}F_1)$ = 218.074

Ethyl 4-fluoromethyl-2-naphthoate, *m/e*: 232.088; $M_r(^{12}C_{14}{}^1H_{13}{}^{16}O_2{}^{19}F_1)$ = 232.090

2-Acetyl-4-fluoromethylnaphthalene, *m/e*: 202.084; $M_r(^{12}C_{13}{}^1H_{11}{}^{16}O_1{}^{19}F_1)$ = 202.079

1-Fluoromethyl-3-nitronaphthalene, *m/e*: 205.072; $M_r(^{12}C_{11}{}^1H_8{}^{14}N_1{}^{16}O_2{}^{19}F_1)$ = 205.054

4-Methoxymethyl-2-naphthonitrile, *m/e*: 197.070; $M_r(^{12}C_{13}{}^1H_{11}{}^{14}N_1{}^{16}O_1)$ = 197.084. *Anal.* calcd. for $C_{13}H_{11}ON$: C 79.14, H 5.62, N 7.10; found: C 79.45, H 6.00, N 7.06

Ethyl 4-methoxymethyl-1-naphthoate, *m/e*: 244.093; $M_r(^{12}C_{15}{}^1H_{16}{}^{16}O_3)$ = 244.101

Ethyl 4-ethoxymethyl-2-naphthoate, *m/e*: 258.142; $M_r(^{12}C_{16}{}^1H_{18}{}^{16}O_3)$ = 258.126

4-Hydroxymethyl-1-naphthamide, *m/e*: 201.068; $M_r(^{12}C_{12}{}^1H_{11}{}^{16}O_2{}^{14}N_1)$ = 201.079. *Anal.* calcd. for $C_{12}H_{11}O_2N$: C 71.63, H 5.50, N 6.96; found: C 71.48, H 5.53, N 6.80

the acid (37.4 g, 91%) was obtained, mp 175–175.5°C (lit. (21) mp 175°C).

4-Methoxy-1-naphthoic acid

4-Methoxy-1-naphthyl magnesium bromide was prepared from magnesium (6.12 g, 0.25 mol) and 1-bromo-4-methoxynaphthalene (59.25 g, 0.25 mol). The Grignard solution was poured onto solid CO_2 (400 g) in 800 cm^3 of ether, with vigorous manual stirring. After work-up the 4-methoxy-1-naphthoic acid was recrystallized twice from acetic acid and dried under reduced pressure to give 24 g (48%), mp 247–247.5°C (lit. (13) mp 248°C).

4-Hydroxymethyl-2-naphthoic acid

4-Hydroxymethyl-2-naphthonitrile was heated under reflux with aqueous NaOH (6 mol dm^{-3}) until only one phase was present in the reaction mixture (15 h). The white solid obtained after work-up was recrystallized from 95% ethanol to give colourless crystals of the acid, mp 293–295°C.

3-Bromo-1-naphthoic acid (14–16)

3-Bromo-1,8-naphthalic anhydride, mp 241–243°C (lit. (15) mp 244°C) was obtained in 23% yield on bromination of 1,8-naphthalic anhydride in concentrated nitric acid (14). Mercuration with yellow mercuric oxide in aqueous acetic acid gave anhydro-3-bromo-8-hydroxymercuri-1-naphthoic acid (100%) which was demercurated by boiling with aqueous hydrochloric acid. Fractional crystallization from acetic acid gave the less soluble 3-bromo-1-naphthoic acid in the early fractions in 50% yield, mp 230.5–232°C (lit. (14) mp 231–232°C). The more soluble 6-bromo isomer remained in the mother liquor.

4-Methyl-1-naphthylcarbinol (19, 22)

4-Methyl-1-naphthoic acid (4.57 g, 0.025 mol) in anhydrous ether (100 cm^3) was added over 45 min to a stirred suspension of $LiAlH_4$ (0.7 g, 0.18 mol) in anhydrous ether (50 cm^3), under an atmosphere of nitrogen, at such a rate that boiling of the solvent was maintained. After stirring under reflux for 3 h and again at

Can. J. Chem. Downloaded from www.nrcresearchpress.com by 210.87.254.40 on 09/06/12
For personal use only.

Can. J. Chem. Downloaded from www.nrcresearchpress.com by 210.87.254.40 on 09/06/12
For personal use only.

room temperature for 14 h the reaction mixture was worked up to give the carbinol. On recrystallization from petroleum ether (bp 60–70°C) 4-methyl-1-naphthylcarbinol (3.4 g, 82%) was obtained as needles, mp 76–77°C (lit. (23) mp 77°C).

3-Nitro-1-naphthylcarbinol

$LiAlH_4$ (0.38 g, 0.01 mol) was suspended in anhydrous ether (10 cm^3). Anhydrous $AlCl_3$ (1.33 g, 0.01 mol) in 15 cm^3 ether was added quickly to the vigorously stirred suspension. A suspension of methyl 3-nitro-1-naphthoate (2.0 g, 8.7 mmol) in ether (50 cm^3) was added dropwise over 30 min. Ice-cold water (100 cm^3) was added cautiously to the mixture, cooled in ice. Work-up gave the 3-nitro-1-naphthylcarbinol (1.26 g, 85%), recrystallized from a mixture of 10% benzene/petroleum ether (bp 100–110°C) as needles, mp 131.5–133.5°C.

1-Bromomethyl-4-methylnaphthalene

4-Methyl-1-naphthylcarbinol (10.3 g, 0.06 mol) was dissolved in dry benzene (100 cm^3) to which was added PBr_3 (19.5 g, 0.072 mol) and two drops of pyridine. The solution was stirred and heated at 50–55°C for 6 h; the reaction mixture was then poured onto ice (100 g), and the organic and aqueous layers were separated. The aqueous layer was extracted with benzene and the benzene solutions combined, washed with water, with 15% Na_2CO_3 solution, and again with water. After drying ($MgSO_4$) and evaporation of the benzene a dark green solid was obtained. Recrystallization (×3) from petroleum ether (bp 35–45°C) gave 1-bromomethyl-4-methylnaphthalene as needles (11.8 g, 84%), mp 77–79°C (lit. (23) mp 80°C).

1-Acetyl-4-bromomethylnaphthalene and 1-Bromoacetyl-4-bromomethylnaphthalene; 1-Bromomethyl-3-methylnaphthalene and 1,3-Bisbromomethylnaphthalene

Recrystallized *N*-bromosuccinimide (133.5 g, 0.75 mol) was added to 1-acetyl-4-methylnaphthalene (93 g, 0.5 mol) in CCl_4 (1250 cm^3) and the suspension stirred under reflux for 48 h. The residue (157.37 g) obtained after work-up contained some unreacted 1-acetyl-4-methylnaphthalene, but was comprised mainly of 1-bromoacetyl-4-bromomethylnaphthalene and 1-acetyl-4-bromomethylnaphthalene in a 1:2 ratio. Chromatography on silica gel (1400 g) and elution with petroleum ether gave in the first 8 fractions (7200 cm^3) 1-acetyl-4-methylnaphthalene (2.59 g). Fractions 9 and 10 contained pure 1-bromoacetyl-4-bromomethylnaphthalene (37.43 g). The next 25 fractions (12 L of petroleum ether/benzene, 90:10) contained both bromomethylnaphthalenes (50 g). The final 3 fractions contained 1-acetyl-4-bromomethylnaphthalene (32.8 g). Recrystallization from petroleum ether (bp 60–75°C) gave colourless platelets of 1-acetyl-4-bromomethylnaphthalene, mp 83–84°C. Fraction 10 was similarly recrystallized to give needles of 1-bromoacetyl-4-bromomethylnaphthalene, mp 118.5–119.5°C.

Bromination of 1,3-dimethylnaphthalene (0.04 mol) with *N*-bromosuccinimide (0.04 mol) in CCl_4 (500 cm^3) gave a mixture of unreacted 1,3-dimethylnaphthalene, 1,3-bisbromomethylnaphthalene, 3-bromomethyl-1-methylnaphthalene, and 1-bromomethyl-3-methylnaphthalene. Chromatography on silica gel using petroleum ether (bp 35–45°C) as eluent gave 1,3-dimethylnaphthalene in the early fractions, two bromomethylmethylnaphthalene isomers in the following fractions, and, in the final fractions, 1,3-bisbromomethylnaphthalene. The bromomethylmethylnaphthalenes were separated by fractional crystallization from petroleum ether (bp 60–75°C).

4-Bromomethyl-1-naphthoic acid

4-Methoxymethyl-1-naphthoic acid (2.16 g, 0.01 mol) was dissolved in dry benzene (300 cm^3). This solution was surrounded by an ice-bath and dry HBr gas bubbled in for 2 h. The suspension was stirred at room temperature for 12 h and at 60–75°C for 3 h, followed by a further 6 h at room temperature. The benzene was removed on a rotary evaporator and the residue was recrystallized from benzene–dichloromethane to give colourless crystals of 4-bromomethyl-1-naphthoic acid (2.65 g, 100%), mp 193–195°C.

1-Fluoromethyl-4-methylnaphthalene

1-Bromomethyl-4-methylnaphthalene (7.25 g, 0.031 mol) dissolved in dry distilled *N*-methylpyrrolidone (25 cm^3) was added over 15 min to anhydrous potassium fluoride (18.0 g, 0.31 mol), suspended in the pyrrolidone (100 cm^3), at 100°C. The reaction temperature was raised to 150°C and maintained at this temperature for 3 h. After cooling, methylene chloride (200 cm^3) was added and the solution washed with water (100 cm^3), and then thoroughly with saturated NH_4Cl solution (6 × 200 cm^3), in order to extract as much of the pyrrolidone as possible. After drying ($MgSO_4$) and evaporation of the solvent the residue (11.3 g) consisted of, by ^1H nmr, pyrrolidone plus naphthalene compounds, over 90% of the latter being the fluoromethylnaphthalene. The relative quantity of fluoromethyl compound in the mixture was estimated by comparing the integration of the readily distinguishable methylene doublet due to the CH_2F function (J_{H-F} = 48 Hz) with that of the methylene of the bromomethylnaphthalene and/or naphthylcarbinol. Chromatography on silica gel (250 g) and elution with pentane, collecting 13 fractions of 150 cm^3, gave the fluoromethylnaphthalene (1.4 g) in fractions 3 to 11.

1-Methyl-4-nitronaphthalene (24, 27)

1-Methylnaphthalene (Aldrich) was nitrated with concentrated nitric acid and the product recrystallized from petroleum ether to give 1-methyl-4-nitronaphthalene, mp 68–71°C (lit. (24) 71–72°C).

1-Acetyl-4-methoxymethylnaphthalene

1-Acetyl-4-bromomethylnaphthalene (0.15 mol) was added gradually to sodium methoxide (from sodium (4.6 g, 0.2 mol) in methanol (2.2 dm^3)) over 3 h. The solution was stirred at room temperature for 3 h and then under reflux for 14 h before work-up. 4-Methoxymethyl-1-naphthonitrile, mp 67.5–68.5°C, was prepared similarly in 90% yield.

4-Hydroxymethyl-1-naphthamide

4-Hydroxymethyl-1-naphthonitrile (1.77 g, 7.5 mmol) was dissolved in 95% ethanol (10 cm^3) and 6*N* NaOH (2 cm^3). The solution was immersed in an ice-bath and cooled to 10–15°C. Hydrogen peroxide (30%) (10 cm^3) was added. The reaction mixture was gradually heated to 55–60°C and stirred for 4 h. Ethanol was removed, the residue allowed to cool, and the solid that precipitated filtered off; the solid was recrystallized twice from warm water to give a quantitative yield of the amide, mp 146–147°C. 4-Hydroxymethyl-2-naphthamide (mp 155–156°C) was prepared in 50% yield by the same method (28).

Methyl 4-Bromomethyl-1-naphthoate

An ice-cold solution of excess diazomethane in ether was added with stirring to a suspension of 4-bromomethyl-1-naphthoic acid in ether. After work-up and recrystallization of the residue from petroleum ether (bp 60–75°C), methyl 4-bromomethyl-1-naphthoate, mp 83–85°C, was obtained in 90% yield.

Similarly were prepared methyl 4-hydroxymethyl-2-naphthoate (mp 79–80°C, 90%) and methyl 3-bromo-1-naphthoate (mp 58–59°C, lit. (14) 59°C, 95%).

Ethyl 4-Methoxymethyl-1-naphthoate

4-Methoxymethyl-1-naphthoic acid in 100% ethanol was esterified using boron-trifluoride etherate catalyst (25). Ethyl-4-methoxymethyl-1-naphthoate was obtained in 62% yield. Ethyl

Can. J. Chem. Downloaded from www.nrcresearchpress.com by 210.87.254.40 on 09/06/12
For personal use only.

4-ethoxymethyl-2-naphthoate and ethyl 4-hydroxmethyl-2-naphthoate were prepared similarly.

1-Bromo-4-methoxynaphthalene (26)

A solution of bromine (25 cm^3, 0.5 mol) and iodine (127.5 g, 0.5 mol) in chloroform (500 cm^3) was added over 30 min to a stirred solution of 1-methoxynaphthalene (Eastman) (80 g, 0.5 mol) in $CHCl_3$ (250 cm^3) at 15–20°C. A constant stream of air removed the HBr as fast as it was formed. The mixture was stirred at 15–20°C for a further 45 min and was filtered to remove precipitated iodine, washed, dried, and evaporated. On distillation under reduced pressure 1-bromo-4-methoxynaphthalene (74%) was collected at 160–163°C/2 Torr (lit. (13) bp 159°C/4 Torr).

2-Acetyl-4-methoxymethylnaphthalene

4-Methoxymethyl-1-naphthonitrile (0.01 mol) in benzene (10 cm^3) was added to a solution of methylmagnesium iodide (0.05 mol) in benzene (20 cm^3). The reaction mixture was stirred under reflux for 7 h. The green reaction mixture was worked up and the residue chromatographed on silica gel using a 10% benzene/petroleum ether (bp 35–45°C) mixture as the eluent. Pure 2-acetyl-4-methoxymethylnaphthalene was obtained as a clear liquid in 77% yield.

Acknowledgements

We are grateful to the National Research Council of Canada for financial support, and to the University of Victoria for the award of a University of Victoria Post-Graduate Fellowship to one of us (E. A. D.).

1. C. Béguin. Bull. Soc. Chim. Fr. 4214 (1967).
2. W. Adcock, M. J. S. Dewar, R. Golden, and M. A. Zeb. J. Am. Chem. Soc. **97**, 2198 (1975).
3. E. A. Dixon. Ph.D. Thesis, University of Victoria, Victoria, B.C. 1974.
4. C. K. Ingold and E. H. Ingold. J. Chem. Soc. 2249 (1928).
5. J. Bernstein, J. S. Roth, and W. T. Miller. J. Am. Chem. Soc. **70**, 2310 (1948).
6. C. G. Swain and R. E. T. Spalding. J. Am. Chem. Soc. **82**, 6104 (1960).
7. J. J. Delpuech and C. Béguin. Bull. Soc. Chim. Fr. 791 (1967).
8. C. Béguin and A. Meary-Tertian. Bull. Soc. Chim. Fr. 795 (1967).
9. T. Yokoyama, G. R. Wiley, and S. I. Miller. J. Org. Chem. **34**, 1859 (1969).
10. T. L. Jacobs, S. Winstein, J. W. Ralls, and J. H. Robson. J. Org. Chem. **11**, 27 (1946).
11. J. E. Callen, C. A. Dornfeld, and G. H. Coleman. Org. Synth. Coll. Vol. III, 26 (1955).
12. M. S. Newman and H. L. Holmes. Org. Synth. Coll. Vol. II, 2015 (1963).
13. G. W. Gray and B. Jones. J. Chem. Soc. 678 (1954).
14. H. G. Rule and S. B. Thompson. J. Chem. Soc. 1764 (1937).
15. G. J. Leuck, R. P. Perkins, and F. C. Whitmore. J. Am. Chem. Soc. **51**, 1831 (1929).
16. F. C. Whitmore and A. L. Fox. J. Am. Chem. Soc. **51**, 3363 (1929).
17. H. C. Brown and B. C. Subba Rao. J. Am. Chem. Soc. **78**, 2582 (1956).
18. R. F. Nystrom. J. Am. Chem. Soc. **77**, 2544 (1955).
19. F. Bergmann and J. Szmuszkovicz. Bull. Soc. Chim. Fr. 566 (1953); Chem. Abstr **48**, 5168 (1954).
20. R. E. Parker. *In* Advances in fluorine chemistry. Vol. 3. *Edited by* M. Stacey, J. C. Tatlow, and A. G. Sharpe. Butterworths. London. 1963. p. 63.
21. K. Dziewonski and M. Marusinska. Bull. Intern. Acad. Polon. Sci. Classic. Math. Nat. 316 (1937); Chem. Abstr. **33**, 1712 (1939).
22. (*a*) R. F. Nystrom and W. A. Brown. J. Am. Chem. Soc. **69**, 2548 (1947); (*b*) L. F. Fieser and M. Fieser. *In* Reagents for organic synthesis. Vol. I. J. Wiley & Sons, New York. 1967. p. 584.
23. R. Robinson and H. W. Thompson. J. Chem. Soc. 2015 (1932).
24. R. Lesser, A. Glaser, and G. Aczél. Ann. Chem. **402**, 1 (1914).
25. J. L. Marshall, K. C. Erickson, and T. K. Folsom. Tetrahedron Lett. 4011 (1970).
26. W. Militzer. J. Am. Chem. Soc. **60**, 256 (1938).
27. H. W. Thompson. J. Chem. Soc. 2310 (1932).
28. C. R. Noller. Org. Synth. Coll. Vol. II, 586 (1963).
29. S. Ruhemann and S. I. Levy. Ber. **53**, 265 (1920).
30. K. Ziegler. Ber. **54**, 739 (1921).
31. E. Bamberger and O. Boekmann. Ber. **20**, 1115 (1887).
32. J. B. Shoesmith and H. Rubli. J. Chem. Soc. 3098 (1927).
33. Buu-Hoi and J. Lecocq. J. Chem. Soc. 830 (1946).
34. N. B. Chapman and J. F. A. Williams. J. Chem. Soc. 5044 (1952).
35. R. H. Mitchell. Tetrahedron Lett. 4331 (1975).

Substituent effects in fluoromethylnaphthalenes by ^{19}F nuclear magnetic resonance

ELISABETH A. DIXON,[1] ALFRED FISCHER, and FRANK P. ROBINSON
Department of Chemistry, University of Victoria, Victoria, B. C., Canada V8W 2Y2

Received January 27, 1981

ELISABETH A. DIXON, ALFRED FISCHER, and FRANK P. ROBINSON. Can. J. Chem. **59**, 2642 (1981).

^{19}F substituent chemical shifts (SCS) are reported for a series of twenty-one 3- and 4-substituted 1-fluoromethylnaphthalenes. The fluoromethylnaphthalenes exhibit an inverse SCS dependence: electron-withdrawing substituents produce upfield shifts. The results correlate well with SCS values previously reported for substituted benzyl fluorides. Hammett correlations are poor with conjugatively electron-withdrawing substituents exhibiting weaker than expected effects in the 3-position and stronger than expected effects in the 4-position. Dual substituent parameter analysis confirms the enhanced substituent–aromatic ring resonance interaction when the substituent is in the 4-position ($\rho_R/\rho_I = 2$). There is no evidence for enhanced resonance interaction between fluoromethyl side-chain and aromatic ring. The ^{19}F chemical shift of 1-fluoromethylnaphthalene is markedly temperature dependent.

ELISABETH A. DIXON, ALFRED FISCHER et FRANK P. ROBINSON, Can. J. Chem. **59**, 2642 (1981).

On rapporte les déplacements chimiques du ^{19}F d'une série de 21 fluoro-1 méthylnaphtalènes substitués en positions 3 et 4. Dans les fluorométhylnaphtalènes les déplacements chimiques subissent une influence inverse: les substituants électro-attracteurs provoquent un déplacement vers les champs forts. Les résultats sont en parfait accord avec les valeurs des déplacements chimiques relatifs aux fluorures de benzyle substitués rapportés antérieurement. Les corrélations de Hammet sont mauvaises en ce qui a trait aux substituants électro-attracteurs conjugués qui en position 3 montrent des effets beaucoup plus faibles que ceux attendus et anormalement plus forts en position 4. L'analyse du paramètre de substituant double confirme l'augmentation de l'interaction de résonance du cycle aromatique substitué lorsque le substituant se trouve en position 4 ($\rho_R/\rho_I = 2$). On n'a pas pu prouver l'augmentation de l'interaction de résonance entre la chaîne latérale fluorométhyle et le cycle aromatique. Le déplacement chimique du ^{19}F du fluoro-1 méthylnaphtalène dépend fortement de la température.

[Traduit par le journal]

Introduction

^{19}F nmr chemical shift studies have formed an integral part of the development of the more modern treatments of substituent effects on the electron distribution within a molecule. The ^{19}F nmr chemical shift parameter, $\Delta\phi$, has been used as a sensitive probe to these electronic effects.

Gutowsky *et al.* (1) in 1952 reported that an empirical correlation of ^{19}F nmr chemical shift values for *meta*- and *para*-substituted fluorobenzenes with the corresponding Hammett substituent σ constants revealed systematic differences which were attributed to the dependence of the σ-values on the nature of the electronic interactions of the substituent. Interpretation of the data by separate solutions demonstrated a fundamental difference in the particular effects operative at the *meta* and *para* positions. With data from aliphatic series, Taft et al. (2–5) defined an inductive parameter, σ_I, which allowed a quantitative separation of the Hammett σ value into independent inductive, σ_I, and resonance, σ_R, contributions. Taft (6) reevaluated the ^{19}F nmr shielding parameters, previously reported by Gutowsky, in these terms and reported excellent correlations. The most recent refinement of the dual substituent parameter treatment was a rigorous and extensive statistical analysis of existing data by Ehrenson *et al.* (7) which led to the recognition of "four practical classes of pi-delocalization behaviour," and four classes of substituent constants. It should be noted that ^{19}F nmr data were prominent among the data sets used in this refinement.

Thus it may be seen that ^{19}F nmr substituent chemical shift studies have been of enormous utility in the development of many of the modern ideas concerning substituent effects and linear free energy relationships. And yet, in retrospect, the original successes and their interpretations appear fortuitous in that confusion did not arise from the now increasing list of examples of "anomalous" systems. Over the past 20 years there have appeared in the literature an increasing number of fluorine containing systems where, contrary to expectation, the introduction of an electron-withdrawing substituent induces a ^{19}F nmr substituent chemical shift to high field of the parent, unsubstituted, compound. We should like to report another such anomalous sytem, the fluoromethylnaphthalenes, and to offer alternative rationalizations of the observed phenomena.

Detailed structure–reactivity correlations have been carried out on the benzene analogues of the

[1]Current address: Department of Chemistry, University of Calgary, Calgary, Alberta T2N 1N4.

0008-4042/81/172642-08$01.00/0
©1981 National Research Council of Canada/Conseil national de recherches du Canada

Can. J. Chem. Downloaded from www.nrcresearchpress.com by 210.87.254.6 on 09/06/12
For personal use only.

Can. J. Chem. Downloaded from www.nrcresearchpress.com by 210.87.254.6 on 09/06/12
For personal use only.

fluoromethylnaphthalenes, the benzyl fluorides (8,9), but the fluoromethylnaphthalenes have only briefly been mentioned in the literature (10). ^{19}F nmr substituent chemical shift (SCS) values from the benzyl fluorides gave good correlations with substituent parameters and were very sensitive to the effect of a substituent, but the sign of the response was opposite to that observed in fluorobenzenes (1), fluoronaphthalenes (11), fluorobiphenyls (12), and fluoroterphenyls (12).

Experimental

The syntheses of the substituted fluoromethylnaphthalenes are described in the previous paper (13). ^{19}F spectra were recorded on a Varian HA-100 spectrometer operating at 94.08 MHz in frequency sweep mode and on a Varian HA-60-IL spectrometer operating at a frequency of 56.45 MHz in frequency sweep mode at a probe temperature of 27.5±1°C. External hexafluorobenzene and trichlorofluoromethane respectively were used as lock and reference peaks. To avoid solvent effects on the chemical shifts as far as possible, measurements of ^{19}F substituent chemical shifts were carried out on carbon tetrachloride solutions containing 8% by weight substituted fluoromethylnaphthalene and 4% by weight 1-fluoromethylnaphthalene. The carbon tetrachloride used was Fisher "Spectranalyzed" and was not purified further before use. The substituent chemical shifts were measured directly from the spectra of these solutions as the distance between the positions of the central peaks of the two triplets. The substituent chemical shift, $\Delta\phi$, was considered to be a positive value if the signal due to the substituted derivative appeared at higher field than that due to the fluoromethylnaphthalene itself. The conditions of measurement of the fluorine substituent chemical shifts and the sign conventions correspond to those described by Béguin (8) for the benzyl fluorides; the sign convention used by Bromilow *et al.* (9) is opposite to this.

Resonance signals were integrated in order to assign signals to either the substituted or unsubstituted derivative and measurements were repeated on solutions containing 4% substituted fluoromethylnaphthalene and 6% 1-fluoromethylnaphthalene. This was done for two reasons: to determine if there were significant solvent shifts, and to confirm the signal assignments made on the criterion of spectral integration. More extensive dilution studies were subsequently carried out, which showed that solvent shift effects cancelled out if all measurements were made at the same concentrations.

The chemical shifts of 1-fluoromethylnaphthalene, 2-fluoromethylnaphthalene, and benzyl fluoride were recorded under the standardization conditions of Filipovich and Tiers (14) who reported a simplified, internally referenced procedure for determining and tabulating reliable fluorine nmr shielding values. They found trichlorofluoromethane to be an excellent solvent for fluorine compounds; at the same time the solvent was used as internal reference and lock. Chemical shifts were recorded on a 5% solution by weight of fluoromethylnaphthalene or benzyl fluoride in trichlorofluoromethane.

Results and Discussion

Fluoromethylnaphthalene ^{19}F nmr Parameters

The chemical shift values of the reference compounds measured under standard conditions are shown in Table 1. ^{19}F nuclear magnetic resonance substituent chemical shifts measured at 94.08 MHz and 56.45 MHz are shown in Table 2. The most obvious point to note from these data is that the direction of the shift is the same as in the benzyl fluorides and opposite to that of the fluorobenzenes and fluoronaphthalenes: an inverse SCS dependence.

TABLE 1. Chemical shift values for reference compounds[a]

Compound	ϕ_0[b]	Reference
1-Fluoromethylnaphthalene	208.7	This study
	209.2	10
2-Fluoromethylnaphthalene	209.2	This study
	209.4	10
Benzyl fluoride	211.0	This study
	205.5[c]	9
	211.3	8

[a]Measured under standard conditions (14).
[b]Measured in ppm relative to CCl_3F.
[c]93.50 ppm upfield from tetrachlorotetrafluorocyclobutane and converted to $CFCl_3$ as a reference according to Emsley and Phillips (15).

In a bisfluoromethyl substituted naphthalene it is possible to view either fluoromethyl group as substituent or side-chain probe. Thus the 3α-derivative is also a 4β-bisfluoromethylnaphthalene.

The β-CH_2F probe measured in 2-fluoromethylnaphthalene resonates at higher field than the α-CH_2F of 1-fluoromethylnaphthalene. The difference is +14.5 Hz, at 56 MHz, or +0.26 ppm (+0.28 ppm for the mean $\Delta\phi$), a considerable shift. Distinct groups of triplets for the 1,3-bis CH_2F compound would therefore be expected. However, the observed shifts for each CH_2F group are similar at 56 MHz, one triplet appears 72.5 Hz towards higher field than the standard, the other triplet at 70.5 Hz, and at 94 MHz the two triplets are superimposed and cannot be resolved. The 56 MHz values correspond to $\Delta\phi$ values of +1.28 and +1.25 respectively. Clearly, in 1,3-bisfluoromethylnaphthalene the substituent chemical shift of the 3-CH_2F substituent acting on the α-CH_2F probe is greater than the substituent chemical shift of the 4-CH_2F substituent acting on the β-CH_2F probe, the difference between the substituent chemical shifts being 0.28 (mean value).

For the β-CH_2F group regarded as a functional group in 1,3-bisfluoromethylnaphthalene the (mean) measured substituent chemical shift (from 1-fluoromethylnaphthalene) is +1.25. Of this, +0.28 is attributed to the fluoromethyl probe being located in the β- rather than the α-position, and the remainder (1.25–0.28 = 0.97) is therefore attrib-

TABLE 2. ^{19}F SCS[a] and σ values for 3- and 4-substituted fluoromethylnaphthalenes

Substituent	$\Delta\phi^{b,c}$	$\Delta\phi^{b,d}$	$\Delta\phi^{e}$	σ^{f}	$\bar{\sigma}^{g}$	$\sigma-\bar{\sigma}$
4-F	−2.81	−2.86	−2.84	0.06	−0.17	+0.23
4-CH_3	−2.51	−2.57	−2.55	−0.17	−0.14	−0.03
4-CH_2OCH_3	−0.19	−0.28	−0.25		+0.09	
3-$COOCH_3$	−0.07	−0.15	−0.09	0.37	+0.11	+0.26
3-$COOC_2H_5$	−0.13	−0.07	−0.14	0.37	+0.11	+0.26
3-CH_3	—	+0.13	+0.15	−0.07	+0.14	−0.21
4-Cl	+0.25	+0.25	+0.23	0.23	+0.14	+0.09
3-$COCH_3$	+0.30	+0.31	+0.31	0.38	+0.15	+0.23
4-Br	+0.76	+0.82	+0.77	0.23	+0.20	+0.03
3-CH_2F	+1.25	+1.25	+1.23		+0.25	
3-CH_2F[h]	+1.25	+1.28	+1.25			
4-CH_2F	+1.30	+1.31	+1.31		+0.26	
3-Br	+2.89	+2.96	+2.92	0.39	+0.42	−0.03
3-NO_2	—	+3.42	+3.36	0.71	+0.47	+0.24
3-CN	+3.95	+3.98	+4.01	0.62	+0.54	+0.08
4-$COOC_2H_5$	+5.56	+5.65	+5.61	0.45	+0.70	−0.25
4-$COCH_3$	+5.67	+5.76	+5.72	0.50	+0.71	−0.21
4-$COOCH_3$	+5.89	+6.05	+5.95	0.45	+0.74	−0.29
4-$COCH_2F$	+6.70	+6.87	+6.80		+0.83	
4-$COCH_2F$[i]	—	+15.85	+15.47			
4-CN	+7.10	+7.09	+7.05	0.66	+0.85	−0.19
4-NO_2	—	+7.46	+7.29	0.78	+0.88	−0.10
2-CH_2F[j]	+0.30	+0.26	+0.28			

[a]SCS (substituent chemical shift): a positive value implies a signal upfield from the unsubstituted compound, $\Delta\phi \equiv -\delta_F$ (1-fluoromethylnaphthalene reference).
[b]Measured on solutions containing 4% by weight unsubstituted fluoromethylnaphthalene and 8% by weight substituted fluoromethylnaphthalene.
[c]In ppm measured at 94.08 MHz.
[d]In ppm measured at 56.45 MHz.
[e]Mean of values measured at 56.45 MHz and 94.08 MHz on solutions containing 4% unsubstituted fluoromethylnaphthalene and 8% of substituted fluoromethylnaphthalene and at 56.45 MHz on solutions containing 6% fluoromethylnaphthalene and 4% substituted fluoromethylnaphthalene.
[f]From ref. 18.
[g]$\bar{\sigma} = (\Delta\phi + 1.16)/9.65$ (see text).
[h]Shift from the β-CH_2F group of 1,3-bisfluoromethylnaphthalene.
[i]Shift for the $COCH_2F$ group.
[j]$-\delta_F$ for 2-fluoromethylnaphthalene (1-fluoromethylnaphthalene reference).

uted to the substituent effect of the 4-CH_2F group acting on the β-CH_2F probe. We may compare this 4β effect (0.97 ppm) with that of 4α (1.31 ppm) and 3α (1.23 ppm). The response of the ^{19}F nmr signal to the substituent effect of the CH_2F function is greater when the functional centre or probe is situated in the α-position in the naphthalene. A similar observation was noted by Wells *et al.* (16) regarding the data of Adcock and Dewar (17) concerning the ^{19}F shifts of substituted fluoronaphthalenes and also for data concerning naphthalene reactivities.

It is impossible to assign the two signals of 1,3-bisfluoromethylnaphthalene on chemical shift criteria and so a comparison of various coupling constants was made. The J_{HF} coupling constants of 1-fluoromethylnaphthalene and 2-fluoromethylnaphthalene are both 48.0 Hz and so J_{HF} appears to be independent of position. For the two signals due to CH_2F in 1,3-bisfluoromethylnaphthalene to appear so close to one another, the 3α (i.e. considering the 3-CH_2F function as the substituent) orientation must be more sensitive to the influence of the substituent than the 4β orientation (the 4-CH_2F function being the substituent in this case). The value of J appeared to correlate with the substituent chemical shift, being larger for negative shifts and smaller as the shifts became more positive. Hence the CH_2F group with the larger J value was the one which had suffered a smaller substituent chemical shift effect, i.e. the β-CH_2F group.

This assignment is supported by the J_{HF} values measured from ^1H nmr spectra. The chemical shifts for these two functions are readily distinguishable in the proton nmr spectrum. The J_{HF} value assigned to the α-CH_2F in the ^1H nmr spectrum was smaller, in agreement with the assignment arrived at above.

Comparison of Fluoromethylnaphthalene and Benzyl Fluoride SCS Values

Correlation of the fluoromethylnaphthalene SCS values with the benzyl fluoride values gives a good linear relationship with slope = 0.885, intercept =

Can. J. Chem. Downloaded from www.nrcresearchpress.com by 210.87.254.6 on 09/06/12
For personal use only.

Can. J. Chem. Downloaded from www.nrcresearchpress.com by 210.87.254.6 on 09/06/12
For personal use only.

-0.13, correlation coefficient $r = 0.992$, standard deviation (SD) = 0.49, and standard deviation of the slope = 0.045. Thus substituent effects in the naphthalene series parallel those in the benzene series at a slightly reduced sensitivity. The largest individual deviation is that for the 3-nitro substituent for which the naphthalene SCS value of +3.36 is 1.02 less than the value predicted by the correlation relatonship.

Single Substituent-parameter Correlations

The correlation of the fluoromethylnaphthalene SCS values with Hammett substituent constants (18) is poor with $\rho = 9.65$, intercept = -1.16, $r = 0.815$, SD = 1.95, SD_ρ (standard deviation of rho) = 1.77. The poor correlation is indicated both by the low value of the correlation coefficient and also by the marked deviation for the hydrogen substituent, i.e., the large value of the intercept. Had the equation been constrained to zero intercept, an even lower correlation coefficient would have been obtained. Effective sigma values ($\bar{\sigma}$) were evaluated from the relationship $\bar{\sigma} = (\Delta\phi + 1.16)/9.65$ and are shown in Table 2 together with σ values and values of $\sigma - \bar{\sigma}$. A positive value of $\sigma - \bar{\sigma}$ indicates that the substituent appears to be more electron-donating or less electron-withdrawing than the Hammett substituent constant would predict and vice versa. It is apparent from Table 2 that conjugatively electron-withdrawing (−M) substituents have much weaker effects in the 3-position (mean σ deviation +0.21) and much stronger effects in the 4-position (mean σ deviation -0.21) than expected. The 4-fluoro substituent is also noticeably deviant to the extent that it exerts an electron-donating effect rather than the expected electron-withdrawing effect. Béguin reported a good correlation of benzyl fluoride SCS values with σ^+ values (8). Using his data we obtained $\rho = 9.92$, $r = 0.982$. However, this result is of questionable significance since (*i*) several of the more strikingly deviant substituents in the naphthalene correlations are not represented in Béguin's data set; (*ii*) the striking difference in the behaviour of the *conjugatively electron-withdrawing* substituents in the 3- and 4-positions of naphthalene cannot be accounted for in terms of differences between the σ and σ^+ scales for those substituents; (*iii*) the excellent naphthalene–benzene correlation discussed above implies that the benzene series would exhibit similar deviations to those of the naphthalene series; (*iv*) we also observed a better correlation of the naphthalene data with σ^+ values than with σ, viz. $\rho = 9.34$, $r = 0.916$; however, this correlation necessarily excludes the data for some of the substituents which are particularly deviant in the σ correlation.

Dual Substituent-parameter Correlations

The fluoromethylnaphthalene SCS values were correlated with the sets of resonance and polar effect parameters ($\sigma_{R(BA)}$, σ_I; σ_R^0, σ_I; σ_R^+, σ_I; $\sigma_{R(A)}^-$, σ_I) described by Ehrenson *et al.* (7), and with the resonance and inductive parameters (*F*, *R*) of Swain and Lupton (19).[2] The correlations were carried out by performing a multiple linear regression and, in contrast to the treatment by Ehrenson *et al.* (7), the fitting of the data was not constrained to zero intercept behaviour. By allowing a free fit and by not restraining the equation to zero intercept behaviour, the magnitude of the intercept provides another measure of the "goodness of fit" of the data. The results of the correlations are shown in Table 3. Important parameters derived from these analyses are the ρ_I and ρ_R parameters and particularly their signs and magnitudes. Insight is also gained into the nature of the interaction between the probe and the substituent by observing which set of the four different resonance parameters in the DSP analysis best describes the observed behaviour.

Values of σ_R and σ_I for the CH_2F and CH_2OCH_3 substituents are not listed in the compilation of Taft and co-workers (7). However, values for these substituents were reported by Sheppard (20) and the effect of including the data for these substituents in the correlations was investigated. As shown by the initial entries in Table 3 a slightly poorer correlation was obtained when these data were included. For the 4-substituted 1-fluoromethylnaphthalenes the best correlation was obtained using the *F* and *R* parameters, with that involving the $\sigma_{R(BA)}$, σ_I set yielding only slightly poorer results. These parameter sets also gave the best correlations for the *p*-substituted benzylfluorides. It is to be noted that the parameters allowing for enhanced resonance interaction, σ_R^+ and $\sigma_{R(A)}^-$, gave somewhat poorer correlations (recalling that both *R* and INT should be taken into account) in both cases, i.e. Ar–Y (aromatic-ring and side-chain) resonance interaction is apparently not significant. This reinforces the conclusion stated above that little significance should be attributed to Béguin's claim of a good correlation of the benzyl fluoride data with σ^+. The blending factor, $\lambda = \rho_R/\rho_I$, for the $\sigma_{R(BA)}$, σ_I correlations is 2.00 for the 4-substituted naphthalenes and 1.67 for the *p*-substituted benzenes. This indicates that the 4- and p-substituents exert enhanced X–Ar resonance effects (i.e. between substituent and aromatic ring)

[2]The reaction series data do not encompass a complete basis set as defined by Ehrenson, *et al.* (7). The data are substantially representative of such a basis set.

Can. J. Chem. Downloaded from www.nrcresearchpress.com by 210.87.254.6 on 09/06/12
For personal use only.

TABLE 3. Multiple linear regression of ^{19}F SCS for 3-substituted 1-fluoromethylnaphthalenes, 4-substituted 1-fluoromethylnaphthalenes, and *m*- and *p*-benzyl fluorides[a]

Series	Parameters	n[b]	R[c]	ρ_I	ρ_R	INT[d]	SD[e]
4-X	$\sigma_{R(BA)},\sigma_I$	10	0.993	8.48	16.91	0.25	0.53
4-X[f]	$\sigma_{R(BA)},\sigma_I$	11	0.993	8.32	16.91	0.34	0.51
4-X[g]	$\sigma_{R(BA)},\sigma_I$	12	0.992	8.03	16.85	0.47	0.51
4-X	σ_R^0,σ_I	10	0.991	7.87	18.91	0.31	0.60
4-X	σ_R^+,σ_I	10	0.992	8.02	13.21	0.97	0.58
4-X	$\sigma_{\bar{R}(A)},\sigma_I$	10	0.986	5.87	10.76	−0.32	0.77
4-X	F,R[h]	10	0.995	4.32	17.73	0.28	0.46
3-X	$\sigma_{R(BA)},\sigma_I$	8	0.899	7.08	−5.34	−0.61	0.92
3-X	σ_R^0,σ_I	8	0.899	7.08	−5.34	−0.61	0.92
3-X	σ_R^+,σ_I	8	0.902	7.00	−3.60	−0.76	0.89
3-X	$\sigma_{\bar{R}(A)},\sigma_I$	8	0.908	7.67	−3.14	−0.43	0.88
3-X	F,R	8	0.829	4.24	−4.75	−0.65	1.17
p-X	$\sigma_{R(BA)},\sigma_I$	8	0.998	9.87	16.51	−0.34	0.35
p-X	σ_R^0,σ_I	8	0.990	9.25	20.41	−0.17	0.87
p-X	σ_R^+,σ_I	8	0.992	9.35	11.23	0.26	0.80
p-X	$\sigma_{\bar{R}(A)},\sigma_I$	8	0.962	6.94	13.04	0.96	1.74
p-X	F,R	8	0.998	4.98	18.92	0.00	0.39
m-X	$\sigma_{R(BA)},\sigma_I$	7	0.996	7.60	2.18	0.09	0.26
m-X	σ_R^0,σ_I	7	0.996	7.48	2.75	0.12	0.25
m-X	σ_R^+,σ_I	7	0.993	7.54	1.45	0.16	0.32
m-X	$\sigma_{\bar{R}(A)},\sigma_I$	7	0.994	7.14	1.80	0.02	0.31
m-X	F,R	7	0.990	4.64	2.16	0.13	0.39

[a] Fluoromethylnaphthalene data measured at 94.08 MHz and 56.45 MHz; benzyl fluoride data from ref. 8.
[b] n: number of substituents in correlation.
[c] R: multiple correlation coefficient.
[d] INT: intercept.
[e] SD: standard deviation.
[f] Includes data for CH_2F substituent using σ_R and σ_I from ref. 20.
[g] Using CH_2F and CH_2OCH_3 data; values of σ_I and σ_R from ref. 20.
[h] Swain and Lupton's parameters (19); these are not on the same scale as the σ values.

as compared with their effects on benzoic acid ionization.[3] For the *m*-substituted benzyl fluorides all of the correlations were excellent, marginally the best being that with the $\sigma_{R(BA)}$, σ_I parameters. The 3-substituted 1-fluoromethylnaphthalenes were distinctly less well correlated. The marginally best correlation was that involving the $\sigma_{\bar{R}(A)}$, σ_I parameters. It is more noteworthy that for the 3-substituted 1-fluoromethylnaphthalene correlations ρ_R is negative whereas all other ρ values, including in particular ρ_R for the *m*-substituted benzyl fluorides, are positive. It is not clear that this represents a real difference between the naphthalene and benzene series since the methoxycarbonyl and ethoxycarbonyl substituents, which were apparently electron-donating (see discussion above) in the 3-substituted naphthalene series, were not investigated in the benzene series. However, some support for the reality of the difference is provided by the fact that in the correlation of the SCS values of the fluoromethylnaphthalenes with those of the benzylfluorides the largest deviation, as mentioned above, was that for the 3-nitro substituent, which was apparently much less electron-withdrawing in the naphthalene series, and the only other −M 3-substituent common to both series, cyano, also exhibited a smaller deviation in the same direction. What is clear from Table 3 is that, whatever the sign of the ρ_R for the *m*- or 3-substituted series, $|\lambda|$ is much smaller than for the *p*- or 4-substituted series; e.g. for the $\sigma_{R(BA)}$, σ_I correlations, λ is −.0.75 for the 3-series and +0.29 for the *m*-series. This is of course in accord with general observations of substituent effects: resonance effects are much smaller for *meta*-substituents than for *para*-substituents.

[3] Because of the use of some different substituents in the two series we hesitate to attribute any significance to the difference between the two λ values; the difference is in the direction consistent with greater relative importance of resonance effects in the 4-substituted naphthalene system.

Discussion and Conclusions

The nature of the nmr response of a ^{19}F probe to the effect of a substituent has long been the subject of discussion. More recently, a great deal of evidence has accrued from model aromatic systems to suggest that in general the main polar effect is field-induced polarization of the aromatic π electron system (21–29). Various analyses of the magnitude of these effects has been proposed, and the more successful of these (22, 23, 29) include use of the Buckingham (30) equation:

$$\Delta\phi = A(\Delta E_z)$$

where ΔE_z is the difference in electric field components acting along the C—F bonds in the substituted and unsubstituted compounds.

No treatments have been entirely convincing in identifying the nature and origin of the inverse substituent dependence of the ^{19}F chemical shift in the systems where this phenomenon has been observed (8–10, 31–35). Anderson and Stock suggested that in the series of 4-substituted bicyclo-[2.2.2.]octyl-1-fluorides substituent-induced structural changes resulted in changes in carbon–fluorine bond order arising from the interaction between the endocylic carbon–carbon orbitals and nonbonding orbitals on fluorine and these were the cause of the inverse SCS response (31, 32). CNDO/2 calculations do not provide an explanation for the inverse substituent dependence of the ^{19}F response in the 4-substituted bicyclo[2.2.2.]-octyl-1-fluorides (36) and do not support the view that π-electronic effects on fluorine are responsible for the phenomenon (35). In 1974 Adcock *et al.* (10) stated that the inverse chemical shift phenomenon was not "explicable in terms of (then) current theoretical treatments of fluorine chemical shifts". Subsequently Adcock and Khor (35) attempted to relate differences in chemical shifts in the fluorobicyclooctane and 1-fluoro-4-phenylbicyclooctane series to field effect differences. Their calculations indicated that field effects alone could not account for the differences and that additional factors were required. More recently Adcock and Abeywickrema (37) reported data derived from 6- and 7-substituted 1-fluoro-4-methyl-1,4-ethano-1,2,3,4-tetrahydronaphthalenes. In these systems the C—F bond is constrained to the nodal plane of the aromatic π-system, thus precluding the possibility of fluorine hyperconjugative interaction of the C—F bond and the π electrons of the aromatic ring. Unlike the cases of the benzyl fluorides and the fluoromethylnaphthalenes, which bear close resemblance to these systems in terms of the relative positions of substituent and fluorine probe, the induced shift is in the "normal" direction and is very small. In benzyl fluorides and fluoromethylnaphthalenes carbon–fluorine hyperconjugation results in polarization of the σ electrons in the $2p_y$ orbital of fluorine, but not the π electrons in the $2p_z$ and $2p_x$ orbitals. They concluded that the overall SCS depends not only on the total fluorine charge density, but also on the symmetry of its distribution, the latter being affected by hyperconjugation. Béguin proposed a similar explanation for the inverse SCS of benzyl fluorides (and analogous compounds) (8). From Hückel molecular orbital calculations he determined that the bond order between aromatic and ring CH_2F group increased in going from benzyl fluoride to *p*-methoxybenzyl fluoride. In contrast the C—F bond order decreased in going from fluorobenzene to 4-fluoroanisole. He proposed that this was the factor which accounted for the different signs of the SCS in the two series.

A striking illustration of the complex relationship between the electron distribution on fluorine and the ^{19}F chemical shift was provided by Bromilow *et al.* (9). They measured both ^{13}C and ^{19}F chemical shifts in a series of substituted benzyl fluorides. Both the CH_2 carbon and the fluorine exhibited inverse SCS effects. The *ipso* carbon exhibited a normal effect. However, electron density calculations showed that substituent-induced changes in electron density at the *ipso* carbon paralleled those at fluorine whereas the electron density at the benzylic carbon exhibited a remarkable variation: inductive electron-withdrawing substituents reduced the electron density whereas resonance electron-withdrawing substituents increased the electron density at this site. The authors refrained from offering an explanation at these phenomena but were able to dismiss other explanations advanced for inverse fluorine SCS effects, such as substituent induced structural distortion.

Theory developed to explain the screening of a fluorine nucleus relates the chemical shift to a number of terms pertaining to the electron distribution around the fluorine (38–40). It is evident that this relationship does not approximate to a relationship involving only the total electron density at fluorine.

We should like to offer two alternative explanations for the inverse SCS effect. Our models, like the hyperconjugative model, would be expected to show some conformational dependence.

Sheppard (33), in rationalizing the +R effect of fluoralkyl groups, proposed an interaction of the *p*-electrons of the fluorine atoms with the π-system of the aromatic ring at either the *ipso* or *ortho* positions. The so-called "fluorine p–π interaction" causes significant return of electron density to the ring, and this return is more effective to the *meta* position than the *para*. Molecular orbital calculations support the feasibility of the feedback through the π-system. The net charge density in benzotrifluoride is calculated to alternate so that the *ortho* and *para* positions appear more deficient in charge density than the *meta* position. Increased electron density at the benzylic carbon reflecting a positive Ar—CH_2 inductive effect would allow

Can. J. Chem. Downloaded from www.nrcresearchpress.com by 210.87.254.6 on 09/06/12
For personal use only.

Can. J. Chem. Downloaded from www.nrcresearchpress.com by 210.87.254.6 on 09/06/12
For personal use only.

increased feedback of the fluorine p electrons to the ring. Alternatively, an Ar—CH_2 resonance effect would, through carbon–fluorine hyperconjugation, increase the electron density at the fluorine atom itself. This charge is centred on $2p_y(\sigma)$ orbitals, rather than $2p_z(\pi)$ orbitals. The electron return via $p-\pi$ interaction would reduce the charge density in the $2p_z(\pi)$ orbitals on fluorine. The π electron density on fluorine rather than total charge density is important in shift correlations. Thus, electron-donating substituents which increase the overall charge density at fluorine do so by increasing the σ charge density which is partially offset by a decrease in π charge density and it is the decrease in π charge density which is of major importance in determining the chemical shift. The signal therefore appears at lower field.

Another possible mechanism for the inversion of the sign of the response of the ^{19}F nmr SCS may arise as a result of hydrogen bonding between the fluorine and the proton in the 2-position on the naphthalene ring (the *ortho* proton). Hydrogen bonding in HF in the condensed phase has been shown to induce a shift in the fluoride resonance towards lower field by 20.5 ppm (41). Similarly Hagne and Reeves (42) showed a downfield shift due to hydrogen bonding in the BF_4^- ion. We suggest that in 1-fluoromethylnaphthalene itself the fluorine appears at an unusually low field position as a result of deshielding through hydrogen-bonding. Introduction of an electron-withdrawing substituent causes a relative increase in the effective electronegativity of the methylene carbon which shortens the C—F bond and thereby reduces the deshielding hydrogen-bonding influence.

Schaefer and co-workers (43–45) have carried out studies in conformational analysis and coupling constants in methyl substituted benzenes (43), in benzyl fluoride (44), and in benzotrifluoride, benzal fluoride, and benzyl fluoride derivatives (45). These studies showed a conformational preference of the C—F bond for the benzene plane by about 260–300 cal/mol in the case of 3,5-dichlorobenzyl fluoride. This value was in close agreement with the results from *ab initio* and MINDO/3 molecular orbital calculations. It is interesting to note that in the same analysis, for the conformation in which the C—F bond lies in a plane perpendicular to the plane of the ring the C—C—F bond angle reduces to 107.2° and the C—C—H angles increase to 116.1°, suggesting conjugation between the C—F bond or the fluorine atom with the π-electrons of the ring. The preferred conformation, however, is one in which maximum hydrogen-bonding would occur.

TABLE 4. Chemical shift temperature dependence at 56.45 MHz

Substituent	Temperature °C	Substituent chemical shift, $\Delta\phi$
4-CH_2OCH_3	+40.0	−14.0 Hz
	+27.5	−14.0 Hz
	+10.0	−12.2 Hz
	0.0	−11.0 Hz
	−10.0	−10.6 Hz
	−20.0	−10.4 Hz
	−30.0	−8.4 Hz
	−40.0	−7.4 Hz
4-$COOCH_3$	+50.0	+305.0 Hz
	+27.5	+332.5 Hz
	+10.0	+352.0 Hz
	0.0	+370.0 Hz
	−10.0	+384.0 Hz
	−20.0	+398.0 Hz
	−30.0	+416.0 Hz
1-CH_2F[a]	+50.0	11797.0 Hz
	+27.5	11780.0 Hz
	+10.0	11766.0 Hz
	0.0	11752.0 Hz
	−10.0	11747.0 Hz
	−20.0	11738.0 Hz
	−30.0	11725.0 Hz
	−40.0	11712.0 Hz

[a]1-Fluoromethylnaphthalene alone i.e. ϕ and not $\Delta\phi$ is recorded.

That the response of the ^{19}F SCS to the substituent is conformationally dependent is suggested by a series of temperature dependent substituent chemical shift studies. The results for three compounds are shown in Table 4. 1-Fluoromethylnaphthalene shows a shift to higher field with increasing temperature reflecting a decrease in the population of the deshielding conformation (by any of the conformation dependent mechanisms). The substituent chemical shift of the ester group is markedly temperature dependent and is smaller at higher temperatures. Brownlee and Craik (46) have investigated the temperature dependence of p-substituted benzyl fluorides and have explained their observations in terms of conformational effects.

Acknowledgements

We are grateful to the National Research Council for financial support, and to the University of Victoria for the award of a University of Victoria Post-Graduate Fellowship to one of us (E.A.D.).

1. H. S. GUTOWSKY, D. W. MCCALL, D. MCGARVEY, and L. H. MEYER. J. Am. Chem. Soc. **74**, 4809 (1952).
2. R. W. TAFT, JR. J. Am. Chem. Soc. **79**, 1045 (1957).
3. R. W. TAFT, JR., E. PRICE, I. R. FOX, I. C. LEWIS, K. K. ANDERSEN, and G. T. DAVIES. J. Am. Chem. Soc. **85**, 709 (1963).
4. R. W. TAFT, JR., E. PRICE, I. R. FOX, I. C. LEWIS, K. K.

ANDERSEN, and G. T. DAVIES. J. Am. Chem. Soc. **85**, 3146 (1963).
5. R. W. TAFT, JR. and J. W. RAKSHYS. J. Am. Chem. Soc. **87**, 4387 (1965).
6. R. W. TAFT, JR. J. Phys. Chem. **64**, 1805 (1960).
7. S. EHRENSON, R. T. C. BROWNLEE, and R. W. TAFT, JR. *In* Progress in physical organic chemistry. Vol. 10. *Edited by* A. Streitwieser and R. W. Taft, Jr. Interscience, New York. 1973. p. 1.
8. C. BÉGUIN. Bull. Soc. Chim. Fr. 4214 (1967).
9. J. BROMILOW, R. T. C. BROWNLEE, and A. V. PAGE. Tetrahedron Lett. 3055 (1976).
10. W. ADCOCK, M. J. S. DEWAR, R. GOLDEN, and M. A. ZEB. J. Am. Chem. Soc. **97**, 2198 (1975).
11. W. ADCOCK, M. J. S. DEWAR, and Y. TAKEUCHI. J. Am. Chem. Soc. **89**, 379 (1967); **89**, 386, (1967); **89**, 390 (1967).
12. M. J. S. DEWAR and A. P. MARCHAND. J. Am. Chem. Soc. **88**, 3318 (1966).
13. E. A. DIXON, A. FISCHER, and F. P. ROBINSON. Can. J. Chem. **59**, preceding paper (1981).
14. G. FILIPOVICH and G. V. D. TIERS. J. Phys. Chem. **63**, 761 (1959).
15. J. W. EMSLEY and L. PHILLIPS. *In* Progress in N.M.R. Vol. 7. *Edited by* J. W. Emsley, J. Feeney, and L. H. Sutcliffe. Pergamon Press, Oxford. 1971. p. 504.
16. P. R. WELLS, S. EHRENSON, and R. W. TAFT, JR. *In* Progress in physical organic chemistry. Vol. 6. *Edited by* A. Streitwieser and R. W. Taft, Jr. Interscience, New York. 1968.
17. W. ADCOCK and M. J. S. DEWAR. J. Am. Chem. Soc. **89**, 379 (1967).
18. D. H. MCDANIEL and H. C. BROWN. J. Org. Chem. **23**, 420 (1958).
19. C. G. SWAIN and E. C. LUPTON, JR. J. Am. Chem. Soc. **90**, 4328 (1968).
20. W. A. SHEPPARD. Tetrahedron, 945 (1971).
21. W. F. REYNOLDS and G. K. HAMER. J. Am. Chem. Soc. **98**, 7296 (1976).
22. W. ADCOCK and T. C. KHOR. Tetrahedron Lett. 2063 (1976).
23. W. ADCOCK and T. C. KHOR. J. Am. Chem. Soc. **100**, 7799 (1978).
24. W. F. REYNOLDS. Tetrahedron Lett. 675 (1977).
25. D. R. EWING, S. SOTHEESWARAN, and K. J. TOYNE. Tetrahedron Lett. 2041 (1977).
26. D. F. EWING and K. J. TOYNE. J. Chem. Soc. Perkin Trans. II, 243 (1979).
27. W. KITCHING, M. BULLPITT, D. GARTSHORE, W. ADCOCK, T. C. KHOR, D. DODDRELL, and I. D. RAE. J. Org. Chem. **42**, 2411 (1979).
28. D. F. EWING. Org. Magn. Reson. **12**, 499 (1979).
29. W. F. REYNOLDS, V. G. GIBB, and N. PLAVAC. Can. J. Chem. **58**, 839 (1980).
30. A. D. BUCKINGHAM. Can. J. Chem. **38**, 300 (1960).
31. G. W. ANDERSON and L. M. STOCK. J. Am. Chem. Soc. **90**, 212 (1968).
32. G. W. ANDERSON and L. M. STOCK. J. Am. Chem. Soc. **91**, 6804 (1969).
33. W. A. SHEPPARD. J. Am. Chem. Soc. **87**, 2410 (1965).
34. C. L. BUMGARDNER. J. Org. Chem. **28**, 3225 (1963).
35. W. ADCOCK and T. C. KHOR. J. Org. Chem. **42**, 218 (1977).
36. R. T. C. BROWNLEE and R. W. TAFT, JR. J. Am. Chem. Soc. **92**, 7077 (1970).
37. W. ADCOCK and A. N. ABEYWICKREMA. Tetrahedron Lett. 1809 (1979).
38. M. KARPLUS and T. DAS. J. Chem. Phys. **34**, 1683 (1962).
39. F. PROSSER and L. GOODMAN. J. Chem. Phys. **38**, 374 (1963).
40. M. J. S. DEWAR and J. KELEMAN. J. Chem. Phys. **49**, 499 (1968).
41. C. D. CORNWELL and D. K. HINDERMANN. J. Chem. Phys. **48**, 2017 (1968).
42. R. HAGNE and L. W. REEVES. J. Phys. Chem. **70**, 2753 (1966).
43. R. WASYLISHEN and T. SCHAEFER. Can. J. Chem. **50**, 1852 (1972).
44. T. SCHAEFER, J. B. ROWBOTHAM, W. J. PARR, K. MARAT, and A. F. JANZEN. Can. J. Chem. **54**, 1322 (1976).
45. T. SCHAEFFER, W. NIEMCZURA, C.-M. WONG, and K. MARAT. Can. J. Chem. **57**, 807 (1979).
46. R. T. C. BROWNLEE and D. J. CRAIK. Tetrahedron Lett. **21** (1980); 1681 (1980).

Can. J. Chem. Downloaded from www.nrcresearchpress.com by 210.87.254.6 on 09/06/12
For personal use only.

A photochemical approach to the synthesis of (±)-biotin

RALPH ALLEN WHITNEY
Department of Chemistry, Queen's University, Kingston, Ont., Canada K7L 3N6

Received March 31, 1981

RALPH ALLEN WHITNEY. Can. J. Chem. **59**, 2650 (1981).

A synthesis of (±)-biotin **1** based on a photochemical cycloaddition reaction of 1,3-diacetylimidazolin-2-one **3** is presented. Oxidative rearrangement of the cyclobutanol **5** has provided the key intermediate **6** having the necessary stereochemical features for elaboration of *n*-pentyl biotin **2**.

RALPH ALLEN WHITNEY. Can. J. Chem. **59**, 2650 (1981).

On présente une synthèse de la (±)-biotine **1** à partir de la réaction de cycloaddition photochimique de la diacétyl-1,3 imidazolinone-2 **3**. La transposition oxydante du cyclobutanol **5** fournit l'intermédiaire principal **6** avec les bonnes caractéristiques stéréochimiques nécessaires à l'élaboration de la *n*-pentyl biotine **2**.

[Traduit par le journal]

Can. J. Chem. Downloaded from www.nrcresearchpress.com by 210.87.254.42 on 09/06/12
For personal use only.

Increased interest in the role of biotin **1** in human nutrition and therapy (1) as well as its importance as a growth factor (2) has led to the development of numerous syntheses (3) in the past decade of this vitamin of the B-complex. Since total synthesis remains as yet the only major source of this compound, the development of new synthetic strategies continues to be of interest. The use of microbiological methods (4) for conversion of *n*-pentyl biotin **2** into biotin has made **2** an important intermediate for the production of biotin. The approach herein described deals with the synthesis of *n*-pentyl biotin via a photochemical reaction (5) of 1,3-diacetylimidazolin-2-one **3** as outlined in Scheme 1.

We have reported (5) that photolysis of **3** in the presence of enol ethers using acetone as solvent and sensitizer leads to high yields of [2+2] cycloaddition products. Using the readily available (6) trimethylsilyl enol ether **4** of heptanal (a mixture of (*E*)- and (*Z*)-isomers), the photolysis was carried out at room temperature under a nitrogen atmo-

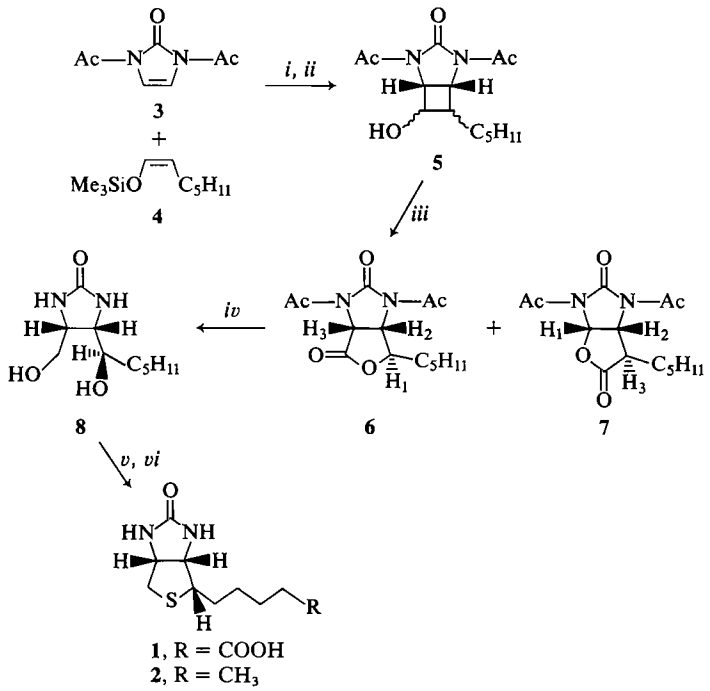

SCHEME 1. Reagents: (*i*) CH_3COCH_3, *hv*; (*ii*) CH_3COCH_3, H_2O, HCl; (*iii*) $RuCl_3$, H_2O, NaOCl, CCl_4; (*iv*) LiBr, $NaBH_4$ diglyme; (*v*) CH_3SO_2Cl, pyridine, −10°C; (*vi*) Na_2S, DMF, 95°C.

0008-4042/81/172650-04$01.00/0
©1981 National Research Council of Canada/Conseil national de recherches du Canada

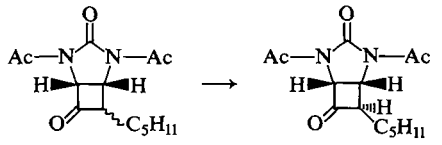

9 10

sphere with a medium pressure mercury lamp to give, after acid hydrolysis, the cyclobutanol **5** in 79% yield upon chromatographic purification. Due to the isomeric composition of the silyl enol ether and the possibility of *syn*- and *anti*-cycloaddition products, the cyclobutanol **5** consisted in principle of four diastereomeric compounds. We expected, however, that the two nitrogen atoms of the cyclic ureido moiety would be in a *cis* stereochemical relationship as desired in the synthetic target **2**. It was intended at this stage to oxidize the cyclobutanol to a cyclobutanone **9** with the anticipated epimerization of the *n*-pentyl group to an exocyclic configuration, as indicated in **10**, prior to Baeyer–Villiger oxidative rearrangement to the lactones **6** and/or **7**. Attempts at oxidation of the alcohol to a ketone using standard methods led repeatedly to complex product mixtures which gave no evidence of cyclobutanone formation. However, chromic acid oxidation (7) gave a low yield of a product identified as the lactone **7**. The regiochemical assignment of the structure was based on proton chemical shift data (8) while the stereochemical assignment was a consequence of proton coupling constants (J_{H_1,H_2} = 6.5 Hz; J_{H_2,H_3} = 1.0 Hz). It was presumed that the reaction was proceeding via a cyclobutanone hydrate **11** (X = H) with the oxidative rearrangement occurring through formation of a chromate ester **11** (X = CrO_3H). Furthermore this suggested that variation of the nature of X might alter the regiochemistry of the rearrangement process. Indeed our expectations were fulfilled when the cyclobutanol **5** was treated with ruthenium tetroxide (9) in carbon tetrachloride in the presence of aqueous hypochlorite solution, the reaction proceeding via the hypochlorite **11** (X = Cl) (10). Examination of the nmr spectrum of the crude reaction product indicated the presence of the lactones **6** and **7** in approximately equal amounts, with purification by column chromatography affording the lactone **6** in a low yield (18%). Again the regiochemistry of the rearrangement product was assigned on the basis of proton chemical shift data (8) and the stereochemistry on the basis of proton coupling constants (J_{H_1,H_2} = 8.9 Hz; J_{H_2,H_3} = 0.9 Hz). It was subsequently established that 1,3-diacetylimidazolin-2-one **3** could be converted to the lactone **6**, without purification of intermediates, in 10% overall yield with the desired product being isolated by recrystallization.

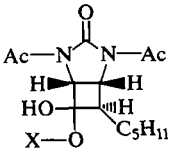

11

Definitive proof of the structure of **6** was provided by facile conversion to *n*-pentyl biotin. Reduction with lithium borohydride in diglyme (12) at room temperature gave the diol **7** as a crystalline material in 78% yield. This was converted, by analogy with literature procedures (3(*i*), (*o*)), to the corresponding bis-mesylate (which was not purified) and then to **2** in 32% yield by treatment with purified sodium sulfide in dimethylformamide at 95°C followed by chromatographic purification. This sample was identical in all respects to an authentic sample of *n*-pentyl biotin.

As stated previously, *n*-pentyl biotin has been converted microbiologically (4) to biotin. Development of this strategy to a totally synthetic route to biotin is, however, under investigation.

Experimental

General

Melting points were determined on a Fisher-Johns or a Thomas Hoover melting point apparatus and are uncorrected. Infrared spectra were recorded on either Perkin Elmer 528 or Acculab 6 instruments. Proton and carbon magnetic resonance spectra were recorded on Varian EM360, Varian HA 100, Bruker HX60, or Bruker CXP 200 spectrometers. Chemical shifts are reported in δ values relative to tetramethylsilane. Column chromatography was performed with Merck 60 mesh silica gel while high performance liquid chromatography was performed on Merck Lobar columns. Unless stated, sodium sulfate was used as drying agent for organic solutions. Microanalyses were performed by Guelph Analytical Laboratories, Guelph, Ontario.

6-Hydroxy-7-pentyl-2,4-diacetyl-2,4-diazabicyclo [3.2.0]heptan-3-one **5**

A solution of 1,3-diacetylimidozalin-2-one (3.0 g, 17.6 mmol) (11) in acetone (250 mL) was placed in a standard immersion well photochemical reactor,[1] then deoxygenated with a stream of nitrogen gas for 0.5 h. Heptanal trimethylsilyl enol ether (22.8 g, 121 mmol) (6) was added and the reaction mixture was photolyzed for 4.5 h with a 450 W Hanovia lamp through a Corex filter. The solvent was then removed by rotary evaporation under reduced pressure. Excess silyl enol ether was removed by Kugelrohr distillation (60°C, 0.5 Torr) and the residue was dissolved in acetone (50 mL) and water (5 mL), cooled in an ice bath, and acidified with dilute aqueous HCl (4 drops). After stirring for 10 h the solution was diluted with methylene chloride

[1]Ace Glass Incorporated, Vineland, NJ 08360.

Can. J. Chem. Downloaded from www.nrcresearchpress.com by 210.87.254.42 on 09/06/12
For personal use only.

Can. J. Chem. Downloaded from www.nrcresearchpress.com by 210.87.254.42 on 09/06/12
For personal use only.

(150 mL), washed with dilute aqueous K_2CO_3, dried, filtered, and evaporated to dryness under reduced pressure to give an oil. Purification by column chromatography (silica gel, CCl_3CH_3) gave a mixture of epimeric cyclobutanols **5** (3.9 g, 13.8 mmol, 79%); ir ($CHCl_3$): 3450 (broad), 2970, 2920, 1755, 1705, 1360, 1270, 1230 cm^{-1}; ^{13}Cmr ($CDCl_3$, one isomer): 171.2, 170.9, 152.9, 78.6, 55.7, 48.0, 47.2, 31.7, 27.8, 25.8, 24.1, 24.1, 22.5, 14.0.

Chromic Acid Oxidation of Cyclobutanol 5

To a stirred solution of the cyclobutanol (0.5 g, 1.77 mmol) in acetone (10 mL) was added dropwise sufficient chromic acid solution (made from 13.4 g CrO_3, 25 mL H_2O, 12 mL H_2SO_4) to sustain an orange colour. After the addition the reaction was stirred for 3 h, then diluted with ether, dried with Na_2SO_4 and K_2CO_3, filtered, and evaporated to dryness. The crude product was chromatographed (silica gel, CCl_3CH_3) to afford the lactone **7** as an oil (0.15 g, 0.51 mmol, 29%); ir ($CHCl_3$): 1780, 1760, 1700, 1460, 1440, 1210 cm^{-1}; ^{1}Hmr ($CDCl_3$): 6.35 (1H, d, J = 6.5 Hz, —OCHN—), 4.45 (1H, d of d, J = 6.5 Hz, 1.0 Hz, —CHN—), 2.9 (1H, d of t, J = 6.0 Hz, 1.0 Hz, —CCH—), 2.58 (3H, s, —CCH$_3$), 2.55 (3H, s, —CCH$_3$), 2.2–0.7 (11H, m); ^{13}Cmr ($CDCl_3$): 175.2, 170.8, 169.6, 150.3, 80.3, 57.1, 45.8, 31.4, 30.6, 25.9, 24.5, 24.1, 22.4, 14.0.

6,8-Diacetyl-2-oxo-4-pentyl-3-oxa-6,8-diazabicyclo[3.3.0]-octan-7-one 6

To a mixture of carbon tetrachloride (15 mL) and water (3 mL) containing $RuCl_3$ (30 mg) was added sufficient aqueous hypochlorite (6%, commercial bleach) to generate a yellow RuO_4 solution (9). The cyclobutanol (1.6 g, 5.67 mmol) in carbon tetrachloride (10 mL) was added dropwise to the rapidly stirred oxidizing solution. Hypochlorite solution was added as required to maintain the yellow oxidizing solution. On completion of the addition the reaction mixture was stirred for 3 h, then the organic layer was separated and washed with dilute aqueous sodium metabisulfite, dried, filtered, and evaporated to dryness. The crude product was purified on a Lobar column (ether) to give the desired lactone **6** (0.31 g, 1.05 mmol, 18%), mp 145–145.5°C (ethyl acetate, ether); ir ($CHCl_3$): 1780, 1760, 1705, 1370, 1345, 1310, 1260, 1215 cm^{-1}; ^{1}Hmr ($CDCl_3$): 5.3 (1H, d, J = 8.9 Hz, —CCHN—), 4.7 (1H, d of t, J = 4.5, 0.9 Hz, —OCH—), 4.5 (1H, d of d, J = 8.9, 0.9 Hz, —CHN—), 2.58 (3H, s, —CCH$_3$), 2.57 (3H, s, —CCH$_3$), 2.0–1.1 (8H, m) 0.9 (3H, m, —CH$_3$); ^{13}Cmr ($CDCl_3$): 171.3, 170.6, 169.0, 150.3, 83.0, 56.3, 50.4, 34.1, 31.3, 24.3, 24.1, 24.1, 22.4, 13.9. *Anal.* calcd. for $C_{14}H_{20}N_2O_5$: C 56.7, H 6.8, N 9.5; found: C 56.4, H 6.8, N 9.5.

4-(1-Hydroxyhexyl)-5-hydroxymethylimidazolidin-2-one 8

To a suspension of sodium borohydride (0.59 g, 15.5 mmol) and lithium bromide (1.28 g, 16.4 mmol) in dry diglyme (8 mL) under a nitrogen atmosphere was added with stirring the lactone **6** (0.54 g, 1.8 mmol) in diglyme (8 mL). The reaction mixture was stirred overnight at room temperature, then methanol (10 mL) was added carefully, followed by acidification with glacial acetic acid. Evaporation to dryness gave a white solid that was dissolved in methanol (20 mL) and evaporated to dryness three times. The residue was partitioned between water (25 mL) and ethyl acetate (75 mL) with the aqueous layer being washed with additional ethyl acetate (75 mL) after separation. The combined organic solutions were dried, filtered, and evaporated to dryness. The residue was crystallized from ethyl acetate to give the diol **8** (0.306 g, 1.42 mmol, 78%), mp 128°C; ir (KBr): 3350, 3290, 1675, 1450, 1310, 1270, 1220, 1105, 1075, 1050 cm^{-1}; ^{1}Hmr (DMSO-d_6): 6.30 (1H, broad s, —NH), 6.17 (1H, broad s, —NH), 5.0 (1H, m, —OH), 4.77 (1H, m, OH), 3.6–3.0 (5H, m), 1.7–0.8 (11H, m); ^{13}Cmr (DMSO-d_6): 162.9 (C=O), 68.7 (—CHOH), 60.1 (—CH$_2$OH), 59.3 (—CHN—), 55.8 (—CHN—), 33.9, 31.3, 24.2, 22.0, 13.8 (CH$_3$). *Anal.* calcd. for $C_{10}H_{20}N_2O_3$: C 55.5, H 9.3, N 13.0; found: C 55.5, H 9.2, N 13.0.

n-*Pentyl Biotin 2*

The diol **8** (50 mg, 0.23 mmol) was dissolved in dry pyridine (3 mL), then cooled in an ice–salt bath while protected by a $CaCl_2$ guard tube. Methane sulfonyl chloride (0.2 g, 0.14 mL) was added dropwise and the reaction mixture was stirred for 20 min at ca. −10°C, then 1.75 h at room temperature. Evaporation to dryness gave a residue that was dissolved in methylene chloride (45 mL), then washed with aqueous HCl (1%, 5 mL) followed by aqueous $NaHCO_3$ (5%, 5 mL), dried, filtered, and evaporated to dryness to give the bis-mesylate (0.085 g), homogeneous by thin-layer chromatography (silica, ethyl acetate); ir ($CHCl_3$): 3460, 3300, 3040, 3020, 2920, 1720, 1370, 1180, 970, 910 cm^{-1}; ^{1}Hmr ($CDCl_3$): 6.2 (broad s, NH); 6.0 (broad s, NH), 5.0–3.6 (m, —CH$_2$O, —CHO, —CHN, —CHN), 3.6 (s, —OSO$_2$CH$_3$), 3.0 (s, —OSO$_2$CH$_3$), 2.0–0.8 (m, C$_5$H$_{11}$).

The bis-mesylate (0.085 g, 0.23 mmol) was dissolved in dry dimethylformamide (2 mL) under nitrogen. Sodium sulfide (0.043 g, purified by crystallization from absolute ethanol) was added, then the reaction mixture was heated at 95°C for 0.5 h. Additional sodium sulfide (0.025 g) was added, the reaction was heated another 0.5 h, then cooled and partitioned between ethyl acetate (50 mL) and water (5 mL). The aqueous layer was washed with additional ethyl acetate (25 mL), then the combined organic layers were dried, filtered, and evaporated to dryness to give a yellow solid (0.053 g). Purification by chromatography on a Lobar column (ethyl acetate) gave *n*-pentyl biotin **2** (0.016 g, 0.075 mmol, 32%) identical with an authentic sample; ^{1}Hmr ($CDCl_3$, DMSO-d_6): 5.64 (1H, s, —NH), 5.44 (1H, s, —NH), 4.49 (1H, d of d, J = 7.5, 5.0 Hz, =CHN—), 4.28 (1H, d of d of d, J = 7.5, 4.5, 1.25 Hz, —CHN—), 3.16 (1H, d of d, J = 7.5, 5 Hz, —CHS—), 2.93 (1H, d of d, J = 12.5, 4.5 Hz, —CH$_2$S—), 2.73 (1H, d of d, J = 12.5, 1.25 Hz, —CH$_2$S—), 1.62 (2H, m, CH$_2$), 1.31 (7H, m, C$_3$H$_7$), 0.86 (3H, m, CH$_3$); ^{13}Cmr ($CDCl_3$, DMSO-d_6): 163.2 (—C—), 61.8 (—CHN—), 60.0 (—CHN—), 55.8 (—CHS—), 40.6 (—CH$_2$S—), 31.6, 28.6, 28.6, 22.3, 13.9.

Acknowledgements

Financial assistance of the Aldrich Chemical Co., Queen's University, and the Natural Sciences and Engineering Research Council of Canada is gratefully acknowledged. I would like to thank Dr. M. R. Uskokovic, Hoffmann–LaRoche Inc., Nutley, New Jersey for an authentic sample of *n*-pentyl biotin.

1. J. P. Bonjour. Int. J. Vitam. Nutr. Res. **47**, 107 (1977); D. B. McCormick. Nutr. Rev. **33**, 97 (1975).
2. R. Blair and C. Whitehead. Feedstuffs, **48**, 30 (1976).
3. (*a*) H. Ohrui and S. Emoto. Tetrahedron Lett. 2765 (1975); (*b*) S. I. Zav'yalov *et al.* Bull. Acad. Sci. USSR, Div. Chem. Sci. **24**, 1533 (1975); (*c*) P. N. Confalone, G.

PIZZOLATO, E. G. BAGGIOLINI, D. LOLLAR, and M. R. USKOKOVIC. J. Am. Chem. Soc. **97**, 5936 (1975); (*d*) P. N. CONFALONE, G. PIZZOLATO, and M. R. USKOKOVIC, Helv. Chim. Acta, **59**, 1005 (1976); (*e*) J. Org. Chem. **42**, 135 (1977); (*f*) J. Org. Chem. **42**, 1630 (1977); (*g*) S. LAVIELLE, S. BORY, B. MOREAU, M. J. LUCHE, and A. MARQUET. J. Am. Chem. Soc. **100**, 1558 (1978); (*h*) M. MARX, F. MARTI, J. REISDORFF, R. SANDMAIER, and S. CLARK. J. Am. Chem. Soc. **99**, 6754 (1977); (*i*) T. OGAWA, T. KAWANO, and M. MATSUI. Carbohydr. Res. **57**, C31 (1977); (*j*) H. OHRUI, N. SUEDA, and S. EMOTO. Agric. Biol. Chem. **42**, 865 (1978); (*k*) P. N. CONFALONE, G. PIZZOLATO, E. G. BAGGIOLINI, D. LOLLAR, and M. R. USKOKOVIC. J. Am. Chem. Soc. **99**, 7020 (1977); (*l*) P. N. CONFALONE, E. D. LOLLAR, G. PIZZOLATO, and M. R. USKOKOVIC. J. Am. Chem. Soc. **100**, 6292 (1978); (*m*) J. VASILEVSKIS, J. A. GUALTIERI, S. D. HUTCHINGS, R. C. WEST, J. W. SCOTT, D. R. PARRISH, F. T. BIZZARRO, and G. F. FIELD. J. Am. Chem. Soc. **100**, 7423 (1978); (*n*) H. KOTAKE, K. INOMATA, Y. MURATA, and H. KINOSHITA. Chem. Lett. **10**, 1973 (1976); (*o*) A. FLIRI and K. HOHENLOHE-OEHRINGEN. Chem. Ber. **113**, 607 (1980).

4. S. OGINO, S. FUJIMOTO, and Y. AOKI. Agric. Biol. Chem. **38**, 275 (1974); **38**, 707 (1974).
5. R. A. WHITNEY. Tetrahedron Lett. In press.
6. L. BLANCO, P. AMICE, and J. M. CONIA. Synthesis, 194 (1976).
7. R. JEANNE-CARTIER and F. BOURELLE-WARGNIER. Bull. Soc. Chim. Fr. 297 (1976).
8. S. WOLFE and M. P. GOELDNER. Tetrahedron Lett. 5131 (1973).
9. S. WOLFE, S. K. HASAN, and J. R. CAMPBELL. Chem. Commun. 1420 (1970).
10. J. A. HORTON, M. A. LAURA, S. M. KALBAG, and R. C. PETTERSON. J. Org. Chem. **34**, 3366 (1969).
11. W. HARTMANN and H.-G. HEINE. Synthesis, 579 (1979).
12. N. K. BOSE and D. N. CHANDHURY. Tetrahedron, **20**, 49 (1964).

Can. J. Chem. Downloaded from www.nrcresearchpress.com by 210.87.254.42 on 09/06/12
For personal use only.

The formation and reactions of carbanionic derivatives of methyl phosphazenes

KEITH D. GALLICANO, RICHARD T. OAKLEY, NORMAN L. PADDOCK,[1] AND RAJENDRA D. SHARMA

Department of Chemistry, The University of British Columbia, 2036 Main Mall, University Campus, Vancouver, B.C., Canada V6T 1Y5

Received January 30, 1981

KEITH D. GALLICANO, RICHARD T. OAKLEY, NORMAN L. PADDOCK, and RAJENDRA D. SHARMA. Can. J. Chem. **59**, 2654 (1981).

The cyclic phosphazenes $N_3P_3Ph_4Me_2$, $N_3P_3Me_6$, and $N_4P_4Me_8$ are deprotonated by alkyllithiums. The resulting carbanions react with monofunctional electrophiles to form phosphazenes carrying the groups PCH_2R (R = Me, Br, I, PhC(O), COOH $AsMe_2$, Me_3M (M = Si, Ge, Sn)). Two phosphazenyl groups can be joined either by the use of a difunctional halide or by oxidative coupling of organo-copper derivatives. The formation of the carbanions, the extent of deprotonation, substituent orientation, and the dependence of reactivity on ring size, are interpreted in terms of a balance between π-electron energies and electrostatic interactions.

KEITH D. GALLICANO, RICHARD T. OAKLEY, NORMAN L. PADDOCK et RAJENDRA D. SHARMA. Can. J. Chem. **59**, 2654 (1981).

Les méthylphosphazènes cycliques $N_3P_3Ph_4Me_2$, $N_3P_3Me_6$ et $N_4P_4Me_8$ sont déprotonés par alkyllithiums. Les carbanions formés reagissent avec des electrophiles monofonctionnels en formant des phosphazènes substitués avec les groupements PCH_2R (R = Me, Br, I, PhC(O), COOH, $AsMe_2$, Me_3M (M = Si, Ge, Sn)). Deux groupements phosphazényliques peuvent être unis, soit par un halogénure bifonctionnel, soit par couplage oxidatif de derivés organocupriens. La formation des carbanions, le degré de la deprotonation, l'orientation du substituent, et la dependence de la reactivité en fonction de la largeur d'anneau, sont interpretés en fonction de l'équilibre entre les énergies des electrons-π et des interactions électrostatiques.

Introduction

The trimeric and tetrameric methylphosphazenes $(NPMe_2)_{3,4}$ were first prepared by the ammonolysis of Me_2PCl_3 (1), and a development of the method (2) allows the relative yields of the two compounds to be controlled. The cyclic compounds $(NPMe_2)_{4,5}$ have been synthesized by the alkylation of the corresponding fluorides (3, 4), and, by the use of Grignard reagents, the series has been extended to $(NPMe_2)_{10}$ (5), and more recently to $(NPMe_2)_{12}$.[2] There is little doubt that the series of ethylphosphazenes $(NPEt_2)_{3,4}$ (6) could be extended in the same way. Until recently, the corresponding high polymers were not available; only partial alkylation of $(NPF_2)_n$ could be carried out without extensive skeletal degradation (7). A polymeric form of $(NPMe_2)_n$ ($n \sim 650$) has now been prepared by the elimination of Me_3SiX from the phosphinimine $Me_2P(X)=NSiMe_3$ (8), so that the available range of alkylphosphazenes is essentially complete.

Many investigations have centred on the behaviour of phosphazenes as donors to organic and inorganic acceptors. The reciprocal withdrawal of electrons from the substituent affects both its ^1H and ^{13}C nmr spectra (9), and separate inductive and conjugative interaction parameters, comparable to those of acyl groups, have been determined for the fluorophosphazenyl groups $N_nP_nF_{2n+1}$ (n = 3–8) (10). Conjugative interactions, especially, are apparent in the near-planarity of the Me_2NP group in the dimethylamidophosphazenes, $N_4P_4(NMe_2)_8$ (11) being the earliest such example.

The synthetic possibilities of the acceptor properties of the phosphazene ring have been exploited only to a limited extent, though they can be seen at their most direct in the reactions of the phosphazenyl anion formed from a hydridophosphazene (12). In a preliminary communication (13) we described the deprotonation of neutral methylphosphazenes, and extended the reaction to the preparation of azaphosphorins from the *N*-methyl quaternary iodides $(NPMe_2)_n \cdot MeI$, (n = 3, 4) (14). Now that alkylphosphazenes can be obtained more easily, a more detailed study of the deprotonation reaction and its synthetic possibilities is justified.

The reaction of alkylphosphazenes with strong bases is similar to the deprotonation of phosphonate esters (15), but it is unusual in that successive deprotonation of methyl groups on different phosphorus atoms occurs easily, and different substituents induce different orientation patterns. We illustrate here the scope of the synthetic possibilities through the reactions of the monocarbanionic derivative $N_3P_3Ph_4Me(CH_2Li)$. In similar reactions of $(NPMe_2)_{3,4}$ the formation of polyfunctional carbanions and the orientational effects are discussed in terms of electronic structure.

Results

The lithio derivative $N_3P_3Ph_4Me(CH_2Li)$ (**2**), re-

[1]Author to whom correspondence may be addressed.

[2]R. T. Oakley, unpublished results.

0008-4042/81/172654-11$01.00/0

©1981 National Research Council of Canada/Conseil national de recherches du Canada

Can. J. Chem. Downloaded from www.nrcresearchpress.com by 210.87.254.40 on 09/06/12
For personal use only.

TABLE 1. $^1H^a$ and $^{31}P^b$ nmr parameters of $N_3P_3Ph_4MeCH_2R$ derivatives

	Compound						
	1[c]	**3a**[d]	**3b**	**3c**	**3d**[h]	**3e**[i]	**3f**[j]
$\delta_P(PMeCH_2R)$	85.2	80.8	87.5	89.0	86.6	83.2	81.86
$\delta_P(PPh_2)$	98.2	99.3	98.3	98.2	96.8	99.4	99.03
$\delta_H(MeP)$	1.58(14.0)[e]	1.52(13.5)	1.75(15.0)	1.72(15.0)[g]	1.76(15.0)	1.40(13.6)	1.68(21.1)
$\delta_H(CH_2P)$	—	1.37(14.0)[f]	3.61(18.0)	3.20(6.5)	2.88(17.0)	1.15(16.1)	1.32

[a] δ(ppm) in $CDCl_3$, reference internal TMS. J_{PH} (Hz) in parentheses.
[b] δ(ppm) in $CDCl_3$, reference external P_4O_6.
[c] See also ref. 24.
[d] $\delta_H(Me_3Sn) = 0.02$ ppm.
[e] $^2J_{PH}$ (long range) = 1.5 Hz.
[f] $^4J_{PH}$ (long range) = 4.0 Hz.
[g] $^2J_{PH}$ (long range) = 1.5 Hz.
[h] $\delta_H(OH) = 9.38$ ppm.
[i] $\delta_H(Me_2Si) = -0.17$ ppm.
[j] Two phosphazenyl groups equivalent; ^1H spectrum of CH_2 groups "deceptively simple" (16); $|^2J_{PH} + {}^3J_{PH}| = 6.1$ Hz.

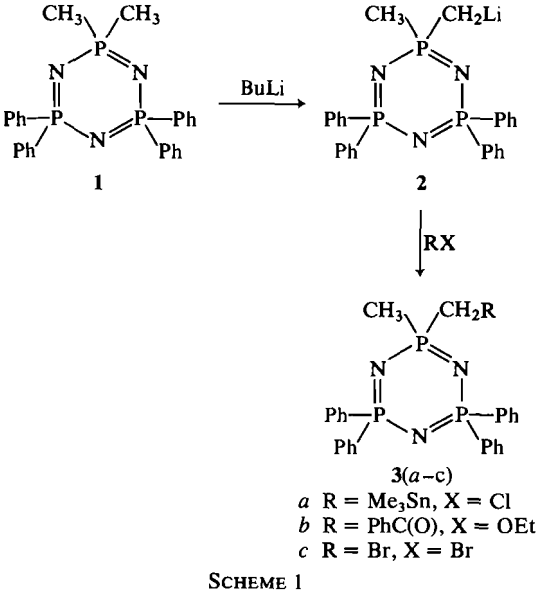

SCHEME 1

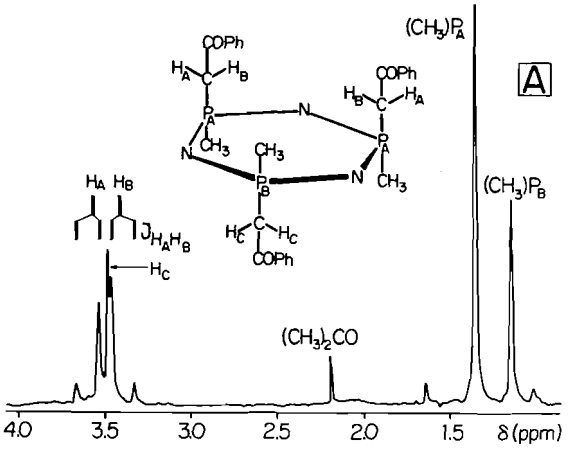

FIG. 1. The ^{31}P-decoupled ^1H nmr spectrum of **5a**. Coupling constants (Hz): P_ACH_3, 14.0; P_AH_A, 13.5; P_AH_B, 14.0, H_AH_B, 13.0; P_BCH_3, 14.6; P_BH_C, 14.9.

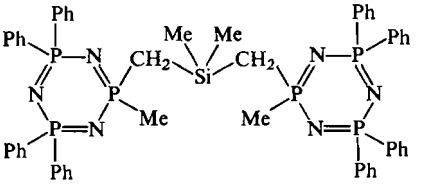

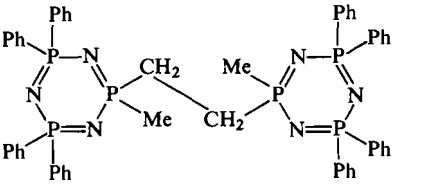

acts with the electrophiles of Scheme 1 to produce the new organophosphazenes $N_3P_3Ph_4Me(CH_2R)$ (**3**). Other derivatives prepared in similar ways include the carboxylic acid (**3d**, R = COOH), and the bridged compound $(Ph_4N_3P_3MeCH_2)_2SiMe_2$ (**3e**). Compound **3f** was prepared from the lithio derivative by an oxidative coupling reaction involving $CuCl/O_2$ (23). The nmr parameters of **1** and **3** (*a*–*f*) are given in Table 1.

Relative to **1**, the methylene protons are shielded by the Me_3Sn group, and deshielded by Br and PhC(O). Since electronegative groups concentrate π-electrons on phosphorus, the phosphorus shifts vary in the opposite sense, and shielding of the nearest phosphorus atom decreases in the order R = Br, PhC(O), COOH, H, $SnMe_3$. In general, **2** has the same synthetic possibilities as other alkyllithiums, but, as will be seen, interactions between a substituent and a phosphazene ring in which multiple deprotonation can occur have an important effect on the orientation of a second substituent.

Can. J. Chem. Downloaded from www.nrcresearchpress.com by 210.87.254.40 on 09/06/12
For personal use only.

Can. J. Chem. Downloaded from www.nrcresearchpress.com by 210.87.254.40 on 09/06/12
For personal use only.

TABLE 2. ^1H and ^{31}P nmr spectra of phosphazenes $N_3P_3Me_3(CH_2R)_3$[f]

R	H	PhC(O)	Br(*cis–cis–cis*)	Br(*cis–trans–trans*)
δ_P	87.0	2P, 89.30 1P, 89.85	88.2	87.1
δ_H (CH_3)	1.46(13.0)	6H, 1.34(14.0) 3H, 1.13(14.6)	1.67(12.6)[a]	6H, 1.72(12.6)[b] 3H, 1.69(12.4)[c]
δ_H (CH_2)	—	2H, A,[g] 3.56(13.5) 2H, B, 3.40(14.0) J_{AB} = 13.0 Hz 2H, C, 3.46(14.9)	3.38(5.4)	4H, 3.38(3.8) 2H, 3.35[d,e]

[a–d]Long range $J_{PH} \sim$ 1.5, 1.4, 1.5, 1.6 Hz.
[e]Coupling not measurable (obscured bands).
[f]In $CDCl_3$.
[g]For A, B, C, see Fig. 1.

TABLE 3. Nuclear magnetic resonance parameters of disubstituted methylcyclotetraphosphazenes[h]

Compound	$\delta_P(PMe_2)$[a]	$\delta_P(PMe)$[a]	$\delta_H(PMe_2)$[b]	$\delta_H(PMe)$[b]	$\delta_H(CH_2)$[b]	$\delta_H(R)$[b]
8*p*[g]	75.8(12)	71.1(12)	2.41(14.0)	2.38(13.0)	2.62(12.0)	1.66(22.0)[c]
8*c*	95.5(12)	99.6(12)	1.42(13.5)	1.45(13.0)	1.18(18.0)	0.11
8*d*	94.4(12)	99.6(12)	1.41(13.5)	1.42(13.5)	1.23(16.5)	0.25
8*e*	92.8(12)	100.0(12)	1.45(13.0)	1.48(12.0)	1.27(14.0)	0.14
8*a*(*i*)[f]	95.4	101.3	1.37(12.6)	1.44(13.2)	3.46(17.0)[d]	—
			1.40(12.7)		3.57(17.4)	—
8*a*(*ii*)[f]	96.6(11.2)	101.6(10.6)	1.47(13.1)	1.44(12.6)	3.50(16.6)[e]	—
					3.61(17.0)	—
6	94.4	—	1.51(11.5)	—	—	—

[a]J_{PP} in parentheses (Hz).
[b]J_{PH} in parentheses (Hz).
[c]J_{HH} = 7.5 Hz.
[d]J_{AB} = 12.4 Hz.
[e]J_{AB} = 12.4 Hz.
[f](*i*), Fresh solution in $CDCl_3$; (*ii*), equilibrated solution in $CDCl_3$ (see text).
[g]$N_4P_4Me_6Et_2 \cdot 2HCl$.
[h]In $CDCl_3$, except **8***p* (D_2O).

Hexamethylcyclotriphosphazene (**4**) forms a tricarbanion, of which a tribenzoyl (**5***a*) and a tribromo derivative (**5***b*) have been prepared. The relative configurations of the benzoyl groups were determined from the ^1H and ^{31}P nmr spectra. If all the benzoyl groups were on the same side of the N_3P_3 plane, they would be equivalent on the nmr time scale, and methyl and methylene signals should appear in the ^{31}P-decoupled spectrum as singlets. The actual ^1H spectrum (Fig. 1) is a pair of singlets, intensities 1:2, for the methyl protons, and a singlet for one methylene group superimposed on an AB pattern characteristic of two equivalent methylene groups each containing diastereotopic protons.

The relative configurations of the benzoyl groups are then *cis–trans–trans*,[3] and the ^{31}P spectrum, consisting of two signals of relative intensity 1:2, shows the expected nonequivalence of the phosphorus atoms. Two forms of **5***b* were obtained. For the first, the proton signal is a pair of simple doublets, so that it is the *cis–cis–cis* isomer. In the

[3]*Cis* and *trans* refer to the relative orientation of groups on successive atoms.

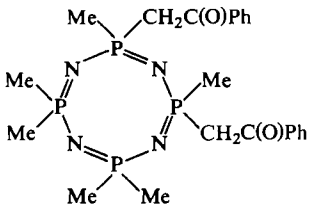

8*a*

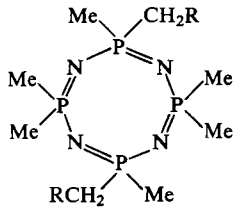

8*b* R = Me
c R = $SiMe_3$
d R = $GeMe_3$
e R = $SnMe_3$

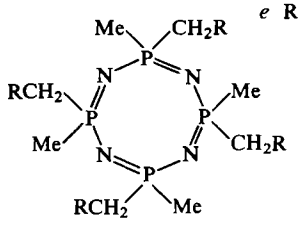

8*f* R = Me
g R = $SiMe_3$
h R = $GeMe_3$
i R = $SnMe_3$
j R = Br
k R = I
l R = $AsMe_2$

SCHEME 2

Can. J. Chem. Downloaded from www.nrcresearchpress.com by 210.87.254.40 on 09/06/12
For personal use only.

TABLE 4. Nuclear magnetic resonance parameters of tetrasubstituted methylcyclotetraphosphazenes[c]

Compound	δ_P	δ_H(PMe)	$\delta_H(CH_2)$	δ_H(R)
8*f*	89.42	1.41(11.5)	1.65(~12.0)	1.10(17.0)
8*g*	100.1	1.46(12.5)	1.19(17.0)	0.24
8*h*	98.1	1.42(12.0)	1.23(17.5)	0.19
8*i*	96.5	1.40(12.5)	1.23(12.3)	0.16
8*j*	99.61	1.62(12.5)	3.35(5.8)	—
8*k*	102.20	1.69(12.3)	3.17(5.9)	—
8*l*	96.53	1.53(11.6)	1.76(11.1)	1.04
8*m*[a]	99.68	2.10(11.6)	3.33(10.2)	2.36
8*n*[b]	71.2	2.39(12.0)	2.62(~12.0)	—

[a] $N_4P_4Me_4(AsMe_2)_4 \cdot 4MeI$; solutions in D_2O.
[b] $N_4P_4Me_4Et_4 \cdot 2HCl$; solutions in D_2O.
[c] In $CDCl_3$.

second isomer, although the ^{31}P signal is apparently a singlet, the differently situated methyl and methylene groups are distinguished, so that its configuration is *cis–trans–trans*. Details are given in Table 2.

The derivatives based on the eight-membered ring show additional features. Deprotonation of $N_4P_4Me_8$ (**6**) gives, in the limit of four equivalents of base, the tetracarbanion derivative $N_4P_4Me_4(CH_2Li)_4$ (**7**). The products of the reaction of this compound with several electrophiles are shown in Scheme 2. The nmr parameters of compounds **8** (*a–e*) are given in Table 3, and those of **8** (*f–l*) in Table 4. The nmr spectra of all the tetrasubstituted derivatives are qualitatively similar, in that the ^{31}P spectrum of each consists of a singlet, and the ^1H spectrum consists of two simple doublets for the methylene and methyl groups respectively. The *cis–cis–trans–trans* structure is ruled out, but no configurational choice can be made between the three more symmetrical possibilities.

The disubstituted derivatives are more generally informative. In the reaction of methyl iodide with the tetracarbanion a small amount of the diethyl derivative was obtained as its dihydrochloride (**8***p*), whose crystal structure (17) showed the molecule to be centrosymmetric, and the ethyl groups to be in *trans*-antipodal orientations. Antipodal substitution is also found in the MMe_3 derivatives (M = Ge, Sn), whose ^{31}P spectra consist of a pair of 1:2:1 triplets; the ^1H methylene and methyl spectra are simple doublets. The reaction of the tetracarbanion with ethyl benzoate is significantly different, in that it goes no further than disubstitution. Moreover, the ^1H and ^{31}P spectra of the dibenzoyl derivative are quite different from those of antipodally substituted derivatives, and depend on both solvent and time. The ^{31}P-decoupled ^1H spectrum of a fresh solution of **8***a* in $CDCl_3$ (Fig. 2A) exhibits a single AB pattern for the two methylene groups,

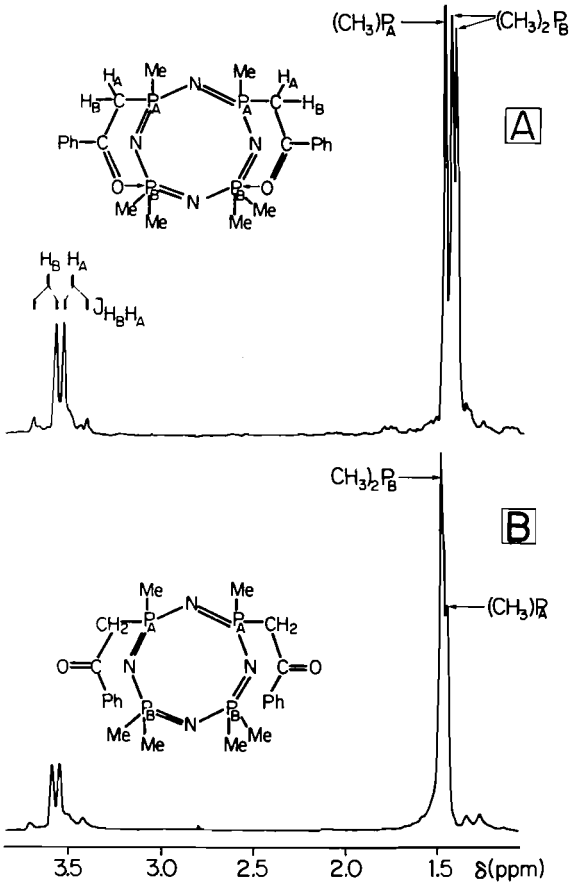

FIG. 2. The ^{31}P-decoupled ^1H nmr spectrum of **8***a* in $CDCl_3$. A, immediately; B, after standing.

and three singlets of relative intensity 1:1:1 in the methyl region, the two methyl groups of the PMe_2 group now being distinguished. The ^{31}P spectrum shows only two broadened singlets of intensity ratio 1:1, and, together with the proton spectrum, indicates vicinal substitution. If the solution is allowed to stand, a slow change occurs (Fig. 2B), and a similar but immediate change takes place in CD_3OD. The methyl signals become two singlets of relative intensity 2:1, and ^{31}P–^{31}P coupling is observed in the ^{31}P spectrum, each signal now being split into a doublet which shows virtual coupling. The AB pattern of the two equivalent methylene groups remains unchanged even at 55°C ($CDCl_3$), thereby confirming the diastereotopic nature of the methylene protons in vicinal positions. The benzoyl groups evidently form weak intramolecular bonds (possibly similar to those in a Wittig intermediate (18), as shown in Fig. 2) which are broken by competitive hydrogen bonding of the carbonyl oxygen atom, slowly with $CDCl_3$, rapidly

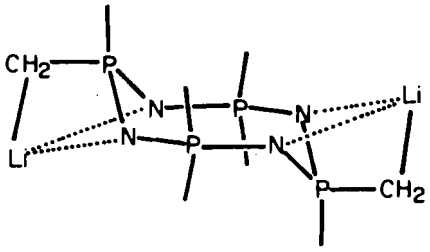

FIG. 3. Possible ion-pairing scheme of di-carbanion.

with CD_3OD. The PMe_2 group thereby becomes (accidentally) symmetrical. Other small changes in the nmr parameters reflect the altered electron distribution, the greatest of which is the upfield shift of the phosphorus signal of the Me_2P groups. Not surprisingly, the methylene protons exchange with CD_3OD. Interaction between a ring nitrogen atom and the carbon atom of a carbonyl group may also occur, as in $N_3P_3F_5(CH_2COPh)$ (19), but the evidence is inconclusive.

Discussion

The reactions of the monofunctional carbanion **2** show the scope of the reaction; it is likely that a much wider range of electrophiles can be used, so that the method should be generally useful for phosphazene synthesis. The same is true of the polyfunctional carbanions of **4** and **6**, but we need to say more about the deprotonation process itself and the orientation of the substituents.

It is striking that no derivatives of the monocarbanion of **4** or **6** could be prepared, whether by a deficit of the base or of the substituting reagent; deprotonation appears to facilitate further deprotonation. Ordinarily, a second deprotonation would be disfavoured by the electrostatic repulsion in the dianion; if the effective dielectric constant is assumed to be 2.5, ΔpK (from this cause alone) for the antipodal protons of $N_4P_4Me_8$ would be about 15, if the two carbon centres are assumed to carry a full negative charge. Two effects, both chemically significant, reduce this difference. First, the effective charge on carbon would be diminished by coordination of the lithium cations, as shown in Fig. 3. Such cation effects are important chemically; in the reaction of phosphonate carbanions with ketones, for instance, such larger cations as Na^+ increase the effective negative charge on oxygen and promote olefin formation (20). The second factor is that conjugation of a carbanionic methylene group can take place by delocalization of its charge into the ring, with consequent changes in both the electrostatic energy and the π-electron levels; these two energy changes often tend to compensate one another. They can be estimated only roughly, but they help in the interpretation of the reactions described here, specifically the occurrence of multiple deprotonation, the dependence of the degree of substitution on substituent electronegativity, the orientation of substituents, and the different reactivities of the carbanions formed from $N_3P_3Me_6$ and $N_4P_4Me_8$ to ethyl benzoate.

The following method was used for the calculations. π-Electron energies and charges were found for molecules based on an N_4P_4 ring by the HMO method (see Fig. 4 for details), and the π-charges so found were used to calculate the intramolecular electrostatic energy of a simplified model, in which all the atoms were assumed to be coplanar (PN = 1.58 Å, PC = 1.80 Å, all ring angles 135°, all exocyclic angles 112.5°; Li^+ 3.2 Å from C, along extended P—C bond). These model calculations have several limitations. The Hückel method, even if its parameters could be relied on, overestimates bond polarity, and the calculated effective electrostatic energies are too great, not only for this reason, but also because of the solvation and ion-pairing effects mentioned above. The neglect of changes in the σ-densities is perhaps a smaller source of error, since the σ-bonds would be less polarizable. For these reasons, the calculations have only qualitative significance, but they help in interpreting the chemistry, and suggest new developments.

Carbanion Formation

Carbon would normally be taken to be more electronegative than phosphorus, but the formal negative charge would raise its energy, and we have assumed $\alpha_C = \alpha_P$. The principal interaction of the carbanion centre is then with the lowest unoccupied level of the N_4P_4 ring, a nonbonding orbital (composed of phosphorus atomic orbitals), to which electrons are transferred on conjugation, as shown in Fig. 4 (level 5). The highest occupied level is appreciably lowered, and the loss of 0.862 electrons from C goes principally to P (0.780 electrons) with a smaller contribution to N (0.082 electrons). The energy changes with progressive conjugation of up to four CH_2^- groups are shown in Fig. 5. The conjugation energies are substantial, and they suggest that the antipodal dianion should be more stable than the vicinal isomer, but since the incremental conjugation energy decreases with increasing number of *exo*-groups, conjugation alone cannot explain the multiple deprotonation which occurs in practice.

An explanation is possible if we also include the electrostatic energy changes which occur as a

Can. J. Chem. Downloaded from www.nrcresearchpress.com by 210.87.254.40 on 09/06/12
For personal use only.

Can. J. Chem. Downloaded from www.nrcresearchpress.com by 210.87.254.40 on 09/06/12
For personal use only.

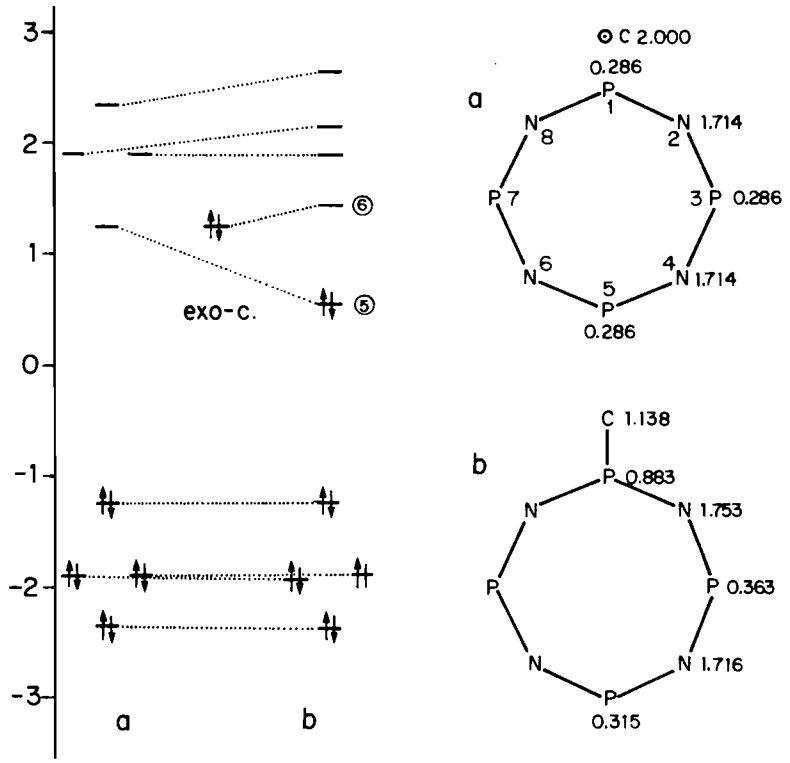

FIG. 4. Energy levels (eV) and π-charge densities of (a) an 8-membered N_4P_4 ring ($\alpha_N = -1.25$, $\alpha_P = 1.25$, $\beta_{endo} = -1$ eV) and (b) the same, but with exocyclic conjugation to form a mono-carbanion, $\beta_{exo} = -1$ eV). Different parameters have been used where stated in the text.

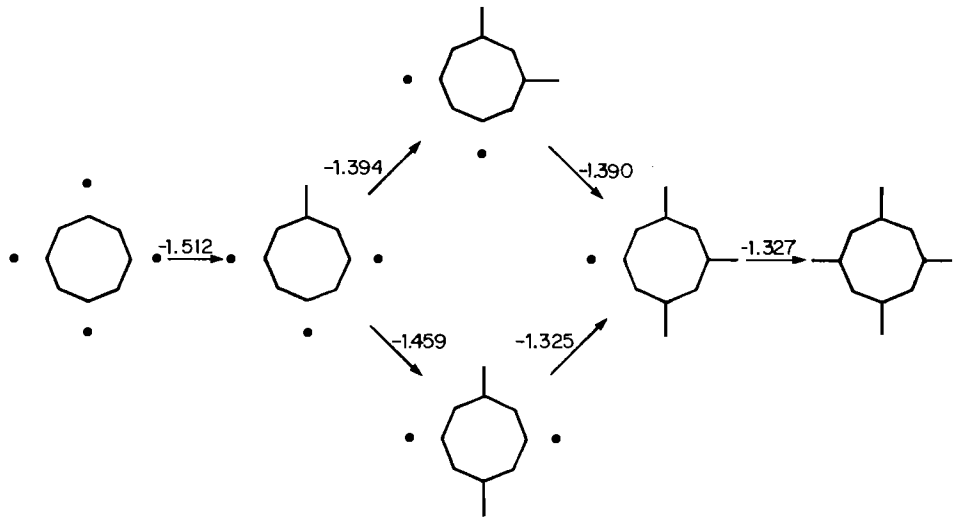

FIG. 5. Changes in conjugation (eV) with progressive conjugation. Parameters as for Fig. 4. Dots represent unconjugated electron pairs.

result of the conjugation. Some typical results are shown in Table 5. Comparison of columns 2 and 3 shows that the transfer of charge to the ring adds a substantial repulsive component to the intra-ring interactions, and a smaller repulsive component to the *exo*-ring interaction. The introduction of a second *exo*-group into the antipodal position increases the *exo*-ring interaction still further, and adds a (small) *exo-exo* contribution. The additional conjugation energy arising from this second

TABLE 5. Calculated electrostatic energies (eV) of N_4P_4 carbanions[a]

Number of formal CH_2^- groups	Charge on *exo*-group	Intra-ring	*Exo*-ring	*Exo–exo*
0	—	−25.32	—	—
1 (localized)	−1.00	−25.32	−1.09	—
1 (delocalized)	−0.11	−16.30	0.38	—
2 (antipodal, delocalized)	−0.45	−14.09	3.44	0.38

[a]$\beta_{exo} = -0.2$ eV.

step is achieved with only a small additional charge delocalization, so that the additional intra-ring repulsive energy is also small. The net changes for the first two deprotonation steps (from rows 1, 3, 4) are 9.40, 5.65 eV, so that, relative to the first step, the second step is exothermic, the energy change more than compensating for the decreased conjugation energy (Fig. 5). If we also include the cation–anion and cation–cation interactions, the conclusion is reinforced; for likely values of β_{exo}, if the added base is strong enough to remove one proton, it will also remove a second.

The third and fourth deprotonation steps can be treated similarly; as a crude approximation, we again consider only the changes in π-energy and electrostatic energy. The third and fourth stages involve increases in the electrostatic energy of the anion alone, the incremental changes for the four steps being (0), −3.75, 1.55, 0.79 eV. However, the negative charge on a single carbanionic centre increases as the number of such groups increases, and if the interactions with the cations are included, the incremental energies are (0), −4.72, −0.03, −0.87 eV. As stated above, the charges are overestimated, but their correction is unlikely to affect the qualitative conclusion that the second and fourth deprotonations should take place more easily than the first and third.

Substitution Reactions

Such calculations are helpful, but not decisive, in the prediction of reaction products. Intramolecular proton transfer in the carbanions evidently occurs more rapidly than reaction of the carbanions with electrophiles, as illustrated by the isolation of only the *cis–trans–trans* form of the tribenzoyl derivative **5***a*; both isomers of the less sterically demanding tribromo derivative **5***b* were obtained. Mostly, the products are what might be expected from equilibrium considerations, though in one case to be discussed below (benzoylation), we need to consider also the nucleophilicity of the carbanion.

Apart from this case, disubstituted derivatives $N_4P_4Me_6(CH_2R)_2$ are obtained only if a deficit of base is used, and if R is at least as electropositive as Me. Electronegative substituents, like bromine, increase the acidity of the methyl group, facilitate removal of the third proton, and displace to the right such equilibria as

[1] $N_4P_4(CH_2R)_2Me_6 + N_4P_4Me_6(CH_2^-)_2 \rightleftharpoons N_4P_4(CH_2R)_2Me_4(CH_2^-)_2 + N_4P_4Me_8$

so promoting the formation of fully-substituted derivatives; in agreement, only a tetrabromo derivative has been isolated. Electropositive groups have the opposite effect. If R = Me, a very small amount of the di-derivative is formed. More strongly electron-releasing groups, like Me_3Si, Me_3Ge, and Me_3Sn, decrease the acidity of the methyl group, and the di-derivatives can be obtained in high yield. The calculated orientation of the two groups is less clear-cut. Conjugation energies favour antipodal, electrostatic energies favour vicinal substitution; the spectroscopic evidence shows that electropositive groups substitute antipodally.

There is an important limitation to the statement that electronegative substituents facilitate full substitution, which arises from the fact that such substituents withdraw charge strongly from the *exo*-group, so that it can eventually cease to be an electrophile. Substitution is thereby restricted, and, since the electrostatic effects are now small, it is possible to make a firmer statement about orientation, on the basis of the π-energies alone. In an antipodal [1, 5] dicarbanion, levels 5 and 6 in Fig. 4 are both stabilized significantly by electronegative perturbation of atoms 3,7, and both levels are occupied. The unperturbed antipodal dicarbanion is more stable than the vicinal isomer, and the relationship is the same for the neutral molecules perturbed identically at the vicinal and antipodal positions. The combination of the two effects (the conjugative interactions in the carbanion and the electronegative perturbation of the phosphorus atoms), reverses the relative energies, for the following reason. The higher energy of the vicinal unperturbed carbanion is associated with a higher negative charge on carbon (−0.48 vs. −0.45 in the antipodal isomer). It therefore has more to gain, through charge delocalization, if the positive

Can. J. Chem. Downloaded from www.nrcresearchpress.com by 210.87.254.40 on 09/06/12
For personal use only.

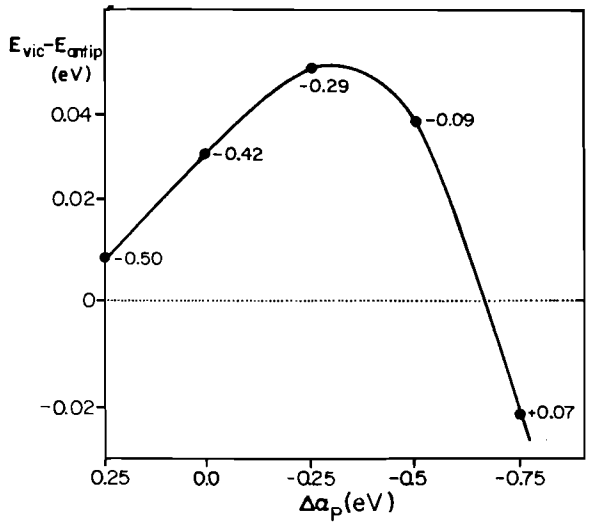

FIG. 6. π-Electron energy of vicinal relative to antipodal $N_4P_4Me_4(CH_2R)_2(CH_2^-)_2$, as a function of the perturbation $\Delta\alpha_P$ induced by R. The residual π-charge on the carbon atoms of the vicinal isomer is marked on the curve; the antipodal charges differ only slightly. The carbanion ceases to be a nucleophile at $\Delta\alpha_P \sim -0.65$ eV.

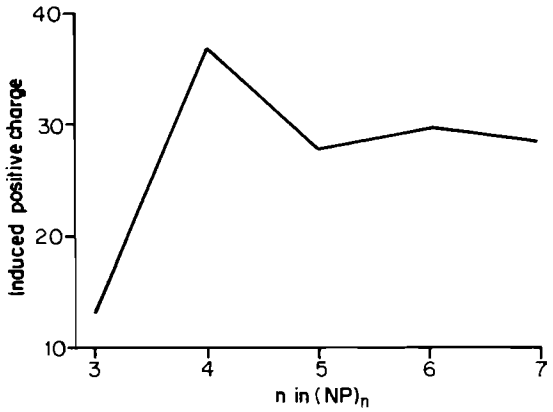

FIG. 7. Positive charge ($\times 10^4$) induced at P(2) by a perturbation of −0.5 eV at P(1). The effect at P(3) is similar, but an order of magnitude smaller.

charge on phosphorus is increased, and the antipodal preference of 0.01 eV is in fact converted to a vicinal preference of 0.02 eV ($\Delta\alpha_P = -0.5\,\beta$, $\beta_{exo} = -0.2$ eV). The energetic effect is not large, but it is accompanied by a dramatic change in charge density on carbon, to −0.03 (vicinal), −0.06 (antipodal). The electron density in nonbonding levels is especially sensitive to electronic changes, and if the substituents are sufficiently electronegative, the dicarbanion is no longer a nucleophile, and the reaction stops at that point. This is evidently what happens in the reaction of $N_4P_4Me_4(CH_2^-)_4$ with ethyl benzoate; it has not been found possible to introduce more than two benzoyl groups, which occupy vicinal positions. Fig. 6 shows the π-energy of vicinal relative to antipodal $N_4P_4(CH_2R)_2$-$Me_4(CH_2^-)_2$ for a particular value of β_{exo}, for which the vicinal form becomes stable for $\Delta\alpha_P \sim -0.65$, the charge on carbon becoming simultaneously close to zero. As in other reactions, the orientation of the substituents appears to be controlled thermodynamically; in an electronegatively monosubstituted carbanion $N_4P_4(CH_2R)Me_4(CH_2^-)_3$, the antipodal carbon carries the highest negative charge, and antipodal substitution would be expected if kinetic effects were dominant. For numerically smaller values of β_{exo}, the vicinal form becomes thermodynamically stable at smaller values of $\Delta\alpha_P$.

As an interesting contrast, the benzoylation of the trimer goes to completion, and this fact, too, has an immediate explanation in terms of π-electron theory. The effect of an electronegative perturbation at phosphorus is to concentrate electron density locally, at the expense of the nearest atoms. Just as (in a homomorphic system) the π-electron energy is an oscillating function of ring size, so is the induced electron density at a particular atom. As Fig. 7 shows, the positive charge is greatest for the eight-membered and least for the 6-membered ring, and the secondary withdrawal from the *exo*-carbon atoms must therefore be greater for the tetramer. If the same parameters are used as for the tetramer, the *exo*-charge on the carbanion of a disubstituted trimer is −0.2, when it is 0.0 in the tetramer. This is indeed much reduced from the value of −0.54 found for the unperturbed molecule, but could well account for the fact that the benzoylation of $N_3P_3Me_6$ goes to completion, whereas the reaction of $N_4P_4Me_8$ stops when two benzoyl groups have been introduced.

Experimental

Most reactions, and operations with products, were carried out under dry nitrogen. Nuclear magnetic resonance spectra were obtained on Varian XL-100, Nicolet-Oxford H-270, Bruker WH-400, and Varian CFT-20 spectrometers. Mass spectra were obtained on a Varian (Atlas) CH 4-B mass spectrometer. Microanalyses were by P. Borda.

Commercial solvents were redistilled and dried, usually over lithium aluminum hydride or sodium-benzophenone. Most reagents, including *n*-butyllithium, were reagent grade commercial products, purified if necessary. Dimethyliodoarsine (21) and the phosphazenes **1**, **4** and **6** were prepared by known methods (2, 4, 22). Methyllithium was prepared as required, by the addition of methyl iodide at −78°C to a slight excess of *n*-butyllithium in hexane (0.5 *M*). The mixture was stirred under an atmosphere of nitrogen and allowed to warm slowly to 0°C. The white precipitate of methyllithium was filtered off under nitrogen and dissolved in dry diethyl ether. The solution so

Can. J. Chem. Downloaded from www.nrcresearchpress.com by 210.87.254.40 on 09/06/12
For personal use only.

Can. J. Chem. Downloaded from www.nrcresearchpress.com by 210.87.254.40 on 09/06/12
For personal use only.

formed was filtered if necessary and standardized by titration with acid. The solutions of methyllithium were used within 24 h.

Reactions of $N_3P_3Ph_4Me(CH_2Li)$ (2)

In a typical preparation, a freshly prepared solution of the alkyllithium (either *n*-butyllithium or methyllithium) in ~10% excess, was added to a solution of **1** in ether. After an induction period of a few minutes, a heavy white precipitate of **2** was formed. To ensure completion of the reaction, the mixture was gently heated under reflux for 2 h.

$N_3P_3Ph_4Me(CH_2SnMe_3)$ (3a)

A solution of Me_3SnCl (0.300 g, 1.50 mmol) in 20 mL ether was added to a slurry of **2** (0.651 mmol) in 100 mL ether. The turbidity was reduced, and the mixture was stirred overnight to ensure that reaction was complete. The mixture was filtered, and evaporation of the filtrate yielded colourless crystals, which were recrystallized from ether–hexane as needles of **3a** (0.861 g, 1.35 mmol, 97%); mp 146–148°C. *Anal.* calcd. for $C_{29}H_{34}N_3P_3Sn$: C 54.8, H 5.4, N 6.6, found: C 54.9, H 5.5, N 6.5.

$N_3P_3Ph_4Me(CH_2COPh)$ (3b)

A solution of ethyl benzoate (0.525 g, 3.5 mmol) in 30 mL ether was added dropwise to **2** (3.17 mmol) in 100 mL ether. The reaction mixture was stirred overnight, shaken with 50 mL of 0.1 *N* H_2SO_4, and the organic layer separated and dried over sodium sulphate. Evaporation of the solvent yielded a white solid, which was recrystallized from benzene–toluene and ether–hexane to give a microcrystalline mass of **3b**; mp 144–146°C; ν(C=O): 1666 cm^{-1}. *Anal.* calcd. for $C_{31}H_{30}N_3OP_3$: C 68.5, H 5.3, N 7.3; found: C 68.7, H 5.4, N 7.1.

$N_3P_3Ph_4Me(CH_2Br)$ (3c)

An ethereal (10 mL) solution (an excess) of bromine was added to **2** (1.66 mmol) in 100 mL ether at −78°C. A dilute solution of NaOH was added at room temperature, the organic layer separated, and the aqueous layer washed with 50 mL CH_2Cl_2. The combined extracts were dried over sodium sulphate and evaporated to white crystals (0.92 g), whose ^1H nmr spectrum showed it to be a mixture (~4:1) of **3c** and **2**. Analytically pure crystals of **3c** were obtained by repeated crystallization of this product from benzene–octane and chloroform–octane; mp 176–178°C. *Anal.* calcd. for $C_{26}H_{25}BrN_3P_3$: C 56.5, H 4.6, Br 14.5, N 7.6; found: C 56.9, H 4.5, Br 14.1, N 7.7.

$N_3P_3Ph_4Me(CH_2COOH)$ (3d)

Carbon dioxide was bubbled for 15 min through a slurry of **2** (0.86 mmol) in 100 mL ether. The clear reaction mixture was shaken with 50 mL of 0.1 *N* H_2SO_4, and the organic layer dried over Na_2SO_4. Evaporation of the solvent yielded a white solid, which was recrystallized from acetone as white flakes of **3d** (0.39 g, 0.75 mmol, 87%); mp 185–186°C (dec.). *Anal.* calcd. for $C_{28}H_{26}N_3O_2P_3$: C 62.7, H 5.1, N 8.1; found: C 62.9, H 5.2, N 8.0.

$(N_3P_3Ph_4MeCH_2)_2SiMe_2$ (3e)

Dimethyldichlorosilane (0.90 g, 0.70 mmol, 20% excess) in 10 mL ether was added to **2** (1.16 mmol) in 75 mL ether at −50°C. The mixture was allowed to warm slowly to room temperature and stirred for 24 h. The lithium chloride was filtered off and the solvent removed. The residual oil was dissolved in ether and eluted with 500 mL ether on a column of Silicar CC-7. The clear pale yellow oil remaining after evaporation of the solvent contained some **1**, which was distilled off at 200°C/0.03 Torr. The brown gummy residue was extracted with 4 × 50 mL hexane, and the product **3e** was freed from traces of **1** by repeated crystallization from hexane; mp 163–164.5°C. *Anal.* calcd. for $C_{54}H_{56}N_6P_6Si$: C 64.7, H 5.6, N 8.4; found: C 64.5, H 5.8, N 8.2.

$(N_3P_3Ph_4MeCH_2)_2$ (3f)

Cuprous chloride (0.296 g, 2.20 mmol) was added to **2** (2.06 mmol) in tetrahydrofuran at −40°C. As the temperature was raised to 0°C, the colour of the solution became reddish brown, which turned to green on bubbling oxygen through the solution for 3 h. The solvent was evaporated off, and the semi-solid product was acidified with dilute sulphuric acid. The greenish-white solid product was filtered off, washed with water, dissolved in ether, and passed through a silica gel column. Evaporation of the solvent from the eluate yielded colourless crystals, which were recrystallized from acetonitrile as colourless blocks of **3f**. *Anal.* calcd. for $C_{52}H_{50}N_6P_6$: C 66.1, H 5.2, N 8.9; found: C 66.5, H 5.3, N 8.8. *Exact mass* calcd.: 944.2514; found (ms): 944.2507.

$N_3P_3Me_3[CH_2C(O)Ph]_3$ (5a)

The trilithio derivative of **4** was prepared by adding 7.3 mmol of *n*-butyllithium in hexane to **4** (0.500 g, 2.22 mmol) in 125 mL ether. The mixture was heated under reflux for 75 min, cooled to −35°C, and ethyl benzoate (1.107 g, 7.37 mmol) in 60 mL ether was added over 10 min. The temperature was allowed to rise, and 75 mL 0.5 *M* aqueous potassium fluoride were added after 16 h. The ether layer was separated off and dried over Na_2SO_4. The excess of ethyl benzoate was removed at 100°C/0.1 Torr, and the residual white solid **5a** was recrystallized twice from acetone; mp 173–177°C; ν (C=O): 1673, 1659 cm^{-1} (intensities 2:1). *Anal.* calcd. for $C_{27}H_{30}N_3O_3P_3$: C 60.3, H 5.6, N 7.8; found: C 60.1, H 5.6, N 7.9.

$N_3P_3Me_3(CH_2Br)_3$ (5b)

Bromopentafluorobenzene (2.322 g, 9.40 mmol, 5% deficit) in 60 mL ether was added to the trilithio derivative (3.30 mmol) in 75 mL ether was −78°C over 15 min. The turbidity decreased, and the reaction mixture became yellow and finally dark brown on being allowed to warm to −20°C over 3.5 h; the addition of 10.2 mmol aqueous HCl removed most of the colour. The ether layer was washed with water and dried over Na_2SO_4. After removal of the solvent, the light brown residue was washed with acetone. The remaining white solid (0.152 g, 10.5%) was identified by its nmr spectra and by tlc (50:50 acetone–hexane) as a mixture of two isomers of $N_3P_3Me_3(CH_2Br)_3$. *Anal.* calcd. for $C_6H_{15}Br_3N_3P_3$: C 15.6, H 3.3, Br 51.9, N 9.1; found: C 15.9, H 3.1, Br 51.5, N 9.0. The isomers (*cis–cis–cis*: *cis–trans–trans* 1:3) were partly separated by crystallization from acetone, in which the latter compound is the more soluble. If *n*-butyllithium and bromopentafluorobenzene are used in excess, some tetrabromo derivatives are formed.

$N_4P_4Me_4Et_4$ (8f)

A solution of methyllithium (39.2 mmol) in 56 mL ether was added dropwise to a solution of **6** (2.712 g, 9.04 mmol) in 50 mL ether. When effervescence had ceased (30 min) the mixture was heated under reflux for 2 h, when a slight turbidity was apparent. An exothermic reaction took place on the addition of a large excess (~25 mL) of methyl iodide. The mixture was heated under reflux for a further 4 h. The solvent and the excess of methyl iodide were distilled off, leaving a white paste (10.75 g) which was dissolved in water and neutralized with sulphuric acid (residual alkalinity 2.15 mmol OH^-). The lithium was precipitated as fluoride, the solvent distilled off the filtered solution, and the residue extracted with 3 × 30 mL hot chloroform. Triethylamine (10 mL) was added to the extract, which was shaken for 5 min and filtered. Evaporation of the solvent from the filtrate left a crystalline mass which was extracted with 3 × 50 mL hot hexane. Evaporation of these extracts yielded colourless crystals of **8f** (2.58 g, 7.2 mmol, 80%) which was purified by sublimation *in vacuo* and by crystalliza-

Can. J. Chem. Downloaded from www.nrcresearchpress.com by 210.87.254.40 on 09/06/12
For personal use only.

tion from hexane; mp 65–67°C. *Anal.* calcd. for $C_{12}H_{32}N_4P_4$: C 40.5, H 9.1, N 15.7; found: C 40.2, H 8.9, N 16.0. The dihydrochloride **8***n* was precipitated from a solution of the phosphazene and HCl in carbon tetrachloride and recrystallized from acetonitrile–benzene as $N_4P_4Me_4Et_4 \cdot 2HCl \cdot H_2O$; mp 180–185°C. *Anal.* calcd. for $C_{12}H_{36}Cl_2N_4OP_4$: C 32.2, H 8.1, Cl 15.9, N 12.5; found: C 32.3, H 8.3, Cl 15.9, N 12.7. If the chloroform extract is not treated with a base, the dihydroiodide is formed, rather than the neutral phosphazene. In one such experiment, the chloroform extract was evaporated to an oil, which was dissolved in water and eluted through an Amberlite CG400 ion exchange column charged with chloride ion. A few crystals of $N_4P_4Me_6Et_2 \cdot 2HCl$ (**8***p*) were obtained on evaporation of the solvent; mp 231–234°C. *Anal.* calcd. for $C_{10}H_{30}Cl_2N_4P_4$: C 29.9, H 7.5, Cl 17.7, N 14.0; found: C 29.6, H 7.6, Cl 18.1, N 14.1.

Trimethylsilyl, -germyl, and -stannyl derivatives of 6

An excess of Me_3SiCl (2.0 mL, 15.9 mmol) was added to **7** (2.52 mmol) in 50 mL ether. The reaction was vigorous and exothermic. The mixture was stirred overnight, the white precipitate filtered off, and the solvent removed. The colourless residual oil was distilled at ~160°/0.01 Torr to give an oil which solidified on standing. The solid was recrystallized from hexane at −23°C, to give colourless blocks of $N_4P_4Me_4(CH_2SiMe_3)_4$ (**8***g*); mp 97–102°C. *Anal.* calcd. for $C_{20}H_{56}N_4P_4Si_4$: C 40.8, H 9.6, N 9.5; found: C 40.5, H 9.6, N 9.5. The trimethylgermyl (**8***h*) and trimethylstannyl (**8***i*) derivatives were prepared similarly (yields 99, 92%). Melting point for **8***h*, 98.5–100°C. *Anal.* calcd. for $C_{20}H_{56}Ge_4N_4P_4$: C 31.3, H 7.4, N 7.3; found: C 31.4, H 7.5, N 7.1. *Anal.* calcd. for $C_{20}H_{56}N_4P_4Sn_4$: C 25.3, H 5.9, N 5.9, Sn 49.9; found: C 25.1, H 5.9, N 6.0, Sn 49.6. The same method was used for the preparation of the disubstituted derivatives, using half-quantities of methyllithium and the halide. $N_4P_4Me_6(CH_2SiMe_3)_2$ (**8***c*): mp 63–65°C. *Anal.* calcd. for $C_{14}H_{40}N_4P_4Si_2$: C 37.8, H 9.1, N 12.6; found: C 38.2, H 9.0, N 12.4. $N_4P_4Me_4(CH_2GeMe_3)_2$ (**8***d*): mp 77–79°C. *Anal.* calcd. for $C_{14}H_{40}Ge_2N_4P_4$: C 31.5, H 7.6, N 10.5; found: C 31.6, H 7.7, N 10.3. $N_4P_4Me_6(CH_2SnMe_3)_2$ (**8***e*): mp 104–106°C. *Anal.* calcd. for $C_{14}H_{40}N_4P_4Sn_2$: C 26.9, H 6.4, N 9.0; found: C 27.1, H 6.5, N 8.7.

$N_4P_4Me_4(CH_2Br)_4$ (8j)

Bromopentafluorobenzene (5.39 g, 21.8 mmol) in 50 mL ether was added to **7** (5.0 mmol) in 90 mL ether at −78°C over 10 min. The temperature was raised to −10°C over 2 h, the solution washed with water, and the golden brown ether layer dried over Na_2SO_4 and evaporated. The product **8***j* was deposited from the residual oil, and was recrystallized from hexane and chloroform (1.85 g, 60%); mp 155–156°C. *Anal.* calcd. for $C_8H_{20}Br_4N_4P_4$: C 15.6, H 3.3, Br 51.9, N 9.1; found: C 15.8, H 3.5, Br 51.8, N 9.1.

$N_4P_4Me_4(CH_2I)_4$ (8k)

Iodine (2.84 g, 11.2 mmol) was added to **7** (2.53 mmol) in 70 mL ether at −78°C. The iodine dissolved as the temperature rose. The reaction mixture was stirred at room temperature for 62 h, the ether was distilled, and the excess of iodine removed with aqueous sodium thiosulphate. The product **8***k* (0.152 g, 14.5%) was precipitated as a white solid on the addition of acetonitrile to the residual red-brown oil; mp 158.5–159.5°C. *Anal.* calcd. for $C_8H_{20}I_4N_4P_4$: C 12.0, H 2.5, I 63.2, N 7.0; found: C 12.1, H 2.4, I 62.9, N 6.9.

$N_4P_4Me_4(CH_2AsMe_2)_4$ (8l)

Dimethyliodoarsine (1.436 g, 6.19 mmol) in 60 mL ether was added to **7** (1.55 mmol) in 80 mL ether at −78°C over 10 min. Aqueous potassium fluoride was added to precipitate the lithium; the ether layer was separated and dried and the solvent evaporated off. The residual clear, colourless, hygroscopic oil was distilled under reduced pressure to yield pure **8***l* (0.61 g, 55%). *Anal.* calcd. for $C_{16}H_{44}As_4N_4P_4$: C 26.8, H 6.2, N 7.8; found: C 27.1, H 6.1, N 7.8. A quaternary salt $N_4P_4Me_4(CH_2AsMe_2)_4 \cdot 4MeI$ (**8***m*) was prepared by the addition of **8***l* to a large excess of methyl iodide. After 3 h, the white solid **8***m* (88%) was filtered off, washed with ether, and recrystallized from water as a monohydrate. It is insoluble in acetonitrile and chloroform; mp 280°C (dec.). *Anal.* calcd. for $C_{20}H_{58}As_4I_4N_4OP_4$: C 18.5, H 4.5, N 4.3; found: C 18.6, H 4.5, N 4.2.

$N_4P_4Me_6[CH_2C(O)Ph]_2$ (8a)

Ethyl benzoate (1.319 g, 8.78 mmol) in 70 mL ether was added to **7** (2.20 mmol) at −78°C over 10 min. On slow warming to room temperature the turbidity rapidly disappeared. After 5 h of stirring, the lithium was precipitated as fluoride and the solvent removed from the dried ether layer. Unchanged ethyl benzoate was distilled from the oily residue *in vacuo*. The addition of acetonitrile to the remaining pasty solid yielded white solid **8***a* (0.27 g, 24%), which was recrystallized from acetonitrile, mp 152.5–156°C; ν(C=O): 1663 cm^{-1}. *Anal.* calcd. for $C_{22}H_{32}N_4O_2P_4$: C 52.0, H 6.3, N 11.0; found: C 52.2; H 6.3, N 11.1.

Acknowledgements

We are grateful to the Natural Sciences and Engineering Research Council of Canada for financial support and for NRC Scholarships (K.D.G., R.T.O.), and to Mr. R. H. Lindstrom for help with some of the preparative work.

1. H. T. Searle. Proc. Chem. Soc. 7 (1959).
2. R. T. Oakley and N. L. Paddock. Can. J. Chem. **53**, 3038 (1975).
3. N. L. Paddock, T. N. Ranganathan, and S. M. Todd. Can. J. Chem. **49**, 164 (1971).
4. H. T. Searle, J. Dyson, T. N. Ranganathan, and N. L. Paddock. J. Chem. Soc. Dalton Trans. 203 (1975).
5. K. D. Gallicano, R. T. Oakley, N. L. Paddock, S. J. Rettig, and J. Trotter. Can. J. Chem. **55**, 304 (1977).
6. A. J. Bilbo. Z. Naturforsch. Teil B, **15**, 330 (1960).
7. H. R. Allcock, D. B. Patterson, and T. L. Evans. J. Am. Chem. Soc. **99**, 6095 (1977).
8. P. Wisian-Nielson and R. H. Neilson. J. Am. Chem. Soc. **102**, 2848 (1980).
9. C. W. Allen and A. J. White. Inorg. Chem. **13**, 1220 (1974); C. W. Allen. J. Organomet. Chem. **125**, 215 (1977).
10. T. Chivers and N. L. Paddock. Inorg. Chem. **11**, 848 (1972).
11. G. J. Bullen. J. Chem. Soc. 3193 (1962).
12. J. Högel and A. Schmidpeter. Z. Anorg. Allg. Chem. **458**, 168 (1979); A. Schmidpeter, K. Blanck, H. Hess, and R. Riffel. Angew. Chem. Int. Ed. Engl. **19**, 650 (1980).
13. H. P. Calhoun, R. H. Lindstrom, R. T. Oakley, N. L. Paddock, and S. M. Todd. Chem. Commun. 343 (1975).
14. R. T. Oakley and N. L. Paddock. Can. J. Chem. **55**, 3651 (1977).
15. A. E. Arbusov and A. A. Dunin. Chem. Ber. **60**, 291 (1947); A. E. Arbusov and A. I. Razumov. J. Russ. Phys. Chem. Soc. **61**, 623 (1929).
16. A. J. Carty and R. K. Harris. Chem. Commun. 234 (1967).
17. H. P. Calhoun, R. T. Oakley, N. L. Paddock, and J. Trotter. Can. J. Chem. **53**, 2413 (1975).
18. G. Chioccola and J. J. Daly. J. Chem. Soc. A, 568 (1968).

19. J. G. DUPONT and C. W. ALLEN. Inorg. Chem. **16**, 2964 (1977).
20. L. HORNER, H. HOFFMANN, and A. G. WIPPEL. Chem. Ber. **91**, 61 (1958).
21. E. ROBERTS, E. E. TURNER, and F. W. BURY. J. Chem. Soc. 1443 (1926).
22. K. D. GALLICANO, R. T. OAKLEY, and N. L. PADDOCK. J. Inorg. Nucl. Chem. **42**, 923 (1980).
23. T. KAUFFMANN, D. KUHLMANN, W. SAHM, and H. SCHRECKEN. Angew. Chem. Int. Ed. Engl. **7**, 541 (1968).
24. R. APPEL and G. SALEH. Chem. Ber. **106**, 3455 (1973).

Can. J. Chem. Downloaded from www.nrcresearchpress.com by 210.87.254.40 on 09/06/12
For personal use only.

The synthesis of the cyathins. Part 1. Synthesis of a tricyclic intermediate

WILLIAM A. AYER, DALE E. WARD, LOIS M. BROWNE, LOUIS T. J. DELBAERE,[1] AND YUMIKO HOYANO

Department of Chemistry, University of Alberta, Edmonton, Alta., Canada T6G 2G2

Received April 14, 1981

This paper is dedicated to Professor W. E. Harris on the occasion of his retirement from the University of Alberta

WILLIAM A. AYER, DALE E. WARD, LOIS M. BROWNE, LOUIS T. J. DELBAERE, and YUMIKO HOYANO. Can. J. Chem. **59**, 2665 (1981).

The tricyclic diketoalcohol **5** (3-phenylthio-6,9,10-trimethyl-12-hydroxytricyclo[7.4.0.0^{2,6}]trideca-2,10-diene-4,8-dione), a potential intermediate in the synthesis of the cyathins, has been prepared starting from 2,5-dimethyl-*p*-benzoquinone. The structure and stereochemistry of **5** was proven by an X-ray crystallographic study of the corresponding *p*-bromobenzoate (**6**). Attempts to isomerize the *cis* BC ring junction in **5** to give the corresponding *trans* compound were unsuccessful. Removal of the thiophenyl group from **5** gave compound **18***a* which on base-catalyzed isomerization provided an equilibrium mixture of the *cis* and *trans* compounds.

WILLIAM A. AYER, DALE E. WARD, LOIS M. BROWNE, LOUIS T. J. DELBAERE et YUMIKO HOYANO. Can. J. Chem. **59**, 2665 (1981).

A partir de la diméthyl-2,5 *p*-benzoquinone on a préparé le dicétoalcool tricyclique **5** (phénylthio-3 triméthyl-6,9,10 hydroxy-12 tricyclo[7.4.0.0^{2,6}]tridécadiène-2,6 dione-4,8) un intermédiaire potentiel dans la synthèse des cyathines. On a établi la structure et la stéréochimie du composé **5** par cristallographie de rayons-X du *p*-bromobenzoate (**6**) correspondant. On a essayé en vain d'isomériser la jonction du cycle BC *cis* du composé **5** en vue d'obtenir le composé *trans*. L'élimination du groupe thiophényle du composé **5** conduit au composé **18***a* qui par une isomérisation catalysée par une base donne un mélange de composé *cis* et *trans* en équilibre.

[Traduit par le journal]

The cyathins are a unique group of diterpenoids produced by the bird's nest fungi *Cyathus helenae* (1–3), *C. africanus* (4), and *C. earlei* (5).[2] Several of the cyathins, especially cyathin B_3 (**1**) and cyathin C_3 (**2**), show strong antibiotic activity (3, 7). The transformation of cyathin A_3 (**3**), the major diterpenoid metabolite of *C. helenae*, into the biologically more active cyathin B_3 (**1**) and cyathin C_3 (**2**), as well as to allocyathin B_3 (**4**), has been achieved (3). Thus, the total synthesis of cyathin A_3 (**3**) would also represent a synthesis of cyathin B_3 (**1**) and cyathin C_3 (**2**). We have briefly described two approaches to the synthesis of these compounds which have failed to reach the tricyclic stage (6). In this paper we describe the synthesis of the tricyclic intermediate **5** and the X-ray crystal structure of its *p*-bromobenzoate **6**.

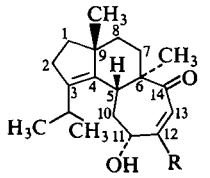

1 R = CHO
3 R = CH_2OH

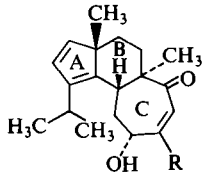

2 R = CHO
4 R = CH_2OH

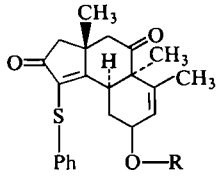

5 R = H
6 R = CO—C_6H_4—Br
16 R = THP

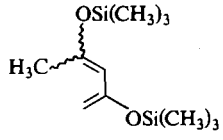

8

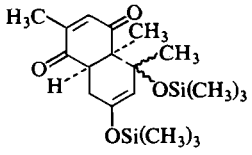

9

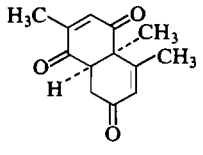

10

The general features of the synthetic strategy are outlined in Scheme 1. We envisioned the A and C rings of the cyathin skeleton to arise through aldol cyclizations of 1,4- and 1,6-diketones, respectively. Since a substituted cyclohexene is a latent 1,6-diketone our initial synthetic target was the substituted octalone **7**. Of crucial importance in the construction of **7**, and in any synthesis of the cyathins, is the generation of the correct *anti*-relationship between the quaternary methyl groups. We felt that by starting with 2,5-dimethyl-*p*-benzoquinone and carrying out two electrocyclic

[1]Present address: Department of Biochemistry, University of Saskatchewan, Saskatoon, Sask., Canada S7N 0W0.

[2]For a review of the structural studies, see ref. 6.

0008-4042/81/172665-08$01.00/0

©1981 National Research Council of Canada/Conseil national de recherches du Canada

Can. J. Chem. Downloaded from www.nrcresearchpress.com by 210.87.254.40 on 09/06/12
For personal use only.

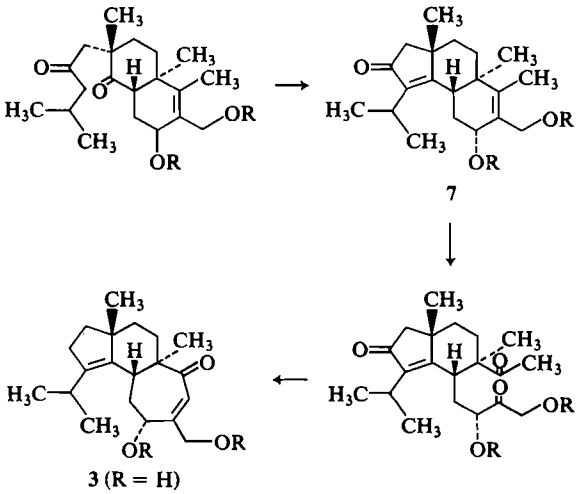

SCHEME 1

additions (one [4 + 2], the other [2 + 2]) the desired stereochemical result could be achieved.

Treatment of 2,5-dimethyl-*p*-benzoquinone with the known (8) 2,4-bistrimethylsilyloxy-1,3-pentadiene (**8**, 2.2 equivalents as a 1:1 mixture of stereoisomers) in refluxing xylene gave the adduct **9** in 91% yield. The ^{1}H nmr and ^{13}C nmr spectra showed that **9** was a single stereoisomer. The relative stereochemistry of the tertiary allylic silyl-ether was not determined, but it is not crucial since at a later stage this group is removed. The adduct **9** was further characterized by hydrolysis to the crystalline trione **10**. In the ^{1}H nmr spectrum of **10** the three nonmethyl aliphatic protons appear as an ABX pattern, with J_{AB} = 4 Hz, J_{AX} = 6 Hz, and J_{BX} = 18 Hz (the ring junction hydrogen is the A proton), confirming the stereo- and regiochemistry of the Diels–Alder addition.

The next stage in the synthesis called for a [2+ 2] photoaddition to the enedione system of **9**. Wiesner has studied the addition of allene and other olefins to enones and has described an empirical rule to predict the stereochemistry of such additions (9). The rule states that the reaction proceeds from a conformationally flexible (at least at the β-carbon) excited state in which the β-substituent of the enone assumes its thermodynamically more stable conformation. This rule is difficult to apply in the case of **9**, since in this flexible system with several sp^2 carbons it is difficult to predict the most stable conformation of the excited state. However, in the photodimerization of these types of compounds it has been shown that the product is the one with the sterically least congested *anti* stereochemistry (10). With this in mind we anticipated that addition of allene to **9** would lead to the product with the desired stereochemistry. Irradiation of a tetrahydrofuran solution of **9** in the presence of excess allene at −40° to −50°C provided a mixture of the adducts **11***a* and **11***b*. This mixture was hydrolyzed to give the triones **12***a* and **12***b* (ratio 4:1) in ca. 60% overall yield from the starting quinone.

In the 270 MHz ^{1}H nmr spectrum of compound **12**, the signals for the *exocyclic* methylene protons at C-5 (δ 5.16, 5.01) are coupled to the 4,6-ring junction proton (C-6, δ 3.70) confirming that the photoaddition had occurred with the desired regiochemistry in the major trione (**12***a*). As well, the coupling constants shown by the C-1 methine proton (δ 3.41, J = 3.8, 4.5 Hz) indicated the presence of a *cis* 6,6-ring junction in **12***a* as shown. Comparison of spectral data (^{1}H nmr and ^{13}C nmr) of the two inseparable isomers (**12***a* and **12***b*) led us to speculate that the minor isomer was the regioisomer **12***b*. This was confirmed by later experiments (*vide infra*). We were unable to assign the relative stereochemistry of the ring junctions (i.e., *cis–anti–cis* or *cis–syn–cis*). This was clarified at a later stage.

The *exocyclic* double bond in **12** was selectively oxidized with *m*-chloroperbenzoic acid to give a mixture of crystalline epoxides **13** in high yield. Hydrolysis of **13** with 1 *N* perchloric acid in refluxing tetrahydrofuran gave, after acetylation, a mixture of two monoacetates. Spectral data (ir, ^{1}H

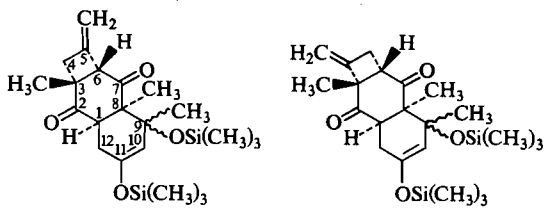

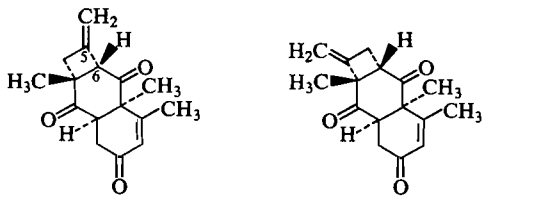

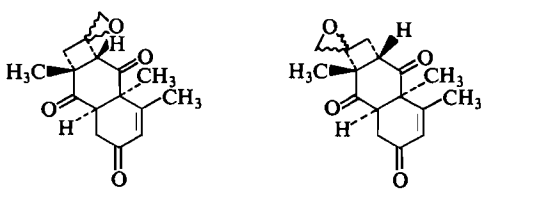

Can. J. Chem. Downloaded from www.nrcresearchpress.com by 210.87.254.40 on 09/06/12
For personal use only.

Can. J. Chem. Downloaded from www.nrcresearchpress.com by 210.87.254.40 on 09/06/12
For personal use only.

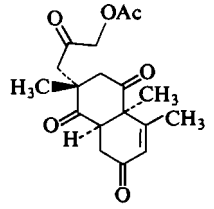

14a

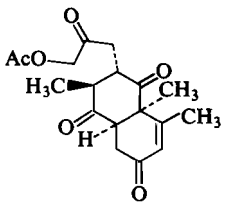

14b

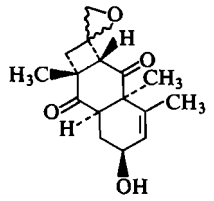

15a

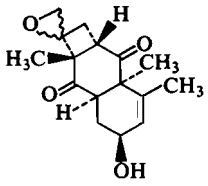

15b

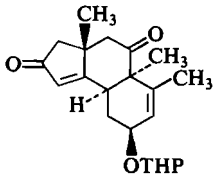

17

nmr) for the mixture was consistent with structures **14***a* and **14***b* present in a ratio of ca. 3 to 1. Significantly, in the ^{1}H nmr spectrum of the mixture, the minor isomer showed a methyl doublet at δ 1.10 which confirms the regioisomeric nature of the minor product in **11**, **12**, and **13**. The formation of **14** is a result of hydrolysis of the epoxide to a diol followed by retro-aldol fragmentation of the resulting β-hydroxyketone.

The next stage in the synthetic sequence involves the elaboration of the cyclobutane ring of compound **12** into the ring A system of the cyathins. Epoxide **13***a* can serve as a latent 1,4-diketone by nucleophilic opening of the epoxide followed by fragmentation as depicted in Scheme 2. Initial experiments suggested that 1,4-addition of the nucleophile to the enone system in ring C was occurring in competition with epoxide opening. To protect the enone system from such addition reactions, the α,β-unsaturated carbonyl group of **13** was selectively reduced with 9-borabicyclo[3.3.1]-nonane (11) to give compound **15** as indicated by the disappearance of the enone carbonyl band at 1670 cm^{-1}. We were unable to effect the desired epoxide opening reaction (cf. Scheme 2) with lithium diisopropylcuprate. However, treatment of **15** with an ethanolic solution of benzenethiol (12) containing 5 mol% aqueous KOH provided the tricyclic dione **5** which was isolated as a single component from the reaction mixture after trituration with ether.

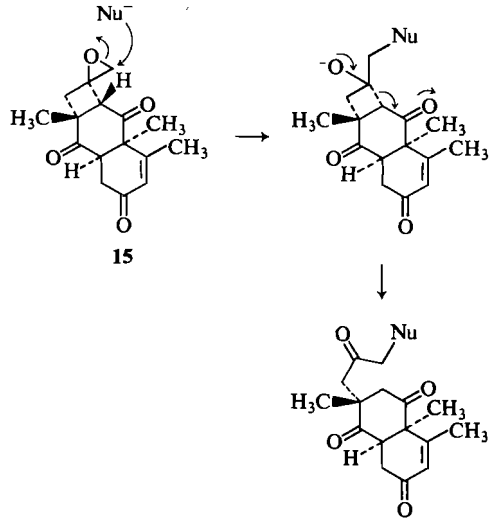

SCHEME 2

In the ^{1}H nmr spectrum of **5** the ring junction hydrogen at C-5 appears as a doublet of doublets at δ 3.62 with axial–equatorial and axial–axial couplings (J = 4, 11 Hz). Examination of Dreiding molecular models of **5** and its diastereoisomers shows that if the methyl groups are *cis*, the most stable conformation should be one in which the C-5 proton would be in a pseudo-equatorial configuration (with respect to the cyclohexene ring) and thus the coupling constants should be small. The large coupling constant observed for the ring junction proton in **5** is indicative of an axial hydrogen and suggested that **5** possessed the desired *anti* relationship of the ring junction methyls. At this point we were unable to unambiguously assign the stereochemistry of the 6,6-ring junction (i.e., *cis* or *trans*). In order to clarify this point and to verify the structure of **5** we undertook an X-ray crystallographic analysis of its *p*-bromobenzoate derivative, **6**. Compound **6** crystallizes in the monoclinic system $P2_1/c$. The crystal structure, which was solved using the heavy atom method and refined to an R index of 0.066, showed that **6** indeed possesses *anti* methyl groups, and that the stereochemistry at the BC ring junction is *cis*. A perspective drawing of the X-ray crystal structure of **6** is shown in Fig. 1.

The cyathins possess a *trans*-fused BC ring system and thus it was desirable to effect epimerization at C-5 in the tricyclic alcohol **5**. Attempted epimerization through deconjugation–conjugation of the ring A enone by treatment with sodium methoxide in refluxing methanol gave only recovered starting compound. Treatment of compound **5**

Can. J. Chem. Downloaded from www.nrcresearchpress.com by 210.87.254.40 on 09/06/12
For personal use only.

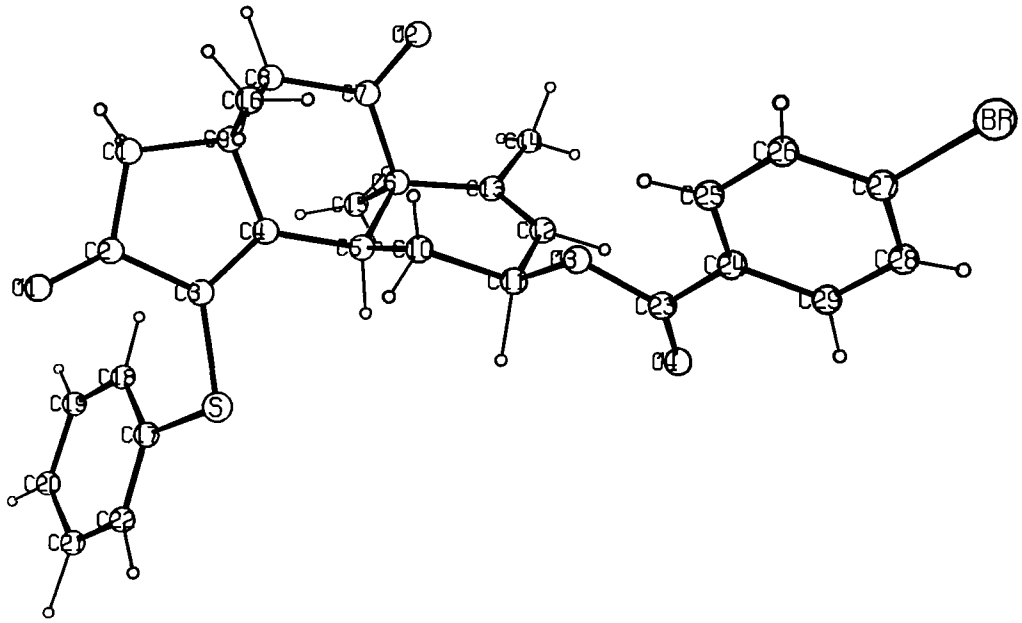

FIG. 1. Perspective drawing of the *p*-bromobenzoate of the tricyclic alcohol **5** (**6**).

using sodium methoxide – methanol-*O*-*d* led to recovery of **5** in which the hydrogens at C-1, C-5, and C-8 had been replaced by deuterium (as evidenced by ^{1}H nmr). These results suggest that the most stable configuration of this compound is that in which the BC ring fusion is *cis*. Inspection of Dreiding molecular models of **5** and its C-5 epimer show that the thiophenyl group at C-3 has a strong nonbonded interaction with the C-9 methylene group in the *trans* epimer, thus making the *cis* epimer thermodynamically more favorable. We reasoned that if the thiophenyl group were removed, then epimerization at C-5 might occur. Tricyclic alcohol **5** was transformed in the usual way to its tetrahydropyranyl ether, **16**, and this was subjected to treatment with Raney nickel, to give, in variable yield, the dione **17**. The THP ether was hydrolyzed in the presence of pyridinium *p*-toluenesulfonate and the resultant alcohol **18***a* was treated with sodium methoxide in hot methanol. The reaction product proved to be a mixture of alcohols in the ratio ca. 1.2:1. Analysis of the ^{1}H nmr spectra of the products **18** and the acetyl derivatives **19** shows that the minor component is the starting alcohol **18***a*.[3]

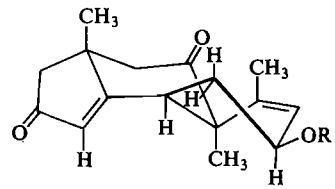

18*a* R = H
19*a* R = Ac

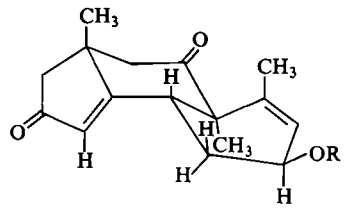

18*b* R = H
19*b* R = Ac

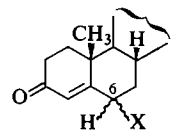

20

The proton at C-5 in **18***a* (δ 3.09) appears as a double doublet (J_5 = 2.5, 13.5 Hz) in the ^{1}H nmr spectrum indicating that ring C adopts a half-chair conformation (as the crystal structure shows to be the case with **6**). In this isomer the carbinyl proton at C-11 (δ 4.20) shows an axial–axial coupling as well as two small couplings ($W_{1/2}$ = 20 Hz (13)). The olefinic proton at C-3 (δ 6.08) appears as a

[3]On the scale on which we were working it was not possible to separate the mixtures **18** and **19**. However, at 400 MHz, it is possible to analyze sufficient portions of the ^{1}H nmr spectra to draw meaningful conclusions especially since spectra of pure **18***a* and **19***a* are available.

Can. J. Chem. Downloaded from www.nrcresearchpress.com by 210.87.254.40 on 09/06/12
For personal use only.

singlet. The major component of the reaction product is the desired *trans*-isomer **18***b*. In the spectrum of **18***b* the signal attributed to the C-5 proton (δ 3.22) is a doublet of doublet of doublets (J = 2, 7.5, 8.5 Hz). The carbinyl proton (δ 4.25) shows $W_{1/2}$ = 15 Hz. If the BC ring junction is indeed *trans*, then one would predict small to medium size couplings for the carbinyl proton. The observed coupling at C-11 ($W_{1/2}$ = 15 Hz) does not allow an unambiguous assignment in this epimer. However, the multiplicity of the C-3 proton (δ 6.0, d, J = 2 Hz) clarifies this point. Theory predicts that allylic coupling, i.e., coupling across one double and three single bonds, is zero when the allylic angle $\theta \approx 0°$ or 180° and reaches a maximum at $\theta = 90°$ (14). This allylic coupling has been amply demonstrated for several series of 6-substituted-Δ^4-3-oxosteroids (**20**) where it was found that olefinic protons at C-4 couple with the β-proton at C-6 ($\theta \sim 85°$) in the 6α-substituted series but not with the α-proton in the 6β-substituted series (allylic angle $\theta \sim 10°$) (14). The observed allylic coupling between the olefinic proton at C-3 and the ring junction proton at C-5 is 2 Hz in the case of **18***b* ($\theta \sim 80°$), confirming that epimerization has occurred. As expected, in the *cis* epimer C-3 appears as a singlet ($\theta \approx 0°$). An analysis of the ^{1}H nmr of the epimeric acetates **19** (see Experimental) is also in agreement with the assignment.

Attempts to completely transform **18***a* to **18***b* were unsuccessful as prolonged heating with sodium methoxide – methanol gave the same mixture of epimeric alcohols. Other methods to effect epimerization of **18** (e.g., through derivatization of the enone) remain to be investigated.

Compound **18** has the necessary stereochemistry for further elaboration to the cyathins. However, removal of the thioether function is undesirable in a synthetic sense, since we had hoped to utilize this functionality in the addition of the C-3 isopropyl group of the cyathins. The experiments described indicate that establishment of the *trans* BC ring junction in the decalin system of **5** is not straightforward and requires modification of the substitution pattern. It is conceivable that cleavage of the C-ring (see Scheme 1) will facilitate epimerization at C-5, or that the greater flexibility of the seven-membered ring C will allow the isomerization. Experiments to test these possibilities are in hand.

Experimental

Analytical thin layer chromatography (tlc) was carried out on glass plates (75 × 25 or 75 × 50 mm) coated (~0.3 mm) with silica gel G (W. Merck, Darmstadt) containing 1% electronic phosphor (General Electric, Cleveland). Preparative thin layer chromatography (ptlc) was carried out on glass plates (20 × 20, 10 × 20, or 5 × 20 cm) coated (0.5 mm) with the same adsorbent. Materials were detected by visualization under an ultraviolet lamp (254 or 350 nm). The plate (only a thin vertical band in the case of ptlc) was then sprayed with a solution of vanillin (1%) in concentrated sulfuric acid and charred using a heat gun.

Mass spectra (ms) were recorded on an A.E.I. MS-50 mass spectrometer coupled to a DS 50 computer, or an A.E.I. MS-9 mass spectrometer (chemical ionization). Data is reported as *m/e* (relative intensity). Unless diagnostically significant, peaks with intensities less than 20% of the base peak are omitted. Infrared spectra were recorded on a Nicolet 7199 FT interferometer or a Perkin-Elmer 297 infrared spectrophotometer and ultraviolet spectra on a Unicam SP 1700 ultraviolet spectrophotometer. The ^{1}H nmr spectra were measured on a Bruker WP-60 spectrometer interfaced to a Digilab FTS/NMR-3 data system, a Bruker WH-200 spectrometer, or a Bruker WH-400 spectrometer. The ^{13}C nmr spectra were measured on the aforementioned Bruker WP-60 instrument or a Bruker HFX-90 spectrometer interfaced to a Nicolet 1085 computer. All nuclear magnetic resonance measurements employed tetramethylsilane as an internal standard. Melting points were recorded on a Fisher-Johns melting point apparatus and are uncorrected. All compounds for which spectral data are reported showed single spots on tlc.

cis-*3,6,7-Trimethyl-7,9-bistrimethylsilyloxybicyclo[4.4.0]deca-3,8-diene-2,5-dione (9)*

A solution of 2,5-dimethyl-*p*-benzoquinone (10 g) and 2,4-bistrimethylsilyloxy-1,3-pentadiene (**8** (8), 40 g) in xylene (300 mL) was heated under reflux for 40 h. The volatiles were removed by evaporation under reduced pressure at 70°C. Bulb to bulb distillation (125°C/0.025 Torr) provided the Diels–Alder adduct **9** as a viscous orange oil (25.5 g). The ^{1}H nmr and ^{13}C nmr data suggested the adduct to be a single stereoisomer: ir (neat): 1684, 1628 cm^{-1}; ^{1}H nmr ($CDCl_3$) δ: 6.40 (1H, q (1.3 Hz), C-4 H), 4.94 (1H, t (1.3 Hz), C-8 H), 3.28 (1H, dd (6.7, 7.3 Hz), C-1 H), 2.22 (2H, m, C-9 H's), 1.95 (3H, d (1.3 Hz), C-3 CH_3), 1.45 (3H, s) and 1.32 (3H, s) (C-6, 7 CH_3's), 0.16 (9H, s) and 0.06 (9H, s) (silyl CH_3's); ^{13}C nmr ($CDCl_3$) δ: 200.4 (s) and 200.2 (s) (C-2, 5), 149.5 (s, C-3), 146.6 (s, C-9), 137.2 (s, C-4), 112.5 (d, C-8), 74.5 (s, C-7), 56.0 (s, C-6), 51.1 (d, C-1), 29.8 (t, C-10), 27.6 (q, C-7 CH_3), 20.1 (q, C-6 CH_3), 15.5 (q, C-3 CH_3), 2.2 (q) and 0.3 (q) (silyl CH_3's); ms *m/e* calcd. for $C_{19}H_{32}O_4Si_2$: 380.1839; found: 380.1834 (2), 244 (55), 230 (21), 229 (100), 73 (31).

cis-*3,6,7-Trimethylbicyclo[4.4.0]deca-3,7-diene-2,5,9-trione (10)*

The Diels–Alder adduct **9** (480 mg) was dissolved in methanol (10 mL) and trifluoroacetic acid (~10 mg) was added. The solution was stirred at room temperature for 3 h, diluted with 10% $NaHCO_3$ (20 mL), extracted with $CHCl_3$, dried (Na_2SO_4), and the solvent evaporated to give the crude **10**. Recrystallization from CCl_4 gave **10** (154 mg, 70%), mp 109–111°C; ir (neat): 1680, 1621 cm^{-1}; ^{1}H nmr ($CDCl_3$) δ: 6.65 (1H, q (1.5 Hz), C-4 H), 5.84 (1H, q (1.5 Hz), C-8 H), 3.17 (2H) and 2.58 (1H) ((ABX 4, 6, 18 Hz), C-1, 10 H's), 2.01 (3H, d (1.5 Hz), C-3 CH_3), 1.81 (3H, d (1.5 Hz), C-7 CH_3), 1.56 (3H, s, C-6, CH_3); ^{13}C nmr ($CDCl_3$) δ: 198.6 (s) and 197.3 (s) (C-2, 5), 194.4 (s, C-9), 159.8 (s, C-7), 150.3 (s, C-3), 136.3 (d, C-4), 127.9 (d, C-8), 54.3 (s, C-6), 53.3 (d, C-1), 34.3 (t, C-10), 21.2 (q, C-6, 7 CH_3's), 16.1 (q, C-3 CH_3); ms *m/e* calcd. for $C_{13}H_{14}O_3$: 218.0942; found: 218.0938 (100), 176 (40), 123 (17), 96 (77), 68 (82). *Anal.* calcd. for $C_{13}H_{14}O_3$: C 71.54, H 6.47; found: C 70.92, H 6.38.

3,8,9-Trimethyl-5-methylene-9,11-bistrimethylsilyloxytricyclo-[6.4.0.0.^{3,6}]dodec-10-ene-2,7-dione (11a)

A solution of the adduct **10** (25 g) and excess allene (250 g) in

Can. J. Chem. Downloaded from www.nrcresearchpress.com by 210.87.254.40 on 09/06/12
For personal use only.

dry THF (500 mL) was irradiated through a Pyrex filter with a 450 W Hanovia mercury vapor lamp for 20 h while nitrogen was bubbled through the solution. The internal temperature was maintained at −40 to −50°C. The excess allene was allowed to evaporate followed by evaporation of the solvent at reduced pressure to afford the crude photoadduct **11** as an oil (27 g). Spectral data (^{1}H and ^{13}C nmr) indicate that **11** is a 4:1 mixture of the 5-methylene (**11***a*) and the 4-methylene (**11***b*) isomers. The later conversion of **11** into **5** indicates that **11***a* possesses the *cis–anti–cis* stereochemistry at the ring junctions; ir (neat): 1708, 1676 cm^{-1}; ^{1}H nmr ($CDCl_3$) δ for major isomer **11***a*: 5.30 (1H, m) and 5.15 (1H, m) (exocyclic methylene H's), 4.96 (1H, t (1.3 Hz), C-10 H), 1.63 (3H, s), 1.52 (3H, s), and 1.37 (3H, s) (C-3, 8, 9 CH_3's), 0.42 (9H, s) and 0.28 (9H, s) (silyl CH_3's); ^{13}C nmr ($CDCl_3$) δ for major isomer **11***a*: 211.3 (s) and 206.2 (s) (C-2, 7), 148.0 (s, C-11), 140.0 (s, C-5), 112.0 (d, C-10), 110.7 (t, C-5 CH_2), 75.1 (s, C-9), 63.1 (d, C-6), 56.8 (s, C-8), 48.9 (d, C-1), 44.9 (s, C-3), 43.3 (t, C-4), 26.0 (t, C-12), 28.0 (q), 24.4 (q), 21.5 (q) (C-3, 8, 9 CH_3's), 2.28 (q) and 0.36 (q) (silyl CH_3's); ms *m/e* calcd. for $C_{21}H_{33}O_4Si_2$ ($M^+ - CH_3$): 405.1917; found: 405.1916 (18), 244 (55), 230 (22), 229 (100), 149 (27), 147 (16), 73 (59).

*3,8,9-Trimethyl-5-methylenetricyclo[6.4.0.0.^{3,6}]dodec-9-ene-2,7,11-trione (12*a)

The photoadduct **11** (27 g) was dissolved in 30% methanol in THF (150 mL) and Rexyn 101 acidic ion exchange resin (~5 g) was added. The mixture was stirred at room temperature for 30 h, poured onto 10% $NaHCO_3$ (300 mL), extracted with $CHCl_3$, washed with saturated $NaHCO_3$, dried (Na_2SO_4), and the solvent evaporated to give the crude trione **12** (17.5 g) which was used in the next step without further purification. In reactions carried out on a smaller scale (i.e., starting with 2 g of the quinone **2**) the crude trione (~3.5 g) was purified by column chromatography (Florosil, ether) to give crystalline **10** (2.2–2.6 g) which was recrystallized from CCl_4–cyclohexane (mp 120–131°C). Spectral data (^{1}H and ^{13}C nmr) indicated that **12** was an ~4:1 mixture of the 5-methylene (**12***a*) and 4-methylene (**12***b*) isomers.[4] The ultimate conversion of **12** into **5** indicates that **12***a* possesses the *cis–anti–cis* stereochemistry at the ring junctions; ir (neat): 1701, 1676, 1619 cm^{-1}; ^{1}H nmr ($CDCl_3$)[5] δ for major isomer **12***a*: 5.83 (1H, q (1.5 Hz), C-10 H), 5.16 (1H, dq (1, 2.7 Hz)) and 5.01 (1H, ddt (1.1, 2.2, 3.3 Hz)) (exocyclic methylene H's), 3.70 (1H, dq (2.2, 2.7 Hz), C-6 H), 3.41 (1H, dd (3.8, 4.5 Hz), C-1 H), 3.08 (1H, dd (3.8, 18 Hz)) and 2.53 (1H, dd (4.5, 18 Hz)) (C-11 H's), 2.86 (2H, m, C-4 H's), 1.80 (3H, d (1.5 Hz), C-9 CH_3), 1.53 (3H, s, C-8 CH_3), 1.37 (3H, s, C-3 CH_3); ^{13}C nmr ($CDCl_3$) δ for major isomer **12***a*: 209.8 (s) and 204.0 (s) (C-2, 7), 157.8 (s, C-9), 139.8 (s, C-5), 128.6 (d, C-10), 110.5 (t, C-5 CH_2), 61.1 (d, C-6), 54.9 (s, C-8), 51.5 (d, C-1), 45.1 (s, C-3), 43.1 (t, C-4), 34.3 (t, C-12), 23.6 (q, C-3, 8 CH_3's), 21.0 (q, C-9, CH_3); ms *m/e* calcd. for $C_{16}H_{18}O_3$: 258.1256; found: 258.1247 (4), 216 (40), 177 (37), 172 (27), 171 (33), 157 (25), 149 (24), 123 (45), 122 (24), 109 (22), 108 (24), 94 (26), 80 (86), 79 (100), 77 (34). *Anal.* calcd. for $C_{16}H_{18}O_3$: C 74.40, H 7.02; found: C 74.08, H 7.03.

*3,8,9-Trimethyltricyclo[6.4.0.0^{3,6}]dodec-9-ene-2,7,11-trione-5-spirooxirane 13*a

The triones **12** (1.75 g) and *m*-chloroperbenzoic acid (85%, 1.75 g) in CH_2Cl_2 (70 mL) were stirred at room temperature for 36 h. The solution was washed with 10% sodium bisulfite, water, saturated $NaHCO_3$, brine, dried (Na_2SO_4), and the solvent evaporated to give a crystalline mixture of epoxides **13** (1.58 g) after trituration with ether. Alternatively, the crude triones **12** could be oxidized as above to give the crystalline epoxides **13** in ~45% overall yield from the quinone without chromatography. Spectral data (^{1}H nmr and ^{13}C nmr) indicated that **13** was an ~4:1 mixture of the 5-spirooxirane (**13***a*) and the 4-spirooxirane (**13***b*) isomers. The conversion of **13** into **5** indicates that **13***a* possesses the *cis–anti–cis* stereochemistry at the ring junctions; ir (neat): 1706, 1674, 1616 cm^{-1}; ^{1}H nmr ($CDCl_3$) δ for major isomer **13***a*: 5.81 (1H, q (1.5 Hz), C-10 H), 3.73 (1H, dd (3, 4 Hz)) and 3.58 (1H, br s) (oxirane CH_2), 2.82 (1H, s, C-6 H), 1.77 (3H, d (1.5 Hz), C-9 CH_3), 1.55 (3H, s, C-8 CH_3), 1.41 (3H, s, C-3 CH_3); ^{13}C nmr ($CDCl_3$) δ for major isomer **13***a*: 208.8 (s) and 204.6 (s) (C-2, 7), 195.0 (s, C-11), 157.7 (s, C-9), 129.1 (d, C-10), 63.8 (s, C-5), 54.4 (s, C-8), 53.3 (t, C-5 CH_2), 48.6 (d) and 46.0 (d) (C-1, 6), 42.2 (s, C-3), 34.1 (t) and 33.2 (t) (C-4, 12), 22.2 (q) and 20.4 (q ×2) (C-3, 8, 9 CH_3's); ms *m/e* calcd. for $C_{16}H_{18}O_4$: 274.1205; found: 274.1212 (17), 259 (14), 246 (13), 232 (39), 191 (20), 188 (22), 187 (22), 173 (21), 158 (20), 152 (27), 124 (28), 123 (49), 96 (32), 95 (28), 94 (54), 93 (24), 91 (35), 82 (51), 79 (100), 77 (59), 68 (37), 66 (38), 65 (32), 55 (26), 54 (24), 53 (44), 51 (21).

Acid Hydrolysis of the Epoxides 13

A solution of the epoxides **13** (541 mg) in THF (15 mL) and 1 *N* $HClO_4$ (5 mL) was heated under reflux overnight and poured onto saturated $NaHCO_3$ (20 mL), extracted with $CHCl_3$ and the solvents evaporated to give a highly insoluble amorphous solid after trituration with ether. The solid was dissolved in CH_2Cl_2 (15 mL) and pyridine (1 mL) and acetic anhydride (1 mL) were added. The resulting solution was stirred at room temperature for 2.5 h and the solvents were evaporated under high vacuum at 50°C to give **14** as an oil (487 mg). This was an ~3:1 mixture of **14***a* and **14***b*, respectively; ir (neat): 1740, 1710 cm^{-1}; ^{1}H nmr ($CDCl_3$) δ for major isomer **14***a*: 5.73 (1H, br s), 4.57 (2H, m), 2.32 (2H, s), 2.12 (3H, s), 1.88 (3H, d (1.5 Hz)), 1.57 (3H, s), 0.98 (3H, s); δ for minor isomer **14***b*: 5.84 (1H, br s), 4.80 (2H, m), 2.16 (3H, s), 1.81 (3H, d (1.5 Hz)), 1.49 (3H, s), 1.10 (3H, d (6)); ms *m/e* calcd. for $C_{18}H_{22}O_6$: 334.1399; found: 334.1425 (7), 218 (37), 123 (100), 122 (42), 94 (33), 91 (20), 79 (47), 77 (25), 55 (45).

Tricyclic Alcohol 5 from the Epoxides 13

To a solution of **13** (275 mg) in dry THF (4 mL) was added 0.5 *N* 9-BBN in THF (2.2 mL). The solution was stirred at room temperature under nitrogen for 1.5 h. The solvent was evaporated at reduced pressure and the resulting oil was dissolved in ether (8 mL). Ethanolamine (70 mg) was added and the mixture was stirred at room temperature for 1 h. The precipitated 9-BBN – ethanolamine complex was removed by centrifuging and the supernatant concentrated under reduced pressure to give the crude allylic alcohol **15** as an oil. To a solution of the crude **15** in ethanol (5 mL) was added benzenethiol (120 mg) and 2 *N* KOH (25 μL). After stirring under nitrogen for 8 h at 0°C a further 25 μL of 2 *N* KOH was added and the solution heated under reflux for 1.5 h. The solution was poured onto saturated $NaHCO_3$ (20 mL), extracted with $CHCl_3$, dried ($NaSO_4$), and the solvent evaporated to give an oil which upon trituration with ether provided the crystalline **5** (200 mg), mp 209–211°C; ir (neat): 3420, 1705 cm^{-1}; ^{1}H nmr ($CDCl_3$) δ: 7.29 (5H, br s, aromatic H's), 5.73 (1H, br s, C-12 H), 4.10 (1H, m, C-11 H), 3.62 (1H, dd (4, 11 Hz), C-5 H), 2.96 (1H, d (13 Hz)) and 2.51 (1H, d (13 Hz)) (C-8 H's), 2.56 (2H, s, C-1 H), 1.78 (3H, d (1.5 Hz), C-13 CH_3), 1.6 (3H, m, C-10, H, OH), 1.35 (3H, s) and 1.32 (3H, s) (C-6, 9 CH_3's); ms *m/e* calcd. for $C_{22}H_{24}O_3S$; 368.1449; found: 368.1444 (100), 350 (33), 335 (27), 285 (45), 284 (21), 199 (23), 198 (27), 185 (21), 175 (20), 109 (37), 91 (48), 77 (45), 65 (22); ^{13}C nmr (DMSO-d_6) δ: 209.8 (s, C-7), 201.5 (s, C-2), 184.1 (s, C-4), 135.4 (s, C-1′), 133.9 (s), and 132.7 (s) (C-3, 13), 130.6 (d, C-12), 129.1 (d ×2) and 128.1 (d ×2), C-2′, 3′), 126.3 (d, C-4′), 65.4 (d, C-11), 52.3 (t, C-8), 51.8 (s) and 49.1 (s) (C-6, 9), 47.4 (d, C-4), 46.7 (t, C-1), 35.0 (C-10), 28.6 (q), 23.9 (q), and 19.6 (q) (C-6, 9, 13 CH_3's).

[4]Compounds **12***a*, **12***b* are co-crystalline and homogeneous by tlc and thus could not be separated.

[5]Spectrum obtained at 270 MHz.

Can. J. Chem. Downloaded from www.nrcresearchpress.com by 210.87.254.40 on 09/06/12
For personal use only.

p-Bromobenzoate of Tricyclic Alcohol (6)

Tricyclic alcohol **5** (100 mg, 0.27 mmol), *p*-bromobenzoyl chloride (65.8 mg, 0.3 mmol), and 4-*N*,*N*-dimethylaminopyridine (60.7 mg, 0.4 mmol) in dry methylene chloride (10 mL) were stirred at room temperature for 1 h under nitrogen. A small amount of water was added and the organic solvent removed. The aqueous residue was extracted twice with ether. The separated ethereal solution was washed successively with 1 *N* hydrochloric acid, sodium bicarbonate, water, then dried and evaporated. The residue was crystallized from ethyl acetate and then from methylene chloride – hexane, mp 126.5–127.5°C; ir: 2990, 1713, 1590, 1280, 1110, 750 cm^{-1}; ^1H nmr ($CDCl_3$) δ: 7.74 (4H, q (9 Hz)), 7.30 (5H, m), 5.70 (1H, s, C-12 H), 5.48 (1H, t (8 Hz), C-11 H), 3.78 (1H, m, C-5 H), 2.78 (2H, q (13 Hz), C-1 H), 2.58 (2H, s, C-8 H), 1.82 (3H, s, C-13 CH_3), 1.37 (6H, s, C-6, 9 CH_3); ^{13}C nmr ($CDCl_3$) δ: 209.7 (s, C-7), 201.4 (s, C-2), 184.1 (s, C-4), 135.4 (s, C-1′), 133.8 (s) and 132.7 (s) (C-3, 13), 130.5 (d, C-12), 129.0 (d ×2) and 128.1 (d ×2) (C-2′, 3′), 126.2 (d, C-4′), 65.4 (d, C-11), 52.3 (t, C-8), 51.8 (s) and 49.1 (s) (C-6, 9), 47.3 (d, C-5), 46.7 (t, C-1), 35.0 (t, C-10), 28.6 (q), 23.9 (q) and 19.6 (q), (C-6, 9, 13 CH_3's); *Anal.* calcd. for $C_{29}H_{21}O_4SBr \cdot 1/4\ CH_2Cl_2$: C 60.07, H 4.69; found: C 59.70, H 4.63.

Compound **6** crystallized in the monoclinic system with the following crystal data:

$C_{29}H_{27}O_4SBr \cdot \frac{1}{4}(CH_2Cl_2)$ f.w. = 551.5

$P2_1/c$, a = 14.118(2), b = 10.987(2), c = 21.534(4), β = 124.24°, V = 2761.3 Å^3, Z = 4, ρ_o = 1.36 g cm^{-3}, ρ_c = 1.33 g cm^{-3}. Radiation Ni-filtered CuK_α, λ = 1.5418 Å, θ – 2θ with scan speed 2° min^{-1} over 1.6° scan range, 10 s stationary background counts on either side of each scan. Data collected: h,k,l; $\bar{h},k,l$, with 6° ≦ 2θ ≦ 100°. Maximum applied absorption correction (15) was 1.49. $R_{sym} = \Sigma_i|\bar{I} - I_i|/\Sigma_i I_i \times 100 = 1.1\%$ for 97 reflections merged. The data set for the crystal structure analysis was limited to the 2114 reflections of the 2824 unique reflections which had net $I > 3\theta$ (I).

The solution of the structure involved examining the Patterson map to obtain the position of the bromine atom of the molecule. Least-squares refinement of the scale factor and the positional parameters of this atom produced an R of 0.497. Four additional atoms were chosen from a subsequent difference Fourier map. The positions of the remaining nonhydrogen atoms were obtained by continually phasing on larger molecular fragments and calculating difference maps. After full matrix isotropic refinement of all of the thirty-five nonhydrogen atoms of the molecule, the R index was 0.156. Further blocked anisotropic refinement produced an R index of 0.127. Twenty-seven hydrogen atoms were located from a difference Fourier map and were assigned isotropic temperature factors of 5–6 Å^2. A disordered methylene chloride molecule was located near the origin of the unit cell corresponding to an electron density peak height of one molecule/unit cell. The chlorine and carbon atoms of this solvent molecule were refined positionally and with isotropic temperature factors. The hydrogen atom positional parameters (but not the temperature factors) were also included in subsequent blocked refinement. Convergence was achieved at an R index of 0.066. These computations were carried out using the X-ray 70 system (16).[6] A perspective drawing of compound **6** is shown in Fig. 1.

Tetrahydropyranyl Ether 16 of the Tricyclic Alcohol

The tricyclic alcohol **5** (100 mg, 0.27 mmol), dihydropyran (33.6 mg, 0.40 mmol, 1.5 equiv.), and *p*-toluenesulfonic acid (0.3 mg) in dry THF (5 mL) were stirred at room temperature for 72 h. The solvent was evaporated and water and ethyl acetate were added to the residue. Extraction with ethyl acetate was repeated twice, then the organic layer was washed with sodium bicarbonate and water, dried, and evaporated to give 168 mg of the tetrahydropyranyl ester **16**. Compound **16** was purified by chromatography over Florosil (10 g). Elution with chloroform (20 × 5 mL) afforded **16** (163 mg) which was recrystallized from methylene chloride – Skellysolve B: (94.2 mg), mp 155–160°C; ir (film): 1735, 1710, 1615 cm^{-1}.

*Preparation of Tricyclic Alcohol 18*a

The THP ether **16** (350 mg, 0.77 mmol) and W-2 Raney nickel (ca. 200 mg) in ethyl acetate were heated under reflux until the starting material disappeared as shown by tlc (approximately one week). The catalyst was removed by careful filtration through Celite and the filtrate was evaporated to give 313 mg of compound **17** which was purified by chromatography over neutral alumina (activity IV) by elution with benzene–chloroform.

The THP ether **17** (100 mg, 0.29 mmol) and pyridinium-*p*-toluenesulfonate (catalytic amount) in 98% ethanol were allowed to stand at room temperature overnight, then heated at 55°C for 2.5 h. The solvent was evaporated and the residue was taken up in methylene chloride, washed with water, dried, and evaporated. The product, compound **18*a***, was purified by preparative tlc and crystallized from methylene chloride – Skelly B: mp 163–165°C; ir: 3580, 1960, 1688, 1610, 1430, 1380 cm^{-1}; ^1H nmr ($CDCl_3$) δ: 6.08 (1H, s, C-3 H), 5.52 (1H, br s, C-12 H), 4.20 (1H, m ($W_{1/2}$ = 20), C-11 H), 3.09 (1H, dd (2.5, 13.5 Hz), C-5 H), 2.68 (2H, q), 2.46 (1H, s), 1.82 (2H, m, C-10 H), 1.76 (3H, s, C-13 CH_3), 1.32 (6H, s, C-6, 9 CH_3's); ms *m/e*: 242 (M^+ – 18, 93), 227 (43), 201 (18), 200 (31), 199 (18), 185 (36), 173 (18), 159 (25), 157 (32), 145 (20), 133 (36).

*Acetylation of Tricyclic Alcohol 18*a

The alcohol **18*a*** (13.1 mg, 0.05 mmol) and 4-*N*,*N*-dimethylaminopyridine (13 mg, 0.08 mmol) in dry methylene chloride (5 mL) were stirred at room temperature overnight. The mixture was diluted with water and extracted with methylene chloride. The organic layer was washed with water, 1 *N* hydrochloric acid, sodium bicarbonate and water, dried, and evaporated to give 17 mg of the acetate **19*a*** as an oil; ir (film): 3400, 1730 (sh), 1705, 1615 cm^{-1}; ^1H nmr ($CDCl_3$) δ: 6.14 (1H, s, C-3 H), 5.68 (1H, s, C-12 H), 5.28 (1H, m ($W_{1/2}$ = 20), C-11 H), 3.17 (1H, dd (2.5, 13.5 Hz), C-5 H), 2.72 (2H, q), 2.52 (2H, m), 2.06 (3H, s, C-11 OCOCH_3), 1.78 (3H, s, C-13 CH_3), 1.35 (6H, s, C-6, 9 CH_3's).

*Epimerization of Tricyclic Alcohol 18*a

The alcohol **18*a*** (12.3 mg, 0.047 mmol) was heated under reflux for 3 h with sodium methoxide (prepared by dissolving sodium (3.5 mg) in dry methanol (5 mL)). The solution was cooled, neutralized with aqueous acetic acid and methanol, then concentrated. The reaction product was extracted with chloroform, washed with water, dried, and evaporated to give 13 mg of an epimeric mixture of alcohols **18*a*** and **18*b*** in the ratio 1:1.2; ^1H nmr ($CDCl_3$) δ for major isomer **18*b***: 6.02 (1H, d (2 Hz), C-3 H), 5.67 (1H, br s, C-12 H), 4.25 (1H, m ($W_{1/2}$ = 15), C-11 H), 3.22 (1H, ddd (2, 7.5, 8.5 Hz), C-5 H), 1.76 (3H, br s, C-13 CH_3), 1.17 (3H, s), 1.11 (3H, s) (C-6, 9 CH_3's).

*Epimerization of Acetate 19*a

The tricyclic acetate **19*a*** was heated with sodium methoxide (prepared by dissolving sodium (11 mg) in dry methanol (10 mL)) for 3 h. After cooling, a few drops of aqueous acetic acid were added and the solution was concentrated. The residue was extracted with methylene chloride, washed with water, dried,

[6]Tables of atomic parameters, bond lengths and angles, and structure factors are available at a nominal charge from the Depository of Unpublished Data, CISTI, National Research Council of Canada, Ottawa, Ont., Canada K1A 0S2.

and evaporated to give 20 mg of a mixture. Purification by chromatography over silica gel and elution with chloroform–ether (1:1) gave a product (15.3 mg) which showed a single spot on tlc. The ^{1}H nmr spectrum showed this to be a mixture of epimeric alcohols **18***a* and **18***b*. Acetylation of this mixture by the method described above gave a mixture of epimeric acetates **19***a* and **19***b*; ^{1}H nmr ($CDCl_3$) δ for major isomer **19***b*: 5.94 (1H, d (2 Hz), C-3 H), 5.64 (1H, d (6 Hz), C-11 H), 5.58 (1H, s, C-12 H), 3.16 (1H, C-5 H), 2.04 (3H, s, C-11 $OCOCH_3$), 1.93 (3H, s, C-13 CH_3), 1.32 (3H, s), 1.22 (3H, s) (C-6, 9 CH_3's).

Acknowledgements

We wish to thank the Natural Sciences and Engineering Research Council of Canada for financial support in the form of an operating grant (W.A.A.) and scholarships (D.E.W.). We also thank Prof. M. James for the use of the equipment used in the collection of the X-ray data and Dr. T. T. Nakashima for his help with the nmr measurements.

1. W. A. Ayer and H. Taube. Can. J. Chem. **51**, 3842 (1973).
2. W. A. Ayer and L. L. Carstens. Can. J. Chem. **51**, 3157 (1973).
3. W. A. Ayer, L. M. Browne, J. R. Mercer, D. R. Taylor, and D. E. Ward. Can. J. Chem. **56**, 717 (1978).
4. W. A. Ayer, T. Yoshida, and D. M. J. van Schie. Can. J. Chem. **56**, 2113 (1978).
5. W. A. Ayer and S. P. Lee. Can. J. Chem. **57**, 3332 (1979).
6. W. A. Ayer, L. M. Browne, S. Fernández, D. E. Ward, and T. Yoshida. Rev. Latinoam. Quim. **9**, 177 (1978).
7. A. D. Allbutt, W. A. Ayer, H. J. Brodie, B. N. Johri, and H. Taube. Can. J. Microbiol. **17**, 1401 (1971).
8. T. Ibaka, Y. Ito, Y. Mori, T. Aoyana, and Y. Inubushi. Synth. Commun. **7**, 131 (1977).
9. (*a*) K. Wiesner. Tetrahedron, **31**, 1655 (1975); (*b*) G. Marini-Bettolo, S. P. Sahoo, G. A. Poulton, T. Y. R. Tsai, and K. Wiesner. Tetrahedron, **36**, 719 (1980).
10. J. R. Scheffer and A. A. Dzakpasa. J. Am. Chem. Soc. **106**, 2163 (1968).
11. H. C. Brown, S. Krishnamunthy, and N. M. Moon. J. Org. Chem. **41**, 1778 (1976).
12. A. G. Schultz, W. Y. Fu, R. D. Lucci, B. G. Korr, K. M. Lo, and M. Boxer. J. Am. Chem. Soc. **100**, 2140 (1978).
13. Alfred Hassner and Clayton Heathcock. J. Org. Chem. **29**, 1350 (1964).
14. L. M. Jackman and S. Sternhell. *In* Applications of nuclear magnetic resonance spectroscopy in organic chemistry. 2nd ed. Pergamon Press, Toronto. 1969. p. 316.
15. A. C. T. North, D. C. Phillips, and F. S. Matthews. Acta Crystallogr. Sect. A, **24**, 351 (1968).
16. J. M. Stewart, F. A. Hundell, and J. C. Baldwin. The X-ray 70 system. Computer Science Center, University of Maryland, College Park, MD, U.S.A. 1970.

Can. J. Chem. Downloaded from www.nrcresearchpress.com by 210.87.254.40 on 09/06/12
For personal use only.

Pyrrole chemistry. XXIII. The cyanation of substituted pyrroles with chlorosulfonyl isocyanate (CSI). New syntheses of pyrrole-3-carbonitriles

CHARLES E. LOADER AND HUGH J. ANDERSON

Department of Chemistry, Memorial University of Newfoundland, St. John's, Nfld., Canada A1B 3X7

Received April 14, 1981

CHARLES E. LOADER and HUGH J. ANDERSON. Can. J. Chem. **59**, 2673 (1981).

Chlorosulfonyl isocyanate (CSI) reacts not only with pyrrole itself but with pyrroles having powerful electron-withdrawing groups in the 2-position. Suitable choice of electron-withdrawing groups allows selective 4-substitution of the pyrrole ring. The *N*-chlorosulfonyl amides formed are readily converted to the corresponding nitriles. The procedure has been used to provide syntheses of pyrrole-3-carbonitrile and its 1-methyl homologue.

CHARLES E. LOADER et HUGH J. ANDERSON. Can. J. Chem. **59**, 2673 (1981).

L'isocyanate de chlorosulfonyle (ISC) réagit non seulement avec le pyrrole lui-même mais également avec les pyrroles ayant des groupes fortement électro-attracteurs en position 2. Un choix convenable des groupes électro-attracteurs permet une substitution sélective du cycle pyrrole en position 4. Les *N*-chlorosulfonylamides qu'on obtient se transforment facilement en nitriles correspondants. On a utilisé la méthode pour réaliser la synthèse du carbonitrile-3 pyrrole et de son analogue méthylé en position 1.

[Traduit par le journal]

Recent improvements in methods for the synthesis of pyrrole-2-carbonitrile have made this useful compound readily available (1). Although pyrrole-3-carbonitrile has been known for many years, the methods available for its preparation give poor yields or are not easily adapted to large scale work (2). In view of the versatility of the nitrile group and the limited amount known about the properties of pyrrole-3-carbonitriles we have developed a synthesis that gives good yields from pyrrole.

Using pyrrole as starting material and making use of our earlier work on the directing properties of substituents at the 2-position of the pyrrole ring (3), the most convenient route to pyrrole-3-carbonitrile appeared to be as shown in Scheme 1.

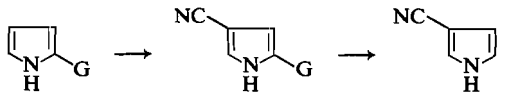

1 **2** **3**

G = suitable electron-withdrawing group directing substitution to the 4-position

a G = —COOH *c* G = —CN *e* G = —$COCCl_3$
b G = —CHO *d* G = —$COOCH_3$

SCHEME 1

Two routes appeared to be particularly attractive, one leading to the decarboxylation of 4-cyanopyrrole-2-carboxylic acid (**2***a*) and the other to the catalytic decarbonylation of 4-cyanopyrrole-2-carboxaldehyde (**2***b*). The main difficulty in this approach was the introduction of the nitrile group in good yield.

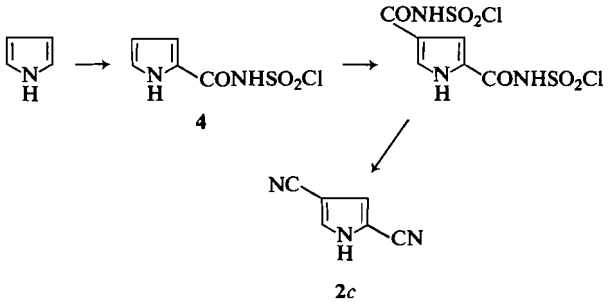

4

2*c*

SCHEME 2

Chlorosulfonyl isocyanate (CSI) has been shown to be a versatile reagent for the introduction of the nitrile group onto active aromatic ring systems (4). CSI is very reactive towards both pyrrole and 1-methylpyrrole and we have reported procedures for the preparation of both pyrrole-2-carbonitrile and 1-methylpyrrole-2-carbonitrile using the reagent (5). The yield of pyrrole-2-carbonitrile was relatively poor and our recent work has led to a modified procedure that gives a much improved yield. *N*,*N*-Dimethylformamide (DMF) does not react with CSI at low temperatures and can be used as a solvent for the reaction. CSI reacts with the pyrrole first and that product, on warming with the DMF, reacts to give the nitrile. This method avoids the formation of by-products, in particular of dicyanopyrroles, that lowered the yield obtained in the earlier procedure.

We also noted that pyrrole with excess CSI followed by treatment with DMF gave a good yield of pyrrole-2,4-dicarbonitrile (**2***c*) (containing a small

0008-4042/81/172673-04$01.00/0

©1981 National Research Council of Canada/Conseil national de recherches du Canada

Can. J. Chem. Downloaded from www.nrcresearchpress.com by 210.87.254.5 on 09/06/12
For personal use only.

Can. J. Chem. Downloaded from www.nrcresearchpress.com by 210.87.254.5 on 09/06/12
For personal use only.

amount of the 2,5-isomer) directly from pyrrole (Scheme 2) (5), indicating that it is capable of disubstituting the pyrrole ring. Because the intermediate amide **4** has an electron-withdrawing group and is further substituted by CSI, we decided to investigate the possibility that CSI would substitute other pyrroles with electron-withdrawing groups.

The reaction between CSI and methyl pyrrole-2-carboxylate (**1***d*) gave, in a very rapid reaction, a mixture of the 4- and 5-substituted products in a ratio of about 2:1. Chromatography of the reaction product allowed the isolation of the two isomers. This poor selectivity is similar to that obtained in the Vilsmeier reaction and the non-Friedel–Crafts acylation of pyrrole-2-esters (6). In earlier unpublished work Dr. Graham H. Barnett of this university showed that in this reaction the use of aluminum chloride as catalyst lowered the yield of product. However, there was no significant change in the ratio of the two isomers in the product. Similar results were obtained for the cyanation of 2-acetylpyrrole. The cyanation of pyrrole-2-carbonitrile with CSI gave a product that was virtually pure pyrrole-2,4-dicarbonitrile (**2***c*). In this latter reaction, the proportion of 2,4-isomer was much greater than obtained from the direct disubstitution of pyrrole where the second substitution actually takes place on the amide **4** rather than the 2-nitrile (**1***c*).

The *N*-chlorosulfonyl amide thus appears to be a weaker 4-directing group than the nitrile. The unsatisfactory selectivity in the cyanation of the ester and the potential difficulties attendant to the selective hydrolysis of the 2-nitrile group in the dinitrile **2***c* (5) led us to look for an alternative, more powerful 4-directing group which could be removed selectively.

The utility of 2-trichloroacetylpyrrole as a starting material for the 4-substituted pyrrole-2-esters and carboxylic acids has been very thoroughly demonstrated by Rapoport and co-workers and by Bélanger (7). CSI reacted very slowly with 2-trichloroacetylpyrrole in acetonitrile but ultimately gave a very good yield of 2-trichloroacetylpyrrole-4-carbonitrile (**2***e*). The reaction was highly selective and no 2,5-substituted product was isolated.

The 2-trichloroacetylpyrrole-4-carbonitrile was easily converted to the 2-carboxylic acid (**2***a*) on treatment with aqueous base followed by acidification. Decarboxylation of the acid was expected to present problems because of the poor results obtained for decarboxylation of similar 4-substituted pyrrole-2-carboxylic acids (3*a*). However, moderate yields (50%) of pyrrole-3-carbonitrile were obtained using copper carbonate as catalyst,

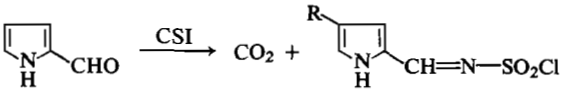

5

a R = H
b R = —CONHSO$_2$Cl
c R = CN

while copper chromite in quinoline gave a 64% yield of the pure product **3**. This compares very well with the yield (59%) obtained by Khan *et al.* (2*a*) for the decarboxylation of 3-cyanopyrrole-2-carboxylic acid by the same method.

Several attempts were made to prepare **2***b*. Cyanation of pyrrole-2-carboxaldehyde was attempted using CSI in acetonitrile and other solvents. CSI reacts vigorously with the aldehyde and the solution becomes highly colored. The ^{1}H nmr spectrum of the reaction mixture shows changes with time that would be expected if 4-substitution was taking place. Work-up of the reaction mixture gave mostly black polymeric material. A small amount (~25%) of the desired product (**2***b*) was isolated. The reaction may involve a predominance of reaction with the aldehyde group rather than with the pyrrole ring. This type of behaviour has been observed and investigated for other aldehydes by Jensen and co-workers (8).

It appears that the CSI first reacts with the aldehyde group to give **5***a* or a precursor, this intermediate then reacts slowly with more CSI to give the 4-(*N*-chlorosulfonylcarboxamido)pyrrole (**5***b*). The conversion of **5***b* to **5***c* on the addition of DMF takes place smoothly, but extensive decomposition occurs in the final work-up. Attempts to improve the hydrolysis of **5***c* to regenerate the 2-carboxaldehyde group have so far been unsuccessful. Similar attempts at the cyanation of 1-methylpyrrole-2-carboxaldehyde gave much better yields (53%) of the desired 1-methyl-4-cyanopyrrole-2-carboxaldehyde. However, in addition to the desired product a small yield of a by-product was obtained which we have tentatively identified as **6**. The formation of **6** requires sulfonylation of the pyrrole ring by the CSI which then reacts with DMF in the work-up. Similar side reactions may be an additional factor in accounting for the poor yield obtained in the reaction of CSI with pyrrole-2-carboxaldehyde.

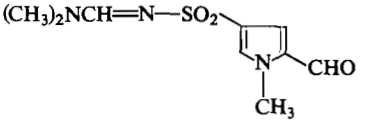

6

Can. J. Chem. Downloaded from www.nrcresearchpress.com by 210.87.254.5 on 09/06/12
For personal use only.

Decarbonylation of 4-cyanopyrrole-2-carboxaldehyde and 1-methyl-4-cyanopyrrole-2-carboxaldehyde using a palladium on carbon catalyst gave high yields of pyrrole-3-carbonitrile and 1-methylpyrrole-3-carbonitrile respectively. As this decarbonylation route appears to be superior to the decarboxylation procedure described earlier, an improved method of synthesis for 4-cyanopyrrole-2-carboxaldehyde now seems to be highly desirable. We shall pursue this problem.

The assigned structures for the new compounds obtained in this work were supported by their spectral properties and satisfactory microanalyses. In particular the coupling constants for the pyrrole ring protons in the ^1H nmr spectra usually allow the identification of the substitution pattern on the pyrrole ring (e.g. **2***a*). In other cases the compounds were converted to known compounds by simple one-step reactions (e.g., **3** was obtained from **2***a* by decarboxylation indicating that **2***a* was 4-cyano- rather than 5-cyano- pyrrole-2-carboxylic acid).

Experimental

Instruments and conditions were as described in ref. 5 except where noted below. All ir spectra are recorded as Nujol mulls unless otherwise indicated.

Pyrrole-2,4-dicarbonitrile (General Method)

Pyrrole-2-carbonitrile (2.00 g, 22 mmol) was dissolved in CH_3CN (5 mL) and cooled in a salt/ice bath. A solution of CSI (4.67 g, 33 mmol) in CH_3CN (5 mL) was added to the stirred solution over about 5 min. The solution rapidly became yellow and solid was deposited. The semi-solid mixture was allowed to warm and was held at room temperature for 2.5 h after which it was again cooled in ice and *N*,*N*-dimethylformamide (DMF) (2 mL) was added. The mixture was heated at 50°C for 15 min and then poured onto ice. Extraction of the aqueous mixture with $CHCl_3$ gave a pale yellow organic extract which was washed with aqueous $NaHCO_3$ (5%), dried ($MgSO_4$), and the solvent was removed.

The crystalline residue (2.03 g) was recrystallized from toluene/petroleum (bp 100–120°C) to give the product as colourless crystals (1.20 g, 47%), mp 181–183°C (lit. (5) mp 181–183°C); mixture mp was undepressed. Spectral properties were identical with those of an authentic sample. The mother liquors from the recrystallization contained traces of the 2,5-substituted isomer. Some material would not dissolve in toluene.

1-Methylpyrrole-2,4-dicarbonitrile

Using the same method described above for pyrrole-2,4-dicarbonitrile, except that the reaction mixture was allowed to stand overnight at room temperature before the DMF was added, 1-methylpyrrole-2-carbonitrile (2.0 g) gave the crude product (1.7 g). Chromatography of the crude product on alumina (Activity 1) and elution with ether/petroleum (bp 30–60°C) followed by sublimation gave the pure product (1.24 g, 50%), mp 108–109°C (lit. (5) mp 108–109°C); mixture mp with authentic 1-methylpyrrole-2,4-dicarbonitrile was undepressed.

Cyanation of Methyl Pyrrole-2-carboxylate

Methyl pyrrole-2-carboxylate under the conditions above gave a mixture (67% yield) of methyl 4- and 5-cyanopyrrole-2-carboxylate in a ratio of about 2:1. The mixture was separated by chromatography on an alumina column.

Methyl 4-Cyanopyrrole-2-carboxylate, mp 168–169°C (lit. (9) mp 168–169°C); ir ν: 2220 (C≡N), 1690 (C=O) cm^{-1}; nmr (acetone-d_6 + D_2O) δ: 3.83 (3H, s), 7.13 (1H, d), 7.70 (1H, d), $J_{3,5}$ = 1.6 Hz; *m/e*: 150.

Methyl 5-Cyanopyrrole-2-carboxylate, mp 173–174°C (lit. (10) mp 170–171°C); ir ν: 3251 (N—H), 2241 (C≡N), 1694 (C=O) cm^{-1}; nmr ($CDCl_3$) δ: 3.94 (3H, s), 6.83 (2H, m), $J_{1,3}$, $J_{1,4}$ = 2.4 Hz; $J_{3,4}$ = 4.4 Hz; *m/e*: 150. *Anal.* calcd. for $C_7H_6N_2O_2$: C 56.00, H 4.03; found: C 56.00, H 4.07.

Cyanation of 2-Acetylpyrrole

2-Acetylpyrrole gave a mixture (56% yield) of 2-acetylpyrrole-4-carbonitrile and 2-acetylpyrrole-5-carbonitrile 7:3. The mixture was separated by repeated crystallization from $CHCl_3$/petroleum (bp 80–100°C) mixtures.

2-Acetylpyrrole-4-carbonitrile, mp 190.5–191°C (from toluene/petroleum (bp 100–120°C)); ir ν: 3245 (N—H), 2235 (C≡N), 1657 (C=O) cm^{-1}; nmr ($CDCl_3$) δ: 2.46 (3H, s), 7.01 (1H, m), 7.36 (1H, m), $J_{3,5}$ = 1.8 Hz; *m/e*: 134. *Anal.* calcd. for $C_7H_6N_2O$: C 62.68, H 4.52, N 20.83; found: C 62.68, H 4.55, N 20.86.

2-Acetylpyrrole-5-carbonitrile, mp 152–153°C (lit. (11) mp 154.5–155.5°C). The mixture melting point with an authentic sample was undepressed; ir ν: 3227 (N—H), 2250 (C≡N), 1654 (C=O) cm^{-1}; nmr ($CDCl_3$ + D_2O) δ: 2.53 (3H, s), 6.80 (2H, s); *m/e*: 134.

Pyrrole-2-carbonitrile

Pyrrole (5.0 g) was dissolved in a mixture of DMF (25 mL) and acetonitrile (25 mL) and the solution was cooled in a solid CO_2/acetone bath. CSI (7.17 mL) in acetonitrile (30 mL) was added dropwise to the stirred solution over 10 min and the mixture formed was allowed to warm to about 5°C over about 1 h. The mixture was then poured onto aqueous NaOH (3 mol L^{-1}, 27 mL), 5% $NaHCO_3$ solution (150 mL), and ice. The aqueous mixture was extracted with dichloromethane. The organic extracts were successively washed with water, dried (anhydrous K_2CO_3), and evaporated to leave an oily residue. The residue (containing approximately equal amounts of the product and DMF) was fractionally distilled (twice) to give the product (5.0 g, 73%) bp 120–123°C/15 Torr (lit. (12) bp 112–114°C/14 Torr). The low boiling fractions contained DMF; no unchanged pyrrole was recovered. Spectral properties were identical with those of an authentic sample.

2-Trichloroacetylpyrrole-4-carbonitrile

2-Trichloroacetylpyrrole (2.0 g) was dissolved in acetonitrile (10 mL) and cooled in ice. A solution of CSI (3.2 g) in acetonitrile (3 mL) was then added dropwise to the stirred solution. When all of the CSI had been added, the ice bath was removed and the solution was stirred at room temperature for 12 h. The stirred mixture was then cooled in an ice bath, DMF (8 mL) was added, heated first to 50°C for 1 h and then stirred at room temperature for a further 3 h. The mixture was then poured onto ice (~50 g) and the aqueous mixture was extracted with $CHCl_3$. The chloroform extracts were washed successively with water and aqueous sodium hydrogen carbonate (1%), and dried ($MgSO_4$). Removal of the solvent gave an oily residue which still contained DMF. Pumping the oil under high vacuum (0.1 Torr) removed the DMF and the residue of crude material crystallized slowly. The crude product was distilled onto a cold finger (130°C/0.5 Torr) where it collected as a solid (1.6 g, 71%), mp 139–140°C; ir ν: 3302 (N—H), 2233 (C≡N), 1672 (C=O) cm^{-1}; nmr (acetone-d_6) δ: 3.07 (1H, s, N—H), 7.63, 7.93 (each 1H, m, pyrrole H), $J_{1,5}$ = 3.6, $J_{1,3}$ = 3.2, $J_{3,5}$ = 1.8 Hz; *m/e*: 236 ($^{35}Cl_3$), 238 ($^{35}Cl_2{}^{37}Cl$). *Anal.* calcd. for $C_7H_3Cl_3N_2O$: C 35.40, H 1.27, N 11.80; found: C 35.31, H 1.36, N 11.94.

Can. J. Chem. Downloaded from www.nrcresearchpress.com by 210.87.254.5 on 09/06/12
For personal use only.

4-Cyanopyrrole-2-carboxylic Acid

2-Trichloroacetylpyrrole-4-carbonitrile (1.00 g) was added to sodium hydroxide (2 mol L^{-1}, 10 mL) cooled in an ice bath. After the addition was complete, the mixture was allowed to warm to room temperature and stirred for a further 2 h during which time a cloudy solution formed. The solution was acidified with concentrated HCl and the white precipitate of product was collected by vacuum filtration, washed with cold water, and dried at 100°C. The product (0.53 g, 92%) was used without further purification for the preparation of pyrrole-3-carbonitrile.

For analysis, the acid was sublimed (130°C/0.1 Torr), mp 279°C (dec.); ir v: 3220 (N—H), 2225 (C≡N), 1670 (C=O) cm^{-1}; nmr (DMSO-d_6) δ: 7.11 (1H, m), 7.70 (1H, m), 12.6 (1H, broad), $J_{3,5}$ = 1.8 Hz; *m/e*: 136. *Anal.* calcd. for $C_6H_4N_2O_2$: C 52.95, H 2.96; found: C 52.93, H 2.98.

Pyrrole-3-carbonitrile

4-Cyanopyrrole-2-carboxylic acid (900 mg) was mixed with quinoline (6 mL) and copper chromite catalyst (600 mg) was added. The stirred mixture was heated in an oil bath to 160°C for 3 h. The resulting brown mixture was cooled, diluted with ether (100 mL), and filtered to remove insoluble material. The ether solution was washed with four portions (30 mL each) of HCl (1 mol L^{-1}) and then with sodium hydrogen carbonate solution (5% aqueous). The pale yellow ether layer was collected, dried (K_2CO_3), and evaporated to leave an oily residue which soon crystallized on cooling. The crystalline residue (486 mg) was recrystallized from a benzene/petroleum (bp 60–80°C) mixture to give pyrrole-3-carbonitrile (388 mg, 64%), mp 56–56.5°C (lit. (2) mp 55–56°C); ir v: 3275 (N—H), 2227 (C≡N) cm^{-1}; nmr ($CDCl_3$) δ: 6.43, 6.77, 7.27 (each 1H, m), 9.1 (1H, broad s, pyrrolic N—*H*); *m/e*: 92.

1-Methyl-4-cyanopyrrole-2-carboxaldehyde

1-Methylpyrrole-2-carboxaldehyde (2.0 g) was dissolved in acetonitrile (10.0 mL) and cooled in a solid CO_2/acetone bath. A solution of CSI (4.83 mL) in acetonitrile (10.0 mL) was added to the stirred solution. The mixture was allowed to warm to room temperature overnight. DMF (7.0 mL) was added to the red coloured product without cooling, and the mixture was warmed to 50°C for 1 h and then poured into a mixture of NaOH (2 mol L^{-1}, 55 mL) and ice. The brown solid that precipitated was collected by vacuum filtration and the filtrate was thoroughly extracted with ethyl ether. The ether extracts were washed with $NaHCO_3$ solution (5% aqueous), dried (K_2CO_3), and the solvent was evaporated. The crystalline residue was combined with the precipitated solid and recrystallized from petroleum (bp 100–120°C) to give the product as very pale yellow crystals (1.3 g, 53%), mp 123–124°C (lit. (9) mp 116–120°C); ir v: 2231 (C≡N), 1670 (C=O) cm^{-1}; nmr ($CDCl_3$) δ: 3.96 (3H, s), 7.09, 7.27 (each 1H, m), 9.53 (1H, s); *m/e*: 134. *Anal.* calcd. for $C_7H_6N_2O$: C 62.68, H 4.52; found: C 62.72, H 4.52.

Chloroform extraction of the aqueous layer from the above preparation gave a small amount of a by-product as a brown solid (88 mg). The solid was sublimed (160°C/0.1 Torr) to give the product **6**, mp 190–191°C; ir v: 1670, 1680 (m, C=N), 1630 (s, C=O) cm^{-1}; nmr (DMSO-d_6) δ: 2.87, 3.10, 3.84 (each 3H, s), 7.14 (1H, d) 7.60 (1H, broad), 8.07 (1H, s), 9.47 (1H, s), $J_{3,5}$ = 1.8 Hz; *m/e*: 243. *Anal.* calcd. for $C_9H_{13}N_3O_3S$: C 44.43, H 5.39, S 13.18; found: C 44.42, H 5.40, S 13.19.

4-Cyanopyrrole-2-carboxaldehyde

The same procedure was used as for the preparation of 1-methyl-4-cyanopyrrole-2-carboxaldehyde. The reaction with CSI required 48 h to reach completion and was easily followed by ^1H nmr of the reaction mixture. The crude product crystallized slowly but contained an impurity (not isolated) which turned black in air making purification difficult. Recrystallization from ether/petroleum (bp 35–60°C) gave the almost pure product as a light brown solid in 27% yield. Sublimation (110°C/0.1 Torr) gave the pure product, mp 177°C (lit. (9) mp 177–177.5°C); ir v: 3228 (N—H), 2233 (C≡N), 1646 (C=O) cm^{-1}; nmr (acetone-d_6) δ: 7.33 (1H, d), 7.82 (1H, dd), 9.58 (1H, d), $J_{3,5}$ = 1.5 Hz, $J_{CHO,5}$ = 1.1 Hz; *m/e*: 120.

1-Methylpyrrole-3-carbonitrile (by decarbonylation)

4-Cyano-1-methylpyrrole-2-carboxaldehyde (1.09 g) was mixed with palladium on charcoal (100 mg) in a pear shaped flask fitted with an air condenser, and then heated in a silicone oil bath at 210°C for 45 min. The black oily mixture formed was distilled to give the product as a colourless oil (0.72 g, 83%), bp 65–70°C/0.1 Torr (lit. (2) bp 135°C/1 Torr); ir (liquid film) v: 3127 (saturated C—H stretch), 2237 (C≡N) cm^{-1}; nmr ($CDCl_3$) δ: 3.64 (3H, s), 6.27, 6.47, 6.96 (each 1H, m); *m/e*: 106.

Pyrrole-3-carbonitrile (by decarbonylation)

Small scale decarbonylation (1) of 4-cyanopyrrole-2-carboxaldehyde (100 mg) gave the product (59 mg, 77%) which was identical to the pyrrole-3-carbonitrile prepared by decarboxylation (above).

Acknowledgements

The authors gratefully acknowledge the financial assistance of the Memorial University of Newfoundland and the Natural Sciences and Engineering Research Council of Canada. They also thank Janet Handrigan and John Drover for technical assistance.

1. H. J. Anderson, C. E. Loader, and A. Foster. Can. J. Chem. **58**, 2527 (1980).
2. (*a*) M. K. A. Khan, K. J. Morgan, and D. P. Morrey. Tetrahedron, **22**, 2095 (1966); (*b*) A. M. van Leusen, H. Siderius, B. E. Hoogenboom, and D. van Leusen. Tetrahedron Lett. 337 (1972).
3. (*a*) H. J. Anderson and C. W. Huang. Can. J. Chem. **45**, 897 (1967); (*b*) C. E. Loader and H. J. Anderson. Tetrahedron, **25**, 3879 (1969); (*c*) H. J. Anderson, C. R. Riche, T. G. Costello, C. E. Loader, and G. H. Barnett. Can. J. Chem. **56**, 654 (1978).
4. G. Lohaus. Chem. Ber. **100**, 2719 (1967); H. Vorbrüggen. Tetrahedron Lett. 1631 (1968); G. Mehta and D. N. Dhar. Synthesis, 374 (1978).
5. G. H. Barnett, H. J. Anderson, and C. E. Loader. Can. J. Chem. **58**, 409 (1980).
6. W. A. M. Davies, A. R. Pinder, and I. G. Morris. Tetrahedron, **18**, 405 (1962); E. Bullock, T.-S. Chen, and C. E. Loader. Can. J. Chem. **44**, 1007 (1966).
7. P. Bélanger. Tetrahedron Lett. 2050 (1979); P. Barker, P. Gendler, and H. Rapoport. J. Org. Chem. **43**, 4849 (1978).
8. K. Clauss, H. J. Friedrich, and H. Jensen. Justus Liebigs Ann. Chem. 561 (1974).
9. P. E. Sonnet. J. Heterocycl. Chem. **10**, 113 (1973).
10. M. Ishikawa, C. Kaneko, I. Yokoe, and S. Yamada. Tetrahedron, **25**, 295 (1969).
11. H. J. Anderson. Can. J. Chem. **46**, 798 (1968).
12. C. E. Loader and H. J. Anderson. Can. J. Chem. **49**, 45 (1971).

Cytotoxic diterpenes triptolide, tripdiolide, and cytotoxic triterpenes from tissue cultures of *Tripterygium wilfordii*

JAMES P. KUTNEY,[1] GARY M. HEWITT, TOSHIO KURIHARA, PHILLIP J. SALISBURY, ROBERT D. SINDELAR, AND KENNETH L. STUART

Department of Chemistry, University of British Columbia, 2036 Main Mall, University Campus, Vancouver, B.C., Canada V6T 1Y6

AND

PHILIP M. TOWNSLEY AND WILLIAM T. CHALMERS

Department of Food Science, Faculty of Agricultural Science, University of British Columbia, 2357 Main Mall, University Campus, Vancouver, B.C., Canada V6T 1Y6

AND

GIULIO G. JACOLI

Laboratory of Biochemistry, Virus Chemistry Section, Research Station, Agriculture Canada, 6660 N. W. Marine Drive, Vancouver, B.C., Canada V6T 1X2

Received April 15, 1981

JAMES P. KUTNEY, GARY M. HEWITT, TOSHIO KURIHARA, PHILLIP J. SALISBURY, ROBERT D. SINDELAR, KENNETH L. STUART, PHILIP M. TOWNSLEY, WILLIAM T. CHALMERS, and GIULIO G. JACOLI. Can. J. Chem. **59**, 2677 (1981).

Plant tissue cultures of *Tripterygium wilfordii* Hook F produced the cytotoxic diterpene triepoxides tripdiolide (**1**) and triptolide (**2**) in yields that were 16 and 3 times greater, respectively, than those observed in the plant itself. Other diterpenes, dehydroabietic acid (**3**) and 15-hydroxy-18-norabieta-3,8,11,13-tetraene-3-oic acid methyl ester (**4**) were also isolated. Co-occuring in these cultures were the cytotoxic quinone-methides, celastrol (**5**), compound **6**, and compound **7**. Other triterpenes produced were oleanolic acid (**8**) and polpunonic acid (**9**). β-Sitosterol (**17**) was also isolated. The proposed structure of **4** was confirmed by synthesis starting from compound **3**. Cytotoxic data are reported, and a possible biosynthetic relationship among dehydroabietic acid, compound **4**, and tripdiolide (**1**) is presented.

JAMES P. KUTNEY, GARY M. HEWITT, TOSHIO KURIHARA, PHILLIP J. SALISBURY, ROBERT D. SINDELAR, KENNETH L. STUART, PHILIP M. TOWNSLEY, WILLIAM T. CHALMERS et GIULIO G. JACOLI. Can. J. Chem. **59**, 2677 (1981).

Les cultures des cellules de la plante *Tripterygium wilfordii* Hook F produisent les triépoxydes diterpéniques cytotoxiques, la tripdiolide (**1**) et la triptolide (**2**) avec des rendements qui sont respectivement 16 et 3 fois plus élevés que ceux que l'on obtient à partir de la plante elle-même. On a également isolé d'autres diterpènes: l'acide déhydroabiétique (**3**) et l'hydroxy-15 norabiéta-18 tétraène-3,8,11,13 oate-3 de méthyle (**4**). On obtient également à partir de ces cultures les méthylures de quinone cytotoxiques: le célastrol (**5**) et les composés **6** et **7**. On a également isolé d'autres triterpènes: l'acide oléanolique (**8**) et l'acide polpunonique (**9**) ainsi que le β-sitostérol (**17**). On a confirmé la structure proposée pour le composé **4** en le synthétisant à partir du composé **3**. On rapporte les données cytotoxiques et on propose une relation biosynthétique possible entre l'acide déhydroabiétique, le composé **4** et la tripdiolide (**1**).

[Traduit par le journal]

In a preliminary communication, we reported the production of tripdiolide (**1**), a novel cytotoxic diterpene triepoxide by tissue cultures of *Tripterygium wilfordii* Hook F (1). We now report the improved production of **1**, the isolation of cytotoxic triptolide (**2**), and the chemical analysis of secondary products obtained from shake-flask cultures.

Examination of shake-flask and stirred fermentor batch cultures (up to 60 L) of our cell line TRP 4a, showed that a modified PRL-4 medium (2) afforded the highest tripdiolide yields. Levels of **1** and **2** were respectively 16 and 3 times greater than those reported for the parent plant source (3). Multistep syntheses of some of these modified abietane-type compounds have been reported recently (4, 5). No synthesis of tripdiolide (**1**) has, however, appeared in the chemical literature.

Three procedures for the isolation of the target cytotoxic diterpenes **1** and **2** are presented in the Experimental. Method 2 proved to be the most efficient for isolating these compounds from the tissue culture broth. Two additional diterpenes, dehydroabietic acid (**3**) and the methyl ester of the novel compound, 15-hydroxy-18-norabieta-3,8,11,13-tetraene-3-oic acid (**4**), were isolated. The isolation of compound **3** and compound **4** has interesting biosynthetic implications. Scheme 1 outlines a possible biosynthetic pathway from geranylgeraniol to tripdiolide. The route from geranylgeraniol to the abietane skeleton has previously been proposed (6). We now suggest that an important step in this pathway involves the rearrange-

[1]Author to whom all correspondence should be addressed.

0008-4042/81/172677-07$01.00/0

©1981 National Research Council of Canada/Conseil national de recherches du Canada

Can. J. Chem. Downloaded from www.nrcresearchpress.com by 210.87.254.42 on 09/06/12
For personal use only.

Can. J. Chem. Downloaded from www.nrcresearchpress.com by 210.87.254.42 on 09/06/12
For personal use only.

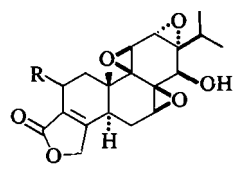

1 R = OH
2 R = H

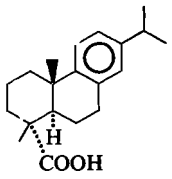

3

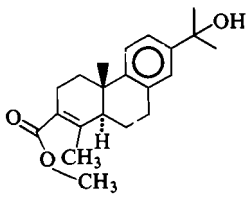

4

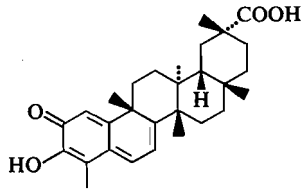

5

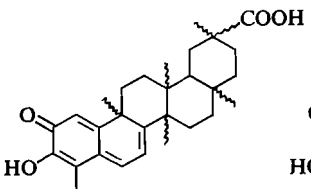

6

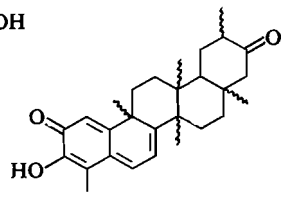

7

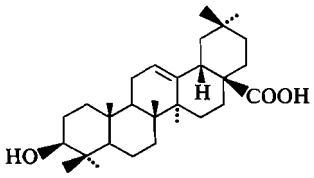

8

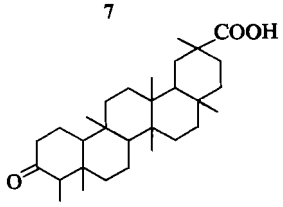

9

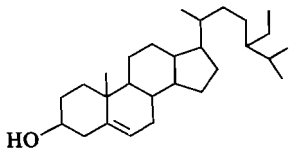

17

ment of dehydroabietic acid to a modified abietane skeleton as is depicted by compound **4**. Subsequent enzymatic oxidations would lead ultimately to tripdiolide (**1**) and triptolide (**2**). With the aid of these high yielding cultures, the possibility of obtaining pertinent biosynthetic information is now very good, and appropriate studies have been initiated.

The quinone-methide type triterpenes, celastrol (**5**), compound **6**, and compound **7** were isolated by method 1 and characterized. Celastrol (**5**) has previously been isolated from the parent plant *Tripterygium wilfordii* (7). Compound **6** had nearly identical nmr, ms, and uv data to those of celastrol, but had different R_f values on tlc. Compound **7** and tingenone had the same relationship. The stereochemistry of both compounds **6** and **7** has yet to be defined.

As a group, the quinone-methides have been of interest because of their antineoplastic activity (8). A recent study of the binding of tingenone to DNA suggests a possible mode of cellular interaction which may elicit antitumor activity (9). The cytotoxic activity of some of these compounds, as measured using the KB cancer cell tissue assay system, is summarized in Table 1.

Oleanolic acid (**8**), which has been found in a wide variety of plants (10), and polpunonic acid (**9**) have also been isolated from these cultures. Polpunonic acid, a friedelane-type triterpene, has been reported from *Plenckia polpunea* (11), and has been recently shown to be present in the tissue

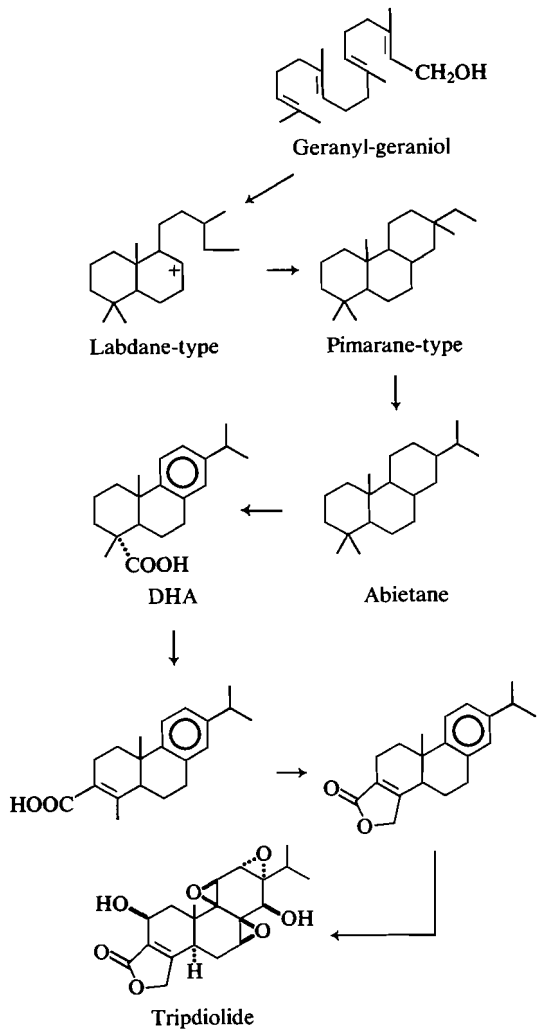

SCHEME 1

Can. J. Chem. Downloaded from www.nrcresearchpress.com by 210.87.254.42 on 09/06/12
For personal use only.

TABLE 1. Cytotoxic activity of some quinone–methide compounds

Compounds (quinone-methides)	Observed ED_{40} values[a]
Celastrol (**5**)	0.55, 1.40 } Two determinations
Pristimerin (**5**, Me acid ester)	0.91
Tingenone	0.27
22-Hydroxytingenone	2.5
Compound **6**	1.8
Diazomethane product of celastrol	1.6

[a] ED_{40} expressed in μg/mL, and is the calculated effective dose which inhibits growth of 50% of control growth. Assays were done using KB cells (human epidermoid carcinoma of the nasopharynx-type 9KB-5). Cytotoxicity and *in vitro* activity were assayed as reported in ref. 18.

cultures of *Maytenus buchananii* (Loes) R. Wilezck (12).

The structure of the diterpene **4** was confirmed by a synthesis which started from dehydroabietic acid **3** (Scheme 2). The ketone **10** obtained from **3**, following the procedure of Huffman (13), was transformed to the corresponding cyanohydrin by refluxing with potassium cyanide in 18-crown-6 ether and dimethyl sulfoxide – dimethyl formamide. This latter compound was immediately dehydrated with thionyl chloride in pyridine to yield a 5:1 mixture of the α,β-unsaturated nitriles **11** and **12** (60% from **10**). Treatment of this mixture with sodium ethoxide in ethanol under reflux gave a 2:1 mixture of **11** and **12**. This mixture was reduced to the aldehydes **13** and **14** by diisobutylaluminium hydride.

Aldehydes **13** and **14** were separated by silica gel column chromatography. Compound **14** was oxidized to the acid **15** by sodium chlorite and resorcinol in acidic dioxane–water (14). This acid was treated with diazomethane to give the corresponding ester (**16**) in 72% yield from **14**. The target compound **4** was prepared by irradiating **16** as a solution in hexane with uv light for 5 h.

Experimental

The *Tripterygium wilfordii* cell line designated TRP 4a was initiated as a 2 mm × 6 mm cutting obtained from a surface-sterilized leaf (a 15 min immersion in a 0.5% sodium hypochlorite solution followed by a sterile distilled water rinse). This explant was placed on $PRD_{2.0}$ Co_{100}[2] medium containing 0.8% agar. The callus obtained through growth on solid medium was used to initiate suspension cultures which have been maintained as stock cultures by regular subculturing with 10% inoculum at 3 week intervals. This TRP 4a cell line has been maintained in stable culture for more than 2.5 years.

Tripdiolide was first detected in callus tissue by tlc. The first 28 L cultivation which was extracted, and products separated (see method 1 below), was grown in $PRD_{2.0}$ Co_{60} without casein hydrolysate. These cultures were incubated in the dark at room temperature (20–26°C) on a rotary shaker (120 rpm). The second (25 L), third (17.5 L), and fourth (22 L) cultivations of TRP 4a (separation method 2) were grown in PRL-4 medium supplemented with 0.5 mg/L of napthaleneacetic acid and 0.5 mg/L kinetin ($PRNA_{0.5}$ $K_{0.5}$). Individual cultures were 500 mL held in 1 L erlenmeyer flasks, and were incubated in the dark at 27°C (±0.5°) with 120 rpm shaking. All cultures were inoculated at 10% of the medium volume with stationary phase stock TRP 4a.

60 L Chemapec Pilot Plant Bioreactor

Fifty liters of TRP 4a were grown in a single batch, using a 60 L capacity Chemapec Inc. fermentor. The medium was $PRNA_{0.5}$ $K_{0.5}$. The incubation conditions were 120 ± 10 rpm agitation, approximately 300 mL/min aeration, and 28°C. The culture was inoculated to 3–5% with a portion of a TRP 4a culture grown in 10 L of $PRD_{2.0}$ Co_{100} in a 12 L Virtis fermentor controlled at 100 rpm agitation, and 50 mL/min aeration at 28°C (±2°), and incubated for 28 days. The Chemapec culture was harvested after 50 days. Due to periodic sampling, the reaped volume was 41 L. The broth was extracted and products separated by method 2 outlined below to give 4.0 mg of tripdiolide. This yield represented 3 times the amount reported from plant material (3).

Ultraviolet spectra were recorded on a Cary 15 spectrophotometer using methanol as the solvent. Circular dichroism (cd) measurements were made on a Jasco J-20 spectropolarimeter. Infrared spectra were recorded either on a Perkin-Elmer 457 or 710 spectrophotometer. The ^{1}Hmr spectra were recorded on Bruker WH-400, Bruker WP-80, Varian XL-100, or Nicolet-Oxford H-270 instruments. Deuteriochloroform was used as the solvent with TMS as internal standard. Mass spectra were recorded on an Atlas CH-4B or AEI MS-902 instrument. Microanalyses were carried out by Mr. P. Borda, Microanalytical Laboratory, University of British Columbia. Column chromatography utilized Merck silica gel 60 (70–230 mesh). Preparative layer chromatography utilized Merck silica gel GF 254 2 mm and 0.25 mm plates, and thin layer chromatography was carried out with Eastman silica chromagram sheets.

Separation Experimental: Method 1

A 28 L shake-flask cultivation of *Tripterygium wilfordii* cell tissue line TRP 4a grown on modified PRL-4 medium was harvested after 6 weeks. The cells (5.9 kg) were extracted with ethanol and ethyl acetate to give 10.0 g of material. The medium yielded another 7.9 g on extraction with ethyl acetate. The material from the medium was separated on a silica column (350 g) packed in benzene. The column was then eluted with benzene (fractions 1 and 2; 500 mL fractions were collected in all cases), followed by 5% benzene – ethyl acetate (fractions 3–5), then 10% benzene – ethyl acetate (fractions 6–8). The % ethyl acetate was gradually increased until the final 3 fractions (fractions 18–20) were eluted with pure ethyl acetate. The analysis showed that tripdiolide (**1**) was present in fractions 19 and 20 (0.88 g), but still was contaminated with other products. A similar column was used to separate the 10.0 g of material obtained from the tissue cells. In this case, tripdiolide was shown to be present in fraction 19 (0.31 g).

Material containing tripdiolide from both columns was absorbed on a silica column (150 g) packed in diethyl ether. Fractions 1–3 were eluted with diethyl ether; fractions 4 and 5 eluted with 1% ethanol–ether; fractions 6–8 (2% ethanol – diethyl ether); fractions 9–11 (3% ethanol – diethyl ether); fractions 12 and 13 (5% ethanol – diethyl ether); fractions 14 and 15 (10% ethanol – diethyl ether). The examination of all fractions on Eastman silica sheets in 3% methanol–chloroform showed the presence of tripdiolide in fractions 11–15.

[2] $PRD_{2.0}$ Co_{100} is the PRL-4 medium of Gamborg and Eveleigh (2) supplemented with 2.0 mg/L of 2,4-dichlorophenoxyacetic acid and 100 mL/L coconut milk.

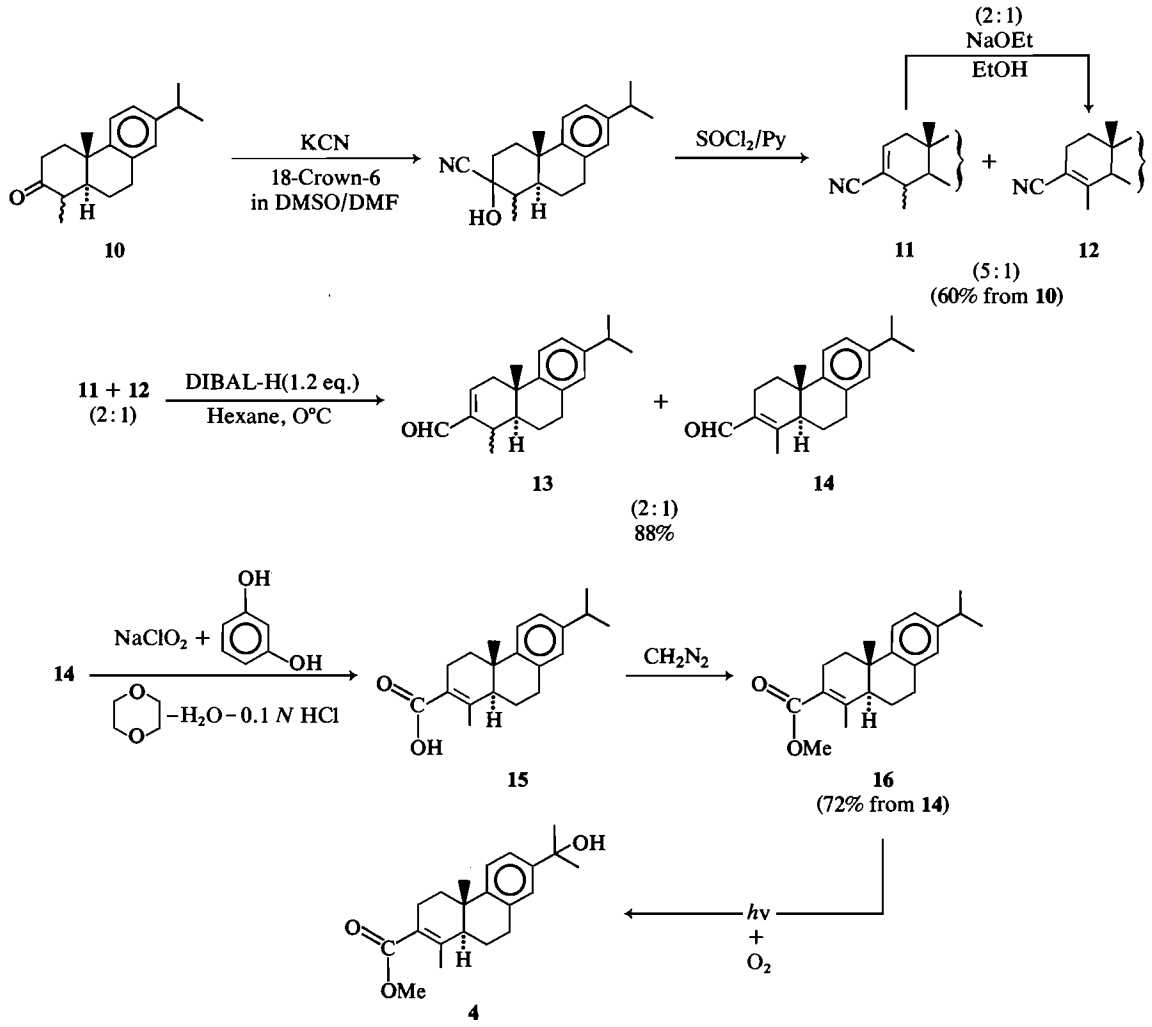

SCHEME 2. Synthetic route to compound **4**.

Tripdiolide 1

Material from fractions 11–15 (96.6 mg) was separated on two 2 mm Merck silica plates developed in 2% ethanol – ethyl acetate to give 14.5 mg of a mixture of compounds which from tlc was mainly tripdiolide. Further purification was on 0.25 mm Merck silica plates. The plates were first developed in ethyl acetate and then four times in diethyl ether. A crystalline compound (4.5 mg) was obtained that had identical tlc behaviour as tripdiolide.

Identity was confirmed by a high resolution ms (M^+, *m/e* 377.1610; calcd. 377.1600 for $C_{20}H_{24}O_7$), mp and mixture mp 211-212°C; 270 MHz ^{1}Hmr, δ: 4.77 (2H, t, J = 1.5 Hz, 19-CH_2), 4.62 (1H, m, 2-C*H*OH), 3.93 (1H, d, J = 3 Hz, 11-CH), 3.66 (1H, dd, J = 3 and 1 Hz, 12-CH), 3.57 (1H, dd, J = 11 and 1 Hz, 14-C*H*OH), 3.55 (1H, d, J = 5 Hz, 7-CH), 2.74 (1H, d, J = 11 Hz, 14-CHO*H*), 2.65 (1H, m, 5-CH), 2.22 (1H, m, 15-CH), 2.10 (1H, 1-CH), 1.83 (1H, d, J = 1 Hz, 1-CH), 1.76 (1H, bs, exchanged with D_2O, 2-CHO*H*), 1.40 (2H, m, 6-CH_2), 1.31 (3H, s, 20-CH_3), 1.01 (3H, d, J = 7 Hz, 17-CH_3), 0.88 (3H, d, J = 7 Hz, 16-CH_3).

Celastrol 5

Fractions from the two earlier columns were pooled based on tlc analysis: fractions 1–9; fractions 10–15 (5.48 g); fractions 16–20; 0.42 g of material from fractions 10–15 was separated on two 2 mm Merck silica plates developed in 3% methanol–chloroform. Thin-layer chromatographic examination of this mixture in several solvent systems showed two major groups of orange colored compounds: group A, which ran close to the solvent front in 3% methanol–chloroform, and consisted of 7 orange compounds; group B, which in the same solvent system was located at approximately R_f 0.4, and consisted of at least 5 orange compounds. One of the orange compounds from group B was isolated in pure form (8 mg), mp 202°C (lit. (15) mp 205°C). The ^{1}Hmr (100 MHz) was characteristic of a quinone-methide type natural product, and the following data identified it as celastrol; δ: 7.09 (1H, dd, J = 7 and 1 Hz, 6-CH), 6.54 (1H, d, J = 1 Hz, 1-CH), 6.36 (1H, d, J = 7 Hz, 7-CH), 2.23 (3H, s, 4-CH_3), 1.44 (3H, s, 9-CH_3), 1.26, 1.24, 1.08 (3 × 3H, s, 13-CH_3, 14-CH_3, 17-CH_3), 0.58 (3H, s, 20-CH_3); ms: 450.2780 (M^+), $C_{29}H_{28}O_4$

Can. J. Chem. Downloaded from www.nrcresearchpress.com by 210.87.254.42 on 09/06/12
For personal use only.

Can. J. Chem. Downloaded from www.nrcresearchpress.com by 210.87.254.42 on 09/06/12
For personal use only.

(33%), 436.2682 ($C_{28}H_{36}O_4$, 8%), 267.1391 ($C_{18}H_{19}O_2$, 6%), 255.1336 ($C_{17}H_{19}O_2$, 2%), 253.1237 ($C_{17}H_{17}O_2$, 13%), 241.1231 ($C_{16}H_{17}O_2$, 38%), 227.1078 ($C_{15}H_{15}O_2$, 16%), 215.1076 ($C_{14}H_{15}O_2$, 15%), 201 ($C_{13}H_{13}O_2$, 51%). *Anal.* calcd. for $C_{29}H_{38}O_4 \cdot H_2O$: C 74.30, H 8.60; found: C 74.06, H 8.62.

Celastrol (3 mg) dissolved in ethyl acetate was treated with excess diazomethane in diethyl ether at room temperature overnight. A light orange product was obtained, mp 183–185°C; ^{1}Hmr (80 MHz), δ: 6.82 (1H, s), 6.70 (1H, d, J = 5 Hz), 6.01 (1H, d, J = 5 Hz), 3.63 (1H, s, C—COOCH_3), 1.84 (3H, s), 1.50 (9H, s), 1.16 (3H, s), 1.13 (3H, s), 1.07 (3H, s), 0.50 (3H, s); ms: 492.3241 (M^+), $C_{32}H_{44}O_4$. *Anal.* calcd. for $C_{32}H_{44}O_4 \cdot CH_3COOCH_2CH_3$: C 74.90, H 9.09; found: C 75.19, H 8.78.

Compound 6

An orange-red compound (9.9 mg), which was more polar than celastrol, was isolated from the group B compounds; mp 200–204°C. Spectral data were similar to those of celastrol; ^{1}Hmr (100 MHz), δ: 7.08 (1H, dd, J = 7 and 1 Hz, 6-CH), 6.56 (1H, d, J = 1 Hz, 1-CH), 6.36 (1H, d, J = 7 H), 2.22 (3H, s, 4-CH_3), 1.45, 1.26, 1.27, 1.12 (4 × 3CH_3, s, 9-CH_3, 13-CH_3, 14-CH_3, 17-CH_3), 0.60 (3H, s, 20-CH_3); ms: 450.2756 ($C_{29}H_{28}O_4$, M^+, 30%), 436.2602 ($C_{28}H_{26}O_4$, 3%), 267.1372 ($C_{18}H_{19}O_2$, 3%), 253.1220 ($C_{17}H_{17}O_2$, 13%), 241.1237 ($C_{16}H_{17}O_2$, 30%), 227.1078 ($C_{15}H_{15}O_2$, 8%), 215.1070 ($C_{14}H_{15}O_2$, 10%), 201.0919 ($C_{13}H_{13}O_2$, 35%), 119.0862 (C_9H_{11}, 11%).

Compound 7

Fractions 10–15 also yielded, from preparative 2 mm Merck silica separation, an orange colored compound (61 mg) in the group A series. The separation was achieved by using 10% methanol–chloroform to first give 200 mg of a mixture of compounds. These were further separated using diethyl ether – benzene (15:85), mp 145–150°C (recrystallized, hexane–benzene–methanol); 210–212°C (recrystallized, benzene); ir, ν_{max} (Nujol): 3300, 1715 cm^{-1}; λ_{max}: 250 (log ε, 4.1535), 262 sh (4.0371), 365 sh (3.2911), 412 (4.1446); cd, λ_{max} (MeOH): 257 (Δε −7.78), 263 (−8.43), 370 (+6.81), 445 (−3.56); ^{1}Hmr (100 MHz), δ: 7.06 (1H, dd, J = 7 and 1.5 Hz, 6-CH), 6.56 (1H, d, J = 2 Hz, 1-CH), 6.4 (1H, d, J = 7 Hz, 7-CH), 2.92 (2H, d, J = 14 Hz, 22-CH_2), 2.21 (3H, s, 4-CH_3), 1.52 (3H, s, 9-CH_3), 1.35 (3H, s, 14-CH_3), 1.02 (3H, s, 13- or 17-CH_3), 1.01 (3H, s, 17- or 13-CH_3), 0.96 (3H, d, J = 6 Hz, 20-CH_3); ms: 420.2666 (M^+), $C_{28}H_{36}O_3$, 405.2425 ($C_{27}H_{33}O_3$, 5.88%), 267.1390 ($C_{18}H_{19}O_2$, 2.69%), 253.1226 ($C_{17}H_{17}O_2$, 7.23%), 241.1231 ($C_{16}H_{17}O_2$, 23.7%), 227.1063 ($C_{15}H_{15}O_2$, 4.87%), 225.1288 ($C_{16}H_{17}O$, 4.54%), 202.0978 ($C_{13}H_{14}O_2$, 12.61%), 201.0910 ($C_{13}H_{13}O_2$, 11.43%), 200.0835 ($C_{13}H_{12}O_2$, 6.39%), 163.1136 ($C_{11}H_{15}O$, 2.18%), 107.0854 (C_8H_{11}, 3.53%), 78.0469 (C_6H_6, 37.65%). Direct tlc comparison with an authentic sample of tingenone, $C_{28}H_{36}O_3$, (16), showed it *not* to be identical, but had a slightly lower R_f value. For the 145–150°C mp sample. *Anal.* calcd. for $C_{28}H_{36}O_3 \cdot 0.5$ MeOH: C 78.39, H 8.77; found: C 78.30, H 8.49.

Further separation of the mixture of compounds in the fractions 10–15 gave small amounts of other orange colored compounds which have not been fully characterized. One of these had spectral properties similar to those of 20-hydroxytingenone; ^{1}Hmr (100 MHz), δ: 7.05 (1H, dd, J = 6.5 and 1.5 Hz), 6.57 (1H, d, J = 1.5 Hz), 6.38 (1H, d, J = 6.5 Hz), 3.00 (2H, d, J = 15 Hz), 2.2 (3H, s), 1.4 (3H, s), 1.35 (6H, s), 1.23 (3H, s), 0.90 (3H, s); ms: 436.2592 (M^+), $C_{28}H_{38}O_4$.

Oleanolic Acid 8

The 0.42 g of material from the fractions 10–15 also yielded 45 mg of a cream colored compound, mp 285°C (recrystallized, ethanol) from plc; ^{1}Hmr (100 MHz), δ: 5.26 (1H, t, J = 1.5 Hz, C=CH), 3.25 (dt, J = 4 and 1.5 Hz, —CHOH), 2.50 (bs, exch. D_2O, —OH), 1.20, 1.10, 0.98, 0.95, 0.92, 0.86, 0.78 (7 × 3H, singlets, 7 × CH_3); ms: 456.3622 (M^+), $C_{30}H_{48}O_3$, base peak at 248.1774 ($C_{16}H_{24}O_2$). Treatment with diazomethane gave a product, mp 193–195°C (lit. (17) mp 196–198°C); ^{1}Hmr (100 MHz), δ: 5.22 (1H, t, J = 1.5 Hz, $\diagdown$C=CH$\diagup$), 3.62 (3H, s, —COOCH_3), 3.15 (1H, dd, J = 11 and 4 Hz), 2.02 (1H, bs, exch. D_2O, —OH), 1.20, 1.15, 1.00, 0.95, 0.92, 0.82, 0.77 (7 × 3H, s, 7 × CH_3); ms: 470.3749 (M^+), $C_{31}H_{50}O_3$ (6.7%), base peak 262.1936 ($C_{17}H_{26}O_2$). *Anal.* calcd. for $C_{31}H_{50}O_3 \cdot H_2O$: C 76.16, H 10.72; found: C 76.17, H 10.72.

Polpunonic Acid 9

Separation on 2 mm Merck silica plates of the 0.42 g mentioned above from fractions 10–15 in 3% methanol–chloroform, gave a fraction which on tlc was shown to contain 5 major and 5 minor compounds. These were further separated by two successive plc runs on three 0.25 mm Merck silica plates in 3% methanol–chloroform. Three milligrams of crystals, mp 242–244°C (lit. (11) mp 246–248°C) were obtained. This was shown to be polpunonic acid by ir, ms, nmr, and mixture mp; ^{1}Hmr (80 MHz), δ: 2.30 (2H, m, CH_2 adjacent to $\diagdown$C=O$\diagup$), 1.27 (3H, s, CH_3), 1.10 (3H, s, CH_3), 1.00 (3H, s, CH_3), 0.87 (3 × 3H, some coupling evident, J = 6.5 Hz, 2 × 3° CH_3 and 1 × 2° CH_3), 0.70 (3H, s, CH_3); ms: 456.3574 (M^+), $C_{30}H_{48}O_3$, (78%).

Compound 4: 15-Hydroxy-18-norabieta-3,8,11,13-tetraene-3-oic Acid Methyl Ester

Fractions 16–19 were recombined and treated with diazomethane in diethyl ether. The product (262 mg) was separated into 29 fractions by hplc using a silica column and solvent system dichloromethane and diethylether–dichloromethane (10:1). Fraction 16 was shown to contain 8 components. Separation on 0.25 mm Merck silica plates in 3% methanol–dichloromethane gave a colorless oil (8 mg) for which structure **4** has been confirmed; ^{1}Hmr (270 MHz), δ: 7.25 (3H, m, aromatic —H), 3.75 (3H, s, $COOCH_3$), 3.0 (2H, m, 7-CH_2), 2.00 (3H, bs, 4-CH_3), 1.57 (6H, s, 17 and 16-CH_3), 1.05 (3H, s, 10-CH_3); ms: M^+ 328 (45%), 313 (65%), 310 (15%), 297 (10%), 295 (10%), 281 (8%), 278 (15%), 269 (5%), 253 (13%), 215 (51%), 197 (17%), 195 (15%), 183 (17%), 157 (19%), 149 (9%), 141 (13%), 91 (11%), 81 (5%), 59 (49%), 43 (100%).

Synthesis of Compound 4: (15-Hydroxy-18-norabieta-3,8,11,13-tetraene-3-oic Methyl Ester)

The ketone **10** was prepared from dehydroabietic acid by a procedure reported by Huffman (13). Scheme 2 outlines the synthetic route to compound **4**.

Compound 10 (18-Norabieta-8,11,13-triene-3-one)

Dehydroabietic acid (25.05 g) was converted by decarboxylation, hydroboration, and oxidation to the ketone **10** (13). The yield of **10** was 8.76 g, mp 60–63°C[3] (yield: 39%). Infrared, ν_{max}: 1705 cm^{-1}; ^{1}Hmr (80 MHz), δ: 7.23 (1H, d, J = 8 Hz), 6.99 (1H, br. d, J = 8 Hz), 6.95 (1H, br. s), 1.33 (3H, s), 1.23 (6H, d, J = 7 Hz), 1.21 (3H, d, J = 8 Hz); ms: 270 (M^+, 15%), 256 (40%), 255 (35%), 241 (100%), 223 (9%), 213 (20%), 199 (11%), 181 (25%), 171 (19%), 155 (9%), 143 (18%), 142 (15%), 141 (18%), 129 (30%), 128 (20%), 117 (14%), 91 (14%), 55 (40%). *Anal.* calcd. for $C_{19}H_{26}O$: C 84.39, H 9.69; found: C 84.01, H 9.71.

[3]The ketone reported by Huffman (13) was an oil.

Can. J. Chem. Downloaded from www.nrcresearchpress.com by 210.87.254.42 on 09/06/12
For personal use only.

Compounds 11 (3-Cyano-18(19)-norabieta-2,8,11,13-tetraene) and 12 (3-Cyano-18(19)-norabieta-3,8,11,13-tetraene)

Potassium cyanide (1.32 g, 20.2 mmol) was added to a solution of 1.0 g (3.70 mmol) of ketone **10** and 18-crown-6 ether in 50 mL of dry dimethyl sulfoxide – acetonitrile (1:3) at room temperature. The mixture was heated at 70–80°C for 1 day.

A saturated solution of sodium chloride was added with ice, and the product extracted 3× with ether. The ether solution was washed successively with aqueous sodium carbonate, water, and brine. The crude cyanohydrin obtained after solvent removal was dissolved in 20 mL of cold pyridine, and the solution treated with 0.5 g (4.20 mmol) of thionyl chloride for 30 min at 0°C under nitrogen. The solution was stirred at room temperature for 24 h and poured into 200 mL of ice and water. The product was extracted with ether and the extract dried with anhydrous sodium sulfate. The oil which remained after solvent removal was chromatographed on silica gel using benzene–hexane (1:1). A mixture of compounds **11** and **12** was obtained. The ^{1}Hmr spectrum indicated that **11** and **12** were present in the ratio of 5:1 (0.66 g; 60% from **10**) respectively. This was changed to a 2:1 ratio (nmr analysis) by the following procedure. Compounds **11** and **12** were dissolved in 50 mL of dry ethanol and treated with excess sodium ethoxide at 80–90°C for 5 h under nitrogen; ir; λ_{max}: 2250 (C≡N) cm^{-1}; ^{1}Hmr (80 MHz), δ: 6.60 (m, C=C—*H*), 1.06 (d, J = 7.0 Hz, C_4—CH_3), 2.08 (br. s, C=C—CH_3); ms: 279 (M^+, 20%), 264 (30%), 250 (18%), 236 (10%), 222 (11%), 199 (10%), 186 (32%), 171 (23%), 159 (24%), 149 (26%), 143 (10%), 141 (9%), 129 (13%), 123 (16%), 121 (70%), 119 (98%), 117 (100%), 115 (6%), 91 (10%), 86 (34%), 84 (41%), 82 (39%). *Anal.* calcd. for $C_{20}H_{25}N$: C 85.96, H 9.01; found: C 86.01, H 8.89.

Compounds 13 (3-Formyl-18(19)-norabieta-2,8,11,13-tetraene) and 14 (3-Formyl-18(19)-norabieta-3,8,11,13-tetraene)

To a solution of 1.28 g (4.58 mmol) of the mixture of **11** and **12** in 50 mL of dry hexane at 0°C under nitrogen was added 5.5 mL (1.0 mmol in hexane) of diisobutylaluminium hydride (DIBAL-H) dropwise. The reaction mixture was allowed to warm to room temperature and stirred for 1 h. The reaction was carefully poured into 100 mL of ice and water, and extracted with ether. After drying, the solvent was removed *in vacuo*. The mixture of aldehydes was separated on a silica gel column using benzene–hexane (3:2) to give 0.71 g of compound **13** (58%) and 0.36 g (30%) of compound **14**, both as colorless oils.

Compound 13: ir, λ_{max}: 1685 cm^{-1}; ^{1}Hmr (80 MHz), δ: 9.51 (1H, s, —C(=O)—*H*), 7.25 (1H, d, J = 9 Hz), 7.07 (1H, br. d, J = 9 Hz), 6.96 (1H, br. s), 6.85 (1H, m), 1.25 (3H, s), 1.24 (6H, d, J = 7.0 Hz), 1.17 (3H, d, J = 7.3 Hz); ms: 282 (M^+, 11%), 267 (10%), 239 (8%), 186 (25%), 171 (10%), 121 (40%), 119 (100%), 117 (92%), 86 (22%), 84 (24%), 82 (30%). *Anal.* calcd. for $C_{20}H_{26}O$: C 85.05, H 9.27; found: C 85.10, H 9.30.

Compound 14: ir, λ_{max}: 1685 cm^{-1}; ^{1}Hmr (80 MHz), δ: 10.19 (1H, s, —C(=O)—*H*), 7.27 (1H, d, J = 9 Hz), 7.06 (1H, br. d, J = 9 Hz), 6.93 (1H, br. s), 2.28 (3H, s), 1.27 (3H, s), 1.22 (6H, d, J = 7 Hz); ms: 282 (M^+, 18%), 267 (15%), 252 (10%), 186 (37%), 171 (10%), 159 (12%), 149 (10%), 121 (50%), 119 (100%), 117 (94%), 86 (42%), 84 (45%), 82 (50%). *Anal.* calcd. for $C_{20}H_{26}O$: C 85.05, H 9.27; found: C 85.01, H 9.30.

Compound 15: (18-Norabieta-3,8,11,13-tetraene-3-oic Acid)

To a solution of 0.36 g of the aldehyde **14** and 1.81 g of resorcinol in 20 mL of dioxane–water (1:1), 0.2 g of sodium chlorite in 5 mL of 0.1 *N* hydrochloric acid was added at room temperature (14). After 30 min stirring, the solution was extracted with ether and the ether extract dried over sodium sulfate. The solvent was removed *in vacuo* to yield compound **15**. Infrared, ν_{max} ($CHCl_3$): 3500, 1688 cm^{-1}; ^{1}Hmr (400 MHz); δ: 7.22 (1H, d, J = 9 Hz), 7.05 (1H, dd, J = 9 and 6 Hz), 6.90 (1H, d, J = 6 Hz), 2.19 (3H, bs), 1.27 (3H, s), and 1.24 (6H, d, J = 7 Hz); ms: 298 (M^+, 45%), 283 (M – CH_3, 50%), 241 (11%), 237 (10%), 223 (10%), 220 (13%), 195 (10%), 186 (100%), 171 (19%), 159 (23%), 149 (10%), 143 (14%), 129 (14%), 117 (11%), 105 (11%), 91 (11%), 87 (10%). *Anal.* calcd. for $C_{20}H_{26}O_2$: C 80.47, H 8.80; found: C 80.47, H 8.73.

Compound 16: (18-Norabieta-3,8,11,13-tetraene-3-oic Acid Methyl Ester)

Compound **15** was treated with excess diazomethane at 0°C in ether overnight. The methyl ester **16** was obtained as a colorless oil (0.28 g), 72% yield from compound **14**; ir, λ_{max}: 1720 cm^{-1}; ^{1}Hmr (80 MHz), δ: 7.25 (1H, d, J = 9.0 Hz), 7.05 (1H, br. d, J = 9.0 Hz), 6.92 (1H, br. s), 3.72 (3H, s), 2.11 (3H, br. s), 1.28 (3H, s), 1.23 (6H, d, J = 7.0 Hz); ms: 312 (M^+, 52%), 297 (27%), 283 (12%), 265 (10%), 257 (12%), 237 (32%), 199 (27%), 186 (49%), 165 (20%), 121 (40%), 119 (100%), 117 (97%), 59 (40%). *Anal.* calcd. for $C_{21}H_{28}O_2$: C 80.72, H 9.03; found: C 80.80, H 9.10.

Compound 4: (15-Hydroxy-18-norabieta-3,8,11,13-tetraene-3-oic Acid Methyl Ester)

The methyl ester **16** (98 mg; 0.298 mmol) was dissolved in 5 mL hexane–water (99:1). The solution was irradiated in a quartz cell with a 650 W Smith-Victor Corp. (Model 700) uv lamp for 5 h. The crude product (18 mg) was purified on 0.25 mm Merck silica plates (solvent: dichloromethane–methanol, 97:3) followed by hplc using a Waters silica column (dichloromethane – petroleum ether, 7:3) to give a colorless oil (8 mg). Infrared, ν_{max} ($CHCl_3$): 3590 and 1606 cm^{-1}; ^{1}Hmr (400 MHz), δ: 7.26 (3H, m, aromatic H), 3.75 (3H, s), 3.0 (2H, m, 7-CH_2), 2.00 (3H, bs, 4-CH_3), 1.57 (6H, s, 17 and 16-CH_3), 1.05 (3H, s, 10-CH_3); ms: 328 (M^+, 50%), 313 (60%), 310 (10%), 297 (12%), 295 (8%), 281 (8%), 278 (11%), 269 (9%), 253 (15%), 215 (66%), 197 (17%), 195 (13%), 183 (13%), 157 (15%), 149 (10%), 141 (12%), 91 (12%), 81 (10%), 59 (60%), 43 (100%). *Exact Mass* calcd. for $C_{21}H_{28}O_3$: 328.2039; found (M^+): 328.2038. *Anal.* calcd. for $C_{21}H_{28}O_3$: C 76.79, H 8.59; found: C 76.81, H 8.62.

β-*Sitosterol*

Material from fractions 1–9 was further fractionated on Merck 2 mm silica plates in benzene. Nine fractions were obtained. Open column chromatography on silica (180 g) of the major fraction, using carbon tetrachloride – benzene, followed by benzene – ethyl acetate, gave 8 fractions. Fraction 5 (867 mg) was further separated on a Waters Associates Prep. 500 HPLC (normal phase Porasil A) in benzene; 26 × 1 L fractions were collected. Fractions 15–18 on tlc showed one compound (116 mg), mp 137–139°C (recrystallized, methanol); nmr, tlc, mixture mp, and ms showed it to be β-sitosterol.

Separation Experimental: Method 2

A 25 L shake-flask cultivation of *T. wilfordii* cells of the TRP 4a line grown on modified PRL-4 medium was harvested after 37 days. Cells were separated from the medium by filtration through Mira cloth (Calbiochem). The broth, pH 5.9, was clarified using a CEPA model LE bench type high speed continuous centrifuge (36 000 rpm). Ethyl acetate was used as the extracting solvent (3 times) to give 2.34 g of an orange-brown solid. This was passed down a short silica column (40 g) in ethyl acetate to yield 1.85 g of a red solid; hplc separation was then performed on a normal phase Porasil A column of a Waters Associates Prep. 500 HPLC apparatus. Benzene, with increasing ethyl acetate as solvent gradient was used. Fifty fractions were collected, and were grouped based on tlc evidence; tlc

Can. J. Chem. Downloaded from www.nrcresearchpress.com by 210.87.254.42 on 09/06/12
For personal use only.

showed the presence of tripdiolide in fractions 25–36 (143 mg). Tripdiolide (9.1 mg) was obtained directly by treatment of these combined fractions with diethyl ether. The residue was separated on 0.25 mm Merck silica plates as outlined in method 1 to give another 12.6 mg. A total of 21.7 mg of crystalline tripdiolide was obtained. This yield represented sixteen times that reported from the plant source (3). The cells were freeze-dried to give 207 g of material. This was extracted with ethanol – ethyl acetate (1:2) and 20.1 g of a dark orange-colored solid was obtained. The open column procedure outlined in method 1 was used to separate 5 g of this extract; 2 mg of tripdiolide was obtained.

A repeat shake culture experiment (17.5 L) of TRP 4a type cells grown for 32 days was also separated by method 2 procedure to yield 18 mg of crystalline tripdiolide.

Separation Experimental Method 3

Part (5.7 g) of the material obtained from the freeze-dried cells as discussed above (20.1 g) was subjected to a solvent partition procedure. Two liters of water were added to the 5.7 g in a large mortar. Petroleum ether was added and the mixture thoroughly mixed. The mixture was next separated in a separating funnel; 0.98 g of a light orange-colored solid was recovered from the petroleum ether. The aqueous layer was successively extracted with benzene (2.11 g of a dark red material obtained), diethyl ether (yield was 0.99 g), ethyl acetate (yield was 0.34 g), and chloroform (yield was 0.20 g). The ethyl acetate fraction was shown by tlc to contain tripdiolide. A short silica column in ethyl acetate, followed by plc on 0.25 mm Merck plates gave 3.1 mg of tripdiolide. By extrapolation, the 20.1 g of extract would contain 10.9 mg or 14 times as much as that obtained by procedure 2. In summary, 32.6 mg of tripdiolide could be obtained from 22.4 g of material extracted from broth and dried cells. This represents a 0.016% yield (based on 207 g of dried cell weight) or 16 times that reported for the plant material (3).

Triptolide 2

A 22 L batch of TRP 4a cell cultures was reaped after 35 days incubation. Ethyl acetate extraction of the medium gave 1.38 g of crude material. A hplc separation procedure similar to that outlined in method 2 above was used to produce 25 fractions. From fractions 9–19. 19.7 mg of tripdiolide was obtained.

Fraction 1 (248 mg) was separated on thirteen 0.25 mm Merck silica plates in 15% acetone–benzene. This gave 9.2 mg of crude material which was further purified on three 0.25 mm Merck silica plates to yield 4.5 mg of triptolide, mp 225–227°C. This yield represented three times the yield reported for the plant material (3); ^{1}Hmr (400 MHz); δ: 4.66 (2H, m, 19-CH_2), 3.89 (1H, d, J = 4 Hz, 11-CH), 3.51 (1H, dd, J = 4 and 1 Hz, 12-CH), 3.41 (1H, dd, J = 11 and 1 Hz, 14-C*H*OH), 3.36 (1H, d, J = 5 Hz, 7-CH), 2.73 (1H, m, 5-CH), 2.32 (1H, d, J = 11 Hz, 14-CHO*H*), 2.24 (1H, m, 1-CH), 2.15 (1H, m, 15-CH), 1.98 (1H, m, 1-CH), 1.56 (2H, m, 2-CH_2), 1.10 (3H, s, 20-CH_3), 1.0 (3H, d, J = 7 Hz, 17-CH_3), 0.88 (3H, d, J = 7 Hz, 16-CH_3); ms: 360.1571 (M^+), $C_{20}H_{24}O_6$, (calcd. 360.1573). Identity was further confirmed by mixture mp, uv, and ir comparison with an authentic sample.

Isolation of Dehydroabietic Acid from TRP-4a Cultures

An aliquot (25 mL) of a 6 day old TRP 4a shake-flask culture (100 mL in a 300 mL flask) in PRL-4 medium was lyophilyzed. This was then powdered and extracted twice with 50 mL of ethyl acetate and once with 50 mL of ethanol. The extracts were combined, and removal of the solvents gave 5.3 mg of product. This was shown to contain 10 compounds by tlc (5% methanol – chloroform containing 0.1% acetic acid). The entire sample was dissolved in ethyl acetate and separated on a 0.25 mm Merck silica gel plate using the solvent system 10% methanol – chloroform with 0.2% acetic acid. The band corresponding to dehydroabietic acid (R_f 0.66) was eluted with ethyl acetate. Solvent removal yielded 1.1 mg of dehydroabietic acid (tlc, ms, methyl ester derivative comparison).

Acknowledgements

Financial support from the National Institutes of Health (Contract NO1-CM-87236) and a grant from the Natural Sciences and Engineering Research Council of Canada is gratefully acknowledged. We thank Professor G. B. Marini-Bettólo for authentic samples of pristimerin, tingenone, and polpunonic acid. We also thank Dr. M. Suffness of NIH for samples of tripdiolide and triptolide, and Dr. J. M. Cassidy, School of Pharmacy, Purdue University, for a sample of tripdiolide. The KB assays were performed by Arthur D. Little.

1. J. P. Kutney, M. H. Beale, P. J. Salisbury, R. D. Sindelar, K. L. Stuart, B. R. Worth, P. M. Townsley, W. T. Chalmers, D. T. Donnelly, K. Nilsson, and G. G. Jacoli. Heterocycles, **14**, 1465 (1980).
2. O. L. Gamborg and D. E. Eveleigh. Can. J. Biochem. **46**, 417 (1968).
3. S. M. Kupchan, W. A. Court, R. G. Dailey, C. J. Gilmore, and R. F. Bryan. J. Am. Chem. Soc. **94**, 7194 (1972).
4. R. S. Buchanin, S. J. Chen, D. M. Frieze, F. T. Sher, and G. A. Berchtold. J. Am. Chem. Soc. **102**, 1200 (1980).
5. E. E. van Tamelen, J. P. Demers, E. G. Taylor, and K. Koller. J. Am. Chem. Soc. **102**, 5424 (1980).
6. T. K. Devon and A. I. Scott. Handbook of naturally occurring compounds. Vol. II. Terpenes. Academic Press, New York. 1972.
7. M. S. Schechter and H. L. Haller. J. Am. Chem. Soc. **64**, 182 (1942).
8. P. Martinod, A. Paredes, F. Delle Monache, and G. B. Marini-Bettólo. Phytochemistry, **15**, 562 (1976).
9. A. R. Campanelli, M. D'Alagni, and G. B. Marini-Bettólo. FEBS Lett. **122**, 256 (1980).
10. D. H. R. Barton and N. J. Holness. J. Chem. Soc. 78, (1952).
11. F. Delle Monache, J. F. de Mello, G. B. Marini-Bettólo, O. Goncalves de Lima, and I. L. d'Albuquerque. Gazz. Chim. Ital. **102**, 636 (1972).
12. J. P. Kutney, M. H. Beale, P. J. Salisbury, K. L. Stuart, B. R. Worth, P. M. Townsley, W. T. Chalmers, K. Nilsson, and G. G. Jacoli. Phytochemistry. In press.
13. J. W. Huffman. J. Org. Chem. **35**, 478 (1970).
14. B. O. Lindgren and T. Nilsson. Acta Chem. Scand. **27**, 888 (1973).
15. R. Harada, H. Kakisana, S. Kobayashi, M. Musya, K. Nakanishi, and Y. Takahashi. Tetrahedron Lett. 603 (1962).
16. (*a*) K. Nakanishi, V. P. Gullo, I. Miura, T. R. Govindachari, and N. Viswanathan. J. Am. Chem. Soc. **95**, 6473 (1973); (*b*) P. M. Brown, M. Moir, R. H. Thomson, T. J. King, V. Krishnamoorthy, and T. R. Seshadri. J. Chem. Soc. Perkin Trans. I, 2721 (1973); (*c*) F. Delle Monache, G. B. Marini-Bettólo, O. Goncalves de Lima, I. L. d'Albuquerque, and J. S. de Barros Coelho. J. Chem. Soc. Perkin Trans. I, 2725 (1973).
17. K. H. Overton and D. J. Picken. Fortsch. Chem. Org. Naturst. **34**, 249 (1977).
18. Cancer Chemother. Rep. **25**, 1 (1962).

Effect of CdI_2 on electrical conductivity and phase transition behavior in AgI

MAHADEVA NATARAJAN AND ETALO A. SECCO[1]

Department of Chemistry, St. Francis Xavier University, Antigonish, N.S., Canada B2G 1C0

Received February 25, 1981

MAHADEVA NATARAJAN and ETALO A. SECCO. Can. J. Chem. **59**, 2685 (1981).

The phase transitions occurring in AgI containing dissolved CdI_2 have been examined by differential thermal analysis (DTA), electrical conductivity technique, and X-ray diffractometry. The electrical conductivity and polymorphic behavior of AgI is significantly modified by low concentrations of CdI_2. The results are interpreted in terms of substitutional Cd^{2+} and Ag^+ vacancies in AgI sublattice.

MAHADEVA NATARAJAN et ETALO A. SECCO. Can. J. Chem. **59**, 2685 (1981).

Faisant appel à l'analyse thermique différentielle (ATD), à la conductivité électrique et à la diffraction de rayons-X, on étudie la transition de phase qui se produit dans le AgI contenant du CdI_2 dissout. La conductivité électrique et le comportement polymorphique du AgI sont modifiés de façon significative par de faibles concentrations de CdI_2. On interprète les résultats en fonction de lacunes provoquées par la substitution de Ag^+ par Cd^{2+} dans le sous réseau de AgI.

[Traduit par le journal]

Introduction

AgI exists in three polymorphic forms at atmospheric pressure α, β, and γ. The high temperature α-form, first investigated by Strock (1) and later by Hoshino (2), is described as an "averaged structure" where the I atoms (ions) occupy a *bcc* arrangement with Ag atoms (ions) distributed statistically over 42 sites; it is stable between 147°C and its melting temperature. The anomalously high ionic conductivity of the α-phase was interpreted earlier in terms of highly mobile Ag^+ in a "quasi-molten" Ag^+ sublattice. Recent results from neutron scattering and microwave studies favor a jump-diffusion model for Ag^+ motion along preferential channels in the lattice as proposed by Gissler and Stump (3) (for review of electrical conductivity in AgI-type compounds see ref. 4).

The β- and γ-phases are identified as hexagonal and cubic structures, respectively. The coexistence of mixed β- and γ-phases at *RT* suggests complex phase interrelationships which are dependent on impurity content (5), thermal history, etc. While conflicting views are reported on the stability of these phases, it is accepted that the β-form is the stable phase at *RT* and the γ-form exists as a metastable phase in the range 25–136°C (6, 7).

The effects of a second component in the different solid phases can be used as a probe to clarify the phase transitions and the conductivity in AgI. CdI_2 was chosen as the component with the expectation that it will enter the AgI substitutionally at low concentrations ($r_{Cd^{2+}} < r_{Ag^+}$); the Cd^{2+} will generate Ag^+ vacancies in the Ag^+ sublattice with a resultant effect on T_t and σ–T behavior.

Experimental

Fused samples of CdI_2 in AgI were prepared by melting physical mixtures of specific compositions in porcelain crucible in air and allowing to equilibrate for an hour at temperature slightly below melting. Samples prepared in a flow of N_2 exhibited similar behavior. The observed loss of small amounts of I_2 due to CdI_2 decomposition was considered inconsequential.

The AgI used was from two sources, A. D. McKay of unspecified grade and Alfa Ventron Corp. of stated purity ≥99.9%; CdI_2 was J. T. Baker "Analyzed" Reagent, 99.9%. No discernible difference in behavior was observed in the two AgI preparations.

X-ray diffraction patterns were obtained on a Norelco diffractometer using CuK_α radiation (8). Electrical conductivity measurements (9) were done on compressed polycrystalline discs, 13 mm diameter and ~2 mm thick, under reduced pressure of 10^{-2} Torr. A thin coating of graphite (Dag #154 Acheson) ensured proper electrical contact with the two Pt disc electrodes. The heating rate was $\leq 15°\,h^{-1}$.

DTA traces were obtained on a duPont 990 Thermal Analyzer in a flowing N_2 (ultrapure) atmosphere using ignited Al_2O_3 as a reference material (10). Thermogravimetric analyses of the fused AgI–CdI_2 samples using TGA-951 accessory showed no weight loss over the temperature region investigated.

Results and Discussion

X-ray diffractogram traces of representative compositions in CdI_2 mole percentages are presented in Fig. 1. Up to 2.5% the characteristic peaks of hexagonal β-AgI remain unaffected but at 5% the (100) peak is shifted slightly to lower *d* spacing with a new peak (*) appearing at $d = 3.65$ Å between (101) and (002) peaks. Higher CdI_2 content effects an intensity drop in all peaks characteristic of AgI and intensity rise in the new peak up to 40%; the latter feature suggests compound formation, γ-

[1]To whom all correspondence should be addressed.

0008-4042/81/182685-04$01.00/0

©1981 National Research Council of Canada/Conseil national de recherches du Canada

Can. J. Chem. Downloaded from www.nrcresearchpress.com by 210.87.254.6 on 09/06/12
For personal use only.

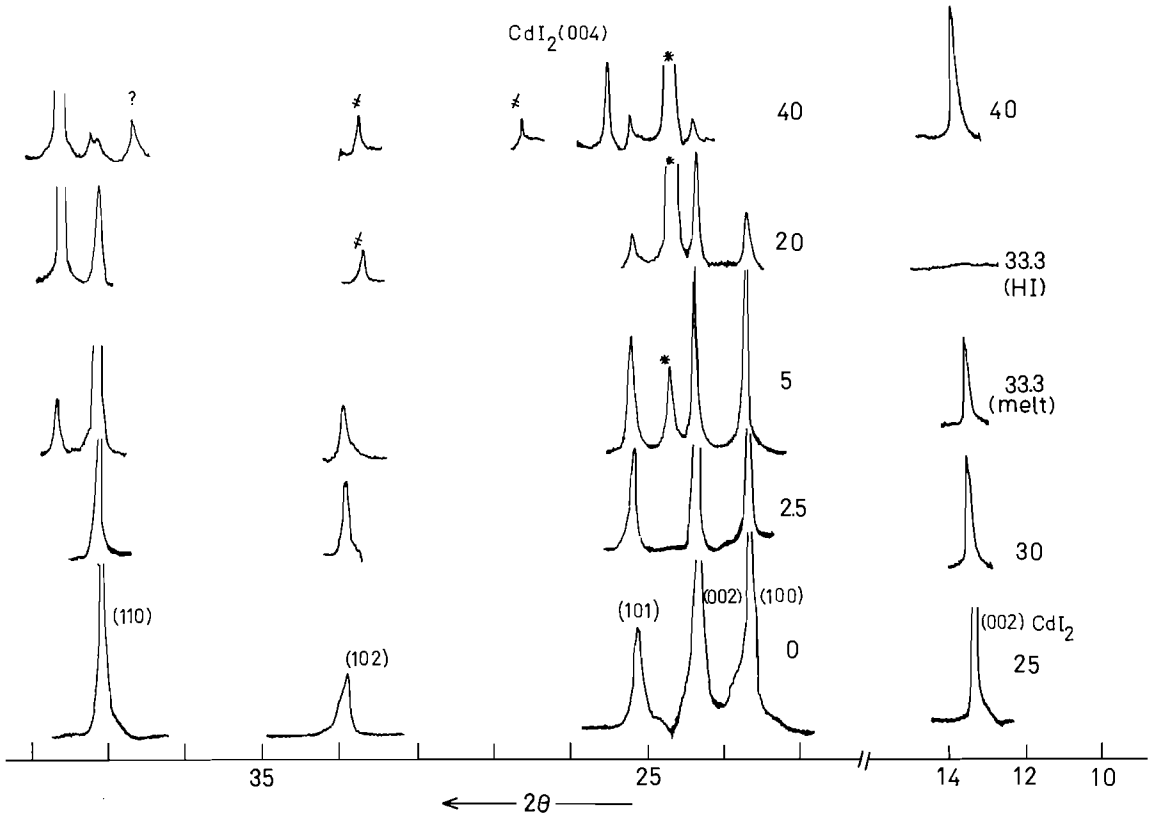

FIG. 1. X-ray diffractometry traces, peak intensity vs. 2θ, with mol% CdI_2 in AgI compositions. The peaks marked * are of possible Ag_2CdI_4 origin.

Ag_2CdI_4 (11). Our efforts to isolate and identify γ-Ag_2CdI_4 from fusion preparations were unsuccessful but γ-Ag_2CdI_4 was identified after evaporating 1:2 CdI_2–AgI in warm HI (57%) in acetic acid. Above 20% the characteristic peaks of CdI_2 intensify, e.g. $2\theta = 12.9°$.

The addition of AgI to CdI_2 effects a displacement of 12.9° peak to lower 2θ, i.e. higher *d* spacing, suggesting that AgI enters CdI_2 lattice substitutionally. Above 15% AgI no further displacement is observed while AgI peaks become evident, indicating saturation of CdI_2 plus undissolved AgI, i.e. solid solution and AgI. No evidence of γ-AgI was discernible in X-ray traces suggesting only β-AgI presence at room temperature.

DTA traces, heat and cool, of representative compositions in CdI_2 mole percentages are given in Fig. 2. The endotherm at 147 ± 1°C for pure AgI represents the β → α transition; the reverse transition reveals a slight hysteresis. However, mixed β and γ phases result on cooling AgI heated above its melting point.

CdI_2 in AgI over 5% increases the number of thermal effects; the doublet on cooling 2.5% does not reappear at higher CdI_2 compositions. The prominent endotherm at 105°C for 10% is assigned to solid–solid transition of the compound $(AgI)_{0.9}$-$(CdI_2)_{0.1}$ or $CdI_2 \cdot 9AgI$ and the broad endotherm at 150–165°C results from the overlapping of a peritectoid yielding Ag_2CdI_4 and β → α AgI transition; the clearly resolved doublet on cooling is consistent with the latter assignment. Above 10%, e.g. 30% the additional endotherm at 135°C is assigned to solid solution or disordering process of the compound in excess CdI_2 which is not reversible. The broad endotherm 225–255°C represents the slow dissolution of Ag_2CdI_4 by AgI; on cooling, the elimination or segregation gives an exotherm at 235°C with subsequent partial recombination to $(AgI)_{0.9}(CdI_2)_{0.1}$ and α → β AgI transition.

Replicate DTA traces on the same sample, heat and cool, reduce the number of thermal effects observed. Since no mass change is observed by TGA to 260°C we conclude that the sample state is determined by kinetic factors.

Can. J. Chem. Downloaded from www.nrcresearchpress.com by 210.87.254.6 on 09/06/12
For personal use only.

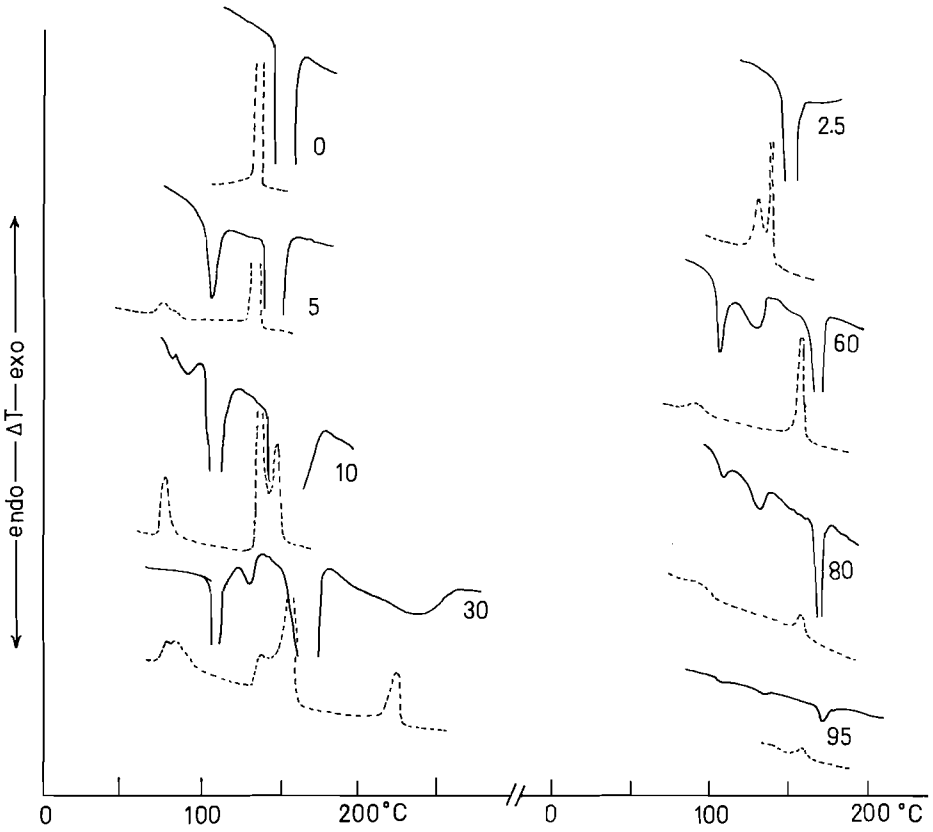

FIG. 2. DTA traces with mol% CdI_2 in AgI compositions with (full line) heat mode and (broken line) cool mode.

Alternate current electrical conductivity measurements at 1 kHz were carried out and cooling plots of representative compositions are presented in Figs. 3 and 4. Although reproducible plots, heat and cool modes, were obtained, heating plots showed non-reversible minor kinks in the unannealed disc.

Pure AgI shows a sharp break at 146°C, $\beta \rightleftarrows \alpha$ transition. 2.5% CdI_2 in AgI effects a higher relative conductivity above 50°C with the break at 125°C and the conductivity remains constant to 230°C. No physical defect in the compressed disc, such as cracking, etc., was observed after the heat–cool cycle. Our results are consistent with the conductivity results of Weiss *et al.* (12) who reported measurements on AgI below 2% CdI_2 and below 140°C. The shape and trend of the $\log\sigma - 1/T$ dependence with CdI_2 are shown by the 5, 50, and 70% plots. The breaks in the plots are consistent with the DTA thermal effects.

The presence of 5% AgI in CdI_2 (95%) has altered significantly the σ–T behavior of CdI_2 presented in Fig. 4.

The physico-chemical property measurements reported herein show a high degree of internal consistency. The AgI lattice can accommodate up to 2.5 mol% CdI_2 substitutionally where CdI_2 enters the α-AgI preferentially lowering the $\beta \rightarrow \alpha$ transition temperature. From the shift to lower d spacing for (100) planes it may be inferred that Cd^{2+} ions and Ag^+ vacancies are on lattice sites affecting (100) planes. This fact suggests that the (100) planes are critically linked to the $\beta \rightarrow \alpha$ transition energy barrier. Higher CdI_2 in AgI compositions result in compound formation and subsequent secondary effects.

The relatively constant E_a values, viz. 0.79 ± 0.07 eV, in the four samples cited, β-AgI, CdI_2, 2.5% CdI_2, 95% CdI_2, suggest a common mode of conductivity bearing in mind that conductivity for a specific charge carrier is a product of its concentration and mobility; our E_a value is consistent with the reported value of 15.4 kcal for KI in AgI (12). The higher conductivity of 2.5% CdI_2 and 5% AgI samples relative to the pure components suggest the presence of Ag^+ vacancies and I^- vacancies,

Can. J. Chem. Downloaded from www.nrcresearchpress.com by 210.87.254.6 on 09/06/12
For personal use only.

Can. J. Chem. Downloaded from www.nrcresearchpress.com by 210.87.254.6 on 09/06/12
For personal use only.

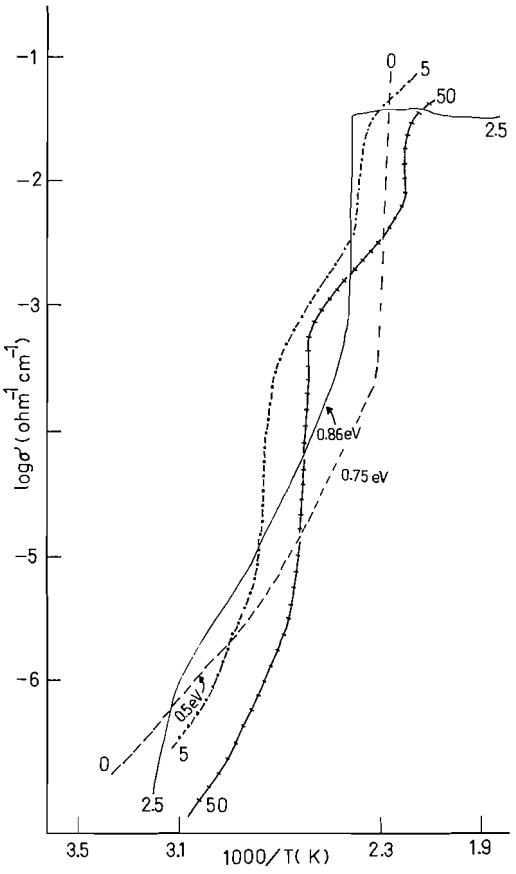

FIG. 3. Logarithm σ versus $1/T$ (K) plots of AgI-rich samples.

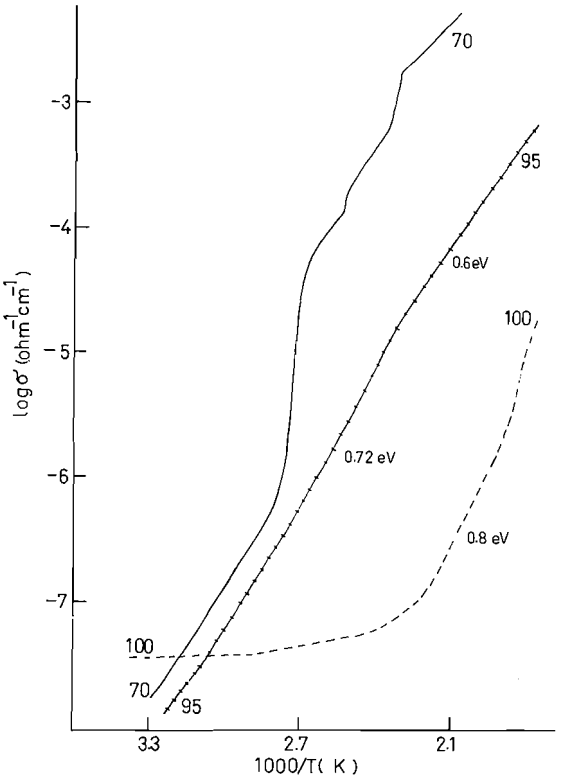

FIG. 4. Logarithm σ versus $1/T$ (K) plots of CdI_2-rich samples.

respectively, in accordance with the electroneutrality requirement.

The temperature-independent conductivity of 2.5% CdI_2 in α-AgI in the 135–230°C region resembles a fast ionic conductor. The presence of Ag^+ vacancies and Cd^{2+} in the sublattice is expected to favor the onset of high ionic conductivity of α-AgI at a lower transition temperature as observed. The jump-diffusion model for high ionic conductivity in α-AgI is consistent with our results. However, the Ag^+ vacancies and Cd^{2+} in the lattice rupture the normal periodicity for the jump-diffusion conductivity mechanism thus imposing a restriction on its simple periodic nature. In other words, the presence of Cd^{2+} in the Ag sublattice has placed a limit on the minimum energy path for Ag^+ motion along a ⟨100⟩ tunnel as proposed by Flygare and Huggins (13).

Acknowledgments

The authors are indebted to the Natural Sciences and Engineering Research Council Canada for financial support and to Allen J. Britten for conductivity and DTA measurements.

1. L. W. STROCK. Z. Physik. Chem. **B25**, 441 (1934); **B31**, 132 (1936).
2. S. HOSHINO. J. Phys. Soc. Jpn. **12**, 315 (1957).
3. W. GISSLER and N. STUMP. Physica, **65**, 109 (1973).
4. K. FUNKE. Prog. Solid State Chem. **11**, 345 (1976).
5. K. YAMADA. Bull. Soc. Sci. Photo Jpn. **11**, 1 (1961).
6. G. BURLEY. J. Phys. Chem. **68**, 1111 (1964).
7. M. NATARAJAN. J. Chem. Soc. A, 3087 (1970).
8. E. A. SECCO. Can. J. Chem. **42**, 2143 (1964).
9. M. NATARAJAN and E. A. SECCO. Can. J. Chem. **52**, 712 (1974).
10. K. RAJESHWAR and E. A. SECCO. Can. J. Chem. **54**, 2509 (1976).
11. Y. OTSUBO, A. NITTA, K. MOTOSHISA, Y. IWATA, and A. UEKI. Kogyo Kagaku Zasshi Jpn. **69**(9), 1716 (1966); Chem. Abstr. **69**, 46412 (1968).
12. K. WEISS, W. JOST, and H. J. OEL. Z. Physik. Chem. Neue Folge, **15**, 429 (1958).
13. W. H. FLYGARE and R. A. HUGGINS. J. Phys. Chem. Solids, **34**, 1199 (1973).

Gas phase basicities of fluorocarbonyl compounds. An ion cyclotron resonance investigation of the effects of fluorine and trifluoromethyl substituents on hydroxy carbonium ion stabilities

C. E. DOIRON AND T. B. MCMAHON

Department of Chemistry, University of New Brunswick, Fredericton, N.B., Canada E3B 5A3

Received February 23, 1981

C. E. DOIRON and T. B. MCMAHON. Can. J. Chem. **59**, 2689 (1981).

Gas phase proton affinities for a number of fluoro- and trifluoromethyl-substituted carbonyl compounds have been obtained using a combination of proton transfer equilibria and bracketing experiments. Absolute and relative substituent effects for F and CF_3 on carbonyl basicities are determined and discussed in terms of inductive, resonance, polarization, and hydrogen bonding interactions. The data are used to interpolate basicities for HCOF and CF_3CHO and are compared to theoretical *ab initio* calculations.

C. E. DOIRON et T. B. MCMAHON. Can. J. Chem. **59**, 2689 (1981).

On a obtenu les affinités pour le proton en phase gazeuse d'une série de composés carbonylés portant un fluor ou un groupement trifluorométhyle, en utilisant les équilibres de transfert de proton combinés à des expériences d'encadrement. On a déterminé les effets de substituants absolus et relatifs du F et du CF_3 sur la basicité du carbonyle et on en discute en fonction des interactions inductives, de résonance, de polarisation et de liaisons hydrogènes. On a utilisé les données pour interpoler les basicités du HCOF et du CF_3CHO et on les a comparées aux calculs *ab initio* théoriques.

[Traduit par le journal]

Introduction

Fluorine and trifluoromethyl substituents have been abundantly demonstrated to be capable of dramatically altering the stabilities of ionic species in both gas and solution phases (1–6). In the gas phase, the true intrinsic substituent effect is revealed since the ion is unencumbered by complicated solvation and ion-pair interactions (7, 8). For example, fluorine substituents are generally presumed, on the basis of solution behaviour, to destabilize positive charge centers via a strong inductive electron withdrawal brought about by the high electronegativity of fluorine (1, 2). However, recent gas phase experiments (4) and theoretical studies (9, 10) have shown that, in fact, fluorine-substituted α to carbonium ion centers gives a net stabilization interaction relative to hydrogen. This is shown to arise from the participation of fluorine 2*p* electrons in back bonding to the vacant *p* lobe of the carbonium ion center which counteracts the σ electron withdrawal (4, 9, 10). In cases where fluorine is substituted in positions other than α to a charge center, only the expected inductive destabilizing effect is observed (11).

Initial *ab initio* calculations by Csizmadia *et al.* (12) appeared to show that fluorine substituents in hydroxy methyl carbonium ions also played a stabilizing role. Their calculations revealed a greater proton affinity for formylfluoride than formaldehyde by a surprising 16 kcal/mol, roughly equal to the stabilizing effect of a methyl group (13).

A subsequent ion cyclotron resonance investigation by us (14) was in substantial disagreement with the theoretical result. Experimentally it was found that the gas phase proton affinity of acetyl fluoride was approximately 8 kcal/mol lower than that of acetaldehyde, indicating a substantial destabilization by fluorine in hydroxy carbonium ions.

More recent, *ab initio* calculations by del Bene and co-workers (15, 17) have shown a strong basis set dependence on the calculated relative basicities of formaldehyde and formyl fluoride. Using an STO-3G basis set formyl fluoride is found to have a proton affinity only 0.8 kcal/mol *lower* than that of formaldehyde (16). However, with the extended 4-31G basis set, a proton affinity difference of 20 kcal/mol was found (16). This is in general agreement with the known tendency of STO-3G calculations to overestimate π back donation (18). An analogous STO-3G study of carbonyl fluoride revealed a 6.4 kcal/mol destabilization relative to formaldehyde. No 4-31G calculation was done in this case (17).

The effects of trifluoromethyl substituents on amine and alcohol basicities have been previously investigated experimentally in the gas phase (19). The CF_3 substituent effect has been shown to be separable into contributions from inductively destabilizing and through space-polarization stabilizing interactions (19), with the destabilizing component dominating in protonated alcohols and amines. A recent *ab initio* investigation has similarly shown a strong destabilizing effect of CF_3 substituents on carbonium ion centers with $CF_3CH_2^+$ predicted to

0008-4042/81/182689-06$01.00/0

©1981 National Research Council of Canada/Conseil national de recherches du Canada

Can. J. Chem. Downloaded from www.nrcresearchpress.com by 210.87.254.40 on 09/06/12
For personal use only.

Can. J. Chem. Downloaded from www.nrcresearchpress.com by 210.87.254.40 on 09/06/12
For personal use only.

TABLE 1. Proton transfer equilibria examined and thermochemical data derived

Equilibrium	K_{eq}	ΔG^0_{298}[a]	ΔS^{0}[b]	ΔH^{0}[c]
[1] $(CF_3)_2COH^+ + SO_2 \rightleftharpoons SO_2H^+ + (CF_3)_2CO$	3.1	−0.7	0	−0.7
[2] $F_2COH^+ + (CF_3)_2CO \rightleftharpoons (CF_3)_2COH^+ + F_2CO$	2.5	−0.5	0	−0.5
[3] $CF_3CFOH^+ + F_2CO \rightleftharpoons F_2COH^+ + CF_3CFO$	0.7	0.2	−1.4	−0.2
[4] $CF_3CFOH^+ + (CF_3)_2CO \rightleftharpoons (CF_3)_2COH^+ + CF_3CFO$	4.8	−0.9	1.4	−0.5
[5] $CF_3CFOH^+ + SO_2 \rightleftharpoons SO_2H^+ + CF_3CFO$	24.9	−1.8	1.4	−1.4
[6] $F_2SO_2H^+ + CF_3CFO \rightleftharpoons CF_3CFOH^+ + F_2SO_2$	1.4	−0.2	−1.4	−0.6
[7] $F_2SO_2H^+ + F_2CO \rightleftharpoons F_2COH^+ + F_2SO_2$	5.6	−1.0	0	−1.0
[8] $F_2SO_2H^+ + (CF_3)_2CO \rightleftharpoons (CF_3)_2COH^+ + F_2SO_2$	6.9	−1.2	0	−1.2

[a] All values in kcal mol^{-1} obtained from $\Delta G^0 = -RT \ln K_{eq}$.
[b] All values in cal K^{-1}mol^{-1}, estimated from changes in rotational entropy due to symmetry.
[c] All values in kcal mol^{-1} obtained from $\Delta G^0 = \Delta H^0 - T\Delta S^0$ at 298 K.

be destabilized by 37 kcal/mol relative to CH_3^+ (18).

In order to clarify and quantify the dual role of both fluorine and trifluoromethyl substituents on carbonium ion centers, we have undertaken the present investigation of gas phase basicities of carbonyl fluoride, trifluoroacetyl fluoride, hexafluoroacetone, 1,1,1-trifluoroacetone, and acetyl fluoride. By comparison of the basicities of fluorinated and non-fluorinated analogues, it is hoped that a resolution of fluorine- and trifluoromethyl-substituent effects into contributions from inductive, resonance, polarization, and hydrogen bonding interactions may be obtained.

Experimental

All experiments were conducted at ambient temperature (20°C) using an ICR spectrometer of basic Varian V-5900 design extensively modified to permit trapped-ion experiments according to the method of McMahon and Beauchamp (20). Details of the design and operation of the trapped-ion ICR technique and conventional ICR single and double resonance experiments have been described in detail previously (21, 22).

All compounds used were commercially available chemicals of the highest purity obtainable. Carbonyl fluoride, trifluoroacetyl fluoride, and acetyl fluoride were obtained from PCR Inc. Hexafluoroacetone and 1,1,1-trifluoroacetone were purchased from ICN Pharmaceuticals Inc.

A typical relative proton affinity determination involved preparation of a mixture of bases of accurately known partial pressures using a Validyne AP-10 absolute pressure gauge attached to a monel vacuum line. This mixture was leaked into the ICR cell region via a high vacuum leak valve. In cases in which no hydrogens were present in either base, methane was also added to generate CH_5^+ to act as a protonation reagent (23). Usually three mixtures of ratios varying by a factor of 10 were examined to make a single relative proton affinity determination.

Equilibrium constants for each proton transfer reaction were calculated from the constant steady state ratio of ionic intensities and the known neutral pressure ratio. A typical example is that shown in Fig. 1 for the proton transfer equilibrium involving CF_2O and CF_3CFO, reaction [1].

[1] $CF_3CFOH^+ + CF_2O \rightleftharpoons CF_2OH^+ + CF_3CFO$

The ΔG^0 values calculated from the equilibrium constants determined were then converted to approximate ΔH^0 values by estimating the entropy changes for each of the proton transfer reactions based solely on changes in rotational entropies due to symmetry changes (24).

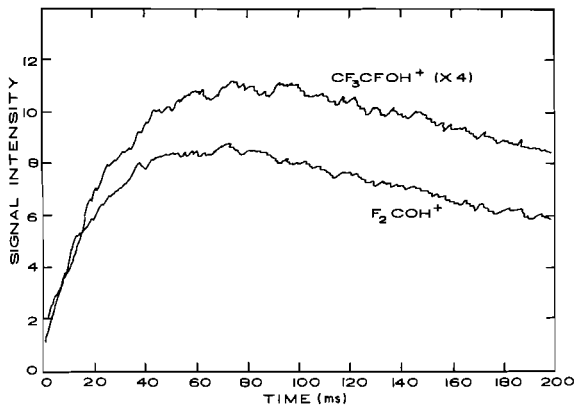

FIG. 1. Variation of relative abundances of F_2COH^+ and CF_3CFOH^+ with time in the CH_4 chemical ionization of a 4:1 mixture of F_2CO:CF_3CFO following a 5 ms, 70 eV electron beam pulse. Methane pressure is 2×10^{-7} Torr and carbonyl mixture pressure is 1.6×10^{-6} Torr. Only the protonated bases are shown.

Results

The equilibrium constants obtained for all proton transfer equilibria examined are summarized in Table 1, together with the ΔG^0 values derived from them, the estimated ΔS^0 values and the resulting ΔH^0 values. The relative proton affinities thus obtained may be placed on an approximate absolute proton affinity scale by a combination of appropriate double resonance experiments with reference bases of accurately known basicity in the gas phase.

The proton affinity of ethylene has recently been redetermined to be 163 ± 2 kcal/mol by two independent investigations (25, 26). Using photoionization and photoion-photoelectron coincidence (PIPECO) experiments, Baer has accurately identified the threshold for production of $C_2H_5^+$ from

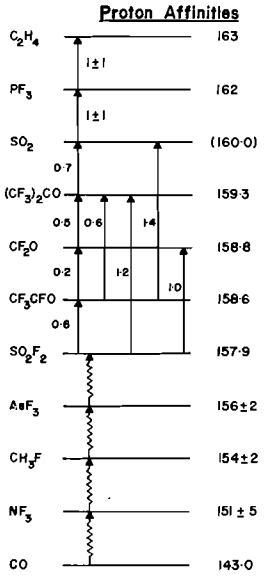

FIG. 2. Proton affinities for fluoro- and trifluoromethyl-substituted carbonyl compounds and various reference bases. A wavy arrow indicates the exothermic direction of proton transfer was identified by double resonance experiment. Numbers beside straight arrows are values of ΔH_{rxn}^0 taken from Table 1 or the text.

C_2H_5I while simultaneously measuring the kinetic energy release, reaction [2] (25).

[2] $C_2H_5I \xrightarrow{h\nu} C_2H_5^+ + I$

This measurement allows a calculation of 215.3 ± 1 kcal/mol for $\Delta H_f^0(298)$ for $C_2H_5^+$ using the known $\Delta H_f^0(298)$ for C_2H_5I and I (27). From the values of $\Delta H_f^0(298)$ for C_2H_4 and H^+ (28) a proton affinity for ethylene of 164.4 ± 1 kcal/mol may be calculated.

This value for the proton affinity of ethylene is in excellent agreement with another that may be derived from a combination of equilibrium experiments (26, 29). Bohme has recently determined the proton affinity of ethane to be 142.1 ± 1.4 kcal/mol from the measurement of the equilibrium constant for reaction [3] (26).

[3] $N_2OH^+ + C_2H_6 \rightleftharpoons C_2H_7^+ + N_2O$

The value of ΔH_f^0 (298) for $C_2H_7^+$ derived from this experiment may be combined with the value of ΔH^0 of −11.8 ± 0.5 kcal/mol determined by Kebarle for reaction [4] (29) to yield a value of $\Delta H_f^0(298)$ for $C_2H_5^+$ of 216.7 ± 2 kcal/mol. This allows a calculation of the proton affinity of ethylene of 163 ± 2 kcal/mol. Since Baer's determination lies within these error limits, we have chosen the reference standard for our absolute proton affinity scale as C_2H_4 with a value of 163 ± 2 kcal/mol.

[4] $C_2H_5^+ + H_2 \rightleftharpoons C_2H_7^+$

Double resonance experiments have shown that the proton affinity of PF_3 is less than that of C_2H_4, but at the same time sufficiently close to it to give an endothermic double resonance response for reaction [5] (23).

[5] $C_2H_5^+ + PF_3 \rightarrow HPF_3^+ + C_2H_4$

Equilibrium could not be established due to the reactivity of $C_2H_5^+$ with C_2H_4 (30).

[6] $HPF_3^+ + SO_2 \rightarrow SO_2H^+ + PF_3$

Similarly, reaction [6] was found to be endothermic to a sufficiently small extent to observe a positive double resonance signal. We have thus arbitrarily assigned a value for the proton affinity of SO_2 as 160 kcal/mol relative to an ethylene value of 163 kcal/mol. This proton affinity for SO_2 is consistent with a prediction by Munson based on a correlation of valence ionization potentials and proton affinities for oxygen-containing species (31).

The fluorocarbonyl compound proton affinities may all be related to that of SO_2 via the equilibrium data summarized in Table 1. The proton affinity scale thus derived from these compounds is given in Fig. 2. It is of interest to note that the value of 159 kcal/mol derived for the proton affinity of hexafluoroacetone is in excellent agreement with predictions based on empirical correlations of fluorinated acetone proton affinities with both the number of fluorine substituents and with vertical ionization potentials of the fluorinated acetones (32).[1]

At the lower end of the proton affinity scale given in Fig. 2, the fluorocarbonyl compounds may be seen to be more basic than AsF_3 with a proton affinity of 156 ± 2 kcal/mol (33).

The basicities of acetyl fluoride and 1,1,1-trifluoroacetone have been previously determined by us (14, 32). Acetyl fluoride may be assigned a proton affinity of 178 ± 2 kcal/mol based on the exothermicity of reactions [7] and [8].

[7] $H_3S^+ + CH_3CFO \rightarrow CH_3CFOH^+ + H_2S$

[8] $CH_3CFOH^+ + HCO_2H \rightarrow HCO_2H_2^+ + CH_3CFO$

As discussed previously, no equilibrium involving CH_3CFO could be obtained due to competing reaction channels. The proton affinity of 1,1,1-trifluoroacetone has been established as 178 kcal/mol based on a value of ΔH^0 of −0.6 ± 0.2 kcal/mol

[1]Reference data are taken to be those of ref. 13 with a $PA(NH_3)$ of 202.3 kcal mol^{-1}.

Can. J. Chem. Downloaded from www.nrcresearchpress.com by 210.87.254.40 on 09/06/12
For personal use only.

Can. J. Chem. Downloaded from www.nrcresearchpress.com by 210.87.254.40 on 09/06/12
For personal use only.

determined for the equilibrium in reaction [9] (32).

[9] $(CF_3COCH_3)H^+ + CH_2(CN)_2 \rightleftharpoons CH_2(CN)_2H^+ + CF_3COCH_3$

Discussion

It is of interest to examine the results obtained for the basicities of fluorocarbonyl compounds both in terms of absolute magnitudes of the fluorine and trifluoromethyl substituents effects, and in terms of the relative magnitudes of the two group effects.

From the results above and those in Table 1, it may be seen that replacement of hydrogen by fluorine at a carbonyl carbon results in a lowering of the carbonyl oxygen basicity of roughly 8 kcal/mol. This may be inferred from the 8 kcal/mol difference in basicity between CH_3CFO and CH_3CHO and from the 16 kcal/mol difference in basicity between F_2CO and H_2CO. This order of substituent effect for fluorine at carbonyl carbon is supported by observations by Taft, who reports a difference of 8.5 kcal/mol between the basicities of $FCO_2C_2H_5$ and $HCO_2C_2H_5$ (34). This magnitude for the fluorine substituent effect allows a prediction of 167 kcal/mol for the proton affinity of formyl fluoride which disagrees with predictions using both the STO-3G and 4-31G basis sets. Thus, the STO-3G basis set appears to overestimate the importance of π back donation from fluorine to the hydroxy carbonium ion center, while the 4-31G basis set must underestimate this contribution.

A comparison of the basicities of acetaldehyde and 1,1,1-trifluoroacetone reveals a difference of 8 $\pm$ 2 kcal/mol in the substitution of a CF_3 group for hydrogen at carbonyl carbon. Alternatively, comparison of 1,1,1-trifluoroacetone with acetone shows a reduction of 17 kcal/mol in proton affinity by substitution of CF_3 for CH_3. These relative data can thus be used to predict a value of the proton affinity of trifluoroacetaldehyde (CF_3CHO) of either 8 kcal/mol less than formaldehyde (167 kcal/mol), or 17 kcal/mol less than acetaldehyde (169 kcal/mol). Thus, the proton affinity of CF_3CHO is expected to be 168 $\pm$ 2 kcal/mol. Similarly, the difference in proton affinity between $(CF_3)_2CO$ and $(CH_3)_2CO$ (36 kcal/mol) is seen to be roughly twice that between CH_3COCF_3 and $(CH_3)_2CO$. In addition, the difference between the basicity of $(CF_3)_2CO$ and the predicted basicity of CF_3CHO is equal to the predicted difference between CF_3CHO and CH_2O.

These comparisons above reveal a remarkable similarity in the effects of F and CF_3 substituents on carbonyl basicities. It may be seen that within the experimental uncertainties, the proton affinities of CH_3CFO and CH_3COCF_3 are equal. The equilibrium experiments carried out in the present study also unambiguously show nearly identical basicities for the disubstituted carbonyls F_2CO, CF_3CFO, and $(CF_3)_2CO$. In addition, as a consequence of these similarities, the basicities of the elusive compounds HCOF and CF_3CHO are predicted to be nearly equal. This rather surprising similarity is not expected from the known substituent behaviour of fluorine and trifluoromethyl groups in solution studies of ionic species. For example, the substituent constant scale developed for electrophilic species by Brown and Okamoto gives a σ^+ value for *m*-CF_3 of 0.52 while that for *m*-F is only 0.35 (35). Thus in solution CF_3, substituents are expected to inductively destabilize positive charge centers more than F. Similarly, the Hammet σ scale gives values of 0.43 and 0.34 for *m*-CF_3 and *m*-F respectively (35). The greater electron-withdrawing effect of CF_3 relative to F is also borne out in both solution and gas phase studies of anionic species. For example, the pK_a's of *meta*- and *para*-substituted benzoic acids and phenols are lower for CF_3 substituents than for F substituents (35). In addition, gas phase acidity data have also shown that *meta*- and *para*-CF_3-substituted phenols are 5 and 9 kcal/mol more acidic than the corresponding F-substituted phenols (36). Obviously then, in the gas phase cationic species investigated in the present work, substituent effects either not present or not important in solution cationic species or gas phase anionic species must be considered to explain the similarity of CF_3 and F effects on carbonyl basicities.

Four distinct types of effect may be identified to operate in the protonated fluorocarbonyl species. The first of these is the normal electron-withdrawing inductive effect which removes electron density from the cationic center through the σ framework, destabilizing the ion. On the basis of the evidence discussed above it is to be expected that CF_3 substituents will exert the greater σ electron-withdrawing effect and inductively destabilize the protonated carbonyl group to a greater extent.

As discussed in the Introduction, in compounds in which fluorine is substituted directly at the carbonyl carbon, a resonance stabilization of the positively charged carbonium ion center may occur via a π interaction between the fluorine 2*p* orbital and the vacant 2*p* lobe on the carbonium ion center typified by the valence bond structures **I–III**. No similar resonance stabilization of CF_3-substituted carbonyls is possible.

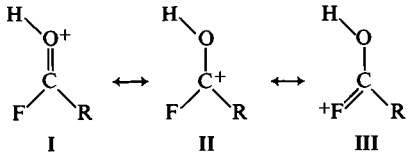

I II III

Both of the above types of interaction should contribute to an enhanced basicity of fluorine-substituted carbonyls relative to the analogous trifluoromethyl-substituted compounds. Since it is experimentally observed that both groups of carbonyls have nearly equal proton affinities, there must be one or more interactions giving rise to a preferential stabilization of the CF_3 substituted systems. One such interaction which immediately suggests itself is a through-space polarization interaction between the substituent and the charge center. This type of stabilization, originally suggested by Braumann (37), depends upon the group polarizability of the substituent and the distance between the substituent and the charge center. The polarizability of the CF_3 group may be estimated to be 2.12 Å^3 while that for a fluorine atom roughly is 0.45 Å^3 compared to a hydrogen atom polarizability of 0.40 Å^3 (38). In charge-delocalized systems such as the protonated carbonyl bases, there is no single site which may be identified as the charge center, although Mulliken population analyses from *ab initio* calculations indicate significant positive charge should reside on the hydrogen (12, 15–17). If such is the case, the distance between hydrogen and substituent would be less for CF_3 than F. These two factors would thus combine to give a significantly greater stabilization for the CF_3-substituted carbonyl via a through-space polarization interaction.

A further interaction likely giving rise to preferential stabilization of protonated CF_3-substituted carbonyls is intramolecular hydrogen bonding. Del Bene has shown that the *cis* form of protonated formylfluoride, **IV**, is more stable than the *trans* form, **V**, by roughly 2.5 kcal/mol (15, 16) due to the formation of a weak intramolecular hydrogen bond. In protonated CF_3 substituted carbonyls intramolecular hydrogen bond formation between the methyl fluorine and hydrogen should be even more facile since the geometry of these species brings the substituent fluorine very close to hydrogen, as in **VI**. This situation is very similar to that found in β-fluoroalcohols and amines where relatively strong intramolecular hydrogen bonds are found (39, 40). In this case, the hydrogen bond interaction should be significantly stronger due to the increased positive charge on the hydrogen and, in addition, should be substantially greater than that found in fluoro-substituted carbonyls.

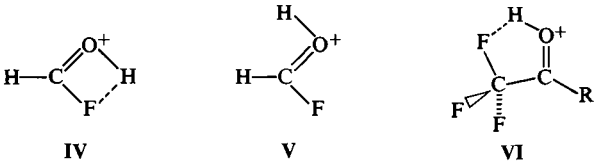

IV V VI

From the experimental observation that CF_3 and F appear to exert the same net substituent effect on carbonyl basicities, it must therefore be the case that the hydrogen bonding and polarization interactions which favour CF_3 basicities are almost exactly counterbalanced by the inductive and resonance interactions favouring F substitution.

Conclusions

Gas phase proton affinities have been determined for a number of fluorine- and trifluoromethyl-substituted carbonyl compounds. From the data obtained, it is evident that these two substituents exert the same net effect on carbonyl basicity. This is shown to be so, however, because of a complex combination of constituent substituent effects including inductive, resonance, polarization, and hydrogen bonding interactions. The inductive and resonance effects are predicted to favour basicities involving fluorine as a substituent rather than trifluoromethyl, while the polarization and hydrogen bonding interactions give rise to a more favourable situation for CF_3 substituents. Coincidentally, these biases appear to cancel each other giving rise to no net advantage for either F or CF_3 in affecting carbonyl basicities.

In addition to quantifying F and CF_3 substituent effects, the present work has provided a number of valuable reference compounds for the intermediate basicity range of the gas phase proton affinity scale. Our continuing proton affinity determinations will be directed toward further elaborating this basicity region.

Acknowledgement

Financial support of this work by the Natural Sciences Engineering and Research Council of Canada is gratefully acknowledged.

1. W. A. Sheppard and C. M. Sharts. Organic fluorine chemistry. Benjamin, New York, NY. 1969.
2. D. Holtz. Prog. Phys. Org. Chem. **8**, 1 (1971).
3. E. Buncel. Carbanions: mechanistic and isotopic aspects. Elsevier, Amsterdam. 1975.
4. T. B. McMahon, R. J. Blint, D. P. Ridge, and J. L. Beauchamp. J. Am. Chem. Soc. **94**, 8934 (1972).

Can. J. Chem. Downloaded from www.nrcresearchpress.com by 210.87.254.40 on 09/06/12
For personal use only.

5. T. B. McMahon and P. Kebarle. J. Am. Chem. Soc. **99**, 2222 (1977).
6. R. Farid and T. B. McMahon. Can. J. Chem. **58**, 2307 (1980).
7. E. M. Arnett and N. J. Pienta. J. Am. Chem. Soc. **102**, 3329 (1980).
8. P. Kebarle, W. R. Davidson, J. Sunner, and S. Meza-Höjer. Pure Appl. Chem. **51**, 63 (1979).
9. N. C. Baird and R. K. Datta. Can. J. Chem. **49**, 3708 (1971).
10. P. A. Kollman, W. F. Trager, S. Rothenberg, and J. E. Williams. J. Am. Chem. Soc. **95**, 458 (1973).
11. T. B. McMahon. Ph. D. Thesis. California Institute of Technology. 1973.
12. A. C. Hopkinson and I. G. Csizmadia. Can. J. Chem. **52**, 546 (1974).
13. J. F. Wolf, R. H. Staley, I. Koppel, M. Taagepera, R. T. McIver, Jr., J. L. Beauchamp, and R. W. Taft. J. Am. Chem. Soc. **99**, 5417 (1977).
14. T. B. McMahon. Can. J. Chem. **56**, 670 (1978).
15. J. E. Del Bene and A. Vaccaro. J. Am. Chem. Soc. **98**, 7526 (1974).
16. J. E. Del Bene. J. Am. Chem. Soc. **100**, 1673 (1978).
17. J. E. Del Bene and S. Radovick. J. Am. Chem. Soc. **100**, 6936 (1978).
18. Y. Apeloig, P. V. R. Schleyer, and J. A. Pople. J. Am. Chem. Soc. **99**, 1291 (1977).
19. R. W. Taft, M. Taagepera, J. L. M. Abboud, J. F. Wolf, D. J. De Frees, W. J. Hehre, J. E. Bartmess, and R. T. McIver, Jr. J. Am. Chem. Soc. **100**, 7765 (1978).
20. T. B. McMahon and J. L. Beauchamp. Rev. Sci. Instrum. **43**, 509 (1972).
21. J. L. Beauchamp. Ann. Rev. Phys. Chem. **22**, 517 (1971).
22. T. A. Lehman and M. M. Bursey. Ion cyclotron resonance spectrometry. Wiley-Interscience, New York. 1976.
23. M. S. B. Munson and F. H. Field. J. Am. Chem. Soc. **88**, 2621 (1966).
24. J. B. Cumming and P. Kebarle. Can. J. Chem. **56**, 1 (1978).
25. T. Baer. J. Am. Chem. Soc. **102**, 2482 (1980).
26. (*a*) D. K. Bohme, G. I. Mackay, and H. I. Schiff. J. Chem. Phys. **73**, 4976 (1980); (*b*) G. I. Mackay and D. K. Bohme. Second Canadian Conference on the Gas Phase Chemistry of Ions, Trent University, June 5–8, 1980.
27. H. M. Rosenstock, K. Draxl, B. W. Steiner, and J. T. Herron. J. Phys. Chem. Ref. Data Suppl. 1, **6** (1977).
28. S. G. Lias. *In* Kinetics of ion molecule reactions. *Edited by* P. Ausloos. Plenum, New York. 1979.
29. K. Hiraoka and P. Kebarle. J. Am. Chem. Soc. **98**, 6119 (1976).
30. T. O. Tiernan and J. H. Futreu. J. Phys. Chem. **72**, 3080 (1968).
31. D. E. Smith and B. Munson. J. Am. Chem. Soc. **100**, 497 (1978).
32. D. F. Drummond and T. B. McMahon. Unpublished results.
33. C. E. Doiron and T. B. McMahon. Inorg. Chem. **19**, 3037 (1980).
34. R. W. Taft. 27th Annual Conference on Mass Spectrometry and Allied Topics, Seattle, Washington, June 3–8, 1979, paper No. TPMO4-2.
35. C. D. Ritchie and W. F. Sager. Prog. Phys. Org. Chem. **2**, 323 (1964).
36. T. B. McMahon and P. Kebarle. Unpublished results.
37. J. I. Brauman and L. K. Blair. J. Am. Chem. Soc. **92**, 5986 (1970).
38. J. O. Hirschfelder, C. F. Curtiss, and R. B. Bird. Molecular theory of gases and liquids. Wiley, New York. 1954.
39. K. S. Buckton and R. G. Azrak. J. Chem. Phys. **52**, 5652 (1970).
40. I. D. Warren and E. B. Wilson. J. Chem. Phys. **56**, 2137 (1972).

Can. J. Chem. Downloaded from www.nrcresearchpress.com by 210.87.254.40 on 09/06/12
For personal use only.

Application of carbon-13 nuclear magnetic resonance to the configurational analysis of stereoisomeric N_α-methyl-N_β-acetylphlegmarines

ANDRZEJ LENIEWSKI[1] AND DAVID B. MACLEAN
Department of Chemistry, McMaster University, Hamilton, Ont., Canada L8S 4M1
AND
JOHN K. SAUNDERS
Département de chimie, Université de Sherbrooke, Sherbrooke (Qué.), Canada J1K 2R1
Received April 10, 1981

ANDRZEJ LENIEWSKI, DAVID B. MACLEAN, and JOHN K. SAUNDERS. Can. J. Chem. **59**, 2695 (1981).

The carbon-13 chemical shifts of isomeric phlegmarines and analogues are presented. The chemical shifts at C-7 and C-9 confirm the assignment of the stereochemistry at C-5. The stereochemistry at C-2′ of the isomeric phlegmarines was assigned by comparing the observed shifts with those predicted from conformer populations and conformer shifts for the various conformers obtained by rotation about the (C-5, C-11) and (C-11, C-2′) bonds. In particular it is possible to assign the relative configuration **1***b* to the naturally occurring N_α-methyl-N_β-acetylphlegmarine.

ANDRZEJ LENIEWSKI, DAVID B. MACLEAN et JOHN K. SAUNDERS. Can. J. Chem. **59**, 2695 (1981).

On présente les déplacements chimiques du ^{13}C des phlegmarines isomères et de leurs analogues. Les déplacements chimiques des carbones en positions 7 et 9 confirment la stéréochimie attribuée au carbone en position 5. On a déduit la stéréochimie du carbone en position 2′ des phlegmarines isomères en comparant les déplacements observés à ceux attendus à partir des populations des conformères et aux déplacements de divers conformères obtenus par la rotation autour des liaisons (C-5, C-11) et (C-11, C-2′). En particulier il est possible d'attribuer la configuration relative **1***b* à la N_α-méthyl N_β-acétylphlegmarine naturelle.

[Traduit par le journal]

We have recently reported a synthesis of (±)-N_α-methyl-N_β-acetylphlegmarine (1) that has established that the compound has the relative stereochemistry shown in structure **1***a* or **1***b*. Here we report an analysis of the ^{13}C spectra of racemic **1***a* and **1***b* that has enabled us to derive the relative stereochemistry at C-2′ in the two compounds and thereby to establish the relative stereochemistry of all five centres of the naturally-occurring alkaloid (2). The configurational assignment is based upon an approach recently developed by Beierbeck and Saunders (3). In the course of this work we also examined the ^{13}C spectra of two other diastereomers of the alkaloid, **2***a* and **2***b*, and several intermediates prepared in the synthetic work. The model compounds, *trans*-7-methyldecahydroquinolines **3**, *trans*-*N*-acetyl-7-methyldecahydroquinoline **4**, and the 2,2,5-trideutero derivatives of each were also prepared and examined to aid in the interpretation of the spectra. The data for all compounds are collected in Table 1.

7-Methyldecahydroquinoline was prepared by lithium aluminum hydride reduction of the tosyl hydrazone of ketolactam **5** according to an established procedure (4). Besides **3** the reduction mixture contained ca. 1% of monounsaturated product, probably the $\Delta^{5,10}$ or $\Delta^{5,6}$ derivative of **3** or a mixture of the two. The trideutero derivative was prepared by reduction with lithium aluminium deuteride. The acetyl compounds, **4**, and **4**-d_3, were prepared in the conventional manner.

In the spectrum of **3** the signals of the *C*-methyl and of the three methine carbon atoms were differentiated from the rest in the off-resonance spectrum. The methine carbon signals at 61.7, 42.8, and 32.1 were assigned to C-9, C-10, and C-7, respectively, based on substituent effects. Of the six signals associated with methylene carbon atoms the signal at lowest field, 47.2, is assigned to C-2. (This signal is absent in the spectrum of the deuterated analogue.) The signal at 32.4 has been assigned to C-5. Not only does it undergo the expected isotopic shift (5) but it also appears as a triplet in the noise decoupled spectrum and is reduced in intensity because of deuteration. Assignments at C-3, C-4, C-6, and C-8 were made by comparison with the published spectra of *trans*-decahydroquinolines (6) and by calculation according to the approach of Beierbeck *et al.* (7). The observed and calculated spectra were in good agreement with the exception of the signal attributed to the C-Me group.

In the *N*-acetyl compound **4** the signals at C-2, C-3, C-4, C-8, and C-10 are shielded with respect to

[1]Present address: Institute of Fundamental Problems of Chemistry, Warsaw University, Pasteura 1, 02-093 Warsaw, Poland.

0008-4042/81/182695-08$01.00/0
©1981 National Research Council of Canada/Conseil national de recherches du Canada

Can. J. Chem. Downloaded from www.nrcresearchpress.com by 210.87.254.5 on 09/06/12
For personal use only.

Can. J. Chem. Downloaded from www.nrcresearchpress.com by 210.87.254.5 on 09/06/12
For personal use only.

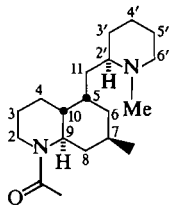

1*a*

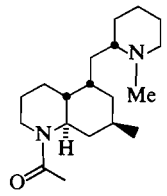

1*b*

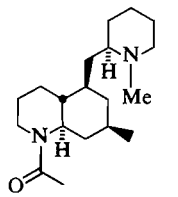

2*a*

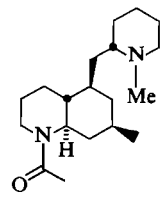

2*b*

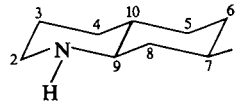

3

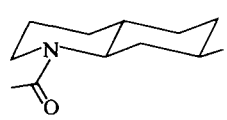

4

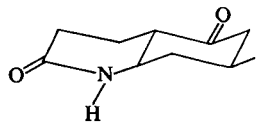

5

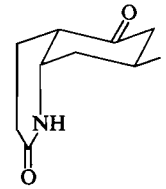

6

the corresponding signals of **3** with the largest effect apparent at C-2. These assignments were made by comparison of the spectrum of **4** with that of **4**-d_3. The signals attributed to C-2 and C-5 are directly affected by deuteration while the signals at C-3, C-6, and C-10 show isotopic shifts. The signals at C-7 and C-9 were easily differentiated from the signals of the methylene carbon atoms in the off-resonance spectrum and were assigned by comparison with the spectrum of **3**. The assignment of signals to C-4 and C-8 was also made by comparison with the spectrum of **3**.

The spectrum of the *trans*-ketolactam **5** was also analysed and assignments were made by comparison with the published spectra of *cis*-ketolactam **6** (8)[2] and 2-piperidine (9).[3] The assignments of signals to C-3 and C-4 were made by comparison with the spectrum of 2-piperidone and those to C-2 and C-5 as a consequence of their carbonyl character. The signals assigned to C-7, C-9, and C-10 are differentiated from the rest in the off-resonance spectrum and assignments made to each on the basis of substituent parameters. Of the two remaining signals, that at lower field is assigned to C-6 because of the proximity to the carbonyl group.

The assignment of signals in the spectra of **7**, **8**, **9**, **10**, and **11** was made by off-resonance studies and by comparison with the spectra of **5**, **3**, α-picoline, and vinyl pyridine (10). The differences observed for the signals in the carbocyclic ring between **8** and **9** on the one hand and **10** and **11** on the other reflect the equatorial and axial character of the substituents at C-5 in the two pairs of isomers and are in accord with predictions (see ref. 5, p. 29).

The assignments made in the spectra of the isomeric pairs **1***a*, **1***b* and **2***a*, **2***b* are based on comparison with the spectra of **4** and 1,2-dimethylpiperidine (12).[4] Again it is possible to differentiate the axial from the equatorial isomers at C-5, i.e. **1***a* and **1***b* from **2***a* and **2***b*, on the basis of the chemical shifts of the carbon atoms at C-7 and C-9 of the carbocyclic ring. The distinction between **1***a* and **1***b* and between **2***a* and **2***b* is not as straightforward. However, inspection of the data in Table 1 reveals that in each series, C-5, C-6, C-11, C-2′, and C-3′ are more shielded in one molecule than in the other. There follows a detailed study of the assignments

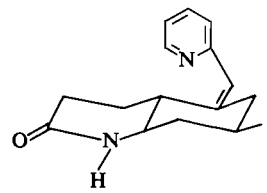

7

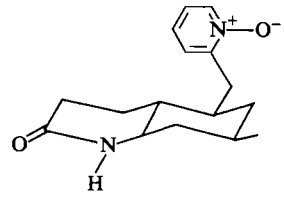

8

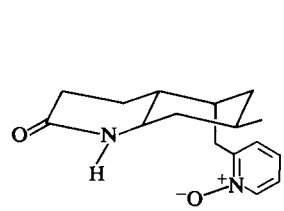

9

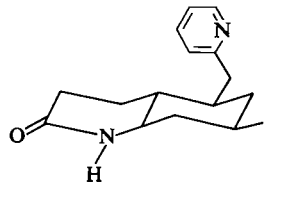

10

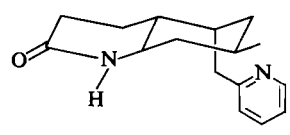

11

[2]In the published spectrum of **6** the assignments at C-8 and C-3 should be reversed.

[3]2-Piperidone: C-2 (173.1); C-3 (31.5); C-4 (21.9); C-5 (22.3); C-6 (42.0).

[4]1,2-Dimethylpiperidine: C-2 (59.4); C-3 (34.9); C-4 (23.7); C-5 (26.4); C-6 (57.2); N-CH_3 (43.4).

Can. J. Chem. Downloaded from www.nrcresearchpress.com by 210.87.254.5 on 09/06/12
For personal use only.

TABLE 1. Carbon-13 chemical shifts of isomeric phlegmarines and model compounds[a]

	Carbon																	
Compound	2	3	4	5	6	7	8	9	10	11	C7-$\overset{*}{\text{M}}$e	CO-$\overset{*}{\text{M}}$e	N-Me	2′	3′	4′	5′	6′
5	172.5	30.6	20.1	207.3	49.3	30.6	40.6	56.3	51.0	—	21.9	—	—	—	—	—	—	—
3 (obs)	47.2	27.1	32.1	32.4	35.0	32.1	42.5	61.7	42.8	—	22.5	—	—	—	—	—	—	—
3 (calcd)	47.4	26.2	33.8	33.8	35.8	31.2	43.8	62.0	44.8	—	25.6	—	—	—	—	—	—	—
3-d_3	—	27.1	32.1	32.1[b]	34.9	32.1	42.6	61.7	42.6	—	22.6	—	—	—	—	—	—	—
4	39.0	23.0	25.9	32.5	35.1	32.1	39.5	61.2	38.1	—	22.2	22.2[c]	—	—	—	—	—	—
4-d_3	—	22.7	25.9	32.1[b]	35.0	32.1	39.6	61.2	38.0	—	22.2	22.2[c]	—	—	—	—	—	—
7	171.9	32.0	25.1	142.4	46.6	31.8	42.1	57.1	45.6	124.9[d]	21.8	—	—	157.6	124.3	135.6	121.5	148.9
8	172.1	31.5	24.6	36.6	40.9[e]	30.1	41.7[e]	57.2	45.0	35.2	21.9	—	—	151.1	125.0	127.1	123.9	140.0
9	171.9	32.1	24.9	34.8	38.2	25.7	43.0	52.2	42.8	28.7	22.0	—	—	151.6	125.1	126.6	123.8	140.1
10	172.0	31.5	24.9	40.1	40.7[f]	30.3	41.9[f]	57.4	44.6	41.9[f]	21.9	—	—	160.7	123.9	136.1	121.2	149.5
11	172.0	32.2	25.4	38.3	37.2	25.4	42.9	52.4	42.9	36.0	22.1	—	—	161.3	123.5	136.4	121.2	149.6
1*a*[g]	37.7	23.0	25.0	36.9	40.2	26.8	39.5	54.7	41.7	30.3	22.3[h]	22.0[h]	42.3	63.5	32.0	22.7	24.3	56.4
1*b*[g]	37.7	22.9	25.7	35.2	38.4	26.5	39.4	54.6	41.2	28.3	22.3[h]	21.9[h]	43.1	62.0	30.6	22.7	23.9	56.7
2*a*[g]	39.0	23.2	26.0	38.2	41.4	31.1	39.0	60.8	43.5	36.3	22.2	22.2	43.2	61.4	30.6	22.1	24.1	57.3
2*b*[g]	38.7	23.1	25.1	40.3	43.0	31.1	38.9	60.8	43.8	38.1	22.2	22.2	42.3	62.5	32.6	22.2	24.3	56.7

[a] All samples were run in solution in $CDCl_3$; values are accurate to ±0.1 ppm from internal TMS.
[b] Triplet (J = 18.4 Hz).
[c] Chemical shift of carbonyl carbon atom = 169.8 (in **4**-d_3 = 169.9 ppm).
[d] A gated decoupling experiment showed that the doublet centered at 124.9 ppm did not have an additional coupling of ca. 7 Hz characteristic of "*meta*" spin interactions (11). In this way this signal was differentiated from those at 124.3 and 121.5 ppm where an additional 7 Hz coupling was observed.
[e] C-6 and C-8 may be reversed.
[f] C-6, C-8, and C-11 may be interchanged.
[g] C-3 and C-4′ as well as C-4 and C-5′ may be reversed.
[h] COMe and N–Me may be reversed.

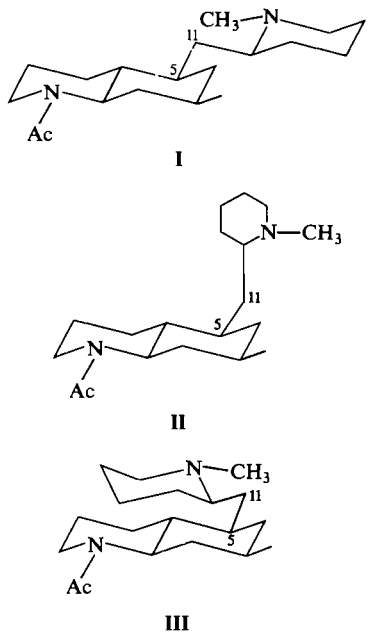

FIG. 1. Various conformations about the (C-5, C-11) bond in **2**.

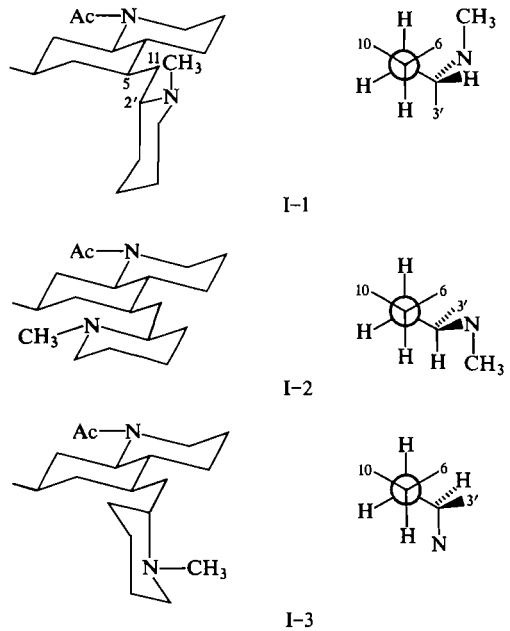

FIG. 2. Conformation about the (C-11, C-2′) bond in **2***a*.

of **2***a* and **2***b* in which the substituent at C-5 occupies the equatorial orientation.

The difference between **2***a* and **2***b* rests in the stereochemistry at C-2′. If one chooses as a reference that enantiomer in which C-5, C-7, C-9, and C-10 have the *R* configuration it is then necessary to determine which isomer, **2***a* or **2***b*, has the *R* and which the *S* configuration at C-2′. This can be accomplished by using the method reported for acyclic hydrocarbons (3). Basically the method consists of determining conformer shifts for each orientation and using the sum of conformer population multiplied by conformer shifts to obtain the predicted shift for each carbon atom in the molecule. For the molecules of interest, rotation is possible about the (C-5, C-11) and the (C-11, C-2′) bonds. Rotamer energies were estimated by considering the number of *gauche* butane interactions (referred to as γ interactions) and the number of δ *syn* interactions. The γ interaction is evaluated at 3.8 kJmol and the δ interaction at 15.4 kJ/mol (13, 14).

There are three possible orientations about the (C-5, C-11) bond and these are shown in Fig. 1. Fortunately two, II and III, can be neglected since these involve more severe steric interactions than those in I. For II the (C-11, C-2′) bond is *gauche* with respect both to the (C-5, C-6) and the (C-5, C-10) bonds. For III, the piperidine ring is *syn* with respect to the nitrogen containing ring and it is impossible for either stereoisomer to possess rotamers without severe steric interactions. Thus only conformers which have the rotamer denoted I about the (C-5, C-11) bond need be considered. The three rotamers about the (C-11, C-2′) bond for both the *R* and *S* stereoisomers are shown in Figs. 2 and 3, respectively.

For the *R* stereoisomer, conformer I-1 has three γ interactions, one between the N-CH_3 and C-11, one between C-3′ and C-5, and one between C-6 and C-2′. The energy is thus evaluated at 11.4 kJ/mol. In conformer I-2, there is an ε interaction between the N-CH_3 and C-6 which is an extremely severe interaction and this rotamer can be neglected. For I-3, there is a δ *syn* interaction between C-6 and C-3′, and γ interactions between the nitrogen and C-5 and between the N-CH_3 and C-11. The relative energy of this conformer is thus evaluated at 23.4 kJ/mol which is significantly higher than that for conformer I-1 and can be neglected. We can therefore conclude that the *R* stereoisomer exists predominantly as conformer I-1.

For the *S* stereoisomer conformer I-1 has a δ interaction between C-3′ and C-6 and a γ interaction between the N-CH_3 and C-11 which gives an estimated energy for this conformer of 19.2 kJ/mol. For conformer I-2, the relative energy is estimated to be 19.2 kJ/mol as this conformer has a δ interaction[5] between the N-CH_3 and C-5 and a γ interaction between C-6 and C-2′. The N-CH_3 could also exist in the axial orientation, conformer I-2′,

[5]The same energy value is estimated for a CH_3 placed on nitrogen as for a CH_3 on a carbon.

Can. J. Chem. Downloaded from www.nrcresearchpress.com by 210.87.254.5 on 09/06/12
For personal use only.

Can. J. Chem. Downloaded from www.nrcresearchpress.com by 210.87.254.5 on 09/06/12
For personal use only.

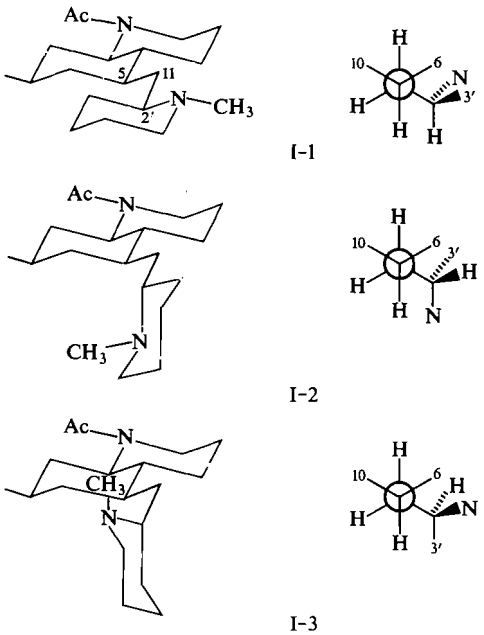

FIG. 3. Conformations about the (C-11, C-2′) bond in **2***b*.

which would alleviate the severe δ interaction. The energy would then be estimated at 19.0 kJ/mol since there are 5 γ interactions involved; N-CH_3 with C-3′, C-5′, and C-11; C-6 with C-2′; and the nitrogen with C-5. The final conformer I-3 has an estimated energy value of 26.8 kJ/mol (1 δ and 3 γ interactions) which is significantly higher than that for I-1 or I-2 and can therefore be neglected. We would thus predict that the *S* stereoisomer exists as a 1:1:1 mixture of I-1, I-2, and I-2′.

From the predicted conformer populations for the two stereoisomers, the predicted chemical shifts for each conformer were calculated. This was accomplished by using the method (7) which takes a reference shift for each carbon atom and takes account of the number of 1,3 diaxial H,H interactions, the number of *gauche* C,C (or C,N) interactions, and the number of δ *syn* interactions present in the molecule which are absent in the reference. The reference shifts for C-5 and C-6 are the corresponding shifts in **4**, for C-11 the shift of the CH_2 of propane, and for the C-atoms of the piperidine ring the corresponding shifts in 1,2-dimethylpiperidine. For C-5, an α shift is also necessary. Each time a 1,3-diaxial H,H interaction (henceforth referred to as an HC interaction) is present in the molecule of interest which was absent in the reference, an increment of +4.5 ppm is added. For each *gauche* interaction present in the molecule which was absent in the reference, a shift of 1.80 ppm is added to the italicized carbon

atom, and finally for each δ interaction introduced a shift of 2.6 ppm is added. The predicted shifts for each carbon atom in I-1 in which C-2′ has been assigned the *R* configuration are as follows

C-5	32.5	(reference)
	6.0	(introduction of C-11)
	−2.7	(replacement of H-4, H-5 interaction in reference by (C-4, C-10), (C-5, C-11) *gauche* interaction)
	1.8	*gauche*, ((C-2′, C-11), (C-5, C-6) interaction)
	37.6	
C-6	35.1	(reference)
	4.5	(HC interaction between H-11 and H-6a)
	39.6	
C-11	17.6	(reference)
	9.0	(HC interactions between H-11 and H-6a and H-10a)
	4.5	(HC interactions between H-11 and H-3′a)
	4.0	(HN interaction between nitrogen lone pair and H-11)
	1.8	*gauche*, (C-6, C-5), (C-11, C-2′)
	1.8	*gauche*, (C-3′, C-2′), (C-11, C-5)
	38.7	
C-2′	59.4	(reference)
	1.8	*gauche*, (C-5, C-11), (C-2′, C-3′)
	61.2	

C-3′	34.9	(reference)
	−4.5	(HC interaction between H-11 and H-3′e removed)
	30.4	

For the *S* stereoisomer, the predicted shifts are

	Rotamer I-1		Rotamer I-2	
C-5	32.5	(reference)	32.5	(reference)
	6.0	(α)	6.0	(α)
	−2.7	(see *R* isomer above)	−2.7	(see *R* isomer above)
	4.5	(H-2′ with H-5)	1.8	*gauche*, (C-2′, C-11), (C-5, C-6)
	1.8	*gauche*, (C-2′, C-11), (C-5, C-6)	2.6	(δ *syn*)
	42.1		40.2	
C-6	35.1	(reference)	35.1	(reference)
	4.5	(H-11 with H-6a)	4.5	(H-11 with H-6)
	2.6	(δ *syn*)		
	42.2		39.6	
C-11	17.6	(reference)	17.6	(reference)
	9.0	(H-11 with H-10 and H-6)	9.0	(H-11 with H-10 and H-6)
	4.5	(H-11 with H-3′)	9.0	(2 × H-11 with 2 × H-3′)
	4.0	(H-11 with N)	4.0	(H-11 with N)
	1.8	*gauche*, (C-3′, C-2′), (C-11, C-5)	1.2	*gauche*, (N-1′, C-2′), (C-11, C-5)
	1.8	*gauche* (C-6, C-5), (C-11, C-2′)	1.8	*gauche*, (C-6, C-5), (C-11, C-2′)
	38.7		42.6	
C-2′	59.4		59.4	
	4.5	(H-2′ with H-5)	1.2	*gauche*, (C-5, C-11), (C-2′, N-1′)
	1.8	*gauche*, (C-5, C-11), (C-2′, C-3′)		
	65.7		60.6	
C-3′	34.9		34.9	
	−4.5	(removal of H-3′ with H-11)		
	2.6	(δ *syn*)		
	33.0		34.9	

The differences between I-2 and I-2′ are the following: for C-5 the δ interaction is absent, C-6 is unchanged, for C-11 the H-11 with N interaction is absent, for C-2′ the HC interaction is replaced by a CC interaction, and for C-3′ the H-3′ with N interaction is removed. The predicted shifts for I-2′ are therefore: C-5, 37.6; C-6, 39.6; C-11, 38.6; C-2′, 57.9; C-3′, 30.9.

If we assume that the *S* isomer exists as a 1:1:1 mixture of I-1, I-2, and I-2′ then the predicted shift for C-5 is 40.0 ppm, for C-6 is 40.5, for C-11 is 40.0 ppm, for C-2′ is 61.4, and for C-3′ is 32.9 ppm. The predicted shifts for all the carbons in the *S* isomer are more deshielded than in the *R* stereoisomer and we can therefore assign configuration. The results are summarized in Table 2.

The neglect of less highly populated conformations will affect the absolute values of the predicted chemical shifts but will not change the sign of the difference between the two configurations.

The difference for the N-CH_3 group between the two stereoisomers is relatively small and for this reason it was not included in the analysis. In the *R* stereoisomer, it should appear at the same position as in 1,2-dimethylpiperidine, which it does. For the *S* stereoisomer, one would predict,

Can. J. Chem. Downloaded from www.nrcresearchpress.com by 210.87.254.5 on 09/06/12
For personal use only.

Can. J. Chem. Downloaded from www.nrcresearchpress.com by 210.87.254.5 on 09/06/12
For personal use only.

TABLE 2. Observed and predicted chemical shifts for **2***a* and **2***b*

	R (**2***a*)		*S* (**2***b*)	
	Observed	Predicted	Observed	Predicted
C-5	38.2	37.6	40.3	40.0
C-6	41.4	39.6	43.0	40.5
C-11	36.3	38.7	38.1	40.0
C-2′	61.4	61.2	62.5	61.4
C-3′	30.6	30.4	32.6	32.9

TABLE 3. Observed and predicted chemical shifts for **1***a* and **1***b*

	R (**1***a*)		*S* (**1***b*)	
	Observed	Predicted	Observed	Predicted
C-5	36.9	34.7	35.2	32.2
C-6	40.2	37.8	38.4	36.9
C-11	30.3	30.8	28.3	29.5
C-2′	63.5	61.4	62.0	61.2
C-3′	32.0	33.4	30.4	30.6

relative to 1,2-dimethylpiperidine, an increment of zero for conformer I-1, an increment of 2.6 ppm (δ interaction) for I-2, and an increment of −9.0 ppm for conformer I-2′. Thus this carbon is predicted to be shielded by 2.1 ppm in the *S* relative to the *R* stereoisomer. Again the predicted sign of the difference between the two stereoisomers for these carbons corresponds to that observed.

The assignment of stereochemistry for the axially substituted compounds **1***a* and **1***b* follows in a logical fashion since the same conformers are present. The *R* stereoisomer of **1** is the mirror image of the *S* for **2** with respect to the chiral centres at C-5 and C-2′ and it is this compound which has the more deshielded carbons at 5, 6, 11, 2′, and 3′. The analysis of the stereoisomers of **1** is summarized in Table 3.

The same situation is present with respect to the N-CH_3 group in the axial isomers, **1***a* and **1***b*, as that already discussed for the equatorial isomers, **2***a* and **2***b*.

The analysis of the carbon-13 chemical shifts has permitted the assignment of the relative stereochemistry at the fifth asymmetric centre of the four molecules examined and has confirmed the assignment at other centres. It should be emphasized that both stereoisomers at C-2′ were necessary to assign the stereochemistry at this carbon since it is the differences which are important rather than the absolute values.

In the previous paper on the phlegmarines (1) it was shown that **1***b* and N_α-methyl-N_β-acetylphlegmarine derived from nature had common physical properties in solution including the same R_f value in several solvent systems. This study has therefore resolved the relative stereochemistry of the alkaloid.

Experimental

Apparatus, Methods, and Materials

The reader is referred to ref. 1 for complete details.

trans-(7H, 10H), trans-(9H, 10H-7-Methyldecahydroquinoline 3 and its 2,2,5-Trideutero Derivative, 3-d_3

Tosylhydrazone of **5**

To a solution of *trans*-ketolactam **5** (905 mg, 5.0 mmol) in warm methanol (16 mL), *p*-toluenesulphonylhydrazide (98%, 950 mg, 5.1 mmol) was added and the mixture kept at 50°C for 2 h. The precipitated product was filtered off when the solution had cooled. The tosylhydrazone (1.50 g, yield 86%) melted at 199–200°C; ir ν_{max} (cm^{-1}): 3405, 3245 and 3180 (NH), 3080, 1605 (aromatic), 1675 (C=N), 1658, 1648 (C=O), 1352, 1169 (SO_2N); ^{1}H nmr $\delta_{80\,MHz}$ (ppm): 1.04 (3H, d, J = 5.6 Hz, CH—CH_3), 2.44 (3H, s, phenyl—CH_3), 5.9 (2H, br. s, NH), 7.3 and 7.8 (4H, AA′BB′ system, aromatic protons).

Hydride (Deuteride) Reduction of Tosylhydrazone of **5**

To a suspension of LAH (300 mg, ~8 mmol) in THF (40 mL), solid hydrazone (1.05 g, 3.0 mmol) was added at room temperature and the solution heated under reflux for 20 h. After cooling the mixture, water (8 mL) and ether (60 mL) were added. A white precipitate was filtered off and from the filtrate 135 mg of a colorless volatile slightly impure (tlc) solid were obtained. The white precipitate was treated with aqueous sodium hydroxide solution and the mixture steam distilled. The distillate (50 mL) was collected and extracted with ether to give 134 mg of the same product isolated above.

By the same procedure but using LAD instead of LAH 312 mg of deuterated compounds were obtained.

Pure **3** and **3**-d_3 were obtained by transformation of the crude products to their *N*-acetyl derivatives, that were purified by chromatographic separation on alumina, and then hydrolysed in 20% H_2SO_4.

N-*Acetylation of* **3** *and* **3**-d_3

The same procedure was used in both cases. Crude **3** (135 mg) was dissolved in absolute pyridine (4 mL) and treated with acetyl chloride (0.3 mL) at 0°C. When the mixture reached room temperature, water was added (50 mL) and most of the pyridine was evaporated at reduced pressure. To the residue 10% aqueous HCl (5 mL) was added and the solution extracted with chloroform. The collected extracts were washed with water and dried over anhydrous $MgSO_4$; 164 mg of undeuterated and 160 mg of deuterated amides were obtained as oils. Column chromatography on neutral alumina (activity 3, 10 g) gave 138 mg of the *N*-acetyl derivative of **3**, and 130 mg of the *N*-acetyl derivative of **3**-d_3, respectively, and 2 mg of *N*-acetyl-5,10- or 5,6)-dehydro derivatives of each or a mixture of both were also obtained.

Compound **4**: colorless oil, solidifying at temperatures below 0°C; ^{1}H nmr $\delta_{90\,MHz}$ (ppm): 0.91 (3H, d, J = 6 Hz, $CHCH_3$), 2.06 (3H, s, $COCH_3$), 3.1 (1H, m, H-2a), 3.30 (1H, m, H-9), 3.70 (1H, m, H-2e); ms: 195 (M^+, 30), 180 (12), 152 (9), 138 (65), 136 (9), 96 (100), 83 (11), 82 (10), 67 (8), 55 (15%).

Compound **4**-d_3: colorless oil, solidifying at temperatures below 0°C; ms: 198 (M^+, 47), 183 (8), 154 (6), 141 (74), 140 (6), 139 (9), 127 (2), 125 (2), 99 (100), 86 (4), 84 (4%).

N-acetyl-5,10(6)-dehydro-2-d_2 derivative, colorless oil; ms: 196 (26), 195 (82), 180 (63), 166 (6), 153 (23), 152 (38), 138 (100), 136 (36), 124 (39%).

Hydrolysis of N-*Acetyl* **3** *and* N-*Acetyl* **3**-d_3

Portions (100 mg) of the pure undeuterated and deuterated acetamides were refluxed separately with 20% aqueous H_2SO_4 (5 mL) for 6 h, 30% aqueous NaOH was carefully added to the cooled solution and the mixture extracted with chloroform yielding **3** and **3**-d_3 as colorless, volatile solids. Compound **3** (68 mg, yield 87%), mp 47–48°C; ^{1}H nmr $\delta_{90\,MHz}$ (ppm): 0.90 (d, J = 6 Hz, CHCH_3), 2.12 (1H, m, H-9), 2.32 (1H, br s, NH), 2.64 (1H, td, J = 11 and 4.5 Hz, H-2a), 3.10 (1H, d of q, J = 11.5 and 2 Hz, H-2e); $\delta_{90\,MHz}$ (C_6D_6) (ppm): 0.88 (d, J = 6 Hz, CHCH_3), 1.93 (1H, m, H-9), 2.48 (1H, m, H-2a), 2.92 (1H, d of q, J = 12 and 3 Hz, H-2e); ms: 153 (M^+, 14), 152 (12), 138 (3), 136 (3), 125 (3), 124 (3), 112 (7), 110 (4), 96 (100), 83 (9), 82 (8), 69 (6), 55 (12%). *Exact Mass* calcd. for $C_{10}H_{19}N$: 153.152; found (hrms): 153.153. Compound **3**-d_3 (66 mg, yield 84%), mp 47.5–48°C; ^{1}H nmr $\delta_{90\,MHz}$ (C_6D_6) (ppm): 0.90 (d, J = 6 Hz, CHCH_3), 1.90 (1H, br s, NH), 2.12 (1H, m, H-9); $\delta_{90\,MHz}$ (C_6D_6) (ppm): 0.89 (d, J = 6 Hz, CHCH_3), 1.94 (1H, t of d, J = 9 and 4 Hz, H-9); ms: 156 (M^+, 16), 155 (7), 99 (100), 98 (5), 85 (7), 84 (7), 58 (5), 56 (3), 55 (4%). *Exact Mass* calcd. for $C_{10}H_{16}D_3N$: 156.170; found (hrms): 156.170.

Acknowledgements

Financial support from the Natural Sciences and Engineering Research Council of Canada is gratefully acknowledged.

1. A. Leniewski, J. Szychowski, and D. B. MacLean. Can. J. Chem. **59**, 2479 (1981).
2. L. Nyembo, A. Goffin, C. Hootele, and J.-C. Braekman. Can. J. Chem. **56**, 851 (1978).
3. H. Beierbeck and J. K. Saunders. Can. J. Chem. **58**, 1258 (1980).
4. L. Caglioti. Tetrahedron, **22**, 487 (1966).
5. R. J. Abraham and P. Loftus. Proton and carbon-13 nmr spectroscopy. Heyden, London. 1979. p. 145.
6. E. L. Eliel and F. W. Vierhapper. J. Org. Chem. **41**, 199 (1976).
7. H. Beierbeck, J. K. Saunders, and J. W. ApSimon. Can. J. Chem. **55**, 2813 (1977).
8. J. Szychowski and D. B. MacLean. Can. J. Chem. **57**, 1631 (1979).
9. K. L. Williamson and J. D. Roberts. J. Am. Chem. Soc. **98**, 5082 (1976).
10. L. F. Johnson and W. Jankowski. Carbon-13 nuclear magnetic resonance spectra. Wiley-Interscience, New York. 1972.
11. F. W. Wehrli and T. Wirthlin. Interpretation of carbon-13 nmr spectra. Heyden, London. 1978. p. 55.
12. G. G. Levy (*Editor*). Topics in carbon-13 nmr spectroscopy. Vol. 3. Wiley, New York. 1979. p. 214.
13. N. L. Allinger and M. A. Miller. J. Am. Chem. Soc. **83**, 2145 (1961).
14. H. Werner, G. Mann, M. Mühlstadt, and H. J. Köhler. Tetrahedron Lett. 3563 (1970).

Can. J. Chem. Downloaded from www.nrcresearchpress.com by 210.87.254.5 on 09/06/12
For personal use only.

Carbon-13 isotopic selectivity in the infrared multiphoton photolysis of CF_2Cl_2–O_2 mixtures[1]

W. S. NIP,[2] P. A. HACKETT, and C. WILLIS

Laser Chemistry Group, Division of Chemistry, National Research Council of Canada, Ottawa, Ont., Canada K1A 0R6

Received April 24, 1981

W. S. NIP, P. A. HACKETT, and C. WILLIS. Can. J. Chem. **59**, 2703 (1981).

The infrared multiphoton chemistry of CF_2Cl_2–O_2 mixtures has been studied at laser frequencies where the product CF_2O is highly enriched in carbon-13. Yield enhancements with no loss of isotopic selectivity are attributed to suppression of radical–atom recombination reactions. It is demonstrated that addition of up to 60 Torr of either excess O_2 or N_2 suppresses a thermal, non-selective channel important at higher fluences. A selectivity factor greater than 30 is observed for 4 Torr CF_2Cl_2 in the presence of 80 Torr of oxygen.

W. S. NIP, P. A. HACKETT et C. WILLIS. Can. J. Chem. **59**, 2703 (1981).

On a étudié la chimie multiphotonique dans l'infrarouge des mélanges de CF_2Cl_2–O_2 à des fréquences laser où le produit CF_2O est fortement enrichi en ^{13}C. On a attribué l'augmentation des rendements sans la perte de sélectivité isotopique, à la suppression des réactions de recombinaison radical–atome. On démontre que l'addition jusqu'à 60 Torr soit d'un excès de O_2 ou de N_2 supprime un canal thermique, non sélectif, mais important à de plus hautes pressions. On a observé un facteur de sélectivité supérieur à 30 à une pression de CF_2Cl_2 de 4 Torr et en présence d'oxygène à une pression de 80 Torr.

[Traduit par le journal]

Introduction

Interest in the infrared multiphoton chemistry of CF_2Cl_2 (1–13) was stimulated by early demonstration of isotope separation (3, 4, 6) and has been sustained by attempts to understand the primary decomposition channels (5, 10, 11) and their relative importance. It now seems clear that the free radical channel ($\rightarrow CF_2Cl + Cl$) dominates (14) because of an exit barrier in the lower enthalpy channel ($\rightarrow CF_2 + Cl_2$). The final decomposition products in the CF_2Cl_2 system are not well understood because of the formation of a complex array of compounds. Early workers (4) and more recently Fettweiss and de Mévergnies (13) noted a simplification in product array caused by addition of small amounts of oxygen; CF_2O and Cl_2 were the only observed products. These latter authors (13) made an additional brief mention that the isotopic enrichment in the products showed a three-fold increase with the addition of oxygen. This, together with the fact that both sets of workers concentrated on measuring selectivities rather than yields, stimulated the present, more detailed, examination of the CF_2Cl_2–O_2 system.

Experimental

The main details of our experiments are similar to those reported elsewhere (15). Briefly, output from a Lumonics (model 103) TEA CO_2 laser was passed through a 1.4 cm aperture to select the central portion of the beam which was then collimated by a 1 m focal length germanium lens. The beam passed through the salt windows of a 18 cm long, 5 cm diameter Pyrex cell. Typically, fluences of 2–5 J cm^{-2} were used.

CF_2Cl_2 (Freon-12, Matheson) was extensively outgassed by several freeze–pump–thaw cycles. The photolyzed mixture was analysed directly by a Hitachi RMU-6D magnetic sector mass spectrometer; relative mass spectrometric responses were determined by calibration with authentic sample mixtures and absolute yields were obtained by relating the sample pressure in the inlet manifold to the relative yields of products in that sample.

Preliminary experiments on neat substrate at the relatively low fluences of our experiments gave very small yields and confirmed that the product array was complex. In addition to the major products, which were C_2F_4, $C_2F_4Cl_2$, and Cl_2, we noticed several three and four carbon-atom-containing species. Addition of small amounts of oxygen suppressed production of molecules containing more than one carbon atom and the dominant products were CF_2O and Cl_2. In the experimental set-up, some of the CF_2O underwent hydrolysis with trace amounts of H_2O (15) (adsorbed or absorbed on glass tubing and metal surfaces of mass spectrometer inlet system) to form CO_2. Therefore, we report CF_2O plus CO_2 as CF_2O and equate the yield of CF_2O directly to the amount of CF_2Cl_2 decomposed. We find justification for this in that no other carbon-containing products were observed and that the product yield increased three- to four-fold with the addition of even trace quantities of O_2.

In a typical experiment, the photolyzed mixture was trapped at liquid nitrogen temperature and excess O_2 was pumped away through a spiral trap also held at liquid nitrogen temperature. The condensed products were then directly transferred to the inlet system of the mass-spectrometer via an isopentane slush bath (−160°C) which prevented Cl_2 and excessive amounts of CF_2Cl_2 from entering the mass spectrometer. The non-condensible fraction contained CF_2O and CO_2 with only traces of CF_2Cl_2. The condensate at −160°C was analysed confirming that Cl_2 was the only other product.

$^{12}CF_2O$ was characterized by its peaks at m/e = 47 and 66. Isotope ratios were determined from the relative peak heights of m/e = 47, 48 and 66, 67. A possible complication in this analysis

[1]NRCC 19463.

[2]Present address: Lumonics Research Limited, 105 Schneider Road, Kanata, Ont., Canada.

0008-4042/81/182703-05$01.00/0

©1981 National Research Council of Canada/Conseil national de recherches du Canada

Can. J. Chem. Downloaded from www.nrcresearchpress.com by 210.87.254.40 on 09/06/12
For personal use only.

Can. J. Chem. Downloaded from www.nrcresearchpress.com by 210.87.254.40 on 09/06/12
For personal use only.

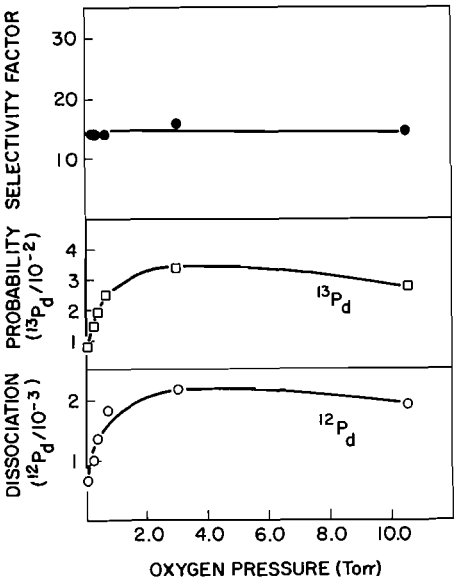

FIG. 1. Effect of oxygen addition on the dissociation probability, P_d. CF_2Cl_2 pressure: 0.5 Torr; laser frequency: 1039 cm^{-1} (9P28); fluence: 5 J cm^{-2}.

was the potential presence of SiF_4 formed after hydrolysis of CF_2O on silicate glass; peaks of $^{28}SiF^+$ at $m/e = 47$ and $^{28}SiF_2^+$ at $m/e = 66$ would negate our interpretation (16). However, we could detect no trace of a peak at $m/e = 86$ ($^{28}SiF_3^+$) and since $[SiF_3^+]/[SiF_2^+]$ is reported to be 10:1 for SiF_4, we conclude that this interference with our analytical method is negligible.

Results

Unlike most previous workers who have attempted to derive product yields and selectivities by analysis of changes in the starting material, we have measured product yields directly and obtain selectivities from ratios of the isotopic variants of the products. The effect of O_2 on the dissociation probability, P_d,

$$\left(P_d = \frac{\text{no. of molecules decomposed per laser pulse}}{\text{no. of molecules irradiated per laser pulse}}\right)$$

is illustrated in Fig. 1. Small additions of O_2 increase the probability of decomposition of both carbon-12- and carbon-13-substituted molecules. The increase is proportionate in each case giving a selectivity factor, α, ($\alpha = {}^{13}P_d/{}^{12}P_d$) which is invariant with added O_2. This constant selectivity indicates that the effect of O_2 is simply reaction with some intermediate rather than initiation or participation of a chain reaction which would be expected to introduce a reduction in selectivity depending on the O_2 mole fraction.

The spectral dependence of the dissociation probability and the consequent variation of isotopic selectivity is shown in Fig. 2. Laser irradiation

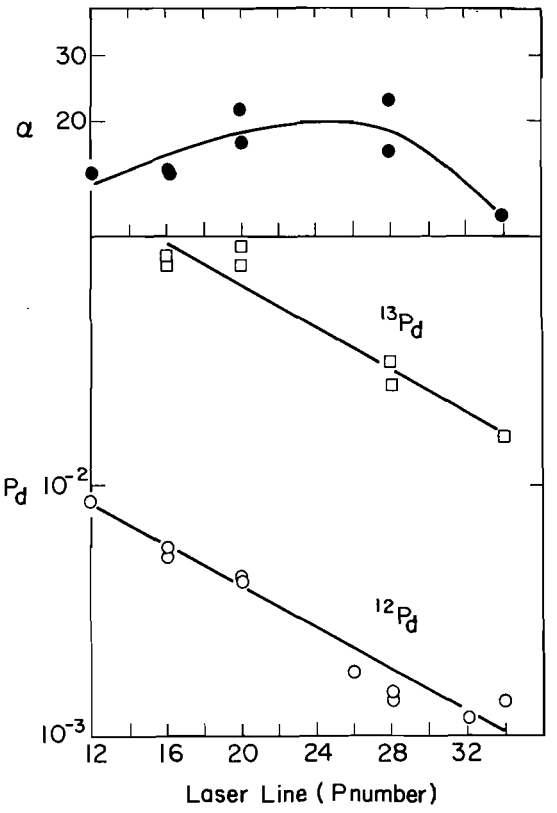

FIG. 2. Effect of laser frequency on dissociation probabilities. Frequency range: 9P12–9P34, 1054–1033 cm^{-1}; CF_2Cl_2 pressure: 0.5 Torr; O_2 pressure: 0.5 Torr; fluence: 5 J cm^{-2}.

progressively further to red of the absorption band (11) results in a steadily declining dissociation probability with small change in isotopic selectivity over the entire range of wavelength; only a small increase in going from 9P12 to 9P28 laser lines is observed. This effect is unusual but not totally unexpected. The carbon-13 isotope shift of the ν_1 band has been estimated (6) to be of the order of 33 cm^{-1} and it is not unreasonable that the frequency range of the present experiments, which is 50–70 cm^{-1} from ν_1 band centre, lies entirely to the red of the peak for multiphoton decomposition of $^{13}CF_2Cl_2$. In the case of CF_3COCF_3 we have observed that C-13 selectivity is frequency independent under these irradiation conditions (17) and such a phenomenon should be general.

Figure 3 compares the effect of pressure for two frequencies, 1050 cm^{-1} 9P16 and 1041 cm^{-1} 9P26 for a constant 1:5::CF_2Cl_2:O_2 mixture. The data are given as a function of the partial pressure of CF_2Cl_2. The outstanding feature in these experiments is the different behaviour of selectivity with pressure. For photolysis at 1050 cm^{-1}, α decreases

Can. J. Chem. Downloaded from www.nrcresearchpress.com by 210.87.254.40 on 09/06/12
For personal use only.

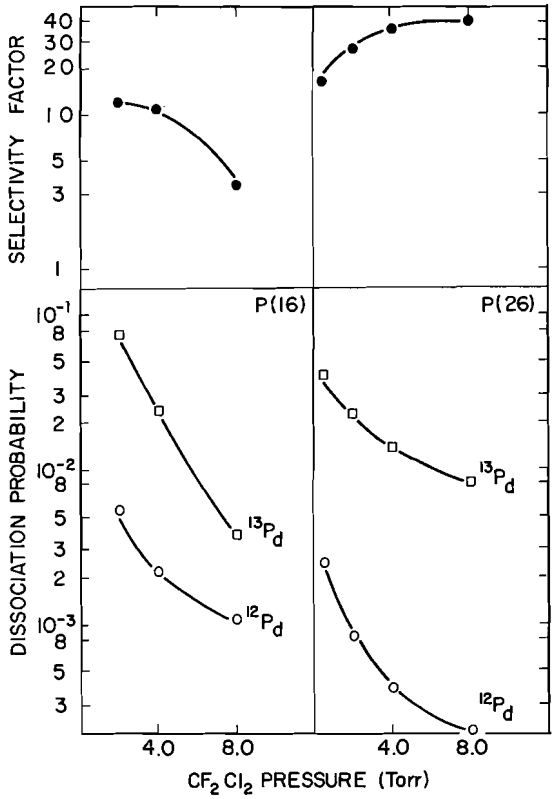

FIG. 3. Effect of sample pressure on dissociation probabilities for 9P16 and 9P26 laser excitation; CF_2Cl_2:O_2 ratio, 1:5; fluence, 5 J cm^{-2}.

as the total pressure of the mixture is raised from 6 Torr to 48 Torr (1 Torr CF_2Cl_2 to 8 Torr CF_2Cl_2) while at 1041 cm^{-1} α increases over the same pressure range. We have observed a similar behaviour in a number of other systems (15, 18, 19).

Figure 4 again compares two frequencies, 1050 cm^{-1} (P16) and 1039 cm^{-1} (P28), but at a constant total pressure (12 Torr) with the proportions of CF_2Cl_2 and O_2 being varied. Increasing partial pressure of CF_2Cl_2 decreases the dissociation probability at both frequencies but once again differential effects lead to a decrease in selectivity at the higher frequency and an increase in selectivity for the lower. We have explained increasing selectivity with pressure in terms of collisional deactivation of molecules with relatively low vibrational energies (19) (in Region I in the three region model of multiphoton decomposition (20)). CF_2Cl_2 is undoubtedly a more efficient quencher of vibrationally excited CF_2Cl_2 than is O_2 and the fact that substitution of CF_2Cl_2 for O_2 leads to an increased selectivity far to the red is entirely consistent with the model we have proposed.

Figure 5 compares an effect of fluence with an inert gas effect. A mixture originally containing 4 Torr CF_2Cl_2 and 8 Torr O_2 is irradiated at progressively increasing fluences (2 to 5 J cm^{-2}). Large increases in yield with consequent drop in selectivity, from $\alpha = 30$ to $\alpha = 2$, are obtained. Taking the system at a constant fluence of 5 J cm^{-2} and adding either extra O_2 or N_2, can essentially reverse the effect. The selectivity is driven up from $\alpha = 2$ to $\alpha \simeq 30$, at 60 Torr of added "inert" gas; O_2 and N_2 behave the same within the precision of the present data. As shown in the figure, this increase is almost entirely due to the suppression of dissociation of carbon-12-bearing species rather than to any increase in the decomposition yield of carbon-13-bearing molecules.

Discussion

The major dissociation channel for CF_2Cl_2, in multiphoton infrared, yields CF_2Cl and Cl. Although the molecular elimination of CF_2 and Cl_2 has a lower reaction enthalpy, there is a significant reverse activation barrier (14). We shall make our points of discussion, then, assuming reaction [1] is

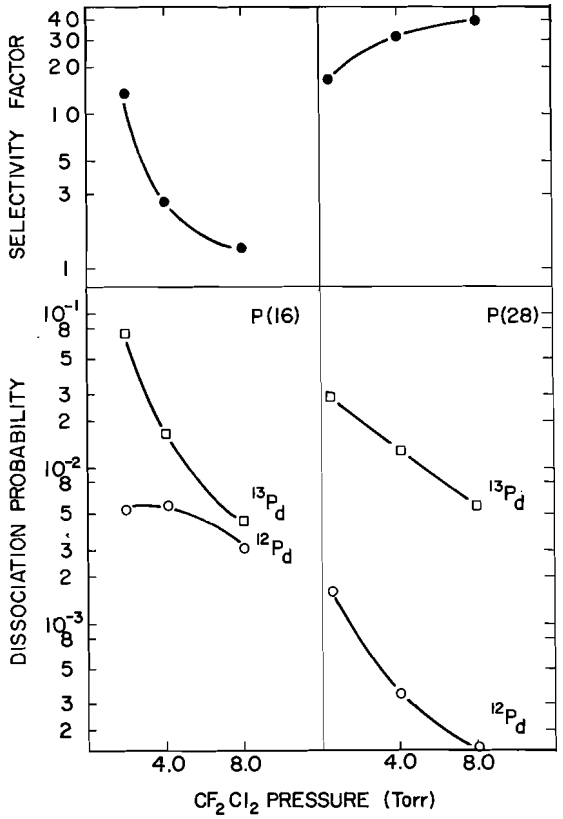

FIG. 4. Effect of CF_2Cl_2:O_2 ratio on dissociation probabilities for 9P16 and 9P28 laser excitation. Total pressure: 12 Torr; fluence: 5 J cm^{-2}.

Can. J. Chem. Downloaded from www.nrcresearchpress.com by 210.87.254.40 on 09/06/12
For personal use only.

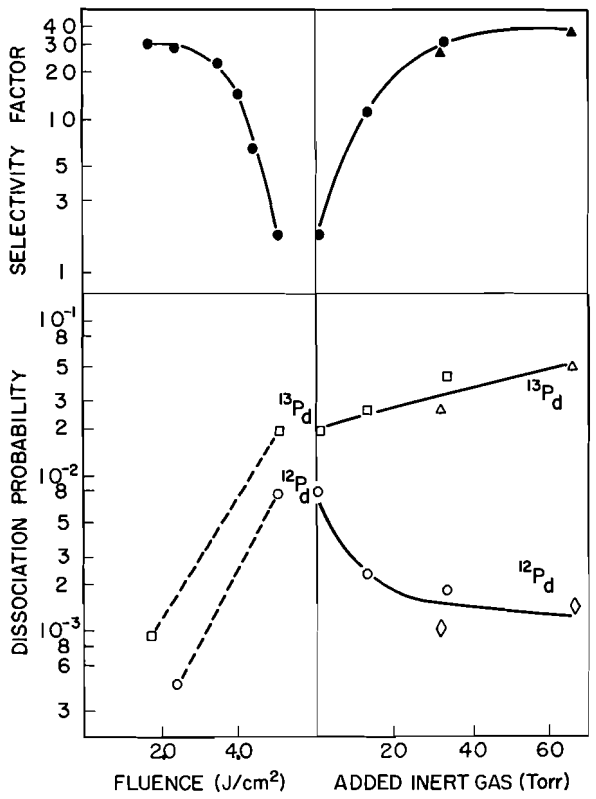

FIG. 5. Effect of fluence and added inert gas on dissociation probabilities; laser frequency: 1050 cm^{-1} (9P16); basic mixture: 4 Torr CF_2Cl_2, 8 Torr O_2; fluence for inert gas experiments: 5 J cm^{-2}; ○, □, ●, added oxygen; △, ◇, ▲, added nitrogen.

the unique primary process, recognizing at the same time that reaction [2] may make contributions to the effects we discuss.

[1] $CF_2Cl_2 \xrightarrow{nh\nu} CF_2Cl + Cl$ $\Delta H_1 = 78$ kcal mol^{-1}

[2] $CF_2Cl_2 \xrightarrow{nh\nu} CF_2 + Cl_2$ $\Delta H_2 = 73$ kcal mol^{-1}

For low conversions, the most important reactions subsequent to decomposition will be those involving radical combination,

[3] $CF_2Cl + CF_2Cl \rightarrow C_2F_4Cl_2$

[4] $CF_2Cl + Cl \rightarrow CF_2Cl_2$

[5] $Cl + Cl \xrightarrow{[M]} Cl_2$

[6] $CF_2Cl + O_2 \rightarrow CF_2O + ClO$

[7] $ClO + ClO \rightarrow Cl_2 + O_2$

These seven reactions are sufficient to explain the present observations. The increase in observed decomposition probabilities simply requires that reaction [4], the back reaction to CF_2Cl_2, occurs with a significant rate, which is not at all unlikely. To test our quantitative data requires a detailed knowledge of the three combination rate constants and these are not available.

Other potential chemical sources of increased yield are (*i*) a chain reaction or (*ii*) reaction of oxygen with highly vibrationally excited species. Both are improbable. The absence of an oxygen effect on the isotopic selectivity of the decomposition, while entirely compatible with the explanation involving suppression of a back reaction, places unreasonable demands on these two alternatives. If a chain reaction is involved, the reaction step where substrate CF_2Cl_2 is consumed must involve reaction only with vibrationally-excited molecules *and* the C-13 to C-12 ratio for consumed species must match closely that for molecules undergoing unimolecular decomposition. This second requirement also applies to a direct reaction (non-chain) of O_2 with vibrationally-excited CF_2Cl_2 molecules. The main problem with envisaging such bimolecular reactions, however, lies in their concerted nature. Reactions of this type are not common because of the large entropy changes in forming the activated complex. There is no reason to expect this constraint to be significantly less severe for vibrationally excited species. The question in point then becomes whether the larger amount of energy possessed by vibrationally excited CF_2Cl_2 can overcome such activation (entropy or energy) barriers. In the absence of further evidence we cannot completely eliminate these two alternatives. However, as long as suppression of the back reaction is sufficient to explain the observations there is no compelling reason to invoke them.

The main points related to variation of selectivity with pressure for conditions covered by the data in Figs. 3 and 4 have been discussed in the Results section or elsewhere (17) and require only brief amplification here. In multiphoton chemistry collisional processes lead to many different effects including rotational redistribution, vibrational quenching, inter- and intra-molecular energy redistribution and so on. In systems, such as those under present study, where only a small fraction of the molecules are excited, collisional deactivition among the first few vibrational levels is very important in controlling the extent of decomposition. Further, in working with the relatively long excitation pulses typical of most TEA CO_2 lasers, multiple deactivation–excitation–deactivation sequences are possible. Because the up-pumping rate depends upon the excitation probability and hence the closeness to resonance for the particular transi-

tion involved, we expect to see apparently different quenching behaviour for differing isotopic species when the off-resonance of the laser radiation is comparable with the isotope shift in the spectrum. This is precisely the case under present discussion and, as reviewed in the Results section, the observed behaviour is qualitatively in agreement with proposed models. We do not attempt a quantitative description because of various uncertainties but with shorter pulse devices becoming available, such a description should be forthcoming.

More interesting perhaps is the contrast displayed in Fig. 5. It is clear that increasing the fluence from 2 to 5 J cm^{-2} leads to a disproportionate increase in yield of C-12-bearing products. In work on other systems, (19, 21) we have attributed this behaviour to the onset of a process loosely described as "pyrolysis", a non-selective, thermally equilibrated decomposition channel whose yield is dependent on the *absorbed* energy per molecule. Addition of increasing amounts of oxygen or nitrogen provides a cold bath gas increasing the heat capacity of the mixture and lowering its effective "temperature". Thus the observed yield of decomposition of C-12 bearing molecules is reduced.

The increase in dissociation probability for C-13 bearing molecules which accompanies increasing inert gas pressure most probably is associated with repopulation of rotational states depleted by the intense laser field. In preliminary experiments where absorption coefficients are measured (22), we observe between a two- and three-fold increase in cross-section for similar conditions when the pressure of nitrogen is increased to 60 Torr. Any parallel effect on C-12 molecules would be buried in the much larger decrease in yield associated with the suppression of the non-selective thermal process.

1. M. P. Freeman, D. N. Travis, and M. F. Goodman. J. Chem. Phys. **60**, 231 (1974).
2. R. N. Zitter, R. A. Lau, and K. S. Wills. J. Am. Chem. Soc. **97**, 2578 (1975).
3. J. L. Lyman and S. D. Rockwood. J. Appl. Phys. **47**, 595 (1976).
4. J. J. Ritter and S. M. Freund. J. Chem. Soc. Chem. Commun. 811 (1976).
5. D. S. King and J. C. Stephenson. Chem. Phys. Lett. **51**, 48 (1977).
6. J. J. Ritter. J. Am. Chem. Soc. **100**, 2441 (1978).
7. V. Slezak, J. Caballero, A. Burgos, and E. Quel. Chem. Phys. Lett. **54**, 105 (1978).
8. J. W. Hudgens. J. Chem. Phys. **68**, 777 (1978).
9. G. Folcher and W. Braun. J. Photochem. **8**, 341 (1978).
10. J. C. Stephenson and D. S. King. J. Chem. Phys. **69**, 1485 (1978).
11. D. S. King and J. C. Stephenson. J. Am. Chem. Soc. **100**, 7151 (1978).
12. M. Nève de Mevérgnies. Appl. Phys. Lett. **34**, 853 (1979).
13. P. Fettweis and M. Nève de Mevérgnies. J. Appl. Phys. **49**, 5699 (1979).
14. D. J. Krajnovich, F. Huisken, Z. Zhang, Y. T. Lee, and Y. R. Shen. Paper C4, 11th International Quantum electronics Conference, June 23 Boston (1980).
15. W. S. Nip, M. Drouin, P. A. Hackett, and C. Willis. J. Phys. Chem. **84**, 932 (1980).
16. A. Cornu and R. Massot. Compilation of mass-spectra data. Heyden, London. 1966.
17. P. A. Hackett, C. Willis, and M. Gauthier. J. Chem. Phys. **71**, 2682 (1979).
18. P. A. Hackett, M. Gauthier, C. Willis, and R. Pilon. J. Chem. Phys. **71**, 546 (1979).
19. M. Gauthier, W. S. Nip, P. A. Hackett, and C. Willis. Chem. Phys. Lett. **69**, 372 (1980).
20. (*a*) D. M. Larsen and N. Bloembergen. Opt. Commun. **17**, 254 (1976); (*b*) D. M. Larsen. Opt. Commun. **19**, 404 (1976); (*c*) S. Mukamel and J. Jortner. Chem. Phys. Lett. **40**, 150 (1976); (*d*) S. Mukamel and J. Jortner. J. Chem. Phys. **65**, 5204 (1976); (*e*) J. G. Black, E. Yablonovitch, N. Bloembergen, and S. Mukamel. Phys. Rev. Lett. **38**, 1131 (1977).
21. M. Gauthier, P. A. Hackett, and C. Willis. Chem. Phys. **45**, 39 (1980).
22. M. Gauthier, S. Asselin, P. A. Hackett, and C. Willis. Unpublished data.

Can. J. Chem. Downloaded from www.nrcresearchpress.com by 210.87.254.40 on 09/06/12
For personal use only.

An electron spin resonance and time-resolved CIDEP study of the oxidation of ascorbic acid by pyruvic acid, duroquinone, and vitamin K_1

M. Catherine Depew, Babatunde B. Adeleke,[1] and Jeffrey K. S. Wan
Department of Chemistry, Queen's University, Kingston, Ont., Canada K7L 3N6

Received February 24, 1981

M. Catherine Depew, Babatunde B. Adeleke, and Jeffrey K. S. Wan. Can. J. Chem. **59**, 2708 (1981).

The photooxidation of vitamin C by pyruvic acid and its derivatives, duroquinone, and vitamin K_1 is systematically studied by the combined esr and time-resolved CIDEP technique. Because of the unique property of the triplet pyruvic acid which is different from that of the duroquinone triplet, the choice of these model systems allowed the CIDEP observations of the initial polarization of the ascorbate radical anion and its counter primary radical in either the enhanced absorptive or the emissive mode. The results demonstrate the efficient photooxidation of vitamin C by the triplet vitamin K_1 and that the latter triplet possesses similar properties as the triplet quinones. In the photooxidation system involving vitamin C and pyruvic acid, the adjustment of the pH of the aqueous solution afforded an opportunity to observe the photochemical reaction between two anions, the pyruvate anion and the ascorbate anion. Arguments were made in favor of an electron transfer mechanism for the oxidation of vitamin C by triplet vitamin K_1 but against the electron transfer mechanism for the oxidation of vitamin C by triplet pyruvate anion. T_1 values of the primary radicals estimated from their CIDEP transient responses at low microwave power are reported and it was suggested that the hydrogen-bonding capacity of the ascorbate radical anion in water does not contribute significantly to the relative difference of T_1's between itself and the counter pyruvic ketyl radical.

M. Catherine Depew, Babatunde B. Adeleke et Jeffrey K. S. Wan. Can. J. Chem. **59**, 2708 (1981).

En faisant appel à la rpe combinée à la technique de PEDIC résolue en fonction du temps, on étudie systématiquement la photooxydation de la vitamine C par l'acide pyruvique et ses dérivés, par la duroquinone et par la vitamine K_1. Compte tenu de la propriété unique du triplet de l'acide pyruvique qui est différente de celle du triplet de la duroquinone, le choix de ces modèles permet des observations de PEDIC de la polarisation initiale de l'anion radical ascorbate et de son radical primaire opposé lors de l'absorption ou de l'émission. Les résultats démontrent l'efficacité de la photooxydation de la vitamine C par le triplet de la vitamine K_1 et que le dernier triplet possède des propriétés identiques à celles du triplet des quinones. Dans la photooxydation qui implique la vitamine C et l'acide pyruvique, l'ajustement du pH de la solution aqueuse fournit l'opportunité d'observer la réaction photochimique entre deux anions, l'anion pyruvate et l'anion ascrobate. On suggère un mécanisme par transfert d'électrons pour l'oxydation de la vitamine C par le triplet de la vitamine K_1, mais on n'admet pas ce mécanisme dans le cas de l'oxydation de la vitamine C par le triplet de l'anion pyruvate. On rapporte les valeurs de T_1 des radicaux primaires évalués à partir de leurs réponses intermédiaires en PEDIC en microondes de faible puissance, et on suggère que la capacité en liaison hydrogènes de l'anion radical ascorbate dans l'eau ne contribue pas de façon significative à la différence relative des T_1 entre cet anion et le radical cétylpyruvique opposé.

[Traduit par le journal]

Introduction

Interest in the biological significance of vitamin C and vitamin E continues to be stimulated by reports of their involvement in many biochemical processes including cancer (1) and iron nutrition (2). It has been established that L-ascorbic acid (vitamin C) is readily oxidized in aqueous solution to a relatively stable radical whose controversial structure has been determined by esr spectroscopy (3). The ascorbic acid radicals generated in non-aqueous and aprotic solvents have also been reported (4). A recent theoretical calculation (5) has confirmed the esr assignments of the ascorbate anion free radical (**1**) in aqueous solution with the following structure

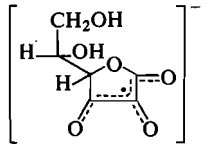

1

In the non-enzymatic systems, formation of the ascorbate free radical may involve either an electron-transfer process and/or a molecular elimination process. For example, a time-resolved esr study of the oxidation of ascorbic acid by hydroxyl radical produced in pulse radiolysis of water (6) has suggested that addition of ȮH at C-2 followed by rapid elimination of a water molecule resulted in the formation of the ascorbate radical anion. However, a direct electron-transfer process between the ascorbate and the ȮH radical

[1]CIDA–NSERC Summer Faculty Research Associate, 1979–1981. Permanent address: Department of Chemistry, University of Ibadan, Ibadan, Nigeria.

0008-4042/81/182708-06$01.00/0

©1981 National Research Council of Canada/Conseil national de recherches du Canada

Can. J. Chem. Downloaded from www.nrcresearchpress.com by 210.87.254.6 on 09/06/12
For personal use only.

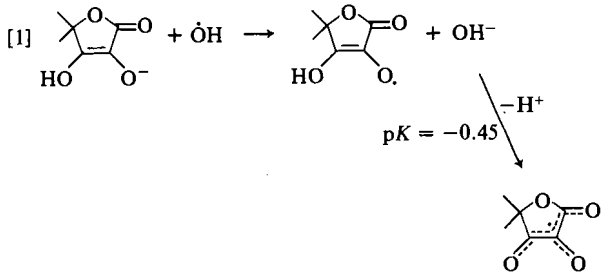

was considered to be also possible.

In the past five years we have extensively used the photoreduction of quinone by phenol as model systems for chemically induced magnetic polarization studies (7). In addition to providing some insights into the mechanistic aspects of free radical reactions, CIDEP could be used to probe the dynamic/structural properties of the transient radicals such as their spin–lattice relaxation times in solution. The interesting ascorbate free radical has a semiquinone-like structure and various probable sites for hydrogen-bonding interaction with the water solvent. It is our hope that a systematic CIDEP study of the photooxidations of vitamin C and vitamin E may yield further valuable information on the mechanism and the dynamic properties of the transient free radicals involved in these processes. In this report we have carefully chosen three model systems: the oxidation of vitamin C by excited pyruvic acid, the oxidation of vitamin C by excited duroquinone, and the oxidation of vitamin C by excited vitamin K_1. The choice of the first two systems is most significant in that the excited triplet states of pyruvic acid and of duroquinone have distinctly different spin dynamic properties (8) which lead to an initial polarization of the ascorbate radical anion being totally enhanced absorptive in the first case and totally emissive in the latter reaction. Spin–lattice relaxation times estimated from both the emissive and the absorptive ascorbate radical anions should be the same and this provides a critical test for the photo-triplet mechanism as well as the reliability of the CIDEP method in estimating T_1 of transient free radicals. Furthermore, by using sodium pyruvate as a control the oxidation of vitamin C by pyruvate affords an interesting opportunity to study a primary photochemical reaction between *two anions*.

Experimental

Pyruvic acid, ethylpyruvate, D-arabascorbic acid, and duroquinone were supplied by Aldrich. L-Ascorbic acid (vitamin C) was purchased from Anachemia and vitamin K_1 was obtained from Sigma. 2,3-Dimethylascorbic acid was custom synthesized and was a gift from Professor W. A. Szarek and Dr. K. S. Kim. The quinones were sublimed before use and laboratory grade benzene and toluene were distilled and dried over $MgSO_4$. A typical organic solution sample was prepared by placing a 0.1 *M* solution of the respective reagents in a Pyrex tubing of 2 mm i.d. and the solution was degassed under high vacuum before being sealed off. For aqueous solution samples, the solution was placed in a quartz flat cell of 0.1 mm thickness and deoxygenated by purging with gaseous nitrogen.

The esr spectra were recorded on a Varian E3 spectrometer equipped with a variable temperature control accessory. The samples were irradiated within the cavity by using a 200 W super pressure mercury lamp. Time-resolved CIDEP experiments were performed on the Varian E3 spectrometer using dc detection. The amplified dc signal was digitized by a Nicolet Explorer III digital scope at 50 ns per point and the digitized data were collected and processed on-line by a Nicolet 1180 computer in a synchronous mode. The design of the dc detection system is similar to that reported by Kim and Weissman (9). The light source used is a Molectron UV24 1-MW nitrogen pulsed laser. A detailed description and evaluation of the present system and the analysis of the data to obtain the spin–lattice relaxation times have been given elsewhere (10).

Results and Discussion

Photooxidation of Vitamin C by Pyruvic Acid in Aqueous Solutions

Photolysis of a saturated aqueous solution of ascorbic acid containing 10% v/v of pyruvic acid at room temperature led to the observation of an esr spectrum which is the superposition of the two primary radicals, the ascorbate radical anion **1** and the pyruvic ketyl radical $CH_3\dot{C}(OH)COOH$. Radical **1** exhibits a hyperfine structure of a doublet (A_H = 1.85 G) which is further split into a triplet (A_{CH_2} = 0.18 G). The pyruvic ketyl radical shows a quartet (A_{CH_3} = 16.9 G) of doublets (A_{OH} = 1.8 G). These assignments are consistent with those reported in the literature (3, 8). Direct inspection of the cw esr spectrum revealed that the low field hyperfine lines of the pyruvic ketyl radical were less intense than the corresponding high field lines. This is typically due to the E/A polarization originating from the radical-pair mechanism of the CIDEP effect (7, 8). Time-resolved CIDEP experiments, however, showed that both primary radicals, **1** and $CH_3\dot{C}(OH)COOH$, exhibit strong *initial* polarization with all hyperfine lines in the enhanced absorption mode. In the time-resolved experiments the effective radical concentrations generated by the 5 ns nitrogen laser pulse were much lower than those achieved by continuous irradiation and thus leading to a predominant *initial* polarization (originated from the photo-triplet mechanism) as observed. The results can be accounted for by the following reactions:

[2] $CH_3COCOOH + h\nu \xrightarrow{ISC} {}^3(CH_3COCOOH)^*$

Can. J. Chem. Downloaded from www.nrcresearchpress.com by 210.87.254.6 on 09/06/12
For personal use only.

Can. J. Chem. Downloaded from www.nrcresearchpress.com by 210.87.254.6 on 09/06/12
For personal use only.

[3] $^3(CH_3COCOOH)^*$ + Ascorbic acid → $CH_3\dot{C}(OH)COOH^*$ + **1***

The * denotes initial electron polarization.

In a neutral solution ascorbic acid exists mainly in the form of an ascorbate anion and its presence suppresses the ionization of pyruvic acid, as confirmed by nmr (the chemical shifts for the methyl protons are different for pyruvic acid and for pyruvic anion). In the pyruvic/ascorbic acid system most of the excitation light at the laser wavelength of 337 nm would be absorbed by the pyruvic acid only. In a previous study of the photochemical reactions between triplet pyruvic acid and lactic acid, the initial polarization originating from the photo-triplet mechanism led to the polarization of the primary radicals in the enhanced absorption mode (8). To the best of our knowledge, this is the only confirmed photochemical system giving a totally absorptive initial polarization for the primary radical pair. Since the mode of the primary radical initial polarization depends upon the triplet property alone (11), it is expected that in the present pyruvic/ascorbic acid system the reaction of the polarized pyruvic acid triplet should lead to an initial polarization in the totally absorptive mode for both the ascorbate radical anion and the pyruvic ketyl radical. According to the photoexcited triplet model (11) in which the population of each of the spin sublevels can be approximated by

$$P_{\pm 1} \propto (P_x + P_y - 2P_z)(D/B_0)$$

the excited triplet pyruvic acid must either have $D > 0$ and $P_z > P_x, P_y$, or $D < 0$ and $P_z < P_x, P_y$, where D is electron dipolar parameter related to the zero-field splittings of the sublevels. Unfortunately, CIDEP studies in liquid solutions alone can not yield the information of the sign of D. But the observed enhanced absorption for both pyruvic ketyl radical and ascorbate radical anion establishes the oxidation of vitamin C by pyruvic acid via an excited triplet mechanism.

The detailed mechanism of the reaction [3] is of great significance. Although triplet pyruvic acid has been found to abstract hydrogen with a rate similar to benzophenone triplet in various alcohols (12) and thus hydrogen abstraction from ascorbate anion could account for the reaction leading to CIDEP of the primary radicals, it must be recognized that the reaction could also proceed rapidly via an electron-transfer mechanism:

[4] $^3(CH_3COCOOH)^*$ + $ascorbate^-$ → $(CH_3COCOOH)^{\dot{-}*}$ + ascorbic acid radical*

[5] Ascorbic acid radical* → Ascorbate radical anion **1*** + H^+

[6] $H^+ + (CH_3COCOOH)^{\dot{-}*} \rightarrow (CH_3\dot{C}(OH)COOH)^*$

In the initial series of experiments the pH of the solutions was at 3.5, so that appreciable concentrations of both the unionized pyruvic acid and the pyruvate anion could be involved in the photooxidation of vitamin C. The triplet property of the unionized pyruvic acid is not expected to be different from that of the triplet pyruvate anion. By adjusting the pH of the solution to 10.2 using KOH, the concentrations of the pyruvate anion and the ascorbate anion would be greatly enhanced so that the actual photooxidation is now represented by the reaction

[7] $^3(CH_3COCOO)^{-*}$ + $ascorbate^-$ → $(CH_3\dot{C}(OH)COO)^{-*}$ + **1***

This presents an interesting opportunity to study the photochemical reaction between two anions and at this time there is no compelling argument that reaction [7] should proceed via an electron-transfer from the ascorbate anion to the excited pyruvate anion as an efficient means to preserve the initial polarization later developed in the observed radicals. The experimental results clearly show that in the basic solution, the CIDEP intensity as well as the mode of polarization were unchanged from those observed in acidic solutions. Similar CIDEP results were obtained in the sodium pyruvate/ascorbic acid system. We thus suggest that the photoredox reaction between triplet pyruvic acid/pyruvate and ascorbate involves mainly a hydrogen abstraction mechanism. The approach of the triplet anion towards another anionic reactant apparently does not slow down the reaction as the triplet anion possesses sufficient excitation energy to overcome any small energy barrier for two approaching anions. We must reiterate that the present results are insufficient to establish the detailed mechanism of the primary process, i.e. whether it involves electron-transfer to be followed by a proton transfer, or it is a direct H atom abstraction. Experimental differentiation of these two mechanisms is extremely difficult at the present time and it is hoped that further technical improvements of the time-resolution to the 10^{-12} s range may help solve the problem.

From the CIDEP observations the T_1's of both the primary radicals/radical ions were estimated and these will be reported and discussed in another section below.

Can. J. Chem. Downloaded from www.nrcresearchpress.com by 210.87.254.6 on 09/06/12
For personal use only.

Photooxidation of Ascorbic Acid by Ethyl Pyruvate, 2-Ketobutyric Acid, and Ethylacetoacetate

To further probe the "unique" triplet property of pyruvic acid which leads to enhanced absorptive initial polarization, a systematic study using various available pyruvic derivatives was carried out. In the cw photolysis of ethyl pyruvate and vitamin C in a mixed ethanol/water solvent between 0 and 10°C, both the ascorbate radical anion **1** and the $CH_3\dot{C}(OH)COOC_2H_5$ radical were observed. The latter was identified by its hyperfine pattern with A_{CH_3} = 16.8G and A_{OH} = 1.9G as reported in literature (13). Time-resolved CIDEP experiments again showed that for both primary radicals all their hyperfine lines were in totally enhanced absorption, as expected from the phototriplet mechanism having the ethyl pyruvate triplet similar to the triplet pyruvic acid in the spin sublevel populations. In the cw photolysis of 2-ketobutyric acid and vitamin C in ethanol/water solvent, again both the radical anion **1** and the $CH_3CH_2\dot{C}(OH)COOH$ radical were observed. The latter radical has hyperfine coupling constants A_{CH_2} = 11.6G, A_{OH} = 2.0G, and A_{CH_3} = 0.8G. In the cw spectrum the 2-ketobutyric ketyl radical also exhibits the E/A type polarization originated from the radical-pair mechanism. Time-resolved CIDEP observations in this system also showed a predominant initial polarization with both primary radicals clearly in the enhanced absorptive mode for all their hyperfine components. However, a similar experiment using ethyl acetoacetate as the triplet precursor failed to yield any CIDEP effects. Thus, we are inclined to believe that the similar and "unique" triplet property of pyruvic acid and its derivatives is characteristic of alkyl carbonyl compounds having a functional group —CO—COO—. It is interesting to speculate here that a substitution of the alkyl group next to the carbonyl by an aromatic group might alter the triplet property and thus leading to a different CIDEP pattern.

The photoredox systems were repeated using D-arabascorbic acid instead of vitamin C. In all cases, no significant differences in CIDEP and the T_1's of the ascorbate radical anions were observed.

Photooxidation of Vitamin C by Duroquinone

The photoredox reactions between quinones and phenols have been extensively used in this laboratory as model systems for CIDEP study. It is generally recognized that photoexcited triplet duroquinone is spin polarized which in subsequent reactions transfers the initial polarization to the primary radicals in a totally emissive mode. Thus, the triplet property of the duroquinone with respect to spin population of the sublevels is directly opposite to that of pyruvic acid. As a comparison the photooxidation of vitamin C by duroquinone was studied in ethanol solution. Continuous photolysis led to the observation of an esr spectrum which is the superposition of the ascorbate radical anion **1** and the durosemiquinone radical. Time-resolved CIDEP experiments showed again the strong initial polarization of both primary radicals. Because of the triplet duroquinone property, the initial polarizations of both radicals were in the totally emissive mode, as expected by the phototriplet mechanism.

The detailed mechanism of the reaction of duroquinone triplet with the ascorbate anion again deserves some attention. It remains probable that the reaction involves an electron transfer from the ascorbate anion to the triplet duroquinone which is a good electron acceptor. In this regard, we have studied the photooxidation of 2,3-dimethyl ascorbate by duroquinone. Here, no radicals nor CIDEP were observed. Although esr negative results can not be used to exclude the possibility of chemical reactions, it is fairly safe to say that under identical experimental conditions the free radical processes involved in the photooxidation of 2,3-dimethyl ascorbate by quinone are insignificant. This can be attributed to the fact that the "efficient" hydrogen abstraction reaction by the triplet quinone from the —OH group on the vitamin C is no longer operative in the case of the 2,3-dimethyl ascorbate. On the other hand, the 2,3-dimethyl ascorbate is probably unionized in solution but an electron transfer mechanism from the substituted ascorbate to the triplet quinone is still possible. A definitive conclusion of the detailed mechanism of the photooxidation of vitamin C by quinone, however, must await further elucidation.

Photooxidation of Vitamin C by Vitamin K_1

Vitamin K_1 is known to form semiquinone radical with the following structure (14):

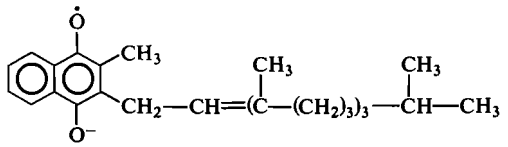

The biochemical importance of vitamin K_1 semiquinone suggested that the possible photooxidation of vitamin C by vitamin K_1 would be of some interest.

When vitamin K_1 was photolyzed alone in ethanol, an esr spectrum of the vitamin K_1 semiquinone radical having the same spectral parameters as reported in the literature (14) was observed. Time-

Can. J. Chem. Downloaded from www.nrcresearchpress.com by 210.87.254.6 on 09/06/12
For personal use only.

resolved CIDEP study of this system revealed no polarization. However, addition of vitamin C to the solution showed the formation of both the vitamin K_1 semiquinone radical and the ascorbate radical anion **1**, and the CIDEP experiments produced totally emissive polarization for both primary radicals. On the whole, these experiments suggest that the photooxidation of vitamin C involves the spin-polarized vitamin K_1 triplet molecule which possesses property similar to that of other 1,4-quinone triplets. The more salient conclusion to be drawn is the experimental fact that the vitamin K_1 triplet is photoreduced much more efficiently by vitamin C than by ethanol, a suggested by the CIDEP triplet mechanism argument (7). Here the electron transfer mechanism from vitamin C to the triplet vitamin K_1 is particularly attractive as it can account for both the direct formation of the semiquinone radical anion and the efficient reaction rate required by the phototriplet mechanism.

The spin–lattice relaxation times of the vitamin K_1 semiquinone radical and the ascorbate radical anion were measured by CIDEP and reported in the next section.

Spin–Lattice Relaxation Times of Ascorbate Radical Anion, Pyruvic Ketyl Radical, Durosemiquinone Radical, and Vitamin K_1 semiquinone Radical Anion

The choice of the two different triplet precursors, the duroquinone and the pyruvic acid, in the photooxidation of vitamin C affords a unique opportunity to produce the *same* ascorbate radical anion with initial polarization in the emissive mode in the case of pyruvic acid. Figure 1 shows the typical transient enhanced absorptive response from the ascorbate radical anion in the photooxidation by pyruvic acid and Fig. 2 gives the typical transient emissive response from the same radical anion in the photooxidation by duroquinone. In all

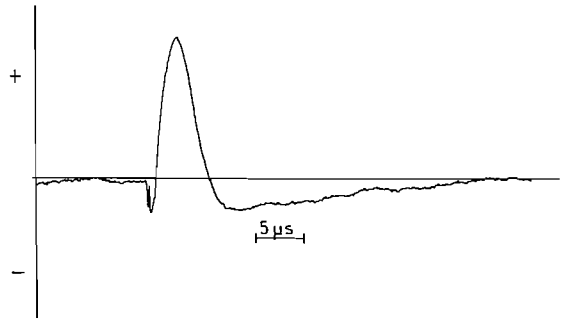

FIG. 1. Transient enhanced absorptive response from the ascorbate radical anion generated in the photooxidation by triplet pyruvic acid in an aqueous solution at 6°C. B_1 is about 40 mG. The curve represents the *difference* between the on-resonance and off-resonance responses.

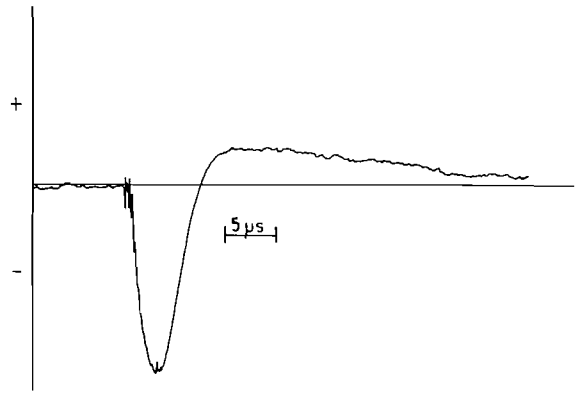

FIG. 2. Transient emissive response from the ascorbate radical anion generated in the photooxidation by triplet duroquinone in an ethanol solvent at −20°C. B_1 is about 40 mG. The curve represents the *difference* between the on-resonance and off-resonance responses.

the CIDEP observations on all systems, the presence of both primary radicals allowed the simultaneous estimates of the T_1's of both radicals under the identical experimental conditions. In all cases, the T_1 measurements used only data obtained from experiments at low microwave power (at or below 1 mW which is equal to B_1 less than 40 mG (10)). Since the Varian E3 is not equipped with a low-power operation configuration, the lowest B_1 usuable is about 15 mG and the extrapolation to $B_1 = 0$ will only provide an estimate of T_1. The estimated values of T_1's for various primary radicals observed in the photooxidation of vitamin C are given in Table 1.

The data show that in general the T_1 of the L-ascorbate radical anion is the same as that of D-arabascorbate radical anion. The apparently shorter spin–lattice relaxation time of the ascorbate radical anion as compared to its counter radicals such as pyruvic ketyl radical under the same experimental conditions is rather surprising. It was expected that in aqueous solutions the ascorbate radical anion may interact with water via substantial hydrogen-bonding and this effect would have increased the value of T_1. In a recent theoretical consideration of T_1's for semiquinone radical in solution (15) it was shown that the T_1 depends upon three major factors which are the orientational correlation time τ_2 for a second rank tensor, the average excitation energy $\Delta\varepsilon$ and some quantities related to **G** tensor deviation. The hydrogen-bonding interaction could conceivably affect the value of τ_2 but Rengan *et al.* (16) have investigated the hydrogen-bonding interaction among semiquinone radicals and obtained a low activation energy, about 4 kJ mol^{-1}. Taking into account that similar hydrogen-bonding interaction is also probable for the counter pyruvic ketyl radical, it is

TABLE 1. Estimated T_1 values from CIDEP measurements of transient radicals in solutions

Radicals in the primary pair	Mode of initial polarization	Temperature (°C)	Solvent	T_1 (μs)
L-Ascorbate radical anion	Absorptive	6	Water	2.1±0.4
Pyruvic Ketyl radical	Absorptive	6	Water	3.4
L-Ascorbate radical anion	Absorptive	29	Water	1.0
Pyruvic Ketyl radical	Absorptive	29	Water	2.3
L-Ascorbic radical anion	Absorptive	27	Water	1.4
Pyruvic Ketyl radical anion	Absorptive	27	(pH = 10.2)	2.5
L-Ascorbate radical anion	Emissive	19	Ethanol	2.0
Vitamin K_1 semiquinone	Emissive	19	Ethanol	4.0
L-Ascorbate radical anion	Emissive	−20	Ethanol	2.4
Durosemiquinone	Emissive	−20	Ethanol	3.0
D-Arabascorbate radical anion	Absorptive	11	Water	2.0
$CH_3CH_2\dot{C}(OH)COO^-$ [a]	Absorptive	11	Water	3.6

[a] T_1 in $CH_3CH_2\dot{C}(OH)COO^-$ radical is slightly dependent on the hyperfine components with T_1 for the center component (0) slightly larger than those associated with the (+1) and (−1) components.

reasonable to argue that the difference in T_1's between the ascorbate radical anion and the pyruvic ketyl radical is not mainly due to hydrogen-bonding. Another factor which comes into the comparison here is the contribution of the hyperfine interaction to the relaxation of these two radicals. Usually the anisotropic contribution is more important because this interaction is readily modulated by the rotational tumbling of the molecule. In the case of the pyruvic ketyl radical with a rotating methyl group, the anisotropic splitting is small and the only contribution to the relaxation will come from the modulation of the isotropic splitting, which is not expected to affect the T_1 significantly. On the other hand, the isotropic hyperfine splitting of the proton at the C-5 position in the ascorbate radical anion may be small but the angular dependence of the anisotropic hyperfine interaction and thus its modulation by the tumbling molecule may contribute to the relaxation in a manner as to reduce the observed T_1. Experimental evidence of such an anisotropic hyperfine interaction contribution to relaxation for the $CH_3CH_2\dot{C}(OH)COO^-$ radical is found in the observed small dependence of T_1's on the hyperfine components with T_1 slightly larger for the central component ($m_I = 0$) than for the outer components having $m_I = \pm 1$. This observation is consistent with those reported for the nitroxide radicals (17). It is hoped that further T_1 studies of vitamin C radical and its derivatives will provide some insight into the dynamics of this class of important radicals.

Another interesting observation is that T_1 of the large vitamin K_1 semiquinone radical appears to be in the same magnitude as the corresponding unsubstituted naphthosemiquinone radical in solution (15). This, however, is not too surprising as the recent theoretical treatments (15) on T_1's of semiquinone radicals in solution showed that a combined argument based upon a modest size effect and upon the extent of the π system provides a better understanding of the T_1 observations than either consideration by itself.

Acknowledgement

This research is supported by the Natural Sciences and Engineering Research Council of Canada.

1. S. LEWIN. Vitamin C; its molecular biology and medical potential. Academic Press, New York. 1976.
2. S. R. LYNCH. Contemporary nutrition. Vol. 5. 1980.
3. G. P. LAROFF, R. W. FESSENDEN, and R. N. SCHULER. J. Am. Chem. Soc. **94**, 9062 (1972); R. D. MCALPINE, M. COCIVERA, and H. CHEN. Can. J. Chem. **51**, 1682 (1973) and references therein.
4. Y. KIRINO. Chem. Lett. 153 (1974); S. STEENKEN and G. OLBRICH. Photochem. Photobiol. **18**, 43 (1973).
5. C. THOMSON. J. Mol. Struct. **67**, 133 (1980).
6. R. W. FESSENDEN and N. C. VERMA. Biophys. J. 95 (1978).
7. J. K. S. WAN and A. J. ELLIOT. Acc. Chem. Res. **10**, 161 (1977); J. K. S. WAN. Advan. Photochem. **12**, 283 (1980).
8. K. Y. CHOO and J. K. S. WAN. J. Am. Chem. Soc. **97**, 7127 (1975).
9. S. S. KIM and S. I. WEISSMAN. J. Magn. Reson. **24**, 167 (1976).
10. J. W. M. DEBOER, T. Y. C. CHANG CHUNG, and J. K. S. WAN. Can. J. Chem. **57**, 2971 (1979) and references therein.
11. J. K. S. WAN, D. A. HUTCHINSON, and S. K. WONG. Acc. Chem. Res. **7**, 58 (1974); J. H. FREED and J. B. PEDERSEN. Advan. Magn. Reson. **8**, 1 (1976).
12. P. A. LEERMAKERS and G. F. VESLEY. J. Am. Chem. Soc. **85**, 3776 (1963); D. S. KENDALL and P. A. LEERMAKERS. J. Am. Chem. Soc. **88**, 2766 (1966).
13. A. SAMUNI, D. BEHA, and R. W. FESSENDEN. J. Phys. Chem. **77**, 777 (1973) and references therein.
14. M. S. BLOIS and J. E. MALING. Biochem. Biophys. Res. Commun. **3**, 132 (1960).
15. D. A. HUTCHINSON, J. RUSSELL, J. W. M. DEBOER, and J. K. S. WAN. Chem. Phys. **53**, 149 (1980).
16. S. K. RENGAN, M. P. KHAKHAR, B. S. PRAHHANADA, and B. VENKATARAMAN. Pramana, **3**, 95 (1974).
17. P. J. HORE, K. A. MCLAUCHLAN, L. PASIMENI, and R. C. SEALY. J. Chem. Soc. Faraday II, **74**, 1662 (1978).

Can. J. Chem. Downloaded from www.nrcresearchpress.com by 210.87.254.6 on 09/06/12
For personal use only.

The direct electrochemical synthesis of triphenylphosphine adducts of Group IB monohalides

MASOOD KHAN, COLIN OLDHAM,[1] AND DENNIS G. TUCK

Department of Chemistry, University of Windsor, Windsor, Ont., Canada N9B 3P4

MASOOD KHAN, COLIN OLDHAM, and DENNIS G. TUCK. Can. J. Chem. **59**, 2714 (1981).

The electrochemical oxidation of copper, silver, or gold into acetonitrile solutions of benzyl chloride or hydrogen halide plus triphenylphosphine leads to the formation of the adducts MXL_n (M = Cu, Ag, Au; X = Cl, Br, I; L = Ph_3P; n = 1, 1.5, 2; not all combinations). The value of n depends markedly on the mole ratio Ph_3P:dissolved metal. The reaction pathway is discussed in the light of measurements of current efficiency. The results of X-ray structural studies of AuCl · L and $AuClL_2$ are briefly reported.

MASOOD KHAN, COLIN OLDHAM et DENNIS G. TUCK. Can. J. Chem. **59**, 2714 (1981).

L'oxydation électrochimique du cuivre, de l'argent ou de l'or dans du chlorure de benzyle ou dans un halogénure d'hydrogène et du triphénylphosphine en solution dans l'acétonitrile conduit à la formation d'adduits du type MXL_n (M = Cu, Ag, Au; X = Cl, Br, I; L = Ph_3P; n = 1, 1,5, 2; on n'obtient pas toutes les combinaisons). La valeur de n dépend fortement du rapport molaire Ph_3P:métal dissout. On discute du cheminement de la réaction à partir des mesures de l'efficacité du courant. On rapporte brièvement les résultats des études par cristallographie de rayons-X du AuCl·L et du $AuClL_2$.

[Traduit par le journal]

Introduction

A number of recent publications from this laboratory have described the preparation of organometallic halides by the electrochemical oxidation of a metal in the presence of the appropriate alkyl or aryl halide. For main group metallic elements, the products are readily stabilised as adducts with various monodentate and bidentate donors (1–4). Amongst the transition metals, we have shown that the Group IVB elements (5), and nickel and palladium (6), can be similarly oxidised to R_2MX_2 or RMX compounds, again conveniently stabilised and characterised as adducts with donor ligands.

The present work was initiated in order to investigate the applicability of the technique of direct electrochemical synthesis to organometallic compounds of the coinage metals. In essence, we find that although each of these metals can be oxidised in the presence of organohalides, the products isolated are in fact inorganic derivatives of the monohalides. A similar conclusion was reached in parallel experiments in which the ultimate products were anionic halogen-complexes of copper (I) (7). We have also found that these MX adducts can be more simply prepared in cells in which the medium is acetonitrile containing approximately 5% concentrated aqueous hydrohalic acid. Such media, which require a lower applied voltage than that required for purely organic solvent systems, have also been successfully used in other electrochemical syntheses (8). Further useful applications of the electrochemical oxidation of noble metals in such quasi-non-aqueous media will no doubt be forthcoming.

[1]Permanent address: Department of Chemistry, University of Lancaster, U.K.

Experimental

General

With gold (M4N) or copper (electrolytically purified), strips of metal approximately 2 × 1 × 0.1 cm suspended on a platinum wire, formed the anode of the cell. Silver metal (Puratonic) was used as a 7 mm rod.

Acetonitrile was dried over calcium hydride, and diethyl ether over sodium. All experiments were carried out in a nitrogen atmosphere. Concentrated aqueous acids (A.R. grade) were used as supplied.

Analysis for silver and gold was by atomic absorption spectrophotometry. Decomposition of the silver chloride derivative by concentrated nitric acid left a deposit of AgCl, which was collected and weighed. Microanalysis was carried out by Guelph Chemical Laboratories Ltd. Analytical results and melting points for triphenylphosphine adducts are given in Table 1.

Electrochemical Synthesis

The electrochemical procedures were similar to those described in earlier papers (1–8). The metal to be oxidised formed the anode of a single cell containing an acetonitrile solution of either the organohalide or a quantity of concentrated aqueous hydrohalic acid, plus the neutral donor triphenylphosphine; details of the solution compositions used in the preparation of triphenylphosphine adducts are shown in Table 2. Tetraethylammonium chloride (ca. 20 mg) was generally added to enhance the conductivity in the benzyl chloride experiments. A major advantage in using solutions of hydrohalic acid in acetonitrile is that a sufficient current flows in the absence of other added electrolyte.

In some cases, products precipitated during the electrolysis, and in the remainder, addition of diethylether led to precipitation. For the Au/benzyl chloride system, addition of an equal volume of diethylether, followed by cooling, resulted in the formation of needle-like crystals of $AuCl(Ph_3P)_2$ together with a small quantity of adherent AuCl · Ph_3P. A crystal of $AuCl(Ph_3P)_2$ was selected from this material for X-ray structural analysis (see

0008-4042/81/182714-05$01.00/0

©1981 National Research Council of Canada/Conseil national de recherches du Canada

Can. J. Chem. Downloaded from www.nrcresearchpress.com by 210.87.254.105 on 09/06/12
For personal use only.

TABLE 1. Analytical results and melting points for Group IB monohalide adducts

Compound[a]	Melting point (Lit.) °C	Analysis % (Calcd)
$AuClL$[b]	248(247)[c]	Au 39.6 (39.8)
$AuClL_2$[b]	210(—)	
$AgClL$	295(294)[d]	AgCl 35.0 (35.4)
$Ag_2Cl_2L_3 \cdot Et_2O$	175(—)	C 59.8 (60.7), H 5.8 (4.8), P 7.0 (8.0)
$CuClL$	245(240)[e]	Cu 17.4 (17.6), C 59.5 (59.8), H 4.1 (4.2), P 8.6 (8.6)
$Cu_2Cl_2L_3$	232(235)[f]	Cu 12.3 (12.9), C 65.5 (65.8), H 4.6 (4.6), P 9.9 (9.4)
$Cu_2Br_2L_3$	224(231)[f]	C 59.9 (60.4), H 4.2 (4.2), P 8.4 (8.7)
$Cu_2I_2L_3$	224(226)[f]	Cu 10.3 (10.9)

[a]L = triphenylphosphine.
[b]Characterised by X-ray crystallography; see text.
[c]Reference 9.
[d]Reference 10.
[e]Reference 11.
[f]Reference 12.

below). Addition of a three-fold excess of diethylether to the filtrate, followed by cooling, produced crystals of $AuCl \cdot Ph_3P$. For the $Au/CH_3CN/HCl$ system, crystals of $AuCl \cdot Ph_3P$ began to grow in the cell approximately 30 min after the beginning of the electrolysis.

The compound $Ag_2Cl_2(Ph_3P)_3$, which precipitated during electrolysis, was purified by reprecipitation from chloroform solution by diethylether.

For the Cu/benzyl chloride system, addition of an equal volume of diethylether to the electrolysis mixture, followed by cooling, produced crystalline $CuCl \cdot Ph_3P$, and this substance was also precipitated when diethylether was added to the $Cu/CH_3CN/HCl$ electrolyte solution. When the volume of this filtrate was reduced, $Cu_2Cl_2(Ph_3P)_3$ precipitated, and similar procedures yielded the corresponding bromide. In the $Cu/CH_3CN/HI$ system a mixture of $Cu_2I_2(Ph_3P)_3$ and $[PPh_3H]^+I^-$ precipitated from the anode, and was separated by extracting the copper(I) complex into acetonitrile and reprecipitating. All products were washed well with ethanol and diethylether, and dried *in vacuo*. Total yields were in the range 40–70%, based upon the quantity of anode metal dissolved.

Ethyl bromide and methyl iodide, in combination with 2,2′-bipyridine, were also used in electrolyses of gold, but in no case was any organogold product isolated.

X-ray Crystallography

X-ray structural procedures were identical to those described in a previous paper (13).

Results and Discussion

As noted in the Introduction, none of the systems investigated gave rise to stable compounds containing M—C bonds, although some evidence was obtained from vibrational spectroscopy for the formation of unstable organogold intermediates. Gold systems were the subject of the most extensive range of experiments, and we discuss the preparative results in order of decreasing atomic number of the metal concerned. The adducts formed all involve triphenylphosphine as donor, but there is no reason to doubt that the electrochemical method can be used with other suitable neutral donors.

Gold

Despite the fact that gold is classically resistant to attack by aqueous mineral acids, the metal is readily oxidised under electrochemical conditions in various media. In addition to the series of experiments involving acetonitrile solutions of benzyl chloride or hydrochloric acid, a number of other organohalides were examined and shown to support the dissolution of gold from the anode. In view of the extensive organometallic chemistry of the element, it is disappointing that no stable organogold species could be isolated. When gold serves as the anode of an electrochemical cell containing an acetonitrile solution of benzyl chloride and triphenylphosphine, the metal readily dissolves under an applied voltage of 20 V at room temperature. No solid material precipitated during the electrolysis, but addition of diethylether to the solution formed by electrolysis threw down a mixture of the 1:1 and 1:2 gold(I) halide triphenylphosphine complexes. When triphenylphosphine was replaced by 2,2′-bipyridine, dissolution of gold again occurred, and precipitation with ether gave an oily material whose principal component was identified as $[AuCl_4]^-$ by vibrational spectroscopy. Thus in neither case was an organogold complex isolated, and qualitatively similar results were obtained with solutions of C_2H_5Br or CH_3I in acetonitrile and other solvents. On the basis of experience with these and related organometallic systems, we tentatively suggest that any organogold halides formed by electrolysis decompose by subsequent reaction with excess organic halide present in the solution phase.

Gold is also easily oxidised electrochemically using a solution phase of acetonitrile + aqueous hydrochloric acid + triphenylphosphine. In the

Can. J. Chem. Downloaded from www.nrcresearchpress.com by 210.87.254.105 on 09/06/12
For personal use only.

Can. J. Chem. Downloaded from www.nrcresearchpress.com by 210.87.254.105 on 09/06/12
For personal use only.

TABLE 2. Experimental conditions for the anodic oxidation of Group IB metals

Solution composition				Initial		Metal dissolved		Mole ratio[b]	Products[c]
Anode	CH_3CN (cm^3)	RX (cm^3)[a]	Ph_3P (mmol)	Voltage (V)	Current (mA)	Time (min)	mg	mmol	PPh_3 : metal	
Au	30	BzCl, 10	1.73	20	20	165	143	0.72	2.4	AuClL, $AuClL_2$
Au	30	HCl, 2	0.68	2	30	120	150	0.76	0.9	AuClL
Ag	40	BzCl, 5	1.97	20	15	270	261	2.42	0.8	AgClL
Ag	30	BzCl, 10	1.87	20	20	138	179	1.66	1.1	$Ag_2Cl_2L_3 \cdot Et_2O$
Cu	30	BzCl, 10	1.87	20	20	180	142	2.22	0.9	CuClL
Cu	50	HCl, 2	1.80	5	50	60	96	1.51	1.2	CuClL, $Cu_2Cl_2L_3$
Cu	50	HBr, 2	1.80	5	50	120	176	2.77	0.6	$Cu_2Br_2L_3$
Cu	30	HI, 2	1.80	5	50	110	158	2.50	0.7	$Cu_2I_2L_3$

[a]HCl, etc., refers to concentrated aqueous acid.
[b]See text.
[c]L = Ph_3P.

experiment reported in Table 2, the quantity of triphenylphosphine used was close to the quantity of gold dissolved, and the only product isolated was the 1:1 complex $AuCl \cdot Ph_3P$.

The current efficiency (E_F), expressed as moles of metal dissolved per Faraday of electricity, was measured for both CH_3CN/benzyl chloride and CH_3CN/HCl. In each case the value was 0.34 ± 0.01 mol F^{-1}, implying that the gold species generated at the anode surface is in the +III state. Following previous discussions (14), the cathode reactions for both systems are written as

[1] $RCl + e \rightarrow R\cdot + Cl^-$

[2] $2R\cdot \rightarrow R_2$

(R = H, $C_6H_5CH_2$), and hydrogen evolution was certainly detected for R = H. At the anode, the process which gives $E_F = 0.33$ most readily is

[3] $3Cl^- + Au \rightarrow AuCl_3 + 3e$

but this should be treated with some reserve, since the essentially simultaneous attack of three anions at one metal site is unlikely at the current densities (ca. 10 mA cm^{-2}) used. An attractive alternative is the sequence of reactions

[4] $Cl^- + Au \rightarrow AuCl + e^-$

[5] $3AuCl \rightarrow AuCl_3 + 2Au$

since gold(I) chloride is known to be unstable with respect to disproportionation (ref. 15, p. 33). Such processes will also give $E_F = 0.33$, provided that reaction [5] occurs sufficiently quickly at the electrode surface for the gold metal formed to be redeposited. The postulated primary anode reaction, [4], is that proposed for the discharge of halide ion at other sacrificial electrodes (14), and confirmed in the particular case of indium (4) by the observation that InI can be detected visually on the anode. In many of these systems, the freshly formed MX is assumed to react with excess RX

[6] $MX + RX \rightarrow RMX_2$

or

[7] $MX + RX \rightarrow RMX + X$

Reaction [6] gives $E_F = 1$; reaction [7] gives $E_F > 1$, since reaction [7] may be followed by the formation of more MX, setting up a repeating sequence. The measured E_F values demonstrate that reaction [7] does not occur in the present case, and in fact there do not appear to be any reports (12) of oxidative insertion reactions of AuX of the type which would be required by reaction [6].

Despite the current efficiency evidence, which as noted above implies the generation of Au(III)

Can. J. Chem. Downloaded from www.nrcresearchpress.com by 210.87.254.105 on 09/06/12
For personal use only.

species at the electrode, the final products are adducts of gold(I) chloride. This is ascribed to the reducing action of triphenylphosphine, used by earlier workers (10) in the preparation of $AuX \cdot PR_3$ adducts:

[8] $AuCl_3 + 2PPh_3 \rightarrow AuCl \cdot PPh_3 + PPh_3Cl_2$

and

[9] $AuCl_3 + 3PPh_3 \rightarrow AuCl(PPh_3)_2 + PPh_3Cl_2$

Such reactions explain the formation of both mono- and bis-triphenylphosphine derivatives at high mole ratio of PPh_3: dissolved metal (c.f. Table 2). The effect of changes in this mole ratio are discussed more fully below for the case of copper. The reaction scheme in reactions [8] and [9] is further supported by the identification of PPh_3Cl_2 among the reaction products (chloride content 19.8, calcd. 21.2; nmr spectroscopy).

Silver

When silver forms the anode of a cell containing acetonitrile + benzyl chloride + triphenylphosphine, dissolution of the metal occurs, with $E_F = 0.9 \pm 0.01$ mol F^{-1}. When the mole ratio PPh_3:dissolved Ag is < 1, colourless needles of $AgCl \cdot PPh_3$ gradually form in the reaction mixture. When this mole ratio is > 1, the addition of diethylether to the reaction mixture precipitates $Ag_2Cl_2(PPh_3)_3 \cdot Et_2O$ from the clear solution. Thus again benzyl chloride appears to be acting as a source of halide ion, with current efficiencies and product stoichiometries implying the reactions

[10] $Ag + Cl^- \rightarrow AgCl + e$

[11] $AgCl + PPh_3 \rightarrow AgCl \cdot PPh_3$

$2AgCl \cdot PPh_3 + PPh_3 \rightleftharpoons Ag_2Cl_2(PPh_3)_3$

Electrolysis with acetonitrile/aqueous hydrochloric acid was unsuccessful, since a dark coating (AgCl?) quickly formed on the anode surface, after which no current flowed at the voltages accessible to us.

Copper

Anodic copper dissolves readily in an electrochemical cell containing acetonitrile + benzyl chloride + triphenylphosphine, with $E_F = 1.0$ mol F^{-1}. Addition of diethylether to the clear solution precipitated $CuCl \cdot PPh_3$. Again no organometallic derivatives are formed, as with previous studies of sacrificial copper electrodes (7), and the reactions involved are presumably the analogues of reactions [10] and [11].

The results obtained when benzyl chloride is replaced by aqueous hydrohalic acid require some discussion. With hydrochloric acid, the addition of diethylether to the clear solution in the cell results in the isolation of $CuCl \cdot PPh_3$ and $Cu_2Cl_2(PPh_3)_3$. When hydrobromic acid is used, crystals of $Cu_2Br_2(PPh_3)_3$ grow from the copper anode; with hydroiodic acid, $Cu_2I_2(PPh_3)_3$ again forms at the anode, sometimes accompanied by $[PPh_3H]^+I^-$.

The current efficiencies for all three hydrohalic acids systems have been determined: X = Cl, $E_F = 0.81$ mol F^{-1}; X = Br, $E_F = 0.75$ mol F^{-1}; X = I, $E_F = 0.73$ mol F^{-1}. A complicating factor here is the slow but visible attack of the cell solution upon the copper metal in the absence of applied voltage, to give copper(II) species. Such chemical attack can only give an artificially high values of E_F and we therefore tentatively conclude that the limiting E_F is 0.5 mol F^{-1}, and that the mechanism for the formation of Cu(II) species at the anode in these systems is probably similar to that proposed above for gold (c.f. reactions [4] and [5]). Reduction by triphenylphosphine then yields CuX, which complexes with excess ligand to give the adducts isolated.

The stoichiometry of the adduct which is isolated must depend, *inter alia*, on the Cu:L ratio in the solution phase, since the adducts of copper(I) halides with neutral donor ligands have a range of stoichiometries (c.f. ref. 17). Tables 1 and 2 show that with copper, as with gold, a mixture of products can be obtained, and that the stoichiometry depends in part on the Cu:Ph_3P ratio in the reaction mixture. The ratios shown in Table 2 are simply $[Ph_3P]_{t=0}$: metal dissolved, and cannot be taken as specifying reaction conditions; in particular no allowance is made for oxidation of triphenylphosphine via reaction [8] or [9], for possible cathodic reduction of Ph_3PCl_2, or for loss of metal by cathodic deposition. Despite these simplifications, the results are in agreement with the reaction scheme proposed. In general, the experiments offer a simple and direct synthesis of adducts of the monohalides of copper, silver, and gold.

X-ray Crystallography of AuCl Complexes

Microscopic examination of the crystalline product obtained from $Au/C_6H_5CH_2Cl/CH_3CN$ systems revealed the presence of two different substances, and subsequent X-ray structural analysis showed these to be chloro(triphenylphosphine) gold(I) and chlorobis(triphenylphosphine) gold(I).

The compound $AuCl \cdot Ph_3P$ was obtained as equi-dimensional cubic crystals. The X-ray analysis yielded a structure which on refinement ($R = 0.041$) proved to be identical with that previously

Can. J. Chem. Downloaded from www.nrcresearchpress.com by 210.87.254.105 on 09/06/12
For personal use only.

reported by Bennett, Soboroff, and Baenziger (18). The second compound had elongated acicular crystals, one of which (dimensions 0.42 × 0.12 × 0.08 mm) was selected for crystal structure analysis. Preliminary results showed that the crystal of $AuCl(Ph_3P)_2$ was twinned, but it was decided to proceed with the analysis in order to establish the structural differences, if any, between this substance and the previously reported chlorobis(triphenylphosphine)gold(I) hemibenzene (19). The orientation matrix for the single crystal component of the twinned crystal was successfully obtained, and the intensity data were collected. We had hoped that overlapping of reflections due to twinning would be negligible in terms of the final analysis, but in the event this proved not to be the case. Various procedures were explored in attempts to overcome this significant overlapping, include assigning an artificially large σ value to the suspect reflections and suppressing the zonal reflections completely, but it was not possible to improve the refinement beyond an R-value of 0.108. This analysis thus served to identify the compound $AuCl(Ph_3P)_2$ beyond any doubt, but did not permit a complete structural determination. In particular, the final difference map showed seven large peaks (3.0–7.0 e Å^{-3}) in the xz plane, which contains the gold atom (0.0327X, 0.0611Y, 0.2739Z), and all approximately 0.06Y from the gold. Table 3 shows the main structural features of $AuCl(Ph_3P)_2$, and the corresponding values for $AuCl(Ph_3P)_2 \cdot 0.5C_6H_6$. Comparison of the two sets of results shows no significant differences in the Au—Cl or Au—P distances, but there are important differences in the bond angles in the coordination kernel, due in part presumably to the presence or absence of benzene in the lattice.

TABLE 3. Important structural features of $AuCl(Ph_3P)_2$ and $AuCl(Ph_3)_2 \cdot 0.5C_6H_6$ (19). Distances in Å, angles in degree

Parameter	Value	
	$AuCl(Ph_3P)_2$	$AuCl(Ph_3P)_2 \cdot 0.5C_6H_6$
Cell dimensions a	11.862(2)	10.187(1)
b	10.921(3)	12.997(1)
c	14.701(2)	16.596(1)
α	113.65(2)	52.54(1)
β	99.35(3)	90.68(1)
γ	109.31(3)	75.00(1)
V (Å^3)	1547.5	1643.2
Space group	$P\bar{1}$	$P\bar{1}$
Z	2	2
Au—Cl	2.526(10)	2.500(4)
Au—P(1)	2.313(8)	2.323(4)
Au—P(2)	2.230(9)	2.339(4)
Cl—Au—P(1)	115.1(3)	118.7(1)
Cl—Au—P(2)	108.1(3)	109.2(1)
P(1)—Au—P(2)	136.4(3)	132.1(1)

Acknowledgements

This work was supported by a Grant (to D.G.T.) from Imperial Oil Ltd. One of us (C.O.) acknowledges the receipt of a travel grant from the Minna–James–Heinemann–Stiftung of Hanover, and the award of sabbatical leave from the University of Lancaster. We thank Dr. A. Osman for the identification of PPh_3Cl_2.

1. J. J. HABEEB and D. G. TUCK. J. Organomet. Chem. **134**, 363 (1977).
2. J. J. HABEEB and D. G. TUCK. J. Organomet. Chem. **146**, 213 (1978).
3. J. J. HABEEB, A. OSMAN, and D. G. TUCK. J. Organomet. Chem. **185**, 117 (1980).
4. J. J. HABEEB, F. SAID, and D. G. TUCK. J. Organomet. Chem. **190**, 325 (1980).
5. F. F. SAID and D. G. TUCK. Can. J. Chem. **58**, 1673 (1980).
6. J. J. HABEEB and D. G. TUCK. J. Organomet. Chem. **139**, C17 (1977).
7. F. F. SAID and D. G. TUCK. Can. J. Chem. **59**, 62 (1981).
8. M. KHAN, C. OLDHAM, M. J. TAYLOR, and D. G. TUCK. Inorg. Nucl. Chem. Lett. **16**, 469 (1980), and unpublished results.
9. C. K. INGOLD and B. J. GREGORY. J. Chem. Soc. B, 276 (1969).
10. F. CARIATI and L. NALDINI. Gazz. Chim. Ital. **95**, 201 (1965).
11. F. H. JARDINE, L. RULE, and A. G. VOHRA. J. Chem. Soc. A, 238 (1970).
12. G. COSTA, G. PELLIZER, and F. RUBESSA. J. Inorg. Nucl. Chem. **26**, 961 (1964).
13. M. KHAN, R. C. STEEVENSZ, D. G. TUCK, J. G. NOLTES, and P. W. R. CORFIELD. Inorg. Chem. **19**, 3407 (1980).
14. D. G. TUCK. Pure Appl. Chem. **51**, 2005 (1979).
15. R. J. PUDDEPHATT. The chemistry of gold. Elsevier, Amsterdam. 1978.
16. R. R. ROULET, N. Q. LAN, W. R. MASON, and G. P. FENSKE. Helv. Chim. Acta, **56**, 2405 (1973).
17. F. H. JARDINE. Adv. Inorg. Radiochem. **17**, 115 (1975).
18. W. E. BENNETT, D. M. SOBOROFF, and N. C. BAENZIGER. Acta Crystallogr. B**32**, 962 (1976).
19. N. C. BAENZIGER, K. M. DITTEMORE, and J. R. DOYLE. Inorg. Chem. **13**, 805 (1974).

Attack of H-atoms on aqueous thionine studied by pulse radiolysis

SONJA SOLAR AND NIKOLA GETOFF
Institut für Theoretische Chemie und Strahlenchemie der Universität Wien, A-1090 Wien, Währingerstr. 38, Austria
WOLFGANG SOLAR
Ludwig Boltzmann Institut für Strahlenchemie, A-1090 Wien, Währingerstr. 38, Austria
AND
FRANZ MARK
Institut für Strahlenchemie am Max Planck Institut für Kohlenforschung, Stiftstraße 34-36, D-4330 Mülheim/Ruhr, FRG

Received September 30, 1980

SONJA SOLAR, NIKOLA GETOFF, WOLFGANG SOLAR, and FRANZ MARK. Can. J. Chem. **59**, 2719 (1981).

The reaction mechanism of the H-attack on thionine (TH^+) in aqueous solutions (5×10^{-6} to 2×10^{-5} mol dm^{-3} TH^+; 2×10^{-2} mol dm^{-3} *t*-butanol, pH 1 and 4) was investigated by pulse radiolysis in combination with simulation by computation. Applying a least-squares fitting procedure it was possible to state that at pH 1, 89.5% of the H-atoms react with TH^+, $k = (8.5 \pm 0.3) \times 10^9$ dm^3 mol^{-1} s^{-1}, to form semiquinone ($^{\cdot}TH_3^{2+}$, $\lambda_{max} = 390$ nm, $\varepsilon_{390} = 685 \pm 20$ m^2 mol^{-1}; $\varepsilon_{770} = 720$ m^2 mol^{-1} and $\lambda_{max} = 790$ nm, $\varepsilon_{790} = 775 \pm 20$ m^2 mol^{-1}), which dismutates to TH^+ and leucodye with $2k = (2.4 \pm 0.1) \times 10^9$ dm^3 mol^{-1} s^{-1}. In addition to this a second H-attack (10.5% H) occurs on the ring carbon of the dye with $k = (1.0 \pm 0.1) \times 10^9$ dm^3 mol^{-1} s^{-1}, resulting in the production of H-adducts. These results are of interest for photogalvanic cells using thionine as a sensitizer.

SONJA SOLAR, NIKOLA GETOFF, WOLFGANG SOLAR et FRANZ MARK. Can. J. Chem. **59**, 2719 (1981).

Utilisant la radiolyse par pulsation combinée avec une simulation obtenue par le calcul, on a étudié le mécanisme de la réaction d'attaque du H sur la thionine (TH^+) dans des solutions aqueuses (5×10^{-6} à 2×10^{-5} mol dm^{-3} TH^+; 2×10^{-2} mol dm^{-3} *tert*-butanol, pH 1 et 4). En utilisant la méthode des moindres carrés il est possible de dire qu'à un pH de 1, 89,5% des atomes d'hydrogène réagissent avec la TH^+, $k = (8{,}5 \pm 0{,}3) \times 10^9$ dm^3 mol^{-1} s^{-1}, pour conduire à la semithionine ($^{\cdot}TH_3^{2+}$, $\lambda_{max} = 390$ nm, $\varepsilon_{390} = 685 \pm 20$ m^2 mol^{-1}, $\varepsilon_{770} = 720$ m^2 mol^{-1} et $\lambda_{max} = 790$ nm, $\varepsilon_{790} = 775 \pm 20$ m^2 mol^{-1}) qui se dismute en TH^+ et en leucocolorant avec $2k = (2{,}4 \pm 0{,}1) \times 10^9$ dm^3 mol^{-1} s^{-1}. De plus, il se produit une deuxième attaque de l'hydrogène (10,5% H) sur le cycle carboné du colorant avec $k = (1{,}0 \pm 0{,}1) \times 10^9$ dm^3 mol^{-1} s^{-1} qui conduit à la formation d'adduits d'hydrogène. Ces résultats intéressants se rapportent aux cellules photogalvaniques qui utilisent la thionine comme sensibilisateur.

[Traduit par le journal]

Introduction

Thionine (TH^+) in aqueous solutions has been the subject of numerous photochemical, photophysical, and photoelectrochemical investigations in respect of both, basic chemistry (1–16) and solar energy utilization (3, 17–22). The main primary photochemical induced intermediate is thionine triplet, $^3TH^+$ ($Q_T = 0.4$ (23), absorption maxima: 375 nm and 665 nm at pH 1 (8)), whereas the fluorescence quantum yield is relatively low ($Q_F = 0.047$ (11)).[1] Special attention was drawn to the formation of semiquinone ($^{\cdot}TH_2^+$) by means of appropriate triplet quenchers. Using, e.g., ferrous ions in acid solution, the process can be summarized as follows:

[1] $TH^+ \longrightarrow {}^1TH^+ \xrightarrow{ISC} {}^3TH^+$

[2] $^3TH^+ + H^+ \rightleftharpoons {}^3TH_2^{2+}$ ($pK_T = 6.3$ (24))

[3] $^3TH_2^{2+} + Fe^{2+} \xrightarrow{k_3} {}^{\cdot}TH_2^+ + Fe^{3+}$
$k_3 = 6 \times 10^7$ dm^3 mol^{-1} s^{-1} (25)

[4] $^{\cdot}TH_2^+ \rightleftharpoons {}^{\cdot}TH + H$ ($pK = 8.1$ (8, 26))

[5] $^{\cdot}TH_2^+ + {}^{\cdot}TH_2^+ \xrightarrow{H_{aq}^+} TH^+ + TH_4^{2+}$

It was further established that semiquinone is formed not only from $^3TH_2^{2+}$, but also from $^1TH^+$ by an electron transfer process (7, 11, 16). The absorption spectrum of $^{\cdot}TH_2^+$ has been measured by some authors, applying the flash photolysis method. Using ferrous ions as the electron donor in aqueous solutions its absorption maxima were found to be at 390–400 nm ($\varepsilon = 650$ to 680 m^2 mol^{-1}) and at >750–770 nm ($\varepsilon = 820$–1200 m^2 mol^{-1}) (7, 13, 27). Applying allythiourea (8, 28) or paraphenylendiamine (9) as triplet quenchers in neutral solutions absorption bands at 400 nm ($\varepsilon = 700$–870 m^2 mol^{-1}) and at 750–775 nm ($\varepsilon = 1360$–1750 m^2 mol^{-1}) were observed. The scattering of the results could be explained by different protonation forms of semiquinone in addition to other factors. Some of these are briefly mentioned, e.g. the kind and concentration of the electron donor can influence the yield of semiquinone (12, 15, 29, 30). Besides, the absorption of the dye triplet interferes significantly with that of semiquinone in the range of 350–450 nm; further, in some cases the absorption

[1] The left superscript indicates the multiplicity of the excited dye state.

0008-4042/81/182719-05$01.00/0
©1981 National Research Council of Canada/Conseil national de recherches du Canada

Can. J. Chem. Downloaded from www.nrcresearchpress.com by 210.87.254.6 on 09/06/12
For personal use only.

Can. J. Chem. Downloaded from www.nrcresearchpress.com by 210.87.254.6 on 09/06/12
For personal use only.

of the donor or its oxidized form is overlapping with that of semiquinone.

A direct formation of semiquinone, avoiding all above mentioned factors can be achieved by reaction of thionine with H-atoms. The pulse radiolysis technique offers this possibility.

In the present paper experimental and simulation computation data concerning the formation and decay kinetics, as well as spectroscopic data of semireduced thionine in strong acid aqueous solutions are presented. Such investigations have been recently performed with aqueous methylene blue (MB^+) at pH = 1 which is the *N,N,N',N'*-tetramethyl derivative of thionine (31).

Experimental section

Chemicals and Preparation of Solutions

The substances (*t*-butanol, $HClO_4$, and H_2SO_4) were of reagent grade (E. Merck) and were used without further purification. Thioninehydrochloride (3,7-diamino-5-phenothiaziniumchloride; MW 263.75; EGA-Chemie, FRG) was recrystallized from 50% water–ethanol solutions (32). The determined molar extinction coefficient, $\varepsilon_{598} = 5480\ m^2\ mol^{-1}$ was in good agreement with that of other authors measured under the same conditions (9, 32). The dye solutions (5×10^{-6} to 2×10^{-5} mol dm^{-3} TH^+, 2×10^{-2} mol dm^{-3} *t*-butanol as OH scavenger with $k(OH + t\text{-butanol}) = 5.5 \times 10^8\ dm^3\ mol^{-1}\ s^{-1}$ (33)) were prepared using water distilled at least four times, and immediately before the experiment, were saturated with high purity argon for about 1 h. For adjusting pH = 1.0 ± 0.1 of the dye solutions, sulfuric acid, or in some cases perchloric acid, was used. Some experiments with the same dye concentrations were also carried out at pH = 4 ± 0.1. No difference between the spectroscopic and kinetic data of the transients was observed by applying either of the two acids in the range of the dye concentrations given above. The solvated electrons were converted rapidly into H-atoms ($k(e_{aq}^- + H_{aq}^+) = 2.3 \times 10^{10}\ dm^3\ mol^{-1}\ s^{-1}$ at pH 1 (34)), hence G_H (total) was taken to be 3.55 (35).

Pulse radiolysis[2]

The pulse radiolysis set-up was previously described in detail (36, 37). A 3 MeV Van de Graaff accelerator (High Voltage Eng. Co, Burlington, type K) provided electron pulses of 0.4 μs duration. The dose per pulse was varied from 1 to 5 J/kg (100–500 rad) producing 0.37×10^{-6} to 1.85×10^{-6} mol dm^{-3} H-atoms. A double monochromator (Zeiss MQ 12) in combination with a wide range photomultiplier (Hamamatsu, type R 955) and an oscilloscope (Tektronix, type 555) were used for registration of the intermediate absorption in the range of 280 to 900 nm. All solutions were irradiated at 20 ± 2°C in a suprasil quartz cell with light path of 3 × 2 cm and were exchanged after each single pulse by means of a remote-controlled valve. The optical density of all measurements has been normalized for 1 cm light path and to a dose of 10 J/kg (1 krad) per pulse.

Simulation Computation

Based on the kinetic and spectroscopic results obtained by pulse radiolysis, calculations were performed on the CDC computer of the Vienna University in order to elucidate the reaction mechanism.

[2]We are indebted to Dipl. Phys. F. Schwörer, Mr. K. H. Toepfer, Mr. F. Reikowski, and Mrs. G. Kampmann for valuable help.

Results and Discussion

Pulse Radiolysis

The absorption spectrum of the intermediates, formed by attack of H-atoms on thionine, was measured in air-free solutions at pH = 1 ± 0.1 using three different dye concentrations (5×10^{-6}, 1×10^{-5}, and 2×10^{-5} mol dm^{-3} TH^+ in the presence of 2×10^{-2} mol dm^{-3} *t*-butanol) in the range from 280 to 900 nm. Two strong absorption maxima at 390 and 790 nm were observed, which correspond to semithionine, in accordance to the above mentioned flash photolysis studies (7–9, 22). In addition to this an absorption at about 300 nm was obtained, after correction for depletion of the dye. This absorption was attributed to the H-adduct, produced by an addition of H-atoms to ring carbon, as previously shown for methylene blue (31) and aromatic amines (38–40).

Preliminary information about the reaction mechanism for the formation and dismutation of semithionine was obtained by kinetic analysis at the absorption maxima at 390 and 790 nm for short (up to about 15 μs) and long times (from 100–1500 μs). The intermediate time range, where the build-up and decay processes overlap, was first neglected. For illustration in this respect typical oscilloscope traces of the transients absorbing at 390 and 770 nm are shown in Fig. 1. It is obvious that the course of

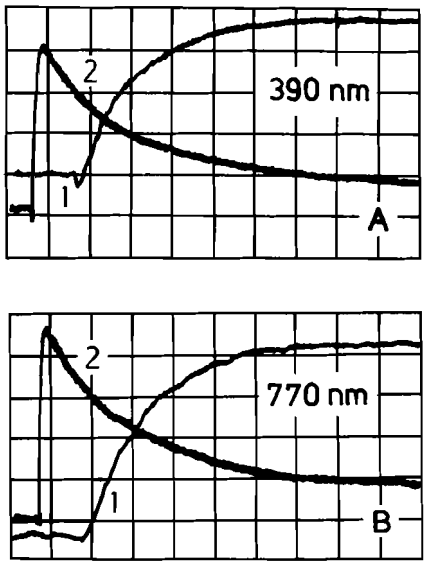

FIG. 1. Oscilloscope traces of transients formed by H-attack on TH^+ (1×10^{-5} mol dm^{-3} dye, 2×10^{-2} mol dm^{-3} *t*-butanol, pH = 1) in airfree aqueous solution. Vertical displacements correspond to the relative absorbance; horizontal displacements represent the time scale: for *A* 1 and *B* 1: 5 μs/div., for *A* 2 and *B* 2: 200 μs/div. (*A*, λ = 390 nm, dose: 4.8 J/kg; *B*, λ = 770 nm, dose: 5.2 J/kg).

Can. J. Chem. Downloaded from www.nrcresearchpress.com by 210.87.254.6 on 09/06/12
For personal use only.

the corresponding traces is similar and the H-attack on TH^+ with formation of semiquinone is completed within 30 μs (Fig. 1, curves 1*A* and 1*B*).

The evaluation of the traces from at least ten individual measurements for each of the above mentioned three thionine concentrations shows purely first-order kinetics, giving a mean value of $k_6 = 1.0 \times 10^{10}$ dm^3 mol^{-1} s^{-1} at both wavelengths. This fact gives evidence that only one short-living species ($\cdot TH_3^{2+}$) absorbs at these wavelength ranges. Thus, there is a difference in the reactivity of H-atoms with TH^+ and MB^+, since in the case of MB^+ the absorption at 400 nm was superimposed by a second transient, resulting from the H-attack by splitting the chromophore group of the dye molecule (31).

Purely second order plots of 1/OD values vs. time (up to about 1.5 ms) were obtained for the dismutation reaction of semithionine at 390, 770, and 790 nm for a number of measurements using all three different dye concentrations. Taking the slopes of these plots of both absorption bands and mean ε-values based on the previously reported flash photolysis data for $\varepsilon_{390} = 650$ m^2 mol^{-1} and $\varepsilon_{770} = 1200$ m^2 mol^{-1} (e.g. ref. 13), no significant difference between the kinetic data at both wavelengths was observed. The resulting mean value for semiquinone decay was $2k_9 = 2.4 \times 10^9$ dm^3 mol^{-1} s^{-1}. This fact supports again the assumption that only one transient with absorption maxima at 390 to 790 nm is produced.

The kinetic evaluation at 300 nm was not carried out graphically, because at this wavelength there is a significant superimposition with the primary absorption of the dye.

Simulation Computation

Both processes, the formation of semiquinone and that of H-adducts (reactions [6] and [7]), are in competition with the combination of H-atoms (reaction [8]), because of the very low dye concentration used. Hence, the reaction scheme at pH = 1 may be summarized as follows (the structure of semithionine is based on esr measurements (41, 42), whereas that of the H-adduct is reasonable in accordance with results for other aromatic compounds (33, 38)):

[6] 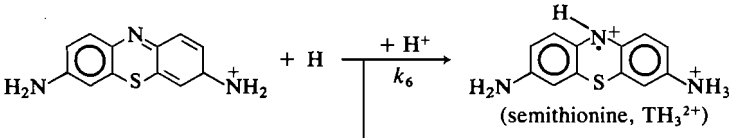

[7] 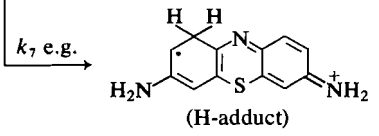

[8] $H + H \longrightarrow H_2$ ($2k_8 = 2.3 \times 10^{10}$ dm^3 mol^{-1} s^{-1} (31))

[9] $\cdot TH_2^{2+} + \cdot TH_3^{2+} \xrightarrow{2k_9} TH_4^{2+} + TH^+ + H^+$

Based on the assumption of a homogeneous distribution of the H-atoms in the acid dye solution one can apply normal chemical kinetics for reactions [6] to [9]. Thus, the following kinetic equations can express the reaction mechanism:

[10] $$d[TH^+]/dt = -(k_6 + k_7)[TH^+][H] + k_9[\cdot TH_3^{2+}]^2$$

[11] $$d[H]/dt = -(k_6 + k_7)[TH^+][H] - 2k_8[H]^2$$

[12] $$d[\cdot TH_3^{2+}]/dt = k_6[TH^+][H] - 2k_9[\cdot TH_3^{2+}]^2$$

[13] $$d[TH_4^{2+}]/dt = k_9[\cdot TH_3^{2+}]^2$$

The unknown model-parameters (rate constants for reactions [6], [7], and [9]), for $\cdot TH_3^{2+}$: ε_{390} and ε_{790}, have been determined by approximating the experimental OD-values to the OD-values calculated for the reaction scheme (reactions [6] to [9]), using a non-linear least-squares fitting procedure (31). The system of non-linear differential equations ([10] to [13]) has been solved numerically by the Runge–Kutta method (43) for various parameter sets, until the sum of the squared deviations between calculated and experimental OD-values was minimised (44). All experimental data obtained by using different dye concentrations were applied for this computation. The parameter data at the beginning of the iterative procedure were: $k_6 = 1.0 \times 10^{10}$ dm^3 mol^{-1} s^{-1} and $2k_9 = 2.6 \times 10^9$ dm^3 mol^{-1} s^{-1}, which were experimentally determined as

TABLE 1. Computed molar extinction coefficients (ε) and rate constants (k) for formation and decay of short-lived species formed by reaction of H-atoms with thionine.

Species	Molar extinction coefficients (ε in m^2 mol^{-1}) ε_{390}	ε_{770}	ε_{790}	Rate constants (dm^3 mol^{-1} s^{-1}) Formation (k)	Decay ($2k$)
Semithionine	685±20	720±20	775±20	$(8.5\pm0.3)\times10^9$	$(2.4\pm0.1)\times10^9$
H-adducts	—	—	—	$(1.0\pm0.1)\times10^9$	—

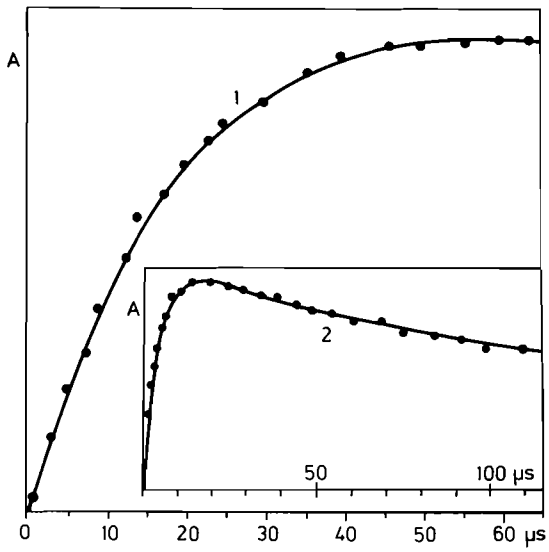

FIG. 2. Absorbance (A; arbitrary scale) as a function of time for experimentally determined (○) and computed data (solid line) for formation and decay of semiquinone ($^{\bullet}TH_3^{2+}$) at 770 nm (*1*) and 390 nm (insert, curve *2*). Solution: (*1*) 5×10^{-6} mol dm^{-3} TH^+, 1×10^{-2} mol dm^{-3} *t*-butanol, pH = 1; dose/pulse: 2.1 J/kg (*2*) 2×10^{-5} mol dm^{-3} TH^+, 2×10^{-2} mol dm^{-3} *t*-butanol, pH = 1; dose/pulse: 4.9 J/kg.

mentioned before. The rate constant for reaction [7] was taken to be the same as in the case of methylene blue, namely $k_7 = 0.6 \times 10^9$ dm^3 mol^{-1} s^{-1} (31).

It might be further mentioned that each pulse radiolysis measurement was performed at least five times, using various doses/pulse for each of the three dye concentrations. Afterwards the obtained measurements were analyzed together in one single computation step. Hence, only one set of rate constants and ε-values, satisfying all individual chosen experimental conditions, was obtained. Typical computer plots of absorbance vs. time (μs) of calculated and experimental data are shown in Fig. 2 for illustration.

The final computed rate constants for formation and decay of the transients together with ε_{390}, ε_{770}, and ε_{790} for $^{\bullet}TH_3^{2+}$ are presented in Table 1, having confidence limits of 99%. Our ε_{390}-value agrees well with those determined by flash photolysis in acid solutions (7, 13), however, their ε_{770}-values are essentially higher than ours. The rate constant for dismutation of $^{\bullet}TH_3^{2+}$ ($2k_9$) is rather similar to some of those determined previously, e.g. $2k_9 = 2.4 \times 10^9$ dm^3 mol^{-1} s^{-1} (7, 8). Based on the results given in Table 1 it was calculated that 89.5% of the H-atoms are reacting with thionine with the production of semithionine (reaction [6]) and that the remaining 10.5% yield H-adducts (reaction [7]). However, the root-mean-square error in the calculated OD-values is about two times larger, if the calculations are performed under the assumption that reaction (7) is negligible.

Simulation computations were also performed with some preliminary pulse radiolysis data obtained with TH^+ at pH = 4. The ε_{390}-values and the kinetic data for formation of semiquinone and H-adducts at both pH's (1 and 4) are found to be rather similar, but at pH 4 $\varepsilon_{770} = 1870$ m^2 mol^{-1}, whereas at pH 1 $\varepsilon_{790} = 775$ m^2 mol^{-1}. The reason for this difference is the two protonation forms of semiquinone, namely $^{\bullet}TH_3^{2+}$ (pH 1) and $^{\bullet}TH_2^{+}$ (pH 4). The semiquinone decay constant ($2k_9$) at pH 4 is about 20% larger than that at pH 1.

Finally it might be mentioned that the presented data are also of interest for photogalvanic and other redox systems, using thionine as a sensitizer for solar energy utilization (3, 21). These devices are still not stable enough for practical use. The electrons ejected from the cathode are converted into H-atoms in acid solution, and lead to formation of semiquinone, leuco-dye, and H-adducts. The first two products can be reversed to the original dye form by a dark reaction with the oxidized electron donor of the system (e.g. Fe^{3+}). The formation of H-adducts on ring carbon, however, is an irreversible process, which could explain at least partly the instability of such devices.

Acknowledgements

The authors (S.S. and N.G.) are indebted to Prof. Dr. D. Schulte-Frohlinde for permission to

Can. J. Chem. Downloaded from www.nrcresearchpress.com by 210.87.254.6 on 09/06/12
For personal use only.

use the facilities of the Institut für Strahlenchemie im Max Planck Institut für Kohlenforschung, Mülheim/Ruhr, FRG and to the Max Planck Gesellschaft for financial support. Financial support by Fonds zur Förderung der wissenschaftlichen Forschung, Vienna and the Bundesministerium für Wissenschaft und Forschung, Austria is gratefully acknowledged.

1. K. WEBER. Z. Phys. Chem. B**15**, 18 (1931).
2. J. WEISS. Nature, **136**, 794 (1935).
3. E. RABINOWITCH. J. Chem. Phys. **8**, 551 (1940).
4. R. HAVEMANN and H. PIETSCH. Z. Phys. Chem. Leipzig, **208**, 98 (1957).
5. C. A. PARKER. Nature, **182**, 245 (1958).
6. R. HARDWICK. J. Am. Chem. Soc. **80**, 5667 (1958).
7. C. G. HATCHARD and G. A. PARKER. Trans. Faraday Soc. **57**, 1093 (1961).
8. H. FISCHER. Z. Phys. Chem. N.F. **43**, 177 (1964).
9. R. BONNEAU, J. FAURE, and J. JOUSSOT-DUBIEN. Ber. Bunsenges. Phys. Chem. **72**, 263 (1968).
10. H. FISCHER, H. E. A. KRAMER, and A. MAUTE. Z. Phys. Chem. N.F. **69**, 113 (1970).
11. M. D. ARCHER, M. I. C. FERREIRA, G. PORTER, and C. J. TREDWELL. Nouv. J. Chim, **1**, 9 (1977).
12. E. VOGELMANN, S. SCHREINER, W. RAUSCHER, and H. E. A. KRAMER. Z. Phys. Chem. N.F. **101**, 321 (1976).
13. P. D. WILDES and N. N. LICHTIN. J. Phys. Chem. **82**, 981 (1978).
14. H. E. A. KRAMER and A. MAUTE. Photochem. Photobiol. **15**, 7 (1972).
15. S. N. GUHA, P. N. MOORTHY, and K. N. RAO. Molec. Photochem. **9**, 183 (1979).
16. G. KÖHLER, S. SOLAR, and N. GETOFF. Z. Naturforsch. **35**a, 1201 (1980).
17. A. E. POTTER and L. H. THALER. Sol. Energy, **3**, 1 (1957).
18. R. A. MANN, C. READ, D. R. ROSSEINSKY, and P. WASSELL. Nature London Phys. Sci. **244**, 126 (1973).
19. W. D. K. CLARK and J. A. ECKERT. Sol. Energy, **17**, 147 (1975).
20. G. PORTER and M. D. ARCHER. Interdisc. Sci. Rev. **1**, 119 (1976).
21. N. GETOFF, K. J. HARTIG, G. KITTEL, G. A. PESCHEK, and S. SOLAR. Wasserstoff als Energieträger. Springer-Verlag, Wien (1977).
22. N. N. LICHTIN. *In* Solar power and fuels. *Edited by* J. R. Bolton. Academic Press Inc., London. 1977. p. 119.
23. J. SCHLAG. Z. Phys. Chem. N.F. **20**, 53 (1959).
24. R. BONNEAU and R. D. S. STEVENS. Chem. Phys. Lett. **13**, 376 (1972).
25. P. D. WILDES, N. N. LICHTIN, M. Z. HOFFMAN, L. ANDREW, and H. LINSCHNITZ. Photochem. Photobiol. **25**, 21 (1970).
26. G. N. LEWIS and J. BIGELEISEN. J. Am. Chem. Soc. **65/II**, 2419 (1943).
27. M. I. C. FERREIRA and A. HARRIMAN. J. Chem. Soc. Faraday Trans. I, **73**, 1085 (1977).
28. U. STEINER, M. HAFNER, S. SCHREINER, and H. E. A. KRAMER. Photochem. Photobiol. **19**, 119 (1974).
29. U. STEINER, G. WINTER, and H. E. A. KRAMER. J. Phys. Chem. **81**, 1104 (1977).
30. K. KIKUCHI, S.-I. TAMURA, CH. IWANAGA, and H. KOKUBUN. Z. Phys. Chem. N.F. **106**, 17 (1977).
31. S. SOLAR, N. GETOFF, W. SOLAR, and F. MARK. Radiat. Phys. Chem. **17**, 107 (1981).
32. G. R. HAUGEN and E. R. HARDWICK. J. Phys. Chem. **67**, 725 (1963).
33. M. GOHN and N. GETOFF. J. Chem. Soc. Faraday Trans. I, **73**, 1207 (1977).
34. L. M. DORFMAN and I. A. TAUB. J. Am. Chem. Soc. **85**, 2370 (1963).
35. J. W. T. SPINKS and R. W. WOODS. An introduction to radiation chemistry. J. Wiley and Sons, New York. 1976.
36. N. GETOFF and F. SCHWÖRER. Raditat. Res. **41**, 1 (1970).
37. N. GETOFF and F. SCHWÖRER. Int. J. Radiat. Phys. Chem. **5**, 101 (1973).
38. H. CHRISTENSEN. Radiat. Phys. Chem. **4**, 311 (1972).
39. J. LICHTSCHEIDL and N. GETOFF. Monatsh. Chem. **110**, 1377 (1979).
40. N. GETOFF and M. PRUCHOVA. To be published.
41. U. STEINER and H. SCHMIDT. Private communication.
42. M. F. CHIU, B. C. GILBERT, and P. HANSON. J. Chem. Soc. B, 1700 (1970).
43. A. RALSTON and H. S. WILF. *In* Mathematical methods for digital computers. Vol. 1. J. Wiley, New York. p. 110.
44. U. HOFFMAN and H. HOFMAN. *In* Einführung in die Optimierung. Verlag Chemie, Weinbein. 1971. p. 178.

Can. J. Chem. Downloaded from www.nrcresearchpress.com by 210.87.254.6 on 09/06/12
For personal use only.

The reaction between carbon disulfide and some α-methylaminonitriles. The supposed isomerism of 4,4-dialkyl-5-imino-3-methylthiazolidine-2-thiones

FRANCIS L. CHUBB AND JOHN T. EDWARD

Department of Chemistry, McGill University, 801 Sherbrooke St. West, Montreal, P.Q., Canada H3A 2K6

Received February 20, 1981

FRANCIS L. CHUBB and JOHN T. EDWARD. Can. J. Chem. **59**, 2724 (1981).

The reaction of carbon disulfide with α-methylaminonitriles **1** yields 5-iminothiazolidine-2-thiones **3**, which on prolonged reaction are converted to 5-methyliminothiazolidine-2-thiones **5** and 2,4-dithiohydantoins **9**. A mechanism for this apparent methyl transfer is advanced. The yellow compounds obtained by prolonged reaction of the aminonitriles **1** ($R^1 = R^2 =$ Me and $R^1 =$ Et, $R^2 =$ Me) are not isomers of the imines **3** ($R^1 = R^2 =$ Me and $R^1 =$ Et, $R^2 =$ Me), but 2:1 complexes of these imines with the corresponding 2,4-dithiohydantoins **9** ($R^1 = R^2 =$ Me and $R^1 =$ Et, $R^2 =$ Me).

FRANCIS L. CHUBB et JOHN T. EDWARD. Can. J. Chem. **59**, 2724 (1981).

Le bisulfure de carbone réagit avec les α-méthylaminonitriles **1** en donnant les imino-5 thiazolidinethiones-2 **3**. En prolongeant le temps de réaction on transforme les composés **3** en méthyl-5 iminothiazolidinethiones-2 **5** et en dithio-2,4 hydantoïnes **9**. On propose un mécanisme pour expliquer ce transfert apparent d'un méthyle. Les composés jaunes obtenus par la réaction prolongée des aminonitriles **1** ($R^1 = R^2 =$ Me et $R^1 =$ Et, $R^2 =$ Me) ne sont pas des isomères des imines **3** ($R^1 = R^2 =$ Me et $R^1 =$ Et, $R^2 =$ Me), mais sont des complexes 2:1 de ces imines avec les dithio-2,4 hydantoïnes correspondants **9** ($R^1 = R^2 =$ Me et $R^1 =$ Et, $R^2 =$ Me).

[Traduit par le journal]

Carrington (1) reported that both α-methylaminoisobutyronitrile (**1**; $R^1 = R^2 =$ Me) and α-methylamino-α-methylbutyronitrile (**1**; $R^1 =$ Et, $R^2 =$ Me) reacted with carbon disulfide to give, after 24 hours, yellow crystalline compounds, formulated as **3** ($R^1 = R^2 =$ Me or $R^1 =$ Et, $R^2 =$ Me). Each yellow compound, he claimed, was converted by warm alcoholic sodium hydroxide into a colourless isomer. The relationship between the yellow and colourless isomers could not be elucidated; both isomers, it was claimed, were hydrolysed by acid to the common product **4** ($R^1 = R^2 =$ Me and $R^1 =$ Et, $R^2 =$ Me). On the other hand, reaction of carbon disulfide with the aminonitriles **1** ($R^1R^2 = (CH_2)_5$ and $CH_3CH\langle[CH_2]_4\rangle$) gave only colourless products **3** ($R^1R^2 = (CH_2)_5$ and $R^1R^2 = CH_3CH\langle[CH_2]_4\rangle$) and no yellow isomer.

In a reinvestigation of Carrington's reactions, we found that α-methylaminoisobutyronitrile (**1**; $R^1 = R^2 =$ Me) after 12 hours reaction with carbon disulfide gave only the colourless product reported by him. Its analysis and spectral characteristics supported his formulation **3** ($R^1 = R^2 =$ Me). However, when the reaction time was prolonged to 30 hours his yellow product was obtained in 38% yield, together with a new colourless product $C_7H_{12}N_2S_2$.

The analysis and spectra of this second colourless compound showed it to be the *N*-methylimine **5** ($R^1 = R^2 =$ Me), a structure following also from the fact that both compounds **3** and **5** ($R^1 = R^2 =$ Me) were hydrolysed by dilute acid to the same carbonyl compound **4** ($R^1 = R^2 =$ Me).

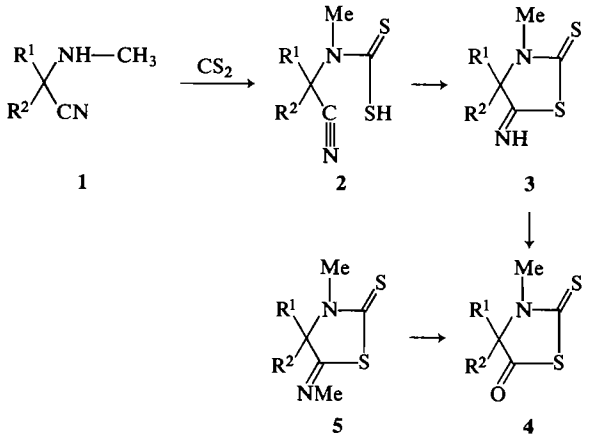

SCHEME 1

The yellow compound proved to be a complex (C-1) made up of one mole of 5,5-dimethyl-2,4-dithiohydantoin (**9**; $R^1 = R^2 =$ Me) (2) and two of the imine **3** ($R^1 = R^2 =$ Me). As reported by Carrington, the yellow solid was converted by dilute aqueous sodium hydroxide to the colourless imine **3** ($R^1 = R^2 =$ Me); however, the alkaline filtrate contained 5,5-dimethyl-2,4-dithiohydantoin (2), which was precipitated by acidification. Furthermore, a yellow product of identical properties (mp, ir) crystallized out when methanolic solutions of the imine **3** ($R^1 = R^2 =$ Me) and the 2,4-dithiohydantoin **5** ($R^1 = R^2 =$ Me) were mixed in varying proportions; its uv spectrum showed that the mole ratio of **3**:**5** in the product was invariably 2:1. It is presumably a hydrogen-bonded complex, dissociated

0008-4042/81/182724-05$01.00/0

©1981 National Research Council of Canada/Conseil national de recherches du Canada

Can. J. Chem. Downloaded from www.nrcresearchpress.com by 210.87.254.5 on 09/06/12
For personal use only.

Can. J. Chem. Downloaded from www.nrcresearchpress.com by 210.87.254.5 on 09/06/12
For personal use only.

completely into its components when dissolved in ethanol (as shown by the uv spectrum of the solution).

A reaction mixture similar to that which had given first **3** ($R^1 = R^2 =$ Me) and later **5** and **9** ($R^1 = R^2 =$ Me) was heated to 50°C, and samples were withdrawn at various intervals of time and examined by nmr and ir spectroscopy. The disappearance of **1** ($R^1 = R^2 =$ Me), and the appearance first of **3** ($R^1 = R^2 =$ Me), and then of **5** ($R^1 = R^2 =$ Me), could be followed by changes in the areas of their *N*-methyl peaks in the nmr spectrum.[1] The results are shown in Fig. 1.[2]

The same changes were apparent when the ir spectrum of the reaction mixture was scrutinized at various times. This spectrum showed that the disappearance of the C≡N band (2220 cm^{-1}) due to **1** ($R^1 = R^2 =$ Me) was accompanied by the appearance of a C=NH band (1630 cm^{-1}) due to **3** ($R^1 = R^2 =$ Me). The latter band increased in intensity up to a maximum after about 24 hours, and then declined, while three new bands became apparent after 18–24 hours; one at 1660 cm^{-1} (C=NMe) due to **5** ($R^1 = R^2 =$ Me); another (somewhat more slowly) at 1530 cm^{-1} (>N—CS—) due to **9** ($R^1 = R^2 =$ Me); and a third at 2050 cm^{-1} (—N=C=S (3)) due to **8**. This last peak is interesting in supplying the first direct experimental evidence for the involvement of an isothiocyanate intermediate (4) **8** in the formation of a 2,4-dithiohydantoin **9** by the route shown in Scheme 2 and pioneered by Carrington (2). Unfortunately, attempts to isolate the compound **8** ($R^1 = R^2 =$ Me) from the complex reaction mixture by chromatography on Florosil failed, possibly because the compound rearranged to **9** ($R^1 = R^2 =$ Me) on the adsorbent. When the reaction mixture was extracted with dilute aqueous acid, basic products such as **3** and **5** ($R^1 = R^2 =$ Me) were removed, as shown by the disappearance of the peaks at 1630 and 1660 cm^{-1}, but the peak at 2050 cm^{-1} remained. However, when the reaction mixture was extracted with dilute aqueous sodium hydroxide, the peaks due to the basic products remained but the peak at 2050 cm^{-1} disappeared. This was to be expected from the weak acidity ($pK_a \sim 10$) (5) which one could anticipate for **8** ($R^1 = R^2 =$ Me).

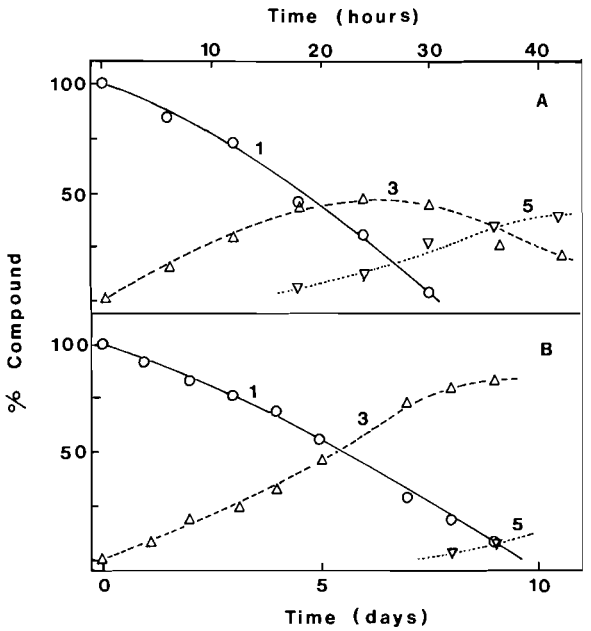

FIG. 1. Rate of disappearance of compound **1** (Scheme 1) and of appearance of compounds **3** and **5**. A: $R^1 = R^2 =$ Me; B: R^1 = Et, R^2 = Me.

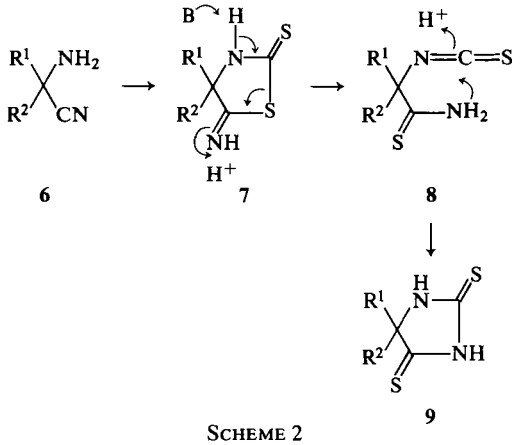

SCHEME 2

However, when the aqueous alkaline extract was acidified only the 2,4-dithiohydantoin **9** ($R^1 = R^2 =$ Me) was obtained, the reaction **8** → **9** evidently being rapid under these conditions.

In considering mechanisms for the general reaction [1] we must postulate

[1] 2 **3** → **5** + **9**

the formation of the aminonitrile **6**, the only plausible precursor to the 2,4-dithiohydantoin **9**. A pos-

[1]No *N*-methyl peak due to **2** ($R^1 = R^2 =$ Me) could be detected, and it seems probable that **2** does not accumulate because **2** → **3** is fast.

[2]The percentages shown in Fig. 1 were obtained first from the relative areas *A* of the *N*-methyl peaks of **1** and **3**; later, when **5** appeared, from the relative areas of the peaks for **1**, **3**, and **5**, with 100% given by the summation

$$A(1) + A(3) + 2A(5) = 100\%$$

as required by the stoichiometry (see below) of

2 **1** → 2 **3** → **5** + (**8** and/or **9**)

Can. J. Chem. Downloaded from www.nrcresearchpress.com by 210.87.254.5 on 09/06/12
For personal use only.

sible route involving **6** is:

[2] $\mathbf{3} \rightleftarrows \mathbf{1} + CS_2$

[3] $\mathbf{1} + NH_3 \rightleftarrows \mathbf{6} + CH_3NH_2$

[4] $\mathbf{6} + CS_2 \rightarrow \mathbf{9}$

[5] $CH_3NH_2 + \mathbf{3} \rightleftarrows \mathbf{5} + NH_3$

four equations which sum up to [1]. We have found that methylamine in aqueous ethanol displaces ammonia from the imine **3** (R^1 = Et, R^2 = Me) to give the *N*-methylimine **5** (R^1 = Et, R^2 = Me), as required by [5]. Under the same conditions, the reaction of methylamine with the imine **3** ($R^1 = R^2$ = Me) gives another compound along with *N*-methylimine **5** ($R^1 = R^2$ = Me); this reaction is being investigated further. The reversibility of [3] seems plausible from the work of Tallaides and Commeyras (6). This mechanism depends on the adventitious presence of traces of ammonia or methylamine (or, equivalently, water) which are regenerated during the overall reaction sequence [2]–[5]. Some evidence was obtained that "spiking" the reaction mixture with small amounts of ammonia or methylamine accelerated overall reaction [1], but systematic studies were not made.

The reaction of the aminonitrile **1** (R^1 = Et, R^2 = Me) with carbon disulfide paralleled precisely that of the aminonitrile **1** ($R^1 = R^2$ = Me), but was much slower, as shown in Fig. 1. Again, the yellow product was found to be a 2:1 complex (C-2) of the imine **3** (R^1 = Et, R^2 = Me) and the dithiohydantoin **9** (R^1 = Et, R^2 = Me), and could be obtained also by mixing warm solutions of appropriate amounts of the imine and of the 2,4-dithiohydantoin in 50% aqueous methanol, and allowing the solution to cool. However, a 1:1 yellow complex (C-3) could also be obtained if different amounts of imine and of 2,4-dithiohydantoin were mixed in solution. Both complexes had similar melting points (121–122° and 122–123°C), but were distinguishable by differing ultraviolet absorption spectra in solution in ethanol.

In agreement with Carrington (1), the aminonitrile **1** ($R^1R^2 = (CH_2)_5$) derived from cyclohexane gave the colourless imine **3** ($R^1R^2 = (CH_2)_5$), but no yellow compound on prolonged reaction. This was not due to the failure of **3** ($R^1R^2 = (CH_2)_5$) to react further: both the *N*-methylimino compound **5** ($R^1R^2 = (CH_2)_5$) and the spiro-2,4-dithiohydantoin **9** ($R^1R^2 = (CH_2)_5$) were obtained on prolonged reaction. However, a methanolic solution of **3** and **9** ($R^1R^2 = (CH_2)_5$) failed to deposit crystals of a yellow complex. This may be due to steric hindrance: yellow complexes of mixed composition could be obtained from methanolic solutions of the imine **3** (R^1 = Et, R^2 = Me) and the dithiohydantoin **9** ($R^1 = R^2$ = Me) (C-4, mole ratio 1:1), and of the imine **3** ($R^1 = R^2$ = Me) and the dithiohydantoin **9** (R^1 = Et, R^2 = Me) (C-5, mole ratio 2:1). On the other hand, no yellow complex could be obtained from methanolic solutions of the imines **3** ($R^1 = R^2$ = Me or R^1 = Et, R^2 = Me) with the dithiohydantoin **9** ($R^1R^2 = (CH_2)_5$), nor from methanolic solutions of the imine **3** ($R^1R^2 = (CH_2)_5$) with the dithiohydantoins **9** (R^1 = Et, R^2 = Me or $R^1 = R^2$ = Me). Furthermore, no yellow complexes could be obtained when 5,5-dimethyl-2- or 4-thiohydantoin was substituted for 5,5-dimethyl-2,4-dithiohydantoin, nor when the *N*-methylimine **5** ($R^1 = R^2$ = Me) was substituted for the imine **3** ($R^1 = R^2$ = Me). It seems likely that formation of the yellow complexes depends upon a very precise alignment of hydrogen bonding donor and acceptor groups, and hence on a very precise packing of imines and of 2,4-dithiohydantoins in the crystal.

Experimental

Reaction of α-Methylaminoisobutyronitrile (1; $R^1 = R^2$ = Me) with Carbon Disulfide

α-Methylaminoisobutyronitrile (18 g) and carbon disulfide (24 g) were heated to 50°C by a water-bath and stirred under reflux for 30 h. After evaporation of carbon disulfide, benzene (15 mL) was added. On standing, 11.5 g (38%) of yellow crystals (C-1) separated, mp 114–118°C, raised to 117–118°C (lit. (1) mp 115–116°C) by recrystallization from aqueous methanol; ir (Nujol): 3210 (N—H), 1620 (C=N), 1530 (2,4-dithiohydantoin) cm^{-1}; ^1H nmr ($CDCl_3$) δ: 1.55 (s, 6H), 1.60 (s, 12H), 3.33 (s, 6H), 8.61 (s, 1H). *Anal.* calcd. for $C_{17}H_{28}N_6S_6$: C 40.13, H 5.55, N 16.52; found: C 40.13, H 5.61, N 16.45.

The benzene filtrate was evaporated and the oily residue extracted with hot petroleum ether (bp 30–60°C). On cooling, the extract yielded 3.75 g (13%) of crude 3,4,4-trimethyl-5-methyliminothiazolidine-2-thione (**5**; $R^1 = R^2$ = Me); mp (after recrystallization from aqueous methanol) 80–81°C; ir (Nujol): 1660 (C=N) cm^{-1}; ^1H nmr ($CDCl_3$) δ: 1.58 (s, 6H), 3.20 (s, 3H), 3.36 (s, 3H). *Anal.* calcd. for $C_7H_{12}N_2S_2$: C 44.64, H 6.43, N 14.88; found: C 44.70, H 6.52, N 14.98.

Alkaline Decomposition of Yellow Complex C-1

Treatment of the yellow complex C-1 (5 g) with 2% sodium hydroxide (50 mL) discharged the yellow colour after a few minutes. After 2 h, white crystals (3.15 g, 92%), of 3,4,4-trimethyl-5-iminothiazolidine-2-thione (**3**; $R^1 = R^2$ = Me), mp 73–75°C (lit. (1) mp 70°C), were removed by filtration; ir (Nujol): 3140 (NH), 1630 (C=N) cm^{-1}; ^1H nmr ($CDCl_3$) δ: 1.66 (s, 6H), 3.33 (s, 3H), 9.59 (s, 1H).

Acidification of the alkaline filtrate yielded 1.35 g (80%) of crude 5,5-dimethyl-2,4-dithiohydantoin, mp 122–135°C, raised by one recrystallization from benzene to 145–147°C (lit. (2) mp 144°C); ir (Nujol): 3140 (NH), 1545 (2,4-dithiohydantoin) cm^{-1}; ^1H nmr (DMSO-d_6) δ: 1.33 (s, 6H), 10.66 (s, 1H), 13.00 (s, 1H).

Hydrolysis of 3,4,4-Trimethyl-5-methyliminothiazolidine-2-thione (5; $R^1 = R^2$ = Me)

3,4,4-Trimethyl-5-methyliminothiazolidine-2-thione (0.5 g) was dissolved in 10 mL of water and 5 mL concentrated hydrochloric acid and heated on the steam bath for 10 min. After

TABLE 1. Yellow complexes formed by direct mixing of imines **3** with 2,4-dithiohydantoins **9**

Complex	3 R¹	3 R²	9 R¹	9 R²	Ratio 3:9	Melting point (°C)	Formula		Analysis C	Analysis H	Analysis N
C-1	Me	Me	Me	Me	2:1	117–118	$C_{17}H_{28}N_6S_6$		—	—	—
C-2	Et	Me	Et	Me	2:1	121–122	$C_{20}H_{34}N_6S_6$		—	—	—
C-3	Et	Me	Et	Me	1:1	122–123	$C_{13}H_{22}N_4S_4$	calcd.	43.05	6.12	15.45
								found	43.05	6.04	15.63
C-4	Et	Me	Me	Me	1:1	119–120	$C_{12}H_{20}N_4S_4$	calcd.	41.35	5.78	16.07
								found	41.34	5.83	16.00
C-5	Me	Me	Et	Me	2:1	121–122	$C_{18}H_{30}N_6S_6$	calcd.	41.35	5.78	16.08
								found	41.33	5.88	16.04

the mixture had cooled, crystalline precipitate (10.43 g, 92%) was removed by filtration; mp 87–89°C (lit. (1) mp 85°C), identical (ir, nmr) with an authentic sample of 3,4,4-trimethylthiazolidine-5-one-2-thione (**4**; $R^1 = R^2 =$ Me); ir (Nujol): 1725 (C=O) cm^{-1}, prepared by hydrolysis of the imine **3** ($R^1 = R^2 =$ Me) according to Carrington (1).

Reaction of α-Methylamino-α-methylbutyronitrile (1; R^1 = Et, R^2 = Me) with Carbon Disulfide

A solution of α-methylamino-α-methylbutyronitrile (23.5 g) in carbon disulfide (27 g) was heated and stirred under reflux at 50°C for 72 h. After evaporation of carbon disulfide the oily residue partially crystallized. The crystals were sucked as dry as possible on the filter and recrystallized from aqueous methanol to yield 8.0 g (20%) of crude 3,4-dimethyl-4-ethyl-5-iminothiazolidine-2-thione (**3**; R^1 = Et, R^2 = Me), mp 72–75°C, raised by recrystallization to 87–89°C (lit. (1) mp 85°C); ir (Nujol): 3080 (N—H) 1620, 1640 (C=N) cm^{-1}; ^1H nmr ($CDCl_3$) δ: (t, J = 7.5 Hz, 3H, CH_2—CH_3), 1.56 (s, 3H, C—CH_3), 1.91 (q, J = 7.5, 2H, CH_2), 3.26 (s, 3H, NCH_3), 9.37 (s, 1H, NH).

The original filtrate on standing deposited yellow crystals (complex C-2), mp 115–116°C, raised by crystallization from aqueous methanol to 121–122°C (lit. (1) mp 117°C); ir (Nujol): 3215, 3200 (NH), 1610 (C=N), 1525 (2,4-dithiohydantoin) cm^{-1}; ^1H nmr ($CDCl_3$) δ: 0.85 (t, 9H), 1.50 (s, 3H), 1.60 (s, 6H), 1.93 (m, 6H), 3.30 (s, 6H), 8.4 (s, 1H), 8.9 (s, 2H). *Anal.* calcd. for $C_{20}H_{34}N_6S_6$: C 43.60, H 6.22, N 15.26; found: C 43.56, H 6.27, N 15.19.

The filtrate from C-2 was concentrated. Extraction of the oily residue with boiling petroleum ether and cooling of the extract yielded 2.0 g (4.8%) of white crystals, mp 74–75°C, of 3,4-dimethyl-4-ethyl-5-methyliminothiazolidine-2-thione (**5**; R^1 = Me, R^2 = Et); ir (Nujol): 1665 (C=N) cm^{-1}; ^1H nmr ($CDCl_3$) δ: 0.80 (t, J = 7.5 Hz, 3H, CH_2—CH_3), 1.53 (s, 3H, C—CH_3), 1.90 (q, J = 7.5 Hz, 2H, CH_2), 3.26 (s, 3H, NCH_3), 3.33 (s, 3H, =NCH_3). *Anal.* calcd. for $C_8H_{14}N_2S_2$: C 47.48, H 6.97, N 13.84; found: C 47.56, H 7.08, N 13.86.

Alkaline Decomposition of Complex C-2

Treatment of C-2 (0.5 g) by the procedure described for C-1 yielded 3,4-dimethyl-4-ethyl-5-iminothiazolidine-2-thione (0.32 g, 94%), mp 85–87°C, and 5-ethyl-5-methyl-2,4-dithiohydantoin (0.08 g, 50%), mp 148–150°C (lit. (2) mp 147–148°C), identical (ir, nmr) to an authentic specimen (2).

Reaction of 3,4-dimethyl-4-ethyl-5-iminothiazolidine-2-thione with Methylamine

The thione **3** (R^1 = Et, R^2 = Me) (1 g) in 40% aqueous methylamine (10 mL) and methanol (5 mL) was heated to reflux overnight. The solution was concentrated to remove methanol, more aqueous methylamine was added, and a solid was removed by filtration. This was crystallized from aqueous methanol to give 0.55 g of *N*-methylimine **5** (R^1 = Et, R^2 = Me), mp 71–73°C, having an ir spectrum identical with that of the authentic compound.

Hydrolysis of 3,4-Dimethyl-4-ethyl-5-methyliminothiazolidine-2-thione (5; R^1 = Et, R^2 = Me)

3,4-Dimethyl-4-ethyl-5-methyliminothiazolidine-2-thione (0.5 g) was dissolved in 5 mL of concentrated hydrochloric acid and 15 mL of water and heated on the steam bath for 15 min. After cooling, crystals (0.43 g, 92%) of 3,4-dimethyl-4-ethylthiazolidine-5-one-2-thione (**4**; R^1 = Et, R^2 = Me), mp 76–77°C (lit. (1) mp 76°C), were removed by filtration. The product was identical (ir (Nujol): 1730 cm^{-1}; nmr) with authentic material prepared according to Carrington (1).

Reaction of 1-Methylamino-1-cyanocyclohexane (1; R^1R^2 = $(CH_2)_5$) with Carbon Disulfide

A solution of 1-methylamino-1-cyanocyclohexane (30 g) and carbon disulfide (28 g) was heated and stirred under reflux at 50°C for 24 h. On removal of carbon disulfide, a crystalline product separated. It was removed by filtration and washed with petroleum ether (30–60°C) to yield 9.5 g of crude 5-imino-5,5-cyclopentamethylene-3-methylthiazolidine-2-thione (**3**; R^1R^2 = $(CH_2)_5$), mp 122–125°C.

After further evaporation of solvent, the residue was stirred under reflux with 28 g of carbon disulfide for another 24 h giving a further 5 g of the imine **3** ($R^1R^2 = (CH_2)_5$). Since the ir of the residue of the reaction still showed a nitrile band, it was stirred under reflux at 50°C for a third 24 h period. An additional 2.9 g of crude imine **3** ($R^1R^2 = (CH_2)_5$) was obtained, making a total yield of 17.4 g (38%); after recrystallization from methanol, mp 126–128°C (lit. (1) mp 125°C); ir (Nujol): 3195 (NH), 1640, 1610 (C=N) cm^{-1}; ^1H nmr ($CDCl_3$) δ: 1.5–1.9 (m, 10H), 3.33 (s, 3H), 9.50 (s, 1H).

Extraction of the residue with boiling petroleum ether (30–60°C) removed 0.1 g of crude *N*-methylimine **5** (R^1R^2 = $(CH_2)_5$). The residue on standing deposited yellow crystals (1.7 g) which, when recrystallized from alcohol, yielded 0.95 g (2.2%) of 5,5-pentamethylene-2,4-dithiohydantoin, mp 274–275°C (lit. (2) mp 276–278°C); ir (Nujol): 3220, 3160 (NH), 1530 (2,4-dithiohydantoin) cm^{-1}; ^1H nmr ($CDCl_3$) δ: 1.57 (s, 10H), 10.9 (s, 1H), 13.0 (s, 1H), identical with authentic material (2).

After removal of the dithiohydantoin, dilution of the residue with 50 mL of methanol resulted in the separation of a crystalline product (2.8 g), which recrystallized from methanol to yield 3-methyl-4,4-pentamethylene-5-methyliminothiazolidine-2-thione (**5**; R^1R^2 = $(CH_2)_5$) (2.1 g, 4.3%), mp 110–112°C; ir (Nujol): 1650, 1660 (C=N) cm^{-1}; ^1H nmr ($CDCl_3$) δ: 1.6–1.8 (m, 10H), 3.17 (s, 3H), 3.33 (s, 3H). *Anal.* calcd. for $C_{10}H_{16}N_2S_2$: C 52.59, H 7.06, N 12.27; found: C 52.67, H 7.23, N 12.23.

Can. J. Chem. Downloaded from www.nrcresearchpress.com by 210.87.254.5 on 09/06/12
For personal use only.

Direct Preparation of Yellow Complexes from Imines 3 and 2,4-Dithiohydantoins 9

Warm aqueous methanol solutions containing imine **3** and 2,4-dithiohydantoin **9** deposited the complexes C-1, C-2, C-3, C-4, and C-5 in 80–90% yield on cooling. C-1 and C-2 proved identical (ir, nmr) to the compounds described above; C-3, C-4, and C-5 are described in Table 1.

Acknowledgements

The financial support of the Natural Sciences and Engineering Research Council of Canada is gratefully acknowledged.

1. H. C. CARRINGTON. J. Chem. Soc. 1619 (1948).
2. H. C. CARRINGTON. J. Chem. Soc. 681 (1947).
3. D. J. PASTO and C. R. JOHNSON. Organic structure determination. Prentice-Hall, Englewood Cliffs, NJ. 1969. p. 463.
4. J. T. EDWARD. The chemistry of organic sulfur compounds. Vol. 2. *Edited by* C. Y. Meyers and N. Kharasch. Pergamon Press, Oxford. 1966. p. 287.
5. J. T. EDWARD and I. C. WANG. Can. J. Chem. **40**, 399 (1962).
6. J. TAILLADES and A. COMMEYRAS. Tetrahedron, **30**, 127 (1974); **30**, 2493 (1974); **30**, 3407 (1974).

Can. J. Chem. Downloaded from www.nrcresearchpress.com by 210.87.254.5 on 09/06/12
For personal use only.

Oxidation products of arachidonic acid. V. The synthesis of 8*R*,11*R*,15(*R* and *S*)-trihydroxy-9*S*,12*S*-oxyeicosa-5*Z*,13*E*-dienoic acids

GEORGE JUST AND HUNSEUNG OH

Department of Chemistry, McGill University, 801 Sherbrooke St. W., Montreal, P.Q., Canada H3A 2K6

Received April 13, 1981

GEORGE JUST and HUNSEUNG OH. Can. J. Chem. **59**, 2729 (1981).

The synthesis of the title compounds is described. It is shown that β-nitro ketals are versatile intermediates for the synthesis of prostaglandin-type C-13 – C-20 side-chains.

GEORGE JUST et HUNSEUNG OH. Can. J. Chem. **59**, 2729 (1981).

La synthèse des composés sus-mentionnés est décrite et l'utilité des β-nitrocétales en tant qu'intermédiaires dans l'introduction de chaînes aliphatiques correspondantes au segment C-13 – C-20 des prostaglandines a été démontrée.

We wish to report the synthesis of title compounds **1** and **2** (1), which confirm the structure proposed for an oxidation product of arachidonic acid by Pace-Asciak and Wolfe (2), without, however, specifying its stereochemistry, since the R_f-values of **1** and **2** are different from that of the natural product.[1]

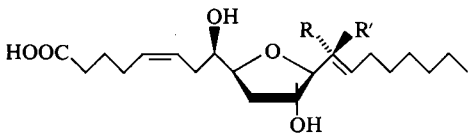

1 R = H, R′ = OH
2 R = OH, R′ = H

The strategy involved in the synthesis was to condense a readily available and suitably protected aldehyde such as ***6a*** with fragment **17**. The nitro function of **17** not only serves to generate the anion which adds to the aldehyde to give a nitro alcohol, but, after dehydration, it also serves as part of a nitro olefin which functions as Michael-acceptor for the tetrahydrofuran formation. Finally, being β to a potential ketone, its β-elimination then gives an α,β-unsaturated ketone, the reduction of which, followed by deblocking of protecting groups, provides title compounds **1** and **2**.

As a model compound, we used the readily available furanose **3** (3), which was transformed by the action of ethanethiol – zinc chloride to dithioacetal **4**, and hence to the corresponding isopropylidene compound **5**. Mercuric ion mediated hydrolysis then gave aldehyde ***6a*** in 75% yield, based on **3**.

Condensation of β-nitro ketal **7** and aldehyde ***6a*** in DMF (4), using diisopropylamine as base, gave a mixture of nitro alcohols **8** and **10** which were separable as their acetates **9** and **11**. Both acetates **9** and **11** were treated with anhydrous potassium carbonate and dicyclohexyl-18-crown-6 in benzene to give nitro olefin **12**. Selective hydrolysis of the isopropylidene group of **12** under various acidic reaction conditions failed because of the instability of dimethyl ketal to acid.

Treatment of nitro acetate **9** with methanolic *p*-toluenesulfonic acid gave bicyclic ketal **15**, probably via monocyclic ketal **13**. In contrast, the same acid treatment of the isomeric nitro acetate **11** gave a more polar product (tlc), which probably had the monocyclic ketal structure **14**, and which gave **16** upon reaction with triethylamine or during work-up ($NaHCO_3$). The structures of **15** and **16** were proven by their ^{1}Hmr, ir, and mass spectra.

These results can best be rationalized in the following manner. It is quite likely that the two nitro alcohols **8** and **10** have the two *threo*-configurations, since the addition ***6a*** + **7** → **8** + **10** is probably reversible, so that the most stable configurations permitting hydrogen bonding of the OH and NO_2 groups should be as depicted.

If these representations are correct, then the acid treatment of acetate **9** derived from **8** should give a mixture of conformers in which conformer **13** is populated to a considerable extent. Extrusion of the methoxy group at C-15, followed by cyclization, would then give **15**. In the case of acetate **11** derived from nitro alcohol **10**, a similar acid catalyzed cyclization would lead to a tetrahydropyran in which all secondary ring-substituents are equatorial. The other conformation being of little importance, no further acid-catalyzed cyclization takes place. Base treatment then results in elimination of the elements of acetic acid and formation of a nitro olefin which then cyclizes to bicyclic ketal **16**. Attempts to transform **16**, which has the carbon frame-work of the desired final product, to ***23a***, failed. Whereas the stereochemical assignments of **10**, **11**, **14**, and **16** are probably correct, is it quite

[1]We wish to thank Dr. C. Pace-Asciak for the chromatographic comparisons.

0008-4042/81/182729-08$01.00/0
©1981 National Research Council of Canada/Conseil national de recherches du Canada

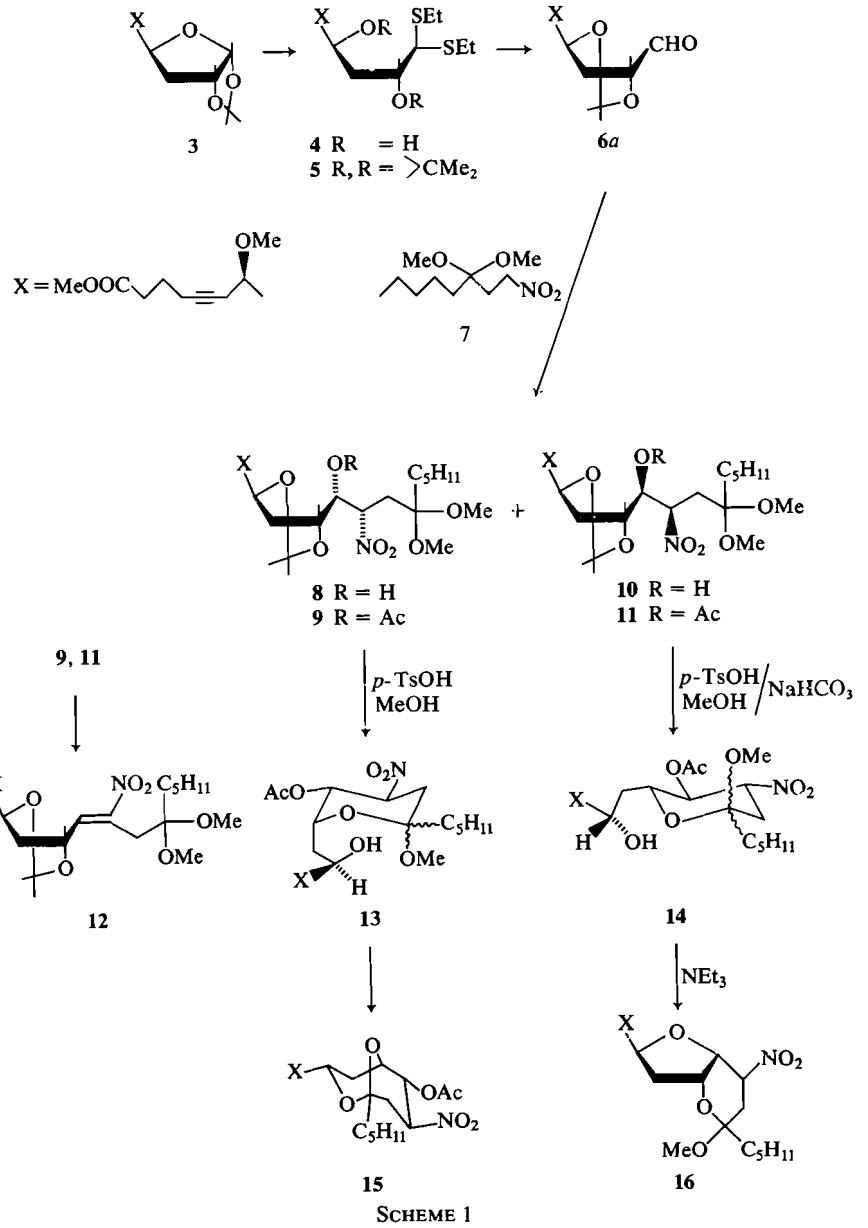

SCHEME 1

possible that the nitro and hydroxyl or acetate groups of **8**, **9**, **13**, and **15** have one of the *erythro*-configurations. A search of the literature revealed that little is known on the configuration of nitro alcohols derived from condensation of nitroalkanes with aldehydes (5).

Since we could not cleave the isopropylidene group in the presence of a dimethyl ketal in compounds of type **12**, the condensation of **6***a* was repeated with β-nitro ketal **17**. The resulting nitro alcohol **18***a* was acetylated, and nitro acetate **19***a* treated with anhydrous potassium carbonate and dicyclohexyl-18-crown-6 to give nitro olefin **20***a*. Mild acid hydrolysis of **20***a* gave the corresponding diol **21***a*, which, upon treatment with triethylamine, gave tetrahydrofuran **22***a* as a mixture of isomers. Acid hydrolysis of the ethylene ketal function gave nitro ketones **23***a*. Upon treatment with triethylamine, both isomers of **23***a* were transformed to one α,β-unsaturated ketone having structure **24***a*, which was characterized as its acetate **25***a*. This leads one to suspect that **23***a* was a mixture of isomers at C-13. Had the isomers of **23***a* differed because of difference of stereo-

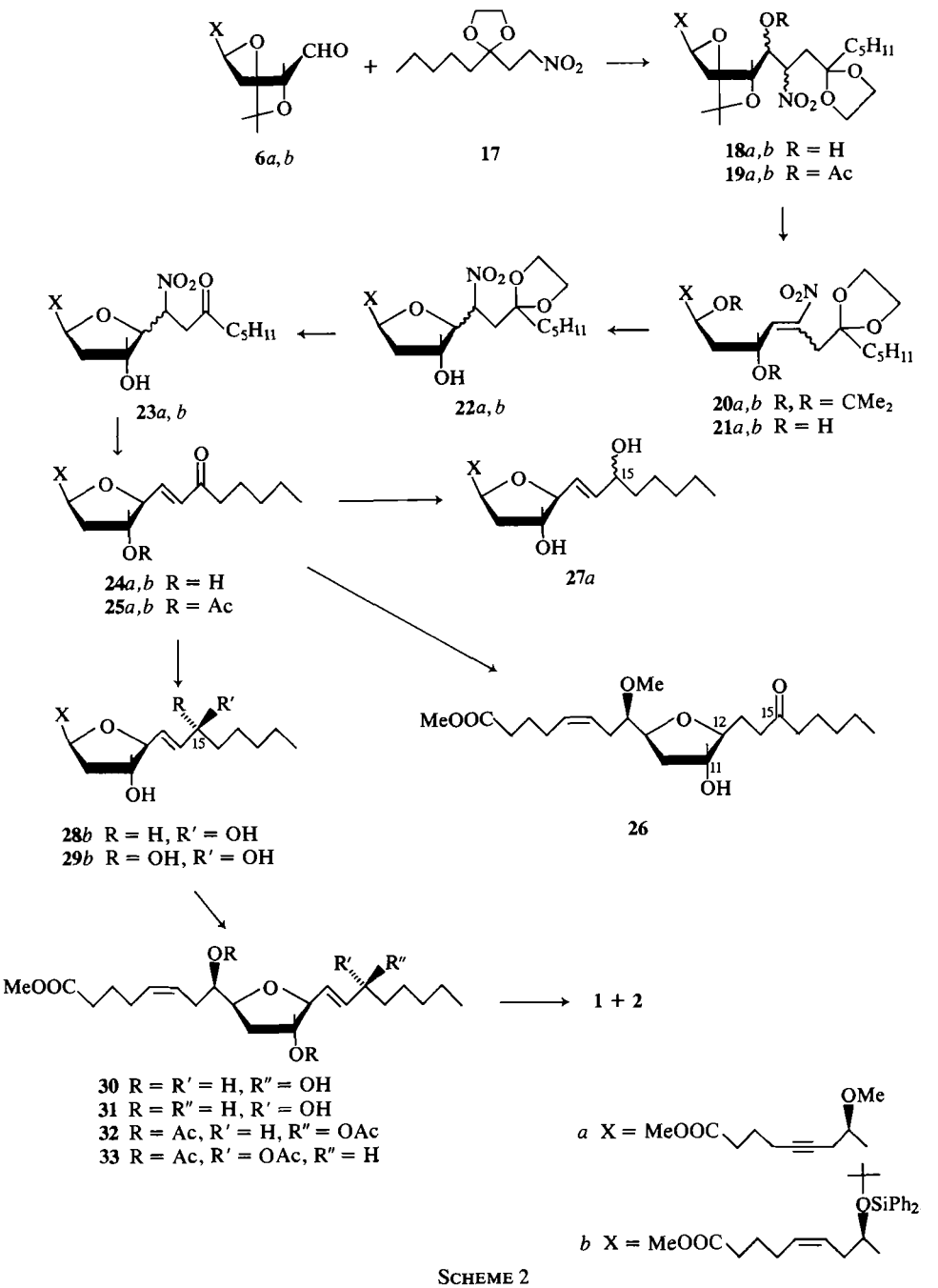

SCHEME 2

chemistry at C-12, or C-12 and C-13, then acid treatment of **22***a* should have led to compounds of type **16**. In order to establish unambiguously the stereochemistry at C-12, **24***a* was hydrogenated with H_2/5% Pd–C to give **26**, which was treated under the same reaction conditions (*p*-TsOH/MeOH, 20°C) as for the transformation of **10** to **16**. No cyclic ketalization between the hydroxyl and the free carbonyl groups was observed, thus proving unambiguously that the structure assigned to **24***a* is correct.

Sodium borohydride reduction of **24***a* gave **27***a*, contaminated with products of 1,4-reduction, as a mixture of isomers at C-15, which were not separable.

Having accomplished the conversion of **6***a* to

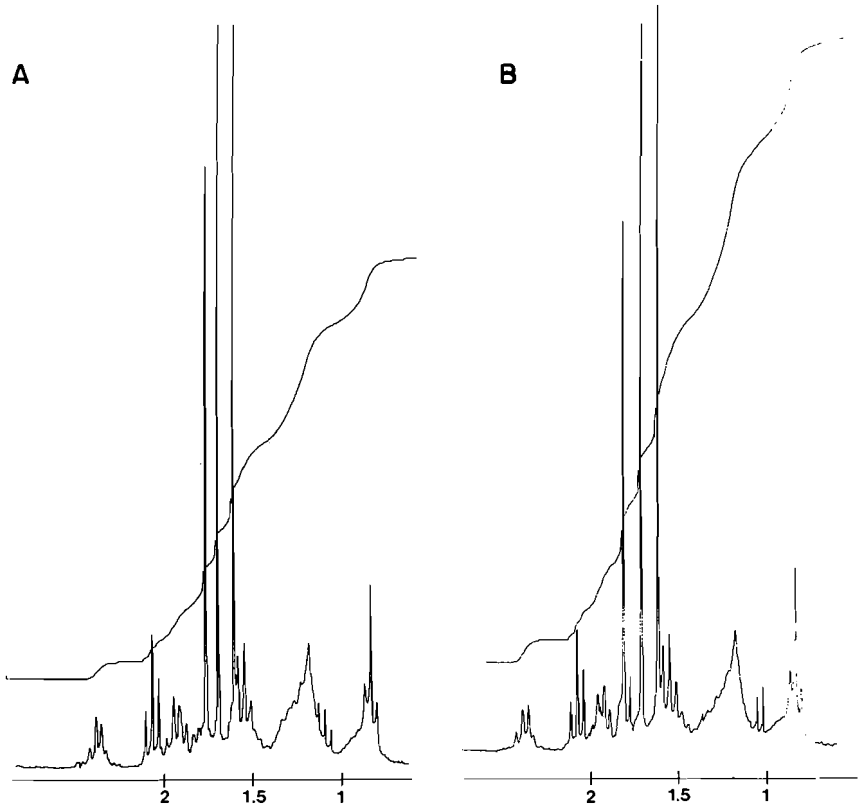

FIG. 1. 200 MHz ^{1}Hmr spectra of 8*R*,11*R*,15*S*-triacetate **32** (A) and 8*R*,11*R*,15*R*-triacetate **33** (B), betwen 0.6 and 2.6 ppm, in benzene-d_6.

27*a*, the sequence was repeated with aldehyde **6***b* (3). Except for minor details and the fact that **22***b* appeared to be one isomer only, the sequence of **24***b* paralleled the one discussed, and is the only one described in the Experimental.

Reduction of **24***b* by diisobornyloxyaluminum isopropoxide (6) gave **28***b* and **29***b* as a mixture of isomers, without contamination by 1,4-reduction products. They were cleanly separable by flash chromatography (7). Removal of the silyl protecting group of both isomers **28***b* and **29***b* by tetra-*n*-butylammonium fluoride gave the corresponding trihydroxy methyl esters **30** and **31**, respectively. They were virtually indistinguishable by mass spectrometry, ir, or ^{1}Hmr. However, the ^{1}Hmr spectra of their acetates **32** and **33** were clearly different and are reproduced in Fig. 1.

Using the method developed in our laboratory (8), the more polar fraction **30** was shown to have the *S*, and the less polar **31** the *R* configuration at C-15. Gas chromatography – mass spectra of tris-trimethylsilyl ether methyl esters of **30** and **31** showed mass spectra identical to that reported by Pace-Asciak and Wolfe (2), except for some minor differences in intensity of some peaks. The ^{1}Hmr (200 MHz) and ir spectra were all consistent with the structure proposed.

Base hydrolysis of trihydroxy methyl ester **30** gave the corresponding trihydroxy carboxylic acid **1**. Here again, the gc – mass spectrum of its tris-trimethylsilyl ether trimethylsilyl ester was identical to that of the natural product isolated by Pace-Asciak and Wolfe (2). This synthesis therefore proves the structure of **1** proposed by Pace-Asciak and Wolfe.

Experimental

Thin-layer chromatography (tlc) was performed on Merck Silica Gel 60 F_{254} aluminum-backed plates. Flash chromatography was done on Woelm Silica (32–63 μ). Melting points (mp) were measured on a Gallenkamp block and are uncorrected, unless specified otherwise. The ^{1}Hmr spectra were recorded on Varian T-60, T-60A, and where noted, XL-200 spectrometers. Infrared (ir) spectra were recorded on Perkin Elmer 257 and 297 spectrophotometers. Mass spectra (ms) were obtained on HP 5984A or LKB 9000 spectrometers, in the direct inlet mode unless indicated otherwise. Elemental analyses were performed by Midwest Microlab Ltd., Indianapolis.

Dihydroxy Dithioacetal **4**

A solution of acetonide **3** (0.978 g, 3 mmol) in ethanethiol

(3.5 mL) was cooled to −15°C in an ice–salt bath. To this was added anhydrous $ZnCl_2$ (1.4 g, 10 mmol). The flask was stoppered and allowed to stand for 30 min at −15°C. The ethanethiol was removed under diminished pressure, keeping temperature below 0°C, and the foamy residue was dissolved in ethyl acetate (30 mL). To this was added 5% aqueous $NaHCO_3$ solution (20 mL), and the white precipitate was filtered off. After separation of the organic layer, the aqueous layer was saturated with NaCl and further extracted with ethyl acetate (2 × 15 mL). The combined extracts were dried ($MgSO_4$) and concentrated to give dihydroxy dithioacetal **4** as a yellowish oil in quantitative yield; $[\alpha]_D^{23}$ −2.6° (*c* 2.65, $CHCl_3$); ir (film) ν_{max}: 3440 (OH), 2920, 1730 ($COOCH_3$) cm^{-1}; ^{1}Hmr ($CDCl_3$) δ: 1.27 (t, 6H, *J* = 7 Hz, 2 SCH_2CH_3), 1.50–2.60 (m, 10H, 5 CH_2), 2.70 (q, 4H, *J* = 7 Hz, 2 SCH_2), 3.07–4.20 (m, 4H, 3 CH—O, SCHS), 3.44 (s, 3H, OCH_3), 3.67 (s, 3H, $COOCH_3$) ppm; ms (70 eV, 40°C), *m/e* (rel. int. %): 374 (0.3, $M^{+\cdot} - H_2O$), 345 (2.0, $M^{+\cdot} - CH_3OH - CH_3^{\cdot}$), 313 (3.8, 374 − $SC_2H_5^{\cdot}$), 257 (56.5, $M^{+\cdot}$ − 135), 239 (36.4, 257 − H_2O), 221 (7.4, 257 − $2H_2O$), 135 (86.2, $CH(SC_2H_5)_2^+$), 75 (100).

Isopropylidene Dithioacetal 5

A solution of dihydroxy dithioacetal **4** (588 mg, 1.5 mmol) and 2,2-dimethoxypropane (2 mL) in acetone (40 mL) containing a catalytic amount of *p*-toluenesulfonic acid was stirred for 30 min at room temperature. The acetone was evaporated under reduced pressure and the residual oil was dissolved in ether (20 mL). The ether solution was washed with 5% aqueous $NaHCO_3$ (2 × 20 mL), water (2 × 10 mL) and brine, dried ($MgSO_4$), and evaporated *in vacuo* to give isopropylidene dithioacetal **5** as a colorless oil in quantitative yield; ir (film) ν_{max}: 2930, 1740 ($COOCH_3$), 1437, 1380 cm^{-1}; ^{1}Hmr ($CDCl_3$) δ: 1.25 (t, 6H, *J* = 7.5 Hz, 2 SCH_2CH_3), 1.38 and 1.43 (s and s, 6H, CMe_2), 1.62–2.63 (m, 10H, 5 CH_2), 2.74 (q, 4H, *J* = 7.5 Hz, 2 SCH_2), 3.02–4.29 (m, 4H, 3 CH—O, SCHS), 3.44 (s, 3H, OCH_3), 3.65 (s, 3H, $COOCH_3$) ppm; ms (70 eV, 52°C), *m/e* (rel. int. %): 432 (1.1, $M^{+\cdot}$), 371 (1.0, $M^{+\cdot} - SC_2H_5^{\cdot}$), 357 (7.8, $M^{+\cdot} - CH_3COOCH_3$), 297 (96.3, $M^{+\cdot}$ − 135), 293 (2.9, $M^{+\cdot} - CH_2C{\equiv}C(CH_2)_3COOCH_3^{\cdot}$), 265 (3.8, 297 − CH_3OH), 239 (34.6), 207 (44.8), 147 (60.8), 135 (32.7, $CH(SC_2H_5)_2^+$), 45 (100).

Aldehyde 6a

To a solution of dithioacetal **5** (216 mg, 0.50 mmol) in acetone (20 mL) and water (2 mL) were added HgO (976 mg, 4.5 mmol) and $HgCl_2$ (406 mg, 1.5 mmol). The heterogeneous mixture was stirred for 3 h at room temperature, and was filtered into 5% aqueous $NaHCO_3$ (20 mL); the HgO cake was washed with acetone (3 × 5 mL). Filtration and concentration to about 20 mL, followed by extraction with $CHCl_3$ (3 × 20 mL), and washing with 5% aqueous KI solution (3 × 10 mL) and water (20 mL), gave, after drying ($MgSO_4$) and evaporation *in vacuo*, crude ***6a***. Purification by flash chromatography, using petroleum ether – ethyl acetate (5:3) as eluant, afforded 123 mg (75%) of aldehyde ***6a*** as a colorless oil; $[\alpha]_D^{23}$ 11.5° (*c* 5.7, $CHCl_3$); ir (film) ν_{max}: 2990, 2935, 2820, 1736 ($COOCH_3$, CH═O), 1436, 1380 cm^{-1}; ^{1}Hmr ($CDCl_3$) δ: 1.47 (s, 6H, CMe_2), 1.60–2.64 (m, 10H, 5 CH_2), 3.03–3.37 (m, 1H, CH—O), 3.45 (s, 3H, OCH_3), 3.68 (s, 3H, $COOCH_3$), 3.85–4.50 (m, 2H, 2 CH—O), 9.37 (s, 1H, CH═O) ppm; ms (70 eV, 41°C), *m/e* (rel. int. %): 311 (3.4, $M^{+\cdot} - CH_3^{\cdot}$), 297 (3.1, $M^{+\cdot} - CHO^{\cdot}$), 239 (2.0, $M^{+\cdot} - CH_2CH_2COOCH_3^{\cdot}$), 183 (7.8, $CH(OCH_3)CH_2C{\equiv}C(CH_2)_3COOCH_3^+$), 143 (25.7), 129 (47.3), 85 (45.1), 59 (46.7, $COOCH_3^+$), 45 (100).

Nitro Alcohols 8 and 10

A solution of aldehyde ***6a*** (326 mg, 1 mmol), β-nitro dimethyl ketal **7** (285 mg, 1.3 mmol), and diisopropylamine (152 mg, 1.5 mmol) in dry dimethylformamide (8 mL) was stirred overnight at room temperature. Water (100 mL) was added to the reaction mixture and the product was extracted with ether (3 × 20 mL). The combined extracts were washed with water (2 × 30 mL) and brine, dried ($MgSO_4$), and evaporated under reduced pressure to give crude adducts **8** and **10**. Purification by flash chromatography, using petroleum ether – ethyl acetate (7:3) as eluant, afforded 490 mg (90%) of nitro alcohols **8** and **10**, which were not separable, as a colorless oil; ir (film) ν_{max}: 3460 (OH), 2990, 2955, 2870, 1740 ($COOCH_3$), 1555 (NO_2), 1380 cm^{-1}; ^{1}Hmr ($CDCl_3$) δ: 0.63–2.67 (m, 29H, 10 CH_2, 3 CH_3), 2.87–4.20 (m, 4H, 4 CH—O), 3.08 and 3.12 (s and s, 6H, $C(OCH_3)_2$), 3.40 (s, 3H, OCH_3), 3.63 (s, 3H, $COOCH_3$), 4.60–5.03 (m, 1H, CH—NO_2) ppm.

Nitro Acetates 9 and 11

To a solution of nitro alcohols **8** and **10** (327 mg, 0.6 mmol) in anhydrous ether (10 mL) were added acetic anhydride (73 mg, 0.72 mmol), triethylamine (85 mg, 0.84 mmol), and 4-dimethylaminopyridine (15 mg, 0.12 mmol). After 30 min at room temperature, the solution was washed with 0.1 *N* aqueous HCl (3 mL), 5% aqueous $NaHCO_3$ (2 × 5 mL), and water (2 × 10 mL), dried ($MgSO_4$), and concentrated under reduced pressure to give a 1:1 mixture of nitro acetates **9** and **11** with R_f = 0.31 and 0.40, respectively, in petroleum ether – ethyl acetate (3:1), in quantitative yield. Their spectroscopic data were virtually identical; ir (film) ν_{max}: 2995, 2960, 1758 and 1742 ($COOCH_3$, $OCOCH_3$), 1560 (NO_2), 1370, 1220 cm^{-1}; ^{1}Hmr ($CDCl_3$) δ: 0.67–2.60 (m, 23H, 10 CH_2, CH_3), 1.37 and 1.41 (s and s, 6H, CMe_2), 2.07 (s, 3H, $OCOCH_3$), 3.03 and 3.07 (s and s, 6H, $C(OCH_3)_2$), 3.34 (s, 3H, OCH_3), 3.61 (s, 3H, $COOCH_3$), 2.90–4.13 (m, 3H, 3 CH—O), 4.80–5.20 (m, 2H, C*H*OAc, C*H*—NO_2) ppm; ms (70 eV, 61°C), *m/e* (rel. int. %): 572 (0.8, $M^{+\cdot} - CH_3^{\cdot}$), 556 (0.4, $M^{+\cdot} - OCH_3^{\cdot}$), 540 (1.3, $M^{+\cdot} - HNO_2$), 516 (3, $M^{+\cdot}$ − 71), 469 (6.3, 540 − 71), 458 (2.1, 516 − $CH_3^{\cdot}$ − $COCH_3^{\cdot}$), 448 (1.3, $M^{+\cdot}$ − 139), 404 (2.8, $M^{+\cdot}$ − 183), 346 (5.6, 404 − $CH_3^{\cdot}$ − $COCH_3^{\cdot}$), 314 (14.8, 404 − HNO_2 − $C_3H_7^{\cdot}$), 297 (12.7, $M^{+\cdot}$ − CH(OAc) − $CH(NO_2)CH_2C(OCH_3)_2C_5H_{11}^{\cdot}$), 286 (2.2, 404 − HNO_2 − 71), 254 (25.5, 314 − CH_3COOH), 183 (7.0, $CH(OCH_3)CH_2C{\equiv}C(CH_2)_3COOCH_3^+$), 145 (100, $C(OCH_3)_2C_5H_{11}^+$), 139 (8.0, $CH_2C{\equiv}C(CH_2)_3COOCH_3^+$), 71 (32, $C_5H_{11}^+$), 43 (88.7, $C_3H_7^+$, $COCH_3^+$).

Nitro Olefin 12

A mixture of nitro acetates **9** and **11** (117 mg, 0.2 mmol), powdered anhydrous K_2CO_3 (138 mg, 1 mmol), and a catalytic amount of dicyclohexyl-18-crown-6 in dry benzene (3 mL) was stirred for 5 h at 75°C under N_2 atmosphere. The solid K_2CO_3 was filtered off and, after evaporation of the solvent, the residual oil was purified by flash chromatography, using petroleum ether – ethyl acetate (8:2) as eluant, to afford 95 mg (90%) of nitro olefin **12** as a mixture of *E*- and *Z*-olefins; ir (film) ν_{max}: 2990, 2950, 1740 ($COOCH_3$), 1534 (NO_2), 1200 cm^{-1}; ^{1}Hmr ($CDCl_3$) δ: 0.67–2.63 (m, 27H, 9 CH_2, 3 CH_3), 3.10 (bs, 2H, C(NO_2)—CH_2), 3.14 and 3.17 (s and s, 6H, $C(OCH_3)_2$), 3.42 (s, 3H, OCH_3), 3.65 (s, 3H, $COOCH_3$), 3.73–4.37 (m, 2H, 2 CH—O), 4.76 (ddd, 1H, *J* = 3, 8, 11 Hz, C═CHC*H*—O), 5.72 and 6.68 (d and d, 1H, *J* = 8 Hz, CH═C) ppm; ms (70 eV, 69°C), *m/e* (rel. int. %): 480 (0.2, $M^{+\cdot} - HNO_2$), 456 (0.6, $M^{+\cdot}$ − 71), 438 (0.3, $M^{+\cdot} - NO_2^{\cdot}$ − $C_3H_7^{\cdot}$), 344 (0.5, $M^{+\cdot}$ − 183), 286 (5.7, 344 − $CH_3^{\cdot}$ − $C_3H_7^{\cdot}$), 183 (1.7, $CH(OCH_3)CH_2C{\equiv}C(CH_2)_3COOCH_3^+$), 145 (100, $C(OCH_3)_2C_5H_{11}^+$), 139 (1.6, $CH_2C{\equiv}C(CH_2)_3COOCH_3^+$), 71 (8.3, $C_5H_{11}^+$), 43 (9.3, $C_3H_7^+$, $COCH_3^+$). *Anal.* calcd. for $C_{27}H_{45}O_9N$: C 61.48, H 8.54, N 2.66; found: C 61.70, H 8.79, N 2.39.

Bicyclic Ketal 15

A solution of more polar nitro acetate **9** (45 mg, 0.077 mmol, R_f = 0.31 in 3:1 petroleum ether – ethyl acetate) in methanol (2 mL, dried over molecular sieves) was stirred overnight at room

temperature with a catalytic amount of *p*-toluenesulfonic acid. The acid was neutralized with 5% aqueous $NaHCO_3$ solution and the methanol removed under reduced pressure. The residue was taken up in ether (20 mL), which was then washed with water (2 × 10 mL). The ether layer was dried ($MgSO_4$) and concentrated under reduced pressure. Purification by flash chromatography, using petroleum ether – ethyl acetate (3:1) as eluant, gave 27 mg (73%) of bicyclic ketal **15** as a colorless oil; ir (film) ν_{max}: 2950, 2870, 1740 ($COOCH_3$ and $OCOCH_3$), 1555 (NO_2), 1440, 1375, 1230 cm^{-1}; ^{1}Hmr 200 MHz ($CDCl_3$) δ: 0.91 (t, 3H, J = 7 Hz, CH_3), 1.13–2.55 (m, 20H, 10 CH_2), 2.07 (s, 3H, $OCOCH_3$), 3.28 (dt, 1H, J = 6, 6 Hz, C*H*—OCH_3), 3.43 (s, 3H, OCH_3), 3.68 (s, 3H, $COOCH_3$), 4.02 (dt, 1H, J = 4, 12 Hz, CH—O), 4.45–4.58 (m, 1H, CH—O), 5.10–5.25 (m, 1H, CH—NO_2), 5.38–5.47 (m, 1H, C*H*OAc) ppm; ms (70 eV, 107°C), *m/e* (rel. int. %): 437 (8.8, $M^{+\cdot} - NO_2^{\cdot}$), 377 (2.4, $M^{+\cdot} - NO_2^{\cdot} - CH_3COOH$), 345 (4.4, 377 – CH_3OH), 300 (27.2, $M^{+\cdot}$ – 183), 253 (9.5, 300 – HNO_2), 252 (8.8, $M^{+\cdot} - CH_3COOH - CH_3OH$ – 139), 240 (8, 300 – CH_3COOH), 237 (21.7, $M^{+\cdot} - CH_3COOH - HNO_2$ – 139), 209 (16.6, 252 – $C_3H_7^{\cdot}$), 196 (16.4, 253 – $C_4H_9^{\cdot}$), 193 (66.4, 253 – CH_3COOH), 183 (21, $CH(OCH_3)CH_2$-$C{\equiv}C(CH_2)_3COOCH_3^+$), 139 (8.6, $CH_2C{\equiv}C(CH_2)_3COOCH_3^+$), 99 (100), 71 (76.8, $C_5H_{11}^+$), 43 (67.7, $C_3H_7^+$, $COCH_3^+$); CI (110°C): 484 (24.5, MH^+), 406 (100, $MH^+ - HNO_2 - OCH_3^{\cdot}$), 377 (65.5, $MH^+ - HNO_2 - CH_3COOH$).

Bicyclic Ketal 16

A solution of less polar nitro acetate **11** (45 mg, 0.077 mmol, R_f = 0.40 in 3:1 petroleum ether – ethyl acetate) in methanol (2 mL, dried over molecular sieves) was stirred overnight at room temperature with a catalytic amount of *p*-toluenesulfonic acid. After neutralization with 5% aqueous $NaHCO_3$ solution and evaporation of the methanol, the residue was partitioned between ether (10 mL) and water (10 mL). The ether layer was dried ($MgSO_4$) and to this was added triethylamine (0.5 mL). The resulting solution was stirred overnight at room temperature. After the usual work-up, the crude product was purified by flash chromatography, using petroleum ether – ethyl acetate (3:1) as eluant, to afford 17 mg (50%) of bicyclic ketal **16**; ir (film) ν_{max}: 2955, 2870, 1738 ($COOCH_3$), 1553 (NO_2), 1385, 1040 cm^{-1}; ^{1}Hmr 200 MHz ($CDCl_3$) δ: 0.92 (t, 3H, J = 7 Hz, CH_3), 1.18–2.36 (m, 18H, 9 CH_2), 2.44 (t, 3H, J = 7 Hz, $COCH_2$), 3.20 (s, 3H, OCH_3), 3.47 (s, 3H, OCH_3), 3.44–3.60 (m, 1H, CH—O), 3.68 (s, 3H, $COOCH_3$), 4.21–4.30 (m, 1H, CH—O), 4.36–4.50 (m, 1H, CH—O), 4.52–4.62 (m, 1H, CH—O), 4.86–5.02 (m, 1H, CH—NO_2) ppm; ms (70 eV, 85°C), *m/e* (rel. int. %): 377 (8.2, $M^{+\cdot} - HNO_2 - OCH_3^{\cdot}$), 345 (2.8, 377 – CH_3OH), 337 (5.9, $M^{+\cdot} - HNO_2$ – 71), 269 (9.9, $M^{+\cdot} - HNO_2$ – 139), 252 (3.1, $M^{+\cdot} - CH_2{=}CHNO_2 - C_5H_{11}COOCH_3$), 237 (21.7, 269 – CH_3OH), 225 (3.4, $M^{+\cdot} - HNO_2$ – 183), 223 (7.6, 269 – $OCH_3^{\cdot} - CH_3^{\cdot}$), 194 (9.3, 225 – $OCH_3^{\cdot}$), 193 (9.6, 225 – CH_3OH), 183 (64.2, $CH(OCH_3)CH_2C{\equiv}C(CH_2)_3COOCH_3^+$), 181 (100, 269 – $OCH_3^{\cdot} - C_4H_9^{\cdot}$), 151 (37.7, 183 – CH_3OH), 139 (16.3, $CH_2C{\equiv}C(CH_2)_3COOCH_3^+$), 71 (38, $C_5H_{11}^+$); CI (80°C): 456 (27.8, MH^+), 377 (100, $MH^+ - HNO_2 - CH_3OH$).

β-*Nitro Ethylene Ketal 17*

A solution of 1-nitro-3-octanone (3.46 g, 0.02 mol), ethylene glycol (1.49 g, 0.024 mol), and *p*-toluenesulfonic acid (20 mg) in benzene (20 mL) was refluxed overnight using a Dean-Stark apparatus. The resulting solution was washed with 5% aqueous $NaHCO_3$ (15 mL) and brine, dried, and evaporated under reduced pressure. Distillation gave 3.34 g (77%) of β-nitro ethylene ketal **17** as a colorless oil (bp 88–90°C/0.02 Torr); ir (film) ν_{max}: 2950, 2870, 1552 (NO_2), 1380 cm^{-1}; ^{1}Hmr ($CDCl_3$) δ: 0.67–1.80 (m, 11H, 4 CH_2, CH_3), 2.40 (t, 2H, J = 7 Hz, C$H_2$$CH_2NO_2$), 3.92 (s, 4H, OCH_2CH_2O), 4.40 (t, 2H, J = 7 Hz, CH_2NO_2) ppm.

Nitro Alcohol **18**b

A solution of aldehyde **6***b* (1.66 g, 3 mmol), β-nitro ethylene ketal **17** (0.847 g, 3.90 mmol), and diisopropylamine (0.455 g, 4.50 mmol) in dry dimethylformamide (25 mL) was stirred overnight at room temperature. Water (250 mL) was added to the reaction mixture and the product was extracted with ether (3 × 60 mL). The combined extracts were washed with water (2 × 100 mL) and brine, dried ($MgSO_4$), and concentrated under reduced pressure to yield crude adduct. Purification by flash chromatography, using petroleum ether – ethyl acetate (2:1) as eluant, afforded 2.08 g (90%) of nitro alcohol **18***b* as a colorless oil; ir (film) ν_{max}: 3450 (OH), 3060, 3040, 2930, 2850, 1730 ($COOCH_3$), 1545 (NO_2) cm^{-1}; ^{1}Hmr ($CDCl_3$) δ: 0.67–3.10 (m, 23H, 10 CH_2, CH_3), 1.08 (s, 9H, *t*-Bu), 1.30 (s, 6H, CMe_2), 3.60 (s, 3H, $COOCH_3$), 3.87 (bs, 4H, OCH_2CH_2O), 3.40–4.04 (m, 4H, 4 CH—O), 4.63–5.10 (m, 1H, CH—NO_2), 5.12–5.40 (m, 2H, CH=CH), 7.13–7.80 (m, 10H, 2 C_6H_5) ppm; ms (20 eV, 95°C), *m/e* (rel. int. %): 608 (0.7, $M^{+\cdot} - 143 - H_2O$), 495 (26.5, $CH(CO)(OSi(t\text{-}Bu)Ph_2)CH_2CH{=}CH(CH_2)_3COOCH_3^+$), 409 (12.7, $CH(OSi(t\text{-}Bu)Ph_2)CH_2CH{=}CH(CH_2)_3COOCH_3^+$), 381 (64.2, $CH(CHO)(OSiPh_2)CH_2CH{=}CH(CH_2)_3COOCH_3^+$), 353 (7.3, 381 – CO), 199 (17.3, 381 – $SiPh_2^{\cdot}$), 143 (100, $C(OCH_2$-$CH_2O)C_5H_{11}^+$), 141 (8.9, $CH_2CH{=}CH(CH_2)_3COOCH_3^+$), 71 (10, $C_5H_{11}^+$).

*Nitro Acetate 19*b

To a solution of nitro alcohol **18***b* (1.02 g, 1.33 mmol) in anhydrous ether (20 mL) were added acetic anhydride (0.163 g, 1.60 mmol), triethylamine (0.188 g, 1.86 mmol), and 4-dimethylaminopyridine (0.033 g, 0.27 mmol). After 30 min at room temperature, the solution was washed with 0.1 *N* aqueous HCl (20 mL), 5% aqueous $NaHCO_3$ (2 × 10 mL), and water (1 × 10 mL), dried ($MgSO_4$), and evaporated *in vacuo* to give nitro acetate **19***b* as a colorless oil in quantiative yield; ir (film) ν_{max}: 3060, 2950, 2850, 1753 and 1735 ($COOCH_3$, $OCOCH_3$), 1550 (NO_2) cm^{-1}; ^{1}Hmr ($CDCl_3$) δ: 0.67–2.90 (m, 23H, 10 CH_2, CH_3), 1.07 (s, 9H, *t*-Bu), 1.35 (s, 6H, CMe_2), 2.01 (s, 3H, $OCOCH_3$), 3.67 (s, 3H, $COOCH_3$), 3.92 (bs, 4H, OCH_2CH_2O), 3.50–4.10 (m, 3H, 3 CH—O), 4.80–5.60 (m, 4H, CH=CH, C*H*OAc, CH—NO_2), 7.27–7.94 (m, 10 H, 2 C_6H_5) ppm; ms (70 eV, 76°C), *m/e* (rel. int. %): 811 ($M^{+\cdot}$), 796 (2.6, $M^{+\cdot} - CH_3^{\cdot}$), 740 (0.4, $M^{+\cdot} - C_5H_{11}^{\cdot}$), 696 (24.4), 693 (1.7, 740 – HNO_2), 682 (9.3), 637 (9.2, $M^{+\cdot}$ – 143 – $OCH_3^{\cdot}$), 636 (9.5, $M^{+\cdot}$ – 143 – CH_3OH), 437 (20.5, $CH(CO)(OSi(t\text{-}Bu)Ph_2)CH_2CH{=}CH(CH_2)_3COOCH_3^+$), 409 (10.1, 437 – CO), 381 (22.8, $CH(CHO)(OSiPh_2)CH_2CH{=}CH(CH_2)_3COOCH_3^+$), 199 (5.1, 381 – $SiPh_2^{\cdot}$), 143 (100, $C(OCH_2CH_2O)C_5H_{11}^+$). *Anal.* calcd. for $C_{44}H_{65}O_{11}NSi$: C 65.10, H 8.01, N 1.73; found: C 64.91, H 8.30, N 1.90.

*Nitro Olefin 20*b

A mixture of nitro acetate **19***b* (1.90 g, 2.34 mmol), powdered anhydrous K_2CO_3 (1.61 g, 11.7 mmol), and a catalytic amount of dicyclohexyl-18-crown-6 was stirred in dry benzene (25 mL) for 6 h at 75°C under a N_2 atmosphere. The solid K_2CO_3 was filtered off and after evaporation of the benzene, the residual oil was purified by flash chromatography, using petroleum ether – ethyl acetate (8:1) as eluant to give 1.67 g (95%) of nitro olefin **20***b* as an oil; ir (film) ν_{max}: 3060, 2950, 2925, 2850, 1735 ($COOCH_3$), 1525 (NO_2), 1423, 1106 cm^{-1}; ^{1}Hmr ($CDCl_3$) δ: 0.67–2.40 (m, 21H, 9 CH_2, CH_3), 1.07 (s, 9H, *t*-Bu), 1.37 and 1.40 (s and s, 6H, CMe_2), 3.10 (bs, 2H, $C(NO_2)$—CH_2), 3.62 (s, 3H, $COOCH_3$), 3.80 (bs, 4H, OCH_2CH_2O), 3.60–4.00 (m, 2H, 2 CH—O), 4.36–4.90 (m, 1H, C=CHC*H*—O), 5.20–5.50 (m, 2H, CH=CH), 6.74 (d, 1H, J = 8 Hz; $C(NO_2){=}CH$), 7.17–7.80 (m, 10H, 2 C_6H_5) ppm; ms (70 eV, 119°C), *m/e* (rel. int. %): 409 (1.1, $CH(OSi(t\text{-}Bu)Ph_2)CH_2CH{=}CH(CH_2)_3COOCH_3^+$), 381 (3.6, $CH(CHO)(OSiPh_2)CH_2CH{=}CH(CH_2)_3COOCH_3^+$), 199 (7.6, 381 – $SiPh_2^{\cdot}$), 143 (100, $C(OCH_2CH_2O)C_5H_{11}^+$).

*Dihydroxy Nitro Olefin 21*b *and Hydroxy Tetrahydrofuran 22*b

A solution of isopropylidene nitro olefin **20***b* (975 mg, 1.30 mmol) in 2 *N* aqueous HCl (8 mL) and methanol (80 mL) was stirred for 2 h at room temperature. To this 5% aqueous $NaHCO_3$ solution was added until the solution became neutral and the methanol was removed under reduced pressure. The residue was partitioned between ethyl acetate (40 mL) and saturated salt solution (20 mL), and the aqueous layer was further extracted with ethyl acetate (2 × 20 mL). The combined extracts were dried ($MgSO_4$) and concentrated *in vacuo* to give a mixture of dihydroxy nitro olefin **21***b* and hydroxy tetrahydrofuran **22***b*. Purification by flash chromatography, using petroleum ether – ethyl acetate (3:1) as eluant, afforded 138 mg (15%) of dihydroxy nitro olefin **21***b* and 555 mg (60%) of hydroxy tetrahydrofuran **22***b*.

A solution of dihydroxy nitro olefin **21***b* (138 mg, 0.194 mmol) and triethylamine (24 mg, 0.234 mmol) in dry THF (3 mL) was stirred overnight at room temperature. The THF was removed under reduced pressure and the residue was taken up in ether (10 mL). The ether solution was washed with 0.1 *N* aqueous HCl (5 mL), 5% aqueous $NaHCO_3$ (5 mL), dried ($MgSO_4$), and concentrated *in vacuo* to give hydroxy tetrahydrofuran **22***b* in quantitative yield.

The separation of **21***b* and **22***b* proved to be unnecessary, and, in general, the mixture of **21***b* and **22***b* was submitted directly to the action of triethylamine.

Dihydroxy nitro olefin **21***b*; ^{1}Hmr ($CDCl_3$) δ: 0.67–3.30 (m, 23H, 10 CH_2, CH_3), 1.07 (s, 9H, *t*-Bu), 3.60 (s, 3H, $COOCH_3$), 3.81 (bs, 4H, OCH_2CH_2O), 3.50–3.97 (m, 2H, 2 CH—O), 4.30–4.76 (m, 1H, C=CHC*H*—O), 5.13–5.40 (m, 2H, CH=CH), 6.78 (d, 1H, J = 8 Hz, $C(NO_2)$=CH), 7.17–7.77 (m, 10H, 2 C_6H_5) ppm.

Hydroxy tetrahydrofuran **22***b*; ir (film) ν_{max}: 3460 (OH), 3065, 3040, 2950, 2925, 2850, 1737 ($COOCH_3$), 1550 (NO_2), 1423, 1105 cm^{-1}; ^{1}Hmr ($CDCl_3$) δ: 0.63–2.93 (m, 23H, 10 CH_2, CH_3), 1.06 (s, 9H, *t*-Bu), 3.61 (s, 3H, $COOCH_3$), 3.84 (bs, 4H, OCH_2CH_2O), 3.53–4.80 (m, 5H, 4 CH—O, CH—NO_2), 5.06–5.43 (m, 2H, CH=CH), 7.17–7.83 (m, 10H, 2 C_6H_5) ppm; ms (70 eV, 96°C), *m/e* (rel. int. %): 711 ($M^{+\cdot}$), 654 (1.2, $M^{+\cdot}$ – *t*-Bu$^\cdot$), 640 (3.9, $M^{+\cdot}$ – $C_5H_{11}{}^\cdot$), 607 (3.9, 654 – HNO_2), 593 (2.3, 640 –HNO_2), 437 (3.3, $M^{+\cdot}$ – *t*-Bu$^\cdot$ – $O_2NCH_2CH_2C(OCH_2CH_2O)C_5H_{11}$), 409 (2,6, $CH(OSi(t\text{-}Bu)Ph_2)CH_2CH$=$CH(CH_2)_3COOCH_3{}^+$), 199 (25.6), 143 (100, $C(OCH_2CH_2O)C_5H_{11}{}^+$).

*Methyl 8*R-tert-*Butyldiphenylsilyloxy-11*R-*hydroxy-13-nitro-15-oxo-9*S,*12*S-*oxyeicosa-5Z-enoate 23*b

A solution of β-nitro ketal **22***b* (426 mg, 0.6 mmol) in acetone (8 mL) containing a catalytic amount of *p*-toluenesulfonic acid was stirred overnight at room temperature. The acetone was removed under reduced pressure and the residue was dissolved in ether (30 mL). The ether solution was washed with 5% aqueous $NaHCO_3$ (2 × 15 mL), water (15 mL) and brine, dried ($MgSO_4$), and concentrated to give crude product. Purification by flash chromatography, using petroleum ether – ethyl acetate (3:1) as eluant, afforded 320 mg (80%) of β-nitro ketone **23***b* as a colorless oil; ir (film) ν_{max}: 3460 (OH), 3065, 3045, 2950, 2930, 2855, 1735 ($COOCH_3$), 1720 (C=O), 1550 (NO_2), 1423, 1107 cm^{-1}; ^{1}Hmr ($CDCl_3$) δ: 0.70–3.33 (m, 23H, 10 CH_2, CH_3), 1.07 (s, 9H, *t*-Bu), 3.60 (s, 3H, $COOCH_3$), 3.77–4.40 (m, 4H, 4 CH—O), 4.66–5.03 (m, 1H, CH—NO_2), 5.10–5.40 (m, 2H, CH=CH), 7.17–7.83 (m, 10H, 2 C_6H_5) ppm; ms (70 eV, 85°C), *m/e* (rel. int. %): 620 (1.1, $M^{+\cdot}$ – HNO_2), 610 (3.4, $M^{+\cdot}$ – *t*-Bu$^\cdot$), 593 (3.6, $M^{+\cdot}$ – CH_3COOCH_3), 563 (9.3, 610 – HNO_2), 545 (10.2, 563 – H_2O), 461 (1.0, 620 – H_2O – CH_2CH=$CH(CH_2)_3COOCH_3{}^\cdot$), 437 (5.6, 610 – $O_2NCH_2CH_2C(O)C_5H_{11}$), 409 (10.2, $CH(OSi(t\text{-}Bu)Ph_2)CH_2CH$=$CH(CH_2)_3COOCH_3{}^+$), 381 (15.3, $CH(CHO)(OSiPh_2)CH_2CH$=$CH(CH_2)_3COOCH_3{}^+$), 199 (83.1, 381 – $SiPh_2{}^\cdot$), 99 (32.8, $C(O)C_5H_{11}{}^+$).

*Methyl 8*R-tert-*Butyldiphenylsilyloxy-11*R-*hydroxy-15-oxo-9*S, *12*S-*oxyeicosa-5Z,13*E-*dienoate 24*b

A solution of β-nitro ketone **23***b* (180 mg, 0.264 mmol) and triethylamine (40 mg, 0.396 mmol) in chloroform (5 mL) was stirred overnight at room temperature. The resulting solution was washed with water (2 × 5 mL) and brine, dried ($MgSO_4$), and concentrated under reduced pressure. The residual oil was purified by flash chromatography, using petroleum ether – ethyl acetate (2:1) as eluant, to give 138 mg (85%) of α,β-unsaturated ketone **24***b* as a colorless oil; $[\alpha]_D{}^{23}$ −16.2° (*c* 1.75, $CHCl_3$); ir (film) ν_{max}: 3440 (OH), 3060, 3035, 2940, 2918, 2842, 1730 ($COOCH_3$), 1670 and 1626 (C=C—C=O), 1420, 1105 cm^{-1}; ^{1}Hmr ($CDCl_3$) δ: 0.67–2.60 (m, 21H, 9 CH_2, CH_3), 1.07 (s, 9H, *t*-Bu), 3.62 (s, 3H, $COOCH_3$), 3.77–4.37 (m, 4H, 4 CH—O), 5.13–5.40 (m, 2H, CH=CH), 6.20 (dd, 1H, J = 1.5, 16 Hz, CH=C*H*—C=O), 6.72 (dd, 1H, J = 4.5, 16 Hz, C*H*=CH—C=O), 7.20–7.87 (m, 10H, 2 C_6H_5) ppm; ms (70 eV, 76°C), *m/e* (rel. int. %): 620 (2.1, $M^{+\cdot}$), 602 (1.1, $M^{+\cdot}$ – H_2O), 563 (19.9, $M^{+\cdot}$ – *t*-Bu$^\cdot$), 545 (19, 563 – H_2O), 531 (1.2, 602 – $C_5H_{11}{}^\cdot$), 409 (14.1, $CH(OSi(t\text{-}Bu)Ph_2)CH_2CH$=$CH(CH_2)_3COOCH_3{}^+$), 381 (20, $CH(CHO)(OSiPh_2)CH_2CH$=$CH(CH_2)_3COOCH_3{}^+$), 199 (100, 381 – $SiPh_2{}^\cdot$), 135 (80.5), 99 (38.1, $C(O)C_5H_{11}{}^+$). *Anal.* calcd. for $C_{37}H_{52}O_6Si$: C 71.62, H 8.39; found: C 71.34, H 8.37.

*Methyl 11*R-*Acetoxy-8*R-tert-*butyldiphenylsilyloxy-15-oxo-9*S, *12*S-*oxyeicosa-5Z,13*E-*dienoate 25*b

A solution of alcohol **24***b* (42 mg, 0.068 mmol), acetic anhydride (8.4 mg, 0.082 mmol), triethylamine (9.0 mg, 0.088 mmol), and a catalytic amount of 4-dimethylaminopyridine in anhydrous ether (3 mL) was stirred for 30 min at room temperature. The resulting solution was partitioned between ether (10 mL) and 0.1 *N* aqueous HCl (3 mL). The ether layer was washed with 5% aqueous $NaHCO_3$ (5 mL), water (5 mL) and brine, dried ($MgSO_4$), and evaporated under reduced pressure to afford 40 mg (90%) of acetate **25***b* as a colorless oil; $[\alpha]_D{}^{23}$ −25.1° (*c* 1.85, $CHCl_3$); ir (film) ν_{max}: 3060, 2945, 2920, 2845, 1735 ($COOCH_3$, $OCOCH_3$), 1670 and 1630 (C=C—C=O), 1420, 1230, 1104 cm^{-1}; ^{1}Hmr 200 MHz ($CDCl_3$) δ: 0.90 (t, 3H, J = 7 Hz, CH_3), 1.06 (s, 9H, *t*-Bu), 1.16–2.37 (m, 14H, 7 CH_2), 2.09 (s, 3H, $OCOCH_3$), 2.21 (t, 2H, J = 7 Hz, CH=CHCOCH_2), 2.47 (t, 2H, J = 7 Hz, CH_2—COO), 3.65 (s, 3H, $COOCH_3$), 3.98 (td, 1H, J = 4,8 Hz, CH—O), 4.06–4.20 (m, 1H, CH—O), 4.39 (ddd, 1H, J = 1.8, 3.5, 4.7 Hz, C*H*—CH=CH—C=O), 4.92–5.04 (m, 1H, C*H*OAc), 5.26–5.48 (m, 2H, CH=CH), 6.26 (dd, 1H, J = 1.8, 16 Hz, CH=C*H*—C=O), 6.72 (dd, 1H, J = 4.7, 16 Hz, C*H*—CH—C=O), 7.32–7.82 (m, 10H, 2 C_6H_5) ppm; ms (70 eV, 79°C), *m/e* (rel. int. %): 662 (0.4, $M^{+\cdot}$), 631 (2.0, $M^{+\cdot}$ – $OCH_3{}^\cdot$), 605 (45.7, $M^{+\cdot}$ – *t*-Bu$^\cdot$), 563 (5, $M^{+\cdot}$ – 99), 545 (33, 605 – CH_3COOH), 521 (1.4, $M^{+\cdot}$ – 141), 461 (11, 521 – CH_3COOH), 409 (17.2, $CH(OSi(t\text{-}Bu)Ph_2)CH_2CH$=$CH(CH_2)_3COOCH_3{}^+$), 381 (52.7, $CH(CHO)(OSiPh_2)CH_2CH$=$CH(CH_2)_3COOCH_3{}^+$), 199 (94.4, 381 – $SiPh_2{}^\cdot$), 141 (8, CH_2CH=$CH(CH_2)_3COOCH_3{}^+$), 135 (78.9), 99 (35.6, $C(O)C_5H_{11}{}^+$), 71 (20.5, $C_5H_{11}{}^+$), 43 (100, $C_3H_7{}^+$, $COCH_3{}^+$).

*Methyl 11*R-*Hydroxy-8*R-*methoxy-15-oxo-9*S,*12*S-*oxyeicosa-5Z-enoate 26*

A solution of α,β-unsaturated ketone **24***a* (64 mg, 0.163 mmol) in absolute ethanol (2 mL) containing 5% Pd–C (13 mg) was hydrogenated for 30 min at atmospheric pressure until hydrogen uptake stopped. After filtration, the ethanol was removed under reduced pressure to give ketone **26** in quantitative yield; ir (film) ν_{max}: 3440 (OH), 2950, 2920, 1730 ($COOCH_3$), 1705 (C=O), 1430 cm^{-1}; ^{1}Hmr ($CDCl_3$) δ: 0.67–2.77 (m, 25H, 11 CH_2, CH_3), 3.33 (s, 3H, OCH_3), 3.58 (s, 3H, $COOCH_3$), 3.0–4.33 (m, 4H, 4 CH—O), 5.20–5.46 (m, 2H, CH=CH) ppm.

*Methyl 8*R-tert-*Butyldiphenylsilyloxy-11*R,*15(*S *and* R)-*dihydroxy-9*S,*12*S-*oxyeicosa-5*Z,*13*E-*dienoates 28*b *and 29*b

To a solution of α,β-unsaturated ketone **24***b* (102 mg, 0.165 mmol) in dry toluene (4 mL) was added a solution of 0.3 *M* diisobornyloxyaluminum isopropoxide (5) in toluene (1.12 mL, 0.336 mmol). The reaction mixture was stirred under a nitrogen atmosphere for 2 h at room temperature and partitioned between ethyl acetate (15 mL) and 5% aqueous KH_2PO_4 (pH = 4.1–4.5, 10 mL). The organic layer was separated and the aqueous layer further extracted with ethyl acetate (10 mL). The combined extracts were washed with water (10 mL) and brine, dried ($MgSO_4$), and concentrated under reduced pressure. Purification by flash chromatography, using petroleum ether – ethyl acetate (1:1) as eluant, afforded 82 mg (80%) of allylic alcohols as an approximately 5.5 : 4.5 isomeric mixture at C-15 (**28***b* R_f = 0.23 and **29***b* R_f = 0.33). The two isomers were cleanly separated by hplc, using petroleum ether – ethyl acetate (2:1) as eluant. Allylic alcohol **28***b* with R_f = 0.23; $[\alpha]_D^{23}$ −16.2° (*c* 2.1, $CHCl_3$); ir (film) ν_{max}: 3395 (OH), 3070, 3050, 2950, 2930, 2855, 1736 ($COOCH_3$), 1585, 1423, 1106 cm^{-1}; ^{1}Hmr ($CDCl_3$) δ: 0.67–2.53 (m, 21H, 9 CH_2, CH_3), 1.06 (s, 9H, *t*-Bu), 3.62 (s, 3H, $COOCH_3$), 3.73–4.38 (m, 5H, 5 CH—O), 5.11–5.45 (m, 2H, *Z* CH=CH), 5.48–5.78 (m, 2H, *E* CH=CH), 7.20–7.84 (m, 10H, 2 C_6H_5) ppm; gc–ms (1.5% OV-101, 280°C, 70 eV, di-trimethylsilylated **28***b*), *m/e* (rel. int. %): 766 (0.6, $M^{+\cdot}$), 751 (0.9, $M^{+\cdot}$ – $CH_3^{\cdot}$), 709 (0.8, $M^{+\cdot}$ – *t*-Bu$^{\cdot}$), 676 (2.1, $M^{+\cdot}$ – Me_3SiOH), 625 (1.3, $M^{+\cdot}$ – 141), 619 (30.6, 676 – *t*-Bu$^{\cdot}$), 586 (1.1, $M^{+\cdot}$ – 2Me_3SiOH), 535 (6.7, 676 – 141), 503 (1.9, 676 – 173), 477 (1.3, 676 – 199), 409 (9, $CH(OSi(t\text{-}Bu)Ph_2)CH_2CH{=}CH(CH_2)_3COOCH_3^+$), 381 (60.5, $CH(CHO)(OSiPh_2)CH_2CH{=}CH(CH_2)_3COOCH_3^+$), 199 (38.1, $CH{=}CHCH(OSiMe_3)C_5H_{11}^+$), 173 (12, $CH(OSiMe_3)C_5H_{11}^+$), 141 (4.4, $CH_2CH{=}CH(CH_2)_3COOCH_3^+$), 135 (63.9), 73 (100, $SiMe_3^+$).

Allylic alcohol **29***b* with R_f = 0.33; $[\alpha]_D^{23}$ −23.4° (*c* 2.5, $CHCl_3$); its ^{1}Hmr, ir, and ms data were virtually the same as compound **28***b* described above.

*Methyl 8*R,*11*R,*15*S-*Trihydroxy-9*S,*12*S-*oxyeicosa-5*Z,*13*E-*dienoate 30*

To a solution of silyl ether **28***b* (50 mg, 0.081 mmol) in dry THF (2 mL) was added a solution of 1 *M* *n*-Bu_4NF in dry THF (0.12 mL, 0.12 mmol) via a syringe, and the resulting solution was stirred for 7 h at 65°C under a N_2 atmosphere. The THF was removed under reduced pressure and the residue was taken up in ethyl acetate (10 mL). The solution was then washed with brine and the aqueous layer was further extracted with ethyl acetate (5 mL). The combined extracts were dried ($MgSO_4$) and concentrated under reduced pressure. The crude product was purified by flash chromatography, using ethyl acetate as eluant, to give 26 mg (85%) of trihydroxy methyl ester **30** as a white solid (mp 44–45.5°C); $[\alpha]_D^{23}$ −16.4° (*c* 0.95, $CHCl_3$); ir (film) ν_{max}: 3400 (OH), 2955, 2930, 2860, 1735 ($COOCH_3$), 1436 cm^{-1}; ^{1}Hmr 200 MHz ($CDCl_3$) δ: 0.89 (t, 3H, *J* = 7 Hz, CH_3), 1.18–2.46 (m, 18H, 9 CH_2), 3.68 (s, 3H, $COOCH_3$), 3.74–4.28 (m, 5H, 5 CH—O), 5.40–5.60 (m, 2H, *Z* CH=CH), 5.66 (dd, 1H, *J* = 8, 16 Hz, *E* C*H*=CH), 5.83 (dd, 1H, *J* = 7, 16 Hz, *E* CH=C*H*) ppm; gc–ms (1.5% OV-101, 220°C, 70 eV, tris-trimethylsilylated **30**), *m/e* (rel. int. %): 600 (2.0, $M^{+\cdot}$), 510 (13.8, $M^{+\cdot}$ – Me_3SiOH), 495 (3.4, 510 – $CH_3^{\cdot}$), 479 (2.8, 510 – $OCH_3^{\cdot}$), 459 (7.6, $M^{+\cdot}$ – $CH_2CH{=}CH(CH_2)_3COOCH_3^{\cdot}$), 439 (5.9, 510 – $C_5H_{11}^{\cdot}$), 420 (2.6, $M^{+\cdot}$ – 2 Me_3SiOH), 369 (53.4, 459 – Me_3SiOH), 357 (6.8, $M^{+\cdot}$ – 243), 337 (14, 510 – 173), 279 (17.6, 459 – 2 Me_3SiOH), 267 (11.7, 510 – 243), 243 (77.3, $CH(OSiMe_3)CH_2CH{=}CH(CH_2)_3COOCH_3^+$), 211 (11.8, 243 – CH_3OH), 199 (10.2, $CH{=}CHCH(OSiMe_3)C_5H_{11}^+$), 173 (23, $CH(OSiMe_3)C_5H_{11}^+$), 147 (20.1), 129 (46.8), 73 (100, $SiMe_3^+$).

Compound **31** was prepared from the corresponding silyl ether **29***b* as described above for the preparation of compound **30** in 90% yield (mp 52–53.5°C); $[\alpha]_D^{23}$ −28.6° (*c* 1.4, $CHCl_3$). Its ^{1}Hmr, ir, and ms data were virtually the same as compound **30**.

*8*R,*11*R, *15*S-*Trihydroxy-9*S,*12*S-*oxyeicosa-5*Z,*13*E-*dienoic acid 1*

To a solution of trihydroxy methyl ester **30** (18 mg, 0.047 mmol) in methanol (0.5 mL) was added 0.5 *N* aqueous methanolic NaOH (CH_3OH–H_2O = 7:3, 0.4 mL) and the resulting solution was stirred overnight at room temperature. NaOH was neutralized with glacial acetic acid. After evaporation of the solvent, the residue was dissolved in ethyl acetate (5 mL). The solution was washed with brine (3 mL) and the aqueous layer was further extracted with ethyl acetate (2 × 3 mL). The combined extracts were dried ($MgSO_4$) and concentrated under reduced pressure to give 15 mg (85%) of trihydroxy carboxylic acid **1**; ir (film) ν_{max}: 3370 (OH), 2960, 2930, 2860, 1710 (C=O) cm^{-1}; ^{1}Hmr 200 MHz ($CDCl_3$) δ: 0.88 (t, 3H, *J* = 7 Hz, CH_3), 1.18–2.50 (m, 18H, 9 CH_2), 3.58–4.44 (m, 5H, 5 CH—O), 5.34–5.94 (m, 4H, 2 CH=CH) ppm; gc–ms (1.5% OV-101, 240°C, 70 eV, fully trimethylsilylated **1**), *m/e* (rel. int. %): 658 (0.9, $M^{+\cdot}$), 643 (1.7, $M^{+\cdot}$ – $CH_3^{\cdot}$), 568 (10.5, $M^{+\cdot}$ – Me_3SiOH), 553 (4.4, 568 – $CH_3^{\cdot}$), 497 (2.7, 568 – $C_5H_{11}^{\cdot}$), 478 (3.1, $M^{+\cdot}$ – 2 Me_3SiOH), 459 (4.3, $M^{+\cdot}$ – $CH_2CH{=}CH(CH_2)_3COOSiMe_3^{\cdot}$), 395 (6.6, 568 – $CH(OSiMe_3)C_5H_{11}^{\cdot}$), 369 (34.6, 459 – Me_3SiOH), 357 (4,6 $M^{+\cdot}$ – 301), 301 (49.3, $CH(OSiMe_3)CH_2CH{=}CH(CH_2)_3COOSiMe_3^+$), 279 (12.1, 459 – 2 Me_3SiOH), 272 (30.6), 267 (12.0, 357 – Me_3SiOH), 211 (22.9, 301 – Me_3SiOH), 199 (9.7, $CH{=}CHCH(OSiMe_3)C_5H_{11}^+$, $CH_2CH{=}CH(CH_2)_3COOSiMe_3^+$), 191 (22.9), 173 (20.0, $CH(OSiMe_3)C_5H_{11}^+$), 147 (29.1), 129 (47.8), 75 (63.0), 73 (100, $SiMe_3^+$).

General Micromethod for the Determination of the Absolute Chemistry at C-15 of 30

Trihydroxy methyl ester **30** (1 mg, 2.6 μmol) was acetylated using a standard method. Ozone was bubbled into a solution of triacetate **32** in dry CH_2Cl_2 (35 mL) at a rate of 8 mmol/h at −78°C for 5 min. After excess ozone was removed by flushing with N_2 at −78°C, dimethylsulfide (2 mL) was added and stirred overnight at room temperature. The residue, after evaporation of the solvent, was taken up in ether (5 mL) and washed with water (2 × 10 mL) and brine. Concentration under reduced pressure gave crude 2-acetoxyheptanal. A solution of 2-acetoxyheptanal thus obtained and excess 1-ephedrine in CH_2Cl_2 (2 mL) was stirred for 1 h at room temperature. It was then diluted with ether (10 mL) and washed with water (3 × 5 mL) and brine. Evaporation and purification by column chromatography, using petroleum ether – ethyl acetate (9:1) as eluant, gave the oxazolidine derivative. Its R_f value (0.33, in petroleum ether – ethyl acetate 5:1) and 200 MHz ^{1}Hmr spectrum were identical with those of the authentic material with known stereochemistry (8).

1. G. Just, H. Oh, and C. Luthe. Tetrahedron Lett. 1001 (1980).
2. C. Pace-Asciak and L. Wolfe. Biochemistry, **10**, 3664 (1971); Chem. Commun. 1234 (1970); 1235 (1970).
3. G. Just and C. Luthe. Can. J. Chem. **58**, 1799 (1980).
4. P. Bakuzis, L. F. Bakuzis, and F. Weingartner. Tetrahedron Lett. 2371 (1978).
5. H. Feuer. The chemistry of the nitro and nitroso groups. Interscience Publishers, New York. 1970. p. 76, and references cited therein.
6. J. Hutton. Synth. Commun. **9**(6), 483 (1979).
7. W. C. Still, M. Kahn, and Abhijit Mitra. J. Org. Chem. **43**, 2923 (1978).
8. G. Just and H. Oh. Tetrahedron Lett. 3667 (1980).

The crystal structure and vibrational spectra of *cis*-dichlorobis(cyclopropylamine)-platinum(II), $PtCl_2(C_3H_5NH_2)_2$

HELEN ELAINE HOWARD-LOCK, COLIN JAMES LYNE LOCK,[1] GRAHAM TURNER, AND MARUTA ZVAGULIS

Institute for Materials Research, McMaster University, Hamilton, Ont., Canada L8S 4M1

Received November 21, 1980

HELEN ELAINE HOWARD-LOCK, COLIN JAMES LYNE LOCK, GRAHAM TURNER, and MARUTA ZVAGULIS. Can. J. Chem. **59**, 2737 (1981).

Crystals of *cis*-dichlorobis(cyclopropylamine)platinum(II), $PtCl_2(C_3H_5NH_2)_2$, are monoclinic, $a = 12.770(5)$, $b = 5.838(2)$, $c = 15.113(6)$ Å, $\beta = 104.46(3)°$, $Z = 4$, space group $P2_1/c$. The structure was solved by Patterson and Fourier syntheses and was refined by full-matrix least-squares to $R = 0.057$, $R_w = 0.055$ for 1577 reflections with $I > 3\sigma(I)$. Bond lengths and angles are normal. A vibrational analysis of the compound and its d_2-deuterated analogue was performed.

HELEN ELAINE HOWARD-LOCK, COLIN JAMES LYNE LOCK, GRAHAM TURNER et MARUTA ZVAGULIS. Can. J. Chem. **59**, 2737 (1981).

Les cristaux de dichloro bis(cyclopropylamine)platine(II) *cis*-$PtCl_2(C_3H_5HN_2)_2$ sont monocliniques et appartiennent au groupe d'espace $P2_1/c$ avec $a = 12,770(5)$, $b = 5,838(2)$, $c = 15,113(6)$ Å, $\beta = 104,46(3)°$, $Z = 4$. On a résolu la structure par les synthèses de Patterson et de Fourier et on l'a affinée par la méthode des moindres carrés (matrice complète) jusqu'a des valeurs de $R = 0,057$ et de $R_w = 0,055$ pour 1577 réflexions avec $I > 3\sigma(I)$. Les angles et les liaisons ont des longueurs normales. On a réalisé une analyse vibrationnelle du composé et de son analogue deutéré d_2.

[Traduit par le journal]

Introduction

cis-Dichlorodiammineplatinum(II) has been shown to be a useful anti-cancer agent both in animals and in man (1–8). Further studies have shown that other amine complexes also show anti-tumor activity in animals (1–8), and in particular, that certain cyclic amine complexes are very effective against some animal tumors (9, 10).[2] It has been suggested that the differences in the efficacies of the various complexes are related to structural features of the complexes (10), but until recently few, if any, accurate structures of these platinum amine complexes had been determined. We are currently determining the crystal structures of selected amine complexes of platinum and report here the results of our studies on *cis*-dichlorobis(cyclopropylamine)-platinum(II).

Experiments

Preparation of cis-*Dichlorobis(cyclopropylamine-*N)-*platinum(II), $PtCl_2(C_3H_5NH_2)_2$*

The method used is a modification of the method of Dhara (11).

An aqueous solution (10 mL) of K_2PtCl_4 (0.4272 g) was mixed with potassium iodide (0.6563 g) and left at room temperature for a few hours. Cyclopropylamine (0.12 g) was added dropwise and the yellow product filtered off after a half-hour. The product was stirred in 0.1 *M* aqueous silver nitrate solution (19 mL) for approximately 6 h. After removal of silver iodide by filtration, potassium chloride (0.15 g) was added to the filtrate. The yellow product separated over the course of a week and was removed by filtration, washed with a small amount of ice water, followed by ethanol and diethyl ether. Crystals suitable for X-ray diffraction studies were obtained by recrystallization from water at 20°C. *Anal.* calcd. for $C_6H_{14}Cl_2N_2Pt$: C 19.0, H 3.7, N 7.4; found: C 19.2, H 3.9, N 7.0.

Preparation of $PtCl_2(ND_2C_3H_5)_2$

Deuterated cyclopropylamine (0.1464 g) was added dropwise to a solution of K_2PtCl_4 (0.5221 g) in D_2O (10 mL) and left overnight at room temperature. The pale yellow powder which formed was collected by filtration, washed with a small amount of D_2O and cold acetone.

Preparation of $C_3H_5ND_2$

Cyclopropylamine (2.3240 g) was reacted with 1 *N* HCl (40 mL). The water was removed under vacuum on a rotary evaporator at ~40°C. The hydrochloride salt was dissolved in D_2O (50 mL) and allowed to stand in a stoppered flask at room temperature for 2 weeks. The D_2O was removed under vacuum on a rotary evaporator and the white powder redissolved in a minimum of D_2O (3 mL). Sodium bicarbonate (3.4319 g) was added and the solution left overnight. The deuterated amine was distilled from the solution at reduced pressure with gentle warming (~40°C).

Spectral Measurements

Infrared spectra of the platinum complexes were measured in Nujol and hexachlorobutadiene mulls suspended between potassium bromide or polyethylene windows. The amines were diluted with CCl_4 and run between potassium bromide windows with a CCl_4 reference. Spectra were recorded on a Perkin-Elmer PE 283 spectrometer between 4000–200 cm^{-1}. The cell compartment was flushed with dry nitrogen for several hours before spectra were recorded in the 400–200 cm^{-1} region.

[1]To whom all correspondence should be addressed.

[2]Reference 6 contains all the papers presented at the 3rd International Conference on Platinum Coordination Complexes in Cancer Chemotherapy, Dallas, TX, Oct. 1976; ref. 8 contains all the papers presented at the Conference on "Chimie de coordination et chimotherapie des Cancers," Toulouse, July 1978.

0008-4042/81/182737-09$01.00/0

©1981 National Research Council of Canada/Conseil national de recherches du Canada

Can. J. Chem. Downloaded from www.nrcresearchpress.com by 210.87.254.42 on 09/06/12
For personal use only.

Can. J. Chem. Downloaded from www.nrcresearchpress.com by 210.87.254.42 on 09/06/12
For personal use only.

Raman spectra were excited with ~100 mW of λ5145 Å radiation from a Spectra-Physics Model 164-02 Argon ion laser. Crystalline samples were contained in glass melting point tubes and liquid samples in nmr tubes. Radiation scattered at 90° to the incident beam was analysed with scanning double monochromators (Coderg PHO or Spex 14018). A rough intensity calibration was obtained by comparison with carbon tetrachloride standards. The spectrometer was calibrated regularly against an indene standard, and had been calibrated previously with a neon lamp; the wavelength readout scale was found not to change. The vibrational spectra are reported in Tables 4 and 5.

Collection of the X-ray Diffraction Data

A pale yellow crystal, chosen after examination under a polarizing microscope for homogeneity, was mounted on a glass fibre with the crystal 061 direction roughly parallel to the fibre axis. Precession photographs were obtained from a fit of χ, ϕ, and 2θ for 15 medium angle ($20° < 2\theta < 35°$) reflections recorded on a Syntex $P\bar{1}$ diffractometer using graphite-monochromated MoKα radiation ($\lambda = 0.71069$ Å at 22°C). Crystal data and other numbers related to data collection are summarized in Table 1. The density was determined by flotation in an aqueous zinc bromide solution. Intensity data were also recorded on the Syntex $P\bar{1}$ diffractometer using a coupled θ(crystal)–2θ(counter) scan. The methods of selection of scan rates and initial data treatment have been described (12, 13). Corrections were made for Lorentz-polarization effects and absorption.

Solution of the Structure

The coordinates of the platinum atom were found from a three-dimensional Patterson synthesis, and three-dimensional electron density difference maps revealed the remaining non-hydrogen atoms. After refinement the temperature factors of all the atoms, which were previously isotropic, were made sequentially anisotropic. Tests were made at each stage to show that the use of the increased parameters was significant (14). Further refinement using full least-squares refinement minimizing $\Sigma w(|F_o| - |F_c|)^2$, was terminated when the maximum shift/error was 0.006. Corrections for secondary extinction were made by the method of Larson (15).

Throughout the refinement, the scattering curves were taken from the International Tables (ref. 16, Table 2.2A, pp. 72ff), and anomalous dispersion corrections from International Tables (ref. 16, Table 2.3.1, pp. 149–150) were applied to the curves for platinum and chlorine. The atom parameters for the non-hydrogen atoms are listed in Table 2.[3]

Crystal data are given in Table 1.

TABLE 1. Crystal data

$C_6H_{14}Cl_2N_2Pt$, formula weight = 380.19, crystal bounded by {010}, separation 0.290 mm, {102} 0.168 mm, {001} 0.136 mm, {100} 0.210 mm, {10$\bar{2}$} 0.162 mm. Systematic absences $h0l$, $l \neq 2n$, $0k0$, $k \neq 2n$. Monoclinic, $a = 12.770(5)$, $b = 5.358(2)$, $c = 15.113(6)$ Å, $\beta = 104.46(3)°$, $V = 1000.3(7)$ Å^3, $P2_1/c$, $Z = 4$, $\rho_{obs} = 2.52(1)$ g cm^{-3}, $\rho_{calcd} = 2.52$ g cm^{-3}, $\mu = 152.1$ cm^{-1}, absorption coefficient limits, A^*, 5.657–15.323, standard reflection −2,1,3, e.s.d. 2.24%. No. of independent reflections 2310, No. $I > 3\sigma(I)$ 1577, No. $3\sigma(I) > I > 0.0$, 526, $I < 0.0$, 207, final $R_1 = 0.0566$, $R_2 = 0.0546$.[a] Final max. shift/error 0.006, g (secondary extinction) $= 8.868 \times 10^{-8}$, error in an observation of unit weight 1.010, weighting scheme $w = [\sigma^2 + (0.03F_o)^2]^{-1}$, final difference peak, location, 1.60 e/Å^3, 0.34,0.0,0.0, valley, location, −1.41 e/Å^3, 0.26,0.24,−0.02. $F_{000} = 6406$.

[a] $R_1 = \Sigma||F_o| - |F_c||/\Sigma|F_o|$; $R_2 = [\Sigma w(|F_o| - |F_c|)^2/\Sigma wF_o^2]^{1/2}$.

Results and Discussion

Our earliest attempts to prepare *cis*-dichlorobis(cyclopropylamine)platinum(II) were based on the method of Connors *et al.* (9), which involves the reaction of cyclopropylamine hydrochloride with K_2PtCl_4 in water in the presence of sodium bicarbonate. We did obtain the mixture of black powder and yellow crystals described by the above authors, but the subsequent recrystallization from hot concentrated hydrochloric acid gave, in our laboratory, ammonium hexachloroplatinate. The product was identified uniquely both by powder and single crystal X-ray diffraction. We have repeated this preparation a number of times with the same result. On one occasion we did obtain a rather impure crystalline mass, where the crystals were needle-like in form, but a subsequent recrystallization, using the method of Connors *et al.* (9), again gave ammonium hexachloroplatinate.

It appears that under the conditions of recrystallization of our compound a reaction is taking place together with oxidation, by air, of Pt(II) to Pt(IV).[4] We did not pursue this further as it proved possible to get crystals, suitable for X-ray purposes, using the preparative method of Dhara (11).

The Structure

The molecule is illustrated in Fig. 1 and selected interatomic distances and angles are given in Table 2. The bonded ligand atoms are in a rough square around the platinum atom. The arrangement of the five atoms is essentially planar. The deviations from the best plane (Pt, 0.006(1); Cl(1), −0.003(4); Cl(2), 0.004(4); N(1), −0.04(1); N(2), 0.03(1) Å) are not significant.

The Pt—N distances (2.05(1), 2.04(1)) (Table 3)

[3] A table of the moduli for F_o and F_c is available, at a nominal charge, from the Depository of Unpublished Data, CISTI, National Research Council of Canada, Ottawa, Ont., Canada K1A 0S2.

All calculations were carried out on CDC 6400 or CYBER 170/730 computers. Initial data treatment used programs from the XRAY 76 package (18). The structure was solved using internally written Fourier and full-matrix least-squares programs SYMFOU and CUDLS written by J. S. Rutherford and J. S. Stephens respectively. The least-squares planes were calculated using NRC-22 (19) and diagrams were prepared using ORTEP II (20).

[4] Discussions with Professor Tobe have revealed that the reason we did not obtain *cis*-dichlorobis(cyclopropylamine)-platinum(II) is that the procedure in the literature (10) is inaccurate. Instead of recrystallization from hot concentrated hydrochloric acid as reported, the correct procedure should call for the product to be leached with hot concentrated hydrochloric acid, when the material insoluble in hydrochloric acid is the desired product. We have confirmed by powder diffraction examination of the product that this is indeed the case.

Can. J. Chem. Downloaded from www.nrcresearchpress.com by 210.87.254.42 on 09/06/12
For personal use only.

TABLE 2

(*a*) Atom parameters for *cis*-dichlorobis(cyclopropylamine)-platinum(II) ($\times 10^3$)*

Atom	*X*	*Y*	*Z*
Pt	260.65(4)	55.3(1)	−5.12(3)
Cl(1)	382.6(3)	−261.5(7)	24.4(3)
Cl(2)	160.2(3)	−114.4(7)	85.6(3)
N(1)	152.6(9)	345(2)	−28.2(8)
N(2)	346.1(8)	215(2)	−87.8(7)
C(1)	88.6(9)	373(3)	−120(1)
C(2)	119(1)	563(3)	−175(1)
C(3)	21(1)	602(3)	−142(1)
C(4)	317(1)	122(3)	−180(1)
C(5)	394(1)	170(4)	−240(1)
C(6)	372(1)	−80(4)	−208(1)

(*b*) Anisotropic temperature factors U_{ij} ($\times 10^3$)†

Atom	U_{11}	U_{22}	U_{33}	U_{12}	U_{13}	U_{23}
Pt	49.3(3)	46.1(3)	40.6(3)	3.5(2)	15.0(2)	−2.3(3)
Cl(1)	54(2)	57(2)	76(2)	10(1)	16(2)	2(2)
Cl(2)	85(2)	60(3)	64(2)	9(2)	42(2)	10(2)
N(1)	77(7)	60(8)	50(6)	26(6)	36(6)	19(6)
N(2)	56(6)	55(7)	48(6)	−3(5)	28(5)	−4(6)
C(1)	42(6)	62(10)	62(9)	−8(6)	21(6)	2(7)
C(2)	70(8)	88(12)	55(8)	19(8)	25(7)	14(9)
C(3)	58(7)	79(12)	94(12)	27(7)	35(8)	46(10)
C(4)	56(7)	86(12)	49(8)	4(8)	20(6)	−2(8)
C(5)	79(10)	116(15)	59(10)	−10(10)	40(8)	−6(11)
C(6)	78(10)	111(16)	76(11)	−12(10)	42(9)	−20(12)

*Estimated standard deviations from the least squares programs are given in parentheses.
†The temperature factor parameters U_{ij} were obtained from $\beta_{ij} - 2\pi^2 b_i b_j U_{ij}$ where β_{ij}'s appear as a temperature effect through $\exp[-(\beta_{11}h^2 + \ldots + \beta_{12}hk + \ldots)]$ in the structure factor expression and b_i are the reciprocal lattice vectors.

are normal as are the Pt—Cl distances (2.273(4), 2.286(5)) (21–24). All distances and angles within the amine group are normal (25). The dihedral angles between the best plane through the ligand atoms and the cyclopropyl groups are relatively small (3.9° for C(1)C(2)C(3) and 26.0° for C(4)C(5)-C(6)), and this is probably caused by crystal packing since there appear to be no intramolecular steric interactions requiring the planes to be parallel (see below). The amine group is in the *gauche* arrangement with respect to the cyclopropyl ring. (Torsion angles PtN(1)C(1)⟨C(2)C(3)⟩, 136(1)°, PtN(2)C(4)⟨C(5)C(6)⟩, 127(1)°), where ⟨C(A)C(B)⟩ is the midpoint of C(A)—C(B)).

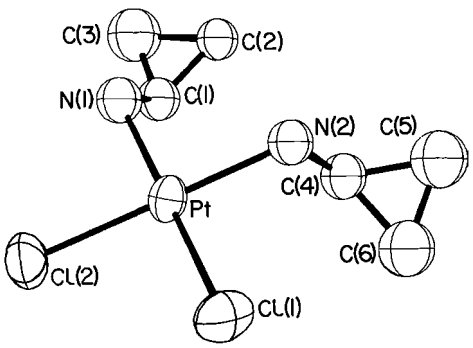

FIG. 1. *cis*-Dichlorobis(cyclopropylamine)platinum(II) showing the atom numbering.

The packing of the molecules within the cell is shown in Fig. 2. In the ***b*** direction molecules related by the *y* translation were packed head to tail, and inclined relative to the ***ab*** plane such that the square ligand planes were stacked roughly like tiles on a roof. The prime contacts were between N(1)···Cl(2), 3.35(1) Å, and N(2)···Cl(1), 3.25(1) Å, suggesting hydrogen bonding between the atom pairs. Hydrogen bonding also played a part in the packing in the ***a*** direction. The molecules related by x,y,z and $1-x, -y, -z$ had Cl(1)···N(2) contacts of 3.37(1) Å. The other contact in the ***a*** direction was between a chlorine atom on one molecule and the cyclopropyl group on the next. Thus the crystal was composed of layers of molecules centred at roughly $z = 0$ and $z = 1/2$ and within the layers rows of molecules arranged so that the dipoles were very roughly parallel to the ***b*** direction. In adjacent rows the dipoles point in opposite directions. Contact between rows (in different layers) was almost entirely between chlorine and platinum atoms of one mole-

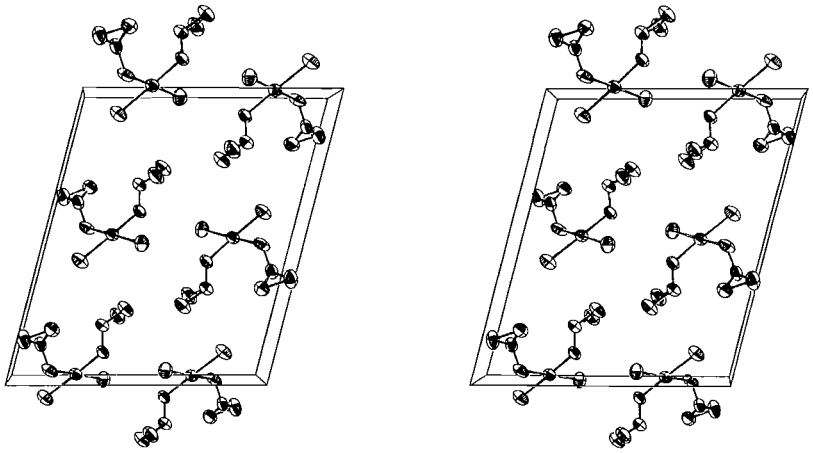

FIG. 2. The packing of the molecule within the unit cell. *a* and *c* are parallel to the bottom and side of the page respectively and the view is down *b*.

cule and the cyclopropyl groups of the adjacent molecule. There was no evidence of hydrogen bonding between layers. Other than the distances specifically enumerated above, all contact distances mentioned were greater than or equal to van der Waals contact distances.

TABLE 3. Selected distances and angles for *cis*-dichlorobis-(cyclopropylamine)platinum(II)

Atoms	Distance (Å)	Atoms	Distance (Å)
	Bonded distances		
Pt—Cl(1)	2.272(4)	C(1)—C(2)	1.43(2)
Pt—Cl(2)	2.287(4)	C(1)—C(3)	1.49(2)
Pt—N(1)	2.05(1)	C(2)—C(3)	1.48(2)
Pt—N(2)	2.04(1)	C(4)—C(5)	1.51(2)
N(1)—C(1)	1.43(2)	C(4)—C(6)	1.41(3)
N(2)—C(4)	1.44(2)	C(5)—C(6)	1.48(3)
	Nonbonded distances		
Cl(1)—Cl(2)	3.295(6)	Cl(2)—N(1)	2.99(1)
Cl(1)—N(2)	3.04(1)	N(1)—N(2)	2.92(2)

Atoms	Angle (deg)	Atoms	Angle (deg)
Cl(1)—Pt—Cl(2)	92.6(1)	N(1)—C(1)—C(2)	118(1)
Cl(1)—Pt—N(1)	178.4(3)	N(1)—C(1)—C(3)	117(1)
Cl(1)—Pt—N(2)	89.3(3)	C(2)—C(1)—C(3)	61(1)
Cl(2)—Pt—N(1)	87.1(4)	C(1)—C(2)—C(3)	62(1)
Cl(2)—Pt—N(2)	178.1(3)	C(1)—C(3)—C(2)	58(1)
N(1)—Pt—N(2)	91.1(5)	N(2)—C(4)—C(5)	118(1)
Pt—N(1)—C(1)	116.1(9)	N(2)—C(4)—C(6)	122(1)
Pt—N(2)—C(4)	113.6(9)	C(5)—C(4)—C(6)	61(1)
		C(4)—C(5)—C(6)	56(1)
		C(4)—C(6)—C(5)	63(1)

Possible H-bond distances

Atoms	Distance
Cl(1)···N(2)[a]	3.25(1)
Cl(1)···N(2)[b]	3.37(1)
Cl(2)···N(1)[a]	3.36(1)

[a] $x, -y, z$.
[b] $1-x, -y, -z$.

The Vibrational Spectra

The infrared and Raman spectra of cyclopropylamine, the d_2-deuterated analogue and platinum complexes of the two ligands were recorded and examined. The cyclopropylamine spectrum was essentially the same as that reported by Kalasinsky *et al.* (26) with minor variations in wave number for some bands. We also report the spectrum of the analogue, deuterated at the amine, and the polarization ratios for both ligands, which have not been reported previously. The spectra are very similar, the only changes being those associated with the ND_2 group. These absorptions are shifted to lower wave number (ND_2 asym. str. 2533 ir, 2520 R, ND_2 sym. str. 2476 ir, 2474 R, ND_2 def. 1231 ir, ND_2 wag, 680 ir, ND_2 rock, 630 ir, ND_2 twist, not observed), the ratio ν_H/ν_D being 1.31–1.34. The complete spectra and assignments are listed in Table 5.

By studying the isotopic shifts in the ligand and the complex as well as bands exclusive to the complex, and by comparison with other platinum complexes, we have been able to assign most of the bands. These assignments together with the observed frequencies are shown in Table 4. The spectra for the complex in the ligand region are much less simple than those for the free ligand, firstly because there is a pair of symmetric and asymmetric modes for each vibration of the pure ligand; secondly because some modes shift on complexing and some do not; and finally because there may be interactions between the vibrations of the crystallographically inequivalent cyclopropylamine groups.

Can. J. Chem. Downloaded from www.nrcresearchpress.com by 210.87.254.42 on 09/06/12
For personal use only.

Can. J. Chem. Downloaded from www.nrcresearchpress.com by 210.87.254.42 on 09/06/12
For personal use only.

NH_2 and CH_2 Stretches and Deformations

The NH_2 stretching vibrations are shifted to lower energies ($\sim 100\,cm^{-1}$) in the complexes as compared with the ligand, as are the deformations ($\sim 50\,cm^{-1}$). The ratio $\nu_{ligand}/\nu_{complex} \cong 1.04$. The ND_2 shifts for these motions are in the ratio $\nu_H/\nu_D = 1.34–1.36$ for the complexes. Similar assignments have been made previously for several ethylenediamineplatinum(II) complexes (27).

The CH_2 stretching vibrational frequencies for the complexes are close to those observed for the ligand (for which the higher one is more intense in the infrared, and the lower one is more intense in the Raman and polarized). The positions are typical for the somewhat strained three-membered ring (28).

The CH stretch was assigned previously (26), on the basis of band contours, to the infrared band at $2975\,cm^{-1}$ for cyclopropylamine vapour. There are no distinct bands in the complexes that can be so assigned, but our $2965\,cm^{-1}$ ligand band disappears in the complexes and it is possible that this vibration occurs at a higher wave number in the complexes because of additional strain and is lost under the $—CH_2$ absorptions. Pairs of bands for the complex at 1462 and $1430\,cm^{-1}$ which do not shift on deuteration are assigned to the CH_2 symmetric and asymmetric deformations. These are very close to the pure ligand frequencies.

The pair of bands at $1370\,cm^{-1}$ is assigned to the CH bend (in-plane); it occurs at slightly higher energy in the complexes ($\nu_{complex}/\nu_{ligand} = 1.01$), and is slightly affected by deuteration, ($\nu_H/\nu_D = 1.01–1.02$). A similar assignment ($1374\,cm^{-1}$) was previously made for the ligand (26). The CH bend (out-of-plane) for the ligand (solid phase spectra) was previously assigned as $1026\,cm^{-1}$ (26). This frequency was not observed in our solution spectra of the ligand; for the complexes, it could be hidden under the $1030\,cm^{-1}$ bands which are broad in the infrared spectra, and the 1010 and $1012\,cm^{-1}$ bands for the d_2-complex have some additional intensity. Such an assignment would give the same $\nu_{complex}/\nu_{ligand}$ and ν_H/ν_D ratios that were noted for the CH in-plane bend.

The middle frequency range of the spectra ($1300\,cm^{-1} - 700\,cm^{-1}$) contains many bands with overlaps, intensity variations, and deuterium shifts in several ratios. There will obviously be some ambiguities and some of the assignments must be considered to be tentative. We have, however, succeeded in making reasonable assignments for all the observed bands, and will indicate where the anomalies lie.

Twisting, Wagging, and Rocking Vibrations

The $—NH_2$ twisting vibration is assigned to the $1267, 1260\,cm^{-1}$ bands (982, 975 d_2-complex, ν_H/ν_D ratio 1.29). This vibration is unique to the complexes. The corresponding motion in the ligand is a hindered rotation which was observed at fairly low energy ($254\,cm^{-1}$) in the infrared spectrum (26).

The NH_2 wags for the complexes are assigned by us to bands at $1122\,cm^{-1}$ ($887\,cm^{-1}$, $\nu_H/\nu_D = 1.26$) and $958\,cm^{-1}$ ($785\,cm^{-1}$, $\nu_H/\nu_D = 1.22$). The NH_2 rocks are assigned to bands at 757, $724\,cm^{-1}$ (618, $593\,cm^{-1}$, $\nu_H/\nu_D = 1.22$). The correlating ligand bands occur at $680\,cm^{-1}$ (ND_2 wag) and 826(630) cm^{-1} (rock), which is in disagreement with previous assignments (26), probably in part because of different nomenclature. The infrared spectrum of the d_2-ligand exhibits a shoulder at $680\,cm^{-1}$ on the broad, very intense $630\,cm^{-1}$ band. We assign $680\,cm^{-1}$ to the ND_2 wag. If the ν_H/ν_D ratios are 1.31 for both the rock and the wag, then the NH_2 wag would have a wave number of $890\,cm^{-1}$, and would be masked by the very broad ($250\,cm^{-1}$) group centred at $826\,cm^{-1}$.

Our ordering for these NH_2 group deformation modes is consistent with the usual ordering for similar CH_2 modes (28). The deuterium shift ratios are less than for the NH_2 stretching vibrations, more so for the complexes than for the ligands, a difference which would be expected as a result of moderately strong coupling with the skeletal motions.

The general order for CH_2 group vibrations is twist > wag > rock (28). Twisting vibrations usually result in lower intensity absorptions than wagging vibrations. We observe ligand bands at 1170, 1100; 1014, 1044; and 759, $826\,cm^{-1}$, which are assigned to pairs of twists, wags, and rocks respectively. These bands show no shifts on deuteration and the assignments are in agreement with previous work (26) except where noted. We observe bands for the complexes at 1170 and 1110, 1094; 1034, 1029 and 1068, 1050; and 744 and 829, 820 which are not affected by deuteration and which are similarly assigned. The 1170 band in the d_2-complex is not observed directly and appears to be lost under the $1180–1158\,cm^{-1}$ group where the upper band is quite broad and has weak components at 1179, 1172, and $1167\,cm^{-1}$. The $820\,cm^{-1}$ group is somewhat weaker in the d_2-complex, and it is possible that this frequency represents two or more overlapping bands, one of which is shifted.

Ring Deformation and CN Vibrations

The ring breathing mode for the ligand is observed at $1210–1214\,cm^{-1}$ in agreement with Kalasinsky *et al.* (26) who assigned the band at this wave number to the more stable *trans* configuration and a vapour phase Raman band at $1220\,cm^{-1}$ to the

TABLE 4. Vibrational spectra of *cis*-$PtCl_2(C_3H_5NH_2)_2$ and *cis*-$PtCl_2(C_3H_5ND_2)_2$[a]

Assignment	*cis*-$PtCl_2(C_3H_5NH_2)_2$		*cis*-$PtCl_2(C_3H_5ND_2)_2$		ν_H/ν_D
	Infrared	Raman	Infrared	Raman	
NH_2 asym.str.	3266(65) 3242(67)	3245(8) 3205(26)	[2432(100)]	[2422(21)]	1.34
NH_2 sym.str.	3205(72) 3138(60)	3197(23) 3135(12)	[2350(89)]	[2367(21)] [2325]	1.36
CH_2 asym.str.	3080(29)	3085(21) 3082(29)	3080(19)	3081(35)	
CH_2 sym.str.	3062(32)	3070(51) 3059(33)		3069(48) 3059(29)	
CH str.	3001(8)	2997(72)	3005(32)	3000(60)	
NH_2 def.	1592(100) 1560(65)	1590(17) 1587(13)	[1180(50)] [1150(91)]	[1179(vw)] [1158(15)]	1.35 1.36
CH_2 sym.def.	1456	1462(21) 1453(14)	1462(47)	1462(15) 1449(15)	
CH_2 asym.def.	1433(34) 1414(21)	1430(14)	1430(55) 1420(72)	1427(8)	
CH bend (in plane)	1388(44) 1385(40)	1382(18) 1378(24)	1370(sh) 1362(81)	1379(12) 1360(18)	1.01 1.02
NH_2 twist	1267(17) 1260(19)	1262(12)	[975(55)]	[982(27)] [975(15)]	1.29 1.29
Ring breathing	1240(38) 1230	1232(16) 1222(27)	1240(sh) 1220(81)	1220(68)br	
CN str.	1215(34) 1204(90)	1210(73) 1204(100)	[1010(87)] [1000(91)]	[1012(95)] [1008(100)]	1.2 1.2
CH_2 twist	1169(12)	1175(4) 1169(4)	hidden under 1180/1150 group		
NH_2 wag	1122(sh)		[887(77)]	[892]	1.26
CH_2 twist	1110(47) 1094(31)	1113(15) 1095(8) 1087(4)	1094(vw)	1110(vw)	
CH_2 wag	1068(19) 1050(19)	1050(8)	1068(49) 1050(47)	1070(6)	
CH bend (out-of-plane)	hidden under 1030		[1010]	[1012]	
CH_2 wag	1034(73)br 1029(79)br	1032(7) 1028(10)	1034(83) 1030	1034(23)	
NH_2 wag	958(20)	961(26)	[785(34)]	[788(23)]	1.22
Ring def.	933(41) 921(27)	934(58) 920(38) 845(12)	[887(77)] [880(71)] 850(41)br	[895(13)] [885(6)] 857(15)br	1.05 1.05
CH_2 rock	829(69) 820(57)br	829(12) 822(21)	830(48) 820(62)	835(5) 828(7)	
Ring def.	810	816(14)	815(76)	815(7)	
NH_2 rock	757(40)	762(23) 758(37)	[618(49)]	[622(21)]	1.22
CH_2 rock	744(42)	744(18)	740(58)	745(42)	
NH_2 rock	724(40)	732(15) 726(13)	[593w]	[590vw]	1.22
Pt—N str.	595(7)	601(55) 593(18)	540w,br	555(35) 549(13)	1.08 1.08

Can. J. Chem. Downloaded from www.nrcresearchpress.com by 210.87.254.42 on 09/06/12
For personal use only.

TABLE 4 (*Concluded*)

Assignment	*cis*-$PtCl_2(C_3H_5NH_2)_2$ Infrared	*cis*-$PtCl_2(C_3H_5NH_2)_2$ Raman	*cis*-$PtCl_2(C_3H_5ND_2)_2$ Infrared	*cis*-$PtCl_2(C_3H_5ND_2)_2$ Raman	ν_H/ν_D
C—N—Pt def.	406(40) 396sh		353(53)br		1.15
Pt—Cl sym.str.	332(88) 321(96)	333(74) 326(88) 317(9)	325(94)br	331(74) 328(85)	
Pt—Cl asym.str.	296(37)	302(61) 291(31)		300(57) 288(29)	
Pt—N def. (in-plane)	225(19)	233(40)		217(16)	1.07
Pt—N def. (out-of-plane)		201(12)br 196(12) 190(11)		192w,br 182 182br	1.07 1.02 1.06
Pt—Cl def. (in-plane) (out-of-plane)		163(83) 123(45)		163(76) 123(38)	
		111(40) 78(46)		115(40) 78(60)	

[a]Relative intensities shown in parentheses. Symbols: br broad, sh shoulder, w weak, v very.

gauche conformer. In the complex the ligand takes on the *gauche* configuration (see Fig. 1), and therefore an intense pair of bands at $\sim 1220\,cm^{-1}$ which shows no shift on deuteration is assigned to the ring breathing mode. This band is intensified in the d_2-complex by the overtone of $618\,cm^{-1}$.

The other two ligand ring deformations have been assigned to bands at $971\,cm^{-1}$ (*gauche*, vapour, ir, and Raman) and $884\,cm^{-1}$ (vapour, ir, and Raman) (26). We observe ligand bands at $968\,cm^{-1}$ and $880\,cm^{-1}$ and assign them as asymmetric (infrared inactive) and symmetric ring deformations respectively. For the complexes one expects considerable coupling between ring modes, CN stretching, and NH_2 group deformations and the assignments must be considered tentative, particularly as there are some changes in relative intensity in the $800\,cm^{-1}$ region: our preferred assignments for the complexes are 933, $921\,cm^{-1}$ (887, $880\,cm^{-1}$, $\nu_H/\nu_D = 1.05$); 845, 850 (850, $857\,cm^{-1}$, no shift). The 933, $921\,cm^{-1}$ bands are so close to the $958\,cm^{-1}$ NH_2 wag that coupling is likely and a slight deuterium shift is reasonable.

Alternatively it is to be noted that the $820\,cm^{-1}$ band which is assigned to the CH_2 rock is broader and has greater relative intensity in the h_2-complex than in the d_2-complex. This fact suggests that it represents more than one band, and that part of it shifts on deuteration. A shift from 820 to $785\,cm^{-1}$ (ratio 1.05), for example, might be reasonable for a ring deformation. The band at $785\,cm^{-1}$, which has been assigned as the ND_2 wag, also has enough intensity and breadth to encompass an extra band.

We assign the intense pair of bands at 1215, $1204\,cm^{-1}$ (1010, $1000\,cm^{-1}$, $\nu_H/\nu_D = 1.2$) to the C—N stretch. The $1215\,cm^{-1}$ region in the h_2-complex is complicated by Fermi resonance with the first overtone of the Pt—N stretch, as well as by strong coupling with both the NH_2 twisting vibration, and particularly the very intense symmetric ring breathing mode. In the ligand a band at $1145\,cm^{-1}$ was assigned to the C—N stretch ($\nu_H/\nu_D = 1.19$) and hence there is a shift to higher energy in the complex in the ratio 1.06.

A C—N—Pt deformation is assigned to the band at $406\,cm^{-1}$ ($353\,cm^{-1}$, $\nu_H/\nu_D = 1.15$).

The platinum–nitrogen stretching motions are exclusive to the complex and occur to the higher end of the frequency range for such vibrations in other platinum–nitrogen complexes (29). The bands at 601, $593\,cm^{-1}$ (555, 549) are assigned as the symmetric and asymmetric vibrations on the basis of Raman intensities. The ν_H/ν_D ratio is 1.08, indicating moderately weak coupling with an NH_2 vibration.

The platinum–chlorine stretching vibrations are observed at $333\,cm^{-1}$ (symmetric) and $302\,cm^{-1}$ (asymmetric) with no shift on deuteration. The predicted chlorine isotope effect is a splitting into three components of relative intensity 9:6:1. A splitting is observed for the totally symmetric vibration (333, 326, $317\,cm^{-1}$) but the middle com-

Can. J. Chem. Downloaded from www.nrcresearchpress.com by 210.87.254.42 on 09/06/12
For personal use only.

TABLE 5. Vibrational spectra of $C_3H_5NH_2$ and $C_3H_5ND_2$ (cm^{-1})[a]

		$C_3H_5NH_2$			$C_3N_5ND_2$			
Assignment	Vibration[b]	Infrared	Raman	ρ[c]	Infrared	Raman	ρ	ν_H/ν_D
NH_2 asym.str.	$3412\,\nu_{16}$	3392(30)	3374(10)	dp	[2533(36)]	[2520(6)]	dp	1.34
NH_2 sym.str.	$3348\,\nu_1$	3320(11)	3327(26)	0.2	[2476(15)]	[2474(17)]	0.16	1.34
2×1210[e]						[2408(16)]	0.13	
CH_2 asym.str.	$3100\,\nu_{17}$ $3100\,\nu_2$	3091(51)	3077(26)	dp	3091(60)	3078(14)	0.17	
CH_2 sym.str.	$3032\,\nu_3$ $3023\,\nu_{18}$	3010(62)	3005(100)	0.15	3010(71)	3006(100)	dp	
CH str.	$2975\,\nu_4$	2966(62)	2965(23)	0.3	2965(66)	2965(19)	0.1	
2×1454[e]			2901(6)	dp		2901(3)	dp	
2×826[e]		1660sh						
NH_2 def.	$1617\,\nu_5$	1615(60)br			[1231(81)]			1.31
CH_2 def.	$1456\,\nu_6$	1454(88)	1455(21)	0.3	1455(92)	1455(11)	0.27	
	$1424\,\nu_{19}$	1420(10)	1417(14)	dp	1419(25)	1421(6)	dp	
CH bend (in-plane)	$1374\,\nu_7$	1370(98)	1372(17)	0.22	1370(100)	1371(16)	0.1	
Ring breathing (*gauche*)	$1214\,\nu_8$ (1220)	1209(46)	1214(75)	0.12	1210(sh)	1215(60)	0.14	
CH_2 twist	$1168\,\nu_9$	1169(2)	1172(3)	dp	1170(4)	1170(8)	dp	
C—N str.	$1150\,\nu_{10}$	1145(38)	1146(15)	0.11	[965(40)]	[969(50)]	0.1	1.19
CH_2 twist	$1104\,\nu_{20}$	1105(32)			1110(30)			
CH_2 sym.wag	$1045\,\nu_{21}$	1040(65)			1044(71)			
CH bend (out-of-plane)	1026[f] ν_{22}	Not observed						
CH_2 asym.wag	$1020\,\nu_{11}$	1014(100)	1014(16)	0.2	1014(93)	1014(8)	0.2	
Ring def.	$989\,\nu_{12}$ (971 *gauche*)	Inactive	989(54)	0.11	Inactive	975(43)	0.1	1.01
			968(17)	0.15		969(50)		
Ring def.	$884\,\nu_{24}$	880(74)	881(16)	dp	840sh	833br		1.05
NH_2 wag	940[f] ν_{24}	890(?)			[680(sh)]			1.31
CH_2 rock (out of phase)	$830\,\nu_{25}$	826(84) v br	826(16)	dp	829(49)br	833(11)v br	dp	
NH_2 rock	$805\,\nu_{13}$ (wag)	826			[630(91)]			1.31
CH_2 sym. rock (in phase)	$762\,\nu_{14}$		759(25)	dp		753(11)	dp	
		704[g](14)						
CN bend (in-plane)	$408\,\nu_{15}$	403(59)	411(9)	dp	390(64)	390(6)v br	dp	
CN bend (out-of-plane)	$396\,\nu_{26}$							
NH_2 torsion	$254\,\nu_{27}$							

[a] Symbols: br, broad; sh, shoulder; v, very; w, weak.
[b] Data from ref. 26.
[c] ρ, polarization ratios; dp, polarized.
[d] Relative intensities (shown in parentheses).
[e] Fermi resonance doublet.
[f] Observed for solid only in ref. 26.
[g] Unassigned.

ponent has the highest intensity. This increased intensity is attributed to coincidence with the first overtone of the Pt—Cl deformation at 163 cm^{-1} ($2 \times 163 = 326\,cm^{-1}$). The frequency separation of the components is the predicted amount.

The Pt—N deformations occur at the usual frequencies and exhibit shifts in the ratio $\nu_H/\nu_D = 1.07$.

The Pt—Cl deformations are observed at 163 and 123 cm^{-1}, with no shifts, and again these are

Can. J. Chem. Downloaded from www.nrcresearchpress.com by 210.87.254.42 on 09/06/12
For personal use only.

very characteristic frequencies for these motions (17).

Acknowledgements

We acknowledge, with thanks, financial support from the Natural Sciences and Engineering Research Council of Canada, National Cancer Institute of Canada, McMaster University Science and Engineering Research Board, and Johnson, Matthey, Mallory Ltd.

1. B. ROSENBERG, L. VANCAMP, J. G. TRASKO, and V. H. MANSOUR. Nature, London, **222**, 385 (1969).
2. T. A. CONNORS. *In* Platinum coordination complexes in cancer chemotherapy. *Edited by* T. A. Connors and J. J. Roberts. Springer-Verlag, New York. 1974. p. 112ff.
3. M. J. CLEARE. Coord. Chem. Rev. **12**, 349 (1974).
4. B. ROSENBERG. Platinum Met. Rev. **15**, 42 (1971).
5. M. J. CLEARE and J. D. HOESCHELE. Bioinorg. Chem. **2**, 187 (1973).
6. J. Clin. Hematol. Oncol. **7** (1977).
7. M. J. CLEARE and J. D. HOESCHELE. Platinum Met. Rev. **17**, 2 (1973).
8. Biochimie, **60** (1978).
9. T. A. CONNORS, M. JONES, W. C. J. ROSS, P. D. BRADDOCK, A. R. KHOKHAR, and M. L. TOBE. Chem.-Biol. Interact. **5**, 415 (1972).
10. P. D. BRADDOCK, T. A. CONNORS, M. JONES, A. R. KHOKHAR, D. H. MELZACK, and M. L. TOBE. Chem.-Biol. Interact. **11**, 145 (1975).
11. S. C. DHARA. Indian J. Chem. **8**, 193 (1970).
12. R. P. HUGHES, N. KRISHNAMACHARI, C. J. L. LOCK, J. POWELL, and G. TURNER. Inorg. Chem. **16**, 314 (1977).
13. B. LIPPERT, C. J. L. LOCK, B. ROSENBERG, and M. ZVAGULIS. Inorg. Chem. **16**, 1525 (1977).
14. W. C. HAMILTON. Acta Crystallogr. **18**, 502 (1965).
15. A. C. LARSON. Acta Crystallogr. **23**, 664 (1967).
16. D. T. CROMER and J. WABER. International tables for X-ray crystallography. Vol. IV. Kynoch Press, Birmingham. 1974.
17. K. NAKAMOTO. Infrared and Raman spectra of inorganic and coordination compounds. 3rd ed. John Wiley and Sons, Inc., New York. 1978. Part III.
18. J. M. STEWART. The XRAY 76 System. Tech. Rep. TR-446. Computer Science Center, Univ. of Maryland, College Park, MD. 1976
19. M. E. PIPPY and F. R. AHMED. Mean planes and torsional angles. Report NRC-22. National Research Council of Canada, Ottawa, Canada.
20. C. K. JOHNSON, ORTEP II. Report ORNL-5138, Oak Ridge National Laboratory, TN. 1976.
21. C. J. L. LOCK and M. ZVAGULIS. Inorg. Chem. **20**, 1817 (1981).
22. C. J. L. LOCK, R. A. SPERANZINI, and M. ZVAGULIS. Acta Crystallogr. B**36**, 1789 (1980).
23. J. P. BRADFORD, R. FAGGIANI, and C. J. L. LOCK. Acta Crystallogr. B**37**, 243 (1981).
24. C. J. L. LOCK and M. ZVAGULIS. Acta Crystallogr. B**36**, 2140 (1980).
25. D. K. HENDERICKSEN and M. D. HARMONY. J. Chem. Phys. **51**, 700 (1969).
26. V. F. KALASINSKY, D. E. POWERS, and W. C. HARRIS. J. Phys. Chem. **83**, 506 (1979).
27. D. B. POWELL and N. SHEPPARD. Spectrochim. Acta, **17**, 68 (1961).
28. JAMES R. DURIG (*Editor*). Vibrational spectra and structure. Vol. 7. Elsevier Scientific Publishing Co., Amsterdam. 1978. Chapt. 1.

Can. J. Chem. Downloaded from www.nrcresearchpress.com by 210.87.254.42 on 09/06/12
For personal use only.

A crystallographic and spectroscopic study of mercury(II) dithiocarbamate

CHUNG CHIEH AND SING KWEN CHEUNG

Guelph–Waterloo Centre for Graduate Work in Chemistry, University of Waterloo, Waterloo, Ont., Canada N2L 3G1

Received February 24, 1981

CHUNG CHIEH and SING KWEN CHEUNG. Can. J. Chem. **59**, 2746 (1981).

Ammonium dithiocarbamate, $H_2NCS_2NH_4$, decomposes easily but the anion forms a stable mercury(II) complex, the crystals of which are orthorhombic with $a = 7.851(3)$, $b = 17.565(7)$, $c = 12.051(3)$ Å, and space group *Pbca*. The structure was solved by the Patterson method and refined by the full-matrix least-squares method to an R of 0.038 for 781 reflections. The structure consists of layers of two-dimensional polymeric networks. The dimeric subunits in the layer containing two each of mutually connected Hg atoms and dithiocarbamates are further linked by other bridging dithiocarbamates forming a sheet-like structure. Each Hg atom bonds to four S atoms from four separate dithiocarbamates with Hg—S distances of 2.499(4), 2.508(4), 2.533(4), and 2.629(4) Å. The ir bands observed were: $\nu(NH_2)$, 3320, 3220, 3125; $\delta(NH_2)$, 1600; ν(C—N), 1395; $\rho_r(NH_2)$, 1172; and ν(C—S), 840 cm^{-1}. The mass spectrum of this polymeric compound gave peaks corresponding to Hg, S_2, CNH_2, HNCS, S, CS_2, S_5, S_4, S_3, and S_8 in the order of their intensities.

CHUNG CHIEH et SING KWEN CHEUNG. Can. J. Chem. **59**, 2746 (1981).

Le dithiocarbamate d'ammonium, $H_2NCS_2NH_4$, se décompose facilement mais l'anion forme un complexe stable de mercure(II) dont les cristaux sont orthorhombiques avec $a = 7,851(3)$, $b = 17,565(2)$, $c = 12,051(3)$ Å, groupe d'espace *Pbca*. On a résolu la structure par la méthode de Patterson et on l'a affinée par la méthode des moindres carrés (matrice complète) jusqu'à une valeur de $R = 0,038$ pour 781 réflexions. La structure comprend des couches d'un réseau polymérisé bidimensionnel. Les sous unités dimères de la couche contiennent deux atomes de Hg et deux dithiocarbamates reliés l'un à l'autre et qui sont de plus reliés à d'autres dithiocarbamates formant ainsi une structure lamellaire. Chaque atome de mercure est lié à 4 atomes de soufre provenant de quatre dithiocarbamates avec les distances Hg—S = 2,499(4), 2,508(4), 2,533(4) et 2,629(4) Å. On a observé les bandes ir suivantes: $\nu(NH_2)$, 3320, 3220, 3125; $\delta(NH_2)$, 1660; ν(C—N), 1395; $\rho_r(NH_2)$, 1172; et ν(C—S), 840 cm^{-1}. Le spectre de masse de ce composé polymérisé donne des pics correspondants à Hg, S_2, CNH_2, HNCS, S, CS_2, S_5, S_4, S_3 et S_8 dans l'ordre de leurs intensités.

[Traduit par le journal]

Introduction

In our study of interaction between mercury(II) ion and tetraethylthiuram disulfide (1), we encountered and reported many crystal structures of dithiocarbamate complexes (2–5). Results from these structures indicate that mercury(II) and dithiocarbamates bond in various ways and the complexes formed depend not only on the solvent used, but also on the concentration of halide ions which are often incorporated into the complex.

Most dithiocarbamate or xanthate complexes of heavy metals have short metal-to-sulfur bonds (6). Their structural features led us to believe that these dithio acids might be potentially useful for removing metal ions from industrial waste waters. Therefore, we have explored further the properties of these dithio acids.

The ammonium salt of the first member of dithiocarbamates, $H_2NCS_2^-$, is not stable at 298 K. Although its formation from reaction between ammonia and carbon disulfide was noted as early as 1850 by Debus (7), and improved methods for its preparation were patented in 1940 and 1941 (8), structural studies on metal complexes of this compound are scarce (9). Two crystal structures of mercury(II) *N*,*N*-diethyldithiocarbamate were reported by Iwasaki (10), who indicated to us in May 1980 that he was refining the structure of mercury(II) *N*,*N*-dimethyldithiocarbamate. The structural features of these compounds and those published by us suggested that mercury(II) ion might form a compound with $H_2NCS_2^-$ through the coordination of sulfur atoms, thus stabilizing the anion. Indeed, mercury(II) dithiocarbamate was the first stable complex obtained in this laboratory and here we report its crystal structure as determined by X-ray diffraction.

Experimental

Chemicals and solvents used in these experiments were of reagent grade from BDH. Ammonium dithiocarbamate was prepared by the method described in ref. 11. The mass spectrum was measured on a VG 7070 (by VG Micromass) by electron bombardment. The ir spectrum was obtained on a Perkin Elmer 457 using KBr pellets.

Preparation of Mercury(II) Dithiocarbamate

This experiment was carried out in a cold room (273 K).

To 15 mL aqueous/ethanol (50/50 by volume) solution of ammonium dithiocarbamate (0.004 mol), 10 mL ethanol solution of $HgCl_2$ (0.002 mol) was added slowly. A white precipitate (A) which formed instantly was filtered off. The clear filtrate was allowed to evaporate slowly and colorless crystals (B) were obtained amongst a black material (HgS) resulting from decomposition. In an attempt to recrystallize the white precipitate A, it was suspended in an aqueous/ethanol solution and the white slurry turned black after a few hours. The filtrate from this yielded crystals similar to B when dried. The crystals were stable with no deterioration even when irradiated by X-rays. Although some well-formed crystals were covered with a thin

0008-4042/81/182746-04$01.00/0

©1981 National Research Council of Canada/Conseil national de recherches du Canada

Can. J. Chem. Downloaded from www.nrcresearchpress.com by 210.87.254.40 on 09/06/12
For personal use only.

Can. J. Chem. Downloaded from www.nrcresearchpress.com by 210.87.254.40 on 09/06/12
For personal use only.

layer of black material, others could be visually identified as colorless.

Crystallographic Study

A prismatic crystal with dimensions of 0.20 × 0.18 × 0.10 mm was mounted on a Syntex $P2_1$ computer-controlled diffractometer and a rotation photograph was taken. Film coordinates of 15 reflections were measured; their angles were calculated and refined by repetitive measurements. These were used to determine cell constants and the orientation matrix. The space group was determined by noting the systematics of unobserved reflections.

Crystal Data

$C_2H_4HgN_2S_4$ fw = 384.9

Orthorhombic, a = 7.851(3), b = 17.565(7), c = 12.051(3) Å, V = 1662(1) Å^3. Space group *Pbca* (D_{2h}^{15} No. 61). D_o = 3.05(4) (by flotation in a mixture of *s*-tetrabromoethane and diiodomethane), Z = 8, D_c = 3.076 g cm^{-3}. mp = 438–439 K, λ(Mo Kα) = 0.71069 Å.

A total of 781 reflections with $2\theta \leq 45°$ was measured; those with F less than $\sigma(F)$ were given a value of $0.25*\sigma(F)$. They were all used in the structural analysis; no absorption correction was made. The structure was solved by the heavy-atom method and refined by full-matrix least-squares using the SHELX system (12). Anisotropic temperature factors were given to all non-hydrogen atoms and positions for the H atoms of the $—NH_2$ group were estimated from a difference Fourier map. These were included in the last cycle of the 93-variable least-squares with the isotropic temperature factor, U, of the H maintained constant at 0.05. The function minimized was $\Sigma w(|F_o| - |F_c|)^2$, with $w = 1/\sigma^2(F)$. The final R and R_w factors were 0.039 and 0.044 respectively. The atomic parameters are given in Table 1.[1]

Results and Discussion

Many methods for the preparation of ammonium dithiocarbamate have been described in the literature, and we have tried various ways. The use of ether/ethanol as a solvent as described in ref. 11 for the reaction between NH_3 and CS_2 gave a reasonably pure crop of $H_2HCS_2NH_4$ and the product was even stable at 298 K for at least a day, provided it remained in the solvent. The yellow ammonium dithiocarbamate crystals changed to a liquid form when they were in contact with air at 298 K, possibly due to the absorption of moisture.

However, the crystal of its mercury complex was stable and the intensities of the checking reflections did not decline throughout the course of data collection. We further examined the stability of mercury(II) dithiocarbamate by carrying out the reactions in either absolute ethanol or water. Mercury(II) dithiocarbamate formed in an absolute ethanol solution was creamy white and no coloration was observed if kept under a dry N_2 atmosphere. This precipitate turned yellow when exposed to air. Mercury(II) chloride reacted with ammonium dithiocarbamate in an aqueous solution giving a similar precipitate, but it turned black in a few hours; these products are being studied. The crystal used in this study was prepared by reaction of $H_2NCS_2NH_4$ and $HgCl_2$ in an aqueous/ethanol solution at 273 K.

TABLE 1. Final atomic coordinates (10^4)

Atom	*x/a*	*y/b*	*z/c*	*B**
Hg	1215(1)	3656.9(3)	5759(1)	2.57
S(1)	3192(5)	4281(2)	4251(3)	2.36
S(2)	246(6)	5189(1)	3470(3)	2.36
S(3)	3040(6)	2986(2)	7147(3)	3.70
S(4)	4466(6)	2432(2)	5016(4)	3.11
N(1)	3034(19)	5768(8)	4356(13)	3.27
N(2)	4612(25)	1692(8)	6928(12)	5.07
C(1)	2222(21)	5143(10)	4106(12)	2.48
C(2)	4083(20)	2315(9)	6397(13)	3.02

*$B = 8\pi^2 \sum_{i=1}^{3} U_{ii}/3$.

The simple formula of mercury dithiocarbamate $Hg(S_2CNH_2)_2$ does not represent the structure in the crystal, which consists of layers of networks as shown in Fig. 1. This network can be understood easily by employing a topological pattern, see Fig. 2. The subunits in the layer are dimers which contain two each of mutually connected mercury atoms, M, and dithiocarbamates, X. The center of this subunit is represented by B in Fig. 1. These dimers are further linked by bridging dithiocarbamate into a two-dimensional sheet extending to the

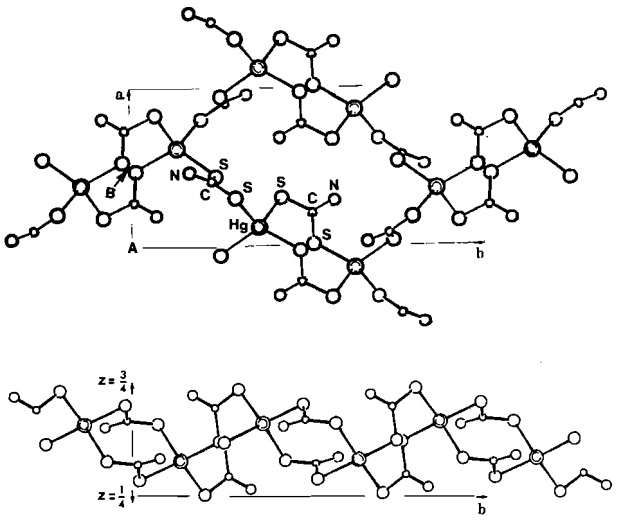

FIG. 1. Two views of the layer, one looking from a direction perpendicular to the layer (top) and one from the side of the layer. The unit cell is given to show the orientation of the layer in it.

[1]A complete set of data is available, at a nominal charge, from the Depository of Unpublished Data, CISTI, National Research Council of Canada, Ottawa, Ont., Canada K1A 0S2.

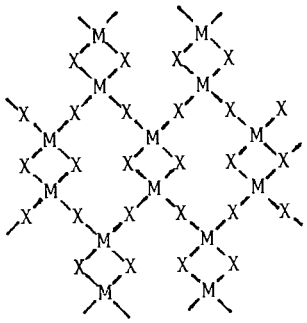

FIG. 2. Topological pattern of the layer structure.

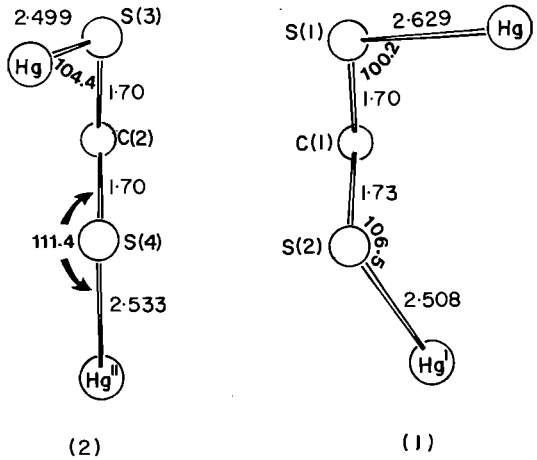

FIG. 3. The relative positions of the mercury atoms as seen from the C—NH_2 direction of the dithiocarbamates. (*1*) The anion bonded to two Hg atoms forming the dimeric subunit. (Hg′ at $-x, 1-y, 1-z$); (*2*) the anion linking the dimeric subunit into a two dimensional sheet. Standard deviations are σ(Hg—S) = 0.004 Å, σ(C—S) = 0.02 Å, σ(Hg—S—C) = 0.5° (Hg″ at $0.5+x, 0.5-y, 1-z$).

sides of the crystals. Two types of rings are found in the sheet structure, an 8-membered ring in the dimeric subunits and a 16-membered ring involving 4 dithiocarbamates and 4 subunits. The centers of these rings are crystallographic centers of symmetry. The 8-membered ring adopted an extended chair form. The *c* axis goes through the centers of the 8- and the 16-membered rings alternately, i.e. layers stack up switching their positions A and B in the [0 0 1] direction.

Each mercury atom is bonded to four sulfur atoms with Hg—S distances ranging from 2.499(4) to 2.629(4) Å (see Fig. 3). The six angles are S(1)HgS(2), 100.9; S(1)HgS(3), 108.7; S(1)HgS(4), 112.3; S(2)HgS(3), 113.3; S(2)HgS(4), 119.9; and S(3)HgS(4), 101.6°, all with standard deviation of 0.1°. Thus the coordination is distorted tetrahedral.

There is an interesting difference in the positions of the bonded mercury atoms with respect to the planes defined by the four atoms of the NCS_2 group. Both the Hg atoms (deviations: Hg, 2.35; Hg′, 1.17A) are on the same side of the NCS_2 plane of the dithiocarbamate in the dimeric subunits as shown in Fig. 3, which shows the views along the C—N bond for the anions. For the other dithiocarbamate, only one Hg atom deviates significantly from the NCS plane, (deviations: Hg, −1.07 and Hg″, 0.14 Å). These differences may account for the nonequivalence of the Hg—S bonds or the SHgS angles as given above. However, the C—S distances are virtually identical, as are the C—N bonds with a mean of 1.32 Å. These distances are in good agreement with those of nickel bis(dithiocarbamate), in which case, the two anions coordinate to one Ni atom as bidentate chelating ligands. The difference between bidentate and bridging coordination is in the SCS angles: for the Ni complex the mean value is 111.8(1.2)°, whereas for the Hg complex, they are 119.2(5) and 121.5(5)° respectively, for the ligands labeled as C(1) and C(2).

Despite the difference in bonding between the nickel and mercury complexes of dithiocarbamate, they exhibit similar ir spectra, which consist of five well separated bands in the sodium chloride optics region (13). A normal coordinate analysis for dithiocarbamate complexes of Pd, Pt, Ni, Co, Cr, and Cd led to the assignment of the bands at ~3200 cm^{-1} to NH_2 stretching, 1600 cm^{-1} to NH_2 bending, 1400 cm^{-1} to C—N stretching, 1225 cm^{-1} to NH_2 rocking, and 800 cm^{-1} to C—S stretching (14). For the mercury complex, these bands have their maxima at 3125 (a triplet with two other maxima at 3320 and 3220), 1600, 1395, 1172, and 840 cm^{-1}, respectively. From the published data on ir spectra, it appears that NH_2 bending and the C—N stretching modes of Ni, Pt, and Pd complexes are 30 cm^{-1} higher, whereas the ν(C—S) is 10 cm^{-1} lower than those of the mercury complex. The Hg—S band was not in this region.

After the crystal structure was determined, we were curious as to whether we could obtain a mass spectrum for such a 2-dimensional polymeric compound. Indeed, its mass spectrum showed some simple, but interesting fragmentations. Using the natural abundances of isotopes as guides, we clearly identified peaks due to Hg, S_2, CNH_2, HNCS, S, S_6, CS_2, S_5, S_4, S_3, and S_8 in the order of their intensities.

It is perhaps interesting to point out that the use of the computer assisted "Self-Training Interpretive and Retrieval System" (STIRS) (15, 16) suggested the possible substructures of azide, NNN, disulfide, SS, and phenothiazine. None of the suggested possible compounds resemble mercury

Can. J. Chem. Downloaded from www.nrcresearchpress.com by 210.87.254.40 on 09/06/12
For personal use only.

dithiocarbamate. The compound does not contain disulfide linkage, but the presence of S_2 peaks led the system to suggest the disulfide as a possible substructure. Although this is a sulfur-rich compound, it might still be a surprise to find the S_6 peak more intense than those of S_4. The formation of the latter can be rationalized by the collapse of the four S atoms after the liberation of the Hg atom. However, there are many ways by which the S_6 can be formed and the stability of this 6-membered species may contribute to its high intensity. If we neglect the total count due to the various isotopes of mercury, S_2 peaks are the strongest. There are two possibilities: fragmentation from a single dithiocarbamate or from two anions.

Acknowledgement

We thank the Natural Sciences and Engineering Research Council of Canada for financial support.

1. C. CHIEH and L. P. C. LEUNG. Can. J. Chem. **54**, 3077 (1976).
2. C. CHIEH. Can. J. Chem. **55**, 1115 (1977).
3. C. CHIEH. Can. J. Chem. **56**, 564 (1978).
4. L. BOOK and C. CHIEH. Acta Crystallogr. B**36**, 300 (1980.
5. C. CHIEH and K. J. MOYNIHAN. Acta Crystallogr. B**36**, 1367 (1980).
6. D. COUCOUVANIS. Prog. Inorg. Chem. **11**, 233 (1969).
7. H. DEBUS. Ann. Chem. (Liebigs) **73**, 26 (1850).
8. R. A. MATHES. B.F. Goodrich Company, U.S. Patent 2,207,627 (1940); W. H. HILL and D. J. SALLEY, American Cyanmid Company, U.S. patent 2,235,747 (1941).
9. G. F. GASPARRI, M. NARDELLI, and A. VILLA. Acta Crystallogr. **23**, 384 (1967).
10. H. IWASAKI. Acta Crystallogr. B**29**, 2115 (1973).
11. C. E. REDEMANN, R. N. ICKE, and G. A. ALLES. Org. Synth. Coll. **III**, 763 (1967).
12. G. M. SEHDRICK. Private communication.
13. D. COUCOUVANIS and J. P. FACKLER. Inorg. Chem. **6**, 2047 (1967).
14. K. NAKAMOTO, J. FUJITA, R. A. CONDRATE, and Y. MORIMOTE. J. Chem. Phys. **39**, 423 (1963).
15. K. S. KWOK, R. VENKATARAGHAVAN, and F. W. MCLAFFERTY. J. Am. Chem. Soc. **95**, 4185 (1978).
16. F. W. MCLAFFERTY. Interpretation of mass spectra. 3rd ed. University Science Books, Mill Valley, CA. 1980. p. 234.

Can. J. Chem. Downloaded from www.nrcresearchpress.com by 210.87.254.40 on 09/06/12
For personal use only.

Quantum yields in the photolytic oxidation of some sulphur compounds

D. F. SHERATON AND F. E. MURRAY

Department of Chemical Engineering, The University of British Columbia, Vancouver, B.C., Canada V6T 1W5

Received August 11, 1980[1]

D. F. SHERATON and F. E. MURRAY. Can. J. Chem. **59**, 2750 (1981).

The photolytic oxidation of methyl mercaptan, dimethyl sulphide, and dimethyl disulphide was studied in a batch photolysis apparatus. Short wavelength ultraviolet light was provided by a deuterium discharge lamp and monitored by a monochromator equipped with an extended response photomultiplyer tube. Sulphide concentrations were determined using a gas chromatograph equipped with a flame photometric detector having a sulphur response at 365 nm.

The rate of photo-oxidation of methyl mercaptan was found to be a linear function of the photon absorption rate and exhibited a quantum yield of 12. The methyl mercaptan photo-oxidation rate was found to be unaffected by increased oxygen concentration, decreased atmospheric pressure, or the presence of sulphur dioxide.

The quantum yield of dimethyl sulphide photo-oxidation was found to be dependent upon air pressure; the quantum yield of 4 at 1 atm pressure increased to 8 at $\frac{1}{4}$ atm.

The quantum yield of dimethyl disulphide photo-oxidation in air was found to be 1.9 at atmospheric pressure and a disulphide concentration of 7.04×10^{-5} *M*.

D. F. SHERATON et F. E. MURRAY. Can. J. Chem. **59**, 2750 (1981).

Utilisant un appareil à photolyse en discontinu, on a étudié l'oxydation photolytique du méthylmercaptan, du sulfure de diméthyle et du disulfure de diméthyle. On a utilisé une lumière ultraviolette de courte longueur d'onde fournie par une lampe à décharge au deutérium et enregistrée par un monochromateur équippé d'un tube photomultiplicateur à réponse prolongée. On a déterminé les concentrations en sulfure à l'aide d'un chromatographe muni d'un détecteur photométrique à flamme sensible au soufre à 365 nm.

On trouve que la vitesse d'oxydation photochimique du méthylmercaptan est linéaire en fonction de la vitesse d'absorption du photon et présente un rendement quantique de 12. On a trouvé que la vitesse d'oxydation photochimique du méthylmercaptan n'est pas affectée par une augmentation de la concentration en oxygène, par la diminution de la pression atmosphérique ou par la présence du bioxyde de soufre.

On a trouvé que le rendement quantique de l'oxydation photochimique du sulfure de diméthyle dépend de la pression d'air; le rendement quantique qui est de 4 à la pression atmosphérique passe à 8 à une pression de 0,25 atmosphère.

Dans le cas du disulfure de diméthyle le rendement quantique dans l'air est de 1,9 à la pression atmosphérique pour une concentration en disulfure de $7,04 \times 10^{-5}$ *M*.

[Traduit par le journal]

Introduction

A number of process industries generate bivalent sulphur compounds, some of which are emitted to the atmosphere. These compounds include methyl mercaptan (CH_3SH), dimethyl sulphide (CH_3SCH_3), and dimethyl disulphide (CH_3SSCH_3). They have odour thresholds in air of 2, 1, and 16 ppb, respectively (1).

The major mode of sulphide removal in the atmosphere is believed to be oxidation to SO_2 and SO_3, likely followed by washout through precipitation. The rate of thermal oxidation at atmospheric temperatures is rather low; however, the gases are capable of absorbing ultraviolet light which leads to oxidation of the sulphur to SO_2. Although the intensity of solar radiation at wavelengths below 300 nm is low at ground level, it is probably significant in the conversion of bivalent sulphur compounds to sulphur dioxide.

Rayner and Murray (2) determined that sulphides in air would oxidize when exposed to solar radiation and more rapidly under ultraviolet light. Short wavelength uv (254 nm) was found to be superior to longer wavelength (360 nm) and the order of reactivities was found to be

$$CH_3SH > (CH_3)_2S_2 \gg (CH_3)_2S$$

The oxidation of $(CH_3)_2S$ was found to be very slow.

In this study, the absorption spectra of CH_3SH,

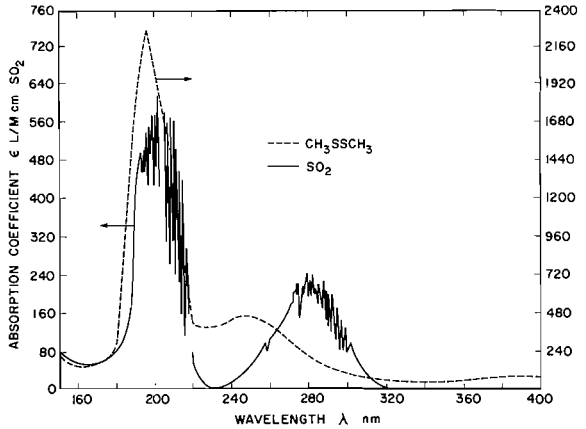

FIG. 1. The polychromatic absorption coefficients for CH_3SSCH_3 and SO_2.

[1]Revision received March 23, 1981.

0008-4042/81/182750-05$01.00/0

©1981 National Research Council of Canada/Conseil national de recherches du Canada

Can. J. Chem. Downloaded from www.nrcresearchpress.com by 210.87.254.6 on 09/06/12
For personal use only.

Can. J. Chem. Downloaded from www.nrcresearchpress.com by 210.87.254.6 on 09/06/12
For personal use only.

SO_2, CH_3SCH_3 and CH_3SSCH_3 were measured using incident radiation from a deuterium source. Results of these measurements are shown in Figs. 1 and 2. For methyl mercaptan, the wavelength at which the maximum absorption of radiant energy occurred was 235 nm, corresponding to a photon energy of 121.6 kcal/einstein. This frequency was dependent not only on the absorbance but also on the radiation intensity from the chosen source at that wavelength. This energy is in excess of the bond energy for the bonds of interest by 32.8 kcal/mol for S—H scission, 46.4 kcal/mol for C—S scission, and 54.6 kcal/mol for S—S scission.

The primary modes of CH_3SH decomposition reported in the literature are:

$$CH_3SH + h\nu \rightarrow CH_3S + H \text{ (refs. 3, 4 to 21)}$$
$$\rightarrow CH_3 + SH$$

$$CH_3SCH_3 + h\nu \rightarrow CH_3S + CH_3 \text{ (refs. 7, 22)}$$

$$CH_3SSCH_3 + h\nu \rightarrow 2CH_3S \text{ (refs. 3, 7, 23 to 25)}$$

The mercaptan scission has been found to occur primarily at the S—H bond with C—S scission becoming more important at shorter wavelengths. This suggests that the photo-energized CH_3SH^* molecule attains a state where the S—H bonding force is repulsive and thus dissociation occurs with the production of the H atom. The dissociation also produces CH_3S, CH_3, and SH fragments, each of which is highly reactive.

Experimental

The reactions were performed in a parallel-ended, grease-free tubular reactor designed to transmit wavelengths down to 180 nm. Illumination was provided by a medium-pressure deuterium discharge lamp collimated by two quartz lenses. The polychromatic illumination passed through a fully illuminated 25-mm diameter, Teflon-sealed, 10 cm Pyrex reaction vessel fitted with 1.5 mm-thick Suprasil windows. Transmitted light was analysed using a Jarrel-Ash 0.25 meter monochromator. Exiting radiation of 0.25 nm bandwidth was measured by an EMT 9558QBM photomultiplyer.

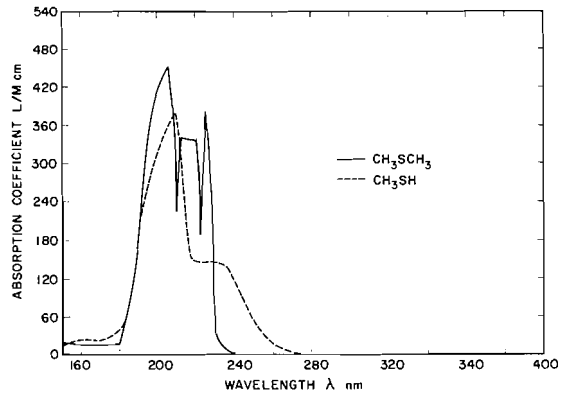

FIG. 2. The polychromatic absorption coefficients for CH_3SCH_3 and CH_3SH.

The sulphide gas concentrations were measured using a Varian gas chromatograph equipped with a Tracor flame photometric detector. The separation was carried out on a Carbopak BHT-100 column (1/8 in. × 5 ft) operated at 65°C. The chromatograph was calibrated for analysis of CH_3SH, CH_3SCH_3, SO_2, and CH_3SSCH_3.

The incident radiation intensity was measured using potassium ferrioxalate solution actinometry operated within the limits recommended by Nicodem *et al.* (26). The total incident intensity from the radiation source was first determined. A borosilicate glass filter was then inserted in the incident beam to eliminate radiant energy of wavelengths shorter than 320 nm. The incident energy in the wavelength range of interest, 180 to 320 nm, was obtained by difference. The ferrioxalate solution absorbed all of the incident radiation in the wavelength range of 180 to 320 nm.

The fraction of the incident radiation, in the wavelength range 180 to 320 nm, which was absorbed by the sulphur compound under study, was obtained by graphical integration. A spectrum of the radiation transmitted through an air-filled cell was used as the baseline. A spectrum of the radiation transmitted through the cell containing a mixture of air and the sulphur compound provided the additional data needed to determine the radiant energy absorbed by the sulphur compound. Rates of photo-oxidation were measured as soon as possible after initiation. No corrections were made for reflection from the cell windows. Calculations based on the refractive index of the windows indicated that the error involved from reflections would be less than 1% of the absorbed energy.

Calibration of the chromatograph was the first step in the experimental procedure. The reaction cells were swept with bottled air passed through drierite, molecular sieve 5A, and filtered through a Whatman Gamma 12 grade 10 filter to remove water vapour, oils, and small particles. The optical path was swept with 1 CFH of dry N_2 for a minimum of 12 h before the start of the run. The air-filled reaction cells were placed in the beam and a transmission spectrum was run on each cell. This measure of the air-filled cell light output for each run was used to correct for lamp changes and end-window fogging.

The CH_3SH was supplied by the Matheson Co. and contained no other components identifiable with the chromatograph. The CH_3SCH_3 and CH_3SSCH_3 were supplied by the Eastman Kodak Co. Gases were transferred by Hamilton Gas-Tite syringes and liquids were transferred using Hamilton micro-litre syringes.

The cells were allowed to sit for 30 min before measurement of the initial concentration. The cell was placed in the reaction position and a second transmission spectrum was measured when the illumination was begun. The area between the spectra when the cell was filled with air and with added sulphide provided the measure of light absorption by the sulphide and formed the basis for calculating quantum yield. The monochromator was then set for continuous measurements at 290 nm to observe the production of gases absorbing at that wavelength. On completion of radiation, the cells were allowed to equilibrate in the dark for ½/h. The contents were then analysed for H_2S, CH_3SH, SO_2, and CH_3SSCH_3. After analysis the cells were flushed with dry air.

Results

(a) Irradiation of Dimethyl Sulphide in Air

The results observed during irradiation of dim-

Can. J. Chem. Downloaded from www.nrcresearchpress.com by 210.87.254.6 on 09/06/12
For personal use only.

TABLE 1. The quantum yield of CH_3SCH_3 photo-oxidation

$[CH_3SCH_3]$ $\times 10^4$ M	Pressure atm	Absorbed photons $\times 10^{-16}$	Reaction rate $\times$ 10^6 g/h	Quantum yield	Std. dev.	No. of expts.
1.71	1.0	7.74	74.2	4.1	1.6	10
1.71	0.25	6.46	64.2	8.0	2.9	6

ethyl sulphide in air are shown in Table 1. The quantum yield of CH_3SCH_3 photo-oxidation was found to increase as the total pressure in the reaction vessel was decreased. Reaction rates were low, coinciding with the low level of energy absorption by CH_3SCH_3. At wavelengths below 300 nm, CH_3SCH_3 absorbed only 4% of the incident radiation.

(b) Irradiation of Dimethyl Disulphide in Air

The quantum yield of CH_3SSCH_3 photo-oxidation was found to be 2 at a concentration of 7.05×10^{-5} M in air at a total pressure of 1 atm. Results obtained with dimethyl disulphide are given in Table 2.

(c) Irradiation of Methyl Mercaptan in Air

Extensive studies on the photolysis of methyl mercaptan in air showed that the reaction rate is a linear function of the photon absorption rate, Fig. 3. The absorption of short wavelength radiation was found also to be a function of CH_3SH concentration, Fig. 4. Thus, it was concluded that the reaction occurred as a result of photon absorption by methyl mercaptan and not by oxygen.

Reactions were conducted in an oxygen atmosphere to assess further the possible role of oxygen initiation. No significant change in the rate of methyl mercaptan photo-oxidation resulted from change in the oxygen partial pressure from 0.2 to 1 atm. These observations also tend to show that ozone is not a significant factor in the photo-oxidation of CH_3SH.

Other experiments of a preliminary nature indicated that unfiltered room air or moist air in the reactor yielded erratic results. This problem was averted by using filtered and dried bottled air. It is apparent that the reaction rate is sensitive to the presence of moisture or other components in the air used.

The results observed for methyl mercaptan photo-oxidation are given in Table 3. The quantum yield indicates the number of CH_3SH molecules decomposed per photon absorbed by the sulphide gas.

TABLE 2. The quantum yield of CH_3SSCH_3 photo-oxidation

$[(CH_3)_2S_2]$ $\times 10^5$ M	Percentage absorbance	Reaction rate $\times$ 10^6 g/h	Quantum yield	Std. dev.	No. of expts.
7.05	28.4	93.6	2.0	0.940	40
14.1	42.8	90.5	1.3	0.825	7

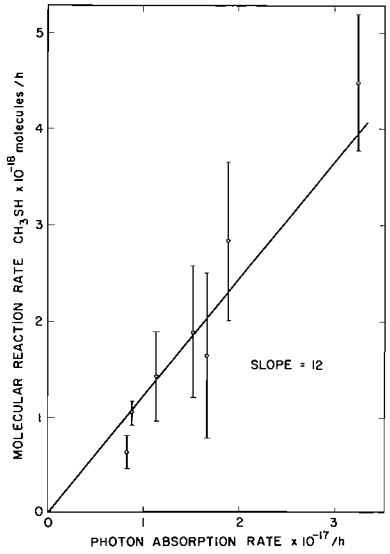

FIG. 3. Molecular reaction rate of CH_3SH as a function of photon absorption rate.

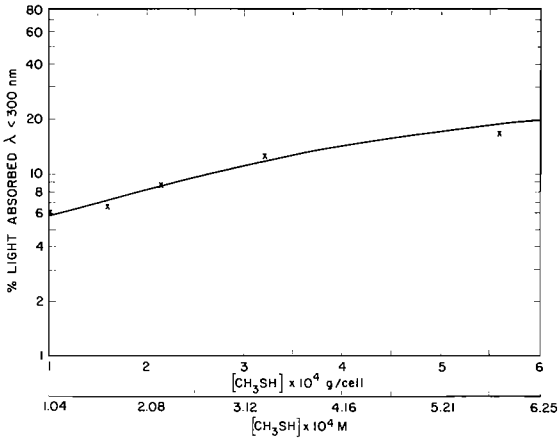

FIG. 4. Polychromatic light absorption as a function of CH_3SH concentration.

The average value of ϕ_{-SH} is 12 so that, in the concentration range studied (5.56×10^{-5} M to 2.78×10^{-4} M), the reaction may be described by the linear relationship:

$$R_{-SH} = 12\, I_a$$

Standard deviation = 4.16

No. of expts. = 85

Changes in air pressure in the reactor did not affect the quantum yield of CH_3SH removal.

The effect of SO_2 on CH_3SH photo-oxidation was studied by adding SO_2 to the air–mercaptan mixture in the photolysis cell. Addition of SO_2 did not cause any significant change in the rate of CH_3SH decomposition. There was, however, absorption of radiation by the SO_2 and the yield of CH_3SH per photon absorbed was reduced, although the quantum yield of mercaptan oxidation remained unchanged (Table 4).

The major reaction products found in all CH_3SH photo-oxidations were SO_2 and CH_3SSCH_3. There were two further unidentified peaks in the chromatographic trace, one after CH_3SH and the other a broad, low peak which emerged from the column after 1 h at 100°C.

A yellow oil appeared on the cell walls concentrated about the entrance end. The oil was likely a polymerized sulphur-containing product. A chromatographic analysis of the reaction products revealed a disulphide to sulphur dioxide formation ratio of $[CH_3SSCH_3]/[SO_2] = 0.633$. This indicates the methyl thiyl combination rate to be 1.26 times the oxidation rate to SO_2 at atmospheric oxygen concentrations.

A sulphur balance was examined using both chromatographic and spectroscopic techniques. The spectroscopic technique relied on the absorption coefficients of the reactant and product gases at 290 nm. The methyl mercaptan has a very low absorption coefficient at 290 nm whereas SO_2 and CH_3SSCH_3 have appreciable absorbancies.

When chromatographic data is used for a sulphur balance, 38.3% of the sulphur lost as CH_3SH appears as CH_3SSCH_3 or SO_2. If chromatographic data for CH_3SH and SO_2 are combined with absorption spectral information at 290 nm to estimate CH_3SSCH_3, the apparent concentration of disulphide obtained exceeds by a factor of 3.24 the disulphide analysis by gas chromatograph indicating the presence of other products which have significant absorption at 290 nm.

TABLE 3. Quantum yields in CH_3SH photolysis*

$[CH_3SH]$ × 10^5 M	I_a eins × 10^{10}	ϕ_{-SH}	Std. dev.	No. of expts.	ϕ_{SO_2}	ϕ_{SS}
5.56	9.29	8.28	2.22	10	—	—
8.35	9.31	12.19	2.03	4	—	—
11.1	20.7	12.73	4.01	11	—	—
11.1	14.6	12.61	4.53	28	—	—
11.1	18.6	15.13	4.43	9	2.35	1.49
16.7	19.3	9.79	5.18	10	—	—
27.8	40.17	12.91	2.07	13	1.58	1.0
Average		11.97	4.16			

*ϕ_{-SH} = quantum yield of CH_3SH removal; ϕ_{SO_2} = quantum yield of SO_2 production; ϕ_{SS} = quantum yield of CH_3SSCH_3 production.

TABLE 4. The effect of added SO_2 on CH_3SH photo-oxidation

$[CH_3SH]$ × 10^5 M	$[SO_2]$ × 10^5 M	CH_3SH Reaction rate × 10^6 g/h	% Absorbed light
5.85	0.	53.05	6.13
5.85	5.85	57.2	15.05
5.85	11.16	53.5	32.3

These other products probably give rise to the chromatographic peak after that of CH_3SH (at 7 min) and to the low broad peak at 1 h at 100°C. The identity of the small peaks has not been established.

The sulphur balance indicates the presence of an appreciable amount of sulphur in forms other than SO_2 or $(CH_3)_2S_2$. These are likely higher polysulphides and are probably involved in forming the oily deposit which clouded the entrance area of the reactant vessel. A similar deposit has been reported by other workers (4, 7, 14, 22, 27–29). The deposit has been reported insoluble in H_2O, CCl_4, $CHCl_3$, CH_3OH, or acetone (30) but is soluble in CS_2 (27). The cell could be cleaned by baking in air at 500°C overnight. Rao and Knight (22) found mass spectral analysis to suggest a molecular weight of about 258 and that the compound contained CH_2S and CH_3S groups.

The deposit caused a gradual decrease in transmission through the reaction cells during the course of a number of photo-oxidation reactions. Microphotographs revealed a series of droplets surrounded by smaller droplets. The X-ray emission spectrum revealed the presence of sulphur in the deposit, which is probably an organic polysulphide.

Acknowledgements

The authors would like to acknowledge financial assistance for the support of this work from the National Research Council of Canada and the Natural Sciences and Engineering Research Council of Canada.

1. Special Report, National Council of the Paper Industry for Air and Stream Improvement, New York, on Miscellaneous Point Source Reduced Sulphur Contributions from the Kraft Pulping Process, P. 4, January, 1972.
2. H. B. RAYNER and F. E. MURRAY. Pulp Pap. Mag. Can. **71**, 75 (1970).
3. T. UENO, and K. U. I. YOSHIMASA TAKEZAKI. Chem. Res. Bull. **36**, 19 (1958).
4. N. P. SKERRETT and N. W. THOMPSON. Trans. Faraday Soc. **37**, 81 (1951).

Can. J. Chem. Downloaded from www.nrcresearchpress.com by 210.87.254.6 on 09/06/12
For personal use only.

5. T. INABA and B. DE B. DARWENT. J. Phys. Chem. **64**, 1431 (1960).
6. B. MILLIGAN, D. E. RIVETT, and W. E. SAVIGE. Aust. J. Chem. **16**, 1020 (1963).
7. A. B. CALLEAR and D. R. DICKSON. Trans. Faraday Soc. **66**, 1907 (1970).
8. J. SKELTON and F. C. ADAM. Can. J. Chem. **49**, 3536 (1971).
9. R. P. STEER, B. L. KALRA, and A. R. KNIGHT. J. Phys. Chem. **71**, 783 (1967).
10. R. P. STEER and A. R. KNIGHT. J. Phys. Chem. **72**, 2145 (1968).
11. R. P. STEER and A. R. KNIGHT. Can. J. Chem. **47**, 1335 (1969).
12. G. L. HEMPHILL and J. M. WHITE. J. Phys. Chem. **76**, 2668 (1972).
13. L. BRIDGES and J. M. WHITE. J. Phys. Chem. **77**, 295 (1973).
14. D. KAMRA and J. M. WHITE. J. Photochem. **4**, 361 (1975).
15. B. G. DZANTIEV and A. V. SHISHKOV. Khim. Vys. Energ. **2**, 119 (1968).
16. B. G. DZANTIEV, A. V. SHISHKOV, and M. S. UNUKOVICH. Khim. Vys. Energ. **3**, 111 (1969).
17. B. G. DZANTIEV, A. V. SHISHKOV, and M. S. UNUKOVICH. Khim. Vys. Energ. **5**, 172 (1971).
18. B. G. DZANTIEV, O. S. SHIMCHUK, and A. V. SHISHKOV. Khim. Vys. Energ. **4**, 361 (1970).
19. G. P. STURM and J. H. WHITE. J. Chem. Phys. **50**, 5035 (1969).
20. J. M. WHITE and G. P. STURN. Can. J. Chem. **47**, 357 (1969).
21. G. P. STURM and J. M. WHITE. J. Phys. Chem. **72**, 3679 (1968).
22. P. M. RAO and A. R. KNIGHT. Can. J. Chem. **50**, 844 (1972).
23. P. M. RAO, J. A. COPECK, and A. R. KNIGHT. Can. J. Chem. **45**, 1369 (1967).
24. K. SAYAMOL and A. R. KNIGHT. Can. J. Chem. **46**, 999 (1969).
25. P. M. RAO and A. R. KNIGHT. Can. J. Chem. **46**, 2462 (1968).
26. D. E. NICODEM, M. L. P. F. CABRAL, and J. C. N. FERREIRA. Molec. Photochem. **8**, 213 (1977).
27. C. LALO and C. VERMEIL. J. Photochem. **1**, 321 (1972/73).
28. C. LALO and C. VERMEIL. J. Photochem. **3**, 441 (1974/75).
29. H. MACKLE. Tetrahedron, **19**, 1159 (1963).
30. M. LURIA, K. J. OLSZYNA, R. G. DE PENA, and S. HEICKLEN. J. Aerosol Sci. **5**, 435 (1975).

Can. J. Chem. Downloaded from www.nrcresearchpress.com by 210.87.254.6 on 09/06/12
For personal use only.

Chemical reactivity of lumazine derivatives. Acid–base and redox reactions of a number of lumazines, deazalumazines, and isoalloxazines. An unusual effect of methyl substitution[1]

ROSS STEWART, R. SRINIVASAN, AND STEWART J. GUMBLEY

Department of Chemistry, University of British Columbia, Vancouver, B.C., Canada V6T 1Y6

Received March 19, 1981

ROSS STEWART, R. SRINIVASAN, and STEWART J. GUMBLEY. Can. J. Chem. **59**, 2755 (1981).

Three lumazines, seven deazalumazines, and two isoalloxazines have been studied and the following chemical properties measured; equilibrium acidity (pK_a), equilibrium basicity (pK_{SH^+}), polarographic reduction potential ($E_{\frac{1}{2}}$), and, where applicable, the rates of the general acid and general base catalyzed dissociation of the protons in the C-5 and C-7 methyl groups ($k_{SH^+ + A^-}$ and $k_{S + A^-}$, respectively). The latter quantities were determined by means of isotope exchange or iodination. Structural variations in the substrate produce compatible results in pK_a and pK_{SH^+} and, to lesser extents, in $E_{\frac{1}{2}}$ and in the catalytic rate data. Anomalies in the rate constants appear when a methyl group is present at C-6; it facilitates ionization of the C-5 and C-7 methyl groups, reversing the quite large effect of more distant methyl. Buttressing effects appear to be absent. The effects of methyl substitution are attributed, in part, to (*a*) resonance stabilization by 5- and 7-methyl groups in the reactant molecules (neutral substrate and conjugate acid), and (*b*) relief of steric strain in going from essentially aromatic reactants to nonplanar intermediates. The significance of the 6-methyl group in the lumazine–flavin conversion is noted.

ROSS STEWART, R. SRINIVASAN et STEWART J. GUMBLEY. Can. J. Chem. **59**, 2755 (1981).

On a étudié trois lumazines, sept déazalumazines et deux isoalloxazines et on a mesuré les propriétés chimiques suivantes: l'acidité à l'équilibre (pK_a), la basicité à l'équilibre (pK_{SH^+}) le potentiel de réduction polarographique ($E_{\frac{1}{2}}$) et là où c'est applicable, les vitesses de dissociation, catalysée en général par un acide ou par une base, des protons des groupes méthyles en C-5 et C-7 ($k_{SH^+ + A^-}$ et $k_{S + A^-}$ respectivement). On a déterminé les dernières propriétés par échange isotopique ou par iodation. Les variations structurelles du substrat donnent des résultats compatibles pour le pK_a et le pK_{SH^+} et à un moindre degré pour $E_{\frac{1}{2}}$ et pour les données de vitesse catalytique. Des anomalies dans les constantes de vitesse apparaissent quand le groupe méthyle est présent en C-6; il facilite l'ionisation au niveau des méthyles en C-5 et en C-7 en inversant le large effect du méthyle le plus éloigné. Les effets de compression semblent être absents. On attribue les effets de substitution du méthyle en partie (*a*) à la stabilisation par résonance due aux groupes méthyles en position 5 et 7 dans les molécules en réaction (substrat neutre et acide conjugué) et (*b*) à une diminution de la contrainte stérique due au passage de réactifs essentiellement aromatiques à des intermédiaires non plans. On a noté l'importance du groupe méthyle en position 6 dans la transformation de lumazine–flavine.

[Traduit par le journal]

Introduction

Lumazines (e.g. **1**)[2] constitute an important class of compounds on several grounds. First, the 6,7-dimethyl-8-ribityl compound (**1***a*) is known to be the precursor in nature of the important oxidative coenzymes, the flavins **2***a* (2). Secondly, they possess many of the structural features of the isoalloxazine ring system of the flavins and can serve as models for these compounds. Moreover, they possess a number of functional groups whose interaction is of general chemical interest.

It is known that the pathway for general conversion of lumazines to flavins, **1** to **2**, involves ionization of the 7-methyl group in the lumazine (2) and that this reaction is catalyzed by general acids and bases (3). Lumazines and to a lesser extent flavins have structural features that activate the methyl protons in question (the R^2 location in both **1** and **2**) and the present work, dealing chiefly with

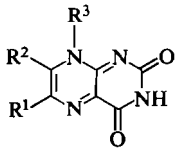

1

1*a* $R^1 = R^2 = CH_3$, R^3 = ribityl
1*b* $R^1 = R^2 = R^3 = CH_3$
1*c* $R^1 = H$, $R^2 = R^3 = CH_3$

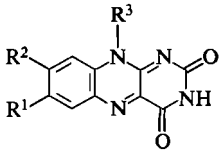

2

2*a* $R^1 = R^2 = CH_3$, R^3 = ribityl or ribityl phosphate
2*b* $R^1 = R^2 = H$, $R^3 = CH_3$

[1]A preliminary account of a portion of this work appeared in ref. 1.

[2]The numbering system for the lumazine and isolloxazine (flavin) ring systems is as follows:

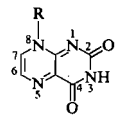

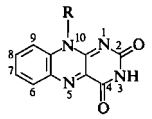

0008-4042/81/182755-11$01.00/0

©1981 National Research Council of Canada/Conseil national de recherches du Canada

Can. J. Chem. Downloaded from www.nrcresearchpress.com by 210.87.254.105 on 09/06/12
For personal use only.

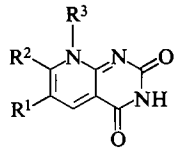
3

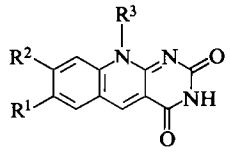
4

5-deazalumazines, **3**, was initiated to obtain more information with regard to such activation.

A further reason for examining the 5-deazalumazine system is the importance of the analogous 5-deazaflavin system **4**. The latter has been used for some years in attempts to fix the location of hydrogen addition in the reduction of flavins, since the exchange characteristics of protons attached to nitrogen preclude the use of isotopic tracers in such reactions (4). Furthermore, it has recently been shown that 5-deazaflavins are the active coenzymes in the biological conversion of carbon dioxide to methane (*4d*, 5).

We report herein the preparation of a series of lumazines and isoalloxazines and a determination of the rate constants for the acetic acid/acetate catalyzed exchange at the compounds' reactive sites.[3] In addition the equilibrium acidity and basicity of the compounds have been determined and their polarographic reduction potentials measured.

Experimental

Materials

6,7,8-Trimethyllumazine (**1***b*) and 6,7-diphenyl-8-methyllumazine (**13**) were prepared as previously described (3, 7). All deazalumazines were prepared by condensing 6-methylaminouracil with either a 1,3-diketone, a 1,3-keto aldehyde, or the corresponding acetals (6). 6-Methylaminouracil (**5**) was prepared from 2,4,6-trichloropyrimidine according to the method of King and King (8), as modified by McAndless (9).

6,7,8-Trimethyl-5-deazalumazine (*6*)

6-Methylaminouracil (**5**) (1.41 g) and 2-methyl-3-oxobutanal (1.0 g) (10) were heated together at 100°C in 16 cm^3 of 1 *M* hydrochloric acid for 2 h. The dark solution was cooled and neutralized with aqueous ammonia. The light yellow solid that formed was filtered off and recrystallized from water giving 1.80 g (88%) of **6**. Ultraviolet maxima: 220, 275, 362 nm (neutral form); 256, 368 nm (anion); 217, 250, 323 nm (cation). Nuclear magnetic resonance in trifluoroacetic acid (TFA), δ: 2.68 (3H, 6-Me), 2.98 (3H, 7-Me), 4.37 (3H, 8-Me), 8.96 (1H, 5-H). *Anal.* calcd. for $C_{10}H_{11}N_3O_2$: C 58.53, H 5.40, N 20.48; found: C 58.41, H 5.39, N 20.36.

Since the condensation might have proceeded to give the isomeric compound **9** a structural assignment was required. This together with the nmr assignments given above was made on the basis of the nuclear Overhauser effect and the observation of hydrogen exchange. The methyl group absorbing at 2.98 δ underwent exchange and hence occupies either the 5 or 7 position. Irradiation of the 8-methyl signal produced a 7% enhancement in the 2.98 signal and hence this corresponds to the methyl group at C-7.

7,8-Dimethyl-5-deazalumazine (*7*)

Acetoacetaldehyde dimethyl acetal (1.32 g) (10) and **5** (1.41 g) were heated together in 20 cm^3 of 0.1 *M* hydrochloric acid for 3 h. After neutralization with aqueous ammonia the volume of the solution was reduced and the product allowed to crystallize. The yellow solid was recrystallized from water to give 0.57 g (30%) of pure product. Ultraviolet maxima: 272, 353 nm (neutral form); 255, 362 nm (anion); 206, 247, 315 nm (cation); nmr in TFA, δ: 3.04 (3H, 7-Me), 4.37 (3H, 8-Me), 7.80 (1H, doublet, J = 8 Hz, 6-H), 9.06 (1H, doublet, J = 8 Hz, 5-H). *Anal.* calcd. for $C_9H_9N_3O_2$: C 56.54, H 4.75, N 21.98; found: C 56.46, H 4.86, N 21.81.

Irradiation of the *N*-methyl signal in $CDCl_3$ caused a 20% enhancement of the *C*-methyl signal relative to the absorption of the lone hydrogen atom at C-5. This compound is thus almost certainly the 7,8-dimethyl compound, not the 5,8-dimethyl isomer. It should be noted that Paterson and Wood (6) assigned a 5-methyl structure to an analogous compound prepared from acetoacetaldehyde.

5,7,8-Trimethyl-5-deazalumazine (*8*)

Acetylacetone (1.5 g) and **5** (2.11 g) were heated at 100°C in 15 cm^3 of 85% aqueous phosphoric acid for 3 h. After dilution with 100 cm^3 of water and neutralization with aqueous ammonia, 1.9 g (64%) of a pale yellow precipitate formed and was recrystallized from hot water. Ultraviolet maxima: 223, 273, 345 nm (neutral form); 222, 258, 352 nm (anion); 222, 255 (sh), 310 nm (cation); nmr in TFA, δ: 2.95 (3H, 7-Me), 3.07 (3H, 5-Me), 4.28 (3H, 8-Me), 7.57 (1H, 6-H). *Anal.* calcd. for $C_{10}H_{11}N_3O_2$: C 58.53, H 5.40, N 20.48; found: C 58.54, H 5.28, N 20.15.

Irradiation of the *N*-methyl resonance at position 8 produced a 6% enhancement of the 2.95 δ signal, relative to the 3.07 signal, enabling the above assignments to be made.

5,6,8-Trimethyl-5-deazalumazine (*9*)

2-Methylbut-2-enal (tiglic aldehyde) (0.85 g) was stirred with 1.41 g of **5** at room temperature for 36 h in 20 cm^3 20% aqueous hydrochloric acid. After neutralization with aqueous ammonia several recrystallizations of the resulting yellow solid were necessary to remove the isomeric impurity (**6**). Ultraviolet maxima: 232, 272, 352 nm (neutral form); 235, 256, 360 nm (anion); 212, 248, 312 nm (cation); nmr in TFA, δ: 2.57 (3H, 6-Me), 3.13 (3H, 5-Me), 4.40 (3H, 8-Me), 8.52 (1H, 7-H). *Anal.* calcd. for $C_{10}H_{11}N_3O_2$: C58.53, H 5.40, N 20.48; found: C 58.33, H 5.30, N 20.22.

Structure assignment and nmr assignments were consistent with the observation that the methyl group at 3.13 δ underwent exchange and that the lone proton at 8.52 δ showed a 38% enhancement (relative to the 5-methyl peak) when the *N*-methyl resonance at position 8 was irradiated.

5,8-Dimethyl-5-deazalumazine (*10*)

Crotonaldehyde diethyl acetal (1.44 g) and **5** (1.41 g) were condensed as for compound **7**. The yield of yellow needles was 41%. Ultraviolet maxima: 228, 271, and 344 nm (neutral form); 228, 254, 353 nm (anion); 222, 249, 303 nm (cation); nmr in TFA, δ: 3.15 (3H, 5-Me), 4.43 (3H, 8-Me), 7.63 (1H, doublet, J = 7.0 Hz, 6-H), 8.58 (1H, doublet, J = 7.0 Hz, 7-H). *Anal.* calcd. for $C_9H_9N_3O_2$: C 56.54, H 4.75, N 21.98; found: C 56.48, H 4.72, N 21.75.

Nuclear Overhauser experiments were inconclusive with this compound partly because of low solubility in $CDCl_3$. However, comparison with the spectra of the 7,8-dimethyl isomer (**7**) shows it to be a different compound.

[3]Wood and co-workers (6), in a search for specific enzyme inhibitors, have prepared a number of 5-deazalumazines that are similar in structure to some of the compounds studied here.

Can. J. Chem. Downloaded from www.nrcresearchpress.com by 210.87.254.105 on 09/06/12
For personal use only.

Can. J. Chem. Downloaded from www.nrcresearchpress.com by 210.87.254.105 on 09/06/12
For personal use only.

5,6,7,8-Tetramethyl-5-deazalumazine (11)

3-Methyl-2,4-pentanedione (11) (1.71 g) and **5** (2.11 g) were heated together in 15 cm^3 of 85% phosphoric acid for 6 h at 100°C. After similar treatment to that accorded **8** a 16% yield of pure product was obtained. Ultraviolet maxima: 227, 274, 353 nm (neutral form); 233, 254, 362 nm (anion); 217, 250, 323 nm (cation); nmr in TFA, δ: 2.59 (3H, 6-Me), 2.97 (3H, 7-Me), 3.13 (3H, 5-Me), 4.32 (3H, 8-Me). *Anal.* calcd. for $C_{11}H_{13}N_3O_2$: C 60.26, H 5.98, N 19.17; found: C 60.06, H 5.93, N 19.01.

The nmr assignments came from the observation that the methyl groups at 2.97 δ and 3.13 δ underwent exchange and hence occupy the 5 and 7 positions and that the 2.97 δ signal showed a 9% enhancement and the 2.59 δ signal a 3% enhancement (relative to the 3.13 δ peak) when the *N*-methyl signal at 4.32 δ was irradiated.

7,8-Dimethyllumazine (1c)

Two cm^3 of a 40% aqueous solution of pyruvaldehyde and 5-amino-6-methylaminouracil (9, 12) (2.5 g) were mixed together in 50 cm^3 of methanol and refluxed for 3 h. A number of attempts to isolate pure product from this mixture were unsuccessful (as were other preparative variations), the best results being obtained as follows. The solvent was removed and the resulting solid dissolved in water and placed immediately on a column of alumina and eluted with water. The green fluorescent band was collected to give a small quantity of yellow crystals. This compound is light sensitive in solution and produces a dark coloured compound on decomposing. Consequently, the above process should be carried out in dim light with fluorescent lighting, in particular, being avoided. Ultraviolet maxima: 254, 272, 394 nm (neutral form); 260, 310, 294 (anion); 245, 350 (cation); nmr in TFA, δ: 3.14 (3H, 7-Me), 4.44 (3H, 8-Me); the upfield peak began decreasing in intensity when D_2O was added. The 6-H resonance is missing in TFA, possibly because of exchange broadening. In DMSO it appears at 8.12 δ, with the two methyl resonances appearing at 2.63 and 3.82. *Anal.* calcd. for $C_8H_8N_4O_2$: C 50.00, H 4.20, N 29.15; found: C 50.22, H 4.24, N 28.91.

This compound was also prepared using pyruvaldehyde dimethyl acetal followed by filtration, concentration, and elution on a silica gel column with 80% aqueous ethanol. A yellow-green fluorescent compound was collected and recrystallized from ethanol. Although sample purity appeared to be lower using this method, as indicated by less satisfactory microanalytical data, samples prepared by the two methods behaved similarly in their chemical reactions.

5,8-Dimethyl-7-ethyl-5-deazalumazine (12)

2,4-Hexanedione (0.52 g) and **5** (0.65 g) were heated together in 5 cm^3 of 85% phosphoric acid at 100°C for 4 h. The red solution was then neutralized with aqueous ammonia and cooled in ice. The cream-coloured product was filtered off and recrystallized from hot water. Ultraviolet maxima: 228, 272, 345 nm (neutral form); 228, 253, 353 nm (anion); 222, 247, 310 nm (cation); nmr in TFA, δ: 1.55 (3H, triplet, J = 7 Hz, 7-Et), 3.10 (3H, 5-Me), 3.24 (2H, quartet, J = 7 Hz, 7-Et), 4.30 (3H, 8-Me), 7.59 (1H, 6-H). *Anal.* calcd. for $C_{11}H_{13}N_3O_2$: C60.26, H 5.98, N 19.17; found: C 59.89, H 6.18, N 18.91.

This compound has been assigned the 7-ethyl-5-methyl structure on the basis of the positions of the nmr resonances. (Signal overlap makes nuclear Overhauser experiments extremely difficult to interpret for this compound.) Table 1 shows the chemical shifts for the various protons in methyldeazalumazines studied herein and it can be seen that the resonances for the 5-methyl groups vary from 3.07 to 3.15 δ, whereas the 7-methyl resonances vary from 2.95 to 3.04 δ. Since this compound has its exchanging methyl group at 3.10 δ we assign it the structure given above.

TABLE 1. Nuclear magnetic resonance chemical shifts (δ) for protons in methyl deazalumazines[a]

Location of methyl group	Compound 6	7	8	9	10	11
5	—	—	3.07	3.13	3.15	3.13
6	2.68	—	—	2.57	—	2.59
7	2.98	3.04	2.95	—	—	2.97
8	4.37	4.37	4.28	4.40	4.43	4.32
Location of ring proton						
5	8.96	9.06[b]	—	—	—	—
6	—	7.80[b]	7.57	—	7.63[c]	—
7	—		—	8.52	8.58[c]	—

[a] In trifluoroacetic acid.
[b] J = 8 Hz.
[c] J = 7 Hz.

9-Aza-10-methylisoalloxazine (14)

Alloxan (0.4 g) was dissolved in glacial acetic acid and 3-amino-2-methylaminopyridine (13) (0.1 g) dissolved in a small quantity of glacial acetic acid was gradually added with stirring. The resulting solution was heated on a steam bath for 30 min. On cooling yellow crystals appeared, which, upon recrystallization from aqueous formic acid, gave a compound that melted with decomposition at 350°C. *Anal.* calcd. for $C_{10}H_7N_5O_2$: C 52.40, H 3.08, N 30.56; found: C 52.13, H 2.95, N 30.21. We thank Dr. K. Oyama for the preparation of this compound.

10-Methylisoalloxazine (2b)

This compound was prepared from alloxan and *N*-methyl-1,2-phenylenediamine essentially by the method of Matsukawa and Shirakawa (14). Recrystallization from 50% aqueous acetic acid gave a high yield of yellow-orange crystals melting above 300°C (15). We thank Dr. J. M. McAndless for the preparation of this compound.

6,7,8-Trimethyl-5-deazalumazine-7-methyl-d_3-3-N-d (15)

Compound **6** was boiled in D_2O (99.7 at.% D) for 24 h. The solution was allowed to cool and the separated crystals removed by filtration. After four such operations the nmr spectrum showed no detectable absorption for the 7-methyl group.

pK Measurements

The acidity constants for loss of the N-3 proton, designated herein as K_a, and gain of a proton at N-1, designated herein as K_{SH^+}, were determined spectrophotometrically at room temperature for all compounds except **2b** and **14**. Good isosbestic points for the pH absorbance curves were obtained in all cases (see Fig. 1).

In the case of the two isoalloxazines, **2b** and **14**, the spectral changes upon protonation and deprotonation are too small to allow pK_a values to be determined in the above way. The values for these compounds were determined by fluorescence measurements, since only the neutral molecules fluoresce. The concentration of the isoalloxazines in aqueous buffer was approximately 10^{-6} M and was such that the fluorescence intensity was linear with concentration. Measurements were made on a Turner 110 fluorometer.

Polarography

The polarographic half-wave potentials, $E_{\frac{1}{2}}$, were measured by the AC modulation method on a Metrohm polarograph E-354 equipped with Polarecord E 261 and AC Modulator E 393. The compounds were dissolved in an aqueous solution that was 0.05 M in phosphate buffer, pH 6.87, and 0.05 M in potassium chloride to give an approximate substrate concentration of

Can. J. Chem. Downloaded from www.nrcresearchpress.com by 210.87.254.105 on 09/06/12
For personal use only.

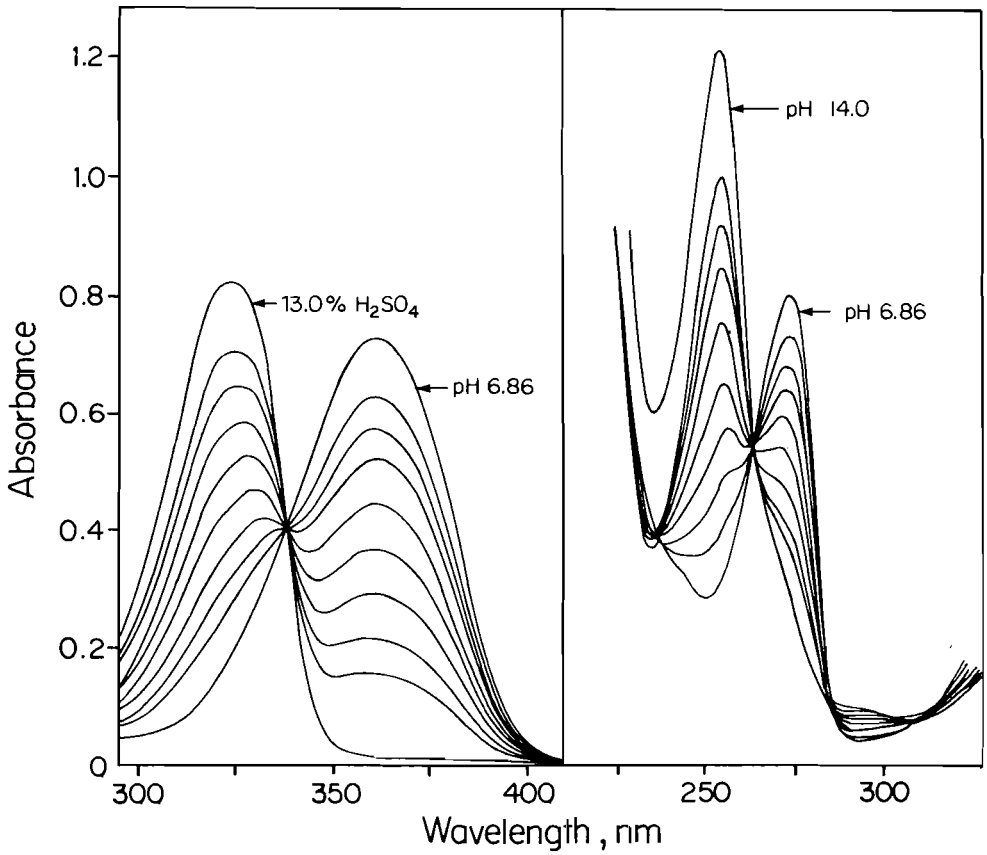

FIG. 1. Isosbestic plots for protonation (left) and deprotonation (right) of **6** in aqueous acid and in aqueous base. Intermediate pH values are, in order, for left-hand plot 1.59, 1.80, 2.01, 2.20, 2.41, 2.61, 2.80, and 3.01; and for right-hand plot 10.73, 11.01, 11.23, 11.40, 11.61, 11.80, 12.00, and 12.20; $pK_{SH^+} = 2.21$, $pK_a = 11.4$.

10^{-4} *M*. The solutions were then deaerated prior to the measurement of $E_{\frac{1}{2}}$ by flushing with N_2 for 15 min.

The instrument was calibrated using a set of metal ion solutions of known $E_{\frac{1}{2}}$ (16). The half-wave potentials obtained for the compounds were corrected using the least-squares line of the calibration graph.

Rate Measurements

The nmr rate measurements were made in D_2O as previously described (17). The iodination measurements (18) were made at 440 nm ($\varepsilon I^- = 1818$) in all cases except 5,8-dimethyl-5-deazalumazine, where the wavelength chosen was 450 nm ($\varepsilon I_3^- = 1340$). The acidity was adjusted using HCl or KOH and measured at approximately 25°C, with a Radiometer pH instrument. The carboxylic acids used as buffer sources were purified by recrystallization before use.

In a typical iodination experiment the substrate was suspended in 50 cm^3 of aqueous buffer of ionic strength 1.2 and the suspension agitated for several minutes in an ultrasonic bath at 35–40°C. (The 5-deaza compounds are much less water soluble than their 5-aza analogs.) After complete dissolution a 10 cm cell was filled with this solution, a fresh solution of sodium iodide added, and the cell allowed to equilibrate in the thermostatted cell compartment (35.7° ± 0.2°C) of a Cary 16 spectrophotometer. The reaction was initiated by adding by syringe 100 μL of a solution of iodine in spectral grade methanol. The concentration of iodine was 3×10^{-5} *M* and of sodium iodide 0.005 *M*. The substrate concentration was varied from 6×10^{-4} to 8×10^{-3} *M*. The ionic strength was kept at 1.2 by adding potassium chloride.

Partitioning of the iodination rates between the two methyl groups in **8** was done by allowing an exchange reaction of **8** in a saturated solution in D_2O to proceed for an extended period and then measuring the degrees of exchange using a 270 MHz spectrometer equipped with Fourier transform. The 7-methyl group (upfield) had undergone 2.4 times more exchange than the 5-methyl group. The same ratio was assumed to hold for the reactive groups in **11**.

Results and Discussion

The rate data for proton loss from the activated methyl groups in the compounds studied are given in Table 2. Two methods were required to obtain this data, isotopic exchange and iodination; the deazalumazines are not sufficiently soluble in water to follow the reaction by nmr, and absorption in the visible spectrum of the lumazines does not allow the iodination process to be monitored. The validity of comparing results obtained by the two

Can. J. Chem. Downloaded from www.nrcresearchpress.com by 210.87.254.105 on 09/06/12
For personal use only.

different methods is considered in the next section. As found in previous work both methods gave satisfactory kinetic plots, the isotopic exchange reactions all being first-order in substrate and the iodination reaction being zero order in iodide to at least 50% of reaction.

Comparison of Isotopic Exchange and Iodination Methods

We have found previously that methylcreatininium ion, whose rate of reaction with bases can be followed both by deuterium exchange and by iodination, gives results by the two methods that are in satisfactory agreement (18). There is an enormous reactivity difference in the present case, however, between the lumazines (isotopic exchange) and the deazalumazines (iodination) and it is only prudent to make any further comparison between the two methods that is possible. Accordingly, we have studied the exchange of the activated methyl group of the deazalumazines in D_2O–D_2SO_4, a medium which will dissolve enough substrate to allow the rate of exchange to be followed by nmr. The first order rate constants are given in Table 2. In this medium (0.96 *M* D_2SO_4) the substrates are almost entirely protonated and the predominant general bases in the medium will be sulfate ion and water, whereas in the iodination studies at higher pH the substrate is only partly protonated, with the predominant general base being acetate ion. Figure 2 shows a comparison of the first-order rate constants for isotopic exchange in D_2O–D_2SO_4 and the second-order rate constants for iodination in water, catalyzed by acetate ion. A reasonably linear relation is obtained in the log–log plot, with the slope being close to unity. The near-unit slope indicates that the acetate rates have about the same sensitivity to structural changes in the substrate as do the combined sulfate and water rates, despite the much lower basicity of the latter bases compared to acetate ion. (On the basis of the work of Edward and Wong (20) and Lietzke and Stoughton (21) the sulfate concentration can be estimated to be of the order of 10^{-1} and at this concentration its considerably greater basicity, compared to D_2O, means that it will make a significant contribution to the exchange rate, though whether it is the more important proton abstractor is problematical.) There is precedent for bases of differing strength and reactivity having parallel but widely separated Brönsted lines (19) and the present results conform to this pattern.

It is well known that many pteridines, of which the lumazines are derivatives, undergo reversible

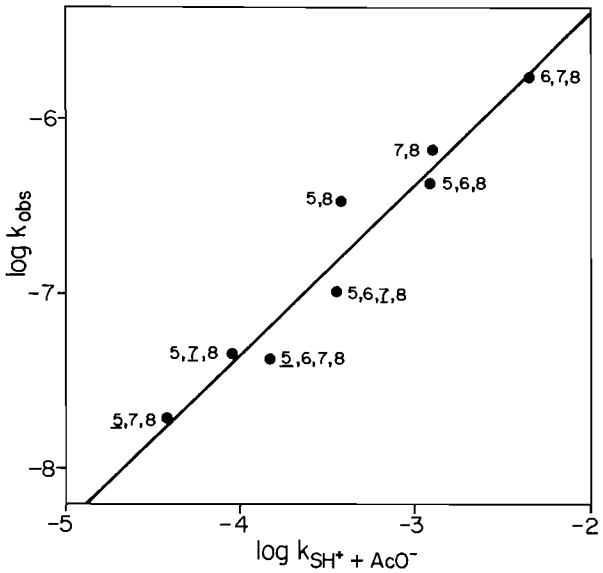

FIG. 2. A comparison of the first-order rate of isotopic exchange in D_2O–D_2SO_4 for 5-deazalumazines (ordinate) with the second-order rate of iodination of the same compounds (abscissa). The positions of the methyl groups are shown by numbers on the plot. In compounds with two exchange sites the position of the exchanging methyl group is underlined. Slope = 0.970, correlation coefficient 0.970.

covalent hydration (22). Both ultraviolet and nmr spectra would reveal this phenomenon if it took place to a significant extent and we saw no evidence for it in any of our experiments, except possibly in strongly basic solutions (pH ~ 14) where some nmr or uv spectra were anomalous. Since no rate measurements were done in this region we have discounted this phenomenon as an explanation for the effects considered below.

Buffer Catalysis and Methyl Reactivity

The way in which a change in pH affects the rate of proton loss from the 7-methyl group in 6,7,8-trimethyllumazine (**1***b*) is shown in Fig. 3 for both unbuffered and phosphate buffered media. The minima in the two curves come at almost the same pH, as expected, since the minimum depends only on the basicity of the substrate and on the proton activating factor (*paf*), which has generally been found to be independent of the base that is involved in the proton-removal step.[4] It can be seen that there is no plateau at the minimum of the curve for the unbuffered system and this indicates that there

[4]The quantity *paf* for any compound Z is the ratio of rate constants for the two reactions Z + B and ZH^+ + B, where B is any base or nucleophile. It can be obtained from buffer catalytic data using the relation $paf = k_{HA} K_{ZH^+}/k_{A^-} K_{HA}$, where HA is the buffer acid and A^- the base.

Can. J. Chem. Downloaded from www.nrcresearchpress.com by 210.87.254.105 on 09/06/12
For personal use only.

TABLE 2. Rate,[a] equilibrium, and electrochemical data for reaction of lumazines, deazalumazines, and isoalloxazines in water

	Compound, S	pK_{SH^+}[b]	pK_a[b]	$10^7 k_{S + AcO^-}$[c] M^{-1} s^{-1}	$10^5 k_{SH^+ + AcO^-}$[c] M^{-1} s^{-1}	$10^8 k$(0.96 M D_2SO_4)[c] s^{-1}	$E_{\frac{1}{2}}$[b]
1*b*	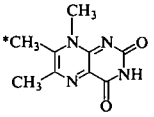	0.93	9.72	142,000[d]	238,000[d]	—	−0.621
1*c*	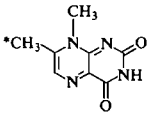	0.15	10.1	19,300	—	—	−0.622
6	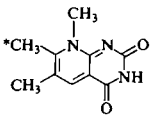	2.21[e]	11.4	230	461	170	−1.190
7	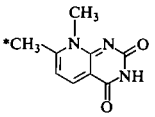	1.81	11.2	95.8	130	64.2	−1.159
8	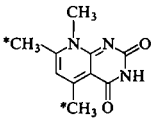	2.26	12.0	9.92 7-CH_3 7.0 5-CH_3 2.9	13.0 7-CH_3 9.2 5-CH_3 3.8	7-CH_3 4.5 5-CH_3 1.9	−1.326
9	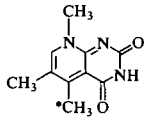	2.46	12.0	87.8	122	42.0	−1.243
10	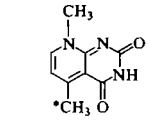	2.14	11.9	25.8	38.6	34.2	−1.200
11	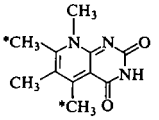	2.57	12.2	39.2 7-CH_3 28 5-CH_3 11	51.2 7-CH_3 36 5-CH_3 15	7-CH_3 10.1 5-CH_3 4.2	−1.321
12	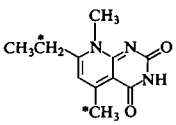	2.26	12.0	—	—	5.7[f]	—
13	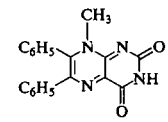	0.20	9.5	—	—	—	−0.542
2*b*	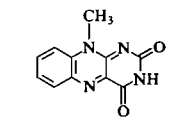	−0.26	9.9	—	—	—	−0.361

TABLE 2. (*Concluded*)

Compound, S	pK_{SH^+}[b]	pK_a[b]	$10^7 k_{S + AcO^-}$[c] M^{-1} s^{-1}	$10^5 k_{SH^+ + AcO^-}$[c] M^{-1} s^{-1}	$10^8 k$(0.96 M D_2SO_4)[c] s^{-1}	E_f^b
14 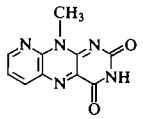	−0.88	9.4	—	—	—	−0.274

[a] Reactive sites shown by asterisks.
[b] Room temperature, approx. 23°C.
[c] T = 35.7°C.
[d] Reference 17*a*, T = 34.5°C. These values were not corrected for isotope effects on K_a or K_{SH^+}. Using the original buffer data the correction in $k_{S + AcO^-}D_2O$ = 1.28 × $10^{-2} M^{-1} s^{-1}$; the correction required for the complex rate term $k_{SH^+ + AcO^-}$ is much more difficult to estimate.
[e] Previously determined at 35°C and reported as 2.12 (1).
[f] Combined rate for 5-methyl and 7-methylene protons.

is not a great difference in the contributions made by the two kinetically equivalent paths shown in reactions [1] and [2] (24).

[1] $S + H_2O \rightarrow$ reactive intermediate

[2] $SH^+ + HO^- \rightarrow$ reactive intermediate

It should be noted that the true minimum for the unbuffered system is probably not as sharp as shown in Fig. 3. The rapid fall-off in rate that begins as the "pH" changes from positive to negative indicates that self-catalysis is important for this system, as observed previously in related systems

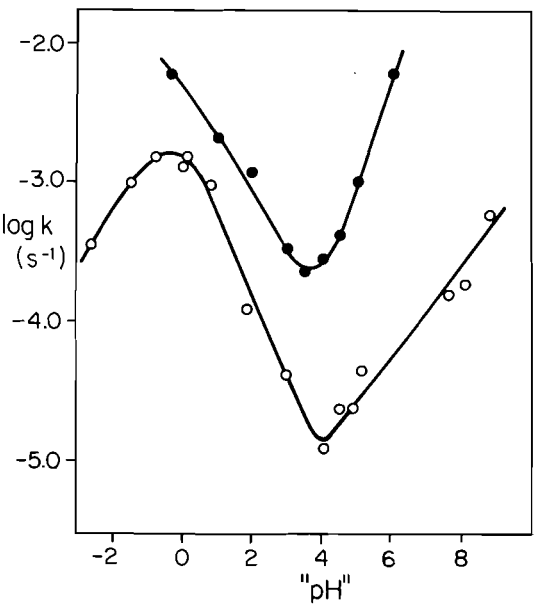

FIG. 3. The effect of acidity on the first-order rate constant for the isotopic exchange of the 7-methyl group of **1***b* in 0.1 M phosphate buffer in D_2O (upper curve) (3) and in unbuffered D_2O (lower curve). The "pH" values are uncorrected glass electrode readings except in highly acidic media where uncorrected H_0 values are used. The acidity of the unbuffered solutions was adjusted using D_2SO_4, DCl, and NaOD.

(25). Self-catalysis, the reaction of substrate S with its conjugate acid SH^+, will be at a maximum when pH = pK = 0.9, thus causing the rates in the pH range 1–3 to be elevated and making the minimum sharper than it would otherwise be.

The effect of replacing the 5-N unit in lumazines to give deazalumazines has a very large deactivating effect on the lone reactive site in lumazines, that at C-7, as can be seen from the results in Table 2. Compare **1***b* with **6** and **1***c* with **7**, where the rate differences are between 10^2 and 10^3. The source of this effect is presumably the electronegativity difference between carbon and nitrogen. It is noteworthy that the same change in reactivity can be seen whether one considers the rate constants $k_{S + AcO^-}$ or $k_{SH^+ + AcO^-}$, that is, whether proton loss involves the neutral molecule or the cation.

The effect of methyl groups elsewhere in the molecule on the activated sites in deazalumazines (positions 5 and 7) is interesting. It can be seen from the results in Table 2 that a methyl group at position 5 has a large deactivating effect on the methyl group at position 7, and vice versa. (We refer to this as next-but-one substitution.) A 5-methyl group lowers the kinetic acidity of a 7-methyl group by factors of 8.2 to 14; a 7-methyl group has a similar effect on the 5-methyl ionization (factors of 8.0–10.2).

The effect of methyl at an *adjacent* site has an *activating* effect on the rate of ionization of both 5-methyl and 7-methyl groups. For the deazalumazines the rate constants for dissociation of the protons of the 7-methyl group are increased by factors of 2.4 to 4.0 for the reaction $S + AcO^-$, 3.5–3.9 for the reaction $SH^+ + AcO^-$, and 2.2–2.6 for the reaction $SH^+ + SO_4^{2-}$ (or H_2O). The dissociation of the 5-methyl protons shows a similar effect, the factor being 3.4–3.8 for $S + AcO^-$, 3.2–3.9 for $SH^+ + AcO^-$, and 1.2–1.9 for $SH^+ + SO_4^{2-}$ (or H_2O).

Can. J. Chem. Downloaded from www.nrcresearchpress.com by 210.87.254.105 on 09/06/12
For personal use only.

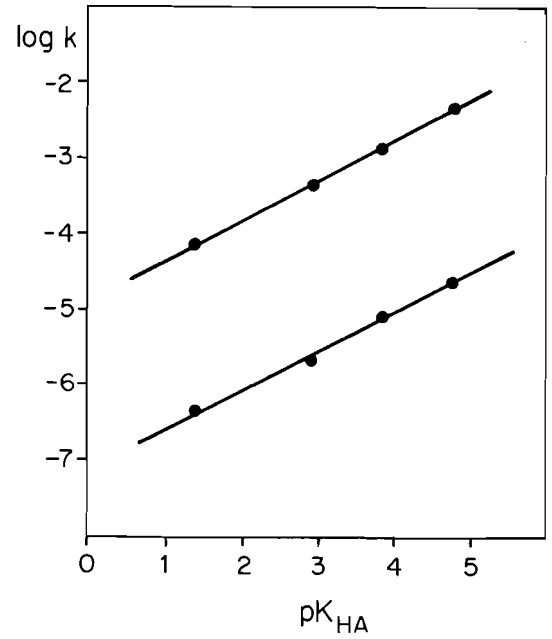

FIG. 4. Brönsted plots for **6**; upper curve log $k_{SH^+ + AcO^-}$; lower curve, log $k_{S + AcO^-}$. The buffer acids HA are, from left to right, dichloroacetic acid, chloroacetic acid, glycollic acid, and acetic acid.

The activating effect of adjacent methyl, a factor of roughly three, is not large but it is remarkable in that it reverses the quite substantial deactivating effect of methyl at a next-but-one location. Perhaps the most striking result of the reversed effect of methyl can be seen by comparing the reactivities of the 6,7,8- and 5,7,8-trimethyl isomers in the deazalumazine series, compounds **6** and **8** in Table 2. The former is 23 to 35 times the more reactive despite having only one reactive methyl group and the latter having two.

In the lumazine series there is only one comparison that can be made, that between compounds **1***b* and **1***c*. Here again an adjacent methyl group has an activating effect, though the difficulty we have had in preparing substantial quantities of pure **1***c* has precluded our gathering completely reliable rate data for this compound.

Brönsted Coefficients and paf *Values*

Brönsted plots for 6,7,8-trimethyl-5-deazalumazine are shown in Fig. 4. The slopes are virtually identical, 0.51 for the plot of log $k_{S + A^-}$ against pK_{HA} and 0.52 for the plot of log $k_{SH^+ + A^-}$ against pK_{HA}. The former is the conventional Brönsted β coefficient for catalysis by bases A^-; the latter can be converted to the Brönsted α coefficient for catalysis by acids HA by substracting from unity, though that makes little difference in the magnitude of the coefficient in the present case. The parallelism of the lines in Fig. 4 means that *paf* is independent of the base used to remove the proton from the 7-methyl group (17*a*), at least within the range of buffer acids used.[4] The *paf*, which can be obtained from the vertical separation of the two lines in Fig. 4, is 180, very near the value of 168 found for the much more reactive aza analog **1***b* (a value of 210 is given in ref. 23). The magnitude of *paf* has been previously linked to the degree of conjugation with the site of proton loss and since this is essentially unchanged in the aza and deaza compounds it is perhaps not surprising that protonation has the same activating effect in the two cases, despite there being a large reactivity difference between the two compounds.

Deuterium Isotope Effect

The protons of the 7-methyl group in **6** were exchanged for deuterium to produce **15** and the rate of ionization determined at 35.7°C in H_2O at pH 6.10 by means of iodometry. At this acidity k_{AcOH} is negligible and the observed rate constant $5.44 \times 10^{-6}\ M^{-1}s^{-1}$ corresponds to $k_{S + AcO^-}$, the isotope effect being 4.3.

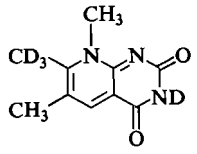

15

Relationships between Acidity, Basicity, and Polarographic Half-wave Potential

The acidity constant K_{SH^+} was required for all compounds in order to convert the catalytic constants k_{HA} into the rate constants $k_{SH^+ + A^-}$ and they were determined in this work. At the same time the acidity constant K_a for dissociation of the 3-N proton in the neutral compound was determined in each case.

Substitution at the 5, 6, and 7 positions of lumazines and deazalumazines produces roughly the same change in pK_{SH^+} as in pK_a, as can be seen from the results in Table 2. It is significant that both pK_{SH^+} and pK_a measurements can be made in the present case in what is essentially an aqueous medium. Attempts to link acidity and basicity in other heterocyclic systems, aminopyrimidines and purines, for example (26), perforce used data acquired largely outside the aqueous standard state by means of acidity function and related extrapolative techniques, the reliability of which are open to question. (See ref. 27 and references therein.)

The polarographic reduction potential becomes

Can. J. Chem. Downloaded from www.nrcresearchpress.com by 210.87.254.105 on 09/06/12
For personal use only.

TABLE 3. Effect of substituents on the reactions of 5-deazalumazines[a]

				7-Methyl		5-Methyl	
Substituent	ΔpK_{SH^+}	ΔpK_a	$\Delta E_{\frac{1}{2}}$	$\Delta pk_{S + AcO^-}$	$\Delta pk_{SH^+ + AcO^-}$	$\Delta pk_{S + OAc^-}$	$\Delta pk_{SH^+ + AcO^-}$
5-Aza	+1.28	+1.7	+0.569	+2.75	+2.71[b]	—	—
	+1.66	+1.1	+0.537	+2.30	—	—	—
5-Methyl	−0.45	−0.8	−0.167	−1.14	−1.15	—	—
	−0.36	−0.8	−0.131	−0.91	−0.89	—	—
6-Methyl[c]	−0.78	−0.4	+0.001	+0.82			
	−0.40	−0.2	−0.031	+0.38	+0.55	+0.53	+0.50
	−0.32	−0.1	−0.043	+0.60	+0.59	+0.58	+0.60
	−0.31	−0.3	+0.005				
7-Methyl	−0.12	−0.1	−0.126	—	—	−0.95	−1.00
	−0.11	0.0	−0.079	—	—	−0.96	−0.91

[a] Obtained from the results shown in Table 2, the order in which the Δ values are listed coming from the order in Table 2; e.g. the first set of values for the effect of 5-aza substitution comes from a comparison of **1***b* and **6**, the second from **1***c* and **7**, and similarly with the other substituents.
[b] Uncorrected for solvent isotope effect.
[c] The boxed values are anomalous (see text).

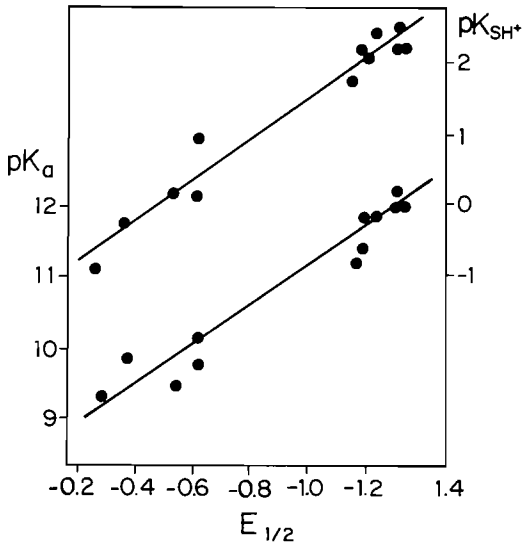

FIG. 5. Variation of polarographic half-wave potential with pK_a and pK_{SH^+} for compounds studied herein. Upper curve and right-hand axis, pK_{SH^+}, slope = −2.92, correlation coefficient = 0.980; lower curve and left-hand axis, pK_a, slope = −2.63, correlation coefficient = 0.966.

more negative the more electron-donating groups there are present in the molecule, as expected. Indeed, roughly linear correlations exist between $E_{\frac{1}{2}}$ and pK_{BH^+} and pK_a. The slopes of such plots (Fig. 5) are $-2.92\ V^{-1}$ and $-3.06\ V^{-1}$ for pK_{BH^+} and pK_a, respectively. The significance of these numbers can be seen by converting them to dimensionless quantities by dividing by $\alpha nF/2.303RT$, where α is the transfer coefficient for the reaction and n is the number of electrons transferred (28). The corrective factor is obtained from the variation of current with potential (29); in our case the average value of αn was 1.16 and $\alpha nF/2.303RT$ was 19.8 V^{-1}. Using this correction the absolute values of the dimensionless slopes in Fig. 5 are 0.15 and 0.16, indicating that proton gain and proton loss in these compounds are processes that are much less sensitive to structural changes than is the one-electron addition process that occurs during polarographic reduction.

The Problem of the 6-Methyl Group

Why does a methyl group at C-6 activate the adjacent sites in lumazines and deazalumazines instead of deactivating them as would be expected from the behaviour of methyl when it is at a next-but-one position? Both the general acid and general base catalyzed reactions are bimolecular with transition states whose geometries at the reaction sites are expected to be virtually identical and the steric effect of an adjacent group should hinder reaction, not facilitate it. If electronic effects are dominant, why is the effect reversed when the position of the group is changed?

The distinctive effect of the 6-methyl group can best be appreciated by considering the results given in Table 3 and those shown in Fig. 6.

Table 3 summarizes the effect of substituting the groups 5-aza, 5-methyl, 6-methyl, and 7-methyl on pK_{SH^+}, pK_a, $E_{\frac{1}{2}}$, $k_{S + AcO^-}$, and $k_{SH^+ + AcO^-}$. Except for perhaps the very modest effect of 7-methyl the pK results are unexceptionable. Likewise, the effect of 5-aza, 5-methyl, and 7-methyl on the rate constants for the general acid and general base reactions is qualitatively reasonable, though a comparison of the appropriate Hammett sigma (σ) values (−0.07 for 3-methyl and +0.65 for 3-aza (30)) suggests that the relative deactivating effect in our system of next-but-one methyl is particularly large. This may well be a result of contributions of

Can. J. Chem. Downloaded from www.nrcresearchpress.com by 210.87.254.105 on 09/06/12
For personal use only.

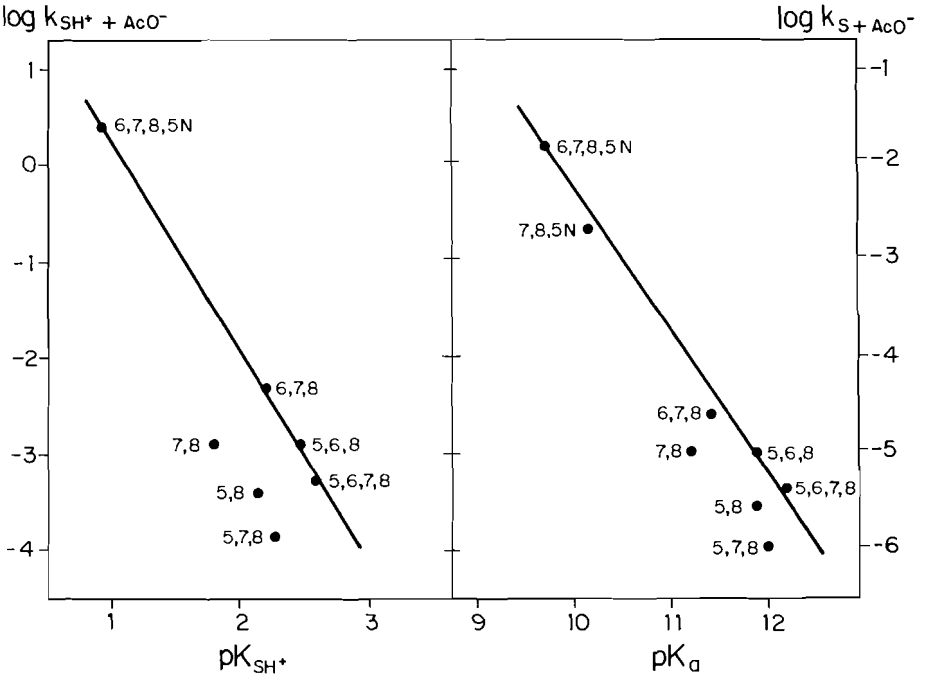

FIG. 6. Logarithm of the rate constant for the reaction of acetate ion with SH^+ as a function of the equilibrium acid strength of SH^+ (left; slope = −2.19, correlation coefficient, 0.999), and with S as a function of the equilibrium acid strength of S (right; slope = −1.46; correlation coefficient 0.994) for the lumazine and deazalumazine series; methyl (and nitrogen) positions indicated by numbers. The straight lines are drawn with respect to the compounds containing a 6-methyl group.

structures such as **16** and **17** (including hyperconjugation) in the neutral molecule and in the conjugate acid, and similarly at C-7.

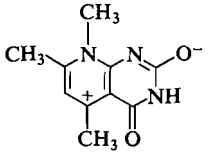

16

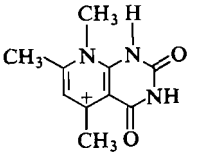

17

If the neutral molecule (and its conjugate acid) has considerable aromatic character as a result of contributions from structures such as **18** it will be closer to planarity than will the reactive intermediate and relief of steric strain may well contribute to the rate increases produced by adjacent methyl (*7b*, 31). If this interaction were dominant, however, we would not expect to find the additivity of effects that is observed with the tetramethyl compound **11**. There the rates can be calculated reasonably accurately on the basis of the rates of the dimethyl and trimethyl compounds. That is, there is no buttressing effect (32, 33).

Turning to Fig. 6, shown there is a plot of the logarithm of the rate of deprotonation by acetate ion against the logarithm of the equilibrium constant for deprotonation for both the neutral substrates and their conjugate acids. (These would be conventional Brönsted plots if the sites of deprotonation were the same in the rate and equilibrium processes.) It can be seen that the compounds that contain a 6-methyl group appear to form a separate series from those that do not; this is particularly noticeable in the case of the protonated substrate.

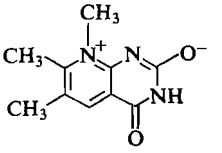

18

In summary we attribute much of the large deactivating effect of next-but-one methyl to hyperconjugative stabilization of the reactant molecule; the reversing of this effect when methyl is moved to an adjacent position we tentatively attribute, at least in part, to relief of steric strain accompanying conversion of reactant molecule to a puckered intermediate, though the lack of buttressing is paradoxical.

Although the polarographic reduction potentials correlate reasonably well with pK, as previously pointed out, a close look at the $E_{\frac{1}{2}}$ values for the 6-methyl compounds shows them to be less negative

Can. J. Chem. Downloaded from www.nrcresearchpress.com by 210.87.254.105 on 09/06/12
For personal use only.

Can. J. Chem. Downloaded from www.nrcresearchpress.com by 210.87.254.105 on 09/06/12
For personal use only.

than would be expected. This can be seen in Table 3 where the effect of a 6-methyl group on $E_{\frac{1}{2}}$ is highlighted and can be seen to be virtually nil. Whether this phenomenon is related to the anomalies in the catalytic rate data, discussed above, is uncertain but it points again to the cryptic role of a 6-methyl group in lumazine and deazalumazine chemistry.

We conclude by referring to the difficulties we had in synthesizing pure 7,8-dimethyllumazine, **1***c*, and the seemingly greater thermal and photochemical stability of the 6,7,8-trimethyl compound, **1***a*. Does the 6-methyl group, which must be present for biological conversion to flavins to take place, play a greater role than simply supplying a carbon atom in the flavin skeleton? Is the 6,7,8-trimethyl-5-deazalumazine, **6**, capable of self-condensation as is the aza analog? What are the effects on the reactive C-5 and C-7 positions of larger alkyl groups at C-6, and indeed at N-8? These questions are currently being addressed.

Acknowledgement

We thank the Natural Sciences and Engineering Research Council of Canada for financial support.

1. R. STEWART, S. J. GUMBLEY, and R. SRINIVASAN. J. Am. Chem. Soc. **102**, 6168 (1980).
2. (*a*) T. PATERSON and H. C. S. WOOD. J. Chem. Soc. Perkin Trans. I, 1051 (1972); (*b*) G. W. E. PLAUT, R. L. BEACH, and T. AOGAICHI. Biochemistry, **9**, 771 (1970); R. L. BEACH and G. W. E. PLAUT. Biochemistry, **9**, 760 (1970); (*c*) G. W. E. PLAUT and R. L. BEACH. *In* Chemistry and biology of pteridines. *Edited by* W. Pfleiderer. de Gruyter, Berlin. 1975.
3. J. M. MCANDLESS and R. STEWART. Can. J. Chem. **48**, 263 (1970).
4. (*a*) M. BRUSTLEIN and T. C. BRUICE. J. Am. Chem. Soc. **94**, 6548 (1972); (*b*) M. S. JORNS and L. B. HERSH. J. Am. Chem. Soc. **96**, 4013 (1974); (*c*) V. MASSEY and P. HEMMERICH. Biochemistry, **17**, 1 (1978); (*d*) C. WALSH, F. JACOBSEN, and C. C. RYERSON. Advances in chemistry. Vol. 191. *Edited by* D. Dolphin, C. McKenna, Y. Murakami, and T. Tabushi. American Chemical Society, Washington, DC. 1980.
5. (*a*) S. T. ZENG, R. WOLFE, and M. BRYANT. J. Bacteriol. **121**, 184 (1975); (*b*) D. EIRICH, W. BALCH, and R. WOLFE. Biochemistry, **17**, 4583 (1979); (*c*) W. T. ASHTON, R. D. BROWN, F. JACOBSEN, and C. WALSH. J. Am. Chem. Soc. **101**, 4419 (1979).
6. T. PATERSON and H. C. S. WOOD. J. Chem. Soc. Perkin Trans. I, 1041 (1972); H. C. S. WOOD, R. WRIGGLESWORTH, D. A. YEOWELL, F. W. GURNEY, and B. S. HURLBERT. J. Chem. Soc. Perkin Trans. I, 1225 (1974).
7. (*a*) R. STEWART and K. OYAMA. J. Am. Chem. Soc. **97**, 6510 (1975); (*b*) W. PFLEIDERER, J. BUNTING, D. D. PERRIN, and G. NUBEL. Chem. Ber. **99**, 3505 (1966).
8. E. KING and T. KING. J. Chem. Soc. 726 (1947).
9. J. M. MCANDLESS. Ph.D. Thesis, University of British Columbia, 1969.
10. E. E. ROYALS and K. C. BRANNOCK. J. Am. Chem. Soc. **75**, 2050 (1953).
11. R. G. KELSO, K. W. GREENLEE, J. M. DOOFER, and C. E. BOORD. J. Am. Chem. Soc. **77**, 1751 (1955).
12. A. J. BIRCH and C. J. MOYE. J. Chem. Soc. 2623 (1958).
13. (*a*) O. V. SCHICKH, A. BINZ, and A. SCHULZ. Chem. Ber. **69**, 2593 (1936); (*b*) K. OYAMA and R. STEWART. J. Chem. Soc. Perkin Trans. I, 673 (1973).
14. T. MATSUKAWA and K. SHIRAKAWA. J. Pharm. Soc. Jpn. **69**, 458 (1949).
15. D. A. WADKE and D. E. GUTTMAN. J. Pharm. Sci. **55**, 1088 (1966).
16. J. HEYROVSKY and J. KUTA. Principles of polarography. Academic Press, New York. 1966. pp. 531–547.
17. (*a*) R. STEWART and J. M. MCANDLESS. J. Chem. Soc. Perkin Trans. II, 376 (1972); (*b*) R. SRINIVASAN and R. STEWART. J. Chem. Soc. Perkin Trans. II, 674 (1976).
18. R. SRINIVASAN and R. STEWART. J. Am. Chem. Soc. **98**, 7648 (1976).
19. F. G. BORDWELL, J. E. BARTMESS, and J. A. HOUTALA. J. Org. Chem. **43**, 3108 (1978).
20. J. T. EDWARD and I. C. WANG. Can. J. Chem. **43**, 2867 (1965).
21. M. H. LIETZKE and T. W. STOUGHTON. J. Phys. Chem. **67**, 652 (1963).
22. A. ALBERT. *In* Advances in heterocyclic chemistry. Vol 20. *Edited by* A. R. Katritzky and A. J. Boulton. Academic Press, New York. 1976. p 117.
23. R. STEWART and R. SRINIVASAN. Acc. Chem. Res. **11**, 271 (1978).
24. R. STEWART and R. SRINIVASAN. Can. J. Chem. **59**, 957 (1981).
25. R. STEWART, S. J. GUMBLEY, and R. SRINIVASAN. Can. J. Chem. **57**, 2783 (1979).
26. R. STEWART and M. G. HARRIS. J. Org. Chem. **43**, 3123 (1978).
27. J. T. EDWARD, M. SJÖSTROM, and S. WOLD. Can. J. Chem. **59**, 2350 (1981).
28. (*a*) P. ZUMAN. Collect. Czech. Chem. Commun. **25**, 3225 (1960); (*b*) A. STREITWIESER and C. PERRIN. J. Am. Chem. Soc. **86**, 4938 (1964); (*c*) J. GRIMSHAW and J. S. RAMSEY. J. Chem. Soc. B, 60 (1968).
29. J. KOUTECKY. Collect. Czech. Chem. Commun. **18**, 597 (1953).
30. (*a*) C. D. JOHNSON. The Hammett equation. Cambridge University Press, Cambridge, U.K. 1973; (*b*) A. D. CAMPBELL, S. Y. CHOOI, L. W. DEADY, and R. A. SHANKS. Aust. J. Chem. **23**, 203 (1970).
31. N. W. JACOBSEN. J. Chem. Soc. C, 1065 (1966).
32. F. H. WESTHEIMER. *In* Steric effects in organic chemistry. *Edited by* M. S. Newman. Wiley, New York. 1956. p. 552.
33. L. A. PAQUETTE and J. M. GARDLIK. J. Am. Chem. Soc. **102**, 5033 (1980).

FOR ERRATA SEE
v.60 #6 19.82 ...p.812...

The crystal and molecular structure of *N,N'*-ethylenebis(benzoylacetoniminato)-nickel(II)[1]

VINCENZO MALATESTA
Division of Chemistry, National Research Council of Canada, Ottawa, Ont., Canada K1A 0R6
AND
ANGELO MUGNOLI
Istituto di Chimica Fisica dell'Università, Corso Europa, Palazzo delle Scienze, 16132 Genova, Italy

Received April 7, 1981

ERRATA

VINCENZO MALATESTA and ANGELO MUGNOLI. Can. J. Chem. **59**, 2766 (1981).

The crystal structure of *N,N'*-ethylenebis(benzoylacetoniminato)nickel(II), Ni^{II}(benacacen), has been determined by X-ray diffraction. Crystals are monoclinic and belong to the space group $P2_1/n$; the cell dimensions are a = 10.793(2), b = 7.910(1), c = 22.020(4) Å, β = 96.68(2)°. Intensity data were measured on a four-circle automatic diffractometer and the structure was solved by combined use of direct and Patterson methods. Full-matrix least-squares refinement converged at R = 0.032 for 3456 observed reflections. The geometry around the Ni atom is square planar; remarkable planarity extends to the whole ligand, aside from the rotation of the phenyl rings and the torsion along the dimethylene bond. Bond distances and bond angles are in agreement with corresponding values found for other Schiff-base type complexes. The packing of the molecules leaves empty channels running through the crystal, a relevant point in the study of chemical models for oxygen carriers of biological interest.

ERRATA

VINCENZO MALATESTA et ANGELO MUGNOLI. Can. J. Chem. **59**, 2766 (1981).

On a déterminé par diffraction de rayons-X, la structure du cristal de *N,N'*éthylènebis(benzoylacétoniminato)nickel(II), Ni^{II}(benacacen). Les cristaux sont monocliniques et appartiennent au groupe d'espace $P2_1/n$; les dimensions de la maille sont; a = 10,793(2), b = 7,910(1), c = 22,020(4) Å, β = 96,68(2)°. On a mesuré les données d'intensité dans un diffractomètre à 4 cercles et on a résolu la structure en combinant la méthode directe à celle de Patterson et on l'a affinée par la méthode des moindres carrés (matrice complète) jusqu'à des valeurs de R = 0,032 pour 3456 réflexions. La géométrie autour de l'atome de Ni est plan carré et la planéarité s'étend remarquablement à tout le ligand à l'exception de la rotation du cycle phényle et de la torsion le long de la liaison diméthylène. Les distances et les angles de liaison sont en accord avec les valeurs correspondantes obtenues pour d'autres complexes de type base de Schiff. L'entassement des molécules laisse des canaux vides qui parcourent tout le cristal, un point important dans l'étude des modèles chimiques des transporteurs d'oxygène ayant une importance biologique.
[Traduit par le journal]

Low molecular weight model substances containing a transition metal center (mono or polynuclear) and being able to combine with oxygen have attracted a great deal of interest. The properties of many of these metal complexes have been extensively investigated with the aim of identifying the structural features which render them suitable model substances for the natural "oxygen carrier" systems (1). Most likely the conclusions drawn from the relationship of the structure to the oxygen binding ability of these model molecules should prove useful when trying to understand the analogous properties of more complex biological systems.

Although many esr studies of tetra- and pentacoordinate Schiff-base complexes have been reported (2–7), the identification of their ground states has been difficult and in some cases (2, 4) controversial. The difficulties stem from the fact that most of the work was done on frozen solutions or powders in which it is not possible to identify and assign, with any degree of confidence, the three g and A values in the spin Hamiltonian to specific molecular axes and/or define the relative orientation of the molecular axes with respect to the crystal axes.

It is, on the other hand, clear that the electronic requirements for the fixation of oxygen of many of the complexes are rather critical and that the elucidation of the electronic configuration (nature of the ground state) and of the intimate details of their crystal structure are of definite importance.

It has been stated that "... the stabilities of dioxygen adducts of Schiff-base complexes of cobalt(II) are very dependent upon the nature of the Schiff base and upon crystal-packing effects"

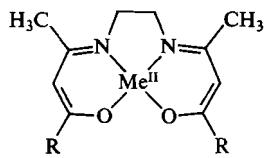

1*a*: R = CH_3, Me^{II}(acacen)
1*b*: R = C_6H_5, Me^{II}(benacacen) or Me^{II}(bzacen)

[1]NRCC No. 19462.

0008-4042/81/182766-05$01.00/0
©1981 National Research Council of Canada/Conseil national de recherches du Canada

Can. J. Chem. Downloaded from www.nrcresearchpress.com by 210.87.254.105 on 09/06/12
For personal use only.

Can. J. Chem. Downloaded from www.nrcresearchpress.com by 210.87.254.105 on 09/06/12
For personal use only.

(8). As reported in a previous esr study (9), crystals of Ni^{II}(benacacen) can be doped with Co^{II}(benacacen) (**1***b*), which absorbs oxygen in the solid state. From that study some crystallographic and structural indication was obtained for the host crystal, Ni^{II}(benacacen). In order to confirm the esr predictions and as a first step in investigating structural features possibly related to the ability of the Co^{II} compound to absorb oxygen, the crystal structure of Ni^{II}(benacacen) has been determined by X-ray diffraction. Preliminary results were reported (10).

Experimental

The compound crystallizes in dark red prisms elongated parallel to the *y* axis. Preliminary film data showed that the crystals are monoclinic, space group $P2_1/n$ ($h0l$, only for $h + l = 2n$; $0k0$, only for $k = 2n$). Lattice constants were obtained from a least-squares fit of 15 reflections (plus their equivalents) measured on a Syntex $P\bar{1}$ automatic diffractometer. The crystal data can be summarized as follows:

$NiC_{22}H_{22}N_2O_2$ fw = 405.1

Monoclinic, space group $P2_1/n$, $a = 10.793(2)$, $b = 7.910(1)$, $c = 22.020(4)$ Å, $\beta = 96.68(2)°$, $V = 1867.1$ Å^3, $D_x = 1.441$, $D_m = 1.445$ g cm^{-3} (by flotation in CCl_4–C_6H_6), $Z = 4$ (20°C; MoKα, $\lambda = 0.71069$ Å), $F(000) = 848$, μ(MoKα) = 10.0 cm^{-1}.

Intensities were collected from a crystal ground in a sphere ($r = 0.25$ mm) with graphite monochromatized MoKα radiation, using the ω-scan technique, total ω scan 1°, variable scan speed between 2 and 12° min^{-1}. The background was counted for half the total scanning time 1° on each side of the Kα position. After every group of 50 reflections three standard reflections were monitored; no significant change in their intensities was observed. In the range explored (2θ between 4 and 55°) 4291 independent reflections were measured, of which 3462 having $I \geq 3\sigma(I)$ were considered observed. Lorentz and polarization factors were applied; absorption corrections were unnecessary (for a spherical specimen with $\mu R = 0.25$, the correction factor remains essentially constant within the explored range of θ).

Some preliminary attempts to solve the structure by direct methods were unsuccessful, until the five central atoms, i.e. Ni, N(1), N(2), O(1), O(2), were introduced in MULTAN 78 (11) in known positions (as determined by a sharpened Patterson synthesis). Using 350 reflections with $|E| \geq 1.56$ the structure solution arose from the set of phases having the best combined figure of merit, in spite of a very high residual (0.77). The corresponding *E*-map allowed recognition of all 27 non-hydrogen atoms.

Refinement on the 3462 observed reflections was performed by full-matrix least-squares process by means of the SHELX 76 system of programs (12), with isotropic and then anisotropic thermal factors, for a total of 244 variable parameters. The function minimized was $\Sigma w(\Delta F)^2$ with weights $w = 1/\sigma^2(F)$. The scattering factors for C, N, O atoms were taken from ref. 13 and for H from ref. 14; the nickel curve was corrected for anomalous dispersion (15).

All hydrogen atoms with the exception of two (whose positions were derived from geometrical considerations) were located on a difference Fourier map. They were not refined, but all were introduced in structure factor calculations with an isotropic thermal parameter $U_H = 0.05$ Å^2. In the last cycles, six very strong low-angle reflections were given zero weight because they were presumably affected by extinction or exper-

TABLE 1. Final atomic coordinates and their standard deviations. The equivalent positions for space group $P2_1/n$ are x, y, z; $-x, -y, -z$; $1/2 - x, 1/2 + y, 1/2 - z$; $1/2 + x, 1/2 - y, 1/2 + z$

(*A*) Nonhydrogen atoms[a]

Atom	*x*	*y*	*z*
Ni	4840(0)	2062(0)	9689(0)
C(1)	7095(2)	2889(3)	9217(1)
C(2)	7614(2)	3517(4)	9769(1)
C(3)	6996(2)	3646(3)	10301(1)
C(4)	7700(3)	4500(4)	10848(1)
C(5)	5223(2)	3460(3)	10862(1)
C(6)	4136(2)	2269(3)	10860(1)
C(7)	2474(2)	1418(3)	10093(1)
C(8)	1600(3)	1356(4)	10583(1)
C(9)	1994(2)	866(3)	9503(1)
C(10)	2686(2)	662(3)	9027(1)
C(11)	7770(2)	2954(3)	8664(1)
C(12)	7335(2)	2002(3)	8151(1)
C(13)	7934(3)	2054(4)	7626(1)
C(14)	8983(3)	3071(4)	7612(1)
C(15)	9415(2)	4027(4)	8106(1)
C(16)	8833(2)	3963(3)	8633(1)
C(17)	2124(2)	−103(3)	8437(1)
C(18)	834(2)	−281(4)	8289(1)
C(19)	357(2)	−1017(4)	7743(1)
C(20)	1129(3)	−1595(4)	7329(1)
C(21)	2408(2)	−1413(4)	7471(1)
C(22)	2895(2)	−671(3)	8020(1)
N(1)	5858(2)	3098(2)	10321(1)
N(2)	3640(2)	1925(2)	10224(1)
O(1)	5987(2)	2237(2)	9125(1)
O(2)	3852(1)	1067(2)	9044(1)

(*B*) Hydrogen atoms[b]

Atom	*x*	*y*	*z*
H(2)	849	393	981
H(4′)	781	373	1121
H(4″)	725	555	1097
H(4‴)	852	480	1071
H(5′)	488	464	1082
H(5″)	583	323	1127
H(6′)	440	112	1112
H(6″)	357	270	1107
H(8′)	191	58	1093
H(8″)	75	134	1039
H(8‴)	144	254	1077
H(9)	115	45	947
H(12)	662	103	821
H(13)	758	118	726
H(14)	935	320	722
H(15)	1012	489	808
H(16)	910	478	897
H(18)	29	33	856
H(19)	−57	−101	757
H(20)	82	−211	694
H(21)	293	−205	721
H(22)	382	−54	813

[a] All coordinates were multiplied by 10^4.
[b] All coordinates were multiplied by 10^3. The numbering of hydrogen atoms refers to the bonded carbon atom (Fig. 1).

Can. J. Chem. Downloaded from www.nrcresearchpress.com by 210.87.254.105 on 09/06/12
For personal use only.

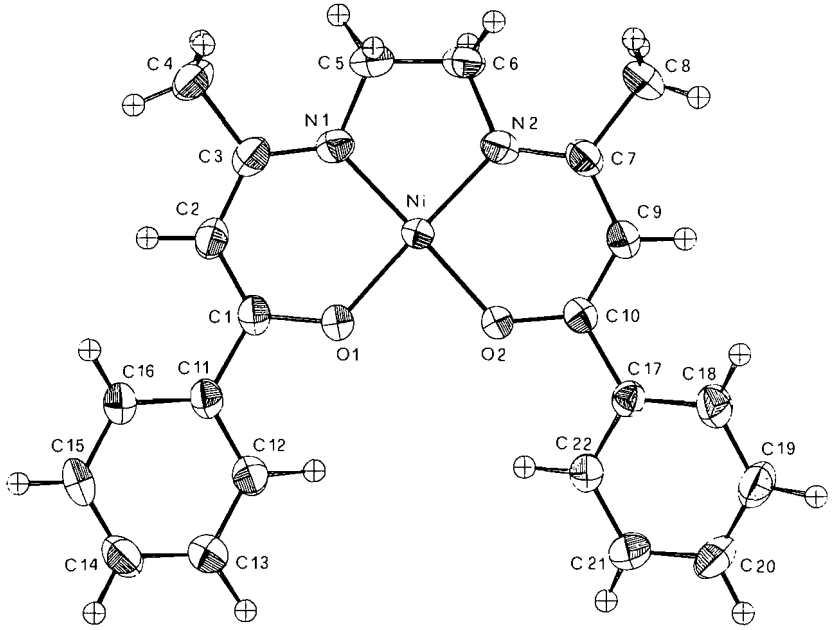

FIG. 1. A molecule of Ni(benacacen) viewed along the direction corresponding to the maximum moment of inertia of the ligand. Temperature ellipsoids of heavy atoms include 50% probability; hydrogen atoms, treated as isotropic, are on an arbitrary scale.

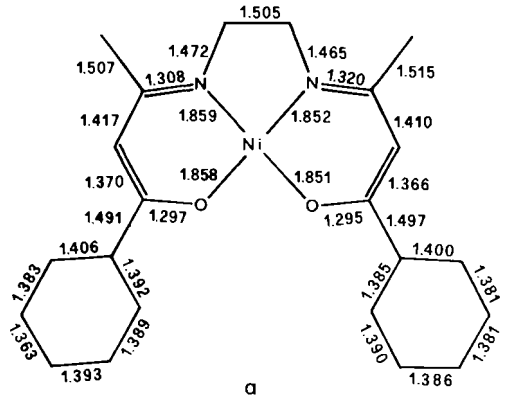

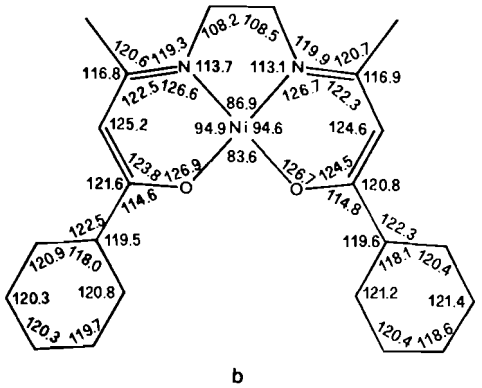

FIG. 2. Molecular geometry: (*a*) bond lengths; esd's are 0.002–0.004 Å; (*b*) bond angles; esd's are about 0.2°.

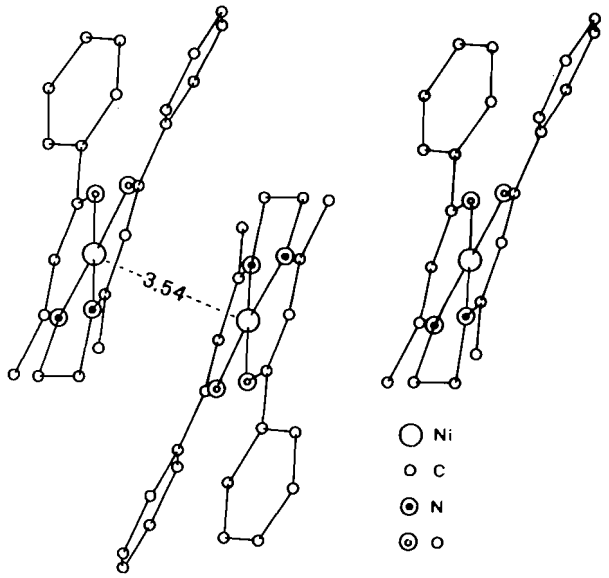

FIG. 3. Coupling of molecules of Ni(benacacen).

imental error. When all the shifts were less than 0.7σ the refinement was considered complete; the residual converged to a final value $R = 0.032$ for 3456 observed reflections. A final difference map showed no significant features. The coordinates are listed in Table 1; lists of anisotropic temperature parameters and of observed and calculated structure factors are available.[2] The overall conformation of the molecule and the numbering of atoms are shown on the thermal ellipsoids plot (16) of Fig. 1.

[2]These tables may be obtained, at a nominal charge, from the Depository of Unpublished Data, CISTI, National Research Council of Canada, Ottawa, Ont., Canada K1A 0S2.

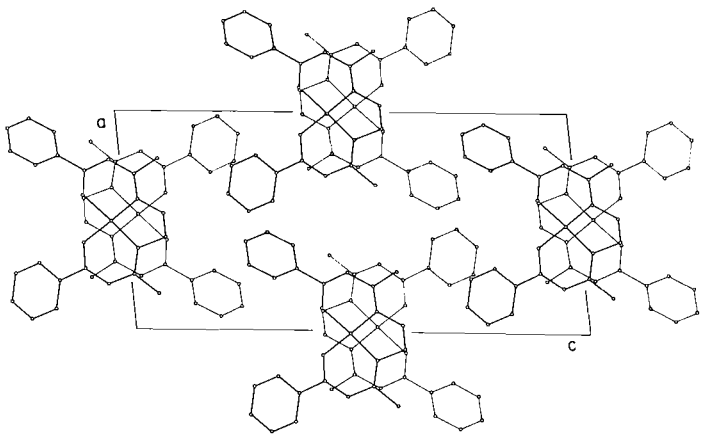

FIG. 4. Packing of molecules in the crystal, as seen along the y axis.

Results and Discussion

Bond distances and bond angles are reported in Fig. 2. The two N=C(—C)—C=C—O chelating chains and the Ni atom are nearly coplanar, the highest deviation from the least-squares plane (17) being 0.13 Å. The geometry around the Ni atom is approximately square planar, the deviations from the mean plane defined by the atoms Ni, N(1), N(2), O(1), and O(2) being within 0.02 Å; the Ni—N, Ni—O distances are in the range 1.85–1.86 Å. Predictions emerging from the previous single crystal esr study (9) have been confirmed: in particular referring to the crystal system, the approximate orientation of the ligand plane with respect to the elongation axis of the crystals, and the lack of coplanarity of the phenyl rings with respect to the chelating chains, the involved torsion angles being −15° for C(12)—C(11)—C(1)—O(1), and +15° for C(22)—C(17)—C(10)—O(2). The torsion angle along the dimethylene bond is −33°. The signs are given following a known convention (18).

Bond lengths along the ligand are in very good agreement with corresponding values found for 8 Schiff-base type complexes of V, Cu, Co (19):

Bond	Length (Å)	
	Average values from ref. 19	This work (average of two values, except for the last figure)
C(1)—O(1)	1.294	1.296
C(1)—C(2)	1.366	1.368
C(2)—C(3)	1.423	1.414
C(3)—N(1)	1.308	1.314
C(3)—C(4)	1.517	1.511
N(1)—C(5)	1.462	1.469
C(5)—C(6)	1.503	1.505

As already pointed out (19), the ligand bond lengths are independent of the nature of the metal. For all these compounds, including the present one, the chelating chains are always found to be planar or nearly planar, with the metal in the plane of the four donor atoms. These facts, along with the feasibility of growing crystals of Ni^{II}(benacacen) doped with Co^{II}(benacacen), support the hypothesis of isostructurality of the two compounds.

In the crystal the molecules are stacked in centrosymmetric pairs by van der Waals forces (Fig. 3), leaving voids between different couples and giving rise to empty channels which run parallel to the y axis through the whole structure (Fig. 4). This feature can be considered an important prerequisite for oxygen absorption in the solid state (20), a relevant point in the study of chemical models of biological interest.

Acknowledgments

We wish to thank Professor M. Simonetta (University of Milano, Italy) for permitting the use of the Syntex P1 diffractometer, and the Italian Consiglio Nazionale delle Ricerche for financial support.

1. G. HENRICI-OLIVÉ and S. OLIVÉ. Angew. Chem. Internat. Edit. **13**, 29 (1974) and references cited therein.
2. B. M. HOFFMAN, F. BASOLO, and D. L. DIEMENTE. J. Am. Chem. Soc. **95**, 6497 (1973); **92**, 61 (1970).
3. B. M. HOFFMAN, F. BASOLO, and D. L. DIEMENTE. Chem. Commun. 467 (1970).
4. F. L. URBACH, R. D. BEREMAN, J. A. TOPICH, M. HARIHARAN, and B. J. KALBACHER. J. Am. Chem. Soc. **96**, 5063 (1974).
5. C. BUSETTO, F. CARIATI, A. FUSI, M. GULLOTTI, F. MORAZZONI, A. PASINI, R. UGO, and V. VALENTI. J. Chem. Soc. Dalton Trans. 754 (1973).
6. E. I. OCHIAI. J. Chem. Soc. Chem. Commun. 489 (1972); J. Inorg. Nucl. Chem. **35**, 1727 (1973).
7. C. BUSETTO, F. CARIATI, P. C. FANTUCCI, D. GALIZZOLI, and F. MORAZZONI. Inorg. Nucl. Chem. Lett. **9**, 313 (1973).

Can. J. Chem. Downloaded from www.nrcresearchpress.com by 210.87.254.105 on 09/06/12
For personal use only.

8. K. J. HALLER and J. H. ENEMARK. Acta Crystallogr. Sect. B, **34**, 102 (1978).
9. V. MALATESTA and B. R. MCGARVEY. Can. J. Chem. **53**, 3791 (1975).
10. V. MALATESTA and A. MUGNOLI. Fifth European Crystallographic Meeting, Copenhagen, August 1979. p. 203.
11. P. MAIN, S. E. HULL, L. LESSINGER, G. GERMAIN, J. P. DECLERCQ, and M. M. WOOLFSON. MULTAN 78, University of York, England. 1978.
12. G. M. SHELDRICK. SHELX 76, University of Cambridge, England. 1976.
13. D. T. CROMER and J. B. MANN. Acta Crystallogr. Sect. A, **24**, 321 (1968).
14. R. F. STEWART, E. R. DAVIDSON, and W. T. SIMPSON. J. Chem. Phys. **42**, 3175 (1965).
15. D. T. CROMER and D. LIBERMAN. J. Chem. Phys. **53**, 1891 (1970).
16. C. K. J.OHNSON. ORTEP, Report ORNL-3794. Oak Ridge National Laboratory, Oak Ridge, TN. 1965.
17. V. SCHOMAKER, J. WASER, R. E. MARSH, and G. BERGMAN. Acta Crystallogr. **12**, 600 (1959).
18. W. KLYNE and V. PRELOG. Experientia, **16**, 521 (1960).
19. M. CALLIGARIS, G. NARDIN, and L. RANDACCIO. Coord. Chem. Rev. **7**, 385 (1972).
20. W. P. SCHAEFER and R. E. MARSH. Acta Crystallogr. Sect. B, **25**, 1675 (1969).

Can. J. Chem. Downloaded from www.nrcresearchpress.com by 210.87.254.105 on 09/06/12
For personal use only.

Erysotrine-*N*-oxide and erythrartine-*N*-oxide, two novel alkaloids from *Erythrina mulungu*

MARIA HELENA SARRAGIOTTO, HERMOGENES LEITÃO FILHO,[1] AND ANITA J. MARSAIOLI[2]

Instituto de Química, Universidade Estadual de Campinas, CP 1170, 13100 Campinas, São Paulo, Brasil

Received February 13, 1981

MARIA HELENA SARRAGIOTTO, HERMOGENES LEITÃO FILHO, and ANITA J. MARSAIOLI. Can. J. Chem. **59**, 2771 (1981).

Erysotrine, erythrartine, hypaphorine, and two novel alkaloids, erysotrine-*N*-oxide and erythrartine-*N*-oxide, were isolated from the flowers of *Erythrina mulungu*. The *N*-oxide structures were determined by spectroscopic analysis (mass, ^{1}H, and ^{13}C nmr) and by partial synthesis.

MARIA HELENA SARRAGIOTTO, HERMOGENES LEITÃO FILHO et ANITA J. MARSAIOLI. Can. J. Chem. **59**, 2771 (1981).

A partir des fleurs de l'*Erythrina mulungu* on a isolé l'érysotrine, l'érythrartine, l'hypaphorine et deux nouveaux alcaloides, les *N*-oxydes d'érysotrine et d'érythrartine. On a déterminé les structures des *N*-oxydes par des analyses spectroscopiques (rmn du ^{1}H et du ^{13}C et spectroscopie de masse) et par synthèse partielle.

[Traduit par le journal]

Erythrina mulungu[3] (Leguminosae) is a medicinal plant used in folk medicine as a nervine sedative, febrifuge, and antiasthmatic (1). These pharmacological activities are very similar to those shown by *E. variegata* (2) and seem to be due to the presence of spiroamine alkaloids. These compounds, usually referred to as Erythrina alkaloids, have been exhaustively investigated from phytochemical (3), synthetic (4), biosynthetic (5), and spectroscopic (mass (6), gc–mass (3), ^{1}H nmr (7)) points of view; ^{13}C nmr spectroscopy, though, has not yet been fully applied (4, 8).

We now wish to report the isolation of five major alkaloids (**1**, **2**, **3**, **4**, and **5**) from the methanol extract of *Erythrina mulungu* flowers, as well as their ^{13}C nmr data.

Compounds **1**, **2**, and **3** were identified as erysotrine **1** (9), erythrartine **2** (10), and hypaphorine **3** (10). Compounds **1–3** are common constituents of the Erythrina species. Their identifications were based on previously published spectroscopic data and confirmed by their ^{13}C nmr spectra analysis.

The shift assignments, listed in Table 1, were made by standard chemical shift theory and analysis of the SFORD and fully coupled spectra (11). 1-(*p*-Methoxybenzyl)-6,7-dimethoxytetrahydroisoquinoline **6** (12) and 1-α-bromo-15,16-dimethoxy-*cis*-erythrinan-2,8-dione-2-ethylenacetal **7** (8) were used as models.

Comparison of the carbon signals of **1** with the corresponding signals of erythrartine **2** shows agreement for all, except for those at 128.3, 64.3, and 51.2 ppm which were assigned to C-12, C-11, and C-10 respectively. Similar changes are observed, in C-α and C-β, when an axial hydroxyl group is introduced to 5-α-cholest-8(14)-en-3-β-ol **8**, i.e. **8** to **9** (13). This corroborates the pseudo axial hydroxyl

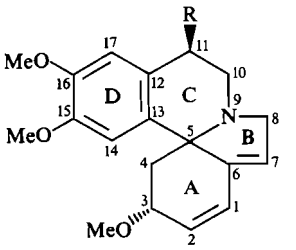

1 R = H
2 R = OH
12 R = OMe

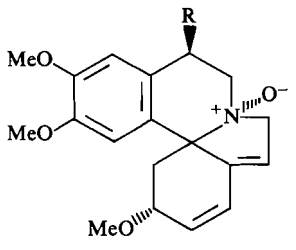

4 R = H
5 R = OH
13 R = OMe

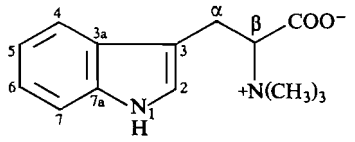

3

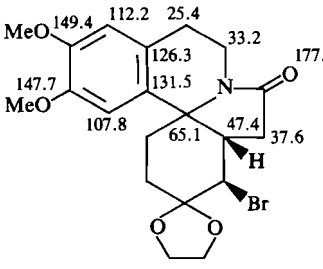

7

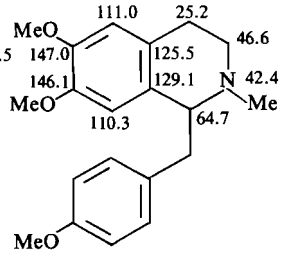

6

[1]Departamento de Morfologia e Sisternatica Vegetais, Instituto de Biologia, UNICAMP, 13100 Campinas, SP, Brasil.

[2]Author to whom correspondence may be addressed.

[3]*E. mulungu* identification is supported by previous works on Brazilian *Erythrina* species (see ref. 18).

0008-4042/81/182771-05$01.00/0

©1981 National Research Council of Canada/Conseil national de recherches du Canada

Can. J. Chem. Downloaded from www.nrcresearchpress.com by 210.87.254.105 on 09/06/12
For personal use only.

Can. J. Chem. Downloaded from www.nrcresearchpress.com by 210.87.254.105 on 09/06/12
For personal use only.

TABLE 1. Carbon shifts of *Erythrina* alkaloids

	1	2	4	5	13
C-1	124.9	125.3	125.6	125.5	125.7
C-2	132.0	131.2	133.5	133.0	133.4
C-3	75.6	75.6	75.4	75.6	75.3
C-4	40.2	40.5	30.8	31.0	30.5
C-5	67.8	66.2	82.5	82.1	81.9
C-6	141.5	141.7	138.3	138.2	138.0
C-7	121.6	123.3	118.1	118.8	118.7
C-8	56.6	58.8	71.7	73.5	72.6
C-10	43.7	51.2	59.6	66.4	59.6
C-11	23.8	64.3	27.2	63.9	74.4
C-12	125.6	128.3	122.0	126.1	122.5
C-13	129.6	129.4	128.5	126.3	127.3
C-14	109.2	108.6	108.7	107.8	107.8
C-15	147.2[a]	148.0[a]	147.8[a]	148.8[a]	149.2[a]
C-16	147.9[a]	148.2[a]	148.6[a]	148.3[a]	149.7[a]
C-17	111.4	110.2	110.5	111.2	111.4
OMe	55.8	55.8	55.7	55.9	55.8

[a] Signals in any vertical column may be reversed.

group at C-11 in erythrartine **2**, previously suggested on the basis of ^{1}H nmr data and $[\alpha]_D$ correlation with related alkaloids (10).

Compound **4** was isolated as an oily brown substance of molecular formula $C_{19}H_{23}NO_4$ (M^+ 329.1595) as determined by high resolution mass spectrometry. The ir (ν_{max} 1610 cm^{-1}) and the uv spectra (λ_{max} 231 (14000) and 278 (2900) nm) were almost identical with those of erysotrine **1** (9) and erythrartine **2** (10). The mass spectrum showed significant ions at *m/e* 329 (M^+), 313 ($M^+ - 16$), 298 ($M^+ - 16 - 15$), 282 ($M^+ - 16 - 31$), 269, 239 (100), 165, 152.

Based on these data an erythrinan carbon skeleton of the 1–6 diene type was assumed. The ^{1}H nmr spectrum of **4**, in deuteriochloroform, revealed two aromatic proton singlets at δ 6.83, 6.76 and three methoxyl group singlets at δ 3.43 (3H), 3.84 (3H), and 3.95 (3H). The presence of three olefinic proton signals at δ 5.92 (broad singlet, H-7), δ 6.30 (broad doublet, J = 10 Hz, H-1), and δ 6.86 (d, J = 3 Hz, low field arm of a double doublet partially covered by one of the aromatic singlets, H-2) corroborated the assumption of a diene system in the molecule. On irradiation at δ 4.10 (H-3) the double doublet at δ 2.14 (H-4e, J_{3e-4e} = 5.5 Hz; J_{4a-4e} = 11 Hz) collapsed to a doublet, the large multiplet at δ 3.08–3.36 (3 superimposed proton signals) was simplified, and the low field arm of the H-2 signal collapsed to a singlet. Further irradiation at δ 3.20 (H-4a) and δ 2.14 (H-4e) allowed the assignment of this ABXY system to that depicted in ring A of **4**.

These results were comparable with those of erythristemine **12** (7) and erythrartine **2** (10) except for the H-4a chemical shift ($\Delta\delta_{4-12}$ 1.12, $\Delta\delta_{4-2}$ 1.35 ppm). Further analysis of the ^{1}H nmr spectrum was not possible due to superimposed signals.

The clue to the structure elucidation of **4** was given by the analysis of the ^{13}C nmr spectrum. The main differences between compound **4** and **1** in the ^{13}C nmr spectra lie in the chemical shifts of the carbon atoms neighboring *N*. The shielding ($\Delta\delta_{1-4}$ 9.4, 3.5, and 3.6 ppm at C-4, C-7, and C-12 respectively) and deshielding ($\Delta\delta_{1-4}$ 14.7, 15.1, and 15.9 ppm at C-5, C-8, and C-10 respectively) effects are consistent with those observed for fumaritine **10** and fumaritine-*N*-oxide **11** (14).

The above arguments, and the presence of an ($M - 16$)$^+$ peak in the mass spectrum (characteristic of *N*-oxides (15)), led us to suggest the erysotrine-*N*-

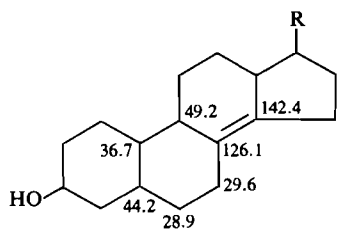

8

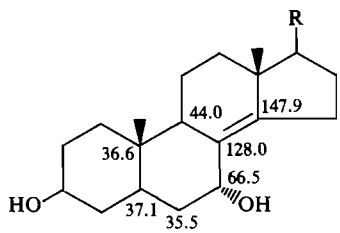

9

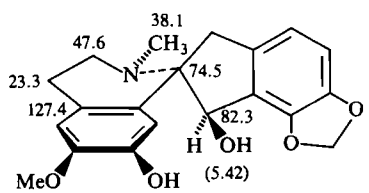

10

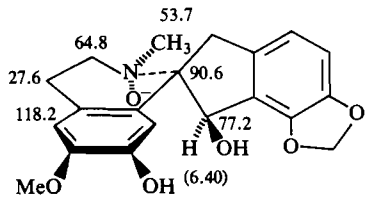

11

Can. J. Chem. Downloaded from www.nrcresearchpress.com by 210.87.254.105 on 09/06/12
For personal use only.

oxide structure for compound **4**. Further confirmation of structure **4** was accomplished by treating **1** with *m*-chloroperbenzoic acid. The resulting *N*-oxide was identical in all aspects (ir, ^{1}H nmr) to the natural product **4**.

Compound **5** was isolated as an oil of molecular formula $C_{19}H_{23}NO_5$ (M^+ 345.1602) as determined by high resolution mass spectrometry. This compound exhibited the uv (λ_{max} 278 (2900), 231 (14000) nm) and ir (ν_{max} 1610, 3250 (OH) cm^{-1}) absorption bands attributable to the 1–6 diene moiety and an hydroxyl group respectively. The ^{1}H nmr spectrum (deuteriochloroform) showed the presence of the following functional groups: three methoxyl groups (δ 3.38, 3.78, and 3.92, each 3H, s), two aromatic protons (δ 6.68 and 7.08, each 1H, s), and three methines (δ 5.82 (broad singlet, 1H), 6.18 (d, J = 10 Hz), and 6.74 (dd, J = 10 and 2 Hz)), the latter characteristic of a 1–6 diene erythrinan skeleton.

On irradiation at δ 2.09 (dd, J_{3a-4e} = 5 Hz, J_{4e-4a} = 10.5 Hz), the triplet at δ 3.16 (J_{4a-4e} = 10.5 Hz, J_{3a-4a} = 10.5 Hz) collapsed to a doublet. Conversely, irradiation of the triplet at δ 3.16 changed the double doublet at δ 2.09 to a doublet. In compound **5**, as in erysotrine-*N*-oxide, H-4a (part of the ABX system of ring A) is shifted downfield (Δδ 1.31 ppm) when compared to that of erythrartine **2**. This supports an *N*-oxide structure. Finally, the existence of a carbinolic proton at C-11 was suggested, based on the signal at δ 5.28 (d, $J_{10a-11a}$ = 15 Hz, H-11a).

The ^{13}C nmr spectrum of **5** (Table 1) when compared to that of **2** revealed deshieldings ($\Delta\delta_{2-5}$ 15.2, 15.9, and 14.7 ppm at C-10, C-5, and C-8 respectively) and shieldings ($\Delta\delta_{2-5}$ 9.5, 4.5, and 2.2 ppm at C-4, C-7, and C-12 respectively) analogous to those observed in the transformation of erysotrine **1** into erysotrine-*N*-oxide **4**. Based on these arguments, we assumed compound **5** was erythrartine-*N*-oxide. Confirmation was obtained by treating erythrartine with *m*-chloroperbenzoic acid. The resultant synthetic *N*-oxide and the natural product **5** showed superimposable ir and ^{1}H nmr spectra.

The absolute configuration at C-3 and C-11 of **5** was established as follows. Methylation of the oily *N*-oxide **5** with sodium hydride – methyl iodide afforded the *O*-methyl derivative **13**, whose ^{1}H nmr spectrum analysis revealed the presence of an additional methoxyl group at δ 3.64. As observed in **4** and **5**, the ABX system of ring A appears at δ 2.00 (dd, J_{4e-4a} = 11 Hz, J_{4e-3a} = 5.5 Hz, H-4e), 3.34 (t, J_{4e-4a} = 11 Hz, J_{4a-3a} = 11 Hz, H-4a). The INDOR technique was used to identify H-3. Using the central peak of the triplet at δ 3.34 as the observed transition, responses were obtained at δ 2.00 and δ 4.30. Consequently H-3 must be at δ 4.30. Using the INDOR technique and observing the peak at δ 5.80 (broad s, H-7), H_{8a} and H_{8e} were detected at δ 4.20. Finally, observing each line of the doublet at δ 5.16 (d, J = 15 Hz, H-11), responses were obtained at δ 4.40. Thus, from δ 4.60 to δ 4.10 are located signals corresponding to H_{10a}, H_{10e}, H_3, H_{8a}, H_{8e}. Finally the large coupling (J = 15 Hz) of the carbinolic proton was indicative of an axial proton at H-11.[4] The analysis of the ^{13}C nmr spectrum of **13** was also carried out. The comparison of the δ values for **13** with the δ values for **5** revealed the concordance of all carbon shifts except for C-10, C-11, and C-13, where the methylation occurred. Furthermore, the C-11 and C-3 shifts (74.4 and 75.3 ppm respectively) suggested equatorial methoxyl groups at both carbons, thus corroborating the pseudo axial H-11.

Treatment of **13** with triethylphosphite in benzene produced the tertiary base erythristemine **12**, which showed $[\alpha]_D$ and ^{1}H nmr data analogous to that reported in the literature (7). The absolute configurations at C-11 and C-3 of **12** were determined by a crystallographic study. This indicates that indeed **5** and **12** have the same absolute configurations at C-3 and C-11.

This is the first time erythrinan *N*-oxides have been reported. The possibility that these *N*-oxides might be artefacts could not be ignored. Therefore fresh flowers were collected and extracted with cold methanol and the crude extract was immediately analyzed by thin layer chromatography. The presence of the *N*-oxides showed that in fact they are natural products. The water solubility of the *N*-oxides and the current methods for isolation of water soluble alkaloids are probably responsible for the lack of examples of erythrinan-*N*-oxides in the literature.

Interestingly, *N*-oxidation of each of the alkaloids erysotrine **1** and erythrartine **2** yielded only one of the two possible (considering inversion at the bridgehead nitrogen (16)) *N*-oxides. In fact the *N*-oxides **4** and **5** are those produced by introduction of oxygen from the more accessible convex face of the molecules **1** and **2**, and this can be shown in the ^{13}C nmr by the C-4 shielding ($\Delta\delta \simeq 9.5$ ppm) and in the ^{1}H nmr by the H-4a deshielding ($\Delta\delta \simeq$ 1.30 ppm) effects produced when *N*-oxidation of the tertiary bases occurs, similar to those observed when going from **10** to **11** (14).

[4]Erythristemine **12** and compound **13** possess the same absolute configuration at C-11 but their solution conformations are different (H-11 is equatorial in **12** and axial in **13**).

Can. J. Chem. Downloaded from www.nrcresearchpress.com by 210.87.254.105 on 09/06/12
For personal use only.

Experimental

The ^{1}H nmr spectra were determined on a Varian T-60 or a Varian XL 100 spectrometer using $CDCl_3$ solutions (unless otherwise indicated) and Me_4Si as an internal standard, chemical shifts are expressed in δ and coupling constants (J) are given in Hertz (s = singlet, d = doublet, t = triplet, m = multiplet). The ^{13}C nmr spectra were recorded in $CDCl_3$ solutions on a Varian XL-100 spectrometer operating at 25.2 MHz in the Fourier transform mode; the values are in parts per million downfield from Me_4Si ($\delta(Me_4Si) = \delta(CDCl_3) + 76.9$); low resolution mass spectra were obtained with a Finnigan Model 1015/SL spectrometer; optical rotations were measured in a Carl Zeiss photoelectric polarimeter. All melting points were determined on a Reichert hot-stage microscope and are uncorrected. Infrared spectra were run on a Perkin-Elmer 337 spectrophotometer using thin films or KBr pellets. Merck silica gel HF was utilized for thin layer plates (tlc) and spots were visualized by spraying Dragendorff solution (17) followed by $MeOH/H_2SO_4$ and heating at 110°C.

The *Erythrina mulungu* flowers were collected in 1979 at "Fazenda Santa Elisa" (Campinas, SP, Brazil) and dried at 40°C for 36 h. The finely ground flowers (690.00 g) were then extracted with methanol yielding 55.60 g of crude extract, which was adsorbed on celulose (120.00 g) and eluted with hexane (5.67 g), chloroform (7.06 g), chloroform–methanol 1:1 (23.33 g), and methanol (7.52 g). Column chromatography through silica gel afforded the alkaloids, further purified using preparative layer chromatography.

Erysotrine **1** (0.17 g) was isolated in 0.31% yield and was identified by ir (9), mass (6), and ^{1}H nmr (9) spectra; uv λ_{max} (EtOH) (ε): 2.30 (12 100), 280 (3300) nm; ir ν(KBr): 1610 cm^{-1}; ^{1}H nmr δ: 6.86 (s, H-14), 6.66 (s, H-17), 6.56 (d, J = 3 Hz, high field arm of a dd, H-2), 6.04 (broad d, J_{1-2} = 10 Hz, H-1), 5.76 (broad s, H-7), 3.86 (s, OMe), 3.76 (s, OMe), 3.34 (s, OMe), 1.89 (t, J_{4a-3a} = 10.5 Hz, H-4a); ms *m/e* (relative intensity): 313 (M^+, 65), 298 (41), 282 (100), 280 (12). The ^{13}C nmr data for **1** are given in Table 1.

Erythrartine **2** (0.17 g) was isolated in 0.31% yield and was identified by ir (10), mass (10), and ^{1}H nmr (10) spectra; $[\alpha]_D^{25}$ 256 (*c* 1.4, $CHCl_3$); uv λ_{max} (EtOH) (ε): 227 (15 135), 275 (3630) nm; ir ν (film) 1610 cm^{-1}; ^{1}H nmr δ: 7.08 (s, H-17), 6.92 (s, H-14), 6.68 (dd, J_{2-1} = 10 Hz, J_{2-3} = 2 Hz, H-2), 6.10 (broad d, J_{1-2} = 10 Hz, H-1), 5.82 (broad s, H-7), 4.80 (t, H-11e), 3.95 (s, OMe), 3.83 (s, OMe), 3.37 (s, OMe), 3.67 (dd, $J_{10a-10e}$ = 15 Hz, $J_{11e-10a}$ = 5 Hz, H-10a), 3.14 (dd, $J_{11e-10e}$ = 4 Hz, $J_{10e-10a}$ = 15 Hz, H-10e), irradiation at δ 4.8 (t) → 3.67 and 3.14 collapsed to a pair of doublets J = 15 Hz; 2.46 (dd, J_{4e-3a} = 5 Hz, J_{4e-4a} = 11 Hz, H-4e), 1.85 (t, $J_{4a-4e} \cong J_{4a-3a}$, H-4a), irradiation at δ 1.85 (t) → 2.46 collapsed to a doublet, conversely, irradiation at δ 2.46 collapsed δ 1.85 to a doublet; ms *m/e* (relative intensity): 329 (M^+, 75), 314 (26), 298 (100), 296 (28), 280 (12); ^{13}C nmr data of **2** are given in Table 1.

Hypaphorine **3** (0.13 g) was isolated in 0.24% yield, mp 247.8–248.8°C (lit. (10) mp 245–247°C); (HCl) 233.1–234.4°C (lit. (10) mp 231–233°C); ir ν_{max}(KBr): 3200, 1640 cm^{-1}; ^{1}H nmr (CF_3COOH) δ: 7.77–7.30 (6 aromatic protons), 4.53 (t, J = 8 Hz, 1H), 3.65 (d, J = 8 Hz, 2H), 3.47 (s, 9H, $3\overset{+}{N}Me$); ^{13}C nmr (D_2O) δ: 172.0 (C=O), 136.9 (C-7a), 127.2 (C-3a), 125.4 (C-2), 122.7 (C-6), 120.1 (C-5), 118.9 (C-4), 112.7 (C-7), 107.9 (C-3), 79.7 (C-β), 52.8 ($\overset{+}{N}Me$), 23.7 (C-α).

Erysotrine-N-*oxide* **4** (0.11 g) was isolated in 0.19% yield; $[\alpha]_D^{25}$ 78.3 (*c* 1, EtOH); uv λ_{max} (EtOH) (ε): 231 (14 000), 278 (2900) nm; ir ν_{max} (KBr): 1610 cm^{-1}; ^{1}H nmr δ: 6.83 (s, 1H), 6.76 (s, 1H), 6.86 (d, J = 3 Hz, low field arm of a double doublet, H-2), 4.60–4.12 (m, 4H), 3.95 (s, 3H, OMe), 3.84 (s, 3H, OMe), 3.43 (s, 3H, OMe), 3.36–3.08 (m, 3H), 2.14 (dd, J_{3e-4e} = 5.5 Hz, J_{4a-4e} = 11 Hz, H-4e); ms *m/e* (relative intensity): 329 (M^+, 5), 313 (10), 311 (10), 298 (12), 282 (20), 269 (90), 254 (36), 239 (100), 224 (55), 165 (62), 152 (52). *Exact Mass* calcd. for $C_{19}H_{23}N_1O_4$: 329.1627; found (ms): 329.1595. The ^{13}C nmr data for **4** are listed in Table 1.

Erythrartine-N-*oxide* **5** (0.089 g) was isolated in 0.16% yield as a yellowish oil; $[\alpha]_D^{25}$ 88.57 (*c* 1.4, EtOH); uv λ_{max} (EtOH) (ε): 231 (14 000), 278 (2900) nm; ir ν_{max} (KBr): 1610 cm^{-1}; ^{1}H nmr δ: 7.08 (s, H-14), 6.68 (s, H-17), 6.74 (dd, J_{1-2} = 10 Hz, J_{2-3e} = 2 Hz, H-2), 6.18 (d, J_{1-2} = 10 Hz, H-1), 5.82 (broad s, H-7), 5.28 (broad d, $J_{10a-11a}$ = 15 Hz, H-11a), 4.4–4.0 (m, 4H), 3.92 (s, 3H, OMe), 3.78 (s, 3H, OMe), 3.38 (s, 3H, OMe), 3.16 (t, J_{4a-4e} = 10.5 Hz, J_{3a-4a} = 10.5 Hz, H-4a), 2.09 (dd, J_{3a-4e} = 5 Hz, J_{4e-4a} = 10.5 Hz, H-4e), irradiation at 2.09 (dd) → 3.16 (t) collapsed to a doublet; conversely, irradiation at 3.16 (t) collapsed 2.09 (dd) to a doublet; ms *m/e* (relative intensity): 345 (M^+, 4), 329 (26), 326 (29), 298 (70), 239 (100), 224 (45), 165 (47), 152 (39). *Exact Mass* calcd. for $C_{19}H_{23}N_1O_5$: 345.1576; found (ms): 345.1602. The ^{13}C nmr data of **5** are given in Table 1.

Erysotrine-N-*oxide* **4**

m-Chloroperbenzoic acid (97.7 mg, 6 × 10^4 mol) was added to a cold stirred mixture (0–5°C) of erysotrine **1** (177.2 mg, 0.0006 mol) in chloroform (5 mL), and the mixture was left at room temperature for 3 h. The $CHCl_3$ solution was evaporated and the residue purified by preparative layer chromatography, developed with $CHCl_3$–MeOH 1:1, affording 110.7 mg (59.4% yield) of synthetic erysotrine-*N*-oxide **4**, which was identical (ir, ^{1}H nmr, uv) to the natural product **4**.

Erythrartine-N-*oxide* **5**

m-Chloroperbenzoic acid (25.28 mg, 1.47 × 10^{-4} mol) was added to a cold stirred mixture (0–5°C) of erythrartine **2** (48.4 mg, 1.47 × 10^{-4} mol) in chloroform (3 mL), and the mixture was left at room temperature for 3 h. The reaction mixture was then worked up as described above (58.7% yield).

O-*Methyl-erythrartine*-N-*oxide* **13**

Sodium hydride (16 mg) was gradually added to a cold stirred solution (5°C) of **5** (120 mg, 3.4 × 10^{-4} mol), followed by addition of ≈ 0.03 mL of methyl iodide and the mixture was left at room temperature for 24 h. Methanol was added to destroy the excess of sodium hydride and then evaporated. The residue was purified by preparative layer chromatography, developed with $CHCl_3$–MeOH 1:1, affording 40.0 mg (32% yield); ^{1}H nmr δ: 6.87 (s, H), 6.78 (s, H), 6.66 (d, J_{2-3} = 2 Hz, high field arm of a dd, H-2), 6.20 (d, J_{1-2} = 10 Hz, H-1), 5.80 (broad s, H-7), 5.16 (d, $J_{11a-10a}$ = 15 Hz, H-11), 4.60–4.10 (m, H-10a, H-10e, H-3, H-8a, H-8e), 3.95 (s, OMe), 3.81 (s, OMe), 3.64 (s, OMe), 3.40 (s, OMe), 3.34 (t, J = 11 Hz, H-4a), 2.00 (dd, J_{4e-4a} = 11 Hz, J_{4e-3a} = 5.5 Hz, H-4e). The ^{13}C nmr data for **13** are listed in Table 1.

Erythristemine **12**

O-Methyl-erythrartine-*N*-oxide **13** (0,040 g, 1.1 × 10^{-4} mol) and 0.025 mL of triethylphosphite in benzene (5 mL) were heated under reflux for one hour. The reaction mixture was then evaporated and the residue purified by preparative layer chromatography, yielding 0.030 g of erythristemine (78.9%); $[\alpha]_D^{25}$ 192 (*c* 0.8, $CHCl_3$) (lit. (7) $[\alpha]_D^{25}$ 189 ($CHCl_3$)); uv λ_{max} (EtOH) (ε): 225 (12 900), 278 (3300) nm; ^{1}H nmr (C_6D_6) δ: 7.12 (s, 1H), 7.00 (s, 1H), 6.35 (dd, J_{1-2} = 10.0 Hz, J_{2-3} = 2.0 Hz, H-2), 5.93 (d, J_{1-2} = 10.0 Hz, H-1), 5.38 (broad s, H-7), 3.42 (s, OMe, 6H), 3.20 (s, OMe, 3H), 3.02 (s, OMe, 3H), 2.52 (dd, J_{4a-4e} = 12.0 Hz, J_{3a-4e} = 5.0 Hz, H-4e, 2.13 (t, $J_{4a-4e} \cong J_{3a-4a}$ = 12.0 Hz, H-4a); ms *m/e*: 343 (M^+).

Acknowledgements

We wish to express our appreciation to Profs.

Fred Fujiwara for the 100 MHz ^1H nmr spectra, to Concetta Kascheres for the mass spectra, to Dr. John A. Stephens from Monsanto Agricultural Products Co., St. Louis, MO, U.S.A. for the high resolution mass spectra, and to Profs. Edmundo A. Ruveda, Francisco de A. M. Reis, and Albert J. Kascheres for helpful suggestions.

We acknowledge financial support from FAPESP (Fundação de Amparo à Pesquisa do Estado de São Paulo) and FINEP (Financiadora de Estudos e Projetos).

1. A. BALBACH. "As Plantas Curam". Edições "A Edificação do Lar". São Paulo, Brasil.
2. S. GHOSAL, S. K. DUTTA, and S. K. BHATTACHARYA. J. Pharm. Sci. **61**, 1274 (1972).
3. R. T. HARGREAVES, R. D. JOHNSON, D. S. MILLINGTON, M. H. MONDAL, W. BEAVERS, L. BECKER, C. YOUNG, and K. L. RINEHART, JR. Lloydia, **37**, 4 (1974).
4. A. MONDON, M. EPE, C. WOLFF, T. CLAUSEN, and H. G. VILHUBER. Chem. Ber. **112**, 1126 (1979).
5. A. G. M. BARRETT, D. H. R. BARTON, G. FRANCKOWIAK, D. PAPAIOANNOU, and D. WIDDOWSON. J. Chem. Soc. Perkin Trans. I, 662 (1979).
6. R. B. BOAR and D. A. WIDDOWSON. J. Chem. Soc. B, 1591 (1970).
7. D. H. R. BARTON, P. N. JENKINS, and D. A. WIDDOWSON. J. Chem. Soc. Chem. Commun. 391 (1970).
8. A. MONDON, H. G. VILHUBER, C. FISCHER, M. EPE, B. EPE, and C. WOLFF. Chem. Ber. **112**, 1110 (1979).
9. K. ITO, M. HARUNA, Y. JINNO, and H. FURUKAWA. Chem. Pharm. Bull **24**, 52 (1976).
10. M. M. EL-OLEMY, A. A. ALI, and M. M. MOTTALEB. Lloydia, **41**, 243 (1978).
11. J. B. STOTHERS. Carbon-13 nmr spectroscopy. Academic Press, New York. 1972; G. C. LEVY and G. L. NELSON. Carbon-13 nuclear magnetic resonance for organic chemists. Wiley–Interscience, New York. 1972.
12. A. J. MARSAIOLI, E. A. RÚVEDA, and F. DE A. M. REIS. Phytochemistry, **17**, 1655 (1978).
13. M. TSUDA, E. J. PARISH, and G. J. SCHROEPFER, JR. J. Org. Chem. **44**, 8 (1979).
14. R. M. PREISNER and M. SHAMMA. Lloydia, **43**, 305 (1980).
15. J. D. PHILLIPSON and S. S. HANDA. Lloydia, **41**, 385 (1970).
16. E. D. BERGMANN and Y. MIGRON. Tetrahedron, **32**, 2617 (1976).
17. J. B. HARBORNE. Phytochemical methods. J. Wiley & Sons Inc., New York. 1973.
18. C. T. RIZZINI. "A Flora do Cerrado", Symposium on "Cerrado". *Edited by* Edgard Blücher and EDUSP. 1971. pp. 105–154; M. B. FERREIRA and W. R. C. D'ASSUMPÇÃO. "Leguminosae em Minas Gerais II. O Gênero *Erythrina* L." XXVIII Botanic National Congress. Belo Horizonte, Brasil. 1978. pp. 59–74.

Can. J. Chem. Downloaded from www.nrcresearchpress.com by 210.87.254.105 on 09/06/12
For personal use only.

The oxidation of phenol and chlorophenols by alkaline permanganate

DONALD G. LEE[1] AND CARLOS F. SEBASTIÁN
Department of Chemistry, University of Regina, Regina, Sask., Canada S4S 0A2

Received October 9, 1980

DONALD G. LEE and CARLOS F. SEBASTIÁN. Can. J. Chem. **59**, 2776 (1981).

A kinetic study has been made of the oxidation of phenol and seven chlorophenols by alkaline permanganate. The initial reaction, which results in the formation of manganate(VI) ion, is first order with respect to permanganate ion, independent of the concentration of hydroxide ion, and of variable order with respect to phenol. At low phenol concentrations the order is unity, but at high concentrations it becomes zero. These observations can be accounted for quantitatively by the following mechanism:

$$Na^+ + PhO^- + MnO_4^- \rightleftharpoons [PhO—Na—OMnO_3]^-$$

$$[PhO—Na—OMnO_3]^- \rightarrow PhO^\cdot + MnO_4^{2-} + Na^+$$

$$PhO^- + [PhO—Na—OMnO_3]^- \rightarrow 2PhO^- + MnO_4^- + Na^+$$

DONALD G. LEE et CARLOS F. SEBASTIÁN. Can. J. Chem. **59**, 2776 (1981).

On a étudié la cinétique de l'oxydation du phénol et de 7 chlorophénols par le permanganate en milieu basique. La réaction initiale qui conduit à la formation de l'ion manganate(VI) est du premier ordre par rapport à l'ion permanganate, elle est indépendante de la concentration de l'ion hydroxyde et est d'un ordre variable par rapport au phénol. A de faibles concentrations de phénol la réaction est d'ordre un, mais elle est d'ordre zéro si les concentrations sont élevées. On peut justifier quantitativement les observations à l'aide des mécanismes suivants:

$$Na^+ + PhO^- + MnO_4^- \rightleftharpoons [PhO—Na—OMnO_3]^-$$

$$[PhO—Na—OMnO_3]^- \rightarrow PhO^\cdot + MnO_4^{2-} + Na^+$$

$$PhO^- + [PhO—Na—OMnO_3]^- \rightarrow 2PhO^- + MnO_4^- + Na^+$$

[Traduit par le journal]

Introduction

Knowledge of the oxidation of phenols by alkaline permanganate is of potential application in both organic synthesis (1) and water purification procedures (2). Previous studies of the mechanism of this reaction indicate that it is initiated by transfer of an electron from the phenolate ion to permanganate (3) as in eq. [1].

[1] $PhO^- + MnO_4^- \rightarrow Ph\dot{O} + MnO_4^{2-}$

The phenoxy free radicals so formed undergo further coupling and oxidation reactions which eventually produce the observed products (a mixture of *o* and *p*-diphenoquinones).

In this paper we wish to report new information that was obtained from a kinetic study of the oxidation of phenol and a number of chlorophenols.

Experimental

The initial reaction between phenolate (or a chlorophenolate) ion and permanganate ion is of such a rate that it can conveniently be monitored using stopped-flow equipment. The inorganic product of the reaction was identified from its uv–vis spectrum to be manganate(VI) ion, MnO_4^{2-}. Although this ion also oxidizes phenolate ions, the reaction rate is several orders of magnitude slower than the permanganate oxidation and thus would not influence the kinetics of the initial reaction (4).

Kinetic Procedure

A solution of sodium hydroxide (about 0.1 *M*) in doubly distilled, degassed water was prepared and standardized against potassium hydrogen phthalate. To part of this solution was added sufficient phenol or chlorophenol to give an appropriate concentration (about 1.5×10^{-3} *M*). Potassium permanganate was dissolved in another portion of the same sodium hydroxide solution to give a concentration of about 6×10^{-4} *M*. These solutions were then placed in the thermostated syringes of a Durrum D-150 stopped-flow apparatus with the wavelength set at 530 nm and plots of voltage against time were recorded. These were converted into plots of permanganate concentration against time by use of a previously prepared calibration curve and the initial reaction rates were obtained by taking a tangent to the curve at time zero (5).

Materials

Distilled water was redistilled from alkaline permanganate (6) and degassed by bubbling through nitrogen, boiling, and cooling under a nitrogen atmosphere. Phenol, obtained from Analar, was purified by distillation (bp 98–100°C/30 Torr) and recrystallization from hexane; mp 40.0–41.5°C, lit. (7) mp 40.9°C. *o*-Chlorophenol, obtained from Aldrich, was purified by fractional distillation. A middle fraction was collected and used; bp 169–170°C, lit. (8) bp 175–176°C. *p*-Chlorophenol, obtained from Aldrich, was first distilled (104–106°C/25 Torr) and then recrystallized from hexane; mp 42.5–44.0°C, lit. (8) mp 43°C. *m*-Chlorophenol, obtained from Aldrich, was recrystallized from hexane; mp 32–34°C, lit. (8) mp 33°C. 2,4-Dichlorophenol, obtained from Aldrich, was first distilled (103–105°C/30 Torr) and then allowed to solidify; mp 41.5–43.0°C, lit. (7) 42–43°C. 2,4,5-Trichlorophenol, obtained from Aldrich, was purified by sublimation; mp 66.0–67.5°C, lit. (7) mp 67°C. 2,4,6-Trichloro-

0008-4042/81/182776-04$01.00/0
©1981 National Research Council of Canada/Conseil national de recherches du Canada

Can. J. Chem. Downloaded from www.nrcresearchpress.com by 210.87.254.42 on 09/06/12
For personal use only.

Can. J. Chem. Downloaded from www.nrcresearchpress.com by 210.87.254.42 on 09/06/12
For personal use only.

phenol, obtained from Aldrich, was recrystallized from acetic acid; mp 67.5–69.5°C, lit. (7) mp 67–68°C. 2,3,4,5-Tetrachlorophenol, obtained from Aldrich, was recrystallized from hexane; mp 117.5– 119.0°C, lit. (8) mp 116–117°C.

Results

Plots of the logarithm of the initial rate against the logarithm of the permanganate concentration (when the phenolate concentration was held constant) indicated that the reaction was first order with respect to oxidant (Fig. 1). However, the order with respect to phenolate concentration, although unity at low concentrations, approached zero order at high concentrations. Typical examples of this phenomenon are illustrated in Figs. 2 and 3. All other chlorophenols gave similar plots.

The reaction rate was unaffected by changes in the concentration of hydroxide ion between 0.04 and 0.8 *M* as the data in Table 1 illustrate.

Discussion

The observed change in order with respect to reductant suggests that the reaction may proceed

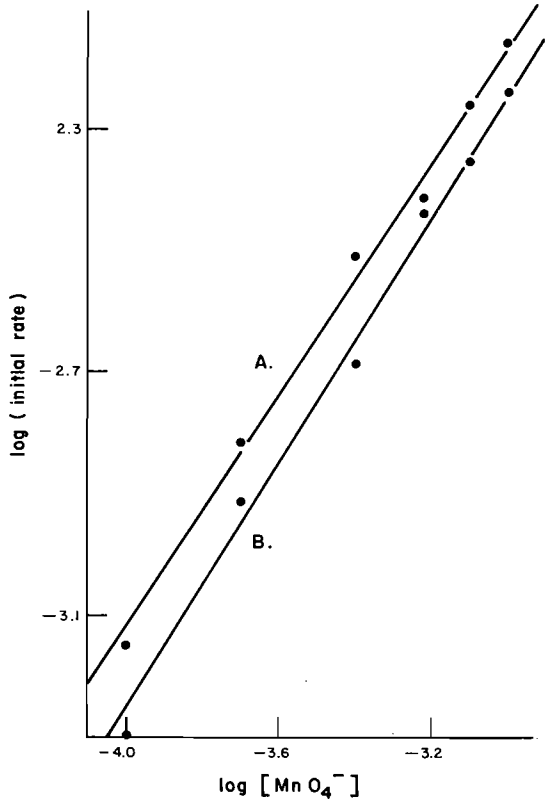

FIG. 1. Plots indicating that the order with respect to permanganate ion is unity. A. $[PhO^-] = 2.09 \times 10^{-2}$ *M*; B. $[PhO^-] = 1.19 \times 10^{-2}$ *M*.

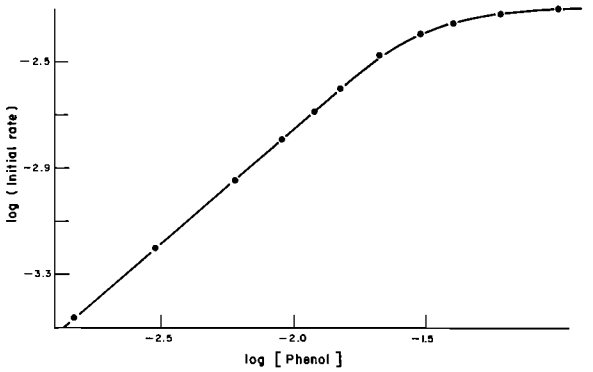

FIG. 2. Plot showing the changing order with respect to phenol concentration.

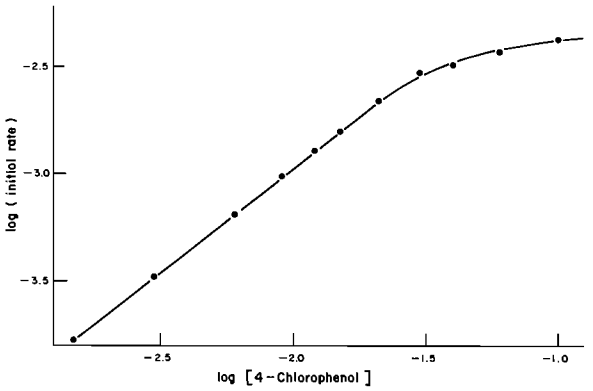

FIG. 3. Plot showing the changing order with respect to 4-chlorophenol.

TABLE 1. The reaction order with respect to hydroxide ion[a]

[NaOH] (*M*)	Initial rate (*M*/s) ($\times 10^4$)	Relative initial rate
0.048	2.32	1.00
0.095	2.28	0.98
0.191	2.30	0.99
0.381	2.35	1.01
0.571	2.19	0.94
0.762	2.30	0.99

[a]The conditions used to determine this order were: [Phenol] = 5.99×10^{-3} *M*, $[MnO_4^-] = 5.99 \times 10^{-4}$ *M*, temperature = 24.6 ± 0.1°C.

with formation of an intermediate that can either decompose to give products or react with phenolate ion to give back the reactants. Such a scheme is depicted in eqs. [2]–[4], where I is an intermediate.

$$[2] \quad MnO_4^- + PhO^- \underset{k_{-1}}{\overset{k_1}{\rightleftharpoons}} I$$

$$[3] \quad I \xrightarrow{k_2} MnO_4^{2-} + Ph\dot{O}$$

Can. J. Chem. Downloaded from www.nrcresearchpress.com by 210.87.254.42 on 09/06/12
For personal use only.

[4] $I + PhO^- \xrightarrow{k_3} 2PhO^- + MnO_4^-$

The rate of disappearance of permanganate ion for this mechanism would be given by eq. [5].

[5] $$-d[MnO_4^-]/dt = k_1[MnO_4^-][PhO^-] - k_{-1}[I] - k_3[PhO^-][I]$$

Assuming I to be a reactive intermediate and applying the steady state approximation gives an expression for the concentration of the intermediate (eq. [6]) that can be substituted into eq. [5] to give eq. [7].

[6] $$[I] = \frac{k_1[MnO_4^-][PhO^-]}{k_{-1} + k_2 + k_3[PhO^-]}$$

[7] $$-d[MnO_4^-]/dt = \frac{k_1k_2[MnO_4^-][PhO^-]}{k_{-1} + k_2 + k_3[PhO^-]}$$

The rate law in eq. 7 is of the required form to account for the observed kinetics. Under limiting conditions in which the concentration of phenolate is low the last term in the denominator could be neglected and the rate law would appear to be second order (eq. [8]), while under conditions of high phenolate concentrations this term could dominate and the reaction would appear to be first order (eq. [9]).

[8] $$-d[MnO_4^-]/dt = \frac{k_1k_2}{k_{-1} + k_2}[MnO_4^-][PhO^-]$$

[9] $$-d[MnO_4^-]/dt = \frac{k_1k_2}{k_3}[MnO_4^-]$$

By recasting eq. [7] in the form of eq. [10] and preparing the appropriate plots one can obtain values for $k_1k_2/(k_{-1} + k_2)$ and k_1k_2/k_3 from the inverses of the slopes and intercepts respectively. The good linearity of such plots (Fig. 4) substantiates the correctness of this approach.

[10] $$\frac{[MnO_4^-]}{-d[MnO_4^-]/dt} = \frac{k_{-1} + k_2}{k_1k_2[PhO^-]} + \frac{k_3}{k_1k_2}$$

From the results collected in Table 2 it can be seen that the values for the composite second order rate constants, $k_1k_2/(k_{-1} + k_2)$, decrease with increasing chlorine substitution. Except for *p*-chlorophenol the values for the composite first order rate constants, k_1k_2/k_3, also decrease regularly as the number of chlorine atoms is increased. These effects are likely of electronic origin, but difficult to understand exactly because of the complex nature of the rate constants. However, it is apparent that the more heavily chlorinated phenols are more resistant to oxidation and that it would be more difficult, for example, to remove them from contaminated water by treatment with permanganate. This observation is consistent with previous work where it was noted that nitrophenols were also difficult to oxidize (9).

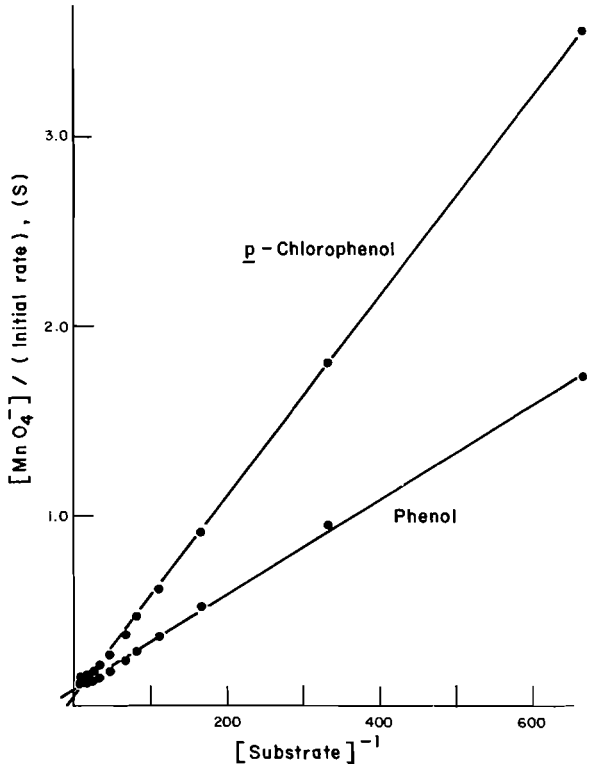

FIG. 4. Plots of eq. [10].

TABLE 2. Composite rate constants[a]

Substrate	$k_1k_2/(k_{-1} + k_2)$[b]	k_1k_2/k_3[c]	r[d]
Phenol	397	12.1	0.999
p-Chlorophenol	189	23.4	0.999
o-Chlorophenol	10.8	7.75	0.997
m-Chlorophenol	9.73	0.368	0.997
2,4-Dichlorophenol	2.44	0.191	0.993
2,4,5-Trichlorophenol;	2.07	0.171	0.995
2,4,6-Trichlorophenol	1.30	0.006	0.999
2,3,4,5-Tetrachlorophenol	0.76	0.005	0.989

[a]Conditions used were: $[MnO_4^-] = 6.0 \times 10^{-4}$ *M*, [NaOH] = 0.10 *M*, temperature = 25.0 ± 0.1°C; substrate concentrations from 0.001 to 0.100 *M*.
[b]M^{-1} s^{-1}.
[c]s^{-1}.
[d]Correlation coefficient for plot of $[MnO_4^-]/(-d[MnO_4^-]/dt)$ against $1/[PhO^-]$.

It should be noted that this analysis applies to the initial rates of reaction only. The entire reaction is not first order in oxidant; for example, linear plots are not obtained when ln (absorbance) is plotted against time for two or more half-lives. This means that the total sequence is complicated by reaction of products with the oxidant or other side reac-

Can. J. Chem. Downloaded from www.nrcresearchpress.com by 210.87.254.42 on 09/06/12
For personal use only.

tions. A likely possibility that could account for this behavior is found if it is assumed that phenoxyl radicals are produced. These radicals would undergo coupling reactions that produce unsaturated compounds which would be attacked by permanganate.

One question that remains to be considered is the nature of the intermediate, I, which is formed from the reaction of permanganate ion with phenolate ion. Two limiting possibilities could be considered. The intermediate could be covalently bonded, having a structure such as **1** whose formation would be facilitated by polarization of the Mn—O bonds (eq. [11]) in the manner recently suggested by Sharpless *et al.* (10). They have presented evidence that all oxidations by transition metal oxy anions could be initiated by formation of similar intermediates. It is difficult, however, to understand how this intermediate could be decomposed by reaction with another phenolate ion as required by reaction [4].

[11] 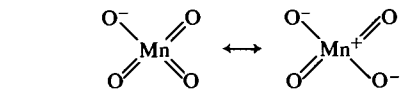

[12] 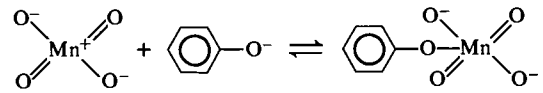

1

On the other hand, permanganate and phenolate could combine to form a complex with sodium ion, **2**. Similar complexes have been proposed for other reactions such as the exchange of electrons between permanganate and manganate which involves the intermediate $[O_3MnO—Na—OMnO_3]^{2-}$ (11), and for a similar reaction between potassium ferricyanide and potassium ferrocyanide where an analogous transition state, $[KFe(CN)_6—K—Fe(CN_6K]^{4-}$, has been proposed (12). Other examples where experimental evidence for the involvement of cations in oxidation reactions has been observed include the exchange of electrons between various organic compounds and their negative ions (12).

[13] 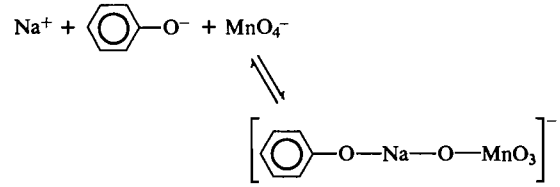

2

Although **2** has been depicted as a sodium bridged complex in analogy with the previous work cited above, it is possible that the role of the cation is simply to reduce the overall charge on the complex which forms prior to electron exchange. In other words, the formation of an intermediate from two anions is facilitated by the presence of a cation which reduces the net charge on the complex.

It would appear that a complex such as **2** is a more likely intermediate than **1** since it could be more easily decomposed by reaction with phenolate ion. Transfer of a sodium cation to a second phenolate ion before electron transfer had taken place would cause **2** to decompose with no net reaction having occurred. The kinetic consequence of this process would require the inclusion of a step such as eq. [4] in the reaction sequence.

Consequently, it is apparent that the reaction sequence depicted in eqs. [2]–[4] adequately accounts for the kinetic data obtained in this study.

Acknowledgements

The authors are grateful for financial support from the Natural Sciences and Engineering Research Council of Canada.

1. W. I. TAYLOR and A. R. BATTERSBY. Oxidative coupling of phenols. Marcel Dekker, New York. 1967.
2. R. G. SPICHER and R. T. SKRINDE. J. Am. Water Works Assoc. **57**, 472 (1965).
3. M. DORÉ, B. LEGUBE, and N. MERLET. J. Fr. Hydrol. **18**, 53 (1975).
4. D. G. LEE and C. F. SEBASTIÁN. Can. J. Chem. **59**, 2780 (1981).
5. K. J. LAIDLER. Chemical kinetics. McGraw-Hill, Toronto. 1950. pp. 14–16.
6. I. M. KOLTHOFF and E. B. SANDELL. Textbook of quantitative inorganic analysis. MacMillan, New York. 1952. p. 181.
7. D. D. PERRIN, W. L. F. ARMAREGO, and D. R. PERRIN. Purification of laboratory chemicals. Pergamon Press, London. 1966.
8. J. R. A. POLLOCK and R. STEVENS (*Editors*). Dictionary of organic compounds. 4th ed. Eyre and Spottiswoode, London. 1965.
9. F. F. MUSGRAVE and E. A. MOELWYN-HUGHES. Trans. Faraday Soc. **29**, 1162 (1933); E. A. ALEXANDER and F. C. TOMPKINS. Trans. Faraday Soc. **35**, 1156 (1939); C. N. HINSHELWOOD and C. A. WINKLER. J. Chem. Soc. 368 (1936).
10. K. B. SHARPLESS, A. Y. TERANISHI, and J. E. BACKVALL. J. Am. Chem. Soc. **99**, 3120 (1977).
11. J. HALPERN. Q. Rev. Chem. Soc. **15**, 207 (1961).
12. F. BASOLO and R. G. PEARSON. Mechanisms of inorganic reactions. Wiley, New York. 1967. pp. 487–489.

The oxidation of phenol and chlorophenols by manganate(VI) ion

DONALD G. LEE[1] AND CARLOS F. SEBASTIÁN

Department of Chemistry, University of Regina, Regina, Sask., Canada S4S 0A2

Received October 9, 1980

DONALD G. LEE and CARLOS F. SEBASTIÁN. Can. J. Chem. **59**, 2780 (1981).

The kinetics of the oxidation of phenol and three chlorophenols have been studied under alkaline conditions. Although the reaction is first order with respect to the oxidant it exhibits a fractional order with respect to the substrates, thus suggesting a free radical chain mechanism (eqs. [3]–[7]). The inverse dependence of the reaction rate on base concentration has been attributed to acid catalysis of the chain initiating step.

DONALD G. LEE et CARLOS F. SEBASTIÁN. Can. J. Chem. **59**, 2780 (1981).

On a étudié la cinétique de l'oxydation du phénol et de trois chlorophénols en milieu basique. Bien que la réaction soit d'ordre un par rapport à l'oxydant, elle montre un ordre fractionnaire par rapport au substrats, ce qui suggère un mécanisme radicalaire libre en chaîne (éqs. [3]–[7]). On a attribué l'influence inverse de la concentration de la base sur la vitesse de réaction à une catalyse acide de l'étape de formation de la chaîne.

[Traduit par le journal]

Introduction

The oxidation of phenols by alkaline permanganate proceeds in two distinct stages. In the first, permanganate ion is rapidly reduced as in eq. [1], while in the second, manganate(VI) ion is more slowly reduced to manganese dioxide (eq. [2]).

[1] $PhO^- + MnO_4^- \longrightarrow Ph\dot{O} + MnO_4^{2-}$

[2] $2PhO^- + MnO_4^{2-} + 2H_2O \longrightarrow 2Ph\dot{O} + MnO_2 + 4OH^-$

The kinetics of the first stage of this reaction have previously been described by ourselves and others (1, 2). In this paper we wish to focus on the kinetics of the second stage.

Experimental

The rates of reduction of manganate(VI) ion were monitored by following the decrease in absorbance at 606 nm using a Perkin-Elmer 356 uv–vis spectrophotometer. In a typical experiment two flasks, one containing a solution of phenol (2×10^{-2} *M*) in 0.1 *M* NaOH and the other containing potassium manganate(VI) (9×10^{-4} *M*), also in 0.1 *M* NaOH, were thermostated for 30 min. Then equal volumes of each solution were mixed and a timer started. This solution was returned to the thermostated bath and aliquots of about 7 mL each were withdrawn periodically. These were first centrifuged (to separate any MnO_2 present) and then transferred to a cuvette for absorbance measurements.

Identical reaction rates were obtained when the reaction was initiated by use of potassium permanganate which rapidly reduces to manganate(VI) ion on contact with the phenolate solution (1).

Materials

Many of the materials used in this study have previously been described (1). Potassium manganate(VI), K_2MnO_4, was obtained from the Carus Chemical Company.

[1]Author to whom correspondence may be addressed.

Results

Under conditions where the substrate and the hydroxide ion were in excess, linear plots of ln (absorbance) against time were obtained thus indicating that the reaction is first order with respect to manganate(VI) ion (Fig. 1).

The order with respect to substrate was then determined by plotting the logarithm of the pseudo first order rate constants (k_s) against the logarithm of the phenolate concentrations. Figures 2 and 3 give typical examples. Orders of 0.6 to 0.8 were obtained for all of the phenols studied (Table 1).

In a similar way the order with respect to hydroxide ion was found to be −0.79 (Fig. 4).

Discussions

Fractional orders such as those found in this study are indicative of radical chain processes and, therefore, it may be expected that the reduction of manganate(VI) ion to manganese(IV) oxide by phenols proceeds by such a mechanism. The reaction would most likely be initiated by the transfer of one electron from manganate(VI) ion to phenolate ion as in reaction [3].

[3] $PhO^- + MnO_4^{2-} \xrightarrow{k_3} Ph\dot{O} + MnO_4^{3-}$

Other studies have shown that the phenoxy radicals formed in this reaction would undergo a rapid dimerization to isomeric dihydroxybiphenyls (3). The manganate(V) ion, which is also formed in reaction [3], would be a very reactive oxidant under these conditions and might be expected to undergo one or more of three possible reactions: (*i*) it could react with water (reaction [4]), (*ii*) it could disproportionate into manganate(VI) ion and manganese

0008-4042/81/182780-07$01.00/0

©1981 National Research Council of Canada/Conseil national de recherches du Canada

Can. J. Chem. Downloaded from www.nrcresearchpress.com by 210.87.254.40 on 09/06/12
For personal use only.

Can. J. Chem. Downloaded from www.nrcresearchpress.com by 210.87.254.40 on 09/06/12
For personal use only.

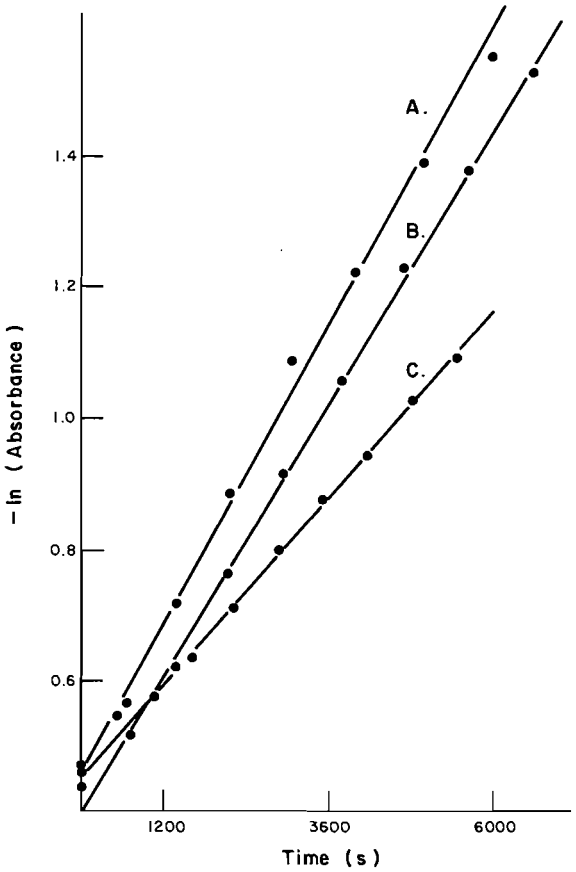

FIG. 1. Pseudo first order plots. $[MnO_4^{2-}] = 4.5 \times 10^{-4}$ *M*; [NaOH] = 0.10 *M*; A, [*o*-chlorophenol] = 6.75×10^{-3} *M*; B, [*o*-chlorophenol] = 6.75×10^{-3} *M*; C, [*m*-chlorophenol] = 4.49×10^{-3} *M*; temperature = 24.5 ± 0.1°C.

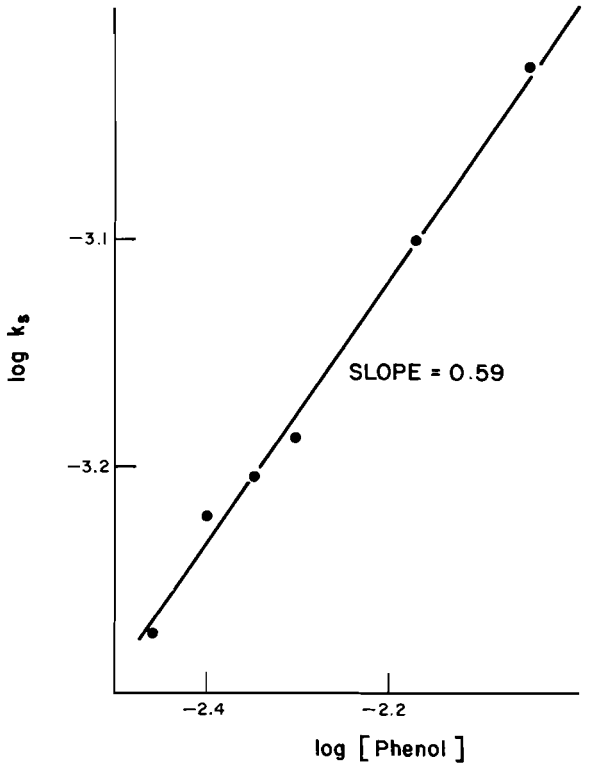

FIG. 2. The apparent order with respect to phenol concentration. $[MnO_4^{2-}] = 4.5 \times 10^{-4}$ *M*; [NaOH] = 0.10 *M*; temperature = 24.5 ± 0.1°C.

dioxide (reaction [4*a*]) (4), or (*iii*) it could react with phenolate ion (reaction [4*b*]).

$$[4]\quad MnO_4^{3-} + H_2O \xrightarrow{k_4} HMnO_4^{3-} + \dot{O}H$$

$$[4a]\quad 2MnO_4^{3-} \longrightarrow MnO_4^{2-} + MnO_4^{4-}$$

$$[4b]\quad MnO_4^{3-} + PhO^- \longrightarrow Ph\dot{O} + MnO_4^{4-}$$

Of these three bimolecular reactions the first is likely to predominate because water, since it is the solvent, is present in very high concentrations. Analogous reactions of transition metal oxides with water are known; for example, ruthenate(VI) ion (which is also a d^2 system) is stable only under very basic conditions and is reduced by water below pH 12 (5). Furthermore, if either [4*a*] or [4*b*] were the predominant reaction following [3], a chain reaction would not be produced.

It may be noted that each of the possible reactions of manganate(V) ion results in the formation of a manganate(IV) anion which would eventually precipitate as manganese dioxide (e.g. $HMnO_4^{3-} + H_2O \rightarrow MnO_2 + 3OH^-$).

TABLE 1. The order with respect to substrate[a]

Substrate	Order	r^b
Phenol	0.59	0.997
p-Chlorophenol	0.79	0.998
o-Chlorophenol	0.69	0.996
m-Chlorophenol	0.71	0.999
2,4-Dichlorophenol	0.67	0.996

[a] $[MnO_4^{2-}] = 4.5 \times 10^{-4}$ *M*; [NaOH] = 0.10 *M*; [Substrate] = 3.5×10^{-3} to 1.6×10^{-2} *M*; temperature = 24.5 ± 0.1°C.
[b] Correlation coefficient.

Previous work (6) has shown that the hydroxyl radical formed in reaction [4] would react readily with phenolate ion (reaction [5]) to give a radical anion (which we shall designate as "J" for the time being). Oxidation of J by manganate(VI) ion (reaction [6]) would then complete the chain propagation sequence.

$$[5]\quad \dot{O}H + PhO^- \xrightarrow{k_5} J$$

$$[6]\quad J + MnO_4^{2-} \xrightarrow{k_6} MnO_4^{3-} + \text{products}$$

Can. J. Chem. Downloaded from www.nrcresearchpress.com by 210.87.254.40 on 09/06/12
For personal use only.

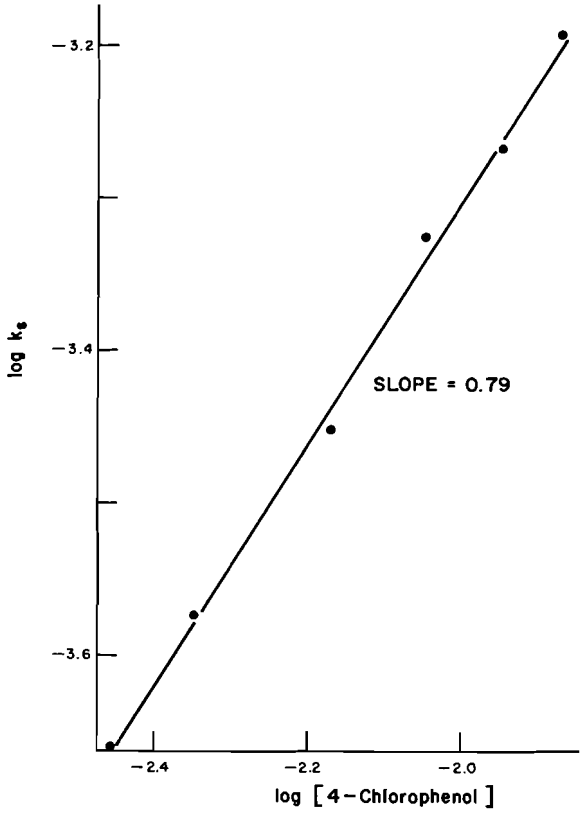

FIG. 3. The apparent order with respect to 4-chlorophenol concentration. $[MnO_4^{2-}] = 4.5 \times 10^{-4}$ *M*; [NaOH] = 0.10 *M*; temperature = 24.5 ± 0.1°C.

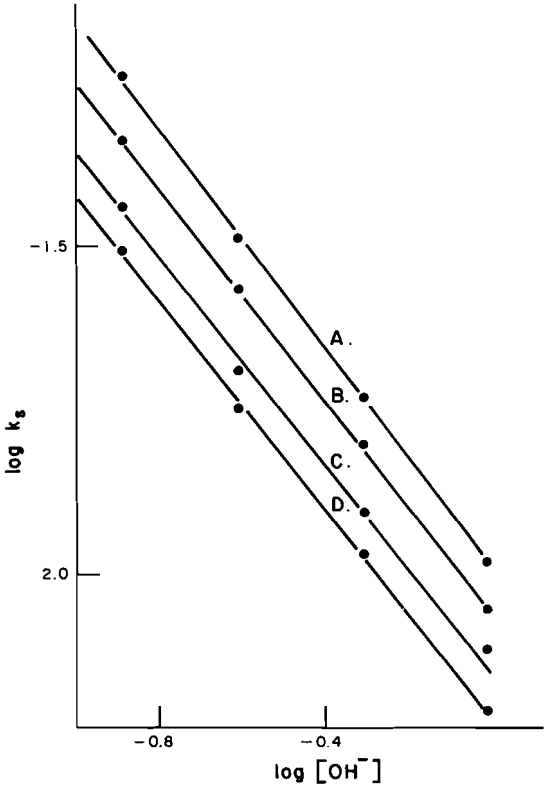

FIG. 4. The apparent order with respect to hydroxide ion concentration. $[MnO_4^{2-}] = 4.5 \times 10^{-4}$ *M*; temperature = 24.5 ± 0.1°C; $[PhO^-] = 3.5 \times 10^{-3}$ *M* (A); 4.5×10^{-3} *M* (B); 6.8×10^{-3} *M* (C); 9.0×10^{-3} *M* (D). Average slope = −0.79.

At least two chain terminating steps could be considered; the intermediate, J, could be oxidized by manganate(V) as in reaction [7], or J could dimerize. The latter possibility cannot be a major contributor to chain termination because its involvement leads to the prediction of a rate law that is not first order in manganate(VI) ion. It is possible that the rate of dimerization of J is suppressed relative to other free radicals because it bears a negative charge which would present an electrostatic barrier to coupling.

[7] $J + MnO_4^{3-} \xrightarrow{k_7} MnO_4^{4-} + \text{products}$

The sequence of reactions [3] to [7] thus describes a chain process, where reaction [3] is the initiation step, reactions [4], [5], and [6] are the chain propagation steps, reaction [7] is the termination step, and J is a reactive intermediate. Furthermore, as shown below, this sequence fits the available kinetic data quantitatively.

The rate of disappearance of the manganate(VI) ion for this scheme would be given by eq. [8].

$$[8] \quad -\frac{d[MnO_4^{2-}]}{dt} = k_3[PhO^-][MnO_4^{2-}] + k_6[J][MnO_4^{2-}]$$

Assuming that the steady-state approximation holds for the intermediates (ȮH, J, and MnO_4^{3-}), their concentrations would be given by eqs. [9]–[11].

$$[9] \quad [J] = \frac{k_5[\dot{O}H][PhO^-]}{k_6\,MnO_4^{2-}] + k_7[MnO_4^{3-}]}$$

$$[10] \quad [\dot{O}H] = k_4[MnO_4^{3-}]/k_5[PhO^-]$$

$$[11]\quad [MnO_4^{3-}] = [MnO_4^{2-}]\left(\frac{k_3[PhO^-] + k_6[J]}{k_4 + k_7[J]}\right)$$

Substitution of eqs. [10] and [11] into [9] gives a solution for [J] of the form depicted in eqs. [12] and [13].

$$[12]\quad [J]^2(2k_6k_7) + [J](k_3k_7[PhO^-]) - (k_3k_4[PhO^-]) = 0$$

$$[13]\quad [J] = \frac{-k_3k_7[PhO^-] \pm \sqrt{(k_3k_7)^2[PhO^-]^2 + 8k_3k_4k_6k_7[PhO^-]}}{4k_6k_7}$$

Substitution of eq. [13] into eq. [8] gives the exact rate law as expressed in eq. [14].

$$[14]\quad -\frac{d[MnO_4^{2-}]}{dt} = [MnO_4^{2-}]\left([PhO^-](k_3 - k_3/4) \pm \frac{k_3k_7}{4k_7}\sqrt{[PhO^-]^2 + \frac{8k_4k_6}{k_3k_7}\ PhO^-]}\right)$$

In order to further simplify eq. [14] one assumption may be made. Since $[PhO^-]$ is small, the square of the substrate concentration will be smaller. Therefore, it may be negligible compared to the other term under the square root sign. Further, the converse assumption (that the term $8k_4k_6[PhO^-]/k_3k_7$ is negligible compared to the $[PhO^-]^2$ term) cannot be accepted because it would predict a rate expression first order with respect to substrate. This cannot be correct, since experimentally it was found that the order was between 0.6 and 0.8, depending on the substrate.

Accepting this assumption, eq. [14] reduces to eq. [15].

$$[15]\quad -\frac{d[MnO_4^{2-}]}{dt} = [MnO_4^{2-}]\left(\frac{3}{4}k_3[PhO^-] \pm \left[\frac{k_3k_4k_6}{2k_7}\right]^{1/2}[PhO^-]^{1/2}\right)$$

It then follows that the pseudo first order rate constant could be equated with the term in parentheses as expressed in eq. [16].

$$[16]\quad k_s = \frac{3}{4}k_3[PhO^-] \pm \left(\frac{k_3k_4k_6}{2k_7}\right)^{1/2}[PhO^-]^{1/2}$$

The correctness of this expression can be tested quantitatively by recasting it in a linear form (eq. [17]) and preparing plots of $k_s/[PhO^-]^{1/2}$ against $[PhO^-]^{1/2}$.

$$[17]\quad \frac{k_s}{[PhO^-]^{1/2}} = \frac{3}{4}k_3[PhO^-]^{1/2} \pm \left(\frac{k_3k_4k_6}{2k_7}\right)^{1/2}$$

Since these plots are linear (Fig. 5) the reaction sequence and assumptions[2] are probably correct, and the values for the rate constants can be calculated from the slopes and intercepts (Table 2).

A perusal of the data in Table 2 shows that the intercepts are all positive, indicating that the positive root in eq. [17] should be considered in the solution.

It must be understood that the mechanism proposed is not necessarily the only possibility. However, it proves that such a free radical scheme can explain the fractional orders obtained experimentally. In this particular case it is found that the derived expression contains a term that is first order in substrate and another that is one-half order, thus accounting for the observation that the apparent order with respect to substrate is found to lie between unity and one-half for all the phenols studied (Table 1).

It was found experimentally that the order with respect to sodium hydroxide was fractional and negative. Such an inverse dependency on base suggests the possibility of acid catalysis in the reaction. (Many other oxidation reactions are also known to be subject to acid catalysis (7, 8).)

It is instructive therefore to consider the possibility that one or more of the steps in the reaction sequence may be subject to acid catalysis. For example, reactions [4] and [7] which both involve MnO_4^{3-} might be considered as likely points at which protonation of the oxidant would accelerate the reaction. Then by following an analysis similar to that described above it can be shown that the concentration of J would be given by eq. [18].

$$[18]\quad [J] = \frac{-k_3k_7[H^+][PhO^-] \pm \sqrt{(k_3k_7[H^+][PhO^-])^2 + 8k_3k_4k_6k_7[PhO^-][H^+]^2}}{4k_6k_7[H^+]}$$

[2]From the data in Table 2 it is possible to calculate values for the term $8k_4k_6/k_3k_7$, which appears in eq. [14]. The calculated values range from 0.02 to 0.80, thus indicating that the approximation will not introduce large errors.

Can. J. Chem. Downloaded from www.nrcresearchpress.com by 210.87.254.40 on 09/06/12
For personal use only.

It can be seen that the proton concentration vanishes from eq. [18], and consequently from the rate expression as well. This result, therefore, allows for the possibility of acid catalysis in these steps, but does not account for the inverse dependence on base concentration.

Furthermore, if eq. [4] is considered to be accelerated by acid, the concentration of J is given by eq. [19].

$$[19]\quad [J] = \frac{-k_3k_7[PhO^-] \pm \sqrt{(k_3k_7)^2[PhO^-]^2 + 8k_3k_4k_6k_7[PhO^-][H^+]}}{4k_7k_8}$$

Following the procedure previously used the rate expression is then given by eq. [20] where $K_w = [H^+][OH^-]$.

$$[20]\quad -d[MnO_4^{2-}]/dt = [MnO_4^{2-}]\left(\frac{3}{4}k_3[PhO^-] \pm \left(\frac{K_wk_3k_4k_6}{2k_7}\right)^{1/2}\frac{[PhO^-]^{1/2}}{[OH^-]^{1/2}}\right)$$

If this approach were correct the observed pseudo first order rate constants should be linearly related to the inverse of the square root of the hydroxide ion concentration. The lack of linearity in the appropriate plots (Fig. 6) therefore indicates that acceleration of step 4 by acid does not adequately account for the observed results.

If, on the other hand, the first step of the sequence (eq. [3]) is considered to be subject to acid catalysis, the inverse dependence on base can be accounted for quantitatively, as shown in the following derivation (eqs. [21]–[26]).

$$[21]\quad [J] = \frac{-k_3k_7[H^+][PhO^-] \pm \sqrt{(k_3k_7[H^+][PhO^-])^2 + 8k_3k_4k_6k_7[H^+][PhO^-]}}{4k_6k_7}$$

$$[22]\quad -\frac{d[MnO_4^{2-}]}{dt} = [MnO_4^{2-}]\left(\frac{3k_3K_w[PhO^-]}{4[OH^-]} \pm \left(\frac{k_3k_4k_6K_w[PhO^-]}{2k_7[OH^-]}\right)^{1/2}\right)$$

Under conditions where the concentration of hydroxide ion is constant, eq. [22] would have the same general form as eq. [15]; i.e.:

$$[23]\quad -\frac{d[MnO_4^{2-}]}{dt} = [MnO_4^{2-}](k_m[PhO^-] \pm k_n[PhO^-]^{1/2})$$

where

$$k_m = 3k_3K_w/(4[OH^-]) \text{ and } k_n = (k_3k_4k_6K_w/(2k_7[OH^-])^{1/2}$$

Under conditions where the concentration of phenolate ion is constant and the hydroxide ion varied, eq. [22] may be rewritten in the form of eq. [24].

$$[24]\quad -\frac{d[MnO_4^{2-}]}{dt} = [MnO_4^{2-}](k_p[OH^-]^{-1} \pm k_q[OH^-]^{1/2})$$

where

$$k_p = \frac{3}{4}k_3K_w[PhO^-] \quad \text{and} \quad k_q = \left(\frac{k_3k_4k_6K_w[PhO^-]}{2k_7}\right)^{1/2}$$

The pseudo first order rate constant can be equated with the term in the parentheses of eq. [24] to give eq. [25].

$$[25]\quad k_s = k_p[OH^-]^{-1} \pm k_q[OH^-]^{-1/2}$$

Equation [25] can then be recast in a linear form (eq. [26]), where the slope and the intercept are given by k_q and k_p, respectively.

$$[26]\quad k_s[OH^-] = k_p \pm k_q[OH^-]^{1/2}$$

A plot of $k_s[OH^-]$ against $[OH^-]^{1/2}$ should be linear if the assumptions and the reaction sequence are correct. The fact that the plots appear to be linear with reasonably good correlation coefficients indicates that there is consistent agreement with the data (see Fig. 7).

Finally, it is necessary to consider a possible structure for the intermediate, J, which is formed by reaction of a hydroxyl radical with a phenolate ion (eq. [5]). This facile reaction, which has been

Can. J. Chem. Downloaded from www.nrcresearchpress.com by 210.87.254.40 on 09/06/12
For personal use only.

Can. J. Chem. Downloaded from www.nrcresearchpress.com by 210.87.254.40 on 09/06/12
For personal use only.

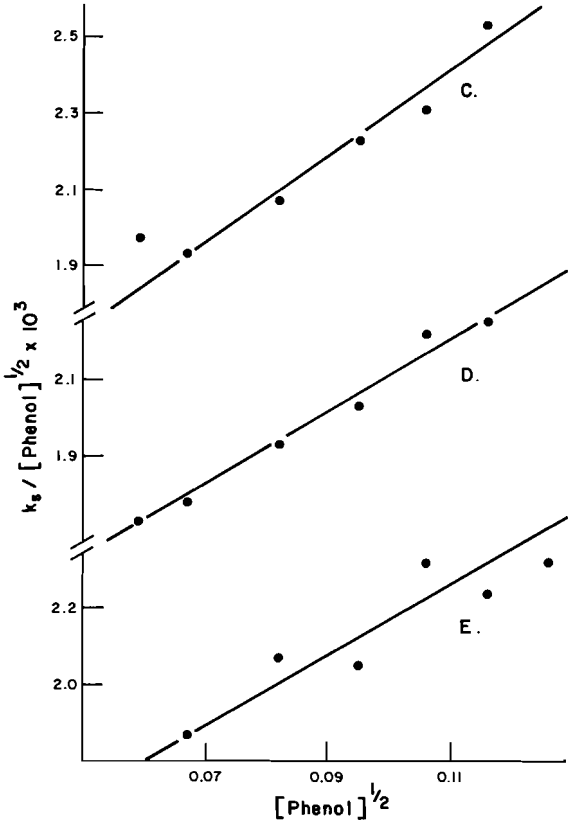

FIG. 5. Plots of eq. [17]. Top (C), *o*-chlorophenol; middle (D), *m*-chlorophenol; bottom (E), 2,4-dichlorophenol.

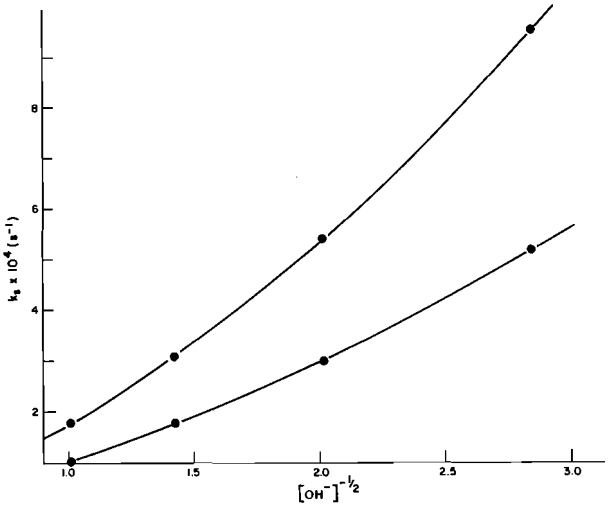

FIG. 6. Plots of the pseudo first order rate constants against $[OH^-]^{-1/2}$. Top, *p*-chlorophenol. Bottom, phenol.

extensively studied (9), takes place predominantly at the *ortho* or *para* positions giving a radical anion which would subsequently lose an electron to an oxidant to give products (eqs. [6] and [7]). As the

TABLE 2. Rate constants obtained from plots of $k_s/[PhO^-]^{1/2}$ against $[PhO^-]^{1/2}$

Substrate[a]	k_3 ($M^{-1}s^{-1}$)	$k_3k_4k_6/k_7$ ($M^{-1}s^{-2}$)	r^b
Phenol	3.37×10^{-2}	1.15×10^{-4}	0.995
p-Chlorophenol	4.33×10^{-2}	6.34×10^{-6}	0.992
o-Chlorophenol	1.64×10^{-2}	2.33×10^{-6}	0.995
m-Chlorophenol	1.22×10^{-2}	2.78×10^{-6}	0.998
2,4-Dichlorophenol	9.43×10^{-3}	4.03×10^{-6}	0.970

[a]Substrate concentrations were varied from 1.6×10^{-2} *M* to 3.5×10^{-3} *M*; $[MnO_2^{2-}] = 4.5 \times 10^{-4}$ *M*; [NaOH] = 0.10 *M*; temperature = 25.0°C
[b]Correlation coefficient.

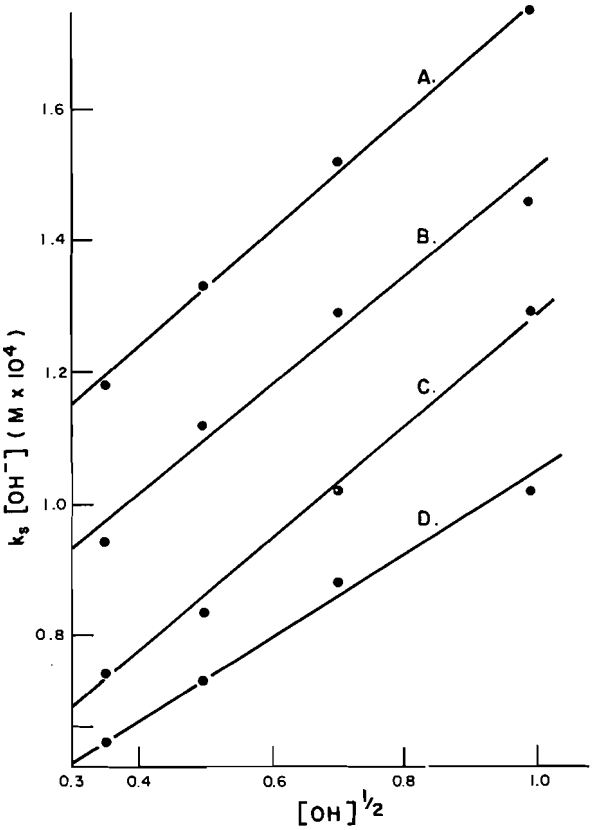

FIG. 7. Plots of eq. [26].

following reactions indicate, such a sequence would lead to formation of two compounds (*o*- and *p*-hydroquinone) that are known to be produced when phenol is oxidized (2).

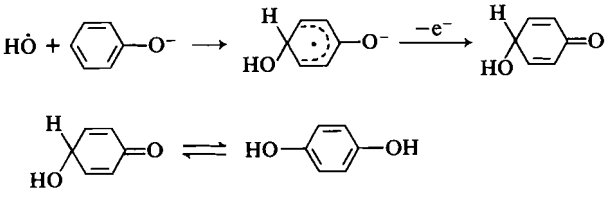

Acknowledgements

The authors are grateful to the Natural Sciences and Engineering Research Council of Canada for financial support.

1. D. G. LEE and C. F. SEBASTIÁN. Can. J. Chem. **59**, 2776 (1981).
2. M. DORÉ, B. LEGUBE, and N. MERLET. J. Fr. Hydrol. **18**, 53 (1975).
3. E. J. LAND and G. PORTER. Trans. Faraday Soc. **59**, 2016 (1963); G. DOBSON and L. I. GROSSWEINER. Trans. Faraday Soc. **61**, 708 (1965); L. R. MAHONEY and S. A. WEINER. J. Am. Chem. Soc. **94**, 585 (1972).
4. B. JEZOWSKA-TRZEBIATOWSKA and J. NAWOJSKA. Bull. Acad. Pol. Sci. Ser. Sci. Chim. **10**, 361 (1962).
5. R. E. CONNICK and C. R. HURLEY. J. Am. Chem. Soc. **74**, 5012 (1952).
6. C. R. E. JEFCOATE and R. O. C. NORMAN. J. Chem. Soc. B, 48 (1968); E. J. LAND and M. EBERT. Trans. Faraday Soc. **63**, 1181 (1967).
7. K. B. WIBERG and R. STEWART. J. Am. Chem. Soc. **77**, 1706 (1955).
8. R. STEWART. *In* Oxidation in organic chemistry. Part A. *Edited by* K. B. Wiberg. Academic Press, New York. 1965. p. 35.
9. D. I. METELITSA. Russ. Chem. Rev. **40**, 563 (1971), and references therein.

Can. J. Chem. Downloaded from www.nrcresearchpress.com by 210.87.254.40 on 09/06/12
For personal use only.

The acid-catalyzed oxido-reduction of spiroketals. Evidence for stereoelectronic control in hydride transfer to cyclic oxenium ions

PIERRE DESLONGCHAMPS, DARYL D. ROWAN, AND NORMAND POTHIER

Laboratoire de Synthèse Organique, Département de Chimie, Faculté des Sciences, Université de Sherbrooke, Sherbrooke (Qué.), Canada J1K 2R1

Received April 3, 1981

PIERRE DESLONGCHAMPS, DARYL D. ROWAN, and NORMAND POTHIER. Can. J. Chem. **59**, 2787 (1981).

Tricyclic spiroketal **1** undergoes an acid-catalyzed oxidation–reduction reaction which yields equatorial bicyclic ether aldehyde **5** specifically. Similarly, spiroketals **2**, **3**, and **4** give equatorial bicyclic ether ketone **12**. These results are interpreted by invoking an internal hydride transfer from an alcohol function to a cyclic oxenium ion which takes place with stereoelectronic control. The reduction of tricyclic ketals **1** and **22** with sodium cyanoborohydride under acidic conditions is also reported.

PIERRE DESLONGCHAMPS, DARYL D. ROWAN et NORMAND POTHIER. Can. J. Chem. **59**, 2787 (1981).

Le spirocétal **1** subit une réaction d'oxydo-réduction acido-catalysée conduisant spécifiquement à l'aldéhyde-éther bicyclique équatorial **5**. De même, les spirocétals **2**, **3** et **4** donnent la cétone-éther bicyclique équatoriale **12**. Ces résultats sont interprétés en faisant appel à un transfert interne d'hydrure d'une fonction alcool à un ion oxénium cyclique qui se ferait avec contrôle stéréoélectronique. On rapporte aussi la réduction des cétals tricycliques **1** et **22** en milieu acide par le cyanoborohydrure de sodium.

We have recently shown that 1,7-dioxaspiro[5.5]-undecane and its derivatives provide a very convenient system for the study of stereoelectronic effects (anomeric and *exo*-anomeric effects) in the acetal function (1, 2). In the course of that study, we observed that these spiroketals undergo an acid-catalyzed oxidation–reduction reaction. We wish to report that investigation.[1]

Results and Discussion

We have studied the tricyclic spiroketal **1** and the three isomeric methyltricyclic spiroketals **2**, **3**, and **4** (Scheme 1).

Treatment of tricyclic spiroketal **1** with hydrogen bromide in ether–pentane gave stereospecifically the bicyclic ether aldehyde **5** (≃ 40% yield). Reduction of compound **5** with lithium aluminium hydride in ether gave the bicyclic ether alcohol **6** which was further characterized by formation of the acetate derivative **7**.

The structure and the stereochemistry of bicyclic ether alcohol **6** was rigorously established by comparison with an authentic sample. Compound **6** and its isomer **8** were obtained from the monocyclic ketone mesylate **9** (4). Reduction of compound **9** with sodium borohydride in methanol gave a mixture of the isomeric alcohols **10** which was transformed (KH, THF) into the isomeric mixture of THP-bicyclic ethers **11**. Acid hydrolysis of the tetrahydropyranyl ethers **11** gave the bicyclic ether alcohols **6** and **8** which were separated by chromatography. The relative stereochemistry of isomers

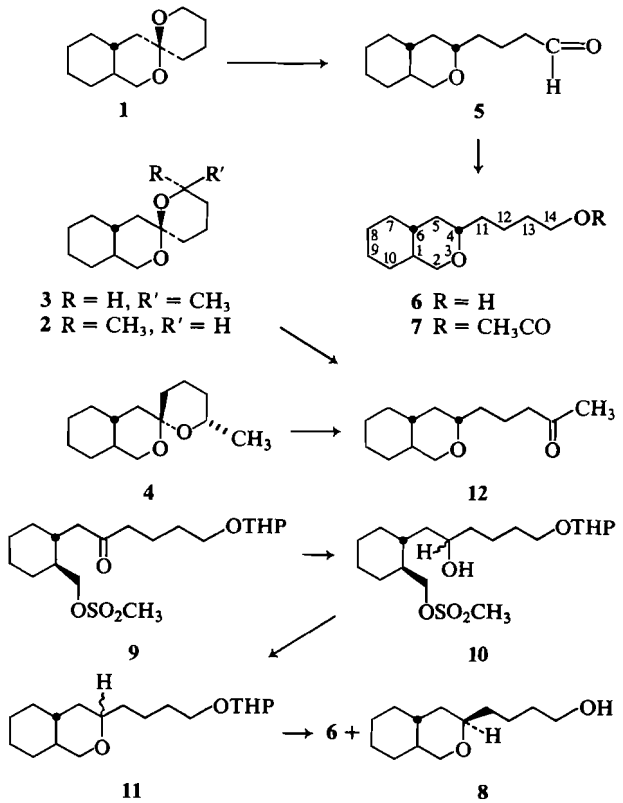

SCHEME 1

6 and **8** was established by carbon nuclear magnetic resonance spectroscopy. In particular, the carbons 2, 4, and 6 which are γ, α, and γ respectively to C(11) of the side chain, show shieldings of 7.7, 4.8, and 5.8 ppm (5) on passing from **6** to its axial epimer **8**.

[1]These results have been reported in a preliminary form, see ref. 3.

0008-4042/81/182787-05$01.00/0

©1981 National Research Council of Canada/Conseil national de recherches du Canada

Can. J. Chem. Downloaded from www.nrcresearchpress.com by 210.87.254.5 on 09/06/12
For personal use only.

Can. J. Chem. Downloaded from www.nrcresearchpress.com by 210.87.254.5 on 09/06/12
For personal use only.

We have also observed that the tricyclic spiroketal **2** or a mixture of isomers **3** and **4** (interconvertible under mild acidic conditions) gave the bicyclic ether methyl ketone **12** (≃100% yield) with aqueous hydrochloric acid under reflux conditions. Similarly, treatment of isomer **4** or isomer **3** with *p*-toluenesulfonic acid in benzene (1), gave compound **12** upon reflux. Isomer **2** proved inert under these conditions. The structure and the stereochemistry of the bicyclic ether methyl ketone **12** was rigorously established by its conversion into bicyclic ether alcohol **6** (NaOBr, NaOH; $LiAlH_4$).

The acid-catalyzed oxido-reduction reactions described above can be readily explained by the opening of the spiroketals giving an hydroxy bicyclic oxenium ion intermediate such as **13** which undergoes an internal hydride transfer to yield the bicyclic ether **5** or **12**.

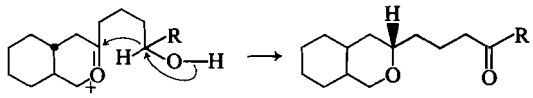

13 **5** R = H; **12** R = CH_3

This mechanism is very similar to the one proposed by Woodward *et al.* (6) to explain the acid-catalyzed interconversion of the normal and the *iso*-sapogenins **14** and **15** (Scheme 2). They have obtained strong support for this mechanism by observing that the isomeric aldehydes **16** and **17** are converted into a mixture of spiroketals **14** and **15** under acidic conditions. Also, Pettit and Boyer (7) have shown that the aldehyde intermediate (**16** or **17**) can be trapped with ethanedithiol.

The stereospecific formation of the equatorial bicyclic ethers **5** and **12** can be explained if stereoelectronic effects (8) are taken into consideration. If we accept that the hydride transfer will take place with minimum energy only when the intermediate oxenium ion can develop an electron pair which will become antiperiplanar to the newly formed C—H bond in the final product, the above results can be easily rationalized.

It can be readily seen that the β-attack on **13** (i.e. **18**) can occur with stereoelectronic control because the ether oxygen has an electron pair oriented antiperiplanar to the newly formed C—H bond in the resulting products **5** or **12** (Scheme 3). On the other hand, the α-attack on **13** with stereoelectronic control cannot yield the axial bicyclic ethers directly in the most stable conformation **21**. The α-attack on **13** (i.e. **19**) must first give conformer **20** of axial bicyclic ether having its ring B twisted in order to fulfill the orbital alignment requirement. Conformer **20** would then undergo a conformational change to the more stable conformation **21**. The transformation **19** → **20** → **21** requires more energy than the transformation **18** → **5** (or **12**). Consequently the formation of axial bicyclic ethers **21** cannot compete with the formation of equatorial bicyclic ethers **5** or **12**.[2]

The above rationalization further indicates that internal delivery of a hydride is not a requisite for the observed stereospecificity. Reduction of the oxenium ion with an external hydride reagent should also give equatorially oriented bicyclic ether only. We have found that this is indeed the case by observing that the reduction of tricyclic spiroketal **1** with sodium cyanoborohydride at pH ≃ 3–4 yields only the equatorial bicyclic ether alcohol **6**. When the reaction was repeated with deuterated sodium cyanoborohydride, compound **6** contained one deuterium which was found to be in α position to the ether oxygen (C(4)).

Finally, no stereospecificity should be expected in the hydride transfer step when the cyclic oxenium ion is conformationally labile. This was confirmed by the reduction ($NaBH_3CN$, pH ≃3–4) of bicyclic spiroketal **22** (1) which gave after acetylation a mixture of cyclic ether acetates **23** and **24** in a 3:1 ratio (Scheme 4). Compounds **23** and **24** were separated by chromatography and their relative stereochemistry was assigned on the basis of their ^{13}C nuclear magnetic resonance spectra. In particular, the minor ether acetate **24** (^{13}C nmr: C(3), 26.0 ppm and C(5), 21.1 ppm) showed a shielded methylene and methine carbon (6.4 and 5.7 ppm respectively) relative to the major isomer **23** (^{13}C nmr: C(3), 32.4 ppm and C(5), 26.8 ppm). This result indicates that the secondary methyl group in the ring of the minor isomer is axially oriented (5).

The above results complement our previous work on the stereoelectronically controlled addition of an hydroxyl group to cyclic oxenium ions, i.e. the kinetically controlled formation of acetal (10). The high stereoselectivity for axial attack in $AlCl_2H$ reduction of substituted 2-alkoxy-1,3-dioxanes has been observed by Eliel and Nader (11) and they have also explained their results on the basis of the principle of stereoelectronic control.

Experimental

Vapor phase chromatography (vpc) was performed on a Varian Aerograph Insrument, model 2800 equipped with a thermal conductivity detector. The following columns were used: column a: 10% APIEZON, 240°C; column b: 3% SE-30, 190°C; column c: 10% SE-30, 190°C; column d: 5% SE-30,

[2]The importance of the nonbonded electron pair on oxygen in $AlHCl_3$ reduction of 2-alkoxytetrahydropyran has been previously suggested (9).

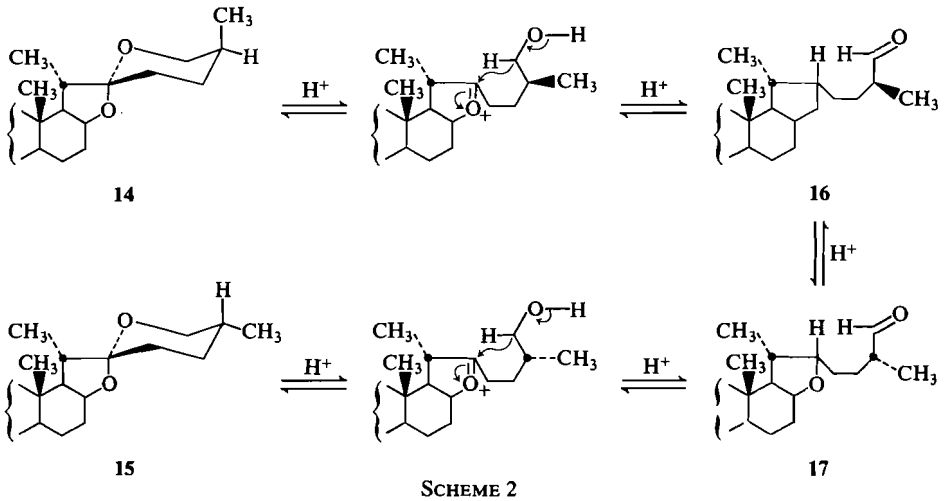

SCHEME 2

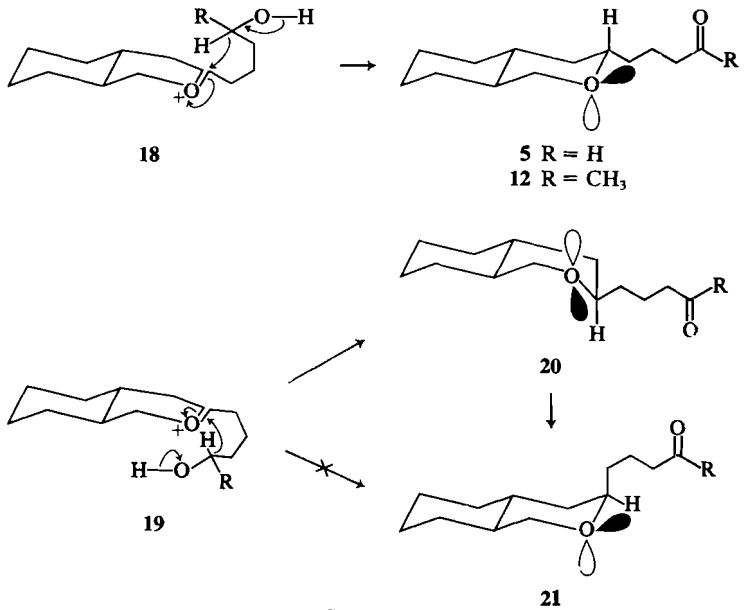

SCHEME 3

190°C. All columns were of dimensions 5 ft × ¼ in. and packed with Chromosorb W 60–80 mesh. The infrared (ir) spectra were obtained in chloroform on a Perkin-Elmer 257 spectrophotometer. Proton nuclear magnetic resonance (^{1}H nmr) spectra were recorded in chloroform on a Bruker WP-60 instrument with TMS as an internal standard. The ^{13}C nmr spectra were recorded in deuterochloroform on a Bruker HX-90 equipped with a Nicolet 1083 computer (8K memory for data) and operating in the Fourier transform mode. Mass spectra were obtained on Hitachi-Perkin-Elmer RMU-6-A and Micromass ZAB-2F machines.

The following abbreviations are used: % E/H: % of ether in hexane; % EA/H: % ethyl acetate in hexane; RT: room temperature; s: singlet; d: doublet; t: triplet, m: multiplet; b: broad; dt: deformed triplet.

Aldehyde 5

To a stirred solution of acetal (**1**) (1) (327 mg, 1.56 mmol) in pentane (15 mL) and ether (15 mL) was added a trace of water (2 drops) and then anhydrous hydrogen bromide gas to saturate the system. After 26 h, the reaction was quenched with saturated sodium bicarbonate and diluted with ether. After washing with brine (1×) and drying (Na_2SO_4) the organic phase was evaporated to give a clear oil (333 mg). Chromatography on silica gel gave, on elution with 5% E/H, unchanged acetal (**1**) (197 mg, 60.2%). Elution with 10% E/H gave aldehyde **5** (89.4 mg, 27.3%). The combined fore-fractions gave an analytical sample (21 mg, 97% by vpc column d, R_f 4.4 min); ir: 2700, 1730, 1176, 1107, and 1062 cm^{-1}; ^{1}H nmr δ: 1.52 (m), 2.46 (dt, $J \simeq 6$ Hz), 3.18 (bm, CH_2OR), 3.68 and 3.89 (2 multiplets, CHOR), 9.76 (t, $J = 1.6$ Hz, CHO); ms *m/e*: 210 (M^+), 165, 152, 139, 121.

Can. J. Chem. Downloaded from www.nrcresearchpress.com by 210.87.254.5 on 09/06/12
For personal use only.

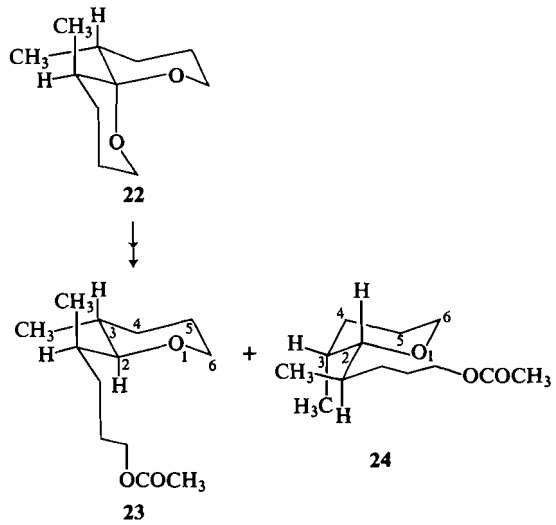

SCHEME 4

The 2,4-DNP of aldehyde **5**, prepared from a crude sample, resisted crystallization but showed ^{1}H nmr δ: 2.41 (2H, m) 3.20 (2H, m, CH_2OR), 3.69 and 3.89 (1H, 2 multiplets, CHOR), 7.53 (1H, t, J = 5 Hz, HCR=NR), isomeric aromatic AMX systems: 8.00 (7.83) (1H, s), 8.22 (8.02) (1H, d, J = 2 Hz), 9.12 (8.42) (1H, *d*, J = 2 Hz), 11.01 (1H, bs, NH).

Attempts to increase the yield of aldehyde **5** by either longer reaction times and/or addition of further hydrogen bromide were usually unsuccessful. It is possible that compounds **1** and **5** are in equilibrium (6).

Reduction of Aldehyde 5

Typically aldehyde **5** (68 mg, 0.34 mmol, the entire aldehyde fraction from the above reaction) in ether (10 mL) was stirred at RT with excess lithium aluminium hydride for 2 h. Excess reagent was destroyed with 10% hydrochloric acid, the reaction was diluted with ether, and the ethereal phase washed with brine (1 ×). Drying (Na_2SO_4) and evaporation gave alcohol **6** (55 mg, 80%). No isomer (**8**) was detected by tlc, vpc (column a), or Cmr; plc (40% EA/H) gave an analytical sample; ir: 3585, 3400, and 1070 cm^{-1}; ^{1}H nmr δ: 1.45 (18H, m), 1.77 (1H, s, OH, D_2O gave HDO δ 4.67), 3.19 (2H, m, CH_2OR), 3.64 (2H, t, J = 6 Hz, CH_2OH), ≃3.70 and 3.78 (1H, 2 multiplets, CHOR); ^{13}C nmr δ: 21.8 (C-12), 25.9 (C-8), 26.3 (C-9), 27.8 (C-10), 32.7 (C-13), 33.0 (C-7), 36.0 (C-11), 39.0 (C-5), 41.2 (C-6), 42.4 (C-1), 62.7 (C-14), 73.2 (C-2), 78.0 (C-4); ms *m/e*: 212.1774 (M^+, $C_{13}H_{24}O_2$ requires 212.1776), 194 ($M^+ - H_2O$).

Acetate 7

Alcohol **6** (25 mg, 0.12 mmol) was stirred with acetic anhydride (100 μL) and pyridine (100 μL) for 2 h at RT. The reaction was diluted with ether and washed successively with 5% sulfuric acid (1 ×), saturated sodium bicarbonate (2 ×), and brine (1 ×). Drying (Na_2SO_4) and evaporation gave acetate (**7**) (8.0 mg, 38%); plc (60% E/H) gave an analytical sample (4.8 mg) as a clear oil; ir: 1724, 1250, and 1082 cm^{-1}; ^{1}H nmr δ: 1.51 (18H, m), 2.05 (3H, s, OAc), 3.20 (2H, m, CH_2OR), 3.68 and 3.89 (1H, 2 multiplets, CHOR), 4.07 (2H, t, J = 6 Hz, CH_2OAc); ms *m/e*: 254 (M^+, weak), 194 (M^+ − HOAc), 165, 152, 139, and 121.

Mesylate-alcohols 10

To ketomesylate **9** (4) (619 mg, 1.58 mmol) in methanol (10 mL) at −18°C was added sodium borohydride (83 mg, 2.2 mmol) and the solution warmed to 0°C over 3½ h. After evaporation of the solvent at or below RT, ether was added and the solution was washed with 5% sulfuric acid (1 ×), saturated sodium bicarbonate (1 ×), and brine (1 ×). Drying (Na_2SO_4) and evaporation gave mesylate-alcohols **10** (580 mg, 84.9%) as a clear oil; ir: 3430, 1354, 1174, 1022, and 937 cm^{-1}; ^{1}H nmr δ: 1.48 (= 25H, m), 1.82 (1H, s; O*H*, D_2O gave HDO δ 4.69), 2.99 and 3.00 (3H, 2 singlets, OMs), 3.66 (5H, m, CHOR), 4.23 (2H, m, CH_2OMs), 4.56 (1H, OCHO).

THP-ethers 11

Mesylate-alcohols **10** (432 mg, 1.10 mmol) in THF (10 mL) were refluxed for 6 h with excess potassium hydride (washed hexane, 3 ×) and then left at RT for 2 days. The reaction was diluted with wet ether and water and saturated ammonium chloride slowly added. Extraction with dichloromethane (3 ×) gave, after drying (Na_2SO_4) and evaporation, the crude product (349 mg, 87.5%). Chromatography on Florisil, eluting with 20% EA/H, gave a midfraction of THP-ethers **11** (146 mg, 36.6%) as a clear oil, "two spot" by tlc; ir: 1319, 1064, and 1021 cm^{-1}; ^{1}H nmr δ: 1.46 (23H, m), 2.34 (1H, m), 2.8–4.1 (7H, m), 4.56 (1H, m, OCHO).

Alcohols 6 and 8

To THP-ethers **11** (138 mg, 0.47 mmol) in THF (5 mL) was added 5% sulfuric acid (0.5 mL). After 6 h at RT the reaction was concentrated and then diluted with ether and the aqueous phase saturated with sodium carbonate. The aqueous phase was adsorbed into sodium sulfate and the solvent filtered and evaporated to give 137 mg of clear oil; plc (2 × 25% EA/H) gave, from highest R_f, (*i*) THP-ethers **11** (45.1 mg, 32.7%) by tlc and ^{1}H nmr; (*ii*) alcohol **6** (35.0 mg, 35.4%) by tlc, vpc, ir, and ^{1}H and ^{13}C nmr identical with previously prepared material; and (*iii*) alcohol **8** (18.1 mg, 18.3%) as a clear oil. Pure by vpc (column 1, R_f 9.5 min) though tlc showed two minor contaminants; ^{13}C nmr δ: 22.5 (C-12), 26.0 (C-8), 26.4 (C-9), 28.1 (C-10), 30.0 (C-11), 32.7 (C-13), 33.3 (C-7), 35.5 (C-6), 36.1 (C-5), 42.7 (C-1), 63.1 (C-14), 65.6 (C-2), 73.2 (C-4); plc (50% EA/H) gave an analytical sample; ir: 3420, 1052, and 1013 cm^{-1}; ^{1}H nmr δ: 1.46 (19H, m), 1.58 (OH, D_2O gave HDO δ 4.68), 3.34 (2H, m, CH_2OR), 3.66 (2H, t, J = 6 Hz, CH_2OH), ≃ 3.83 (1H, m, CHOR); ms *m/e*: 212.1783 (M^+, $C_{13}H_{24}O_2$ requires 212.1776).

Bicyclic Ether Methyl Ketone 12

Spiroketal **2** (224 mg, 1 mmol) (1) in 2.4 *M* hydrochloric acid (10 mL) was refluxed for 24 h. Dilution with water (25 mL) and ether extraction (3 ×) gave, after drying ($MgSO_4$) and evaporation, bicyclic ether methyl ketone **12** quantitatively as a clear oil, melting below RT; ir: 1708, 1357, 1165, 1080, and 1065 cm^{-1}; ^{1}H nmr δ: 1.49 (16H, m), 2.09 (3H, s, CH_3CO), 2.40 (2H, dt, J ≃ 6 Hz, CH_2CO), 3.17 (2H, bm, CH_2OR), 3.64 and 3.83 (1H, 2 multiplets, CHOR); ^{13}C nmr δ: 20.1 (C-12), 25.9 (C-8), 26.2 (C-9), 27.8 (C-10), 29.8 (C-15), 33.0 (C-7), 35.7 (C-11), 39.0 (C-5), 41.2 (C-6), 42.2 (C-1), 43.7 (C-13), 73.2 (C-2), 77.7 (C-3), 208.9 (C-14); ms *m/e*: 224 (M^+).

Similarly reflux of a mixture of acetals **3** and **4** (1) (224 mg) for 6 h gave bicyclic ether methyl ketone **12** quantitatively (ir, ^{1}H and ^{13}C nmr superimposable).

Alternatively either acetal **3** or acetal **4** (224 mg, 1 mmol) was refluxed overnight in benzene (50 mL) with a trace of *p*-toluenesulfonic acid. Drying ($MgSO_4/K_2CO_3$) and evaporation gave **12** in each case (ir, ^{1}H and ^{13}C nmr). Acetal **2** was recovered unchanged under these conditions.

Bromoform Degradation of Ketone 12

Bromine (1.0 mL) was slowly added to a stirred solution of sodium hydroxide (2.18 g) in water (11 mL), maintained at 0°C. After 20 min, 1.5 mL of this solution was added at 0°C to ketone **12** (40 mg, 0.18 mmol) in dioxane (1 mL). The system was

Can. J. Chem. Downloaded from www.nrcresearchpress.com by 210.87.254.5 on 09/06/12
For personal use only.

allowed to warm to RT over 4 h and then heated to 40°C for 90 min. The reaction was diluted with 5% sodium bicarbonate and washed with ether (1 ×). The ethereal phase was extracted with saturated sodium bicarbonate and the combined aqueous phases were acidified with 5% sulfuric acid. Extraction with dichloromethane (3 ×), drying (Na_2SO_4), and evaporation gave the corresponding acid (41 mg), 101%) as a clear oil; ir: 3540–2400 (b), 1708 and 1240 (b); ^{1}H nmr δ: 1.58 (≃ 16H, m), 2.38 (2H, t, J = 6 Hz, CH_2COOR), 3.20 (2H, bm, CH_2OR), 3.69 and 3.87 (1H, 2 multiplets, CHOR), 8.59 (1H, b, OH).

The derived acid (81 mg, 0.36 mmol) in tetrahydrofuran (10 mL) was refluxed under nitrogen with excess lithium aluminium hydride for 5 h and then left at RT for 2 days. With stirring, sufficient saturated ammonium chloride was added to destroy excess hydride and then ether. Filtration through Celite and evaporation gave alcohol **6** (55 mg, 72%) by tlc, vpc (column a), and ^{13}C nmr. Isomeric alcohol **8** was not observed; plc (50% EA/H) gave pure **6** (43 mg, 33%) by ir, and ^{13}C and ^{1}H nmr.

Cyanoborohydride Reduction of Acetal 1

A stirred solution of acetal **1** (104 mg, 0.50 mmol) in methanol (9 mL) and water (1 mL) was acidified to methyl orange by dropwise addition of a solution of hydrochloric acid (2 *N*) in 80% methanol. Portions of sodium cyanoborohydride, together with further acid and indicator as required, were added over a period of 4 days to give complete reduction of the acetal. the solution was concentrated under reduced pressure, then diluted with water and extracted with dichloromethane (2 ×). Drying (Na_2SO_4) and evaporation gave alcohol **6** (97.4 mg, 92.9%) as a clear oil, crystalline below RT (vpc, tlc, ir, ^{1}H, and ^{13}C nmr). Although tlc indicated that a trace of isomeric alcohol **8** was present, none was observed by vpc (column a) or ^{13}C nmr.

Cyanoborodeuteride Reduction of Acetal 1

A stirred solution of acetal **1** (104 mg, 0.50 mmol) in methanol-d_1 (9 mL) and deuterium oxide (1 mL) was acidified to methyl orange by dropwise addition of a solution of deuterium chloride (2 *N*) in 80% methanol-d_1 – 20% deuterium oxide. Portions of sodium cyanoborodeuteride, together with further acid and indicator as required, were added over a period of 24 h to give reduction of the acetal. The solution was concentrated under reduced pressure, then diluted with water and extracted with dichloromethane (2 ×). Drying (Na_2SO_4) and evaporation gave alcohol **6** (95 mg, 90%) as a clear oil. It was shown by ^{13}C nmr spectroscopy that carbon-4 of alcohol **6** has a deuterium atom axially oriented.

Cyanoborohydride Reduction of Acetal 22

A stirred solution of acetal **22** (152 mg, 0.83 mmol) (1) in methanol (12 mL) and water (2 mL) was acidified to methyl orange by dropwise addition of a solution of hydrochloric acid (2 *N*) in 80% methanol. Portions of sodium cyanoborohydride, together with further acid and indicator as needed, were added over 10 days. The solution was concentrated under reduced pressure, then diluted with water and continuously extracted with dichloromethane. Evaporation gave a clear oil (175 mg, 101%) which was acetylated in acetic anhydride (10 mL) and pyridine (10 mL) at RT overnight. The reaction was diluted with ether (100 mL) and washed sequentially with 5% sulfuric acid (1 ×), saturated sodium bicarbonate (2 ×), and brine (1 ×). Drying (Na_2SO_4) and evaporation gave acetates **23** and **24** with residual acetic anhydride (229 mg, 122%). A sample (84 mg) was separated by plc (3 × 15% E/H) to give (*i*) at higher R_f, acetate **23** (52 mg, 62%) as a clear oil; vpc (column d, R_t 4.5 min); ir: 1727, 1245, and 1082 cm^{-1}; ^{1}H nmr δ: 0.75 (3H, d, *J* = 5.5 Hz, CH_3), 0.85 (3H, d, *J* = 5.7 Hz, CH_3), 1.47 (10H, m), 2.03 (3H, s, OAc), 2.90 and 2.75 (1H, 2 multiplets), 3.26 (1H, bm), 4.04 (3H, deformed t, *J* = 6 Hz, CH_2OAc and CHOR); ^{13}C nmr δ: 12.8, 18.7, 21.0, 26.8, 26.9, 30.6, 32.4, 33.2, 33.5, 65.0, 68.7, 85.9, 171.2; ms *m/e*: 288.1706 ($C_{13}H_{24}O_3$ requires 228.1725). (*ii*) At lower R_f, acetate **24** (17 mg, 20%) as a clear oil; vpc (column d, R_t 7.1 min); ir: 1730, 1237, and 1040 cm^{-1}; ^{1}H nmr δ: 0.79 (3H, d, *J* = 6.8 Hz, CH_3), 0.93 (3H, d, *J* = 6.3 Hz, CH_3), 1.69 (10H, m), 2.04 (3H, s, OAc), 2.91 (1H, dd, *J* = 9 Hz, *J* ≃ 2 Hz), 3.36 (1H, deformed t, *J* ≃ 9 Hz), 4.05 (3H, deformed t, *J* = 6 Hz, CH_2OAc and CHOR); ^{13}C nmr δ: 11.3, 14.6, 21.1, 21.1, 26.0, 28.8, 29.8, 31.4, 34.8, 65.2, 69.5, 84.5, 171.2; ms *m/e*: 228.1702 (M^+, very weak), 227.1640 ($M^+ - 1$, $C_{13}H_{23}O_3$ requires 227.1646), 168 (M^+ – HOAc).

Acknowledgements

We wish to thank Professor John K. Saunders for the interpretation of ^{13}C nmr spectra. This research was supported by the Natural Sciences and Engineering Research Council of Canada (NSERCC) and by the Ministère de l'Education of Québec.

1. P. Deslonghamps, D. D. Rowan, N. Pothier, G. Sauve, and J. K. Saunders. Can. J. Chem. **59**, 1105 (1981).
2. N. Pothier, D. D. Rowan, P. Deslongchamps, and J. K. Saunders. Can. J. Chem. **59**, 1132 (1981).
3. P. Deslongchamps, D. D. Rowan, and N. Pothier. Heterocycles, **15**, 1093 (1981).
4. P. Deslongchamps, D. D. Rowan, N. Pothier, and J. K. Saunders. Can. J. Chem. **59**, 1122 (1981).
5. J. B. Stothers. *In* Carbon-13 nmr spectroscopy. Academic Press, New York, NY. 1972. p. 65.
6. R. B. Woodward, F. Sondheimer, and Y. Mazur. J. Am. Chem. Soc. **80**, 6693 (1958).
7. G. R. Pettit and W. J. Boyer. J. Org. Chem. **25**, 84 (1960).
8. P. Deslongchamps. Pure Appl. Chem. **43**, 351 (1975); Tetrahedron, **31**, 2463 (1975); Heterocycles, **7**, 1271 (1977).
9. E. L. Eliel, B. E. Nowak, R. A. Daigneault, and V. G. Badding. J. Org. Chem. **30**, 2441 (1965).
10. N. Beaulieu, R. A. Dickinson, and P. Deslongchamps. Can. J. Chem. **58**, 2531 (1980).
11. E. L. Eliel and F. W. Nader. J. Am. Chem. Soc. **92**, 3045 (1970).

Can. J. Chem. Downloaded from www.nrcresearchpress.com by 210.87.254.5 on 09/06/12
For personal use only.

Conditions for excited-state Raman and absorption processes during optical pumping[1]

B. HALPERIN
Soreq Nuclear Research Center, Yavne, Israel
AND
J. A. KONINGSTEIN
Department of Chemistry, Carleton University, Ottawa, Ont., Canada K1S 5B6

Received February 13, 1981

B. HALPERIN and J. A. KONINGSTEIN. Can. J. Chem. **59**, 2792 (1981).

A theoretical analysis is presented for conditions of optical pumping of an electronic excited state and the subsequent induction of Raman scattering thereof, using the radiation of a tunable laser with a specific λ for pumping and Raman probing.

The analysis shows that the number of excited states created by the optical pump can be estimated as a function of the photon flux from the (non-linear) behaviour of the transmission of the sample at the selected laser wavelength. It is shown that such transmission studies are a prerequisite before attempts are made to record any excited level Raman spectrum.

B. HALPERIN et J. A. KONINGSTEIN. Can. J. Chem. **59**, 2792 (1981).

On propose une analyse théorique des conditions de pompage optique d'un état électronique excité et de l'induction subséquente de la diffusion de Raman qui en découle, en utilisant un laser ajustable avec un λ spécifique pour le pompage et la recherche Raman.

L'analyse montre que l'on peut évaluer le nombre d'états excités, créés par la pompe optique, en fonction du courant de photons à partir du comportement (non linéaire) de la transmission produit par l'échantillon à la longueur d'onde du laser où l'on opère. On montre que de telles études de transmission sont un prérequis avant d'essayer d'enregistrer n'importe quel niveau de spectre Raman.

[Traduit par le journal]

I. Introduction

With the advent of tunable pulsed lasers, another area in Raman spectroscopy has become accessible in addition to spectra which involve transitions of the ground state. Recently, light-scattering (1–9) transitions from short-lived excited states of molecules and atoms or ions in solids have been observed. Due to the tunability of present-day lasers it is, in fact, possible to employ one particular frequency of the laser in order to both populate and scatter (2–7, 9) from the optically pumped excited state. It can be shown that by using cw lasers, only excited states with lifetimes of $\tau \geq 100$ μs may be populated, while with the radiation of an N_2-pumped dye laser, light-scattering of excited states having $\tau \geq 10$ ps has been detected (9, 10). From the experimental data presently available, one may even predict that by means of picosecond lasers, this limit could eventually be lowered towards states having $\tau > 1$ fs. However, in all cases one has to rely on the capability of the (Raman) detection system to process weak light pulses having a duration of a few nano or picoseconds.

Presently we are interested in the details of the optical pumping process, and in particular the types of calculations which have to be performed (2, 11–13) before such light-scattering experiments can be carried out. The calculations in this paper refer to the conditions for saturation population of the excited states, and a discussion is given of some experimental measurements which form the basis for an excited-state Raman study.

II. Absorption Models and Effective Absorption Cross Sections

We consider the experimental situation where a beam of coherent photons is travelling through a medium which shows some absorption at the frequency of the laser. We distinguish between two different cases which are schematically illustrated in Fig. 1. In both cases, the incident frequency is in resonance with a vibronic side-band of an electronic transition, and the energy of the laser reaches the excited state E. From there fluorescence (or radiationless) transitions $E \rightarrow A$ (ground-state) may provide a downward channel for the energy. If enough population of E is obtained, absorption of another laser photon may occur to raise the system indirectly into a higher-laying excited state Y (via pumping into a vibronic side band $E \rightarrow Y'$). The difference between the two cases I and II is in the relaxation process from Y. In case I, the system relaxes directly from Y into A. In case II we consider the situation where the relaxation from Y to A occurs via E.

[1]Research supported by the Natural Sciences and Engineering Research Council of Canada.

0008-4042/81/182792-11$01.00/0
©1981 National Research Council of Canada/Conseil national de recherches du Canada

Can. J. Chem. Downloaded from www.nrcresearchpress.com by 210.87.254.6 on 09/06/12
For personal use only.

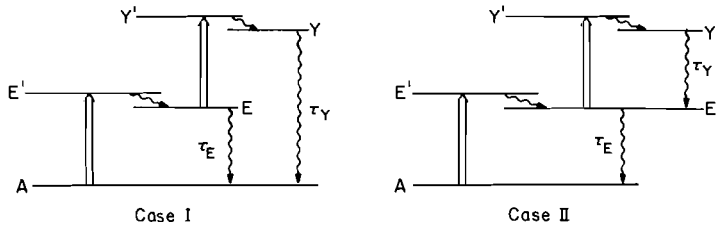

FIG. 1. Optical pumping and energy relaxation for the two cases considered in this paper. The levels E' and Y' are vibronic levels of the electronic states E and Y and it is assumed here that these vibronic levels relax instantaneously into E or Y. The energy difference of E' and A is equal to that of Y' and E and the corresponding absorption cross sections are σ_A and σ_E.

In both cases, we assume that the absorption is not directly into the states E or Y but rather into their vibronic side-bands (or other intermediate states E', Y') which immediately relax into E and Y. In what follows, the relaxations from E' into E and Y' into Y are considered to be instantaneous and accordingly, they do not explicitly appear in the equations which describe the kinetics of the system. This "short-circuiting" model resembles actual systems (e.g. ruby) and has the advantage that the pump field does not give rise to stimulated emission from E to A (or from Y to E).

Let us denote by N that total concentration (density) of absorbing centers, which we assume to be uniform throughout the medium. We have

$$[1] \quad N = n_A(x) + n_E(x) + n_Y(x)$$

where $n_A(x)$, $n_E(x)$, and $n_Y(x)$ are the densities of absorbing centers in the states A, E, and Y, respectively, measured at depth x inside the sample. The point $x = 0$ is the front edge where the laser beam enters the medium, and $0 \leq x \leq L$. The change in populations with time for case I is given by the following expressions:

$$[2] \quad \dot{n}_A(x) = \frac{1}{\phi}\left(\frac{dI(x)}{dx}\right)_A + \frac{n_E(x)}{\tau_E} + \frac{n_Y(x)}{\tau_Y}$$

$$[3] \quad \dot{n}_E(x) = -\frac{1}{\phi}\left(\frac{dI(x)}{dx}\right)_A - \left(\frac{dI(x)}{dx}\right)_E - \frac{n_E(x)}{\tau_E}$$

and

$$[4] \quad \dot{n}_Y(x) = -\frac{1}{\phi}\left(\frac{dI(x)}{dx}\right)_E - \frac{n_Y(x)}{\tau_Y}$$

In these expressions ϕ is the cross-sectional area of the laser beam, τ_E and τ_Y are, respectively, the lifetimes of the states E and Y, and $(dI(x)/dx)_A$ $(dI(x)/dx)_E$ describe the attenuation of the incident intensity due to absorptions from states A and E, respectively. For case II, the only difference in the above expressions is that the last term in the right hand side of eq. [2] should be deleted and transferred to eq. [3]. For both cases we have, in addition, the relations

$$[5] \quad \left(\frac{dI(x)}{dx}\right)_A = -\sigma_A[N - n_E(x) - n_Y(x)]I(x)$$

$$[6] \quad \left(\frac{dI(x)}{dx}\right)_E = -\sigma_E n_E(x) I(x)$$

where σ_A, σ_E are the absorption cross-sections of the centers in states A and E, respectively.

If the duration of the laser pulse is long compared to the lifetimes of the pertinent states, steady-state conditions exist, i.e.

$$[7] \quad \dot{n}_A(x) = \dot{n}_E(x) = \dot{n}_Y(x) = 0$$

By eliminating $n_E(x)$ and $n_Y(x)$ from the equations we obtain the following result for case I:

Can. J. Chem. Downloaded from www.nrcresearchpress.com by 210.87.254.6 on 09/06/12
For personal use only.

$$[8]\quad \frac{dI(x)}{dx} = \left(\frac{dI(x)}{dx}\right)_A + \left(\frac{dI(x)}{dx}\right)_E = -\frac{\sigma_A N I(x)[1 + 2\sigma_E\tau_E I(x)/\phi]}{1 + \tau_E(\sigma_A + \sigma_E)\frac{I(x)}{\phi} + \sigma_A\sigma_E\tau_E\tau_Y\frac{I^2(x)}{\phi^2}}$$

The corresponding result for case II is:

$$[9]\quad \frac{dI(x)}{dx} = -\frac{\sigma_A N I(x)[1 + \sigma_E\tau_E I(x)/\phi]}{1 + \tau_E\sigma_A\frac{I(x)}{\phi} + \sigma_A\sigma_E\tau_E\tau_Y\frac{I^2(x)}{\phi^2}}$$

Integration of eqs. [8] and [9] over the path of the laser beam through the medium yields transcendental expressions for the transmission $T \equiv I(L)/I(0)$, as functions of the incident intensity $I(0)$. For case I we get

$$[10]\quad T = \left[\frac{1 + 2\sigma_E\tau_E T I(0)/\phi}{1 + 2\sigma_E\tau_E I(0)/\phi}\right]^{[(\sigma_E - \sigma_A)/2\sigma_E + \tau_Y\sigma_A/4\sigma_E\tau_E]} \exp\left(-N\sigma_A L + \frac{\tau_Y\sigma_A}{2}\frac{I(0)}{\phi}(1 - T)\right)$$

whereas for case II we find:

$$[11]\quad T = \left[\frac{1 + \sigma_E\tau_E T I(0)/\phi}{1 + \sigma_E\tau_E I(0)/\phi}\right]^{[(\sigma_E - \sigma_A)/\sigma_E + \tau_Y\sigma_A/\sigma_E\tau_E]} \exp\left(-N\sigma_A L + \tau_Y\sigma_A\frac{I(0)}{\phi}(1 - T)\right)$$

Equations [10] and [11] have been solved numerically for the transmissions T as functions of the incident flux $I(0)/\phi$, assuming characteristic values for the absorption cross sections and relaxation times. The results obtained in case I are presented in Fig. 2 and those for case II are presented in Fig. 3. In each figure, two curves are shown, one for the situation where the ground-state absorption cross section is greater than the excited-state absorption cross section ($\sigma_A > \sigma_E$) and the other for the inverse situation ($\sigma_E > \sigma_A$). As seen from the figures, the curves tend to flatten at extremely low as well as at extremely high intensities of the incident radiation. In the low-intensity limit $I(0)/\phi \to 0$, the simple Beer's law for ground-state absorption alone

$$[12]\quad T = T_A \equiv \exp(-N\sigma_A L)$$

is recovered from both eqs. [10] and [11].

In order to analyse the behaviour of the transmission curves in the high intensity regime, consider first case I, represented by eq. [10] and Fig. 2. The flattening of the curve occurs when the incident flux $I(0)/\phi$ obeys

$$[13]\quad \frac{I(0)}{\phi} \gg \frac{1}{\tau_E\sigma_E}$$

In the particular example which is represented in the figure, we have chosen $\tau_E = 1$ ns and $\sigma_E \gtrsim 10^{-18}$ cm^2, so that in order to obey condition [13], $I(0)/\phi$ should be greater than 10^{27} photons s^{-1} cm^{-2}. This is achieved by present-day N_2-pumped dye lasers which can deliver 10^{14}–10^{15} photons per pulse of 1 ns, provided the beam is focused down to a cross section $\phi \lesssim 10^{-4}$ cm^2. In the limit described by eq. [13], the attenuation of the incident radiation, eq. [8] becomes

$$[14]\quad \frac{dI(x)}{dx} = -N I(x)\frac{2\sigma_A\sigma_E}{\sigma_A + \sigma_E + \tau_Y\sigma_A\sigma_E I(x)/\phi}$$

One immediately realizes that if the additional condition

$$[15]\quad \tau_Y\sigma_A\sigma_E I(0)/\phi \ll \sigma_A + \sigma_E$$

holds as well, eq. [14] reduces to the form of an effective Beer's law where

$$[16]\quad T = T_{\text{eff}} \equiv \exp(-N\sigma_{\text{eff}}L)$$

with the effective absorption cross-section given by

$$[17]\quad \sigma_{\text{eff}} = (2\sigma_A\sigma_E)/(\sigma_A + \sigma_E)$$

Can. J. Chem. Downloaded from www.nrcresearchpress.com by 210.87.254.6 on 09/06/12
For personal use only.

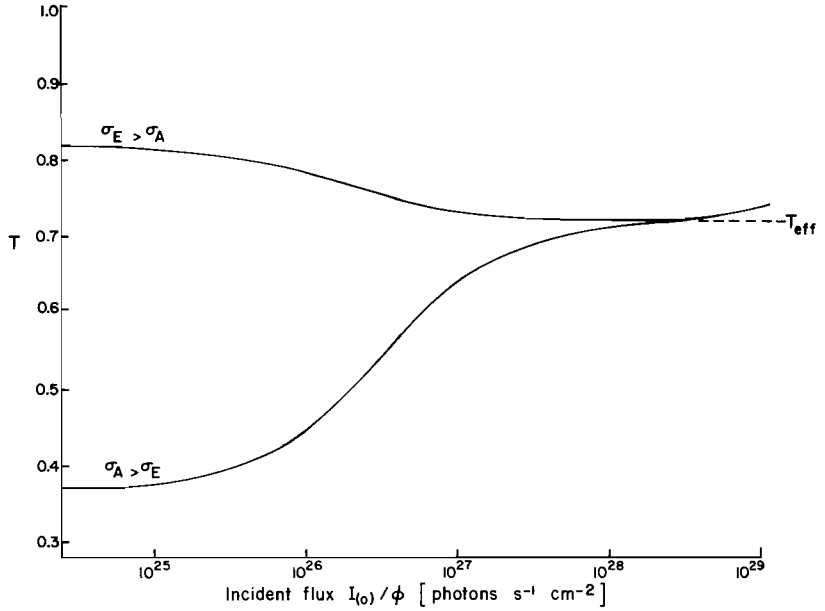

FIG. 2. The dependence of the transmission T of the sample on the incident photon flux for a molecular system in which energy transfer is that depicted in Fig. 1, case I where $\tau_E = 1$ ns, $\tau_Y = 1$ ps, and N (number of molecules) $\times$ L (length of cuvette) = 2×10^{17} cm^{-2}. The upper curve is for $\sigma_A = 10^{-18}$ cm^2. $\sigma_E = 5 \times 10^{-18}$ cm^2 and the lower curve is for a situation where the absorption cross sections for the transitions $E' \leftarrow A$ and $Y' \rightarrow E$ (see Fig. 1) are respectively $\sigma_A = 5 \times 10^{-18}$ cm^2 and $\sigma_E = 10^{-18}$ cm^2. T_{eff} is the value of the transmission where Beer's Law applies (see eq. [16]).

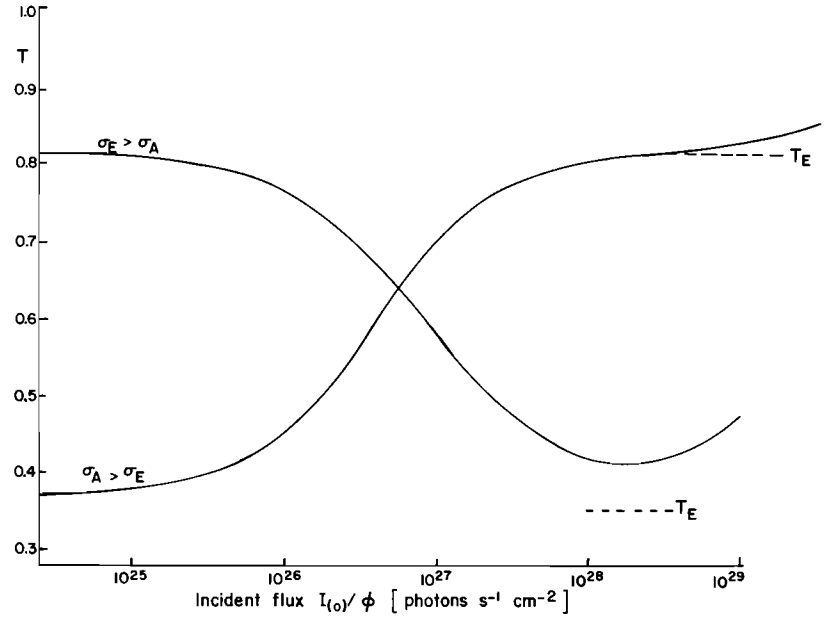

FIG. 3. The dependence of the transmission on I_{laser} for a system which follows case II of Fig. 1, assuming $\tau_E = 1$ ns, $\tau_Y = 1$ ps and $N \times L = 2 \times 10^{17}$ cm^2. Upper curve $\sigma_A = 10^{-18}$ cm^2, $\sigma_E = 5 \times 10^{-18}$ cm^2, lower curve $\sigma_A = 5 \times 10^{-18}$ cm^2, $\sigma_E = 10^{-18}$ cm^2.

Can. J. Chem. Downloaded from www.nrcresearchpress.com by 210.87.254.6 on 09/06/12
For personal use only.

In the particular example represented in Fig. 2, we have assumed $\tau_Y = 1$ ps and σ_A, $\sigma_E \gtrsim 10^{-18}$ cm^2. Hence, condition [15] holds as long as $I(0)/\phi$ does not exceed values of $\sim 10^{29}$ photons s^{-1} cm^{-2}. This is well realised by the deviation from an effective Beer's law behaviour, which is observed for higher flux values in Fig. 2.

In the extreme case where $\sigma_E \gg \sigma_A$; we have, from eq. [17], $\sigma_{eff} = 2\sigma_A$, whence

$$[18] \quad T_{eff} = (T_A)^2$$

On the other hand, for $\sigma_A \gg \sigma_E$ we have $\sigma_{eff} = 2\sigma_E$ and

$$[19] \quad T_{eff} = (T_E)^2 \equiv \exp(-2N\sigma_E L).$$

Equations [18] and [19] demonstrate that a determination of σ_E from the asymptotic behaviour of an excited-state absorption spectrum is much less straightforward than determining σ_A from a ground-state absorption experiment.

Returning to case II and assuming condition [13] to hold (for $1/\tau_E\sigma_A$ as well) we have from eq. [9]

$$[20] \quad \frac{dI(x)}{dx} = -NI(x)\frac{\sigma_E}{1 + \tau_Y\sigma_E I(x)/\phi}$$

and with the additional condition

$$[21] \quad \tau_Y\sigma_E I(0)/\phi \ll 1$$

We find an effective Beer's law of the form

$$[22] \quad T = T_E \equiv \exp(-N\sigma_E L)$$

This lends itself to a direct interpretation as a pure excited-state absorption spectrum due to a complete degree of excitation. The limiting degree of population in the excited state E and the conditions for saturation in both models are calculated in the next section. This kind of information is essential whenever an excited-state light-scattering experiment is proposed.

III. Excited-state Population and Effective Saturation

At steady-state conditions the density of absorbing centers in the excited state E is found to be

$$[23] \quad n_E(x) = -\frac{1}{\phi}\frac{dI(x)}{dx}\frac{\tau_E}{1 + \nu\sigma_E\tau_E I(x)/\phi}$$

where $\nu = 2$ in case I, $\nu = 1$ in case II.

From eqs. [8] and [9] we then have

$$[24] \quad n_E(x) = \frac{N\frac{I(x)}{\phi}\sigma_A\tau_E}{1 + \tau_E[\sigma_A + (\nu - 1)\sigma_E]\frac{I(x)}{\phi} + \tau_Y\tau_E\sigma_A\sigma_E\left[\frac{I(x)}{\phi}\right]^2}$$

In the limits described by eqs. [13], [15], and [21] this turns out to be

$$[25] \quad n_E(x) \simeq \begin{cases} N\dfrac{\sigma_A}{\sigma_A + \sigma_E} & \text{in case I} \\ N & \text{in case II} \end{cases}$$

The result, eq. [25] for case II, was anticipated in view of the Beer's law behaviour represented by eq. [22]. On the other hand, for case I, the Beer's law transmission represented by eq. [16] is not just exp $(-n_E\sigma_E L)$ but rather, exp $(-2n_E\sigma_E L)$. The factor 2 here manifests the fact that at saturation conditions in case I, the ground and excited states give rise to equal absorptions. In the ground state, the population is $N\sigma_E/(\sigma_A + \sigma_E)$ and the absorption cross-section is σ_A, whereas in the excited state the population is $N\sigma_A/(\sigma_A + \sigma_E)$ and the cross section is σ_E. We note in passing that in both cases $n_Y(x)$ is proportional to τ_Y and is therefore negligibly small.

Can. J. Chem. Downloaded from www.nrcresearchpress.com by 210.87.254.6 on 09/06/12
For personal use only.

Can. J. Chem. Downloaded from www.nrcresearchpress.com by 210.87.254.6 on 09/06/12
For personal use only.

IV. Population Numbers of Excited and Ground State in Relation to Photon Densities

We now wish to assess the number of photons N_{ph} (per unit time and unit volume of the sample) required in order to maintain the steady-state saturation population given by eq. [25]. This is defined by

$$[26] \quad N_{ph} \equiv \frac{I(0)}{L\phi}(1 - \bar{T})$$

where $\bar{T}$ is the asymptotic value of the transmission in the limit described by eqs. [13], [15], and [21]. By expanding eqs. [10] and [11] in terms of $[I(0)/\phi]^{-1}$, we find for case I

$$[27] \quad \bar{T} = T_{eff} + \frac{(1 - T_{eff})}{2\sigma_E\tau_E}\frac{(\sigma_E - \sigma_A)}{(\sigma_E + \sigma_A)}\frac{1}{I(0)/\phi} + O\left(\frac{1}{I(0)^2}\right)$$

where T_{eff} is defined in eqs. [16], [17]. For case II we find

$$[28] \quad \bar{T} = T_E + \frac{(1 - T_E)}{\sigma_E\tau_E}\frac{(\sigma_E - \sigma_A)}{\sigma_A}\frac{1}{I(0)/\phi} + O\left(\frac{1}{I(0)^2}\right)$$

where T_E is defined in eq. [22].

From an experimental point of view, one can always make sure that $\sigma_{eff}NL \ll 1$ and $\sigma_E NL \ll 1$, in which situation we find for case I

$$[29] \quad N_{ph} \simeq \frac{I(0)}{\phi} N \frac{2\sigma_A\sigma_E}{\sigma_A + \sigma_E} + \frac{\sigma_A(\sigma_A - \sigma_E)}{(\sigma_A + \sigma_E)^2}\frac{N}{\tau_E}$$

and for case II

$$[30] \quad N_{ph} \simeq \frac{I(0)}{\phi} N\sigma_E + \frac{(\sigma_A - \sigma_E)}{\sigma_A}\frac{N}{\tau_E}$$

If $I(0)/\phi \gg [(\sigma_A + \sigma_E)\tau_E]^{-1}$ in case I, or $I(0)/\phi \gg (\sigma_A\tau_E)^{-1}$ in case II (the necessary conditions to get the saturation limits of eq. [25]), we formally have

$$[31] \quad N_{ph} \gg \frac{\sigma_A}{(\sigma_A + \sigma_E)}\frac{N}{\tau_E} \quad \text{in case I}$$

and

$$[32] \quad N_{ph} \gg \frac{N}{\tau_E} \quad \text{in case II}$$

A closer inspection of the transmission curves in Figs. 2 and 3 reveals that the steepness of the curves is the highest when $I(0)/\phi$ is equal to $[(\sigma_A + \sigma_E)\tau_E]^{-1}$ in case I or to $(\sigma_A\tau_E)^{-1}$ in case II. In other words, at these values of the incident flux the transmission is most susceptible to any additional increment in $I(0)/\phi$, whereas at higher values the susceptibility is reduced. Hence, these incident flux values may effectively be considered as giving rise to the onset of saturation. The actual excited-state population (eq. [24]) is then half of the saturation population (eq. [25]). It is instructive to point out that eqs. [31], [32] only yield lower limits on N_{ph} but do not determine its magnitude. On the other hand, for a model system where the ground state alone absorbs ($\sigma_E = 0$), eq. [32] becomes a strict equality.

From a practical point of view, the incident flux values which give rise to the onset of saturation can be utilized in order to determine the values of the lifetimes τ_E. Apparently, an alternative way to determine τ_E is to plot the transmission as a function of $[I(0)/\phi]^{-1}$ for very high incident flux values, and use eqs. [27], [28] to obtain the relation between τ_E and the slope of such curves. However, at high flux values, population inversion occurs and stimulated emission may already play a noticeable role. As will be shown in the next section, this will give rise to an effective value τ_E' which is smaller than the intrinsic lifetime τ_E.

V. Optical Pumping and Stimulated Emission

Stimulated emission from a vibronic level of E, which is in resonance with that of the optical pump, was excluded in the discussion above because we assumed that the vibronic level of E' relaxes instantaneously

into E. Now, this level can emit radiation, and the lifetime of the radiative process $E \rightarrow A$ is denoted by τ_E. However, the results presented in section III, eq. [25], suggest that population inversion of the levels E and A can occur, and this in combination with the availability of a photon flux I_F/ϕ at the wavelength λ_{EA}, can result in stimulated emission from $E \rightarrow A$. In the following discussion, we shall assume that the population numbers n_A, n_E, and n_Y are all small compared to the number of photons in the pumping laser beam, and that population inversion of the level Y versus either E or A does not take place. The dynamical equation (14) describing the rate change of n_E becomes:

$$[33] \quad \dot{n}_E = -\frac{1}{\phi}\left(\frac{dI(x)}{dx}\right)_A - \left(\frac{dI(x)}{dx}\right)_E - \frac{n_E}{\tau_E} - \frac{1}{\phi} I_F(x)\sigma_E'(n_E - n_A)$$

where σ_E' is the gain cross section for stimulated emission. In the absence of the latter, the photon flux in the x direction may be obtained by a decay rate from a segment dx,

$$[34] \quad \frac{1}{\phi}\frac{dI_F(x)}{dx} = \Omega(x)\frac{n_E}{\tau_E}$$

where $\Omega(x)$ is a probability of a photon being emitted in the direction of propagation of the optical pump. It is normally assumed that the emitted photons experience exponential stimulated amplification so that eq. [34] is replaced by

$$[35] \quad \frac{1}{\phi}\frac{dI_F(x)}{dx} = \Omega(x)\frac{n_E}{\tau_E}\{\exp(n_E - n_A)\sigma_E' x\}$$

Integration of eq. [35] over length L and substitution of the result in eq. [33] gives:

$$[36] \quad n_E = -\frac{1}{\phi}\left(\frac{dI(x)}{dx}\right)_A - \left(\frac{dI(x)}{dx}\right)_E - \frac{n_E}{\tau_E'}$$

where

$$\frac{1}{\tau_E'} \approx \frac{1}{\tau_E}(1 + \Omega\{\exp[(n_E - n_A)\sigma_E' L] - 1\})$$

The difference between $\Omega(x)$ and Ω is that the latter represents a small solid angle in which light amplification occurs.

A comparison of eqs. [3] and [36] shows that formally the effect of stimulated emission is represented by replacing τ_E with τ_E' as given by eq. [36]. If the condition $n_E - n_A \rightarrow 0$ applies, the expressions of sections II and III remain useful.

The substitution of τ_E' for τ_E can still be valid if $n_E - n_A$ is finite, as long as $n_E - n_A < 1/\sigma_E' L$, because from eq. [36] it follows that $1/\tau_E \approx 1/\tau_E'$. Light amplification in the x direction can occur if $\sigma_E' L > 1/(n_E - n_A)$, and in that case, the term n_E/τ_E, which appears in the right hand side of eq. [33] is small compared to the stimulated emission term and a comparison of eqs. [3] and [36] cannot be made anymore. However, the assumption that the emitted photons experience stimulated exponential amplification may not hold anymore if the cross section σ_E'' for a transition $Y'' \leftarrow E$, which occurs at the same wavelength as that of the $E \rightarrow A$ fluorescence, becomes large.

In any case, from a practical point of view one does not want to generate laser action at the wavelength λ_{EA} because this would interfere with the Stokes part of the Raman spectrum excited with the tunable laser which serves simultaneously as an optical pump and Raman probe. From Fig. 1, it follows that the wavelength of the Raman probe is always smaller than that of the fluorescence $E \rightarrow A$.

Having in mind that one of the purposes of this paper is related to study the conditions which would make it possible to record an excited-level Raman (E.L.R.) spectrum, we emphasize that one should have $\sigma_A \neq 0$ in order that population of the E level can take place. This means that in all cases the intensity of Raman bands of the ground state A are resonance enhanced. In the case where eq. [25] is valid, conditions are favourable for the recording of the E.L.R. spectrum, in particular if $\sigma_E \rightarrow 0$. On the other hand, if $\sigma_E \neq 0$ one also deals with a resonance Raman effect which enhances intensities in the Raman spectrum of E, although the population number n_E of this level is reduced (case I only), and ground- and excited-level scattering can both contribute to the recorded spectrum. It is clear that the E.L.R. spectrum can be made to dominate over that of the spectrum associated with the electronic ground state after a judicious choice is made of the wavelength and power of the pulsed tunable laser.

Can. J. Chem. Downloaded from www.nrcresearchpress.com by 210.87.254.6 on 09/06/12
For personal use only.

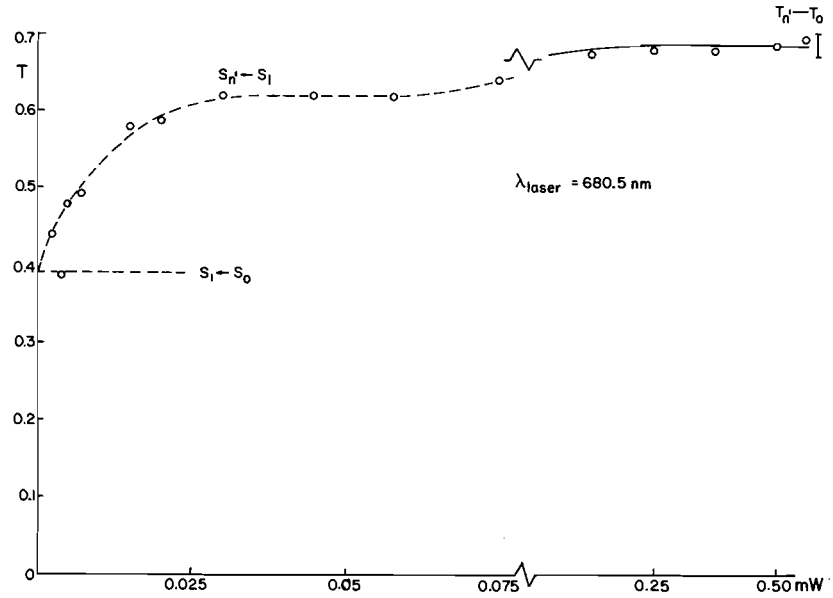

FIG. 4. The transmission T as function of the average power of a dye laser (repetition rate 25 Hz, pulse duration 3.2×10^{-9} s) at $\lambda = 680.5$ nm of a 1.45×10^{-4} M solution of chlorophyll a in pyridine. For the focused laser beam and $I_{laser} \approx 0.025$ mW (corresponding to $\sim 4 \times 10^{24}$ photons s^{-1} cm^{-2}) effective saturation occurs of the singlet S_1 state while for $I_{laser} \approx 0.50$ mW ($\sim 8 \times 10^{25}$ photons s^{-1} cm^{-2}) saturation of the T_0 triplet state occurs. Also indicated is the value of T for the ground state absorption process $S_1 \leftarrow S_0$ (laser beam not focused).

VI. Some Experimental Results

The absorption spectrum of chlorophyll a in pyridine in the visible spectral region is well known (15, 16). Its main features are two bands at ~ 680 nm and 440 nm, which are due to transitions from the singlet S_0 ground state to the excited singlets S_1 at $\sim 14\,780$ cm^{-1} and S_4 at $\sim 22\,280$ cm^{-1} above S_0.

When chlorophyll a is exposed to radiation with wavelengths < 680 nm, one finds that S_1 can be populated via vibrational relaxation. From there, part of the energy returns to the ground state S_0 giving rise to the well-known red fluorescence, while part of the absorbed *energy reaches* the lowest lying triplet state which is at $\sim 10\,150$ cm^{-1} above the ground state. From the decay time of the red fluorescence, a lifetime $\tau_{S_1} = 45$ ns was established (17) while $\tau_{T_0} \approx 70$ μs. Both lifetimes are longer than the duration of the pulses of a tunable dye laser used in the experiments described below (duration 3.2 ns at a repetition rate of 25 Hz).

Figure 4 shows the behaviour of transmission of the sample (1.45×10^{-4} M) when pumping at $\lambda = 680.5$ nm, that is, in the wing of the $S_1 \leftarrow S_0$ absorption band (towards longer wavelength). The transmission (~ 0.4) for low laser power is the value for T in the singlet spectrum when measurements of T are carried out with a non-focused laser beam. If, however, this beam is focused and its intensity is increased, one records an increase in T. Conditions for which Beer's law applies are met if 0.03 mW $< l <$ 0.06 mW and if $I \geq 0.25$ mW (average power). The value of the transmission $T = 0.69$ for the latter case is equal to that for T at 680.5 nm in the *triplet excited* (16) state absorption spectrum of chlorophyll a in pyridine (1.45×10^{-4} M). These experiments prove that with pumping at 680.5 nm, energy is transferred into the triplet system and that population of T_0 takes place. The value of the transmission $T = 0.62$ for 0.03 mW $< l <$ 0.06 mW agrees with the value of T in the *singlet–singlet* (and not triplet–triplet) absorption spectrum (16) and effective population of S_1 is achieved. It was found that while increasing the intensity of the focused laser beam a decrease was observed in the intensity of the $S_1 \rightarrow S_0$ red fluorescence. This suggests that the absorbed energy in the singlet excited-state spectrum does not return again to S_1 but reaches the ground state via another path. Hence the energy transfer within the singlet system maybe an example of case I, Fig. 1, except that the effect of intersystem crossing from $S_1 \rightarrow T_0$ (which occurs for chlorophyll) is not included. This effect may be incorporated in the equations of section II as playing the role of radiationless transitions from $E \rightarrow A$, ($E \equiv S_1$ and $A \equiv S_0$) representing another path for the return of energy to the ground state, in competition with the stimulated emission process. The introduction of radiationless transitions and energy transfer may be incorporated

Can. J. Chem. Downloaded from www.nrcresearchpress.com by 210.87.254.6 on 09/06/12
For personal use only.

Can. J. Chem. Downloaded from www.nrcresearchpress.com by 210.87.254.6 on 09/06/12
For personal use only.

in the reduction of the stimulated gain σ_E', see eqs. [33] and [35]. This means that the effective lifetime τ_E' ($\tau_E' < \tau_E$) takes on another meaning without affecting the derivations of section II.

Equation [31] cannot be directly applied to obtain an estimate of the lifetimes τ_{S_1} from the data shown in Fig. 4. This equation states that the number of photons per second delivered in the lifetime τ_E should exceed the number of molecules times $\sigma_A/(\sigma_A + \sigma_E)$ in the path of the laser beam. Pulsed lasers do not deliver photons per second but rather photons per duration of the laser pulse ($\hat{N}_{ph}$). Hence the lifetime τ_E can only be computed in terms of a fraction f, where

$$f = \frac{\sigma_A}{\sigma_A + \sigma_E} \frac{N}{\hat{N}_{ph}}$$

of the duration of the laser pulse t_p as can be seen from the following. In the situation where the duration of the pulse becomes equal to the lifetime τ_E, one finds from eq. [31] that the following expression applies:

$$[37] \quad \frac{\hat{N}_{ph}}{t_p} \gtrsim \frac{\sigma_A}{\sigma_A + \sigma_E} \frac{N}{\tau_E}$$

However, if $t_p \leq \tau_E$, we find that in order to reach conditions for the applicability of Beer's law, the number of photons $\hat{N}_{ph}$ has to be increased by the factor t_E/t_p, and the relevant expression now becomes

$$[38] \quad \hat{N}_{ph} \gtrsim \frac{\sigma_A}{\sigma_A + \sigma_E} N$$

Figure 5 shows the result of transmission studies with pulsed and cw lasers operating at 488.0 nm. For high laser powers, the transmission again approaches the value at 488.0 nm previously found in the triplet absorption spectrum. Because eq. [38] is valid for the pulsed case and eq. [37] for the cw measurements, we obtain $\tau_{T_0} \approx 70$ μs. One also notes that whereas for lower intensities of the pulsed laser, the S_1 state becomes populated. This is not the case with the cw laser. This is because the number of photons per second is not large enough to reach conditions for which eq. [31] applies. We also find that in the region $0.2 < I < 0.3$ mW the relation $(T_{S_1-S_0})^2 \sim T_{S^*-S_1}$ is valid. The singlet excited state spectrum of chlorophyll *a* in pyridine was recently recorded (16) and $\sigma_{S^*-S_1} \sim 10\,\sigma_{S_1-S_0}$ at 488.0 nm. The fact that conditions exist for which eq. [18] is valid is taken as another proof that case I of Fig. 1 applies to energy transfer within the singlet system. On the other hand, because we find, consistently, for large laser intensities that the value of the transmission is, within experimental error, equal to that found in the

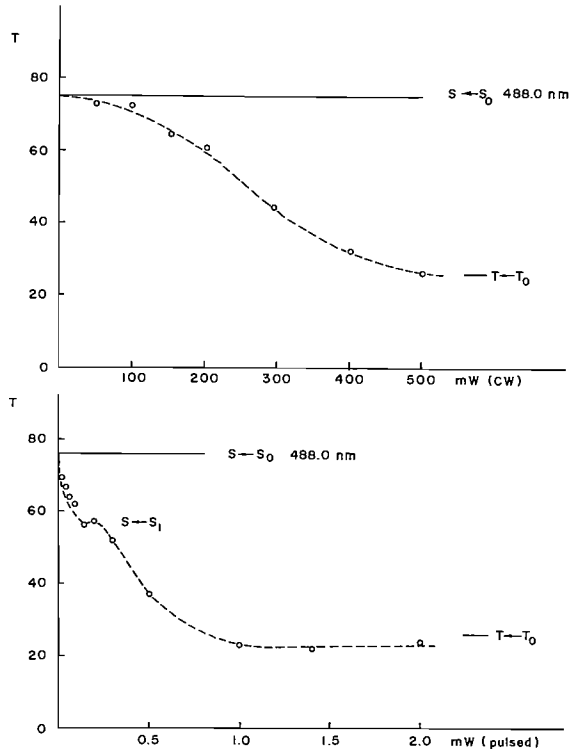

FIG. 5. Transmission studies at $\lambda = 488.0$ nm of a 1.45×10^{-4} *M* solution of chlorophyll *a* in pyridine. Top: studies with a cw laser, bottom: T as function of I_{laser} (pulsed). The horizontal solid line represents the value of T measured with a non-focused beam, the broken line is obtained if the laser is focused down to an effective radius of $r \approx 50$ μ. Population of the singlet excited state S_1 (via a rapid vibrational relaxation process) can be detected with the pulsed laser only because if given a lifetime of $\tau_{S_1} = 45$ ns of S_1, population of this state cannot be achieved with the cw laser (maximum incident flux at 500 mW is $\sim 6.25 \times 10^{21}$ photons s^{-1} cm^{-2}).

triplet excited spectrum, eq. [22] is seen to be valid. The energy flow inside the triplet system is an example of case II, Fig. 2. The data displayed in Fig. 6 represent transmission studies as function of the intensity of a non-focused, and of a focused, pulsed laser beam near the absorption maximum of the Soret band in the blue for a 1.45×10^{-5} *M* of chlorophyll *a* in pyridine in a 1 cm cell. We note that even for the unfocused beam an increase of T is recorded upon an increase of the intensity of the laser beam. From a comparison of photon densities in the focused and non-focused beams leading to the same value of the transmission, it follows that the former is ~250 times more effective than the latter. The effective radius of the unfocused beam amounts to ~1.0 mm, hence the effective radius of the focused beam in the absorbing medium is ~63 μ. A simple calculation shows that there are $N = 2.2 \times 10^{11}$ chlorophyll *a* molecules in the path of the laser beam

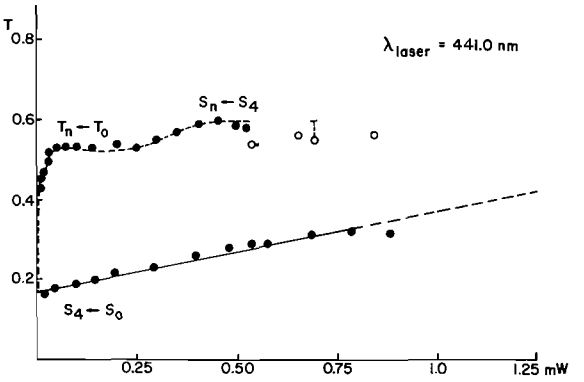

FIG. 6. Transmission studies of a 1.45×10^{-5} molar solution of chlorophyll *a* in pyridine at 441.0 nm. Even for non-focused radiation (solid line) of the pulsed laser one observes an increase in *T*. The rate of the data shows that the focused laser beam (broken curve) is $\sim 250 \times$ more effective than the non-focused beam with regard to the optical pumping process. For $I_{laser} > 0.50$ mW photo-decomposition of the solution occurs and the data become less reliable.

and employing eq. [37] yields $\tau_{S_4} \leq 160$ ps because population of S_4 occurs at $I \approx 0.4$ mW (which corresponds to 0.35×10^{14} photons per pulse of 3.2 ns at a repetition of 25 Hz). The observation of excited state Raman spectra of normal modes in either T_0, S_0, or S_4 for specific values of the intensity and wavelength of the pulsed laser is made difficult because of a strong background due to the $S_1 \rightarrow S_0$ and also an $S_4 \rightarrow S_0$ fluorescence.

Excited state spectra of several other molecular systems have been recorded in the past (1–10) but transmission studies before or during the time that Raman spectra were recorded were carried out only in a few isolated cases (2, 7, 9).

The recent study of (9) the excited state Raman spectrum of tris(2,2′-bipyridine) Cr(III) complex is a case in point. The energy level diagram of this complex is discussed in terms of that of Cr^{3+} in a distorted octahedral surrounding, and the states of interest here are the $^4A_2$ ground state, the ^2E excited at $\sim 13\,740$ cm^{-1} and $^4T_2$ at $\sim 17\,000$ cm^{-1}. This complex fluoresces at ~ 740 nm ($^2E \rightarrow {}^4A_2$) and the spectrum is quenched if the complex is exposed to radiation of $\lambda = 457.9$ nm of the tunable dye laser mentioned in the above. The quenching of the said fluorescence is interpreted on the basis that the energy transfer of the Cr complex is an example of case II, Fig. 1, because if exposed to the same power level at 457.9 nm of a cw laser, strong $^2E \rightarrow {}^4A_2$ fluorescence is recorded. Transmission measurements reveal that the $^4T_2$ state (with a ~ 10 ps lifetime) is populated during the experiments with the pulsed laser and absorption of radiation at 457.9 nm in the $^4T_2$ excited state spectrum takes place. The absorbed radiation reaches another high-lying excited state ^4Y and returns to the ground state via a path which does not involve the $^4T_2$ and (via intersystem crossing) ^2E excited states of $Cr(bpy)_3{}^{3+}$. The above interpretation of energy transfer is consistent with the fact that at 457.9 nm $(T_{4_{T_2}-4_{A_2}})^2 \approx T_{4Y-4_{T_2}}$. Consequently the intensity of vibrational Raman bands of $^4T_2$:$Cr(bpy)_3{}^{3+}$ are resonance enhanced to a larger degree than the corresponding modes of $^4A_2$:$Cr(bpy)_3{}^{3+}$ although, according to eq. [25], there are more ground state than optically pumped excited-state scattering centers in the laser beam. In the case of $^4T_2$:$Cr(bpy)_3{}^{3+}$, however, the assignment of the excited-state Raman scattering is made easier because of a larger band width for Raman shifts of modes in the excited state, compared to the width of the corresponding modes in the ground state.

The excited state electronic Raman effect of Cr^{3+}:αAl_2O_3 and Cr^{3+} in other solids was also recorded (18) after transmission studies were made, but the assignment here was straightforward in that there does not occur an electronic Raman process of the ground state which can interfere with that of the optically-pumped excited state. Earlier results (19) obtained by Szabo for the excited-state absorption cross section in ruby, by means of saturation-transmission measurements, indicate that ruby may well be an example of the situation depicted by case II in Fig. 1. The limiting transmission obtained at high incident flux values follows a Beer's Law of the form given by eq. [22], with a value of σ_E which equals excited-state absorption cross sections obtained by other methods.

VII. Summary

An attempt is made to lay down the ground rules for excited level Raman spectroscopy. It is shown that in order to record scattering from one specific excited state one must carry out transmission studies at some specific laser (which position is in resonance with an absorption band of the molecule) wavelength as function of laser power. The E.L.R. spectrum may then become detectable only after a judicious choice is made of (*i*) the wavelength and (*ii*) the intensity of the laser radiation. In addition to the above it appears that measurement of the transmission at a specific wavelength as function of I_l allows one to obtain the lifetime of an excited state. At the same time an insight is obtained of the energy transfer between excited states of the absorbing molecules, ions or atoms.

1. R. WILBRANDT, N. H. JENSEN, P. PAGSBERG, A. H. SILLISEN, and K. B. HANSEN. Nature, **276**, 167 (1978).

Can. J. Chem. Downloaded from www.nrcresearchpress.com by 210.87.254.6 on 09/06/12
For personal use only.

2. L. V. HALEY, B. HALPERIN, and J. A. KONINGSTEIN. Chem. Phys. Lett. **54**, 389 (1978); B. HALPERIN and J. A. KONINGSTEIN. J. Chem. Phys. **69**, 3302 (1978).
3. J. P. DEVLIN and M. G. ROCKEY. Chem. Phys. Lett. **56**, 608 (1978).
4. J. HERRMANN and M. LANDMANN. Opt. Quantum Electron. **11**, 161 (1979).
5. W. WERNCKE, H. J. WEIGMAN, J. PÄTZOID, A. LAU, K. LENZ, and M. PFEIFFER. Chem. Phys. Lett. **61**, 105 (1979).
6. R. F. DALLINGER and W. H. WOODRUFF. J. Am. Chem. Soc. **101**, 4391 (1979).
7. M. ASANO, D. MONGEAU, D. NICOLLIN, R. SASSEVILLE, and J. A. KONINGSTEIN. Chem. Phys. Lett. **65**, 293 (1979).
8. G. H. ATKINSON and L. R. DOSSER. J. Chem. Phys. **72**, 2195 (1980).
9. M. ASANO, J. A. KONINGSTEIN, and D. NICOLLIN. J. Chem. Phys. **73**, 688 (1980).
10. M. ASANO and J. A. KONINGSTEIN. Picosecond phenomena II. Springer Verlag. 1980. p. 351.
11. M. O. BULANIN, A. P. BURTSEV. Opt. Spectrosk. **47**, 663 (1979).
12. M. HERCHER. Appl. Opt. **6**, 947 (1967).
13. R. ARSENAULT and M. M. DENARIES-ROBERGE. Chem. Phys. Lett. **40**, 84 (1976).
14. P. V. AVIZONIS and W. R. WILLOUGHBY. J. Appl. Phys. **37**, 682 (1956).
15. H. LINSCHITZ and K. SARKANEN. J. Am. Chem. Soc. **80**, 4826 (1958).
16. J. BAUGHER, J. C. HINDMAN, and J. J. KATZ. Chem. Phys. Lett. **63**, 159 (1979).
17. M. ASANO and J. A. KONINGSTEIN. Chem. Phys. To be published.
18. B. HALPERIN, D. NICOLLIN, and J. A. KONINGSTEIN. Chem. Phys. **42**, 277 (1979).
19. A. SZABO. Optics Commun. **12**, 366 (1974).

Can. J. Chem. Downloaded from www.nrcresearchpress.com by 210.87.254.6 on 09/06/12
For personal use only.

Electron trapping in alcohol clusters in γ-irradiated *n*-propanol–hydrocarbon glasses at 77 K

MASAYA ITO, TOYOAKI KIMURA, AND KENJI FUEKI

Department of Synthetic Chemistry, Faculty of Engineering, Nagoya University, Chikusa-ku, Nagoya, Japan

Received December 22, 1980

MASAYA ITO, TOYOAKI KIMURA, and KENJI FUEKI. Can. J. Chem. **59**, 2803 (1981).

A study has been made of trapped electrons in *n*-propanol–hydrocarbon mixture glasses at 77 K by the optical absorption method. The yields of electrons trapped in alcohol clusters (e_{alc}^-) were measured for several γ-irradiated *n*-propanol–hydrocarbon glasses, where the yields of trapped electrons in these neat hydrocarbon glasses at 77 K are known to range from 0.015 to 1.1 G units. The results show that the yields of e_{alc}^- in the mixture glasses do not depend on the trapped electron yields in neat hydrocarbon glasses. Thus, it is concluded that electron migration from relaxed hydrocarbon matrix traps into alcohol clusters is not the major process for e_{alc}^- formation in the systems studied here. The major process for e_{alc}^- formation may be attributed to quasi-free electron scavenging by alcohol clusters and electron migration from unrelaxed hydrocarbon traps into alcohol clusters. Both ir-induced and isothermal changes in the e_{alc}^- yield have also been investigated. These investigations indicate that there is a correlation between the observed change in the e_{alc}^- yield and the matrix viscosity.

MASAYA ITO, TOYOAKI KIMURA et KENJI FUEKI. Can. J. Chem. **59**, 2803 (1981).

Utilisant la méthode d'absorption optique, on a étudié le piégeage d'électrons dans un mélange de *n*-propanol–hydrocarbure à l'état vitreux à 77 K. On a mesuré les rendements en électrons piégés dans les agrégats d'alcool pour plusieurs verres de *n*-propanol hydrocarbure irradiés au rayons γ et pour lesquels les rendements en électrons piégés dans ces verres d'hydrocarbures homogènes à 77 K sont de l'ordre de 0,015 à 1,1 unités G. Les résultats indiquent que les rendements dans le mélange de verre ne dépendent pas des électrons piégés dans les verres d'hydrocarbures homogènes. On en conclut alors que la migration de l'électron à partir des pièges de la masse hydrocarbonée en relaxation dans les agrégats d'alcool ne consittue pas le processus fondamental dans la formation des systèmes étudiés. On peut attribuer le processus principal de formation au piégeage des électrons à partir des pièges hydrocarbonés non relaxés aux agrégats d'alcool. On a également étudié le rendement des changements induits par ir et par des changements isothermiques. Ces études indiquent qu'il existe une corrélation entre le changement observé dans le rendement et la viscosité de la gangue.

[Traduit par le journal]

Introduction

Solvated and trapped electrons in γ-irradiated alcohol–hydrocarbon mixtures have been investigated in the liquid (1–6) and glassy states (7–14). Optical absorption bands were observed in the visible and ir region in a glassy alcohol–hydrocarbon mixture at 77 K, and they were, respectively, ascribed to electrons (e_{hc}^-) trapped in the hydrocarbon matrix and those (e_{alc}^-) trapped in alcohol clusters (8), the existence of which was confirmed by the infrared absorption method (15–17). The formation of e_{alc}^- has also been proposed in liquid alcohol–hydrocarbon mixtures from a study of free ion yields, suggesting that a fraction of electrons generated in a hydrocarbon region are probably scavenged by alcohol clusters (1).

Concerning the mechanism of e_{alc}^- formation in alcohol–hydrocarbon glasses the following findings seem to give us some suggestions on the mechanism: in a pulse radiolysis study of *n*-propanol (*n*-PrOH) – 3-methylpentane (3MP) mixture glasses Mayer *et al.* have shown the interesting result that an absorption peak in the visible region grows at 107 K after the pulse accompanied by decay of a peak in the ir region (11). This can be explained in terms of electron migration from 3MP matrix traps into *n*-PrOH clusters. However, the visible peak was not observed separately from the ir peak at 90 K during 500 μs after the pulse (11). On the other hand, both absorption peaks corresponding to e_{alc}^- and e_{hc}^- were observable in γ-irradiated *n*-PrOH–3MP glasses at 77 K (12). Shimizu *et al.* have reported that electron migration from 3MP matrix traps into *n*-PrOH clusters occurs within tens of minutes in γ-irradiated *n*-PrOH–3MP glasses at 77 K (18). These results seem to indicate a mechanism of e_{alc}^- formation in which electrons migrate from hydrocarbon matrix traps, in which electrons are originally trapped, into alcohol clusters. Thus, if this kind of electron migration is the major process of e_{alc}^- formation in alcohol–hydrocarbon mixture glasses, then yields of e_{alc}^- can be expected to depend on the trapped electron yield in the neat hydrocarbon glass: the higher the trapped electron yield in the hydrocarbon glass, the higher the e_{alc}^- yield in the alcohol–hydrocarbon glasses. In order to look at this point we have measured yields of e_{alc}^- and e_{hc}^- in *n*-PrOH–hydrocarbon glasses at 77 K. The matrices used are 2-methylpentane (2MP), 3-methylhexane (3MHx), methyl-

0008-4042/81/182803-05$01.00/0

©1981 National Research Council of Canada/Conseil national de recherches du Canada

Can. J. Chem. Downloaded from www.nrcresearchpress.com by 210.87.254.42 on 09/06/12
For personal use only.

Can. J. Chem. Downloaded from www.nrcresearchpress.com by 210.87.254.42 on 09/06/12
For personal use only.

cyclohexane (MCH) – 31 mol% cyclopentane (CP), MCH and isopropylcyclohexane (*i*-PrCHx). The electron fraction (e.f.) of *n*-PrOH in these mixtures was varied from 0.01 to 0.2. We have chosen these hydrocarbons because the trapped electron yields in these neat hydrocarbon matrices at 77 K are known to range from 0.015 to 1.1 G units (19). In addition, we have investigated the isothermal growth of the optical absorption band of e_{alc}^- after γ-irradiation and the effect of ir illumination on the growth of e_{alc}^-.

Experimental

Hayashi Pure Chemical *n*-PrOH (extra pure) was refluxed over sodium borohydride under argon atmosphere for 70 h at 340 K, distilled, and then further purified *in vacuo* three times using molecular sieves 4A which were heated at 550 K *in vacuo* for 12 h before use. Tokyo Kasei 3MHx and *i*-PrCHx (extra pure), and Tokyo Kagaku Seiki MCH, CP, and 2MP (standard purity) were purified using molecular sieves 13X by the procedure described above. The hydrocarbons were taken by a volumetric flask *in vacuo* and vacuum-distilled into optical cells which contained the desired amount of *n*-PrOH taken by a microsyringe. Samples were sealed off a vacuum line. Optical cells were made of Suprasil quartz. γ-Irradiation was carried out by ^{60}Co γ-rays. The dose was 1.0–3.4 × 10^5 rad. Optical absorption spectra were measured on a Hitachi 323 spectrophotometer. γ-Irradiation and optical absorption measurements were made at 77 K. Photobleaching was carried out using a 300 W tungsten lamp with a Toshiba IR-DIA filter which cuts off light with wavelengths shorter than 900 nm.

Results and Discussion

γ-Irradiated *n*-PrOH–hydrocarbon glasses give two characteristic optical absorption bands due to e_{alc}^- with $\lambda_{max} \simeq 560$ nm and e_{hc}^- with $\lambda_{max} \simeq 1700$ nm. With increasing *n*-PrOH concentration the visible band increases whereas the ir band decreases. Figure 1 shows the optical densities of e_{alc}^- and e_{hc}^- at λ_{max} (560 and 1730 nm, respectively) vs. electron fraction of *n*-PrOH for *n*-PrOH–3MHx systems. The ir illumination reduces the ir absorption band to zero without any significant decrease in the visible band. In some cases the visible band increases with a slight blue shift of the peak as will be described later.

1. Trapped Electrons (e_{alc}^-) in Alcohol Clusters

The optical absorption spectrum of e_t^- in a neat hydrocarbon glass has a long tail towards the high energy side. Thus, the absorption spectrum of e_{alc}^- in a *n*-PrOH–hydrocarbon glass may overlap with the tail of the e_{hc}^- absorption spectrum. Since it is difficult to separate these two absorption bands, we use the observed optical density at λ_{max} in the visible region as a measure of the yield of e_{alc}^-. The error due to the neglect of such overlapping e_{hc}^- absorption is estimated to be at most 10% at a lower

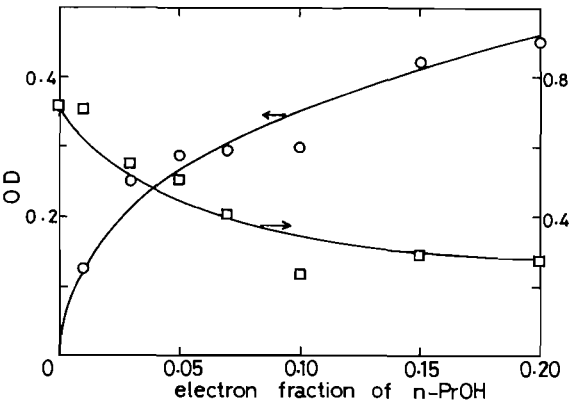

FIG. 1. Optical densities of e_{alc}^- (○) and e_{hc}^- (□) at λ_{max} (560 and 1730 nm, respectively) in *n*-PrOH–3MHx systems vs. electron fraction of *n*-PrOH. The dose is normalized to 1.1 × 10^5 rad and the optical path length to 3 mm.

n-PrOH concentration (0.03 e.f.) but less than 5% at a higher concentration (0.07 e.f.).

Optical densities of e_{alc}^- in *n*-PrOH–hydrocarbon glasses studied are shown in Fig. 2 as a function of the electron fraction of *n*-PrOH. The dashed line is the one extrapolation of which to pure *n*-PrOH (e.f. = 1.0) gives the observed optical density of e_t^- in pure *n*-PrOH. In view of the lack of data on the molar extinction coefficient, ε, for e_{alc}^-, we make an assumption that ε for e_{alc}^- in the systems studied here are all the same. It should be noted in Fig. 2 that the observed optical density of e_{alc}^- in each system lies far above the dashed line. Thus, we may say that a major part of e_{alc}^- formation can be ascribed to electron migration from hydrocarbon matrix into alcohol clusters via

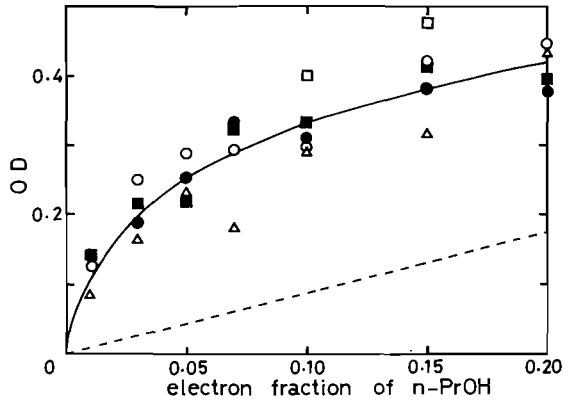

FIG. 2. Optical density of e_{alc}^- at λ_{max} (560 nm) in *n*-PrOH–hydrocarbon glasses vs. electron fraction of *n*-PrOH. The dose is normalized to 1.1 × 10^5 rad and the optical path length to 3 mm. ■: *n*-PrOH–2MP; ○: *n*-PrOH–3MHx; △: *n*-PrOH–MCH–CP; ●: *n*-PrOH–MCH; □: *n*-PrOH–*i*-PrCHx.

Can. J. Chem. Downloaded from www.nrcresearchpress.com by 210.87.254.42 on 09/06/12
For personal use only.

the "trap to cluster" migration (18) and/or the quasi-free electron scavenging process (1).

It is seen from Fig. 2 that the yield of e_{alc}^- does not differ very much among the *n*-PrOH–hydrocarbon systems at specified alcohol concentration. On the other hand, the yields of e_t^- in these neat hydrocarbon glasses determined by the steady-state γ-radiolysis differ by two orders of magnitude as shown in the first and second column in Table 1 (19, 20). If e_{alc}^- is formed as a result of electron migration from relaxed hydrocarbon matrix traps into alcohol clusters, the yield of e_{alc}^- should depend on that of e_t^- in each neat hydrocarbon glass, namely, the yield of e_{alc}^- should be the highest in 2MP and lowest in *i*-PrCHx as shown in Table 1. However, this is not the case as seen from the experimental results in Fig. 2. Therefore it can be said that electron migration from relaxed hydrocarbon traps into alcohol clusters is not the major process for e_{alc}^- formation in our systems studied here.

The possibility of electron migration from unrelaxed hydrocarbon matrix traps, which can exist only transiently, into alcohol clusters has to be considered. Klassen *et al.* have shown that optical absorption bands in pulse irradiated hydrocarbon glasses decay to some extent within a short time after the pulse and that the absorption at a longer wavelength region decreases more than that at shorter wavelength region (21, 22). Thus, this part of electrons which decay within a short time after the pulse in a neat hydrocarbon system may migrate into alcohol clusters to form e_{alc}^- in alcohol–hydrocarbon systems. In the last column of Table 1 values of $G(e_t^-)\varepsilon \times 10^{-4}$ determined by the pulse radiolysis at 73 K (22) are listed. If one assumes that ε_{max} is roughly the same for all the hydrocarbon matrices, then the comparison of the values in the first and third columns in Table 1 leads to the conclusion that there is considerable decay of e_t^- in 2,4-dimethylpentane (2,4DMP). At present, we cannot exclude the possibility of electron migration from unrelaxed hydrocarbon traps into alcohol clusters, leading to e_{alc}^- formation. However, one cannot explain the results in Fig. 2 in terms of this mechanism alone: the value of $G(e_t^-)\varepsilon \times 10^{-4}$ in 2MP in Table 1 differs by a factor of about two from that in MCH, which means that the initial trapped electron yield in 2MP is roughly twice as high as that in MCH. Nevertheless, the yields of e_{alc}^- in *n*-PrOH–2MP systems are nearly the same as those in *n*-PrOH–MCH systems as seen from Fig. 2. Therefore, quasi-free electron scavenging by alcohol clusters may be another significant process for e_{alc}^- formation.

TABLE 1. Trapped electron yield in neat hydrocarbon glasses

Hydrocarbon	$G(e_t^-)$ γ-radiolysis (77 K) Ref. 19	$G(e_t^-)$ γ-radiolysis (77 K) Ref. 20	$G(e_t^-)\varepsilon \times 10^{-4}$ pulse (73 K) ref. 22
2MP*	1.1	—	3.3
3MP	0.7	0.67	3.1
3MHx*	0.7	0.73	2.9
3MO	—	0.41	2.8
MCH*	0.44	0.34	1.8
2,4DMP	0.16	—	1.9
i-PrCHx*	0.015	—	—
MCH-CP*	0.65	—	—

*Matrices used in the present work.

2. *Photobleaching of Trapped Electrons (e_{hc}^-) in Hydrocarbon Matrices*

Photobleaching of trapped electrons in γ-irradiated *n*-PrOH–hydrocarbon glasses by ir light ($\lambda > 900$ nm) reduces the absorption band in the ir region and increases the visible band for 2MP, 3MHx, and MCH–CP matrices. As an example, the effect of ir illumination on the e_{alc}^- yield in *n*-PrOH–2MP systems is shown in Fig. 3. On the other hand, in *n*-PrOH–MCH and *n*-PrOH–*i*-PrCHx glasses no increase in the e_{alc}^- absorption band could be observed as a result of ir photobleaching of e_{hc}^-. The effect of ir photobleaching on the optical density of the e_{alc}^- absorption for samples containing 0.07 e.f. *n*-PrOH (in the case of *i*-PrCHx matrix containing 0.1 e.f. *n*-PrOH) is given in Table 2. The increment of the e_{alc}^- yield due to ir photobleaching appears to depend on the rigidity (or viscosity) of the matrix except for 3MHx. The viscosities of the matrices at 77 K are given in Table

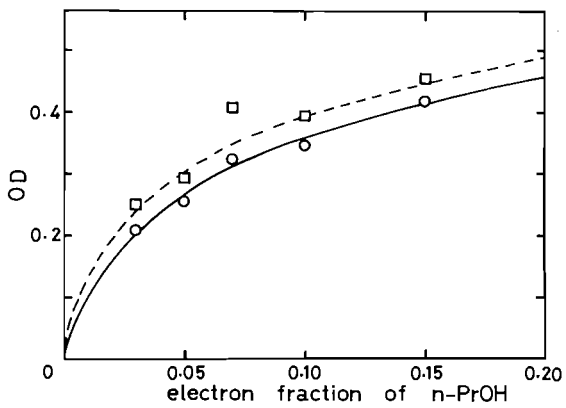

FIG. 3. Effect of ir photobleaching on the optical densities of e_{alc}^- at λ_{max} (560 nm) in *n*-PrOH–2MP systems. The dose is normalized to 1.1×10^5 rad and the optical path length to 3 mm. ○: OD at λ_{max} before ir photobleaching; □: OD at λ_{max} after ir photobleaching.

Can. J. Chem. Downloaded from www.nrcresearchpress.com by 210.87.254.42 on 09/06/12
For personal use only.

TABLE 2. Effect of ir photobleaching on the optical density of the e_{alc}^- absorption for *n*-PrOH (0.07 e.f.)–hydrocarbon glasses

Matrix	OD_a*	OD_b†	$\frac{OD_b - OD_a}{OD_a} \times 100$
2MP	0.32_7	0.41_4	27
3MHx	0.29_2	0.33_4	14
MCH–CP	0.17_7	0.20_6	16
MCH	0.34_1	0.34_1	0
i-PrCHx‡	0.40_5	0.40_5	0

*OD at λ_{max} (560 nm) before ir photobleaching.
†OD at λ_{max} (560 nm) after ir photobleaching.
‡The electron fraction of *n*-PrOH was 0.1 in this case.

TABLE 3. Viscosities of the matrices and $\tau_{2/3}$ of e_t^- at 77 K

Matrix	Viscosity* (poise)	$\tau_{2/3}$
2MP	2.4×10^{13}	42 min†
MCH–CP		22 min†
MCH	1.2×10^{18}	$\gg$ 1 h†
3MHx	3.2×10^{18}	$>$ 1 h‡
i-PrCHx		$\gg$ 1 h†
3MP	2.2×10^{12}	15 min†

*Reference 23.
†Reference 24.
‡This work.

3 together with the time, $\tau_{2/3}$, required for the e_t^- yield to decay to 2/3 of its initial value. For comparison 3MP is also included in Table 3. Trapped electrons in 3MHx decay slowly and they decay in MCH and *i*-PrCHx too slowly to be observed within a few hours. The viscosity of the MCH–CP mixture is not available but may be estimated to be a value close to that of 3MP, because the value of $\tau_{2/3}$ for these two matrices are close to one another. Although the viscosity of *i*-PrCHx at 77 K is not known, *i*-PrCHx presumably has the highest viscosity among the matrices studied here, since it is most difficult to make a clear glass from this compound.

The data from Tables 2 and 3 indicate that ir photobleaching causes the e_{alc}^- yields to increase in the matrices which have lower viscosities and in which the decay of trapped electrons is observable. Although the viscosity of 3MHx is higher than that of MCH, the decay of e_t^- in 3MHx is faster than that in MCH and slight increase in the e_{alc}^- yield is observable in *n*-PrOH–3MHx glasses as a result of ir photobleaching but not in *n*-PrOH–MCH glasses. This exception might be explained in terms of the local viscosity, which is possibly different from the bulk viscosity. Since the value of the viscosity for MCH was obtained by the extrapolation from viscosities of MCH–3MP mixtures to that of MCH (25), the true viscosity of MCH might be higher than that of 3MHx. Then, this case may not be an exception.

The correlation between the change in the e_{alc}^- yield and the viscosity of the matrix may indicate that reorientation of alcohol molecules is necessary for electrons photoejected from electron traps that consist of hydrocarbon molecules to be retrapped in alcohol clusters. The lower is the viscosity of the matrix, the higher is the increase of the e_{alc}^- yield arising from ir photobleaching.

3. *Isothermal Growth of the e_{alc}^- Absorption Band*

The absorption bands of e_{alc}^- in *n*-PrOH–MCH and *n*-PrOH–*i*-PrCHx glasses did not change during at least 2 h after γ-irradiation. On the other hand, when 3MHx, 2MP, or MCH–CP was used as a matrix in *n*-PrOH–hydrocarbon systems, the e_{alc}^- absorption band grew during 30 min after γ-irradiation. As an example, the isothermal increase in the e_{alc}^- yield in *n*-PrOH–2MP glasses is shown in Fig. 4. The results on the isothermal increase in the e_{alc}^- absorption band are summarized in Table 4. The optical densities were not measured at the same specified time after γ-irradiation for each system. Also we did not measure systematically the growth of the e_{alc}^- absorption band as a function of time. Nevertheless, we can say that the e_{alc}^- absorption bands grow mainly within the first 30 min in these matrices. It can be seen from Table 4 that the isothermal increase in the e_{alc}^- absorption band is larger in *n*-PrOH–2MP and *n*-PrOH–MCH–CP glasses than that in *n*-PrOH–3MHx glasses. It should be noted that the isothermal increase in the e_{alc}^- yield occurs in low viscosity matrices such as 2MP and MCH–CP,

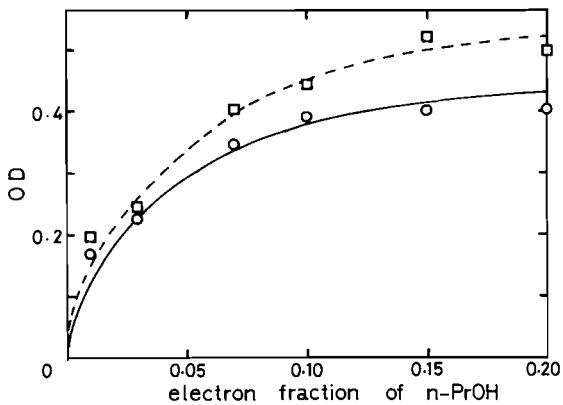

FIG. 4. Isothermal increase in the optical densities of e_{alc}^- at λ_{max} (560 nm) in *n*-PrOH–2MP systems. The dose is normalized to 1.1×10^5 rad and the optical path length to 3 mm. ○: OD at λ_{max} obtained at 3 min after γ-irradiation; □: OD at λ_{max} obtained at 93 min after γ-irradiation.

TABLE 4. Isothermal increase in the e_{alc}^- absorption for *n*-PrOH (0.07 e.f.)–hydrocarbon glasses

Matrix	OD_0*	OD_t†	$\frac{OD_t - OD_0}{OD_0} \times 100$
2MP	0.34_9	0.40_7§	17
3MHx	0.29_2	0.30_8‖	5.5
MCH–CP‡	0.22_7	0.26_6¶	17
MCH	0.34_1	0.34_1¶	0
i-PrCHx	0.40_5	0.40_5¶	0

*OD at λ_{max} (560 nm) obtained at 3 min after γ-irradiation.
†OD at λ_{max} (560 nm) at the specified time after γ-irradiation.
‡The electron fraction of n-PrOH was 0.05 in this case.
§Value obtained at 93 min after γ-irradiation.
‖Value obtained at 33 min after γ-irradiation.
¶Value obtained at 123 min after γ-irradiation.

but not in high viscosity matrices such as MCH and *i*-PrCHx. Thus, it appears that reorientation of alcohol molecules plays an important part for the isothermal incease in the e_{alc}^- yield, as is the case for ir photobleaching already described.

In the preceding section we have shown that the e_{alc}^- yield is increased by ir illumination in the low viscosity matrices but not in high viscosity matrices and explained this in terms of reorientation of alcohol molecules in a cluster. However, since the visible band of e_{alc}^- in γ-irradiated *n*-PrOH–hydrocarbon glasses of high viscosity at 77 K is observed, reorientation of alcohol molecules occurs even in these rigid systems, although it takes rather a long time (500 μs (11, 14)) for alcohol molecules to reorient even at 90 K. Then the question arises as to why ir illumination does not lead to the increase in the e_{alc}^- yield in these rigid matrices. Further study is required to resolve this problem.

1. G. R. FREEMAN. J. Phys. Chem. **76**, 944 (1972).
2. J. H. BAXENDALE and E. J. RASBURN. J. Chem. Soc. Faraday Trans. I, **70**, 705 (1974).
3. J. H. BAXENDALE and P. H. G. SHARPE. Chem. Phys. Lett. **41**, 440 (1976).
4. J. R. BRANDON and R. F. FIRESTONE. J. Phys. Chem. **78**, 792 (1974).
5. G. A. KENNEY-WALLACE and C. D. JONAH. Chem. Phys. Lett. **47**, 362 (1977).
6. T. E. GANGWER, A. O. ALLEN, and R. A. HOLROYD. J. Phys. Chem. **81**, 1469 (1977).
7. L. SHIELDS. J. Phys. Chem. **69**, 3186 (1965).
8. A. EKSTROM and J. E. WILLARD. J. Phys. Chem. **72**, 4599 (1968).
9. T. SAWAI and W. H. HAMILL. J. Phys. Chem. **73**, 3452 (1969).
10. T. ITO, N. UJIKAWA, and K. FUEKI. J. Phys. Chem. **79**, 2479 (1975).
11. J. MAYER, J. L. GEBICKI, and J. KROH. Radiochem. Radioanal. Lett. **36**, 299 (1978).
12. J. MAYER, J. KROH, and E. WOJCIECHOWSKA. Nukleonika, **21**, 267 (1976).
13. J. MAYER, J. L. GEBICKI, and J. KROH. Radiat. Phys. Chem. **11**, 101 (1978).
14. J. MAYER, J. L. GEBICKI, and J. KROH. Radiat. Phys. Chem. **16**, 335 (1980).
15. A. N. FLETCHER and C. A. HELLER. J. Phys. Chem. **71**, 3742 (1967).
16. B. J. BROWN, N. T. BAKER, and D. F. SANGSTER. Aust. J. Chem. **26**, 2089 (1973).
17. W. M. BARTCZAK. Ber. Bunsenges. Phys. Chem. **83**, 987 (1979).
18. K. SHIMIZU, M. OGASAWARA, and H. YOSHIDA. Presented at the 22nd annual meeting of the Japanese Society of Radiation Chemistry. Oct. 1979, Nagoya, Japan.
19. T. KIMURA, N. BREMER, and J. E. WILLARD. J. Chem. Phys. **66**, 1127 (1977).
20. J. LIN, K. TSUJI, and F. WILLIAMS. J. Am. Chem. Soc. **90**, 2766 (1968).
21. N. V. KLASSEN, H. A. GILLIS, and G. G. TEATHER. J. Phys. Chem. **76**, 3847 (1972).
22. N. V. KLASSEN and G. G. TEATHER. J. Phys. Chem. **83**, 326 (1979).
23. L. KEVAN. Advances in radiation chemistry. Vol. 4. *Edited by* M. Burton and J. L. Magee. Wiley-Interscience, New York. 1974. p. 188.
24. T. KIMURA and J. E. WILLARD. Unpublished results.
25. A. C. LING and J. E. WILLARD. J. Phys. Chem. **72**, 3349 (1968).

Can. J. Chem. Downloaded from www.nrcresearchpress.com by 210.87.254.42 on 09/06/12
For personal use only.

Enzymic aromatization of deuterium labelled testosterone and androst-4-ene-3,17-dione

HERBERT L. HOLLAND AND GREGG J. TAYLOR
Department of Chemistry, Brock University, St. Catharines, Ont., Canada L2S 3A1

Received March 24, 1981

HERBERT L. HOLLAND and GREGG J. TAYLOR. Can. J. Chem. **59**, 2809 (1981).

The preparation and aromatization by human placental microsomes of androst-4-ene-3-ones labelled with deuterium at C-4, C-6α, C-6β, C-16, and C-19 is described. Deuterium nmr spectra are reported for these compounds and for a sample of a 1,2-dideuterated androst-4-ene-3-one; the latter is formed nonstereospecifically by reduction of the C-1(2) double bond of a $\Delta^{1,4}$-diene-3-one. Aromatization by placental microsomes occurs with retention of deuterium at C-4 and C-6, but with some loss from C-16. The aromatization of 19-d_1 and 19,19,19-d_3 steroids in the presence of 16,16-d_2 steroids has been carried out to determine the deuterium isotope effect for the oxidative removal of C-19. The values obtained (k_H/k_D for 19-d_1 = 2.3, k_H/k_D for 19,19,19-d_3 = 3.2) are a combination of primary and secondary effects, but suggest that oxidation at C-19 is a rate-limiting reaction of the biosynthetic sequence.

The fungus *Pellicularia filamentosa* NRRL 2727, reported to hydroxylate androst-4-ene-3,17-dione at C-19, gave only the products of hydroxylation at C-11α, C-11β, and C-14.

HERBERT L. HOLLAND et GREGG J. TAYLOR. Can. J. Chem. **59**, 2809 (1981).

On décrit la préparation et l'aromatisation par les microsomes du placenta humain, d'androstène-4 ones-3 marquées au deutérium en C-4, C-6α, C-6β, C-16 et C-19. On rapporte les spectres de rmn du ^2H de ces composés ainsi que celui d'un échantillon d'androstène-4 one-3 dideutéré en positions 1 et 2. On a obtenu ce dernier de façon non stéréospécifique par la réduction de la double liaison en C-1(2) d'une Δ-diène-1,4 one-3. L'aromatisation par les microsomes du placenta se produit avec une rétention de configuration des deutérium en C-4 et en C-6 mais avec quelques pertes au niveau du C-16. On a réalisé l'aromatisation des stéroides deutérés 19-d_1 et 19,19,19-d_3 en présence de stéroides 16,16-d_2 dans le but de déterminer l'effet isotopique du deutérium lors de l'élimination oxydante de C-19. Les valeurs obtenues (k_H/k_D pour 19-d_1 = 2,3, k_H/k_D pour 19,19,19-d_3 = 3,2) sont une combinaison d'effets isotopiques primaires et secondaires mais elles suggèrent que l'oxydation au niveau de C-19 est l'étape déterminante de cette série de réactions biosynthétiques.

Le champignon *Pellicularia filamentosa* NRRL 2727 responsable de l'hydroxylation de l'androstène-4 dione-3,17 au niveau du C-19 donne seulement des produits d'hydroxylation en C-11α, C-11β et C-14.

[Traduit par le journal]

Introduction

In spite of the intense effort which has been expended over the last two decades on investigation of the later stages of the biosynthesis of estradiol (estra-1,3,5(10)-triene-3,17β-diol, **1***a*) and estrone (estra-1,3,5,(10)-triene-3-ol-17-one, **1***b*), several aspects of the conversion of testosterone (androst-4-ene-17β-ol-3-one, **2***a*) or androst-4-ene-3,17-dione (**2***b*), the C_{19} substrates of the aromatase enzyme system, to the estrogens, remain obscure. The established route for this conversion by human placental microsomes is presented in Fig. 1 (1–6).

The key features of this pathway are (*i*) the intermediacy of the 19-alcohol **21** and aldehyde **22**, and their formation by the action of a monooxygenase type enzyme utilizing molecular oxygen and NADPH (two equivalents); (*ii*) the apparent involvement of a third equivalent of oxidizing potential (O_2/NADPH); and (*iii*) the release of C-19 of the substrate as formic acid, the stereochemistry of oxidation at C-19 being that shown in Fig. 1.

Less well defined from a mechanistic standpoint are the following; firstly, the function of the third oxidizing equivalent and the pathway for conversion of **22** to **1***a* or **1***b*. Pathways have been postulated which involve 1β hydroxylation to give intermediate **23** (Fig. 2) (7–9), 2β hydroxylation to give **24** (10, 11), enzymic "Baeyer–Villiger" oxidation to give the ester **25** (12), or epoxidation to **26** (13, 14). The possible involvement of a Δ^5 steroid via a 5,6 epoxide has also been suggested (13). The proposed pathways for the aromatization of the aldehyde **22** are based on the experimental observations of the release of C-19 as formate (Fig. 1), and a stereospecific loss of hydrogen from C-1β and C-2β (15–18). Secondly, the relative rates of the steps shown in Fig. 1 have been the subject of some discussion, complicated by the possible distinction between "free" and enzyme-bound intermediates, which now seems to indicate that the transformations occur at a single enzyme site, with little dissociation of intermediates from the enzyme, and that hydroxylation at C-19 is rate limiting in the overall pathway (5, 6, 19).

Although the stereochemistry of loss of hydrogen from C-1 and C-2 of substrate during aromatization has been investigated (15–18), the possible fate of the hydrogens attached to C-4 and C-6 has

0008-4042/81/192809-11$01.00/0
©1981 National Research Council of Canada/Conseil national de recherches du Canada

Can. J. Chem. Downloaded from www.nrcresearchpress.com by 210.87.254.105 on 09/06/12
For personal use only.

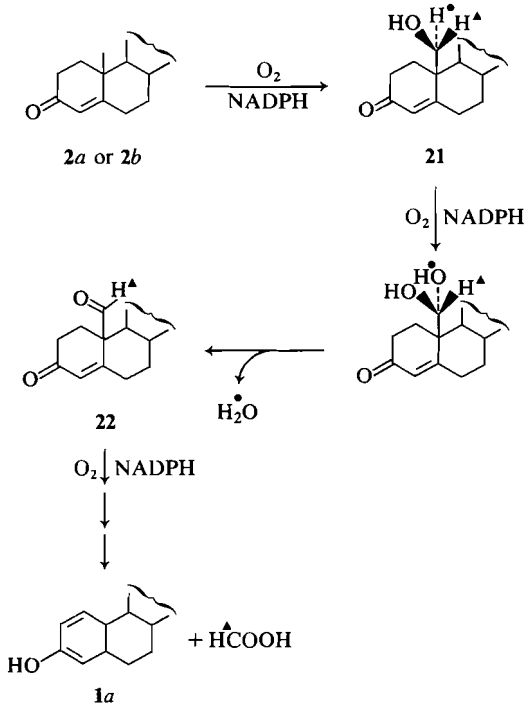

FIG. 1. Established mechanism of the aromatization of C_{19} steroids (1–6)

not hitherto been considered. Several of the mechanisms proposed for the aromatization of **22** have included intermediates in which the Δ^4 double bond is rearranged to the $\Delta^{5(10)}$ position (1, 13) or the $\Delta^{5(6)}$ position (13), and so a knowledge of the fate of the C-4 and C-6 hydrogens of **2***a* or **2***b* during conversion to the estrogens is desirable. In addition, the use of C-19-deuterium labelled steroids enables the kinetic isotope effect, k_H/k_D at C-19, for the aromatization to be determined. This information may provide additional evidence for the identity of the rate-limiting step of the overall process, and for the nature of the oxidation reaction occurring at C-19.

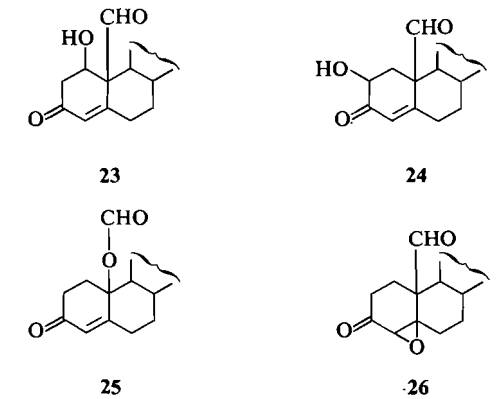

FIG. 2. Proposed intermediates in the conversion of **22** to **1***a*

Results and Discussion

The deuterium labelled steroids used in this study are listed in Table 1, and were prepared as outlined in the Experimental. The preparation of substrates labelled at C-2β, C-4, C-6α, and C-6β was straightforward, and ^2H nmr spectra of the products (Table 1) confirmed the essential integrity of the label. The presence of a small amount of additional deuterium in 4-d_1-**2***b*, presumably at C-6β, and in 6β-d_1-**2***b*, is apparent from both mass spectral and ^2H nmr data, but does not affect the conclusions discussed below. The ^2H nmr chemical shifts observed are consistent with those reported for analogous ^2H (20) and ^3H (21) labelled steroids. The 19-d_1 labelled steroids were prepared by two routes (see Experimental). The material obtained by route A (Scheme 1) was of slightly higher isotopic enrichment and was subsequently used for biotransformation. The 19,19,19-d_3 labelled testosterone was synthesized (Scheme 2) by a procedure similar to that of Baba *et al.* (22), and was obtained in high isotopic purity.

Synthesis of 1β,2β-d_2-testosterone was undertaken for comparative purposes. Reduction of androsta-1,4-diene-17β-ol-3-one (**27**) by deuterium gas gave a low yield of **2***a*. Although the sample was chemically pure and the predominant labelled species was dideuterated, ^2H nmr spectral analysis revealed the presence of deuterium in at least four different locations in **2***a*. The spectra were not sufficiently well resolved to allow quantification of the results, but a recent ^3H nmr study (21) of the product of reduction of **27** by tritium gas identified the presence of label at 1β (36.6%), 2β (2.3%), 1α,2α (12.3%), and 1β,2β (48.8%). Our results confirm that this reduction is indeed nonstereospecific. The substrates "specifically" labelled at C-1β which were originally used to demonstrate stereospecific removal of the C-1β hydrogen during estrogen biosynthesis were made by catalytic reduction of a $\Delta^{1(2)}$ bond (15), but more recent work with C-1α labelled material has confirmed the stereospecific loss of the C-1β hydrogen in this process (23).

By assignment of different chemical shifts to axial and equatorial deuterium (20) and tritium (21), the presence of two deuteron signals in the ^2H nmr spectra of steroids labelled at C-16 (Table 1) confirms the presence of stereochemically distinct deuterons. If ring D were predominantly in the planar or the envelope conformations then both C-16 deuterons would be virtually equivalent and only one signal would be expected. If ring D were conformationally mobile, a single average resonance might be expected. However, if ring D were

Can. J. Chem. Downloaded from www.nrcresearchpress.com by 210.87.254.105 on 09/06/12
For personal use only.

TABLE 1. Isotope content and ^2H nmr chemical shifts for **2***a* and **2***b*

Compound	Isotope content (%)									δ(ppm)
	d_8	d_7	d_6	d_5	d_4	d_3	d_2	d_1	d_0	
2β-d_1-**2***a*						7	9	38	46	2.19
4-d_1-**2***b*						2	22	58	18	2.39(minor), 5.59
6α-d_1-**2***b*						1	4	87	8	2.27
6β-d_1-**2***b*						1	18	70	10	2.34
19-d_1-**2***a* (Route A)						3	6	69	22	1.20
19-d_1-**2***b* (Route A)						4	9	68	19	1.19
19-d_1-**2***a* (Route B)						7	12	62	19	1.19
19-d_1-**2***b* (Route B)						9	10	60	21	1.19
1β,2β-d_2-**2***a*				7	8	10	28	15	32	1.28, 1.66, 2.05, 2.23
16,16-d_2-**2***a*					1	6	63	6	24	
16,16-d_2-**2***b*					1	5	54	33	7	1.95, 2.32
19,19,19-d_3-**2***a*						>99				1.19
2,2,4,6,6,16,16-d_7-**2***b*	1	24	36	24	9	2	2	1	1	1.90(br), 2.25(br), 5.59

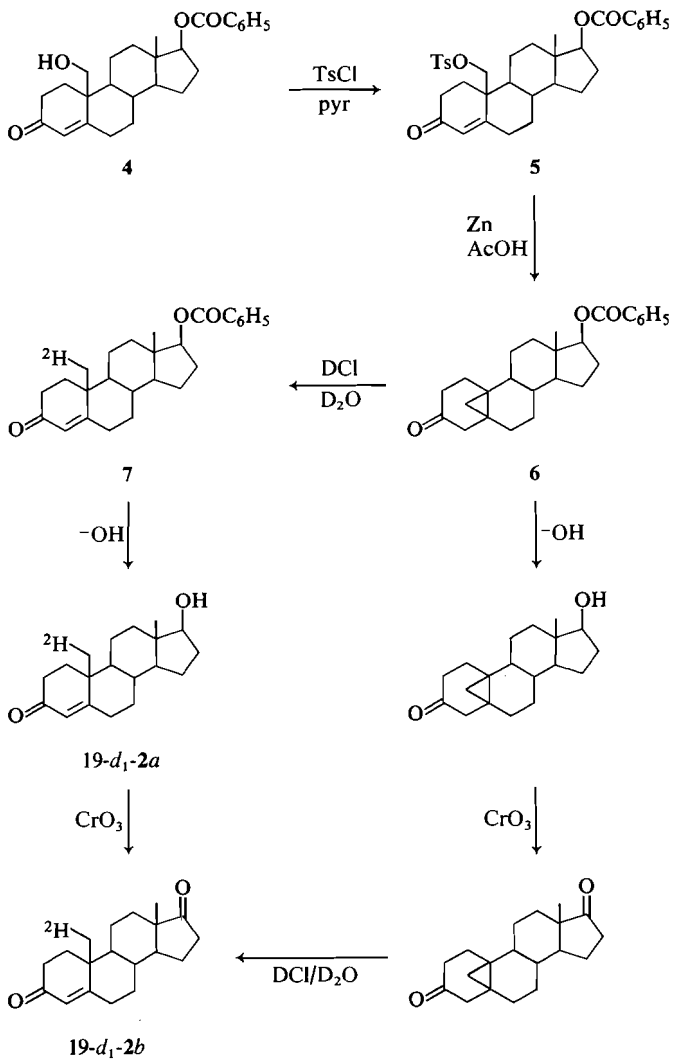

SCHEME 1. Preparation of 19-d_1-**2***a* and 19-d_1-**2***b*

Can. J. Chem. Downloaded from www.nrcresearchpress.com by 210.87.254.105 on 09/06/12
For personal use only.

Can. J. Chem. Downloaded from www.nrcresearchpress.com by 210.87.254.105 on 09/06/12
For personal use only.

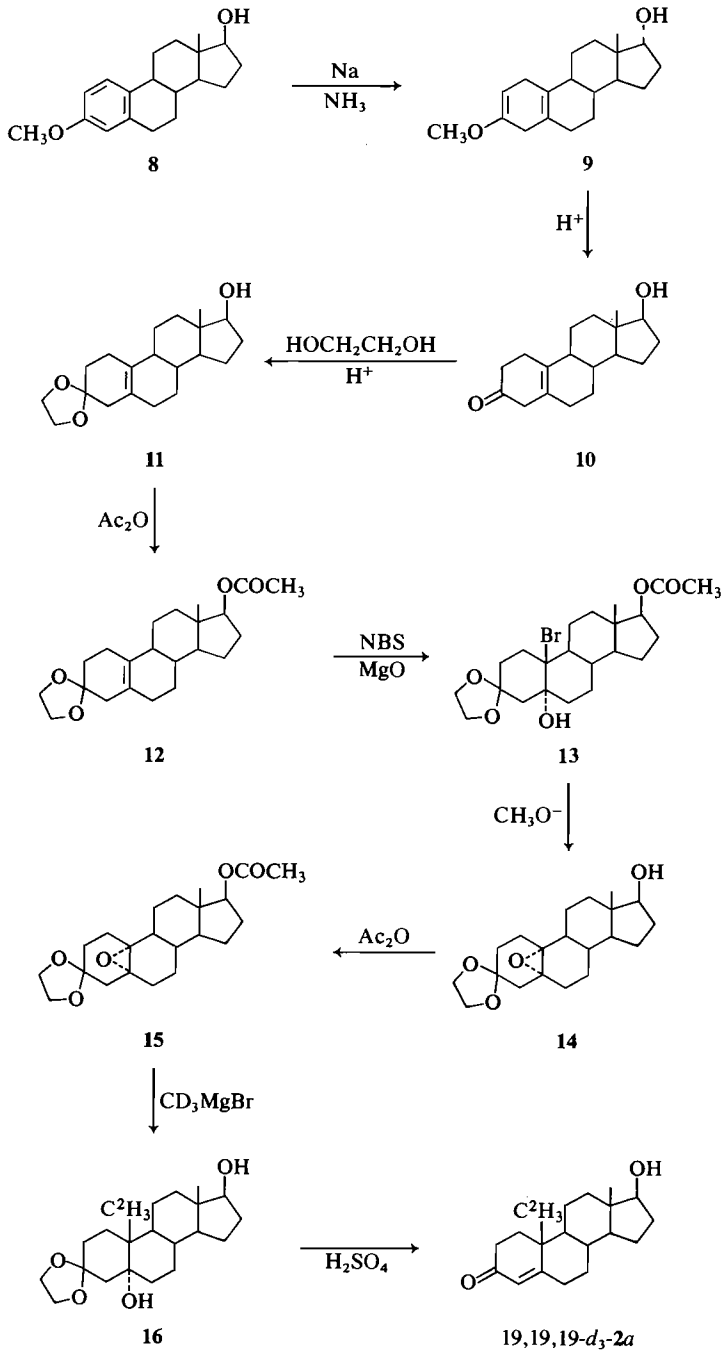

SCHEME 2. Preparation of 19,19,19-d_3-2*a*

predominantly in the half-chair conformation, both pseudo-axial and pseudo-equatorial deuterons would be present. This compares favourably with X-ray crystallographic data (24) where, in the crystalline state, ring D adopts a conformation intermediate between the half-chair and envelope forms.

The results of the aromatization of deuterium labelled **2***a* and **2***b* are presented in Table 2. Both substrates are transformed by the same enzyme, at the same site (25, 26), and in both cases only a single product of aromatization (estradiol, **1***a*) is obtained. We have therefore used both 17β-alcohol and 17-keto substrates in the present study.

The values in Tables 1 and 2 indicate that

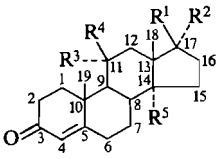

2

a $R^1 = OH, R^2 = R^3 = R^4 = R^5 = H$
b $R^1 + R^2 = O, R^3 = R^4 = R^5 = H$
c $R^1 + R^2 = O, R^3 = OH, R^4 = R^5 = H$
d $R^1 + R^2 = O, R^3 = R^5 = H, R^4 = OH$
e $R^1 + R^2 = O, R^3 = R^4 = H, R^5 = OH$

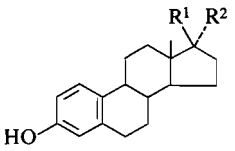

1

a $R^1 = OH, R^2 = H$
b $R^1 + R^2 = O$

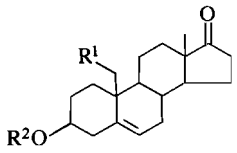

3

a $R^1 = R^2 = H$
b $R^1 = OH, R^2 = H$
c $R^1 = H, R^2 = Ac$
d $R^1 = OTr, R^2 = Tr$

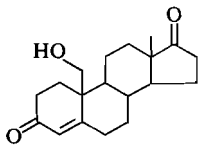

21

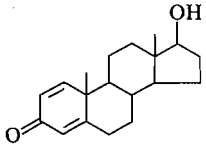

27

aromatization occurs with no loss of label from C-4 or C-6β. There is an apparent loss of some label from the C-6α position, the reason for which is not clear; its stereochemistry is inconsistent with a loss by enolization, in which major loss from C-6β should occur (27). The degree of retention is high, however, and this, together with the retention at C-4 and C-6β, eliminates from consideration any mechanism of aromatization in which the substrate may bind to the enzyme as a $\Delta^{3,5}$ enol (13) with loss of the C-6 hydrogen to the environment. The alternative binding as a $\Delta^{2,4}$ enol is consistent with the specific loss of the axial C-2β hydrogen (17), and thus appears to be the preferred mode of attachment of substrate to the enzyme (7, 15).

Transformations of substrates labelled at C-16 were carried out for control purposes to enable their use as internal rate standards in the determination of isotope effects at C-19 (*vide infra*). Surprisingly, there was a small but consistent loss of label from C-16 during aromatization. Recovered starting material in these experiments showed little or no loss of deuterium. In accord with this, substrate **2***b* labelled at all enolizable positions (2, 2, 4, 6, 6, 16, 16) also showed a greater deuterium loss on aromatization than could be accounted for by the known loss of the C-2β deuterium atom, and aromatizations of **2***b* in 50% and 95% D_2O produced estradiol with deuterium label appreciably greater than that of recovered substrate. The location of exchange of label was not determined in the latter experiments, but by inference is predominantly C-16, since previous work and the results discussed above rule out significant exchange at C-2, -4, or -6. Engel and co-workers (6) have reported appreciable loss of deuterium from C-17α of testosterone during conversion to estradiol by placental microsomes, and have demonstrated that reversible oxidation–reduction at C-17 may occur at any of the intermediate stages of the pathway shown in Fig. 1. We therefore attribute loss of label from C-16 to enolizable exchange, the loss from labelled **2***a* occurring at the carbonyl level at C-16.

In order to determine isotope effects at C-19, equimolar proportions of testosterone labelled at C-16 and at C-19 were incubated with placental microsomes, and the resulting estradiol assayed for deuterium. The deuterium content of product was then used to calculate the deuterium isotope effect for the oxidative removal of C-19 by the procedure of McMullen and Thode (28). The calculations were complicated by the loss of deuterium from C-16 discussed above, and so in order to establish the validity of the method, testosterone labelled at C-16 was co-incubated with unlabelled material, and deuterium content of product, corrected for the expected loss from C-16, was used to calculate the amounts of estradiol produced from labelled and unlabelled substrate (predicted ratio 1.0). The values obtained (1.02 ± 0.05 and 1.03 ± 0.05) demonstrate that correction of the observed deuterium content of product for the expected loss from C-16 could be confidently carried out in experiments with mixed C-16 and C-19 labelled substrates to give accurate values for the deuterium isotope effect at C-19. The values so obtained are listed in Table 2. These are intermolecular "mixed-labelling" effects which circumvent the problem of differential activities of individual microsome preparations. As the enzyme preparations used in studies on aromatization are not purified to homogeneity, individual batches can vary considerably in activity. This must be taken into account in studies which use only the absolute reaction velocities in order to study the kinetics of this system. In addition, during the preparation of labelled substrate, trace amounts of contaminants may be present which may act as inhibitors of the enzyme. In the mixed-labelling studies, such an inhibitor, if present, would be expected to act equally on the

Can. J. Chem. Downloaded from www.nrcresearchpress.com by 210.87.254.105 on 09/06/12
For personal use only.

Can. J. Chem. Downloaded from www.nrcresearchpress.com by 210.87.254.105 on 09/06/12
For personal use only.

TABLE 2. Transformations of labelled **2***a* and **2***b* by placental microsomes

Substrate	Recovered substrate (% label)[a]									Estra-1,3,5(10)-triene-3,17β-diol (**1***a*) (% label)								k_H/k_D[b]
	d_8	d_7	d_6	d_5	d_4	d_3	d_2	d_1	d_0	d_7	d_6	d_5	d_4	d_3	d_2	d_1	d_0	
4-d_1-**2***b*						9	13	58	19					8	9	59	23	
															18	58	24	
6α-d_1-**2***b*						2	3	88	8						8	73	19	
6β-d_1-**2***b*						3	17	72	9						14	69	16	
						3	16	74	8						18	64	19	
															13	68	19	
16,16-d_2-**2***a*					3	7	60	7	23						54	23	23	
															51	22	27	
															51	20	29	
16,16-d_2-**2***b*						3	52	32	11						46	36	18	
					1	3	50	37	10						48	36	16	
2,2,4,6,6,16,16-d_7-**2***b*	2	21	35	26	11	3	1	1	1	5	15	26	20	13	7	7	8	
	3	21	32	21	9	5	2	3	3[d]	4	17	26	16	17	7	7	6	
19,19,19-d_3-**2***a* + 16,16-d_2-**2***a*					2	36	37	8	17						47	14	38	3.0 ±0.2
					5	35	35	8	16						49	16	35	3.9 ±0.2
															49	10	42	2.8 ±0.2
19-d_1-**2***a*[e] + 16,16-d_2-**2***a*														7	39	10	44	2.3 ±0.1
														6	39	10	45	2.3 ±0.1
2*a* + 16,16-d_2-**2***a*[c]														11	29	10	51	1.02±0.05
														10	31	8	52	1.03±0.05
2*b* in 95% D_2O						5	5	14	76						12	30	58	
							6	10	84						10	22	68	
2*b* in 50% D_2O							2	5	93						9	20	71	

[a] Values are accurate to ±2%.
[b] Value calculated for **2***a* → **1***a* (28).
[c] For control purposes.
[d] Isolated as androst-4-ene-17β-ol-3-one.
[e] Route A material (see Table 1).

Can. J. Chem. Downloaded from www.nrcresearchpress.com by 210.87.254.105 on 09/06/12
For personal use only.

conversion of both labelled and unlabelled substrate.

Previous studies on intermolecular isotope effects of cytochrome (cyt) P-450-dependent hydroxylations have generally shown deuterium isotope effects of 2 or less. The benzylic hydroxylation of phenylethane by liver microsomes was determined to proceed with a deuterium isotope effect of 1.8 (29). The 7β-hydroxylation of estr-4-ene-3,17-dione by *Botryodiplodia malorum* was found to have an isotope effect (k_H/k_D) of 1.4 (30), and the 21-hydroxylation of pregn-4-ene-3,20-dione was determined to proceed with an intramolecular isotope effect of 1.3 (31), whereas no isotope effect was observed in the 3-hydroxylation of estra-1,3,5(10)-triene-2,17β-diol when examined by mixed-labelling studies (32).

All of the above hydroxylations are presumed to involve cyt P-450. Some hydroxylations, however, are not mediated by carbon monoxide-sensitive cyt P-450; this appears to be the case for 19-hydroxylation during aromatization (33). Another such hydroxylation, the 7α-hydroxylation of taurodeoxycholic acid was determined to proceed with a tritium isotope effect of 3.8 (34), equivalent to a deuterium isotope effect of 2.5 (based on $(k_H/k_D)^{1.44} = k_H/k_T$).

The 16α-hydroxylation of pregn-5-ene-3β-ol-20-one and the 24-hydroxylation of 5β-cholestane-3α,7α,21α-triol were determined to proceed with a deuterium isotope effect of 3 to 4. These two processes appear to be insensitive to inhibition by carbon monoxide (35). Conney *et al.* (36) suggested a correlation between the degree of sensitivity toward carbon monoxide and the nature of the rate-limiting step in hydroxylation.

The rate-limiting step in these reactions has been identified in some cases as decomposition of the cyt P-450 – O_2-substrate complex to products (37). It has also been suggested (31, 37) that hydroxylations occurring at unactivated positions proceed by an oxene-type mechanism involving direct insertion of activated oxygen into a C—H bond. The analogous chemical insertion of carbene into a C—H or C—D bond proceeds with an observed isotope effect of 1.8 (38). This mechanism is consistent with the low observed isotope effects, and the retention of configuration observed in such processes (39, 40).

The results from the incubation of a 1:1 mixture of the 19-d_1 and 16,16-d_2 labelled steroids verified the presence of an isotope effect ($k_H/k_D = 2.3$) operating at the level of 19-hydroxylation. The complexity of this enzymic process makes unambiguous interpretation of the apparent isotope effect difficult. As expected, the effect observed for the 19-d_1 steroid was less than that for the 19-d_3 substrate. This may be the result of an isotope effect operating for a single hydroxylation at C-19 or the result of cumulative primary and secondary isotope effects incurred during both initial hydroxylation and subsequent hydroxylation (alcohol to aldehyde) at C-19. Equilibrium effects could result in the reduction of the intrinsic isotope effect of an early step in the reaction sequence, but in the absence of evidence for reversibility of any of the steps of the process, this would seem unlikely.

It is apparent from the observed isotope effects that a carbon–hydrogen bond cleavage during oxidation at C-19 is at least a partially rate-determining process in aromatization. This is consistent with previous proposals (6, 19) concerning the rate-determining step of aromatization.

It was our original intention to compare the isotope effect of aromatization with that observed for hydroxylation of **2***b* at C-19 by the fungus *Pellicularia filamentosa* (*Corticium microsclerotia*) NRRL 2727, a micro-organism reported to produce the desired alcohol **21** in high yield from **2***b* (41). However, in our hands this fungus yielded only products of C-11α, -11β, and -14 hydroxylation. Hasegawa and Takahashi (42) previously identified the 11α- and 11β-hydroxylated products from the incubation of pregn-4-ene-17α,21-diol-3,20-dione with another fungus of the same family, *Corticium sasakii*, and Takahashi (43) only found the 11β-hydroxylated product upon the incubation of the same substrate with *P. filamentosa*. It therefore appears that earlier claims of C-19 hydroxylation of C_{19} steroids by *P. filamentosa* are unsubstantiated, and that the microbial 19-hydroxylation of **2***a* or **2***b* is unknown (44, 45).

Experimental

Apparatus, Materials, and Methods

Melting points were determined on a Kofler heating stage and are uncorrected. Infrared spectra were recorded with a Perkin-Elmer 237B spectrometer. Proton nmr spectra were obtained with a Varian A-60 or Bruker WP-60 at 60 MHz using $CDCl_3$ or DMSO-d_6 as solvent and TMS as internal standard, ^{13}C nmr spectra with a Bruker WP-60 at 15.18 MHz using $CDCl_3$ as solvent and TMS as internal standard, and ^2H nmr spectra at McMaster University, Hamilton, Ont., with a Bruker WH-90 at 13.8 MHz using CS_2 as solvent and $CDCl_3$ or acetone-d_6 as external standard. Mass spectra were obtained with an AEI MS30 spectrometer. Isotopic composition was determined by repetitive scanning of the relevant ions and application of the appropriate corrections for natural abundances; values are accurate to ±2%. Column chromatography was performed on silica gel (60–200 mesh), thin layer chromatography on Merck silica gel 60 F-254 (0.25 mm), and preparative layer chromatography on Merck silica gel F-254 (2.0 mm). Microanalyses were performed by the Guelph Chemical Laboratories, Guelph, Ontario. Human placental microsomes were obtained and

Can. J. Chem. Downloaded from www.nrcresearchpress.com by 210.87.254.105 on 09/06/12
For personal use only.

stored as previously described (46). *Pellicularia filamentosa* NRRL 2727 was maintained on slopes composed of malt agar (1.5%), tomato paste (2.0%), and oatmeal (2.0%).

Preparation of Substrates

Androst-4-ene-3,17-dione (**2***b*), androst-5-ene-3β-ol-17-one (**3***a*), androst-4-ene-17β-ol-3-one (testosterone) (**2***a*), estra-1,3,5(10)-triene-3-ol-17-one (estrone) (**1***b*), estra-1,3,5(10)-triene-3,17β-diol (estradiol) (**1***a*), androst-4-ene-3,17-dione-11β-ol (**2***d*), androst-4-ene-17β,19-diol-3-one, 17-benzoate (**4**), and androst-5-ene-3,19-diol-17-one (**3***b*) were commercial samples.

Authentic samples of androst-4-ene-3,17-dione-11α-ol, (**2***c*) and androst-4-ene-3,17-dione-14α-ol (**2***e*) were available in our laboratories from incubations of **2***b* with *Rhizopus arrhizus* ATCC 11145 (47) and *Mucor griseocyanus* ATCC 1207 (48), respectively.

The following substrates were prepared by published procedures (47) and gave satisfactory spectral and analytical data: androst-4-ene-3,17-dione, 4-*d*, (4-*d*-**2***b*), androst-4-ene-3,17-dione, 6α-d_1, (6α-d_1-**2***b*), androst-4-ene-3,17-dione, 2,2,4,6,6,16,16-d_7, and androst-4-ene-3,17-dione, 16,16-d_2.

Androst-4-ene-17β-ol-3-one, 19-d_1*, (19-*d_1*-2a) and Androst-4-ene-3, 17-Dione, 19-*d_1 *(19-*d_1*-2b) (Scheme 1)*

Route A: From Androst-4-ene-17β,19-diol, 17-Benzoate (4)

Androst-4-ene-17β,19-diol-3-one, 17-Benzoate, 19-Tosylate (5)

Toluene *p*-sulphonyl chloride (2.9 g) was added to a solution of androst-4-ene-17β,19-diol-3-one, 17-benzoate (**4**) (2 g) (Maybridge Chemical Co., U.K.) in pyridine (5 mL). The mixture was allowed to stand at room temperature overnight and then poured into ice water. The resultant precipitate was collected by filtration and treated briefly with refluxing ether (40 mL). Filtration of the mixture afforded the product (2.41 g, 88%), mp 142–147°C, which was used directly in the preparation of **6**.

5β,19-Cycloandrostan-17β-ol-3-one, 17-Benzoate (6)

The tosylate **5** (1.4 g) was dissolved in aqueous acetic acid (350 mL, 50%) and zinc dust (17 g, Shawinigan) added to the solution. The resulting suspension was stirred and refluxed for 90 min, then filtered. The zinc was washed with methanol and the total filtrate evaporated. The residue was crystallized from acetone–ether, and recrystallized from methanol to give the product (0.4 g, 41%), mp 184–186°C; ^{1}H nmr included signals at δ 0.50 (2H, s, C-19H), 0.97 (3H, s, C-18H), 2.55 (2H, br s, C-4H), 4.9 (1H, t, C-17H), and 7.3–8.3 (5H, m, aromatic H) ppm; ms *m/e* (%): 392 (6), 287 (3), 270 (13), 255 (6), 105 (100). *Anal.* calcd. for $C_{26}H_{32}O_3$: C 79.59, H 8.16%; found: C 79.26, H 8.42%.

Androst-4-ene-17β-ol-3-one, 17-Benzoate, 19-d_1 *(7)*

Conversion of **6** to **7** was performed by a modification of the procedure of Rakhit and Gut (49). To a solution of **6** (540 mg) in dried dioxan (10 mL) was added D_2O (80 mg) and DCl (1 mL, 38% in D_2O). The mixture was refluxed for 24 h, and the solvents then removed under vacuum. The crude residue was purified by column chromatography (benzene/ether gradient elution) affording **7** (460 mg, 85%), mp 187–190°C (lit. (50) mp 190°C); ^{1}H nmr included signals at δ 0.99 (3H, s, C-18H), 1.21 (2H, s, C-19H), 4.9 (1H, t, C-17H), 5.8 (1H, s, C-4H), and 7.3–8.3 (5H, m, aromatic H) ppm.

Androst-4-ene-17β-ol-3-one, 19-d_1 *(19-*d_1*-2a)*

A solution of **7** (0.17 g) in methanolic sodium hydroxide (5 mL, 5%) was refluxed for 1 h. The mixture was cooled, neutralized with acetic acid, and worked up in the usual way to give 19-d_1-**2***a* (0.12 g, 96%), mp 152–154°C (lit. (50) mp 154°C); ^{1}H nmr included signals at δ 0.81 (3H, s, C-18H), 1.22 (2H, s, C-19H), 3.75 (1H, t, C-17H), and 5.9 (1H, s, C-4H) ppm; ms *m/e* (%): 289 (28), 273 (5), 247 (28), 125 (100). Isotopic content: see Table 1.

Androst-4-ene-3,17-dione, 19-d_1 *(19-*d_1*-2b)*

Jones' oxidation of 19-d_1-**2***a* (0.16 g) afforded 19-d_1-**2***b* (0.12 g, 76%); ^{1}H nmr included signals at δ 0.92 (3H, s, C-18H), 1.22 (2H, s, C-19H), and 5.8 (1H, s, C-4H) ppm; ^{2}H nmr: see Table 1; ms *m/e* (%): 287 (100), 272 (14), 269 (13), 259 (20), 245 (96). Isotopic content: see Table 1.

Route B. From Androst-4-ene-3,17-dione, 19-ol (27) (Scheme 1)

An analogous series of reactions and conditions to those of the route described above for the conversion of **4** into **7** (Scheme 1) was used to convert the 19-ol **27** into androst-4-ene-3,17-dione, 19-d_1 (19-d_1-**2***b*). Alternatively, 19-d_1-**2***b* was available by the following procedure.

5β,19-Cycloandrostan-17β-ol-3-one

The benzoate **6** (0.5 g) was dissolved in methanolic sodium hydroxide (15 mL, 5%) and the solution refluxed for 1 h. Conventional work-up gave the product (81%), which was used in the next step without further purification.

5β,19-Cycloandrostan-3,17-dione

Jones' oxidation of the aforegoing alcohol (0.3 g) afforded the product (0.24 g, 81%), identical in all respects with an authentic sample (49).

Androst-4-ene-3,17-dione-19-d_1*, (19-*d_1*-2b)*

The cyclopropyl ketone was treated with DCl in D_2O by the procedure described above for the conversion of **6** into **7**. The product was then refluxed briefly in 5% methanolic sodium hydroxide to ensure removal of any enolizable deuterium. Conventional work-up afforded 19-d_1-**2***b* identical in physical and spectral properties with an authentic sample of unlabelled material. Isotope content is presented in Table 1.

Androst-4-ene-17β-ol-3-one, 19-d_1*(19-*d_1*-2a)*

The conversion of 19-d_1-**2***b* into 19-d_1-**2***a* was performed by a published procedure (51). The product was purified by preparative layer chromatography and obtained in 60% yield. Isotope content is presented in Table 1.

Androst-4-ene-17β-ol-3-one, 19,19,19-d_3 *(19,19,19-*d_3*-2a) (Scheme 2)*

The procedure followed was similar to that of Baba *et al.* (22).

Estra-2,5(10)-diene-3,17β-diol, 3-Methyl Ether (9) (52)

Isopropanol (30 mL) and a solution of estra-1,3,5(10)-triene-3,17β-diol, 3-methyl ether (5.0 g) in THF (30 mL) were added to redistilled ammonia (80 mL). To this mixture, sodium metal (total 4.5 g) was added in portions. After the addition was complete and all of the sodium consumed (ca. 1 h), methanol (20 mL) was added. The ammonia was then allowed to evaporate and the THF subsequently removed by distillation under reduced pressure. The precipitated product was collected, washed with water, and dried to give a product (5.0 g, 99%), mp 110–112°C (lit. (53) mp 118–119.5°C) of sufficient purity to be useable directly in the next step; ^{1}H nmr included signals at δ 0.77 (3H, s, C-18H), 2.69 (4H, m, C-1 and C-4H), 3.65 (1H, t, C-17H), 3.66 (3H, s, OCH_3), and 4.7 (1H, m, C-2H) ppm.

Estr-5(10)-ene-17β-ol-3-one (10)

The enol ether **9** (5.0 g) was dissolved in a mixture of THF (25 mL), water (12 mL), and sulphuric acid (96%, 1.5 mL), and the resulting solution stirred at room temperature for 45 min. Ammonium sulphate was then added until the solution became saturated, and the product was extracted into dichloromethane. The extract was washed (saturated $NaHCO_3$/$(NH_4)_2SO_4$), dried, and evaporated to afford the product **10** (4.10 g). Crystallization from ethyl acetate/hexane gave 3.84 g, mp 178–181°C (lit. (54) mp 181–182°C); ^{1}H nmr included signals at δ 0.79 (3H, s,

Can. J. Chem. Downloaded from www.nrcresearchpress.com by 210.87.254.105 on 09/06/12
For personal use only.

C-18H), 2.47 (4H, m, C-1 and C-2 H's), 2.75 (2H, m, C-4H), and 3.65 (1H, t, C-17H) ppm.

5α-Estran-17β-ol-3-one-5α,10α-oxide, 17-Acetate, 3-Cyclic Ethylene Ketal (15)

Conversion of the ketone **10** to the title compound **15** as outlined in Scheme 2 was carried out precisely as described (22).

5α-Androstan-5,17β-diol-3-one, 3-Cyclic Ethylene Ketal (16)

The reagent CD_3MgBr (1 *M* in THF) was prepared by condensing CD_3Br (2.0 g, 99.5 at.% ^2H), by means of a cold-finger condenser, into an ice-cooled reaction flask containing dry THF (20 mL) and magnesium turnings (0.5 g). To this reagent was added dropwise a solution of the epoxide **15** (0.5 g) in dry THF (5 mL). The solution was refluxed for 2 h and then cooled, whereupon 10 mL 1.5 *M* NH_4Cl solution was added dropwise. The resultant mixture was diluted with water, extracted with methylene chloride, and washed successively with 3 *N* HCl, 5% $NaHCO_3$, and water. Drying over Na_2SO_4 followed by evaporation yielded 490 mg crude product. Purification by column chromatography (benzene/ether gradient elution) yielded 260 mg product (55%), identified by comparison with an authentic sample of unlabelled material prepared by reaction of (5,6α)-epoxytestosterone ethylene ketal with lithium aluminum hydride.

Androst-4-ene-17β-ol-3-one, 19,19,19-d_3 (19,19,19-d_3-2a)

The ketal **16** (0.26 g) was dissolved in a mixture of methanol (7 mL) and sulphuric acid (0.7 mL, 1 *M*), and the solution refluxed for 30 min. The solution was then cooled and diluted with ether and water and the organic layer removed. The aqueous layer was re-extracted with ether and the combined organic extract washed (5% $NaHCO_3$, water), dried, and evaporated to yield 180 mg of crude product. Column chromatography followed by preparative layer chromatography afforded 75 mg of pure product, identified by spectral and mp comparison with an authentic sample of unlabelled material. Isotope content is presented in Table 1.

Androst-4-ene-17β-ol-3-one, 16,16-d_2 (16,16-d_2-2a) (Scheme 3)

Androst-5-ene-17β-ol-3-one, 3-Cyclic Ethylene Ketal (17)

Androst-4-ene-17β-ol-3-one (**2***a*, 1.5 g) was dissolved in a mixture of dry benzene (80 mL), ethylene glycol (1.5 g), and *p*-toluene sulphonic acid (100 mg), and the solution refluxed for 24 h under a Dean–Stark trap. Conventional work-up gave 1.43 g (82%) product.

Androst-5-ene-3,17-dione, 3-Cyclic Ethylene Ketal (18)

The above ketal (1.4 g) was dissolved in pyridine (15 mL) to which Sarett reagent was added (15 mL, 0.1 g CrO_3 per mL). The mixture was stirred for 20 h and then diluted with dichloromethane. The resulting mixture was washed (5% HCl, water), dried, and evaporated to yield crude **18** (900 mg), which was purified by column chromatography and then crystallized from ethyl acetate/hexane to afford the title compound (0.6 g, 43%), mp 175–180°C (lit. (55) mp 197–198°C); ^1H nmr included signals at δ 0.90 (3H, s, C-18H), 1.08 (3H, s, C-19H), 3.98 (4H, s, $-OCH_2$), and 5.4 (1H, m, C-6H) ppm.

Androst-5-ene-3,17-dione, 3-Cyclic Ethylene Ketal, 16,16-d_2 (19)

A solution of **18** (0.5 g) in dry benzene (10 mL) was added to a solution of tetra *n*-butyl ammonium bromide (0.5 g) in basic D_2O (5% NaOD, 10 mL), and the resulting mixture stirred and refluxed for 20 h. Normal work-up afforded **19** (0.45 g), identified by comparison with an authentic sample of **18**.

Androst-5-ene-17β-ol-3-one, Cyclic Ethylene Ketal, 16,16-d_2 (20)

A solution of the ketal **19** (0.45 g) in benzene/ether (1:1, 25 mL) was added to a suspension of lithium aluminum hydride (0.45 g) in ether (30 mL) and the mixture refluxed for 3.5 h. Conventional work-up afforded **20** (0.4 g, 88%), identified by comparison with an authentic sample of **17**.

Androst-4-ene-17β-ol-3-one, 16,16-d_2 (16,16-d_2-2a)

The above ketal **20** (0.4 g) was dissolved in a mixture of methanol (6 mL) and dilute sulphuric acid (6%, 1 mL) and the solution refluxed for 30 min, diluted with water, and the product extracted into ether. The extract was dried and evaporated, and the residue crystallized from acetone/hexane to give 16,16-d_2-**2***a* (0.3 g, 86%), mp 149–151°C (lit. (50) mp 154°C). Isotope content is listed in Table 1.

Androst-4-ene-17β-ol-3-one, 2β-d, (2β-d_1-2a)

A solution of androst-4-ene-17β-ol-3-one (**2***a*, 0.25 g) in dry benzene (5 mL) was added to a solution of tetra *n*-butyl ammonium bromide (0.25 g) in basic D_2O (5% NaOD, 5 mL), and the mixture stirred at room temperature for 45 h. Conventional work-up afforded the title compound (0.18 g). Isotope content is listed in Table 1.

Androst-4-ene-17β-ol-3-one, 1β,2β-d_2 (1β,2β-d_2-2a)

A mixture of androsta-1,4-diene-17β-ol-3-one (**27**) (0.2 g) and 10% Pd/C (0.2 g) in ethyl acetate (10 mL) was stirred under deuterium gas at atmospheric pressure for 6 min. Conventional work-up afforded 0.2 g crude product, which was subjected to preparative layer chromatography (4% methanol in ether as solvent) to give the desired product (40 mg, 20%), identified by comparison with an authentic sample of unlabelled material. Isotope content is listed in Table 1. A reaction time of 25 min resulted in the production of 5β-androstan-17β-ol-3-one as major product.

Androst-4-ene-3,17-dione-19-ol (21)

Method A. From Androst-5-ene-3β,19-diol-17-one (3b) by Oppenauer Oxidation (56)

A solution of androst-5-ene-3β,19-diol-17-one (**3***b*, 0.5 g) (Bader Chemical Co.) and aluminum isopropoxide (0.5 g) in toluene (40 mL) and cyclohexanone (10 mL) was refluxed for 10 min. Work-up and chromatography afforded a 6–15% yield of **21** in several experiments; ^1H nmr included signals at δ 0.92 (3H, s, C-18H), 3.90 (2H, ABq, C-19H), and 5.7 (1H, s, C-4H) ppm.

Method B. From 3b via bis *Trityl Ether (3d) (57)*

Conversion of **3***c* to the ether **3***d* was performed as described (58). The product was obtained in 92% yield. Triphenylmethylfluoroborate (1.3 g) (59) was added to a solution of **3***d* (2.93 g) in dichloromethane. The mixture was stirred for 12 h, then washed ($NaHCO_3$), dried, and evaporated to yield 1.6 g crude product. This was dissolved in a mixture of ethanol (100 mL), benzene (25 mL), and dilute sulphuric acid (2 *N*, 10 mL) and the mixture refluxed for 4 h. The product was isolated by extraction and purified by column chromatography to give **21** in 35% yield, mp 163–167°C (lit. (60) mp 164–166°C).

Method C. From Androst-5-ene-3β-ol-17-one, 3-Acetate (3c)

The conversion of **3***c* to **21** was performed as described (60) in an overall yield of 18%. The last step described in ref. 60 proceeded in acceptable yield in our hands only with the use of MCB zinc dust as a reagent.

Incubation with P. filamentosa *NRRL 2727*

The fungus was grown in 1-L Erlenmeyer flasks as described (41). After 3 to 4 days of fungal growth at room temperature, androst-4-ene-3,17-dione (**2***b*) in ethanol solution (80 mg in 0.5 mL ethanol per flask) was added, and growth allowed to continue for a further 8–12 h. The medium and mycelia were then separated by filtration, and each extracted with dichloromethane. The combined extract was dried and evaporated, and

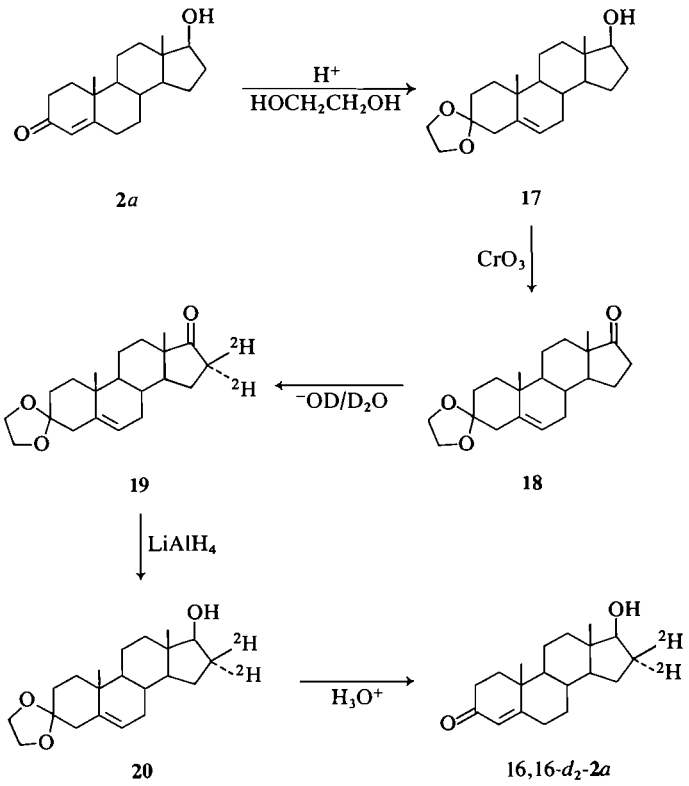

SCHEME 3. Preparation of 16,16-d_2-**2***a*

the residue subjected to column chromatography (benzene/ether gradient elution) to give recovered starting material (typically 30–40%), androst-4-ene-3,17-dione-11α-ol (**2***c*, typically 35%), androst-4-ene-3,17-dione-11β-ol (**2***d*, typically 15%), and androst-4-ene-3,17-dione-14α-ol (**2***e*, typically 10%), all of which were identical in all respects with corresponding samples of authentic material.

Incubations with Placental Microsomes

Incubations of androst-4-ene-3,17-dione (**2***b*) and androst-4-ene-17β-ol-3-one (**2***a*) with a microsomal suspension from human placentae were performed as previously described (46). Isolated yields of estra-1,3,5(10)-triene-3,17β-diol were typically 5–10%. Isotope content of substrates and products are presented in Table 2.

Acknowledgements

We thank the Natural Sciences and Engineering Research Council of Canada for a research studentship (to G.J.T.) and for financial support of this project. We are also grateful to Dr. P. H. Buist of McMaster University, Hamilton, Ontario, for preliminary work on the conversion of **3***c* into **21**, and to Dr. M. Gut of the Worcester Foundation for Experimental Biology for providing an authentic sample of 5β,19-cycloandrostan-3,17-dione. Thanks are also due to Drs. J. N. Wood and J. Lo of the St. Catharines General Hospital for their invaluable cooperation in obtaining placentae for use in this study, to Dr. P. Morand of the University of Ottawa for helpful discussions, and to T. Jones of Brock University and B. Sayer of McMaster University for their assistance in obtaining nmr spectra.

1. L. L. ENGEL. Handbook of physiology, section 7.2, part 1. Endocrinology: female reproductive system. American Physiological Society, 1973. Chapt. 20.
2. Y. OSAWA. Endocrinology. Proceedings of the fourth International Congress of endocrinology, Washington, D.C. June 18–24, 1972. *Edited by* R. O. Scow. American Elsevier Publishing, New York, NY. 1973. p. 814.
3. E. CASPI, E. SANTANIELLO, K. PATEL, T. ARUNACHALAM, and C. ECK. J. Am. Chem. Soc. **100**, 5223 (1978).
4. E. A. THOMPSON and P. K. SIITERI. J. Biol. Chem. **249**, 5373 (1974).
5. W. G. KELLY, D. JUDD, and A. STOLEE. Biochemistry, **16**, 140 (1977).
6. W. E. BRASELTON, L. L. ENGEL, and J. C. ORR. Eur. J. Biochem. **48**, 35 (1974).
7. J. D. TOWNSLEY and H. J. BRODIE. Biochemistry, **7**, 33 (1968).
8. M. GANGULY, K. L. CHEO, and H. J. BRODIE. Biochim. Biophys. Acta, **431**, 326 (1976).
9. H. J. BRODIE, A. K. PILLAI, and C. E. HAY. Biochim. Biophys. Acta, **187**, 275 (1969).
10. H. HOSODA and J. FISHMAN. J. Am. Chem. Soc. **96**, 7325 (1974).
11. J. GOTO and J. FISHMAN. Science, **197**, 80 (1977).
12. M. AKHTAR, D. CORINA, J. PRATT, and T. SMITH. J. Chem. Soc. Chem. Commun. 854 (1976).

Can. J. Chem. Downloaded from www.nrcresearchpress.com by 210.87.254.105 on 09/06/12
For personal use only.

13. P. MORAND, M. KALAPURACKAL, L. LOMPA-KRZYMIEN, and A. VAN TONGERLOO. J. Theoret. Biol. **56**, 503 (1976).
14. P. MORAND, D. G. WILLIAMSON, D. S. LAYNE, L. LOMPA-KRZYMIEN, and J. SALVADOR. Biochemistry, **14**, 635 (1975).
15. T. MORATO, K. RAAB, H. J. BRODIE, M. HAYANO, and R. I. DORFMAN. J. Am. Chem. Soc. **84**, 3764 (1962).
16. H. J. BRODIE, K. J. KRIPALANI, and G. PASSANZA. J. Am. Chem. Soc. **91**, 1241 (1969).
17. J. FISHMAN, H. GUZIK, and D. DIXON. Biochemistry, **8**, 4304 (1969).
18. Y. OSAWA and D. G. SPAETH. Biochemistry, **10**, 66 (1971).
19. R. B. WILCOX and L. L. ENGEL. Steroids Suppl. **1**, 49 (1965).
20. D. J. COLLINS, B. M. K. GATEHOUSE, W. R. JACKSON, G. A. KAKOS, and R. N. TIMMS. J. Chem. Soc. Chem. Commun. 138 (1980).
21. L. J. ALTMAN and N. SILBERMAN. Steroids, **29**, 557 (1977).
22. S. BABA, Y. SHINOHARA, and Y. KASUYA. J. Labelled Compd. Radiopharm. **14**, 783 (1978).
23. J. FISHMAN and M. S. RAJU. J. Biol. Chem. **256**, 4472 (1981).
24. W. L. DUAX, C. M. WEEKS, and D. C. ROHRER. *In* Topics in stereochemistry. Vol. 9. *Edited by* N. L. Allinger and E. L. Eliel. John Wiley, Toronto. 1976.
25. W. GIBB and J.-C. LAVOIE. Steroids, **36**, 507 (1980).
26. K. C. REED and S. OHNO. J. Biol. Chem. **251**, 1625 (1976).
27. G. SUBRAHMANYAM, S. K. MALHOTRA, and H. J. RINGOLD. J. Am. Chem. Soc. **88**, 1332 (1966).
28. C. C. MCMULLEN and H. G. THODE. Mass Spectrometry. *Edited by* C. A. McDowell. McGraw Hill, Toronto. 1963.
29. R. E. MCMAHON, H. R. SULLIVAN, J. C. CRAIG, and W. E. PEREIRA. Arch. Biochem. Biophys. **132**, 575 (1969).
30. I. KIM, C. E. HAY, and H. J. BRODIE. J. Biol. Chem. **248**, 2134 (1973).
31. H. L. HOLLAND and B. J. AURET. Can. J. Chem. **53**, 845 (1975).
32. M. NUMAZAWA, N. SOEDA, S. MORO, and T. NAMBARA. Biochem. Pharmacol. **26**, 769 (1977).
33. R. A. MEIGS and K. J. RYAN. Biochim. Biophys. Acta, **165**, 476 (1968).
34. I. BJÖRKHEM. Eur. J. Biochem. **18**, 299 (1971).
35. I. BJÖRKHEM. Eur. J. Biochem. **27**, 354 (1972).
36. A. H. CONNEY, W. LEVIN, M. IDEDA, and R. KUNZMAN. J. Biol. Chem. **243**, 3912 (1968).
37. Y. ISHIMURA. *In* Cytochrome P-450. *Edited by* R. Sato and T. Omura. Academic Press, New York, NY. 1978. p. 209.
38. V. FRANZEN and R. EDENS. Ann. Chem. **729**, 33 (1969).
39. M. HAYANO, M. GUT, R. I. DORFMAN, O. K. SEBEK, and D. H. PETERSON. J. Am. Chem. Soc. **80**, 2336 (1958).
40. E. J. COREY, G. A. GREGORIOU, and D. H. PETERSON. J. Am. Chem. Soc. **80**, 2338 (1958).
41. T. HASEGAWA, T. TAKAHASHI, M. NISHIKAWA, and H. HAGIWARA. U.S. Pat. No. 2,966,444 (Dec. 27, 1960); Chem. Abstr. **55**, 14816e (1961).
42. T. HASEGAWA and T. TAKAHASHI. Agric. Biol. Chem. **22**, 212 (1958).
43. T. TAKAHASHI. Agric. Biol. Chem. **27**, 633 (1963); **27**, 639 (1963).
44. W. CHARNEY and H. L. HERZOG. Microbial transformations of steroids: a handbook. Academic Press, New York, NY. 1967.
45. L. L. SMITH. Terpenes and steroids. Vol. 4. The Chemical Society, London. 1974. p. 394.
46. H. L. HOLLAND and G. J. TAYLOR. Can. J. Chem. **58**, 2326 (1980).
47. H. L. HOLLAND and P. R. P. DIAKOW. Can. J. Chem. **56**, 694 (1978).
48. K. SINGH, S. N. SEHGAL, and C. VEZINA. Can. J. Microbiol. **13**, 1271 (1967).
49. S. RAKHIT and M. GUT. J. Am. Chem. Soc. **86**, 1432 (1964).
50. Dictionary of Organic Compounds. 4th ed. Eyre and Spottiswoode, London. 1965.
51. H. L. HOLLAND. Can. J. Chem. **59**, 1651 (1981).
52. H. L. DRYDEN. *In* Organic reactions in steroid chemistry. Vol. 1. *Edited by* J. Fried and J. A. Edwards. Van Nostrand Reinhold Co., Toronto. 1972. p. 50.
53. A. L. WILDS and N. A. NELSON. J. Am. Chem. Soc. **75**, 5366 (1953).
54. S. DANISHEFSKY and P. CAIN. J. Am. Chem. Soc. **98**, 4975 (1976).
55. H. J. DAUBEN, B. LÖKEN, and H. J. RINGOLD. J. Am. Chem. Soc. **76**, 1359 (1954).
56. T. JEN and M. E. WOLFF. J. Org. Chem. **28**, 1573 (1963).
57. M. E. JUNG and L. M. SPELTZ. J. Am. Chem. Soc. **98**, 7882 (1976).
58. D. R. BAIGENT and K. G. LEWIS. Aust. J. Chem. **27**, 323 (1974).
59. H. J. DAUBEN, L. R. HONNEN, and K. M. HARMON. J. Org. Chem. **25**, 1442 (1960).
60. J. M. NASCIMENTO and M. E. FAUSTINO. Rev. Port. Quim. **8**, 133 (1966); Chem. Abstr. **67**, 91000x (1967).

Can. J. Chem. Downloaded from www.nrcresearchpress.com by 210.87.254.105 on 09/06/12
For personal use only.

Approaches to the synthesis of lycoxanthol and similar natural products. Synthesis of coleon U

ROBERT H. BURNELL,[1] ANDRÉ ANDERSEN, MARTINE NÉRON-DESBIENS, AND SYLVAIN SAVARD
Département de chimie, Université Laval, Québec (Qué.), Canada G1K 7P4

Received March 16, 1981

ROBERT H. BURNELL, ANDRÉ ANDERSON, MARTINE NÉRON-DESBIENS, and SYLVAIN SAVARD. Can. J. Chem. **59**, 2820 (1981).

Using suitable models the various problems anticipated in preparing lycoxanthol from podocarpic acid have been resolved. Five oxygen atoms are introduced by methods involving direct oxidation, ring fission, and after suitable functionalization, recyclization and nucleophilic substitution of intermediate *p*-quinones. The validity of this approach has been demonstrated in a synthesis of coleon U (as the tri- and tetra-*O*-methyl ethers).

ROBERT H. BURNELL, ANDRÉ ANDERSON, MARTINE NÉRON-DESBIENS et SYLVAIN SAVARD. Can. J. Chem. **59**, 2820 (1981).

En utilisant des modèles appropriés on a résolu les divers problèmes qui pourraient intervenir au cours de la préparation du lycoxanthol à partir de l'acide podocarpique. On a introduit 5 atomes d'oxygène par des méthodes qui impliquent une oxydation directe, une ouverture de cycle suivie d'une fonctionalisation convenable, d'une recyclisation et d'une substitution nucléophile sur les *p*-quinones intermédiaires. On démontre la validité de cette approche en synthétisant le coléon U (sous forme d'éthers tri- et tétra-*O*-méthyle).

[Traduit par le journal]

Can. J. Chem. Downloaded from www.nrcresearchpress.com by 210.87.254.40 on 09/06/12
For personal use only.

During our preparation of dehydrocycloroyleanone **1** (1) we entertained the idea of continuing the synthesis to lycoxanthol (**2**) (2) or to coleon C (**3***a*) which has been previously converted to lycoxanthol (3). The last step of our synthesis of **1** involved the per-acid oxidation of the benzodihydrofuran **4***a* but this afforded only poor yields of the quinone **1** so a significant improvement was called for. Alternate approaches (4) did prove slightly more rewarding but when coupled with our inability to oxidize the benzylic methylene (C.7) in hydroquinone derivatives of dehydrocycloroyleanone **4***b* (a difficulty which others have observed in similar systems (5)) we were forced to explore other avenues leading to lycoxanthol.

After some experimentation and a literature search we concluded that no single reaction could be of direct utility so we imagined the use of "sequences of reactions" which could be performed without rigorous purification of the intermediates. In the "reaction suites" certain of the products were purified and characterized as confirmation that the sequence proceeded as predicted.

The aim of our first "reaction suite" was to convert the ketone **8***a* in which the aromatic ring bears one methoxyl residue to the ketone **10***a* in which there are two (neither in the original position, however). The ketone **8***a* is readily available from methyl-*O*-methyl podocarpate **7***a* by described methods (6*a* and *b*) and using this ketone as a model starting material, the synthesis of a lycoxanthol type molecule (lycoxanthol has a *gem* dimethyl grouping at C.4) involves the introduction of oxygen functions at C.6, C.11, C.14, and C.16. In the following series of experiments we have demonstrated methods which systematically affect these oxidations.

Baeyer–Villiger oxidation of the ketone **8***a* afforded a lactone which on acid catalysed methanolysis lead to the phenol ester **9***a*. *O*-Methylation of the latter gave the neutral hydroquinone diether **9***b* which by dilute basic hydrolysis was converted to the acid **9***c*. Trifluoroacetic anhydride at room temperature cyclized the acid with "rotation" of the aromatic ring to give the ketone **10***a*. This sequence, which in principle introduces one oxygen atom, was carried through without rigorous purification at each step and was inspired by similar results obtained by Pelletier and Ohtsuka (7) in another context. The overall yield was about 4.5% without any attempt to optimize the individual steps. When compared with the direct oxidation (above), and since the C.7 ketone is already incorporated, this result was considered encouraging so we sought to modify the "suite" to include the introduction of another oxygen function.

When the oxidation of the starting ketone **8***a* was performed with per-acetic acid prepared *in situ* from acetic anhydride, sulfuric acid, and hydrogen peroxide (rather than the *m*-chloroperbenzoic acid used previously) the only product isolated was the quinone **11***a*. 2,5-Dialkylquinones are often reluctant to react under Thiele acetylation conditions and such was the case with compound **11***a*. We had hoped that this method of introducing an *O*-acetyl residue (to give **12**) might be accompanied by

[1]Author to whom all correspondence should be addressed.

0008-4042/81/192820-06$01.00/0
©1981 National Research Council of Canada/Conseil national de recherches du Canada

Can. J. Chem. Downloaded from www.nrcresearchpress.com by 210.87.254.40 on 09/06/12
For personal use only.

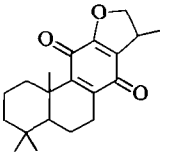

1

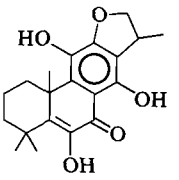

2

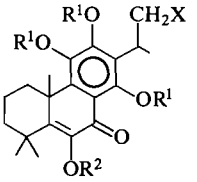

3*a* R¹ = H, R² = H, X = OH
3*b* R¹ = H, R² = H, X = H
3*c* R¹ = Me, R² = H, X = H
3*d* R¹ = Me, R² = Me, X= H

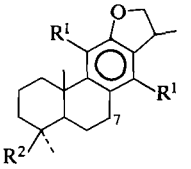

4*a* R¹ = H, R² = Me
4*b* R¹ = OH, R² = Me
4*c* R¹ = H, R² = COOMe
4*d* R¹ = H, R² = CH_2OH
4*e* R¹ = H, R² = CHO

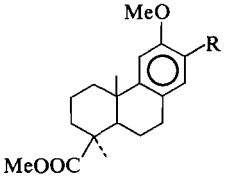

7*a* R = H
7*b* R = *iso*-Pr

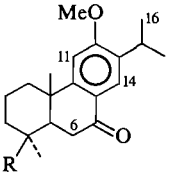

8*a* R = COOMe
8*b* R = Me

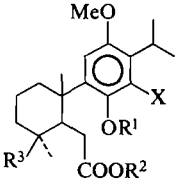

9*a* R¹ = H, R² = Me, R³ = COOMe, X = H
9*b* R¹ = Me, R² = Me, R³ = COOMe, X = H
9*c* R¹ = Me, R² = H, R³ = COOMe, X = H
9*d* R¹ = Me, R² = Me, R³ = COOMe, X = OMe
9*e* R¹ = Me, R² = H, R³ = COOMe, X = OMe
9*f* R¹ = Me, R² = Me, R³ = Me, X = OMe
9*g* R¹ = Me, R² = H, R³ = Me, X = OMe

cyclization especially if trifluoroacetic anhydride were used in the Thiele reaction. To confirm the structure of the quinone **11***a* and to provide an alternate pathway in the aromatic ring rotation sequence, the quinone was catalytically reduced and methylated while still under an atmosphere of hydrogen. The product, ester **9***b*, had already featured in the sequence described above.

We achieved in another reaction suite what we hoped the Thiele reaction would do directly. The quinone acid **11***a* was treated with bromine in acetic acid affording the dibromo addition product **13***a*. We could not detect any quantity of the product arising from the addition to the other double bond. An ether solution of the dibromo derivative and diethylamine affected the elimination of hydrogen bromide allowing the isolation of the bromoquinone **11***b* in high yield. The latter was treated with dilute methanolic sodium hydroxide which replaced the bromo substituent by an hydroxyl group but, rather than isolate the product (**11***c*), dimethyl sulfate was added to the basic solution which probably partially methylated both the hydroxyl and carboxyl residues (**11***d*). The isolated product was reduced catalytically and methylated *in situ* to afford two products (5:1). The major neutral fraction showed five *O*-methyl peaks in the nmr spectrum and was identified as the ester **9***d* while the minor acid product proved to be the corresponding carboxylic acid **9***e*. The former was hydrolysed in mild aqueous base to the acid **9***e* which when stirred for several hours with trifluoroacetic anhydride gave the aromatic ketone **10***b*. The molecule now contains the C.7 carbonyl group and the fully substituted aromatic ring as in lycoxanthol. The overall yield from the ketone **8***a* to ketone **10***b* was 28% which implies an average yield of over 80% for each reaction and certainly shows the reaction suite to be manageable and effective.

Other than the sidechain hydroxyl, there remains one position where oxygen should be introduced to obtain the lycoxanthol (**2**) or coleon C (**3***a*) substitution pattern, that at C.6 which is an enolized ketone moiety. A different model was used for this transformation. The ketone **14** was obtained from the ester **4***c* prepared in another context, by reduction to the primary alcohol **4***d*, oxidation to the aldehyde **4***e*, and Huang–Minlon reduction which gave **4***a*. Chromium trioxide – acetic acid oxidation of the latter afforded **14**. The method of choice for introducing the enolized ketone function proved to be oxygenation in anhydrous strong base (*t*-BuOK in *t*-BuOH). The diosphenol (**15** in this case) was invariably accompanied by the neutral starting ketone which could be recycled to improve the yield. The use of other models such as ketone **8***a*, **10***a*, and **10***b* (which we tried first) was misleading since under these conditions, while there appears to be formation of a diosphenol, the C.4 carbomethoxy substituent is lost during the reaction.[2] The precise nature of the product is unknown at present.

The approach elaborated on these models was applied to the synthesis of coleon U (**3***b*) as the

[2]R. H. Burnell and M. Neron-Desbiens, unpublished results.

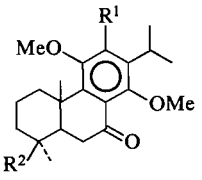

10a $R^1 = H, R^2 = COOMe$
10b $R^1 = OMe, R^2 = COOMe$
10c $R^1 = OMe, R^2 = Me$

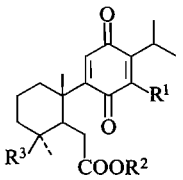

11a $R^1 = H, R^2 = H, R^3 = COOMe$
11b $R^1 = Br, R^2 = H, R^3 = COOMe$
11c $R^1 = OH, R^2 = H, R^3 = COOMe$
11d $R^1 = OMe, R^2 = Me, R^3 = COOMe$
11e $R^1 = H, R^2 = H, R^3 = Me$
11f $R^1 = Br, R^2 = H, R^3 = Me$
11g $R^1 = OH, R^2 = H, R^3 = Me$

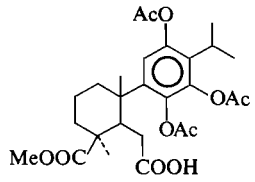

12

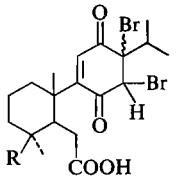

13a R = COOMe
13b R = Me

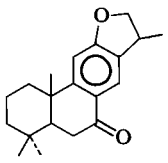

14

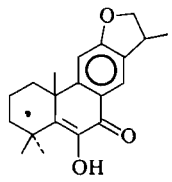

15

tri- and tetra-*O*-methyl ethers (**3***c* and **3***d*). The naturally occurring diterpene (8) is one of the simplest coleons with no oxygen function in the isopropyl sidechain and has recently been synthesized by Matsumoto and Takeda (9) following a somewhat longer and different route. In our case the necessary starting material **8***b* (sugiol-*O*-methyl ether) was prepared from podocarpic acid (via **7***b*: see Experimental for references). Peracetic acid oxidation of **8***b* afforded the expected quinone **11***e* in excellent yield and the sequence of bromine addition (→**13***b*) and dehydrobromination gave regiospecifically the bromo-quinone **11***f*. The facile exchange of the bromo substituent by hydroxyl (→**11***g*) followed by catalytic reduction and immediate *O*-methylation *in situ*, following the procedures optimized for some of the models, gave a mixture which proved to be composed of partially *O*-methylated hydroquinone acids and methyl esters. Since the mixture had already been separated the individual fractions were further methylated to give the methyl ester **9***f*. The only base sensitive functionality in the latter is the ester itself which hydrolyzed readily to the corresponding acid **9***g* which smoothly cyclized in trifluoroacetic anhydride to the expected ketone **10***c*. The remaining oxygen function was introduced by oxygenation in strong base. The product, the enolic α-diketone **3***c* (coleon U tri-*O*-methyl ether) was *O*-methylated to give coleon U tetra-*O*-methyl ether **3***d*.

Neither of these ethers (**3***c* nor **3***d*) is described in the literature since in the methylation of naturally occurring coleon U the strongly chelated C.14 phenolic hydroxyl is unaffected by the conditions employed. However, the spectral characteristics of the products and the nonambiguity of the synthetic route (comparison with the model systems) leave no doubt as to the identity of the products. Particularly convincing is the Cmr spectrum summarized in Fig. 1 which with suitable adjustment for the presence of methoxyl rather than hydroxyl groups, is in excellent agreement with values in the literature (8).

The overall yield of the synthesis from sugiol methyl ether **8***b* is 18% in the case of the tri-*O*-methyl derivative **3***c* and 17.6% for the tetra-*O*-methyl derivative **3***d*. In another synthetic approach we prepared the quinone **11***e* from abietic acid. After reduction of the acid residue to methyl and benzylic oxidation to give the ketone analogous to **8***b* but with no methoxyl group at position 12, the quinone **11***e* was obtained by peracetic oxidation

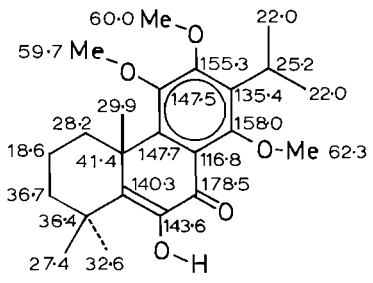

FIG. 1. Summary of Cmr spectrum of **3***c*.

Can. J. Chem. Downloaded from www.nrcresearchpress.com by 210.87.254.40 on 09/06/12
For personal use only.

Can. J. Chem. Downloaded from www.nrcresearchpress.com by 210.87.254.40 on 09/06/12
For personal use only.

but the time necessary for reaction to provide a reasonable yield was considerably longer than cases where the aromatic ring bears a methoxyl substituent.

Experimental

Unless otherwise stated the conditions and instruments used to characterize the products were: melting points, Electrothermal, uncorrected; ultraviolet spectra, ethanol solutions (ε in parenthesis), Beckman DK-1A; infrared spectra, carbon tetrachloride solutions, Beckman IR 12 and Perkin Elmer 457; proton magnetic resonance spectra, deuteriochloroform solutions, TMS internal standard, (multiplicity, integrated peak areas, coupling constants and assignments in parenthesis), Bruker HX 90; mass spectra, Varian M 66 (only molecular ions are given). Extraction in a procedure implies several extractions with the appropriate solvent, suitable washing, drying over anhydrous magnesium sulfate, and evaporation *in vacuo*. Elemental analyses were by Chemalytics, Arizona and Galbraith Laboratories, Knoxville. The high resolution mass spectrum was recorded on an A.E.I. model MS-50 at the University of Alberta, Edmonton.

*Reaction Suite from Ketone 8*a *to Ketone 10*a *(Methyl 7-Oxo-11,14-dimethoxy-13-isopropylpodocarpate)*

The ketone **8***a* was prepared from methyl-*O*-methyl podocarpate **7***a* following procedures described by Campbell and Todd (6*a*) and Cambie *et al.* (6*b*). The product showed mp 144–146°C (from ether, lit. (6*b*) mp 144–144.5°C).

To the ketone **8***a* (1.0 g) in $CHCl_3$ (5 mL) was added dropwise a solution of *m*-chloroperbenzoic acid (1.133 g) in $CHCl_3$ (18 mL). After stirring for 4 days at room temperature, the solution was washed (Na_2CO_3, NaCl) and filtered through a short column of silica gel. Evaporation gave a lactone as an orange foam (1.03 g) showing ir: 1770 and 1730 (lactone and ester) cm^{-1}.

The lactone (1.03 g) was refluxed in absolute MeOH (50 mL) containing concentrated H_2SO_4 (0.5 mL) for 30 min. After adding water, most of the MeOH was removed *in vacuo* and the solution then extracted with ether to afford a phenolic fraction (0.88 g) as a yellow foam. Normally this was used as such in the following steps but a portion of **9***a* recrystallized from hexane showed mp 134–136°C; ir: 3600–3200 (phenol OH), 1720 and 1705 (esters) cm^{-1}; H nmr δ: 7.10 (s, D_2O, phenol OH), 6.79 and 6.68 (2s, Ar—H), 3.81 (s, Ar—O—Me), 3.72 and 3.31 (2s, 2 COOMe), 1.30 and 1.18 (2s, 2 C—Me), 1.26 and 1.15 (2d, J = 7 Hz, isopropyl methyls).

To the preceding diester **9***a* (0.329 g) in dry acetone (33 mL) containing K_2CO_3 (3.29 g) was added dimethyl sulfate (3.0 mL). After 20 h at reflux, water (100 mL) was added and most of the acetone removed at the pump. Extraction with ether afforded a pale yellow oil (0.325 g), a portion of which was chromatographed over silica gel and gave pure **9***b* as a low melting waxy solid; ir: 1720 (br), 1610 and 1570 cm^{-1}; H nmr δ: 6.67 (s) and 6.79 (s, 2 Ar—H), 3.83 (s), 3.78 (s), 3.67 (s) and 3.23 (s, 4—OMe), 1.21 (s), 1.17 (d, J = 7 Hz) and 1.14 (s, 4 C—Me); *m/e*: 420 (M^+).

The crude fully methylated diester **9***b* (2.02 g) was taken up in MeOH (90 mL) to which aqueous KOH was added (90 mL of 10%). After 2 h at reflux, the MeOH was mostly removed *in vacuo* and the solution extracted to afford an acid fraction (1.08 g) which was purified by dry column chromatography over silica gel affording the acid **9***c* (0.780 g) as a pale yellow foam; ir: 3200–2900 (br acid trough), 1725 (ester), 1705 (COOH), 1510, 1240, 1210, and 865 cm^{-1}; H nmr δ: 6.76 (s) and 6.62 (s, 2 Ar—H), 3.78 (s) and 3.76 (s, 2 Ar—O—Me), 3.70 (s, COOMe), 1.20 (s) and 1.15 (s, 2C—Me), 1.15 (d, J = 7 Hz) and 1.11 (d, J = 7 Hz, isopropyl methyls).

The acid **9***c* (0.490 g) was dissolved in trifluoroacetic anhydride (4.9 mL) and stirred at room temp for 3.5 h. After pouring into ice-water, ether extraction gave the intermediate enol trifluoroacetate (0.390 g, ir 1805 cm^{-1}) which was hydrolysed by stirring in MeOH (39 mL) containing aqueous KOH (3.9 mL of 10%) for 1 h. After adding water, partial evaporation of the MeOH, and ether extraction, the aromatic *ketone* **10***a* (0.300 g) was obtained as a foam which crystallized on standing. Chromatography over silica gel gave the pure compound, mp 131–132°C (white needles, hexane); uv: 257 (6100) and 375 (4700) nm; ir: 1730 (ester), 1695 (aromatic ketone), 1600, 1235, 1160, 1145, and 870 cm^{-1}; H nmr δ: 6.98 (s, Ar—H), 3.82 (s) and 3.77 (s, 2Ar—O—Me), 3.69 (s, COOMe), 1.21 (d, 6H, J = 7 Hz, isopropyl methyls), 1.26 (s) and 1.18 (s, 2 C—Me); *m/e*: 388 (M^+). *Anal.* calcd. for $C_{23}H_{32}O_5$: C 71.10, H 8.30; found: C 71.40, H 8.27.

*Quinone 11*a *(2[6-Methoxycarbonyl-2(2-isopropyl-1,4-benzoquinone-5-yl)-2,6-dimethylcyclohexyl] Acetic Acid)*

Hydrogen peroxide (10 mL of 30%) was added dropwise to a solution of acetic anhydride (33 mL) and concentrated H_2SO_4 (0.2 mL) at 0°C. After stirring overnight, the ketone **8***a* (1.0 g) dissolved in acetic anhydride (20 mL) was added slowly with cooling and the mixture was allowed to come to room temperature and stirred for an additional 20 h. A yellow solid precipitated on pouring the solution onto ice (200 g) and this was collected by filtration after stirring for 2 h, dried *in vacuo*, and the quinone **11***a* crystallized from ethanol (0.850 g), mp 194–195°C; uv: 260 (15 600) nm; ir (br acid trough): 1730 (br), 1668, 1615 cm^{-1}; H nmr δ: 9.11 (br s, D_2O, COOH), 6.62 (s, 2H, 2=CH—), 3.72 (s, COOMe), 1.28 (s) and 1.01 (s, 2 C—Me), and 1.15 and 1.13 (2d, J = 7 Hz, isopropyl methyls); *m/e*: 376 (M^+) and 316 (base). *Anal.* calcd. for $C_{21}H_{28}O_6$: C 67.12, H 7.38; found: C 67.00, H 7.50.

*Diester 9*b *(by Reduction and Methylation of Quinone 11*a*)*

The quinone **11***a* (0.800 g) was hydrogenated at atmospheric pressure over prehydrogenated Adams catalyst (0.100 g). The uptake ceased after 47.5 mL. Aqueous NaOH (1 mL of 30%) was introduced while the mixture was still under hydrogen, followed 5 min later by dimethyl sulfate (1 mL). Similar portions of NaOH and dimethyl sulfate were added every hour (total 11 mL each) and the mixture then stirred for 30 h. Dilution with water and evaporation of much of the MeOH facilitated the benzene extraction of the basic solution which afforded a neutral fraction (0.230 g) while acidification and extraction of the aqueous layer gave the starting acid quinone **11***a* (0.580 g). Chromatography of the neutral product gave the *ester* **9***b* (0.204 g) identical with that obtained previously.

*Reaction Suite: Quinone 11*a *to Aromatic Ketone 10*b *(Methyl 7-Oxo-11,12,14-trimethoxy-13-isopropylpodocarpate)*

*(a) Bromoquinone 11*b *via Dibromo Compound 13*a

To the quinone (1.70 g) in acetic acid (20 mL) was added dropwise a solution of bromine (0.4 mL) in acetic acid (5 mL). After stirring for 5 h at room temperature the mixture was poured into water (200 mL) and the precipitated solid filtered, well washed, and dried *in vacuo*. The pale yellow powdery dibromo derivative **13***a* (2.03 g) showed ir (acid trough): 1720, 1696, 1610 cm^{-1}; H nmr δ: 6.52 (s, 1H, =CH—), 4.78 (s, —CHBr—), 3.71 (s, COOMe). No molecular ion was detectable in the mass spectrum which was identical with that of **11***b*.

The crude dibromo compound **13***a* (2.0 g) was taken up in ether (40 mL) and cooled to 10°C. With vigorous stirring, diethylamine (0.7 mL) in ether (5 mL) was slowly added. After 2 h at room temperature the reaction mixture was poured into water and the acid fraction obtained by suitable extraction

Can. J. Chem. Downloaded from www.nrcresearchpress.com by 210.87.254.40 on 09/06/12
For personal use only.

afforded the bromoquinone **11***b* as a yellow glass (1.70 g); ir (acid trough): 1720 br, 1678, 1660, 1588 cm^{-1}; H nmr δ: 6.53 (s, 1H, =C—), 3.69 (s, COOMe), 1.25 (s, C—Me), 1.27 and 1.24 (2d, J = 7 Hz, isopropyl methyls), 1.02 (s, 3H, C—Me); *m/e*: 456 and 454 (M^+).

(b) The Diester **9***d via Hydroxyquinone* **11***c*

The bromoquinone **11***b* (1.70 g) was treated with a solution of NaOH (4.0 g) in water (30 mL) and methanol (30 mL) at room temperature for 1 h. Extraction of an acidified aliquot at this stage gave the hydroxyquinone **11***c* as an oil; ir: 3400, 1730, 1645, 1610 cm^{-1}; H nmr δ: 7.70 (br s, OH), 6.50 (s, =CH—), 3.71 (s, COOMe), 1.29 (s) and 1.02 (s, C—Me), 1.21 (d, J = 7 Hz, isopropyl methyls); *m/e*: 392 (M^+). The product showed a typical intense violet coloration in NaOH solution.

To the bulk of the basic solution of the hydroxyquinone **11***c* was added dimethyl sulfate (4.0 mL) and the mixture stirred at room temperature overnight. Dilution with water, acidification, and ether extraction of the solution gave a product (1.50 g) which appeared to be only partially methylated. Without further purification the crude material was taken up in MeOH (30 mL) and hydrogenated over Adams catalyst (0.050 g) at atmospheric pressure. After a rapid uptake of 90 mL of hydrogen, aqueous NaOH (1.5 mL of 30%) was introduced in a manner to keep the reaction mixture protected by an atmosphere of hydrogen and 10 min later dimethyl sulfate (1 mL) was added. These additions were repeated every hour up to a total of 10 mL of dimethyl sulfate and then stirring was continued at room temperature for 12 h. The catalyst was filtered, the solution diluted with water (50 mL), and most of the methanol removed at the pump before extracting with benzene. The neutral product obtained was chromatographed over silica gel affording the diester **9***d* (0.920 g) as a very pale yellow glass; ir: 1735 br, 1612, 1575 cm^{-1}; H nmr δ: 6.56 (s, Ar—H), 3.92 (s), 3.78 (s), 3.76 (s), 3.70 (s) and 3.37 (s, 5 O—Me), 1.33 (s, C—CH_3), 1.22 (d, J = 7 Hz, isopropyl methyls), 1.20 (s, 3H, C—Me); *m/e*: 450 (M^+).

Acidification of the basic solution from the extraction above and extraction with benzene provided an acidic compound (0.596 g) which contained the *acid* **9***e* (0.180 g) (see step (*c*)).

(c) Ketone **10**b *(Methyl 7-Oxo-11,12,14-trimethoxy-13-isopropylpodocarpate) via the Acid* **9**e

The diester **9***d* (0.040 g) was hydrolyzed with NaOH in MeOH—H_2O as described for **9***b*. The acid **9***e* obtained by extraction (0.035 g) showed the following, ir (acid trough): 1735, 1720, 1620 cm^{-1}; H nmr δ: 6.57 (s, Ar—H), 3.86 (s), 3.73 (s), 3.68 (s) and 3.67 (s, 4 OMe).

The acid **9***e* (0.120 g) was stirred with trifluoroacetic anhydride (5 mL) for 16 h at room temperature. The reaction mixture was decomposed with ice-water and extracted with ether and well washed. The intermediate product, the enol trifluoroacetate of the required ketone was hydrolyzed at room temperature in MeOH (40 mL) containing aqueous KOH (4 mL of 10%). After 1 h and dilution with water, most of the MeOH was removed at the pump and the solution then extracted with ether. The resulting pale yellow oil (0.091 g) was chromatographed over silica gel affording the pure ketone **10***b* (0.080 g); ir: 1731 (ester), 1695 (aromatic ketone) cm^{-1}; H nmr δ: no aromatic H, 3.79 (s, 3H), 3.76 (s, 6H), and 3.66 (s, 3H, 4 OMe), 3.61 (sept, J = 7 Hz, CH in isopropyl), 1.30 (d, J = 7 Hz, isopropyl methyls), 1.24 (s) and 1.22 (s, C—Me); *m/e*: 418.2354 (M^+). *Mol. Wt.* calcd. for $C_{24}H_{34}O_6$: 418.2355.

Preparation of Ketone **14** *(5-Oxo-3,7,7,10a-tetramethyl-2,3,5,6,6a,7,8,9,10,10a-decahydrophenanthro[2,3-b]furan) from* **4**c

The methyl ester group of the benzodihydrofuran **4***c* was reduced with $LiAlH_4$ following essentially the procedure of Zeiss *et al.* (10) in 85% yield. The primary *alcohol* **4***d* showed mp 86–88°C; ir: 3340, 1638, 1605 cm^{-1}; H nmr δ: 6.82 (s) and 6.72 (s, 2 Ar—H), 4.63 (t, J = 8.5 Hz) and 3.99 (t, J = 8.5 Hz, CH_2—O—R), 3.86 (d, J = 10 Hz) and 3.50 (d, J = 10 Hz, —CH_2—O(H), 3.44 (s, OH), the m for the *CH*—Me is hidden under the peaks in this area (integrated area 4.1 to 3.3 = 5H), 2.83 (m, 2H, C.7 benzylic protons), 1.29 (d, J = 7 Hz, CH—*Me*), 1.17 (s) and 1.06 (s, 2 C—Me). *Anal.* calcd. for $C_{20}H_{28}O_2$: C 79.95, H 9.39; found: C 79.95, H 8.95.

The alcohol **4***d* was oxidized with chromium trioxide – pyridine (the procedure of Matsumoto *et al.* (11)) and gave the *aldehyde* **4***e* in 93% yield, mp 123–124°C (from ethanol); ir: 2740, 1718, 1630, 1597 cm^{-1}; H nmr δ: 9.70 (d, J = 1.5 Hz, —CHO), 6.75 (s) and 6.61 (s, 2 Ar—H), 4.64 (t, J = 9 Hz) and 4.01 (dd, J = 9 and 8 Hz, —CH_2—O—R), 3.36 (sex, —*CH*—Me), 2.90 (m, 2H, C.7 benzylic protons), 1.30 (d, J = 6.5 Hz, CH—*Me*), 1.10 and 1.06 (s, C—Me). *Anal.* calcd. for $C_{20}H_{26}O_2$: C 80.49, H 8.78; found: C 80.19, H 9.08.

Huang–Minlon reduction (11) of aldehyde **4***e* afforded the cyclic ether **4***a*, identical in all respects with that described previously (1).

A solution of chromium trioxide (0.70 g) in 80% aqueous acetic acid (21.5 mL) was added slowly to the cyclic ether **4***a* (1.3 g) in acetic acid (35 mL). After 1 h, the reaction mixture was poured into ice-water and extracted with ether. Chromatography of the oily product gave the *ketone* **14** (1.10 g), mp 99–100°C; uv: 236 (8,550), 280 (6,400) and 305 (6,800) nm; ir: 1670, 1625, 1595 cm^{-1}; H nmr δ: 7.86 (s, C.14-H), 6.72 (s, C.11-H), 4.72 (t, J = 9 Hz) and 4.09 (dd, J = 9 and 7.5 Hz, CH_2—O—R), 3.49 (sex, J = 9, 7.5 and 7 Hz, *CH*—Me), 1.32 (d, J = 7 Hz, CH—*Me*), 1.20 (s), 0.98 (s) and 0.92 (s, 3 C—Me); *m/e*: 298 (M^+). *Anal.* calcd. for $C_{20}H_{26}O_2$: C 80.49, H 8.78; found: C 80.51, H 8.99.

Oxidation of **14** *to Diosphenol* **15** *(5-Oxo-6-hydroxy-3,7,7,10a-tetramethyl-2,3,5,7,8,9,10,10a-octahydrophenanthro-[2,3-b] furan)*

The ketone **14** (0.310 g) in *tert*-butanol (10 mL) was added to the cooled solution prepared by dissolving potassium (1.5 g) in *tert*-butanol (40 mL). The mixture was stirred in an atmosphere of oxygen for 2 h which resulted in the uptake of 30.6 mL. The solution was poured into dilute HCl and extracted with chloroform affording a yellow oil (0.350 g) which by chromatography over silica gel gave the *diosphenol* **15** (0.220 g), mp 90–91°C; uv: 232 (9,500), 262 (10 400), 295 (6,200) and 310 (6,000) nm; ir: 3380, 3040, 1635, 1610, 1600 cm^{-1}; H nmr δ: 7.98 (br s, C.14-H), 7.20 (s, D_2O, enol OH), 6.89 (s, C.11-H), 4.79 (t, J = 9 Hz) and 4.17 (dd, J = 9 and 7.5 Hz, —CH_2—O—R), 3.58 (sex, J = 9, 7.5 and 7 Hz, *CH*—Me), 1.51 (s), 1.44 (s) and 1.42 (s, 3 C—Me), 1.39 (d, J = 7 Hz, CH—*Me*); *m/e*: 312 (M^+).

Synthesis of Coleon U (Tri- and Tetra-O-methyl Ethers, **3**c *and* **3**d)

The starting material was prepared from methyl-*O*-methyl podocarpate **7***a* by published methods. The isopropyl residue was introduced (**6***a*) to give **7***b* and the methyl ester was converted to methyl (10, 11) (ferruginol methyl ether). The latter was oxidized with CrO_3/HOAc (see preparation of **14**) to afford **8***b* (sugiol methyl ether).

Quinone **11**e *(2[2(2-Isopropyl-1,4-benzoquinone-5-yl)-2,6,6-trimethylcyclohexyl] Acetic Acid)*

The ketone **8***b* was oxidized as described in the preparation of **11***a*. The crude product obtained by filtration was dried and purified by dry column chromatography (silica gel). After crystallization from ether the yield was 76%, mp 209–210°C (pale yellow needles); ir: 1710, 1640, 1590 cm^{-1}; H nmr δ: 6.54 (s, 1H, =CH—), 6.42 (d, J = 1 Hz, =CH—), 2.84 (sept, J = 7 Hz, 1H, CH in iso-Pr), 1.18 (s, 3H, C—CH_2), 1.11 (d, J = 7 Hz, 6H,

Can. J. Chem. Downloaded from www.nrcresearchpress.com by 210.87.254.40 on 09/06/12
For personal use only.

iso-Pr methyls), 0.93 (s, 6H, 2 C—CH_3); *m/e*: 332 (M^+). *Anal.* calcd. for $C_{20}H_{28}O_4$: C 72.26, H 8.49; found: C 72.40, H 8.60.

Bromoquinone 11f (2[2(2-Bromo-3-isopropyl-1,4-benzoquinone-6-yl)-2,6,6-trimethylcyclohexyl] Acetic Acid)

The quinone **11***e* was brominated with Br_2 (1 mol) in acetic acid (see bromoquinone **11***b*) and the dibromo derivative **13***b* obtained was dried and treated immediately with diethylamine (see **11***b*). The bromoquinone **11***f* was obtained by dry column chromatography in 92% yield from quinone **11***e*, orange needles, mp 182–183°C; ir: 1720, 1670, 1645, 1580 cm^{-1}; H nmr δ: 9.62 (s, 1H, COOH), 6.51 (s, 1H, =CH—), 3.35 (sept, J = 7 Hz, 1H, CH in iso-Pr), 1.29 and 1.26 (2d, J = 7 Hz, 6H, iso-Pr methyls), 1.21 (s, 3H, C—CH_3), 0.95 (s, 6H, 2 C—CH_3); *m/e*: 412 and 410 (M^+). *Anal.* calcd. for $C_{20}H_{27}O_4Br$: C 58.40, H 6.62, Br 19.43; found: C 58.38, H 6.70, Br 19.35.

Hydroxyquinone 11g (2[2(2-Hydroxy-3-isopropyl-1,4-benzoquinone-6-yl)-2,6,6-trimethylcyclohexyl] Acetic Acid)

The product, prepared in the same manner as **11***b*, was purified by dry column chromatography (90%), orange needles, mp 168–170°C (from ether/hexane); ir: 3320, 1715, 1660, 1640, 1600 cm^{-1}; H nmr δ: 7.39 (s, 1H, OH), 6.41 (s, 1H, =CH—), 3.12 (sept, J = 7 Hz, 1H, CH in iso-Pr), 1.19 (d, J = 7 Hz, 6H, iso-Pr methyls), 1.17 (s, 3H, C—CH_3), 0.92 (s, 6H, 2 C—CH_3). *Anal.* calcd. for $C_{20}H_{28}O_5$: C 68.94, H 8.10; found: C 69.19, H 8.21.

Ketone 10c (7-Oxo-11,12,14-trimethoxy-13-isopropyl-podocarpa-8,11,13-triene)

The hydroxyquinone **11***g* was catalytically reduced and methylated while still under hydrogen, as described for diester **9***d*. The product **9***f*, which has never crystallized, was purified by dry column chromatography (yield 79%); ir: 1730 cm^{-1}; H nmr δ: 6.54 (s, 1H, aromatic H), 3.93, 3.77, 3.74 and 3.29 (4s, 3H each, 4 OMe), 1.33 (s, 3H, C—CH_3), 1.27 (d, J = 7 Hz, 6H, iso-Pr methyls), 0.97 (s, 3H, C—CH_3), 0.91 (s, 3H, C—CH_3); *m/e*: 406 (M^+).

Without further purification the ester **9***f* was hydrolyzed to the acid **9***g* (see preparation of **9***e*). The crude product, obtained by suitable extraction (ir: 1705 cm^{-1}; H nmr: 11.1 (s, COOH), only three OMe resonances) was immediately cyclized in trifluoroacetic anhydride (see **10***b*). The product **10***c* was purified by dry column chromatography and crystallized from ether, 73% from **9***f*: needles, mp 93–95°C; ir: 1680 cm^{-1}; H nmr δ: no aromatic protons, 3.81, 3.73 and 3.72 (3s, 3H each, 3 OMe), 1.33 (s, 3H, C—CH_3), 1.31 (d, J = 7 Hz, 6H, iso-Pr methyls), 0.98 (s, 3H, C—CH_3), 0.94 (s, 3H, C—CH_3); *m/e*: 374 (M^+). *Anal.* calcd. for $C_{23}H_{34}O_4$: C 73.76, H 9.15; found: C 73.90, H 9.30.

Coleon U Tri-O-methyl Ether 3c

The oxidation of ketone **10***c* followed the same procedure used to prepare diosphenol **15**. Dry column chromatography afforded a neutral fraction (mostly the starting ketone **10***c*) and the oxidized product **3***c* (50%), needles, mp 148–150°C; ir: 3300, 1670, 1630 cm^{-1}; H nmr δ: 7.41 (s, OH), 3.82 (2s, 6H, 2 OMe), 3.72 (s, 3H, OMe), 3.54 (sept, J = 7 Hz, 1H, CH of iso-Pr), 1.62 (s, 3H, C—CH_3), 1.44 (s, 6H, 2 C—CH_3), 1.33 and 1.31 (2d, J = 7 Hz, 3H each, iso-Pr methyls); *m/e*: 383 (M^+). *Anal.* calcd. for $C_{23}H_3O_5$: C 71.10, H 8.30; found: C 71.38, H 8.46.

Coleon U Tetra-O-methyl Ether 3d

Methylation of **3***c* with methyl iodide and potassium carbonate in acetone afforded the tetra-*O*-methyl ether **3***d* which was purified by dry column chromatography (97%), needles, mp 145–146°C; ir: 1645; H nmr δ: 3.81 (2s, 6H, 2 OMe), 3.75 (s, 3H, OMe), 3.74 (s, 3H, OMe), 3.52 (sept, J = 7 Hz, 1H, CH of iso-Pr), 1.64 (s, 3H, C—CH_3), 1.43 (s, 6H, 2 C—CH_3), 1.36 and 1.34 (2d, J = 7 Hz, 3H each, iso-Pr methyls).

Acknowledgements

We acknowledge gratefully financial assistance from the Natural Sciences and Engineering Research Council of Canada in the form of operating grants and a graduate bursary (S.S.). We thank also the Ministère d'Education du Québec for continued operating grants.

1. R. H. Burnell and M. Ringuet. Can. J. Chem. **56**, 517 (1978).
2. R. H. Burnell, L. Mo, and M. Moinas. Phytochemistry, **11**, 2815 (1972).
3. P. Rüedi and C. H. Eugster. Helv. Chim. Acta, **54**, 1606 (1971).
4. M. Ringuet. Thèse Doctorat en Sciences, Université Laval, Quebec, 1976.
5. T. Matsumoto, Y. Tachibana, M. Hayashi, and K. Fukui. J. Sci. Hiroshima Univ. Ser. A, **39**, 111 (1975).
6. (*a*) W. P. Campbell and D. Todd. J. Am. Chem. Soc. **62**, 1287 (1940); (*b*) R. C. Cambie, L. N. Mander, A. K. Bose, and M. S. Manhas. Tetrahedron, **20**, 409 (1964).
7. S. W. Pelletier and Y. Ohtsuka. Tetrahedron, **33**, 1021 (1977).
8. T. Miyase, P. Rüedi, and C. H. Eugster. Helv. Chim. Acta, **60**, 2270 (1977).
9. T. Matsumoto and S. Takeda. Chem. Lett. 409 (1979).
10. H. H. Zeiss, C. E. Slimowicz, and V. Z. Pasternak. J. Am. Chem. Soc. **70**, 1981 (1948).
11. T. Matsumoto, Y. Ohsuga, S. Harada, and K. Fukui. Bull. Chem. Soc. Jpn. **50**, 266 (1977).

Deaminative electrochemical reduction of pyrazolo[1,5-*a*]pyrimidine-7-amines

CHRISTIAN BELLEC AND PIERRE MAITTE

Laboratoire de Chimie des Hétérocycles, Université Pierre et Marie Curie, 4, Place Jussieu, 75230 Paris, Cedex 05, France

JOSEPH ARMAND

Laboratoire de Physicochimie des solutions, Université Pierre et Marie Curie, 4, Place Jussieu, 75230 Paris, Cedex 05, France

AND

JEAN PINSON

Laboratoire d'Electrochimie, Université Paris VII, 4, Place Jussieu, 75251 Paris, Cedex 05, France

Received January 21, 1981

CHRISTIAN BELLEC, PIERRE MAITTE, JOSEPH ARMAND, and JEAN PINSON. Can. J. Chem. **59**, 2826 (1981).

The pyrazolo[1,5-*a*]pyrimidine-7-amines are electrochemically reduced in hydroorganic medium at low pH into the corresponding 4,5-dihydro compounds. A mechanism is proposed featuring the intermediacy of the parent pyrazolo[1,5-*a*]pyrimidine itself. The 4,5-dihydroderivatives can be rearomatized, thus offering a facile synthetic route to the pyrazolo[1,5-*a*]pyrimidines.

CHRISTIAN BELLEC, PIERRE MAITTE, JOSEPH ARMAND et JEAN PINSON. Can. J. Chem. **59**, 2826 (1981).

Les amino-7 pyrazolo[1,5-*a*] pyrimidines peuvent être réduites électrochimiquement en milieu hydroorganique acide, elles conduisent par désamination et réduction aux dérivés 4,5-dihydro. Le mécanisme de cette réduction a été étudié; on propose la formation intermédiaire de la pyrazolo[1,5-*a*] pyrimidine correspondante. Les dihydro-4,5 pyrazolo[1,5-*a*] pyrimidines ont été réaromatisées. L'ensemble de ces deux étapes constitue une voie d'accès facile aux pyrazolo[1,5-*a*] pyrimidines.

Introduction

The reaction of hydrazine and of its derivatives with β-ketonitriles leads generally to 5-aminopyrazoles through the hydrazones or enehydrazines which can be isolated (1). However, under certain conditions it is possible to prepare fused heterocyclic compounds: the pyrazolo[1,5-*a*]pyrimidine-7-amines (2–5).

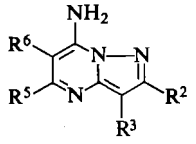

The synthesis of pyrazolo[1,5-*a*]pyrimidines (6–11) has been the subject of recent interest in pharmacological activities. Central nervous system depressor, tranquilizer, anticoagulant, and antiinflammatory properties have been found for some members of the series.

Therefore, the interest of an electrochemical investigation of pyrazolo[1,5-*a*]pyrimidine-7-amines was twofold: on the one hand, the opportunity of studying the reduction mechanism of a new fused heterocyclic system and, on the other hand, the possibility of preparing new compounds.

Compounds **1**(*a–f*) have been prepared and investigated (Table 1).

Electrochemical Behaviour of 1(a–f)

In an acidic buffered hydroorganic solution (50% acetonitrile, pH 1.15) all these compounds, or more likely a protonated form, present a single polarographic wave; the height is close to 4 F and the half wave potential lies between −1.20 V and −1.30 V (Table 1).

These waves are very close to the background. The precise measurement of their half-wave potential and of their height is rather difficult. This was achieved according to the following procedure: the half-wave potentials were measured by ac polarography ($E_p = E_{1/2}(12)$) and the height of the wave was obtained by multiplying by two the height at the level of the half-wave potential. Upon increasing the pH these waves disappeared.

A coulometry carried out at a potential corresponding to the foot of the wave (e.g. for **1***a*, pH = 1.38, $E = -1.25$ V) indicated the consumption of 4 F per mole. A preparative electrolysis under the same experimental conditions ($c = 9 \times 10^{-3}$ *M*) yielded 4,5-dihydropyrazolo[1,5-*a*]pyrimidines **2** (*a–f*) in good yields (Table 2).

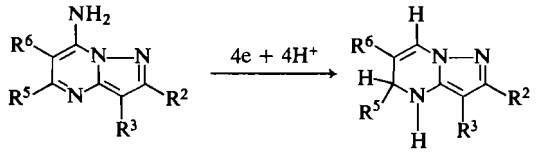

1(*a–f*) **2**(*a–f*)

The cyclic voltammetry of **1***a* on a vitreous carbon electrode (Fig. 1) (starting from +0.9 V, v =

0008-4042/81/192826-07$01.00/0

©1981 National Research Council of Canada/Conseil national de recherches du Canada

Can. J. Chem. Downloaded from www.nrcresearchpress.com by 210.87.254.5 on 09/06/12
For personal use only.

Can. J. Chem. Downloaded from www.nrcresearchpress.com by 210.87.254.5 on 09/06/12
For personal use only.

0.2 V s^{-1}) shows on the first cathodic scan the single peak I_c of **1***a* and two small anodic peaks II_a (E_p = +0.22 V) and III_a (E_p = +0.48 V) identical with those observed for the corresponding dihydroderivative **2***a*. On the second and successive cathodic scans, a small cathodic peak IV_c (E_p = −1.05 V) is observed, which is that of the pyrazolo[1,5-*a*]pyrimidine **3***a*. This same peak IV_c can be observed both on a vitreous carbon and on a hanging mercury drop electrode (Fig. 2; E_{p_c} = −0.975 V) when starting from −0.4 V and scanning at 200 V s^{-1}.

This could allow the determination of the rate of the chemical deamination step if one could measure the height of the peak of **1***a*, which should decrease from 4 to 2 F per mole (13). In our case, the peak of **1***a* is too close to the background to allow such a determination. However, the relative height of the peaks of **1***a* and **3***a* allows one to estimate the order of magnitude of this rate constant which is about 100 s^{-1}.

When the electrolysis is carried out on mercury in a thin layer cell inside a uv spectrophotometer, the spectrum of **1***a* (λ_{max} = 285 nm, ε = 18 400; 346 nm, ε = 5700; 50% CH_3CN) progressively disappears at the expense of that of **2***a* (λ_{max} = 275 nm, ε = 12 000; 325 nm, ε = 18 600) (Fig. 3). The spectrum presents two isobestic points at 306 and 350 nm.

The pyrazolo[1,5-*a*]pyrimidine **3***a* was also investigated by cyclic voltammetry on vitreous carbon; on the cathodic scan (starting from +0.8 V, v = 0.2 V s^{-1}) peak IV_c is observed, while peaks II_a and III_a appear on the anodic scan. Besides, a preparative electrolysis of **3***a* under the same conditions as for **1***a* (E = −1.15 V) furnished **2***a* in 87% yield.

Aromatization of 4,5-Dihydropyrazolo[1,5-a]-pyrimidines

As the pyrazolo[1,5-*a*]pyrimidines unfunctionalized on the 7-position have never been described in the literature, attempts were made to prepare them through the rearomatization of their dihydroderivatives. From the voltammogram of Fig. 1 this reoxidation seems possible by electrochemistry. However, it was more convenient to achieve the

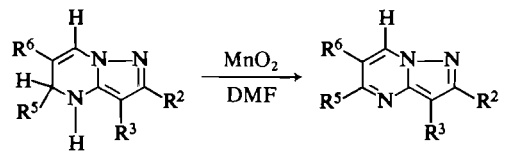

2(*a*–*f*) **3**(*a*–*f*)

TABLE 1. Properties of compounds **1** (*a*–*f*)

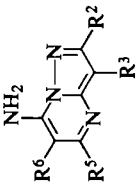

Compound	R^2	R^3	R^5	R^6	Yield (%)	Melting point (°C)	$E_{1/2}$ (V) at pH 1.15	δR^2	δR^3	δR^5	δR^6	δNH_2
1*a*[a]	H	C_6H_5	H	C_6H_5	73	223–224	−1.21	8.62 s	7.1–7.7 m	8.25 s	7.1–7.7 m	8.15 s[c]
1*b*[b]	CH_3	C_6H_5	H	C_6H_5	81	215–216	−1.21	2.67 s	7.55–7.62 m	8.17 s	7.55–7.62 m	—
1*c*[a]	CH_3	H	H	C_6H_5	68	186–187	−1.30	2.47 s	6.21 s	8.06 s	7.50 s	7.12 s[c]
1*d*[b]	C_6H_5	H	H	C_6H_5	76	236–237	−1.31	7.1–8.0 m	6.87 s	8.03 s	7.1–8.0 m	—
1*e*[a]	H	C_6H_5	CH_3	C_6H_5	70	241–242	−1.22	8.61 s	7.3–8.2 m	2.33 s	7.3–8.2 m	6.6 s[c]
1*f*[b]	C_6H_5	C_6H_5	H	C_6H_5	89	240	−1.29	7.25–7.8 m	7.25–7.8 m	8.17 s	7.25–7.8 m	—

[a]Solvent DMSO-d_6.
[b]Solvent trifluoroacetic acid.
[c]Broad signal exchanges with D_2O.

TABLE 2. Properties of compounds **2** (*a–f*)

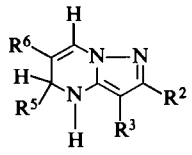

Compound	Yield (%)	Melting point (°C)	δR²	δR³	δR⁵	δR⁶	δ7-H
2*a*[a]	80	234–235	8.18 s	7.56 s 7.68 s	5.41 s	7.56 s 7.68 s	7.07 s
2*b*[a]	78	135–136	2.50 s	7.2–7.7 m	5.27 s	7.2–7.7 m	6.88 s
2*c*[a]	82.5	200–201	2.47 s	5.93 s	5.17 s	7.35 s	6.83 s
2*d*[a]	70	185–186	7.45–7.75 m	6.37 s	5.25 s	7.45–7.75 m	6.90 s
2*e*[b]	74	157	[c]	6.9–7.7 m	1.05 d 4.33 q	6.9–7.7 m	[c]
2*f*[a]	60.7	143	7.2–7.75 m	7.2–7.75 m	5.31 s	7.2–7.75 m	6.86 s

[a]Solvent trifluoacetic acid.
[b]Solvent $CDCl_3$.
[c]In aromatic signal.

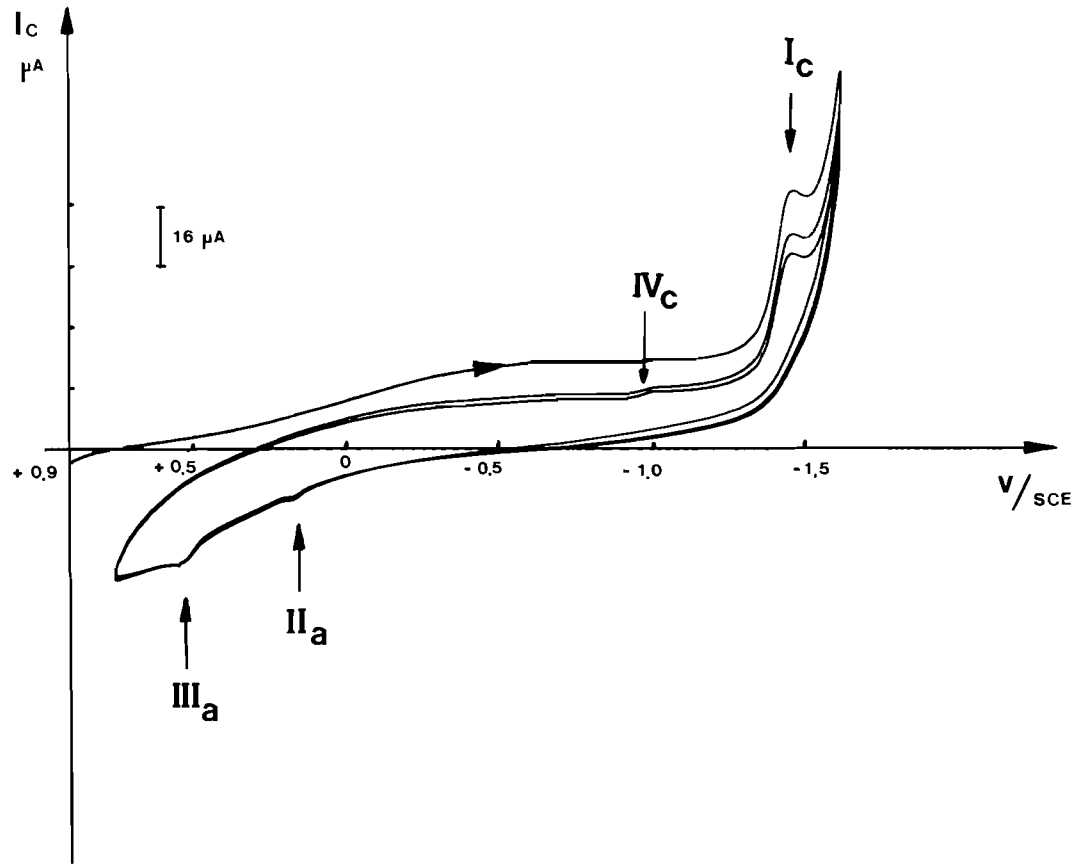

FIG. 1. Cyclic voltammogram of **1***a* at pH 1. 15 (60% DMF) on a vitreous carbon electrode. Scan rate 200 mV s^{-1}.

Can. J. Chem. Downloaded from www.nrcresearchpress.com by 210.87.254.5 on 09/06/12
For personal use only.

Can. J. Chem. Downloaded from www.nrcresearchpress.com by 210.87.254.5 on 09/06/12
For personal use only.

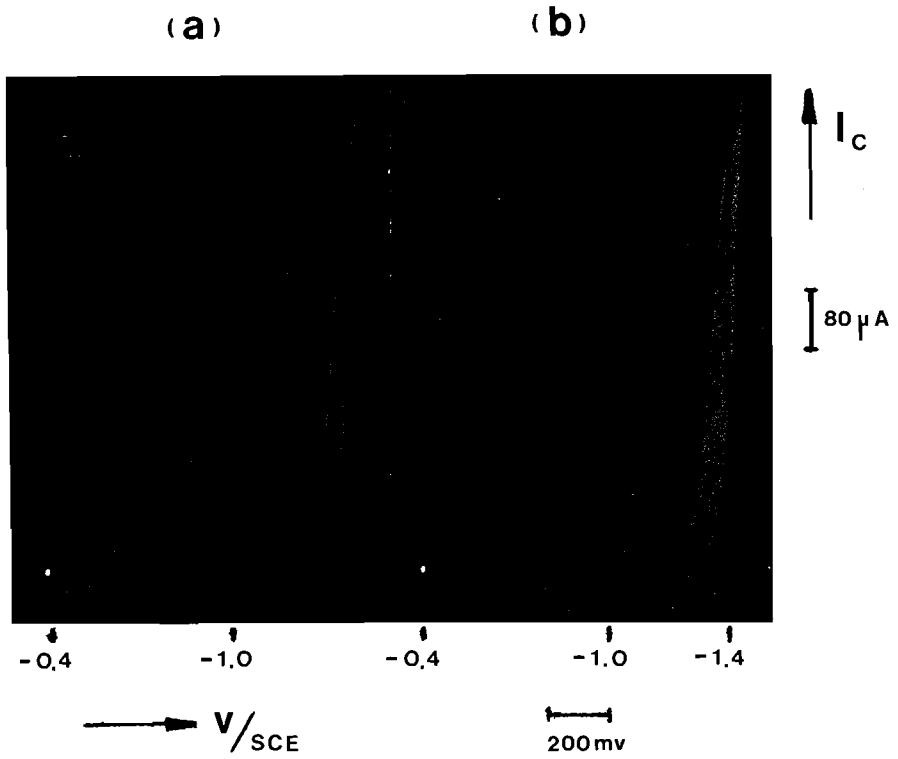

FIG. 2. Cyclic voltammogram of **1***a* at pH 1.15 (60% DMF) on a hanging mercury drop electrode. Scan rate 200 V s^{-1}. (a) First scan; (b) first and successive scans.

TABLE 3. Properties of compounds **3** (*a–f*)

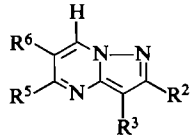

Compound	Yield (%)	Melting point (°C)	δ R^2	δ R^3	δ R^5	δ R^6	δ 7-H
3*a*[a]	75	197–198	8.63 s	7.3–7.9 m	9.51 s	7.3–7.9 m	9.25 s
3*b*[a]	59	143–144	2.73 s	7.4–7.8 m	9.71 s	7.4–7.8 m	9.25 s
3*c*[a]	50	164–165	2.80 s	7.08 s	9.77 s	7.66 s	9.33 s
3*d*[a]	65	195–196	7.4–8.1 m	7.38 s	9.80 s	7.4–8.1 m	9.21 s
3*e*[a]	62	172–173	8.40 s	7.1–7.5 m	2.53 s	7.1–7.5 m	9.20 s
3*f*[a]	72	160	7.3–7.8 m	7.3–7.8 m	9.82 s	7.3–7.8 m	9.25 s

[a]Solvent trifluoroacetic acid.

oxidation by MnO_2 in dimethylformamide according to an experimental procedure derived from that used for the aromatization of dihydropyrazines (14).

The yields and melting points of the compounds **3**(*a–f*) are given in Table 3.

Discussion

Reduction Mechanism

Three reduction pathways can be envisaged for the reduction of **1** into **2** as shown in Scheme 1.

The results of the fast scan cyclic voltammetry experiments indicate that **3** must be an intermediate

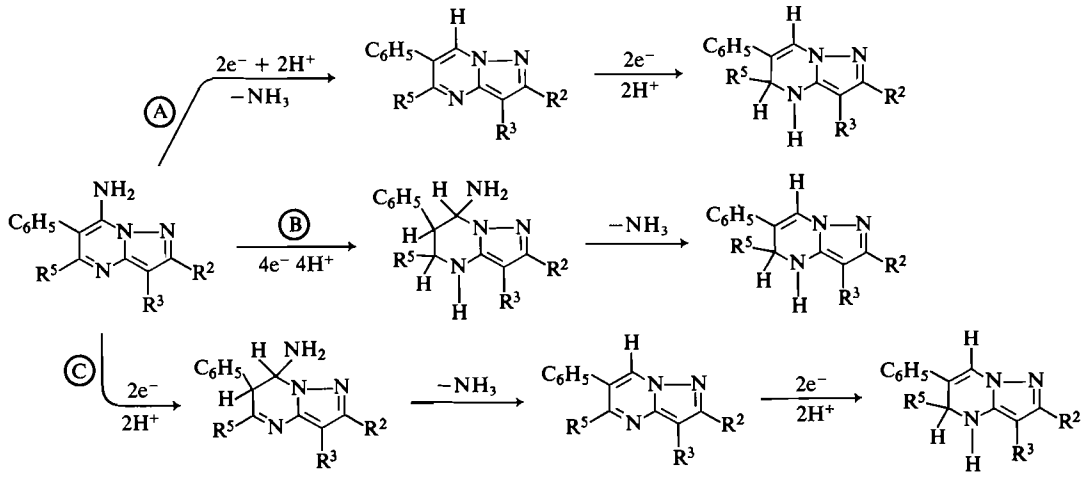

SCHEME 1

on the way from **1** to **2**. This allows one to exclude route B. Compound **3**, as it is easier to reduce than **1**, is converted into **2** during the electrolysis. The deamination of the 7-amino-6,7-dihydro intermediate must be fast as the spectra recorded during the electrolysis show an isobestic point. This was confirmed by cyclic voltammetry as no additional peak, which could have been assigned to this intermediate, could be observed up to a scan rate of 200 V s^{-1} at room temperature or up to 20 V s^{-1} at −17°C.

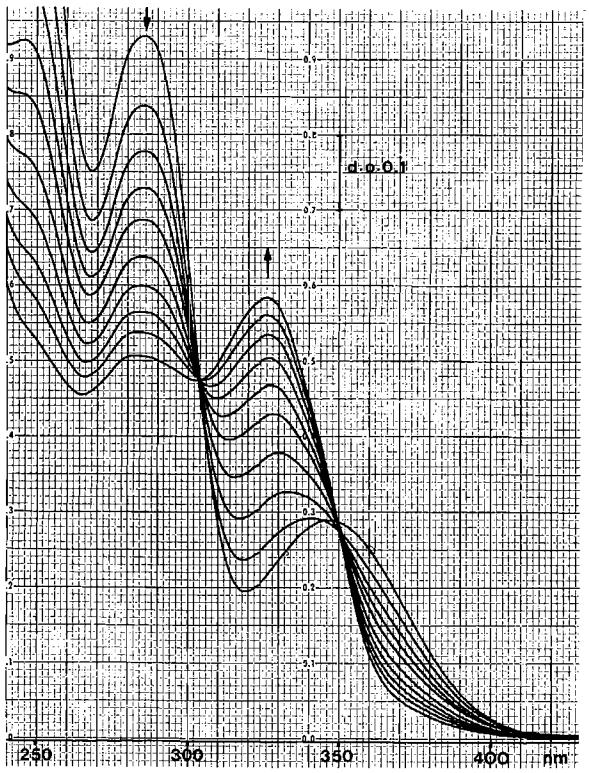

FIG. 3. Ultraviolet spectral changes during the electrolysis of **1***a* at pH 1. 15 (50% CH_3CN) at $E = -1.25$ V.

In the case of 4-amino-2,6-dimethylpyrimidine (15), 4-aminoquinazoline (16), and cytosine (17) a reduction path similar to route C was proposed. In the case of adenine, Smith and Elving (17) had suggested a mechanism analogous to route B, but it was shown later by Kwee and Lund (18) that a reduction scheme similar to C was more likely. For example, in the case of 4-aminoquinazoline (16) the mechanism was supported by the increase of the reduction wave from 2 to 4 F per mole upon increasing the pH.

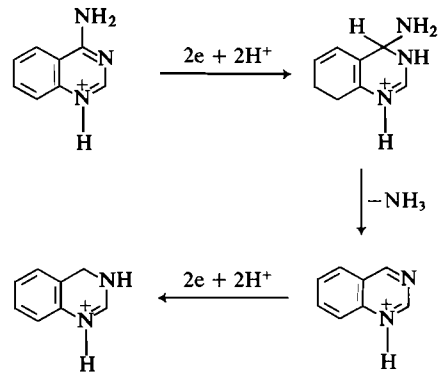

There is, to the best of our knowledge, no published example of a mechanism similar to route A, featuring a C—N electrochemical cleavage. On the other hand, route C implies that a C=C bond be reduced before a C=N bond. Therefore, it is not possible at the present time to discriminate soundly between path A and path C.

Synthetic Interest

Although some derivatives dihydrogenated in the 4,7-position have been prepared recently by

Can. J. Chem. Downloaded from www.nrcresearchpress.com by 210.87.254.5 on 09/06/12
For personal use only.

Can. J. Chem. Downloaded from www.nrcresearchpress.com by 210.87.254.5 on 09/06/12
For personal use only.

reaction of sodium borohydride with pyrazolopyrimidines having an ester group on the 6-position (11), no 4,5-dihydropyrazolo[1,5-*a*]pyrimidines have ever been described. The same situation occurs for 6-aryl substituted pyrazolo[1,5-*a*]pyrimidines that we have obtained through the rearomatization of the dihydrogenated compounds.

As the pyrazolo[1,5-*a*]pyrimidine-7-amines are easily obtained from the β-ketonitriles, the electrochemical reduction provides a new and simple route to the 4,5-dihydropyrazolo[1,5-*a*]pyrimidines. These can be rearomatized into pyrazolo-[1,5-*a*]pyrimidines.

Experimental

The apparatus and techniques used for polarography and electrolysis have been described previously (19, 20). The reference electrode was a saturated calomel electrode. The pH values were measured with a Radiometer model 4 pHmeter equipped with a combined glass–calomel electrode GK 2302B standardized in aqueous buffer. The high scan rate voltammograms were recorded with the help of an apparatus composed of a Tacussel GSTP3 signal generator, a fast-rise wide bandpass potentiostat provided with an ohmic drop compensation device (21), and a memory oscilloscope Tektronix 7313. A vitreous carbon electrode (3 mm diameter) was used, and it was polished with 1 μ diamond paste before each experiment. The ac polarograms (10 mV, 320 Hz ac signal) were recorded on a Tacussel PRG3 polarograph. The uv spectra were recorded on a Cary 219 spectrophotometer by withdrawing samples from an electrolysis at regular intervals ($c = 5 \times 10^{-4}$ *M*; 50% CH_3CN, H_2SO_4 *N*/10; quartz cell 0.5 mm diameter). The microanalyses were performed by the "Service de Microanalyse du CNRS" (Gif sur Yvette). All the compounds described gave correct elemental analyses. The following abbreviations are used in reporting the nmr results: s = singlet, d = doublet; t = triplet, q = quadruplet, and m = multiplet.

Preparation of Pyrazolo[1,5-a]pyrimidine-7-amines

7-Amino-3,6-diphenylpyrazolo[1,5-a]pyrimidine (1a) was obtained by condensation in acidic medium of 5-amino-4-phenylpyrazole (22) with 2-formyl-2-phenylacetonitrile according to ref. 4; mp 224°C, $C_{18}H_{14}N_4$. A erroneous assignment has been proposed (4) for nmr data.

7-Amino-2-methyl-3,6-diphenylpyrazolo[1,5-a]pyrimidine (1b)

A mixture of 1.8 g of 3-methyl-4-phenyl-5-aminopyrazole and 1.5 g of 2-formyl-2-phenylacetonitrile was heated during 6 h in 60 mL of ethanol and 3 mL of concentrated hydrochloric acid. After cooling, the hydrochloride did not precipitate. The solution was poured into 300 mL of water and sodium carbonate was added until pH 7–8. The white precipitate was filtered, washed with water, and dried; 81% yield, mp 215–216°C (ethanol), $C_{19}H_{16}N_4$.

7-Amino-2-methyl-6-phenylpyrazolo[1,5,-a]pyrimidine: (1c) was obtained, as in the case of 1*b*, by condensation of 1.3 g of 5-amino-3-methylpyrazole (4) with 2 g of 2-formyl-2-phenylacetonitrile; 68% yield, mp 186–187°C (C_6H_6–ligroin 80:20), $C_{13}H_{12}N_4$.

7-Amino-2,6-diphenylpyrazolo[1,5-a]pyrimidine: (1d) was obtained under the same conditions as above with a mixture of 1.35 g of 5-amino-3-phenylpyrazole and 1.2 g of 2-formyl-2-phenylacetonitrile: 76% yield, mp 236–237°C (benzene), $C_{18}H_{14}N_4$.

7-Amino-5-methyl-3,6-diphenylpyrazolo[1,5-a]pyrimidine: (1e) was prepared by condensation of 2 g of 5-amino-4-phenylpyrazole and 1.8 g of 2-acetyl-2-phenylacetonitrile: 70% yield, mp 241–242°C (benzene), $C_{19}H_{16}N_4$.

7-Amino-2,3,6-triphenylpyrazolo[1,5-a]pyrimidine: (1f) was obtained by condensation of 1 g of 5-amino-3,4-diphenylpyrazole and 0.6 g of 2-formyl-2-phenylacetonitrile: 89% yield, mp 240–241°C (benzene–ligroin 80:20), $C_{24}H_{18}N_4$.

Electrochemical Reductions of Pyrazolo[1,5-a]pyrimidine-7-amines: Preparation of Dihydro Derivatives

Electrolysis of 7-Amino-3,6-diphenylpyrazolo[1,5-a]pyrimidine (1a): Preparation of (2a)

A solution (250 mL) was prepared from 125 mL of CH_3CN, 25 mL of a 1 *M* solution of sulfuric acid, and water; 200 mL of this solution and 500 mg ($c = 8.75 \times 10^{-3}$ *M*) of **1***a* were used to fill the cathodic compartment while the remainder was used in the anodic compartment, pH 1.38; $E = -1.25$ V. After consumption of 650 C (4 F = 675 C) the current decreased to 40 mA. A precipitate appeared in the cell at 700 C and the current increased to attain 100 mA at 900 C. The electrolysis was stopped, CH_3CN was evaporated, and the solution was filtered. The precipitate was washed with water and dried; 380 mg (80% yield) of 4,5-dihydro-3,6-diphenylpyrazolo[1,5-*a*]pyrimidine (**2***a*) were obtained, mp 234–235°C ($CHCl_3$), $C_{18}H_{15}N_3$.

Electrolysis of 7-Amino-2-methyl-3,6-diphenylpyrazolo[1,5-a]pyrimidine (1b): Preparation of 2b

A solution was prepared as in the case of **1***a*. Compound **1***b*, 600 mg ($c = 10^{-2}$ *M*) was reduced in 200 mL of this solution, pH 1.40; $E = -1.3$ V. After consumption of 800 C (772 C = 4 F) the current decreased to 15 mA and the electrolysis was stopped. Acetonitrile was evaporated to give a precipitate (440 mg, 78% yield) of 4,5-dihydro-2-methyl-3,6-diphenylpyrazolo[1,5-*a*]pyrimidine (**2***b*), mp 135–136°C, $C_{19}H_{17}N_3$.

Electrolysis of 7-Amino-2-methyl-6-phenylpyrazolo[1,5-a]pyrimidine (1c): Preparation of 2c

In the same condition as above, the electrolysis was carried out with 700 mg ($c = 1.6 \times 10^{-2}$ *M*) of **1***c*, pH 1.46; $E = -1.25$ V. After consumption of 1300 C (1206 C = 4 F) the current dropped to 30 mA. The electrolysis was stopped and acetonitrile was evaporated. Sodium carbonate was added to the solution until pH 7–8. A white solid precipitated: 545 mg (82.5% yield) of 4,5-dihydro-2-methyl-6-phenylpyrazolo[1,5-*a*]pyrimidine (**2***c*), mp 200–201°C, $C_{13}H_{13}N_3$.

Electrolysis of 7-Amino-2,6-diphenylpyrazolo[1,5-a]pyrimidine (1d): Preparation of 2d

Electrolysis was carried out with 590 mg ($c = 10^{-2}$ *M*) of **1***d*, pH 1.35; $E = -1.3$ V. After consumption of 760 C (772 C = 4 F) the electrolysis was stopped. A solid was obtained after evaporation of acetonitrile: 4,5-dihydro-2,6-diphenylpyrazolo-[1,5-*a*]pyrimidine (**2***d*), 390 mg (70% yield), mp 185–186°C (C_6H_6), $C_{18}H_{15}N_3$.

Electrolysis of 7-Amino-5-methyl-3,6-diphenylpyrazolo[1,5-a]pyrimidine (1e): Preparation of 2e

Electrolysis was carried out at $E = -1.30$ V with 700 mg of **1***e*, pH 1.20. After consumption of 2800 C (4 F = 906 C) the current was still 200 mA. This high intensity was due to the reduction of H^+. The electrolysis was stopped, CH_3CN evaporated, and Na_2CO_3 added until pH 7. A white solid precipitated: 4,5-dihydro-5-methyl-3,6-diphenylpyrazolo[1,5-*a*]pyrimidine (**2***e*): 520 mg (74% yield), mp 157°C, $C_{19}H_{17}N_3$.

Electrolysis of 7-Amino-2,3,6-triphenylpyrazolo[1,5-a]-pyrimidine (1f): Preparation of 2f

Electrolysis was carried out at $E = -1.30$ V with 700 mg of **1***f*. A solid precipitated during the electrolysis. After consumption of 1200 C the current was stopped. The precipitate was filtered

and dried: 4,5-dihydro-2,3,6-triphenylpyrazolo[1,5-*a*]pyrimidine (**2***f*), 410 mg (61% yield), mp 143°C, $C_{24}H_{19}N_3$.

Aromatization of 4,5-Dihydropyrazolo[1,5-a]pyrimidines
General Procedure

Three hundred milligrams of 4,5-dihydropyrazolo[1,5-*a*] pyrimidine (200 mg in the case of **3***b*) were dissolved in 10 mL of dimethylformamide; 300 mg of MnO_2 were added to the solution. The mixture was stirred and heated at 50°C during 12 h. The solution was filtered and 300 mL of water were added. The solid was washed with water and dried.

1. P. Souchay, S. Deswarte, and Ch. Bellec. C.R. Acad. Sci. Ser. C, **276**, 1457 (1973).
2. F. Eiden and G. Evers. Arch. Pharm. Weinheim, **304**, 121 (1971).
3. V. Sprio, R. Vicenzo. Atti Accad. Sci. Lett. Arti Palermo, **61**, 206 (1971).
4. E. Alcade, J. Demendoza, C. Almera, and J. Elguero. J. Heterocycl. Chem. **11**, 423 (1974).
5. A. McKillop and R. J. Kobylecki. Heterocycles, **6**, 1355 (1977).
6. R. Robins, D. E. O'Brien, T. Novinson, and R. H. Springer. Ger. Patent No. 2,257,547 (June, 1973); Chem. Abstr. **79**, 78840 (1973).
7. M. Elnagdi, S. M. Fahmy, and E. Zayed. Z. Naturforsch. Teil B, **31**, 795 (1976).
8. W. E. Kirkpatrick, T. Okabe, I. W. Hillyard, and R. K. Robins. J. Med. Chem. **20**, 386 (1977).
9. Y. Van Haverbeke, A. Maquestiau, and J. J. Vanden Eynde. J. Heterocycl. Chem. **16**, 773 (1979).
10. G. Auzzi, L. Cecchi, A. Constanzo, and F. Bruni. Farmaco Ed. Sci. **34**, 478 (1979).
11. G. Auzzi, L. Cecchi, A. Costanzo, L. Vettori, L. Pecori, and F. Bruni. Farmaco Ed. Sci. **34**, 751 (1979).
12. A. J. Bard and L. R. Faulkner. Electrochemical methods. J. Wiley and Sons, New York. 1980. p. 332.
13. L. Mastragostino, L. Nadjo, and J. M. Saveant. Electrochim. Acta, **13**, 721, (1968).
14. Y. Ohtsuka, E. Tohma, S. Kojima, and N. Tomita. J. Org. Chem. **44**, 4871 (1979).
15. D. L. Smith and P. J. Elving. J. Am. Chem. Soc. **84**, 2741 (1962).
16. S. Kwee and H. Lund. Acta Chem. Scand. **25**, 1818 (1971).
17. D. L. Smith and P. J. Elving. J. Am. Chem. Soc. **84**, 1412 (1962).
18. S. Kwee and H. Lund. Acta Chem. Scand. **26**, 1195 (1972).
19. J. Armand and L. Boulares. Bull. Soc. Chim. Fr. 336 (1975).
20. J. Pinson and J. Armand. Collect. Czech. Chem. Commun. **36**, 585 (1971).
21. D. Garreau and J. M. Saveant. J. Electroanal. Chem. **35**, 309 (1972).
22. C. Alberti. Gazz. Chim. Ital. **89**, 1017 (1959).

Can. J. Chem. Downloaded from www.nrcresearchpress.com by 210.87.254.5 on 09/06/12
For personal use only.

Preparation and reactions of 4b-acetoxy-4b,9b-dihydroindeno[2,1-*a*]indene-5,10-dione

STANLEY WAWZONEK

Department of Chemistry, University of Iowa, Iowa City, IA 52242, U.S.A.

Received March 25, 1981

STANLEY WAWZONEK. Can. J. Chem. **59**, 2833 (1981).

4b-Acetoxy-4b,9b-dihydroindeno[2,1-*a*]indene-5,10-dione prepared by treating 4b,9b-dihydroindeno[2,1-*a*]indene-5,10-dione with lead tetraacetate was hydrolyzed to the alcohol, 4b-hydroxy-4b,9b-dihydroindeno[2,1-*a*]indene-5,10-dione with hydrochloric acid and converted to 4b-methoxy-4b,9b-dihydroindeno[2,1-*a*]indene-5,10-dione with sodium hydroxide in methanol. The alcohol was stable to base and could not be converted to dibenzo[*a*,*c*]cyclooctadiene-5,6,11-trione. Attempts to form the epoxydiketone from the acetate with sodium hydroxide and hydrogen peroxide gave benzil dicarboxylic acid, 11-keto[1,2-*c*]isocoumarin and 4b-methoxy-4b,9b-dihydroindeno[2,1-*a*]indene-5,10-dione.

STANLEY WAWZONEK. Can. J. Chem. **59**, 2833 (1981).

L'acétoxy-4b dihydro-4b,9b indéno[2,1-*a*] indènedione-5,10, obtenu par la réaction des dihydro-4b,9b indéno[2,1-*a*] indènedione-5,10 avec le tétraacétate de plomb est hydrolysé en hydroxy-4b dihydro-4b,9b indéno[2,1-*a*] indènedione-5,10 sous l'influence de l'acide chlorhydrique et ce acétate soumis à l'action de l'hydroxyde de sodium en présence de méthanol conduit au méthoxy-4b dihydro-4b,9b indéno[2,1-*a*] indènedione-5,10. L'alcool est stable en milieu basique et ne peut être transformé en dibenzo [*a*,*c*] cyclooctadiène trione-5,6,11. On a essayé de former l'époxycétone à partir de l'acétate avec l'hydroxyde de sodium et l'eau oxygénée mais on obtient l'acide benzyle dicarboxylique, le céto-11[1,2-*c*] isocoumarin et la méthoxy-4b dihydro-4b,9b indéno[2,1-*a*] indènedione-5,10.

[Traduit par le journal]

Can. J. Chem. Downloaded from www.nrcresearchpress.com by 210.87.254.5 on 09/06/12
For personal use only.

Attempts to prepare dibenzo[*a*,*e*]cyclooctadien-5,6,11-trione (**3**) from dibenzo[*a*,*e*]cyclooctadien-5,11-dione were not successful; the product obtained was 11-keto[1,2-*c*]isocoumarin (**4**) (1). In the present work the product from the reaction of 4b,9b-dihydroindeno[2,1-*a*]indene-5,10-dione with lead tetraacetate, 4b-acetoxy-4b,9b-dihydroindeno[2,1-*a*]indene-5,10-dione, was investigated as a means of preparing this elusive compound. It was hoped that conversion of this acetate to the corresponding alcohol followed by a reverse aldol would yield the desired triketone.

Experimental

All melting points are uncorrected. Infrared (ir) spectra were recorded with a Perkin-Elmer Infracord spectrometer. The nmr spectra were obtained using tetramethylsilane as an internal standard with a Varian A60 NMR spectrometer.

4b-Acetoxy-4b,9b-dihydroindeno[2,1-a]indene-5,10-dione (1b)

The diketone (**1***a*) (11.7 g, 0.05 mol) was heated with lead tetraacetate (25 g, 0.056 mol) in acetic acid (200 mL) upon a steam bath for 48 h. The acetic acid was removed under reduced pressure and the resulting solid was treated with water and extracted with benzene. Removal of the benzene gave a solid (**1***b*) which was recrystallized from benzene; yield, 5.9 g; mp 120–124°C (gas evolution). The filtrate was chromatographed using benzene and silica and gave an additional 4.04 g of **1***b*. Two recrystallizations from a mixture of benzene and petroleum ether (bp 60–70°C) gave a sample melting at 125–127°C. Occasionally the sample obtained melted at 150–151°C. The lower melting sample upon remelting gave the higher melting point. Both samples gave the same ir and nmr spectra and elemental analysis.

The use of a two-fold amount of lead tetraacetate in this reaction did not change the nature of the product.

Infrared (Nujol): 5.68 (CH_3COO), 5.8–5.82 (CO), 8.26 (C—O) μ; nmr (chloroform-*d*), δ: 2.13 (s, 3H, CH_3), 4.45 (s, 1H, CH), 7.4–8.1 (m, 8H, aromatic). *Anal.* calcd. for $C_{18}H_{12}O_3$: C 73.97, H 4.11; found: 73.67, H 3.96.

4b-Hydroxy-4b,9b-dihydroindeno[2,1-a]indene-5,10-dione (1c)

The acetate (**1***b*) (0.74 g) was refluxed in a mixture of methanol (30 mL), water (10 mL), and 6 *N* hydrochloric acid (5 mL) for 25 h. Addition of water followed by removal of the solvent under reduced pressure gave a solid which was treated with water and filtered; yield, 0.62 g. Recrystallization from benzene gave the hydroxy ketone **1***c* melting at 140–142°C; ir (Nujol): 2.97 (OH), 5.82 (shoulder), 5.90 (C=O); nmr (chloroform-*d*), δ: 4.23 (s, 1H, CH), 4.50 (broad s, 1H, OH), 7.3–8.0 (m, 8H, aromatic). The broad singlet at 4.50 disappeared in the presence of D_2O. *Anal.* calcd. for $C_{16}H_{10}O_3$: C 76.80, H 4.00; found: C 76.99, H 4.21.

The alcohol (**1***c*) was stable to treatment with an aqueous methanol solution of sodium carbonate, *o*-phenylenediamine, and sodium hydroxide and benzaldehyde.

The alcohol (**1***c*) (0.09 g) upon treatment with acetic anhydride (2.5 mL) and potassium acetate (0.01 g) at 100°C for 2 h gave the acetate (**1***b*) (0.09 g) melting at 125–128°C after recrystallization from methanol.

Solvolysis of Acetate 1b

The acetate **1***b* (0.05 g) was heated at reflux in methanol (15 mL) and water (5 mL) for 41 h. The solution upon cooling gave a red solid (0.006 g) melting at 285–287°C (lit. (2) mp 284°C). The filtrate upon concentration gave the starting acetate (**1***b*) (0.03 g).

4b-Methoxy-4b,9b-dihydroindeno[2,1-a]indene-5,10-dione (1d)

A solution of the acetate (**1***b*) (0.12 g) in methanol (25 mL) was treated with 1.5 mL of 0.004 *N* sodium hydroxide and allowed to stand for 4 h at room temperature. The resulting solution was filtered from a small amount of high melting solid and the methanol was removed under reduced pressure. The resulting pink solid was triturated with water and filtered. Extraction of this solid (0.106 g) with hot petroleum ether (bp 60–68°C) gave 0.03 g of the methyl ether **1***d* which on heating softened at 85°C

0008-4042/81/192833-02$01.00/0

©1981 National Research Council of Canada/Conseil national de recherches du Canada

and melted at 91–94°C. Recrystallization from the same solvent gave a sample which softened at 85°C and melted at 96–97°C; ir (Nujol): 5.85 (CO); nmr (chloroform-*d*), δ: 3.35 (s, 3H, CH_3O), 4.35 (s, 1H, CH), 7.3–8.1 (m, 8H, aromatic). *Anal.* calcd. for $C_{17}H_{12}O_3$: C 77.27, H 4.55; found: C 77.13, H 5.03.

Higher melting products in this reaction were not investigated.

*Oxidation of Acetate 1*b

The acetate (**1***b*) (2.92 g) was dissolved in methanol (150 mL) by heating and the resulting solution after cooling was treated successively with 15% hydrogen peroxide (5 mL) and 4 *N* sodium hydroxide (7.5 mL). The solution turned dark red and was stirred at room temperature for 6 h and then allowed to stand for an additional 21 h; no change in color occurred in this period. Acidification with dilute acetic acid followed by concentration of the solution gave 1.40 g of *o*,*o*′-benzildicarboxylic acid melting at 250–254°C dec. Recrystallization from ethanol gave a sample melting at 261–265°C dec. (lit. (3) mp 265–270°C). Identification was made by the ir spectrum and formation of diphthalyl and phthalic anhydride upon melting (3).

The methanol filtrate was evaporated to dryness and the residue was dissolved in benzene. Chromatography on silica gave 11-keto[1,2-*c*]isocoumarin (**4**) (0.03 g) and the methyl ether **1***d* (0.15 g). Identification of these two compounds was made by comparison with authentic samples.

The use of 2.3 mL of 15% hydrogen peroxide and 5 mL of 4 *N* sodium hydroxide gave similar products to the above, but the amount of indenoisocoumarin **4** formed was larger.

Results and Discussion

Treatment of 4b,9b-dihydroindeno[2,1-*a*]indene-5,10-dione (**1***a*) with lead tetraacetate gave 4b-acetoxy-4b,9b-dihydroindeno[2,1-*a*]indene-5,10-dione (**1***b*); only monoacetylation occurred even when an excess of lead tetraacetate was used.

The acetate (**1***b*) was hydrolyzed by dilute hydrochloric acid to the alcohol **1***c* without dehydration of **1***c* to the unsaturated diketone **2** or its

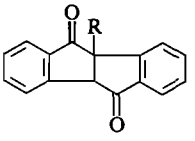

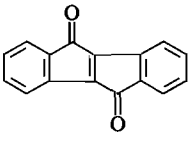

2

1*a* R = H
1*b* R = $OCOCH_3$
1*c* R = OH
1*d* R = OCH_3

Diels–Alder dimer, which loses carbon monoxide readily (2). Such a dehydration is prevented in this reaction by the *cis* configuration of the alcohol **1***c* and the inability to form a planar carbonium ion in this system. The acetate (**1***b*) behaves differently under solvolytic conditions and slowly yields the dimer of **2**.

Alcohol **1***c* is the intramolecular aldol product expected from dibenzo[*a*,*c*]cyclooctan-5,6,11-trione (**3**) and could not be converted to the latter with sodium carbonate or sodium hydroxide. Attempts to trap the triketone (**3**) with *o*-phenylenediamine or benzaldehyde were likewise unsuccessful. These results suggest that the triketone (**3**) will be stable only under acid-free or base-free conditions.

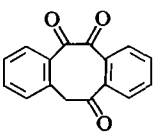

3

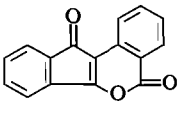

4

The reaction of the acetate **1***b* with sodium hydroxide in methanol was abnormal and gave the methyl ether (**1***d*) instead of the alcohol **1***c*. This product (**1***d*) is formed by elimination of acetic acid from **1***b* with the formation of the diketone **2**. Addition of methanol or methoxide ion to the conjugated system occurs before the diketone **2** can dimerize. This elimination of acetic acid and formation of the intermediate diketone **2** is similar to the dehydrobromination of the 4b-bromo derivative (**1**, R = Br) observed by others (4); the intermediate diketone **2** in this example was trapped with furan.

The availability of a facile method for the formation of the transient diketone **2** using alkaline conditions suggested a study of its (**2**) conversion to an epoxide. Such an intermediate would be useful in the preparation of the tetraketone in the dibenzocyclooctane series.

Treatment of the acetate (**1***b*) in methanol sequentially with 15% hydrogen peroxide and sodium hydroxide gave a mixture of *o*,*o*′-benzil dicarboxylic acid (3), 11-keto[1,2-*c*]isocoumarin (**4**) (5), and the methyl ether **1***c*. These results suggest a preferential attack of the hydroperoxide ion on the carbonyl groups of **1***b* before elimination can occur to the unsaturated ketone **2**. This addition is followed by a Dakin Reaction (6) with subsequent elimination of acetic acid. 11-Keto[1,2-*c*]isocoumarin (**4**) is probably the precursor of *o*,*o*′-benzil dicarboxylic acid since more of it is formed if less base and hydrogen peroxide are used in the oxidation.

1. E. Lewars, J. K. Stowell, S. Wawzonek, and P. Yates. Chem. Ind. 344 (1968).
2. K. Brand and H. W. Stephan. Chem. Ber. **72**, 2168 (1939).
3. C. Graebe and F. Honigsberger. Justus Liebigs Ann. Chem. **311**, 257 (1900).
4. E. Le Goff and R. B. Lacount. J. Org. Chem. **33**, 2529 (1968).
5. S. Wawzonek and J. K. Stowell. J. Org. Chem. **33**, 896 (1968).
6. C. A. Buton. *In* Peroxide reaction mechanisms. *Edited by* J. O. Edwards. Interscience, New York. 1962. pp. 14–15.

Can. J. Chem. Downloaded from www.nrcresearchpress.com by 210.87.254.5 on 09/06/12
For personal use only.

Fluorosulfates of palladium. Part 3. The tetrakis(fluorosulfato)palladate(II) ion

KEITH C. LEE AND FRIEDHELM AUBKE[1]

Department of Chemistry, The University of British Columbia, Vancouver, B.C., Canada V6T 1Y6

Received April 10, 1981

KEITH C. LEE and FRIEDHELM AUBKE. Can. J. Chem. **59**, 2835 (1981).

The reduction of ternary fluorosulfato complexes of palladium(IV) like cesium hexakis(fluorosulfato)palladate(IV) by bromine in liquid sulfur dioxide at room temperature or at slightly elevated temperatures results in the formation of cesium tetrakis(fluorosulfato)palladate(II), according to:

$$Cs_2[Pd(SO_3F)_6] + Br_2 \xrightarrow[25°C]{Br_2/SO_2} Cs_2[Pd(SO_3F)_4] + 2BrSO_3F$$

In contrast to all previously reported palladium(II) fluorosulfato derivatives, Pd^{2+} is found in a square planar environment resulting in diamagnetism.

KEITH C. LEE et FRIEDHELM AUBKE. Can. J. Chem. **59**, 2835 (1981).

La réduction des complexes ternaires de fluorosulfato de palladium(IV) tel l'hexakis(fluorosulfato) palladate(IV) de cesium. Par le brome dans le bioxyde de soufre liquide à la température ambiante ou à des températures légèrement supérieures conduit à la formation du tétrakis(fluorosulfato) palladate(II) de césium selon l'équation

$$Cs_2[Pd(SO_3F)_6] + Br_2 \xrightarrow[25°C]{Br_2/SO_2} Cs_2[Pd(SO_3F)_4] + 2BrSO_3F$$

Contrairement à tout ce qui a été publié antérieurement sur les dérivés fluorosulfato de palladium(II) on a trouvé que l'ion Pd^{2+} est dans un environnement carré plan résultant du diamagnétisme.

[Traduit par le journal]

Introduction

In the two preceding publications in this series we have reported on the synthesis, the spectroscopic and the magnetic properties of a number of paramagnetic palladium(II) fluorosulfates (1, 2). Most divalent palladium compounds are diamagnetic and, consistent with a d^8 electron configuration, have the metal in a square planar, or more rarely a five coordinate environment.

Octahedral coordination, resulting in a $^3A_{2g}$ groundstate for the central atom, is found in $Pd(SO_3F)_2$ (1), where the fluorosulfate group acts as a tridentate, weak field oxygen donor ligand, and in ternary fluorosulfates of the type $Pd^{II}M^{IV}(SO_3F)_6$ (2), where M = Pd, Pt, or Sn. In these compounds the fluorosulfate group acts as an anisobidentate ligand, seemingly strongly coordinated to the tetravalent metal and more weakly linked to palladium(II), again producing a regular octahedral environment and a $^3A_{2g}$ groundstate. Both $Pd(SO_3F)_2$ and the palladium(II) hexakis(fluorosulfato)metallates(IV), may be viewed as coordination polymers, with polydentate fluorosulfate groups as bridges between the metallic centers. Octahedral coordination to Pd(II) produces a weak ligand field, reflected in the measured D_q, B, and β parameters (1, 2) and the magnetic susceptibilities.

Comparable structures as well as magnetic and spectroscopic properties are reported for palladium(II) fluorides. PdF_2(3) has a rutile structure (4), with antiferromagnetic coupling (5) producing a lower magnetic moment than the one found for $Pd(SO_3F)_2$ (2). An octahedral environment and paramagnetism are also found for a number of ternary fluorides of the type Pd(II)M(IV)F_6, with M = Pd, Pt, Ge, or Sn (6). However, in addition, a number of anionic fluorocomplexes of Pd(II) have been synthesised and characterised, which show diverging magnetic properties. While both $CsPdF_3$ (7) and $ZnPdF_4$ (8) are paramagnetic for two unpaired electrons, $BaPdF_4$ is reported to be diamagnetic with a square planar environment for palladium.

Therefore we became interested in synthesising and characterising analogous anionic complex compounds of Pd(II) with possibly monodentate fluorosulfate groups. The similarity of F^- and SO_3F^- as weakly coordinating ligands in coordination chemistry (9) would suggest the possible existence of square planar, diamagnetic fluorosulfate complexes as well.

Results and Discussion

(i) *Synthesis*

A number of initial attempts at the synthesis of palladium(II) fluorosulfato complexes were unsuc-

[1]To whom all correspondence should be addressed.

0008-4042/81/192835-04$01.00/0

©1981 National Research Council of Canada/Conseil national de recherches du Canada

Can. J. Chem. Downloaded from www.nrcresearchpress.com by 210.87.254.6 on 09/06/12
For personal use only.

Can. J. Chem. Downloaded from www.nrcresearchpress.com by 210.87.254.6 on 09/06/12
For personal use only.

cessful. Complexation according to

[1] $Pd(SO_3F)_2 + nCsSO_3F \xrightarrow{HSO_3F} Cs_n[Pd(SO_3F)_{2+n}]$, $n = 1$ or 2

did not proceed, because $Pd(SO_3F)_2$ was virtually insoluble in HSO_3F even up to 120°C. The starting materials were recovered after removal of HSO_3F *in vacuo*.

The attempted solvolysis of nitrosonium tetrachloropalladate(II) in either HSO_3F or $BrSO_3F$ was unsuccessful as well. In HSO_3F a precipitate of $PdCl_2$ occurred according to:

[2] $(NO)_2[PdCl_4] + 2HSO_3F \rightarrow 2(NO)SO_3F + PdCl_2 + 2HCl$

while in $BrSO_3F$ insoluble $Pd(SO_3F)_2$ was formed and some partial oxidation to Pd(IV) was noted.

A more feasible approach was suggested by the previously (1) reported thermal decomposition of $Pd(II)Pd(IV)(SO_3F)_6$ according to

[3] $Pd(II)Pd(IV)(SO_3F)_6 \xrightarrow{+160°C} 2Pd(II)(SO_3F)_2 + S_2O_6F_2$

a decomposition mode subsequently also found for complexes of the type $M_2[Pd(IV)(SO_3F)_6]$, where M = K or Cs. This decomposition and the rather uncommon (10) release of bis(fluorosulfuryl)peroxide pointed to the strong oxidizing ability of palladium(IV) fluorosulfate derivatives and while the resulting solid pyrolysis products were insufficiently pure, a reduction reaction with bromine provides a suitable synthetic route:

[4] $Pd(II)Pd(IV)(SO_3F)_6 + Br_2 \xrightarrow[30\ min]{100°C} 2Pd(II)(SO_3F)_2 + 2BrSO_3F$

Palladium(II) fluorosulfate so obtained is analytically pure. Coupled with the fast and efficient oxidation of palladium metal in a $HSO_3F/S_2O_6F_2$ mixture according to:

[5] $2Pd + 3S_2O_6F_2 \xrightarrow[3\ days]{100°C} Pd(II)Pd(IV)(SO_3F)_6$

the subsequent reduction to $Pd(II)(SO_3F)_2$ provides a more convenient route to this compound than the original oxidation of Pd by $BrSO_3F$, where reaction temperatures of 110°C and reaction times of two weeks are required (1). The ability of bromine to reduce Pd(IV) to Pd(II) under these conditions also provides an explanation as to why only $Pd(II)(SO_3F)_2$ was formed in the original reaction (1):

[6] $Pd + 2BrSO_3F \xrightarrow[14\ days]{100°C} Pd(II)(SO_3F)_2 + Br_2$

Surprisingly the complex $Cs_2[Pd(IV)(SO_3F)_6]$ does not react with bromine under similar conditions. A more reactive reducing agent is found in the mixture of Br_2 and SO_2. Like Br_2, sulfur dioxide does not reduce $Cs_2[Pd(IV)(SO_3F)_6]$, but mixtures of both provide a fast and efficient reaction medium, affording analytically pure $Cs_2[Pd(SO_3F)_4]$ according to:

[7] $Cs_2[Pd(IV)(SO_3F)_6] + Br_2 \xrightarrow[25°C,\ 1\ day]{Br_2/SO_2} Cs_2[Pd(II)(SO_3F)_4] + 2BrSO_3F$

followed by a subsequent reaction as evident from vibrational spectra:

[8] $2BrSO_3F + SO_2 \rightarrow Br_2 + S_3O_8F_2$

This procedure employing Br_2/SO_2 as the reducing agent can also be applied to the preparation of $Pd(SO_3F)_2$ and $Ba[Pd(SO_3F)_4]$ as well as of $(NO)_2[Pd(SO_3F)_4]$. All reactions proceed to completion at 25°C within a day.

Attempts to study the ionic dissociation of the palladium(II) fluorosulfato complexes in fluorosulfuric acid result in the instantaneous quantitative formation of insoluble polymeric $Pd(SO_3F)_2$ according to:

[9] $Cs_2[Pd(II)(SO_3F)_4] \xrightarrow{HSO_3F} 2Cs^+ + 2SO_3F^- + Pd(II)(SO_3F)_2$

which explains why all initial attempts to obtain tetrakis(fluorosulfato) complexes by reactions in HSO_3F had been unsuccessful.

Interestingly our efforts to extend the reduction method to corresponding platinum(IV) complexes or to $Pt(SO_3F)_4$ were unsuccessful even under more stringent conditions. This failure reflects the differences in oxidizing ability between Pd(IV) and Pt(IV).

(ii) Vibrational Spectra

The brown color of the samples containing the $[Pd(SO_3F)_4]^{2-}$ precluded the recording of Raman spectra. The observed infrared frequencies for $Ba[Pd(SO_3F)_4]$, $(NO)_2[Pd(SO_3F)_4]$, and $Cs_2[Pd(SO_3F)_4]$, as well as for $Cs[Au(SO_3F)_4]$ and the Raman bands for $Cs_2[Pd(SO_3F)_6]$ are listed in Table 1 together with a tentative assignment.

The observed band positions, in particular in the SO and SF stretching range are consistent with the presence of monodentate —OSO_2F groups in complex anions for all complexes. However, the relatively small splitting of the SO_2 stretching frequencies of $\sim 150\,cm^{-1}$, the occurrence of the highest frequency SO stretch at $\sim 1340\,cm^{-1}$, the position of the bridging SO stretch at a relatively high 1000 to $1035\,cm^{-1}$, and the low SF stretch at $800\,cm^{-1}$, all are indicative of the retention of ionic character and weak covalent interaction with the metal in the

TABLE 1. Infrared frequencies for $[Pd(SO_3F)_4]$ complexes and related compounds

ν^a (cm^{-1})					
$Ba[Pd(SO_3F)_4]$	$(NO)_2[Pd(SO_3F)_4]$	$Cs_2[Pd(SO_3F)_4]$	$Cs[Au(SO_3F)_4]^b$	$Cs_2[Pd(SO_3F)_6]^c$	Assignment
	2330 w				νNO
1340 vs, b	1345 vs, b	1340 vs, b	1400 s, b	1405 w, 1395 w	νSO_2 as.
1255 vw	1285 vw	1290 vw	1245 s	1300 wv	
1215 vs, sh	1210 vs, sh	1215 s, sh	1208 vs	1236 vs	νSO_2 sym.
1195 vs	1200 vs, b	1190 vs, b		1212 m	
1075 vw	1035 ms, sh	1040 m, sh	1010 w, sh	1020 vs	
1035 vs	1022 vs	1005 vs	970 s, sh	995 ms	$\nu S\text{-}O_b$
			930 vs, b	975, 960 vw	
815 s	810 s	800 s	830 s, sh	835 vw	νSF
803 vs	795 s	775 s	810 s	805 w, 785 w	
642 s	655 s	655 s	678 s	618 ms	νMO
	610 vw	645 s			
580 vs	582 s	575 s	585 s	585 vw, sh	SO_2 bend
552 s	555 s	550 s	550 s	542 w	SO_2 rock
452 s	445 s	440 s	456 ms	441 ms	νMO

[a] Estimated intensity: s, strong; m, medium; w, weak; v, very; sh, shoulder; b, broad.
[b] See ref. 11.
[c] Reference 2. Raman shifts additional bands at: 400 w, sh, 283s, and 215ms.

tetrakis(fluorosulfato)palladate(II) complexes. Somewhat stronger covalent interaction is apparent for both $[Au(SO_3F)_4]^-$ and $[Pd(SO_3F)_6]^{2-}$, where the central metal has a +3 and a +4 formal oxidation state, but generally some strong similarity in the observed spectra is apparent. The observed band positions for the $[Pd(SO_3F)_4]^{2-}$ complexes are inconsistent with the presence of mere mixtures of $Pd(SO_3F)_2$ and the corresponding ionic fluorosulfates.

Finally, strong ir bands at ~ 650 and 450 cm^{-1} are assigned as M—O skeletal stretching vibrations, but obviously as argued by us previously (2, 11) for similar complexes, strong mixing with SO_3F deformation modes is probably present here as well.

(iii) Magnetic Susceptibilities

Consistent with a square planar environment and a d^8 electron configuration, the tetrakis(fluorosulfato)palladate(II) complexes are found to be diamagnetic. Detailed measurements for $Cs_2[Pd(SO_3F)_4]$ at room temperature give a molar magnetic susceptibility of $-214 \pm 18 \times 10^{-6}$ cgs units per mol. The χ_M value calculated from Pascal's constants of -247×10^{-6} cgs units per mol is in reasonable agreement with the experimental value. Appreciable contributions from temperature independent paramagnetism or from paramagnetic impurities to the molar magnetic susceptibility appear to be absent.

(iv) Electronic Spectra

The observed band positions for $Cs_2[Pd(SO_3F)_4]$ and $Ba[Pd(SO_3F)_4]$ are listed in Table 2 and compared to values for solid $K_2[PdCl_4]$, discussed previously by Gray and Ballhausen (12). All three bands found are assignable to *d–d* transitions, and charge transfer bands found in solution spectra of $[PdCl_4]^{2-}$ at 36 000 and 44 000 cm^{-1} were not observed for the fluorosulfates and are possibly outside the range of our instrument.

TABLE 2. Electronic spectra and ligand field parameters for $[Pd(SO_3F)_4]^{2-}$

	Value (cm^{-1})		
Parameter	$Cs_2[Pd(SO_3F)_4]$	$Ba[Pd(SO_3F)_4]$	$[PdCl_4]^{2-}$
ν_1, $^1A_{1g} \rightarrow {}^1A_{2g}$	−15 400 w	15 400 w	16 700
ν_2, $^1A_{1g} \rightarrow {}^1B_{1g}$	−20 000 s, sh	−20 000 s, sh	21 500
ν_3, $^1A_{1g} \rightarrow {}^1E_{1g}$	22 200 s	−22 700 s	23 300
Charge transfer			36 000
Charge transfer			44 900
Δ_1	17 850	17 850	19 150
Δ_2	6 000	6 000	6 200
Δ_3	1 850	2 350	1 450

Following a procedure previously applied to $PdCl_4^{2-}$ and using assumptions shown in Fig. 1, the ligand field parameters Δ_1, Δ_2, and Δ_3 were calculated and are listed also in Table 2. The Δ_1 value indicative of the energy separation of d_{xy} and $d_{x^2-y^2}$ is at the lower end of such values reported for

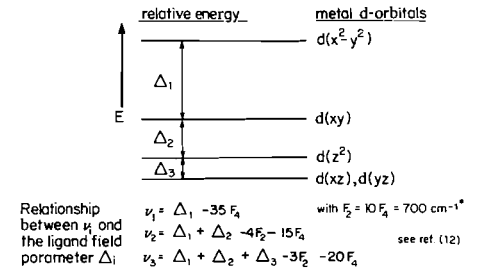

FIG. 1. Energy level diagram for a square planar complex.

Can. J. Chem. Downloaded from www.nrcresearchpress.com by 210.87.254.6 on 09/06/12
For personal use only.

square planar palladium(II) complexes (13), in keeping with the weak field character of the SO_3F group, even in a monodentate environment. Obviously the ligand field parameters so derived for the $[Pd(SO_3F)_4]^{2-}$ ion are rather approximate since the observation of only three spin-allowed bands does not permit an accurate determination of the actual interelectronic repulsion parameter, valid for the complex.

While a direct comparison between ν_1 of $\sim 15\,400\,cm^{-1}$ or Δ_1 of $17\,850\,cm^{-1}$ for the $[Pd(SO_3F)_4]^{2-}$ complexes studied here and the ligand field parameter $10D_q$ for octahedral Pd(II) fluorosulfates (1, 2) found to range from 1105 to 1177 cm^{-1} is rather crude and open to criticism, it seems clear that a monodentate SO_3F group exerts a greater ligand strength than either bi- or tridentate fluorosulfate groups.

Experimental

(*a*) *Chemicals*

Palladium powder, 60 mesh and 99.95% purity, was obtained from Ventron Corporation. Technical grade fluorosulfuric acid from Allied Chemicals was doubly distilled at atmospheric pressure. Bis(fluorosulfuryl)peroxide (14) was synthesized from SO_3 (Allied Chemicals) and F_2 (Air Products) with AgF_2 as catalyst. Bromine was purified by treatment with P_4O_{10} and KBr and distilled before use. The synthesis of complexes containing the $[Pd(SO_3F)_6]^{2-}$ ion has been described previously (2).

(*b*) *Instrumentation*

The infrared spectrophotometer, equipment to record electronic and diffuse reflectance spectra and the Gouy apparatus to measure bulk magnetic susceptibilities have all been described in the two preceding articles in this series (1, 2).

All reactions were performed in Pyrex reaction vials of about 40 mL contents, fitted with Kontes Teflon stem values. Volatile materials were handled using vacuum line techniques. Moisture-sensitive solids were stored and manipulated in a Vacuum Atmosphere Corporation "Dri Lab" Model No. HE-43-2 filled with purified dry nitrogen, equipped with a "Dri Train" Model NO. HE-93-B circulating unit. Filtration of moisture-sensitive materials was carried out in an apparatus described by Shriver (15).

(*c*) *Synthetic Reactions*

(*i*) $Cs_2[Pd(SO_3F)_4]$

$Cs_2[Pd(SO_3F)_6]$ was prepared by the reaction of palladium metal (100 mg, 0.940 mmol) and CsCl (316 mg, 1.877 mmol) with $S_2O_6F_2/HSO_3F$ (2). After all volatile materials were removed *in vacuo*, SO_2 (~4 mL) and Br_2 (~1 mL) were added to the solid. The reaction mixture was stirred at room temperature for 1 day. The removal of all volatile materials gave a light brown material which analyzed as $Cs_2[Pd(SO_3F)_4]$ (721 mg, 938 mmol).

$Cs_2[Pd(SO_3F)_4]$ is a light brown hygroscopic powder which melts with decomposition at ~195°C. It is slightly soluble in HSO_3F, but deposits $Pd(SO_3F)_2$ immediately; the filtered solid shows only the ir spectrum of $Pd(SO_3F)_2$. *Anal.* calcd. for $Cs_2[Pd(SO_3F)_4]$: Cs 34.59, Pd 13.85, S 16.69, F 9.89; found: Cs 34.68, Pd 13.66, S 16.54, F 10.01.

(*ii*) $Ba[Pd(SO_3F)_4]$

In a manner analogous to the preparation of $Cs_2[Pd(SO_3F)_4]$ (196 mg, 0.941 mmol), $Ba[Pd(SO_3F)_6]$, prepared from the reaction of $BaCl_2$ and palladium metal (100 mg, 0.940 mmol) with $S_2O_6F_2/HSO_3F$, was reduced with a mixture of Br_2/SO_2 to give a compound suggesting the formulation of $Ba[Pd(SO_3F)_4]$ (602 mg, 0.941 mmol).

$Ba[Pd(SO_3F)_4]$ is a very light brown hygroscopic powder. It decomposes at ~200°C to a purple solid. It is insoluble in HSO_3F. *Anal.* calcd. for $Ba[Pd(SO_3F)_4]$: Ba 21.46, Pd 16.63, S 20.04, F 11.88; found: Ba 21.22, Pd 16.82, S 20.03, F 11.92. $(NO)_2[Pd(SO_3F)_4]$ can also be prepared in a similar manner.

Acknowledgement

Financial support by the Natural Sciences and Engineering Council of Canada in form of an operating grant and a postgraduate scholarship to one of us (K.C.L.) is gratefully acknowledged. Microanalyses on $Cs_2[Pd(SO_3F)_4]$ and on $Ba[Pd(SO_3F)_4]$ were performed by Analytische Laboratorien, vorm. A. Bernhardt, Gummersbach, West Germany.

1. K. C. Lee and F. Aubke. Can. J. Chem. **55**, 2473 (1977).
2. K. C. Lee and F. Aubke. Can. J. Chem. **57**, 2058 (1979).
3. N. Bartlett and M. A. Hepworth. Chem. Ind. 1425. (1956).
4. N. Bartlett and R. Maitland. Acta Crystallogr. **11**, 747 (1958).
5. R. S. Nyholm and A. G. Sharpe. J. Chem. Soc. 3579 (1952).
6. N. Bartlett and P. R. Rao. Proc. Chem. Soc. 393 (1964); A. Tressaud, M. Winterberger, N. Bartlett, and P. Hagenmuller. C. R. Acad. Sci. Ser. C, **282**, 1069 (1976).
7. N. Bartlett and J. W. Quail. J. Chem. Soc. 3728 (1961).
8. D. Paus and R. Hoppe. Z. Anorg. Allg. Chem. **372**, 119 (1970).
9. D. A. Edwards, M. J. Stiff, and A. A. Woolf. Inorg. Nucl. Chem. Lett. **3**, 427 (1967).
10. A. A. Woolf. *In* New pathways in inorg. chemistry. *Edited by* E. B. Ebsworth, A. G. Maddock, and A. G. Sharpe. Cambridge Press. 1968. p. 357.
11. K. C. Lee and F. Aubke. Inorg. Chem. **18**, 389 (1979).
12. H. B. Gray and C. J. Ballhausen. J. Am. Chem. Soc. **85**, 260 (1963).
13. H. B. Gray. *In* Transition metal chemistry. Vol. 1. *Edited by* R. L. Carlin, Marcel Dekker Inc., New York. 1965. p. 278.
14. G. H. Cady and J. M. Shreeve. Inorg. Synth. **7**, 116 (1963).
15. D. R. Shriver. The manipulation of air-sensitive compounds. McGraw-Hill, New York. 1969.

Can. J. Chem. Downloaded from www.nrcresearchpress.com by 210.87.254.6 on 09/06/12
For personal use only.

Excess volumes of binary mixtures of tetrahydrofuran with various hydrocarbons at 313.15 K

S. K. SURI

Chemistry Department, Indian Institute of Technology, New Delhi 110016, India

Received January 6, 1981

S. K. SURI. Can. J. Chem. **59**, 2839 (1981).

Molar excess volumes of binary mixtures of tetrahydrofuran with *n*-propylbenzene, isopropylbenzene, 1,3,5-trimethylbenzene, 1,2,3,4-tetramethylbenzene, diphenylmethane, *n*-hexane, *n*-octane, 2,2,4-trimethylpentane, *n*-nonane, 3,3-diethylpentane, *n*-dodecane, 2,2,4,6,6-pentamethylheptane, cyclohexane, and methylcyclohexane at 313.5 K have been computed from the experimental density data. The systematic variation of V^E with the change in size, substitution, and molecular geometry of the hydrocarbon has been discussed.

S. K. SURI. Can. J. Chem. **59**, 2839 (1981).

A partir des données expérimentales de densité, on a calculé à 313,15 K les volumes molaires en excès des mélanges binaires de tétrahydrofuranne avec les composés suivants: *n*-propylbenzène, isopropylbenzène, triméthyl-1,3,5 benzène, tétraméthyl-1,2,3,4 benzène, diphénylméthane, *n*-hexane, *n*-octane, triméthyl-2,2,4 pentane, *n*-nonane, diéthyl-3,3 pentane, *n*-dodécane, pentaméthyl-2,2,4,6,6 heptane, cyclohexane et méthylcyclohexane. On discute de la variation systématique de V^E avec les variations de la grosseur, de la substitution et de la géométrie moléculaire de l'hydrocarbure.

[Traduit par le journal]

Introduction

In the earlier papers, we reported the excess volumes for the binary mixtures of tetrahydrofuran with alcohols (1), amides (2), various aliphatic compounds having different functional groups (3), and a few aromatic hydrocarbons, namely benzene, toluene, ethylbenzene, and the isomeric xylenes (4). As an extension of that work, we have determined the excess volumes for the mixtures of tetrahydrofuran with *n*-pyropylbenzene, isopropylbenzene, 1,3,5-trimethylbenzene, 1,2,3,4-tetramethylbenzene, diphenylmethane, *n*-hexane, *n*-octane, 2,2,4-trimethylpentane, *n*-nonane, 3,3-diethylpentane, *n*-dodecane, 2,2,4,6,6-pentamethylheptane, cyclohexane, and methylcyclohexane. The purpose of these investigations is to provide some information about the thermodynamic properties of tetrahydrofuran–hydrocarbon mixtures with a view to understand the factors determining the unlike interactions between molecules in such mixtures.

Experimental

Fisher (A.C.S. Certified) tetrahydrofuran was purified by the procedure described in the earlier paper (4). The samples of *n*-nonane (ir and gc analysed grade) supplied by Aldrich, and 3,3-diethylpentane supplied by Chemical Samples Company, OH, were dried over molecular sieves and fractionally distilled at a reflux ratio of 1:10 immediately before use. The densities and refractive indexes of tetrahydrofuran, *n*-nonane, and 3,3-diethylpentane have been compared with the accepted literature values (5–7) in Table 1. The purification procedure and criterion of purity of other hydrocarbons used in the present investigations have been described elsewhere (8).

The molar excess volumes of mixing, V^E, were calculated from the experimental density data. The solutions for the measurement of densities were prepared by weight, and the corrections for buoyancy were applied. The densities were measured with a vibrating flow densitometer (Sodev. Inc.). The details of the experimental technique for the preparation of solutions and measurement of densities have been described earlier (8). Each data point reported is an average of at least two different measurements. Duplicate densities agreed to within 1×10^{-5} g cm^{-3}. The maximum uncertainty in the molar excess volumes is expected to be less than ± 0.005 cm^3 mol^{-1}.

Results and Discussion

V^E values for the binary mixtures at 313.15 K are recorded in Table 2 and a graphical representation is given in Figs. 1–3. The data have been fitted to a smoothing equation:

$$[1]\quad V^E/(\text{cm}^3\ \text{mol}^{-1}) = X_1(1 - X_1)[A + B(2X_1 - 1) + C(2X_1 - 1)^2 + D(2X_1 - 1)^3]$$

where X_1 is the mole fraction of tetrahydrofuran. Values of the parameters A, B, C, and D and the standard deviations for the excess volumes, $\sigma(V^E)$, are given in Table 3.

It is observed from Figs. 1–3 that V^E varies almost symmetrically with the mole fraction of tetrahydrofuran (and shows a maximum somewhere between $X_{THF} = 0.4$ to 0.6) for all the binary mixtures studied except those containing *n*-hexane and 2,2,4-trimethylpentane. The V^E versus composition plots for these two binary mixtures are skewed towards the hydrocarbon and tetrahydrofuran axis respectively (Fig. 2). Geier and Bittrich (9) reported V^E for tetrahydrofuran solutions containing *n*-hexane and cyclohexane at 313.15 K. For *n*-hexane solutions, their results show a symmetrical V^E versus compo-

0008-4042/81/192839-06$01.00/0

©1981 National Research Council of Canada/Conseil national de recherches du Canada

Can. J. Chem. Downloaded from www.nrcresearchpress.com by 210.87.254.5 on 09/06/12
For personal use only.

Can. J. Chem. Downloaded from www.nrcresearchpress.com by 210.87.254.5 on 09/06/12
For personal use only.

TABLE 1. Densities and refractive indexes of some liquids

Liquid	Density at 313.15 K (g cm^{-3}) Our value	Density at 313.15 K (g cm^{-3}) Literature value	Refractive index at 298.15 K Our value	Refractive index at 298.15 K Literature value
Tetrahydrofuran	0.86567	0.86554 (ref. 4)	1.4048	1.40474 (ref. 5)
n-Nonane	0.70235	0.7020 (ref. 6)	1.4032	1.40311*
3,3-Diethylpentane	0.73908	0.73923*	1.4185	1.41837*

*Extrapolated value from data given in ref. 7.

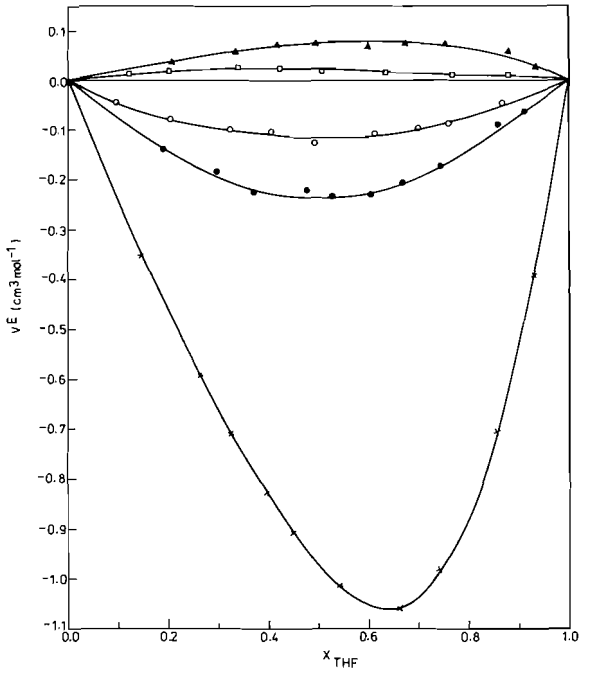

FIG. 1. Molar excess volumes of mixing at 313.15 K for the binary mixtures of tetrahydrofuran (THF) + *n*-propylbenzene (○), + isopropylbenzene (●), + 1,3,5-trimethylbenzene (▲), + 1,2,3,4-tetramethylbenzene (□), and + diphenylmethane (×).

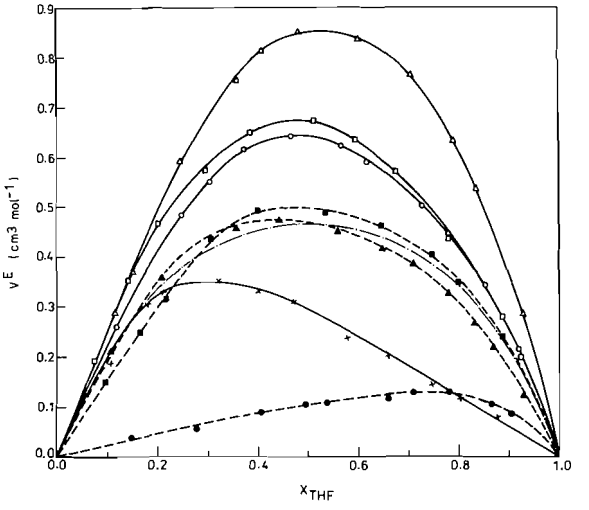

FIG. 2. Molar excess volumes of mixing at 313.15 K for the binary mixtures of tetrahydrofuran (THF) + *n*-hexane (×), + *n*-octane (○), + 2,2,4-trimethylpentane (●), + *n*-nonane (□), + 3,3-diethylpentane (■), + *n*-dodecane (△), and + 2,2,4,6,6-pentamethylheptane (▲). ------ Geier and Bittrich values for THF + *n*-hexane mixtures (ref. 9).

sition plot. Their V^E values for the two sets of binary mixtures are consistently higher over the entire composition range than the ones reported by us. A similar observation was made by us for tetrahydrofuran solutions containing benzene (4). Excess volumes for tetrahydrofuran + cyclohexane mixtures reported by Geier and Bittrich (9) at 298.15 K show poor agreement with the other available literature values (10–12) whereas their data at 303.15 K show a reasonably good agreement with the report of Deshpande and Oswal (13). To the best of our knowledge, no V^E data have been reported in the literature for the other binary mixtures considered in this paper.

It is established that the sign and magnitude of V^E give a good estimate of the strength of the unlike

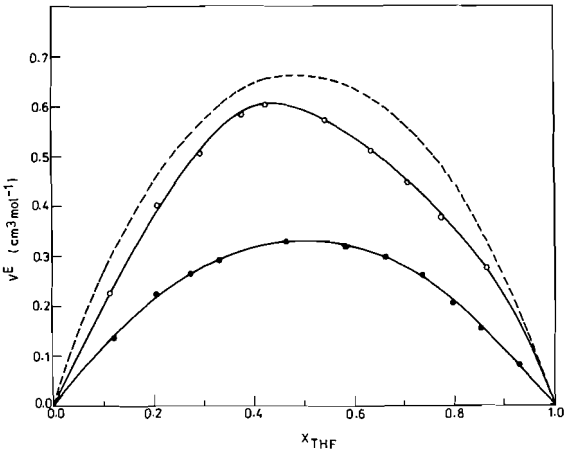

FIG. 3. Molar excess volumes of mixing at 313.15 K for the binary mixtures of tetrahydrofuran (THF) + cyclohexane (○) and + methylcyclohexane (●). Dotted line indicates Geier and Bittrich values for THF + cyclohexane mixtures (ref. 9).

Can. J. Chem. Downloaded from www.nrcresearchpress.com by 210.87.254.5 on 09/06/12
For personal use only.

interactions in a binary mixture (14). Large positive V^E's are taken as indicative of weak intermolecular interactions whereas large negative values of V^E are usually found when these interactions are strong and intermolecular "complexes" are believed to be present. We considered it worthwhile to compare the V^E values at equimolar concentration for the binary mixtures of tetrahydrofuran with some hydrocarbons. In Fig. 4, excess volumes at the equimolar concentration, $V^E_{0.5}$, has been plotted as a function of the number of carbon atoms in the hydrocarbon. A plot of $V^E_{0.5}$ versus molar volume of the hydrocarbon yields a similar plot. Our results lead to the following conclusions:

Cyclic Hydrocarbons

The n–π interactions: it is observed that a marked change in V^E occurs on changing from cyclohexane to benzene, which is indicative of specific interactions occurring between the lone pair of the electrons on the oxygen atom of tetrahydrofuran and the π-electron system of benzene. These interactions appear to be fairly strong.

Substituted Benzenes

The methyl substitution in cyclohexane or benzene produces structural changes in the hydrocarbon and in the case of benzene, a weakening of the like π–π interactions, resulting in increased n–π interactions. A comparison of curve *A* and the first part of curve *E* of Fig. 4 suggests that the volumetric effects caused by structural changes predominate over the change in n–π interactions caused by methyl substitution.

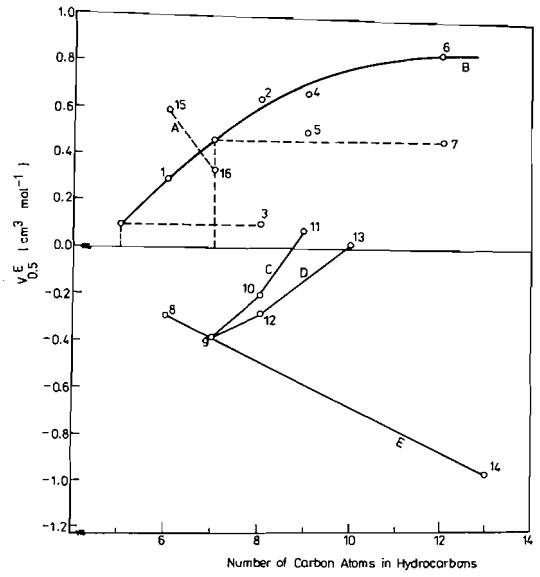

FIG. 4. Excess volumes at equimolar concentration, $V^E_{0.5}$ at 313.15 K plotted against the number of carbon atoms in the hydrocarbon: (*1*) *n*-hexane, (*2*) *n*-octane, (*3*) 2,2,4-trimethylpentane, (*4*) *n*-nonane, (*5*) 3,3-diethylpentane, (*6*) *n*-docecane, (*7*) 2,2,4,6,6-pentamethylheptane, (*8*) benzene (data from ref. 4), (*9*) toluene (data from ref. 4), (*10*) *m*-xylene (data from ref. 4), (*11*) *o*-xylene (data from ref. 4), (*12*) 1,3,5-trimethylbenzene, (*13*) 1,2,3,4,-tetramethylbenzene, (*14*), diphenylmethane, (*15*) cyclohexane, and (*16*) methylcyclohexane.

We find that when substitution in the benzene ring is restricted to one alkyl group, V^E increases for mixtures of tetrahydrofuran with the *n*-alkylbenzenes in the series from toluene to *n*-propylbenzene which is indicative of a significant decrease in n–π interactions. The effect on the π-electron density due to increase in the size of the alkyl substituents from methyl to *n*-propyl is relatively small, we may attribute the increase in V^E to: (*i*) the decrease in aromatic proportion of the total molecule, and (*ii*), the decrease in n–π interactions resulting from decrease in the number of contacts (due to increase in distance of closest approach) between the tetrahydrofuran and the aromatic part of the hydrocarbon because of the structural changes in the aromatic ring produced by alkyl substitution. Thus, although increasing the length of the side chain is likely to make the molecule more polarizable, and presumably therefore more strongly interacting through dispersion forces with the tetrahydrofuran molecule, V^E increases rather than decreases for the reasons given above.

The substitution of a second methyl group to benzene, likewise, because of structural changes in the ring, increases the distance of closest approach of the tetrahydrofuran and the hydrocarbon molecules, resulting in a decrease in n–π interactions, the magnitude of which is determined by the position of the substituent methyl group. It is observed that the value of V^E is higher for solutions containing *m*-xylene and *o*-xylene as compared to those containing *p*-xylene where we expect minimum steric repulsion. The substitution of a methyl group at the *meta* position deactivates the aromatic ring for n–π interactions as compared to substitution at *ortho* position (15). The plots of $V^E_{0.5}$ versus number of methyl groups on the ring (curves *C* and *D* of Fig. 4) are linear in each case. This further supports the conclusion that the volumetric effects caused by structural changes are significant in the binary solutions of tetrahydrofuran. The smaller V^E for isopropylbenzene solutions as compared to *n*-propylbenzene solutions may possibly be due to the steric factors facilitating the packing of the isopropylbenzene molecules in the tetrahydrofuran lattice. Diphenylmethane, because of the large

TABLE 2. Excess volumes of mixing, V^E (cm^3 mol^{-1}) for the binary mixtures at 313.15 K

X_1	V^E	X_1	V^E
Tetrahydrofuran (1) + *n*-propylbenzene (2)		Tetrahydrofuran (1) + isopropylbenzene (2)	
0.0946	−0.045	0.1905	−0.138
0.2049	−0.077	0.2982	−0.183
0.3243	−0.097	0.3690	−0.225
0.4065	−0.103	0.4472	−0.219
0.4932	−0.125	0.5285	−0.233
0.6123	−0.108	0.6045	−0.230
0.7002	−0.096	0.6665	−0.206
0.7606	−0.087	0.7439	−0.172
0.8679	−0.047	0.8568	−0.089
		0.9124	−0.066
Tetrahydrofuran (1) + 1,3,5-trimethylbenzene (2)		Tetrahydrofuran (1) + 1,2,3,4-tetramethylbenzene (2)	
0.2064	0.036	0.1214	0.014
0.3344	0.057	0.2019	0.017
0.4164	0.070	0.3407	0.025
0.4959	0.071	0.4217	0.023
0.6003	0.065	0.5088	0.017
0.6747	0.072	0.6342	0.012
0.7544	0.073	0.7696	0.011
0.8797	0.057	0.8791	0.012
0.9335	0.024		
Tetrahydrofuran (1) + diphenylmethane (2)		Tetrahydrofuran (1) + *n*-hexane (2)	
0.1464	−0.352	0.1066	0.185
0.2636	−0.593	0.1816	0.304
0.3245	−0.708	0.2128	0.328
0.3949	−0.826	0.3217	0.350
0.4501	−0.907	0.4031	0.331
0.5399	−1.014	0.4727	0.309
0.6605	−1.061	0.5776	0.235
0.7410	−0.981	0.6574	0.199
0.8554	−0.704	0.7445	0.143
0.9294	−0.391	0.8025	0.116
		0.8769	0.077
Tetrahydrofuran (1) + *n*-octane (2)		Tetrahydrofuran (1) + 2,2,4-trimethylpentane (2)	
0.1213	0.258	0.1468	0.038
0.2502	0.482	0.2768	0.054
0.3085	0.548	0.4086	0.087
0.3750	0.615	0.4954	0.106
0.4672	0.640	0.5364	0.105
0.5641	0.623	0.6606	0.113
0.6164	0.589	0.7075	0.127
0.7284	0.501	0.7804	0.129
0.7824	0.443	0.8643	0.103
0.8538	0.342	0.9031	0.084
0.9199	0.212		
Tetrahydrofuran (1) + *n*-nonane (2)		Tetrahydrofuran (1) + 3,3-diethylpentane (2)	
0.0747	0.191	0.0998	0.148
0.1418	0.352	0.1657	0.247
0.2028	0.466	0.2186	0.312
0.2983	0.573	0.3077	0.432
0.3846	0.650	0.4006	0.491
0.5129	0.672	0.5359	0.487
0.5923	0.635	0.6464	0.460
0.6748	0.569	0.7471	0.403
0.7993	0.434	0.7984	0.348
0.8884	0.278	0.8897	0.238
0.9217	0.198		

Can. J. Chem. Downloaded from www.nrcresearchpress.com by 210.87.254.5 on 09/06/12
For personal use only.

TABLE 2 (*Concluded*)

X_1	V^E	X_1	V^E
Tetrahydrofuran (1) + *n*-dodecane (2)		Tetrahydrofuran (1) + 2,2,4,6,6-pentamethylheptane (2)	
0.1148	0.288	0.1065	0.209
0.1502	0.371	0.2104	0.357
0.2487	0.591	0.3566	0.456
0.3575	0.755	0.4433	0.472
0.4081	0.813	0.5598	0.451
0.4868	0.850	0.6468	0.418
0.6002	0.834	0.7134	0.387
0.7044	0.764	0.7782	0.324
0.7869	0.630	0.8319	0.265
0.8363	0.536	0.8692	0.218
0.9273	0.284	0.9286	0.123
Tetrahydrofuran (1) + cyclohexane (2)		Tetrahydrofuran (1) + methylcyclohexane (2)	
0.1123	0.224	0.1216	0.134
0.2077	0.399	0.2062	0.223
0.2944	0.504	0.2748	0.262
0.3786	0.583	0.3319	0.291
0.4244	0.602	0.4648	0.327
0.5429	0.570	0.5815	0.318
0.6352	0.511	0.6646	0.298
0.7070	0.446	0.7369	0.261
0.7757	0.377	0.7988	0.204
0.8640	0.274	0.8557	0.154
		0.9310	0.081

TABLE 3. Parameters of eq. [1] and standard deviation $\sigma(V^E)$ of experimental values at 313.15 K

System (1) + (2)	Parameters of eq. [1]				$\sigma(V^E)$ ($cm^3\ mol^{-1}$)
	A	*B*	*C*	*D*	
Tetrahydrofuran + n-propylbenzene	−0.4667	−0.074	0.048	0.210	0.005
Tetrahydrofuran + isopropylbenzene	−0.9365	−0.062	0.175	0.255	0.007
Tetrahydrofuran + 1,3,5-trimethylbenzene	0.2814	0.071	0.091	0.215	0.005
Tetrahydrofuran + 1,2,3,4-tetramethylbenzene	0.0718	−0.103	0.069	0.173	0.002
Tetrahydrofuran + diphenylmethane	−3.9242	−2.407	−0.696	0.824	0.006
Tetrahydrofuran + *n*-hexane	1.1607	−1.200	0.463	0.553	0.007
Tetrahydrofuran + *n*-octane	2.5566	−0.161	0.093	0.719	0.005
Tetrahydrofuran + 2,2,4-trimethylpentane	0.4005	0.327	0.335	0.175	0.005
Tetrahydrofuran + *n*-nonane	2.6702	−0.253	0.241	0.324	0.006
Tetrahydrofuran + 3,3-diethylpentane	2.0055	−0.098	0.051	1.025	0.007
Tetrahydrofuran + *n*-dodecane	3.4214	0.422	0.065	0.647	0.005
Tetrahydrofuran + 2,2,4,6,6-pentamethylheptane	1.8760	−0.183	0.401	−0.161	0.006
Tetrahydrofuran + cyclohexane	2.3491	−0.575	−0.126	1.117	0.006
Tetrahydrofuran + methylcyclohexane	1.3243	0.017	−0.056	−0.091	0.005

aromatic proportion in the molecule, offers appreciable volumetric effects as expected (curve *E*, Fig. 4).

n-*Alkanes*

The binary solutions of tetrahydrofuran with *n*-alkanes show expansion on mixing. The magnitude of V^E in these solutions increases sharply initially with the number of carbon atoms in the straight chain and has a tendency to reach a limiting positive value (curve *B* of Fig. 4). This feature for solutions containing *n*-alkanes is also observed from the data for solutions containing benzene (16), tetrabutyltin (17), triethylamine (8), alkyl nitriles (18), etc. The initial trend in the increase in V^E with number of C-atoms in the *n*-alkane chain can be explained on the basis of the packing property and the shape of the straight-chain molecules which allow them to fit into the lattice of the other component. Nevertheless, it is apparent that the volumetric behaviour of solutions containing higher *n*-alkanes is not solely due to the large size of the *n*-alkane molecule.

Branched Chain Alkanes

The solutions containing methyl substituted

Can. J. Chem. Downloaded from www.nrcresearchpress.com by 210.87.254.5 on 09/06/12
For personal use only.

structural isomers exhibit smaller V^E values than those containing *n*-alkanes. The excess volumes for solutions of 2,2,4-trimethylpentane and 2,2,4,6,6-pentamethylheptane are of the same order of magnitude as one would expect for *n*-pentane and *n*-heptane respectively (from curve *B* of Fig. 4). A similar observation was made by plotting data for alkane solutions of tetrabutyltin (17) and of triethylamine (8). It is therefore evident that the magnitude of V^E in these solutions is determined by the chain length of the alkane molecule and the number of methyl substitutions in the molecule plays an almost insignificant role (8). This, however, does not hold when a relatively bulky alkyl group is substituted in the *n*-alkane chain as is apparent from V^E values for 3,3-diethylpentane solutions. Apparently the lattice of tetrahydrofuran is large enough to allow similar packing affinity to a methyl substituted alkane molecule as it does to an *n*-alkane molecule having the same chain length. This is not true for ethyl-substituted alkane molecules for steric reasons.

Acknowledgement

The author wishes to thank Professor R. H. Wood of Chemistry Department, University of Delaware for providing laboratory facilities.

1. B. CHAWLA and S. K. SURI. Thermochim. Acta, **41**, 147 (1980).
2. S. K. SURI. Thermochim. Acta, **39**, 325 (1980).
3. S. K. SURI and B. CHAWLA. J. Chem. Eng. Data. In press.
4. Y. P. RAO. Private communication.
5. O. KIYOHARA and G. C. BENSON. Can. J. Chem. **55**, 1354 (1977).
6. J. TIMMERMANS (*Editor*). Physiochemical constants. Elsevier, Amsterdam. 1965.
7. American Petroleum Institute, Research Project 44, Chemical Thermodynamic Properties Center, Texas A & M University, College Station, TX.
8. S. K. SURI. J. Chem. Eng. Data, **25**, 390 (1980).
9. V. K. GEIER and H.-J. BITTRICH. Z. Phys. Chem. **255**, 305 (1974).
10. H. ARM and D. BANKAY. Helv. Chim. Acta, **52**, 279 (1969).
11. J. ROVEILLO and M. GOMEL. D.R. Acad. Sci. Ser. C, **266**, 1655 (1968).
12. R. MEYER, G. GIUSTI, M. MEYER, and E. J. VINCENT. Thermochim. Acta, **13**, 379 (1975).
13. D. D. DESHPANDE and S. L. OSWAL. J. Chem. Thermodyn. **7**, 155 (1975).
14. R. J. POWELL and F. L. SWINTON. J. Chem. Thermodyn. **2**, 87 (1970).
15. Y. P. RAO and S. K. SURI. J. Chem. Eng. Data, **25**, 388 (1980).
16. M. DIAZ PENA and J. N. DELGADO. J. Chem. Thermodyn. **7**, 201 (1975).
17. G. DELMAS, P. S. ROMANIA, and P. PURVES. J. Chem. Soc. Faraday Trans. 1, **71**, 1181 (1975).
18. I. A. MCLURE and A. T. RODRIGUEZ. J. Chem. Thermodyn. **12**, 745 (1980).

Can. J. Chem. Downloaded from www.nrcresearchpress.com by 210.87.254.5 on 09/06/12
For personal use only.

The dependence of acid dissociation constants in water on temperature as expressed by the Gurney equation

MICHAEL J. BLANDAMER, JOHN BURGESS, AND PHILIP P. DUCE
Department of Chemistry, The University, Leicester, England
ROSS E. ROBERTSON
Department of Chemistry, University of Calgary, Calgary, Alta., Canada T2N 1N4
AND
JOHN W. M. SCOTT
Department of Chemistry, Memorial University, St John's, Nfld., Canada A1B 3X7

Received February 13, 1981

MICHAEL J. BLANDAMER, JOHN BURGESS, PHILIP P. DUCE, ROSS E. ROBERTSON, and JOHN W. M. SCOTT. Can. J. Chem. **59**, 2845 (1981).

The dependence on temperature of the acid dissociation constants in water for a range of carboxylic acids has been fitted to the Gurney equation using a modified Gauss–Newton method. The equation fits the data reasonably well and identifies the dependence on temperature of the electrical and non-electrical contributions to ln K.

MICHAEL J. BLANDAMER, JOHN BURGESS, PHILIP P. DUCE, ROSS E. ROBERTSON et JOHN W. M. SCOTT. Can. J. Chem. **59**, 2845 (1981).

On a introduit, dans l'équation de Gurney en utilisant une méthode de Newton-Gauss modifiée, l'effet de la température sur les constantes de dissociation dans l'eau d'une série d'acides carboxyliques. L'équation s'ajuste raisonnablement bien aux données et dentifie l'effet de la température sur les contributions électriques et non électrique à ln K.

[Traduit par le journal]

Over many years, extensive efforts have been aimed at formulating equations which describe the dependence of acid dissociation constants, K, on temperature (1). For the most part these equations have expressed the dependence of ln K on temperature T, in an equation which contains several terms each being a different function of T. Moreover, these equations have often been written in such a way that the data can be fitted to the final expression using a linear least-squares technique. A rather different approach to the problem is to start out with a model which attempts to describe those factors which determine the value of K at temperature T. Thus Gurney (2) suggested that ln K for a given acid is determined by two contributions arising from electrical interaction between solutes and solvent and from other non-electric forces. In this way, Gurney attempted to account for the observation that in many cases plots of ln K against T show a maximum value at some temperature, T_m, characteristic of the acid. The resulting equation, the Gurney equation, contains three parameters, C, a, and the Gurney temperature θ (eq. [1]).

$$[1] \quad \ln K = -C[a + \exp(T/\theta)]/T$$

This equation can be rewritten as follows:

$$[2] \quad \ln K = a_1T^{-1} + a_2T^{-1} \exp(T/\theta)$$

Although the Gurney equation is often mentioned in the literature, as far as we are aware no attempt has been made to fit the data to either eqs. [1] or [2] in any quantitative fashion apart from various comments on the general dependence of the two terms in eq. [2] on temperature. An explanation of this omission stems from the observation that the analysis cannot be based on a conventional least-squares technique to yield estimates of a_1, a_2, and θ. This paper reports the results of an attempt to fit the data for several acids to eq. [2].

Analysis

The basis of analysis described here is the Gauss–Newton method (3) which, starting with guessed values of a_1, a_2, and θ, obtains the estimates of these parameters which minimise the residual sum of squares, $[\ln K(\text{obs}) - \ln K(\text{calcd})]^2$. A computer program (FORTRAN-CDC Cyber 73 at the University of Leicester) contained subroutines which calculated the first and second derivatives of ln K with respect to a_1, a_2, and θ. The assumption is made that the local minimum obtained from a range of initial estimates is also the global minimum (3). From the best-fitted parameters the dependences on temperature of both a_1T^{-1} and $a_2T^{-1} \exp(T/\theta)$ were calculated.

Results

The results of the analysis are summarised in Table 1 for 15 carboxylic acids in water. We also

0008-4042/81/192845-03$01.00/0
©1981 National Research Council of Canada/Conseil national de recherches du Canada

Can. J. Chem. Downloaded from www.nrcresearchpress.com by 210.87.254.6 on 09/06/12
For personal use only.

Can. J. Chem. Downloaded from www.nrcresearchpress.com by 210.87.254.6 on 09/06/12
For personal use only.

TABLE 1. Derived parameters for the dependence on temperature of acid-dissociation constants according to the Gurney equation

Acid	10^2C	a	θ/K	$10^5\Delta^a$
Acetic[b]	4.066	3.000	184.6	3.190
Acetic-d_3[c]	4.644	2.418	194.4	4.434
Formic[d]	1.143	12.692	130.3	10.579
Propionic[e]	4.724	2.394	192.9	9.449
Isobutyric[f]	6.349	1.124	211.8	10.535
Cyanoacetic[g]	0.4923	18.74	108.3	1.052
Isopropylcyanoacetic[h]	2.900	0.1426	174.3	35.466
Diisopropylcyanoacetic[i]	7.481	−1.259	232.5	0.3859
Dimethylcyanoacetic[h]	1.493	2.879	141.2	0.4407
Fluoroacetic[j]	0.0818	134.36	71.0	23.247
Chloroacetic[j]	0.5888	17.74	108.4	1.047
Bromoacetic[j]	1.317	6.098	135.5	0.037
Iodoacetic[j]	3.052	1.604	174.2	0.052
Water[k]	0.8996	94.47	118.4	25.94
Acetic[l,m]	4.231	3.530	183.2	1.171
Acetic-d_4[l,n]	4.538	3.180	188.2	0.827
Deuteriumoxide[l,o]	0.8163	116.6	112.6	6.501

[a] Residual sum of squares on ln K.
[b] H. S. Harned and R. W. Ehlers. J. Am. Chem. Soc. **55**, 652 (1933).
[c] M. Paabo, R. G. Bates, and R. A. Robinson. J. Phys. Chem. **70**, 540 (1966).
[d] H. S. Harned and N. D. Embree. J. Am. Chem. Soc. **50**, 1042 (1934).
[e] H. S. Harned and R. W. Ehlers. J. Am. Chem. Soc. **55**, 2379 (1933).
[f] D. H. Everett, D. A. Landsman, and B. R. W. Pinsent. Proc. R. Soc. A, **215**, 403 (1952).
[g] F. A. Feates and D. J. G. Ives. J. Chem. Soc. 2798 (1956).
[h] D. J. G. Ives and P. G. N. Moseley. J. Chem. Soc. B, 1656 (1970).
[i] D. J. G. Ives and P. D. Marsden. J. Chem. Soc. 649 (1965).
[j] D. J. G. Ives and J. H. Pryor. J. Chem. Soc. 2104 (1955).
[k] A. K. Covington, M. I. A. Ferra, and R. A. Robinson. J. Chem. Soc. Faraday Trans. I, **73**, 1721 (1977).
[l] In deuterium oxide.
[m] R. S. Gary, R. G. Bates, and R. A. Robinson. J. Phys. Chem. **70**, 2073 (1966).
[n] A. K. Covington, R. A. Robinson, and R. S. Bates. J. Phys. Chem. **70**, 3820 (1966).

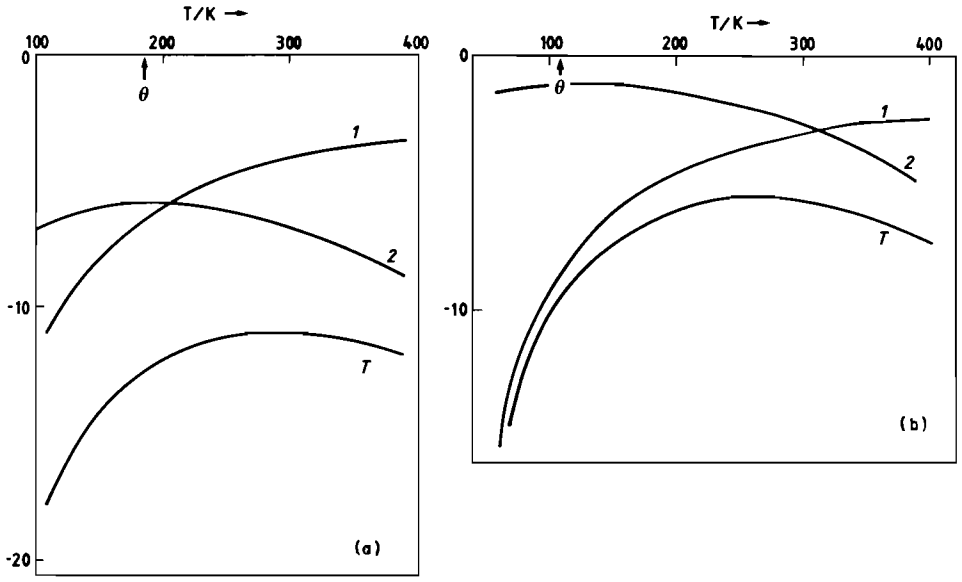

FIG. 1. Analysis of the dependence on temperature of ln K for (*a*) acetic and (*b*) cyanoacetic acids in water. Curve *1* shows the dependence on temperature of a_1T^{-1}, curve *2* shows that for $a_2T^{-1}\exp(T/\theta)$, and curve *T* indicates the dependence of their sum on temperature.

include for comparison the parameters calculated for the self-dissociation of water and deuterium oxide but we will not comment on these further because the chemical process is quite different, and it is not obvious that Gurney included these systems in his analysis. The fit, as measured by the residual sum of squares, is satisfactory.

The dependences on temperature of both a_1T^{-1} and $a_2T^{-1}\exp(T/\theta)$ for cyanoacetic and acetic acids in water are shown in Fig. 1 together with the

sum of the two curves over an extended temperature range to include θ where $a_2T^{-1}\exp(T/\theta)$ is a maximum. Thus for acetic acid, the non-electrostatic term shifts the maximum from 184 K to around 298 K, bringing it within the measured range. For cyanoacetic acid, θ is lower and hence the resulting curve (Fig. 1*b*) has its maximum near 270 K, just below the measured range.

Discussion

The most striking feature is the ability of the eqs. [1] and [2] to fit the data for a range of systems having quite marked differences in their dependence of ln K on T. Nonetheless, the residual sum of squares is, in all cases, larger than that obtained if the data are fitted using three parameters using, for example, the Valentiner (4) or the Clarke–Glew (5) equations. Thus for cyanoacetic acid, the residual sum of squares obtained from the latter two equations is 0.22×10^{-5}. In general we find that the residual sum of squares is only slightly larger than that obtained from the Valentiner equation, an equation which is less constrained than the Gurney equation. However, the optimism generated by these comments is dispelled to some extent following examination of the derived parameters in light of the points made by Gurney (2). Thus it is assumed that the non-electrical contribution to $\Delta G^\ominus$ ($= -RT \ln K$) is independent of temperature; the dependence of $\Delta G^\ominus$ on temperature is related to the temperature-dependent relative permittivity of the solvent, ε_r. For a range of solvents, ε_r^{-1} is directly proportional to $\exp(T/\theta)$ where θ is a characteristic property of the solvent (2). A plot of $-\exp(T/\theta)/T$ passes through a maximum at θ. When this electrical contribution is combined with the non-electrical contribution, the actual maximum in ln K is shifted away from θ (Fig. 1). For water, θ is 219 K but the maximum in ln K for acetic acid is shifted to 298 K. However, for cyanoacetic acid, the shift is less marked and so the maximum is below 273 K. However, the theory requires (2) that for all acids in water θ should be constant at 219 K (218 K for D_2O). This turns out not to be the case, and in most systems the calculated value is less than the theoretical value. Nonetheless, the disagreement is certainly not marked with the possible exception of fluoroacetic acid. Thus of the 15 carboxylic acids, 9 have values of θ within 50 K of the required temperature. Perhaps the most dramatic assumption in the Gurney treatment is the independence of temperature for the non-electrical contributions to $\Delta G^\ominus$. Unfortunately, even with the increase in understanding of solute–solvent interactions in aqueous systems, it is still not strikingly obvious how this equation should be modified. In this sense our criticism of the Gurney equation is not so harsh as that advanced by King (1), whose comments were based on a qualitative examination of the data. Moreover, the Gurney equation may provide a convenient basis for calculating ln K at other temperatures using the derived parameters.

Acknowledgements

We thank SRC for a maintenance grant to P.P.D., and the Royal Society for a travel grant to M.J.B.

1. E. J. KING. Acid–base equilibria. Academic Press, New York. 1965. Chapt. 8.
2. R. W. GURNEY. Ionic processes in solution. McGraw-Hill, New York. 1953.
3. P. R. ADBY and M. A. H. DEMPSTER. Introduction to optimization methods. Chapman and Hall, London. 1974.
4. S. VALENTINER. Z. Physik. Chem. **42**, 853 (1907).
5. E. C. W. CLARKE and D. N. GLEW. Trans. Faraday Soc. **64**, 539 (1966).

Can. J. Chem. Downloaded from www.nrcresearchpress.com by 210.87.254.6 on 09/06/12
For personal use only.

The 1,3-dimethoxytrimethylene bridge as two latent carboxyl groups: synthesis of *cis*-isoaposantenic and *cis*-apocamphoric acids

PELAYO CAMPS[1] AND CARLOS JAIME

Departamento de Química Orgánica, Universidad Autónoma de Barcelona, Bellaterra, Barcelona, Spain

Received February 16, 1981

PELAYO CAMPS and CARLOS JAIME. Can. J. Chem. **59**, 2848 (1981).

The syntheses of *cis*-cyclopentane-1,3-dicarboxylic acid, *cis*-cyclohexane-1,3-dicarboxylic acid, *cis*-isoaposantenic acid, and *cis*-apocamphoric acid are described. The key step of each synthesis is the bromine oxidation of an appropriate bicyclic compound in which a 1,3-dimethoxytrimethylene bridge is converted into two *cis*-carboxyl groups.

PELAYO CAMPS et CARLOS JAIME. Can. J. Chem. **59**, 2848 (1981).

On décrit la synthèse des acides suivants: cyclopentane dicarboxylique-1,3 *cis*, cyclohexane dicarboxylique-1,3 *cis* isoaposanténique *cis* et apocamphorique *cis*. L'étape principale de chaque synthèse est l'oxydation par le brome d'un composé bicyclique approprié dans lequel un pont diméthoxy-1,3 triméthylène est transformé en deux groupes carboxyliques *cis*.

[Traduit par le journal]

Can. J. Chem. Downloaded from www.nrcresearchpress.com by 210.87.254.5 on 09/06/12
For personal use only.

We have recently described a one-step synthesis of 2,4-dialkoxybicyclo[3.*n*.1]alkan-(*n*+6)-ones (*n* = 2, 3) (1, 2). We describe in this communication the easy, one-pot, medium yield bromine oxidation of the 1,3-dimethoxytrimethylene bridge to two *cis*-carboxyl groups.

This transformation could be carried out in three steps by cleavage of the ether functions at the methyl–oxygen bond, oxidation of the 1,3-diol to a 1,3-diketone, and haloform reaction. Although in recent years several sophisticated methods to selectively cleave dialkyl ethers have been described (Me_3SiI (3), BBr_3 (4)), the expected yield for such a three-step transformation would be low. Deno and Potter (5) reported the oxidation of dialkyl ethers to carbonyl compounds in moderate to good yields, depending on the particular substrates, by reaction with bromine in aqueous solution at pH 5 (acetic acid – sodium acetate buffer). Carrying out this reaction on a bicyclic compound having a 1,3-dimethoxytrimethylene bridge, followed by an haloform reaction, a *cis*-cycloalkane-1,3-dicarboxylic acid could conceivably be obtained and possibly in a one-pot reaction. The simplicity of the method makes it attractive in spite of the expected low yield.

We have studied the reaction of 2,4-dimethoxybicyclo[3.2.1]octane,[2] **1***a*, with bromine, first in aqueous buffer solutions at different pH and then in alkaline medium. After the work-up described in the Experimental, we have isolated either *cis*-cyclopentane-1,3-dicarboxylic acid, **5***a*, or its dimethyl ester, **5***b*. The yields of **5***a* or **5***b* obtained from **1***a* show a great dependence on the pH of the solution before the haloform reaction, the best results being obtained at pH 6–7 or, even better, using deficiency of buffer solution of pH 7–8, which makes the solution become acidic during the course of the reaction. The yields of the products isolated from the reaction of **1***a* with bromine at different pH conditions before the haloform reaction are shown in Table 1.

As by-products, we isolated in some of these reactions variable amounts (5–31.5%) of 3-(2,2-dibromoethenyl)cyclopentanecarboxylic acid, **9***a*, or its methyl ester, **9***b*, depending on the work-up. Both must be *cis* because of their origin, and on one occasion we isolated, in 8.5% yield, 3-bromobicyclo[3.2.1]oct-3-en-2-one, **10**. Compounds **9***a* and **10** might have been formed as depicted in Scheme 2, which implies that α-keto bromination takes place, at least in part, before the complete oxidation of the ether functions. No defined products were isolated when the reaction of **1***a* with bromine was carried out in a 1.2 *M* HBr aqueous solution. As can be seen from Table 1, we isolated 44.0% yield of **5***a* by reaction of 2,4-diethoxybicyclo[3.2.1]octane, **1***b*, with bromine using a deficiency of buffer solution of pH 7, which indicates that the 1,3-diethoxytrimethylene bridge can also be used as two latent carboxyl groups.

The reactions of 2,4-dimethoxybicyclo[3.3.1]nonane, **2**, *syn*-2,4-dimethoxy-8-methylbicyclo[3.2.1]octane, **3**, and 2,4-dimethoxy-8,8-dimethylbicyclo[3.2.1]octane, **4**, with bromine using deficiency or excess of buffer solution of pH 7

[1]Author to whom correspondence may be addressed.

[2]Compounds **1***a*, **3**, **4**, **14**, and **15** are mixtures of stereoisomers prepared as described in the Experimental from **12***a*, which in turn is a mixture of stereoisomers in which the nonsymmetric ones are the major components (1, 2). The same applies to **1***b* obtained from **12***b* and to **2** obtained from **13** (1, 2).

0008-4042/81/192848-05$01.00/0

©1981 National Research Council of Canada/Conseil national de recherches du Canada

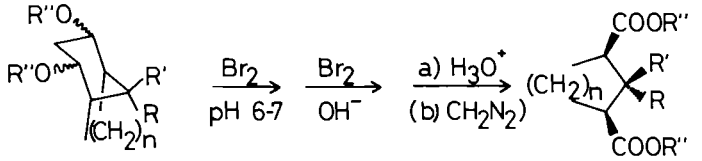

1a, n=2, R=R'=H, R''=Me
1b, n=2, R=R'=H, R''=Et
2, n=3, R=R'=H, R''=Me
3, n=2, R=H, R'=R''=Me
4, n=2, R=R'=R''=Me

5a, n=2, R=R'=R''=H
5b, n=2, R=R'=H, R''=Me
6a, n=3, R=R'=R''=H
6b, n=3, R=R'=H, R''=Me
7a, n=2, R=R''=H R'=Me
7b, n=2, R=H, R'=R''=Me
8a, n=2, R=R'=Me R''=H
8b, n=2, R=R'=R''=Me

SCHEME 1

followed by haloform reaction and esterification gave medium yields of the corresponding dicarboxylic esters, dimethyl *cis*-cyclohexane-1,3-dicarboxylate, **6***b*, dimethyl (1*R*, 2*s*, 3*S*)-2-methylcyclopentane-1,3-dicarboxylate, **7***b*, and dimethyl *cis*-2,2-dimethylcyclopentane-1,3-dicarboxylate, **8***b*, respectively (see Table 1). Hydrolysis of compounds **6***b*, **7***b*, and **8***b* gave the known dicarboxylic acids **6***a*, **7***a*, and **8***a*, respectively.

Noteworthy is the isolation in 38% yield of 3-bromobicyclo[3.3.1]nonan-2,4-dione, **11**, which exists essentially in the enol form, from the reaction of **2** with bromine using excess buffer solution of pH 7 before the haloform reaction.

Compounds **1***a*, **1***b*, and **2** were prepared by Wolff–Kishner reduction of 2,4-dimethoxybicyclo[3.2.1]octan-8-one (1), **12***a*, 2,4-diethoxybicyclo[3.2.1]octan-8-one (1), **12***b*, and 2,4-dimethoxybicyclo[3.3.1]nonan-9-one (2), **13**, respectively (see Scheme 3). Compounds **3** and **4** were prepared from **12***a* by the sequence depicted in Scheme 3. Wittig reaction of **12***a* with methylenetriphenylphosphorane gave 2,4-dimethoxy-8-methylenebicyclo[3.2.1]octane, **14**, which on hydrogenation gave **3**. Compound **3** must be *syn* because of its correlation with **7***a*. Simmons–Smith reaction of **14** with methylene iodide and Zn gave 2,4-dimethoxy-8,8-ethylenebicyclo[3.2.1]octane, **15**, which on hydrogenation gave **4**.

Thus, the use of the 1,3-dimethoxytrimethylene bridge as two latent carboxyl groups has allowed us to bring about the first total synthesis of *cis*-isoaposantenic acid (6), **7***a*, and *cis*-apocamphoric acid (7), **8***a*, products previously obtained by degradation of natural products. Further work is in progress in order to apply this latent functionality.

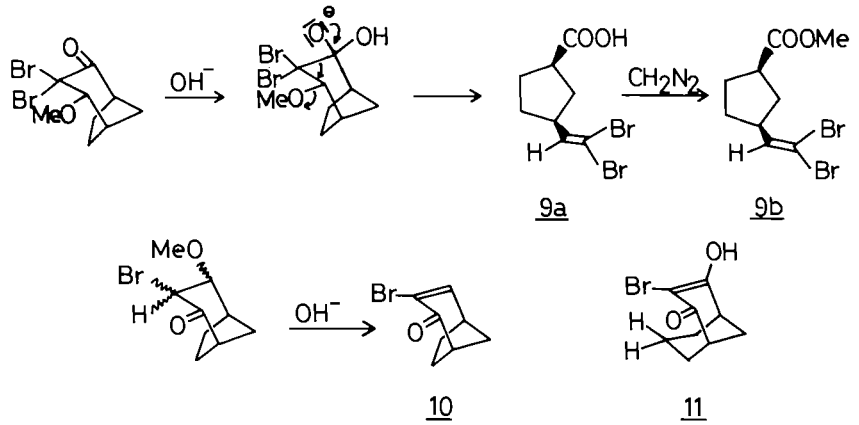

SCHEME 2

Can. J. Chem. Downloaded from www.nrcresearchpress.com by 210.87.254.5 on 09/06/12
For personal use only.

Can. J. Chem. Downloaded from www.nrcresearchpress.com by 210.87.254.5 on 09/06/12
For personal use only.

TABLE 1. Products and yields obtained by bromine oxidation of compounds **1***a*, **1***b*, **2**, **3**, and **4** at different pH conditions followed by haloform reaction

		Data of the buffer solution					
Reaction	Substrate	M_{acid}	M_{base}	Initial pH	mol base/ Ratio mol substrate	Final pH	Compound (yield%)[a]
1	**1***a*	0.17 *M* AcOH	0.30 *M* AcO^-	5	6	~ 5	**5***b* (34.4%), **11***b* (21%)
2	**1***a*	1.20 *M* $PO_4H_2^-$	0.15 *M* PO_4H^{2-}	6	6	~ 6	**5***b* (43.0%), **11***b* (5%).
3	**1***a*	0.32 *M* $PO_4H_2^-$	0.42 *M* PO_4H^{2-}	7	7	~ 7	**5***b* (31.0%), **11***b* (7.0%), **12** (8.5%)
4	**1***a*	0.026 *M* $PO_4H_2^-$	0.036 *M* PO_4H^{2-}	7	0.2	Acidic	**5***a* (46.7%)[c]
5	**1***a*	0.032 *M* PO_4H^{2-}	0.012 *M* PO_4^{3-}	8	0.1	Acidic	**5***b* (44.0%)
6	**1***b*	0.026 *M* $PO_4H_2^-$	0.036 *M* PO_4H^{2-}	7	0.36	Acidic	**5***a* (44.0%)[c]
7	**2**	0.026 *M* $PO_4H_2^-$	0.036 *M* PO_4H^{2-}	7	0.36	Acidic	**6***b* (42.0%)
8	**2**	0.32 *M* $PO_4H_2^-$	0.42 *M* PO_4H^{2-}	7	6.6	~ 7	**6***b* (38.0%), **13** (38.0%)[c]
9	**3**	0.026 *M* $PO_4H_2^-$	0.036 *M* PO_4H^{2-}	7	0.4	Acidic	**7***b* (45.0%)[b]
10	**3**	0.32 *M* $PO_4H_2^-$	0.42 *M* PO_4H^{2-}	7	6.2	~ 7	**7***b* (51.0%)
11	**4**	0.026 *M* $PO_4H_2^-$	0.036 *M* PO_4H^{2-}	7	0.4	Acidic	**8***b* (43.0%)[b]
12	**4**	0.32 *M* $PO_4H_2^-$	0.42 *M* PO_4H^{2-}	7	8.7	~ 7	**8***b* (34.5%)

[a]Where not indicated, yield refers to chromatographed product.
[b]Chromatographed and distilled product.
[c]Chromatographed and crystallized or crystallized product.

Experimental

Infrared spectra were recorded on a Perkin-Elmer spectrophotometer model 720, mass spectra on a Hewlett-Packard spectrometer model 5930A, and nmr spectra on a Perkin-Elmer spectrometer model R-12A. Chemical shifts are given in ppm relative to internal TMS (δ scale). Melting points were determined on a Kofler hot-stage and are corrected.

*2,4-Dimethoxybicyclo[3.2.1]octane, 1*a

In a 50 mL flask to which a distillation apparatus was connected, 2.042 g (11.1 mmol) of **12***a*, 2.0 g (32.7 mmol) of 80% $NH_2NH_2.H_2O$, and 2.67 g (46.7 mmol) of KOH in 18 mL diethyleneglycol were placed. The mixture was heated at 110°C for 1 h and at 180°C for 17 h. Water (25 mL) was added to the cold solution and it was extracted with CH_2Cl_2 (4 × 20 mL). Evaporation of the dried organic extracts and distillation gave 1.65 g (9.72 mmol) of **1***a*, bp 110–120°C (oven)/18 Torr, 87.6% yield; ir: spectrum not definitive; nmr (CCl_4), δ: 3.8–3.0 (broad), 3.17 (s) (total 8H), 2.5–2.1 (broad, 2H), 2.1–0.9 (broad, 8H); ms: 139 (M^+ − MeO, 3), 138 (M^+ − MeOH, 10), 107 (M^+ − MeOH − MeO, 6), 106 (M^+ − 2MeOH, 5), 103 (MeO—$\overset{+}{C}$H—CH_2—CH_2—OMe, 87), 101 (MeO—$\overset{+}{C}$H—CH=CH—OMe, 100), 71 (MeO—$\overset{+}{C}$H—CH=CH_2, 76). *Anal.* calcd. for $C_{10}H_{18}O_2$: C 70.55, H 10.66; found: C 70.69, H 10.68.

*2,4-Diethoxybicyclo[3.2.1]octane, 1*b

The title compound was prepared as described for **1***a*. From 1.15 g (5.45 mmol) of **12***b*, 0.65 g (3.3 mmol) of distilled **1***b* was obtained, bp 128–132°C (oven)/16 Torr, 61% yield; ir: spectrum not definitive; nmr (CCl_4), δ: 3.7–3.1 (complex m, 6H), 2.25 (broad, 2H), 2.1–1.0 (broad), 1.12 (t, J = 7 Hz) and 1.10 (t, J = 7 Hz) (total 14 H); ms: 198 (M^+, 2), 152 (M^+ − EtOH, 79), 131 (EtO—$\overset{+}{C}$H—CH_2—CH_2—OEt, 28), 129 (EtO—$\overset{+}{C}$H—CH=CH—OEt, 100), 85 (EtO—$\overset{+}{C}$H—CH=CH_2, 36). *Anal.* calcd. for $C_{12}H_{22}O_2$: C 72.68, H 11.18; found: C 71.74, H 11.14.

2,4-Dimethoxybicyclo[3.3.1]nonane, 2

The title compound was prepared as described for **1***a*. From 2.17 g (11 mmol) of **13**, 1.85 g (10.1 mmol) of distilled **2** was obtained, bp 95–100°C (oven)/12 Torr, 92% yield; ir: spectrum not definitive; nmr ($CDCl_3$), δ: 3.8–3.0 (broad), 3.31 (s), 3.29 (s) (total 8H), 2.5–1.0 (broad, 12H); ms: 184 (M^+, 3), 152 (M^+ − MeOH, 50), 103 (MeO—$\overset{+}{C}$H—CH_2—CH_2—OMe, 73), 101 (MeO—$\overset{+}{C}$H—CH=CH—OMe, 100), 71 (MeO—$\overset{+}{C}$H—CH=CH_2, 65). *Anal.* calcd. for $C_{11}H_{20}O_2$: C 71.70, H 10.94; found: C 71.53, H 10.79.

2,4-Dimethoxy-8-methylenebicyclo[3.2.1]octane, 14

In a one-liter three-necked flask fitted with mechanical stirrer, reflux condenser, and argon atmosphere, 400 mL of anhydrous DME and 6.23 g (115 mmol) of anhydous sodium methoxide were placed. Methyltriphenylphosphonium iodide (46.1 g, 114 mmol) was slowly added (30 min) and the mixture was heated at reflux for 2 h. Then 7.0 g (38 mmol) of **12***a* in 20 mL of anhydrous DME was added at once and reflux was continued for 21 h. Four hundred milliliters of water were added and the mixture was extracted with hexane (3 × 150 mL). Evaporation of the dried hexane extracts and distillation of the residue gave 5.35 g (29.4 mmol) of **14**, bp 80–85°C (oven)/12 Torr, 77% yield; ir (CCl_4), ν: 3025 (m), 1095 (vs) cm^{-1}; nmr (CCl_4), δ: 4.7–4.5 (broad, 2H), 3.7–3.2 (broad), 3.23 (s) (total 8H), 2.62 (broad, 2H), 2.1–1.1 (broad, 6H); ms: 182 (M^+, 1), 167 (M^+ − Me, 1.5), 150 (M^+ − MeOH, 100), 135 (6), 124 (61), 118 (M^+ − 2MeOH, 85), 109 (54), 101 (MeO—$\overset{+}{C}$H—CH=CH—OMe, 58), 94 (61), 91 (58), 79 (55). *Anal.* calcd. for $C_{11}H_{18}O_2$: C 72.49, H 9.95; found: C 72.14, H 9.66.

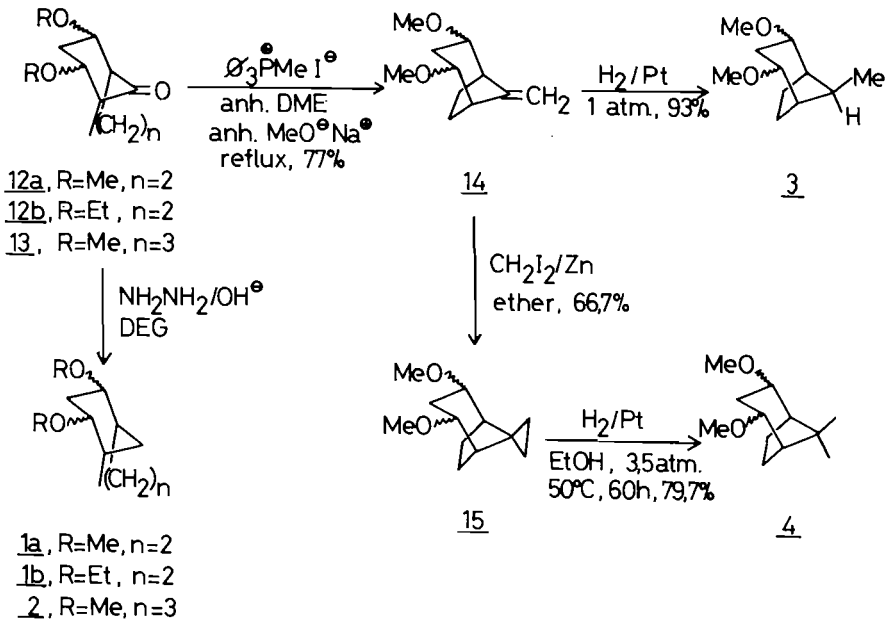

SCHEME 3

syn-2,4-Dimethoxy-8-methylbicyclo[3.2.1]octane, 3

A solution of 0.266 g (1.46 mmol) of **14** in 5 mL ethyl acetate was hydrogenated at atmospheric pressure using 25 mg PtO_2 as catalyst in 15 min. Filtration of the suspension through 1 g silica gel and evaporation of the solvent gave 0.249 g (1.35 mmol) of **3**, bp 90–95°C (oven)/20 Torr, 93% yield; ir: spectrum not definitive; nmr (CCl_4), δ: 3.8–3.2 (broad), 3.30 (s), 3.28 (s) (total 8H), 2.4–0.9 (broad), 1.24 (d, J = 8 Hz) (total 12H); ms: 184 (M^+, 2), 152 (M^+ − MeOH, 17), 101 (MeO—$\overset{+}{C}$H—CH=CH—OMe, 100), 71 (MeO—$\overset{+}{C}$H—CH=CH_2, 58). *Anal.* calcd. for $C_{11}H_{20}O_2$: C 71.70, H 10.94; found: C 71.62, H 10.89.

2,4-Dimethoxy-8,8-ethylenebicyclo[3.2.1]octane, 15

In a 250-mL three-necked flask fitted with mechanical stirrer, addition funnel, reflux condenser, and N_2 atmosphere, 7.25 g (110 mmol) Zn dust, 1.08 g (5.5 mmol) of Cu_2Cl_2, and 60 mL anhydrous ether were placed. The suspension was refluxed for 1 h and 2.0 g (11 mmol) of **14** were introduced, then 14.72 g (55 mmol) of CH_2I_2 were slowly added (1 h) and the mixture was refluxed for 16 h. To the cold mixture (ice was introduced), 60 mL of 3*N* HCl and 16 mL concentrated HCl were added. The organic phase was separated and the aqueous one was extracted with ether (3 × 60 mL). The combined extracts were successively washed with 1 *N* HCl (3 × 20 mL), saturated $NaHCO_3$ aqueous solution (2 × 10 mL), and water (2 × 10 mL). Evaporation of the dried extracts gave 1.92 g of crude product which was filtered through 20 g silica gel (ether as eluent) and distilled to give 1.44 g (7.34 mmol) of **15**, bp 128–132°C (oven)/15 Torr, 66.7% yield; ir: spectrum not definitive; nmr (CCl_4), δ (external TMS): 3.9–3.0 (broad), 3.18 (s) (total 8H), 2.1–1.0 (broad, 8H), 1.0–(−0.1) (complex m, 4H); ms: 196 (M^+, 1), 195 (M^+ − 1, 1), 165 (M^+ − MeO, 4), 164 (M^+ − MeOH, 16), 132 (M^+ − 2MeOH, 32), 106 (100), 101 (MeO—$\overset{+}{C}$H—CH=CH—OMe, 52), 91 (52), 71 (MeO—$\overset{+}{C}$H—CH=CH_2, 23). *Anal.* calcd. for $C_{12}H_{20}O_2$: C 73.43, H 10.27; found: C 73.10, H 10.58.

2,4-Dimethoxy-8,8-dimethylbicyclo[3.2.1]octane, 4

A solution of 0.342 g (1.73 mmol) of **15** in 10 mL ethanol was hydrogenated in a Parr apparatus at 4.5 atm and 50°C during 60 h, using 34 mg PtO_2 as catalyst. The suspension was filtered through 1 g silica gel; evaporation of the solvent and distillation gave 0.273 g (1.38 mmol) of **4**, bp 130–134°C (oven)/18 Torr, 79.7% yield; ir: spectrum not definitive; nmr (CCl_4), δ: 3.9–3.1 (broad), 3.25 (s) (total 8H), 2.3–1.3 (broad), 1.23 (s) (total 11H), 0.98 (s, 3H); ms: 198 (M^+, 1), 182 (1), 166 (M^+ − MeOH, 3), 101 (MeO—$\overset{+}{C}$H—CH=CH—OMe, 100), 71 (MeO—$\overset{+}{C}$H—CH=CH_2, 63). *Anal.* calcd. for $C_{12}H_{22}O_2$: C 72.68, H 11.18; found: C 72.51, H 10.82.

General Procedure for the Bromine Oxidation of the 1,3-Dialkoxytrimethylene Bridge to Two Carboxyl Groups

One mmol of the compound to be oxidized, 8 mmol of Br_2, and the required number of mL of buffer solution[3] were placed in a flask. The flask was stoppered and the mixture was magnetically stirred at room temperature for 62 h. The solution was basified by addition of NaOH; 2.5 mmol of Br_2 was added and it was stirred at room temperature for 24 h more. The solution was diluted with 20 mL water, acidified with concentrated HCl, the excess Br_2 destroyed by addition of solid Na_2SO_3, and extracted thoroughly with ether. Evaporation of the dried extracts yielded the crude product which was chromatographed through silica gel (mixture $CHCl_3$/ether as eluent) and crystallized. Alternatively, the crude product was esterified by reaction with ethereal diazomethane or by reaction with MeOH/HCl and then chromatographed.

*cis-Cyclopentane-1,3-dicarboxylic acid, 5*a (Reaction 4 from Table 1)

From 0.500 g (2.94 mmol) of **1***a*, 0.637 g of crude product was obtained, which on chromatography through 3 g silica gel, eluting with $CHCl_3$/ether, and crystallization from benzene gave 0.217 g (1.37 mmol) of **5***a*, mp 118–121°C (lit. (8) mp 121°C), 46.7% yield.

[3]The number of mL of buffer solution per mmol substrate for each reaction may be obtained from Table 1 by dividing the ratio mol base/mol substrate by the corresponding molar concentration of base (M_{base}).

Can. J. Chem. Downloaded from www.nrcresearchpress.com by 210.87.254.5 on 09/06/12
For personal use only.

Can. J. Chem. Downloaded from www.nrcresearchpress.com by 210.87.254.5 on 09/06/12
For personal use only.

Methyl cis-*3-(2,2-Dibromoethenyl)cyclopentanecarboxylate,* **9**b (Reaction 1 from Table 1)

From 0.251 g (1.36 mmol) of **1***a*, 0.277 g of crude acid was obtained which on methylation with ethereal solution of diazomethane and chromatography through 30 g silica gel, eluting with hexane/ether 9:1, yielded 0.089 g (0.28 mmol) of **9***b* (21% yield); ir ($CHCl_3$), ν: 1725 (s), 1620 (w) cm^{-1}; nmr ($CDCl_3$), δ: 6.41 (d, J = 10 Hz, 1H), 3.70 (s, 3H), 3.2–2.5 (broad, 2H), 2.5–1.2 (broad, 6H); ms: 310 (M^+, 3), 279 (M^+ − MeO, 4), 278 (M^+ − MeOH, 6), 251 ($M^+ - CO_2Me$, 6), 250 ($M^+ - HCO_2Me$, 7), 231 (M^+ − Br, 24), 210 ($C_4H_4Br_2^+$, 9), 197 ($C_3H_3Br_2^+$, 12), 171 ($M^+ - CO_2Me$ − HBr, 50), 151 (M^+ − HBr − Br, 25), 91 ($C_7H_7^+$, 100). *Anal.* calcd. for $C_9H_{12}Br_2O_2$: C 34.65, H 3.88, Br 51.22; found: C 34.92, H 3.75, Br 50.30.

Eluting with hexane–ether 8:2, 0.087 g (0.47 mmol) of **5***b* was obtained. Its spectroscopic data were identical with those reported by James and Stille (9).

3-Bromobicyclo[3.2.1]oct-3-en-2-one, ***10*** (Reaction 3 from Table 1)

From 0.405 g (2.38 mmol) of **3***a*, 0.432 g of crude product was obtained which was esterified by reaction with 20 mL of anhydrous MeOH and 3 drops of concentrated HCl. The solvent and HCl were evaporated and the crude liquid was chromatographed through 30 g silica gel. There were obtained successively 0.052 g (0.167 mmol, 7.0% yield) of **9***b* (hexane/ether 9:1), 0.040 g (0.20 mmol, 8.5% yield) of **10** (hexane/ether 17:3), and 0.137 g (0.73 mmol, 31.0% yield) of **5***b* (hexane/ether 8:2). Spectroscopic and analytical data of **10**: ir ($CHCl_3$), ν: 1690 (s), 1590 (w) cm^{-1}; nmr ($CDCl_3$), δ: 7.58 (d, J = 8 Hz, 1H), 3.4–2.7 (broad, 2H), 2.5–1.0 (broad, 6H); ms: 200 (M^+, 34), 172 (16), 159 (50), 131 (31), 93 (100), 91 (100), 77 (75). *Anal.* calcd. for C_8H_9BrO: C 47.81, H 4.51, Br 39.76; found: C 47.77, H 4.79, Br 39.71.

Dimethyl cis-*Cyclohexane-1,3-dicarboxylate,* **6**b (Reaction 7 from Table 1)

From 0.184 g (1.0 mmol) of **2**, 0.217 g of crude product was obtained which, after esterification with ethereal diazomethane and two chromatographies through 20 g silica gel, gave 0.084 g (0.42 mmol) of **6***b* (hexane/ether 8:2), in 42.0% yield. Its spectroscopic data were identical with those reported by James and Stille (9).

cis-*Cyclohexane-1,3-dicarboxylic Acid,* **6**a

Hydrolysis of **6***b* by refluxing with dilute aqueous HCl for 16 h gave **6***a* in quantitative yield, mp 165–167°C (lit. (8) mp 167–167.8°C).

3-Bromobicyclo[3.3.1]nonan-2,4-dione, ***11*** (Reaction 8 from Table 1)

From 0.233 g (1.26 mmol) of **2**, 0.240 g of crude product was obtained which was refluxed with 12 mL anhydrous MeOH and 2 drops of concentrated H_2SO_4 for 16 h. Water was added, the acid was neutralized with aqueous $NaHCO_3$, and the mixture was extracted with $CHCl_3$ (3 × 15 mL). Evaporation of the dried extracts gave 0.224 g of a semisolid crude which by crystallization from $CHCl_3$ gave 0.110 g (0.48 mmol, 38% yield) of **11** which exists essentially in the enol form; ir (KBr), ν: 3400–2500 (m), 1690 (s), 1650 (m) cm^{-1}; nmr ($CDCl_3$), δ: 9.9–7.7 (broad, 1H), 2.9–0.7 (broad, 10H); ms: 230 (M^+, 26), 151 (M^+ − Br, 59), 150 (M^+ − HBr, 11), 133 (14), 123 (21), 109 (29), 108 (26), 97 (14), 95 (26), 83 (26), 82 (33), 81 (100). *Anal.* calcd. for $C_9H_{11}BrO_2$: C 46.78, H 4.80, Br 34.58; found: C 46.69, H 4.75, Br 34.30.

Evaporation of the mother liquors of the crystallization gave 0.097 g (0.48 mmol, 38% yield) of **6***b* pure by nmr.

Dimethyl (*1*R,*2s*,*3*S)-*2-methylcyclopentane-1,3-dicarboxylate,* **7**b (Reaction 9 from Table 1)

From 0.249 g (1.35 mmol) of **3**, 0.205 g of crude ester was obtained after esterification with MeOH/HCl. This crude was chromatographed through 30 g silica gel to give 0.139 g (0.69 mmol, 51% yield) of **7***b* eluting with hexane/ethyl acetate 17:3, bp 80–85°C (oven)/15 Torr; ir ($CHCl_3$), ν: 1725 (s) cm^{-1}; nmr ($CDCl_3$), δ: 3.58 (s, 6H), 3.1–2.5 (broad, 3H), 2.5–1.5 (broad, 4H), 0.73 (d, J = 7 Hz, 3H); ms: 169 (M^+ − MeO, 18), 168 (M^+ − MeOH, 11), 140 ($M^+ - HCO_2Me$, 55), 108 (M^+ − MeOH − HCO_2Me, 45), 81 ($M^+ - HCO_2Me - CO_2Me$, 100). *Anal.* calcd. for $C_{10}H_{16}O_4$: C 59.99, H 8.05; found: C 59.72, H 8.05.

cis-*Isoaposantenic Acid,* **7**a

Hydrolysis of 0.266 g of **7***b* by refluxing in 12 mL of dilute aqueous HCl for 16 h gave, after crystallization from ethyl acetate/hexane, 0.192 g (1.12 mmol) of **7***a*, mp 160–163°C (lit. (6) mp 155°C), 84.0% yield. The cyclic anhydride, obtained by reaction of **7***a* with acetyl chloride, melts at 175–176°C (lit. (6) mp 174°C), and the monoanilide, obtained by reaction of this anhydride with aniline, melts at 197–198°C (lit. (6) mp 197–198°C).

Dimethyl cis-*2,2-Dimethylcyclopentane-1,3-dicarboxylate,* **8**b (Reaction 11 from Table 1)

From 0.256 g (1.30 mmol) of **4**, 0.367 g of crude product was obtained after esterification with ethereal diazomethane. This crude product was chromatographed through 30 g silica gel to give 0.147 g of **8***b* eluting with hexane/ether 9:1. It distilled at 116–120°C (oven)/13 Torr, giving 0.120 g (0.56 mmol) of **8***b*, pure by nmr (43.0% yield); ir (film), ν: 1730 (s) cm^{-1}; nmr ($CDCl_3$) δ: 3.8 (s, 6H), 2.9–1.6 (broad, 6H), 1.38 (s, 3H), 0.82 (s, 3H); ms: 214 (M^+, 1), 183 (M^+ − MeO, 12), 182 (M^+ − MeOH, 9), 154 ($M^+ - HCO_2Me$, 54), 122 (M^+ − MeOH − HCO_2Me, 57), 96 ($M^+ - 2\,CO_2Me$, 32), 95 ($M^+ - HCO_2Me - CO_2Me$, 100), 94 ($M^+ - 2\,HCO_2Me$, 49), 55 (62). *Anal.* calcd. for $C_{11}H_{18}O_4$: C 61.66, H 8.47; found: C 61.49, H 8.64.

cis-*Apocamphoric Acid,* **8**a

Hydrolysis of 0.118 g of **8***b* by refluxing with dilute aqueous HCl (5 mL) for 23 h, gave 0.071 g of **8***a* (70% yield), mp 206–208°C (water/ethanol) (lit. (7) mp 203 and 209°C).

Acknowledgments

A fellowship from the "Ministerio de Educacion y Ciencia" to C. Jaime is gratefully acknowledged. We gratefully thank M. Guerra for elemental analysis.

1. P. Camps and C. Jaime. Tetrahedron, **36**, 393 (1980).
2. P. Camps and C. Jaime. Org. Magn. Reson. **14**, 177 (1980).
3. M. E. Jung and M. A. Lyster. J. Org. Chem. **42**, 3761 (1977).
4. J. F. W. McOmie, M. L. Watts, and D. E. West. Tetrahedron, **24**, 2289 (1968).
5. N. C. Deno and N. H. Potter. J. Am. Chem. Soc. **89**, 3550 (1967).
6. G. Komppa and S. Beckmann. Ann. Chem. **523**, 68 (1936).
7. Beilstein. Handbuch der Organischen Chemie. **H9**, 741.
8. R. C. Weast (*Editor*). Handbook of chemistry and physics, 56th ed. Chemical Rubber Co., Cleveland. 1975–1976.
9. D. E. James and J. K. Stille. J. Am. Chem. Soc. **98**, 1810 (1976).

The hydrolyses of benzamides, methylbenzimidatium ions, and lactams in aqueous sulfuric acid. The excess acidity method in the determination of reaction mechanisms[1]

ROBIN A. COX AND KEITH YATES

Department of Chemistry, University of Toronto, 80 St. George St., Toronto, Ont., Canada M5S 1A1

Received March 6, 1981

ROBIN A. COX and KEITH YATES. Can. J. Chem. **59**, 2853 (1981).

The excess acidity method has been applied to hydrolysis rate data for a number of benzamides, methylbenzimidatium ions, and lactams, obtained as a function of sulfuric acid concentration and temperature. All of the substrates studied except β-propiolactam (**8**) and methyl-2,6-dimethylbenzimidatium ion (**7**) were found to follow the A_0T2 mechanism at all acidities. The excess acidity method provided considerable mechanistic detail; in dilute acid the transition state contains *O*-protonated (or methylated) substrate and three water molecules (large negative ΔS^*), but in more concentrated solutions a one-water-molecule mechanism takes over (smaller negative ΔS^*). In strong acid bisulfate ion acts as the nucleophile (positive ΔS^*). *N*-protonated intermediates are not involved for "normal" substrates, being observed in this work only for **8**, which follows the A_ND1 pathway. Observed differences between benzamide and methylbenzimidatium ion (**4**) hydrolyses are due to their differing activity coefficient behaviour, the mechanism being the same for both. The hydrolysis of **7** involves a one-water-molecule S_N2 displacement at the *O*-methyl group. Comparison with **7** shows that this displacement is not likely to occur under the reaction conditions for **4**; however, for the *N*-methyl and *N*,*N*-dimethyl derivatives studied it is probably an important reaction pathway. A comprehensive mechanistic framework for amide hydrolyses in strong acid media is given.

ROBIN A. COX et KEITH YATES. Can. J. Chem. **59**, 2853 (1981).

On a appliqué la méthode d'acidité en excès aux données relatives aux vitesses d'hydrolyse d'une série de benzamides, d'ions méthylbenzimidatium et de lactames obtenues en fonction de la concentration en acide sulfurique et de la température. On a trouvé que tous les substrats étudiés, à l'exception du β propiolactame (**8**) et de l'ion méthyle diméthyl-2,6 benzimidatium (**7**) suivent le mécanisme A_0T2 pour toutes les acidités. La méthode d'acidité en excès fournit beaucoup de détails sur le mécanisme de réaction; en solution diluée d'acide, l'état de transition implique un substrat *O*-protoné (ou méthylé) et trois molécules d'eau (forte valeur négative du ΔS^*), mais dans des solutions plus concentrées un mécanisme à une molécule d'eau prédomine (valeur négative plus faible du ΔS^*). En milieu acide fort, l'ion bisulfate agit comme nucléophile (ΔS^* positif). Les intermédiaires *N*-protonés ne sont pas impliqués dans le cas des substrats "normaux"; dans ce travail, on les a remarqués seulement dans le cas du composé **8** qui suit un mécanisme A_ND1. Les différences observées entre l'hydrolyse du benzamide et de l'ion méthylbenzimidatium **4** sont dues au comportement différent de leur coefficient d'activité, le mécanisme étant le même dans les deux cas. L'hydrolyse du composé **7** fait intervenir une substitution S_N2 du groupe *O*-méthyle par une molécule d'eau. La comparaison avec le composé **7** révèle que ce déplacement ne se produit ordinairement pas dans les conditions de la réaction de **4**; cependant dans le cas des dérivés *N*-méthyle et *N*,*N*-diméthyle étudiés, il est probablement un mécanisme réactionnel important. On propose un mécanisme de base pour l'hydrolyse des amides en milieu acide fort.

[Traduit par le journal]

Introduction

Excess acidities (*X*-functions (1, 2) or M_C functions (3)) are used in a method for the evaluation of protonation acidity constants of weak bases, from ionization ratio measurements in strong acid solutions, by extrapolation to the aqueous standard state. Excess acidity analyses give accurate, reliable pK_{BH^+} values either in the absence (1, 2) or the presence (4, 5) of medium effects on the spectra used to obtain the ionization ratios. The method is also of considerable value in the analysis of rate data obtained in these media; the appropriate kinetic equations are derived and illustrated elsewhere (6). So far it has provided valuable mechanistic information concerning acid-catalyzed ketone enolizations (7), sterically crowded ester hydrolyses (8) and aromatic nitrations (9), and in this paper it is applied to amide hydrolyses in sulfuric acid.

Amide hydrolysis in acid media has been widely studied; the early work has been summarized (10). The consensus today (10, 11) would probably be that normal amides hydrolyze via the A_0T2 (acid-catalyzed, oxygen-protonated, tetrahedral intermediate, bimolecular (12)) mechanism shown in eq. [1] (11, 13–15). This mechanism received strong support when a small but detectable amount of ^{18}O exchange was observed into benzamide under the reaction conditions (16), as would be expected if a tetrahedral intermediate is formed. Also the oxygen-protonated amide involved in mechanism [1] is the only detectable protonated species present at any acidity, as we have discussed elsewhere (4, 5). The number of water molecules taking part in the hydrolysis, *n* in eq. [1], has been found in several cases to be three (17). Apart from eq. [1], well-established amide hydrolysis

[1]Presented at the International Symposium on Physical Organic Chemistry, Toronto, Ont., August, 1979, No. 40.

0008-4042/81/192853-11$01.00/0

©1981 National Research Council of Canada/Conseil national de recherches du Canada

Can. J. Chem. Downloaded from www.nrcresearchpress.com by 210.87.254.42 on 09/06/12
For personal use only.

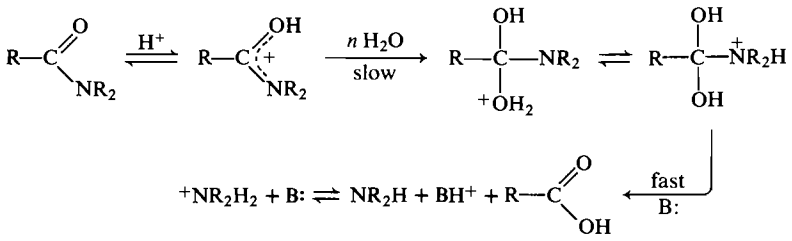

[1]

mechanisms include that of *N-tert*-butyl amides via alkyl carbon–nitrogen bond fission (13, 18), that of some acetanilides via A-1 acylium ion formation (19), and that of *N*-nitroso amides via an *N*-protonated species (20).

However, despite this general agreement it has often been suggested that reaction occurs via the *N*-protonated amide, either partially (21–24) or exclusively (12, 25–27). This species, although present in much lower concentration than the *O*-protonated amide (14), is attractive as an intermediate, being susceptible to nucleophilic attack or acylium ion formation (13). It is involved in some reactions; Perrin invokes it to explain the mechanism of rotation about the carbonyl–nitrogen bond in *N*-substituted amides (28). It is true that eq. [1] does not explain all the details of the kinetic behaviour; Yates *r*-plots (29), for instance, are often curved (25, 30). Bunton *et al.* (22) developed a kinetic equation based on parallel reactions via *N*- and *O*-protonated amides, as did Vinnik (21). Giffney and O'Connor (26) give an equation based on exclusive *N*-protonation which correlates the data well at low acidity, but is not easy to interpret mechanistically (26). Because of this situation we decided to apply the excess acidity method, which is capable of providing considerable mechanistic information (6–8), to this process.

Amides are protonated in dilute acid (4, 5), and so come under Case 2 in ref. 6; the appropriate kinetic equation for an A-2 reaction is reproduced here as eq. [2] (6). For an A-1 reaction the equation

$$[2]\quad \log k_\psi - \log (C_{SH^+}/(C_S + C_{SH^+})) = (m^\ddagger - 1)\, m^* X + \log a_{Nu} + \log k_0$$

is the same except that the term $\log a_{Nu}$ is not present (6). The observed pseudo-first-order rate constant is k_ψ, and C_{SH^+} and C_S are concentrations of protonated and unprotonated substrates, respectively; the protonation correction term containing these is negligible for full protonation. X is the excess acidity, and a_{Nu} is the activity of the nucleophile or base involved in the A-2 reaction, water or bisulfate ion in sulfuric acid (6–8, 31). m^* and $m^\ddagger$ are slope parameters, expressing the sensitivity of the substrate and transition state, respectively, to the changing acidity (6), and k_0 is the medium-independent second-order rate constant. Although the equivalent equations for predominantly unprotonated substrates have been used extensively (6–8), eq. [2] has not, and one of the aims of this work was to test this equation thoroughly.

The compounds involved in this study were benzamide, **1**, *N*-methylbenzamide, **2**, and *N*,*N*-dimethylbenzamide, **3** (23, 25, 34), with the corresponding methylbenzimidatium ions used as *O*-protonated models, **4**, **5**, and **6** (12); methyl-2,6-dimethylbenzimidatium ion **7** (32), used as a check for S_N2 displacement at the *O*-methyl group in these ions; and the 4-, 5-, 6-, and 7-membered ring lactams **8**, **9**, **10**, and **11**, with the open-chain compound *N*-ethylacetamide, **12** (33). With rate

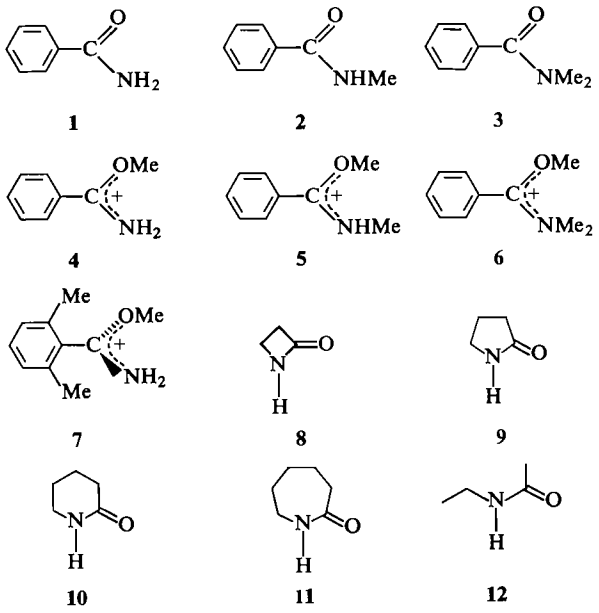

data available at different temperatures (T), activation parameters can be obtained by substituting eq. [3] into eq. [2]; R is the gas constant and θ is

$$[3]\quad \log k_0 = 10.3188 + \log T - \Delta G^\ddagger_{25°}/R\theta \ln 10 + (\Delta H^\ddagger_{25°}/R\theta \ln 10) \times (T - \theta)/T$$

Can. J. Chem. Downloaded from www.nrcresearchpress.com by 210.87.254.42 on 09/06/12
For personal use only.

Can. J. Chem. Downloaded from www.nrcresearchpress.com by 210.87.254.42 on 09/06/12
For personal use only.

298.15 K (35). Equation [3] provides slightly more accurate $\Delta G^{\neq}$ and $\Delta H^{\neq}$ values (35) than does the equation used previously (8). $\Delta S^{\neq}$ is easily obtained via $\Delta G^{\neq} = \Delta H^{\neq} - \theta\Delta S^{\neq}$. All the activation parameters obtained in this study, using eqs. [2] and [3], are valid at 25°C in the aqueous standard state (6–8).

Experimental

The rate constants k_ψ for **1**, **2**, and **3** were taken from Smith and Yates (25), who give extensive data covering the 6–60% H_2SO_4 and 25–85°C ranges, with some additional measurements in stronger acid at 85°C by Smith (34); and from Bunton *et al.* (23), whose measurements were at 100.4°C and extended to 96% H_2SO_4 in the case of **1**. For **4**, **5**, and **6** the rate data in the 12–63% H_2SO_4 and 25–85°C ranges given by Smith and Yates (12) were used. McClelland (32) gives hydrolysis rates for **7** in the regions 0–60% H_2SO_4 and 86–108°C. Data for **9**, **10**, and **11** in the 5–60% and 65–97°C ranges were taken from Wan *et al.* (33), as were data for **8** between 5% and 46% H_2SO_4 at 33°C and for **12** between 5% and 60% at 25°C. The hydrolysis reaction products are detailed in the references cited.

Values of $\log (C_{SH^+}/(C_S + C_{SH^+}))$, i.e. $\log (I/(1 + I))$, are also required for eq. [2]. These were obtained using eq. [4] (1), listed values of X and $\log C_{H^+}$ (1) and the recently obtained accurate

$$[4] \quad \log I - \log C_{H^+} = m^*X + pK_{SH^+}$$

m^* and pK_{SH^+} values for **1–3** and **8–12** (5). X and $\log C_{H^+}$ were corrected to the reaction temperature as previously described (8). Little information is available concerning the temperature dependence of amide and lactam pK_{SH^+} values, and so these were corrected to the reaction temperature by assuming that $\Delta S^0 = 0$ and $\Delta H^0 = \Delta G^0$ for the protonation process, as assumed previously for esters (8), which was felt to be better than using the same pK_{SH^+} at different temperatures. Protonation corrections were not needed for **4–7**, which are positive ions under the reaction conditions (32, 36). Temperature-corrected log water activities in molarity units were obtained as before (8), and temperature-corrected log bisulfate ion concentrations were estimated from Raman spectroscopy measurements by Chen and Irish at 25°C (37) and by Young *et al.* at 0°, 25°, and 50°C (38). The computer program used for fitting eqs. [2] and [3], either for a single reaction or simultaneously for two or three parallel reactions, was the same as that used before (8).

Results

Inspection of eq. [2] reveals that if $m^{\neq} = 1$, i.e. the activity coefficients f_{SH^+} and $f_{\neq}$ for the protonated amide and for the hydrolysis transition state exactly cancel (6), and if the nucleophile is water, a plot of the left hand side (LHS) against log water activity will be linear with slope r, where r is the number of water molecules involved in the hydrolysis (29). In this case r-plots are curved (25, 33, 34); for the amides and lactams (excluding **8**) they vary from about slope 3 in dilute acid to about slope 1 in more concentrated solutions, and deviate still more in strong acid. Either the molarity-based water activities used in this work (7, 8) or the mole-fraction-based ones used before (25) give essentially the same result. This curvature has been suggested (25) to be due to an activity coefficient effect; in the terminology used here this means $m^{\neq} \neq 1$. Accordingly the LHS of eq. [2], minus r log a_{H_2O}, should be linear when plotted against X. However, when this was tried no value of r produced a linear plot. For instance for benzamide, with $r = 3$ (the most likely value (17)) the plots are horizontal until about half-way and then deviate upward; with $r = 1$ they curve down before levelling out. In view of the consistent linearity found before with plots of this type (6–8) this can only mean that a gradual mechanism change is occurring at intermediate acidities.

A computer program was available which enables dissection of k_ψ for two parallel reactions into its components (8), and this was used to investigate the change in mechanism, by trying various combinations of possible mechanisms (A-2 with 3 H_2O + A-1, A-2 with 3 H_2O + A-2 with 1 H_2O, A-2 with 2 H_2O + A-2 with 1 HSO_4^-, etc.) until the combination which fitted the data best was found. Equations [2] and [3] combine to form a multiple linear regression (8). In this work r was given a fixed value (see above), leaving an intercept term and two slopes, from which $\Delta H^{\neq}_{25°}$, $\Delta G^{\neq}_{25°}$, and $(m^{\neq} - 1)m^*$ can be calculated. Thus if one mechanism is sufficient to fit the data three coefficients are obtained; if two are necessary six coefficients result, and so on.

By far the best combination of mechanisms, for compounds **2–6** and **9–12**, was found to be an A-2 reaction with 3 H_2O in the dilute acid region and another A-2 process, this time using only one H_2O, in the more concentrated region, as suggested by the r-plots and in full agreement with the previous proposal for lactam hydrolysis (33). These mechanisms also fitted the experimental data well for benzamide, **1**, except in the highly concentrated acid region; it was found that inclusion of a third mechanism, involving one bisulfate ion, produced an excellent fit in this case. Benzamide is the only compound in the study that has been adequately investigated at high acidity. Indications of a bisulfate mechanism could be seen for **2** and **3** also, but not enough data points at high acidity were present to enable parameters to be calculated. No evidence for a 2 H_2O pathway was found in this work; neither substituting it for one of the 3 H_2O or 1 H_2O reactions, nor adding a 2 H_2O process as a third mechanism, resulted in reasonable fits of the experimental data. For **7** only one A-2 mechanism, involving one water molecule, was found. Compound **8** follows an A-1 pathway; a plot of the LHS of eq. [2] against X is linear, meaning that nucleo-

Can. J. Chem. Downloaded from www.nrcresearchpress.com by 210.87.254.42 on 09/06/12
For personal use only.

philes are not involved in the rate-determining step in this case (6).

The excellent agreement found in this work between the calculated curves due to the different mechanisms and the experimental data is illustrated for compounds **1**, **4**, **7**, and **9** in Figs. 1–6. Figures 1–3 concern benzamide; Fig. 1 covers hydrolysis in the 0–60% H_2SO_4 region at four different temperatures (25). For the 25°C data individual curves for the 3 H_2O and 1 H_2O mechanisms are given, along with the curve through the data points for the two in combination. All the lines curve downward, normal for an A-2 reaction involving water (6); it can be seen that the 3 H_2O mechanism is dominant in media more dilute than about 45% H_2SO_4, and that the 1 H_2O mechanism takes over in more concentrated solutions. Figure 2 illustrates benzamide hydrolysis data at 85°C in 0–80% H_2SO_4 (25, 34); the 1 H_2O mechanism is the dominant one in the 45–75% region, at which point the HSO_4^- mechanism begins to appear. This can be more clearly seen in Fig. 3, with data at 100.4°C extending to 96% H_2SO_4 (23), at which point only the HSO_4^- hydrolysis is occurring. This is to be expected, since the water activity is very low and the HSO_4^- concentration high in this acidity region (31).

Figure 4 shows that exactly the same hydrolysis mechanisms apply to the methylbenzimidatium ion **4** (12), but that the downward slope of the curves is much sharper; the m^+ values (i.e. activity coefficient behaviour) for **1** and **4** are quite different. In Fig. 5 it can be seen that only one mechanism, a 1 H_2O A-2 reaction, is sufficient to explain the hydrolysis of **7** (32) in 0–60% H_2SO_4. Figure 6 shows that the hydrolysis data for the lactam **9** (33)

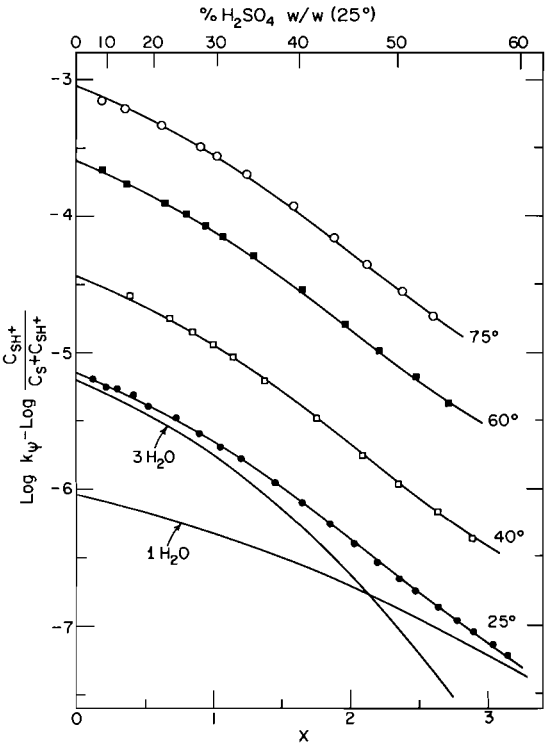

FIG. 1. Graphs according to eq. [2] for the hydrolysis of benzamide in sulfuric acid at several temperatures (25). Points are experimental, curves theoretical, assuming two parallel A-2 reactions, one involving three water molecules and the other one. Theoretical curves for the two individual reactions at 25°C are also shown.

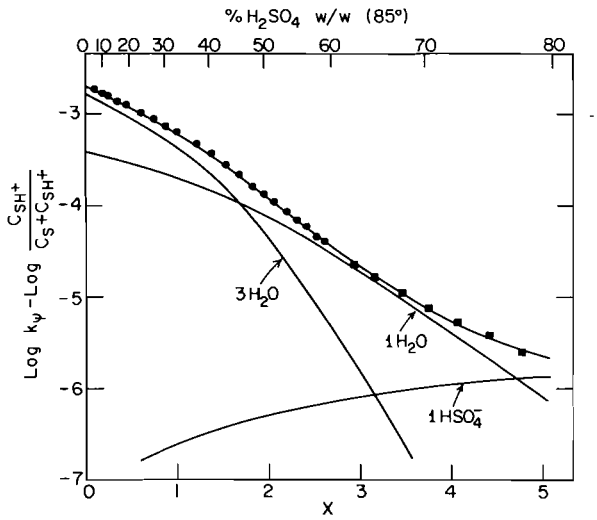

FIG. 2. The hydrolysis of benzamide in sulfuric acid at 85°C. Data from (●) Smith and Yates and (■) Smith (25, 34), plotted according to eq. [2]. Theoretical curves are shown for the three parallel A-2 reactions occurring in this medium; when these are combined the curve through the points results.

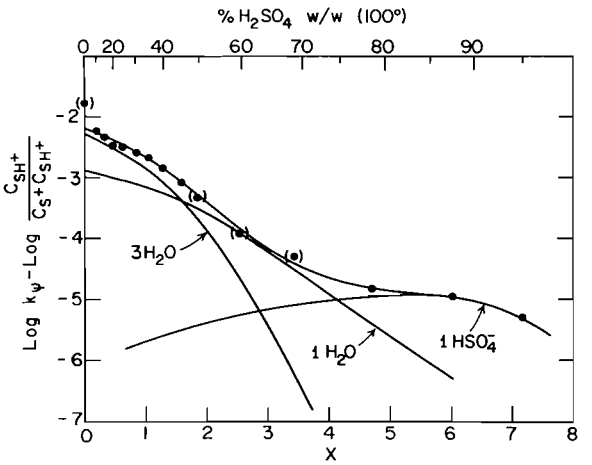

FIG. 3. The hydrolysis of benzamide in sulfuric acid at 100.4°C. Data from Bunton *et al.* (23); see Fig. 2.

Can. J. Chem. Downloaded from www.nrcresearchpress.com by 210.87.254.42 on 09/06/12
For personal use only.

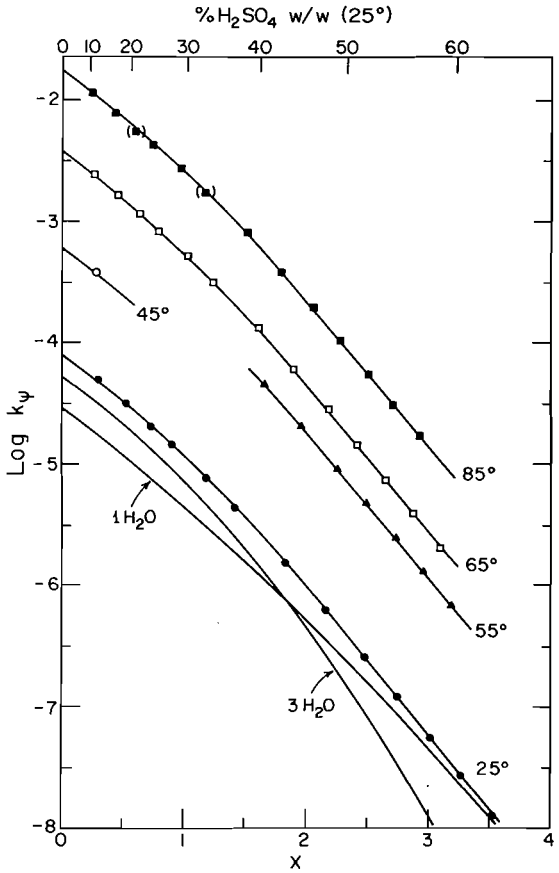

FIG. 4. The hydrolysis of methylbenzimidatium ion **4** in sulfuric acid at various temperatures (12), plotted according to eq. [2]. The theoretical curves assume two parallel reactions, as indicated for the 25°C data.

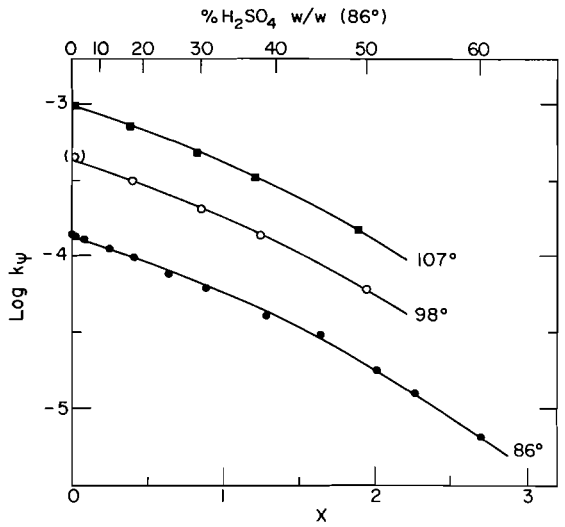

FIG. 5. The hydrolysis of methyl-2,6-dimethylbenzimidatium ion **7** in sulfuric acid at 86°, 98°, and 107°C (32), plotted according to eq. [2]. The theoretical curves shown assume a single A-2 reaction involving one water molecule.

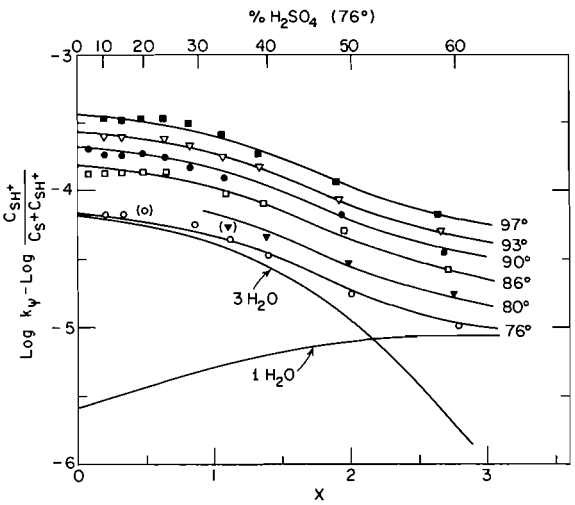

FIG. 6. The hydrolysis of 2-pyrrolidone **9** in sulfuric acid at various temperatures (33), plotted according to eq. [2]. The theoretical curves assume two parallel reactions, as indicated for the 76°C data.

is also fitted well by a combination of 3 H_2O and 1 H_2O hydrolysis mechanisms, the latter dominant above about 50% H_2SO_4.

The parameters found using the computer curve-fitting process are presented for all the compounds in Table 1. Rather than $\Delta G^{\ddagger}_{25°}$, the more familiar log k_0 at 25°C in water is quoted, along with aqueous standard state $\Delta H^{\ddagger}$ and $\Delta S^{\ddagger}$ values, for each mechanism. Combined log k_0 values, including all mechanisms, are also given. $m^{\ddagger}$'s for **1–3** and **8–12** can be obtained from the $(m^{\ddagger} - 1)m^*$ slopes listed in Table 1 using the known m^*'s (5), and these are given in Table 2. Although the m^* concept has little meaning for the preformed positive ions **4–7** (especially **6**), an m^* value of 1.0 can be used for the $m^{\ddagger}$ calculation, since benzimidates protonate in the pH region (32, 36). Table 1 also contains the number of data points included and the root-mean-square error of the fit, used as a criterion of goodness of fit for the various combinations of mechanisms tried; for the ones in Table 1 these are well within the estimated experimental error on each point. Two compounds, **8** and **12**, were only studied at one temperature, so activation parameters could not be obtained. For **12** the data were only sufficient to permit calculation of a combined $(m^{\ddagger} - 1)m^*$, assumed to apply to both mechanisms.

Discussion

The combination of the excess acidity method with the curve-fitting procedure described above

Can. J. Chem. Downloaded from www.nrcresearchpress.com by 210.87.254.42 on 09/06/12
For personal use only.

provides detailed insights into the various amide hydrolysis mechanisms, and good quantitative information about the rate-determining step for each of them; the $\Delta H^{\ddagger}$, $\Delta S^{\ddagger}$, etc. given by eqs. [2] and [3] are aqueous standard state values, directly comparable with those obtained in aqueous buffer media (6). As can be seen the method works very well; none of the alternative rate equations proposed (21, 22, 26) fit experimental data over the wide ranges of acidity and temperature covered in this work. The various mechanistic possibilities will now be considered.

The $3\,H_2O$ process is probably best visualized as proceeding through a cyclic transition state as shown in eq. [5].

[5]

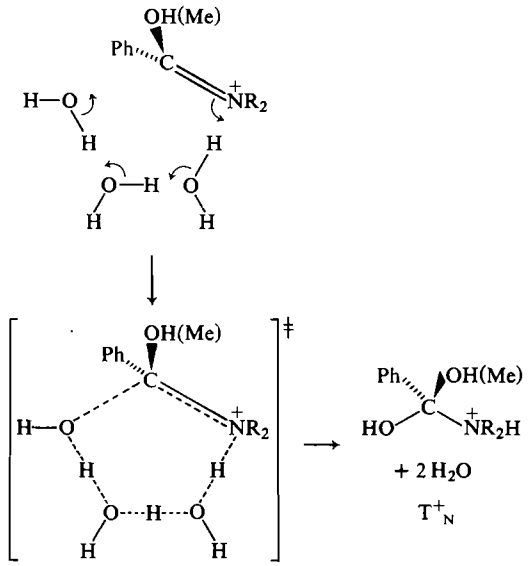

This involves an oxygen-protonated (or methylated) intermediate, shown in the canonical form with the positive charge on nitrogen, and three water molecules, in a five-membered ring (C, N, and 3 O's; hydrogen bonds are collinear). This differs somewhat from previous proposals for the role of two of the water molecules in these reactions (17, 25). Certainly the very large negative entropies of activation, −40 to −55 eu, only seem consistent with a highly structured transition state such as the one shown. The observed very small extent of ^{18}O exchange into benzamide under the reaction conditions (16) would be expected if an intermediate with the good leaving group $^{+}NR_2H$, T^{+}_{N} in eq. [5], were formed directly in the rate-determining step, rather than subsequently as in eq. [1]. Collapse of T^{+}_{N} to product would then be very much faster than the reverse of reaction [5]. Cyclic mechanisms of this type are not unknown; one involving four water molecules has recently been proposed for the water-catalyzed hydrolysis of 1-acetyl-1,2,4-triazole, following a proton inventory study (39). The fact that the *O*-methylated ions **4**, **5**, and **6** react via the same $3\,H_2O$ pathway in dilute acid, giving the corresponding ester and its acid hydrolysis product (25), is strong evidence against the involvement of an *N*-protonated amide in the benzamide and lactam $3\,H_2O$ hydrolyses.

The $1\,H_2O$ reaction can be understood with reference to the reaction scheme given in eq. [6], which applies to the amides, all the lactams except **8**, and, at least partially, to all of the methylbenzimidatium ions except **7**. (Another hydrolysis mechanism, discussed below, is possible for these.) The rate-determining step is attack of a water molecule on the *O*-protonated or methylated amide to give tetrahedral intermediate T^{+}_{O}, deprotonation of which gives the neutral species T^{0}; further proton transfers result in the intermediates T^{+}_{N} and $T^{\pm}$.

Intermediate T^{0} can protonate in three places. By far the most probable is protonation at N to give T^{+}_{N}; however, if protonation at O occurs loss of water or alcohol may result as shown to give the protonated amide (the stable form in the acid solutions in which the $1\,H_2O$ reaction is important (5)). If the substrate is an amide this leads to ^{18}O exchange; the likely basicity difference between N and O in T^{0} would account quite well for the small amount actually observed, $k_{hydrolysis}/k_{exchange}$ being 320 for benzamide in 6% H_2SO_4 at 85°C (16). If the substrate is a benzimidatium ion, amide formation is the result; McClelland and Potter have shown that the hydrolysis of *O*-ethyl-*N*,*N*-dimethyl-4-nitrobenzimidatium ion in 48% H_2SO_4 at 25°C gives 10% amide product, and that all of it is formed via the T^{0} pathway in eq. [6], as shown by ^{18}O exchange (40).

Protonation of T^{0} at nitrogen gives T^{+}_{N} (eq. [6]), and this is the major fate of T^{0}. In acid media strong enough to support the formation of protonated ester, T^{+}_{N} can lose NR_2H directly, as shown. More probable at moderate and low acid concentrations (40) is loss of an OH proton to give the zwitterion $T^{\pm}$, which then readily loses NR_2H to give the acid or ester product. As indicated in scheme [6], the $3\,H_2O$ pathway of eq. [5] is a "short cut" leading directly to T^{+}_{N}. This means that ^{18}O exchange in amides, or amide formation from benzimidatium ions, is an unlikely result of the $3\,H_2O$ pathway. Thus, since the relative importance of the $3\,H_2O$ and $1\,H_2O$ mechanisms changes as the acidity changes (Figs. 1–6), the extent of ^{18}O exchange into amides and the amount of amide formation

Can. J. Chem. Downloaded from www.nrcresearchpress.com by 210.87.254.42 on 09/06/12
For personal use only.

[6]

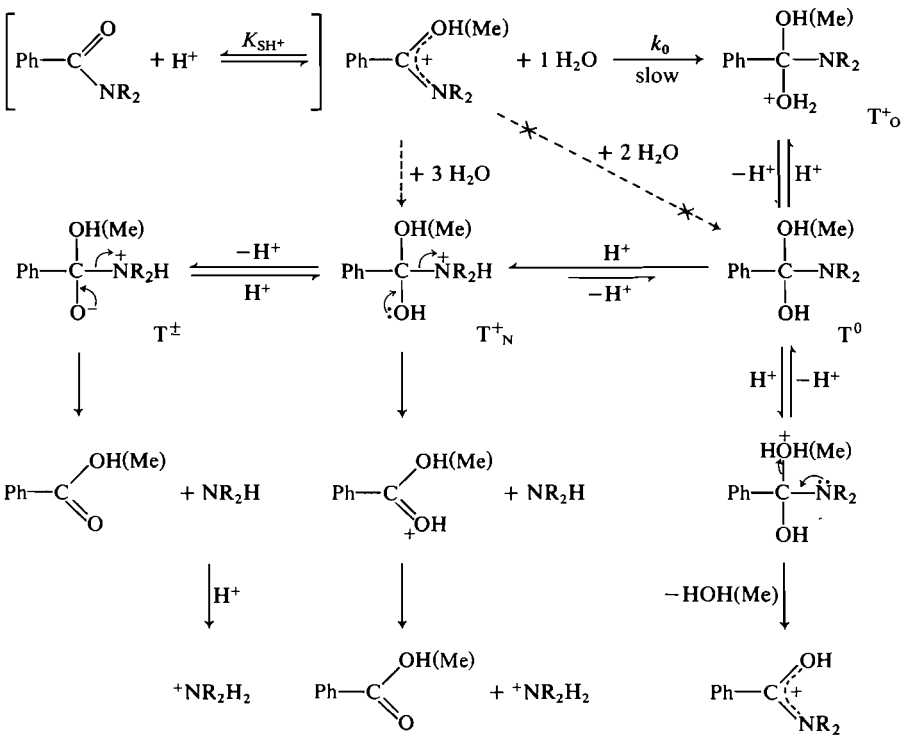

from benzimidatium ions should both increase with acidity. Evidence for the former is lacking, but experimental results support the latter prediction (12, 40).

No evidence for a $2\,H_2O$ reaction was found. By analogy with the ester hydrolysis mechanism (8) a $2\,H_2O$ process would lead to formation of T^0 from protonated amide directly, see scheme [6]. Here, however, it would seem that $T^+{}_O$ has to be formed first, with proton removal to T^0 occurring subsequently, rather than the two steps being concerted.

For the benzimidatium ions the situation is more complex, however, because an alternative hydrolysis pathway exists for them, S_N2 attack at the *O*-methyl group as in eq. [7], leading to amide formation. Product analysis shows that amide is the

[7]

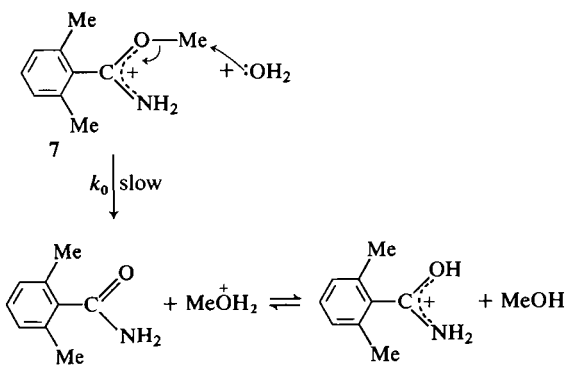

exclusive hydrolysis product for **7** (32); presumably the eq. [5] and eq. [6] mechanisms leading to ester/carboxylic acid products are greatly retarded because of steric hindrance to the approach of water at the carbonyl carbon by the ring methyl groups (32). As can be seen from Fig. 5, only one mechanism, involving one H_2O, is observed for **7**, presumably eq. [7] above.

Reactions [6] and [7] are not kinetically distinguishable. However, a comparison of relative rates and activation parameters (Table 1) for **7** and the unsubstituted analog **4** shows that eq. [7] is an unlikely mechanism for **4**; in water the one-water-molecule process for **7** is slower than that for **4** by nearly $2\frac{1}{2}$ orders of magnitude. In contrast, the $1\,H_2O$ rates for **5** and **6** are much slower, in the latter case approaching that of the identified eq. [7] process for **7**, so presumably the S_N2 hydrolysis is much more important for these compounds. Product studies which have been made in 65% H_2SO_4 at 85°C (12, 34, 41), conditions under which the $3\,H_2O$ hydrolysis is negligible (Fig. 4), enable a more quantitative evaluation. Direct product analysis shows that amide is present (25), but since this is also hydrolyzed to carboxylic acid under the reaction conditions the amount of amide formed initially is best estimated from the kinetics. In this way it was found that amide is the *only* significant initial hydrolysis product for **6** under these condi-

TABLE 1. Standard state rate constants and activation parameters for the hydrolyses of **1–12** in aqueous sulfuric acid[a]

Mechanism	log k_0,	25°C[b]	$\Delta H^{\ddagger}$, kcal/mol	$\Delta S^{\ddagger}$, eu	$(m^{\ddagger} - 1)m^{*}$	N[c]	$\pm \sigma_y$[d]
Benzamide, **1**							
3 H_2O	−5.198	−5.140	19.52±0.08	−40.8±0.3	−0.086±0.010	98 (4)	0.017
1 H_2O	−6.039		20.99±0.10	−23.7±0.5	−0.126±0.020		
HSO_4^-	−11.65[e]		35.8±1.8	+8.2±6.2	0.045±0.013		
N-methylbenzamide, **2**							
3 H_2O	−6.623	−6.538	21.09±0.15	−42.0±0.5	−0.191±0.022	57 (3)	0.014
1 H_2O	−7.288		21.62±0.13	−27.3±0.5	−0.014±0.017		
N,*N*-dimethylbenzamide, **3**							
3 H_2O	−5.828	−5.788	17.86±0.18	−49.2±0.6	−0.219±0.022	51 (3)	0.018
1 H_2O	−6.843		19.71±0.15	−31.7±0.6	0.045±0.016		
Methylbenzimidatium ion, **4**							
3 H_2O	−4.269	−4.078	17.67±0.49	−42.7±1.7	−0.403±0.015	48 (2)	0.018
1 H_2O	−4.528		20.40±0.19	−18.8±0.8	−0.666±0.033		
N,*O*-dimethylbenzimidatium ion, **5**							
3 H_2O	−3.951	−3.944	16.14±0.24	−46.4±0.8	−0.545±0.042	27 (1)	0.024
1 H_2O	−5.717		22.15±0.62	−18.4±2.4	−0.418±0.068		
N,*N*,*O*-trimethylbenzimidatium ion, **6**							
3 H_2O	−4.255	−4.254	15.38±0.31	−50.3±1.0	−0.962±0.056	25 (1)	0.034
1 H_2O	−6.917		22.85±0.48	−21.5±1.8	−0.283±0.044		
Methyl-2,6-dimethylbenzimidatium ion, **7**							
1 H_2O	−6.976		24.40±0.26	−16.6±0.9	−0.205±0.005	22 (1)	0.017
β-Propiolactam, **8**							
A-1	−2.654±0.077[f]		—	—	0.726±0.061	7	0.106
2-Pyrrolidone, **9**							
3 H_2O	−6.302	−6.295	19.36±0.56	−46.4±1.9	0.318±0.032	47 (2)	0.030
1 H_2O	−8.121		23.20±1.28	−25.9±4.7	0.479±0.116		
δ-Valerolactam, **10**							
3 H_2O	−5.251	−5.186	18.16±0.96	−45.6±3.2	−0.167±0.064	35 (1)	0.037
1 H_2O	−6.045		17.24±1.55	−36.4±5.3	0.117±0.064		
ε-Caprolactam, **11**							
3 H_2O	−5.563	−5.543	15.82±1.54	−54.9±5.2	−0.114±0.100	34	0.040
1 H_2O	−6.878		22.63±1.18	−22.1±4.3	0.037±0.088		
N-ethylacetamide, **12**							
3 H_2O	−6.700±0.072	−6.593	—	—	0.16±0.14[g]	8	0.035
1 H_2O	−7.25±0.46		—	—			

[a]Obtained using eqs. [2] and [3]. Errors quoted are standard deviations.
[b]In pure water, which is 55.34 *M* at 25°C, rather than in 1 *M* water. Given both for the individual mechanisms, and combined to illustrate overall reactivity.
[c]Number of data points. Any rejected by the program used as being too far off the best regression curve are in parentheses, both here and in Figs. 3–6.
[d]Root-mean-square deviation between experimental points and fitted curve.
[e]1 *M* HSO_4^-.
[f]At 33°C.
[g]Both mechanisms combined.

tions, and that amide predominated by a factor of 2:1 for **5**, but that for **4** nearly 90% of the initial product was methyl benzoate (immediately hydrolyzed to benzoic acid (8)) (12, 34). For **5** and **6** ^{18}O exchange studies show that essentially all of this amide results from the S_N2 process of eq. [7] (41). Mechanism [6] can produce as much as 10% amide in favourable cases (40) (see above), but mechanism [7] produces only amide. So we may conclude, at least in 65% H_2SO_4 at 85°C, that almost all of the 1 H_2O pathway for **6** and two-thirds of it for **5** is the S_N2 mechanism [7], but that the reaction between one water molecule and **4** has an 80–90% probability of being mechanism [6]. In more dilute acid where the 3 H_2O process predominates, the amide-forming reactions are not available; the exclusive product found for **4**, **5**, and **6** in 5% H_2SO_4 at 25°C is methyl benzoate (25).

The β-lactam **8** hydrolyzes via a unimolecular route. The only reasonable mechanism for this would seem to be the A_NP1 (13) pathway of eq. [8] (33); reaction is very fast (Table 1), presumably due to the large relief of strain involved. This is the only compound in the study which reacts by way of a

Can. J. Chem. Downloaded from www.nrcresearchpress.com by 210.87.254.42 on 09/06/12
For personal use only.

TABLE 2. m^* values for the various hydrolysis mechanisms[a]

	A-2 Mechanism			
Substrate	3 H_2O	1 H_2O	1 HSO_4^-	A-1
1	0.8	0.8	1.1	—
2	0.6	1.0	—	—
3	0.6	1.1	—	—
4	0.6	0.3	—	—
5	0.5	0.6	—	—
6	0.1	0.7	—	—
7	—	0.8	—	—
8	—	—	—	4.5
9	1.5	1.7	—	—
10	0.8	1.1	—	—
11	0.8	1.1	—	—
12	1.4		—	—

[a] From $(m^* - 1)m^*$ values in Table 1 and known m^*'s, see text.

nitrogen-protonated intermediate. It will probably be argued that the 3 H_2O and 1 H_2O hydrolyses discussed above proceed via *O*- and *N*-protonated intermediates, respectively, rather than via exclusive *O*-protonation as proposed here. The major arguments against this can be summarized (see also refs. 10, 14, 15): a transition-state activity coefficient study of several amides showed that amide

[8] 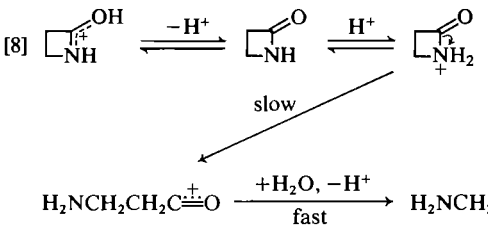

hydrolysis transition states behave similarly to ester hydrolysis ones over the whole acidity range, as scheme [6] would predict (13); the 1 H_2O process is important in the strong acid region where even the opponents of *O*-protonation (27) would agree that the concentration of *N*-protonated amide is very small, and decreasing; 90% of the 1 H_2O hydrolysis for methylbenzimidatium ion **4** occurs via scheme [6], at rates even faster than those for the benzamides and lactams (Table 1), and reaction via *N*-protonation for this species is unlikely in the extreme; the one *N*-protonation hydrolysis found in this work (eq. [8]) is not even bimolecular.

The bisulfate ion mechanism found in concentrated H_2SO_4 can best be represented by eq. [9]. The activation enthalpy is very high (HSO_4^- is a poor nucleophile compared to water (7)) so the reaction is only apparent at high temperatures, 85° and 100°C here (Figs. 2 and 3). On the other hand the nucleophilic attack in eq. [9] involves charge

[9] 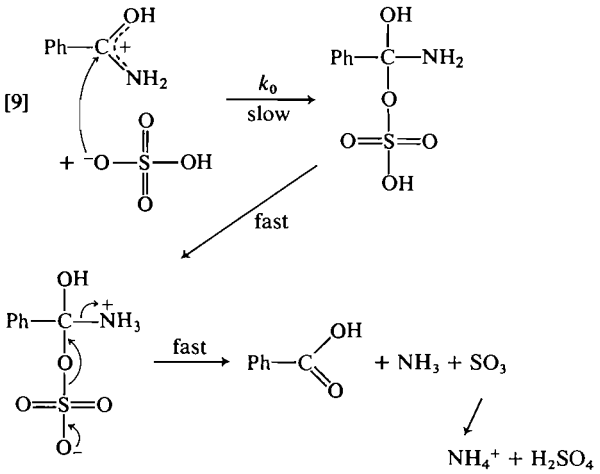

destruction, freeing solvating species, in agreement with the observed positive activation entropy, +8 eu. Fast breakup of the tetrahedral intermediate involving SO_3 loss as shown has precedent in these media (31, 42).

The trends in ΔH^* and ΔS^* in Table 1 are in accord with expectation, with some exceptions. The 3 H_2O process has the lower ΔH^*, i.e. eq. [5] is a lower energy route than eq. [6] or eq. [7], with the possible exception of the δ-lactam **10**. Increasing methyl substitution on nitrogen causes increasingly negative ΔS^* values for both mechanisms in the series **1–3** and **4–6**, in accord with decreasing probability for the favourable orientation of approaching water molecules, and with other reasonable expectations (25). Methyl substitution would be expected to increase ΔH^*, inductive effects and increasing steric repulsion both reducing the electrophilicity of the carbon centre (25); in fact the 3 H_2O hydrolyses of **4**, **5**, and **6** show a decrease and the 1 H_2O ones an increase (remembering the contribution of mechanism [7]). The ΔH^* of **3** is low compared to **1** and **2**, probably because the nonplanarity of **3** (5) enhances the carbon electrophilicity by reducing positive charge delocalization into the phenyl ring. Ring size effects in the lactams have been discussed elsewhere (33).

The values of m^* given in Table 2 reflect the sensitivity of the transition state to the changing medium acidity, as compared with the protonated substrate (6). Typical values for A-2 reactions are around 1.0 (6, 7), and the closer to it they are, the better for the success of the *r*-parameter treatment (see above). Increasing divergence from 1.0 means that the activity coefficient behaviour of the protonated substrate is an increasingly poor model for that of the transition state. All of the A-2 mechanism values in Table 2 lie between 0 and 2, but this

Can. J. Chem. Downloaded from www.nrcresearchpress.com by 210.87.254.42 on 09/06/12
For personal use only.

Can. J. Chem. Downloaded from www.nrcresearchpress.com by 210.87.254.42 on 09/06/12
For personal use only.

encompasses a very wide range of medium sensitivity. The activity coefficient variations which these values reflect account quite well for the previously puzzling differences between the medium sensitivities of **1–3** and **4–6**; the mechanisms are, in fact, the same, as shown here, but the rate–acidity profiles and *r*-plot behaviour are quite different (12, 25). A-1 reactions have quite large m^* values (6), and the 4.5 observed for **8** is added confirmation of the eq. [8] mechanism for this compound.

Trends are apparent in Table 2; increasing methyl substitution in **1–3** and **4–6** increases m^* for the 1 H_2O mechanism and decreases it for the 3 H_2O one. The eq. [7] mechanism seems to have m^* closer to one than does the eq. [6] mechanism. Increasing lactam ring size decreases m^* for both mechanisms. All of this probably reflects differing degrees of positive charge dispersal at the transition state. For instance in mechanism [5] it has to change from its initial state of delocalization over the oxygen, nitrogen, and phenyl in the protonated amide reactant, to a positive charge localized entirely on nitrogen in the T^+_N product, and in mechanism [6] to a position localized on the incoming oxygen in T^+_O. In view of this the supposition that the transition state does not closely resemble the protonated amide reactant if half-way or more along the reaction coordinate does not seem unreasonable; the activation entropies are indicative of a high degree of solvent orientation, and thus a late rather than an early transition state. At this time care in not overinterpreting the actual m^* magnitudes seems advisable, but it is apparent that once a large enough body of data for different reactions is available, m^* could well have the utility of other linear free energy relationship slope values.

In dilute acid where the water concentration is high, nucleophilic addition of water to the carbonyl group requires three water molecules for amide hydrolysis, compared to two for esters (6, 8, 29) and thiol- and thionesters (6, 43). This is understandable as the esters do not have an adjacent nitrogen to accept positive charge as in eq. [5], so this is dispersed onto the second H_2O, which becomes H_3O^+ (8). Even when water acts as a base some charge dispersal appears to be necessary, with observed *r*-values approaching two for acid-catalyzed acetophenone enolizations (7). However, when water takes part in a nucleophilic *substitution* as in eq. [7] above, only one water molecule appears in the transition state, even in dilute acid (Fig. 5). Evidently charge dispersal into the solvent is minimal, which may mean an early transition state, with little charge buildup on the incoming water, for this reaction. This receives some support from the observed m^* values, at least as far as the comparison between eqs. [6] and [7] is concerned, and it is consistent with Hammond's postulate (44), which predicts late transition states for eqs. [5] and [6], with their relatively high energy intermediates T^+_N and T^+_O, and an earlier one for eq. [7], which goes directly to product.

In summary, delineation of a comprehensive mechanistic framework for amide hydrolyses in strong acid media is now possible, based on the $A_O{}^T2$ mechanism and scheme [6]. In dilute acid the 3 H_2O pathway of eq. [5] is followed, and in concentrated sulfuric acid the bisulfate ion hydrolysis of eq. [9] can take place. For sterically crowded methylbenzimidatium ions the S_N2 displacement at the *O*-methyl group of eq. [7] becomes favourable. Hydrolysis via an *N*-protonated species is not a common reaction, being observed in this work only for the highly strained β-lactam **8**, which reacts via the $A_N{}^D1$ mechanism of eq. [8].

Acknowledgements

Financial support of this research by the Natural Sciences and Engineering Research Council of Canada is gratefully acknowledged. We thank Professor R. A. McClelland for valuable discussions.

1. R. A. Cox and K. Yates. J. Am. Chem. Soc. **100**, 3861 (1978).
2. R. A. Cox and K. Yates. Can. J. Chem. **59**, 2116 (1981).
3. N. C. Marziano, P. G. Traverso, A. Tomasin, and R. C. Passerini. J. Chem. Soc. Perkin Trans. II, 309 (1977).
4. R. A. Cox and K. Yates. Can. J. Chem. **59**, 1560 (1981).
5. R. A. Cox, L. M. Druet, A. E. Klausner, T. A. Modro, P. Wan, and K. Yates. Can. J. Chem. **59**, 1568 (1981).
6. R. A. Cox and K. Yates. Can. J. Chem. **57**, 2944 (1979).
7. R. A. Cox, C. R. Smith, and K. Yates. Can. J. Chem. **57**, 2952 (1979).
8. R. A. Cox, M. F. Goldman, and K. Yates. Can. J. Chem. **57**, 2960 (1979).
9. P. G. Traverso, N. C. Marziano, and R. C. Passerini. J. Chem. Soc. Perkin Trans. II, 845 (1977); N. C. Marziano, P. G. Traverso, and G. G. Cimino. J. Chem. Soc. Perkin Trans. II, 574 (1980).
10. C. O'Connor. Q. Rev. Chem. Soc. **24**, 553 (1970); C. H. Rochester. Acidity functions. Academic Press, London. 1970. p. 132; B. C. Challis and J. A. Challis. *In* The chemistry of amides. *Edited by* J. Zabicky. Interscience, London. 1970. p. 731; M. Liler. Reaction mechanisms in sulfuric acid. Academic Press, London. 1971. p. 189.
11. J. March. Advanced organic chemistry. 2nd. ed. McGraw-Hill, Toronto. 1977. p. 353.
12. C. R. Smith and K. Yates. J. Am. Chem. Soc. **94**, 8811 (1972).
13. T. A. Modro, K. Yates, and F. Beaufays. Can. J. Chem. **55**, 3050 (1977).
14. A. Williams. J. Am. Chem. Soc. **98**, 5645 (1976).
15. A. J. Hall and D. P. N. Satchell. Chem. Ind. London, 527 (1974); A. J. Kresge, P. H. Fitzgerald, and Y. Chiang. J. Am. Chem. Soc. **96**, 4698 (1974); A. J. Waring. J. Chem. Soc. Perkin Trans. II, 1029 (1979).

16. R. A. McCLELLAND. J. Am. Chem. Soc. **97**, 5281 (1975).
17. R. B. MOODIE, P. D. WALE, and T. J. WHAITE. J. Chem. Soc. 4273 (1963); K. YATES and J. B. STEVENS. Can. J. Chem. **43**, 529 (1965); K. YATES and J. C. RIORDAN. Can. J. Chem. **43**, 2328 (1965); J. T. EDWARD, G. D. DERDALL, and S. C. WONG. J. Am. Chem. Soc. **100**, 7023 (1978).
18. T. YAMANA, Y. MIZUKAMI, A. TSUJI, and M. IKUTA. Chem. Pharm. Bull. Tokyo, **20**, 1778 (1972).
19. J. A. DUFFY and J. A. LEISTEN. J. Chem. Soc. 853 (1960); J. W. BARNETT and C. J. O'CONNOR. J. Chem. Soc. Perkin Trans. II, 2378 (1972).
20. B. C. CHALLIS and S. P. JONES. J. Chem. Soc. Chem. Commun. 748 (1974).
21. M. I. VINNIK. Izv. Akad. Nauk SSSR, Ser. Khim. 799 (1978); Engl. Transl. 689 (1978).
22. C. A. BUNTON, C. J. O'CONNOR, and T. A. TURNEY. Chem. Ind. London, 1835 (1967).
23. C. A. BUNTON, S. J. FARBER, A. J. G. MILBANK, C. J. O'CONNOR, and T. A. TURNEY. J. Chem. Soc. Perkin Trans. II, 1869 (1972).
24. C. J. HYLAND and C. J. O'CONNOR. J. Chem. Soc. Perkin Trans. II, 1402 (1973); C. J. GIFFNEY and C. J. O'CONNOR. J. Chem. Soc. Perkin Trans. II, 1203 (1975).
25. C. R. SMITH and K. YATES. J. Am. Chem. Soc. **93**, 6578 (1971).
26. C. J. GIFFNEY and C. J. O'CONNOR. Aust. J. Chem. **29**, 307 (1976).
27. M. LILER. J. Chem. Soc. Perkin Trans. II, 816 (1972).
28. C. L. PERRIN. J. Am. Chem. Soc. **96**, 5628 (1974).
29. K. YATES. Acc. Chem. Res. **4**, 136 (1971).
30. V. C. ARMSTRONG, D. W. FARLOW, and R. B. MOODIE. J. Chem. Soc. B, 1099 (1968).
31. R. A. COX. J. Am. Chem. Soc. **96**, 1059 (1974).
32. R. A. McCLELLAND. J. Am. Chem. Soc. **97**, 3177 (1975).
33. P. WAN, T. A. MODRO, and K. YATES. Can. J. Chem. **58**, 2423 (1980).
34. C. R. SMITH. Ph.D. Thesis, University of Toronto. 1971.
35. E. C. W. CLARKE and D. N. GLEW. Trans. Faraday Soc. **62**, 539 (1966).
36. J. T. EDWARD and S. C. R. MEACOCK. J. Chem. Soc. 2009 (1957).
37. H. CHEN and D. E. IRISH. J. Phys. Chem. **75**, 2672 (1971).
38. T. F. YOUNG, L. F. MARANVILLE, and H. M. SMITH. *In* The structure of electrolytic solutions. *Edited by* W. J. Hamer. Wiley, New York. 1959. p. 35.
39. J. F. PATTERSON, W. P. HUSKEY, and J. L. HOGG. J. Org. Chem. **45**, 4675 (1980).
40. R. A. McCLELLAND and J. P. POTTER. Can. J. Chem. **58**, 2318 (1980).
41. R. A. McCLELLAND. J. Am. Chem. Soc. **96**, 3690 (1974).
42. E. BUNCEL and W. M. J. STRACHAN. Can. J. Chem. **47**, 911 (1969).
43. J. T. EDWARD and S. C. WONG. J. Am. Chem. Soc. **99**, 7224 (1977); J. T. EDWARD, S. C. WONG, and G. WELCH. Can. J. Chem. **56**, 931 (1978).
44. G. S. HAMMOND. J. Am. Chem. Soc. **77**, 334 (1955).

Can. J. Chem. Downloaded from www.nrcresearchpress.com by 210.87.254.42 on 09/06/12
For personal use only.

Aminobenzylation d'aldéhydes phosphoniques: préparation d'acides aminoalkylphosphoniques

GENEVIÈVE FABRE et NOËL COLLIGNON
Laboratoire de Chimie Organique I.N.S.C.I.R., B.P. 08, 76130 Mont-Saint-Aignan, France
ET
PHILIPPE SAVIGNAC
Equipe CNRS-SNPE, 2–8 rue Henry Dunant, B. P. N° 28, 94320 Thiais, France
Reçu le 2 février 1981

GENEVIÈVE FABRE, NOËL COLLIGNON et PHILIPPE SAVIGNAC. Can. J. Chem. **59**, 2864 (1981).

La réaction des aldéhydes phosphoniques avec la benzylamine, en présence de $NaBH_3CN$, conduit aux *N*-benzylaminoalkylphosphonates qui sont débenzylés par hydrogénation catalytique. Lorsque l'amination est effectuée en présence d'hydrogène et de palladium, la réduction et la débenzylation sont simultanées. En l'absence de réducteur, l'énaminobenzylphosphonate peut être isolé puis alkylé à l'azote. L'hydrolyse des aminoesters phosphoniques par HCl dilué libère les amino-acides phosphoniques. L'ordre de déroulement de chacune des opérations, ainsi que le choix du catalyseur, sont étudiés.

GENEVIÈVE FABRE, NOËL COLLIGNON and PHILIPPE SAVIGNAC. Can. J. Chem. **59**, 2864 (1981).

The reaction of phosphonic aldehydes with benzylamine in presence of $NaBH_3CN$ yields benzylaminoalkylphosphonates which, submitted to catalytic hydrogenation, lead to phosphonic amino esters. When reductive amination is carried out with H_2/Pd reduction and debenzylation are observed simultaneously. In the absence of reducing agent the enaminobenzylphosphonate can be isolated and *N*-alkylated. Hydrolysis of phosphonic amino-esters with dilute HCl gives phosphonic amino acids. The order of occurrence of each operation, as well as the choice of the catalyst is discussed.

Introduction

L'étude de la biosynthèse de l'acide amino-2 éthylphosphonique (AEPA ou ciliathine), simultanément réalisée par plusieurs équipes (1), a montré que l'oxo-2 éthylphosphonate de diéthyle est un précurseur de cet acide. Cependant malgré sa disponibilité et sa réactivité, les possibilités synthétiques offertes par cet aldéhyde n'ont pas été exploitées; seule une préparation, due à Isbell *et al.* (2), le met en jeu. Son emploi ainsi que celui de ses homologues nécessitent la mise au point de réactions spécifiques permettant d'introduire sélectivement une fonction amine, primaire, secondaire ou tertiaire.

Dans le but d'accéder aux acides à fonction primaire, nous avons étudié l'aminobenzylation du phosphonoacétaldéhyde et des homologues. Cette réaction, quel que soit l'aldéhyde, conduit aux acides aminophosphoniques recherchés; avec le phosphonacétaldéhyde l'intermédiaire de l'aminobenzylation possèdant un hydrogène échangeable par un métal, elle conduit également aux acides aminoéthylphosphoniques secondaires. Le schéma réactionnel suivi, ainsi que les acides préparés, sont décrits dans la figure 1.

Résultats

L'ensemble des résultats est rassemblé dans le Tableau 1.

(a) Acides aminoalkylphosphoniques primaires

La synthèse est divisible en trois étapes: l'aminobenzylation, la débenzylation et l'hydrolyse. L'étude et la mise au point de ces réactions nous ont conduits à l'établissement de deux méthodes séquencées et d'une méthode directe. Les méthodes séquencées se différencient au niveau de l'ordre de réalisation des étapes (**1** → **2** → **3** → **4** → **5**) ou (**1** → **2** → **4** → **5**) qui sont chacune consécutives alors que dans la méthode directe les deux premières étapes sont simultanées (**1** → **2** → **3**) et la troisième (**3** → **5**) distincte. En prenant le phosphonoacétaldéhyde comme modèle, nous avons comparé chacune des méthodes. Dans les méthodes séquencées nous réalisons l'aminobenzylation (**1** → **2**) dans le méthanol à pH 7 en présence de $NaBH_3CN$ commercial. Le rendement est régulier mais n'excède pas 85%.

La débenzylation (**2** → **3**) s'effectue sur le composé brut dans l'éthanol à 20°C en présence du couple $H_2/Pd(OH)_2/C$; elle est totale au bout d'environ 16 h sans aucune autre dégradation apparente de l'aminophosphonate. Cependant, il est utile de préciser que l'emploi d'hydroxyde de palladium sur charbon, même fraîchement préparé, ne donne pas des réactions reproductibles et la débenzylation est fréquemment incomplète. Nous attribuons le déroulement irrégulier de cette réaction à un empoisonnement du catalyseur par l'aminophos-

0008-4042/81/192864-06$01.00/0
©1981 National Research Council of Canada/Conseil national de recherches du Canada

Can. J. Chem. Downloaded from www.nrcresearchpress.com by 210.87.254.105 on 09/06/12
For personal use only.

Can. J. Chem. Downloaded from www.nrcresearchpress.com by 210.87.254.105 on 09/06/12
For personal use only.

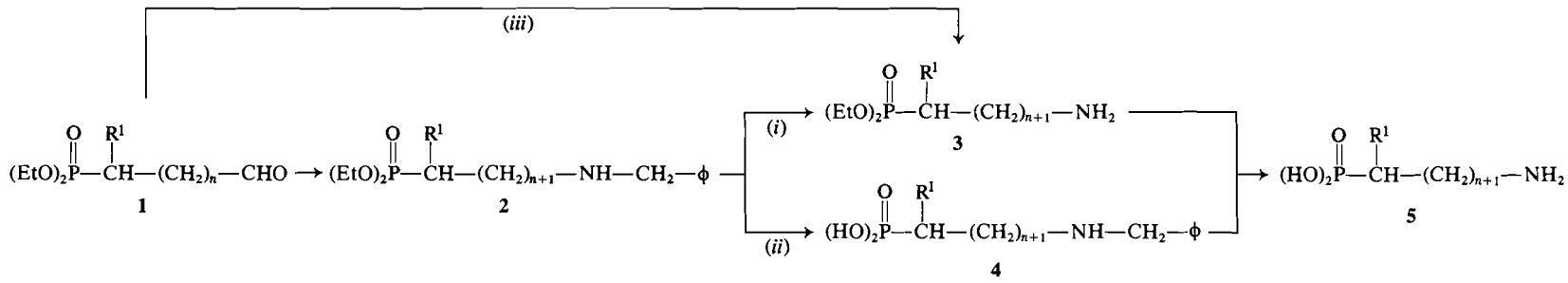

	n	R^1
a	0	H
b	1	H
c	1	Me

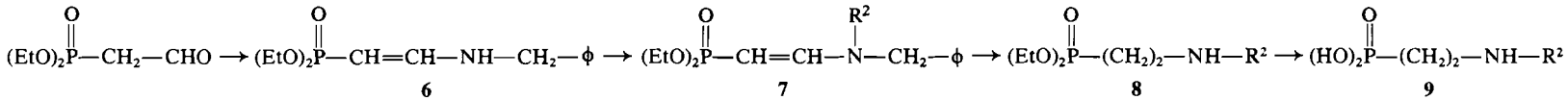

	R^2
d	Me
e	Et
f	Pr

FIG. 1

Can. J. Chem. Downloaded from www.nrcresearchpress.com by 210.87.254.105 on 09/06/12
For personal use only.

TABLEAU 1. Amino-acides phosphoniques

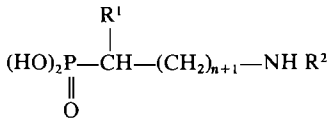

Essai	n	R^1	R^2	Rdt %[a] (global)
5a	0	H	H	34[b]
5a′	0	H	H	47[c]
5a″	0	H	H	56[d]
5a‴	0	H	H	46
5b	1	H	H	89
5c	1	Me	H	86
9d	0	H	Me	34
9e	0	H	Et	36
9f	0	H	Pr	53

[a]Par rapport à l'aldéhyde de départ.
[b]Méthode (*i*).
[c]Méthode (*ii*).
[d]Méthode (*iii*).

phonate dont la qualité n'est pas toujours constante. Le remplacement de l'hydroxyde de palladium par le catalyseur commercial Pd/C s'est révélé inefficace quelles que soient les conditions opératoires (temps ou T^0). Dans les cas favorables, le rendement de débenzylation en présence d'hydroxyde de palladium est de 95%.

L'étape (**3** → **5**) utilise les procédés d'hydrolyse et de purification sur résines échangeuses d'ions précédemment décrits (3) (essai 5a).

Les difficultés rencontrées lors de l'emploi de l'hydroxyde de palladium sur charbon nous ont amenés à inverser l'ordre des réactions afin d'éviter son emploi. Ainsi après isolement de **2**, on procède à l'hydrolyse acide (**2** →**4**) (70%) puis à la débenzylation de l'acide aminobenzylphosphonique (**4** → **5**). Dans cette dernière étape, seul le catalyseur commercial Pd/C dans l'eau à 100°C permet une débenzylation complète (79%) (essai 5a′). L'emploi de $Pd(OH)_2/C$ que se soit dans l'eau ou l'acide acétique, conduit toujours à des mélanges d'aminophosphonates partiellement débenzylés.

Cette seconde séquence, qui utilise un catalyseur commercial stable dont chaque étape est reproductible et dont les rendements sont réguliers, est préférable à la première.

Dans la méthode directe, nous réalisons simultanément l'aminobenzylation et la débenzylation (**1** → **3**). Nous opérons dans l'éthanol à 60°C en présence du couple $H_2/Pd/C$ avec un léger excès de benzylamine afin d'éviter la formation d'aminodiphosphonates (4). Cette opération conduit à l'isolement de **3** totalement débenzylé avec un très bon rendement (88%); on procède à l'hydrolyse sans purification préalable et obtient ainsi des acides **5** avec une pureté et un rendement supérieurs à ceux des deux précédentes méthodes (essai 5a″). Cette voie directe, qui est simple, rapide et également économique, est plus avantageuse que les deux précédentes.

L'extension de la réaction d'aminobenzylation aux homologues du phosphonoacétaldéhyde a été réalisée par la séquence directe (essais 5b, 5c). Ces structures moins énolisables et moins fragiles donnent à chaque opération des résultats très supérieurs à ceux observés avec le phosphonoacétaldéhyde. A la suite d'un travail récemment publié (5) nous avons substitué la dibenzylamine à la benzylamine. Son emploi n'apporte aucune amélioration sensible justifiant cette substitution (essai 5a‴).

(b) Acides aminoéthylphosphoniques secondaires

L'action d'une amine primaire sur l'oxo-2 éthylphosphonate de diéthyle conduit à un iminophosphonate dont Nagata et Hayase (6) ont montré qu'en solution il s'isomérisait en énaminophosphonate. L'existence de cet équilibre tautomère, dû à la présence du groupe phosphoryle, permet d'obtenir une métallation en α du phosphore conduisant ensuite, suivant l'électrophile engagé, soit à une alkylation, soit à une élimination.

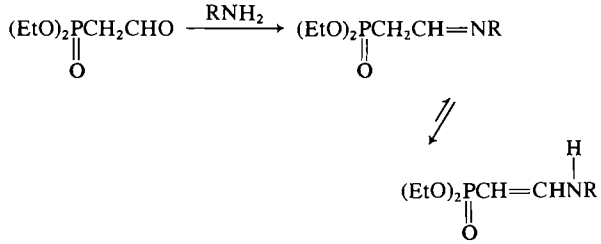

Nous avons étudié cette réaction dans le cas du couple phosphonoacétaldéhyde–benzylamine, qui en solution, conduit à la formation prépondérante d'énaminophosphonate **6**. La géométrie de cette énamine phosphonique (7), lorsqu'elle est réalisée dans le benzène anhydre à la température ambiante, est majoritairement *cis*.

L'action de d'hydrure de sodium dans le THF sur **6** conduit à l'anion mésomère **10** dont l'alkylation fournit un énaminophosphonate **7** totalement substitué à l'azote. Trois alkylations ont été faites (R^2 = Me (67%), Et (80%), allyle (84%)).

A l'opposé du sodium et ainsi qu'il avait été observé par Nagata et Hayase (6) le magnésium ne donne jamais une réaction complète. L'énaminophosphonate **7** est réduit et débenzylé en **8** soit par le procédé séquencé, soit par le procédé direct puis hydrolysé en acides **9** (essais 9d, 9e, 9f).

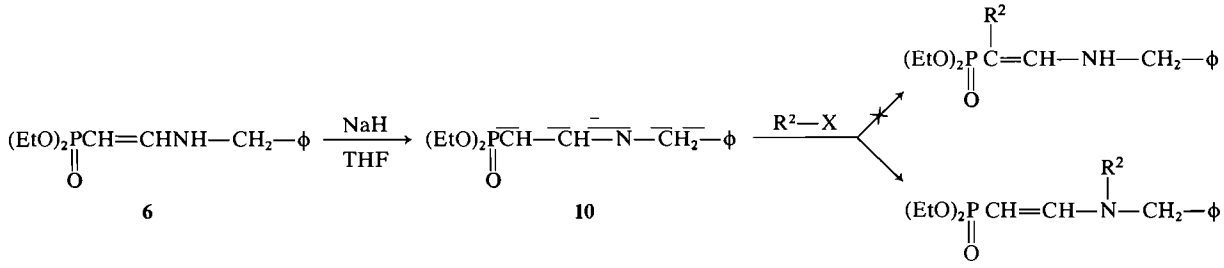

6 10 7

Conclusion

Cette voie d'accès aux acides phosphoniques aminés en position β ou γ n'avait, à notre connaissance, jamais été décrite. Son emploi soustrait l'aldéhyde aux réactions de polycondensation qui constituent l'écueil principal des préparations d'amines primaires à partir d'une fonction bivalente. Elle représente la seule préparation spécifique d'amino-acides primaires à partir des précurseurs naturels.

Partie expérimentale

Les spectres rmn ^1H sont enregistrés à 60 MHz sur Varian T60 ou A60; les solvants sont $CDCl_3$, CCl_4 ou D_2O; le Me_4Si sert de référence interne; les abréviations suivantes sont utilisées: s = singulet, d = doublet, t = triplet, q = quadruplet, qi = quintuplet, m = massif, mu = multiplet. Les spectres ir sont tracés sur Beckman Acculab TM2 (liquide pur ou pastilles de KBr). Les chromatographies en phase gazeuse (cpg) ont été réalisées sur Girdel 300 FN1 (colonnes SE30 ou OV1). Les points de fusion sont déterminés sur banc Kofler et ne sont pas corrigés. La purification des acides aminoalkylphosphoniques est réalisée sur résine Amberlite IRA 410. Les analyses élémentaires (C, H, N) sont déterminées sur un appareil Technicon. Les hydrogénations sont effectuées avec un hydrogénateur simple de laboratoire sous la pression atmosphérique.

Préparation des matières premières et réactifs

Les aldéhydes phosphoniques

L'oxo-2 éthylphosphonate de diéthyle, l'oxo-3 propylphosphonate de diéthyle et le méthyl-1 oxo-3 propylphosphonate de diéthyle sont préparés suivant des procédés récemment décrits (8).

Les catalyseurs

Le palladium (Pd/C 10%) est le catalyseur commercial Merck. L'hydroxyde de palladium ($Pd(OH)_2/C$) est préparé suivant la méthode adaptée de Pearlman (9).

Séquence 1 → 2 → 3 → 5

Synthèse du N*-benzylamino-2 éthylphosphonate de diéthyle* (**2**, $n = 0$, $R^1 = H$)

A un mélange d'oxo-2 éthylphosphonate de diéthyle (2 g, 1.1×10^{-2} mol) et de benzylamine (1.2 g, 1.1×10^{-2} mol) en solution dans 20 mL de méthanol, on ajoute une solution de cyanoborohydrure de sodium (0.7 g, 1.1×10^{-2} mol) dans 20 mL de méthanol. Le pH de la solution est amené à 7–7,5 par addition d'une solution (≃ 10 *M*) de HCl gazeux dans le méthanol. Le mélange est agité magnétiquement à température ambiante dans un erlenmeyer bouché par un septum et la réaction suivie en cpg. La réduction est presque complète après l'addition d'HCl. L'agitation est poursuivie pendant 1 h environ. Le mélange est acidifié à pH ≃ 1 par HCl concentré. Le méthanol est évaporé et le résidu repris par 25 mL d'eau. Cette phase aqueuse est lavée à l'éther (3 × 30 mL), alcalinisée à pH ≃ 10 par KOH en pastilles, saturée avec NaCl et extraite par CH_2Cl_2 (4 × 25 mL). L'extrait séché et évaporé donne 2,6 g (86%) d'une huile brute à laquelle nous avons attribué la structure du *N*-benzylamino-2 éthylphosphonate de diéthyle, après examen des spectres ir et de rmn ^1H, résumés ci-dessous. Infrarouge ir (liq. pur) ν : 3280 (NH), 1230, 1050–1020 et 950 (O—P(O)), 730 et 680 (Ph) cm^{-1}; rmn ^1H (CCl_4) δ(ppm): 1.25 (t, 6H, CH_3—CH_2O, $J = 7$ Hz), 1,8 (2 t, 2H, P(O)CH_2, $J = 7$ Hz, $J_{PH} = 18$ Hz), 2.0(s, 1H, *NH*), 2.8(2 t, 2H, CH_2NH, $J = 7$ Hz, $J_{PH} = 17$ Hz), 3.7 (s, 2H, CH_2Ph), 4.0(qi, 4H, OCH_2CH_3, $J = 7$ Hz, $J_{PH} = 7$ Hz), 7.2 (s large, 5H, H_{ar}).

Synthèse de l'amino-2 éthylphosphonate de diéthyle (**3**, $n = 0$, $R^1 = H$)

Au *N*-benzylamino-2 éthylphosphonate de diéthyle (2.5 g, 9.2×10^{-3} mol) en solution dans 50 mL d'éthanol, on ajoute le catalyseur $Pd(OH)_2/C$ (1.21 g) fraichement préparé et hydrogène à température ambiante pendant 16 h. Le catalyseur est séparé par filtration sur Célite, l'éthanol est évaporé. L'huile brute obtenue pèse 1.56 g (94%); nous lui avons attribué la structure de l'amino-2 éthylphosphonate de diéthyle après examen de ses spectres ir et de rmn ^1H que nous résumons: ir (liq. pur) ν: 3360, 3280 et 1610 (NH_2), 1230, 1050–1020 et 950 (O—P(O)) cm^{-1}; rmn ^1H (CCl_4) δ (ppm): 1.3 (t, 6H, CH_3—CH_2O, $J = 7$ Hz), 1.9 (2t, 2H, P(O)CH_2, $J = 7$ Hz, $J_{PH} = 18$ Hz), 1.9 (s, 2H, NH_2), 2.9 (2t, 2H, CH_2—NH_2, $J = 7$ Hz, $J_{PH} = 15$ Hz), 4.1 (qi, 4H, OCH_2CH_3, $J = 7$ Hz, $J_{PH} = 7$ Hz).

Synthèse de l'acide amino-2 éthylphosphonique (ou AEPA) (**5**, $n = 0$, $R^1 = H$)

L'amino-2 éthylphosphonate de diéthyle (1.4 g, 7.7×10^{-3} mol) est porté au reflux dans 25 mL d'HCl 8 M pendant 18 h. La solution refroidie est lavée par CH_2Cl_2 (2 × 30 mL), puis évaporée. Le résidu est remis en solution dans 30 mL d'eau, puis la solution est évaporée à nouveau; cette opération est répétée 4 fois. Le résidu est remis en solution dans 100 mL d'eau et éventuellement décoloré à chaud au noir animal. La solution obtenue est passée sur colonne de résine Amberlite IRA 410 (sous forme OH^-) qui fixe les ions Cl^- et l'acide aminophosphonique. Après un lavage à l'eau de la résine, l'acide aminophosphonique est sélectivement décroché par une solution d'acide acétique à 5% en poids. L'évaporation de la fraction de pH 7–3 fournit 0.42 g (43%) de cristaux blancs, pF > 260°C, dont le spectre de rmn ^1H correspond à la structure de l'AEPA: rmn ^1H (D_2O) δ (ppm): 2.0 (2t, 2H, P(O)CH_2, $J = 8$ Hz, $J_{PH} = 17$ Hz), 3.2 (2t, 2H, CH_2NH_2, $J = 8$ Hz, $J_{PH} = 10$ Hz), mais dont l'analyse (à 1.2% près sur C et 0.7% près sur N) est médiocre.

Le rendement global de la séquence **1 → 2 → 3 → 5** s'établit à 34% (essai 5a).

Séquence 1 → 2 → 4 → 5

L'étape **1 → 2** est identique à celle de la séquence précédente.

Synthèse de l'acide N*-benzylamino-2 éthylphosphonique* (**4**, $n = 0$, $R^1 = H$)

Le *N*-benzylamino-2 éthylphosphonate de diéthyle (2.2 g, 8.1×10^{-3} mol) est porté au reflux dans 25 mL d'HCl 8 *M* pendant

Can. J. Chem. Downloaded from www.nrcresearchpress.com by 210.87.254.105 on 09/06/12
For personal use only.

Can. J. Chem. Downloaded from www.nrcresearchpress.com by 210.87.254.105 on 09/06/12
For personal use only.

18 h. La suite du traitement est identique à celui de la synthèse de l'AEPA. On isole 1.21 g (69,5%) de cristaux blancs, pF > 260°C, auxquels nous avons attribué la structure de l'acide *N*-benzylamino-2 éthylphosphonique; rmn ^1H (D_2O) δ (ppm): 2.2 (2t, 2H P(O)CH_2, J = 8 Hz, J_{PH} = 18 Hz), 3.5 (2t, 2H, CH_2—NH, J = 8 Hz, J_{PH} = 18 Hz), 4.3 (s, 2H, CH_2Ph), 7.5 (s, 5H, H_{ar}). *Anal.* calc. pour $C_9H_{14}NO_3P$: C 50.23, H 6.51, N 6.51; trouvé: C 50.09, H 6.56, N 6.59.

Synthèse de l'AEPA (**5**, n = 0, R^1 = H)

L'acide *N*-benzylamino-2 éthylphosphonique (1.2 g, 5.6 × 10^{-3} mol), le catalyseur commercial Pd/C 10% (0.6 g) et 20 mL d'eau sont placés dans un ballon équipé d'un réfrigérant à reflux, d'un agitateur magnétique et d'un capillaire de barbotage. Le mélange est dégazé par barbotage d'argon pendant 1 h 30 à température ambiante. L'argon est remplacé par l'hydrogène (≃ 50 mL/min) et on porte à 100°C en maintenant une agitation vigoureuse pendant 10 h. Le catalyseur est séparé par filtration sur Célite, le filtrat, évaporé à sec donne 0.55 g (79%) de cristaux blancs, pF > 260°C dont le spectre de rmn ^1H (dans D_2O) est analogue à celui de l'AEPA décrit ci-dessus. L'analyse est à 0.7% près sur N.

Le rendement global de la séquence **1** → **2** → **4** → **5** s'établit à 47% (essai 5a').

Méthode directe **1** → **3** → **5**

Synthèse de l'AEPA (**5**, n = 0, R^1 = H)

L'oxo-2 éthylphosphonate de diéthyle (3 g, 1.7 × 10^{-2} mol), la benzylamine (2.35 g, 2.2 × 10^{-2} mol), le catalyseur commercial Pd/C 10% (0.6 g) et 100 mL d'éthanol sont placés dans la fiole à hydrogéner et agités magnétiquement pendant 19 h à 65°C. Après séparation du catalyseur et évaporation de l'alcool et de la benzylamine en excès, on isole 2.7 g (88%) d'une huile brute à laquelle nous avons attribué la structure de l'amino-2 éthylphosphonate de diéthyle (**3**, n = 0, R^1 = H) grâce aux spectres ir et rmn ^1H analogues à ceux décrits ci-dessus. Cette huile brute est hydrolysée comme précédemment par HCl 8 M au reflux et l'acide obtenu, purifié sur résine Amberlite IRA 410 (Rdt d'hydrolyse: 64%); le spectre de rmn ^1H (dans D_2O) des cristaux blancs isolés est analogue à celui de l'AEPA décrit ci-dessus. L'analyse donne les résultats suivants. *Anal.* calc. pour $C_2H_8NO_3P$: C 19.20, H 6.40, N 11.20; trouvé: C 19.13, H 6.69, N 10.98.

Le rendement global s'établit à 56% (essai 5a'').

Synthèse de l'acide amino-3 propylphosphonique (**5**, n = 1, R^1 = H)

Le mélange d'oxo-3 propylphosphonate de diéthyle (2 g, 10^{-2} mol), de benzylamine (1.43 g, 1.3 × 10^{-2} mol), de catalyseur Pd/C 10% (0.4 g) et d'éthanol (50 mL) est hydrogéné pendant 17 h à 55°C. Après traitement, l'huile brute pèse 2 g (≃ 100%); nous lui avons attribué la structure de l'amino-3 propylphosphonate de diéthyle (**3**, n = 1, R^1 = H) d'après ses spectres ir et de rmn ^1H: ir (liq. pur) ν: 3380, 3300 et 1600 (NH_2), 1220, 1020 et 940 (O—P(O))cm^{-1}; rmn ^1H (CCl_4) δ (ppm): 1.25 (t, 6H, CH_3—CH_2O, J = 7 Hz), 1.3 à 1.4 (s large, 2H, NH_2), 0.9 à 2.0 (mu mal résolu, 4H, P(O) CH_2—CH_2), 2.6 (t, 2H, CH_2NH_2, J = 6 Hz), 4.0 (qi, 4H, OCH_2CH_3, J = 7 Hz, J_{PH} = 7 Hz). L'huile brute précédente (1.9 g, 9.7 × 10^{-3} mol) est hydrolysée dans 30 mL d'HCl 8 *M* au reflux 18 h. Après traitement, on isole 1.2 g (89%) de cristaux blancs, pF > 260°C auxquels nous avons attribué la structure de l'acide amino-3 propylphosphonique; rmn ^1H (D_2O) δ (ppm): 1.3 à 2.3 (mu mal résolu, 4H, P(O) CH_2—CH_2), 3.2 (t, 2H, CH_2—NH_2, J = 7 Hz). *Anal.* calc. pour $C_3H_{10}NO_3P$: C 25.89, H 7.19, N 10.07; trouvé: C 25.55, H 7.40, N 9.90.

Le rendement global s'établit à 89% (essai 5b).

Synthèse de l'acide amino-3 méthyl-1 propylphosphonique (**5**, n = 1, R^1 = Me)

Le mélange de méthyl-1 oxo-3 propylphosphonate de diéthyle (2 g, 9.6 × 10^{-3} mol), de benzylamine (1.33 g, 1.24 × 10^{-2} mol), de catalyseur Pd/C 10% (0.35 g) et d'éthanol (75 mL) est hydrogéné pendant 15 h à 60°C. Après traitement, l'huile brute pèse 2 g (≃ 100%): nous lui avons attribué la structure de l'amino-3 méthyl-1 propylphosphonate de diéthyle (**3**, n = 1, R^1 = Me) après examen de ses spectres ir et de rmn ^1H; ir (liq. pur) ν: 3340, 3280 et 1600 (NH_2), 1220, 1050–1020 et 950 (O—P(O)) cm^{-1}; rmn ^1H (CCl_4) δ (ppm): 1.1 (2d, 3H, —CH(CH_3), J = 7 Hz, J_{PH} = 18 Hz), 1.3 (t, 6H, CH_3—CH_2O, J = 7 Hz), 1.3 à 2.3 (m, 5H, P(O)—CH(CH_3)—CH_2 et NH_2, s large à 1.7), 2.7 (t mal résolu, 2H, CH_2NH_2, J ≃ 6 Hz); 4.0 (qi, 4H, OCH_2CH_3, J = 7 Hz, J_{PH} = 7 Hz).

L'huile brute précédente (1.9 g, 9.1 × 10^{-3} mol) est hydrolysée dans 25 mL d'HCl 8 *M* au reflux 15 h. Après traitement, on isole 1.2 g (86%) de cristaux blancs, pF > 260°C auxquels nous avons attribué la structure de l'acide amino-3 méthyl-1 propylphosphonique; rmn ^1H (D_2O) δ (ppm): 1.3 (2d, 3H, CH(CH_3), J = 6 Hz), J_{PH} = 17 Hz), 1.7 (mu mal résolu, 3H, P(O)CH(CH_3)-CH_2), 3.3 (t, 2H, CH_2NH_2, J = 7 Hz) *Anal.* calc. pour $C_4H_{12}NO_3P$: C 31.37, H 7.84, N 9.15; trouvé: C 31.12, H 7.68, N 9.00.

Le rendement global s'établit à 86% (essai 5c).

Synthèse d'acides aminoéthylphosphoniques secondaires

Nous décrivons la synthèse de l'acide *N*-propylamino-2 éthylphosphonique (essai 9f).

Synthèse de l'énaminophosphonate

L'oxo-2 éthylphosphonate de diéthyle (2 g, 1.1 × 10^{-2} mol) et la benzylamine (1.18 g, 1.1 × 10^{-2} mol) sont mélangés dans 30 mL de benzène anhydre et portés au reflux pendant 2 h avec distillation azéotropique. L'évaporation du benzène donne 2.95 g (≃ 100%) d'une huile brute à laquelle nous avons attribué la structure du *N*-benzylamino-2 vinylphosphonate de diéthyle après examen de ses spectres ir et de rmn ^1H: ir (liq. pur) ν: 3260 (NH), 3050 (=CH), 1615 (C=C *cis* majoritaire), 1585 (C=C *trans* minoritaire), 1190, 1055–1030 et 955 (O—P(O)), 750 et 700 (Ph) cm^{-1}; rmn ^1H (CCl_4) δ (ppm): 1.1 et 1.2 (2t imbriqués dont les intensités relatives sont dans le rapport ≃ 85/15, 6H, CH_3—CH_2O, J = 7 Hz), 3.8 (qi, 4H, OCH_2CH_3, J = 7 Hz), 3.7 à 4.5 (mu, > 3H, P(O)—CH=, CH_2Ph et NH de la forme *trans*), 6.7 à 7.6 (s large et mu, > 6H, =CH—NH, H_{ar} et NH de la forme *cis*).

Alkylation de l'énaminophosphonate

Dans un tricol équipé d'un agitateur magnétique, d'un thermomètre, d'un réfrigérant à reflux, d'une ampoule isobare et relié à un gazomètre, on place l'hydrure de sodium (0.58 g de la suspension commerciale à 50% dans l'huile, 1.2 × 10^{-2} mol) préalablement dégraissé, le THF anhydre (30 mL) et le bromure d'allyle (1.6 g, 1.3 × 10^{-2} mol). L'énaminophosphonate (2.9 g, 1.1 × 10^{-2} mol) en solution dans le THF (20 mL) est ajouté goutte à goutte sous agitation, la température atteint 27°C. Après addition, on chauffe à 30°C pendant 4 h jusqu'à obtention du volume théorique d'hydrogène. Après hydrolyse et traitement habituel, on isole 2.8 g (84%) d'une huile brute à laquelle nous avons attribué la structure du *N*-allyl, *N*-benzylamino-2 vinylphosphonate de diéthyle après examen des spectres ir et de rmn ^1H; ir (liq. pur) ν: 1620 (C=C), 1240, 1065–1040 et 960 (O—P(O)), 745 et 700 (Ph)cm^{-1}; rmn ^1H (CCl_4) δ (ppm): 1.2 (t, 6H, CH_3—CH_2O, J = 7 Hz), 3.9 (qi, 4H, OCH_2CH_3, J = 7 Hz, J_{PH} = 7 Hz), 4.3 (s, 2H, CH_2Ph), 3.5 à 4.5 (mu, 3H, P(O)—CH=, N—CH_2—CH=), 4.6 à 6.2 (mu, 3H, —CH=CH_2), 6.7 à 7.8 (s large et mu, 6H, H_{ar} et =CH—N).

Réduction–débenzylation du N-*alkylénaminophosphonate*

Le *N*-allyle *N*-benzylamino-2 vinylphosphonate de diéthyle (2.7 g, 8.7 × 10^{-3} mol) est hydrogéné en présence de catalyseur commercial Pd/C 10% (0.33 g) dans 50 mL d'éthanol, à 60°C pendant 15 h. Après filtration du catalyseur et évaporation, on isole 1.75 g (90%) d'une huile brute à laquelle nous avons attribué la structure du *N*-propylamino-2 éthylphosphonate de

diéthyle à l'examen de ses spectres ir et de rmn ^1H; ir (liq. pur) ν: 3300 (NH), 1240, 1060–1035 et 960 (O—P(O)) cm^{-1}; rmn ^1H (CCl_4) δ (ppm): 0.9 (t, 3H, CH_2—CH_2—CH_3, J = 7 Hz), 1.3 (t, 6H, CH_3—CH_2O, J = 7 Hz), 1.1 à 2.3 (mu, 4H, P(O)—CH_2 et CH_2—CH_2—CH_3), 2.1 (s, 1H, *NH*), 2.5 (t, 2H, N—CH_2—CH_2—CH_3, J = 7 Hz), 2.7 (2t, 2H, P(O) CH_2—CH_2—NH, J = 7 Hz, J_{PH} = 17 Hz), 4.0 (qi, 4H, OCH_2CH_3, J = 7 Hz, J_{PH} = 7 Hz).

Hydrolyse du N-*alkylamino-2 éthylphosphonate*

Le *N*-propylamino-2 éthylphosphonate de diéthyle (1.7 g, 7.6 × 10^{-3} mol) est hydrolysé dans 23 mL d'HCl 8 *M* au reflux 19 h. Après traitement et purification habituels, on isole 0.9 g (71%) de cristaux blancs, pF > 260°C auxquels nous avons attribué la structure de l'acide *N*-propylamino-2 éthylphosphonique; rmn ^1H (D_2O) δ (ppm): 1.1 (t, 3H, CH_2—CH_2—CH_3, J = 7 Hz), 1.3 à 2.4 (mu, 4H P(O)—CH_2 et CH_2—CH_2—CH_3), 3.2 (t, 2H, N—CH_2—CH_2—CH_3, J = 7 Hz), 3.3 (2t, 2H, (P(O)CH_2—CH_2—NH), J = 7 Hz, J_{PH} = 10 Hz). *Anal.* calc. pour $C_5H_{14}NO_3P$: C 35.93, H 8.38, N 8.38; trouvé: C 36.24, H 8.09, N 8.00.

Le rendement global de l'opération s'établit à 53%.

1. A. Trebst et F. Geike. Z. Naturforsch. Teil B, **22**, 989 (1967); H. Horiguchi, J. S. Kittredge et E. Roberts. Biochim. Biophys. Acta, **165**, 164 (1968); W. A. Warren. Biochim. Biophys. Acta, **156**, 437 (1968); H. Horiguchi. Biochim. Biophys. Acta, **261**, 102 (1972); H. Horiguchi et H. Rosenberg. Biochim. Biophys. Acta, **104**, 333 (1975).
2. A. F. Isbell, L. F. Englert et H. Rosenberg. J. Org. Chem. **34**, 755 (1969).
3. D. Brigot, N. Collignon et P. Savignac. Tetrahedron, **35**, 1345 (1979).
4. N. Collignon, G. Fabre, J. M. Varlet et P. Savignac. Phosphorus Sulfur. A paraître.
5. W. Szczepaniak et K. Kuczynski. Phosphorus Sulfur, **7**, 333 (1979).
6. W. Nagata et Y. Hayase. Tetrahedron Lett. 4359 (1968); W. Nagata et Y. Hayase. J. Chem. Soc. C, 460 (1969).
7. J. Y. Merour, N. T. Thuong et P. Chabrier. C.R. Acad. Sci. Ser C, **280**, 473 (1975).
8. J. M. Varlet, G. Fabre, F. Sauveur, N. Collignon et P. Savignac. Tetrahedron. **37**, 1377 (1981).
9. L. F. Fieser et M. Fieser. Reagents for organic synthesis. Vol 1. Wiley-Interscience. 1967; p. 782. W. M. Pearlman. Org. Synth. Coll. Vol. V. 1973. p. 671.

Can. J. Chem. Downloaded from www.nrcresearchpress.com by 210.87.254.105 on 09/06/12
For personal use only.

Carbon-13 magnetic resonance: hydrogen involvement in γ-*anti* substituent effects

T. P. FORREST AND J. THIEL[1]

Department of Chemistry, Dalhousie University, Halifax, N.S., Canada B3H 4J3

Received October 27, 1980[2]

T. P. FORREST and J. THIEL. Can. J. Chem. **59**, 2870 (1981).

Chemical shifts have been determined for the carbons in a series of 3,3-dimethylcyclohexyl derivatives, (substituent = H, CH_3, NH_2, OH, Cl, Br, I). Comparison of the γ-*anti* substituent effects at carbons 3 and 5 indicates that presence of axial protons on these carbons causes increased shielding by all of the above substituents. The shielding by γ-*anti* substituents is decreased by the replacement of either the α or γ protons by methyl groups; the extent of the decrease is dependent upon the substituent and upon the position of the hydrogen which is replaced.

T. P. FORREST et J. THIEL. Can. J. Chem. **59**, 2870 (1981).

On a déterminé les déplacements chimiques du carbone de dérivés du diméthyl-3,3 cyclohexyle (les substituants sont: H, CH_3, NH_2, OH, Cl, Br, I). La comparaison des effets de substituants γ-*anti* au niveau des carbones 3 et 5 indique que la présence de proton axiaux sur ces carbones provoque une augmentation du blindage par tous les substituants mentionnés. Le blindage par les substituants γ-*anti* diminue lorsqu'on remplace le proton α ou γ par des groupes méthyles; le taux de diminution dépend du substituant et de la position de l'hydrogène qui est remplacé.

[Traduit par le journal]

Carbon-13 chemical shifts have proven to be sensitive probes for the determination of the structure and stereochemistry of organic compounds. The effects of structural changes on chemical shift may be very complex, but satisfactory empirical correlations (1) have been established in many cases that allow the prediction of the chemical shifts. These empirical correlations continue to be developed and refined. The substituent parameter for a group in a γ-*anti* orientation has recently been purported to be dependent upon the presence or absence of hydrogens in a *syn* orientation on the α and γ carbons (2). We had observed (2*c*) in a series of compounds that shielding increased with increasing electronegativity of a γ-*anti* substituent, regardless of whether the *syn* α and γ protons were present, when the substituent was a higher row halogen (Cl, Br, I), whereas for the first row elements (CH_3, NH_2, OH, F) shielding increased with increasing electronegativity when the *syn* α and γ hydrogens were present, but decreased when they were absent. This observation of the change in electronegativity dependence of the substituent parameter for the first row elements rested solely on compounds with bridgehead substituents for those cases without the H–H interaction. We have now measured the γ-*anti* effect in a series of compounds without bridgehead substituents to determine the effect of the H–H interaction in these cases, and to attempt to quantify the effect.

For this purpose we prepared a series of 3,3-dimethylcyclohexyl derivatives to test the electronegativity dependence of the γ-substituent effect at carbons 3 and 5. This series was chosen because it gives a conformationally homogeneous system with the substituent *anti* to two γ-carbons, the one (C-5) which has an axial proton and the second (C-3) which does not. The synthetic scheme employed in the preparation of these compounds is shown in Scheme 1; preparation of derivatives by direct nucleophilic substitution reactions was not successful, nor were attempts to prepare the fluoro derivative.

Results

Chemical shifts for the carbons of each derivative are given in Table 1. Assignments were made on the basis of off-resonance decoupling and correlations with established empirical parameters (1) for cyclohexane chemical shifts. The chemical shifts of the methylene carbons (C-2, C-4, C-5, C-6) were different enough so that each assignment could be made unequivocally except in the case of C-4 and C-6 of the chloride and bromide. In each compound the methyl group with the higher field chemical shift (lower δ) was assigned the axial orientation (γ-*gauche* effect).

Discussion

Parameters for the substituent effects of the different groups are given in Table 2. The values for the α, β, and δ effects for the ring carbons are similar to values reported for these substituent parameters (ref. 1*c*, p. 45).

[1]Postdoctoral fellow from Adam Mickiewicz University, Institute of Chemistry, 60780, Poznan, Poland.

[2]Revision received June 11, 1981.

0008-4042/81/192870-06$01.00/0

©1981 National Research Council of Canada/Conseil national de recherches du Canada

Can. J. Chem. Downloaded from www.nrcresearchpress.com by 210.87.254.105 on 09/06/12
For personal use only.

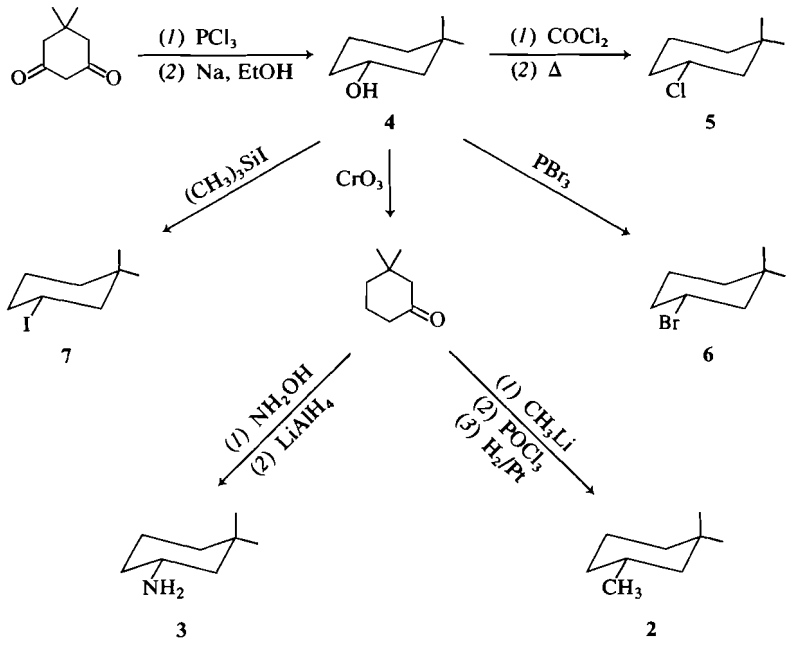

SCHEME 1

The γ-*anti* parameters observed for the two ring carbons (C-3 and C-5) are plotted against electronegativity (electronegativity values from ref. 3) in Figs. 1 and 2. In each case an approximately linear correlation is obtained for the halogens, and another with a different slope is obtained for the first row elements. The plots of the chemical shifts of C-5 are similar to those obtained from the simple cyclohexyl derivatives (4), whereas the plot of the C-3 shifts is characteristic of the γ carbon of the bridgehead substituted compounds (5). In the latter case the first-row elements have a reversed slope,

TABLE 1. Chemical shifts[a] of carbons in 3,3-dimethylcyclohexyl derivatives

Compound	X	C-1[b]	C-2	C-3	C-4	C-5	C-6	C_{eq}	C_{ax}
1	H	22.58	39.67	30.25	39.67	22.58	26.55	28.89	
2	CH_3[c]	28.41	48.90	30.97	39.21	22.64	35.44	33.59	24.85
3	NH_2	46.92	49.27	31.51	38.36	21.37	36.32	33.10	24.82
4	OH	66.98	48.08	31.73	38.17	20.60	35.29	32.76	24.99
5	Cl	57.70	50.00	33.26	37.84[d]	22.44	37.33[d]	32.81	24.55
6	Br	50.01	51.02	34.09	37.75[d]	23.49	38.27[d]	32.83	24.29
7	I	27.25	53.32	34.70	37.73	24.74	40.45	32.79	23.96

[a] In ppm relative to TMS.
[b] The carbons in all compounds are numbered relative to the substituent under consideration: i.e. C-3 is the quaternary carbon in all cases.
[c] Similar values for the chemical shifts of this compound are reported in ref. 12.
[d] Values for C-4 and C-6 may be interchanged.

TABLE 2. Substituent effects (Δδ) in 3,3-dimethylcyclohexyl derivatives

Compound	X	γ_3[a]	γ_5[a]	$\Delta\gamma$[b]	α_1[a]	β_2[a]	β_6[a]	δ_4[a]
2	CH_3	+0.72	+0.06	−0.66	+5.83	+9.23	+8.89	−0.46
3	NH_2	+1.26	−1.21	−2.47	+24.34	+9.60	+9.77	−1.31
4	OH	+1.48	−1.98	−3.46	+44.40	+8.41	+8.74	−1.50
5	Cl	+3.01	−0.14	−3.15	+35.12	+10.33	+10.78[c]	−1.83[c]
6	Br	+3.84	+0.91	−2.93	+27.43	+11.35	+11.72[c]	−1.92[c]
7	I	+4.45	+2.16	−2.29	+4.67	+13.65	+13.90	−1.94

[a] Δδ in ppm relative to the equivalent position in compound **1** (substituent = H).
[b] $\gamma_5 - \gamma_3$.
[c] The values for C-4 and C-6 may be interchanged, with consequent change in β_6 and δ_4.

Can. J. Chem. Downloaded from www.nrcresearchpress.com by 210.87.254.105 on 09/06/12
For personal use only.

Can. J. Chem. Downloaded from www.nrcresearchpress.com by 210.87.254.105 on 09/06/12
For personal use only.

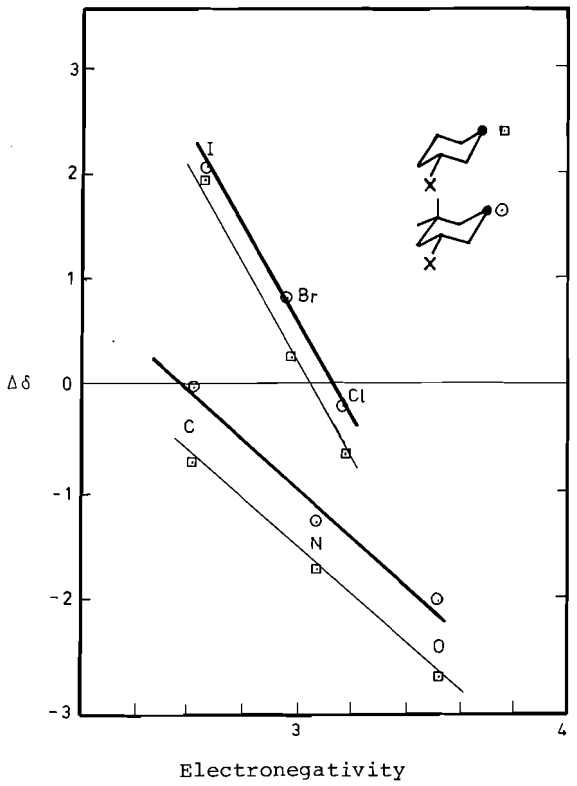

FIG. 1. γ-*anti* substituent effect on a methylene group vs. substituent electronegativity.

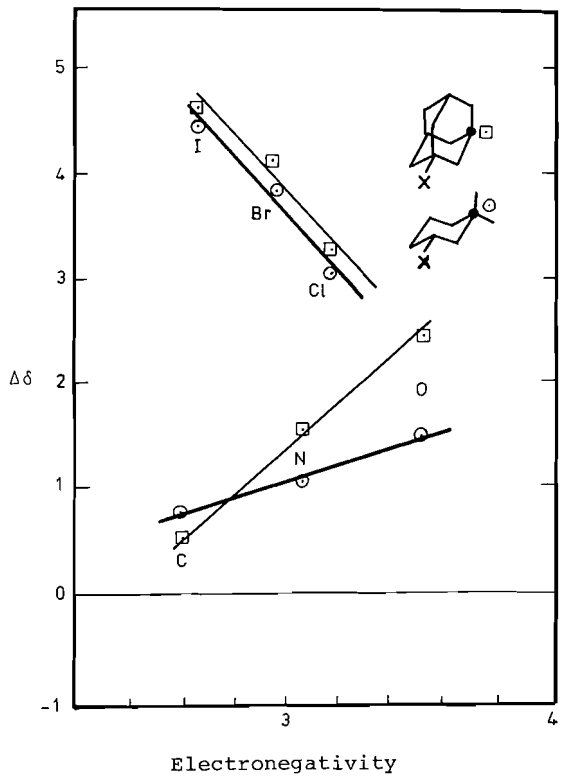

FIG. 2. γ-*anti* substituent effect on a quaternary carbon vs. substituent electronegativity.

the substituent effect becoming less shielding with increasing electronegativity. This observation supports the conclusion (2*b*) that the difference in effect is due to the substitution pattern rather than a pecularity of bridgehead substitution.

A quantification of the effect of the presence of the 1,3-diaxial hydrogen–hydrogen interaction may be sought in the difference $(\gamma_5 - \gamma_3)$ ($\Delta\gamma$ in Table 2), in the substituent effect on carbons 5 and 3. If this difference is attributed to the transmission of the substituent effect through the protons, it may be seen that this pathway contributes a shielding effect for all substituents. A plot of $\Delta\gamma$ against electronegativity shows once again that the first-row and higher-row elements have linear plots with different slopes, but in both cases the shielding increases with increasing substituent electronegativity.

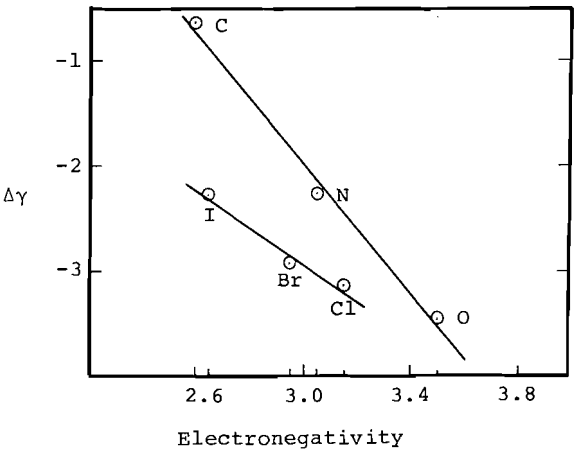

FIG. 3. Difference in γ-*anti* substituent effect with and without γ hydrogens vs. substituent electronegativity.

It might be argued that the equatorial methyl on C-3 could also be responsible, at least in part, for the change in the γ-anti substituent effect. The effect of an equatorial methyl may be detected in the chemical shift difference between C-5 and C-3 in the *cis*-3-methylcyclohexyl derivatives. As may be seen from Table 3, replacement of the equatorial hydrogen by a methyl group causes a decrease in the shielding effect of the substituents, but the decrease is significantly less than that caused by the replacement of both hydrogens of the γ carbons. The effect of the replacement of the α hydrogen by a methyl group can be seen in the comparison of the chemical shift of C-3 of 4-*tert*-butyl and *1*-methyl-

Can. J. Chem. Downloaded from www.nrcresearchpress.com by 210.87.254.105 on 09/06/12
For personal use only.

TABLE 3. Effect of α and γ protons on substituent parameters

Substituent	Change in γ effect by presence of		
	both γ H's[a]	equatorial γ H[b]	α − H[c]
CH_3	−0.66	−0.40	—
NH_2	−2.47	−0.99	—
OH	−3.46	−1.44	−5.87
Cl	−3.15	−1.41	−4.29
Br	−2.93	−0.66	−3.45
I	−2.29	−0.66	−1.69

[a] $\gamma_5 - \gamma_3$ in 3,3-dimethylcyclohexyl derivatives.
[b] $\gamma_5 - \gamma_3$ in *cis*-3-methylcyclohexyl derivatives (ref. 2*b*).
[c] γ_3 in *trans*-4-*tert*-butylcyclohexyl derivatives (**8**) minus the γ_3 in the analogous 1-methyl-4-*tert*-butylcyclohexyl derivatives (**9**) (ref. 2*b*)

4-*tert*-butyl cyclohexyl derivatives **8** and **9** (Table 3). Loss of the α hydrogen causes the substituent to be less effective in shielding the γ carbons; the substituent effects reported for **9** (OH, Cl, Br, I, F) are in fact all deshielding (2*b*).

From the above examples it can be clearly seen that the presence of *syn* diaxial α and γ hydrogens can be directly correlated with increased shielding by γ-*anti* substituents. Removal of either of these hydrogens causes decreased shielding by the substituent, but the effect of replacing the separate protons by methyl groups is not the same numerically, thus vitiating the use of a single parameter assignable to the 1,3-*syn* hydrogen effect for γ-*anti* substituents.

Because substituent effects on carbon chemical shifts can represent a small difference between large opposing paramagnetic and diamagnetic effects, it is often difficult to rationalize the effect in

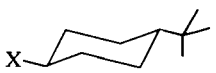

8

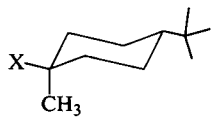

9

terms of factors familiar to the organic chemist. Casual observation of the plot in Fig. 3 indicated a striking similarity with the plot of the proton chemical shift of the methyl group bearing those substituents. Indeed, a plot of $\Delta\gamma$, $(\gamma_5 - \gamma_3)$, against the chemical shift of CH_3X yields a straight line (correlation coefficient = 0.995) (Fig. 4).

The observation of the direct correlation between the proton chemical shift of the simplest possible compounds in which the substituent effect on the α hydrogen can be observed is curious and perhaps entirely fortuitous; however, it does illustrate a case in which the "heavy atom effect" can be experienced by a γ carbon to the same extent as by an α proton.

A difference in the γ-*anti* effect of first-row

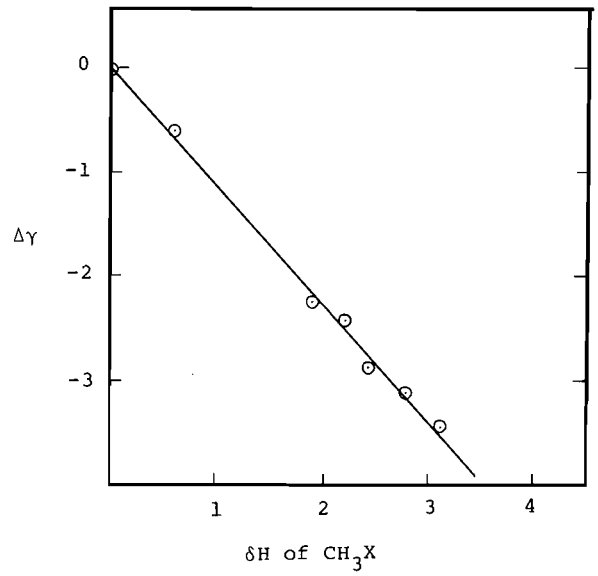

FIG. 4. Difference in γ-*anti* substituent effect vs. proton chemical shift of methyl X (ref. methane).

heteroatoms (N, O, F) and higher-row elements was well established by Eliel *et al.* (6). They concluded that first-row heteroatoms were shielding because of a hyperconjugative interaction involving the nonbonded electrons of the heteroatoms, and that this interaction would not be effective with higher-row elements. This conclusion seemed to be sound and was widely acknowleged (4), but later measurements on additional compounds indicated that the first-row heteroatoms were not always shielding as had been thought, and thus the proposed shielding mechanism is now considered unlikely (ref. 1*d*, p. 205). It is now clear that in the absence of α and γ hydrogens both first-row and higher-row elements are deshielding (Fig. 2), and that the additional shielding associated with the presence of the hydrogens is effective with the higher-row elements as well as with the first-row elements (Fig. 3 and Table 2). However, in both cases, that is in the presence or absence of α and γ hydrogens, the first-row elements are more shielding than the higher-row elements (Figs. 1 and 2 and Table 2), an observation which could be used to support the hyperconjugative donation mechanism as a contributor to the shielding mechanism.

Whatever the reasons, it would appear that the heavy atom effect may be detected at the γ-*anti* carbon through the participation in some way by the α and γ hydrogens. The nature of this participation is difficult to ascertain, but it is not essential to postulate a direct interaction between the two protons. The protons on the two carbons may

indeed act independently; polarization of either could increase the electron density at the γ carbon thus increasing the shielding effect. Although the rationalization of the effect must be speculative, the empirical observation is straightforward in that all γ-*anti* substituents cause increased shielding when α and γ protons are present compared to their effect when these protons are absent. The fact that the substituent shielding effect is decreased by replacement of any one of the three hydrogens attached to the α and γ carbons but by different amounts for the different hydrogens does not offer direct support to the proposal that the substituent effect is transmitted through a *syn* α–γ proton–proton interaction.

Experimental

Nuclear magnetic resonance spectra were determined on a Varian CFT-20 spectrometer using approximately 15% solutions in $CDCl_3$ with tetramethylsilane as internal reference. Mass spectra were determined on a CEC 21-104 mass spectrometer using a direct inlet system with a source temperature of 50°C and an ionization potential of 70 eV.

3,3-Dimethylcyclohexanol (**4**) was prepared from 5,5-dimethyl-1,3-cyclohexanedione (dimedone) by reaction with phosphorous oxychloride followed by reduction with sodium according to the procedure of Crossley *et al.* (7).

3,3-Dimethylcyclohexyl Chloride (**5**)

3,3-Dimethylcyclohexyl chloroformate was prepared (8) by the addition of excess phosgene to 3,3-dimethylcyclohexanol (5 g). The crude chloroformate was pyrolyzed at 150°C for 7 h and the product washed with concentrated sulfuric acid to remove alkenyl products. Distillation at 172–179°C at atmospheric pressure yielded 3.8 g (57%); ^{1}H nmr: 0.93 (s, 3H), 0.96 (s, 3H), 1.2–2.3 (m, 8H), 3.7–4.3 (m, 1H); mass spectrum: 148 (2.5), 146 (8.8), 133 (7.6), 131 (20.2), 111 (10.1), 110 (12.6), 95 (100), 69 (41.7), 67 (12.6), 56 (16.4), 55 (20.2), 43 (6.3), 41 (23).

3,3-Dimethylcyclohexyl Bromide (**6**)

Phosphorous tribromide (0.3 mL) was added dropwise to 3,3-dimethylcyclohexanol (1 mL) with stirring and the mixture was stirred at room temperature for 20 h. The reaction mixture was then shaken with pentane and ice water and the pentane layer washed with aqueous bicarbonate solution. The pentane solution was dried over calcium chloride and washed with concentrated sulfuric acid. Removal of the solvent *in vacuo* yielded 0.7 g of **6**; ^{1}H nmr: 0.97 (s, 3H), 0.94 (s, 3H), 1.2–2.5 (m, 8H), 3.9–4.5 (m, 1H); mass spectrum: 192–190 (1), 177–175 (0.4), 111 (4.5), 110 (100), 94 (26), 79 (50), 68 (72), 55 (34), 41 (30), 39 (14).

3,3-Dimethylcyclohexyl Iodide (**7**)

Trimethylsilyl iodide (9) (3 mL) was added by a syringe through a serum cap to 3,3-dimethylcyclohexanol (1.4 g) under nitrogen. The reaction mixture was poured into ice/pentane and the pentane layer washed with sodium bisulfite solution and water and then dried over magnesium sulfate. The product (2.7 g, 95%) was used without distillation as it decomposes rapidly on heating; ^{1}H nmr: 0.8 (s, 6H), 1–2.5 (m, 8H), 4.1–4.6 (m, 1H).

3,3-Dimethylcyclohexanone

3,3-Dimethylcyclohexanol (2 g) in acetone (40 mL) was cooled to 0°C and Jones reagent (10) (9 mL) was added with stirring over a 2 h period. After 2 h at room temperature the solvent was removed *in vacuo*, water (10 mL) was added, and the mixture extracted with ethyl acetate. The extract was dried over magnesium sulfate, the solvent removed, and the product distilled at atmospheric pressure at 175–180°C yielding 1.4 g (70%).

3,3-Dimethylcyclohexylamine (**3**)

3,3-Dimethylcyclohexanone (1 g) in methanol (4 mL) was added to a solution of hydroxylamine hydrochloride (2 g) and sodium acetate (4 g) in water (20 mL). The mixture was heated under reflux for one hour and then extracted with ether. The ether layer (15 mL) was dried with magnesium sulfate and then added to a stirred suspension of lithium aluminium hydride (2.2 g) in ether (60 mL) over 15 min. After heating under reflux for 24 h the excess hydride was decomposed by slow addition of 5% aqueous sodium hydroxide (25 mL). The resultant slurry was extracted four times with ether and the combined ether extract shaken with aqueous 1 *M* hydrochloric acid. The aqueous layer was made basic and extracted twice with ether. The ether layer was dried over anhydrous potassium carbonate and the solvent removed to yield an oil (0.4 g, 40%); ^{1}H nmr: 0.90 (s, 3H), 0.96 (s, 3H), 1.1–1.8 (m, 8H), 2.06 (bs, 2H), 2.5–3.1 (m, 1H); mass spectrum: 127 (26), 126 (5), 112 (19), 110 (2), 95 (14), 84 (100), 70 (13), 69 (10), 56 (89), 43 (32).

1,3,3-Trimethylcyclohexanol

3,3-Dimethylcyclohexanone (12 g) in dry ether (5 mL) was added under nitrogen over 10 min to a 0.6 *M* ethereal solution (30 mL) of methyl lithium while cooling with acetone – Dry Ice. After the addition was complete the cooling bath was removed and the solution heated under reflux for ½ h. The excess methyl lithium was decomposed by careful addition of water while stirring vigorously. The ether solution was washed with water, dried over magnesium sulfate, and the solvent removed to yield 1.26 g (93%) of a crystalline solid (mp 72°C); ^{1}H nmr: 0.90 (s, 3H), 1.10 (s, 3H), 1.20 (s, 3H), 1.27–2.06 (m, 8H), 2.2 (bs, 1H).

1,1,3-Trimethylcyclohexane (**2**)

Phosphorous oxychloride (1.5 mL) was added dropwise with stirring to a solution of 1,3,3-trimethylcyclohexanol (1.26 g) in pyridine (15 mL) which was maintained at 0°C. After the addition was complete the mixture was allowed to come to room temperature and after 4 h at room temperature was heated under reflux for 1.5 h. The reaction mixture was then cooled and poured onto cracked ice and then extracted three times with pentane. The combined pentane extracts were successively washed with dilute hydrochloric acid and water and after drying over potassium carbonate the solvent was removed to yield 1.08 g of mixed alkene. This dehydration product was then dissolved in acetic acid (30 mL) and hydrogenated by shaking with Adams catalyst (PtO_2) (0.25 g) under hydrogen (26 psi) at room temperature for 3 h. The catalyst was then removed by filtration and the filtrate poured into excess dilute sodium hydroxide solution containing crushed ice. The aqueous layer was extracted with pentane yielding, after evaporation of the solvent, 0.7 g of **2**; ^{1}H nmr: 0.90 (s, 6H), 0.85 (d, 3H overlaps with singlet), 1.15–1.90 (m, 9H); mass spectrum (11): 126 (7), 111 (82), 97 (4), 95 (3), 83 (44), 70 (22), 69 (100), 57 (15), 56 (30), 55 (56), 43 (15), 41 (37), 39 (11).

Acknowledgements

The authors wish to acknowledge the financial assistance of the Natural Sciences and Engineering Research Council of Canada, and of the Committee

Can. J. Chem. Downloaded from www.nrcresearchpress.com by 210.87.254.105 on 09/06/12
For personal use only.

on Development of Research in the Sciences of Dalhousie University.

1. (*a*) J. B. STOTHERS. Carbon-13 nmr spectroscopy. Academic Press, New York. 1972; (*b*) G. C. LEVY, R. L. LICHTER, and G. L. NELSON. Carbon-13 nuclear magnetic resonance spectroscopy. 2nd ed. Wiley-Interscience, New York. 1980; (*c*) F. W. WERHLI and T. WIRTHLIN. Interpretation of carbon-13 nmr spectra. Heyden, London. 1976; (*d*) E. L. ELIEL and K. M. PIETRUSIEWICZ. *In* Topics in carbon-13 nmr spectroscopy. *Edited by* G. C. Levy. John Wiley & Sons, New York. 1979.
2. (*a*) H. BEIERBECK, J. K. SAUNDERS, and J. W. APSIMON. Can. J. Chem. **55**, 2813 (1977); (*b*) H. J. SCHNEIDER and V. HOPPEN. J. Org. Chem. **43**, 3866 (1978); (*c*) T. P. FORREST and J. G. K. WEBB. Org. Magn. Reson., **12**, 371 (1979).
3. M. L. HUGGINS, J. Am. Chem. Soc. **75**, 4123 (1953).
4. H.-J. SCHNEIDER and V. HOPPEN. Tetrahedron Lett. 579 (1974).
5. G. E. MACIEL, H. C. DORYN, R. C. GREEN, W. A. KLESCHICK, M. R. PETERSON, and G. H. WAHL. Org. Magn. Reson. **6**, 178 (1974).
6. E. L. ELIEL, W. F. BAILEY, L. D. KOPP, R. L. WILSON, D. M. GRANT, R. BERTRAND, K. A. CHRISTENSEN, D. K. DALLING, H. W. DUCH, E. WENKERT, F. M. SCHELL, and D. W. COCHRAN. J. Am. Chem. Soc. **97**, 322 (1975).
7. (*a*) A. W. CROSSLEY and H. R. LE SUEUR. J. Chem. Soc. **83**, 117 (1903); (*b*) A. W. CROSSLEY and N. RENOUF. J. Chem. Soc. **87**, 1494 (1905); (*c*) J. Chem. Soc. **91**, 70 (1907).
8. E. L. ELIEL and R. J. L. MARTIN. J. Am. Chem. Soc. **90**, 689 (1968).
9. M. E. JUNG and P. L. ORNSTEIN. Tetrahedron Lett. 2659 (1977).
10. K. BOWDEN, I. M. HEILBORN, E. R. H. JONES, and B. C. L. WEEDON. J. Chem. Soc. 39 (1946).
11. E. STENHAGEN, S. ABRAHAMSON, and F. W. MCLAFFERTY (*Editors*). Atlas of mass spectral data. Vol. 1. Wiley, New York. 1969. p. 540.
12. D. K. DALLING and D. M. GRANT. J. Am. Chem. Soc. **89**, 6612 (1967).

Can. J. Chem. Downloaded from www.nrcresearchpress.com by 210.87.254.105 on 09/06/12
For personal use only.

The synthesis and X-ray crystal structure of triiodotellurium(IV) hexafluoroarsenate(V), TeI_3AsF_6

JACK PASSMORE, GEORGE SUTHERLAND, AND PETER S. WHITE
Department of Chemistry, University of New Brunswick, Fredericton, N.B., Canada E3B 6E2

Received February 20, 1981

JACK PASSMORE, GEORGE SUTHERLAND, and PETER S. WHITE. Can. J. Chem. **59**, 2876 (1981).

TeI_3AsF_6 was prepared quantitatively from the reaction of iodine, tellurium, and arsenic pentafluoride in sulphur dioxide solution. Single crystals of TeI_3AsF_6 are monoclinic, $a = 8.243(2)$, $b = 10.755(2)$, $c = 12.660(2)$ Å; $\beta = 100.91(2)°$, $V = 1102$ Å^3. The structure was refined in the space group $P2_1/c$ to a conventional R factor of 0.075 for 1551 independent reflections with $I \geq 2\sigma(I)$. The structure consists of essentially discrete TeI_3^+ cations and AsF_6^- anions with some cation–anion interaction. The TeI_3^+ cation has approximate C_{3v} symmetry with an average Te—I distance of 2.667 Å and I—Te—I angle of 99.90°.

JACK PASSMORE, GEORGE SUTHERLAND et PETER S. WHITE. Can. J. Chem. **59**, 2876 (1981).

On a préparé quantitativement le composé TeI_3AsF_6 à partir de la réaction entre l'iode, le tellure et le pentafluorure d'arsenic dans une solution de bioxyde de soufre. Les cristaux simples de TeI_3AsF_6 sont monocliniques et appartiennent au groupe d'espace $P2_1/c$ avec $a = 8{,}243(2)$, $b = 10{,}755(2)$, $c = 12{,}660(2)$ Å, $\beta = 100{,}91(2)°$, $V = 1102$ Å^3. Le facteur d'accord R est de 0,075 pour 1551 réflexions indépendantes avec $I > 2\sigma(I)$. La structure comprend essentiellement des cations TeI_3^+ et des anions AsF_6^- discrets avec quelques interactions cation–anion. Le cation TeI_3^+ a approximativement une symétrie C_{3v} avec une distance moyenne Te—I de 2,667 Å et un angle I—Te—I de 99,90°.

[Traduit par le journal]

Introduction

Salts of MF_3^+, MCl_3^+, and MBr_3^+ (M = S, Se and Te) have been prepared, and (with the exception of SBr_3^+) their structures determined by X-ray diffraction methods (1–9). The only related iodine cation known is SeI_3^+ in SeI_3AsF_6 (10) for which preliminary X-ray data were reported; however, no structural data, spectroscopic or crystallographic, were obtained. Attempts to prepare SI_3^+ salts were unsuccessful and lead initially (11) to the isolation of S_7IMF_6 (M = As, Sb). We report below the preparation and X-ray crystal structure of TeI_3AsF_6.

The structures of the binary tellurium iodides, α- and β-TeI (12), Te_2I (13), $(TeI_4)_4$ (14), the anionic tellurium iodide TeI_6^{2-} contained in K_2TeI_6 (15), and various neutral and anionic organo-tellurium iodides (16–25) are known. As far as we are aware, this is the first report on the structure of a tellurium–iodine cation.

Experimental

Apparatus, reagents, and techniques have been previously reported (10). Tellurium sticks (99.998%) supplied by Alfa-Ventron were ground to a powder before use.

In one reaction, AsF_5 (1.73 g, 10.2 mmol) was condensed onto a mixture of excesses of Te (3.90 g, 30.6 mmol) and I_2 (3.80 g, 14.9 mmol) in SO_2 (6.61 g), in a two-bulbed vessel incorporating a coarse sintered glass frit. The red–brown solution was stirred for 36 h and then filtered. The volatile material was then condensed back across the frit and the solution refiltered. TeI_3AsF_6 has a low solubility in the SO_2/AsF_3 mixture, and 38 filtrations were necessary for complete separation. On removal of the volatiles over an 8 h period 4.750 g of a highly crystalline red–black soluble product (essentially 100% yield based on AsF_5) and 3.95 g of insoluble product (excess Te and I_2) was obtained. In other preparations with shorter reaction times, yields were less than 100%.

X-Ray Data Collection

A suitable crystal was mounted in a capillary tube under dry nitrogen as previously described (10), except that the crystals were examined and manipulated with the aid of a Wild M3 microscope of long focal length mounted outside the dry box. A preliminary photographic investigation showed the space group to be $P2_1/c$ and the compound to be isostructural with $TeBr_3AsF_6$. The crystal was mounted on a Picker FACS-I diffractometer equipped with a molybdenum tube ($\lambda(K\alpha) = 0.71069$ Å) and a graphite monochromator. Final cell dimensions were obtained by a least-squares fit to the coordinates of 14 Friedel pairs of well centered reflections.

Intensity data were collected using an ω–2θ scan of 2 deg (2θ) corrected for dispersion of the Kα doublet with a scan rate of 2 deg (2θ) min^{-1}. Backgrounds were estimated from a stationary count of 1/10 of the scan time at each end of the scan. If the net intensity was greater than $2\sigma(I)$ then an analysis of the scan profile was performed and those portions which were not part of the peak were included in the background estimate. Data were collected for $2\theta \leq 50°$ which resulted in 1941 unique reflections of which 1551 were considered observed ($I \geq 2\sigma(I)$) and included in the subsequent refinement. Three standard reflections monitored every 100 reflections throughout data collection showed no significant change in their intensities. The crystal data are:

TeI_3AsF_6 fw = 697.2
Monoclinic, $P2_1/c$, $a = 8.243(2)$, $b = 10.755(2)$, $c = 12.660(2)$ Å, $\beta = 100.91(2)°$, $V = 1102$ Å^3, $Z = 4$, $\rho_c = 4.20$ Mg m^{-3}, $F(000) = 1192$, μ(Mo Kα) = 14.48 mm^{-1}, crystal size = 0.13 × 0.17 × 0.08 mm, $\lambda = 0.71069$ Å (20(±2)°C).

Structure Refinement

After correction of the data for absorption the atomic coordinates of $TeBr_3AsF_6$ were used as a starting point for

0008-4042/81/192876-03$01.00/0
©1981 National Research Council of Canada/Conseil national de recherches du Canada

Can. J. Chem. Downloaded from www.nrcresearchpress.com by 210.87.254.6 on 09/06/12
For personal use only.

Can. J. Chem. Downloaded from www.nrcresearchpress.com by 210.87.254.6 on 09/06/12
For personal use only.

TABLE 1. Atomic coordinates for TeI_3AsF_6[a]

Atom	X	Y	Z	B_{iso}[b]
Te(1)	0.18367(11)	0.16568(8)	0.19199(7)	3.21(4)
I(1)	0.29695(15)	0.04568(11)	0.37508(9)	4.73(6)
I(2)	0.22727(16)	0.40428(10)	0.24693(12)	5.45(7)
I(3)	0.44520(16)	0.15120(11)	0.09570(9)	5.03(5)
As(1)	0.82913(18)	0.27381(14)	0.41901(11)	3.39(6)
F(1)	0.8768(14)	0.2159(10)	0.3020(7)	5.5(6)
F(2)	0.7538(22)	0.1336(12)	0.4413(12)	9.7(14)
F(3)	0.7862(15)	0.3304(13)	0.5375(8)	6.4(8)
F(4)	0.6351(18)	0.3122(21)	0.3591(13)	9.9(14)
F(5)	0.8963(19)	0.4176(12)	0.3907(12)	8.3(9)
F(6)	1.0225(14)	0.2399(15)	0.4855(10)	7.9(11)

[a]Standard deviations in parentheses.
[b]$B_{iso} = (8\pi^2/3)(U_{11} + U_{22} + U_{33})$.

refinement. The structure was refined by a block diagonal least-squares routine using anisotropic thermal parameters for all atoms. The function minimised was $\Sigma w(\Delta F)^2$ where $w = 1/(\sigma^2(F) + pF^2)$; the measurements of the standards indicated a value of 0.005 for p. Atomic scattering factors were taken from the International tables for X-ray crystallography (26) and were corrected for anomalous dispersion. The final values of $R = \Sigma|\Delta F|/\Sigma|F_0|$ and $R_w = (\Sigma w|\Delta F|^2/\Sigma w|F_0|^2)^{1/2}$ were 0.075 and 0.100 (0.089 and 0.106 including unobserved reflections) respectively. Final positional and isotropic thermal parameters are given in Table 1.[1] All computations were performed on a PDP8/A computer using the programs of Gabe *et al.* (27).

Discussion

TeI_3AsF_6 was prepared quantitatively, in sulphur dioxide solution, according to reaction [1].

[1] $2Te + 3I_2 + 3AsF_5 = 2TeI_3AsF_6 + AsF_3$

As far as we are aware, this is the first report of a salt of TeI_3^+.

TeI_3AsF_6 is isostructural with MBr_3AsF_6 (M = Se, Te) (9), and isomorphous and probably isostructural with SBr_3AsF_6 (9) and SeI_3AsF_6 (10). Figure 1 shows the TeI_3^+ cation with anion contacts; corresponding bond distances and angles are presented in Tables 2 and 3. The closest Te···F and I···F contacts of 2.88(1) and 3.04(1) Å respectively indicate that the structure is essentially ionic, with some cation–anion interaction (c.f. sum of van der Waals radii of Te and F (3.55 Å), and I and F (3.50 Å) (28)).

The TeI_3^+ cation is of very approximately C_{3v} symmetry, with an average bond distance of 2.667(1)[2] Å and I—Te—I angle of 99.90(3)° in reasonable agreement with predictions (9) (2.65 Å, 99.2°) made by extrapolation of structural data for Group V trihalides and Group VI trihalide cations.[2] The bond distance is shorter than that found in the isoelectronic SbI_3 (g) (29) (2.719(1) Å), a consequence of the greater charge and smaller size of tellurium (formally Te^{IV}) than antimony (formally Sb^{III}). Although the TeI_3^+ bond angles vary (see Table 3), the average is larger (95.8(3)°) than that found for SbI_3(s) (30), consistent with the general observation, that chalcogen trihalide cation angles are larger than those of the corresponding Group V trihalide neutral isoelectronic partners (9).

Three fluorine contacts give a distorted octahed-

TABLE 2[a]

(*a*) Bond distances for TeI_3AsF_6 (Å)

Bond	Distance	Bond	Distance
Te—I(1)	2.663(1)	As—F(1)	1.720(9)
Te—I(2)	2.665(2)	As—F(2)	1.675(11)
Te—I(3)	2.674(2)	As—F(3)	1.716(9)
		As—F(4)	1.687(15)
		As—F(5)	1.704(12)
		As—F(6)	1.695(11)

(*b*) Interionic (Te···F ≤ 3.24, I···F ≤ 3.36 Å)

Atoms	Distance	Atoms	Distance
Te···F(1)	3.16(1)	I(1)···F(2)	3.11(1)
Te···F(5)	2.90(1)	I(3)···F(3)	3.04(1)
Te···F(6)	2.88(1)		

[a]Standard deviations in parentheses.

TABLE 3. Bond angles for TeI_3AsF_6 (deg)[a]

Bonds	Angle
I(1)—Te—I(2)	103.40(5)
I(1)—Te—I(3)	100.86(5)
I(2)—Te—I(3)	95.42(5)
F(1)—As—F(2)	88.4(6)
F(3)	178.6(6)
F(4)	93.0(7)
F(5)	90.6(6)
F(6)	90.2(6)
F(2)—As—F(3)	91.6(7)
F(4)	86.9(10)
F(5)	176.8(9)
F(6)	93.8(9)
F(3)—As—F(4)	88.4(7)
F(5)	89.5(7)
F(6)	88.4(6)
F(4)—As—F(5)	90.1(9)
F(6)	176.7(7)
F(5)—As—F(6)	89.3(8)

[a]Standard deviations in parentheses.

[1]Tables of anisotropic thermal parameters and observed and calculated structure factors have been deposited and may be obtained, at a nominal charge, from the Depository of Unpublished Data, CISTI, National Research Council of Canada, Ottawa, Ont., Canada K1A 0S2.

[2]The standard deviation of the averages quoted in this paper are approximated by $\bar{\sigma}/\sqrt{n}$ since the standard deviations of the bond lengths in a given structure are similar, i.e., $\sigma_i \simeq \sigma_j$.

TABLE 4. Comparison of cation–anion contacts in TeX_3^+ species, X = F, Cl, Br, I[a]

Compound	Avg. Te–anion contact, Å	% less than sum of van der Waals radii (Pauling)	Avg. X–anion contact, Å[e]	% less than sum of van der Waals radii
$TeF_3Sb_2F_{11}$[b]	2.59	27	—	—
$TeCl_3AlCl_4$[c]	3.06	23.5	—	—
$TeBr_3AsF_6$[d]	2.837	20.1	3.06(1)	7.3
TeI_3AsF_6	2.980	15.8	3.075(7)	12.1

[a] Standard deviations in parentheses.
[b] Reference 4.
[c] Reference 7.
[d] Reference 9.
[e] The numbers quoted are the average of two Te—X···F contacts only, see Fig. 1.

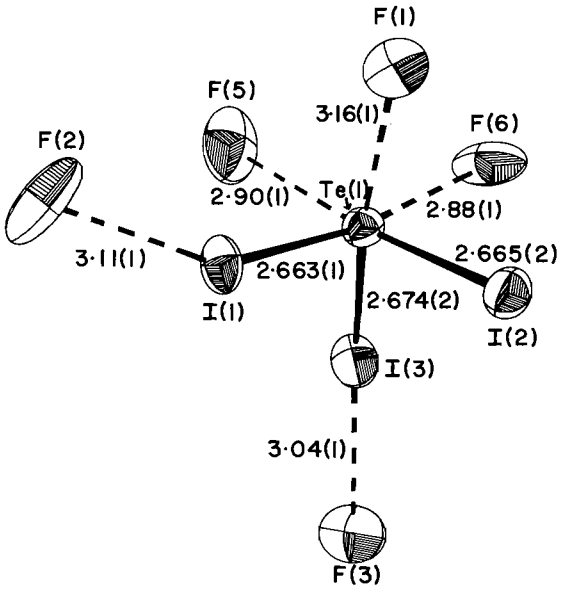

FIG. 1. TeI_3^+ with anion contacts.

ral arrangement about tellurium atom in TeI_3^+ (see Fig. 1). The strengths of contacts to TeX_3^+ cations (see Table 4) are proportional to the effective charge on tellurium. Two of the iodine atoms in TeI_3^+ have weak fluorine contacts that are somewhat stronger than the corresponding contacts to $TeBr_3^+$, consistent with the more positive character of iodine.

The AsF_6^- anions are approximately octahedral with an average As—F distance of 1.70 Å and F—As—F angle of 90.0°.

Acknowledgement

We wish to thank the Natural Sciences and Engineering Research Council of Canada for financial support.

1. D. D. GIBLER, C. J. ADAMS, M. FISCHER, A. ZALKIN, and N. BARTLETT. Inorg. Chem. **11**, 2325 (1972).
2. A. J. EDWARDS and G. R. JONES. J. Chem. Soc. A, 1891 (1970).
3. A. J. EDWARDS and G. R. JONES. J. Chem. Soc. A, 1491 (1970)
4. A. J. EDWARDS and P. TAYLOR. J. Chem. Soc. Dalton Trans. 2150 (1973).
5. A. J. EDWARDS. J. Chem. Soc. Dalton Trans. 1723 (1978).
6. B. A. STORK-BLAISSE and C. ROMERS. Acta Crystallogr. B**27**, 386 (1971).
7. B. KREBS, B. BUSS, and D. ALTENA. Z. Anorg. Allg. Chem. **386**, 257 (1971).
8. W. V. F. BROOKS, J. PASSMORE, and E. K. RICHARDSON. Can. J. Chem. **57**, 3230 (1979).
9. J. PASSMORE, E. K. RICHARDSON, T. K. WHIDDEN, and P. S. WHITE. Can. J. Chem. **58**, 851 (1980).
10. J. PASSMORE and P. TAYLOR. J. Chem. Soc. Dalton Trans. 804 (1976).
11. J. PASSMORE, P. TAYLOR, T. K. WHIDDEN, and P. S. WHITE. J. Chem. Soc. Chem. Commun. 689 (1976); Inorg. Chem. In press.
12. R. KNIEP, D. MOOTZ, and A. RABENAU. Angew. Chem. Internat. Edit. **13**, 403 (1974).
13. R. KNIEP, D. MOOTZ, and A. RABENAU. Angew. Chem. Internat. Edit. **12**, 499 (1973).
14. V. B. KREBS and V. PAULAT. Acta Crystallogr. B**32**, 1470 (1976).
15. S. SYOYAMA, K. OSAKI, and S. KUSANAGI. Inorg. Nucl. Chem. Lett. **8**, 181 (1972).
16. J. D. MCCULLOUGH. Inorg. Chem. **12**, 2669 (1973).
17. G. Y. CHAO and J. D. MCCULLOUGH. Acta Crystallogr. **15**, 887 (1962).
18. C. KNOBLER, J. D. MCCULLOUGH, and H. HOPE. Inorg. Chem. **9**, 797 (1970).
19. F. EINSTEIN, J. TROTTER, and C. WILLISTON. J. Chem. Soc. A, 2018 (1967).
20. L. Y. Y. CHAN and F. W. B. EINSTEIN. J. Chem. Soc., Dalton Trans. 316 (1972).
21. J. D. MCCULLOUGH. Inorg. Chem. **14**, 1142 (1975).
22. H. HOPE, C. KNOBLER, and J. D. MCCULLOUGH. Inorg. Chem. **12**, 2665 (1973).
23. J. D. MCCULLOUGH. Inorg. Chem. **16**, 2318 (1977).
24. H. PRITZKOW. Inorg. Chem. **18**, 311 (1979).
25. O. FOSS, H. M. KJØGE, and K. MARØY. Acta Chem. Scand. **19**, 2349 (1965).
26. C. H. DAUBEN and D. H. TEMPLETON. International tables for X-ray crystallography. Vol. III. Kynoch Press, Birmingham. 1962.
27. A. C. LARSON and E. J. GABE. *In* Computing in crystallography. *Edited by* H. Schenk, R. Olthof-Hazekamp, H. van Koningsveld, and G. C. Bass. Delft University Press. 1978.
28. F. A. COTTON and G. WILKINSON. Advanced inorganic chemistry. 3rd ed. Interscience. 1972.
29. A. ALMENNINGEN and T. BJORVATTEN. Acta Chem. Scand. **17**, 2573 (1963).
30. J. TROTTER and T. ZOBEL. Z. Kristallogr. **123**, 67 (1966).

Can. J. Chem. Downloaded from www.nrcresearchpress.com by 210.87.254.6 on 09/06/12
For personal use only.

The crystal and molecular structure of 1,4-bis(1-oxa-4,10-dithia-7*H*-7-azonia cyclododecan-7-ylmethyl)benzene tetrachlorooxotetrahydrofuran molybdate(V) $[C_{24}H_{42}N_2O_2S_4]^{2+}[MoOCl_4(THF)]_2^-$

PETER H. BIRD[1] AND WASANTHA A. WICKRAMASINGHE

Department of Chemistry, Concordia University, Montreal, P.Q., Canada H3G 1M8

Received September 11, 1980

PETER H. BIRD and WASANTHA A. WICKRAMASINGHE. Can. J. Chem. **59**, 2879 (1981).

The title compound is prepared by the consecutive reaction of $MoOCl_4$ with THF and then the bismacrocyclic compound 1,4-bis(1-oxa-4,10-dithia-7-azacyclododecan-7-ylmethyl) benzene. The crystals are triclinic, space group $P\bar{1}$ (No. 2), $a = 11.993(7)$, $b = 13.196(8)$, $c = 7.928(5)$ Å, $\alpha = 104.54(4)$, $\beta = 94.89(3)$, $\gamma = 81.59(1)°$, $V = 1199.9$ Å^3, $Z = 1$. The final R factor was 0.059 for 2846 reflections where $I > 3\sigma(I)$. The compound is ionic with the macrocycles protonated on both the nitrogen atoms while the anions are octahedral $[MoOCl_4(THF)]^-$ units. These units have the oxo group (Mo═O, 1.655(7) Å) *trans* to THF (Mo—O, 2.331(5) Å). The cations adopt a centrosymmetric *trans* conformation with no strong interactions with the molybdenum.

PETER H. BIRD et WASANTHA A. WICKRAMASINGHE. Can. J. Chem. **59**, 2879 (1981).

On a préparé le composé mentionné dans le titre par la réaction du $MoOCl_4$ avec le THF, puis avec le composé bismacrocyclique bis(oxa-1 dithia-4,10 aza-7 cyclododécanyl-7 méthyl)-1,4 benzène. Les cristaux sont tricliniques et appartiennent au groupe d'espace $P\bar{1}$ (No. 2) avec $a = 11,993(7)$, $b = 13,196(8)$, $c = 7,928(5)$ Å, $\alpha = 104,54(4)$, $\beta = 94,89(3)$, $\gamma = 81,59(1)°$, $V = 1199,9$ Å^3, $Z = 1$. Le facteur d'accord R est de 0,059 pour 2846 réflexions avec $I > 3\sigma(I)$. Le composé est ionique avec les macrocyles protonés sur les deux atomes d'azote tandis que les anions sont des unités octaédriques de $[MoOCl_4(THF)]^-$. Ces unités ont le groupe oxo (Mo═O, 1,655(7) Å) en position *trans* par rapport au THF(Mo—O, 2,331(5) Å). Les cations adoptent une conformation centrosymétrique *trans* sans interactions fortes avec le molybdène.

[Traduit par le journal]

Introduction

The ligand 1,4-bis(1-oxa-4,10-dithia-7-azacyclododecan-7-ylmethyl) benzene which contains two macrocyclic $C_8H_{16}NOS_2$ rings has shown some promise for the synthesis of bimetallic complexes.

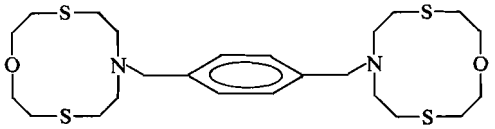

In such compounds metal–metal interaction is possible and vacant coordination sites are available, thus conferring on the molecule a potential for novel catalytic activity (1, 2). The molecule whose structure is reported here was prepared as part of a general screening process intended to establish the range of metal ions which the ligand may complex. Molybdenum in oxidation states V and VI was selected as a candidate for investigation since it is involved in a number of biochemical systems where binuclear complexes are implicated (3, 4).

Experimental Section

In a typical preparation, $MoOCl_4$ 0.17 g (0.67 mmol) (Alfa Products, used as purchased) were dissolved in 5 mL of dry, deoxygenated THF. The solution, initially brown, became green in about 5 min at room temperature. To this solution was added 0.05 g (0.097 mmol) of $C_{24}H_{40}N_2O_2S_4$ (2) dissolved in 5 mL of THF. A pale green precipitate was formed immediately and separated by centrifugation. Crystals suitable for a crystal structure analysis were grown by dissolving the precipitate in CH_3CN and reprecipitating with THF: a small quantity of the CH_3CN solution contained in a test tube was placed in a closed jar containing THF which diffused slowly into the solution, leading to slow crystallization. Elemental analysis (Service Central de Microanalyse, CNRS, France) gave C 32.60, H 4.99, N 2.56, Cl 23.96, S 9.91, Mo 16.32, calcd for $C_{32}H_{58}Cl_8Mo_2N_2O_6S_4$: C 32.83, H 4.99, N 2.39, Cl 24.23, S 10.95, Mo 16.39.

Crystal Data

$C_{32}H_{58}Cl_8Mo_2N_2O_6S_4$ f.w. = 1168.65

Triclinic, $a = 11.993(7)$, $b = 13.196(8)$, $c = 7.928(5)$ Å, $\alpha = 104.54(4)$, $\beta = 94.89(3)$, $\gamma = 81.59(1)°$, $V = 1199.9$ Å^3, $Z = 1$, $\rho_o = 1.61(2)$, $\rho_c = 1.58$ g cm^{-3} (MoK_α $\lambda = 0.71069$ Å, 20°C, $\mu = 11.7$ cm^{-1}.

Preliminary Weissenberg and precession photographs showed only $\bar{1}$ Laue symmetry and no systematic absences which limited the space group to $P1$ (No. 1) or $P\bar{1}$ (No. 2). The latter choice leads to a successful structure solution and refinement.

Accurate cell dimensions were obtained on a fully automated Picker FACS-1 4 circle diffractometer, equipped with a graphite monochromator and coupled to a PDP-8S minicomputer, by centering 12 reflections widely scattered in the reciprocal space ($20° < 2\theta < 30°$: the α_1/α_2 doublet was not resolved). Each reflection was centered at both positive and negative 2θ values. The 2θ, ω, χ, and ϕ values thus obtained were appropriately averaged. These were used in the least-squares refinement to obtain the final unit cell parameters with their estimated standard deviations. These cell parameters were used in subsequent calculations.

Data were collected using a 2θ scan routine in a unique hemisphere of $4.0° < 2\theta < 45°$ for $\pm h$, $\pm k$, $\pm l$ using MoK_α

[1]To whom all correspondence should be addressed.

0008-4042/81/192879-04$01.00/0

©1981 National Research Council of Canada/Conseil national de recherches du Canada

Can. J. Chem. Downloaded from www.nrcresearchpress.com by 210.87.254.5 on 09/06/12
For personal use only.

Can. J. Chem. Downloaded from www.nrcresearchpress.com by 210.87.254.5 on 09/06/12
For personal use only.

radiation. The reflection intensity was computed as

$$I = [N - Bt_s/t_b]$$

and $\sigma(I)$ the standard deviation was computed as

$$\sigma(I) = [N + B(t_s/t_b)^2 + 0.02N^2]^{1/2}$$

where N is the total counts accumulated during the scan time t_s and B is the total background counts accumulated in time t_b.

Instrument and crystal stability were monitored by measuring the intensities of 3 standard reflections after every 50 cycles. These reflections showed a random deviation of not more than ±3%. Data for which $I < 3\sigma(I)$, (1123 reflections) were considered as unobserved and discarded. The remaining 2846 intensities were corrected for crystal absorption[2] and for Lorentz and polarization effects, thus:

$$(Lp)^{-1} = \sin 2\theta_s (\cos^2 2\theta_m + 1)/(\cos^2 2\theta_m + \cos^2 2\theta_s)$$

where $2\theta_m$ and $2\theta_s$ are the diffraction angles at the monochromator and the sample crystal respectively. Transmission factors ranged from 0.70 to 0.83 for the sample which was approximately brick shaped (0.2 × 0.5 × 0.8 mm, longest dimension parallel to diffractometer ϕ axis).

Structure Determination

A 3-dimensional Patterson[3] synthesis yielded the positions of molybdenum and the four chlorine atoms bound to it. The remaining non-hydrogen atoms were found from successive structure factor and Fourier calculations. Full-matrix isotropic refinement[4] (five cycles) converged at the rather high R value of 0.20. We were unable to find any obvious reason for this other than signs of considerable anisotropic motion particularly of the cation. Indeed, anisotropic refinement (5 cycles) reduced the residual F to 0.069. At this stage of refinement, a geometry calculation and a difference Fourier synthesis revealed disordering of the macrocyclic rings at C(7), C(8), C(9), and C(10). Thus, bond distances within this portion of the ring were all too short, and, whereas the hydrogen atoms were clearly visible in other parts of the difference map, the region around the disordered atoms showed a confused collection of minor peaks. In addition atoms C(7), C(8), C(9), and C(10) had abnormally elongated thermal ellipsoids. An attempt to resolve the disordered atoms into pairs of atoms with fractional occupancy did not improve the R values or produce a satisfactory geometry. Anisotropic refinement was continued for 3 more cycles with hydrogen atoms placed in calculated positions (C—H and N—H, 0.98 Å) on all carbon atoms except those exhibiting the disorder. The final unweighted and weighted residuals are: $R_1 = 0.059$, $R_2 = 0.065$ and the "goodness of fit" = 6.3. The entire structure was re-refined in space group $P1$, but the residuals were not significantly improved. There was no evidence for systematic variation of $\omega(|F_o| - |F_c|)^2$ with $\sin\theta/\lambda$ or $|F_o|$ or h, k, and l, therefore we attribute the high value of the goodness of fit to inadequacies in the structure model in the regions of disordering. Indeed, a final difference Fourier map showed numerous peaks of residual electron density (0.8 e/A^3 maximum) in regions around the disordered atoms C(7), C(8), C(9), and C(10), and around the chlorine atoms of the anion, which also display large thermal motion. Table 1 contains the final positions of all non-hydrogen atoms. Tables of observed and calculated structure amplitudes and of temperature factors are available.[5]

TABLE 1. Final positional parameters for $C_{32}H_{58}Cl_8Mo_2N_2O_6S_4$*

Atom	x/a	y/b	z/c
Mo	2715.0(5)	3080.7(5)	1336.3(11)
Cl(1)	1682.5(21)	2044.9(17)	−931(5)
Cl(2)	3776.2(18)	4376.8(18)	3069(3)
Cl(3)	1026.1(17)	4188.5(22)	2102(4)
Cl(4)	4409.9(16)	2173.6(15)	−16(3)
S(1)	9443.2(14)	257.0(14)	2544(3)
S(2)	7431.5(22)	1866.1(21)	7116(3)
O(1)	2705(5)	2364(5)	2773(10)
O(2)	2721(3)	4099(3)	−677(7)
O(3)	8972(4)	2587(3)	4730(7)
N	6987(4)	1372(3)	3141(6)
C(1)	5634(5)	215(5)	3771(9)
C(2)	4475(5)	533(5)	3799(10)
C(3)	3847(5)	328(5)	5030(10)
C(4)	6305(5)	456(5)	2427(9)
C(5)	7558(5)	1562(5)	1639(8)
C(6)	8458(6)	680(5)	921(9)
C(7)	10351(6)	1276(7)	3120(14)
C(8)	10038(8)	2167(10)	4349(17)
C(9)	8914(12)	3051(14)	6421(22)
C(10)	8321(10)	2921(8)	7635(13)
C(11)	6203(6)	2726(6)	6016(11)
C(12)	6315(5)	2376(5)	4120(9)
C(13)	3690(6)	4400(7)	−1252(13)
C(14)	3296(8)	5245(9)	−2064(15)
C(15)	2123(7)	5163(8)	−2589(12)
C(16)	1806(7)	4365(7)	−1827(14)

*The estimated standard deviations are given in parentheses, right justified to the least significant digit. Figures are multiplied by 10^4.

Results and Discussions

Figure 1 shows the unit cell packing diagram, Fig. 2 shows the anion $[MoOCl_4(THF)]^-$, and Fig. 3 depicts the cation $[C_{24}H_{42}NOS_2]^+$. Selected bond lengths and angles are collected in Table 2.

A study of the interaction of $MoOCl_4$ with a variety of common solvents (9) has shown that $MoOCl_4$ probably reacts with diethyl ether to give a chloroether and HCl. An analogous reaction with THF is adequate to rationalize the isolation of the title compound, indeed it seems probable that the species $[MoOCl_4(THF)]^-$ is already present in the solution prior to the addition of the base/ligand.

The anion $[MoOCl_4(THF)]^-$ has not been described previously. However, there are a number of similar $[MoOX_4L]^{n-}$ complexes whose structures have been reported: where X = Cl, L = H_2O or Cl (10), or $OP(OMe)_2$ (11); where X = CN and L is H_2O or OH (12), or O (13); and the ion $[MoOBr_4(OH_2)]^-$ (14). A structure of the parent square

[2]Using GNABS by Burnam (5).

[3]Fourier and Patterson calculations were performed using FORDAP by A. Zalkin.

[4]Structure factor and least squares calculations were performed using SFLS-5 by C. W. Prewitt. The quantity minimized in least squares calculations was: $w(|F_o| - |F_c|)^2$ where $w = [\sigma(F_o)]^{-2}$. Scattering factors used were those of Cromer and Waber (6) (non-hydrogen atoms) and Churchill, De Boer, and Donovan (7) for hydrogen. The anomalous dispersion corrections for Mo, Cl, and S were applied (8).

[5]The supplementary tables are available at a nominal charge, from the Depository of Unpublished Data, CISTI, National Research Council of Canada, Ottawa, Ont., Canada K1A 0S2.

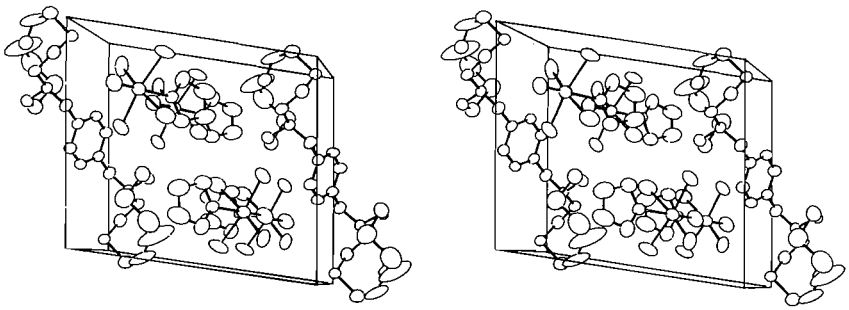

FIG. 1. Crystal packing in $[C_{24}H_{42}N_2O_2S_4]^{2+}[MoOCl_4(THF)]_2^-$ (viewed down c, with a vertical).

TABLE 2. Selected distances (Å) and angles (deg)* in $C_{32}H_{58}Cl_8Mo_2N_2O_6S_4$

(a) The cation $C_{24}H_{42}N_2S_4O_2$

Bond	Length	Bond	Length
C(1)—C(2)	1.393(9)	S(1)—C(7)	1.800(9)
C(2)—C(3)	1.383(10)	C(7)—C(8)	1.354(16)
C(3)—C(1′)	1.384(10)	O(3)—C(8)	1.344(11)
C(1)—C(4)	1.508(10)	O(3)—C(9)	1.330(18)
N—C(4)	1.523(8)	C(9)—C(10)	1.302(20)
N—C(5)	1.513(8)	S(2)—C(10)	1.821(12)
N—C(12)	1.512(8)	S(2)—C(11)	1.807(8)
C(5)—O(6)	1.500(9)	C(11)—C(12)	1.504(11)
S(1)—C(6)	1.800(9)		

Bonds	Angle	Bonds	Angle
C(1)—C(2)—C(3)	120.6(7)	S(2)—C(10)—C(9)	119.1(10)
C(2)—C(3)—C(1′)	120.0(6)	S(2)—C(11)—C(12)	115.7(5)
C(2)—C(1)—C(4)	119.7(6)	N—C(12)—C(11)	114.1(6)
C(1)—C(4)—N	114.0(6)	C(4)—N—C(5)	108.1(5)
N—C(5)—C(6)	112.8(5)	C(4)—N—C(12)	114.6(4)
S(1)—C(6)—C(5)	114.8(5)	C(5)—N—C(12)	111.1(5)
S(1)—C(7)—C(8)	119.2(7)	C(6)—S(1)—C(7)	102.9(4)
O(3)—C(8)—C(7)	125.9(10)	C(10)—S(2)—C(11)	102.8(4)
O(3)—C(9)—C(10)	132.5(14)	C(8)—O(3)—C(9)	110.6(9)

(b) The anion $MoOCl_4(THF)$

	Length			Length	
Bond	Uncorrected	Corrected	Bond	Uncorrected	Corrected
Mo—O(1)	1.655(7)	1.673	O(2)—C(13)	1.425(9)	1.593
Mo—O(2)	2.331(5)	2.356	O(2)—C(16)	1.427(11)	1.522
Mo—Cl(1)	2.348(3)	2.379	C(13)—C(14)	1.426(15)	1.507
Mo—Cl(2)	2.364(2)	2.398	C(14)—C(15)	1.445(13)	1.554
Mo—Cl(3)	2.347(2)	2.366	C(15)—C(16)	1.448(14)	1.544
Mo—Cl(4)	2.394(2)	2.417			

Bonds	Angle	Bonds	Angle
Cl(1)—Mo—Cl(2)	165.02(10)	O(1)—Mo—O(2)	179.6(3)
Cl(1)—Mo—Cl(3)	88.12(10)	O(2)—Mo—Cl(1)	82.97(14)
Cl(1)—Mo—Cl(4)	88.51(9)	O(2)—Mo—Cl(2)	82.07(13)
Cl(2)—Mo—Cl(3)	80.74(9)	O(2)—Mo—Cl(3)	82.76(13)
Cl(2)—Mo—Cl(4)	88.95(8)	O(2)—Mo—Cl(4)	83.06(12)
C(13)—Mo—Cl(4)	165.73(10)	C(13)—O(2)—C(16)	105.5(6)
O(1)—Mo—Cl(1)	97.2(3)	O(2)—C(13)—C(14)	106.8(7)
O(1)—Mo—Cl(2)	97.8(3)	C(13)—C(14)—C(15)	106.8(9)
O(1)—Mo—Cl(3)	96.9(2)	C(14)—C(15)—C(16)	106.2(9)
O(1)—Mo—Cl(4)	97.3(2)	C(15)—C(16)—O(2)	107.5(7)

*Estimated standard deviations, in parentheses, are right justified to the last significant digit of the preceding number. The standard deviations are based on the diagonal elements of the inverse least-squares matrix.

Can. J. Chem. Downloaded from www.nrcresearchpress.com by 210.87.254.5 on 09/06/12
For personal use only.

Can. J. Chem. Downloaded from www.nrcresearchpress.com by 210.87.254.5 on 09/06/12
For personal use only.

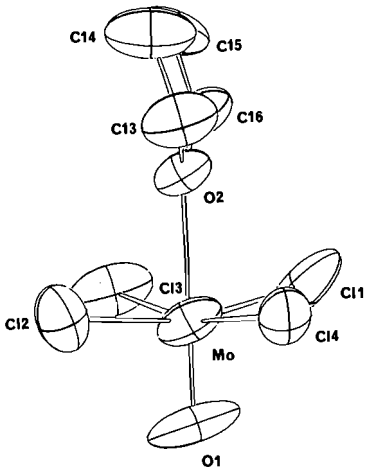

FIG. 2. The anion $[MoOCl_4(THF)]^-$.

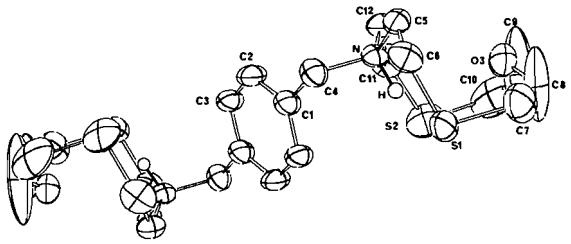

FIG. 3. The cation $[C_{24}H_{42}N_2O_2S_4]^{2+}$.

pyramidal $[MoOCl_4]^-$ ion is also available (15). The Mo—O multiple bond which is 1.61(1) Å long in the five coordinate $[MoOCl_4]^-$ ion is lengthened to 1.655(7) Å in the THF complex. The *trans* influence of the THF is thus most similar to that of coordinated water; in such complexes the Mo—O bond lengths range from 1.64(7) Å to 1.672(15) Å (10, 12). This bond is lengthened to 1.698(7) Å in $[MoO(CN)_4(OH)]^{3-}$ and 1.834(9) Å in $[MoO_2(CN)_4]^{4-}$. Comparison with the short distance 1.604(23) Å quoted for $[MoOCl_4OP(OMe)_2]^{n-}$ is difficult because of the disorder of the phosphite ligand and the ambiguity concerning the oxidation state of the Mo in this ion. The THF oxygen (O(2)) is 2.331(5) Å from the Mo, within the range of 2.27 to 2.39 Å observed in the aquo complexes. The THF moiety which is folded in an envelope conformation with O(2) as the out-of-plane atom, has quite high thermal motion (Fig. 2). It is commonly observed (16) that all bond lengths within this ligand appear unreasonably short. A libration correction (17) for the THF moiety produced much more plausible values (Table 2). The Mo—Cl distances in these six-coordinate complexes are quite insensitive to changes in L and range from 2.35 to 2.37 Å: the average uncorrected distance in $[MoOCl_4(THF)]^-$ is 2.363 Å, but there is a considerable spread in values; 2.347(2) to 2.394(2) Å. There are no unusual intermolecular contacts involving the chlorine atoms. Correction for librational motion of the $MoCl_4O_2$ moiety reduced but did not eliminate the spread, while consistently indicating longer Mo—Cl bonds.

The cation has crystallographically imposed transoid symmetry and presents no particularly striking features except the method of folding of the macrocycles. The adopted conformation, clearly visible in Fig. 3, places the hydrogen atom of the quaternary nitrogen so that it hydrogen bonds weakly to the two sulphur atoms, at about 2.4 Å from S1 and 2.6 Å from S2 (a normal Van der Waals contact lies between 2.9 and 3.1 Å (18, 19)).

Acknowledgements

The authors would like to thank Professor J. A. Osborn of l'Institut le Bel, Université Louis Pasteur de Strasbourg for the use of his laboratories and the Natural Sciences and Engineering Research Council of Canada for financial support.

1. J. E. BULKOWSKI, P. L. BURK, M-F. LUDMANN, and J. A. OSBORN. J. Chem. Soc. Chem. Commun. 498 (1977).
2. D. BLACK and I. MCLEAN. Austral. J. Chem. **24**, 1401 (1971).
3. E. I. STIEFEL. Prog. Inorg. Chem. **22**, 1 (1977).
4. B. SPIVACK and Z. DORI. Coord. Chem. Rev. **17**, 99 (1975).
5. C. W. BURNAM. Am. Mineral. **51**, 159 (1966).
6. D. T. CROMER and J. T. WABER. Acta Crystallogr. **104**, 18 (1965).
7. M. R. CHURCHILL, B. G. DE BOER, and D. J. DONOVAN. Inorg. Chem. **3**, 617 (1975).
8. International tables for X-ray crystallography. Vol. III. Kynoch Press, Birmingham, England. 1962. p. 215.
9. C. G. BARRACLOUGH and D. J. KEW. Austral. J. Chem. **23**, 2387 (1970).
10. C. D. GARNER, L. H. HILL, F. E. MABBS, D. L. MCFADDEN, and A. T. MCPHAIL. J. Chem. Soc. Dalton, 1202 (1977) and references cited therein.
11. M. G. B. DREW and J. D. WILKINS. J. Chem. Soc. Dalton, 1984 (1975).
12. P. R. ROBINSON, E. O. SCHLEMPER, and R. K. MURMANN. Inorg. Chem. **14**, 2035 (1975).
13. V. W. DAY and J. L. HOARD. J. Am. Chem. Soc. **90**, 3374 (1968).
14. J. G. SCANE. Acta Crystallogr. **23**, 85 (1967).
15. C. D. GARNER, L. H. HILL, F. E. MABBS, D. L. MCFADDEN, and A. T. MCPHAIL. J. Chem. Soc. Dalton, 853 (1977).
16. R. R. RIETZ, N. M. EDELSTEIN, H. W. RUBEN, D. H. TEMPLETON, and A. ZALKIN. Inorg. Chem. **17**, 658 (1978) and references cited therein.
17. VERNER SCHOMAKER and K. N. TRUEBLOOD. Acta Crystallogr. **B24**, 63 (1968).
18. W. C. HAMILTON and J. A. IBERS. Hydrogen bonding in solids. W. A. Benjamin, New York. 1968.
19. J. D. LEE and G. W. GOODACRE. Acta Crystallogr. **B26**, 507 (1970).

Contribution à l'étude par spectroscopie ultra-violette de Δ-4 imidazolinethiones-2 et d'alkylthio-2 imidazoles. Calculs théoriques

D. BOUIN-ROUBAUD, J. KISTER, M. RAJZMANN et L. BOUSCASSE

Laboratoire de Chimie Organique A, Faculté des Sciences et Techniques de St-Jérôme, Université d'Aix-Marseille III, 13397 – Marseille, Cedex 13, France

Reçu le 20 janvier 1980

D. BOUIN-ROUBAUD, J. KISTER, M. RAJZMANN et L. BOUSCASSE. Can. J. Chem. **59**, 2883 (1981).

L'incidence des interactions stériques sur les transitions électroniques de Δ-4 imidazolinethiones-2 et d'alkyl-1 méthylthio-2 imidazoles et de méthyl-1 alkylthio-2 imidazoles est décrite. Les transitions électroniques étudiées sont toutes de type $\pi \rightarrow \pi^*$ et leur localisation dans les systèmes électroniques **1** et **2** est précisée au moyen de calculs CNDO/S.

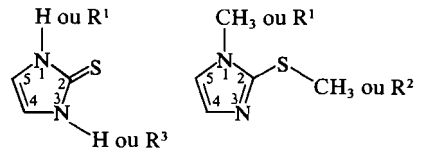

1 **2**

D. BOUIN-ROUBAUD, J. KISTER, M. RAJZMANN, and L. BOUSCASSE. Can. J. Chem. **59**, 2883 (1981).

Steric effects on electronic transitions for the systems **1** and **2** are reported. The $\pi \rightarrow \pi^*$ transitions studied are defined precisely by means of CNDO/S calculations.

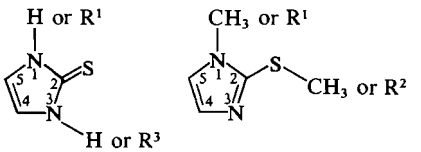

1 **2**

Introduction

Nous nous proposons, dans le présent mémoire, de décrire l'influence de la compression stérique sur les transitions électroniques. Les Δ-4 imidazolinethiones-2, substituées soit en 1, soit en 1 et 3 par des groupements alkyles encombrants, ainsi que les alkyl-1 méthylthio-2 imidazoles et les méthyl-1 alkylthio-2 imidazoles sont les substrats de base pour cette étude.

Conditions expérimentales et méthode de calcul

La préparation des produits a été décrite ailleurs (1–3). Les produits de type **1** sont des solides bien cristallisés; les produits de type **2** dont la synthèse a été réalisée par catalyse par transfert de phase ont été distillés sur hydrure de calcium ou sur potasse et conservés en ampoules scellées à l'abri de la lumière.

L'enregistrement des spectres ultra-violets a été réalisé sur spectrophotomètre Cary 14. L'éthanol utilisé a été purifié, le chlorure de méthylène est un produit pour spectroscopie.

La géométrie du cycle imidazole a été estimée et compte tenu des résultats cristallographiques obtenus par Ansell *et al.* (4) la molécule a été supposée plane.

La paramétrisation de la méthode CNDO/S utilisée a été décrite ailleurs (5–7).

L'interaction de configuration est limitée aux 30 configurations de plus basse énergie. Pour l'atome de soufre, nous avons tenu compte des orbitales *d*. Pour le traitement de celles-ci nous avons employé le procédé de Schulte et Schweig (5) dans lequel le recouvrement est multiplié par 0,3 quand intervient une orbitale *d*.

Résultats expérimentaux

Seules les bandes susceptibles d'être pointées précisément seront discutées dans ce qui suit. L'ensemble du spectre des systèmes de base, ici étudiés, a déjà été discuté (8, 9). Les résultats sont consignés dans les tableaux 1 et 2.

De façon générale, l'effet de substitution par un substituant de plus en plus encombrant ne se manifeste qu'à partir du groupement tertiobutyle.

D'autre part, nous constatons un effet bathochrome lors du passage d'un solvant protique à un solvant aprotique.

Discussion des résultats théoriques

Δ-4 *Imidazolinethione-2*

Les résultats sont consignés dans le tableau 3. Nous constatons une bonne coïncidence entre les résultats expérimentaux et les résultats des calculs.

La paramétrisation adoptée (5, 6), compte tenu de la géométrie choisie, paraît mieux convenir que celle utilisée par Arbelot *et al.* (10) pour décrire ce même type de molécule.

0008-4042/81/192883-08$01.00/0

©1981 National Research Council of Canada/Conseil national de recherches du Canada

Can. J. Chem. Downloaded from www.nrcresearchpress.com by 210.87.254.105 on 09/06/12
For personal use only.

Can. J. Chem. Downloaded from www.nrcresearchpress.com by 210.87.254.105 on 09/06/12
For personal use only.

TABLEAU 1. Absorption dans le domaine de l'ultraviolet d'alkyl-1 alkyl-3 Δ-4 imidazolinethiones-2

		Solvant CH_2Cl_2		Solvant EtOH	
R^1	R^3	λ (nm)	log ε	λ (nm)	log ε
H	H	270	4,458	259	4,134
				228(e)	
		217	3,756	200	3,745
Me	H	270	4,215	260	4,191
				228(e)	
		223	3,756	200	3,632
Et	H	270	3,704	261,5	4,136
		240(e)		230(e)	
				207	3,693
*i*Pr	H	270	4,192	260	4,197
		245(e)		225(e)	
		220	3,86	200	3,765
t-Bu	H	275	4,165	267	4,130
		225	3,81		
Phényl	H	292	3,737	283	3,635
		255(e)		245(e)	
Me	Me	267	4,339	260	4,186
		d	—	234(e)	
		220	3,912	210(e)	
Me	Et	266	4,177	262	4,136
		d	—	230(e)	
		225	3,815	210(e)	
Me	*i*Pr	266	4,127	262	4,119
		d	—	230(e)	
		222	3,751	210(e)	
Me	*t*-Bu	273	4,074	265	4,052
				233(e)	3,751
Me	Phényl	288,5	4,346	279	4,307
		255(e)		245(e)	
		230(e)		210(e)	

TABLEAU 2. Absorption dans le domaine de l'ultraviolet d'alkyl-1 alkylthio-2 imidazole

		Solvant CH_2Cl_2		Solvant EtOH	
R^1	R^2	λ (nm)	log ε	λ (nm)	log ε
H	CH_3	255,0	3,684	250,5	3,605
		225	3,411	220	3,936
Me	CH_3	255,3(e)		250	3,684
		226	3,886	223	3,846
Et	CH_3	255	3,633	250	3,647
		226	3,810	224	3,834
*i*Pr	CH_3	255	3,584	250	3,635
		226,5	3,160	224	3,281
t-Bu	CH_3	256,5	3,560	253,5	3,635
		230	3,790	225	3,792
Phényl	CH_3	263	3,662	260	3,678
		226	4,060		
Me	Et	244,5(e)		250	3,330
		222,4	3,491	222,9	3,747
Me	*i*Pr	248,8(e)		249,5	3,646
		224,4	3,834	225	3,800
Me	*t*-Bu	245,3(e)		250	3,728
		223,5	3,883	222,3	3,846
Me	Phényl	252,6(e)		257	3,740
		216,2	4,103	215	4,041

Le schéma 1 donne les valeurs des carrés des coefficients des orbitales atomiques intervenant dans l'orbitale moléculaire correspondante (multipliés par 10^2). La première transition calculée est de type $n \rightarrow \pi^*$. Elle n'a pas été retrouvée expérimentalement. La transition suivante est de type $\pi \rightarrow \pi^*$. Elle a été calculée à 4,58 eV et apparaît dans le chlorure de méthylène à 4,57 eV. Cette transition correspond principalement au passage d'un électron de la plus haute orbitale moléculaire occupée vers la plus basse orbitale moléculaire vide. Elle met en jeu dans l'orbitale moléculaire occupée le soufre exocyclique, et dans l'orbitale moléculaire virtuelle le carbone du groupement thiocarbonyle.

Pour cette transition, caractéristique du groupement thiocarbonyle, la charge de l'atome de soufre exocyclique à l'état excité est inférieure à celle de l'état fondamental.

Cet atome de soufre étant le site de protonation de la molécule, l'utilisation de la discussion des effets de solvant conduite par Brealey et Kasha (11) nous permet de conclure que la différence de basicité de l'atome de soufre entre l'état excité et l'état fondamental rend bien compte de l'effet hypsochrome observé lors du passage d'un solvant aprotique à un solvant protique.

La transition suivante est calculée à 5,15 eV. Elle a un caractère de transfert de charge du soufre exocyclique vers les carbones doublement liés. Elle n'apparaît pas dans le chlorure de méthylène, mais se retrouve sous forme d'épaulement dans l'éthanol.

Nous notons ensuite une transition de type $n \rightarrow \sigma^*$ à 5,88 eV (210,6 nm) dont la force oscillatrice est de $0{,}122 \times 10^{-3}$ cgs. Cette transition met en jeu dans l'orbitale moléculaire occupée presque exclusivement les électrons de l'atome de soufre exocyclique. Dans l'orbitale moléculaire virtuelle, on remarque une forte participation des orbitales *d* ($d_{x^2-y^2}$ et d_{z^2}) de l'atome de soufre.

Can. J. Chem. Downloaded from www.nrcresearchpress.com by 210.87.254.105 on 09/06/12
For personal use only.

TABLEAU 3. Détermination expérimentale (solvant CH_2Cl_2) et calcul CNDO/S des spectres uv d'alkyl-1 Δ-4 imidazolinethione-2

Nature de la transition	R							
	H		Me		Et		*t*-Bu	
	Théor.	Exp.	Théor.	Exp.	Théor.	Exp.	Théor.	Exp.
$n \rightarrow \pi^*$	470,5 (0,000)		465,3 (0,000)		467,3 (0,000)			
$\pi \rightarrow \pi^*$	270,5 (0,443)	270 (4,458)	272,4 (0,434)	270 (4,215)	273,1 (0,4409)	270 (3,704)	276,1 (0,4288)	275 (4,165)
$\pi \rightarrow \pi^*$	240,4 (0,153)		242,3 (0,155)		243,5 (0,1536)	240(e)	245,0 (0,1630)	
$n \rightarrow \sigma^*$	210,6 (0,0001)		201,2 (0,0001)		201,7 (0,000)		197,2 (0,0002)	
$\pi \rightarrow \pi^*$	183,5 (0,205)	217 (3,756)	183,2 (0,221)	223 (3,756)	183,9 (0,1325)		186,1 (0,1552)	225 (3,81)

La dernière transition à 6,75 eV (183,5 nm) de type $\pi \rightarrow \pi^*$ se retrouve à 5,68 eV (217 nm) dans le chlorure de méthylène. Elle fait intervenir les deux carbones doublement liés dans l'état fondamental et le carbone du groupement thiocarbonyle dans l'état excité.

Méthyl-1 Δ-4 imidazolinethione-2

Géométrie

Nous avons conservé la valeur des angles de valence utilisée pour la Δ-4 imidazolinethione-2.

Résultats

Si nous comparons les résultats expérimentaux avec les résultats théoriques, nous voyons un bon accord, comparable à celui que nous trouvions pour la molécule non substituée. Le calcul indique, tout de même, un effet bathochrome de 1,9 nm qui n'est pas mis en évidence expérimentalement. La nature et les positions relatives des transitions restent inchangées par rapport au composé non substitué.

Ethyl-1 Δ-4 imidazolinethione-2

Géométrie

L'introduction dans la molécule d'un substituant non symétrique nous a amenés à effectuer une

Nature de la transition	Carré du coefficient de la configuration principale	Orbitale moléculaire occupée de la configuration principale	Orbitale moléculaire virtuelle de la configuration principale
$n \rightarrow \pi^*$ 2,63 eV	0,96	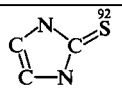	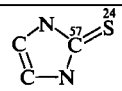
$\pi \rightarrow \pi^*$ 4,58 eV	0,96	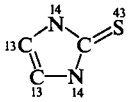	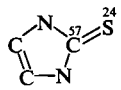
$\pi \rightarrow \pi^*$ 5,15 eV	0,96	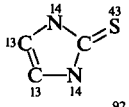	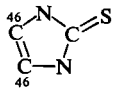
$n \rightarrow \sigma^*$ 5,88 eV	0,53	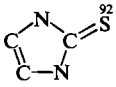	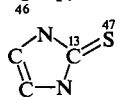
$\pi \rightarrow \pi^*$ 6,75 eV	0,90	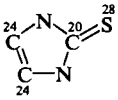	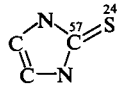

Les nombres attenant aux schémas des molécules sont les carrés des coefficients des orbitales atomiques intervenant dans l'orbitale moléculaire correspondante multipliés par 10^2

SCHÉMA 1

Can. J. Chem. Downloaded from www.nrcresearchpress.com by 210.87.254.105 on 09/06/12
For personal use only.

minimisation de l'énergie à l'aide de la méthode EHT, en faiant tourner le groupement éthyle autour de l'axe C–N tout en conservant constants les autres éléments.

Le choix de la méthode EHT est justifié par le fait que la méthode CNDO/S n'est pas adaptée à l'étude de l'état fondamental. Nous signalons d'autre part que la méthode EHT s'avère moins coûteuse du point de vue temps de calcul que les méthodes CNDO.

Le calcul EHT montre que le minimum d'énergie correspond à un angle de 90°, c'est-à-dire à la représentation de Newman suivante.

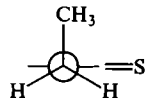

Les résultats du calcul CNDO/S obtenus pour cette conformation sont consignés dans le tableau 3.

Tertiobutyl-1 Δ-4 imidazolinethione-2

Géométrie

La variation assez importante de la longueur d'onde d'absorption de la bande principale (de 270 à 275 nm dans le chlorure de méthylène) quand on passe de la Δ-4 imidazolinethione-2 à la tertiobutyl-1 Δ-4 imidazolinethione-2, pouvait laisser penser que cette substitution entraînait soit une déformation du cycle, soit une modification des angles valentiels. Ce phénomène avait déjà été observé par rmn ^{13}C, et la question était donc déjà posée (12).

Une étude en rmn ^{1}H basée sur les signaux observés pour les atomes 4 et 5 du cycle imidazolique diversement substitué en 1, nous montre que suivant la nature du solvant, on observe soit un singulet dans $CDCl_3$ (les deux protons 4 et 5 équivalents), soit deux doublets dans l'acétone-d_6, excepté pour le tertiobutyle où on constate la non équivalence magnétique quel que soit le solvant (13). Ceci se traduit numériquement par une variation de la différence de glissement chimique entre les deux protons 4 et 5 dans l'acétone-d_6.

TABLEAU 4. Détermination expérimentale (solvant CH_2Cl_2) et calcul CNDO/S du spectre uv de la phényl-1 Δ-4 imidazolinethione-2

Nature de la transition	Théorique		Expérimental	
	λ (nm)	F.O.	λ (nm)	log ε
$n \rightarrow \pi^*$	465,1	0,0000		
$\pi \rightarrow \pi^*$	282,9	0,2720	292	3,737
$\pi \rightarrow \pi^*$	272,3	0,0067		
$\pi \rightarrow \pi^*$	258,6	0,2439	250(e)	
$\pi \rightarrow \pi^*$	244,4	0,1297		
$n \rightarrow \pi^*$	202,0	0,2274		

	Δδ (acétone-d_6) ppm	Δδ ($CDCl_3$) ppm
Me	0,10	0
Et	0,14	0
*i*Pr	0,17	0
t-Bu	0,25	0,20

Nous remarquons une variation régulière d'environ 0,04 ppm correspondant à l'introduction d'un méthyle supplémentaire quand on passe du méthyle à l'isopropyle. La variation de 0,08 ppm quand on passe de l'isopropyle au tertiobutyle est bien en accord avec l'introduction d'une dissymétrie supplémentaire que nous allons essayer de mettre en évidence.

Nous avons, dans un premier temps, étudié la déformation de la planéité du cycle par la méthode EHT. Pour cela nous avons plié la molécule autour de l'axe C-2 C-5, en maintenant l'hydrogène porté par le carbone en 5 dans le plan formé par les atomes N-1, C-5, C-4 et la liaison C=S dans le plan formé par N-1, C-2, C-3. Un autre type de déformation a été introduit, cette fois autour de l'axe N-1 N-3.

C'est toujours la molécule plane qui présente l'énergie minimum. La méthode EHT a été utilisée pour optimiser les angles valentiels formés par les substituants avec le cycle dont la géométrie est laissée invariante. Les valeurs obtenues sont les suivantes:

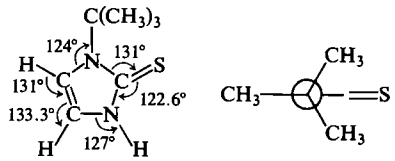

Parallèlement à cette étude théorique, une détermination complète de cette molécule a été réalisée par cristallographie (14). Les résultats de cette mesure confirment en tous points nos hypothèses à la fois sur la conservation de la planéité du cycle et sur la valeur des angles de valence.

D'autre part, nous avons déterminé la conformation du groupement tertiobutyle par rapport au plan de la molécule représentée par les atomes C-2, C-5 et S. Cette conformation a été confirmée par cristallographie.

La même méthode EHT utilisée pour la Δ-4 imidazolinethione-2 donne les valeurs suivantes pour les angles HN-1, C-5 = 127°; SC-2, N-1 = 126,8°; HC-5, C-4 = 133,3°.

Nous observons donc que l'angle de valence de

Can. J. Chem. Downloaded from www.nrcresearchpress.com by 210.87.254.105 on 09/06/12
For personal use only.

la liaison C=S augmente, tandis que l'angle C-5, N-1H diminue, traduisant ainsi un effet de répulsion entre le soufre et le groupement tertiobutyle. Cet effet s'observe aussi pour l'atome d'hydrogène porté par le carbone en 5, ce qui explique les résultats obtenus en rmn ^{1}H. L'utilisation de cette géométrie nous permet d'obtenir les résultats consignés dans le tableau 3. Ils traduisent bien l'effet bathochrome observé expérimentalement.

Nature de l'effet bathochrome

Pour déterminer la participation de l'effet stérique et de l'effet inductif, nous avons effectué les calculs CNDO/S suivants.

Tout d'abord le calcul de la molécule de tertiobutyl-1 Δ-4 imidazolinethione-2 a été effectué en utilisant la géométrie de base, c'est-à-dire sans optimisation des angles de valence. La transition principale est calculée à 278,8 nm (au lieu de 276,1 nm avec optimisation de géométrie). Ceci tend à montrer que la déformation des angles de valence produit un effet inverse de l'effet bathochrome observé.

Nous avons ensuite effectué le calcul des transitions électroniques pour la molécule d'*i*Pr-1 Δ-4 imidazolinethione-2 en utilisant trois conformations, conservant ainsi constant l'effet inductif dû aux différents groupements méthyles.

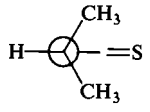

1

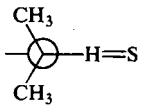

2

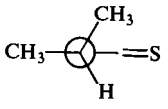

3

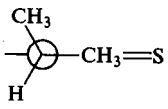

4

Les transitions n'ont pas été calculées pour la forme *4* qui est selon le calcul EHT extrémement défavorisée énergétiquement du fait de l'interaction entre l'un des méthyles et l'atome de soufre. La transition principale $\pi \rightarrow \pi^*$ qui apparaît expérimentalement dans le chlorure de méthylène à 270 nm se retrouve par le calcul à 274,2 nm pour la conformation *1*, à 273,1 nm pour la *2* et à 276,2 nm pour la *3*. Le calcul EHT montre d'ailleurs que la conformation *2* est la plus favorisée énergétiquement. La diminution de l'interaction stérique entre le soufre et les groupes méthyles quand on passe de la forme *1* à la forme *2* se traduit par un abaissement de 1 nm de la longueur d'onde d'absorption de la transition principale.

Dans la conformation *3*, un groupement méthyle éclipse et donc devient plus proche du motif C-5—H du cycle, et le calcul donne un effet bathochrome de 3 nm par rapport à la conformation *2*. Or la conformation la plus favorisée de la molécule substituée par un tertiobutyle correspond à la conformation *3* dans laquelle l'hydrogène est substitué par un méthyle. On peut donc dire que l'effet bathochrome observé pour cette molécule est principalement dû à une interaction stérique entre une groupe méthyle et le motif C-5—H. Il est également causé par une accumulation d'effet inductif et, dans une moindre mesure, par un effet de contact entre le soufre et les groupements méthyles.

Phényl-1 Δ-4 imidazolinethione-2

Nous avons effectué un calcul EHT de minimisation d'énergie pour déterminer la valeur de l'angle entre le plan de l'hétérocycle et le plan du groupement phényle. Des travaux précédents (15) ont montré que la méthode EHT sous-estime l'énergie de conjugaison et qu'il est nécessaire de diviser le sinus de l'angle par un facteur 1,2. L'application de ce facteur ramène l'angle de 68° à 58°. La valeur des angles de valence, calculée par cette même méthode est la suivante: angle SC-2, N-1 = 127,8°; angle HN-3, C-4 = 127°; angle C-Ph, N-1, C-5 = 124,5°. La valeur donnée par le calcul pour la transition de plus basse énergie coïncide avec la valeur obtenue dans l'éthanol et diffère de 9 nm de la valeur obtenue dans le chlorure de méthylène. Cet écart plus important que pour les autres composés peut s'expliquer en considérant que la valeur de l'angle est probablement surestimée malgré le facteur appliqué.

Méthylthio-2 imidazole et dérivés alkyles

Ces composés résultent d'une réaction de transposition catalysée par des sels quaternaires (obtenus par quaternisation des thioéthers par ICH_3) (2). Du fait de la faible différence de longueur d'onde d'absorption entre les bandes caractéristiques d'absorption uv des thiones et des thioéthers *N*-méthylés, c'est le dosage par rmn ^{1}H (16) qui a été retenu pour l'étude de la transposition SR ⇌ NR.

Les résultats de l'étude spectroscopique sont consignés dans le tableau 5. Nous notons tout d'abord que les dérivés thioéthers absorbent à longueur d'onde plus faible que leurs homologues thiones. Comme pour les thiones nous constatons une invariance de la transition lors d'une substitution de l'hydrogène en position 1 par un groupement méthyle ou éthyle. Le passage d'un solvant protique (éthanol) à un solvant aprotique (CH_2C1_2) produit un effet bathochrome.

TABLEAU 5. Détermination expérimentale (solvant EtOH) et calcul CNDO/S des spectres uv d'alkyl-1 alkylthio-2 imidazoles

R^2 =	Me		Me		Me		Et	
R^1 =	H		Me		Et		Me	
Nature de la transition	Théor.	Exp.	Théor.	Exp.	Théor.	Exp.	Théor.	Exp.
$\pi \rightarrow \pi^*$	252,9 (0,3321)	250,5 (3,605)	253,8 (0,3132)	250 (3,684)	256,7 (0,2395)	250 (3,647)	252,0 (0,3039)	250 (3,330)
$\pi \rightarrow \pi^*$	219,5 (0,0455)		221,4 (0,0343)		219,4 (0,0308)		220,9 (0,0363)	
$\pi \rightarrow \pi^*$	186,1 (0,1548)	220 (3,936)	192,9 (0,118)	224 (3,846)	188,4 (0,3362)	224 (3,834)	188,9 (0,1425)	222,9 (3,747)

Nature de la transition	Carré du coefficient de la configuration principale	Orbitale moléculaire occupée de la configuration principale	Orbitale moléculaire virtuelle de la configuration principale
$\pi \rightarrow \pi^*$ 4,90 eV	0,88	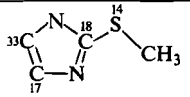	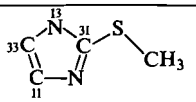
$\pi \rightarrow \pi^*$ 5,64 eV	0,60	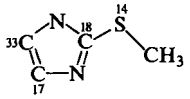	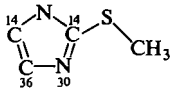
$\pi \rightarrow \pi^*$ 6,65 eV	0,22	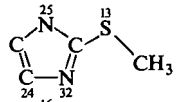	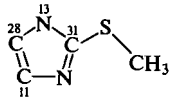
	0,21	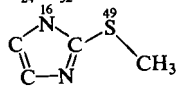	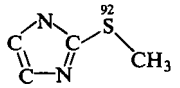

Les nombres attenant aux schémas des molécules sont les carrés des coefficients des orbitales atomiques intervenant dans l'orbitale moléculaire correspondante multipliés par 10^2

SCHÉMA 2

Toutes les transitions calculées sont de type $\pi \rightarrow \pi^*$ (Schéma 2). La première transition qui apparaît à 4,90 eV met en jeu l'ensemble du cycle à la fois à l'état fondamental et à l'état excité. La transition suivante calculée à 4,64 eV (219,5 nm) met aussi en jeu l'ensemble du cycle à l'état fondamental et à l'état excité. La transition correspondante apparaît dans l'éthanol à 220 nm. Elle est en partie recouverte par la transition qui apparaît à plus grande longueur d'onde. La dernière transition calculée à 6,65 eV est un mélange de deux configurations de type $\pi \rightarrow \pi^*$.

Conclusion

La transition caractéristique du groupement thiocarbonyle des Δ-4 imidazolinethione-2 est de type $\pi \rightarrow \pi^*$. Pour cette transition la charge de l'atome de soufre exocyclique à l'état excité est inférieure à celle de l'état fondamental. Ceci est en accord avec le déplacement hypsochrome observé lorsque l'on passe du chlorure de méthylène à l'éthanol. En effet l'état fondamental est stabilisé dans les solvants protiques.

L'optimisation des angles valentiels et l'étude des conformations nous a permis de constater que l'effet stérique est moins important que l'effet électronique et par là même, de rendre compte de la quasi invariance des longueurs d'onde des transitions observées. L'importance relativement faible du déplacement bathochrome dans le cas du dérivé phénylé a été expliqué par le défaut de la conjugaison dû à l'angle de 58° que font les plans des deux cycles entre eux.

Les résultats obtenus dans le présent travail montrent que la méthode CNDO/S conduit, sur l'ensemble des composés que nous avons étudiés, à des résultats satisfaisants pour l'étude des transitions électroniques aussi bien sur le plan qualitatif que quantitatif.

1. J. KISTER, G. ASSEF, G. MILLE et J. METZGER. Can. J. Chem. **57**, 813 (1979).

Can. J. Chem. Downloaded from www.nrcresearchpress.com by 210.87.254.105 on 09/06/12
For personal use only.

2. J. KISTER, G. ASSEF, G. MILLE et J. METZGER. Can. J. Chem. **57**, 822 (1979).
3. P. HASSANALY, H. DOU, J. METZGER, G. ASSEF et J. KISTER. Synthesis, **4**, 253 (1977).
4. B. ANSELL, D. M. FORKEY et D. W. MOORE. Chem. Commun. 56 (1970).
5. Y. W. SCHULTE et A. SCHWEIG. Theor. Chim. Acta, **33**, 19 (1974).
6. J. DEL BENE and H. H. JAFFE. J. Chem. Phys. **48**, 1807 (1968).
7. M. RAJZMANN et P. FRANCOIS. Q.C.P.E. No 382 (1979).
8. G. ASSEF, D. BOUIN-ROUBAUD, J. KISTER et J. METZGER. C.R. Acad. Sci. Ser. C, **283**, 143 (1976).
9. J. KISTER, D. BOUIN-ROUBAUD, P. HASSANALY, H. DOU et J. METZGER. C.R. Acad. Sci. Ser. C, **287**, 201 (1978).
10. M. ARBELOT, C. GUIMON, D. GOMBEAU et G. PFISTER-GUILLOUZO. J. Mol. Struct. **20**, 487 (1974).
11. G. J. BREALEY et M. KASHA. J. Am. Chem. Soc. **77**, 4462 (1955).
12. R. FAURE, E. J. VINCENT, G. ASSEF, J. KISTER et J. METZGER. Org. Magn. Reson. **9**, 688 (1977).
13. J. KISTER. Spectres 30100 M à 30110 M. Catalogue Sadtler 1980.
14. M. HOSPITAL, J. KISTER et D. BOUIN-ROUBAUD. Travaux en cours.
15. T. AVIGNON, L. BOUSCASSE et J. ELGUERO. Tetrahedron, **34**, 1139 (1978).
16. J. KISTER, G. ASSEF, H. DOU et J. METZGER. Tetrahedron, **32**, 1395 (1976).

Annexe 1

Géométrie des molécules **1** et **2**

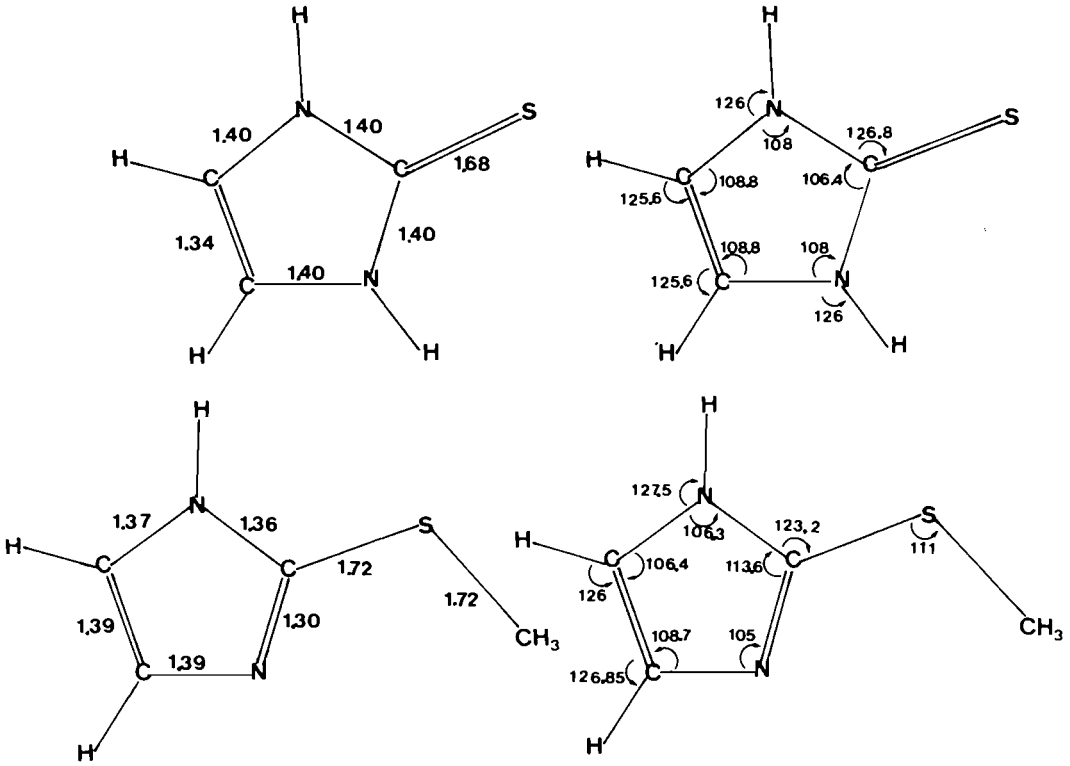

Can. J. Chem. Downloaded from www.nrcresearchpress.com by 210.87.254.105 on 09/06/12
For personal use only.

Annexe 2

Spectres de la Methyl-1 Δ-4 imidazolinethione-2 et du methyl-1 méthylthio-2 imidazole dans l'ethanol

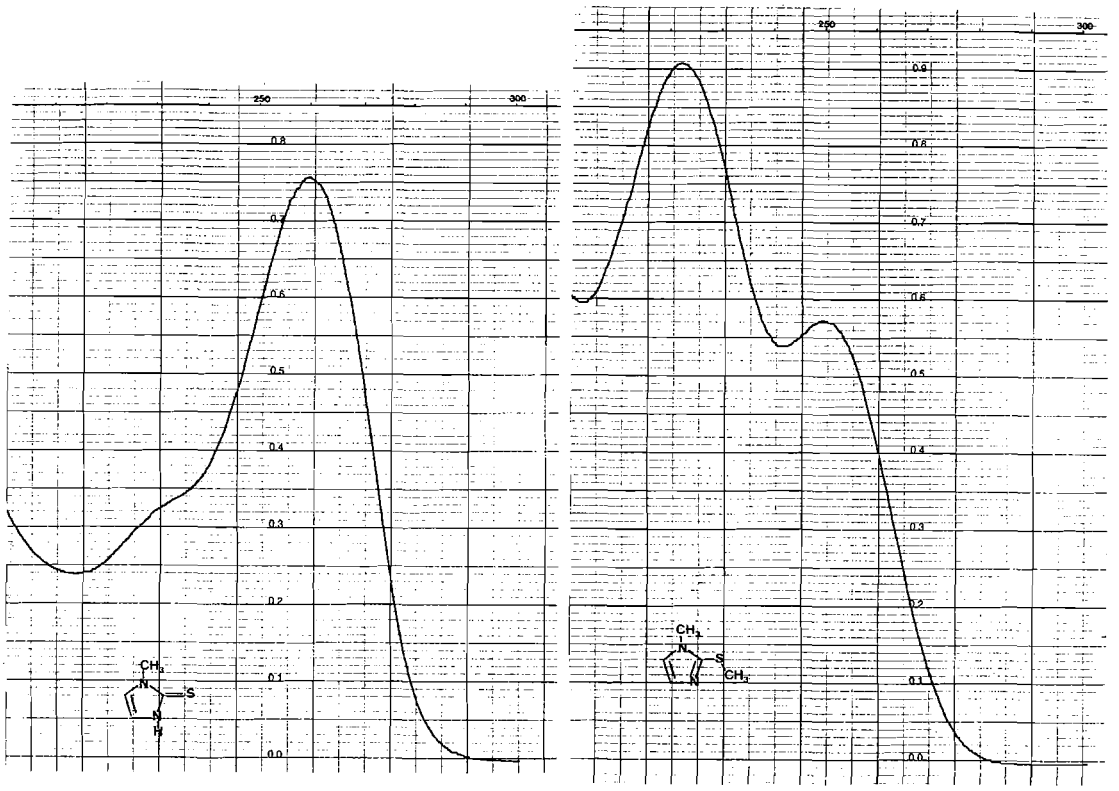

Can. J. Chem. Downloaded from www.nrcresearchpress.com by 210.87.254.105 on 09/06/12
For personal use only.

Action des hydroxyurées sur les maléate et fumarate de méthyle. Obtention des carbométhoxy-5 oxa-6 dihydrouraciles; transposition en carbométhoxyméthylène-5 hydantoïnes

CHAKIB BENNOUNA, FRANÇOISE PETRUS ET JEAN VERDUCCI[1]

Laboratoire de synthèse et d'étude physicochimique d'hétérocycles azotés, Université des Sciences et Techniques du Languedoc, Place E. Bataillon, 34060 Montpellier Cédex, France

ET

CHRISTIAN HAUW ET JACQUES GAULTIER

Laboratoire de Cristallographie et de Physique Cristalline, Université de Bordeaux I, 351 Cours de la Libération, 33405 Talence, France

Reçu le 3 décembre 1980

CHAKIB BENNOUNA, FRANÇOISE PETRUS, JEAN VERDUCCI, CHRISTIAN HAUW et JACQUES GAULTIER. Can. J. Chem. **59**, 2891 (1981).

Ce travail décrit l'addition de type Michael des hydroxyurées sur les maléate et fumarate de méthyle. La cyclisation des uréidoxydiesters ainsi obtenus conduit aux carbométhoxyméthyl-5 oxa-6 dihydrouraciles dont la structure est prouvée par analyse au rayons X. Ces derniers, relativement instables, se transposent en carbométhoxyméthylène-5 hydantoïnes par traitement en milieu basique.

CHAKIB BENNOUNA, FRANÇOISE PETRUS, JEAN VERDUCCI, CHRISTIAN HAUW, and JACQUES GAULTIER. Can. J. Chem. **59**, 2891 (1981).

We describe in this paper the Michael-type addition of hydroxyureas with methyl maleate and fumarate. The cyclization of the ureidoxyester intermediates obtained leads to the isolation of 5-carbomethoxy 6-oxadihydrouracils; their structure is proved by X-ray analysis. These relatively unstable compounds undergo transposition under basic conditions and give 5-carbomethoxyhydantoins.

Les travaux précédents réalisés dans notre laboratoire ont permis de mettre en évidence le caractère "hydroxylamine *N*-protégée" des hydroxyurées: une attaque par l'atome d'oxygène est observée dans les réactions d'addition sur les nitriles α-éthyléniques (1), les esters α-éthyléniques (2), les cétones α-éthyléniques (3, 4) ainsi que dans les réactions de substitution sur les α-bromoesters (5).

Ces résultats permettent de prévoir *à priori* une addition-1,4 des hydroxyurées sur les maléate et fumarate de méthyle.

Résultats

L'action des hydroxyurées sur ces esters insaturés conduit aux mêmes résultats quel que soit l'isomère de départ. La réaction, réalisée dans des conditions douces (en absence de base ou en présence de triéthylamine), conduit à l'α-uréidoxysuccinate de méthyle **1** ou à un mélange de **1** et de carbométhoxyméthyl-5 oxa-6 dihydrouracile **2** (tableau 1, schéma 1). En présence d'une base plus forte telle que le méthylate de sodium et avec un temps de réaction de 30 min, l'uréidoxydiester **1** n'est plus isolé; la réaction conduit soit à **2**, soit à un mélange de **2** et de carbométhoxyméthylène-5 hydantoïne **3**. Si le temps de réaction est prolongé à

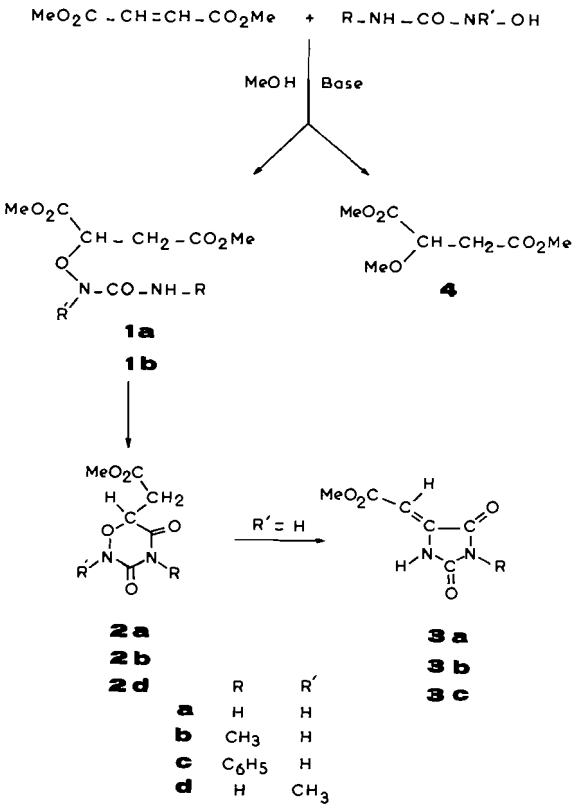

SCHÉMA 1

[1]Auteur à qui toute correspondance sera adressée.

0008-4042/81/192891-07$01.00/0

©1981 National Research Council of Canada/Conseil national de recherches du Canada

Can. J. Chem. Downloaded from www.nrcresearchpress.com by 210.87.254.5 on 09/06/12
For personal use only.

TABLEAU 1. Action de R—NH—CO—N(R')—OH sur les maléate et fumarate de méthyle dans le méthanol

No	R	R'	Base*	Temps	%1	%2	%3	%4	Rdt. global %
1	H	H	—	4 jours	100	0	0	0	5
2	H	H	NEt_3	4 jours	100	0	0	0	30
3	H	H	MeONa	30 min	0	60	20	20	90
4	H	H	MeONa	24 h	0	0	70	30	90
5	CH_3	H	NEt_3	16 h	40	60	0	0	40
6	CH_3	H	MeONa	30 min	0	85–90	0	10–15	90
7	CH_3	H	MeONa	24 h	0	0	80	20	75
8	H	CH_3	MeONa	24 h	0	30	0	70	95
9	C_6H_5	H	MeONa	24 h	0	0	70	30	70

*Le nombre d'équivalents de base est en général égal à celui de l'hydroxyurée et du diester, sauf pour l'expérience 1 (absence de base) et l'expérience 5 où la quantité de base est le dixième du nombre d'équivalents des autres réactifs.

24 h, seule l'hydantoïne est isolée, sauf **3***d* à partir de la *N*(1)-méthylhydroxyurée. Il faut en outre noter la formation d'un certain pourcentage d'α-méthoxysuccinate de méthyle **4** lorsque la réaction est réalisée en présence de méthylate de sodium.

Discussion

L'emploi de différentes conditions expérimentales dans cette réaction permet d'isoler, dans certains cas, les composés **1** et **2** qui sont bien les intermédiaires de la réaction puisque, traités par une solution de méthylate de sodium, ils conduisent à **3** (excepté **2***d*).

La première étape correspond à l'addition-1,4 des hydroxyurées pour conduire aux α-uréidoxysuccinates de méthyle **1** dont la caractérisation sera donnée plus loin. La seconde étape de la réaction, correspondant à la cyclisation de **1**, conduit à un composé dont la détermination de structure présente des difficultés; en effet, trois types de cyclisation peuvent être envisagés pour **1** (schéma 2):

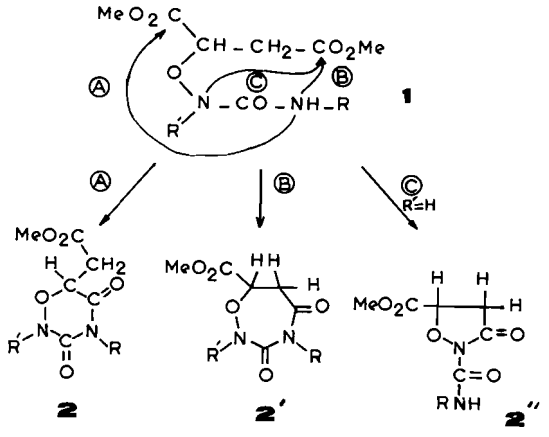

SCHÉMA 2

Le processus C, par attaque de l'azote N(1) sur l'ester en β de la fonction uréidoxy, doit être envisagé puisque c'est le seul type de cyclisation observé dans le cas des β-uréidoxymonoesters (2). Cependant un tel processus ne peut avoir lieu dans le cas où R' = CH_3; or, les composés cycliques obtenus (*a*, *b* et *d*) présentent tous des caractéristiques spectrales tout à fait comparables, permettant d'exclure le processus C et par suite la structure *N*-carboxamidoisoxazolidinone **2″**. Ce résultat est confirmé par l'absence de couplage entre le N(3)—CH_3 et le N(3)—H qui aurait dû être observé pour la structure **2″***b*.

Le processus B, déjà observé pour certaines β-uréidoxycétones (4), implique l'azote N(3) et le carbonyle en β de la fonction uréidoxy pour conduire à l'hétérocycle à 7 chaînons **2′**.

Le processus A, conduisant à **2** par attaque de l'azote N(3) sur l'ester en α de la fonction uréidoxy, doit aussi être envisagé; ce type de cyclisation à 6 chaînons, en général favorable, a été obtenu dans le cas α-uréidoxyesters (5).

Par régression de cycle, **2** et **2′** sont susceptibles de se transposer en hydantoïne **3**. Compte tenu de la fragilité de la molécule, les méthodes chimiques (hydrolyse, décarboxylation, réduction, etc.) ne nous ont pas permis de trancher entre les structures **2** et **2′**. Il en est de même pour les études ir et de rmn qui apportent peu de renseignements comme nous le verrons plus loin. Seule une analyse par rayons X prouve que nous avons à faire à la structure **2**.

La troisième étape de la réaction correspond à la transposition de **2** en carbométhoxyméthylène-5 hydantoïne **3**. Celle-ci se fait par perte d'une molécule d'eau impliquant l'atome d'oxygène intracyclique. Un tel mécanisme a déjà été proposé pour la formation des carbométhoxy-2 pyrroles à partir des carbométhoxydihydrooxazines (6). En milieu basique, la formation d'un carbanion en

Can. J. Chem. Downloaded from www.nrcresearchpress.com by 210.87.254.5 on 09/06/12
For personal use only.

Can. J. Chem. Downloaded from www.nrcresearchpress.com by 210.87.254.5 on 09/06/12
For personal use only.

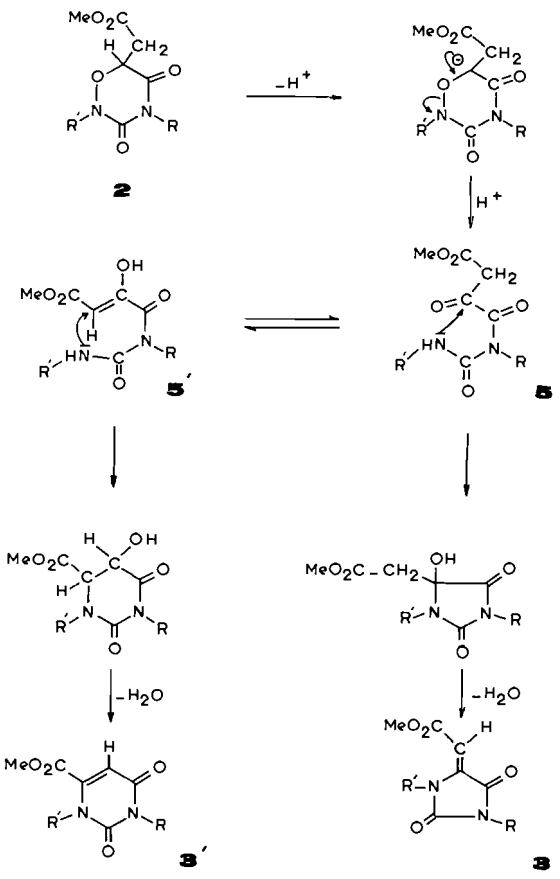

SCHÉMA 3

position 5 induit la rupture de la liaison N—O pour conduire à l'intermédiaire ouvert **5** (schéma 3). Dans le cas du composé **2***d* (R′ = CH_3), le réarrangement n'est pas observé; en milieu méthylate de sodium à température ambiante, **2***d* reste inchangé; à reflux, il conduit à des produits de dégradation non identifiés. Une plus grande stabilité de la liaison N—O due à l'effet donneur du N(1)—CH_3 peut expliquer ce résultat. La cyclisation de **5** conduit après déshydratation à l'hydantoïne **3**, mais on ne pouvait *à priori* rejeter la cyclisation de la forme énol tautomère **5′**, conduisant à l'ester orotique **3′** (schéma 3). La distinction des composés **3** et **3′** est difficile vu la similitude de leurs points de fusion (7–9) et de leurs caractéristiques physicochimiques. D'autre part, l'hydrolyse basique de la carbométhoxyméthylène-5 hydantoïne conduit à l'ester orotique (10–12). Seule la comparaison de plusieurs composés diversement substitués avec les dérivés cités dans la littérature nous a permis de prouver la structure hydantoïne de ces produits de réarrangement.

Caracterisation des composés

Uréidoxyesters 1

Les uréidoxyesters **1** sont caractérisés sans ambiguité par ir et rmn. En ir, les bandes observées pour les fonctions ester et uréide sont tout à fait comparables à celles données pour les α-uréidoxyesters (5) (tableau 2).

Les spectres de rmn sont en accord avec la structure uréidoxyester (tableau 3).

Caractérisation des carboxyméthyl-5 oxa-6 dihydrouraciles 2

Les méthodes physicochimiques classiques se sont révélées peu efficaces pour trancher entre les structures carbométhoxyméthyl-5 oxa-6 dihydrouracile **2** et carbométhoxy-6 oxa-7 hexahydrodiazépinedione **2′**. Les spectres ir (large bande entre 1680 et 1740 cm^{-1} et ν_{NH} à 3395 cm^{-1}) et de rmn ^1H (tableau 4) sont compatibles avec les structures **2** et **2′**.

Seule l'étude des spectres de rmn ^{13}C (tableau 5) apporte quelque argument en faveur de la structure **2**. Pour l'attribution des deux pics dans la région des 170 ppm, on note une faible variation du déplacement chimique de l'un d'eux en fonction de la nature des substituants sur les azotes du cycle, l'autre signal étant pratiquement inchangé; ce dernier est attribué au carbonyle de la fonction ester, plus éloigné des modifications apportées par les substituants, le signal le plus perturbé correspondant au C(4). Cette attribution est confirmée par l'étude du spectre du dérivé *O*-méthylé **6** obtenu simultanément avec **2***e* lors de la méthylation de **2***b*; l'introduction d'un O—CH_3 et d'une double liaison dans le cycle modifie le déplacement chimique du C(4) (de l'ordre de 2 ppm) laissant pratiquement inchangé le signal du carbonyle de la fonction ester. D'autre part, l'intensité nettement supérieure des signaux de la fonction ester par rapport à celle du C(4) (sauf pour **2***a* où les bandes sont confondues) est un élément en faveur de la présence d'un CH_2 en α de la fonction ester, donc de la structure **2**.

TABLEAU 2. Spectres ir* des urëidoxy-2 succinates de méthyle **1**

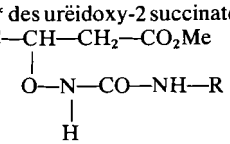

No	R	ν_{CO} ester	ν_{CO} uréide	ν_{NH2}	ν_{NH2}	ν_{NH}
1*a*	H	1735	1700	1590	3510	3335
1*b*	CH_3	1750 1730	1685	1550	3365	—

*Les spectres ir ont été réalisés en solutions chloroformiques; la position des bandes est exprimée en cm^{-1}.

Can. J. Chem. Downloaded from www.nrcresearchpress.com by 210.87.254.5 on 09/06/12
For personal use only.

TABLEAU 3. Spectres de rmn des uréidoxy-2 succinates de méthyle **1** dans $CDCl_3$

No	R	CO_2CH_3	CH	CH_2	N(3)R	N(3)H	N(1)H
1*a*	H	3,65 3,70	H_X 4,73 J_{AX} = 12,8 J_{BX} = 0,6	H_A 2,81 H_B 2,87 J_{AB} = 17,7	8,18		10,83
1*b*	CH_3	3,76 3,81	4,68 (m)	2,86 (m)	2,90 (d) 6,78 (q) J = 5 Hz		7,96

TABLEAU 4. Spectres de rmn ^1H*

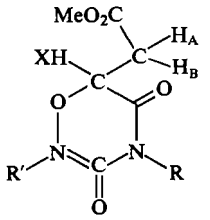

No	R	R′	CO_2Me	CH	CH_2	NR′	NR
2*a*	H	H	3,65	H_X 4,75 J_{AX} = 4,3 J_{BX} = 7,7	H_A 2,93 H_B 2,78 J_{AB} = 17,1	10,97	
2*b*	CH_3	H	3,75	H_X 4,93 J_{AX} = 2,3 J_{BX} = 9,5	H_A 3,03 H_B 2,90 J_{AB} = 17,1	8,50	3,19
2*d*	H	CH_3	3,74	H_X 4,92 J_{AX} = 3,4 J_{BX} = 8,4	H_A 3,05 H_B 2,82 J_{AB} = 17,1	3,22	10,80
2*e*	CH_3	CH_3	3,73	H_X 4,98 J_{AX} = 4,3 J_{BX} = 8,7	H_A 3,04 H_B 2,84 J_{AB} = 17,2	3,16 3,21	

*Les spectres ont été enregistrés dans le DMSO-d_6 pour **2***a* et dans le $CDCl_3$ pour les trois autres composés.

TABLEAU 5. Spectres de rmn ^{13}C*

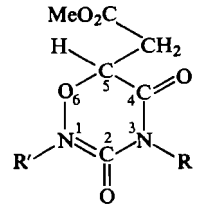

No	R	R′	CO_2Me	C(4)	C(2)	C(5)	CH_2	OMe	N—R	N—R′
2*a*	H	H	169,5		155,0	75,2	32,8	51,8	—	—
2*b*	CH_3	H	169,8	169,1	155,7	76,1	33,6	51,9	25,9	—
2*d*	H	CH_3	169,5	169,3	154,8	75,8	32,8	51,8	—	34,9
2*e*	CH_3	CH_3	169,5	168,6	155,6	76,8	36,0	52,2	27,0	33,8

*Les spectres ont été enregistrés en solution dans le DMSO-d_6 sauf **2***e* pour lequel le $CDCl_3$ a été utilisé.

Pour lever toute ambiguïté nous avons procédé à une étude par diffraction des rayons X du dérivé **2***b* ($C_7H_{10}N_2O_5$; M = 202 g) dont il a été possible d'obtenir des cristaux de bonne qualité.

Ces cristaux de symétrie monoclinique sont caractérisés comme suit, à la température ambiante: groupe spatial $P2_1/c$, a = 9,943(4), b = 10,447(4), c = 8,886(3) Å; β = 101.78(8)°, V = 906 Å^3, ρ_o = 1,48(2), Z = 4, ρ_c = 1,481.

Les coordonnées des atomes et leurs coefficients d'agitation thermique sont données (tableau 6). Les coefficients d'agitation anisotrope des atomes de carbone, d'azote et d'oxygène ainsi que la liste des

Can. J. Chem. Downloaded from www.nrcresearchpress.com by 210.87.254.5 on 09/06/12
For personal use only.

TABLEAU 6. Coordonnées atomiques (et écarts-type) en fraction de maille; facteurs de Debye–Waller

Atome	x	y	z	BI
O(6)	0,9369(3)	0,7867(3)	0,4183(3)	4,0
N(1)	0,9464(3)	0,6533(3)	0,3956(4)	4,0
C(2)	0,8292(4)	0,5863(4)	0,3869(5)	3,7
N(3)	0,7080(3)	0,6518(3)	0,3365(4)	3,4
C(4)	0,7071(4)	0,7719(4)	0,2716(5)	3,7
C(5)	0,8453(4)	0,8351(4)	0,2878(5)	3,9
C(7)	0,8378(5)	0,9779(4)	0,3046(5)	4,4
O(8)	0,6038(3)	0,8213(3)	0,2038(4)	5,7
C(9)	0,5791(4)	0,5822(4)	0,3210(6)	4,7
O(10)	0,8306(3)	0,4719(3)	0,4144(4)	4,9
C(11)	0,7693(4)	1,0190(4)	0,4329(5)	4,2
O(12)	0,7370(4)	0,9498(3)	0,5252(4)	6,4
O(13)	0,7495(3)	1,1435(3)	0,4282(4)	4,8
C(14)	0,6883(6)	1,1969(4)	0,5478(7)	5,9
H(52)	1,012	0,619	0,490	3,8
H(56)	0,882	0,817	0,193	3,8
H(57)	0,934	1,015	0,325	3,8
H(67)	0,786	1,017	0,206	3,8
H(59)	0,500	0,647	0,300	4,8
H(69)	0,557	0,531	0,210	4,8
H(79)	0,575	0,500	0,390	4,8
H(54)	0,600	1,147	0,560	5,5
H(64)	0,658	1,288	0,522	5,5
H(74)	0,760	1,195	0,645	5,5

facteurs de structure observés et calculés sont déposés.[2]

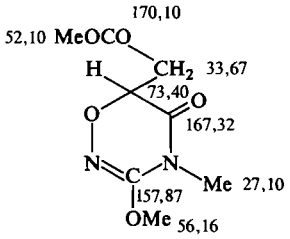

6

Les résultats de l'analyse radiocristallographique confirment, sans ambiguïté, les propositions précédentes d'une structure cyclique à 6 chaînons. Une représentation de la molécule est donnée (schéma 4), les longueurs de liaisons sont reportées; les écarts-type sont de 0,003 Å pour les liaisons entre atomes "lourds" et 0,02 Å pour les liaisons mettant en jeu un atome d'hydrogène.

L'hétérocycle n'est pas plan; les deux liaisons N(1)—C(2) et C(4)—C(5) sont sensiblement parallèles et l'hétérocycle apparaît plié autour de la direction N(1) ... C(5). Ces observations sont consignées (tableau 7) qui donne les écarts des atomes au plan moyen de l'hétérocycle d'équation $-0{,}3877x + 0{,}250y + 0{,}8870z' = 1{,}650$ (référentiel a, b, ab).

[2]On peut obtenir la série complète des données à un prix nominal, en s'adressant au Dépôt des données non publiées, ICIST, Conseil national de recherches du Canada, Ottawa, Canada K1A 0S2.

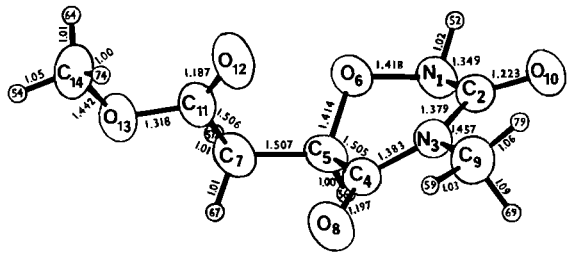

SCHÉMA 4

TABLEAU 7. Ecarts des atomes au plan moyen de l'hétérocycle

Atome	Å	Atome	Å
O(6)	0,33	C(5)	−0,29
N(1)	−0,25	C(7)	0,25
C(2)	−0,05	O(8)	−0,10
N(3)	0,17	C(9)	0,35
C(4)	−0,06	O(10)	−0,12

La structure cristalline est caractérisée par l'existence de colonnes de molécules de direction c; ces colonnes sont associées entre elles par liaisons hydrogène ainsi définies: distance N ... O = 2,82 Å; angle N—H ... O = 152,4°.

Une représentation de l'organisation structurale est donnée dans le schéma 5.

Caractérisation des carbométhoxyméthylène-5 hydantoïnes 3

La caractérisation des carbométhoxyméthylène-5 hydantoïnes **3** est réalisée par comparaison aux dérivés décrits dans la littérature. En ir, l'attribution des différentes bandes est faite en

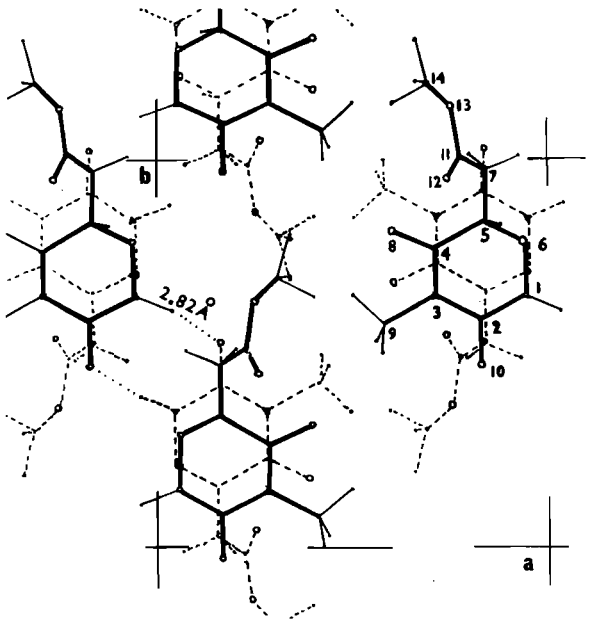

SCHÉMA 5

TABLEAU 8. Spectres ir* des carbométhoxy 3 et carbéthoxy 7 méthylènehydantoïnes

No	N(3)R	Solvant	ν_{CO} ester	ν_{CO} en 4	ν_{CO} en 2	$\nu_{C=C}$
3*a*	H	DMS	1740	1705	1770	1660
3*b*	CH_3	DMS	1730	1705	1785	1665
3*c*	ϕ	DMS	1735	1705	1785	1665
7*a*	H	Nujol	1740	1700	1775	1665
7*b*	CH_3	Nujol	1740 (1740)	1695 (1695)	1795 (1795)	1665 (1665)
7*c*	ϕ	Nujol	1730 (1725)	1695 (1690)	1780 (1775)	1670 (1665)

*Les valeurs entre parenthèses sont celles de Lemieux et Puskas (8).

TABLEAU 9. Spectres de rmn (DMS-d_6)

No	R	R′	CH	CO_2R'	N(1)—H	N(3)—R
3*a*	H	CH_3	5,48	3,72	10,67 11,55	
3*b*	CH_3	CH_3	5,58	3,71	10,95	2,95
3*c*	ϕ	CH_3	5,90	3,90	11,10	7,76 (m)
7*a*	H	C_2H_5	5,51	CH_2 4,20 CH_3 1,25	8,50	
7*b*	CH_3	C_2H_5	5,60	CH_2 4,20 CH_3 1,29	10,90	2,95
7*c*	ϕ	C_2H_5	5,68	CH_2 4,23 CH_3 1,26	11,16	7,50 (m)

accord avec les résultats de Ivin *et al.* (13) et Lemieux et Puskas (10) pour les carbéthoxy-5 hydantoïnes. Dans le but d'obtenir les mêmes composés, nous avons réalisé la transestérification de 3*b* et 3*c* conduisant à 7*b* et 7*c* dont les spectres ir sont identiques à ceux de la littérature (tableau 8); par contre, le spectre de 3*a* est différent de celui de l'orotate de méthyle (8).

De même en rmn (tableau 9), le déplacement chimique du proton éthylénique de 3*a* (5,48 ppm) est différent de celui observé pour l'orotate de méthyle (6,04 ppm) (8). Par contre, les spectres de rmn des composés 7*a* et 7*b* sont identiques à ceux des hydantoïnes (13, 14) à l'exception des déplacements chimiques de l'éthyle de la fonction ester de 7*a*; ceux-ci sont donnés à des valeurs différentes dans deux publications (13, 14) et de ce fait ne sont pas crédibles.

Conclusion

En conclusion, le caractère "hydroxylamine *N*-protégée" des hydroxyurées est confirmé par l'étude de leur action sur les maléate et fumarate de méthyle qui conduit aux uréidoxyesters correspondants. Ces derniers, bien que présentant trois types de cyclisation possibles (à 5, 6 et 7 chaînons) donnent uniquement les carbométhoxyméthyl-5 oxa-6 dihydrouraciles (cycle à 6 chaînons) dont la structure est prouvée par une analyse aux rayons X. Ces composés, relativement instables, conduisent en milieu basique aux carbométhoxyméthylène-5 hydantoïnes par une régression de cycle correspondant à la perte d'une molécule d'eau impliquant l'atome d'oxygène intracyclique.

Partie expérimentale

Les points de fusion non corrigés ont été pris en capillaire. Les analyses ont été déterminées par le laboratoire Central de Microanalyse du CNRS.

Les spectres rmn ^1H ont été réalisés au moyen d'un appareil Varian modèle T 60; les spectres rmn ^{13}C ont été réalisés par le laboratoire de Résonance Magnétique Nucléaire de l'U.S.T.L., au moyen d'un appareil JEOL PS 100 ou Bruker WP 80. Les déplacements chimiques sont exprimés en ppm par rapport au TMS pris comme référence interne.

Les spectres ir ont été enregistrés sur un appareil Perkin Elmer 457.

Analyse radiocristallographique

Les mesures de diffraction des rayons X (mesures en cinq points) ont été effectuées sur diffractiomètre automatique Siemens; 1003 réflextions indépendantes d'indices *hkl* et $\bar{h}kl$ ont été observées dans l'espace limité à $\theta < 26°$. La longueur d'onde Kα du molybdène a été utilisée ($\lambda = 0{,}71069$ Å). Les dimensions de cristal choisi pour ces mesures étant comprises entre 0.2 et 0.25 mm aucune correction d'absorption n'a été effectuée. La structure a été résolue par méthodes statistiques (programmes MULTAN). L'affinement a porté sur les paramètres de positions atomiques, d'agitation thermique anisotrope des atomes de carbone, d'azote et d'oxygène. Les atomes d'hydrogène ont été positionnés sur cartes de densité électronique. Le facteur de reliabilité final est $R = 0.058$ avec $R = (\Sigma |F_o| - |F_c|)/\Sigma |F_o|$

Une méthode de moindres carrés, utilisant l'approximation par blocs diagonaux, a été adoptée pour minimiser la fonction $w(F_o - F_c)^2$. Le facteur de pondération w a été choisi selon le schéma: $w = 1$ si $|F_o| < P$; $w = P/|F_o|$ si $F_o > P$ avec $P = |F_{max}|/3$.

Les facteurs de diffusion atomiques utilisés pour les calculs des facteurs de structure sont issus de International Tables for X-ray Crystallography Vol. IV, 1974.

Synthèse des hydroxyurées

Hydroxyurée: elle a été obtenue par action de l'hydroxylamine sur le carbamate d'éthyle suivant le mode opératoire décrit par Deghenghi (15).

β-*Méthylhydroxyurée*: préparée par action de l'hydroxylamine sur l'isocyanate de méthyle suivant le mode opératoire décrit par Kjellin (16) pour la β-phénylhydroxyurée. Ce composé avait $F = 130$–132°C. *Anal.* calc. pour $C_2H_6N_2O_2$: C 26,67, H 6,67, N 31,11; trouvé: C 26,68, H 6,58, N 31,23.

α-*Méthylhydroxyurée*: préparée par action du cyanate de potassium sur la *N*-méthylhydroxylamine suivant le mode opératoire décrit par Mathieson (17).

Action des hydroxyurées sur le maléate (ou fumarate) de méthyle

A une solution de 0,1 mol de base dans 150 cm³ de méthanol on ajoute 0,1 mol d'hydroxyurée; après solubilisation complète,

Can. J. Chem. Downloaded from www.nrcresearchpress.com by 210.87.254.5 on 09/06/12
For personal use only.

TABLEAU 10. Caractéristiques physiques et analyses des différents produits obtenues

No	F °C	Solvant de recristallisation	Formule	Analyse C% calc. C% tr.	Analyse H% calc. H% tr.	Analyse N% calc. N% tr.
1*a*	86–88	MeOH/$CHCl_3$	$C_7H_{12}N_2O_6$	38,18 37,98	5,45 5,39	12,72 12,78
1*b*	72	MeOH/$CHCl_3$	$C_8H_{14}N_2O_6$	41,02 40,80	5,98 6,04	11,96 12,08
2*a*	135–137	MeOH	$C_6H_8N_2O_5$	38,30 38,20	4,24 4,29	14,89 14,66
2*b*	66–68	$CHCl_3$	$C_7H_{10}N_2O_5$	41,58 41,55	4,95 5,03	13,86 13,83
2*d*	105	$CHCl_3$	$C_7H_{10}N_2O_5$	41,58 41,30	4,95 5.09	13,86 13,97
3*a*	245	MeOH	$C_6H_6N_2O_4$	42,35 42,27	3,53 3,50	16,47 16,32
3*b*	225	MeOH	$C_7H_8N_2O_4$	45,65 45,56	4,34 4,43	15,21 15,43
3*c*	227	MeOH	$C_{12}H_{10}N_2O_4$	58,53 58,62	4,06 4,17	11,38 11,28

une solution de 0,1 mol de maléate (ou fumarate) de méthyle dans 40 cm^3 de méthanol est ensuite ajoutée goutte à goutte. Le mélange est agité à température ambiante, puis le solvant est évaporé sous pression réduite. Le résidu, repris par un minimum d'eau, est neutralisé par une solution d'acide chlorhydrique (40%). Le précipité de carbométhoxyméthylène-5 hydantoïne est filtré; la phase aqueuse est extraite à l'acétate d'éthyle; la phase organique est séchée (Na_2SO_4) et concentrée sous vide. Le résidu est chromatographié sur un appareil Waters Prep LC 500 muni de deux colonnes de silice en série, en utilisant comme éluant un mélange hexane–chloroforme 6:4 à 7:3 suivant la nature des composés.

Les différents résultats obtenus suivant la nature de la base, le temps de réaction et les substituants sont résumés dans le tableau 1 discuté dans la partie théorique.

Les caractéristiques physiques et les analyses centésimales des différents produits obtenus sont données dans le tableau 10.

Méthylation du méthyl-3 carbométhoxyméthyl-5 oxa-6 dihydrouracile, 2b

A une solution de 5 g (0,025 mol) de 2*b* dans 100 cm^3 d'éther on ajoute à 0°C 75 cm^3 d'une solution 0,66 *M* de diazométhane (0,05 mol). La solution est agitée pendant 4 h à cette température puis ramenée à la température ambiante. Le solvant est évaporé sous pression réduite et le résidu chromatographié sur l'appareil Waters Prep LC 500, muni de deux colonnes de silice, en utilisant comme éluant un mélange hexane – acétate d'éthyle 7:3. On obtient, par ordre d'élution: (*1*) le diméthyl-1,3 carbométhoxyméthyl-5 oxa-6 dihydrouracile **2***e* (1,6 g, 30%); $Eb_{0,2}$ = 95–98°C; *Anal.* calc. pour $C_8H_{12}N_2O_5$: C 44,44, H 5,55, N 12,96; trouvé: C 44,16, H 5,32, N 13,12; et (*2*) le méthoxy-2 méthyl-2 carbométhoxyméthyl-5 oxa-4 diazine-1,3 one-6 **6** (1 g; 20%); *F* = 69–70°C (éther); ir ($CHCl_3$): 1630 et 1730 cm^{-1}; rmn ($CDCl_3$): 3,75 (s, 3H, CO_2CH_3), 3,90 (s, 3H, OCH_3), 3,16 (s, 3H, N—CH_3), CH_2—CH: système ABX: H_A 2,74, H_B 3,00, H_X 4,50, J_{AX} = 4,3 Hz, J_{BX} = 7,4 Hz, J_{AB} = 16,3 Hz. *Anal.* trouvé pour $C_8H_{12}N_2O_5$: C 44,50, H 5,60, N 12,93.

Transestérification des carboxyméthylène-5 hydantoïnes 3a–c

A 20 cm^3 d'éthanol anhydre saturé d'acide chlorhydrique gazeux on ajoute 0,01 mol de **3**; le mélange est porté à reflux pendant 10–12 h. Le solvant est ensuite évaporé sous vide et le résidu repris par l'eau est neutralisé. La carbéthoxyméthylène-5 hydantoïne **7** qui précipite est recristallisée dans l'éthanol. La réaction est pratiquement quantitative.

Les composés ont été caractérisés par comparaison aux données de la littérature: 7*a*: 190°C; litt. (18): 186–187°C; 7*b*: 144°C; litt. (10): 141°C; 7*c*: 190°C; litt. (10): 191°C.

1. J.-L. OLIVE, C. PETRUS et F. PETRUS. Bull. Soc. Chim. Fr. 1138 (1973).
2. J.-L. OLIVE, C. PETRUS et F. PETRUS. Bull. Soc. Chim. Fr. 1589 (1976).
3. R. JACQUIER, J.-L. OLIVE, C. PETRUS et F. PETRUS. Tetrahedron Lett. 2337 (1975).
4. R. JACQUIER, J. OLIVE, C. PETRUS et F. PETRUS. Tetrahedron Lett. 2979 (1975).
5. C. BENNOUNA, F. PETRUS et J. VERDUCCI. J. Heterocycl. Chem. **16**, 161 (1979).
6. H. VAN DER PLAS. Ring transformation of heterocycles. Vol. 2. Academic Press, London et New York. 1973. p. 183.
7. K. CHKHIVADZE, N. BRITIKOVA et O. MAGIDSON. Zhur. Obshchei. Khim. **34**, 161, (1964).
8. R. YIP et W. RIDDELL. Can. J. Chem. **48**, 987 (1970).
9. M. SUMI et K. KAZAMA. Chem. Abstr. **58**, 7956e (1963).
10. R. LEMIEUX et I. PUSKAS. Can. J. Chem. **42**, 2909 (1964).
11. B. IVIN, G. RUTKOVSKII, T. RUSAVSKAYA, N. SMORIGO et E. SOCHILIN. Khim. Geterotsikl. Soedin. 1527 (1974).
12. B. IVIN, G. RUTKOVSKII, A. D'YACHKOV et E. SOCHILIN. Zh. Org. Khim. **12**, 1836 (1976).
13. B. IVIN, G. RUTKOVSKII, N. SMORIGO et E. SOCHILIN. Zh. Org. Khim. **6**, 2601 (1970).
14. G. RUTKOVSKII, B. IVIN, E. SOCHILIN et I. TSERETELI. Zh. Obshch. Khim. **40**, 389 (1970).
15. R. DEGHENGHI. Org. Synth. **40**, 60 (1960).
16. C. KJELLIN. Ber. **26**, 2377 (1893).
17. O. MATHIESON. Chem. Abstr. **60**, 2789h (1964).
18. V. GUNAR, L. OVECHKINA, I. MIKHAILOPULO et S. ZOV'YALOV. Chem. Abstr. **70**, 376 (1969).

Can. J. Chem. Downloaded from www.nrcresearchpress.com by 210.87.254.5 on 09/06/12
For personal use only.

Phosphine–borane derivatives. 10[1]. Vibrational spectra of the dimethylphosphine adducts of boron trihalides

JOHN E. DRAKE, J. LAWRENCE HENCHER, AND LAYLA N. KHASROU
Department of Chemistry, University of Windsor, Windsor, Ont., Canada N9B 3P4

Received February 25, 1981

JOHN E. DRAKE, J. LAWRENCE HENCHER, and LAYLA N. KHASROU. Can. J. Chem. **59**, 2898 (1981).

The infrared (200–4000 cm^{-1}) and Raman (0–3100 cm^{-1}) spectra of $(CH_3)_2PHBX_3$, $(CH_3)_2PDBX_3$, and $(CD_3)_2PHBX_3$, where X = Cl, Br, I, have been recorded in solid state and in solutions at room temperature. The fundamentals have been assigned on the basis of C_s molecular symmetry. A modified Urey–Bradley force field model has been used in calculating the frequencies and potential energy distributions as well as the force constants. The (P—B) force constant was found to be consistent with the structural change upon adduct formation.

JOHN E. DRAKE, J. LAWRENCE HENCHER et LAYLA N. KHASROU. Can. J. Chem. **59**, 2898 (1981).

On a enregistré les spectres infrarouges (200–4000 cm^{-1}) et Raman (0–3100 cm^{-1}) des composés suivants: $(CH_3)_2PHBX_3$, $(CH_3)_2PDBX_3$ et $(CD_3)_2$ $PHBX_3$ ou X = Cl, Br, I à l'état solide et en solution à la température ambiante. On a identifié les vibrations fondamentales à partir de la symétrie moléculaire C_s. On a utilisé un modèle de champ de force de Urey–Bradley modifié pour calculer les fréquences, les distributions de l'énergie potentielle ainsi que les constantes de force. On a trouvé que la constante de la force (P—B) est en accord avec les changements de structure résultant de la formation d'un adduit.

[Traduit par le journal]

Introduction

In recent years, several vibrational spectroscopic investigations on phosphorus donor molecules $(CH_3)_nPH_{3-n}$ $n = 0$–3 with the boron acceptor BH_3 have appeared in the literature (1–4). These studies reflect the interest in understanding the nature of the coordinate link between phosphorus and boron in adducts. Vibrational analyses have been reported on the PH_3BX_3 (5) where X = Cl, Br, I, and on the $(CH_3)_3PBX_3$ (6) series, but none as yet involving partially methylated phosphines. We report on the vibrational analysis of the series $(CH_3)_2PHBX_3$ and the specifically deuterated analogues $(CH_3)_2PDBX_3$ and $(CD_3)_2PHBX_3$.

Experimental

The preparation of dimethylphosphine $(CH_3)_2PH$ was by modification (7) of the procedure described by Jolly (8). The purity was checked by its ir (9) and ^1H nmr spectra (10, 11). Dimethylphosphine-d_1, $(CH_3)_2PD$, was prepared in >98 mole% by exchange between $(CH_3)_2PH$ and KOD in D_2O and its purity also checked by its ir (12) and ^1H nmr spectra (11). The procedure was similar to that used for the preparation of $(CH_3)_2AsD$ (13). The boron trihalides were checked for purity as previously reported (5). The preparation of all adducts $(CH_3)_2PHBX_3$, $(CH_3)_2PDBX_3$, $(CD_3)_2PHBX_3$ (X = Cl, Br, I) was by the direct combination of reactants at room temperature. The reactions were carried out on a conventional Pyrex–glass vacuum system, using the same method and equipment used in the formation of H_3PBX_3 and $(CH_3)_3PBX_3$ adducts (5, 6). Raman spectra were recorded on solid samples in thin-walled glass tubes on a Spectra-Physics Model 700 spectrometer in conjunction with a Model 164 Argon-ion laser and Model 265 Exciter Unit. Typical power output was varied between 100 and 300 mW, using the 488.0 nm line. Polarization data were secured by use of MeI and CH_2Cl_2 solutions of the adducts. These solvents are far from ideal but were the only ones that gave significant, though low, solubility for solution spectra. The low solubility of the adducts required high instrument gain and laser output between 300 and 700 mW. Infrared spectra were recorded on a Beckman IR-12 spectrometer using CsI pellets. Far ir spectra were recorded, as Nujol mulls between polyethylene plates, on a Perkin–Elmer 180 spectrometer operating in conjunction with an Interdata model 6/16 computer.

Normal coordinate analysis was carried out using a computer program (Larmol) (14) in which the normal coordinates are expressed as mass-weighted Cartesian coordinates. The Cartesian coordinates were calculated with the aid of Euclidean construction devised by Hilderbrandt (15), from the following geometric parameters: bond lengths (in Å = 100 pm) C—H (1.093), P—H (1.410), P—B (1.901), P—C (1.819), B—Cl (1.840), B—Br (2.020), B—I (2.265), and bond angles (in degrees) XBP (109.5), HCP (109.5), CPC (105.4), HPC (103.6), and HPB (111.5). These parameters were obtained from structural studies on related molecules, $(CH_3)PH_2BH_3$, $(CH_3)_3PBH_3$ (16), $(CH_3)_3P$ (17), $(CH_3)_2PHBH_3$ (18), and PH_3BX_3 (9, 19).

Results and Discussion

Raman spectra of solid $(CH_3)_2PHBCl_3$ (Fig. 1), $(CH_3)_2PDBCl_3$ and $(CD_3)_2PHBCl_3$ (Fig. 2), and their infrared spectra between 1100 and 200 cm^{-1} (Fig. 3) are displayed as representative samples. The approximate description, with point group classification and symmetry species, of the fundamental vibrations are given in Table 1. The assignments of the fundamental vibrations are given for $(CH_3)_2PHBCl_3$, $(CH_3)_2PDBCl_3$, and $(CD_3)_2PHBCl_3$ (Table 2), $(CH_3)_2PHBBr_3$, $(CH_3)_2PDBBr_3$ and $(CD_3)_2PHBBr_3$ (Table 3), and $(CH_3)_2PHBI_3$, $(CH_3)_2PDBI_3$ and $(CD_3)_2PHBI_3$ (Table 4). The force constant numbering and evaluation is in Table 5 and the potential energy distributions in Tables 6, 7, and 8

[1]For Part 9, see ref. 6.

0008-4042/81/192898-11$01.00/0
©1981 National Research Council of Canada/Conseil national de recherches du Canada

Can. J. Chem. Downloaded from www.nrcresearchpress.com by 210.87.254.6 on 09/06/12
For personal use only.

Can. J. Chem. Downloaded from www.nrcresearchpress.com by 210.87.254.6 on 09/06/12
For personal use only.

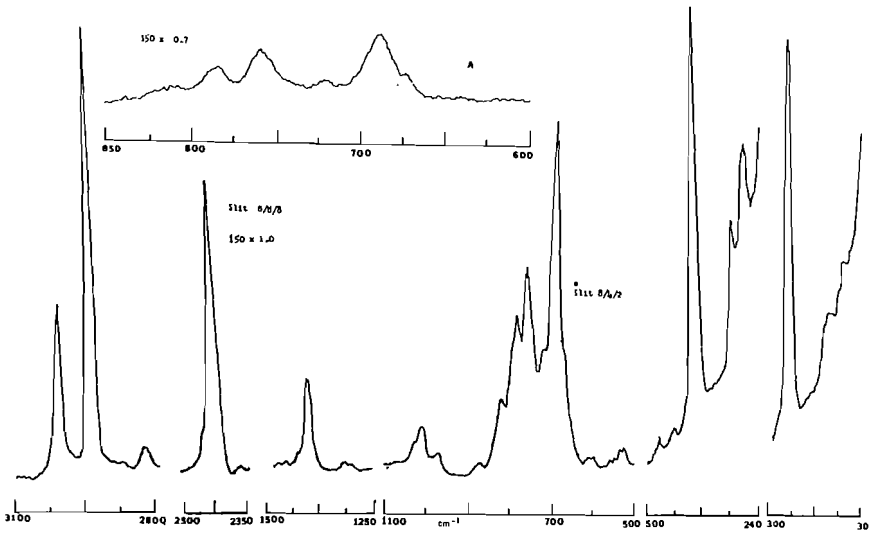

FIG. 1. The Raman spectrum of solid $(CH_3)_2PHBCl_3$.

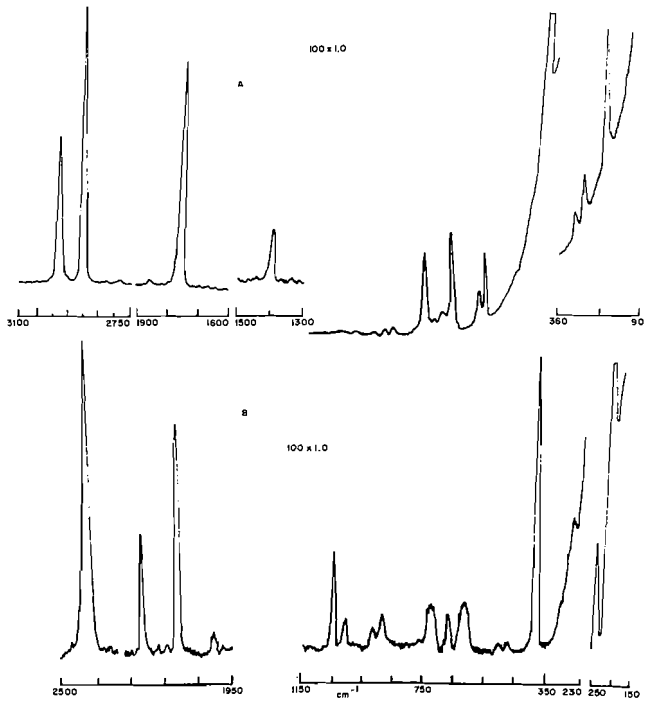

FIG. 2. The Raman spectrum of *A*, solid $(CH_3)_2PDBCl_3$, *B*, solid $(CD_3)_2PHBCl_3$.

for the chloride, bromide, and iodide series, respectively.

The adducts are assumed to have C_s symmetry so that the thirty-six vibrations are divided into twenty *a'* and sixteen *a"*, all being active in both effects. In general, there is good agreement between the solid and solution Raman and infrared data indicating that the influence of torsional and/or translational lattice modes in the solid state is minimal. One obvious feature in the spectra is the unaltered position of the BX_3 symmetric stretch on deuteration. This indicates that appreciable cou-

Can. J. Chem. Downloaded from www.nrcresearchpress.com by 210.87.254.6 on 09/06/12
For personal use only.

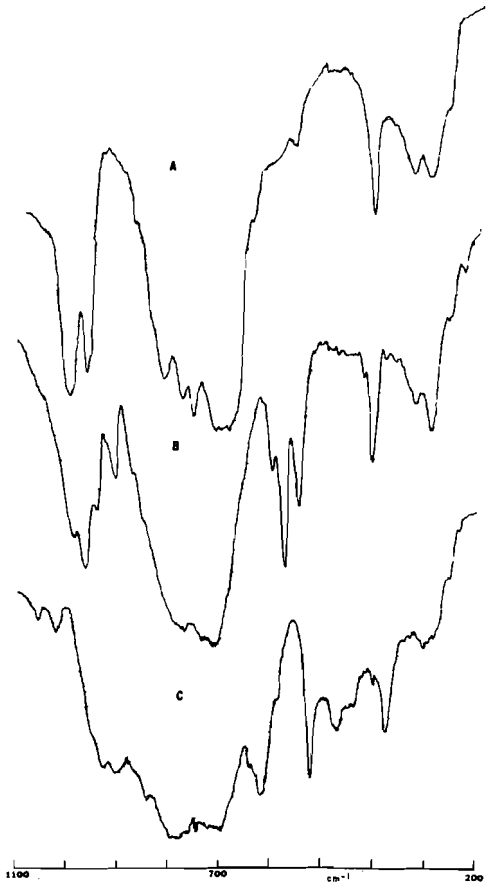

FIG. 3. Selected region of the infrared spectrum (CsI pellet) of *A*, $(CH_3)_2PHBCl_3$; *B*, $(CH_3)_2PDBCl_3$; and *C*, $(CD_3)_2PHBCl_3$.

TABLE 1. Approximate description, with point group classification and symmetry species of the fundamental vibrations of $(CH_3)_2PHBX_3$, X = Cl, Br, I

Species		
a'	*a"*	Description
ν_1, ν_2	ν_{21}, ν_{22}	CH_3 stretch (asym)
ν_3	ν_{23}	CH_3 stretch (sym)
ν_4		PH stretch
ν_5, ν_6	ν_{24}, ν_{25}	CH_3 def. (asym)
ν_7	ν_{26}	CH_3 def. (sym)
ν_8, ν_9	ν_{27}, ν_{28}	CH_3 rock
ν_{10}		P—B stretch
ν_{11}	ν_{29}	PC_2 stretch
ν_{12}	ν_{30}	BX_3 stretch (asym)
ν_{13}		BX_3 stretch (sym)
ν_{14}	ν_{31}	PH def.
ν_{15}		PC_2 def.
ν_{16}	ν_{32}	CPB bend
ν_{17}	ν_{33}	BX_3 def. (asym)
ν_{18}		BX_3 def. (sym)
ν_{19}	ν_{34}	BX_3 rock
ν_{20}	ν_{35}, ν_{36}	Torsions

pling of donor and acceptor group vibrational modes is not dominant and, as with previous studies, the vibrations can be treated as essentially group frequencies.

The previous vibrational assignments of $(CH_3)_2PH$, $(CH_3)_2PD$, $(CD_3)_2PH$, (9, 12, 20), H_3PBX_3 (5), $(CH_3)_3PBX_3$ (6), $(CH_3)H_2PBH_3$ (1), and $(CH_3)_2PHBH_3$ (2), provided the background to the assignments of these dimethylphosphine adducts. Thus in the spectra of $(CH_3)_2PHBCl_3$ and $(CH_3)_2PDBCl_3$ the two features that correspond to the asymmetric CH_3-stretching modes (ν_1, ν_2, ν_{21}, ν_{22}) at ca. 3000 cm^{-1} and the symmetric CH_3-stretches (ν_3, ν_{23}) at ca. 2924 cm^{-1} and clearly polarised in the Raman effect, can be described as typical (Figs. 1, 2 and Table 2). The same can be said for $(CH_3)_2PHBr_3$, $(CH_3)_2PDBBr_3$, $(CH_3)_2PHBI_3$, and $(CH_3)_2PDBI_3$ (Tables 3, 4). The expected shifts to lower wave-numbers for the $(CD_3)_2PHBX_3$ species are also clearly seen (e.g. in Fig. 2). The asymmetric and symmetric methyl deformation modes appear for all of the d_0 and d_1 adducts at around 1400 and 1300 cm^{-1} respectively with the shift to 1060 and 1025 cm^{-1} for the d_6 adducts. In the past, some uncertainty existed in the assignments of the CH_3 rocks and PH deformations in free dimethylphosphine (9, 20). Recently, the vibrational assignments of $(CH_3)_2PH$ has been reassessed (12) and the CH_3 rocking modes placed between 1003 and 801 cm^{-1} (well above the PH deformations). We have recently received a pre-print of a paper in which it is proposed that the CH_3-rocks be placed between 947 and 991 cm^{-1} (21). The CH_3-rocks were also assigned in $(CH_3)_2AsH$ and $(CH_3)_2AsD$ (22) in the region 933–862 cm^{-1}, with the corresponding CD_3-modes between 672 and 496 cm^{-1}. Thus the assignment of the CH_3-rocks, ν_8, ν_9, ν_{27}, ν_{28}, in the $(CH_3)_2PHBX_3$ and $(CH_3)_2PDBX_3$ adducts to the features immediately below 1000 cm^{-1} is reasonable, as is the assignment of the CD_3-rocks in $(CD_3)_2PHBX_3$ to the region 770–550 cm^{-1}.

The PH stretching frequencies are unambiguously assigned to the sharp band, clearly polarised in the Raman effect, at ca. 2400 cm^{-1} in all $(CH_3)_2PHBX_3$ and $(CD_3)_2PHBX_3$ species and at ca. 1750 cm^{-1} in $(CH_3)_2PDBX_3$ compounds. This is at considerably higher wave-numbers than in the corresponding free dimethylphosphine (12, 21).

The two P—H asymmetric and symmetric deformation modes have been assigned in free $(CH_3)_2PH$ at 729 and 714 cm^{-1} respectively and in $(CH_3)_2PD$ at 590 and 561 cm^{-1}, which at least conforms with the polarisation data (12). Recently an alternate assignment has been proposed, placing these modes at 1012 and 729 cm^{-1} for $(CH_3)_2PH$ and 709 and

Table 2. Observed IR and Raman frequencies of solid dimethylphosphine-boron trichloride $(CH_3)_2PHBCl_3$, with Raman polarisation taken from CH_3I and CH_2Cl_2 solutions

Assignment	$(CH_3)_2PHBCl_3$ IR (Solid)[d]	$(CH_3)_2PHBCl_3$ Raman (Solid)	$(CH_3)_2PHBCl_3$ Raman (Soln.)[a]	$(CH_3)_2PDBCl_3$ IR (Solid)[d]	$(CH_3)_2PDBCl_3$ Raman (Solid)	$(CH_3)_2PDBCl_3$ Raman (Soln.)[a]	$(CD_3)_2PHBCl_3$ IR (Solid)[d]	$(CD_3)_2PHBCl_3$ Raman (Solid)	$(CD_3)_2PHBCl_3$ Raman (Soln.)[a]
$\nu_1, \nu_2, \nu_{21}, \nu_{22}$	3000 m	3002 m	solvent	2999 w	2999 m	solvent	2250 w	2253 m	2242 m, dp
ν_3, ν_{23}	2924 m	2925 s	2924[b] s, p	2920 w	2923 s	2920 m, p	2130 w	2137 m	2139 s, p
$2\nu_5, 2\nu_7, 2\nu_{25}$	2865} w 2806}	2840 w	2840[b] mw, p	2810 vw	2842 w	2840} w, p 2819}	2091 w	2086} vw 2059}	---
PH impurity	---	---	---	2420 w	2419 vw	---	---	---	---
ν_4	2415 mw	2422 vs	2426 m,p	1760 mw	1757 s	1755 m, p	2430 w	2435 vs	2439 mw, p
$(\nu_5 + \nu_{29})$	2230 w	---	2245[b] vw	2250 w, sh	---	2245[b] vw	---	---	---
$2\nu_8, (\nu_9 + \nu_{26})$	2040 w	2010 vw	---	---	1840 w	---	1872	1790	---
$2\nu_9, (\nu_9 + \nu_8)$	---	1765 w	---	---	---	---	960 w	944 vw	960 w
$\nu_5, \nu_6, \nu_{24}, \nu_{25}$	1450} m 1417}	1442	solvent	1450} m, br 1412}	1407 m	solvent	1050 sh	1063 m, br	1061 m, dp
ν_7, ν_{26}	1313}[c] 1298}	1310 w	1290 w, p	1312 m 1298 sh	1394 1308	---	1035 mw	1023 mw	1020 m, p
impurity	1070[c] vw	1063 vw, sh	1060 w, p	---	---	1037 w, p	---	---	---
$\nu_8, \nu_9, \nu_{27}, \nu_{28}$	1005 vw 971 vs 877 w, sh	1007 w 965 w 865 w	998 w, p 970 w solvent	1000 sh 965} m 950}	990 w --- 941 w	970 w --- 950 w	770 vw 750 w 642 m, br	762 vw, sh 750 w, sh 645} br 630}	750 w, sh,dp 645 m, p 632 w, ?
ν_{31}, ν_{14}	850 vw 820	810 w, sh	solvent	615 vw, sh 594 mw 574 m	581 mw 570 m	581[b] mw, dp 570[b] m, p	928* mw 901 m	920* mw, sh 901 m	solvent
ν_{10} (^{10}B)	780 mw	786 mw	---	785 mw	780 w, sh	---	---	---	---
ν_{10} (^{11}B)	765 s	760 s	765[b] mw, p	775 m, br	775 ms	775[b] mw, p	735 w	743} m 731}	740[a] m, p
ν_{29}	735 vs	740 w	740[b] w, dp	770 m, br	741 mw	730 w, dp	720 sh	719 mw, sh	725[b] w, dp
ν_{30}, ν_{12}	720} s 710} w, sh	720 w 712 w	719[b] m, dp 710 vw, sh	725 m, br	715 w	710 w, ?	712 mw	710 w	712 sh, dp
ν_{11}	698 s	696 vs	697 m, p	680 ms	683 ms	682 mw, p	681 mw	678 m	680 m, p
(see text)	670 mw	674 sh	---	---	---	---	---	---	---
$2\nu_{15}$	550 w 520 w	552 w	412 vw	540 w	---	---	552} 530} w 490}	---	---
ν_{13}	400 m	399 vs	399 s, p	391 s	391 vs	393 m, p	392 vs	392 vs	393 s, p
$(\nu_{17} + \nu_{19})$	365 w	365 w	356 w, dp	360 vw	---	350 vw	---	---	---
ν_{15}	277 m	277 m, sh	282 m, p	---	271 m	276 m, p	276 w	277 w	280 mw, p
ν_{17}, ν_{33}	265} sh 240} w, sh	260} m 242} m	--- 243 m, dp	260 w 235 w	250 w 222 sh	--- 234 s, dp	--- 235 mw	265 w 239 s	256 w, dp 239 m, dp
ν_{16}, ν_{32}	--- ---	203 s, br 180 sl	191 mw, dp ---	--- ---	200 vs ---	195 s, dp ---	--- ---	199 vs 170 sh	198 m, dp 178 mw
ν_{18}	---	171 vw	178 mw, p	---	166 w	165 w, p	---	---	158 sh, p
ν_{19}, ν_{34}	---	136 mw	140 vw, dp	---	135 w	---	---	147 w	136 w, dp
Lattice mode	--- ---	106 90	--- ---	--- ---	120 sh ---	--- ---	--- ---	--- ---	--- ---

[a]Spectrum in CH_3I, [b]In CH_2Cl_2, [c]Nujol mull, [d]CsI pellet, *PH_2 bending impurity

556 cm^{-1} for $(CH_3)_2PD$ (21). In these $(CH_3)_2PDBX_3$ adducts, two peaks at ca. 590 (depolarised) and 561 cm^{-1} (polarised) are assigned to the asymmetric, ν_{31}, and symmetric, ν_{14}, P—H deformation modes. These two features are clearly fundamentals and cannot be sensibly assigned to any other modes. The calculations that agree with these assignments suggest that the P—H deformations should be above the 730 cm^{-1} region but below the 1000 cm^{-1} region and they are assigned accordingly. It is notable that in any case, both ν_{31} and ν_{14} apparently appear at considerably different positions in the adducts $(CH_3)_2PHBX_3$ and $(CD_3)_2PHBX_3$ relative to the free phosphine, whereas they are virtually unchanged when $(CH_3)_2PDBX_3$ spectra are compared with $(CH_3)_2PD$. This could be associated with the fact that the P—D deformations are "purer" modes and so show less change on adduct formation than does the P—H deformation. This is indicated in the normal coordinate analysis where force constant values for $f(CPH^2)$, $f(HPB^2)$, $f(HCP)^2$ that correspond well to literature values for related systems (5, 6) produce good agreement between the observed and calculated P—D deformations. These same values predict that the corresponding P—H deformations will be in the region of 800–900 cm^{-1} in $(CH_3)_2PHBX_3$ and $(CD_3)_2PHBX_3$ rather than either the 720 or 1000 cm^{-1} regions.

The PC_2 asymmetric and symmetric stretching

Can. J. Chem. Downloaded from www.nrcresearchpress.com by 210.87.254.6 on 09/06/12
For personal use only.

Table 3. Observed IR and Raman frequencies* of solid dimethylphosphine-borontribromide $(CH_3)_2PHBBr_3$, with Raman polarisation data taken from CH_3I and CH_2Cl_2 solutions

Assignment	$(CH_3)_2PHBBr_3$ IR(solid)[d]	$(CH_3)_2PHBBr_3$ Raman(solid)	$(CH_3)_2PHBBr_3$ Raman (soln)[a]	$(CH_3)_2PDBBr_3$ IR(solid)[d]	$(CH_3)_2PDBBr_3$ Raman(solid)	$(CH_3)_2PDBBr_3$ Raman(soln)[a]	$(CD_3)_2PHBBr_3$ IR(solid)[d]	$(CD_3)_2PHBBr_3$ Raman(solid)	$(CD_3)_2PHBBr_3$ Raman(soln)[a]
$\nu_1,\nu_2,\nu_{21},\nu_{22}$	2997 mw	2997 m	solvent	2995 m	2999 ms	solvent	2242	2239 m	2240 m, dp
ν_3,ν_{23}	2912 m	2915 s	2920 s, p	2910 m	2916 vs	2914 m, p	2122	2123 ms	2120 s, p
$2\nu_5,2\nu_{25}$	2802 w	2800 w	---	2804	2804	2800 w, p	2060 vw 2009 vw	2065 vw 2001 w 1978 vw	---
ν_4	2410 w	2409 vs	2402 m, p	1750 w	1752 m, p	1752 m, p	2400 w	2405 vs	2400 m, p
$(\nu_6 + \nu_{29})$	2153 w 2041 vw	2150 vw 2041 vw	solvent	2022 vw	2039 vw 1810 vw	---	1790 vw	1828 vw	---
$(\nu_9 + \nu_{26}),\ 2\nu_8$	1806	1811 w	---	---	---	---	1700 vw	1729 vw	---
$\nu_5,\nu_6,\nu_{24},\nu_{25}$	1400 mw	1439 w 1397 1377 } mw	solvent	1402 m	1404 mw	solvent	1052 m	1057 m	1050 m, dp
ν_7,ν_{26}	1309 1275 w	1310 1278 mw	1270 w, p	1300 mw	1300 w, sh 1278 w	solvent	1015 mw	1018 mw	1018 m, p
$\nu_8,\nu_9,$ } ν_{27},ν_{28}}	999 m 960 ms	998 m 960 w	998 w, p 956 w	978 w 870 m	970 mw 950 w, sh 873 mw, br	970 w, p 877 w, dp	760 m	752 sh 648 w 590 m	solvent
ν_{31},ν_{14}	820 mw	840 ms 810 sh	solvent	590 sh 552 m	607 mw 554 mw	582 w, dp 550 mw, p	925* m 901 mw 815 mw	917* w, sh 900 mw 818 mw	920* w, p 900 w, ?
$\nu_{10}(^{10}B)$	770 w, sh	775 w	solvent	775 m	775 ms	---	769 w,sh	---	---
$\nu_{10}(^{11}B)$	765 s	768 s	760 w, p	770 m	775 ms	765 m, p	745 m	743 s	740 m, p
ν_{29}	730} ms 710} sh	735} w 715} w	735} w, dp 710} vw	729 mw	730 w	720 mw, dp	725 m	723} w 712} sh	725 w, dp
ν_{11}	690 m	694 vs	692 m, p	685 m	680 ms, br	682 m, p	690 m	695 s	690 m, p
ν_{30},ν_{12}	620 ms	625} sh 614} m	solvent	635 ms	640} 617} m	solvent	625 m	613 m	solvent
$(\nu_{19} + \nu_{15})$ $(\nu_{19} + \nu_{13})$	536 351	530} 505} w 385}	---	350	492	solvent	---	469} 394} w	solvent
ν_{13}	278 m	278 s	276 s, p	275 m	276 ms	276 s, p	276 m	276 vs	275 s, p
ν_{15}	252 w	245 m	240 m, p	241 w	242 sh	240 w, p?	240 w	242 m, sh	240 mp
ν_{16},ν_{32}	230 2	230 m 215 sh	225 m, p 190	---	221} 210} m	215 ms, p	---	213} 186} m	220 m, p
ν_{17},ν_{33}	---	178 w	---	---	160 mw	---	---	160 mw	160 w, p
ν_{18}	---	144 w	---	---	141 w, dp 130 sh	---	---	145 w 127 sh	---
ν_{19},ν_{34}	---	102 sh	---	---	95 sh	---	---	100 sh	---

*See footnote to Table 2

modes, ν_{29} and ν_{11}, were assigned at ca. 704 and 660 cm^{-1} respectively in $(CH_3)_2PH$ with the former hardly shifting at all in $(CH_3)_2PD$ but the latter moving very slightly to higher wave-numbers. There are features in all the spectra of the adducts that correspond to these modes slightly shifted to higher wave-numbers. Thus, for example, there is a strong, polarised band at 696, 683, and 682 cm^{-1} in the Raman spectra of $(CH_3)_2PHBCl_3$, $(CH_3)_2PDBCl_3$, and $(CD_3)_2PHBCl_3$, respectively, corresponding to the symmetric PC_2 stretch, ν_{11}, and a medium-strong band in the infrared spectrum at 740, 741, and 743 cm^{-1}, corresponding to the asymmetric PC_2 stretch.

The only mode remaining to be assigned in the region above 700 cm^{-1} is the P—B stretch, ν_{10}. This is usually observed as a pair of lines, with the lower frequency, more intense line assigned to the stretch attributed to the ^{11}B isotope and the weak shoulder at higher frequency attributed to the ^{10}B—P stretch. In the spectra of the adducts, these pairs of frequencies are observed at 780, 765; 785, 775; 750, 743 cm^{-1} in d_0, d_1, d_6 $(CH_3)_2PHBCl_3$; 775, 765; 775, 770; 762, 742 cm^{-1} in d_0, d_1, d_6 $(CH_3)_2PHBBr_3$ and 790 (?), 756; 775, 759; n.o., 723 cm^{-1} in d_0, d_1, d_6 $(CH_3)_2PHBI_3$. Thus in the PD-containing compound the principal ^{11}B—P stretch is shifted to slightly higher wave-numbers (3–10 cm^{-1}) whereas in the $(CD_3)_2PH$-containing series it is shifted by over 20 cm^{-1} to lower wave-numbers. Such features have been noted for related compounds (3, 5, 6).

The assignment of the BX_3 symmetric stretch is straightforward in the spectra of all adducts; showing up as an intense and strongly polarised band. The position is not affected by deuteration and it is consistently lower than the corresponding free boron trihalides (23, 24). Relative to other phosphine adducts with BX_3, such as PH_3BX_3 (5) and

Can. J. Chem. Downloaded from www.nrcresearchpress.com by 210.87.254.6 on 09/06/12
For personal use only.

Table 4. Observed IR and Raman frequencies* of solid dimethylphosphine-borontriiodide, with Raman polarisation data taken from CH_3I and CH_2Cl_2 solutions

Assignment	$(CH_3)_2PHBI_3$ IR (solid)	$(CH_3)_2PHBI_3$ Raman (solid)	$(CH_3)_2PHBI_3$ Raman (soln)	$(CH_3)_2PDBI_3$ IR (solid)	$(CH_3)_2PDBI_3$ Raman (solid)	$(CH_3)_2PDBI_3$ Raman (soln)	$(CD_3)_2PHBI_3$ IR (solid)	$(CD_3)_2PHBI_3$ Raman (solid)	$(CD_3)_2PHBI_3$ Raman (soln)
$\nu_1,\nu_2,\nu_{21},\nu_{22}$	2995	2996 m	solvent	2996 m	2996 m	solvent	2239 mw	2247 m	2250 w, dp
ν_3,ν_{23}	2920 w	2925 s 2905 w, sh	2918 m, p	2920 s	2922 s	2920 w, p	2125 vw	2129 s	2137 m, p
$2\nu_5,2\nu_{25}$	2865	2780 vw	2870 vs, p	2870 w 2770 vw	2865 w 2775	---	2062 vs	2050 2013 w	---
PH_2 impurity	2400 w, sh	2410 vw	---	---	---	---	2406 vw	2401 vw	---
ν_4	2385 m, br	2390 vs	2400 mw, p	1740 w	1738 ms, br	1745 m, p	2397 mw	2398 vs	2390 m, p
$(\nu_6+\nu_{29})$ $(\nu_9+\nu_{26})2\nu_8$	1820 w	2260 w 2220 w 1815 w	---	---	2250 w	2265 w 2220 vw	---	---	---
$\nu_5,\nu_6,\nu_{24},\nu_{25}$	1409	1480 w, sh 1406 m	solvent	1410 mw	1410 m	solvent	1051 mw 1048 sh	1081 ms 1041 sh	1050 mw, dp
ν_7,ν_{26}	1310 1296	1310 vw 1298 mw	1309 w, p	1306 mw 1298 mw	1308 mw, sh 1295 mw	solvent	1015 ms	1019 ms	1020, mw, p
$\nu_8,\nu_9,$ ν_{27},ν_{28}	982 ms 950 s --- ---	984 m 950 w --- ---	990 m, p 952 w, dp --- ---	986 w, sh 940 m --- ---	982 m 942 w --- ---	990 m, p 940 w, dp --- ---	742 w 700 mw --- ---	740 w 710 mw 630 w 550 sh	solvent 700 w, dp solvent 540 m, dp
ν_{31},ν_{14}	820 mw	818 808 w	solvent	575 mw	590 w, sh 578 m	590 sh 572 s, p	930* 905 m 790 w	929* m, sh 909 m 800 w, sh	solvent
$\nu_{10}(^{10}B)$	790 w, sh	790 vw	---	770 vw	775 w	---	---	---	---
$\nu_{10}(^{11}B)$	756 s	758 m	760 mw, p	765 m	759 m	760 mw, p	---	723 ms	725 m, p
ν_{29}	732 702 s	748 w, sh	740 w, dp 712 w	738 s	---	740 w, dp 720 vw	735 m 665 w	620 w	---
ν_{11}	687 m	689 sh 682 m	680 m	689 m	689 m	690 m, p	680 m	680 ms	682 w, p
ν_{12},ν_{30}	570 w, sh 540 s	573 sh 545 ms	570 w, sh	542 ms	547 s	540 ms	530 s	539 s	530 sh, dp
PH_2 rock impurity	460 vw	468 vw	solvent	---	468 vw	---	460 vw	450 vw	solvent
ν_{15}	250	254 ms	254 m, p	251 sh	250 sh	252 sh	240 w	298 vw 245 m	243 m, p
$(\nu_{19}+\nu_{18})$	220 w	225 w, sh	---	225 w	220 w	---	---	210 w, sh	---
ν_{13}	207 w	200 vs	202 s, p	205 w	205 s	202 s, p	---	201 vs	200 m, p
ν_{32},ν_{16}	---	182 w	---	---	178 w	170 w, dp?	---	168 m	159 w, dp
ν_{17},ν_{33}	---	130 ms	131 sh	---	---	122 m	---	134 m	135 m, dp
ν_{18}	---	112 mw	112 w, dp	---	110 mw	---	---	117 w, sh	---
ν_{19},ν_{34}	---	104 mw 95 mw	105 vw 97 sh	---	100 mw	---	---	86 mw	---

*See footnote to Table 2

$(CH_3)_3PBX_3$ (6), the position of the symmetric BCl_3 stretch, ν_{13}, at ca. 399, 391, and 392 cm^{-1} in $(CH_3)_2PHBCl_3$ (d_0, d_1, d_6) virtually remains unchanged throughout the series $H_n(CH_3)_{3-n}PBX_3$. However, its location is somewhat lower by ca. 30–40 cm^{-1} in comparison with the H_3PBX_3 and $(CH_3)_3PBX_3$ adducts, where X = Br and I.

The BX_3 asymmetric vibrations, ν_{30}, ν_{12}, are assigned in the $(CH_3)_2PHBI_3$ adducts to the broad band in the infrared spectra, with a corresponding apparently depolarised band in the Raman, at ca. 540 cm^{-1} for all species. The breadth of this band is probably related to a slight loss of degeneracy. In the bromide this loss of degeneracy is sufficient for the peak to be split (centered around 616 cm^{-1}) and this appears to be a general feature of related BBr_3 adducts (25). Unfortunately, solvent peaks obscure this region of the spectrum so that polarisation data are not available. The BCl_3 asymmetric stretch, as with related BCl_3 adducts, appears in a crowded region of the spectrum, but it shows up as a strong band in the infrared spectrum at 720 cm^{-1} in $(CH_3)_2PHBCl_3$.

In the skeletal region, the PC_2 deformation, ν_{15}, is assigned to a medium-strong, polarised band at ca. 276 cm^{-1} in all $(CH_3)_2PHBCl_3$ analogues, while the corresponding PC_2 rocking modes, ν_{16} and ν_{32}, are assigned at 203, 180; 200, 195; 199, 178 cm^{-1} in the d_0, d_1, and d_6 $(CH_3)_2PHBCl_3$ compounds respectively. The PC_2 deformation mode is seen at slightly lower wave-numbers (ca. 25 cm^{-1}) for all of the bromide and iodide adducts. By contrast, the rocking modes are seen at progressively lower wave-numbers in the bromides and iodides as is expected since the rocking modes involve more motions of the B—X bonds. The order of the BX_3

Can. J. Chem. Downloaded from www.nrcresearchpress.com by 210.87.254.6 on 09/06/12
For personal use only.

Can. J. Chem. Downloaded from www.nrcresearchpress.com by 210.87.254.6 on 09/06/12
For personal use only.

TABLE 5. Modified Urey–Bradley force fields for $(CH_3)_2PHBX_3$* and the force constant values for uncoordinated $(CH_3)_2PH$

	Force constant	Value			
		$(CH_3)_2PHBX_3$[a]			
		X = Cl	X = Br	X = I	$(CH_3)_2PH$[a]
1	fCH[2][b]	4.800(2)	4.792(4)	4.789(1)	4.766(5)
2	fPH[2]	3.345(4)	3.336(2)	3.325(9)	2.890(3)
3	fHCH[2]	0.423(2)	0.420(4)	0.420(2)	0.460(2)
4	fHCP[2]	0.588(4)	0.571(1)	0.567(2)	0.559(1)
5	fCP[2]	3.225(4)	3.232(9)	3.247(7)	2.785(2)
6	fCPH[2]	0.538(6)	0.538(6)	0.540(4)	0.589(9)
7	fCPC[2]	0.810(2)	0.801(6)	0.801(6)	0.926(4)
8	fHPB[2]	0.423(5)	0.4074	0.412(1)	
9	fCPB[2]	0.674(2)	0.712(3)	0.736(2)	
10	K_{PB}	1.755(4)	1.825(6)	1.901(5)	
11	K_{BX}	1.521(8)	1.380(8)	1.224(8)	
12	H_{XBX}	0.37(4)	0.36(7)	0.35(7)	
13	H_{PBX}	0.59(4)	0.61(4)	0.64(5)	
14	F_{XX}	0.49(2)	0.50(1)	0.53(3)	
15	F_{PX}	0.27(4)	0.26(3)	0.25(7)	
16	fCH/CH	0.045(5)	0.045(5)	0.045(5)	0.040(2)
17	fHCP/HCP	−0.079(8)	−0.070(8)	−0.069(3)	−0.049(5)
18	fCP/CP	0.27(4)	0.25(9)	0.25(5)	0.30(7)
19	fCPH/CPH	0.025(6)	0.025(6)	0.025(6)	0.038(4)
20	fT—HCP/CPH[c]	0.135(1)	0.112(6)	0.090(8)	0.202(6)
21	fC—HCP/CPH	−0.067(5)	−0.045(4)	−0.045(4)	−0.078(8)
22	fXBX/XBX	0.06(7)	0.08(1)	0.10(2)	
23	fPB/HPB	−0.09[d]	−0.09[d]	−0.09[d]	
24	fPC/BP	0.00	0.00	0.00	
25	fPB/PBX	0.08(2)	0.08(2)	0.08(2)	

[a] Units: stretching constants in mdyn Å^{-1} (10^2 N m^{-1}), bending constants mdyn Å rad^{-2} (10^2 N m rad^{-2}) and stretch/bend interaction constant mdyn rad^{-1} (uncertainties in parentheses).
[b] General valence force constants f_{ij}; Urey–Bradley force constants K (stretch), H (bend), and F (repulsion). Linear constant $F' = (1/10)F$ assumed.
[c] Interaction of HCP and CPH angles which are *trans* and *cis* to each other.
[d] Fixed value in least-squares analysis.

deformation and rocking modes is consistent with the earlier work on similar boron trihalides (26). Generally, good agreement is observed between our spectra and the spectra reported for H_3PBX_3 (5) and Me_3PBX_3 (6). The lowest mode is given to the BX_3 rocking at 147–140 cm^{-1} in the chloride; 110–95 cm^{-1} in the bromide and 97–85 cm^{-1} in the iodide. The BX_3 asymmetric and symmetric deformations are assigned to the Raman bands at 260, 242, and 178 cm^{-1}; 178, 160, and 144 cm^{-1}; and 130, 130, and 112 cm^{-1} in the dimethylphosphine adducts with boron trichloride, -bromide, -iodide, respectively. The corresponding deuterated analogues have slightly lower assignments.

Finally, *overtone and combination bands* are included in the comprehensive listings of the vibrational spectra, but they are not of particular use in this study as confirmations of the assignments of the fundamentals.

Normal Coordinate Analysis

The calculated frequencies and potential energy distributions are presented in Tables 6, 7, and 8 for the chloride, bromide, and iodide adducts, respectively. The force-field model can be claimed to be reasonable judging by the good correspondence between calculated and experimental frequencies for all $(CH_3)_2PHBX_3$ series and the good transfer to the $(CH_3)_2PDBX_3$ and $(CD_3)_2PHBX_3$ analogues. The potential-energy distribution reveals that there is no pure P—B bond stretching frequency because it is involved in the BX_3 and PC_2 symmetric modes. The degree of this involvement differs in the deuterated as well as in the iodide and bromide species. The ^{10}B-substituted frequencies are included in brackets. The potential energy distributions also indicate extensive vibrational coupling between the P—C and P—B stretching modes. The extent of this coupling is different in the deuterated

Table 6. Calculated frequencies and potential energy distribution* of $(CH_3)_2PHBCl_3$, $(CH_3)_2PDBCl_3$ and $(CD_3)_2PHBCl_3$

Assignment	$(CH_3)_2PHBCl_3$		$(CH_3)_2PDBCl_3$		$(CD_3)_2PHBCl_3$		P.E.D.[a]
	Obs.	Calc.	Obs.	Calc.	Obs.	Calc.	
CH_3 st. (asym)	3001	2998	2999	2998	2253	2248	100(1)
CH_3 st. (sym)	2925	2923	2922	2923	2137	2132	98(1)
PH st.	2420	2422	1755	1746	2431	2422	100(2)
CH_3 def. (asym)	1418	1410	1412	1410	1063	1060	94(3) + 6(4) + 10(17)
CH_3 def. (sym)	1313	1310	1312	1310	1023	1020	52(2) + 54(3) - 11(17)
	1298	1299	1298	1299	----	1018	(52(2) + 54(3) - 10(17))
							[56(2) + 43(3) + 15(5) - 12(17)]
CH_3 rock	1005	995	998	978	770	775	58(4) + 14(6) + 13(8) + 7(20)
	971	972	965	955	750	738	(48(14) + 6(3) + 5(20))
							[43(4) + 20(5) + 20(6) + 6(20)]
	---	950	950	937	645	654	88(4) + 6(3) - 6(21)
	---	933	---	925	630	642	(92(4) + 5(3) - 9(21)
							[54(4) + 30(6) + 18(5) + 10(10) - 10(21)]
PH def.	850	850	595	590	901	901	49(6) + 29(5) + 27(4) - 9(20)
	820	786	574	569	---	840	22(6) + 10(5) + 34(8) + 26(4) - 6(20)
							(95(6) + 11(5) - 9(20))
							(45(6) + 33(8) - 5(20))
							[67(6) + 17(4) + 28(8) - 9(20)]
							[36(6) + 13(4) + 34(5) - 5(20)]
P-B^{10}[c]	{786}	{780}	{780}	{785}	---	{780}	73(10) + 24(5) + 13(11) + 7(4) - 5(23)
P-B^{11}	765	760	776	772	743	740	(32(10) + 30(5) + 19(11) - 4(23))
							[32(10) + 30(4) + 16(11) + 5(13) - 5(23)]
PC_2 st. (asym)	735	730	741	758	719	715	57(5) + 36(6) - 7(18)
							(76(5) + 12(11) - 5(18)
							[48(5) + 30(4) - 4(18) - 2(20)]
PC_2 st. (sym)	690	680	690	725	678	674	48(5) + 36(6) + 8(10) + 7(18)
							(47(5) + 13(10) + 11(8) + 4(18))
							[44(5) + 28(4) + 4(18)]
BX_3 st. (asym)	720	723	725	719	712	709	61(11) + 7(12) + 16(6)
	710	693	710	700	---	687	(62(11) + 6(12) + 12(10))
							[45(11) + 5(12) + 15(6) + 16(5)]
BX_3 st. (sym)	397	393	391	391	392	386	36(11) + 33(14) + 11(10) + 10(15)
							(36(11) + 34(14) + 10(10) + 10(15))
							[36(11) + 35(14) + 11(10) + 11(15)]
PC_2 def.	277	269	271	276	276	270	70(7) + 5(9) + 10(14)
							(65(7) + 7(9) + 10(14) + 6(15))
							[46(7) + 16(12) + 7(13) + 11(15)]
BX_3 def. (asym)	265	256	260	265	256	252	26(12) + 60(14) + 10(15) + 2(22)
	240	235	235	236	232	239	
PC_2 rock.	204	202	200	197	199	190	33(9) + 14(12) + 23(14) + 11(13)
							(34(9) + 10(12) + 19(14) + 13(13))
							[30(9) + 12(12) + 19(14) + 19(13)]
BX_3 def. (sym)	178	170	170	173	158	168	19(12) + 35(14) + 19(15) + 16(9) - 5(22)
BX_3 rock.	140	136	135	132	136	133	27(13) + 46(15) + 20(9) - 3(22)

* Contribution greater than 5% except for significant interactions, [a]P.E.D. for $(CH_3)_2PDBCl_3$ in parentheses (), and $(CD_3)_2PHBCl_3$ in []; [b]Observed values are the average of i.r. and Raman frequencies; [c]{} give values for B^{10}.

analogues as illustrated in the tables. Generally, the asymmetric modes are relatively pure. The "whiplash" *cis*- and *trans-f* HCP/CPH force constant is crucial in allowing for splitting of the methyl rocks and in lowering the PH deformation mode to an acceptable value.

The force-constants associated with the C—H stretching and H—C—H bending are similar to those calculated for the trimethylphosphine adducts (6). The values of the P—H constants are fairly similar for all three adducts but significantly higher than the value in free Me_2PH. This is entirely consistent with conclusions based on the value of J_{PH} in the nmr spectra where its value was considerably higher, 426 ± 6 Hz, for the adducts than in the free phosphine, 191.03 ± 0.03 Hz (11). This, in turn, is consistent with an increase of *s*-character in the P—H bond on adduct formation

Can. J. Chem. Downloaded from www.nrcresearchpress.com by 210.87.254.6 on 09/06/12
For personal use only.

Table 7. Calculated frequencies and potential energy distribution* of $(CH_3)_2PHBBr_3$, $(CH_3)_2PDBBr_3$ and $(CD_3)_2PHBBr_3$

Assignment	$(CH_3)_2PHBBr_3$		$(CH_3)_2PDBBr_3$		$(CD_3)_2PHBBr_3$		P.E.D.
	Obs.	Calc.	Obs.	Calc.	Obs.	Calc.	
CH_3 st. (asym)	2997	2996	2999	2996	2240	2236	100(1)
CH_3 st. (sym)	2918	2920	2919	2920	2130	2125	98(1)
PH st.	2410	2410	1742	1737	2405	2410	100(2)
CH_3 def. (asym)	1417	1410	1412	1410	1057	1060	94(3) + 6(4) + 8(17)
CH_3 def. (sym)	1310	1310	1309	1310	1018	1020	54(2) + 52(3) - 11(17)
	1298	1299	1298	1299	----	1018	(54(2) + 52(3) - 10(17))
							[54(2) + 46(3) + 15(5) - 12(17)]
CH_3 rock.	998	986	978	957	760	764	53(4) + 16(6) + 9(8) + 8(20)
	960	956	950	938	---	735	(82(4) + 5(3) + 5(6) + 5(20))
							[50(4) + 24(5) + 8(9) + 2(20)]
	---	937	873	917	648	650	92(4) + 5(3) - 5(21)
	---	918	---	902	592	630	(92(4) + 5(3) - 9(21))
							[62(4) + 20(6) + 10(5) - 10(21)]
PH def.	840	852	607	598	900	901	34(6) + 17(5) + 20(4) - 6(20)
	810	783	559	547	815	830	30(6) + 32(8) + 21(5) - 5(20)
							(95(6) + 8(4) - 9(20))
							(42(6) + 35(8) - 5(20))
							[52(6) + 29(4) - 10(20)]
							[30(6) + 32(8) + 16(4) - 5(20)]
P-B[10c]	(770)	(775)	(775)	(775)	(762)	(756)	41(10) + 13(11) + 26(5) - 5(23)
P-B st.	765	760	765	770	743	749	(35(10) + 32(11) + 8(8) - 4(23))
							[30(10) + 45(4) + 8(11) - 3(23)]
PC_2 st. (asym)	735	740	745	750	723	720	49(5) + 30(6) + 17(4) - 7(18)
							(87(5) + 6(4) - 7(18))
							[46(5) + 27(4) + 19(11) - 5(18)]
PC_2 st. (sym)	694	699	698	707	689	680	49(5) + 20(10) + 7(8) + 5(4) + 4(18)
							(48(5) + 9(4) + 15(10) + 5(18))
							[30(5) + 13(4) + 8(10) + 17(11) + 3(18)]
BX_3 st. (asym)	625	630	640	635	613	623	64(11) + 10(12) + 8(5) + 5(13)
	614	618	617	622	---	610	(67(11) + 14(12) + 7(5) + 10(10))
							[33(11) + 13(12) + 9(5) + 9(8)]
BX_3 st. (sym)	278	276	276	275	275	274	26(11) + 10(14) + 21(10) + 9(9)
							(26(11) + 10(14) + 20(10) + 8(9))
							[29(11) + 12(14) + 23(10) + 9(9)]
PC_2 def.	252	260	242	256	241	240	60(7) + 9(6) + 6(8) + 7(15)
							(66(7) + 9(6) + 7(8) + 5(15))
							[67(7) + 9(6) + 6(8) + 5(15)]
PC_2 rock.	232	226	221	255	214	219	43(9) + 16(11) + 18(15) + 13(14)
	190	200	180	199	186	190	(54(9) + 15(11) + 15(15) + 7(14))
							[53(9) + 15(11) + 16(15) + 6(14)]
BX_3 def. (asym)	178	170	165	165	160	163	25(12) + 60(14) + 5(9) + 4(22)
	---	165	---	160	---	158	(25(12) + 61(14) + 6(9) + 4(22))
							[18(12) + 57(14) + 9(9) + 4(22)]
BX_3 def. (sym)	144	147	140	145	145	141	18(12) + 37(14) + 10(9) + 15(15) - 7(22)
BX_3 rock	102	98 96	95	97 96	95	93 90	30(13) + 47(15) - 8(22)

*See footnote in Table 6.

as a result of reorganization towards tetrahedral angles. The increase in *s*-character would be expected to lead to higher J_{PH} values and a stronger bond as also reflected by the force constants. An analogous increase in the value of the C—P stretching force constant is then to be expected, and indeed is found, on comparing the free phosphine with the adducts. The value of K_{PB} associated with the stiffness of the P—B stretch, also suggests a successive strengthening of the P—B bond along with the series $BCl_3 < BBr_3 < BI_3$ which is in accord with the increased Lewis acidity of the BX_3 groups (27). The trend is identical to that observed in the H_3PBX_3 (5) and Me_3PBX_3 series (6). It is also notable that the values of K_{PB} in this Me_2PHBX_3 series do fall between those of the PH_3BX_3 and

Can. J. Chem. Downloaded from www.nrcresearchpress.com by 210.87.254.6 on 09/06/12
For personal use only.

Table 8. Calculated frequencies and potential energy distribution* of $(CH_3)_2PHBI_3$, $(CH_3)_2PDBI_3$ and $(CD_3)_2PHBI_3$

Assignment	$(CH_3)_2PHBI_3$		$(CH_3)_2PDBI_3$		$(CD_3)_2PHBI_3$		P.E.D.
	Obs.	Calc.	Obs.	Calc.	Obs.	Calc.	
CH_3 st. (asym)	2999	2994	2997	2994	2239	2232	100(1)
CH_3 st. (sym)	2915	2915	2918	2915	2125	2120	98(1)
PH st.	2398	2398	1740	1735	2398	2397	100(2)
CH_3 def. (asym)	1409	1409	1410	1409	1052	1051	94(3) + 6(4) + 9(17)
CH_3 def. (sym)	1310	1310	1308	1310	1015	1019	54(2) + 52(3) - 11(17)
	1296	1298	1296	1298		1015	(54(2) + 52(3) - 10(17))
							[54(2) + 46(3) + 15(5) - 13(17)]
CH_3 rock.	984	980	982	954	740	738	61(4) + 14(6) + 8(8) + 7(20)
	950	966	940	937	700	717	(82(4) + 4(20))
							[34(4) + 21(5) + 18(10) + 7(20)
	---	919	---	918	630	581	91(4) + 6(3) - 6(21)
	---	905	---	882	550	559	(91(4) + 6(3) - 10(21))
							[48(4) + 13(5) + 8(6) - 11(21)]
PH def.	818	808	590	582	905	900	45(6) + 25(5) + 18(4) - 9(20)
	790	780	574	567	---	835	30(6) + 10(5) + 30(8) + 17(4) - 5(20)
							(90(6) + 10(5) - 9(20))
							(42(6) + 36(8) - 5(20))
							[60(6) + 17(4) + 25(5) - 9(20)]
							[35(6) + 12(4) + 32(8) - 5(20)]
P-B st.	756	745	758	753	724	729	40(10) + 31(5) + 7(13) - 5(23)
							(42(10) + 11(5) + 20(11) + 10(13) - 3(23))
							[46(10) + 15(4) + 8(11) - 3(23)]
PC_2 st. (asym)	732	736	733	745	735	720	46(5) + 24(4) - 4(18)
							(78(5) + 8(4) + 8(6) - 6(18))
							[48(5) + 21(4) + 10(6) - 4(18)]
PC_2 st. (sym)	687	690	689	702	678	680	36(5) + 23(10) + 11(8) + 4(18)
							(47(5) + 18(10) + 5(8) + 5(18))
							[34(5) + 24(10) + 15(4) + 21(18)]
BX_3 st. (asym)	570	557	560	560	539	542	53(11) + 7(12) + 4(14) + 13(13)
	540	545	545	547	529	531	(55(11) + 7(12) + 3(14) + 12(13))
							[30(11) + 10(12) + 18(4) + 5(13)]
BX_3 st. (sym)	207	200	201	199	201	198	32(11) + 37(14) + 11(9) + 6(15)
							(30(11) + 38(14) + 11(9) + 6(15))
							[31(11) + 40(14) + 7(9) + 11(15)]
PC_2 def.	254	256	250	254	245	237	60(7) + 8(6) + 8(8)
							(55(7) + 7(6) + 5(8))
							[62(7) + 5(6) + 5(8)]
PC_2 rock.	182	190	---	185	168	178	57(9) + 19(11) + 12(15)
							(56(9) + 20(11) + 11(15))
							[49(9) + 20(11) + 15(15)]
BX_3 def. (asym)	130	132	122	130	134	130	22(12) + 65(14) + 5(22)
BX_3 def. (sym)	112	120	110	115	117	115	10(12) + 14(14) + 26(13) + 9(11) - 8(22)
							(9(12) + 32(14) + 16(13) - 8(22))
							[9(12) + 28(14) + 15(13) - 8(22)]
BX_3 rock.	104	102	100	101	86	95	36(13) + 27(15) + 11(9) + 8(14) - 9(22)
	95	100		96		84	

* See Footnote in Table 6

Me_3PBX_3 series; again consistent with an increase in Lewis basicity along the series $PH_3 < Me_2PH < Me_3P$.

Acknowledgement

We wish to thank the Natural Sciences and Engineering Research Council for financial support.

1. J. R. Durig, V. F. Kalasinsky, Y. S. Li, and J. D. Odom. J. Phys. Chem. **79**, 468 (1975).
2. J. R. Durig, B. A. Hudgens, Y. S. Li, and J. D. Odom. J. Chem. Phys. **61**, 4890 (1974).
3. J. D. Odom, B. A. Hudgens, and J. R. Durig. J. Phys. Chem. **77**, 1972 (1973).
4. J. Davis and J. E. Drake. J. Chem. Soc. A, 2959 (1970).
5. J. E. Drake, J. L. Hencher, and B. Rapp. J. Chem. Soc. Dalton, 595 (1974).

Can. J. Chem. Downloaded from www.nrcresearchpress.com by 210.87.254.6 on 09/06/12
For personal use only.

6. J. E. DRAKE, J. L. HENCHER, and B. RAPP. Inorg. Chem. **16**, 2289 (1977).
7. B. RAPP. Ph.D. Thesis, University of Windsor. 1973.
8. W. L. JOLLY. Inorg. Synth. **11**, 126 (1968).
9. H. C. BEACHALL and B. KATLAFSKY. J. Chem. Phys. **27**, 182 (1957).
10. G. M. WHITESIDES, J. L. BEAUCHAMP, and J. D. ROBERTS. J. Am. Chem. Soc. **85**, 2665 (1963).
11. S. L. MONATT, G. L. JUVINALL, R. I. WAGNER, and D. D. ELLEMAN. J. Am. Chem. Soc. **88**, 2689 (1966).
12. A. J. F. CLARK and J. E. DRAKE. Spectrochim. Acta, **34**A, 307 (1978).
13. A. L. ALLREA and R. L. DEMING. Inorg. Nucl. Chem. Lett. **6**, 39 (1970).
14. J. L. HENCHER. Ph.D. Thesis, McMaster University. 1964.
15. R. L. HILDERBRANDT. J. Chem. Phys. **51**, 1654 (1969).
16. P. S. BRYAN and R. L. KUCZKOWSKI. Inorg. Chem. **11**, 553 (1972).
17. L. S. BARTELL and L. O. BROCKWAY. J. Chem. Phys. **32**, 512 (1960).
18. A. B. BURG. Inorg. Chem. **3**, 1325 (1964).
19. J. R. DURIG, Y. S. LI, L. A. CARREIRA, and J. D. ODOM. J. Am. Chem. Soc. **95**, 2491 (1973).
20. J. R. DURIG and J. E. SAUNDERS. J. Raman Spectrosc. **4**, 121 (1975).
21. J. R. DURIG, S. D. HUDSON, M. R. JALILAN, and Y. S. LI. J. Chem. Phys. **74**, 772 (1981).
22. A. J. F. CLARK, J. E. DRAKE, and Q. SHEN. Spectrochim. Acta, **34**A, 311 (1978).
23. R. E. SCRUBY, J. R. LACHER, and J. D. PARK. J. Chem. Phys. **19**, 386 (1951).
24. T. WENTINK, JR. and V. H. TIENSUU. J. Chem. Phys. **28**, 826 (1958).
25. G. HERZBERG. Molecular spectra and molecular structure. Vol. II. Van Nostrand, Princeton, NJ. 1968. p. 491.
26. P. D. H. CLIPPARD. Ph.D. Thesis, University of Michigan. 1969.
27. D. C. MENTE, J. L. MILLS, and R. E. MITCHELL. Inorg. Chem. **14**, 123 (1975).

Can. J. Chem. Downloaded from www.nrcresearchpress.com by 210.87.254.6 on 09/06/12
For personal use only.

Studies of silyl and germyl group VI species. Part VI. Synthesis and vibrational spectra of methylthiosilanes

JOHN E. DRAKE, BORIS M. GLAVINČEVSKI,[1] AND LAYLA N. KHASROU
Department of Chemistry, University of Windsor, Windsor, Ont., Canada N9B 3P4

Received March 10, 1981

JOHN E. DRAKE, BORIS M. GLAVINČEVSKI, and LAYLA N. KHASROU. Can. J. Chem. **59**, 2909 (1981).

Methylthiosilanes of the type $(CH_3)_nH_{3-n}SiSCH_3$, $n = 0$–3, and $(CH_3)HSi(SCH_3)_2$ have been prepared. Their ir and Raman spectra were recorded and assigned. The assignments were supported by normal coordinate analyses based on a modified valence force field.

JOHN E. DRAKE, BORIS M. GLAVINČEVSKI et LAYLA N. KHASROU. Can. J. Chem. **59**, 2909 (1981).

On a préparé des méthylthiosilanes du type $(CH_3)_nH_{3-n}SiSCH_3$, $n = 0$–3 et $(CH_3)HSi(SCH_3)_2$. On a enregistré et identifié leurs spectres ir et Raman. Pour identifier les spectres on a fait appel à des analyses de coordonnées normales à partir du champ de force de valence modifié.

[Traduit par le journal]

Can. J. Chem. Downloaded from www.nrcresearchpress.com by 210.87.254.6 on 09/06/12
For personal use only.

Introduction

The versatility of bisgermylcarbodiimides as convenient starting materials for germylchalcogenides has been demonstrated for various compounds including methylthiogermanes (1–3). However, the corresponding cleavage of the Si—N bond in bissilylcarbodiimides by protic species containing S—H, Se—H, or Te—H bonds is less effective as a synthetic route (1, 4) despite its ready cleavage by H_2O and ROH (2, 3, 5). The use of complex aluminates as synthetic reagents (6–8) suggested that $LiAl(SCH_3)_4$ might provide a convenient route to methylthiosilanes and indeed we find this method leads to high yields of the series $(CH_3)_nH_{3-n}SiSCH_3$, $n = 0 \rightarrow 3$, in a relatively short time. The characterisation of the fully methylated or protonated species did include some mention of their spectroscopic properties (9–11) although more extensive studies have been reported on the methoxymethylsilanes and $((CH_3)_nH_{3-n}Si)_2S$ series (12–14). We report herein the preparation and detailed vibrational analyses of the series $(CH_3)_nH_{3-n}SiSCH_3$ and also of $(CH_3)HSi(SCH_3)_2$ while ^1H and ^{13}C nmr, as well as mass spectra, are used to confirm the purity of the monomeric species.

Experimental

Reagents and Apparatus

All manipulations were carried out on a conventional vacuum line equipped with greaseless stopcocks. Iodosilanes were prepared from the corresponding hydrides with hydrogen iodide in presence of AlI_3 (15). Lithium tetramethylthioaluminate was obtained from recrystallized $Li(AlH_4)$ and methanethiol (Matheson) in dimethylether (16).

The ^1H nmr spectra were recorded on a JEOL C60-HL instrument. The ^{13}C nmr spectra were recorded under ^1H noise decoupling, using a Bruker CPX 100 (FT model) spectrometer operating at a resonance frequency of 22.639 MHz, at a probe temperature of 35°C. Neat samples were in sealed capillaries which were then placed in 5 mm nmr tubes containing $CDCl_3$ (as a lock) and TMS (as standard). The ir spectra were recorded on a Beckman IR-12 instrument, using gas cells of 9 mm path-length fitted with KBr windows. Raman spectra were recorded on a Spectra-Physics 700 spectrometer using the argon ion laser exciting line at 488.0 nm. The mass spectra were recorded at 70 eV on a Varian GMAT-CH5 spectrometer, fitted with a greaseless vacuum inlet system. The normal co-ordinate analysis was performed using an IBM S/360-50 series computer with a program written by Dr. J. L. Hencher of this department. The assignments are made for all molecules on the basis of C_s symmetry (17). All angles were assumed to be tetrahedral, the other dimensions: C—H, 110 pm; Si—C, 186.7 pm; S—C, 182 pm; Si—C, 215 pm; and Si—H, 148.4 pm were based on related molecules (7). The descriptions of the fundamental vibrations of $(CH_3)_nH_{3-n}SiSCH_3$ and $(CH_3)HSi(SCH_3)_2$ are presented in Tables 1 and 2, respectively.

Synthesis

All methylthiosilanes were prepared from $Li[Al(SCH_3)_4]$ and the corresponding iodosilane in a similar way to $(Me_nH_{3-n}Si)_2S,Se$ as previously reported (36). In a typical reaction, H_3SiI (1.020 mmol) was condensed at −196°C into the reaction vessel containing an excess of $Li[Al(SCH_3)_4]$ (1.285 mmol) and dimethyl ether (ca. 8.00 mL). The reactants were allowed to react at −45°C for ca. 2–3 h with occasional shaking of the reaction vessel. Fractionation of the volatile material through U-traps held at −78, −96, and −196°C gave pure H_3SiSCH_3 (1.00 mmol, 98%; *m/e* 75–80 $(H_nCSiS)^+$ 78 (100%)). Similar sets of experiments using $(CH_3)H_2SiI$ (2.201 mmol), $(CH_3)_2HSiI$ (2.456 mmol), $(CH_3)HSiI_2$ (1.791 mmol), and $(CH_3)_3SiI$ with an excess of $Li[Al(SCH_3)_4]$ at room temperature for ca. 3–4 h afforded the corresponding methylthiosilane: $(CH_3)H_2SiSCH_3$ (97%; *m/e* 90–94 $(H_nC_2SiS)^+$ 92 (50%); $(CH_3)_2HSiSCH_3$ (99%; *m/e* 105–108 $(H_nC_3SiS)^+$ 106 (20%)); $(CH_3)HSi(SCH_3)_2$ (98%; *m/e* 137–141 $(H_nC_3SiS_2)^+$ 138 (100%)); $(CH_3)_3SiSCH_3$ (94%; *m/e* 120–122 $(H_nC_4SiS)^+$ 120 (38%)).

Results and Discussion

In recent years some alkylthiosilanes have been

[1]Present address: Division of Chemistry, National Research Council of Canada, Ottawa, Ont., Canada K1A 0R6.

0008-4042/81/192909-12$01.00/0

©1981 National Research Council of Canada/Conseil national de recherches du Canada

Can. J. Chem. Downloaded from www.nrcresearchpress.com by 210.87.254.6 on 09/06/12
For personal use only.

TABLE 1. Description of the expected fundamental vibrations of $(CH_3)_nH_{3-n}SiSCH_3$* $n = 0$–3

H_3SiSCH_3			$(CH_3)H_2SiSCH_3$			$(CH_3)_2HSiSCH_3$			$(CH_3)_3SiSCH_3$		
Vibration	a'	a''	Vibration	a'	a''	Vibration	a'	a''	Vibration	a'	a''
CH_3st(a).	ν_1	ν_{14}	CH_3(Si)st(a).	ν_1	ν_{19}	CH_3(Si)st(a).	ν_1, ν_2	ν_{23}, ν_{24}	CH_3(Si)st(a).	ν_1, ν_2, ν_3	$\nu_{28}, \nu_{29}, \nu_{30}$
CH_3st(s).	ν_2		CH_3(Si)st(s).	ν_2		CH_3(Si)st(s).	ν_3	ν_{25}	CH_3(Si)st(s).	ν_4, ν_5	ν_{31}
SiH_3st(a).	ν_3	ν_{15}	CH_3(S)st(a).	ν_3	ν_{20}	CH_3(S)st(a).	ν_4	ν_{26}	CH_3(S)st(a).	ν_6	ν_{32}
SiH_3st(s).	ν_4		CH_3(S)st(s).	ν_4		CH_3(S)st(s).	ν_5		CH_3(S)st(s).	ν_7	
CH_3def(a).	ν_5	ν_{16}	CH_3(Si)def(a).	ν_5	ν_{21}	Si—H st.	ν_6		CH_3(Si)def(a).	ν_8, ν_9, ν_{10}	$\nu_{33}, \nu_{34}, \nu_{35}$
CH_3def(s).	ν_6		CH_3(Si)def(s).	ν_6		CH_3(Si)def(a).	ν_7, ν_8	ν_{27}, ν_{28}	CH_3(Si)def(s).	ν_{11}, ν_{12}	ν_{36}
CH_3 rock	ν_7	ν_{17}	CH_3(S)def(a).	ν_7	ν_{22}	CH_3(Si)def(s).	ν_9	ν_{29}	CH_3(S)def(a).	ν_{13}	ν_{37}
SiH_3def(a).	ν_8	ν_{18}	CH_3(S)def(s).	ν_8		CH_3(S)def(a).	ν_{10}	ν_{30}	CH_3(S)def(s).	ν_{14}	
SiH_3def(s).	ν_9		CH_3(Si) rock	ν_9	ν_{23}	CH_3(S)def(s).	ν_{11}		CH_3(S) rock	ν_{15}	ν_{38}
S—C st.	ν_{10}		CH_3(S) rock	ν_{10}	ν_{24}	CH_3(Si) rock	ν_{12}, ν_{13}	ν_{31}, ν_{32}	CH_3(Si) rock	$\nu_{16}, \nu_{17}, \nu_{18}$	$\nu_{39}, \nu_{40}, \nu_{41}$
SiH_3 rock.	ν_{11}	ν_{19}	SiH_2st.	ν_{11}	ν_{25}	CH_3(S) rock	ν_{14}	ν_{33}	C—S st.	ν_{19}	
Si—S st.	ν_{12}		SiH_2 bend	ν_{12}		SiC_2st.	ν_{15}	ν_{34}	C—Si st (a).	ν_{20}	ν_{42}
SiSC bend	ν_{13}		SiH_2 wag	ν_{13}		SiH def.	ν_{16}	ν_{35}	C—Si st (s).	ν_{21}	
SiH_3 torsion		ν_{20}	SiH_2 twist		ν_{26}	Si—S st.	ν_{17}		Si—S st.	ν_{22}	
CH_3 torsion		ν_{21}	SiH_2 rock		ν_{27}	S—C st.	ν_{18}		SiSC bend.	ν_{23}	
			C—S st.	ν_{14}		SiC_2def.	ν_{19}		SiC_3def(a).	ν_{24}	ν_{43}
			Si—S st.	ν_{15}		CSiS def.	ν_{20}	ν_{36}	SiC_3def(s).	ν_{25}	
			S—C st.	ν_{16}		SiSC bend	ν_{21}		SiC_3 rock	ν_{26}	ν_{44}
			CSiS bend	ν_{17}		torsions	ν_{22}	$\nu_{37}, \nu_{38}, \nu_{39}$	CH_3 torsion	ν_{27}	$\nu_{45}, \nu_{46}, \nu_{47}$
			SiSC bend	ν_{18}					frame torsion		ν_{48}
			torsions		$\nu_{28}, \nu_{29}, \nu_{30}$						

Can. J. Chem. Downloaded from www.nrcresearchpress.com by 210.87.254.6 on 09/06/12
For personal use only.

TABLE 2. Description of the expected fundamental vibrations of $(CH_3)HSi(SCH_3)_2$*

Vibration	a'	a''
CH_3(S) stretch (a)	ν_1, ν_2	ν_{24}, ν_{25}
CH_3(Si) stretch (a)	ν_3	ν_{26}
CH_3(S) stretch (s)	ν_4	ν_{27}
CH_3(Si) stretch (s)	ν_5	
Si—H stretch	ν_6	
CH_3(S) deformation (a)	ν_7, ν_8	ν_{28}, ν_{29}
CH_3(Si) deformation (a)	ν_9	ν_{30}
CH_3(S) deformation (s)	ν_{10}	ν_{31}
CH_3(Si) deformation (s)	ν_{11}	
CH_3(S) rocking	ν_{12}, ν_{13}	ν_{32}, ν_{33}
CH_3(Si) rocking	ν_{14}	ν_{34}
Si—C stretch	ν_{15}	
S—C stretch	ν_{16}	ν_{35}
SiH deformation	ν_{17}	ν_{36}
Si—S stretch	ν_{18}	ν_{37}
CSSi bending	ν_{19}	ν_{38}
CSiS bending	ν_{20}	ν_{39}
SSiS bending	ν_{21}	
Torsions	ν_{22}, ν_{23}	$\nu_{40}, \nu_{41}, \nu_{42}$

*C_s symmetry.

prepared by reaction of appropriate halogenosilanes with CH_3SMgI (10), RSNa (18), and CH_3SH in the presence of base (9, 10). The use of complex aluminates as synthetic reagents has been studied considerably (8, 19). In this study, these were extended to $Li[Al(SCH_3)_4]$ to include a convenient preparation of a series of methylthiosilanes by the general reaction:

$$[1]\quad Li[AlH_4] + 4CH_3SH \xrightarrow{Me_2O} Li[Al(SCH_3)_4] + 4H_2$$

$$[2]\quad Li[Al(SCH_3)_4] + 4(CH_3)_2HSiI \rightarrow 4(CH_3)_2HSiSCH_3 + AlI_3 + LiI$$

The formation of $Li[Al(SCH_3)_4]$ is rapid and it undergoes facile exchange with iodosilanes to give essentially quantitative yields of the corresponding methylthiosilane. All methylthiosilanes are clear, colorless liquids sufficiently volatile that they can be easily handled under vacuum line conditions. The silicon–sulfur linkage is known to be moisture-sensitive (20) to give the corresponding disiloxane. The Si—S bond is apparently less readily attacked in $(CH_3)HSi(SCH_3)_2$ and in $(CH_3)_2Si(SCH_3)_2$ than in the $(CH_3)_nH_{3-n}SiSCH_3$ species.

The methylthiosilanes all give first-order ^1H nmr spectra (Table 3) consistent with free rotation about the C—Si and Si—S bonds. The ^1H and ^{13}C chemical shifts and coupling constants correlate well with those of previously reported disilthianes (21), halogenosilanes (22, 23), methyltelluro-silanes and -germanes (24, 25) and provide the initial confirmation of the molecular species.

Vibrational Spectra

The Raman spectrum of H_3SiSCH_3 is shown in Fig. 1 and tabulated in Table 4, along with the previously published ir data (9). The polarisation data are very clear in establishing the asymmetric and symmetric CH_3 stretches and deformations as well as the SiH_3 stretches. Three rather weak overlapping bands are seen in the Raman spectrum in the region 900–970 cm^{-1}. However, the calculations and comparisons with related compounds such as CH_3SiH_3 and CH_3SiD_3 (26), SiH_4 (27), $(H_3Si)_2S$ (25), and organosulfur derivatives (28) allow us to assign the symmetric SiH_3 deformation, ν_9, to the sharper, more intense line at 914 cm^{-1}, the asymmetric SiH_3 deformations, ν_8 and ν_{18}, to the depolarised feature at 943 cm^{-1} and the CH_3 rocking vibrations, ν_7 and ν_{17}, to the shoulder at 968 cm^{-1}. The Si—C and Si—S stretches, ν_{10} and ν_{12}, are unambiguously assigned to the strong polarised maxima in the Raman at 695 and 507 cm^{-1}, respectively. The two SiH_3 rocking motions, ν_{19} and ν_{11}, are found as usual only slightly separated at 631 and 645 cm^{-1}. The remaining band, the SiSC bend, ν_{13}, appears as a broad feature at ca. 205 cm^{-1}. The weak feature at 406 cm^{-1} could be its overtone.

The Raman and infrared spectra of $(CH_3)H_2SiSCH_3$ are displayed in Figs. 1 and 2 while the assignment is in Table 5. The two types of methyl groups lead to overlapping bands in the ir spectrum so that band contours are not of much assistance. However, the presence of both methyl groups is clear for both the stretching and deformation modes in the Raman effect. In accord with the assignments on organic sulfur compounds (28), the bands at higher wave-number 2990dp and 2926p cm^{-1} are assigned to the CH_3—S asymmetric (ν_3 and ν_{20}) and symmetric (ν_4) stretches. The corresponding CH_3—Si stretches, ν_1, ν_{19}, and ν_2, are seen at 2967 and 2907 cm^{-1}, respectively. The small splitting of the asymmetric (ν_{25}) and symmetric (ν_{11}) SiH_2 stretches of about 20 cm^{-1} is typical of the $(CH_3)SiH_2$ group (29, 30). Similarly, the CH_3 deformations for the methyl group attached to sulfur ν_7, ν_{22}, and ν_8 are at higher wave-number than for that attached to silicon ν_5, ν_{21}, and ν_6, giving two sets of bands at ca. 1430 and 1319 for the former and 1417 and 1250 cm^{-1} for the latter. As with H_3SiSCH_3, the CH_3—S rocking modes, ν_{10} and ν_{24}, are placed at ca. 960 cm^{-1} while the CH_3—Si rocks are placed at 891 and 876 cm^{-1}. This leaves the band at 929 cm^{-1} to be assigned as the SiH_2 bend, ν_{12}, which compares favourably with the HSiH angle deformation in SiH_4 (27). The most prominent features in the Raman spectrum can be readily assigned to the Si—C, S—C and Si—S stretches, ν_{14}, ν_{16}, and ν_{15}, at 734, 701, and

TABLE 3. ^{13}C and ^{1}H—nmr spectra* of $(CH_3)_nH_{3-n}SiSCH_3$ and $(CH_3)HSi(SCH_3)_2$

Compounds	$\delta^{13}C(CH_3)$	$\delta^{13}C(SCH_3)$	$\delta^{1}H(CH_3)$	$\delta^{1}H(SiH)$	$\delta^{1}H(SCH_3)$	$J^{13}CH$	$J^{29}SiH$
H_3SiSCH_3	—	10.68	—	4.29	2.02	—	213.7
$(CH_3)H_2SiSCH_3$	−5.98	9.61	0.42	4.45	2.03	123.0	211.3
$(CH_3)_2HSiSCH_3$	−2.47	8.38	0.34	4.58	1.98	122.3	205.1
$(CH_3)_3SiSCH_3$	−0.13	7.34	0.26	—	1.92	121.5	—
$(CH_3)HSi(SCH_3)_2$	—	—	0.49	5.01	1.99	124.2	—

*All chemical shifts are in ppm referenced to TMS, positive values denoting down field shifts. Coupling constants are in Hz.

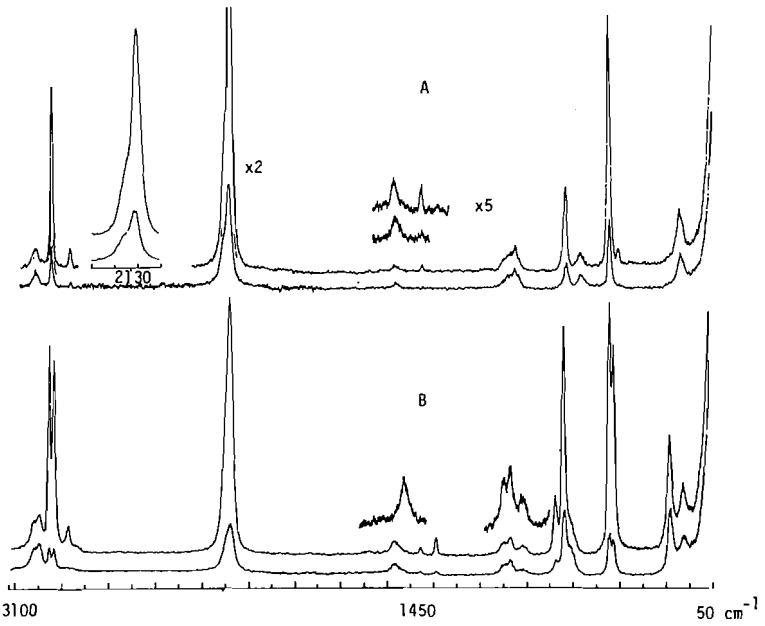

FIG. 1. The Raman spectra of H_3SiSCH_3 (*A*) and $(CH_3)H_2SiSCH_3$ (*B*).

500 cm^{-1}, respectively. All are, as expected, sharp, polarised bands. The placing of the Si—C stretch at higher wave-number than the S—C is consistent with data on related sulfides (10). In organic sulfides, the S—C stretch typically appears as a strong Raman band with a corresponding rather weak infrared feature (28), and the value of 701 cm^{-1} is close to that in H_3SiSCH_3 where there is no ambiguity. The SiH_2 wag, ν_{13}, and twist, ν_{26} are then appropriately assigned to the relatively weak features around 669 cm^{-1} by comparison with the methylsilyhalides (23). The SiH_2 rock, ν_{27}, is to be expected in the same region as the Si—S stretch, but with much less intensity in the Raman effect. The peak at 500 cm^{-1} is apparently split and this pair at 500 cm^{-1} and 483 cm^{-1} are both polarised. An assignment of the peak at 483 cm^{-1} to the SiH_2 rock ignores this polarisation and also ignores the fact that the splitting occurs in the same peak in $(CH_3)_2SiHSCH_3$ in which there is no SiH_2 rock. Alternately, the splitting could arise from Fermi resonance between the Si—S stretch and $2\nu_{18}$, or be an indication that two conformers exist. Finally, the SiSC, ν_{18}, and CSiC, ν_{17}, skeletal deformations are assigned to 241 and 177 cm^{-1}, respectively.

The Raman spectrum of $(CH_3)_2HSiSCH_3$ is displayed in Fig. 3, its ir spectrum in Fig. 2 and its assignment in Table 6. The SiH stretch, ν_6, is clearly seen in both effects at ca. 2130 cm^{-1}. The number and position of the bands associated with CH_3 stretches and deformations remain the same as noted for $(CH_3)H_2SiSCH_3$. There is an increase in the relative intensity of the band at 1265 cm^{-1} which is assigned to the CH_3—Si symmetrical deformation. There is also an increase in the relative intensity of the features assigned to CH_3—Si rocking modes at around 765 and 870 cm^{-1} relative to the CH_3—S rocks at 970 cm^{-1}. The band at 712 cm^{-1} in the ir spectrum which has no significant counterpart in the Raman effect is assigned as the

Can. J. Chem. Downloaded from www.nrcresearchpress.com by 210.87.254.6 on 09/06/12
For personal use only.

TABLE 4. The vibrational spectra of H_3SiSCH_3

Infrared* (gas)	Raman (liquid)	Calcd.	Assignment	P.E.D.†
	2995 mw, dp	2990	ν_1, ν_{14}	101(1)
2910 w	2927 s, p	2930	ν_2	97(1)+3(17)
2840 vw	2899 w, p		$2\nu_5, 2\nu_{16}$	
	2179 sh, dp	2180	ν_3, ν_{15}	100(3)
2160 s	2151 vs, p	2145	ν_4	101(3)
1440 w	1441 wbr, dp	1443	ν_5, ν_{16}	91(7)+6(9)
1320 w	1319 w, p	1319	ν_6	49(7)+61(9)+4(5)−8(28)−4(23)
959 m	968 sh	965 960	ν_7, ν_{17}	90(9)+6(7)
	943 sh, dp	940	ν_8, ν_{18}	92(10)+8(13)
915 s	914 mw	911	ν_9	46(10)+43(13)+4(29)
695 w	695 ms, p	701	ν_{10}	95(5)+3(6)
645 m	631 w, dp	630 625	ν_{19} ν_{11}	87(13)+11(10) 82(13)+10(10)
	406 w?			
	507 vs, p	501	ν_{12}	89(6)+6(13)+5(10)−6(29)
	ca. 205 mp, dp	204	ν_{13}	95(16)+4(6)

*Reported infrared (9).
†Contribution greater than 3%.

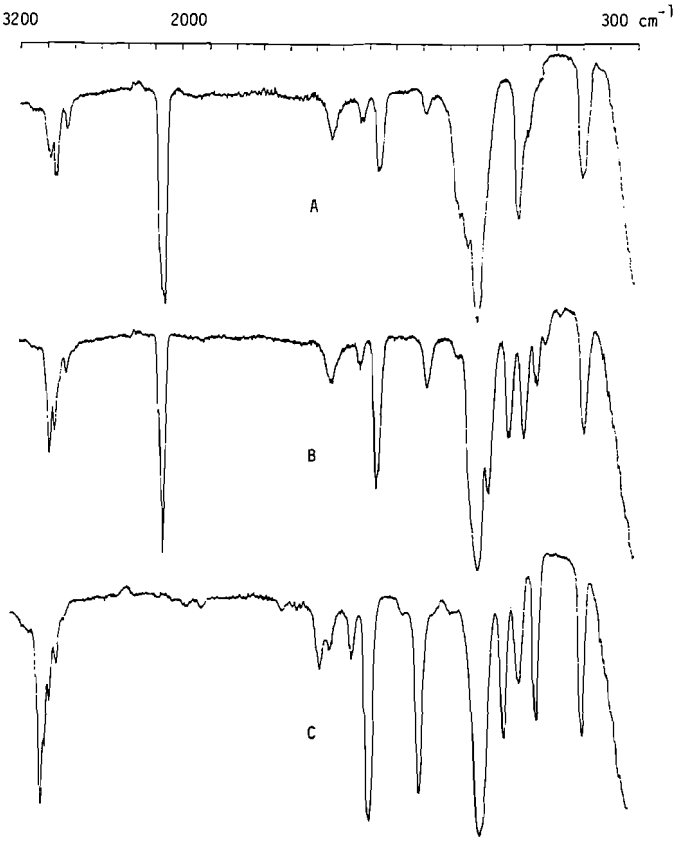

FIG. 2. The infrared spectra of $(CH_3)H_2SiSCH_3$ (*A*), $(CH_3)_2HSiSCH_3$ (*B*), and $(CH_3)_3SiSCH_3$ (*C*).

Can. J. Chem. Downloaded from www.nrcresearchpress.com by 210.87.254.6 on 09/06/12
For personal use only.

TABLE 5. The vibrational spectra of $(CH_3)H_2SiSCH_3$*

Infrared (gas)	Raman (liquid)	Calcd.	Assignment	P.E.D.†
	2990 sh, dp	2989	ν_3, ν_{20}	100(1)
2974 mw	2967 m, dp	2970	ν_1, ν_{19}	101(2)
2939 s	2926 vs, p	2930	ν_4	97(1)+4(17)
2921 s	2907 vs, p	2905	ν_2	97(2)+4(17)
2844	2850 mw, p		$2\nu_7, 2\nu_{22}$	
	2802 vw, br		$2\nu_5, 2\nu_{21}$	
2179 sh	2162 sh, dp	2170	ν_{25}	100(3)
2154 sh				
C 2146 Q, s	2142 vs, p	2143	ν_{11}	100(3)
1441 mw	1430 w, dp	1443	ν_7, ν_{22}	91(7)+7(9)
1415 vw, sh	1417 w, dp	1417	ν_5, ν_{21}	93(8)+5(11)
1326 w	1319 w, p	1320	ν_8	50(7)+60(9)+4(5)−4(23)−8(28)
1320 w				
1270 m	1250 w, p	1260	ν_6	54(8)+55(11)+4(4)−9(27)
1261 m				
1254 m				
972 w	960 sh	965	ν_{10}	89(9)+7(7)+4(23)
960 w	958 w, dp	959	ν_{24}	90(9)+7(7)+5(23)
929 m, sh	929 w, p	929	ν_{12}	68(10)+9(13)+10(11)+8(25)
899				
A/B 892 Q, vs	876 w, p	891	ν_{23}	90(11)+5(8)+5(25)
885		878	ν_9	82(11)+4(8)+7(13)+4(25)
742 ms	734 m, p	730	ν_{14}	50(4)+8(6)+20(12)+15(13)−4(26)
737 ms				
710 w, sh	701 vs, p	704	ν_{16}	64(5)+17(4)−4(26)
698 w, sh	669 w, sh, dp	667	ν_{26}	29(13)+36(12)+31(4)−4(22)−10(25)
662 w, sh		650	ν_{13}	61(13)+46(12)−8(22)
502 s	500 vs, p	501	ν_{15}	84(6)+5(16)+4(15)
498 s	483 vs, p			
470 w, sh	—	470	ν_{27}	39(13)+53(12)+7(22)
	241 s, p	239	ν_{18}	65(16)+19(15)+9(6)
	177 w	174	ν_{17}	26(16)+63(15)+4(13)

*Spectra recorded at room temperature.
†See footnote to Table 4.

SiH deformation, ν_{35}. This leaves the strong polarised peak at 699 cm^{-1}, which is seen as a weak shoulder on the 712 cm^{-1} infrared feature, to be assigned as the S—C stretch, ν_{18}, in essentially the same position as observed in H_3SiSCH_3 and $(CH_3)H_2SiSCH_3$. Similarly, the symmetric Si—C stretch, ν_{15}, can be unambiguously placed at 661 cm^{-1} where there is a polarised, reasonably strong band. The position of the asymmetric Si—C stretch, ν_{34}, is less obvious. By comparison with some previous assignments of $(CH_3)_nSiX_{4-n}$ species (31, 32), it could be placed as coincident with the bands at ~765 cm^{-1} or even 840 cm^{-1}. However, more recent work on Me_3SiCl (33), $(CH_3)_2SiX_2$ (34), and $(CH_3)_2SiHX$ (23) suggests that the splitting between the Si—C asymmetric and symmetric stretching modes is small. This is confirmed by normal coordinate analysis. It is not possible, using a reasonable set of force constants, to produce a large calculated splitting of these two modes. Thus, the assignment of ν_{34} to the shoulder at 672 cm^{-1} in the infrared spectrum is made with some confidence. As was mentioned in discussing the spectrum of $(CH_3)H_2SiSCH_3$, the Raman band assignable to the Si—S stretching mode ν_{17}, is clearly split (481 and 472 cm^{-1}). In this molecule there is no obvious overtone to suggest as a candidate for Fermi resonance although the combination of ν_{19} at 229 cm^{-1} and ν_{21} at 261 cm^{-1} cannot be definitely excluded. Thus, again, this could be the result of two conformers being present. The asymmetric SiC_2 deformation, ν_{36}, and SiC_2 rocking mode, ν_{20}, are assigned to the bands of lowest wave-number at 208 cm^{-1} and 150 cm^{-1} in accord with the normal coordinate analysis.

The Raman and ir spectra of $(CH_3)_3SiSCH_3$ are displayed in Figs. 3 and 2 respectively. The assignment in Table 7, but for minor details, is essentially in agreement with the earlier partial assignment made along with those of other methylsilylsulfides (10). The relative intensity increase of the CH_3 stretching and deformation modes for the

Can. J. Chem. Downloaded from www.nrcresearchpress.com by 210.87.254.6 on 09/06/12
For personal use only.

TABLE 6. The vibrational spectra of $(CH_3)_2HSiSCH_3$

Infrared (gas)	Raman (liquid)	Calcd.	Assignment	P.E.D.
A/C 2990 vw, sh	2991 sh, dp	2989	ν_4, ν_{26}	101(1)
2970 s	2967 m, dp	2970	$\nu_{11}, \nu_{12}, \nu_{23}, \nu_{24}$	101(2)
2931 ms	2928 s, p	2929	ν_5	97(1)+3(17)
2900 sh	2904 vs, p	2904	ν_3, ν_{25}	97(2)+3(17)
2850 mw	2848 mw, p		$2\nu_{30}, 2\nu_{10}$	
	2760		$2\nu_7, 2\nu_8$	
2175 sh				
2157 sh				
C 2130 Q, vs	2126 vs, p	2139	ν_6	100(3)
1440 mw	1435 w, dp	1438	ν_{30}, ν_{10}	
1430 w, sh	1425 w, sh	1420	ν_7, ν_8	91(7)+7(9)
1422		1415	ν_{27}, ν_{28}	95(8)+5(11)
A/B 1329 Q, m	1318 vw, p	1322	ν_{11}	51(7)+50(9)+4(5)−4(23)−8(28)
A/C 1265 Q, s	1251 w, p	1263	ν_9, ν_{29}	53(8)+50(11)+5(21)+3(4)−8(27)
1075 m	1060 v, vw		$\nu_{36}+\nu_{31}$	
970 sh, w	970 vw	964	ν_{14}, ν_{33}	89(9)+6(7)+3(23)
B 870 vs	870 w	868	ν_{12}, ν_{31}	89(11)+4(8)+3(4)+9(25)
840 ms	840 vw	854		
770		790		
765 Q, m	763 mw, dp	772	ν_{13}, ν_{32}	99(11)+5(12)+3(6)−15(21)+5(25)
760				
712 m	—	707	ν_{16}	35(13)+30(4)+18(12)+10(11)−4(22)−5(5)
705 w, sh	699 s, p	699	ν_{18}	68(5)+30(6)
672 sh	661 ms, p	690	ν_{34}	65(4)+31(12)+7(11)−3(27)−5(25)
665 m		660	ν_{15}	39(4)+38(12)+3(11)+3(13)−5(25)
635 w	630 w, dp	620	ν_{35}	50(12)+40(4)+9(11)+18(13)−4(22)
489 ms	481 vs	480	ν_{17}	74(6)+11(4)+7(13)+3(15)
	472 m, sh			
	261 m, p	264	ν_{21}	45(16)+29(15)+7(14)
	229 s, p	223	ν_{19}	80(14)+12(15)+4(16)
	208 ms, dp	190	ν_{36}	101(15)
	150 w, p	143	ν_{20}	35(15)+42(16)

$(CH_3)_3Si$ group relative to those of CH_3S underlines the placing of the latter modes to higher wave-number. The band at 960 cm^{-1} in the Raman (965 cm^{-1} in the ir) can be considered characteristic of the CH_3—S rocking motion while the $(CH_3)_3$—Si rocks can be placed, again characteristically, in the range 750–870 cm^{-1}. Consistent with the assignment of the previous three molecules, their normal coordinate analyses, and distinct features in the Raman spectrum, the S—C stretch, ν_{19}, can be placed at 702 cm^{-1} and the Si—C symmetric stretch, ν_{21}, at 632 cm^{-1}. The asymmetric Si—C stretches, ν_{20} and ν_{42}, might well be expected to be between these two vibrations. However, in the absence of any peaks in either effect, it must be assumed that they are coincident with one. Although assignments of SiC asymmetric modes have been made to the region ca. 700 cm^{-1} (35), the normal coordinate analyses and the expectation of a small separation from the Si—C symmetric stretch (23, 33, 34) suggests that near coincidence with the latter mode is more probable. Unlike the case in the mixed hydrido-methyl compounds, the Si—C symmetric stretch is seen, as in the case of H_3SiSCH_3, as a single sharp band (at 466 cm^{-1} in the Raman) with no sign of splitting. There are skeletal modes that could, in principal, provide overtones or combinations of the correct wave-number to lead to Fermi resonance, yet no splitting is observed. Thus, if the splitting in the cases of $(CH_3)H_2SiSCH_3$ and $(CH_3)_2HSiSCH_3$ can be interpreted as resulting from the presence of conformers, these are only observed for mixed hydrido-methyl silanes. In $(CH_3)H_2PBH_3$ the structural determination has shown (36) that the $(CH_3)H_2P$ group is not symmetrical but is askew of the "C_3" axis. Possibly in mixed hydrido-methyl species a slight distortion leads to conformers which could be exchanging much too rapidly to be observed on the nmr time-scale. Similar splitting of the Si—E (E = S, Se and Te) symmetric stretch was observed for the compounds $[(CH_3)H_2Si]_2E$ and $[(CH_3)_3Si]_2E$ (14).

The Raman and infrared spectra of $(CH_3)HSi(SCH_3)_2$ are assigned in Table 8. These assign-

Can. J. Chem. Downloaded from www.nrcresearchpress.com by 210.87.254.6 on 09/06/12
For personal use only.

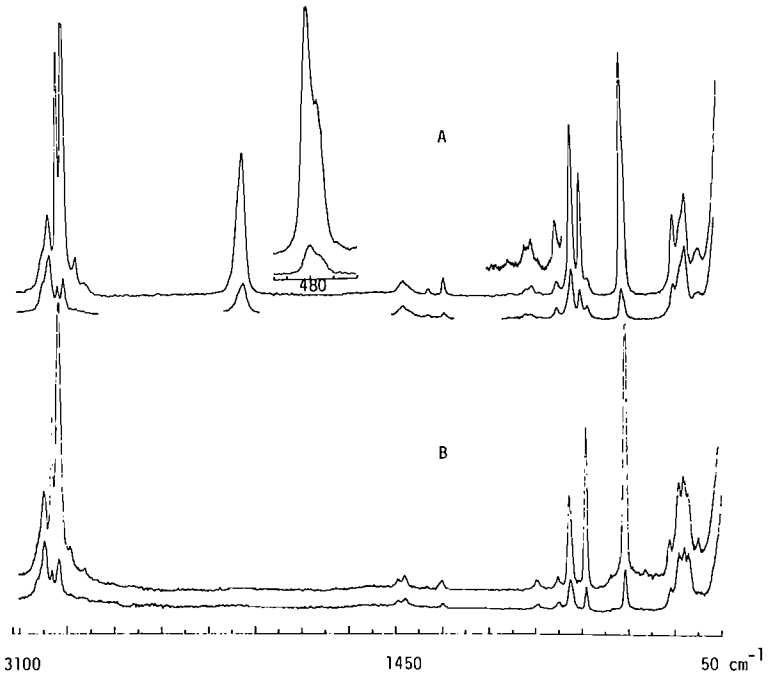

FIG. 3. The Raman spectra of $(CH_3)_2HSiSCH_3$ (*A*) and $(CH_3)_3SiSCH_3$ (*B*).

ments can be readily made by comparison with those of the $(CH_3)_nH_{3-n}SiSCH_3$ series and supported by the normal coordinate analysis. The molecule is assumed to have C_s symmetry with the two methyl groups on sulfur eclipsed relative to each other and a plane of symmetry passing through silicon and the H and C atoms attached to it. This model minimizes the non-bonding interactions. The forty-two fundamental vibrations break down into twenty-one a' and sixteen a'' modes that are both ir- and Raman-active. The five torsional modes were not observed. The methyl stretching, bending, and rocking modes all follow the pattern established for $(CH_3)_nH_{3-n}SiSCH_3$ with the relative intensities now reflecting the presence of two SCH_3 groups. The Si—H stretch is clearly seen at 2147 cm^{-1} in the Raman spectrum. The infrared spectrum in this region is slightly broadened because of the overlap of a combination of bands presumably enhanced by Fermi resonance. The methyl H_3C—S rocking frequencies are still characteristically weak in both effects and the Si—CH_3 rocking modes strong in the infrared spectrum appearing in regions of the spectrum anticipated from $(CH_3)_nH_{3-n}SiSCH_3$. The S—C stretching vibrations, ν_{16} and ν_{35}, are placed, as in the aforementioned series, at 698 (Raman) and 702 cm^{-1} (ir) while the Si—C stretch, ν_{15}, is clearly identifiable at ca. 730 cm^{-1}. Similarly, the S—Si stretching vibrations, ν_{18} and ν_{37}, are placed at 451 (Raman) and 479 cm^{-1} (ir) respectively. There is no sign of splitting in the sharp Raman band associated with ν_{18}. The only features remaining to be assigned in the region at 666 and 530 cm^{-1} are therefore given as Si—H deformation modes. These are considerably lower than those observed in the $(CH_3)_nH_{3-n}SiSCH_3$ compounds.

The skeletal deformations all appear below 300 cm^{-1} and are assigned on the basis of the polarisation data. The remaining mode, ν_{20}, is calculated to be at 182 cm^{-1}, but it is not clearly visible in the spectrum and could be essentially coincident with ν_{39}.

Normal Coordinate Analysis

The force field uses twenty-nine force constants in the $(CH_3)_nH_{3-n}SiSCH_3$ series and twenty-five in $(CH_3)HSi(SCH_3)_2$ (see Tables 9 and 10 respectively). The stretch–bend interactions involving a common bond (e.g. the force constant fX—C/HCX in X—CH_3 where X = S or Si) are important in calculating the CH_3 deformations. Two bend–bend interactions, fHCX/HCX and fHCH/HCH, keep the CH_3 deformations and rocks in the correct order. To avoid the number of force constants exceeding the number of frequencies, certain restrictions are placed on these interactions. Either two or three constants are set to zero, or one is

Can. J. Chem. Downloaded from www.nrcresearchpress.com by 210.87.254.6 on 09/06/12
For personal use only.

TABLE 7. Vibrational spectra of $(CH_3)_3SiSCH_3$

Infrared					
Liquid film*	Gas	Raman (liquid)	Calcd.	Assignment	P.E.D.
	3025 sh	2990 w, sh, dp	2989	ν_6, ν_{23}	101(1)
2965 m	2970 vs	2963 m, dp	2970	$\nu_1, \nu_2, \nu_3, \nu_{28}, \nu_{29}, \nu_{30}$	101(2)
2932 m	2929 sh	2930 s, p	2929	ν_7	97(1)+3(17)
	2908 sh	2900 vs, p	2904	ν_4, ν_5, ν_{31}	97(2)+3(17)
	2858 w	2850 w, p		$2\nu_{13}, 2\nu_{37}, 2\nu_8, 2\nu_{35}$	
		2750 vw, p			
1436 w	1445 m	1442 w, dp	1440	ν_{13}, ν_{37}	95(7)+7(9)
1401 w	1410 m	1411 w, dp	1409	$\nu_8, \nu_9, \nu_{10}, \nu_{33}, \nu_{34}, \nu_{35}$	97(8)+4(11)
	1326 m	1323 vw	1320	ν_{14}	53(7)+60(9)+3(5)−9(28)−6(23)
1246 s	1260 vs	1252 w, p	1260	$\nu_{11}, \nu_{12}, \nu_{36}$	48(8)+54(11)−10(27)+6(21)
	1075 m			$\nu_{39}+\nu_{43}$	
950 vw	965 vw	960 vw	966 / 960	ν_{15}, ν_{38}	87(9)+7(7)+4(23)
		863 sh	870	ν_{16}	83(11)+4(8)+4(21)
839 vs	845 vs	839 w	842	ν_{17}, ν_{39}	90(11)+5(8)+4(21)
			777	ν_{18}, ν_{40}	98(11)+12(4)−17(21)
749 m	755 ms	752 w	768	ν_{41}	100(11)+4(8)−21(21)
690 m	700 m	702 ms, p	704	ν_{19}	97(5)+4(6)−4(28)
629 s	638 m	—	640 / 637	ν_{20} / ν_{42}	89(4)+17(11)−10(27) / 92(4)+16(11)−10(27)
—	—	632 s, p	630	ν_{21}	58(4)+31(6)+7(11)+4(14)−7(27)
		522 vw		$2\nu_{23}$	
461 mw	467 m	466 m, p	460	ν_{22}	48(6)+43(4)+5(16)−5(27)
		375 vw		$\nu_{43}+\nu_{26}$	
		272 w, p	265	ν_{23}	38(16)+22(15)+32(14)+6(4)
		231 m, dp	240	ν_{43}	91(14)+4(4)
			233	ν_{24}	76(14)+14(15)+5(16)
		207 m, p	205	ν_{25}	50(15)+11(16)+28(14)+9(6)
		190 mw, dp	192	ν_{44}	94(15)+4(14)
		146, w, p	145	ν_{26}	52(15)+41(16)

*Reported ir (10).

fixed and the other two allowed to change. The force constant, fHCS/HCS, is used with fSC/HCS because the former constant is found to have a significant effect on reducing the frequency of the a' mode of the CH_3S deformations as well as the CH_3S rocking modes, while fSC/HCS only effects the CH_3S deformations. Generally, in the absence of fHCX/XC, unreasonably large values are required for fXC/HCX to establish an agreement between the observed and calculated CH_3X deformations. The force constant, *fcis*-HCSi/HCSi, is introduced when there is more than one methyl group attached to silicon, in an attempt to produce some splitting in the rocking modes of the $(CH_3)_nSi$, n = 2–3 groups. In the molecule $(CH_3)HSi(SCH_3)_2$ with only one methyl group, this interaction is replaced by a corresponding interaction *fcis*-HCSi/CSiS, to give partial splitting of the CH_3Si rocking modes. In some recent reports (23, 37, 38), a reasonable match between the calculated and observed frequencies for the deformation and rocking CH_3 modes (e.g., in the normal coordinate analysis of $(CH_3)_2HSiX$ (23)) was achieved by separating the HCM (where M = Si or Ge) angles into those in the plane of the molecule ($HCM^{||}$), and those that are approximately perpendicular to the symmetry plane ($HCM^{\perp}$). This was based on the assumption that there is a considerable interaction between the deformations of the HCSi and CSiH angles *trans* to each other. However, with the introduction of substituents onto silicon, the HCSi angles are no longer equivalent. The results indicate that this alternative method is less satisfactory than that used in this work. Extensive mixing between CSiH and HCSi angle bending is observed and required the introduction of another very important interaction constant; namely, *ftrans*-HCSi/CSiH which describes the "whiplash" motion of the hydrogen atom in the *trans* position. As in the calculation reported on CH_3SiH_3, CD_3SiH_3,

Can. J. Chem. Downloaded from www.nrcresearchpress.com by 210.87.254.6 on 09/06/12
For personal use only.

TABLE 8. The vibrational spectra of $(CH_3)HSi(SCH_3)_2$

Infrared (gas)	Raman (liquid)	Calcd.	Assignment	P.E.D.
2998 w	2995 mw, dp	2997 2996	$\nu_1, \nu_2, \nu_{24}, \nu_{25}$	101(1)
2970 w	2970 mw, dp	2970	ν_3, ν_{26}	101(2)
2930 m	2927 vs, p	2925	ν_4, ν_{27}	97(1)
2907 vw, sh	2905 vs, p	2902	ν_5	97(2)
2846 w	2843 w, dp		$2\nu_7, 2\nu_8, 2\nu_{28}, 2\nu_{29}$	
2160 w, sh 2151 Q, m, sh 2130 Q, s	2147 m, p	2150	ν_6	99(7)
2100 vw, sh			$(\nu_{14}+\nu_{11})$	
1440 w	1435 w, dp	1439	$\nu_7, \nu_8, \nu_{28}, \nu_{29}$	91(3)+7(5)
1410 vw	1403 w, br	1406	ν_9, ν_{30}	93(4)+4(6)
1325 w	1318 w, p	1321	ν_{10}, ν_{31}	50(3)+60(5)+4(9)−8(24)−4(19)
1261 m	1255 w, p	1258	ν_{11}	54(6)+54(4)+5(10)−9(25)−4(18)
1100 vw			$2\nu_{17}$	
969 mw	972 w, p	970 962	ν_{12}, ν_{32} ν_{13}, ν_{33}	89(5)+6(3)+4(19)
865 s	862 w	865	ν_{34}	92(6)+4(4)
820 vs	814 w, p	830	ν_{14}	95(6)+4(4)−6(22)−4(20)
735 m	730 m, p	732	ν_{15}	78(10)+11(9)+4(8)
702 w	698 s, p	698 690	ν_{35} ν_{16}	96(9) 87(9)+12(10)
	666 sh, dp	668	ν_{36}	89(13)+8(8)
540 ms	530 w	530	ν_{17}	59(12)+40(13)−4(20)
479 w	472 m, sh, dp	474	ν_{37}	83(8)+76(11)+10(13)−4(23)
456 w	451 vs, p	455	ν_{18}	87(8)+3(11)+19(15)+5(14)−9(23)
	294 w, p	270	ν_{19}	45(15)+29(11)+10(9)+5(23)−5(22)
	252 m, dp	254	ν_{38}	94(15)+5(11)−5(22)
	199 w	197	ν_{39}	85(11)+7(8)+4(15)
	180 sh	182	ν_{20}	49(11)+29(15)+10(19)+5(13)+5(12)−6(22)
	133 w, p	135	ν_{21}	83(14)+5(15)+9(11)

CD_3SiD_3 (25), this interaction is prominent in the degenerate CH_3 modes and in SiH bending activity. When the force constant, *fcis*-HCSi/CSiH is used, a lesser but similar effect is also noticed, and this force constant plays an important role in splitting the two CH_3Si rocking modes ν_{14} and ν_{34} (Raman 814 and 862 cm^{-1} and ir 820 and 865 cm^{-1}) in the compound $(CH_3)HSi(SCH_3)_2$.

The values of the force constants for the $(CH_3)_n$-$H_{3-n}SiSCH_3$ series show a consistency that suggests the force field is probably a good approximation. The values of fCH are essentially constant throughout the series, except for a higher value still for fC—H(S) in H_3SiSCH_3, emphasizing the C—H bond is apparently stronger (stiffer) when attached to the more electronegative sulfur atom. The force constants fSi—H, fSi—C and fSi—S get smaller as methyl groups are substituted for hydrogen atoms. The same phenomenon can be seen when methyl groups are substituted for halide atoms in series such as $(CH_3)_{4-n}SiX_n$ (31, 32, 34) or $(CH_3)_{4-n}$-GeX_n (20, 39), indicating that the effect of the hydrogen atom is that of a "weakly electronegative halogen". Thus, when attached to silicon, hydrogen is more electron-withdrawing than a methyl group, as has been pointed out previously (40), and the effect of substituting the less electronegative methyl group is to loosen up all the bonds to silicon. By contrast, the force constant fS—C has a slightly higher value in the two mixed compounds than in the hydride or trimethyl derivative. The only stretching force constant that is significantly different in $(CH_3)HSi(SCH_3)_2$ relative to those in the $(CH_3)_nH_{3-n}SiSCH_3$ series, is fSi—S which has a lower value. On the basis that SCH_3 is expected to be more electron-withdrawing than CH_3, an increase might have been expected. The lowering could be indicative of a significant change from approximately all tetrahedral angles about silicon arising from a combined effect of the steric requirements of the two SCH_3 groups and the possible distortion arising from mixed hydrido-methyl groups mentioned earlier.

In general, the fit between calculated and ob-

Can. J. Chem. Downloaded from www.nrcresearchpress.com by 210.87.254.6 on 09/06/12
For personal use only.

Can. J. Chem. Downloaded from www.nrcresearchpress.com by 210.87.254.6 on 09/06/12
For personal use only.

TABLE 9. Force constant values* for $(CH_3)_nH_{3-n}SiSCH_3$, $n = 0-3$

No.	Force constant	Value			
		H_3SiSCH_3	$(CH_3)H_2SiSCH_3$	$(CH_3)_2SiHSCH_3$	$(CH_3)_3SiSCH_3$
1	*f*C—H(S)	4.972	4.785	4.785	4.785
2	*f*C—H(Si)	—	4.735	4.735	4.735
3	*f*Si—H	2.672	2.655	2.615	
4	*f*Si—C		2.909	2.845	2.811
5	*f*S—C	2.939	2.990	2.990	2.955
6	*f*Si—S	2.409	2.375	2.346	2.302
7	*f*HCH(S)	0.507	0.507	0.510	0.519
8	*f*HCH(Si)	—	0.489	0.489	0.513
9	*f*HCS	0.613	0.613	0.603	0.603
10	*f*HSiH	0.445	0.427		
11	*f*HCSi	—	0.495	0.480	0.459
12	*f*CSiH	—	0.387	0.387	—
13	*f*HSiS	0.506	0.475	0.443	—
14	*f*CSiC	—	—	0.629	0.629
15	*f*CSiS	—	0.600	0.600	0.592
16	*f*CSSi	0.789	0.929	0.813	0.813
17	*f*CH/CH	0.075	0.069	0.065	0.060
18	*f*Si—H/Si—H	−0.025	−0.020	—	—
19	*f*Si—C/Si—C	—	—	0.030	0.040
20	*f*HCH/HCH	−0.010	−0.010	−0.010	−0.010
21	*fcis*—HCSi/HCSi	—	—	0.070	0.081
22	*f*CSiH/HSiS	—	0.029	0.029	—
23	*f*HCS/HCS	−0.015	−0.017	−0.019	−0.025
24	*fcis*—HCSi/CSiH	—	−0.023	−0.011	—
25	*ftrans*—HCSi/CSiH	—	0.047	0.023	—
26	*f*Si—C/CSiH	—	0.083	0.066	—
27	*f*Si—C/HCSi	—	0.235	0.228	0.255
28	*f*S—C/HCS	0.204†	0.211†	0.213†	0.234†
29	*f*Si—S/HSiS	−0.088†	0.017†	0.00	

*Units are: mdyne $Å^{-1}$ for stretching $\times (10^2) = N\ m^{-1}$, mydn Å rad^{-2} for bending $\times (10^2) = N\ m\ rad^{-2}$, mdyn rad^{-1} for stretch/bend constants.
†Fixed values.

TABLE 10. The force constant values for $(CH_3)HSi(SCH_3)_2$

No.	Description	Value	No.	Description	Value
1	*f*C—H(S)	4.800	14	*f*SSiS	0.595
2	*f*C—H(Si)	4.719	15	*f*CSSi	0.963
3	*f*HCH(S)	0.507	16	*f*CH/CH	0.050
4	*f*HCH(Si)	0.499	17	*f*Si—S/Si—S	0.040
5	*f*HCS	0.613	18	*f*HCH/HCH	−0.011
6	*f*HCSi	0.490	19	*f*HCS/HCS	−0.017
7	*f*Si—H	2.600	20	*fcis*—HCSi/CSiH	0.047
8	*f*Si—S	2.152	21	*ftrans*—HCSi/CSiH	−0.023
9	*f*C—S	2.976	22	*fcis*—HCSi/CSiS	0.090
10	*f*Si—C	2.925	23	*f*Si—S/CSSi	0.196*
11	*f*CSiS	0.720	24	*f*S—C/HCS	0.211*
12	*f*HSiC	0.367	25	*f*Si—C/HCSi	0.209
13	*f*HSiS	0.424			

*Fixed values.

served frequencies is good, but it is best for H_3SiSCH_3 and $(H_3C)_3SiSCH_3$ molecules (Tables 4–8). The extent of mixing between the Si—C stretch and the CSiH, HCS, and S—C modes is demonstrated in the potential energy distribution in the mixed species. Thus, in $(CH_3)H_2SiSCH$, the "Si—C stretch" is, in fact, made up of 50% *f*(Si—C), 20% *f*CSiH, 15% *f*HCS, and 8% *f*SiC. The Si—H bending modes, which appear in $(CH_3)_2HSiSCH_3$ in similar positions to those of other mixed hydrides, namely, ~710 and ~630 cm^{-1}, are much lower in $(CH_3)HSi(SCH_3)_2$ at 668 and 530 cm^{-1}. The values of the force constants *f*HSiC and *f*HSiS are only slightly lower; the decrease mainly

arises because, in the latter case, there is much less mixing with the SC or SiC stretch. In addition, relatively pure Si—C, S—C, and Si—S vibrations are observed in $(CH_3)HSi(SCH_3)_2$. Also, no extensive mixing is noted for the Si—S mode in all members of the series $H_nMe_{3-n}SiSMe$, and molecular skeletal motions are essentially decoupled from the motions involving hydrogen. Finally, in general, vibrations involving symmetrical motions show mixing of force constants while those involving more asymmetrical motions are essentially "pure".

Acknowledgement

We thank the Natural Sciences and Engineering Research Council for financial support.

1. J. E. DRAKE, R. T. HEMMINGS, and H. E. HENDERSON. J. Chem. Soc. 366 (1976).
2. J. E. DRAKE, R. T. HEMMINGS, and H. E. HENDERSON. Inorg. Nucl. Chem. Lett. **12**, 563 (1976).
3. J. E. DRAKE, H. E. HENDERSON, and R. T. HEMMINGS. Inorg. Chem. **16**, 1682 (1977).
4. E. A. V. EBSWORTH. *In* Organometallic compounds of the group IV elements. Vol. 1. *Edited by* A. G. MacDiarmid. Dekker, New York. 1968. Part 1.
5. T. TANAKA. J. Inorg. Nucl. Chem. **13**, 225 (1960); A. E. BEEZER and C. T. MORTIMER. J. Chem. Soc. A, 514 (1966).
6. C. GLIDEWELL. J. Chem. Soc. A, 823 (1971).
7. R. W. KILB and L. PIERCE. J. Chem. Phys. **27**, 108 (1957).
8. G. K. BARKER. Ph.D. Thesis, University of Windsor. 1972.
9. B. STERNBACH and A. G. MACDIARMID. J. Inorg. Nucl. Chem. **23**, 225 (1961).
10. K. A. HOOTON and A. L. ALLRED. Inorg. Chem. **4**, 671 (1965).
11. E. W. ABEL and D. B. BRADY. J. Organomet. Chem. **11**, 145 (1968); C. H. YODER and R. SCHENCK. J. Inorg. Nucl. Chem. **33**, 2699 (1971); R. A. N. MCLEAN and J. D. UMPLEBY. Can. J. Chem. **48**, 3769 (1970).
12. R. O. SAUER. J. Am. Chem. Soc. **66**, 1707 (1944); C. W. N. CUMPER, A. MELNIKOFF, and A. I. VOGEL. J. Chem. Soc. A, 246 (1966); J. DEDIER, A. MARCHAND, M. T. FOREL, and E. FRAINNET. J. Organomet. Chem. **81**, 161 (1974).
13. S. SORRISO. J. Organomet. Chem. **67**, 369 (1974).
14. J. E. DRAKE, B. M. GLAVINČEVSKI, and R. T. HEMMINGS. Can. J. Chem. **58**, 2161 (1980).
15. J. E. DRAKE, B. M. GLAVINČEVSKI, R. T. HEMMINGS, and H. E. HENDERSON. Inorg. Synth. **19**, 268 (1979).
16. J. E. DRAKE and B. M. GLAVINČEVSKI. Inorg. Synth. In press.
17. L. N. KHASROU. Ph.D. Thesis, University of Windsor. 1980.
18. E. W. ABEL and D. A. ARMITAGE. Adv. Organomet. Chem. **5**, 1 (1967).
19. J. W. ANDERSON, G. K. BARKER, J. E. DRAKE, and R. T. HEMMINGS. Can. J. Chem. **49**, 2931 (1971).
20. E. W. ABEL. J. Chem. Soc. 4406 (1966).
21. J. E. DRAKE, B. M. GLAVINČEVSKI, R. E. HUMPHRIES, and A. MAJID. Can. J. Chem. **57**, 3253 (1979); **57**, 1426 (1979).
22. E. A. V. EBSWORTH and S. G. FRANKISS. Trans. Faraday Soc. 1574 (1967).
23. A. J. F. CLARK. Ph.D. Thesis, University of Windsor. 1979.
24. J. E. DRAKE and R. T. HEMMINGS. Inorg. Chem. **19**, 1879 (1979).
25. S. CRADOCK, E. A. V. EBSWORTH, and D. W. H. RANKIN. J. Chem. Soc. A, 1628 (1969); S. CRADOCK. J. Chem. Soc. A, 1426 (1968).
26. A. J. F. CLARK and J. E. DRAKE. Can. J. Spectrosc. **22**, 79 (1977).
27. D. F. HEATH, J. W. LINNETT, and P. J. WHEATLEY. Trans. Faraday Soc. **146**, 137 (1950); D. F. BALL and D. C. MCKEAN. Spectrochim. Acta, **81**, 1019 (1962).
28. D. W. SCOTT and J. P. MCCALLOUGH. J. Am. Chem. Soc. **80**, 3554 (1958).
29. D. F. BALL, T. CARTER, D. C. MCKEAN, and L. A. WOODWARD. Spectrochim. Acta, **20**, 1721 (1964).
30. M. RANDIC. Spectrochim. Acta, **18**, 115 (1962).
31. T. SHIMANOUCHI, I. TSUCHIYA, and Y. MIKAWA. J. Chem. Phys. **18**, 1306 (1950).
32. H. MURATA and S. HAYASHI. J. Chem. Phys. **19**, 1217 (1951).
33. H. HÖFLER. Z. Naturforsch. **27a**, 760 (1972).
34. H. KRIEGSMANN. Z. Elektrochem. **62**, 1033 (1958).
35. H. KRIEGSMANN. Z. Elektrochem. **61**, 1088 (1957).
36. P. S. BRYAN and R. L. KUCZKOWSKI. Inorg. Chem. **11**, 553 (1972).
37. G. K. BARKER, J. E. DRAKE, R. T. HEMMINGS, and B. RAPP. J. Chem. Soc. A, 3291 (1971); Spectrochim. Acta, **28**, 1113 (1972).
38. G. K. BARKER, J. E. DRAKE, and R. T. HEMMINGS. Can. J. Chem. **51**, 302 (1973).
39. D. F. VAN DE VONDEL, G. P. VAN DER KELEN, and G. VAN HOOYDONK. J. Organomet. Chem. **23**, 431 (1970).
40. J. E. DRAKE, C. RIDDLE, B. GLAVINČEVSKI, K. GORZELSHA, and H. E. HENDERSON. Inorg. Chem. **17**, 2333 (1978).

Can. J. Chem. Downloaded from www.nrcresearchpress.com by 210.87.254.6 on 09/06/12
For personal use only.

Effects of organic solvents on immobilized enzyme catalyses.[1] Chymotrypsin immobilized on porous glass

J. Bryan Jones and Diana H. Pliura

Department of Chemistry, University of Toronto, Toronto, Ont., Canada M5S 1A1

Received January 30, 1981

J. Bryan Jones and Diana H. Pliura. Can. J. Chem. **59**, 2921 (1981).

The esterolytic activity of native chymotrypsin (CT) immobilized on ionically neutral porous glass beads has been studied in the presence of up to 20% (v/v) of the organic solvents methanol, ethanol, 2-propanol, *tert*-butyl alcohol, dioxane, and DMSO. In marked contrast to the variations observed with native CT, inhibition of CT immobilized on glass (CT–glass) was independent of the nature of the organic solvent. The overall activity, as indicated by $k_c(app)/K_m(app)$, decreased by 35–50% as the concentration of all solvents surveyed was increased up to 20%. In general, high organic solvent concentration accelerated the rate of protein release from the insoluble catalyst. For practical applications in aqueous organic solvents CT–glass conjugates are inferior to those of the enzyme attached to Sephadex.

J. Bryan Jones et Diana H. Pliura. Can. J. Chem. **59**, 2921 (1981).

On a étudié l'activité estérolytique de la chymotypsine naturelle (CT) immobilisée sur un lit de verre poreux ioniquement neutre en présence de solvants organiques tel le méthanol, l'éthanol, le propanol-2, le *tert*-butanol, le dioxanne et le DMSO à des concentrations allant jusqu'à 20% (v/v). L'inhibition de la CT immobilisée sur le verre (CT–verre) est indépendante de la nature du solvant organique ce qui contraste fortement avec les variations observées dans le cas de la CT naturelle. L'activité globale telle qu'indiquée par le $k_c(app)/k_m(app)$ décroît de 35 à 50% lorsque la concentration de tous les solvants utilisés augmente jusqu'à 20%. En général une forte concentration de solvant organique accélère la vitesse de libération de la protéine à partir du catalyseur insoluble. Du point de vue des applications pratiques dans des solvants organiques aqueux, les CT conjugées à des verres sont moins utiles que les enzymes immobilisés sur du Séphadex.

[Traduit par le journal]

The potential of enzymes as chiral catalysts for asymmetric synthesis is attracting increasing attention in both academic and industrial laboratories. A broad spectrum of applications has already been documented (1*b*), but future exploitation of enzymes in organic synthesis will undoubtedly require more extensive use of organic cosolvents in order to ensure the solubility of hydrophobic substrates in the predominantly aqueous reaction media. While the effects of organic cosolvents on enzymes are usually detrimental (2) their adverse influences can be mitigated by using immobilized enzyme preparations (3–7). Furthermore, the use of enzymes in insolubilized form offers considerable practical advantage since problems of product separation, and catalyst recovery and reuse, are greatly reduced, particularly for processes where continuous operation is required (8).

In a previous report (1*c*) we described the influences of representative water-miscible organic solvents on the catalytic properties of chymotrypsin (CT)[2] bound to Sephadex. Hydrophilic gels such as Sephadex shrink in aqueous organic solvent solutions (1*c*, 9, 10). The enzyme embedded within the gel thus becomes less accessible to substrate and the activity of the immobilized enzyme preparation decreases. Deleterious solvent effects of this kind are avoided when ionically neutral but rigid supports such as porous glass are employed. In this paper we report on the effects of up to 20% (v/v) methanol, ethanol, 2-propanol, *tert*-butyl alcohol, dioxane, and DMSO on CT–glass preparations.

Experimental

Materials

α-Chymotrypsin (EC 3.4.21.1) from bovine pancreas was obtained as a lyophilized powder from Worthington Biochemical Corporation and was used without further purification. The porous glass supports (CPG-1350 and CPG-550) and γ-aminopropyltriethoxysilane were purchased from Pierce Chemicals. Alkylamine glass derivatives were prepared by a general procedure outlined by the Corning Bioorganic Technology Group (11).[3] *N*-Acetyl-L-tyrosine ethyl ester (NATEE) was purchased from Sigma Chemical Co. All other chemicals were of the highest purity available.

Preparation of CT–Glass Derivatives

(a) CT–Glass–Glu

The CT–glass–glu derivatives were prepared by the standard method of coupling protein to glutaraldehyde-activated alkylamine glass beads (11, 12). The conjugates were washed exhaustively with 0.1 *M* aqueous potassium phosphate buffer

[1]Enzymes in Organic Syntheses 21. For Part 20 see ref. 1*a*. Abstracted from the Ph.D. thesis of D.H.P., University of Toronto, 1977.

[2]Abbreviations used: CT, chymotrypsin; CT–Sephadex, CT immobilized on Sephadex; CT–glass–glu, CT linked to glass via glutaraldehyde method; CT–glass–azo, CT coupled to glass via diazo method; NATEE, *N*-acetyl-L-tyrosine ethyl ester; (app), apparent; DMSO, dimethyl sulfoxide; CPG, controlled pore glass.

[3]R. A. Messing, Cornell Bioorganic Technology Group, personal communication.

0008-4042/81/192921-05$01.00/0

©1981 National Research Council of Canada/Conseil national de recherches du Canada

(pH 7) until no enzyme was detected in the effluent by monitoring the absorbance at 280 nm.

(b) CT–Glass–Azo

Diazotized glass beads were prepared from alkylamine glass by *p*-nitrobenzoylation, reduction, and diazotization according to the usual procedure (12). The diazotized glass beads were then coupled to CT by reaction at pH 8.5 at 20°C for 1 h. After the coupling reaction was complete, the CT–glass–azo (10 g) was transferred to a fritted glass filtering funnel and washed with 0.05 *M* aqueous $NaHCO_3$ (350 mL) under suction. The following sequence of wash media was then supplied by a peristaltic pump: 0.05 *M* aqueous $NaHCO_3$ (1 L); 1 m*M* aqueous HCl (100 mL); 0.5 *M* aqueous NaCl (200 mL); and finally distilled water until no enzyme was detected in the wash media.

Both of the CT–glass conjugates were stored at 4°C in a minimum of distilled water. Their protein contents were determined by amino acid analysis as before (1*c*).

Kinetic Measurements

The rates of CT–glass-catalyzed hydrolysis of NATEE were determined using a Radiometer Automatic Titrator at 25°C under a nitrogen stream in a 10 mL capacity reaction vessel as described previously (1*c*, 13).

Specific Activities

The specific activities of CT–glass derivatives (0.1–0.5 mL of wet packed beads) were assayed using 9 mL of a solution of NATEE (11 m*M*) in 0.1 *M* aqueous KCl containing 2% (v/v) methanol. The total assay volume was brought up to 10 mL by the addition of doubly distilled water.

pH–Activity Profiles

The esterolytic activity as a function of the pH of the reaction mixtures was assayed at 25°C against NATEE (10 m*M*) in 2% (v/v) methanol or 20% (v/v) organic solvent, 1.0 *M* in KCl at 25°C. Typically, the enzyme concentration was 2.6×10^{-6} *M* based on the total protein content of the CT–glass derivatives. Rates of hydrolysis were measured from the linear portions of the titration curves and, when necessary, were corrected for nonenzymic hydrolysis at very high pH.

Determination of Apparent Kinetic Parameters

The kinetic parameters K_m(app) and k_c(app) were determined at pH(app) 9.8 at 25°C for 1.0 *M* KCl solutions containing different concentrations of organic solvent. Typically, a substrate concentration range of 0.7–8 m*M* NATEE and an enzyme concentration of 3×10^{-6} *M* were employed. No nonenzymic ester hydrolysis was detected under the experimental conditions. Rates were measured from the initial slopes of the titration curves and rate constants in each hydroorganic reaction mixture were determined by linear regression analysis of a Lineweaver–Burk plot.

Stability of the CT–Glass–Azo Conjugate

To determine the stability of the conjugate, CT–glass–azo (1–1.5 mL of beads) was stored in water or in 20% (v/v) organic solvent, 0.1 *M* KCl, pH(app) 9.8 at 20°C in a stoppered flask. The activity of CT–glass–azo (0.2–0.3 mL of beads, 0.8–0.7 mL of incubation medium) was assayed periodically against NATEE (9 mL, 11 m*M* in substrate). After each activity determination the glass beads were filtered, washed with distilled water (60 mL), and returned to the incubation flask. After two months, the glass beads were washed with acetone, air-dried, and analyzed for protein content by amino acid analysis.

Results and Discussion

The two principal methods for the covalent coupling of proteins to porous glass are the diazo and glutaraldehyde methods (11, 12). The results of experiments evaluating the two methods for coupling CT to porous glass of 550 Å and 1350 Å pore diameters are shown in Table 1. For all four CT–glass conjugates, a considerable portion of the immobilized CT does not contribute to the catalytic activity. All subsequent work was carried out with the most active conjugate, CT–glass–azo on CPG 1350.

Contrary to the observations of Tanizawa and Bender (4), the pH optimum for the esterolytic activity of CT–glass–azo was displaced two pH units towards more alkaline pH values relative to the optimum pH of 7.8 for native CT (Fig. 1). These conflicting observations are accounted for by differences in assay conditions. Tanizawa and Bender (4) measured their pH–activity profiles in highly buffered solutions, whereas the present experiments were done in unbuffered media. It is known that displacements of pH–activity profiles toward alkaline pH values of the form seen in Fig. 1 are characteristic of enzymically generated pH gradients when the catalyst is operating under diffusional restrictions (6*b*, 14). These displacements can be negated by using buffered solutions (6*c*, 15) or by decreasing the reactivity of the enzyme toward substrate (16). Although concentrations of organic solvent up to 20% decrease the measurable catalytic activity of CT–glass–azo, no shift in pH–activity profiles back toward pH 7.8, the optimum pH for native CT, was observed. On the contrary, for the three solvents surveyed, namely 2-propanol, *tert*-butyl alcohol, and DMSO, addition of 20% organic solvent further displaced the pH optimum toward more alkaline pH values (Fig. 1).[4] Unlike the CT–Sephadex conjugates in the previous study (1*c*), increasing the pH of the 20% aqueous DMSO solution did not reverse the DMSO-induced inhibition of the catalytic activity of CT–glass–azo.

For CT–Sephadex conjugates, the intrinsic catalytic parameters of the enzyme are not altered by the immobilization procedure (16, 17). Unfortunately, similar assurances regarding the effect of azo-coupling of CT to glass on the intrinsic k_c and K_m constants are not available. Substrate and product diffusion limitations of enzymes bound to

[4]The measured pH of the carbonate–borate buffer solutions used is shifted toward more alkaline values with increasing concentration of organic solvent, presumably due to modification of the buffer pK_a as the dielectric constant of the aqueous medium is progressively altered (7). These perturbations of the apparent pH are greatest (up to 0.7 pH units) when the solvent is DMSO and it is significant that the most pronounced pH optimum shift observed is for CT–glass–azo in 20% DMSO.

TABLE 1. Characterization of glass-bound CT derivatives

Support	Coupling method	Protein content[a] (mg enzyme/g support)	Specific activity[b] (μmol/min/mg enzyme)	Residual activity of CT after coupling[c]
550 Å CPG[d]	Glutaraldehyde	31.1±1.2	15	5
	Azo	8.7±0.6	50	17
1350 Å CPG[e]	Glutaraldehyde	8.1±0.2	29	10
	Azo	7.9±0.5	68	23

[a] Determined by amino acid analysis (1*b*).
[b] Activity assayed against NATEE (10 m*M*), 0.1 *M* KCl, 2% methanol at 20°C, pH(app) 9.8.
[c] Specific activity of native CT under assay conditions: 294 μmol/min/mg enzyme.
[d] Surface area 70 m^2/g.
[e] Surface area 34 m^2/g.

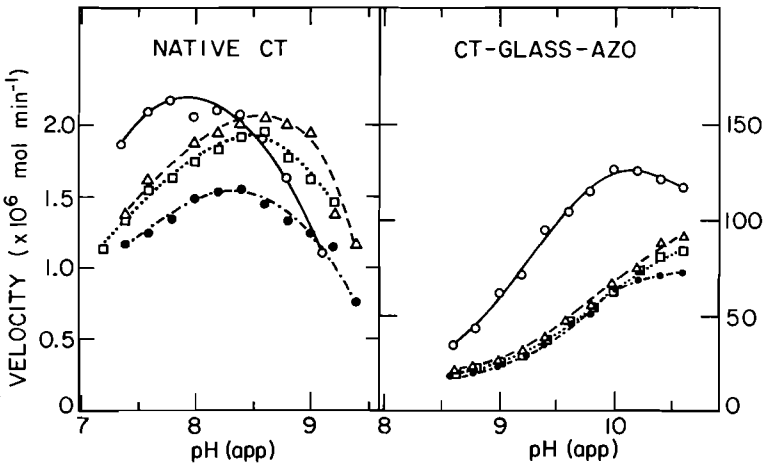

FIG. 1. Effects of 20% organic solvent on the pH–activity profiles for native CT and CT–glass–azo. The enzyme activities were assayed against NATEE (10 m*M*) in 2% methanol (○), 20% 2-propanol (●), 20% *tert*-butyl alcohol (□) and 20% DMSO (△) solutions 1.0 *M* in KCl at 25°C.

glass (18, 19) also complicate interpretation of the apparent k_c and K_m values obtained directly from Lineweaver–Burk plots[5] (21). However, the apparent specificity constants $k_c(app)/K_m(app)$ remain useful overall indicators of the relative catalytic activities under the various organic solvent conditions. These data are summarized in Table 2. The catalytic activity of CT–glass–azo is seen to be dramatically lower than that of native CT under all conditions assayed. Furthermore while the activities decrease monotonically as the concentration of each solvent is increased, CT–glass–azo is surprisingly insensitive to both the nature and concentration of the organic solvent used.[6] The apparent specificity constants for the immobilized enzyme vary by a factor of only ~4-fold under any of the conditions surveyed.

For long term practical applications, immobilized enzymes must retain their activity for extended periods (8). The half-lives for native CT and CT–glass–azo in different organic solvent media are compared in Table 3. With the exception of its behaviour in 20% aqueous dioxane and DMSO, the CT–glass–azo conjugate is somewhat more stable than the native enzyme. However, the half-lives observed are generally well below the levels necessary for an immobilized catalyst to be practicable.

The glass-immobilized enzyme suffers considerable loss of activity on storage for two months (Table 4) under normal operating conditions. Part of the instability of CT–glass–azo can be accounted for by the known susceptibility of porous glass to degradation under alkaline conditions (22) but the higher levels of protein loss in 20% solvent solutions than in water were unexpected. Although in each case the overall activity of CT–glass–azo drops as protein is lost during storage, the rate of activity loss is significantly slower than in water for all solvents except dioxane. Paradoxically, this results in conjugates of increased specific activity

[5] Recently, Brown *et al.* (20) have demonstrated that immobilization of CT to glass via a thioester linkage does not alter the intrinsic catalytic parameters. However, diffusion limitations of the catalytic activity still remained.

[6] Reduced availability of water in the higher organic solvent concentrations (4) is clearly not a significant factor here.

TABLE 2. Effects of organic solvents on the specificity constants for native CT and CT–glass–azo catalyzed hydrolyses[a]

Solvent (%v/v)	Native CT[b] k_c/K_m (mM^{-1} s^{-1})	CT–glass–azo $k_c(app)/K_m(app)$ (mM^{-1} s^{-1})
0	268± 8	
Methanol		
2		5.2±1.4
4.5	114± 6	4.4±0.7
10	39± 5	3.6±0.7
15	30± 3	2.5±0.6
20	11± 2	2.2±0.5
Ethanol		
2		7.5±1.0
4.5	98±10	6.9±0.7
10	55± 5	5.3±0.9
15	38± 6	3.5±0.5
20	19± 2	2.8±0.5
2-Propanol		
2		4.9±0.8
4.5	130±16	4.9±0.9
10	94± 9	3.8±0.9
15	73± 4	3.2±0.7
20	45± 4	2.3±0.4
tert-Butyl alcohol		
2		9.9±1.6
4.5	196±15	10.1±1.3
10	79± 7	8.4±1.2
15	66±13	5.5±0.9
20	35± 4	3.9±0.5
Dioxane		
2		8.5±1.5
4.5	61± 7	6.8±0.9
10	24± 3	5.0±1.2
15	16± 4	4.2±1.0
20	8± 1	2.9±0.5
DMSO		
2		9.4±1.7
4.5	130± 6	8.8±1.6
10	94± 9	7.8±2.1
15	73± 4	6.4±1.8
20	45± 4	4.6±1.0

[a]For hydrolyses of NATEE in aqueous organic solvent solutions, 1.0 *M* in KCl at 25°C and pH(app) 7.8 for native CT or pH(app) for CT–glass–azo.
[b]From ref. 1c.

TABLE 3. Half-lives of native CT and CT–glass–azo[a]

Solvent	Half-life (days) Native CT[b]	CT–glass–azo
H_2O	14	33
20% Methanol	16	21
20% Ethanol	9	26
20% 2-Propanol	7	20
20% *tert*-Butyl alcohol	2.5	16
20% Dioxane	13	8
20% DMSO	>200 (est.)	>150 (est.)

[a]Determined for pH(app) 7.8 solutions, 0.1 *M* in KCl, at 20°C for native CT and at pH(app) 9.8 for CT–glass–azo.
[b]From ref. 1b.

TABLE 4. Properties of CT–glass–azo conjugate after storage for two months[a]

Solvent	% Protein retained[b]	% Activity remaining[c]
H_2O	30±2	40
20% Methanol	19±2	26
20% Ethanol	15±2	30
20% 2-Propanol	13±2	21
20% *tert*-Butyl alcohol	13±2	17
20% Dioxane	9±1	3
20% DMSO	48±3	74

[a]Storage was at pH(app) 9.8 in 0.1 *M* KCl solutions at 20°C.
[b]Relative to initial protein content of 10.2 ± 0.3 mg enzyme/g conjugate.
[c]Relative to initial specific activity of 42.4 μmol/min/mg bound enzyme.

in terms of catalytic power per mg of the bound protein remaining in the aged preparations. A similar increase in specific activity on partial protein removal has been observed for CT bound to glass via thioester linkages (20). With protic solvents, the apparent stability of CT–Sephadex increases with increasing hydrophobic character of the organic solvent (1c). As Table 4 shows, the converse is true for CT–glass–azo. Both the stability of the covalent link (as reflected by the proportion of retained protein) and the stability of the catalyst (as measured by the residual activity) decrease with increasing hydrophobic character of the alcoholic solutions.

From the data obtained, it is evident that porous glass is not a suitable immobilized enzyme support for general use in aqueous organic solutions. Its rigid character does extend the viability of CT–glass–azo at high organic solvent concentrations, thereby avoiding the shrinkage problems encountered with Sephadex (1c). Nevertheless, overall CT–Sephadex is much preferable as a practical catalyst. Coupling of CT to Sephadex rather than porous glass provides a conjugate that has two-fold higher specific activity and that is considerably more stable, particularly in aqueous *tert*-butyl alcohol and DMSO for which the half-lives of CT–Sephadex are in excess of three months and 1 year respectively (1c). Clearly, however, many other carriers must be evaluated before optimum supports and coupling methods can be recommended with confidence for immobilized enzyme operations in aqueous organic solvents. Further work on this is to be carried out.

Acknowledgements

We are grateful to the Natural Sciences and Engineering Research Council of Canada for finan-

cial support of this work and for the award of a Science Scholarship to one of us (D.H.P.).

1. (*a*) J. B. JONES and I. J. JAKOVAC. Can. J. Chem. Submitted; (*b*) J. B. JONES. *In* Enzyme and non-enzymic catalysis. *Edited by* P. Dunnill, A. Wiseman, and N. Blakeborough. Ellis Horwood/J. Wiley, Rochester/New York. 1980. pp. 54–83; (*c*) D. H. PLIURA and J. B. JONES. Can. J. Chem. **58**, 2633 (1980).
2. M. DIXON and E. C. WEBB. Enzymes. 2nd ed. Longmans, London. 1964.
3. P. DOUZOU and C. BALNY. Proc. Natl. Acad. Sci. U.S.A. **74**, 2297 (1977).
4. K. TANIZAWA and M. L. BENDER. J. Biol. Chem. **249**, 2130 (1974).
5. C. R. LOWE. Eur. J. Biochem. **76**, 401 (1977).
6. (*a*) J.-M. ENGASSER and C. HORVATH. Biochemistry, **13**, 3845 (1974); **13**, 3849 (1974); (*b*) *In* Applied biochemistry and bioengineering. Vol. I. *Edited by* L. B. Wingard, Jr., E. Katchalski-Katzir, and L. Goldstein. Academic Press, New York. 1976. pp. 127–220; (*c*) Biochim. Biophys. Acta, **358**, 178 (1974); (*d*) J.-M. ENGASSER. Biochim. Biophys. Acta, **526**, 301 (1978).
7. H. WAN and C. HORVATH. Biochim. Biophys. Acta, **410**, 135 (1975).
8. K. MOSBACH (*Editor*). Methods Enzymol. **44** (1976).
9. J. F. KENNEDY and A. ROSEVEAR. J. Chem. Soc. Perkin Trans. II, 747 (1974).
10. M. A. MITZ and L. J. SUNMARIA. Nature, **189**, 576 (1961).
11. H. H. WEETALL. Methods Enzymol. **44**, 134 (1976).
12. L. GOLDSTEIN and G. MANECKE. *In* Applied biochemistry and bioengineering. Vol. I. *Edited by* L. B. Wingard, Jr., E. Katchalski-Katzir, and L. Goldstein. Academic Press, New York. 1976. pp. 23–127.
13. C. F. JACOBSEN, J. LEONIS, K. LINDERSTROM-LANG, and M. OTTENSEN. Methods in biochemical analysis. Vol. 4. *Edited by* D. Glick. Wiley-Interscience, New York. 1957. p. 171.
14. L. GOLDSTEIN. Methods Enzymol. **44**, 397 (1976).
15. R. GOLDMAN, O. KEDEM, I. H. SILMAN, S. R. CAPLAN, and E. KATCHALSKI. Biochemistry, **7**, 487 (1968).
16. R. AXEN, P.-A. MYRIN, and J. C. JANSON. Biopolymers, **9**, 401 (1970).
17. J. LASCH, L. BESSMETNAYA, L. V. KOZLOV, and V. K. ANTONOV. Eur. J. Biochem. **63**, 591 (1976).
18. M. K. WEIBEL and H. J. BRIGHT. Biochem. J. **124**, 801 (1971).
19. B. J. ROVITA and J. R. KITTRELL. Biotechnol. Bioeng. **15**, 143 (1973).
20. R. J. BROWN, H. E. SWAISGOOD, and H. R. HORTON. Biochemistry, **18**, 4901 (1979).
21. I. A. WEBSTER. Biotechnol. Bioeng. **22**, 2455 (1980).
22. A. M. FILBERT. Immobilized enzymes for industrial reactors. *Edited by* R. A. Messing. Academic, New York. 1975.

Clay chemistry: Investigation of thermodynamics of ion exchange reactions by titration calorimetry

GAVIN J. EWIN,[1] BRIAN P. ERNO,[2] AND LOREN G. HEPLER

Department of Chemistry and Oil Sands Research Laboratory, University of Lethbridge, Lethbridge, Alta., Canada T1K 3M4

Received November 19, 1980[3]

GAVIN J. EWIN, BRIAN P. ERNO, and LOREN G. HEPLER. Can. J. Chem. **59**, 2927 (1981).

We have built a titration calorimeter that is suitable for measurements on colloidal suspensions as well as more conventional chemical reactions in solution. This calorimeter has been used for investigation of a number of ion exchange reactions involving kaolinite and montmorillonite clays. Results of these measurements have led to cation exchange capacities, to enthalpies of ion exchange reactions, and also to equilibrium constants for some of these same reactions. These calorimetrically determined cation exchange capacities and equilibrium constants agree well with corresponding quantities obtained by way of conventional methods based on chemical analyses. It has been demonstrated that titration calorimetry is a useful and convenient method for investigation of ion exchange in clays.

GAVIN J. EWIN, BRIAN P. ERNO et LOREN G. HEPLER. Can. J. Chem. **59**, 2927 (1981).

Nous avons construit un calorimètre de titrage qui convient à la mesure des suspensions colloidales aussi bien qu'à celle des réactions chimiques conventionnelles en solution. On a utilisé ce calorimètre pour étudier un certain nombre de réactions d'échange d'ions impliquant des argiles à base de kaolinite et de montmorillonite. Les résultats de ces mesures ont conduit aux capacités d'échange de cations, aux enthalpies des réactions d'échange d'ions et également aux constantes d'équilibre de ces réactions. Ces constantes d'équilibre et ces capacités d'échange de cations déterminées par calorimétrie s'accordent bien avec les quantités correspondantes obtenues par des méthodes conventionnelles s'appuyant sur des analyses chimiques. On a démontré que le titrage par calorimétrie est une méthode utile et pratique d'étude de l'échange d'ions dans les argiles.

[Traduit par le journal]

Introduction

Ion exchange equilibria involving clays (also other minerals and synthetic substances) are important in such diverse fields as soil chemistry, disposal of radioactive wastes, treatment of industrial and municipal waste waters, properties of tailings from mineral extraction and oil sands plants, etc. Thermodynamic investigations of these ion exchange equilibria are useful in several ways. Knowledge of enthalpies and volumes permits calculation of the effects of temperature and pressure on such equilibria; conversely, investigations of ion exchange equilibria at different temperatures and pressures permit evaluation of enthalpies and volumes. Knowledge of thermodynamic quantities associated with ion exchange reactions can be combined with theoretical models to improve our understanding of such systems and processes. Also, as shown later in this paper, experimental methods that are commonly thought of as "thermodynamic" can be used as analytical tools.

Many investigations of ion exchange reactions of clay minerals are reviewed in excellent books (1–4). Various methods based on chemical analyses have been applied usefully to evaluation of equilibrium constants for ion exchange in clay systems. Some of these equilibrium investigations have been carried out at two or more temperatures with subsequent calculation of enthalpies and entropies. Although sound in principle, this latter approach is not entirely satisfactory in practice. Partly from studies (5, 6) of such "simple" equilibria as ionization of aqueous acids, it is now well known that very accurate equilibrium constants are required to withstand the magnification of uncertainties and errors that goes with differentiation as in $d \ln K/dT$.

Various investigators have applied ampoule or batch mixing calorimetry to the measurement of enthalpies of ion exchange reactions. Early investigations of this kind were carried out by Coleman (7, 8). Others, a few of whom we cite later, have applied similar calorimetric methods. These investigators have used the method of common final states, which requires multiple calorimetric measurements, or have used a combination of calorimetric results with results of separate equilibrium measurements on the same systems. Although such investigations have yielded useful results, we point out that these well established calorimetric methods are limited in that they lead only to enthalpies; other useful quantities such as cation exchange capacities and equilibrium constants must be determined separately.

Modern methods of titration calorimetry offer several advantages for investigation of ion ex-

[1]Present address: BP Australia Ltd., Port Melbourne, Victoria, Australia.

[2]Present address: PetroCanada, Calgary, Alta., Canada.

[3]Revision received June 26, 1981.

0008-4042/81/202927-07$01.00/0

©1981 National Research Council of Canada/Conseil national de recherches du Canada

Can. J. Chem. Downloaded from www.nrcresearchpress.com by 210.87.254.42 on 09/06/12
For personal use only.

Can. J. Chem. Downloaded from www.nrcresearchpress.com by 210.87.254.42 on 09/06/12
For personal use only.

change reactions. First, titration calorimeters are relatively easy to build or inexpensive to buy as compared to the microcalorimeters that have been used in many previous calorimetric investigations of ion exchange reactions. Second, previous applications (9–12) of titration calorimetry have demonstrated that this method can lead to both thermodynamic and analytical information about complex systems.

Ragland (13) has applied titration calorimetry to investigation of enthalpies of reaction of hydrogen and aluminum bentonites with aqueous sodium hydroxide. Because of uncertainties in the characterization of the clays used by Ragland and complications associated with acid–base reactions of clays, we will not be concerned with the details of his reported results, but we do emphasize that Ragland's early investigation demonstrated that titration calorimetry could lead to enthalpies *and* to cation exchange capacities of clays.

It is now well established (9–12) that calorimetric titrations can have endpoints similar to the endpoints observed in traditional titrimetry. As shown by Ragland (13) and also later in this paper, it is possible to use the endpoints observed in certain calorimetric titrations for evaluation of cation exchange capacities of clays.

Results of some calorimetric titrations also permit simultaneous evaluation of the enthalpies and equilibrium constants of reactions. The quantity of heat evolved or absorbed (enthalpy decrease or increase) as a result of mixing reactants is given by the molar ΔH of the calorimetric reaction multiplied by the number of moles that react. The number of moles that react is determined by the amounts and concentrations of various chemicals and by the equilibrium constant for the reaction. The results of appropriate calorimetric titrations can therefore be used in solving simultaneous equations for both the enthalpy and equilibrium constant for the calorimetric reaction. We call particular attention to the work of Christensen, Izatt, and colleagues (14–16), who have applied the method extensively and developed useful calculational procedures. A principal aim of the present investigation has been to apply this kind of titration calorimetry to the simultaneous determination of equilibrium constants and enthalpies for ion exchange reactions involving clays.

Experimental

The calorimetric reaction vessel consists of an inexpensive and replaceable 250 cm^3 polypropylene beaker suspended inside a stainless steel canister, which is submerged in a constant temperature bath maintained at 25.00°C for this investigation. Bath temperature was held constant to ±0.001°C for times longer than the duration of one calorimetric run.

The titration burette consists of a motor driven syringe having 20 cm^3 capacity and delivery rates adjustable from 0.5 to 20 cm^3 min^{-1}. Test experiments with different delivery rates, including halts in the titration, showed that chemical and thermal changes in most of our systems could keep up with a delivery rate of about 1 cm^3 min^{-1}. Most measurements were made with a delivery rate of 1.1258 ± 0.0014 cm^3 min^{-1}, accurately determined by weighing samples of water collected during accurately timed delivery intervals. Delivery of titrant from syringe to calorimeter is by way of a coil of Teflon tubing submerged in the constant temperature bath to ensure that titrant is at the temperature of the bath as it enters the calorimeter.

Our calorimeter has been constructed throughout to have low heat capacity along with minimal thermal lags and consequent rapid response. Because the systems we have expected to investigate are known to have widely different viscosities and mixing characteristics, we have included variable speed stirring with a choice of several different stirrer blade sizes and shapes.

Temperature in the calorimeter is measured with a 2000 ohm Fenwall rapid response thermistor enclosed in Teflon heat shrink tubing. This thermistor forms one arm of an operational amplifier self-balancing Wheatstone bridge (17). Noise and shunting effects were reduced by means of a 1 Hz single pole low pass filter (18). Temperature sensitivity varied from (1–5) × 10^{-5} K, depending on the stirring characteristics of the clay suspension in the calorimeter.

The calorimeter was calibrated electrically for each experiment. All timing was done automatically by electrical coupling with a Standard Electric clock, accurate to ±0.02 s.

Output data (bridge voltage or temperature versus volume of titrant added) from our first series of experiments were collected with a strip chart recorder. Readings from the strip chart were then used as input for a computer program[4] that calculates "corrected" enthalpy changes by allowing for enthalpies of dilution, which were measured separately, and for stirring effects. Output data from later experiments were obtained directly in digital form by way of an automatic digital printer.

Experimental accuracy and procedures for calculation were tested using the neutralization of dilute excess NaOH with HCl. Our results led to $\Delta H^0 = -55.80 \pm 0.20$ kJ mol^{-1}, in which ± indicates standard deviation, as compared with the previously selected (20, 21) best value, $\Delta H^0 = -55.815$ kJ mol^{-1}.

All chemicals used were of analytical reagent grade. Solutions of cations used in calorimetric titrations were made from corresponding chlorides dissolved in distilled water and analyzed by thermometric titration with suitable titrants as described by Vaughan (10) and also by more traditional volumetric methods. Sodium and potassium determinations were carried out with a Corning 450 Flame Photometer.

Fisher K-3 "colloidal kaolin" from Florida was used as starting material for preparation of Na^+-kaolinite and NH_4^+-kaolinite, following procedures similar to those previously described by Ferris and Jepson (22).

Wyoming montmorillonite (VOLCLAY KWK, American Colloid Co.) was thoroughly dispersed in distilled water by stirring for several hours. The resulting suspension contained about 4% clay. Centrifuging this suspension for an hour at 2000 g gave a sediment consisting of a small amount of coarse black particles at the bottom of the centrifuge bottle and two other well

[4]Our computer program is a modified version of a procedure reported earlier by Christensen and Izatt (19).

Can. J. Chem. Downloaded from www.nrcresearchpress.com by 210.87.254.42 on 09/06/12
For personal use only.

defined layers. The upper yellow–white layer was removed for further treatment. This yellow–white clay was mixed with acetic acid – sodium acetate buffer (pH = 3.8 at room temperature) and then maintained with stirring at 70°C for 3 h to remove soluble impurities. The suspension was then allowed to stand at room temperature for 3 days before the clay was recovered by centrifuging. The recovered clay was dispersed in 1 *M* NaCl solution, adjusted to pH = 7 with NaOH, and recovered by centrifuging again. This NaCl treatment was repeated and followed by several washings with distilled water. Finally, suspensions of the clay in distilled water were concentrated to 2% clay by use of an Amicon Model DC3 hollow fiber ultrafiltration unit.

All solutions in which clays were suspended were analyzed for Na^+, for which concentrations were found to range between 0.0008 and 0.011 *M*.

Most calorimetric measurements described in this paper were carried out with 20 g of Na^+-kaolinite suspended in 180 g of water or with 2 g of Na^+-montmorillonite suspended in 198 g of water. Most calorimetric titrant solutions were 0.1 *M* solutions of MCl_n salts.

Results

Calorimetric titrations of suspensions of Na^+-clays with solutions of divalent or trivalent chlorides lead to nearly linear endothermic thermograms that show moderately sharp "breaks" typical of endpoints in many kinds of titrations. We analyze these thermograms in terms of ion exchange reactions represented generally by

[1] $M^{n+}(aq) + nNa^+\text{-clay} = M^{n+}\text{-clay}_n + nNa^+(aq)$

The straight part of the thermogram is consistent with the equilibrium constant for the exchange reaction [1] being sufficiently large that nearly all added $M^{n+}(aq)$ is exchanged up to the break. Taking the exchange reaction to be complete at the break, which we now call an endpoint, permits calculation of the cation exchange capacity from our knowledge of the amount and concentration of added titrant and the amount of clay in the calorimeter. Results of these determinations of cation exchange capacities are summarized in Table 1. We have also determined cation exchange capacities of these same clays by means of conventional chemical analyses, with results in agreement (better than ±4%) with those shown in Table 1. We also note that our calorimetrically determined cation exchange capacities are within the ranges of values found by previous investigators of similar clays, as summarized by Marshall (1) and Grim (23).

TABLE 1. Cation exchange capacities of Na^+-clays

Clay	Replacing cation	Cation exchange capacity, μmol Na^+ g^{-1}
Kaolinite	Mg^{2+}	35.2±0.6
	Ca^{2+}	35.6±0.5
Montmorillonite	Mg^{2+}	780±40
	Ca^{2+}	800±50
	La^{3+}	730±30

As stated above, we have interpreted the breaks in our thermograms as endpoints associated with M^{n+}/Na^+ exchange reactions. Subsequent measurements and data analyses by Schramm and Kwak (24) have shown that effects of tactoid formation and not-quite-complete exchange should also be considered. Although it is probable that detailed consideration of these effects (24) would improve the agreement (now better than ±4%) between our calorimetrically evaluated cation exchange capacities and those obtained more accurately (and more laboriously) by chemical analyses, we will in this paper retain our initial simple interpretation and use the values for cation exchange capacities listed in Table 1.

Because nearly all of the added $M^{n+}(aq)$ is exchanged at any point along the linear portion of the titration thermogram (before the endpoint), it is also possible to obtain the desired enthalpy for the exchange reaction [1] quite simply from

[2] $\Delta H = Q/r$

in which Q represents the total heat evolved or absorbed at any point and r represents the number of moles of $M^{n+}(aq)$ that have exchanged (reacted), with r being almost exactly equal to the number of moles of $M^{n+}(aq)$ added. Results are summarized in Table 2.

Calorimetric titrations of suspensions of Na^+-clays with solutions of monovalent chlorides lead to curved thermograms, which do not exhibit endpoints. It is intended to obtain from such thermograms the enthalpies *and* equilibrium constants of the ion exchange reactions represented generally by

[3] $M^+(aq) + Na^+\text{-clay} = M^+\text{-clay} + Na^+(aq)$

The equilibrium constant for the exchange reaction [3] is

[4] $K = (a_{M^+\text{-clay}})(a_{Na^+})/(a_{Na^+\text{-clay}})(a_{M^+})$

in which the terms in parentheses represent the indicated thermodynamic activities. We will take ratios of activity coefficients for $Na^+(aq)/M^+(aq)$ and for M^+-clay/Na^+-clay to be unity so that [4] becomes

[5] $K = [M^+\text{-clay}][Na^+]/[Na^+\text{-clay}][M^+]$

and thence

[6] $K = (f_{M^+})[Na^+]/(f_{Na^+})[M^+]$

TABLE 2. Thermodynamics of exchange of M^{n+} on Na^+-clays at 25°C, as represented by eq. [1][a]

Clay	M^{n+}	ΔH kJ (mol M^{n+})$^{-1}$			
Kaolinite	Mg^{2+}	5.65±0.25			
	Ca^{2+}	5.48±0.30			
	Ba^{2+}	4.10±0.30			
	La^{3+}	15.6±0.4			
Montmorillonite	Mg^{2+}		2.4±0.4	(10.9)[b]	
	Ca^{2+}	3.4±0.8	(10.2)[b]	(3.44, 2.82)[c]	(3.3)[d]
	Ba^{2+}		3.2±0.4	(5.7)[b]	
	La^{3+}		9.7±0.5		

[a] All values without superscripts are based on our present work.
[b] Reference 27.
[c] Reference 28.
[d] Reference 24.

in which square brackets indicate molarities and f_{M^+} and f_{Na^+} represent fractions of the clay in the M^+ and Na^+ forms. The equilibrium constant for the exchange reaction [3] can also be expressed as

$$[7] \quad K = [r][r + (Na^+)_i V_i]/[W \cdot CEC - r][TV_a - r]$$

in which the symbols have the following meanings and are conveniently expressed in the indicated units: r: number of moles of M^+ that react (exchange), in mol; $(Na^+)_i$: initial concentration of Na^+(aq) in the suspending solution in mol/L; V_i: the initial volume of suspension in L; W: the mass of Na^+-clay initially present in g; CEC: cation exchange capacity; moles exchangeable Na^+/g of clay; T: concentration of titrant solution in mol/L; and V_a: volume of titrant solution added in L.

It is possible to use the values of Q and V_a from any two points on a thermogram in eqs. [2] and [7] to obtain the desired values of K and ΔH^0; we have carried out such calculations using a large number (usually 28) of such points as follows. First, we have chosen an arbitrary value of K and then used eq. [7] in calculating the values of r that correspond to each of the selected points along the titration thermogram. Next, these values of r were used with corresponding values of Q in eq. [2] to obtain a value of ΔH corresponding to each of the selected points along the titration thermogram. This sequence of calculations was then repeated with various other selected values of K. Finally, the "best" value of K was taken to be the value that leads to the most consistent (as judged by standard deviation) ΔH. Some practical procedures for carrying out these calculations have been cited by Eatough, Izatt, and Christensen (15). Our results are summarized in Table 3.

Several tests of the results summarized in Table 3 are possible; we have done the following. First, we have determined equilibrium constants for all of the exchange reactions by means of chemical analyses for Na^+(aq) and M^+(aq) in various solutions at equilibrium. Values of these conventionally determined equilibrium constants, which have uncertainties smaller than those indicated in Table 3, are all in agreement with the listed values that have been determined calorimetrically. It is also possible to use these conventionally determined equilibrium constants in eq. [7] for calculation of values of r at various points along the thermogram and then apply eq. [2] to obtain ΔH values. All ΔH values so obtained are in good agreement with the values listed in Table 3. The values of ΔH calculated in this latter way have somewhat smaller uncertainties than the values listed in Table 3, because the latter procedure requires evaluation of only one quantity (ΔH) instead of two (K and ΔH) from a single thermogram.

Next, we have combined results from Table 3 for exchange of Cs^+(aq) and NH_4^+(aq) with Na^+-kaolinite to obtain the following calculated equilibrium constant and ΔH for exchange of Cs^+(aq) with NH_4^+-kaolinite:

$$[8] \quad Cs^+(aq) + NH_4^+\text{-kaol} = Cs^+\text{-kaol} + NH_4^+(aq)$$

$$K = 3.2$$

$$\Delta H = -8.4 \pm 1.4 \text{ kJ mol}^{-1}$$

Direct calorimetric titration of NH_4^+-kaolinite with a solution of CsCl led to $K = 3.2$ and $\Delta H = -10.7 \pm 1.3$ kJ mol^{-1} for the reaction represented by eq. [8]. The two independent K values are in excellent agreement and the two ΔH values agree within their stated uncertainties.

Discussion

Test measurements with our calorimeter on "simple" chemical systems, such as the acid–base neutralization reaction mentioned earlier, have demonstrated that purely calorimetric uncertain-

Can. J. Chem. Downloaded from www.nrcresearchpress.com by 210.87.254.42 on 09/06/12
For personal use only.

TABLE 3. Thermodynamics of exchange of M^+ on Na^+-clays at 25°C, as represented by eq. [3][a]

Clay	M^+	K	ΔH kJ mol^{-1}	ΔS^0 J K^{-1} mol^{-1}
Kaolinite	K^+	1.5±0.2	−12.1±1	−37±3
	NH_4^+	1.0±0.1	−11.9±1	−40±3
	Cs^+	3.2±0.5	−20.3±1	−58±4
Montmorillonite	K^+	1.9±0.4	−5.3±0.4	−12±2
			(−4.1)[b]	
			(−4.9)[c]	
			(−4.8, −4.5, −2.5)[d]	
			(−5.9)[e]	
	Cs^+	2.6±0.3	−18.4±0.8	−54±3
			(−16.3)[b]	
			(−11.0)[c]	
			(−11.1, −16.1, −18.2)[d]	
			(−14.3)[e]	

[a] All values without superscripts are based on our present work.
[b] Reference 29.
[c] Reference 30.
[d] Reference 31.
[e] Reference 24.

ties for homogeneous systems without stirring problems range from about 0.2% to about 1% for ΔT values in the range we have investigated. Actual uncertainties in results we have reported in Tables 2 and 3 are larger than these purely calorimetric uncertainties, for reasons that are outlined below.

Our application of eq. [2] to the linear portions of thermograms from titration of Na^+-clay with M^{n+}(aq) implies that the enthalpy of exchange is independent of the extent of exchange that is represented by r. Partly because this implication is not exactly correct and partly because of a small scatter in our results that we attribute mostly to heats of stirring, the standard deviations indicated by ± in Table 2 are significantly larger than purely calorimetric uncertainties cited in the preceding paragraph. All of these ΔH values in Table 2 are to be regarded as average values for fraction exchanged equal to zero up to fraction exchanged nearly equal to unity.

We have assumed in our derivation of eq. [7] that the ratios of activity coefficients for Na^+(aq)/M^+(aq) and for M^+-clay/Na^+-clay are unity. This assumption for Na^+(aq)/M^+(aq) is quite accurate for the dilute solutions used in this investigation and can be neglected as a source of significant error. On the other hand, Argersinger, Davidson, and Bonner (25) and Gaines and Thomas (26) have shown that the ratio of activity coefficients for M^+-clay/Na^+-clay is not necessarily unity, which means that the equilibrium "constants" we have used are not necessarily independent of the extent of exchange of M^+ for Na^+. Similarly, the enthalpies of exchange are not necessarily constant, being expected to vary a little with extent of exchange.

At the beginning of a calorimetric titration of Na^+-clay with MCl(aq) all of the clay is in the sodium form and the fraction converted to the M^+ form (f_{M^+}) is zero. At the end of a calorimetric titration ($V_a \leq 0.020$ L), f_{M^+} (calculated conveniently as $r/\text{CEC}\cdot W$) might be as large as 0.6 but was typically less than 0.5. Our analyses of calorimetric titration thermograms in terms of eqs. [2] and [7] therefore yield average values of the equilibrium "constant" and enthalpy of exchange that refer to f_{M^+} values in the range from zero to less than 0.5. The standard deviations indicated by ± values in Table 3 are expected to be a good indication of uncertainties in these *average* values for equilibrium "constants" and corresponding enthalpies of exchange. Results of a considerable number of investigators who have applied the method of Gaines and Thomas (26) to determination of true thermodynamic equilibrium constants permit us to estimate that the further uncertainties resulting from our approximation concerning the activity ratio for M^+-clay/Na^+-clay are approximately the same size as the cited standard deviations, thus making the *total* uncertainties in our thermodynamic K and ΔH values equal to about twice the standard deviations.

We now turn to comparison of some of our results in Tables 2 and 3 with results of earlier investigations.

Our ΔH values for exchange of M^{2+} on Na^+-montmorillonite (Table 2) are distinctly smaller than corresponding values reported by Laudelot, Van Bladel, Bolt, and Page (27), but are in close agreement with more recently reported values from

Can. J. Chem. Downloaded from www.nrcresearchpress.com by 210.87.254.42 on 09/06/12
For personal use only.

Can. J. Chem. Downloaded from www.nrcresearchpress.com by 210.87.254.42 on 09/06/12
For personal use only.

Maes and Cremers (28) and Schramm and Kwak (24).

Our ΔH value for exchange of K^+ on Na-montmorillonite (Table 3) is in good agreement with the results of four investigations (24, 29–31) of five different montmorillonites. However, our ΔH is considerably more exothermic than the value found in one investigation (31) of one montmorillonite.

Our ΔH value for exchange of Cs^+ on Na-montmorillonite is in good agreement with results of two other investigations (29, 31) of three montmorillonites. However, our ΔH is also considerably more exothermic than the values reported for three other montmorillonites (24, 30, 31).

On the basis of the above comparisons and also the results of our test of internal consistency involving exchanges of Cs^+, NH_4^+, and Na^+ on kaolinite, we conclude that our ΔH values have about the same accuracy and reliability as similar values from other calorimetric investigations. In this connection we note that only a few previous investigators have carried out consistency checks similar to our investigations of exchange of Cs^+, NH_4^+, and Na^+ on kaolinite; of these, we call attention to four such investigations (24, 29, 30, 32) leading to internal consistencies about the same as ours.

The enthalpies of exchange of M^{2+}(aq) and La^{3+}(aq) with Na^+-clay are all endothermic. Because the equilibrium constants for these exchanges are all larger than unity, corresponding to negative values of ΔG^0, we see that all of these exchanges are "entropy driven" with values of $T\Delta S^0$ that are larger than the corresponding values of ΔH.

The results in Table 3 for M^+/Na^+ exchange show that there is partial compensation between ΔH and $T\Delta S^0$ so that ΔG^0 is nearer zero than either ΔH or $T\Delta S^0$. This kind of enthalpy–entropy compensation has been observed before for ion exchange reactions and also for many other reactions (33–44).

Summary

The principal point of this paper has been to demonstrate that titration calorimetry can lead to satisfactorily accurate determinations of cation exchange capacities and equilibrium constants for ion exchange reactions as well as the enthalpies of exchange that are commonly determined by other calorimetric methods. Further, it is our experience that such determinations using titration calorimetry can be carried out more quickly than the traditional determinations that depend heavily on various chemical analyses.

We have also provided some thermodynamic results for ion exchange in certain clay systems.

Finally, we suggest that application of methods similar to those described here to ion exchange reactions on various synthetic substances is likely to be useful.

Acknowledgements

We are grateful to the Alberta Oil Sands Technology and Research Authority and the Natural Sciences and Engineering Research Council of Canada for support of different parts of our research on clay chemistry.

1. C. E. MARSHALL. The physical chemistry and mineralogy of soils. Vol. I: soil materials. Robert E. Krieger Publ. Co., Huntington, N.Y. 1975. Reprint of 1964 edition.
2. R. M. GARRELS and C. L. CHRIST. Solutions, minerals, and equilibria. Harper and Row, New York. 1965.
3. W. STUMM and J. J. MORGAN. Aquatic chemistry: an introduction emphasizing chemical equilibria in natural waters. Wiley–Interscience, New York. 1970.
4. S. YARIV and H. CROSS. Geochemistry of colloid systems. Springer-Verlag, New York. 1979.
5. J. W. LARSON and L. G. HEPLER. *In* Solute–solvent interactions. *Edited by* J. F. Coetzee and C. D. Ritchie. Marcel Dekker, New York. 1969. chapt. 1.
6. L. G. HEPLER and E. M. WOOLLEY. *In* Water: a comprehensive treatise. Vol. 3. *Edited by* F. Franks. Plenum, New York. 1973. Chapt. 3.
7. N. T. COLEMAN. Soil Sci. **74**, 115 (1952).
8. N. T. COLEMAN and M. E. HARWARD. J. Am. Chem. Soc. **75**, 6045 (1953).
9. H. J. V. TYRRELL and A. E. BEEZER. Thermometric titrimetry. Chapman and Hall, London. 1968.
10. G. A. VAUGHAN. Thermometric and enthalpimetric titrimetry. Van Nostrand Reinhold, London. 1973.
11. L. D. HANSEN, R. M. IZATT, and J. J. CHRISTENSEN. *In* New developments in titrimetry. *Edited by* J. Jordan. Marcel Dekker, New York. 1975.
12. R. N. HEISTAND. Rev. Anal. Chem. **2**, 195 (1974/5).
13. J. J. RAGLAND. Soil Sci. Soc. Am. Proc. **26**, 133 (1962).
14. R. M. IZATT, D. EATOUGH, R. L. SNOW, and J. J. CHRISTENSEN. J. Phys. Chem. **72**, 1208 (1968).
15. D. J. EATOUGH, R. M. IZATT, and J. J. CHRISTENSEN. Thermochim. Acta, **3**, 233 (1972).
16. R. M. IZATT, J. D. LAMB, N. E. IZATT, B. E. ROSSITER, JR., J. J. CHRISTENSEN, and B. L. HAYMORE. J. Am. Chem. Soc. **101**, 6273 (1979).
17. O. GINSTRUP. Chem. Script. **3**, 97 (1973).
18. L. D. BOWER and P. W. CARR. Thermochim. Acta, **10**, 129 (1974).
19. J. J. CHRISTENSEN and R. M. IZATT. J. Phys. Chem. **66**, 1030 (1962).
20. G. OLOFSSON and L. G. HEPLER. J. Solution Chem. **4**, 127 (1975).
21. P. J. CERUTTI, H. C. KO, K. G. MCCURDY, and L. G. HEPLER. Can. J. Chem. **56**, 3084 (1978).
22. A. P. FERRIS and W. B. JEPSON. J. Coll. Interf. Sci. **51**, 245 (1975).
23. R. E. GRIM. Clay mineralogy. 2nd ed. McGraw-Hill, New York. 1968.
24. L. L. SCHRAMM and J. C. T. KWAK. To be published; L. L. SCHRAMM. Ph.D. Thesis, Dalhousie University. 1980.

25. W. J. ARGERSINGER, JR., A. W. DAVIDSON, and O. D. BONNER. Trans. Kansas Acad. Sci. **53**, 404 (1950).
26. G. L. GAINES, JR. and H. C. THOMAS. J. Chem. Phys. **21**, 714 (1953).
27. H. LAUDELOT, R. VAN BLADEL, G. H. BOLT, and A. L. PAGE. Trans. Faraday Soc. **64**, 1477 (1968).
28. A. MAES and A. CREMERS. J. Chem. Soc. Faraday Trans. I, **73**, 1807 (1977).
29. H. MARTIN and H. LAUDELOT. J. Chim. Phys. Phys.-Biol. **76**, 1086 (1963).
30. R. G. GAST. Soil Sci. Soc. Am. Proc. **36**, 14 (1972).
31. A. MAES and A. CREMERS. J. Chem. Soc. Faraday Trans. I, **74**, 1234 (1978).
32. R. J. LEWIS and H. C. THOMAS. J. Phys. Chem. **67**, 1781 (1963).
33. W. B. PERSON. J. Am. Chem. Soc. **84**, 536 (1962).
34. O. EXNER. Coll. Czech. Chem. Commun. **29**, 1094 (1964).
35. I. P. GOL'DSHTEIN, E. GUR'YONOVA, and E. S. SHCHERBAKOVA. Russ. J. Gen. Chem. **40**, 166 (1968).
36. R. LUMRY and S. RAJENDER. Biopolymers, **9**, 1125 (1970).
37. L. G. HEPLER. J. Am. Chem. Soc. **85**, 3089 (1963); J. Phys. Chem. **68**, 2645 (1964); Can. J. Chem. **49**, 2803 (1971).
38. C. JOLICOEUR and P. R. PHILIP. Can. J. Chem. **52**, 1834 (1974).
39. A. K. CHATTOPADHYAY, A. BHATTACHARYYA, and S. C. LAHIRI. Z. Phys. Chem. N. F. **102**, 151 (1976).
40. D. PATTERSON and M. BARBE. J. Phys. Chem. **80**, 2435 (1976).
41. J. W. LARSON, W. J. PLYMALE, and A. F. JOSEPH. J. Phys. Chem. **81**, 2074 (1977).
42. G. I. MUKHAYER and S. S. DAVIS. J. Coll. Interf. Sci. **61**, 582 (1977).
43. W. R. FAWCETT and T. M. KRYGOWSKI. J. Electronanal. Chem. **77**, 47 (1977).
44. P. C. CHUN, E. E. SAFFEN, JR., and J. Q. OESWEIN. Biophys. Chem. **10**, 129 (1979).

Can. J. Chem. Downloaded from www.nrcresearchpress.com by 210.87.254.42 on 09/06/12
For personal use only.

Synthesis of fluorescent probe – carbohydrate conjugates[1]

MANSUR YALPANI[2] AND LAURANCE D. HALL
Department of Chemistry, University of British Columbia, Vancouver, B.C., Canada V6T 1Y6

Received May 6, 1981

MANSUR YALPANI and LAURANCE D. HALL. Can. J. Chem. **59**, 2934 (1981).

A new type of luminescent label has been synthesized and a range of carbohydrates has been derivatized with various fluorescent probes. Amine-containing labels were readily transformed with chloroacetylchloride into the corresponding fluorescent chloroacetamide reagents **1–4**. Suitably blocked monosaccharides containing either a free thio **9**, hydroxyl **11**, or carboxyl **17** functionality have been conjugated with (*a*) 4-chloroacetamido labels **1** and **2**, (*b*) with 4-aminobenzophenone **5**, and (*c*) with 1-dimethyl-1-aminonaphthalene-5-sulfonylchloride **21**, to form the fluorescent carbohydrate conjugates **10**, **16**, **18**, and **20**. Direct derivatization of the unblocked disaccharides **22** and **23** was achieved by reductive amination with amines **5** and **7** and sodium cyanoborohydride affording the 1-deoxyglycit-1-yl derivatives **24–26**, which were characterized by ^{13}C nmr spectroscopy. The synthesis of fluorescent polysaccharides is exemplified by the condensation of 9-anthraldehyde with chitosan either via Schiff's base formation to afford **32**, or via reductive alkylation to form **33**.

MANSUR YALPANI et LAURANCE D. HALL. Can. J. Chem. **59**, 2934 (1981).

On a synthétisé un nouveau type de marqueur luminescent et l'on a attaché divers groupes fluorescents à des hydrates de carbone. Les marqueurs contenant des amines réagissent facilement avec le chlorure de chloroacétyle et donnent les réactifs chloroacétamides correspondants **1–4**. On a fait réagir des monosaccharides convenablement protégés comportant soit des groupes thio (**9**) soit des groupes hydroxyles (**11**) ou des groupes carbonyles (**17**) (*a*) avec les marqueurs chloroacétamido-4 **1** et **2**, (*b*) avec l'amino-4 benzophénone **5** et (*c*) avec le chlorure de diméthylamino-1 naphthalène sulfonyle-5 **21** pour former des hydrates de carbone conjugués fluorescents **10**, **16**, **18** et **20**. On a formé des dérivés des disaccharides non protégés **22** et **23** en procédant à une amination réductrice par les amines **5** et **7** en présence de cyanoborohydrure de sodium; il y a formation de dérivés déoxy-1 glycityle-1 **24–26** que l'on a caractérisé par la spectroscopie de rmn du ^{13}C. On a utilisé comme exemple de synthèse de polysaccharides fluorescents, la condensation de l'anthraldehyde-9 avec le chitosane soit par l'intermédiaire de la formation d'une base de Schiff qui conduit au composé **32** ou par l'alkylation réductrice pour aboutir au composé **33**.

[Traduit par le journal]

Introduction

The complexity of many biologically important carbohydrates has prompted the development in recent years of new analytical techniques for their characterization. Spectroscopic methods based on either fluorescence or magnetic resonance are particularly attractive in this regard in view of the wealth of information which they can provide at the molecular level. Fluorescent carbohydrate conjugates have received considerable attention in a variety of fields ranging from studies of cell surface topography (2), membrane transport (3), polysaccharide mobility (4), and gelling mechanism (5), to the analysis of glycoproteins (6). Concurrently, the need has arisen for a broader spectrum of labelling methods and reagents (7, 8).

As part of our interest in synthetic methods for the specific labelling of complex, carbohydrate-containing systems (9), we describe here the synthesis of a new type of luminescent reagent as well as typical protocols whereby mono-, oligo-, and poly-saccharides can be transformed into the corresponding luminescent derivatives. Emphasis was directed in this work towards methods which require relatively mild reaction conditions, including some which operate in aqueous media.

Results and Discussion

A series of luminescent probes **1–4** were readily prepared by the reaction of the luminescent amines (10) **5–8** with chloroacetylchloride in ethyl acetate or diethyl ether under reflux, followed by concentration at ambient temperature using a stream of dry nitrogen. The chloroacetamide derivatives **1–4** were obtained in good to high yields (59–100%), and constitute a versatile type of reagent which can be employed for the alkylation of thiol, amino, or hydroxyl functionalities under appropriate reaction conditions. Being less reactive than the equivalent iodoacetamides (11), these reagents offer the advantage of greater selectivity.

This selectivity was demonstrated using as an exemplar label **1**, which readily condensed with the thiosugar tetraacetate **9** in boiling chloroform in the presence of solid sodium bicarbonate to afford **10** in good yield. In contrast, neither *N*- or *O*-alkylation could be accomplished under similar conditions; thus, the luminescent probes **1** and **2** failed to react when either the partially blocked primary and

[1]Aspects of this work were presented at the 62nd Canadian Chemical Conference, Vancouver, Canada, June 3–9, 1979; for a preliminary communication on this work, see ref. 1.

[2]Present address: Department of Pathology, University of British Columbia, Vancouver, B.C., Canada V6T 1W5.

0008-4042/81/202934-06$01.00/0
©1981 National Research Council of Canada/Conseil national de recherches du Canada

Can. J. Chem. Downloaded from www.nrcresearchpress.com by 210.87.254.5 on 09/06/12
For personal use only.

Can. J. Chem. Downloaded from www.nrcresearchpress.com by 210.87.254.5 on 09/06/12
For personal use only.

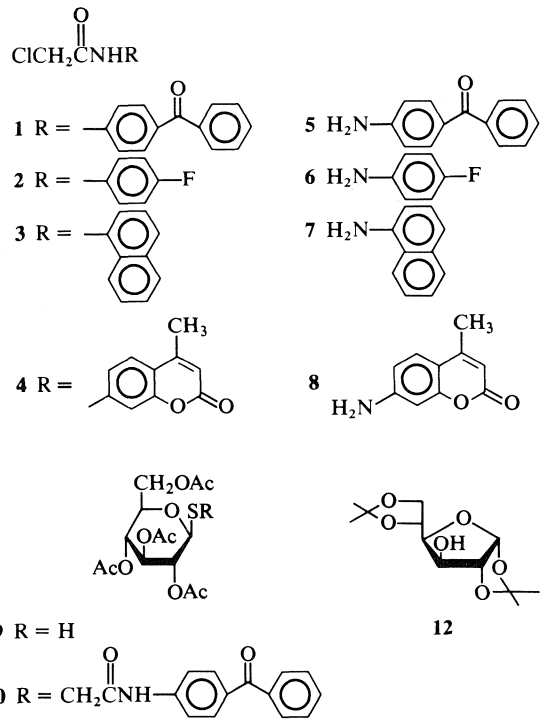

secondary alcohols **11–14** or the amino sugar **15** were used. However, the ether **16** was produced, from condensation of the diisopropylidene galacto derivative **11** and **2** using sodium hydride in dimethyl formamide (12).

Amide-linked luminescent derivatives were obtained via carbodiimide-mediated coupling (13); for example, reaction of the D-galacturonic acid derivative **17** with amine **5** in dichloromethane solution gave the amide **18** in acceptable yield[3] (48%) upon treatment with dicyclohexylcarbodiimide.

The intense fluorescence of 5-dimethylamino-1-naphthalene sulfonyl (DANSYL) derivatives has previously been exploited for the investigation of several carbohydrate systems (7, 14) and in this study the sulfonate ester derivative **20** was prepared in high yield (73%) by condensation of the D-galactose derivative **11** with DANSYL-chloride **21** in acetone with triethylamine as base acceptor. However, because attempts to remove the isopropylidene blocking groups of the crystalline derivative **20** were unsuccessful, this particular approach was not pursued further. More recently, Zissis and Glaudemanns (7) have reported methods for the direct dansylation of the primary hydroxyl function of methyl-β-D-galactopyranoside to afford an amorphous product.

Complementary to the foregoing procedures are methods for selectively labelling unprotected sugars in polar media. Aldehydo- or keto-sugars, for example, are readily derivatized using the versatile reductive amination reaction (15). We found that condensation of amine-containing fluorescent probes with disaccharides proceeded in excellent yields in refluxing methanol with sodium cyanoborohydride as reducing agent. Facile conversion of lactose **22** and cellobiose **23** into the corresponding luminescent derivatives **24** and **25**, and **26**, respectively, was observed. These products were obtained even under conditions which were not strictly anhydrous, e.g. by employing commercial samples of β-lactose or nonanhydrous methanol. The luminescent disaccharide derivatives were isolated by column chromatography on silica gel and were further characterized as their nonaacetates.

The 1-deoxyglycit-1-yl derivatives were also characterized by ^{13}C nmr spectroscopy. The ^{13}C chemical shifts of the carbohydrate moieties together with their assignments are gathered in Table 1. The assignments are based on off-resonance

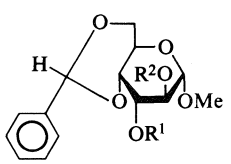

13 R^1 = H, R^2 = Me
14 R^1 = Me, R^2 = H

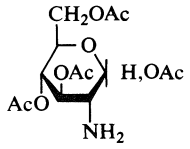

15

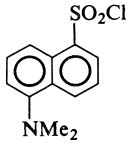

21

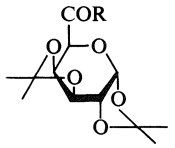

17 R = OH

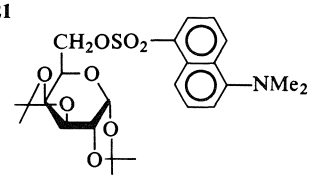

20

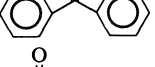

19 R = $N(C_6H_{11})CNHC_6H_{11}$

[3]We have generally obtained essentially quantitative yields for amidations of various water soluble carbohydrates, including polysaccharides, by employing the equivalent water soluble carbodiimides (e.g. 1-ethyl-3-(3-dimethylaminopropyl)-carbodiimide; the higher yields may be chiefly attributed to suppression of *N*-acylurea by-product formation (e.g. **19**) (13).

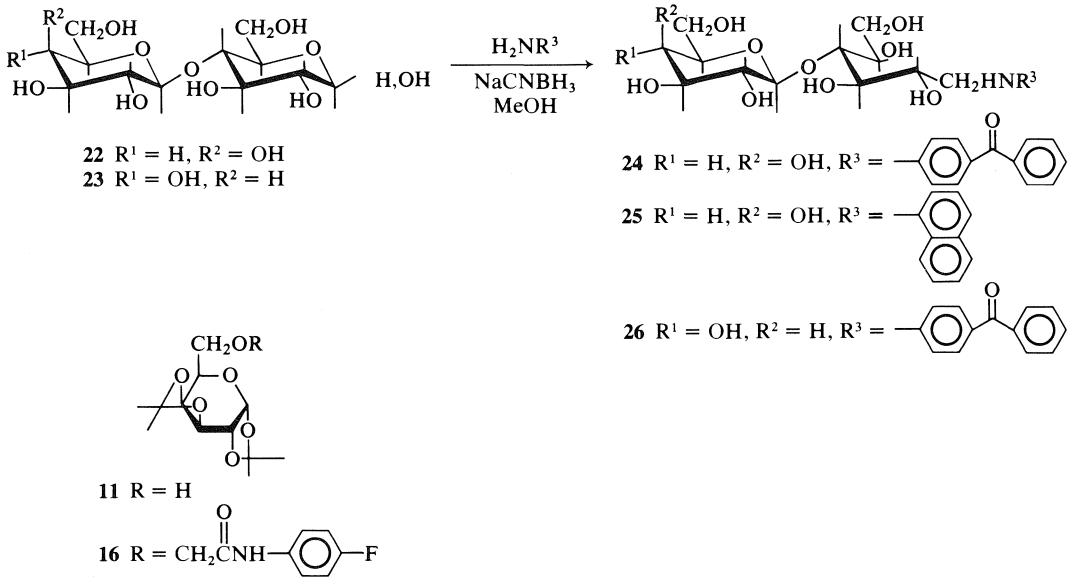

decoupling experiments and comparison with data recently reported by Pfeffer *et al.* (16) as well as from ^{13}C nmr results obtained from branched 1-deoxyglycit-1-yl chitosan derivatives (9, 17). The fact that the C-1′ resonances of the fluorescent derivatives exhibit a downfield shift relative to the corresponding alkyl derivatives of Hoagland *et al.* (18) can be attributed to the presence of the aromatic moieties.

The luminescent disaccharide derivatives exhibited a pH-dependence, similar to that observed by Hoagland *et al.* (18) at high pH, in which peak-splitting was observed on lowering the pH from 7.5 to 6.5. These pH-induced splittings occurred for the resonances of C-1, C-1′, C-4′, C-5, C-6, and C-6′ of all three derivatives. We are unable, however, to offer a plausible explanation for this effect, which Hoagland *et al.* (18) proposed to be due to "restricted intermolecular interactions".

The selective labelling of chitosan was accomplished using the reductive amination procedure. Thus, condensation of chitosan **28** with 9-anthraldehyde **29** in aqueous acetic acid – methanol (1:1) produced a stiff gel, which, after purification by extensive washing, afforded the fluorescent Schiff's

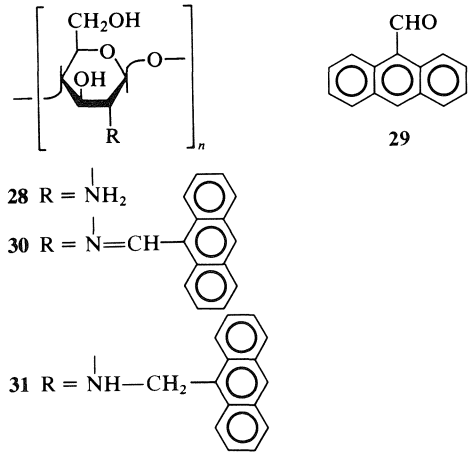

TABLE 1. ^{13}C chemical shifts (ppm) of carbohydrate residues of luminescent 1-deoxyglycit-1-yl derivatives[a]

	β-D-galactopyranosyl						1-Deoxy-D-glycit-1-yl					
Compound	C-1	C-2	C-3	C-4	C-5	C-6	C-1′	C-2′	C-3′	C-4′	C-5′	C-6′
24[b,c]	104.13	71.95	73.47	69.35	75.79	61.56	46.14	71.06	72.25	82.20	71.17	62.97
25[b,c]	103.87	71.76	73.39	69.28	75.78	61.54	47.44	70.65	72.09	81.87	71.17	62.94
	β-D-glucopyranosyl						1-Deoxy-D-glycit-1-yl					
	C-1	C-2	C-3	C-4	C-5	C-6	C-1′	C-2′	C-3′	C-4′	C-5′	C-6′
26[d]	103.54	74.21	76.44	70.13	76.69	61.33	46.14	72.18	75.79	80.94	71.39	62.94

[a] In D_2O referenced to internal 1,4-dioxane at 67.40 ppm.
[b] $(Ph)_2C{=}O$ 198.28 ppm.
[c] Twelve resonances of aromatic carbons between 133.60 and 154.35 ppm (21).
[d] Nine resonances of aromatic carbons between 131.85 and 147.17 ppm (22).

Can. J. Chem. Downloaded from www.nrcresearchpress.com by 210.87.254.5 on 09/06/12
For personal use only.

Can. J. Chem. Downloaded from www.nrcresearchpress.com by 210.87.254.5 on 09/06/12
For personal use only.

base derivative **30**. The degree of substitution (ds 0.73) of **30** was determined by elemental microanalysis. The imine moiety of **30** could be further stabilized against hydrolysis by reduction with sodium cyanoborohydride to yield **31**. Alternatively **31** was obtained directly by reductive alkylation of **28**.

Conclusions

Of the above methods for labelling partially blocked monosaccharide derivatives, alkylation with luminescent chloroacetamide reagents seems to offer a somewhat greater potential, in terms of overall facility and selectivity, than either dansylations or carbodiimide-mediated amidations. Based on the results described here and in the literature (14), we consider specific derivatization of the reducing end of mono- or oligo-saccharides, via either Schiff's base formation or reductive amination using sodium cyanoborohydride, to be the method of choice in view of the mild reaction conditions, the excellent yields, and the convenience of using unblocked sugars. The advantages of the latter approach are further emphasized when complex carbohydrate-containing systems, such as polysaccharides, are to be labelled. Insofar as the yields reported here for chitosan are typical of those we have obtained for other similar polysaccharide derivatizations (9, 17, 19), we believe that this method will find general application in covalent labelling of many sugar-containing systems.

Experimental

General Methods and Materials

All solutions were concentrated using a Buchi rotary evaporator unless otherwise stated. All melting points were measured using a Thomas Hoover Unimelt instrument (Model 6406-K) and are corrected. Optical rotations were determined on a Perkin-Elmer Polarimeter (Model 241-MC).

Thin-layer chromatography (tlc) was performed on silica gel plates (Baker-flex Silica gel 1B2-F) using the following solvent systems: (A), 1-butanol – acetic acid – water (6:3:1); (B), benzene – methanol – ethyl acetate (4:3:1); (C), toluene–ether (2:1); (D), toluene – ethyl acetate (2:1 or 1:1); (E), benzene–methanol (4:1); (F), methanol–chloroform (5:1). The fluorescent chloroacetamide derivatives (**1–4**) were checked for purity by tlc in solvents (E) and (C) and were detected as dark nonfluorescent spots under uv light. The corresponding blocked acetamido sugar derivatives (tlc solvents (C), (D), or (E)) were fluorescent under uv light and were also checked by charring with H_2SO_4–EtOH. The fluorescent disaccharide derivatives (**24–26**) were checked by tlc using solvent (A) and were also tested by spraying with 2% ninhydrin in acetone. Column chromatography was performed using 100–200 ASTM mesh silica (Fisher) packed in columns approximately 2.5 × 50 cm and solvents (B), (C), or (F) as eluants.

All microanalyses were carried out by Mr. P. Borda of this Department. The mass spectra were obtained from an Atlas CH-4B mass spectrometer and high resolution measurements were performed using an AE1 MS-9 or an MS-50 mass spectrometer. Proton nmr spectra were obtained from the following instruments: Varian T-60 (60 MHz); Bruker WP-80 (80 MHz), WH-400 (400 MHz); or at 270 MHz from the prototype of a homebuilt spectrometer based on a Bruker WP-60 console, a Nicolet 1180 computer (40K), a Nicolet 293 A′ pulse controller unit, a Diablo Disk, and an Oxford Instruments Superconducting Solenoid.

Carbon-13 nmr spectra were obtained using a Varian CFT-20 spectrometer equipped with a 16K computer. All deuterated solvents were purchased from Merck Sharp & Dohme (Montreal, Canada). Tetramethylsilane and *p*-dioxane (67.40 ppm) were used as standards for proton and carbon nmr, respectively.

4-Aminobenzophenone, *p*-fluoroaniline, 9-anthraldehyde, 1-dimethylaminonaphthalene-5-sulfonylchloride (DANSYL-Cl), 1-aminonaphthalene, and sodium cyanoborohydride were obtained from Aldrich Chemical Co.; chloroacetyl chloride, lactose, and *N*,*N*-dicyclohexylcarbodiimide were from Eastman Chemical Co. Sodium periodate and propionic acid were purchased from Fisher Scientific Co.; benzoic acid, acetic anhydride, and pyridine from Mallinckrodt; sodium hydride from Metal Hydride Inc. 7-Amino-4-methylcoumarin was obtained from Chemical Dynamics Corp. 1,2:3,4-di-*O*-isopropylidene galactopyranose and 1,2:5,6-di-*O*-isopropylidene glucofuranose were from Koch Light Laboratories Ltd. Chitosan was purchased from Sigma Chemical Co. Alginate (Keltone) was a gift from Kelco Co. 2,3,4,6-Tetra-*O*-acetyl-thio-α-D-glucopyranoside (**9**) was prepared by Ms. L. Evelyn of this laboratory; 1,2:3,4-di-*O*-isopropylidene-α-D-galactopyranuronic acid (**17**) was prepared by permanganate oxidation of the corresponding galactopyranose derivative according to known procedures.

Preparation of Fluorescent Chloroacetamide Labels

General Procedure

To a solution of chloroacetyl chloride (0.95 mL, 12 mmol) in either diethyl ether or ethyl acetate (10 mL) was added a solution of the fluorescent amine (6 mmol) in anhydrous diethyl ether or ethyl acetate (4–5 mL), causing immediate precipitation. The reaction mixture was then refluxed for 2–3 h under anhydrous conditions and subsequently filtered; the filtrate was concentrated using a slow stream of dry N_2 at ambient temperature. The crystalline material separating out of solution was filtered and dried, being analytically pure in most cases.

4-Chloroacetamido Benzophenone (1)

White crystals were obtained (90%) using ethyl acetate as solvent; mp 133.5°C (from toluene); tlc: solvent (C); nmr (270 MHz, $CDCl_3$) δ: 10.0 (s, 1H, NH), 7.99–7.61 (m, 9H, arom. H's), 4.35 (s, 2H, —CH_2—); ms *m/e* (relative intensity): 273 (64) M^+, 238 (13) $M^+ - Cl$, 198 (70), 197 (31), 196 (100) $M^+ - C_6H_5^+$, 167 (14), 140 (11), 120 (32) $(COC_6H_4NH)^+$, 119 (78) *m/e* 120 − H^+, 105 (49) $C_6H_5CO^+$, 77 (28). *Anal.* calcd. for $C_{15}H_{12}NO_2Cl$: C 65.82, H 4.42, N 5.12; found: C 66.00, H 4.38, N 5.18.

p-*Fluorochloroacetamidoaniline (2)*

The reaction was carried out in ethyl acetate yielding (100%) white crystals, mp 131–131.5°C (dec., from toluene); tlc: solvent (E); nmr (60 MHz, $CDCl_3$) δ: 7.95 (s, 1H, NH), 7.35–6.60 (m, 4H, arom. H's), 4.05 (s, 2H, —CH_2—); ms *m/e* (relative intensity): 189 (2) $M^+ + 2$, 188 (18) $M^+ + 1$, 187 (54) M^+, 138 (17), 112 (10), 111 (100), 100 (16). *Anal.* calcd. for C_8H_7FNOCl: C 51.22, H 3.76, N 7.47; found: C 51.02, H 3.73, N 7.54.

1-Chloroacetamidonaphthalene 3

Using ethyl acetate as solvent a white crystalline material was obtained (75%); mp 92°C; tlc: solvent (E); nmr (270 MHz, $CDCl_3$) δ: 8.88 (s, 1H, NH), 7.9–7.5 (m, 7H, arom. H's), 4.4 (s, 2H, —CH_2—); ms *m/e* (relative intensity): 219 (89) M^+, 170 (33), 144 (45), 143 (100), 142 (21), 127 (14), 115 (54), 50 (15). *Exact Mass* calcd. for $C_{12}H_{10}NOCl$: 219.0452 amu; found (hrms): 219.0452.

Can. J. Chem. Downloaded from www.nrcresearchpress.com by 210.87.254.5 on 09/06/12
For personal use only.

7-Chloroacetamido-4-methylcoumarin ***4***

The reaction proceeded in diethyl ether or ethyl acetate yielding a white product (59%) soluble in DMSO; mp 240–241°C; tlc: solvent (E); nmr (270 MHz, DMSO-d_6) δ: 8.9 (s, 1H, NH), 6.76 (d, 1H, H6), 6.65 (d, 1H, H8), 6.52 (dd, 1H, H5), 5.54 (q, 1H, H3), 4.36 (s, 2H, —CH_2—), 2.32 (d, 3H, Me); ms *m/e* (relative intensity): 251 (100), 175 (55), 174 (42), 147 (60), 119 (87). *Exact Mass* calcd. for $C_{12}H_{10}NO_3Cl$: 251.0349 amu; found (hrms): 251.0346.

*Preparation of 2,3,4,6-Tetra-*O*-acetyl-(4-acetamidobenzophenone)-1-thio-α-*D*-glucopyranoside (**10**)*

A solution of the chloroacetamide label **1** (0.82 g, 3 mmol) in a 1:2 mixture of ethyl acetate – $CHCl_3$ (15 mL) was added to a mixture of 2,3,4,6-tetra-*O*-acetyl-1-thio-α-D-glucopyranoside (**9**), (1.09 g, 3 mmol), and sodium bicarbonate (0.5 g) in ethyl acetate (15 mL). After refluxing for 18 h, the reaction mixture was cooled and concentrated yielding a yellow syrup from which white crystals separated on standing overnight at 22°C. The product was recrystallized once from 95% EtOH; yield 67%, mp 130°C, $[\alpha]_D^{22}$ −30° (*c* 1.6, $CHCl_3$); tlc: solvent (E); nmr (270 MHz, $CDCl_3$) δ: 8.80 (s, 1H, NH), 7.82–7.48 (m, 9H, arom. H's), 5.25 (t, 1H, H-4), 5.16–5.09 (m, 2H, H-2 and H-3), 4.64 (d, 1H, H-1), 4.11–4.03 (m, 2H, H-6's), 3.81–3.75 (m, 1H, H-5), 3.68–3.41 (2d, 2H, SCH_2—), 2.09–1.87 (3s, 12H, —OAc); ms *m/e* (relative intensity): 601 (16) M^+, 422 (30), 421 (37), 408 (33), 380 (34), 379 (38), 367 (29), 366 (38), 331 (37), 276 (33), 275 (50), 274 (43), 273 (66), 272 (35), 271 (46), 240 (35), 239 (54), 238 (31), 229 (32), 224 (42), 223 (40), 211 (40), 210 (38), 199 (44), 198 (75), 197 (68), 196 (82), 169 (77), 105 (77), 77 (80), 45 (65), 44 (64), 43 (100) $COCH_3^+$. *Anal.* calcd. for $C_{29}H_{31}NO_{11}S$: C 57.89, H 5.19, N 2.33; found: C 57.97, H 5.27, N 2.44.

*Preparation of 1,2:3,4-Di-*O*-isopropylidine-6-*O*-(4-fluoroacetamidoaniline)-α-*D*-galactopyranose (**16**)*

Sodium hydride (0.49 g, 20.5 mmol) was added to a stirred, cooled (0°C) solution of 1,2:3,4-di-*O*-isopropylidine-α-D-galactopyranose (**11**) in dry dimethyl formamide (DMF) (30 mL). After 1 h, a solution of *p*-fluorochloroacetamidoaniline (**2**, 1.5 g, 8 mmol) in DMF (25 mL) was added in portions to the mixture. After 0.5 h, the product began to form as indicated by a fluorescent spot (tlc: solvent (D)) which was also carbohydrate positive (H_2SO_4–EtOH). The reaction mixture was left stirring overnight. After addition of dry methanol (15 mL) the solution was concentrated to dryness at 0.01 Torr pressure and 80°C. The crude product thus obtained was extracted with 1:1 chloroform–water (100 mL). The organic layer was washed with water (3 × 40 mL), dried over magnesium sulfate, and concentrated. The crude product was purified by silica gel column chromatography (eluant: solvent (F)), to yield 390 mg (39%) of a brown syrup which decomposed on prolonged air exposure, mp 128°C (from isopropanol); $[\alpha]_D^{22}$ − 12° (*c* 1.1, benzene); nmr (80 MHz, $CDCl_3$) δ: 8.75 (s, 1H, NH), 7.65–6.91 (m, 5H, arom. H's), 5.59 (d, 1H, H-1), 4.65 (q, 1H, H-5), 1.55–1.36 (3s, 12H, CH_3); *Exact Mass* calcd. for $C_{20}H_{26}FNO_7$: 411.1685 amu; found (hrms): 411.1693 amu.

Attempted Synthesis

The above reaction failed to proceed under the following conditions: (*a*) using the same starting material with benzene as solvent together with crushed KOH pellets; (*b*) using 1,2:5,6-di-*O*-isopropylidene-α-D-glucofuranose **12** and 4-chloroacetamidobenzophenone (**1**), under the same conditions as in (*a*); (*c*) using 1,3,4,6-tetra-*O*-acetyl-(2-deoxy-2-amino)-D-glucopyranose (**15**) and 4-fluorochloroacetamidoaniline in chloroform with pyridine; (*d*) using methyl (1-*O*-methyl-2-*O*-methyl-4,6-benzylidene)-α-D-altropyranoside (**13**) or methyl (1-*O*-methyl-3-*O*-methyl-4,6-benzylidene)-α-D-altropyranoside (**14**) and 4-chloroacetamidobenzophenone (**1**) in chloroform with solid sodium bicarbonate.

*Preparation of 4-(1,2:3,4-Di-*O*-isopropylidine-α-D-galactopyranuronamide)benzophenone (**18**)*

A mixture of 4-aminobenzophenone (243 mg, 1.1 mmol) and *N,N*-dicyclohexylcarbodiimide (277 mg, 12 mmol) in dry CH_2Cl_2 (15 mL) was cooled to 0°C. To this mixture was added in portions a solution of 1,2:3,4-di-*O*-isopropylidene-α-D-galactpyranuronic acid (17) (329 mg, 1.2 mmol) in CH_2Cl_2 (10 mL). After keeping the reaction mixture at 0°C for 1 h, it was left standing at room temperature for 35 h. The precipitated dicyclohexylurea side-product was filtered off, the filtrate containing some unreacted amine (tlc: solvent (C)). After silica gel column chromatography (solvent (C)), the product was obtained in 48% yield, mp 117°C (dec.); $[\alpha]_D^{22}$ −16.0 (*c* 0.4, $CHCl_3$); nmr (270 MHz, $CDCl_3$) δ: 8.37 (s, 1H, NH), 7.77–7.40 (m, 9H, arom. H's), 5.61 (d, 1H, H-1), 4.68 (q, 1H, H-4), 4.65 (q, 1H, H-3), 4.38 (d, 1H, H-5), 4.36–4.33 (q, 1H, H-2), 1.30–1.25 (4s, 12H, Me); ms *m/e* (relative intensity): 454 (8)M^+ + 1, 453 (26) M^+, 438 (8) $M^+ - CH_3$, 326 (10), 279 (10), 197 (9), 167 (19), 155 (100), 149 (50), 127 (46), 113 (10), 100 (12), 85 (11), 57 (13). *Exact Mass* calcd. for $C_{25}H_{27}NO_7$: 453.1788 amu; found (hrms): 453.1795.

*Preparation of 1,2:3,4-Di-*O*-isopropylidine-6-*O*-(5-dimethylamino-1-naphthalenesulfonyl)-α-*D*-galactopyranose (**20**)*

A solution of DANSYL-Cl (1.21 g, 4.5 mmol) in dry acetone (5 mL) was added to a mixture of 1,2:3,4-di-*O*-isopropylidine-α-D-galactopyranose (**11**), (1.18 g, 4.5 mmol) and triethylamine (3 mL) in dry acetone (15 mL). The reaction mixture was stirred for 2 h in the dark at 22°C, yielding a yellow crystalline product which was filtered and dried. Two recrystallizations from isopropanol yielded 1.62 g (73%) green needle-shaped crystals, mp 146–147°C; $[\alpha]_D^{22}$ −55 (*c* 0.9, acetone); tlc: solvent (C); ^{1}H nmr (270 MHz, $CDCl_3$) δ: 8.6–8.3 (m, 3H, arom. H's), 7.6–7.2 (m, 3H, arom. H's), 5.36 (d, 1H, H-1), 4.53 (q, 1H, H-3), 4.30 (q, 1H, H-2), 4.16–4.05 (m, 2H, H-4 and H-6), 4.00 (m, 1H, H-5), 2.90 (d, 6H, NMe_2), 1.34–1.14 (4s, 12H, Me); ms *m/e* (relative intensity): 494 (20) M^+ + 1, 493 (52) M^+, 478 (14) $M^+ - CH_3$, 252 (16), 251 (100), 250 (15), 171 (10), 170 (25), 168 (10). *Anal.* calcd. for $C_{24}H_{31}NO_8S$: C 58.40, H 6.33, N 2.84; found: C 58.26, H 6.35, N 2.86.

Preparation of Fluorescent Disaccharide Derivatives

General Procedure

Method A: to a solution of the disaccharide (3.18 g, 9.3 mmol) in dry methanol (20 mL) was added the fluorescent amine derivative (14 mmol), the solution was acidified with acetic acid to pH 4[4] and then brought to reflux under anhydrous conditions. A solution of sodium cyanoborohydride (2.86 g, 45.5 mmol) in methanol (15 mL) was added to the refluxing mixture over a 20 min period. The initially clear solution formed some precipitate after a few hours. The reflux was continued for ca. 18 h. The reaction mixture was cooled and then concentrated under diminished pressure yielding a syrupy material which was diluted with aqueous methanol (10 mL) and poured into a large volume of acetone (250 mL). The precipitated product was collected, dried, and purified by silica gel column chromatography (eluant (C)), yielding a crystalline material, which could be further characterized as its nona-acetate; tlc: solvent (A).

Method B: this was the procedure of Hoagland *et al.* (18).

*Preparation of 4-[(1-Deoxylactit-1-yl)-amino]benzophenone (**24**)*

Method A: the crude yellow product isolated after 18 h reflux was purified by column chromatography yielding 4.10 g (78%), mp 156–159°C; $[\alpha]_D^{22}$–16° (*c* 1.1, H_2O).

Method B: 3.90 g (74%) material was isolated after refluxing for 23 h; ms *m/e* (relative intensity): 523 (4) M^+, 343 (1) M^+ −

[4]Efforts to substitute IR-120 (H^+ form) resin for the organic acids were unsuccessful.

Can. J. Chem. Downloaded from www.nrcresearchpress.com by 210.87.254.5 on 09/06/12
For personal use only.

$HNC_6H_4COC_6H_5^+$, 305 (2) $M^+ - C_6H_5NH^+$, 281 (12), 210 (21), 197 (15), 122 (92), 120 (42) $C_6H_5NH^+$; 106 (10), 105 (100) $C_6H_5CO^+$; 77 (33).

Preparation of Nona-acetate Derivative

Compound **24** (1.08 g) was acetylated according to the procedure of Wolfrom and Thompson (20). The acetylated product was recrystallized three times from 95% ethanol to yield yellowish crystals (0.82 g), mp 61–63°C; $[\alpha]_D^{22}$ 26°, (*c* 1.1, $CHCl_3$); tlc: solvent (D). *Anal.* calcd. for $C_{43}H_{51}NO_{20}$: C 57.21, H 5.70, N 1.55; found: C 57.00, H 5.80, N 1.64.

Preparation of 1-[(1-Deoxylactit-1-yl)-amino]naphthalene (25)

Method A: the reaction proceeded in 83% yield after 18 h reflux. After chromatography, a pink product was obtained, mp 148–150°C (dec.); $[\alpha]_D^{22}$ −16° (*c* 1.7, MeOH); ms *m/e* (relative intensity): 469 (7) M^+, 452 (10), 451 (34) $M^+ - H_2$, 331 (19), 307 (14), 289 (28), 271 (45), 229 (12), 228 (39), 180 (25), 168 (39), 157 (79), 143 (100). *Exact Mass* calcd. for $C_{22}H_{31}NO_{10}$: 469.1948 amu; found (hrms): 469.1917 amu.

Preparation of 4-[(1-Deoxycellobiit-1-yl)-amino]benzophenone (26)

Method A: after 27 h reaction time and column chromatography, 4.0 g (76%) yellow product was obtained, mp 82–85°C; $[\alpha]_D^{22}$ 39° (*c* 1, H_2O); ms *m/e* (relative intensity): 550 (0.2) M^+, 211 (1), 199 (3), 198 (54), 197 (2), 184 (13), 183 (10), 168 (2), 166 (3), 121 (100). *Anal.* calcd. for $C_{25}H_{33}NO_{11}\cdot 1.5H_2O$: C54.52, H 6.59, N 2.54; found: C 54.40, H 6.62, N 2.46.

A 1 g portion of this material was acetylated to give 0.95 g of the nona-acetate derivative, mp 71–74°C (from 95% EtOH); $[\alpha]_D^{22}$ 20° (*c* 1, $CHCl_3$); ms *m/e* (relative intensity): 910 (0.1) M^+, 901 (0.1) $M^+ - 1/2H_2O$, 859 (2), 549 (1), 331 (3), 323 (3), 295 (5), 279 (4), 240 (3), 239 (4), 43 (100). *Exact Mass* calcd. for $C_{43}H_{51}NO_{20}$: 901.2988 amu; found (hrms): 901.2994.

Preparation of N-*methylene[-9-anthracenyl]-chitosan (32)*

To chitosan (500 mg, 3.0 mmol) dissolved in 2% aqueous acetic acid (25 mL) was added dropwise with vigorous stirring a solution of 9-anthraldehyde (1.15 g, 5.5 mmol) in methanol (25 mL). The reaction mixture was left standing for 12 h until a soft yellow gel had formed, which was treated repeatedly with methanol (100 mL) and diethyl ether (100 mL). The product had a ds of 0.73, after drying. *Anal.* calcd. for $[(C_{21}H_{19}NO_4)_{0.73}(C_6H_{11}NO_4)_{0.27}]\cdot 0.99\ H_2O$: C 64.31, H 6.00, N 4.43; found: C 64.12, H 5.90, N 4.46.

Preparation of N-*methyl-[9-anthracenyl]-chitosan (33)*

The same procedure as for **32** was followed using sodium cyanoborohydride (0.84 g, 13.4 mmol). A stiff porous gel formed in this case after 3 h reaction time. The product had ds 0.5. *Anal.* calcd. for $[(C_{21}H_{21}NO_4)_{0.5}(C_6H_{11}NO_4)_{0.5}]\cdot 0.43H_2O$: C 61.41, H 6.44, N 5.31; found: C 61.36, H 6.21, N 5.21.

Acknowledgements

This work was supported by the Natural Sciences and Engineering Research Council of Canada via operating grants to LDH (A 1905).

1. L. D. Hall and M. Yalpani. Carbohydr. Res. **78**, C4 (1980).
2. R. D. Berlin, J. M. Pliver, T. E. Ukena, and H. H. Yin. Nature (London), **247**, 45 (1974); J. S. Becker, J. M. Oliver, and R. D. Berlin. Nature (London), **254**, 152 (1975); N. Sharon. Sci. Am. **236**, 108 (1977).
3. J. P. Reeves, E. Shechter, R. Weil, H. R. Kaback. Proc. Natl. Acad. Sci. U.S.A. **70**, 2722 (1973).
4. S. Claesson and H. Odani. J. Chem. Soc. Faraday Disc. **49**, 268 (1970); W. Brown, G. Kloow, K. Chitumbo, and T. Amu. J. Chem. Soc. Faraday Trans. I, **72**, 485 (1976); G. Holzwarth. Carbohydr. Res. **68**, 173 (1978).
5. A. Hayashi, K. Minoshita, and M. Kuwano. Polym. J. **9**, 219 (1977).
6. S. Hase, T. Ikenaka, and Y. Matsushima. J. Biochem. **85**, 989 (1979).
7. E. Zissis and C. P. J. Glaudemans. Carbohydr. Res. **63**, 99 (1978).
8. M. Claeyssens, E. Saman, and C. K. de Bruyne. J. Carbohydr. Nucleos. Nucleot. **5**, 33 (1978); H. Wada, H. Nakamura, and K. Miyatake. J. Carbohydr. Nucleos. Nucleot. **4**, 231 (1977).
9. L. D. Hall and M. Yalpani. Carbohydr. Res. **81**, C10 (1980); J. Chem. Soc. Chem. Commun. 1153 (1980).
10. E. J. O'Connell. J. Chem. Soc. Chem. Commun. 571 (1969); J. W. Bridges and R. T. Williams. Nature (London), **196**, 59 (1962).
11. E. N. Hudson and G. Weber. Biochemistry, **12**, 4154 (1973); P. Faerber and W. Vizethum. J. Carbohydr. Nucleos. Nucleot. **3**, 15 (1976).
12. J. S. Brimacombe. Methods Carbohydr. Chem. **6**, 376 (1972).
13. D. F. Detar, R. Silverstein, and E. F. Rogers. J. Am. Chem. Soc. **88**, 1024 (1966); K. Holmberg and B. Hansen. Acta Chem. Scand. Ser. B, **33**, 410 (1979).
14. G. Avigad. J. Chromatogr. **139**, 343 (1977); G. Schepers, Y. Blatt, K. Himmelspach, and I. Pecht. Biochemistry, **17**, 2239 (1978); R. V. Wenn. Biochem. J. **145**, 281 (1975).
15. R. F. Borch, M. D. Bernstein, and H. D. Durst. J. Am. Chem. Soc. **93**, 2897 (1971); G. R. Gray. Methods Enzymol. **50**, 155 (1978).
16. P. E. Pfeffer, K. M. Valentine, and F. W. Parrish. J. Am. Chem. Soc. **101**, 1265 (1979).
17. M. Yalpani. Ph.D. Thesis, University of British Columbia, 1980.
18. P. D. Hoagland, P. E. Pfeffer, and K. M. Valentine. Carbohydr. Res. **74**, 135 (1979).
19. L. D. Hall and M. Yalpani. Carbohydr. Res. **83**, C5 (1980).
20. M. L. Wolfrom and A. Thompson. Methods Carbohydr. Chem. **2**, 211 (1963).
21. V. Formacek, L. Desnoyer, H. P. Kellerhals, T. Keller, and J. T. Clerc. ^{13}C Data Bank. Vol. 1. Bruker, Karlsruhe. 1976. p. 171.
22. L. F. Johnson and W. C. Jankowski. Carbon-13 nmr spectra. J. Wiley, New York. 1972. p. 414.

Antimony-121 nuclear magnetic resonance study of hexahaloantimonate anions

R. GARTH KIDD AND H. GARTH SPINNEY

Department of Chemistry, University of Western Ontario, London, Ont., Canada N6A 5B7

Received March 3, 1981

R. GARTH KIDD and H. GARTH SPINNEY. Can. J. Chem. **59**, 2940 (1981).

The seven hexahaloantimonate anions in the series $[SbCl_nBr_{6-n}]^-$ have been prepared and their antimony-121 nmr spectra show that for $[SbCl_4Br_2]^-$, $[SbCl_3Br_3]^-$, and $[SbCl_2Br_4]^-$, only the *cis* isomers are present in acetonitrile solution. The pairwise additivity model for central atom shielding has been used for configuration assignments. Models relevant to the higher incidence of *cis* over *trans* isomers are discussed. The nuclear shielding of ^{121}Sb is the most sensitive to halogen substitution of all the elements whose halide chemical shifts have been studied. Antimony shieldings exhibit normal halogen dependence, with bromine substitution causing *upfield* shifts relative to chlorine substitution.

R. GARTH KIDD et H. GARTH SPINNEY. Can. J. Chem. **59**, 2940 (1981).

On a préparé les sept anions hexahaloantimonates de la série $[SbCl_nBr_{6-n}]^-$; leurs spectres rmn du Sb-121 révèlent que seuls les isomères *cis* des anions $[SbCl_4Br_2]^-$, $[SbCl_3Br_3]^-$ et $[SbCl_2Br_4]^-$ sont présents en solution dans l'acétonitrile. On a utilisé le modèle d'additivité par paire du blindage de l'atome central pour attribuer les configurations. On discute de modèles appropriés pour expliquer la présence prépondérante des isomères *cis* sur les isomères *trans*. De tous les éléments dont on a étudié les déplacements chimiques des halogènes, le blindage nucléaire du Sb^{121} est le plus sensible à la présence des halogènes. L'effet de l'halogène sur le blindage de l'antimoine est normal par rapport au chlore alors que le brome provoque un déplacement vers les champs forts.

[Traduit par le journal]

It was established some time ago (1, 2) that when mixed halide complexes of metals having $MX_4Y_2^{n-}$ stoichiometry are prepared, it is the *cis* isomers which crystallize from solution.[1] What remains to be established is whether the higher incidence of *cis*-isomers in the solid state reflects an enthalpic bonding preference for *cis*-isomers or merely the lower solubility of *cis*-isomers present as the minor fraction in an equilibrium solution mixture of the two. Although electronic and vibrational spectroscopy will distinguish *cis*- and *trans*-isomers when only one or the other is present, there are few techniques capable of making the distinction in an equilibrium mixture that might contain both along with eight other redistribution products. The possibility of drawing invalid bond energy conclusions from distinctions that may only reflect solubility differences is thus a recurring problem for chemists.

This paper reports molecular structure determinations *in solution* for seven hexahaloantimonate anions. The experimental method used is ^{121}Sb nmr spectroscopy. The chemical shift data obtained has been analyzed in terms of the pairwise additivity model and the results indicate exclusively *cis*-isomers in solution. The implications of this *cis*-isomer preference are discussed in terms of bonding models which emphasize ligand-to-metal π-bonding and steric repulsion, respectively.

While some early skepticism concerning the existence of six-coordinate mixed chlorobromoantimonate(V) species of the type $[SbCl_nBr_{6-n}]^-$ was expressed (3, 4) the $[SbCl_5Br]^-$ ion has now been characterized in the solid state (5), and the octahedral geometry of six-coordinate antimony(V) halides has been verified by single-crystal X-ray analysis (6). In the present study all seven stoichiometries in the series $[SbCl_nBr_{6-n}]^-$ have been prepared for the first time and seven out of the ten possible configurations have been identified in the equilibrium mixture.

The noteworthy fact that bromine substitution leads to higher magnetic shielding of the ^{121}Sb nucleus than does chlorine substitution is demonstrated in this study and serves to place antimony in that class of elements whose nuclear shielding exhibits *normal halogen dependence*. The 2430 ppm chemical shift of $[SbBr_6]^-$ relative to $[SbCl_6]^-$, however, establishes ^{121}Sb as the nucleus whose sensitivity to halogen substitution is the largest of all those elements whose halides have undergone nmr measurement.

Experimental

All the antimony compounds subjected to nmr study were prepared under anhydrous conditions using high purity $SbCl_5$, $SbCl_3$, and $SbBr_3$ obtained from Alfa Inorganics. Acetonitrile solvent was purified and dried by fractional distillation from calcium hydride. Et_4NSbCl_6 was prepared by the method of Furlani and Zinato (7) from $SbCl_5$ and Et_4NCl in thionyl chloride. Et_4NSbBr_6 was prepared by the method of Lawton

[1]For the $[SbCl_3Br_3]^-$ complex, the structure of the *mer*-isomer is characterized by two *trans* relationships while the *fac*-isomer contains only *cis* relationships. In order that the generality of the behaviour observed in this study be recognized, statements about *cis*-isomers will only be made if they are also valid for the *fac*-isomer case.

0008-4042/81/202940-05$01.00/0

©1981 National Research Council of Canada/Conseil national de recherches du Canada

Can. J. Chem. Downloaded from www.nrcresearchpress.com by 210.87.254.5 on 09/06/12
For personal use only.

Can. J. Chem. Downloaded from www.nrcresearchpress.com by 210.87.254.5 on 09/06/12
For personal use only.

and Jacobson (8) in which a mixture of $SbBr_3$ and Et_4NBr in acetonitrile is oxidized with Br_2. The shapes and positions of ^{121}Sb nmr lines for acetonitrile solutions of hexachlorobromoantimonate(V) anions were found to be independent of total antimony concentration and Cl:Br:Sb ratio. For all solutions studied, antimony concentration was about 0.5 *M* and Cl:Br:Sb ratios producing the best spectra were selected.

Acetonitrile solutions containing mixed hexahaloantimonates were prepared by mixing constituents in the following proportions:

$$n\,Et_4NSbCl_6 + (6\text{-}n)\,Et_4NSbBr_6 \quad (1 \leq n \leq 5)$$

$$Et_4NSbCl_6 + n\,KBr \text{ (or } Et_4NBr) \quad (1 \leq n \leq 10)$$

$$Et_4NSbBr_6 + n\,KCl \text{ (or } Et_4NCl) \quad (1 \leq n \leq 6)$$

The rates of halogen exchange were slow; redistribution half-life for Et_4NSbCl/Et_4NSbBr_6 at 28°C was ca. 40 h while that for bromide ion exchange with Et_4NSbCl_6 was ca. 20 h. In the latter case the exchange could be observed visually as the solution colour changed from the very pale yellow of $[SbCl_6]^-$/MeCN to light orange as the concentration of the deep orange–red $[SbBr_6]^-$/MeCN increased. Solubility decreased with increasing bromide content of the complex.

^{121}Sb nmr spectra were measured at 14.37 MHz using a modified Varian 4200B spectrometer which has been described elsewhere (9). Spectra were recorded as dispersion mode derivatives and calibration was effected by the generation of audio-frequency sidebands. Chemical shifts are reported relative to $[SbCl_6]^-$ in acetonitrile as internal reference, and negative shifts represent increased shielding. Experimental uncertainty in line positions was ±5 ppm.

Results and Discussion

The pattern of ^{121}Sb resonances obtained from acetonitrile solutions containing hexahaloantimonate(V) anions is shown in Fig. 1. For the solution prepared from a 1:1 mole ratio Et_4NSbCl_6:Et_4NSbBr_6, all seven resonances were observed with intensity ratios proportional to the binomial coefficients and indicating random distribution of halogens among antimony atoms. While spectra with different line intensities were obtained from solutions prepared with different Cl:Br ratios (see Experimental Section), no new resonances were observed, and the line positions for all resonances from all solutions studied coincided with those in Fig. 1 within experimental uncertainty.

Spectral Assignments to Stoichiometries

Spectral assignments of the seven lines in Fig. 1 to specific stoichiometries (*n*-values) were made on the basis of linewidth differences, the correlation between signal intensity and Cl:Br ratio of the solution, and the established monotonic variation in halogen dependence of metal shieldings generally. Previous nmr studies of ^{27}Al (10), ^{73}Ge (11), and ^{93}Nb (12) have established that successive replacement of Cl^- by Br^- in $[AlCl_4]^-$, $GeCl_4$, and $[NbCl_6]^-$ causes a monotonic change in metal atom chemical shift regardless of whether this shift is

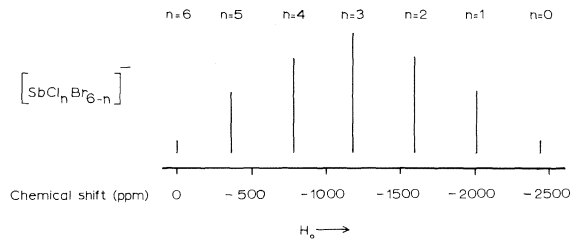

FIG 1. Line positions and relative intensities of ^{121}Sb resonances for $[SbCl_nBr_{6-n}]^-$ anions in acetonitrile solution.

upfield as in the ^{27}Al and ^{73}Ge cases or downfield as in the ^{93}Nb case. The chemical shift pattern in Fig. 1 is similar to that seen in these other systems and indicates a monotonic change in Sb shielding with successive Br^- substitution in $[SbCl_6]^-$. Those solutions having high Br:Cl ratios yielded spectra in which the high-field signals underwent intensity enhancement, while the low-field signal intensities were enhanced by low Br:Cl ratios. This enables the assignment of the −2430 resonance to $[SbBr_6]^-$. With an electric quadrupole moment of −0.8 barn, the ^{121}Sb nucleus is expected to yield broad nmr lines in environments of lower than cubic symmetry. While the resonances for $n = 0, 6$ were relatively narrow ($\nu_{1/2} \simeq 350$ Hz), the others were much broader, consistent with $\delta = 0$ for $[SbCl_6]^-$ and $\delta = -2430$ for $[SbBr_6]^-$ assignments.

Spectral Assignments to Configurations

Random redistribution of Cl^- and Br^- among the six coordination sites around Sb would give rise to the seven stoichiometries shown in Fig. 1 and the 10 configurations shown in Table 1. If all 10 configurations were formed in solution, 10 different ^{121}Sb resonances should be observed in the spectra. The fact that only seven resonances are seen indicates that only seven configurations are present in detectable concentrations. The detailed argument presented below leading to specific configurational assignments will show that rapid isomerization of *cis–trans* pairs leading to a single time-averaged resonance is *not* operating to reduce the number of observed lines.

Were the ^{121}Sb shieldings to show a first-order halogen dependence it would be possible to calculate ^{121}Sb chemical shifts by evaluating substituent constants for Cl^- and Br^- as has been attempted in Table 1 and Fig. 2. The lack of agreement between the substituent additive δ-values and the observed δ-values indicates that halide ions do not contribute independently to ^{121}Sb shielding and that a second-order model is required to explain the observed behaviour.

Can. J. Chem. Downloaded from www.nrcresearchpress.com by 210.87.254.5 on 09/06/12
For personal use only.

TABLE 1. ^{121}Sb chemical shifts for $[SbCl_nBr_{6-n}]^-$ anions in acetonitrile solution

Species	Coefficients, C_{ij} Cl,Cl	Cl,Br	Br,Br	δ calcd[a] ($\Sigma C_{ij}\eta_{ij}$)	δ obsd[b]	δ calcd[c] (substituent additive)
$[SbCl_6]^-$	12	0	0	+1	0	(0)
$[SbCl_5Br]^-$	8	4	0	−383	−380	−405
$[SbCl_4Br_2]^-$						−810
cis	5	6	1	−778	−780	
trans	4	8	0	−767		
$[SbCl_3Br_3]^-$						−1215
fac	3	6	3	−1183	−1180	
mer	2	8	2	−1172		
$[SbCl_2Br_4]^-$						−1620
cis	1	6	5	−1589	−1590	
trans	0	8	4	−1578		
$[SbClBr_5]^-$	0	4	8	−2005	−2005	−2025
$[SbBr_6]^-$	0	0	12	−2432	−2430	(−2430)

[a] Pairwise additivity parameter values (ppm): $\eta_{Cl,Cl} = +0.1$; $\eta_{Cl,Br} = -95.9$; $\eta_{Br,Br} = -202.7$ (uncertainty limits ±0.2 in each case).
[b] Negative shifts designate higher shielding. Experimental uncertainty ±5 ppm.
[c] Substituent constants (ppm): Cl = 0; Br = −405.

The pairwise additive model for metal-atom shieldings has been used to assign configurations to six-coordinate niobium(V) complexes (12), and its application to the present system of antimony complexes is shown in Fig. 2. The halides are regarded as contributing to the antimony shielding in pairs, with 12 independent contributions corresponding to the 12 edges of the octahedron. The chemical shift calculated according to this model is given by the sum of three $C_{ij}\eta_{ij}$ terms in which η_{Cl-Cl}, η_{Br-Cl}, and η_{Br-Br} are the three pairwise additivity parameters and C_{ij} are the numerical coefficients determined by the structure and summing to 12. Whereas the substituent additive model yields the same calculated shift for *cis*- and *trans*-isomers of the same complex, the pairwise additivity model gives calculated shifts that differ by more than the uncertainty in the observed shift, thus providing a method for identifying specific isomers in a solution mixture of several.

With seven observed resonance positions, one can set up seven linear equations containing the three η_{ij} as unknowns, and a multiple linear regression analysis yields the η_{ij} values listed at the bottom of Table 1. The configuration assignments shown in Table 1 are the only ones yielding a set of calculated shifts all of which lie within the uncertainty interval of the observed shifts. In particular the δ = −780, δ = −1180, and δ = −1590 resonances all lie within 3 ppm of the theoretical values calculated for *cis*-isomers. If rapid *cis*–*trans* isomerization were occurring, the calculated positions for the time-averaged resonances would be δ = −773, δ = −1177, and δ = −1583. For $[SbCl_4Br_2]^-$ and $[SbCl_2Br_4]^-$ these values lie 7 ppm from the observed positions thereby rendering the

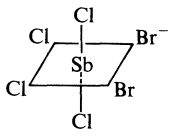

cis-isomer

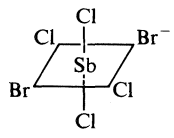

trans-isomer

Isomer	$\eta_{Cl,Cl}$	$\eta_{Cl,Br}$	$\eta_{Br,Br}$	Calculated ^{121}Sb shift (ppm) Pairwise additive	Substituent additive
cis-$SbCl_4Br_2^-$	5	6	1	−778	−810
trans-$SbCl_4Br_2^-$	4	8	0	−767	−810

FIG 2. Pairwise additivity model (octahedral complex) for ^{121}Sb nuclear shielding in a hexahalo-environment.

Can. J. Chem. Downloaded from www.nrcresearchpress.com by 210.87.254.5 on 09/06/12
For personal use only.

possibility of time-averaged signals unlikely on chemical shift grounds. The extremely slow rate observed for intermolecular redistribution of halide, while not ruling out the possibility of rapid intramolecular rearrangement, also makes it unlikely.

For the $n = 2, 3, 4$ members of the $[SbCl_nBr_{6-n}]^-$ system which could potentially adopt both *cis* and *trans* configurations, all of the experimental evidence supports the hypothesis that only the *cis*-isomers are present in solution. This observation provides us with a better understanding of the antimony–halogen bond.

Models for Configurational Preference

Antimony is not alone in showing this preference for *cis* halides. Among the transition metals, titanium(IV) (1) and niobium(V) (12) favour *cis*-configurations, while among the representative elements, tin(IV) (1) follows this same pattern. The traditional view has been that *cis* interactions between bulky ligands (in this case, Br^-) occasion destabilizing steric repulsions that are larger than those arising from *trans* interactions and, other things being equal, *trans* isomers will predominate. Where *cis* isomers predominate, other things are apparently not equal, and a number of workers (1, 16, 17) have taken a preference for *cis* isomers to indicate a higher order of ligand → metal π-bonding than could be achieved in the *trans*-isomer where the two (stronger) π-donor ligands are competing for the same vacant t_{2g}-orbital on the central atom. This model uses a preference for *cis*-isomers as evidence for the existence of π-bonding.

An alternative view presented by Zahrobsky (18) argues on geometrical grounds that steric factors alone favour the formation of *cis*-isomers by six-coordinate mixed halide complexes, thereby undercutting the argument for π-bonding contained in the traditional view of steric repulsion.

The *cis*-bonding preference observed in the present study, while consistent with the pattern observed previously for analogous systems, does not provide a basis for mediating between these two models.

Halogen Dependence of Antimony Shieldings

The nuclear shielding of all atoms is particularly sensitive to halogen substitution. For antimony compounds containing no bromine, all ^{121}Sb chemical shifts reported to date lie in the 1000 ppm region downfield of $[SbCl_6]^-$ (9). The six compounds containing bromine reported in this study extend the ^{121}Sb shielding range by another 2400 ppm and, together with $[SbCl_6]^-$, span 70% of the total shielding range for this nucleus. While the effect of iodine substitution on ^{121}Sb shielding has not yet been tested, one can safely extrapolate from the halogen dependence patterns for other shieldings that the $[SbI_6]^-$ resonance will lie another ca. 5300 ppm upfield of $[SbBr_6]^-$. The 2430 ppm MCl_6–MBr_6 chemical shift difference for ^{121}Sb is 1.3 times the difference for the ^{195}Pt halides (13),[2] and 3.3 times the difference for the ^{93}Nb halides (12), establishing ^{121}Sb as the nucleus most sensitive to halogen substitution among the 25 or so elements whose halides have undergone nmr investigation. Only ^{205}Tl exhibits a halogen dependence whose magnitude rivals that of ^{121}Sb (14), and the oxidative instability of thallium(III) has precluded to date the preparation of analogous $[TlCl_6]^{3-}$ and $[TlBr_6]^{3-}$ compounds. While ^{59}Co at 18 000 ppm has the largest chemical shift range of any nucleus, this span is achieved by virtue of the large variety of chemical environments adopted by cobalt. Its halogen dependence appears to be intermediate in magnitude, but the test of analogous compounds is again precluded, this time because $[CoCl_6]^{3-}$ and $[CoBr_6]^{3-}$ are high-spin d^6 configurations and hence paramagnetic.

Normal halogen dependence (NHD) is that in which a central atom M is more highly shielded by a bromide than by a chloride. The MX_4^{n-} tetrahalides of the representative elements from periodic groups III and IV all show NHD. The only MX_6^{n-} hexahalides reported heretofor involve transition metals; ^{93}Nb shows inverse halogen dependence (IHD) (12) and ^{195}Pt shows NHD (13). With ^{121}Sb here becoming a documented case of six-coordinate NHD among the representative elements, the possibility of a correlation between IHD and six-coordination is further discounted. A satisfactory explanation for the cause of inverse halogen dependence has yet to be fully worked out, but the topic has been explored elsewhere (15).

Acknowledgements

This work was supported by the National Research Council of Canada through Operating Grant No. A-1906 to R.G.K. and through an NRCC scholarship to H.G.S.

1. R. J. H. Clark, L. Maresca, and R. J. Puddephatt. Inorg. Chem. **7**, 1603 (1968).
2. D. C. Bradley and C. E. Holloway. Chem. Commun. 284 (1965).
3. L. Kolditz. Adv. Inorg. Chem. Radiochem. **7**, 13 (1965).
4. L. Kolditz. Halogen Chem. **2**, 133 (1967).
5. F. F. Bentley, A. Finch, P. N. Gates, and F. J. Ryan. Inorg. Chem. **11**, 413 (1972).

[2]The chemical shift sign convention used to report data in ref. 13 is the reverse of that stated by the authors.

6. M. L. HACKERT, R. J. JACOBSON, and T. A. KEIDERLING. Inorg. Chem. **10**, 1075 (1971).
7. C. FURLANI and E. ZINATO. Z. Anorg. Allgem. Chem. **351**, 219 (1967).
8. S. L. LAWTON and R. A. JACOBSON. Inorg. Chem. **7**, 2124 (1968).
9. R. G. KIDD and R. W. MATTHEWS. J. Inorg. Nucl. Chem. **37**, 661 (1975).
10. R. G. KIDD and D. R. TRUAX. J. Am. Chem. Soc. **90**, 6867 (1968).
11. R. G. KIDD and H. G. SPINNEY. J. Am. Chem. Soc. **95**, 88 (1973).
12. R. G. KIDD and H. G. SPINNEY. Inorg. Chem. **12**, 1967 (1973).
13. J. J. PESEK and W. R. MASON. J. Magn. Reson. **25**, 519 (1977).
14. B. N. FIGGIS. Trans. Faraday Soc. **55**, 1075 (1959).
15. R. G. KIDD. *In* Annual reports on nmr spectroscopy. Vol. 10*a*. *Edited by* G. A. Webb. Academic Press, London. 1980. p. 6.
16. H. H. JAFFÉ. J. Phys. Chem. **58**, 185 (1954).
17. D. C. BRADLEY and C. E. HOLLOWAY. Chem. Commun. 284 (1965).
18. R. F. ZAHROBSKY. J. Am. Chem. Soc. **93**, 3313 (1971).

Can. J. Chem. Downloaded from www.nrcresearchpress.com by 210.87.254.5 on 09/06/12
For personal use only.

Studies related to antitumor antibiotics. Part XXIV. High field ^{1}H nmr analysis and conformations of saframycins A and C

J. William Lown, Alummoottil V. Joshua, and Hsiao-Hsiung Chen
Department of Chemistry, University of Alberta, Edmonton, Alta., Canada T6G 2G2

Received January 20, 1981

J. William Lown, Alummoottil V. Joshua, and Hsiao-Hsiung Chen. Can. J. Chem. **59**, 2945 (1981).

A detailed analysis of the high field (400 MHz) ^{1}H nmr spectra of the basic antitumor antibiotics saframycin A and C in $CDCl_3$, C_6D_6, and in aqueous DMSO solutions has been carried out. Selective double irradiation experiments permitted the unambiguous assignment of all the proton chemical shifts and coupling constants. Consideration of the magnitudes of the latter together with specific nOe experiments permits assignment of molecular geometry and average conformations in solution. Selective shifts occurring in DMSO–D_2O solutions upon addition of CF_3COOD identified the 12-N atom as the site of protonation which result bears directly on the acid promoted binding of these antibiotics to DNA templates as part of their cytotoxic action.

J. William Lown, Alummoottil V. Joshua et Hsiao-Hsiung Chen. Can. J. Chem. **59**, 2945 (1981).

On a effectué une analyse complète des spectres de rmn à haut champ (400 MHz) des antibiotiques antitumescents fondamentaux, les saframycines A et C dans le $CDCl_3$, le C_6D_6 et dans des solutions aqueuses de DMSO. Des expériences d'irradiation double sélective ont permis d'identifier sans ambiguité les déplacements chimiques de tous les protons et toutes les constantes de couplage. En se basant sur l'amplitude des constantes de couplage et sur des expériences de eOn spécifiques on a pu établir la géométrie moléculaire et les conformations moyennes en solution. Les déplacements sélectifs que l'on observe dans les solutions de DMSO–D_2O lors de l'addition du CF_3COOD ont permis d'identifier l'azote en position 12 comme étant le site de la protonation; ce résultat établit donc directment le site de liaison en milieu acide de ces antibiotiques aux modèles de ADN dans le cadre de leur action cytotonique.

[Traduit par le journal]

Introduction

Saframycins (Fig. 1) are members of a new family of antibiotics isolated from the streptothricin-producing strain of *Streptomyces* lavendulae (1–3). The saframycins are yellow crystalline solids structurally related to the heterocyclic quinone antibiotics which include mitomycin C (4), streptonigrin (5), and naphthyridinomycin (6). Unlike the latter the saframycins contain two heterocyclic quinone moieties. Saframycin A differs from saframycin C by the fact that the former has a cyano group on C-21 (orientation not known), while the latter has a methoxy group on C-14. Saframycin S has a hydroxy group on C-21 and has been proposed as a precursor to saframycin A in the biosynthetic process (3). Saframycins A and S have also been interconverted chemically (3). Saframycin B has no substituents at these positions. The structures of saframycins D and E have not been established yet. The X-ray crystallographic structures of saframycins B and C have been determined, although such studies could not distinguish between the two possible optical antipodes (7). The structure of saframycin A has been established by ^{13}C nmr studies and by chemical means (8).

The saframycins exhibit wide-spectrum antimicrobial activity, but more particularly saframycin A is attracting interest because it exhibits extreme cytotoxicity towards cultured cells and shows antitumor activity against several experimental tumors including leukemias L1210 and P388 and Ehrlich carcinoma both in ascites and solid forms (2, 9). Saframycin A has been shown to block RNA synthesis in cultured L1210 cells (9). The mode of action, in common with that of other quinone-containing antibiotics, has been shown to involve direct interaction with a DNA template rather than interference with replicative enzymes

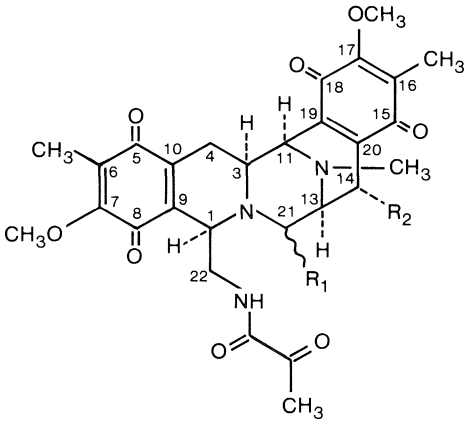

Saframycin A	R_1 = CN,	R_2 = H
B	R_1 = H,	R_2 = H
C	R_1 = H,	R_2 = OCH_3
S	R_1 = OH,	R_2 = H

FIG. 1. Structural formulae of saframycins A, B, C, and S.

0008-4042/81/202945-08$01.00/0
©1981 National Research Council of Canada/Conseil national de recherches du Canada

Can. J. Chem. Downloaded from www.nrcresearchpress.com by 210.87.254.42 on 09/06/12
For personal use only.

Can. J. Chem. Downloaded from www.nrcresearchpress.com by 210.87.254.42 on 09/06/12
For personal use only.

(9). However, the precise nature of the interaction between the saframycins and DNA has not been elucidated and it has been suggested that in order to clarify the reaction a more sensitive assay employing covalently closed circular DNA should be carried out to detect any DNA strand scission (9).

Since any discussion of molecular recognition between the antibiotics and duplex DNA should also take into account the conformation of the antibiotics in solution, we have undertaken a detailed high field ^1H nmr analysis of saframycins A and C, which we report here. Also, since our preliminary studies on the binding of these antibiotics to DNA showed a pH dependence, it was necessary to establish the relative ease of protonation of the two basic nitrogens in the molecules. Therefore we report the ^1H nmr spectra of these antibiotics in aqueous acidic solutions. The 100 MHz ^1H nmr spectra of the saframycins have been reported (2, 3) although no assignments have been made.

Materials and Methods

Saframycins A and C were kindly supplied by Dr. K. Ishiguro, Division of Chemotherapy, Chiba Cancer Centre Research Institute, Japan. Saframycins A and C were further purified by preparative thin layer chromatography on silica gel using ethyl acetate as eluent and by recrystallization from a mixture of ethyl acetate and petroleum ether (1:1).

The nmr measurements were carried out in the Fourier transform mode using the Bruker WH-400/DS NMR spectrometer and the Aspect 2000 Data System utilizing 16 or 32K of data memory. The spectra were measured in appropriate deuterated solvents at ambient temperature (298 K). The deuterium resonance of the solvent was used for the lock signal. The homonuclear decoupling experiments were also performed in the pulse mode. The chemical shifts and coupling constants were calculated to first order at 400 MHz and are reported with an accuracy of ± 0.01 ppm and ± 0.20 Hz, respectively.

Results and Discussion

For the purposes of discussion of the nmr spectra of saframycins A and C, the twelve protons in each (excluding the methyl groups) have been assigned as shown in the figures. Irradiation of the dd absorption at δ 6.33 (H-1) in saframycin A in benzene-d_6 led to the collapse of the signal at δ 3.76 (H-2) from a ddd to a dd as well as the simplification of the signal at δ 2.50 (H-3) from a ddd to a dd. The same simplification was obtained by D_2O exchange. The signal at δ 3.76, which is overlapped by two methoxy signals, can be resolved by changing the solvent from benzene-d_6 to $CDCl_3$. Double irradiation of the ddd signal at δ 3.76 (H-2) led to the collapse of the signal at δ 2.50 (H-3) from a ddd to a dd. Further, double irradiation of the ddd at δ 2.50 (H-3) leads to a d signal at δ 6.33 (H-1) from its original dd and also decouples the H-2 signal at δ 3.76 from a ddd to a dd. These double irradiation experiments together with inspection of the spectra permitted the measurement of the following coupling constants: $J_{1,2} = 9.5$ Hz, $J_{1,3} = 4.0$ Hz, and $J_{2,3} = 14$ Hz. Values for J(H–C–N–H) have been observed to be in the range from 9 to 5 Hz (10*a*). Double irradiation of the signal at δ 3.76 (H-2) simplified the complex signal at δ 3.87 (H-4) to a dd. Similarly irradiation of the ddd signal at δ 2.50 (H-3) caused the collapse of the multiplet at δ 3.87 (H-4) to a dd, permitting the measurement of $J_{2,4} = 1.5$ Hz, $J_{3,4} = 4.0$ Hz. Irradiation of the signal at δ 3.87 (H-4) led to a simplification of the absorption at δ 1.32 (H-5) from a ddd to a dd while the δ 3.76 signal is simplified to a dd and the δ 2.50 signal (H-3) is simplified to a dd.

Stereochemical relationships among H-1, H-2, H-3, and H-4 may be analyzed by considering the relative populations of the three staggered rotamers a, b, and c. The magnitudes of *trans* vicinal

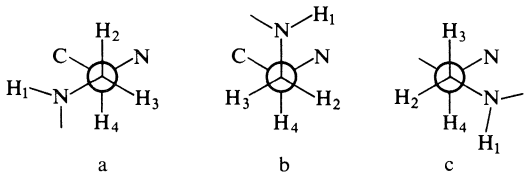

a b c

proton–proton coupling constants in ethane systems are about 9–10 Hz while *gauche* couplings are about 3–4.5 Hz (10*b*). While the magnitudes of these J values undoubtedly vary according to substituent pattern, for ethane derivatives the electronegativity dependence is rather low (10*c*), illustrated in this case by the observed "normal" geminal coupling $J_{2,3} = 14.0$ Hz. The observed values of $J_{2,4} = 1.5$ and $J_{3,4} = 4.0$ Hz would seem to preclude a high population of either rotamer a or c but suggest rather an average conformation of the side chain grouping as the slightly skewed rotamer b depicted in d, with the H_2–H_4 dihedral angle closer to 90° than is the H_3–H_4 dihedral angle.

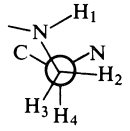

d

Although $J_{1,2} = 9.5$ is $> J_{3,1} = 4.0$ there are insufficient model systems reported for one to draw stereochemical inferences of the disposition of H-1 relative to H_3 or H_2 and this is not implied in the depiction d. It is noteworthy that very similar values for all these coupling constants are observed in D_2O, $CDCl_3$, and C_6D_6.

Double irradiation of the ddd signal at δ 1.32

Can. J. Chem. Downloaded from www.nrcresearchpress.com by 210.87.254.42 on 09/06/12
For personal use only.

(H-5) led to the collapse of the signal at δ 2.89 (H-6) from a dd to a d which is overlapped with the H-12 doublet signal and in addition caused the collapse of the H-7 absorption at δ 3.02 from a ddd to a dd. In $CDCl_3$ H-7 resonates at δ 3.14 which is closely comparable with a similarly situated and axially oriented proton at δ 3.17 in the model compound 1-azabicyclo[3.3.0]decane (10*d*). Spin decoupling of the dd resonance at δ 2.89 (H-6) not only leads to the collapse of the ddd signal at δ 1.32 (H-5) to a dd, but also simplifies the ddd absorption at δ 3.02 (H-7) to a dd. Irradiation of the H-7 ddd signal at δ 3.02 caused simplification of the H-5, H-6, and H-8 signals at δ 1.32, 2.89, and 3.90, respectively. In the ^1H nmr spectrum of saframycin A the chemical shifts between H-4, H-5, H-6, and H-7 are quite large and double irradiation of each in turn produces clean d or dd signals. Therefore by normal criteria this system may be treated to a high degree of approximation as first order and this permits the estimation of the coupling constant values and assignment of $J_{4,5} = 3.0$, $J_{4,6} = 0.0$, $J_{5,6} = 17.0$, $J_{5,7} = 11.0$, and $J_{6,7} = 3.0$ Hz. The magnitude of the coupling between H-4 and H-5 over five bonds is consistent with such long range coupling over a W path (10*e*) and demands that H-4 and H-5 be *trans* to each other permitting unambiguous stereochemical assignment of H-4 and H-5.

Double irradiation of the signal at δ 3.90 ascribed to H-8 simplifies the ddd resonance at δ 3.02 (H-7) to a dd as well as the ddd signal at δ 2.57 (H-11) to a dd through a W – long range coupling effect. This permitted assignment of the coupling constants $J_{7,8} = 3.0$ and $J_{8,11} = 2.5$ Hz. Double irradiation of H-8 at δ 3.90 had no effect on the H-9 absorption at δ 2.83 nor on the H-10 absorption at δ 2.30 so there is

TABLE 1. Proton chemical shifts and coupling constants for saframycin A in C_6D_6 and $CDCl_3$

Proton	Chemical shifts[a] δ (ppm) C_6D_6	Chemical shifts[a] δ (ppm) $CDCl_3$	Coupling constants[b] (Hz)
1	6.33	6.70	$J(1-2) = 9.5$
			$J(1-3) = 4.0$
2	3.76	3.84	$J(2-1) = 9.5$
			$J(2-3) = 14.0$
			$J(2-4) = 1.5$
3	2.50	3.26	$J(3-1) = 4.0$
			$J(3-2) = 14.0$
			$J(3-4) = 4.0$
4	3.87	3.98	$J(4-2) = 1.5$
			$J(4-3) = 4.0$
			$J(4-5) = 3.0$
			$J(4-6) = 0.0$
5	1.32	1.28	$J(5-4) = 3.0$
			$J(5-6) = 17.0$
			$J(5-7) = 11.0$
6	2.89	2.87	$J(6-5) = 17.0$
			$J(6-7) = 3.0$
			$J(6-4) = 0.0$
7	3.02	3.14	$J(7-5) = 11.0$
			$J(7-6) = 3.0$
			$J(7-8) = 3.0$
8	3.90	4.06	$J(8-7) = 3.0$
			$J(8-11) = 2.5$
9	2.31	2.83	$J(9-10) = 20.5$
			$J(9-11) = 7.5$
10	1.68	2.30	$J(10-9) = 20.5$
			$J(10-11) < 0.5$
11	2.57	3.44	$J(11-9) = 7.5$
			$J(11-10) < 0.5$
			$J(11-12) = 2.5$
12	2.90	3.99	$J(11-12) = 2.5$

[a] The chemical shifts were obtained at 400 MHz and are given relative to internal TMS as reference.
[b] The coupling constants were obtained by double irradiation experiments.

TABLE 2. Proton chemical shifts and coupling constants for saframycin C in C_6D_6 and $CDCl_3$

Proton	Chemical shifts[a] δ (ppm) C_6D_6	Chemical shifts[a] δ (ppm) $CDCl_3$	Coupling constants[b] (Hz)
1	6.64	6.74	$J(1-2) = 9.5$
			$J(1-3) = 3.0$
2	3.89	3.77	$J(2-1) = 9.5$
			$J(2-3) = 14.0$
			$J(2-4) = 1.5$
3	2.64	3.20	$J(3-1) = 3.0$
			$J(3-2) = 14.0$
			$J(3-4) = 4.0$
4	3.38	3.63	$J(4-2) = 1.5$
			$J(4-3) = 4.0$
			$J(4-5) = 3.0$
5	1.36	1.18	$J(5-4) = 3.0$
			$J(5-6) = 17.5$
			$J(5-7) = 11.0$
6	2.91	2.75	$J(6-5) = 17.5$
			$J(6-7) = 3.0$
7	2.40	2.67	$J(7-5) = 11.0$
			$J(7-6) = 3.0$
			$J(7-8) = 3.0$
8	4.10	4.10	$J(8-7) = 3.0$
			$J(8-10) = 1.0$
9	3.79	3.85	$J(9-10) < 0.5$
10	2.94	3.27	$J(10-9) < 0.5$
			$J(10-8) = 1.0$
			$J(10-11) = 2.0$
			$J(10-12) = 3.0$
11	2.36	2.83	$J(11-10) = 2.0$
			$J(11-12) = 11.0$
12	2.38	3.03	$J(12-10) = 3.0$
			$J(12-11) = 11.0$

[a] The chemical shifts were obtained at 400 MHz. Internal TMS was used as the reference compound.
[b] The coupling constants were obtained from the related proton decoupling spectra.

Can. J. Chem. Downloaded from www.nrcresearchpress.com by 210.87.254.42 on 09/06/12
For personal use only.

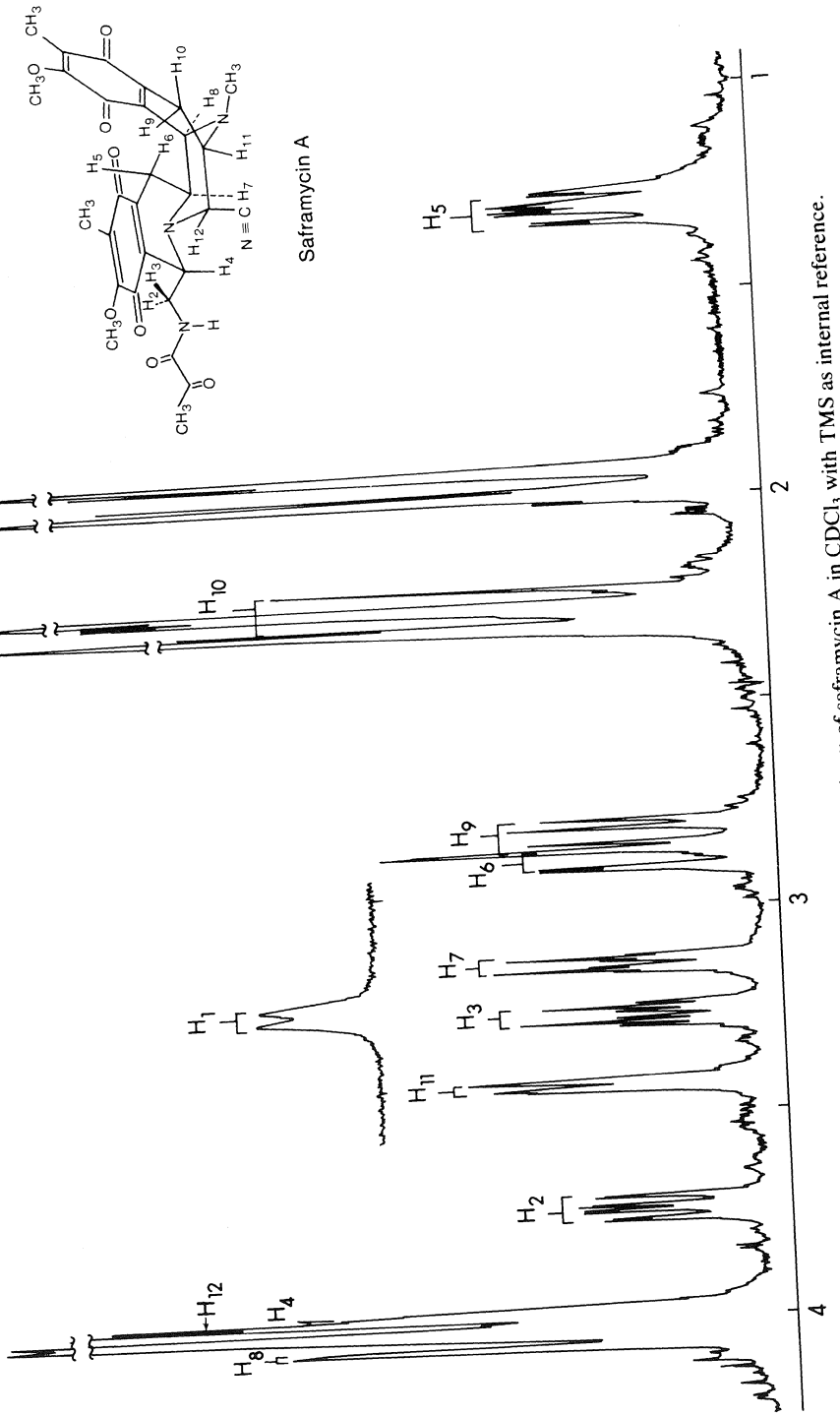

FIG. 2. High field (400 MHz) ^{1}H nmr spectrum of saframycin A in $CDCl_3$ with TMS as internal reference.

Can. J. Chem. Downloaded from www.nrcresearchpress.com by 210.87.254.42 on 09/06/12
For personal use only.

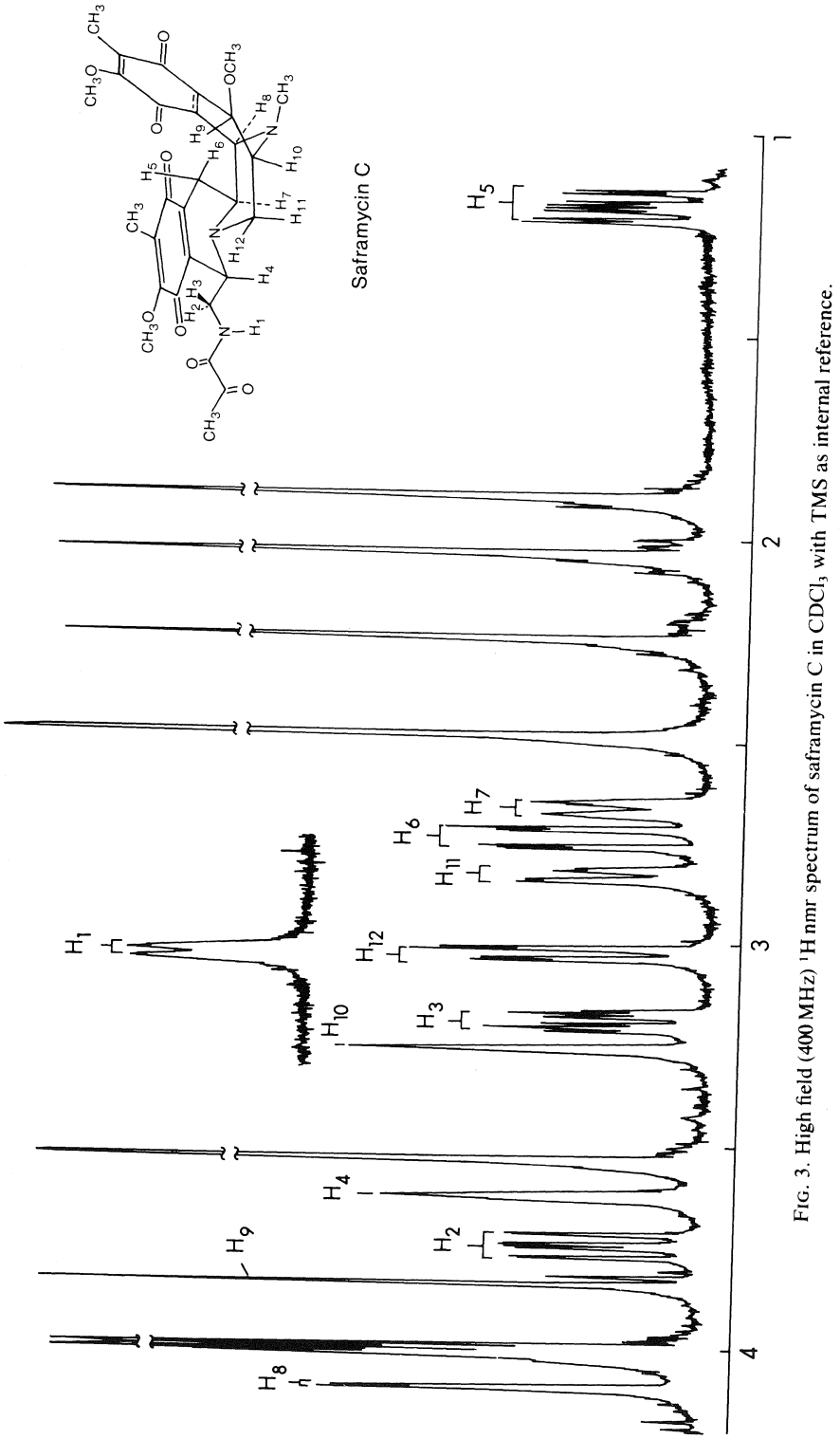

FIG. 3. High field (400 MHz) ^{1}H nmr spectrum of saframycin C in $CDCl_3$ with TMS as internal reference.

Can. J. Chem. Downloaded from www.nrcresearchpress.com by 210.87.254.42 on 09/06/12
For personal use only.

TABLE 3. Proton chemical shifts and coupling constants for saframycin A in DMSO-d_6 – D_2O and DMSO-d_6 – D_2O–CF_3COOD

	DMSO-d_6 – D_2O		DMSO-d_6 – D_2O–CF_3COOD	
Proton	Chemical shifts[a] δ (ppm)	Coupling constants[b] (Hz)	Chemical shifts[a] δ (ppm)	Coupling constants[b] (Hz)
H-2	3.0	J(2–3) = 14.0 J(2–4) = 2.0	3.07	J(2–3) = 14.0 J(2–4) = 1.5
H-3	3.63	J(3–2) = 14.0 J(3–4) = 4.0	3.61	J(3–2) = 14.0 J(3–4) = 4.0
H-4	3.74	J(4–2) = 2.0 J(4–3) = 4.0 J(4–5) = 3.0 J(4–6) = 0.0	3.94	J(4–5) = 2.5 J(4–3) = 4.0 J(4–2) = 1.5 J(4–6) = 0.0
H-5	1.13	J(5–6) = 17.0 J(5–7) = 11.0 J(5–4) = 3.0	1.29	J(5–6) = 17.5 J(5–7) = 11.0 J(5–4) = 2.5
H-6	2.57	J(6–5) = 17.0 J(6–7) = 3.0 J(6–4) = 0	2.77	J(6–5) = 17.5 J(6–7) = 3.0 J(6–4) = 0
H-7	2.80	J(7–5) = 11.0 J(7–6) = 3.0 J(7–8) = 3.0	3.24	J(5–7) = 11.0 J(7–6) = 3.0 J(7–8) = 2.5
H-8	3.79	J(8–7) = 3.0 J(8–11) = ~ 1.0	4.70	J(8–7) = 2.5 J(8–11) = ~ 1.0
H-9	2.62	J(9–11) = 7.5 J(9–10) = 20.5	3.06	J(9–11) = 7.5 J(9–10) = 21.0
H-10	2.24	J(10–9) = 20.5 J(10–11) = < 0.5	2.86	J(10–9) = 21.0 J(10–11) = <0.5
H-11	3.36	J(11–9) = 7.5 J(11–12) = 2.5 J(11–10) = < 0.5 J(11–8) = ~ 1.0	4.31	J(11–9) = 7.5 J(11–12) = 2.5 J(11–10) = < 0.5 J(11–8) = ~ 1.0
H-12	4.30	J(11–12) = 2.5	4.75	J(12–11) = 2.5
N-Me	2.08	—	2.74	—

[a] The chemical shifts were obtained at 400 MHz and are given relative to that of DMSO taken as δ 2.50.
[b] The coupling constants were obtained by double irradiation experiments.

no evidence for long range coupling between H-8 and H-9 or H-10 through the quinone ring. Irradiation of the dd absorption at δ 2.31 (H-9) collapsed the H-10 signal at δ 1.68 (which is partially overlapped by the methyl signals) as well as the ddd signal at δ 2.57 (H-11) to a dd. Irradiation of the H-10 resonance at δ 1.68 caused the H-9 absorption at δ 2.31 to change from a dd to a d and the H-11 signal at δ 2.57 from a ddd to a dd. In turn irradiation of the ddd signal of H-11 at δ 2.57 caused the collapse of the dd signal of H-9 at δ 2.31 to a d and of the H-10 signal at δ 1.68 and of the H-8 signal at δ 3.90. From these decoupling experiments it was possible to deduce $J_{9,10} = 20.5$, $J_{9,11} = 7.5$, and $J_{10,11} < 0.5$ Hz. Finally, irradiation of the H-11 resonance at δ 2.57 led to the collapse of the d signal of H-12 at δ 2.90 to an s and double irradiation of H-12 d in turn leads to a simplification of the H-11 signal at δ 2.57 giving $J_{11,12} = 2.5$ Hz. (See Fig. 2 and Table 1).

A similar analysis of the high field nmr spectrum of saframycin C in $CDCl_3$ employing extensive double irradiation gave the spectral parameters shown in Table 2. The accurate chemical shifts and coupling constants for the protons of saframycin C in benzene-d_6 and $CDCl_3$ were obtained in a similar manner (see Fig. 3 and Table 2).

The nuclear Overhauser effect (nOe) difference experiments (11*a*) involve the measurement of the intensity change of a proton resonance upon saturating another proton (or group of protons) within the same molecule. Ordinarily an nOe change indicates that the two protons are in close proximity. However, the relaxation mechanisms available to the protons in question need to be considered. The experiments selected involved a dilute and degassed sample and irradiation of the methyl group of the α-dione amide side chain and inspection of the other methine and methylene protons in

TABLE 4. Proton chemical shifts and coupling constants for saframycin C in DMSO-d_6 – D_2O and DMSO-d_6 – CF_3COOD

	DMSO-d_6 – D_2O		DMSO-d_6 – D_2O–CF_3COOD	
Proton	Chemical shifts[a] δ (ppm)	Coupling constants[b] (Hz)	Chemical shifts[a] δ (ppm)	Coupling constants[b] (Hz)
H-2	3.16	$J(2-3) = 14.0$ $J(2-4) = \sim 1.5$	3.09	$J(2-3) = 14.0$ $J(2-4) = \sim 1.5$
H-3	3.54	$J(3-2) = 14.0$ $J(3-4) = 4.0$	3.55	$J(3-2) = 14.0$ $J(3-4) = 4.0$
H-4	3.46	$J(4-3) = 4.0$ $J(4-2) = \sim 1.5$ $J(4-5) = 3.0$ $J(4-6) = 0$	3.59	$J(4-3) = 4.0$ $J(4-2) = \sim 1.5$ $J(4-5) = 3.0$ $J(4-6) = 0$
H-5	0.96	$J(5-6) = 17.5$ $J(5-7) = 11.0$ $J(5-4) = 3.0$	1.02	$J(5-6) = 17.5$ $J(5-7) = 11.0$ $J(5-4) = 3.0$
H-6	2.42	$J(6-5) = 17.5$ $J(6-7) = 3.0$ $J(6-4) = 0$	2.54	$J(6-5) = 17.5$ $J(6-7) = 2.5$ $J(6-4) = 0$
H-7	2.54	$J(7-5) = 11.0$ $J(7-6) = 3.0$ $J(7-8) = 3.0$	2.94	$J(7-5) = 11.0$ $J(7-6) = 2.5$ [c]
H-8	3.86	$J(8-7) = 3.0$ $J(8-10) = \sim 1.0$	4.68	[c] [c]
H-9	3.89	$J(9-10) =$ very small	4.40	$J(9-10) =$ very small
H-10	3.18	$J(10-11) = 2.5$ $J(10-12) = 2.5$ $J(10-8) = \sim 1.0$ $J(10-9) =$ very small	3.98	[c] [c] [c] [c]
H-11	2.60	$J(11-12) = 11.0$ $J(11-10) = 2.5$	2.95	$J(11-2) = 11.5$ [c]
H-12	3.10	$J(12-11) = 11.0$	3.35	$J(12-11) = 11.5$
N-Me	2.24	—	2.84	—

[a] The chemical shifts were obtained at 400 MHz and are given relative to that of DMSO taken as δ 2.50.
[b] Coupling constants were obtained by double irradiation experiments.
[c] Coupling constants could not be measured either because of poor resolution or overlapping.

the molecule. The expression for the nOe phenomenon involves two terms (*i*) a direct dipolar term and (*ii*) an indirect term via polarization nOe transmission from adjacent protons (11*b*). In these situations the expression for nOe implies a dependence predominantly on the relaxation parameters of the protons being observed. The predominant relaxation mechanisms for the geminal protons H_{11} and H_{12} in saframycin C will be dipole–dipole (11*c*). A reported example of irradiation of the methyl groups in crotonaldehyde (*Z* and *E*) resulted in nOe enhancement of the adjacent protons implying molecular proximity (12). In the present application irradiation of the side-chain methyl group at 400 MHz produced no detectable nOe change in any of the methine or methylene protons in either saframycin A or C. Since nOe experiments can show a frequency dependence in the direction of increased enhancement at lower frequencies (13) the experiment was repeated at 200 MHz. Again no nOe changes were detected. It is tentatively concluded that the antibiotics in solution adopt conformations in which the side-chain methyl group is remote from other protons, which result is in accord with the conclusion drawn earlier from the rotamer analysis. Although we could not ascertain the orientation of the nitrile group in saframycin A on the basis of nmr coupling constants it is assigned the α-orientation as shown, which explains the easy elimination of the nitrile on mild acid treatment (3). This requires that the lone pair on N-2 be *trans* to the nitrile group. The problem of distinguishing between the two optical antipodes of the saframycins has to await a more refined X-ray crystallographic study.

The above conformation predicts that H-5 be placed in the strongly shielding zone of the quinone ring (adjacent to H-8) and also in close proximity to

Can. J. Chem. Downloaded from www.nrcresearchpress.com by 210.87.254.42 on 09/06/12
For personal use only.

Can. J. Chem. Downloaded from www.nrcresearchpress.com by 210.87.254.42 on 09/06/12
For personal use only.

the lone pair of the bridging central nitrogen atom (see Figs. 2, 3). These two shielding influences may account for the unusually high field position of H-5 in both antibiotics.

The resonance positions of the protons of the lower half of both antibiotics suffer a remarkable downfield shift in changing the solvent from benzene-d_6 to $CDCl_3$. In the case of saframycin A, the most affected protons are H-3 (0.76 ppm), H-9 (0.52 ppm), H-10 (0.62 ppm), H-11 (0.87 ppm), and H-12 (1.09 ppm) and for saframycin C, they are H-3 (0.56 ppm), H-10 (0.33 ppm), H-11 (0.47 ppm), and H-12 (0.65 ppm). The chemical shifts of the other protons and the coupling constants of all the protons are relatively unaffected. This downfield shift may be due to the change in the orientation of the α-dione amide side chain with respect to the methylene group in the two solvents.

To study any conformational change in aqueous solution and relative ease of protonation of the two basic nitrogen atoms in the saframycin molecules, the spectra of both antibiotics were recorded in DMSO-d_6 – D_2O (7:3) and DMSO-d_6 – D_2O–CF_3COOD (~ 5% CF_3COOD). The chemical shifts of the various protons were determined by extensive double irradiation studies as described before (see Tables 3 and 4). No conformational change could be ascertained from the spectra, except possibly for the α-dione amide side chain with respect to the methylene group, because the relative resonance positions of H-2 and H-3 were reversed in aqueous solution compared to those in benzene-d_6 and $CDCl_3$. This conclusion is based on the coupling constants $J_{2,4}$ and $J_{3,4}$.

In the presence of CF_3COOD, the resonance positions of H-8, H-11, and the N-Me in saframycin A and H-8, H-10, and N-Me in saframycin C were shifted relatively more downfield (0.91, 0.95, and 0.68 ppm, respectively for saframycin A and 0.82, 0.80, and 0.60 ppm respectively for saframycin C) compared to H-7 and H-12 in saframycin A and H-7, H-11, and H-12 in saframycin C, indicating preferential protonation of N-12 in both antibiotics. The chemical shift of H-4 was hardly affected. Examination of models indicates that the lone pair on N-12 is more accessible than on N-2.

The significance of the conformation of the saframycins as discussed above and the preferential protonation of N-12 over N-2 in both antibiotics in the molecular recognition process in their mode of action on duplex DNA will be discussed in a subsequent publication.

Acknowledgements

This investigation was supported by grants from the National Cancer Institute of Canada, the Natural Sciences and Engineering Research Council of Canada, and the Department of Chemistry of the University of Alberta. We wish to thank Mr. Glen Bigam for technical assistance in obtaining the decoupled high field nmr spectra.

1. T. Arai, K. Yazawa, Y. Mikami, A. Kubo, and K. Takahashi. J. Antibiot. Tokyo, **29**, 398 (1976).
2. T. Arai, K. Takahashi, and A. Kubo. J. Antibiot. Tokyo, **30**, 1015 (1977).
3. T. Arai, K. Takahashi, K. Ishiguro, and K. Yazawa. J. Antibiot. Tokyo, **33**, 951 (1980).
4. W. Szybalski and V. N. Iyer. The mitomycins and profiromycins. *In* Antibiotics I. Mechanism of Action. *Edited by* D. Gottlieb and P. D. Shaw. Springer Verlag, New York. 1967. pp. 211–245.
5. K. V. Rao, K. Biemann, and R. B. Woodward. J. Am. Chem. Soc. **85**, 2532 (1963).
6. D. Kluepfel, H. A. Baker, G. Piattoni, S. N. Sehgal, A. Sidorowicz, K. Singh, and S. Vezina. J. Antibiot. Tokyo, **28**, 497 (1975).
7. T. Arai, K. Takahashi, A. Kubo, S. Nakahara, S. Sato, K. Aiba, and C. Tamura. Tetrahedron Lett. 2355 (1979).
8. T. Arai, K. Takahashi, S. Nakahara, and A. Kubo. Experientia, **36**, 1025 (1980).
9. K. Ishiguro, S. Sakiyama, K. Takahashi, and T. Arai. Biochemistry, **17**, 2545 (1978).
10. (*a*) L. M. Jackman and S. Sternhell. Applications of nuclear magnetic resonance spectroscopy in organic chemistry. 2nd ed. Pergamon, New York. 1969. p. 299; (*b*) p. 280; (*c*) p. 283; (*d*) p. 240; (*e*) p. 333.
11. (*a*) J. H. Noggle and R. E. Schirmer. The nuclear Overhauser effect – chemical applications. Academic Press, New York. 1971; (*b*) pp. 46–48; (*c*) pp. 25–26.
12. R. Rowan, J. A. McCammon, and B. D. Sykes. J. Am. Chem. Soc. **96**, 4773 (1974).
13. J. D. Glickson, S. L. Glickson, T. P. Pitner, D. G. Agresti, and R. Walter. Biochemistry, **15**, 5721 (1976).

Studies in partial miscibility: the systems triethylamine–dimethylsulfoxide–methylethylketone and triethylamine–formamide–methylethylketone

ALAN N. CAMPBELL AND ELINOR M. KARTZMARK

Department of Chemistry, University of Manitoba, Winnipeg, Man., Canada R3T 2N2

Received April 14, 1981

ALAN N. CAMPBELL and ELINOR M. KARTZMARK. Can. J. Chem. **59**, 2953 (1981).

The systems triethylamine–methylethylketone–dimethylsulfoxide and triethylamine–methylethylketone–formamide have been studied by the methods of isothermal equilibrium and thermal analysis. At least in the case of the system triethylamine–methylethylketone–dimethylsulfoxide, the equilibrium conditions have been completely established with respect to concentration and temperature. From these data a solid model can be constructed, as was previously done for the system nicotine–water–methylethylketone. It appears that the miscibility is greater in the system involving dimethylsulfoxide than in the system involving formamide.

ALAN N. CAMPBELL et ELINOR M. KARTZMARK. Can. J. Chem. **59**, 2953 (1981).

Faisant appel à l'équilibre isothermique et à l'analyse thermique, on a étudié les systèmes suivants: triéthylamine–méthyléthylcétone–diméthylsulfoxyde et triéthylamine–méthyléthylcétone–formamide. On a établi complètement, du moins, dans le cas du premier système, les conditions d'équilibre en fonction de la concentration et de la température. A partir de ces données, on a construit un modèle solide comme celui trouvé antérieurement pour le système nicotine–eau–méthyléthylcétone. Il semble que la miscibilité est plus grande dans le système impliquant le diméthylsulfoxyde que dans celui contenant le formamide.

[Traduit par le journal]

Introduction

The well known, completely closed, egg-shaped equilibrium diagram of the system nicotine–water (2) has a close analogue in the system methylethylketone–water, except that, in the case of the latter system, the lower critical solution temperature is unattainable, at least at atmospheric pressure: the curve of mutual solubility is intersected by the ice line (3). These two systems have been combined in a study of the ternary system nicotine–water–methylethylketone (1). In the ternary system, the heterogeneous (two liquid) region forms a tunnel, without ternary maximum.

In the present paper, the systems triethylamine–methylethylketone–dimethylsulfoxide and triethylamine–methylethylketone–formamide are investigated. The completely miscible pair in these two systems is triethylamine–methylethylketone, while triethylamine forms two layers with formamide and with dimethylsulfoxide.

Experimental

Triethylamine was determined conductometrically by titration with standard hydrochloric acid. The densities of numerous homogeneous mixtures were determined and plotted on a large triangular diagram. Points of equal density were joined. The lines of equal triethylamine content were of necessity parallel to the base of the triangle and were crossed by the curves of equal density at a sharp angle (for both systems).

The temperatures of homogeneity in the two-component systems were determined with the apparatus shown in Fig. 1. The apparatus was charged with various known compositions of mixture and heated on a Fisher Thermix apparatus, which permits simultaneous and vigorous (magnetic) stirring, while heating. Below the temperature of homogeneity, mixtures were turbid under vigorous stirring but promptly settled into two layers when the stirring was stopped. The transitions from turbid to clear (one homogeneous liquid) and conversely were quite sharp.

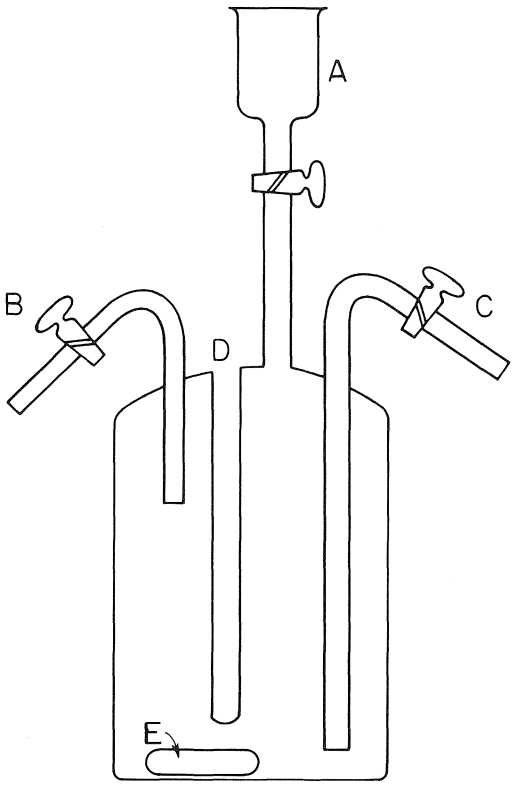

FIG. 1. Equilibrium apparatus.

For the system formamide–triethylamine, the critical solution

0008-4042/81/202953-04$01.00/0

©1981 National Research Council of Canada/Conseil national de recherches du Canada

Can. J. Chem. Downloaded from www.nrcresearchpress.com by 210.87.254.6 on 09/06/12
For personal use only.

Can. J. Chem. Downloaded from www.nrcresearchpress.com by 210.87.254.6 on 09/06/12
For personal use only.

temperature is not realisable because, although the compositions of congruent layers are approaching with rising temperature and would therefore become identical at some high temperature, the L ⇋ V critical point intervenes before this temperature can be reached. This was confirmed by observations in thick-walled capillary tubes.

The technique whereby a heterogeneous mixture is observed in the field of a telescope while the mixture is being heated in an electric furnace has been frequently described (4). At room temperature, two menisci are clearly visible. On heating the system formamide–triethylamine there is a sudden disappearance of the $L_2 \leftrightharpoons V$ meniscus, leaving only $L_1 \leftrightharpoons V$ below the temperature at which $L_1 \leftrightharpoons L_2$ disappears. L_2 is the layer rich in triethylamine, L_1 is the layer rich in formamide.

For the high temperature study of the ternary system, the apparatus in Fig. 1 was used (approximately) isothermally. By careful manipulation of the rheostat controlling the heating element of the thermix an approximately constant temperature could be maintained for a short time and this is all that is necessary because (*a*) equilibrium is rapidly attained and (*b*) the effect of temperature on both the binary and ternary systems is not great. It is obvious from Fig. 1 how samples of both the equilibrium layers can be removed for analysis.

Thermal analysis of both systems was carried out, using a copper–constantan thermocouple and liquid nitrogen as cooling agent. In a binary system, after the appearance of a solid phase, the temperature (at constant pressure) remains constant, while the process $L_2 \rightarrow L_1 + S$ is taking place. In a three component system, the temperature should continue to fall while the above transformation is taking place and the compositions of the two liquid layers should change progressively (5). In practice, however, the compositions of the two layers differ so greatly that there is little or no change of temperature while the transformation goes to completion. Thermal analysis should yield two significant temperatures, that at which the above transformation takes place and, if continued to sufficiently low temperature, that of the ternary eutectic.

Results

The temperatures of homogeneity (temperature rising) in the binary system dimethylsulfoxide–triethylamine are listed in Table 1 and are expressed graphically in Fig. 2. The critical solution temperature is seen to be 122°C and corresponds to a composition of 75% triethylamine.

The temperatures of homogeneity in the binary system formamide–triethylamine are listed in Table 2 and are expressed graphically in Fig. 3.

In the experiments in sealed tubes on the system formamide–triethylamine, the $L_1 \leftrightharpoons L_2$ transition was never observed, but the critical point $L_1 \leftrightharpoons V$ or $L_2 \leftrightharpoons V$ occasionally was around a temperature of 270°C. The critical temperatures are given as 259°C for triethylamine (6) and 260°C for methylethylketone (7); it is probable that all mixtures of these liquids have critical temperatures around 260°C. At this temperature, the tubes frequently exploded. It seems clear that in the system formamide–triethyl-

TABLE 1. Temperatures of homogeneity in the binary system dimethylsulfoxide–triethylamine

Wt.% triethylamine	Temperature of homogeneity (°C)
8.5	25
10.0	52
20.0	91
51.5	118
80.0	120
90.0	100
95.0	85
96.0	25

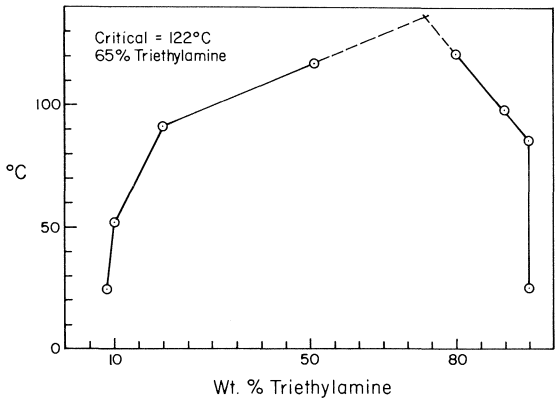

FIG. 2. The system triethylamine–dimethylsulfoxide at various temperatures.

TABLE 2. Temperatures of homogeneity in the binary system formamide–triethylamine

Temperature (°C)	Wt.% triethylamine	
	Layer I	Layer II
0	9.0	81.4
25	11.0	79.0
60	12.5	77.5
100	16.4	74.2
140	17.0	73.0

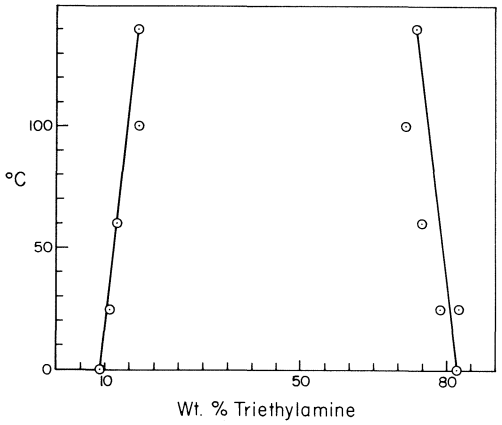

FIG. 3. The system triethylamine–formamide at various temperatures.

Can. J. Chem. Downloaded from www.nrcresearchpress.com by 210.87.254.6 on 09/06/12
For personal use only.

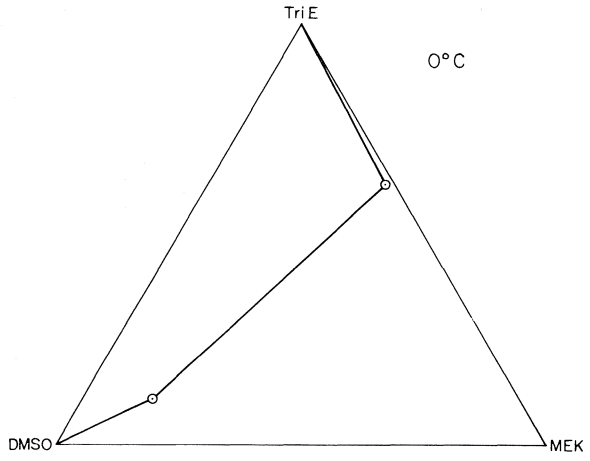

FIG. 4. The system triethylamine–dimethylsulfoxide–methylethylketone at 0°C.

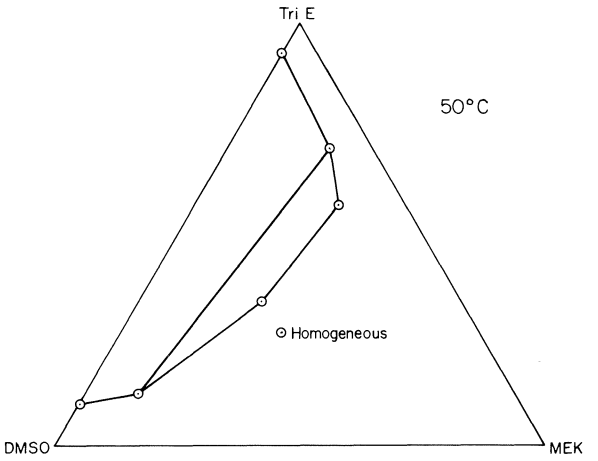

FIG. 6. The system triethylamine–dimethylsulfoxide–methylethylketone at 50°C.

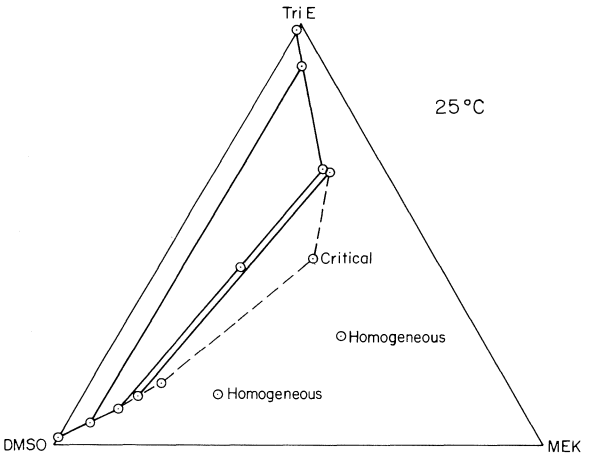

FIG. 5. The system triethylamine–dimethylsulfoxide–methylethylketone at 25°C.

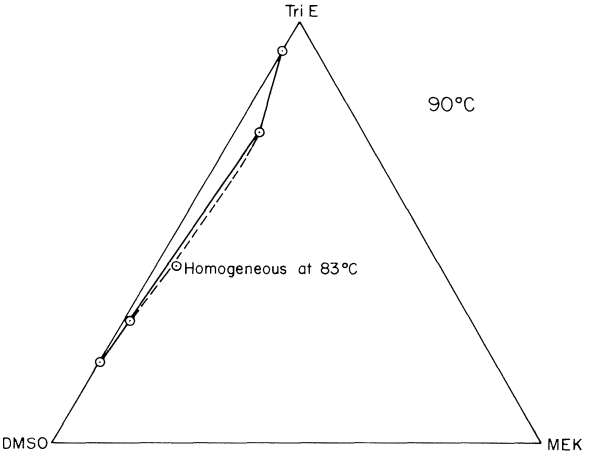

FIG. 7. The system triethylamine–dimethylsulfoxide–methylethylketone at 90°C.

amine, the critical solution temperature lies above the critical temperature L ⇋ V.

The results of the equilibrium studies are expressed graphically in Figs. 4–9. The numerical results are to be found in Depository.[1]

The thermal analysis figures for the system triethylamine–methylethylketone are listed in Table 3. When these results are plotted, a simple eutectic diagram results, with the eutectic lying at −146°C and 79 wt.% triethylamine.

The data referring to the system triethylamine–dimethylsulfoxide are listed in Table 4. When these results are combined with Fig. 2 (diagrammatic),

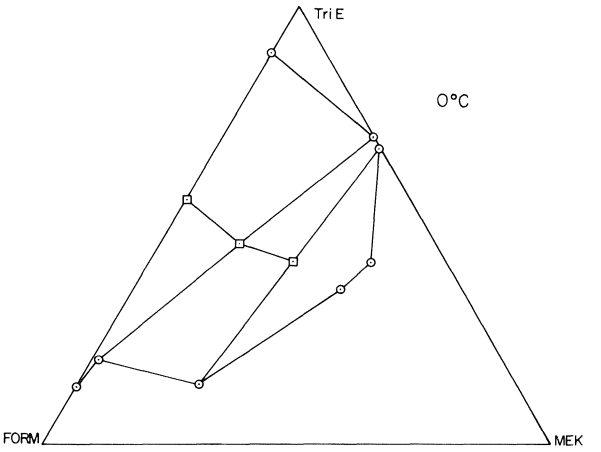

FIG. 8. The system triethylamine–formamide–methylethylketone at 0°C.

[1]Complete set of data may be obtained, at a nominal charge, from the Depository of Unpublished Data, CISTI, National Research Council of Canada, Ottawa, Ont., Canada K1A 0S2.

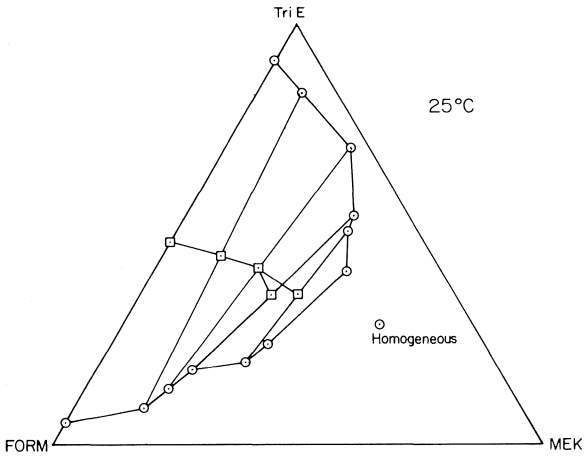

FIG. 9. The system triethylamine–formamide–methylethylketone at 25°C.

TABLE 3. Thermal analysis figures of the system triethylamine–methylethylketone

Wt.% triethylamine	Freezing point (°C)	Eutectic (°C)
0.0	−87	—
9.0	−91	—
19.0	−97	−145
27.0	−103	−142
53.0	−108	−146
78.5	−146	−146
90.0	−116	—
100.0	−115	—

TABLE 4. Thermal analysis figures of the system triethylamine–methylethylketone

Wt.% triethylamine	First halt (°C)	Eutectic (°C)
22.76	16.31	−181
85.64	15	−181

Fig. 10 is obtained. If any mixture of triethylamine and dimethylsulfoxide lying between 5 and 95% triethylamine is cooled, a first halt is observed at 16°C, 2° below the freezing point of pure dimethylsulfoxide. The temperature remains constant while the change

$$L_1 \rightarrow L_2 + \text{solid DMSO}$$

is taking place. Cooling then continues to the eutectic temperature, at which both components are present in the solid state.

Experiments similar to the above on the system triethylamine–formamide were not successful. The temperature of the transition

$$L_1 \rightarrow L_2 + \text{solid formamide}$$

appears to lie at −24°C, but the eutectic temperature did not appear, perhaps due to a slow rate of crystallisation.

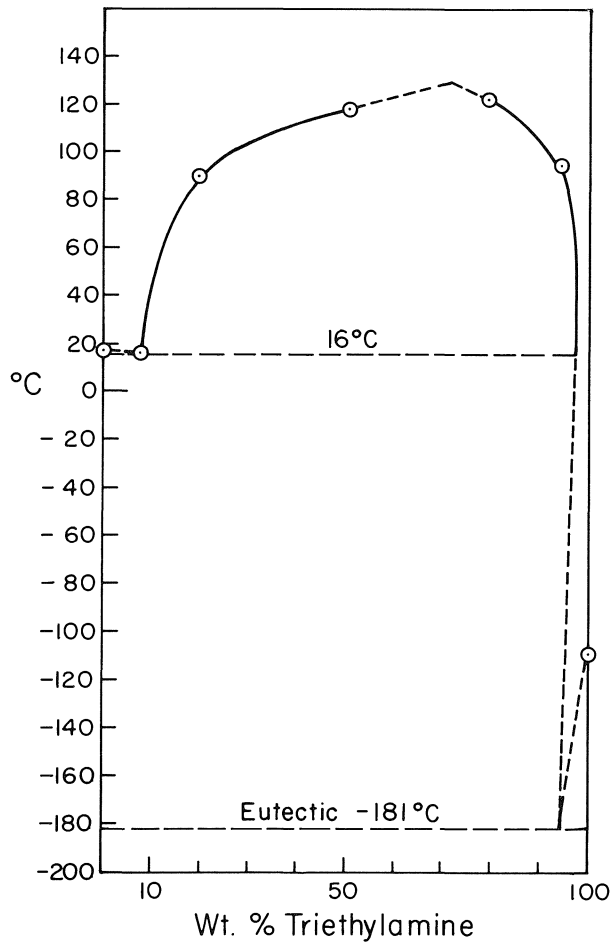

FIG. 10. The system triethylamine–dimethylsulfoxide at various temperatures.

Sufficient data are given in this paper for the construction of a solid model at least for the system dimethylsulfoxide–triethylamine–methylethylketone as was done for the system nicotine–water–methylethylketone (3).

1. A. N. CAMPBELL, E. M. KARTZMARK, and W. E. FALCONER. Can. J. Chem. **36**, 1475 (1958).
2. C. HUDSON. Z. Phys. Chem. **47**, 113 (1904).
3. P. KOHNSTAMM and J. TIMMERMANS. Proc. K. Akad. Wetensch. Amsterdam, **15**, 1021 (1913).
4. A. N. CAMPBELL and E. M. KARTZMARK. Can. J. Chem. **41**, 1058 (1963).
5. G. MASING. Ternary systems. *Translated by* B. A. Rogers. Dover Publishers, New York, NY. 1960. p. 112.
6. C. VINCENT and J. CHAPPIUS. J. Phys. **5**, 58 (1886).
7. M. ROSENBAUM. M.S. Thesis, University of Texas. 1951.

Can. J. Chem. Downloaded from www.nrcresearchpress.com by 210.87.254.6 on 09/06/12
For personal use only.

Successive electron transfers to dibiphenylene-ethene molecule — effect of solvent and electrolyte

ELŻBIETA WAGNER, TERESA PAROL, AND MAREK K. KALINOWSKI[1]

Department of Chemistry, University of Warsaw, 1 Pasteur Street, 02-093 Warszawa, Poland

Received December 10, 1980

Can. J. Chem. Downloaded from www.nrcresearchpress.com by 210.87.254.40 on 09/06/12
For personal use only.

ELZBIETA WAGNER, TERESA PAROL, and MAREK K. KALINOWSKI. Can. J. Chem. **59**, 2957 (1981).

The polarographic and voltammetric behaviour of dibiphenylene-ethene (DBPE) has been studied in benzonitrile, acetonitrile, propylene carbonate, acetone, *N*,*N*-dimethylformamide, *N*,*N*-dimethylacetamide, dimethylsulfoxide, *N*,*N*-diethylformamide, pyridine, and ethylenediamine. The two successive reversible electron transfers have been observed in all these solvents. The separation between the formal potentials of DBPE/DBPE$^{-\cdot}$ and DBPE$^{-\cdot}$/DBPE^{2-} systems was found to vary with the properties of solvents and with the kind of supporting elecrtrolyte cations (tetraethylammonium and sodium perchlorates were used as electrolytes). The variation of redox potentials both with the solvent and the cation is discussed in terms of the donor–acceptor concept for solvent–solute interaction. Numerical analysis using both the values of the donor numbers and the acceptor numbers leads to successful description of experimental results. It has further been observed that DBPE^{2-} dianion is protonized in ethylenediamine solutions.

ELZBIETA WAGNER, TERESA PAROL et MAREK K. KALINOWSKI. Can. J. Chem. **59**, 2957 (1981).

On a étudié le comportement polarographique et voltamétrique du dibiphénylène-éthène (DBPE) dans le benzonitrile, l'acétonitrile, le carbonate de propylène, l'acétone, la *N*,*N*-diméthylformamide, la *N*,*N*-diméthylacétamide, le diméthylsulfoxyde, la *N*,*N*-diéthylformamide, la pyridine et l'éthylène diamine. Dans tous ces solvants on a observé les deux transferts réversibles successifs d'électrons. On a trouvé que la séparation entre les potentiels formels de systèmes DBPE/DBPE$^{-\cdot}$ et DBPE$^{-\cdot}$/DBPE^{2-} varie avec la propriété des solvants et avec le type de cation de l'électrolyte de support (comme électrolytes on a utilisé les perchlorate de tétraéthylammonium et de sodium). On discute de la variation des potentiels rédox avec le cation et le solvant en fonction du concept de donneur–accepteur pour l'interaction solvent–soluté. L'analyse numérique utilisant à la fois les valeurs des différents donneurs et des différents accepteurs conduit à une description satisfaisante des résultats expérimentaux. On a de plus observé que le dianion DBPE^{2-} est protoné dans les solutions d'éthylènediamine.

[Traduit par le journal]

Introduction

The problem of successive electron transfers to organic molecules has been studied by many workers (1–8) and corresponding theoretical analysis has been presented (3, 4, 9, 10). According to Ammar and Savéant (3), the difference between the formal potentials for the first and second electron transfer steps is influenced both by structural and medium effects. These authors first pointed out that for the molecules containing two identical but completely isolated electroactive groups, $\Delta E_{1/2}$ values are only connected with entropic factors. On the other hand if these centers interact two possibilities should be differentiated: (*i*), the first electron transfer hinders the second one, for example, by a coulombic interaction, and (*ii*), the first electron transfer promotes the second transfer, because of solvation and ion pairing phenomena. Now, in the first case the second wave will move towards more extreme potentials causing an increase in $\Delta E_{1/2}$, whereas in the second case $\Delta E_{1/2}$ values will be diminished.

The purpose of this paper is to describe the medium effects on the separation of reversible

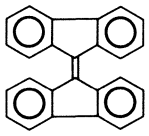

potentials for the first and second electron transfers. Thus, we report here electrochemical studies of dibiphenylene-ethene (DBPE) in a series of organic solvents. The perchlorates of $(C_2H_5)_4N^+$ and Na^+ were used as supporting electrolytes. The molecule of DBPE may be formally treated as two fluorene moieties joined together by a double bond, therefore it is an example of the molecule containing two identical and strongly interacting electroactive centers.

Experimental

Polarographic and stationary electron voltammetric measurements were carried out in a three-electrode system using a Radelkis OH-105 polarograph. For higher scan rates (up to 20 V s^{-1}) the digiscope polarograph OP-3 Unitra-Telpod (Poland) and Luggin capillary were applied. The working electrode was either a mercury drop electrode characterized by drop time 2.0 s (a drop timer was used throughout experiments) or a hanging mercury drop electrode of the design of Kemula and Kublik (11) with diameter 0.71 mm. The potentials were measured against an aqueous SCE using a two-part salt bridge. In one arm of this bridge, there was a solvent and electrolyte exactly as in the

[1]To whom all correspondence should be addressed.

0008-4042/81/202957-05$01.00/0

©1981 National Research Council of Canada/Conseil national de recherches du Canada

TABLE. 1. Solvent parameters and essential characteristics of dibiphenylene-ethene in various solvents

Solvent	DN[a]	AN[b]	E_T[c]	$(C_2H_5)_4NClO_4$				$NaClO_4$	
				$-E^{I}_{1/2}$, V	I^{I}_d	$-E^{II}_{1/2}$, V	I^{II}_d	$-E^{I}_{1/2}$, V	$-E^{II}_{1/2}$, V
Benzonitrile	11.9	15.5	42.0	1.005	1.30	1.410	1.30	1.010	1.420
Acetonitrile	14.1	18.9	46.0	1.050	2.45	1.450	2.30	1.050	1.440
Propylene carbonate	15.1	18.3	46.6	1.020	0.89	1.425	0.85	1.025	1.435
Acetone	17.0	12.5	42.2	1.045	2.66	1.465	2.57	1.040	1.485
N,*N*-dimethylformamide	26.6	16.0	43.8	0.980	1.55	1.425	1.52	0.980	1.450
N,*N*-dimethylacetamide	27.8	13.6	43.7	0.990	1.35	1.435	1.29	0.990	1.465
Dimethylsulfoxide	29.8	19.3	45.0	0.935	1.00	1.365	0.98	0.940	1.380
N,*N*-diethylformamide	30.9			0.980	1.48	1.440	1.48	0.980	1.485
Pyridine	33.1	14.2	40.2	1.015	1.45	1.465	1.50	1.010	1.485
Ethylenediamine	55		42.0	0.950	1.06	1.225	1.05	0.955	1.240

[a] DN stands for Gutmann's donor number in kcal mol^{-1} (19).
[b] AN = acceptor number (19).
[c] Dimroth and Reichardt parameter of solvent polarity in kcal mol^{-1} (20).
[d] Diffusion current constant. $I_d = i_d/m^{2/3}t^{1/6}C$ in μA $mg^{-3/2}$ $s^{1/2}$ mM^{-1}.

polarographic vessel. Coulometric measurements were made by means of a Radelkis OH-404 apparatus.

DBPE of very high purity was kindly given by Dr. M. Jawdosiuk. Tetraethylammonium perchlorate was prepared (12) and recrystallized from triply distilled water and dried *in vacuo* at 60°C. $NaClO_4$ (AR grade) was dried at 120°C over P_2O_5 under reduced pressure. The solvents were dried and purified immediately before use according to the standard procedures (13). The water content in the solvents, analysed by Karl Fisher method, was about 10^{-3} *M*. All experiments were run at 23.0 ± 0.1°C. Before electrochemical measurements the solutions were deoxygenated with solvent-presaturated pure argon. The concentrations of the depolarizer and supporting electrolyte were usually 5.0×10^{-4} and 0.10 *M*, respectively.

Results

Two cathodic waves were observed in all solvents during the studies of DBPE on the dropping mercury electrode. Semi-logarithmic analysis gives $\Delta E/\Delta \log \{i/(i_d - i)\}$ slopes close to theoretical values for reversible one-electron transfer. Measurements of the wave height as a function of depolarizer concentration (in the range 0.08–0.75 m*M*) and as a function of the square root of a mercury height indicate that the limiting currents of both waves are controlled by diffusion. Coulometric determination yields one as the number of electrons for each electroreduction step. Such a behaviour was found in solutions containing $(C_2H_5)_4NClO_4$ and $NaClO_4$, respectively. The main difference in both these cases consists only in the different half-wave potentials of the second reduction step determined in some solvents. Essential characteristics of the polarographic waves of DBPE are summarized in Table 1. This table also contains some physicochemical parameters proper for the solvents.

Cyclic voltammograms of DBPE confirm reversible one-electron transfers for both electroreduction steps. Typical curve recorded at scan rate 0.1 V s^{-1} is presented in Fig. 1. On this curve one

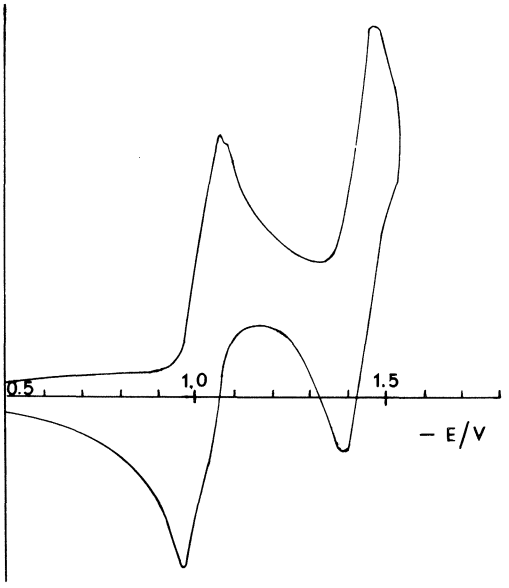

FIG. 1. Cyclic voltammetric curve of 5.0×10^{-4} *M* dibiphenylene-ethene in acetone containing 0.10 *M* $(C_2H_5)_4NClO_4$. Scan rate 0.05 V s^{-1}.

can observe corresponding pairs of cathodic and anodic peaks with i_{pa}/i_{pc} values close to unity and with theoretical separation (within ±5 mV). The ratios i_{pa}/i_{pc} and the peak potentials are independent of scan rate, v. We have observed that all these values remained practically constant when v changed from 0.05 to 10 V s^{-1}. It should also be pointed out that quite identical results were obtained in all remaining solvents applied in this work (both in the presence of $(C_2H_5)_4NClO_4$ and $NaClO_4$) with the exception of ethylenediamine.

Polarographic behaviour of DBPE in ethylenediamine differs markedly. Reversibility was only found for the first electroreduction step, whereas no anodic peak was recorded for the second wave

Can. J. Chem. Downloaded from www.nrcresearchpress.com by 210.87.254.40 on 09/06/12
For personal use only.

Can. J. Chem. Downloaded from www.nrcresearchpress.com by 210.87.254.40 on 09/06/12
For personal use only.

(using HMDE) even at $v = 20\,V\ s^{-1}$ (Fig. 2). Moreover, $E^{II}_{1/2}$ value was found to depend on the drop time ($\Delta E_{1/2}/\Delta \log t_1 = 28.5 \pm 3$ mV in solution containing tetraethylammonium perchlorate and in the t_1 range 1.0–10.0 s) but it is independent of the depolarizer concentration, at least in the range 0.1–1.2 m*M*. It should be noted that identical picture was observed when, instead of tetraethylammonium perchlorate, 0.10 *M* $NaClO_4$ was used.

Discussion

It follows from our experiments that relatively stable radical anions and dianions are produced during the electroreduction of DBPE in acetonitrile, acetone, propylene carbonate, *N*,*N*-dimethylformamide, dimethylsulfoxide, *N*,*N*-diethylformamide, pyridine, *N*,*N*-dimethylacetamide, and benzonitrile independently of electrolytes applied in this work. Thus, the general mechanism represented by scheme:

$$DBPE + e \rightleftharpoons DBPE^{-\cdot} \qquad E^{I}_{1/2}$$

$$DBPE^{-\cdot} + e \rightleftharpoons DBPE^{2-} \qquad E^{II}_{1/2}$$

is in agreement with the results reported previously in dimethylformamide solutions (14). The different behaviour of DBPE in ethylenediamine thus calls for an explanation.

Evidently, the irreversibility of the second wave under these conditions is connected with the protonization of $DBPE^{2-}$ dianions. We assume that the proton source are the molecules of the solvent, similarly it was demonstrated in the case of the electrochemistry of aromatic azo-compounds (15).[2] Accordingly, dibiphenylene-ethane was polarographically and spectrophotometrically identified as the product of the potentiostatic reduction (macroscale electrolysis) at the potential of the second wave of DBPE. It should be noted that taking into account these observations, we have not considered the values of $\Delta E_{1/2} = E^{I}_{1/2} - E^{II}_{1/2}$ for ethylenediamine solutions in the analysis presented below.

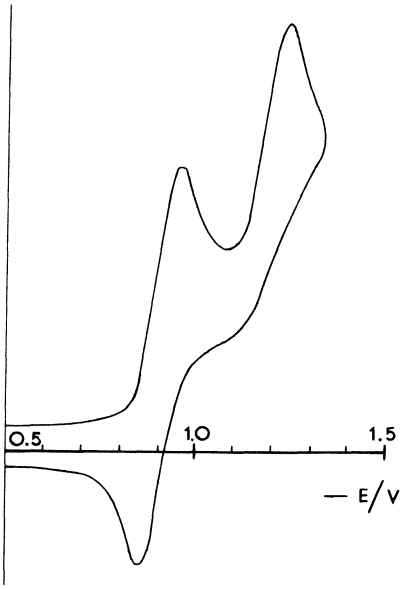

FIG. 2. Cyclic voltammogram of 5.0×10^{-4} *M* dibiphenylene-ethene registered in ethylenediamine solution containing 0.10 *M* $(C_2H_5)_4NClO_4$ at scan rate 10 V s^{-1}.

It was of particular interest in this study to obtain information on the environmental effects on $\Delta E_{1/2}$ values of DBPE. As clearly seen from the data presented in Table 1 these values are dependent both on the properties of solvent and on the nature of electrolyte cation. The possible reason can be that the difference between the formal potentials of DBPE is influenced by the effects of solvation and by ion pairing phenomena. We suppose that the role of ion pairs $DBPE^{-\cdot}...M^+$ (M^+ stands for a counter ion) may be neglected. It follows from the observation that $E^{I}_{1/2}$ values are identical within experimental error both in the presence of $(C_2H_5)_4NClO_4$ and $NaClO_4$ in a given solvent. These values are also indendent of electrolyte concentration (in the range 0.02–0.15 *M*). On the other hand, the half-wave potentials of the second reduction step are, in many solvents, dependent on the nature of cations (Table 1) and on their concentration in solutions. Thus, in the case of $DBPE^{2-}$ the solvent–anion interaction is overlapped by cation–anion interactions.

At present, it is not easy to discuss in detail the structural aspects of $DBPE^{2-}...(M^+)_n$ systems; anyway this is not important in our present work. Therefore, we only suppose that the ionic associates $DBPE^{2-}...(M^+)_n$ have most probably loose structure, because $E^{II}_{1/2}$ values of DBPE are generally shifted towards negative direction when sodium perchlorate is used instead of $(C_2H_5)_4NClO_4$. This problem requires, however, additional investigations.

In the light of the facts described above, it was of interest to investigate whether $\Delta E_{1/2}$ values of DBPE can be correlated with solvent parameters. Plots of these values versus the dielectric permittivity or the dipole moments showed no correlations, indicating that the simplest electrostatic models do not satisfy our experimental results.

[2]Very recently Sock *et al.* demonstrated that (amino-2-ethyl) carbamic acid is produced by the fixation of CO_2 gas from the air dissolved in ethylenediamine (16). Obviously, this acid can also react as an effective proton source.

TABLE 2. Application of the equation $\Delta E_{1/2} = \alpha DN + \beta AN + \gamma$ to $\Delta E_{1/2}$ values of dibiphenylene-ethene[a]

Supporting electrolyte	$\alpha \times 10^3$	$\beta \times 10^3$	γ	r^b
$(C_2H_5)_4NClO_3$	2.16±0.27[c]	−2.47±0.89	0.417±0.016	0.975
$NaClO_4$	3.18±0.48	−6.70±0.15	0.467±0.028	0.974

[a] Multiparametric equation for calculating the solvent dependence of chemical systems using DN and AN values has been introduced by Mayer (21).
[b] Correlation coefficient.
[c] Errors are standard deviations.

Thus, we have analyzed the relations between $\Delta E_{1/2}$ and the parameters approximating Lewis basicity and acidity of solvents. Accordingly, we have applied an empirical model proposed by Krygowski and Fawcett (17, 18) in which the solvent effect on a given physicochemical property is a linear function of the Gutmann donor number (DN) (19) and of the Dimroth and Reichardt parameter (E_T) (20). In our case, the appropriate expression of this relationship is

$$\Delta E_{1/2} = \alpha DN + \beta E_T + \gamma$$

where α and β describe (after normalization) the sensitivity of the half-wave potential to changes in solvent basicity and acidity, respectively. Applying this relation to the results collected in Table 1, we have found that the correlation coefficients are 0.945 and 0.902 for the values determined in solutions containing tetraethylammonium and sodium perchlorates, respectively. The correlations were much better if instead of E_T, corresponding Gutmann's acceptor numbers (19) were used. The results of calculations in this case are listed in Table 2. It must be pointed out that DN and AN values are not collinear, in the case investigated by us the correlation coefficient between between them is $r = 0.165$.

As can be seen from Table 2, α is positive whereas β is negative in solutions containing both $(C_2H_5)_4NClO_4$ and $NaClO_4$ as electrolytes. This means that the separation between two successive electron transfers decreases with the decrease of Lewis basicity and with the increase of Lewis acidity of a solvent. This observation can easily be explained in terms of ion pairing and solvation phenomena.

Generally, ion pairing is expected to favor the disproportionation of $DBPE^{-\cdot}$ radical ions, and, consequently, to diminish the $\Delta E_{1/2}$ value, similarly as in many cases decribed in literature (for review see e.g. ref. 22). Obviously, the donicity plays the major role in ion pair formation (23), a high DN value of the solvent increases the degree of dissociation of $DBPE^{2-}...(M^+)_n$ into free ions owing to the solvation of M^+. On the other hand, the solvation of anionic species, particularly of $DBPE^{2-}$, drives disproportionation, according to the donor–acceptor concept (19), the free energies of the solvation of anions increase with an increase in AN. On this basis, the positive sign of α and negative sign of β in the correlations we obtained is fully comprehensible.

Evidently, the thermodynamical aspects of successive electron transfers should be analyzed in consideration of enthalpy and entropy terms for ion pairing and solvation. Such a treatment was described in the case of electrochemistry of some dinitrocompounds but only in dimethylformamide solutions (24). How is it in a series of various solvents? Are ΔH and ΔS collinearly changed with their Lewis basicity and acidity? Further investigations will be to explain these questions.

1. J. E. HARRIMAN and A. H. MAKI. J. Chem. Phys. **39**, 778 (1963).
2. A. J. BARD and J. PHELPS. J. Electroanal. Chem. **25**, App. 2 (1970).
3. F. AMMAR and J. M. SAVÉANT. J. Electroanal. Chem. **47**, 115 (1973).
4. F. AMMAR and J. M. SAVÉANT. J. Electroanal. Chem. **47**, 215 (1973).
5. B. S. JENSEN and V. D. PARKER. J. Am. Chem. Soc. **97**, 5211 (1975).
6. B. S. JENSEN and V. D. PARKER. J. Am. Chem. Soc. **97**, 5619 (1975).
7. T. SAJI, N. F. PASCH, S. E. WEBBER, and A. J. BARD. J. Phys. Chem. **82**, 1101 (1978).
8. K. ITAYA, A. J. BARD, and M. SZWARC. Z. Phys. Chem. Neue Folge, **112**, 1 (1978).
9. R. L. MYERS and I. SHAIN. Anal. Chem. **41**, 980 (1969).
10. J. B. FLANAGAN, S. MARGEL, A. J. BARD, and F. C. ANSON. J. Am. Chem. Soc. **100**, 4248 (1978).
11. W. KEMULA and Z. KUBLIK. Anal. Chim. Acta, **18**, 104 (1958).
12. I. M. KOLTHOFF and J. F. COETZEE. J. Am. Chem. Soc. **79**, 850 (1957).
13. C. K. MANN. *In* Electroanalytical chemistry. Vol. 3. *Edited by* A. J. Bard. Marcel Dekker, New York. 1969. Chapt. 2.
14. A. C. ATEN, G. J. HOIJTINK, and C. BÜTHKER. Trans. Faraday Soc. **55**, 324 (1959).

Can. J. Chem. Downloaded from www.nrcresearchpress.com by 210.87.254.40 on 09/06/12
For personal use only.

15. E. WAGNER and M. K. KALINOWSKI. Bull. Acad. Polon. Sci. Ser. Sci. Chim. **27**, 777 (1979).
16. O. SOCK, P. LEMOINE, and M. GROSS. Electrochim. Acta, **25**, 1025 (1980).
17. T. M. KRYGOWSKI and W. R. FAWCETT. J. Am. Chem. Soc. **97**, 2143 (1975).
18. W. R. FAWCETT and T. M. KRYGOWSKI. Aust. J. Chem. **28**, 2115 (1975).
19. V. GUTMANN. The donor–acceptor approach to molecular interaction. Plenum Press, New York. 1978.
20. C. REICHARDT. Angew. Chem. Intern. Ed. **18**, 98 (1979).
21. U. MAYER. Monats. Chem. **109**, 421 (1978).
22. M. SZWARC and J. JAGUR-GRODZINSKI. *In* Ions and ion pairs in organic reactions. Vol. 2. *Edited by* M. Szwarc. John Wiley, New York. 1974. Chapt. 1.16.
23. U. MAYER. Coord. Chem. Rev. **31**, 159 (1976).
24. C. P. ANDRIEUX and J. M. SAVÉANT. J. Electroanal. Chem. **57**, 27 (1974).

Can. J. Chem. Downloaded from www.nrcresearchpress.com by 210.87.254.40 on 09/06/12
For personal use only.

Formylation en série arylpyrrolique

JEAN-PAUL BOUKOU-POBA, MICHEL FARNIER ET ROGER GUILARD

Laboratoire de Synthèse et d'Electrosynthèse organométallique associé au C.N.R.S., Faculté des Sciences "Gabriel", 21100 Dijon, France

Reçu le 23 janvier 1981

JEAN-PAUL BOUKOU-POBA, MICHEL FARNIER et ROGER GUILARD. Can. J. Chem. **59**, 2962 (1981).

La formylation d'aryl-2 pyrroles et d'aryl-5 pyrrolecarboxylates-2 de méthyle (avec aryl = benzyl, thiényl-2′, thiényl-3′, furyl-2′, furyl-3′) est décrite par la méthode de Vilsmeier. L'orientation de cette substitution électrophile est discutée. La structure des aldéhydes obtenus est précisée à l'aide des données de rmn protonique.

JEAN-PAUL BOUKOU-POBA, MICHEL FARNIER, and ROGER GUILARD. Can. J. Chem. **59**, 2962 (1981).

The formylation of 2-arylpyrroles and methyl 5-arylpyrrole-2-carboxylates (with aryl = benzyl, 2′-thienyl, 3′-thienyl, 2′-furyl, and 3′-furyl) is performed by the Vilsmeier reaction. The orientation of this electrophilic substitution is discussed. The structure of the aldehydes obtained is established by proton nmr data.

Introduction

Dans une précédente publication (1), nous avons indiqué une méthode générale pour la synthèse d'aryl-2 pyrroles. Ces systèmes hétérocycliques peuvent être le siège de divers types de réactions et en particulier de substitutions électrophiles. Or, dans ce domaine, aucune étude systématique de l'effet de la présence d'un groupe aryle sur la réactivité d'un hétérocycle donné n'a été signalée.

Pour préciser cette influence, nous avons examiné l'une des diverses substitutions possibles et nous avons fait choix de la formylation. Ce choix a été dicté par les deux considérations suivantes: d'une part les formyl aryl-2 pyrroles peuvent être des précurseurs d'analogues de prodigiosines (2); d'autre part, si on peut obtenir des diformyl-αα′ aryl-2 pyrroles, ceux-ci opposés à des diacides dérivés du dipyrrolylméthane doivent permettre l'accès à des isostères de corrines (3).

Résultats

Nous décrivons ici la synthèse de formyl aryl-2 pyrroles selon la méthode de Vilsmeier.

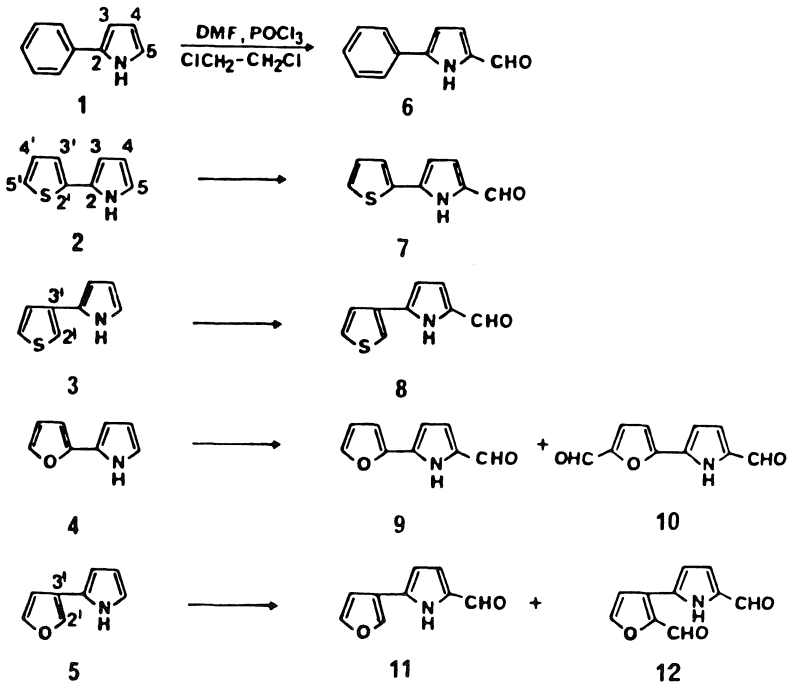

SCHÉMA 1

0008-4042/81/202962-06$01.00/0

©1981 National Research Council of Canada/Conseil national de recherches du Canada

Can. J. Chem. Downloaded from www.nrcresearchpress.com by 210.87.254.40 on 09/06/12
For personal use only.

Can. J. Chem. Downloaded from www.nrcresearchpress.com by 210.87.254.40 on 09/06/12
For personal use only.

Formylation des aryl-2 pyrroles eux-mêmes

Nous avons examiné le comportement des phényl-2 **1**, (thiényl-2′)-2 **2**, (thiényl-3′)-2 **3**, (furyl-2′)-2 **4** et (furyl-3′)-2 **5** pyrroles. A l'exception du phényl-2 pyrrole **1**, le lien valentiel unissant le reste pyrrolyl-2 à l'autre noyau hétérocyclique intéresse des sommets de réactivité très différente et on pouvait s'attendre à ce que les résultats varient, non seulement d'un hétérocycle à l'autre, mais également pour un même hétérocycle selon que le reste arylique est en position α ou β. Les résultats que nous avons observés sont indiqués sur le schéma 1 et le rendement global des réactions est de l'ordre de 80%.

La formylation du (furyl-2′)-2 pyrrole **4** conduit aux aldéhydes **9** et **10** dans les proportions relatives de 81 et 19%. Lors de la formylation du dérivé **5**, outre les aldéhydes **11** et **12**, on isole un composé **13** pour lequel les caractéristiques analytiques et rmn sont en accord avec la structure suivante:

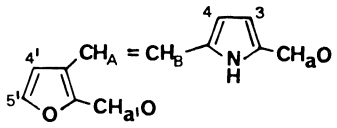

13

Par ailleurs, le spectre de masse de ce dérivé **13** montre une nette similitude avec celui du dialdéhyde **12**, les fragments correspondants différant de 26 unités. Ainsi, outre le pic moléculaire à 215 (100%), on relève les principaux fragments suivants M^+ 186 (72), 158 (22), 130 (21), 104 (18), 103 (28) et 77 (28). Ces fragments correspondent aux coupures des fonctions aldéhydiques (par perte de CHO$^\bullet$ et de CO), des cycles furannique et pyrrolique (par perte de CO et de HCN) et à la perte de C_2H_2 pour conduire vraisemblablement à l'ion phényle $C_6H_5^+$. A noter que les dérivés **11**, **12** et **13** sont obtenus dans les proportions relatives de 73, 16 et 11%.

De l'ensemble des résultats observés se dégagent les remarques suivantes:

(*1*) Le groupe formyle se fixe électivement ou très majoritairement sur le cycle pyrrolique et uniquement en α. Ce résultat est conforme à celui attendu: en effet, on retrouve le fait bien connu (4) que parmi les hétérocycles fondamentaux, thiophène, furanne, pyrrole, c'est le pyrrole qui est le plus sensible aux attaques électrophiles, puis le furanne, enfin le thiophène; le benzène non substitué est quant à lui peu sensible au réactif utilisé lors de la formylation selon Vilsmeier. Par ailleurs, la position α est toujours plus réactive que la position β.

(*2*) C'est d'ailleurs sur cette position α la plus réactive que se fixe le second groupe formyle dans le cas des dialdéhydes **10** et **12**; dans le cas du (furyl-3′)-2 pyrrole **5** pour lequel les deux positions α furanniques sont libres, la fixation du second groupe formyle en position 2′ est conforme à l'orientation généralement observée (4).

Formylation d'aryl-5 pyrrolecarboxylates-2 de méthyle

La formylation d'un ester α pyrrolique a été étudiée (5); le groupe formyle s'introduit très majoritairement en position β′ et α′ (les proportions relatives des isomères obtenus dépendant largement des modalités opératoires). Compte tenu de l'effet électro-attracteur d'un groupe ester et des résultats de l'étude précédente, on pouvait prévoir que la formylation des esters précurseurs des arylpyrroles intéresserait et le noyau pyrrolique et le reste aryle qui lui est lié; c'est effectivement ce qui est observé, les divers synthèses réalisées figurant au schéma 2.

Les résultats obtenus s'interprètent là-aussi assez aisément en tenant compte des diverses réactivités des hétérocycles fondamentaux vis à vis d'une substitution électrophile. La position α pyrrolique étant occupée par un groupe carboxylate de méthyle, par suite de l'effet orientant de ce substituant, le groupe formyle doit être introduit en position β′ sur le cycle pyrrolique; c'est ce qui se passe de façon très préférentielle pour les phényl et thiényl pyrroles. Cependant dans le cas des thiénylpyrroles **15** et **16** on observe conjointement, mais minoritairement, la formylation en α du cycle thiophénique (proportions relatives des dérivés **20** et **21** d'une part, **22** et **23** d'autre part: 95 et 5%).

Les dérivés minoritaires obtenus en série thiénylpyrrolique sont en fait les produits uniques en série furannique; en effet, l'on sait (4) que la différence de réactivité entre le pyrrole et le furanne vis-à-vis d'une substitution électrophile est la plus faible; il est alors plus aisé de formyler en α du furanne qu'en β′ du pyrrole.

Spectres de résonance magnétique nucléaire

La structure de chacun des produits obtenus a pu être généralement établie par analyse des spectres de rmn protonique.

(a) Aldéhydes dérivés des aryl-2 pyrroles

Les caractéristiques rmn observées pour les mono et dialdéhydes arylpyrroliques obtenus ont été regroupées dans le tableau 1.

Pour tous les produits étudiés, la constante de couplage des protons pyrroliques correspond à

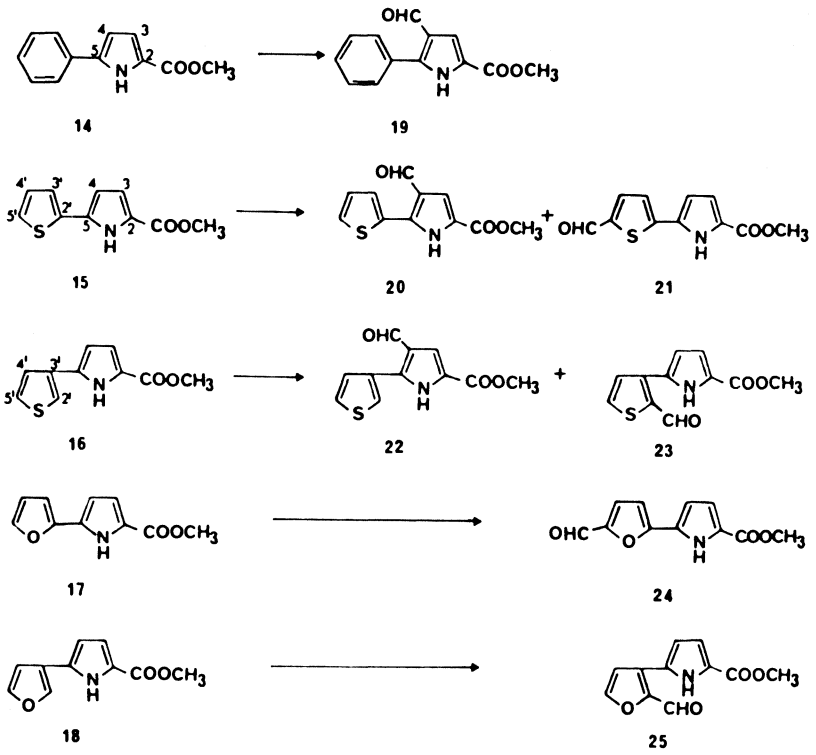

SCHEMA 2

celle signalée pour des protons ββ′ pyrroliques (5, 7). Dans le cas des monoaldéhydes, les positions des signaux et les constantes de couplage correspondent à celles de protons αββ′ ou αα′β′ thiophéniques (8) ou furanniques (9). Pour les dialdéhydes, les valeurs des constantes de couplage des protons furanniques impliquent que ces protons soient respectivement en position ββ′ pour le dérivé **10** et αβ pour le dérivé **12**. Pour ce dialdéhyde **12**, le proton du groupe formyle en 2′ est également couplé (^5J) avec $H_{5'}$ et (^5J) avec $H_{4'}$; aussi à température ambiante et dans le diméthylsulfoxyde hexadeutérié comme solvant, la molécule présente l'équilibre conformationnel suivant:

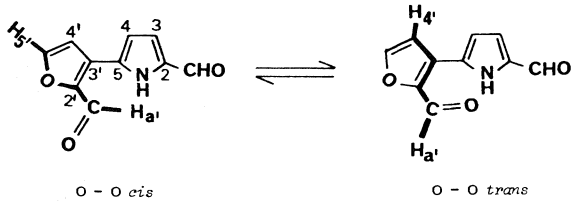

O - O *cis* O - O *trans*

En se référant aux constantes de couplage observées pour les conformères *cis* et *trans* du furfural (10) on aurait les proportions suivantes: environ 60% de conformère *trans* et 40% de *cis*.

Enfin le spectre rmn du dialdéhyde **13**, vinylogue du composé **12**, présente les caractéristiques suivantes: δ: 7.10 (d, $J_{4'5'}$ = 1.7 Hz, $H_{4'}$), 8.05 (2d, $J_{4'5'}$ = 1.7 et $J_{a'5'}$ = 0.6 Hz, $H_{5'}$), 7.05 (d, J_{34} = 3.6 Hz, H_3), 6.59 (d, J_{34} = 3.6 Hz, H_4), 9.47 (s, H_a), 9.90 (d, $J_{a'5'}$ = 0.6 Hz, $H_{a'}$), 7.15 et 7.81 (deux doublets, J_{AB} = 16.4 Hz, H_A et H_B).

(b) Aldéhydes dérivés des aryl-5 pyrrolecarboxylates-2 de méthyle

Dans le tableau 2 ont été rassemblées les caractéristiques rmn des esters aldéhydes **19** à **25**.

Pour les composés **19**, **20** et **22**, le singulet situé entre 7.2 et 7.3 ppm est attribuable au proton pyrrolique. En considérant l'effet orientant du groupe carboxylate de méthyle, le groupe formyle doit occuper la position 4. Nous avons vérifié la validité de cette conclusion dans le cas de l'ester aldéhyde **20**; soumis à une hydrolyse suivie d'une décarboxylation, il donne naissance à un aldéhyde **26**:

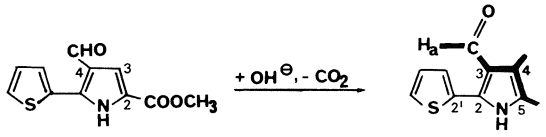

20 **26**

La constante de couplage des protons pyrroliques de l'aldéhyde **26** correspond à un couplage αβ. De plus on observe le couplage du proton aldéhydique

Can. J. Chem. Downloaded from www.nrcresearchpress.com by 210.87.254.40 on 09/06/12
For personal use only.

Can. J. Chem. Downloaded from www.nrcresearchpress.com by 210.87.254.40 on 09/06/12
For personal use only.

TABLEAU 1. Caractéristiques rmn des aldéhydes 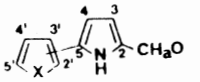 et dialdéhydes 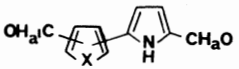

		Déplacement chimique des protons (ppm)[a]								Constantes de couplage (Hz)			
		Thiophéniques ou furanniques				Pyrroliques		Aldéhydiques					
Composé	X	$H_{2'}$	$H_{3'}$	$H_{4'}$	$H_{5'}$	H_3	H_4	H_a	$H_{a'}$				
7	S		7.65(2d)	7.08(2d)	7.52(2d)	7.01(d)	6.49(d)	9.42(s)		3.9(J_{34})	3.6($J_{3'4'}$)	1.1($J_{3'5'}$)	5.0($J_{4'5'}$)
8	S	7.98(t)		7.59(d)	7.59(d)	7.10(d)	6.68(d)	9.42(s)		3.9(J_{34})	2.1($J_{2'4'} = J_{2'5'}$)		
9	O		7.05(2d)	6.64(2d)	7.78(2d)	7.07(d)	6.57(d)	9.50(s)		3.9(J_{34})	3.4($J_{3'4'}$)	0.8($J_{3'5'}$)	1.7($J_{4'5'}$)
10	O		7.64(d)	7.29(d)		7.11(d)	6.79(d)	9.57(s)	9.57(s)	4.0(J_{34})	3.8($J_{3'4'}$)		
11	O	8.22(2d)		6.99(2d)	7.71(2d)	7.07(d)	6.57(d)	9.40(s)		3.8(J_{34})	0.8($J_{2'4'}$)	1.5($J_{2'5'}$)	1.9($J_{4'5'}$)
12[b]	O			7.37(2d)	8.18(2d)	7.15(d)	7.05(d)	9.57(s)	9.85(2d)	3.8(J_{34})	1.8($J_{4'5'}$)	0.35($J_{a'5'}$)	0.5($J_{a'4'}$)
		Benzéniques											
			H_o	$H_{m,p}$									
6[c]	CH=CH		7.89(m)	7.37(m)		7.07(d)	6.70(d)	9.49(s)		4.0(J_{34})			

[a]s, singulet; d, doublet; t, triplet; m, multiplet.
[b]Pour le dérivé **12**, l'attribution proposée pour les protons pyrroliques H_3 et H_4 ne peut être certaine en raison de la faible différence de glissement chimique entre ces deux protons.
[c]Valeurs en bon accord avec celles de Berner *et al.* (6).

TABLEAU 2. Caractéristiques rmn des esters aldéhydes **19** à **25** 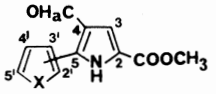 ou 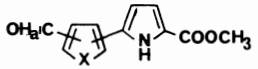

		Déplacement chimique des protons (ppm)								Constantes de couplage (Hz)			
		Thiophéniques ou furanniques				Pyrroliques		Aldéhydiques	Méthyliques				
Composé	X	$H_{2'}$	$H_{3'}$	$H_{4'}$	$H_{5'}$	H_3	H_4	H_a ou $H_{a'}$	CO_2CH_3				
20[a]	S		7.65	7.23	7.22	7.29(s)		9.89(s)	3.83(s)	3.6($J_{3'4'}$)	1.2($J_{3'5'}$)	5.0($J_{4'5'}$)	
21	S		7.80(d)	7.97(d)		6.87(d)	6.70(d)	9.86(s)	3.81(s)	3.8(J_{34})	4.1($J_{3'4'}$)		
22[a]	S	8.10		7.58	7.67	7.26(s)		9.84(s)	3.84(s)	1.3($J_{2'4'}$)	2.9($J_{2'5'}$)	5.0($J_{4'5'}$)	
23	S			7.58(d)	8.13(2d)	6.78(d)	6.71(d)	9.92(d)	3.82(s)	3.8(J_{34})	1.1($J_{a'5'}$)	5.0($J_{4'5'}$)	
24	O			7.28(d)	7.62(d)	6.91(d)	6.70(d)	9.56(d)	3.82(s)	3.9(J_{34})	3.8($J_{3'4'}$)		
25	O			7.36(2d)	8.17(2d)	7.02(d)	6.99(d)	9.82(2d)	3.82(s)	3.9(J_{34})	0.65($J_{a'4'}$)	1.8($J_{4'5'}$)	0.15($J_{a'5'}$)
25[b]	O			6.88(2d)	7.66(d)	6.93(2d)	6.63(2d)	9.84(d)	3.92(s)	3.9(J_{34})	0.9($J_{a'4'}$) 2.4(J_{NH-4})	1.8($J_{4'5'}$)	2.5(J_{NH-3})
		Benzéniques											
			H_o	$H_{m,p}$									
19	CH=CH		7.68(m)	7.52(m)		7.22(s)		9.74(s)	3.83(s)				

[a]Les protons thiophéniques apparaissent sous forme d'un système **ABX**.
[b]Spectre relevé dans $CDCl_3$.
NOTE: l'attribution de $H_{3'}$ et $H_{4'}$ pour le composé **21** et l'attribution de H_3 et H_4 pour les systèmes AB pyrroliques est incertaine.

TABLEAU 3. Modalités de synthèse et caractéristiques des composés synthétisés

Composé	Eluant de chromatographie[a]	Solvant de recristallisation[a]	Rendement (%)	Point de fusion (°C)	Formule moléculaire	Analyses Calculé / Trouvé C	H	N	O	S
6	A–B(9:1)	C–D(2:1)	71	142–144[b]	$C_{11}H_9NO$	77.17 76.97	5.30 5.22	8.18 8.28	9.35 9.52	
7	A–B(9:1)	A–D(1:1)	85	167–168	C_9H_7NOS	60.99 60.74	3.98 3.98	7.90 8.04	9.03 9.14	18.10 17.81
8	A–B(9:1)	A–D(6:1)	81	191	C_9H_7NOS	60.99 60.99	3.98 3.95	7.90 7.86	9.03 8.99	18.10 18.15
9	A–B(9:1)	D	62	106	$C_9H_7NO_2$	67.07 66.81	4.38 4.33	8.69 8.63	19.86 20.13	
10	A–B(9:1)	A	14	219	$C_{10}H_7NO_3$	63.49 63.28	3.73 3.76	7.41 7.43	25.37 25.55	
11	A–B(9:1)	A–D(3:1)	56	151	$C_9H_7NO_2$	67.07 66.90	4.38 4.38	8.69 8.67	19.86 20.20	
12	A–B(9:1)	A–D(2:1)	12	161	$C_{10}H_7NO_3$	63.49 63.70	3.73 3.78	7.41 7.47	25.37 25.19	
13	A–B(9:1)	A–D(4:1)	8	176	$C_{12}H_9NO_3$	66.97 67.09	4.22 4.30	6.51 6.45	22.30 22.38	
9	A–B(9:1)	G–H(2:1)	62	177	$C_{13}H_{11}NO_3$	68.14 68.16	4.84 5.01	6.10 5.91	20.92 21.19	
20	A–B(9:1)	A–D(2:1)	85	176	$C_{11}H_9NO_3S$	56.16 55.84	3.86 3.80	5.95 5.85	20.40 20.46	13.63 13.35
21	A–B(9:1)	A–D(7:1)	4	235	$C_{11}H_9NO_3S$	56.16 55.91	3.86 3.85	5.95 5.88	20.40 20.62	13.63 13.18
22	A–B(9:0.5)	C–D(2:1)	85	173	$C_{11}H_9NO_3S$	56.16 56.10	3.86 3.92	5.95 6.08	20.40 20.52	13.63 13.10
23	A–B(9:0.5)	A	4	169–170	$C_{11}H_9NO_3S$	56.16 56.42	3.86 3.93	5.95 5.94	20.40 20.26	13.63 13.54
24	A–B(9:1)	E	88	193	$C_{11}H_9NO_4$	60.27 59.55	4.14 4.29	6.39 6.16	29.20 29.15	
25	A–B(9:1)	F–D(2:1)	56	156	$C_{11}H_9NO_4$	60.27 59.99	4.14 4.23	6.39 6.55	29.20 29.29	

[a]A, chloroforme; B, acétone; C, benzène; D, hexane; E, dichloro-1,2 éthane; F, toluène; G, méthanol; H, eau.
[b]Litt. (6), pf 99–101°C.

avec à la fois le proton H_4 (^4J) et le proton H_5 (^5J) du noyau pyrrolique; or ces deux couplages ne peuvent apparaître simultanément (11) que dans la mesure où le groupe formyle est en position 3; l'aldéhyde **26** est donc le (thiényl-2′)-2 pyrrolecarbaldéhyde-3 (son groupe formyle a été représenté dans l'état conformationnel majoritaire).

Pour le dérivé thiophénique **23**, le proton aldéhydique n'apparaît couplé qu'avec le proton $H_{5'}$ ($J_{a'5'}$ = 1.1 Hz); le groupe formyle est donc pratiquement totalement conformé en S—O *cis*. Nous avons étudié le [(formyl-2′) furyl-3′]-5 pyrrolecarboxylate-2 de méthyle **25** en solution dans le diméthylsulfoxyde hexadeutérié et dans le deutériochloroforme. Dans le premier solvant le couplage intéresse à la fois $H_{5'}$ (^5J = 0.15 Hz) et $H_{4'}$ (^5J = 0.65 Hz); dans le second, seul $H_{4'}$ est couplé (^5J = 0.9 Hz). A température ambiante on peut donc envisager l'existence de l'équilibre conformationnel suivant:

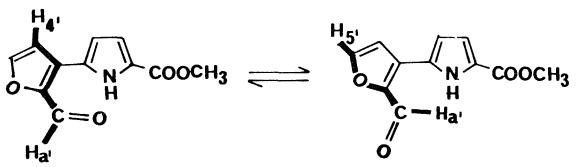

O – O *trans* O – O *cis*

Dans le deutériochloroforme, le groupe formyle est pratiquement totalement conformé en O—O *trans*, conformation vraisemblablement privilégiée en raison de l'existence d'une liaison intramoléculaire NH—O (aldéhydique). Par contre, dans un solvant polaire (type DMSO-d_6), la liaison

Can. J. Chem. Downloaded from www.nrcresearchpress.com by 210.87.254.40 on 09/06/12
For personal use only.

est partiellement rompue; le groupe formyle, bien que toujours préférentiellement en conformation O—O *trans*, existe alors en proportion non négligeable sous la conformation O—O *cis*.

Partie expérimentale

Les analyses élémentaires ont été effectuées par le Laboratoire Central de Microanalyse du C.N.R.S. Les spectres rmn ont été relevés sur un appareil JEOL FX 100 en utilisant le TMS comme référence interne et, sauf indication contraire, le DMSO-d_6 comme solvant. Le couplage des protons pyrroliques avec l'hydrogène iminique a été supprimé par ajout d'eau lourde.

La synthèse des aryl-2 pyrroles et aryl-5 pyrrolecarboxylates-2 de méthyle utilisés a été décrite précédemment (1).

Formylation des aryl-2 pyrroles et aryl-5 pyrrolecarboxylates-2 de méthyle

Toutes les formylations ont été conduites selon la même méthode exposée ci-dessous de façon générale.

Dans 1.7 cm³ (0.022 mol) de diméthylformamide on verse, à 0°C, goutte à goutte et sous agitation, 2 cm³ (0.022 mol) d'oxychlorure de phosphore. On laisse revenir à température ambiante tout en maintenant l'agitation puis, à 0°C, 40 cm³ de dichloro-1,2 éthane anhydre sont ajoutés. On introduit alors 0.02 mol d'aryl-2 pyrrole ou d'ester en solution dans 100 cm³ de dichloro-1,2 éthane. L'addition terminée (1 h environ), on porte à reflux 1 h. On laisse revenir à température ambiante et ajoute lentement et avec précaution 15 g d'acétate de sodium trihydraté en solution dans 40 cm³ d'eau tout en maintenant une agitation efficace. Le mélange réactionnel est porté à reflux 1 h. A température ambiante, la phase organique est séparée. La phase aqueuse est extraite deux fois par 100 cm³ de chloroforme. Les phases organiques réunies sont traitées par une solution saturée d'hydrogénocarbonate de sodium, puis à l'eau jusqu'à neutralité. Les solvants sont évaporés et le résidu obtenu est chromatographié sur colonne d'acide silicique.

Les modalités opératoires utilisées et les caractéristiques des produits obtenus sont indiquées dans le tableau 3.

Préparation du (thiényl-2')-2 pyrrolecarbaldéhyde-3 ***26***

(a) Hydrolyse du (thiényl-2')-5 formyl-4 pyrrolecarboxylate-2 de méthyle ***20***

On porte à reflux durant 30 min une solution de 1.175 g (0.005 mol) de (thiényl-2')-5 formyl-4 pyrrolecarboxylate-2 de méthyle **20** et 0.57 g (0.01 mol) de potasse dans 10 cm³ d'eau. Après retour à la température ambiante, on acidifie à 0°C par de l'acide chlorhydrique 5 *N*. Le précipité obtenu est essoré, lavé à l'eau froide jusqu'à neutralité. On récupère 0.85 g (77%) d'acide (thiényl-2')-5 formyl-4 pyrrolecarboxylique-2, pf 278°C.

(b) Décarboxylation de l'acide (thiényl-2')-5 formyl-4 pyrrolecarboxylique-2

On chauffe à 90°C 10 cm³ de quinoléïne et 0.796 g de l'acide précédent et maintient cette température jusqu'à dissolution totale de l'acide. On ajoute alors 0.120 g de chromite de cuivre (activé par du baryum), puis on porte la température à 158–162°C jusqu'à ce que l'on n'observe plus de dégagement de CO_2. On refroidit brutalement dans un mélange eau–glace, ajoute 80 cm³ de chloroforme et filtre le catalyseur. On élimine la quinoléïne par lavage à l'acide chlorhydrique 5 *N* jusqu'à pH 2. La phase chloroformique est lavée à l'eau bicarbonatée jusqu'à neutralité. On recueille après chromatographie sur acide silicique (éluant chloroforme–acétone (9:1)) et recristallisation dans un mélange benzène–hexane (1:1), 0.250 g (40%) de (thiényl-2')-2 pyrrolecarbaldéhyde-3 **26**, pf 120–122°C; rmn (DMSO-d_6, D_2O) δ: 6.56 (2d, J_{45} = 3.0 et J_{a4} = 0.37 Hz, H_4), 6.96 (2d, J_{45} = 3.0 et J_{a5} = 0.73 Hz, H_5), 7.19 (2d, $J_{3'4'}$ = 3.7 et $J_{4'5'}$ = 5.1 Hz, $H_{4'}$), 7.50 (2d, $J_{3'4'}$ = 3.7 et $J_{3'5'}$ = 1.2 Hz, $H_{3'}$), 7.67 (2d, $J_{3'5'}$ = 1.2 et $J_{4'5'}$ = 5.1 Hz, $H_{5'}$), 9.94 (2d, J_{a4} = 0.37 et J_{a5} = 0.73 Hz, H_a). *Anal.* calc. pour C_9H_7NOS: C 60.99, H 3.98, N 7.90, O 9.03, S 18.10; trouvé: C 61.08, H 3.92, N 7.82, O 9.10, S 17.95.

1. J. P. Boukou-Poba, M. Farnier et R. Guilard. Tetrahedron Lett. 1717 (1979).
2. (*a*) W. R. Hearn, M. K. Elson, R. H. Williams et J. Medina-Castro. J. Org. Chem. **35**, 142 (1970); (*b*) N. N. Gerber. Crit. Rev. Microbiol. 469 (1975); (*c*) H. Berner, G. Schulz et H. Reinshagen. Monatsh. Chem. **108**, 233 (1977).
3. (*a*) R. Grigg. The porphyrins. Vol. II. Structure and Synthesis, Part B. *Edité par* D. Dolphin. Academic Press, New York. 1978. p. 327. (*b*) A. W. Johnson. Porphyrins and metalloporphyrins. *Edité par* K. M. Smith. Elsevier Scientific Publishing Company, Amsterdam. 1975. p. 729.
4. J. A. Joule et G. F. Smith. Heterocyclic chemistry. Van Nostrand Reinhold Company, London. 1972. p. 184.
5. P. Fournari, M. Farnier et C. Fournier. Bull. Soc. Chim. Fr. 283 (1972).
6. H. Berner, G. Schulz et H. Reinshagen. Monatsh. Chem. **108**, 285 (1977).
7. (*a*) C. E. Loader et H. J. Anderson. Tetrahedron, **25**, 3879 (1969); (*b*) S. Gronowitz, A.-B. Hörnfeldt, B. Gestblom et R. A. Hoffman. Ark. Kemi. **18**, 133 (1961); (*c*) K. J. Morgan et D. P. Morrey. Tetrahedron, **27**, 245 (1971).
8. R. A. Hoffman et S. Gronowitz. Ark. Kemi. **16**, 563 (1960).
9. S. Gronowitz, G. Sorlin, B. Gestblom et R. A. Hoffman. Ark. Kemi. **19**, 483 (1962).
10. (*a*) K.-I. Dahlqvist et S. Försen. J. Phys. Chem. **69**, 4062 (1965); (*b*) B. Roques, S. Combrisson, C. Riche et C. Pascard-Billy. Tetrahedron, **26**, 3555 (1970).
11. (*a*) M. Farnier et T. Drakenberg. Tetrahedron Lett. 429 (1973); (*b*) M. Farnier et T. Drakenberg. J. Chem. Soc. Perkin Trans. II, 333 (1975).

Can. J. Chem. Downloaded from www.nrcresearchpress.com by 210.87.254.40 on 09/06/12
For personal use only.

Volume fraction statistics and the surface tensions of non-electrolyte solutions

DOUGLAS E. GOLDSACK AND CARMEN DESIRRIE SARVAS

Department of Chemistry, Laurentian University, Sudbury, Ont., Canada P3E 2C6

Received November 14, 1980[1]

DOUGLAS E. GOLDSACK and CARMEN DESIRRIE SARVAS. Can. J. Chem. **59**, 2968 (1981).

Explicit and implicit surface tension equations have been derived using both mole fraction and volume fraction statistics and have been applied to a variety of binary polar–polar, non-polar–non-polar, and non-polar–polar organic systems with good success. Average errors of less than 1% are found for a large variety of such systems with the assumption of ideal chemical potential equations and molar surface areas calculated from bulk density values. These equations are found to be valid for those systems with surface tension differences of 20 ergs/cm^2 or less. Systems with surface tension differences larger than this value would require the inclusion of activity coefficient effects.

DOUGLAS E. GOLDSACK et CARMEN DESIRRIE SARVAS. Can. J. Chem. **59**, 2968 (1981).

Faisant appel aux statistiques de la fraction molaire et de la fraction volumique on a déduit les équations de tensions de surface implicites et explicites et on les a appliqué avec succès à une série de systèmes organiques binaires: polaire–polaire, non-polaire–non-polaire et non-polaire–polaire. On a trouvé que la moyenne des erreurs est inférieure à 1% pour une grande variété de ces systèmes en supposant que les équations de potentiel chimique idéal et les domaines de surface molaire sont calculées à partir des valeurs de densité de volume. On a trouvé que les différences de tension de surface sont de 20 ergs/cm^{-1}. Les systèmes ayant des différences de tension de surface plus grandes que cette valeur nécessitent l'inclusion des effets de coefficient d'activité.

[Traduit par le journal]

Can. J. Chem. Downloaded from www.nrcresearchpress.com by 210.87.254.5 on 09/06/12
For personal use only.

Introduction

At present there are no simple explicit formulae for calculating the surface tension of mixtures of organic compounds of a wide range of polarity from the bulk parameters of the individual components (1). The thermodynamics of the surface tension of such systems has been treated in a variety of fashions in the literature in an attempt to formulate such an explicit equation for the concentration dependence of the surface tension of these solutions with a minimum number of adjustable parameters (2–6). These approaches have generally involved arbitrary assumptions of equal or average molar surface areas of the components and use of regular solution theory to approximate activity coefficient effects. In some cases (7, 8), other arbitrary assumptions in the formulation of the thermodynamics have led to incorrect equations for the concentration dependence of the surface tension of these mixtures (9).

In all of these attempts mole fraction statistics have been applied to both the surface and bulk phases. The effect of molecular size on the surface tension of mixtures has been tentatively explored (ref. 4, chapt. 13, ref. 10) and has also been shown to have a significant effect on adsorption isotherms (11, 12). Hence a detailed comparison of mole fraction and volume fraction statistics on the surface tension of binary solutions of nonelectrolytes over a wide range of polarity would seem to be warranted.

Theory

The starting point for obtaining any relation involving the surface tension of a mixture is to assume (4, 9, 13, 14) that the surface layer can be treated thermodynamically as a phase separate from the bulk phase.

The chemical potential of a component i in the bulk liquid phase (B) of a solution is given by:

$$[1] \qquad \mu_{i,B} = \mu^0_{i,B} + RT \ln (a_{i,B})$$

where $\mu^0_{i,B}$ is the standard state chemical potential of component i in the bulk phase, $a_{i,B}$ is the activity of component i in the bulk phase, and R and T are the gas constant and absolute temperature respectively. In the surface phase (S), the chemical potential of component i is similarly given by:

$$[2] \qquad \mu_{i,S} = \mu^0_{i,S} + RT \ln (a_{i,S}) - \sigma A_i$$

where σ is the surface tension of the mixture of activity $a_{i,S}$ and A_i the molar surface area of component i. For a pure component

$$[3] \qquad \mu^0_{i,S} - \mu^0_{i,B} = \sigma_i A_i$$

At equilibrium

$$[4] \qquad \mu_{i,S} = \mu_{i,B}$$

Combining eqs. [1] through [4] leads to the Butler equation (13):

$$[5] \qquad \sigma = \sigma_i + \frac{RT}{A_i} \ln \left(\frac{a_{i,S}}{a_{i,B}}\right)$$

This equation can also be written as

$$[6] \qquad a_{i,S} = a_{i,B} \exp \left[(\sigma - \sigma_i)\frac{A_i}{RT}\right]$$

[1]Revision received June 26, 1981.

0008-4042/81/202968-13$01.00/0

©1981 National Research Council of Canada/Conseil national de recherches du Canada

where exp stands for the Napierian base e. If the surface and bulk phases over the whole concentration range are similar in properties, e.g. the heat of mixing of the components are similar as a function of concentration, then to a first approximation, the activity coefficients, f_i, in the surface and bulk phases are approximately equal over the whole concentration range and as a result the following relation is approximately valid:

$$[6a] \quad \frac{a_{i,S}}{a_{i,B}} = \frac{f_{i,S}X_{i,S}}{f_{i,B}X_{i,B}} \simeq \frac{X_{i,S}}{X_{i,B}}$$

and therefore [6] can be rewritten as

$$[6b] \quad X_{i,S} = X_{i,B} \exp\left[(\sigma - \sigma_i)\frac{A_i}{RT}\right]$$

Since the sum of the mole fractions of all components in the surface phase is unity, then

$$[7] \quad \sum X_{i,S} = \sum X_{i,B} \exp\left[(\sigma - \sigma_i)\frac{A_i}{RT}\right] = 1$$

This general equation has been obtained previously by a variety of authors (9, 14). It can also be rearranged in a different fashion to obtain the concentration dependence of the surface tension. For a binary solution

$$[8] \quad X_{1,B}\left\{\exp\left[(\sigma - \sigma_1)\frac{A_1}{RT}\right]\right\} + X_{2,B}\left\{\exp\left[(\sigma - \sigma_2)\frac{A_2}{RT}\right]\right\} = 1$$

Since the sum of the mole fractions in the bulk phase is unity, this equation can also be rearranged into:

$$[9] \quad \sigma = \sigma_1 - \frac{RT}{A_1}\left\{\ln\left\{1 + X_2\left[\exp\left(\frac{\sigma(A_2 - A_1)}{RT} + \frac{\sigma_1 A_1 - \sigma_2 A_2}{RT}\right) - 1\right]\right\}\right\}$$

If $A_2 = A_1 = A$, which is an approximation often used in the literature, then an equation of a form similar to the Szyszkowski equation (4) results.

$$[10] \quad \sigma = \sigma_1 - \frac{RT}{A}\left\{\ln\left\{1 + X_2\left[\exp\left(\frac{(\sigma_1 - \sigma_2)A}{RT}\right) - 1\right]\right\}\right\}$$

This latter equation has one adjustable parameter and has been used to fit the concentration dependence of the surface tension of binary mixtures of non-electrolytes. The values of A so found have sometimes been unreasonable (15), and this is not unexpected since [9] is an implicit equation for which some approximate value for σ on the right-hand side must be given before it can be used.

Schuchowitsky (2) first showed how it was possible to obtain an explicit equation for σ using the Butler equation [5] as the starting point. We will therefore show how, taking his approach, one can derive both explicit and implicit equations for the surface tension of a binary mixture on both the mole fraction and volume fraction scales and indicate both theoretically and practically the limits of applications of both the explicit and implicit forms.

In order to use the Butler equation one must first have an estimate of the molar surface area, A_i, of each component. If it is assumed that the surface phase is a monolayer (1), then the individual molar surface areas of each component, A_i, can be related to bulk molar volumes V_i. To do so requires the further assumption that the molecules of each component can be approximated as spheres and that the cross sectional area of each molecule is the appropriate geometrical area presented at the surface. In that case

$$A_i = \pi\left(\frac{3}{4\pi}\right)^{2/3} N^{1/3} V_i^{2/3} = 1.02 \times 10^8 V_i^{2/3}$$

where N is Avogadro's number. This relation also assumes that the bulk density and the surface density of component i are equal — an assumption which may bear further investigation since it may not necessarily, and is most probably not, valid in general (16). But, for a first approximation, this assumption is useful since it enables the surface tension of mixtures to be calculated from known bulk properties of each component.

It is also useful to note that the value of RT/A_i for most organic components with molar volumes in the range of 50 to 150 cm^3/mol is of the order of 10 to 20 ergs/cm^2. This factor is of importance in limiting the usefulness of the explicit equations to be derived for σ.

Can. J. Chem. Downloaded from www.nrcresearchpress.com by 210.87.254.5 on 09/06/12
For personal use only.

Explicit Equations for σ on Mole Fraction Scale

The Butler equations on the mole fraction scale for components 1 and 2 of a binary mixture are:

$$[11a] \quad \sigma = \sigma_1 + \frac{RT}{A_1} \ln \left(\frac{X_{1,S}}{X_{1,B}}\right)$$

$$[11b] \quad \sigma = \sigma_2 + \frac{RT}{A_2} \ln \left(\frac{X_{2,S}}{X_{2,B}}\right)$$

Multiplying [11*a*] by $X_{1,B}$ and [11*b*] by $X_{2,B}$ and adding results in an equation yielding an ideal surface tension term and a term involving the free energy of mixing per unit area, one gets

$$[12] \quad \sigma = \sigma_1 X_{1,B} + \sigma_2 X_{2,B} + X_{1,B} \frac{RT}{A_1} \ln \left(\frac{X_{1,S}}{X_{1,B}}\right) + X_{2,B} \frac{RT}{A_2} \ln \left(\frac{X_{2,S}}{X_{2,B}}\right)$$

Equation [12] cannot be used to calculate the surface tension of a mixture unless the surface mole fractions $X_{1,S}$ and $X_{2,S}$ are known. Prigogine *et al.* (ref. 4, p. 202 *ff*) have introduced a difference function which enables a relation between the surface and bulk mole fractions to be established under certain conditions. If we define a dimensionless difference term Δ such that:

$$[13] \quad X_{1,S} = X_{1,B} + X_{1,B}X_{2,B}\Delta$$

and since

$$[14] \quad X_{1,S} + X_{2,S} = X_{1,B} + X_{2,B} = 1$$

$$[15] \quad X_{2,S} = X_{2,B} - X_{1,B}X_{2,B}\Delta$$

Applying these equations to the Butler equations for each component gives

$$[16a] \quad \sigma = \sigma_1 + \frac{RT}{A_1} \ln (1 + X_{2,B}\Delta)$$

$$[16b] \quad \sigma = \sigma_2 + \frac{RT}{A_2} \ln (1 - X_{1,B}\Delta)$$

Subtracting [16*a*] from [16*b*], and expanding the logarithmic terms to their first term under the conditions that $X_{2,B}\Delta$ and $X_{1,B}\Delta$ are much less than one, yields the following relation for Δ:

$$[17] \quad \Delta = -\frac{(\sigma_2 - \sigma_1)A_1A_2}{(A_1X_1 + A_2X_2)RT}$$

where the mole fractions now apply to the bulk phase only. If this equation for Δ is now put into eq. [12] then the following explicit equation for the surface tension of a binary mixture is obtained (the mole fractions refer to the bulk phase only):

$$[18] \quad \sigma = \sigma_1X_1 + \sigma_2X_2 + \frac{X_1RT}{A_1} (\ln (1 + X_2\Delta)) + \frac{X_2RT}{A_2} (\ln (1 - X_1\Delta))$$

The same restriction on the derivation of the equation for Δ should apply to this general equation for the surface tension, however, i.e. that $X_2\Delta$ or $X_1\Delta$ must be less than one. As noted previously, because of the size of the molecular volumes of most molecules, the term RT/A_i is of the order of 10–20 cm^2/ergs and hence the use of the Δ function approach should be restricted to systems with $(\sigma_2 - \sigma_1)$ generally less than 10 ergs/cm^2 in order that the expansion approximation used in deriving [17] be valid.

For such systems, however, [18] can be simplified by expanding the logarithmic terms. To the second approximation the surface tension then becomes:

$$[19] \quad \sigma = (\sigma_1X_1 + \sigma_2X_2) + RTX_1X_2\Delta\left[\frac{(A_2 - A_1)}{A_1A_2}\right] - \frac{RT}{2} X_1X_2\Delta^2\left[\frac{A_1X_1 + A_2X_2}{A_1A_2}\right]$$

Equation [19] has not been derived previously and shows that for unequal molar surface areas, a first order deviation term can either add to or cause a negative deviation from the ideal surface tension relation. Gener-

Can. J. Chem. Downloaded from www.nrcresearchpress.com by 210.87.254.5 on 09/06/12
For personal use only.

ally it is found on application of [19] to real systems, as will be discussed later, that the second order term in Δ^2 dominates over the first order term causing an overriding negative deviation from the simple linear relation for surface tension as is observed for real systems.

Schuchowitsky (2) also showed how a different weighting for the ideal term could be obtained on the mole fraction scale. If the Butler equations are written as:

$$[20a] \quad \sigma A_1 = \sigma_1 A_1 + RT \ln \left(\frac{X_{1,S}}{X_{1,B}}\right)$$

$$[20b] \quad \sigma A_2 = \sigma_2 A_2 + RT \ln \left(\frac{X_{2,S}}{X_{2,B}}\right)$$

and are multiplied by $X_{1,B}$ and $X_{2,B}$ respectively, added, the Δ notation introduced to eliminate the surface mole fractions and the logarithmic terms expanded as before, then the first term approximation in the logarithmic expansion yields:

$$[21] \quad \sigma = \sigma_1 \left(\frac{A_1 X_1}{A_1 X_1 + A_2 X_2}\right) + \sigma_2 \left(\frac{A_2 X_2}{A_1 X_1 + A_2 X_2}\right)$$

This equation implies that the ideal surface tension relation is affected strongly by the ratio of the molar surface area A_2/A_1. The second term approximation will be given by

$$[22] \quad \sigma = \sigma_1 \frac{A_1 X_1}{A_1 X_1 + A_2 X_2} + \sigma_2 \frac{A_2 X_2}{A_1 X_1 + A_2 X_2} - \frac{RTX_1 X_2}{A_1 X_1 + A_2 X_2} \frac{\Delta^2}{2}$$

These equations should also be expected to apply to systems with $(\sigma_2 - \sigma_1)$ less than 20 ergs/cm^2.

Volume Fraction Statistics and Explicit Surface Tension Equations

So far only mole fraction statistics have been used to derive equations for the surface tension of binary mixtures. Volume fraction statistics can be applied to the surface and bulk phases assuming that the entropy of mixing for each phase is given by:

$$[23] \quad \Delta S_{mix} = -R[N_1 \ln \phi_1 + N_2 \ln \phi_2]$$

where N_1 and N_2 are the number of moles of components 1 and 2 and ϕ_1 and ϕ_2 are the volume fractions of each component as defined by:

$$[24a] \quad \phi_1 = \frac{X_1 V_1}{X_1 V_1 + X_2 V_2}$$

$$[24b] \quad \phi_2 = \frac{X_2 V_2}{X_1 V_1 + X_2 V_2}$$

where V_1 and V_2 are the molar volumes of components 1 and 2 respectively. The chemical potentials for components 1 and 2 in the bulk and surface phases then become (13):

$$[25a] \quad \mu_{1,B} = \mu^0_{1,B} + RT \left[\ln \phi_{1,B} + \left(1 - \frac{V_1}{V_2}\right)\phi_{2,B}\right]$$

$$[25b] \quad \mu_{2,B} = \mu^0_{2,B} + RT \left[\ln \phi_{2,B} + \left(1 - \frac{V_2}{V_1}\right)\phi_{1,B}\right]$$

$$[25c] \quad \mu_{1,S} = \mu^0_{1,S} + RT \left[\ln \phi_{1,S} + \left(1 - \frac{V_1}{V_2}\right)\phi_{2,S}\right] - \sigma A_1$$

$$[25d] \quad \mu_{2,S} = \mu^0_{2,S} + RT \left[\ln \phi_{2,S} + \left(1 - \frac{V_2}{V_1}\right)\phi_{1,S}\right] - \sigma A_2$$

Equating the chemical potentials in each phase and recognizing that the surface free energies of each component are given by the difference in chemical potentials of the pure components in the surface and bulk phases, then the surface tension equations can be written as:

Can. J. Chem. Downloaded from www.nrcresearchpress.com by 210.87.254.5 on 09/06/12
For personal use only.

$$[26a]\quad \sigma = \sigma_1 + \frac{RT}{A_1}\left[\ln\left(\frac{\phi_{1,S}}{\phi_{1,B}}\right) + \left(1 - \frac{V_1}{V_2}\right)(\phi_{2,S} - \phi_{2,B})\right]$$

$$[26b]\quad \sigma = \sigma_2 + \frac{RT}{A_2}\left[\ln\left(\frac{\phi_{2,S}}{\phi_{2,B}}\right) + \left(1 - \frac{V_2}{V_1}\right)(\phi_{1,S} - \phi_{1,B})\right]$$

We can now proceed in a fashion similar to that carried out for the mole fraction statistics in order to eliminate the unknown surface volume fractions in [26*a*] and [26*b*]. Defining the difference function Δ (13) as:

$$[27a]\quad \phi_{1,S} = \phi_{1,B} + \phi_{1,B}\phi_{2,B}\Delta$$

$$[27b]\quad \phi_{2,S} = \phi_{2,B} - \phi_{1,B}\phi_{2,B}\Delta$$

and introducing these definitions into [26*a*] and [26*b*] yields (dropping the B subscript since all volume fractions are now bulk volume fractions):

$$[28a]\quad \sigma = \sigma_1 + \frac{RT}{A_1}\left[\ln(1 + \phi_2\Delta) - \phi_1\phi_2\Delta\left(1 - \frac{V_1}{V_2}\right)\right]$$

$$[28b]\quad \sigma = \sigma_2 + \frac{RT}{A_2}\left[\ln(1 - \phi_1\Delta) + \phi_1\phi_2\Delta\left(1 - \frac{V_2}{V_1}\right)\right]$$

Expanding the logarithms to a first term and subtracting [28*a*] from [28*b*] yields the following expression for Δ on the volume fraction scale:

$$[29]\quad \Delta = \frac{(\sigma_2 - \sigma_1)A_1A_2}{\left\{\phi_1A_1\left[1 - \phi_2\left(1 - \frac{V_2}{V_1}\right)\right] + \phi_2A_2\left[1 - \phi_1\left(1 - \frac{V_1}{V_2}\right)\right]\right\}RT}$$

For many systems, as will be shown in the Discussion section, the denominator of this expression for Δ can be approximated as $(\phi_1A_1 + \phi_2A_2)$ to within 2 to 3% or less over the whole range of composition. This can be readily seen from the denominator expression which can be rearranged as:

$$[30]\quad (\phi_1A_1 + \phi_2A_2) - \phi_1\phi_2\frac{(V_2 - V_1)(A_2V_1 - A_1V_2)}{V_1V_2}$$

Since the molar volumes of most organic molecules are generally within 10 to 20% of each other and since the last term of eq. [30] is the product of two difference terms and a concentration variable, $\phi_1\phi_2$, whose maximum value is 0.25, then for most organic mixtures the Δ function on the volume fraction basis is given by

$$[31]\quad \Delta \simeq \frac{(\sigma_2 - \sigma_1)A_1A_2}{(\phi_1A_1 + \phi_2A_2)RT}$$

For either Δ function, however, explicit equations for the surface tension of a binary mixture on the volume fraction scale can be derived similar to [19] and [22] for the mole fraction scale. Multiplying [28*a*] and [28*b*] by ϕ_1 and ϕ_2, respectively, and expanding logarithmic terms yield the following equations for the surface tension of a binary mixture:

$$[32]\quad \sigma = (\sigma_1\phi_1 + \sigma_2\phi_2) + RT\phi_1\phi_2\left\{\frac{\left[\phi_2\left(1 - \frac{V_2}{V_1}\right) - 1\right]}{A_2} - \frac{\left[\phi_1\left(1 - \frac{V_1}{V_2}\right) - 1\right]}{A_1}\right\}\Delta - RT\frac{\phi_1\phi_2}{2}\left(\frac{A_1\phi_1 + A_2\phi_2}{A_1A_2}\right)\Delta^2$$

It may be noted that the ideal term $(\sigma_1\phi_1 + \sigma_2\phi_2)$ is effectively weighting the surface tension, i.e. the surface free energy per unit area, linearly with the volume fraction. On the other hand, if the revised Butler equations [26*a*] and [26*b*] are weighted according to molar surface free energies, i.e., σ_1A_1 and σ_2A_2, by multiplying [26*a*] and [26*b*] by ϕ_1A_1 and ϕ_2A_2 respectively, and if the logarithmic term is then expanded after the Δ notation has been introduced, then the following equation results:

Can. J. Chem. Downloaded from www.nrcresearchpress.com by 210.87.254.5 on 09/06/12
For personal use only.

$$[33]\quad \sigma = \sigma_1\left(\frac{A_1\phi_1}{A_1\phi_1 + A_2\phi_2}\right) + \sigma_2\left(\frac{A_2\phi_2}{A_1\phi_1 + A_2\phi_2}\right) + \frac{RT\phi_1\phi_2}{(A_1\phi_1 + A_2\phi_2)} \times \left\{\left[\phi_2\left(1 - \frac{V_2}{V_1}\right) - \phi_1\left(1 - \frac{V_1}{V_2}\right)\right]\Delta - \frac{\Delta^2}{2}\right\}$$

It is to be noted that the ideal term of this equation now reflects the difference in molar surface areas through the molar surface area ratio A_2/A_1 and furthermore that this total expression should be limited to those systems for which the explicit Δ equation derivation is applicable, viz. those systems with $\sigma_2 - \sigma_1 < 10$ to 20 ergs/cm^2.

Implicit Surface Tension Equations on Mole and Volume Fraction Scales and Their Application to Systems of Large Polarity Difference

It has been mentioned several times that the Δ function approach to obtaining explicit surface tension equations for binary systems is inherently limited to systems of low polarity differences, i.e. for those systems with $(\sigma_2 - \sigma_1) < 10$ ergs/cm^2. This is due to the need for expansion of the logarithmic expression to its first order term in Δ in order to derive an explicit expression for Δ in terms of the bulk system parameters. A second approach to overcome this limitation is to use the implicit equation [9] with first or second order approximations to the implicit σ term on the right-hand side of equation, which were derived from the explicit Δ function approach, such as [19] and [21]. Since [9] has been derived using mole fraction statistics, by analogy a volume fraction statistic implicit equation should also be readily generated for comparison and the appropriate implicit σ term in this new implicit equation can be approximated by the first or second approximations for σ on the volume fraction scale.

To obtain this implicit equation on the volume fraction scale [26*a*] and [26*b*] are rewritten in terms of the volume fractions in the surface phase as:

$$[34a]\quad \phi_{1,S} = \phi_{1,B}\left\{\exp\left[(\sigma - \sigma_1)\frac{A_1}{RT}\right]\exp\left[(\phi_{2,S} - \phi_{2,B})\left(\frac{V_1}{V_2} - 1\right)\right]\right\}$$

$$[34b]\quad \phi_{2,S} = \phi_{2,B}\left\{\exp\left[(\sigma - \sigma_2)\frac{A_2}{RT}\right]\exp\left[(\phi_{1,S} - \phi_{1,B})\left(\frac{V_2}{V_1} - 1\right)\right]\right\}$$

We have previously defined the differences $(\phi_{i,S} - \phi_{i,B})$ as $|\phi_i\phi_j\Delta|$. The parameter Δ is generally of the order of 1 or less and $\phi_i\phi_j$ has a maximum of 0.25. Furthermore, $(V_2/V_1 - 1)$ and $(V_1/V_2 - 1)$ are generally of the order of 0.1 to 0.2 for most systems. Hence the second exponential in [34*a*] and [34*b*] are of the character e^x where x is much smaller than 1 over the whole range of composition. Expanding this term of e^x to $(1 + x)$ and defining the following terms for ease of derivation,

$$[35]\quad \exp\left[(\sigma - \sigma_1)\frac{A_1}{RT}\right] = B_1 \quad \text{and} \quad \exp\left[(\sigma - \sigma_2)\frac{A_2}{RT}\right] = B_2$$

and noting that $(\phi_{2,S} - \phi_{2,B})$ equals $-(\phi_{1,S} - \phi_{1,B})$, then [34*a*] and [34*b*] become:

$$[36a]\quad \phi_{1,S} = \phi_{1,B}B_1\left[1 + (\phi_{1,S} - \phi_{1,B})\left(1 - \frac{V_1}{V_2}\right)\right]$$

$$[36b]\quad \phi_{2,S} = \phi_{2,B}B_2\left[1 + (\phi_{2,S} - \phi_{2,B})\left(1 - \frac{V_2}{V_1}\right)\right]$$

These two equations enable explicit functions for $\phi_{1,S}$ and $\phi_{2,S}$ to be obtained by rearrangement and since the sum of these volume fractions in the surface phase is unity, we obtain the following explicit relation for the surface tension of the mixture in terms of bulk parameters alone:

$$[37]\quad \phi_{1,B}B_1\frac{\left[1 - \phi_{1,B}\left(1 - \frac{V_1}{V_2}\right)\right]}{\left[1 - \phi_{1,B}B_1\left(1 - \frac{V_1}{V_2}\right)\right]} + \phi_{2,B}B_2\frac{\left[1 - \phi_{2,B}\left(1 - \frac{V_2}{V_1}\right)\right]}{\left[1 - \phi_{2,B}B_2\left(1 - \frac{V_2}{V_1}\right)\right]} = 1$$

Can. J. Chem. Downloaded from www.nrcresearchpress.com by 210.87.254.5 on 09/06/12
For personal use only.

Dropping the bulk subscripts since all volume fractions now refer to the bulk phase, it can be shown that [37] can be rearranged into the following form:

$$[38]\quad \phi_1 B_1\left[1+\phi_2\left(1-\frac{V_1}{V_2}\right)\right]+\phi_2 B_2\left[1+\phi_1\left(1-\frac{V_2}{V_1}\right)\right]-\phi_1\phi_2 B_1 B_2\left[\left(1-\frac{V_1}{V_2}\right)+\left(1-\frac{V_2}{V_1}\right)\right]=1$$

For most organic systems $(1 - V_1/V_2)$ is of the order of 0.1 to 0.2 and is approximately equal to $(V_2/V_1 - 1)$. Furthermore the last term of this equation is the product of several terms all of which are less than 1. To a good approximation therefore, this term is smaller than the first two terms. Neglecting this term yields:

$$[39]\quad B_1\left[\phi_1+\phi_1\phi_2\left(1-\frac{V_1}{V_2}\right)\right]+B_2\left[\phi_2+\phi_1\phi_2\left(1-\frac{V_2}{V_1}\right)\right]=1$$

Again we note that the terms $\phi_1\phi_2(1 - V_1/V_2)$ and $\phi_1\phi_2(1 - V_2/V_1)$ are of the order of 0.025. Neglecting these terms as a further approximation and replacing the B_1 and B_2 terms with their definitions yields:

$$[40]\quad \phi_1 \exp\left[(\sigma-\sigma_1)\frac{A_1}{RT}\right]+\phi_2\exp\left[(\sigma-\sigma_2)\frac{A_2}{RT}\right]=1$$

This last equation is the volume fraction equivalent to [8] and is applicable only to systems for which the above detailed approximations are valid. Just as [8] can be rearranged into its implicit form, so can [40], [39], and [38].

The following equations are the implicit forms of these last three equations and can be tested for those systems with $(\sigma_2 - \sigma_1)$ greater than 10 ergs/cm^2 by using an approximate value (on the volume fraction scale) for the σ on the right-hand side of each equation to obtain an explicit function in each case. The approximate σ is indicated by σ' in these formulae.

$$[41]\quad \sigma=\sigma_1-\frac{RT}{A_1}\left\{\ln\left\{1+\phi_2\left\{\exp\left[\frac{\sigma'(A_2-A_1)}{RT}\right]\exp\left[\frac{(\sigma_1A_1-\sigma_2A_2)}{RT}\right]-1\right\}\right\}\right\}$$

$$[42]\quad \sigma=\sigma_1-\frac{RT}{A_1}\left\{\ln\left\{\phi_1\left[1+\phi_2\left(1-\frac{V_1}{V_2}\right)\right]+\phi_2\left[1+\phi_1\left(1-\frac{V_2}{V_1}\right)\right]\exp\left[\frac{\sigma'(A_2-A_1)}{RT}\right]\times\exp\left[\frac{(\sigma_1A_1-\sigma_2A_2)}{RT}\right]\right\}\right\}$$

$$[43]\quad \sigma=\sigma_1-\frac{RT}{A_1}\left\{\ln\left\{\phi_1\left[1+\phi_2\left(1-\frac{V_1}{V_2}\right)\right]+\phi_2\left[1+\phi_1\left(1-\frac{V_2}{V_1}\right)\right]\exp\left[\frac{\sigma'(A_2-A_1)}{RT}\right]\times\exp\left[\frac{\sigma_1A_1-\sigma_2A_2}{RT}\right]-\phi_1\phi_2\left[\left(1-\frac{V_1}{V_2}\right)+\left(1-\frac{V_2}{V_1}\right)\right]\exp\left[(\sigma'-\sigma_2)\frac{A_2}{RT}\right]\right\}\right\}$$

These implicit and explicit equations for the surface tensions of binary mixtures have been tested to determine the practical usefulness of these equations for a large variety of binary organic systems for large and small polarity differences.

Discussion and Conclusions

A variety of binary systems were chosen from the literature with increasing $(\sigma_2 - \sigma_1)$ values. Table 1 details the average percentage error found using different explicit functions to account for the concentration dependence of the surface tension of these binary solutions. There is generally some improvement in accuracy using the volume fraction ideal equation G over the corresponding ideal mole fraction statistics form A. With increasing $(\sigma_2 - \sigma_1)$ difference, there is an increasing deviation from ideal equations behaviour no matter what form of ideal equation is used, i.e., mole fraction statistics, area fraction statistics or volume fraction statistics (columns A, B, G, and H respectively). Columns J and K (volume fraction statistics) indicate what effect the first and second order perturbation terms (eqs. [19] and [22] and eqs. [32] and [33]) have when added to the linear ideal surface tension equation. As is observed, the resultant equations are able to account for the concentration dependence of the surface tension of binary solutions with a wide range of polarity (polar–polar, non-polar–non-polar, and non-polar–polar) to within an average error of less than 1%.

For some systems, however, (e.g. $BrCH_2CH_2Br$ +

Can. J. Chem. Downloaded from www.nrcresearchpress.com by 210.87.254.5 on 09/06/12
For personal use only.

Can. J. Chem. Downloaded from www.nrcresearchpress.com by 210.87.254.5 on 09/06/12
For personal use only.

TABLE 1. Average percent error of explicit functions for the surface tension of binary organic mixtures*

System	T (°C)	Ref.	$\sigma_2 - \sigma_1$	Mole fraction						Volume fraction					
				A	B	C	D	E	F	G	H	I	J	K	L
Dioxane + C_6H_5Cl	30	25	−0.14	0.14	0.13	0.13	0.13	0.13	0.14	0.13	0.13	0.13	0.13	0.13	0.13
MeOH + *s*-BuOH	25	19	+0.90	0.15	0.20	0.20	0.18	0.18	0.16	0.36	0.18	0.20	0.19	0.17	0.35
n-BuOH + EtAc	25	20	−1.22	0.51	0.47	0.47	0.43	0.43	0.47	0.45	0.47	0.47	0.43	0.43	0.41
CCl_4 + $C_6H_5CH_3$	20	21	+1.83	0.66	0.60	0.60	0.68	0.68	0.74	0.57	0.60	0.60	0.68	0.68	0.65
MeOH + *n*-BuOH	25	19	+2.08	0.77	0.16	0.16	0.18	0.17	0.86	0.36	0.15	0.16	0.16	0.17	0.28
n-HxOH + *n*-DeOH	25	19	+2.47	0.48	0.19	0.19	0.32	0.33	0.66	0.17	0.20	0.19	0.33	0.35	0.21
$EtCO_3$ + C_6H_6	25	22	+2.51	0.86	0.60	0.60	0.46	0.46	0.72	0.47	0.60	0.60	0.46	0.46	0.33
n-BuOH + $C_6H_5CH_3$	25	20	+3.35	0.23	0.42	0.42	0.42	0.13	0.13	0.11	0.52	0.42	0.42	0.13	0.23
C_6H_6 + C_6H_{12}	30	23	−3.70	1.48	1.19	1.19	0.84	0.83	1.12	1.05	1.19	1.19	0.84	0.84	0.69
C_5H_{10} + CCl_4	25	24	+4.28	0.28	0.33	0.33	0.22	0.22	0.26	0.35	0.33	0.33	0.22	0.22	0.20
Dioxane + *m*-xylene	30	25	−4.57	1.27	0.79	0.79	0.59	0.56	0.87	0.65	0.79	0.79	0.55	0.55	0.43
C_6H_5Cl + *m*-xylene	20	26	−4.57	1.08	0.80	0.80	0.31	0.31	0.59	0.66	0.80	0.80	0.31	0.32	0.18
C_6H_6 + acetone	25	27	−4.82	0.65	0.52	0.52	0.72	0.71	1.04	0.46	0.52	0.52	0.71	0.71	0.64
C_6H_{12} + *t*-decalin	25	24	+5.59	0.29	0.50	0.50	0.41	0.41	1.20	0.90	0.49	0.50	0.39	0.39	0.12
C_5H_{10} + $C_6H_5CH_3$	25	24	+6.09	1.23	1.55	1.55	0.47	0.47	0.17	1.71	1.55	1.55	0.47	0.47	0.63
CCl_4 + C_6H_5Cl	20	21	+6.53	0.94	1.06	1.06	0.18	0.19	0.22	1.12	1.06	1.06	0.20	0.21	0.20
C_6H_{12} + $Cl_2C{=}CCl_2$	25	24	+6.92	2.18	2.03	2.03	0.80	0.80	0.95	1.96	2.03	2.03	0.81	0.81	0.73
C_6H_{12} + C_6H_5Cl	20	21	+8.22	2.83	2.65	2.65	0.99	0.98	1.15	2.56	2.65	2.65	0.98	0.98	0.90
C_6H_5Cl + C_6H_{12}	20	26	−8.35	1.29	1.11	1.11	0.73	0.72	0.60	1.02	1.11	1.11	0.72	0.71	0.80
C_5H_{10} + $Cl_2C{=}CCl_2$	25	24	+9.45	1.65	1.94	1.94	0.42	0.45	0.62	2.09	1.94	1.94	0.47	0.51	0.40
C_6H_6 + *n*-C_8H_{18}	30	31	−10.05	5.77	4.23	4.23	1.47	1.42	3.00	3.46	4.25	4.23	1.48	1.54	0.71
$BrCH_2CH_2Br$ + C_6H_6	25	28	−11.40	5.07	4.95	4.95	2.44	2.44	2.56	4.89	4.95	4.95	2.44	2.44	2.38
$BrCH_2CH_2Br$ + $C_6H_5CH_3$	25	28	−11.62	4.05	3.28	3.28	0.74	0.61	1.31	2.90	3.29	3.28	0.59	0.62	0.54
C_6H_5OH + C_6H_6	25	32	−12.04	6.97	6.89	6.89	3.61	3.61	3.69	6.85	6.89	6.89	3.61	3.61	3.57
C_6H_6 + DMSO	25	29	+14.38	5.22	4.25	4.25	1.08	0.91	1.70	3.76	4.25	4.25	0.87	0.79	0.66
C_6H_6 + $C_6H_5NO_2$	20	23	+14.55	2.70	3.29	3.29	0.89	0.98	1.37	3.59	3.29	3.29	1.01	1.11	0.84
C_6H_6 + $C_6H_5NO_2$	30	23	+14.65	3.07	3.68	3.68	1.12	1.25	1.47	3.99	3.68	3.68	1.30	1.41	1.17
$BrCH_2CH_2Br$ + C_6H_{12}	25	28	−14.90	5.82	4.68	4.68	0.61	0.57	0.94	4.11	4.68	4.68	0.60	0.74	0.84
Quinoline + C_6H_{12}	20	30	−16.30	3.83	5.02	5.02	0.43	0.61	0.85	5.62	5.01	5.02	0.75	1.04	0.96
C_6H_{12} + $C_6H_5NO_2$	30	23	+18.40	6.70	6.42	6.42	1.17	1.07	1.15	6.29	6.42	6.42	1.02	0.91	1.03

*Key to equations for Tables 1, 2, 3: *explicit mole fraction*: A, $\sigma^A = \sigma_1 x_1 + \sigma_2 x_2$; B, eq. [21]; C, $\sigma^c = \sigma^A + x_1 x_2(\sigma_2 - \sigma_1)(A_2 - A_1)/(X_1 A_1 + X_2 A_2)$; D, eq. [19]; E, eq. [22]; F, $\sigma^F = \sigma^A - (x_1 x_2)[(\sigma_2 - \sigma_1)^2 A_1 A_2/(x_1 A_1 + x_2 A_2)RT]$. *Explicit volume fraction*: G, $\sigma^G = \sigma_1\phi_1 + \sigma_2\phi_2$; H, eq. [33], first and second term; I, eq. [32], first and second term; J, eq. [32] total; K, eq. [33] total; L, $\sigma^L = \sigma^G - \phi_1\phi_2(\sigma_2 - \sigma_1)^2 A_1 A_2/2(\phi_1 A_1 + \phi_2 A_2)RT$. *Implicit equations*: a, eq. [9]; b, eq. [43]; c, eq. [42]; d, eq. [41].

Can. J. Chem. Downloaded from www.nrcresearchpress.com by 210.87.254.5 on 09/06/12
For personal use only.

TABLE 2. Average percent error of implicit functions for the surface tension of binary organic mixtures

System	T (°C)	Ref.	$\sigma_2 - \sigma_1$	Mole fraction				Volume fraction							
				A	a	F	a	G	b	c	d	L	b	c	d
$C_6H_6 + C_6H_{12}$	30	23	−3.70	1.48	0.79	1.12	0.81	1.05	0.82	1.11	0.36	0.69	0.85	1.14	0.39
$CS_2 + CCl_4$	25	27	−5.89	3.85	1.91	2.23	2.22	2.42	2.25	4.30	0.68	1.75	2.40	4.41	0.72
Et_2O + acetone	30	17	+6.23	3.19	1.13	1.93	1.04	1.44	1.03	2.03	0.82	0.78	0.96	1.91	0.89
n-$C_6H_{14} + C_6H_{12}$	25	33	+6.28	1.60	0.20	0.51	0.16	0.94	0.18	0.33	0.49	0.22	0.14	0.28	0.54
$CCl_4 + C_6H_5Cl$	20	21	+6.53	0.94	0.17	0.22	0.17	1.12	0.17	0.17	0.27	0.20	0.17	0.18	0.28
$C_6H_{12} + Cl_2C{=}CCl_2$	25	24	+6.92	2.18	0.84	0.95	0.83	1.96	0.84	0.86	0.63	0.73	0.83	0.84	0.61
$C_6H_{12} + C_6H_5Cl$	20	21	8.22	2.83	1.02	1.15	1.00	2.56	1.02	1.04	0.76	0.90	1.00	1.02	0.74
C_6H_{12} + dioxane	30	23	+8.35	3.09	0.79	1.39	0.70	1.95	0.75	1.12	0.36	0.31	0.67	1.02	0.41
$C_5H_{10} + Cl_2C{=}CCl_2$	25	24	+9.45	1.65	0.33	0.42	0.29	2.09	0.33	0.29	0.18	0.40	0.29	0.25	0.21
Dioxane + $C_6H_5NO_2$	20	23	+9.65	0.24	0.94	0.94	0.90	0.97	0.96	0.81	0.25	0.71	0.89	0.75	0.19
$BrCH_2CH_2Br$ + p-xylene	35	28	11.29	6.60	1.86	3.78	2.39	4.58	2.34	3.18	0.63	1.86	2.90	3.67	0.80
$BrCH_2CH_2Br + C_6H_5CH_3$	30	28	11.56	4.30	0.95	1.56	1.15	3.13	1.04	1.12	0.70	0.76	1.23	1.31	0.86
$C_6H_6 + C_6H_5NO_2$	20	23	+14.55	2.70	0.66	1.37	0.56	3.59	0.66	0.57	0.21	0.84	0.56	0.48	0.28
$C_6H_6 + C_6H_5NO_2$	30	23	+14.65	3.07	0.64	1.47	0.63	3.99	0.64	0.61	0.61	1.17	0.62	0.61	0.69
$C_6H_{12} + C_6H_5NO_2$	20	23	+18.40	6.07	0.93	1.15	0.93	6.29	0.93	0.93	0.84	1.03	0.94	0.94	0.84
α-Bromonapthalene + C_6H_6	20	30	−15.00	0.88	0.98	3.19	1.82	3.42	0.66	0.54	1.51	0.55	1.09	0.62	0.73
	40	30	−15.60	0.38	1.55	4.23	2.75	2.91	1.21	0.68	0.85	1.41	1.99	1.48	0.14
Quinoline + C_6H_6	20	30	−16.30	3.83	0.93	0.85	0.28	5.62	1.23	1.49	2.63	0.96	0.63	0.84	2.01
Quinoline + C_6H_6	40	30	−16.60	3.05	0.36	1.84	0.65	4.91	0.53	0.63	1.77	0.57	0.31	0.15	1.15
$Br_2CHCHBr_2 + C_6H_6$	20	30	−20.30	3.30	1.13	3.54	2.09	5.30	0.79	0.57	0.71	1.80	1.69	1.53	0.34
$Br_2CHCHBr_2 + C_6H_6$	40	30	−20.40	2.35	2.17	4.57	3.10	4.41	1.83	1.60	0.27	2.50	2.71	2.54	1.17
Quinoline + Trimethylpentane	20	30	−26.30	26.78	7.68	16.91	9.77	23.44	7.93	8.70	5.42	13.66	11.11	11.54	6.97
	40	30	−25.80	36.78	6.04	13.76	11.17	30.11	7.32	8.16	3.60	9.78	13.44	13.89	7.22
C_6H_6 + DMSO	30	29	+14.44	5.19	0.91	1.62	0.79	3.68	0.90	1.19	0.55	0.58	0.80	1.02	0.66
C_6H_6 + DMSO	50	29	+14.70	4.98	0.56	1.29	0.44	3.28	0.54	0.80	1.20	0.53	0.45	0.65	1.35
MeOH + DMSO	30	29	+20.30	1.61	3.91	7.40	3.41	3.98	4.16	1.64	1.58	2.08	3.39	1.21	2.14
MeOH + DMSO	50	29	+19.55	2.68	4.69	8.25	4.19	3.03	4.98	2.21	1.11	2.80	4.22	1.77	1.58
EtOH + DMSO	20	29	+20.97	6.59	0.59	1.64	0.80	8.75	0.57	0.84	2.55	1.73	0.83	1.05	2.78
EtOH + DMSO	40	29	+20.59	5.21	0.64	2.29	0.57	7.37	0.65	0.51	1.44	1.62	0.54	0.47	1.67
EtOH + DMSO	60	29	+20.06	3.91	1.31	2.70	1.10	5.93	1.34	1.05	0.95	1.73	1.10	0.89	1.15

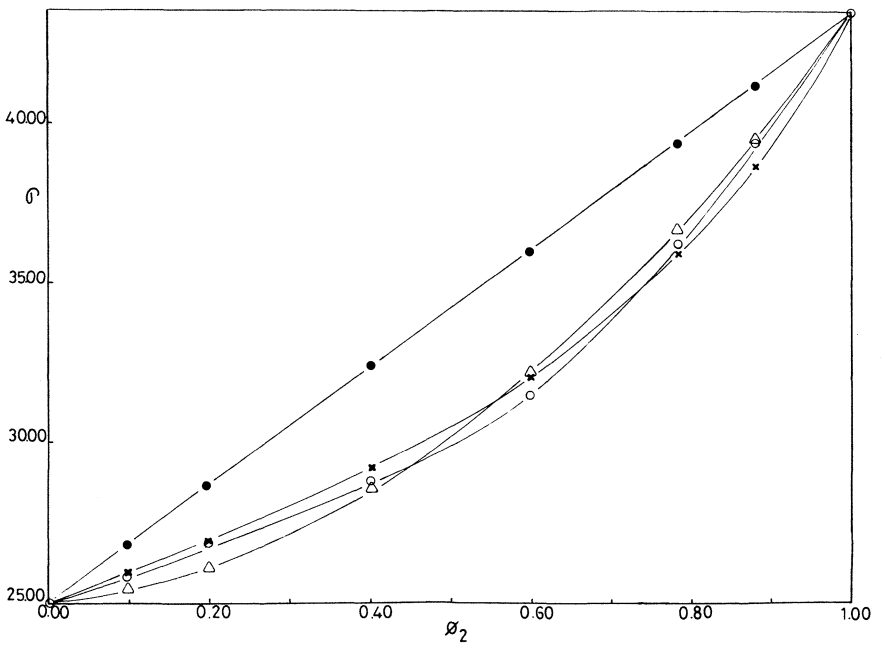

FIG. 1. Test of surface tension equations for cyclohexane–nitrobenzene (data of Table 3*b*) on volume fraction scale ϕ: Experimental ○, G, ●, △, L; ×, L, d. Letters refer to equations detailed in footnote to Table 1.

C_6H_6; $C_6H_5OH + C_6H_6$), the average error is substantially larger. This most probably is due to surface orientation effects which would require molar area values A_i much different (generally smaller) than those calculated using the assumption that the bulk density gives a good first estimate of these molar area values. The other possible explanation of this deviation is that the mixtures do not form ideal solutions to a first approximation. Activity coefficient effects could be invoked to account for this, possibly by using regular solution behaviour. For over 90% of the binary systems studied, however, the ideal solution approximation coupled with the use of bulk densities for calculating molar area values has been shown to be useful.

For those systems with $(\sigma_2 - \sigma_1)$ values greater than 20 as indicated in the theory section, substantial errors are found when using the explicit forms of these surface tension equations. Furthermore, the higher order expansion terms generally show diverging values. For such systems the implicit surface tension equations were tested and examples of this test are given in Table 2. On comparing the average error for calculating surface tensions of the same system either by the explicit or implicit methods, it is generally found that a decrease in error is found by using the less complex implicit equations (e.g. $C_6H_6 + C_6H_{12}$; $C_6H_{12} + C_6H_5Cl$; $C_6H_6 + C_6H_5NO_2$). Furthermore, it is generally found that equations based on volume fraction statistics give

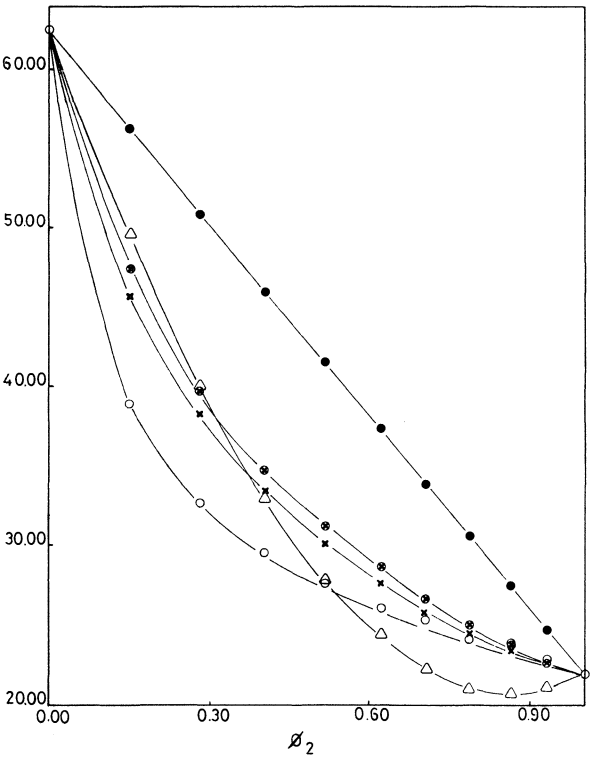

FIG. 2. Test of surface tension equation for glycerin–ethanol (data of Table 3*b*) on volume fraction scale ϕ: Experimental ○, G; ●, △, L; ×, L, b; ⊗, L, d. Letters refer to equations detailed in footnote to Table 1.

Can. J. Chem. Downloaded from www.nrcresearchpress.com by 210.87.254.5 on 09/06/12
For personal use only.

Can. J. Chem. Downloaded from www.nrcresearchpress.com by 210.87.254.5 on 09/06/12
For personal use only.

TABLE 3

(*a*) Comparison of calculated surface tensions by explicit and implicit functions, on the mole fraction scale, for the systems glycerin + ethanol and cyclohexane + nitrobenzene

		Mole fraction statistics											
X_2	σ_{obs}	A	a	B	a	C	a	D	a	E	a	F	a
Glycerin + ethanol (18) at 25°C: $\sigma_2 - \sigma_1 = -40.50$ dynes/cm													
1.0000	22.00	22.00	22.00	22.00	22.00	22.00	22.00	22.00	22.00	22.00	22.00	22.00	22.00
0.9473	22.90	24.13	23.00	24.45	23.04	24.45	23.04	21.12	22.59	21.53	22.65	21.21	22.60
0.8888	23.90	26.50	24.16	27.13	24.24	27.13	24.24	20.71	23.37	21.39	23.46	20.76	23.37
0.8235	24.20	29.15	25.50	30.06	25.63	30.06	25.63	20.90	24.39	21.70	24.49	20.79	24.37
0.7499	25.40	32.13	27.11	33.29	27.26	33.29	27.26	21.86	25.73	22.63	25.83	21.47	25.68
0.6666	26.10	35.50	29.06	36.86	29.24	36.86	29.24	23.82	27.50	24.39	27.58	23.03	27.40
0.5713	27.70	39.36	31.50	40.84	31.69	40.84	31.69	27.07	29.89	27.29	29.91	25.81	29.72
0.4614	29.60	43.81	34.68	45.29	34.87	45.29	34.87	31.98	33.17	31.76	33.14	30.28	32.95
0.3332	32.70	49.01	39.12	50.30	39.27	50.30	39.27	39.05	37.92	38.42	37.84	37.13	37.68
0.1817	38.90	55.14	46.17	55.99	46.26	55.99	46.26	48.93	45.53	48.21	45.46	47.37	45.37
0.0000	62.50	62.50	62.50	62.50	62.50	62.50	62.50	62.50	62.50	62.50	62.50	62.50	62.50
Ave. % error		25.54	8.56	28.63	8.96	28.63	8.96	10.27	5.82	8.59	5.82	9.66	5.52
Stand. Dev.		10.17	3.84	11.16	3.96	11.16	3.96	4.35	3.02	3.86	2.99	3.80	2.90
Cyclohexane + nitrobenzene (23) at 20°C: $\sigma_2 - \sigma_1 = +18.40$ dynes/cm													
1.0000	43.40	43.40	43.40	43.40	43.40	43.40	43.40	43.40	43.40	43.40	43.40	43.40	43.40
0.8863	39.38	41.31	38.81	41.24	38.81	41.24	38.81	39.58	38.78	39.62	38.78	39.69	38.70
0.7916	36.32	39.57	36.11	39.45	36.11	39.45	36.11	36.76	36.07	36.82	36.07	36.93	36.07
0.6616	31.51	36.25	32.35	36.09	32.34	36.09	32.34	32.29	32.31	32.32	32.31	32.49	32.32
0.4146	28.80	32.63	29.37	32.46	29.37	32.46	29.37	28.67	29.35	28.64	29.35	28.81	29.35
0.2068	26.83	28.81	26.95	28.69	26.95	28.69	26.95	26.19	26.94	26.13	26.94	26.24	26.94
0.1012	25.81	26.86	25.91	26.80	24.91	26.80	25.91	25.91	25.43	25.94	25.39	25.91	25.91
0.0000	25.00	25.00	25.00	25.00	25.00	25.00	25.00	25.00	25.00	25.00	25.00	25.00	25.00
Ave. % error		6.70	0.93	6.42	0.93	6.42	0.93	1.07	0.94	1.17	0.94	1.15	0.93
Stand. Dev.		2.84	0.45	2.73	0.45	2.73	0.45	0.45	0.45	0.49	0.45	0.52	0.45

Can. J. Chem. Downloaded from www.nrcresearchpress.com by 210.87.254.5 on 09/06/12
For personal use only.

TABLE 3 (*Concluded*)

(*b*) Comparison of calculated surface tensions by explicit and implicit functions on the volume fraction scale, for the systems glycerin + ethanol, and cyclohexane + nitrobenzene

		Volume fraction statistics															
ϕ_2	σ_{obs}	G	b	c	d	I	b	c	d	K	b	c	d	L	b	c	d
Glycerin + ethanol (18) at 25°C: $\sigma_2 - \sigma_1 = -40.50$ dyn/cm																	
1.0000	22.00	22.00	22.00	22.00	22.00	22.00	22.00	22.00	22.00	22.00	22.00	22.00	22.00	22.00	22.00	22.00	22.00
0.9351	22.90	24.63	23.07	23.07	23.24	24.45	23.05	23.05	23.21	20.90	22.56	22.56	22.73	21.08	22.59	22.59	22.75
0.8650	23.90	27.47	24.29	24.30	24.64	27.13	24.25	24.25	24.59	20.37	23.33	23.34	23.67	20.71	23.38	23.38	23.72
0.7891	24.20	30.54	25.71	25.72	26.24	30.06	25.64	25.66	26.18	20.54	24.36	24.37	24.89	21.03	24.43	24.43	24.96
0.7062	25.40	33.90	27.38	27.40	28.11	33.29	27.30	27.32	28.03	21.57	25.73	25.74	26.46	22.18	25.82	25.83	26.54
0.6158	26.10	37.56	29.38	29.42	30.33	36.86	29.29	29.33	30.23	23.68	27.56	25.57	28.94	24.38	27.65	27.66	28.58
0.5165	27.70	41.58	31.86	31.92	33.02	40.84	31.82	32.93	32.93	27.13	30.00	30.03	31.15	27.88	30.10	30.12	31.25
0.4072	29.60	46.01	35.04	35.15	36.44	45.29	34.94	35.05	36.35	32.25	33.35	33.39	34.72	32.97	33.45	33.49	34.81
0.2860	32.70	50.92	39.44	39.60	41.04	50.30	39.38	39.53	40.97	39.46	38.15	38.22	39.70	40.08	39.22	38.30	39.77
0.1511	38.90	56.38	46.37	46.60	48.01	55.99	46.33	46.56	47.97	49.31	45.73	45.88	47.32	49.70	45.77	45.92	47.36
0.0000	62.50	62.50	62.50	62.50	62.50	62.50	62.50	62.50	62.50	62.50	62.50	62.50	62.50	62.50	62.50	62.50	62.50
Ave. % error		30.20	9.29	9.47	11.92	28.63	9.09	9.27	11.72	11.03	6.06	6.14	8.25	10.55	6.21	6.29	8.39
Stand. dev.		11.66	4.07	4.16	5.08	11.16	4.01	4.10	5.02	4.60	3.14	3.19	4.07	4.68	3.18	3.23	4.12
Cyclohexane + nitrobenzene (23) at 20°C: $\sigma_2 - \sigma_1 = +18.40$ dyn/cm																	
1.0000	43.40	43.40	43.40	43.40	43.40	43.40	43.40	43.40	43.40	43.40	43.40	43.40	43.40	43.40	43.40	43.40	43.40
0.8806	39.38	41.20	38.81	38.82	38.63	41.24	38.81	38.82	38.63	39.55	38.78	38.79	38.60	39.52	38.78	38.79	38.59
0.7823	36.32	39.39	36.11	36.12	35.88	39.45	36.11	36.12	35.88	36.73	36.07	36.08	35.84	36.68	36.07	36.08	35.84
0.5983	31.51	36.01	32.35	32.35	32.12	36.09	32.35	32.36	32.12	32.28	32.32	32.32	32.09	32.20	32.32	32.32	32.09
0.4012	28.80	32.38	29.37	29.37	29.19	32.46	29.37	29.37	29.19	28.68	29.35	29.36	29.18	28.60	29.35	29.36	29.18
0.1979	26.83	28.64	26.95	26.95	26.85	28.69	26.95	26.95	26.85	26.22	26.94	26.95	26.85	26.16	26.94	26.94	26.85
0.0963	25.81	26.77	25.91	25.91	25.86	26.80	25.91	25.91	25.86	25.45	25.91	25.91	25.86	25.42	25.91	25.91	25.86
0.0000	25.00	25.00	25.00	25.00	25.00	25.00	25.00	25.00	25.00	25.00	25.00	25.00	25.00	25.00	25.00	25.00	25.00
Ave. % error		6.29	0.93	0.93	0.84	6.42	0.93	0.93	0.84	1.02	0.94	0.94	0.84	1.03	0.94	0.94	0.84
Stand. dev.		2.67	0.45	0.45	0.43	2.73	0.45	0.45	0.43	0.43	0.45	0.45	0.44	0.43	0.45	0.45	0.44

Can. J. Chem. Downloaded from www.nrcresearchpress.com by 210.87.254.5 on 09/06/12
For personal use only.

better fits to the observed surface tension data than do equations based on mole fraction statistics.

For those systems where the explicit higher order terms in the equations for the surface tension showed divergence, it was found that the implicit forms of the surface tension equations gave excellent fits to the data, i.e. less than 1% average error.

Table 3 *a* and *b* illustrate a detailed set of calculations for two systems for all the explicit and implicit formulae derived in the theory section (the large capital letters indicate explicit surface tension functions and the small capital letters indicate implicit surface tension functions). The cyclohexane–nitrobenzene systems illustrate for a non-polar–polar system how well the simple explicit functions as well as the more complex implicit functions are able to account for the data with the elementary assumptions made about the system. These same data are displayed in Fig. 1.

The system glycerin–ethanol was chosen to illustrate the fact that for very large differences in $(\sigma_2 - \sigma_1)$ e.g. greater than 30, neither the explicit nor the implicit equations are able to account for the data. This is particularly true of aqueous systems. Obviously for such systems the assumption of ideal or near-ideal solutions is not valid and activity coefficients in the surface and bulk chemical potential equations would have to be taken into account in deriving surface tension equations for such mixtures. A systematic approach to this problem is presently underway. These data are displayed in Table 3 *a* and *b* as well as in Fig. 2.

In conclusion, the surface tension equations which have been derived both in their implicit and explicit forms are able to account for the composition dependence of the surface tension of a wide variety of binary organic systems with $(\sigma_2 - \sigma_1)$ values 20 or less. This includes polar–non-polar mixtures which have not been accounted for previously (1). Surface orientation effects seem to be insignificant for most systems studied, although a small percentage of the systems, where larger errors persist no matter what form of the surface tension is used, may indicate the presence of such orientation factors. A detailed study of surface entropy effects in such systems is also underway in order to elucidate this factor.

Acknowledgement

We would like to thank the Natural Sciences and Engineering Research Council of Canada for support of this project and the Ontario Government for a scholarship for one of us (C.S.).

1. R. C. Reid, J. M. Prausnitz, and R. K. Sherwood. The properties of gases and liquids. 3rd ed. McGraw Hill Co., New York. 1977. Chapt. 12.
2. A. Schuchowitsky. Acta Physicochim. URSS, **19**, 176 (1944).
3. A. Schuchowitsky. Acta Physicochim. URSS, **19**, 508 (1944).
4. R. Defay, I. Prigogine, A. Bellemans, and D. H. Everett. Surface tension and adsorption. John Wiley and Sons, New York. 1966.
5. F. B. Sprow and J. M. Prausnitz. Can. J. Chem. Eng. **45**, 25 (1967).
6. E. A. Guggenheim. Trans. Faraday Soc. **41**, 150 (1945).
7. J. G. Eberhardt. J. Phys. Chem. **70**, 1183 (1966).
8. J. L. Shereshefsky. J. Coll. Interfac. Sci. **24**, 317 (1967).
9. R. S. Hansen and L. Sogar. J. Coll. Interfac. Sci. **40**, 424 (1972).
10. J. Marechal. Trans. Faraday Soc. **48**, 601 (1952).
11. B. E. Conway and H. P. Dhar. Surface Sci. **44**, 261 (1974).
12. H. P. Dhar, B. E. Conway, and K. M. Joshi. Electrochim. Acta, **18**, 789 (1973).
13. J. A. V. Butler. Proc. R. Soc. A, **135**, 348 (1932).
14. J. C. Eriksson. Adv. Chem. Phys. **6**, 145 (1964).
15. M. M. Chaudhri, P. K. Katti, and M. N. Baliga. Trans. Faraday Soc. **55**, 2013 (1959).
16. B. E. Conway. Croatica Chem. Acta **48**, 573 (1976).
17. I. Prigogine. Trans. Faraday Soc. **44**, 626 (1948).
18. R. C. Ernst, C. H. Watkins, and H. H. Ruwe. J. Phys. Chem. **40**, 627 (1936).
19. G. C. Benson and V. T. Lam. J. Col. Int. Sci. **38**, 294 (1972).
20. E. E. Litkenhous, J. D. Van Arsdale, and J. W. Spanyer, Jr. J. Phys. Chem. **44**, 377 (1940).
21. M. Siskova and V. Secova. Coll. Czech. Chem. Commun. **35**, 2702 (1970).
22. S. T. Bowden and E. T. Butler. J. Chem. Soc. London, 79 (1939).
23. S. K. Suri and V. Ramakrishna. J. Phys. Chem. **72**, 3073 (1968).
24. V. T. Lam and G. C. Benson. Can. J. Chem. **48**, 3773 (1970).
25. K. Chand and V. Ramakrishna. Ind. J. Chem. **7**, 698 (1969).
26. M. S. Dhillon and B. S. Mahl. Z. Phys. Chem. Leipzig, **259**, 249 (1978).
27. W. E. Shipp. J. Chem. Eng. Data, **15**, 308 (1970).
28. M. S. Dhillon and H. S. Chugh. Thermochim. Acta, **16**, 185 (1976).
29. E. Tommila and T. Autio. Suom. Kemistil. **42**, 107 (1969).
30. A. P. Toropov. Uzbek. Khim. Zhur. **1**, 23 (1971).
31. R. L. Schmidt, J. C. Randall, and H. L. Clever. J. Phys. Chem. **70**, 3912 (1966).
32. L. E. Swearingen. J. Phys. Chem. **32**, 1346 (1928).
33. H. L. Clever and W. E. Chase Jr. J. Chem. Eng. Data, **8**, 291 (1963).

β-Lactams. IX. The synthesis of 7-β-phenylacetamido-3′-hydroxybenzo-[3,4]-*O*-2-isocephem, a weak antibacterial β-lactam antibiotic

GEORGE JUST, YOULA S. TSANTRIZOS, AND ANTONIO UGOLINI[1]
Department of Chemistry, McGill University, Montreal, P.Q., Canada H3A 2K6
Received January 22, 1981

GEORGE JUST, YOULA S. TSANTRIZOS, and ANTONIO UGOLINI. Can. J. Chem. **59**, 2981 (1981).
The synthesis of the title compound is described.

GEORGE JUST, YOULA S. TSANTRIZOS et ANTONIO UGOLINI. Can. J. Chem. **59**, 2981 (1981).
La synthèse du produit nommé est décrite.

[Traduit par le journal]

As part of a continuing program to prepare nonclassical β-lactam antibiotics (for rationale, see ref. 1), in which a phenolic group replaces the carboxylic function of penicillins and cephalosporins, we wish to describe the synthesis of title compound **18** and its nitro analogues. Recently, Doyle (2) has described a similar compound differing from **18** only in the nature of the side-chain and the position of the phenolic hydroxy group, which was attached *para* to the ether function.

o-Aminophenol **1** and 2-aminoresorcinol **4** were transformed to their dimethyl-*tert*-butylsilyl ethers **2** and **5**. Amines **2** and **5** were converted to their cinnamylidene Schiff bases **3** and **6**, and, without purification, treated with azidoacetyl chloride and triethylamine at −20°C.

β-Lactams **7**, mp 84–85°C, and **8**, mp 95–96°C, were obtained in good yield after column chromatography and crystallization. The presence of the azide and β-lactam functions was confirmed by ir absorption bands at 2100, and 1760 and 1770 cm^{-1} respectively. The stereochemistry could not be assigned at this point because of overlapping signals in the ^{1}Hmr spectrum. However, all ^{1}Hmr spectra of compounds **9**–**21** showed $J_{3,4} \simeq 5$ Hz, indicating that the substituents on the β-lactam ring were *cis* (3).

Ozonolysis of **7** in methanol at −78°C, followed by sodium borohydride reduction (−40° → +20°C), gave alcohol **9**, mp 77°C. Alcohol **9** was converted with little difficulty to the corresponding mesylate **11**, and, by means of thionyl chloride – pyridine in boiling benzene, to chloride **13**.

In order to study the cyclization reaction, mesylate **11** and chloride **13** were used as model compounds. Treatment of a tetrahydrofuran solution of either mesylate **11** or chloride **13** with freshly prepared tetra-*n*-butylammonium fluoride (4) gave instantaneously a quantitative yield of tricyclic azide **15**, mp 77–78°C.

This sequence was then applied to the disilylazido-β-lactam **8**. Ozonolysis of **8** in methanol at −78°C as described for monosilyl-β-lactam **7** proceeded in very poor yield. However, when the reaction was carried out in ethanol – methylene chloride (4:1) at −78°C, and the crude ozonide reduced with sodium borohydride (−40° → +20°C), alcohol **10** was obtained in good yield. Treatment of **10** with methanesulfonyl chloride and triethylamine in methylene chloride at −78°C gave mesylate **12**.

Reaction of mesylate **12** with exactly one equivalent of tetra-*n*-butylammonium fluoride in dry tetrahydrofuran gave tricyclic azide **16**, mp 69–70°C. Since the amount of fluoride added turned out to be extremely critical, and the reaction was virtually a titration with no easily determined end-point except by tlc, a more controllable set of reaction conditions was sought. Treatment of an acetonitrile solution of disilylether **12** with 1.2 equiv. of potassium fluoride and 0.3 equiv. of 18-crown-6 effected the same transformation to **16** in about 6 hours, permitting easy monitoring of the reaction. The reaction conditions turned out not to be critical, and the amounts of 18-crown-6 and potassium fluoride could be varied with impunity.

Tricyclic azido-β-lactam **15** exhibited a clean, nearly first-order ^{1}Hmr spectrum in deuterobenzene at 100 MHz for protons A–D. Proton A appeared at 4.18 ppm (J_{AB} = 5.0 Hz). Proton B (3.10 ppm) was coupled to A (J_{BA} = 5.0 Hz), C (J_{BC} = 3.5 Hz), and D (J_{BD} = 10 Hz). Protons C (3.36 ppm) and D (3.87 ppm) showed geminal coupling of 10 Hz, giving the spectrum a deceptively simple appearance reproduced below (Fig. 1). Hydrogen

[1]Holder of a NSERC Scholarship, 1978–1980 and DGES Scholarship, 1978–1981.

0008-4042/81/202981-07$01.00/0
©1981 National Research Council of Canada/Conseil national de recherches du Canada

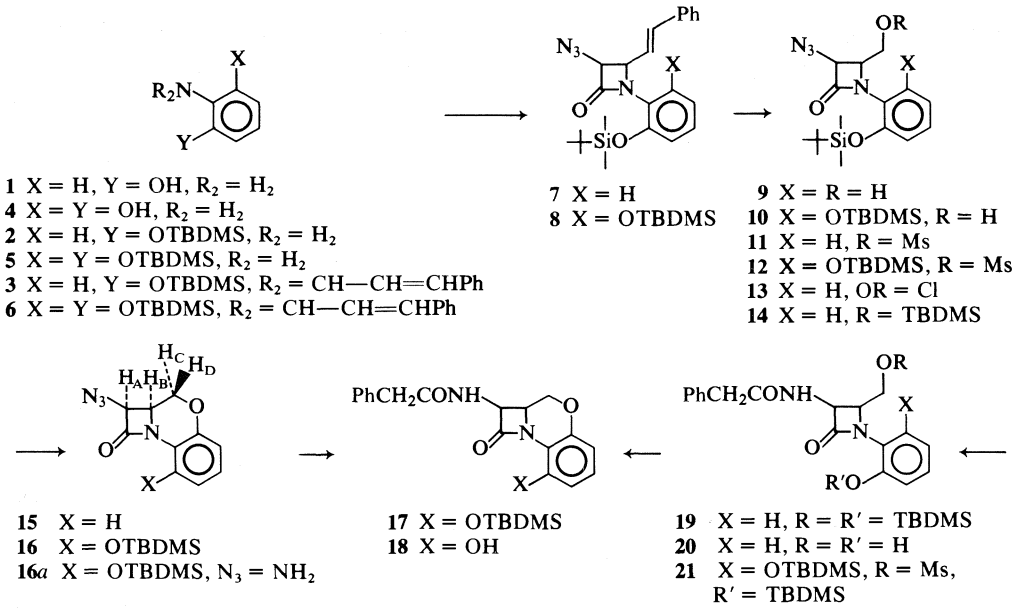

1 X = H, Y = OH, $R_2 = H_2$
4 X = Y = OH, $R_2 = H_2$
2 X = H, Y = OTBDMS, $R_2 = H_2$
5 X = Y = OTBDMS, $R_2 = H_2$
3 X = H, Y = OTBDMS, R_2 = CH—CH=CHPh
6 X = Y = OTBDMS, R_2 = CH—CH=CHPh

7 X = H
8 X = OTBDMS

9 X = R = H
10 X = OTBDMS, R = H
11 X = H, R = Ms
12 X = OTBDMS, R = Ms
13 X = H, OR = Cl
14 X = H, R = TBDMS

15 X = H
16 X = OTBDMS
16*a* X = OTBDMS, $N_3 = NH_2$

17 X = OTBDMS
18 X = OH

19 X = H, R = R′ = TBDMS
20 X = H, R = R′ = H
21 X = OTBDMS, R = Ms, R′ = TBDMS

sulfide – triethylamine reduction of **16** followed by acylation with phenylacetyl chloride, gave amide **17** in 54% yield, based on **8**. Removal of the silyl group gave tricyclic amide **18**, mp 194–195°C. The same compound could be obtained using the alternate route **12** → **21** → **17** → **18**. It should be noted that the potassium fluoride/18-crown-6 cyclization method could not be used for the transformation **21** → **17**, and the tetra-*n*-butylammonium fluoride method had to be employed.

For comparison purposes, alcohol **9** was silylated, and the resulting silyl ether **14** transformed by the methods described to the phenylacetamido-β-lactam **19**, which was hydrolyzed to **20**. Whereas bicyclic β-lactam **20** showed no biological activity, when tested against a variety of microorganisms in concentrations up to 256 μg/mL (MIC), tricyclic β-lactam **18** inhibited the growth of *S.aureus* (Q74-1) and *S.lutea* (PCI-1001) at 128 and 64 μg/mL respectively.

High anti-bacterial activity has usually been associated with chemical reactivity of the β-lactam ring, which is normally induced by steric strain. In a system such as **18**, increased reactivity of the β-lactam ring can, in principle, be induced by substituting the phenyl ring with an electron-withdrawing substituent such as a nitro group. In order to obtain a tricyclic β-lactam in which a nitro group is substituted *para* to the β-lactam nitrogen (see **15**), one would have to use as starting material an *o*,*o*′-disilyloxy-*p*-nitroaniline. We have shown

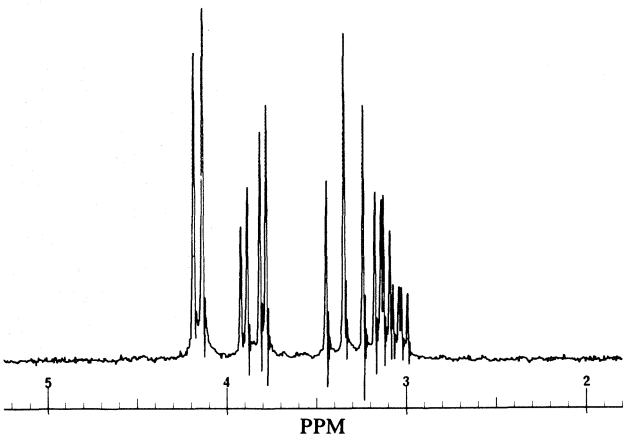

FIG. 1

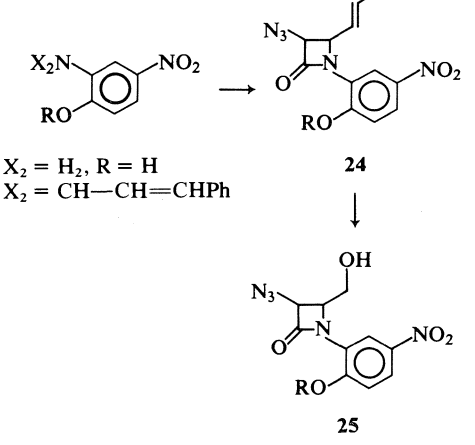

22 $X_2 = H_2$, R = H
23 X_2 = CH—CH=CHPh

24

25

a, R = *t*-BuSiMe_2
b, R = *t*-BuSiPh_2

that *o*-dimethyl-*tert*-butylsilyloxy-*p*-nitroaniline is converted to the corresponding *trans*-fused β-lactam only (5).

We therefore used 2-hydroxy-5-nitroaniline **22** as model. Silylation with either *tert*-butyldimethyl or *tert*-butyldiphenylsilyl chloride gave silyl ethers **22***a* and **22***b*, which were converted via their cinnamylidene derivatives **23***a* and **23***b* to β-lactams **24***a* and **24***b*. Both **24***a* and **24***b* were extremely labile to reductive ozonolysis reaction conditions, and little **25** could be isolated, the side-products being silanol and other unidentified products. Because of the lability of the *p*-nitrosilyl ethers to reductive ozonolysis conditions, we next investigated the nitration of the relatively unstrained β-lactam **12**, and cyclization of the resulting nitro derivatives, **26** and **27**.

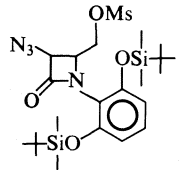

12

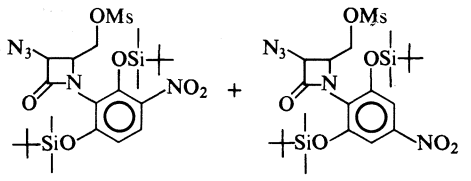

26 **27**

β-Lactam **12** was treated with nitronium tetrafluoroborate at −20°C and, as expected, two compounds (**26** and **27**) were detected in the reaction mixture. Attempts to purify the mixture, which was well separated on thin layer chromatography, proved unsuccessful, resulting in complete decomposition of **27** and extensive desilylation of **26**.

It is known that *p*-nitrophenols ($pK_A = 7.2$) (7) behave almost like carboxylic acids, and it is therefore to be expected that the *p*-nitrosilyl ether **26** would be extremely unstable to hydrolysis, as are silyl esters. In **27**, the nitro substituent *para* to the β-lactam ring introduces so much chemical reactivity that the amide linkage is easily hydrolyzed on contact with silica gel.

Nitration of silyloxy azido-β-lactam **16** showed very similar complications. The ^{1}Hmr spectrum of the crude reaction mixture clearly showed the presence of three compounds (**28**, **29**, and **30**), characterized by three sets of doublets, two having a large coupling constant ($J = 9$ Hz), as would be expected for *ortho* protons (**28**, **30**), and one set at about 7.4 ppm with the two doublets overlapping and a small coupling constant of 3 Hz indicating *meta* protons (**29**). Attempts to separate the three compounds by chromatography lead to complete decomposition of **29** and some desilylation of **28** and **30**. The latter were found to be sensitive to moisture and traces of acid, even after crystallization. The ^{1}Hmr spectra of **28** and **30** in deuterobenzene were virtually identical. However, in deuterochloroform the two methyl groups attached to silicon appeared in **28** as two 3H singlets at approximately 0.2 ppm downfield from the corresponding 6H singlet in **30**, indicating hindered rotation of the silyloxy group in **28**. This assignment was further corroborated by mass spectrometric data: *o*-nitro substituted phenyl ethers and amines are characterized by intense ions of mass $M^{+\cdot} - OR^{\cdot}$ (6).

The very intense peak at *m/e* 260 ($M^{+\cdot}$ − $OSiMe_2$-*tert*-butyl$^{\cdot}$) seen in the mass spectrum of compound **28** is almost completely absent from the spectrum of **30**.

Both compounds show intense ions at *m/e* 334 (base peak, $M^{+\cdot}$ − *tert*-butyl$^{\cdot}$), 306 (334 − $N_2^{\cdot}$, from the azide group), 251 (334 − 83, 83 = COCH—N_3), and 205 (251 − $NO_2^{\cdot}$).

A mixture of **28** and **30** was reacted with hydrogen sulfide – triethylamine to obtain the unstable amines **31** and **33***a* in good yield. Further reaction of **31** or **33***a* with phenylacetyl chloride was unsuccessful, initially leading to hydrolysis of the silyl ether, followed by hydrolysis of the β-lactam ring, as evidenced by ^{1}Hmr, which showed the presence of silanol, and ir, which showed a decrease in intensity of the β-lactam absorption with time.

We then thought that protection of the phenol group with diphenyl-*tert*-butylsilyl chloride would give a more stable β-lactam. It was found that treatment of phenol **30***a* with diphenyl-*tert*-butylsilyl chloride – triethylamine gave compound **30***b* which was well characterized by its ^{1}Hmr spectrum. However, phenol **28***a* was unreactive under the same conditions, further confirming that the phenolic group was sterically hindered by the presence of an *ortho* nitro substituent. The azide function of diphenyl-*tert*-butylsilyl ether **30***b* was then reacted with hydrogen sulphide – triethylamine and the progress of the reaction was followed by the disappearance of the infrared absorption of the azide. Upon complete formation of amine **33***b*,

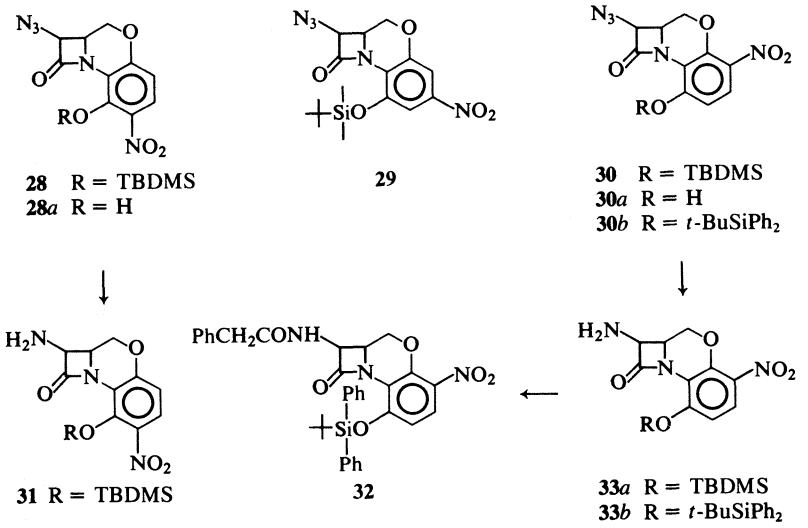

an equivalent of triethylamine was added along with an equivalent of phenylacetyl chloride to form final product **32**.

The ^{1}Hmr spectrum of **32** clearly showed the presence of all expected proton resonances: a singlet at 3.5 ppm (—COCH_2Ph), a multiplet at 3.3–3.6 ppm due to H_B, two sets of doublets at 3.8 to 4.6 ppm, coupled to each other and each integrating to one proton (H_C and H_D). H_A was found as a doublet of doublets at 5.1 to 5.3 ppm with one of its coupling constants equal to that of the broad doublet (due to NH) at 8.0 ppm. Finally, two doublets (6.6 and 8.7 ppm) were seen coupled to each other by a large coupling constant of 9 Hz, characteristic of the *ortho* protons on the nitrobenzene ring.

The infrared spectrum of **26** was also consistent with the structure given, with an absorption of 1790 cm^{-1} for the carbonyl group of the β-lactam.

Unfortunately, mass spectrometry and elemental analysis could not be used to further support the structure of **32** due to the extreme instability of this compound. It was observed through ^{1}Hmr and ir studies that even the traces of moisture or acid found in DMSO-d_6 would cause rapid decomposition of the silyl ether, followed by hydrolysis of the β-lactam ring, within half an hour.

Biological studies of these compounds were inconclusive due to complete decomposition of these compounds within a short time. We therefore showed that a nitro substituent introduces greater reactivity than desired and perhaps replacement of this group with a less electron withdrawing substituent such as an ester might lead to more stable and perhaps biologically active products.

Experimental

Thin-layer chromatography (tlc) was performed on Merck Silica Gel 60 F_{254} aluminum-backed plates. Flash chromatography was done on Woelm Silica (32–63 μ). Melting points (mp) were measured on a Gallenkamp block and are uncorrected, unless specified otherwise. The nmr spectra were recorded on Varian T-60, T-60A, and where noted, HA-100 and XL-200 spectrometers. Infrared (ir) spectra were recorded on Pye Unicam SP-1000, Perkin Elmer 257 and 297 spectrophotometers. Mass spectra (ms) were obtained on HP 5984A or LKB 9000 spectrometers, in the direct inlet mode unless indicated otherwise. Elemental analyses were performed by Midwest Microlab Ltd., Indianapolis.

*Di-*tert*-butyldimethylsilyl-2-aminoresorcinol 5*

A suspension of 2-nitroresorcinol (15 g, 97 mmol) and PtO_2 (1 g) in absolute ethanol (250 mL) was hydrogenated in a Parr apparatus at 40 psi. Filtration through Celite and evaporation of the rapidly darkening filtrate afforded 12 g of amine **4** as a brown solid. This amine was added to *tert*-butyldimethylsilyl chloride (32 g, 211 mmol) and imidazole (33 g, 485 mmol) in dry DMF (75 mL), and let stir overnight at room temperature. Then water (300 mL) was added and the solution extracted thrice with ether (300, 50, 50 mL). The ether extract was washed with water (3 × 100 mL), then brine (100 mL), then dried ($MgSO_4$) and evaporated. Chromatography of the residue on SiO_2 (250 g) afforded 20 g (59%) of amine **5** as a brownish oil; ^{1}Hmr ($CDCl_3$) δ: 0.2 (s, 12H, $SiMe_2$), 1.0 (s, 18H, *t*-BuSi), 3.47 (bs, 2H, NH_2), 6.27 (s, 3H, C_6H_3).

β-Lactam Azide 8

Amine **5** (14.2 g, 40 mmol) and cinnamaldehyde (5.6 g, 42 mmol), in benzene (150 mL), with a trace of *p*-TsOH, were refluxed overnight using a Dean–Stark trap. Evaporation of the solvent afforded Schiff base **6** as a thick brown oil. To this Schiff base, in CH_2Cl_2 (250 mL) containing triethylamine (5.3 g, 52 mmol), at −20°C was added dropwise azidoacetyl chloride (6.2 g, 52 mmol) in CH_2Cl_2 (50 mL), over 1 h. The red-brown solution was stirred for an additional hour at −20°C, and then allowed to warm up. Washing with water (2 × 150 mL) and brine (150 mL), then drying ($MgSO_4$) and evaporation of the solvent afforded, after chromatography on SiO_2 (300 g, $CHCl_3$), 13 g (59%) of β-lactam **8** as a thick brown oil, which crystallized upon trituration with

petroleum ether, mp 95–96°C; ir (film) ν_{max}: 2900, 2100 (N_3), 1770 (β-lactam), 1580 cm^{-1}; ^{1}Hmr ($CDCl_3$) δ: 0.24, 0.3 (2s, 12H, $SiMe_2$), 1.03 (s, 18H, *t*-BuSi), 4.8–5.0 (m, 2H, CH—CHN_3), 6.4–7.3 (m, 10H, C_6H_3 and CH=CH—C_6H_5).

β-Lactam Azide **7** was prepared as described for **8**; 63% yield, mp 84–85°C; ir ($CHCl_3$) ν_{max}: 2100 (N_3), 1760 (β-lactam) cm^{-1}; ^{1}Hmr ($CDCl_3$) δ: 0.28 (s, 6H, $SiMe_2$), 1.03 (s, 9H, *t*-BuSi), 4.88 (d, 1H, CHN_3), 5.02 (dd, 1H, C*H*—CHN_3), 6.1 (dd, 1H, C*H*=CH—Ph, *J* = 7, 15 Hz), 6.57 (d, 1H, C*H*—Ph, *J* = 15 Hz), 6.6–7.5 (m, 9H, C_6H_5 and C_6H_4).

Azido Alcohol ***10***

Ozone was bubbled through a solution of β-lactam **8** (7 g, 12.7 mmol) in EtOH (200 mL) and CH_2Cl_2 (50 mL) at −78°C. Excess ozone was flushed out with N_2 and $NaBH_4$ (0.95 g, 25 mmol) was added at −40°C. After warming to room temperature, pH 4.5 buffer (200 mL) was added and the ethanol removed under reduced pressure. The aqueous residue was extracted with ether (3 × 100 mL) and the ether washed with brine (100 mL), dried ($MgSO_4$), and evaporated to a yellow oil, which was chromatographed on SiO_2 to give 4.5 g (74%) of a viscous pale yellow oil. Crystallization was induced, by addition of a little pentane, giving β-lactam **10** as white needles, mp 99.5–100°C; ir (film) ν_{max}: 3500 (OH), 2100 (N_3), 1765 (β-lactam), 1590 cm^{-1}; ^{1}Hmr ($CDCl_3$) δ: 0.26, 0.30 (2s, 12H, $SiMe_2$), 1.05 (s, 18H, *t*-BuSi), 2.5 (bs, 1H, OH), 3.8 (bs, 2H, CH_2), 4.1 (dt, 1H, C*H*—CH_2—OH, *J* = 5, 5 Hz), 4.7 (d, 1H, CH—N_3, *J* = 5 Hz), 6.4–7.2 (m, 3H, C_6H_3).

Azido Alcohol **9** was prepared as described for **10**; 88% yield, mp 77–77.5°C; ^{1}Hmr ($CDCl_3$) δ: 0.25 (s, 6H, $SiMe_2$), 0.98 (s, 9H, *t*-BuSi), 2.30 (bt, 1H, OH), 3.83 (bdd, 2H, CH_2), 4.46 (dt, 1H, C*H*—CH_2, *J* = 4, 5 Hz), 4.87 (d, 1H, CHN_3, *J* = 5 Hz), 6.7–7.7 (m, 4H, C_6H_4).

Azido Mesylate ***12***

To alcohol **10** (4 g, 8.4 mmol) in CH_2Cl_2 (100 mL) and Et_3N (1 g, 10 mmol) at −78°C was added dropwise MsCl (1.1 g, 10 mmol) in CH_2Cl_2 (10 mL). The solution was stirred for 0.5 h at −78°C and allowed to warm to room temperature. After 1 h the solution was washed with water (2 × 75 mL), then brine (75 mL), dried ($MgSO_4$), and evaporated to give a pale yellow oil, which crystallized *in vacuo*. Trituration with petroleum ether yielded 4.4 g (95%) of mesylate **12** as white crystals, mp 69–70.5°C; ir (film) ν_{max}: 2900, 2100 (N_3), 1780 (C=O) cm^{-1}; ^{1}Hmr ($CDCl_3$) δ: 0.24, 0.27 (2s, 12H, 2$SiMe_2$), 1.0 (s, 18H, 2*t*-BuSi), 2.86 (s, 3H, SCH_3), 4.45 (bm, 3H, CH—CH_2), 4.94 (m, 1H, CHN_3), 6.4–7.2 (m, 3H, C_6H_3).

Azido Mesylate β-Lactam **11** was prepared as described for **12**; 85% yield; ir (film) ν_{max}: 2110 (N_3), 1770 (β-lactam) cm^{-1}; ^{1}Hmr ($CDCl_3$) δ: 0.28 (s, 6H, $SiMe_2$), 1.02 (s, 9H, *t*-BuSi), 2.87 (s, 3H, SO_2CH_3), 4.47 (m, 2H, CH_2), 4.80 (m, 1H, C*H*—CH_2), 5.10 (d, 1H, CHN_3, *J* = 4.5 Hz), 6.8–7.8 (m, 4H, C_6H_4).

Chloro β-Lactam ***13***

Alcohol **9** (0.5 g, 1.4 mmol) was refluxed for 2 h in benzene (25 mL), containing thionyl chloride (0.2 g, 1.7 mmol) and pyridine (0.14 g, 1.7 mmol). This mixture was added to ether (25 mL) and then washed with water (2 × 30 mL) and brine (30 mL). Treatment with charcoal and drying ($MgSO_4$), followed by filtration and evaporation of the solvent afforded 0.46 g (87%) of chloride **13** as a white solid, mp 77–78°C (Et_2O–hexane); ir (film) ν_{max}: 2110 (N_3), 1765 (β-lactam) cm^{-1}; ^{1}Hmr ($CDCl_3$) δ: 0.32 (s, 6H, $SiMe_2$), 1.03 (s, 9H, *t*-BuSi), 3.75 (m, 2H, CH_2), 4.75 (m, 1H, C*H*—CH_2), 5.05 (d, 1H, CHN_3, *J* = 4.5 Hz), 6.8–7.8 (m, 4H, C_6H_4).

Disilyl Ether **14** was prepared according to the procedure described by Corey and Venkoteswarlu (8); ^{1}Hmr ($CDCl_3$) δ: −0.10, −0.15 (2s, 6H, $SiMe_2$), 0.20 (s, 6H, $SiMe_2$), 0.75, 0.92 (2s, 18H, 2*t*-BuSi), 3.75 (d, 2H, CH_2, *J* = 5 Hz), 4.40 (dt, 1H, C*H*—CH_2, *J* = 5,5 Hz), 4.65 (d, 1H, C*H*N_3, *J* = 5 Hz), 6.6–7.6 (m, 4H, C_6H_4).

β-Lactam Amide **19** was prepared as described for **21**; ir ($CHCl_3$) ν_{max}: 3400 (NH), 1755 (β-lactam), 1680 (amide) cm^{-1}; ^{1}Hmr ($CDCl_3$) δ: −0.37, −0.23 (2s, 6H, $SiMe_2$), 0.20, 0.24 (2s, 6H, $SiMe_2$), 0.80, 0.95 (2s, 18H, 2*t*-BuSi), 3.52 (s, 2H, CH_2Ph), 3.72 (broad *ABX*, 2H, CH_2O), 4.47 (bd, 1H, C*H*—CH_2, *J* = 5.5 Hz), 5.60 (dd, 1H, C*H*—NH, *J* = 5.5, 10 Hz), 6.5–7.9 (m, 10H, C_6H_4, C_6H_5, NH).

Tricyclic β-Lactam **15** was prepared from **11** or **13** as described for **16**, mp 77–78°C; ir (KBr) ν_{max}: 2120 (N_3), 1780 (β-lactam) cm^{-1}; ^{1}Hmr 100 MHz (C_6D_6) δ: 3.10 (ddd, 1H, C*H*—CH_2, *J* = 3.5, 5.0, 10 Hz), 3.36 (dd, 1H, CH—C*H*H, *J* = 10,10 Hz), 3.87 (dd, 1H, CH—CH*H*, *J* = 3.5, 10 Hz), 4.18 (d, 1H, CHN_3, *J* = 5.0 Hz), 6.6–7.4 (m, 4H, C_6H_4); ms (70 eV, 30°C), *m/e* (‰): 216 (330, $M^{+\cdot}$), 188 (250, $M^{+\cdot} - N_2$), 135 (1000), 133 (455, $M^{+\cdot}$ − O=C=CH—N_3), 84.4 (M*, 216 → 135).

Tricyclic β-Lactam ***16***

To mesylate **12** (400 mg, 0.72 mmol) in dry THF (30 mL) at 0°C was added dropwise *n*-Bu_4NF (0.76 mmol) in dry THF (10 mL), over 15 min. Dilution with pH 4.5 buffer (KH_2PO_4, 40 mL) and extraction with ether (3 × 50 mL) afforded, after chromatography of the residue on SiO_2 (CH_2Cl_2), 226 mg (91%) of tricyclic β-lactam **16** as a pale yellow oil which crystallized on standing, mp 69–70°C; ir (film) ν_{max}: 2900, 2100 (N_3), 1775 (C=O) cm^{-1}; ^{1}Hmr ($CDCl_3$) δ: 0.22, 0.30 (2s, 6H, $SiMe_2$), 1.0 (s, 9H, *t*-BuSi), 3.95 (m, 2H, CH_2), 4.56 (m, 1H, C*H*—CH_2), 5.24 (d, 1H, CHN_3, *J* = 5 Hz), 6.55–6.94 (m, 3H, C_6H_3).

Procedure B

To mesylate **12** (3.42 g, 6.2 mmol) in dry CH_3CN (80 mL) was added anhydrous KF (0.43 g, 7.4 mmol) and 18-crown-6 (0.49 g, 1.9 mmol). Upon completion of the reaction, as indicated by tlc (6–8 h), the solution was diluted with water (100 mL) and extracted with CH_2Cl_2 (3 × 80 mL), which was then washed with brine (100 mL), dried ($MgSO_4$), and evaporated to give 2.0 g (95%) of tricyclic β-lactam **16**, after chromatography.

Amino β-Lactam ***16a***

Into azide **16** (2.1 g, 6.1 mmol) dissolved in CH_2Cl_2 (80 mL) and Et_3N (0.61 g, 6.1 mmol) at 0°C was bubbled H_2S for 10 min. The solution was allowed to warm, and after stirring for 1 h at room temperature, nitrogen was bubbled through the solution for 0.5 h. The solution was then washed with H_2O (2 × 50 mL) and brine (50 mL), then dried ($MgSO_4$), and evaporated. The oily residue was flash chromatographed on silica gel, using ethyl acetate – petroleum ether (3:1), affording 1.65 g (85%) of amine **16*a*** as a white solid, mp 135–136°C (recrystallized from ether); ir (film) ν_{max}: 3400 and 3330 (NH_2), 2900, 1765 (C=O) cm^{-1}; ^{1}Hmr (C_6D_6) δ: 0.22, 0.30 (2s, 6H, $SiMe_2$), 0.9 (bs, 2H, NH_2), 1.13 (s, 9H, *t*-BuSi), 3.15 (ddd, 1H, O—CH_2—C*H*, *J* = 3.5, 4.6, 10 Hz), 3.5 (dd (apparent triplet), 1H, O—C*H*H—CH, *J* = 10, 10 Hz), 3.95 (bs, 1H, C*H*NH_2), 4.1 (dd, 1H, O—CH*H*—CH, *J* = 3.5, 10 Hz), 6.4–6.9 (m, 3H, C_6H_3); ms (70 eV, 51°C), *m/e* (‰): 320 (22, $M^{+\cdot}$), 305 (54, $M^{+\cdot} - CH_3$), 292 (428), 263 (1000, $M^{+\cdot} - 57$), 248 (290, $M^{+\cdot} - 15 - 57$), 235 (314), 216.2 (M*, 320 → 263), 189.1 (M*, 292 → 235). *Anal.* calcd. for $C_{16}H_{24}N_2O_3Si$: C 59.97, H 7.55, N 8.74; found: C 59.59, H 7.61, N 8.74.

β-Lactam Amide ***17***

To amine **16*a*** (640 mg, 2 mmol) and Et_3N (242 mg, 2.4 mmol)

in CH_2Cl_2 (20 mL) at 0°C was added dropwise phenylacetyl chloride (370 mg, 2.4 mmol) in CH_2Cl_2 (5 mL), over a period of 5 min. The solution was allowed to warm and, after stirring for 1 h at room temperature, was washed with pH 4.5 buffer (20 mL) and H_2O (20 mL), dried ($MgSO_4$), and evaporated. Chromatography of the residue on SiO_2, eluting successively with CH_2Cl_2, $CHCl_3$, and ether, afforded 750 mg (86%) of amide **17** as fine needles from ether, mp 161–162°C; ir (film) ν_{max}: 3300 (NH), 2900, 1780 (β-lactam), 1670 (amide) cm^{-1}; ^{1}Hmr 200 MHz ($CDCl_3$) δ: 0.15, 0.22 (2s, 6H, $SiMe_2$), 0.96 (s, 9H, *t*-BuSi), 3.56 (s, 2H, CH_2Ph), 3.62 (dd, 1H, C*H*H—CH, J = 10, 10 Hz), 3.93 (ddd, 1H, CH_2CH, J = 3.5, 5.0, 10 Hz), 4.38 (dd, 1H, CH*H*—CH, J = 3.5, 10 Hz), 5.46 (dd, 1H, C*H*NH, J = 5, 7 Hz), 6.4 (2 dd, 2H, C*H*—CH—C*H* on C_6H_3, J = 1, 8 Hz), 6.53 (bd, 1H, NH, J = 7 Hz), 6.83 (dd, 1H, CH—C*H*—CH, on C_6H_3, J = 8, 8 Hz), 7.25 (m, 5H, C_6H_5); ms (70 eV, 91°C), *m/e* (‰): 438 (311, $M^{+\cdot}$), 423 (26, $M^{+\cdot} - CH_3^{\cdot}$), 381 (130, $M^{+\cdot} - t$Bu$^{\cdot}$), 264 (1000), 206 (732), 159.1 (M*, 438 → 264), 111.4 (M*, 381 → 206).

Phenol β-*Lactam* ***18***

To silyl ether **17** (240 mg, 0.55 mmol) in dry THF (15 mL) at 0°C was added *n*-Bu_4NF (0.61 mL, 1 *M*), in dry THF (4 mL), dropwise over 10 min. After stirring for 15 min, pH 4.5 buffer (15 mL) was added, and half the THF removed under reduced pressure. Extraction with ethyl acetate (30 mL) followed by evaporation afforded 92 mg (52%) of phenolic β-lactam **18** as fine needles, mp 194–195°C, from ethyl acetate – petroleum ether; ir (Nujol) ν_{max}: 3280 (NH, OH), 1760 (β-lactam), 1655 (amide) cm^{-1}; ^{1}Hmr 200 MHz ($OC(CD_3)_2$) δ: 3.62 (s, 2H, CH_2Ph), 4.07 (dd, 1H, C*H*HCH, J = 10, 10 Hz), 4.18 (ddd, 1H, CH_2CH, J = 3.3, 4.5, 10 Hz), 4.47 (dd, 1H, CH*H*CH, J = 3.3, 10 Hz), 5.66 (dd, 1H, C*H*NH, J = 4.5, 8 Hz), 6.50 (2dd, 2H, C*H*—CH—C*H* on C_6H_3, J = 1, 8 Hz), 6.92 (dd, 1H, CH—C*H*—CH on C_6H_3, J = 8, 8 Hz), 7.32 (m, 5H, C_6H_5), 7.99 (bd, 1H, NH, J = 8 Hz); ms (70 eV), *m/e*(‰): 324 (103, $M^{+\cdot}$), 205 (12, $M^{+\cdot} - PhCH_2CO^{\cdot}$), 175 (30), 149 (54), 150 (1000), 91 (398).

Hydroxy Phenol β-*Lactam* **20** was prepared as described for **18**, 97% yield, mp 174–175°C dec. (corr.); ir (CH_3CN) ν_{max}: 3400 (OH, NH), 1720 (β-lactam), 1680 (amide) cm^{-1}; ^{1}Hmr ($OC(CD_3)_2$) δ: 3.1 (b, 2H, 2 OH), 3.80 (s, 2H, CH_2Ph), 4.07 (*ABCX*, 2H, CH_2OH, J = 2.5, 3.0, 12.5 Hz), 4.75 (ABC*X*, 1H, C*H*—CH_2, J = 2.5, 3.0, 5.0 Hz), 5.72 (ABC*X*, dd, 1H, C*H*—NH, J = 5.0, 10 Hz), 6.8–7.7 (m, 10H, C_6H_4, C_6H_5, NH); gc–ms (TMS derivative) (70 eV), *m/e* (‰): component 1: 542 (4, $M^{+\cdot}$, tri-TMS derivative), 527 (17, $M^{+\cdot} - CH_3^{\cdot}$), 439 (30, $M^{+\cdot}$ – TMS—O—$CH_2^{\cdot}$), 335 (210, $M^{+\cdot}$ – TMS—O—Ar—N=C=O); component 2: 470 (56, $M^{+\cdot}$, di-TMS derivative), 455 (24, $M^{+\cdot} - CH_3^{\cdot}$), 296 (1000, $M^{+\cdot} - 174$).

Amide Mesylate 21

Hydrogen sulfide was bubbled through a solution of azido mesylate **12** (796 mg, 1.4 mmol) and Et_3N (0.2 mL, 1.4 mmol) in CH_2Cl_2 (75 mL) at 0°C for 10 min. The cooling bath was removed and stirring continued for 1 h, then nitrogen was flushed through the solution for 0.5 h. To this solution at 0°C was added Et_3N (0.26 mL, 1.8 mmol) followed by dropwise addition of phenylacetyl chloride (287 mg, 1.8 mmol) over 5 min. After stirring for 1 h at ambient temperature, the solution was washed with H_2O (3 × 50 mL) and brine (50 mL), then treated with $MgSO_4$ and charcoal, filtered, and evaporated to give 735 mg (79%) of crystalline amide **21**, upon trituration with hexane, mp 129–130°C; ir (CH_2Cl_2) ν_{max}: 3310 (NH), 1775 (β-lactam), 1685 (amide) cm^{-1}; ^{1}Hmr ($CDCl_3$) δ: 0.20 (s, 12H, $SiMe_2$), 0.95 (s, 18H, *t*-BuSi), 2.80 (s, 3H, CH_3SO_2), 3.68 (s, 2H, CH_2Ph), 4.15–4.60 (m, 3H, CH_2CH), 5.35 (dd, 1H, C*H*NH, J = 4.4, 7 Hz), 6.0 (bd, 1H, NH, J = 7 Hz), 6.4–7.2 (m, 3H, C_6H_3), 7.37 (s, 5H, C_6H_5); ms (70 eV, 116°C), *m/e* (‰): 537 (8), 512 (23, $M^{+\cdot} - t$Bu$^{\cdot} - SO_2CH_3^{\cdot}$), 495 (131), 322 (1000).

Azido β-*Lactam* ***24***a

2-*tert*-Butyldimethylsiloxy-5-nitroaniline (7.5 g, 28 mmol) and cinnamaldehyde (4.1 g, 31 mmol), in benzene (100 mL) containing a trace of *p*-TsOH, were refluxed for 2 days using a Dean–Stark trap. The solvent was then evaporated and replaced by CH_2Cl_2 (250 mL). To this solution, at −20°C, was added triethylamine (3.7 g, 36 mmol) followed by dropwise addition of azidoacetyl chloride (4.3 g, 36 mmol), in CH_2Cl_2 (50 mL), over 1 h. The red-brown solution was stirred for an additional hour at −20°C, then allowed to warm up. Washing with water (2 × 200 mL), brine (200 mL), and drying ($MgSO_4$), then treating with charcoal and evaporating the solvent afforded 6.9 g (53%) of β-lactam ***24a*** as a pale yellow solid; mp 109–110°C (ether – petroleum ether); ir (film) ν_{max}: 2100 (N_3), 1770 (β-lactam) cm^{-1}; ^{1}Hmr (C_6D_6) δ: 0.10 (s, 6H, $SiMe_2$), 0.93 (s, 9H, *t*-BuSi), 4.35 (d, 1H, CH—N_3, J = 5.5 Hz), 4.58 (dd, 1H, C*H*—CHN_3, J = 5.5, 7.0 Hz), 5.9–6.7 (m, 2H, CH=CH), 6.42 (d, 1H, C_6H_3), 7.16 (m, 5H, C_6H_5), 7.60 (dd, 1H, C_6H_3), 8.46 (d, 1H, C_6H_3).

Azido β-*Lactam* ***24***b

tert-Butyldiphenylsilyl ether β-lactam ***24b*** was obtained, using the same procedure as for ***24a***, in 58% yield as fine white crystals, mp 159.5–160°C corr. (ether – petroleum ether); ir (film) ν_{max}: 2100 (N_3), 1780 (β-lactam) cm^{-1}; ^{1}Hmr (C_6D_6) δ: 1.22 (s, 9H, *t*-BuSi), 4.50 (m, 2H, CH—CHN_3), 6.33 (m, 3H, CH=CH, and C_6HH_2), 7.16 and 7.76 (2m, 16H, 3 C_6H_5 and C_6HH_2), 8.16 (d, 1H, C_6H_3).

Nitro Derivatives: 28 and 30

To a solution of **16** (574 mg, 1.6 mmol) in dry acetonitrile (20 mL) under nitrogen atmosphere at −20°C, nitronium tetrafluoroborate (3.2 mL, 0.5 *M* solution in sulfolane) was added dropwise. After 1 h, dry benzene (10 mL) was added and the mixture was stirred for 10 more minutes. The reaction mixture was then poured (while still very cold) into 30 mL of pH 4.5 buffer and extracted twice, dried ($MgSO_4$), and evaporated. The *ortho*-, *nitro*-, and *para*-nitrosilyl ether compounds were isolated and crystallized, after flash chromatography. The remaining mixture of nitrophenols was separated from sulfolane via Kugelrohr distillation, resilylated, and purified by flash chromatography to afford more of the desired products.

ortho-Silyl ether **28**, mp 109–110°C; ir (film) ν_{max}: 2100 (N_3), 1795 (β-lactam) cm^{-1}; ^{1}Hmr (C_6D_6) δ: 0.2 (s, 3H, $SiCH_3$), 0.3 (s, 3H, $SiCH_3$), 1.1 (s, 9H, *t*-Bu), 2.6–2.9 (ddd, 1H, CH_2—C*H*), 2.9–3.3 (dd, 1H, CH*H*—CH, J = 10, 10 Hz), 3.8–4.0 (dd, 1H, C*H*H—CH, J = 3, 10 Hz), 4.05 (d, 1H, CHN_3, J = 4.5 Hz), 6.15 (d, 1H, C_6HH, J = 9 Hz), 7.43 (d, 1H, C_6HH, J = 9 Hz); ms, *m/e*: 334 ($M^{+\cdot} - t$-Bu$^{\cdot}$), 306 ($M^{+\cdot} - t$-Bu$^{\cdot} - N_2^{\cdot}$), 260 ($M^{+\cdot} - OSi(CH_3)_2C(CH_3)_3^{\cdot}$), 251 ($M^{+\cdot} - t$-Bu$^{\cdot}$ – O=C=CHN_3).

para-Silyl ether **30**, mp 122–123°C; ir (film) ν_{max}: 2100 (azide), 1785 (β-lactam) cm^{-1}; ^{1}Hmr (C_6D_6) δ: 0.03 (s, 3H, $SiCH_3$), 0.15 (s, 3H, $SiCH_3$), 1.7 (s, 9H, *t*-Bu), 2.66–3.0 (ddd, 1H, CH_2—C*H*, J = 4, 5, 10 Hz) 3.15–3.45 (dd, 1H, C*H*H—CH, J = 10, 10 Hz), 3.7–3.9 (dd, 1H, CH*H*—CH, J = 4, 10 Hz), 4.1 (d, 1H, CHN_3, J = 5 Hz), 6.15 (d, 1H, C_6HH, J = 9 Hz), 7.35 (d, 1H, C_6HH, J = 9 Hz); ms *m/e*: 334 ($M^{+\cdot} - t$-Bu$^{\cdot}$), 306 ($M^{+\cdot} - t$-Bu$^{\cdot} - N_2^{\cdot}$), 251 ($M^{+\cdot} - t$-Bu$^{\cdot}$ – O=C=CHN_3). *Anal.* calcd. for $C_{16}H_{21}N_5O_5Si$: C 49.10, H 5.37, N 17.90; found: C 48.91, H 5.50, N 17.72.

p-*Nitro Silyl Ether* ***30***b

A mixture of *ortho*- and *para*-nitrophenols ***28a*** and ***30a*** (138 mg, 0.5 mmol), *tert*-butyldiphenylsilyl chloride (165 mg, 0.6 mmol), and imidazole (82 mg, 1.2 mmol), in dry dimethylformamide (5 mL) was stirred at room temperature for 15–20 h.

The reaction mixture was then added to ethyl ether (100 mL), washed with water and brine, dried ($MgSO_4$), and evaporated to dryness to give crude product **30***b* which was crystallized from CH_2Cl_2 – petroleum ether (100 mg, 45%), mp 153–154°C. The water–brine layer was further extracted with ethyl acetate in order to isolate *ortho*-nitrophenol **28***a* and decomposition products; ^{1}Hmr (C_6D_6) δ: 1.1 (s, 9H, $C(CH_3)_3$), 3.15–3.5 (ddd, 1H, CH_2—C*H*, *J* = 4, 5, 10 Hz), 3.65–4.0 (dd, 1H, C*H*H—CH, *J* = 10, 10 Hz), 4.3–4.55 (dd, 1H, CH*H*—CH, *J* = 4, 10 Hz), 4.65 (d, 1H, CHN_3, *J* = 5 Hz), 6.47 (d, 1H, C_6HH, *J* = 9 Hz), 7.2–7.7 (m, 11H, C_6HH, 2Ph).

β-*Lactam Amines 31 and 33*a

Hydrogen sulphide was bubbled into a solution of azides **28** and **30** (mixture) (170 mg, 0.45 mmol) and triethylamine (49 mg, 0.5 mmol) in dry methylene chloride (10 mL) at 0°C. After 1 h of stirring at room temperature the solution was purged with nitrogen, washed with water (2 × 10 mL), dried, and evaporated to give a crude yellow oily product (140 mg); ir (film) ν_{max}: 3350 (amine), 1780 (β-lactam) cm^{-1}; ^{1}Hmr (acetone-d_6) δ: 0.3 (2s, 6H, $Si(CH_3)_2$), 1.0 (s, 9H, $C(CH_3)_3$), 2.9 (bs, 2H, NH_2), 4.0–4.3 (m, 2H), 4.7–4.9 (m, 1H), 5.5–5.6 (dd, 1H, C*H*NH_2), 6.5–6.7 (2d, 1H, C_6HH), 7.6 (d, 1H, C_6HH).

Phenylacetamido Silyl Ether 32

Hydrogen sulphide was bubbled into a solution of azide **30***b* (140 mg, 0.3 mmol) and triethylamine (0.05 mL) in methylene chloride (10 mL) at 0°C for 3–5 min. After 1 h, the solution was purged with nitrogen. To the crude product **33***b*, in methylene chloride (10 mL) and triethylamine (0.05 mL) at 0°C, was added dropwise phenylacetyl chloride (0.06 g, 0.4 mmol). After stirring for 1 h the solution was washed with pH 4.5 buffer (10 mL), water (10 mL), dried ($MgSO_4$), and concentrated. The crude product **32** was crystallized from ethyl acetate – petroleum ether several times to obtain 100 mg (60%) of pale yellow crystalline product, mp 190–191°C; ir (film) ν_{max}: 1790 (β-lactam), 1710 (amide) cm^{-1}; ^{1}Hmr (DMSO-d_6) δ: 1.1 (s, 9H, $C(CH_3)_3$), 3.5 (s, 2H, $COCH_2Ph$), 3.3–3.7 (m, 1H, CH_2—C*H*), 3.8–4.2 (dd, 1H, C*H*H—CH, *J* = 10, 10 Hz), 4.3–4.6 (dd, 1H, CH*H*—CH, *J* = 4, 10 Hz), 5.1–5.3 (dd, 1H, C*H*—NHCO, *J* = 5, 8 Hz), 6.6 (d, 1H, C_6HH, *J* = 9 Hz), 7.2 (s, 10H, $SiPh_2$), 7.2–7.7 (m, 5H, —CH_2Ph), 8.0 (bd, 1H, NH, *J* = 8 Hz), 8.7 (d, 1H, C_6HH, *J* = 9 Hz).

Acknowledgements

We wish to thank the Natural Sciences and Engineering Research Council of Canada and Lederle Laboratories for financial support, Ms. Kuck for biological tests, Roger Simoneau for the 100 MHz spectrum, and Dr. O Mamer for the mass spectra.

1. G. JUST and R. ZAMBONI. Can. J. Chem. **56**, 2720 (1978).
2. T. W. DOYLE. Can. J. Chem. **55**, 2714 (1977).
3. H. B. KAGAN, J. J. BASSELIER, and J. L. LUCHE. Tetrahedron Lett. 941 (1964).
4. J. PLESS. J. Org. Chem. **39**, 2644 (1974).
5. G. JUST, A. UGOLINI, and R. ZAMBONI. Synth. Commun. **9**, 117 (1979).
6. H. BUDZIKIEWICZ, C. DJERASSI, and D. H. WILLIAMS. Mass spectrometry of organic compounds. Holden-Day, Inc., U.S.A. 1967.
7. A. J. GORDON and R. A. FORD. The chemist's companion. John Wiley & Sons, New York. 1972.
8. E. J. COREY and A. VENKOTESWARLU. J. Am. Chem. Soc. **94**, 6190 (1972).

Cation mobilities in C_1–C_4 hydrocarbon gases at densities up to the critical

NORMAN GEE AND GORDON R. FREEMAN

Chemistry Department, University of Alberta, Edmonton, Alta., Canada T6G 2G2

Received February 5, 1981

This paper is dedicated to Professor W. E. Harris on the occasion of his retirement from the University of Alberta

NORMAN GEE and GORDON R. FREEMAN. Can. J. Chem. **59**, 2988 (1981).

The temperature coefficient of cation mobility, $d\mu/dT$, at constant gas density n, is positive and increases with increasing n. The increase of temperature coefficient is attributed to the clustering of molecules about the ion. However, the temperature coefficient is positive even for the mass-identified, unclustered CO_3^- ion in N_2 gas (Eisele, Perkins, and McDaniel. J. Chem. Phys. 1980). The energy dependence of the cross section for the scattering of CO_3^- by N_2 was deconvoluted from the $(\mu n, T)$ data. The cross section decreases with increasing energy in a manner that implies sticky collisions (associative interactions) at energies < 0.1 eV, and essentially hard core collisions at higher energies. The scattering of CH_5^+(?) ions by CH_4 behaves similarly. The cross section in methane is larger than that predicted by the simple polarization potential at all energies. In the low density gas the ion mobility is controlled by collision with one molecule at a time, and $\mu n \approx$ constant. In the dense liquid the mobility is governed mainly by viscosity, and $\mu\eta \approx$ constant. The transition region is $0.3 \lesssim n/n_c \lesssim 2.0$, which corresponds to $0.5 \lesssim \eta/\eta_c \lesssim 3$. A plot of $\mu\eta$ against η for several hydrocarbons ranging from methane to n-hexane is nearly independent of molecular size in both the liquid and gas phases.

NORMAN GEE et GORDON R. FREEMAN. Can. J. Chem. **59**, 2988 (1981).

Le coefficient de température de la mobilité du cation, $d\mu/dT$, pour une densité constante n de gaz est positif et augmente avec n. On attribue l'augmentation du coefficient de température à l'entassement des molécules autour de l'ion. Cependant le coefficient de température est positif même pour l'ion CO_3^- dans l'azote gazeux qui d'après la masse ne subirait pas d'entassement des molécules (Eisele, Perkins, and McDaniel. J. Chem. Phys. 1980). A partir des données $(\mu n, T)$, on a déduit l'effet de l'énergie sur la section droite lors de la dispersion du CO_3^- par l'azote. On déduit de la relation entre la diminution de la section droite avec une augmentation de l'énergie qu'il existe des collisions avec association (interactions associatives) à des énergies $< 0{,}1$ eV et ces collision sont essentiellement fortes qu'aux énergies plus grandes. La dispersion des ions CH_5^+(?) par le CH_4 présente un comportement semblable. La section droite dans le méthane est plus grande que celle prévue par le potentiel de polarisation simple à toutes les énergies. Dans les gaz à faible densité, la mobilité de l'ion est contrôlée par la collision avec une molécule a la fois et à un $\mu n \approx$ constante. Dans le cas des liquides denses la mobilité dépend principalement de la viscosité et de $\mu n \approx$ constante. La région de transition est de $0{,}3 \lesssim n/n_c \lesssim 2{,}0$ qui correspond à $0{,}5 \lesssim \eta/\eta_c \lesssim 3$. Une courbe de $\mu\eta$ en fonction η pour plusieurs hydrocarbures allant du méthane au n-hexane est presqu'indépendante de la taille des molécules dans les phases liquide et gazeuse.

[Traduit par le journal]

Introduction

The mobility μ of cations is chiefly limited by the viscosity η in the liquid phase (1–9) and by the density n in the dilute gas (6, 7, 10, 11). Relatively few attempts have been made to connect the liquid and gas phase behaviors (10, 12). We had recently examined the variation of $\mu\eta$ over the entire liquid range up to the critical region for eight C_1 to C_4 hydrocarbons (9). The $\mu\eta$ values were only slightly dependent on the nature of the molecules. Plots of $\mu\eta$ against η^{-1} usually contained a broad maximum with $\mu\eta \approx 3 \times 10^{-3}$ cm^2 mP/V s in the vicinity of 1 mP^{-1}. With increasing temperature and concomitant decreasing liquid density and viscosity, $\mu\eta$ first increases due to increasing ion mean free path, then decreases as the critical region is approached, due to increasing liquid compressibility and consequent electrostriction about the ion (9). The study has now been extended through the critical fluid into the dense gas and to progressively lower densities.

Measurements of mobility were also made as a function of temperature at several constant densities.

Experimental

The experimental procedures have been previously reported (5–7, 9). The electrodes in the present cells were always in the gas phase.

Briefly, the fluid in a parallel plate cell was irradiated by a 100 ns pulse of 1.7 MeV X rays ($\approx 1 \times 10^{10}$ eV/g). Data collection was controlled by a Texas Instruments 980A minicomputer. The electrons were swept from the gas by the electric field in a time about 1000-fold less than the ion time. Both the electron and ion currents were integrated, giving a charge vs. time signal. The signal was amplified with a Princeton Applied Research 113 preamplifier. From 4 to 32 signals were averaged using a Fabritek 1062 or Nicolet 1170 signal averager. The final result was drawn on a Zeta Research Incorp. 1200 plotter. Representative traces are given in Fig. 1. The initial sharp rise is due to collection of the electrons. The collection time of the ions equals the drift time of the ions. The ion mobility is given by the drift distance (cell gap) divided by the product of drift time t_D and electric field strength. Both the drift distance and electric field strength have errors of less than 1%. The major source of error is the determination of t_D from the charge vs. time plots.

Gas densities were obtained from ref. 13, except for cyclopropane which were obtained as described in ref. 14. Viscosities were obtained from ref. 15, except for ethene which were taken

0008-4042/81/202988-09$01.00/0

©1981 National Research Council of Canada/Conseil national de recherches du Canada

Can. J. Chem. Downloaded from www.nrcresearchpress.com by 210.87.254.5 on 09/06/12
For personal use only.

Can. J. Chem. Downloaded from www.nrcresearchpress.com by 210.87.254.5 on 09/06/12
For personal use only.

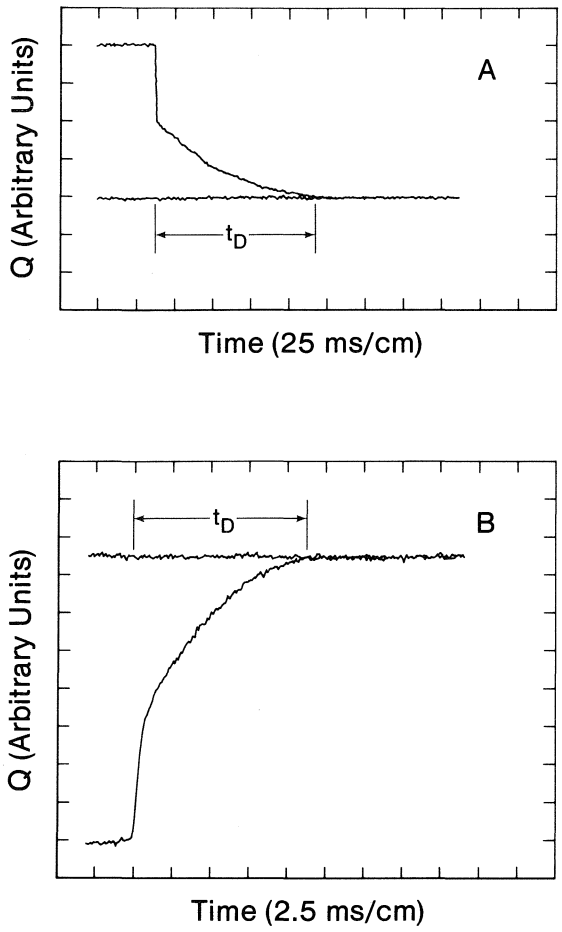

FIG. 1. Collected charge as a function of time. The densities (10^{20} molecules/cm^3), temperatures (K), and applied voltages (V) were: *A*, 3.4, 365, −20; *B*, 8.2, 349, +500. The sample *A* was *n*-butane and *B* was propene. The drift distance was 0.322 ± 0.003 cm.

from ref. 16, and liquid *i*-butane which were obtained as described in ref. 9. Only viscosities based on experimental measurements were used. The critical temperatures, densities, and viscosities are listed in Table 1.

Results

The cation mobilities in each of the eight gases at all densities were independent of applied electric field strength up to the highest field used, ~ 1 Td. Examples of the data are shown in Fig. 2. Each point is the average of the positive and negative applied voltage results. The average deviation of μ for the ~ 6 data points at a given n and T was usually ~ 3%, but ranged from 1–6%.

Arrhenius plots of the mobilities at different densities are displayed for methane and ethane (Fig. 3), ethene and propene (Fig. 4), propane and cyclopropane (Fig. 5), *n*-butane and *i*-butane (Fig. 6). The number beside each constant density curve is n (10^{20} molecules/cm^3). The highest density for each system is the critical. The triangles represent mobilities in the coexistence vapors, the densities of which increase with temperature.

At constant density $d\mu/dT$ was positive in all systems. The coefficient increases with density (Figs. 3–6). This density effect was previously observed for cations in benzene and toluene vapors and was attributed to clustering of molecules about the cations (7).

The upper half of the coexistence curve (triangles) for each compound in Figs. 3–6 corresponds to a negative Arrhenius parameter ($-E$ = 8.4 kJ/mol for methane, ~ 15 kJ/mol for the C_2's, ~ 20 kJ/mol for the C_3's, and 24 kJ/mol for the C_4's) that is 5–20% larger than the heat of vaporization of the compound at the corresponding temperature. If there were no clustering of molecules about the ion, the positive $d\mu/dT$ at constant n would have caused the negative Arrhenius parameter from the triangles in Figs. 3–6 to be slightly smaller than the heat of vaporization of the corresponding compound.

The density normalized mobility μn is plotted against n for the coexistence vapors and liquids (9) in Fig. 7. The slightly negative slopes at low densities are consistent with the clustering, but the concomittant increase of temperature with n keeps the overall effect on μn small. At $n/n_c \gtrsim 0.3$ the value of μn increases. There is no special effect at

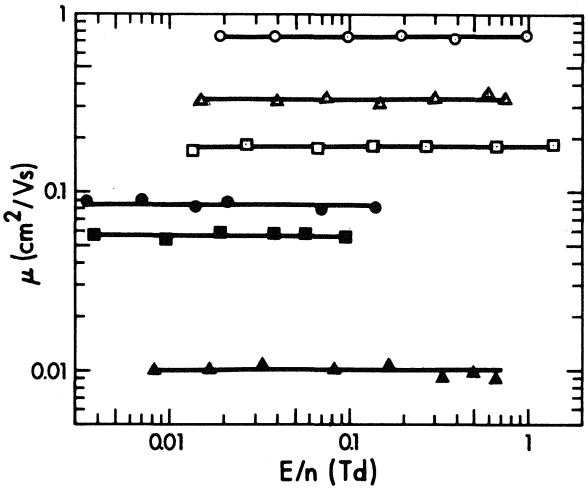

FIG. 2. Cation mobilities μ as functions of density normalized electric field strength E/n in gaseous hydrocarbons. The densities (10^{20} molecules/cm^3) and temperatures (K) were as follows: CH_4: ○, 0.53, 108; ●, 4.66, 144; C_2H_6: △, 0.68, 197; ▲, 19.0, 296; *n*-C_4H_{10}: □, 0.76, 370; ■, 1.64, 333. The average % deviations are (top to bottom): 1.2, 1.9, 2.0, 4.8, 2.7, and 5.6.

Can. J. Chem. Downloaded from www.nrcresearchpress.com by 210.87.254.5 on 09/06/12
For personal use only.

TABLE 1. Gas phase ion mobilities compared to the polarization limit. Values of T_c, n_c, and η_c are listed for convenience

Gas	T_c (K)	n_c (10^{19} molecules/cm^3)	η_c (μP)	α[a] (10^{-24} cm^3)	M_r[b] (g/mol)	$n\mu_{pol}$[c] (10^{19} molecules/cm V s)	$n\mu_{expt}$[d] (10^{19} molecules/cm V s)	expt/pol
CH_4	190.6	608	162	2.6	16	5.8	3.8	0.66
C_2H_4	282.7	472	216	4.0	28	3.5	1.8	0.52
C_2H_6	305.5	407	210	4.4	30	3.3	1.8	0.55
C_3H_6-1	365.1	333	230	5.8	42	2.4	1.2	0.50
c-C_3H_6	398	354		5.5[e]	42	2.5	1.4	0.56
C_3H_8	370.0	301	226	6.2	44	2.3	1.2	0.52
n-C_4H_{10}	425.2	236	243	8.0	58	1.73	0.92	0.53
i-C_4H_{10}	408.1	230	215	8.0	58	1.73	0.95	0.55
c-C_5H_{10}[b]	511.8	232		9.0	70	1.49	0.93	0.63
C_6H_6[g]	562.6	233		9.9	78	1.34	0.63	0.47
c-C_6H_{12}[f]	554	195		10.8	84	1.24	0.80	0.65
n-C_6H_{14}[f]	507.8	164	272	11.6	86	1.18	0.64	0.54
$CH_3C_6H_5$[g]	594.0	190		12.0	92	1.12	0.60	0.53

[a] Reference 24.
[b] Assuming heavily clustered ions, M_r = molecular mass. For monomeric ions M_r = 0.5 molecular mass, $n\mu_{pol}$ would be 1.41 times and (expt/pol) would be 0.71 times the values listed.
[c] Equation [4].
[d] At the minimum of $n\mu$, near $n = 4 \times 10^{20}$ molecules/cm^3 in the coexistence vapor (Fig. 6).
[e] Reference 25.
[f] Reference 6.
[g] Reference 7.

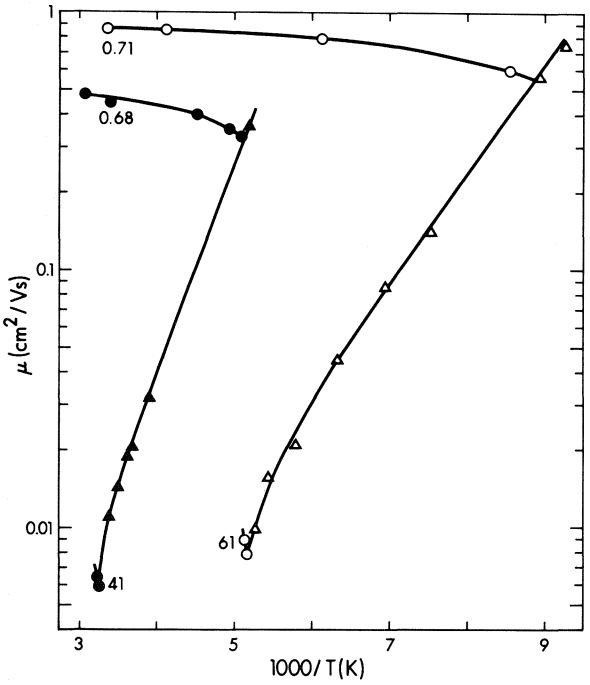

FIG. 3. Arrhenius plots of cation mobilities in methane (open symbols) and ethane (solid symbols). Triangles represent vapor in equilibrium with liquid. Circles represent constant density gas; the numbers labelling the curves give the density n in units of 10^{20} molecules/cm^3.

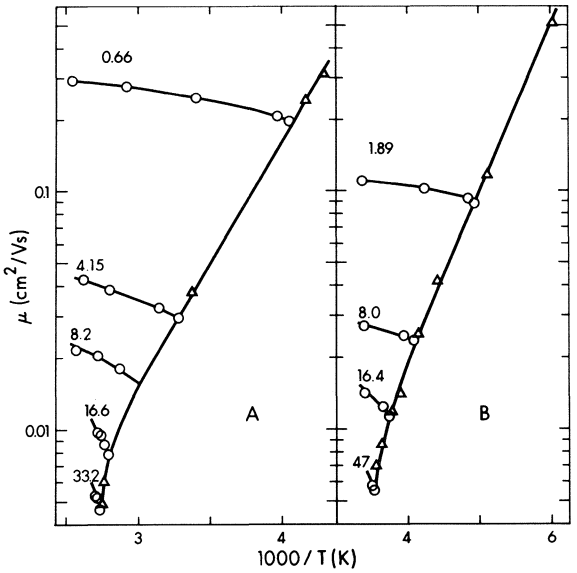

FIG. 4. Arrhenius plots of cation mobilities in propene (A) and ethene (B). The symbols have the same meanings as in Fig. 2.

the critical point (7, 17), in agreement with theory (18).

The density variation of μn at constant temperature (T_c + 2) K is shown in Fig. 8. The curves are similar to those in Fig. 7, but the low density ends are raised somewhat.

The uncertainty in n is ~6% at $n < 1 \times 10^{20}$ molecules/cm^3, and is smaller at higher n for all the gases. The uncertainty in μn is therefore ~9%.

Discussion

(A) Low Density Gas

Previous measurements indicated that the mobility was independent of field strength below about 600 Td in methane (19) and below about 130 Td in ethane (20) at 293 K and $n < 10^{19}$ molecules/cm^3. The present measurements (Fig. 2) were at fields two orders of magnitude lower than those used

Can. J. Chem. Downloaded from www.nrcresearchpress.com by 210.87.254.5 on 09/06/12
For personal use only.

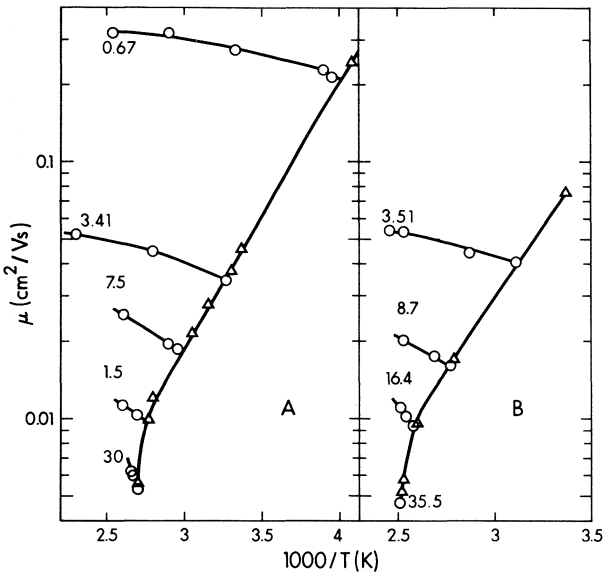

FIG. 5. Arrhenius plots of cation mobilities in propane (*A*) and cyclopropane (*B*). The symbols have the same meanings as in Fig. 2.

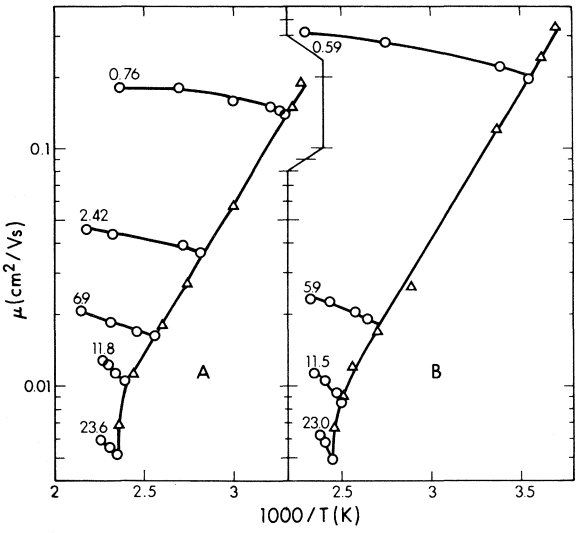

FIG. 6. Arrhenius plots of cation mobilities in *n*-butane (*A*) and *i*-butane (*B*). The symbols have the same meanings as in Fig. 2.

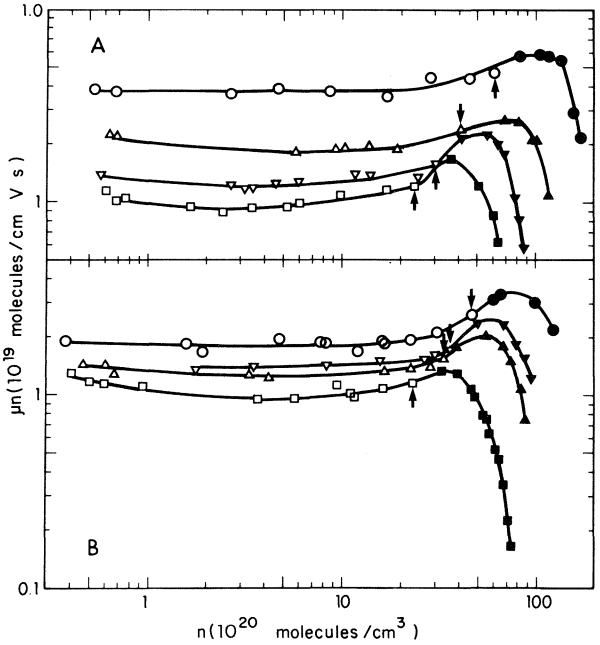

FIG. 7. Density normalized mobility μn as a function of n in the coexistence vapors (open points) and liquids (solid points). The arrows indicate n_c. *A*: ○, methane; △, ethane; ▽, propane; □, *n*-butane. *B*: ○, ethene; △, propene; ▽, cyclopropane; □, *i*-butane.

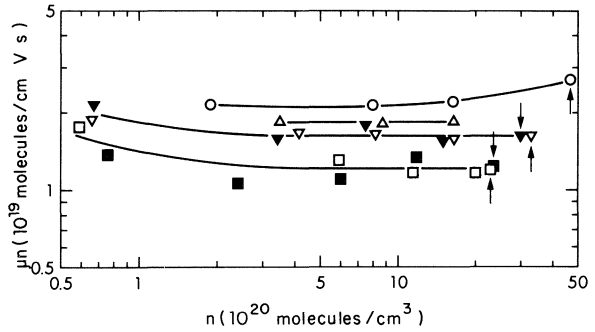

FIG. 8. Density normalized mobility μn as a function of n in the gas at $(T_c + 2)$ K. The arrows indicate n_c. ○, ethene; △, cyclopropane; ▽, propene; ▼, propane; □, *i*-butane; ■, *n*-butane.

earlier and were far below the field dependence threshold. The previously reported low field mobilities correspond to μn (10^{19} molecules/cm V s) values of 6.9 (19), 6.0 (21*a*), and 5.9 (21*b*) in methane, compared to the present 6.1, 2.5 (20) in ethane compared to the present 3.1, and 1.6 (21*a*) in isobutane compared to the present 1.3, in the low density gases at 294 ± 1 K. The differences between the sets are ±2 to 23%. The high value for methane in ref. 19 is attributed to the high field used (see later). The gas densities used in ref. 21*a* were two orders of magnitude lower than our lowest, so clustering in our isobutane sample at 295 K probably contributed to the lower value of μn for that compound.

The present ion drift times were $\sim 10^{-3}$ s. Ion–molecule reaction cross sections in hydrocarbons are typically 10^{-15}–10^{-14} cm² (22), so at $n \approx 10^{20}$ molecules/cm³ and $T \approx 10^2$ K the initial ions would be altered by reaction in $\sim 10^{-10}$ s. Clustering would also reach equilibrium at a time $\ll 10^{-3}$ s. One may therefore assume that the mobilities

Can. J. Chem. Downloaded from www.nrcresearchpress.com by 210.87.254.5 on 09/06/12
For personal use only.

measured were those of ions that could not undergo charge exchange, but whose masses and sizes changed several times according to [1] during the drift period:

[1] $M_m^+ + M \rightleftharpoons M_{m+1}^+$

where $m = 1, 2, \ldots$. The mass and size changes caused by ion–molecule reactions such as [2] may be neglected, while reactions such as [3] simply affect the value of m.

[2] $CH_4^+ + CH_4 \rightarrow CH_5^+ + CH_3$

[3] $C_2H_4^+ + C_2H_4 \rightarrow C_4H_8^+$

Scattering cross sections extracted from the mobilities are average values for the clusters present at the particular n and T.

(1) Scattering Cross Sections

Scattering by the polarization potential would give (23):

[4] $n\mu_{pol} = 3.73 \times 10^{20}/(\alpha M_r)^{1/2}$ molecules/cm V s

where α is the polarizability of the gas molecules M in units of 10^{-24} cm^3 (24, 25), M_r is the reduced mass of the drifting ion and a gas molecule in units of g/mol. The observed values of $n\mu$ are approximately half those predicted by [4], as illustrated in Table 1. It was assumed that the ions were heavily clustered, with M_r = molecular mass. If the ions are less heavily clustered the reduced mass is less than the molecular mass, for example, $M_r = 0.67 \times$ molecule mass when $m = 2$, then the ratio (expt/pol) is somewhat lower than the values listed in Table 1. The simple polarization potential is too small to explain the ion scattering, as had been noted in many other systems (6, 7, 23). The ratio $(n\mu_{expt}/n\mu_{pol})$ equals 0.53 ± 0.02 for nine of the thirteen alkanes, alkenes, cycloalkanes, and aromatics listed in Table 1. The exceptions were methane, cyclopentane, and cyclohexane for which (expt/pol) = 0.65 ± 0.02, and benzene for which the ratio equalled 0.47. The polarization interaction makes a major contribution to ion scattering in hydrocarbon vapors, but something else makes an approximately equal contribution.

Calculated mobilities can be brought into closer agreement with experimental values by adding a hard core to the polarization potential (23). This adjusts mainly for the facts that the ion is not a point charge and the molecule is not a perfectly polarizable sphere. The correction is especially important for polyatomic ions and molecules. However, when the cross section has been doubled by adding a hard core to the polarization potential the model predicts a negative temperature coefficient for the mobility (Fig. 1, ref. 23, $\mu/\mu_{pol} \approx 0.5$), which is the opposite of that observed experimentally (Figs. 3–6 and refs. 6, 7). Positive temperature coefficients have also been observed for certain simple ions such as CO_3^- (26), Rb^+ (27), and H_3^+ (28) in gases such as N_2, Ar, and H_2, respectively. The positive temperature coefficients might be interpreted in terms of short-lived association complexes (sticky collisions).

In low density gases the normalized mobility may be represented by the Chapman–Enskog equation (29, 30):

$$[5a] \quad n\mu = \frac{\frac{3e}{8M_r}\sqrt{\pi}\left(\frac{2kT}{M_r}\right)^{5/2}}{\int_0^\infty v^5\sigma_v \exp\left(-\frac{M_r v^2}{2kT}\right) dv}$$

or

$$[5b] \quad n\mu = \frac{\frac{3e}{8}(kT)^{5/2}\left(\frac{2\pi}{M_r}\right)^{1/2}}{\int_0^\infty \varepsilon^2\sigma_\varepsilon \exp\left(-\frac{\varepsilon}{kT}\right) d\varepsilon}$$

where e is the charge on the ion, M_r is the reduced mass, k is Boltzmann's constant, T is the absolute temperature, v is the relative velocity of the ion with respect to the molecule, and σ_v (or σ_ε) is the ion–molecule scattering cross section for velocity v (or energy ε). Equation [5] is equivalent to using an average cross section σ_{av} represented by [6].

[6] $\sigma_{av} = \langle v^3\sigma_v\rangle/\langle v^3\rangle = \langle \varepsilon^{3/2}\sigma_\varepsilon\rangle/\langle\varepsilon^{3/2}\rangle$

Sets of experimental ($n\mu$, T) values in the lowest density gases were used to extract apparent values of σ_v as functions of v in the trial and error manner described for electrons (31, 32). Data for the mass identified, unclustered CO_3^- ion in N_2 gas (ref. 26 and Fig. 9) were first analyzed to see the shape of a cross section curve for ions. The value of σ_v decreases with increasing v up to about 1.0 km/s (ε = 0.1 eV), then is relatively constant up to about 2.5 km/s or 0.6 eV (Fig. 10). The simple polarization potential leads to (ref. 33, eq. [42], $S^{(1)}$):

$$[7] \quad \sigma^{pol} = (2.2\pi/v)(e^2\alpha/M_r)^{1/2} = \pi\,(2.42e^2\alpha/\varepsilon)^{1/2} = 1.86 \times 10^{-15}\,(\alpha/\varepsilon)^{1/2} \quad \text{cm}^2$$

where α is in units of 10^{-24} cm^3 and ε is in eV. For CO_3^- in N_2 one obtains

[8] $\sigma^{pol} = 2.47 \times 10^{-15}\varepsilon^{-1/2}$ cm^2

Equation [8] cuts through the empirical cross

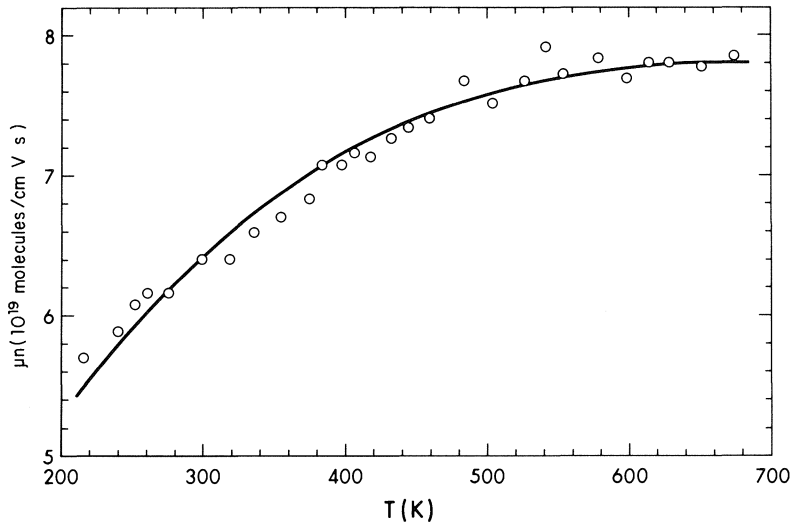

FIG. 9. Temperature dependence of μn for unclustered CO_3^- ions in N_2 gas (26). $n = (1.2 \pm 0.4) \times 10^{18}$ molecules/cm^3. The line was calculated from the cross sections in Fig. 10, using eq. [5].

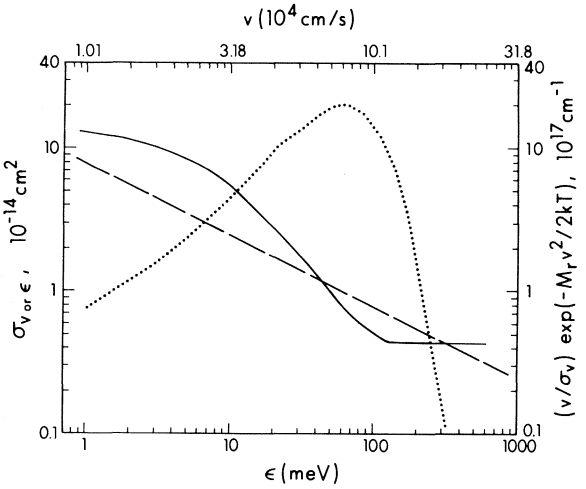

FIG. 10. Momentum transfer cross sections for CO_3^- collisions with N_2, as a function of energy ε and relative velocity v. —, obtained from Fig. 9 and eq. [5]. ---, σ^{pol}, eq. [8], obtained from polarization potential; ···, (v/σ_v) exp $(-M_r v^2/2kT)$, at 446 K, using σ_v from the full curve.

sections (Fig. 10). The sensitivity of the empirical fitting of $(n\mu, T)$ data to eq. [5] is greatest in the vicinity of the maximum of the transport distribution. The latter may be approximated as

$$[9] \quad \text{Maxwellian}/v\sigma_v = (v/\sigma_v) \exp(-M_r v^2/2kT)$$

The sensitivity of the data in Fig. 9 to σ_v is greatest between about 0.010 and 0.16 eV (Fig. 10). The empirical cross sections are progressively less accurate as the distance from this central energy region increases.

The interpretation of the hydrocarbon ion mobilities is complicated by clustering and its effect on M_r and σ_v. The Maxwellian energy distribution is independent of M_r, whereas the velocity distribution is not, so eq. [5*b*] is the more convenient form for examining the effect of clustering on the mobility. Clustering increases M_r and therefore decreases $n\mu$. The reduction of n would be negligible at the low ion concentrations used. Increasing the cluster size would increase the stiff core portion of the scattering potential, but the polarization portion might decrease due to shielding, so the effect of clustering is not simple. The net effect is probably to increase σ_ε and thereby further decrease $n\mu$. Changing from a monomer ion to a dimer would decrease $n\mu$ by a factor of about 1.5. In a mixture the smaller clusters make a proportionately larger contribution to the mobility than do the larger clusters. We assume that the exchange time of reaction [1] is much smaller than the drift time and that the measured time is the average drift time of the distribution.

For a given set of $(n\mu, T)$ data the *apparent* values of the cross sections vary as $M_r^{-1/2}$. Thus if the ions are assumed to be monomeric (M_r = 0.5 molecular mass) the apparent values of σ_ε are 1.4 times those that would be obtained by assuming that the ions are heavily clustered (M_r = molecular mass).

In the temperature studies of the hydrocarbons at constant low density, the methane sample had the lowest value of n/n_c (0.012) and highest value of T/T_c (up to 1.6). The extent of clustering should

Can. J. Chem. Downloaded from www.nrcresearchpress.com by 210.87.254.5 on 09/06/12
For personal use only.

Can. J. Chem. Downloaded from www.nrcresearchpress.com by 210.87.254.5 on 09/06/12
For personal use only.

therefore be smaller in methane than in the other hydrocarbons under the conditions used. The low density methane results were analyzed in two stages: (*a*) the main ion was assumed to be CH_5^+ at all temperatures; (*b*) clustering was assumed to have a significant effect on $n\mu$ at 117 K, which is near the coexistence curve at this density, and a minor effect at $T \geq 143$ K. The apparent cross sections obtained from these treatments are displayed in Fig. 11. The calculated and experimental values of $n\mu$ are compared in Fig. 12. The full line in Fig. 11 represents the more realistic cross sections; at 117 K the ratio of μ calculated from this curve to the experimental value is 1.20, which is equivalent to about half of the ions being dimers if the rest are monomers.

It is curious that the dash–dot curve in Fig. 11 is similar in shape to the full curve in Fig. 10. The former is thought to be distorted by ion–molecule clustering at low temperatures. The latter represents ions that were identified by mass and no clustering was observed (26). In both cases a better fit to the experimental mobilities could have been obtained by putting a minimum in the cross section near the energy where the present curves become flat, then having σ_ε increase at higher ε.

The cross sections extracted from the mobilities in methane are greater than σ^{pol} at all energies (Fig. 11). This implies that the contribution of sticky collisions to ion scattering in the methane system is greater than in the scattering of CO_3^- by N_2. The latter system had a much lower value of n/n_c (1.8×10^{-4}) and larger T/T_c (1.7–5.4), which might explain the lower contribution of associative interactions. We do not understand the shape of the cross section curve in Fig. 10 relative to those in Fig. 11.

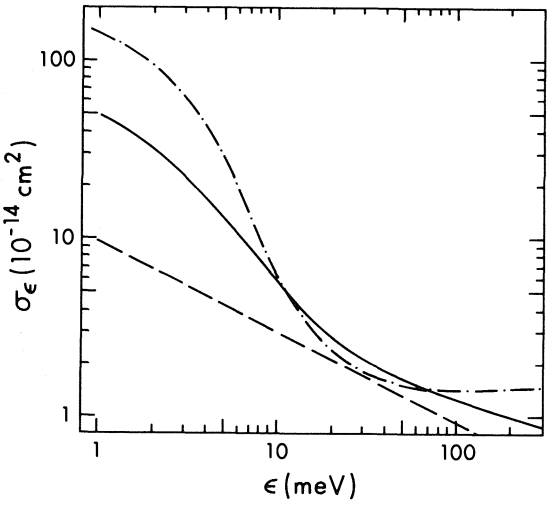

FIG. 11. Momentum transfer cross sections in methane, assuming the ions to be CH_5^+, -·-·-, estimated by ignoring an effect of clustering; —, estimated after discarding the point at 117 K in Fig. 12; ---, $\sigma^{pol} = 3.00 \times 10^{-15}\ \varepsilon^{-1/2}$ cm^2, where ε is in eV.

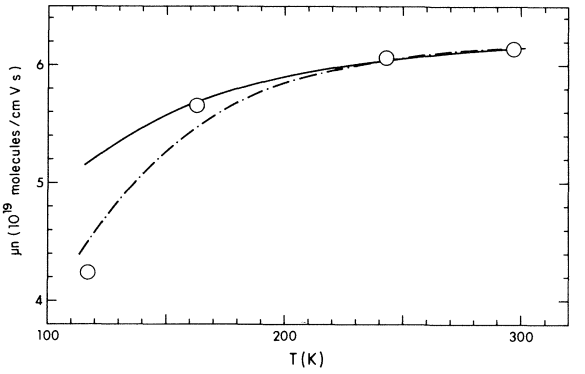

FIG. 12. Comparison of calculated and experimental (○) values of ion mobilities in methane. $n = 7.1 \times 10^{19}$ molecules/cm^3. The lines were calculated from eq. [5], assuming the ions to be CH_5^+: -·-·- and —, using the corresponding curves in Fig. 11.

All the other hydrocarbons were studied at larger relative densities, $n/n_c \geq 0.02$, and lower relative temperatures, T/T_c up to only 1.04 ± 0.04. Fitting the ($n\mu$, T) data to eq. [5] in each case gave a minimum in the *apparent* σ_ε at $\varepsilon = 0.05 \pm 0.01$ eV. The minima are artifacts attributed to the effects of clustering on the temperature dependence of μ. In each hydrocarbon gas at the lowest density the change of mobility with temperature is approximately equivalent to that expected if the average value of m in M_m^+ were reduced by half on going from the coexistence curve to 1.1 T_c. Assuming $m < 10$ a few K above the coexistence curve at the lowest gas density, the average association energy of a molecule to an ion is roughly 3 kJ/mol, within a factor of about two.

(2) Field Dependence

When the drift velocity of the ions is equal to or greater than the random velocities of the molecules, v_{mol}, it is no longer reasonable to assume that the temperature of the ions equals that of the gas. An upper limit to the threshold field, above which the mobility should be field dependent if the thermal ion mobility is temperature dependent, may be estimated from eq. [10].

$$[10] \quad (E/n)_{thr} \lesssim v_{mol}/\mu n \text{ (thermal)}$$

where $v_{mol} = (3kT/M_{mol})^{1/2}$ and M_{mol} is the molecular mass. To connect eq. [10] with earlier comments on this matter (34), v_{mol} is approximately equal to the speed of sound in the gas. One obtains for ethane at 293 K, $(E/n)_{thr} \lesssim 4.9 \times 10^4/3.1 \times 10^{19} = 1.60 \times 10^{-15}$ V cm^2/molecule, or 160 Td. This is

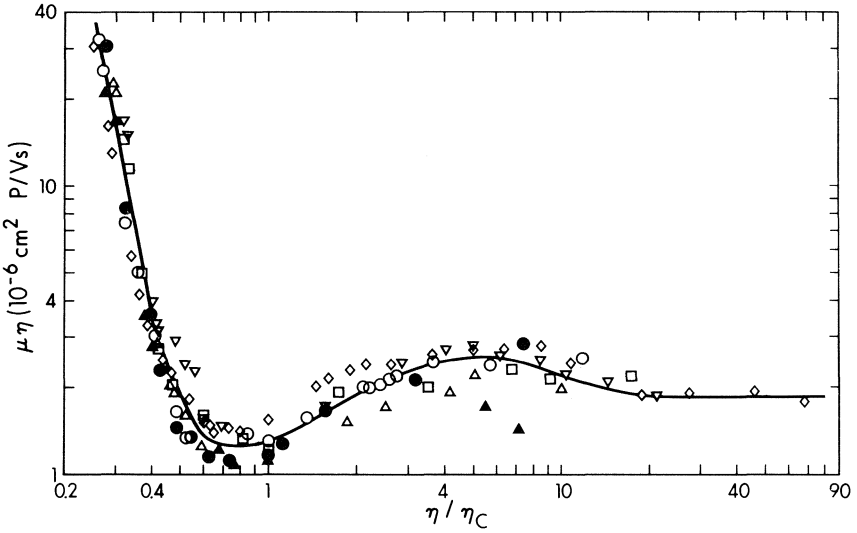

FIG. 13. Cation mobilities normalized for differences in fluid viscosities η, plotted against η/η_c, where $\eta_c \approx 0.2$ mP refers to the critical fluid. The fluid is a gas at $\eta/\eta_c < 1.0$ and a liquid at $\eta/\eta_c > 1.0$. ○, methane; ●, ethene; △, ethane; ▲, propene; ▽, propane; □, *n*-butane; ◇, *n*-hexane, ref. 6. The liquid phase data are from ref. 9. The vapor and liquid are coexistent fluids.

consistent with the observed threshold at 120 Td (20). The threshold predicted from the speed of sound, 311 m/s, would be 100 Td.

For methane at 293 K, eq. [10] predicts $(E/n)_{thr} \lesssim 6.8 \times 10^4/6.1 \times 10^{19} = 1.1 \times 10^{-15}$ V cm²/molecule, or 110 Td. In the study where the threshold in methane was reported to be 600 Td the lowest field used was 170 Td (19), and $d\mu/dE$ was negative above the reported threshold. We predict that the true threshold lies at ~80 Td and that $d\mu/dE$ is positive just above it. This could explain why Schlumbohm's (19) value for μn for methane is 13% larger than ours. The values of μn obtained at less than 20 Td (21) were within 3% of ours.

(B) Effect of Density Along the Coexistence Curve

At $n/n_c \geq 0.3$ the value of μn increases (Fig. 7), due to the mutual interference of the long range interactions of an ion with more than one molecule at the same time. The increase continues through the critical fluid and into the low density liquid. At $n/n_c \approx 1.7$ the value of μn passes through a maximum, and decreases rapidly at $n/n_c \geq 2.2$ (Fig. 7). The decrease of μn at the higher densities is due to transition to a different mechanism of ion transport. At low densities, where the ion mean free path is much greater than the molecular diameter, the drift of the ion in the direction of the electric field is disturbed by collisions with single molecules. Under these conditions $\mu n \approx$ constant. At high densities, where the mean free path is less than a molecular diameter, the ion interacts continuously with one or more molecules. Under these conditions the *viscosity* η dominates and $\mu\eta \approx$ constant. In Fig. 13, μη is plotted against η/η_c for the liquids and gases, where η_c is the viscosity of the critical fluid. The general behavior is similar for the alkanes from methane to *n*-hexane. Ethene and propene also fall near the alkane curve (Fig. 13). As noted earlier (9), at high viscosities in the liquids μη is approximately constant. The viscosity was reduced by heating the liquid under its vapor pressure. The value of μη passed through a slight maximum at $\eta/\eta_c \approx 5$ and decreased gently until the critical fluid was reached. Upon passing to the coexistence vapor the viscosity was decreased by decreasing the temperature and concomittant density. The value of μη passed through a shallow minimum at $\eta/\eta_c \approx 0.8$ and increased rapidly at $\eta/\eta_c < 0.6$. At the lowest densities the curve becomes vertical, because for an ideal gas η is independent of density.

Thus in the region where $\mu n \approx$ constant the value of μη varies rapidly (compare Figs. 7 and 13), and where $\mu\eta \approx$ constant the value of μn varies rapidly. The analogous regions in fluid mechanics are sometimes called the kinetic (low density) and hydrodynamic (high density) regimes (35). The transition region in our work is $0.3 \lesssim n/n_c \lesssim 2.0$, or $0.5 \lesssim \eta/\eta_c \lesssim 3$.

In ref. 8 it was suggested that μη was constant for cations in liquid ethane up to the critical point. However, they used η values from Gallant (36), which are too high for ethane and many other compounds near the critical region (15). Insertion of correct viscosities shows that μη decreases as

Can. J. Chem. Downloaded from www.nrcresearchpress.com by 210.87.254.5 on 09/06/12
For personal use only.

the critical region is approached, in agreement with our result (9).

There is no systematic dependence of $\mu\eta$ on molecular size (Fig. 13). This had been noted earlier for the liquid phase (9, 37) and attributed to electrostriction being greater around smaller ions. Electrostriction increases the local viscosity around the ions and tends to make $\eta R \approx$ constant, where R is the ion radius. By contrast, in the low density gases μn is strongly dependent upon molecular size (Table 1).

Acknowledgment

We would like to thank the staff of the Radiation Research Center for aid with the electronics.

1. P. WALDEN and H. ULICH. J. Phys. Chem. **107**, 219 (1923).
2. H. ULICH. Trans. Faraday Soc. **23**, 388 (1927).
3. A. HUMMEL, A. O. ALLEN, and F. H. WATSON, JR. J. Chem. Phys. **44**, 3431 (1966).
4. I. ADAMCZEWSKI and B. JACHYM. Acta Phys. Polon. **30**, 767, (1966) and references therein.
5. J.-P. DODELET and G. R. FREEMAN. Can. J. Chem. **53**, 1263 (1975).
6. S. S.-S. HUANG and G. R. FREEMAN. J. Chem. Phys. **70**, 1538 (1979).
7. S. S.-S. HUANG and G. R. FREEMAN. J. Chem. Phys. **72**, 1989 (1980).
8. W. DÖLDISSEN, W. F. SCHMIDT, and G. BAKALE. J. Phys. Chem. **84**, 1179 (1980).
9. N. GEE and G. R. FREEMAN. Can. J. Chem. **58**, 1490 (1980).
10. J. J. THOMSON and G. P. THOMSON. Conduction of electricity through gases. Vol. 1. 3rd ed. Cambridge University Press. 1928.
11. E. W. MCDANIEL and E. A. MASON. The mobility and diffusion of ions in gases. J. Wiley and Sons, New York. 1973.
12. E. CUNNINGHAM. Proc. R. Soc. London, A**83**, 357 (1910).
13. L. N. CANJAR and F. S. MANNING. Thermodynamic properties and reduced correlations for gases. Gulf Publ. Co., Houston TX. 1967.
14. N. GEE and G. R. FREEMAN. Rad. Phys. Chem. **15**, 267 (1980).
15. (*a*) Y. S. TOULOUKIAN, S. C. SAXENA, and P. PETERMANS. Viscosity, thermophysical properties of matter. Vol. 11, IFI/Plenum, New York. 1975; (*b*) N. B. VARGAFTIG. Tables on the thermophysical properties of liquids and gases. 2nd ed. J. Wiley, Halsted Press. 1975.
16. S. ANGUS, B. ARMSTRONG, and K. J. DE REUCK (*Editors*). IUPAC, International thermodynamic tables of the fluid state: ethylene, 1972. Butterworth, London, 1974.
17. G. R. FREEMAN. J. Phys. Soc. Jpn. **48**, 683 (1980).
18. S. WATANABE. J. Phys. Soc. Jpn. **46**, 1819 (1979).
19. H. SCHLUMBOHM. Z. Phys. **182**, 317 (1965).
20. M. P. WATTS and A. E. D. HEYLEN. J. Phys. D, **12**, 695 (1979).
21. (*a*) G. SCHULTZ, G. CHARPAK, and F. SAULI. Rev. Phys. Appl. **12**, 67 (1977); (*b*) C. W. POLLEY JR., A. J. ILLIES, and G. G. MEISELS. Anal. Chem. **52**, 1797 (1980).
22. F. W. LAMPE, J. L. FRANKLIN, and F. H. FIELD. Prog. Reac. Kinet. **1**, 67 (1961).
23. E. A. MASON, H. O'HARA, and F. J. SMITH. J. Phys. B, **5**, 169 (1972).
24. (*a*) H. STUART. *In* Landolt-Börnstein, Zahlenwerte und Funktionen, I. Band, 3. Teil, Molekeln II. *Edited by* A. Eucken and K. H. Hellwege. Springer-Verlag, Berlin. 1951. p. 511; (*b*) N. J. BRIDGE and A. D. BUCKINGHAM. Proc. R. Soc. London, A**295**, 334 (1966); (*c*) R. J. W. LEFÈVRE. Rev. Pure Appl. Chem. **20**, 67 (1970).
25. M. J. AVOEY, R. J. W. LE FÈVRE, W. LUETTKE, G. L. D. RITCHIE, and P. J. STILLS. Aust. J. Chem. **21**, 2551 (1968).
26. F. L. EISELE, M. D. PERKINS, and E. W. MCDANIEL. J. Chem. Phys. **73**, 2517 (1980).
27. I. R. GATLAND, D. R. LAMM, M. G. THACKSTON, W. M. POPE, F. L. EISELE, H. W. ELLIS, and E. W. MCDANIEL. J. Chem. Phys. **69**, 4951 (1978).
28. H. W. ELLIS, R. Y. PAI, E. W. MCDANIEL, E. A. MASON, and L. A. VIEHLAND. Atomic data and nuclear data tables. Academic Press, New York. **17**, 177 (1976).
29. S. CHAPMAN and T. G. COWLING. The mathematical theory of non-uniform gases. 2nd ed. Cambridge University Press, London. 1952. Chapt. 9.
30. F. W. MORRISON, G. R. AKRIDGE, H. W. ELLIS, R. Y. PAI, E. W. MCDANIEL, L. A. VIEHLAND, and E. A. MASON. J. Chem. Phys. **63**, 2238 (1975).
31. L. S. FROST and A. V. PHELPS. Phys. Rev. **127**, 1621 (1962).
32. G. R. FREEMAN, I. GYÖRGY, and S. S.-S. HUANG. Can. J. Chem. **57**, 2626 (1979).
33. G. HEICHE and E. A. MASON. J. Chem. Phys. **53**, 4687 (1970).
34. S. S.-S. HUANG and G. R. FREEMAN. J. Chem. Phys. **68**, 1355 (1978).
35. V. GHAEM-MAGHAMI and A. D. MAY. Phys. Rev. A, **22**, 692 (1980).
36. R. W. GALLANT. Physical properties of hydrocarbons. Vol. 1, Gulf Publication Co., Houston TX. 1970.
37. D. L. GOODSTEIN. J. Low Temp. Phys. **33**, 137 (1978).

Can. J. Chem. Downloaded from www.nrcresearchpress.com by 210.87.254.5 on 09/06/12
For personal use only.

Diels–Alder adducts of 2-acetoxyfuran as a route to 2,3-functionalized 4-hydroxycyclohexanones. Application of X-ray diffraction to the problem of regio- and stereochemistry

D. GRAVEL[1] AND R. DEZIEL[2]

Département de Chimie, Université de Montréal, C.P. 6210, Succ. A, Montréal (Qué.), Canada H3C 3V1

AND

F. BRISSE[1] AND L. HECHLER[3]

Laboratoire de Rayons X, Département de Chimie, Université de Montréal, C.P. 6210, Succ. A, Montréal (Qué.), Canada H3C 3V1

Received March 18, 1981

D. GRAVEL, R. DEZIEL, F. BRISSE, and L. HECHLER. Can. J. Chem. **59**, 2997 (1981).

The Diels–Alder adducts of 2-acetoxyfuran and maleic anhydride and 2-acetoxyfuran and chloromethylmaleic anhydride have been obtained and their dihydro derivatives manipulated in high yield to various 2,3-functionalized 4-hydroxycyclohexanones. In all cases the hemiketal acetate bridge of the oxabicyclo[2.2.1] derivatives was cleaved smoothly using sodium methoxide in methanol at 0°C; however, in the case of the chloromethyl compounds the reaction proceeds further to give an almost quantitative yield of the corresponding fused cyclopropane derivatives. These sequences, starting from the readily accessible but seldom used 2-acetoxyfuran, are therefore extremely advantageous to gain rapid and efficient access to a number of 2,3-functionalized 4-hydroxycyclohexanones. In the case of the adduct involving chloromethylmaleic anhydride, stereochemistry and regiochemistry were established by X-ray diffraction on the dihydro derivative.

D. GRAVEL, R. DEZIEL, F. BRISSE et L. HECHLER. Can. J. Chem. **59**, 2997 (1981).

Les adduits de Diels–Alder de l'anhydride maléique et de l'anhydride chlorométhylmaléique avec l'acétoxy-2 furanne ont été obtenus et leur dérivé dihydro transformé en excellent rendement en diverses hydroxy-4 cyclohexanones fonctionnalisées aux positions-2,3. Dans chaque cas l'acétate du pont hémicétal des dérivés oxabicyclo[2.2.1] a été facilement scindé en utilisant le méthylate de sodium dans le méthanol à 0°C. Toutefois, dans le cas des composés chlorométhylés la réaction progresse plus loin pour donner un rendement presque quantitatif des dérivés cyclopropaniques fusionnés correspondants. Ces séquences à partir du réactif très accessible mais peu utilisé qu'est l'acétoxy-2 furanne sont donc très avantageuses pour préparer rapidement et efficacement certaines hydroxy-4 cyclohexanones fonctionnalisées en -2,3. Dans le cas de l'adduit impliquant l'anhydride chlorométhylmaléique, la stéréochimie et la régiochimie furent établies par diffraction des rayons X sur le dérivé dihydro.

Introduction

Over the years, the Diels–Alder reaction has been developed to the state of being probably the greatest tool available to organic chemists to quickly and efficiently assemble relatively complex synthons, be they bridged polycyclics, aromatics, or cyclohexane derivatives (1). Recent important developments on this topic have been in the areas of understanding and predicting regioselectivity (2), reversing regioselectivity by using Lewis acid catalysis (3), improving rate of reaction by the use of Lewis acids (4) or very high pressures (5), and broadening the spectrum of functionalities available on the enophile (6).

The problem at hand in the present case was the need for a simple, efficient, and selective method to generate various 2,3-functionalized 4-hydroxycyclohexanones required as potential starting material in a synthetic problem currently under study in our laboratory. Of the different methods envisaged or explored, it appeared that the Diels–Alder reaction might provide an advantageous solution.

Currently, the most frequently employed diene to generate 1,4-dioxygenated 2,3-functionalized cyclohexanes is *trans-trans*-1,4-diacetoxybutadiene (**1**) in conjunction with suitable dienophiles (7). An alternate, slightly less reactive but also less expensive, diene is 2-acetoxyfuran (**2**) which in the presence of suitable dienophiles leads to the usual [4 + 2] adduct which by opening of the hemiketal acetate bridge should lead *directly* to 2,3-disubstituted 4-hydroxycyclohexanones as required in the present study (see Scheme 1). As is readily apparent, both types of dienes could possibly be applicable to the synthetic objective pursued and both are under study. The results we wish to report in the present paper pertain to the use of 2-acetoxyfuran (**2**) as starting diene.

An examination of the literature reveals that 2-acetoxyfuran (**2**) was first reported by Clauson-Kaas and Elming (8) in 1952 who described its preparation and formation of an adduct **3** with maleic anhydride. A few years later, Cava *et al.* (9) reported a study of its preparation and its behavior

[1]Authors to whom correspondence should be addressed.
[2]Fellow NSERC, Canada and MEQ, Quebec.
[3]Fellow FDR, Université de Montréal.

0008-4042/81/202997-10$01.00/0
©1981 National Research Council of Canada/Conseil national de recherches du Canada

Can. J. Chem. Downloaded from www.nrcresearchpress.com by 210.87.254.42 on 09/06/12
For personal use only.

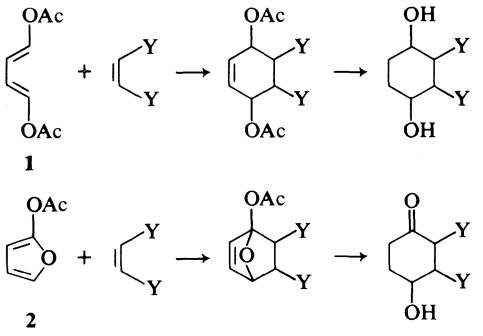

SCHEME 1

as a diene with the conclusion that: "The reactivity of 2-acetoxyfuran as a diene in the Diels–Alder reaction is as great as, though not noticeably greater than, that of furan itself".

To our knowledge, there is only one report in the literature (10) describing the use of a Diels–Alder adduct of 2-acetoxyfuran (**2**) to generate a 4-hydroxycyclohexanone derivative and this is the base induced hydrolysis of the dihydro adduct **4** of maleic anhydride and 2-acetoxyfuran (**2**). As depicted in Scheme 2, the reaction leads to hydrolysis of the anhydride, saponification of the hemiketal acetate, and decarboxylation of the resulting β-ketoacid moiety to yield 2-hydroxy-5-oxocyclohexane carboxylic acid (**5**). According to the authors (10*a*) the latter experiment was performed as a model to devise conditions to carry out the same sequence of transformations on the isopropylidene derivative

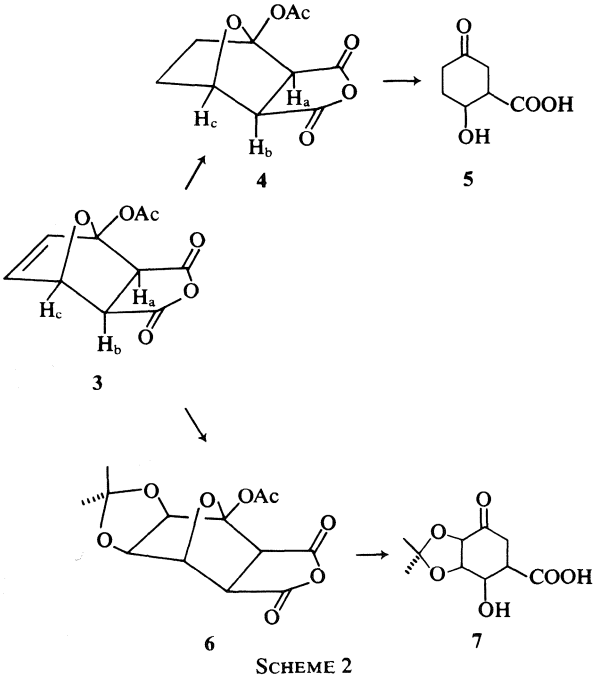

SCHEME 2

6 to obtain **7**; unfortunately, aromatization was invariably present to a large extent, forcing the authors to modify their strategy and to use *trans-trans*-1,4-diacetoxybutadiene (**1**) as starting diene.

Since then there appears to have been no other report of the use of 2-acetoxyfuran (**2**) as diene in Diels–Alder reactions although 2-methoxyfuran, which is commercially available, and 2-trialkylsilyloxyfuran, which has been reported recently (11), have both been used as dienes a number of times (11, 12) but only to generate aromatic synthons.

Results and Discussion

For strategic, practical, and economic reasons we chose to investigate the potential of 2-acetoxyfuran (**2**) first. In our initial study we repeated the preparation of the known (8, 9) adduct **3** with maleic anhydride and verified by nmr the *exo* configuration which had correctly been assigned by McCrindle *et al.* (10*a*) on the basis of analogy with the furan – maleic anhydride adduct reported by Woodward and Baer (13).[4] In the adduct **3** the *endo* protons H_a and H_b appear (acetone-d_6) as a pair of AB doublets ($\Delta\nu \simeq 8$ Hz) centered at δ 3.95 with $J =$ 8 Hz and no evidence of vicinal coupling with H_c, the bridgehead proton, as expected in such bicyclo[2.2.1] systems (15). The same observation holds for the dihydro adduct **4** where H_a and H_b again appear (acetone-d_6) as a pair of AB doublets ($\Delta\nu \simeq 20$ Hz) centered at δ 4.0 with $J = 8.0$ Hz and no evidence of vicinal coupling with H_c, the bridgehead proton (see Scheme 2).

As stated earlier, our synthetic objective was to develop access to various 2,3-substituted 4-hydroxycyclohexanones and therefore, contrary to McCrindle *et al.* (10), opening of the anhydride had to be achieved without decarboxylation of the β-ketoacid. In a first sequence of reactions (see Scheme 3), the anhydride **4** was heated in water at 70°C for 1 h and the crude diacid esterified with ethereal diazomethane to yield 91% overall of the bicyclotriester **8**. The delicate step of opening the bicyclotriester **8** to the corresponding cyclohexanone derivative was achieved in methanolic sodium methoxide at 0°C to yield 96% of the desired *trans*-2,3-dicarbomethoxy-*cis*-4-hydroxycyclohexanone **9**, as evidenced by the nmr spectrum which shows the 2, 3,

[4]In a recent paper Herndon and Lee (14) showed that, in accord with the typical kinetic and thermodynamic pattern for Diels–Alder reactions, maleic anhydride and furan react to give the *endo* adduct as the kinetically preferred product, but since the reaction is reversible and since the *exo* adduct (**3**) is 1.9 kcal/mol more stable than the *endo* adduct, the former is eventually the final product isolated.

Can. J. Chem. Downloaded from www.nrcresearchpress.com by 210.87.254.42 on 09/06/12
For personal use only.

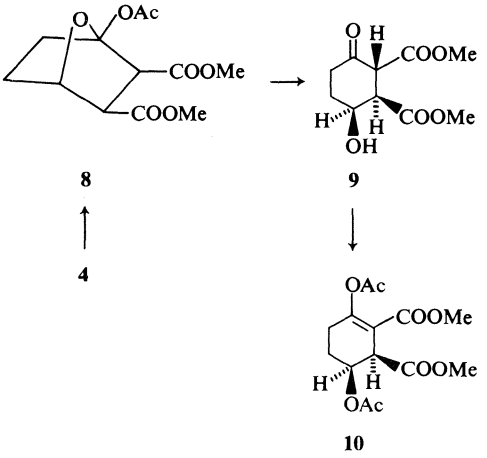

SCHEME 3

and 4 protons in the form of an ABX portion where J_{AB} = 12.3 Hz and J_{AX} = 2.6 Hz. Acetylation of **9** under the usual pyridine – acetic anhydride conditions yielded 81% of diacetate **10**, providing additional evidence for the proposed structure **9**.

In a second sequence of reactions (see Scheme 4) we aimed at regioselectively manipulating the fused anhydride ring prior to hemiketal acetate cleavage in order to have chemically differentiated functional groups at the 2,3-positions. There was of course the possibility of opening the anhydride by a nucleophile such as an alcohol or an amine in order to achieve differentiation, but our objective here was to generate two groups differing in their oxidation state. There are many reports in the literature pertaining to the regioselective reduction of nonsymmetrical fused anhydrides by sodium borohydride (16, see also 10*b*), and although regioselection is almost invariably observed, explanations differ as to its origin (16*a*). Be that as it may, at this early stage of the work, our strategy could

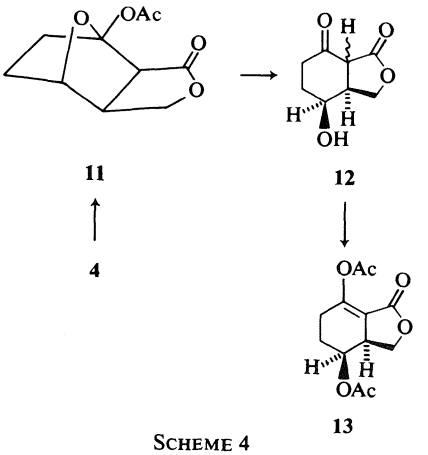

SCHEME 4

accommodate itself to either mode of regioselection so long as it were complete.

In the event, reduction of the fused anhydride **4** with sodium borohydride in absolute ethanol yielded 85% of a single (tlc, nmr) crystalline fused lactone of known (10*b*) structure **11**, as shown unambiguously by the formation of a diacetate **13** after base cleavage of the hemiketal acetate bridge (*vide infra*). As in the former case, opening of the hemiketal acetate **11** was carried out in methanolic sodium methoxide at 0°C and the expected hydroxyketolactone **12** isolated in 85% yield as an epimeric mixture. Acetylation in pyridine – acetic anhydride yielded a single crystalline diacetate **13** in a 94% yield. The formation of a diacetate (**13**) in the reaction shows conclusively that reduction of the fused anhydride **4** had taken place *only* at the carbonyl *opposite* the hemiketal acetate moiety. In the nmr, diacetate **13** shows clearly the two acetate methyl singlets at δ 2.10 and 2.27 and in the infrared, two characteristic carbonyl absorptions appear at 1750 and 1725 cm^{-1}.

Having thus found anhydrous basic conditions to efficiently open the hemiketal acetate ring, and thus avoiding loss of functionality at the 2-position by decarboxylation, and also having observed total regioselectivity in the reduction of the fused anhydride, we decided to attempt to increase the complexity of the dienophile in order to achieve a more elaborate synthon. An interesting such dienophile is chloromethyl maleic anhydride (**14**), the synthesis of which was reported by Eschenmoser *et al.* (17). Again, as in the case of maleic anhydride, the conditions to be met were (*i*) stereoselective adduct formation, (*ii*) regioselective manipulation of the anhydride function, and (*iii*) efficient opening of the hemiketal acetate plus a new condition due to the nonsymmetrical nature of the dienophile, namely, regioselective adduct formation.

Diels–Alder addition of chloromethylmaleic anhydride (**14**) to 2-acetoxyfuran (**2**) took place smoothly in refluxing dichloromethane to yield 76%[5] of a single (tlc, nmr) adduct which was shown by chemical correlation (*vide infra*) to have structure **15**, i.e. a *meta* adduct where the fused anhydride has the *exo* configuration, which by analogy with the former case should be the thermodynamically most stable product (see Scheme 5).

The nmr of the adduct **15**, although quite simple, is of little help to determine regio- and stereochemistry in this case; indeed, the key proton H_a appears as a sharp singlet which means it is not coupled

[5]Lower yields were obtained when the reaction was scaled up.

Can. J. Chem. Downloaded from www.nrcresearchpress.com by 210.87.254.42 on 09/06/12
For personal use only.

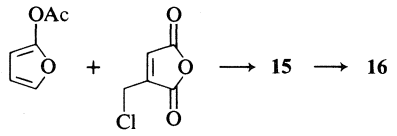

2 14

SCHEME 5

appreciably to any other proton in the molecule. Of the four possible adducts (*exo-ortho*, *exo-meta*, *endo-ortho*, and *endo-meta*) it therefore results that only one, the *endo-ortho* structure, can safely be eliminated as H_a and H_b form a dihedral angle of approximately 45° and therefore should be coupled by 3–4 Hz.

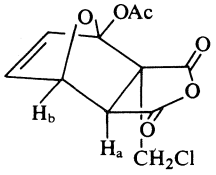

exo-ortho

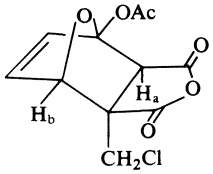

exo-meta **15**

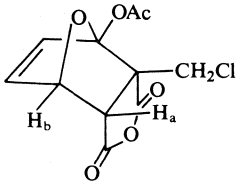

endo-ortho

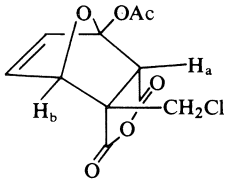

endo-meta

Hydrogenation of the adduct over 10% palladium on charcoal in ethyl acetate gave 87% of the crystalline dihydroadduct **16** (*exo-meta*) whose structure was conclusively established by X-ray diffraction as described below (*vide infra*).

As in the former case, the nmr spectrum is of little help in establishing the structure since the H_a proton again appears as a sharp singlet and therefore, of the three remaining possible structures for the dihydro adduct, only the *endo-meta* dihydro adduct may possibly be eliminated since H_a and H_c should normally show a long-range W coupling of 1–2 Hz as in the norbornyl systems. Be that as it may, there nevertheless remain two possible structures, perhaps three, and since the carbon-13 spectra of these compounds which were recorded did not allow us to unambiguously solve the problem, we resorted, as mentioned earlier, to the method of X-ray diffraction (*vide infra*).

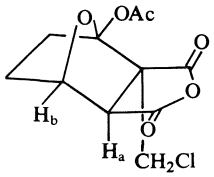

exo-ortho

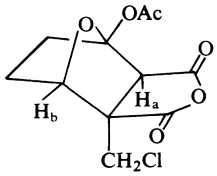

exo-meta **16**

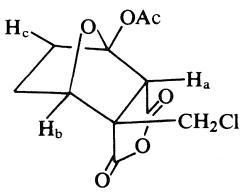

endo-meta

Again, in analogy with the first adduct discussed, a few sequences of reactions were carried out in order to assess the possibilities of the intermediate for further elaboration. Firstly, heating anhydride **16** in water for 30 min at 70°C and then leaving it at room temperature for 12 h yielded the corresponding crystalline diacid which was characterized as its dimethyl ester by treating it with diazomethane. The crystalline diester **17** was obtained in an overall yield of 72% (see Scheme 6). As in the previous cases, the *endo* proton, α to carbomethoxy, appears as a sharp singlet at δ 3.3. Cleavage of the hemiketal acetate group of dimethylester **17** took place smoothly as in the previous case but, however, yielded 95% of the undesired hydroxyketodiester **18**, i.e. where the desired chloromethyl group had been transformed into a fused cyclopropane ring by internal displacement of chlorine by the β-ketoester anion even under the mild conditions (0°C) used. Such behavior for somewhat similar systems has been exploited by Eschenmoser *et al.* in their synthesis of colchicine (17*a*) and by Greenlee and Woodward in their synthesis of marasmic acid (17*b*); in these cases, however, more basic conditions were used (*t*-BuOK – benzene). Acetylation of the product (**18**) in pyridine – acetic anhydride at room temperature for 24 h yielded 94% of the corresponding crystalline monoacetate **19**, thus corroborating the proposed structure **18** for the hydroxyketodiester. It is important to note at this point that, regarding the ultimate objective pursued in this work, loss of the chloromethyl side chain renders the intermediate useless.

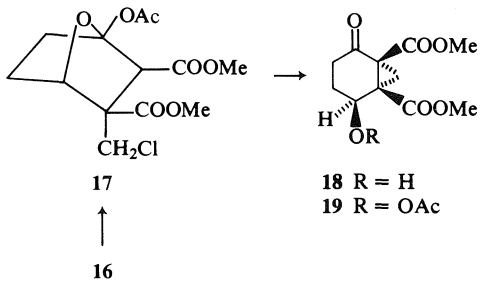

17 **18** R = H
19 R = OAc

16

SCHEME 6

Can. J. Chem. Downloaded from www.nrcresearchpress.com by 210.87.254.42 on 09/06/12
For personal use only.

Can. J. Chem. Downloaded from www.nrcresearchpress.com by 210.87.254.42 on 09/06/12
For personal use only.

It therefore becomes imperative that the bicyclic derivative **17** be elaborated further before hemiketal acetate opening and/or that an alternative method of hemiketal acetate cleavage be found which avoids cyclopropanation (*vide infra*).

In a second sequence, dihydro adduct **16** was reduced with sodium borohydride in ethanol to yield 80% of the corresponding crystalline fused lactone **20** where a sharp singlet at δ 3.10 is typical of the *endo* proton α to carbonyl; also, an AB system (J = 9.7 Hz) centered at δ 4.36, and which shows no vicinal coupling, both demonstrate conclusively that reduction took place in a totally regioselective manner on the chloromethyl side of the anhydride (see Scheme 7). Interestingly, reduction of dihydroadduct **16** using lithium tri-*tert*-butoxyaluminium hydride in tetrahydrofuran gave 83% of an epimeric mixture of lactols **21** as evidenced by nmr; however, the sharpness of the melting point suggests that in the crystalline form only one diastereoisomer of the lactol is present. In the nmr, the epimeric mixture of lactols shows a singlet at δ 2.07 for the *endo* proton α to carbonyl and two singlets at δ 3.22 and 3.27 integrating for one hydrogen and attributable to the lactol carbinol. However, the final and conclusive evidence showing that the site of reduction is identical to that observed with sodium borohydride was obtained by reducing the epimeric lactol mixture **21** to obtain the fused lactone **20** described above.

Finally, cleavage of the hemiketal acetate group of fused lactone **20** in methanolic sodium methoxide at 0°C and acetylation at room temperature of the crude product afforded the crystalline 4-acetoxycyclohexanone derivative **22** in 80% yield. As in the previous case, chlorine was displaced by the β-ketolactone anion resulting in the formation of a fused cyclopropane ring, thus again imposing the condition of elaborating bicyclic intermediate **20** further prior to hemiketal acetate opening and/or of finding an alternative method of hemiketal acetate cleavage which avoids cyclopropanation. Such a method was indeed found simply by treating anhydride **16** with methanolic hydrogen chloride which yields 71% of the desired 2,3-disubstituted 4-hydroxycyclohexanone **23**. Further work is therefore in progress on this and related series.

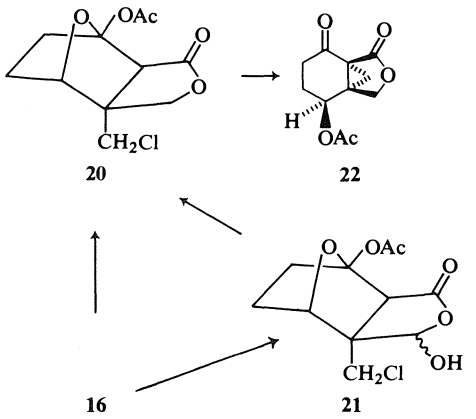

SCHEME 7

[1] **16** ⟶ 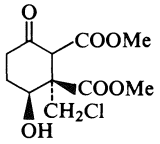

23

X-Ray Structure Determination of the Dihydro Adduct of 2-Acetoxyfuran and Chloromethylmaleic Anhydride (16)

Final atomic coordinates and their standard deviations are given in Table 1.[6] The molecular structure is represented by the pair of stereoscopic drawings in Fig. 1. The molecule consists of a six-membered ring A (atom C(1) through C(6)) in the boat conformation *cis* fused to a five-membered ring B made up of the anhydride group of atoms. In addition, an oxygen atom O(7) bridges atoms C(1) and C(4) of ring A. Finally the acetate group is on the bridgehead at C(1) while the chloromethyl group is *endo* at C(3).

Bond Distances and Angles

The interatomic distances and angles calculated from the final refined coordinates are summarized in Fig. 2. The estimated standard deviations are of the order of 0.004 Å and 0.3° for bond distances and angles between nonhydrogen atoms. When one H atom is implied, these values become 0.03 Å and 2° respectively. The two bridging C—O bond lengths are significantly different 1.447(3) and 1.422(3) Å. Although no explanation is given, a similar situation has been found for an analogous oxabicyclo-[2.2.1]heptane derivative where the corresponding distances have the values of 1.442(3) and 1.425(3) Å (22).

The C(sp^3)—C(sp^3) bond distances, ranging from 1.504 to 1.550 Å, average 1.530 Å, and the C(sp^3)—Cl distance of 1.782(3) Å are all normal. Except for angles C(2)–C(1)–C(6) = 109.5(3)° and C(3)–C(4)–C(5) = 110.9(3)°, the other bond angles in the bicyclo[2.2.1] system are smaller than usual; they

[6]The structure factor table and the anisotropic temperature factors are available, at a nominal charge, from the Depository of Unpublished Data, CISTI, National Research Council of Canada, Ottawa, Canada, K1A 0S2.

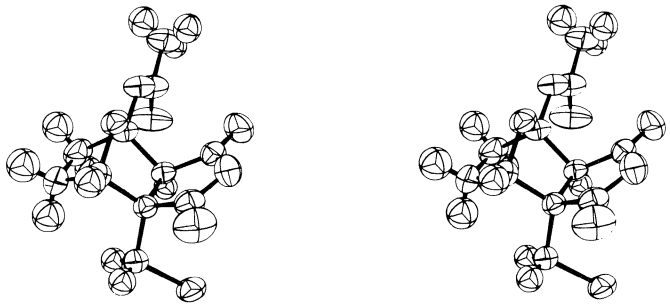

FIG. 1. Stereoscopic view of dihydro adduct **16**.

TABLE 1. Fractional coordinates and their esd's ($\times 10^4$, $\times 10^3$ for H atoms) and thermal parameter U_{eq} ($\times 10^4$) and U_{iso} ($\times 10^3$ for H atoms)

Atom	x	y	z	U_{eq}
Cl(1)	5460(1)	8843(1)	436(1)	520
O(1)	−182(3)	10353(1)	−3122(2)	523
O(2)	1461(3)	9150(1)	−3074(2)	492
O(3)	2972(3)	7832(2)	−2662(2)	723
O(4)	−3421(3)	9352(1)	−3127(2)	479
O(5)	−2349(3)	10299(2)	−1454(2)	892
O(7)	−1939(2)	8085(1)	−3106(2)	426
C(1)	−1756(3)	8772(2)	−2262(2)	395
C(2)	444(3)	9128(2)	−1652(2)	356
C(3)	1573(3)	8257(2)	−1464(2)	323
C(4)	−199(4)	7569(2)	−2057(3)	411
C(5)	−743(5)	7401(2)	−1113(3)	513
C(6)	−1749(4)	8286(3)	−1185(3)	592
C(7)	491(4)	9641(2)	−2660(3)	421
C(8)	2120(4)	8349(2)	−2425(3)	459
C(9)	3483(4)	8045(2)	−81(3)	375
C(10)	−3570(4)	10105(2)	−2595(3)	598
C(11)	−5400(5)	10632(2)	−3624(3)	658
H(2)	97(3)	945(1)	−91(2)	394
H(4)	2(4)	707(2)	−241(3)	655
H(51)	48(4)	727(2)	−19(3)	714
H(52)	−170(4)	694(2)	−144(3)	911
H(61)	−104(4)	868(2)	−41(3)	682
H(62)	−307(4)	820(2)	−150(3)	781
H(91)	400(3)	749(2)	−6(2)	559
H(92)	320(3)	809(2)	56(2)	493
H(111)	−531(4)	1118(2)	−327(3)	901
H(112)	−654(4)	1033(2)	−395(3)	829
H(113)	−531(4)	1075(2)	−429(3)	818

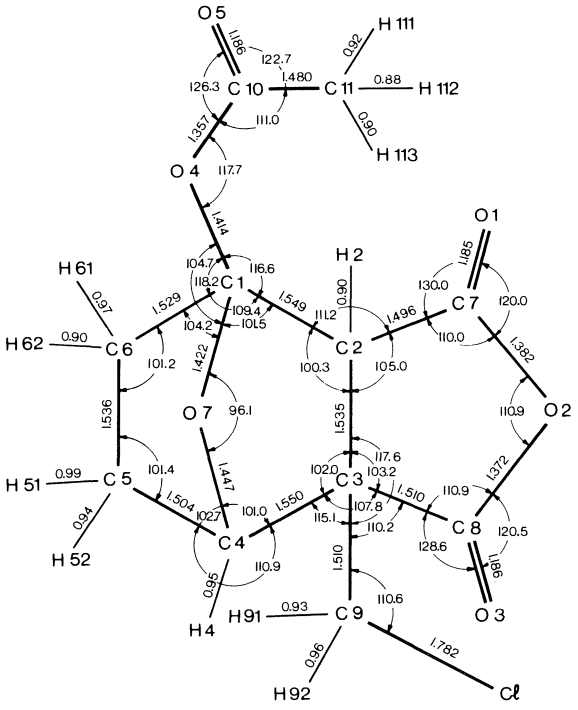

FIG. 2. Bond distances and angles of dihydro adduct **16**.

range in values from 100.3 to 102.0° and average 101.2°.

Mean Planes

The least-squares plane computed for the anhydride group reveals that C(2) deviates from the plane by about 10σ; when C(2) is omitted the groups of atoms are planar (Table 2). The acetate group including C(1) is also planar. Other various planes have been defined and the angles between them are compared in Fig. 3 with the corresponding dihedral angles in the *anti*-8-tricyclo[3.2.1.$0^{2,4}$] octyl derivative (23).

TABLE 2. Mean planes*

Plane 1 Atoms	$x^2 = 12.7$ Deviations, Å	Plane 2 Atoms	$x^2 = 12.8$ Deviations, Å
O(1)	0.004(3)	O(4)	0.005(2)
O(2)	−0.005(2)	O(5)	0.003(3)
O(3)	0.005(3)	C(1)	−0.006(3)
C(7)	0.000(3)	C(10)	−0.005(4)
C(8)	−0.005(3)	C(11)	−0.007(5)
C(2)†	0.029(3)		
C(3)	0.004(3)		

*Equations for the least-squares planes:

Plane 1 $-0.558X - 0.410Y - 0.722Z + 5.369 = 0$

Plane 2 $0.851X + 0.479Y - 0.215Z - 7.056 = 0$

†This atom was not included in the least-squares plane calculation.

Can. J. Chem. Downloaded from www.nrcresearchpress.com by 210.87.254.42 on 09/06/12
For personal use only.

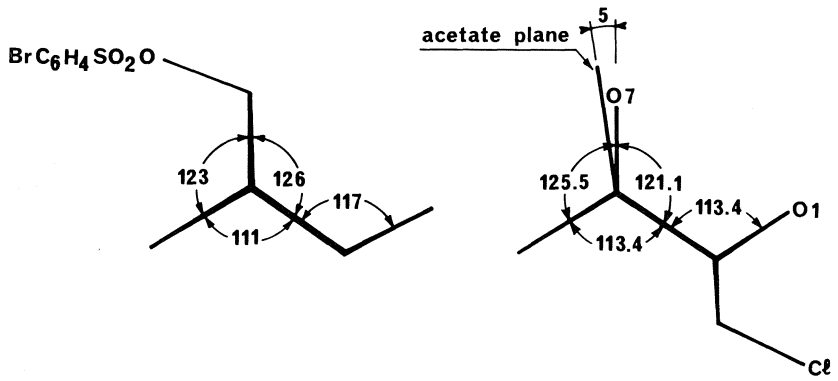

FIG. 3. Comparison of dihedral angles in dihydro adduct **16** with those observed in *anti*-8-tricyclo[3,2,1,$0^{2,4}$]octyl-*p*-bromobenzenesulfone (ref. 23).

TABLE 3. Ring torsion angles (°)*

Endocyclic torsion angles		Boat	Exocyclic torsion angles	
C(1)–C(2)–C(3)–C(4)	2.4	0	C(3)–C(2)–C(1)–O(4)	−151.2
C(2)–C(3)–C(4)–C(5)	−75.2	−60	C(5)–C(6)–C(1)–O(4)	146.0
C(3)–C(4)–C(5)–C(6)	69.5	60	C(5)–C(4)–C(3)–C(9)	53.2
C(4)–C(5)–C(6)–C(1)	4.6	0	C(1)–C(2)–C(3)–C(9)	−124.4
C(5)–C(6)–C(1)–C(2)	−77.4	−60	C(6)–C(5)–C(7)–O(7)	−37.7
C(6)–C(1)–C(2)–C(3)	71.6	60	C(5)–C(6)–C(1)–O(7)	30.4
C(6)–C(1)–C(2)–C(7)	−177.8		C(2)–C(3)–C(4)–O(7)	33.2
C(5)–C(4)–C(3)–C(8)	176.6		C(3)–C(2)–C(1)–O(7)	−38.2
C(1)–C(2)–C(7)–O(2)	−106.2		H(4)–C(4)–C(3)–C(9)	−80.
C(4)–C(3)–C(8)–O(2)	108.2			

*The esd's are of the order of 0.4° except for the torsion angle involving a H atom for which the esd is of 3°.

Torsion Angles

The torsion angles of interest are listed in Table 3. In the six-membered ring the torsion angles do correspond to the boat conformation but with deviations of up to 17° from the theoretical values. Two other torsion angles, C(6)–C(1)–C(2)–C(7) and C(5)–C(4)–C(3)–C(8), nearly 180°, indicate that all light atoms C(1) to C(8) are very nearly coplanar. The torsion angle H(4)–C(4)–C(3)–C(9) has a value of 80° which supports nicely the fact that no coupling is observed in the nmr between protons H_b and H_c in structures **3** and **4** (*vide supra*).

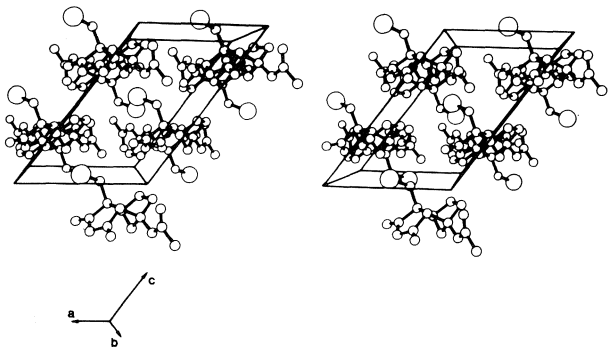

FIG. 4. Stereoscopic view of the packing of the molecule of dihydro adduct **16**.

Packing of Molecules

The organisation of the molecules in the crystal is shown in Fig. 4. There are no contacts shorter than 3.30 Å, hence the molecules are held in the crystal by van der Waals forces only.

Experimental

Melting points (mp) were taken on a Büchi apparatus and are uncorrected. The nmr spectra were recorded on a Bruker WH-90 apparatus and tetramethylsilane used as internal standard; deuterated solvents used are indicated in the experimental. The chemical shifts (δ) are expressed in parts per million (ppm) and the coupling constants (*J*) in Hertz (Hz). The following notation has been used throughout: s for singlet, d for doublet, t for triplet, m for multiplet, dd for doublet of doublets, br s for broadened singlet and unres. m for unresolved multiplet. The infrared spectra (ir) were recorded on a Perkin-Elmer 710A apparatus using the 1601 cm^{-1} band of a polystyrene film as reference. The EI mass spectra were taken on a AEI MS902 spectrometer and the CI spectra taken on a AEI MS25 apparatus. Finally, the combustion analyses were done by Guelph Chemical Laboratories Ltd., Guelph, Ont.

exo-*1-Acetoxy-7-oxabicyclo[2.2.1]heptane-2,3-dicarboxylic Anhydride (4)*

Catalytic hydrogenation of **3** (8, 9) (7.2 g, 33.6 mmol) in ethyl

Can. J. Chem. Downloaded from www.nrcresearchpress.com by 210.87.254.42 on 09/06/12
For personal use only.

Can. J. Chem. Downloaded from www.nrcresearchpress.com by 210.87.254.42 on 09/06/12
For personal use only.

acetate over 10% Pd/C catalyst gave, after filtration through Celite and recrystallization from mixtures of dichloromethane–hexane, 7.2 g (94%) of colourless crystals **4**, mp 143–144°C (lit. (10) mp 165–166°C (AcOEt)).[7] Infrared ($CHCl_3$): 1870, 1790 and 1760 cm^{-1}; nmr (acetone-d_6), δ: 2.2 (s, 3H), 1.7–2.3 (m, 4H), 3.85 (A of AB, d, 1H, J_{AB} = 8 Hz), 4.20 (B of AB, 1H), and 5.0 (unres. m, 1H); ms, CI, *m/e*: 227 (M + 1).

Dimethyl exo-*1-Acetoxy-7-oxabicyclo[2.2.1]heptane-2,3-dicarboxylate (8)*

A suspension of anhydride **4** (10) (210 mg, 0.93 mmol) in 4 mL of water was heated at 70°C for 1 h. After the reaction mixture had cooled to room temperature, the white crystalline diacid was filtered and dried *in vacuo* at room temperature. The crude diacid was esterified with an excess of ethereal diazomethane at room temperature to afford diester **8** (230 mg, 91%) as colourless crystals, mp 128–129°C; ir ($CHCl_3$): 1760–1750 cm^{-1}; nmr $CDCl_3$), δ: 2.1 (s, 3H), 1.6–2.4 (m, 4H), 3.4 (AB, 2H, J_{AB} = 9.4 Hz, Δν = 58 Hz), 3.6 (s, 3H), and 5.0 (br d, 1H); ms, CI, *m/e*: 273 (M + 1).

2,3-Dicarbomethoxy-4-hydroxycyclohexanone (9)

To a solution of triester **8** (1.7 g, 6.25 mmol) in 25 mL of dry methanol at 0°C were added 40 mL of 0.61 *N* methanolic sodium methoxide. The solution was stirred for 60 min under argon at 0°C and then quenched by the addition of an excess of acidic resin (Dowex 50W-X8). The resulting mixture was stirred for 10 min, filtered, and the resin washed with 100 mL of methanol. After drying ($MgSO_4$) and removal of the methanol *in vacuo*, the residual colourless oil was crystallized from mixtures of ether–hexane to afford 1.37 g (96%) of colourless crystals **9**, mp 108–109°C; ir ($CHCl_3$): 3500, 1760, 1735, and 1260 cm^{-1}; nmr $CDCl_3$), δ: 1.9–2.9 (m, 4H), 3.0 (s, 1H, —OH), 3.30 (A of ABX, dd, 1H, J_{AB} = 12.3 Hz, J_{AX} = 2.6 Hz), 3.74 (s, 3H), 3.77 (s, 3H), 4.10 (B of ABX, d, 1H), and 4.6 (unres. m, 1H); ms, CI, *m/e*: 231 (M + 1). *Anal.* calcd. for $C_{10}H_{14}O_6$: C 52.17, H 6.13; found: C 52.45, H 6.31.

1,4-Diacetoxy-2,3-dicarbomethoxycyclohexene (10)

Ketoester **9** (450 mg, 1.96 mmol) was dissolved in 5 mL of dry pyridine and 1 mL of acetic anhydride added. After stirring for 12 h at room temperature the volatile components were removed *in vacuo* and the residual oil chromatographed on 28 g of silica gel. Elution with ethyl acetate afforded 550 mg of diacetate **10** as a white solid. Recrystallization from mixtures of ether–hexane gave 500 mg (81%) of colourless crystals **10**, mp 106–107°C; ir (CH_2Cl_2): 1780, 1730, 1650, and 1220 cm^{-1}; nmr ($CDCl_3$), δ: 1.9 (m, 2H), 2.05 (s, 3H), 2.22 (s, 3H), 2.42 (m, 2H), 3.68 (s, 3H), 3.72 (s, 3H), 3.98 (m, 1H), and 5.2 (m, 1H); ms, *m/e*: 314 (M^+).

Sodium Borohydride Reduction of Anhydride 4

A suspension of anhydride **4** (16*b*) (1 g, 4.44 mmol) in 5 mL of absolute ethanol at 0°C was treated, in small portions, with sodium borohydride (200 mg, 5.28 mmol). The reaction mixture was allowed to warm slowly to 20°C by permitting the ice to melt (2 h). The solution was then cooled to 0°C and acidified with 10% hydrochloric acid to pH 5. The resulting solution was extracted with dichloromethane (3 × 50 mL) and the combined extracts dried ($MgSO_4$). Removal of the volatile components *in vacuo* gave an oil which easily crystallized in ether to afford 800 mg (85%) of white crystalline lactone **11**, mp 139–140°C (lit. (10*b*) mp 142–143°C); ir (CH_2Cl_2): 1770, 1750, and 1220 cm^{-1}; nmr ($CDCl_3$), δ: 1.6–2.5 (m, 4H), 2.20 (s, 3H), 2.9 (A of AB, m, 1H), 3.50 (B of AB, d, 1H, J_{AB} = 8.5 Hz), 4.14 (A of AB, m, 1H, J_{AB} = 9.4 Hz), 4.37 (d, 1H), and 4.51 (B of AB, d, 1H); ms, *m/e*: 169 ($M^+ - CH_3CO\cdot$).

[7]Recrystallization of our material in ethyl acetate did not raise the mp.

Base Cleavage of Hemiketal Acetate 11

To a solution of lactone **11** (900 mg, 4.28 mmol) in 15 mL of dry methanol at 0°C were added 27 mL of 0.61 *N* methanolic sodium methoxide. The solution was stirred for 40 min under argon at 0°C and then quenched by the addition of an excess of acidic resin (Dowex 50W-X8). The mixture was worked up as before and the resulting clear oil crystallized easily from chloroform to yield 610 mg (85%) of white crystalline lactone **12** as an epimeric mixture; ms, CI, *m/e*: 171 (M + 1).

Acetylation of Hydroxy Keto Lactone 12

Lactone **12** (500 mg, 2.94 mmol) was dissolved in 10 mL of dry pyridine and 1.2 mL of acetic anhydride added. After stirring for 8 h at room temperature the volatile components were removed *in vacuo* and the residual oil chromatographed on 80 g of silica gel. Elution with ethyl acetate afforded 700 mg (94%) of diacetate **13** as a white solid, mp 139–140°C; ir (CH_2Cl_2): 1750, 1725, 1690, and 1220 cm^{-1}; nmr ($CDCl_3$), δ: 1.6–2.5 (m, 4H), 2.10 (s, 3H), 2.27 (s, 3H), 3.44 (X of ABX, m, 1H), 3.92 (B of ABX, m, 1H), 4.44 (A of ABX, m, 1H), and 5.25 (m, 1H); ms, *m/e*: 254 (M^+).

exo-*1-Acetoxy-3-chloromethyl-7-oxabicyclo[2.2.1]hept-5-ene-2,3-dicarboxylic Anhydride (15)*

To a solution of chloromethylmaleic anhydride (**14**) (17) (580 mg, 4 mmol) in 25 mL of dry dichloromethane was added 500 mg (4 mmol) of 1-acetoxyfuran (**2**) (8, 9) and the solution was heated to reflux for 18 h. Removal of the volatile components *in vacuo* gave a crude crystalline adduct which was recrystallized from mixtures of dichloromethane–hexane to afford 820 mg (76%) of colourless crystals **15**, mp 125–126°C; ir (CH_2Cl_2): 1860, 1790, 1760, and 1200 cm^{-1}; nmr ($CDCl_3$), δ: 2.18 (s, 3H), 3.22 (A of AB, d, 1H, J_{AB} = 11.4 Hz), 3.62 (s, 1H), 4.01 (B of AB, d, 1H), 5.13 (d, 1H), 6.66 (A of AB, dd, 1H, J_{AB} = 5.9 Hz), and 6.90 (B of AB, 1H); ms, *m/e*: 272 (M^+).

exo-*1-Acetoxy-3-chloromethyl-7-oxabicyclo[2.2.1]heptane-2,3-dicarboxylic Anhydride (16)*

Application of the same hydrogenation procedure as described above for the preparation of **4** gave 350 mg (87%) of **16** (recrystallized from mixtures of dichloromethane–hexane) as colourless crystals, mp 175–176°C; ir (CH_2Cl_2): 1860, 1780, 1760, and 1220 cm^{-1}; nmr ($CDCl_3$), δ: 1.6–2.3 (m, 4H), 2.22 (s, 3H), 3.60 (A of AB, d, 1H, J_{AB} = 11.5 Hz), 3.79 (s, 1H), 3.85 (B of AB, 1H), and 4.75 (d, 1H, *J* = 4.7 Hz); ms, *m/e*: 274 (M^+). *Anal.* calcd. for $C_{11}H_{11}O_6Cl$: C 48.10, H 4.04, Cl 12.91; found: C 48.10, H 4.19, Cl 12.10.

Dimethyl exo-*1-Acetoxy-3-chloromethyl-7-oxabicyclo[2.2.1]-heptan-2,3-dicarboxylate (17)*

A suspension of anhydride **16** (600 mg, 2.18 mmol) in 4 mL of water was heated at 70°C for 30 min and then left at room temperature for 12 h. The reaction mixture was cooled to 0°C and the white crystalline diacid filtered, dried, and esterified with ethereal diazomethane to afford diester **17** (500 mg, 72%) as colourless crystals, mp 122–123°C; ir ($CHCl_3$): 1760 and 1750 cm^{-1}; nmr ($CDCl_3$), δ: 1.6–2.4 (m, 4H), 2.08 (s, 3H), 3.24 (s, 1H), 3.51 (A of AB, d, 1H, J_{AB} = 11.4), 3.66 (s, 3H), 3.76 (s, 3H), 4.28 (B of AB, 1H), and 5.15 (br d, 1H); ms, CI, *m/e*: 321, 323 (M + 1, M + 3).

Base Cleavage of Hemiketal Acetate 17[8]

To a solution of diester **17** (300 mg, 0.94 mmol) in 10 mL of dry methanol at 0°C were added 8 mL of 0.61 *N* methanolic sodium methoxide. The solution was stirred for 30 min under argon at 0°C, then quenched by the addition of an excess of acidic resin (Dowex 50 W-X8). The mixture was worked up as above, giving

[8]The reaction time is crucial in this case as the product evolves further with longer reaction times.

Can. J. Chem. Downloaded from www.nrcresearchpress.com by 210.87.254.42 on 09/06/12
For personal use only.

pure alcohol **18** as a clear oil (247 mg, 95%); ir ($CHCl_3$): 3600, 1750, 1720, 1700, and 1260 cm^{-1}; nmr ($CDCl_3$), δ: 1.86 (A of AB, d, 1H, J_{AB} = 6.4 Hz), 2.30 (B of AB, 1H), 1.6–2.7 (m, 4H), 3.73 (s, 3H), 3.75 (s, 3H), 3.90 (s, 1H, —OH), and 4.70 (t, 1H); ms, *m/e*: 228 (M^+).

Acetylation of Hydroxyketodiester 18

Alcohol **18** (50 mg, 0.18 mmol) was dissolved in 1 mL of dry pyridine and 1 mL of acetic anhydride added. After stirring for 24 h at room temperature, the volatile components were removed *in vacuo* and the residual oil chromatographed on 10 g of silica gel. Elution with ethyl acetate afforded 55 mg (94%) of acetate **19** as a white solid, mp 153–155°C; ir ($CHCl_3$): 1740, 1730, and 1700 cm^{-1}; nmr ($CDCl_3$), δ: 1.82 (A of AB, d, 1H, J_{AB} = 6.5 Hz), 2.10 (s, 3H), 2.21 (B of AB, 1H), 2.0–2.5 (m, 4H), 3.71 (s, 3H), 3.78 (s, 3H), and 5.91 (t, 1H); ms, *m/e*: 284 (M^+).

Sodium Borohydride Reduction of Anhydride 16

A suspension of anhydride **16** (750 mg, 2.72 mmol) in 10 mL of absolute ethanol at 0°C was treated, in small portions, with sodium borohydride (140 mg, 3.7 mmol). The reaction mixture was allowed to warm slowly to 20°C (2 h). The solution was then cooled to 0°C and acidified with 10% hydrochloric acid to pH 3. The resulting solution was extracted with dichloromethane (3 × 20 mL) and the combined extracts dried ($MgSO_4$). Removal of the volatile components *in vacuo* gave a crude crystalline lactone which was recrystallized from mixtures of ether–dichloromethane to afford 600 mg (80%) of colourless crystals **20**, mp 194–195°C; ir ($CHCl_3$): 1770 and 1750 cm^{-1}; nmr ($CDCl_3$), δ: 1.6–2.5 (m, 4H), 2.18 (s, 3H), 3.10 (s, 1H), 3.73 (A of AB, d, 1H, J_{AB} = 11.7 Hz), 3.84 (B of AB, 1H), 4.23 (A of AB, d, 1H, J_{AB} = 9.7 Hz), 4.46 (d, 1H), and 4.49 (B of AB, 1H); ms, *m/e*: 262 and 260 (M + 2, M^+).

*Lithium Tri-*tert*-butyoxyaluminium Hydride Reduction of Anhydride 16*

To a suspension of lithium tri-*tert*-butoxyaluminium hydride (7 g, 27.5 mmol) in 100 mL of dry tetrahydrofuran at −20°C was added a solution of anhydride **16** (6 g, 21.9 mmol) in 100 mL of dry tetrahydrofuran at −20°C. The solution was stirred for 8 h under argon at −20°C, then 50 mL of water–tetrahydrofuran (1:1) were added followed by the addition of 100 mL of hydrochloric acid (1.2 *N*). The resulting solution was extracted with methylene chloride (3 × 20 mL) and the combined organic layers dried ($MgSO_4$) and filtered through Celite. The volatile components were removed *in vacuo* and the residual colourless oil dissolved in 50 mL of methylene chloride and then cooled at −10°C to afford 5.0 g (83%) of an epimeric mixture of lactols **21** as colourless crystals, mp 183–185°C; ir (CH_2Cl_2): 3600, 1775, and 1755 cm^{-1}; nmr (acetone-d_6), δ: 1.6–2.5 (m), 2.07 (s superimposed over residual nondeuterated acetone), 3.22 and 3.27 (2s, 1H), 3.77–4.95 (m, 2H), 4.95 (m, 1H), 5.80 (m, 1H), and 7.0 (m, 1H, —OH); ms, *m/e*: 278 and 276 (M + 2, M^+). The mixture of lactols **21** can be converted to lactone **20** under conditions identical to those described for the reduction of anhydride **16** to lactone **20**.

Base Cleavage of Hemiketalacetate 20

To a solution of lactone **20** (120 mg, 0.461 mmol) in 5 mL of dry methanol at 0°C were added 3 mL of 0.61 *N* methanolic sodium methoxide at 0°C. The solution was stirred for 30 min[8] under argon at 0°C followed by the addition of an excess of acidic resin (Dowex 50W-X8). The mixture was worked up as above and the resulting clear oil dissolved in 2 mL of dry pyridine and treated with 0.3 mL of acetic anhydride. The resulting mixture was stirred for 18 h at room temperature after which 0.2 mL of methanol was added. The volatile components were removed *in vacuo* and the residual oil chromatographed on 20 g of silica gel. Elution with ethyl acetate afforded 96 mg (80%) of colourless crystals of acetate **22**, mp 194–195°C; ir ($CHCl_3$): 1780, 1740, and 1700 cm^{-1}; nmr ($CDCl_3$), δ: 1.67 (A of AB, d, 1H, J_{AB} = 6.2 Hz), 2.05 (B of AB, 1H), 2.15 (s, 3H), 1.96–2.5 (m, 4H), 4.25 (s, 2H), and 5.64 (t, 1H); ms, *m/e*: 224 (M^+). *Anal.* calcd. for $C_{11}H_{12}O_5$: C58.92, H 5.39; found: C 58.76, H 5.43.

Acidic Methanolysis of Hemiketal Acetate 16

To a suspension of anhydride **16** (500 mg, 1.82 mmol) in 10 mL of dry methanol at 0°C was added 10 mL of 5% methanolic hydrogen chloride. The reaction mixture was allowed to warm slowly to 25°C and then stirred 30 min at this temperature. The solution was then cooled to 0°C and neutralized with aqueous sodium bicarbonate. The resulting mixture was extracted with ether (3 × 30 mL) and the combined extracts dried ($MgSO_4$). Removal of the volatile components *in vacuo* gave a white solid which was recrystallized from mixtures of chloroform–hexane to afford 360 mg (71%) of colourless crystals **23**, mp 165–166°C; nmr ($CDCl_3$), δ: 1.6–1.8 (m, 2H), 2.26 (s, 1H, —OH), 2.3–2.6 (m, 2H), 2.96 (s, 1H), 3.51 (s, 3H), 3.80 (A of AB, d, 1H, J_{AB} = 11.7 Hz), 3.79 (s, 3H), 4.23 (B of AB, d, 1H), and 4.15 (m, 1H); ms, CI, *m/e*: 279, 281 (M + 1, M + 3). *Anal.* calcd. for $C_{11}H_{15}O_6Cl$: C 47.41, H 5.43, Cl 12.72; found: C 47.69, H 5.58, Cl 12.36.

X-Ray Structure Determination of Dihydro Adduct 16

Well developed clear prismatic crystals were obtained by slow evaporation from a chloroform–hexane (80:20) solution. Precession photographs revealed that the crystals belonged to the monoclinic system, space group $P2_1/c$ (systematic absences for $0k0$, $K \neq 2n$; $h0l$, $l \neq 2n$). The unit cell dimensions were obtained by a least-squares refinement of the angular measurements of 25 reflections centered on the Nonius CAD4 diffractometer using graphite monochromatized MoKα radiation.

Crystal data:

$C_{11}H_{11}ClO_6$ f.w. = 274.66

Monoclinic, a = 8.059(3), b = 15.079(3), c = 12.474(4) Å, β = 126.66(3)°, V = 1216.0 $Å^3$, ρ_0 = 1.49 Mg/m^3, ρ_c = 1.500 Mg/m^3, Z = 4, $F(000)$ = 568 e, μ(MoKα) = 0.326 mm^{-1}, λ(MoKᾱ) = 0.71068 Å, mp = 447–448 K.

Three dimensional intensity data were collected on the Nonius CAD4 diffractometer using a graphite monochromator and MoKα radiation. The reflection intensities were measured with an ω − 2θ scan, Δω = (0.80 + 0.35 tan θ) degrees, and an aperture 4 mm high and 2 mm wide. Each reflection was measured with a prescan acceptance limit such that $\sigma(I)/I$ = 0.010 at a minimum scanning speed, S, of 6.67 deg min^{-1}, and a maximum scanning time of 120 s. The intensities of three standard reflections were monitored every hour; these did not vary to any significant degree during the entire period of the data collection. No trend was detected although the crystal had turned orange by the end of the measurement. The fluctuations of the reference reflections remained constant to within ±1.5% over the duration of the measurements. Of the 2138 reflections measured out to $2\theta \leq 50°$ (hkl and $hk\bar{l}$), 1556 of them (72%) were such that $I/\sigma(I) > 1.90$, with $\sigma^2(I) = (I_T + 4B)S^2 + (0.04\ I_N)^2$ where I_T is the total intensity, I_N the net intensity, and B the background. Lorentz and polarization corrections were applied but, since the crystal was of small dimensions (0.22 × 0.30 × 0.50 mm) and the linear absorption coefficient was low, no absorption correction was applied.

A set of normalized structure factors $|E|$ was obtained after isotropic temperature factor correction. The statistical averages of the normalized structure factors indicated a centrosymmetrical distribution in agreement with the space group determination. The signs of 305 reflections with $|E| \geq 1.50$ were determined using the MULTAN multisolution programme (18). The E-map, calculated with the set of phases having the highest combined figures of merit coordinates and isotropic temperature

factor led to an R-value of 0.205, ($R = \Sigma||F_o| - |F_c||/\Sigma|F_o|$). The function minimized was $\Sigma w(|F_o| - |F_c|)^2$. Following anisotropic temperature factor refinement of Cl, O, and C atoms, which was concluded when R reached 0.086, the H atoms were located on a Fourier difference map. The refinement of the atomic coordinates, anisotropic temperature factors for Cl, O, and C atoms, and isotropic temperature factors for H atoms proceeded normally using the block diagonal approximation and unit weights for all reflections. When the refinement process was terminated $R = 0.039$ and the mean error in an observation of unit weight $\sigma_F = [\Sigma w \Delta F^2/(m - n)]^{1/2} = 2.01$, where m is the number of reflections and n, the number of refined parameters. When all measured reflections were included, $R = 0.060$. The mean shift/error in the final least-squares cycle was 0.3. The difference Fourier synthesis following the last cycle showed electron density fluctuations in the range -0.18 + to 0.23 Å^{-3}. Weighting analyses confirmed the suitability of unitary weights over those derived from counting statistics. Scattering factors for the H atoms were taken from Stewart *et al.* (19) and all others from Cromer and Waber (20). The anomalous dispersion for the chlorine atom was taken from Cromer and Liberman (21).

Acknowledgements

Financial assistance from the Natural Sciences and Engineering Research Council of Canada and le Ministère de l'Education du Québec is gratefully acknowledged.

The authors are also indebted to Professor M. Bertrand, Université de Montréal, for obtaining the chemical ionization mass spectra.

1. (*a*) H. Wollweber. Diels–Alder reaction. George Thieme Verlag, Stuttgart. 1972; (*b*) J. Sauer. Angew. Chem. Int. Ed. Engl. **5**, 211 (1966).
2. (*a*) L. E. Overman, G. F. Taylor, K. N. Houk, and L. N. Domelsmith. J. Am. Chem. Soc. **100**, 3182 (1978), and references cited therein; (*b*) J. Sauer and R. Sustmann. Angew. Chem. Int. Ed. Engl. **19**, 779 (1980), and references cited therein.
3. (*a*) Z. Stojanac, R. A. Dickinson, N. Stojanac, R. J. Woznow, and Z. Valenta. Can. J. Chem. **53**, 616 (1975); (*b*) N. Stojanac, A. Sood, Z. Stojanac, and Z. Valenta. Can. J. Chem. **53**, 619 (1975); (*c*) M. Kakushima, J. Espinosa, and Z. Valenta. Can. J. Chem. **54**, 3304 (1976); (*d*) B. M. Trost, J. Ippen, and W. C. Valaduchick. J. Am. Chem. Soc. **99**, 8116 (1977).
4. (*a*) P. Yates and P. Eaton. J. Am. Chem. Soc. **82**, 4436 (1960); (*b*) J. Sauer. Angew. Chem. Int. Ed. Engl. **5**, 16 (1967), and references cited therein.
5. W. G. Dauben and H. O. Krabbenhoft. J. Org. Chem. **42**, 282 (1977), and references cited therein.
6. (*a*) S. Danishefsky, T. Kitahara, C. F. Yan, and J. Morris. J. Am. Chem. Soc. **101**, 6996 (1979); (*b*) S. Danishefsky, C. F. Yan, R. K. Singh, R. B. Gammill, P. M. McCurry, Jr., N. Fritsch, and J. Clardy. J. Am. Chem. Soc. **101**, 7001 (1979).
7. (*a*) T. A. Eggelte, H. de Koning, and H. O. Huisman. J. R. Neth. Chem. Soc. **98**, 267 (1979); (*b*) G. W. Holbert and B. Ganem. J. Org. Chem. **41**, 1655 (1976), and references cited therein.
8. N. Clausen-Kaas and N. Elming. Acta Chem. Scand. **6**, 560 (1952).
9. M. P. Cava, C. L. Wilson, and C. J. Williams, Jr. J. Am. Chem. Soc. **78**, 2303 (1956).
10. (*a*) R. McCrindle, K. H. Overton, and R. A. Raphael. J. Chem. Soc. 1560 (1960); (*b*) J. Chem. Soc. 4798 (1962).
11. (*a*) E. Yoshii, T. Koizumi, E. Kitatsuji, T. Kawazoe, and T. Kaneko. Heterocycles, **4**, 1663 (1976); (*b*) M. Asaoka, K. Miyake, and H. Takei. Chem. Lett. 167 (1977).
12. (*a*) J. J. Krutak, R. D. Burpett, W. H. Moore, and J. A. Hyatt. J. Org. Chem. **44**, 3847 (1979); (*b*) E. Sherman and P. Dunlop. J. Org. Chem. **25**, 1309 (1960); (*c*) G. F. D'Alelio, C. J. Williams, Jr., and C. L. Wilson. J. Org. Chem. **25**, 1028 (1960).
13. R. B. Woodward and H. Baer. J. Am. Chem. Soc. **70**, 1161 (1948).
14. M. W. Lee and W. C. Herndon. J. Org. Chem. **43**, 518 (1978).
15. L. M. Jackman and S. Sternhell. Applications of nuclear magnetic resonance spectroscopy in organic chemistry. 2nd ed. Pergamon Press, London. 1969. pp. 288–289.
16. (*a*) M. M. Kayser and P. Morand. Can. J. Chem. **58**, 2484 (1980), and references cited therein; (*b*) D. M. Bailey and R. E. Johnson. J. Org. Chem. **35**, 3574 (1970); M. E. Birckelbaw, P. W. LeQuesne, and C. K. Wocholski. J. Org. Chem. **35**, 558 (1970), and references cited therein.
17. (*a*) H. Eschenmoser, J. Schreiber, W. Leimgruber, M. Pesaro, and P. Schudel. Helv. Chim. Acta, **44**, 540 (1961); (*b*) W. J. Greenlee and R. B. Woodward. Tetrahedron, **36**, 3367 (1980).
18. P. Main, M. M. Woolfson, L. Lessinger, G. Germain, and J. P. Declercq. MULTAN A system of computer programs for the automatic solution of crystal structures from X-ray diffraction data. Univs. of York, England, and Louvain, Belgium. 1978.
19. R. F. Stewart, E. R. Davidson, and W. T. Simpson. J. Chem. Phys. **42**, 3175 (1965).
20. D. T. Cromer and J. T. Waber. Acta Crystallogr. **18**, 104 (1965).
21. D. T. Cromer and D. Liberman. J. Chem. Phys. **53**, 1891 (1970).
22. C. L. D. Jennings-Clive, A. B. Holmes, and P. R. Raithby. J. Chem. Soc. Chem. Commun. 542 (1979).
23. A. C. MacDonald and J. Trotter. Acta Crystallogr. **18**, 243 (1965).

Can. J. Chem. Downloaded from www.nrcresearchpress.com by 210.87.254.42 on 09/06/12
For personal use only.

^{13}C lithiation shifts in aldimines and ketimines. Evidence on the configuration of lithiated *N-tert*-butylimines

ROBERT R. FRASER AND NOEMI CHUAQUI-OFFERMANNS

Department of Chemistry, University of Ottawa, Ottawa, Ont., Canada K1N 9B4

Received April 15, 1981

ROBERT R. FRASER and NOEMI CHUAQUI-OFFERMANNS. Can. J. Chem. **59**, 3007 (1981).

The ^{13}C shieldings for a series of aldimines and ketimines have been measured along with the shifts for their 1-lithio derivatives. For those aldimines with a primary or secondary alkyl group attached to nitrogen, the "lithiation shifts" for the attached carbon (C-4) were all upfield due to the change from *anti* to *syn* configuration on lithiation. In the ketimines and in the *N-tert*-butyl aldimines and ketimines, the lithiation shifts for the C-4 carbon failed to provide stereochemical information. The shifts at C-1 and C-2 proved similar to those previously observed for lithiated alkenes.

ROBERT R. FRASER et NOEMI CHUAQUI-OFFERMANNS. Can. J. Chem. **59**, 3007 (1981).

On a mesuré les blindages du ^{13}C d'une série d'aldimines et de cétimines ainsi que les déplacements chimiques de leurs dérivés lithiés en position 1. Pour les aldimines ayant un groupe alkyle primaire ou secondaire fixé sur l'azote, les déplacements conduits par la lithiation du carbone (C-4) se font tous vers les champs forts par suite d'un changement de configuration de *anti* à *syn* lors de la lithiation. Dans le cas des cétimines, des *N*-butylaldimines et cétimines, les déplacements provoqués par la lithiation sur le carbone en position 4 n'ont pas apporté d'information sur la stéréochimie. Les déplacements chimiques des carbones en positions 1 et 2 sont identiques à ceux observés antérieurement pour les dérivés lithiés des alcènes.

[Traduit par le journal]

Can. J. Chem. Downloaded from www.nrcresearchpress.com by 210.87.254.5 on 09/06/12
For personal use only.

In a series of studies of the stereochemistry of lithiation and alkylation of aldimines and ketimines, we have described evidence for a very marked energetic preference for the formation of a *syn*[1] lithiated intermediate on the basis of formation of *syn* alkylation products (1, 2), *ab initio* calculations (3), and the observation of extraordinarily large barriers to rotation about the N—C-4 single bond of several 1-lithio-3-azapent-2-enides (4). Distinction between configurations at the C=N bond of these imines having the formulae shown below is readily provided by the large *syn–anti* differential shielding which appears as preferential upfield shifts of 5 to 11 ppm (5) for either C-1 or C-4 when *syn* to each other.

In this paper we wish to describe the ^{13}C shielding parameters for a variety of lithiated imines. Comparison with the shieldings of their neutral precursors provides a measure of the "lithiation shifts" whose magnitudes appear to be significantly influenced by substituent effects and by the stereochemistry at the C=N bond. A more unique class of sterically congested aldimines and ketimines bearing an *N-tert*-butyl substituent was also studied. One of these, acetone *N-tert*-butylimine was observed to undergo lithiation and methylation to give only *syn* product, indicative of

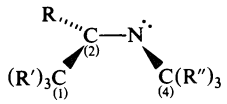

a *syn* lithiated intermediate. Unfortunately, similar alkylation experiments on *N-tert*-butylaldimines were inconclusive.[2] Measurement of the ^{13}C spectra of these aldimines and lithio derivatives gave "lithiation shift" data which failed to provide any clear stereochemical evidence.

Experimental

Imines **1–10** were synthesized from the parent aldehyde or ketone and primary amine as described previously (5). For the ketimine derived from *tert*-butyl amine (60 mmol scale) pentane (10 mL) was used in place of ether and two drops of pyridine were added to shorten the reaction time to 16 h. Yields of distilled imine varied from 30 to 50%. For the *N-tert*-butyl aldimines only one hour of reaction time was required to produce similar yields. Much of the loss in yield is thought to be manipulative, resulting from the high volatility of these imines. Compound **11** was synthesized (in 62% yield) by the method of Etienne and Correia (6). The product, bp 64°C (18 Torr) exhibited proton and ^{13}C nmr properties (5) consistent with structure. Imine **14** has been described previously (7).

The solutions of all anions, 1 *M* in THF, were prepared as reported previously for 1-lithio-4-methyl-3-azapent-2-enide (4).

The ^{13}C spectra were recorded on a Varian FT-80 nmr spectrometer operating at a frequency of 20 MHz and at a temperature of 29°C. The assignments were made on the basis of

[1]The use of *syn–anti* nomenclature to describe the configuration at the C=N function will be continued herein as it serves to pinpoint the location at the C—N bond while *E–Z* nomenclature can be employed to delineate stereochemistry at the C-1—C-2 bond in lithiated derivatives.

[2]The single product observed in the alkylation of lithiated aldimines had the *anti* configuration. However, it is possible that a *syn* alkylation product was formed which then rapidly isomerized to *anti*. This isomerization would be expected to be faster in the *tert*-butyl series than in the isopropyl series ($t_{1/2}$ = 1 h at −20°C (2)).

0008-4042/81/203007-05$01.00/0

©1981 National Research Council of Canada/Conseil national de recherches du Canada

Can. J. Chem. Downloaded from www.nrcresearchpress.com by 210.87.254.5 on 09/06/12
For personal use only.

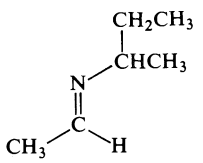
1

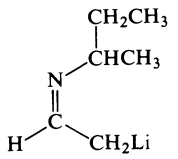
1-Li

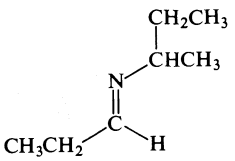
2

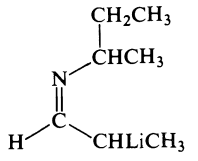
2-Li

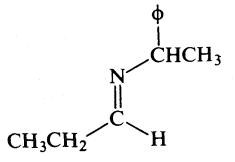
3

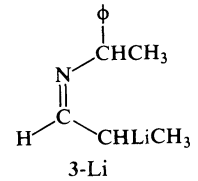
3-Li

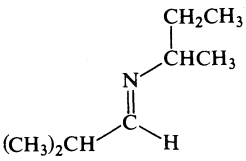
4

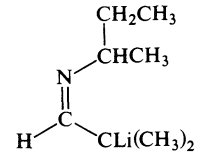
4-Li

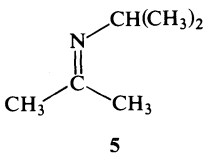
5

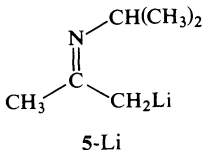
5-Li

off-resonance decoupling experiments and known substituent effects. To verify the signal assignment in **1** by an unambiguous method, a sample of 2-deutero-2-aminobutane was prepared by the reduction of 2-butanone oxime with lithium aluminum deuteride. Reaction of this amine with acetaldehyde gave 4-deutero-4-methyl-3-azahex-2-ene, **1**-d_1. The change in the appearance of the ^{13}C absorption of C-4 due to coupling with deuterium verified its signal assignment in the spectra of this imine and its lithio derivative.

Results and Discussion

Before discussing the nmr data of imines **1** to **15** and their lithio derivatives, one point must be emphasized. The formulae given to represent the lithiated imines are simply a formal representation of their gross structure. They are not meant to indicate a definitive position of the lithium counterion. Whether it is C-coordinated, N-coordinated, π-coordinated, or fully solvated cannot be determined at this time.

The ^{13}C shielding parameters, listed in Table 1, represent imines belonging to four classifications, each of which we will consider in sequence. The shieldings presented are those for carbons C-1, C-2, and C-4 of the common structural unit of all the imines which possess the C-1—C-2=N—C-4 or 3-azabut-2-ene fragment. These are the only absorptions which are consistently free from overlap with the peaks of solvent or other reaction components.

A. Aldimines

Compounds **1** to **4** are aldimines, all of which possess the more stable *anti* configuration. Previously we have found a consistent difference in the shifts for C-1 in several closely related *syn* and *anti* aldimines (5). The signal for C-1 in the *syn* form appeared 6 ppm to higher field. Assuming comparable shift differences in **1** to **4**, we have listed the estimated shifts for C-1 of each *syn* isomer in brackets.

The lithiation shifts at C-1 can be seen to be downfield shifts which show an increasing magnitude with the change from primary site (50 ppm) to a secondary (55 ppm) or a tertiary one (62 ppm). It is possible that this decrease in shielding at the lithiated carbon reflects a decrease in electron density and thus greater double bond character between C-1 and C-2. House *et al.* (8) proposed the same explanation to account for similar trends in

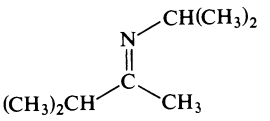
6

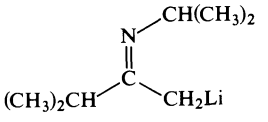
6-Li

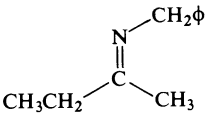
7-*anti*

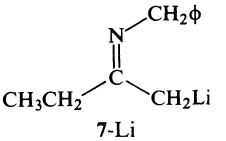
7-Li

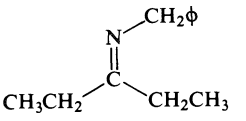
8

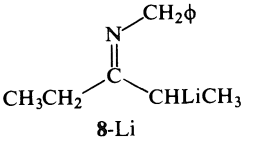
8-Li

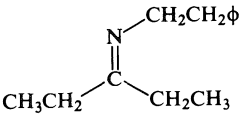
9

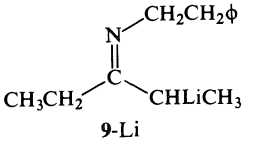
9-Li

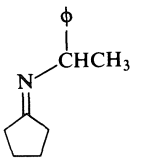
10

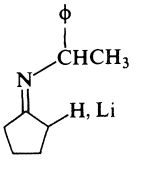
10-Li

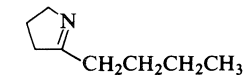

11

11-Li

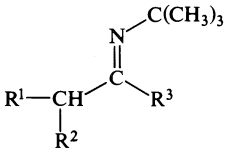

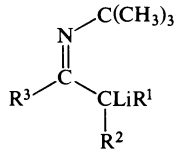

12 $R^1 = R^2 = R^3 = H$ — **12-Li**
13 $R^1 = CH_3$, $R^2 = R^3 = H$ — **13-Li**
14 $R^1 = R^2 = CH_3$, $R^3 = H$ — **14-Li**
15 $R^1 = R^2 = H$, $R^3 = CH_3$ — **15-Li**
16-*syn* $R^1 = R^2 = H$, $R^3 = CH_2CH_3$
16-*anti* $R^1 = R^3 = CH_3$, $R^2 = H$

the chemical shifts of lithium enolates. The shifts at C-2 are consistent with this explanation, moving progressively upfield with substitution and also showing behavior parallel to the enolates (8). In the structurally related enamines, methyl substitution effects at C-1 and C-4 are also remarkably similar (9). The most consistent change in the aldimines occurs at C-4 which in each case shifts upfield by 8 to 9 ppm on lithiation. The major cause for this upfield shift is undoubtedly the change from the *anti* configuration in the aldimine to the *syn* configuration in the organolithium derivative. This change at the C-2—N bond introduces a γ-effect of steric origin. Shifts smaller in size can be seen in the data for C-4 of the carbon analogs given in Table 1. For example, comparing C-4 in **17**-Li versus **18** and **19**-Li versus **20** shows upfield lithiation shifts of 3.3 and 4.5 ppm respectively.

B. Acyclic Ketimines

The lithiation shifts at C-1, the primary carbon in **5**, **6**, and **7**, behave similarly to that of primary aldimine **1**, and the lithiation shifts for **8** and **9** at their secondary carbon, C-1, are comparable to that in **2**. The C-2 carbons of the imines **5** and **6** shift on lithiation, but by only a small amount (±3 ppm) as also found in **1**. Again C-2 undergoes a substantial upfield shift upon lithiation at the secondary α carbon in **9** just as occurs for C-2 in **2**. A striking difference in ketimine lithiation shifts vs. aldimines

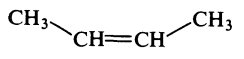

17

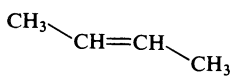

18

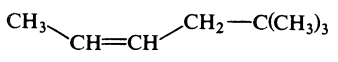

19

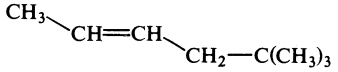

20

TABLE 1. ^{13}C shieldings in imines and lithiated imines

Compound	C-1*s*	C-1*a*	C-2(=N)	C-4(—N=)	
A. Aldimines					
1	(17)	23.1	157.9	69.5	
1-Li	67.0		155.2	61.5	
2	(23)	30.4	163.1	69.4	
2-Li	76.8		152.0	60.5	
3	(23)	30.5	164.4	71.5	
3-Li	80.0		151.5	62.4	
4	(28)	35.3	167.2	69.2	
4-Li	90.7		145.1	60.9	
B. Acyclic ketimines					
5	17.8	30.1	163.6	50.5	
5-Li	67.9		160.7	50.0	
6-*anti*	15.3	41.0	169.9	51.3	
6-Li	61.3		171.1	49.2	
7-*anti*	17.8	36.2	—	55.7	
7-*syn*	27.2	26.4	—	55.3	
7-Li	64.5	33.8	—	55.7	
8	25.6	33.1	—	54.7	
8-Li	74.9	30.1	—	55.8	
9	25.6	33.2	174.2	53.8	
9-Li	76.6	30.4	159.8	54.3	
C. Cyclic ketimines					
10	29.6	37.9	178.1	63.7	
10-Li	79.5	37.7	162.1	61.0	
11	37.2	33.6	178.2	60.9	
11-Li (major)		74.6	165.4	56.2	
11-Li (minor)		78.3	162.5	57.2	
D. *N-tert*-butylimines					
12		23.1	154.2	57.8	
12-Li	66.0		154.0	53.8	
13		30.9	158.9	57.6	
13-Li	77.8		150.4	53.2	
14		35.6	162.9	57.3	
14-Li	93.3		142.7	53.3	
15	22.5	32.1	163.6	55.7	
15-Li	67.6		158.1	52.9	
16-*anti*[a]		38.2	166.2	55.5	
16-*syn*[a]	21.2	36.3	168.4	55.5	
Lithiation shifts in allyl lithiums[b]					Ref.
17	10.6	124	124	10.6	10
17-Li	30	143	76	14	11
18	17.3	125	125	17.3	10
18-Li	32	145	79	19	11
19	12.8	125.3	127.8	41.1	12
19-Li	31.0	142.5	81.9	43.2	12
20	17.9	127.1	128.7	47.7	12
20-Li	—	146.0	79.6	50.7	12

[a] Shifts for the related hydrazonium iodides of 2-butanone were recently reported (14).
[b] Shifts in ppm from TMS. All shifts measured in THF except for **17** and **18** which were measured in chloroform-*d*.

is seen at C-4 where all ketimines give negligible shifts (±1 ppm) in contrast to the 9 ppm upfield shifts of aldimines. This is of course a result of the lack of any *anti* to *syn* configurational change in the ketimine series and therefore no introduction of a γ-shielding factor.

Can. J. Chem. Downloaded from www.nrcresearchpress.com by 210.87.254.5 on 09/06/12
For personal use only.

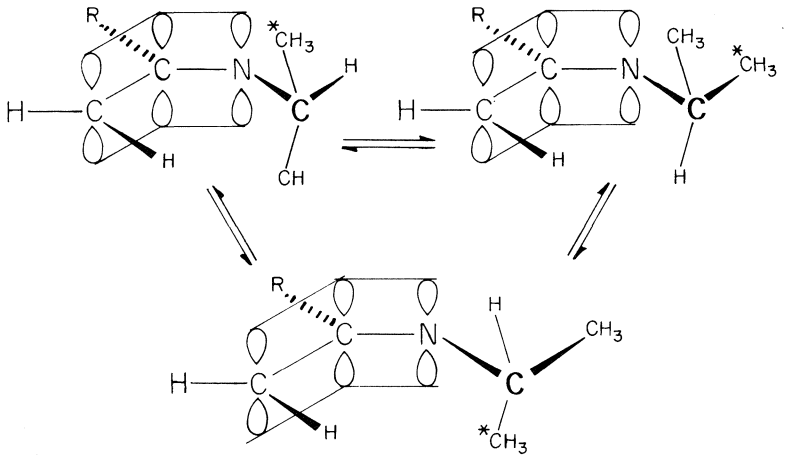

SCHEME 1

C. Cyclic Ketimines

The lithiation shifts for the exocyclic imine, **10**, do not differ significantly from those of either the open ketimine, **9**, or the endocyclic imine, **11**. One might attempt to utilize the fact that the shift for the *anti* lithiated α carbon in **11** is at higher field (δ 78) than would be expected for a *syn* lithiated carbon (i.e., the *syn*-lithiated carbon of **9** shifted 51 ppm downfield in **9**-Li), while the *anti*-lithiated carbon of **11**-Li is only shifted 41 and 45 ppm downfield in the two lithiation products (which differ in configuration at the C-1—C-2 bond). The magnitude of the downfield shift could be considered as diagnostic of the stereochemistry. However, the mobility of **9**, which surely changed on lithiation, precludes its use as a model for comparison with the data of the rigid imine **11**.

D. N-tert-*Butylimines*

Only one configuration in this category, that for **15**-Li has been established as *syn* by means of chemical evidence. Methylation of **15**-Li gave a single product **16** which was assigned the *syn* configuration on the basis of its slow subsequent isomerization to a mixture dominant in its *anti* configurational isomer, *anti* being expected to be the more stable isomer on the basis of steric interactions. Examination of the ^{13}C spectral data for **12–15** in comparison with **1**, **2**, **4**, and **5**, which are the *N*-isopropyl or *N-sec*-butyl imines of the same carbonyl compounds, provides little firm evidence regarding the configuration about the C-2—N bond in the lithiated *tert*-butyl imines. A comparison of the *syn* **15**-Li with **5**-Li reveals similar shielding parameters for both. Only at C-4 is the effect of the extra methyl group (an α effect) different in the ketimines (5.2 ppm) versus the lithiated species (2.9 ppm). Gamma effects at C-2 and δ effects at C-1 are both small. Indeed, δ effects in sterically crowded environments have generally been found to vary in an unpredictable fashion, up to ±3 ppm (13), so that their potential for providing stereochemical evidence is small. Comparing the lithiation shifts in **1**, **2**, and **4** with those of **12**, **13**, and **14** reveals differences in the upfield shift at C-4 on lithiation. They are smaller in the *tert*-butyl (4 ppm) series than in the isopropyl series (8 ppm) but no conclusion can be made since the lithiation shifts for **15** → **15**-Li (*syn*) and **11** → **11**-Li (*anti*) are also similar (2–4 ppm). Even the similarities at C-1 at lithiated **1**, **2** and **4** (all *syn*) in comparison with C-1 in lithiated **12**, **13**, and **14**, though suggestive, are not conclusive evidence of like configuration. Additional evidence will be required to prove the configurations in these lithiated *N-tert*-butylaldimines. An independent argument can be made for the *syn* configuration in all these species. We have described elsewhere the detection of two rotamers of equivalent energy for **12**-Li as shown in Scheme 1 (4). Since location of one methyl or two methyls "inside" or close to C-1 does not affect the relative energies of the two conformers, it would suggest that replacement of the remaining hydrogen at C-4 by a methyl would not introduce any steric destabilization of the *syn* configuration. This lack of change in steric effect in the lithiated *tert*-butyl imines versus isopropyl imines can in part be attributed to the very large N–C-2–C-1 bond angle of about 133° (3). It is also important to recognize that the smaller N–C-2–C-1 angle calculated to be 128° in the neutral *syn* imine should cause the *syn* isomer of the neutral *tert*-butyl imines to be strained more than their isopropyl counterparts as suggested in footnote 2.

Can. J. Chem. Downloaded from www.nrcresearchpress.com by 210.87.254.5 on 09/06/12
For personal use only.

Acknowledgements

The authors thank the Natural Sciences and Engineering Research Council of Canada for their financial support.

1. R. R. FRASER, J. BANVILLE, and K. L. DHAWAN. J. Am. Chem. Soc. **100**, 7999 (1978).
2. R. R. FRASER and J. BANVILLE. J. Chem. Soc. Chem. Commun. 47 (1979).
3. K. N. HOUK, R. W. STROZIER, N. G. RONDAN, R. R. FRASER, and N. CHUAQUI-OFFERMANNS. J. Am. Chem. Soc. **102**, 1426 (1980).
4. R. R. FRASER, N. CHUAQUI-OFFERMANNS, K. N. HOUK, and N. G. RONDAN. J. Organomet. Chem. **206**, 131 (1981).
5. R. R. FRASER, J. BANVILLE, F. AKIYAMA, and N. CHUAQUI-OFFERMANNS. Can. J. Chem. **59**, 705 (1981).
6. A. ETIENNE and Y. CORREIA. Bull. Soc. Chim. Fr. 3704 (1969).
7. H. O. HOUSE, W. C. LIANG, and P. D. WEEKS. J. Org. Chem. **39**, 3102 (1974).
8. H. O. HOUSE, A. V. PRABHU, and W. V. PHILLIPS. J. Org. Chem. **41**, 1209 (1976).
9. M. P. STROBEL, L. MORIN, D. PAQUER, and C. C. PHAM. Nouv. J. Chim. **5**, 27 (1981).
10. J. B. STOTHERS. Carbon-13 nmr spectroscopy. Academic Press, New York. 1972.
11. J. P. C. M. VAN DONGEN, H. W. D. VAN DIJKNIAN, and M. J. A. DE BIE. Recl. Trav. Chim. Pays-Bas, **93**, 29 (1974).
12. S. BYWATER and D. J. WORSFOLD. J. Organomet. Chem. **159**, 229 (1978).
13. J. W. BLUNT and J. B. STOTHERS. Org. Magn. Reson. **9**, 439 (1977).
14. S. ARSENIYADIS, A. LAURENT, and P. MISON. Bull. Soc. Chim. Fr. II, 233 (1980).

Can. J. Chem. Downloaded from www.nrcresearchpress.com by 210.87.254.5 on 09/06/12
For personal use only.

Complexing and exchange of boron, aluminum, and gallium chlorides with some Lewis bases[1]

BORIS GLAVINCEVSKI AND SYDNEY K. BROWNSTEIN
Division of Chemistry, National Research Council, Ottawa, Ont., Canada K1A 0R9

Received March 31, 1981

BORIS GLAVINCEVSKI and SYDNEY K. BROWNSTEIN. Can. J. Chem. **59**, 3012 (1981).

Boron trichloride and dimethyl sulfide form a 1:1 complex. It exchanges with excess boron trichloride by a displacement mechanism with an activation energy of 5.0 ± 0.5 kcal/mol and with excess dimethyl sulfide by a dissociation mechanism which has an activation energy of 20 ± 1 kcal/mol. The 1:1 complex of $AlCl_3$ and dimethyl sulfide exchanges very rapidly with excess dimethyl sulfide. Equilibria and exchange reactions of $AlCl_3[(CH_3)_2O]$, $AlCl_3[(CH_3)_2O]_2$, and $(CH_3)_2O$ are described. Rapid exchange is always found in the analogous gallium systems. BCl_3 reacts with chloride ion to give BCl_4^- and $B_2Cl_7^-$, which exchange rapidly with excess BCl_3. $AlCl_3$ reacts with Cl^- and BCl_4^- to give $AlCl_4^-$ which does not exchange with $AlCl_3$.

BORIS GLAVINCEVSKI et SYDNEY K. BROWNSTEIN. Can. J. Chem. **59**, 3012 (1981).

Le trichlorure de bore donne un complexe 1:1 avec le sulfure de méthyle. En présence d'un excès de trichlorure de bore, il y a un échange suivant un mécanisme de déplacement avec une énergie d'activation de 5,0 ± 0,5 kcal/mol et en présence d'un excès de sulfure de méthyle suivant un mécanisme de dissociation avec une énergie d'activation de 20 ± 1 kcal/mol. Le complexe 1:1 formé entre $AlCl_3$ et le sulfure de méthyle échange très rapidement avec le sulfure de méthyle en excès. Des équilibres et des réactions d'echange de $AlCl_3$ $[(CH_3)_2O]$ et $AlCl_3[(CH_3)_2O]_2$ avec $(CH_3)_2O$ sont décrits. On a toujours trouvé un échange rapide dans les systèmes semblables du gallium. BCl_3 réagit avec l'ion chlorure pour donner BCl_4^- et $B_2Cl_7^-$, complexes qui échangent rapidement avec le BCl_3 en excès. $AlCl_3$ réagit avec Cl^- et BCl_4^- pour donner $AlCl_4^-$ qui n'échange pas avec $AlCl_3$.

Introduction

Lewis acid–base interactions involving boron trihalides have been widely studied and a variety of exchange rates and mechanisms have been reported (1–6). Exchange of the acid–base complex with excess of Lewis acid has only been reported for boron trifluoride and occurs by a displacement mechanism. Exchange of the complex with an excess of Lewis base has been found to occur via a dissociation mechanism with acetonitrile and trimethylamine as bases and BCl_3 and BBr_3 as Lewis acids (4, 5). Thus far, studies of aluminum halide complexes have been limited to the solid state and to solutions of the halide in acetonitrile, a strongly coordinating solvent (7–14). In acetonitrile both cationic and anionic aluminum species have been identified. It is possible that different results might be obtained if the aluminum halide and Lewis base are allowed to react in an inert solvent. Sulfur dioxide, a good solvent for $AlCl_3$ and its complexes, was chosen for this study. This solvent is not truly inert since it forms a molecular complex with aluminum trichloride (15). The structure of the complex has not been determined although a dimer with SO_2 coordinated to chlorine at each end of the Al_2Cl_6 chain has been suggested.

The tetrachloroborate anion is well known but thus far no evidence has been reported for $B_2Cl_7^-$ although the existence of the analogous $B_2F_7^-$ is well established (16). With aluminum as central atom equilibria have been reported between $AlCl_3$, Cl^-, $AlCl_4^-$, and $Al_2Cl_7^-$ (17, 18). The positions of the equilibria depend upon the solvent.

Experimental

Boron trichloride and aluminum trichloride were purified by fractional distillation and stored in containers on the vacuum system used for sample preparation. Sulfur dioxide and tetramethylammonium chloride were purified and manipulated as previously reported (19).

Proton, ^{11}B, ^{27}Al, and ^{71}Ga resonance spectra were obtained on a Varian Associates XL100 spectrometer equipped with Nicolet Fourier Transform and multinuclear attachments. All spectra are referenced with respect to internal tetramethylsilane (20). For cross-comparison with existing compilations of boron resonance spectra (21), we find Ξ BCl_3 of 32,085,482 (lit. 32,085,486)[2] and Ξ $B(OCH_3)_3$ of 32,084,591 (lit. 32,084,565),[2] well within the variation which may be caused by solvent effects. The most common reference for ^{27}Al has been $Al(H_2O)_6^{3+}$. In order to compare our results with previous literature values Ξ $Al(H_2O)_6^{3+}$ was measured and found to be 26,056,780 (lit 26.057 × 1(

Infrared spectra of potassium bromide pellets of some products were obtained on Beckman Acculab 4 and Perkin–Elmer 283 spectrometers. Raman spectra of solids and sulfur dioxide solutions were obtained by excitation with the 514.5 nm line of a Coherent Radiation argon ion laser and recorded with a Jarrell–Ash 25–100 double monochromator equipped with photon counting detection. Lifetimes in the exchanging systems were determined by comparison of experimental spectra with those calculated by a stochastic method (22).

Tetramethylammonium (TMA) chloroborate: 227.2 mg (2.073 mmol) of well dried TMACl were dissolved in sulfur dioxide and

[1]NRCC No. 19604.

[2]These values are calculated from the various types of results reported in ref. 21.

0008-4042/81/203012-04$01.00/0
©1981 National Research Council of Canada/Conseil national de recherches du Canada

Can. J. Chem. Downloaded from www.nrcresearchpress.com by 210.87.254.6 on 09/06/12
For personal use only.

ERRATA

Can. J. Chem. Downloaded from www.nrcresearchpress.com by 210.87.254.6 on 09/06/12
For personal use only.

2.073 mmol of BCl_3 were added to the solution. All volatile materials were removed under vacuum to give 458.5 mg (2.073 mmol) of product. *Anal.* calcd: B 4.77, Cl 62.5; found: B 4.58, Cl 61.2%.

Results and Discussion

Sulfur dioxide and methylene chloride solutions with a ratio of boron trichloride to dimethyl sulfide from 3:1 to 1:2 and a mole fraction of complex from 0.022 to 0.149 were studied by proton, ^{11}B, and ^{13}C resonance spectroscopy over a temperature range from 245 to 299K. The rate constants as a function of temperature are shown in Fig. 1. The relationships between reaction rates, rate constants, and lifetimes via nuclear magnetic resonance studies have been known for many years (1, 2). Exchange between a free and complexed species, as in eq. [1], can occur either by dissociation of the complex or by displacement of one species in the complex by excess of the free species. In the former case the activation enthalpy for exchange equals the heat of dissociation and the lifetime of the complex is independent of the concentration of the free species. For exchange by displacement the activation enthalpy will be less than the heat of dissociation and the lifetime of the complex will be inversely proportional to the concentration of the free species.

[1] $A^* + A{:}B \rightleftharpoons A^*{:}B + A$

In the present study, we have determined the energetics and exchange mechanisms for exchange of both excess Lewis acid and base upon the same complex, boron trichloride – dimethyl sulfide. From ^{11}B resonance spectroscopy it was possible to obtain the lifetimes of free and complexed boron trichloride as a function of temperature and concentration. At a given temperature the lifetime of complexed BCl_3 varied with concentration of free BCl_3 and a constant value for the rate constant could only be obtained for the kinetics of a displacement reaction. Results for three samples are shown in Fig. 1. The Arrhenius activation energy for BCl_3 exchange was calculated to be 5.0 ± 0.5 kcal/mol.

The second exchange reaction for this system, exchange of free and complexed dimethyl sulfide, was studied by ^1H and ^{13}C spectroscopy. It was found that the lifetime of complexed dimethyl sulfide was independent of the concentration of free dimethyl sulfide and a constant value of the rate constant for exchange was obtained by assumption of a dissociation mechanism. These kinetic results, also shown in Fig. 1, yield an Arrhenius activation energy for dimethyl sulfide exchange of

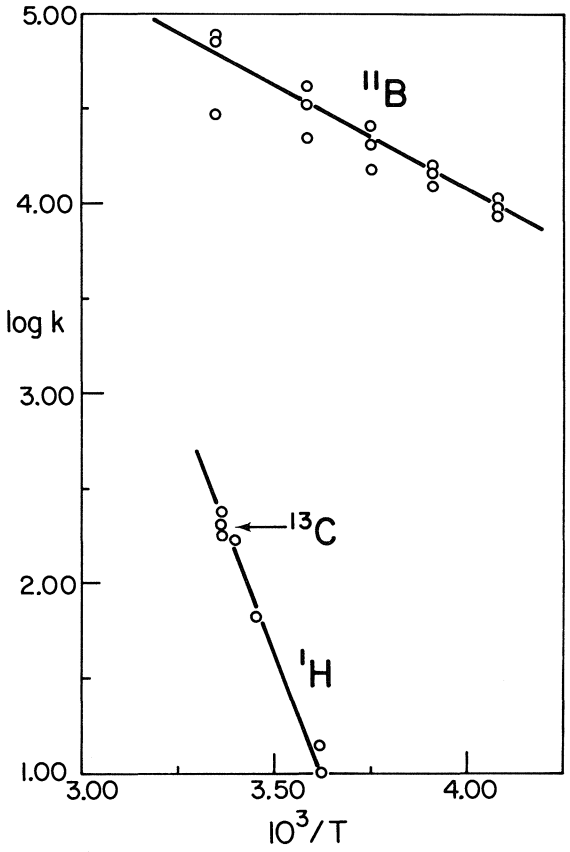

FIG. 1. Temperature dependence for exchange rates with the complex $(CH_3)_2S{\cdot}BCl_3$.

20 ± 1 kcal/mol. The order of activation energies also agrees with the proposed mechanisms.

It therefore appears that exchange of excess Lewis acid by a displacement mechanism and excess Lewis base by a dissociation mechanism may be the usual mechanisms for complexes of boron trihalides. A possible route for exchange with excess boron trichloride is via tetra-coordinate sulfur with the incoming BCl_3 coordinating to the remaining lone pair of electrons on sulfur followed by departure of BCl_3. This possibility would allow a low energy pathway for exchange via displacement. It is difficult to visualize two molecules of dimethyl sulfide coordinated to a single boron trichloride. The higher energy dissociation mechanism of exchange with excess dimethyl sulfide indicates that a lower energy pathway via a displacement reaction is not available. Thus the mechanistic results for dimethyl sulfide exchange are also consistent with chemical intuition.

It would be useful to determine if the mechanisms for exchange with BCl_3 as Lewis acid were

TABLE 1. Chemical shifts of species in the exchange studies

Compound	δ^1H^a	$\Xi^{11}B^b$	$\delta^{13}C^c$	$\Xi^{27}Al^d$	$\Xi^{71}Ga$
$(CH_3)_2S$	2.084		16.62		
$(CH_3)_2SBCl_3$	2.540	32,091,085	20.30		
$(CH_3)_2SAlCl_3$	2.508		19.63	26,059,260	
$(CH_3)_2SGaCl_3$	2.143		18.22		30,515,003
$(CH_3)_2O$	3.232		58.20		
$[(CH_3)_2O]_2AlCl_3$	3.883		64.31	26,059,461	
$(CH_3)_2OAlCl_3$	4.157		65.35	26,059,489	
$CH_3CNAlCl_3$	0.45		2.79	26,059,272	
			44.9 (CN)		
$[CH_3CN]_nAlCl_4^-$	2.7		3.2	26,059,536	
			50 (CN)		
$[CH_3CN]_mAlCl^{2+}$	2.7		3.2	26,056,131	
			50 (CN)		
BCl_3		32,085,482			
TMA BCl_4		32,084,185			
TMA B_2Cl_7		32,084,373			
$AlCl_3$				26,058,956	
$TMAAlCl_4$				26,059,270	
$GaCl_3$					30,514,807
$TMAGaCl_4$					30,514,359

[a] In ppm to low field of TMS.
[b] Ξ for $(CH_3O)_3B$ is 32,084,591.
[c] In ppm to low field of TMS.
[d] Ξ for $(CH_3CH_2)Al$ is 26,060,416 in CH_2Cl_2.

Can. J. Chem. Downloaded from www.nrcresearchpress.com by 210.87.254.6 on 09/06/12
For personal use only.

also followed by $AlCl_3$ and $GaCl_3$. For the aluminum chloride – dimethyl sulfide system in sulfur dioxide solution and for the systems $GaCl_3$–$(CH_3)_2S$ and $GaCl_3$–$(CH_3)_2O$ exchange was too fast to be measured by the nmr technique. The shielding parameters are listed in Table 1. It is to be noted that a complex $2(CH_3)_2S \cdot AlCl_3$ has been reported (21), suggesting that a low energy displacement pathway for exchange of dimethyl sulfide may be available in this system.

Although exchange in the system $AlCl_3$–$(CH_3)_2S$ was too fast to study, in the system $AlCl_3$–$(CH_3)_2O$ the rates were in a convenient range. The geometry of 2:1 complexes of an ether with $AlCl_3$ was found to be a trigonal bipyramid with the ethers at the axial sites (23). Only a 1:1 complex between diethyl ether and $AlCl_3$ was reported for a mixture of the reactants (13). We found both 2:1 and 1:1 complexes of dimethyl ether with $AlCl_3$ in sulfur dioxide solution. Their nuclear magnetic resonance parameters are listed in Table 1.

Samples were prepared with from 4.0 to 1.5 equivalents of $(CH_3)_2O$ for each $AlCl_3$. In those samples containing more than two equivalents of dimethyl ether, signals are observed only for the 2:1 complex and for free ether. There is no evidence for the 1:1 complex. Therefore the kinetics of the exchange between at least one of the dimethyl ether species in the 2:1 complex and free dimethyl ether can be measured directly. The exchange rates for $(CH_3)_2O$ in the 2:1 complex are listed in Table 2. Since they are independent of the

TABLE 2. Exchange rates for dimethyl ether in the 2:1 complex with free dimethyl ether and that in the 1:1 complex

Mole fraction		T (°C)	k s^{-1}
$[(CH_3)_2O]_2AlCl_3$	$(CH_3)_2O$		
0.020	0.040	−60	2
		−50	67
		−40	690
0.011	0.011	−60	3
		−50	50
		−40	1,000
$[(CH_3)_2O]_2AlCl_3$	$(CH_3)_2OAlCl_3$		
0.018	0.011	−60	10
		−50	180
0.042	0.018	−60	12

concentration of free dimethyl ether this implies that exchange occurs via a dissociation of at least one bound ether from the 2:1 complex. From an Arrhenius plot of the average rate for these samples an activation energy of 29.3 ± 0.5 is obtained. The limited temperature range and number of data points precludes an accurate measure but an activation energy of about 30 kcal/mol is reasonable for a dissociation process. It compares reasonably well with the value of 20 kcal/mol for the dissociation mechanism found for $BCl_3 \cdot (CH_3)_2S$.

In those samples containing less than two equivalents of ether per $AlCl_3$ only signals of the 2:1 and 1:1 complexes are observed. The exchange between these species can then be determined without interference. The exchange rates for $(CH_3)_2O$ in the 2:1 complex with that in the 1:1 complex are

Can. J. Chem. Downloaded from www.nrcresearchpress.com by 210.87.254.6 on 09/06/12
For personal use only.

also listed in Table 2. Within the rather large limits of error the rates are the same for exchange of the 2:1 complex with either free ether or the 1:1 complex. This is also strong confirmation that the exchange occurs via dissociation of one dimethyl ether from the 2:1 complex.

Disproportionation and ionization to yield $AlCl_4^-$ and $AlCl^{2+}$, both solvated, have been reported when $AlCl_3$ is dissolved in acetonitrile (7). Very recent results present evidence for some $CH_3CN \cdot AlCl_3$ and various solvated CH_3CN species (24). Since the behaviour of neat acetonitrile is rather different from that found for dimethyl ether and dimethyl sulfide in sulfur dioxide as solvent, the system $AlCl_3$–acetonitrile was investigated in SO_2 solvent. With an excess of aluminum trichloride only the complex $CH_3CN \cdot AlCl_3$ and uncomplexed $AlCl_3$ were observed via ^1H, ^{13}C, and ^{27}Al resonance spectroscopy. The shielding parameters are listed in Table 1. With approximately equal concentrations of $AlCl_3$ and CH_3CN both the 1:1 complex and the ionized species previously reported were observed via their ^{27}Al resonances. The shielding parameters for $AlCl_4^-$ and $AlCl^{2+}$ are also listed in Table 1 and agree with the previously reported values (7). With ratios of two or three CH_3CN for each $AlCl_3$ only the ionized species were observed. At −60°C in the proton resonance spectra of these solutions considerable fine structure was observed for the coordinated acetonitrile, suggesting different environments for these species. These results show that CH_3CN, in an inert solvent, with an excess of $AlCl_3$, behaves similarly to $(CH_3)_2S$ and $(CH_3)_2O$ as a Lewis base. The rather different behaviour when acetonitrile is in excess is presumably due to its strong coordinating tendency for the aluminum ion.

It is possible to study exchange and competitive complexing of the Group III chlorides BCl_3, $AlCl_3$, and $GaCl_3$ with the common Lewis base, chloride ion. The reaction of chloride ion and BCl_3 to give BCl_4^- is long established but further reaction to give $B_2Cl_7^-$ has not been previously reported. There is rapid boron exchange on the nmr time scale between BCl_4^- and BCl_3. The chemical shift for the boron resonance in a solution of composition $B_2Cl_7^-$ is not the weighted average of those for BCl_3 and BCl_4^-. With an excess of BCl_3 the chemical shift of the single line observed is that of a weighted average for $B_2Cl_7^-$ and BCl_3. The shielding parameters are listed in Table 1. These results suggest, but do not prove, the existence of $B_2Cl_7^-$ in solution. It was not possible to isolate $TMAB_2Cl_7$ since a reaction with the solvent occurred upon concentration, or standing at room temperature, to yield an insoluble product with a very different elemental composition.

In sulfur dioxide as solvent $AlCl_3$ and $AlCl_4^-$ are observed as separate ^{27}Al resonances with no evidence of reaction or exchange. Perhaps the complex of $AlCl_3$ with the SO_2 solvent is stronger than that which might be formed with $AlCl_4^-$. In a competition experiment for chloride ion it was found that for an initially equimolar mixture of Cl^-, BCl_3, and $AlCl_3$ only BCl_3 and $AlCl_4^-$ were observed at equilibrium. There was no evidence for BCl_4^- nor $BAlCl_7^-$. Shielding parameters for these and the corresponding gallium species are given in Table 1.

1. S. Brownstein, A. M. Eastham, and G. A. Latremouille. J. Phys. Chem. **67**, 1028 (1963).
2. J. B. De Roos and J. P. Oliver. Inorg. Chem. **4**, 1741 (1965).
3. A. H. Cowley and J. L. Mills. J. Am. Chem. Soc. **91**, 2911 (1969).
4. J. Fogelman and J. M. Miller. Can. J. Chem. **50**, 1262 (1972).
5. J. R. Blackborow. J. Chem. Soc. Dalton Trans. 2139 (1973).
6. M. J. Bula and J. S. Hartman. J. Chem. Soc. Dalton Trans. 1047 (1973).
7. I. R. Beattie, P. J. Jones, J. A. K. Howard, L. E. Smart, C. J. Gilmore, and J. W. Akitt. J. Chem. Soc. Dalton Trans. 528 (1979).
8. T. Okuda, H. Ohta, H. Ishihara, K. Yamada, and H. Negita. Bull. Chem. Soc. Jpn. **53**, 2721 (1980).
9. J. E. Hon. Mol. Phys. **15**, 57 (1968).
10. H. Haraguchi and S. Fujiwara. J. Phys. Chem. **73**, 3467 (1969).
11. J. W. Akitt and R. H. Duncan. J. Magn. Reson. **25**, 391 (1977).
12. J. F. O'Brian and M. Alei. J. Phys. Chem. **74**, 743 (1970).
13. R. L. Richards and A. Thompson. J. Chem. Soc. A, 1244 (1967).
14. R. L. Richards and A. Thompson. J. Chem. Soc. A, 1248 (1967).
15. H. Gerding and E. Smit. Z. Physik. Chem. Abt. B, **51**, 200 (1942).
16. S. Brownstein and J. Paasivirta. Can. J. Chem. **43**, 1645 (1965).
17. R. J. Gale, B. Gilbert, and R. A. Osteryoung. Inorg. Chem. **17**, 2728 (1978).
18. U. Anders and J. Plambeck. J. Inorg. Nucl. Chem. **40**, 387 (1978).
19. S. Brownstein and G. Latremouille. Can. J. Chem. **56**, 2764 (1978).
20. S. Brownstein and J. Bornais. J. Magn. Reson. **38**, 131 (1980).
21. R. K. Harris and B. E. Mann. NMR and the periodic table. Academic Press, London. 1978.
22. R. A. Sack. Mol. Phys. **1**, 163 (1958).
23. A. H. Cowley, M. C. Cushner, R. E. Davis, and P. E. Riley. Inorg. Chem. **20**, 1179 (1981).
24. F. W. Wehrli and R. Hoerdt. J. Magn. Reson. **42**, 334 (1981).

Can. J. Chem. Downloaded from www.nrcresearchpress.com by 210.87.254.42 on 09/06/12
For personal use only.

The effect of the leaving group on the nature of the E2 transition state for reaction of 2-aryl-1-phenylethylammonium ions with ethoxide in ethanol

SHUNE-LONG WU AND PETER JAMES SMITH[1]

Department of Chemistry and Chemical Engineering, University of Saskatchewan, Saskatoon, Sask., Canada S7N 0W0

Received May 29, 1981

SHUNE-LONG WU and PETER JAMES SMITH. Can. J. Chem. **59**, 3016 (1981).

The reaction of 2-aryl-1-phenylethylammonium salts with ethoxide in ethanol at 40°C for five different amine leaving groups has been investigated. A significant dependence of the rate of reaction on the basicity of the leaving group was found. The variation of the primary hydrogen–deuterium isotope effect and pK_a of the leaving group was not linear and it is concluded that the proton is less than one-half transferred to base at the transition state for reactions involving the best two leaving groups. In support of this conclusion is the observed opposite variation of k^H/k^D with ring substituents for the various leaving groups, i.e., for *N*-methylpyrrolidine, $k^H/k^D = 4.58$, 4.72, and 5.01 for *p*-Me, H, and *p*-Cl, respectively; for *N*-methylmorpholine, $k^H/k^D = 6.13$, 5.73, and 5.50 for *p*-Me, H, and *p*-Cl, respectively.

SHUNE-LONG WU et PETER JAMES SMITH. Can. J. Chem. **59**, 3016 (1981).

Opérant à 40°C, on a étudié la réaction des sels d'aryl-2 phényléthyl-1 ammonium portant cinq groupes amino nucléofugues différents sous l'influence de l'ion éthanolate dans l'éthanol. On a trouvé que la basicité du groupe nucléofugue affecte de façon marquée la vitesse de la réaction. L'effet isotopique primaire hydrogène-deutérium ne varie pas d'une façon linéaire avec le pK_a du groupe nucléofugue; on en conclut que le proton est transferré très partiellement à la base pendant l'étape de transition de la réaction qui fait intervenir les deux meilleurs groupes labiles. A l'appui de cette conclusion, on a observé une variation contraire de k^H/k^D avec les substituants du cycle pour différents groupes nucléofugues, ainsi avec la *N*-méthylpyrolidine, le k^H/k^D varie de 4,58 à 4,72 et à 5,01 pour les groupes *p*-Me, H et *p*-Cl. Dans le cas de *N*-méthylmorpholine, ces valeurs sont respectivement de 6,13, 5,73 et 5,50.

[Traduit par le journal]

Elimination reactions have been investigated in considerable detail. The effect of β and α substituents as well as changes in the abstracting base and solvent on the nature of the E2 transition state have been extensively studied. However, detailed studies on the effect of changes in the leaving group on the E2 transition state have been limited (1, 2).

Alunni and Jencks (2) studied the reaction of 2-phenylethylammonium salts with ethoxide in ethanol for various substituted quinuclidines as leaving group and found $\beta_{lg} = -0.28$. The results of Schmid and Bourns (1) in a study on the same system with substituted anilines as leaving groups give $\beta_{lg} = -0.26$ to -0.31. As well, we have recently investigated the same reaction for nine different amine leaving groups where the pK_a was varied over 6 units and found a value of $\beta_{lg} = -0.28$.[2]

Due to the dependence of the rate of reaction on the pK_a of the leaving amine a transition state with significant carbon leaving-group rupture is indicated. In order to investigate in more detail the effect of the leaving group on the nature of the E2 transition state we have studied the reaction of 2-aryl-1-phenylethylammonium ions with five different amine leaving groups with ethoxide at 40°C to give the more stable stilbene product as compared with styrene obtained in the earlier studies (1, 2). In all cases elimination was the sole reaction and only *trans* 4-substituted stilbenes were formed. The rate constant (measured by the spectrophotometric procedure), primary hydrogen–deuterium isotope effects, rho (ρ), and the pK_a for the different amine leaving groups are shown in Table 1.

A plot of log k_2 versus pK_a (determined in H_2O) was made in order to determine the Bronsted β for the leaving group. There was no apparent correlation, in contrast to the 2-phenylethyl series (1, 2), and this observation will be discussed in a subsequent publication. It is seen that the ρ values are the same within experimental error for the first three leaving groups, but they are significantly greater than the values obtained for the two best leaving groups, *N*,*N*-dimethylbenzylamine and *N*-methylmorpholine. The fact that ρ decreases as the pK_a of the leaving group decreased suggests that the better

[1]Author to whom correspondence should be addressed.

[2]T. S. Grover and P. J. Smith, unpublished results.

0008-4042/81/203016-03$01.00/0

©1981 National Research Council of Canada/Conseil national de recherches du Canada

TABLE 1. Rate constants, primary k^H/k^D, rho (ρ), and the pK_a for the different amine leaving groups for the reaction of 2-aryl-1-phenylethylammonium ions with ethoxide in ethanol at 40°C

Leaving group	$k_2 \times 10^4$ (M^{-1} s^{-1})[a]	pK_a	k^H/k^D	rho (ρ)
N-methylpyrrolidine	1.48±0.01	10.32	4.72±0.04[b]	2.74±0.24
Trimethylamine	4.29±0.04	9.81	5.60±0.05	2.80±0.21
N-methylpiperidine	4.98±0.02	10.08	6.32±0.03	2.67±0.19
N,*N*-dimethylbenzylamine	14.3±0.1	9.02	6.61±0.05	2.17±0.17
N-methylmorpholine	22.1±0.1	7.40	5.73±0.03	2.15±0.18

[a] Rate constants are for aryl = phenyl.
[b] Deviation = $\pm k^H/k^D[(r^H/k^H)^2 + (r^D/k^D)^2]^{\frac{1}{2}}$, where r is the standard deviation in k.

TABLE 2. Rate constants and primary hydrogen–deuterium isotope effects for reaction of 2-aryl-1-phenylethylammonium ions with ethoxide in ethanol at 40°C

Leaving group	*para* Substituent	$k_2 \times 10^4$ (M^{-1} s^{-1})	(k^H/k^D)[a]
N-methylpyrrolidine	Me	0.618±0.002	4.58±0.04
	H	1.48±0.01	4.72±0.04
	Cl	7.56±0.03	5.01±0.04
Trimethylamine	MeO	0.685±0.003	5.20±0.03
	Me	1.87±0.01	—
	H	4.29±0.04	5.60±0.05
	Cl	19.6±0.3	5.80±0.10
N-methylpiperidine	MeO	0.960±0.002	5.08±0.03
	Me	2.39±0.02	6.15±0.03
	H	4.98±0.02	6.32±0.03
	Cl	23.4±0.3	5.91±0.05
N,*N*-dimethylbenzylamine	Me	7.06±0.04	6.76±0.06
	H	14.3±0.1	6.61±0.05
	Cl	51.6±0.2	6.02±0.04
N-methylmorpholine	Me	11.1±0.1	6.13±0.06
	H	22.1±0.1	5.73±0.03
	Cl	79.2±0.3	5.50±0.08

[a] Deviation = $\pm k^H/k^D[(r^H/k^H)^2 + (r^D/k^D)^2]^{\frac{1}{2}}$ where r is the standard deviation in k.

leaving groups lead to an E2 transition state where there is less carbon–hydrogen bond weakening.

The variation of k^H/k^D with the pK_a of the leaving group is of particular significance. It is seen that k^H/k^D *increases* initially when the leaving group becomes less basic, but a further decrease in pK_a leads to a *decrease* in the magnitude of the hydrogen–deuterium isotope effect. This behaviour suggests that at least when the leaving group is *N*-methylmorpholine the proton is less transferred to base at the transition state (3). The theoretical treatments of both Winey and Thornton (4) and More O'Ferrall (5) predict less C—H bond rupture for an E2 transition state when the leaving group is made better.

In order to investigate further the degree of proton transfer, a series of 2-aryl-1-phenylethylammonium salts and their β,β-d_2 analogues were prepared and the rate constants and k^H/k^D were determined for reaction with ethoxide in ethanol at 40°C, Table 2. It is noted that for reactions involving the two poorest leaving groups, *N*-methylpyrrolidine and trimethylamine, the magnitude of k^H/k^D increases when the ring substituent is changed from electron-donating to electron-withdrawing. This behaviour is expected for a transition state where the proton is more than one-half transferred to base (6).

On the other hand, however, for the better leaving group, *N*-methylpiperidine, the magnitude of k^H/k^D increases when the ring substituent is changed from MeO to H, but *decreases* when electron-withdrawing chlorine is the substituent. This behaviour suggests that the proton is approximately one-half transferred to base, slightly more for the *p*-MeO reaction and slightly less for the *p*-Cl process.

For the best two leaving groups, where the consideration of ρ and k^H/k^D indicated the least degree of C—H bond weakening for the various leaving groups studied, the trend of k^H/k^D with variation of ring substituent is exactly the opposite

Can. J. Chem. Downloaded from www.nrcresearchpress.com by 210.87.254.42 on 09/06/12
For personal use only.

to that found for the two poorest leaving groups (k^H/k^D is the least for electron-withdrawing substituents). The conclusion is reached that for the two best leaving groups, the proton is *less* than one-half transferred to base at the transition state.

Acknowledgement

The authors gratefully acknowledge the financial support of this work by the Natural Sciences and Engineering Research Council of Canada.

1. P. SCHMID and A. N. BOURNS. Can. J. Chem. **53**, 3513 (1975).
2. S. ALUNNI and W. P. JENCKS. J. Am. Chem. Soc. **102**, 2052 (1980).
3. F. H. WESTHEIMER. Chem. Rev. **61**, 265 (1961).
4. D. A. WINEY and E. R. THORNTON. J. Am. Chem. Soc. **97**, 3102 (1975).
5. R. A. MORE O'FERRALL. J. Chem. Soc. B, 274 (1970).
6. P. J. SMITH and A. N. BOURNS. Can. J. Chem. **52**, 749 (1974).

Can. J. Chem. Downloaded from www.nrcresearchpress.com by 210.87.254.42 on 09/06/12
For personal use only.

The structure of ravidomycin

JOHN A. FINDLAY AND JIA-SEN LIU
Department of Chemistry, University of New Brunswick, Fredericton, N.B., Canada E3B 6E2
LAJOS RADICS
NMR Laboratory, Central Research Institute for Chemistry, P.O. Box 17, H-1525 Budapest, Hungary
AND
S. RAKHIT
Ayerst Research Laboratories, P.O. Box 6115, Montreal, P.Q., Canada H3C 3J1

Received May 8, 1981

JOHN A. FINDLAY, JIA-SEN LIU, LAJOS RADICS, and S. RAKHIT. Can. J. Chem. **59**, 3018 (1981).
The structure **1***a* is proposed for ravidomycin on the basis of chemical and spectroscopic data.

JOHN A. FINDLAY, JIA-SEN LIU, LAJOS RADICS et S. RAKHIT. Can. J. Chem. **59**, 3018 (1981).
En se basant sur les données chimiques et spectroscopiques on propose la structure **1***a* pour la ravidomycine.
[Traduit par le journal]

Ravidomycin, isolated from the fermentation broth of *Streptomyces ravidus*, possesses strong inhibitory effect on gram positive organisms and potent antitumor activity (1). We propose structure **1***a* for ravidomycin[1] based on chemical and spectral information.

Ravidomycin, $C_{31}H_{33}NO_9$ (M^+ 563.2148), mp 248–250°C, $[\alpha]_D^{26}$ −105.5°, has an infrared (ir) spectrum which shows the presence of two carbonyls (1740, 1720 cm^{-1}), an aromatic system (1620, 1600, 1580 cm^{-1}), and hydroxyl groups (3380 cm^{-1}). Its ultraviolet (uv) spectrum λ_{max}(MeOH) nm (log ε): 244 (4.68), 263 (4.54, sh), 277 (4.60), 285 (4.65), 308 (4.33), 320 (4.30), 335 (4.20), 350 (4.08), 392 (4.24) reveals the presence of a substituted naphthalene system (2). The ^1H nmr spectra of ravidomycin **1***a* and its diacetate **1***b* (see Table 1) attest to the presence of *ortho* (one pair), *meta* (one pair), and isolated (one) aromatic protons, which features can only be accommodated by inclusion of two tetrasubstituted and one pentasubstituted aromatic rings. Fusion of ravidomycin with alkali affords the aglycone **2***a* which features in its ^1H nmr ($CDCl_3$) spectrum six aromatic hydrogens, three of which (H-6, δ 7.00, dd, J = 8.0/0.8; H-7, δ 7.50, dd, J = 8.0/8.0; H-8, δ 8.04, dd, J = 8.0/0.8) are in a 1,2,3 relationship clearly demonstrating the position of the *C*-glycosidic moiety relative to the *ortho* hydrogens. This aglycone can be hydrogenated (Pt/glacial acetic acid) to a desoxohexahydro derivative **3** in which the original aglycone-containing ring has suffered reduction and has also been the site of hydrogenolysis of the phenolic hydroxyl. Alkali fusion of ravidomycin also furnishes diastereomeric hemiacetal carboxylic acids (~ 1:1) **4***a*, which provides compelling evidence for the relationship of the *C*-glycosidic bond and the

[1]Ravidomycin **1***a* possesses the same aglycone moiety as the newly reported antibiotics toromycin (4) and gilvogarcin V (5).

0008-4042/81/203018-03$01.00/0
©1981 National Research Council of Canada/Conseil national de recherches du Canada

to that found for the two poorest leaving groups (k^H/k^D is the least for electron-withdrawing substituents). The conclusion is reached that for the two best leaving groups, the proton is *less* than one-half transferred to base at the transition state.

Acknowledgement

The authors gratefully acknowledge the financial support of this work by the Natural Sciences and Engineering Research Council of Canada.

1. P. SCHMID and A. N. BOURNS. Can. J. Chem. **53**, 3513 (1975).
2. S. ALUNNI and W. P. JENCKS. J. Am. Chem. Soc. **102**, 2052 (1980).
3. F. H. WESTHEIMER. Chem. Rev. **61**, 265 (1961).
4. D. A. WINEY and E. R. THORNTON. J. Am. Chem. Soc. **97**, 3102 (1975).
5. R. A. MORE O'FERRALL. J. Chem. Soc. B, 274 (1970).
6. P. J. SMITH and A. N. BOURNS. Can. J. Chem. **52**, 749 (1974).

Can. J. Chem. Downloaded from www.nrcresearchpress.com by 210.87.254.5 on 09/06/12
For personal use only.

The structure of ravidomycin

JOHN A. FINDLAY AND JIA-SEN LIU
Department of Chemistry, University of New Brunswick, Fredericton, N.B., Canada E3B 6E2
LAJOS RADICS
NMR Laboratory, Central Research Institute for Chemistry, P.O. Box 17, H-1525 Budapest, Hungary
AND
S. RAKHIT
Ayerst Research Laboratories, P.O. Box 6115, Montreal, P.Q., Canada H3C 3J1

Received May 8, 1981

JOHN A. FINDLAY, JIA-SEN LIU, LAJOS RADICS, and S. RAKHIT. Can. J. Chem. **59**, 3018 (1981).
The structure **1***a* is proposed for ravidomycin on the basis of chemical and spectroscopic data.

JOHN A. FINDLAY, JIA-SEN LIU, LAJOS RADICS et S. RAKHIT. Can. J. Chem. **59**, 3018 (1981).
En se basant sur les données chimiques et spectroscopiques on propose la structure **1***a* pour la ravidomycine.
[Traduit par le journal]

Ravidomycin, isolated from the fermentation broth of *Streptomyces ravidus*, possesses strong inhibitory effect on gram positive organisms and potent antitumor activity (1). We propose structure **1***a* for ravidomycin[1] based on chemical and spectral information.

Ravidomycin, $C_{31}H_{33}NO_9$ (M^+ 563.2148), mp 248–250°C, $[\alpha]_D^{26}$ −105.5°, has an infrared (ir) spectrum which shows the presence of two carbonyls (1740, 1720 cm^{-1}), an aromatic system (1620, 1600, 1580 cm^{-1}), and hydroxyl groups (3380 cm^{-1}). Its ultraviolet (uv) spectrum λ_{max}(MeOH) nm (log ε): 244 (4.68), 263 (4.54, sh), 277 (4.60), 285 (4.65), 308 (4.33), 320 (4.30), 335 (4.20), 350 (4.08), 392 (4.24) reveals the presence of a substituted naphthalene system (2). The ^1H nmr spectra of ravidomycin **1***a* and its diacetate **1***b* (see Table 1) attest to the presence of *ortho* (one pair), *meta* (one pair), and isolated (one) aromatic protons, which features can only be accommodated by inclusion of two tetrasubstituted and one pentasubstituted aromatic rings. Fusion of ravidomycin with alkali affords the aglycone **2***a* which features in its ^1H nmr ($CDCl_3$) spectrum six aromatic hydrogens, three of which (H-6, δ 7.00, dd, J = 8.0/0.8; H-7, δ 7.50, dd, J = 8.0/8.0; H-8, δ 8.04, dd, J = 8.0/0.8) are in a 1,2,3 relationship clearly demonstrating the position of the *C*-glycosidic moiety relative to the *ortho* hydrogens. This aglycone can be hydrogenated (Pt/glacial acetic acid) to a desoxohexahydro derivative **3** in which the original aglycone-containing ring has suffered reduction and has also been the site of hydrogenolysis of the phenolic hydroxyl. Alkali fusion of ravidomycin also furnishes diastereomeric hemiacetal carboxylic acids (~ 1:1) **4***a*, which provides compelling evidence for the relationship of the *C*-glycosidic bond and the

[1]Ravidomycin **1***a* possesses the same aglycone moiety as the newly reported antibiotics toromycin (4) and gilvogarcin V (5).

0008-4042/81/203018-03$01.00/0
©1981 National Research Council of Canada/Conseil national de recherches du Canada

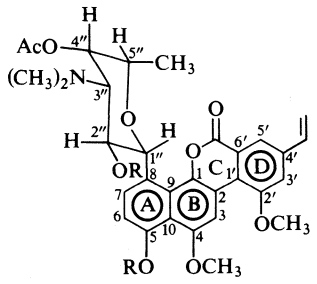

1*a* R = H
1*b* R = Ac

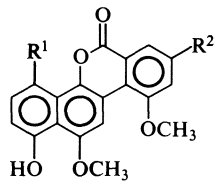

2*a* R^1 = H, R^2 = —CH=CH_2
2*b* R^1 = —CH_2CHO, R^2 = —CH_2CH_3

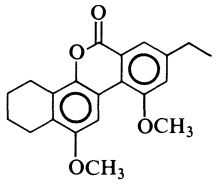

3

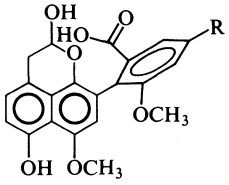

4*a* R = —CH=CH_2
4*b* R = —CH_2—CH_3

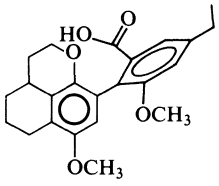

5

ethereal oxygen of the original lactone system in **1**. Thus the mixture **4***a* displays in its ^{1}H nmr ($CDCl_3$) spectrum signals at δ 5.38 (dd, 0.5H, J = 3.0/7.2) and δ 5.67 (dd, 0.5H, J = 3.0/3.0) corresponding to the hemiacetal proton coupled to the CH_2-8 multiplet at δ 3.00–3.30. The existence of **4***a* in diastereomeric form is no doubt due to restricted rotation around the C2—C1′ bond. Transformation of **4***a* by catalytic hydrogenation (Pt/glacial acetic acid) into the dihydropyran **5** parallels the reduc-

TABLE 1. ^{1}H nmr parameters* of ravidomycin **1***a* and its diacetate **1***b*

Proton	**1***a*	**1***b*
H-3	8.47 (s)	8.59 (s)
H-7	7.99 (AB, $J_{6,7}$ = 8.4)	7.98† (AB, $J_{6,7}$ = 8.4)
H-6	7.07 (AB, $J_{6,7}$ = 8.4)	7.22† (AB, $J_{6,7}$ = 8.4)
H-5′	8.11 (d, $J_{3',5'}$ = 1.5)	8.16 (d, $J_{3',5'}$ = 1.5)
H-3′	7.36 (d, $J_{3',5'}$ = 1.5)	7.42 (d, $J_{3',5'}$ = 1.5)
OCH_3-4	4.11 (s)	4.00 (s)
OCH_3-2′	4.11 (s)	4.13 (s)
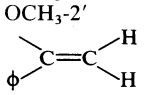	5.47 (d, J_{cis} = 10.9) 5.96 (d, J_{trans} = 17.5)	5.49 (d, J_{cis} = 10.9) 5.98 (d, J_{trans} = 17.5)
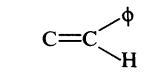	6.82 (dd, J_{cis} = 10.9, J_{trans} = 17.5)	6.84 (dd, J_{cis} = 10.9, J_{trans} = 17.5)
H-1″	5.87 (d, $J_{1'',2''}$ = 9.0)	6.31 (d, $J_{1'',2''}$ = 10.0)
H-2″	4.46 (dd, $J_{1'',2''}$ = 9.0, $J_{2'',3''}$ = 10.3)	5.75 (dd, $J_{1'',2''}$ = 10.0, $J_{2'',3''}$ = 10.3)
H-3″	3.10 (dd, $J_{3'',4''}$ = 2.4, $J_{2'',3''}$ = 10.3)	3.25 (dd, $J_{3'',4''}$ = 2.4, $J_{2'',3''}$ = 10.3)
H-4″	5.57 (dd, $J_{3'',4''}$ = 2.4, $J_{4'',5''}$ = 1.0)	5.60 (dd, $J_{3'',4''}$ = 2.4, $J_{4'',5''}$ = 1.0)
H-5″	4.51 (qd, J_{5'',CH_3} = 6.4, $J_{4'',5''}$ = 1.0)	4.44 (qd, J_{5'',CH_3} = 6.4, $J_{4'',5''}$ = 1.0)
CH_3-5″	1.07 (d, J_{5'',CH_3} = 6.4)	1.15 (d, J_{5'',CH_3} = 6.4)
	2.51 (s)	2.42 (s)
Ac-4″	2.13 (s)	2.17 (s)
Ac-2″		1.60 (s)
Ac-5		2.40 (s)
OH-5	9.83 (s)	
OH-2″	3.57 (br)	

*In $CDCl_3$. Chemical shifts, δ, in ppm relative to internal TMS. Coupling constants, J, in Hz.
†May be interchanged.

Can. J. Chem. Downloaded from www.nrcresearchpress.com by 210.87.254.5 on 09/06/12
For personal use only.

tion and hydrogenolysis of **2***a* to **3** and confirms the fact that the hemiacetal ring in **4***a* utilizes the phenolic oxygen derived from opening of the lactone. The lactone aldehyde **2***b* is obtainable by heating **4***b* in quinoline at 180°C in the presence of copper affording corroboration of the relationship of lactone and sugar in **1***a*.

The lactone ring in ravidomycin must unite the tetrasubstituted phenyl ring bearing the *meta* hydrogens to the pentasubstituted naphthalene ring and placement of the substituents on this ring D follows from the juxtaposition of groups on the known anisole-2,3,5-tricarboxylic acid obtainable by hot alkaline permanganate treatment of **1***a*, together with analysis of ^{1}H nmr chemical shift data on various compounds. For example, in compound **3** the solvent-induced chemical shift for the *meta* protons, $\Delta_{C_6H_6}(CDCl_3) = -0.23$ ppm for H-5′ and +0.46 ppm for H-3′ is as predicted by the "carbonyl plane rule" (3). Mutual proton decoupling experiments on ravidomycin diacetate **1***b* give rise to a significant narrowing of the resonance lines due to H-3′ (δ 7.42) and the OCH_3-2′ (δ 4.13) which indicates an *ortho* relationship between the respective carbons. In a similar manner it was shown that the isolated aromatic proton H-3 is *ortho* to the remaining methoxyl group. Furthermore, when the lactone ring is opened, as in **4***a*, the isolated aromatic proton and one methoxyl are shifted 1.58 ppm and 0.32 ppm upfield, respectively, relative to the corresponding signals in **2***a* and this can only be explained if the isolated aromatic proton and one methoxyl are located at C-3 and C-2′, respectively, where both are deshielded when the lactone ring is closed and shielded when it is open and the angle between the planes of the two aromatic systems is changed substantially.

The structure of the amino sugar moiety follows from consideration of ^{1}H nmr data on ravidomycin and its diacetate, together with a full set of appropriate decoupling experiments which confirmed the presence of the 3,6-dideoxy-3-*N*,*N*-dimethylamino pseudo altropyranose in the conformation (with H-7 and H-1″ *S-trans*) indicated in **1***a*. The absolute configuration of the molecule has yet to be determined.

The structures of all compounds are fully supported by infrared, ultraviolet, and mass spectral data and are consistent with ^{13}C nmr chemical shift, multiplicity data and selective ^{13}C–{^{1}H} decoupling experiments.

1. (*a*) S. N. SEHGAL and CLAUDE VEZINA. Current chemotherapy and infectious disease. Proceedings of the 11th I.C.C. and the 19th I.C.A.C., American Society of Microbiology. 1980. p. 1553; (*b*) S. N. SEHGAL and CLAUDE VEZINA. U.S. Patent No. 4,230,692 (1980).
2. E. S. STERN and C. J. TIMMONS. Electronic absorption spectroscopy in organic chemistry. 3rd ed. St. Martin's Press, New York. 1971. pp. 113–141.
3. (*a*) F. A. L. ANET and RAGINI ANET. Determination of organic structures by physical methods. Vol. 3. *Edited by* F. C. Nachod and J. J. Suckerman. 1971. p. 383; (*b*) F. SCHEINMANN. Chem. Commun. 1015 (1967).
4. SATOSHI HORII, HIROSHI FUKASE, EIJI MIZUTA, KAZUNORI HATANO, and KOMEI MIZUNO. Chem. Pharm. Bull. **28**, 3601 (1980).
5. KEIICHI TAKAHASHI, MAYUMI YOSHIDA, FUSAO TOMITA, and KUNIKATSU SHIRAHATA. J. Antibiot. **34**, 271 (1981).

Can. J. Chem. Downloaded from www.nrcresearchpress.com by 210.87.254.5 on 09/06/12
For personal use only.

Information from stereospecific spin–spin couplings about the relative absorptivities of the hydroxyl stretching bands in 2-iodophenol solutions

TED SCHAEFER, RUDY SEBASTIAN, and TIMOTHY A. WILDMAN
Department of Chemistry, University of Manitoba, Winnipeg, Man., Canada R3T 2N2

Received May 15, 1981

TED SCHAEFER, RUDY SEBASTIAN, and TIMOTHY A. WILDMAN. Can. J. Chem. **59**, 3021 (1981).

The stereospecific spin–spin coupling constants between the hydroxyl proton and the ring protons for 2-iodophenol in various solvents yield some free energy differences between the *cis* and *trans* conformations of this molecule at 305 K. Comparison with areas of the hydroxyl stretching bands in the same or similar solvents shows that the ratio of the absorptivity coefficients for the two conformers is sensitive to solvent. It is suggested that this ratio is temperature dependent and therefore apparent enthalpy differences must be considered tentative for at least some solutions. Molecular orbital calculations are consistent with the arguments concerning the absorptivity coefficients.

TED SCHAEFER, RUDY SEBASTIAN et TIMOTHY A. WILDMAN. Can. J. Chem. **59**, 3021 (1981).

Les constantes de couplage stéréospécifique entre le proton hydroxylique et les protons du cycle de l'iodo-2 phénol dans divers solvants donnent quelques différences d'énergie libre entre les conformations *cis* et *trans* de cette molécule à 305 K. La comparaison avec les bandes d'élongation de l'hydroxyle dans les mêmes solvants ou dans des solvants identiques montre que le rapport des coefficients d'absorption des deux conformères est sensible au solvant. On suggère que ce rapport dépend de la température et que par conséquent on doit considérer les différences d'enthalpie apparente comme des valeurs expérimentales du moins pour quelques solutions. Les calculs d'orbitales moléculaires sont en accord avec les faits relatifs aux coefficients d'absorption.

[Traduit par le journal]

Can. J. Chem. Downloaded from www.nrcresearchpress.com by 210.87.254.6 on 09/06/12
For personal use only.

Introduction

Infrared spectroscopy is still used for the conformational analysis of intramolecular hydrogen bonding in dilute solutions. A recent review is available (1). In particular, the *trans–cis* equilibrium in 2-iodophenol has been investigated extensively by infrared spectroscopy (1–8), both in the gas phase and in a variety of solvents. The equilibrium constant, K, is given by $(A_c/A_t)(\alpha_t/\alpha_c)$, where A is the area of the hydroxyl stretching band for a conformer and α is its integrated absorption coefficient. This relationship is correct if Beer's law holds.

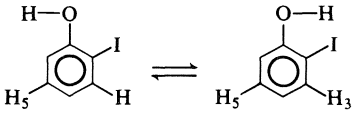

trans, **1***a* *cis*, **1***b*

If α_t/α_c is temperature independent, then the enthalpy difference between the conformers, ΔH, is obtainable from the usual van't Hoff plot. ΔH values were measured in this way for twelve solvents (4). It was also argued that K was given reasonably well by the ratio of band areas (4), thereby yielding free energy differences, ΔG, at 298 K.

In addition, if α_c and α_t are each independent of temperature, then a plot of A_c against A_t is linear and gives α_c/α_t and therefore ΔG (9). The precise data (4) for a CCl_4 solution indicated (9) that α_c/α_t is 13 and that ΔG is very nearly zero for this solution.

In this paper, stereospecific spin–spin couplings are used to derive some ΔG values for the equilibrium in a number of solvents. Comparison with the thermodynamic parameters obtained from the infrared data suggests that α_c/α_t is probably less than one in relatively polar solvents and that it is temperature dependent. These criticisms of the infrared method, as applied to 2-iodophenol, need not apply to the gas phase nor to 2,6-dihalo-substituted phenol derivatives.

Experimental

Solutions of 2-iodophenol (K and K Laboratories) in various solvents contained some tetramethylsilane (TMS) and were transferred to 5 mm od nmr sample tubes. The samples were degassed by the freeze–pump–thaw procedure and were then flame-sealed. ^1H nmr spectra were recorded at a probe temperature of 305 K on an HA100 spectrometer. Calibrations of peak positions were made in the frequency-sweep mode at a center-band frequency of 100.001 MHz (10). Sweep rates were 0.02 and 0.01 Hz/s. Intermolecular proton exchange was retarded in the manner described previously. Linewidths at half height were 0.10 Hz and were no doubt determined by the residual magnetic field inhomogeneity.

Results and Discussion

Spectral Analysis

The spectra for the CCl_4, C_6F_6, CD_2Cl_2, CH_2Br_2, and C_6H_{12} solutions were analyzed precisely with the computer program LAME (11, 12). Spectral parameters appear in Table 1. The $^5J_m^{H,OH}$ obtained by analysis is indistinguishable from the splitting of the OH peaks, no doubt because of the relatively large chemical shift dispersion for the

0008-4042/81/213021-05$01.00/0
©1981 National Research Council of Canada/Conseil national de recherches du Canada

TABLE 1. Chemical shifts and coupling constants for the ring protons in 2-iodophenol at 305 K

Parameter	CCl_4 (4.7 mol%)	C_6F_6 (4.7 mol%)	CH_2Br_2 (0.7 mol%)	CD_2Cl_2 (0.9 mol%)	C_6H_{12} (1.3 mol%)
ν_3[a]	756.789(2)	750.826(2)	766.571(4)	766.441(3)	752.492(3)
ν_4	658.562(2)	633.126(2)	668.772(4)	666.964(3)	652.023(3)
ν_5	715.884(2)	721.949(2)	724.771(4)	723.436(3)	709.590(3)
ν_6	692.968(2)	678.664(2)	697.478(4)	696.835(3)	689.592(3)
$^3J_{34}$	7.950(3)	7.952(3)	7.949(6)	7.952(5)	7.969(4)
$^3J_{45}$	7.307(3)	7.328(3)	7.322(5)	7.318(5)	7.302(4)
$^3J_{56}$	8.164(3)	8.189(3)	8.141(5)	8.151(5)	8.177(4)
$^4J_{35}$	1.557(3)	1.553(3)	1.564(5)	1.558(5)	1.551(4)
$^4J_{46}$	1.514(3)	1.492(3)	1.505(5)	1.491(5)	1.515(4)
$^5J_{36}$	0.282(3)	0.287(3)	0.269(6)	0.283(5)	0.285(4)
Root mean Square deviation	0.006	0.008	0.013	0.012	0.010
Assigned peaks	79	80	66	72	71

[a]In Hz at 100.001 MHz to low field of internal TMS, numbers in parentheses being standard deviations in the last significant figure.

ring protons. Accordingly, for the other solutions $^5J_m{}^{H,OH}$ was found directly from the OH resonance and from splittings in the peaks from H-5.

Because $^5J_m{}^{OH,H_3}$ is clearly very small (when not zero), showing that the *cis* form, **1***b*, is preponderant in all solutions, decoupling experiments were used to investigate the existence of hydroxyl proton couplings other than $^5J_m{}^{OH,H_5}$. It was expected that some coupling to H-6 would be present, $^4J_0{}^{OH,H}$ in phenol being ± 0.07 Hz (13).

The smallest $\Delta\nu_{1/2}$ obtainable in all solutions was 0.10 Hz. In Fig. 1*a*, the OH resonance is displayed for a 2 mol% solution in CCl_3CF_3, showing $\Delta\nu_{1/2}$ as $0.10 + 0.01$ Hz. This was also the linewidth for the ring proton transitions. Decoupling the OH resonance did not decrease the linewidth of any ring proton peaks. By way of comparison, Fig. 1*b* displays the OH doublet for the CCl_4 solution. The width, a $\Delta\nu_{1/2}$ of 0.13 Hz, indicates additional coupling to ring protons other than H-5. As shown, in Fig. 1 *c* and *c'* a multiplet from H-3 shows no change in $\Delta\nu_{1/2}$ when the OH resonance is irradiated; $\Delta\nu_{1/2}$ is 0.10 Hz in both single and double resonance conditions. However, a multiplet from H-6 in Fig. 1 *d* and *d'* displays a change in $\Delta\nu_{1/2}$ from 0.13 to 0.10 Hz under such conditions. Therefore $^4J_0{}^{OH,H_6}$ appears to be a maximum of $\pm 0.03 \pm 0.01$ Hz.

A series of such experiments yielded the data in Table 2. In C_6D_6, CH_2Br_2, and CD_2Cl_2 solutions there was evidence for coupling between H-3 and the hydroxyl proton. A series of simulations of spectral peaks, assuming $\Delta\nu_{1/2}$ as 0.10 Hz in the absence of extra coupling, were useful in the estimation of the magnitudes of the very small couplings.

Because $^5J_m{}^{H_3,OH}$ is so very small, when present at all, the present method is not suitable for a reliable study of the temperature dependence of the equilibrium constant.

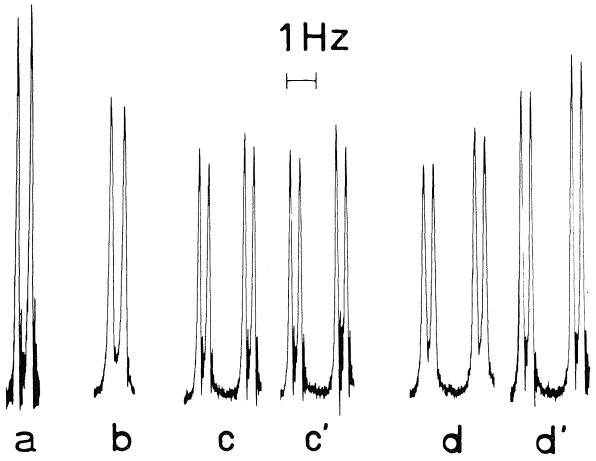

FIG. 1. (*a*) A display of the hydroxyl proton resonance at 100.001 MHz (centerband) and 305 K of a 2.0 mol% solution of 2-iodophenol in CCl_3CF_3. The linewidth at half height is 0.10 Hz. In (*b*) the same resonance is shown for a 4.7 mol% solution in CCl_4. In (*c*) and (*c'*) a multiplet from H-3 is recorded in single resonance and when the hydroxyl proton is decoupled. From (*d*) and (*d'*) it is clear that a multiplet from H-6 changes its linewidth from 0.13 to 0.10 Hz when the hydroxyl proton is irradiated.

Thermodynamic Parameters

(a) Equilibrium Constants

The ΔG values in Table 3, determined from the $^5J^{H,OH}$ magnitudes in Table 2, depend on the experience (13–16) that $^5J_m{}^{OH,H_3} \equiv {}^5J_c$ in the *cis* form is indistinguishable from zero and that $^5J_m{}^{OH,H_5} \equiv {}^5J_t$ is finite; and that a similar statement holds for the *trans* form. Accordingly,

$$\Delta G = G_c - G_t = -RT \ln {}^5J_t/{}^5J_c$$

Can. J. Chem. Downloaded from www.nrcresearchpress.com by 210.87.254.6 on 09/06/12
For personal use only.

TABLE 2. Hydroxyl proton chemical shifts and coupling constants in 2-iodophenol

Solvent	Concentration (mol %)	Chemical shift[a]	$^5J_m^{OH,H_5}$	$^5J_m^{OH,H_3}$	$^4J_o^{OH,H_6}$
c-C_6H_{12}	1.3	504.29[b]	0.450(5)[c]	<0.02	≤0.02
CCl_3CF_3	2.0	506.46	0.457(5)	<0.02	<0.02
C_6F_6	4.7	504.54	0.439(3)	<0.02	0.04±0.01
C_6D_6	2.0	489.2_0	0.40±0.02	0.04±0.01	0.02±0.01
CCl_4	4.7	512.15	0.469(3)	<0.02	0.03±0.02
$CDCl_3$	2.0	523.11	0.437(5)	≤0.02	0.03±0.01
CH_2Br_2	0.7	527.71	0.435(6)	0.03±0.01	0.03±0.01
CD_2Cl_2	0.9	528.40	0.421(5)	0.02±0.01	0.03±0.01

[a] In Hz at 100.001 MHz (centerband) to low field of internal TMS at 305 K.
[b] For a 0.2 mol% solution the shift is 502.0_4 Hz.
[c] Numbers in parentheses are standard deviations in the last significant figure.

TABLE 3. Thermodynamic parameters for 2-iodophenol from infrared intensities and nmr coupling constants for the *trans–cis* equilibrium

Solvent	$-\Delta G^a$ (kcal) Infrared[b] (298 K)	$-\Delta G^a$ (kcal) Nmr (305 K)	$-\Delta H^c$ (kcal) (ir)	ΔS^e (cal/deg) (ir)
c-C_6H_{12}	—	>1.88	—	—
iso-C_8H_{12}	1.88	—	1.40±0.05	1.6
CCl_3CF_3	—	>1.86	—	—
$CFCl_2CF_2Cl$	1.72	—	1.17	1.8
CCl_4	1.54	>1.86	0.99	1.8
	−0.02[d]	—	0.99	−3.4
C_6F_6	1.25	>1.86	0.31	3.1
$CDCl_3$	0.98	≥1.86	0.3	2.3
CH_2Br_2	0.77	1.6±0.3	0.18	2.0
CD_2Cl_2	—	1.8±0.4	—	—
C_6D_6	—	1.4±0.2	—	—
Vapor[f]	—	—	2.75±0.07	—

[a] 1 kcal ≡ 4.184 kJ.
[b] From band areas.
[c] Assuming α_t/α_c to be temperature independent (4).
[d] From the same data, where α_c/α_t is 13 (9).
[e] From ΔG and ΔH.
[f] Reference 5, using peak heights of the infrared bands.

This relationship has led to consistent equilibrium constants for a wide variety of phenol derivatives.

The ΔG values in Table 3 also assume that the sum of the $^5J_m^{OH,H}$ numbers in Table 2 are independent of solvent or, perhaps less stringently, that an intrinsic solvent-induced increase or decrease in one coupling is accompanied by a proportional increase or decrease, respectively, in the other coupling. If the standard deviations in $^5J_m^{OH,H_5}$ (numbers in parentheses in Table 2) are multiplied by 2 to obtain the 95% confidence limits and the errors in $^5J_m^{OH,H_3}$ are taken as 0.01 Hz also, then the sum of the two couplings ranges from $0.43_9 \pm 0.01_9$ to $0.46_9 \pm 0.01_9$ Hz.

The errors in ΔG for the C_6D_6, CH_2Br_2, and CD_2Cl_2 solutions are estimated by writing, for the CD_2Cl_2 solution for example

$$\Delta G = -RT \ln (0.42 \pm 0.01)/(0.02 \pm 0.01)$$
$$= -1850 \pm 400 \text{ cal/mol}$$

Were it to be argued that the small magnitudes of $^5J_m^{OH,H_3}$ are overestimated, then the magnitudes of ΔG in Table 3 would all be too small, and the disagreement with the magnitudes from infrared band areas would become larger than indicated. Again, in order to obtain agreement between the nmr data and the infrared data for the CH_2Br_2 solution, for example, $^5J_m^{OH,H_3}$ would have to be 0.12 Hz, easily resolvable in spectra of the present quality. If the coupling were this large, the sum of the two $^5J_m^{H,OH}$ values would become 0.55_5 Hz, in stark contrast to the other solutions in Table 2.

The solute concentrations (Table 2) in the nmr samples are much higher than those employed in the infrared measurements. Note, however, that a change in concentration from 1.3 to 0.2 mol% in C_6H_{12} entails an upfield shift of only 0.022 ppm. Because the dimerization of 2-iodophenol is expected to be largest in C_6H_{12} (17), and because the shift for the dimer would certainly be as large as 7.0 ppm

Can. J. Chem. Downloaded from www.nrcresearchpress.com by 210.87.254.6 on 09/06/12
For personal use only.

Can. J. Chem. Downloaded from www.nrcresearchpress.com by 210.87.254.6 on 09/06/12
For personal use only.

(17), comparison with the observed shift of 5.04 ppm clearly indicates that dimerization is not an important consideration in a discussion of the data in Table 2.

Table 3 also contains the ΔG values as given in ref. 4 and obtained from band areas. Comparison of the ΔG numbers demonstrates the inadequacy of the underlying assumption that α_t/α_c is near unity in all solvents. In fact, in CH_2Br_2 near 300 K, α_t/α_c must be approximately 4 (K_{nmr} is 14 and K_{area} is 3.5). Rough values of α_t/α_c near 300 K are ~ 4 for $CDCl_3$, >2.5 for C_6F_6, >1.5 for CCl_4, and ≥ 1 for *iso*-C_8H_{12} (*c*-C_6H_{12}).

(b) The Enthalpy Differences, ΔH

The enthalpy differences in Table 3 assume that α_t/α_c is temperature independent and that they can therefore be derived from a van't Hoff plot involving apparent K values.

Consider, however, that the absolute intensity of the hydroxyl stretching band of phenol is dependent on solvent (18, 19), being twice as intense in CCl_4 as in hexane, for example. Furthermore, intensities of a number of hydroxyl bands decrease roughly linearly with an increase in temperature (20, 21) and the solvent dependence of the intensity of a *trans* band is greater than for a *cis* band (18). If, therefore, the temperature dependence of α_t for 2-iodophenol in solution is larger than that of α_c and if the temperature dependence of α_t/α_c is roughly linear over a limited temperature range; then it follows that a van't Hoff plot using band areas may be linear but the slope includes a contribution from the decrease in α_t/α_c. The magnitude of ΔH deduced from the plot will be less than the true magnitude.

It is interesting that the smallest ΔH magnitudes in Table 3 correspond to the largest magnitudes of α_t/α_c deduced from the nmr and infrared ΔG data near 305 K.

Previous corrections to ΔH values by means of estimates of α values at 298 and 348 K in CCl_4 solution (6) were about 0.1 kcal/mol and were not applied in the detailed study of 2-iodophenol (4).

It is concluded that, at least for a number of the solvents (4), both ΔG and ΔH are unreliable.

In consequence, nothing very reliable can be stated about ΔS for the *trans–cis* equilibrium in many of the solvents. If ΔS were zero, as is apparently true for 2-alkylphenols in CCl_4 (18), then the J data would suggest a maximum solvent stabilization of the *trans* form by ca. 1 kcal/mol (enthalpy) in CH_2Br_2 solution, because in the vapor phase the *cis* form is favoured by 2.7 kcal/mol in enthalpy. The high dielectric constant of CH_2Br_2 would favor the more polar *trans* conformer.

In C_6D_6, hydrogen bonding to the π electrons would account for the increased population of the *trans* form. Enthalpies for the interaction of phenolic hydroxyl groups with π bases can evidently be as large as 1.7 kcal/mol (22, 23). The shift to high field of the hydroxyl proton in C_6D_6 solution is consistent with such an interaction. In C_6F_6 solution the solute protons do not experience high field shifts (compare C_6F_6 and C_6H_{12} solutions in Tables 1 and 2). These results are in keeping with the charge distribution in C_6D_6 and C_6F_6 deduced from the signs of their quadrupole moments (24).

(c) Plots of A_c *versus* A_t *for* CCl_4 *Solutions*

If α_c and α_t are *not* dependent on temperature, a plot of A_c versus A_t should be linear with a slope equal to α_c/α_t. The precise data in ref. 4 yield (9) α_c/α_t as 13 for the CCl_4 solution and therefore a ΔG of 0.02 kcal/mol. Yet we have $\Delta G < -1.86$ kcal/mol (Table 3). It must be concluded that, in fact, none of ΔG, ΔH, ΔS is known for 2-iodophenol in CCl_4 solution. We know only that ΔG is smaller than -1.86 kcal/mol at 305 K. Unfortunately, the present method is not suitable for a *reliable* determination of ΔH.

Molecular Orbital Calculations of α

The CNDO/2 and INDO MO methods (25) available in this laboratory are not parameterized for iodine. However, calculations on an Amdahl 470/V7 system for 2-chlorophenol gave $\delta\mu_{OH}/\delta r_{OH}$ as 0.91 D/Å for the *cis* and as 0.66 D/Å for the *trans* form; implying 1.9 for α_c/α_t in the free molecule. Approach of a CH_3F molecule along the O—H direction of the *trans* conformer to give a linear F ··· H—O arrangement led to a dipole derivative of 1.1 D/Å; larger than for the *cis* form.

Although the E versus r_{OH} plots were parabolic near the minimum and μ_{OH} versus r_{OH} plots were nicely linear (correlation coefficients of 0.999 for 13 points), the calculations suggest only that α_t/α_c is sensitive to solvent and that ΔG is not available from band areas for 2-halophenols. The calculations do support the suggestion (18) that the intrinsic intensity of the *trans* band in such compounds in the vapor is lower than in solution.

A referee does not believe the CNDO MO calculations are useful in this type of problem, emphasizing the caution with which we view the numbers quoted in this section.

Acknowledgment

We are grateful to the Natural Sciences and Engineering Research Council of Canada for financial support.

1. H. S. AARON. Top. Stereochem. **11**, 1 (1979).
2. A. W. BAKER and W. W. KAEDING. J. Am. Chem. Soc. **81**, 5904 (1959).
3. H. BOURASSA-BATAILLE, P. SAUVAGEAU, and C. SANDORFY. Can. J. Chem. **41**, 2240 (1963).
4. A. W. BAKER and A. T. SHULGIN. Spectrochim. Acta, **22**, 95 (1965).
5. T-S. LIN and E. FISHMAN. Spectrochim. Acta, Part A, **23**, 491 (1967).
6. A. W. BAKER and A. T. SHULGIN. Can. J. Chem. **43**, 650 (1965).
7. G. L. CARLSON, W. G. FATELEY, A. S. MANOCHA, and F. F. BENTLEY. J. Phys. Chem. **76**, 1553 (1972).
8. J. H. RICHARDS and S. WALKER. Trans. Faraday. Soc. **57**, 412 (1961).
9. K. O. HARTMAN, G. L. CARLSON, R. E. WITKOWSKI, and W. G. FATELEY. Spectrochim. Acta, Part A, **24**, 157 (1968).
10. T. SCHAEFER and R. SEBASTIAN. J. Magn. Reson. **41**, 395 (1980).
11. S. CASTELLANO and A. A. BOTHNER-BY. J. Chem. Phys. **41**, 3863 (1964).
12. C. W. HAIGH and J. M. WILLIAMS. J. Mol. Spectrosc. **32**, 398 (1969).
13. T. SCHAEFER, J. B. ROWBOTHAM, and K. CHUM. Can. J. Chem. **54**, 3666 (1976).
14. J. B. ROWBOTHAM and T. SCHAEFER. Can. J. Chem. **52**, 3037 (1974).
15. T. SCHAEFER and K. CHUM. Can. J. Chem. **56**, 1788 (1978).
16. T. SCHAEFER, R. SEBASTIAN, and T. A. WILDMAN. Can. J. Chem. **57**, 3005 (1979).
17. A. J. DALE and T. GRAMSTAD. Spectrochim. Acta, Part A, **28**, 639 (1972).
18. K. U. INGOLD. Can. J. Chem. **40**, 111 (1962).
19. K. SZCZEPIANAK and W. J. ORVILLE-THOMAS. J. Chem. Soc. Faraday Trans. II **70**, 1175 (1974).
20. U. LIDDELL and E. D. BECKER. J. Chem. Phys. **25**, 173 (1956).
21. R. H. HUGHES, R. J. MARTIN, and N. D. COGGESHALL. J. Chem. Phys. **24**, 489 (1956).
22. M. OKI and H. IWAMURA. Bull. Chem. Soc. Jpn. **33**, 717 (1960).
23. Z. YOSHIDA and E. OSAWA. J. Am. Chem. Soc. **87**, 1467 (1965).
24. J. URBANCICH and G. L. D. RITCHIE. J. Chem. Soc. Faraday II, **76**, 648 (1980).
25. P. A. DOBOSH. QCPE, **11**, 141 (1979).

Can. J. Chem. Downloaded from www.nrcresearchpress.com by 210.87.254.6 on 09/06/12
For personal use only.

The σ–π transmitted coupling over five and six bonds in pyridine–borane complexes. MO calculations on structure and spin–spin couplings

TED SCHAEFER, RUDY SEBASTIAN, AND SALMAN R. SALMAN[1]

Department of Chemistry, University of Manitoba, Winnipeg, Man., Canada R3T 2N2

Received May 26, 1981

TED SCHAEFER, RUDY SEBASTIAN, and SALMAN R. SALMAN. Can. J. Chem. **59**, 3026 (1981).

The spin–spin coupling over six bonds between borane and ring protons in the borane complexes of pyridine and 2,6-lutidine has the same magnitude as in toluene. This σ–π transmitted coupling suggests that the hyperfine parameters Q_{CCH} and Q_{NBH} have the same magnitude. Comparison of INDO MO FPT calculations of ^6J for these compounds and the methyl borazines with experiment indicates the relative degree of electron delocalization in these systems. An STO-3G structure is calculated for pyridine–borane. Almost free rotation about the B—N bond is predicted (sixfold barrier). The calculated $^6J^{H,BH_3}$ depends exponentially on the B—N bond length. Solvent effects on the proton chemical shift are in qualitative agreement with the reaction field model.

TED SCHAEFER, RUDY SEBASTIAN et SALMAN R. SALMAN. Can. J. Chem. **59**, 3026 (1981).

La constante de couplage spin–spin à travers six liaisons entre le borane et les protons du cycle dans les complexes du borane avec la pyridine et la lutidine-2,6 est du même ordre de grandeur que dans le toluène. Ce couplage σ–π suggère que les paramètres hyperfins Q_{CCH} et Q_{NBH} ont le même ordre de grandeur. La comparaison des calculs INDO MO FPT des ^6J de ces composés et des méthylborazines avec les résultats expérimentaux indiquent le degré de délocatisation relative des électrons dans ces systèmes. En utilisant les calculs STO-3G on a calculé une structure pour la pyridine–borane. On a prédit une rotation presque libre autour de la liaison B—N (barrière du sixième ordre). Les constantes $^6J^{H,BH_3}$ calculées varient d'une façon exponentielle avec la longueur de la liaison B—N. Les effets de solvant sur le déplacement chimique du proton sont qualitativement en accord avec le modèle de champ réactionnel.

[Traduit par le journal]

Introduction

Theory and experiment agree that the spin–spin coupling constant over six bonds between the methyl protons and the ring proton in the *para* position of toluene is transmitted via a σ–π electron mechanism. The experimental value of −0.62 Hz for $^6J_p^{H,CH_3}$ in toluene (1) is reproduced by INDO MO FPT computations (2), which also predict a $\sin^2\theta$ dependence; θ is the angle by which the methyl C—H bond is rotated out of the benzene plane. Accordingly, $^6J^{H,CH_3}$ is proportional to $Q_{CH}Q_{CCH}$, the hyperfine interaction constants between unpaired spin in the π electron system and the aromatic C—H and aliphatic C—H bonds, respectively. The fact that $^6J_p^{H,CH_3}$ in toluene equals $-{}^7J_p^{CH_3,CH_3}$ in *p*-xylene (3, 4) suggests that $Q_{CH} \sim -Q_{CH}$.

$^7J_p^{CH_3,CH_3}$ is insensitive to ring substituents and indeed to the presence of heteroatoms in the ring (4). For example, it is 0.59 ± 0.02 Hz in 2,5-dimethylpyridine and sinks only to 0.53 ± 0.02 Hz in 1,4-dimethylpyridinium iodide. However, it is 0.0 ± 0.04 Hz in 2,5-dimethyl-*p*-benzoquinone, showing that ^7J is also a good test of electron delocalization in these six-membered rings.

In fact, for borazine such tests suggest very small if not negligible delocalization (aromaticity), in agreement with INDO MO FPT calculations of $^6J^{H,CH_3}$ for *N*-methyl and *B*-methyl borazines (4), giving an average of ^7J of 0.06 Hz in *p*-dimethylborazine. The possibility that Q_{BH} and Q_{NH} or Q_{NCH} and Q_{BCH} are very small, thereby accounting for the very small observed and calculated ^6J and ^7J, can be partly negated by the ^7J (4) and ^6J observed in pyridine derivatives (5) and by the known Q_{NH} from esr data (6).

Little is known about σ–π interactions for B—H bonds. The present measurements of $^6J_p^{H,BH_3}$ in the borane complexes of pyridine and 2,6-lutidine are therefore of interest because delocalization in the pyridine fragment of the complexes must still occur. Calculations at the STO-3G (7) and INDO (8*a*) levels of molecular orbital theory are reported, yielding a partially optimized structure of the pyridine complex and spin–spin couplings.

Experimental

The complexes were insoluble in CCl_4 or CS_2. Approximately 5 mol% solutions of the borane complexes of pyridine and 2,6-lutidine (Aldrich) in $CDCl_3$, containing some tetramethylsilane, were degassed by the freeze–pump–thaw technique and were then sealed into 5 mm od nmr sample tubes. The ^{1}H nmr spectra were recorded in the frequency sweep mode on an HA100 spectrometer at a probe temperature of 305 K. Calibrations were performed by reading sweep and manual oscillator frequencies of markers placed at ca. 5 Hz intervals. Repetition of this procedure at sweep rates of 0.02 Hz/s and a dispersion of 1 Hz/cm yielded peak frequencies by an interpolation procedure. The precision of the frequencies was about 0.02 Hz for

[1]University of Baghdad, Iraq.

0008-4042/81/213026-04$01.00/0

©1981 National Research Council of Canada/Conseil national de recherches du Canada

Can. J. Chem. Downloaded from www.nrcresearchpress.com by 210.87.254.6 on 09/06/12
For personal use only.

TABLE 1. Some spectral parameters for the borane complexes of pyridine and 2,6-lutidine at 305K

Parameter	Py·BH_3[a]		2,6-Lut·BH_3[a]	
	$CDCl_3$	$(CD_3)_2C{=}O$	$CDCl_3$	$(CD_3)_2C{=}O$
ν_2[b]	859.8	862.6	279.1[c]	273.0[c]
ν_3	751.9	770.3	722.5	740.3
ν_4	795.3	814.4	763.5	781.3
ν_{BH_3}	264.0	260.3	229.5	279.3
$^3J_{23}$	5.5	5.5	—	—
$^3J_{34}$	7.72	7.7	7.78	—
$^4J_{24}$	1.56	1.6	—	—
$^6J_p^{H,CH_3}$	$(-)0.59_7$[d]	(−)0.6	-0.62_3[e]	—

[a] 5.0 mol% solutions.
[b] In Hz at 100.00 MHz to low field of internal TMS.
[c] Shifts of the methyl protons.
[d] $^5J_m^{H,BH_3}$ is (+)0.24 ± 0.03 Hz.
[e] $^5J_o^{BH_3,CH_3}$ is 0.22 ± 0.02 Hz.

those peaks not broadened by partially relaxed couplings to ^{14}N or ^{11}B nuclei (T_2 effects on H-2 and *B*-H protons).

The borane protons of the pyridine complex displayed strong broadening (about 40 Hz) of the quartet arising from $^1J(^{11}B{-}H)$, so that ^1J could not be deduced accurately (see, for example, Fig. 7 of ref. 8*b*). However, a 5 mol% solution in acetone-d_6, having a lower viscosity, displayed no overlap of these peaks ($\Delta\nu_{1/2} \sim 18$ Hz) and yielded $^1J(^{11}B{-}H)$ as 97.4 ± 1.0 Hz, close to the value of 98 Hz reported for a benzene solution (9).

STO-3G and INDO MO FPT computations were made on an Amdahl 470/V7 system.

Results and Discussion

Spectral Analysis

The width of the H-2 transitions in the pyridine complex (partially relaxed coupling to ^{14}N) precluded a thorough analysis of the ring proton spectrum. The parameters extractable with some accuracy are given in Table 1 and involved the use of the computer program LAME (10, 11). The sign of $^6J_p^{H,BH_3}$ could not be determined but is no doubt negative.

Decoupling of the methyl protons in the 2,6-lutidine complex allowed extraction of the parameters in Table 1. The value of $^5J_o^{CH_3,BH_3}$ could then be obtained by simulation of the methyl proton resonance, using $^nJ^{H,CH_3}$ parameters reliably determined for some 2,6-lutidine derivatives (5).

STO-3G and INDO MO Computations on Structures

The most striking parameter is $^6J_p^{H,BH_3}$, whose magnitude is the same as $^6J_p^{H,CH_3}$ in toluene, to within experimental error. The latter is reproduced by INDO MO PFT procedures (2) and therefore MO calculations were performed on the structure and *J* values as follows.

The microwave geometry of pyridine (12) was assumed for the ring skeleton. Minimization procedures with respect to all other bond lengths and angles yielded the two STO-3G structures in Scheme 1. Local threefold symmetry was maintained for the BH_3 group. The structure with a B—H bond in a plane perpendicular to the ring plane (90°) had an energy (−269.7749994 au) lower by 24.5 J/mol than the other structure in Scheme 1. It may probably be concluded that the sixfold barrier to internal rotation about the B—N bond is very small and similar to the 59 J/mol in toluene (13). The calculated dipole moment is 7.06 D for both structures, somewhat larger than the benzene solution value of 5.86 D (14). The B—N bond length of 1.647 Å appears rather large, when compared to the X-ray value of 1.56 Å in $NH_3{\cdot}BH_3$ (15) or to the microwave value of 1.609 Å in $(CH_3)N{\cdot}BH_3$ (16). In the latter the B—H length is 1.21 Å and the NBH angle is 105.3°.

The minimization procedures also suggested that the B—N bond makes an angle of 2° with the ring plane so as to move the unique B—H bond closer to the ring in the 90° structure.

The INDO//STO 3G computations agree that the 90° structure is the most stable, but by 543 J/mol and with a dipole moment of 7.36 D. That this rather significant barrier is an artifact, is indicated by INDO calculations for the averaged STO 3G geometry (average of all bond lengths and angles in the two structures of Scheme 1), which yield a preference of only 25 J/mol for the 90° structure. Variation of the B—N bond length in the INDO// STO 3G calculations gave a minimum at 1.56_5 Å.

For all these calculations it must be noted that the ring skeleton was that of pyridine and that further, rather expensive, STO 3G or, better, 4-31G computations are needed.

INDO MO FPT Calculations of J

These were performed for various B—N bond lengths and θ, where θ is the angle by which a B—H bond is rotated out of the ring plane.

Can. J. Chem. Downloaded from www.nrcresearchpress.com by 210.87.254.6 on 09/06/12
For personal use only.

Can. J. Chem. Downloaded from www.nrcresearchpress.com by 210.87.254.6 on 09/06/12
For personal use only.

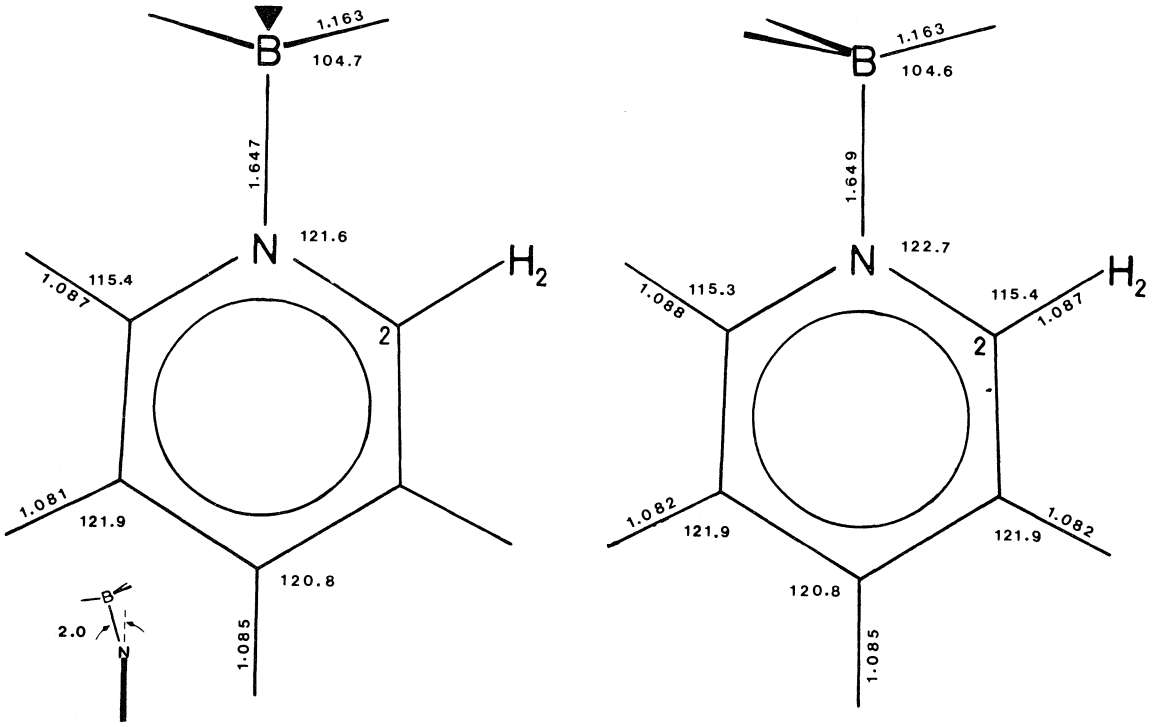

SCHEME 1

The most interesting results are perhaps those for ${}^6J_p^{H,BH_3}$. They can be written as

[1] $${}^6J^{H,BH_3} = {}^6J_o{}^r + {}^6J_{90}{}^r \sin^2\theta$$

where ${}^6J_o{}^r$ is the value at $\theta = 0°$ (B—H in ring plane) for a given value of r, the B—N bond length. Table 2 summarizes the calculated data for four r values. Note that ${}^6J_o{}^r$ is very small and that a σ–π mechanism is indicated, as for toluene (2). In Table 2, $\langle J \rangle$ is the average of J over θ. The observed ${}^6J^{H,BH_3}$ of -0.59_7 Hz is reproduced at $r = 1.600$ Å, probably a reasonable number (of course, this r value need not correspond to a minimum in the energy, being dependent on the FPT parameterization).

It is also true that $|{}^6J_o{}^r + J_{90}{}^r|$ in Hz is reproduced by the function 1266.5 exp $-4.366r$ (correlation coefficient of 0.99998) where r is in Å. This fact may indicate the way in which Q_{NBH} depends on overlap between the B—H orbitals and the π orbitals of the ring. The magnitude of ${}^6J^{H,BH_3}$ implies that Q_{CCH} in toluene is very nearly the same as Q_{NBH} in pyridine–borane. Recent esr data (17) on pyridinyl radicals are compatible with $Q_{NCH} \sim Q_{CCH}$. The present results do not alter our previous conclusions (4) about the very low degree of electron delocalization in borazine.

The calculations on ${}^5J_m{}^{H,BH_3}$ are not reproduced here. Qualitatively they follow previous results (2) for toluene. $\langle J_m{}^{H,BH_3} \rangle$ is calculated as 0.78 $\langle J_m{}^{H,CH_3} \rangle$. Then the observed value of 0.36 Hz in toluene perhaps implies a ${}^5J_m{}^{H,BH_3}$ of 0.28 Hz in pyridine–borane, in acceptable agreement with experiment. If it is remembered that ${}^5J^{H,BH_3}$ is expected to have a substantial σ component, in addition to a σ–π component apparently as large as in toluene (see above), then it follows that the σ component is smaller in the complex than in toluene.

${}^4J_o{}^{H,BH_3}$ could not be measured in the pyridine complex. In the 2,6-lutidine complex, ${}^5J_o{}^{BH_3,CH_3}$ is (+)0.22 Hz as compared to 0.45 Hz in *o*-xylene (3, 4). In addition to σ and σ–π components, these couplings contain contributions from direct or through-space mechanisms (2) very sensitive to interproton distances.

Because the INDO calculations of J for boron are apparently reliable in other systems (18), some such values are given in Table 3 for two B—N distances. The computed numbers are insensitive to θ. ${}^1J({}^{11}B–H)$ is overestimated by 10%. The small ${}^1J({}^{11}B–{}^{14}N)$ of near +5 Hz is compatible with the surmise (19) that a positive coupling occurs between nuclei if the electronegativity difference between the corresponding atoms is less than 1.5,

TABLE 2. INDO MO FPT values[a] for $^6J^{H,BH_3}$ in the pyridine–borane complex[b,c]

r_{BN}, Å	$^6J_o{}^r$	$^6J_{90}{}^r$	$\langle {}^6J \rangle$
1.648	−0.02	−0.93	-0.48_5
1.600	−0.02	−1.15	-0.59_5
1.550	-0.02_5	−1.43	−0.74
1.500	−0.03	−1.79	-0.92_5

[a] In Hz.
[b] $^6J_0{}^r$ and $^6J_p{}^r$ are defined in eq. [1] of the text.
[c] $\langle {}^6J \rangle$ is the value averaged over the rotation about the B—N bond.

TABLE 3. INDO NO FPT values for coupling to ^{11}B in the pyridine–borane complex[a]

Nucleus	1.60 Å	1.55 Å	Nucleus	1.60 Å	1.55 Å
^{14}N	4.63	4.79	H_2	0.60	0.68
C_2	−3.37	−3.90	H_3	−0.32	−0.39
C_3	1.17	1.30	H_4	0.39	0.46
C_4	−1.25	−1.47	$H_{(B)}$	110.1	109.3

[a] In Hz at two values of the B—N length.

and is negative if the difference is greater than 1.5. The other couplings to ^{11}B alternate in sign with the number of formal intervening bonds.

Other Parameters

The available couplings between ring protons in the pyridine complex (Table 1) fall between those in pyridine (20) and the pyridinium ion (21), as expected (22) on the basis of electronegativity of the *N*-substituent.

The ^{14}N spin lattice relaxation rate is lower in the complex than in the free base, yielding broader H-2 resonances, and therefore the other ring proton parameters are not reliably available.

The ^{11}B and ^{14}N shifts fall between those of the free base and the pyridinium ion (23). They indicate no steric hindrance to the addition of BH_3 to the lutidine, as is confirmed by $^6J^{H,BH_3}$ for the complexes. According to these numbers (Table 1) and those in Table 2, the B—N bond lengths in the two complexes should be the same to within 0.01 Å.

Solvent Shifts

Their striking aspect is the (small) shift to high field of the BH_3 and CH_3 peaks as the dielectric constant of the solution increases and the corresponding, rather larger, low-field shift for H-3 and H-4. These observations are in qualitative agreement with a reaction field model (24). From geometrical considerations, however, it is clear that quantitative agreement with this model cannot be had for these solvents.

1. M. P. WILLIAMSON, R. KOSTELNIK, and S. M. CASTELLANO. J. Chem. Phys. **49**, 2218 (1968).
2. R. WASYLISHEN and T. SCHAEFER. Can. J. Chem. **50**, 1852 (1972).
3. C. J. MACDONALD and W. F. REYNOLDS. Can. J. Chem. **48**, 1002 (1970).
4. J. B. ROWBOTHAM and T. SCHAEFER. Can. J. Chem. **52**, 489 (1974).
5. J. B. ROWBOTHAM and T. SCHAEFER. Can. J. Chem. **50**, 2344 (1972).
6. B. L. BARTON and G. K. FRAENKEL. J. Chem. Phys. **41**, 695 (1964); **41**, 1455 (1964).
7. W. J. HEHRE, W. A. LATHAN, R. DITCHFIELD, M. D. NEWTON, and J. A. POPLE. Quantum Chemistry Program Exchange, **11**, 236 (1979).
8. (*a*) P. A. DOBOSH. Quantum Chemistry Program Exchange, **11**, 141 (1979); (*b*) E. K. MELLON, B. M. COKER, and P. B. DILLON. Inorg. Chem. **11**, 852 (1972).
9. T. P. ONAK, H. LANDESMAN, R. E. WILLIAMS, and I. SHAPIRO. J. Phys. Chem. **63**, 1533 (1959).
10. S. M. CASTELLANO and A. A. BOTHNER-BY. J. Chem. Phys. **41**, 3863 (1964).
11. C. W. HAIGH and J. M. WILLIAMS. J. Mol. Spectrosc. **32**, 398 (1969).
12. B. BAK, L. HANSEN-NYGAARD, and J. RASTRUP-ANDERSEN. J. Mol. Spectrosc. **2**, 361 (1958).
13. H. RUDOLPH, H. DREIZLER, A. JAESCHKE, and P. WENDLING. Z. Naturforsch. Part A, **22**, 940 (1967).
14. C. M. BOX, A. R. KATRITZKY, and L. E. SUTTON. J. Chem. Soc. London, 1254 (1958).
15. R. P. BURNS, G. DEMARIA, J. DROWART, and R. T. GRIMLEY. J. Chem. Phys. **32**, 1363 (1960).
16. J. R. DURIG, Y. S. LIU, and J. D. ODOM. J. Mol. Struct. **16**, 443 (1973).
17. K. AKIYAMA, S. KUBOTA, and Y. IKEGAMI. J. Phys. Chem. **85**, 120 (1981).
18. A. J. ZOZULIN, H. J. JAKOBSEN, T. F. MOORE, A. R. GARBER, and J. D. ODOM. J. Magn. Reson. **41**, 458 (1980).
19. J. SCHAEFER and R. YARIS. Chem. Phys. Lett. **1**, 173 (1967).
20. S. CASTELLANO, C. SUN, and R. KOSTELNIK. J. Chem. Phys. **46**, 327 (1967).
21. J. B. MERRY and J. H. GOLDSTEIN. J. Am. Chem. Soc. **88**, 5560 (1966).
22. S. CASTELLANO and R. KOSTELNIK. J. Am. Chem. Soc. **90**, 141 (1968).
23. H. NOTH and B. WRACKMEYER. Chem. Ber. **107**, 3070 (1974).
24. A. D. BUCKINGHAM. Can. J. Chem. **38**, 300 (1960).

Can. J. Chem. Downloaded from www.nrcresearchpress.com by 210.87.254.6 on 09/06/12
For personal use only.

Standard electrode potentials of the silver – silver phosphate and silver – silver arsenate electrodes in formamide at different temperatures

UPENDRA NATH DASH[1] AND SURENDRA KUMAR NAYAK
Department of Chemistry, G.M. College, Sambalpur (Orissa), India

Received January 12, 1981

UPENDRA NATH DASH and SURENDRA KUMAR NAYAK. Can. J. Chem. **59**, 3030 (1981).

For the emf measurements of cells of the type Ag, AgCl/NaCl(m)|Na_3X(m/3)/Ag_3X, Ag where X is PO_4 or AsO_4, the standard potentials of the silver – silver phosphate and silver – silver arsenate electrodes have been determined in formamide at five different temperatures ranging from 5 to 45°C. The standard molal potentials of the electrodes have been expressed through the equations

$$E_m^0(Ag,Ag_3PO_4) = (2.0565 \pm 0.0001) - (5.1627 \pm 0.0001) \times 10^{-2}T + (88.974 \pm 0.039) \times 10^{-4}T \ln T - (29.892 \pm 0.054) \times 10^{-6}\, T^2/2$$

$$E_m^0(Ag,Ag_3AsO_4) = (2.0771 \pm 0.0001) - (5.3252 \pm 0.0013) \times 10^{-2}T + (91.743 \pm 0.016) \times 10^{-4}\, T \ln T - (31.116 \pm 0.029) \times 10^{-6}\, T^2/2$$

The standard thermodynamic quantities, ΔG^0, ΔH^0, ΔS^0, and $\Delta C_p{}^0$ for the respective electrode reactions have been evaluated from the $E_m{}^0$'s of the electrodes at these temperatures. The solubility products of silver phosphate and silver arsenate have also been calculated in formamide at these temperatures.

UPENDRA NATH DASH et SURENDRA KUMAR NAYAK. Can. J. Chem. **59**, 3030 (1981).

On a déterminé les potentiels normaux des électrodes de phosphate d'argent/argent et d'arsénate d'argent/argent dans le formamide à 5 températures différentes allant de 5 à 45°C pour mesurer la fem des cellules du type Ag, AgCl/NaCl(m)| Na_3X(m/3)/Ag_3X, Ag, où X = PO_4 ou AsO_4. On exprime les potentiels molaires normaux des électrodes par les équations:

$$E_m^0(Ag,Ag_3PO_4) = (2.0565 \pm 0.0001) - (5.1627 \pm 0.0001) \times 10^{-2}T + (88.974 \pm 0.039) \times 10^{-4}T \ln T - (29.892 \pm 0.054) \times 10^{-6}\, T^2/2$$

$$E_m^0(Ag,Ag_3AsO_4) = (2.0771 \pm 0.0001) - (5.3252 \pm 0.0013) \times 10^{-2}T + (91.743 \pm 0.016) \times 10^{-4}\, T \ln T - (31.116 \pm 0.029) \times 10^{-6}\, T^2/2$$

On a évalué les quantités thermodynamiques normales ΔG^0, ΔH^0, ΔS^0 et $\Delta C_p{}^0$ des diverses réactions aux électrodes, à partir des $E_m{}^0$ des électrodes à ces températures. On a également calculé les produits de solubilité du phosphate d'argent et de l'arsenate d'argent dans la formamide à ces températures.

[Traduit par le journal]

Introduction

No work seems to have been done on the determination of the standard potentials of the silver – silver phosphate and silver – silver arsenate electrodes in aqueous and non-aqueous media. However, from this laboratory Dash and Padhi (1) have reported the standard potentials of these electrodes in aqueous and aqueo-organic solvent systems over a range of temperature. The present work has been undertaken as a part of our programme of the determination of standard potentials of some electrodes of the second kind of the inorganic tribasic acids in formamide.

As in previous communications (2), the cells with liquid junction

[A] Ag,AgCl/NaCl(m)|Na_3X(m/3)/Ag_3X,Ag

where X is PO_4 or AsO_4, have been studied in formamide for the determination of standard potentials of the silver – silver phosphate and silver – silver arsenate electrodes.

Experimental

Sodium chloride (BDH, AnalaR) was dried above 100°C for 2 h before use. Formamide (BDH, LR) was purified as described earlier (3). Sodium phosphate (E. Merck) and sodium arsenate (BDH, AnalaR) were dried at 120°C, and kept in vacuum desiccator before use.

Silver phosphate and silver arsenate were prepared from silver nitrate (BDH, AnalaR) and sodium phosphate or

[1]Present address: Bhadrak College, Bhadrak 756100 (Orissa), India.

0008-4042/81/213030-04$01.00/0
©1981 National Research Council of Canada/Conseil national de recherches du Canada

Can. J. Chem. Downloaded from www.nrcresearchpress.com by 210.87.254.42 on 09/06/12
For personal use only.

Can. J. Chem. Downloaded from www.nrcresearchpress.com by 210.87.254.42 on 09/06/12
For personal use only.

arsenate, and the precipitates were repeatedly washed with conductivity water, and were kept in conductivity water in amber coloured bottles for use.

The preparation of silver – silver chloride electrodes has been described earlier (4). Silver – silver phosphate and silver – silver arsenate electrodes were prepared by a method similar to that of the silver – silver oxalate, malonate, succinate, adipate, or chromate electrodes (5) by applying a paste of silver phosphate or arsenate on the spongy silver obtained by the thermal decomposition of silver oxide (6). The electrodes thus prepared were stored in 0.05 *M* aqueous sodium phosphate or arsenate solution for 24 h and then rinsed with sodium phosphate or arsenate solution in formamide before use. Only those electrodes which showed a potential difference of 0.01 mV or less on mutual comparison were used.

Solutions for emf measurements were prepared by dissolving the appropriate weighed amounts of salts in known weights of formamide.

Setting up of the cells and emf and conductance measurements was essentially similar to that described earlier (2, 7). The cells were kept in the water thermostat at the required temperature with a precision of ±0.1°C. The reproducibility of emf measurements was of the order of ±0.2 mV.

Results and Discussion

The emf, E, of cell [A] is given by the expression

$$[1]\quad E = E^0_{cell} + (2RT/3F)\ln(3m) + (RT/3F)\ln[\gamma^3(Cl^-)/\gamma(X^{3-})] + E_j$$

where the symbols have their usual significance.[2]

The standard molal potential, E_m^0 of the silver – silver phosphate or arsenate electrodes was obtained by the method of extrapolating (2) the auxiliary function, $E_m^{0\prime}$ given by

$$[2]\quad E_m^{0\prime} = E - \tfrac{2}{3}k\log(3m) - k[(3A\sqrt{2m}/1 + \sqrt{2m}) - (A\sqrt{m}/1 + \sqrt{m})] + E_m^0(Ag/AgCl) - E_j = E_m^0(Ag/Ag_3X) + bm$$

to the molality, $m = 0$, (Figs. 1 and 2) where $E_m^0(Ag/AgCl)$ is the standard potential of the silver – silver chloride electrode and A is the Debye–Hückel constant, and are known (8) over the temperature range under investigation. In eq. [2] $k = (2.3026RT/F)$ and $b = k\{\beta_{Cl^-} - \tfrac{2}{3}\beta_{X^{3-}}\}$ where β is the usual constant ($2b$) in the Debye–Hückel expression for the activity coefficient, i.e.,

$$-\log\gamma_i = \frac{AZ_i^2\mu^{1/2}}{1 + \mu^{1/2}} - \beta_i\mu$$

where i is Cl^- or X^{3-}.

[2]Complete set of original data is available, at a nominal charge, from the Depository of Unpublished Data, CISTI, National Research Council of Canada, Ottawa, Ont., Canada K1A 0S2.

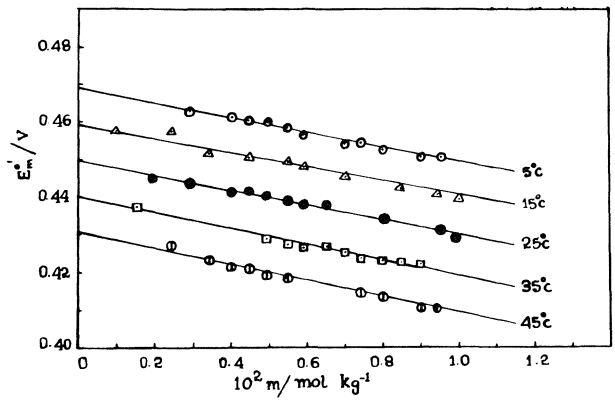

FIG. 1. Plot of $E_m^{0\prime}$ of Ag/Ag_3PO_4, PO_4^{3-} electrode vs. molality in formamide at different temperatures.

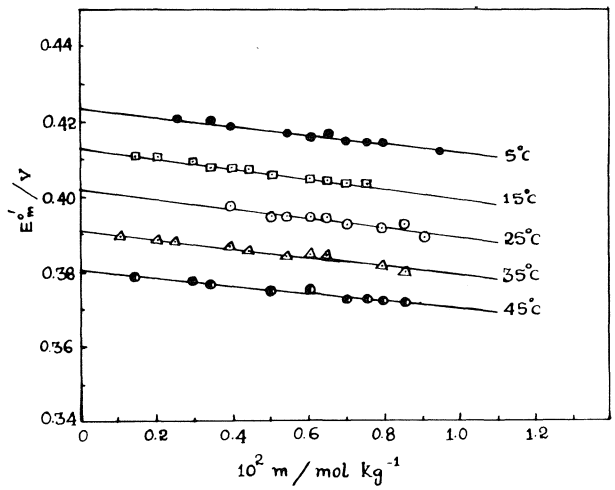

FIG. 2. Plot of $E_m^{0\prime}$ of Ag/Ag_3AsO_4, AsO_4^{3-} electrode vs. molality in formamide at different temperatures.

As usual (2), the values of the liquid junction potentials, E_j, were calculated from the equivalent conductance of sodium phosphate or arsenate and sodium chloride by means of the Henderson equation. The values of E were found to be in the range 0.02–0.03 V at all temperatures.

From the E_m^0 values of the silver – silver phosphate or arsenate electrodes the values for the standard potential on the molar (E_c^0) and mole-fraction (E_N^0) scales have also been calculated at experimental temperatures by the usual equations (9). The variation of the standard potential in molal (E_m^0), molar (E_c^0), and mole-fraction (E_N^0) scales with temperature has been expressed through the equations of the type (7),

$$[3]\quad E_x^0 = A + BT + CT\ln T + DT^2/2$$

TABLE 1. Values for the parameters A, B, C, and D in eq. [3]

X	A	$\sigma(A)$	-10^2B	$\sigma(B)$	10^4C	$\sigma(C)$	-10^6D	$\sigma(D)$
				(X = PO_4)				
m	2.0565	0.0001	5.1627	0.0001	88.974	0.039	29.892	0.054
c	1.9681	0.0001	4.8748	0.0007	84.236	0.025	28.967	0.153
N	1.9584	0.0002	4.7924	0.0007	81.357	0.031	26.999	0.109
				(X = AsO_4)				
m	2.0771	0.0001	5.3252	0.0013	91.743	0.016	31.116	0.029
c	1.9757	0.0002	4.9911	0.0015	86.206	0.014	29.943	0.308
N	1.9788	0.0002	4.9118	0.0017	83.214	0.034	27.623	0.303

TABLE 2. Standard thermodynamic quantities, ΔG^0, ΔH^0, ΔS^0, and $\Delta C_p{}^0$ (on the molal scale) for the electrode reaction [4] at different temperatures*

	ΔG^0 (kJ mol^{-1})		$-\Delta S^0$ (J mol^{-1} K^{-1})		$-\Delta H^0$ (kJ mol^{-1})		$\Delta C_p{}^0$ (J mol^{-1} K^{-1})	
T (°C)	PO_4	AsO_4	PO_4	AsO_4	PO_4	AsO_4	PO_4	AsO_4
5	135.7	122.7	280.3	318.0	213.7	211.0	170	152
15	133.0	119.5	275.8	314.2	212.4	210.0	84	62
25	130.2	116.3	274.5	314.7	212.0	209.8	−3	−28
35	127.5	113.2	276.0	316.1	212.5	210.5	−90	−111
45	124.7	110.0	280.2	321.3	213.8	212.2	−176	−209

*Uncertainties in ΔG^0, ±0.6 kJ mol^{-1}; ΔS^0, ±2 J mol^{-1} K^{-1}; ΔH^0, ±0.9 kJ mol^{-1}; and $\Delta C_p{}^0$, ±2 J mol^{-1} K^{-1}.

where x is m, c, or N, and T is the temperature in K. The parameters A, B, C, and D in eq. [3] on different scales are presented in Table 1 along with their standard deviations calculated by the least-squares method.

The thermodynamic quantities, ΔG^0, ΔH^0, ΔS^0, and $\Delta C_p{}^0$ for the electrode reaction

[4] $Ag_3X(s) + 3\ e \rightleftharpoons 3\ Ag(s) + X^{3-}$ (solvated)

have been calculated by the usual relations (7), and are given in Table 2 at different temperatures.

A comparison of the standard potentials of these electrodes ($E_m{}^0(Ag/Ag_3PO_4)$ = 0.4498 V and $E_m{}^0(Ag/Ag_3AsO_4)$ = 0.4019 V) at 25°C in formamide with those reported in water (1) ($E_m{}^0(Ag/Ag_3PO_4)$ = 0.4524 V and $E_m{}^0(Ag/Ag_3AsO_4)$ = 0.4079 V) shows that the $E_m{}^0$ values are higher in water than in formamide, lending support to the earlier studies on the determination of standard potentials of the electrodes of the second kind in formamide (6, 10). The lowering of $E_m{}^0(Ag/Ag_3PO_4)$ may be explained by the lower basicity of formamide which increases $\Delta G^0(\Delta G^0(Ag_3PO_4)$ = −130.2 kJ and $\Delta G^0(Ag_3AsO_4)$ = −116.3 kJ at 25°C in comparison with $\Delta G^0(Ag_3PO_4)$ = −131 kJ and $\Delta G^0(Ag_3AsO_4)$ = −118.1 kJ at 25°C in water) of the cell reaction [4] by increasing the Gibbs free energy of $PO_4{}^{3-}$ (solvated) or $AsO_4{}^{3-}$ (solvated) in formamide. As expected the ΔH^0 and ΔS^0 values for the cell reaction [4] are negative in both water and formamide but they are less negative in formamide than in water (1) ($\Delta S^0(Ag_3PO_4)$ = −450.1 J mol^{-1} K^{-1} and $\Delta S^0(Ag_3AsO_4)$ = −483.3 J mol^{-1} K^{-1}) pointing to the fact that the net amount of order created by $PO_4{}^{3-}$ or $AsO_4{}^{3-}$ ions is less in formamide than in water. In other words, the formamide molecules become more associated than water suggesting that $PO_4{}^{3-}$ or $AsO_4{}^{3-}$ ions "break down more structure" in formamide than in water.

The solubility products, $K_s{}^0$, of silver phosphate and silver arsenate in formamide have been calculated from the values of standard potentials of the silver – silver phosphate or arsenate, and of the silver electrodes by means of the equation

$$[5]\quad \ln K_s{}^0 = (E_m{}^0\,(Ag/Ag_3X) - E_m{}^0(Ag/Ag^+))(3F/RT)$$

where $E_m{}^0(Ag/Ag^+)$ is the standard molal potential of silver electrode and is given by the equation (11)

$$[6]\quad E_m{}^0(Ag/Ag^+) = (1.7073 \pm 0.0019) - (3.5171 \pm 0.0026) \times 10^{-2}T + (62.486 \pm 0.017) \times 10^{-4}\,T \ln T - (25.492 \pm 0.013) \times 10^{-6}\,T^2/2$$

over the temperature range under investigation. The values for $K_s{}^0$ in the molality ($K_s{}^{0m}$) and molarity ($K_s{}^{0c}$) scales are shown in Table 3 at the experimental temperatures. The data for $K_s{}^{0c}$ calculated from $K_s{}^{0m}\ \rho^2$ where ρ is the density of

Can. J. Chem. Downloaded from www.nrcresearchpress.com by 210.87.254.42 on 09/06/12
For personal use only.

TABLE 3. Values of the solubility products, K_s^0, of Ag_3PO_4 and Ag_3AsO_4 in formamide at different temperatures

	X = PO_4		X = AsO_4	
T (°C)	$10^{13}\ K_s^{0m}$ (mol^2 kg^{-2})	$10^{13}\ K_s^{0c}$ (mol^2 dm^{-6})	$10^{16}\ K_s^{0m}$ (mol^2 kg^{-2})	$10^{16}\ K_s^{0c}$ (mol^2 dm^{-6})
5	0.27	0.36	0.94	1.24
15	0.48	0.62	1.75	2.27
25	1.12	1.43	4.16	5.30
35	3.36	4.23	12.84	16.13
45	11.85	14.67	46.51	57.56

formamide at the various temperatures. The solubility product data were fitted by least-squares to the following equations.

[7] $\log K_s^{0m}(Ag_3PO_4) = -3624/T - 0.658\ (\sigma = 0.10)$

$\log K_s^{0c}(Ag_3PO_4) = -3567/T - 0.745\ (\sigma = 0.10)$

$\log K_s^{0m}(Ag_3AsO_4) = -3733/T - 2.721\ (\sigma = 0.10)$

$\log K_s^{0c}(Ag_3AsO_4) = -3676/T - 2.807\ (\sigma = 0.10)$

where σ is the standard deviation of the least-squares fit: the correlation coefficient for these relations is 0.993.

1. U. N. DASH and M. C. PADHI. Thermochim. Acta. In press.
2. (*a*) U. N. DASH. Thermochim. Acta, **13**, 105 (1975); (*b*) R. C. DAS, U. N. DASH and K. N. PANDA, Electrochim. Acta, **24**, 99 (1979); (*c*) U. N. DASH and M. C. PADHI. Thermochim. Acta, **39**, 335 (1980); (*d*) U. N. DASH and M. C. PADHI. J. Electroanal. Chem. **122**, 147 (1981); (*e*) U. N. DASH and M. C. PADHI. Thermochim. Acta. **45**, 245 (1981).
3. U. N. DASH and B. NAYAK. Indian J. Chem. **8**, 659 (1970).
4. R. K. AGARWAL and B. NAYAK. Aust. J. Chem. Phys. **70**, 2568 (1966).
5. (*a*) U. N. DASH and B. NAYAK. Aust. J. Chem. **28**, 1373 (1975); (*b*) U. N. DASH and P. C. RATH. Thermochim. Acta. **13**, 250 (1975); (*c*) U. N. DASH and U. K. NAYAK. Can. J. Chem. **58**, 323 (1980); (*d*) U. N. DASH. Thermochim. Acta, **16**, 177 (1976).
6. U. N. DASH and B. NAYAK. J. Electroanal. Chem. **41**, 323 (1973).
7. U. N. DASH and S. K. NAYAK. Can. J. Chem. **58**, 992 (1980).
8. (*a*) R. K. AGARWAL and B. NAYAK. J. Phys. Chem. **71**, 2062 (1967); (*b*) U. N. DASH and B. NAYAK. Aust. J. Chem. **28**, 793 (1975).
9. R. A. ROBINSON and R. H. STOKES. Electrolyte solutions. Butterworths, London. 1959.
10. (*a*) U. N. DASH. Electrochim. Acta, **21**, 279 (1975); **21**, 1061 (1976); (*b*) U. N. DASH. Thermochim. Acta, **30**, 73 (1979).
11. U. N. DASH. Ph.D. Thesis. Indian Institute of Technology, Kharagpur. India. 1973.

Can. J. Chem. Downloaded from www.nrcresearchpress.com by 210.87.254.42 on 09/06/12
For personal use only.

The kinetics of proton and deuteron transfer from 4-nitrophenylnitromethane and 1-(4-nitrophenyl)-1-nitroethane to 2,7-dimethoxy-1,8-bis(dimethylamino)naphthalene in acetonitrile solvent[1]

KENNETH T. LEFFEK AND PRZEMYSLAW PRUSZYNSKI[2]

Department of Chemistry, Dalhousie University, Halifax, N.S., Canada B3H 4H6

Received April 3, 1981

KENNETH T. LEFFEK and PRZEMYSLAW PRUSZYNSKI. Can. J. Chem. **59**, 3034 (1981).

4-Nitrophenylnitromethane reacts with 2,7-dimethoxy-1,8-bis(dimethylamino)naphthalene in acetonitrile in a bimolecular proton transfer, which shows a primary deuterium isotope effect, $k_H/k_D = 12.2$ at 25°C. The large isotope effect on the enthalpy of activation, $(\Delta H_D^{\ddagger} - \Delta H_H^{\ddagger}) = 4.6 \pm 0.3$ kcal mol^{-1} is consistent with a significant contribution of proton tunnelling to the reaction rate of the protium substrate.

The analogous reaction of 1-(4-nitrophenyl)-1-nitroethane with the same base in acetonitrile gives contrasting kinetics and reaction parameters. The reaction is first order, showing no dependence on base concentration. While the isotope effect $k_H/k_D = 9.3$ at 25°C, the enthalpy of activation difference $(\Delta H_D^{\ddagger} - \Delta H_H^{\ddagger})$ is only 0.5 ± 0.1 kcal mol^{-1}. It is concluded that the 1-(4-nitrophenyl)-1-nitroethane undergoes a slow dissociation, with a very small dissociation constant, followed by a fast association with the base to yield the carbanion ion-pair.

KENNETH T. LEFFEK et PRZEMYSLAW PRUSZYNSKI. Can. J. Chem. **59**, 3034 (1981).

Le nitro-4 phenylnitrométhane réagit avec le diméthoxy-2,7 bis(diméthylamino)-1,8 naphtalène dans l'acétonitrile selon un transfert de proton bimoléculaire avec un effet isotopique primaire du deutérium de $k_H/k_D = 12{,}2$ à 25°C. Le grand effet isotopique sur l'enthalpie d'activation $(\Delta H_D^{\ddagger} - \Delta H_H^{\ddagger}) = 4{,}6 \pm 0{,}3$ kcal mol^{-1} est en accord avec une contribution importante de l'effet tunnel du proton à la vitesse de réaction de l'hydrogène du substrat.

La réaction analogue du (nitro-4 phényl)-1 nitro-1 éthane avec la même base dans l'acétonitrile donne des cinétiques et des paramètres de réaction qui s'opposent. La réaction est d'ordre un et est indépendante de la concentration de la base. L'effet isotopique k_H/k_D est égal à 9,3 à 25°C tandis que la différence d'enthalpie d'activation $(\Delta H_D^{\ddagger} - \Delta H_H^{\ddagger})$ est seulement de $0{,}5 \pm 0{,}1$ kcal mol^{-1}. On en conclut que le (nitro-4 phényl)-1 nitro-1 éthane subit une dissociation lente avec une très faible constante de dissociation, suivie d'une association rapide avec la base pour conduire au carbanion sous forme de paire d'ions.

[Traduit par le journal]

Introduction

An earlier study of the proton transfer from 4-nitrophenylnitromethane to 1,8-bis(dimethylamino)naphthalene in isopropyl alcohol and *tert*-butyl alcohol solvents showed only small primary isotope effects and fairly high enthalpies of activation (1). Subsequent calculations in which the results were fitted to Bell's equation (2–4) for quantum mechanical tunnelling of the proton through a parabolic potential energy barrier yielded a wide barrier of 3.3 Å and indicated no significant proton tunnelling (5).

In aprotic solvents, in which larger isotope effects may be expected, the base abstracts a proton from 4-nitrophenylnitromethane and 1-(4-nitrophenyl)-1-nitroethane to yield a coloured carbanion in measurable yield only at high concentration; i.e. the reactions have very low equilibrium constants. Therefore, in order to study this type of reaction it is necessary to use 2,7-dimethoxy-1,8-bis(dimethylamino)naphthalene, which is one of the strongest neutral bases (6) and also very sterically hindered. The high steric hindrance should make the reaction very sensitive to steric crowding in the acid molecule and perhaps give a reaction with a narrow potential energy barrier. This would give a large tunnelling contribution to the proton transfer relative to the deuteron transfer and hence a high primary isotope effect. The nitroethane substrate has been used to test this hypothesis.

Results and Discussion

The reactions of 4-nitrophenylnitromethane (4-NPNM) and 1-(4-nitrophenyl)-1-nitroethane (4-NPNE) with 2,7-dimethoxy-1,8-bis(dimethylamino)naphthalene (2,7-DMDAN) in acetonitrile give single absorption peaks in the visible region at 500 nm and 520 nm respectively. Caldin and Mateo (7) found $\lambda_{max} = 493$ nm for 4-NPNM reacting with tetramethylguanidine in acetonitrile. The intensity of the absorbance varied very little with base concentration indicating that the equilibrium constants for the reactions were large.

[1]Presented at the Fast Reactions in Solution meeting of The Chemical Society held at Göttingen, Germany, September 3–5, 1980.

[2]Postdoctoral Fellow 1979–1980.

0008-4042/81/213034-05$01.00/0

©1981 National Research Council of Canada/Conseil national de recherches du Canada

Can. J. Chem. Downloaded from www.nrcresearchpress.com by 210.87.254.5 on 09/06/12
For personal use only.

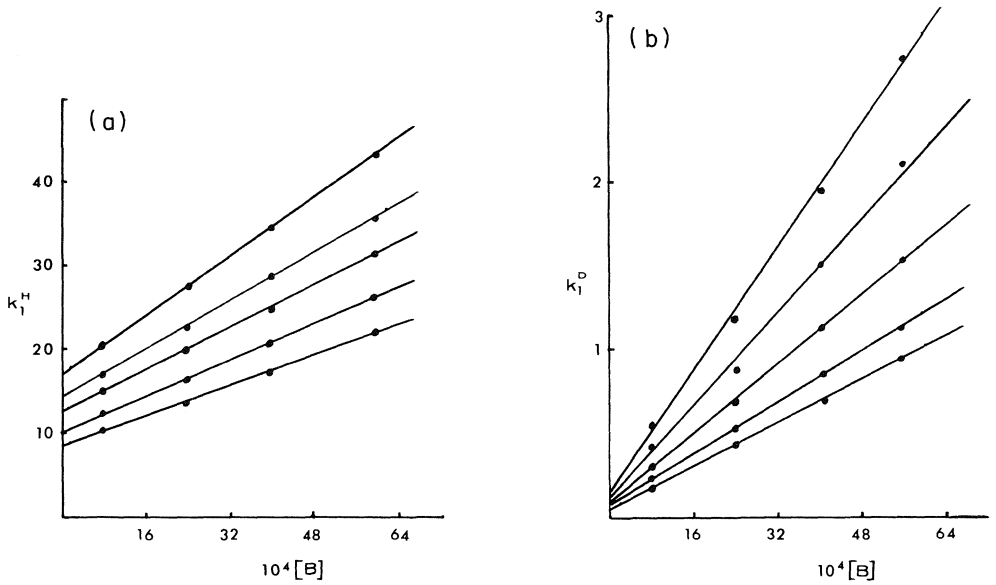

FIG. 1. Pseudo-first order rate constants (a) k_H and (b) k_D in s^{-1} vs. base concentration for the proton and deuteron transfer from *p*-nitrophenylnitromethane and its α-deuterated analogue to 2,7-dimethoxy-1,8-bis(dimethylamino)naphthalene. Rate constant measurements were made at 15, 20, 25, 30, and 35°C.

The 4-Nitrophenylnitromethane Reaction

For the 4-NPNM and 4-NPNM-d_2 reactions, pseudo first-order rate constants were determined using an acid concentration of 2×10^{-5} *M* and a series of base concentrations ranging from 8×10^{-4} *M* to 6×10^{-3} *M*. Figures 1(a) and (b) show these first-order rate constants plotted against base concentration. The slopes of these lines are the second-order rate constants and are collated in Table 1, together with the isotopic rate ratios. These values yield the activation parameters shown in Table 2.

The isotopic rate ratio of 12.2 at 25°C is the same within experimental error as that found by Caldin and Mateo (7) for the reaction of 4-NPNM with tetramethylguanidine in acetonitrile, and isotope effects of this magnitude have been observed for a number of other proton transfer reactions of this acid (8–13). This value may be indicative of proton tunnelling in that it is considerably greater than the value of ~7 which is obtained by the assumption of the complete loss of one C—H stretching vibration during the activation process. The activation parameter differences are considerably larger than the maximum values which can be accounted for without assuming a large contribution to the reaction by proton tunnelling. The enthalpy of activation difference of more than 4 kcal mol^{-1} and log A_D/A_H in excess of 2 are very similar to such values recorded by Caldin and Mateo (7) for the 4-NPNM reaction with tetramethylguanidine, although these workers obtained such results mostly in nonpolar solvents where the equilibrium constants were fairly small. Furthermore, their values were associated with very high isotopic rate ratios.

TABLE 1. Second order rate constants for the reaction of 4-nitrophenylnitromethane and its deuterated analogue and 2,7-dimethoxy-1,8-bis(dimethylamino)naphthalene in acetonitrile

Temperature (°C)	$10^{-2} k_{2H}$ ($L\ mol^{-1}\ s^{-1}$)	$10^{-2} k_{2D}$ ($L\ mol^{-1}\ s^{-1}$)	k_{2H}/k_{2D}
15	22.6±1	1.56±0.05	14.5
20	26.1±1	1.90±0.07	13.7
25	31.0±1	2.55±0.09	12.2
30	35.1±1.5	3.54±0.15	9.9
35	40.5±2	4.61±0.18	8.8

The results have been fitted to Bell's equation (2–4) using the technique of Caldin and Mateo (7) and the tunnelling parameters are shown in Table 3, together with the values reported (7) for the reaction 4-NPNM with TMG. Thus, although the isotope effect on the second-order rate constants is not exceptionally large, tunnelling of the proton appears to contribute to the proton transfer reaction to a significant extent.

The 1-(4-Nitrophenyl)-1-nitroethane Reaction

Pseudo first-order rate constants were determined in the same manner as for the 4-NPNM reaction. The 4-NPNE initial concentration was 1×10^{-5} *M* and the base concentration was varied

Can. J. Chem. Downloaded from www.nrcresearchpress.com by 210.87.254.5 on 09/06/12
For personal use only.

TABLE 2. Activation parameters for the reaction of 4-NPNM and 4-NPNM-d_2 with 2,7-DMDAN in acetonitrile at 25°C

Parameter	Proton transfer	Deuteron transfer
$\Delta H^{\ddagger}$ (kcal mol^{-1})	4.6±0.1	9.2±0.5
$\Delta S^{\ddagger}$ (cal mol^{-1} K^{-1})	−27.2±0.4	−16.5±1.7
$(\Delta H_D^{\ddagger} - \Delta H_H^{\ddagger})$ (kcal mol^{-1})	4.6±0.5	
$(\Delta S_D^{\ddagger} - \Delta S_H^{\ddagger})$ (cal mol^{-1} K^{-1})	10.7±1.8	
$\log_{10} A$	7.3±0.1	9.6±0.4
$\log_{10} A_D/A_H$	2.3	

TABLE 3. Tunnelling and barrier parameters for the reaction of 4-NPNM in acetonitrile

Parameter	4-NPNM + 2,7-DMDAN	4-NPNM + TMG*
$E_{H_{obs}}$ (kcal mol^{-1})	5.1	5.0
$E_{D_{obs}}$ (kcal mol^{-1})	9.7	6.4
$E_{H_{calc}}$ (kcal mol^{-1})	9.5	5.85
$E_{D_{calc}}$ (kcal mol^{-1})	10.5	7.00
$2b$ (Å)	0.75	0.96
$E_{H_{obs}}/E_{H_{calc}}$	0.54	0.85
$E_{D_{obs}}/E_{D_{calc}}$	0.92	0.92

*Reference 7.

between 1.2×10^{-4} and 6.1×10^{-3} M. The first-order rate constants showed no change when the base concentration was changed by a factor of 50. At 20°C measurements at eight different base concentrations gave $k_{1H} = 2.6 \pm 0.2 \times 10^{-2}$ s^{-1} and for the deuteron transfer five determinations gave $0.32 \pm 0.01 \times 10^{-2}$ s^{-1}. This insensitivity of the first-order rate constant could arise in a second order reaction with a very small equilibrium constant. For such a reaction the observed first-order rate constant k_{obs} is given by eq. [1], where k_2 and k_{-2} are the second-order rate constants for the forward and reverse reactions respectively and b is the base concentration. If the equilibrium constant, k_2/k_{-2}, is very small, the k_{obs} is approximately equal to k_{-2}. However, if the equilibrium constant were very small an increase in the base concentration would give a proportionate increase in the carbanion concentration at equilibrium and hence a proportionate increase in the intensity of the absorbance at 520 nm. In our reaction, an increase in the base concentration by a factor of 10 increased the intensity of the absorbance by only about 4% indicating that the equilibrium constant is large, about 5000 dm^3 mol^{-1}. This value would give a very marked dependence of k_{obs} on base concentration if the reaction were indeed second order. It is concluded, therefore, that the reaction of 2,7-DMDAN with 4-NPNE is a first-order reaction.

$$[1] \quad k_{obs} = k_2 b + k_{-2}$$

Table 4 shows the temperature dependence of k_{obs} and the isotopic rate ratios. These values yield the activation parameters in Table 5.

TABLE 4. Observed first-order rate constants for the reaction of 4-nitrophenylnitroethane* and 2,7-dimethoxy-1,8-bis(dimethylamino)naphthalene* in acetonitrile

Temperature	$10^2 k_{H_{obs}}$ (s^{-1})	$10^2 k_{D_{obs}}$ (s^{-1})	k_H/k_D
15	2.54	0.250	10.2
20	2.94	0.321	9.2
25	3.75	0.405	9.3
30	4.59	0.500	9.2
35	5.82	0.649	9.0

*Initial concentrations 4-NPNE 1×10^{-5} M, 2,7-DMDAN 6.12×10^{-3} M.

TABLE 5. Activation parameters for the reaction of 4-NPNE and 4-NPNE-d_2 with 2,7-DMDAN in acetonitrile at 25°C

Parameter	Proton transfer	Deuteron transfer
$\Delta H^{\ddagger}$ (kcal mol^{-1})	6.8±0.4	7.7±0.2
$\Delta S^{\ddagger}$ (cal mol^{-1} K^{-1})	−42.1±1.3	−43.7±0.6
$(\Delta H_D^{\ddagger} - \Delta H_H^{\ddagger})$	0.9±0.4	
$(\Delta S_D^{\ddagger} - \Delta S_H^{\ddagger})$	−1.6±1.4	
$\log_{10} A$	4.0±0.3	3.7±0.1
$\log_{10} A_D/A_H$	−0.3	

The results show that, although the values of k_H/k_D are not very different for the two acids 4-NPNM and 4-NPNE, the activation parameters and the isotope effects on the activation parameters show no similarity at all and reinforce the conclusion dictated by the difference in the kinetics that the two reactions have different mechanisms. The p-nitrophenylnitromethane reaction is not markedly different from proton transfer from this substrate to other bases (7) and may, therefore, be assumed to follow the same mechanism, a bimolecular reaction. The p-nitrophenylnitroethane reaction, on

Can. J. Chem. Downloaded from www.nrcresearchpress.com by 210.87.254.5 on 09/06/12
For personal use only.

Can. J. Chem. Downloaded from www.nrcresearchpress.com by 210.87.254.5 on 09/06/12
For personal use only.

the other hand, shows a significant isotope effect on the rate of the reaction and also an isotope effect on the enthalpy of activation about equal to the maximum effect associated with the loss of one C–H stretching vibration. Despite this, the concentration of the base does not appear in the kinetic equation. The proton transfer must, therefore, be a two-step process in which the step involving the base is not rate determining.

There are two possibilities. In the first, the base associates with the acid in a rapid step with a large equilibrium constant to yield a hydrogen-bonded complex which subsequently undergoes a proton transfer from acid to base to yield the colored anion in a second rate-determining step. In the second possible mechanism, the acid dissociates in an initial slow step to give an ion-pair which then is captured by the base in a second rapid proton transfer.

The second of these two mechanisms fits the data better than the first because the two-step mechanism is not observed with the methane substrate. This may be accounted for by the fact that the methane substrate is less sterically hindered in its reaction with the base, hence the direct bimolecular reaction can be observed. For the ethane substrate, the bimolecular reaction is blocked by the additional steric hindrance, allowing the slower dissociation to be observed.

In the first possible mechanism, if it is assumed that the base associates rapidly with the ethane substrate, it would also associate rapidly with the less crowded methane substrate and hence the same kinetics would be found for both acids.

It is, therefore, concluded that the 4-nitrophenylnitroethane undergoes a slow dissociation followed by a fast association with the base to yield the carbanion ion-pair. The isotope effect on the dissociation, $\Delta H_D^{\ddagger} - \Delta H_H^{\ddagger} = 0.9$ kcal mol^{-1} shows no contribution from tunnelling. This result contrasts markedly with the bimolecular proton transfer from 4-nitrophenylnitromethane which shows a narrow energy barrier for reaction of 0.75 Å and an isotope effect enhanced by proton tunnelling.

The fact that 4-nitrophenylnitroethane transfers a proton to the solvent faster than it does to 2,7-DMDAN is a dramatic demonstration of the observation by Alder *et al.* (6) that, despite the very high base strength of 2,7-DMDAN, proton transfers to and from it are exceptionally slow.

Experimental

Materials

4-Nitrophenylnitromethane and its deuterated analogue were prepared as described previously (14). 1-(4-Nitrophenyl)-1-nitroethane was prepared from *p*-nitroacetophenone via the oxime as described by Boyle (15) and earlier workers (16, 17). The 1-deuterated material was made by the same procedure as that used for the methane.

2,7-Dimethoxy-1-8-bis(dimethylamino)naphthalene was obtained from 2,7-dihydroxynaphthalene by methylation with dimethylsulphate (18) to give the 2,7-dimethoxy derivative, followed by nitration at the 1 and 8 positions with 90% nitric acid in acetic acid. The nitro groups were reduced to amino groups with stannous chloride (19) and these were methylated by refluxing the material with excess methyl iodide and potassium hydride in tetrahydrofuran (16). The crude base was purified by repeated crystallization from *n*-hexane at low temperature; mp 67–68.5°C. The nmr spectrum showed two doublets each from two protons at 2.52 τ and 2.94 τ ($J = 9.0$ Hz), a singlet for 6 protons from the methoxy groups at 6.11 τ, and a singlet for 12 protons from the four methyl groups at 7.11 τ. The values are in good agreement with those of Alder *et al.*[3]

Acetonitrile, reagent grade, was purified by the method of O'Donnell *et al.* (20) and fractionally distilled over P_2O_5.

Kinetic Measurements

The reaction rates were measured with a Durrum–Gibson stopped-flow spectrophotometer using the standard technique previously described (21). Some of the rate measurements with deuterated substrates were made both with the stopped-flow spectrophotometer and a standard uv–vis spectrophotometer and the results showed good agreement between the two instruments. A sample run is given in Table 6.

TABLE 6. Run #185; temperature 15.0°C; initial concentration $NO_2C_6H_4CH_2NO_2 = 2 \times 10^{-5}$ *M*; initial concentration 2,7-dimethoxy-1,8-bis(dimethylamino)naphthalene $= 4.05 \times 10^{-3}$ *M*

Time (ms)	x_1*	x_2*
0	271.0	129.0
10	241.5	117.5
20	218.0	112.0
30	197.5	107.0
40	180.5	103.0
50	164.0	99.0
60	152.5	95.5
70	141.5	92.5

Guggenheim analysis yields $k_1 = 17.6$ s^{-1}

*x_1 and x_2 are readings in mm from the enlarged reaction trace corresponding to transmittance decreasing with time.

Acknowledgements

The authors are grateful for financial support by the Natural Sciences and Engineering Research Council of Canada.

1. A. JARCZEWSKI, P. PRUSZYNSKI, and K. T. LEFFEK. J. Chem. Soc. Perkin Trans. II, 814 (1977).
2. R. P. BELL. Trans. Faraday Soc. **55**, 1 (1959).
3. R. P. BELL, W. H. SACHS, and R. L. TRAINER. Trans. Faraday Soc. **67**, 1995 (1971).
4. R. P. BELL. *In* The proton in chemistry. 2nd ed. Chapman and Hall, London. 1973. p. 275.
5. A. JARCZEWSKI, P. PRUSZYNSKI, and K. T. LEFFEK. Can. J. Chem. **57**, 669 (1979).
6. R. W. ALDER, N. C. GOODE, N. MILLER, F. HIBBERT, P. P. HUNTE, and H. J. ROBBINS. J. Chem. Soc. Chem. Commun. 89 (1978).

[3]R. W. Alder, private communication.

7. E. F. CALDIN and S. MATEO. J. Chem. Soc. Faraday Trans. I, 1876 (1975).
8. E. F. CALDIN and S. MATEO. J. Chem. Soc. Faraday Trans. I, 112 (1976).
9. O. ROGNE. Acta Chem. Scand. Ser. A, **32**, 559 (1978).
10. J. H. BLANCH and O. ROGNE. J. Chem. Soc. Faraday Trans. I, 1254 (1978).
11. I. HEGGEN, J. LINDSTROM, and O. ROGNE. J. Chem. Soc. Faraday Trans. I, 1263 (1978).
12. E. F. CALDIN, O. ROGNE, and C. J. WILSON. J. Chem. Soc. Faraday Trans. I, 1796 (1978).
13. E. F. CALDIN and O. ROGNE. J. Chem. Soc. Faraday Trans. I, 2065 (1978).
14. E. F. CALDIN, A. JARCZEWSKI, and K. T. LEFFEK. Trans. Faraday Soc. **67**, 110 (1971).
15. W. BOYLE, JR. Ph.D. dissertation, Northwestern University, 1971.
16. D. E. PEARSON and J. D. BRUTON. J. Org. Chem. **19**, 957 (1954).
17. W. D. EMMONS and A. S. PAGANO. J. Am. Chem. Soc. **77**, 4557 (1955).
18. O. FISCHER and W. KERN. J. Prakt. Chem. **94**, 34 (1916).
19. S. N. CHAKRAVATI and V. PASUPATI. J. Chem. Soc. 1859 (1937).
20. J. F. O'DONNELL, J. T. AYERS, and C. K. MANN. Anal. Chem. **37**, 1161 (1965).
21. A. JARCZEWSKI and K. T. LEFFEK. Can. J. Chem. **50**, 24 (1972).

Can. J. Chem. Downloaded from www.nrcresearchpress.com by 210.87.254.5 on 09/06/12
For personal use only.

Erratum: Hydrogen–deuterium exchange of heteroaromatics in neutral D_2O at elevated temperatures

NICK HENRY WERSTIUK AND GEORGE TIMMINS
Department of Chemistry, McMaster University, Hamilton, Ont., Canada L8S 4M1

(Ref.: Can. J. Chem. **59**, 1022 (1981))
Received July 22, 1981

Page 1023, column 1, line 23: entries 1, 5, 8, and 12 should read entries 1, 4, 6, 9, and 12.
Page 1023, column 2, line 14: entry 15 should read entry 11.
Page 1024, column 1, line 25: entries 4 and 11 should read entries 4 and 8.
Page 1024, column 2, line 4: entry 9 should read entry 7.

Table 1 should read as follows:

TABLE 1. Hydrogen–deuterium exchange of heteroaromatics in neutral D_2O

Entry	Substrate	Temp. °C (±5°C)	Time (h)	Percent exchange[a] C2	C3	C4	C5	C6	CH_3
1	**1**	225	4	71	3[b]	10	3	71	
2	**1**	280	96	94[c]	59	53	59	94	
3	**1**	300	15	97	68	69	68	97	
4	**2**	180	9	—	7[d]	5	—	43	93
5	**2**	280	96	—	54[d]	53	—	96	96
6	**3**	180	9	11	—	1	1	11	1
7	**3**	280	96	97	—	25	46	97	79
8	**4**	180	8	32	3	—	3	32	63
9	**4**	195	12	44	5	—	5	44	78
10	**4**	280	96	99	48	—	48	99	96
11	**4**	300[e]	168	95	95	—	95	95	95
12	**5**	250	5	96	9	13	<5[f]		
13	**5**	300	66	96	96	96	96[f]		

[a] For runs up to 225°C the substrate (0.4 g) in 6 mL of D_2O was heated in a sealed tube in a Carius oven. For runs above 225°C the heterocycle was heated in a sealed tube in a bomb which contained water to equalize pressure. The deuterated substrates were isolated by preparative glpc and the yields ranged between 40–70%.
[b] Determined by ^1H nmr as averages of six integrals. Since the precision is not better than ±5%, incorporations of around 5% are not meaningful.
[c] Exchanges of >90% reflect equilibration with the deuterium pool.
[d] Total exchange at C3 and C5. Based on pyridine chemical shifts and analysis of ^1H nmr spectra of partially deuterated substrates.
[e] See text for experimental.
[f] Total exchange at C2(9), C3(8), C4(7), and C5(6).

Rearrangements during deamination of 4-amino-4-des(oxymethylene)anhydrolycoctonam[1,2]

O. E. EDWARDS

Division of Chemistry, National Research Council of Canada, Ottawa, Ont., Canada K1A 0R6

Received April 21, 1981

O. E. EDWARDS. Can. J. Chem. **59**, 3039 (1981).

The diterpenoid alkaloid lycoctonine was transformed into 4-amino-4-des(oxymethylene)anhydrolycoctonam. Nitrous acid deamination of this led to two unexpected products, an aldehydo-lactam acid and a hydroxy-keto lactam, both involving skeletal rearrangement. The origin of these products is discussed on the basis of structures determined by X-ray crystallography.

O. E. EDWARDS. Can. J. Chem. **59**, 3039 (1981).

On a transformé la lycoctonine, un alkaloide diterpénique, en amino-4 des(oxyméthylène)-4 anhydrolycoctoname. La désamination nitreuse de ce composé conduit à deux produits inattendus, un acide aldéhydo-lactame et une hydroxy-céto lactame impliquant tous deux une transposition du squelette. On discute de l'origine de ces produits en fonction des structures déterminées par cristallographie de rayons-X.

[Traduit par le journal]

Introduction

The first determination of the structure of a polyoxygenated diterpene alkaloid was made possible by the X-ray analysis of the structure of des(oxymethylene)lycoctonine hydriodide **1** (1). In our search, prior to this analysis, for methods which might help to define the skeleton of the parent alkaloid lycoctonine (**2**)[3] we explored reactions of its derivative lycoctonamic acid **3** (2).

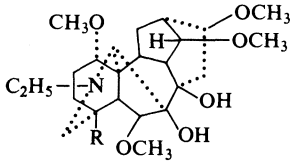

1 R = H
2 R = CH_2OH

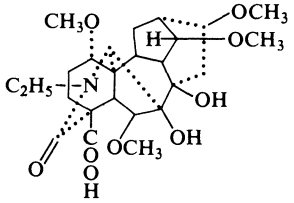

3

An improved method of preparing the product of its pinacolic dehydration, anhydrolycoctonamic acid **4**, involved the action of very dilute sulfuric acid in acetic acid on **3**. Acid **4** was converted into 4-amino-4-des(oxymethylene)anhydrolycoctonam **5** by Curtius or Hofmann degradation. Nitrous acid deamination of **5** gave as main products a hydroxy-keto lactam (50%) and a crystalline acid (20%). The skeletal rearrangements involved in their formation, and the nature of the oxidation leading to the acid are of considerable interest.

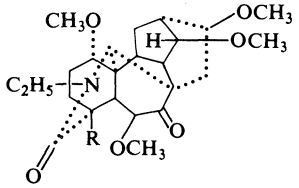

4 R = COOH
5 R = NH_2

Structures

Because of a number of difficulties in interpreting the structural evidence, recourse was had to X-ray crystallographic analysis of the derivatives of the two major products. The exposition is simplified by assuming the correct structures.

The acid from the deamination proved to be an aldehydo-lactam acid (δ 9.9, 1H singlet, doublet at 201 ppm in its ^{13}C nmr spectrum), with empirical formula $C_{22}H_{31}NO_7$. Since it contained no C—C double bond (^{13}C nmr) it was pentacyclic. It only contained three methoxyl groups, hence it appeared probable that ring B had undergone fission with loss of C-6 and its attached methoxyl. This and the facts that the aldehyde group was attached to a quaternary carbon and that a γ-lactam (ν_{max} 1686 cm^{-1}) was probably present, coupled with mechanistic considerations, made structure **6** one of the likely possibilities.

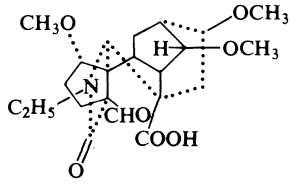

6

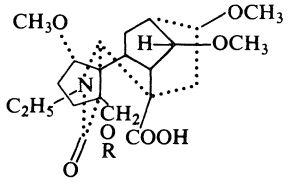

7

The aldehyde function of **6** hydrated or formed hemiacetals on handling, resulting in the, at first puzzling, disappearance of the group. The mass spectrum of the methyl ester of **6**, prepared using

[1]NRCC No. 19608.

[2]Presented in part at the Annual Conference of the Chemical Institute of Canada, Ottawa, June 8–11, 1980.

[3]The C-1 configuration has been changed to conform to the new X-ray information (see Discussion).

0008-4042/81/213039-05$01.00/0

©1981 National Research Council of Canada/Conseil national de recherches du Canada

Can. J. Chem. Downloaded from www.nrcresearchpress.com by 210.87.254.105 on 09/06/12
For personal use only.

Can. J. Chem. Downloaded from www.nrcresearchpress.com by 210.87.254.105 on 09/06/12
For personal use only.

diazomethane in methanol–ether, gave an apparent molecular ion of *m/e* 449. This could possibly be due to small amounts of homologous aldehyde or epoxide formed by reaction with diazomethane. This, and ambiguity of many analyses, hampered structural work.

The aldehyde group was reduced to the primary alcohol, then this acetylated, giving an acetoxy acid. An X-ray analysis (3) showed that the acetoxy acid had structure **7** (R = OAc) and that **6** was the correct representation of the aldehydo acid.

The neutral deamination products contained some very polar components, nitrite esters (slow release of oxides) and at least three similar components separated by preparative thin layer chromatography. The main one (51% yield) was a hydroxy-keto-lactam (ν_{max}: 3470, 1729, and 1633 cm^{-1}) with formula $C_{24}H_{35}NO_7$. Since it had a saturated skeleton (^{13}C nmr) it was hexacyclic. The hydroxyl was readily acetylated, hence was primary or secondary. Jones' reagent oxidized it into a mixture of neutral and acidic products. The main acid (up to 52% yield) was a crystalline keto-lactam acid with formula $C_{24}H_{33}NO_8$. X-ray analysis[4] showed that it had the surprising structure **8** and hence that the hydroxy-keto lactam was **9**.

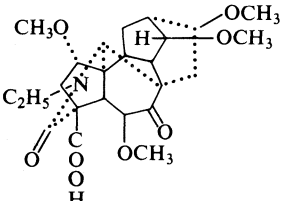

8

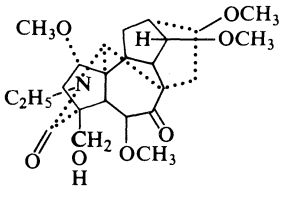

9

The ^{13}C spectrum of **9** had a triplet at 66 ppm, now attributable to the CH_2OH group. However the main neutral product from the Jones' oxidation (14%) appeared to be a diketo γ-lactam (ν_{max}: 1732, 1711, and 1693 cm^{-1}, no aldehyde proton in its ^1H nmr spectrum). This proved to be a stumbling block to interpretation. Despite the clean spectra of **9**, it may have contained an impurity which gave rise to this product.

The keto-lactam acid **8** showed strong internal hydrogen bonding (lactam carbonyl at 1604 cm^{-1}) as expected for a malonamic acid (see lycoctonamic and anhydrolycoctonamic acids (2)). Unlike these malonamic acids, however, it did not decarboxylate below 255°C.

Discussion

The X-ray analyses of **7** (3) and **8**[4] gave totally unexpected information that the C-1 configuration in lycoctonine was opposite to what had been assumed on the basis of the X-ray analysis of "des(oxymethylene)lycoctonine" hydriodide (1). This point will be discussed in a separate communication. The skeletal rearrangement involved in formation of the aldehyde was expected to be the main one observed, since the bond antiparallel to the departing nitrogen migrates, giving a secondary cation. However, the cleavage to the aldehydo acid was unexpected. One possible explanation is the formation of an intermediate nitrite ester, which fragments (eq. [1]). Subsequent oxidative cleavage

[1] 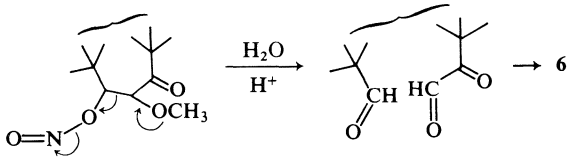

by nitrous acid or oxides of nitrogen could give **6**. Fragmentation giving hyponitrous acid has been demonstrated in nitrosamide photolysis in acid (4*a*).

We are grateful to a referee for suggesting an alternate mechanism outlined in eq. [2]. This would require formation of the secondary alcohol from the rearranged cation, then retroaldol fission of the rather rigid ring B. This might relieve strain and increase entropy. The nitrosation of the resulting enol also seems possible. However, the second order Beckmann reaction of α-oximino ketones normally requires the action of strong acid (sulfuric, trifluoroacetic), or the action of base on the oxime esters (4*b*). The actual medium for the deamination was partially neutralized (amine, $NaNO_2$) 2 *N* sulfuric acid. Hence the fragmentation under such mild conditions would be unusual.

The formation of the primary alcohol **9** as a major

[2] 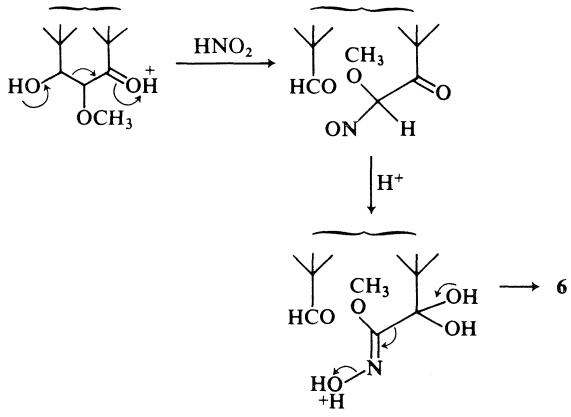

product of the deamination is surprising. In model studies related to this work, we demonstrated ring contraction of α-aminocyclohexanones to hydroxy-

[4]M. Cygler and M. Przybylska, unpublished work.

cyclopentanones and the related enones (5, 6). But the process was clearly a downhill one energetically, since the secondary cations were involved (eq. [3]).

[3] 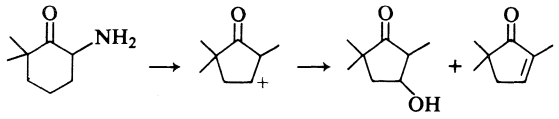

The driving force for the ring contraction was the avoidance of a high energy cation adjacent to the positive end of the carbonyl dipole (6). Even though the bridgehead cation at C-4 would probably be more destabilized than the cations adjacent to the ketone carbonyls of our model compounds, it seems improbable that a high energy primary cation[5] would form from it. Hence, as in our model studies (6) we invoke formation of a specific edge-protonated cyclopropane as a less energetic intermediate. This would form by C2—C3 bond participation in the ionization followed by proton migration to give **10** with the proton on the more basic bond of the cyclopropane (6). This would then be preferentially attacked by water at C-3 for steric reasons and the proximity of solvent molecules to the face near the departing nitrogen and the lactam carbonyl (eq. [4]).

[4] 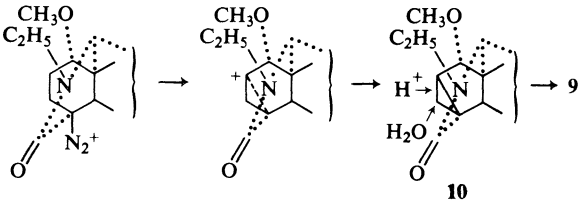

10

The failure of the malonamic acid **8** to decarboxylate below 250°C, in contrast to the behaviour of lycoctonamic (**3**) and anhydrolycoctonamic (**4**) acids (2) could be interpreted as due to the very high energy of a transition state with bridgehead double bond character (see **11**) in this rigid fused system. However, Ferris and Miller (8) suggested that the transition state resembles a zwitterion such as **12** in these cases, and that the energy of this state diminishes to the extent that overlap of the anion with the π orbitals of the carbonyl becomes possible.

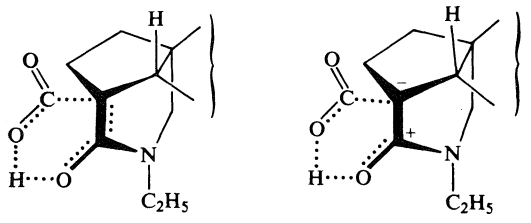

11 **12**

[5]A primary cation is around 27 kcal/mol less stable than a simple tertiary cation, and around 10 kcal/mol less stable than an isolated secondary cation (7).

Experimental

Unless otherwise mentioned, infrared spectra were of chloroform solutions and nmr spectra of deuterochloroform solutions containing TMS as reference. All plate separations were done on silica gel plates with fluorescent indicator. Spectra were obtained on a Perkin–Elmer model 157 infrared spectrometer, and Varian EM-360 and CFT-20 spectrometers.

Anhydrolycoctonamic Acid 4

An improved method of preparing this acid (2) follows. The trihydrate of lycoctonamic acid (**3**) (1.01 g) in 15 mL of glacial acetic acid containing 0.015 mL of concentrated sulfuric acid was heated at 85–90°C for 5.5 h. The sulfuric acid was neutralized by the addition of solid sodium carbonate, then the acetic acid removed under reduced pressure. The residue was taken up in water and the acid extracted into chloroform. The acid crystallized when 1 mL of methanol was added. A first crop of crystals (600 mg) melted at 181°C (dec.) and gave no mixture mp depression with the product prepared using acetyl chloride (2). Its ^{1}H nmr spectrum had signals at δ 4.02 (1H, d?, J = 3 Hz), 3.48 (3H, s), 3.38 (3H, s), 3.26 (6H, s), 2.96 (1H, s), 2.78 (1H, s), 1.17 (3H, t, J = 7 Hz), and its ^{13}C nmr spectrum had signals at δ 203.4, 174.1, 172.9, 88.3(d), 82.6(d), 82.0(d), 80.4(d), 64.7(d), 59.9(q), 58.6(s), 57.1(s), 56.7(q), 56.6(q), 55.5(t or s), 48.7(s), 47.6(d), 46.9(d), 43.9(t), 42.2(d), 38.8(d), 32.3(t), 25.6(t), 23.1(t), and 11.5(q).

Anhydrolycoctonamide

Anhydrolycoctonamic acid (910 mg) was added to 15 mL of thionyl chloride containing 0.2 mL of pyridine. The solution was refluxed for 45 min, the reagents removed under reduced pressure, then the residue cooled to 0°C. Ice-cold concentrated ammonia (28%, 15 mL) was added rapidly. A white gum formed, which gradually crystallized. After 30 min this was extracted into chloroform and the chloroform washed with dilute ammonia. The 757 mg of neutral product from the chloroform crystallized from ether giving 716 mg of amide, mp 190–200°C. Some unchanged acid was recovered from the ammonia solutions.

The amide was recrystallized from methanol–ether. After drying 3.5 h at 100°C *in vacuo* it had mp 210–214°C. It had ν_{max}: 3480, 3320, 1728, 1675, 1632, and 1553 cm^{-1}. Its ^{1}H nmr spectrum gave signals at δ 8.66 (1H, broad), 5.85 (1H, broad), 3.98 (1H, d, J = 3 Hz), 3.50 (3H, s), 3.40 (3H, s), 3.30 (6H, s), 3.08 (1H, s), 2.85 (1H, s), 1.13 (3H, t, J = 7 Hz). *Anal.* calcd. for $C_{25}H_{36}N_2O_7$: C 63.00, H 7.61; found: C 63.09, H 7.64.

4-Amino-4-des(oxymethylene)anhydrolycoctonam 5

Anhydrolycoctonamide (680 mg) was added to 15 mL of an ice-cold solution of potassium hypobromite (2 g of potassium hydroxide, 260 mg of bromine). The bulk of the amide dissolved rapidly. The solution was allowed to warm gradually until only a trace of undissolved solid remained (15 min), then heated at 75°C for 50 min. Sodium bisulfite was added to the solution, which was then acidified using sulfuric acid. Extraction of the solution with chloroform removed 36 mg of neutral material. The aqueous layer was basified and the base extracted into methylene chloride. The 580 mg of base crystallized from ether giving 550 mg, mp 194–202°C. It had ν_{max} (CH_2Cl_2): 3380 (very weak), 1726, and 1648 cm^{-1} and $[\alpha]_D$ 16° (*c* 1.03, absolute ethanol). Its ^{1}H nmr spectrum had signals at δ 4.36 (1H, s), 3.93 (1H, s), 3.52 (3H, s), 3.36 (3H, s), 3.26 (3H, s), 3.25 (3H, s), 1.1 (3H, t, J = 7 Hz), and its ^{13}C nmr spectrum had signals at δ 204.2, 173.0, 84.3, 83.4, 82.8, 64.0, 60.4, 59.2, 57.9, 56.9, 56.5, 56.2, 54.2, 49.9,

Can. J. Chem. Downloaded from www.nrcresearchpress.com by 210.87.254.105 on 09/06/12
For personal use only.

Can. J. Chem. Downloaded from www.nrcresearchpress.com by 210.87.254.105 on 09/06/12
For personal use only.

47.9, 43.7, 43.4, 38.8, 33.2, 26.4, 25.5, and 12.3. Its pK_a in 50% aqueous methanol was 5.5. *Anal.* calcd. for $C_{24}H_{36}N_2O_6$: C 64.26, H 8.09, N 6.25; found: C 64.19, H 8.21, N 6.32.

The amine was also prepared by converting anhydrolycoctonamic acid into its chloride using thionyl chloride, then its azide (ν_{max} 2145 cm^{-1} in methylene chloride) using a cold saturated solution of sodium azide in 50% aqueous acetone. The azide was converted to isocyanate by heating in refluxing benzene for 1 h. The isocyanate had ν_{max}: 2235, 1731, and 1656 cm^{-1}. This was hydrolysed, using 1 *N* sulfuric acid in 50% aqueous acetone, to give a crystalline amine identical to **5**.

Deamination of 5

Five hundred milligrams of the amino-lactam were dissolved in 15 mL of 2 *N* sulfuric acid. After addition of 400 mg of sodium nitrite the flask was loosely stoppered. After 40 min and 70 min two further 100 mg portions of nitrite were added. At the end of 95 min total reaction time the mixture was concentrated under reduced pressure to remove nitrogen oxides. The neutral and acidic products were extracted into methylene chloride, then the acids removed from the methylene chloride by two sodium carbonate washes. The neutral product weighed 400 mg and the acids 115 mg (1). Only a trace of base was recovered.

Aldehydo Acid 6

After purification by preparative tlc on silica gel plates, using 15% methanol in chloroform for development, the main acid from deamination of **5** crystallized from methanol as needles, mp 230°C. It had ν_{max}: 1711 and 1656 cm^{-1} with intermediate shoulders. Its ^1H nmr spectrum had signals at δ 9.9 (1H, s), 4.4 (1H, s), 3.36, 3.24 (singlets), and a distorted triplet centered at δ 1.13 (3H, J = 7 Hz). Its ^{13}C nmr spectrum had signals at δ 201.1(d), 177.1(s), 174.6(s), 84.6(d), 83.8(d), 81.8(d), 71.5(d), 69(s), 63.5(s), 57.5(q), 56.7(q), 56.3(q), 54.5(s), 48.9(d), 43.1(d), 40.14(d), 38.6(t), 33.8(t), 30.1(t), 28.8(t), 27.5(t), and 12.3(q). *Anal.* calcd. for $C_{22}H_{31}NO_7$: C 62.69, H 7.41, N 3.32, OCH_3 22.09; found (average of three analyses): C 63.43, H 7.66, N 3.44, OCH_3 21.68. Occasionally a hydrated form of the aldehyde was obtained (lactol?) distinguished by the absence of the ^1H nmr signal at δ 9.9. It could be reconverted to the aldehydo acid by recycling through the sodium salt.

Aldehydo Acid Methyl Ester (and its homologue?)

This was prepared by action of an ether solution of diazomethane on a solution of the acid in methanol. After purification by preparative tlc on silica gel plates, using 5% methanol in chloroform as developing solvent, it crystallized from ether–hexane mixture as thin rectangular plates, mp 118°C. It had ν_{max}: 1727 and 1683 cm^{-1}. Its ^1H nmr spectrum gave signals at δ 9.95 (1H, s), 4.36 (1H, s), 3.68, 3.34, 3.20 (3H singlets), 1.07 (3H, t, J = 6 Hz). *Anal.* calcd. for $C_{23}H_{33}NO_7$: C 63.43, H 7.64, N 3.32; found: C 63.90, H 7.72, N 3.18. Its mass spectrum gave peaks at *m/e*: 449 (calcd. for $C_{24}H_{35}NO_7$ = 449; $C_{23}H_{33}NO_7$ = 435), 417, 408, 407 (intense). However, a later determination on an MS-9 instrument gave *m/e* 449 and 435 in the ratios of 1 to 1.8.

Hydroxy and Acetoxy Acids 7

Sodium borohydride (60 mg) was added in five portions to a solution of 32 mg of aldehydo acid in 2 mL of methanol over the course of 20 min. The solution was evaporated to dryness on a rotating evaporator. After addition of dilute sulfuric acid, the product was recovered by extraction with methylene chloride, giving crystalline hydroxy acid **7** (R = H). This gave ^1H nmr signals at δ 7.75 (2H, br), 4.3 (1H, s), 3.35, 3.3, 3.26 (OCH_3 singlets), 1.08 (3H, t, J = 7 Hz). This was not further characterized. It was acetylated overnight in 1 mL of 1:1 pyridine – acetic anhydride at room temperature, giving 4 mg of neutral product and 35 mg of acetoxy acid **7** (R = Ac) which crystallized readily from ether–hexane mixture. It was purified by preparative tlc on silica gel plates using 15% methanol in chloroform for development. After three recrystallizations from ether–hexane (small prisms) it had mp 199–202°C. Its ^1H nmr spectrum in C_6D_6 had signals at δ 9.95 (1H, br), 4.8 (2H, s), 4.49 (1H, s), 3.2 (6H, s), 2.93 (3H, s), 1.91 (3H, s), 1.07 (3H, t). Its ^{13}C nmr spectrum had signals at δ 177.0, 176.0, 170.8, 85.5, 84.3, and 81.2, 71.9, 63.8, 61.0, 58.2, 57.65, 56.4, 54.6, 49.2, 42.9, 40.3, 38.5, 34.4, 29.6, 27.9, 27.5, 20.9, and 12.0. *Anal.* calcd. for $C_{24}H_{35}NO_8$: C 61.92, H 7.58, N 3.01; found: C 62.36, H 7.68, N 2.97.

Methyl Ester of Acetoxy Acid 7

Excess ethereal diazomethane was added to a solution of the acetoxy acid in methanol. After a few minutes the solvent was removed on a rotating evaporator. After purification by preparative tlc on a silica gel plate, using 5% methanol in chloroform, it crystallized as lustrous prisms from ether–hexane mixture, mp 111–114°C. It had ν_{max}: 1726 and 1681 cm^{-1} and gave ^1H nmr signals at δ 4.38 (2H, s), 4.28 (1H, s), 3.64 (3H, s), 3.35 (3H, s), 3.32 (3H, s), 3.22 (3H, s), 2.08 (3H, s), 1.03 (3H, t, J = 7 Hz). Its mass spectrum had peaks at *m/e*: 479 (M^+), 447, and 392 (M^+ calcd. for $C_{25}H_{37}NO_8$: 479). *Anal.* calcd. for $C_{25}H_{37}NO_8$: C 62.61, H 7.78, N 2.92; found: C 62.39, H 7.87, N 2.80.

Hydroxy-keto Lactam 9

The neutral product from the deamination was a mixture that was separated by preparative tlc on silica gel plates using 10% methanol in chloroform for development. The main band with R_f near 0.6 represented 68% of the neutral product (50% yield). After replating for final purification the substance was still amorphous. It had ν_{max}: 3470, 1729, and 1633 cm^{-1}. Its ^1H nmr spectrum had signals at δ 3.9 (1H, s), 3.48 (3H, s), 3.39 (3H, s), 3.27 (6H, s), and 1.07 (3H, t, J = 7 Hz). In C_6D_6 it gave signals at δ 3.90 (1H, s), 3.40 (3H, s), 3.18 (3H, s), 3.12 (3H, s), 2.90 (3H, s), and 1.06 (3H, t, J = 7 Hz). Its ^{13}C nmr in deuterobenzene had signals at δ: 204.2(s), 175.8(s), 83.3(d), 83.2(d), 80.0(d), 66.4(t), 62.0(d), 59.9(q), 57.6(q), 57.4(q), 57.3(q), 56.8(s), 56.0(s), 53.7(d), 53.4(s), 45.8(d), 45.2(d), 41.2(t), 40.0(d), 38.8(t), 30.2(t), 26.9(t), and 12.3(q). This fits structure **9** if there is accidental superposition of two methine carbons carrying methoxyl groups (ca. 83 ppm).

The amorphous solid did not give satisfactory analysis, but a sample distilled at 170°C, 1×10^{-4} Torr did. Its electron impact mass spectrum had peaks at *m/e*: 449 (M^+), 434, 417, 406, 402, 390, 389, 373, 359, 358, and 357 (M^+ calcd. for $C_{24}H_{35}O_7N$: 449). *Anal.* calcd. for $C_{24}H_{35}O_7N$: C 64.12, H 7.85; found: C 63.98, H 8.08.

Acetoxy-keto Lactam

The hydroxy-keto lactam **9** was completely acetylated overnight at room temperature in 1:1 acetic anhydride – pyridine. The amorphous product had ν_{max}: 1735 and 1651 cm^{-1} and gave ^1H nmr signals at δ 4.38 (2H, s), 3.88 (1H, s), 3.45 (3H, s), 3.37 (3H, s), 3.25 (3H, s), 3.22 (3H, s), 2.07 (3H, s), and 1.05 (3H, t, J = 7 Hz). When heated in a bath at 250°C under 0.1 Torr the acetate refluxed but did not significantly decompose.

Keto-lactam Tosylate

Sixty milligrams of **9** were added to a solution of 159 mg of *p*-toluenesulfonyl chloride in 1 mL of dry pyridine. After 40 h at room temperature, 0.5 mL of water was added, then the mixture left for 1 h. The solvents were then removed on a rotating evaporator, the residue taken up in methylene chloride and this washed with dilute sulfuric acid, then saturated sodium bicarbonate solution. The 80 mg of product was purified by preparative tlc on silica gel using 5% methanol and chloroform. The main band (R_f 0.7) contained 53 mg. A chloroform solution of this was filtered through a short bed of activity I neutral alumina

giving 47 mg of colorless amorphous product. An ether solution of this was filtered for analysis, giving on evaporation a colorless froth. This had ν_{max}: 1731 and 1649 cm^{-1} and gave ^1H nmr signals (C_6D_6) at δ 7.72 (2H, d, J = 8 Hz), 6.75 (2H, d, J = 8 Hz), 4.78 (1H, d, J = 11 Hz), 4.25 (1H, d, J = 11 Hz), 3.88 (1H, s), 3.28 (3H, s), 3.18 (3H, s), 3.08 (3H, s), 2.82 (3H, s), 1.88 (3H, s), and 0.98 (3H, t, J = 7 Hz). *Anal.* calcd. for $C_{31}H_{41}NO_9S$: C 61.67, H 6.84, N 2.32; found: C 61.50, H 6.72, N 2.49.

A solution of the 80 mg of tosylate in 1 mL of toluene containing 107 mg of DBN was refluxed under argon for 2 h. Relatively pure starting material (70 mg) was recovered.

Oxidation of Hydroxy-keto Lactam **9**

A solution of 150 mg of **9** in 2 mL of acetone was titrated with a dilute solution of Jones' reagent (9) in acetone until excess reagent persisted for 10 min. The solvent was decanted from precipitate, then evaporated. The residue was taken up in methylene chloride and the acids removed by two extractions with sodium carbonate solution. The aqueous layers were back-washed with methylene chloride. The methylene chloride gave 60 mg of neutral products while the sodium carbonate solution gave 106 mg of acid.

Combined neutral products from 334 mg of hydroxy-keto lactam (123 mg) were purified by separation on a 1000 μm tlc plate using 10% methanol in chloroform under argon. Only 46 mg were recovered in the main zone. After replating this, 25 mg were recovered, which gave sharp spectra: ν_{max}: 1732, 1711, and 1693 cm^{-1}; ^1H nmr signals in C_6D_6 at δ 4.08 (1H, d, J = 12 Hz), 3.37 (3H, s), 3.07 (6H, s), 2.77 (3H, s), and 0.97 (3H, t, J = 7 Hz). Addition of $Eu(dpm)_3$ shift reagent resulted in separation of the methoxyl signals, but gave no more information about the medium-field hydrogens.

No further work was done on this material.

Keto-lactam Acid **8**

The acid from the Jones' oxidation of **9** crystallized from ether as thin plates, mp 154°C, with no gas evolution below 255°C; $[\alpha]_D$ +39° (*c* 0.89, ethanol); ν_{max}: 1736 and 1604 cm^{-1}; for a Nujol mull, ν_{max}: 1747, 1734, and 1606 cm^{-1}. Its ^1H nmr spectrum had signals at δ 3.98 (1H, s), 3.48 (3H, s), 3.38 (3H, s), 3.26 (6H, s), 1.10 (3H, t). In C_6D_6 the signals were shifted to δ 3.86 (1H, s), 3.38 (3H, s), 3.16 (3H, s), 3.09 (3H, s), 2.73 (3H, s), 0.91 (3H, t, J = 7 Hz). *Anal.* calcd. for $C_{24}H_{33}NO_8$: C 62.19, H 7.18, N 3.02 (mol. wt. 463.5; $4OCH_3$ 26.77); found: C 62.07, H 7.43, N 2.97; equivalent wt. by titration 465; OCH_3 27.58. Its pK_a in 50% aqueous methanol was 5.0.

The same acid was produced less efficiently by oxidation of **9** with chromium trioxide in wet acetic acid, or by potassium permanganate in acetone containing a small amount of acetic acid.

Methyl Ester of Keto-lactam Acid **8**

This was prepared by addition of excess diazomethane in ether to a methanol solution of acid **8**. After purification on silica gel plates (5% MeOH in chloroform), it crystallized from ether as sheaves of fine needles with mp 196°C. It had ν_{max}: 1728 and 1657 cm^{-1} and gave ^1H nmr signals at δ 4.14 (1H, s), 3.78 (3H, s), 3.52 (3H, s), 3.26 (6H, s), 1.03 (3H, t, J = 7 Hz). In pyridine-d_5 the signals were at δ 4.61 (1H, s), 4.14 (1H), 3.92 (1H), 3.72 (3H, s), 3.63 (3H, s), 3.33 (3H, s), 3.26 (3H, s), 3.14 (3H, s), 1.13 (3H, t, J = 7 Hz). Its ^{13}C nmr spectrum in C_6D_6 had signals at δ: 203.9, 170.9, 169.5, 82.8(d), 78.6(d), 61.5(d), 59.9(q), 59.7(s), 56.9(d), 56.7(q), 56.3(q), 55.5(t?), 54.5(d), 51.9(q), 45.4(d), 44.5(d), 41.2(t), 39.6(d), 38.1(t), 29.8(t), 26.3(t), and 11.7(q). *Anal.* calcd. for $C_{25}H_{35}NO_8$: C 62.87, H 7.39, N 2.93 (mol. wt. 477.54); found: C 62.06, H 7.45, N 2.93. Its mass spectrum gave M^+ 477, with the next significant peak at *m/e* 462. The analysis was repeated several times on different samples with no better agreement.

Acknowledgements

The author wishes to thank Drs. M. H. Benn and Z. Antkowiak for early attempts to deduce the structure of the deamination products, Dr. D. G. Garratt for the ^{13}C nmr spectra and help with their analysis, Mr. H. Seguin for microanalyses, and M. Bednas and Prof. John Holmes for the mass spectra.

1. M. Przybylska and L. Marion. Can. J. Chem. **34**, 185 (1956).
2. O. E. Edwards and L. Marion. Can. J. Chem. **30**, 627 (1952).
3. M. Cygler, M. Przybylska, and O. E. Edwards. Acta Crystallogr. In press.
4. (*a*) Y. L. Chow. Can. J. Chem. **45**, 53 (1967); Y. L. Chow and A. C. H. Lee. Can. J. Chem. **45**, 311 (1967); (*b*) A. H. Ferris. J. Org. Chem. **24**, 580 (1959); **25**, 1813 (1960); R. K. Hill. J. Org. Chem. **27**, 29 (1962).
5. O. E. Edwards and M. Lesage. Can. J. Chem. **41**, 1592 (1963)
6. O. E. Edwards, J. Dixon, J. W. Elder, R. J. Kolt, and M. Lesage. Can. J. Chem. **59**, 2096 (1981).
7. E. M. Arnett and C. Petro. J. Am. Chem. Soc. **100**, 5408 (1978); J. L. Franklin. *In* Carbonium ions. Vol. 1. *Edited by* G. A. Olah and P. von R. Schleyer. Interscience Publishers, New York. 1968. p. 85.
8. J. A. Ferris and N. C. Miller. J. Am. Chem. Soc. **88**, 3522 (1966).
9. K. Bowden, J. M. Heilbron, E. R. H. Jones, and B. C. L. Weedon. J. Chem. Soc. 39 (1946).

Can. J. Chem. Downloaded from www.nrcresearchpress.com by 210.87.254.105 on 09/06/12
For personal use only.

A theoretical study on the bimolecular hydrogen exchange aminonitrene → *trans*-diimide. Comparison with formaldehyde photochemistry

M. J. H. KEMPER AND H. M. BUCK

Laboratory for Organic Chemistry, Eindhoven University of Technology, Eindhoven, The Netherlands

Received April 22, 1981

M. J. H. KEMPER and H. M. BUCK. Can. J. Chem. **59**, 3044 (1981).

Ab initio calculations on the rearrangement aminonitrene → *trans*-diimide are reported. It is shown that a bimolecular hydrogen exchange is much easier than a unimolecular 1,2 hydrogen shift: the reactions have activation energies of 4 and 94 kcal/mol, respectively. The hydrogen exchange starts from dimers which have a fairly large stabilization energy. Infrared and Raman frequencies of these dimers are calculated in order to facilitate experimental studies. Some striking similarities are indicated between diimide chemistry and the photochemistry of formaldehyde. It is shown that results from one field are transferable to the other one. From this, some new experiments are suggested.

M. J. H. KEMPER et H. M. BUCK. Can. J. Chem. **59**, 3044 (1981).

On rapporte les calculs *ab initio* relatifs à la transposition aminonitrène → diimide *trans*. On a montré que la réaction bimoléculaire d'échange d'hydrogène est plus facile que le glissement d'hydrogène-1,2 unimoléculaire: les énergies d'activation de ces deux réactions sont respectivement de 4 et de 94 kcal/mol. L'échange d'hydrogène se fait à partir des dimères qui ont une énergie de stabilisation assez élevée. On a calculé les fréquences ir et Raman de ces dimères en vue d'en faciliter les études expérimentales. On indique des similarités frappantes entre la chimie des diimides et la photochimie de la formaldéhyde. On montre que ces résultats sont transférables d'un champ à l'autre. On suggère de nouvelles expériences à partir de ces données.

[Traduit par le journal]

I. Introduction

There are three different equilibrium structures of N_2H_2: *trans*-diimide (**1**), *cis*-diimide (**2**), and the nitrene-structure (**3**) (aminonitrene or 1,1-diazine).

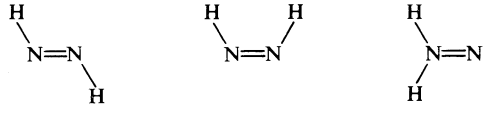

1 **2** **3**

The thermochemistry of these isomers has been the subject of intense theoretical and experimental interest (1). A reason for this is the fact that diimide, generated *in situ*, is widely used as a reagent in the hydrogenation of double bonds. The observation that this reduction of alkenes and alkynes occurs in a highly stereoselective *syn* manner resulted in a concerted mechanism, via a six-centered transition state, which requires *cis*-diimide. However, only *trans*-diimide has been definitely observed by spectroscopic means (2). The probable stereochemistry of the molecules produced in the various reactions giving diimide is not clarified. The thermal cycloreversion of diimide–anthracene adducts (3) produces directly *cis*-diimide. The stereochemistry of the products from microwave discharges (4) or oxidation (5) of hydrazine, however, is unclear, although energetic considerations suggest that *trans*-diimide should be the dominant isomer formed. It can also be argued (6), that a nitrene is the expected product of the decomposition of unsymmetrically substituted hydrazine derivatives:

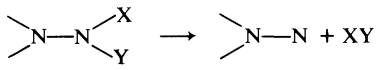

The same holds for reactions involving the decomposition of hydrazine derivatives containing the R_1R_2—N—N—Z fragment. The nitrene rearranges then to the azo compound:

$$R_1R_2\text{—N—N} \rightarrow R_1\text{—N—N—}R_2$$

So, a very central point in the chemistry of N_2H_2 is the question how an easy interconversion between the isomers **1**, **2**, and **3** is possible. The most stable isomer is singlet *trans*-diimide, which lies 6–7 kcal/mol below the *cis* structure (7, 8). Much calculational attention has been paid to the *trans*–*cis* isomerization which is considered to be the rate-controlling step in gas phase reactions of diimide. An experimental activation energy of 4.2 kcal/mol has been reported for this process (9). Unimolecular isomerizations, however, including both concerted and dissociation–recombination mechanisms, have much too high energy barriers (1). Therefore, Casewit and Goddard III (1) proposed a bimolecular radical-chain mechanism, initiated by:

$$\textit{trans}\text{-HNNH} + \textit{trans}\text{-HNNH} \rightarrow \text{H}\cdot + \text{N}_2 + \text{H}_2\text{N}\dot{\text{N}}\text{H}$$
$$\Delta H = -15.0\ \text{kcal/mol}$$

The experimentally observed activation energy for the diimide reactions is consistent with the rate-

0008-4042/81/213044-05$01.00/0

©1981 National Research Council of Canada/Conseil national de recherches du Canada

Can. J. Chem. Downloaded from www.nrcresearchpress.com by 210.87.254.42 on 09/06/12
For personal use only.

Can. J. Chem. Downloaded from www.nrcresearchpress.com by 210.87.254.42 on 09/06/12
For personal use only.

determining step in their scheme:

$$H_2N\dot{N}H + \textit{trans}\text{-}HNNH \rightarrow \textit{cis}\text{-}HNNH + H_2N\dot{N}H \qquad \Delta H = 4.7\,\text{kcal/mol}$$

A similar problem occurs for the unimolecular rearrangement aminonitrene → *trans*-diimide:

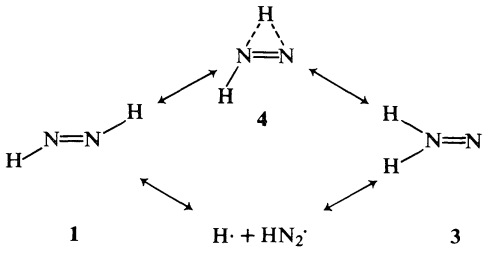

Sophisticated calculations including electron correlation give rather ultimate values for the barrier (relative to **1**) of the 1,2 hydrogen shift: 83.0 (7) and 82.6 (8) kcal/mol. The dissociation–recombination is a little easier: the N—H bond energy of **1** is predicted (1) to be (at 298 K) 71.5 kcal/mol. So, also in this case the unimolecular barriers are too high to agree with the easy nitrene–azo rearrangement.

We will show in Section II that there is, just as for the *trans–cis* isomerization, a bimolecular mechanism which easily produces *trans*-diimide from aminonitrene. We also give in that section calculated infrared and Raman frequencies of **1**, **3**, and dimers of these isomers. Details of the calculation are described in Section III. In Section IV we offer some comments on the similarities between the systems H_2N_2–HNNH and H_2CO–HCOH.

II. Results

Figure 1 gives the structures and relative energies of **1**, **3**, and the two cyclic dimers of these isomers, which are important here. The dimers are considerably stabilized, relative to two non-interacting monomers:

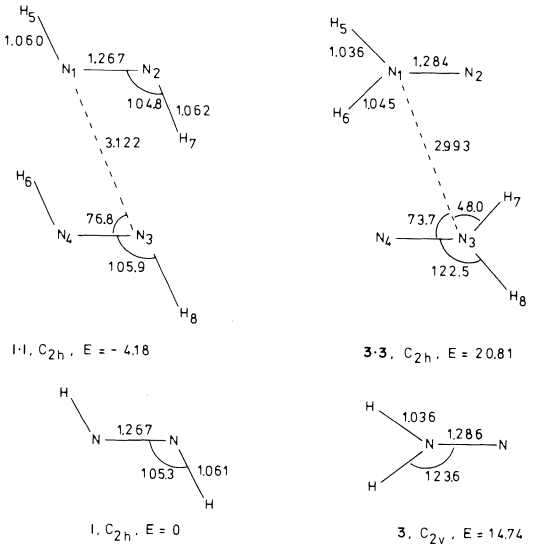

FIG. 1. STO-3G monomers and dimers of trans-diimide and aminonitrene. Geometries are in Å and deg. Energies are in kcal/mol; the dimer energies are relative to two non-interacting *trans*-diimides.

4.18 and 8.67 kcal/mol for **1·1** and **3·3**, respectively. This stabilization energy is caused by the formation of —N···H— hydrogen bonds. This is seen from the equilibrium geometries: the hydrogens H_6 and

TABLE 1. Calculated infrared and Raman frequencies (cm^{-1}) for *trans*-diimide (**1**), aminonitrene (**3**), and their dimers

		Frequency				
		1				
Assignment		Exp[b]	Calcd	**1·1**	**3·3**	**3**
NH sym.	(+)[a]	3128	2915.0	2926.3 (+) 2920.1 (−)	2860.1 (−) 2844.8 (+)	2944.5
Bend sym.	(+)	1583	1681.9	1693.0 (+) 1691.3 (−)	1807.5 (−) 1759.8 (+)	1831.7
NN	(+)	1529	1512.5	1511.4 (+) 1506.6 (−)	1346.8 (+) 1328.7 (−)	1279.3
NH asym.	(−)	3131	2939.1	2959.7 (+) 2931.8 (−)	3129.6 (−) 3099.6 (+)	3146.6
Bend asym.	(−)	1286	1353.7	1388.4 (−) 1356.0 (+)	1290.7 (−) 1249.6 (+)	1214.6

[a] The (±) sign denotes the inversion symmetry in the C_{2h} group (+ is Raman active, while − is infrared active); the bands of **3** (C_{2v}) are both Raman and infrared active.
[b] N_2-matrix values from ref. 11; the gas-phase value of NH asym. is 3120 cm^{-1} (12).

Can. J. Chem. Downloaded from www.nrcresearchpress.com by 210.87.254.42 on 09/06/12
For personal use only.

H_7 interact with the directed nitrogen lone pairs. This interaction is reflected in the small, but significant electron densities[1] between the hydrogen bonded atoms (N_1H_6 and N_3H_7 in **1·1**; N_4H_6 and N_2H_7 in **3·3**).

The most promising way to study, in an experimental manner, dimer formation is infrared and Raman spectroscopy. Therefore, we calculated the in-plane vibrational frequencies of the structures in Fig. 1. The results are shown in Table 1. We used some empirical corrections in our method, which were calibrated on the formaldehyde molecule (13, 14) (see also Section III). This method reproduces the experimental frequencies of *trans*-diimide with an average deviation of 5%. A more refined calibration on diimide itself is not possible, because the experimental values are nitrogen matrix frequencies. What is more important is the calculated difference between monomeric and dimeric spectra. As a consequence of dimer formation the frequencies of **1** and **3** shift. The largest change occurs for the asymmetric bonding modes. This is by far the strongest *trans*-diimide absorption (11). Also, every vibration is split into two bands: one infrared and one Raman band. So, **1·1** might be detectable because of the appearance (near 1360 cm^{-1}) of the Raman-active component of the asymmetrical band. This statement needs, of course, the reservation that the spectra are not perturbed by *cis*-diimide, that should have frequencies (both infrared and Raman active), close to the *trans* isomer (15).

As might be clear already from the dimers given in Fig. 1, the reaction

aminonitrene → *trans*-diimide

involves a bimolecular hydrogen exchange via the transition state (TS):

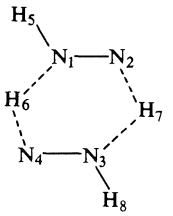

In Fig. 2 we give the STO-3G energetics of this process. We calculated the potential energy surface as a function of the N_1H_6 and N_3H_7 distances. All the other parameters were optimized with respect to the total energy of the supermolecule. The system retains C_{2h} symmetry; relaxation of this symmetry constraint is not expected to give a considerable lowering of TS. This will be discussed in Section III, together with possible changes due to larger basis sets. The interatomic electron densities (10) show that in TS the migrating hydrogens are equally shared by the two nitrogens; the six-centered transition state has an "aromatic" character, in the sense that the migration of 6 electrons is involved in it. We also compare in Fig. 2 the bimolecular energetics with the concerted unimolecular 1,2 hydrogen shift (**3** → **4** → **1**), as calculated with the same method. The hydrogen exchange mechanism is clearly in favour:

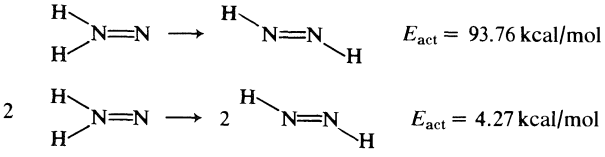

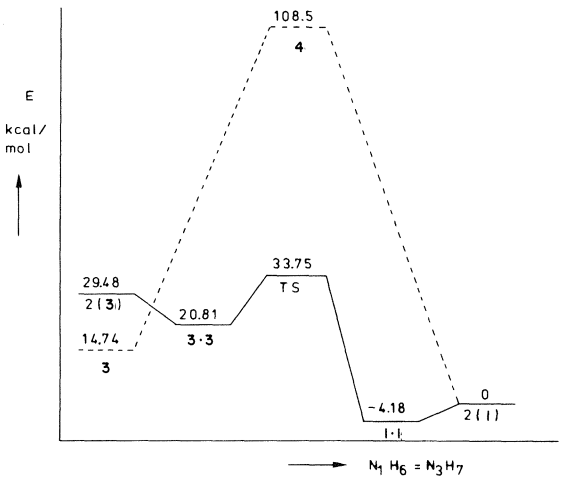

FIG. 2. STO-3G energetics of 2 aminonitrene → (aminonitrene)$_2$ → TS → (HNNH-*trans*)$_2$ → 2 HNNH-*trans*. The broken line gives the energy of the unimolecular 1,2 hydrogen shift (**3** → **4** → **1**).

III. Methods of Calculation

Ab-initio structures and energies were calculated with the widely used GAUSSIAN 70 program (16) and the STO-3G (17) basis set. These methods are well described and documented (18) in the literature and need no further comment here. We do not expect that larger basis sets will give a qualitative change of the picture given in Fig. 2. We extensively studied (13, 14) the analogous hydrogen exchange in the isoelectronic formaldehyde system:

2HCOH-*trans* → $2H_2CO$

The results were virtually the same in going from minimal STO-3G up to complete optimization with 6-31 G* (19). We also found in the case of formaldehyde that the hydrogen exchange is nearly symmet-

[1]The electron density indicates the strength of a bond between two atoms and is calculated similar to the so-called Reduced Overlap Population as defined in ref. 10.

Can. J. Chem. Downloaded from www.nrcresearchpress.com by 210.87.254.42 on 09/06/12
For personal use only.

ric. Relaxation of the C_{2h} symmetry constraint resulted in almost the same reaction path and barrier.

To obtain vibrational frequencies, we calculated the STO-3G force constants. We used internal coordinates (bond distances and angles). Diagonal constants are obtained from:

$$F_{xx} = \frac{\partial^2 E}{\partial x^2} \simeq E(x_0 + \Delta x) - 2E(x_0) + E(x_0 - \Delta x)/\Delta x^2$$

The interaction constants are calculated from:

$$F_{xy} = \frac{\partial^2 E}{\partial x \partial y} \simeq E(x_0 + \Delta x, y_0 + \Delta y) + E(x_0 - \Delta x, y_0 - \Delta y) - E(x_0 + \Delta x, y_0 - \Delta y) - E(x_0 - \Delta x, y_0 + \Delta y)/4\Delta x \Delta y$$

Here, x_0 and y_0 are the values of the internal coordinates in the equilibrium structure. The displacements Δ are chosen (by some trial and error) neither too large for anharmonicity to matter nor too small for numerical inaccuracies to appear. The force constants are transformed to frequencies using the conventional **FG** method (20). The obtained symmetry of the normal mode movement shows whether the vibration is infrared and/or Raman active. As shown by Pulay (21), the prediction of diagonal force constants to experimental accuracy is not easily possible from single determinant Hartree–Fock wave functions. Fortunately, however, the errors are near-systematic and allow for correction factors to improve significantly the agreement with experiment. The method that was used here was calibrated on formaldehyde (13). We scaled down the diagonal stretching constants by a factor 0.65; for the diagonal bendings we used 0.9. The interaction constants were left unchanged. Another important improvement is made by using spectroscopic masses defined by (22, 23):

$$M_{sp} = M + 0.0795M^{1/2}$$

This partially corrects for anharmonicity and improves primarily H-stretching modes.

IV. Some Similarities with Formaldehyde Photochemistry

It will be clear from the foregoing that this study on the reaction

aminonitrene → *trans*-diimide

was heavily inspired from our studies on formaldehyde. There, the hydroxycarbene molecule (HCOH) is supposed to be a good candidate for the long searched intermediate state in formaldehyde photochemistry (13, 14, 24). HCOH has a much higher energy than H_2CO and can only be produced via the excited formaldehyde S_1 state. A direct experimental verification of the existence of this intermediate has not yet been published in the literature. Indirect evidence comes from matrix experiments (25, 26). The addition products, which are formed out of formaldehyde dimers, can be explained with the HCOH intermediate (13, 14). A hydrogen exchange mechanism was shown to explain the rearrangement

trans-HCOH → H_2CO

In this section we want to point out some other striking similarities between these two fields. Pasto and Chipman (27, 28) calculated reactions of ethene with diimide species, and disproportionation reactions of N_2H_2. Diimide and ethene are isoelectronic with formaldehyde, so it might not be too surprising that the reactions are completely analogous to our formaldehyde results. For instance:

$$\left.\begin{array}{l} H_2C{=}CH_2 + \textit{cis}\text{-HNNH} \rightarrow H_3C - CH_3 + N_2 \\ H_2C{=}O \quad + \textit{cis}\text{-HCOH} \rightarrow H_3COH \quad + CO \end{array}\right\}$$

or:

$$\left.\begin{array}{l} H_2C{=}CH_2 + \textit{trans}\text{-HNNH} \rightarrow \text{1-ethyl-1,1-diazine} \\ H_2C{=}O \quad + \textit{trans}\text{-HCOH} \rightarrow \text{glycoaldehyde} \end{array}\right\}$$

So, it is seen that the results from one field are transferable to the other one; this study is, in fact, the first example. Pasto's (28) theoretical results on disproportionation reactions of N_2H_2 species ($2N_2H_2 \rightarrow N_2H_4 + N_2$) can be a guide for analogous reactions between two hydroxycarbenes. Perhaps more important (and it is the main purpose of this section to indicate this), is the fact that these results might stimulate two kinds of experiments. Firstly, suited photochemical studies of diimide can give information about the behaviour of the mysterious hydroxycarbene. Secondly, photoinduced gas-phase reactions between formaldehyde and alkenes should be studied; such experiments can give valuable information concerning the involvement of HCOH in addition reactions.

1. C. J. Casewit and W. A. Goddard, III. J. Am. Chem. Soc. **102**, 4057 (1980) and references therein.
2. M. Carlotti, J. W. C. Johns, and A. Trombetti. Can. J. Chem. **52**, 340 (1974).
3. E. J. Corey and W. L. Mock. J. Am. Chem. Soc. **84**, 685 (1962).
4. C. Willis and R. A. Back. Can. J. Chem. **51**, 3605 (1973).
5. E. J. Corey, W. L. Mock, and D. J. Pasto. Tetrahedron Lett. 347 (1961).
6. B. V. Ioffe and M. A. Kuznetsov. Russ. Chem. Rev. **41**, 131 (1972).
7. J. A. Pople, R. Krishnan, H. B. Schlegel, and J. S. Binkley. Int. J. Quant. Chem. **XIV**, 545 (1978).
8. C. A. Parsons and C. E. Dijkstra. J. Chem. Phys. **71**, 3025 (1979).

9. C. WILLIS, R. BACK, and J. G. PURDON. Int. J. Chem. Kinet. **9**, 787 (1977).
10. A. G. TURNER. Methods in molecular orbital theory. Prentice-Hall, NJ. 1974.
11. V. E. BONDYBEY and J. W. NIBLER. J. Chem. Phys. **58**, 2125 (1973).
12. A. TROMBETTI. Can. J. Phys. **46**, 1005 (1968).
13. M. J. H. KEMPER. Thesis, Eindhoven University of Technology. 1980.
14. M. J. H. KEMPER, C. H. HOEKS, and H. M. BUCK. J. Chem. Phys. **74**, 5744 (1981).
15. C. POUCHAN, A. DARGELOS, and M. CHAILLET. J. Mol. Spectrosc. **76**, 118 (1979).
16. W. J. HEHRE *et al.* QCPE **11**, 236 (1973).
17. W. J. HEHRE, R. F. STEWART, and J. A. POPLE. J. Chem. Phys. **51**, 2657 (1969).
18. W. A. LATHAN, L. A. CURTISS, W. J. HEHRE, J. B. LISLE, and J. A. POPLE. Prog. Phys. Org. Chem. **11**, 175 (1974).
19. (*a*) P. C. HARIHARAN, W. A. LATHAN, and J. A. POPLE. Chem. Phys. Lett. **14**, 385 (1972); (*b*) P. C. HARIHARAN and J. A. POPLE. Chem. Phys. Lett. **16**, 217 (1972); (*c*) P. C. HARIHARAN and J. A. POPLE. Theoret. Chim. Acta, **28**, 213 (1973).
20. E. B. WILSON, J. C. DECIUS, and P. C. CROSS. Molecular vibrations. McGraw-Hill, New York. 1955.
21. P. PULAY. *In* Modern theoretical chemistry. Vol. 4. *Edited by* H. F. Schaefer. Plenum Press, New York and London. 1977.
22. A. RYTEL and M. RYTEL. Opt. Spektrosk. **21**, 61 (1966).
23. M. RYTEL. Opt. Spektrosk. **16**, 402 (1964).
24. M. J. H. KEMPER, J. M. F. VAN DIJK, and H. M. BUCK. J. Am. Chem. Soc. **100**, 7841 (1978).
25. M. DIEM and E. K. C. LEE. Chem. Phys. **41**, 373 (1979).
26. J. R. SODEAU and E. K. C. LEE. Chem. Phys. Lett. **57**, 71 (1978).
27. D. J. PASTO and D. M. CHIPMAN. J. Am. Chem. Soc. **101**, 2290 (1979).
28. D. J. PASTO. J. Am. Chem. Soc. **101**, 6852 (1979).

Can. J. Chem. Downloaded from www.nrcresearchpress.com by 210.87.254.42 on 09/06/12
For personal use only.

Heat capacities and volumes of NaCl, $MgCl_2$, $CaCl_2$, and $NiCl_2$ up to 6 molal in water

GÉRALD PERRON, ALAIN ROUX[1], AND JACQUES E. DESNOYERS[2]
Department of Chemistry, Université de Sherbrooke, Sherbrooke (Qué.), Canada J1K 2R1

Received April 2, 1981

GÉRALD PERRON, ALAIN ROUX, and JACQUES E. DESNOYERS. Can. J. Chem. **59**, 3049 (1981).

It has been claimed by Enderby and co-workers that changes in long-range order occur in $NiCl_2$ aqueous solutions at high concentrations. To investigate the possibility of a transition, the partial molar heat capacities and volumes of $NiCl_2$, $CaCl_2$, $MgCl_2$, and NaCl were measured and compared in water at 25°C up to 6 mol kg^{-1}. In the case of NaCl, data were also measured at 5 and 45°C. A slight change in slope of $\bar{C}_{p,2}$ is observed for $NiCl_2$ around 4 mol kg^{-1} which may suggest a third or higher order transition. However, the change is too small to support unambiguously any particular model for the high concentration region.

GÉRALD PERRON, ALAIN ROUX et JACQUES E. DESNOYERS. Can. J. Chem. **59**, 3049 (1981).

Enderby et ses collaborateurs ont prétendu qu'il se produit des changements très importants dans des solutions aqueuses très concentrés de $NiCl_2$. Afin d'étudier la possibilité d'une transition, on a mesuré les capacités calorifiques molaires partielles et les volumes molaires partiels du $NiCl_2$, du $CaCl_2$, du $MgCl_2$ et du NaCl et on les a comparés dans l'eau à 25°C jusqu'à 6 mol, kg^{-1}. Dans le cas du NaCl, on a également mesuré les données à 5°C et à 45°C. On a observé un léger changement dans la pente de $\bar{C}_{p,2}$ pour le $NiCl_2$ à environ 4 mol kg^{-1} ce qui suggère une transition d'ordre trois ou une transition d'ordre plus élevée. Cependant le changement est trop faible pour servir de preuve formelle à tout modèle particulier dans la région de forte concentration.

[Traduit par le journal]

Introduction

Enderby and co-workers (1, 2) reported in 1974 data on the neutron scattering of aqueous solutions of $NiCl_2$ and concluded that, at high concentration, the Ni ions were arranged in a quasi-lattice and that the solutions possessed a substantial degree of long-range order. This unexpected conclusion has prompted numerous investigations, namely, Raman scattering (3, 4), thermodynamic measurements (5), viscosity (6), diffusion (7), and X-ray scattering (8). However, the interpretation of many of these data is subject to criticism and other explanations can be offered to explain the anomalous neutron scattering (9).

Of all the thermodynamic properties, heat capacity is probably the most sensitive to transitions in the condensed state. On a suggestion from Professor H. L. Friedman, we therefore decided to make a careful investigation of this property up to the region where the transitions are said to occur. Our flow microcalorimeter measures heat capacities per unit volume, and densities of comparable precision are required to calculate apparent and partial molar heat capacities. The densities were therefore measured with a flow densimeter on the same solutions.

It will be necessary to compare the data on $NiCl_2$ with other systems where such transitions are not expected to occur. $CaCl_2$ seems to be a good reference for this purpose. If the hydration of Ni^{++} is responsible for any anomalous behavior, then similar trends would be expected for $MgCl_2$. Data on these two electrolytes are available in the literature. For example, data in our own laboratory were reported on these two salts at low concentration (10). However, it is important to compare the properties of all these electrolytes under very similar experimental conditions.

Volumes and heat capacities of NaCl have been measured as a function of temperature up to 3 mol kg^{-1} (11). Many authors interested in the data of this salt have asked us to extend our measurements to higher concentration. We therefore measured these properties up to 6 mol kg^{-1} at 5, 25, and 45°C. A comparison with the 1:2 electrolytes might also prove to be informative.

Experimental

The techniques for measuring heat capacities and densities by flow microcalorimetry (12, 13) and flow densimetry (14) have been well described, and the method of calculating apparent molar heat capacities (ϕ_C) and volumes (ϕ_V) are given therein.

The origin and purification procedure of the chemicals are the following. NaCl (Fisher Certified) was used as such after drying under vacuum at 150°C. $NiCl_2$ (Ultra-pur Alfa Product), $MgCl_2$ (Analar, BDH Chemicals), and $CaCl_2$ (Fisher Certified) were recrystallized in water at a pH of 5. $NiCl_2$ was analyzed by precipitation with EDTA and also by conductometric titration with $AgNO_3$ with a concentrated and with two dilute samples. $MgCl_2$ and $CaCl_2$ were analyzed gravimetrically and conductometrically with $AgNO_3$. In all cases the analyses agreed within 0.05%. All solutions were prepared by weight dilution of the same stock solution. The uncertainty in the concentration plus the 0.5% uncertainty in the relative change in heat capacity per unit volume limits the precision in ϕ_C to ± 0.8 J K^{-1} mol^{-1}. At low concentration this uncertainty may increase.

[1]Present address: Laboratoire de thermodynamique et cinétique chimique, U.E.R. Sciences, Université de Clermont II, B.P. 45, 63170 Aubière, France.

[2]Author to whom correspondence should be addressed.

0008-4042/81/213049-06$01.00/0

©1981 National Research Council of Canada/Conseil national de recherches du Canada

Can. J. Chem. Downloaded from www.nrcresearchpress.com by 210.87.254.6 on 09/06/12
For personal use only.

TABLE 1. Apparent molar volumes and heat capacities of some electrolytes in water

m mol kg^{-1}	$10^3 \Delta d$ g cm^{-3}	ϕ_V cm^3 mol^{-1}	$10^3 \Delta\sigma/\sigma_o$	ϕ_C JK^{-1} mol^{-1}
NaCl T=5°C				
0.78747	33.011	15.99		
0.99472	41.216	16.33	-35.94	-85.8
1.26100	51.558	16.70	-41.96	-72.8
1.50180	60.708	16.99	-46.42	-61.8
1.78240	71.123	17.31	-51.28	-51.9
1.96500	77.759	17.51	-53.67	-45.1
2.00340	79.162	17.54	-54.38	-44.4
2.25170	88.012	17.79	-57.62	-37.1
2.47330	95.765	18.00	-59.49	-29.9
2.76250	105.692	18.25	-61.83	-22.1
2.95140	112.029	18.42	-63.20	-17.5
2.98360	113.137	18.44	-63.38	-16.7
3.48710	129.623	18.83	-65.42	-4.9
3.94470	144.121	19.15	-66.83	3.9
4.44730	159.548	19.46	-67.48	12.5
4.93030	173.896	19.74	-66.92	20.3
5.38390	187.054	19.96	-66.10	26.8
5.95180	202.893	20.24	-64.02	34.4
NaCl T=25°C				
0.99472	38.933	18.52	-27.35	-39.9
1.26102	48.796	18.77	-32.77	-32.9
1.50179	57.540	18.98	-36.81	-26.3
1.78243	67.528	19.20	-41.45	-20.5
1.96500	73.894	19.35	-43.60	-15.6
2.00338	75.235	19.38	-44.32	-15.3
2.25174	83.760	19.55	-47.54	-10.6
2.47333	91.243	19.70	-50.08	-6.6
2.76245	100.841	19.88	-52.29	-0.6
2.95143	106.970	20.01	-53.89	2.6
2.98355	108.045	20.02	-54.39	2.7
3.48710	124.038	20.31	-57.42	10.9
3.94470	138.134	20.54	-59.64	17.3
4.44730	153.162	20.78	-61.02	24.0
4.93030	167.162	20.99	-61.67	29.8
5.38590	180.036	21.16	-61.89	34.7
5.95180	195.522	21.38	-61.09	40.8
NaCl T=45°C				
0.78747	30.189	19.33	-20.14	-28.5
0.99472	37.797	19.52	-24.57	-24.4
1.26100	47.402	19.74	-29.86	-19.7
1.50180	55.928	19.91	-33.91	-14.7
1.78240	65.688	20.10	-38.24	-9.6
1.96500	71.859	20.26		
2.00340	73.161	20.28	-41.45	-6.0
2.25170	81.496	20.43	-44.59	-2.0
2.47330	88.817	20.55	-47.79	0.2
2.76250	98.209	20.71	-51.19	3.9
2.95140	104.236	20.81		
2.98360	105.274	20.82	-53.22	7.2
3.48710	120.966	21.07	-57.49	13.3
3.94470	134.814	21.27	-60.18	18.9
4.44730	149.576	21.48	-62.51	24.6
4.93030	163.353	21.66	-64.23	29.4
5.38590	175.984	21.82	-64.98	34.0
5.95180	191.239	22.00	-65.13	39.4

m mol kg^{-1}	$10^3 \Delta d$ g cm^{-3}	ϕ_V cm^3 mol^{-1}	$10^3 \Delta\sigma/\sigma_o$	ϕ_C JK^{-1} mol^{-1}
$NiCl_2$ T=25°C				
0.09554	11.512	8.70	-6.83	-262.6
0.19580	23.414	9.49	-13.40	-246.9
0.29750	35.366	10.07	-19.77	-236.6
0.48690	57.290	11.02	-30.99	-221.5
0.73680	85.659	12.03	-44.19	-202.7
1.00290	115.224	12.94	-56.70	-185.2
1.23200	140.167	13.64	-66.20	-171.4
1.48740	167.411	14.37	-76.00	-158.2
1.73150	192.981	14.99	-83.90	-145.3
1.97440	217.878	15.59	-91.10	-133.8
2.23800	244.369	16.20	-97.60	-121.3
2.51100	271.402	16.73	-103.20	-109.3
2.64100	283.848	17.04	-105.10	-102.8
2.74500	294.130	17.16	-107.70	-100.2
2.97800	316.279	17.59	-111.20	-91.0
3.22700	339.690	17.99	-114.60	-82.0
3.42100	357.570	18.30	-116.40	-74.9
3.53200	367.901	18.43	-118.20	-72.1
3.89200	400.428	18.92	-121.60	-61.4
4.53900	457.652	19.59	-127.00	-45.6
4.98900	495.902	20.05	-130.70	-36.6
5.38400	528.696	20.04	-133.70	-30.2
$MgCl_2$ T=25°C				
0.13680	10.691	16.71	-9.80	-229.8
0.23310	18.038	17.34	-16.20	-218.6
0.29790	22.932	17.64	-20.60	-216.9
0.48210	36.606	18.44	-32.10	-203.7
0.97080	71.421	20.06	-58.90	-174.8
1.49900	106.905	21.46	-84.70	-154.2
1.93600	134.699	22.46	-103.00	-138.4
2.32500	158.461	23.25	-117.10	-125.0
3.07900	202.018	24.53	-140.70	-103.1
3.44500	222.136	25.06	-150.50	-93.9
4.07400	255.301	25.85	-167.20	-81.8
4.18700	261.104	25.97	-169.90	-79.7
4.71200	287.275	26.53	-181.20	-70.4
5.02800	302.481	26.84	-187.50	-65.0
$CaCl_2$ T=25°C				
0.05001	4.568	19.34	-3.97	-251.5
0.09583	8.700	19.82	-7.42	-241.9
0.50190	44.042	22.07	-35.10	-204.0
0.95590	81.498	23.62	-61.60	-176.9
1.52060	125.468	25.15	-88.29	-147.1
2.02090	162.196	26.30	-108.15	-125.9
2.29340	181.401	26.86	-117.00	-114.4
3.35450	251.240	28.73	-141.80	-73.9
3.55790	263.800	29.05	-145.20	-67.1
3.92350	285.686	29.59	-148.30	-53.0
4.93050	341.557	31.01	-152.90	-20.2
5.54980	372.586	31.87	-153.40	-3.1
5.92220	390.022	32.39	-153.80	5.7
6.46440	413.788	33.16	-157.90	14.3

Results

The measured densities and heat capacities per unit volume and the derived ϕ_V and ϕ_C are given in Table 1.

The volumes and heat capacities of $MgCl_2$, $CaCl_2$, and NaCl have been well investigated at low concentration and need not be discussed here. On the other hand, only one set of reliable data seems to exist for $NiCl_2$ (15). This electrolyte was therefore studied to fairly low concentration. The values of $\phi_V - A_V m^{1/2}$ and $\phi_C - A_C m^{1/2}$, where A_V and A_C are the theoretical slopes of the limiting Debye–Hückel theory, are plotted against m and compared with the data of Hepler *et al.* (15*a*) in Fig. 1.

Two sets of measurements, corresponding to two different stock solutions of $NiCl_2$, agree well inside the expected uncertainty. Our data are also in reasonably good agreement with those of Hepler *et al.*, especially at their higher concentrations. An extrapolation of the straight lines at low concentration to infinite dilution will give the standard partial molal values at 25°C.

Can. J. Chem. Downloaded from www.nrcresearchpress.com by 210.87.254.6 on 09/06/12
For personal use only.

$$\bar{V}_2^0 = 6.20 \pm 0.05\ \text{cm}^3\ \text{mol}^{-1}$$
$$\bar{C}_{p,2}^0 = -306 \pm 1\ \text{J K}^{-1}\ \text{mol}^{-1}$$

The data of all the electrolytes up to 6 mol kg^{-1} were fitted with eq. [1]:

$$[1]\quad \phi_Y = \phi_Y^0 + A_Y m^{1/2} + B_Y m + C_Y m^{3/2} + D_Y m^2 + \ldots$$

where Y stands for V or C_p. In eq. [1] ϕ_Y^0 should be equal to $\bar{Y}_2^0$, the standard value, and A_Y should be the Debye–Hückel limiting slope. However, ϕ_Y varies significantly at low concentration and much less at high concentration. As a result, if ϕ_Y^0 and A_Y are fixed before the least-squares analysis, many parameters are required to fit the data. A better extended form of the Debye–Hückel theory would probably give a better fit. However, since in the present case we are not interested in the high dilution region, it was found simpler to treat ϕ_Y^0 and A_Y as adjustable parameters like the other coefficients since this allowed a very good representation of all our high concentration data with a minimum of parameters. Parameters such as A_Y then include any specific interactions such as a small degree of association.

The coefficients of eq. [1] are given in Table 2. Again we stress that no physical significance should be given to the parameters ϕ_Y^0 and A_Y.

The uncertainty in the data and a comparison with the literature are best illustrated through deviation plots $\Delta(\phi_Y^{obs} - \phi_Y^{calc})$, where ϕ_Y^{calc} is obtained from eq. [1] and the parameters in Table 2.

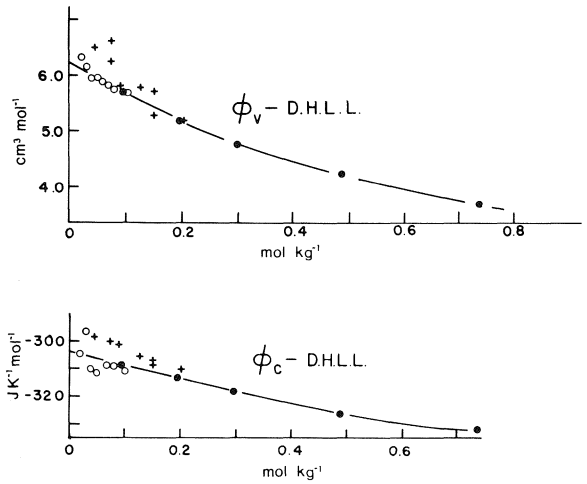

FIG. 1. Apparent molal volumes and heat capacities of $NiCl_2$ at low concentrations at 25°C; ○: present data, low concentration stock solution; ●: present data, high concentration stock solution; +: ref. 15*a*.

These plots are shown in Fig. 2 for ϕ_V and in Fig. 3 for ϕ_C. These functions will be discussed separately.

The scatter of data points for ϕ_V of NaCl is about 0.01 cm^3 mol^{-1} at 5 and 45°C and somewhat higher at 25°C. At 5° and 25°C the present data agree with our earlier ones within 0.02 cm^3 mol^{-1}. At 45°C the difference is more of the order of 0.10 cm^3 mol^{-1}. Recently, Rogers and Pitzer (15*b*) have analyzed the literature data of volumetric properties of NaCl over a large range of temperature and pressure. They proposed parametric equations to represent ϕ_V as a function of concentration up to about saturation. These predicted ϕ_V are systematically lower than ours, the mean deviation being 0.046 cm^3 mol^{-1}. Our weights were not corrected for vacuum. This can cause an error of about 0.06% in m and of about 0.02 cm^3 mol^{-1} in ϕ_V. Assuming the predicted ϕ_V data are the correct ones then the probable source of error in our data would be in the calibration of the densimeter. Dry nitrogen and distilled water were used for this purpose (14). Probably aqueous NaCl solutions should be used as a standard instead. For the present purpose a recalculation of our data is not warranted since a maximum error of 0.05 cm^3 mol^{-1} in ϕ_V causes a negligible error in ϕ_C.

Our volume data for $MgCl_2$ and $CaCl_2$ are in very good agreement with most literature values (16–19). The data of Wirth and Bangert for $MgCl_2$ (19, 20) (not shown) show a scatter of 0.20 cm^3 mol^{-1} but overlap our data. The data of Vasilëv *et al.* (21) for $MgCl_2$ diverge by as much as 1.4 cm^3 mol^{-1} and cannot be considered reliable. Their data for $CaCl_2$ are better but still show much scatter.

It was shown in Fig. 1 that our low concentration data for ϕ_V of $NiCl_2$ were in good agreement with those of Hepler *et al.* (15). At high concentration (see Fig. 2) a systematic difference of 0.10 cm^3 mol^{-1} is observed with the data of Stokes *et al.* (22). The agreement would be worse if corrections such as those discussed for NaCl were made on our data. It is therefore more probable that the observed difference could be accounted for by the uncertainty in the analyses of the $NiCl_2$ stock solutions in both laboratories. The data of Karapet'yants *et al.* (23) are quite different from ours and those of Stokes *et al.*

The heat capacities are shown in Fig. 3. The present data for NaCl are in excellent agreement with our earlier data (11) at all temperatures and also with the recent data of Tanner and Lamb (24) at 25 and 45°C. A difference of about 2 J K^{-1} mol^{-1} is observed at 5°C. For $CaCl_2$ the agreement with the literature (21, 25) is acceptable. With $MgCl_2$ the

Can. J. Chem. Downloaded from www.nrcresearchpress.com by 210.87.254.6 on 09/06/12
For personal use only.

TABLE 2. Parameters of eq. [1] for the volumes and heat capacities of various electrolytes in water at 25°C

Solute	T°C	ϕ_V°	A_V	B_V	C_V	D_V	σ^a
NaCl	5	13.4228	2.91796	−0.088435	0.121670	−0.043552	0.007
	25	17.2928	0.074893	1.658656	−0.581732	0.061657	0.004
	45	18.5501	−0.310934	1.91820	−0.730121	0.095913	0.007
$MgCl_2$	25	15.0030	4.38801	0.792211	0.107646	−0.127300	0.02
$CaCl_2$	25	18.3549	4.03473	2.42792	−1.26686	0.230971	0.03
$NiCl_2$	25	6.8372	6.2164	−1.05872	1.36201	−0.429651	0.04

Solute	T°C	ϕ_C°	A_C	B_C	C_C	D_C	σ
NaCl	5	−204.667	132.187	−12.069	−0.92839	0.049905	0.3
	25	−85.46	25.072	30.116	−10.6986	1.16001	0.3
	45	−50.768	4.4499	31.577	−10.8616	1.38434	0.4
$MgCl_2$	25	−252.545	50.8894	36.2508	−9.63046		1.0
$CaCl_2$	25	−278.326	133.147	−67.3016	47.7742	−9.44019	1.0
$NiCl_2$	25	−295.270	114.882	−33.0619	38.4626	−10.5031	0.5

[a]Standard deviation.

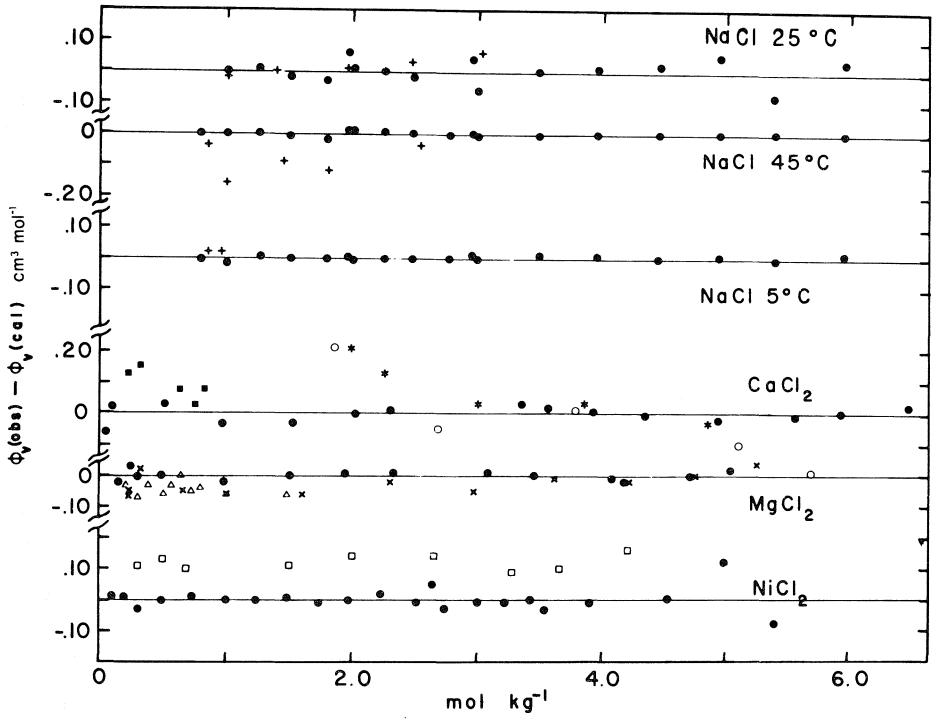

FIG. 2. Apparent molal volumes of various electrolytes in water. Deviation plots from eq. [1]: ●: present data; +: ref. 11; ○: Vasilëv *et al.* (21); *: I.C.T. (18); ×: Phang and Stokes (16); △: Chen *et al.* (17); □: Stokes *et al.* (22); ■: Dunn (20).

agreement is less satisfactory since the data of Fedyainov *et al.* (25) and of Rutskov (26) diverge by as much as 6 J K^{-1} mol^{-1}. Since the densities from the same laboratory (21) showed large differences, such disagreement is not unexpected. We could not find any reliable data for $NiCl_2$ at high concentration for comparison. Our scatter of points is of the order of 0.5 J K^{-1} mol^{-1}.

Discussion

Transitions in aqueous solutions have been well investigated by heat capacity measurements, especially in the case of the micellization process (27). If the partial molar heat capacities of the initial and final states are different and if there is a corresponding enthalpy change, then the transition can be considered of first order and $\bar{C}_{p,2}$ will go through a

Can. J. Chem. Downloaded from www.nrcresearchpress.com by 210.87.254.6 on 09/06/12
For personal use only.

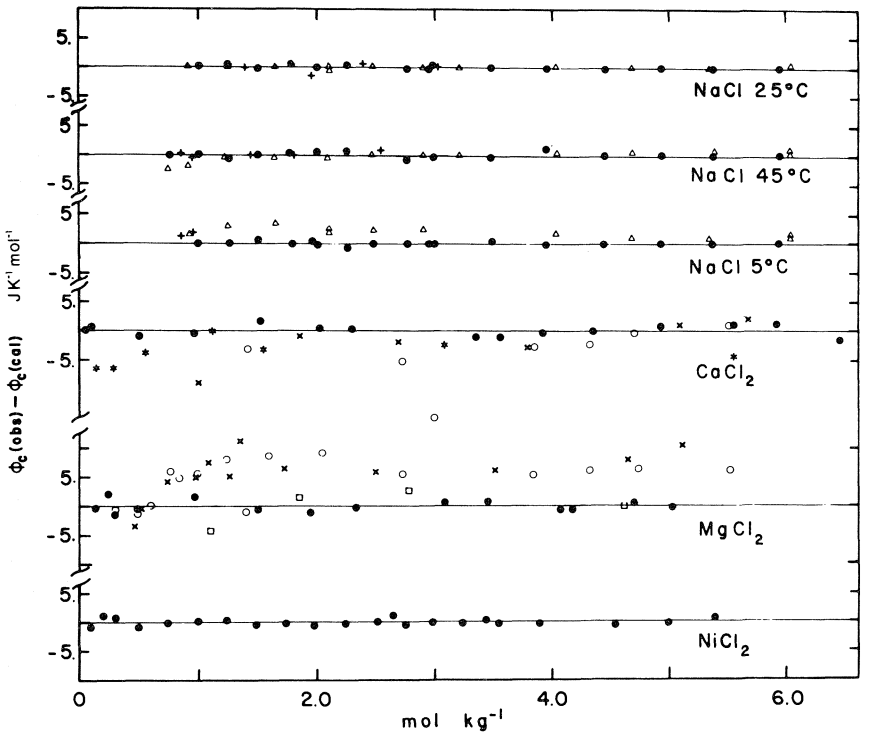

FIG. 3. Apparent molal heat capacities of various electrolytes in water. Deviation plots from eq. [1]: ○: present data; △: Tanner and Lamb (24); +: Perron *et al.* (11); ○: Fedyainov *et al.* (25); ×: Vasilëv *et al.* (21); *: Ruskov (26); □: Ruskov (26).

hump or maximum before dropping rapidly to its final value as the concentration crosses the transition zone. If there is no corresponding enthalpy change, $\bar{C}_{p,2}$ will still change rapidly in the transition concentration but no hump (relaxational contribution) will be observed. This would be a second order transition. A break in a $\bar{C}_{p,2}$ curve would therefore indicate a transition of a higher order.

The partial molar volumes $\bar{V}_2$ and heat capacities $\bar{C}_{p,2}$ of the solutes were calculated in two ways: from eq. [1] knowing that $d(\phi_V m)/dm = \bar{V}_2$ and from a plot of $\Delta(\phi_V m)/\Delta m$ against the mean molality. The first technique is the simplest but may lead to erroneous results at the concentration limits since the least-squares analysis may not be reliable at these edges unless many data points were available. For example, the $\bar{C}_{p,2}$ of rare earth chlorides of Spedding *et al.* (28), obtained by this technique, give very pronounced curvature at high concentrations which may not be real. In our case both approaches to the calculation of $\bar{V}_2$ gave the same results except at very high concentrations where the graphical procedure was better. The values of $\bar{V}_2$ and $\bar{C}_{p,2}$ are shown in Figs. 4 and 5.

The trends in $\bar{V}_2$ of $NiCl_2$, $MgCl_2$, and $CaCl_2$ are quite similar at intermediate concentrations as seen from Fig. 4. At concentrations above 3 mol kg^{-1} the data for $NiCl_2$ and $MgCl_2$ level off more rapidly than those for $CaCl_2$. However, no break in these $\bar{V}_2$ curves can be seen. NaCl shows less curvature than the 1:2 electrolytes.

The $\bar{C}_{p,2}$ data are shown in Fig. 5. The trends with NaCl, $MgCl_2$, and $CaCl_2$ are all quite smooth while $\bar{C}_{p,2}$ of $NiCl_2$ levels off at about 4 mol kg^{-1}. The derivative of this curve, $d\bar{C}_{p,2}/dm$ suggests that there might be a change in slope with $NiCl_2$ at about that concentration. However, this may also be true of $CaCl_2$ near 6 mol kg^{-1}.

The present data therefore exclude the possibility of a sharp transition in aqueous $NiCl_2$ near 4 mol kg^{-1} but not a transition of a high order. It would be of course possible to find methods of plotting our data so as to show a definite break with our heat capacities (6), but unless the function has a sound scientific justification such plots are meaningless. The heat capacity is very sensitive to local average structure but the effect of long-range ordering is small. The structures proposed by Enderby *et al.* (1, 2) are long range and the transitions could be gradual. Under such circumstances heat capacities, or any other thermodynamic properties, would not be expected to change significantly. There are

Can. J. Chem. Downloaded from www.nrcresearchpress.com by 210.87.254.6 on 09/06/12
For personal use only.

Can. J. Chem. Downloaded from www.nrcresearchpress.com by 210.87.254.6 on 09/06/12
For personal use only.

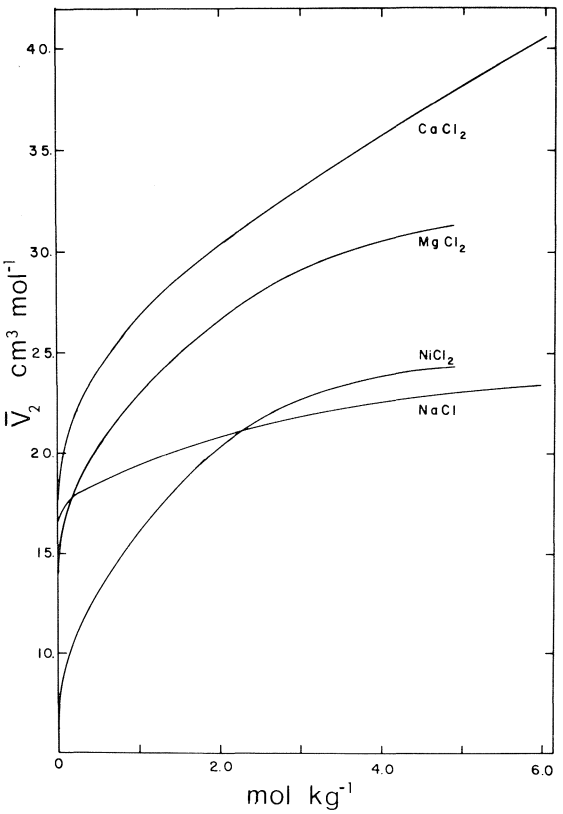

FIG. 4. Partial molal volumes of various electrolytes in water at 25°C.

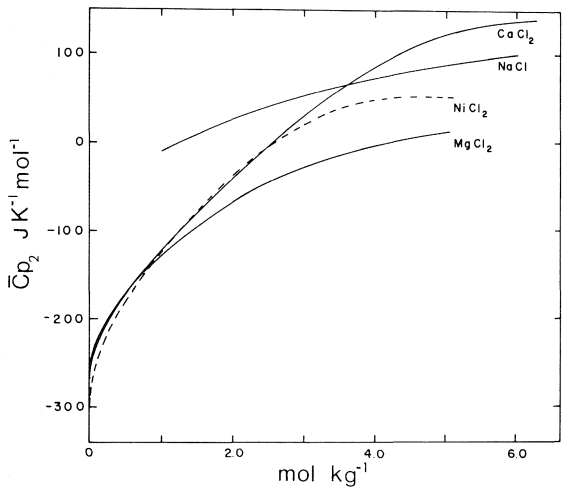

FIG. 5. Partial molal heat capacities of various electrolytes in water at 25°C.

also many ways of interpreting the changes in $\bar{C}_{p,2}$ of these electrolytes at high concentration, including a partial dehydration of the ions, complex formation, and ionic association. We can therefore conclude that while heat capacity data do not exclude the possibility of a smooth transition in aqueous $NiCl_2$, they do not offer strong evidence for such changes.

Acknowledgements

We are grateful to the Natural Sciences and Engineering Research Council of Canada for financial support and to NATO for a fellowship to one of us (A.R.). We would also like to thank Daniel Hétu for his help with some of these measurements.

1. R. A. HOWE, W. S. HOWELLS, and J. E. ENDERBY. J. Phys. C, **7**, L111 (1974).
2. J. E. ENDERBY and G. W. NEILSON. *In* Water, a comprehensive treatise. *Edited by* F. Franks. Plenum Press, New York. 1979.
3. M. P. FONTANA. Solid State Commun. **18**, 765 (1976).
4. M. P. FONTANA, G. MAISANO, P. MIGLIARDO, and F. WANDERLICH. Phys. Chem. Liq. **8**, 45 (1978).
5. G. CUBIOTTI, G. MAISANO, P. MIGLIARDO, and F. WANDERLICH. J. Phys. C, **10**, 4689 (1977).
6. G. MAISANO, P. MIGLIARDO, F. WANDERLICH, and M. P. FONTANA. J. Chem. Phys. **68**, 5594 (1978).
7. R. MILLS, N. H. MARCH, P. V. GIAQUINTA, M. PARRINELLO, and M. P. TOSI. Chem. Phys. **26**, 237 (1977).
8. R. CAMINITI, G. LICHERI, G. PICCALUGA, and G. PINNA. Faraday Disc. **64**, 62 (1978).
9. N. L. FRIEDMAN and J. B. DUDOWICZ. Aust. J. Chem. **33**, 1889 (1980).
10. G. PERRON, J. E. DESNOYERS, and F. MILLERO. Can. J. Chem. **52**, 3738 (1974).
11. G. PERRON, J. L. FORTIER, and J. E. DESNOYERS. J. Chem. Thermodyn. **7**, 1177 (1975).
12. P. PICKER, P. A. LEDUC, P. PHILIP, and J. E. DESNOYERS. J. Chem. Thermodyn. **3**, 631 (1971).
13. J. E. DESNOYERS, C. DE VISSER, G. PERRON, and P. PICKER. J. Solution Chem. **5**, 605 (1976).
14. P. PICKER, E. TREMBLAY, and C. JOLICOEUR. J. Solution Chem. **3**, 377 (1974).
15. (*a*) J. J. SPITZER, P. P. SINGH, K. G. MCCURDY, and L. G. HEPLER. J. Solution Chem. **7**, 81 (1978); (*b*) F. S. Z. ROGERS and K. S. PITZER. J. Chem. Phys. Ref. Data. Submitted.
16. S. PHANG and R. H. STOKES. J. Solution Chem. **9**, 497 (1980).
17. C.-T. A. CHEN, J. H. CHEN, and F. J. MILLERO. J. Chem. Eng. Data, **25**, 307 (1980).
18. E. W. WASHBURN (*Editor*). International Critical Tables 3:71. McGraw-Hill. 1928.
19. L. A. DUNN. Trans. Faraday Soc. **62**, 2348 (1966).
20. H. E. WIRTH and F. H. BANGERT. J. Phys. Chem. **76**, 3488 (1972).
21. Y. A. VASILËV, N. V. FEDYAINOV, and V. V. KURENKOV. Russ. J. Phys. Chem. **47**, 1570 (1970).
22. R. H. STOKES, S. PHANG, and R. MILLS. J. Solution Chem. **8**, 489 (1979).
23. M. KH. KARAPET'YANTS, V. A. VASILËV, and E. S. SANAEV. Russ. J. Phys. Chem. **51**, 1281 (1977).
24. J. E. TANNER and F. W. LAMB. J. Solution Chem. **7**, 303 (1978).
25. N. V. FEDYAINOV, V. A. VASILËV, and M. KH. KARAPET'YANTS. Russ. J. Phys. Chem. **44**, 1026 (1970).
26. A. RUTSKOV. Chem. Zhur. Priklad. Khim. **21**, 820 (1948).
27. J. E. DESNOYERS, R. DELISI, and G. PERRON. Pure Appl. Chem. **52**, 433 (1980).
28. F. H. SPEDDING, J. P. WALTERS, and J. L. BAKER. J. Chem. Eng. Data, **20**, 438 (1975).

Synthesis of phthalideisoquinolines from 3-halophthalides and 3,4-dihydroisoquinolinium salts[1]

CLARKE E. SLEMON,[2] LOUISE C. HELLWIG, JEAN-PIERRE RUDER, ERIC W. HOSKINS, AND DAVID B. MACLEAN[3]

Department of Chemistry, McMaster University, Hamilton, Ont., Canada L8S 4M1

Received May 20, 1981

CLARKE E. SLEMON, LOUISE C. HELLWIG, JEAN-PIERRE RUDER, ERIC W. HOSKINS, and DAVID B. MACLEAN. Can. J. Chem. **59**, 3055 (1981).

Phthalideisoquinoline alkaloids have been synthesized by coupling appropriately substituted 3-halophthalides and 2-methyl-3,4-dihydroisoquinolinium salts in the presence of Zn(Cu) couple or metallic Zn. Both *erythro* and *threo* isomers are formed in the reaction. The nmr spectra of the (±)-*erythro*- and (±)-*threo*-isocordrastines have been reinvestigated. The results, which differ from those previously reported, lead to a different conclusion regarding the conformation of the molecules.

CLARKE E. SLEMON, LOUISE C. HELLWIG, JEAN-PIERRE RUDER, ERIC W. HOSKINS et DAVID B. MACLEAN. Can. J. Chem. **59**, 3055 (1981).

On a synthétisé des alkaloides du type phtalideisoquinoleines en faisant réagir des halo-3 phtalides convenablement substitués avec les sels de méthyl-2 dihydro-3,4 isoquinolinium en présence du couple Zn(Cu) ou du Zn métallique. Il se forme les deux isomères *érythro* et *thréo* au cours de la réaction. On a étudié de nouveau les spectres de rmn des isocordrastines (±) *érythro* et (±) *thréo*. Les résultats, qui diffèrent de ceux rapportés antérieurement, conduisent à une conclusion différente en ce qui a trait à la conformation des molécules.

[Traduit par le journal]

Can. J. Chem. Downloaded from www.nrcresearchpress.com by 210.87.254.40 on 09/06/12
For personal use only.

The first successful synthesis of a phthalideisoquinoline alkaloid was realized by Perkin and Robinson (1) in 1911 by direct coupling of an isoquinoline moiety and a suitably activated phthalide moiety. In the interim, but particularly in the past decade, many new but less direct approaches to the construction of this ring system have been reported (2–18). In the past year, two syntheses using the strategy of Perkin and Robinson have been reported in which improved methods of joining the two moieties have been developed. Shono *et al.* (19) have shown that bromophthalides and *N*-methyl-3,4-dihydroisoquinolinium salts may be coupled electrochemically, while Mooney *et al.* (20) have shown that phthalide anions add to isoquinolinium salts. In a similar vein we report here the coupling of 3-halophthalides **1** with *N*-methyl-3,4-dihydroisoquinolinium salts **2** in the presence of Zn(Cu) couple or metallic Zn to give a mixture of *erythro*- and *threo*-*N*-methylphthalidetetrahydroisoquinolines, **3** and **4**, respectively (Scheme 1). In a different context Granelli and Leander (21) found that Zn(Cu) couple could be used to couple an α-bromoester and an iminium salt.

We have used this method successfully in the preparation of the following racemic diastereomeric pairs, β-hydrastine **5** and α-hydrastine **6**, corlumine **7** and adlumine **8**, bicuculline **9** and adlumidine **10**, and the *erythro* **11** and *threo* **12** isocordrastines.[4] However, we have studied the reaction in detail only in the case of the isocordrastines. In this instance we have found that optimum yields were obtained when the ratio of halophthalide **1** to iminium salt **2** to Zn(Cu) was 2:1:2. In the preparation of other compounds different reactant ratios were used and no attempt was made to find conditions for optimum yields. It is likely that better yields might be obtained in the latter cases by altering the reactant ratio but these experiments were not attempted.

In the condensation of **1***a* and **2***a* the optimum yield of *erythro* and *threo* isomers was 35% and 28% respectively. Reaction periods longer than those normally used had no effect on yield but higher temperatures caused a decrease. Yields were equally good when Zn metal was used instead of Zn(Cu) couple but Cu metal was ineffective in promoting condensation. An increase in the amount of metal used above the stoichiometric quantity had no effect. When **1***a* was treated with Zn under Reformatsky conditions, followed by introduction of **2***a*, coupling of the two components did

[1]A preliminary account of this work was reported. D. B. MacLean, 11th Int. Symp. Chem. Nat. Prod. Golden Sands Bulgaria, Symp. Papers 4(2) 204 (1979).

[2]Present address: Canada Packers Research Centre, 2211 St. Clair Ave. W., Toronto, Ont., Canada M6N 1K4.

[3]Author to whom correspondence may be directed.

[4]The name isocordrastine is proposed for these compounds that differ from cordrastine in the position of the OMe groups in the phthalide moiety.

0008-4042/81/213055-06$01.00/0

©1981 National Research Council of Canada/Conseil national de recherches du Canada

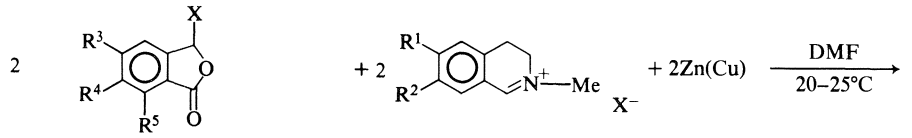

1*a* $R^3 = R^4 = OCH_3$; $R^5 = H$; X = Br
1*b* $R^4 = R^5 = OCH_3$; $R^3 = H$; X = Br
1*c* $R^4 + R^5 = OCH_2O$; $R^3 = H$; X = Cl
1*d* $R^4 = R^5 = OCH_3$; $R^3 = H$; X = Cl

2*a* $R^1 = R^2 = OCH_3$
2*b* $R^1 + R^2 = —OCH_2O—$

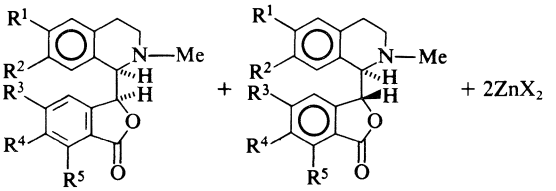

3 (*erythro*) **4** (*threo*)

5 and **6** $R^1 = R^2 = OCH_2O$; $R^4 = R^5 = OCH_3$; $R^3 = H$
7 and **8** $R^1 = R^2 = OCH_3$; $R^4 + R^5 = OCH_2O$; $R^3 = H$
9 and **10** $R^1 + R^2 = R^4 + R^5 = OCH_2O$; $R^3 = H$
11 and **12** $R^1 = R^2 = R^3 = R^4 = OCH_3$; $R^5 = H$

SCHEME 1

not occur. From these observations we conclude that the reaction proceeds on the metal surface through formation of a phthalide anion which reacts directly with the iminium salt at the surface. However, a radical mechanism for the reaction cannot be excluded on the basis of the present data. The only by-products isolated and identified were *m*-meconin **13** and compound **14** but their formation in no way helps to clarify the mode of coupling.

In the course of these studies we examined the ^1H nmr spectra of the isocordrastines, **11** and **12**. The compounds had been previously studied by Shamma and St. Georgiev (8, 11) who assigned the resonances of the aromatic protons using conformational arguments. However, they provided no experimental justification for their assignments. We have reached a different conclusion regarding the aromatic resonances based upon double irradiation experiments. As a result we are led to a different conclusion concerning the favoured conformation of the molecules from that proposed earlier.

The coupling constants between H-1 and H-1′ are 4.2 Hz for **11** and 3.5 Hz for **12**, indicating dihedral angles of approximately 45°, 135°, 225°, or 315° for **11** and 50°, 130°, 230°, or 310° for **12**. The absorptions of the aromatic protons were assigned unambiguously by double irradiation experiments. Thus in **11**, irradiation at δ 5.57, assigned to H-1′ in analogy to other phthalideisoquinoline alkaloids (7, 12), collapses the H-1 doublet at δ 4.10 and sharpens the signal of H-7′ at δ 6.22 from $w_{\frac{1}{2}}$ = 1.6 Hz to $w_{\frac{1}{2}}$ = 1.3 Hz. Irradiation of the H-1 resonance at δ 4.10 collapses the H-1′ doublet at δ 5.57 and sharpens the aromatic singlet at δ 6.46 from $w_{\frac{1}{2}}$ = 1.6 Hz to $w_{\frac{1}{2}}$ = 1.4 Hz, attributed therefore to H-8. In addition, irradiation at δ 2.49 causes a sharpening of the proton at δ 6.62 from $w_{\frac{1}{2}}$ = 1.8 Hz to $w_{\frac{1}{2}}$ = 1.3 Hz which must therefore be assigned to H-5.

In **12**, irradiation at δ 5.64, attributed to H-1′, collapses the doublet at δ 4.12 to a singlet and also sharpens the aromatic singlet at δ 7.14 ($w_{\frac{1}{2}}$ = 1.5 Hz before irradiation and $w_{\frac{1}{2}}$ = 1.2 Hz during irradiation), which may now be assigned to H-7′. Irradiation at δ 4.12 collapses the doublet at δ 5.64 and affects the aromatic singlet at δ 6.67 ($w_{\frac{1}{2}}$ = 1.5 Hz before irradiation and $w_{\frac{1}{2}}$ = 1.3 Hz during irradiation), which is assigned to H-8. Assignment of the resonance at δ 6.34 to H-5 was confirmed by another double irradiation experiment in which the signal at 6.34 sharpened from $w_{\frac{1}{2}}$ = 1.8 Hz to $w_{\frac{1}{2}}$ = 1.2 Hz when the sample was irradiated at δ 2.68, presumably at the protons at C-4 (Table 1).

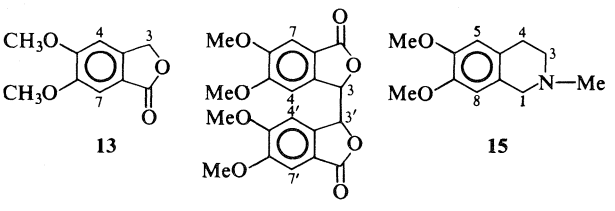

13 **14** **15**

Can. J. Chem. Downloaded from www.nrcresearchpress.com by 210.87.254.40 on 09/06/12
For personal use only.

TABLE 1. The ^{1}H nmr chemical shifts of compounds **11** and **12**, and of model compounds **13** and **15** (80 MHz, $CDCl_3$, δ from TMS)[a]

	11 *erythro*			**12** *threo*			**13**	**15**
H-1	4.10	d	$J = 4.2$ Hz	4.12	d	$J = 3.5$ Hz		
H's at C-3 H's at C-4	2.14-3.07[b]	m		2.21-3.24[c]	m			
H-5	6.62	s		6.34	s			6.55
H-8	6.46	s		6.67	s			6.47
H-1′	5.57	d	$J = 4.2$ Hz	5.64	d	$J = 3.5$ Hz		
H-4′	7.24	s		7.02	s		7.26 (H-7)	
H-7′	6.22	s		7.14	s		6.97 (H-4)	
N—Me	2.59	s		2.71	s			
6 OMe	3.73[d]	s		3.73[e]	s			
7 OMe	3.78[d]	s		3.78[e]	s			
5′ OMe	3.85[d]	s		3.83[e]	s			
6′ OMe	3.91[d]	s		3.92[e]	s			

[a] It is noteworthy that the nmr of **11** is very susceptible to Zn(Cu) impurities present.
[b] H's at C-4 from decoupling experiment: δ 2.49.
[c] H's at C-4 from decoupling experiment: δ 2.68.
[d,e] Assignments may be interchanged.

The aromatic proton resonances of **11** and **12** may be compared with those of 2-methyl-1,2,3,4-tetrahydroisoquinoline **15** and *m*-meconin **13** in Table 1. Whereas the protons at H-5, H-8, and H-4′ of the alkaloids **11** and **12** are not affected very much relative to the models, the protons at H-7′ show a big change in chemical shift. In **11**, H-7′ is shielded more than 0.7 ppm to δ 6.22, indicating that it must be located somewhere above the plane of the aromatic ring of the isoquinoline moiety. This is the case only with a dihedral angle of approximately 45°, and qualitative calculations using a Dreiding model and the method of Johnson and Bovey (22) suggest conformation **11***a*. In the case of **12** a dihedral angle of ca. 130° between H-1 and H-1′ leads to conformation **12***a* where there is minimum interaction between the two aromatic rings and, as expected, little change in chemical shift in the alkaloids relative to the corresponding signals in **13** and **15** (See Scheme 2).

The general procedure for the preparation of the alkaloids **5** to **10** is given in the Experimental. In these preparations chlorophthalides prepared by standard methods were sometimes used instead of bromophthalides. In cases where both phthalides were available the reactions were carried out with each halide but there was no appreciable difference in yield. The choice of chloro or bromophthalide is therefore a matter of preparative convenience. In all cases mixtures of the *erythro* and *threo* isomers were isolated. The isomers were easily separated from one another and from by-products by flash chromatography. These yields (30–35%) are comparable to those of the isocordrastines (combined yield 34%) when prepared under similar conditions.

This preparative method provides a convenient route to alkaloids of this family from readily available starting materials. In the one case where optimum reaction conditions for the condensation were established the yields are comparable to those obtained in the electrochemical coupling reaction (19).

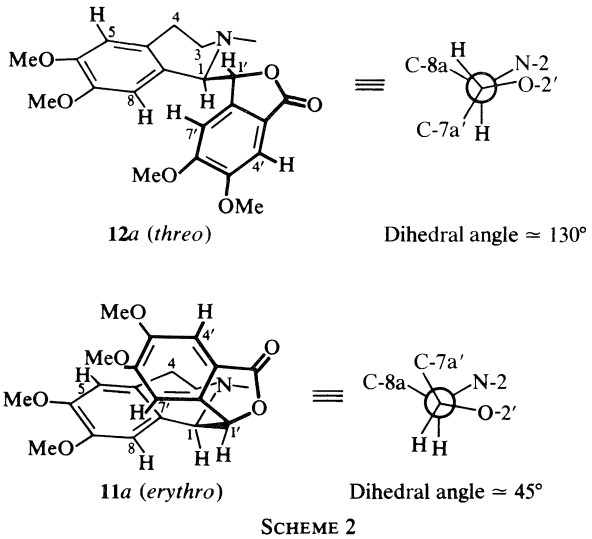

SCHEME 2

Experimental

Apparatus, Materials, and Methods

Continuous wave ^{1}H nmr spectra were run on a Varian EM 390 or T-60 spectrometer and Fourier transform nmr spectra on either a Bruker WP 80 or WH 90 spectrometer. Unless otherwise specified, the samples were dissolved in chloroform-*d* using tetramethylsilane (TMS) as the internal standard. Chemical shifts, quoted as δ values, were measured in relation to TMS. The symbols s = singlet, d = doublet, t = triplet, q = quartet, m = multiplet, and br = broad are used in reporting spectra.

Mass spectra were recorded on a V.G. Micromass 7070 F mass spectrometer, at 70 eV. Infrared spectra were recorded on a Perkin Elmer 283 spectrometer in chloroform solution.

Can. J. Chem. Downloaded from www.nrcresearchpress.com by 210.87.254.40 on 09/06/12
For personal use only.

Can. J. Chem. Downloaded from www.nrcresearchpress.com by 210.87.254.40 on 09/06/12
For personal use only.

Melting points were determined on a Kofler micro hot stage and are uncorrected.

Column and thin layer chromatography (tlc) were performed using silica gel 60 as the adsorbent. Gravity columns were run using Baker 60–200 mesh silica, and "flash" columns prepared as described in the literature (23). Zn(Cu) couple (Ventron, Alfa Products) was activated by washing with 10% aqueous HCl, rinsed with water until neutral, flushed with acetone, and dried at 120°C at reduced pressure. Zn dust (Matheson, Coleman, and Bell) was activated by washing with dilute aqueous NaOH, water, dilute acetic acid, water, ethanol, acetone, and ether in this sequence, and dried at 100°C under reduced pressure (24).

The following compounds were prepared by standard methods and gave satisfactory physical and spectral data: *m*-meconin (25), meconin (26), 6,7-dimethoxy-2-methyl-3,4-dihydroisoquinolinium iodide (27), 2-formyl-5,6-methylenedioxybenzoic acid (28), and opianic acid, prepared from lithiated 2,3-dimethoxy-*N*,*N*-diethylbenzamide and dimethyl formamide using the procedure of Snieckus and co-workers (29).

Preparation of Hydrastinine Iodide, **2**b

(a) 3,4-Methylenedioxydihydrocinnamoyl Chloride

3,4-Methylenedioxydihydrocinnamic acid (30) prepared by standard methods from piperonal (12.9 g, 66.5 mmol) was treated with excess thionyl chloride on a steam bath for one hour. The excess thionyl chloride was removed on the rotary evaporator and the residue was distilled at 100–110°C/0.15 Torr to give 12.2 g (86%) of the acid chloride as a viscous yellow liquid.

(b) 2-(3,4-Methylenedioxyphenyl)-ethyl Isocyanate

3,4-Methylenedioxydihydrocinnamoyl chloride (12.116 g, 57 mmol) was dissolved in mesitylene (50 mL) and brought to reflux. Trimethylsilyl azide (11.2 mL, 84.5 mmol) was added and refluxing continued for 40 h. The reaction solution was cooled, the excess trimethylsilyl azide and mesitylene were distilled off at reduced pressure, and the residue was distilled at 82–100°C/0.15 Torr to give 9.93 g (91%) of the isocyanate: ir (neat): 2900, 2260, 1610, 1503, 1490, 1440, 1250, 1040 cm^{-1}; ^1H nmr ($CDCl_3$) δ: 6.58–6.83 (3H, m, arom), 5.90 (2H, s, OCH_2O), 3.45 (2H, t, J = 7.0 Hz), 2.78 (2H, t, J = 7.0 Hz).

(c) Homopiperonyl Formamide

2-(3,4-Methylenedioxyphenyl)-ethyl isocyanate (5.6 g, 29.4 mmol) was dissolved in dry ether (34 mL) and cooled to −78°C. Diisobutylaluminum hydride (32.6 mL, 20% in hexane, 95% active, 1.5 equiv.) was added via syringe, and the solution was allowed to warm to 0°C over 4 h. The mixture was quenched with water (5 mL). After the vigorous reaction had subsided aqueous hydrochloric acid (100 mL) was added to dissolve the aluminum salts. The solution was extracted with ether (2 × 50 mL) and the aqueous layer basified to pH 10 with solid potassium carbonate and extracted with diethyl ether (5 × 50 mL). The combined ether extract (350 mL) was dried to give 4.24 g (75%) of the formamide as a white solid which was recrystallized from ether–acetone to give white crystals, mp 60–62°C (lit. (31) mp 62–63°C); ir ($CHCl_3$): 3450, 2860, 1685 cm^{-1}; ^1H nmr ($CDCl_3$) δ: 8.05 (1H, d, J = 2.0 Hz, CHO), 7.26 (1H, br s, NH, exchangeable in D_2O), 6.53–6.83 (3H, m, arom), 5.80 (2H, s, OCH_2O), 3.39 (2H, "quintet", J = 6 Hz, CH_2NH), 2.70 (2H, t, J = 6 Hz, benzylic).

(d) 6,7-Methylenedioxy-3,4-dihydroisoquinoline (Norhydrastinine)

To a refluxing solution of homopiperonyl formamide (2.46 g, 12.7 mmol) in acetonitrile (18 mL, freshly distilled from calcium hydride) was added phosphorus oxychloride (1.23 mL, 13.38 mmol, 1.05 equiv.) After two hours, the dark solution was cooled in an ice bath and washed with petroleum ether. The acetonitrile layer was diluted with water (20 mL), and this acidic layer (pH 1) was washed with benzene (3 × 30 mL) before being basified to pH 11 with 10% sodium hydroxide solution, and then extracted with benzene (3 × 50 mL). The combined basic organic extract was dried and evaporated to give 1.02 g (46%) of norhydrastinine as a beige solid; ^1H nmr ($CDCl_3$) δ: 8.14 (1H, br s, CH=N), 6.70 (1H, s, arom), 6.60 (1H, s, arom), 5.90 (2H, s, OCH_2O), 3.67 (2H, triplet split into doublets, J = 7.0 and 2 Hz, HC=NCH_2), 2.6 (2H, t, J = 7.0 Hz, benzylic).

(e) Hydrastinine Iodide

A solution of norhydrastinine (3.2 g, 18.3 mmol) in benzene (50 mL) was swirled with methyl iodide (3 mL) and left overnight. Filtration yielded 5 g (86%) of hydrastinine iodide, mp 220–230°C. A sample was recrystallized from EtOH to give shiny yellow plates, mp 232–237°C (lit. (32) mp 234°C); ^1H nmr (CD_3OD) δ: 8.90 (1H, s, CH=N), 7.27 (1H, s, arom), 7.03 (1H, s, arom), 6.19 (2H, s, OCH_2O), 4.03 (2H, t, J = 8.0 Hz, CH_2N), 3.27 (2H, t, J = 8.0 Hz benzylic), 3.78 (3H, s, N—CH_3).

5,6-Dimethoxy-3-bromophthalide, **1**a

A mixture of *m*-meconin (2.0 g, 10.3 mmol) and *N*-bromosuccinimide (1.73 g, 9.7 mmol) in dry benzene (40 mL) was treated with a few mg of dibenzoyl peroxide and the solution heated under reflux for 3.5 h under a nitrogen atmosphere. The mixture was cooled to 5°C, the succinimide removed by filtration, and the filtrate washed with water (2 × 25 mL). The benzene solution was dried (anhydrous $MgSO_4$) and evaporated to give a crystalline residue which was used directly in subsequent steps. Yield: 80%. Recrystallization from CCl_4 gave a sample melting at 108–109°C; ^1H nmr ($CDCl_3$) δ: 7.39 (1H, s), 7.34 (1H, s), 7.07 (1H, s), 4.05 (3H, s, OMe), 3.95 (3H, s, OMe).

6,7-Dimethoxy-3-bromophthalide, **1**b

A solution of meconin (0.458 g, 2.36 mmol) and *N*-bromosuccinimide (0.448 g, 2.52 mmol) in carbon tetrachloride (39 mL) was refluxed with a catalytic amount of dibenzoyl peroxide under the illumination of a 100-W light bulb for 4 h. The suspension was cooled in an ice bath, filtered, and the filtrate evaporated to give a quantitative yield of the bromophthalide as a brownish solid which was used without further purification; ^1H nmr ($CDCl_3$) δ: 7.31 (1H, s), 7.26 (2H, s), 4.12 (3H, s, OMe), 3.93 (3H, s, OMe).

6,7-Methylenedioxy-3-chlorophthalide, **1**c

2-Formyl-5,6-methylenedioxybenzoic acid (0.39 g, 2 mmol) was heated with excess thionyl chloride on a steam bath for 10 min. When all the acid had gone into solution, the excess thionyl chloride was removed at reduced pressure to give a quantitative yield of the chlorophthalide as a brownish white solid which was used without further purification; ^1H nmr ($CDCl_3$) δ: 7.10 (1H, s), 7.07 (1H, s), 7.03 (1H, s), 6.20 (2H, s, OCH_2O).

6,7-Dimethoxy-3-chlorophthalide, **1**d

This compound was prepared in the same manner as the above from opianic acid; ^1H nmr ($CDCl_3$) δ: 7.25 (2H, s), 6.98 (1H, s), 4.05 (3H, s, OMe), 3.90 (3H, s, OMe).

Preparation of the Isocordrastines, **11** *and* **12**

3-Bromo-*m*-meconin (255 mg, 0.93 mmol) and 6,7-dimethoxy-2-methyl-3,4-dihydroisoquinolinium iodide (154 mg, 0.46 mmol) were dissolved in dimethylformamide (7 mL, distilled from CaH_2). To the clear yellow solution 61 mg of Zn or 67 mg Zn(Cu) (0.94 mmol) were added yielding a greenish-black mixture. The mixture was stirred at room temperature yielding first a yellow green solution and after 3 days a clear solution. The solution was filtered to remove any solid impurity, the solvent removed under reduced pressure, and the residue taken up in $CHCl_3$ (15 mL). The chloroform solution was extracted first with water (1 × 15 mL) and then with 10% aqueous HCl (5 × 7 mL). The now light yellow chloroform layer was evaporated and the brownish-

Can. J. Chem. Downloaded from www.nrcresearchpress.com by 210.87.254.40 on 09/06/12
For personal use only.

yellow residue was dissolved in dry benzene (10 mL). This solution was washed with 10% aqueous HCl, 5 × 7 mL, leaving behind a slightly beige benzene layer. The combined greenish-yellow acidic aqueous layers from the chloroform and the benzene extractions were basified with concentrated NH_4OH (to pH 9) after cooling to 0–5°C. The now alkaline solution was extracted with 10 × 10 mL dry ether and the yellow combined ethereal layers were dried over $MgSO_4$ overnight, filtered, and evaporated, leaving behind 135 mg of a yellow oil, which showed 4 spots on tlc (R_f in EtOAc: 0.45, 0.41, 0.38, 0.07).

Flash chromatography (23) (12 mm column, 15 cm silica gel 37–53 μm, eluants CH_2Cl_2–Et_2O (15:1) 90 mL, EtOAc 45 mL, EtOAc–acetone (1:1) 30 mL, and acetone 50 mL (in this sequence), speed 5 cm/min, fraction size 1 mL) yielded 4 pure compounds: *m*-meconin **13** (4 mg, R_f 0.45), *m*-meconin dimer **14** (3 mg, R_f 0.41), *threo*-isocordrastine **12** (51 mg, 28%, R_f 0.38), and *erythro*-isocordrastine **11** (65 mg, 35%, R_f 0.07). *m*-Meconin **13** was identified by comparison with an authentic sample. *m*-Meconin dimer **14** had the following physical properties: ^{1}H nmr ($CDCl_3$) δ: 3.83 (6H, 2 × OMe); 3.90 (6H, 2 × OMe); 5.94 (2H, s, H-3 and H-3′), 6.93 (2H, s, H-4 and H-4′), 7.07 (2H, s, H-7 and H-7′); ms (70 eV, probe) *m/e*: 386 M^+, 193, 165, 149, 122. (±)-*erythro*-Isocordrastine **11** had the following physical properties: mp 169–170°C (from EtOH) (lit. (8) mp 157–159°C, (13) mp 166–167°C); ir ν_{max} ($CHCl_3$): 1755 cm^{-1}; ^{1}H nmr, see Table 1. (±)-*threo*-Isocordrastine **12** had the following physical properties: mp 144–146°C (from EtOH) (lit. (8, 13)[5] mp 115–117°C); ir ν_{max} ($CHCl_3$): 1758 cm^{-1}; ^{1}H nmr, see Table 1.

Preparation of the Alkaloids, 5 to 10

(a) General Procedure

The halophthalide (2 mmol) and the imminium iodide (1.69 mmol) were dissolved in dimethylformamide (10 mL, freshly distilled from calcium hydride). The Zn(Cu) couple (0.2 g, ca. 3 mmol) was added and the reaction was left stirring in a stoppered flask overnight. The solvent was removed at reduced pressure. The solid residue was taken up in chloroform and washed with 10% hydrochloric acid (5 × 50 mL). The combined aqueous layers were basified to pH 10 with ammonium hydroxide and extracted with ether (5 × 25 mL). The combined ethereal layers were dried to give a mixture of *erythro* and *threo* compounds, hereafter referred to as "the product of the first work-up". The chloroform layer was evaporated and the residue taken up in benzene and 10% hydrochloric acid (50 mL of each). The benzene layer was further washed with 10% hydrochloric acid (4 × 50 mL). The combined aqueous layers were basified to pH 10 with ammonium hydroxide and extracted with ether (5 × 25 mL). The combined ethereal layers were dried to give a mixture of *erythro* and *threo* compounds, hereafter referred to as "the product of the second work-up".

(b) Preparation of (±)-β-Hydrastine 5 and (±)-α-Hydrastine, 6

The product of the first work-up, 0.320 g (47%), was subjected to column chromatography (silica gel, 10 g, column diameter 5/8 in., eluting with methylene chloride gradually changing to 30% ether – methylene chloride) to give 0.086 g (13%) of (±)-α-hydrastine identical by nmr with an authentic sample. Recrystallization from methanol gave a sample melting at 150–154°C (lit. (2, 33) mp 150–152°C) identical with an authentic sample[6] by ir and tlc. The product of the second work-up (0.134 g, 20%) was essentially pure (±)-β-hydrastine. It was recrystallized from methanol yielding a sample melting at 136–140°C (lit. (2, 34) mp 138–139°C) identical with authentic sample by nmr, ir, and tlc.

(c) Preparation of (±)-Corlumine 7 and (±)-Adlumine 8

The product of the first work-up, 0.282 g (43%), was subjected to flash chromatography (column diameter 25 mm, eluting with 2% acetone – ethyl acetate) to yield 0.127 g (20%) of pure (±)-adlumine as a pale yellow foam, identical with an authentic sample by nmr. Crystallization from chloroform–methanol yielded pale yellow crystals melting at 191.5–193.5°C (lit. (35) mp 190°C), identical by tlc and ir with authentic adlumine. The product of the second work-up, 0.063 g (10%) of (±)-corlumine, was identical with an authentic sample of corlumine by nmr. Recrystallization from methanol yielded yellow crystals, mp 178–181°C (lit. (27) mp 193.5–195°C dec.) identical with an authentic sample by ir and tlc.

(d) Preparation of (±)-Bicuculline 9 and (±)-Adlumidine 10

This preparation was done using 3 mmol of the imminium iodide, 3.55 mmol of the halophthalide, and 5 mmol of the Zn(Cu) couple. The product of the first work-up, 0.616 g (56%), was subjected to flash chromatography (column diameter 25 mm, eluting with ethyl acetate – acetone, then acetone) to yield 0.240 g (22%) of (±)-adlumidine as a yellow foam which was crystallized from chloroform–methanol to yield colorless crystals melting at 200–203°C (lit. (35) mp 205°C), identical with authentic adlumidine by nmr, ir, and tlc. A second fraction contained 0.134 g (12%) of (±)-bicuculline as a white foam which was crystallized from chloroform–methanol to give colorless crystals melting at 217–220°C (lit. (36) mp 215°C) identical with authentic bicuculline by nmr, ir, and tlc.

The product of the second work-up (0.06 g, 5%) was discarded.

[5]The melting point was consistently higher than values reported in the literature whereas the spectroscopic data were in accord with reported values (8, 13). We conclude therefore that (±)-*threo*-isocordrastine must be dimorphic.

[6]In this and in subsequent cases comparisons were made with samples of the natural alkaloids. All spectra were recorded in solution.

Acknowledgements

We thank the Natural Sciences and Engineering Research Council of Canada for financial support of this work. One of us, J.-P. Ruder, wishes to express his gratitude to the Swiss National Science Foundation for financial assistance. We are indebted to Dr. B. C. Nalliah, formerly of this laboratory, for suggesting the method used in the preparation of homopiperonylformamide.

1. W. H. Perkin, Jr. and R. Robinson. J. Chem. Soc. **99**, 775 (1911).
2. R. D. Haworth and A. R. Pinder. J. Chem. Soc. 1776 (1950).
3. R. Bognar and P. Kerekes. Biochem. Physiol. Alkaloide. 4th Int. Symp. 1969 (Publ. 1972). p. 307; Chem Abstr. **77**, 140368r (1972).
4. P. Kerekes and R. Bognar. J. Prakt. Chem. 313, 923 (1971); Chem Abstr. **76**, 113410w (1972).
5. P. Kerekes and R. Bognar. Magy. Kem. Foly. **77**, 655 (1971); Chem Abstr. **76**, 141100p (1972).
6. W. Kloetzer, S. Teitel, J. Blount, and A. Brossi. Monatsh. Chem. **103**, 435 (1972).
7. V. Smula, N. E. Cundasawmy, H. L. Holland, and D. B. MacLean. Can. J. Chem. **51**, 3287 (1973).
8. M. Shamma and V. St. Georgiev. Tetrahedron Lett. 2339 (1974).
9. T. Kametani, T. Honda, H. Inoue, and K. Fukumoto. Heterocycles, **3**, 1091 (1975).
10. J. L. Moniot and M. Shamma. J. Am. Chem. Soc. **98**, 6714 (1976).

11. M. SHAMMA and V. ST. GEORGIEV. Tetrahedron, **32**, 211 (1976).
12. B. C. NALLIAH, D. B. MACLEAN, R. G. A. RODRIGO, and R. H. F. MANSKE. Can. J. Chem. **55**, 922 (1977).
13. T. KAMETANI, T. OHSAWA, S. HIRATA, M. S. PREMILA, M. IHARA, and K. FUKUMOTO. Chem. Pharm. Bull. **25**, 321 (1977).
14. M. SHAMMA, D. M. HINDENLANG, T.-T. WU, and J. L. MONIOT. Tetrahedron Lett. 4285 (1977).
15. T. KAMETANI. Chem. Abstr. **88**, 22661k (1978).
16. P. KEREKES, G. HORVATH, G. GAAL, and R. BOGNAR. Acta Chim. Acad. Sci. Hung. **97**, 353 (1978); Chem Abstr. **90**, 39085q (1979).
17. B. C. NALLIAH, D. B. MACLEAN, H. L. HOLLAND, and R. RODRIGO. Can. J. Chem. **57**, 1545 (1979).
18. S. O. DE SILVA, I. AHMAD, and V. SNIECKUS. Can. J. Chem. **57**, 1598 (1979).
19. T. SHONO, Y. USUI, and H. HAMAGUCHI. Tetrahedron Lett. 1351 (1980).
20. B. MOONEY, T. V. HUNG, R. H. PRAGER, J. M. TIPPETT, and A. D. WARD. 12th Int. Symp. Chem. Nat. Prod., Puerto de la Cruz, Tenerife, Spain, 1980; Symp. Abstr. 56 (1980).
21. I. GRANELLI and K. LEANDER. Acta Chem. Scand. **24**, 1108 (1970).
22. C. E. JOHNSON, JR. and F. A. BOVEY. J. Chem. Phys. **29**, 1012 (1958).
23. W. C. STILL, M. KAHN, and A. MITRA. J. Org. Chem. **43**, 2923 (1978).
24. C. R. HAUSER and D. S. BRESLOW. Org. Synth. Coll. Vol. III, 408 (1955).
25. G. A. EDWARDS, W. H. PERKIN, JR., and F. W. STOYLE. J. Chem. Soc. **127**, 195 (1925).
26. J. W. WILSON, C. L. ZIRKLE, E. L. ANDERSON, J. J. STEHLE, and G. E. ULLYOT. J. Org. Chem. **16**, 792 (1951).
27. W. M. WHALEY and M. MEADOW. J. Chem. Soc. 1067 (1953).
28. F. E. ZIEGLER and K. W. FOWLER. J. Org. Chem. **41**, 1564 (1976).
29. S. O. DE SILVA, M. WATANABE, and V. SNIECKUS. J. Org. Chem. **44**, 4802 (1979).
30. W. H. PERKIN, JR. and R. ROBINSON. J. Chem. Soc. **91**, 1073 (1907).
31. E. SPATH and N. POLGAR. Monatsh. Chem. **51**, 190 (1929).
32. S. ISHIWATA and T. NOZAKI. J. Pharm. Soc. Jpn. **71**, 1257 (1951).
33. E. HOPE, F. L. PYMAN, F. G. REMFRY, and R. ROBINSON. J. Chem. Soc. 236 (1931).
34. R. D. HAWORTH, A. R. PINDER, and R. ROBINSON. Nature, **165**, 529 (1950).
35. R. H. F. MANSKE and H. L. HOLMES. The alkaloids Vol. IV. Academic Press Inc., New York. 1954. p. 188.
36. P. W. G. GROENEWOUD and R. ROBINSON. J. Chem. Soc. 199 (1936).

Can. J. Chem. Downloaded from www.nrcresearchpress.com by 210.87.254.40 on 09/06/12
For personal use only.

Merostabilization in radical ions, triplets, and biradicals. 6. The excited state behaviour of *para*-substituted tetraphenylethylenes

WILLIAM J. LEIGH AND DONALD R. ARNOLD[1]

Department of Chemistry, Dalhousie University, Halifax, N.S., Canada B3H 4J3

Received April 3, 1981

This paper is dedicated to Prof. G. Hammond on the occasion of his 60th birthday

WILLIAM J. LEIGH and DONALD R. ARNOLD. Can. J. Chem. **59**, 3061 (1981).

The half-wave oxidation and reduction potentials, measured by cyclic voltammetry, of tetraphenylethylene and a series of *para*-substituted (cyano, methyl, and methoxy) derivatives are found to correlate with σ^+ and σ^- values respectively. The deviations from these correlations that are observed for one of the derivatives (unsymmetrically substituted) are attributed to merostabilization.

The nature of the first excited singlet state of these compounds is investigated by spectroscopic and photochemical means. Quantum yields for the direct *cis–trans* photoisomerization demonstrate that this provides the dominant pathway for decay of the singlet state. The π,π^* triplet energies are estimated from a qualitative investigation of the relative efficiencies of triplet-sensitized *cis–trans* isomerization as a function of sensitizer triplet energy.

WILLIAM J. LEIGH et DONALD R. ARNOLD. Can. J. Chem. **59**, 3061 (1981).

On a trouvé que les potentiels d'oxydation et de réduction à demi-onde, mesurés par voltométrie cyclique, du tétraphénylethylène et d'une série de dérivés (cyano, méthyle et méthoxy) substitués en position *para*, sont respectivement en accord avec les valeurs σ^+ et de σ^-. On attribue à la mérostabilisation les écarts observés par rapport à ces corrélations dans le cas des dérivés dissymétriquement substitués.

On a étudié la nature du premier état singulet excité de ces composés par la photochimie et la spectroscopie. Les rendements quantiques de la photoisomérisation directe *cis–trans* démontrent le mécanisme principal de la désintégration de l'état singulet. On a évalué les énergies du triplet π,π^* à partir d'une recherche qualitative sur l'efficacité relative de l'isomérisation *cis–trans* sensibilisée par un triplet en fonction de l'énergie du triplet sensibilisateur.

[Traduit par le journal]

Introduction

We have recently reported the synthesis, separation, characterization, and kinetics of the thermal *cis–trans* isomerization of a series of uniquely substituted tetraphenylethylenes (**1***a–d*) (1). These results were significant in many respects. The variation in the rates and energetics of thermal isomerization of the three disubstituted derivatives (**1***a–c*) is consistent with the transition state having distinct biradical character; the rates of isomerization in benzene solution correlate with a series of parameters $\sigma^\cdot$, which reflect the effect of the substituents on benzylic radical stabilities (2). While it is commonly accepted that the transition state for thermal isomerization of symmetrically substituted (1,2- across the double bond) olefins is 1,2- biradical-like in nature (3, 4), this study provides experimental evidence of the validity of this idea.

The rate of isomerization of **1***d* was found to be significantly faster than what would be expected based on the normal radical-stabilizing effects of the substituents (i.e. their $\sigma^\cdot$ values). This was attributed to increased stability of the biradical-like transition state due to merostabilization (5, 6). The effect of merostabilization was also evident in the Arrhenius activation energies for the isomerization of **1***a–d*. While the activation energies for thermal isomerization of **1***a–c* were identical (35.3 kcal mol^{-1}) within experimental error, that of **1***d* was found to be about 2 kcal mol^{-1} lower. This value provides an assessment of the contribution from merostabilization to the ground state rotational barrier in the cyano, methoxy substituted tetraphenylethylene derivative **1***d*.

Further support for the biradical nature of the transition state was provided by the agreement between these experimental values and an empirical calculation of the rotational barrier using radical stability arguments. The resonance stabilization energy of the radicals was estimated from esr spin density data (7). The rotational barrier of tetraphenylethylene, for example, was calculated by simply subtracting twice the difference between the resonance stabilization energies of the benzyl and diphenylmethyl radicals from the activation energy for thermal isomerization of *cis*-stilbene. This calculated rotational barrier agreed quite closely with the value (35.5 kcal mol^{-1}) estimated by extrapolation from the activation energies found for **1***a–c*. Good agreement was also found in similar comparisons of calculated and experimental rotat-

[1]Author to whom correspondence may be addressed.

0008-4042/81/213061-15$01.00/0

©1981 National Research Council of Canada/Conseil national de recherches du Canada

Can. J. Chem. Downloaded from www.nrcresearchpress.com by 210.87.254.105 on 09/06/12
For personal use only.

Can. J. Chem. Downloaded from www.nrcresearchpress.com by 210.87.254.105 on 09/06/12
For personal use only.

ional barriers in the related compounds 9,9′-bisfluorenylidene and bixanthylidene.

We were also interested in characterizing the first excited states (singlet and triplet) of this series. In contrast to the stilbenes, which have been well characterized (8), very little work has been done by way of mapping out the excited state behaviour of tetraphenylethylene, in spite of considerable interest in the thermo- and photochromic properties of related, heavily arylated olefin systems (9). Previous investigations of the first excited singlet state of tetraphenylethylene have focussed on the minor pathways for decay of the excited state, i.e. fluorescence emission (10) and electrocyclic ring closure (11). Substitution as in **1***a–d* enables an investigation of the direct *cis–trans* photoisomerization process, which is believed to be the dominant pathway for decay of the first excited singlet state of tetraphenylethylene (11). The π,π^* triplet state has been neglected, with the exception of one early experimental estimate of its energy (12).

In this paper, we describe our initial attempts to characterize the first excited (singlet and triplet) states of tetraphenylethylene and the *para*-substituted derivatives **1***a–f*. The nature of the singlet state is characterized by absorption and fluorescence emission spectroscopy and determinations of the photostationary states and quantum yields for *cis–trans* isomerization. The half-wave oxidation and reduction potentials of this series provide further information about the HOMO and LUMO in this system, as well as providing further examples illustrating the effect of merostabilization on the stabilities of radical-like species, i.e., the radical ions. A preliminary examination of the nature of the π,π^* triplet state of tetraphenylethylene is also described. These results are used in conjunction with our previous report (1) to characterize the nature of the ground and the excited state surfaces of tetraphenylethylene.

Results and Discussion

Half-wave Oxidation and Reduction Potentials

The electrochemical behaviour of tetraphenylethylene (TPE) has been reasonably well studied with respect to both its oxidation (13) and reduction (14) processes. The oxidative cyclic voltammogram of TPE in acetonitrile solution exhibits two closely-spaced separate anodic waves, each corresponding to irreversible one-electron transfer. A cathodic wave associated with the first anodic wave is evident at high scan rates (13). The reduction of TPE has been investigated by cyclic voltammetry in dimethylformamide solution (16). The single "reversible" wave that was observed was interpreted as being due to two reversible one-electron transfers at potentials separated by less than 0.1 V. A similar rationale has been extended to account for the reversible oxidative cyclic voltammetric behaviour of tetraanisylethylene (**1***e*) in acetonitrile (15). The radical cations of TPE (16) and **1***e* (17) and the radical anion of TPE (18) have been observed by esr spectroscopy.

In this study, the half-wave oxidation and reduction potentials of TPE and the substituted derivatives **1***a–f* were measured in acetonitrile solution using a platinum working electrode and a Ag/0.1 *M* $AgNO_3$ reference electrode. The cyclic voltammetric behaviour of these compounds varied within the series.

Since we are interested primarily in the variation in stability of the radical cation and anion with substituent, we will confine our attention to the first oxidative and reductive waves in the cyclic voltammograms of the series (**1***a–f*). For those derivatives which exhibited reversible electrolytic behaviour, redox potentials were calculated as the midpoints of the forward and reverse waves and are thermodynamically significant (19). Redox potentials of those derivatives exhibiting irreversible behaviour were estimated as 0.03 V less than the peak position of the voltammogram using a 0.1 V s^{-1} sweep rate. Although redox potentials calculated in this way have no strict thermodynamic significance (19), it has been shown that they can, in fact, provide reasonable estimates of the thermodynamic redox potentials and are therefore useful for comparison within a closely related series (20). The voltammetric behaviour and oxidation–reduction potentials of TPE and **1***a–f* are summarized in Table 1.

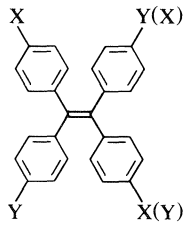

1

a X = H, Y = CH_3
b X = H, Y = OCH_3
c X = H, Y = CN
d X = OCH_3, Y = CN
e X = Y = OCH_3
f X = Y = CN

The radical cation of tetraphenylethylene can be represented by the parent valence bond structure **2**. The substituent effect on the stability of this species is naively expected to be roughly the composite of a polar effect on the stability of the diphenylmethyl cation and a radical-stabilizing effect on the stability of the diphenylmethyl radical. Since, as is well known, the stability of an ion is much more profoundly affected by substituents

Can. J. Chem. Downloaded from www.nrcresearchpress.com by 210.87.254.105 on 09/06/12
For personal use only.

TABLE 1. The half-wave oxidation and reduction potentials of tetraphenylethylene (TPE) and 1*a*–*f* in acetonitrile solution[a,b]

1	X	Y	Ox.	$E_{\frac{1}{2}}^{ox}$ (ev)[c]	Red.	$-E_{\frac{1}{2}}^{red}$ (ev)[c]
TPE	H	H	irrev.	1.02	irrev.	2.49
a	H	CH_3	irrev.	0.93	irrev.	2.56
b	H	OCH_3	rev.	0.69	irrev.	2.63
c	H	CN	irrev.	1.24	rev.	1.95
d	CN	OCH_3	rev.	0.84	rev.	2.00
e	OCH_3	OCH_3	rev.	0.52	—	—
f	CN	CN	irrev.	1.56	rev.	1.55

[a] 27°C vs. Ag/0.1 *M* $AgNO_3$/0.1 *M* TEAP.
[b] The voltammogrammes of the *cis* and *trans* isomers of 1*d* were identical; mixtures of isomers of 1*a*–*c* were used.
[c] For reversible processes $E_{\frac{1}{2}} = (E_p^f - E_p^r)/2$; error = ±0.05 (abs), ±0.01 (rel). For irreversible processes, $E_{\frac{1}{2}} = E_p^f - 0.03$; error = ±0.10 V.

than the stability of the corresponding radical (21, 22), polar factors are expected to dominate the observed substituent effect on radical cation stability.

We can similarly represent the radical anion of tetraphenylethylene by the parent valence bond structures **3**. The substituent effect in this case is expected to be dominated by a polar effect on the stability of the diphenylmethyl anion.

We have plotted the half-wave oxidation and reduction potentials of TPE and 1*a*–*f* versus $\Sigma\sigma^+$ and $\Sigma\sigma^-$, respectively, in Figs. 1 and 2. The reasonable correlations observed in both cases illustrate the additive nature of the effect of substituents on the stabilities of **2** and **3**, and as expected,

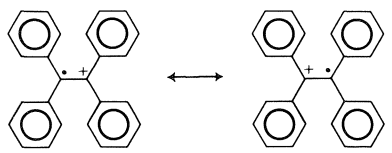

2

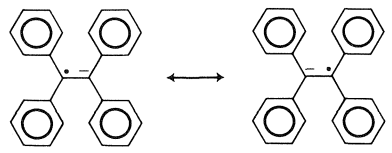

3

polar factors are seen to dominate in both cases. The points for 1*d* in Figs. 1 and 2 deviate significantly from the best lines drawn for the other derivatives, $E_{\frac{1}{2}}^{ox}$ and $E_{\frac{1}{2}}^{red}$, both being lower than what would be expected based on the normal effects of the substituents on the stabilities of the radical cation and the radical anion as defined by σ^+ and σ^- values. It is tempting to attribute these deviations of 0.1–0.15 eV (2–3 kcal mol^{-1}) from normal behaviour to merostabilization of the radical-like species. Our interpretation, however, is tempered by the known effect of substituents on the rate of solvolysis of

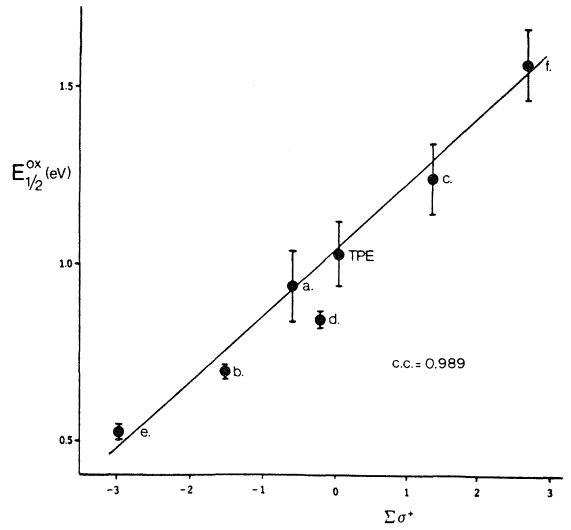

FIG. 1. Hammett correlation: $E_{\frac{1}{2}}^{ox}$ vs. σ^+ for substituted tetraphenylethylenes. The correlation coefficient was derived excluding point 1*d*.

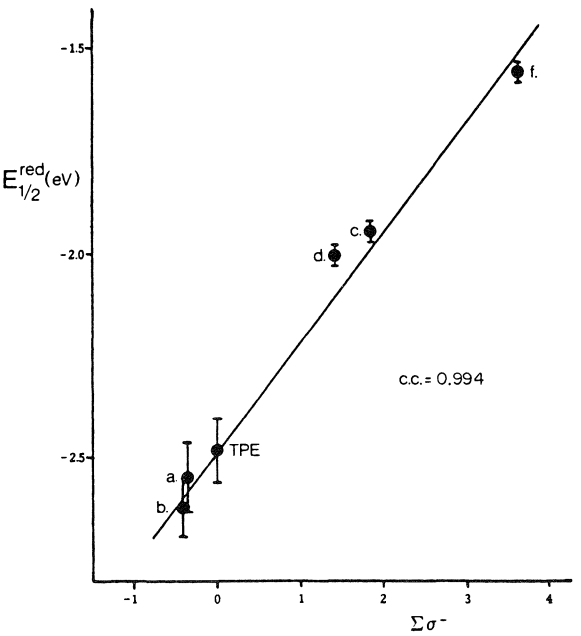

FIG. 2. Hammett correlation: $E_{\frac{1}{2}}^{red}$ vs. σ^- for substituted tetraphenylethylenes. The correlation coefficient was derived excluding point 1*d*.

diphenylmethyl chloride (23). The effects of substituents on the stability of the diphenylmethyl cation are *not* strictly additive; a plot of relative rate of solvolysis versus $\Sigma\sigma^+$ for a variety of substituents gives a series of lines, each characteristic of a given electron-donating group (23). It is clear that the solvolysis of those diphenylmethyl

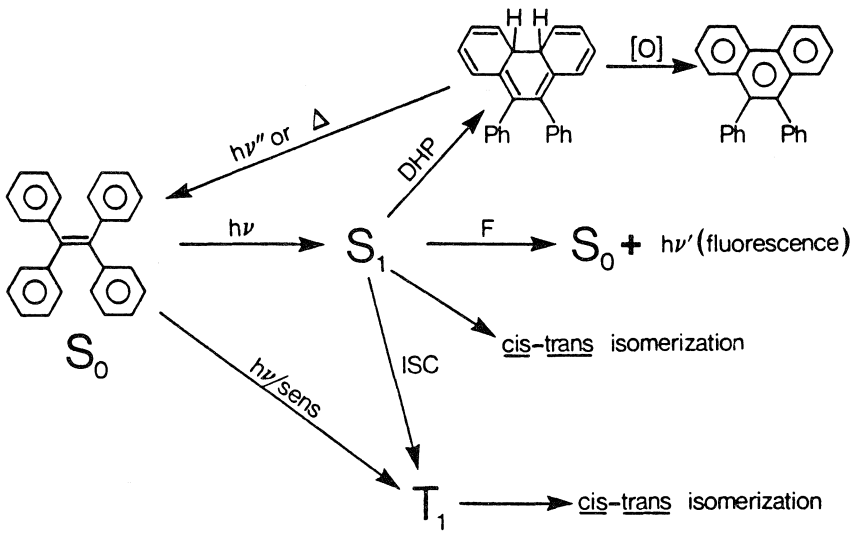

FIG. 3. Summary of the decay processes available to the excited states of tetraphenylethylene.

chlorides substituted in the *para*- and *para'*-position with electron donating and electron withdrawing groups (e.g., *para*-methoxy-*para'*-nitrobenzhydrylchloride) proceed with an anomalously fast rate. Since the substituent effects on the stabilities of the radical cation and anion of TPE are clearly dominated by polar factors, it may be that the anomalous behaviour of **1***d* is the result of some factor other than merostabilization, analogous to the situation with the diphenylmethyl cation.

The Excited Singlet State; Spectroscopic Singlet Energies

The behaviour of the stilbenes upon direct irradiation has been investigated thoroughly (8), and the character of the excited states in this system is well understood. The excited state behaviour of *cis*-stilbene is considerably different from that of the *trans* isomer, and it is widely accepted that this difference is primarily the result of steric factors. It is reasonable to expect that the excited state behaviour of tetraphenylethylene will parallel that of *cis*-stilbene in many respects. The various processes by which the excited states of these olefins can decay are shown in Fig. 3.

The ultraviolet absorption spectra of tetraphenylethylene (Fig. 4) and the stilbenes have been discussed in some detail by Suzuki (24). According to his nomenclature, the three absorption bands in these spectra are designated the A, B, and C bands in order of decreasing wavelength. The A-band, or the so-called conjugation band, corresponds to the transition to the first excited singlet state in these molecules. The absorption spectrum of TPE shows marked similarities to that of *cis*-stilbene, and it has

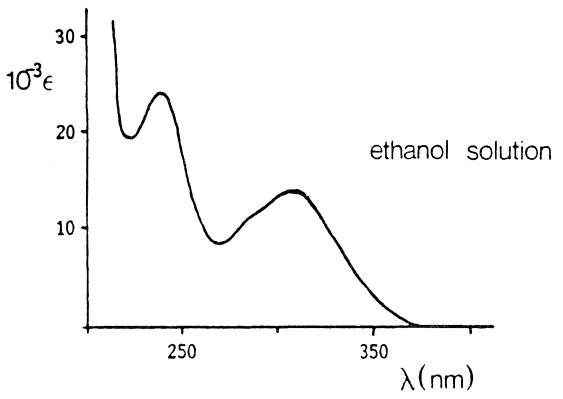

FIG. 4. The ultraviolet absorption spectrum of tetraphenylethylene.

been concluded that the preferred conformation is one in which all the phenyl groups are rotated out of the plane of the ethylenic bond (24). This is in agreement with X-ray crystallographic data (25),[2] and accounts for the relative intensities of the A- and B-bands in the spectrum.

In Fig. 5 are shown the ultraviolet (uv) absorption spectra of the *para*,*para'*-disubstituted derivatives **1***a*–*c*. Substitution by methyl or methoxy groups in the *para*-positions has little effect on the general appearance of the spectrum (Fig. 5a, b). These substituents do shift the positions of the A- and B-bands to slightly longer wavelengths, the shift being greatest for methoxy substitution. There are no significant differences between the spectra of the *cis* and *trans* isomers of either **1***a* or **1***b*.

[2]T. S. Cameron, unpublished results.

Can. J. Chem. Downloaded from www.nrcresearchpress.com by 210.87.254.105 on 09/06/12
For personal use only.

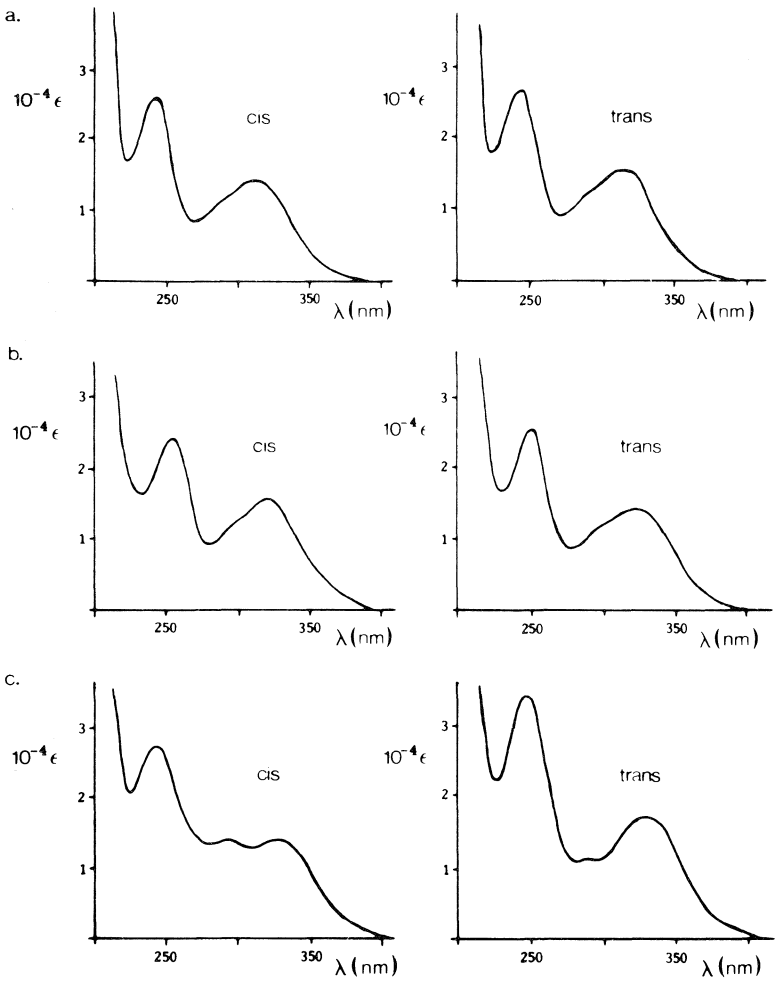

FIG. 5. Ultraviolet absorption spectra (ethanol solution) of disubstituted tetraphenylethylene derivatives 1*a*(a), 1*b*(b), and 1*c*(c).

Furthermore, the spectra of *cis*- and *trans*-1*b* are closely similar to that of tetraanisylethylene (1*e*, Fig. 6b), except the positions of the absorption bands in the latter are shifted to slightly longer wavelengths.

Interesting differences become evident in the spectra of the isomeric dicyano-derivatives 1*c* (Fig. 5c); a new absorption band, positioned between the A- and B-bands, appears. This band may correspond to the shoulder on the short wavelength side of the A-bands in the spectra of 1*a*, *b*, *e*, and TPE, in which case its position would appear to be insensitive to substitution. Its appearance in the spectra of 1*c* as a distinct absorption band is a result of the fact that the A-band has been shifted considerably from its position in the spectra of the other derivatives. There are now distinct differences between the spectra of *cis*- and *trans*-1*c*, in that the intensities of the A- and B-bands in *trans*-1*c* are significantly greater than those for *cis*-1*c*. The opposite effect is noted for the intermediate band. The spectrum of *cis*-1*c* is very similar to that of 1*f* (Fig. 6c), both in the positions and relative intensities of the bands.

The uv absorption spectra of the tetrasubstituted tetraphenylethylene derivatives 1*d*–*f* are shown in Fig. 6. The A-bands in the spectra of *cis*- and *trans*-1*d* (Fig. 6a) are identical in position and intensity, but are shifted to considerably longer wavelengths than in the other derivatives. The big difference between the two isomers appears in the short wavelength region of the spectra. There is very little fine structure in the spectrum of *trans*-1*d*, and the B-band has shifted to considerably longer wavelengths from its position in the spectrum of *trans*-1*c*. This band appears to be masking the intermediate band which was noted in the spectra of *cis*- and *trans*-1*c*. In *cis*-1*d*, the B-band is similar

Can. J. Chem. Downloaded from www.nrcresearchpress.com by 210.87.254.105 on 09/06/12
For personal use only.

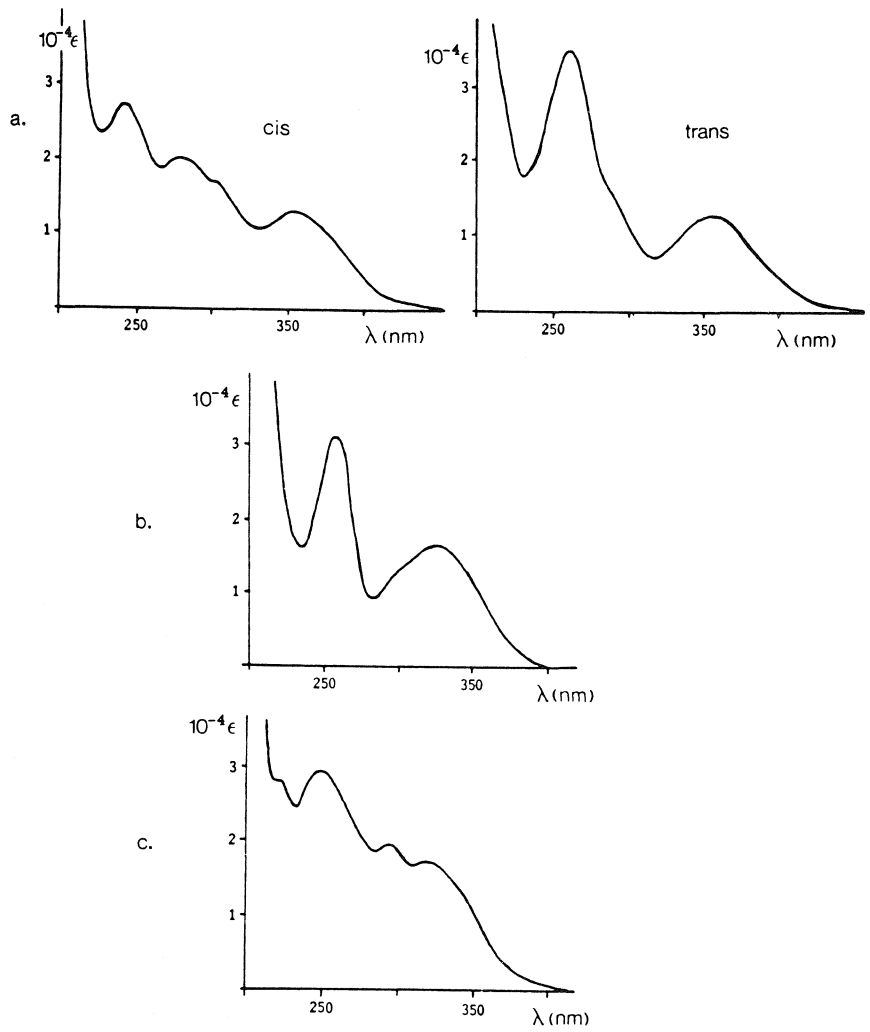

FIG. 6. Ultraviolet absorption spectra (ethanol solution) of tetrasubstituted tetraphenylethylene derivatives 1*d*(a), 1*e*(b), and 1*f*(c).

in both position and intensity to that in the spectrum of *cis*-1*c*. There are now two bands situated at intermediate wavelengths, one of which presumably corresponds to the band observed in the spectra of *cis*- and *trans*-1*c*. The effect of substituents on the absorption spectrum of TPE provides evidence for the existence of two closely spaced transitions within the long wavelength A-band. A similar conclusion has been reached for *trans*-stilbene on the basis of absorption and fluorescence emission studies with a series of substituted derivatives (26).

The use of benzene as a solvent is known to have a remarkable effect on the absorption spectra of stilbene derivatives, causing the A-band to shift to longer wavelengths and blurring its vibrational fine structure in the case of *trans*-stilbene (24). This has been attributed to an interaction between the π-orbitals of the olefin and those of the solvent. The magnitude of the shift appears to be related to the preferred conformation of the molecule, being considerably smaller for nonplanar derivatives such as *cis*-stilbene and TPE than for planar ones (24). This solvent shift amounts to about +3 nm for TPE. The A-bands in the spectra of 1*a–f* in benzene are shifted to a similar extent relative to the spectra in ethanol.

The fluorescence emission spectrum of *cis*-1*d* was measured in alcohol solution at room temperature, and this is shown in Fig. 7, along with the fluorescence excitation spectrum. The appearance of the excitation spectrum does not match that of the absorption spectrum in the short wavelength

Can. J. Chem. Downloaded from www.nrcresearchpress.com by 210.87.254.105 on 09/06/12
For personal use only.

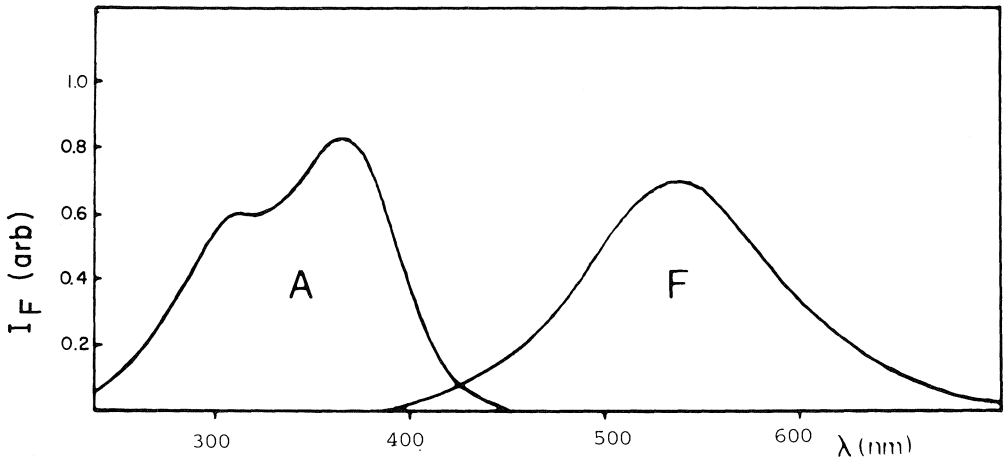

FIG. 7. Fluorescence emission (F) and excitation (A) spectra of *cis*-**1***d* (alcohol, 25°C; uncorrected).

region due primarily to the spectral distribution of the excitation source. The large Stokes shift ($\bar{\nu}_{max}^{ex.} - \bar{\nu}_{max}^{F} \sim 9000\,cm^{-1}$) is similar to that observed for TPE itself (10*a*), and indicates a substantial difference in the preferred geometries of S_0 and S_1. From these spectra, the position of the 0–0 band is estimated to be 425 ± 5 nm. Noting that the extinction coefficient (ε) at 425 nm in the absorption spectrum of *cis*-**1***d* is ca. 100, we estimate the positions of the 0–0 band in the other derivatives as the wavelength at which ε ~ 100. This data is collected in Table 2. The energies listed in Table 2 are believed to correspond to the energies of the vertical (Franck–Condon) transitions between the stable ground state, slightly nonplanar S_0 and the corresponding S_1, (i.e. ${}^0t \rightarrow {}^1t$, ${}^0c \rightarrow {}^1c$) (8).

Included in Table 2 for comparison are the π- and π*-orbital energy differences calculated from the half-wave oxidation and reduction potentials of these compounds. Singlet excitation energies are related to the redox potentials by eq. [1] (27), where J_{12} is the Coulomb repulsion integral and K_{12} is the exchange integral. The term $(-J_{12} + 2K_{12})$ represents the difference between the energy of the lowest unoccupied molecular orbital when it is occupied by an electron after excitation and when it is empty in the closed shell (i.e. ground state) configuration. The close agreement between the spectroscopic singlet energies and $(E_{\frac{1}{2}}^{ox} - E_{\frac{1}{2}}^{red})$ for this series indicates that this term is very small. A similar result was obtained by Loutfy and Loutfy (27*b*) for an extensive series of polynuclear aromatic hydrocarbons.

TABLE 2. Estimated energies of the spectroscopic π,π* singlet states for TPE and **1***a*–*f*[a]

1		λ_{max} (nm)[b]	λ_{0-0} (nm)[c]	E_{S_1}[d,e]	$E_{\frac{1}{2}}^{ox} - E_{\frac{1}{2}}^{red}$[d,f]
TPE		306	366	79	81±4
a	*cis*	312	372	77	80±4
	trans	312	372		
b	*cis*	318	384	75	76±3
	trans	318	384		
c	*cis*	326	392	73	74±3
	trans	329	391		
d	*cis*	353	425	68	65±2
	trans	354	425		
e		324	390	73	—
f		319	391	73	72±3

[a] In 95% ethanol; 25°C.
[b] λ_{max} of the A-band in the absorption spectrum.
[c] Wavelength of absorption onset (ε ~ 100) from the absorption spectrum; error = ±4 nm.
[d] In kcal mol^{-1}.
[e] Calculated from λ_{0-0}; error ~ ±2 kcal mol^{-1}.
[f] From the data in Table 1.

[1] $E_s = E_{\frac{1}{2}}^{ox} - E_{\frac{1}{2}}^{red} - J_{12} + 2K_{12}$

Fluorescence Emission

Trans-stilbene fluoresces at room temperature (φ ~ 0.05) (8), and this competes with *cis–trans* isomerization. The fluorescence quantum yield increases considerably in viscous media and at low temperatures. This is known to be due both to hindrance to rotation by the rigidity of the medium and to the presence of a small activation barrier (~ 3 kcal mol^{-1}) for twisting to the ${}^1p$ conformer, from which *cis–trans* isomerization occurs.

Cis-stilbene, on the other hand, is nonfluorescent at room temperature owing to rapid (unactivated) rotation to the ${}^1p$ conformer. Electrocyclic ring closure to dihydrophenanthrene also occurs (ϕ_{DHP} ~ 0.1). In rigid media, *cis*-stilbene fluoresces efficiently due to an inhibition of bond rotation. The fluorescence exhibits a large Stokes shift ($\bar{\nu}_{max}^{ex} - \bar{\nu}_{max}^{F} \sim 12\,000\,cm^{-1}$), which implies that the geometry of the fluorescent state is much different from the preferred ground state geometry.

The situation is a bit different for the case of

Can. J. Chem. Downloaded from www.nrcresearchpress.com by 210.87.254.105 on 09/06/12
For personal use only.

Can. J. Chem. Downloaded from www.nrcresearchpress.com by 210.87.254.105 on 09/06/12
For personal use only.

tetraphenylethylene, although many parallels with *cis*-stilbene can be drawn. Tetraphenylethylene is visibly fluorescent at room temperature, though this process is not very efficient ($\phi_F < 0.01$) (10) and the Stokes shift is only about 9000 cm^{-1} (10*a*). The fluorescence is shifted to shorter wavelengths (10*a*) and ϕ_F increases considerably in more viscous solvents (10*b*). From studies of the fluorescence quantum yield as a function of temperature and solvent viscosity, it has been concluded that bond rotation in S_1 is an unactivated process (10*b*). Dihydrophenanthrene formation ($\phi_{DHP} = 0.022$) competes with fluorescence at room temperature (11), and by analogy with *cis*-stilbene, this is expected to be subject to a modest activation barrier. It has furthermore been suggested that *cis–trans* isomerization is the most efficient decay process in fluid media (11).

The dependence of $\bar{\nu}_{max}{}^F$ and ϕ_F on solvent viscosity has led to the suggestion that the geometry of the luminescent species is different in viscous and nonviscous media (10*a*). According to the "classical" explanation, bond rotation can occur within the lifetime of S_1 in solvents of low viscosity, and emission therefore occurs from the favoured (lowest energy) twisted conformation. On the other hand, bond rotation is hindered considerably in viscous solvents, so that fluorescence occurs mainly from conformations close to those originally populated during excitation, and with considerably higher efficiency. This explanation is apparently supported by the observation that the fluorescence spectrum of tetraphenylethylene in highly viscous solvents is strongly dependent on the excitation wavelength (10*c*). Also, in solvents of intermediate viscosities (where the time required for double bond rotation is presumably of the same order of magnitude as the fluorescence) the fluorescence lifetime is longer in the lower energy end of the emission spectrum (10*d*).

Two recent studies, utilizing picosecond absorption (28) and fluorescence emission (29) spectroscopy, point to a different explanation for these results. Rentzepis and co-workers argue that the viscosity dependent spectral shift of the fluorescence is a result of rotation of the phenyl rings in tetraphenylethylene, and *not* to rotation about the carbon–carbon double bond in S_1. They do, however, favor the classical explanation for the dependence of the fluorescence quantum yield and total lifetime on solvent viscosity (29). Greene has observed two transient absorptions after picosecond excitation of tetraphenylethylene in solution at room temperature (28). The long wavelength absorption ($\lambda_{max} = 640$ nm) is characterized by a lifetime of 5 ps, and is attributed to absorption by a nearly planar S_1 geometry, which decays as rotation about the double bond proceeds. The lifetime of this absorption corresponds rather closely with the fluorescence lifetime of TPE in solution at room temperature (6 ps (29)). The short wavelength absorption ($\lambda_{max} = 417$ nm) decays with a lifetime of 3 ns, and is attributed to absorption from a long-lived twisted geometry. These results seem to indicate that the twisted singlet (^1p) of TPE, although a factor of ca. 500 longer-lived than the planar singlet, is nonfluorescent.

We have attempted to measure fluorescence quantum yields for **1***c*, *d* (*cis* and *trans*), **1***e*, and **1***f* in benzene solution at room temperature. The emission spectra were measured under standard conditions with solutions whose concentrations were adjusted so that their optical densities matched at the excitation wavelength (370 nm). The relative fluorescence quantum yields (measured by determining the areas beneath the emission spectra) varied by less than a factor of two within the series: **1***e* > **1***f* > **1***c* > **1***d*. The *cis* and *trans* isomers of both **1***c* and **1***d* fluoresce with equal efficiencies. On an absolute scale, $\phi_F \sim 0.001$ for these compounds since 9,10-diphenylanthracene fluorescence[3] (measured under comparable conditions) was more than a factor of 10^3 more intense.

cis–trans *Isomerization*

Direct irradiation of *cis*- or *trans*-**1***a–d* in benzene solution (10°C) results in rapid *cis–trans* isomerization. The photostationary states obtained upon irradiation of the long wavelength absorption tail of these derivatives are collected in Table 3. In all cases, attainment of the photostationary state was ensured by approaching it from both directions. By analogy with the stilbenes (8), the photostationary states obtained upon direct irradiation will be given by eq. [2], where the partitioning constant, β, defines the fraction of twisted singlets that decay to the *trans* isomer (8). The major simplifying assumption made here is that isomerization proceeds from an excited singlet state and does not involve intersystem crossing to the triplet, prior to decay to the ground state. The validity of this assumption will be discussed later.

$$[2]\quad (t/c)_{pss} = \frac{\varepsilon_c}{\varepsilon_t} \cdot \frac{\phi_{c \to t}}{\phi_{t \to c}} = \frac{\varepsilon_c}{\varepsilon_t} \cdot \frac{(1 - \phi_F{}^c)}{(1 - \phi_F{}^t)} \times \frac{(1 - \phi_{DHP}{}^c)}{(1 - \phi_{DHP}{}^t)} \cdot \frac{\beta}{1 - \beta}$$

[3]Using the value of $\phi_F = 0.85$ for 9,10-diphenylanthracene in benzene (30).

TABLE 3. Photostationary states obtained by direct irradiation of **1***a*–*d*[a]

	1*a*	**1***b*	**1***c*	**1***d*
λ_{irr} (nm)	> 390	> 400	> 400	> 400
$(t/c)_{pss}$	1.20	1.28	1.35	8.33[b]
β[c]	0.55	0.56	0.57	0.89

[a] Degassed benzene solution; 10°C. Solutions were generally 10^{-3} *M*.
[b] The same photostationary state obtains with $\lambda_{irr} > 350$ nm.
[c] Calculated according to eq. [2] (see text).

TABLE 4. Quantum yields for the direct *cis*–*trans* photoisomerization of **1***b*–*d*[a]

Structure	$\phi_{c \rightarrow t}$	$\phi_{t \rightarrow c}$
1*b*[b]	0.56±0.02	0.42±0.02
1*c*[b]	0.54±0.02	0.40±0.02
1*d*[c]	0.24±0.02	0.03±0.01

[a] Benzene solution, 25°C.
[b] Average of two determinations.
[c] Average of three determinations.

Enough data are now available to further simplify eq. [2]. The A-bands in the absorption spectra of the isomeric pairs are virtually identical in each case and therefore $\varepsilon_c/\varepsilon_t \sim 1$. We have seen that ϕ_F for tetraphenylethylene is very small at room temperature (~ 0.001) (10), as is also the case for **1***c*. Furthermore, $\phi_F^c \sim \phi_F^t$ for **1***c*, *d*, and if we assume this to be the case as well for **1***a*, *b*, the term involving fluorescence quantum yields drops out of eq. [2]. Olsen and Buckles have shown that dihydrophenanthrene formation proceeds with a very low quantum yield (~ 0.02) for TPE and several substituted derivatives (11). This term in eq. [2] will therefore also be very close to unity, even if $\phi_{DHP}^c \neq \phi_{DHP}^t$. The photostationary states obtained upon direct irradiation of **1***a*–*d* can thus be almost totally accounted for by the partitioning ratio describing the decay of ^1p to the ground state:

$$[3] \quad (t/c)_{pss} = \frac{\phi_{c \rightarrow t}}{\phi_{t \rightarrow c}} \sim \frac{\beta}{1 - \beta}$$

The partitioning constants (β), calculated according to eq. [3], are collected in Table 3.

The value of β is essentially constant for **1***a*–*c* (0.55–0.57). The indication that ^1p decays to give almost equal amounts of *cis* and *trans* olefins is expected, since the geometry of ^1p should be approximately perpendicular and decay to the ground state should be vertically down (i.e. to the point on the S_0 surface corresponding to the transition state for thermal isomerization). The behaviour of **1***d* upon direct excitation is obviously very different from that of the other derivatives, since in this case the photostationary state consists of 90% of the *trans* isomer.

In order to test the validity of eq. [3], we have determined quantum yields for the direct photoisomerization of **1***b*–*d* in benzene solution at 25°C, with 370 nm excitation (31). These data, collected in Table 4, further illustrate the anomalous behaviour of **1***d* upon direct excitation. *cis*–*trans* Isomerization does indeed prove to be the major pathway for decay of the first excited singlet state of **1***b* and **1***c*. In these cases, the sum of the quantum yields for *cis* → *trans* and *trans* → *cis* interconversion are only slightly less than unity, and the photostationary state is hence described adequately by eq. [3]. On the other hand, *cis*–*trans* isomerization appears to account for less than one-third of the total light absorbed at 370 nm in the case of **1***d*. Hence, the assumptions leading to the simplification of eq. [2] are not justifiable in this case, and eq. [3] does not adequately describe the photostationary state. Obviously, some other nonradiational decay process is responsible for the reduced efficiency of *cis*–*trans* isomerization in this derivative.

Two possibilities are vibrational deactivation, taking place before complete twisting to ^1p can occur, and dihydrophenanthrene formation. These processes are expected to be of increased importance when rotation in S_1 is an activated process. Although it is believed that, in S_1, bond rotation in TPE itself is unactivated (11), we cannot rule out the possibility of an activation barrier for twisting in the first excited singlet state of **1***d*.

Theory predicts the first excited singlet state of olefins to have zwitterionic character (4). A zwitterionic configuration in tetraphenylethylene will be especially stabilized when the molecule bears *both* cyano and methoxy substituents, through the contribution of resonance structures such as those illustrated below in **1***d*′. This may also account for the significantly lower singlet energy observed for **1***d* than the other derivatives. The barrier to rotation in S_1 may then arise as a result of a stabilizing charge-transfer-like interaction across the rings, the barrier being higher, of course, for *trans* ^1p than *cis* ^1p rotation. This sort of interaction may also constrain the most stable conformation of ^1p to have an angle of twist less than 90° (i.e. transoid), which would result in an anomalously high value of β, the partitioning constant.

Although we have not determined the quantum yields for dihydrophenanthrene formation from *cis*- and *trans*-**1***d*, qualitative experiments indicate that they are relatively low. Thus, irradiation (370 nm) of oxygen-saturated benzene solutions of either *cis*- or *trans*-**1***d* (10^{-5} *M*) does not result in any detectable change of the uv absorption spectrum during the time required to achieve partial (ca.

Can. J. Chem. Downloaded from www.nrcresearchpress.com by 210.87.254.105 on 09/06/12
For personal use only.

TABLE 5. Sensitizers used for the triplet-sensitized isomerization of **1***a–d*

Sensitizer		E_T[a]	λ_{max}[b]	λ_c[b,c]	ϕ_{isc}	Ref.
3,3′-Carbonyl-*bis*(5,7-diethoxycoumarin)	(**4**)	56	395 (41 000)	435	0.99	34
3,3′-Carbonyl-*bis*(7-diethylaminocoumarin)	(**5**)	51	449 (88 000)	498	0.94	34
Benzanthrone	(**6**)	47	385 (11 000)	435	—	32
Phenazine	(**7**)	43.8	364 (13 000)	420	0.21	33*a* 35
Michler's thioketone	(**8**)	43.4	575 (550)	630	—	36
3,4-Benzopyrene	(**9**)	41.9	388 (33 000)	412	—	33*a*
9-Methylanthracene	(**10**)	40.6	390 (10 000)	403	0.67	33*a*

[a] In kcal mol^{-1}.
[b] From the absorption spectra in benzene; in nm. The figure in parentheses refers to the extinction coefficient at this wavelength.
[c] The cutoff wavelength is taken as the wavelength at which the extinction coefficient has fallen to ~ 100.

10%) *cis–trans* photoequilibration. Therefore, it does not appear that the decreased efficiency of *cis–trans* photoisomerization of **1***d* relative to the other derivatives can be attributed to dihydrophenanthrene formation. It must be stressed, however, that this interpretation is based on the assumptions that oxygen serves only to trap the initially formed dihydrophenanthrene and, furthermore, that it would do so with high efficiency.

The Triplet-sensitized cis–trans *Isomerization of* 1a–d

Since one of our primary interests in the investigation of the excited state behaviour of **1***a–d* was an examination of the effect of substituents (and merostabilization) on the π,π^* triplet energy of tetraphenylethylene, our initial efforts were directed toward spectroscopic determination of the triplet energy of **1***d*.

A low intensity $S_0 \rightarrow T$ absorption band could not be found in the absorption spectrum of a saturated solution of **1***d* in ethanol, even with cells of path-length as high as 15 cm. The use of a heavy atom solvent (ethyl iodide) was also fruitless. Phosphorescence emission could not be detected from **1***d* in either an ethanol/methanol or ethanol/ethyl iodide glass at 77 K. Sensitized phosphorescence was also undetectable upon irradiating a benzophenone glass containing ca. 10^{-4} *M* **1***d* at 77 K.

We therefore turned to indirect methods of determining the triplet energies of this series. The simplest method involves examination of the triplet-sensitized isomerization of the olefin using a series of sensitizers of varying triplet energy (32) and this is the approach we have used to estimate the triplet energies of **1***a–d*. It should be emphasized, however, that this method affords only a qualitative indication of an olefin's triplet energy.

A major problem in this study was that our choice of sensitizers was severely restricted by the fact that the absorption spectra of **1***a–d* (**1***d* in particular) tail out to quite long wavelengths. In order to ensure that the sensitizer absorbs at least 99% of the incident light, the relative concentrations of sensitizer/olefin would have to be as high as 200:1 for many of the common, well characterized triplet sensitizers in frequent use (33, 34). This presented analytical problems in most cases. Particular attention was therefore paid to choosing a series of sensitizers which each absorb at fairly long wavelengths. These are listed in Table 5, along with their triplet energies, absorption maxima, long wavelength cutoffs, and intersystem crossing efficiencies (where known).

We can use the well-defined stilbene system (8) to aid in the analysis of our results. We assume that the behaviour of the triplet states of **1***a–d* will correspond more closely to that of *cis*-stilbene than *trans*-stilbene. Thus, the twisted triplet (^3p) is expected to be lower in energy than both planar triplets (^3t and ^3c), and conversion of ^3t and ^3c to ^3p will be irreversible in both cases. Furthermore, nonvertical endothermic energy transfer is expected to occur for both isomers.

The photostationary states obtained upon triplet-sensitized isomerization will be given by eq. [4], by analogy with the stilbenes (8),

$$[4] \quad (t/c)_{pss} = \frac{k_{et}^c}{k_{et}^t} \frac{\alpha}{1-\alpha}$$

where the partitioning constant, α, represents the percentage of twisted triplets that decay to the *trans* isomer. With high energy sensitizers, energy

Can. J. Chem. Downloaded from www.nrcresearchpress.com by 210.87.254.105 on 09/06/12
For personal use only.

TABLE 6. Approximate times required to effect equilibrium in the photosensitized isomerization of **1***a–d*[a]

Sensitizer (Filter system[b])	E_T^{sens} (kcal mol^{-1})	Irradiation time (h)			
		1*a*[c]	**1***b*[d]	**1***c*[d]	**1***d*[d]
4 (A)	56.0	< 0.5	< 0.5	< 0.5	< 0.5
6 (A)	47.0	1	1	< 0.5	< 0.5[e]
7 (A)	43.8	1–2	1–2	1[e,f]	1[e,f]
8 (B)	43.4	> 8	> 8	> 8	< 0.5[g]
9 (C)	41.9	—	[h,i]	[h,i]	5[e,h]
10 (D)	40.6	—	—	—	[i,k]
$(t/c)_{pss,\ sens}$		1.10	1.07	1.06	1.14
$(t/c)_{pss,\ direct}$		1.21[j]	1.28[k]	1.35[k]	8.35[k,l]

[a] Degassed benzene solution (10°C); 1 kW medium pressure Hg lamp.
[b] Corning glass filters: A, CS 3-73; B, CS 3-69; C, CS 0-51/7-60; D, CS 3-75/7-60.
[c] Olefin/sensitizer concentrations = 0.15 *M*/0.01–0.05 *M*; analysed by ir.
[d] Olefin/sensitizer concentrations = 0.001 *M*/0.001 *M* unless otherwise noted; analysed by hplc.
[e] $(t/c)_{pss}$ was slightly higher than that listed due to partial direct irradiation.
[f] Olefin/sensitizer concentrations = 0.0005 *M*/0.001 *M*.
[g] $(t/c)_{pss}$ was identical to that obtained with **5** (E_T = 52 kcal mol^{-1}) under conditions where the sensitizer absorbs all the light.
[h] Olefin/sensitizer concentrations = 0.001 *M*/0.01 *M*.
[i] $(t/c)_{pss}$ was that observed in direct irradiations.
[j] Using Corning CS 3-74 glass filter.
[k] Filter system A.
[l] Filter system C.

transfer to both isomers should be diffusion-controlled, and the photostationary state (pss) ratio will be given by the decay ratio $\alpha/(1-\alpha)$.

Exploratory photolyses revealed that the $(t/c)_{pss}$ ratios for **1***a–d* are *invariant* as a function of

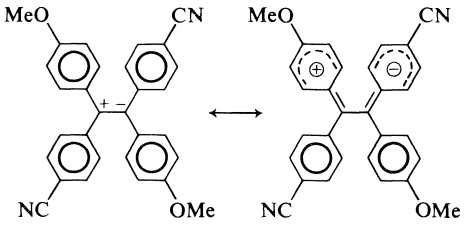

1*d′*

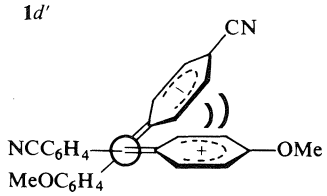

sensitizer triplet energy in every case. This implies that the rates of energy transfer to the *cis* and *trans* isomers are equal regardless of the sensitizer's triplet energy, and hence that the spectroscopic triplet energies of the *cis* and *trans* isomers are very nearly the same. The result of this observation is that a Saltiel plot ($(t/c)_{pss}$ vs. E_T^{sens}) will contain no fine structure, and hence yield no information regarding the olefins' triplet energies.

We therefore turned to a qualitative examination of the relative efficiencies of triplet-sensitized isomerization of **1***a–d* as a function of sensitizer triplet energy. This was done by simply comparing the times required to effect photoequilibrium for each olefin with a given sensitizer, and these results are collected in Table 6. While little significance can be attached to the variation in irradiation time for a particular olefin with the different sensitizers (i.e. proceeding down the columns in Table 6), the irradiation times required for each olefin to reach the photostationary state with a given sensitizer (i.e. proceeding across the rows in Table 6) do reflect the relative quenching efficiencies. Assuming that the quenching process responsible for isomerization is indeed triplet energy transfer, the data then provide estimates of the triplet energies of **1***a–d*. We assume that nonvertical excitation transfer should be observable by this method when triplet energy transfer is endothermic by ca. 5 kcal mol^{-1} or less; triplet (^3p) energies are then obtained by simply adding 5 kcal mol^{-1} to the triplet energy of the lowest energy sensitizer that effects isomerization.

Examining Table 6, we see that energy transfer is efficient in all cases with the high energy sensitizer (**4**, E_T = 56 kcal mol^{-1}), isomerization being complete in less than 0.5 h in all cases. A drop in the relative isomerization efficiencies of **1***a*, *b* becomes evident with **6** (E_T = 47 kcal mol^{-1}), and this becomes even more pronounced with **7** (E_T = 43.4 kcal mol^{-1}). Energy transfer from Michler's thioketone (**8**, E_T = 43.4 kcal mol^{-1}) to **1***a–c* is very inefficient compared to **1***d*, and we thus estimate the triplet (^3p) energies of **1***a–c* to be about 48 kcal mol^{-1}. This estimate is in excellent agreement with the value of 47 kcal mol^{-1} which was estimated for tetraphenylethylene (12). Energy transfer to **1***d*

Can. J. Chem. Downloaded from www.nrcresearchpress.com by 210.87.254.105 on 09/06/12
For personal use only.

appears to be inefficient with **9** (E_T = 41.9 kcal mol^{-1}), although we have nothing to compare it to. However, since the $(t/c)_{pss}$ ratio obtained in this case is intermediate between the high energy limit (1.14) and the direct irradiation value (8.35), we are reasonably certain that triplet energy transfer is indeed occurring.[4] Since triplet sensitized isomerization of **1***d* does not occur (detectably) with **10** (E_T = 40.6 kcal mol^{-1}) as sensitizer (the photostationary state was the same as that obtained upon direct irradiation[4]), we estimate the triplet (^3p) energy of **1***d* to be about 46 kcal mol^{-1}.

This study provides only qualitative estimates of the triplet (^3p) energies of **1***a–d*, as was emphasized earlier. Although these estimates provide only upper limits for the triplet energies of **1***a–d*, it does seem safe to conclude that the triplet energies of **1***a–c* are in fact similar (±1 kcal mol^{-1}) while that of **1***d* is about 2 kcal mol^{-1} lower. This difference between the estimated triplet energies of **1***a–c* and **1***d* compares favourably with the difference in the activation energies for thermal isomerization of these compounds (1). We attribute this difference to additional stabilization of the twisted, biradicaloid triplet state as a result of merostabilization.

Summary and Conclusions

We are now in a position to define the potential energy curves for twisting about the double bond in the ground and first excited singlet and triplet states of tetraphenylethylene, and the effect of substituents on these energy surfaces. Mulliken diagrams for the 1,2-diphenyl-1,2-ditolylethylenes (**1***a*) and the 1,2-dianisyl-1,2-di(4-cyanophenyl)ethylenes (**1***d*) are shown in Fig. 8.

The most stable ground state conformation in tetraphenylethylene is twisted about the double bond by about 8° (25). The difference in thermodynamic stability between *cis* and *trans* isomers of **1***a–d* is less than 0.5 kcal mol^{-1}, the *trans* isomer being more stable in every case (1). The transition state for thermal isomerization, which presumably occurs at an angle of twist of about 90°, lies 35–36 kcal mol^{-1} for **1***a–c*, and about 33 kcal mol^{-1} for **1***d*, above the energies of the stable S_0 conformers (1).

We were not able to determine the spectroscopic triplet energies of *cis*- and *trans*-**1***a–d*, so these points in Fig. 8 are uncertain. We assume, however, that like *cis*-stilbene (8), the planar triplets are higher in energy than the twisted triplet (^3p). The

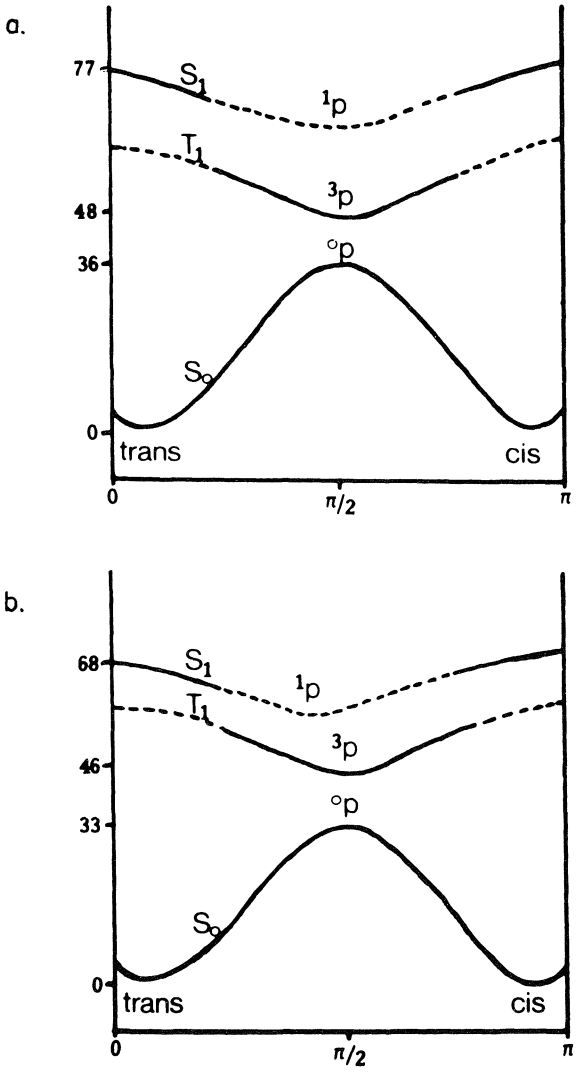

FIG. 8. Mulliken diagrams for **1***a* (a) and **1***d* (b).

angle of twist in ^3p is presumably about 90° in **1***a–d*, since the photostationary states obtained upon triplet-sensitized isomerization indicate that the partitioning ratio $\alpha/(1-\alpha)$ is about unity in each case. The energy of ^3p in TPE and **1***a–c* is estimated to be about 48 kcal mol^{-1} (12). The effect of substituents on the energy of ^3p in tetraphenylethylene parallels that on the ground state rotational barrier, which supports the notion that the triplet state of symmetrical olefins is biradical-like in nature. Merostabilization contributes about 2 kcal mol^{-1} additional stabilization of ^3p in **1***d* relative to the other derivatives. *Cis–trans* isomerization is the major pathway for decay of the triplet state.

The relative energies of the twisted triplet (^3p)

[4]Direct irradiation of **1***d* could not be avoided in this case. It is estimated that the sensitizer absorbed at least 90% of the incident light.

Can. J. Chem. Downloaded from www.nrcresearchpress.com by 210.87.254.105 on 09/06/12
For personal use only.

Can. J. Chem. Downloaded from www.nrcresearchpress.com by 210.87.254.105 on 09/06/12
For personal use only.

and the twisted ground state (^0p) conformers are a cause of concern. We were not expecting ^3p to be so much higher in energy than ^0p (12 kcal mol^{-1}). Theory predicts the triplet to be the ground state for simple olefins in the twisted geometry (4). In the stilbenes, however, ^3p and ^0p are known to be nearly isoenergetic, with ^0p slightly lower in energy than ^3p (8), and the difference is apparently even greater in tetraphenylethylene. Radical stability arguments (1) would lead to the prediction that ^3p in tetraphenylethylene should be 8–10 kcal mol^{-1} lower in energy than the corresponding state in the stilbene system. The apparent similarity between the energies of the ^3p states in stilbene and TPE thus appears to be incompatible with the biradical nature of these species. We do not understand this relatively major discrepancy, however, we hasten to stress that the triplet energies of **1***a–d* estimated in this way are *upper limits*, so the true values may actually be considerably less.

The spectroscopic singlet energy of tetraphenylethylene is about 79 kcal mol^{-1}. Substituents in the *para* positions lower this value somewhat, although isomeric pairs are not different enough electronically to cause their singlet energies to differ appreciably in the cases studied thus far. The singlet energy of **1***d* is considerably lower than those of the other derivatives studied. Twisting in S_1 is apparently unactivated (28, 29) (at least for TPE and **1***a–c*), and leads to a lower-energy, nonfluorescent twisted singlet from which *cis–trans* isomerization occurs. Although we have identified this low energy twisted singlet as ^1p (i.e. part of the S_1 potential energy surface), it is now accepted that this state in the stilbene system is, in fact, a doubly excited one, populated by internal conversion from S_1 as twisting proceeds (8, 38). In any case, we are not able to estimate the energy of this conformer from our data. In **1***a–c*, the angle of twist in ^1p is presumably about 90°, since decay to the ground state results in the formation of both *cis* and *trans* isomers in almost equal amounts.

Minor pathways of decay from the first excited singlet state of TPE and **1***a–f* are fluorescence and electrocyclic ring closure (DHP formation). At room temperature, fluorescence presumably occurs mainly from a conformer in which the phenyl rings have rotated somewhat from their arrangement in S_0, but in which very little rotation about the double bond has occurred (29).

Cis–trans isomerization occurs as a result of decay of ^1p to the ground state. This decay must not involve intersystem crossing to the triplet state, since the photostationary states obtained upon direct and triplet-sensitized excitation conditions are different, particularly in the case of **1***d*. Although *cis–trans* isomerization accounts for essentially all the decay of the singlet states of **1***a–c* (and, by analogy, tetraphenylethylene), it is much less important in **1***d*. This may be due to the presence of an activation barrier to twisting in the first excited singlet state of this derivative.

Much remains to be done in this area. Although the singlet state decay processes of TPE and **1***a–c* are now completely accounted for, further investigation is required in order to fully understand the unusual behaviour of **1***d*. An examination of the temperature and viscosity dependence of the quantum yields for *cis–trans* isomerization of **1***a–d* would obviously go a long way towards a full understanding of the first excited singlet state of TPE. A more careful study of the triplet state is also necessary. Quenching rate studies and sensitized isomerization quantum yields will give a more accurate indication of the triplet energies of this compound. Although the triplet energies of **1***a–d* are apparently not as low as we had originally expected, these compounds may nevertheless prove to be useful as triplet counters for sensitizers whose triplet energies are too low for them to be conveniently investigated with the widely used stilbene system.

Experimental

All melting points are corrected. The ^{1}Hmr spectra were recorded on Varian T60 or CFT20 nmr spectrometers and are reported in parts per million downfield from TMS. Infrared spectra were recorded on a Perkin–Elmer 180 grating infrared spectrometer and are reported in wavenumbers, calibrated against the 1601.8 cm^{-1} polystyrene absorption. Ultraviolet absorption spectra were recorded on a Cary–Varian 219 ultraviolet spectrometer and reported in nanometers. Fluorescence emission and excitation spectra were recorded on an Aminco–Bowman Model 4-8202 spectrophotofluorometer. All spectra were calibrated with a Pen-ray low pressure mercury vapour lamp. Suprasil optical cells (1 cm path length) were used for room temperature measurements, while evacuable Suprasil tubes (4 mm od) were used with a quartz Dewar for those at 77 K.

Half-wave oxidation and reduction potentials were measured by cyclic voltammetry using the apparatus and method described previously (2). Substrate concentrations were typically 20 mg/25 mL 0.1 *M* tetraethylammonium perchlorate (TEAP) in acetonitrile. The voltammograms were scanned at 20, 50, 100, and 200 mV s^{-1}. For reversible waves the half-wave redox potentials were calculated as the average of the midpoints between the forward and reverse waves for the 50, 100, and 200 mV s^{-1} scans. For irreversible waves, the half-wave potentials were calculated as 0.03 V less than the peak potential of the forward scan at 100 mV s^{-1}.

Acetonitrile was refluxed with calcium hydride under dry nitrogen for three days and distilled as required. Benzene was stirred with concentrated sulfuric acid for 24 h, washed thrice with distilled water, once with saturated aqueous bicarbonate, refluxed over sodium for 8 h, distilled, and stored over 4A molecular sieves. Absolute ethanol was obtained by refluxing

Can. J. Chem. Downloaded from www.nrcresearchpress.com by 210.87.254.105 on 09/06/12
For personal use only.

95% ethanol over magnesium turnings and iodine for 24 h followed by distillation. Ethyl iodide was Fisher reagent grade, and was passed down an alumina column and stored over copper wire.

Silver nitrate was Engelhard A.C.S. grade and was recrystallized three times from aqueous ethanol and stored in the dark. Tetraethylammonium perchlorate (TEAP; Aldrich) was recrystallized three times from 90% ethanol.

Tetraphenylethylene (mp 224–225°C) was obtained from Aldrich and recrystallized twice from chloroform–ethanol. The preparation, purification, and characterization of **1***a–d* have been previously described (1). Tetraanisylethylene (**1***e*) was prepared in a similar manner and was recrystallized four times from chloroform–methanol to yield colourless plates (mp 189–190°C; lit. (39) mp 179–180°C).

1,1,2,2-Tetra(4-cyanophenyl)ethylene (**1***f*) was prepared by the same procedure used for **1***a–e* (1). The crude product, a brown, oily solid (3 g), was chromatographed on a silica gel (150 g) column with ether (0 → 10%)–benzene. Elution with pure benzene brought unreacted 4,4′-dicyanobenzophenone (0.9 g) off the column. The olefin was eluted with 10% ether. Evaporation of solvent yielded the product as a yellow solid (0.7 g), which was recrystallized three times from chloroform–methanol to yield **1***f* as light yellow needles (mp 363–366°C); ir (KBr): 2230(s), 1500(s), 1401(m), 1172(w), 1108(w), 1010(m), 826(m, br), 806(m), 750(m), 675(m, br); uv λ_{max} (ethanol): 220(sh, 28 300), 254(29 600), 305(19 500), 319(17 100); ^{1}Hmr ($CDCl_3$): 7.09(d, 1H), 7.53(d, 1H). *Anal.* calcd. for $C_{30}H_{16}N_4$: C 83.31, H 3.73; found: C 83.35, H 3.83.

3,3′-Carbonyl-bis*(5,7-diethoxycoumarin)* (**4**) was prepared by the method of Farid and Specht (35*b*), and recrystallized twice from chloroform–ethanol (1:1) to yield bright yellow crystals (mp 237–239°C).

3,3′-Carbonyl-bis*(7-diethylaminocoumarin)* (**5**) was prepared in a similar fashion (35*b*), and recrystallized twice from acetonitrile–ethanol (1:3) to yield orange needles, mp 213–214°C (lit. (35*b*) mp 213°C).

Benzanthrone (**6**, K & K, 15 g) was treated with Norite (3 g) in refluxing 1,1,2,2-tetrachloroethane for 15 min and filtered. Hot ethanol (200 mL) was added and the solution was allowed to cool slowly. The dark yellow crystals were collected by vacuum filtration and the process was repeated. A portion of this material (5 g) was then chromatographed on a silica gel (125 g) column, using benzene (80%) – hexane as the eluant, and finally recrystallized twice from ethanol, mp 169.5–170°C.

Phenazine (**7**, Aldrich) was recrystallized once from ethanol, mp 180–180.5°C.

Michler's thioketone (**8**, Fisher) was recrystallized thrice from chloroform–methanol, mp 203–204°C.

3,4-Benzopyrene (**9**, Sigma) was sublimed (150°C, 0.1 Torr), chromatographed on alumina (benzene (70%) – hexane), and recrystallized from benzene, mp 183–184°C.

9-Methylanthracene (**10**, Aldrich) was recrystallized once from methanol and sublimed (85°C, 0.1 Torr), mp 81–81.5°C.

All sensitizers were shown to be pure by tlc or hplc.

Direct and Triplet-sensitized Photoisomerization of **1**a–d

All irradiations were carried out in degassed (bubbling N_2, 15 min) benzene solution in 5 or 7 mm Pyrex tubes, using the appropriate Corning glass filter. The tubes were clamped in a water bath (10°C) 2 in. away from the light source, which was a 1 kW GE medium pressure mercury vapour lamp. The photostationary states were approached from both directions, progress of the isomerization being monitored by ir spectroscopy (**1***a*) or hplc (**1***b–d*) (see ref. 1 for analytical procedures). Each sample was analysed at least twice, and the results were averaged. Further experimental details are listed as footnotes in Tables 3 and 6.

Quantum Yield Determinations

Quantum yields were determined with an apparatus which is conceptually similar to that described by Zimmerman *et al.* (40), the major difference being that the photomultiplier tubes used to measure the intensities of the main and reference beams are replaced with phototransistors (41). The light source is an Osram 450 W high pressure xenon lamp, powered by a PRA Model 302 power supply. A Spex Minimate monochromator, fitted with 1.25 mm entrance and exit slits is used to isolate excitation light of the desired wavelength. After entering the sample/phototransistor compartment, the light passes through a Corning CS7-37 glass filter to remove the long wavelength component, and then passes through the beam splitter. The apparatus was calibrated daily by ferrioxalate actinometry.

A 10 mL volume of a benzene solution of the olefin was pipetted into a 2 cm Suprasil optical cell, the cell was sealed with a rubber septum, and the solution was degassed by bubbling dry nitrogen through a syringe for at least 30 min. The concentration of the solution was chosen such that its optical density would be between 1 and 2. After degassing, the optical density of the solution at 370 nm was measured, the cell was placed in the main beam of the quantum yield apparatus, and irradiated. At suitable time intervals, irradiation was stopped, the number of accumulated counts (from the reference phototransistor) was recorded, the photolysis cell was shaken vigorously, and a 70 μL aliquot of the solution was removed by syringe for hplc analysis. The cell was then replaced and irradiation was continued. After a suitable number of aliquots (usually ten) had been taken, irradiation was continued to evaluate the photostationary state.

Analysis of the data is based on the treatment developed by Zimmerman *et al.* (31). Since $\varepsilon^{370}_{trans} = \varepsilon^{370}_{cis}$,

$$[5] \quad \ln (X_c^e - X_c) = \ln (X_c^e - X_c^0) - \frac{\theta \phi_{t \rightarrow c} D}{V c_0 X_c^e \left(1 + \frac{D}{2} + \frac{D^2}{12}\right)} I$$

where X_c = mole fraction of the *cis* isomer, θ = light intensity in einsteins/count, D = optical density of the solution, I = accumulated counts absorbed = $SI_{ref} - I_{main}$, where S = splitting ratio, V = initial volume in photolysis cell, and C_0 = total olefin concentration. Plots of $\ln (X_c^e - X_c)$ vs. I were linear, and the correlation coefficients better than 0.990 in all cases. $\phi_{t \rightarrow c}$ and $\phi_{c \rightarrow t}$ were then calculated from the slope of the plot and the photostationary state composition, and are collected in Table 4. For **1***b* and **1***c*, both *trans* → pss and *cis* → pss were examined and the results averaged, while for **1***d*, only *cis* → pss was examined. The quantum yields in this case are the average of three determinations.

Acknowledgements

This work was supported by a grant from the Natural Sciences and Engineering Research Council of Canada. D.R.A. thanks the Guggenheim Foundation for a Fellowship.

1. W. J. Leigh and D. R. Arnold. Can. J. Chem. **59**, 609 (1981).
2. W. J. Leigh, D. R. Arnold, R. W. R. Humphreys, and P. C. Wong. Can. J. Chem. **58**, 2537 (1980).
3. (*a*) H. O. Kalinowski and H. Kessler. Top. Stereochem. **7**, 295 (1973); (*b*) S. W. Benson. Thermochemical kinetics. John Wiley and Sons, Inc., New York. 1968. p. 72.
4. (*a*) L. Salem and C. Rowland. Angew. Chem. Int. Ed. Engl. **11**, 92 (1972); (*b*) L. Salem. Pure Appl. Chem. **33**, 317 (1973).
5. (*a*) M. J. S. Dewar. J. Am. Chem. Soc. **74**, 3353 (1952); (*b*)

R. W. BALDOCK, P. HUDSON, A. R. KATRITZKY, and F. SOTI. J. Chem. Soc. Perkin Trans. I, 1422 (1974).
6. (*a*) D. R. ARNOLD and R. W. R. HUMPHREYS. J. Chem. Soc. Chem. Commun. 181 (1978); (*b*) R. W. R. HUMPHREYS and D. R. ARNOLD. Can. J. Chem. **57**, 2652 (1979); (*c*) W. J. LEIGH and D. R. ARNOLD. J. Chem. Soc. Chem. Commun. 406 (1980).
7. A. R. BASSINDALE, A. J. BOWLES, A. HUDSON, R. A. JACKSON, K. SCHREINER, and A. BERNDT. Tetrahedron Lett. 3185 (1973).
8. (*a*) J. SALTIEL, J. D'AGOSTINO, E. D. MEGARITY, L. METTS, K. R. NEUBERGER, M. WRIGHTON, and O. C. ZAFIRIOU. Organic photochemistry. Vol. 3. *Edited by* O. E. Chapman. Marcel Dekker, Inc., New York. 1973. p. 1; (*b*) J. SALTIEL and J. L. CHARLTON. Rearrangements in ground and excited states. Vol. 3; *Edited by* P. de Mayo. Academic Press, New York. 1980.
9. (*a*) J. H. DAY. Chem. Rev. **63**, 65 (1963); (*b*) D. L. Ross and J. BLANC. *In* Photochromism, Tech. of Chem. Vol. 3. *Edited by* G. H. Brown. Wiley-Interscience, New York. 1971. Chapt. 5.
10. (*a*) H. STEGEMEYER. Ber. Bunsenges. Phys. Chem. **72**, 335 (1972); (*b*) S. SHARAFY and K. A. MUSZKAT. J. Am. Chem. Soc. **93**, 4119 (1971); (*c*) N. H. KLINGENBERG and W. RAPP. Z. Physik. Chem. N.F. **84**, 92 (1973); (*d*) N. H. KLINGENBERG, E. LIPPERT, and W. RAPP. Chem. Phys. Lett. **18**, 417 (1973).
11. R. J. OLSEN and R. E. BUCKLES. J. Photochem. **10**, 215 (1979).
12. E. F. ULLMAN and W. A. HENDERSON, JR. J. Am. Chem. Soc. **89**, 4390 (1967).
13. J. D. STUART and W. E. OHNESORGE. J. Am. Chem. Soc. **93**, 4531 (1971).
14. (*a*) B. L. FUNT and D. G. GRAY. J. Electrochem. Soc. **117**, 1020 (1970); (*b*) T. TROLL and M. M. BAIZER. Electrochim Acta, **19**, 951 (1974).
15. A. J. BARD and J. PHELPS. Electroanal. Chem. Interfac. Elect. **25**, App. 2, (1970).
16. I. C. LEWIS and L. S. SINGER. J. Chem. Phys. **43**, 2712 (1965).
17. J. A. VALENZUELA and A. J. BARD. J. Phys. Chem. **72**, 286 (1968).
18. C. PAN, K. FU, K. HOU, and Y. HUANG. Chem. Abstr. **62**, 11311f (1965).
19. (*a*) C. K. MANN and K. K. BARNES. Electrochemical reactions in nonaqueous solvents. Marcel Dekker, Inc., New York. 1970; (*b*) A. J. FRY. Synthetic organic electrochemistry. Harper and Row, Inc., New York. 1972.
20. D. R. ARNOLD and P. C. WONG. Can. J. Chem. **57**, 2098 (1979).
21. W. A. PRYOR, T. H. LIN, J. P. STANLEY, and R. W. HENDERSON. J. Am. Chem. Soc. **95**, 6993 (1973).
22. E. M. KOSOWER. An introduction to physical organic chemistry. J. Wiley and Sons, Inc., New York. 1968. p. 49.
23. J. R. FOX and G. KOHNSTAM. Proc. Chem. Soc. 115 (1964).
24. H. SUZUKI. Electronic absorption spectra and geometry of organic molecules. Academic Press, New York. 1967. p. 325.
25. A. HOEKSTRA and A. VOS. Acta Crystallogr. Sect. B, **31**, 1716 (1975); **31**, 1722 (1975).
26. J. BERNSTEIN. Spectrochim. Acta. Part A, **29**, 147 (1973).
27. (*a*) R. DITCHFIELD, J. E. DEL BENE, and J. A. POPLE. J. Am. Chem. Soc. **94**, 703 (1972); (*b*) R. O. LOUTFY and R. O. LOUTFY. Can. J. Chem. **54**, 1454 (1976).
28. B. I. GREENE. Chem. Phys. Lett. **79**, 51 (1981).
29. P. F. BARBARA, S. D. RAND, and P. M. RENTZEPIS. J. Am. Chem. Soc. **103**, 2156 (1981).
30. J. B. BIRKS and D. J. DYSON. Proc. R. Soc. London Ser. A, **275**, 135 (1963).
31. G. ZIMMERMAN, L. Y. CHOW, and U. J. PAIK. J. Am. Chem. Soc. **80**, 3528 (1958).
32. G. S. HAMMOND, J. SALTIEL, A. A. LAMOLA, N. J. TURRO, J. S. BRADSHAW, D. O. COWAN, R. C. COUNSELL, V. VOGT, and C. DALTON. J. Am. Chem. Soc. **86**, 3197 (1964).
33. W. G. HERKSTROETER and G. S. HAMMOND. J. Am. Chem. Soc. **88**, 4769 (1966).
34. (*a*) P. S. ENGEL and B. M. MONROE. Adv. Photochem. **8**, 245 (1971); (*b*) W. G. HERKSTROETER. J. Am. Chem. Soc. **97**, 4161 (1975).
35. (*a*) S. FARID, P. A. MARTIC, R. C. DALY, D. R. THOMPSON, D. P. SPECHT, S. E. HARTMAN, and J. L. R. WILLIAMS. Pure Appl. Chem. **51**, 241 (1979); (*b*) S. FARID and D. P. SPECHT. U.S. Patent No. 4, 147, 552, (1979).
36. S. M. JAPAR and E. W. ABRAHAMSON. J. Am. Chem. Soc. **93**, 4140 (1971).
37. D. BLACKWELL, C. C. LIAO, R. O. LOUTFY, P. DE MAYO, and S. PASZYE. Mol. Photochem. **4**, 171 (1972).
38. (*a*) G. ORLANDI and W. SIEBRAND. Chem. Phys. Lett. **30**, 352 (1975); (*b*) T. M. STACHELEK, T. A. PAZOHA, W. M. MCCLAIN, and R. P. DRUCKER. J. Chem. Phys. **66**, 4540 (1977); (*c*) K. FUKE, S. SAKAMOTO, M. UEDA, and M. ITOH. Chem. Phys. Lett. **74**, 546 (1980).
39. D. BETHELL and J. D. CALLISTER. J. Chem. Soc. 3801 (1963).
40. H. E. ZIMMERMAN, T. P. CUTLER, V. R. FITZGERALD, and T. J. WEIGH. Mol. Photochem. **8**, 379 (1977).
41. J. A. PINCOCK. To be published.

Can. J. Chem. Downloaded from www.nrcresearchpress.com by 210.87.254.105 on 09/06/12
For personal use only.

The least-squares triangle: a new method for evaluation of solid phase compositions from solubility measurements

JOHN W. LORIMER

Department of Chemistry, University of Western Ontario, London, Ont., Canada N6A 5B7

Received February 5, 1981

JOHN W. LORIMER. Can. J. Chem. **59**, 3076 (1981).

A least-squares method is described for calculating compositions of equilibrium solid phases from data on solubilities and either wet residues or initial compositions for systems of three or more thermodynamic components. The method minimizes the squares of areas of triangles formed by the solubility, wet residue (or initial composition), and solid composition points. Full descriptions of error analyses and hypothesis tests are given, along with an illustrative example and detailed comparisons with the traditional extrapolation method.

JOHN W. LORIMER. Can. J. Chem. **59**, 3076 (1981).

On décrit une méthode impliquant les moindres carrés qui permet de calculer des compositions de phases solides à l'équilibre à partir de données de solubilité ainsi que des restes ou des compositions initiales des systèmes thermodynamiques à trois composants ou plus. La méthode minimise les carrés des aires des triangles formés par les points de solubilité, de reste (ou de composition initiale) et de composition solide. On donne une description complète des erreurs d'analyse et des vérifications, des hypothèses ainsi qu'un exemple et des comparaisons détaillées avec la méthode d'extrapolation directe.

[Traduit par le journal]

Can. J. Chem. Downloaded from www.nrcresearchpress.com by 210.87.254.105 on 09/06/12
For personal use only.

Introduction

In determinations of solubilities of solids in liquids, it is important, but not always easy, to establish accurately the composition of the equilibrium solid phase or phases. A general way of finding the composition of a solid phase while it is in contact with a saturated solution was devised by Schreinemakers (1) in 1893, and his "method of wet residues" has found wide use up to the present. Bancroft (2) rediscovered the method independently in 1902. In Fig. 1a, A, B, and C are three components whose compositions (as mass or mole fractions at constant temperature and pressure) are represented on the triangle ABC. The curves ab, bc are the solubility curves, respectively, of the binary compound A' and the ternary compound B'. If x' is a point on the solubility curve bc, then all points on tie-line $x'B'$ represent systems containing solid B' and solution x' saturated with B'. If a sample of solution is removed and analyzed to give the composition x', then the remaining solid and solution (the "wet residue") will have a composition x'' lying on the tie-line. This composition may be determined by analysis of the complete wet residue, and the tie-line $x'x''$ may be drawn. Other tie-lines such as $z'z''$ can be found in a similar way, and their intersection gives the composition B'. The points x'', z'' can equally well be the initial overall compositions of the system, and Hill and Ricci (3) have recommended using these compositions, called by them the "initial complexes", to avoid errors due to loss or gain of solvent in transferring the wet residues from the solubility bottles to the containers used for analysis. It is also possible to determine two wet residue compositions by successive sampling of different proportions of solid and liquid or to use one wet residue and the initial composition. The three points obtained thus for a given tie-line should improve the precision of the extrapolation, but the method has been used infrequently; for examples, see Delyon (4) and Filipescu and Filipescu (5). Other points such as p'' lie on tie-lines within three-phase regions, and these tie-lines intersect at the eutonic (isothermally invariant) point b. In principle, such tie-lines can be used to obtain a more precise value for the eutonic composition, but no instances of this application have been found in the literature.

Extrapolation of tie-lines is usually done graphically, even in modern work, but Hill and Ricci (3) have used an algebraic method. The two points x', x'', with coordinates x_A', x_B' and x_A'', x_B'' for coordinate axes A, B are used to find the equation of the tie-line. The intersection of the tie-line with a line through a vertex and the assumed composition of the compound, such as lines CA or CB', is then calculated. These reference lines fix the relative proportions of components A and B in the compound; component B is absent along line CA. The points of intersection of all p tie-lines constitute a univariate population of random variables with mean $\bar{x}_x$ (the relative amount of the one independent component X in the compound) and standard deviation σ. If x_x^0 is a theoretical value for x_x, the hypothesis $x_x = x_x^0$ can be tested by computing the statistic $|\bar{x}_x - x_x^0|p^{\frac{1}{2}}/\sigma$. If this value exceeds the

0008-4042/81/213076-08$01.00/0

©1981 National Research Council of Canada/Conseil national de recherches du Canada

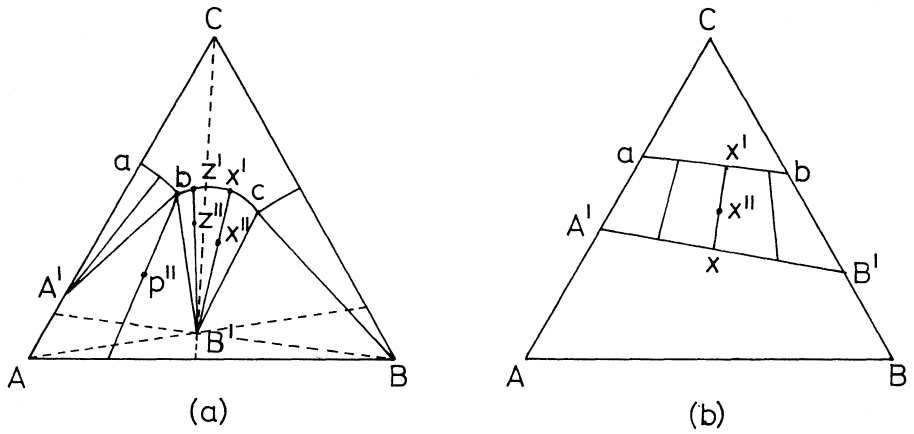

FIG. 1. Schematic solubility curves for ternary systems of A, B, and C where: (a) binary compound A' with solubility curve ab and ternary compound B' with solubility curve bc appear; (b) isomorphic solid solutions $A'B'$ appear, with solubility curve ab. Lines such as aA', $x'x''$ are tie-lines.

tabulated value of Student's t for $p - 1$ degrees of freedom, the hypothesis can be rejected (6). The existence of this simple statistical test does not appear to have been realized previously. It is also possible to find the point of intersection of pairs of tie-lines without making any assumption concerning the ratio of components in the compound. The data for the $p(p-1)/2$ pairs of tie-lines give rise to a set of nonlinear conditions which can be linearized and used to find least-squares estimates of the point of intersection by an iterative procedure (7). This approach is being investigated.[1] The point of intersection will be more precise if the points x' and x'' are widely separated as possible (1, 3), whatever method of extrapolation, graphical or analytical, is used.

It is also possible to extrapolate the tie-lines to intersect line BB', along which the ratio of components C to A is fixed, or to intersect line AB', along which the ratio of components B to C is fixed. Only two of these lines will give independent estimates of the composition of the solid phase, because the intersection of any two of the lines AB', BB', CB' is sufficient to determine point B'. If C is a solvent component, then the usual practice is to use line CB'. If, as shown in Fig. 1a, the tie-lines are roughly parallel to CB', intersections with AB' or BB' will tend to give a more precise estimate of the solid composition than intersections with CB'. Similar considerations hold for point A', except that only two reference lines, CA' and BA', are possible. These considerations of precision appear not to have been recognized.

A variation of the analytical extrapolation procedure which uses projections of the points x' and x'' on the coordinate axes has been proposed independently by Smith (8) and by Schott (9), but Heric (10) has pointed out that nothing is gained by this method. Filipescu and Filipescu (5) fitted least-squares equations of the form $\hat{y}_{ij} = n_i + m_i x_{ij}$ to tie-lines i defined by three points x_{ij}, y_{ij} (one solubility, one initial composition, one wet residue) with parameters n_i, m_i. The point of intersection x_s, y_s was then found by minimizing $\Sigma_i(y_s - \hat{y}_{si})^2 = \Sigma(y_s - n_i - m_i x_s)^2$ with respect to x_s and y_s. The method was also applied to two-dimensional projections of four-component reciprocal salt systems. The statistical properties of the method were not investigated, but the assumption that the variance of x_{ij} is negligible compared to that of y_{ij} is implied in the theory. In practice, both variances are of comparable magnitude, so the statistical basis of the procedure is unsatisfactory.

The various procedures outlined above (with the probable exception of the iterative least-squares procedure) are all deficient in one or more respects. What is required is a method which: (a) allows for equal or pre-assigned weights for each coordinate; (b) makes no assumptions about the composition of a solid phase, and thereby permits estimation of n coordinates of the point of intersection in an $n + 1$ component system; (c) permits estimation of the variance–covariance matrix for the point of intersection; (d) permits statistical tests for the significance of the point of intersection; and (e) can be

[1]The author wishes to thank a referee for pointing out the relevance of Mikhail's book.

Can. J. Chem. Downloaded from www.nrcresearchpress.com by 210.87.254.105 on 09/06/12
For personal use only.

Can. J. Chem. Downloaded from www.nrcresearchpress.com by 210.87.254.105 on 09/06/12
For personal use only.

generalized to multicomponent systems. The method described below satisfies all these criteria, and does not require iterations. It has proved of value in analyzing critically the large body of solubility data which exists for the alkaline earth sulfates (11). In practice, it is restricted to three-component systems in which continuous series of solid solutions do not occur, or to ternary sections or ternary projections of higher-component systems. If isomorphic solid solutions occur ($A'B'$ in Fig. 1b), tie-lines such as $x'x''$ have no common intersection, but can be extrapolated algebraically (12, 13) to find the composition x of the conjugate solid solution. In four-component systems, tie-lines may exist between points on a three-dimensional solubility surface and the composition point of a solid phase. However, most solubility experiments on four-component systems are conducted by adding the fourth component to a three-component eutonic system. The tie-lines for these isothermally univariant four-component systems are not collinear. Similar considerations hold for systems of five or more components.

Theory

(a) *The Least-squares Triangle*

In Fig. 2, A, B, and C are three points in n-dimensional space which represent, respectively, the compositions (as mass or mole fractions) of the solid phase ($\boldsymbol{x}$), the saturated solution ($\boldsymbol{x}_k'$) and the wet residue ($\boldsymbol{x}_k''$) for an $(n + 1)$-component system. The coordinates of the points in terms of their components x_{ik} $(i = 1, \ldots, n)$ and a set of n orthogonal unit basis vectors $\boldsymbol{e}_i$ are

$$[1] \quad \boldsymbol{x} = \sum_{i=1}^{n} \boldsymbol{e}_i x_i, \boldsymbol{x}_k' = \sum_{i=1}^{n} \boldsymbol{e}_i x_{ik}'$$

and similarly for $\boldsymbol{x}_k''$. The line segments AB, AC form two sides of a triangle the area of which is the length of the vector

$$[2] \quad \boldsymbol{a}_k = \tfrac{1}{2}(\boldsymbol{x}_k' - \boldsymbol{x}) \wedge (\boldsymbol{x}_k'' - \boldsymbol{x})$$

where $\wedge$ is the exterior (vector) product. Define

$$[3] \quad \boldsymbol{y}_k \equiv \boldsymbol{x}_k' - \boldsymbol{x}_k''$$

Then, eq. [2] can be written as

$$[4] \quad 2\boldsymbol{a}_k = (\boldsymbol{x} - \boldsymbol{x}_k') \wedge \boldsymbol{y}_k$$

or, in terms of its components,

$$[5] \quad 2\boldsymbol{a}_k = \sum_{i<j=1}^{n} \boldsymbol{e}_i \wedge \boldsymbol{e}_j\{(x_i - x_{ik}')y_{jk} - (x_j - x_{jk}')y_{ik}\}$$

Now consider the set of lines $k = 1, \ldots, p$ each of which is determined uniquely by two points $\boldsymbol{x}_k'$ and $\boldsymbol{x}_k''$; the set is approximately collinear through point $\boldsymbol{x}$. If $p > n$, the coordinates of $\boldsymbol{x}$ are overdetermined, and it is desired to find estimates of these coordinates. If $\boldsymbol{a}_k = 0$, points $\boldsymbol{x}_k'$, $\boldsymbol{x}_k''$, and $\boldsymbol{x}$ are exactly collinear. If B lies as shown in Fig. 2, $\boldsymbol{a}_k$ is negative; if B lies on the opposite side of AC, $\boldsymbol{a}_k$ is positive. The coordinates $\boldsymbol{x}$ can then be estimated by minimizing the sum of squares of the areas $\boldsymbol{a}_k$, a procedure suggested to the author by Prof. M. M. Ali.

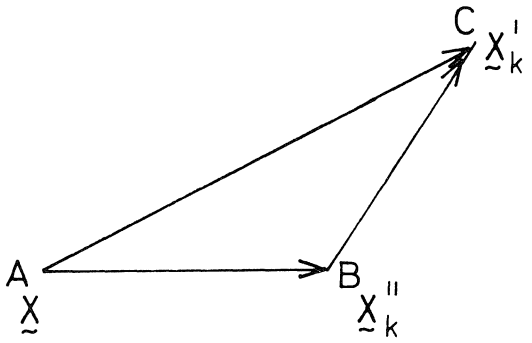

FIG. 2. Vector relations among a solubility coordinate $\mathbf{x}_k'$, a wet residue coordinate $\mathbf{x}_k''$, and a solid phase coordinate $\mathbf{x}$.

(b) *The Least-squares Normal Equations*

Vector notation (bold face italic type) is now abandoned, and the problem is recast in matrix terms. (Matrices are in bold face Roman type.) The skew symmetric matrix

$$[6] \quad 2\mathbf{A}_k = (\mathbf{x}\mathbf{y}_k^t - \mathbf{y}_k\mathbf{x}^t) - (\mathbf{x}_k'\mathbf{y}_k^t - \mathbf{y}_k\mathbf{x}_k''), \quad k = 1, \ldots, p$$

contains as its elements all components of the area given by eq. [5]. Here, the superscript t after a matrix indicates the transpose; lower case letters represent column matrices, upper case letters square matrices. Thus, $\mathbf{x}$, $\mathbf{x}_k'$, $\mathbf{y}_k$ are $n \times 1$ matrices (n rows, 1 column), $\mathbf{x}^t$, etc. are $1 \times n$ row matrices, and $\mathbf{A}_k$ is a $n \times n$ matrix. There are only $n(n-1)/2$ distinct components of area, but their signs are undefined, so that each component appears twice with a different sign in eq. [6]. The quantity

$$[7] \quad \alpha_k = \pm\{\tfrac{1}{2} \operatorname{tr} \mathbf{A}_k^t\mathbf{A}_k\}^{1/2}, \quad k = 1, \ldots, p$$

is the square root of the sum of squares of all components of area, and thus its magnitude is that of the area $\boldsymbol{a}_k$ in eq. [2]. The sign of α_k is undefined, so that the matrix $\boldsymbol{\alpha}$ with elements α_k is a matrix of random variables with zero means and finite variances. The corresponding variance–covariance matrix of $\boldsymbol{\alpha}$ is

$$[8] \quad \mathbf{M}_\alpha = \langle \boldsymbol{\alpha}\boldsymbol{\alpha}^t \rangle$$

where angular brackets indicate the expectation

Can. J. Chem. Downloaded from www.nrcresearchpress.com by 210.87.254.105 on 09/06/12
For personal use only.

value. In practice, this matrix is diagonal, with elements $\sigma_{A_k}^2$, because individual areas are uncorrelated. In addition, only relative variances are known, so that

[9] $\mathbf{M}_\alpha = \sigma^2\mathbf{P}^{-1}$

where σ^2 is the variance of unit weight, and $\mathbf{P}$ is the weight matrix, which may itself be the unit matrix $\mathbf{I}$. The weighted sum of squares of all areas is given by the scalar

[10] $S = \boldsymbol{\alpha}^t\mathbf{M}_\alpha^{-1}\boldsymbol{\alpha} = \sum_{k=1}^{p} \frac{1}{2}\,\mathrm{tr}\,\mathbf{A}_k^t\mathbf{A}_k/\sigma_{A_k}^2$

where a diagonal weight matrix has been assumed in the second term. This quantity can be expanded using eq. [6] and simplified by multiplying out such products as

$$\mathrm{tr}\,(\mathbf{x}\mathbf{y}_k^t)^t(\mathbf{x}\mathbf{y}_k^t) = \mathrm{tr}\,(\mathbf{y}_k\mathbf{x}^t\mathbf{x}\mathbf{y}_k^t) = \mathbf{x}^t\mathbf{y}_k^t\mathbf{y}_k\mathbf{x}$$

to give finally

[11] $4S = \mathbf{x}^t\mathbf{B}\mathbf{x} - 2\mathbf{x}^t\mathbf{C} + D$

where

[12] $\mathbf{B} = \mathbf{B}^t = \left[\sum_{k=1}^{p} (\lambda_k^2\delta_{ij} - y_{ik}y_{kj})/\sigma_{A_k}^2\right]$

with

[13] $\lambda_k^2 = \sum_{i=1}^{n} y_{ik}^2$

[14] $\mathbf{C} = \left[\sum_{j=1}^{n}\sum_{k=1}^{p} (\lambda_k^2\delta_{ij} - y_{ik}y_{jk})x_{kj}/\sigma_{A_k}^2\right]$

[15] $D = \sum_{i,j=1}^{n}\sum_{k=1}^{p} (\lambda_k^2\delta_{ij} - y_{ik}y_{jk})x_{ik}'x_{jk}'/\sigma_{A_k}^2$

with δ_{ij} the Kronecker delta. Matrix $\mathbf{B}$ has dimensions $n \times n$, $\mathbf{C}$ has dimensions $n \times 1$, and D is a scalar.

The least-squares estimator $\hat{\mathbf{x}}$ for matrix $\mathbf{x}$ is found in the usual way by setting a variation in scalar S equal to zero:

$$4\delta S = \delta\mathbf{x}^t\mathbf{B}\hat{\mathbf{x}} + \mathbf{x}^t\mathbf{B}\delta\mathbf{x} - 2\delta\mathbf{x}^t\mathbf{C} = 0$$

or

[16] $4\delta S = 2\delta\mathbf{x}^t(\mathbf{B}\hat{\mathbf{x}} - \mathbf{C}) = 0$

from which

[17] $\mathbf{B}\hat{\mathbf{x}} = \mathbf{C}$ or $\hat{\mathbf{x}} = \mathbf{B}^{-1}\mathbf{C}$

Equations [17] are the required least-squares normal equations, and give estimates of the point of intersection $\hat{\mathbf{x}}$ in terms of the matrices $\mathbf{B}$ and $\mathbf{C}$, which are known if the $\sigma_{A_k}^2$ are known. If $\mathbf{P} = \mathbf{I}$ in eq. [9], then the weights $\sigma_{A_k}^2$ in eqs. [12] to [15] may all be set equal to unity, as they cancel in eq. [17]. An estimate $\hat{S}$ of the weighted sum of squares can now be found by substituting eq. [17] into eq. [11] to give

[18] $4\hat{S} = D - \mathbf{C}^t\mathbf{B}^{-1}\mathbf{C} = D - \hat{\mathbf{x}}^t\mathbf{B}\hat{\mathbf{x}}$

For a 3-component system, the specific equations are as follows, where all sums are over the p pairs of experimental points with coordinates (x_{1k}', x_{2k}'), (x_{1k}'', x_{2k}''), and $\sigma_{A_k}^2 = 1$.

[19] $\mathbf{B}^{-1}\Delta = \begin{bmatrix} \sum y_{1k}^2 & \sum y_{1k}y_{2k} \\ \sum y_{1k}y_{2k} & \sum y_{2k}^2 \end{bmatrix}$

[20] $\Delta = \sum y_{1k}^2 \sum y_{2k}^2 - (\sum y_{1k}y_{2k})^2$

[21] $\mathbf{C} = \begin{bmatrix} \sum y_{2k}(y_{2k}x_{1k}' - y_{1k}x_{2k}') \\ \sum y_{1k}(y_{1k}x_{2k}' - y_{2k}x_{1k}') \end{bmatrix}$

The correlation coefficient between the coordinates (x_1, x_2) of the point of intersection is

[22] $\hat{\rho}_{12} = \sum y_{1k}y_{2k}/\{\sum y_{1k}^2 \sum y_{2k}^2\}^{1/2}$

(c) *Errors in the Estimated Parameters*

The variance–covariance matrix of the parameter estimates $\hat{\mathbf{x}}$ is

[23] $\mathbf{M}_x = \langle(\mathbf{x} - \hat{\mathbf{x}})(\mathbf{x} - \hat{\mathbf{x}})^t\rangle = 4\langle\mathbf{B}^{-1}\rangle$

where angular brackets indicate the expectation value. It has not been possible to find a direct proof of eq. [23], but an indirect proof can be given readily by making use of the theorem that (6), if $\mathbf{X}$ is the matrix of a set of random variables with zero means, finite variances, and variance–covariance matrix $\mathbf{M}$ of rank q, then

[24] $\langle\mathbf{X}^t\mathbf{M}^{-1}\mathbf{X}\rangle = q$

Subtract eq. [11] from eq. [18] and use eq. [17]:

[25] $4(S - \hat{S}) = \mathbf{x}^t\mathbf{B}\mathbf{x} + \hat{\mathbf{x}}^t\mathbf{B}\hat{\mathbf{x}} - 2\mathbf{x}^t\mathbf{B}\hat{\mathbf{x}}$

Because the product $\mathbf{x}^t\mathbf{B}\hat{\mathbf{x}}$ is a scalar,

[26] $\mathbf{x}^t\mathbf{B}\hat{\mathbf{x}} = (\mathbf{x}^t\mathbf{B}\hat{\mathbf{x}})^t = \hat{\mathbf{x}}^t\mathbf{B}\mathbf{x}$

and thus

[27] $4\langle\hat{S}\rangle = 4\langle S\rangle - \langle(\mathbf{x} - \hat{\mathbf{x}})^t\mathbf{B}(\mathbf{x} - \hat{\mathbf{x}})\rangle$

Now,

[28] $\langle S\rangle = \langle\boldsymbol{\alpha}^t\mathbf{M}_\alpha^{-1}\boldsymbol{\alpha}\rangle = p$

since $\boldsymbol{\alpha}$ is a matrix of random variables with zero means and variance–covariance matrix $\mathbf{M}_\alpha$ of rank p. Similarly, if $4\ \mathbf{B}^{-1}$ is the variance–covariance

matrix for the random variables $\mathbf{x} - \hat{\mathbf{x}}$ with zero means, its rank is n, and thus

$$[29] \quad \langle \hat{S} \rangle = p - n = \left\langle \sum_k \tfrac{1}{2} \mathrm{tr}\,(\mathbf{A}_k{}^t\mathbf{A}_k) \right\rangle \Big/ \sigma^2$$

An estimate of the variance of an observation of unit weight is therefore

$$[30] \quad \hat{\sigma}^2 = \sum_k \tfrac{1}{2}\,\mathrm{tr}\,(\mathbf{A}_k{}^t\mathbf{A}_k)/(p - n)$$

and an unbiased estimate of $\mathbf{M}_x$ is

$$[31] \quad \hat{\mathbf{M}}_x = 4\hat{\sigma}^2\mathbf{B}^{-1}$$

Equations [23] and [29] are what one would expect by comparison with other least-square problems (6). It should be noted that p is the number of *pairs* of points $\mathbf{x}_k'$, $\mathbf{x}_k''$, or the number of tie-lines, and n is the number of dimensions, or one less than the number of thermodynamic components.

(d) *Multivariate Linear Hypothesis*

The theory of the least-squares triangle, as formulated above, is formally similar to general linear least-squares theory (6). The only differences are in the actual form of the defining equation for the parameters. This formal similarity means that all the results concerning the multivariate distribution function and the distribution properties of quadratic forms can be taken over directly. Only one result is of interest here, the test of the null hypothesis

$$[32] \quad \mathbf{x} = \mathbf{x}^0$$

where $\mathbf{x}^0$ is a set of theoretical parameters. The quantity to be tested is (6)

$$[33] \quad u = (\hat{\mathbf{x}} - \mathbf{x}^0)^t\hat{\mathbf{M}}_x{}^{-1}(\hat{\mathbf{x}} - \mathbf{x}^0)/n$$

and this quantity is distributed as $F_{n,\,p-n,\,\alpha}$ the F-distribution (14) for a significance level α. If the computed value of u exceeds $F_{n,p-n,\alpha}$ the hypothesis that the set $\hat{\mathbf{x}}$ is equal to the set $\mathbf{x}^0$ may be rejected at significance level α; otherwise, it may be accepted.

If a given value of F is chosen, then (cf. ref. 6, sect. 4–2)

$$[34] \quad (\mathbf{x} - \hat{\mathbf{x}})^t\hat{\mathbf{M}}_x{}^{-1}(\mathbf{x} - \hat{\mathbf{x}}) = nF_{n,p-n,\alpha} \equiv w$$

defines a hyperellipsoid of constant probability centred on $\mathbf{x} = \hat{\mathbf{x}}$. Setting $x_i - \hat{x}_i = \delta_i$ gives

$$[35] \quad \delta_1{}^2/\hat{\sigma}_1{}^2 + \delta_2{}^2/\hat{\sigma}_2{}^2 - 2\hat{\rho}_{12}\delta_1\delta_2/\hat{\sigma}_1\hat{\sigma}_2 = w(1 - \hat{\rho}_{12}{}^2)$$

as the equation of the projection of the hyperellipsoid on the (δ_1, δ_2) coordinate plane, where $\hat{\sigma}_1$, $\hat{\sigma}_2$ are the estimated standard deviations for parameters $\hat{x}_1$, $\hat{x}_2$ and $\hat{\rho}_{12}$ is the parameter correlation coefficient. The following properties of this ellipse are easy to establish, and permit a sketch to be made (compare ref. 6, p. 133). The ellipse is inscribed in a rectangle

$$[36] \quad \delta_1 = \pm w^{1/2}\hat{\sigma}_1,\ \delta_2 = \pm w^{1/2}\hat{\sigma}_2$$

The axis α of the ellipse makes an angle β with the δ_2-axis, where

$$[37] \quad \tan 2\beta = 2\hat{\rho}_{12}\hat{\sigma}_1\hat{\sigma}_2/(\hat{\sigma}_1{}^2 - \hat{\sigma}_2{}^2)$$

If $\hat{\rho}_{12} = 0$, $\beta = 0$; if $\hat{\sigma}_1 = \hat{\sigma}_2$ and $\hat{\rho}_{12} \neq 0$, $\beta = \pm 45°$. The sign of the angle in [37] is given by the sign of $\hat{\rho}_{12}\hat{\sigma}_2/\hat{\sigma}_1$, which is the slope of the ellipse at $\delta_1 = 0$, or the slope of the regression line of δ_2 on δ_1. Alternatively, the slope of the ellipse at $\delta_2 = 0$, or the slope of the regression line of δ_1 on δ_2, is $\hat{\sigma}_2/\hat{\rho}_{12}\hat{\sigma}_1$. The semi axes a and b of the ellipse are given by

$$[38] \quad a^2 = w(\hat{\sigma}_1{}^2\cos^2\beta + \hat{\sigma}_2{}^2\sin^2\beta + \hat{\rho}_{12}\hat{\sigma}_1\hat{\sigma}_2\sin 2\beta)$$

and

$$[39] \quad b^2 = w(\hat{\sigma}_1{}^2\sin^2\beta + \hat{\sigma}_2{}^2\cos^2\beta - \hat{\rho}_{12}\hat{\sigma}_1\hat{\sigma}_2\sin 2\beta)$$

where β is given by eq. [37]. The ellipse defined by these equations will be called the 100(1-α)% confidence ellipse. The probability that the true values x_1, x_2 lie within this ellipse is 100(1-α)%. The ratio of the axes of the confidence ellipse is $a/b = \hat{\sigma}_1/\hat{\sigma}_2$ if $\hat{\rho}_{12} = 0$ (when $\beta = 0$) and zero or infinite if $\hat{\rho}_{12} = 1$ (when $\tan\beta = -\hat{\sigma}_1/\hat{\sigma}_2$ or $\hat{\sigma}_1/\hat{\sigma}_2$). Thus for no correlation between the coordinates of the point of intersection, one axis of the ellipse is parallel to a coordinate axis, and the axial ratio is simply the ratio of the standard deviations. From eq. [22], zero correlation is highly unlikely, because for values of y_{1k} near a coordinate axis (and thus small), the correlation coefficient remains finite. Perfect correlation between the coordinates of the point of intersection occurs only if y_{1k} and y_{2k} are proportional, i.e., when the points $\mathbf{x}'$ and $\mathbf{x}''$ lie on a reference line. In general, finite correlation coefficients are therefore to be expected, and the confidence ellipse will be more elongated if all tie-lines are nearly parallel to a reference line.

For the extrapolation method, the coordinates of the points of intersection for a two-component system are proportional: $\hat{x}_2 = r_i M_i \hat{x}_1/M_1$ where r_i is the mole ratio of components i and 1 in the solid and M_i is the molar mass, and

$$[40] \quad \tan\beta = r_i M_i/M_1 \quad \text{or} \quad -M_1/r_i M_i$$

The confidence limits for the theoretical point of

Can. J. Chem. Downloaded from www.nrcresearchpress.com by 210.87.254.105 on 09/06/12
For personal use only.

Can. J. Chem. Downloaded from www.nrcresearchpress.com by 210.87.254.105 on 09/06/12
For personal use only.

intersection x_i constitute a straight line segment with slope β and extending between $\hat{x}_i - \hat{\sigma}_i\, t_{p-1,\alpha}/p^{\frac{1}{2}} < x_i < \hat{x}_i + \hat{\sigma}_i\, t_{p-1,\alpha}/p^{\frac{1}{2}}$, $i = 1, 2$. The experimental point of intersection lies on this line or on its extension.

(e) *Errors in and Distribution of Individual Data Points*

It is of interest to investigate how the variance–covariance matrix, eq. [23], depends on the separation of the solubility and wet residue points. To simplify the problem, consider the case where the ratio, L, of the distance between any pair of solubility and wet residue points to the distance between the solubility point and the theoretical point of intersection is constant. Thus, $\mathbf{y}_k = L\,(\mathbf{x}_k' - \mathbf{x})$, an equation that also holds for each coordinate component, but implies that all three points are collinear. To represent experimental data it is necessary to add a random error $\delta\mathbf{y}_k$ whose magnitude is determined by the errors in $\mathbf{x}_k'$ and $\mathbf{x}_k''$, but is independent of L:

$$[41] \quad \mathbf{y}_k = L(\mathbf{x}_k' - \mathbf{x}) + \delta\mathbf{y}_k$$

If $\delta\mathbf{y}_k \ll L\,(\mathbf{x}_k' - \mathbf{x})$, substitution of eq. [41] in eq. [23] shows that $\mathbf{M}_x$ is inversely proportional to L^2, while eq. [17] shows that $\hat{\mathbf{x}}$ is independent of L. Similar conclusions are found for the estimated variance–covariance matrix, $\hat{\mathbf{M}}_x$, eq. [31]. In particular, the contribution of the first term of eq. [41] to S (and also to $\hat{S}$; see eqs. [11], [18]) is zero, and there is a finite contribution to S which involves the products $\delta y_i \delta y_j$, $i, j = 1, \ldots, n$. It is expected, therefore, that the standard deviations of the parameter estimates are inversely proportional to L.

For the extrapolation method, the standard deviation in $\hat{x}_i$ can be calculated in terms of $\mathbf{x}_k'$ and $\mathbf{y}_k$, and it is also found, by use of eq. [41], to be approximately inversely proportional to L, while $\hat{x}_i$ itself is independent of L, under the condition $|\delta y_{2k} - r\delta y_{1k}| \ll L|x_{2k}' - r\,x_{1k}'|$, where r is the mole ratio of components 2 to 1 in the solid.

These predictions were all confirmed by computer simulations based on two different sets of six solubility points and a theoretical point of intersection which corresponded approximately to the experimental data used in the application section below. Values of $\delta\mathbf{y}_k$ were chosen as random numbers in the range ± 0.1, a choice which was found to simulate typical experimental data. Values of $\mathbf{y}_k$ were then calculated from eq. [41], and points of intersection were calculated using both the least-squares triangle and extrapolation methods for a series of values of L between 0.025 and 0.975. For $L \leq 0.1$, the parameter estimates themselves became unreliable. This behaviour is expected, since such small values of L cause both terms in eq. [41] to be of comparable magnitude. Again as predicted, standard deviations were independent of the distribution of data points relative to a reference line for the least-squares triangle method, but not for the extrapolation method.

Zero correlation among individual points $\mathbf{x}_k'$, $\mathbf{x}_k''$ is in accord with the way in which experiments are carried out, but correlations among the components of these points can arise. In a three-component system, if analyses in terms of masses of components 1 and 2 are carried out on the same weighed sample, there is a correlation (usually small) between the two mass fractions w_i. If mole fractions x_i are now calculated from these mass fractions, strong correlations automatically appear because of the occurrence of both w_1 and w_2 in the denominator of

$$[42] \quad x_i = w_i/M_i\{1/M_3 + w_1(1/M_1 - 1/M_3) + w_2(1/M_2 - 1/M_3)\}$$

where M_i is the molar mass of thermodynamic component i. For this reason, data analysis should be based on mass fractions rather than derived mole fractions (cf. ref. 10).

(f) *The Formula of the Solid*

For a three-component system, the data for the point of intersection can be used to calculate the formula of the solid in the form $A{\cdot}r_2B{\cdot}r_3C$ where

$$[43] \quad r_2 = x_2M_1/x_1M_2,\ r_3 = (1 - x_1 - x_2)M_1/x_1M_3$$

Using standard methods, the estimated variances in r_2 and r_3 are found to be:

$$[44] \quad \hat{\sigma}^2(r_2)/r_2^2 \simeq \hat{\sigma}_1^2/x_1^2 + \hat{\sigma}_2^2/x_2^2 - 2\hat{\sigma}_1\hat{\sigma}_2\hat{\rho}_{12}/x_1x_2$$

and

$$[45] \quad \hat{\sigma}^2(r_3)/r_3^2 \simeq \hat{\sigma}_2^2/x_3^2 + \hat{\sigma}_1^2(1/x_3 + 1/x_1)^2 + 2\hat{\rho}_{12}\hat{\sigma}_1\hat{\sigma}_2(1/x_3 + 1/x_1)/x_3$$

if component 1 has a coefficient of unity in the formula, or

$$[46] \quad \hat{\sigma}^2(r_3)/r_3^2 \simeq \hat{\sigma}_1^2/x_3^2 + \hat{\sigma}_2^2(1/x_3 + 1/x_2)^2 + 2\hat{\rho}_{12}\hat{\sigma}_1\hat{\sigma}_2(1/x_3 + 1/x_2)/x_2$$

if component 2 has a coefficient of unity in the formula, where $\hat{\sigma}_1$, $\hat{\sigma}_2$, and $\hat{\rho}_{12}$ are the least-square estimates of the standard deviations in the coordinates of the point of intersection and of the correlation coefficient.

Application and Discussion

Recent measurements (15) of solubilities and wet

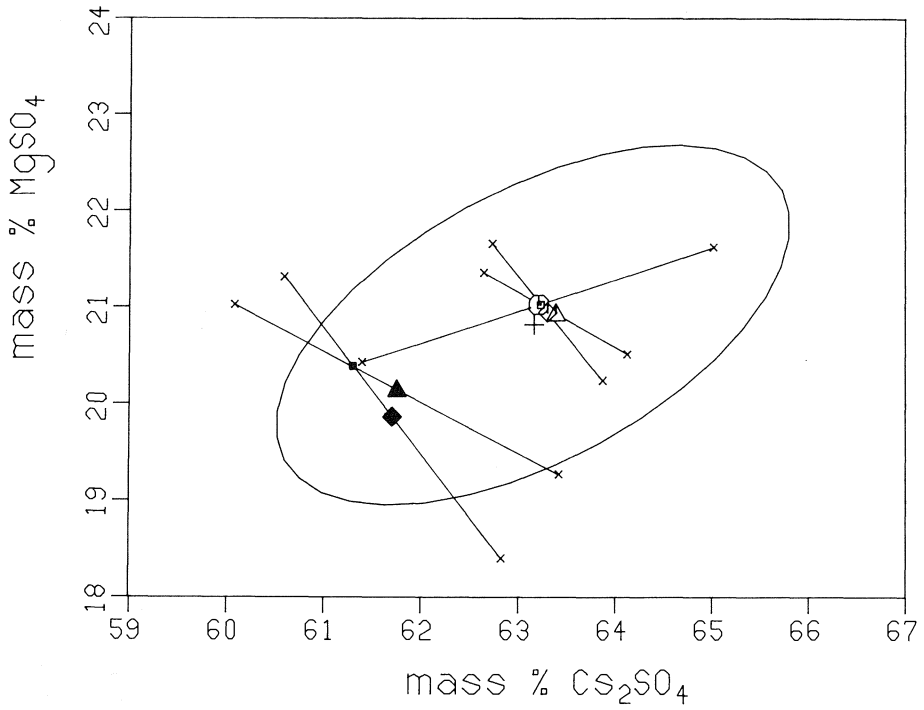

FIG. 3. The 95% confidence ellipses and confidence limits for formation of the compound $Cs_2SO_4 \cdot MgSO_4 \cdot r\ H_2O$ at 100°C. Theoretical solid compositions: ■, $r = 6$; □, $r = 5$. Calculated solid compositions: by least squares, +; by extrapolation, (a) assuming $Cs_2SO_4/MgSO_4 = 1{:}1$, ○; (b) assuming $H_2O/MgSO_4 = 6{:}1$, ▲; (c) assuming $H_2O/Cs_2SO_4 = 6{:}1$, ◆; (d) assuming $H_2O/MgSO_4 = 5{:}1$, △; (e) assuming $H_2O/Cs_2SO_4 = 5{:}1$, ◇. The 95% confidence lines for the extrapolation method each point to a vertex of the composition triangle, terminate in the points marked ×, and are centred on the extrapolated values. The confidence ellipse is centred on the least-squares value.

residue compositions for the system Cs_2SO_4–$MgSO_4$–H_2O will be used to illustrate use of the theory given above. The authors have tabulated data for 19 compositions of this system at 100°C. A plot of these data on a triangular diagram indicates four compositions which, from graphical intersection of tie-lines, appear to correspond to solutions saturated with respect to the solid phase $Cs_2SO_4 \cdot MgSO_4 \cdot 6H_2O$. All subsequent calculations are based on these original data (14) (given as mass fractions of Cs_2SO_4 and $MgSO_4$), and have been carried out using the author's computer program SOLUB, which is a general BASIC/MAXBASIC program for processing solubility data.

Matrices **B**, **C**, and scalar D are computed first, using eqs. [12]–[15], and have the values

$$\mathbf{B} = \begin{bmatrix} 234.227 & -216.085 \\ -216.085 & 1028.58 \end{bmatrix}$$

$$\mathbf{C} = \begin{bmatrix} 10296.2 \\ 7763.42 \end{bmatrix} \qquad D = 812060$$

Components 1, 2 are Cs_2SO_4, $MgSO_4$ respectively. The coefficients of the point of intersection of the tie-lines are, from eq. [17], $\hat{x}_1 = 63.16\ (0.53)$; $\hat{x}_2 = 20.82\ (0.25)$ mass%, with estimated standard deviations in parentheses, correlation coefficient $\hat{\rho}_{12} = 0.4402$ and overall standard deviation 3.643 (mass%)^2 (eqs. [30], [31]). The individual contributions to the area, eq. [6], are $2A_k = 5.540, -8.356, 2.141, 1.039$ (mass%)^2. If the theoretical point of intersection corresponds to $Cs_2SO_4 \cdot MgSO_4 \cdot 6H_2O$, then $x_1^0 = 61.30$, $x_2^0 = 20.39$ mass%, and the quantity $u = 6.186$ can be calculated from eq. [33]. From tables (14), the critical value of $F_{2,2,0.05} = 19.00$, so the hypothesis that the calculated point of intersection coincides with the theoretical point is acceptable at the 95% confidence level. The semi-axes of the 95% confidence ellipse are $a = 1.402$, $b = 2.923$ (eqs. [38], [39]), and a lies at an angle 28.8° with coordinate axis 2 (eq. [37]). Figure 3 shows this confidence ellipse centred on the calculated point of intersection. The calculated formula of the solid, with standard deviations in parentheses and component 2 as a reference, is 1.009 (0.011) $Cs_2SO_4 \cdot MgSO_4 \cdot$ 5.14 (0.27) H_2O, and suggests that a pentahydrate double salt would represent the solid phase equally well. This is in fact the case. The parameters are $x_1^0 = 63.23$, $x_2^0 = 21.03$, $u =$

Can. J. Chem. Downloaded from www.nrcresearchpress.com by 210.87.254.105 on 09/06/12
For personal use only.

Can. J. Chem. Downloaded from www.nrcresearchpress.com by 210.87.254.105 on 09/06/12
For personal use only.

0.396 (see Fig. 3). The authors have also analyzed a synthetic sample of the double salt, and found 45.32 mass% Cs, 4.120 Mg, 11.01 S (theory for hexahydrate: 45.03 Cs, 4.117 Mg, 10.86 S; for pentahydrate; 46.45 Cs, 4.247 Mg, 11.20 S). The analyses correspond more closely to the hexahydrate, and thus provide independent evidence for its existence.

If the same data are now analyzed by algebraic extrapolation, two cases are possible. (a) If the ratio $Cs_2SO_4/MgSO_4$ is fixed at unity, $\hat{x}_1 = 63.21$ (1.14), $\hat{x}_2 = 21.03$ (0.38) mass% (eq. [40]), and $t = 3.358$ using $x_1^0 = 61.30$, or $t = 0.027$ using $x_1^0 = 63.23$ mass%. The critical value of $t_{3,\,0.05} = 3.182$, so the pentahydrate is an acceptable formula at a 95% confidence level, but the hexahydrate is not. The calculated formula of the salt is $Cs_2SO_4 \cdot MgSO_4 \cdot 5.01$ (0.057) H_2O, and the 95% confidence limits on the theoretical values are $\pm$ 1.81 mass%. (b) If the ratio $H_2O/MgSO_4$ is fixed at 6, $\hat{x}_1 = 61.76$ (1.05), $\hat{x}_2 = 20.15$ (0.55) mass%, and $t = 0.863$ using $x_1^0 = 61.30$. If the ratio is 5, $\hat{x}_1 = 63.39$ (0.47), $\hat{x}_2 = 20.94$ (0.27), and $t = 0.668$ using $x_1^0 = 63.23$ mass%. Thus, both pentahydrate and hexahydrate are acceptable formulae at the 95% confidence level. The formula of the salt is 1.019 (0.045) $Cs_2SO_4 \cdot MgSO_4 \cdot 6H_2O$ or 1.007 (0.020) $Cs_2SO_4 \cdot MgSO_4 \cdot 5H_2O$.

Figure 3 illustrates the data given above, and includes as well the nonindependent points found by extrapolation, the 95% confidence limits for all extrapolated values, and the 95% confidence ellipse. The figure shows clearly that, in this case, much the same information can be obtained from either least squares or extrapolation. However, in all generality, the least-squares triangle gives a unique point of intersection and one confidence ellipse for each theoretical point of intersection. By contrast, the extrapolation method gives three independent points of intersection and three sets of confidence limits for the two theoretical values, and it is useful to examine all five different points of intersection and the corresponding confidence limits to obtain a complete picture of the results.

In summary, the least-squares triangle provides a convenient and unambiguous method of finding compositions of solid phases from solubility and wet residue or initial composition data which is free from the ambiguities and assumptions inherent in the extrapolation method. More generally, the least-squares triangle can be used to find the point of intersection of any family of straight lines, each member of which is determined by two points.

Acknowledgements

The author wishes to thank Prof. M. M. Ali, Dept. of Statistics, University of Western Ontario, for making the suggestion that the least-squares triangle might provide a useful approach to this problem. This research was supported in part by a grant from the Natural Sciences and Engineering Research Council of Canada (NSERC).

1. F. A. H. Schreinemakers. Z. Phys. Chem. Stoechiom. Verwandtschaftsl. **11**, 75 (1893).
2. W. D. Bancroft. J. Phys. Chem. **6**, 178 (1902).
3. A. E. Hill and J. E. Ricci. J. Am. Chem. Soc. **53**, 4305 (1931).
4. M. L. Delyon. Bull. Soc. Chim. Fr. **3**, 1811 (1936).
5. L. Filipescu and M. Filipescu. Rev. Chim. Bucharest, **28**, 538 (1977).
6. W. C. Hamilton. Statistics in physical science. Ronald Press, New York. 1964. Chapt. 4; sect. 5.
7. E. M. Mikhail and F. Ackermann. Observations and least squares. IEP, New York. 1976. Chapt. 6; sect. 6.1, 6.2; chapt. 11, sect. 11.1.
8. A. S. Smith. Chem. Eng. **54**, 123 (1947).
9. H. Schott. J. Chem. Eng. Data, **6**, 324 (1961).
10. E. L. Heric. J. Chem. Eng. Data, **7**, 467 (1962).
11. J. W. Lorimer, C. Kalidas, and K. S. Johnson. Solubility data series. Alkaline earth sulfates in all solvents. Pergamon Press, London. In preparation.
12. G. I. Gorshtein and N. I. Silantyeva. Zh. Obshch. Khim. **23**, 1920 (1953); J. Gen. Chem. USSR (Engl. Transl.) **23**, 1355 (1953).
13. D. Trandefelov and Chr. Balarew. Izv. Otd. Khim. Nauki, Bulg. Akad. Nauk, **1** (2), 73 (1968).
14. M. Abramowitz and I. A. Stegun (*Editors*) Handbook of mathematical functions. Natl. Bureau of Standards, Washington. 1964. Table 26.9.
15. V. G. Shevchuk, D. A. Storozhenko, and N. M. Lazorenko. Zh. Neorg. Khim. **24**, 3140 (1979); Russ. J. Inorg. Chem. (Engl. Transl.) **24**, 1747 (1979).

Ultrasonic dispersion studies in 3-methylcyclohexanone

BUDIDETI ANANDA REDDY AND NAGINENI PRABHAKARA RAO
Sri Venkateswara University Physical Laboratories, Tirupati 517 502, India

Received February 13, 1981

BUDIDETI ANANDA REDDY and NAGINENI PRABHAKARA RAO. Can. J. Chem. **59**, 3084 (1981).

Using a variable path interferometer, ultrasonic velocity dispersion in 3-methylcyclohexanone was studied in the temperature range 323.15 K to 363.15 K and in the frequency range 0.5 MHz to 5.0 MHz. The relaxation parameters were evaluated from the experimental data. These values were utilised to evaluate the energy parameters; the differences in the enthalpy (ΔH_0), the free energy (ΔG_0), and the entropy (ΔS_0) are 2.79 kcal/mol, 0.88 kcal/mol, and 5.9 cal/mol K, respectively. The enthalpy (ΔH_r) for the backward reaction was 7.63 kcal/mol.

BUDIDETI ANANDA REDDY et NAGINENI PRABHAKARA RAO. Can. J. Chem. **59**, 3084 (1981).

Utilisant un interféromètre à trajectoire variable on a étudié la vitesse ultrasonique de dispersion de la méthyl-3 cyclohexanone dans l'intervalle de temperature allant de 323,15 K à 363,15 K et à des fréquences variant de 0,5 à 5,0 MHz. A partir des données expérimentales, on a évalué les paramètres de relaxation. On a utilisé ces valeurs pour évaluer les paramètres énergétiques tels les variations d'enthalpie (ΔH_0), l'énergie libre (ΔG_0) et l'entropie (ΔS_0) qui sont respectivement 2,79 kcal/mol, 0,88 kcal/mol et 5,9 cal/mol/K. L'enthalpie (ΔH_r) de la réaction inverse est de 7,63 kcal/mol.

[Traduit par le journal]

Introduction

Ultrasonic relaxation phenomena have been studied in alicyclic compounds, mainly substituted cyclohexanes, by many workers (1–6) who suggested that the mechanism involved the perturbation of equilibrium by ultrasonic wave.

Physico-chemical (7) evidence indicates that the substituted cyclic compounds take mainly a chair configuration with the substituted atom in the equatorial position. This isomer is believed to be in equilibrium with another having a chair configuration and an axial substituent, the two isomers being rapidly interconvertible by a process often called ring inversion in which no bonds are broken. The energy difference between the two isomers could be evaluated from the measured variation with temperature of the magnitude of the dispersion. The barrier hindering rotation could be found from the associated variation of the relaxation frequency with temperature.

In the present work, the dispersion and the relaxation frequency for 3-methylcyclohexanone at different temperatures were calculated using ultrasonic velocity measurements. These values are used to evaluate the energy parameters.

Experimental

Ultrasonic velocities were measured using a variable path interferometer technique (8). To obtain the velocities at frequencies 0.5, 1, 2, 3, and 5 MHz, a tri-tet (9) crystal controlled rf oscillator was used to excite the quartz transducers of fundamental frequencies of 0.5, 1, and 2 MHz.

To obtain the measurements at different temperatures, the interferometer was immersed in a thermostatic water bath whose temperature could be maintained with an accuracy of ± 0.1°C. The accuracy in measurement of velocity is $\pm 0.003\%$.

3-Methylcyclohexanone was supplied by Riedel-Dehaen Ag seelze-Hanover and was of purity 97%.

Theory

The equilibrium between the equatorial and axial conformers is equivalent to a two state process of the kind $A \rightleftharpoons B$ with A having the lower energy. Such a two-state process is characterized by a single relaxation time and at any given temperature the ultrasonic relaxation arising from the perturbation of the above equilibrium is accompanied by a variation in velocity given by [1],

$$[1] \quad \frac{C_\infty^2 - C^2}{C_\infty^2 - C_0^2} = \frac{1}{1 + (f/f_r)^2}$$

where C is the velocity at frequency f, C_0 is the velocity at low frequency ($f \ll f_r$), C_∞ is the velocity at high frequencies ($f \gg f_r$) and f_r is the relaxation frequency.

If C_1, C_2, and C_3 are the velocities at 1, 2, and 3 MHz, respectively, substituting these values in [1] we get

$$[2] \quad C_\infty^2 = \frac{5C_2^2C_3^2 - 8C_1^2C_3^2 + 3C_1^2C_2^2}{8C_2^2 - 5C_1^2 - 3C_3^2}$$

Using the above equation C_∞ was calculated from the experimental data.

The equilibrium parameters ΔH_0, ΔG_0, ΔS_0, and ΔV_0, the differences in enthalpy, Gibbs free energy, entropy and volume, respectively, between 1 mol of axial and equatorial isomers are related to C_0 and C_∞ as follows (10).

$$[3] \quad F = (2C_p^2J(C_\infty - C_0)/\theta^2C_i^2RTM)^{1/2}$$

0008-4042/81/213084-03$01.00/0
©1981 National Research Council of Canada/Conseil national de recherches du Canada

Can. J. Chem. Downloaded from www.nrcresearchpress.com by 210.87.254.105 on 09/06/12
For personal use only.

Can. J. Chem. Downloaded from www.nrcresearchpress.com by 210.87.254.105 on 09/06/12
For personal use only.

$$[4] \quad = \left(\frac{\Delta H_0}{RT} - \frac{\Delta V_0 C_p}{\theta V_0 RT}\right)\left[\frac{\exp(\Delta G_0/2RT)}{1 + \exp(\Delta G_0/RT)}\right]$$

Assuming ΔV_0 equals zero, [4] becomes

$$[5] \quad F = \frac{\Delta H_0}{RT}\frac{\exp(\Delta G_0/2RT)}{1 + \exp(\Delta G_0/RT)}$$

In these equations C_p is the molar specific heat capacity at constant pressure, J the conversion factor from joules to ergs, θ the thermal expansion coefficient, R the gas constant, T the absolute temperature, M the molecular weight, V_0 the molar volume, and C_i is equal to $(C_\infty + C_0)/2$. If ΔH_0 and ΔS_0 are both independent of the temperature, the algebraic solution of [5] is

$$[6] \quad \frac{\Delta G_0}{RT} = 2 \ln\left[\frac{(\xi_1 + 1) + [F_1^2 + (\xi_1 + 1)^2]^{1/2}}{F_1}\right]$$

and

$$[7] \quad \frac{\Delta H_0}{RT} = 2[F_1^2 + (\xi_1 + 1)^2]^{1/2}$$

where

$$\xi_1 = \frac{T_1}{F_1}\left[\frac{dF}{dT}\right]_1$$

In the above equation subscript 1 refers to the value for a given temperature T_1. The value of ΔS_0 was obtained from the relation

$$[8] \quad \Delta S_0 = (\Delta H_0 - \Delta G_0)/T$$

The slope of the plot of $1/T$ vs. $\log f_r$ yields the value of activation enthalpy for the backward reaction.

Results

For a single relaxation process at a given temperature and pressure, the shape of $\log(C_\infty^2 - C^2)$ vs. $\log f$ is independent of the numerical values of the relaxation parameters; i.e. f_r and $(C_\infty^2 - C_0^2)$. Hence a template of this theoretical curve with the relaxation frequency marked on it was made on transparent material. This template was moved parallel to the axis and the theoretical curves fitting the experimental data are shown in Fig. 1. The relaxation frequency was read directly from the graph. The value of the ordinate asymptote attained at $f \ll f_r$ as read from the graph gave values of $(C_\infty^2 - C_0^2)$. C_∞^2 was calculated using [2].

The velocity data measured at different frequencies from 0.5 MHz to 5.0 MHz and at different temperatures from 323.15 K to 363.15 K are presented in Table 1 and the relaxation parameters evaluated are

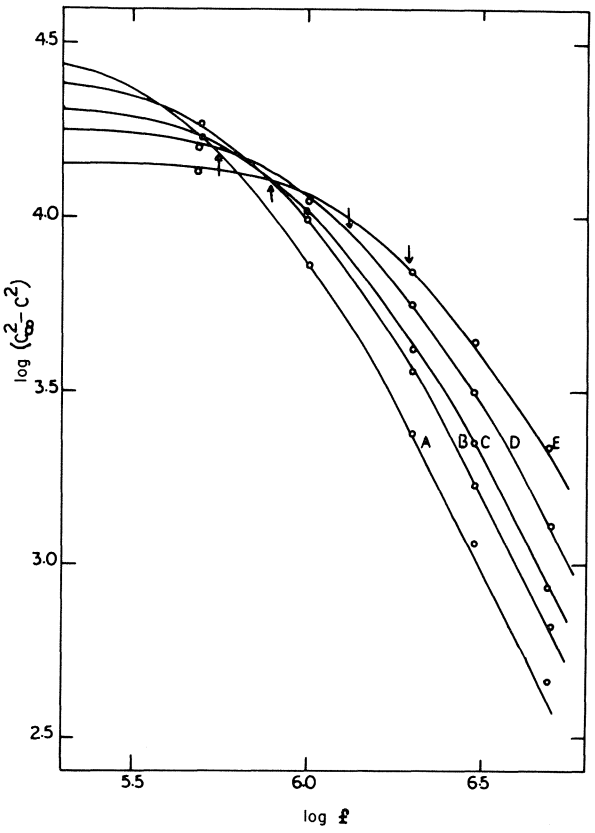

FIG. 1. Variation of $\log(C_\infty^2 - C^2)$ vs. $\log f$ in 3-methylcyclohexanone. *A*, 323.15 K; B, 333.15 K; *C*, 343.15 K; *D*, 353.15 K; *E*, 363.15 K.

TABLE 1. Ultrasonic velocity variation with frequency and temperature in 3-methylcyclohexanone

	Ultrasonic velocities (m/s)				
T (K)	0.5 MHz	1 MHz	2 MHz	3 MHz	5 MHz
323.15	1287.45	1279.59	1281.46	1281.95	1282.30
333.15	1238.51	1242.81	1244.58	1245.33	1245.74
343.15	1203.83	1206.62	1208.69	1209.14	1210.57
353.15	1170.24	1172.10	1173.98	1175.65	1176.44
363.15	1137.44	1138.17	1140.20	1141.22	1142.13

TABLE 2. Relaxation frequencies and dispersion values for 3-methylcyclohexanone

T (K)	f_r (MHz)	C_∞ (m/s)	C_0 (m/s)	$C_\infty - C_0$ (m/s)	F
323.15	0.5623	1282.42	1271.88	10.83	1.2719
333.15	0.7943	1246.00	1236.84	9.66	1.2323
343.15	1.0000	1210.86	1202.59	8.27	1.1736
353.15	1.3180	1176.99	1169.41	7.58	1.1222
363.15	1.9498	1143.09	1136.89	6.20	1.0668

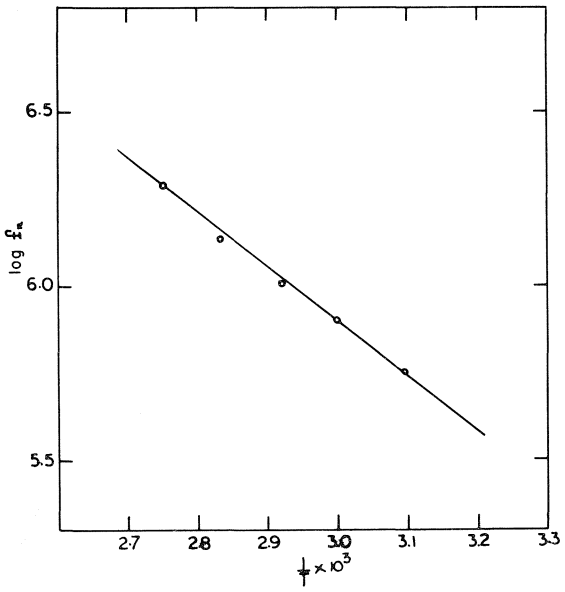

FIG. 2. Variation of $1/T$ vs. log f_r for 3-methylcyclohexanone.

given in Table 2. The plots of log $(C_\infty{}^2 - C^2)$ vs. log f at different temperatures and the plot of $1/T$ vs. log f_r for 3-methylcyclohexanone are shown in Figs. 1 and 2, respectively. The energy parameters ΔG_0, ΔH_0, and ΔS_0, the change in free energy, enthalpy and entropy between two isomers, evaluated from [6]–[8], are 0.88 kcal/mol, 2.79 kcal/mol, and 5.9 cal/mol K, respectively. The activation enthalpy for the backward reaction, calculated from the slope of the plot of $1/T$ vs. log f_r, was 7.63 kcal/mol.

Discussion

Replacement of the equatorial hydrogen atom by a methyl group at C_3 in cyclohexanone would set up additional steric repulsion, as a result of which the difference in energy between 3-methylcyclohexanones with equatorial and axial methyl should be less than the normal difference of 1.7 kcal/mol (11) between equatorial and axial methyl groups in cyclohexane. This supposed reduction in ΔG_0 was called the 3-methyl ketone effect (12) and was estimated to amount to about 0.85 kcal/mol (11). Therefore, in the present relaxation process the free energy of 0.88 kcal/mol between two isomers is in agreement with the above result. The relaxation frequency observed in 3-methylcyclohexanone is of the same order as that observed in substituted cyclohexanes (1, 2, 4). Hence the molecular mechanism in the present relaxation process may be attributed to ring inversion.

Acknowledgement

The authors thank Professor K. Sreerama Murthy for his encouragement and interest in this work.

1. J. KARPOVICH. J. Chem. Phys. **22**, 1767 (1954).
2. J. E. PIERCY. J. Acoust. Soc. Am. **33**, 198 (1961).
3. J. E. PIERCY and S. V. SUBRAHAMANYAM. J. Chem. Phys. **42**, 4011 (1965).
4. N. P. RAO and K. C. REDDY. Acustica, **40**, 54 (1978).
5. V. HYDERKHAN and S. V. SUBRAHAMANYAM. Acustica, **29**, 350 (1973).
6. J. LAMB and J. W. C. SHERWOOD. Trans. Faraday Soc. **51**, 1674 (1955).
7. W. G. DAUBEN and K. S. PITZER. Conformational analysis of steric effects in organic chemistry. John Wiley and Sons, New York. 1954.
8. K. V. SIVAKUMAR, K. C. REDDY, and S. V. SUBRAHAMANYAM. Z. Physik. Chem. Neue Folge. **83**, 141 (1973).
9. J. J. DE FRANCE. General electronics circuits, Holt, Rinehart and Winston, New York. 1966. p. 398.
10. G. ALLEN. Molecular structure and properties. MTP International review of science, physical chemistry series one. Vol. 2. University Park Press Inc. U.S.A. and Canada.
11. E. L. ELIEL, N. L. ALLINGER, S. J. ANGYAL, and G. A. MORRISON. Conformational analysis. John Wiley and Sons, Inc., New York. 1965.
12. N. L. ALLINGER, H. M. BLATTER, L. A. FREIBERG, and G. M. KARKOWSTI. J. Am. Chem. Soc. **88**, 2999 (1966).

Can. J. Chem. Downloaded from www.nrcresearchpress.com by 210.87.254.105 on 09/06/12
For personal use only.

Photolysis of 5,5-dimethyl-4-phenyl-Δ^1-1,2,4-triazolin-3-one. Fragmentation to nitrogen, carbon monoxide, and isopropylidene phenyl amine

LUBOMIRA M. CABELKOVA-TAGUCHI AND JOHN WARKENTIN

Department of Chemistry, McMaster University, Hamilton, Ont., Canada L8S 4M1

Received December 2, 1980[1]

LUBOMIRA M. CABELKOVA-TAGUCHI and JOHN WARKENTIN. Can. J. Chem. **59**, 3087 (1981).

Photolysis of 5,5-dimethyl-4-phenyl-Δ^1-1,2,4-triazolin-3-one (**2**) produces the same products as thermolysis; namely, nitrogen, carbon monoxide, and isopropylidene phenyl amine (acetone anil). The quantum yield for direct photolysis of **2** in methanol with 313 nm light is 0.066. Sensitization with benzophenone in the same solvent, and quenching with 1,3-cyclohexadiene, revealed that photolysis of **2** involves a triplet excited state. The most likely photo processes are thought to involve initial cleavage of the C3—N4 bond or the C3—N2 bond (Norrish, type 1 cleavage).

LUBOMIRA M. CABELKOVA-TAGUCHI et JOHN WARKENTIN. Can. J. Chem. **59**, 3087 (1981).

La photolyse de la diméthyl-5,5 phényl-4 Δ^1 triazoline-1,2,4 one-3 (**2**) conduit aux mêmes produits que la thermolyse; soit en particulier, l'azote, le monoxyde de carbone et l'isopropylidene phénylamine (acétone anil). Le rendement quantique de la photolyse directe du composé **2** dans le méthanol à 313 nm est de 0,066. La sensibilisation avec la benzophénone dans le même solvant et le piégeage par le cyclohexadiène-1,3 indiquent que la photolyse du composé **2** implique un état excité triplet. On pense que les procédés photolytiques les plus communs font intervenir la rupture initiale de la liaison C3—N4 ou de la liaison C3—N2 (rupture de type I de Norrish).

[Traduit par le journal]

Introduction

The thermolysis behaviour of a number of 5-membered heterocyclic rings (**1**) has been reported (1–7). Some of them undergo competitive fragmentations according to paths A and B, eq. [1],[2] and the

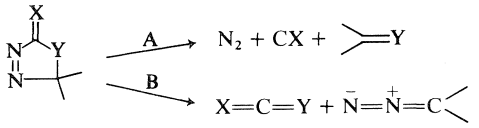

[1]

1*a* X = Y = O
b X = N—N=CR_2, Y = O
c X = NAr, Y = O
d X = S, Y = NAr
e X = O, Y = NAr

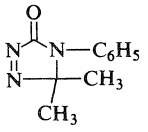

2

diazoalkane fragment from path B can undergo subsequent reactions which have some synthetic utility (2, 3, 4).

Others fragment largely or exclusively by path A only[3] while still others fragment exclusively according to path B.[4] In view of this intriguing and potentially exploitable chemistry we became interested in finding out which pathway, A or B, is followed during photolysis or if photolysis actually involves a third set of products. To this end we chose to study 5,5-dimethyl-4-phenyl-Δ^1-1,2,4-triazolin-3-one (**2**).

Experimental

Compound **2**, prepared by oxidative cyclization of acetone-4-phenylsemicarbazone on alumina (7, 8), melted at 142–143°C (lit. (8) mp 143–144°C); uv (95% EtOH, λ_{max}, log ε): 275 nm (3.35), 375 nm (2.63); ^{1}H nmr (δ, $CDCl_3$) : 1.58 (s, 6H), 7.0–7.6 (m, 5H).

For product studies, **2** (0.15 g, 0.77 mmol) in methanol (50 mL, spectroscopic grade) was irradiated through quartz in a Srinivasan–Griffin Photochemical Reactor (Rayonet) fitted with 12 lamps (253.7 nm). The solution was purged with argon before and during irradiation and 1 mL aliquots were withdrawn at 1 h intervals to monitor the reaction. To an aliquot was added 1 mL of a stock solution of 1,3,5-trimethoxybenzene (**3**) in methanol, most of the solvent was evaporated with a rotary evaporator, and the height of the methyl singlet in the ^{1}H nmr spectrum of **2** was compared to that of the internal standard (**3**). After 5 h irradiation, when **2** could no longer be detected, the solution was divided into two parts, one of which was analyzed by glpc, which showed only acetone and aniline. The liquid residue left after removal of the volatile components, under vacuum, from the second portion, was examined by ^{1}H nmr, ir, and uv. All three spectra were those of aniline.

Quantum yield experiments were done with an optical bench and a Bausch and Lomb Model 33-86-01 high intensity monochromator fitted with an achromatic condenser lens and coupled to an Osram HBO 200 W super pressure mercury lamp[5] (9). The slits of the grating were set to give a band pass of 15 nm at 313 nm. Absorbances of ferrioxalate actinometry solutions

[1]Revision received July 16, 1981.

[2]Compounds which show this duality are **1***a* (2, 4, 6), **1***b* (1), and **1***c* (2).

[3]For example **1***d* (5).

[4]For example **1***e* (7).

[5]We thank Professor J. J. McCullough for the loan of this equipment.

0008-4042/81/213087-03$01.00/0

©1981 National Research Council of Canada/Conseil national de recherches du Canada

Can. J. Chem. Downloaded from www.nrcresearchpress.com by 210.87.254.42 on 09/06/12
For personal use only.

Can. J. Chem. Downloaded from www.nrcresearchpress.com by 210.87.254.42 on 09/06/12
For personal use only.

were determined with a Bausch and Lomb Precision Spectrophotometer, Model 33-26-50. The latter was calibrated by the procedure of Hatchard and Parker (10).

The concentration of **2** in aliquots was determined by ^{1}H nmr, using **3** as internal standard, by measuring peak heights. The latter were converted to concentrations using calibration charts prepared from standard solutions containing both **2** and **3**. Thus, irradiation for 10 h at 313 nm, with absorption of 7.3×10^{-4} Einstein of light, led to disappearance of 9.0 mg (4.8×10^{-5} mol) from a solution containing initially 39 mg (2.1×10^{-4} mol) of **2** in 13 mL of methanol, corresponding to a quantum yield of 0.066. A duplicate run gave the same value.

For benzophenone-sensitized photolysis, the solution cell contained 39 mg (2.1×10^{-4} mol) of **2** and 234 mg (1.29×10^{-3} mol) of benzophenone (Anal. Reagent, BDH) in a solution prepared with 13 mL of methanol. The quantum efficiency of conversion of ferrioxalate was taken to be 1.23.

Duplicate quantum yield determinations using ^{1}H nmr to monitor consumption of **2**, as described above, gave apparent values of 0.20 and 0.22. Correction of these for the fraction (ca. 1/3) of light absorbed by **2** under the experimental conditions gave a quantum yield of 0.3 for benzophenone-sensitized photolysis of **2**.

Analogous photolysis of **2** (39 mg, 2.1×10^{-4} mol) in the presence of freshly-distilled 1,3-cyclohexadiene (84 mg, 1.0×10^{-2} mol) and methanol (13 mL) for 10 h did not result in any detectable consumption of **2**.

Discussion

Previous work on the thermolysis of **2** showed that it fragments cleanly to nitrogen, carbon monoxide, and isopropylidene phenyl amine (7). However, the latter is very sensitive to hydrolysis and it was obtained free from acetone and aniline only if carefully dried hydrocarbon solvents were used (7). It was partly hydrolyzed during handling; for example, during analysis by glpc (7). Freshly prepared **4** was converted to acetone and aniline when small amounts of **4** were added to the methanol used in the present study. Since there is no straightforward mechanism for the clean formation of acetone and aniline as primary photoproducts from **2**, we conclude that **2** is converted to **4**, which is then hydrolyzed to the products observed.

The higher quantum yield for triplet-sensitized photolysis of **2**, compared to that for direct photolysis, and the suppression of direct photolysis by a known triplet quencher (1,3-cyclohexadiene) (11), indicates that **2** fragments from a triplet excited state. Since that triplet state can be populated by energy transfer from benzophenone triplets (E_t = 69 kcal mol^{-1}), it probably lies less than 69 kcal mol^{-1} above the energy of the ground state of **2**. Moreover, intersystem crossing (isc) (S → T) appears to be inefficient for **2**, since the quantum yield for triplet-sensitized fragmentation of **2** is between 4 and 5 times as large as that for direct photolysis.

Other conclusions are more tentative. The most likely intermediates, by analogy to the known

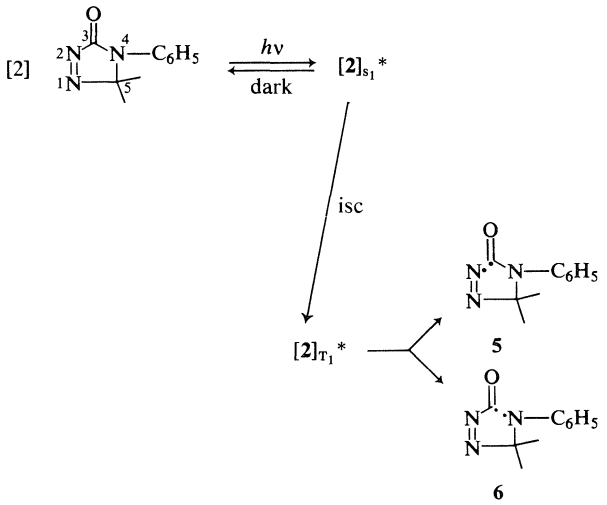

Norrish Type 1 cleavage of carbonyl compounds[6] are diradicals **5** and **6** (eq. [2]). A choice between **5** and **6** on the basis of the present results does not seem possible. Initial cleavage of the N1—C5 bond cannot be excluded either, but a fully-concerted process, involving simultaneous rupture of three bonds from the triplet state of **2**, is symmetry forbidden and can presumably be ignored as a possible mechanism.

From the standpoint of synthetic application, the photolysis of **2**, like its thermolysis, holds little promise. We plan to examine the photolysis of other members of the family **1**, in a search for sources of photogenerated heterocumulenes (eq. [1], path B).

Acknowledgements

This work was financed from a grant provided by the Natural Sciences and Engineering Research Council of Canada. We gratefully acknowledge helpful discussions with Professor J. J. McCullough, who also allowed us to use some of his equipment.

1. P. R. West and J. Warkentin. J. Org. Chem. **33**, 2089 (1968).
2. S. L. Lee, A. M. Cameron, and J. Warkentin. Can. J. Chem. **50**, 2326 (1972).
3. P. C. Ip, K. Ramakrishnan, and J. Warkentin. Can. J. Chem. **52**, 3671 (1974).
4. G. A. MacAlpine and J. Warkentin. Can. J. Chem. **56**, 308 (1978).
5. D. C. Frosst, N. P. C. Westwood, N. H. Werstiuk, L. M. Cabelkova-Taguchi, and J. Warkentin. Can. J. Chem. **55**, 3677 (1977).

[6]There is precedent for Norrish Type 1 cleavage of amides (12, 13) and lactams (14), as well as for N—CO bond cleavage of azocarbonyl compounds (15, 16).

6. A. J. PAINE and J. WARKENTIN. Can. J. Chem. **57**, 2681 (1979).
7. L. M. CABELKOVA-TAGUCHI and J. WARKENTIN. Can. J. Chem. **59**, 100 (1981).
8. J. K. LANDQUIST. J. Chem. Soc. C, 63 (1970).
9. R. M. BOWMAN, T. R. CHAMBERLAIN, C.-W. HUANG, and J. J. MCCULLOUGH. J. Am. Chem. Soc. **96**, 692 (1974).
10. G. C. HATCHARD and C. A. PARKER. Proc. R. Soc. London Ser. B, **140**, 470 (1953).
11. A. A. LAMOLA and N. J. TURRO. Technique of organic chemistry. Vol. 14. *Edited by* P. Leermakers and A. Weissberger. Interscience Publishers, New York. 1969. pp. 99–104.
12. C. H. NICHOLLS and P. A. LEERMAKERS. J. Org. Chem. **35**, 2754 (1970).
13. P. H. MAZZOCCHI and M. BOWEN. J. Org. Chem. **41**, 1279 (1976).
14. P. H. MAZZOCCHI, M. W. BOWEN, and J. KACHINSKY. J. Chem. Soc. Chem. Commun. 53 (1977).
15. P. STILBS, G. AHLGREN, and B. ÅKERMARK. Tetrahedron Lett. 2387 (1972).
16. D. MACKAY, U. F. MARX, and W. A. WATERS. J. Chem. Soc. 4793 (1964).

Can. J. Chem. Downloaded from www.nrcresearchpress.com by 210.87.254.42 on 09/06/12
For personal use only.

Isotope effects in the diphenylpicrylhydrazyl-inhibited thermal polymerization of 2,6-dideuteriostyrene[1]

KARL R. KOPECKY AND MICHAEL C. HALL
Department of Chemistry, University of Alberta, Edmonton, Alta., Canada T6G 2G2

Received March 6, 1981

KARL R. KOPECKY and MICHAEL C. HALL. Can. J. Chem. **59**, 3090 (1981).

There is an inverse isotope effect in the reaction between 2,2-diphenyl-1-picrylhydrazyl DPPH and 2,6-dideuteriostyrene of 0.75 ± 0.07 at 75°C in degassed neat styrene. This result is consistent with the proposal that the reaction involves hydrogen transfer to DPPH from a Diels–Alder dimer of styrene. The rate constant for dimerization of styrene to this dimer is calculated to be 1.8×10^{-10} L mol^{-1} s^{-1} at 75°C.

KARL R. KOPECKY et MICHAEL C. HALL. Can. J. Chem. **59**, 3090 (1981).

Lors de la réaction entre le diphényl-2,2 picryl-1 hydrazyle (DPPH) et le dideutéro-2,6 styrène dégasé agissant comme solvant il y a un effet isotopique inverse de $0,75 \pm 0,07$ à 75°C. Ce résultat est en accord avec la proposition qui stipule que la réaction fait intervenir un transfert d'hydrogène du dimère de Diels–Alder du styrène au DPPH. On a calculé que la constante de vitesse de dimérisation du styrène est de $1,8 \times 10^{-10}$ L mol^{-1} s^{-1} à 75°C.

[Traduit par le journal]

Introduction

The rate of initiation of the polymerization of styrene can be calculated (1) from eq. [1]

[1] $$R_p^2 - R_{p,th}^2 = k_p^2[M]^2R_i/2k_t$$

where R_p is the total rate of polymerization, $R_{p,th}$ is the rate of thermal polymerization, k_p and k_t are the rate constants for propagation and termination, respectively, [M] is the monomer concentration, and R_i is the rate of initiation due to monoradical producing catalysts (initiators). For moderate concentrations of initiators $R_{p,th}$ may be neglected and eq. [1] reduces to eq. [2].

[2] $$R_p^2 = k_p^2[M]^2R_i/2k_t$$

DPPH

In the presence of the stable free radical 2,2-diphenyl-1-picrylhydrazyl, DPPH, there is an induction period during which no polymerization occurs and DPPH is consumed. The rate of disappearance of DPPH, R_{DPPH}, is equal to the value of R_i determined from eq. [2] (2). In the absence of added initiator DPPH still inhibits the thermal polymerization of styrene (3) and is consumed in a zero order process above a concentration of $\sim 1 \times 10^{-4}$ *M* at 60°C. Under these conditions R_{DPPH} is 1.1×10^{-8} *M* s^{-1} (3*a*). This is 85 times greater than the calculated rate of the thermal initiation of radicals, $R_{i,th} = 1.3 \times 10^{-10}$, which can be obtained from eq. [3] (3*a*).

[3] $$R_{p,th} = k_p^2[M]^2R_{i,th}/2k_t$$

The tentative explanation for this discrepancy proposed that a small fraction of the 1,4-diphenyl-1,4-butadiyl diradical **1**, reaction [4], which had

[4] 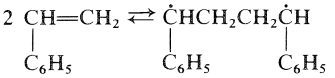

1

been suggested earlier (1) to be responsible for the thermal initiation, is intercepted by DPPH. However, **1** cyclizes too rapidly to be involved in the formation of high polymer (4) and it is unlikely that it could be scavenged by the low concentration of DPPH used.

The inhibition by DPPH of the thermal polymerization might be accounted for in terms of the currently accepted mechanism for the thermal initiation, reactions [5]–[7] (5), where $M_n\cdot$ is a growing polymer chain.

[5] 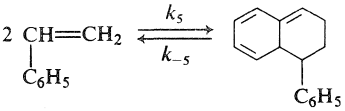

2

[6] 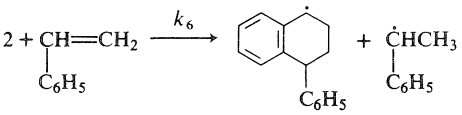

3

[1]This research was supported by a grant from the National Research Council of Canada.

0008-4042/81/213090-05$01.00/0
©1981 National Research Council of Canada/Conseil national de recherches du Canada

Can. J. Chem. Downloaded from www.nrcresearchpress.com by 210.87.254.40 on 09/06/12
For personal use only.

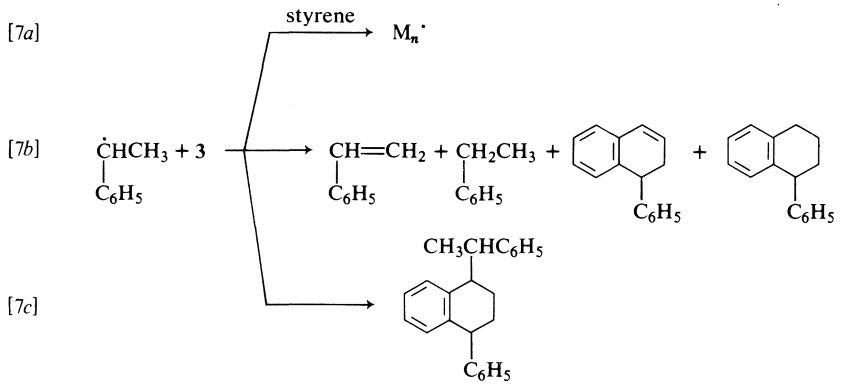

In this mechanism hydrogen atom transfer from the reversibly formed styrene Diels–Alder dimer **2** to a third styrene molecule results in the formation of a pair of radicals, some of which initiate polymer chains. On the basis of this mechanism for the thermal initiation the inhibition by DPPH occurs as the result of hydrogen atom abstraction from the Diels–Alder adduct **2**, reaction [8] (6), to produce the radical **3**

[8] DPPH + **2** → **3** + DPPH—H

[9] DPPH + **3** → products

and the hydrazine DPPH—H. The radical **3** would then consume a second DPPH, reaction [9].

The present study was undertaken to test this proposal by determining the isotope effect in the thermal reaction between DPPH and styrene using 2,6-dideuteriostyrene. The accompanying paper reports the products of the reaction (7).

Results

The rates of disappearance of DPPH in both normal styrene and in 2,6-dideuteriostyrene (91.7 mol% styrene-d_2, 8.3 mol% styrene-d_1, prepared as previously described (8)), Table 1, were initially zero order with respect to DPPH, Fig. 1. The point at which the rates deviated from zero order dependence varied with the initial concentration of DPPH and was $\sim 7 \times 10^{-5}\,M$ DPPH in ordinary styrene when the initial DPPH concentration was $1.8 \times 10^{-4}\,M$, and $\sim 2 \times 10^{-4}\,M$ DPPH in the styrene-d_2 when the initial concentration of DPPH was $7 \times 10^{-4}\,M$. The rates were monitored by following the decrease in absorption of DPPH at 525 nm in degassed, neat styrene at 75°C. The rate of disappearance of DPPH in a sample of synthetic styrene prepared by the route used for the preparation of the deuterated material was the same as that in purified commercial styrene. The rate is quite reproducible and the average value, 2.42×10^{-8} mol $L^{-1}\,s^{-1}$, compares with a value 30% greater than this 3.19×10^{-8} mol $L^{-1}\,s^{-1}$ at 75°C, as estimated from a figure given in the original study (3*a*). The reason for this discrepancy is not known, but the rate of disappearance of DPPH is sensitive to oxygen (3*a*) and presumably to other impurities.[2]

In the deuterated styrene the rate was found to be significantly greater, $R'_{DPPH} = 3.19 \times 10^{-8}$ mol $L^{-1}\,s^{-1}$, than in normal styrene. Correcting (9) for isotopic purity, the isotope effect R_{DPPH}/R'_{DPPH} is 0.75 ± 0.07.

Discussion

The isotope effect found here for the disappearance of DPPH in styrene in the absence of added initiators lends support to the proposal (6) that reactions [5] and [8] are involved in which the first formed Diels–Alder dimer of styrene **2** suffers hydrogen atom transfer to DPPH to produce the radical **3** and DPPH—H as initial products. Further support results from a product study of the reaction (7). The order of the reaction with respect to styrene was not determined in this work but the original report (3*a*) that the reaction is second order with respect to styrene has been confirmed (10). In this sequence of reactions hydrogen atom transfer to DPPH will be the fast step since the rate of disappearance of DPPH obeys a zero order dependence on the concentration of DPPH. The formation of the Diels–Alder adduct **2** will then be the rate determining step, and the isotope effect observed is the isotope effect for formation of **2**. The inverse isotope effect that is found for this reaction is consistent with what is expected for the effect of deuterium substitution on a carbon atom which is undergoing sp^2 rehybridization during the

[2]A referee has suggested that a possible reason for this discrepancy is the fact that the earlier work was done before it was recognized that DPPH complexes with solvents and that DPPH was not purified nor freed from complexed solvent.

Can. J. Chem. Downloaded from www.nrcresearchpress.com by 210.87.254.40 on 09/06/12
For personal use only.

Can. J. Chem. Downloaded from www.nrcresearchpress.com by 210.87.254.40 on 09/06/12
For personal use only.

TABLE 1. Rates of disappearance of DPPH in degassed styrene at 75°C

Monomer	Run	[DPPH] × 10^4	R_{DPPH} × 10^8 (mol L^{-1} s^{-1})
Styrene	9	1.39	2.14
	10[a]	1.86	2.54
	11	1.87	2.48
	12	1.87	2.50
	23	1.90	2.70
	41	1.82	2.46
	42	1.90	2.10
			Average 2.42±0.16[b]
2,6-Dideuteriostyrene	34	8.83	3.05
	35	9.95	3.21
	36	6.64	3.14
	37	8.83	3.19
	46	6.97	3.23
	47	7.17	3.35
			Average 3.19±0.07[b]

[a]Synthetic styrene.
[b]Average error.

course of the reaction (9, 11). While the magnitude of the inverse isotope effect found here is greater than usually observed for cycloaddition reactions, $k_H/k_D \sim 0.85$–0.95 per deuterium (10), it is still well within the maximum predicted for an inverse secondary isotope effect of 0.46 (12).

Since two DPPH radicals are consumed each time a molecule of **2** is intercepted the rate of formation of **2** is $(1/2)R_{DPPH}$ or 1.2×10^{-8} mol L^{-1} s^{-1} at 75°C. The rate constant k_5 for the dimerization of styrene to **2** is then 1.8×10^{-10} L mol^{-1} s^{-1} (calculated using a value of 0.855 for the density of styrene at 75°C (12)).[3] This value is in good agreement with the value of 7×10^{-11} L mol^{-1} s^{-1} at 64°C which was obtained by monitoring the increase at 320 nm of an absorption in neat styrene that was attributed to the dimer **2** (13).

The factor of 85 between R_{DPPH} and $R_{i,th}$ at 60°C can be explained in terms of reactions [5] to [9] (10). In the presence of sufficient DPPH all the molecules of **2** are consumed by reaction [8] as soon as they are formed. In the absence of DPPH only a small fraction of the **2** molecules formed will initiate polymerization. Several reactions occur that make **2** a very inefficient initiator. In the mechanism considered here $R_{i,th}$ is given by eq. [10],

$$[10] \quad R_{i,th} = 2k_5k_6f[M]^3/(k_{-5} + \Sigma k_s)$$

[3]This should be a minimum number for the value of k_5. There will be some reaction in the original solvent cage between **3** and DPPH—H to produce DPPH and 1-phenyl-1,2,3,4-tetrahydronaphthalene. Thus less than 1 mole of DPPH is consumed for each mole of **2** that is intercepted. When the concentration of DPPH—H is great enough it can compete with DPPH for **3** outside the solvent cage as well. This results in a decrease in the rate of disappearance of DPPH after a time which depends upon the initial concentration of DPPH.

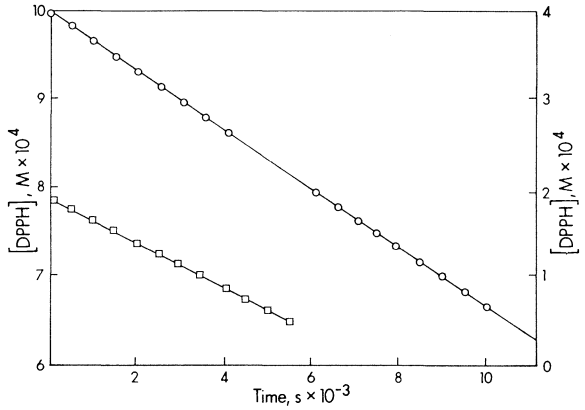

FIG. 1. Disappearance of DPPH in normal (□) and in 2,6-dideuteriostyrene (○).

where k_5 and k_{-5} are the rate constants for formation of **2** and for reversion of **2** to styrene, respectively, k_6 is the rate constant for hydrogen atom transfer from **2** to styrene, Σk_s is the sum of the rate constants for other reactions that consume **2** and f is the fraction of the radicals which are formed according to reaction [6] that reacts with styrene to form growing polymer chains, reaction [7*a*]. With the radical initiator azoisobutyronitrile only 50–55% of the radicals produced react with styrene to initiate polymerization (14). The remainder undergoes coupling and disproportionation within the solvent cage. The radical pair produced according to reaction [6] will undergo coupling and disproportionation reactions to a greater extent than that from azoisobutyronitrile because the former is born without an intervening nitrogen molecule. This leaves a smaller fraction left to initiate polymerization. An alternate route to the trimer of

Can. J. Chem. Downloaded from www.nrcresearchpress.com by 210.87.254.40 on 09/06/12
For personal use only.

reaction [7*c*] is an ene reaction between styrene and **2** (15) which would, of course, divert some more of **2** from initiation. Another contributor to the inefficiency of **2** as an initiator is the reversal of the reaction that forms **2**. The overall rate of initiation is third order in styrene which requires that most **2** formed must revert to monomer (6). Another reaction which will divert **2** from initiating polymerization is hydrogen atom transfer to a growing polymer chain (16). Although it is not possible to assess quantitatively the effect of these reactions on the efficiency of **2** as an initiator it is clear qualitatively that only a small fraction of **2** formed will initiate polymer chains.

A more quantitative assessment may be made as follows. The consumption of two molecules of DPPH for each molecule of **2** formed in the presence of DPPH accounts for 50% of the discrepancy between R_{DPPH} and $R_{i,th}$. This leaves a factor of 42 which is the difference between the rate of formation of **2** and $R_{i,th}$ at 60°C. Thus, only about 1.2% of the molecules of **2** that are formed actually initiate polymerization (two radicals are formed from each molecule of **2**). This is in excellent agreement with the value of 1.1% which was obtained recently using a different analysis (17). In this analysis the fraction of **2** that reacts to produce polymer chains was calculated from the ratio of the rate of thermal initiation of polymerization (3*a*) over the rate of disappearance of **2**. The latter value was based on the steady-state concentration of **2** as determined from the steady-state absorption at 320 nm (attributed to **2**) in the thermal polymerization. This absorption builds up in the initial stages of the polymerization and on this basis it was calculated (17) that the instantaneous rate of polymerization should increase during the first few hours of reaction. The values of $R_{p,th}$ at 0.25, 0.5, 1.0, and 1.5 h were calculated to be about 0.5, 0.75, 1.03, and 1.22×10^{-6} mol L^{-1} s^{-1}, respectively, at 60°C. As was pointed out, this change in rate should be detectable experimentally. However, this was not observed in a study of the rate of the thermal polymerization of styrene and some deuterated styrenes (8). The rates were measured accurately using a dilatometer. Although a changing rate of polymerization during the initial stages of polymerization was not sought at that time a review of the data shows that all rates were followed from 0.25 or 0.5 h after the dilatometer was placed in the constant temperature bath for a total of 8 to 12 h. In several runs measurements were made initially at 0.25 h intervals and at 0.5 h intervals in all other runs. There was no change in the rate of polymerization in the initial 1 to 2 h period in any of the 40 runs that were made (except for several runs in which the rate appeared to be variable for several hours) and the rates were linear for the entire time during which they were followed. The reason for the discrepancy between the predicted and observed initial rates is not clear.

While the evidence that **2** is the critical intermediate in the thermal initiation seems compelling it must be pointed out that 5-methylene-1,3-cyclohexadiene, prepared as a model for **2**, does not initiate styrene polymerization (15, 17) although it does react rapidly with styrene in an ene reaction. A possible explanation for the discrepancy in the behaviour of **2** and the model compound has been offered (17), and other model compounds do initiate styrene polymerization (18).[4]

Experimental

General

Mass spectra were obtained on an A.E.I. model MS-9 mass spectrometer using an ionizing voltage of 10.5 eV.

All glassware used in the distillation of monomer and in kinetic measurements was cleaned in a mixture of concentrated nitric and sulfuric acids, 1:3, washed thoroughly with distilled water, placed in ammonium hydroxide solution for several hours, washed with distilled water, and finally dried at 110°C. The cuvette used for kinetic measurements was washed with benzene and rinsed with acetone after each run prior to the neutralization procedure.

The method previously described (8) was used to prepare 2,6-dideuteriostyrene. It was stored under nitrogen at 0°C.

Commercial styrene was freed from inhibitor by washing three times with an equal volume of 10% sodium hydroxide and then with saturated aqueous sodium chloride until free from alkali. The styrene was dried with magnesium sulfate and distilled through a 12 in Vigreux column at 41°C (14 Torr) in a current of nitrogen. A middle cut was collected and stored under nitrogen at 0°C. For the kinetic runs samples of normal and deuterated styrene that had been freshly distilled through a 12 in. Vigreux column in a stream of nitrogen were used.

DPPH was recrystallized by dissolving 50 mg in a minimum amount of benzene, adding a few drops of purified ($KMnO_4$) ligroin and allowing the resulting solution to stand in an open flask. After a day the crystals were filtered and dried under vacuum for 8 h to give 45 mg bright, violet crystals, mp 128–129°C (lit. (20) mp 127–129°C for a 1:1 DPPH-benzene complex).

---

[4]Citing unpublished work it is reported in an excellent review article (19) that there is a normal isotope effect, R_{DPPH}/R'_{DPPH}, of 2 when the rate of disappearance of DPPH in 2,3,4,5,6-pentadeuteriostyrene was compared with that in styrene. It was concluded that this isotope effect resulted from the abstraction of a hydrogen atom from a position originally in the phenyl ring in the rate-determining step and supported the proposal that the reaction involves hydrogen atom abstraction from **2** by DPPH. However, this result is not compatible with the results of the present study. Also, since the reaction is zero order in DPPH it is impossible for the hydrogen abstraction step to be rate determining, as is pointed out in the present paper. Thus, the dimerization of styrene to give **2** must be rate determining and a primary isotope effect is not to be expected. An inverse secondary isotope effect should result as is reported in the present paper.

Kinetics

A solution of DPPH in spectro grade benzene was placed in a reservoir that was attached to a glass tube which also had attached to it a 0.1 mm cuvette and another reservoir for styrene. This apparatus was then sealed onto a high vacuum rack and the benzene was evaporated under 0.2 Torr pressure. The styrene reservoir was removed, filled with 2.0 mL styrene, and resealed to the apparatus. The styrene was degassed by three freeze–thaw cycles under 0.01 Torr pressure and then distilled into the DPPH reservoir. The styrene reservoir was sealed off and the resulting solution was degassed once more, allowed to warm to 22°C, and inverted into the cuvette. The cuvette was placed into a Bausch and Lomb dual cell constant temperature cell holder kept at 75.0°C in a Bausch and Lomb Spectronic 600 Spectrophotometer. The reaction was followed by the decay in the absorbance at 525 nm of DPPH. The rate of decomposition of DPPH is less than 0.1%/h under these conditions (7). Small corrections were made to the rates for the absorption of DPPH—H type molecules formed in the reaction. It was assumed that no DPPH—H was present initially and that all the DPPH which reacted was converted into DPPH—H type molecules. At 525 nm ε = 500 and 11 900 for DPPH—H and DPPH, respectively. Initial concentrations of DPPH were determined from the initial absorbance readings.

1. P. J. Flory. J. Am. Chem. Soc. **59**, 241 (1937).
2. (*a*) P. D. Bartlett and H. Kwart. J. Am. Chem. Soc. **72**, 1051 (1950); (*b*) M. S. Matheson, E. E. Auer, E. B. Bevilacqua, and E. J. Hart. J. Am. Chem. Soc. **71**, 497 (1949); (*c*) M. S. Matheson, E. E. Auer, E. B. Bevilacqua, and E. J. Hart. J. Am. Chem. Soc. **71**, 2610 (1949).
3. (*a*) K. E. Russell and A. V. Tobolsky. J. Am. Chem. Soc. **75**, 5052 (1953); (*b*) F. Tudos and V. Furst. Acta Chim. Acad. Sci. Hung. **15**, 441 (1958). Chem. Abstr. **52**, 21220*c* (1958).
4. (*a*) R. N. Haward. Trans. Faraday Soc. **46**, 204 (1950); (*b*) B. H. Zimm and J. K. Bragg. J. Polym. Sci. **9**, 476 (1952).
5. (*a*) F. R. Mayo. J. Am. Chem. Soc. **75**, 6132 (1953); (*b*) F. R. Mayo. J. Am. Chem. Soc. **90**, 1289 (1968).
6. R. R. Hiatt and P. D. Bartlett. J. Am. Chem. Soc. **81**, 1149 (1959).
7. K. R. Kopecky and M. C. Hall. Can. J. Chem. **59**, 3095 (1981).
8. K. R. Kopecky and S. Evani. Can. J. Chem. **47**, 4049 (1969).
9. E. A. Halevi. *In* Progress in physical organic chemistry. Vol. 1. *Edited by* S. G. Cohen, A. Streitweiser, and R. W. Taft. Interscience, New York. 1963. p. 109.
10. J. Wiesner and P. Mehnert. Koll. Z.u.Z. Polymere **251**, 607 (1973).
11. W. R. Dolbier, Jr. *In* Isotopes in organic chemistry. Vol. 1. *Edited by* E. Buncel and C. C. Lee. Elsevier, Amsterdam. 1975. p. 27
12. K. J. Laidler. Chemical kinetics. 2nd ed. McGraw Hill, New York. 1965. p. 98.
13. K. Bucholz and K. Kirchner. Makromol. Chem. **177**, 935 (1976).
14. J. C. Bevington. Trans. Faraday Soc. **51**, 1392 (1955).
15. K. R. Kopecky and M. P. Lau. J. Org. Chem. **43**, 524 (1978).
16. K. F. Müller. Makromol. Chem. **79**, 128 (1964).
17. (*a*) W. A. Pryor, W. D. Graham, and J. G. Green. J. Org. Chem. **43**, 526 (1978); (*b*) W. D. Graham, J. G. Green, and W. A. Pryor. J. Org. Chem. **44**, 907 (1979).
18. (*a*) W. A. Pryor, J. H. Coco, W. H. Daly, and K. N. Houk. J. Am. Chem. Soc. **96**, 5591 (1974); (*b*) T. Sato, M. Abe, and T. Otsu. Makromol. Chem. **178**, 1061 (1977).
19. W. A. Pryor and L. D. Lasswell. *In* Advances in free radical chemistry. Vol. 5. *Edited by* G. H. Williams. Academic Press, New York. 1975. p. 27.
20. R. H. Poirier, E. J. Kahler, and F. Benington. J. Org. Chem. **17**, 1437 (1952).

Can. J. Chem. Downloaded from www.nrcresearchpress.com by 210.87.254.40 on 09/06/12
For personal use only.

Products of reaction between styrene and some radicals with 2,2-diphenyl-1-picrylhydrazyl[1,2]

KARL R. KOPECKY AND MICHAEL C. HALL

Department of Chemistry, University of Alberta, Edmonton, Alta., Canada T6G 2G2

Received March 6, 1981

KARL R. KOPECKY and MICHAEL C. HALL. Can. J. Chem. **59**, 3095 (1981).

Addition of 2,2-diphenyl-1-picrylhydrazyl DPPH to styrene at 75°C results in little change in the amounts of *cis*- and *trans*-1,2-diphenylcyclobutane and 1,2,3,4-tetrahydro-1-phenylnaphthalene, in a slightly smaller amount of 1-phenylnaphthalene, and in a considerable increase in the amount of 1,2-dihydro-1-phenylnaphthalene that are formed. Formation of the styrene trimer 1,2,3,4-tetrahydro-1-phenyl-4-(1-phenylethyl)naphthalene is eliminated completely. Products derived from DPPH are 1-(4-nitrophenyl)-1-phenyl-2-picrylhydrazine **9** and 1-[2,6-dinitro-4-(1,2,3,4-tetrahydro-4-phenyl-1-naphthyl)phenyl]-2,2-diphenylhydrazine, **10**. DPPH intercepts the thermally formed Diels–Alder dimer of styrene as soon as it is formed to give the 1,2,3,4-tetrahydro-4-phenyl-1-naphthyl radical.

Thermolysis of bis(1,2,3,4-tetrahydro-4-phenyl-1-naphthyl)diazene in the presence of DPPH yields 20% of **10**, 10% of 1-[2,6-dinitro-4-(1,2,3,4-tetrahydro-4-phenyl-1-naphthyl)phenyl]-2-(4-nitrophenyl)-2-phenylhydrazine and **9** while thermolysis of 1,2-bis(1-phenylethyl)diazene in the presence of DPPH yields **9** and 44% of 1-[2,6-dinitro-4-(1-phenylethyl)phenyl]-2,2-diphenylhydrazine showing that substituted benzyl radicals efficiently displace the 4-nitro group of DPPH. The nitro group is transferred to an unsubstituted phenyl group of DPPH.

KARL R. KOPECKY et MICHAEL C. HALL. Can. J. Chem. **59**, 3095 (1981).

L'addition du diphényl-2,2 picrylhydrazyle (DPPH) au styrène à 75°C ne change que faiblement les quantités de diphényl-1,2 cyclobutane *cis* et *trans* et de tétrahydro-1,2,3,4 phényl-1 naphtalène, mais conduit à une quantité légèrement plus faible de phényl-1 naphtalène et à une augmentation considérable de dihydro-1,2 phényl-1 naphtalène. On élimine complètement la formation du trimère du styrène, le tétrahydro-1,2,3,4 phényl-1 (phényl-1 éthyl)-4 naphtalène. Les produits obtenus à partir du DPPH sont la (nitro-4 phényl)-1 phényl-1 picryl-2 hydrazine (**9**) et la [dinitro-2,6 (tétrahydro-1,2,3,4 phényl-4 naphtyl-1)-4 phényl]-1 diphényl-2,2 hydrazine (**10**). Le DPPH intercepte le dimère du styrène, formé thermiquement selon une réaction de Diels–Alder au fur et à mesure qu'il se forme en donnat le radical tétrahydro-1,2,3,4 phényl-4 naphtyl-1.

La thermolyse du bis(tétrahydro-1,2,3,4 phényl-4 naphtyl-1) diazène en présence du DPPH conduit à 20% du composé **10** et à 10% de [dinitro-2,6 (tétrahydro-1,2,3,4 phényl-4 naphtyl-1)-4 phényl]-1 (nitro-4 phényl)-2 phényl-2 hydrazine et au composé **9** tandis que la thermolyse du bis(phényl-1 éthyl)-1,2 diazène en présence de DPPH conduit au composé **9** et à 44% de [dinitro-2,6 (phényl-1 éthyl)-4 phényl]-1 diphényl-2,2 hydrazine montrant ainsi que le radical portant un substituant benzyle déplace efficacement le groupe nitro du DPPH. Le groupe nitro est transféré au group phényl non substitué du DPPH.

[Traduit par le journal]

Introduction

The generally accepted mechanism for the thermal initiation of the polymerization of styrene is given by reactions [1]–[3] (1), where $M_n^{\cdot}$ is a growing polymer chain. According to this mechanism hydrogen atom transfer from the reversibly formed Diels–Alder dimer **1** of styrene to a third molecule of styrene yields a pair of radicals, a fraction of which initiate styrene polymerization. The radical pair also undergoes coupling and disproportionation reactions. The products **3**, **4**, and **5** of these reactions have been isolated from thermolysis of styrene as have the isomeric 1,2-diphenylcyclobutanes, *cis*- and *trans*-**6** and 1-phenylnaphthalene (1, 2).

The stable free radical 2,2-diphenyl-1-picrylhydrazyl DPPH inhibits the thermal polymerization and is consumed during the inhibition period (3). The rate of disappearance of DPPH is ~ 85 times the rate of the thermal initiation of polymer chains at 60°C (3*a*), is zero order with respect to DPPH in styrene, and is second order with respect to styrene in benzene or toluene (3*a*, 4). It has been proposed that DPPH intercepts the dimer as soon as it is formed (1*b*, 5). Presumably the initial products of this reaction would be those resulting from hydrogen atom transfer, 1,1-diphenyl-2-picrylhydrazine DPPH—H and **2**, reaction [4]. Consistent with this proposal is the finding of an inverse isotope effect, $k_H/k_D = 0.75$, on the rate of disappearance of DPPH in 2,6-dideuteriostyrene (6). The radical **2** would then consume a second molecule of DPPH, reaction [5].

The present study was undertaken to determine the effect of DPPH on the distribution of the dimers and trimers formed during the thermal polymerization (2, 7), and to identify the products from the DPPH that has been consumed. Products of the reaction between DPPH and the two radicals

[1]This work was supported by the National Research Council of Canada.

[2]Presented in part at the 55th Chemical Conference of the Chemical Institute of Canada, Quebec, P.Q., Canada. June 5–7, 1972. Abstract p. 46.

0008-4042/81/213095-10$01.00/0

©1981 National Research Council of Canada/Conseil national de recherches du Canada

Can. J. Chem. Downloaded from www.nrcresearchpress.com by 210.87.254.6 on 09/06/12
For personal use only.

Can. J. Chem. Downloaded from www.nrcresearchpress.com by 210.87.254.6 on 09/06/12
For personal use only.

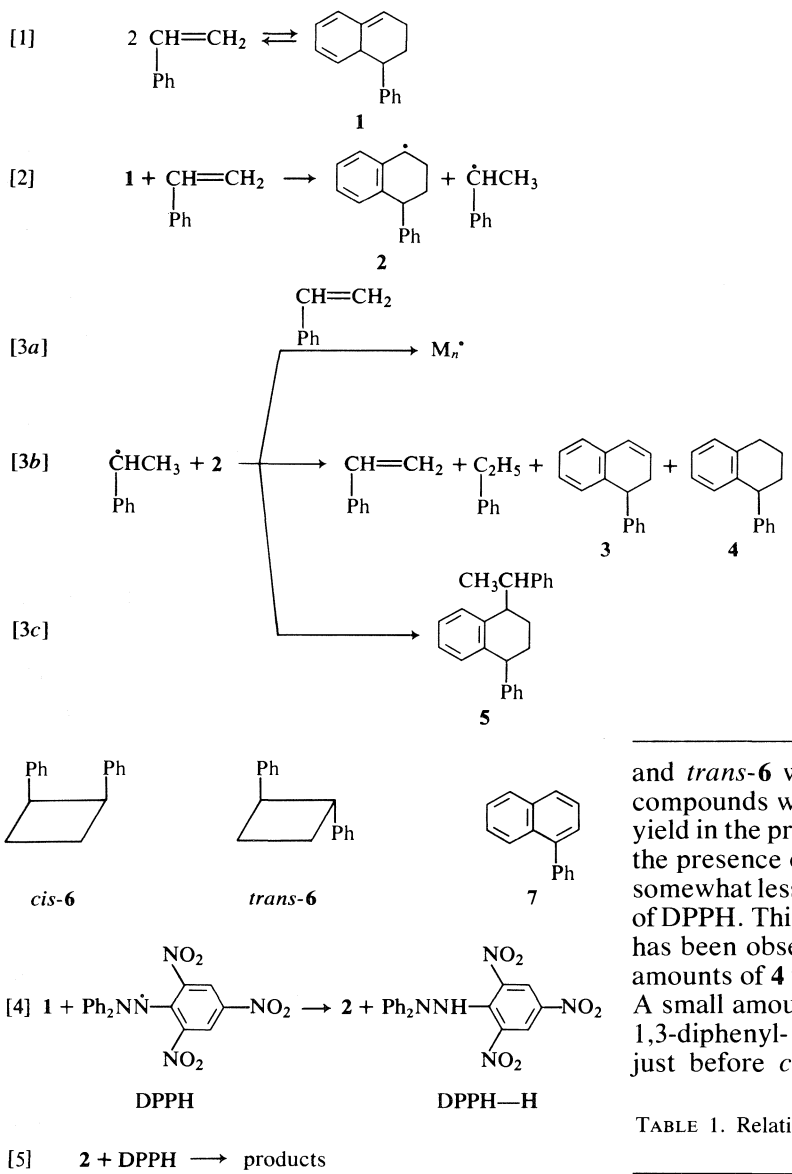

1-phenylethyl and **2**, generated by thermolysis of the appropriate diazenes, were also identified.

Results

DPPH in Styrene

The relative yields, Table 1, of dimeric compounds that were formed on heating pure styrene and styrene containing 1% DPPH, both degassed, at 75°C for 72 h were determined by gas chromatography (gc). Not all the DPPH was consumed under these conditions. Styrene dimers were separated from DPPH and its derivatives by column chromatography on silica gel. The relative amounts of *cis*- and *trans*-**6** were essentially the same and these compounds were formed in qualitatively the same yield in the presence as in the absence of DPPH. In the presence of DPPH relatively much more **3** and somewhat less **7** were produced than in the absence of DPPH. This effect of DPPH on the formation of **3** has been observed before (*7b*, *c*, *d*). Very similar amounts of **4** were formed in the two experiments. A small amount of an unknown material, possibly 1,3-diphenyl-1-butene (*7a*), that eluted from the gc just before *cis*-**6** was formed in the uninhibited

TABLE 1. Relative amounts of styrene dimers formed under various conditions

Conditions	Compound, relative amount				
	Unknown	**3**	**4**	*cis*-**6**	*trans*-**6**
Neat styrene, 75°C[a]	0.19	0.82	0.07	1	2.8
Neat styrene + 1% DPPH, 75°C[a]	0.0	2.7	0.09	1	2.6
Neat styrene, 137°C[b]	—	—	0.4	1	2
Neat styrene, 30°C[c]	—	0.2	1.1	1	1.5
0.2 *M* styrene in benzene, 110°C[d]	—	0.22	6.6	1	2.3
Neat styrene, 130°C[e]	—	—	4.6	1	

[a] This work.
[b] Reference 7*a*.
[c] Reference 7*b*, *c*, *d*.
[d] Reference 2*b*, *c*.
[e] Reference 2*a*.

Can. J. Chem. Downloaded from www.nrcresearchpress.com by 210.87.254.6 on 09/06/12
For personal use only.

reaction, but was not formed at all in the presence of DPPH. Also, material, presumably the styrene trimer **5** (2*d*), with a much longer retention time than those of the dimeric products was formed in the absence of DPPH, but could not be detected among the products formed in the presence of DPPH.

It has been found in previous studies, Table 1, that *trans*-**6** predominates over *cis*-**6** and that the formation of these compounds is not suppressed in the presence of DPPH (7). The relative amounts of **4** formed vary considerably among the various studies and has been found to be as low as 2% (2*d*), as in the present work, to as high as 70% (2*a*) of the total dimeric fraction. The greater amounts of **4** formed in some experiments must result from isomerization of the initial dimer **1** by adventitious acid. A model of **1**, 5-methylene-1,3-cyclohexadiene **8**, has been found to be extremely sensitive to acid and is isomerized to toluene, reaction [6] (8).

[6] 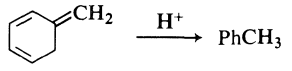

8

The finding that similar amounts of **4** are formed in the presence and in the absence of DPPH is in contrast to an earlier report that the formation of **4** is completely suppressed by DPPH (7*b*, *c*, *d*).

The products derived from DPPH were isolated from a larger scale run by column chromatography followed by preparative tlc. Three main fractions were isolated: 21% of 1-(4-nitrophenyl)-1-phenyl-2-picrylhydrazine, **9**, 5% of 1-[2,6-dinitro-4-(1,2,-3,4-tetrahydro-4-phenyl-1-naphthyl)-phenyl]-2,2-diphenylhydrazine, **10**, and 50% DPPH—H. The

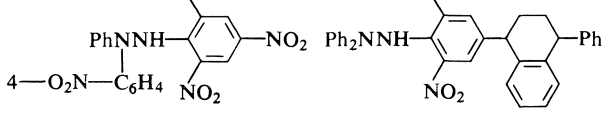

9 **10**

yields are based on starting DPPH and the products isolated represent 76% of the initial DPPH. The amount of **10** isolated from heating 100 mL of styrene with DPPH for 30 h at 75°C was 0.04 g. Compounds **9** and **10** were identified as described below. A large number of other compounds derived from DPPH was formed as evidenced by colored bands on the chromatogram but all were present in very small amounts and were not identified.

The Radicals 2 and 1-Phenylethyl with DPPH

To aid in the identification of the products derived from reaction of DPPH in styrene the product analyses of the decomposition of the diazenes **11** and **12** in the presence of DPPH were carried out.

Degassed benzene solutions 0.4 *M* in **11** and 1.6 *M* in DPPH or 0.6 *M* in **12** and 1.2 *M* in DPPH were heated at 84°C for 72 h, about 4 half-lives of decomposition for **11** (9). Initial product studies were made on the products derived from **11** which generates the 1-phenylethyl radical which might give products that are easier to identify than the products derived from **12** which generates the radical **2**.

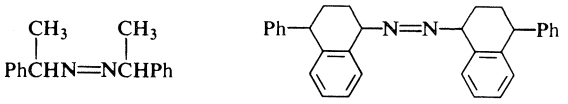

11 **12**

The determination of the structures of the DPPH—1-phenylethyl products was greatly facilitated by the fortuitous discovery that appreciable amounts of volatile N—N cleavage products were formed at high temperature in the gc. In a preliminary attempt to measure the scavenger efficiency of DPPH under these conditions and to estimate the cage effect in the thermolysis of **11** by this method a sample of the reaction mixture from thermolysis of **11** was analyzed by gc at 220°C column temperature. Four compounds designated **A**, **B**, **C**, and **D** in order of increasing retention time, were eluted after the radical coupling products *meso*- and *dl*-2,3-diphenylbutane. Injection of a benzene solution of DPPH into the gc also resulted in formation of **A**, **B**, and **C**, but not **D**, indicating that **D** might be derived from a DPPH—1-phenylethyl radical adduct. The thermal decomposition of DPPH has not been reported, but it has long been known that tetraphenylhydrazine decomposes to diphenylamine **13** among other products (10). By analogy thermolysis of DPPH and of DPPH—H might yield **13** and 2,4,6-trinitroaniline, reaction [7].

[7] 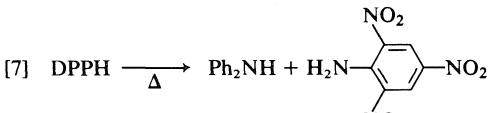

13 **14**

Compounds **A** and **B** were identified as **13** and **14**, respectively, **A** by coinjection of authentic **13** with the reaction mixture, and **B** by isolation from the effluent of the gc and comparison of this with authentic **14**. The compounds **C** and **D** were analyzed by mass spectrometry as they eluted from the gc. The mass spectrum of **C** has a parent peak at *m/e* 214 and was identical with that (11) of 4-nitrodiphenylamine. The mass spectrum of **D** has a

Can. J. Chem. Downloaded from www.nrcresearchpress.com by 210.87.254.6 on 09/06/12
For personal use only.

parent peak at *m/e* 287 and prominent peaks at *m/e* 272 ($M^{+\cdot} - 15$), 180 ($M^{+\cdot} - 107$) and 152 ($M^{+\cdot} - 135$). The odd molecular weight indicates that **D** contains an odd number of nitrogen atoms. The peak at *m/e* 180 is attributed to a fragment that has lost a methyl and two nitro groups. The most intense peak is at *m/e* 272 which indicates loss of a methyl group. Other small peaks correspond to ($M^{+\cdot} - 17$) and ($M^{+\cdot} - 48$) which, by analogy to the cracking pattern of 2,4,6-trinitroaniline, suggests that **D** has an amino group with two *ortho* nitro groups on an aromatic ring. The ready loss of methyl indicates the presence of a benzylic carbon, perhaps *para* to the amino group, which bears a methyl group. Such compounds readily undergo loss of benzylic substituents to give a quinoid species (12), reaction [8].

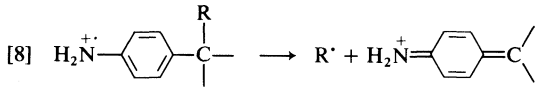

This prompted the assignment of the structure of 2,6-dinitro-4-(1-phenylethyl)aniline **15** to **D**. The mass spectrum of authentic **15**, prepared as shown in Scheme 1, was identical with that of **D**.

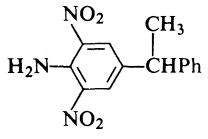

15

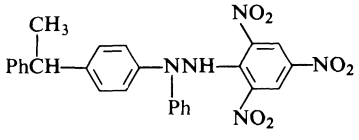

16

These results indicate that 1-phenylethyl radicals couple with DPPH at the 4-position of the picryl ring with displacement of a nitro group which then becomes attached to the 4-position of the phenyl group of DPPH or a substituted DPPH. However, capture of a variety of radicals by DPPH had previously been proposed to take place either at the 4-position of the phenyl ring or at the radical nitrogen atom in every instance studied (13). If this occurred with the 1-phenylethyl radical the hydrazines **16** or **17** would be formed which would cleave under the gc conditions to yield either the diphenylamine **18** or the N-substituted picramine **19**. Authentic samples of **18** and **19** were prepared but no materials with similar retention times could be detected by gc of the reaction mixture of the thermolysis of **11** in the presence of DPPH. Thus, the DPPH–radical adducts formed from thermolysis of **11** and **12** should have the structures **20** and **10**, respectively.

Authentic samples of **10** and **20** were prepared as shown in Schemes 1 and 2. The reactions were all straightforward and will not be discussed here. However, the compounds in the sequence leading

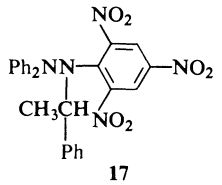

17

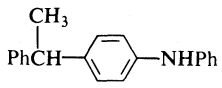

18

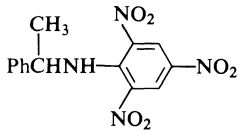

19

to **10** were all syrups which could not be crystallized and a satisfactory analysis was not obtained for any of these. Also **10** was an amorphous solid which could not be crystallized and a satisfactory analysis was not obtained either. The presence of two chiral carbon atoms in these compounds results in diastereomeric mixtures which may be responsible for the failure to obtain crystalline materials. The structures of these compounds are assigned on the basis of the similarity of the reactions used to make them to those of Scheme 1, and on the basis of their nmr spectra. These spectra showed no evidence of impurities and were consistent with the structures. The mass spectrum of **10** was also consistent with its proposed structure.

The electron impact mass spectra of **10** and **20** did not contain the molecular ion peaks, but only peaks due to fragments of the molecular ions. The chemical ionization (CH_5^+) mass spectra did contain the parent ($M^+ + 1$) peaks at *m/e* 557 for **10** and *m/e* 455 for **20**. In both spectra peaks at ($M^+ + 1$) − 46 and ($M^+ + 1$) − 63, resulting from loss of NO_2 and NO_2 + OH, respectively, from the parent ion were present. The most intense peaks in both spectra were those due to the ions resulting from N—N bond cleavage at *m/e* 390 from **10** and *m/e* 288 from **20**. These correspond to the protonated forms of **15** and **21**, respectively.

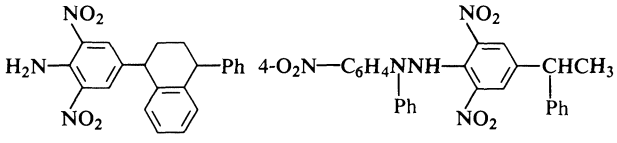

21 **22**

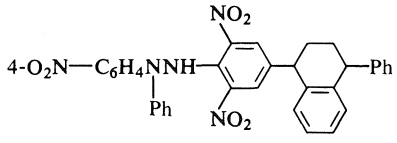

23

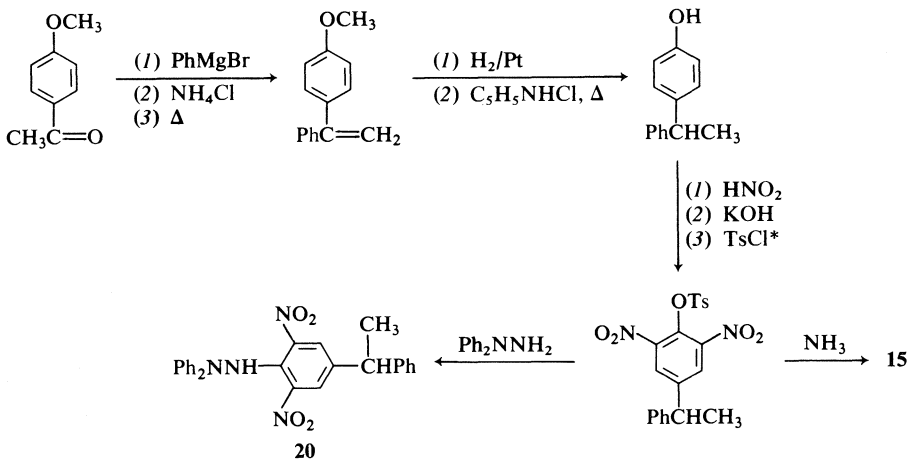

SCHEME 1

The products from the thermolysis of **11** in the presence of DPPH were isolated by a combination of column chromatography on cellulose and preparative tlc on silica gel. There was obtained 23% of **20**, 11% of **9**, both yields based on DPPH, and 22% recovered DPPH, accounting for 56% of the initial DPPH. Based on **11** the yield of **20** was 44%. The structure of **9** was determined by comparison with an authentic sample (13*b*), and **20** isolated from the reaction mixture was identical with synthetic material.

A number of other products derived from DPPH was formed but each was present in very small amount, except for a few mg of material tentatively identified as **22** on the basis of its nmr spectrum.

The products from the thermolysis of **12** in the presence of DPPH were separated by preparative tlc on silica gel. There was obtained 20% of **10** and 27% of **9**, based on DPPH, and 35% recovered DPPH. Also isolated was ~10%, based on DPPH, of a compound tentatively assigned structure **23** on the basis of its nmr and mass spectra. These products account for 92% of the initial DPPH. The total yield, based on **12**, of **10** and **23** is 30%. Again, a number of other products derived from DPPH was formed but all these were present in very small amounts.

The structure of **10** was determined by comparison with synthetic material. The nmr spectrum of **23** is almost identical with that of **10** except that the

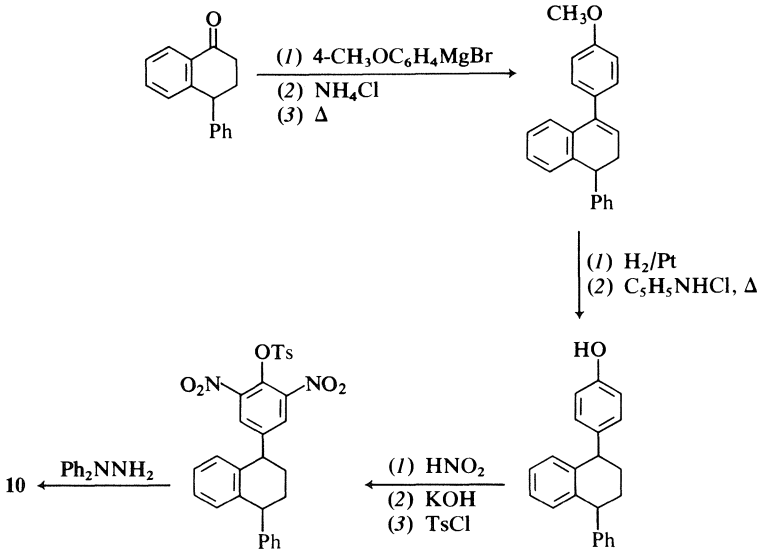

SCHEME 2

Can. J. Chem. Downloaded from www.nrcresearchpress.com by 210.87.254.6 on 09/06/12
For personal use only.

Can. J. Chem. Downloaded from www.nrcresearchpress.com by 210.87.254.6 on 09/06/12
For personal use only.

aromatic region contains an A_2B_2 system that is identical with that observed for the 4-nitrophenyl group in the nmr spectrum of **9**. The chemical ionization (CH_5^+) mass spectrum of **23** has the highest mass peak of *m/e* 556 which is assigned as $(M^+ + 1) - 46$, resulting from loss of NO_2 from the molecular ion. The most intense peak was at *m/e* 390, as in the mass spectrum of **10**, which is due to the protonated form of **21**.

A ~25% yield of a mixture of **3** and **4**, identified by gc, and a ~25% yield of viscous material, presumably the products of coupling of the radicals **2** in the original solvent cage, were isolated as well from the thermolysis of **12** in the presence of DPPH.

Discussion

The main effect of the addition of DPPH to styrene on the distribution of styrene dimers and trimers is the three-fold increase in the relative amount of **3** formed and the elimination of the formation of the trimer **5** and of a presumed styrene dimer of undetermined structure. The formation of other products is relatively unaffected. The results are consistent with the mechanism of the thermal initiation of polymerization given by reactions [1]–[3]. Interception of the initial styrene dimer **1** by DPPH, reaction [4], as soon as it is formed would prevent hydrogen transfer to a third molecule of styrene, reaction [2] and thereby eliminate formation of **5**. Subsequent rapid reaction between **2** and DPPH would prevent any addition of **2** to styrene to initiate polymer chains. This mechanism for the inhibitory effect of DPPH is supported by the isolation of **10**, the product of coupling of DPPH with the radical **2**. Reaction between **2** and DPPH—H could also lead to the disproportionation products **3** and DPPH. Although the relative amount of **3** formed is greater by a factor of ~3 in the presence of DPPH the coupling reaction must predominate. If disproportionation were the predominant reaction the amount of **3** formed would be increased by as much as 40-fold in the presence of DPPH. This number is obtained in the following way. In the absence of DPPH most of **1** that is formed reverts to styrene and some undergoes chain transfer (2*a*) with growing polymer chains. A portion of the molecules of **1** that are formed undergo hydrogen atom transfer with styrene to give a pair of radicals, reaction [2], and only a fraction of these radicals initiate polymerization. DPPH intercepts all the molecules of **1** as they are formed. This accounts for the much greater rate of disappearance of DPPH as compared with the rate of initiation of polymerization, a factor of 85 at 60°C. Half the DPPH that is consumed is converted to DPPH—H by hydrogen atom transfer from **1**, reaction [4]. The remainder reacts by disproportionation or coupling with **2**.

The results of the thermolysis of **11** and **12** in the presence of DPPH confirm that half or more of 1-phenylethyl radicals and of **2** react with DPPH by coupling. The coupling products were isolated in 44 and 30% yields, respectively. The cage effect in the thermolysis of **11** at ca. 110°C is over 30% (14) and must be at least as great for **12**, so that the majority of the radicals which escape the cage must couple with DPPH.

The maximum amount of **10** that could have been formed in styrene if **2** and DPPH gave only **10** can be calculated. The rate of disappearance of DPPH in styrene at 75°C is $2.2 \times 10^{-8} M\ s^{-1}$ (6). A maximum of half the DPPH consumed can be converted to **10**, so that from 100 mL of styrene at 75°C after 30 h the theoretical yield of **10** would be ~0.06 g. This compares well with the 0.04 g which was isolated under these conditions, considering that about half the molecules of **2** and DPPH that react with each other form **10** as found from thermolysis of **12** in the presence of DPPH.

In neat styrene **4** can be formed by a disproportionation reaction, [3*b*], and by isomerization of **1** by adventitious acid. With care the latter route to **4** can be minimized, and in the presence of DPPH reaction [3*b*] cannot occur. **4**, which is formed in the presence of DPPH, likely results from a hydrogen atom transfer from DPPH—H to **2**, which are the initial products of reaction [4], in the original solvent cage in which they are formed. Such a reaction between DPPH—H and radicals is known to occur (15).

The finding that **2** and 1-phenylethyl radicals react with DPPH at the 4-position of the picryl ring stands in contrast to all studies of reactions between radicals and DPPH which had been carried out when this work was completed (13). For every system studied the radical was claimed to become bound to the nitrogen containing the free valence or to an unsubstituted phenyl group. In each instance in which reaction at the unsubstituted phenyl ring was claimed the only evidence available was the observation that the products could be oxidized to hydrazyls. This oxidation reaction is also available to products of reaction at the picryl ring and does not distinguish between reaction at the two different positions.

Since the present work was completed there have been three reports of displacement of a nitro group from an aromatic ring: from DPPH by the thiyl radical derived from 2,4,6-tri-*t*-butylbenzenethiol (16*a*, *b*), and by bromine (16*c*) and from

Can. J. Chem. Downloaded from www.nrcresearchpress.com by 210.87.254.6 on 09/06/12
For personal use only.

a series of *p*-substituted nitrobenzenes by 1-adamantyl radicals (17).

However, 2-cyano-2-propyl radicals and ethylthiyl radicals are reported to react with DPPH at the 4-position of an unsubstituted phenyl group (18). The evidence for the structure of the 2-cyano-2-propyl—DPPH adduct **24** is based on the mass spectrum of the product. A peak at *m/e* 462 was present, but this is also consistent with the isomeric structure **25**, a secondary product formed after

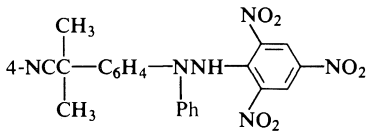

24

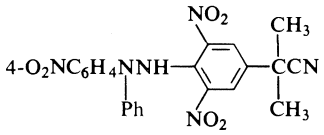

25

attack of the 2-cyano-2-propyl radical at the picryl ring. In the present study adducts corresponding to **25** were formed in the reactions between both **2** and 1-phenylethyl radical and DPPH. A fragment with *m/e* 236, attributed to the product **26** of the N—N cleavage of the molecular ion obtained from **24** was also detected in the mass spectrum (18). However, an ($M^{+\cdot}$ + 1) peak is present in the mass spectrum of 2-nitroaniline (19). N—N cleavage of the corresponding ion derived from **25** might form **27** which would lose CH_3 to give **28** which has *m/e* 235. A

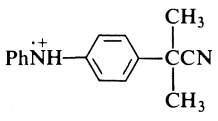

26

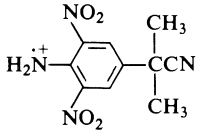

27

corresponding fragmentation of the (M^+ + 1) ion from **25** would produce a fragment with *m/e* 236. Thus the mass spectral evidence is ambiguous.

The structure of the ethylthiyl–DPPH adduct seems to be more secure as it was degraded chemically to 4-ethylthiodiphenylamine.

Coupling of radicals at the unsubstituted phenyl group of DPPH is certainly a feasible reaction and does occur with nitrogen dioxide, at least, as evidenced by the formation of **9** (13*b*) and **23** in the present work. It is possible that nitrogen dioxide reacts preferentially with DPPH at the picryl ring, a process undetectable in the absence of suitably labelled materials, and more slowly at the unsubstituted phenyl group to form **9**.

There are thus at least three sites in DPPH at which radical attack may occur and careful characterization of the products is required to distinguish between reaction at the picryl ring and the unsubstituted phenyl group.

Experimental

General

Melting points and boiling points are uncorrected. Refractive indices were measured on a Bausch and Lomb Abbe-3L refractometer. Infrared spectra were recorded on a Beckman IR-7 recording spectrophotometer. Ultraviolet spectra were recorded on a Bausch and Lomb Spectronic 600 spectrophotometer. Nuclear magnetic resonance spectra were recorded on Varian Analytical Spectrometers, Models A-60 and HR-100 with tetramethylsilane as internal standard. Mass spectra were recorded on A.E.I. Models MS-2, MS-9, and MS-12 mass spectrometers. Gas chromatographic – mass spectra were obtained using a Varian Series 1200 gc connected to the MS-12 mass spectrometer. Gas–liquid chromatographic analyses were carried out on an Aerograph-202 Gas Chromatograph. Elemental analyses were performed in the microanalytical laboratories in the Chemistry Department under the supervision of Mrs. Darlene Mahlow.

Solutions were dried with magnesium sulfate.

All reactions involving the heating of styrene were conducted in apparatus that had been soaked several hours in ammonium hydroxide solution and then baked at 120°C for several hours.

cis- and *trans*-**6** (20), **4** (20), and **11** (9) were prepared as described in literature, while **7** was obtained commercially. Styrene and DPPH were purified as described (6).

1,2,3,4-Tetrahydro-4-phenyl-1-naphthol

A mixture of 10 g of 4,4-diphenyl-3-butenoic acid and the corresponding lactone (21) in 150 mL methanol was hydrogenated over 500 mg palladium on charcoal at 710 Torr. Hydrogenation was complete in 3 h. The solid remaining after removal of catalyst and solvent was recrystallized from benzene to give 9.2 g large prisms, mp 107°C (lit. (22) mp 107°C), of 4,4-diphenylbutanoic acid. This material was preheated to 70°C and added in one lot to 40 g polyphosphoric acid at 90°C and the resulting mixture was kept at 90°C for 3 min and stirred vigorously for 4 min more. Then 40 g polyphosphoric acid preheated to 90°C was added with stirring and the resulting mixture was kept at 90°C for 1 h. After cooling to 60°C ice water was added and the product was taken up in ether. Further workup yielded a solid which was recrystallized to give 7.6 g of 1,2,3,4-tetrahydro-4-phenylnaphthalen-1-one, mp 76–77°C (lit. (23) mp 75.5–76°C). Reduction of 5.0 g of this material with excess sodium borohydride in ethanol provided 4.8 g white powder after workup which was recrystallized from carbon tetrachloride, mp 96–100°C. A portion of this material was recrystallized from pentane to give long white needles, mp 121.5–123°C; nmr ($CDCl_3$: τ 2.72 (m, 9 H), 5.16 (m, 1 H), 5.91 (m, 1 H), 7.75 (s, O—*H*), 8.0 (broad m, 5 H). *Anal.* calcd. for $C_{16}H_{16}O$: C 85.68, H 7.19; found: C 85.98, H 7.11.

1,2-Dihydro-1-phenylnaphthalene, ***3***

A mixture of 4.8 g of the above alcohol and 10 g phosphoric acid was heated at 120–130°C for 2 h and then poured into ice water. The product was taken up in ether and the ether solution washed with sodium bicarbonate solution, with water, and then dried. Ether was removed and the residue distilled to give 3.4 g (70%) of a viscous oil, bp 87°C/0.08 Torr, n_D^{25} 1.6225. The

Can. J. Chem. Downloaded from www.nrcresearchpress.com by 210.87.254.6 on 09/06/12
For personal use only.

infrared spectrum matched that reported (1*b*). *Anal.* calcd. for $C_{16}H_{14}$: C 93.16, H 6.84; found: C 93.45, H 6.94.

Bis(1,2,3,4-tetrahydro-4-phenyl-1,1-naphthylene)diazane

A mixture of 2.5 g (0.011 mol) of 1,2,3,4-tetrahydro-4-phenylnaphthalen-1-one, 0.32 g (0.011 mol) of 85% hydrazine hydrate and a drop of acetic acid in 25 mL 98% ethanol was heated under reflux for 3.5 h during which time the product precipitated. This was filtered, washed with ethanol, and dried to yield 2.35 g (84%) of fine yellow powder, mp 207–210°C; ir ($CHCl_3$): 1690 (C=N) cm^{-1}; nmr ($CDCl_3$): τ 1.80 (m, 2 H), 2.90 (m, 16 H), 5.87 (m, 2 H), 7.25 (m, 4 H), and 7.80 (m, 4 H). *Anal.* calcd. for $C_{32}H_{28}N_2$: C 87.24, H 6.41, N 6.36; found: C 87.06, H 6.49, N 6.54.

Bis(1,2,3,4-tetrahydro-4-phenyl-1-naphthyl)diazene

A mixture of 1.7 g of the above diazane and 500 mg 5% palladium on charcoal in 300 mL benzene was stirred under hydrogen at 710 Torr until hydrogen uptake ceased. Catalyst and solvent were removed to give a sticky white solid which was immediately taken up in 125 mL ether. The resulting solution was stirred under oxygen for 24 h. The white solid which had formed was filtered and the ether cooled to 0°C to give more precipitate. A total of 0.78 g (46%) of white powder was obtained, mp 121–124°C; nmr ($CDCl_3$): τ 2.87 (m, 18 H), 5.82 (m, 2 H), and 7.80 (broad m, 8 H); uv (ether): 362 (110) nm. *Anal.* calcd. for $C_{32}H_3ON_2$: C 86.84, H 6.83, N 6.33; found: C 86.79, H 6.50, N 6.09.

The infrared spectrum showed no absorptions due to NH or to C=N. Addition of a drop of hydrochloric acid to the ether solution used for the uv spectrum rapidly gave a new absorption at 286 (11000) nm.

1-(4-Hydroxyphenyl)-1-phenylethane

Hydrogenation of 1-(4-methoxyphenyl)-1-phenylethene (24) gave 1-(4-methoxyphenyl)-1-phenylethane (25) and 39.5 g of this material was added to molten pyridinium hydrochloride at 140°C for the cleavage reaction (26). The mixture was heated under reflux under nitrogen for 3 h and then cooled. To the warm solution was added 80 mL water and this mixture was poured into 600 mL water. The product was taken up in ether. The ether solution was dried, the solvent removed, and the residue distilled to give 33 g (91%) of a viscous liquid that solidified at 0°C, bp 133–134°C/0.5 Torr, mp 54–56°C (lit bp 185–190°C/10 Torr (27), mp 64°C (28)); nmr (CCl_4): τ 2.92 (s, 5 H), 7.07 (d, J = 9 Hz, 2 H), 7.36 (d, J = 9 Hz, 2 H), 3.95 (broad, 1 H, O—*H*), 6.05 (q, J = 7 Hz, 1 H) and 8.50 (d, J = 7 Hz, 3 H). *Anal.* calcd. for $C_{14}H_{14}O$: C 84.81, H 7.12; found: C 84.88, H 6.90.

2,6-Dinitro-4-(1-phenylethyl)phenyl-p-*toluenesulfonate*

Nitration of 9.75 g of 1-(4-hydroxyphenyl)-1-phenylethane with nitrous acid in buffered solution (29) followed by shaking the benzene extract of the diluted reaction mixture with 10% potassium hydroxide produced 7.8 g orange–red precipitate. This was recrystallized from boiling water to give 7.6 g (50%) potassium 2,6-dinitro-4-(1-phenylethyl)phenoxide as long orange needles. A mixture of 1.6 g (0.005 mol) of this salt, 1.0 g (0.005 mol) *p*-toluenesulfonyl chloride, and 15 mL acetone was stirred under reflux for 4 h. The dark red solution gradually lost its color and became light yellow. The reaction mixture was filtered and solvent removed from the filtrate. The residual solid was treated with charcoal in methanol and recrystallized from methanol to give 1.8 g (81%) white needles, mp 114–115°C; nmr ($CDCl_3$): τ 0.41 (s, 2 H), 0.68 (d, J = 8.5 Hz, 2 H), 1.12 (d, J = 8.5 Hz, 2 H), 1.23 (m, 5 H), 4.84 (q, J = 7.3 Hz, 1 H), 7.03 (s, 3 H), and 7.97 (d, J = 7.3 Hz, 3 H). *Anal.* calcd. for $C_{21}H_{18}N_2O_7S$: C 57.01, H 4.10, N 6.33, S 7.25; found: C 57.20, H 4.11, N 6.05, S 7.33.

2,6-Dinitro-4-(1-phenylethyl)aniline, ***15***

Anhydrous ammonia was bubbled through a solution of 1.8 g of the above tosylate in 20 mL diglyme kept at 160°C. After 3 h the solution had turned dark red and fine white needles had precipitated. The reaction mixture was filtered and solvent removed from the filtrate. The residue was recrystallized from methanol to give 0.94 g (81%) bright orange prisms, mp 115°C; ir ($CHCl_3$): 3485 and 3370 cm^{-1}; nmr ($CDCl_3$): τ 1.58 (s, 2 H), 1.60 (broad, 2 H), 5.89 (q, J = 7.5 Hz, 1 H), and 8.33 (d, J = 7.5 Hz, 3 H); ms (70 eV) *m/e*: 287 ($M^{+\cdot}$), 272, 180, 152. *Anal.* calcd. for $C_{14}H_{13}N_3O_4$: C 58.53, H 4.56, N 14.63; found: C 58.40, H 4.75, N 14.50.

1-[2,6-Dinitro-4-(1-phenylethyl)phenyl]-2,2-diphenylhydrazine, ***20***

To a stirred mixture of 0.5 g (0.0023 mol) of 1,1-diphenylhydrazine hydrochloride in 10 mL ethanol was added 0.5 g (0.006 mol) sodium bicarbonate. When gas evolution ceased 1.0 g (0.0023 mol) of 2,6-dinitro-4-(1-phenylethyl)phenyl-*p*-toluenesulfonate was added and the resulting mixture heated under reflux for 2.5 h. The mixture was cooled, filtered, the filtrate concentrated and the residue recrystallized from 98% ethanol to give 0.72 g red prisms, mp 133°C (char 131°C); ir ($CHCl_3$): 3310 cm^{-1}; nmr ($CDCl_3$): τ 0.52 (s, 1 H), 2.18 (s, 2 H), 2.80 (m, 17 H), 5.93 (q, J = 7 Hz, 1 H) and 8.42 (d, J = 7 Hz, 3 H); ms (CH_5^+) *m/e*: 455 (M^+ + 1), 409, 392, 288. *Anal.* calcd. for $C_{26}H_{22}N_4O_4$: C 68.71, H 4.88, N 12.11; found: C 68.81, H 4.83, N 12.11.

1,2-Dihydro-1-phenyl-4-(4-methoxyphenyl)naphthalene

A solution of 6.2 g (0.028 mol) of 1,2,3,4-tetrahydro-4-phenylnaphthalen-1-one in 100 mL ether was added to the Grignard reagent made from 2.4 g (0.1 mol) magnesium and 18.7 g (0.1 mol) 4-bromo-1-methoxybenzene. The reaction was carried out in the usual way, hydrolyzed with saturated ammonium chloride, and worked up in the usual way. Removal of solvent left an oily residue which was heated at 210°C under 60 Torr for 30 min to leave a viscous oil, 8.5 g (89%) which could not be crystallized, nmr (CCl_4): τ 2.85 (m, 9 H), 2.95 (d, J = 8.5 Hz, 2 H), 3.18 (d, J = 8.5 Hz, 2 H), 4.10 (t, J = 4.5 Hz, 1 H), 5.90 (t, J = 8.5 Hz, 1 H), 6.26 (s, 3 H), and 7.35 (d of d, J = 4.5 Hz, 8.5 Hz, 2 H). A satisfactory analysis was not obtained. At least a three-fold excess of Grignard reagent was required to consume all the ketone.

1,2,3,4-Tetrahydro-4-(4-methoxyphenyl)-1-phenylnaphthalene

The above material was hydrogenated in ethyl acetate using platinum oxide and the reaction worked up in the usual way, except that the product was warmed to 80°C under 20 Torr for 0.5 h, to give 100% of a viscous oil that could not be crystallized, nmr (CCl_4): τ 3.0 (broad m, 13 H), 5.90 (broad m, 2 H), 6.28 (s, 3 H), and 8.0 (m, 4 H). A satisfactory analysis was not obtained.

1,2,3,4-Tetrahydro-4-(4-hydroxyphenyl)-1-phenylnaphthalene

Cleavage of 7.5 g of the above ether with pyridinium hydrochloride (26) yielded 6.2 g (86%) of a viscous oil that could not be crystallized, ir (CCl_4): 3350 cm^{-1}; nmr (CCl_4): τ 3.0 (broad m, 13 H), 5.90 (broad m, 2 H), 6.70 (s, 1 H), and 8.0 (m, 4 H). A satisfactory analysis was not obtained.

1-[2,6-Dinitro-4-(1,2,3,4-tetrahydro-4-phenyl-1-naphthyl)-phenyl]-2,2-diphenylhydrazine, ***10***

Nitration (29) of 3.05 g (0.01 mol) of the above phenol with nitrous acid in buffered solution gave, after work up and conversion of the product to the potassium salt, 0.8 g (18%) of a sticky red solid. This was dissolved in 10 mL acetone containing 0.4 g (0.02 mol) *p*-toluenesulfonyl chloride and the resulting solution was heated under reflux until the red color disappeared. The reaction mixture was filtered and the filtrate concentrated to give a tan syrup which could not be crystallized. The material was added to a mixture of 0.45 g (0.02 mol) of 1,1-diphenylhydrazine hydrochloride and 0.45 g sodium carbonate in 10 mL ethanol. The mixture was heated under reflux for 2.5 h, filtered,

Can. J. Chem. Downloaded from www.nrcresearchpress.com by 210.87.254.6 on 09/06/12
For personal use only.

and the solvent removed. The residue was applied to a 20 × 20 cm plate coated with 2 mm of silica gel. The plate was developed six times with 1:8 acetone–hexane which resulted in a well separated red–brown band. This was removed and extracted with benzene. Removal of the benzene left 73 mg of a brittle orange–red solid, which could not be crystallized, mp 69–72°C; nmr (CCl_4): τ 0.50 (s, 1 H), 2.35 (overlapping s, 2 H adjacent to NO_2), 2.90 (m, 19 H), 5.85 (broad m, 2 H), and 8.10 (broad m, 4 H); ms (CH_5^+) *m/e*: 557 ($M^+ + 1$), 511, 494, 390. A satisfactory analysis was not obtained.

2,4,6-Trinitro-N-(1-phenylethyl)aniline, ***19***

A mixture of 2.0 g (8 mmol) of picryl chloride, 1.0 g (8 mmol) 1-phenylethylamine, and 1 g sodium carbonate in 50 mL chloroform was heated under reflux for 30 min. The dark red reaction mixture was shaken with water, dried, and concentrated. The residue was recrystallized from ethanol to give 2.45 g (89%) bright yellow needles, mp 108–109°C, nmr ($CDCl_3$): τ 1.10 (s, 2 H), 2.75 (s, 5 H), 5.70 (q, J = 6.5 Hz, 1 H), 7.25 (broad s, 1 H, N*H*), and 8.30 (d, J = 6.5 Hz, 3 H). *Anal.* calcd. for $C_{14}H_{12}N_4O_6$: C 50.45, H 3.64, N 16.86; found: C 50.47, H 3.69, N 17.02.

4-(1-Phenylethyl)diphenylamine

The method used is a modification of that described (30) for the preparation of 4-benzyldiphenylamine. A mixture of 11.2 g (0.08 mol) of 1-chloro-1-phenylethane, 13.6 g (0.04 mol) of diphenylamine, and 13.6 g zinc chloride was heated at 100°C for 80 min when gas evolution ceased. The dark brown reaction mixture was mixed twice with 100 mL boiling water, cooled, and taken up in ether. The resulting solution was dried and concentrated to a viscous oil which was distilled to give 3 g of an oil, bp 190–220°C/1 Torr, which deposited white crystals of diphenylamine. The crystals were separated and a portion of the oil chromatographed on a 3 × 30 cm column of silica gel using 1:8 acetone–hexane as eluent. Concentration of the first fraction, 150 mL, left a clear oil, nmr (CCl_4) τ 2.8–3.5 (broad, 14 H), 5.05 (broad s, 1 H, N—*H*), 5.82 (q, J = 7 Hz, 1 H) and 8.40 (d, J = 7 Hz, 3 H). This material was not analyzed further.

*Thermolysis of **11** in the presence of DPPH*

A solution of 0.207 g (9 mmol) of **11** and 1.34 g (34 mmol) of DPPH in 20 mL benzene was degassed with four freeze–thaw cycles under 0.001 Torr and then kept at 84°C for 72 h. Analysis by gc on a 5 ft × 0.25 in. column of 15% SF 96 on 60/80 Chromosorb W at 220°C, 60 mL/min helium flow rate, and injector temperature of 275°C indicated four components with retention times of 6.0, 14.4, 25.4, and 43.5 min. The retention time of the first component coincided with those of diphenylamine and of *meso-* and *dl*-2,3-diphenylbutane. The second compound was isolated by preparative gc, mp, and mixed mp with 2,4,6-trinitroaniline 187°C. The third and fourth components were analyzed by mass spectrometry of the effluent of the gc. The ms of the third component matched that of 4-nitrodiphenylamine and the ms of the fourth component matched that of **15**.

Diphenylamine, *meso-* and *dl*-2,3-diphenylbutane were separated on a 5 ft × 0.25 in. column of 20% PDEAS on 60/80 Chromosorb W temperature programmed from 90 to 225°C over 20 min. The retention times were 36.0, 17.2, and 17.7 min, respectively, and the compounds were identified by coinjection with authentic materials.

Removal of benzene left 1.6 g residue, 0.800 g of which was chromatographed on a 5 × 38 cm column of microcrystalline cellulose. Washing with heptane eluted a brown–red and, overlapping with it, a violet band. Removal of solvent left 0.40 g dark solid which was taken up in the minimum amount of benzene and applied to four 20 × 20 cm plates coated with 2 mm silica gel. The plates were developed six times at 5°C with 1:10 acetone–hexane to separate two strong bands, the first red–brown, the second violet, and a number of minor, highly colored, more slowly moving bands. The materials from the bands were extracted into chloroform. The first gave 178 mg of red–brown solid whose nmr spectrum showed only broad signals. Addition of a drop of a solution of hydroquinone resulted in a spectrum with sharp lines that was identical with that of authentic **20**. The second band gave 146 mg of violet solid whose nmr spectrum, after addition of a little hydroquinone, was identical with that of authentic DPPH—H.

Further elution of the cellulose column with 1:1 benzene–heptane removed further material which was collected in 250 mL fractions. The first three fractions contained 0.105 g material which was shown by tlc to consist mainly of DPPH and **20** along with a small amount of an unidentified indigo colored material. The next three fractions contained 77 mg material which was separated on a preparative tlc plate using 1:8 acetone–hexane as eluent. After six developments three bands were separated. The major band was extracted with chloroform to give 16 mg solid whose nmr spectrum, after addition of some hydroquinone, indicated that it was a mixture of **9** and 1-[2,6-dinitro-4-(1-phenylethyl)phenyl]-2-(4-nitrophenyl)-2-phenylhydrazine, **22**. The nmr spectrum of the mixture contained peaks that were present in the spectra of both **9** and **20**, but **20** was shown by tlc not to be present.

Fractions 7–11 contained 0.285 g material 0.085 g of which was chromatographed on a preparative tlc plate. After six developments with 1:6 acetone–hexane a brown band and a violet band were separated. Extraction with chloroform and removal of solvent gave 48 and 33 mg, respectively, of **9** and the corresponding hydrazyl. These were identified by their nmr spectra, after the addition of some hydroquinone, which matched that of authentic **9** (13*b*).

*Thermolysis of **12** in the Presence of DPPH*

A solution of 0.076 g (1.7 mmol) **12** and 0.134 g (3.4 mmol) DPPH in 3 mL benzene was degassed as described above and heated at 84°C for 72 h. The benzene was removed, the residue taken up in the minimum volume of acetone, and the resulting solution was applied to three 20 × 20 cm plates coated with 2 mm silica gel. The plates were developed six times with 1:8 acetone–hexane at 5°C. Four well defined colored bands and two closely spaced colorless bands which were near the solvent front were resolved at this time. The organic material of each band was taken up in chloroform and analyzed in order of decreasing R_f value as follows:

Fraction 1, 20 mg oil shown to contain **3** and **4** by gc.

Fraction 2, 20 mg viscous oil, presumably products of coupling of **2**.

Fraction 3, 38 mg orange brown solid whose nmr and mass spectra matched those of authentic **10**.

Fraction 4, 47 mg orange red solid whose nmr and mass spectra matched those of DPPH—H.

Fraction 5, 23 mg orange red solid assigned structure **23** on the basis of its nmr spectrum (CD_3COCD_3): τ 0.75 (s, 1 H, N*H*), τ 1.90 (d, J = 9 Hz, 2 H, half of A_2B_2 of 4-O_2N—C_6H_4) 2.08 (s, 2 H), 2.80 (broad, 16 H), 5.75 (broad, 2 H), 8.05 (broad, overlapping with solvent); and mass spectrum (CH_5^+): *m/e* 556 (P − 46), 415, 390, 386, 360, 206.

Fraction 6, 40 mg red–brown solid whose nmr spectrum matched that of authentic **9**.

Fraction 7, 8 mg material remaining at the base line which was not identified.

Thermolysis of Styrene

(a) With DPPH

A 250 mL long-necked round-bottomed flask with a side arm reservoir containing 0.8 g DPPH–benzene complex was filled with 100 mL freshly distilled styrene which was then degassed with three freeze–thaw cycles under 0.02 Torr. The DPPH was

taken up in styrene and the sidearm sealed off. The flask was then immersed in a 75°C bath for 30 h in the dark. Styrene was then removed at 80°C/23 Torr to leave 1.35 g residue which was chromatographed on a 3 × 60 cm column of silica gel using 1:4 acetone–hexane as eluent. Fractions were collected in 20 mL portions and analyzed by tlc. Those containing similar products were combined and rechromatographed, if necessary, using a ratio of 1:100 compound – silica gel. The following materials were obtained: 0.520 g of a hydrocarbon mixture whose nmr spectrum indicated it to be 90% styrene and which was analyzed by gc as described in *b*, below; 0.04 g of **10** identified on the basis of its nmr spectrum; 0.048 g of DPPH—H, and 0.190 g **9**, identified on the basis of their nmr spectra.

(b) Without DPPH

A 100 mL portion of freshly distilled styrene was heated under the conditions as given in (*a*), except that no DPPH was present, and then poured into 250 mL benzene. The resulting solution was poured into 500 mL methanol. The sticky polymer was filtered and leached several times with methanol. The leachings and filtrate were combined and concentrated under 23 Torr to a yellow viscous residue which was chromatographed on 100 g silica gel. Elution with 1:4 acetone–hexane and removal of the eluent gave 0.36 g of a pale yellow viscous oil whose nmr spectrum indicated it was ~90% styrene.

This material and the hydrocarbon fraction from (*a*) were analyzed by gc using a 10 ft × 0.125 in. column of 10% Apiezon L on 60/80 Firebrick at 202°C with 85 mL/min helium flow rate. The products were identified by comparison of their retention times and mass spectra with those of authentic materials. Several mass spectra were recorded as each component eluted to ensure that no other materials were eluted at the same time.

Thermolysis of DPPH

A solution of 134 mg DPPH in 3 mL benzene was degassed and then heated at 84°C for 72 h. The resulting solution was applied to two 20 × 20 cm plates coated with 2 mm silica gel and the plates developed six times with 1:10 acetone – petroleum ether at 5°C to give three resolved bands. The most intense was extracted into chloroform and the solvent removed to give 127 mg (95%) DPPH. The other two bands were identified as **9** and the corresponding hydrazyl by comparison of their R_f values with those of authentic samples.

1. (*a*) F. R. MAYO. J. Am. Chem. Soc. **75**, 6132 (1953); (*b*) F. R. MAYO. J. Am. Chem. Soc. **90**, 1289 (1968); (*c*) W. A. PRYOR and L. D. LASSWELL. *In* Advances in free radical chemistry. Vol. 5. *Edited by* G. H. Williams. Academic Press, New York. 1975. p. 27.
2. (*a*) K. F. MÜLLER. Makromol. Chem. **79**, 128 (1964); (*b*) W. G. BROWN. J. Am. Chem. Soc. **90**, 1916 (1968); (*c*) W. G. BROWN. Mackromol. Chem. **128**, 130 (1969); (*d*) J. KURZE, D. J. STEIN, P. SIMAK, and R. KAISER. Angew. Makromol. Chem. **12**, 25 (1970).
3. (*a*) K. E. RUSSELL and A. V. TOBOLSKY. J. Am. Chem. Soc. **75**, 5052 (1953); (*b*) F. TUDOS and V. FURST. Acta Chim. Acad. Sci. Hung. **15**, 441 (1958); Chem. Abstr. **52**, 21220*c* (1958).
4. J. WIESNER and P. MEHNERT. Koll. Z. Z. Polym. **251**, 607 (1973).
5. R. R. HIATT and P. D. BARTLETT. J. Am. Chem. Soc. **81**, 1149 (1959).
6. K. R. KOPECKY and M. C. HALL. Can. J. Chem. **59**, 3090 (1981).
7. (*a*) K. KIRCHNER and K. BUCHOLZ. Angew. Makromol. Chem. **13**, 127 (1970); (*b*) J. WIESNER and P. MEHNERT. Kolloid Z. Z. Polym. **251**, 607 (1973); (*c*) J. WIESNER and P. MEHNERT. Markromol. Chem. **165**, 1 (1973); (*d*) J. WIESNER and P. MEHNERT. Chem. Ing. Tech. **45**, 1269 (1973).
8. K. R. KOPECKY and M.-P. LAU. J. Org. Chem. **43**, 525 (1978).
9. S. G. COHEN, S. J. GROSZOS, and D. B. SPARROW. J. Am. Chem. Soc. **72**, 3947 (1950).
10. H. WIELAND and A. H. LECHER. Justus Liebigs Ann. Chem. **392**, 156 (1912).
11. E. STENHAGEN, S. ABRAHAMSSON, and F. W. MCLAFFERTY (*Editors*). Atlas of mass spectral data. Interscience, New York. 1969. p. 1524.
12. J. H. BEYNON. Mass spectrometry and its application to organic chemistry. Elsevier, Amsterdam. 1960. p. 395.
13. (*a*) S. GOLDSCHMIDT and K. RENN. Chem. Ber. **55**, 628 (1927); (*b*) R. H. POIRIER, E. J. KAHLER, and F. BENINGTON. J. Org. Chem. **17**, 1437 (1952); (*c*) A. HENGLEIN. Makromol. Chem. **15**, 188 (1955); (*d*) B. G. TARGLADIS and A. W. SCHOENMAKERS. Nature, **210**, 1151 (1956); (*e*) D. VERDIN. Trans. Faraday Soc. **56**, 823 (1960); (*f*) J. A. WEIL, K. V. SANE, and J. M. KINKADE. J. Phys. Chem. **65**, 710 (1961); (*g*) C. E. H. BAWN and D. VERDIN. Trans. Faraday Soc. **56**, 815 (1960); (*h*) D. W. OVENALL. J. Polym. Sci. **49**, 225 (1961); (*i*) T. MRZEWINSKI and K. OKON. Buil. Wojskowej Akad. Tech. **13**, 35 (1964); (*j*) K. MARUYAMA and T. OTSUKI. Tetrahedron Lett. 3705 (1966); (*k*) K. MARUYAMA, T. OTSUKI, and T. IWAS. J. Org. Chem. **32**, 82 (1967); (*l*) L. DULOG and G. BAUM. Chem. Ber. **104**, 661 (1971).
14. F. D. GREENE, M. A. BERWICK, and J. C. STOWELL. J. Am. Chem. Soc. **92**, 867 (1970).
15. (*a*) G. S. HAMMOND, J. N. SEN, and C. E. BOOZER. J. Am. Chem. Soc. **77**, 3244 (1955); (*b*) J. C. BEVINGTON. J. Chem. Soc. 1127 (1956).
16. (*a*) J. FLOOD, K. E. RUSSELL, and J. A. STONE. J. Chem. Soc. Chem. Commun. 482 (1972); (*b*) J. FLOOD and K. E. RUSSELL. Can. J. Chem. **53**, 1123 (1975); (*c*) P. F. CURRIE, J. W. QUAIL, and J. A. WEIL. Can. J. Chem. **58**, 723 (1980).
17. L. TESTAFERRI, M. TIECCO, M. TINGOLI, M. FIORENTINO, and L. TROISI. J. Chem. Soc. Chem. Commun. 93 (1978).
18. D. G. HAWTHORN and D. H. SOLOMON. J. Macromol. Sci. A. **6**, 661 (1972).
19. J. H. BENYON. Mass spectrometry and its application to organic chemistry. Elsevier, Amsterdam. 1960. p. 268.
20. K. R. KOPECKY and S. EVANI. Can. J. Chem. **47**, 4041 (1969).
21. W. S. JOHNSON, J. W. PETERSEN, and W. P. SCHNEIDER. J. Am. Chem. Soc. **69**, 74 (1947).
22. J. E. EIJKMAN. Chem. Weekbl. **1**, 421 (1904).
23. S. WAWZONEK and J. KOSIKOWSKI. J. Am. Chem. Soc. **76**, 1641 (1954).
24. C. D. HURD and C. N. WEBB. J. Am. Chem. Soc. **49**, 549 (1927).
25. D. Y. CURTIN and M. J. HURWITZ. J. Am. Chem. Soc. **74**, 5381 (1952).
26. J. J. CURPHEY, E. J. HOFFMAN, and C. M. DONALD. Chem. Ind. London, 1138 (1967).
27. J. V. BRAUN. Justus Liebigs Ann. Chem. **507**, 14 (1933).
28. M. E. MCGREAL and C. B. NIEDERL. J. Am. Chem. Soc. **57**, 2625 (1935).
29. J. GASPARIC. Chem. Ind. London, 43 (1962).
30. R. MELDOLA. J. Chem. Soc. **41**, 200 (1882).

Can. J. Chem. Downloaded from www.nrcresearchpress.com by 210.87.254.6 on 09/06/12
For personal use only.

Some chemical and analytical aspects of polysaccharide modifications. I. Nitroxide spin-labelling studies of alginic acid, cellulose, and xanthan gum[1]

MANSUR YALPANI[2] AND LAURANCE D. HALL

Department of Chemistry, University of British Columbia, Vancouver, B.C., Canada V6T 1Y6

Received May 7, 1981

MANSUR YALPANI and LAURANCE D. HALL. Can. J. Chem. **59**, 3105 (1981).

Nitroxide spin labels have been employed as model reagents for evaluating several aspects of the synthesis of covalently modified polysaccharide derivatives using alginic acid **1**, xanthan gum **19**, and cellulose **23** as exemplars. Modifications were accomplished both nonspecifically, by the alkylation of hydroxyl groups, and specifically, either by direct transformation of the carboxylate function of **1** and **19** or after introduction of appropriate prominent functions, such as aldehydes or amines. Thus, the acetamido ether **3** was obtained from **1** and chloroacetamide **2**. The carboxylate functions of **1** and **19** were condensed with amines to yield the corresponding amides **8**, **10**, **20**, **21**, and **22** either by direct reaction, by carbodiimide-mediated coupling, or by transesterification. The amine derivatives **12**, **13**, **25**, and **18** were obtained either from dialdehyde derivatives via periodate oxidation or from *s*-triazine intermediates, using sodium cyanoborohydride. Similarly, the keto spin label **15** reacted with hydrazide intermediates **14** and **29** in the presence of sodium cyanoborohydride to afford the hydrazide derivatives **16** and **30**. The cellulose urethane derivative **27** was obtained via the cyclic carbonate precursor. The products were characterized by esr and other spectroscopic techniques.

MANSUR YALPANI et LAURANCE D. HALL. Can. J. Chem. **59**, 3105 (1981).

On a utilisé des marqueurs de spin de type nitroxyde comme réactifs modèles pour évaluer plusieurs aspects de la synthèse de dérivés de polysaccharides modifiés de façon covalente en utilisant comme exemples l'acide alginique (**1**), la gomme xanthane (**19**) et la cellulose (**23**). On a réalisé ces modification de façon non spécifique en alkylant les groupes hydroxyles et de façon spécifique soit par la transformation directe de la fonction carboxylate des composés **1** et **19** soit après l'introduction de fonctions appropriées telles les aldehydes ou les amines. Dans ces conditions, on obtient l'éther acétamido **3** à partir du composé **1** et du chloroacétamide (**2**). Les fonctions carboxylates des composés **1** et **19**, par condensation sur les amines, donnent les amides correspondants **8**, **10**, **20**, **21** et **22** soit par réaction directe soit par couplage en présence de carbodiimide ou par transestérification. On a obtenu les dérivés d'amines **12**, **13**, **25** et **18** soit à partir des dérivés dialdéhydes au moyen d'une oxydation par le periodate ou à partir des intermédiaires *s*-triazines en utilisant le cyanoborohydrure de sodium. D'une manière analogue, le marqueur de spin de type cétone (**15**) réagit avec les hydrazines intermédiaires **14** et **29** en présence du cyanoborohydrure de sodium en donnant les dérivés de l'hydrazide **16** et **30**. On a obtenu le dérivé uréthane de la cellulose **27** par l'intermédiaire d'un précurseur cyclique. On a caractérisé les produits par la rpe et par d'autres techniques spectroscopiques.

[Traduit par le journal]

Introduction

Polysaccharides are increasingly being recognized for their immense value in many areas of academe, industry, and medicine (1). With their rich abundance, low cost, and general versatility, natural polysaccharides can be expected to be of even greater significance in future, particularly in view of possible discoveries of new types of polymers from bacterial sources. At the same time, there is a growing demand for the preparation of modified polysaccharides which display specific properties such as viscosity (2), gelling ability (3), metal-chelating capacity (4), or drug-releasing potential (5). However, despite the substantial amount of work which has been directed at evaluating both native and modified polysaccharides (6), the predictive understanding of the important relationship between their structure and function is still rather imperfect (7). This is partially a consequence of the limitations both of the "traditional" analytical methods and of the chemical methodology used for modification (8); developments in both of these areas would clearly advance such an understanding.

There are several distinct protocols for the chemical modification of polysaccharides: (*i*) "statistical chemistry", until recently the prevailing trend, which involves the use of nonselective chemical reagents for random derivatizations (8); and (*ii*) specific modifications which can be accomplished either (*a*) by derivatizing polysaccharide sites which have intrinsic selective chemical reactivities (e.g. —COOH, —NH_2, etc.) (9), or, (*b*) in the absence of such sites, by selectively introducing reactive functions using either chemical or enzymic methodology (10).

The reagents commonly used in category (*i*) include strong alkalis and alkylating or acylating agents, as, for example, in the preparation of carboxyalkyl derivatives; these can lead to partial degradation of the polysaccharide (3), which is undesirable.

[1]Aspects of this work were presented at the 63rd Canadian Chemical Conference, Ottawa, June 3–9, 1980.

[2]Present address: Department of Pathology, University of British Columbia, Vancouver, B.C., Canada V6T 1W5.

0008-4042/81/213105-15$01.00/0

©1981 National Research Council of Canada/Conseil national de recherches du Canada

Can. J. Chem. Downloaded from www.nrcresearchpress.com by 210.87.254.6 on 09/06/12
For personal use only.

Can. J. Chem. Downloaded from www.nrcresearchpress.com by 210.87.254.6 on 09/06/12
For personal use only.

Characterization and detailed structural determinations of the modified products by the conventional methods of monosaccharide chemistry are in most cases complicated, if not precluded, by the intrinsic properties of polysaccharides, such as high solution viscosity, gel formation, polydispersity, or polymolecularity. There is, consequently, a need for the development of new analytical techniques whereby the chemistry of these complex systems can be followed.

In this study we have chosen to emphasize the use of nitroxide spin-labelling for evaluating various aspects of polysaccharide derivatizations. The basic concept involves the use of nitroxide probes as model reagents either to monitor the course of a particular reaction, or to optimize the reaction conditions, in order to establish criteria for processes involving diamagnetic analogues. Among the important advantages of this approach is the facility with which products in either the solid state or in the hydrated forms (solution, gel) can be investigated, and "covalently-bound" species can be distinguished from even relatively low concentrations of "adsorbed" or "trapped" spin-labelled reagents.

In the present paper we attempt to survey various aspects of some selective and nonselective modification procedures. In view of the substantial versatility and efficiency of the reductive amination reaction (11), most of the modifications described herein were designed to introduce either carbonyl or amine functionalities into the polysaccharides for subsequent derivatizations. The choice of synthetic procedures was further guided by the following main considerations: (*i*) to maintain the polysaccharide chain largely, if not completely, intact and to avoid acid hydrolysis of the nitroxide spin labels; and (*ii*) to form covalent linkages between the nitroxide labelled reagents and the polymers in the simplest and most direct way. As a consequence, strongly acidic or basic conditions were avoided and the reactions were conducted at ambient temperature and pressure.

Three important polysaccharides were used as exemplars: cellulose, the most abundant neutral polymer; alginic acid, a linear uronic acid derivative; and xanthan gum, a branched, high-molecular-weight acidic species. The reactions reported herein afforded in all cases covalently-linked derivatives, confirmation of which was obtained by esr and other spectroscopic methods.

Results

A. *Alginic Acid*

Of the three polysaccharides discussed here, alginic acid **1**, provided the greatest challenge for modifications because of its susceptibility to degradation and low reactivity; as a result mild reaction conditions were employed to preserve structural integrity. Various workers (12) had earlier noted that the acetylation of alginic acid never proceeded to completion, introducing no more than one acetyl group per uronic acid residue. However, Schweiger (13) discovered that a peracetylated product could be obtained with minimal polymer degradation if alginic acid was first partially (80–90%) dehydrated. This procedure reduces the extensive hydrogen-bonding in **1** thereby rendering the hydroxyl groups available for reactions, whereas complete dehydration leads to inactivation of **1**. Thus, following

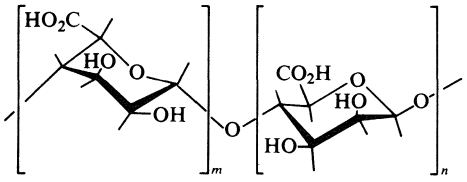

1

1 **2**

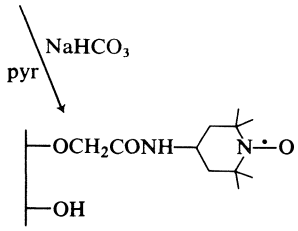

3

Schweiger's method (13), partially dehydrated alginic acid was obtained by treatment of **1** with cold, glacial acetic acid, and used for subsequent reactions.

Alkyl ether

Stable acetamido ethers **3** were prepared from activated alginic acid **1** using 4-chloroacetamido-2, 2,6,6-tetramethylpiperidine-1-oxyl **2** in either pyridine or aqueous acetone (65%), with solid sodium bicarbonate as base. The mild conditions which were employed to minimize degradation of **1** led to very low degrees of substitution, ds (0.03–0.04).

The esr spectrum of **3** in aqueous solution (Fig. 1a) reveals a very mobile nitroxide moiety (τ_c 1.1×10^{-11} s); at least part of this relatively high mobility can be ascribed to the rotational freedom associ-

Can. J. Chem. Downloaded from www.nrcresearchpress.com by 210.87.254.6 on 09/06/12
For personal use only.

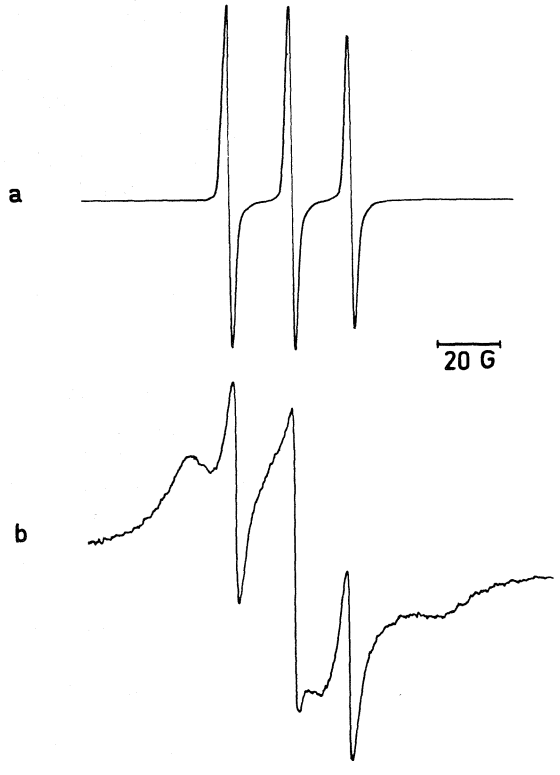

FIG. 1. Room temperature esr spectra of **3**: (a) aqueous solution; (b) powder.

ated with the four-bond linkage between the polymer and probe.

The powder spectrum of **3** (Fig. 1b) resembles that of a polycrystalline sample and also indicates presence of a small percentage of free label which could not be removed by dialysis. The amount of free label did not vary with time, i.e. no "leakage" could be detected after periods of several weeks.

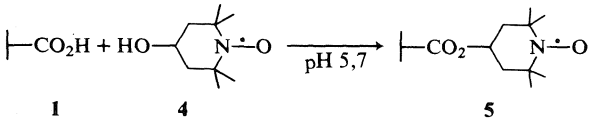

1 **4** **5**

Alkyl ester

The esterification of partially dehydrated alginic acid **1** was accomplished using 4-hydroxy-2,2,6,6-tetramethylpiperidine-1-oxyl **4** in aqueous acetone, to afford the ester **5** (ds 0.05). The τ_c value of **5** in aqueous solution was 20 ns (Fig. 2a). Evidence[3] for the formation of **5** was derived from the esr spectrum of the powder under methanol (Fig. 2b) which revealed a broad "bound" component together with a superimposed signal arising from

[3]Attempts to verify the formation of **5** by ir were unsuccessful.

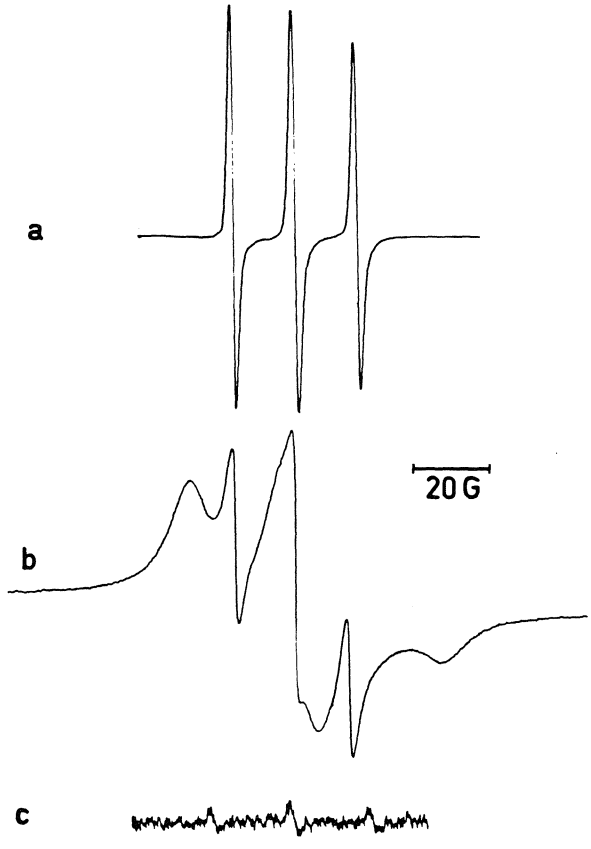

FIG. 2. Room temperature esr spectra of **5**: (a) aqueous solution; (b) powder; (c) control experiment: **1** treated with **6** under identical conditions.

"free" label (despite extensive dialysis of the product!). This "free" label may be present as the salt to which previous workers have alluded (14, 15). Additional evidence for the occurrence of esterification was derived from a control experiment in which the spin label **4** was replaced by the unreactive analogue **6**. Only a very small proportion of **6** remained in the sample after dialysis, as indicated in Figure 2c.

The above reaction appears to provide a viable alternative to the known esterification procedures for alginic acid which involve the use of alkyne oxides (16) or the alginic acid chloride intermediate proposed by Wypych (17).

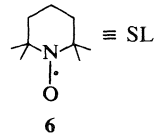

6

Amides

(a) Via Carbodiimide Coupling

Amide derivatives of alginic acid could be readily

Can. J. Chem. Downloaded from www.nrcresearchpress.com by 210.87.254.6 on 09/06/12
For personal use only.

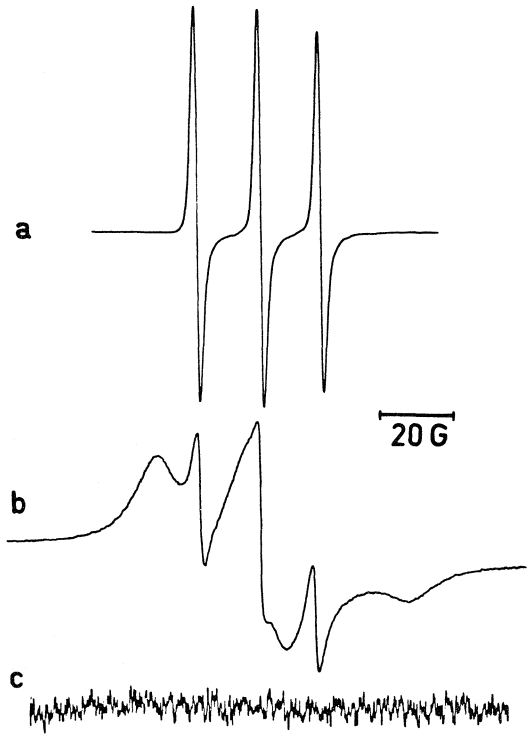

FIG. 3. Room temperature esr spectra of **8**: (a) aqueous solution; (b) powder; (c) control experiment: **1** treated with **6** under identical conditions.

prepared by carbodiimide-mediated coupling in organic, or mixed aqueous–organic media. As in the previous reactions, however, alginic acid is only reactive in its partially dehydrated form (18). Amidation could be achieved using *N*,*N*′-dicyclohexylcarbodiimide (DCC) in dimethylformamide (DMF), or with *N*-ethyl-*N*′-dimethylaminopropylcarbodiimide (EDC) in 65% aqueous acetone to afford the amide **8** with ds 0.10 and 1.00, respec-

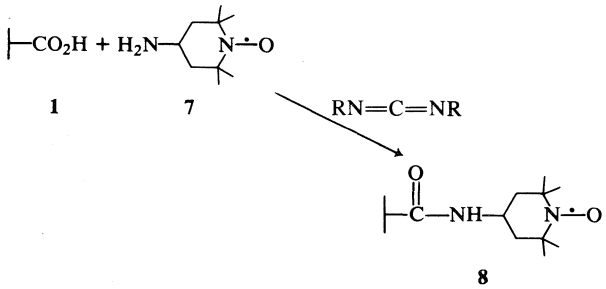

1 **7** **8**

tively; clearly, EDC is the preferred reagent for high ds products. The esr spectra of **8** provide evidence for the covalent nature of the linkage (Fig. 3); in the control experiment with label **6** no signal was detectable after identical treatment (Fig. 3c). The nitroxide moiety of **8** is moderately immobile in aqueous solution, (τ_c 15 ns) (Fig. 3a).

(b) Via Nucleophilic Substitution of Alginic Esters

Propylene glycol esters of alginate **9** have been reported to react with amines to form amides in high yields at ambient temperature (14, 15, 19). Two commercial samples of propylene glycol alginate (PGA) with different degrees of esterification (ds 0.80–0.85 and ds 0.50–0.60, respectively)

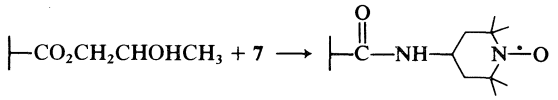

9 **10**

were condensed with amine spin label **7** in DMF in the presence of small amounts of water to yield the amide **10**. Reactions of this type are of considerable utility since they can be reportedly (15) performed with a wide range of amines such as primary or secondary aliphatic, cycloaliphatic, aromatic, and diamines. The resulting products are of interest for their gel-forming properties.

The esr spectra of amides of the type **10** in aqueous solution (Fig. 4a) indicate moderately immobile nitroxide moieties (τ_c 33 ns) and the corresponding powder spectra reveal not only the covalent nature of the linkages to the polymer, but also strong dipolar interactions (Fig. 4b). Similar information can be derived from rapidly frozen (77 K) samples (Fig. 4c). The control experiment with label **6** revealed no detectable esr signal (Fig. 4d).

Amines

Following the methods of Painter and coworkers (20), dialdehyde alginates **11** with varying degrees of oxidation (do) were prepared by periodate oxidation. These were subsequently converted to the corresponding amine derivatives **12** using reductive amination with label **7**; typically, amines with ds 0.05 (**12***a*) and 0.13 (**12***b*) were obtained from dialdehyde precursors with do 0.10 and 0.44, respectively. The esr spectra of **12***a* and **12***b* in aqueous solution (Fig. 5a) revealed substantial line broadening and τ_c values of 51 ns and 57 ns, respectively. When these solutions were frozen, dipolar broadening was again apparent (Fig. 5c). The powder spectra of the respective materials at 298 K

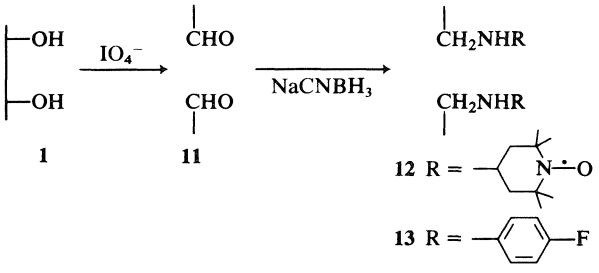

1 **11**

Can. J. Chem. Downloaded from www.nrcresearchpress.com by 210.87.254.6 on 09/06/12
For personal use only.

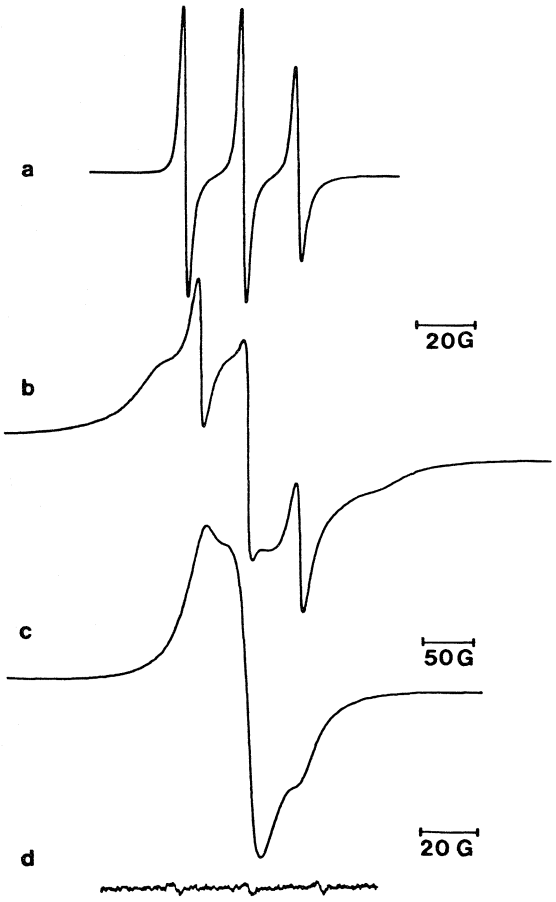

FIG. 4. The esr spectra of **10**: (a) aqueous solution (298 K); (b) powder (298 K); (c) powder (77 K); (d) control experiment: **9** treated with **6** under identical conditions.

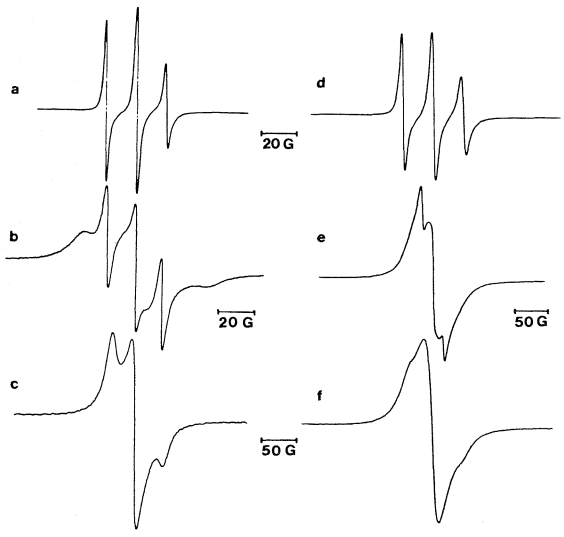

FIG. 5. The esr spectra of **12***a*: (a) aqueous solution (298 K); (b) powder (298 K); (c) powder (77 K); and **12***b*: (d) aqueous solution (298 K); (e) powder (298 K); (f) powder (77 K).

show the presence of small proportions of free label (Fig. 5b). The above findings seem to implicate the presence of two spin-label units per periodate-cleaved hexuronic acid residue of **12** since, even at low ds, dipolar interactions are evident. Possible contributions to the observed lineshapes from interactions between nitroxides attached to different chains or to neighbouring uronide residues should be negligible, at least for derivatives of **12** with low overall ds. If the above inference is correct, it would be in contrast to several observations of other dialdehyde reaction products for which incorporation of only one amine-bearing unit per dialdehyde has been found (see for example ref. 21). The reaction of equivalent dialdehyde cellulose derivatives will be discussed in section C.

A sample of periodate-oxidized alginate (do 0.10) was treated with *p*-fluoroaniline under identical conditions as above, to produce a derivative **13**, the 100.6 MHz ^{13}C nmr spectrum of which showed the aromatic resonances at 117 ppm. Fluorine-19 nmr studies of this derivative at 96.4 MHz indicated that ^{19}F is well suited for distinguishing covalently-bound material from reactant; thus, when *p*-fluoroaniline was added to an aqueous solution of the fluoroaniline-alginate derivative, the free and bound species were found to have resonances separated by ca. 1 ppm in chemical shift.

Hydrazide

Pfannemüller *et al.* (22) have recently reported a series of polysaccharide-hydrazide derivatives which they employed for the synthesis of branched-chain derivatives. In the present work, alginic acid hydrazide **14** was prepared, in adaptation of their method, from propylene glycol alginate **9** and hydrazine hydrate. Reductive amination of **14**, using 4-oxy-2,2,6,6-tetramethylpiperidine-1-oxyl **15** afforded the spin-labelled derivative **16** (ds 0.21),

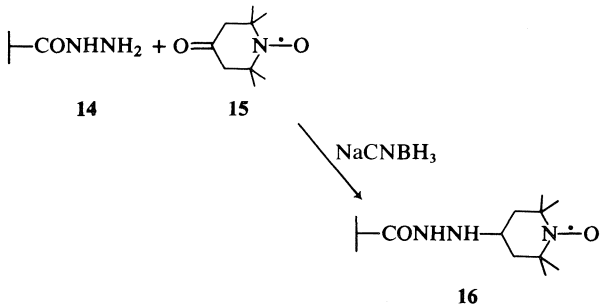

whose aqueous solution spectrum is shown in Fig. 6a. This method is potentially useful for the preparation of polysaccharide intermediates since it introduces a very short spacer group between the polymer and other molecules to be attached to it.

Can. J. Chem. Downloaded from www.nrcresearchpress.com by 210.87.254.6 on 09/06/12
For personal use only.

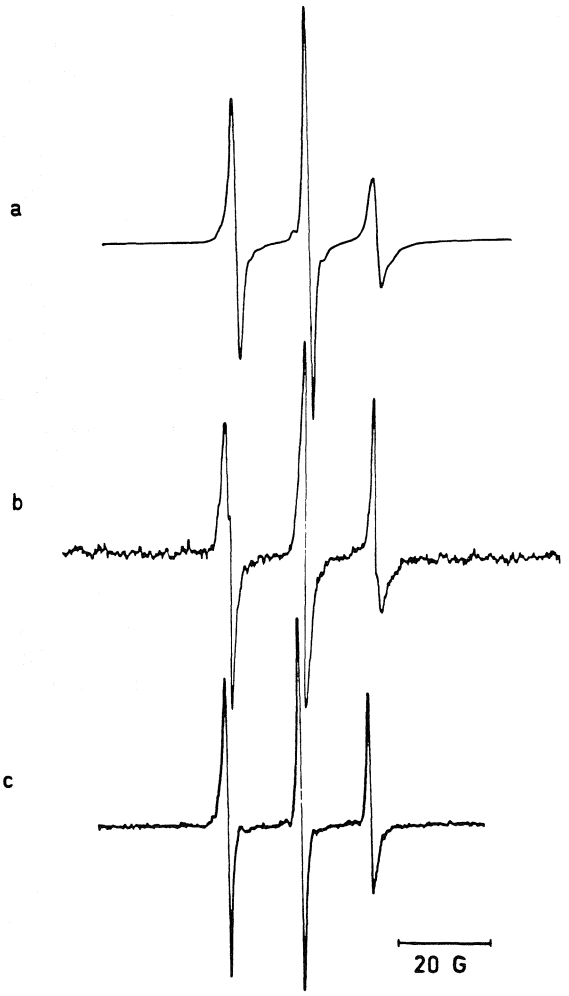

FIG. 6. Room temperature esr spectra of: (a) **16** in aqueous solution (b) **18** in aqueous solution; (c) **30** in aqueous solution.

s-*Triazine Derivative*

Lee and Maekawa (23) have reported a method for incorporating the carboxyl groups of polyuronides into *s*-triazine rings using dimethylbiguanidine hydrochloride. Following their method, **17** (ds 0.12) was prepared from propylene glycol alginate **9** and subsequently labelled using **15** to afford a product **18** (ds 0.02) whose aqueous solution spectrum (Fig. 6b) revealed a relatively slow tumbling nitroxide moiety (τ_c 31 ns). The *s*-triazine type derivative may be of interest for applications in which a partial masking of the carboxylate groups of polyuronides is desired.

B. *Xanthan Gum*

The carboxyl functions of the glucuronic acid and pyruvic acid residues are the most prominent candidates for specific derivatizations of xanthan gum, and should undergo the same reactions as their counterparts in alginate; this is demonstrated here by the carbodiimide-mediated preparation of the carboxamide derivative.

Amide

(a) Via Carbodiimide Coupling

Purified xanthan gum **19** was activated via the carbodiimide procedure using EDC, and subsequently condensed with amine label **7** to afford the amide **20** in which 43% of the carboxyl groups had been transformed. In light of the mild reaction conditions employed, it is likely that derivatization of the pyruvic acid acetal groups has also occurred.

The esr spectrum of **20** in aqueous solution (Fig. 7a) reveals a fast tumbling (τ_c 6.1×10^{-11} s) nitroxide moiety, the motion of which is presumably attributable to the motional freedom enjoyed by the sidechains.

(b) Via Direct Condensation

A procedure has been described (24) for the preparation of "amine" alginates which involves the condensation of amines with solid alginate in the presence of small amounts of water. Since no further information was provided it is unclear, however, from this report what the term "amine alginates" actually implies in terms of the structure of such derivatives; assuming the formation of covalent linkages between the amines and hexuronide carboxylates, such products should be more appropriately classified as amides. Nevertheless, the procedure appeared to be interesting enough to warrant investigation using xanthan gum as substrate. Thus, xanthan gum **19** was condensed with amine label **7** following this procedure to yield a product **21** whose esr spectrum (Fig. 8b) revealed the presence of both "bound" and some "free" label, after purification by dialysis.

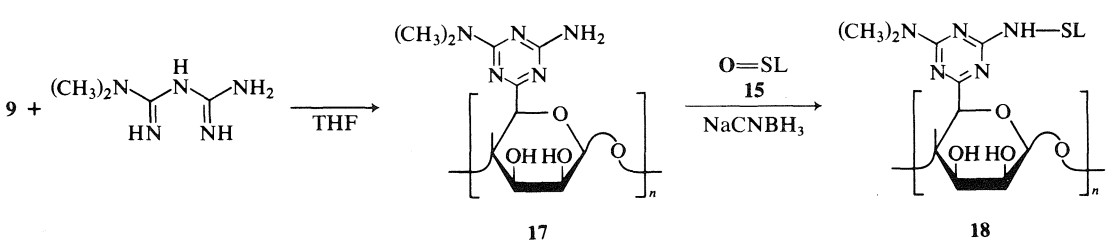

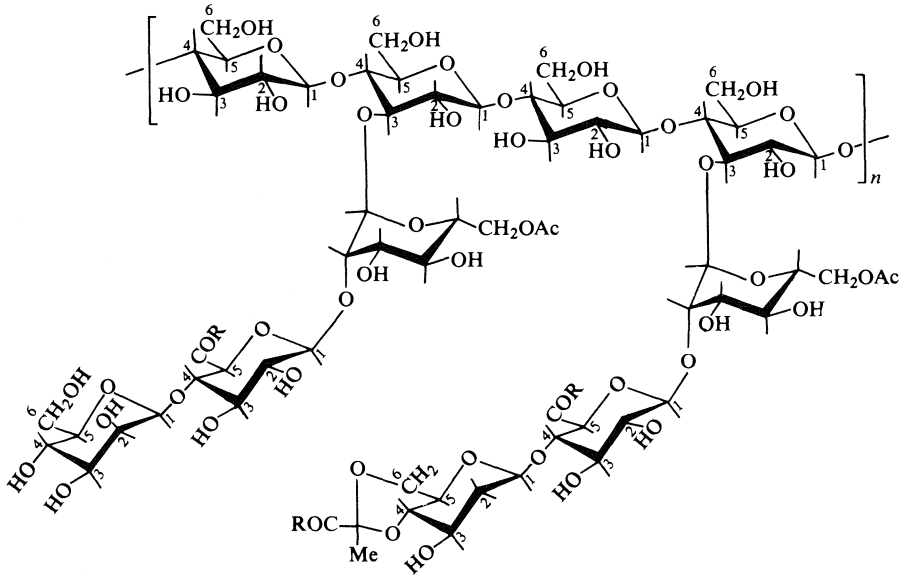

19 R = OH

20, 21 R = NH—

22 R = $NH(CH_2)_{17}CH_3$

Encouraged by this evidence for the formation of a covalent derivative, the reaction was performed using a diamagnetic analogue, *n*-octadecylamine. Carbon-13 nmr measurements of the resulting product **22**, both in the solid state as well as in aqueous solution, confirmed the presence of the amide substituent (25). The ds of **22** could not, however, be accurately established; the C/N ratio found by combustion analysis corresponded approximately to a fully substituted product.

C. *Cellulose*

Amines via Reductive Amination of Dialdehyde Cellulose

Following Nevell's procedure (26), cellulose **23** was oxidized with periodate to the dialdehyde derivative **24** to obtain products with three different degrees of oxidation (do), 0.05, 0.19, and 0.34, respectively. Subsequent reductive amination of these materials produced the spin-labelled derivatives **25**. As in the case of alginate, the conversion into spin-labelled amines **25** did not seem to linearly correspond to the increasing do of the precursors. Degree of substitution values of 0.01, 0.063, and 0.065 were obtained for **25** from the dialdehyde samples with do 0.05, 0.19, and 0.34, respectively. The low overall spin-label incorporations can probably be attributed to the fact that the cellulose samples exhibit differential accessibility to the bulky nitroxide probes. Such reasoning seems justifiable in light of a recent esr study of the accessibility of cellulose which came to similar conclusions (18, 27). Interestingly, the esr spectra of **25** in aqueous suspension (Fig. 9a), indicate two distinct nitroxide populations of which one enjoys a substantially greater freedom of motional reorientation than the other; this finding gives further credence to the above "accessibility" arguments.

As for the corresponding alginate derivatives

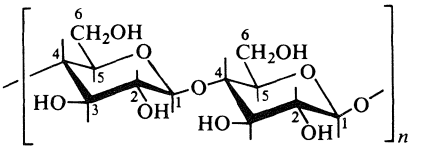

23

(**12**), the esr powder spectra (Fig. 9b) of the cellulose derivatives **25** reveal dipole–dipole interactions between neighbouring spins from which it may again be inferred that structures containing two nitroxides per periodate-cleaved glucose residue **25***a* predominate over those bearing only one label, as exemplified (from a series of other possibilities) by **25***b*. The strongest evidence for this inference derives from the observation of dipolar interactions for cellulose derivatives with low ds. Assuming random oxidation and subsequent label-

Can. J. Chem. Downloaded from www.nrcresearchpress.com by 210.87.254.6 on 09/06/12
For personal use only.

Can. J. Chem. Downloaded from www.nrcresearchpress.com by 210.87.254.6 on 09/06/12
For personal use only.

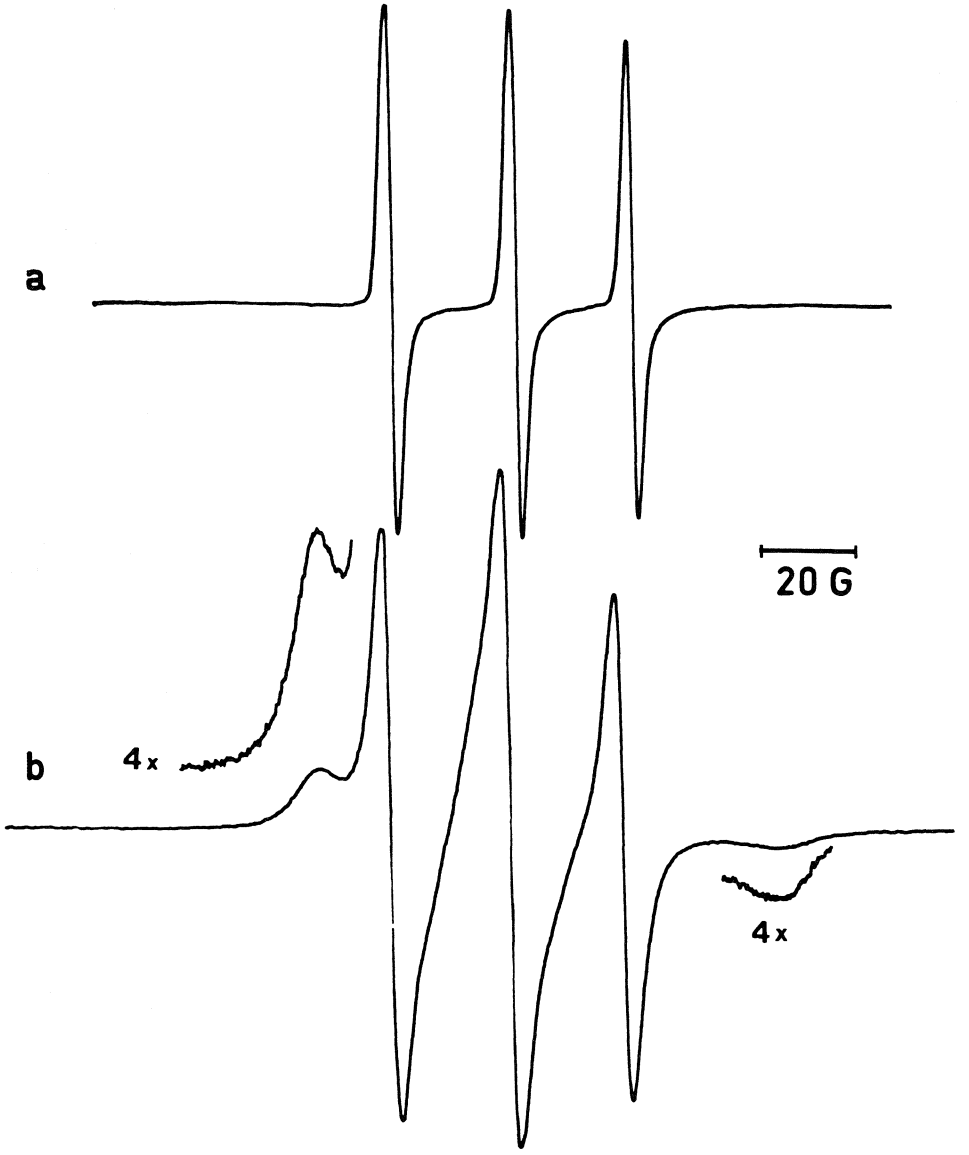

FIG. 7. Room temperature esr spectra of **20**: (a) aqueous solution; (b) powder (insert: receiver gain × 4).

ling of the polymer and with due consideration of the aforementioned "accessibility" factor, it is reasonable to expect the separation between single nitroxides attached to different hexose units to be too great for significant contributions to the dipolar interactions to arise from this source. Thus, it would seem that these findings are best accommodated by structural units of the type **25***a*.

Urethanes

Five-membered cyclic carbonate derivatives, obtained from the reaction of ethylchloroformate with vicinal diols, have been reported for a number of carbohydrates including polysaccharides (28). These derivatives form stable urethane products upon reaction with amine nucleophiles. Commercial cellulose carbonate (ds 0.21) **26** was derivatized in aqueous medium to afford the spin-labelled derivative **27** (ds 0.08).

It is interesting to note that (as for **25**) an aqueous suspension of **27** produced a complex spectrum consisting of a partially resolved broad component and a more mobile (τ_c 9.1×10^{-11} s) one (Fig. 10a). Differences in the morphology of **27** are therefore again indicated; indeed, the properties of **27** varied with its history: when prepared from methanol, the

Can. J. Chem. Downloaded from www.nrcresearchpress.com by 210.87.254.6 on 09/06/12
For personal use only.

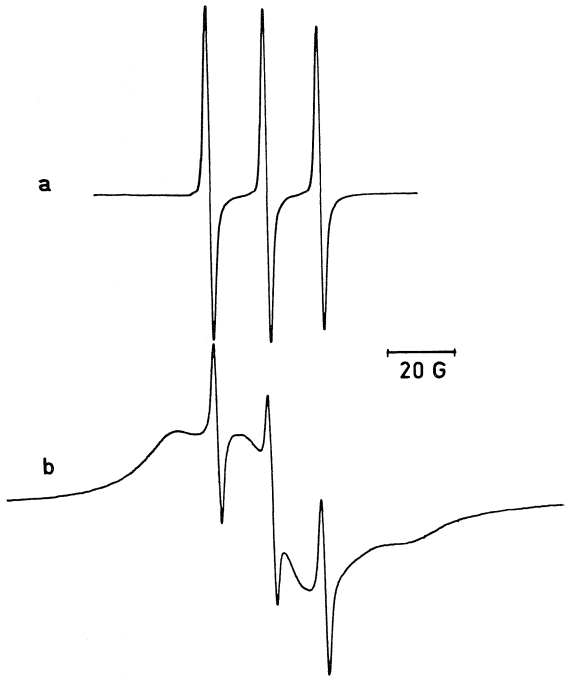

FIG. 8. Room temperature esr spectra of **21**: (a) aqueous solution; (b) powder.

product had a lower ds and its esr spectrum (Fig. 10b) resembled that of a polycrystalline sample, whereas the product obtained from reaction in aqueous medium revealed strong dipolar interactions (Fig. 10c). It can therefore be suggested that these differences are attributable to the greater accessibility of **26** to aqueous solvent. A control experiment in which **26** was treated with the unreactive label **6**, proved that no adsorption phenomena were present in this set of experiments (Fig. 10d).

Finally, it should be noted that in methanol **26** may possibly undergo side-reactions (formation of

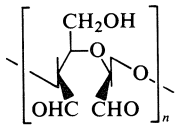

24

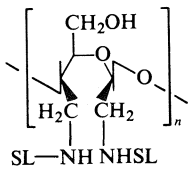

25*a*

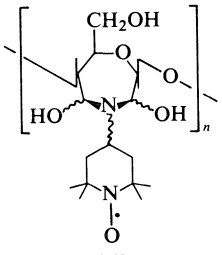

25*b*

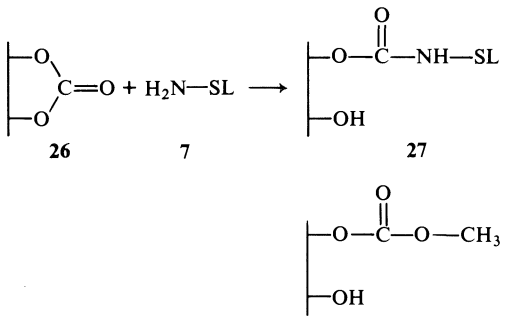

26 **7** **27**

28

O-methoxycarbonyl derivatives **28**) which could be partially responsible for the lower ds of **27** obtained from this medium.

Hydrazide

Cellulose hydrazide derivatives have found various applications as reactive intermediates (22) for enzyme immobilization (30), or for metal collection (31). Their synthesis can be achieved via the *C*-6-chlorodeoxy derivative (31) or, more conveniently, via commercially available carboxymethyl cellulose (32). Using the latter method, cellulose hydrazide **29** (ds 0.5) was prepared and subsequently reductively aminated, using **15**, to yield the hydrazide derivative **30** (ds 0.003) whose aqueous solution spectrum is shown in Fig. 6c. The nitroxide moiety of **30** displayed a relatively slow motional reorientation time (τ_c 17 ns).

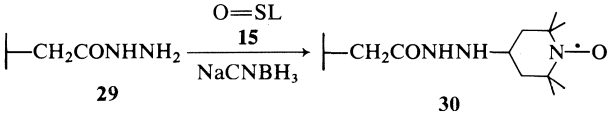

29 **30**

Discussion

In view of the fact that some of the reactions described here, for example the amidation or esterification of alginate derivatives, occur under conditions which have no formal analogy in monosaccharide chemistry, it is appropriate to summarize the criteria used herein to establish the existence of covalent linkages. The esr spectra of nitroxide-labelled derivatives are highly informative in this regard for the following reasons.

1. The spectral lineshapes and widths from derivatives (in most cases, in aqueous solution) at ambient temperature are a well-established measure of the degree of motional immobilization of nitroxide moieties attached to polymers (33), allowing for facile distinction between these species and unbound spin label which is tumbling freely in solution. Whereas the latter species gives rise to three sharp lines of essentially equal intensity, the

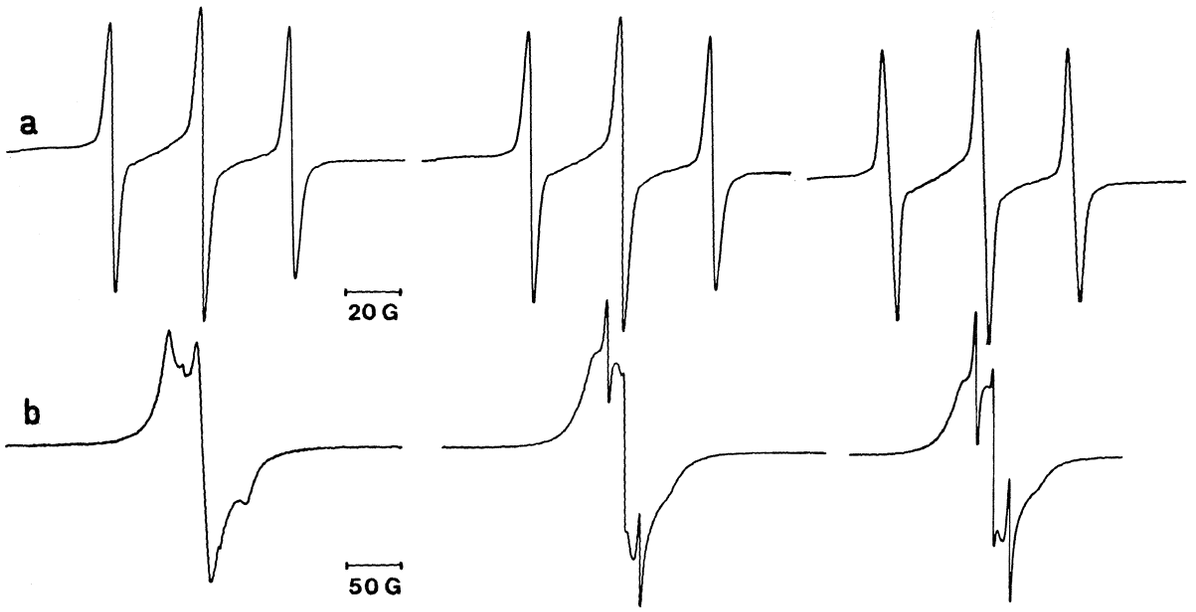

FIG. 9. Room temperature esr spectra of **25** with ds 0.03 (left), 0.063 (centre), and 0.065 (right): (a) aqueous suspension; (b) powder.

former exhibit varying intensity ratios and degrees of linewidth. This differential is important because even after extensive washing or dialysis, the esr spectra of several derivatives revealed the presence of small quantities of adsorbed species (see also item 4 below).

2. Similarly, the spectral lineshapes obtained from powder samples at 77 K facilitate distinction of "bound" and "free" labels (in the former case). Additional information regarding interactions between attached, proximate spin labels can, as we have described elsewhere (10, 18, 27, 34), be extracted from these spectra.

3. The τ_c values of nitroxide moieties provide, of course, another useful indication for the presence of covalent linkages, since values differing by several orders of magnitude are commonly found between species which are covalently associated as compared with species tumbling freely in solution. Due to the apparent complexity of many of the esr spectra (e.g. Fig. 6b) the corresponding τ_c values derived here merely serve for comparative purposes.

4. Control experiments in which an "unreactive" spin label was employed under identical reaction conditions as its reactive counterparts demonstrated that very few, if any, noncovalent associations or other phenomena such as trapping within a polysaccharide matrix occur for the various derivatives studied here. The absence of esr signals in experiments involving label **6** does, of course, not necessarily preclude ionic interactions in reactions involving amine- and hydroxy-bearing nitroxides and polyelectrolytes, such as alginate. Evidence for such phenomena derives from the relatively small, albeit significant, contribution of "free" label to the esr spectra (e.g. Figs. 2 and 4) of several derivatives where the corresponding control experiments produced only very weak esr signals. Thus, nitroxide labels can also be employed, as we will describe elsewhere, to probe polyelectrolyte interactions.

5. Whenever "free" nitroxide was suspected to coexist with bound label the leakage of such species from the polymer systems was monitored with time.

While fulfilment of only one of the above criteria may not always be considered sufficient proof for the existence of a polymer-bound nitroxide probe, a combination of several criteria, in conjunction with other spectroscopic evidence (such as nmr, ir, etc.) establishes such species unambiguously. Our attempts to use (standard) ir spectroscopy were generally unsuccessful mainly because the levels of probe incorporation were often too small to be detected.

Our confidence in the reliability of the esr technique for the purposes outlined above derives from a series of studies of polysaccharide derivatizations using spin labels (10, 18, 27, 35), in addition to the host of esr literature on a variety of other polymer systems (33).

Although some reactions proceeded in essentially quantitative fashion, for many others the

For personal use only.

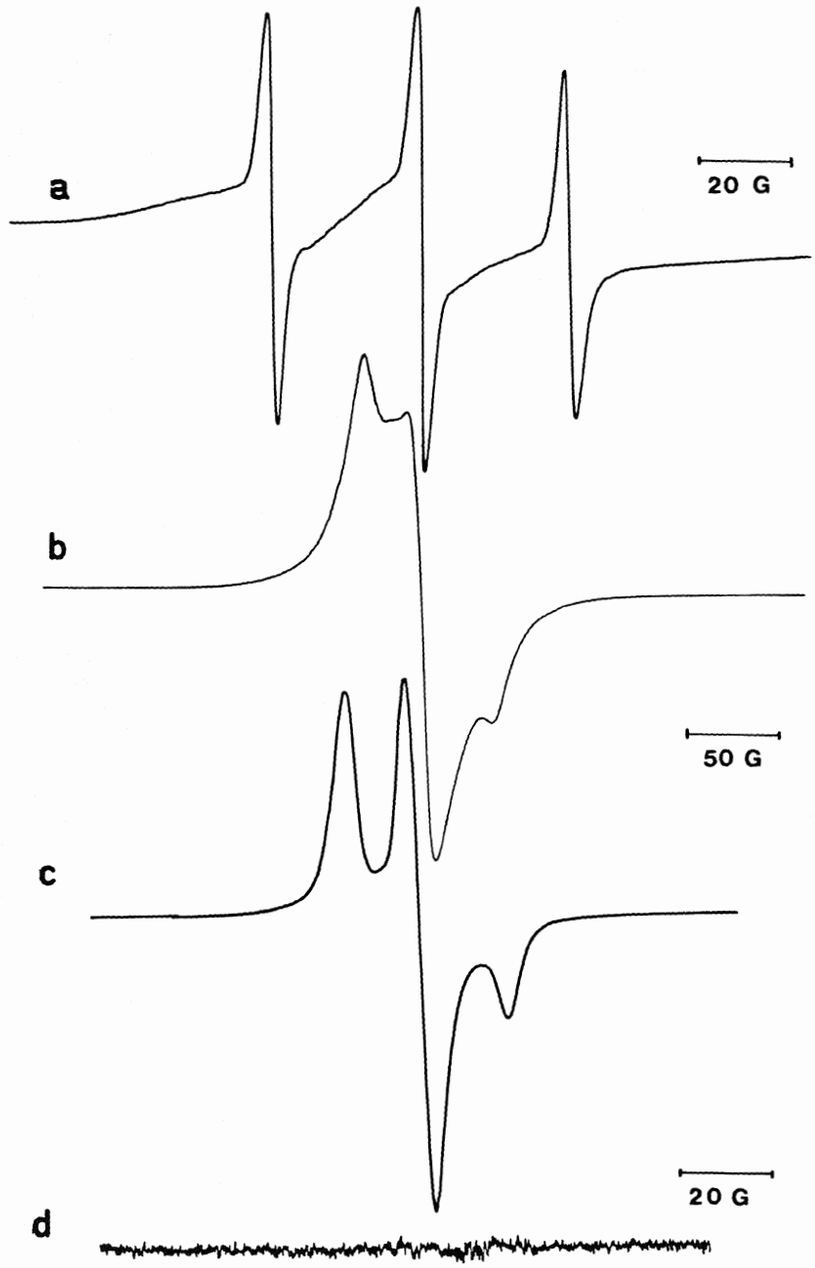

FIG. 10. The esr spectra of **27**: (a) aqueous suspension (298 K); (b) powder (298 K); (c) powder (77 K); (d) control experiment: **26** reated with **6** under identical conditions.

:onversion yields were relatively low. For two easons no attempts were made here to fully ptimize the reaction conditions in such cases: on ıe one hand, these studies were intended largely to rove the formation of covalent derivatives, and, ı the other hand, industrial procedures (36) for the eparation of high ds polysaccharide derivatives ere not followed to avoid factors, such as a certain degree of polymer degradation or additional chemical species, which might complicate the interpretation of our data.

In view of the low ds values obtained in many reactions, esr double integration was used to determine the levels of spin-label incorporation. Although this method is satisfactory for water-soluble polysaccharide derivatives, we have generally ob-

personal use only.

Can. J. Chem. Downloaded from www.nrcresearchpress.com by 210.87.254.6 on 09/06/12
For personal use only.

tained (with the instrumentation available to us) somewhat less reliable results from double integration of *solid* samples. From calibration studies we estimate the accuracy of the esr double integration to range from a few percent for solutions, to approximately 10–15 percent for powder samples, depending on the ds values of the derivatives.

For the case of derivatives with higher ds values, particularly for those containing nitrogen, routine microanalysis offers, of course, a highly reliable method for ds determinations; a certain small (generally less than one percent) uncertainty in the ds values is, however, usually encountered here, as a consequence of the extremely hygroscopic character of polysaccharides (37).

It is evident from the above that a number of reactions satisfied the requirements for specific and medium- to high-efficient conversion of polysaccharides. The carbodiimide-mediated amidation falls into this category, as does the formation of reactive intermediates via the hydrazide derivatives. The modification of vicinal diols via periodate oxidation or cyclic carbonate formation is less specific; however, the former procedure may, if performed under controlled conditions, be a useful method. Among the other methods examined, the esterification of alginic acid with alcohols seems to be promising and deserves investigation for some other polysaccharide systems; the same holds true for the amidation reactions of alginic esters.

In conclusion, we wish to note that the particular merit of the spin-labelling approach derives not solely from the fact that it provides information regarding polymer bound versus free species. As will be demonstrated in future publications, the esr method can also be employed for probing important molecular parameters, such as surface homogeneity and area, as well as the proximity of spin probes tethered to polysaccharide substrates.

Experimental

General Methods and Materials

All polysaccharide modification reactions were conducted at ambient temperature. All concentrations were performed on a Büchi rotary evaporator. Polysaccharide reaction products were purified by dialysis (unless indicated otherwise) using Spectropore #1 or #2 tubing from Spectrum Medical Inc. (Los Angeles, CA), against 0.01 *M* EDTA/0.01 *M* NaCl solutions or distilled water with 0.02% NaN_3 for 4–6 days, and subsequently lyophilized. All samples were stored refrigerated with desiccation.

C, H, N microanalyses were carried out by Mr. P. Borda of the Microanalytical Laboratory, Department of Chemistry, University of British Columbia, following careful and extensive (1–2 days) drying of the samples *in vacuo* (56°C, 0.01 Torr) over sodium hydroxide.

The following alginate samples were a gift from Kelco Co., San Diego, CA: sodium alginate (Keltone), alginic acid (Kelacid), and propylene glycol alginate esterified 50–60% (Kelcoloid-HVF) and 80–85% (Kelcoloid-O). Sodium alginate was purified following Schweiger's method (38). Cellulose carbonate was purchased from Sigma Chemical Co., cellulose powder (Whatman CF11) from W. & R. Balston Ltd., U.K. Carboxymethylcellulose (12M31P) was a gift from Hercules Inc., Wilmington, DE. Xanthan gum samples were gifts from Kelco Co. (Keltrol) and Tate & Lyle Ltd, London ($77A_3$). The former samples were purified according to the method of Holzwarth (39) while the latter were supplied in purified form.

1-Ethyl-3-(3-dimethylaminopropyl)carbodiimide HCl (EDC) was purchased from Sigma Chemical Co., and *N,N'*-dicyclohexylcarbodiimide (DCC) from Eastman Chemical Co. Dimethylbiguanidine HCl was from Aldrich Chemical Co., sodium periodate was from Fisher Scientific Co. Hydrazine hydrate was purchased from Mallinckrodt Co. Sodium cyanoborohydride, 4-amino-2,2,6,6-tetramethylpiperidine-1-oxyl, 4-oxo-2,2,6,6-tetramethylpiperidine-1-oxyl, and the spin label analogue, 4-amino-2,2,6,6-tetramethylpiperidine were purchased from Aldrich Chemical Co. The other spin labels, 4-hydroxy-2,2,6,6-tetramethylpiperidine-1-oxyl and 4-chloroacetamido-2,2,6,6-tetramethylpiperidine-1-oxyl, were synthesized by Ms. L. Evelyn of this lab using the method of McConnell and co-workers (40).

Electron Spin Resonance

The esr spectra were recorded at *X*-band using a Varian E-3 instrument in the derivative adsorption mode, and integrated using a Pacific Precision Co. MO-1012A integrator. The second integration was performed by peak cutting and weighing and comparison with freshly prepared, standard solutions of 4-hydroxy-2,2,6,6-tetramethylpiperidine-1-oxyl. Spectral lineshape distortions were avoided by careful choice of spectrometer settings (modulation amplitude, filter time constant, and scan rate); nonsaturating power levels were used. Linewidths and correlation times for rotational reorientation (τ_c) were measured using the smallest possible scan range (generally not that shown in the diagrams) and at least two to three scans in each case. τ_c values were calculated from the quadratic term of the ratio-of-heights method of McConnell and co-workers (41). No computer simulation of spectra was used since only estimates for relative comparisons were required here. A flat high-quality quartz cell (73 μL) with ground glass joints at both ends (J. Scanlon Co.) was used for aqueous solutions; aqueous suspensions and gels of polysaccharides were measured using a Teflon insert which was designed by Dr. F. G. Herring of this Department.

Nuclear Magnetic Resonance

Carbon-13 nmr spectra of aqueous and solid polysaccharide samples were recorded with a Bruker WH-400 and CXP 200 spectrometer at 100.6 MHz and 50.3 MHz, respectively, at ambient temperature (25). Fluorine-19 nmr spectra were obtained with a Varian XL-100 spectrometer (at 96.4 MHz).

Preparation of (4-Acetamido-2,2,6,6-tetramethylpiperidine-1-oxyl) Alginic Acid (3)[4]

Alginic acid was partially dehydrated following Schweiger's

[4]The application of systematic nomenclature to most of the polysaccharide derivatives reported here is not feasible due to the heterogeneity in the structure of the original polymers or in the substitution pattern of the reaction products; in a number of cases, such as for the products derived from periodate-oxidized materials, the exact structure of the product is unknown (see text). The nomenclature system adapted here attempts to indicate the substituent(s) introduced followed by the name of the native polysaccharide.

Can. J. Chem. Downloaded from www.nrcresearchpress.com by 210.87.254.6 on 09/06/12
For personal use only.

method (13) but with some modifications. Alginic acid (1 g) was swelled in glacial acetic acid (5 mL) and then centrifuged in a desk-top centrifuge. The supernatant was decanted, and the procedure repeated several times. The wet material thus obtained was used for subsequent reactions.

A solution of chloroacetamide label **2** (130 mg, 5.3 mmol) in pyridine (4 mL) was added to partially dehydrated alginic acid (40 mg, 0.23 mmol) and the dispersion was adjusted with solid $NaHCO_3$ to pH 7.5. The reaction mixture was gently shaken for 18 h. The resulting product **3** had ds 0.04. When 65% aqueous acetone was used as solvent instead of pyridine the ds of **3** was lowered to 0.01.

Preparation of [4-(2,2,6,6-Tetramethylpiperidine-1-oxyl)] Alginate (5)

Partially dehydrated alginic acid (150 mg, 0.85 mmol) was suspended in 65% aqueous acetone (5 mL). After addition of hydroxy label **4** (300 mg, 1.7 mmol) the pH was adjusted to 6 using $NaHCO_3$ and the mixture was shaken for 18 h. The product **5** had ds 0.05.

Preparation of [4-(2,2,6,6-Tetramethylpiperidine-1-oxyl)] Alginamides (8, 10)

(i) Carbodiimide Coupling

(a) EDC coupling. To partially dehydrated alginic acid (150 mg, 0.85 mmol) was added a 65% aqueous acetone solution of EDC (240 mg, 1.25 mmol, 5 mL), and after adjustment of the pH to 6.5 using Na_2CO_3, a solution of amine label **7** (270 mg, 1.6 mmol, 2 mL). The mixture was shaken for 18 h and the resulting product **8** had ds 1.00.

(b) DCC coupling. The reaction conditions were the same as in the EDC coupling procedure with the exception of using DCC (100 mg, 0.48 mmol), and DMF (3 mL) as solvent. This reaction, however, proceeded in lower (ca. 10%) yields than the EDC coupling.

(ii) Via Propylene Glycol Esters

A solution of amine label **7** (276 mg, 1.6 mmol) in DMF (2 mL) was added to a suspension of propylene glycol alginate (PGA) with a degree of esterification 0.80–0.85 (193 mg, 0.86 mmol) in DMF (2 mL). The mixture was shaken for 14 h to yield a product **10** with ds 0.15 (18% conversion of available ester groups). For PGA with a lower degree of esterification (0.5–0.6) a product with ds 0.10 (18% conversion) was obtained.

Preparation of [4-N-(2,2,6,6-Tetramethylpiperidine-1-oxyl)] Alginamine (12)

Sodium alginate was periodate-oxidized according to the procedure of Painter and co-workers (20). In a typical experiment, a 0.78% aqueous solution of sodium alginate was oxidized with 0.25 *M* $NaIO_4$ in the presence of 1-propanol at 4°C in the dark for 24 h. The oxidation was terminated by addition of ethylene glycol. Reductive amination was performed by addition of an aqueous solution of amine spin label **7** (3- to 5-fold molar excess) and sodium cyanoborohydride (7- to 10-fold molar excess). The reaction mixture was shaken for 24 h. For alginate samples oxidized 10%, products with ds 0.05 (52% conversion of available aldehyde groups) were obtained, while for samples oxidized 44% the products **12** had ds 0.13 (30% conversion).

Preparation of N-[4-(2,2,6,6-Tetramethylpiperidine-1-oxyl)] Algin Hydrazide (16)

(a) The method of Andresz *et al.* (22) was modified to prepare the hydrazide derivatives. Samples of propylene glycol alginate (Kelcoloid-O, 0.5 g, 2.2 mmol) were mixed with hydrazine hydrate, (10 mL, 0.2 *M*), in a 50 mL Erlenmeyer flask. The reaction mixture was gently shaken overnight at 22°C, affording a viscous solution which was diluted with water (25 mL). The product was precipitated in methanol (300 mL), the precipitate was collected after centrifugation (9000 rpm, 50 min), and dialyzed against 0.01 *M* EDTA for 2 days before lyophilization. Elemental analysis showed a product **14** with ds 0.76, i.e., 92% conversion of the ester. *Anal.* calcd. for $[(C_6H_8O_6)_{0.17}(C_9H_{14}O_7)_{0.07}(C_6H_{10}N_2O_5)_{0.76}]\cdot 0.88\ H_2O$: C 36.25, H 5.74, N 10.35 (C/N 3.53); found: C 36.01, H 5.37, N 10.36 (C/N 3.48).

Similarly, for PGA with lower degrees of esterification, products **14** with ds 0.45 (i.e., 80% conversion) were obtained (C/N 5.71). These ds obtained here correspond well with those of Andresz *et al.* (22) (ds 0.67).

(b) Reductive amination of hydrazide alginate **14** (ds 0.76) was carried out by dissolving it (27 mg, 0.13 mmol) in water (10 mL) and adding a solution (7 mL) of keto spin label **15** (102 mg, 0.58 mmol) and $NaCNBH_3$ (140 mg, 2.2 mmol). The reaction mixture was left on a shaker overnight. The hydrazide product **16** had ds 0.21.

Preparation of [(2-Amino-4-N-dimethylamino)-s-triazin-6-yl] Alginate (17) and [4-(N-Dimethylamino)-2-(4-amino-2,2,6,6-tetramethylpiperidine-1-oxyl)-s-triazin-6-yl] Alginate (18)

(a) The *s*-triazinyl derivate was prepared according to Lee and Maekawa (23) using propylene glycol alginate (Kelcoloid-O) instead of the methyl ester of alginate. Kelcoloid-O (1 g, 5.44 mmol) was suspended in MeOH (100 mL) at 0°C and dimethylbiguanidine hydrochloride (1 g, 6.1 mmol) in THF/MeOH (1:1) (60 mL) was added with stirring to the suspension over a 20 min period. After one hour, the reaction mixture was allowed to warm to room temperature and left stirring for four days. The mixture was concentrated to dryness, and distilled water (20 mL) was added affording a gel, which was purified by dialysis. The product had ds ca. 0.12 (i.e., 15% conversion of esters) as determined by microanalysis. *Anal.* calcd. for $[(C_6H_8O_6)_{0.2}(C_9H_{14}O_7)_{0.68}(C_{10}H_{15}N_5O_4)_{0.12}]\cdot 2.01\ H_2O$: C 38.88, H 6.50, N 3.20 (C/N 12.2); found: C 38.59, H 5.70, N 3.05, (C/N 12.7).

(b) The *s*-triazinyl alginate **17** was labelled by dissolving 40 mg (0.18 mmol) in water (10 mL) and adding a solution of keto label **15** (80 mg, 0.47 mmol) and $NaCNBH_3$ (100 mg, 1.5 mmol) to the mixture, which was shaken for 13 h. The product **18** had ds 0.02.

Preparation of [4-N-(2,2,6,6-Tetramethylpiperidine-1-oxyl)] Xanthan Amide 20

To xanthan gum (150 mg, 0.16 mmol) dissolved in water (10 mL) was added EDC (100 mg, 0.78 mmol) and the reaction mixture (pH 5) was cooled to 5°C for 10 min before the amine label **7** (80 mg, 0.47 mmol) was added with stirring. The reaction was continued for 12 h, yielding a product **20** with ds 0.43 (based on carboxyl groups) after dialysis (4 days).

Preparation of [4-N-(2,2,6,6-Tetramethylpiperidine-1-oxyl)] Xanthan Amide (21)

Following a method reported for the synthesis of "amine alginates" (24), xanthan gum (50 mg, 0.05 mmol) was mixed in a 25 mL Erlenmeyer flask with solid amine spin label **7** (57 mg, 0.33 mmol) using a spatula. Three drops of water were added and mixed in to produce a heavy paste, which was shaken for 11 h, and then dialysed (4 days). The product **21** had ds 0.05 (based on carboxyl groups).

Preparation of [18-N-(n-Octadecyl)] Xanthan Amide (22)

Following the above procedure, octadecylamine (60 mg, 0.22 mmol) was admixed with xanthan gum (75 mg, 0.08 mmol) to afford (22), after precipitation from ethanol (twice), and dialysis (3 days), **22**. The microanalytical results (C 48.04, H 7.99, N 2.27) could not be matched with a corresponding molecular formula but the C/N ratio corresponds roughly to a ds 1.0.

Can. J. Chem. Downloaded from www.nrcresearchpress.com by 210.87.254.6 on 09/06/12
For personal use only.

*Preparation of [4-*N*-(2,2,6,6-Tetramethylpiperidine-1-oxyl)] Cellulose Amine (25)*

(a) The periodate oxidation method of Nevell (26) was used. Three samples (500 mg, 3.1 mmol) of cellulose powder were each reacted with $NaIO_4$ (0.01 *M*, 0.05 *M*, and 0.10 *M*) in distilled water (25 mL) in the dark for 60 h at 20°C in a constant temperature shaker to afford products which had a degree of oxidation (do) of 5%, 19%, and 34%, respectively. The reaction was quenched by mixing the dispersions with distilled water (250 mL) and decanting the supernatant. This process was repeated 6–7 times. The samples were left in distilled water overnight, then washed with water (100 mL) and subsequently dried *in vacuo* at 56°C.

(b) Periodate-oxidized cellulose samples (1 mmol) were labelled in MeOH (7 mL) by adding 2.6 equivalents of amine spin label **7** and 6.4 equivalents $NaCNBH_3$ and a few drops of water. After gentle shaking (28 h) the samples were successively washed on a fritted glass filter with 100 mL each of water, ethanol, acetone, and ether, and subsequently dried under vacuum for 24 h at 56°C. The following ds were obtained (do): (A) ds 0.03 (5%); (B) ds 0.063 (19%); (C) ds 0.065 (34%). *Anal.* calcd. for (A) $[(C_6H_{10}O_5)_{0.93}(C_6H_8O_5)_{0.04}(C_{13}H_{27}N_2O_5)_{0.03}]\cdot 0.13\ H_2O$: C 44.30, H 6.43, N 0.50; found: C 44.01, H 6.38, N 0.51. *Anal.* calcd. for (B) $[(C_6H_{10}O_5)_{0.81}(C_6H_8O_5)_{0.127}(C_{13}H_{27}N_2O_5)_{0.063}]\cdot 0.14\ H_2O$: C 44.81, H 6.49, N 1.02; found: C 44.70, H 6.49, N 1.03. *Anal.* calcd. for (C) $[(C_6H_{10}O_5)_{0.66}(C_6H_8O_5)_{0.275}(C_{13}H_{27}N_2O_5)_{0.065}]\cdot 0.21\ H_2O$: C 44.61, H 6.37, N 1.05; found: C 44.33, H 6.25, N 1.04.

*Preparation of [4-*N*-(2,2,6,6-Tetramethylpiperidine-1-oxyl)] Cellulose Urethane (27)*

A solution of the amine label **7** (366 mg, 2.1 mmol) in phosphate buffer (0.5 *M*, pH 7, 2 mL) was added to a suspension of cellulose carbonate (ds 0.21, 80 mg, 0.48 mmol) in the buffer (10 mL). The reaction mixture was stirred overnight at 5°C, and then dialyzed (5 days) at the same temperature to afford a product **27** with ds 0.08. *Anal.* calcd. for $[(C_6H_{10}O_5)_{0.74}(C_7H_8O_6)_{0.18}(C_{16}H_{27}N_2O_6)_{0.08}]\cdot 0.75\ H_2O$: C 43.22, H 6.50, N 1.16; found: C 43.08, H 6.54, N 1.10.

When the reaction was carried out in methanol a product with lower ds (0.05) was obtained. *Anal.* calcd. for $[(C_6H_{10}O_5)_{0.8}(C_7H_8O_6)_{0.15}(C_{16}H_{27}N_2O_6)_{0.05}]\cdot 0.34\ H_2O$: C 44.06, H 6.25, N 0.77; found: C 43.86, H 6.16, N 0.75.

Preparation of N*-[4-(2,2,6,6-Tetramethylpiperidine-1-oxyl)] Cellulose Hydrazide (30)*

(a) The cellulose hydrazide derivative **29** was prepared following the method of Andresz *et al.* (22) using sodium carboxymethylcellulose (ds 1.2–1.4) as starting material. The product had a ds value of ca. 0.5 (lit. (22) ds 0.68) as calculated from elemental analysis. *Anal.* calcd. for $[(C_8H_{12}O_7)_{0.5}(C_8H_{14}N_2O_6)_{0.5}]\cdot 2.9\ H_2O$: C 34.37, H 6.78, N 5.01 (C/N 6.86); found: C 34.20, H 5.87, N 4.90 (C/N 6.98).

(b) Cellulose hydrazide (40 mg, 0.16 mmol) was labelled in phosphate buffer (0.5 *M*, ph 7, 10 mL) using keto spin label **15** (97 mg, 0.6 mmol) and $NaCNBH_3$ (100 mg, 1.6 mmol). The mixture was shaken for 15 h and then dialyzed (4 days), to afford **30**, ds 0.003 (from esr double integration).

Acknowledgements

This work was supported by the Natural Sciences and Engineering Research Council of Canada via operating grants to L.D.H. (A 1905). It is a pleasure to thank Kelco Co., Hercules Inc., and Tate & Lyle Ltd. for polysaccharide samples.

1. R. L. Whistler (*Editor*). Industrial gums. Academic Press, New York. 1973; I. W. Cottrell and K. S. Kang. Dev. Ind. Microbiol. **19**, 117 (1978); R. M. Rowell and R. A. Young (*Editors*). Modified cellulosics. Academic Press, New York. 1978; R. A. A. Muzzarelli. Chitin. Pergamon Press, New York. 1977.
2. R. G. Schweiger. Carbohydr. Res. **70**, 185 (1979).
3. Y. L. Meltzer. Water-soluble resins and polymers. Noyes Data Corp., London. 1976.
4. B. Tabushi, Y. Kobuke, and T. Nishiya. Nature, **280**, 665 (1979).
5. H. Moldenhauer and H. J. Loh. Pharmazie, **33**, 216 (1978).
6. J. F. Kennedy. Adv. Carbohydr. Chem. Biochem. **29**, 305 (1974); J. F. Kennedy. *In* Carbohydrate chemistry (Specialist Periodical Reports of the Chemical Society). **11**, 445 (1979), and references cited therein.
7. D. A. Rees. Polysaccharide shapes. Chapman and Hall, London. 1977; E. M. Morris. *In* Techniques and applications of fast reactions in solution. *Edited by* W. J. Gettins and E. Wyn-Jones. Wiley, New York. 1979. p. 379.
8. R. L. Whistler (*Editor*). Methods in carbohydrate chemistry. Vols. III, IV. Academic Press, New York. 1963.
9. D. Horten and T. Usui. *In* Carbohydrate sulfates. *Edited by* R. G. Schweiger. ACS Symp. Ser. **77**, 95 (1978); L. D. Hall and M. Yalpani. J. Chem. Soc. Chem. Commun. 1153 (1980).
10. L. D. Hall and M. Yalpani. Carbohydr. Res. **81**, C10 (1980).
11. R. F. Borch, M. D. Bernstein, and H. D. Durst. J. Am. Chem. Soc. **88**, 1024 (1966); G. R. Gray. Methods Enzymol. **50**, 155 (1978).
12. A. Wassermann. Nature, **158**, 271 (1946); N. H. Chamberlain, G. E. Cunningham, and J. B. Speakman. Nature, **158**, 553 (1946).
13. R. G. Schweiger. J. Org. Chem. **27**, 1786 (1962).
14. R. H. McDowell. J. Soc. Cosmet. Chem. **21**, 441 (1970).
15. R. Kohler and W. Dierichs. U.S. Pat. No. 1,881,161 (1959); (Chem. Abstr. **54**, 7926d (1960)); Brit. Pat. No. 768,309 (1957).
16. A. B. Steiner and W. H. McNeely. Ind. Eng. Chem. **43**, 2073 (1951).
17. Z. Wypych. Rocz. Chem. **43**, 1616 (1969).
18. J. D. Alpin. Ph.D. thesis, University of British Columbia (1979).
19. K. W. Kirby. Ph.D. thesis, Purdue University (1958).
20. I. L. Andresen, T. Painter, and O. Smidsrød. Carbohydr. Res. **59**, 563 (1977), and references therein.
21. J. C. Lee, H. L. Weith, and P. T. Gilham. Biochemistry, **9**, 113 (1970); Z. I. Kuznetsova, E. G. Ivanova, and A. I. Usov. Izvest. Akad. Nauk SSSR, Ser. Khim. 1858 (1973).
22. H. Andresz, G. C. Richter, and B. Pfannemüller. Makromol. Chem. **179**, 301 (1978).
23. C. S. Lee and K. Maekawa. Agric. Biol. Chem. **40**, 785 (1976).
24. Kelco Algin. 2nd ed. Kelco Co., San Diego, CA. 1976. p. 41.
25. L. D. Hall and M. Yalpani. Carbohydr. Res. **91**, C1 (1981).
26. P. T. Nevell. Methods Carbohydr. Chem. **3**, 164 (1963).
27. L. D. Hall and J. D. Aplin. J. Am. Chem. Soc. In press.
28. W. M. Doane, B. S. Shasha, E. I. Stout, C. R. Russell, and C. E. Rist. Carbohydr. Res. **11**, 321 (1969); J. F. Kennedy and T. C. Tun. Antimicrob. Agents Chemother. **3**, 575 (1975).

29. E. I. STOUT, W. M. DOANE, B. S. SHASHA, C. R. RUSSELL, and C. E. RIST. Tetrahedron Lett. **45**, 4481 (1967).
30. E. JUNOWICZ and S. E. CHARM. Biochim. Biophys. Acta, **428**, 157 (1976).
31. S. MACHIDA and Y. SUEYOSHI. Angew. Makromol. Chem. **49**, 171 (1976).
32. H. L. WEITH, J. L. WIEBERS, and P. T. GILHAM. Biochemistry, **9**, 4396 (1970).
33. A. T. BULLOCK and G. G. CAMERON. *In* Structural studies of macromolecules by spectroscopic methods. *Edited by* K. J. Ivin. Wiley, New York. 1976; H. M. MCCONNELL. *In* Spin labeling. *Edited by* L. J. Berliner. Academic Press, New York. 1976; H. DUGAS. Acc. Chem. Res. **10**, 47 (1977); P. TORMALA. J. Macromol. Sci. Rev. Macromol. Chem. **17**, 297 (1979).
34. L. D. HALL and J. C. WATERTON. J. Am. Chem. Soc. **101**, 3697 (1979).
35. J. D. APLIN and L. D. HALL. Carbohydr. Res. **75**, 17 (1979); J. D. APLIN and L. D. HALL. Eur. J. Biochem. **110**, 195 (1980); M. YALPANI. Ph.D. thesis, University of British Columbia (1980).
36. C. P. IOVINE and D. K. RAY-CHAUDHURI. U.S. Pat. No. 4,129,722 (1978).
37. R. L. WHISTLER. *In* Carbohydrates in solution. ACS Symp. Ser. **117**, 242 (1973).
38. R. G. SCHWEIGER. J. Org. Chem. **41**, 90 (1976).
39. G. HOLZWARTH. Biochemistry, **19**, 4333 (1976).
40. W. G. STRUVE and H. M. MCCONNELL. Biochem. Biophys. Res. Commun. **49**, 1631 (1972); H. W. WIEN, J. D. MORRISETT, and H. M. MCCONNELL. Biochemistry, **11**, 3707 (1972).
41. T. J. STONE, T. BUCKMAN, P. L. NORDIO, and H. M. MCCONNELL. Proc. Natl. Acad. Sci. U.S.A. **54**, 1010 (1965).

Can. J. Chem. Downloaded from www.nrcresearchpress.com by 210.87.254.6 on 09/06/12
For personal use only.

Can. J. Chem. Downloaded from www.nrcresearchpress.com by 210.87.254.6 on 09/06/12
For personal use only.

COMMUNICATION

A thermal [1,3] sigmatropic rearrangement: thermolysis of 2,2-bis(ethylthio)-3,3-dimethyl-4-pentenal

GORDON S. BATES[1] AND S. RAMASWAMY

Department of Chemistry, University of British Columbia, Vancouver, B.C., Canada V6T 1Y6

Received June 12, 1981

GORDON S. BATES and S. RAMASWAMY. Can. J. Chem. **59**, 3120 (1981).

2,2-Bis(ethylthio)-3,3-dimethyl-4-pentenal was found to quantitatively isomerize to 2,2-bis(ethylthio)-5-methyl-4-hexenal over a wide temperature range (130–170°C). This rearrangement can formally be regarded as a [1,3] sigmatropic shift. The reaction, which could be conveniently monitored by ^{1}Hmr spectroscopy, was found to obey first order kinetics. The substantial positive entropy of activation (+ 61.5 J deg^{-1} mol^{-1}) for the reaction and the negligible solvent effect (decane vs. DMF) are both consistent with a proposed diradical pathway.

GORDON S. BATES et S. RAMASWAMY. Can. J. Chem. **59**, 3120 (1981).

On a trouvé que le bis(éthylthio)-2,2 diméthyl-3,3 pentène-4 al s'isomérise quantitativement en bis(éthylthio)-2,2 méthyl-5 hexène-4 al à des températures allant de 130 à 170°C. On peut considérer formellement cette transposition comme étant un glissement sigmatropique [1,3]. Cette réaction qu'on peut suivre convenablement par la spectroscopie de rmn, est d'ordre un. La forte entropie positive d'activation (+61,5 J deg^{-1} mol^{-1}) de la réaction et l'effet négligeable du solvant (décane vs. DMF) sont en accord avec le mécanisme biradicalaire proposé.

[Traduit par le journal]

The alkylation of the anions of various enamines of bis(ethylthio)acetaldehyde (1) with 2-methyl-4-bromo-2-butene gives exclusively, after hydrolysis of the enamine, the S_N2 product **1**, whereas alkylation of the anion of the aldehyde yields the S_N2' product **2**. This latter compound is likely formed by initial S_N2 alkylation of one of the sulphur atoms of the anion followed by a [2,3] sigmatropic rearrangement of the resulting ylide.[2] Compound **2** appeared to be an ideal substrate to provide an example of a rare thermal carbon–carbon [1,3] alkyl shift (5) in an *acyclic* system. Rearrangement of **2** into **1** should be favoured since the transformation would be accompanied by relief of the steric strain associated with the two adjacent quaternary centres in **2**, as well as by formation of the more highly substituted alkene in **1**. Indeed, upon heating an *n*-decane solution of **2** at 170°C for one hour, the desired rearrangement occurred to provide **1** in virtually quantitative yield.[3] This rearrangement may be rationalized in terms of several different mechanisms as shown in Scheme 1.

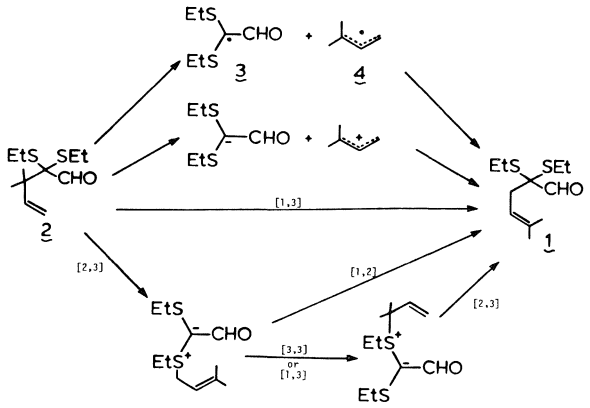

SCHEME 1

Any of the concerted processes must involve ordered transition states which should be reflected in a relatively large negative entropy of activation ($\Delta S^{\ddagger}$).[4] The $\Delta S^{\ddagger}$ for the ionic pathway could vary greatly. If there is considerable freedom in the transition state then $\Delta S^{\ddagger}$ would be positive. However, a negative $\Delta S^{\ddagger}$ is also possible due to electrostriction of the solvent around the ions produced (11). The diradical process should have a substantial positive $\Delta S^{\ddagger}$ (12). If the rearrangement proceeds by way of an ionic, or indeed, via any process involving significant charge development

[1]Author to whom correspondence should be addressed.

[2]For similar transformations see refs. 2, 3, and 4 and references cited therein.

[3]Thermal [1,3] rearrangements of several 4-dimethylaminobutenes have been reported. See refs. 6 and 7.

[4]For example, the Cope rearrangement has $\Delta S^{\ddagger}$'s ranging from −46.4 to −58.6 J deg^{-1} mol^{-1} (8–10).

0008-4042/81/213120-03$01.00/0

©1981 National Research Council of Canada/Conseil national de recherches du Canada

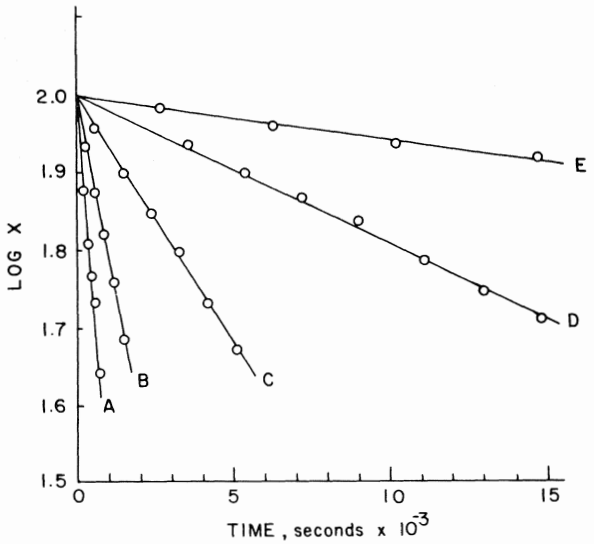

FIG. 1. Rate of rearrangement of **2**: X = 100 ([2]/[1 + 2]) as determined by ^{1}Hmr spectroscopy. A, t = 170°C, $k = 1.10 \times 10^{-3}$ s^{-1}; B, t = 160°C, $k = 4.73 \times 10^{-4}$ s^{-1}; C, t = 150°C, $k = 1.46 \times 10^{-4}$ s^{-1}; D, t = 140°C, $k = 4.51 \times 10^{-5}$ s^{-1}; E, t = 130°C, $k = 1.35 \times 10^{-5}$ s^{-1}.

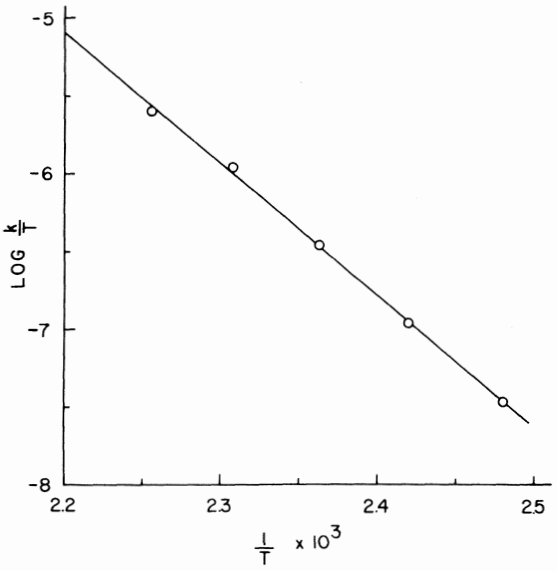

FIG. 2. Dependence on temperature of rate constants for rearrangement of **2**.

in the transition state, there should be a definite solvent effect. The rate of a concerted or of a diradical process should be relatively independent of solvent (13). A determination of the activation parameters of the reaction as well as the presence or absence of a solvent effect will thus allow a mechanistic choice to be made.

The ^{1}Hmr spectra of **1** and **2** are very different.[5] The progress of the rearrangement was conveniently monitored by observing the change in the relative intensities of the singlets in the ^{1}Hmr spectrum due to the aldehyde protons of **1** (δ 9.10) and **2** (δ 9.20). The thermolyses were carried out in degassed, spectral grade *n*-decane under an argon atmosphere. The reactions were quenched at various intervals by immersing the samples in an ice–water slurry. Figure 1 clearly indicates that the rearrangement follows first order reaction kinetics. The enthalpy (162.3 kJ mol^{-1}) and entropy (+ 61.5 J deg^{-1} mol^{-1}) of activation for the reaction were calculated from the Eyring equation (14) using the data obtained from Fig. 2. The rearrangement was also carried out in *N*,*N*-dimethylformamide (DMF) (t = 140°C, $k = 6.59 \times 10^{-5}$ s^{-1}). Since the rate of the rearrangement changes by a factor of less than 1.5 with the drastic change in solvent from *n*-decane to DMF, we feel that the rearrangement is not accompanied by any charge separation and thus the ionic process may be ruled out.[6] The substantial positive $\Delta S^{\ddagger}$ for the reaction appears to be inconsistent with a concerted mechanism. On the basis of the sign and magnitude of the $\Delta S^{\ddagger}$ for the reaction and the lack of any significant solvent effect we propose that **2** undergoes homolytic cleavage to form two stabilized radicals, the tertiary allylic fragment **3** and capto-dative stabilized (16) radical **4**. These two radicals then undergo smooth recombination to give **1**.

Preliminary studies have shown that 3,3-dimethyl-2,2-(1,3-dithiane)-4-pentenal (3) undergoes a similar [1,3] rearrangement. Further work on this and several other related systems will be reported in due course.

Acknowledgements

This work was supported by the Natural Sciences and Engineering Research Council of Canada and in part by a Cottrell Research Grant provided by Research Corporation.

1. G. S. BATES and S. RAMASWAMY. Chem. Commun. 904 (1980).
2. K. OGURA, S. FURUKAWA, and G. TSUCHIHASHI. J. Am. Chem. Soc. **102**, 2125 (1980).
3. S. R. WILSON and J. MATHEW. Synthesis, 625 (1980).

[5]Compound **1** ^{1}Hmr δ ($CDCl_3$): 1.20 (t, 6, J = 7), 1.65 (s, 3), 1.75 (d, 3, J = 1.5), 2.50 (q, 4, J = 7), 2.58 (d, 2, J = 7), 5.30 (tq, 1, J = 7, 1.5), 9.10 (s, 1); **2** ^{1}Hmr δ ($CDCl_3$): 1.20 (t, 6, J = 7), 1.25 (s, 6), 2.5 (m, 4), 5.00 (dd, 1, J = 18, 1.5), 5.02 (dd, 1, J = 10, 1.5), 6.10 (dd, 1, J = 18, 10), 9.20 (s, 1).

[6]See ref. 15 for an alternate view on the mechanistic significance of the lack of a solvent effect on the rate of a reaction.

Can. J. Chem. Downloaded from www.nrcresearchpress.com by 210.87.254.6 on 09/06/12
For personal use only.

4. R. W. JEMISON, T. LAIRD, W. D. OLLIS, and I. O. SUTHERLAND. J. Chem. Soc. Perkin Trans. I, 1450 (1980).
5. C. W. SPANGLER. Chem. Rev. **76**, 187 (1976).
6. R. W. JEMISON, T. LAIRD, W. D. OLLIS, and I. O. SUTHERLAND. J. Chem. Soc. Perkin Trans. I, 1458 (1980).
7. R. W. JEMISON, W. D. OLLIS, I. O. SUTHERLAND, and J. TANNOCK. J. Chem. Soc. Perkin Trans. I, 1462 (1980).
8. E. G. FOSTER, A. C. COPE, and F. DANIELS. J. Am. Chem. Soc. **69**, 1893 (1947).
9. G. R. ALDRIDGE and G. W. MURPHY. J. Am. Chem. Soc. **73**, 1158 (1951).
10. H. M. FREY and R. K. SOLLY. Trans. Faraday Soc. **64**, 1858 (1968).
11. R. STEWART. The investigation of organic reactions. Prentice-Hall, Inc., Englewood Cliffs, NJ. 1966. pp. 74–76.
12. W. VON E. DOERING and E. K. G. SCHMIDT. Tetrahedron, **27**, 2005 (1971).
13. D. C. WIGFIELD and S. FEINER. Can. J. Chem. **48**, 855 (1970).
14. H. EYRING. J. Chem. Phys. **3**, 107 (1935); W. F. K. WYNNE-JONES and H. EYRING. J. Chem. Phys. 492 (1935); A. J. GORDON and R. A. FORD. The chemist's companion. John Wiley and Sons, Inc., New York, NY. 1972. p. 136.
15. D. C. WIGFIELD and B. LEM. Tetrahedron, **31**, 9 (1975).
16. H. G. VIEHE, R. MERÉNYI, L. STELLA, and Z. JANOUSEK. Angew. Chem. Int. Ed. Engl. **18**, 917 (1979).

Can. J. Chem. Downloaded from www.nrcresearchpress.com by 210.87.254.6 on 09/06/12
For personal use only.

Manganese, molybdenum, and tungsten carbonyl derivatives incorporating the dimethylbis(1-pyrazolyl)gallate ligand, $[Me_2Ga(N_2C_3H_3)_2]^-$

SHARON E. ANSLOW, KENNETH S. CHONG, STEVEN J. RETTIG, ALAN STORR, AND JAMES TROTTER

Department of Chemistry, University of British Columbia, 2036 Main Mall, Vancouver, B.C., Canada V6T 1Y6

Received March 27, 1981

SHARON E. ANSLOW, KENNETH S. CHONG, STEVEN J. RETTIG, ALAN STORR, and JAMES TROTTER. Can. J. Chem. **59**, 3123 (1981).

The synthesis of a number of six-coordinate manganese, molybdenum, and tungsten carbonyl compounds incorporating both the bidentate bispyrazolyl gallate ligand, $[Me_2Ga(N_2C_3H_3)_2]^-$, and a neutral pyrazole ligand in a facial coordination arrangement are described. Variable temperature ^1H nmr studies have revealed interestingly different behaviours in solution for the valence isoelectronic species $[Me_2Ga(N_2C_3H_3)_2](N_2C_3H_4)Mn(CO)_3$ and $[Me_2Ga(N_2C_3H_3)_2](N_2C_3H_4)Mo(CO)_3^-$. X-ray structural analyses of crystalline samples of the two compounds have been carried out in an effort to shed light on these behavioural differences. Crystals of $[Me_2Ga(N_2C_3H_3)_2](N_2C_3H_4)Mn(CO)_3$ are monoclinic, $a = 31.053(2)$, $b = 8.0503(4)$, $c = 15.8629(8)$ Å, $\beta = 108.164(2)°$, $Z = 8$, space group $C2/c$ and crystals of $[(C_2H_5)_4N]^+\{[Me_2Ga(N_2C_3H_3)_2](N_2C_3H_4)Mo(CO)_3\}^-$ are monoclinic, $a = 10.058(1)$, $b = 20.6488(5)$, $c = 13.533(1)$ Å, $\beta = 93.800(5)°$, $Z = 4$, space group $P2_1/n$. Both structures were solved by Patterson and Fourier syntheses and were refined by full-matrix least-squares procedures to final R values of 0.028 and 0.023 for 2613 and 4388 observed reflections for the Mn and Mo complexes, respectively. The neutral Mn complex and the complex Mo anion both have approximate mirror symmetry and both metal atoms have trigonally distorted octahedral coordination geometry. Important bond distances (corrected for thermal vibration) are: Mn—N, 2.074(3)–2.086(3), Mn—C, 1.795(4)–1.809(5), Mo—N, 2.291(2)–2.295(2), and Mo—C, 1.918(3)–1.936(3) Å. Although structural differences between these two species do offer plausible explanations for the differences observed in solution, it appears that other factors are more important.

SHARON E. ANSLOW, KENNETH S. CHONG, STEVEN J. RETTIG, ALAN STORR et JAMES TROTTER. Can. J. Chem. **59**, 3123 (1981).

On décrit la synthèse d'une série de composés carbonylés hexacoordonnés du manganèse, du molybdène et du tungstène, incorporant le ligand bidentate bispyrazolyl gallate $[Me_2Ga(N_2C_3H_3)_2]^-$ et un ligand neutre pyrazole coordonné de façon faciale. Les études de rmn du ^1H à température variable ont révélé de façon intéressante les comportements différents de la valence des espèces isoélectroniques $[Me_2Ga(N_2C_3H_3)_2](N_2C_3H_4)Mn(CO)_3$ et $[Me_2Ga(N_2C_3H_3)_2](N_2C_3H_4)Mo(CO)_3^-$ en solution. On a étudié les cristaux par cristallographie de rayons-X afin de comprendre ces différences de comportement. Les cristaux de $[Me_2Ga(N_2C_3H_3)_2](N_2C_3H_4)Mn(CO)_3$ sont monocliniques et appartiennent au groupe d'espace $C2/c$ avec $a = 31,053(2)$, $b = 8,0503(4)$, $c = 15,8629(8)$ Å, $\beta = 108,164(2)°$, $Z = 8$. Les cristaux de $[(C_2H_5)_4N]^+\{Me_2Ga(N_2C_3H_3)_2](N_2C_3H_4)Mo(CO)_3\}^-$ sont monocliniques avec $a = 10,058(1)$, $b = 20,6488(5)$, $c = 13,533(1)$ Å, $\beta = 93,800(5)°$, $Z = 4$, groupe d'espace $P2_1/n$. On a résolu les deux structures par les synthèses de Patterson et de Fourier et on les a affinées par la méthode des moindres carrés (matrice complète) jusqu'à des valeurs de $R = 0,028$ et 0,023 pour 2613 et 4388 réflexions observées pour les complexes de Mn et de Mo respectivement. Le complexe neutre de Mn et le complexe anionique de Mon sont approximativement l'image l'un de l'autre dans un mirroir et les deux atomes métalliques ont une géométrie de coordination octaédrique déformée de façon trigonale. Les longueurs importantes de liaison (corrigés pour la vibration thermique) sont Mn—N, 2,074(3)–2,086(3), Mn—C, 1,795(4)–1,809(5), Mo—N, 2,291(2)–2,295(2) et Mo—C, 1,918(3)–1,936(3) Å. Bien que les différences structurales entre ces deux espèces offrent des explications plausibles des différences observées en solution, il semble que d'autres facteurs sont plus importants.

[Traduit par le journal]

Introduction

Earlier reports have detailed the synthesis of bidentate chelating anionic pyrazolyl gallate ligands of the type $[Me_2Ga(N_2C_3H_3)_2]^-$ and their complexation with divalent transition metal ions (1–4). More recently a series of allylic derivatives of Ni and Pd incorporating these ligands has been characterized (5). The present account describes the use of these bidentate ligands in the preparation of a number of manganese, molybdenum, and tungsten carbonyl complexes. The properties of the compounds prepared are compared with and contrasted to the properties of similar pyrazolyl borate complexes. X-ray structural studies have been carried out on two of the complexes in an attempt to explain their variable temperature ^1H nmr spectra.

Experimental

Starting Materials

Air-sensitive materials were handled in a glove box under an atmosphere of oxygen-free dry nitrogen or in a nitrogen-blanketed apparatus. Tetrahydrofuran (THF) was dried by refluxing over sodium/benzophenone and was used immediately following distillation. Benzene was dried by refluxing over molten potassium followed by distillation. Pyrazole (Aldrich), molybdenum and tungsten hexacarbonyls, (Strem) and tetraethylammonium chloride (Eastman) were used as supplied. $Mn(CO)_5Br$ (6), $(MeCN)_3M(CO)_3$, M = Mo or W (7), $(C_7H_7)Mo(CO)_2I$ (8) and $(C_7H_7)W(CO)_2I$ (9) were prepared as described in the literature. The bidentate gallium ligand $Na^+[Me_2Ga(N_2C_3H_3)_2]^-$ was prepared as described previously (4) and used as a THF solution. Analytical and ir data for the complexes described below are given in Table 1. Proton nmr data are given in Table 2.

Preparation of $[Me_2Ga(N_2C_3H_3)_2](N_2C_3H_4)Mn(CO)_3$

To a stirred solution of $Mn(CO)_5Br$ (1.07 g, 3.9 mmol) in THF

0008-4042/81/223123-13$01.00/0

©1981 National Research Council of Canada/Conseil national de recherches du Canada

Can. J. Chem. Downloaded from www.nrcresearchpress.com by 210.87.254.40 on 09/06/12
For personal use only.

TABLE 1. Analytical data for 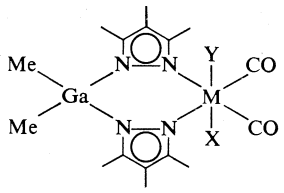 complexes

M	X	Y	Color	Calculated (%) C	H	N	Found (%) C	H	N	ν_{CO} (cm^{-1}) cyclohexane (Nujol)	ν_{HN} (cm^{-1}) (Nujol)
Mn	CO	$N_2C_3H_4$	Yellow	38.1	3.6	19.1	38.2	3.6	18.9	2022, 1940, 1922	3435
Mn	CO	$N_2C_5H_8$	Yellow	41.0	4.3	17.9	41.3	4.3	18.2	2020, 1944, 1926	3415
Mo[a]	CO	CO	Bright yellow	42.0	5.6	12.3	41.8	5.5	12.4	(1998, 1877, 1852, 1800)	
W[a]	CO	CO	Bright yellow	36.4	4.9	10.6	36.5	5.1	10.9	(1990, 1865, 1842, 1792)	
Mo[a]	CO	$N_2C_3H_4$	Pale yellow	43.2	5.9	16.0	42.8	6.0	15.8	(1896, 1764, 1735)	3422
W[a]	CO	$N_2C_3H_4$	Pale yellow	37.7	5.1	14.0	37.3	5.1	13.9	(1885, 1748, 1722)	3410
Mo	C_3H_5	$N_2C_3H_4$	Golden yellow	38.8	4.2	17.0	39.0	4.3	17.0	1950, 1865	3430
W	C_3H_5	$N_2C_3H_4$	Golden yellow	33.0	3.6	14.4	33.3	3.9	14.1	1942, 1858	3415
Mo	C_7H_7	$N_2C_3H_4$	Red–brown	44.1	4.3	15.4	43.8	4.3	15.0	1949, 1874	3417
W	C_7H_7	$N_2C_3H_4$	Red–brown	37.9	3.6	13.3	38.0	3.7	13.0	1942, 1863	3403

[a]Isolated as tetraethylammonium salts.

Can. J. Chem. Downloaded from www.nrcresearchpress.com by 210.87.254.40 on 09/06/12
For personal use only.

was added a solution of $Na^+[Me_2Ga(N_2C_3H_3)_2]^-$ (3.9 mmol) in the same solvent. Pyrazole (0.27 g, 3.9 mmol) was added immediately and the reaction mixture stirred overnight. The solvent was then removed *in vacuo* and the remaining yellow residue recrystallized from benzene to give bright yellow crystals of the product. Yield 0.91 g (53%). The corresponding compound incorporating the 3,5-dimethylpyrazole molecule, $[Me_2Ga(N_2C_3H_3)_2](N_2C_5H_8)Mn(CO)_3$, was prepared in a similar manner.

Preparation of $Et_4N^+[Me_2Ga(N_2C_3H_3)_2M(CO)_4]^-$ where M = Mo, W

To a THF solution of the appropriate hexacarbonyl $M(CO)_6$ was added an equimolar amount of the ligand $Na^+[Me_2Ga(N_2C_3H_3)_2]^-$ in the same solvent. The reaction mixture was refluxed overnight. After cooling the reaction mixture to room temperature a CH_2Cl_2 solution of $Et_4N^+Cl^-$ was added. The resultant mixture was filtered and slow evaporation of the filtrate produced bright yellow crystals of the product (yield 80–90%).

Preparation of $Et_4N^+[Me_2Ga(N_2C_3H_3)_2](N_2C_3H_4)M(CO)_3^-$ where M = Mo, W

An equimolar amount of $Et_4N^+Cl^-$ dissolved in CH_2Cl_2 was added to a 1:1:1 mixture of $(MeCN)_3M(CO)_3$, $Na^+[Me_2Ga(N_2C_3H_3)_2]^-$, and $N_2C_3H_4$ in THF. The reaction mixture was stirred for approximately 1 h and then filtered. Slow evaporation of the filtrate gave golden yellow crystals of the product in 80% yield.

Preparation of $[Me_2Ga(N_2C_3H_3)_2](N_2C_3H_4)M(CO)_2(C_3H_5)$ where M = Mo, W

To a 1:1:1 mixture of $(MeCN)_3M(CO)_3$, $Na^+[Me_2Ga(N_2C_3H_3)_2]^-$ and $N_2C_3H_4$ in THF was added an excess of allyl bromide. After stirring the reaction mixture for 2 h, the solvent was removed *in vacuo*. The yellow residue was recrystallized from benzene to give yellow crystals of the product in 20% yield. These compounds may also be prepared by the reaction of $Na^+[Me_2Ga(N_2C_3H_3)_2]M(CO)_4^-$ with allyl bromide but this alternate route gives even lower yields of the desired product.

Preparation of $[Me_2Ga(N_2C_3H_3)_2](N_2C_3H_4)M(CO)_2(C_7H_7)$ where M = Mo, W

An equimolar amount of $Na^+[Me_2Ga(N_2C_3H_3)_2]^-$ in THF was added to $(C_7H_7)M(CO)_2I$ in the same solvent. An equimolar amount of pyrazole was then added immediately. The reaction mixture was stirred overnight and the solvent then removed *in vacuo*. The resultant solid was extracted with and recrystallized from benzene. The desired product was isolated as red–brown crystals (yield 60%).

Spectra

Mass spectra were recorded on a Varian MAT CH4 mass spectrometer at 70 eV with an ion source temperature of 100–180°C. Infrared spectra were recorded on a Perkin-Elmer 457 spectrophotometer and ^1H nmr spectra on a Varian XL-100 spectrometer using FT techniques.

TABLE 2. ^{1}H nmr data for 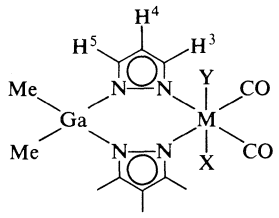 complexes

			τ (ppm)					
M	X	Y	H^3	H^5	H^4	X	Y	GaMe
Mn[a]	CO	$N_2C_3H_4$	2.40d	2.77d	3.91t		1.99s br (NH) 2.70t (H^3) 4.30t (H^5), 4.50q (H^4)	9.62s, 9.92s
Mn[a]	CO	$N_2C_5H_8$	2.45d	2.54d	3.89t		2.30s br (NH), 4.79s br (H^4) 7.83s (Me^3), 9.07s (Me^5)	9.67s, 10.05s
Mo[b,c]	CO	CO	2.01d	2.38d	3.73t			10.19s
W[b,c]	CO	CO	1.99d	2.39d	3.74t			10.16s
Mo[b,c]	CO	$N_2C_3H_4$	2.24d	2.41d	3.86t		See discussion	10.15s
W[b,c]	CO	$N_2C_3H_4$	2.24d	2.42d	3.88t		See discussion	10.10s
Mo[a]	C_3H_5	$N_2C_3H_4$	2.27d	2.64d	4.07t	5.61m (H unique) 6.81d (H syn) J = 6 Hz 8.49d (H anti) J = 9 Hz	1.78s br (NH), 2.27 (H^3) 4.33t (H^5), 4.66q (H^4)	9.97s, 10.06s
W[a]	C_3H_5	$N_2C_3H_4$	2.19d	2.71d	4.15t	6.41m (H unique) 7.02d (H syn) J = 6 Hz 8.19d (H anti) J = 9 Hz	1.37s br (NH), 2.56t (H^3) 4.32t (H^5), 4.78q (H^4)	9.99s, 10.07s
Mo[a]	C_7H_7	$N_2C_3H_4$	2.01d	2.56d	3.98t	4.69s	1.63s br (NH), 2.65t (H^3) 4.38t (H^5), 4.78q (H^4)	9.86s, 10.05s
W[a]	C_7H_7	$N_2C_3H_4$	2.01d	2.64d	4.06t	4.91s	1.04s br (NH), 2.66 (H^3) 3.98t (H^5), 4.84q (H^4)	9.96s, 10.11s

[a]Measured in C_6D_6 ($\tau_{C_6H_6}$ = 2.84 ppm).
[b]Measured in acetone-d^6 ($\tau_{acetone}$ = 7.89 ppm), J_{HCCH} (for $N_2C_3H_3$ and $N_2C_3H_4$ groups) = 2 Hz.
[c]Et_4N^+ salts $\tau_{NCH_2CH_3} \cong$ 6.52q (J_{HCCH} = 7 Hz); $\tau_{NCH_2CH_3} \cong$ 8.61t (J_{HCCH} = 7 Hz, $J_{HCC^{14}N}$ = 2 Hz). s = singlet, d = doublet, t = triplet, q = quartet, br = broad, m = multiplet.

X-ray Crystallographic Analyses

[Dimethylbis(1-pyrazolyl)gallato(N,N)](pyrazole)-tricarbonylmanganese(I)

A crystal ca. 0.18 × 0.50 × 0.53 mm in size was mounted in a general orientation. Unit-cell parameters were refined by least-squares on 2 sin θ/λ values for 25 reflections measured on a diffractometer with Mo K_α radiation (λ = 0.71073 Å). Crystal data at 22°C are:

$C_{14}H_{16}GaMnN_6O_3$ fw = 440.98
Monoclinic, a = 31.053(2), b = 8.0503(4), c = 15.8629(8) Å, β = 108.164(2)°, V = 3767.9(3) Å^3, Z = 8, ρ_c = 1.555 g cm^{-3}, $F(000)$ = 2016, μ(Mo K_α) = 20.93 cm^{-1}. Absent reflections: hkl, $h + k \neq 2n$ and $h0l$, $l \neq 2n$, space group $C2/c$ (C_{2h}^6, No. 15) from structure analysis.

Intensities were measured with graphite-monochromated Mo K_α radiation on an Enraf-Nonius CAD4-F diffractometer. An ω–2θ scan at 1.18–10.26° min^{-1} over a range of (0.65 + 0.35 tan θ) degrees in ω (extended by 25% on both sides for background measurement) was employed. Data were measured to 2θ = 60°. The intensities of 3 check reflections, measured every 3600 s throughout the data collection, decreased uniformly during the data collection to final values about 3% less than the initial values. An isotropic decay correction was applied. After data reduction, an absorption correction was applied using the Gaussian integration method (10, 11). Transmission factors ranged from 0.342 to 0.575 for 200 sampling points. Of the 5476 independent reflections measured, 2613 (47.7%) had intensities greater than 3σ(I) above background where $\sigma^2(I) = S + 2B + (0.04(S - B))^2$ with S = scan count and B = background count.

The systematic absences allow space groups Cc or $C2/c$, the latter being chosen on the basis of the E-statistics and the number of molecules in the unit-cell. The coordinates of the metal atoms were determined from the Patterson function and those of the remaining non-hydrogen atoms from a subsequent difference map. After full-matrix least-squares refinement of the non-hydrogen atoms with anisotropic thermal parameters to R = 0.044, a difference map gave the coordinates of all 16 hydrogen atoms which were included in subsequent cycles of refinement with isotropic thermal parameters. The scattering factors of ref. 12 were used for non-hydrogen atoms and those of ref. 13 for hydrogen atoms. Anomalous scattering factors from ref. 14 were used for the Ga and Mn atoms. The weighting scheme, $w = 1/\sigma^2(F)$ where $\sigma^2(F)$ is derived from the previously defined $\sigma^2(I)$ gave uniform average values of $w(|F_o| - |F_c|)^2$ over ranges of $|F_o|$ and was employed in the final stages of refinement. An isotropic Type I extinction correction (Thornley–Nelmes definition of mosaic anisotropy with a Lorentzian distribution) was applied (15–17). The final value of g was 2.5(2) × 10^4. Convergence was reached at R = 0.028 and R_w = 0.034 for 2613

Can. J. Chem. Downloaded from www.nrcresearchpress.com by 210.87.254.40 on 09/06/12
For personal use only.

Can. J. Chem. Downloaded from www.nrcresearchpress.com by 210.87.254.40 on 09/06/12
For personal use only.

reflections with $I \geq 3\sigma(I)$. For all 5476 reflections $R = 0.102$. The function minimized was $\Sigma w(|F_o| - |F_c|)^2$, $R = \Sigma||F_o| - |F_c||/\Sigma|F_o|$ and $R_w = (\Sigma w(|F_o| - |F_c|)^2/\Sigma w|F_o|^2)^{1/2}$.

On the final cycle of refinement the mean and maximum parameter shifts corresponded to 0.02 and 0.21σ respectively. The mean error in an observation of unit weight was 1.050. A final difference map showed no unusual features. The final positional and thermal parameters appear in Tables 3 and 4[1] respectively. Measured and calculated structure factors have been placed in the Depository of Unpublished Data.[1]

Tetraethylammonium [dimethylbis(1-pyrazolyl)gallato-(N,N)](pyrazole)tricarbonylmolybdate(0)

Experimental details are as above except where noted. Crystal dimensions were ca. 0.24 × 0.53 × 0.55 mm. Crystal data are:

$C_{22}H_{36}GaMoN_7O_3$ fw = 612.24

Monoclinic, $a = 10.058(1)$, $b = 20.6488(5)$, $c = 13.533(1)$ Å, $\beta = 93.800(5)°$, $V = 2804.4(4)$ Å^3, $Z = 4$, $\rho_c = 1.450$ g cm^{-3}, $F(000) = 1256$, μ(Mo K$_\alpha$) = 14.27 cm^{-1}. Absent reflections: $h0l$, $h + l \neq 2n$ and $0k0$, $k \neq 2n$ uniquely indicate the space group $P2_1/n$ (non-standard setting of $P2_1/c$, C_{2h}^5, No. 14).

An ω–2θ scan at 1.12–10.06° min^{-1} over a range of (0.60 + 0.35 tan θ)° in ω was employed. Corrections were made for an isotropic decay of ~6% during data collection. Of 8120 independent reflections measured (to 2θ = 60°), 4388 (54.0%) had intensities greater than 3σ(*I*) above background. An absorption correction yielded transmission factors ranging from 0.521 to 0.734 for 244 sampling points.

The coordinates of the metal atoms were determined from the Patterson function and those of the remaining non-hydrogen atoms from a subsequent Fourier synthesis. After full-matrix least-squares refinement of the non-hydrogen atoms with anisotropic thermal parameters to $R = 0.043$, a difference map revealed disordering of the α-carbons of the Et_4N^+ cation and positions of all hydrogen atoms except those associated with the low occupancy methyl groups of the cation (although the methyl carbon atoms themselves are not disordered, the methyl hydrogens are). Site occupancies for the disordered carbon atoms were initially estimated from relative peak heights on a Fourier map and were later adjusted to yield comparable isotropic thermal parameters for corresponding atoms. Final occupancies were fixed at 0.78 and 0.22. In the final stages of refinement the low-occupancy carbon atoms and all hydrogen atoms were refined with isotropic thermal parameters. Anomalous scattering terms were included for the Mo and Ga atoms. No extinction correction was applied. Convergence was reached at $R = 0.023$ and $R_w = 0.029$ for 4388 reflections with $I \geq 3\sigma(I)$, for all 8120 reflections $R = 0.080$. The mean and maximum parameter shifts on the final cycle of refinement corresponded to 0.08 and 0.97σ respectively and the mean error in an observation of unit weight was 0.8756. A final difference map showed no unusual features.

Analysis of Thermal Motion

The thermal motion in $[Me_2Ga(N_2C_3H_3)_2](N_2C_3H_4)Mn(CO)_3$, in the $[Me_2Ga(N_2C_3H_3)_2](N_2C_3H_4)Mo(CO)_3^-$ anion and in the Et_4N^+ cation (shown in Figs. 1 and 2) has been analysed in terms of the rigid-body modes of translation, libration, and screw-motion (18). The rms errors in the U_{ij} (derived from the least-squares analysis) are 0.0023 and 0.0019 Å^2 respectively for the Mn and Mo complexes. For the Mn complex and the molybdate anion two successful analyses were carried out, one rigid group consisting of all non-hydrogen atoms except the methyl carbon atoms and carbonyl oxygen atoms and the second consisting of the Ga atom and the four atoms bonded to it (rms $\Delta U_{ij} = 0.0047$ and 0.0013 for Mn, 0.0045 and 0.0025 Å^2 for Mo). The Et_4N^+ cation was analysed as a five atom group consisting of the N and four high-occupancy α-carbon atoms (rms $\Delta U_{ij} = 0.0017$ Å^2). The appropriate bond distances have been corrected for libration (19), using shape parameters q^2 of 0.08 for all atoms involved. Corrected bond lengths appear in Table 5 along with the uncorrected values; corrected bond angles do not differ by more than 1σ from the uncorrected values given in Table 6. Intra-annular torsion angles defining the conformations of six-membered chelate rings are listed in Table 7.

[1]The structure factor table and Table 4 (anisotropic thermal parameters) are available, at a nominal charge, from the Depository of Unpublished Data, CISTI, National Research Council of Canada, Ottawa, Ont., Canada K1A 0S2.

Results and Discussion

Manganese Compounds

The two manganese tricarbonyl derivatives prepared in this study, $[Me_2Ga(N_2C_3H_3)_2](N_2C_3H_4)Mn(CO)_3$ and $[Me_2Ga(N_2C_3H_3)_2](N_2C_5H_8)Mn(CO)_3$, were characterized as monomeric octahedral complexes having the three CO groups in a facial arrangement. Mass spectral analysis of the complexes displayed the monomer parent ion signal as the highest mass peak with the most intense signal arising from the parent ion minus the three CO groups and the "pyrazole" ligand. Other signals observed could be assigned to ions arising from predictable fragmentation patterns. The ir spectra of both compounds in cyclohexane solution showed three strong bands of equal intensity in the ν_{CO} region of the spectrum. This pattern indicates that the three CO groups are facially coordinated in the octahedral complexes since a meridional arrangement of the carbonyl groups would lead to two weak and one strong ν_{CO} bands in the ir spectra (20). The ^{1}H nmr spectra of the two complexes in C_6D_6 solution are also consistent with a *fac* arrangement of the three CO groups. The ^{1}H nmr spectrum of the complex $[Me_2Ga(N_2C_3H_3)_2](N_2C_3H_4)Mn(CO)_3$ is shown in Fig. 3. The signals due to the two equivalent pyrazolyl groups of the chelating gallate ligand can easily be distinguished from those of the pyrazole ligand by virtue of their relative intensities (2:1). A *mer* arrangement of the three CO groups would lead to a different ^{1}H nmr pattern since the two pyrazolyl moieties of the gallate ligand would no longer be equivalent. The N—H proton on the pyrazole ring gives rise to a broad singlet at low field in the spectrum. It is noteworthy that the C—H protons of the coordinated pyrazole in this, and all of the complexes studied, show an additional coupling above the expected J_{HCCH} interaction. A triplet–triplet–quartet pattern is observed, presumably caused by an interaction with the N—H proton. The octahedral structure proposed for the complexes in the vapor phase and in solution has been demonstrated unequivocally in the solid state through a crystal structure analysis

TABLE 3. Final positional (fractional × 10^5, H and low-occupancy C × 10^4) and isotropic thermal parameters ($U \times 10^3$ Å^2) with estimated standard deviations in parentheses

Atom	x	y	z	U_{eq}/U_{iso}	Atom	x	y	z	U_{eq}/U_{iso}
				$[Me_2Ga(N_2C_3H_3)_2](N_2C_3H_4)Mn(CO)_3$					
Ga	20562(1)	50717(5)	54947(2)	50	C(10)	18328(18)	10358(62)	68880(28)	70
Mn	8438(2)	34162(7)	47609(3)	47	C(11)	20837(16)	22754(60)	67108(25)	64
O(1)	2610(13)	21836(53)	57739(27)	114	C(12)	4770(16)	1594(69)	36981(39)	84
O(2)	−27(11)	45436(52)	34523(22)	101	C(13)	6253(17)	−11889(70)	33407(39)	88
O(3)	8188(11)	66627(45)	56078(22)	86	C(14)	10775(17)	−10238(63)	35690(33)	74
N(1)	12359(9)	41853(38)	39862(17)	44	H(N6)	1439(16)	817(60)	4312(30)	87(16)
N(2)	16719(9)	47419(37)	42624(17)	48	H(4a)	2794(22)	3778(84)	5956(44)	147(29)
N(3)	14116(9)	24881(37)	57260(18)	48	H(4b)	2667(20)	4176(80)	5021(47)	141(25)
N(4)	18334(9)	31585(38)	60141(18)	49	H(4c)	2842(21)	5354(73)	5787(40)	118(23)
N(5)	8139(9)	11530(39)	41268(20)	53	H(5a)	1663(25)	7660(84)	5725(43)	156(29)
N(6)	11820(12)	3783(48)	40367(26)	65	H(5b)	2136(21)	7849(81)	6113(42)	144(27)
C(1)	4957(14)	26452(57)	53869(30)	70	H(5c)	1843(19)	6931(68)	6524(38)	120(20)
C(2)	3332(13)	41009(61)	39400(27)	66	H(6)	823(14)	3818(49)	2798(25)	72(13)
C(3)	8523(13)	54094(57)	52891(25)	58	H(7)	1418(14)	5052(46)	2200(28)	70(12)
C(4)	26871(15)	45868(92)	55469(40)	73	H(8)	2056(14)	5498(46)	3596(25)	60(12)
C(5)	19315(22)	71769(70)	59877(42)	74	H(9)	1197(12)	608(45)	6165(23)	42(11)
C(6)	11037(14)	42567(60)	31013(24)	60	H(10)	1888(14)	291(47)	7333(27)	65(12)
C(7)	14388(15)	48438(56)	27952(27)	66	H(11)	2389(12)	2563(44)	6969(23)	56(11)
C(8)	17903(14)	51270(56)	35421(26)	60	H(12)	194(17)	497(57)	3622(30)	86(15)
C(9)	14197(18)	12023(56)	62611(30)	66	H(13)	446(15)	−2055(61)	2989(30)	92(15)
					H(14)	1289(15)	−1737(56)	3501(30)	84(15)
				$[(C_2H_5)_4N]^+\{[Me_2Ga(N_2C_3H_3)_2](N_2C_3H_4)Mo(CO)_3\}^-$				
				equivalent positions: $\pm(x, y, z; 1/2 - x, 1/2 + y, 1/2 - z)$				
Mo	19976(2)	39581(1)	21489(2)	42	C(18′)	370(14)	2714(7)	4340(11)	67(3)
Ga	48776(3)	37341(1)	42273(2)	51	H(N6)	2616(33)	5358(16)	3204(24)	90(11)
O(1)	−8206(23)	33591(14)	19122(21)	109	H(4a)	6087(41)	3909(20)	5824(33)	120(16)
O(2)	19654(27)	39893(13)	−1386(16)	96	H(4b)	6918(39)	4168(17)	5061(25)	100(13)
O(3)	27148(21)	25159(9)	18791(15)	69	H(4c)	5837(37)	4511(21)	5425(29)	108(15)
N(1)	40886(19)	43988(9)	23239(15)	47	H(5a)	4256(39)	2664(19)	3536(30)	117(14)
N(2)	50812(19)	42642(10)	30276(15)	51	H(5b)	5691(39)	2726(19)	3743(29)	107(15)
N(3)	20215(20)	40713(9)	38309(15)	47	H(5c)	5049(38)	2573(18)	4626(29)	114(14)
N(4)	30597(21)	40004(10)	45164(15)	49	H(6)	4138(27)	4894(14)	1157(21)	66(9)
N(5)	12865(19)	50096(9)	22198(15)	48	H(7)	6480(28)	5100(15)	1580(22)	69(9)
N(6)	18506(23)	54672(10)	28085(17)	54	H(8)	6903(31)	4550(15)	3155(22)	77(10)
N(7)	6773(21)	20258(10)	46907(16)	53	H(9)	177(28)	4322(14)	3995(20)	62(8)
C(1)	2254(30)	36054(14)	20002(23)	64	H(10)	946(29)	4388(15)	5768(22)	69(10)
C(2)	19649(29)	39743(13)	7190(21)	61	H(11)	3162(30)	4134(15)	5907(22)	71(10)
C(3)	25012(26)	30680(12)	20259(18)	49	H(12)	−216(27)	5075(15)	1283(21)	72(9)
C(4)	60692(41)	41303(21)	52826(30)	72	H(13)	−368(32)	6274(16)	1783(24)	87(11)
C(5)	49714(41)	28000(17)	39894(33)	72	H(14)	1448(28)	6372(14)	2990(21)	64(9)
C(6)	46396(31)	47874(14)	16726(23)	60	H(15a)	697(33)	1353(17)	5708(26)	92(11)
C(7)	59422(33)	49073(16)	19317(27)	70	H(15b)	244(35)	1102(17)	4496(28)	97(12)
C(8)	61871(30)	45683(16)	27802(27)	66	H(16a)	2501(31)	2349(15)	5123(22)	78(9)
C(9)	9777(31)	42622(15)	43295(24)	62	H(16b)	1392(31)	2916(17)	5009(23)	84(10)
C(10)	13335(37)	43166(16)	53177(26)	71	H(17a)	2092(34)	2019(16)	3689(25)	96(11)
C(11)	26326(36)	41482(15)	54060(23)	65	H(17b)	783(26)	2628(14)	3548(21)	66(8)
C(12)	2713(28)	53100(14)	17405(22)	59	H(18a)	−1179(36)	1811(18)	4403(27)	105(13)
C(13)	1967(33)	59507(14)	20266(24)	68	H(18b)	−814(29)	2028(14)	5516(23)	68(9)
C(14)	12158(32)	60365(14)	27043(23)	60	H(19a)*	3029(33)	1395(17)	4898(25)	42(11)
C(15)*	9060(53)	13223(20)	50051(35)	75	H(19b)*	2525(49)	1094(22)	4200(39)	102(18)
C(16)*	15852(41)	24768(21)	53283(32)	66	H(19c)*	2362(51)	715(27)	5115(37)	109(20)
C(17)*	9860(43)	21348(20)	36289(28)	64	H(20a)*	1565(50)	2097(26)	6675(36)	96(20)
C(18)*	−7749(42)	21739(24)	48514(39)	74	H(20b)*	537(42)	2590(20)	6493(31)	78(14)
C(19)	23440(61)	11004(27)	48776(45)	104	H(20c)*	1990(69)	2695(37)	6500(55)	142(37)
C(20)	13297(65)	24477(39)	64273(35)	102	H(21a)*	101(54)	1363(26)	2932(39)	76(21)
C(21)	1269(64)	17336(34)	28809(36)	101	H(21b)*	−824(39)	1757(17)	2997(26)	68(11)
C(22)	−11749(53)	28654(26)	45625(54)	102	H(21c)*	412(50)	1867(25)	2309(39)	114(19)
C(15′)	2196(14)	1907(7)	4541(11)	64(3)	H(22a)*	−1891(55)	2874(27)	4716(39)	113(22)
C(16′)	359(16)	1901(8)	5729(12)	77(4)	H(22b)*	−609(56)	3144(28)	4929(42)	130(24)
C(17′)	−159(16)	1527(8)	3987(12)	78(4)	H(22c)*	−1163(51)	2911(27)	3867(40)	117(21)

*Occupancy 0.78, primed atoms have occupancy 0.22.

Can. J. Chem. Downloaded from www.nrcresearchpress.com by 210.87.254.40 on 09/06/12
For personal use only.

Can. J. Chem. Downloaded from www.nrcresearchpress.com by 210.87.254.40 on 09/06/12
For personal use only.

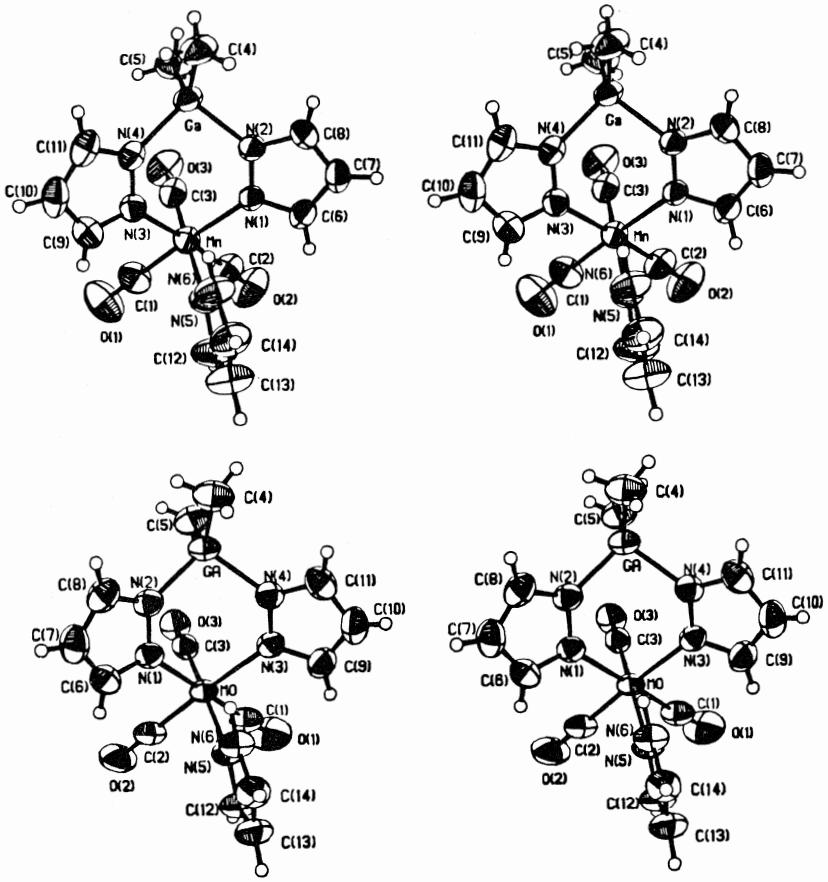

FIG. 1. Stereo views of $[Me_2Ga(N_2C_3H_3)_2](N_2C_3H_4)Mn(CO)_3$ (top) and the $[Me_2Ga(N_2C_3H_3)_2](N_2C_3H_4)Mo(CO)_3^-$ anion (bottom). 50% probability thermal ellipsoids are shown for non-hydrogen atoms. Hydrogen atoms have been assigned artifically small thermal parameters for the sake of clarity.

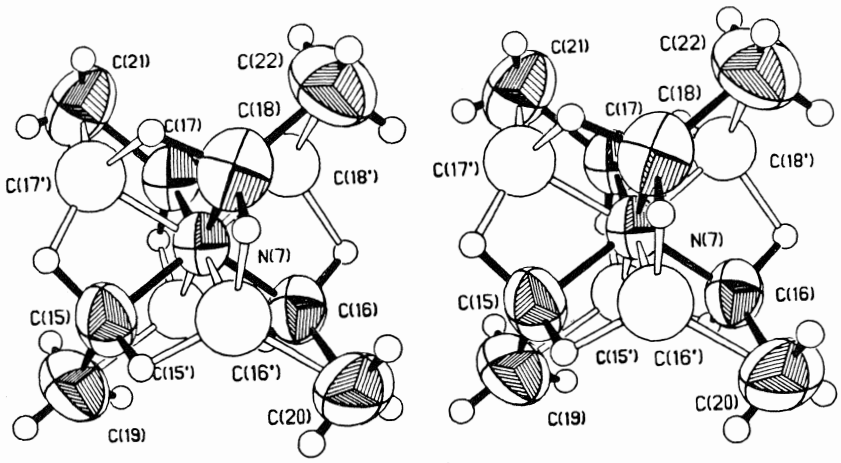

FIG. 2. Stereo view of the disordered Et_4N^+ cation in $[(C_2H_5)_4N]^+\{[Me_2Ga(N_2C_3H_3)_2](N_2C_3H_4)Mo(CO)_3\}^-$.

of the complex $[Me_2Ga(N_2C_3H_3)_2](N_2C_3H_4)Mn(CO)_3$ (see below). It is noteworthy that in earlier studies it was found that the complex $[H_2B(N_2C_3H_3)_2](N_2C_3H_4)Mn(CO)_3$ was formed by the reaction of the ligand $H_2B(N_2C_3H_3)_2^-$ with $Mn(CO)_5Br$ in the absence of pyrazole (21). In the present study reaction of $[Me_2Ga(N_2C_3H_3)_2]^-$ with $Mn(CO)_5Br$ in the absence of pyrazole did yield the complex

TABLE 5. Bond lengths (Å) with estimated standard deviations in parentheses

Bond	Length		Bond	Length	
	Uncorr.	Corr.		Uncorr.	Corr.
			$[Me_2Ga(N_2C_3H_3)_2](N_2C_3H_4)Mn(CO)_3$		
Mn —N(1)	2.076(3)	2.083	N(3) —C(9)	1.334(5)	1.336
Mn —N(3)	2.080(3)	2.086	N(4) —C(11)	1.340(5)	1.341
Mn —N(5)	2.069(3)	2.074	N(5) —N(6)	1.348(4)	1.351
Mn —C(1)	1.791(4)	1.795	N(5) —C(12)	1.324(5)	1.326
Mn —C(2)	1.796(4)	1.799	N(6) —C(14)	1.334(6)	1.335
Mn —C(3)	1.807(5)	1.809	C(1) —O(1)	1.151(5)	1.151
Ga —N(2)	1.965(3)	1.969	C(2) —O(2)	1.145(5)	1.145
Ga —N(4)	1.971(3)	1.977	C(3) —O(3)	1.148(5)	1.148
Ga —C(4)	1.974(5)	1.974	C(6) —C(7)	1.363(6)	1.364
Ga —C(5)	1.955(5)	1.956	C(7) —C(8)	1.357(6)	1.359
N(1) —N(2)	1.362(4)	1.366	C(9) —C(10)	1.363(6)	1.364
N(1) —C(6)	1.335(4)	1.337	C(10)—C(11)	1.349(6)	1.352
N(2) —C(8)	1.341(5)	1.341	C(12)—C(13)	1.369(7)	1.370
N(3) —N(4)	1.357(4)	1.361	C(13)—C(14)	1.343(6)	1.345
			$[(C_2H_5)_4N]^+\{[Me_2Ga(N_2C_3H_3)_2](N_2C_3H_4)Mo(CO)_3\}^-$		
Mo —N(1)	2.289(2)	2.295	N(3) —C(9)	1.344(3)	1.346
Mo —N(3)	2.287(2)	2.291	N(4) —C(11)	1.340(3)	1.341
Mo —N(5)	2.290(2)	2.293	N(5) —N(6)	1.338(3)	1.340
Mo —C(1)	1.924(3)	1.926	N(5) —C(12)	1.327(3)	1.328
Mo —C(2)	1.934(3)	1.936	N(6) —C(14)	1.341(4)	1.342
Mo —C(3)	1.917(3)	1.918	C(1) —O(1)	1.167(3)	1.168
Ga —N(2)	1.980(2)	1.986	C(2) —O(2)	1.161(3)	1.161
Ga —N(4)	1.973(2)	1.979	C(3) —O(3)	1.179(3)	1.180
Ga —C(4)	1.980(3)	1.985	C(6) —C(7)	1.356(4)	1.358
Ga —C(5)	1.959(3)	1.965	C(7) —C(8)	1.353(5)	1.355
N(1) —N(2)	1.362(3)	1.364	C(9) —C(10)	1.366(5)	1.367
N(1) —C(6)	1.339(3)	1.340	C(10)—C(11)	1.350(5)	1.352
N(2) —C(8)	1.339(3)	1.339	C(12)—C(13)	1.382(4)	1.383
N(3) —N(4)	1.358(3)	1.360	C(13)—C(14)	1.341(4)	1.343
N(7) —C(15)	1.527(5)	1.539	N(7) —C(15′)	1.573(14)	
N(7) —C(16)	1.530(4)	1.542	N(7) —C(16′)	1.485(16)	
N(7) —C(17)	1.507(4)	1.519	N(7) —C(17′)	1.603(16)	
N(7) —C(18)	1.522(5)	1.535	N(7) —C(18′)	1.524(14)	
C(15)—C(19)	1.538(7)	1.548	C(15′)—C(19)	1.731(15)	
C(16)—C(20)	1.527(7)	1.537	C(16′)—C(20)	1.732(15)	
C(17)—C(21)	1.530(6)	1.540	C(17′)—C(21)	1.602(17)	
C(18)—C(22)	1.527(7)	1.537	C(18′)—C(22)	1.633(15)	

$[Me_2Ga(N_2C_3H_3)_2](N_2C_3H_4)Mn(CO)_3$ but the yield was considerably lower than that obtained from the preparative route above. In addition, isolation of the desired complex was complicated by the formation of $Mn_2(CO)_{10}$ and other carbonyl containing products. The desired product obtained from the reaction involving pyrazole as a reactant was the only carbonyl-containing product formed.

Molybdenum and Tungsten Compounds

The tetracarbonyl anions, $[Me_2Ga(N_2C_3H_3)_2]M(CO)_4^-$, M = Mo and W, were isolated as their tetraethylammonium salts. The room temperature proton nmr spectra (Table 2) of the complexes displayed one signal for the $GaMe_2$ moiety suggesting that the octahedral species possess either a planar M—(N—N)$_2$—Ga six-membered chelate ring or a rapidly inverting boat conformation for this part of the molecule. Even at −80°C there is no indication of the $GaMe_2$ singlet separating into a doublet, so either inversion of the boat conformation is very fast even at low temperature or the planar arrangement is preferred. The ir spectra (Table 1) of the two anions in the ν_{CO} region show a four band pattern typical of a *cis* tetracarbonyl octahedral species (20).

The tricarbonyl anions, $[Me_2Ga(N_2C_3H_3)_2](N_2C_3H_4)M(CO)_3^-$, M = Mo and W, isolated as their tetraethylammonium salts, were shown to possess the three CO groups facially coordinated. Thus the ir spectrum of the complexes showed three strong bands in the ν_{CO} region of the spectrum. In addition a sharp singlet ν_{NH} band gave evidence for the presence of a coordinated pyraz-

Can. J. Chem. Downloaded from www.nrcresearchpress.com by 210.87.254.40 on 09/06/12
For personal use only.

Can. J. Chem. Downloaded from www.nrcresearchpress.com by 210.87.254.40 on 09/06/12
For personal use only.

TABLE 6. Bond angles (deg) with estimated standard deviations in parentheses, non-hydrogen atoms

Bonds	Angle (deg)	Bonds	Angle (deg)
	$[Me_2Ga(N_2C_3H_3)_2](N_2C_3H_4)Mn(CO)_3$		
N(1)—Mn —N(3)	91.4(1)	Ga —N(2) —C(8)	125.0(3)
N(1)—Mn —N(5)	85.4(1)	N(1) —N(2) —C(8)	108.1(3)
N(1)—Mn —C(1)	176.5(2)	Mn —N(3) —N(4)	127.8(2)
N(1)—Mn —C(2)	91.6(1)	Mn —N(3) —C(9)	126.2(3)
N(1)—Mn —C(3)	94.8(2)	N(4) —N(3) —C(9)	105.6(3)
N(3)—Mn —N(5)	86.6(1)	Ga —N(4) —N(3)	126.7(2)
N(3)—Mn —C(1)	89.3(2)	Ga —N(4) —C(11)	124.8(3)
N(3)—Mn —C(2)	176.2(2)	N(3) —N(4) —C(11)	108.5(3)
N(3)—Mn —C(3)	95.2(1)	Mn —N(5) —N(6)	123.2(2)
N(5)—Mn —C(1)	91.2(2)	Mn —N(5) —C(12)	133.6(3)
N(5)—Mn —C(2)	91.3(2)	N(6) —N(5) —C(12)	103.1(4)
N(5)—Mn —C(3)	178.1(1)	N(5) —N(6) —C(14)	112.5(4)
C(1)—Mn —C(2)	87.7(2)	Mn —C(1) —O(1)	177.8(4)
C(1)—Mn —C(3)	88.6(2)	Mn —C(2) —O(2)	176.3(4)
C(2)—Mn —C(3)	86.9(2)	Mn —C(3) —O(3)	174.2(4)
N(2)—Ga —N(4)	97.3(1)	N(1) —C(6) —C(7)	111.8(4)
N(2)—Ga —C(4)	107.6(2)	C(6) —C(7) —C(8)	104.1(4)
N(2)—Ga —C(5)	112.4(2)	N(2) —C(8) —C(7)	110.2(4)
N(4)—Ga —C(4)	107.5(2)	N(3) —C(9) —C(10)	111.6(4)
N(4)—Ga —C(5)	111.8(2)	C(9) —C(10)—C(11)	104.4(4)
C(4)—Ga —C(5)	118.2(3)	N(4) —C(11)—C(10)	109.9(4)
Mn —N(1)—N(2)	128.0(2)	N(5) —C(12)—C(13)	112.2(4)
Mn —N(1)—C(6)	126.2(3)	C(12)—C(13)—C(14)	105.6(4)
N(2)—N(1)—C(6)	105.9(3)	N(6) —C(14)—C(13)	106.6(4)
Ga —N(2)—N(1)	126.8(2)		
	$[(C_2H_5)_4N]^+\{[Me_2Ga(N_2C_3H_3)_2](N_2C_3H_4)Mo(CO)_3\}^-$		
N(1)—Mo —N(3)	84.69(7)	N(6) —N(5) —C(12)	104.1(2)
N(1)—Mo —N(5)	84.61(7)	N(5) —N(6) —C(14)	112.1(2)
N(1)—Mo —C(1)	178.8(11)	Mo —C(1) —O(1)	176.4(3)
N(1)—Mo —C(2)	92.9(11)	Mo —C(2) —O(2)	178.9(3)
N(1)—Mo —C(3)	98.27(9)	Mo —C(3) —O(3)	173.6(2)
N(3)—Mo —N(5)	81.03(7)	N(1) —C(6) —C(7)	112.0(3)
N(3)—Mo —C(1)	95.2(1)	C(6) —C(7) —C(8)	104.1(3)
N(3)—Mo —C(2)	173.1(1)	N(2) —C(8) —C(7)	110.3(3)
N(3)—Mo —C(3)	101.49(9)	N(3) —C(9) —C(10)	110.7(3)
N(5)—Mo —C(1)	94.2(1)	C(9) —C(10)—C(11)	104.8(3)
N(5)—Mo —C(2)	92.34(9)	N(4) —C(11)—C(10)	110.2(3)
N(5)—Mo —C(3)	176.31(9)	N(5) —C(12)—C(13)	111.4(3)
C(1)—Mo —C(2)	87.0(1)	C(12)—C(13)—C(14)	105.4(3)
C(1)—Mo —C(3)	82.9(1)	N(6) —C(14)—C(13)	107.1(3)
C(2)—Mo —C(3)	85.2(1)	C(15)—N(7) —C(16)	110.4(3)
N(2)—Ga —N(4)	98.98(8)	C(15)—N(7) —C(17)	111.8(3)
N(2)—Ga —C(4)	105.8(1)	C(15)—N(7) —C(18)	106.2(3)
N(2)—Ga —C(5)	113.6(1)	C(16)—N(7) —C(17)	107.1(2)
N(4)—Ga —C(4)	105.4(2)	C(16)—N(7) —C(18)	109.9(3)
N(4)—Ga —C(5)	111.2(1)	C(17)—N(7) —C(18)	111.5(3)
C(4)—Ga —C(5)	119.5(2)	C(15′)—N(7)—C(16′)	111.5(8)
Mo —N(1)—N(2)	128.1(1)	C(15′)—N(7)—C(17′)	107.4(8)
Mo —N(1)—C(6)	126.0(2)	C(15′)—N(7)—C(18′)	106.5(8)
N(2)—N(1)—C(6)	105.4(2)	C(16′)—N(7)—C(17′)	108.2(9)
Ga —N(2)—N(1)	125.1(1)	C(16′)—N(7)—C(18′)	113.9(9)
Ga —N(2)—C(8)	126.7(2)	C(17′)—N(7)—C(18′)	109.1(8)
N(1)—N(2)—C(8)	108.2(2)	N(7) —C(15)—C(19)	112.2(4)
Mo —N(3)—N(4)	128.8(1)	N(7) —C(16)—C(20)	113.1(4)
Mo —N(3)—C(9)	124.9(2)	N(7) —C(17)—C(21)	114.0(4)
N(4)—N(3)—C(9)	106.2(2)	N(7) —C(18)—C(22)	113.0(4)
Ga —N(4)—N(3)	125.1(2)	N(7)—C(15′)—C(19)	100.6(8)
Ga —N(4)—C(11)	126.7(2)	N(7)—C(16′)—C(20)	104.7(10)
N(3)—N(4)—C(11)	108.1(2)	N(7)—C(17′)—C(21)	105.3(10)
Mo —N(5)—N(6)	125.0(1)	N(7)—C(18′)—C(22)	107.2(9)
Mo —N(5)—C(12)	130.9(2)		

TABLE 7. Intra-annular torsion angles (deg) chelate rings

Atoms	Value	Atoms	Value
N(3)—Mn —N(1)—N(2)	−32.8(2)	N(1)—Mo —N(3)—N(4)	−35.9(1)
Mn —N(1)—N(2)—Ga	−2.7(3)	Mo —N(3)—N(4)—Ga	−2.8(2)
N(1)—N(2)—Ga —N(4)	36.1(2)	N(3)—N(4)—Ga —N(2)	42.8(1)
N(2)—Ga —N(4)—N(3)	−30.2(2)	N(4)—Ga —N(2)—N(1)	−36.0(1)
Ga —N(4)—N(3)—Mn	−8.5(3)	Ga —N(2)—N(1)—Mo	−9.8(2)

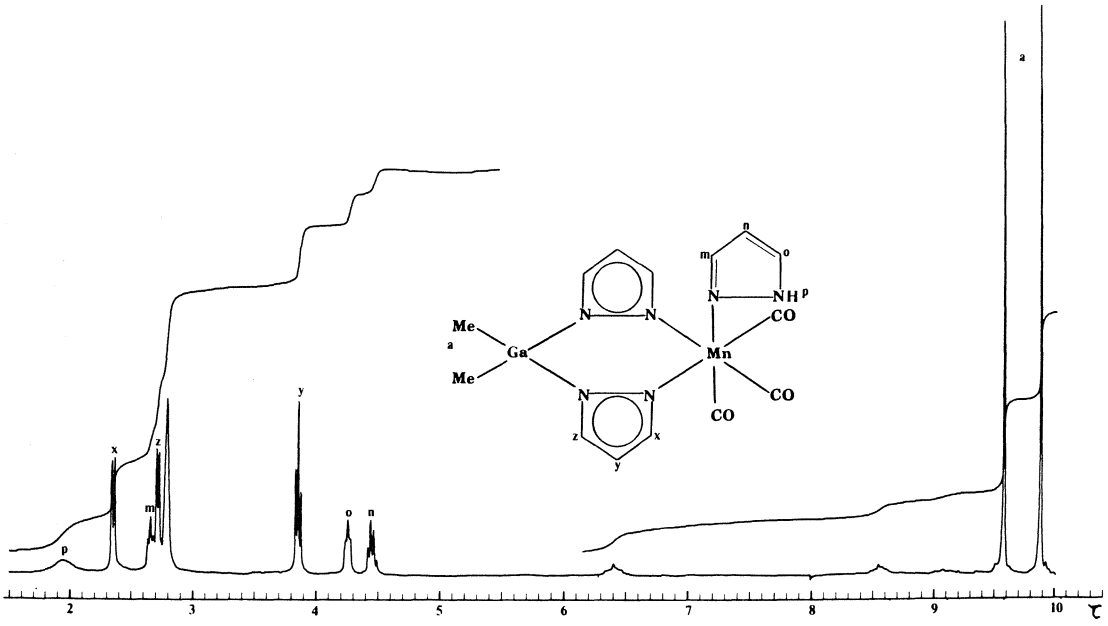

FIG. 3. Room temperature 100 MHz ^{1}H nmr spectrum of $[Me_2Ga(N_2C_3H_3)_2](N_2C_3H_4)Mn(CO)_3$ in C_6D_6 solution.

ole ligand. However, the ^{1}H nmr spectra of these complex anions were somewhat surprising in that they showed only one GaMe signal and one set of signals due to both the pyrazolyl groups and the pyrazole group (see Fig. 4). No signal could be found in the region where the NH proton of the pyrazole group might be expected. A possible explanation for these observations is that there is a rapid exchange of roles between the pyrazolyl groups and pyrazole group which makes all three of these groups equivalent and the methyl groups on the gallium equivalent on the nmr time scale. A proposed mechanism is shown in Fig. 5. In this mechanism the structure displayed in the solid state (Fig. 1) must initially undergo an inversion of the GaN_4M six-membered ring to bring the two pyrazolyl moieties and the coordinated pyrazole group in close proximity. The "Ga" and "M" portions of the molecule could then remain relatively fixed while the pyrazolyl units breathe in and out while the H atom exchanges among the three nitrogen atoms. It is interesting that the neutral $[Me_2Ga(N_2C_3H_3)_2](N_2C_3H_4)Mn(CO)_3$ compound does not show this type of fluxionality since it is valence isoelectronic with the Mo and W tricarbonyl anions, the only difference being the charge on the latter species. The ^{1}H nmr spectrum of the Mn compound was run in d_6-acetone to establish the absence of a solvent effect and indeed the spectrum obtained displayed the same type of pattern as shown in Fig. 3 for the C_6D_6 solution of the complex. Even at −80°C the $GaMe_2$ singlet in the spectra of the Mo and W tricarbonyl anions showed no signs of splitting into the doublet pattern observed in the room temperature spectrum of the Mn derivative. It was thought that a structural difference in the two complexes might be responsible for the observed difference in solution behaviour. Consequently X-ray structural analyses of the manganese compound $[Me_2Ga(N_2C_3H_3)_2](N_2C_3H_4)Mn(CO)_3$ and the corresponding Mo tricarbonyl anion $[Me_2Ga(N_2C_3H_3)_2](N_2C_3H_4)Mo(CO)_3^-$ were carried out and the results are discussed below. The Mo and W tricarbonyl anions of the present study are closely

Can. J. Chem. Downloaded from www.nrcresearchpress.com by 210.87.254.40 on 09/06/12
For personal use only.

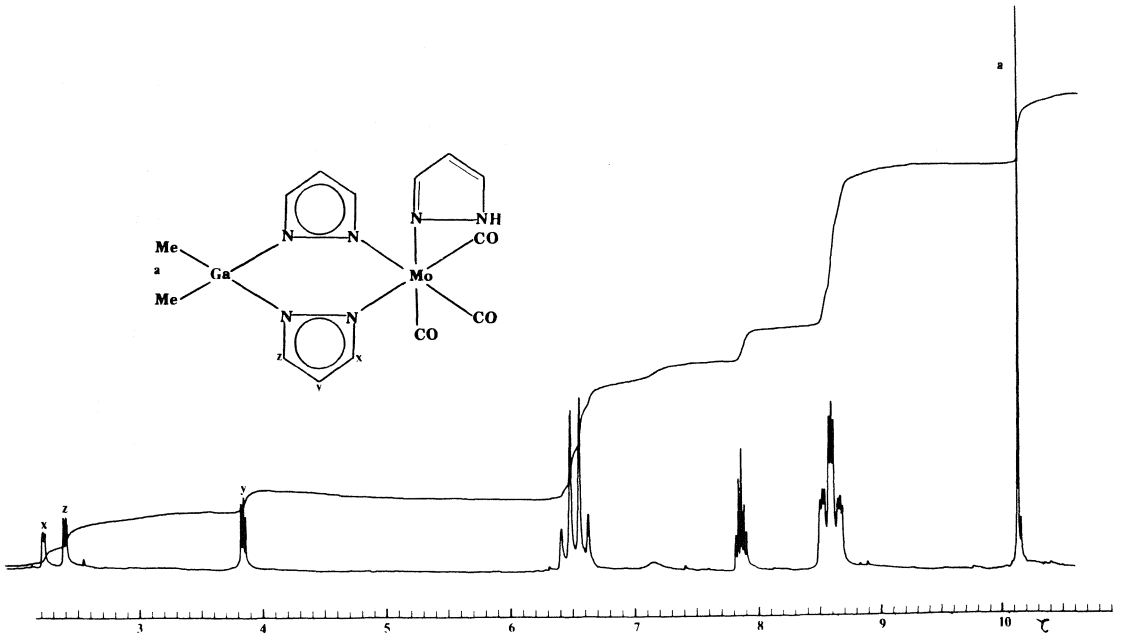

FIG. 4. Room temperature 100 MHz ^{1}H nmr spectrum of $[(C_2H_5)_4N]^+\{[Me_2Ga(N_2C_3H_3)_2](N_2C_3H_4)Mo(CO)_3\}^-$ in d_6-acetone solution.

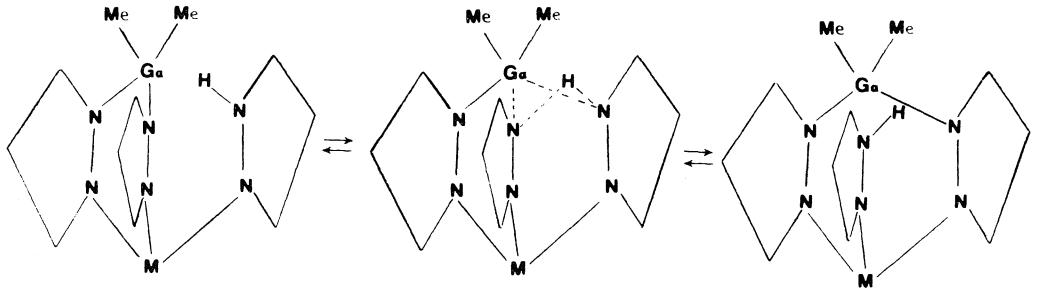

FIG. 5. Proposed mechanism for exchange of pyrazole and pyrazolyl groups in solutions of $[(C_2H_5)_4N]^+\{[Me_2Ga(N_2C_3H_3)_2](N_2C_3H_4)Mo(CO)_3\}^-$.

related to the anions incorporating the trispyrazolylborate and trispyrazolylgallate ligands, viz. $RE(N_2C_3H_3)_3M(CO)_3^-$ (where R = H, E = B; R = Me, E = Ga; M = Mo and W). It has already been shown that these symmetrical anions react with allyl bromide or diazald to give the corresponding neutral species $RE(N_2C_3H_3)_3M(CO)_2D$ (where D = η^3-C_3H_5 or NO) (22, 23). Consequently it was not surprising that the reaction of $[Me_2Ga(N_2C_3H_3)_2](N_2C_3H_4)Mo(CO)_3^-$ with allyl bromide in THF produced the monomeric six-coordinate complex $[Me_2Ga(N_2C_3H_3)_2](N_2C_3H_4)Mo(CO)_2(\eta^3\text{-}C_3H_5)$ in good yield. The ^{1}H nmr of this complex in C_6D_6 solution is shown in Fig. 6. Assuming that the facial configuration of the $[Me_2Ga(N_2C_3H_3)_2]$ and $N_2C_3H_4$ ligands is retained during the substitution reaction the allyl group may be positioned either opposite the pyrazole ligand or opposite one of the pyrazolyl moieties of the chelating gallate ligand. The ^{1}H nmr pattern shown in Fig. 6 shows two sets of signals for the pyrazolyl and pyrazole protons in the ratio 2:1. This means that the pyrazolyl groups of the gallate ligand must be equivalent and hence the allyl group must be positioned opposite to the pyrazole ligand as shown. The ^{1}H nmr signals due to the allyl protons also indicate this positioning for the allyl groups since there is one signal only for the two *anti* protons and one signal only for the two *syn* protons. In this position the allyl group must be either symmetrically attached or undergoing a rapid rotation about the molybdenum–allyl bond axis. If the allyl group were positioned opposite to

Can. J. Chem. Downloaded from www.nrcresearchpress.com by 210.87.254.40 on 09/06/12
For personal use only.

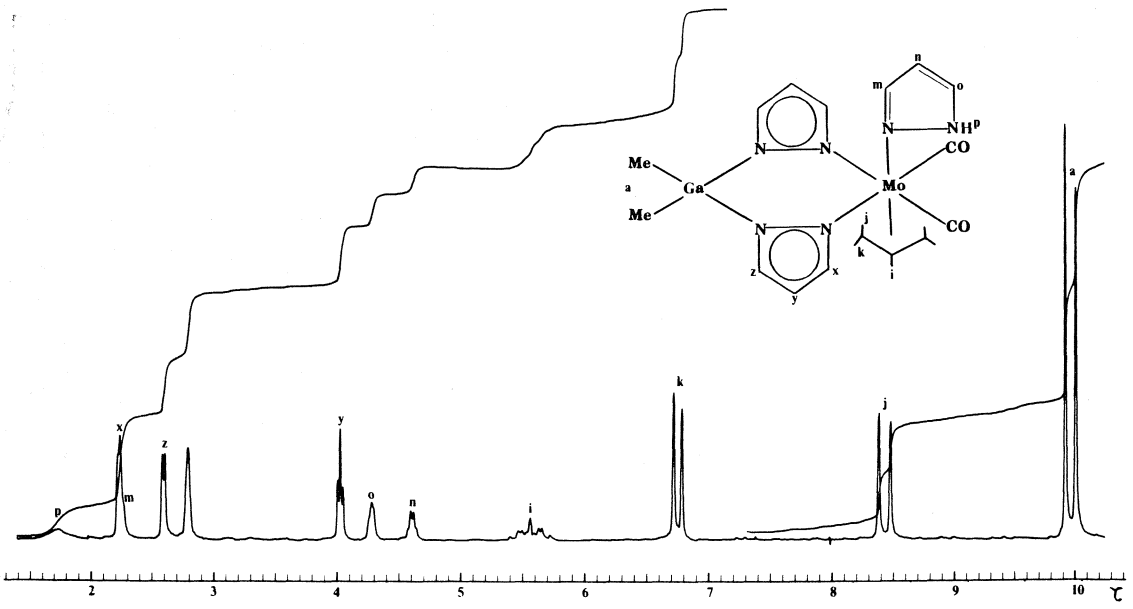

FIG. 6. Room temperature 100 MHz ^{1}H nmr spectrum of $[Me_2Ga(N_2C_3H_3)_2](N_2C_3H_4)Mo(CO)_2$ (η^3-C_3H_5) in C_6D_6 solution.

one of the pyrazolyl moieties two signals should be seen for the *syn* protons and for the *anti* protons even if a rapid rotation of the allyl group is occurring.

In contrast to the allylating experiments, attempts to nitrosylate the tricarbonyl anions met with only marginal success. Reactions of the Mo tricarbonyl anion with Diazald in THF resulted in the evolution of CO and a color change from yellow to orange. A small amount of orange solid (<1% yield) was obtained on workup of the reaction mixture and this was shown by mass spectrometry to contain the desired nitrosyl compound $[Me_2Ga(N_2C_3H_3)_2](N_2C_3H_4)Mo(CO)_2NO$. However, attempts to prepare the nitrosyls on a larger scale were unsuccessful.

The related cycloheptatrienyl compounds $[Me_2Ga(N_2C_3H_3)_2](N_2C_3H_4)M(CO)_2(\eta^3\text{-}C_7H_7)$, M = Mo and W, were prepared by the reaction of $[Me_2Ga(N_2C_3H_3)_2]^-$ with $(C_7H_7)M(CO)_2I$ in the presence of pyrazole in THF solution. As with the allyl compound discussed above, two structural isomers are possible but again the ^{1}H nmr spectra (Table 2) of the complexes establish that the position of substitution of (C_7H_7) is *trans* to the pyrazole ligand. The room temperature spectra also display but one signal for the C_7H_7 group indicating that this ligand is involved in a rapid fluxional process, a phenomenon observed recently in another series of η^3-C_7H_7 complexes (24). It should be noted that in earlier studies involving the bispyrazolylborate ligands it was found that the $H_2B(N_2C_3H_3)_2^-$ anion frequently acted as a tridentate ligand in molybdenum complexes by utilizing a 3c–2e B—H—Mo bonding interaction in addition to coordination via the two pyrazolyl groups. For example, the reaction of the ligand $H_2B(N_2C_3H_3)_2^-$ with $(C_7H_7)Mo(CO)_2I$ gave the complex $[H_2B(N_2C_3H_3)_2]Mo(CO)_2(\eta^3\text{-}C_7H_7)$ which contains a trihapto cycloheptatrienyl ligand and a B—H—Mo bond (25, 26). In addition, substitution of ethyl groups for hydrogens on the B atom of the ligand gave a novel B—CH···H···Mo 3c–2e bonding interaction in the complex $Et_2B(N_2C_3H_3)_2Mo(CO)_2(\eta^3\text{-}C_7H_7)$ (27–29). In the present study there was no evidence for a similar type of interaction involving the gallate ligand. Indeed, when $(C_7H_7)Mo(CO)_2I$ was reacted with the gallate ligand $[Me_2Ga(N_2C_3H_3)_2]^-$ in THF, in the absence of pyrazole, an intractable black tar resulted. As pointed out by a referee, a much closer analogy to the "Et_2B" complex would be possible if the $Et_2Ga(N_2C_3H_3)_2^-$ ligand were utilized in the above reaction. Even with this ligand, however, the longer Ga—N bond, compared to the B—N bond lengths, might well preclude the formation of such a 3c–2e interaction.

Crystal Structures of $[Me_2Ga(N_2C_3H_3)_2](N_2C_3H_4)Mn(CO)_3$ and $[(C_2H_5)_4N]^+\{[Me_2Ga(N_2C_3H_3)_2](N_2C_3H_4)Mo(CO)_3\}^-$

The crystal structure of $[Me_2Ga(N_2C_3H_3)_2](N_2C_3H_4)Mn(CO)_3$ consists of discrete neutral molecules (Fig. 1) separated by normal van der Waals distances. The structure of $[(C_2H_5)_4N]^+\{[Me_2Ga-$

Can. J. Chem. Downloaded from www.nrcresearchpress.com by 210.87.254.40 on 09/06/12
For personal use only.

Can. J. Chem. Downloaded from www.nrcresearchpress.com by 210.87.254.40 on 09/06/12
For personal use only.

$(N_2C_3H_3)_2](N_2C_3H_4)Mo(CO)_3\}^-$ consists of discrete cations (Fig. 2) and anions (Fig. 1), all anion–cation and cation–cation contacts corresponding to normal van der Waals interactions while screw-related anions interact via possible weak C—H···O hydrogen bonds (C(14)—H(14)···O(3) ($1/2 - x$, $1/2 + y$, $1/2 - z$), H···O = 2.51(3), C···O = 3.275(4) Å, C—H···O = 156(3)°).

The metal atoms in both structures are coordinated by three mutually *cis* carbonyl ligands, two pyrazolyl nitrogen atoms of the $[Me_2Ga(N_2C_3H_3)_2]^-$ ligand and by the non-protonated nitrogen of the pyrazole ligand. The resulting coordination geometry is trigonally distorted octahedral, the distortion from "ideal" octahedral geometry being greater for the Mo complex anion. The inner coordination group in each case has approximate C_{3v} symmetry while both the Mn complex and the Mo complex anion have approximate mirror symmetry. The distortions from mirror symmetry in both structures involve a twist of the pyrazole ligand such that the N—H is closer to one of the two pyrazolyl groups of the $[Me_2Ga(N_2C_3H_3)_2]^-$ ligand. The chemically equivalent pyrazolyl groups also differ slightly, one having a larger torsional twist about the N—N bond than the other. On this basis the C(1) and C(2) carbonyl groups and the N(1) and N(3) pyrazolyl groups of the Mn complex correspond to the C(2) and C(1) carbonyl groups and the N(3) and N(1) pyrazolyl groups respectively in the Mo complex anion as shown in Fig. 1. Average bond angles about the central metal atoms are: C—M—C, 87.7 and 85.0, N—M—N, 87.5 and 83.4, *cis*-N—M—C, 92.3 and 95.7, *trans*-N—M—C, 176.9 and 176.1° for M = Mn and Mo respectively. In the Mn complex the Mn—N distances involving the gallate ligand are equal within experimental error and their mean[2] of 2.085(2) Å is longer by about 3σ than the Mn—N distance of 2.074(3) Å to the pyrazole ligand. A corresponding trend is observed for the Mn—CO distances, that *trans* to the pyrazole ligand being slightly longer than the two others (1.809(5) compared to a mean of 1.797(2) Å). In the Mo anion all three Mo—N distances are equal within experimental error (mean Mo—N = 2.293(2) Å) and the trend in the Mo—CO distances is opposite to that observed in the Mn complex with Mo—C(3), 1.918(3) Å, being shorter than the others (mean 1.931(5) Å). The carbonyl C—O distances in the Mn complex are equal within experimental error (mean C—O = 1.148(3) Å) while in the Mo anion the extreme values are significantly different, the longest involving O(3) which is involved in the postulated weak hydrogen bond. All of the C—O distances in the Mo complex (mean C—O = 1.170(10) Å) are significantly longer than in those in the Mn structure in accord with the markedly different ν_{CO} values for these species in solution (see Table 1).

The gallium atoms in both structures have distorted tetrahedral coordination geometry with bond angles in the range 97.3(1)–119.5(2)°. The bonds to gallium in the Mo complex are longer than those in the Mn analog by an average of 0.01 Å even though all other intraligand bond distances and angles are essentially equal. This observation as well as the differences in the C—O distances mentioned above indicate stronger binding of all ligands in the Mo structure and may result, at least in part, from the greater steric crowding about the smaller Mn centre. The Ga—C(4) distances are longer than the Ga—C(5) distances in both cases (by 0.018(7) and 0.020(4) Å respectively for Mn and Mo), bond angles at Ga indicating that this is primarily a result of σ-hybridization effects. The chemically equivalent Ga—N distances also differ by a small but possibly significant amount, Ga—N(4) being longer than Ga—N(2) by 0.008(4) Å in the Mn complex and the corresponding bonds in the Mo anion differing in the same sense by 0.007(3) Å. The longer Ga—N bond is associated in both structures with the nitrogen atom involved in the larger Ga—N—N—M torsion angle (see Table 7).

The pyrazolyl and pyrazole rings in both structures are planar within experimental error (χ^2 values range from 0.5 to 3.8) and in each case the metal atoms are significantly displaced from the mean planes. The six-membered chelate rings have slightly twisted asymmetric boat conformations, that in the Mo complex being somewhat steeper (corresponding intra-annular torsion angles are presented side-by-side in Table 7). The angles between normals to the pyrazolyl mean planes of the gallate ligand (180° for a planar chelate ring) are 139.8 and 128.1° respectively for the Mn and Mo structures. Corresponding values for the square-planar metal complexes $[Me_2Ga(N_2C_3H_3)_2]_2M$ (M = Ni (1) or Cu (3)) are 116.4 and 117.1° respectively, indicating that the GaN_4M rings in the present octahedral complexes are less steep. This is as expected in view of the greater steric hindrance in the octahedral complexes. The cross-ring M···Ga distances are 3.818 and 3.929 Å for M = Mn and Mo respectively.

The structures of $[Me_2Ga(N_2C_3H_3)_2](N_2C_3H_4)$-$Mn(CO)_3$ and $[Me_2Ga(N_2C_3H_3)_2](N_2C_3H_4)Mo(CO)_3^-$ are remarkably similar, especially in view of the

[2]Here and elsewhere in this report mean values refer to weighted means with rms deviations from the mean in parentheses.

fact that the local environments of these species in the solid state are quite different. The major structural differences noted above arise from the different sizes of the central metals. It may be argued that in the case of the more sterically crowded Mn complex the exchange mechanism of Fig. 5, which requires an initial inversion of the six-membered chelate ring (see Fig. 1) through a planar (or nearly planar) transition state, is inhibited by short (2.7 Å) intramolecular contacts between the atom pairs C(1)···H(9) and C(2)···H(6) which are increased to at least 2.93(3) Å in the Mo complex. However, an impure sample of $[Me_2Ga(N_2C_3H_3)_2](N_2C_3H_4)Cr(CO)_3^-$ (the Cr being comparable to Mn in size) gave a ^1H nmr spectrum which indicated fluxional behaviour in solution, an observation which tends to discount the steric argument presented above.[3] The ^1H nmr data in Table 2 show that all fluxional species reported here are anionic, a feature which may be of overriding importance. It should be noted in this regard that the neutral Mo and W complexes reported in Table 2 are not fluxional.

Acknowledgments

We thank the Natural Sciences and Engineering Research Council of Canada for financial support and the University of British Columbia Computing Centre for assistance. We are grateful to Mr. P. Borda for C, H, N analyses, Mr. J. Nip for mass spectra, and to Ms. L. Evelyn for the ^1H nmr spectra.

1. D. F. Rendle, A. Storr, and J. Trotter. J. Chem. Soc. Dalton Trans. 176 (1975).
2. F. G. Herring, D. J. Patmore, and A. Storr. J. Chem. Soc. Dalton Trans. 711 (1975).
3. D. J. Patmore, D. F. Rendle, A. Storr, and J. Trotter. J. Chem. Soc. Dalton Trans. 718 (1975).
4. K. R. Breakell, D. J. Patmore, and A. Storr. J. Chem. Soc. Dalton Trans. 749 (1975).
5. K. S. Chong, S. J. Rettig, A. Storr, and J. Trotter. Can. J. Chem. **59**, 996 (1981).
6. E. W. Abel and G. Wilkinson. J. Chem. Soc. 1501 (1959).
7. D. P. Tate, W. R. Knipple, and J. M. Augl. Inorg. Chem. **1**, 433 (1962).
8. R. B. King. Organomet. Synth. **1**, 169 (1965).
9. R. B. King and A. Fronzaglia. Inorg. Chem. **5**, 1837 (1966).
10. P. Coppens, L. Leiserowitz, and D. Rabinovich. Acta Crystallogr. **18**, 1035 (1965).
11. W. R. Busing and H. A. Levy. Acta Crystallogr. **22**, 457 (1967).
12. D. T. Cromer and J. B. Mann. Acta Crystallogr. Sect. A, **24**, 321 (1968).
13. R. F. Stewart, E. R. Davidson, and W. T. Simpson. J. Chem. Phys. **42**, 3175 (1965).
14. D. T. Cromer and D. Liberman. J. Chem. Phys. **53**, 1891 (1970).
15. P. J. Becker and P. Coppens. Acta Crystallogr. Sect. A, **30**, 129 (1974); **30**, 148 (1974); **31**, 417 (1975).
16. P. Coppens and W. C. Hamilton. Acta Crystallogr. Sect. A, **26**, 71 (1970).
17. F. R. Thornley and R. J. Nelmes. Acta Crystallogr. Sect. A, **30**, 748 (1974).
18. V. Schomaker and K. N. Trueblood. Acta Crystallogr. Sect. B, **24**, 63 (1969).
19. D. W. J. Cruickshank. Acta Crystallogr. **9**, 747 (1956); **9**, 754 (1956); **14**, 896 (1961).
20. D. M. Adams. Metal–ligand and related vibrations. Edward Arnold Ltd. London. 1967. Chapt. 3.
21. A. Bond and M. Green. J. Chem. Soc. Sect. A, 682 (1971).
22. S. Trofimenko. J. Am. Chem. Soc. **91**, 588 (1969).
23. K. R. Breakell, S. J. Rettig, D. L. Singbeil, A. Storr, and J. Trotter. Can. J. Chem. **56**, 2099 (1978).
24. K. S. Chong and A. Storr. Can. J. Chem. **58**, 2278 (1980).
25. S. Trofimenko. Inorg. Chem. **9**, 2493 (1970).
26. F. A. Cotton, M. Jeremic, and A. Shaver. Inorg. Chim. Acta, **6**, 543 (1972).
27. S. Trofimenko. J. Am. Chem. Soc. **90**, 4754 (1968).
28. F. A. Cotton, T. LaCour, and A. G. Stanislowski. J. Am. Chem. Soc. **96**, 754 (1974).
29. F. A. Cotton and V. W. Day. J. Chem. Soc. Chem. Commun. 415 (1974).

[3]Note added in proof: The Re complex $[Me_2Ga(N_2C_3H_3)_2](N_2C_3H_4)Re(CO)_3$ has been prepared and shown by ^1H nmr studies to be non-fluxional in both C_6D_6 and d_6-acetone solutions.

Can. J. Chem. Downloaded from www.nrcresearchpress.com by 210.87.254.40 on 09/06/12
For personal use only.

Erratum: On cardioactive steroids. IV. A new synthesis of cardenolides

Rinaldo Marini-Bettolo, Petr Flecker, Thomas Y. R. Tsai, and Karel Wiesner

Natural Products Research Centre, University of New Brunswick, Bag Service #45222, Fredericton, N.B., Canada E3B 6E2

(Ref.: Can. J. Chem. **59**, 1403 (1981))

Received August 14, 1981

The melting point of compound **8** has been given erroneously as 157–159°C. It should be 129–131°C.

Crystal and molecular structure of *cis,anti,cis*-*N,N'*-dibenzoyl-3,12-diazatricyclo[6.4.0.0^{2,7}]dodecan-6,12-dione and *cis,anti,cis*-*N,N'*-dibenzoyl-3,9-diazatricyclo[6.4.0.0^{2,7}]dodecan-6,9-dione. Photodimers of *N*-benzoylcyclohex-2-ene-4-one

T. Stanley Cameron and Ruth E. Cordes
Department of Chemistry, Dalhousie University, Halifax, N.S., Canada B3J 4J3
and
B. Mario Pinto and Walter A. Szarek
Department of Chemistry, Queen's University, Kingston, Ont., Canada K7L 3N6

Received March 19, 1980[1]

T. Stanley Cameron, Ruth E. Cordes, B. Mario Pinto, and Walter A. Szarek. Can. J. Chem. **59**, 3136 (1981).

The products of photodimerization of *N*-benzoylazacyclohex-2-ene-4-one (**1**) have been investigated by X-ray crystallography. Irradiation of a benzene solution of compound **1** leads to a mixture of head-to-head and head-to-tail, *cis,anti,cis* adducts, namely, *cis,anti,cis*-*N,N'*-dibenzoyl-3,12-diazatricyclo[6.4.0.0^{2,7}]dodecan-6,12-dione and *cis,anti,cis*-*N,N'*-dibenzoyl-3,9-diazatricyclo-[6.4.0.0^{2,7}]dodecan-6,9-dione, compounds **2** and **3** respectively.

T. Stanley Cameron, Ruth E. Cordes, B. Mario Pinto et Walter A. Szarek. Can. J. Chem. **59**, 3136 (1981).

On a étudié par cristallographie de rayons-X les produits résultant de la photodimérisation de la *N*-benzoylcyclohexène-2 one-4 (**1**). L'irradiation du composé **1** en solution dans le benzène conduit à un mélange d'adduits *cis*, *anti*, *cis* tête à tête et tête à queue soit la *N,N'*-dibenzoyldiaza-3,12 tricyclo[6,4,0,0^{2,7}]dodécanedione-6,12-*cis*, *anti*, *cis* (**2**) et la *N,N'*-dibenzoyldiaza-3,9 tricyclo[6,4,-0,0^{2,7}]dodécanedione-6,9 *cis*, *anti*, *cis* (**3**).

[Traduit par le journal]

Introduction

Numerous reports have appeared in the literature on the photochemical [2 + 2] cycloaddition dimerization reactions of α,β-unsaturated carbonyl compounds both in solution (1, 2) and in the solid state (3–5). The photochemical reactions of enamides and dienamides have also been extensively studied (6). In particular dienamides have been shown to undergo 6π-electron photocyclization to form polycyclic heterocycles when irradiated (6) with ultraviolet light. However, the photodimerization of *N*-substituted enaminones (R_1R_2N—C=C—C=O) has not been the subject of much investigation. We report here the photodimerization of an *N*-acyl enaminone, *N*-benzoylazacyclohex-2-ene-4-one (**1**), and the determination of the regiochemistry and the stereochemistry of the products by X-ray crystallography.

Results and Discussion

N-Benzoylazacyclohex-2-ene-4-one (**1**) was prepared from the saturated amide, *N*-benzoylazacyclohexan-4-one by an adaptation of the peroxyester reaction of Kharasch and Sosnovsky (6).

Irradiation of a 0.005 *M* solution of compound **1** in benzene with light of wavelengths greater than 3000 Å leads to a mixture of two possible cyclobutane dimers, namely the head-to-head and the head-to-tail adducts **2** and **3** respectively.

Crystal structure of 2

Crystal data

$C_{24}H_{22}N_2O_4$ fw = 402.24

Monoclinic $P2_1/c$, a = 18.568(4), b = 11.396(4), c = 19.374(5) Å, β = 150.75(2)°, V = 2003 Å^3, Z = 4, ρ_c = 1.334 g cm^{-3} (22 ± 1°C; MoKα_1, λ = 0.71069 Å (graphite monochromator) μ = 0.53 cm^{-1}), F(000) = 848.

A crystal about 0.3 × 0.3 × 0.8 mm was mounted along its long axis. The cell dimensions were refined from 25 general reflections with the Bragg angle θ in the range of 14–15° on a CAD4 diffractometer. 3113 independent reflections were measured in the range θ = 2–25° of which 1188 had $I > \sigma(I)$. The data were reduced to a standard scale by routine procedures (7) and were corrected for Lorentz and polarisation, but not for extinction or absorption, factors. Reflections with $|E| > 1.2$ were used to solve the structure by an application of the tangent formula that examined 4096 (2^{12}) sets of starting phases and eliminated successively all but the most likely. This procedure is part of an X-ray system written by Sheldrick (8). The positions of all but the hydrogen atoms were found on the resultant E map.

The structure was refined by least-squares pro-

[1]Revision received June 15, 1981.

0008-4042/81/223136-05$01.00/0
©1981 National Research Council of Canada/Conseil national de recherches du Canada

Can. J. Chem. Downloaded from www.nrcresearchpress.com by 210.87.254.6 on 09/06/12
For personal use only.

Can. J. Chem. Downloaded from www.nrcresearchpress.com by 210.87.254.6 on 09/06/12
For personal use only.

cedures, minimising $\Sigma w\{\Delta F\}^2$ with isotropic temperature factors on all the atoms. The H atom positions were located from a difference Fourier synthesis when R was 0.09. Refinement was continued with anisotropic temperature factors on all but these hydrogen atoms, and it converged with $R = 0.026$. Weights were calculated from $w = (\sigma|F_0| + 0.003252F_0^2)^{-1}$ where σ is the standard deviation for each reflection and is determined from the diffractometer counting statistics.

Table 1 gives the final atomic coordinates.[2] The atomic scattering factors are taken from International Tables for X-ray Crystallography (1974), and the scattering factors of all but the hydrogen atoms were corrected for the real part of the anomalous dispersion effect. The interatomic distances and interbond angles are given in Table 2, while the torsional angles are given in Table 3.[2] Figure 1*a* shows a view of the molecule projected onto the least-squares best plane through the four-membered ring, and Fig. 2 shows the packing of the molecules in the unit cell viewed along the *a* axis.[2]

The crystal is constructed from isolated molecules of **2** with the head-to-head configuration. Within the molecule there are two types of C—C bonds. Those in the phenyl rings exhibit typical bond lengths for a conjugated system; the lengths are in the range 1.374(7) to 1.396(10), with a mean of 1.383(3) Å, and are not significantly different. The other type of C—C bond is in the heterocyclic and four-membered rings and these are all saturated. The C—C bond lengths, unique to the heterocyclic rings, C(12) to C(15) and C(22) to C(25), are equivalent with a mean value of 1.510 (3) Å. The lengths of the C—N bonds at N(1) and N(2) are also equivalent and have a mean value of 1.456 (5) Å. The C—C bonds C(11)—C(12) and C(21)—C(22) which are common to both the six- and the four-membered rings have a mean length of 1.555 (6) Å. This four-membered ring is sterically strained and in these circumstances C—C bond lengths of bonds common to several rings are often somewhat longer (10, 11). The other two bonds in the four-membered ring, C(11)—C(21) and C(12)—C(22), are shorter (mean 1.542 (6) Å) but the difference is not significant. The four-membered ring itself is not quite planar, C(21) for example is 0.045 (3) Å out of the plane of the other three atoms. There are four

TABLE 1. Atomic parameters (× 10^4) for compound **2**

Name	*X*/*a*	*Y*/*b*	*Z*/*c*	Mod (*U*)
C(1)	1874 (3)	105 (3)	−512 (3)	523
O(1)	646 (3)	503 (3)	−1653 (2)	816
N(1)	2640 (2)	424 (2)	695 (2)	483
C(11)	3824 (3)	−255 (3)	1980 (3)	436
C(12)	3609 (3)	−699 (3)	2558 (3)	439
C(13)	2538 (3)	2 (3)	2088 (3)	587
C(14)	1334 (4)	624 (3)	683 (4)	730
C(15)	1963 (4)	1267 (3)	601 (3)	643
O(3)	2619 (3)	24 (3)	2775 (3)	966
C(2)	6723 (3)	1168 (3)	3721 (3)	473
O(2)	5814 (2)	1955 (2)	2915 (2)	633
N(2)	6542 (2)	275 (2)	4036 (2)	476
C(21)	5261 (3)	333 (3)	3405 (3)	434
C(22)	5260 (3)	−426 (3)	4066 (3)	483
C(23)	6255 (3)	−1489 (3)	4891 (3)	506
C(24)	7612 (3)	−1362 (3)	5597 (3)	596
C(25)	7253 (4)	−881 (3)	4585 (3)	620
O(4)	5973 (3)	−2362 (2)	4985 (2)	730
C(31)	2590 (3)	−709 (3)	−413 (3)	509
C(32)	3880 (4)	−430 (3)	336 (3)	684
C(33)	4466 (4)	−1173 (4)	331 (4)	868
C(34)	3772 (5)	−2221 (4)	−405 (4)	863
C(35)	2487 (4)	−2511 (3)	−1149 (3)	724
C(36)	1888 (4)	−1757 (3)	−1171 (3)	601
C(41)	8083 (3)	1185 (3)	4419 (3)	510
C(42)	9476 (3)	1171 (3)	5871 (3)	592
C(43)	10699 (4)	1318 (3)	6482 (3)	662
C(44)	10542 (5)	1457 (3)	5650 (5)	839
C(45)	9156 (5)	1474 (3)	4206 (4)	842
C(46)	7925 (3)	1353 (3)	3582 (3)	599

carbonyl C=O bonds in the molecule, two of these are ketonic (C(13)—O(3) and C(23)—O(4)) and have a mean length of 1.206 (6) Å and the other two (C(1)—O(1) and C(2)—O(2)) are amidic with a mean length of 1.228 (6) Å. The difference in length is barely significant, but it is normal for the carbonyl C=O bond to be longer in an amide than in an alkyl ketone; for example, the amide C=O bond length in N^{α}-acetylaza-α′-homo-L-valine methylamide (12) is 1.228 (3) Å while the ketone carbonyl length in cyclomethylenomycin (13) is 1.210 (5) Å.

Crystal structure of ***3***

Crystal data:

$C_{24}H_{22}N_2O_4$ fw = 402.24

Monoclinic $P2_1/c$, $a = 8.392$ (1), $b = 13.602$ (5), $c = 8.839$ (2) Å, $\beta = 92.93$ (1)°, $V = 1007$ Å^3, $Z = 2$, $\rho_c = 1.326$ g cm^{-3} (20 ± 2°C, MoKα_1, $\lambda = 0.71069$ Å (graphite monochromator) $\mu = 0.53$ cm^{-1}), F (000) = 424. Crystal size about 0.2 × 0.2 × 0.9 mm.

The cell dimensions were refined from 25 general reflections with θ in the range 14–15° on a CAD4 diffractometer. 1391 unique reflections with θ in the range 2–25° were measured of which only 445 had I

[2]A complete list of atomic parameters (Table 1), selected torsional angles (Table 3), a view of the unit cell projected down *a*, and a list of the structure factors (Table 4) are available from the Depository of Unpublished Data, CISTI, National Research Council of Canada, Ottawa, Ont., Canada K1A 0S2.

Can. J. Chem. Downloaded from www.nrcresearchpress.com by 210.87.254.6 on 09/06/12
For personal use only.

TABLE 2. (*a*) Interatomic distances for compound **2**

Atoms	Distance	Atoms	Distance
C(1)–O(1)	1.230 (7)	C(21)–C(22)	1.547 (7)
C(1)–N(1)	1.353 (6)	C(22)–C(23)	1.514 (7)
C(1)–C(31)	1.489 (7)	C(23)–C(24)	1.494 (7)
N(1)–C(11)	1.448 (6)	C(23)–O(4)	1.210 (6)
N(1)–C(15)	1.463 (7)	C(24)–C(25)	1.522 (8)
C(11)–C(12)	1.562 (7)	C(31)–C(32)	1.375 (7)
C(11)–C(21)	1.536 (7)	C(31)–C(36)	1.396 (7)
C(12)–C(13)	1.507 (7)	C(32)–C(33)	1.386 (9)
C(12)–C(22)	1.558 (7)	C(33)–C(34)	1.386 (11)
C(13)–C(14)	1.521 (8)	C(34)–C(35)	1.374 (11)
C(13)–O(3)	1.202 (7)	C(35)–C(36)	1.377 (8)
C(14)–C(15)	1.499 (8)	C(41)–C(42)	1.389 (7)
C(2)–O(2)	1.226 (6)	C(41)–C(46)	1.385 (7)
C(2)–N(2)	1.371 (6)	C(42)–C(43)	1.379 (8)
C(2)–C(41)	1.503 (7)	C(43)–C(44)	1.3 (11)
N(2)–C(21)	1.445 (6)	C(44)–C(45)	1.382 (11)
N(2)–C(25)	1.471 (7)	C(45)–C(46)	1.377 (9)

(*b*) Interbond angles for compound **2**

Bonds	Angle	Bonds	Angle
O(1) —C(1) —N(1)	121.3(5)	N(2) —C(21)—C(22)	117.5(4)
O(1) —C(1) —C(31)	120.8(5)	C(12)—C(22)—C(21)	88.7 (3)
N(1) —C(1) —C(31)	117.9(4)	C(12)—C(22)—C(23)	114.8(4)
C(1) —N(1) —C(11)	124.4(4)	C(21)—C(22)—C(23)	116.1(4)
C(1) —N(1) —C(15)	117.8(4)	C(22)—C(23)—C(24)	115.1(4)
C(11)—N(1) —C(15)	114.7(4)	C(22)—C(23)—O(4)	121.7(5)
N(1) —C(11)—C(12)	116.9(4)	C(24)—C(23)—O(4)	123.2(5)
N(1) —C(11)—C(21)	121.1(4)	C(23)—C(24)—C(25)	111.0(4)
C(12)—C(11)—C(21)	89.0 (3)	N(2) —C(25)—C(24)	111.3(4)
C(11)—C(12)—C(13)	115.0(4)	C(1) —C(31)—C(32)	122.1(5)
C(11)—C(12)—C(22)	88.1 (3)	C(1) —C(31)—C(36)	119.1(5)
C(13)—C(12)—C(22)	115.6(4)	C(32)—C(31)—C(36)	118.7(5)
C(12)—C(13)—C(14)	115.9(5)	C(31)—C(32)—C(33)	120.5(5)
C(12)—C(13)—O(3)	121.1(5)	C(32)—C(33)—C(34)	120.1(6)
C(14)—C(13)—O(3)	122.9(5)	C(33)—C(34)—C(35)	119.7(6)
C(13)—C(14)—C(15)	110.6(5)	C(34)—C(35)—C(36)	120.1(6)
N(1) —C(15)—C(14)	109.3(4)	C(31)—C(36)—C(35)	120.8(5)
O(2) —C(2) —N(2)	120.7(4)	C(2) —C(41)—C(42)	121.9(4)
O(2) —C(2) —C(41)	120.5(4)	C(2) —C(41)—C(46)	118.1(4)
N(2) —C(2) —C(41)	118.8(4)	C(42)—C(41)—C(46)	119.6(5)
C(2) —N(2) —C(21)	116.8(4)	C(41)—C(42)—C(43)	120.5(5)
C(2) —N(2) —C(25)	124.9(4)	C(42)—C(43)—C(44)	119.9(6)
C(21)—N(2) —C(25)	115.6(4)	C(43)—C(44)—C(45)	119.6(6)
C(11)—C(21)—N(2)	120.3(4)	C(44)—C(45)—C(46)	121.1(6)
C(11)—C(21)—C(22)	89.5 (3)	C(41)—C(46)—C(45)	119.3(5)

$> \sigma (I)$ and only 278 reflections had $I > 3\sigma (I)$. The data were reduced to a common scale and were corrected for Lorentz and polarisation, but not for extinction or absorption, effects. The structure was solved in a way similar to that for compound **2**. The positions of the C, N, and O atoms were located from an E Map and the structure was refined by full-matrix least-squares with isotropic temperature factors on these atoms; it converged with $R = 0.09$.

The X-ray data for this compound are few in number and weak in intensity so the resultant atomic resolution is poor. However, enough detail of the structure can be seen to establish that the molecule has the head-to-tail configuration **3** (Fig. 1*b*) and that there is a crystallographic inversion centre in the middle of the four-membered ring. The ring is apparently planar though disorder remains a possibility. The interatomic distances and interbond angles do not differ significantly in

Can. J. Chem. Downloaded from www.nrcresearchpress.com by 210.87.254.6 on 09/06/12
For personal use only.

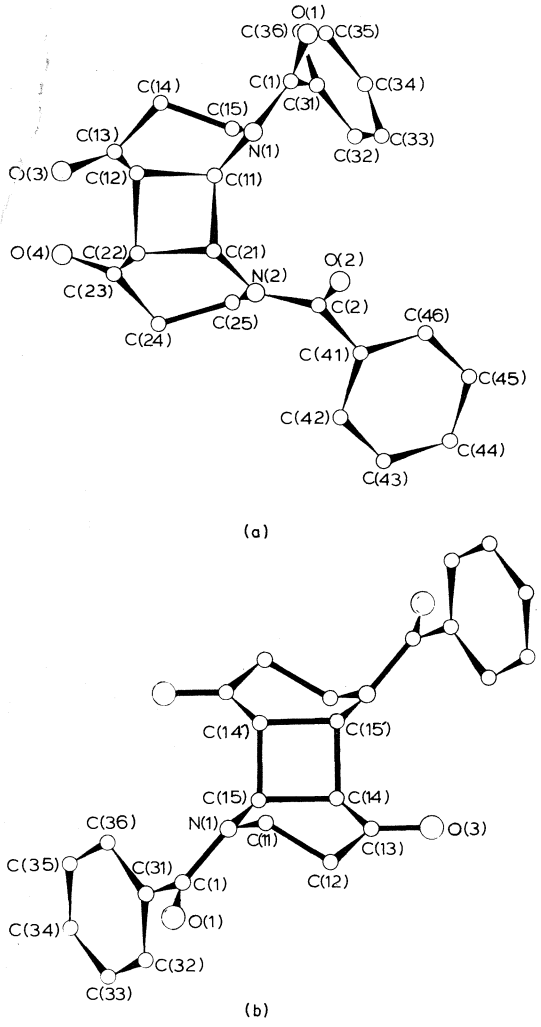

FIG 1. The assymmetric unit viewed perpendicular to the least-squares best plane through (*a*) atoms C (11), C (12), C (21), and C (22), compound **2** and (*b*) atoms C (14), C (15), C (14'), and C (15') compound **3**.

this compound from those observed in compound **2**; the atomic parameters are given in Table 5, and distances and angles are given in Table 6.[3]

The reaction that produced compounds **2** and **3** (reaction [1]) is analogous to the photodimerization reaction of 2-cyclohexenone which also gives only the *cis*-fused products (1). The observed ratio of the head-to-head and head-to-tail products (1.5:1)

[3]A complete list of atomic parameters (Table 5), a list of interatomic distances and interbond angles (Table 6), selected torsional angles (Table 7), a view of the unit cell projected down *b*, and a list of the structure factors (Table 8) are available at a nominal charge from the Depository of Unpublished Data CISTI, National Research Council of Canada, Ottawa, Ont., Canada K1A 0S2.

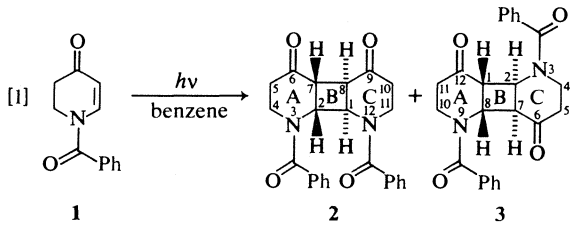

suggests that there is little preference for the direction of photodimerization of compound **1** in a 0.005 *M* benzene solution.

A process, analogous to the intramolecular photocyclization reactions of dienamides (6), in which compound **1** would undergo an intermolecular 6π-electron photocyclization reaction, is shown in reaction [2].

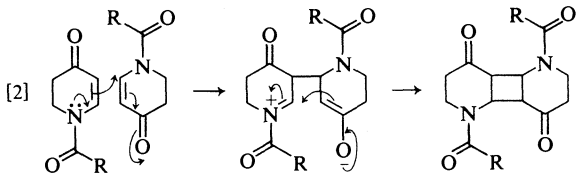

This reaction would, however, only give rise to the head-to-tail products. It is therefore likely that the photodimerization reaction of compound **1** is analogous to the photodimerization reactions of enones and not to the photocyclization reactions of dienamides. The reaction is a rare example of the photodimerization of an *N*-acyl enaminone. Since the photodimerization of *N*-benzoylazacyclohex-2-ene-4-one (**1**) proceeds in excellent yield, it is conceivable that the more general photocycloaddition reactions of *N*-acyl enaminones will be of potential synthetic utility.

TABLE 5. Atomic parameters (× 10^4) for compound **3**

Name	*X/a*	*Y/b*	*Z/c*	U_{iso}
O(1)	6546 (15)	7840 (9)	2200 (16)	369
C(1)	5512 (18)	7350 (11)	1636 (19)	597
N(1)	5705 (13)	6357 (8)	1387 (13)	420
C(11)	7317 (17)	5970 (9)	1632 (15)	557
C(12)	8286 (16)	6008 (10)	191 (18)	612
C(13)	7607 (19)	5341 (11)	−996 (19)	544
O(3)	8446 (14)	4910 (8)	−1934 (14)	756
C(14)	5805 (16)	5230 (10)	−934 (14)	461
C(15)	4833 (14)	5782 (9)	335 (15)	343
C(31)	3904 (17)	7798 (10)	1375 (18)	476
C(32)	3960 (16)	8660 (11)	497 (17)	574
C(33)	2605 (23)	9194 (12)	260 (20)	799
C(34)	1211 (17)	8849 (12)	802 (21)	694
C(35)	1091 (18)	7973 (14)	1648 (24)	901
C(36)	2495 (20)	7455 (11)	1932 (19)	666

Can. J. Chem. Downloaded from www.nrcresearchpress.com by 210.87.254.6 on 09/06/12
For personal use only.

Experimental

Melting points were determined with a Fisher–Johns melting point apparatus and are uncorrected. Thin layer chromatography was performed with silica gel G as the adsorbent in the following solvent systems (v/v): (*A*) benzene – ethyl acetate, 1:1; (*B*) 1:2. The developed plates were air dried and exposed to uv light and/or sprayed with a solution of cerium sulfate (1.0%) and molybdic acid (1.5%) in 10% aqueous sulfuric acid, and heated at ~ 150°C. Column chromatography was performed on Brinkmann silica gel 60 (E. Merck). Preparative thin layer chromatography was performed on plates pre-coated with silica gel F-254 (E. Merck). Solvents were evaporated under reduced pressure below 40°C.

Proton (^{1}H nmr) spectra were recorded on a Varian HA-100 spectrometer in toluene-d_8 with TMS as internal standard. The mass spectra were recorded on a CEC 21-104 mass spectrometer operating at 70 eV ionizing voltage.

The irradiation was performed in a borosilicate glass reaction vessel in which a 450-W Hanovia medium-pressure mercury-arc lamp was mounted. It was contained in a water-cooled quartz immersion-well fitted with a Pyrex filter-sleeve. Nitrogen gas was passed over the solution throughout the course of the irradiation.

N-*Benzoylazacyclohex-2-ene-4-one* (*1*)

Tert-butyl peracetate (0.8 equiv.) in benzene (15 mol) was added over a period of 3 h to a stirred solution of *N*-benzoylazacyclohexan-4-one (1.0 g, 4.9 mmol) in benzene (40 mL) containing cuprous chloride (20 mg), under an atmosphere of nitrogen at 81°C. The mixture was stirred at 81°C for an additional 3.5 h, then cooled, diluted with benzene (30 mL), washed successively with aqueous sodium hydrogen carbonate (2 × 25 mL) and water (25 mL), and dried over anhydrous sodium sulfate. The solvent was evaporated to give a syrup. Thin layer chromatography (solvent B) indicated the presence of a component with an R_F value of 0.51 together with unreacted starting material (R_F 0.34). After column chromatography with solvent B as eluant, the component with the R_F value of 0.51 was isolated as a syrupy solid and was identified as *N*-benzoylazacyclohex-2-ene-4-one (**1**) (0.278 g, 74%). Compound **1** was obtained from ethanol as white plates; mp 121–122°C; ^{1}H nmr data (195.5 K): δ 1.55 min, 2.04 maj (m's, 2H, H5, 5′), 2.82 min, 3.44 maj (m's, 2H, H6, 6′), 4.88 maj, 5.31 min (d's, 1H, H3), 6.45 maj, 7.77 min (d's, 1H, H2), 7.1 (m, 5H, Ph); *m/e* calcd. for $C_{12}H_{11}NO_2$: 201; found: 201. The second component (R_F 0.34) was isolated as a syrup and was identified as unreacted starting material (0.621 g).

Irradiation of N-*benzoylazacyclohex-2-ene-4-one* (*1*)

Compound **1** (0.066 g, 0.33 mmol) was dissolved in dry benzene and the solution was irradiated for 5 h under nitrogen. Thin layer chromatography (solvent A) showed that starting material had been consumed and also showed the presence of two slower moving components with R_F values of 0.28 and 0.14; the mixture was concentrated and the two components were isolated by preparative thin layer chromatography with solvent A as eluant. Compound **2** (R_F 0.28) was isolated as a white solid (0.035 g, 53%); it was recrystallized from ethyl acetate, and has mp 259.5–260.5°C (decomp.). Compound **3** (R_F 0.14) was isolated as a white solid (0.024 g, 36%). It was recrystallized from ethyl acetate, and has mp 276.5–278.5°C (decomp.). The crystals of compounds **2** and **3** used for X-ray crystallographic analysis were obtained by repeated recrystallization of the compounds from ethyl acetate.

Acknowledgement

The authors are grateful to the National Research Council of Canada for its generous financial support of this work in the form of a scholarship (to B.M.P.) and grants (to W.A.S. and to T.S.C.).

1. P. E. Eaton. Acc. Chem. Res. **1**, 50 (1968).
2. P. de Mayo. Acc. Chem. Res. **4**, 41 (1971).
3. G. M. J. Schmidt. Pure Appl. Chem. **27**, 647 (1971).
4. J. Sinnreich and H. Batzer. Helv. Chim. Acta, **56**, 2760 (1973; H.-C. Mez and G. Riks. Helv. Chem. Acta, **56**, 2766 (1973); **56**, 2772 (1973).
5. M. J. Begley, L. Crombie, and T. F. W. B. Knapp. J. Chem. Soc. Perkin I, 976 (1979).
6. G. R. Lenz. Synthesis, 489 (1978).
7. T. S. Cameron and R. E. Cordes. Acta Crystallogr. B**35**, 748 (1979).
8. G. Sheldrick. X-ray system report. University Chemical Laboratory, Lensfield Rd., Cambridge, England. 1976.
9. J. Karle and I. L. Karle. Acta Crystallogr. **21**, 849 (1966).
10. A. W. Hanson. Acta Crystallogr. **15**, 956 (1962).
11. T. S. Cameron and A. W. Hanson. J. Chem. Res. M, 4201 (1980).
12. A. A. Kemme, A. E. Svets, J. J. Blejdelis, J. E. Ancans, and G. I. Cipens. Z. Strukt. Khim. **17**, 1132 (1976).
13. B. H. Toder and A. B. Smith. J. Cryst. Mol. Struct. **7**, 8 (1978).

Thermodynamics of autoionization of aqueous tetrahydrofuran and 1,2-dimethoxyethane and the structuredness of solvents

JAYATI DATTA[1] AND KIRON K. KUNDU[2]

Department of Chemistry, Jadavpur University, Calcutta-700 032, India

Received July 24, 1980[3]

JAYATI DATTA and KIRON K. KUNDU. Can. J. Chem. **59**, 3141 (1981).

Autoionization constants (K_s) of aqueous mixtures of tetrahydrofuran (THF) and 1,2-dimethoxyethane (DME) containing 10, 30, and 50 wt.% cosolvent in each case have been determined from emf measurements of the cell: Pt, H_2 (g, 1 atm)|KOH (m_1), KBr (m_2), solvent|AgBr, Ag at seven equidistant temperatures ranging from 5 to 35°C. The standard free energies (ΔG^0), entropies (ΔS^0), and enthalpies (ΔH^0) of autoionization of the solvents were also evaluated from these data. Relative free energy data, $\delta\Delta G^0(\equiv {}_s\Delta G^0 - {}_w\Delta G^0)$, for these solvents as well as those for dioxane (D) – water mixtures taken from the literature, when coupled with the previously determined transfer free energies of H^+, $\Delta G_t^0(H^+)$, yielded $\Delta G_t^0(OH^-)_{app}$ ($\equiv \Delta G_t^0(OH^-) - \Delta G_t^0(H_2O)$) values in the mixed solvents. Relative magnitudes of $\Delta G_t^0(H^+)$ and $\Delta G_t^0(OH^-)_{app}$ and their non-Born parts, $\Delta G_{t,ch}^0(H^+)$ and $\Delta G_{t,ch}^0(OH^-)_{app}$ in particular, suggest that the "basicity" of these aqueous cosolvents decreases in the order DME > THF > D and their "acidity" in the reverse order, as expected from structural and electronic consideration of these cosolvent molecules. Analysis of the relative entropic contributions, $T\delta$ (ΔS^0) ($\equiv T({}_s\Delta S^0 - {}_w\Delta S^0)$, for the autoionization of these aqueous cosolvents and in particular $\Delta S_t^0(H_2O)$ values derived therefrom, suggests that while THF promotes three dimenstional (3D) ice-like water structures at initial compositions and D induces breakdown of the 3D structures right from the beginning, DME breaks down water structures at initial compositions, but induces some order around 4–14 mol% DME by forming the possible H-bonded bidentate DME–water complexes. And beyond certain compositions, depending upon the relative size and shape, all the cosolvents break down water structure due to packing imbalance.

JAYATI DATTA et KIRON K. KUNDU. Can. J. Chem. **59**, 3141 (1981).

A partir de mesures de la fem de la cellule: Pt, H_2 (g, 1 atm)|KOH (m_1), KBr (m_2) solvant|AgBr, Ag à sept températures équidistantes allant de 5 à 35°C, on a déterminé les constantes d'auto-ionisation (K_s) des mélanges aqueux de tétrahydrofuranne (THF) et de diméthoxy-1,2 éthane (DME) contenant dans chaque cas 10, 30 et 50% en poids de cosolvant. A partir de ces données on a également évalué les énergies libres (ΔG^0), les entropies (ΔS^0) et les enthalpies (ΔH^0) standards d'auto-ionisation des solvants. Les données d'énergie libre relative, $\delta\Delta G^0(\equiv {}_s\Delta G^0 - {}_w\Delta G^0)$ de ces solvants aussi bien que celles des mélanges de dioxanne–eau existantes, combinées aux énergies libres de transfert déterminées antérieurement pour H^+, $\Delta G_t^0(H^+)$, conduisent aux valeurs de $\Delta G_t^0(OH^-)_{app}$ ($\equiv \Delta G_t^0(OH^-) - \Delta G_t^0(H_2O)$ des solvants mixtes. Les grandeurs relatives de $\Delta G_t^0(H^+)$ et de $\Delta G_t^0(OH^-)_{app}$ et leurs éléments qui ne sont pas du type Born, $\Delta G_{t,ch}^0$ (H^+) et $\Delta G_{t,ch}^0(OH^-)_{app}$ en particulier, suggèrent que la basicité de ces co-solvants aqueux décroît dans l'ordre DME > THF > D et que leur acidité est dans l'ordre inverse conformément aux considérations structurales et électroniques des molécules de cosolvant. L'analyse des contributions entropiques relatives, $T\delta$ (ΔS^0) ($\equiv T({}_s\Delta S^0 - {}_w\Delta S^0)$, d'auto-ionisation des cosolvants aqueux et en particulier les valeurs de $\Delta S_t^0(H_2O)$ qui en dérivent suggèrent que le THF favorise des structures tridimensionnelles (3D) comme celle de l'eau glacée pour les compositions initiales tandis que D induit une rupture de ces structures 3D au moment où elles s'établissent. Le DME au contraire rompt les structures de l'eau au départ mais favorise un agencement ordonné pour une composition allant de 4 à 14 mol% de DME en formant possiblement les complexes bidentates de DME–eau liés par des liaisons hydrogène. Au-delà de certaines compositions compte tenu de la taille relative et de la forme, tous les cosolvants rompent la structure de l'eau par suite d'un entassement désordonnée.

[Traduit par le journal]

Introduction

The autoionization constants (K_s) of aquo-organic solvents at different temperatures and the related thermodynamic parameters not only help give the thermodynamic measures of acidity but also help throw some important reflections on their structural features (1). The basis of these structural reflections stems from the fact that while the ionization of water accompanying the production of order-producing H_3O^+ and OH^- ions imparts negative magnitudes to $T\Delta S^0$(ΔS^0 = entropy of ionization), the required configurational changes, including depolymerization of the three dimensional (3D) ice-like structure prior to self-ionization, contribute positive magnitudes to $T\Delta S^0$. These render the observed overall magnitude of $T\Delta S^0$ for water less negative than that for alcohols or glycols (2), where the 3D H-bonded structures are likely to be absent. The observed decreased order of the maximum in $T\delta$ (ΔS^0) ($\equiv T({}_s\Delta S^0 - {}_w\Delta S^0)$) – composition profiles (subscripts s and w refer to the solvent and water respectively) for the aqueous *t*-BuOH, 2-propanol, ethanol etc. (1), which results from the relative effects of the initial promotion and subsequent breakdown of 3D hydrogen-bonded (H-bonded) networks of water (3), also corroborates the same conclusion. Unlike alcohols, as aprotic cosolvents

[1]Née Sinha. Holder of a Research Fellowship of the University Grants Commission, New Delhi.

[2]Author to whom all correspondence should be addressed.

[3]Revision received April 14, 1981.

0008-4042/81/223141-08$01.00/0

©1981 National Research Council of Canada/Conseil national de recherches du Canada

Can. J. Chem. Downloaded from www.nrcresearchpress.com by 210.87.254.5 on 09/06/12
For personal use only.

Can. J. Chem. Downloaded from www.nrcresearchpress.com by 210.87.254.5 on 09/06/12
For personal use only.

like dioxane (D), tetrahydrofuran (THF), 1,2-dimethoxyethane (DME), etc. will not contribute to autoionization of the mixed solvents, similar studies in aqueous mixtures of these aprotic cosolvents should be of particular interest and utility. The present paper therefore deals with similar studies in aqueous mixtures of two ethereal cosolvents, namely THF and DME, as the corresponding data for the closely related D–water mixtures are already known (4).

As in previous studies (1, 2, 5–7) the thermodynamics of autoionization of these mixed solvents have been evaluated from the autoionization constant (K_s) of these mixed solvents as determined by measuring the emf's (E) of the cell [A]

[A]: Pt, H_2 (g, 1 atm)|KOH (m_1), KBr (m_2), solvent|AgBr, Ag

at seven equidistant temperatures ranging from 5 to 35°C. The solvents used contained 10, 30, and 50 wt.% of the cosolvents in each case.

Since the autoionization of aqueous solutions of these aprotic cosolvents involves the ionization of water alone, the general expression of the equilibrium in the different mixed solvents can be written as [1]

[1] $H_2O\ (s) \rightleftharpoons H^+\ (s) + OH^-\ (s)$

where (s) denotes that the respective species are in the standard state in each of the solvent mixtures. H^+ (s) counts all H^+ (solvated) including H_3O^+ and otherwise that are "seen" (2) by the H_2-electrode in the mixed solvents. In the case of pure water, (s) in the process [1] will be replaced by (w) meaning that the species will be in the standard state in pure water.

Experimental

Both THF (Reidel) and DME (Reidel) were first purified by refluxing successively with metallic sodium (Merck) and $LiAlH_4$ (Merck) for about 10–12 h followed by distillation after each refluxing. The twice-distilled solvents were then stored in a desiccator and used within 10 days, redistilling every time from $LiAlH_4$ before the preparation of the cell solutions. The bp, density, and refractive index of the solvents compared fairly well with the corresponding values in the literature (8, 9). Water used was triple distilled and made free from CO_2 by collecting the final distillate under N_2 atmosphere. Solvents of different compositions were made by weight. KBr (Merck, G.R.) was used after drying at 200–300°C and cooling in a vacuum desiccator. Stock KOH solutions were prepared by adding carbonate-free KOH (Merck, G.R.) to the weighed amounts of the solvent and the molalities were determined by titration using phenolphthalein as indicator. The method of preparation of the cell solutions was essentially similar to that described earlier (10). Adequate care was taken to avoid exposure of the solutions to the atmosphere by using a chamber flushed with N_2 whenever possible.

General experimental procedures, including the preparation of the electrodes and the measurements of emf, were similar to those described earlier (1, 2, 5, 7, 10). The equilibrium was attained in about 5–6 h. The constancy of emf readings to about ± 0.1 mV for 1 h was taken as the criterion of equilibrium. The emf's of the cell were measured by a Leeds and Northrup K_4 potentiometer using a moving coil galvanometer (Cambridge Instrument Co.) as the null point detector. Readings at 5°C were taken first and then at successively higher temperatures. Readings at lower temperatures, when checked, were found to agree within the experimental error of ± 0.3 mV. The alkali concentrations were often checked after the experiments and no significant changes were detected.

Results

The emf data (E) of cell [A] at different temperatures and the corresponding molalities of KOH and KBr for each of the solvent mixtures are given elsewhere.[4] The required corrections of the observed emf's corresponding to $p_{H_2} = 1$ were made using the partial pressures reported by Roy *et al.* (11, 12). The pK_s values (molal scale) in these mixed solvents were obtained by extrapolating the observed linear plots of pK_s' values defined by eq. [2] (1, 2, 5, 10).

$$[2] \quad pK_s' = F\,[E - (E_m^0)_{Ag,AgBr}]/2.3026\,RT + \log m_{Br^-}/m_{OH^-} = pK_s - \log a_{H_2O}\,\gamma_{Br^-}/\gamma_{OH^-} = pK_s + f(\mu)$$

against the ionic strength μ to $\mu = 0$. Here a, m, and γ denote activity, molality, and molal activity coefficient of the species subscripted. As in previous studies (1, 2, 4, 5, 10*a*), the standard state is so chosen that at infinite dilution in a given solvent $\gamma_{Br^-} = \gamma_{OH^-} = a_{H_2O} = 1$. And as in aqueous D (4), since the term $-\log \gamma_{Br^-} a_{H_2O}/\gamma_{OH^-}$ in dilute solutions of each solvent is likely to be proportional to μ, the pK_s' function would be linear with μ, as has been observed. Also in the standard state the autoionization constant of the solvent, defined by $K_s = a_{H^+}\,a_{OH^-}/a_{H_2O}$, becomes equal to $m_{H^+}\,m_{OH^-}$.

Assuming that the electrolytes KOH and KBr are completely dissociated in these mixed solvents, m_{OH^-} and m_{Br^-} were taken as equal to m_1 and m_2 respectively and $\mu = (m_1 + m_2)\,d_s$, where d_s is the density of the mixed solvent. The required values of density and E_m^0 of the Ag–AgBr electrode in the solvents were obtained from the literature (11, 12). The pK_s values at different temperatures for all the mixed solvents are listed in Table 2. The average standard deviation in pK_s values is of the order of ± 0.005 unit.

[4] A complete set of the actual experimental data is available, at a nominal charge, from the Depository of Unpublished Data, CISTI, National Research Council of Canada, Ottawa, Ont., Canada K1A 0S2.

TABLE 1. pK_s values (molal scale) for the autoionization of THF–water and DME–water mixtures at different temperatures

	pK_s values at different temperatures (°C)						
Wt.% THF	5	10	15	20	25	30	35
10	14.984	14.789	14.596	14.410	14.224 (14.27)[a]	14.060	13.899
30	15.449	15.244	15.042	14.847	14.659 (14.76)	14.488	14.328
50	15.984	15.820	15.645	15.467	15.303 (15.46)	15.154	15.017
Wt.%DME							
10	14.971	14.784	14.587	14.409	14.226	14.059	13.890
30	15.683	15.455	15.254	15.059	14.870	14.703	14.544
50	16.537	16.342	16.154	15.969	15.776	15.612	15.438

[a] Values within parentheses are Woolley *et al.*'s data (molal scale) obtained by glass electrode (ref. 13).

TABLE 2. Coefficients of eq. [2] and the values of ΔG^0, ΔH^0, and ΔS^0 (molal scale) at 25°C for the autoionization of the aqueous mixtures of THF, DME, and D

Wt.% cosolvent	A	B	C × 10^2	ΔG^0 kJ mol^{-1}	ΔH^0 kJ mol^{-1}	ΔS^0 J K^{-1} mol^{-1}
			THF–water			
0[a]	4471.33	0.0850	1.70500	79.80	56.48	−78.2
10	3791.17	0.83445	0.78811	81.19	59.13	−74.0
30	4739.52	6.5103	1.77026	83.67	60.58	−77.5
50	3558.41	−0.74934	0.88098	87.35	53.09	−114.9
			DME–water			
10	2712.08	−6.4692	−0.39199	81.20	57.62	−79.1
30	6306.19	16.9014	3.56336	84.88	60.06	−83.2
50	2513.43	−9.5535	−0.73736	90.05	60.62	−98.7
			D–water[a]			
20	4596.78	6.3108	1.84867	83.44	56.55	−90.2
45	4641.08	5.7231	1.97840	89.85	55.17	−116.3

[a] Reference 22, p. 759. Assuming that maximum uncertainty in pK_s values in all the solvents used is of the order ± 0.005 unit, the estimated (45) maximum uncertainties in the values of ΔG^0, ΔH^0, and ΔS^0 at 25°C are of the order: ± 0.03 kJ mol^{-1}, ±0.4 kJ mol^{-1}, ±1 J K^{-1} mol^{-1} respectively.

Notably, pK_s values of THF–water mixtures at 25°C compare fairly well at low cosolvent compositions but deviate significantly at higher compositions from the corresponding values reported by Woolley *et al.* (13), as obtained by use of a glass electrode (cf. the data in parentheses of Table 1). Similar discrepancies were also observed between the H_2-electrode data of Harned and Fallon (4) and the glass electrode data of Wooley *et al.* (6) in D–water mixtures. The same is true of the results obtained by H^+/Rb^+-sensitive glass electrodes (14) and those obtained by H_2- (15, 16) and Rb(Hg)- (17, 18) electrodes respectively, especially at higher cosolvent compositions of some aqueous dipolar aprotic cosolvents (14, 19). Now considering the observed larger liquid junction potentials (20), especially across water and dipolar aprotic solvents compared to those across water and alcohols, it is perhaps reasonable to doubt that if the ion-sensitive glass electrodes containing aqueous solutions inside and a large proportion of aprotic cosolvents outside the glass membrane should be free from complications.

The pK_s values at different temperatures were fitted to the Harned–Robinson expression (21).

$$[3] \quad pK_s = A/T - B + CT$$

by the method of least squares. The values of the coefficients A, B, and C for the solvents are given in Table 2. Computed pK_s values using eq. [3] are found to be reproducible within ± 0.005 unit in each solvent mixture.

The thermodynamic quantities, namely ΔG^0, ΔS^0, and ΔH^0 accompanying the autoionization of 1 mol of each of the solvent mixtures, were evaluated by using the standard relations (22) comprising the coefficients of eq. [3]. These values (molal scale) are presented in Table 2.

Can. J. Chem. Downloaded from www.nrcresearchpress.com by 210.87.254.5 on 09/06/12
For personal use only.

TABLE 3. Values of $(pK_s)_N$, $\delta(\Delta G_N^0)$, $\Delta G_t^0(H^+)$, $\Delta G_{t,el}^0(H^+)$, $\Delta G_t^0(OH^-)_{app}$, $\Delta G_{t,el}^0(OH^-)_{app}$, $T\delta(\Delta S_N^0)$, and $\Delta S_t^0(H_2O)$ for aqueous mixtures of THF, DME, and D at 25°C

Wt.%	Mol%	$(pK_s)_N$	$\delta(\Delta G_N^0)$	$\Delta G_t^0(H^+)^a$ kJ mol^{-1}	$\Delta G_{t,el}^0(H^+)$ kJ mol^{-1}	$\Delta G_t^0(OH^-)_{app}$ kJ mol^{-1}	$\Delta G_{t,el}^0(OH^-)_{app}$ kJ mol^{-1}	$T\delta(\Delta S_N^0)$ kJ mol^{-1}	$\Delta S_t^0(H_2O)$ J K^{-1} mol^{-1}
THF–water									
0	0	17.485	0	0	0	0	0	0	0
10	2.70	17.645	0.91	−3.56	0.40	4.47	0.54	1.63	−11
30	9.68	17.927	2.52	−7.26	1.24	9.78	2.20	1.47	−16
50	20.00	18.384	5.13	−9.07	3.09	14.20	5.46	−8.63	16
DME–water									
10	2.17	17.641	0.89	−2.01	−0.48	2.90	−0.85	0.13	13
30	7.89	18.120	3.62	−5.94	−0.50	9.56	−0.89	−0.16	1
50	16.66	18.820	7.62	−10.53	1.88	18.15	3.33	−3.60	−7
D–water[b]									
10	2.22	(17.713)	(1.3)	−1.59	0.42	2.89	0.73	(−1.1)	4
20	4.87	17.958	2.70					−2.74	9
30	8.06	(18.274)	(4.5)	−5.65	1.65	10.15	2.92	(−4.6)	11
45	14.33	18.847	7.77					−9.24	12
50	16.98	(19.132)	(9.4)	−4.32	4.15	13.72	7.34	—	—

[a] $\Delta G_t^0(H^+)$ values in THF–water and D–water mixtures have been taken from ref. 25*b* and those for DME–water mixtures from ref. 25*a*.
[b] Values in parentheses have been obtained by interpolation and conversion of the corresponding data of Harned *et al.* (ref. 22, p. 759), as the values for H^+ have been determined at these compositions.

Free Energy Changes

The standard free energy changes accompanying the autoprotolytic reaction [1] in the mixed solvent, ${}_s\Delta G_N^0$, relative to that in pure water, ${}_w\Delta G_N^0$, have been computed on the mole fraction scale using [4]

$$[4]\quad \delta(\Delta G_N^0) = {}_s\Delta G_N^0 - {}_w\Delta G_N^0$$
$$= 2.3026\,RT\,[p({}_sK_s)_N - p({}_wK_s)_N]$$
$$= 2.3026\,RT\left[(p_sK_s + 2\log 1000/M_s) - \left(p_wK_s + 2\log\frac{1000}{M_w}\right)\right]$$

The subscript s refers to the solvent, w to water, and N to the mole fraction scale. M_w and M_s are the molar and mean molar mass of water and the mixed solvent respectively. The values of $\delta(\Delta G_N^0)$ are presented in Table 3.

Figure 1 illustrates the variations of $\delta(\Delta G_N^0)$ values with mol% of the cosolvent for these solvent systems. For the sake of comparison the corresponding profile for the D–water system is also shown. The required data were obtained from Harned and Fallon (4) after due interpolation and conversion. As for aqueous mono-ols (6), $\delta(\Delta G_N^0)$ values for all these mixed solvents are found to be increasingly positive and at any cosolvent composition these are in the order D > DME > THF. It is well known that $\delta(\Delta G_N^0)$ values are the result of the combined effects of dielectric constant as well as the acidity and basicity of the mixed solvents (1). Since the dielectric constant of DME increases up

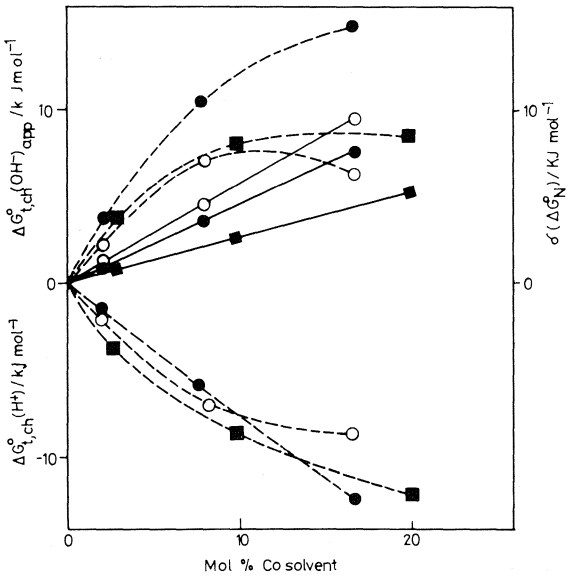

FIG. 1. Variation of $\delta(\Delta G_N^0)$ (solid line), $\Delta G_{t,ch}^0(H^+)$ and $\Delta G_{t,ch}^0(H^-)_{app}$ (dotted line) in aqueous ethers (■ THF, ● DME, and ⊙ dioxane).

to 30 wt.% and then decreases (12), whilst that for D (23) and THF (11) decreases monotonically, the relative positions of $\delta(\Delta G_N^0)$ suggest that the effects of acidity and basicity are apparently more predominant than that of the dielectric constant. So, derivation of these effects should be more informative.

As indicated in previous studies (1, 10) the quantity $\delta(\Delta G_N^0)$ represents the standard free energy changes accompanying the reaction [1] rela-

Can. J. Chem. Downloaded from www.nrcresearchpress.com by 210.87.254.5 on 09/06/12
For personal use only.

Can. J. Chem. Downloaded from www.nrcresearchpress.com by 210.87.254.5 on 09/06/12
For personal use only.

tive to that in pure water, i.e. of the process [5]

[5] $H^+(w) + OH^-(w) + H_2O(s) = H^+(s) + OH^-(s) + H_2O(w)$

Since this process is equivalent to the sum of the processes [6] and [7]

[6] $H^+(w) = H^+(s)$

[7] $OH^-(w) + H_2O(s) = OH^-(s) + H_2O(w)$

$\delta(\Delta G_N^0)$ would be given by

[8] $\delta(\Delta G_N^0) = \Delta G_t^0(H^+) + \Delta G_t^0(OH^-)_{app}$

where $\Delta G_t^0(H^+)$ denotes the transfer free energy accompanying the process [6] and $\Delta G_t^0(OH^-)_{app}$ that for the process [7]. As indicated in earlier papers (2, 10*a*), $\Delta G_t^0(OH^-)_{app}$ referred to above is equivalent to $\Delta G_t^0(OH^-)$, the standard free energy change accompanying the transfer of OH^- alone from water to the mixed solvent, i.e. the transfer process OH^- (w) $\rightarrow$ OH^- (s). This is because $\Delta G_t^0(H_2O)$ embedded in $\Delta G_t^0(OH^-)_{app}$ referred to here is formally zero due to the involved assumption that a_{H_2O} in the standard state of each solvent mixture $(a_{H_2O})_s^s$ is unity. If, however, the said activity of water $(a_{H_2O})_w^s$ be referred to that in pure water, $(a_{H_2O})_w^w$ as unity, then $-RT \ln (a_{H_2O})_w^s$ would give a measure of $\Delta G_t^0(_{H_2O})$. Obviously, while $\Delta G_t^0(H^+)$ gives a thermodynamic measure of basicity of the mixed solvent relative to that of water, $\Delta G_t^0(OH^-)_{app}$ gives the corresponding measure for the relative acidity of the mixed solvents. Consequently dissection of $\delta(\Delta G_N^0)$ to $\Delta G_t^0(H^+)$ and $\Delta G_t^0(OH)_{app}$ is in order.

Utilizing the $\Delta G_t^0(H^+)$ values based on the widely used reference electrolyte assumption (24): $\Delta G_t^0(Ph_4As^+) = \Delta G_t^0(Ph_4B^-) = \frac{1}{2}\Delta G_t^0(Ph_4AsBPh_4)$ reported earlier for these solvent systems (25), we have evaluated $\Delta G_t^0(OH^-)_{app}$ for all these mixed solvents. The values of $\Delta G_t^0(H^+)$ and $\Delta G_t^0(OH^-)_{app}$ are given in Table 3. Moreover, in order to make these data free from Born-type electrostatic effects (26) $\Delta G_{t,el}^0(i)$, these values were computed tentatively by use of the simple Born equation (26) taking $r_{H^+} \approx r_{H_3O^+} = 0.276$ nm (27), $r_{OH^-} = 0.156$ nm (28), and ε values as given in the literature (11, 12, 23). These values when subtracted from the respective $\Delta G_t^0(i)$ values yielded the chemical or non-Born type contributions (26): $\Delta G_{t,ch}^0(H^+)$ and $\Delta G_{t,ch}^0(OH^-)_{app}$, which are plotted against the cosolvent composition in Fig. 1.

Notably, in all the solvent systems, while $\Delta G_{t,ch}^0(H^+)$ are increasingly negative the corresponding values of $\Delta G_{t,ch}^0(OH^-)_{app}$ are increasingly positive. This implies that the "basicity" of the mixed solvent increases and the "acidity" decreases with the increased proportion of the cosolvents. Moreover, while the order of increased "basicity" especially at higher compositions is D < THF < DME, that of decreased "acidity" is D > THF > DME. Structural and electronic consideration of the cosolvent molecules also indicates that these three ethers, unlike water, are incapable of acting as electron acceptor or donating H^+, and hence aprotic. But, because of the electron-releasing tendency of the $(-CH_2-)$ or $(-CH_3)$ groups, the molecules are capable of acting as stronger electron donors and H^+ acceptors or "bases" than water. Also, the negative charge density will be much more intense on the single O-centre of the THF molecule than on the two O-centres of the D molecule. And, the DME molecule being effectively a 1,4 dioxane with the ring opened up, each of the electron donating $(-CH_3)$ groups induces large negative charge density on the respective O-centre to which it is attached so that the flexible chain so produced imparts more H-bond donating propensity compared to D and THF. As a result, the "basicity" or "cation–O-centre" interacting capacities of the cosolvents (28) are likely to increase in the order: D < THF < DME and their "acidity" or "anion–H-centre" interacting capacities (28) in the reverse order, as observed. Besides, since the "basicity" and "acidity" of the cosolvents are likely to be relayed through cooperative H-bonding between the cosolvents and H_2O molecules (28*a*, *b*) in their aqueous solutions, the possible H-bonded cosolvent–water complexes and their aqueous solutions should be more "basic" and less "acidic" than water. At low compositions of the DME–water system the contrary behaviour of H^+ seemingly stems from the possible structural changes due to the formation of H-bonded bidentate intercomponent complexes peculiar to this cosolvent, as indicated by Roy *et al.* (12) to explain the observed increased dielectric constant up to 30 wt.% DME.

Entropy Changes

Since entropy changes rather than enthalpy changes are a better indicator of the structural implications of a process in any aquo-organic solvents (29), analysis of the entropy changes in the present study should be useful. The values of entropy of autoionization on the mole fraction scale, ΔS_N^0, were computed at 25°C by use of eq. [9]

[9] $\Delta S_N^0 = \Delta S^0 - 2R \ln 1000/M_s$

The variations of the values of $T\Delta S_N^0$ at 25°C relative to that in water, $T\delta(\Delta S_N^0)$ ($\equiv T\ (_s\Delta S_N^0 - {}_w\Delta S_N^0)$), for these solvent systems are shown in Fig. 2 in which the corresponding profile for D–

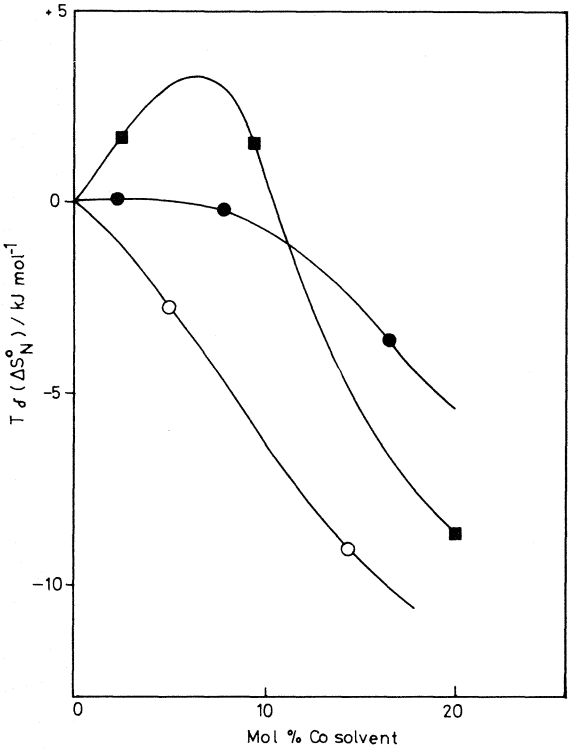

FIG. 2. Variation of $T\delta(\Delta S_N^0)$ accompanying the autoionization of water in aqueous ethers (■ THF, ● DMe, and ⊙ dioxane).

water mixtures has also been shown. The required data were obtained from Harned and Fallon's work on pK_s values at different temperatures (4).

Since the depolymerization of water molecules prior to self-ionization contributes positive entropy changes to the overall entropy of autoionization, the larger the extent of 3D ice-like water structures in the aquo-organic solvents, the larger is this contribution. Consequently, the appearance of a maximum in $T\delta(\Delta S_N^0)$–composition profiles would imply that the mixed solvents are more structured than pure water and a downward trend would imply less structured. Evidently the observed profile for THF–water mixtures implies that the addition of THF initially promotes the 3D-structure of water, possibly due to the strong hydrophobicity of 4 ($-CH_2-$) groups, but breaks down the same beyond 10 mol% THF due to packing imbalance. This contention is also in fair agreement with that arrived at from various other studies (30–33) in this solvent system.

In the case of D–water mixtures, as the $T\delta(\Delta S_N^0)$–composition (x) profile (Fig. 2) takes a sharply downward trend from $x_D = O$, it appears to suggest that the addition of D, unlike THF, breaks down the 3D-water structure even at the water-rich composition, as has been concluded from various other studies (34–39). The genesis of this destabilizing effect is possibly the effect of H-bonded intercomponent interactions, as has been indicated by ir and nmr studies (40, 41). The symmetrically placed ethereal O atoms with pronounced H-bond-donating propensity, caused by the cooperative inductive effect of the $-CH_2-$ groups (42), and also the high quadrupole moment of D (43) possibly help in such interactions. These, in effect, shift the $(\text{water})_{\text{bulky}} \leftrightarrow (\text{water})_{\text{dense}}$ equilibrium towards the right.

In the case of DME–water mixtures, the observed slight hump followed by a sharp negative trend of $T\delta(\Delta S_N^0)$ (Fig. 2) with increased cosolvent composition apparently suggests that the small addition of DME to water possibly does not alter water structure to a significant extent, unlike both THF and D, although like both of these cosolvents DME at higher composition breaks down 3D structure due to the packing imbalance. However, as the H-bonding capability of the DME molecule (because of its two flexible methoxy O-centres) exceeds that of D, the observed slight hump possibly stems from the unusual dielectric behaviour (12) and its reverse temperature dependence (12) compared to the D–water system (23).

Moreover, in view of the fact that $T\delta(\Delta S_N^0)$ is more involved by having a contribution of $\Delta S_t^0(H_2O)$ as well (cf. eq. [10]), if pK_s values for all the solvents be referred to $(a_{H_2O})_w^w = 1$ instead of $(a_{H_2O})_s^s = 1$, it would be of interest to see the structural implications of $T\delta(\Delta S_N^0)$ from another angle. Since $\delta(\Delta S_N^0)$ is given by

$$[10] \quad \delta(\Delta S_N^0) = {}_s\Delta S_N^0 - {}_w\Delta S_N^0 = \Delta S_t^0(H^+) + \Delta S_t^0(OH^-) - \Delta S_t^0(H_2O)$$

and the contributions of $\Delta S_t^0(H^+) + \Delta S_t^0(OH^-)$ could be tentatively obtained from another source which is free from a_{H_2O}, it would be possible to estimate $\Delta S_t^0(H_2O)$ by subtracting the contributions of the sum: $(\Delta S_t^0(H^+) + \Delta S_t^0(OH^-))$ from $\delta(\Delta S_N^0)$. In fact, in the following paper (44) we have collected the values of the sum: $(\Delta S_t^0(H^+) + \Delta S_t^0(X^-))$ where $X^- = Cl^-$, Br^-, and I^-, for these solvent mixtures. So, plotting $(\Delta S_t^0(H^+) + \Delta S_t^0(X^-))$ values against $(r_{x^-})^{-1}$ and reading out the values corresponding to $(r_{OH^-})^{-1}$ (by slight extrapolation of the smooth plots) yielded the tentative values of $(\Delta S_t^0(H^+) + \Delta S_t^0(OH^-))$. The values of $\Delta S_t^0(H_2O)$ so obtained for all these solvent mixtures are given in Table 3 and their variations with cosolvent compositions are shown in Fig. 3.

Simple consideration of order–disorder phenomena indicates that the negative trend of the $\Delta S^0(H_2O)$ – composition profile would imply more

Can. J. Chem. Downloaded from www.nrcresearchpress.com by 210.87.254.5 on 09/06/12
For personal use only.

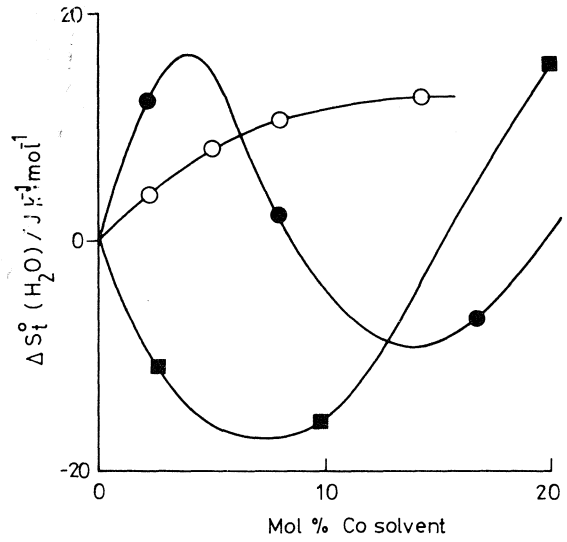

FIG. 3. Variation of ΔS_t^0 (H_2O) in aqueous ethers (■ THF, ● DMe, and ⊙ dioxane).

order and hence more "structure" or "cluster" in the mixed solvents than in water. But the reverse is true when the $\Delta S_t^0(H_2O)$–composition profile has a positive trend. The observed results in Fig. 3 therefore suggest that addition of THF initially enhances the 3D structure of water while at higher composition breaks down the same, conforming to what has been indicated earlier. On the other hand, addition of D to water induces breaking down of the 3D water structure right from the beginning as has also been indicated earlier. But in the case of the DME–water system the observed sharp increases of $\Delta S_t^0(H_2O)$ with the addition of DME are indicative of the effect of the predominant structure-breaking propensity of DME. And the observed downward trend of $\Delta S_t^0(H_2O)$ around 4–14 mol% DME is possibly the result of the increased order accompanying the formation of relatively more stable H-bonded bidentate DME–water complexes peculiar to this cosolvent, as referred to earlier. Lastly, the observed upward trend at still higher composition is the reflection of increased disorder due to the packing imbalance as common to all other cosolvents.

Acknowledgement

Thanks are due to the University Grants Commission, Government of India for awarding a research fellowship to J. Datta (nee Sinha).

1. K. K. KUNDU, P. K. CHATTOPADHYAY, D. JANA, and M. N. DAS. J. Phys. Chem. **74**, 2635 (1970).
2. A. K. DAS and K. K. KUNDU. J. Phys. Chem. **79**, 2604 (1975).
3. F. FRANKS and D. J. G. IVES. Q. Rev. **20**, 1 (1966).
4. H. S. HARNED and L. D. FALLON. J. Am. Chem. Soc. **61**, 2374 (1939).
5. I. N. BASU MULLICK and K. K. KUNDU. Ind. J. Chem. **18A**, 1 (1979).
6. E. M. WOOLLEY, D. G. HURKOT, and L. G. HEPLER. J. Phys. Chem. **74**, 3908 (1970).
7. S. K. BANERJEE, K. K. KUNDU, and M. N. DAS. J. Chem. Soc. 166 (1967).
8. W. J. WALLACE and A. L. MATHEWS. J. Chem. Eng. Data, **8**, 496 (1963); **13**, 376 (1966).
9. J. MATOUS, J. P. NOVAK, J. SOBR, and J. PICK. Collect. Czech. Chem. Commun. **37**, 2653 (1972).
10. (*a*) K. K. KUNDU and A. K. DAS. J. Chem. Soc. Faraday Trans. I, **69**, 730 (1973); (*b*) K. BOSE and K. K. KUNDU. Can. J. Chem. **57**, 2470 (1979).
11. R. N. ROY, E. E. SWENSSON, and G. LA CROSS, Jr. J. Chem. Thermodyn. **7**, 4566 (1975).
12. R. N. ROY, E. E. SWENSSON, G. LA CROSS, Jr., and C. W. KRUEGER. *In* Adv. Chem. Ser. 155. *Edited by* W. F. Furter. 1976.
13. E. M. WOOLLEY, J. TOMKINS, and L. G. HEPLER. J. Solution Chem. **41**, 341 (1972).
14. R. SMITH, D. L. MASSART, J. JULLIARD, and J. P. MOREL. Electrochim. Acta, (*a*) **21**, 437 (1976); (*b*) **21**, 431 (1976).
15. T. MUSSINI, R. LONGHI, and P. GIAMMARIO. Chim. Ind. Milan, **53**, 124 (1971).
16. K. H. KHOO. J. Chem. Soc. A, 2932 (1971).
17. (*a*) K. DAS, A. K. DAS, and K. K. KUNDU. Electrochim. Acta, **26**, 471 (1981); (*b*) A. K. DAS and K. K. KUNDU. J. Chem. Soc. Faraday Trans. I, **70**, 1452 (1974).
18. D. FEAKINS. J. Chem. Soc. Faraday Trans. I, **74**, 381 (1978).
19. C. F. WELLS. J. Chem. Soc. Faraday Trans. I, **74**, 1569 (1978).
20. J. W. DIGGLE and A. J. PARKER. Aust. J. Chem. **27**, 1617 (1974).
21. H. S. HARNED and R. A. ROBINSON. Trans. Faraday Soc. **36**, 973 (1941).
22. H. S. HARNED and B. B. OWEN. Physical chemistry of electrolyte solutions. Reinhold, New York. 1958.
23. G. J. AKERLOF. J. Am. Chem. Soc. **54**, 4125 (1932).
24. B. G. COX, G. R. HEDWIG, A. J. PARKER, and D. W. WATTS. Aust. J. Chem. **27**, 477 (1974).
25. (*a*) A. BHATTACHARYA, A. K. DAS, and K. K. KUNDU. Ind. J. Chem. **20A**, 353 (1981); (*b*) A. BHATTACHARYA, J. DATTA, K. DAS, and K. K. KUNDU. Ind. J. Chem. In press.
26. U. SEN, K. K. KUNDU, and M. N. DAS. J. Phys. Chem. **71**, 3665 (1967).
27. M. PAABO, R. G. BATES, and R. A. ROBINSON. J. Phys. Chem. **70**, 247 (1966).
28. (*a*) D. FEAKINS. *In* Physico-chemical processes in mixed aqueous solvents. *Edited by* F. Franks. Heinemann, London. 1967; (*b*) D. FEAKINS. *In* Hydrogen-bonded solvent systems. *Edited by* A. K. Covington and P. Jones. Taylor and Francis, London. 1968.
29. E. M. ARNETT, W. G. BENTRUDE, J. J. BURKE, and P. MAC DUGGLEBY. J. Am. Chem. Soc. **87**, 1541 (1965).
30. (*a*) O. KIYOHARA and G. C. BENSON. Can. J. Chem. **55**, 1354 (1977), and references therein; (*b*) **57**, 1006 (1979), and references therein.
31. K. W. MORCOM and R. W. SMITH. Trans. Faraday Soc. **66**, 1073 (1970).
32. R. E. ROBERTSON and S. R. SUGAMARI. Can. J. Chem. **50**, 1353 (1972), and references therein.
33. D. N. GLEW, H. D. MAK, and N. S. RATH. *In* Hydrogen-bonded solvent systems. *Edited by* A. K. Covington and P. Jones. Taylor and Francis, London. 1968.

Can. J. Chem. Downloaded from www.nrcresearchpress.com by 210.87.254.5 on 09/06/12
For personal use only.

34. (*a*) C. G. HAMMES and W. KNOCHE. J. Chem. Phys. **45**, 404 (1966); (*b*) K. ARAKAWA and N. TANAKA. Bull. Chem. Soc. Jpn. **42**, 5 (1969).
35. H. SCOTT. J. Chem. Eng. Data, **6**, 19 (1961).
36. J. A. GEDDES. J. Am. Chem. Soc. **55**, 4832 (1933).
37. G. WADA and S. UMEDA. Bull. Chem. Soc. Jpn. **35**, 1797 (1962).
38. A. BEN NAIM and G. MORAN. Trans. Faraday Soc. **61**, 821 (1965).
39. R. K. MOHANTY, T. S. SARMA, S. SUBRAMANIAN, and J. C. AHLUWALIA. Trans. Faraday Soc. **67**, 305 (1971); R. K. MOHANTY and J. C. AHLUWALIA. J. Solution Chem. **1**, 531 (1972).
40. (*a*) N. GORDY. J. Chem. Phys. **4**, 769 (1936); (*b*) J. ERREA, R. GASPART, and H. SACK. J. Chem. Phys. **8**, 63 (1940); (*c*) A. FRATIELIO and J. P. LUONGO. J. Am. Chem. Soc. **85**, 3072 (1963); (*d*) G. R. CHOPPIN and M. R. VIOLANTE. J. Chem. Phys. **56**, 5890 (1972).
41. A. FRATIELIO and D. C. DOUGLAS. J. Mol. Spectrosc. **11**, 465 (1963).
42. E. M. ARNETT and C. Y. WU. J. Am. Chem. Soc. **84**, 1864 (1962).
43. O. KIYOHARA, G. PERRON, and J. E. DESNOYERS. Can. J. Chem. **53**, 2591 (1975).
44. J. DATTA and K. K. KUNDU. Can. J. Chem. **59**, 3149 (1981).
45. N. W. PLEASE. Biochem. J. **56**, 196 (1954).

Can. J. Chem. Downloaded from www.nrcresearchpress.com by 210.87.254.5 on 09/06/12
For personal use only.

Free energies and entropies of transfer of hydrogen halides from water to aqueous solutions of tetrahydrofuran, dioxane, and 1,2-dimethoxyethane and the structuredness of the solvents

JAYATI DATTA[1] AND KIRON K. KUNDU[2]

Physical Chemistry Laboratories, Jadavpur University, Calcutta – 700 032, India

Received July 24, 1980[3]

JAYATI DATTA and KIRON K. KUNDU. Can. J. Chem. **59**, 3149 (1981).

Standard free energies (ΔG_t^0) and entropies (ΔS_t^0) of transfer of hydrogen iodide from water to some aqueous solutions of tetrahydrofuran (THF), dioxane (D), and 1,2-dimethoxyethane (DME) have been determined by measuring the emf's of the cell: Pt, H_2 (g, 1 atm)|KOH (m_1), KI (m_2), solvent|AgI, Ag at seven equidistant temperatures ranging from 5 to 35°C. In each of these ethereal solvent systems ΔG_t^0 values of HI, as well as of HCl and HBr obtained from the literature, and particularly of the individual ions, suggest that while H^+ is increasingly stabilized, halide ions are increasingly destabilized due to the influence of cosolvent-induced larger "basicity" and smaller "acidity" of the mixed solvents compared to that of water, and both conformed to the expected order: D < THF < DME. Moreover, the relative order: $Cl^- > Br^- > I^-$ in all the solvent systems is ascribable to the combined effects of "acid–base" and "soft–soft" interactions and the superimposed quadrupolar interactions in the case of D and the charge transfer to solvent (CTTS) complexation effect, especially on I^- in the case of THF. Analysis of the entropic contributions, $T\Delta S_t^0$, and particularly of the relative order of ΔY ($\equiv T\Delta S_t^0(H^+) + T\Delta S_{t,ch}^0(X^-)$) for X = Cl, Br, and I, in the light of the semi-quantitative theory proposed earlier by Kundu *et al.*, reveals that at initial compositions, while THF promotes 3D structures of water, both D and DME break down the same; at higher compositions all the cosolvents disrupt the structure as usual due to packing imbalance. The nature and relative positions of ΔY–composition profiles also suggest that while increase of hydrophobic groups of the cosolvents increases the stabilization, increase in hydrophilicity or H-bonding sites decreases the stabilization of the 3D structure of water.

JAYATI DATTA et KIRON K. KUNDU. Can. J. Chem. **59**, 3149 (1981).

A partir de mesures de la fem de la cellule: Pt, H_2 (g, 1 atm)|KOH (m_1), KI (m_2), solvant|AgI, Ag à sept températures équidistantes allant de 5 à 35°C, on a déterminé les énergies libres (ΔG_t^0) et les entropies (ΔS_t^0) standards de transfert, de l'iodure d'hydrogène, de l'eau aux solutions aqueuses de tétrahydrofuranne (THF), de dioxanne (D) et de diméthoxy-1,2 éthane (DME). Dans chacun de ces systèmes de solvants les valeurs de ΔG_t^0 de HI aussi bien que celles de HCl et de HBr déjà existantes, et en particulier celles des ions individuels, suggèrent que tandis que H^+ est stabilisé de façon accru, les ions halogénures sont déstabilisés par suite de l'influence de la plus grande "basicité" induite du cosolvant et d'une plus faible "acidité" des solvants mixtes comparés à celles de l'eau, les deux propriétés étant dans l'ordre prévu: D < THF < DME. De plus, l'ordre relatif: $Cl^- > Br^- > I^-$ dans tous les systèmes de solvants est attribuable aux effets combinés d'interactions de type "acide–base" et "doux–doux" et d'interactions quadrupolaires additionnées dans le cas de D et à l'effet de complexation du transfert de charge au solvant (CTTS), spécialement avec I^- dans le cas du THF. L'analyse des contributions entropiques $T\Delta S_t^0$ et en particulier l'analyse de l'ordre relatif de ΔY ($\equiv T\Delta S_t^0(H^+) + T\Delta S_{t,ch}^0(X^-)$) pour X = Cl, Br et I, à la lumière de la théorie semi-quantitative de Kundu *et al.* proposé antérieurement, révèle que pour des compositions initiales le THF favorise les structures 3D de l'eau tandis que le D et le DME au contraire détruisent cette structure 3D pour des compositions plus élevées, tous les cosolvants rompent la structure comme d'habitude par suite d'un entassement déséquilibré. La nature et les positions relatives des profils de composition–ΔY suggèrent également que, tandis que l'augmentation des groupes hydrophobes des cosolvants augmente la stabilisation, l'augmentation de l'hydrophilicité ou des sites de liaisons hydrogène diminue la stabilisation de la structure 3D de l'eau.

[Traduit par le journal]

Introduction

As part of evolving some knowledge on solvating and structural characteristics of certain aqueous ethers we have reported in the preceding paper (1) the autoionization constants of tetrahydrofuran (THF) – water and 1,2-dimethoxyethane (DME) – water mixtures at different temperatures. The related thermodynamic parameters gave some insight into the acidity and basicity as well as the structural aspects of these aqueous ethers.

Recent studies by Kundu and co-workers (2) have shown that standard potentials (E^0) of the Ag–AgX electrodes at different temperatures in different aquo-organic solvents are not only valuable in various electrochemical studies involving these electrodes in the solvents, but the related transfer free energies of HX from water to those solvents, ΔG_t^0 (HX), also furnish useful measures of the relative ion–solvent interactions, and the transfer entropies, ΔS_t^0 (HX), serve as an effective probe for the structural aspects of the solvents relative to that of water. In fact, the observed characteristic "maximum" of $T\Delta S_t^0$(HX)–composition profiles and the relative order of the

[1]Née Sinha. Holder of a Research Fellowship of the University Grants Commission, New Delhi.

[2]Author to whom all correspondence should be addressed.

[3]Revision received April 20, 1981.

0008-4042/81/223149-08$01.00/0

©1981 National Research Council of Canada/Conseil national de recherches du Canada

Can. J. Chem. Downloaded from www.nrcresearchpress.com by 210.87.254.40 on 09/06/12
For personal use only.

Can. J. Chem. Downloaded from www.nrcresearchpress.com by 210.87.254.40 on 09/06/12
For personal use only.

function ΔY ($\equiv T\Delta S_t^0(H^+) + T\Delta S_{t,ch}^0(X^-)$) (2): HI > HBr > HCl in the water-rich compositions of aqueous *t*-BuOH, 2-propanol, and ethanol, the well known promoters of three-dimensional (3D) ice-like structure of water (3), and the observed downward trends of ΔY values and their reverse order at higher cosolvent compositions where the 3D structures collapse due to packing-imbalance (3), led Kundu *et al.* (2) to propose a semi-quantitative theory relating $T\Delta S_t^0(HX)$ or rather ΔY as a structural probe for aquo-organic solvents. According to that theory (*a*) when solvent structure > pure water structure, $\Delta Y > 0$, and ΔY (X = I) > ΔY (X = Br) > ΔY (X = Cl), and (*b*) when solvent structure < pure water structure, $\Delta Y < 0$, and ΔY (X = I) < ΔY (X = Br) < ΔY (X = Cl).

Applying the above-noted tenets as the structural probe Kundu and co-workers also derived important conclusions regarding the structural features of some other solvents, viz. glycol–water (2), glycerol–water (4), etc. which are in fair agreement with those derived from various other studies in the respective solvents. So it should be highly interesting and useful to apply the said probe in elucidating the structural features of these aqueous ethers as well.

As the E^0 values of the Ag–AgX (X = Cl or Br) electrodes at different temperatures are already known in these solvents (5, 6), we are reporting the same for X = I. Since I^- is highly susceptible to oxidation at low pH solutions of these cosolvents, cell [A]

[A] Pt, H_2 (g, 1 atm)|KOH (m_1), KI (m_2), solvent| AgI, Ag

has been used. The required autoionization constants (K_s) of the solvents are of course already known (1). Moreover, although E^0 values of the Ag–AgX (X = Cl, Br, and I) at different temperatures are already known (7–9) in the aqueous mixtures of dioxane (D), another widely used and closely related ethereal cosolvent, the values of the Ag–AgI electrode are, however, based on emf measurements of cells with liquid junction (8*c*). So it would be useful to extend the present study to D–water mixtures as well. In all these aqueous ether solvents E^0 values have been determined at seven equidistant temperatures ranging from 5° to 35°C. The compositions studied for DME are 10, 30, and 50 wt.% DME and for THF are restricted to 10, 20, and 30 wt.% THF, while those for D are restricted to 20 and 45 wt.% D, as the required pK_s data available from Harned and Fallon's work (10) are restricted to these compositions only where the compositions of ion-association are likely to be absent.

Experimental

The quality and the method of purification of the solvents DME and THF have been described (1). Dioxane (Merck, G.R.) was purified by refluxing over pieces of Na for about 24 h and then distilling twice. The physical properties, viz. bp, density, and refractive index, compared fairly well with those given in the literature (6, 11, 12). The solvents so purified were stored in a desiccator not more than 10 days and redistilled every time before use after refluxing with Na for some time. Water used was, as before (1), triple distilled. KI (Merck, G.R.) was used after drying at about 150°C and then over a vacuum desiccator for about 12 h. The purity of the sample was checked by gravimetric estimation of I^-. Ag–AgI electrodes were of the thermal type and prepared by the method described by Ives and Janz (13). Other experimental details including the preparation of solvents, solutions, and the platinized electrodes and also the methods of measurements were exactly as described in the preceding paper (1). The behaviour of the electrodes, the time for attainment of the equilibrium, and criteria of equilibrium of the cells were also essentially similar to that described in the said paper.

Results

The emf (E) of the cell [A] at any solvent mixture is given by

$$[1] \quad E = E^0 - 2.303\frac{RT}{F}\log(a_{H^+}a_{I^-})$$

where the terms have the usual significance. Replacing a_{H^+} in terms of K_s by $K_s\, a_{H_2O}/a_{OH^-}$ (1, 10), a_i of the ionic species by the product of molality (m_i) and the molal activity coefficient (γ_i), and $2.303RT/F$ by k, we have an extrapolation function, $E^{0\prime}$ defined by [2]

$$[2] \quad E^{0\prime} \equiv E + k\log m_{I^-}/m_{OH^-} + k\log K_s = E^0 - k\log a_{H_2O}\gamma_{I^-}/\gamma_{OH^-} = E^0 + f(\mu)$$

As in the previous cases (1, 10, 11*b*), the standard states are so chosen that at infinite dilution in each solvent mixture the activity coefficients of the ions concerned as well as the activity of water (a_{H_2O}) are unity. Also, as the term $\log a_{H_2O}\gamma_{I^-}/\gamma_{OH^-}$ in dilute solution in each solvent mixture is, as before (1, 10, 11), likely to be proportional to the ionic strength, μ, extrapolation of the function $E^{0\prime}$ to $\mu = 0$ would yield the E^0 values on the molal scale, henceforth denoted as E_m^0. It may be noted that since the effect of the a_{H_2O} term in eq. [2] gets cancelled by that contained in the K_s term, the E^0 value is effectively free from the involved assumption that $a_{H_2O} = 1$.

The E values of cell [A] at different temperatures and the corresponding molalities of KOH and KI for each of the solvent mixtures are given else-

TABLE 1. The values of E_m^0 of the Ag–AgI electrode at different temperatures for aqueous mixtures of THF, DME, and D

Wt.% cosolvent	5°C	10°C	15°C	20°C	25°C	30°C	35°C
			THF–water mixtures				
10	−0.1416	−0.1424	−0.1436	−0.1451	−0.1460	−0.1472	−0.1489
20	−0.1302	−0.1315	−0.1323	−0.1337	−0.1359	−0.1386	−0.1408
30	−0.1142	−0.1174	−0.1206	−0.1234	−0.1266	−0.1296	−0.1328
			DME–water mixtures				
10	−0.1375	−0.1390	−0.1393	−0.1407	−0.1432	−0.1443	−0.1458
30	−0.1252	−0.1261	−0.1278	−0.1298	−0.1327	−0.1358	−0.1395
50	−0.1066	−0.1121	−0.1186	−0.1238	−0.1297	−0.1353	−0.1403
			D–water mixtures				
20	−0.1423	−0.1433	−0.1449	−0.1476	−0.1500 (−0.1513)[a]	−0.1568	−0.1556
45	−0.1421	−0.1455	−0.1504	−0.1540	−0.1594 (−0.1603)[a]	−0.1638	−0.1696

[a]Reference 15*a*.

TABLE 2. The values of constants a (in V), b (in V(°C)$^{-1}$), and c (in V(°C)$^{-2}$) of eq. [3] for Ag–AgI electrodes in THF + water, DME + water, and D + water mixtures

Wt.% cosolvent	a	$-b \times 10^4$	$-c \times 10^6$
	THF + water mixtures		
0[a]	−0.1508	2.94	3.29
10	−0.1448	2.42	1.57
20	−0.1340	3.54	7.43
30	−0.1235	6.16	0.10
	DME + water mixtures		
10	−0.1411	2.81	2.95
30	−0.1299	4.80	10.86
50	−0.1240	11.33	−2.67
	D + water mixtures		
20	−0.1479	5.14	6.86
45	−0.1543	9.15	6.24

[a]Computed from the data reported in ref. 27.

where.[4] The required partial pressures of the mixed solvents for correcting P_{H_2} = 1 atm were taken from data of Roy *et al.* for THF–water (5*b*) and DME–water (6*c*) mixtures and from Akerlof's paper (14) for D–water mixtures. The required values of pK_s for computing $E^{0\prime}$ values were obtained from the previous paper for most of the compositions of DME and THF and by interpolating the appropriate data at 20 wt.% THF, and those for D–water mixtures were taken from Harned and Fallon's data (10).

Assuming as before (1, 10, 11) that KOH and KI are completely dissociated in all these mixed solvents, m_{OH^-} and m_{I^-} were taken as equal to m_1 and m_2 respectively, and $\mu = (m_1 + m_2)d_s$, where d_s is the density of the mixed solvent. The values of d_s were obtained from the literature (5*b*, 6*c*, 10). The values of $E^{0\prime}$ computed by use of eq. [2] at any temperature for any composition were then fitted to linear plots by the method of least squares and the values of E_m^0 so obtained are given in Table 1. The uncertainties in the values of E_m^0 as obtained from the standard deviations lie within ±0.3 mV. The E_m^0 values of D–water mixtures at 25°C compare fairly well with the data of Feakins *et al.* (15*a*), as shown in parentheses beside the respective data in the table.

The E_m^0 values at different temperatures for each solvent mixture were then fitted into the E_m^0–temperature quadratic equation

$$[3] \quad E_m^0 = a + b(t - 20) + c(t - 20)^2$$

by the method of least squares where t is the temperature in degree Celsius. The coefficients a, b, and c for each of the solvent mixtures are listed in Table 2. The coefficients of eq. [3] for water were also obtained by use of data of Bates and coworkers (27) and are included in Table 2.

The free energy change ΔG_t^0 accompanying the transfer of 1 mole of HI from the standard state in water (w) to that in each of the mixed solvents (s), i.e. of the process HI (w) → HI (s), were computed on the mole fraction scale at t = 25°C, using the relation

$$[4] \quad \Delta G_t^0(\mathrm{HI}) = -F[(E_m^0)_s^{25°} - (E_m^0)_w^{25°}] - 2RT \log M_s/M_w$$

where T = 298.15, and M_s and M_w are the average and pure molar mass of the mixed solvent and

[4]A complete set of the data referred to above is available at a nominal charge from the Depository of Unpublished Data, CISTI, National Research Council of Canada, Ottawa, Ont., Canada K1A 0S2.

Can. J. Chem. Downloaded from www.nrcresearchpress.com by 210.87.254.40 on 09/06/12
For personal use only.

Can. J. Chem. Downloaded from www.nrcresearchpress.com by 210.87.254.40 on 09/06/12
For personal use only.

TABLE 3. Standard free energies (ΔG_t^0), entropies (ΔS_t^0), and the related quantities of transfer $\Delta Y = T\Delta S_t^0(H^+) + T\Delta S_{t,ch}^0(X^-)$ of HX (X = Cl, Br, I) from water to THF + water, DME + water, and D + water mixtures at 25°C (mol fraction scale)

Wt.% cosolvent	Mol.% cosolvent	ΔG_t^0 (kJ mol^{-1})							ΔS_t^0 (J K^{-1} mol^{-1})			ΔY ($\equiv T\Delta S_t^0(H^+) + T\Delta S_{t,ch}^0(X^-)$) (kJ mol^{-1})		
		H^+	HCl	Cl^-	HBr	Br^-	HI	I^-	HCl	HBr	HI	HCl	HBr	HI
							THF + water mixtures							
10	2.70	−3.6[a]	(0.7)[c]	4.3	−0.11	3.5	−1.00	2.6	(2.3)	3.1	7.8	1.79	1.94	3.22
20	5.88	—	—	—	—	—	−2.40	—	—	—	−7.3	—	—	−0.17
30	9.68	−7.3[a]	(1.8)	9.1	−0.33	6.9	−3.78	3.5	(−11.7)	−20.3	−23.9	0.71	−2.14	−3.62
50	20.00	−9.1[a]	(3.2)	12.3	0.62	9.7	(−6.4)	2.7	(−38.6)	−53.1	(−67.8)	1.0	−4.35	—
							DME + water mixtures							
10	2.17	−2.0[b]	(0.30)	2.3	−0.40	1.6	−1.30	0.71	(7.4)	5.9	2.7	−8.15	−7.81	−7.90
30	7.89	−5.9[b]	(1.0)	6.9	−0.92	5.0	−3.26	2.6	(−9.1)	−13.4	−20.9	−13.22	−13.73	−14.99
50	16.66	−10.5[b]	(2.2)	12.7	−0.48	10.1	−4.72	5.8	(−45.3)	−51.5	−66.9	−14.04	−15.81	−20.39
							D + water mixtures							
10	2.22	−1.6[a]	(0.4)	2.0	0.13	1.7	(0.5)	1.1	—	—	—	—	—	—
20	4.87	—	1.01	—	0.19	—	−1.09	—	−8.4	−14.8	−21.9	0.54	−1.58	−4.19
30	8.06	−5.7[a]	(1.6)	7.3	(0.40)	6.1	(−1.4)	4.2	—	—	—	—	—	—
45	14.33	—	3.48	—	1.34	—	−1.52	—	−39.9	−46.2	−55.6	−1.85	−4.47	−8.37
50	16.98	−4.3[a]	(4.4)	8.7	(1.8)	6.2	(−1.2)	3.1	—	—	—	—	—	—

[a] Reference 18.
[b] Reference 11.
[c] Values in parentheses are interpolated values.

Can. J. Chem. Downloaded from www.nrcresearchpress.com by 210.87.254.40 on 09/06/12
For personal use only.

water respectively. The corresponding entropy changes ΔS_t^0(HI) at 25°C were obtained by use of eq. [5]

$$[5]\quad \Delta S_t^0(\mathrm{HI}) = F(b_s - b_w) + 2F(t - 20)(c_s - c_w) + 2R \ln M_s/M_w$$

The values of ΔG_t^0 and ΔS_t^0 so obtained for HI for all these solvents are presented in Table 3. The average estimated uncertainties in ΔG_t^0 and ΔS_t^0 at 25°C for these mixed solvents are respectively $\pm$ 0.03 kJ mol^{-1} and $\pm$ 3 J K mol^{-1}.

For the sake of comparison, the corresponding values for HBr were also computed in a similar manner. As E_m^0 values of the Ag–AgBr electrodes in THF–water (5*b*) and DME–water (6*c*) mixtures reported by Roy *et al.* are based on a polynomial curve-fitting technique, these might differ from those based on an extrapolation procedure. We have therefore first reevaluated E^0 values from the primary emf data of Roy *et al.* by the usual extrapolation procedure. The observed E_m^0 values at seven equidistant temperatures in the range 5–35°C were then fitted into eq. [3], the coefficients of which were used to calculate ΔG_t^0 and ΔS_t^0 values for HBr. In the case of D–water mixtures, as values of Mussini *et al.* (9) are already based on an extrapolation procedure, these values were fitted into eq. [3] and the coefficients so obtained yielded the ΔG_t^0 and ΔS_t^0 values. All these values are given in Table 3. Notably, these values agree with Roy's data (Table 3) within the limits of experimental error, namely $\pm$3 J K^{-1}. But the E^0 values of the Ag–AgCl electrode in THF–water (5*a*) and DME–water (6*a*, *b*) systems are, however, given at equidistant temperatures from 15 to 35°C and at 10° intervals, and also at other compositions. So, similar treatment of the data would involve interpolations and hence is likely to incur extra uncertainties. In view of these intrinsic limitations, data of Johnson and Sen (6*a*), though based on a polynomial curve-fitting technique, were not reevaluated by extrapolation procedure. Instead, E_m^0 values at intermediate temperatures at 20° and 30°C were first obtained by careful interpolation of the large scale plots of E_m^0 between 15° and 35°C. E_m^0 values at these 5 temperatures were then fitted into eq. [3] for the reported compositions and also for water. The coefficients so obtained were used for computing ΔG_t^0 and ΔS_t^0 values for HCl. And the values at desired compositions were then collected by interpolation and are given in Table 3. In the case of D–water mixtures, however, corresponding values were obtained by treating Harned *et al.*'s extrapolation data (7) at seven equidistant temperatures in the range 5–35°C.

In Fig. 1 $T\Delta S_t^0$(HX)–composition profiles for HCl, HBr, and HI in D–water mixtures as obtained from the data of Harned *et al.* (7), Mussini *et al.* (9), and the present study respectively have been compared with the corresponding profiles obtained from data of Das and co-workers (8). Notably, the former set of profiles are increasingly negative and their order HCl > HBr > HI conforms to what is expected from Kundu and co-workers' theory (2) if D has the structure-breaking propensity implied by various other studies referred to in the preceding paper (1). But curiously enough, the latter set of profiles are not only widely divergent from the respective profiles of the former set but their order: HI > HBr > HCl at any composition is also not akin to their behaviour in the cosolvents studied so far. This questions the reliability of the entropy data of Das and co-workers.

Discussion

Free Energies of Transfer

A perusal of ΔG_t^0(HX) values in Table 3 reveals that the variation of ΔG_t^0(HX) with cosolvent composition of the three aquo-ether systems is essentially similar to that of aqueous alcohols (2), glycol (2), glycerol (4), etc., and at any composition $\Delta G_t^0(\mathrm{HCl}) > \Delta G_t^0(\mathrm{HBr}) > \Delta G_t^0(\mathrm{HI})$. This is expected if the halide ions become destabilized on passing from water to any of these mixed solvents, being influenced by decreased dielectric constant and the decreased acidity (15*b*, 16) of the solvents. For better understanding of the involved ion–sol-

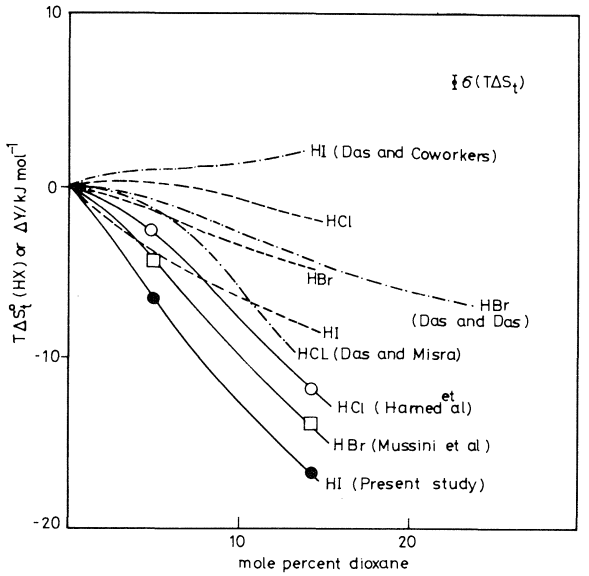

FIG. 1. Variation of ΔS_t^0 (HX) (solid lines) and ΔY ($\equiv T\Delta S_t^0$ (H^+) + $T\Delta S_{t,ch}^0$ (X^-)) (dotted lines) of hydrogen halides in dioxane + water mixtures at 25°C (Das *et al.*'s data refer to ΔS_t^0 (HX)).

Can. J. Chem. Downloaded from www.nrcresearchpress.com by 210.87.254.40 on 09/06/12
For personal use only.

vent interactions, $\Delta G_t^0(HX)$ values were broken down into individual ion contributions by the use of the tetraphenyl arsonium tetraphenyl boride reference electrolyte data for these solvent systems reported earlier (11, 16) and are given in Table 3. In all these cosolvent systems, while $\Delta G_t^0(H^+)$ values are more or less increasingly negative, indicating increased "basicity" or "cation – O-centre" type interactions with the possible H-bonded aquo-ether complexes (15, 16) in the mixed solvents, $\Delta G_t^0(X^-)$ values are increasingly positive, reflecting the decreased "acidity" or "anion–H-centre" type interactions with the aquo-ether complexes (15, 16) in the mixed solvents. These increased "basicity" and decreased "acidity" values of the mixed solvents compared to that of water, and their relative orders: D < THF < DME, are in conformity with what is expected from structural and electronic consideration of these aprotic ethereal cosolvents, as discussed in the preceding paper (1). And the relative order of destabilization of the halide ions in each of the cosolvent systems is the combined result (16–18) of the decreasing strength of anion – H-centre type interactions and the possible increasing strength of soft–soft interactions (17–19) between the increasingly polarizable anions and the softer cosolvent or their aquo-complex bases than water. The observed trend of less destabilization of I^- compared to Br^- and Cl^- at higher compositions of THF (Table 3) is possibly indicative of the superimposed effect of charge transfer to solvent (CTTS) (20) complexation of I^- with THF molecules or their aquo-complexes. On the other hand, the observed downward trend of $\Delta G_t^0(X^-)$ for all the halide ions in D–water mixtures (Table 3) is possibly the result of the effect of enhanced quadrupolar interactions arising from the high quadrupole moment of D (21).

Entropies of Transfer

Since $T\Delta S_t^0(HX)$ rather than $\Delta H_t^0(HX)$ should be more informative regarding the structuredness of the solvents (22), we have illustrated the variation of $T\Delta S_t^0(HX)$ values at 25°C with cosolvent composition for all three solvent systems in Figs. 1–3. In the case of THF–water mixtures the observed $T\Delta S_t^0(X)$–composition profiles (Fig. 2) exhibit the characteristic maxima at initial compositions and their downward trends at higher cosolvent compositions. Also, while the relative order of the maxima is the regular one: HI > HBr > HCl, that at the higher compositions is, as usual, the reverse one. In DME–water mixtures, however, $T\Delta S_t^0(HX) - T\Delta S_{t,el}^0(X^-)$ (2) for this system, as well as ing small maxima at the initial composition, take

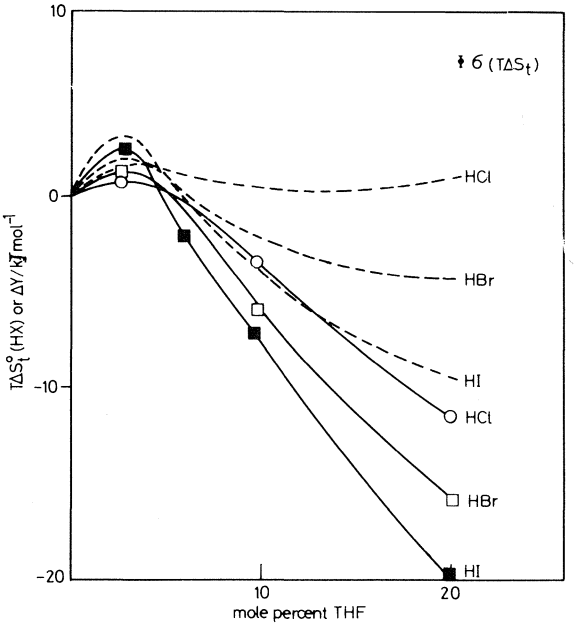

FIG. 2. Variation of $T\Delta S_t^0$ (HX) (solid lines) and ΔY ($\equiv T\Delta S_t^0(H^+) + T\Delta S_{t,ch}^0(X^-)$) (dotted lines) of hydrogen halides in THF + water mixtures at 25°C.

sharply downward trends at higher compositions. But their relative order being HCl > HBr > HI throughout the whole composition, the observed small maxima are possibly due to the effect of increased dielectric constant of the mixtures at that region, compared to water (6*c*). That this is particularly true becomes all the more evident when we consider the partly rationalized quantities ΔY ($\equiv T\Delta S_t^0(H^+) + T\Delta S_{t,ch}^0(X^-)$) presented in Table 3 and depicted in Fig. 3. These values of ΔY ($\equiv T\Delta S_t^0(HX) - T\Delta S_{t,el}^0(X^-)$) (2) for this system, as well as those for other cosolvent systems, were obtained by subtracting the Born-type electrostatic contributions of the halide ions, $\Delta S_{t,el}^0(X^-)$, which were tentatively computed in a manner described earlier (23). The required values of $\theta^{-1} = -d \ln \varepsilon/dT$ for water and the mixed solvents were obtained from data of Roy *et al.* on DME–water (6*c*) and THF–water (5*b*) mixtures and from Akerlof's paper (14) on D–water mixtures. Figures 1 and 2 illustrate the variation of ΔY–composition profiles for the other two solvent systems.

Notably, while ΔY–composition profiles for both THF–water and D–water mixtures are simply raised without undergoing an essential change in their nature, those for DME–water mixtures move sharply downward in the scale and undergo a significant change by being concave upward in place of the convex-downward nature of the $T\Delta S_t^0(HX)$–composition profiles. Evidently θ^{-1} values

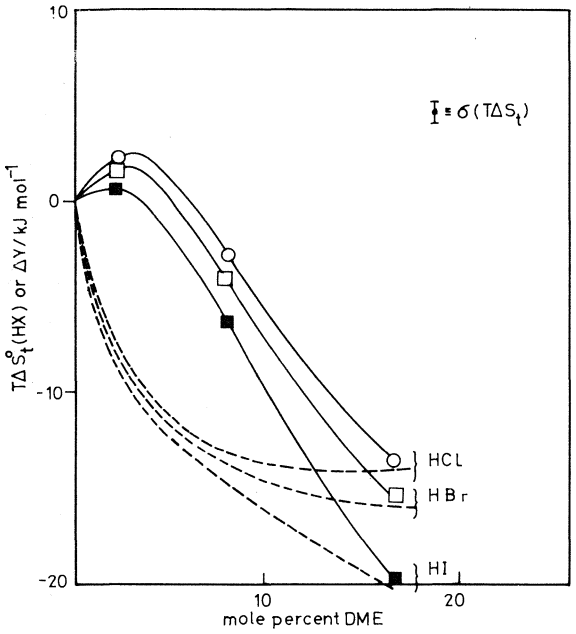

FIG. 3. Variation of $T\Delta S_t^0$ (HX) (solid lines) and ΔY ($\equiv T\Delta S_t^0$ (H^+) + $T\Delta S_{t,ch}^0$ (X^-)) (dotted lines) of hydrogen halides in DME + water mixtures at 25°C.

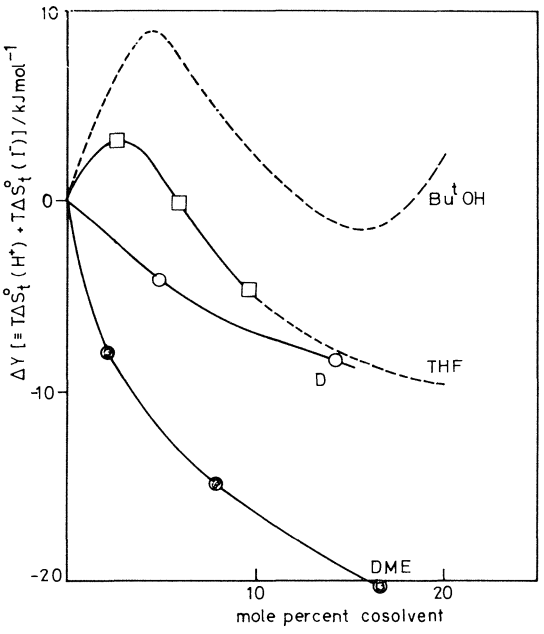

FIG. 4. Variation of ΔY ($\equiv T\Delta S_t^0$ (H^+) + $T\Delta S_{t,ch}^0$ (X^-)) of HI in aqueous ethers (□, THF; ●, DME; ○, dioxane) (solid lines) and *t*-BuOH + water mixtures (dotted line).

in the latter case, which are in reverse order to those for other cosolvent systems, are responsible for this.

Referring to Fig. 4, where we have illustrated ΔY–composition profiles for HI for all these cosolvent systems as well as for *t*-BuOH–water mixtures (24) for drawing meaningful implications of the results, we find that as in *t*-BuOH–water mixtures, the profile for THF–water mixtures exhibits a maximum around 2–4 mol% of THF and then a sharply downward trend at higher compositions. But the profiles for both D–water and DME–water systems move downward right from the beginning, with the relative position for the former system being above that for the latter.

Following the dictates of the semi-quantitative theory proposed by Kundu and co-workers (2) referred to earlier, it may be concluded that like *t*-BuOH and also other mono-ols, the well known promoters of the 3D-structure of water (3), the THF molecule promotes the same at initial compositions but beyond 3–4 mol% it starts breaking down the same due to onset of packing imbalance, as is usual in the cases of other nonelectrolytes (3). Moreover, the relative order of ΔY viz. HI > HBr > HCl (Fig. 2) in the region of the maximum and the reverse order at the structure-breaking region also substantiate the above contention. Evidently, like *t*-BuOH and other mono-ols, the structure-inducing hydrophobicity of four (—CH_2—) groups of the THF molecule overcomes the structure-breaking hydrophilicity of the ethereal O-atom. Similarly, the observed downward trends of ΔY values for HX and their relative order: HCl > HBr > HI right from zero cosolvent composition in both D + water and DME + water solvent systems (Figs. 1, 2) imply that the addition of D or DME induces the breakdown of the 3D structure of water right from their initial compositions. Evidently, in D–water mixtures the hydrophilic effect of two symmetrically placed ethereal O-centres with a pair of free orbitals on each D molecule overcomes the structure-making propensity of the two hydrophobic (—CH_2—CH_2—) groups in between. But in DME–water mixtures the observed relatively sharp downward trends of ΔY compared to that of D–water mixtures reflect the stronger structure-breaking effect of DME compared to that of D. Seemingly, the inductive effect of two (—CH_3) groups attached to the two flexible ethereal O-atoms of the DME molecule makes it more hydrophilic than the D molecule. Moreover, as in THF or other cosolvent systems, the downward trends of ΔY values and their relative order: HCl > HBr > HI at higher compositions also reflect the structure-breaking effect of these cosolvents due to packing imbalance.

Thus, the contentions of the present study are in

Can. J. Chem. Downloaded from www.nrcresearchpress.com by 210.87.254.40 on 09/06/12
For personal use only.

fair agreement with those drawn from our earlier studies (1) on the behaviour of $T\delta(\Delta S_N^0)$ or ($\equiv T({}_s\Delta S^0 - {}_w\Delta S^0)$), i.e. T times the relative entropy of autoionization of water, as well as of $\Delta S_t^0(H_2O)$ derived therefrom, and also that from various other studies referred to therein for all these cosolvent systems. Notably, however, the structural changes reflected from the observed downward trends of $\Delta S_t^0(H_2O)$ around 4–14 mol% of DME referred to in the previous paper are not reflected in the behaviour of ΔY(HX) values. Seemingly, the behaviour of $\Delta S_t^0(H_2O)$ values, if free from uncertainties, is more informative than that of $T\Delta S_t^0$(HX) or ΔY values which, after all, contain the Born-type electrostatic contributions (25). Nevertheless, the present results are indicative of the fact that, at initial compositions, the THF molecule because of the larger hydrophobicity of its 4 (—CH_2—) groups, compared to the hydrophilicity of its one ethereal O-group, shifts the $(water)_{bulk} \leftrightarrow (water)_{dense}$ equilibrium towards the left. But the D molecule, because of its larger hydrophilicity of two ethereal O-centres over the two structure-promoting hydrophobic (—CH_2—CH_2—) groups, and the DME molecule, with its two CH_3-induced strongly negative and flexible O-centres, being more hydrophilic, shift the said equilibrium towards the right. Thus, the present results substantiate the observation of Ahluwalia and co-workers (26) that the initial structuring or destructuring ability of a cosolvent depends upon the ratio of hydrophobic to hydrophilic effects of the cosolvents. Increase in hydrophobic groups in the cosolvent increases the stabilization while increase in the hydrophilicity of H-bonding sites decreases the stabilization of the 3D structure of water.

Acknowledgement

Thanks are due to the University Grants Commission, Government of India, for awarding a research fellowship to J. Datta.

1. J. Datta and K. K. Kundu. Can. J. Chem. **59**, 3141 (1981).
2. K. Bose, K. Das, A. K. Das, and K. K. Kundu. J. Chem. Soc. Faraday Trans. I, **74**, 1051 (1978), and references therein.
3. F. Franks and D. J. G. Ives. Q. Rev. **20**, 1 (1966).
4. I. N. Basu Mullick and K. K. Kundu. Can. J. Chem. **57**, 961 (1979).
5. (*a*) R. N. Roy and B. Sen. J. Chem. Eng. Data, **12**, 584 (1967); (*b*) R. N. Roy, E. E. Swensson, and G. LaCross, Jr. J. Chem. Thermodyn. **7**, 4566 (1975).
6. (*a*) D. A. Johnson and B. Sen. J. Chem. Eng. Data, **13**, 376 (1969); (*b*) R. N. Roy and A. L. M. Bothwell. J. Chem. Eng. Data, **16**, 347 (1971); (*c*) R. N. Roy, E. E. Swensson, G. LaCross, Jr., and C. W. Krueger. *In* Adv. Chem. Ser. 155. *Edited by* W. F. Furter. 1976.
7. (*a*) H. S. Harned and J. O. Morrison. J. Am. Chem. Soc. **59**, 1908 (1936); Am. J. Sci. **33**, 161 (1937); (*b*) H. S. Harned. J. Am. Chem. Soc. **60**, 336 (1938); (*c*) H. S. Harned and C. Caimon. J. Am. Chem. Soc. **60**, 2130 (1936); (*d*) H. S. Harned, F. Walker, and C. Caimon. J. Am. Chem. Soc. **61**, 44 (1939).
8. (*a*) P. K. Das and U. C. Misra. Electrochim. Acta, **22**, 59 (1977); (*b*) B. K. Das and P. K. Das. J. Chem. Soc. Faraday Trans. I, **74**, 22 (1978); (*c*) U. C. Misra, B. K. Das, and P. K. Das. Thermochim. Acta, **28**, 217 (1979).
9. T. Mussini, C. M. Formaro, and P. Andrigo. J. Electroanal. Chem. **33**, 171 (1971).
10. H. S. Harned and L. D. Fallon. J. Am. Chem. Soc. **61**, 2374 (1939).
11. A. Bhattacharya, A. K. Das, and K. K. Kundu. Can. J. Chem. **59**, 1153 (1981).
12. A. K. Covington and T. Dickinson (*Editors*). Physical chemistry of organic solvents. Plenum Press, New York. 1973.
13. D. J. G. Ives and G. J. Janz. Reference electrodes – theory and practice. Academic Press, New York. 1969. p. 208.
14. G. Akerlof. J. Am. Chem. Soc. **54**, 4125 (1932).
15. (*a*) D. Feakins and O. J. Turner. J. Chem. Soc. 4906 (1965); (*b*) D. Feakins. *In* Hydrogen-bonded solvent system. *Edited by* A. K. Covington and P. Jones. Taylor and Francis, London. 1968.
16. A. Bhattacharya, J. Datta, K. Das, and K. K. Kundu. Ind. J. Chem. In press.
17. D. Feakins and P. J. Voice. J. Chem. Soc. Faraday Trans. I, **68**, 1340 (1972).
18. A. K. Das and K. K. Kundu. J. Solution Chem. **5**, 431 (1976).
19. R. G. Pearson. J. Am. Chem. Soc. **85**, 3533 (1963).
20. M. C. R. Symons and M. J. Blandamer. *In* Hydrogen-bonded solvent systems. *Edited by* A. K. Covington and P. Jones. Taylor and Francis, London. 1968.
21. O. Kiyohara, G. Perron, and J. E. Desnoyers. Can. J. Chem. **53**, 2591 (1975).
22. E. M. Arnett, W. G. Bentrude, J. J. Burke, and P. MacDuggleby. J. Am. Chem. Soc. **87**, 1541 (1965).
23. U. Sen, K. K. Kundu, and M. N. Das. J. Phys. Chem. **71**, 3665 (1967).
24. K. Bose, A. K. Das, and K. K. Kundu. J. Chem. Soc. Faraday Trans. I, **71**, 1835 (1975).
25. R. G. Bates. *In* Hydrogen-bonded solvent systems. *Edited by* A. K. Covington and P. Jones. Taylor and Francis, London. 1968.
26. R. K. Mohanty, T. S. Sarma, S. Subramanian, and J. C. Ahluwalia. Trans. Faraday Soc. **67**, 305 (1971).
27. H. B. Hetzer, R. A. Robinson, and R. G. Bates. J. Phys. Chem. **68**, 1929 (1964).

Can. J. Chem. Downloaded from www.nrcresearchpress.com by 210.87.254.40 on 09/06/12
For personal use only.

The reaction of tetrasulphur tetranitride with bis(fluorosulphuryl) peroxide: the electronic structure of the tetrathiazyl dication

RAJENDRA D. SHARMA, FRIEDHELM AUBKE, AND NORMAN L. PADDOCK

Department of Chemistry, University of British Columbia, 2036 Main Mall, Vancouver, B.C., Canada V6T 1Y6

Received May 1, 1981

RAJENDRA D. SHARMA, FRIEDHELM AUBKE, and NORMAN L. PADDOCK. Can. J. Chem. **59**, 3157 (1981).

Tetrasulphur tetranitride is oxidized quantitatively at room temperature to tetrathiazyl di(fluorosulphate) $S_4N_4(SO_4F)_2$. Conductance measurements in HSO_3F show this compound to dissociate into ions. The vibrational spectra of the cation are uniquely consistent with a flexible planar structure of D_{4h} symmetry, and the anion bands are characteristic of ionic SO_3F^-. CNDO and EHMO calculations indicate that the planar form of the cation is stable but easily deformable.

RAJENDRA D. SHARMA, FRIEDHELM AUBKE et NORMAN L. PADDOCK. Can. J. Chem. **59**, 3157 (1981).

On a oxydé quantitativement le tétranitrure de tétrasulfure à la température ambiante en di(fluorosulphate) de tétrathiazyle $S_4N_4(SO_4F)_2$. Les mesures de conductivité dans le HSO_3F montrent que ce composé se dissocie en deux ions. Les spectres de vibration du cation sont en accord avec une structure plane flexible de symétrie D_{4h} et les bandes de l'anion sont caractéristiques de l'espèce ionique SO_3F^-. Les calculs CNDO et EHMO indiquent que la forme plane du cation est stable mais se déforme facilement.

[Traduit par le journal]

Can. J. Chem. Downloaded from www.nrcresearchpress.com by 210.87.254.6 on 09/06/12
For personal use only.

Introduction

Tetrasulphur tetranitride S_4N_4 occupies a central position in sulphur–nitrogen chemistry; very many derivatives can be made from it by reaction at sulphur or nitrogen. The length of the bonds between opposing sulphur atoms (2.60 Å) (1) (Fig. 1) is significantly greater than the length of the bonds in S_8 (2.06 Å) (2), and at least one of these bonds is usually broken on reaction. If the cross bonds are appreciably weaker than single bonds, as the structural evidence suggests, homolytic bond cleavage and reaction with radicals can be expected to take place easily. Some reactions of this type have been reported. S_4N_4 reacts with an excess of the radical $(CF_3)_2NO$ to give $N_4S_4[ON(CF_3)_2]_4$ (3), the $(CF_3)_2NO$ group being linked through oxygen to sulphur (4). The reaction of S_4N_4 with molecular chlorine, under carefully controlled conditions, gives first $N_4S_4Cl_2$ (5), and may be of the same type, but the dissociation energy of Cl_2 is high (239 kJ/mol), and it is possible that the first step in the reaction is the electrophilic attack of the chlorine molecule on sulphur. Bis(fluorosulphuryl) peroxide is a more likely source of radicals, since it is extensively dissociated at 100°C; even at −25°C, it abstracts hydrogen from dichloromethane, a reaction typical of free radicals (6). Its dissociation energy (91.3–97.6 kJ/mol) (7) is much less than that of chlorine, so that the mechanistic ambiguity, though still present, is less significant. In the experiments described here, $S_2O_6F_2$ was found to react smoothly and completely with S_4N_4 at room temperature to give $S_4N_4(SO_3F)_2$ (**1**). Since the electron affinity of the fluorosulphate radical is high (it has been estimated as 1060 kJ/mol (8) and 1110 kJ/mol (9)), the product is ionic, $S_4N_4^{2+}(SO_3F^-)_2$. The overall reaction is an an oxidation, the cation being the same as that produced in the oxidation of S_4N_4 by SbF_5 or $SbCl_5$ (10).

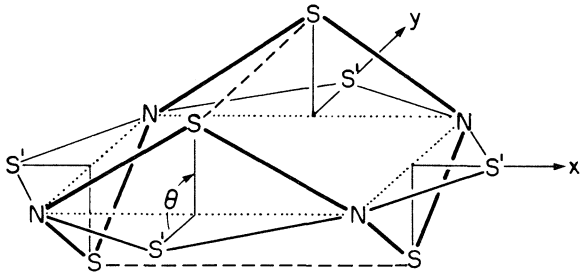

FIG. 1. Relation of normal conformation of S_4N_4 (D_{2d}, heavy lines) to planar $S_4'N_4^{2+}$ (D_{4h}). The cross bonds in S_4N_4 are shown by dashed lines. The rings are interconverted by local rotations ± θ about successive NN vectors.

Experimental

Tetrasulphur tetranitride was prepared by the ammonolysis of sulphur dichloride (11) and sublimed twice *in vacuo*. Bis(fluorosulphuryl) peroxide, prepared by the fluorination of SO_3 with AgF_2 as a catalyst (12), was stirred over a large quantity of anhydrous KF for 48 h and distilled *in vacuo*. Fluorosulphuric acid (Allied Chemicals) was doubly distilled (13). All manipulation was carried out in a dry atmosphere; the reaction vessels were fitted with greaseless Kontes Teflon stem valves. Infrared spectra were recorded from thin films on AgCl, AgBr, or KRS-5 windows on a Perkin–Elmer 457 grating spectrophotometer, and Raman spectra on a Spex Ramalog 5 spectrometer equipped with an argon ion laser (514.5 nm). The esr spectra were recorded on a Varian Associates E-3 spectrometer, electronic spectra on a Cary 17 spectrophotometer, and ^{19}F nmr spectra on an EM360 instrument. Electrical conductance measurements were carried out with a Wayne–Kerr Universal Bridge, Type B221. The measuring temperature of 25.00 ± 0.01°C was maintained in an oil bath equipped with a Sargent Thermonitor

0008-4042/81/223157-05$01.00/0

©1981 National Research Council of Canada/Conseil national de recherches du Canada

Can. J. Chem. Downloaded from www.nrcresearchpress.com by 210.87.254.6 on 09/06/12
For personal use only.

Model ST temperature control unit. The conductivity cell, similar to that described by Barr *et al.* (13), was scaled down to allow measurements on small volumes (~ 50 mL).

Tetrathiazyl Di(fluorosulphate)

A large excess (~12 g) of $S_2O_6F_2$ was distilled on to S_4N_4 (0.020 g, 5 mmol) at −196°C. The reactor was warmed first to −78°C, and then very slowly to room temperature, when the orange colour of S_4N_4 changed to black (radical, 5 line esr spectrum) in about ten minutes, then to brown and finally to bright yellow in approximately 48 h. The excess of $S_2O_6F_2$ was distilled off *in vacuo*, leaving **1** as a very hygroscopic pale yellow powder (1.914 g, 100%); dec. 110°C. *Anal.* calcd. for $F_2N_4O_6S_6$: F 10.1, N 14.7, S 50.0; found: F 9.9, N 14.3, S 50.3. A solution of **1** in fluorosulphuric acid (from which the solute can be recovered) showed a single ^{19}F nmr signal characteristic of solvent in equilibrium with the fluorosulphate anion. A plot (Fig. 2) of the electrical conductance of **1** in HSO_3F as a function of concentration is slightly steeper than that for $Ba(SO_3F)_2$ (13), indicating higher conductance at the same concentration. Ionic association is presumably reduced by the larger size of the $S_4N_4^{2+}$ ion. The vibrational spectra of **1** are summarized in Tables 1 and 2. The electronic spectrum of the cation is shown in Fig. 3.

Results and Discussion

The synthesis of **1** described above is straightforward and quantitative. The oxidative addition reaction

[1] $S_4N_4 + S_2O_6F_2 \rightarrow S_4N_4(SO_3F)_2$

when performed with the peroxide in excess, requires no solvent, and the easy isolation of very pure **1** is ensured by the high volatility of $S_2O_6F_2$

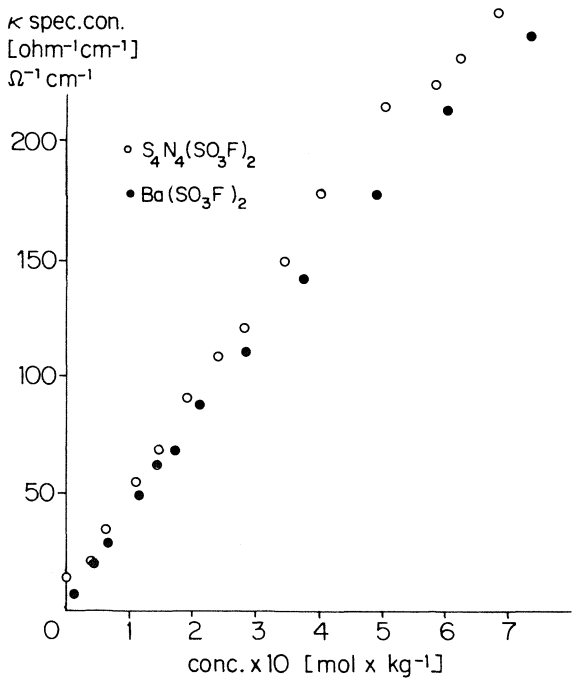

FIG. 2. The electric conductance of **1** and $Ba(SO_3F)_2$ in HSO_3F at 25°C.

TABLE 1. Vibrational frequencies of SO_3F^- (cm^{-1})[a]

$S_4N_4(SO_3F)_2$ (s)		$NOSO_3F$ (s)	
Raman	Infrared	Raman	Assignment
1292 mw 1265 m	1285 vs, b 1260 vs, b	1278 mw 1265 m	ν_4, E, ν_{as} (SO_3)
1072 s	1065 s	1075 s	ν_1, A_1, ν_{sym} (SO_3)
710 vw	715 s, b	745 s	ν_2, A_1, ν (SF)
585 w 570 w, sh	580 s, sh 575 s	600 ms 588 ms	ν_5, E, δ_{as} (SO_3)
561 m	550 s	570 m	ν_3, A_1, δ_{sym} (SO_3)
406 ms 400 m, sh	402 mw	416 m 403 m	ν_6, E, ρ (SO_3F)

[a] Abbreviations: s = strong, m = medium, w = weak, v = very, b = broad, sh = shoulder.

TABLE 2. Vibrational frequencies of $S_4N_4^{2+}$ (cm^{-1})

Raman, **1**, solid	Raman, **1**, solution	Infrared, **1**, solid
1205 vs	1206 s, pol. (0.63)[a]	
		1035 s, sh 1015 ms
808 vw (768 vw, 744 vw)[b]	808 mw	
689 m	682 w	
664 mw	—	
623 ms	624 m	
510 vw, sh 502 vw	500 vs, pol. (0.08)	
		440 s, sh 434 s 378 s
225 vs 207 vw, sh	229 vs dp (0.74)	
167 m	155 w, b	

[a] Depolarization measurements on this band are affected by solvent bands at 1220 and 1180 cm^{-1}.
[b] Impurity bands.

and the absence of by-products. In addition, solutions of **1** in HSO_3F are stable, and the solute may be recovered quantitatively by removing the solvent *in vacuo*.

The vibrational frequencies of the anion are all comparable to those in the ionic $NOSO_3F$ (14), and the weakness of ionic polarization in **1** is attested not only by the small splitting of the E modes (e.g. by 27 cm^{-1} for $\nu_{as}(SO_3)$) but also by the particularly low value of ν(SF), characteristic of an isolated SO_3F^- ion. To a good approximation, the spectra of $S_4N_4^{2+}$ are those of an isolated cation, only slightly perturbed by the anion. Molecular symmetries C_{4h}, C_{4v}, and D_{2d} are ruled out, since they require both a larger number of bands and 4, 7, and 7 coincidences respectively between the Raman and infrared frequencies, and there are none. Symmetry D_{4h} requires two polarised Raman bands (A_{1g}) and five depolarized bands ($2B_{1g} + 2B_{2g} + E_g$) and four infrared bands ($A_u + 3E_u$), in agreement

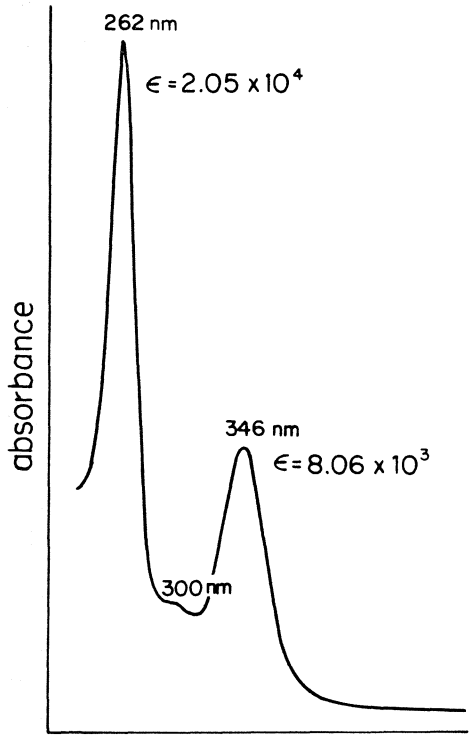

FIG. 3. The electronic spectrum of $S_4N_4^{2+}$ in HSO_3F.

with experiment, if the pair of infrared bands at 434/440 cm^{-1} is taken to be a partly resolved degenerate band. The Raman spectrum of the cation in solution shows no splitting of the degenerate band; the splitting found in the infrared spectrum of the solid may be a result of a low site symmetry or weak ionic polarization. We conclude that in solution, at least, $S_4N_4^{2+}$ is planar, with equal bond lengths, though the molecule appears to be flexible, and may be deformed in the crystal; the high symmetry may be attained statistically. The high value of ν(SN) (1205 cm^{-1}; cf. 1160 cm^{-1} in $S_4N_3^+$ (15)) shows that the SN bond is strong. The electronic spectrum of $S_4N_4^{2+}$ (Fig. 3) is quite different from that of S_4N_4 in organic solvents (16). Tetrasulphur tetranitride is oxidized by sulphuric acid (17), but the spectrum of the unidentified cation so produced varies with time, and shows fine structure near 400 nm; the product is evidently not $S_4N_4^{2+}$, because neither feature is found in the spectrum of $S_4N_4^{2+}$ in HSO_3F.

It is not possible to write a single canonical form for $S_4N_4^{2+}$ which reflects its high symmetry. The electronic structure of S_4N_4 itself has received considerable attention; an extensive list of references is given in ref. 18, which illuminates many of the features of S—N bonding through extensive *ab*

TABLE 3. Bond populations[a]

	D_{4h}			D_{2d}		
Molecule	S—N	S—S	Total	S—N	S—S	Total
S_4N_4	0.672	0.001	5.378	0.597	0.471	5.718
$S_4N_4^{2+}$	0.681	0.001	5.450	0.609	0.297	5.466

[a] EHMO, sp basis. Mulliken analysis.

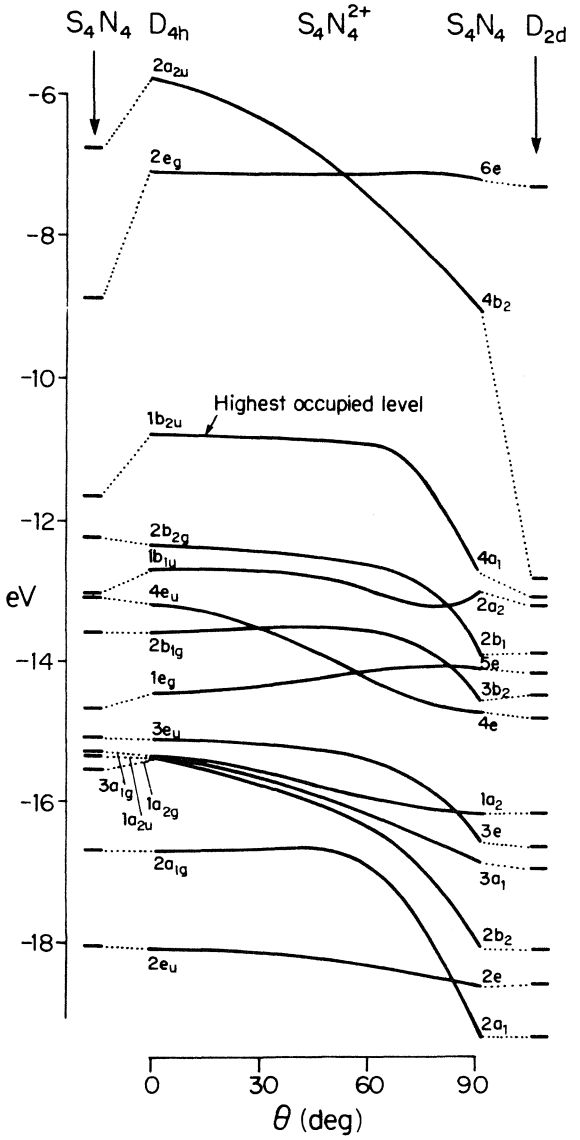

FIG. 4. The energy levels of $S_4N_4^{2+}$ (CNDO) as a function of θ. For comparison, the levels of S_4N_4 (D_{4h}) and S_4N_4 (D_{2d}) are given at the LH and RH sides, respectively. The lowest levels ($1a_1$, $1e$, $1b_1$, $1b_2$ in D_{2d}) are not shown; their relative positions are independent of charge and conformation. The calculated levels for the neutral molecule are lowered by 6.30 (D_{4h}), 7.14 eV (D_{2d}) to match the lowest levels shown for the cation.

Can. J. Chem. Downloaded from www.nrcresearchpress.com by 210.87.254.6 on 09/06/12
For personal use only.

TABLE 4. Calculated electronic levels of $S_4N_4^{2+}$ (CNDO)

Level	Energy (eV)	Description[a]	Level	Energy (eV)	Description
$3e_u$	−15.08	ip b	$3a_{1g}$	−5.29	ip ab
$3a_{1g}$	−15.36	ip ab	$2a_{2u}$	−5.77	op ab
$1a_{2u}$	−15.37	op b	$5e_u$	−5.82	ip ab
$1a_{2g}$	−15.40	ip b	$2e_g$	−7.06	op ab LUMO
$2a_{1g}$	−16.69	ip b	$1b_{2u}$	−10.79	op n(s) HOMO
$2e_u$	−18.02	ip b	$2b_{2g}$	−12.32	ip n(N)
$1b_{1g}$	−20.03	ip b	$1b_{1u}$	−12.68	op n(N)
$1b_{2g}$	−22.18	ip b	$4e_u$	−13.15	ip ab
$1e_u$	−23.78	ip b	$2b_{1g}$	−13.54	ip b
$1a_{1g}$	−25.10	ip b	$1e_g$	−14.39	op b

[a] In (ip) or out of (op) plane: bonding (b), antibonding (ab) and nonbonding (n).

initio studies. We have found simpler methods helpful in considering the conformational effects of the ionization of S_4N_4.

The relation between the planar ring of $S_4N_4^{2+}$ and the saddle shape of S_4N_4 is shown in Fig. 1. All conformations with $\theta \neq 0$ have symmetry D_{2d}, but for convenience we reserve this symbol for the experimental conformation of S_4N_4 (1), for which $\theta = 93°$. If the interactions are restricted to pπ-orbitals at each atom, the energy of the highest antibonding level (a_{2u}) drops sharply as θ increases, eventually acquiring significant S—S bonding character through the interactions of opposing sulphur atoms (19). More detailed treatments of S_4N_4 (20) show that the energy of this orbital (b_2 in D_{2d}) is comparable to those of the highest occupied a_1, a_2, and b_1 combinations, which correspond to nonbonding S, N, N combinations in D_{4h}. The calculated energy range of the four orbitals is about 1 eV. The energies of the highest two occupied orbitals, at least, cannot be distinguished by photoelectron spectroscopy, which places them at −9.5 eV (20*c*) or −9.36 eV (20*e*), but the b_2 orbital is still formally antibonding with respect to the SN bonds, and ionization of electrons from it should strengthen the molecule, in agreement with the high value of ν(SN) in $S_4N_4^{2+}$.

The changes in the bond parameters, as a consequence of ionization, have been estimated by a population analysis of the EH molecular orbitals (Table 3).[1] We draw the following conclusions. (1) Ionization of S_4N_4 in either conformation increases the S—N bond population, consistent with the release of electrons from an orbital with partial antibonding character. (2) In the $D_{4h} \rightarrow D_{2d}$ transformation, the S—S bonds are made partly at the expense of the S—N bonds, but, for S_4N_4, there is a large net increase in total bond population (0.34) (3). In the same transformation of $S_4N_4^{2+}$, the S—S bonds are formed almost wholly at the expense of the S—N bonds.

More nearly quantitative results have been obtained through CNDO calculations on both S_4N_4 and $S_4N_4^{2+}$ over the whole conformation range, using the program of ref. 21. The energies and approximate descriptions of the molecular orbitals are given for the D_{4h} limit of $S_4N_4^{2+}$ in Table 4. They are shown in Fig. 4 as a function of θ; the levels of neutral S_4N_4 at the limiting conformations are also shown. Ionization stabilizes all the levels of either conformation, and, to a first approximation, to the same extent, without altering their order. The matching, to within an additive constant, is good for all orbitals except the HOMO, which is (relatively) destabilized in the ion, presumably because it is shielded better by the more contracted inner electrons. The LUMO (b_2) is strongly destabilized in the D_{2d} conformation, so that it is no longer competitive with the a_1, a_2 orbitals. An appreciable part of the S—S bonding is thereby lost, again in agreement with the EH results, and confirming that ionization is effectively from the $4b_2$ level.

Figure 4 shows, principally, the important influence of conformation on the energy levels. As the planar molecule approaches the cluster conformation, most of the bonding levels are lowered, not only those ($2a$, $3a$, $3b_2$, $4a_1$) with an appreciable b(SS) component. This is presumably a general result of improved overlap in the more compact molecule; its effect on the total electronic energy is partly offset by the π-bonding in the planar molecule, though this is weaker for 3pπ than for 2pπ-orbitals. Nuclear repulsion destabilizes the D_{2d} relative to the D_{4h} conformation, so that as the planar molecule is deformed, the total energy (CNDO) increases until the shorter range valence forces supervene near $\theta = 60°$, when the energy decreases again. At their face value, the CNDO

[1] We are grateful to Professor L. S. Bartell for the EHMO program, and to Dr. J. D. Head for the Mulliken analysis program.

Can. J. Chem. Downloaded from www.nrcresearchpress.com by 210.87.254.6 on 09/06/12
For personal use only.

calculations on $S_4N_4^{2+}$ predict stability of the D_{2d} relative to the D_{4h} conformation. This result is not reliable, because the CNDO method is known to overestimate bonding contributions; the energy minimum found for S_4N_4 itself corresponds to much too short an S—S bond (22). The EH method frequently gives better results on conformational problems. In this case it, too, shows an energy maximum, but the planar form has the highest stability. The energy varies very slowly near $\theta = 0°$, and the ion can be expected to be flexible. Crystal structure determinations (R. J. Gillespie, personal communication), improving on the preliminary work (10), show that $S_4N_4^{2+}$ is frequently, but not always, quite planar in the crystal. More refined calculations, like those by X_α (20*b*) or *ab initio* methods (20*e*) are required both for a full discussion of the electronic spectrum of $S_4N_4^{2+}$, and for a more reliable assessment of conformational stability.

Acknowledgements

We are grateful to Dr. K. C. Lee for his help in recording the Raman spectra, and to the Natural Sciences and Engineering Research Council of Canada (NSERC) for financial support.

1. M. L. DeLucia and P. Coppens. Inorg. Chem. **17**, 2336 (1978); B. D. Sharma and J. Donohue. Acta Crystallogr. **16**, 891 (1963).
2. S. C. Abraham. Acta Crystallogr. **8**, 661 (1955); G. S. Pawley and R. P. Rinaldi. Acta Crystallogr. Sect. B, **28**, 3605 (1972).
3. H. J. Emeléus and A. J. Poulet. J. Fluorine Chem. **1**, 13 (1971/2).
4. R. A. Forder and G. M. Sheldrick. J. Fluorine Chem. **1**, 23 (1971/2).
5. L. Zbořilová and P. Gebauer. Z. Anorg. Chem. **448**, 5 (1979).
6. R. A. DeMarco and J. M. Shreeve. Adv. Inorg. Chem. Radiochem. **16**, 109 (1974).
7. F. B. Dudley and G. H. Cady. J. Am. Chem. Soc. **85**, 3375 (1963); E. Castellano, R. Gatti, J. E. Sicre, and H. L. Schumacher. Z. Phys. Chem. (Frankfurt), **42**, 174 (1964).
8. A. B. Cornford. Ph.D. thesis, University of British Columbia, 1971.
9. P. C. S. Leung. Ph.D. thesis, University of British Columbia, 1979.
10. R. J. Gillespie, D. R. Slim, and J. D. Tyrer. Chem. Commun. 253 (1977).
11. M. Becke-Goehring. Inorg. Synth. **6**, 123 (1960).
12. J. M. Shreeve and G. H. Cady. Inorg. Synth. **7**, 124 (1963).
13. J. Barr, R. J. Gillespie, and R. C. Thompson. Inorg. Chem. **3**, 1149 (1964).
14. A. M. Qureshi, H. A. Carter, and F. Aubke. Can. J. Chem. **49**, 35 (1971).
15. R. T. Bailey and E. R. Lippincott. Spectrochim. Acta, **20**, 1327 (1964).
16. P. S. Braterman. J. Chem. Soc. 2297 (1965).
17. S. A. Lipp and W. L. Jolly. Inorg. Chem. **10**, 33 (1971).
18. R. C. Haddon, S. R. Wasserman, F. Wudl, and G. R. J. Williams. J. Am. Chem. Soc. **102**, 6687 (1980).
19. R. Gleiter. J. Chem. Soc. A, 3174 (1970).
20. (*a*) A. G. Turner and F. S. Mortimer. Inorg. Chem. **5**, 906 (1966); (*b*) D. R. Salahub and R. P. Messmer. J. Chem. Phys. **64**, 2039 (1976); (*c*) W. R. Salaneck, J. W.-P. Lin, A. Paton, C. B. Duke, and G. P. Ceasar. Phys. Rev. Sect. B, 4517 (1976); (*d*) S. Millefiori and A. Millefiori. Inorg. Chim. Acta, **45**, L19 (1980); (*e*) R. H. Findlay, M. H. Palmer, A. J. Downs, R. G. Edgell, and R. Evans. Inorg. Chem. **19**, 1307 (1980).
21. P. A. Dobosh. QCPE **11**, 141 (1969).
22. P. Cassoux, O. Glemser, and J. F. Labarre. Z. Naturforsch. Teil B, **32**, 41 (1977).

Can. J. Chem. Downloaded from www.nrcresearchpress.com by 210.87.254.6 on 09/06/12
For personal use only.

Erratum: The action of hypochlorite on *m*-cresol. Part 2. Muconic acid derivatives

George M. Strunz, Masatoshi Kakushima, and Alan D. Gibson
Canadian Forestry Service, P.O. Box 4000, Fredericton, N.B., Canada E3B 5P7
Archibald W. McCulloch
Atlantic Regional Laboratory, National Research Council of Canada, Halifax, N.S., Canada B3H 3Z1
AND
Peter S. White
Department of Chemistry, University of New Brunswick, Fredericton, N.B., Canada E3B 6E2

(Ref.: Can. J. Chem. **58**, 2765 (1980))
Received June 23, 1981

The hydroxyl groups in structure **1** should be *cis* (cf. ref. 6).

Chemistry of thujone. IV.[1] Cyclopropane derivatives and analogs of pyrethrins

JAMES P. KUTNEY, MANASH K. CHOUDHURY, JOHN M. DECESARE, HELEN JACOBS, ASHOK K. SINGH, AND BRIAN R. WORTH

Department of Chemistry, University of British Columbia, 2036 Main Mall, University Campus, Vancouver, B.C., Canada V6T 1Y6

Received April 8, 1981

JAMES P. KUTNEY, MANASH K. CHOUDHURY, JOHN M. DECESARE, HELEN JACOBS, ASHOK K. SINGH, and BRIAN R. WORTH. Can. J. Chem. **59**, 3162 (1981).

Thujone **1** was degraded to the thujaketonic acids **5** and **18** which were used as starting materials for the synthesis of pyrethroid analogs **8**, **12–17**, **21–24**, and **27–35**.

JAMES P. KUTNEY, MANASH K. CHOUDHURY, JOHN M. DECESARE, HELEN JACOBS, ASHOK K. SINGH et BRIAN R. WORTH. Can. J. Chem. **59**, 3162 (1981).

On a dégradé la thujone **1** en acides thujacétoniques **5** et **18** qui sont utilisées comme produits de départ dans la synthèse des analogues de la pyréthroide: **8**, **12–17**, **21–24** et **27–35**.

[Traduit par le journal]

Can. J. Chem. Downloaded from www.nrcresearchpress.com by 210.87.254.5 on 09/06/12
For personal use only.

Introduction

Previous communication from these laboratories described the uses of thujone **1**, readily available from Western Red Cedar leaf oil, in the preparation of acyclic juvenoid analogs (e.g. **2**) (1, 2) and of bicyclic natural products (e.g. (+)-β-cyperone **3**)

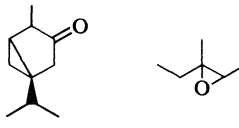

1

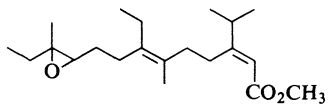

2

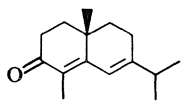

3

(3). In those experiments the propensity for opening of the cyclopropane ring was utilized to generate required functionality. In the synthesis of **3**, the optical purity of thujone enabled the preparation of (+)-β-cyperone with an optical purity > 98.8%. Here we report the preparation of several analogs of the biologically active pyrethrins in which the cyclopropane function of thujone has been retained (and, accordingly, the optical activity), or a new cyclopropane ring generated.

Pyrethroid insecticides, with general structure **4**, have pioneered a vast new area of insect control methods and in this light we set out to prepare *analogs*, readily derived from thujone **1**. Using α-thujaketonic acid (**5**) (obtained from **1** by permanganate cleavage) and its open chain derivatives, the following modifications (cf. **4**) in the

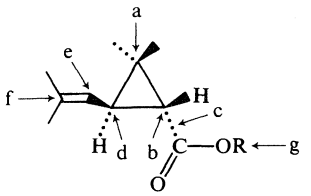

4

pyrethroid skeleton were envisaged: (*a*) optional *gem*-dimethyl substitution on the cyclopropane ring; (*b*) incorporation of an isopropyl group on the ring; (*c*) introduction of a methylene unit between the ring and the carboxyl group; (*d*) use of both *cis* and *trans* orientation of substituents on the cyclopropane ring; (*e*) alkyl substitution at the α-carbon of the side chain; (*f*) variation in the nature of the unsaturated side chain; (*g*) variation in the nature of the ester function, R.

The utility of α-thujaketonic acid (**5**), as an intermediate in pyrethroid synthesis, can be seen from the simple transformations indicated in the following schemes. In our initial studies (Scheme 1), Wittig reaction of the sodium salt of **5** with methyltriphenylphosphorane in dimethylsulphoxide (DMSO) gave the vinyl cyclopropane **6** in very

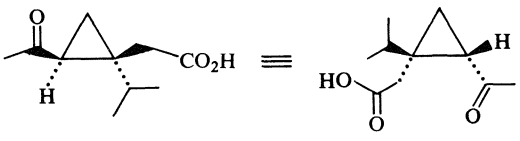

5

high yield. Subsequent reaction of the sodium salt of **6** with oxalyl chloride provided the labile acid chloride **7** which, on treatment with (±)*m*-phenoxybenzaldehyde cyanohydrin, gave the required analog **8**. Elliott *et al.* (4) have discussed the use of

[1]For part III, see ref. 3.

0008-4042/81/223162-06$01.00/0

©1981 National Research Council of Canada/Conseil national de recherches du Canada

m-phenoxybenzaldehyde cyanohydrin as ester function in the preparation of pyrethrin insecticides with a "new order of activity"; e.g. NRDC 161, (**9**).

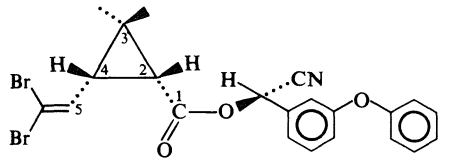

9

Pyrolysis of **8** at 130–140°C (e.g. under distillation) allowed facile conversion to the diene **10** which could also be obtained during the preparation of **8** over prolonged reaction periods. Treatment of **10** in petroleum ether with neutral alumina gave a low yield (ca. 25%) of the conjugated diene **11**. Elliott *et al.* (5) have also discussed the crucial 2*R* configuration for active pyrethroids, e.g. NRDC 161, (**9**), as well as the usefulness of both *cis* and *trans* orientation of groups about the cyclopropane ring. Analog **8**, although lacking in the required configuration at C-2, was nevertheless deemed a useful inclusion in our biological screening program.

Scheme 2 illustrates the derivation of cyclopropane carboxylic acids and esters with the appropriate configuration at C-2. Here the acetyl cyclopropane function of α-thujaketonic acid methyl ester (**12**) was oxidized with NaOBr to give a mixture of the acid ester **13** (13%) and the diacid **14** (77%).

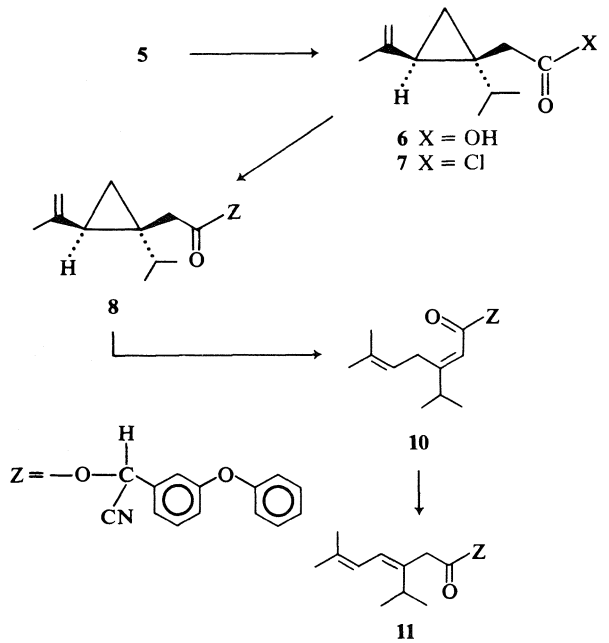

SCHEME 1

Esterification of **14** (CH_2N_2) gave the diester **15**, while reaction with Ac_2O provided the cyclic anhydride **16** in 89% yield. Treatment of **16** with pyridine in dry methanol solution gave a mixture of acid esters **17** and **13** in the ratio 6:4, not readily separated by standard chromatographic methods.

Thermolysis of **5** in boiling water gave the known (*E*)β-thujaketonic acid (**18**) in high yield (1). Wittig reaction of methyltriphenylphosphorane and the sodium salt of **18** gave the terminal olefin **19** which

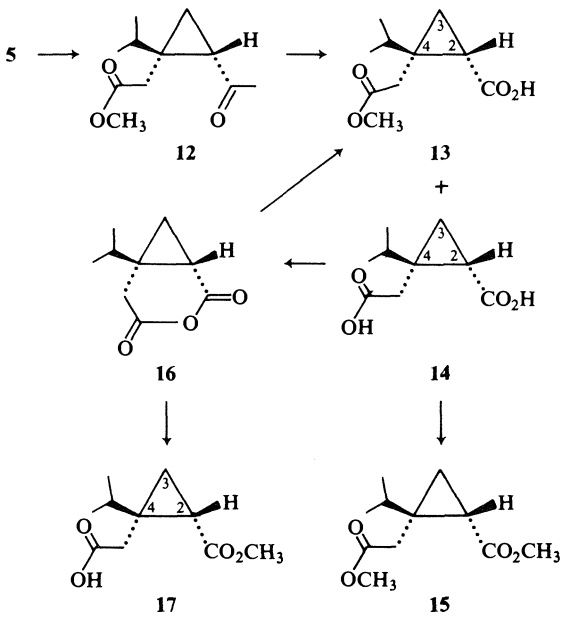

SCHEME 2

on subsequent esterification with CH_2N_2 provided **20** in almost quantitative yield. Cyclopropanation using methyl diazoacetate, in the presence of copper sulphate catalyst, gave the racemic cyclopropane derivatives **21** and **22** in approximately equal amounts. Analogous treatment with ethyl diazoacetate provided **23** and **24** (Scheme 3).

The ^1H nmr spectra of **21**–**24** (Table 1) enable tentative assignment of *cis* (**22** and **24**) and *trans* (**21** and **23**) stereochemistry to the appropriate isomers. The significant downfield shifts (0.2–0.3 ppm) of three of the four methylene protons on C-5, C-6 in **22** and **24**, due to the influence of the proximate C-1 carboxyl group, was possible only in a *cis* orientation. The cyclopropane ring protons showed the usual 5 Hz *geminal* and *trans* coupling and 7 Hz *cis* relationships.

The preparation of cyclopropane derivatives carrying a *gem*-dimethyl function is described in Scheme 4. Here thermolysis of the acid **6** gave **25**

Can. J. Chem. Downloaded from www.nrcresearchpress.com by 210.87.254.5 on 09/06/12
For personal use only.

Can. J. Chem. Downloaded from www.nrcresearchpress.com by 210.87.254.5 on 09/06/12
For personal use only.

TABLE 1. The ^{1}H nmr signals[a] for *cis* and *trans* cyclopropane derivatives: **21–24**

	21 (*trans*)	**22** (*cis*)	**23** (*trans*)	**24** (*cis*)
H-2	1.63 (dd, 7, 5)	1.53 (dd, 7, 5)	1.61 (dd, 7, 5)	1.53 (dd, 7, 5)
H-3a	1.11 (t, 5)	1.15 (t, 5)	1.11 (t, 5)	1.15 (t, 5)
H-3b	0.98 (dd, 7, 5)	0.89 (dd, 7, 5)	0.96 (dd, 7, 5)	0.88 (dd, 7, 5)
H-5a	1.42 (td, 12, 12, 5)	1.61 (td, 12, 12, 5)	1.45 (td, 12, 12, 5)	1.65 (td, 12, 12, 5)
H-5b	1.45 (td, 12, 12, 5)	1.72 (td, 12, 12, 5)	1.45 (td, 12, 12, 5)	1.74 (td, 12, 12, 5)
H-6a	2.66 (td, 12, 12, 5)	2.89 (td, 12, 12, 5)	2.67 (td, 12, 12, 6)	2.92 (td, 12, 12, 5)
H-6b	2.66 (td, 12, 12, 5)	2.30 (td, 12, 12, 5)	2.67 (td, 12, 12, 5)	2.32 (td, 12, 12, 5)
H-8	5.65	5.61	5.67	5.64
—OCH_3	3.67	3.67	3.71	3.71
—OCH_3	3.68	3.68	—	—
—OCH_2	—	—	4.15 (q, 7)	4.14 (q, 7)
—OCH_2CH_3	—	—	1.27 (t, 7)	1.27 (t, 7)
—CH_3	1.27	1.25	1.27	1.26
—$CH(CH_3)_2$	2.36 (septet, 7)	2.33 (septet, 7)	2.36 (septet, 7)	2.35 (septet, 7)
—$CH(CH_3)CH_3$	1.08 (d, 7)	1.04 (d, 7)	1.08 (d, 7)	1.04 (d, 7)
—$CH(CH_3)CH_3$	1.08 (d, 7)	1.06 (d, 7)	1.08 (d, 7)	1.06 (d, 7)

[a]Chemical shift values are given in δ ppm. Values in parentheses represent signal multiplicity and coupling constants in Hz.

and subsequent esterification provided **26** in high yield. Cyclopropanation of **26** provided a *cis*/*trans* mixture of esters **27** which after ozonolysis gave the ketones **28** and **29**, separable by chromatography on silica gel.

The ^{1}H nmr spectra of **28** and **29** again provided sufficient information for assignment of stereochemistry. Here the *cis* isomer **28** was characterized by a coupling of 9 Hz between H-2 (δ 1.58, d) and H-4 (δ 1.46, dt, J = 6, 6, 9) while in **29**, H-2 (δ 1.25, d) was coupled to H-4 (δ 1.67, dt, J = 6, 6, 8) with J = 6 Hz. Again the methylene protons on C-5 in the *cis* isomer were shifted downfield by ca. 0.2–0.4 ppm relative to the *trans* isomer **29**. The relatively high field absorbance of H-2 in **29** is attributed to its relationship to the shielding zone of the C-6 carbonyl group.

Reduction of **28** with $NaBH_4$ gave the alcohol **30**. The derived tosylate **31** readily eliminated TsOH to give **32**. A similar sequence from **29** (viz. **29** → **33** → **34** → **35**) provided the *trans* isomer **35**.

These final racemic products, **32** and **35**, represent the closest analogs to the pyrethrins, generalized as **4**.

The synthetic sequences described in Schemes 1–4 form the basis of preparation of a wide variety of pyrethrin analogs from the relatively inexpensive versatile starting material thujone (**1**). Biological evaluation of these compounds is presently underway.

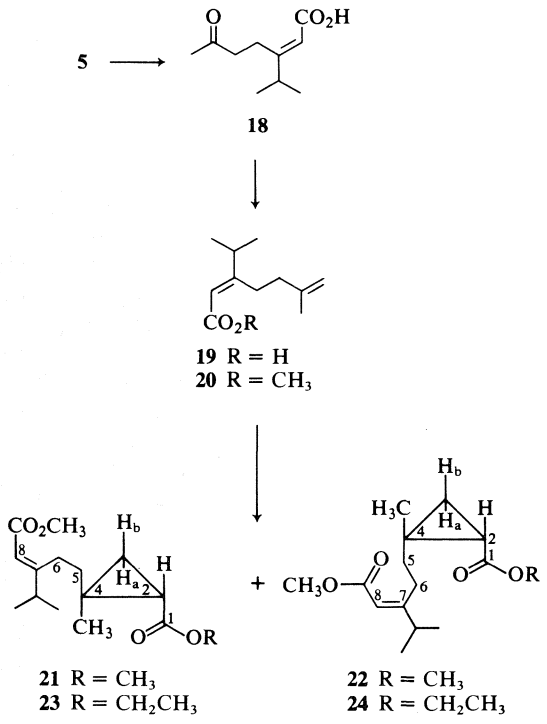

SCHEME 3

Experimental

Ultraviolet spectra were recorded on a Cary 15 spectrophotometer using methanol as the solvent. Infrared spectra were recorded on a Perkin–Elmer 457 spectrophotometer with samples as neat films. The ^{1}H nmr spectra were recorded on a Varian HA- or XL-100 or Nicolet Oxford H-270 or a 400 MHz instrument. The ^{13}C nmr spectra were recorded on a Varian CFT-20 instrument. Deuterochloroform was used as the solvent with TMS as internal standard. Mass spectra were recorded using an Atlas CH-4B or AEI MS-902 instrument. Microanalyses were carried out by Mr. P. Borda, Microanalytical Laboratory, University of British Columbia. Column chromatography utilized Merck silica gel GF_{254} or Woelm neutral alumina grade I. Petroleum ether refers to the fraction with boiling range 30–60°C.

Isopropenyl Derivative ***6*** *(1)*

A solution of methyltriphenylphosphonium bromide (75 g) in dimethylsulphoxide (DMSO, 400 mL) was added to NaH (7.5 g) in DMSO (100 mL) at ambient temperature under nitrogen. The mixture was stirred for 15 min, cooled to 10°C and treated with

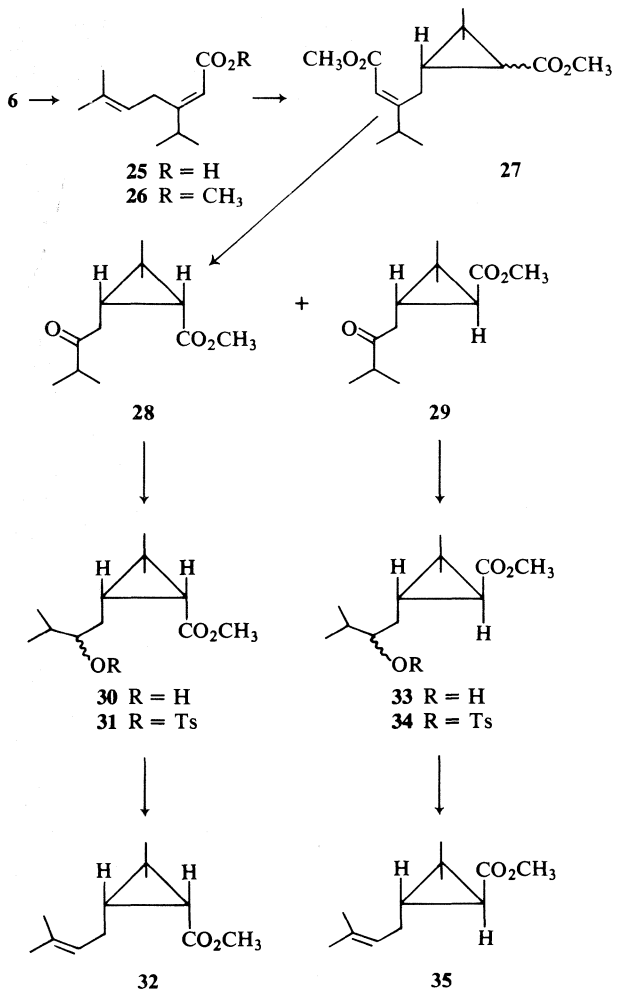

SCHEME 4

the sodium salt of α-thujaketonic acid (**5**) (14 g), and the solution stirred 20 h at ambient temperature. The solution was cooled, diluted with cold water (500 mL), and washed with dichloromethane (1 L). The aqueous layer was acidified with 10% H_2SO_4 and extracted with petroleum ether (2 L). This extract was washed with water (1 L), dried ($MgSO_4$), and concentrated *in vacuo* to give **6** (11.6 g, 94%); bp 249–250°C; ir ν_{max}: 1706, 1646; ^{1}H nmr δ: 4.93 (1H, bs), 4.63 (1H, bs), 2.27 (2H, ABq, J = 16), 1.78 (3H, s), 0.98 (3H, d, J = 7), 0.91 (3H, d, J = 7); ms *m/e*: 182 (M^+), 139, 93, 69 (100%).

Ester 8 via 7

Oxalyl chloride (1.5 mL) was added, slowly, to a stirred suspension of the sodium salt of **6** (221 mg) in benzene (8 mL) and pyridine (0.03 mL) at ca. 5°C under nitrogen. The mixture was stirred 2 h at 5°C, filtered, and concentrated *in vacuo* to give the crude acid chloride **7** (159 mg, 73%); ir ν_{max}: 1801. A solution of *m*-phenoxybenzaldehyde cyanohydrin (463 mg) and pyridine (0.096 mL) in benzene (8 mL) was added to **7** in benzene (3 mL) and the mixture refluxed under nitrogen for 45 min. The solvent was removed *in vacuo* and the residue partitioned between water and ether. The ether extract was washed, dried ($MgSO_4$), and concentrated. The oily residue was chromatographed on silica gel to give the ester **8** (115 mg, 37%); ir ν_{max}: 1749, 1643; ^{1}H nmr δ: 7.0–7.5 (9H, envelope), 6.39 (1H, s), 4.90 (1H, bs), 4.60 (1H, bs), 2.30 (2H, ABq, J = 16), 1.76 (3H, s), 0.89 (3H, d, J = 7), 0.87 (3H, d, J = 7); ms *m/e*: 389.1996 (M^+, $C_{25}H_{27}NO_3$ requires 389.1991). *Anal.* calcd. for $C_{25}H_{27}NO_3$: C 77.12, H 6.94, N 3.59; found: C 76.90, H 6.87, N 3.66.

Refluxing in toluene instead of benzene gave a mixture of **8** and **10** (see below) in approximately equal amounts.

Ester 10

The ester **8** (2.7 g) was heated at 130–140°C for 3 h under vacuum (ca. 0.04 Torr), cooled, and filtered (as solution in petroleum ether) through a short column of silica gel to give **10** (2.43 g, 90%); ir ν_{max}: 1723; ^{1}H nmr δ: 7.0–7.5 (9H, envelope), 6.46 (1H, s), 5.73 (1H, s), 5.06 (1H, t, J = 7), 3.43 (2H, d, J = 7), 2.45 (1H, septet, J = 7), 1.69 (6H, s), 1.07 (6H, d, J = 7); ms *m/e*: 389.1998 (M^+, $C_{25}H_{27}NO_3$ requires: 389.1991). *Anal.* calcd. for $C_{25}H_{27}NO_3$: C 77.12, H 6.94, N 3.59; found: C 77.19, H 6.87, N 3.70.

Ester 11

A mixture of the ester **10** (66.5 mg) and Woelm neutral alumina, grade I (3.3 g) was stirred in petroleum ether (30 mL) for 5 min, filtered, and concentrated *in vacuo*. The residue was chromatographed on silica gel to give starting material **10** (27 mg) and **11** (17 mg, 26%); uv λ_{max}: 234 nm (28 000); ir ν_{max}: 1748; ^{1}H nmr δ: 6.95–7.55 (9H, envelope), 6.40 (1H, s), 6.05 (2H, s), 3.1 (2H, s), 3.03 (1H, septet, J = 7), 1.80 (3H, s), 1.70 (3H, s), 0.95 (6H, d, J = 7); ms *m/e*: 389.1992 (M^+, $C_{25}H_{27}NO_3$ requires: 389.1991). *Anal.* calcd. for $C_{25}H_{27}NO_3$: C 77.12, H 6.94, N 3.59; found: C 77.43, H 7.23, N 3.46.

Acid Ester 13 and Diacid 14

Bromine (24 g) was added to a solution of NaOH (15 g) in water (200 mL) at −5°C. A solution of the ketoester **12** (9.7 g) in dioxane (100 mL) was added and the mixture stirred 1 h at −5°C. Saturated Na_2SO_3 solution (50 mL) was added and the mixture acidified with dilute HCl and extracted with dichloromethane. The organic layer was dried and concentrated *in vacuo* to give a viscous oil. Chromatography on silica gel gave the diacid **14** (7.2 g, 77%); mp 135–136°C (dichloromethane); ir ν_{max}: 3400–2400, 1715, 1690; ^{1}H nmr (acetone-d_6) δ: 2.68 and 2.57 (2H, ABq, J = 18), 1.63 (1H, dd, J = 8, 6), 1.41 (1H, septet, J = 7), 1.02–1.10 (2H, m), 0.96 (3H, d, J = 7), 0.95 (3H, d, J = 7); ^{13}C nmr (acetone-d_6) δ: 174.6, 174.2, 36.1, 32.5, 31.3, 24.4, 20.3, 19.5; ms *m/e*: 97, 96, 81, 69 (100), 68, 55, 41. *Anal.* calcd. for $C_9H_{14}O_4$: C 58.06, H 7.53; found: C 58.08, H 7.55.

Also obtained was the acid ester **13** (1.1 g, 13%); bp 150°C (0.1 Torr); ir ν_{max}: 3500–2400, 1735, 1695; ^{1}H nmr δ: 9.30 (1H, bs), 3.65 (3H, s), 2.74 and 2.59 (2H, ABq, J = 16.5), 1.64 (1H, dd, J = 8, 6), 1.26 (2H, m), 1.07 (1H, dd, J = 8, 4), 0.94 (3H, d, J = 7), 0.92 (3H, d, J = 7); ^{13}C nmr δ: 179.3, 173.0, 51.3, 36.2, 33.7, 32.4, 24.7, 21.0, 19.2; ms *m/e*: 200 (M^+), 126, 96, 81, 55 (100), 41. *Anal.* calcd. for $C_{10}H_{16}O_4$: C 60.00, H 8.00; found: C 59.80, H 8.06.

Diester 15

Esterification of **14** (2.1 g) with excess CH_2N_2 in ether gave the diester **15** (2.0 g, 80%); bp 140°C (0.1 Torr); ir ν_{max}: 1725; ^{1}H nmr δ: 3.69 (3H, s), 3.63 (3H, s), 2.72 and 2.56 (2H, ABq, J = 16), 1.67 (1H, dd, J = 8, 6), 1.26 (1H, septet, J = 7), 1.17 (1H, t, J = 5), 0.98 (1H, m), 0.94 (3H, d, J = 7), 0.92 (3H, d, J =7); ^{13}C nmr δ: 173.3, 172.9, 51.6, 51.3, 36.0, 32.3, 24.6, 20.1, 19.3, 19.1; ms *m/e*: 182, 154, 122, 96, 95, 69 (100), 68, 55, 41. *Anal.* calcd. for $C_{11}H_{18}O_4$: C 61.58, H 8.41; found: C 61.50, H 8.58.

Anhydride 16

A solution of the diacid **14** (1.7 g) in acetic anhydride (50 mL) was heated at 110°C for 24 h. The solvent was removed by distillation and the residue distilled *in vacuo* to give **16** (1.4 g,

Can. J. Chem. Downloaded from www.nrcresearchpress.com by 210.87.254.5 on 09/06/12
For personal use only.

Can. J. Chem. Downloaded from www.nrcresearchpress.com by 210.87.254.5 on 09/06/12
For personal use only.

89%); bp 120°C (0.1 Torr); mp (petroleum ether) 42–43°C; ir ν_{max}: 1800, 1760; ^{1}H nmr δ: 2.98 and 2.84 (2H, ABq, J = 16.5), 1.98 (1H, dd, J = 9, 4), 1.38 (2H, m), 1.17 (1H, t, J = 4), 1.04 (6H, d, J = 7); ^{13}C nmr δ: 167.9, 165.3, 33.9, 31.4, 28.7, 22.9, 20.8, 18.8; ms *m/e*: 168 (M^+), 126, 96, 71, 55 (100), 41. *Anal.* calcd. for $C_9H_{12}O_3$: C 64.28, H 7.14; found: C 63.99, H 7.29.

Conversion of ***16*** *to* ***13*** *and* ***17***

The anhydride **16** (5.0 g) was stirred in pyridine (1 mL) and methanol (50 mL) for 16 h at ambient temperature. The reaction mixture was poured into ice water (200 mL) and extracted with dichloromethane. The extract was dried and evaporated to give a mixture (5.2 g, 86%) of **13** (identical with that obtained above) and **17** (ratio 2:3); ^{1}H nmr δ: 9.1 (1H, bs), 3.67 (3H, s), 2.75 and 2.61 (2H, ABq, J = 16.5), 1.67 (1H, dd, J = 8, 6), 0.95 (3H, d, J = 7), 0.94 (3H, d, J = 7).

Acid ***19***

A mixture of sodium hydride (4.5 g) and dry DMSO (150 mL) was stirred at 70°C for 1 h under N_2. Methyltriphenylphosphonium bromide (68 g) in DMSO (150 mL) was added at room temperature and the solution stirred for 30 min. The sodium salt of (*E*)β-thujaketonic acid (**18**) (9.13 g) was added and the mixture stirred at 65°C for 20 h, diluted with ice-cold water (1.2 L), and washed with ether. The aqueous layer was acidified (5°C) with 6 *N* HCl and extracted with petroleum ether. The extract was dried (Na_2SO_4) and concentrated. Distillation *in vacuo* gave **19** (8.69 g, 98%); bp. 80–90°C (0.03 Torr); mp 46–48°C; ^{1}H nmr δ: 5.74 (1H, bs), 4.76 (2H, bs), 2.45 (1H, septet, J = 7), 1.80 (3H, bs), 1.12 (6H, d, J = 7); ms *m/e*: 182 (M^+). *Anal.* calcd. for $C_{11}H_{18}O_2$: C 72.49, H 9.95; found: C 72.34, H 9.69.

Ester ***20***

Esterification of **19** with CH_2N_2 gave **20** (quantitative); uv λ_{max}: 215 (log ε 3.89); ^{1}H nmr δ: 5.71 (1H, s), 4.7 (2H, bs), 3.71 (3H, s), 2.40 (1H, septet, J = 7), 1.86 (3H, bs), 1.10 (6H, d, J = 7); ms *m/e*: 196 (M^+). *Anal.* calcd. for $C_{12}H_{20}O_2$: C 73.43, H 10.27; found: C 73.43, H 10.15.

Cyclopropanes ***21*** *and* ***22***

Methyl diazoacetate (15 g) was added slowly (10 h) to a mixture of **20** (8.15 g) and anhydrous copper sulphate (0.8 g) at 0–5°C. The mixture was stirred until the evolution of gases ceased, then heated to 100°C. Additional methyl diazoacetate (5 g) was added at this temperature during 1 h. The mixture was cooled to room temperature, diluted with dichloromethane and filtered. The filtrate was evaporated and the residue extracted into petroleum ether. The extract was concentrated *in vacuo* and filtered through a short plug of silica gel. The eluate was then chromatographed (preparative hplc, Waters Associates LC-500) on silica gel to give **21** (3.54 g); uv λ_{max}: 217 (log ε 3.2); ir ν_{max}: 3065, 1710–1732, 1635, 1015, 870; ^{1}H nmr, see Table 1; ms *m/e*: 268 (M^+), 209, 208, 150. *Anal.* calcd. for $C_{15}H_{24}O_4$: C 67.14, H 9.01; found: C 67.60, H 9.20; and **22** (2.68 g); uv λ_{max}: 218 (log ε 3.2); ir ν_{max}: 3068, 1710–1735, 1638, 1025, 870; ^{1}H nmr, see Table 1; ms *m/e*: 268 (M^+), 209, 208, 150. *Anal.* calcd. for $C_{15}H_{24}O_4$: C 67.14, H 9.01; found: C 67.33, H 9.18.

Esters ***23*** *and* ***24***

Similarly, reaction of **20** with ethyl diazoacetate gave **23**; ir ν_{max}: 3035, 1720, 1640; ^{1}H nmr, see Table 1; ms *m/e*: 282 (M^+). *Anal.* calcd. for $C_{16}H_{26}O_4$: C 68.08, H 9.22; found: C 67.99, H 9.38; and **24**; ir ν_{max}: 3040, 1725, 1645, 790; ^{1}H nmr, see Table 1; ms *m/e*: 282 (M^+). *Anal.* calcd. for $C_{16}H_{26}O_4$: C 68.08, H 9.22; found: C 68.00, H 9.28.

Acid ***25***

The acid **6** (9.0 g) was heated, *in vacuo*, at 140°C for 6 h. The crude product was then chromatographed on silica gel to give **25** (6.65 g, 74%); mp 42–45°C; uv λ_{max}: 216 (log ε 4.07); ir ν_{max}: 3500–2600, 1690, 1635; ^{1}H nmr δ: 5.72 (1H, s), 5.18 (1H, bt, J = 7), 3.40 (2H, bd, J = 7), 2.42 (1H, septet, J = 7), 1.69 (6H, bs), 1.08 (6H, d, J = 7); ms *m/e*: 182 (M^+), 139, 41. *Anal.* calcd. for $C_{11}H_{18}O_2$: C 72.49, H 9.95; found: C 72.30, H 9.99.

Ester ***26***

Esterification of **25** with CH_2N_2 gave **26** (98%); uv λ_{max}: 218 (log ε 4.28); ir ν_{max}: 1720, 1630; ^{1}H nmr δ: 5.63 (1H, s), 5.04 (1H, bt, J = 7), 3.64 (3H, s), 3.39 (2H, bd, J = 7), 2.34 (1H, septet, J = 7), 1.63 (6H, bs), 1.00 (6H, d, J = 7); ms *m/e*: 196 (M^+), 165, 164, 154, 153, 149, 137, 121, 95, 93, 91, 81, 79, 77, 69, 67, 41. *Anal.* calcd. for $C_{12}H_{20}O_2$: C 73.43, H 10.27; found: C 73.23, H 10.21.

Cyclopropane Esters ***27***

Reaction of **26** (6.96 g) with methyldiazoacetate and copper sulphate, as described above, gave a *mixture* of the isomeric esters **27** (7.22 g, 76%); uv λ_{max}: 219 (log ε 3.99); ir ν_{max}: 1715, 1635, 1015, 870; ^{1}H nmr δ: 5.68 (2 × 1H, s), 3.66, 3.65, 3.62, 3.61 (4 × 3H, s), 3.03 (1H, dd, J = 14, 6), 2.90 (1H, dd, J = 13, 6), 2.85 (1H, dd, J = 13, 6), 2.80 (1H, dd, J = 14, 9), 2.48 (1H, septet, J = 7), 2.37 (1H, septet, J = 7), 1.51 (1H, dt, J = 9, 6, 6), 1.39 (1H, d, J = 6), plus overlapping methyl signals; ms *m/e*: 268 (M^+), 236, 193, 177, 154, 153, 135, 133, 107, 95, 67, 43, 41. *Anal.* calcd. for $C_{15}H_{24}O_4$: C 67.14, H 9.01; found: C 66.99, H 8.95.

Ozonolysis of ***27*** *to* ***28*** *and* ***29***

A solution of **27** (3 g) in dichloromethane (100 mL) was treated, at 0°C, with an excess of ozone for 30 min. The solution was washed with 5% Na_2SO_3 solution, dried (Na_2SO_4), and concentrated *in vacuo*. Chromatography on silica gel gave the isomeric ketones **28** (0.65 g); ir ν_{max}: 1720, 1000, 855; ^{1}H nmr δ: 3.64 (3H, s), 2.94 (1H, dd, J = 16, 6), 2.91 (1H, dd, J = 16, 6), 2.63 (1H, septet, J = 7), 1.58 (1H, d, J = 9), 1.46 (1H, dt, J = 6, 6, 9), 1.23 (3H, s), 1.16 (3H, s), 1.11 (3H, d, J = 7), 1.09 (3H, d, J = 7); ms *m/e*: 212 (M^+), 153, 152. *Anal.* calcd. for $C_{12}H_{20}O_3$: C 67.89, H 9.50; found: C 67.59, H 9.51; and **29** (0.84 g); ir ν_{max}: 1720, 1000, 875; ^{1}H nmr δ: 3.70 (3H, s), 2.65 (1H, septet, J = 7), 2.66 (1H, dd, J = 16, 6), 2.49 (1H, dd, J = 16, 8), 1.67 (1H, dt, J = 8, 6, 6), 1.28 (3H, s), 1.25 (1H, d, J = 6), 1.12 (3H, s), 1.11 (6H, d, J = 7); ms *m/e*: 212 (M^+), 153, 152. *Anal.* calcd. for $C_{12}H_{20}O_3$: C 67.89, H 9.50; found: C 67.75, H 9.44.

Alcohol ***30***

Reduction of **28** with $NaBH_4$ in methanol gave the alcohol **30** (88%); ir ν_{max}: 3440, 1725, 865; ^{1}H nmr δ: 3.64 (3H, s), 3.34 (1H, m), 1.92 (1H, m), 1.68 (2H, m), 1.62 (1H, bs, D_2O exchangeable), 1.20 (3H, s), 1.19 (3H, s), 0.91 (6H, d, J = 7); ms *m/e*: 196 (M − 18), 137, 136. *Anal.* calcd. for $C_{12}H_{22}O_3$: C 67.26, H 10.35; found: C 67.10, H 10.38.

Alcohol ***33***

Similarly, **29** gave **33**; ir ν_{max}: 3410, 1725, 865; ^{1}H nmr δ: 3.67 (3H, s), 3.44 (1H, m), 1.81 (1H, bs, D_2O exchangeable), 1.69 (1H, m), 1.60 (1H, m), 1.45 (2H, m), 1.24 (3H, s), 1.16 (3H, s), 0.92 (3H, d, J = 7), 0.91 (3H, d, J = 7), most signals were doubled due to the presence of two diastereomers; ms *m/e*: 214 (M^+), 196, 137, 136. *Anal.* calcd. for $C_{12}H_{22}O_3$: C 67.26, H 10.35; found: C 67.36, H 10.40.

The Olefin ***32*** *via* ***31***

Alcohol **30** (130 mg) and *p*-toluenesulphonyl chloride (140 mg) were heated in dry pyridine (1 mL) at 110°C for 6 h. The mixture was cooled, poured into ice-water, and extracted with ether. The extract was washed with $CuSO_4$ solution, dried (Na_2SO_4), and concentrated *in vacuo*. The residual oil was distilled *in vacuo* (0.2 Torr) at 50–60°C to yield **32** (94 mg, 79%); ir ν_{max}: 1725, 855; ^{1}H nmr δ: 5.05 (1H, bt, J = 8), 3.63 (3H, s), 2.33 (2H, bm), 1.99 (1H, bm), 1.69 (3H, bs), 1.62 (3H, bs), 1.24 (3H, s), 1.15 (3H, s); ms *m/e*: 196 (M^+), 137, 136. *Anal.* calcd. for $C_{12}H_{20}O_2$: C 73.43, H 10.27; found: C 73.23, H 10.19.

*The Olefin **35** via **34***

Similarly, **33** gave the olefin **35** (85%); ir ν_{max}: 1725, 820; ^{1}H nmr δ: 5.13 (1H, bt, $J = 8$), 3.68 (3H, s), 1.70 (3H, bs), 1.60 (3H, bs), 1.22 (3H, s), 1.17 (3H, s); ms *m/e*: 196 (M^+), 137, 136. *Anal.* calcd. for $C_{12}H_{20}O_2$: C 73.43, H 10.27; found: C 73.31, H 10.16.

Acknowledgements

Financial aid from the Science Council of British Columbia is gratefully acknowledged. The authors would also like to thank MacMillan Bloedel Limited for generous samples of cedar leaf oil.

1. J. P. KUTNEY, J. BALSEVICH, R. CARRUTHERS, A. MARKUS, M. J. MCGRATH, R. N. YOUNG, and B. R. WORTH. Biorg. Chem. **7**, 289 (1978).
2. J. P. KUTNEY, M. J. MCGRATH, R. N. YOUNG, and B. R. WORTH. Can. J. Chem. **57**, 3145 (1979).
3. J. P. KUTNEY, J. BALSEVICH, and P. GRICE. Can. J. Chem. **58**, 2641 (1980).
4. M. ELLIOTT, A. W. FARNHAM, N. F. JANES, P. H. NEEDHAM, and D. A. PULMAN. Nature, **248**, 710 (1974).
5. M. ELLIOTT, A. W. FARNHAM, N. F. JANES, P. H. NEEDHAM, and D. A. PULMAN. A.C.S. Symposium Series, No. 2, 80 (1974).

Can. J. Chem. Downloaded from www.nrcresearchpress.com by 210.87.254.5 on 09/06/12
For personal use only.

1,3-Dinitrobenzene – hydroxide ion interactions. Equilibrium constants for σ-complex formation in the dimethylformamide–water solvent system

ERWIN BUNCEL AND ALLEN W. ZABEL

Department of Chemistry, Queen's University, Kingston, Ont., Canada K7L 3N6

Received April 30, 1981

Can. J. Chem. Downloaded from www.nrcresearchpress.com by 210.87.254.40 on 09/06/12
For personal use only.

ERWIN BUNCEL and ALLEN W. ZABEL. Can. J. Chem. **59**, 3168 (1981).

The results of a uv–visible spectroscopic study of the interaction of 1,3-dinitrobenzene (DNB) with hydroxide ion in aqueous dimethylformamide (DMF) media are reported. Formation of several spectral species has been discerned, depending on factors such as the relative concentrations of the reactants, the time scale of the experiments, and the medium composition. The principal interaction is formation of the 1-hydroxy-2,4-dinitrocyclohexadienate anion. The molar absorptivities of this σ-complex, and the equilibrium constants (K_e) for its formation, have been determined as a function of medium composition. Values of K_e increase from 7.5 M^{-1} to 3×10^5 M^{-1} as the DMF content of the medium is changed from 57.4 to 95.8 mol% DMF. A solvent isotope effect, $K_e(D_2O)/K_e(H_2O)$, of ca. 0.4 has been observed. Structural and medium effects in this and related systems are evaluated. Correlations between log K_e and H_- are examined using the stoichiometric as well as the calculated free hydroxide ion concentrations. Attention is drawn to an important condition for equilibrium constant measurement in systems where one of the interacting species contributes significantly to the overall basicity, or to another property of the medium.

ERWIN BUNCEL et ALLEN W. ZABEL. Can. J. Chem. **59**, 3168 (1981).

On rapporte les résultats de l'étude de la spectroscopie dans l'uv visible de l'interaction du dinitro-1,3 benzène (DNB) avec l'ion hydroxyde dans du diméthylformamide aqueux. On a décelé la formation de plusieurs expèces spectrales dépendant de facteurs tels les concentrations relatives des réactifs, la durée des expériences et la composition du milieu. La formation de l'anion hydroxy-1 dinitro-2,4 cyclohexadiénate est la réaction principale. On a déterminé, en fonction de la composition du milieu, les absorptions molaires de ce complexe σ et la constante d'équilibre (K_e) de sa formation. Les valeurs de K_e augmentent de 7,5 M^{-1} à $3 \times 10^5 M^{-1}$ lorsque la teneur en DMF du milieu passe de 57,4 à 95,8 mol% de DMF. On a observé un effet isotopique du solvant $K_e(D_2O)/K_e(H_2O)$ d'environ 0,4. On a évalué dans ce système et dans des systèmes apparentés, les effets de structure et les effets du milieu. On a examiné les corrélations entre log K_e et H_- en utilisant les concentrations stoechiométriques aussi bien que les concentrations calculées de l'ion hydroxyle libre. On a porté une attention particulière à une condition importante de la mesure de la constante d'équilibre dans les systèmes où l'une des espèces en interaction peut contribuer d'une façon importante soit à la basicité globale soit à une autre propriété du milieu.

[Traduit par le journal]

In the interaction of aromatic nitro compounds with bases such as alkoxides or amines, the predominant mode of interaction is Meisenheimer or σ-complex formation, although various other types of interaction have also been substantiated, viz. proton transfer, electron transfer processes, etc. (1–5). Our work in this area has attempted to delineate the conditions under which given interactions occur and to identify structurally the nature of the species that are formed. One aspect of this work has focussed on the effect of medium changes on these processes. Of particular interest have been the dipolar aprotic media dimethyl sulfoxide (DMSO) and dimethylformamide (DMF), and how these media affect the balance between hydrogen isotope exchange and σ-complex formation (6, 7).

For 1,3,5-trinitrobenzene (TNB) in DMF–D_2O media containing NaOD, we have found that deuterium exchange, occurring via carbanion **1** as the intermediate, was intimately related to formation of the σ-complex **2** (8, 9). The present work is concerned with a parallel approach to the case of 1,3-dinitrobenzene (DNB) in basic DMF media. We have shown in the accompanying paper that, with respect to deuterium exchange, the behaviour of DNB contrasts to that of TNB in a number of important aspects (10). The present paper describes the uv–vis spectroscopic results for DNB in alkaline DMF systems. The spectral behaviour is found to be much more complex than in the case of TNB (9).

The diversity of spectral behaviour found in the present system required a systematic variation of

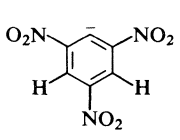

1

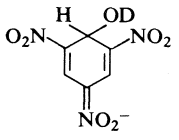

2

parameters such as the medium composition, the relative concentrations of DNB and OH^-, etc. The principal species present has been identified, however, and the conditions for its formation are shown to parallel the accompanying study of deuterium exchange (10).

0008-4042/81/223168-09$01.00/0

©1981 National Research Council of Canada/Conseil national de recherches du Canada

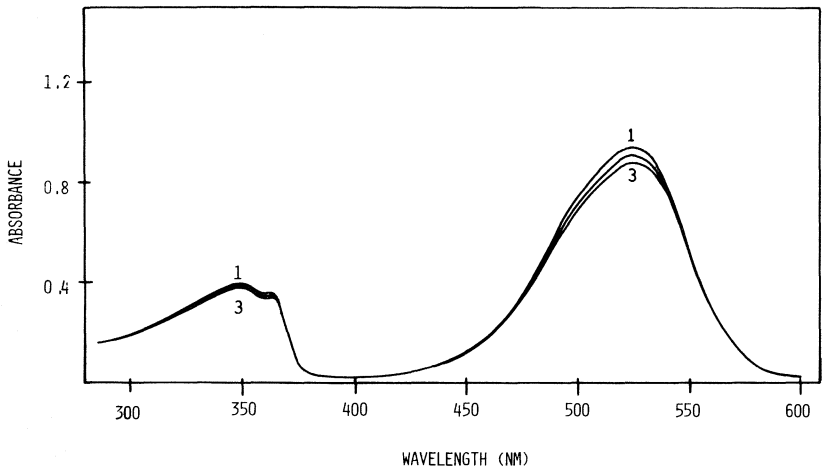

FIG. 1. Spectra of solution containing DNB (0.004 *M*) and Me_4NOH (0.004 *M*) in 91 mol% DMF taken at various times after preparation in 0.1 mm cuvette. (1) 1 min, (3) 20 min.

Results and Discussion

Characterization of Spectral Species

In Fig. 1 are shown the spectra of a solution of DNB (0.004 *M*) and tetramethylammonium hydroxide (0.004 *M*) in 91 mol% DMF taken at various intervals from the time of mixing. The spectra are characterized by a main absorption occurring at 526 nm and a minor absorption with maxima at 350 and 364 nm. It is seen that a uniform decrease in the absorptions, to the extent of 3%, has taken place over the entire spectral region over this period. This decrease continues thereafter at about the same rate until eventually there is no absorption in the visible region.

The decay in the absorptions as a function of time which is displayed in Fig. 1 can be ascribed to the removal of hydroxide ion from the equilibrium as a result of reaction with solvent DMF (11). The rate of decay of the spectral species is dependent on the free OH^- concentration and varies with solvent composition. In media of relatively low DMF content, where K_e is relatively small, the decay is relatively fast, while the converse holds for media of relatively high DMF content (e.g. Fig. 1).

The type of spectral behaviour shown in Fig. 1 was found to obtain in solvent compositions varying from ca. 96 mol% DMF, the upper limit studied, down to ca. 70 mol% DMF. However, in media of still lower DMF content another type of spectral behaviour was observed and this will be described subsequently. Increasing the concentrations of DNB and OH^- had no effect on the principal absorption at 526 nm under the condition that $[DNB] \geq [OH^-]$, but for $[DNB] < [OH^-]$ a different type of behaviour was observed (*vide infra*). At a relatively large DNB concentration and with the nitroaromatic in excess, the absorption maxima in the 350 nm region could not be seen, being swamped by the end absorption due to DNB. In the high DMF region, the rate of decay of the spectrum when DNB was in large excess over OH^- (0.5 *M* and 0.004 *M* respectively) was identical to that when the reagents were equimolar (0.004 *M*).

Addition of a slight excess (25%) of acid to a solution containing 0.004 *M* Me_4NOH and 0.1 *M* DNB led to instantaneous collapse of the entire visible spectrum. Addition to this solution, after an interval of 10 min, of an aliquot of base equivalent to the acid added earlier quantitatively restored the original spectrum. This type of behaviour is characteristic of Meisenheimer complex formation (1–5).

The stoichiometry of the colored species was investigated by means of a continuous variation (Job) plot (12) and the results for 81.8 mol% DMF are shown in Fig. 2. The two curves in this plot correspond to absorbances at 490 and 526 nm, which were chosen to determine whether changes in absorbance are dependent on the wavelength selected. In fact the curves in both cases are quite similar. Extrapolation in each case produces an apex corresponding to 0.47 mole fraction DNB, as opposed to 0.50 which would be expected for a 1:1 complex. However, careful scrutiny of the spectra upon which this plot is based reveals that more than one type of spectral behaviour is present. When $[DNB] \geq [OD^-]$, a single absorption at 526 nm occurs, which then slowly decreases with time. On

Can. J. Chem. Downloaded from www.nrcresearchpress.com by 210.87.254.40 on 09/06/12
For personal use only.

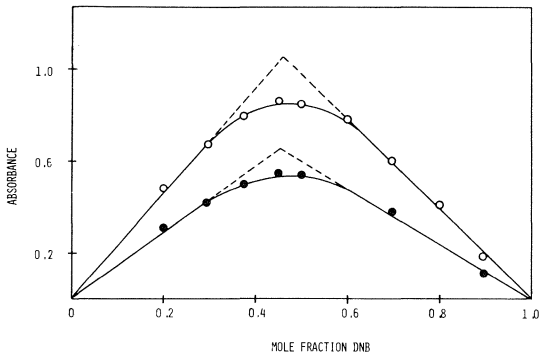

FIG. 2. Continuous variations plot for DNB + Me_4NOD system (total concentrations, 0.01 *M*) in 81.8 mol% DMF; absorbances in 0.1 mm cuvette at 526 nm (open circles) and 490 nm (closed circles).

the other hand, when [DNB] < [OD^-], the 526 nm absorption shifts with time to 533 nm, via an isosbestic point, and then slowly decreases. This suggests that another spectral species is formed when the base is in excess. The presence of this species, which could possibly result from addition of two hydroxide ion moieties to DNB, is presumably responsible for the lack of symmetry in the plots in Fig. 2. Since the isotopic exchange studies (10) were carried out under the conditions [DNB] ≫ [OD^-], the presence of only a 1:1 complex in those systems seems highly probable. It should be noted, however, that the Job method does not distinguish between a single 1:1 complex, and two (or more) 1:1 complexes coexisting in the same system.

Another, minor, spectral species could be discerned under some conditions in media containing <70 mol% DMF, and became somewhat more prominent as the DMF content was further decreased. A hint of this new species was first seen in the 68 mol% DMF medium, containing 2×10^{-4} *M* DNB and 1×10^{-2} *M* hydroxide ion, as a minor shoulder absorption at ca. 500 nm. This absorption remained following decay of the main absorption, λ_{max} 526 nm. The new species is visible more clearly in Fig. 3 which is applicable to 57.4 mol% DMF and [DNB] = [Me_4NOD] = 10^{-2} *M*. It is also seen that the spectra in this figure show an initial increase with time and upon reaching a maximum value begin to decay. This type of behaviour was found for all solutions containing <70 mol% DMF.

It was not possible to find conditions under which the 500 nm species predominated in the absence of the 526 nm species. As a result, the nature and stoichiometry of the former species could not be determined, though a possibility is σ-complex formation with the dimethylamine liberated in this system. This species should be unimportant under the typical conditions pertaining to the accompanying isotopic exchange study (10), namely in media of high DMF content and with DNB in large excess over the hydroxide (deuteroxide) ion concentration.

The increase in the 526 nm absorption in media containing <70 mol% DMF can be ascribed to a decrease in the forward rate constant for σ-complex formation as the aqueous component is increased. Such an effect was found in DMSO–methanol media where the rate of formation of the methoxide ion adduct of TNB and other nitroaromatics increased very greatly when the DMSO content was increased, but the rate of decomposition of the adduct was not appreciably affected

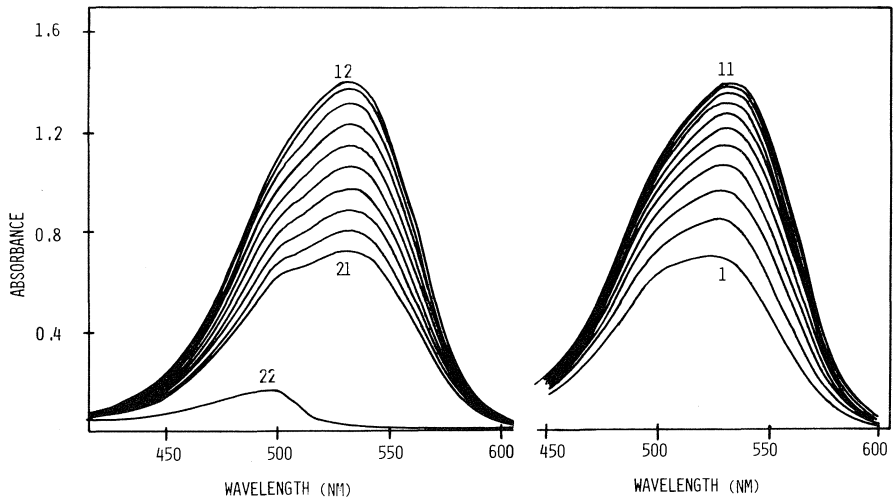

FIG. 3. Spectra of solution of DNB (0.01 *M*) and Me_4NOD (0.01 *M*) in 57.4 mol% DMF taken in 1 mm cuvette at various times after preparation: (1) 1 min, (11) 9 min, (12) 10 min, (21) 33 min, (22) 24 h.

Can. J. Chem. Downloaded from www.nrcresearchpress.com by 210.87.254.40 on 09/06/12
For personal use only.

thereby (12, 13). This is consistent with the present results.

The 1-Hydroxy-2,4-dinitrocyclohexadienate Anion and Other Species in DNB–Base Systems

Our results show that in media of relatively high DMF content one species predominates. It is concluded that this species is the 1-hydroxy-2,4-dinitrocyclohexadienate anion, **4**, formed by the addition of OH^- (OD^-) to a carbon *para* to one of the NO_2 groups in DNB, for which the absorption maximum occurs at 526 nm (Fig. 1). The isomeric structure **3** could be formed only as a transient species. The evidence which points to this conclusion is as follows.

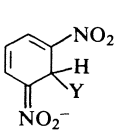

3

Y = OH or OD

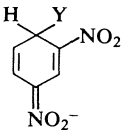

4

Unambiguous evidence concerning the structures of σ-complexes has been obtained by nmr spectroscopy for a variety of structural types (15–23). However, the nmr method has been found unworkable in the present system. This may be due in part to the generally low value of the equilibrium constant for formation of σ-complexes of DNB, simultaneously with its high affinity for electron transfer leading to the radical anion $DNB^{\cdot-}$ (24–28). Bellobono *et al.* (25) obtained evidence for the formation of $DNB^{\cdot-}$ by action of methanolic sodium methoxide on DNB, but only at very large MeONa concentrations (2.9–5 *M*). They reported a λ_{max} value of 500 nm for this species, which was also characterized by its esr spectrum. It was shown that $DNB^{\cdot-}$ was a reaction intermediate in the reduction of DNB to 3,3′-dinitroazoxybenzene, the final product. In contrast to the study of Bellobono *et al.* (25), under the conditions of the present study the spectral species with λ_{max} 348, 360, 526 nm was found to be formed reversibly, and DNB could be isolated in high yield on acidification (e.g. in the deuteration experiments). We can therefore exclude the formation of $DNB^{\cdot-}$ in the present system, except as a minor species.

Can one distinguish through uv–vis spectroscopy between the two σ-complexes **3** and **4**? Pollitt and Saunders (29) found that in σ-complex formation by 2,6- and 2,4-dinitroanisoles, the uv–vis spectra of adducts of type **5** were characteristically different from those of type **6** (for **5**, R = Me, λ_{max} 358, 586 nm; for **6**, R = Me, λ_{max} 348, 358, 503 nm), the longest wavelength absorption being the most intense in each case.

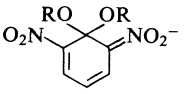

5

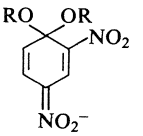

6

There was close similarity between the uv–vis spectra of **5** and **7**, and those of **6** and **8**. These structural assignments were confirmed in subsequent nmr studies on the σ-complexes **5**–**8** (28, 30).

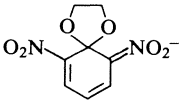

7

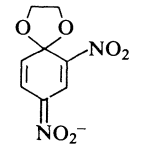

8

The uv–vis spectrum that we have observed in the DNB–DMF–H_2O–OH^- system, as shown in Fig. 1, fits closely the characteristics given for **6** but not for **5**.

Following the discovery by Servis (31) that 2,4,6-trinitroanisole (TNA) reacts with MeO^- to yield the C-3 adduct in a kinetically preferred process and the C-1 adduct by thermodynamic control, a number of studies have confirmed this type of behaviour in related systems (2–5). It has been shown by Hasegawa and Abe (32) that this applies equally to the dinitrobenzene series, including DNB and 2,4-dinitroanisole. In these cases, uv–vis spectra taken by means of a rapid scan spectrophotometer showed that the initial spectrum taken ≤ 1 s after mixing had the characteristics ascribed above to species **3** (Y = OMe) and **5** (R = Me), while spectra taken at later times corresponded to **4** (Y = OMe) and **6** (R = Me), respectively. Since in our work initial spectra were taken ~ 1 min after mixing, only the σ-complex **4** would be detectable.

Equilibrium Parameters and Medium Effects

Preliminary experiments indicated that the equilibrium constants for formation of σ-complex **4** increase greatly with an increase in the DMF content of the medium. In Fig. 4 is shown a qualitative measure of this effect, as a plot of absorbance vs. [DNB] at constant [OD^-], for two different medium compositions. Both plots show an initial increasing portion when the reactant concentrations are in the order [DNB] < [OD^-], and a plateauing when [DNB] > [OD^-]. The sharpness of the transitional region in these plots is an indication of the magnitude of K_e. In 88.6 mol% DMF, the absorbance has reached virtually its maximum value when DNB is only in slight excess over OD^-, in accord with a very large value of K_e.

Can. J. Chem. Downloaded from www.nrcresearchpress.com by 210.87.254.40 on 09/06/12
For personal use only.

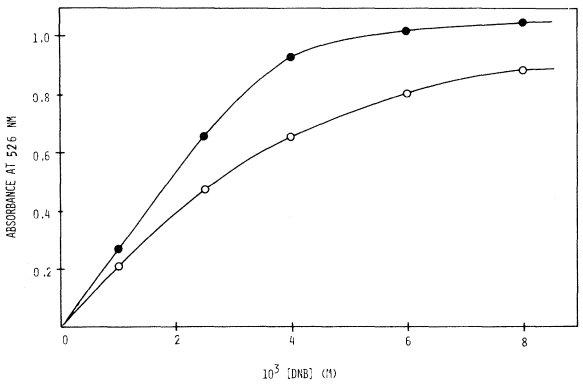

FIG. 4. Plot of absorbance vs. [DNB] at constant [Me_4NOD] (0.004 *M*) in 0.1 mm cuvette, for 81.8 mol% DMF (open circles) and 88.6 mol% DMF (closed circles).

Therefore, when K_e is large, that is in media of high DMF content, the molar absorptivity should readily be determined by the overload procedure, using a large excess of DNB over OH^- (or OD^-). Accordingly, typical measurements (Table 1) were performed using [Me_4NOD] = 0.004 *M* and [DNB] = 0.5 *M*, that is for [DNB]/[Me_4NOD] = 125:1. For the media with >70 mol% DMF, absorbance values at 526 nm were extrapolated with reasonable accuracy back to zero time, in order to correct for the decay of the spectra as a result of the reaction of OH^- with DMF. As noted earlier, in the 68.1 and 57.4 mol% DMF systems there was an initial increase in the absorbance prior to the slow decrease (Fig. 3). Since in these systems the absorbance passed through a maximum, this presented difficulty in determining the value to be used in subsequent calculations of K_e. An iterative method was adopted for this purpose (33) and gave results for the two solvent compositions which were consistent with expected trends (e.g. variation of K_e with solvent composition).

In Table 1 and Fig. 5 is shown the variation of the absorbance at 526 nm due to the σ-complex with the solvent composition, as determined in the above manner. It is seen that the absorbance rises steeply at first, reaching a near plateau at ca. 75 mol% DMF, and thereafter increases only very slightly as the DMF content is increased still further. The levelling off in absorbance indicates that beyond ca. 75 mol% DMF virtually all of the base has been complexed, the slight increase in absorbance in media richer in DMF being the result of a solvent effect on the extinction coefficient (9). The molar absorptivity (ε) at the absorption maximum in ≥75 mol% DMF is thus readily calculated from the relationship $A = \varepsilon cl$, where l is the cell path length and c is the hydroxide ion concentration which (as the species in deficit) will be equal to the stoichiometric concentration of σ-complex. For media containing ≥75 mol% DMF, A is the measured (limiting) absorbance value corresponding to the linear portion of the plot in Fig. 5. In media more aqueous than 75 mol% DMF, an extrapolated value from the linear plot was used, shown as the dotted line in Fig. 5. Because of the possibility of error in this procedure, it was only employed for media with >50 mol% DMF.

TABLE 1. Medium dependence of absorbance and molar absorptivities at 526 nm in DMF–D_2O system at 25°C (0.476 *M* DNB, 0.0038 *M* Me_4NOD)

Mol% DMF	A^a	ε M^{-1} cm^{-1}
57.4	0.286	26 600[b]
68.1	0.853	26 800[b]
73.3	0.993	27 000[c]
75.8	1.020	27 100[c]
81.8	1.033	27 200[c]
91.1	1.049	27 500[c]
95.8	1.050	27 700[c]

[a] Average values of absorbance, using 0.1 mm cuvette, extrapolated to zero time (see text).
[b] Extrapolated values based on dashed line in Fig. 5.
[c] Data from linear portion in Fig. 5.

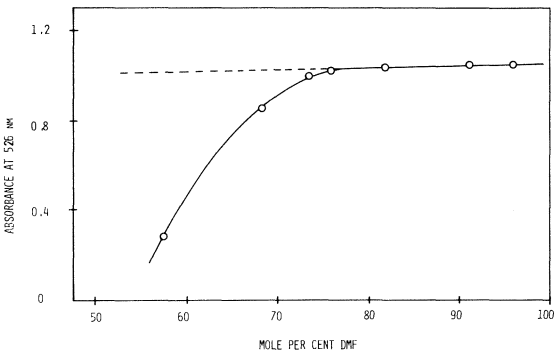

FIG. 5. Determination of molar absorptivity as function of medium composition by overload method for DNB = 0.5 *M*, Me_4NOD = 0.0038 *M*. Absorbances at 526 nm given relative to 0.1 mm cuvette.

The molar absorptivity values of **4** determined by the above procedure are given in Table 1 for a range of DMF–water solvent compositions. Another series of measurements was performed using H_2O as the aqueous component. The corresponding values were found to be identical within the error limits of these measurements (±2%).

With the molar absorptivity at λ_{max} for the σ-complex **4** in the various solvent compositions having been determined, the equilibrium constant for σ-complex formation could then be evaluated as a function of solvent composition. For this pur-

Can. J. Chem. Downloaded from www.nrcresearchpress.com by 210.87.254.40 on 09/06/12
For personal use only.

Can. J. Chem. Downloaded from www.nrcresearchpress.com by 210.87.254.40 on 09/06/12
For personal use only.

pose, the absorbance of a series of solutions containing equimolar concentrations of DNB and Me_4NOD was determined as a function of DMF composition, at 25°C. The concentration of **4** in these solutions can be obtained from the relationship $A = \varepsilon[\mathbf{4}]l$. The expression [1] for K_e containing the equilibrium species concentrations

$$[1] \quad K_e = \frac{[\mathbf{4}]}{[DNB]_e[OH^-]_e}$$

is then transformed into eq. [2] by substituting $[DNB]_e = [DNB]_0 - [\mathbf{4}]$ and $[OH^-]_e = [OH^-]_0 - [\mathbf{4}]$.

$$[2] \quad K_e = \frac{[\mathbf{4}]}{([DNB]_0 - [\mathbf{4}])([OH^-]_0 - [\mathbf{4}])}$$

The resulting K_e values are presented in Table 2. The uncertainty limits in these K_e values are considerable when K_e is large. For example in the 95.8 mol% DMF system (K_e ca. 10^5) a change of 1% in the absorbance value leads to a change of ca. 100% in K_e. However, in 75.8 mol% DMF an uncertainty of ±5% in the absorbance leads to uncertainty limits of ±10% in K_e. A noteworthy point is that in the several instances where a range of equimolar concentrations of the reagents was used, there was only moderate effect on the equilibrium constant. This suggests that the orders of magnitude of the K_e values might be generally applicable to other concentration values (10).

TABLE 2. Dependence of equilibrium constant for σ-complex formation on medium composition in DMF–D_2O system at 25°C[a]

Mol% DMF	$10^3[DNB]_0$ ($10^3[OD^-]_0$) M	$10^3[\mathbf{4}]$[b] M	K_e[c] M^{-1}
57.4	10.0	0.526	7.5[d]
68.1	10.0	2.55	62[d]
68.1	4.0	0.472	55[d]
73.3	10.0	3.64	90
73.3	4.0	0.882	91
75.8	10.0	4.59	1.6×10^2
75.8	4.0	1.18	1.5×10^2
81.8	2.0	0.875	6.9×10^2
81.8	4.0	2.33	8.9×10^2
81.8	5.0	3.12	9.9×10^2
81.8	8.0	5.86	1.3×10^3
85.0	4.0	2.97	2.8×10^3
88.6	3.0	2.41	6.9×10^3
88.6	4.0	3.41	9.9×10^3
91.1	4.0	3.67	3.6×10^4
95.8	4.0	3.88	3.1×10^5

[a]Results given are mean values of several measurements (see text for error limits).
[b]Concentration of σ-complex, calculated from expression $A = \varepsilon[\mathbf{4}]l$ where $l = 0.01$ cm, using values of A extrapolated to zero time (see text).
[c]Calculated via eq. [2].
[d]Values obtained by iteration procedure (see text). Uncorrected K_e values based on maximum absorbances reached are $5.9\,M^{-1}$ for 57.4 mol% DMF and $41\,M^{-1}$ for 68.1 mol% DMF.

A second series of experiments was performed for the DMF–H_2O–Me_4NOH system as a function of solvent composition, using equimolar DNB and base solutions ($0.004\,M$), which yielded K_e values for the undeuterated media. The results are summarized in Table 3, which also gives the corresponding K_e values for the deuterated media, as well as the equilibrium constant ratio, that is the solvent isotope effect. The results for the 68.1 and 75.8 mol% solvent compositions are subject to error owing to the facility of the reaction of OH^- with DMF when K_e is relatively small, while in 95.8 mol% DMF the very large K_e value magnifies the error inherent in the experimental method. These considerations lead to a $K_e(D_2O)/K_e(H_2O)$ ratio in the region of 0.35–0.40 for this process.

Previous work has yielded solvent isotope effects for σ-complex formation processes varying between 0.38 and 0.54 (34–36). Use of Bunton and Shiner's model (37) led to a theoretical solvent isotope effect of 0.47 for the formation of **6** (R = Me), in close agreement with the experimental value of 0.38 (35).

Structural, Medium, and Basicity Correlations in Complexation

Table 2 shows that the medium effect on K_e is very large, that is K_e increasing from $7.5\,M^{-1}$ to $3.1 \times 10^5\,M^{-1}$ as the DMF content is increased from 57.4 to 95.8 mol%. In our previous work with TNB it was found that K_e increased from $5\,M^{-1}$ to $2 \times 10^4\,M^{-1}$ on increasing the DMF content of the medium from 1 to 33.8 mol% (9). In order to compare the data for the two systems more directly, one can extrapolate the log K_e vs. H_- plot (Fig. 6) for DNB to the H_- value for 33.8 mol% DMF (i.e. $H_- = 14.8$), yielding $K_e = 0.2\,M^{-1}$. This leads to an equilibrium constant ratio, $K_e(TNB)/K_e(DNB)$, of 10^5. The greater stability of σ-complexes derived from trinitroaromatic substrates, compared with corresponding dinitroaromatics has been noted in previous work (35, 38).

TABLE 3. Solvent isotope effect data on equilibrium constant for σ-complex formation[a]

Mol% DMF	$K_e(H_2O)$ M^{-1}	$K_e(D_2O)$ M^{-1}	$K_e(D_2O)/K_e(H_2O)$
68.1	33	55	0.60
75.8	1.2×10^2	1.5×10^2	0.80
81.8	3.5×10^2	8.9×10^2	0.39
88.6	3.5×10^3	9.9×10^2	0.35
91.1	1.2×10^4	3.6×10^4	0.33
95.8	9.5×10^4	3.1×10^5	0.31

[a]See footnotes to Table 2 for conditions and methods pertaining to measurement of K_e's.

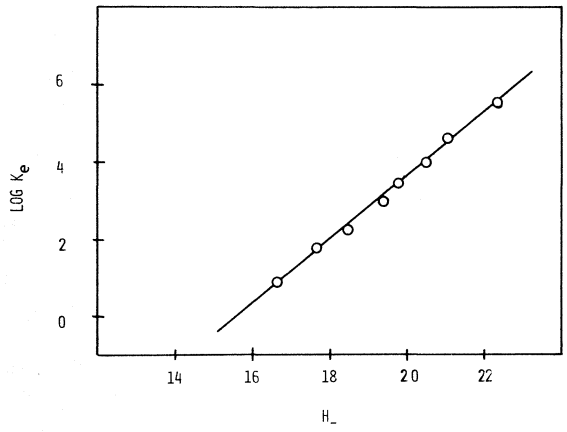

FIG. 6. Plot of log K_e for σ-complex formation vs. H_- acidity function in aqueous DMF system.

An estimate of the medium effect on K_e for the DNB·OH^- σ-complex can be extended to the entire DMF–water solvent system. Extrapolating the plot in Fig. 6 to more aqueous media, using the known H_- values applicable to this system (39), yields an estimated K_e in purely aqueous medium of $4 \times 10^{-4}\ M^{-1}$. One hence obtains for the increase in K_e on going from aqueous to 96 mol% DMF, a factor of ca. 10^9. Using an extrapolation procedure, Crampton estimated that formation of the TNB·OMe^- σ-complex is subject to an enhancement of 10^8 on going from methanol to DMSO medium (40). The generally held explanation of these very large medium effects considers desolvation of charge localized anions such as OH^- or OMe^- in dipolar aprotic media as the main factor, being supplemented in part by increased solvation of the σ-complex, with charge delocalized over the aromatic system (6, 41).

It appears from Fig. 6 that there is a reasonably satisfactory correlation between log K_e and H_-, as a measure of medium basicity (slope of plot, 0.83). However, H_- is referenced with respect to proton abstraction by hydroxide ion, whereas the present process is concerned with hydroxide ion addition. On the other hand, the J_- function has been proposed as a measure of the addition of base to an aromatic system (42). Only scant measurements of this function have been reported so far (42, 43) and no data are available for the aqueous DMF system. It would be desirable to extend the measurement of various solvent parameters (44) to DMF and its mixtures with hydroxylic solvents.

An unusual aspect of the present system is that in the series of measurements designed to evaluate the effect of medium changes on K_e, as depicted in Tables 1 and 2, the increased extent of σ-complex formation results in continuously decreasing concentration of free (uncomplexed) hydroxide ion. On the other hand, the medium basicity, as measured by the conventional H_- function, refers to constant hydroxide ion concentration (0.01 *M*). It is possible to take into account the variation in [OH^-], using the known K_e values in the various media (Table 2), and thereby calculate values of a new function, H_- (equil), as given in Table 4. These data allow one to construct the corresponding log K_e vs. H_- (equil) plot, which is also found to show fair linearity, slope 1.30. In this way account is taken of the changing OH^- concentration as well as the changing hydroxide ion activity as the medium is changed, whereas the conventional treatment reflects only the changes in the latter. However, a drawback of this approach is its limited applicability, since H_- (equil) will vary from one system to another depending on the values of K_e. On the other hand a plot, for example, of log K_e vs. mol% DMF would afford little insight since one can conceive that the decreasing base concentration could more than compensate for the increased base activity. In that case K_e could diminish with increasing DMF content, which would be puzzling indeed unless the change in free OH^- were noted.

An interesting possibility which should be considered is that the σ-complex itself would contribute to the basicity of the medium in these systems. Thus as K_e increases in magnitude and the free [OH^-] becomes very small, the contribution to medium basicity from the σ-complex would become increasingly significant relative to that of OH^-. This would tend to stabilize the medium basicity, since at very large K_e values the concentration of the σ-complex changes only slightly (Table 2). This reasoning would also serve to justify the use of the conventional H_- function in

TABLE 4. Variation of H_- function in aqueous DMF systems: (a) using constant [OH^-]; (b) under conditions where σ-complex formation occurs to significant extent

Mol% DMF	H_-[a]	H_- (equil)[b]
57.4	16.65	16.00
68.1	17.65	16.22
73.3	18.20	16.56
75.8	18.50	16.65
81.8	19.40	16.80
91.1	21.05	16.90
95.8	22.35	17.19

[a]Calculated from data in ref. 39 by means of correction factor for change in [Me_4NOH] from 0.019 *M* to 0.0038 *M* applicable to present system. Data for 91.1 and 95.8 mol% DMF are estimated values.

[b]Calculated H_- values based on the free (uncomplexed) hydroxide ion concentration in DNB–OH^- – DMF–H_2O systems where a significant proportion of OH^- is tied up as the DNB·OH^- σ-complex. The uncomplexed [OH^-] is calculated using K_e values in Table 2(3) for media containing $[DNB]_0 = [OH^-]_0 = 0.004$ *M*.

Can. J. Chem. Downloaded from www.nrcresearchpress.com by 210.87.254.40 on 09/06/12
For personal use only.

Can. J. Chem. Downloaded from www.nrcresearchpress.com by 210.87.254.40 on 09/06/12
For personal use only.

correlations with reaction parameters (e.g. Fig. 6), rather than H_- values based on free hydroxide ion concentrations in systems where extensive complexation has occurred.

Finally, our discussion is also pertinent with respect to the two widely used methods for evaluating complexation constants, namely the Benesi–Hildebrand method (45) and the presently used method based on absorbance measurements of equimolar solutions of the interacting species (12*b*). A unique difficulty arises in the application of these methods to systems where one of the species partaking in the equilibrium contributes significantly to the overall basicity (or another property) of the medium. It is apparent that K_e determined by such methods should be dependent on the actual concentration values of the species (e.g. OH^-) which are employed. A moderate effect of $[OH^-]$ on K_e values in the present work has already been noted (Table 2). Previous work has also demonstrated the dependence of K_e for σ-complex formation on [NaOMe] for various nitroaromatics (35, 46), but such results have generally been ascribed to salt effects or ion pairing effects (47).

Experimental

Tetramethylammonium hydroxide (Matheson, Coleman & Bell), purchased as a 25% solution, was diluted to 2 *M* and titrated with standard acid. A solution of Me_4NOD was prepared by evaporating the 25% Me_4NOH solution *in vacuo* until syrupy, followed by two treatments with D_2O (99.5%) and its removal *in vacuo* at 25°C, before the final dilution with D_2O to 1.9 *M*. DNB (Fisher Certified Reagent) was recrystallized twice from ethanol, mp 89.0–89.5°C (uncorrected), λ(ε) 234 nm (17 800 M^{-1} cm^{-1}). DMF (Fisher Certified Reagent) was distilled from P_2O_5 under vacuum.

In preparation of the reaction solutions for spectrophotometric measurement, stock solutions of $DMF/Me_4NOH/H_2O$ were not used in order to minimize the basic hydrolysis of DMF. The following procedure was hence adopted. DNB was weighed into a 25 mL volumetric flask, which was placed in a thermostated bath at 25°C, an appropriate volume of H_2O (D_2O) was added and made up to mark with DMF, weighing after each addition. The Me_4NOH (Me_4NOD) solution was added by means of a 50 μL syringe fitted with a Chaney adaptor and, after shaking to mix, an aliquot was transferred to a cuvette (0.01 to 1 cm) for spectrophotometric measurement. A Unicam SP800B spectrophotometer equipped with a thermostated cell holder was used. Spectral scans were run over the 300–600 nm region at regular intervals in those cases where the spectra exhibited a decrease (increase) as a function of time.

Acknowledgments

We thank the Natural Sciences and Engineering Research Council of Canada for a grant and Queen's University for a scholarship (A.Z.).

1. R. Foster and C. A. Fyfe. Pure Appl. Chem. Australia, **16**, 61 (1966).
2. M. R. Crampton. Adv. Phys. Org. Chem. **7**, 211 (1969).
3. M. J. Strauss. Chem. Rev. **70**, 667 (1970); Acc. Chem. Res. **7**, 181 (1974).
4. C. F. Bernasconi. MTP Int. Rev. Sci.: Org. Chem. Ser. One, **3**, 33 (1973).
5. E. Buncel. The chemistry of functional groups. Nitro and nitroso groups. Supplement F. *Edited by* S. Patai. Interscience, London. 1981.
6. E. Buncel and H. Wilson. Adv. Phys. Org. Chem. **14**, 133 (1977); E. Buncel and H. Wilson. Acc. Chem. Res. **12**, 42 (1979).
7. E. Buncel, A. R. Norris, K. E. Russell, and R. Tucker. J. Am. Chem. Soc. **94**, 1646 (1972); E. Buncel, A. R. Norris, K. E. Russell, and H. Wilson. Can. J. Chem. **52**, 2306 (1974).
8. E. Buncel and E. A. Symons. J. Org. Chem. **38**, 1201 (1973).
9. E. A. Symons and E. Buncel. Can. J. Chem. **50**, 1729 (1972).
10. E. Buncel and A. W. Zabel. Can. J. Chem. **59**, 3177 (1981).
11. E. Buncel and E. A. Symons. J. Chem. Soc. Chem. Commun. 164 (1970); E. Buncel, S. Kesmarky, and E. A. Symons. J. Chem. Soc. Chem. Commun. 120 (1971).
12. (*a*) P. Job. C. R. Acad. Sci. **180**, 928 (1925); (*b*) M. M. Jones. Elementary coordination chemistry. Prentice Hall, Englewood Cliffs, NJ. 1964. Chapt. 8.
13. E. J. Fendler, J. H. Fendler, C. E. Griffin, and J. W. Larsen. J. Org. Chem. **35**, 287 (1970).
14. F. Terrier and F. Millot. Bull. Soc. Chim. Fr. 2694 (1969); 1743 (1970).
15. C. F. Bernasconi and M. C. Muller. J. Am. Chem. Soc. **100**, 5530 (1978).
16. E. J. Fendler, J. H. Fendler, N. L. Arthur, and C. E. Griffin. J. Org. Chem. **37**, 812 (1972).
17. M. R. Crampton and M. J. Willison. J. Chem. Soc. Chem. Commun. 215 (1973).
18. A. R. Norris. J. Org. Chem. **34**, 1486 (1969).
19. J. A. Chudek and R. Foster. J. Chem. Soc. Perkin Trans. II, 628 (1979).
20. C. A. Fyfe, M. Cocivera, and S. W. H. Damji. Acc. Chem. Res. **11**, 277 (1978).
21. S. Sekiguchi, T. Itagaki, T. Hirose, K. Matsui, and K. Sekine. Tetrahedron, **29**, 3527 (1973).
22. G. Doddi, G. Illuminati and F. Stegel. J. Chem. Soc. Chem. Commun. 953 (1969); P. Mencarelli and F. Stegel. J. Chem. Soc. Chem. Commun. 564 (1978).
23. E. Buncel and J. G. K. Webb. Can. J. Chem. **52**, 630 (1974); E. Buncel, A. Jonczyk, and J. G. K. Webb. Can. J. Chem. **53**, 3761 (1975); E. Buncel, N. Chuaqui-Offermanns, R. Y. Moir, and A. R. Norris. Can. J. Chem. **57**, 494 (1979).
24. G. A. Russell, E. G. Janzen, and E. T. Strom. J. Am. Chem. Soc. **86**, 1807 (1964).
25. I. R. Bellobono, A. Gamba, G. Sala, and M. Tampieri. J. Am. Chem. Soc. **94**, 5781 (1972).
26. E. Buncel and B. C. Menon. J. Am. Chem. Soc. **102**, 3499 (1980).
27. R. D. Guthrie. Comprehensive carbanion chemistry. Vol. 1. *Edited by* E. Buncel and T. Durst. Elsevier, Amsterdam. 1980.
28. R. Foster and C. A. Fyfe. Tetrahedron, **21**, 3363 (1965); C. A. Fyfe. The chemistry of the hydroxyl group. Part. 1. *Edited by* S. Patai. Interscience, London. 1971.
29. R. J. Pollitt and B. C. Saunders. J. Chem. Soc. 1132 (1964); 4615 (1965).
30. M. R. Crampton and V. Gold. J. Chem. Soc. B, 893 (1966).
31. K. L. Servis. J. Am. Chem. Soc. **87**, 5495 (1965); **89**, 1508 (1967).
32. Y. Hasegawa and T. Abe. Bull. Soc. Chem. Jpn. **46**, 2756 (1973).

33. A. W. ZABEL. Ph.D. Thesis, Queen's University.
34. J. H. FENDLER, E. J. FENDLER, and C. E. GRIFFIN. J. Org. Chem. **34**, 689 (1969).
35. C. F. BERNASCONI. J. Am. Chem. Soc. **90**, 4982 (1968).
36. I. R. BELLOBONO, P. BELTRAME, M. G. CATTANIA, and M. SIMONETTA. Tetrahedron Lett. 2673 (1968).
37. C. A. BUNTON and V. J. SHINER. J. Am. Chem. Soc. **83**, 3207 (1961).
38. V. GOLD and C. H. ROCHESTER. J. Chem. Soc. 1687 (1964); F. TERRIER, P. PASTOUR, and R. SCHAAL. C. R. Acad. Sci. **260**, 5783 (1965); J. H. FENDLER, W. L. HINZE, and L. J. LIU. J. Chem. Soc. Perkin Trans. II, 1768 (1975).
39. E. BUNCEL, E. A. SYMONS, D. DOLMAN, and R. STEWART. Can. J. Chem. **48**, 3354 (1970).
40. M. R. CRAMPTON. J. Chem. Soc. 1208 (1968).
41. A. J. PARKER. Chem. Rev. **69**, 1 (1969).
42. C. H. ROCHESTER. Acidity functions. Academic Press, London. 1970.
43. M. R. CRAMPTON, M. A. EL GHARIANI, and H. A. KHAN. J. Chem. Soc. Perkin Trans. II, 1178 (1972).
44. C. REICHARDT. Solvent effects in organic chemistry. Verlag Chemie, Weinheim, 1979; Angew. Chem. Int. Ed. Engl. **18**, 98 (1979).
45. H. A. BENESI and J. H. HILDEBRAND. J. Am. Chem. Soc. **71**, 2703 (1949).
46. J. H. FENDLER, E. J. FENDLER, W. E. BYRNE, and C. E. GRIFFIN. J. Org. Chem. **33**, 977 (1968); M. R. CRAMPTON and H. A. KHAN. J. Chem. Soc. Perkin Trans. II, 1173 (1972).
47. E. BUNCEL and W. EGGIMANN. J. Chem. Soc. Perkin Trans. II, 673 (1978).

Can. J. Chem. Downloaded from www.nrcresearchpress.com by 210.87.254.40 on 09/06/12
For personal use only.

Hydrogen exchange studies. XIV.[1] Kinetics and mechanism of base-catalyzed hydrogen exchange in 1,3-dinitrobenzene in aqueous dimethylformamide and relationship with σ-complex formation[2]

ERWIN BUNCEL AND ALLEN W. ZABEL
Department of Chemistry, Queen's University, Kingston, Ont., Canada K7L 3N6

Received April 30, 1981

ERWIN BUNCEL and ALLEN W. ZABEL. Can. J. Chem. **59**, 3177 (1981).

Kinetic data have been evaluated for hydrogen exchange in 1,3-dinitrobenzene (DNB), occurring at the 2-position, in dimethylformamide (DMF) – D_2O mixtures containing deuteroxide ion. The pseudo first order rate constants for exchange, k_{obs}, show inverse dependence on the initial DNB concentration, which can be quantitatively related to the extent of σ-complex formation in these systems. The profile for k_{obs} as function of medium composition exhibits a maximum at ca. 70 mol% DMF, and ε_{app} for σ-complex formation reaches a plateau at about the same medium composition. The equilibrium constants for σ-complex formation, K_e, are used to calculate the free, or uncomplexed, deuteroxide ion concentrations, which then allow one to calculate k_2, the second order rate constants for exchange. The k_2 values show a uniformly increasing tendency with increased DMF content. Correlations with medium basicity are examined, and the nature of the log k_2 and log K_e vs. H_- plots afford insight into the origin of the medium dependence of proton exchange. The results of the present study are consistent with the σ-complex being an unreactive form of the substrate towards exchange, which occurs via uncomplexed DNB present in small concentration. The study also rules out the possibility that the colored species present in these systems is the carbanion formed on deprotonation of DNB.

ERWIN BUNCEL et ALLEN W. ZABEL. Can. J. Chem. **59**, 3177 (1981).

On a évalué les données cinétiques de l'échange d'hydrogène se produisant en position 2 du dinitro-1,3 benzène (DNB) dans des mélanges de diméthylformamide (DMF) – D_2O contenant l'ion deutéroxyde. La constante de vitesse de pseudo ordre un de l'échange k_{obs}, révèle un effet inverse de la concentration initiale de DNB qui peut être relié quantitativement aux taux de formation du complexe σ dans ces systèmes. Le profil de k_{obs} en fonction de la composition du milieu montre un maximum pour environ 70 mol% de DMF et le ε_{app} de la formation du complexe σ atteint un plateau pour environ la même composition du milieu. On a utilisé la constante d'équilibre de la formation du complexe σ K_e, pour calculer les concentrations de l'ion deutéroxyde libre, ou non complexé qui permettent de calculer k_2 la constante de vitesse d'ordre deux de l'échange. Les valeurs de k_2 montrent une tendance d'augmentation uniforme avec la teneur en DMF. On a examiné les corrélations avec la basicité du milieu; la nature des courbes de log k_2 et log K_e en fonction de H_- fournit des renseignements sur l'origine de l'effet du milieu lors de l'échange de proton. Les résultats de la présente étude sont en accord avec un complexe σ qui ne donnerait pas de réaction d'échange celui-ci se produisant par l'intermédiaire du DNB non complexé présent à une concentration faible. L'étude écarte également la possibilité que l'espèce colorée présente dans ces systèmes soit le carbanion formé par la protonation du DNB.

[Traduit par le journal]

The capability of aromatic nitro compounds to interact with bases by a number of mechanisms has led to controversy regarding the occurrence and importance of nuclear hydrogen exchange (1–6). In the case of 1,3-dinitrobenzene (DNB), the species that have been postulated to be formed at different times through action of a base Y: are a charge transfer complex **1**, a radical anion **2**, covalent adducts (also known as Meisenheimer or σ-complexes) **3** and **4**, as well as the carbanions **5** and **6** which are the presumed intermediates in proton exchange.

1

2

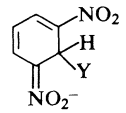

3

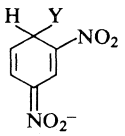

4

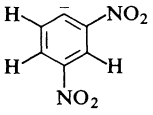

5

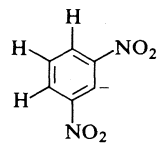

6

The characteristic appearance of color on addition of base to DNB does not immediately serve to distinguish between these species; there is evidence that most of these species are colored. For example, the appearance of a new band characteristic of the charge-transfer type of interaction has been well documented (7–9). Similarly, radical anions of nitroaromatics formed via electron transfer processes have also been spectrally characterized (10–12). A variety of σ-complexes which are

[1]Parts X–XIII are refs. 40, 59, 29, and 60, respectively.

[2]Presented in part at the 5th International Conference on Solute–Solvent Interactions, Florence, Italy, 1980.

0008-4042/81/223177-11$01.00/0

©1981 National Research Council of Canada/Conseil national de recherches du Canada

Can. J. Chem. Downloaded from www.nrcresearchpress.com by 210.87.254.42 on 09/06/12
For personal use only.

Can. J. Chem. Downloaded from www.nrcresearchpress.com by 210.87.254.42 on 09/06/12
For personal use only.

closely analogous to **3** and **4** have been characterized by nmr as well as uv–vis spectroscopy (1–6, 13–22). However, there is as yet no unambiguous uv–vis or nmr evidence for the carbanions **5** and **6**.

In one of the original studies of deuterium exchange in DNB, as catalyzed by deuteroxide ion in dimethylformamide (DMF) – D_2O medium, the solution color was in fact ascribed to species **5** and/or **6** (23).[3] However, in a subsequent study but using methanolic dimethyl sulfoxide (DMSO) solutions, Crampton and Gold (24) disagreed with the earlier interpretation (*vide infra*).

In a preliminary communication we have described some initial results on hydrogen–deuterium exchange in DNB in a number of basic systems (25). Subsequently we carried out a detailed kinetic study of deuterium exchange in 1,3,5-trinitrobenzene (TNB) in the DMF–D_2O–OD^- system (26). An unusual kinetic behaviour was observed and discussed on the basis of σ-complex formation (27) competing with proton exchange. We now report a complementary study for the case of DNB. In the accompanying paper we describe pertinent results on σ-complex formation in this system (28).

Results and Discussion

Proton Exchange vs. σ-Complex Formation

We have found that the deuteroxide ion catalyzed proton exchange in DNB in DMF–D_2O mixtures occurs readily, under mild conditions. For example, in 68 mol% DMF, a solution of 0.5 *M* DNB containing 0.004 *M* NaOD, at 25°C, undergoes virtually complete exchange in ~ 20 min. Only the proton in the 2-position was found to exchange, as shown by nmr on the recovered substrate following acidification of the reaction solution; there was no detectable exchange at the 4(6)-positions. This is in agreement with the earlier report by Pollitt and Saunders (23) for exchange in DNB in DMF–D_2O–NaOD. However, in a recent study (29) of tritium exchange in DNB we found, through tritium nmr spectroscopy, that whereas under mild conditions (CH_3ONa–HTO–dioxan) exchange was confined to the 2-position, under more strongly basic conditions (CH_3ONa–HTO–HMPT) exchange occurred also at the equivalent 4(6)-positions (30). We then showed that the reactivity of the C-2 proton was ca. 2000 times greater than that of the C-4(6) protons, which would explain the lack of observation of C-4 proton exchange in the present work, as monitored by the relatively insensitive nmr method.

[3]Though exchange occurs largely from the 2-position of DNB, Pollitt and Saunders (23) considered that the uv–vis spectrum was more readily explained in terms of proton loss from the 4-position.

The reaction solutions undergoing exchange were found to be strongly colored, varying from pink to dark ruby red depending on the DMF composition and NaOD concentration. This brings into question the nature of the colored species and its role in the exchange process.

In the accompanying paper (28) we have reported on a uv–vis spectroscopic study of σ-complex formation between DNB and hydroxide or deuteroxide ion in DMF media containing H_2O or D_2O. Evidence was presented that the major covalent interaction is formation of σ-complex **7**, through addition of OD^- (OH^-) at C-4. Minor processes yielding **8** and other complexes may occur under some conditions. However, these interactions are not considered important under typical exchange conditions and will hence be disregarded in our subsequent discussions.

What will be the effect of σ-complex formation on proton exchange? The question of the interrelationship between these two processes will be central to most of the considerations in this paper.

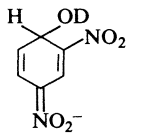

7

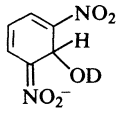

8

Apparent Reaction Orders in Deuteroxide and Dinitrobenzene

The effect of varying the deuteroxide ion and DNB concentrations on the exchange rate was first examined at constant medium composition. The solvent composition of 68.1 mol% DMF was chosen since with a DNB concentration of 0.50 *M*, which was its maximum value throughout the study, the exchangeable D/H ratio in the system would be 20:1 on the basis of one labile hydrogen in the substrate. This would then allow exchange to reach 95% completion ignoring any possible equilibrium isotope effects.

Two series of exchange runs were performed, at 25°C, in which the initial sodium deuteroxide concentration, $[NaOD]_0$, was varied at two given DNB concentrations, namely at $[DNB]_0 = 0.50\,M$ and 0.25 *M*. The pseudo first order rate constants, k_{obs}, are given in Table 1. A typical kinetic plot is displayed in Fig. 1 and shows fairly good linear behaviour in the pseudo first order plot up to ca. 75% exchange.

A plot of $\log k_{obs}$ vs. $\log [NaOD]_0$ is shown in Fig. 2, corresponding to the results for 0.5 *M* DNB. The slope of the line drawn is 1.0. The data for 0.25 *M* DNB yield a plot with slope 1.2. It appears that the order with respect to OD^- is close to unity,

Can. J. Chem. Downloaded from www.nrcresearchpress.com by 210.87.254.42 on 09/06/12
For personal use only.

TABLE 1. Kinetic data for proton exchange in DNB as function of initial substrate and deuteroxide ion concentration in 68.1 mol% DMF at 25°C

	$10^3[NaOD]_0$ M	$10^3 k_{obs}$ s^{-1}
0.50 M	2.48	2.66
	4.97	7.59
	4.97	6.91
	7.45	8.34
	9.94	11.8
	9.94	12.5
	9.94	13.3
	12.5	16.4
	12.5	15.8
	13.2	17.0
	14.9	19.3
	16.2	21.7
	17.5	22.6
	19.8	23.5
	22.4	25.9
	22.4	24.9
0.25 M DNB	2.48	4.05
	3.73	8.37
	4.97	12.9
	4.97	11.1
	7.45	18.4
	7.45	20.2
	9.94	27.5

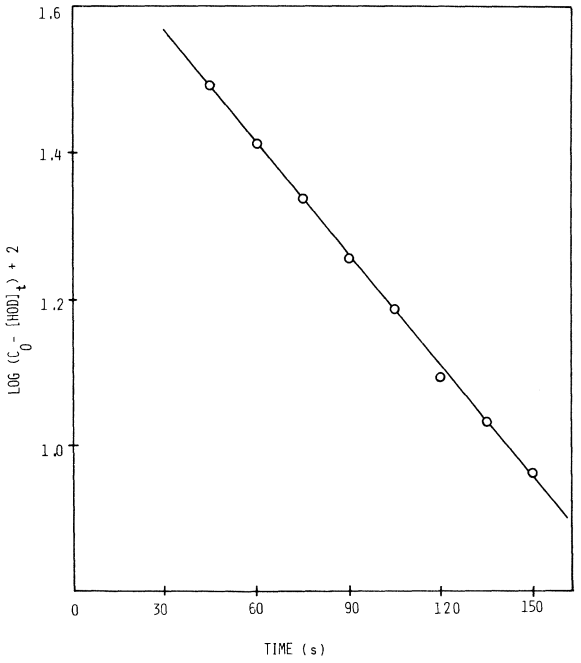

FIG. 1. Pseudo first order plot for proton exchange in DNB (0.5 M) in 68.1 mol per cent DMF containing 9.8 × 10^{-3} M NaOD/D_2O at 25°C.

although the meaning of these plots will be reexamined subsequently.

Inspection of the data in Table 1 shows that k_{obs} is not independent of the initial, stoichiometric DNB concentration as might have been expected for a pseudo first order process. In fact, at constant $[NaOD]_0$, the rate approximately doubles when $[DNB]_0$ is halved. These results are reminiscent of the situation encountered previously with TNB (26) and suggest the following analogous explanation.

We consider that isotopic exchange occurs only through interaction between the uncomplexed, or free DNB and OD^- entities. With the concurrent equilibrium yielding the σ-complex (7) established, i.e. DNB + $OD^- \rightleftarrows$ DNB.OD^-, one has to evaluate the free, or uncomplexed concentrations, $[DNB]_e$ and $[OD^-]_e$, as a function of $[DNB]_0$ and $[NaOD]_0$. The details of the method of calculation are given in the Appendix. The results, summarized in Table 2, indicate an approximately inverse relationship between $[DNB]_0$ and $[OD^-]_e$, which is in accord with the observation of approximately inverse dependence between k_{obs} and $[DNB]_0$ at constant $[NaOD]_0$ (Table 1).

This treatment points also to a reinterpretation of the significance of the log k_{obs} vs. log $[NaOD]_0$ plot (Fig. 2). As seen in Table 2, the $[OD^-]_e$ values show approximately direct proportionality to $[NaOD]_0$

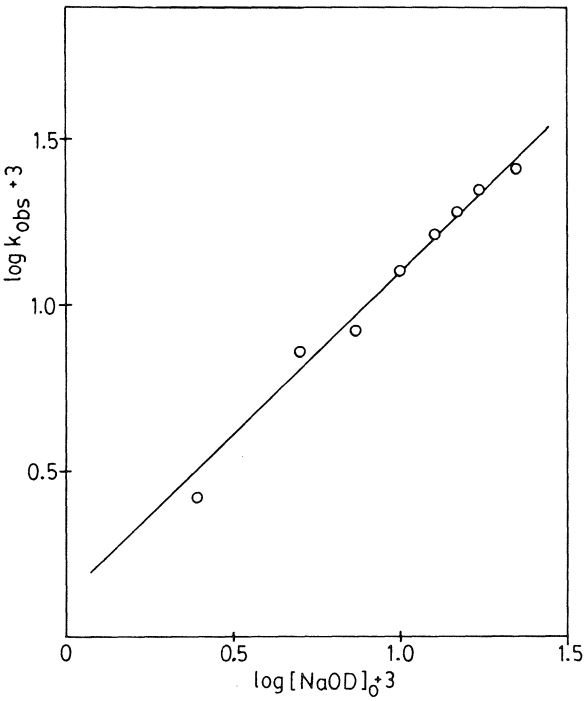

FIG. 2. Plot of log k_{obs} vs. log $[NaOD]_0$ for proton exchange in DNB in 68.1 mol per cent DMF at 25°C.

Can. J. Chem. Downloaded from www.nrcresearchpress.com by 210.87.254.42 on 09/06/12
For personal use only.

TABLE 2. Calculation of uncomplexed (free) deuteroxide ion concentration under conditions of proton exchange in DNB, in 68.1 mol% DMF (K_e = 55 L mol^{-1})[a]

$[DNB]_0$ *M*	$[NaOD]_0$ *M*	$10^3[DNB.OD^-]$ *M*	$10^3[OD^-]_e$ *M*
0.50	0.0040	3.859	0.141
0.50	0.0080	3.725	0.275
0.25	0.0040	7.715	0.285
0.25	0.0080	7.442	0.558

[a]See Appendix for method of calculation.

values, at constant $[DNB]_0$. Hence an increase in $[NaOD]_0$ will be reflected in proportional increase in k_{obs}.

Thus the results on the variation of k_{obs} with reactant concentrations (Table 1) are self-consistent and in accord with the σ-complex being an unreactive form of DNB as well as of OD^-. The observed rate behaviours as a function of initial reactant concentrations are a consequence of the relatively large value of the equilibrium constant for σ-complex formation, as well as the large excess of DNB over OD^-, thus resulting in the OD^- being essentially tied up in the form of the unreactive σ-complex.

Medium Dependence of Proton Exchange

Base catalyzed proton exchange processes are generally strongly accelerated in dipolar aprotic media such as DMSO or DMF, relative to typical hydroxylic solvents such as water or methanol (31, 32). The magnitude of such rate enhancement can, however, vary greatly depending on the system involved. Thus whereas a number of processes in which proton transfer from substrate to base is rate-determining exhibit rate enhancements of 10^{10} or more when the medium is changed from aqueous (or alcoholic) to ~ 99 mol% DMSO (33–38), exchange of D_2 in the DMSO–H_2O–OH^- system is accelerated only by ~ 10^4 when the medium is changed from purely aqueous to 99.5% DMSO (39, 40).

We have evaluated the effect of changing medium composition on the rate of proton exchange in DNB for the DMF–D_2O system. Thus a series of exchange reactions was performed in DMF–D_2O solvent mixtures ranging from 47.5 mol% DMF to 95.8 mol% DMF, keeping the DNB and OD^- concentrations constant, at 0.476 *M* and 0.0038 *M* respectively. In solvent compositions containing more than ~ 70 mol% DMF, the base employed was Me_4NOD due to the limited solubility of NaOD in DMF-rich media. The two bases gave identical exchange rates, within experimental error, in the 68.1 mol% DMF solvent system. The combined results are listed in Table 3 and shown graphically in Fig. 3 in the form of a plot of k_{obs} as a function of medium composition.

TABLE 3. Pseudo first order rate constants for proton exchange in DNB (0.48 *M*) as function of medium composition (DMF–D_2O), at constant NaOD concentration (0.0038 *M*), 25°C

Mol% DMF	10^3 k_{obs} s^{-1}
47.5	0.492
47.5	0.539
47.5	0.524
47.5	0.553
56.1	2.57
56.1	2.49
68.1	6.30
68.1	6.08
73.3	6.70
75.8	6.26
75.8	6.40
81.8	3.98
81.8	4.51
91.1	1.99
91.1	1.96
95.8	0.752
95.8	0.782

It is seen from Fig. 3 that the rate of proton exchange, while increasing initially, passes through a maximum at ~ 70 mol% DMF and then decreases. This type of medium dependence of the rate of *base catalyzed* proton exchange is quite unusual and possibly unprecedented.

A qualitative explanation of the present results can, however, be given in terms of the two main factors bearing on this system. These are the medium effect on the exchange process itself, and the medium effect on the concurrent equilibrium

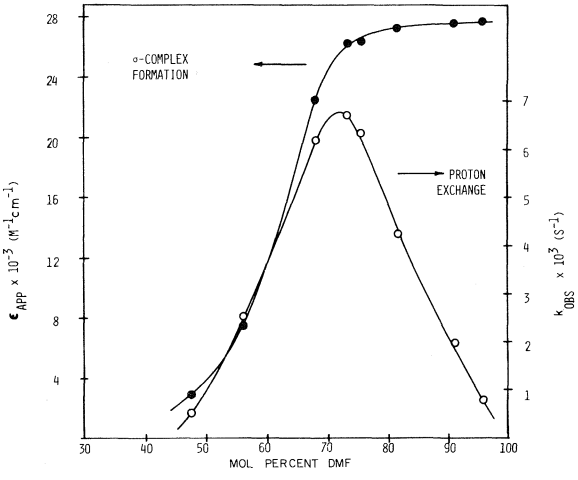

FIG. 3. Dependence of k_{obs} (exchange) and ε_{app} (σ-complex formation) on medium composition.

Can. J. Chem. Downloaded from www.nrcresearchpress.com by 210.87.254.42 on 09/06/12
For personal use only.

σ-complex formation. We have already shown that K_e for σ-complex formation increases markedly with increasing DMF content (28). It follows that as the DMF content of the medium is increased, deuteroxide ion will become increasingly tied up in the form of the unreactive σ-complex towards proton exchange. Qualitatively, this could result in the type of behaviour which has been observed, since the decrease in the effective OD^- concentration as the DMF content is increased could eventually overcome the anticipated increase in exchange rate due to the effect of the dipolar aprotic component. However, the overall balance between these two opposing tendencies cannot be predicted *a priori*.

In Fig. 3 we have represented the σ-complex formation process by including the curve for the variation of ε_{app} with solvent composition, in addition to k_{obs}. ε_{app} is the apparent molar extinction coefficient at λ_{max} for the σ-complex **7** (28), and is a measure of the degree of complex formation in a given system. It is seen that the ε_{app} function shows initially increasing tendency but levels off at ca. 70 mol% DMF, and then remains practically constant. The latter portion corresponds to virtually complete tying up of OD^- in the form of the σ-complex with DNB, which is the component present in large excess. It is interesting to note that σ-complex formation attains ~99% of its maximum value about the same medium composition (~70 mol% DMF) that the maximum in k_{obs} is found (Fig. 3).

Further assessment of the importance of σ-complex formation as a factor pertinent to the exchange process requires that k_{obs} be dissected into its constituent terms. However, before proceeding with this treatment, we consider the possible implications of the concurrent basic hydrolysis of the solvent DMF.

Effect of Basic Hydrolysis of DMF on Proton Exchange

We had previously observed (41, 42) that DMF reacts readily with hydroxide ion, to give formate ion and dimethylamine, despite a statement in the literature suggesting the contrary.[4] In the present work a sharp odour characteristic of amine was evident in the "infinity" solutions following exchange. Thereafter, sodium formate was isolated and characterized following reaction of 0.1 *N* NaOH in 68 mol% DMF at room temperature for 24 h. The possible effect of the DMF hydrolysis reaction on the proton exchange process must be critically examined. However, as in the case of our study of proton exchange with TNB in the DMF–D_2O–OD^- system, it can readily be shown that the concurrent hydrolysis of DMF has little effect on proton exchange in the majority of cases.

In Table 4 are shown the half-lives for the DMF hydrolysis and for the proton exchange process in DNB. It is seen that except for the lowest DMF solvent composition, proton exchange is the faster of the two processes. The data for OD^-_e pertain to the uncomplexed deuteroxide ion under the exchange conditions and are estimated from the equilibrium constants for σ-complex formation. Thus, considering for example the 68.1 mol% DMF system, the loss in the overall OD^- concentration during one exchange half-life as a result of the reaction with DMF will be ~1%, assuming that only free base is consumed by reaction with DMF. The effect of this loss in OD^- on the exchange process should be small, as is evidenced by the linearity of the first order plot for exchange over >75% reaction. In media of lower DMF content, however, the effect of the competing DMF hydrolysis is greater and only initial rates can be determined in proton exchange. In all the exchange reactions the effect of the DMF hydrolysis was minimized in practice through addition of the $NaOD/D_2O$ solution as the final component to the reaction mixture.

Quantitative Evaluation of the Effect of σ-Complexing on Exchange Rates as Function of Medium Composition

The maximum in rate of exchange which is observed as the medium composition is varied, Fig. 3, represents quite unusual behaviour for base catalyzed proton exchange. The implication of σ-complex formation as influencing proton exchange has already been made apparent, but a quantitative relationship between the two processes still remains to be formulated. One approach is clearly to consider the rate law which should be applicable to this system of competing processes, in place of the phenomenologically evaluated k_{obs} which has been considered so far.

We have already drawn the conclusion on the basis of the available evidence that proton exchange occurs via reaction between the free, or uncomplexed, DNB and OD^- entities. The rate of exchange is hence given by the expression in eq. [1]

$$[1] \qquad \text{rate} = k_{obs}\,[\text{DNB}]_0 = k_2\,[\text{DNB}]_e\,[\text{OD}^-]_e$$

where $[DNB]_0$ is the initial, or stoichiometric, concentration of DNB, while $[DNB]_e$ and $[OD^-]_e$ are the concentrations under conditions where the σ-complexing equilibrium DNB + OD^- ⇄ DNB.OD^-

[4]DMF Product Information Bulletin, E. I. duPont de Nemours and Co. (Inc.).

TABLE 4. Comparative data for basic hydrolysis of DMF and proton exchange in DNB as function of medium composition at 25°C

Mol% DMF	$T_{\frac{1}{2}}$ (min)[a] DMF hydrolysis	$T_{\frac{1}{2}}$ (min)[b] proton exchange	% $OD^-{}_e$[c]	1st order plot linearity (% rxn.)
47.5	12	23	95	~ 20
56.1	17	4.6	70	~ 35
68.1	26	1.9	15	> 75
81.8	53	2.7	< 1	> 75

[a] Reference 41.
[b] Using data from Table 2.
[c] Per cent of $[OD^-]_0$, as calculated by method given in Appendix for $[DNB]_0 = 0.48\,M$; $[NaOD]_0 = 0.0038\,M$, using K_e values from ref. 28.

TABLE 5. Kinetic data for proton exchange and equilibrium data for σ-complex formation in reactions of DNB (0.476 *M*) with Me_4NOD (3.81×10^{-3} *M*) in DMF–D_2O mixtures at 25°C

Mol% DMF	H_-[a]	$10^3\,k_{obs}$ s^{-1}	K_e[b] L mol^{-1}	$10^3[OD^-]_e$[c] *M*	k_2[d] L $mol^{-1}\,s^{-1}$
57.4	16.65	2.53	7.5	0.838	3.0
68.1	17.65	6.19	55	0.141	44
73.3	18.20	6.70	91	0.087	77
75.8	18.50	6.33	1.5×10^2	0.053	1.2×10^2
81.8	19.40	4.24	8.5×10^2	0.0095	4.5×10^2
91.1	21.05	1.97	3.8×10^4	0.00021	9.3×10^3
95.8	22.35	0.767	3.1×10^5	0.000026	3.0×10^4

[a] Data from ref. 47 after correction for reduced $[OD^-]$ value (from 0.019 to 0.0038 *M*); H_- data for 91.1 and 95.8 mol% DMF are estimated values.
[b] Data from ref. 28.
[c] Calculated by method given in Appendix.
[d] $k_2 = k_{obs}/[OD^-]_e$.

is established. It is recalled that the results in Fig. 3 have been obtained using the reactant concentrations $[DNB]_0 = 0.48\,M$ and $[OD^-]_0 = 0.0038\,M$, i.e. $[DNB]_0 \gg [OD^-]_0$. Under these conditions, and with the equilibrium constant for σ-complex formation being typically large, one has $[DNB]_e \approx [DNB]_0$. Rewriting eq. [1] in the form [2], one then obtains eq. [3] for the second order rate coefficient for exchange.

$$[2] \quad k_{obs} = \frac{k_2[DNB]_e\,[OD^-]_e}{[DNB]_0}$$

$$[3] \quad k_2 \approx \frac{k_{obs}}{[OD^-]_e}$$

The variation of k_2 with DMF content should provide a more valid measure of the medium effect on exchange than is given by k_{obs} in Fig. 3. To this end, we have calculated the $[OD^-]_e$ values at the various DMF compositions listed in Table 3 by the method detailed in the Appendix, using measured K_e values (28) to calculate $[DNB.OD^-]$ and subtracting this from $[OD^-]_0$ to obtain $[OD^-]_e$. The appropriate data are given in Table 5 for the DMF–D_2O compositions corresponding to Fig. 3. It is seen that the k_2 values so derived exhibit a uniform increase with increasing DMF content of the medium. Thus correction for σ-complex formation leads to disappearance of the rate maximum which appeared in the k_{obs}–solvent composition profile in Fig. 3. The calculated k_2 values exhibit an increase of 4 powers of 10 as the DMF content is increased from 57 to 96 mol% DMF, which is entirely consistent with expectation from the known effect of dipolar aprotic media on OD^- catalyzed proton exchange in carbon acids (31–33).

Further insight into the origin of these phenomena can be gained by considering the dependence of the second order rate constant on some property measuring more directly the basicity of the medium than is represented by the per cent DMF composition. Also this will allow us to draw more valid comparisons with other systems. A measure of medium basicity which is generally used is that given by the H_- acidity function (43–46). We have previously evaluated an H_- scale for the DMF–H_2O–OH^- system, based on the deprotonation of very weak acid indicators (47), and in Table 5 we have listed the appropriate H_- values corresponding to the given solvent compositions. Using these data we have constructed the plots for the variation of log k_2 and log K_e with medium basicity, i.e. with H_-, as shown in Fig. 4. It is seen that the log k_2 vs. H_- plot exhibits an initial linear portion followed by a downward curving plot. However, the plot of log K_e vs. H_- remains linear over the entire range of

Can. J. Chem. Downloaded from www.nrcresearchpress.com by 210.87.254.42 on 09/06/12
For personal use only.

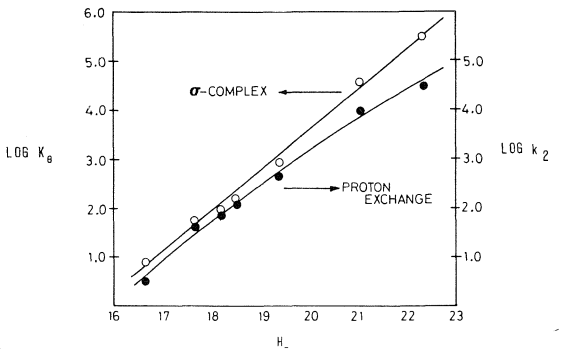

FIG. 4. Dependence of log k_2 (exchange) and log K_e (σ-complex formation) on H_- function.

medium composition. It is this steeper dependence of σ-complex formation on medium basicity, compared to proton exchange, which is thus the underlying cause for the decreasing exchange rate in media of high DMF content.[5]

Comparison with Other Systems

We first draw comparison between the results obtained in the present study and our previously reported work for TNB (26) which is also applicable to the DMF–D_2O–OD^- system. Interestingly, it was found (26) that k_{obs} *decreased* with increasing DMF content over the entire solvent composition range studied (25–80 mol% DMF), which contrasts with the results obtained in the DNB system (Fig. 3).

The principles governing the DNB and TNB systems should, however, be analogous, and the apparent differences in behaviour will arise at the quantitative level, from the different degrees of complexation in the two systems and as a function of medium basicity. That is, in the TNB case, predominant (say 99%) σ-complex formation has set in at a much lower DMF composition (~ 20 mol% DMF). Therefore if one were to extrapolate the plot for exchange in TNB to lower DMF composition, one would expect to observe an initial rise in k_{obs}, as in the DNB system. Hence, even though the experimental method used (26) did not allow measurement of exchange rates in < 25 mol% DMF , due to limited solubility of TNB, it can be predicted that use of an appropriate method (such as tritium exchange), which would be sensitive at low TNB concentrations, would reveal analogous behaviour in the k_{obs} vs. mol% DMF profile for the two substrates. This prediction of behaviour for TNB, which follows from the present results for DNB, will be tested in future work.

Comparison is also drawn between the present study and that reported by Crampton and Gold (24) for DNB in DMSO–MeONa–MeOT mixtures. In that work [MeONa], as well as [DNB], was kept constant and the DMSO content was varied in order to change the basicity of the medium. The plot of log k_{obs} vs. H_- showed an initial linear portion (slope 0.73) but then levelled off at an H_- value corresponding to practically complete (~ 99%) conversion to colored species. The plot of log ε_{app} vs. H_- was also linear initially (slope 1.22) and then levelled off as conversion of DNB to the σ-complex became virtually complete. The levelling off in rate was consistent with the σ-complex representing an unreactive form of the substrate and that exchange occurred via uncomplexed DNB present in very small concentrations. Although a maximum in the log k_{obs} vs. H_- plot was not observed, Crampton and Gold showed that such would be expected under either of the following assumptions: (*i*) the σ-complex is as effective as methoxide ion in catalyzing exchange; (*ii*) the σ-complex is totally ineffective as a catalyst. The authors allowed that an intermediate situation could obtain.

The suggestion by Crampton and Gold (24) that the σ-complex could act as a catalyst in exchange is pertinent also to our study. It would then follow that the σ-complex could also contribute to the basicity of the medium, which would serve to justify our current use of the H_- function in its normally accepted sense (43–46). Thus whereas H_- values are taken to refer to constant hydroxide (deuteroxide)[6] ion concentration (0.01 *M*), in the present system the free OD^- concentration is continually diminishing as a result of σ-complex formation. One could then envisage that as the free, or uncomplexed, deuteroxide ion concentration becomes very small, the contribution by the σ-complex to medium basicity could become significant. Since the concentration of the σ-complex remains essentially constant in media of high DMF content, the basicity of these media would also remain effectively constant. It is also possible that some other acidity function might represent better the medium basicity in the present case than H_-, as

[5]Closer examination of the plots in Fig. 4 suggests that in the initial region of low H_- values the points representing log K_e lie on a line whose slope is smaller than that of the log k_2 plot over the same H_- region, whereas in the region of high H_- values the opposite relationship holds. If this apparent relationship could be confirmed, it would likewise have the effect of favoring proton exchange relative to σ-complex formation in media of low DMF content, and vice versa in media of high DMF content, as is observed.

[6]The H_- function in D_2O/OD^- systems is expected to be larger by ca. 0.5 unit than in the H_2O/OH^- system (48); this, however, will not have an appreciable effect on the present discussion.

Can. J. Chem. Downloaded from www.nrcresearchpress.com by 210.87.254.42 on 09/06/12
For personal use only.

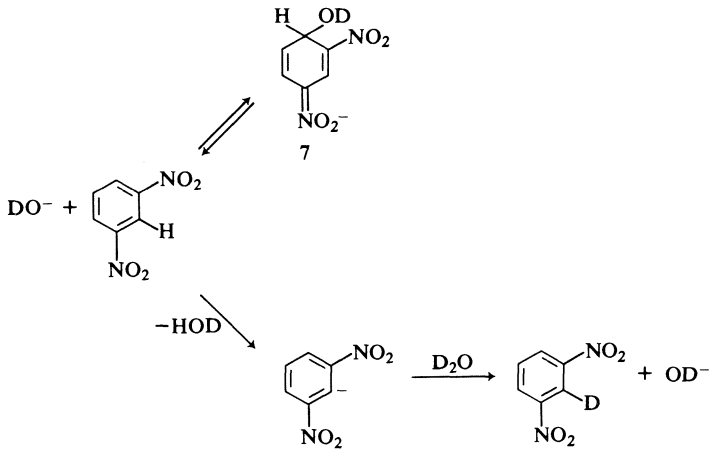

SCHEME 1

for example the J_- function (49, 50). However, such a function has so far not been determined for the system under study and our recourse has been to use the known H_- function but to point out the limitations in its applicability to the present system.

Mechanism of Exchange

The overall conclusion of our work is that the dominant interaction in the DNB–DMF–D_2O–OD^- system is equilibrium formation of σ-complex **7**, and that exchange occurs by proton abstraction from uncomplexed DNB via carbanion **6**, according to Scheme 1.

The possibility that the solution color could be due to the anion **6** (or **5** (23)) can be discounted, as shown by the relationship between k_{obs} and ε_{app} as a function of medium composition, Fig. 3, and discussed earlier. Direct evidence on this point was obtained by quenching with D_2SO_4–D_2O a solution of DNB in DMF–H_2O–OH^- under conditions where substantial conversion to colored species occurred. The DNB which was isolated from the reaction mixture was not detectably labelled with deuterium, thus eliminating the possibility that the carbanion **6** (or **5**) was present in appreciable concentration.

As to the detailed mechanism of exchange it should be pointed out that Scheme 1 is only an approximate representation and that the intimate mechanism must be discussed in terms of eqs. [4]–[6] (51):

$$[4] \quad ArH + OD^- \underset{k_{-a}}{\overset{k_a}{\rightleftarrows}} Ar^- \ldots HOD$$

$$[5] \quad Ar^- \ldots HOD + DOD \underset{k_{-b}}{\overset{k_b}{\rightleftarrows}} Ar^- \ldots DOD + HOD$$

$$[6] \quad Ar^- \ldots DOD \underset{k'_a}{\overset{k'_{-a}}{\rightleftarrows}} ArD + OD^-$$

However, we have no evidence as to the importance of these hydrogen-bonded species, and which of the various steps is rate determining. There has been some discussion whether log k–H_- plots can be informative in this regard, views for and against this notion being expressed (52–54). Recent work (55–57) suggests that kinetic isotope effects might shed light on this question, and we hope to undertake such studies in future work.

Experimental

Reagents

1,3-Dinitrobenzene (Fisher Certified Reagent) was recrystallized twice from ethanol, mp 89.0– 89.5°C (uncorrected), λ(ε) 234 nm (17 800 M^{-1} cm^{-1}). DMF (Fisher Certified Reagent) was distilled under vacuum from P_2O_5. The middle fraction, bp 40°C/7 Torr, was stored in the dark under N_2. A solution of NaOD (1 *M*) was prepared by adding freshly cut sodium metal to 99.5–99.8% D_2O (Diaprep or Stohler) under N_2. The HOD content was checked periodically by monitoring the O–H stretching band at 3400–3500 cm^{-1} in the ir spectrum. A solution of Me_4NOD was prepared by evaporating a solution of Me_4NOH under vacuum at 25°C until syrupy, followed by two treatments with D_2O and its removal under vacuum, before the final dilution with D_2O to 1.9 *M*.

Site of Isotopic Exchange in DNB

The nmr spectrum of normal DNB and of the material recovered following exchange in DMF– D_2O–NaOD are shown in Figs. 5A and 5B respectively. It is seen that the signal appearing in Fig. 5A at δ 8.75 (t), ascribable to H-2 in DNB, is greatly diminished in the spectrum shown in Fig. 5B (maximum exchange under the conditions was 94%). The ratios of the integral heights corresponding to H-4(6) (δ 8.45) and H-5 (δ 7.75) remain constant at 2:1 in Figs. 5A and 5B, indicating that these hydrogens do not undergo exchange. This deduction follows also from our observation that under the more strongly basic conditions of the tritium exchange experiment (29), H-4(6) but not H-5 was found to exchange.

Can. J. Chem. Downloaded from www.nrcresearchpress.com by 210.87.254.42 on 09/06/12
For personal use only.

Can. J. Chem. Downloaded from www.nrcresearchpress.com by 210.87.254.42 on 09/06/12
For personal use only.

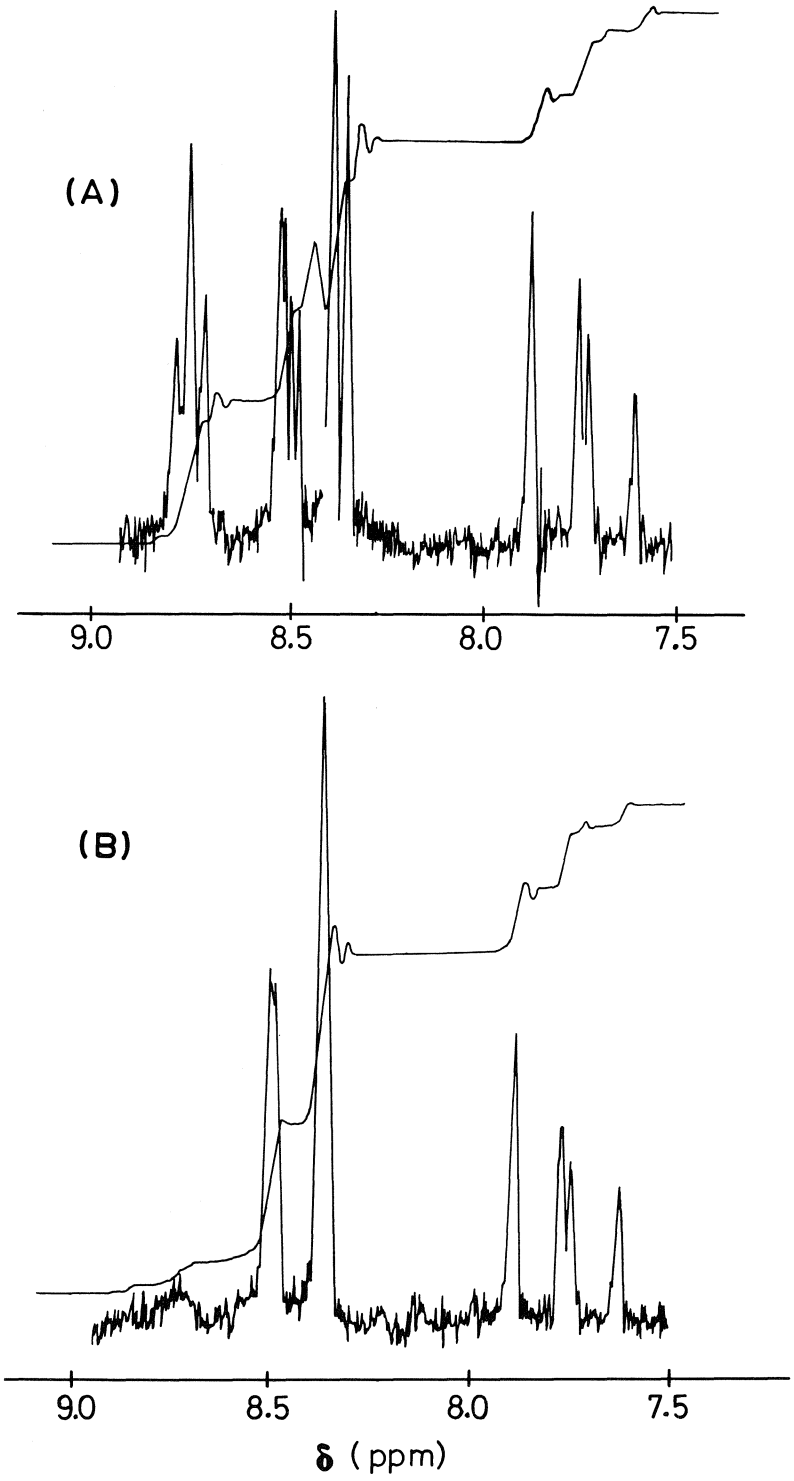

FIG. 5. The nmr spectra of normal DNB (A) and of material following exchange in DMF–NaOD–D_2O system (B).

Kinetic Method

Proton exchange was monitored by ir by following the development in the reaction solution of the O–H stretching band in HOD at 3480 ± 50 cm^{-1}, depending on the DMF–D_2O composition. Measurements were made in a thermostatted CaF_2 cell (0.1 or 0.2 mm pathlength), the temperature being measured by means of a thermocouple, with air in the reference beam to eliminate the possibility of adventitious introduction of moisture in a reference cell. A calibration curve was first prepared using standard solutions of HOD in DMF–D_2O, which yielded a linear Beer's law plot up to 0.5 *M* HOD. The measurements were taken on a Perkin Elmer 21 infrared spectrometer.

In a typical kinetic run, DNB was weighed into a 25 mL volumetric flask, an appropriate volume of D_2O was added and then made up to mark with DMF, weighing after each addition. Ten milliliters of this solution in a glass stopped flask were placed in a constant temperature bath and after equilibration the NaOD(Me_4NOD)–D_2O solution (1–2 *M*) was added by means of a syringe. After vigorous shaking of the reaction solution an aliquot was transferred by syringe to the thermostatted, carefully dried ir cell. The increase in the HOD band was followed until completion of reaction (10 half-lives). The concentration of HOD, obtained from the transmittance value via the calibration curve, yielded the extent of reaction, from which the pseudo first order plot (e.g. Fig. 1) was constructed. The C_0 used in these plots was generally the initial, stoichiometric concentration of DNB. However, use of this C_0 value leads to curvature in the first order plot since the initial effectively infinite deuterium pool becomes diluted by the exchanged hydrogen from the DNB as the reaction proceeds, leading to a back reaction. Alternatively, a C_0 value based on the labile deuterium to hydrogen ratio was chosen and a correction factor applied to k_{obs} using the method of Streitwieser *et al.* (58). This procedure led to first order plots which were linear for longer periods of time and was preferred for the solvent systems where relatively small labile deuterium to hydrogen ratio was present.

Acknowledgments

We thank Queen's University for a scholarship (A. Z.) and the Natural Sciences and Engineering Research Council of Canada for a grant in aid of this research.

1. E. Buncel, A. R. Norris, and K. E. Russell. Q. Rev. Chem. Soc. **22**, 123 (1968).
2. F. Pietra. Q. Rev. Chem. Soc. **23**, 504 (1969).
3. P. Buck. Angew. Chem. Int. Ed. Engl. **8**, 120 (1969).
4. T. N. Hall and C. F. Poranski, Jr. The chemistry of the nitro and nitroso groups. Part 2. *Edited by* H. Feuer. Interscience, London. 1970.
5. C. A. Fyfe. The chemistry of the hydroxyl group. Part 1. *Edited by* S. Patai. Interscience, London. 1971.
6. E. Buncel. The chemistry of functional groups. Nitro and nitroso groups. Supplement F. *Edited by* S. Patai. Interscience, London. 1981.
7. R. S. Mulliken. J. Am. Chem. Soc. **74**, 811 (1952).
8. G. Briegleb. Electronen–Donator–Acceptor Komplexe. Springer-Verlag, Berlin. 1961.
9. R. Foster. Organic charge transfer complexes. Academic Press, London. 1969.
10. C. K. Mann and K. K. Barnes. Electrochemical data in nonaqueous systems. Marcel Dekker, New York. 1970.
11. R. D. Guthrie. Comprehensive carbanion chemistry. Vol. 1. *Edited by* E. Buncel and T. Durst. Elsevier, Amsterdam. 1980.
12. E. Buncel and B. C. Menon. J. Am. Chem. Soc. **102**, 3499 (1980).
13. K. T. Leffek and P. H. Tremaine. Can. J. Chem. **51**, 1659 (1973).
14. M. J. Strauss. Chem. Rev. **70**, 667 (1970); Acc. Chem. Res. **7**, 181 (1974).
15. C. F. Bernasconi. MTP Int. Rev. Sci.: Org. Chem. Ser. One, **3**, 33 (1973); C. F. Bernasconi and M. C. Muller. J. Am. Chem. Soc. **100**, 5530 (1978).
16. F. Terrier, J. Morel, M. J. Pouet, and M. P. Simonnin. Can. J. Chem. **58**, 65 (1980).
17. J. H. Fendler, W. L. Hinze, and L. J. Liu. J. Chem. Soc. Perkin Trans. II, 1768 (1975).
18. C. A. Fyfe, A. Koll, S. W. H. Damji, C. D. Malkiewich, and P. A. Forte. Can. J. Chem. **55**, 1468 (1977); R. Foster and C. A. Fyfe. Pure Appl. Chem. Australia, **16**, 61 (1966).
19. M. R. Crampton. Adv. Phys. Org. Chem. **7**, 211 (1969); J. Chem. Soc. Perkin Trans. II, 1442 (1977).
20. E. Buncel and J. G. K. Webb. Can. J. Chem. **52**, 630 (1974); E. Buncel, A. Jonczyk, and J. G. K. Webb. Can. J. Chem. **53**, 3761 (1975); E. Buncel and W. Eggimann. J. Am. Chem. Soc. **99**, 5958 (1977).
21. L. H. Gan and A. R. Norris. Can. J. Chem. **52**, 1 (1974); **52**, 8 (1974); **52**, 18 (1974); M. E. Moir and A. R. Norris. Can. J. Chem. **58**, 1691 (1980).
22. E. Buncel, N. Chuaqui-Offermanns, R. Y. Moir, and A. R. Norris. Can. J. Chem. **57**, 494 (1979); E. Buncel, M. Hamaguchi, and A. R. Norris. Can. J. Chem. **58**, 1609 (1980); **58**, 1615 (1980).
23. R. J. Pollitt and B. C. Saunders. Proc. Chem. Soc. 176 (1962); J. Chem. Soc. 4615 (1965).
24. M. R. Crampton and V. Gold. J. Chem. Soc. B, 498 (1966).
25. E. Buncel and A. W. Zabel. J. Am. Chem. Soc. **89**, 3082 (1967).
26. E. Buncel and E. A. Symons. J. Org. Chem. **38**, 1201 (1973).
27. E. A. Symons and E. Buncel. Can. J. Chem. **50**, 1729 (1972).
28. E. Buncel and A.W. Zabel. Can. J. Chem. **59**, 3168 (1981).
29. E. Buncel, J. A. Elvidge, J. R. Jones, and K. T. Walkin. J. Chem. Res. (S), 272 (1980).
30. I. R. Bellobono and G. Sala. J. Chem. Soc. Perkin Trans. II, 169 (1972).
31. D. J. Cram. Fundamentals of carbanion chemistry. Academic Press, New York. 1965.
32. E. Buncel. Carbanions, mechanistic and isotopic aspects. Elsevier, Amsterdam. 1975.
33. J. R. Jones and R. Stewart. J. Chem. Soc. (B), 1173 (1967).
34. A. J. Parker. Chem. Rev. **69**, 1 (1969).
35. C. Reichardt. Solvent effects in organic chemistry. Verlag Chemie, Weinheim. 1979; Angew. Chem. Int. Ed. Engl. **18**, 98 (1979).
36. E. Buncel and H. Wilson. Adv. Phys. Org. Chem. **14**, 133 (1977).
37. E. Buncel and H. Wilson. Acc. Chem. Res. **12**, 42 (1979).
38. E. Buncel and H. Wilson. J. Chem. Educ. **57**, 629 (1980).
39. E. A. Symons and E. Buncel. Can. J. Chem. **51**, 1673 (1973).
40. E. Buncel and E. A. Symons. J. Am. Chem. Soc. **98**, 656 (1976).
41. E. Buncel and E. A. Symons. J. Chem. Soc. Chem. Commun. 164 (1970).
42. E. Buncel, S. Kesmarky, and E. A. Symons. J. Chem. Soc. Chem. Commun. 120 (1971).
43. K. Bowden. Chem. Rev. **66**, 119 (1966).

Can. J. Chem. Downloaded from www.nrcresearchpress.com by 210.87.254.42 on 09/06/12
For personal use only.

44. L. P. HAMMETT. Physical organic chemistry. 2nd ed. McGraw Hill, New York. 1970.
45. D. DOLMAN and R. STEWART. Can. J. Chem. **45**, 911 (1967).
46. C. H. ROCHESTER. Acidity functions. Academic Press, London. 1970.
47. E. BUNCEL, E. A. SYMONS, D. DOLMAN, and R. STEWART. Can. J. Chem. **48**, 3354 (1970).
48. E. HOGFELDT and J. BIGELEISEN. J. Am. Chem. Soc. **82**, 15 (1960).
49. V. GOLD and B. W. V. HAWES. J. Chem. Soc. 2102 (1951).
50. C. H. ROCHESTER. Q. Rev. Chem. Soc. **20**, 511 (1966).
51. M. EIGEN. Angew. Chem. Int. Ed. Engl. **3**, 1 (1964).
52. R. STEWART, J. P. O'DONNELL, D. J. CRAM, and B. RICKBORN. Tetrahedron, **18**, 917 (1962).
53. W. D. KOLLMEYER and D. J. CRAM. J. Am. Chem. Soc. **90**, 1784 (1968).
54. A. STREITWIESER, JR., J. A. HUDSON, and F. MARES. J. Am. Chem. Soc. **90**, 648 (1968).
55. L. MELANDER and W. H. SAUNDERS, JR. Reaction rates of isotopic molecules. Wiley, New York. 1980.
56. H. F. KOCH, J. G. KOCH, W. TUMAS, D. J. MCLENNAN, B. DOBSON, and G. LODDER. J. Am. Chem. Soc. **102**, 7955, (1980).
57. A. J. KRESGE and M. F. POWELL. J. Am. Chem. Soc. **103**, 201 (1981).
58. A. STREITWIESER, JR., D. E. VAN SICKLE, and W. C. LANGWORTHY. J. Am. Chem. Soc. **84**, 244 (1962).
59. E. BUNCEL, E. A. SYMONS, and R. A. MORE O'FERRALL. J. Am. Chem. Soc. **100**, 1084 (1978).
60. E. BUNCEL, A. R. NORRIS, J. A. ELVIDGE, J. R. JONES, and K. T. WALKIN. J. Chem. Res. (S), 326 (1980).

Appendix

Calculation of Uncomplexed (Free) Deuteroxide Ion Concentrations under Exchange Conditions in DNB–DMF–D_2O–NaOD Systems

Let the reaction between DNB and OD^- yielding the DNB.OD^- σ-complex (eq. [7]) be associated with an equilibrium constant K_e as given in eq. [8]:

[7] $$DNB + OD^- \rightleftarrows DNB.OD^-$$

[8] $$K_e = \frac{[DNB.OD^-]}{[DNB]_e[OD^-]_e}$$

The quantities $[DNB]_e$ and $[OD^-]_e$ are the concentrations when equilibrium is established, while $[DNB]_0$ and $[OD^-]_0$ are the initial, stoichiometric concentration values. Then eq. [8] can be rewritten as eq. [9]

[9] $$K_e = \frac{[DNB.OD^-]}{([DNB]_0 - [DNB.OD^-])([OD^-]_0 - [DNB.OD^-])}$$

which can be recast into quadratic form,

[10] $$px^2 + qx + r = 0$$

The concentration of σ-complex, [DNB.OD^-], is given by x, while the coefficients p, q, and r are given by known quantities as follows:

$$p = K_e$$

$$q = -K_e[DNB]_0 + K_e[OD^-]_0 + 1$$

$$r = K_e[DNB]_0[OD^-]_0$$

Thus [DNB.OD^-] can be evaluated via solution of the quadratic eq. [10]. One then obtains $[OD^-]_e$ by subtraction of [DNB.OD^-] from $[OD^-]_0$.

In Table 2 are given the calculated $[OD^-]_e$ data corresponding to two sets of values of $[DNB]_0$ and $[OD^-]_0$, and using K_e = 55 L mol^{-1} which is applicable to 68.1 mol% DMF. These results pertain to the discussion of the apparent order in deuteroxide and DNB, and lead to the following conclusions.

1. At constant $[DNB]_0$ of 0.50 *M*, doubling $[OD^-]_0$ from 0.004 to 0.008 *M* increases $[OD^-]_e$ by a factor of 2.02.
2. At constant $[DNB]_0$ of 0.25 *M*, doubling $[OD^-]_0$ from 0.004 to 0.008 *M* increases $[OD^-]_e$ by 2.03.
3. At constant $[OD^-]_0$ of 0.004 *M*, halving $[DNB]_0$ from 0.50 to 0.25 *M* increases $[OD^-]_e$ by 1.95.
4. At constant $[OD^-]_0$ of 0.008 *M*, halving $[DNB]_0$ from 0.50 to 0.25 *M* increases $[OD^-]_e$ by a factor of 1.96.

These conclusions are completely in accord with the observed effect of varying $[DNB]_0$ and $[OD^-]_0$ on k_{obs} (data in Table 1).

Can. J. Chem. Downloaded from www.nrcresearchpress.com by 210.87.254.42 on 09/06/12
For personal use only.

Ozonolysis of substituted 1,2-dichloroethylenes in methanol: products and reaction course

TAE-SEONG HUH,[1] JOACHIM NEUMEISTER, AND KARL GRIESBAUM[2]

Engler-Bunte-Institut, Bereich Petrochemie, Universität Karlsruhe (TH), D-7500 Karlsruhe, West Germany

Received June 12, 1981

TAE-SEONG HUH, JOACHIM NEUMEISTER, and KARL GRIESBAUM. Can. J. Chem. **59**, 3188 (1981).

Ozonolysis of *trans*-2,3-dichloro-2-butene (**5***a*), of *trans*-3,4-dichloro-3-hexene (**5***b*), and of 1,2-dichlorocyclohexene in methanol and in solutions of sodium methoxide in methanol have been examined. They afforded in high yields the corresponding ester fragments methyl acetate (**6***a*), methyl propionate (**6***b*), and dimethyl adipate (**8**), respectively. By trapping with phenylacetylene and formation of 1,1-dichloro-2,2-dimethoxy-2-phenylethane, the presence of methyl hypochlorite in the ozonolysis products was established. A reaction course has been proposed which is in accord with these results.

TAE-SEONG HUH, JOACHIM NEUMEISTER et KARL GRIESBAUM. Can. J. Chem. **59**, 3188 (1981).

On a étudié l'ozonolyse du dichloro-2,3 butène-2 *trans* (**5***a*), du dichloro-3,4 hexène-3 *trans* (**5***b*) et du dichloro-1,2 cyclohexène dans le méthanol et dans des solutions de méthanolate de sodium dans le méthanol. Ils conduisent avec d'excellents rendements aux esters correspondants aux diverses fragmentations soit l'acétate de méthyle (**6***a*), le propionate de méthyle (**6***b*) et l'adipate de diméthyle (**8**). Le piégeage avec le phénylacétylène et la formation de dichloro-1,1 diméthoxy-2,2 phényl-2 éthane ont permis d'établir la présence de l'hypochlorite de méthyle parmi les produits de l'ozonolyse. On propose un schéma réactionnel qui s'accorde avec ces résultats.

[Traduit par le journal]

Introduction

The course and the products of the ozone cleavage of olefins containing monochloro-substituted double bonds in methanol have been described recently (1). By contrast, ozone cleavage of olefins having symmetrically dichloro-substituted double bonds in alcoholic media has been only reported at substrates having specific structures. Thus, ozonolysis of the cyclodiene insecticide-like compounds **1** and **2** in methanol has been found to afford the dimethylesters **3** and **4**, respectively, in virtually quantitative yields (2).

For the course of these reactions, we have advanced a proposal which at that time could not be substantiated by experimental evidence (2). The present paper describes the ozonolysis of the simple substrates **5***a*, **5***b*, and **7** in methanol, as well as experimental evidence for the previously proposed reaction course.

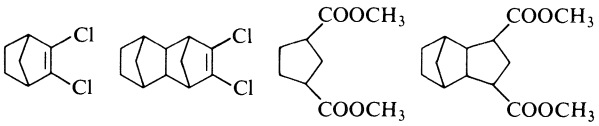

1 **2** **3** **4**

Organic Reaction Products

The ozonolysis reactions were carried out at ca. 1.3 *M* solutions of the substrates in methanol. The acyclic substrates **5***a* and **5***b* were ozonized at −40°C, the cyclic substrate **7** at ambient temperatures. In each case the reactions were slow and required an excess of ozone. After completion of the double bond cleavage and removal of dissolved ozone, the peroxidic solutions were stirred at ambient temperatures until the peroxide content had disappeared. Then, the crude mixtures were analyzed by nmr spectroscopy with the help of 1,1,1-trichloroethane as a standard. By this method, the ester fragments **6***a* and **6***b* have been identified in the crude reaction mixtures in yields of 90% and 92%, respectively. The dimethyl ester **8** has been isolated in a yield of 84%. These results are in agreement with those obtained in the ozonolysis of the bicyclic and tetracyclic substrates **1** and **2**, respectively, and they may well indicate a general mode of reaction for the ozonolysis of olefins having such structural moieties.

Reaction Course

Considerable evidence has been accrued in recent years for a Criegee-type cleavage pattern during the ozonolysis of substituted 1,2-dichloroethylenes in nonparticipating solvents (3–5). In a preliminary rationalization we have, therefore, also proposed a Criegee-type reaction mode for the

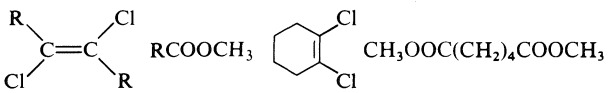

5 **6** **7** **8**

a R = CH_3; *b* R = CH_3CH_2

[1]On leave from Song Sim College for Women, Gang Won Do, Korea.

[2]Author to whom correspondence should be addressed.

0008-4042/81/223188-04$01.00/0

©1981 National Research Council of Canada/Conseil national de recherches du Canada

Can. J. Chem. Downloaded from www.nrcresearchpress.com by 210.87.254.5 on 09/06/12
For personal use only.

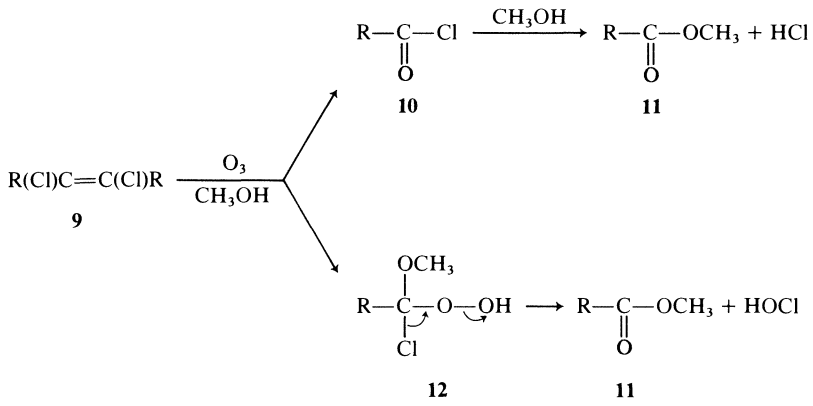

SCHEME 1

ozonolysis of dichloro olefins of structure **9** in methanol as depicted in Scheme 1 (2). In the double bond cleavage step, acyl chloride (**10**) and α-chloro-α-methoxyalkylhydroperoxide (**12**) were postulated as the primary reaction products. Obviously, the acyl chloride (**10**) undergoes rapid solvolysis with methanol to afford methyl ester **11** and hydrogen chloride. Although to our knowledge compounds of type **12** and their chemistry are largely unknown, it is reasonable to assume that they may be rather labile. We have proposed that they decompose in the way indicated in Scheme 1, viz. by loss of hypochlorous acid and formation of a second molecule of methyl ester (**11**). This proposal was based on a similar, albeit slower reaction of the α-chloro peroxide **13** to form diacetyl peroxide (**14**) and chlorine (3).

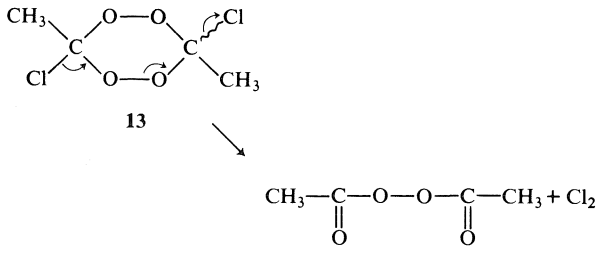

All our attempts at detecting **12** have been unsuccessful. Therefore we have tried to prove the formation of its postulated decomposition product, hypochlorous acid. It is known that hypochlorous acid and methanol react to form methyl hypochlorite (**15**), and it is furthermore established that the latter undergoes facile addition to phenylacetylene to yield the stable adduct **16** (6).

Consequently, addition of phenylacetylene to the ozonolysis reaction products of substituted 1,2-dichloroethylenes in methanol should be a suitable test for the formation of hypochlorous acid. Indeed, addition of excess phenylacetylene to the crude reaction mixtures from the ozonolysis of **5***a*, of **5***b*, and of **7** afforded in each case adduct **16**, which was identified by glc and by nmr analysis with the help of an authentic sample. However, adduct **16** was also formed, albeit in smaller yield,

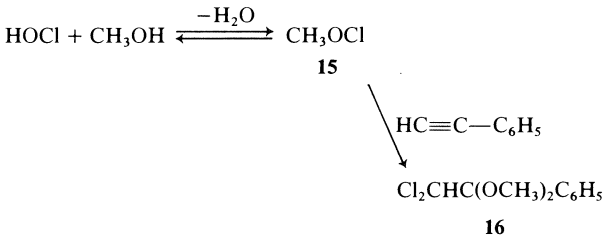

when the crude product from the ozonolysis of 1-chlorocyclohexene (**17**) was treated with phenylacetylene, although this reaction was not expected to co-produce hypochlorous acid but has been shown to proceed via the sequence **17** → **18** → **19** by co-production of hydrogen chloride (1).

This apparent discrepancy showed that there is obviously an alternate source for methyl hypochlorite (**15**) than the postulated intermediate of structure **12**, and that under the prevailing conditions the formation of adduct **16** could not be taken as an unequivocal proof for the transient existence

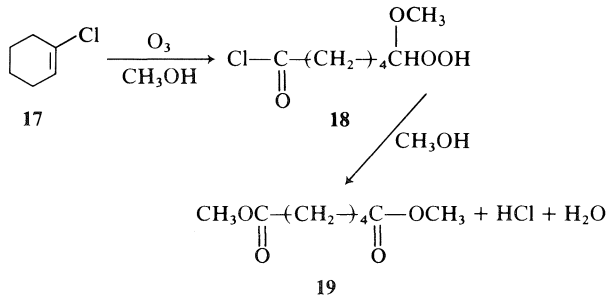

Can. J. Chem. Downloaded from www.nrcresearchpress.com by 210.87.254.5 on 09/06/12
For personal use only.

Can. J. Chem. Downloaded from www.nrcresearchpress.com by 210.87.254.5 on 09/06/12
For personal use only.

of **12**. Based on some observations in other ozonolysis experiments, we had reason to assume that the alternate source for methyl hypochlorite originated from the ozone-initiated oxidation of methanol and from subsequent oxidation of hydrogen chloride by the peroxidic oxidation product to form chlorine. The latter, in turn, could react with methanol to form **15**. The above assumption could be verified by control experiments. Ozone treatment of a 0.35 *M* solution of anhydrous hydrogen chloride in methanol gave a peroxidic reaction mixture. When phenylacetylene was added, adduct **16** was formed, as evidenced by glc and by nmr analysis.

This alternate mode of formation of methyl hypochlorite (**15**) can be effectively prevented if the ozonolysis of chloro olefins is carried out in the presence of sodium methoxide. In its presence, hydrogen chloride is immediately neutralized and the sodium chloride, which is largely precipitated, appears to be resistant towards oxidation. Indeed, under these conditions ozonolysis of 1-chlorocyclohexene and subsequent treatment with phenylacetylene did not afford any detectable amounts of adduct **16**. By contrast, ozonolysis of **5***a*, **5***b*, and **7** and subsequent treatment with phenylacetylene afforded **16** in isolated yields of 92%, 66%, and 95%, respectively. It is felt that these results are good support for the reaction course proposed in Scheme 1 for the ozonolysis of dichloro olefins of type **9**.

Materials and Methods

Materials

The substrates **5***a* (3), **5***b* (7), and **7** (8) were prepared by known procedures. Methanol was of analytical grade. Stock solutions of hydrochloric acid in methanol were prepared by introducing gaseous anhydrous hydrogen chloride into methanol at 0°C and titration of the solutions with aqueous sodium hydroxide using phenolphthalein as indicator. Stock solutions of sodium methoxide were prepared by adding the appropriate amount of sodium to anhydrous methanol.

Analytical Methods

Gas–liquid chromatographic analyses were carried out on a Shimadzu GC-6A unit with flame ionization detector; glass columns: 0.3 × 100 cm, 2.5% Nitrilesiliconoil on Chromosorb G. Conditions: 60°C to 160°C at 4°C per min. Nuclear magnetic resonance spectra were recorded on a Bruker WP 60 spectrometer.

Ozonolysis Reactions in Methanol

trans-*2,3-Dichloro-2-butene* (*5*a)

A mixture of 5.00 g (0.04 mol) of **5***a* in 30 mL of methanol was ozonized at −40°C. Ozone uptake was slow and incomplete and 0.14 moles of ozone were applied over a period of 3 h until the substrate had disappeared. The solution was purged with nitrogen, kept stirring at ambient temperatures for 40 h, and admixed with 5.3 g (0.04 mol) of 1,1,1-trichloroethane as a standard. Nuclear magnetic resonance analysis showed the presence of methyl acetate (**6***a*; δ = 3.70, CH_3CO) in ca. 90% yield.

Phenylacetylene was added to a sample of the freshly ozonized solution and the mixture was stirred for 48 h. In the solution, adduct **16** was identified by co-injection and by comparison of the nmr data with those of an authentic sample (see below).

trans-*3,4-Dichloro-3-hexene* (*5*b)

A mixture of 6.24 g (0.041 mol) of **5***b* in 30 mL of methanol was treated with a total of 0.14 moles of ozone at −40°C within 3 h and then worked up as described above. Methyl propionate (**6***b*; δ = 1.13, t, 3H) was detected in 92% yield by nmr analysis. In a sample treated with phenylacetylene as described above, glc and nmr analysis revealed again the presence of adduct **16**.

1,2-Dichlorocyclohexene (*7*)

A mixture of 7.30 g (0.084 mol) of **7** in 30 mL of methanol was treated with a total of 0.23 moles of ozone within 5 h at ambient temperatures and purged with nitrogen. A small sample of the solution was treated with phenylacetylene as described above and analyzed by glc to afford the peak of adduct **16**. The major part of the ozonized solution was stirred at ambient temperatures for 48 h. Then methanol was removed at 15 Torr and 25°C and the residue was distilled from a micro distillation apparatus to yield 1.02 g (84%) of dimethyl adipate (**8**); bp 114°C/17 Torr. Identification occurred by glc co-injection and by nmr analysis.

1-Chlorocyclohexene (*17*)

A solution containing 1.16 g (0.01 mol) of **17** in 30 mL of methanol was ozonized to completion at ambient temperatures, then purged with nitrogen and stirred for 48 h at ambient temperatures. A sample of the solution was treated with phenylacetylene as described above; glc and nmr analysis showed the presence of adduct **16**.

Anhydrous HCl in Methanol

A solution of 0.25 g (0.007 mol) of hydrogen chloride in 20 mL of methanol was treated with a total of 0.046 moles of ozone within 1 h at ambient temperatures. Then 1.0 g (0.01 mol) of phenylacetylene was added and the mixture was kept stirring for 48 h. Adduct **16** was detected in approximately 18% in the mixture by co-injection with an authentic sample.

Ozonolysis Reactions in Methanol in the Presence of Sodium Methoxide

1-Chlorocyclohexene (*17*)

A solution of 1.16 g (0.01 mol) of **17** and 0.01 mol of sodium methoxide in 30 mL of methanol was ozonized to completion at ambient temperatures within 1 h. The mixture was purged with nitrogen, the precipitated sodium chloride was filtered off, the filtrate was cooled to 0°C, and 1.0 g (0.01 mol) of phenylacetylene was added. Then the solution was acidified to a pH of approximately 3 with a 13 *N* solution of anhydrous HCl in methanol and kept stirring at ambient temperatures for 48 h. The solution was neutralized with solid sodium bicarbonate, filtered, and distilled at 40°C and 15 Torr to remove the methanol. The distillation residue was dissolved in 30 mL of ether, washed with 15 mL of water, dried over sodium sulfate, and then distilled at ambient temperatures and 15 Torr to remove the ether. The residue (1.83 g) was analyzed by nmr spectroscopy. It showed the signals of dimethyl adipate (**19**) as the major component, along with some minor signals of unidentified assignment, however, not the signals of the adduct **16**. The residue was purified by column chromatography (silica gel; 200 mL of *n*-pentane/CH_2Cl_2 = 5:1; 200 mL of *n*-pentane/CH_2Cl_2 = 2:1; 400 mL of ether) to give 1.60 g (92%) of dimethyladipate (**19**) from the ether fraction.

trans-*2,3-Dichloro-2-butene* (*5*a)

A solution of 1.24 g (0.01 mol) of **5***a* and 0.1 mol of sodium

methoxide in 30 mL of methanol was ozonized to completion at ambient temperatures within 4 h and treated further as described above. After neutralization with sodium bicarbonate and filtration, the methanol was distilled off at 40°C and 15 Torr. From the residue 1.38 g of a solid precipitated at ambient temperatures within 30 h. It was recrystallized from methanol to give 1.08 g (92%) of 1,1-dichloro-2,2-dimethoxy-2-phenylethane (**16**); mp 62°C (lit. (6) mp 62°C); nmr (CCl_4, TMS), δ: 3.37 (s, 6H), 6.00 (s, 1H), 7.50 (mc, 5H).

trans-*3,4-Dichloro-3-hexene (5*b*)*

A solution of 1.52 g (0.01 mol) **5***b* and 0.1 mol of sodium methoxide in 30 mL methanol was ozonized to completion at ambient temperatures within 4 h and treated further as described above for **5***a*. After recrystallization from methanol 0.76 g (66%; mp 62°C) of **16** was obtained.

1,2-Dichlorocyclohexene (7)

A solution of 1.50 g (0.01 mol) of **7** and 0.1 mol of sodium methylate in 30 mL of methanol was ozonized to completion at ambient temperatures within 9 h and treated further as described for **5***a* above. After neutralization with sodium bicarbonate and removal of the methanol, the residue was dissolved in 30 mL of ether, washed with water, dried, and the ether distilled off at 40°C and 15 Torr. The viscous liquid residue was analyzed by glc and nmr. It contained 46% of dimethyl adipate (**19**) and 37% of 1,1-dichloro-2,2-dimethoxy-2-phenylethane (**16**).

Acknowledgment

Prof. T. S. Huh thanks the International Seminar at the University of Karlsruhe for a fellowship.

1. H. KEUL and K. GRIESBAUM. Can. J. Chem. **58**, 2049 (1980).
2. G. NAGENDRAPPA and K. GRIESBAUM. J. Agric. Food Chem. **26**, 581 (1978).
3. K. GRIESBAUM and P. HOFMANN. J. Am. Chem. Soc. **98**, 2877 (1976).
4. S. GÄB, S. NITZ, H. PARLAR, and F. KORTE. Chem. Ber. **111**, 1440 (1978).
5. H. SELTZER, S. GÄB, and F. KORTE. Angew. Chem. **92**, 483 (1980); Angew. Chem. Int. Ed. Engl. **19**, 474 (1980).
6. E. L. JACKSON. J. Am. Chem. Soc. **56**, 977 (1934).
7. K. GRIESBAUM, H. KEUL, R. KIBAR, B. PFEFFER, and M. SPRAUL. Chem. Ber. **114**, 1858 (1981).
8. K. GRIESBAUM, R. KIBAR, and B. PFEFFER. Justus Liebigs Ann. Chem. 214 (1975).

Can. J. Chem. Downloaded from www.nrcresearchpress.com by 210.87.254.5 on 09/06/12
For personal use only.

Conformational effects on the enthalpy of formation of straight and branched-chain alkanes

JOHN T. EDWARD
Department of Chemistry, McGill University, 801 Sherbrooke St. West, Montreal, P.Q., Canada H3A 2K6

Received May 11, 1981

JOHN T. EDWARD. Can. J. Chem. **59**, 3192 (1981).

Benson's scheme for calculating the enthalpy of formation of straight and branched-chain alkanes by addition of increments for methyl, methylene, methine, and quaternary carbon groups, and by correction (where necessary) for steric effects, has been modified by a more detailed consideration of the effect of *gauche* interactions.

JOHN T. EDWARD. Can. J. Chem. **59**, 3192 (1981).

Le schéma développé par Benson pour calculer l'enthalpie de formation des alcanes linéaires et ramifiés qui fait appel à l'addition d'incréments pour les groupes méthyle, méthylène, méthine et carbone quaternaire et qui introduit des corrections (quand c'est nécessaire) pour les effets stériques a été modifié en faisant intervenir une considération plus détaillée des effets des interactions gauche.

[Traduit par le journal]

Can. J. Chem. Downloaded from www.nrcresearchpress.com by 210.87.254.5 on 09/06/12
For personal use only.

Benson (1) has developed an additive scheme for calculating the enthalpy of formation ΔH_f^0 of straight and branched-chain alkanes under standard conditions. His group values I and steric correction terms S are listed in Table 1. (Benson uses a different symbolism.) Benson takes account of the effect of *gauche* interactions, but only for branched-chain alkanes: in effect, he considers *n*-alkanes such as *n*-butane (C_4) only in their extended or all *anti* (*a*) conformations. In fact, at 25°C a 0.18 mole fraction of all *n*-butane molecules exist in the g^+, and a 0.18 mole fraction in the g^- conformation, so that the mole fraction Z_g of *gauche* conformations is 0.36. This has the effect of raising the enthalpy of *n*-butane by 0.36 × 700 cal/mol[1] over what it would be if it were completely in the *anti* conformation. This need not be serious in an additive scheme restricted to *n*-alkanes: Z_g increases regularly by 0.29 (corresponding to 0.20 kcal/mol) for each additional CH_2 group (4), and hence the effect of *gauche* interactions can be absorbed into the I value of this group. (Compare I values for CH_2 of Benson and of Edward in Table 1.) However, the limitations of such an approach become more apparent when isomeric branched alkanes are considered. Thus, according to Benson, $Z_g = 2.00$ for both 3-methyloctane (3-MeC_8) and 4-methyloctane (4-MeC_8). In fact, when contributions from the various folded conformations present at 25°C are also taken into account, $Z_g = 3.08$ for 3-MeC_8 and $Z_g = 2.92$ for 4-MeC_8 (4).

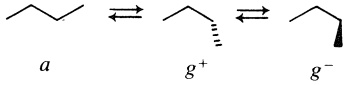

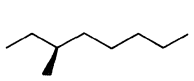

3-MeC_8

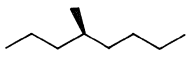

4-MeC_8

These and other steric factors are considered in the values of ΔH_f^0 calculated by the equation

$$[1] \quad \Delta H_f^0 = \sum_1^m n^k I^k + \sum_1^n m^l S^l$$

and recorded in Table 2. Values of I and S are given in Table 1. Z_g (which in [1] becomes m^1) was calculated by reported procedures (3, 4) when it was not already available in the literature (3, 4). In this calculation we have followed Mann (3) in neglecting any conformations containing a g^+g^- or g^-g^+ segment[2] where they could be avoided. However, in some compounds (e.g., 2,2,4-Me_3C_5: Fig. 1) such a segment is unavoidable if the staggered arrangement of the molecule is to be preserved. The value of S^2 reported in Table 1 for such g^+g^- or g^-g^+ arrangements has been adopted on empirical grounds, and agrees with other esti-

[1]More recent work would indicate a ΔH of about 900 cal/mol for the $a \rightarrow g$ conversion of *n*-butane in the gas phase (2). We have, however, retained the value of 700 cal/mol (S^1 in Table 1) used by Mann (3) because of the convenience of using the large number of Z_g values calculated by him, which depend on this value.

[2]Two conformations **A** and **B**, in which **B** has a g^+g^- segment but is otherwise similar to **A**, will be present in the ratio **A**/**B** of 28:1 (assuming the value of S^2 in Table 1). The enthalpy of the compound made up of the two conformations **A** and **B** will be 0.07 kcal/mol higher than if it were made up of **A** alone.

0008-4042/81/223192-03$01.00/0
©1981 National Research Council of Canada/Conseil national de recherches du Canada

Can. J. Chem. Downloaded from www.nrcresearchpress.com by 210.87.254.5 on 09/06/12
For personal use only.

TABLE 1. Group values I and steric correction terms S for calculation of ΔH_f^0

Group	I (kcal mol^{-1}) Benson	Edward	Correction	S (kcal mol^{-1}) Benson	Edward
—CH_3	−10.20	−10.06	$g(S^1)$	0.80	0.70
>CH_2	−4.93	−5.13	$g^{\pm}g^{\mp}(S^2)$	1.5	2.2
>CH—	−1.90	−2.14	2,2,3-$Me_3(S^3)$	—	1.4
—C(—)—	0.50	−0.11	2,2,3,3-$Me_4(S^4)$	—	2.9

TABLE 2. Comparison of experimental and calculated heats of formation ΔH_f^0 (in kcal/mol) using eq. [1]

Compound	Z_g	$-\Delta H_f^0$ Calcd	Exptl[a]
C_2	—	20.12	20.04±0.07
C_3	—	25.27	25.02±0.12
C_4	0.36	30.15	30.03±0.16
2-MeC_3	—	32.32	32.07±0.15
C_5	0.66	35.07	35.08±0.14
2-MeC_4	1.13	36.66	36.73±0.14
2,2-Me_2C_3	—	40.35	40.14±0.15
C_6	0.96	39.99	39.90±0.18
2-MeC_5	1.31	41.68	41.75±0.24
3-MeC_5	2.29	40.98	41.11±0.24
2,2-Me_2C_4	2.00	44.08	44.45±0.24
2,3-Me_2C_4	2.64	42.67	42.59±0.24
C_7	1.25	44.91	44.85±0.22
2-MeC_6	1.64	46.56	46.53±0.28
3-MeC_6	2.47	45.98	45.73±0.47
3-EtC_5	3.58	45.20	45.24±0.33
2,2-Me_2C_5	2.00	49.10	49.19±0.37
2,3-Me_2C_5	3.55	47.16	47.32±0.20
2,4-Me_2C_5	2.00	48.25	48.20±0.29
3,3-Me_2C_5	4.00	47.81	48.07±0.29
2,2,3-$Me_3C_4(S_3)$	4.00	48.4	48.86±0.33
C_8	1.54	49.84	49.90±0.44
2-MeC_7	1.93	51.49	51.47±0.36
3-MeC_7	2.79	50.89	50.79±0.33
4-MeC_7	2.65	50.98	50.66±0.33
3-EtC_6	3.75	50.21	50.36±0.32
2,2-Me_2C_6	2.38	54.07	53.67±0.32
2,3-Me_2C_6	4.30	51.77	51.10±0.40
2,4-Me_2C_6	3.23	52.53	52.40±0.33
2,5-Me_2C_6	2.34	53.14	53.18±0.40
3,3-Me_2C_6	4.00	52.94	52.58±0.32
3,4-Me_2C_6	4.69[c]	51.50[c]	50.87±0.40
	4.72[d]	51.52[d]	
2-Me-3-EtC_5	5.00	51.28	50.44±0.35
3-Me-3-EtC_5	6.00	51.54	51.35±0.35
2,2,3-$Me_3C_5(S_3)$	5.00	52.7	52.57±0.40
2,2,4-$Me_3C_5(S_2)$	3.00	53.3	53.54±0.37
2,3,3-$Me_3C_5(S_3)$	6.00	52.0	51.69±0.38
2,3,4-Me_3C_5	5.00	53.22	51.94±0.43
2,2,3,3-$Me_4C_4(S_4)$	6.00	53.5	53.95±0.28
C_9	1.84	54.76	54.55±0.25
4-MeC_8	2.97	55.77	56.19[b]
2,2-Me_2C_7	2.66	59.01	58.83±0.38

TABLE 2. (*Concluded*)

Compound	Z_g	$-\Delta H_f^0$ Calcd	Exptl[a]
3,3-Et_2C_5	8.00	55.16	55.72±0.43
2,2,3,3-$Me_4C_5(S_4)$	8.00	57.2	56.68±0.39
2,2,3,4-$Me_4C_5(S_2 + S_3)$	6.00	56.9	56.81[b]
2,2,4,4-$Me_4C_5(2S_2)$	4.00	58.5	57.74±0.34
2,3,3,4-$Me_4C_5(2S_3)$	8.00	56.3	56.68[b]
C_{11}	2.42	64.62	64.73±0.64
2,2,5,5-Me_4C_7	6.00	71.77	72.71[b]
3,3,5,5-$Me_4C_7(2S_2)$	8.00	65.9	66.84[b]
2,2,4,4,5-$Me_5C_6(2S_2 + S_3)$	6.00	68.1	67.83[b]
C_{12}	2.72	69.54	69.23±0.36
3,3,6,6-Me_4C_8	8.00	75.50	76.76[b]
4,4,6,6-$Me_4C_9(2S_2)$	8.00	76.2	75.63[b]
3,5-Me_2-3,5-$Et_2C_7(2S_2)$	10.00	74.8	73.20[b]
5,5,7,7-$Me_4C_{11}(2S_2)$	8.75	86.0	88.31[b]
4,6-Me_2-4,6-$Et_2C_9(2S_2)$	10.00	85.1	84.06[b]
C_{16}	3.89	89.24	89.57±0.49
C_{32}	8.58	168.01	166.49[b]

[a] Experimental data from ref. 5, except those marked footnote *b*.
[b] Reference 6.
[c] *meso*-Isomer.
[d] *dl*-Isomer.

mates in the literature (3) (if not with Benson's (1)). The same is true for the S^3 and S^4 correction terms, taking into account the additional strain introduced by a *gem*-dialkyl group[3] vicinal to one or two alkyl groups. The S^2, S^3, and S^4 correction terms are based on a very limited amount of experimental

[3] The mutual repulsions of *gauche* methyl groups in the C_2 form of 2,3-dimethylbutane (**1**; R = H) are relieved by movement in the direction indicated by the arrows, slight increases in torsional and angle strain relieving a large strain energy due to non-bonded repulsions (8). Such relief is not possible for the top methyl group when the distant carbon atom is geminally disubstituted, as in 2,2,3-trimethylbutane (**1**; R = Me).

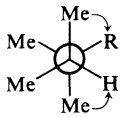

1

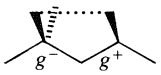

2,2,4-Me_3C_5

FIG. 1. The 2- and 4-methyl groups in a g^-g^+ relationship would be 2.54 Å apart (dotted line) in an undistorted staggered molecule, as compared with a 4.0 Å separation required by their van der Waals radii (7).

data, and may require revision in future. The occasions when they were used in calculating ΔH_f^0 are indicated in Table 2.

The values of ΔH_f^0 thus calculated generally agree with experimental values within the limits of experimental error.[4] For compounds with slight steric congestion (2,2-Me_2C_4 or $EtCMe_3$, 3,3-Me_2C_5 or Et_2CMe_2, 3-Et-3-MeC_5 or Et_3CMe, 2,2,4-Me_3C_5) agreement is better than that found in most other additive schemes (9). For compounds with severe steric congestion, agreement is poorer, but for these compounds other schemes fail completely (10, 11). However, the chief virtue of the present scheme lies in its simplicity and its concreteness. Some other additive schemes are mind-boggling in their complexity (10). Even the relatively simple Allen–Skinner scheme (11) has five steric terms for 2,2,3-trimethylpentane, in comparison with our two (m^1S^1 and m^3S^3). The schemes of Scott (5) and of Somolayajulu and Zwolinski (6) incorporate the steric terms S^1, S^2, S^3, and S^4 (in our terminology) and several more but, like all other schemes up to now, assume the molecule to have a fully extended conformation of the longest chain. Somolayajulu and Zwolinski recognize the limitations of this assumption, and the present paper shows how a realistic assessment of the conformational composition (Z_g) of a hydrocarbon leads to a simple and feasible scheme for calculating ΔH_f^0.

[4]A referee has written that it is doubtful if any ΔH_f^0 for an alkane is known to be better than ± 0.1 kcal mol^{-1} per C atom in absolute or relative terms, and that the uncertainties quoted in Table 2 are experimental precisions, which tend to be unrelated to accuracies.

Acknowledgement

The financial support of the Natural Sciences and Engineering Research Council of Canada is gratefully acknowledged.

1. S. W. BENSON. Thermochemical kinetics. 2nd ed. John Wiley and Sons, New York. 1976. p. 28.
2. J. R. DURIG and D. A. C. COMPTON. J. Phys. Chem. **83**, 265 (1979).
3. G. MANN. Tetrahedron, **23**, 3375 (1967); G. MANN, M. MUHLSTADT, J. BRABAND, and E. DORING. Tetrahedron, **23**, 3393 (1967).
4. J. T. EDWARD, P. G. FARRELL, and F. SHAHIDI. J. Phys. Chem. **82**, 2310 (1978).
5. D. W. SCOTT. J. Chem. Phys. **60**, 3144 (1974).
6. G. R. SOMOLAYAJULU and B. J. ZWOLINSKI. J. Chem. Soc. Faraday Trans. II, **68**, 1971 (1972).
7. J. T. EDWARD. J. Chem. Educ. **47**, 261 (1970).
8. N. L. ALLINGER, J. A. HIRSCH, M. A. MILLER, I. J. TYMINSKI, and F. A. VANCATLEDGE. J. Am. Chem. Soc. **90**, 1199 (1968); R. H. BOYD. J. Am. Chem. Soc. **97**, 5353 (1975).
9. H. HENRY, S. FLISZÁR, and A. JULG. Can. J. Chem. **54**, 2085 (1976).
10. H. A. SKINNER and G. PILCHER. Q. Rev. Chem. Soc. **17**, 264 (1963).
11. H. A. SKINNER. J. Chem. Soc. 4386 (1962).

Can. J. Chem. Downloaded from www.nrcresearchpress.com by 210.87.254.5 on 09/06/12
For personal use only.

Substituent effects upon cation–pseudobase equilibration for isoquinolinium and phthalazinium cations

JOHN W. BUNTING, VIVIAN S.-F. CHEW, AND SHINTA SINDHUATMADJA

Department of Chemistry, University of Toronto, Toronto, Ont., Canada M5S 1A1

Received June 4, 1981

JOHN W. BUNTING, VIVIAN S.-F. CHEW, and SHINTA SINDHUATMADJA. Can. J. Chem. **59**, 3195 (1981).

pK_{R+} values have been measured for cation–pseudobase equilibration by 4-X-2-methylisoquinolinium cations (**1**) (X = Br, $CONH_2$, COC_6H_5, CN, NO_2) at 25°C, ionic strength 0.1. These pK_{R+} values are well correlated by Hammett equations using either σ or σ^- *para* substituent constants. The best correlation gives: $pK_{R+} = -8.8\ (\pm 0.3)\sigma_p^- + 16.5\ (\pm 0.2)$ ($r = 0.998$). The value $pK_{R+} = 16.29$ measured by Cook *et al.* (Tetrahedron, **32**, 1773 (1976)) for the 2-methylisoquinolinium cation in dimethyl sulfoxide – water solutions is in reasonable agreement with this correlation equation. For the 2-methyl-5-nitrophthalazinium cation, $pK_{R+} = 7.87$, and $pK_{RO-} = 12.10$ for alkoxide ion formation by the pseudobase of this cation.

The pH dependence of the pseudo first-order rate constants (k_{obs}) for cation–pseudobase equilibration has been measured for **1**:X = $CONH_2$, COC_6H_5, CN and for the 2-methylphthalazinium cation (**3**) and its 5-NO_2 derivative (**4**). For each of these cations, $k_f = k_{OH}[^-OH] + k_{H_2O}$ and $k_d = k_1[H^+] + k_2$ and the parameters k_{OH} k_{H_2O}, k_1, and k_2 have been evaluated. For **1**:X = $CONH_2$ and CN and **3**, k_{OH} is consistent with a correlation line between log k_{OH} and pK_{R+} established for other isoquinolinium cations (J. Am. Chem. Soc. **99**, 1189 (1977)). For **1**:X = COC_6H_5, k_{OH} is seven-fold smaller, and for **4**, k_{OH} is five-fold greater than predicted by this correlation line.

JOHN W. BUNTING, VIVIAN S.-F. CHEW et SHINTA SINDHUATMADJA. Can. J. Chem. **59**, 3195 (1981).

On a mesuré les valeurs de pK_{R+} de l'équilibre pseudobase/cation provoquée par les cations X-4 méthyl-2 isoquinolénium (**1**) (X = Br, $CONH_2$, COC_6H_5, CN, NO_2) à 25°C et à une force ionique de 0,1. L'équation de Hammett permet d'établir une bonne corrélation entre ces valeurs de pK_{R+} et les valeurs σ et σ^- des substituants en *para*. La meilleure corrélation donne: $pK_{R+} = -8.8\ (\pm 0.3)\sigma_p^- + 16.5\ (\pm 0.2)$ ($r = 0.998$). La valeur de $pK_{R+} = 16{,}29$ mesurée par Cook *et al.* (Tetrahedron, **32**, 1773 (1976)) pour le cation méthyl-2 isoquinolinium dans des solutions de diméthylsulfoxyde–eau est raisonnablement en accord avec cette corrélation. Dans le cas du cation méthyl-2 nitro-5 phtalazinium, le $pK_{R+} = 7{,}87$ alors que le $pK_{RO-} = 12{,}10$ pour la formation de l'ion alcoolate par la pseudobase de ce cation. Pour le composé **1** où X = $CONH_2$, COC_6H_5, CN, ainsi que pour le cation méthyl-2 phtalazinium (**3**) et son dérivé nitré en position 5 (**4**), on a mesuré l'effet du pH sur la constante de vitesse de pseudo ordre un (k_{obs}) de l'équilibre cation/pseudobase. Pour chacun de ces cations, on a évalué $k_f = k_{OH}[OH^-] + k_{H_2O}$ et $k_d = k_1[H^+] + k_2$ et les paramètres k_{OH}, k_{H_2O}, k_1 et k_2. Pour le composé **1** où X = $CONH_2$ et CN et pour le composé **3**, k_{OH} est en accord avec la corrélation linéaire entre le log k_{OH} et pK_{R+} qu'on a établie pour d'autres cations isoquinoliniums (J. Am. Chem. Soc. **99**, 1189 (1977)). Pour les composés **4** et **1** où X = COC_6H_5, les valeurs de k_{OH} sont respectivement cinq et sept fois les valeurs prévues par cette ligne de corrélation.

[Traduit par le journal]

The phenomenon of pseudobase formation by heteroaromatic cations has been recognized for over 80 years (1–3). However, it is only during the past fifteen years that systematic quantitative studies of the equilibria and kinetics of cation–pseudobase equilibration have been attempted (4). In the present work, we report substituent effects upon equilibrium constants for cation–pseudobase equilibration for 2-methylisoquinolinium cations (**1**) bearing a variety of substituents at C-4, and also the pH dependence of the rates of equilibration in this system for those **1** which display cation–pseudobase equilibration rates that are sufficiently slow to allow measurement by the stopped-flow technique. We also report rates of cation–pseudobase equilibration for the 2-methylphthalazinium cation (**3**) and its 5-nitro derivative (**4**). These data allow the first comparison of rates of this phenomenon for the closely related isoquinolinium and phthalazinium cations.

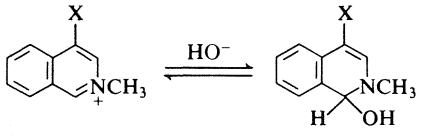

1 **2**

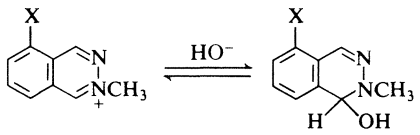

3: X = H
4: X = NO_2

5: X = H
6: X = NO_2

Experimental

Isoquinoline, 4-bromoisoquinoline, and phthalazine were purchased from Aldrich Chemical Co. 4-Cyanoisoquinoline was prepared by treatment of 4-bromoisoquinoline with cuprous cyanide as described by Tyson (5). 5-Nitrophthalazine was prepared by nitration of phthalazine by the method of Kanahara (6).

4-Isoquinolinecarboxamide

4-Cyanoisoquinoline (2.0 g) and Amberlite IRA-400 OH ion exchange resin (2.0 g) were refluxed for two hours in water

0008-4042/81/223195-05$01.00/0

©1981 National Research Council of Canada/Conseil national de recherches du Canada

Can. J. Chem. Downloaded from www.nrcresearchpress.com by 210.87.254.105 on 09/06/12
For personal use only.

Can. J. Chem. Downloaded from www.nrcresearchpress.com by 210.87.254.105 on 09/06/12
For personal use only.

(15 mL) containing acetonitrile (1 mL). The resin was removed from the hot solution by filtration and the solvent evaporated on the steam bath to give 4-isoquinolinecarboxamide (1.7 g), mp 170–171°C (lit. (7) mp 168–172°C).

4-Benzoyl-2-methylisoquinolinium Perchlorate

2-Methylisoquinolinium bromide in basic aqueous acetone was treated with benzoyl chloride as described by Chen and Bradsher (8). The red oily product was stirred with aqueous perchloric acid (30%) to give a pale yellow solid which was filtered off, dried, and stirred with ether. Several recrystallizations of the solid product from ethanol after treatment with decolourizing charcoal gave white crystals of the desired perchlorate salt. *Anal.* calcd. for $C_{17}H_{14}NO_5Cl$: C 58.71, H 4.06, N 4.03; found: C 58.71, H 4.21, N 4.11.

Methylation of Isoquinolines

An acetone solution of the substituted isoquinoline was stirred with excess methyl bromide in a pressure bottle overnight. The white solid was filtered off and recrystallized several times from ethanol.

4-Aminocarbonyl-2-methylisoquinolinium Bromide

Anal. calcd. for $C_{11}H_{11}N_2OBr$: C 49.45, H 4.15, N 10.49; found: C 49.58, H 4.21, N 10.49.

4-Cyano-2-methylisoquinolinium Bromide

Anal. calcd. for $C_{11}H_9N_2Br$: C 53.04, H 3.64, N 11.12; found: C 52.91, H 3.72, N 11.21.

2-Methyl-5-nitrophthalazinium Iodide

This compound was prepared by methylation of 5-nitrophthalazine with methyl iodide and fractional crystallization to separate the 5-nitro and 8-nitro isomers as described by Kanahara (6).

Determination of pK_{R+} Values

All pK_{R+} values were determined spectrophotometrically at a suitable wavelength by the general method of Albert and Serjeant (9) in aqueous buffers of ionic strength 0.1 at 25°C. Reported pK_{R+} values are averages of the values calculated from at least eight different pH solutions in the range $pK_{R+} \pm 1$.

Kinetic Studies

All kinetic studies were made on a Durrum–Gibson stopped-flow spectrophotometer by mixing solutions of the heterocyclic cation (or pseudobase) with suitable aqueous buffers (ionic strength 0.1 after mixing) at 25°C. Absorbance vs. time curves at an appropriate wavelength were digitized (118 data points), and the data were collected and fitted to first-order rate equations in a Tektronix 4051 Minicomputer. The observed first-order rate constants (k_{obs}) for cation–pseudobase equilibration were separated into the individual rate constants for pseudobase formation (k_f) and pseudobase decomposition (k_d) back to the cation by the relationships (10):

$$k_f = k_{obs}/(1 + [H^+]/K_{R+})$$
$$k_d = k_{obs}/(1 + K_{R+}/[H^+])$$

Results and Discussion

pK_{R+} for Isoquinolinium Cations (1)

Each of the 2-methylisoquinolinium cations **1**:X = Br, $CONH_2$, COC_6H_5, CN display pH-dependent electronic absorption spectra in basic aqueous solutions. These spectra display clean isosbestic points and are readily reversible upon acidification of the solutions. Evaluation of pK_{R+} for each cation from the pH dependence of the absorbance at an appropriate wavelength gave the values collected in Table 1. Also included in Table 1 are a previously measured pK_{R+} for **1**:X = NO_2 and estimated and experimental values for **1**:X = H. This latter cation undergoes irreversible spectral changes in the concentrated basic solutions required to generate its pseudobase (11). An earlier estimate (11) of $pK_{R+} = 15.3$ for **1**:X = H was based upon substituent effects upon pK_{R+} values in the 4-bromo and 5-bromo-2-cyanoisoquinolinium cations and relatively uncertain pK_{R+} values for the corresponding 2-methylisoquinolinium cations. Our current estimate in Table 1 for **1**:X = H is based upon the current accurate pK_{R+} for **1**:X = Br and $\Delta pK_{R+} = -1.7$ for a 4-bromo substituent in the 2-cyanoisoquinolinium cation (12). This estimate remains somewhat lower than $pK_{R+} = 16.29$ measured for **1**:X = H by Cook *et al.* in dimethyl sulfoxide – water mixtures (13, 14).

TABLE 1. pK_{R+} for pseudobase formation by **1**[a]

X	pK_{R+}
H	15.5,[b] 16.29[c]
Br	13.81±0.02[d]
$CONH_2$	11.49±0.05
COC_6H_5	9.34±0.07
CN	7.80±0.05
NO_2	5.11[e]

[a] At 25°C, ionic strength 0.1.
[b] Estimated as described in text.
[c] Measured (13, 14) in dimethyl sulfoxide – water mixtures.
[d] Ionic strength 1.0.
[e] From ref. 10.

The X-dependence of the pK_{R+} values in Table 1 is consistent with a Hammett equation based upon either σ values for *para* substituents (σ_p) derived from benzoic acid ionization constants or σ^- values for *para* substituents (σ_p^-) derived from anilinium cation acidity constants (15).

$$[1] \quad pK_{R+} = -13.4\,(\pm 1.1)\sigma_p + 16.1\,(\pm 0.5) \qquad (r = 0.987)$$

$$[1a] \quad pK_{R+} = -14.2\,(\pm 0.9)\sigma_p + 16.5\,(\pm 0.4) \qquad (r = 0.992)$$

$$[1b] \quad pK_{R+} = -14.8\,(\pm 1.4)\sigma_p + 16.9\,(\pm 0.8) \qquad (r = 0.987)$$

$$[2] \quad pK_{R+} = -8.3\,(\pm 0.4)\sigma_p^- + 16.0\,(\pm 0.3) \qquad (r = 0.994)$$

$$[2a] \quad pK_{R+} = -8.8\,(\pm 0.3)\sigma_p^- + 16.5\,(\pm 0.2) \qquad (r = 0.998)$$

$$[2b] \quad pK_{R+} = -9.0\,(\pm 0.4)\sigma_p^- + 16.7\,(\pm 0.3) \qquad (r = 0.997)$$

Equations [1] and [2] are obtained using $pK_{R+} =$

Can. J. Chem. Downloaded from www.nrcresearchpress.com by 210.87.254.105 on 09/06/12
For personal use only.

15.5 for **1**:X = H, while eqs. [1*a*] and [2*a*] result from using $pK_{R+} = 16.29$ for this cation as reported by Cook *et al.* (13, 14). Equations [1*a*] and [2*a*] produce better fits to the experimental data than eqs. [1] and [2] respectively on the basis of the correlation coefficients obtained. Equations [1*b*] and [2*b*] result when the data point for X = H is excluded. All the above correlation equations predict pK_{R+} for **1**:X = H to be somewhat greater than the estimates extrapolated from substituent effects with the 2-cyanoisoquinolinium cation, and we conclude that the value obtained by Cook *et al.* (13, 14) is most consistent with the data obtained for the other substituents in the current study.

Attempted correlations of pK_{R+} data using any form of *meta* substituent constants give much poorer correlations than those reported above, with the bromine substituent in particular showing a large deviation in any correlation line based upon *meta* substituent constants. The somewhat better correlations with σ_p^- (eqs. [2]–[2*b*]) than with σ_p (eqs. [1]–[1*b*]) are readily reconciled in terms of the importance of resonance contributors such as **7** to

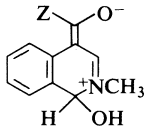

7

the electronic structure of the pseudobase species (**2**). Such resonance interaction of the X substituent with the ring nitrogen atom is not possible in the isoquinolinium cation (**1**). This resonance interaction of a substituent with the neutral nitrogen atom in the pseudobase but not in the heteroaromatic cation is analogous to the situation in the equilibration of neutral anilines and anilinium cations from which the σ_p^- values used in the present correlations have been derived. In fact, eq. [2*a*] for pK_{R+} for **1** can be combined with $pK_a = -2.89\,\sigma_p^- + 4.58$ for anilinium cation acidities (16) in the form of eq. [3].

[3] $\quad pK_{R+} = 3.0\,pK_a + 2.6$

Equation [3] can then be used to directly predict pK_{R+} values for all 4-X-2-methylisoquinolinium cations from the pK_a values for the corresponding 4-X-anilinium cations.

We note that the data of Terrier *et al.* (17) for substituent effects upon the equilibrium constants for Meisenheimer complex (**9**) formation from 4-X-2,6-dinitroanisoles (**8**) can also be correlated with σ_p or σ_p^-. Such observations provide quantitative support for the analogy between Meisenheimer complex formation from electron-deficient

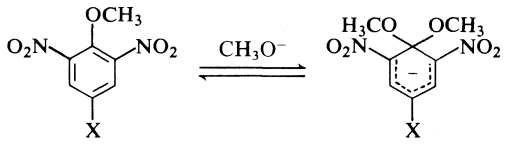

8 **9**

aromatic molecules and pseudobase formation from heteroaromatic cations (4).

pK_{R+} for the 2-Methyl-5-nitrophthalazinium Cation (4)

From the pH dependence of the electronic absorption spectrum of this cation we have calculated $pK_{R+} = 7.87 \pm 0.03$. In more basic aqueous solutions the spectrum of the pseudobase undergoes pH-dependent changes that are consistent with a further acid–base equilibration. We have calculated $pK_{RO-} = 12.10 \pm 0.03$ for this equilibration which we assign to alkoxide ion (**10**) formation

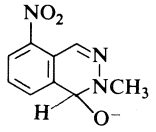

10

by the pseudobase **6**. Analogous pH-dependent spectral changes have been observed previously for the 2-methylphthalazinium cation **3** with $pK_{R+} = 11.0$ and $pK_{RO-} = 13.0$ having been reported (11). The influence of the 5-nitro group on each of these ionizations is qualitatively consistent with expectation. The $\Delta pK_{R+} = 3.13$ for the 5-nitro substituent effect in these phthalazinium cations is somewhat smaller than $\Delta pK_{R+} = 16.29 - 11.7 = 4.59$ calculated for a 5-nitro substituent in the 2-methylisoquinolinium cation ($pK_{R+} = 11.7$ for the 2-methyl-5-nitroisoquinolinium cation (18)).

Kinetics of Cation–Pseudobase Equilibration

Pseudo first-order rate constants (k_{obs}) for cation–pseudobase equilibration were evaluated at intervals of approximately 0.5 pH units for each cation over the pH range in which equilibration rates were sufficiently slow to allow measurement on the stopped-flow spectrophotometer. For **1**:X = Br equilibration was too rapid to allow rate measurements at any pH. Significant pH ranges were accessible for **1**:X = $CONH_2$, COC_6H_5, and CN and also **3** and **4**, and the experimentally derived pH dependences of k_{obs} for each of these cations are displayed in Figs. 1 and 2. In all cases k_{obs} vs. pH passes through a minimum as observed in previous studies (10, 19). Figures 1 and 2 dramatically indicate the influence of pK_{R+} on the overall shape of the k_{obs} vs. pH profiles. High pK_{R+} values lead to a relatively broad plateau region bounded by first-

Can. J. Chem. Downloaded from www.nrcresearchpress.com by 210.87.254.105 on 09/06/12
For personal use only.

order dependence on $[H^+]$ and $[^-OH]$ in low and high pH regions respectively. For low pK_{R+} values, the plateau region is essentially eliminated.

As discussed previously (10), k_{obs} may be converted into separate rate constants for pseudobase formation (k_f) from the cation and pseudobase decomposition (k_d) to the cation. For each cation, k_f and k_d display individual pH dependences exemplified by that for **1**:X = COC_6H_5 in Fig. 3. These pH dependences can be described by equations of the form:

$$[4] \quad k_f = k_{OH}[^-OH] + k_{H_2O}$$

$$[5] \quad k_d = k_1[H^+] + k_2$$

Values of the parameters k_{OH}, k_{H_2O}, k_1, and k_2 were evaluated for each cation and are collected in Table 2. For **1**:X = $CONH_2$ and **3** (i.e. cations of high pK_{R+}) values of k_{H_2O} and k_1 are not accessible within the pH range for which rate data are available. The k_{OH}/k_{H_2O} ratios for **1**:X = COC_6H_5 and CN and **4** are within experimental error of $10^7\ M^{-1}$ as observed for many other quinolinium and isoquinolinium cations (19).

Substituent effects upon k_{OH} and k_{H_2O} indicate that these rate constants increase with the substituent electron-withdrawing effect in both the isoquinolinium and phthalazinium cations. A linear correlation (eq. [6]) between log k_{OH} and pK_{R+} has previously been established (19) for pseudobase formation from a variety of substituted isoquinolium cations. Comparison of experimental and calculated (from eq. [6]) log k_{OH} values gives satisfactory agreement for **1**:X = $CONH_2$ (4.45 (exptl), 4.70 (calcd.)) and **1**:X = CN (5.90 (exptl.), 6.03 (calcd.)). However, for **1**:X = COC_6H_5, $k_{OH} = 4.1 \times 10^4\ M^{-1}\ s^{-1}$ is almost an order of magnitude smaller than the value of $3 \times 10^5\ M^{-1}\ s^{-1}$ derived from eq. [6]. Inspection of k_1 and k_2 values in Table 2 also indicates that these rate constants are smaller for X = COC_6H_5 than expected on the basis of k_1 and k_2 values for other **1** and the X-dependence of pK_{R+}. Since the pK_{R+} value for **1**:X = COC_6H_5 is well correlated with pK_{R+} for other X substituents in **1**, these rate constant anomalies for X = COC_6H_5 appear to reflect a transition state phenomenon of some type.

$$[6] \quad \log k_{OH} = -0.36\ pK_{R+} + 8.84$$

The experimental value of $k_{OH} = 6.0 \times 10^4\ M^{-1}\ s^{-1}$ for **3** is within experimental error of $k_{OH} = 7.6 \times 10^4\ M^{-1}\ s^{-1}$ predicted for this cation on the assumption that eq. [6] is also applicable to phthalazinium cations. However, eq. [6] underestimates ($1.0 \times 10^6\ M^{-1}\ s^{-1}$) k_{OH} for **4** by a factor of five. It has been established (19) that quinolinium and isoquinolinium cations require quite different log k_{OH} vs. pK_{R+} correlation lines. Thus it is possible that the close

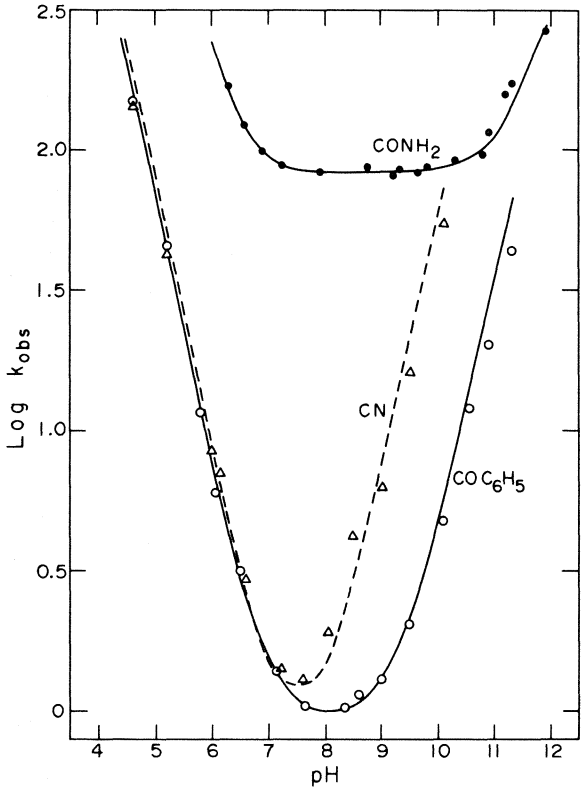

FIG. 1. The pH dependence of k_{obs} (s^{-1}) for the equilibration **1** ⇌ **2** for X = $CONH_2$, COC_6H_5, CN.

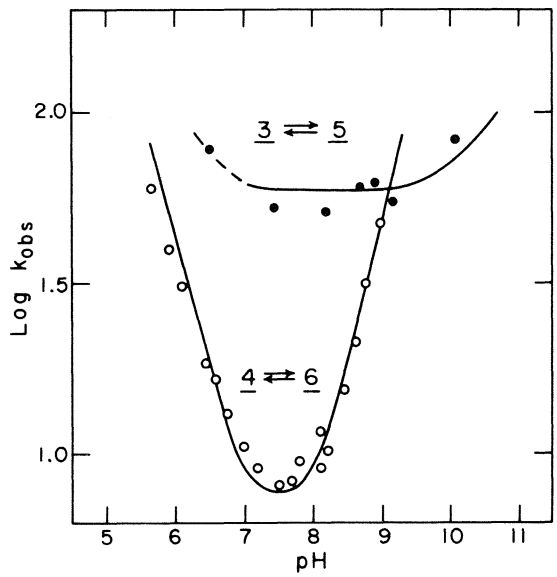

FIG. 2. The pH dependence of k_{obs} (s^{-1}) for the equilibrations **3** ⇌ **5** and **4** ⇌ **6**.

TABLE 2. Rate constants[a] for cation–pseudobase equilibration

Cation	X	k_{OH} (M^{-1} s^{-1})	k_{H2O} (s^{-1})	k_{OH}/k_{H2O} (M^{-1})	k_1 (M^{-1} s^{-1})	k_2 (s^{-1})
1	$CONH_2$	$(2.8\pm0.3)\times10^4$	—	—	(1.5×10^8)[c]	85±10
1	COC_6H_5	$(4.1\pm0.4)\times10^4$	$(3.1\pm0.4)\times10^{-3}$	1.3×10^7	$(6.9\pm0.6)\times10^6$	0.88±0.08
1	CN	$(8.0\pm1.0)\times10^5$	0.10±0.01	8.0×10^6	$(8.2\pm0.8)\times10^6$	0.3±0.1
1	NO_2[b]	8.8×10^6	1.04	8.7×10^6	1.3×10^5	0.011
3	H	$(6.2\pm1.1)\times10^4$	—	—	—	62±11
4	NO_2	$(4.7\pm0.5)\times10^6$	0.55±0.06	8.5×10^6	$(4.4\pm0.5)\times10^7$	3.5±0.5

[a] As defined in eqs. [4] and [5] at 25°C, ionic strength 0.1.
[b] Data from ref. 10.
[c] Based on only two data points.

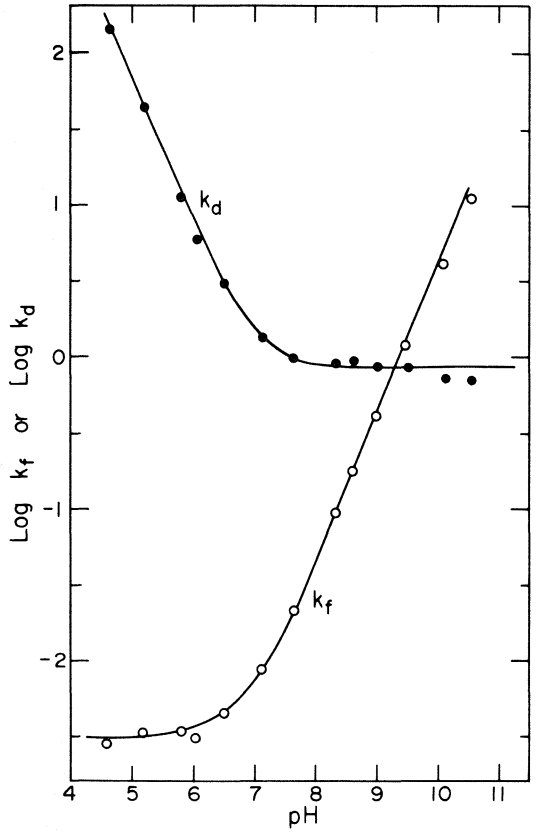

FIG. 3. The pH dependence of k_f (s^{-1}) and k_d (s^{-1}) for **1**:X = COC_6H_5.

prediction for **3** above is fortuitous and that in general isoquinolinium and phthalazinium cations cannot be included on the same correlation line. Further data for phthalazinium cations will be required for a further exploration of this point. However, it should be noted that k_{OH} for **4** is sixfold larger than for **1**:X = CN even though these two cations have very similar pK_{R+} values.

Acknowledgements

This research was supported by an operating grant to J.W.B. from the Natural Sciences and Engineering Research Council of Canada. We thank Ms. Anoma Gunasekara for a number of syntheses, and Dr. Tetsuo Takemura for a translation of ref. 6.

1. H. DECKER. J. Prakt. Chem. (NS) **47**, 28 (1893).
2. A. HANTZSCH. Chem. Ber. **32**, 575 (1899).
3. D. BEKE. Adv. Heterocycl. Chem. **1**, 167 (1963).
4. J. W. BUNTING. Adv. Heterocycl. Chem. **25**, 1 (1979).
5. F. T. TYSON. J. Am. Chem. Soc. **61**, 183 (1939).
6. S. KANAHARA. J. Pharm. Soc. Jpn. **84**, 489 (1964).
7. G. THUILLIER, B. MARCOT, A. VILAR, and P. RUMPF. Bull. Soc. Chim. Fr. 1763 (1966).
8. T.-K. CHEN and C. K. BRADSHER. Tetrahedron, **29**, 2951 (1973).
9. A. ALBERT and E. P. SERJEANT. Ionization constants of acids and bases. Methuen, London. 1962.
10. J. W. BUNTING and W. G. MEATHREL. Can. J. Chem. **51**, 1965 (1973).
11. J. W. BUNTING and W. G. MEATHREL. Can. J. Chem. **50**, 917 (1972).
12. C. J. COOKSEY and M. D. JOHNSON. J. Chem. Soc. B, 1191 (1968).
13. M. J. COOK, A. R. KATRITZKY, P. LINDA, and R. D. TACK. Tetrahedron Lett. 5019 (1972).
14. M. J. COOK, A. R. KATRITZKY, A. D. PAGE, R. D. TACK, and H. WITEK. Tetrahedron, **32**, 1773 (1976).
15. J. CLARK and D. D. PERRIN. Q. Rev. Chem. Soc. **18**, 295 (1964).
16. A. I. BIGGS and R. A. ROBINSON. J. Chem. Soc. 388 (1961).
17. F. TERRIER, F. MILLOT, and J. MOREL. J. Org. Chem. **41**, 3892 (1976).
18. J. W. BUNTING and W. G. MEATHREL. Can. J. Chem. **52**, 962 (1974).
19. J. W. BUNTING and D. J. NORRIS. J. Am. Chem. Soc. **99**, 1189 (1977).

Can. J. Chem. Downloaded from www.nrcresearchpress.com by 210.87.254.105 on 09/06/12
For personal use only.

Geometries of the ground and first excited triplet states of thioformaldehyde[1]

JOHN D. GODDARD

Division of Chemistry, National Research Council of Canada, Ottawa, Ont., Canada K1A 0R6

Received June 3, 1981

JOHN D. GODDARD. Can. J. Chem. **59**, 3200 (1981).

The geometries of the S_0 and T_1 states of thioformaldehyde are determined by *ab initio* SCF calculations with Gaussian basis sets ranging from minimal to double ζ plus both diffuse and polarization functions. The ground state geometries are all in reasonable agreement with experiment but for the $n \rightarrow \pi^*$ triplet state split valence or double ζ basis sets yield unreasonably long CS bond distances.

JOHN D. GODDARD. Can. J. Chem. **59**, 3200 (1981).

On a déterminé les géométries des états S_0 et T_1 de la thioformaldehyde en utilisant les calculs *ab initio* SCF avec des ensembles de base de Gauss allant du minimum à double ζ auxquels on ajoute les fonctions de diffusion et de polarisation. Les géométries de l'état fondamental sont raisonnablement en accord avec l'expérience mais dans le cas de l'état triplet $n \rightarrow \pi^*$, les ensembles de base impliquant le dédoublement de la valence ou le double ζ conduisent à de liaison CS qui sont anormalement longues.

[Traduit par le journal]

Can. J. Chem. Downloaded from www.nrcresearchpress.com by 210.87.254.40 on 09/06/12
For personal use only.

Introduction

Considerable experimental interest exists in the electronic spectrum of thioformaldehyde (1, 2). Although an accurate microwave structure for the ground state of H_2CS has been available for some time (3), only very recently has an analysis of the $\tilde{a}^3A_2 \leftarrow \tilde{X}^1A_1$ absorption band yielded an r_0 structure for the lowest triplet state (2). A number of *ab initio* theoretical studies of the geometries of both the ground and lowest triplet states of thioformaldehyde have appeared (4–6) and very high level calculations on the ground state are also available (7). In the studies which considered the lowest triplet state geometry, only an approximate SCF calculation with a STO-2G + S $3d_\pi$ basis set (4) gave a CS bond length (1.675 Å) in very good agreement with the experimental result of 1.683 Å (2). An STO-3G CS bond length of 1.8075 Å has been reported for the lowest triplet state of thioformaldehyde (6). The CS bond lengths for the $^3n \rightarrow \pi^*$ state using double ζ (DZ) basis sets were 1.783 Å (SCF) and >1.783 Å (CI) (5) and thus at least 0.1 Å greater than experiment. These studies did predict geometries for the ground state in good agreement (e.g. CS bond length within 0.04 Å of the experimental value) with the microwave result.

For molecules containing only H, C, N, and O, it is known that SCF geometry predictions with split-valence or double ζ basis sets usually yield bond lengths within ~0.02 Å and bond angles within ~2° of experiment (18). However, for molecules containing heavier atoms such as S, the picture regarding the effects of the basis set on SCF structural predictions is not so clear (8, 9). It might be anticipated that at the SCF level, but possibly with more extensive basis sets, a similar agreement between experiment and theory could be recovered for a molecule such as thioformaldehyde. In this work, both the ground and lowest triplet state geometries of thioformaldehyde have been determined at the SCF level with basis sets ranging from minimal to double ζ plus diffuse and polarization functions. It is shown that medium sized basis sets without polarization functions such as 3-21G, 4-31G or double ζ yield CS bond lengths in the lowest triplet state of thioformaldehyde which are in very poor agreement with experiment.

Theoretical Methods

References for the Gaussian basis sets used are: STO-3G (S, ref. 10(*a*); C, H, ref. 10(*b*)), STO-3G* (8), 3-21G (S, ref. 12(*a*); C, H, ref. 12(*b*)), 4-31G (S, ref. 11(*a*); C, H, ref. 11(*b*)), and DZ (13). In adding diffuse functions on S, the orbital exponents were chosen to be $\alpha(4s) = 0.023$, $\alpha(4p) = 0.020$, and $\alpha(3d) = 0.015$ (13). The values chosen for the polarization function exponents were $\alpha(d)C = 0.75$, $\alpha(d)S = 0.55$ (7), and $\alpha(p)H = 1.0$. Except for the STO-3G* calculations the sixth *s*-type combination of the Cartesian *d*-type Gaussians was retained in the basis set. All geometries were fully optimized employing energy gradient methods (14, 15). The triplet state was calculated within the Unrestricted Hartree Fock approximation and satisfactory values of the $\hat{S}^2$ operator were obtained (footnote *f*, Table 2). Most calculations were carried out with MONSTERGAUSS 80 (16) which is an extensively modified version of GAUSSIAN 76 (17).

Results and Discussion

The optimized geometries and total energies for

[1]NRCC No. 19667.

0008-4042/81/223200-04$01.00/0

©1981 National Research Council of Canada/Conseil national de recherches du Canada

TABLE 1. SCF optimized geometries and total energies (in hartree) for the $^1A_1$ ground state of thioformaldehyde; bond lengths in Å and bond angles in degrees

Basis set	r_e (CS)	r_e (CH)	θ_e (HCH)	E
STO-3G	1.574	1.090	112.0	−431.67137
STO-3G*[a]	1.551	1.093	111.7	−431.70875
3-21G	1.638	1.073	116.5	−434.33624
4-31G	1.629	1.073	115.5	−435.99188
DZ	1.637	1.075	115.9	−436.45884
DZ + DIFFUSE[b]	1.637	1.075	116.1	−436.46069
DZ**[c]	1.601	1.080	115.7	−436.51163
DZ** + DIFFUSE[b,c]	1.602	1.080	115.8	−436.51332
Experiment[d]	1.6108 (9)	1.0925 (9)	116.87 (5)	—

[a] 5*d* functions on S with exponent 0.39 (8).
[b] *s*, *p*, and *d* functions on S with exponents, 0.023, 0.020, and 0.015 (13).
[c] 6*d* functions on C and S with exponents 0.75 and 0.55 (7) and *p* functions on H with exponent 1.0.
[d] Completely substituted structure (3).

TABLE 2. SCF optimized geometries and total energies (in hartree) for the $^3A''$ ($n \rightarrow \pi^*$) excited state of thioformaldehyde; UHF–SCF;[f] bond lengths in Å and bond angles in degrees

Basis set	r_e (CS)	r_e (CH)	θ_e (HCH)	α_e (oop)	E
STO-3G	1.740	1.082	115.8	27.0	−431.66508
STO-3G*[a]	1.699	1.083	116.5	20.3	−431.69327
3-21G	1.802	1.071	121.7	18.1	−434.31271
4-31G	1.792	1.069	122.2	4.6	−435.97018
DZ	1.783	1.072	121.2	13.2	−436.43532
DZ + DIFFUSE[b]	1.782	1.071	121.8	9.9	−436.43724
DZ**[c]	1.732	1.075	119.6	20.6	−436.48129
DZ** + DIFFUSE[d]	1.732	1.075	119.7	20.6	−436.48292
Experiment[e]	1.683 (5)	1.082 (8)	119.6 (1.7)	16.0 (2.9)	—

[a,b,c,d] See footnotes in Table 1.
[e] r_0 structure (2).
[f] Expectation values of $\hat{S}^2$ were: 2.0083, 2.0242, 2.0123, 2.0132, 2.0138, 2.0148, 2.0216, 2.0221; and differ from the ideal value of 2.000 by ~ 1%.

the ground and lowest triplet excited state are collected in Tables 1 and 2. The experimental results of refs. 2 and 3 are included for comparison although for the triplet state the r_0, θ_0 structure (averaged over zero-point vibrational motion), of ref. 2 is *not* strictly comparable to the calculated r_e, θ_e (actual potential minimum) values (18). In addition, the invariance of the geometrical structure on isotopic substitution (CD_2S) was assumed in calculating the r_0 structure of $^3A_2$ thioformaldehyde from the observed rotational constants of the O_0^0 band (2).

For ground state thioformaldehyde all the Gaussian basis sets used predict r_e (CH) within 0.02 Å of the experimental value. STO-3G and STO-3G* predict HCH angles of 112.0° and 111.7° which are 4.9° and 5.1° smaller than experiment. All other basis sets predicted angles within 1.1° of the measured value. The CS bond lengths from the STO-3G and STO-3G* SCF calculations are shorter than experiment by ~ 0.04 Å and ~ 0.06 Å while the split valence (3-21G, 4-31G) or double ζ basis sets give CS bonds ~ 0.02 Å too long. The addition of diffuse functions on S (DZ to DZ + DIFFUSE) has very little effect on geometry with a change in the HCH angle of 0.2°. The extension of the basis set to include polarization functions on C, S, and H has a dramatic effect on the CS bond length decreasing it by nearly 0.04 Å to a value of 1.601 Å. For the S_0 state the STO-3G result of this work agrees (within small differences due to different geometry optimization criteria) with results previously reported (6). The split-valence, double ζ, and double ζ plus polarization geometries for H_2CS ($^1A_1$) are comparable to calculations with similar types of basis sets (5, 7, 19). It appears that with the possible exception of the STO-3G and STO-3G* results for the CS bond lengths, very reasonable SCF level geometries for ground state H_2CS are predicted.

Properties other than geometry will not be discussed in detail in this article although brief mention will be made of (*1*), the Koopmans theorem ionization potentials for removal of an electron from the sulfur lone pair and (*2*), the Mulliken net atomic charges on C and S. The experimental result

Can. J. Chem. Downloaded from www.nrcresearchpress.com by 210.87.254.40 on 09/06/12
For personal use only.

Can. J. Chem. Downloaded from www.nrcresearchpress.com by 210.87.254.40 on 09/06/12
For personal use only.

for the n_S ionization potential of thioformaldehyde is 9.38 eV (20). STO-3G and STO-3G* basis sets give Koopmans theorem values of 6.59 and 6.39 eV for this quantity and thus differ very markedly (by 2.79 and 2.99 eV) from experiment. All the other Gaussian basis sets considered in this work predict Koopmans theorem ionization potentials for n_S greater than but within 0.4 eV of experiment (3-21G: 9.66 eV, 4-31G: 9.41 eV, DZ + DIFFUSE: 9.75 eV, DZ**: 9.47 eV, DZ** + DIFFUSE: 9.55 eV).

The Mulliken net atomic charges are consistent with the greater electronegativity of C as compared to S as the C is always more negatively charged. The split valence or double ζ basis sets overemphasize charge separation (3-21G: C −0.703, S +0.168, Δq = 0.871; 4-31G: C −0.518, S +0.082, Δq = 0.600). Polarization functions provide a mechanism for charge transfer from C to S and thus reduce the bond polarity (DZ**: C −0.268, S −0.043, Δq = 0.225). The dramatic reduction of the polarity of the CS bond with the inclusion of polarization functions has been noted (7). Interestingly, STO-3G and STO-3G* basis set also yield smaller charge separations (STO-3G: C −0.236, S +0.007, Δq = 0.355; STO-3G*: C −0.107, S +0.007, Δq = 0.114) particularly for the basis set including *d* functions on S.

The geometries for the lowest triplet state of thioformaldehyde (Table 2) are unexpected as the STO-3G geometry is very different from that reported in ref. 6 where due to UHF-SCF convergence difficulties it appears that a $^3(\pi \rightarrow \pi^*)$ state was actually optimized rather than the lowest triplet ($n \rightarrow \pi^*$) state. The split valence (3-21G, 4-31G) and double ζ basis sets yield CS bond lengths at least 0.1 Å greater than experiment for triplet thioformaldehyde. A double ζ type basis also yielded a CS bond length for triplet H_2CS which was far too long in ref. 5. The addition of polarization functions very significantly reduces the CS bond length (by ~0.05 Å) to a value of 1.732 Å (DZ**) which is in reasonable agreement with the experimental result of 1.683(5) Å. It is noteworthy that the small STO-3G and STO-3G* basis sets yield values for *r*(CS) in the triplet state equally as good as the most extensive SCF calculations in this work. The STO-3G* result of 1.699 Å is clearly reminiscent of the good agreement reported with an STO-2G + $3d_\pi$ basis set (4) and suggests that *d* orbitals on S are effective in bringing the CS bond length into reasonable agreement with experiment. The STO-3G and STO-3G* results for the HCH angles are less satisfactory being 3.8° and 3.1° less than experiment. The largest basis set calculations (DZ** and DZ** + DIFFUSE) predict θ_e(HCH) within 0.1° of the experimental value. All basis sets yielded reasonable values for r_e(CH) which were usually slightly too short. The out-of-plane angle (α_e(oop)) is the most poorly defined quantity experimentally due to the very small barrier to pyramidal inversion at carbon (see below) and thus the extreme "floppiness" of nuclear motion in this coordinate. The STO-3G*, 3-21G, DZ, DZ**, and DZ** + DIFFUSE basis sets predict values for α_e in reasonable agreement with experiment (2) (i.e. within 2° of the limits of 13.1 to 18.9° given by the error bars). The STO-3G result is too pyramidal by 11.0° and the 4-31G too planar by 11.4°. The diffuse functions added on S which would normally be expected to cause small effects on the geometry change α_e by 3.3° (DZ to DZ + DIFFUSE) suggesting the weakness of the inversion potential and its extreme sensitivity to basis set effects.

The Mulliken net atomic charges for the T_1 state indicate greater polarization than in S_0 reflecting the charge transfer from a n-type orbital largely localized on S to a π^* orbital with significant C AO character. For example for the DZ** basis set in the T_1 state the net charges are C −0.391 and S +0.057 while for S_0 the same basis predicts C −0.268 and S −0.043. The split valence basis sets predict a very polar CS bond in the T_1 state (e.g. 3-21G: C −0.728, S +0.215). Polarization functions again provide a mechanism for reducing the large charge separation.

The relaxed planar transition states for the pyramidal inversion at C of T_1 thioformaldehyde were calculated for the STO-3G and DZ** + DIFFUSE basis sets. The calculated inversion barriers are STO-3G: 174 cm^{-1} and DZ** + DIFFUSE: 48 cm^{-1} which may be compared with the value of 13 cm^{-1} extracted from experimental data (2). A CI calculation but without full geometry optimization has reported a barrier of 108 cm^{-1} (5). The transition state geometrical parameters undergo small changes relative to the equilibrium results. For both the STO-3G and DZ** + DIFFUSE basis sets the CS bonds contract by 0.003 Å in the transition state. The HCH angles open up at the planar geometry from 115.8° to 118.6° (STO-3G) or 119.6° to 121.4° (DZ** + DIFFUSE) and the CH bond shorten slightly (1.082 Å to 1.079 Å, STO-3G; 1.075 Å to 1.074 Å (DZ** + DIFFUSE)).

This study further emphasizes that the split valence or double ζ basis sets which have proven so useful for molecules containing only first row atoms (C, N, O, H) have a much more limited value when the molecular species contains the second row atom sulfur.

1. R. H. JUDGE and G. W. KING. Can. J. Phys. **53**, 1928 (1975); R. H. JUDGE and G. W. KING. J. Mol. Spectrosc. **74**, 175 (1979); D. J. CLOUTHIER, C. M. L. KERR, and D. A. RAMSAY. Chem. Phys. **56**, 73 (1981).
2. R. H. JUDGE, D. C. MOULE, and G. W. KING. J. Mol. Spectrosc. **81**, 37 (1980).
3. D. R. JOHNSON, F. X. POWELL, and W. H. KIRCHHOFF. J. Mol. Spectrosc. **39**, 136 (1971).
4. N. C. BAIRD and J. R. SWENSON. J. Phys. Chem. **77**, 277 (1973).
5. P. J. BRUNA, S. D. PEYERIMHOFF, R. J. BUENKER, and P. ROSMUS. Chem. Phys. **3**, 35 (1974).
6. A. KAPUR, R. P. STEER, and P. G. MEZEY. J. Chem. Phys. **70**, 745 (1979).
7. R. JAQUET, W. KUTZELNIGG, and V. STAEMMLER. Theoret. Chim. Acta, **54**, 205 (1980).
8. J. B. COLLINS, P. v. R. SCHLEYER, J. S. BINKLEY, and J. A. POPLE. J. Chem. Phys. **64**, 5142 (1976).
9. Y. SAKAI, H. TATEWAKI, and S. HUZINAGA. J. Comput. Chem. **2**, 108 (1981).
10. (*a*) W. J. HEHRE, R. DITCHFIELD, R. F. STEWART, and J. A. POPLE. J. Chem. Phys. **52**, 2769 (1970); (*b*) W. J. HEHRE, R. F. STEWART, and J. A. POPLE. J. Chem. Phys. **51**, 2657 (1969).
11. (*a*) W. J. HEHRE and W. A. LATHAN. J. Chem. Phys. **56**, 5255 (1972); (*b*) R. DITCHFIELD, W. J. HEHRE, and J. A. POPLE. J. Chem. Phys. **54**, 724 (1971).
12. (*a*) M. S. GORDON, J. S. BINKLEY, J. A. POPLE, W. J. PIETRO, and W. J. HEHRE. J. Am. Chem. Soc. In press; (*b*) J. S. BINKLEY, J. A. POPLE, and W. J. HEHRE, J. Am. Chem. Soc. **102**, 939 (1980).
13. T. H. DUNNING, JR. and P. J. HAY. *In* Modern theoretical chemistry. Vol 3. *Edited by* H. F. Schaefer. Plenum, New York. 1977. p. 1.
14. P. PULAY. *In* Modern theoretical chemistry. Vol. 4. *Edited by* H. F. Schaefer. Plenum, New York. 1977. p. 153.
15. H. B. SCHLEGEL. Ph.D. Thesis. Queen's University, Kingston, Ont. 1975.
16. M. R. PETERSON and R. A. POIRIER. MONSTERGAUSS 80. Department of Chemistry, University of Toronto, Toronto, Ont. 1980.
17. J. S. BINKLEY, R. A. WHITESIDE, P. C. HARIHARAN, R. SEEGER, J. A. POPLE, W. J. HEHRE, and M. D. NEWTON. GAUSSIAN 76. QCPE 368, Department of Chemistry, Indiana University, Bloomington, IN.
18. J. A. POPLE. *In* Modern theoretical chemistry. Vol. 4. *Edited by* H. F. Schaefer. Plenum, New York. 1977. p. 1.
19. E. FLOOD and J. E. BOGGS. J. Mol. Struct. **34**, 147 (1976).
20. B. SOLOUKI, P. ROSMUS, and H. BOCK. J. Am. Chem. Soc. **98**, 6054 (1976).

Can. J. Chem. Downloaded from www.nrcresearchpress.com by 210.87.254.40 on 09/06/12
For personal use only.

The three conformations of 3,5-dichloro-2-hydroxythiophenol in solution

TED SCHAEFER, RICHARD P. VEREGIN, AND DAVID M. MCKINNON
Department of Chemistry, University of Manitoba, Winnipeg, Man., Canada R3T 2N2

Received June 4, 1981

TED SCHAEFER, RICHARD P. VEREGIN, and DAVID M. MCKINNON. Can. J. Chem. **59**, 3204 (1981).

The long-range spin–spin coupling constants for the sidechain protons in 3,5-dichloro-2-hydroxythiophenol show that the compound exists as a mixture of three conformers in CCl_4 solution at 305 K. The conformer, in which the S—H bond is held roughly perpendicular to the ring plane by an OH···3*p* hydrogen bond, is 13% abundant. The other two conformers, of roughly equal proportions, contain an OH···Cl hydrogen bond. One of these has the S—H bond *cis* to the OH group, the other has it *trans*. The chemical shifts of the SH proton and of H-6 are in agreement with these conclusions. The free energy preference of the OH···Cl over the OH···S bond is 1140 ± 100 cal/mol at 305 K. The five-bond coupling between the sidechain protons is negative and very likely involves proximate interactions via lone pairs on oxygen and/or sulfur.

TED SCHAEFER, RICHARD P. VEREGIN et DAVID M. MCKINNON. Can. J. Chem. **59**, 3204 (1981).

Les constantes de couplage à longue distance des protons de la chaîne latérale du dichloro-3,5 hydroxy-2 thiophénol révèlent que ce composé, en solution dans le CCl_4, à 305 K, est un mélange de trois conformères. Le conformère, dans lequel la liaison S—H est à peu près perpendiculaire au plan du cycle par une liaison hydrogène OH···3*p*, a une abondance de 13%. Les deux autres conformères en proportions à peu près égales contiennent une liaison hydrogène OH···Cl. Dans un des conformères, la liaison S—H est en position *cis* par rapport au groupement OH, l'autre conformère est son isomère *trans*. Les déplacements chimiques du proton SH et du proton en position 6 s'accordent avec ces conclusions. A 305 K, la liaison OH···Cl est favorisée par une énergie libre de 1140 ± 100 cal/mol par rapport à la liaison OH···S. Le couplage à travers cinq liaisons entre les protons de la chaîne latérale est négatif et implique vraisemblablement des interactions de proximité approchées par l'intermédiaire du doublet libre de l'oxygène ou du soufre ou des deux à la fois.

[Traduit par le journal]

Introduction

The novel perpendicular conformation of 2-hydroxythiophenol, **1** (X = H), deduced from spin–spin couplings, *J*, in CCl_4 at 305 K, can be rationalized with *ab initio* MO calculations (1). A qualitative explanation recognizes that the mainly 3*s* lone pair on sulfur is diffuse but the directional 3*p* lone pair is twisted into the benzene plane by electrostatic fields from the polar O—H bond. Hence the S—H bond now occupies the plane preferred by the 3*p* lone pair in thiophenol itself.

The strength of the OH···S bond could not be measured. The free energy advantage of **1** (X = H) over the three likely planar forms was at least 2 kcal/mol (1 kcal ≡ 4.184 kJ), in semiquantitative agreement with STO 3G results and with Schroeder–Lippencott potential functions (2).

Stereospecific coupling constants in phenol derivatives (3–5) allow the ordering of *ortho* substituents as to their attraction for the O—H dipole. In this work, such couplings for the SH and OH protons in 3,5-dichloro-2-hydroxythiophenol (DDHT) show that conformers **1** to **3** (X = Cl) occur in CCl_4 solution at 305 K. Their relative abundance is related only indirectly to the relative strengths of OH···Cl and OH···S hydrogen bonds. A negative $^5J^{OH,SH}$ is compared with theoretical predictions.

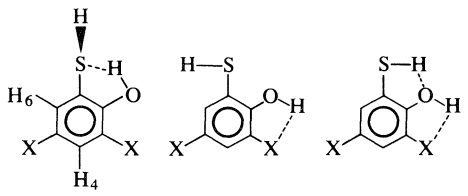

1 **2** **3**

Experimental

DDHT was prepared from the corresponding sulfonyl chloride (Aldrich) by reduction with zinc and hydrochloric acid. It gave the correct mass spectrum. A 2.0 mol% solution in CCl_4, containing 4 mol% tetramethylsilane (TMS), was degassed by the freeze–pump–thaw technique in a 5 mm od nmr tube. The tube was flame-sealed and intermolecular proton exchange was retarded in the usual way (4). There was no doubt that, as for 2-hydroxythiophenol (1), exchange was too slow to contribute to the peak widths. The latter were ≤ 0.10 Hz at half height and were determined by magnetic field inhomogeneity. The ^1H nmr spectrum was calibrated at 305 K on an HA100 spectrometer in the manner recently described in detail (6). Partial decoupling (7) and tickling (8) experiments determined the signs of the coupling constants. A similar solution in C_6D_6 was also examined. It displayed chemical shift degeneracy for the ring protons.

Solutions of 2,6-dichloro-, 2,6-dichloro-4-chloromethyl-, and 2,6-dichloro-4-mercaptophenol in CCl_4 were also examined.

INDO and CNDO/2 MO FPT (9) computations were made on an Amdahl 470/V7 system.

Results and Discussion

Spectral Analysis

Performed with the computer program LAME

0008-4042/81/223204-04$01.00/0
©1981 National Research Council of Canada/Conseil national de recherches du Canada

Can. J. Chem. Downloaded from www.nrcresearchpress.com by 210.87.254.40 on 09/06/12
For personal use only.

Can. J. Chem. Downloaded from www.nrcresearchpress.com by 210.87.254.40 on 09/06/12
For personal use only.

(10, 11), the analysis gave the spectral parameters in Table 1. Figure 1 illustrates the spectral quality and one of the many double irradiation experiments. The analysis was highly precise because the linewidths were small and all of the calculated transitions were assigned.

The Conformational Equilibrium

$^5J_m^{OH,H_6}$ is 0.550 ± 0.012 and $^5J_m^{OH,H_4}$ is 0.084 ± 0.012 Hz (errors given as three times the standard deviations in Table 1, presumably at the 99% confidence level (6, 12)). The sum of the two couplings is 0.634 ± 0.024 Hz, a number expected on the basis of those observed for trihalophenol derivatives (3).

With reference to previous discussions (3–5, 13), one may write $\Delta G = -RT \ln 0.55_0/0.08_4 = -1140 \pm 100$ cal/mol for the free energy favoring **2** + **3** over **1**. The quoted error assumes an uncertainty of 0.012 Hz in each of the couplings. In previous competition experiments of this kind for 2,4,6-trisubstituted phenols (3–5), the free energy preferences were found as Cl ~ Br > F > I > CF_3. Relative to iodine, they were −75 ± 20 for F, −460 ± 60 for Cl and Br, and +1230 ± 200 cal/mol for CF_3. Therefore SH appears to fall between I and CF_3 in this sequence.

Of course, the order of hydrogen bond strengths in these compounds need not be the same as in monosubstituted phenols. Solvent and dimerization perturbations are probably lower for the 2,4,6-trisubstituted compounds. Nevertheless, for 2-iodophenol (14) and 2-hydroxythiophenol (1), the couplings provide no evidence for other than an intramolecularly hydrogen bonded conformer in CCl_4 at 305 K, suggesting a free energy preference of not less than 1.9 kcal/mol. The present competition experiment would then imply a free energy preference of about 3 kcal/mol for the OH···Cl bond of 2-chlorophenol in CCl_4, but this number must be treated with circumspection. Our CNDO/2 calculations give dipole moments of 1.2 D for each of **2** and **3**, and 1.8 D for **1** (X = Cl). The electrostatic theory of solvent stabilization of polar conformers (15) then yields not more than 100 cal/mol for the increased stability of **1** relative to **2** or **3** in CCl_4 solution.

Note, however, that while both of the OH···Cl and OH···S bonds may well involve an OH···3*p* interaction, the OH···S bond is formed at the expense of 3*p*,π conjugation. The latter amounts to about 0.8 kcal/mol (16, 17). Therefore the intrinsic OH···S bond strength may be nearly as large as the OH···Cl interaction (relative to **2** + **3**, there is *not* an entropy of *R* ln 2 favoring **1**). This discussion

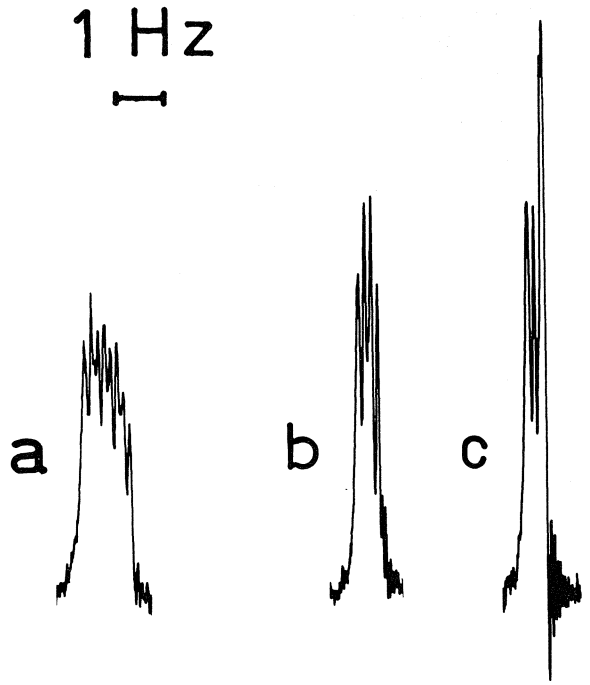

FIG. 1. In (a) the hydroxyl proton resonance at 305 K and 100.001_2 MHz is shown for a 2.0 mol% solution of 3,5-dichloro-2-hydroxythiophenol in CCl_4. The band spans 1 Hz and all 8 peaks expected from coupling to the other three protons are observed. In (b) the S—H proton resonance displays the four peaks expected when the hydroxyl protons are decoupled. In (c) an additional partial decoupling field is applied at 716.39 Hz in order to decouple H-6 from S—H for one spin state of H-4. The experiment shows that $^6J^{H,SH}/^4J_{46} < 0$. The smallest splitting in (b) and (c) is 0.12 Hz.

TABLE 1. The ^{1}H nmr spectral parameters for some thiophenol derivatives in CCl_4 solution at 305 K

Parameter	3,5-diCl-2-OH[a]	2-OH[b]	3,5-diCl-4-OH[c]
ν_{SH}	373.302(2)[d]	281.333(3)	330.447(2)[f]
ν_{OH}	582.090(2)	603.326(2)	560.936(2)
ν_4	711.726(3)	715.560(2)	—
ν_6	714.867(3)	738.209(2)	719.753(2)
$^4J_{46}$	2.402(3)[e]	1.669(2)	—
$^5J_m^{OH,H_4}$	0.084(4)	0.421(3)	—
$^5J_m^{OH,H_6}$	0.550(4)	0.00	—
$^4J_o^{SH,H}$	−0.115(4)	−1.089(3)	−0.590(2)
$^6J_p^{SH,H}$	−0.271(4)	−0.973(3)	—
$^5J_o^{SH,OH}$	−0.253(3)	−0.142(4)	—
Root mean square error	0.005	0.009	0.004

[a] 2.0 mol%.
[b] 1.9 mol%.
[c] 5 mol%.
[d] In Hz at 100.001_2 MHz to low field of internal TMS.
[e] Numbers in parentheses are standard deviations in the last significant figure.
[f] A 1 mol% solution of 3,5-dichlorothiophenol has δ_{SH} as 3.41 ppm and $\delta_{2,4}$ as 7.12 ppm. In a 5 mol% solution of 2,6-dichlorophenol, ν_{OH} is 565.68 Hz and $^5J_m^{H,OH}$ is 0.30 Hz. A 1.9 mol% solution of 2,4,6-trichlorophenol has ν_{OH} as 561.84 Hz. In 2,6-dichloro-4-chloromethylphenol, 5 mol% in CCl_4, ν_{OH} is 570.80 Hz.

Can. J. Chem. Downloaded from www.nrcresearchpress.com by 210.87.254.40 on 09/06/12
For personal use only.

assumes that perpendicular **1** is indeed the conformer representing 13% of the population. Verification goes as follows.

Conformational Deductions about 1 to 3 (X = Cl)

Conformers **2** and **3** are analogous to those present in almost equal abundance in 2-methoxythiophenol (18). The exact *relative* abundance of **2** and **3** is not important in the following discussion, but it must be very nearly the same as the 43 and 57%, respectively, in 2-methoxythiophenol in order to reach the ensuing good agreement between calculated and observed parameters.

One has $P_1 = 0.13$ and $P_2 + P_3 = 0.87$. For a 1.9 mol% solution of 2-hydroxythiophenol in CCl_4, existing as **1** (X = H), $^6J_p^{H,SH}$ is -0.97_3 Hz (1) and is -0.13_6 Hz in 2-methoxythiophenol (18). Therefore $^6J_p^{H,SH}$ in DDHT should be $0.13 \times (-0.97) + 0.87 \times (-0.14)$ or -0.25 Hz. The observed value is -0.27 Hz. Similarly, $^4J_o^{H,SH}$ is calculated as -0.14 Hz and the observed number is -0.11_5 Hz.

In these calculations it is assumed that the chlorine substituents do not alter the reference values of $^6J_p^{H,SH}$ and $^4J_o^{H,SH}$, i.e., those observed in 2-hydroxythiophenol and in 2-methoxythiophenol. If these substituents, placed *meta* to the SH group, were to alter the rotational barrier about the C—S bond, the two couplings would also alter (17–19). Unfortunately, chemical shift degeneracy disallows the extraction of the couplings in 3,5-dichlorothiophenol (19). However, in 3,4-dichlorothiophenol, $^4J_o^{H,SH}$ is the same as in thiophenol (19), suggesting minor perturbations by chlorine substituents placed *meta* or *para* to SH. Yet, in 3,5-dichloro-4-hydroxythiophenol, $^4J_o^{H,SH}$ is -0.59_0 Hz in CCl_4 and is -0.64_9 Hz in *p*-methoxythiophenol (17). Here the perturbation by the chlorine substituents is roughly 0.59/0.65. If this reduction is applied in the calculation above, $^4J_o^{H,SH}$ becomes -0.12 Hz.

$^6J_p^{H,SH}$ is a $\sigma-\pi$ transmitted coupling. For another such coupling, $^6J_p^{H,CH}$ in toluene, no perturbation by *meta* substituents has been observed. Any perturbation of $^6J_p^{H,SH}$ should therefore be no larger than that observed for $^4J_o^{H,SH}$ (conformational changes) and then the calculated $^6J_p^{H,SH}$ becomes -0.23 Hz, still within cumulative experimental error of the observed value.

In view of a referee's remarks, it should be pointed out that **2** + **3** includes any contributions from nonplanar orientations of the S—H group *in* **2** + **3**, including an orientation in which the S—H group lies in a plane perpendicular to the molecular plane. This orientation is unfavorable energetically because the barrier to rotation about the C—S bond in **2** + **3** is substantial (18).

In 2-hydroxythiophenol, δ_{SH} is 2.82 (1) and is 3.66 ppm in 2-methoxythiophenol (18). Weighting these shifts according to the population distribution yields δ_{SH} as 3.55 ppm. The correction for the chlorine substituents is 0.18 ppm (δ_{SH} is 3.41 ppm for 3,5-dichlorothiophenol as a 1 mol% solution in CCl_4 at 305 K[1] and is 3.23 for thiophenol (20)). Dilution shifts are very small for thiophenol derivatives[1] and therefore the observed shift of 3.73 ppm agrees satisfactorily with the calculated shift of 3.73 ppm. The agreement is expected because the local environment of the SH proton is similar in **1**, **2**, and **3** and in the reference compounds (note that **2** and **3** are therefore implied to have the same relative populations as in 2-methoxythiophenol).

By way of contrast, the reference compounds for the hydroxyl proton shifts are not available. For example, δ_{OH} in 2,4-dichlorophenol is 5.40 ppm,[1] is 5.66 ppm in 2,6-dichlorophenol, and is 5.61 ppm in 2,4,6-trichlorophenol (all in CCl_4 at 305 K). In 2,4-dichlorophenol the OH·Cl conformer is at least 96% abundant in dilute solution (3) and the 4-chloro substituent causes only a small shift perturbation. Probably the best explanation for these observations invokes a small repulsion between lone pairs on oxygen and the lone pairs on the non-hydrogen-bonded, *ortho* chlorine substituent. If such repulsions are loosely labeled as steric crowding,[2] it then becomes apparent that δ_{OH} in **1** and **2** (X = Cl) should be larger than δ_{OH} in, respectively, **1** (X = H) and 2,4-dichlorophenol. The perturbation of δ_{OH} by SH in **3** is also quantitatively unknown.

If the δ_{OH} values of 6.03 ppm in **1** (X = H) and of 5.40 ppm in 2,4-dichlorophenol are weighted by 13 and 87%, respectively, then the calculated shift becomes 5.48 ppm for DDHT. The observed shift is 5.82 ppm. The excess shift of 0.34 ppm to low field is reasonably attributable to steric or other perturbations of the type exemplified above. This discussion is only meant to ensure that the observed δ_{OH} in DDHT is *not* taken as evidence against the conformational populations derived above.

The ring proton shifts in 3,5-dichlorothiophenol are[1] both 7.12 ppm. In DDHT, δ_6 is 7.15 ppm and is 7.14 ppm in 2-methoxythiophenol. Therefore H-6 does not display the substantial shift to low field of 7.36 ppm observed in 2-hydroxythiophenol. In the

[1]Unpublished measurement in this laboratory.

[2]Electric fields from the second *ortho* substituent cannot explain the increased shifts to low field. Replacement of Cl-6 by F or Br and I in 2,4,6-trichlorophenol causes high and low field shifts,[1] respectively, in opposite directions to the change in dipole moment of the C—X bond! Steric crowding by 6-X is also evident in the proximate $^4J^{OH,F}$ values for 2-F-4-diX-phenols, where X = Cl, Br, I (4).

latter the 3*p* orbital of sulfur lies approximately in the ring plane and may well turn out (21) to account for the large deshielding of H-6; its $n \rightarrow \pi^*$ excitation energy will be lower in this orientation. In DDHT conformer **1** is a minor constituent. The shifts of H-6 in these three compounds (Table 1) vary by only 0.03 ppm.

The Negative Coupling, $^5J_o^{OH,SH}$

In DDHT this coupling is −0.25 Hz and is −0.14 Hz in 2-hydroxythiophenol. Proton couplings over five bonds are usually positive. In DDHT it is likely that direct (22) or proximate interactions, probably involving lone pairs on sulfur and oxygen, are important, in a way similar to those observed and calculated for the hydroxyl proton and fluorine nuclei in the *cis* forms of 2-fluorophenol and 2-hydroxybenzotrifluoride (4, 23).

INDO MO FPT calculations tend to exaggerate the magnitudes of five-bond couplings in benzene derivatives (4). CNDO/2 calculations on the partially optimized geometries for the conformers of 2-hydroxythiophenol yield $^5J_o^{OH,SH}$ as −0.11, −0.11, and −1.38 Hz for **1**, **2**, and **3** (X = H) respectively. They are insensitive to the chlorine substituents, decreasing by less than 4% in their presence. If the C–S–H angle in **3** is increased by 5° (to 100.4°), $^5J^{OH,SH}$ changes to −0.84 Hz. The H···O distance changes by 0.1 Å. In other words, the coupling is very sensitive to the H···O distance in **3**, as anticipated for proximate interactions (4, 23).

Note that **1** has a calculated $^5J^{OH,SH}$ of −0.11 Hz, close to the observed value of 2-hydroxythiophenol. The present calculations cannot give the proportion of **2** and **3**, even though **3** has a large calculated magnitude for $^5J_o^{OH,SH}$ and **2** a small one. They do indicate that this coupling should be enhanced in magnitude relative to 2-hydroxythiophenol, as observed.

Acknowledgments

We thank a referee for thoughtful criticism and are grateful to the Natural Sciences and Engineering Research Council of Canada for financial assistance.

1. T. SCHAEFER, T. A. WILDMAN, and S. R. SALMAN. J. Am. Chem. Soc. **102**, 107 (1980).
2. W. R. SNYDER, H. D. SCHREIBER, and J. N. SPENCER. Spectrochim. Acta, Part A, **29**, 1225 (1973).
3. J. B. ROWBOTHAM and T. SCHAEFER. Can. J. Chem. **52**, 3037 (1974).
4. J. B. ROWBOTHAM, M. SMITH, and T. SCHAEFER. Can. J. Chem. **53**, 986 (1975).
5. T. SCHAEFER and J. B. ROWBOTHAM. Can. J. Chem. **54**, 2243 (1976).
6. T. SCHAEFER and R. SEBASTIAN. J. Magn. Reson. **41**, 395 (1980).
7. J. P. MAHER and D. F. EVANS. Proc. Chem. Soc. London, 208 (1961).
8. R. FREEMAN and W. A. ANDERSON. J. Chem. Phys. **37**, 2053 (1962).
9. P. A. DOBOSH. Quantum Chemistry Program Exchange, **11**, 141 (1979).
10. S. CASTELLANO and A. A. BOTHNER-BY. J. Chem. Phys. **41**, 3863 (1964).
11. C. W. HAIGH. Ann. Rep. NMR Spectrosc. **4**, 311 (1971).
12. R. LAATIKAINEN. J. Magn. Reson. **27**, 169 (1977).
13. T. SCHAEFER, R. SEBASTIAN, and T. A. WILDMAN. Can. J. Chem. **57**, 3005 (1979).
14. T. SCHAEFER, R. SEBASTIAN, and T. A. WILDMAN. Can. J. Chem. **59**, 3021 (1981).
15. R. J. ABRAHAM and E. BRETSCHNEIDER. *In* Internal rotation in molecules. *Edited by* W. J. Orville-Thomas. Wiley, New York. 1974. Chapt. 13.
16. N. W. LARSEN and F. M. NICOLAISEN. J. Mol. Struct. **22**, 29 (1974).
17. T. SCHAEFER and W. J. E. PARR. Can. J. Chem. **55**, 552 (1977).
18. T. SCHAEFER and T. A. WILDMAN. Can. J. Chem. **57**, 450 (1979).
19. T. SCHAEFER and W. J. E. PARR. Can. J. Chem. **57**, 1421 (1979).
20. W. J. E. PARR and T. SCHAEFER. J. Magn. Reson. **25**, 171 (1977).
21. M. KARPLUS and J. A. POPLE. J. Chem. Phys. **38**, 2803 (1963); J. A. POPLE. Mol. Phys. **7**, 301 (1964).
22. M. BARFIELD and M. KARPLUS. J. Am. Chem. Soc. **91**, 1 (1969).
23. T. SCHAEFER and J. B. ROWBOTHAM. Chem. Phys. Lett. **29**, 633 (1974).

Can. J. Chem. Downloaded from www.nrcresearchpress.com by 210.87.254.40 on 09/06/12
For personal use only.

Heat capacity measurements of liquids with a Picker mixing flow microcalorimeter

MARC-ANDRÉ SIMARD AND JEAN-LUC FORTIER

Centre d'applications en calorimétrie et thermodynamique, Département de Chimie, Université de Sherbrooke, Sherbrooke (Que.), Canada J1K 2R1

Received March 31, 1981

MARC-ANDRÉ SIMARD and JEAN-LUC FORTIER. Can. J. Chem. **59**, 3208 (1981).

The Picker mixed flow microcalorimeter has been used without modification as a differential thermal balance to measure the volumetric heat capacity of liquids. The precision on volumetric heat capacity change is evaluated to be ±0.5% or better, and the limit of detection is $\pm 5 \times 10^{-5}$ J K^{-1} cm^{-3}. As a check, the apparent molar heat capacities of an aqueous solution of NaCl in the range 0.01 to 6 mol kg^{-1} were measured at 298.15 K. The performance of this instrument is compared with that of the Picker heat capacity flow microcalorimeter.

MARC-ANDRÉ SIMARD et JEAN-LUC FORTIER. Can. J. Chem. **59**, 3208 (1981).

Un microcalorimètre dynamique Picker pour chaleur de mélange a été utilisé, sans modification, comme balance thermique différentielle pour mesurer la capacité calorifique volumétrique de liquides. La précision sur un changement de capacité calorifique volumétrique est évaluée à ±0.5% ou mieux et la limite de détection est de $\pm 5 \times 10^{-5}$ J K^{-1} cm^{-3}. Pour vérifier la méthode, les capacités calorifiques molaires apparentes de solutions aqueuses de NaCl entre 0.01 et 6 mol kg^{-1} ont été mesurées à 298.15 K. L'utilisation de cet instrument pour mesurer la capacité calorifique est comparée à celle du microcalorimètre dynamique Picker "capacité calorifique".

Can. J. Chem. Downloaded from www.nrcresearchpress.com by 210.87.254.105 on 09/06/12
For personal use only.

Introduction

Heats of mixing and heat capacities are fundamental properties in the study of solute–solute and solute–solvent interactions in solution. Precise enthalpies have been measured for many years, but it is only recently, with the development of new microcalorimeters (1–3), that the heat capacity of solutions have received much attention. In the last decade, the literature shows an extraordinary expansion in this field. It is known that the temperature dependence of the excess enthalpy can be derived from the excess heat capacity. The possibility of measuring both the excess enthalpy and heat capacity of solutions with the same calorimeter is then a very interesting option. It is also known that C_p can be measured using a mixing microcalorimeter (4, 5), but a high precision on C_p is required (2) since an error of only 0.01% on specific heat capacities causes an uncertainty of about 40 J K^{-1} mol^{-1} on the apparent molal heat capacity (ϕ_C) of an aqueous solution at 0.01 mol kg^{-1}.

The purpose of this paper is to show that the sensitivity and stability of the commercial version of the Picker mixing flow microcalorimeter (1) is such that this instrument can be used, without modification, for the measurement of changes in the volumetric heat capacity of liquids (σ) with a sensitivity of $\pm 5 \times 10^{-5}$ J K^{-1} cm^{-3} and a precision of ±0.5% or better. To establish the performance of this technique, we carried out measurements on aqueous solutions of NaCl in the concentration range 0.01 to 6 mol kg^{-1} at 298.15 K. These values have been evaluated by many authors (2, 6–11) involving the use of different types of calorimeter.

Experimental

In this work, we used the commercial version[1] of the Picker mixing flow microcalorimeter. The principle of operation has been described in details elsewhere (1). Figure 1*A* shows schematically how it is used to measure the volumetric heat capacity of liquids. The calorimeter is differential, so the two cells are of identical construction. One inlet of both flow cells, marked X, was sealed-off. This calorimeter is fitted with mini-mixing device installed at the merging junction of the two inlets to ensure an efficient mixing of the liquids. With most of the aqueous solutions, this mixing device has negligible friction effect, but with viscous liquids it may be necessary to remove it for the present application. In the present work, measurements were made without these mixing devices. As with the Picker heat capacity flow microcalorimeter (1, 2), the two calorimetric cells are connected in series to ensure equal flow rates, and a delay loop is placed between these two cells. An identical heating power (W_0) is applied to heating elements of each cell to produce a temperature increase (ΔT) of about 2 K. The difference in temperature between the two cells is measured with a modulated thermal detector (1), which consists of a modulating flow device, feeding alternatively the heat exchanging fluid in the reference and observation branches, and the thermal detector at the common return of these branches. For the present application, the mixing calorimeter has to operate in adiabatic mode; this was achieved by the use of methanol as heat exchanging fluid with a total flow rate ($2f_E$) of 0.03 cm^3 s^{-1} and a liquid sample flow rate (f_s) of about 0.01 cm^3 s^{-1} in the calorimetric cells. With the heating power (W_0) applied on each cell, large thermal pulses are induced by the pulsation of the heat exchanging fluid, which may lead to saturation of the electronic detection; to avoid this problem the modulated thermal detection is set on a low sensitivity scale, the desired sensitivity is then obtained by increasing the recorder sensitivity.

[1]Sodev Inc., Sherbrooke, P.Q., Canada.

0008-4042/81/223208-04$01.00/0

©1981 National Research Council of Canada/Conseil national de recherches du Canada

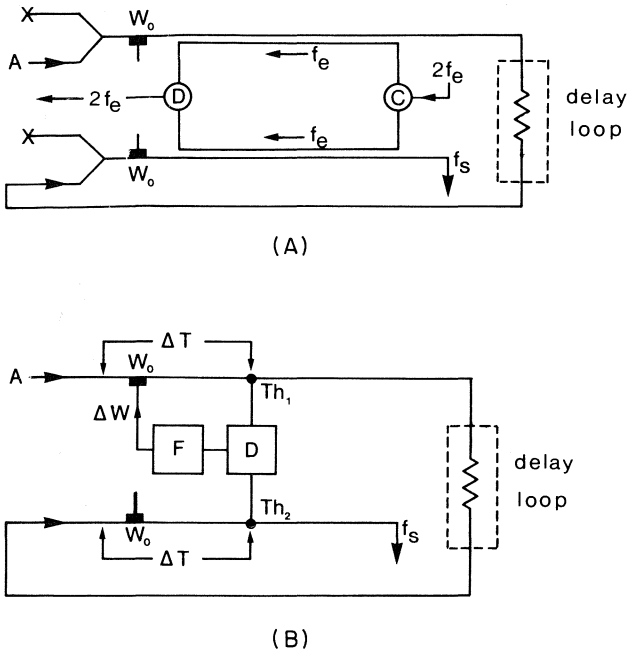

FIG. 1. Schematics. (*A*), The heat of mixing flow microcalorimeter used as a thermal balance for the measurement of the volumetric heat capacity of liquids; (*B*), the heat capacity flow microcalorimeter.

With this set-up the experimental procedure to measure the volumetric heat capacity of a liquid (σ) is similar to the one used with the Picker heat capacity flow microcalorimeter (2). First, a base line is recorded with a reference liquid of known volumetric heat capacity flowing through both cells, then the liquid to be measured is introduced. The difference in volumetric heat capacity ($\Delta\sigma = \sigma - \sigma_0$) between the reference and the sample liquid circulating in the two calorimetric cells is monitored by the difference in the temperature gradient ($\delta(\Delta)$) between these. Since there is no thermal feedback (2) to cancel this change of temperature, the measurement will depend on the flow of liquid. Therefore, this flow has to be kept constant during a run, but its value is not required in the calculations if a calibration is made in the same experimental conditions. With calibration made on the sample liquid, the change of power required to produce an identical $\delta(\Delta T)$ value will be equal to ΔW_s. If the calibration is made on the reference liquid, this change of power will then be different and identified as ΔW_R. The change of volumetric heat capacity between the sample and the reference liquid is evaluated using either eq. [1] or eq. [2] as appropriate.

$$[1] \quad \Delta\sigma/\sigma_0 = \Delta W_s/W_0$$

$$[2] \quad \Delta\sigma/\sigma_0 = \Delta W_R/(W_0 + \Delta W_R)$$

Densities of the solution were measured to within $\pm 3 \times 10^{-6}$ g cm^{-3} with a vibrating tube densimeter (12). All solutions were prepared by mass from distilled water and Fisher certified NaCl that had been dried in a vacuum oven at 150°C for 48 h.

Results and Discussion

If we compare the principle of measurement of the heat capacity flow microcalorimeter (Fig. 1*B*) with the one involved when we used the mixing flow microcalorimeter (Fig. 1*A*) as a thermal balance for the volumetric heat capacity measurement of liquids, we note two main differences. First, there is no heat exchanging device, the ΔT produced by the heating elements are monitored with two thermistors (Th_1, Th_0); second, instead of measuring $\delta(\Delta T)$, there is a thermal feedback circuit (F), connected to the heating elements of the working cell and controlled by the detection bridge (D), which changes the power supplied to the working cell by ΔW to keep the temperature gradient, ΔT_1, equal to the one in the reference cell, ΔT_0. With this thermal feedback and the series connection between the two calorimetric cells, the measurement is independent of the flow of liquids, assuming that there is no mixing effect in the delay loop which may produce an expansion or a contraction of the liquids. As already observed by Fortier *et al.* (13), this mixing effect may produce a significant error on the measured $\Delta\sigma$. This situation is not unique to the heat capacity flow microcalorimeter but it is also valid in the present technique.

For the limit of detection and the precision in the measurements, both techniques are equivalent, the values being respectively ± 5 J K^{-1} mol^{-1} and $\pm 0.5\%$. In the present technique, there is no thermal feedback to maintain a constant temperature gradient during a run, thus in a series of measurements, when the calibrations are made on the reference liquid, a shift of the mean temperature (δT_m) will be observed if the heating power (W_0), the flow rate (f), and the reference liquid are kept the same (single reference procedure). Under these conditions, the temperature gradient in the working cell (ΔT_1) will be directly proportional to the volumetric heat capacity of the measured liquids (σ) as shown in eq. [3], where the subscript 0 refers to the liquid in the reference cell.

$$[3] \quad \Delta T_1\sigma_1 = W_0/f = \Delta T_0\sigma_0$$

From this relation, the shift of the mean temperature can be expressed as

$$[4] \quad \delta T_m = \frac{\Delta T}{2}\left(\frac{\sigma_0}{\sigma} - 1\right)$$

With the aqueous solutions of NaCl, this shift is negligible since at $m = 5.320$, δT_m is only 0.062 K. For systems involving high values of $\Delta\sigma/\sigma_0$, this problem can be avoided by a proper flow adjustment between each run, or by making the calibration on the sample liquid.

The apparent molar heat capacities (ϕ_C) and

Can. J. Chem. Downloaded from www.nrcresearchpress.com by 210.87.254.105 on 09/06/12
For personal use only.

Can. J. Chem. Downloaded from www.nrcresearchpress.com by 210.87.254.105 on 09/06/12
For personal use only.

volumes (ϕ_V) of aqueous solutions were calculated using respectively eq. [5] and eq. [6].

$$[5]\quad \phi_C = Mc_p + 1000\,\frac{(c_p - c_{p0})}{m}$$

$$[6]\quad \phi_V = \frac{M}{d} - 1000\,\frac{(d - d_0)}{mdd_0}$$

in which M is the molecular weight of the solute, m is the molality of the solution (mol/kg solvent), d and d_0 are the densities of the solution and of the pure water ($d_0 = 0.997047$ g cm^{-3}), c_p and c_{p0} are the specific heat capacity of the solution and of pure water ($c_{p0} = 4.1793$ J K^{-1} g^{-1}). The apparent molar volumes and heat capacities results are given in Table 1 with the values of m, d, and $\Delta\sigma/\sigma_0$.

Our ϕ_C results were fitted using the following polynomial equation

$$[7]\quad \phi_C - 28.99(d_0m)^{1/2} = \phi_C^0 + Bm + Cm^2 + Dm^3 + Em^4$$

where the parameter 28.99 is the limiting slope of the Debye–Hückel theory for 1:1 electrolytes in water at 298.15 K (15). The other parameters were obtained with an unweighted least-squares fit, and the number of parameters was fixed by a statistical F-test (16). To represent the results at molalities up to 1 mol kg^{-1}, terms in m are sufficient ($\phi_C^0 = -85.6$, $B = 17.7_8$), but terms in m^4 are required to extend the fit up to 6 mol kg^{-1} ($\phi_C^0 = -86.0$, $B = 21.2_6$, $C = -4.09$, $D = 0.55_3$, $E = -0.034$). The interdependence of the parametric terms B, C, D, E, F explains the difference for the term in m and for the extrapolated value ϕ_C^0. This effect has been observed previously (8). In a residual plot ($\phi_C - \phi_C$ calculated with eq. [7]), the results agreed inside the experimental error which has been estimated to ± 0.5 J K^{-1} mol^{-1} for $m > 0.1$; at concentration below 0.1 m, this uncertainty increases significantly and reaches approximately ± 5 J K^{-1} mol^{-1} around 0.01 m.

In Fig. 2 we compare our experimental values with those from the literature. The graph represents the difference between our value calculated with eq. [7] and the values of different authors. Our experimental values are in good agreement with those from Olofsson (6) obtained with an LKB reaction solution calorimeter, Randall and Rossini (7), Tanner and Lamb (9), Perron *et al.* (10), and Fortier *et al.* (11) (corrected as mentioned by Desnoyers *et al.* (17)).

Sources of errors, such as heat losses, with the prototype and some early commercial versions of the Picker heat capacity flow microcalorimeter have been noted by some authors (6, 14, 17). It must be pointed out that with the Picker mixing flow microcalorimeter, heat losses proportional to the difference in temperature, if occurring, have no effect on the measured heat capacity values; since there is no thermal feedback, the heating power W_0 and calibration power ΔW_c are affected in the same way by these heat losses.

TABLE 1. Apparent molar volumes and heat capacities of NaCl in water at 298.15 K[a]

m	d / g cm^{-3}	ϕ_V / (cm^3 mol^{-1})	$10^3\,\Delta\sigma/\sigma_0$	ϕ_C / (J K^{-1} mol^{-1})
0.01126	0.997516	16.66	−0.411	−84.0
0.02023	0.997887	16.81	−0.748	−83.1
0.02076	0.997908	16.87	−0.751	−80.9
0.04051	0.998716	17.13	−1.452	−77.7
0.06187	0.999596	17.12	−2.179	−75.8
0.06404	0.999673	17.28	−2.292	−77.9
0.1133	1.001728	16.98	−3.95	−74.5
0.1418	1.002847	17.36	−4.90	−71.8
0.2066	1.005462	17.50	−6.99	−69.0
0.2594	1.007578	17.59	−8.57	−65.4
0.4076	1.013450	17.84	−13.04	−60.1
0.5574	1.010307	18.04	−17.02	−53.6
0.6007	1.020983	18.10	−18.12	−51.9
0.7608	1.027140	18.27	−22.11	−47.0
0.9720	1.035155	18.47	−26.78	−40.1
0.9889	1.035767	18.51	−27.24	−40.0
1.5215	1.055271	19.01	−37.0	−25.4
2.0485	1.073833	19.41	−44.8	−14.05
2.0630	1.074346	19.42	−45.0	−13.80
3.0316	1.106639	20.05	−54.5	3.90
4.1420	1.141163	20.63	−60.1	20.16
5.3250	1.175395	21.14	−61.5	34.5

[a] In obtaining these tabulated quantities, we have used $\sigma_0 = 4.1670$ J K^{-1} cm^{-3} and $d_0 = 0.997047$ g cm^{-3}.

To pursue the application of using the mixing flow microcalorimeter as a thermal balance for the measurement of volumetric heat capacity of liquids, we have also verified that this instrument can be used as a differential flowmeter in the same way it has been done with the heat capacity flow microcalorimeter for the direct continuous measurements of the thermal expansion coefficients of liquids and solids (18). The experimental procedure is similar but the equations have to be modified to take into account the absence of the thermal feedback. In doing so, eq. [4] of ref. 8, becomes:

$$[8]\quad \alpha = \frac{f_0}{V}\,\frac{\Delta W}{W_0 + \Delta W}\left(\frac{dT}{dt}\right)^{-1} + \alpha_{cell} + \alpha_e$$

For the meaning of each term, the reader is referred to ref. 18.

Conclusion

As shown in the previous section, the Picker mixing flow microcalorimeter can be used as a

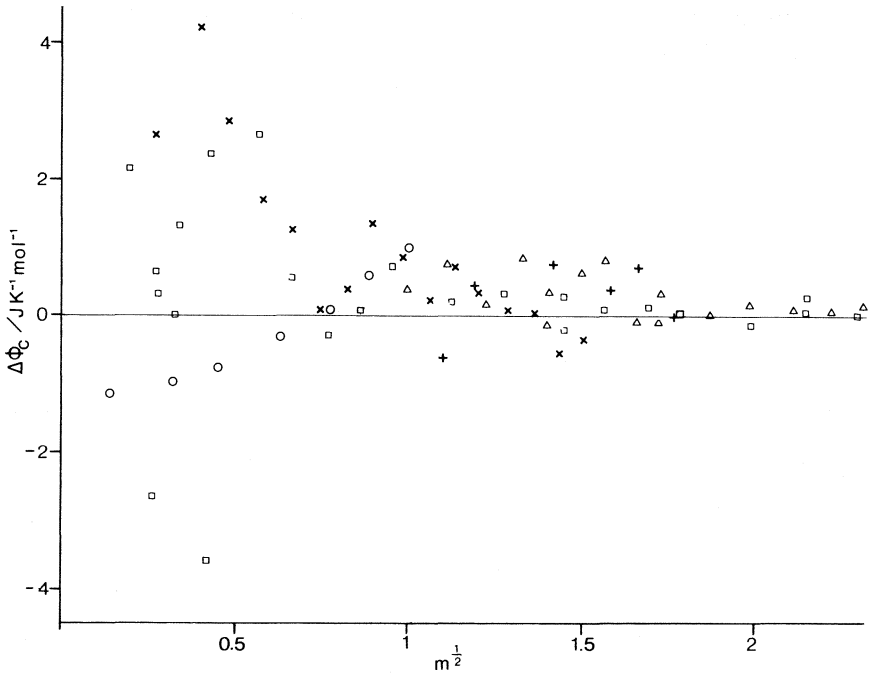

FIG. 2. Apparent molar heat capacity of aqueous NaCl solutions at 298.15 K. The difference between our values calculated with eq. [7] and the values of different authors. Experiment points: +, Olofsson (6), results with LKB calorimeter; ×, Randall and Rossini (7); □, Tanner and Lamb (9); △, Perron *et al.* (10); ○, Fortier *et al.* (11), corrected as mentioned by Desnoyers *et al.* (17).

differential thermal balance to measure the change in volumetric heat capacities of liquids with a sensitivity of $\pm 5 \times 10^{-5}$ J K^{-1} cm^{-3} and a precision of $\pm 0.5\%$. The results obtained are in good agreement with those measured with other types of calorimeter. Compared to the heat capacity flow microcalorimeter, the present technique is more time consuming, mainly due to the calibration which has to be done for each run; furthermore, the operation of the mixing flow microcalorimeter requires greater attention on the part of the user. But these little disadvantages are out-weighed by the possibility of measuring with the same instrument three of the most important thermodynamic properties in the study of solutions: heats, specific heats, and expansibilities.

Acknowledgements

The authors are grateful to Patrick Picker for technical information in some aspects of this application and to Carmel Jolicoeur and Jacques E. Desnoyers for useful discussion. Support from "Le Ministère de l'Education du Québec" is also acknowledged.

1. P. PICKER. Can. Res. Dev. **7**, 11 (1974).
2. P. PICKER, P.-A. LEDUC, P. R. PHILIP, and J. E. DESNOYERS. J. Chem. Thermodyn. **3**, 631 (1971).
3. J. SUURKUUSK and I. WADSO. J. Chem. Thermodyn. **6**, 667 (1974).
4. A. J. B. CRUICKSHANK, P. A. GIGUERE, and TH. ACKERMANN. *In* Experimental thermodynamics. Vol. 1. *Edited by* J. P. McCullough and D. W. Scott. Butterworths, London. 1968. Chapt. 12.
5. C. DEVISSER and G. SONSEN. Z. Phys. Chem. **92**, 159 (1974).
6. I. V. OLOFSSON. J. Chem. Thermodyn. **11**, 1005 (1979).
7. M. RANDALL and F. D. ROSSINI. J. Am. Chem. Soc. **51**, 323 (1929).
8. G. PERRON, J.-L. FORTIER, and J. E. DESNOYERS. J. Chem. Thermodyn. **7**, 1177 (1975).
9. J. E. TANNER and F. W. LAMB. J. Solution Chem. **7**, 303 (1978).
10. G. PERRON, A. ROUX, and J. E. DESNOYERS. Can. J. Chem. **59**, 3049 (1981).
11. J.-L. FORTIER, P.-A. LEDUC, and J. E. DESNOYERS. J. Solution Chem. **3**, 323 (1974).
12. P. PICKER, E. TREMBLAY, and C. JOLICOEUR. J. Solution Chem. **3**, 377 (1974).
13. J.-L. FORTIER, G. C. BENSON, and P. PICKER. J. Chem. Thermodyn. **8**, 289 (1976).
14. J.-L. FORTIER and G. C. BENSON. J. Chem. Thermodyn. **8**, 411 (1976).
15. P. R. PHILIP and J. E. DESNOYERS. J. Solution Chem. **1**, 353 (1972).
16. P. H. BEVINGTON. Data reduction and error analysis for the physical sciences. McGraw-Hill, New York. 1969.
17. J. E. DESNOYERS, D. DEVISSER, G. PERRON, and P. PICKER. J. Solution Chem. **5**, 605 (1976).
18. J.-L. FORTIER, M.-A. SIMARD, P. PICKER, and C. JOLICOEUR. Rev. Sci. Instrum. **50**, 1474 (1979).

Can. J. Chem. Downloaded from www.nrcresearchpress.com by 210.87.254.105 on 09/06/12
For personal use only.

Electron paramagnetic resonance characterization and conformation of daunorubicin semiquinone intermediate implicated in anthracycline metabolism, cardiotoxicity, and anticancer action[1]

J. William Lown and Hsiao-Hsiung Chen
Department of Chemistry, University of Alberta, Edmonton, Alta., Canada T6G 2G2

Received June 4, 1981

Can. J. Chem. Downloaded from www.nrcresearchpress.com by 210.87.254.42 on 09/06/12
For personal use only.

J. William Lown and Hsiao-Hsiung Chen. Can. J. Chem. **59**, 3212 (1981).

The antitumor antibiotic daunorubicin, upon reduction in aqueous solution, gives a transient resolved epr spectrum of linewidth 17.0 G and g value of 2.0024. This is ascribed to the semiquinone previously tentatively assigned in the unresolved epr spectrum obtained by microsomal activation of the antibiotic. By reference to the epr spectrum of quinizarin semiquinone in aqueous solution the individual proton hyperfine splitting constants in both spectra were tentatively assigned by computer simulation. LCAO–MO calculations of one-electron wave function spin densities in both species gave good agreement between calculated and observed hfs for values of the parameters $\beta_{CO}/\beta_{CC} = 1.8$, $\delta\alpha = 1.4$, allowing definite assignment of the aromatic protons. By considering the angular dependence of the ring A benzylic proton hfs it was possible to discriminate between two alternative half-chair conformations of daunorubicin semiquinone. The preferred conformation of the intermediate is tentatively assigned as that which places both 7 and 9 oxygen functions equatorial and the C-9 acetyl group axial.

J. William Lown et Hsiao-Hsiung Chen. Can. J. Chem. **59**, 3212 (1981).

La réduction en solution aqueuse de la daunorubicine, un antibiotique antitumoral, permet d'observer un spectre de rpe d'un composé transitoire présentant une largeur de bandes de 17,0 G et avec une valeur de g de 2,0024. On attribue ceci à la semiquinone dont on avait supposé antérieurement l'existence en se basant sur un spectre de rpe non résolu obtenu par activation microsomique de l'antibiotique. En se référant au spectre de rpe de la semiquinone de la quinizarine en solution aqueuse et d'une simulation par ordinateur, on a attribué d'une façon préliminaire les constantes de couplage hyperfin. Les calculs LCAO–MO des densités de spin de la fonction d'onde d'un électron des deux espèces donnent une bonne corrélation entre les couplages hyperfins calculés et observés pour les valeurs des paramètres $\beta_{CO}/\beta_{CC} = 1.8$, $\delta\alpha = 1.4$ permettant ainsi une identification nette des protons aromatiques. En considérant la dépendance angulaire des couplages hyperfins du proton benzylique du cycle A, il est possible de distinguer entre les deux conformations demi-chaise possibles pour la semiquinone de la daunorubicine. On considère, sans l'avoir prouvé, que la conformation privilégiée de l'intermédiaire est celle dans laquelle les fonctions oxygénées 7 et 9 sont équatoriales et le groupe acétyle en C-9 est axial.

[Traduit par le journal]

Introduction

The anthracycline antibiotics, especially daunorubicin (**1**) and adriamycin, are among the most promising clinically effective agents currently in use against a range of neoplasms (1, 2). Consequently considerable and widespread interest has been shown in their synthesis, biochemical pharmacology, and mechanism of action (1, 2). The antitumor properties in many cases correlate with the ability of the chromophore of the antibiotics to effect intercalative inhibition of DNA template functions (1–4). However, it is being recognized that other mechanisms, including the generation of free radical intermediates (5, 6) and possibly bioreductive covalent attachment to biomolecules, may also be significant (7). These agents suffer from two serious disadvantages: (*i*) a tendency to undergo reductive deglycosidation to produce the inactive 7-deoxyaglycones (1, 2), and (*ii*) a severe dose-related cardiotoxicity (8, 9). Evidence has accumulated to indicate that both effects require initial one-electron reduction of the chromophore and that in the second effect there is subsequent generation of reactive oxygen species including hydrogen peroxide, superoxide anion, and hydroxyl radicals (Fig. 1) (5, 6, 10–12). The susceptibility of cardiac tissue to lipid peroxidation by the latter species may be accounted for by the substantially lowered concentration of the cell protective enzymes superoxide dismutase, catalase, and glutathione peroxidase in the heart compared with other organs (10, 13, 14). A number of the species in the scheme (Fig. 1), which is central to the many in vivo reactions of the anthracyclines, have been

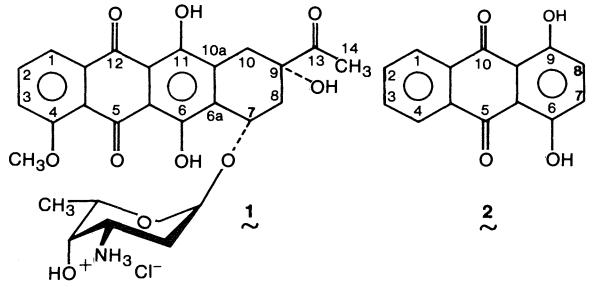

1

2

[1]Studies related to antitumor antibiotics, Part XXVI.

0008-4042/81/223212-06$01.00/0
©1981 National Research Council of Canada/Conseil national de recherches du Canada

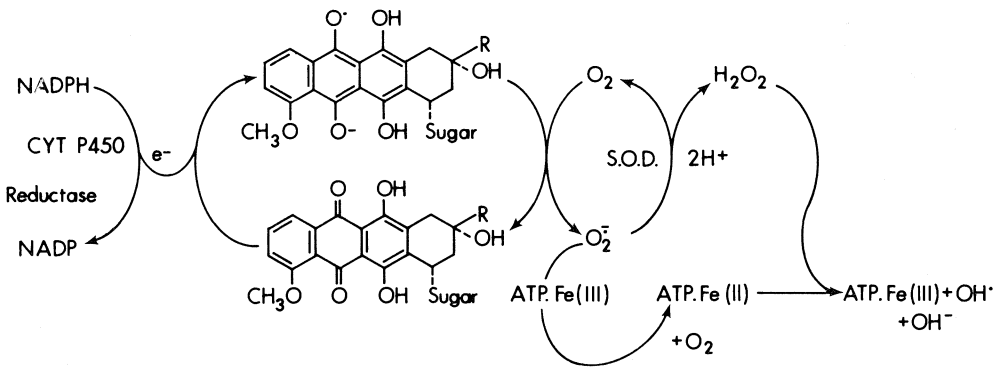

FIG. 1. Scheme for intracellular enzymatic reductive activation of the anthracycline chromophore and subsequent generation of superoxide anion, hydrogen peroxide and hydroxyl radicals.

identified. For example the intermediacy of $O_2^{\cdot-}$ and of H_2O_2 in the action of reductively activated anthracyclines on DNA is unambiguously established by their selective enzymatic removal by superoxide dismutase and by catalase, respectively (7). In addition the superoxide anion generated from daunorubicin in microsomal incubations has been spin-trapped (15). The hydroxyl radical generated from quinone antibiotics has also been spin-trapped in epr experiments (16). Moreover we recently provided evidence using kinetic criteria in conjunction with epr spectroscopy for the generation of free hydroxyl radicals from the anthracyclines as well as certain other antibiotics (17). The remaining species, the anthracycline semiquinone, is strongly implicated in the above processes. Hitherto characterization of this species in aqueous solution has been difficult owing to its transient nature (5, 18). While a steady-state electron paramagnetic resonance (epr) signal generated in vivo during the rat liver microsomal activation of daunorubicin has been tentatively attributed to the semiquinone, the poorly resolved spectrum obtained did not permit unambiguous identification (5, 18). An epr spectrum attributed to daunorubicin semiquinone (18, 19) and a somewhat different spectrum attributed to daunomycinone semiquinone (7) have been obtained in dimethyl sulfoxide solutions, which solvent in general has a stabilizing effect on organic radicals. Because of the profound effects of solvents on the conformation of daunorubicin (2, 20, 21) we have attempted to obtain the epr spectra in aqueous solution with a view to obtaining the unperturbed conformation of the radical. This necessitates some sacrifice in stability of the semiquinone species and some loss of resolution of the narrow splittings. The hyperfine splittings arising from the chromophore could be assigned by computer simulation and an LCAO–MO calculation and by comparison with quinizarin semiquinone as a model compound. By reference to the angular dependence of the hyperfine couplings arising from the protons of ring A a distinction was possible between two possible conformations of the semiquinone.

Experimental

Materials and Methods

Daunorubicin hydrochloride was a generous gift from Dr. F. Arcamone, Farmitalia, Milan. Peroxylamine disulfonate was purchased from Aldrich Chemical Co. Quinizarin was obtained from Aldrich Chemical Co. and was purified by recrystallization just before use.

Electron Paramagnetic Resonance Spectroscopy

The epr spectra were obtained on a Bruker ER-400 epr spectrometer fitted with a Varian V3601 12-inch magnet with VFR Hall effect controller. Hyperfine couplings were obtained by comparison with peroxylamine disulfonate (triplet, spacing 13.0 G) and g values were obtained by direct Fieldial measurements.

Generation and Detection of Daunorubicin and Quinizarin Semiquinones

Stock solutions containing 8×10^{-2} M of the quinones were prepared in triply distilled water. The reactions were performed at room temperature in a total volume of 500 μL in a quartz flat cell containing 4×10^{-3} M quinone, 4×10^{-3} M aqueous sodium borohydride in 50 mM potassium phosphate buffer, pH 7.4, with free access to atmospheric oxygen, and the epr spectra of the semiquinones rapidly recorded. While the spectrum of quinizarin semiquinone was stable, owing to the transient nature of daunorubicin semiquinone, several trials were necessary to obtain the resolved spectrum of the latter in aqueous solution.

Results and Discussion

Daunorubicin semiquinone gave an epr spectrum of spectral width ca. 17.0 G with g value estimated at 2.0024 (Fig. 2). This corresponds in field position to the broad unresolved single line signal obtained by rat liver microsomal activation of daunorubicin

Can. J. Chem. Downloaded from www.nrcresearchpress.com by 210.87.254.42 on 09/06/12
For personal use only.

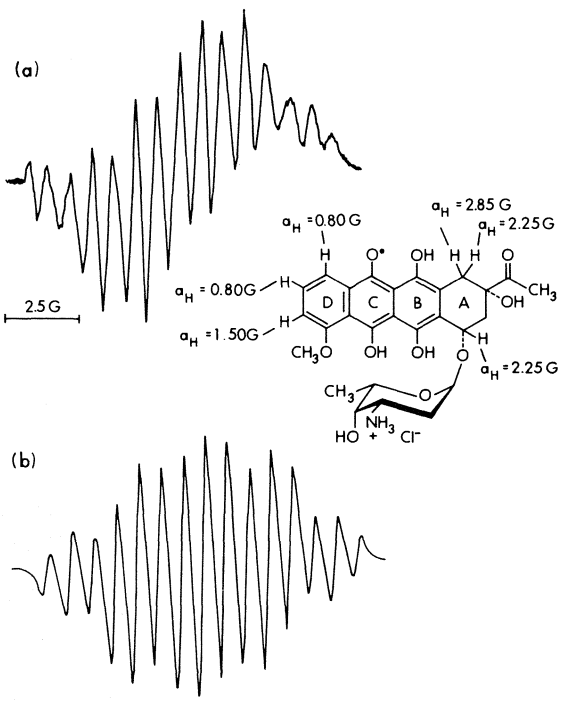

FIG. 2. The epr spectrum (microwave power 4 mW, modulation amplitude 0.06 G, scan time 500 s) obtained from 1×10^{-4} *M* daunorubicin in aqueous solution with reduction by 1×10^{-4} *M* sodium borohydride in 50 m*M* phosphate buffer, pH 7.4, in the presence of atmospheric oxygen. (a) Observed epr spectrum. (b) Computer simulation with Lorentzian line shapes and with line widths of 0.4 G and the hfs shown.

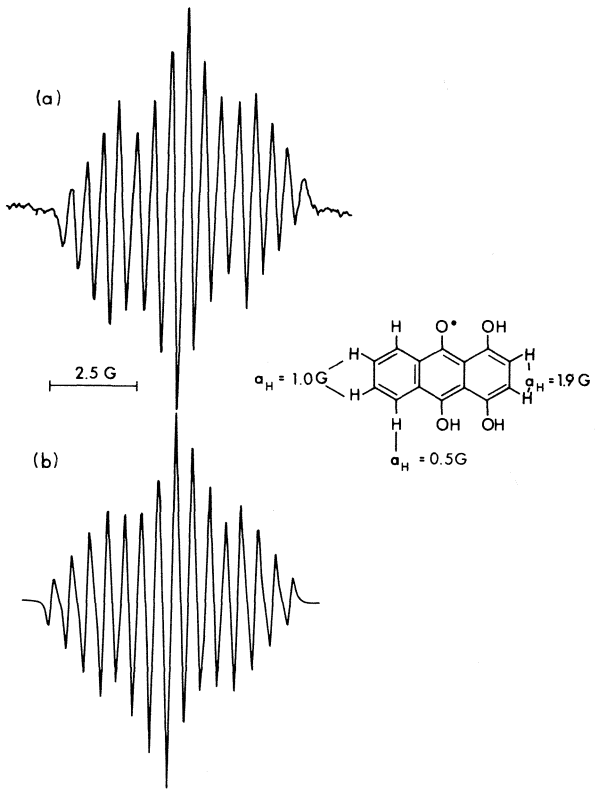

FIG. 3. The epr spectrum (microwave power 4 mW, modulation amplitude 0.06 G, scan time 1000 s) obtained from 1×10^{-4} *M* quinizarin in aqueous solution with reduction by 1×10^{-4} *M* sodium borohydride in 50 m*M* phosphate buffer, pH 7.4, in the presence of atmospheric oxygen. (a) Observed epr spectrum. (b) Computer simulation with Lorentzian line shapes and with line widths of 0.2 G and the hfs shown.

which was tentatively attributed to the antibiotic semiquinone (5, 18). The epr signal was quite short-lived under these conditions in accord with previous estimates of the upper limit of the average lifetime of this species of ca. 1 ms obtained electrochemically (22).

The multiplicity observed in the hyperfine coupling indicated that the unpaired spin density extended to the three benzylic protons of ring A and to the three aromatic protons of ring D of the chromophore. Owing to the lack of symmetry in the anthracycline chromophore, however, it was necessary to examine a model compound in order to assign the individual hyperfine splitting constants (hfs).

Quinizarin **2** has a similar substitution pattern to rings B and C of daunorubicin. Under similar reaction conditions quinizarin gave rise to a stable and well-resolved fifteen-line spectrum with an overall spacing of 7.8 G and a g value of 2.0026 (Fig. 3). Computer simulation gave an accurate match for hyperfine splitting by three pairs of equivalent protons with values for a_H of 0.5, 1.0, and 1.9 G respectively and assigned as shown in Fig. 3. The epr spectrum of quinizarin semiquinone has been obtained previously but under different reaction conditions (23). Although the two semiquinones have been depicted in Figs. 2 and 3 as the neutral species at pH 7, the pK_a values of the phenolic OH groups anticipated to be in the region of 3 to 4 (1, 2) may well result in the neutral species being in equilibrium with the radical anion forms under these conditions. However, since identical spectra were obtained in deuterium oxide solutions this indicates no additional coupling from the OH protons due to rapid exchange in aqueous solution, so the equilibrium level of protonation cannot be ascribed with certainty. In contrast, generation of the anthracycline semiquinone species in dimethyl sulfoxide solution (18, 19) may be expected to result in additional hyperfine splitting from the OH protons as a result of reduced rate of exchange.

On the basis of the tentative quinizarin hfs assignments (which indicate substantial unpaired spin density extending to ring B of the anthracy-

Can. J. Chem. Downloaded from www.nrcresearchpress.com by 210.87.254.42 on 09/06/12
For personal use only.

Can. J. Chem. Downloaded from www.nrcresearchpress.com by 210.87.254.42 on 09/06/12
For personal use only.

cline chromophore), the epr spectrum of daunorubicin semiquinone was analyzed as shown in Fig. 2. Computer simulation gives a match for hyperfine splittings the individual magnitudes of which are tentatively assigned as shown in Fig. 2.

Huckel Molecular Orbital Calculation of Unpaired Spin Densities Permitting Individual Hyperfine Splitting Constant Assignments

Theoretical studies have shown a direct proportionality between proton hyperfine splitting a_i and the calculated density of the unpaired electron ρ_i at the carbon adjacent to the proton (24–26)

[1] $a_i = Q\rho_i$

where Q is a constant. It has been pointed out by Vincow and Fraenkel (23) that although a molecular orbital theory calculation with neglect of configuration interaction cannot be expected to give reasonable results for radicals similar to odd-alternate hydrocarbons, however, the results for the even-alternate hydrocarbon radicals give fair agreement, sufficiently so to give one confidence in the accuracy of individual assignments.

One-electron LCAO – molecular orbital theory calculations were performed using the Huckel approximation for the BCD semiquinone aromatic ring system of the anthracycline as a 19 center pi (π) system, and on the quinizarin semiquinone as an 18 center π system. Molecular wave functions were calculated for a range of values of β_{CO}/β_{CC} from 1.55 to 2.0 and of $\delta\alpha = (\alpha_o - \alpha_C)/\alpha_{CC}$ and where α_C and β_{CC} are the Coulomb and resonance integrals for carbon, respectively. The unpaired spin densities computed as the squares of one-electron wave function coefficients for the carbons of interest in **1** and **2** are summarized in Table 1.[2] To obtain the predicted hfs a_H values from eq. [1], the widely accepted (23, 26, 27) value of $Q = 22.5$ was used for the aromatic protons in each case. For the benzylic protons in ring A of the anthracyclines it was then necessary to consider the angular dependence of axial or equatorial positions relative to the π orbitals at positions 6a and 10a in **2**. It has been argued that if the hyperfine coupling of C_β protons (β to the site of spin density) occurs by a hyperconjugative mechanism it should be proportional to $\cos^2\theta$, where θ is the angle between projections of the $2p_x$-orbital of C_α and the C_β—H bond on a plane perpendicular to the C_α—C_β bond (28). It has been found that, although the simple relationship between β-proton coupling and θ suggested above ($a_H \propto \cos^2\theta$) is fitted reasonably satisfactorily in some examples, closer agreement is obtained by modification of this relationship to form eq. [2]

[2] $a_H = \rho(B_0 + B\cos^2\theta)$

where B_0 is a constant between 3 and 4 G and B is in the range 45–50 (refs. 29–31). For alicyclic systems values of $B_0 = 3.5$ and $B = 45.6$ G have been found to be satisfactory (31, 32) and are therefore used here.

In eq. [2] due account is taken of spin-density values on C_α. Such spin-density transmission for the anthracycline semiquinone reflects the contribution of canonical forms of the type shown in Fig. 4, and which has been suggested to be involved in the enzymatic reductive deglycosidation of anthracyclines (34). The good agreement between calculated and observed a_H values for the aromatic protons of quinizarin and of the anthracycline chromophore given by the values $\beta_{CO}/\beta_{CC} = 1.8$ and $\delta\alpha = 1.4$ (Tables 1, 2)[2] gives one confidence that the unpaired spin densities are reasonably accurate. Therefore we felt justified in using the corresponding calculated spin densities for positions 7a and 10a in daunorubicin obtained by using $\beta_{CO}/\beta_{CC} = 1.8$ and $\delta\alpha = 1.4$ to make some deductions concerning the average conformation of ring A in daunorubicin semiquinone.

It has correctly been pointed out in a comparable conformational analysis of the parent antibiotic by proton magnetic resonance that the Karplus relationship should not be used to determine accurately dihedral angles from vicinal coupling constants (15). It should, however, be possible to use it (or the equivalent relationship in epr spectroscopy) to distinguish between alternative conformations. Two such conformations (Fig. 5, **a** and **b**) of the A ring need to be considered by analogy with daunorubicin itself. These correspond to two possible half-chair conformations of ring A of the antibiotic (2, 15, 20). The conformation **a** is favored for the anthracycline in solution in which the two oxygen functions are pseudo-equatorial (15). By contrast, conformation **b** is found in the crystal structure of

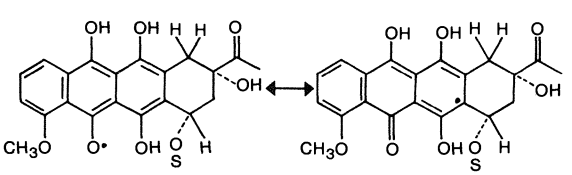

FIG. 4. Suggested transmission of unpaired spin density in daunorubicin semiquinone during enzymatic reductive deglycosidation (ref. 33).

[2]Tables 1 and 2 are submitted as Supplementary Material; copies are available, at a nominal charge, from the Depository of Unpublished Data, CISTI, National Research Council of Canada, Ottawa, Canada K1A 0S2.

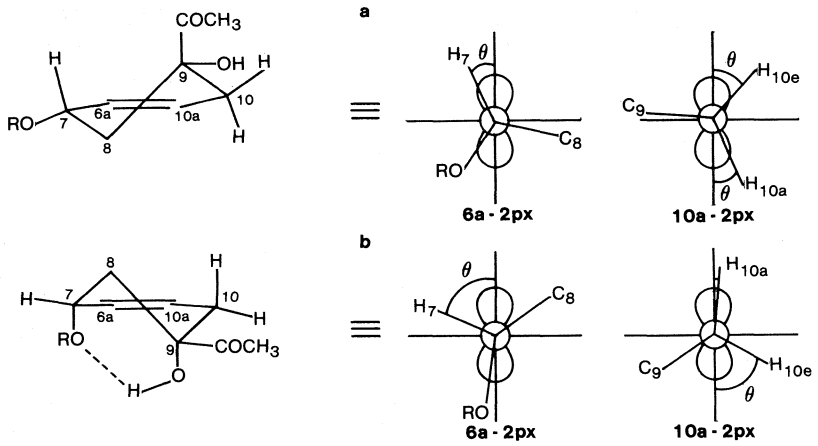

FIG. 5. Possible conformations of ring A in daunorubicin and the corresponding dihedral angles to the unpaired electron in $2p_x$ orbital at the carbons 6a and 10a of ring junction A/B.

the pyridine adduct of daunorubicin where strong hydrogen bonding is permitted between the two axial oxygen functions (35). Considerations of the geometries of the two corresponding conformations of the daunorubicin semiquinone permit certain predictions to be made concerning the relative magnitudes of the benzylic proton hyperfine couplings in ring A. As seen from Fig. 5, viewing along the C_7—C_{6a} bond and along the C_{10}—C_{10a} bond for conformation **a** predicts roughly comparable small values for θ for the respective axial protons at positions 7 and 10 and the equatorial proton at position 10. These values of θ are estimated to be in the 30–40° range. By contrast, the corresponding dihedral angles in conformation **b** are two large (ca. 75°) and one very small (~5°) in the hydrogen bonded structure **b**. In relating calculated hfs to observed it is recognized that initially at least the individual benzylic protons are assigned arbitrarily. The predicted unpaired spin densities at positions 6a and 10a are closely similar (see Table 1).[2] Moreover, since either conformation **a** or **b** predicts two axial and one equatorial or two equatorial and one axial, the two similar observed couplings (2.25 G) are assigned one to each of the 7 and 10 positions. By employing eq. [2] we can estimate the dihedral angles θ for the LCAO calculation with $\beta_{CO}/\beta_{CC} = 1.8$ and $\delta\alpha = 1.4$

$$a_{H_{10e}} = \rho_{10a}(B_0 + B\cos^2\theta)$$
$$2.85 = 0.08509\,(3.5 + 45.6\cos^2\theta)$$

which gives $\cos\theta = 0.81102$ or $\theta_{10e} \approx 36°$.

Similarly $a_{H_{10a}} = 2.25 = 0.08509\,(3.5 + 45.6\cos^2\theta)$, which gives $\cos\theta = 0.70931$ or $\theta_{10a} \approx 45°$. The corresponding dihedral angle for the proton at position 7 is derived from $a_{H_{7a}} = 2.25 = 0.08037\,(3.5 + 45.6\cos^2\theta)$, which gives $\cos\theta = 0.73292$ or $\theta_{7a} \approx 43°$. In contrast, conformation **b**, which requires dihedral angles of ca. 75° for the equatorial protons at positions 7 and 10 and of about 5° for H_{10a}, predicts hfs values of $a_{H_{7a}} = 0.53$, $a_{H_{10e}} = 0.56$, and $a_{H_{10a}} = 4.1$ G, respectively. Even allowing for some distortions in the rings these observations indicate that the conformation **a** depicted in Fig. 5 is in better agreement with the experimental data. It should be emphasized, however, that the epr spectra, owing mainly to the lack of resolution in aqueous media, may be subject to more than one analysis. For this reason the interpretation given must be regarded as tentative.

In view of its recognized role in the metabolism, cardiotoxicity, and possibly the molecular mechanisms of anticancer action of daunorubicin, this result may assist in the interpretation of the biochemical pharmacology of this important antibiotic. For example, the daunorubicin semiquinone has been described as a "site-specific" radical (5) and there is some evidence for its binding to DNA (7). A knowledge of the preferred conformation of this intermediate should be of assistance in delineating the geometry of the molecular recognition process in its interaction with DNA.

Acknowledgements

This research was supported by grants to the authors from the National Cancer Institute of Canada and the University of Alberta. The authors wish to thank Dr. R. E. D. McClung and Mr. Kam Kong for assistance in obtaining the molecular orbital computations and epr computer simulations and Mr. Glen Bigam for assistance in obtaining the epr spectra.

Can. J. Chem. Downloaded from www.nrcresearchpress.com by 210.87.254.42 on 09/06/12
For personal use only.

1. A. DI MARCO, F. ARCAMONE, and F. ZUNINO. *In* Antibiotics, III. Mechanism and action of antimicrobial and antitumor agents. *Edited by* J. W. Corcoran and F. E. Hahn. Springer, New York. 1975. pp. 101–128.
2. F. ARCAMONE. *In* Topics in antibiotic chemistry. *Edited by* P. Sammes. Wiley, New York. 1978. pp. 102–239.
3. F. ZUNINO, R. A. GAMBETTA, A. DI MARCO, and A. ZACCARA. Biochim. Biophys. Acta, **277**, 489 (1972).
4. A. DI MARCO, F. ZUNINO, R. SILVESTRINI, C. GAMBARUCCHI, and R. A. GAMBETTA. Biochem. Pharmacol. **20**, 1323 (1971).
5. N. R. BACHUR, S. L. GORDON, and M. V. GEE. Mol. Pharmacol. **13**, 901 (1977).
6. J. W. LOWN, S. K. SIM, K. C. MAJUMDAR, and R. Y. CHANG. Biochem. Biophys. Res. Commun. **76**, 705 (1977).
7. B. K. SINHA. Chem. Biol. Interact. **30**, 67 (1980).
8. G. BONADONNA and S. MONFARDINI. Lancet, **1**, 837 (1964).
9. B. SMITH. Br. Heart J. **31**, 607 (1969).
10. T. H. DOROSHOW, G. Y. LOCKER, and C. E. MYERS. J. Clin. Invest. **65**, 128 (1980).
11. T. KISHI, T. WATANABE, and K. FOLKERS. Proc. Natl. Acad. Sci. U.S.A. **73**, 4653 (1976).
12. Y. IWAMOTO, I. G. HANSEN, T. H. PORTER, and K. FOLKERS. Biochem. Biophys. Res. Commun. **58**, 633 (1974).
13. T. GOODMAN and P. HOCHSTEIN. Biochem. Biophys. Res. Commun. **77**, 797 (1977).
14. A. V. PESKIN, YA. M. KOEN, I. B. ZBARSKY, and A. A. KONSTANTINOV. FEBS Lett. **78**, 41 (1977).
15. B. KALYANARAMAN, E. PEREZ-REYES, and R. F. MASON. Biochim. Biophys. Acta, **630**, 119 (1980).
16. J. W. LOWN, S. K. SIM, and H. H. CHEN. Can. J. Biochem. **56**, 1042 (1978).
17. J. W. LOWN and H. H. CHEN. Can. J. Chem. **59**, 390 (1981).
18. S. SATO, M. IWAIZUMI, K. HANDA, and Y. TAMURA. Gann, **68**, 603 (1977).
19. S. K. SINHA and C. F. CHIGNELL. Chem. Biol. Interact. **28**, 301 (1979).
20. S. NEIDLE. *In* Topics in antibiotic chemistry. *Edited by* P. Sammes. Wiley, New York. 1978. p. 260.
21. M. E. NUSS, T. L. JAMES, M. A. APPLE, and P. A. KOLLMAN. Biochim. Biophys. Acta, **609**, 136 (1980).
22. G. M. RAO, J. W. LOWN, and J. A. PLAMBECK. J. Electrochem. Soc. **125**, 534 (1978).
23. G. VINCOW and G. K. FRAENKEL. J. Chem. Phys. **34**, 1333 (1961).
24. E. DE BOER and S. I. WEISSMAN. J. Am. Chem. Soc. **80**, 4549 (1938).
25. A. CARRINGTON, F. DRAVNIEKS, and M. C. R. SYMONS. J. Chem. Soc. 947 (1959).
26. H. M. MCCONNELL. J. Chem. Phys. **24**, 632 (1956).
27. P. B. AYSCOUGH. Electron spin resonance in chemistry. Methuen, London. 1967. p. 259.
28. M. C. R. SYMONS. Tetrahedron, **18**, 333 (1962).
29. A. HORSFIELD, J. R. MORTON, and D. H. WHIFFEN. Mol. Phys. **4**, 425 (1961).
30. M. C. R. SYMONS. *In* Advances in physical organic chemistry: Vol. 1. *Edited by* V. Gold. Academic Press, London and New York. 1963. p. 284.
31. E. W. STONE and A. H. MAKI. J. Chem. Phys. **37**, 1326 (1962).
32. W. T. DIXON and R. O. C. NORMAN. J. Chem. Soc. 4850 (1964).
33. D. GRILLER and K. U. INGOLD. Acc. Chem. Res. **8**, 13 (1976).
34. T. KOMIYAMA, T. OKI, and T. INUI. J. Antibiot. **32**, 1219 (1979).
35. S. NEIDLE and G. TAYLOR. Biochim. Biophys. Acta, **474**, 450 (1977).

Can. J. Chem. Downloaded from www.nrcresearchpress.com by 210.87.254.42 on 09/06/12
For personal use only.

Can. J. Chem. Downloaded from www.nrcresearchpress.com by 210.87.254.40 on 09/06/12
For personal use only.

COMMUNICATION

Hydrogen–deuterium exchange and rearrangement of polycyclic aromatic hydrocarbons in dilute acid medium at elevated temperatures

NICK HENRY WERSTIUK AND GEORGE TIMMINS

Department of Chemistry, McMaster University, Hamilton, Ont., Canada L8S 4M1

Received July 8, 1981

NICK HENRY WERSTIUK and GEORGE TIMMINS. Can. J. Chem. **59**, 3218 (1981).

The high temperature – dilute acid (HTDA) method has been applied to the preparation of perdeuterated polycyclic aromatic hydrocarbons. Naphthalene (**1**), 1-methylnaphthalene (**2**), 2-methylnaphthalene (**3**), anthracene (**4**), phenanthrene (**5**), chrysene (**6**), pyrene (**7**), benz[*a*]anthracene (**8**), benzo[*a*]pyrene (**9**), 1,1′-binaphthyl (**10**), 1,2′-binaphthyl (**11**), and 2,2′-binaphthyl (**12**) have been perdeuterated in high yield in dilute DCl–D_2O solutions at elevated temperatures (240–280°C). **2**, **3**, **10**, **11**, and **12** also rearrange.

NICK HENRY WERSTIUK et GEORGE TIMMINS. Can. J. Chem. **59**, 3218 (1981).

On a préparé des hydrocarbures aromatiques polycycliques perdeutérés en opérant en milieu acide dilué et à haute température (ADHT). Utilisant des solutions diluées de DCl dans D_2O et opérant à des températures allant de 240 à 280°C, nous avons perdeutéré les hydrocarbures suivants avec d'excellents rendements: naphtalène (**1**) méthyl-1 naphtalène (**2**), méthyl-2 naphtalène (**3**), authracène (**4**), phénanthrène (**5**), chrysène (**6**), pyrène (**7**), benz [*a*] anthracène (**8**), benzo [*a*] pyrène (**9**), binaphtyl-1,1′ (**10**), binaphtyl-1,2 (**11**) et binaphtyl-2,2′ (**12**). Les composés **2**, **3**, **10**, **11** et **12** subissent aussi des transpositions.

[Traduit par le journal]

In continuing our study of the scope of the high temperature – dilute acid (HTDA) method of hydrogen isotope exchange (1–5) we examined the H–D exchange of naphthalene (**1**), 1-methylnaphthalene (**2**), 2-methylnaphthalene (**3**), anthracene (**4**), phenanthracene (**5**), chrysene (**6**), pyrene (**7**), benz[*a*]anthracene (**8**), benzo[*a*]pyrene (**9**), 1,1′-binaphthyl (**10**), 1,2′-binaphthyl (**11**), and 2,2′-binaphthyl (**12**). All substrates are perdeuterated in near-quantitative yield in a single reaction and **2**, **3**, **10**, **11**, and **12** rearrange. The results of our preliminary study are listed in Table 1.

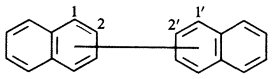

10–12

Typically, substrate (0.030 g) was added to 5 mL of 2% w/v DCl–D_2O in a thick-walled glass tube, the solution was degassed via three freeze–pump–thaw cycles and sealed under vacuum. The tube was placed in a 600 mL Parr pressure apparatus which contained water to equalize pressure and heated for an appropriate period. Solid products were isolated by filtration and 1-methylnaphthalene was isolated by ether extraction. Deuterium content was determined mass spectrometrically at low ionizing voltage.

From Table 1 it can be seen that all compounds can be equilibrated with the deuterium pool and perlabelled in excellent yield in a single reaction at 250–280°C. Benzo[*a*]pyrene which chars substantially at 250°C in 2% w/v DCl–D_2O can be perdeuterated in 1% w/v DCl–D_2O at 240°C (entry 11). Exchange of **10**, **11**, and **12** occurs slowly in neutral D_2O at 280°C (for example entry 15). **1**, **5**, and **6** are also stable and undergo complete H–D exchange at 300°C in neutral D_2O (for example entry 2). With methylnaphthalenes **2** and **3**, the methyl groups also equilibrate with the deuterium pool under these conditions (entries 4 and 5). In a previous study of H–D exchange of toluene and xylenes at 250°C for shorter reaction times, little exchange of the methyl groups and no isomerization were observed (1, 3, 4). We expect that the methylnaphthalenes can similarly be selectively ring deuterated at lower temperatures.

Under HTDA conditions rearrangement of the methylnaphthalenes (entries 3–5) and binaphthyls (entries 12–17) also occurs. The rearrangements are subject to an isotope effect, rearrangement being faster in D_2O than in H_2O (entries 3 and 4 or

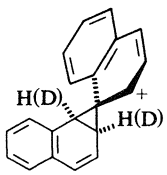

13

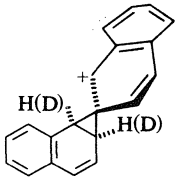

14

0008-4042/81/223218-02$01.00/0

©1981 National Research Council of Canada/Conseil national de recherches du Canada

TABLE 1. Hydrogen–deuterium exchange and rearrangement of polycyclic aromatic hydrocarbons

Entry	Substrate	Conditions[a]	Percent yield[b]	Relative % yields[c]			% exchange (excess D atoms/molecule)[d]		
1	**1**	D, 250°C, 50h	90				99.4 (7.95)		
2	**1**	D_2O, 300°C, 168h	89	**2**	**3**		97.2 (7.78)		
3	**2**	H, 280°C, 50h	Not det.	77.0	23.0				
4	**2**	D, 280°C, 50h	87[e]	67.6	32.4		99.3 (9.93)[f]		
5	**3**	D, 280°C, 50h	88	12.4	87.6		99.4 (9.94)[f]		
6	**4**	D, 250°C, 50h	88				99.4 (9.94)		
7	**5**	D, 250°C, 50h	91				99.4 (9.94)		
8	**6**	D, 250°C, 50h	89				99.3 (11.92)		
9	**7**	D, 250°C, 50h	89				99.4 (9.94)		
10	**8**	D, 250°C, 50h	92				99.4 (11.93)		
11	**9**	D, 1% w/v DCl–D_2O 240°C, 50h	97				89.2 (10.70)		
				10	**11**	**12**			
12	**10**	H, 280°C, 114h	99	34.5	31.7	33.8			
13	**10**	D, 250°C, 72h	93	92.5	7.5	<0.1	98.3 (13.76)	98.0 (13.72)	Not det.
14	**10**	D, 280°C, 114h	93	15.3	26.8	57.9	98.0 (13.72)	98.2 (13.75)	98.2 (13.75)
15	**10**	D_2O, 280°C, 50h	97	100.0			3.5 (0.49)		
16	**11**	D, 250°C, 72h	92	1.2	92.8	6.1	98.1 (13.73)	98.2 (13.75)	98.1 (13.73)
17	**12**	D, 280°C, 50h	97	2.2	19.4	78.4	97.9 (13.71)	98.0 (13.72)	98.3 (13.76)

[a] Reactions were carried out in 2% w/v DCl–D_2O = D or 2% w/v HCl–H_2O = H solutions unless otherwise stated.
[b] Yields of crude product are reported.
[c] The values, average of at least three determinations, were obtained by glpc using electronic integrations.
[d] Deuterium content was determined mass spectrometrically (or, for mixtures, gc–ms) at low ionizing voltage (9 eV).
[e] **2** was isolated by ether extraction, the solution was dried and the ether removed under vacuum.
[f] Since the compounds could not be completely separated, the values quoted are averages of at least eight measurements of peak intensities as both compounds exited the gas chromatograph.

12 and 14). In our view, the binaphthyls rearrange via naphthalene naphthonium ions **13** and **14**. As far as we are aware, this is the first report of naphthyl shifts on aromatic rings via naphthonium ions although ethene naphthonium ions have been implicated as intermediates in the solvolysis of 1- and 2-naphthylethyl sulfonates (6–8).

Acknowledgements

We thank the Natural Sciences and Engineering Research Council of Canada for financial support and Dr. S. Banerjee and Mr. D. Evans for developing a computer program used for deuterium analysis.

1. N. H. WERSTIUK and T. KADAI. Can. J. Chem. **51**, 1485 (1973).
2. N. H. WERSTIUK and T. KADAI. Can. J. Chem. **52**, 2169 (1974).
3. N. H. WERSTIUK and T. KADAI. U.S. Patent 3,989,705 (1976).
4. N. H. WERSTIUK and T. KADAI. Canadian Patent 1048556 (1979).
5. N. H. WERSTIUK and G. TIMMINS. Can. J. Chem. **59**, 1022 (1981).
6. D. J. CRAM and C. K. DALTON. J. Am. Chem. Soc. **85**, 1268 (1963).
7. C. C. LEE and A. G. FORMAN. Can. J. Chem. **43**, 3387 (1965).
8. C. C. LEE and A. G. FORMAN. Can. J. Chem. **44**, 841 (1966).

Can. J. Chem. Downloaded from www.nrcresearchpress.com by 210.87.254.40 on 09/06/12
For personal use only.

A ^{113}Cd nuclear magnetic resonance study of some complexes of cadmium with phosphine oxides, sulfides, and selenides[1,2]

PHILIP A. W. DEAN

Department of Chemistry, University of Western Ontario, London, Ont., Canada N6A 5B7

Received April 7, 1981

Can. J. Chem. Downloaded from www.nrcresearchpress.com by 210.87.254.5 on 09/06/12
For personal use only.

PHILIP A. W. DEAN. Can. J. Chem. **59**, 3221 (1981).

$^{113}Cd(AsF_6)_2$ has been synthesized from ^{113}CdO by treatment in SO_2 with PF_5 then AsF_5. From the ^{113}Cd-enriched salt have been prepared $[Cd(EPR_3)_4]^{2+}$ (E = O, R = C_6H_{11}; E = S or Se, R = Ph), $[Cd(SP(C_6H_{11})_3)_x(SeP(C_6H_{11})_{n-x}]^{2+}$ (n = 4, x = 0–4; n = 3, x = 0–3), $[Cd(EP(o\text{-}C_6H_4Me)_3)_n]^{2+}$ (E = S, n = 4 or 2; E = Se, n = 3 or 2), $[Cd(Ph_2P(O)(CH_2)_nP(O)Ph_2)_3]^{2+}$ (n = 1 or 2), and $[Cd(Ph_2P(O)((CH_2)_2P(O)Ph_2)_2)_2]^{2+}$ in liquid SO_2. The reduced temperature slow exchange ^{31}P and ^{113}Cd nmr spectra have been measured and are discussed. The ^{31}P nmr are as expected from previous work on complexes containing ^{113}Cd at natural abundance except that several values of $^2J(^{113}Cd—O—^{31}P)$ have been measured. From the ^{113}Cd spectra the most important shielding sequences observed are $\delta_O \ll \delta_{Se} < \delta_S$ for $[Cd(EP(C_6H_{11})_3)_4]^{2+}$, $\delta_{2:1} < \delta_{3:1} < \delta_{4:1}$ for $[Cd(EPR_3)_n]^{2+}$ (E = S or Se, n = 1–4, constant R), and $\delta_{CdO_4} > \delta_{CdO_6}$ for the various phosphine oxide complexes studied.

The synthesis of SO_2-insoluble $Cd(SbF_6)_2 \cdot 3(OP(C_6H_{11})_3)$ is reported.

PHILIP A. W. DEAN. Can. J. Chem. **59**, 3221 (1981).

On a synthétisé le $^{113}Cd(AsF_6)_2$ en faisant réagir le ^{113}CdO dans le SO_2 avec du PF_5 puis avec du AsF_5. Utilisant des sels enrichis en ^{113}Cd et opérant dans le SO_2 liquide, on a préparé les composés suivants: $[Cd(EPR_3)_4]^{2+}$ (E = O, R = C_6H_{11}; E = S ou Se, R = Ph), $[Cd(SP(C_6H_{11})_3)_x(SeP(C_6H_{11})_{n-x}]^{2+}$ (n = 4, x = 0–4; n = 3, x = 0–3), $[Cd(EP(o\text{-}C_6H_4Me)_3)]_n^{2+}$ (E = S, n = 4 ou 2; E = Se, n = 3 ou 2), $[Cd(Ph_2P(O)(CH_2)_nP(O)Ph_2)_3]^{2+}$ (n = 1 ou 2), et $[Cd(Ph_2P(O)((CH_2)_2P(O)Ph_2)_2)_2]^{2+}$. On a mesuré et on discute des spectres rmn du ^{31}P et du ^{113}Cd dans lesquels des échanges lents sont observés à basse température. Les spectres rmn du ^{31}P correspondent à prévus par les travaux antérieurs sur les complexes contenant du ^{113}Cd en l'abondance naturelle, on a toutefois mesuré plusieurs valeurs de $^2J(^{113}Cd—O^{31}P)$. Les séquences de blindage les plus importantes observées dans les spectres du ^{113}Cd sont dans l'ordre suivant $\delta_O \ll \delta_{Se} < \delta_S$ pour le $[Cd(EP(C_6H_{11})_3)_4]^{2+}$, $\delta_{2:1} < \delta_{3:1} < \delta_{4:1}$ pour le $[Cd(EPR_3)_n]^{2+}$ (E = S ou Se, n = 1–4, R constant) et $\delta_{CdO_4} > \delta_{CdO_6}$ pour les différents complexes d'oxyde de phosphine étudiés. On rapporte la synthèse du composé $Cd(SbF_6)_2 \cdot 3(OP(C_6H_{11})_3)$ insoluble dans le SO_2.

[Traduit par le journal]

Introduction

Previously, we have used reduced temperature ^{31}P nmr to characterize, in SO_2 solution, a wide range of cadmium complexes with phosphine oxides, sulfides, or selenides, as well as some mixtures of these, as ligands (1, 2). Our intention was to establish a series of related complexes of Group VIA donor ligands in which the kernel could be varied methodically, so providing a basis for a ^{113}Cd nmr study in which the effect of systematic change about the cadmium could be investigated. There is general agreement on the need for more and better model compound studies to advance the application of ^{113}Cd nmr to less straightforward situations, but relatively few detailed studies of model series have appeared (e.g. refs. 3–15), and some of these (e.g. refs. 4, 9, 11) have been complicated by the necessity of working with mixtures undergoing rapid intermolecular exchange.

In this paper we present ^{113}Cd nmr results for selected members from among the cadmium complexes we characterized earlier (1, 2). Unambiguous slow exchange ^{113}Cd spectra have been observed, allowing us to assess the effect on the ^{113}Cd resonance of change of donor atom only, change in ligation number only, change of substituents on the phosphorus atom of the phosphine chalcogenides, and change in the number and size of chelate rings in six-coordinate complexes of chelating phosphine oxides.

Experimental

Materials

Isotopically-enriched CdO (96.3% ^{113}Cd), obtained from Oak Ridge National Laboratory, was dried by heating *in vacuo* prior to use, as were CdO (Mallinckrodt, Analytical Grade), HgO (Shawinigan, Reagent Grade), and ZnO (Fisher, Certified A.C.S. Grade). Arsenic pentafluoride (Ozark-Mahoning, Inc.) and phosphorus pentafluoride (Matheson) were used as received, while antimony pentafluoride (PCR, Inc.) was purified by double distillation in a nitrogen atmosphere. The literature routes (16) to $Cd(AsF_6)_2$ and $Cd(SbF_6)_2$ were used to prepare the salts containing ^{113}Cd in natural abundance, and the preparations of the ligands, except $OP(C_6H_{11})_3$, have been given earlier also (1, 2, 17). Tricyclohexylphosphine oxide was prepared from $S_2C \cdot P(C_6H_{11})_3$ (Strem Chemicals, Inc.) according to Issleib and Brack (18).

Sulfur dioxide (Matheson, Anhydrous Grade) was stored in

[1]No reprints available.

[2]Presented in part at the 64th Chemical Conference, Chemical Institute of Canada, Halifax, N.S., June 1981.

0008-4042/81/233221-05$01.00/0

©1981 National Research Council of Canada/Conseil national de recherches du Canada

Can. J. Chem. Downloaded from www.nrcresearchpress.com by 210.87.254.5 on 09/06/12
For personal use only.

the gas phase over Linde 3A Molecular Sieves for at least 12 h before use.

General Manipulative Procedure

Glove box and vacuum line manipulations and preparations of sealed nmr samples were carried out as described in earlier publications from this laboratory (e.g. refs. 1 and 16).

Preparation of $Cd(AsF_6)_2$ from CdO

Isotopically-enriched cadmium was available only as the oxide, so an alternative to the previously reported route to $Cd(AsF_6)_2$ (16), which relies on anhydrous CdF_2 as a starting material, was necessary.

In a sealed glass H-apparatus of a type described earlier (19), CdO, suspended in SO_2, was treated with AsF_5 using AsF_5/CdO = 4. Within 15 min, the CdO dissolved to give a colourless solution.[3] Filtration, followed by removal of volatiles *in vacuo*, left colourless crude $Cd(AsF_6)_2$. *Anal.* calcd. for As_2CdF_{12}: As 30.56, Cd 22.93, F 46.51; found: As 29.79, Cd 22.42, F 45.28.

Samples of "$^{113}Cd(AsF_6)_2$" prepared by the preceding method gave ^{113}Cd, and with R_3PE (E = O, S, or Se), ^{31}P nmr spectra consistent with those reported earlier (1, 2, 16) for samples containing ^{113}Cd at natural abundance, and the cadmium salt prepared in this way were used in the earlier part of the present work. However, the nmr samples with R_3PE usually contained some insoluble material not present when authentic $Cd(AsF_6)_2$ was used.

The 193 K ^{19}F nmr spectra of SO_2 solutions in which AsF_5/CdO (or ZnO or HgO) = 4 show a broad ($\nu_{1/2} \sim 50$ Hz) line with $\delta_F \approx -48$ ppm and an AX_4 pattern ($\delta_A = -68.3$, $\delta_X = -37.5$ ppm, $J(F—F) = 130 \pm 2$ Hz). The latter spectrum can reasonably be attributed to a species with an AsF_5O kernel, with AsF_5O^- or $F_5AsOAsF_5^-$ (or their SO_2 solvates, O-sulfito complexes) being most likely. This oxygen-containing species may well be the contaminant in $Cd(AsF_6)_2$ prepared from CdO and AsF_5.

A better synthesis of $Cd(AsF_6)_2$ involves two stages. In the initial stage, CdO, suspended in SO_2, is treated with excess PF_5. Over a period of several days at room temperature, the colour of the CdO is blanched and POF_3, identified in the supernatant liquor by ^{19}F nmr, and white $CdF_2 \cdot nPF_5$ formed. From the $CdF_2 \cdot nPF_5$, CdF_2 can be obtained by removal of volatiles *in vacuo*. *Anal.* calcd. for CdF_2: Cd 74.73, F 25.27; found: Cd 74.45, F 25.56. (This proves a convenient route to anhydrous CdF_2 and other metal fluorides.) Normally the $CdF_2 \cdot nPF_5$ was not isolated, but, instead, treated with AsF_5 (AsF_5/Cd $\geq$ 2) in a second stage, causing its rapid (few min) dissolution. $Cd(AsF_6)_2$ was isolated from the colourless solution on removal of volatiles. *Anal.* calcd. for As_2CdF_{12}: see above; found: As 30.62, Cd 22.70, F 46.62. Samples of $Cd(AsF_6)_2$ prepared by this second route had properties identical with a sample prepared from CdF_2 and AsF_5, and this was the preferred synthesis of $^{113}Cd(AsF_6)_2$.

In brief attempts to prepare $M(SbF_6)_2$ (M = Zn, Cd, or Hg) we found that the appropriate metal oxides dissolve in SO_2 on treatment with SbF_5 (SbF_5/MO = 4). These solutions were shown by reduced temperature ^{19}F nmr to contain $Sb_2F_{11}^-$, $SbF_5 \cdot SO_2$ and a species with a *cis*-SbF_4O_2 kernel (A_2X_2 spectrum with $\delta_A = -115.5$, $\delta_X = -89.6$ ppm, $J(F—F) = 135 \pm 2$ Hz) (c.f. ref. 20). The complexity of this mixture deterred us from further efforts, but the desired salts could probably be prepared by a two stage synthesis with PF_5 then SbF_5, analogous to that used for $Cd(AsF_6)_2$ from CdO (see above).

[3]The reaction of metal oxides with MF_5 (M = P, As or Sb) does not seem to have been investigated previously, but a preliminary survey suggests that the reactions reported here may be quite general.

Preparation of $Cd(MF_6)_2 \cdot 3(OP(C_6H_{11})_3)$ (M = As or Sb)

In a sealed H-apparatus, an SO_2 solution of $Cd(MF_6)_2$ was added to a like solution of $OP(C_6H_{11})_3$, with $3 < L/M < 4$. The white *product* precipitated, and was filtered off, washed with several small portions of SO_2 and dried *in vacuo*. Both salts are similar; only the hexafluoroantimonate was analyzed. *Anal.* calcd. for $C_{54}H_{99}CdF_{12}O_3P_3Sb_2$: C 44.02, H 6.77, Cd 7.63, P 6.31; found: C 42.17, 41.97, H 6.70, 6.62, Cd 7.78, P 6.34.

Nuclear Magnetic Resonance Spectra

All nmr spectra were measured using a Varian XL-100-12 spectrometer system operating at 22.34 and 40.54 MHz in the FT mode for ^{113}Cd and ^{31}P, respectively, and 94.19 MHz in the CW mode for ^{19}F. Typically, for the ^{113}Cd spectra several thousand transients were accumulated with a spectral window of 12.5 kHz, tip angle of 30°, and a repetition rate of 14 min^{-1}. A 32 K Fourier transform was performed. Conditions for measurement of ^{31}P spectra have been given before (17).

In all cases shifts to higher frequency than the reference are taken as positive. For ^{19}F and ^{31}P nmr the 10 mm o.d. sample tube was fixed coaxially in a 12 mm o.d. nmr tube with the lock/reference mixture ($(CD_3)_2CO/CFCl_3$ for ^{19}F, $(CD_3)_2CO/OP(OMe)_3$ for ^{31}P) in the outer annulus. For ^{113}Cd nmr, external $(CD_3)_2CO$ was again used as a lock substance, but no external ^{113}Cd reference material, suitable for low temperature nmr, was available. Therefore the shifts in Table 2 are reported relative to the frequency of 4 *M* aqueous $Cd(NO_3)_2$ at ambient probe temperature. In none of the nmr was correction for susceptibility differences made.

Elemental Microanalyses

Carbon, hydrogen analyses were performed by Guelph Chemical Laboratories Ltd., all other analyses were performed by Analytische Laboratorien, Elbach, W. Germany.

Results and Discussion

Isotopically-enriched $^{113}Cd(AsF_6)_2$ was prepared from commercially available ^{113}CdO (96.3% ^{113}Cd) by treatment of the oxide in SO_2 firstly with PF_5 and secondly with AsF_5:

$$^{113}CdO + PF_5 \text{ (excess)} \xrightarrow[RT]{SO_2} {}^{113}CdF_2 \cdot xPF_5 + POF_3$$

$$^{113}CdF_2 \cdot xPF_5 + AsF_5 \text{ (excess)} \xrightarrow[RT]{SO_2} {}^{113}Cd(AsF_6)_2 + PF_5$$

Full details of this preparation, and other preparations attempted are given in the Experimental section (above).

The complexes for study by ^{113}Cd nmr were prepared as reported (1, 2), except that $^{113}Cd(AsF_6)_2$ was used as the source of cadmium. The contents of each solution were verified by reduced temperature ^{31}P nmr prior to the ^{113}Cd measurements. All of the complexes except $[Cd(OP(C_6H_{11})_3)_4]^{2+}$ had been characterized by ^{31}P nmr earlier (1, 2). The $OP(C_6H_{11})_3$ complex is new, although similar complexes of other trialkyl and related phosphine oxides are known (21). It is formed from $Cd(AsF_6)_2$ (or $Cd(SbF_6)_2$) and an excess[4] of the ligand in liquid

[4]When $3 \leq OP(C_6H_{11})_2/Cd \leq 4$, insoluble $Cd(MF_6)_2 \cdot 3(OP(C_6H_{11})_3)$ is formed (see Experimental section).

Can. J. Chem. Downloaded from www.nrcresearchpress.com by 210.87.254.5 on 09/06/12
For personal use only.

TABLE 1. Some values of $^2J(^{113}Cd—O—^{31}P)$ for phosphine oxide complexes of cadmium in SO_2 solution

Complex	T (K)	$^2J(^{113}Cd—O—^{31}P)$ (Hz)[a]
$[Cd(OP(C_6H_{11})_3)_4]^{2+}$	209	25.6[b]
	308	28.0[c]
$[Cd((OPPh_2)_2CH_2)_3]^{2+}$	220	2.4
$[Cd((OPPh_2)_2(CH_2)_2)_3]^{2+}$	205	14.2
$[Cd(triphos\ O_3)_2]^{2+}$[d]	205	~20[e]

[a] Estimated error ±0.5 Hz except where noted.
[b] $\delta_{OP(OMe)_3(ext)} = 62.6$ ppm. ($\delta_{OP(OMe)_3(ext)} = \delta_{H_3PO_4(ext)} - 1.7$ ppm.)
[c] $\delta_{OP(OMe)_3(ext)} = 62.4$ ppm; the free ligand resonance has $\delta_{OP(OMe)_3(ext)} = 55.5$ ppm.
[d] triphos O_3 = (tridentate) $(O)PPh(CH_2CH_2P(O)Ph_2)_2$.
[e] Using the notation of ref. 1, this is probably $^2J(^{113}Cd—P_C)$. $^2J(^{113}Cd—P_A)$ and $^2J(^{113}Cd—P_B)$ were not observed.

SO_2, and is characterized by the ^{31}P nmr spectral parameters included in Table 1. An interesting feature of the ^{31}P spectrum of this cation, even when made with isotopically normal cadmium, is the very clear $^{111}/^{113}Cd$ satellite spectrum, from two-bond Cd—O—P coupling, which is not completely collapsed even at 308 K. In our previous work (1), ^2J(Cd—O—P) could not be seen in the reduced temperature, slow-exchange ^{31}P spectra of complexes with $Ph_2P(O)(CH_2)P(O)Ph_2$, $Ph_2P(O)(CH_2)_2P(O)Ph_2$, or $PhP(O)((CH_2)_2P(O)Ph_2)_2$ as ligands. When $^{113}Cd(AsF_6)_2$ is used as a starting material, however, some of these couplings do become evident. They are given in Table 1, and represent the only new features found for all the phosphine oxide complexes restudied with ^{113}Cd-enrichment. As we have suggested (1), ^2J(Cd—O—P) is significantly smaller in magnitude than ^2J(Cd—E—P) (E = S or Se) for compounds of analogous ligands. The basis for the considerable variation in ^2J(Cd—O—P) shown by the data in Table 1 is not clear, and a more detailed investigation of this phenomenon might be instructive.

For comparison with the ^{113}Cd nmr of complexes with mixed chalcogenide ligands (ref. 2 and see below) we attempted to characterize the mixed ligand complexes $[Cd(OP(C_6H_{11})_3)_x(EP(C_6H_{11})_3)_{4-x}]^{2+}$ (E = S or Se), but both ^{31}P and ^{113}Cd nmr show that ligand distribution in these mixed systems is far from statistical: the parent complexes $[Cd(OP(C_6H_{11})_3)_4]^{2+}$ and $[Cd(EP(C_6H_{11})_3)_4]^{2+}$ were the predominant species at all $OP(C_6H_{11})_3/E(P(C_6H_{11})_3$ ratios when (total L)/Cd = 4. This appears to be an example of the "symbiotic" nature of ligands, i.e. the tendency of ligands of similar "hardness" or "softness" (22) ("class *a*" or "class *b*" behaviour (23)) to "flock" together, noted by Jørgensen (24).

Details of the ^{113}Cd nmr spectra of the various species studied are given in Tables 2–4. In all cases the low temperature spectra had the multiplicity expected on the basis of the known ^{31}P nmr spectra, confirming that slow exchange conditions prevailed. Unfortunately $[Cd(SeP(o\text{-}C_6H_4Me)_3)_4]^{2+}$ and $[Cd(SP(o\text{-}C_6H_4Me)_3)_3]^{2+}$ had solubilities too low to observe the expected ^{113}Cd multiplets: no signal for the former could be obtained in several

TABLE 2. ^{113}Cd nmr spectra of complexes of cadmium with some phosphine oxides, sulfides and selenides in liquid SO_2

Complex	T (K)	δ_{Cd}[a]	Type of spectrum[b]
$[Cd(Ph_2P(O)(CH_2)P(O)Ph_2)_3]^{2+}$	213	58	0
	306	43	0
$[Cd(Ph_2P(O)(CH_2)_2P(O)Ph_2)_3]^{2+}$	203	38	7
$[Cd(Ph_2P(O)(CH_2)_2P(O)Ph_2)_2]^{2+}$(?)	203	52	0
$[Cd(PhP(O)((CH_2)_2P(O)Ph_2)_2)_2]^{2+}$	203	83	3
	306	69	0
$[Cd(OP(C_6H_{11})_3)_4]^{2+}$	213	159	5
	306	140	5
$[Cd(SPPh_3)_4]^{2+}$	203	642	5
$[Cd(SePPh_3)_4]^{2+}$	203	597	5
$[Cd(SP(o\text{-}C_6H_4Me)_3)_4]^{2+}$	198	683	5
$[Cd(SP(o\text{-}C_6H_4Me)_3)_3]^{2+}$	198	530(?)	
$[Cd(SP(o\text{-}C_6H_4Me)_3)_2]^{2+}$	198	242	3
$[Cd(SeP(o\text{-}C_6H_4Me)_3)_3]^{2+}$	198	505	4
$[Cd(SeP(o\text{-}C_6H_4Me)_3)_2]^{2+}$	198	195	3
$[Cd(SP(C_6H_{11})_3)_4]^{2+}$	213	655	5
$[Cd(SP(C_6H_{11})_3)_3]^{2+}$	213	568	4
$[Cd(SeP(C_6H_{11})_3)_4]^{2+}$	213	587	5
$[Cd(SeP(C_6H_{11})_3)_3]^{2+}$	213	515	4

[a] ±1 ppm; relative to the resonance frequency of 4 *M* aqueous $Cd(NO_3)_2$ at 306 K. ($\delta_{0.1M\ Cd(ClO_4)_2} = \delta_{4M\ Cd(NO_3)_2} - 65$ ppm (4)). Shifts to higher frequency than the reference are taken as positive.
[b] 0 = no fine structure observed in ^{113}Cd spectrum; 2 = doublet; 3 = triplet; 4 = quartet; 5 = quintet; 7 = septet.

Can. J. Chem. Downloaded from www.nrcresearchpress.com by 210.87.254.5 on 09/06/12
For personal use only.

TABLE 3. Incremental ^{113}Cd nmr chemical shifts, $\Delta\delta_{Cd}$[a] of $[Cd(SP(C_6H_{11})_2)_x(SeP(C_6H_{11})_3)_{4-x}]^{2+}$ at 213 K in liquid SO_2

x	$\Delta\delta_{Cd}$ (ppm)
0	0.0
1	14.5
2	30.3
3	48.1
4	68.0

[a] $\Delta\delta_{Cd} = \delta_{CdS_xSe_{4-x}} - \delta_{CdSe_4}$. Shifts to increasing frequency are taken as positive.

TABLE 4. Incremental ^{113}Cd nmr chemical shifts, $\Delta\delta_{Cd}$ of $[Cd(SP(C_6H_{11})_3)_x(SeP(C_6H_{11})_3)_{3-x}]^{2+}$ at 213 K in liquid SO_2

x	$\Delta\delta_{Cd}$ (ppm)
0	0.0
1	15.9
2	33.3
3	52.1

[a] $\Delta\delta_{Cd} = \delta_{CdS_xSe_{3-x}} - CdSe_3$. Shifts to increasing frequency are taken as positive.

hours, though ^{31}P nmr (taken in ca. 30 min) showed the presence of the species, and only a weak (but reproducible) signal was seen in the region where the resonance of the latter (known from ^{31}P nmr to be present) was expected.

The data in Table 2 show that for the tetrahedral complexes $[Cd(EP(C_6H_{11})_3)_4]^{2+}$ (E = O, S, or Se), shielding is in the order O $\gg$ Se > S, and the data for $[Cd(EPPh_3)_4]^{2+}$ (E = S or Se) confirm the generality of the shielding pattern Se > S. The cyclohexyl complexes are the first series of analogous, discrete, tetrahedral complexes of first, second, and third row Group VIA donor atoms which have been scrutinized by ^{113}Cd nmr. However, in solid CdS and CdSe, in which the cadmium has a tetrahedral kernel, $\delta_{CdS} > \delta_{CdSe}$ (7). In addition, considerable evidence is available to show that replacement of an oxygen donor to cadmium by a sulfur donor frequently leads to extensive deshielding of the ^{113}Cd resonance (ref. 15 summarizes much of the previous data). Further, the sequence $\delta_{\text{2nd row donor}} > \delta_{\text{3rd row donor}}$ is the same one found for the tetrahalocadmates (11, 13, 14). In addition, $\delta_{\text{3rd row donor}} > \delta_{\text{4th row donor}}$ for CdX_4^{2-} (11, 13); the sequence $\delta_{\text{2nd row donor}} > \delta_{\text{3rd row donor}} > \delta_{\text{4th row donor}}$ has very recently been reported for $\delta_{^{199}Hg}$ of HgX_4^{2-} also (13), as has the sequence $\delta_{\text{2nd row donor}} > \delta_{\text{3rd row donor}}$ for $\delta_{^{199}Hg}$ of $Hg(SCN)_2(EPBu_3)_2$ (25).

The effect of varying the number of R_3PE ligands bound may be deduced by a consideration of results for the series $[Cd(EP(C_6H_{11})_3)_n]^{2+}$ (E = S or Se, n = 3 or 4) and $[Cd(EP(o\text{-}C_6H_4Me)_3)_n]^{2+}$ (E = S, n = 2, 3(?), or 4; E = Se, n = 2 or 3). With the reasonable assumption that, like the resonance of $[Cd(SP(o\text{-}C_6H_4Me)_3)_4]^{2+}$ compared with that of $[Cd(SPPh_3)_4]^{2+}$, the resonance of $[Cd(SeP(o\text{-}C_6H_4Me)_3)_4]^{2+}$ is deshielded from that of $[Cd(SePPh_3)_4]^{2+}$, then for the chalcogenide complexes the sequence $\delta_{4:1} > \delta_{3:1} > \delta_{2:1}$ is found. A similar sequence has been deduced for the series $CdCl_n(aq)^{(2-n)-}$ (9, 11) by an analysis of the variation of δ_{Cd} with Cl^-/Cd^{2+} in rapidly exchanging systems. (In ref. 11, δ_{Cd} for $CdCl_4^{2-}$ in the solid state has been used as a "benchmark".) Such analyses depend on a knowledge of the formation constants of all species present in the various mixtures and therefore it is hardly surprising that there is some doubt about the relative shifts of $CdBr_n(aq)^{(2-n)-}$ (9, 11). Because we have observed slow-exchange spectra here, there is no ambiguity in the shielding sequence found. One ambiguity we have been unable to resolve, however, is the extent to which the solvent and/or counterion are involved in the coordination sphere of $[Cd(EPR_3)_n]^{2+}$ ($n < 4$). We have previously suggested, from the variation of $^2J(^{111}/^{113}Cd—E—P)$ with the number of ligands coordinated, that solvent/anion involvement is slight (2). At the same time it must be recognized that $\delta_{Cd} \approx -230$ ppm for $Cd(AsF_6)_2$ or $Cd(SbF_6)_2$ in SO_2 (16), so replacement of EPR_3 (E = S or Se) by SO_2/AsF_6^- might well lead to extensive shielding of the cadmium resonance. A similar quandary exists with regard to the extent of solvation of the species $CdX_n(aq)^{(2-n)-}$ (X = Cl, Br, or I) (9, 11).

For the complexes $[Cd(EPR_3)_n]^{2+}$ (n = 4, E = S, R = C_6H_{11}, Ph, or $o\text{-}C_6H_4Me$; n = 4, E = Se, R = C_6H_{11} or Ph; n = 3, E = Se, R = C_6H_{11} or $o\text{-}C_6H_4Me$) there is a measurable dependence of δ_{Cd} on R (see Table 2). Surprisingly, the R-dependence of the sulfides and selenides is dissimilar. Within the rather limited series of data available, there is no overlap of chemical shifts for complexes having different E, n combinations, but for complexes of given n, the separation of the ranges for E = S and Se is comparable to the spread observed for constant n and E as R is varied, and it seems probable that for a wider range of R some overlap would occur, meaning that for the type of ligand studied here the cadmium chemical shift may not be interpretable unambiguously in terms of sulfur or selenium coordination. We see, for instance, that the chemical shifts observed for the mixed complexes $[Cd(SP(C_6H_{11})_3)_x(SeP(C_6H_{11})_3)_{4-x}]^{2+}$ (Table 3) fall, in some cases, very close to the range for n = 4, E = S or Se. Presumably overlap or near

Can. J. Chem. Downloaded from www.nrcresearchpress.com by 210.87.254.5 on 09/06/12
For personal use only.

overlap would also occur between the shifts of the mixed complexes $[Cd(SP(C_6H_{11})_3)_x(SeP(C_6H_{11})_3)_{3-x}]^{2+}$ (Table 4) and a wider range of data for $n = 3$, E = S or Se. The incremented shifts within the two series of mixed complexes (Tables 3 and 4) change monotonically but not linearly with x; for the four coordinate species the deviation from linearity at $x = 2$ is ca. 4 ppm, which is comparable to the 3 ppm found by McFarlane *et al.* (26) for the ^{119}Sn chemical shifts of the series $Sn(SMe)_x(SeMe)_{4-x}$. However, the total spread of δ_{Sn} found for the tin complexes (ca. 240 ppm) is much larger than the total spread of δ_{Cd} (68 ppm) for the tetrahedral mixed ligand complexes given in Table 3, and hence the deviation from first order chemical shift additivity is more pronounced for the CdS_xSe_{4-x} kernel studied here. The chemical shift data for both CdS_xSe_{4-x} and CdS_xSe_{3-x} kernels can be correlated empirically using the concept of pairwise additivity (27): the data for CdS_xSe_{4-x} (Table 3) can be reproduced using $\Delta\delta_{S-S} = 11.3$ ppm, $\Delta\delta_{S-Se} = 4.8$ ppm, while the corresponding parameters for CdS_xSe_{3-x} (Table 4) have values 17.4 and 8.0 ppm, respectively.

The cadmium chemical shift range covered by the six-coordinate complexes of chelating polyphosphine oxides is relatively small, 45 ppm at ca. 210 K (Table 1), and separate from the chemical shift of the only unambiguous tetrahedral phosphine oxide complex studied, $[Cd(OP(C_6H_{11})_3]_4^{2+}$. (A lack of fine structure renders structural assignment for $[Cd(Ph_2P(O)(CH_2)_2P(O)Ph_2)_2]^{2+}$ impossible.) Both decrease in chelate ring size (in the two tris(bidentate) complexes) and increase in the number of chelate rings ($[Cd(PH_2P(O)(CH_2)_2P(O)Ph_2)_3]^{2+}$ vs. $[Cd(PhP(O)((CH_2)_2P(O)Ph_2)_2)_2]^{2+}$) appear to cause slight deshielding of cadmium resonance, but the basicity of the donor site(s) must change from ligand to ligand too, and this creates an ambiguity which can only be resolved by further study. Also, more detailed study of a wider range of phosphine oxide complexes will be necessary to ascertain whether overlap of resonance ranges for octahedral and tetrahedral species can occur.

Acknowledgements

This work was made possible by an operating grant from the Natural Sciences and Engineering Research Council of Canada. Mrs. Heather Schroeder of this Department provided expert technical assistance in obtaining some of the nmr spectra.

1. P. A. W. Dean and M. K. Hughes. Can. J. Chem. **58**, 180 (1980).
2. P. A. W. Dean and L. Polensek. Can. J. Chem. **58**, 1627 (1980).
3. G. E. Maciel and M. Borzo. Chem. Commun. 394 (1973).
4. R. J. Kostelnik and A. A. Bother-By. J. Magn. Reson. **14**, 141 (1974).
5. R. A. Haberkorn, L. Que, Jr., W. O. Gillum, R. H. Holm, C. S. Lui, and R. C. Lord. Inorg. Chem. **15**, 2408 (1976).
6. J. D. Kennedy and W. McFarlane. J. Chem. Soc. Perkin Trans. II, 1187 (1977).
7. A. Nolle. Z. Naturforsch. **33a**, 666 (1978).
8. D. B. Bailey, P. D. Ellis, A. D. Cardin, and W. D. Behnke. J. Am. Chem. Soc. **100**, 5236 (1978).
9. T. Drakenberg, N.-O. Björk, and R. Portanova. J. Phys. Chem. **82**, 2423 (1978).
10. T. Maitani and K. T. Suzuki. Inorg. Nucl. Chem. Lett. **15**, 213 (1979).
11. J. J. Ackerman, J. V. Orr, V. J. Bartuska, and G. E. Maciel. J. Am. Chem. Soc. **101**, 341 (1979).
12. E. A. H. Griffith and E. L. Amma. J. Chem. Soc. Chem. Commun. 1013 (1979); Abstr. INOR 17, 181st Am. Chem. Soc. Natl. Meeting, Atlanta, GA, 1981.
13. R. Colton and D. Dakternieks. Aust. J. Chem. **33**, 2405 (1980).
14. R. S. Honkonen and E. L. Amma. Abstr. INOR 144, 181st Am. Chem. Soc. Natl. Meeting, Atlanta, GA, 1981.
15. G. K. Carson, P. A. W. Dean, and M. J. Stillman. Inorg. Chim. Acta, **56**, 59 (1981); G. K. Carson and P. A. W. Dean. Abstr. IN-MP5, 64th Chem. Conf., Chemical Institute of Canada, Halifax, N.S., June 1981.
16. L. C. Damude and P. A. W. Dean. J. Organomet. Chem. **168**, 123 (1979).
17. P. A. W. Dean. Can. J. Chem. **57**, 754 (1979).
18. K. Issleib and A. Brack. Z. Anorg. Allgem. Chem. **277**, 258 (1954).
19. T. Birchall, P. A. W. Dean, and R. J. Gillespie. J. Chem. Soc. A, 1777 (1971).
20. P. A. W. Dean and R. J. Gillespie. J. Am. Chem. Soc. **91**, 7264 (1969) and references therein.
21. M. W. G. de Bolster, C. Boutkan, T. A. van der Knaap, L. van Zweeden, I. E. Kortram, and W. L. Groeneveld. Z. Anorg. Allg. Chem. **443**, 269 (1978) and references therein.
22. R. G. Pearson. J. Am. Chem. Soc. **85**, 3533 (1963).
23. S. Ahrland, J. Chatt, and N. R. Davies. Q. Rev. Chem. Soc. **5**, 265 (1958).
24. C. K. Jørgensen. Inorg. Chem. **3**, 1201 (1964).
25. I. J. Colquhoun and W. McFarlane. J. Chem. Soc. Dalton, 658 (1981).
26. J. D. Kennedy, W. McFarlane, G. S. Pyne, P. L. Clarke, and J. L. Wardell, J. Chem. Soc. Perkin II, 1234 (1975).
27. E. R. Malinowski. J. Am. Chem. Soc. **91**, 4701 (1969) and references therein.

Reaction of hydrogen atoms with diethylsulfide

MBANEFO MBONU EKWENCHI, IMRE SAFARIK, AND OTTO PETER STRAUSZ
Department of Chemistry, University of Alberta, Edmonton, Alta, Canada T6G 2G2

Received March 2, 1981

This paper is dedicated to Professor W. E. Harris on the occasion of his retirement from the University of Alberta

MBANEFO MBONU EKWENCHI, IMRE SAFARIK, and OTTO PETER STRAUSZ. Can. J. Chem. **59**, 3226 (1981).

In the reactions of H atoms, generated by the $Hg(^3P_1)$-sensitized decomposition of H_2, with $C_2H_5SC_2H_5$ the primary reaction has been established to be $H + C_2H_5SC_2H_5 \xrightarrow{[1]} C_2H_5SH + C_2H_5$ with $k_1 = (4.7 \pm 0.9) \times 10^{13} \exp[-(3797 \pm 152)/RT]$ cm^3 mol^{-1} s^{-1} relative to the rate constant of the $H + C_2H_4 \rightarrow C_2H_5$ reaction. The mechanism postulated explains adequately all the experimental observations. The entropy of activation for the primary reaction, −22.1 eu is close to the value obtained for the $H + CH_3SCH_3$ reaction, suggesting a transition state with similar structure. H atoms do not abstract hydrogen from diethylsulfide, but the ethyl radicals from reaction [1] do with a rate coefficient of $k = (7.4 \pm 0.5) \times 10^{13} \exp[-(6860 \pm 98)/RT]$ cm^3 mol^{-1} s^{-1}.

MBANEFO MBONU EKWENCHI, IMRE SAFARIK et OTTO PETER STRAUSZ. Can. J. Chem. **59**, 3226 (1981).

Les atomes d'hydrogène produits par la décomposition du H_2 sensibilisée par le $Hg(^3P_1)$ réagissent avec le $C_2H_5SC_2H_5$; on a établi que la réaction primaire est la suivante $H + C_2H_5SC_2H_5 \xrightarrow{[1]} C_2H_5SH + C_2H_5$ avec $k_1 = (4{,}7 \pm 0{,}9) \times 10^{13} \exp[-(3797 \pm 152)/RT]$ cm^3 mol^{-1} s^{-1} par rapport à la constante de vitesse de la réaction $H + C_2H_4$. Le mécanisme proposé explique adéquatement tous les faits expérimentaux. La valeur de l'entropie d'activation de la réaction primaire, −22,1 ue, est près de celle obtenue pour la réaction de $H + CH_3SCH_3$; ceci suggère un état de transition ayant une structure similaire. Les atomes d'hydrogène n'enlèvent pas d'hydrogène du sulfure de diéthyle, mais les radicaux éthyles produits dans la réaction 1, enlèvent l'hydrogène avec un coefficient de vitesse $k = (7{,}4 \pm 0{,}5) \times 10^{13} \exp[-(6860 \pm 98)/RT]$ cm^3 mol^{-1} s^{-1}.

[Traduit par le journal]

In the course of our continuing studies on the gas phase reactions of hydrogen atoms with organosulfur compounds, the H + COS (1) and the H + thiirane (2) reactions have been first examined. The common feature that was found for these reactions is that the sulfur atom is abstracted by the hydrogen atom in a concerted single step attack on the substrate to yield SH. Further studies have revealed that in the reactions $H + CH_3SCH_3$ (3), $H + CH_3SSCH_3$ (4), and $H + C_2H_5SSC_2H_5$ (5) the hydrogen atom also attacks exclusively at the sulfur atom, forming the corresponding thiol in a metathetical displacement reaction. With thiols the occurrence of an analogous step, $H + RSH \rightarrow R + H_2S$, had been established earlier by Pryor and Olson (6) in the liquid phase and by Hori, Nishino, and Amano (7) in the gas phase. This step proceeds parallel and in competition with the hydrogen abstraction step $H + RSH \rightarrow H_2 + RS$.

In a continuation of our studies we have investigated the $H + C_2H_5SC_2H_5$ reaction in order to establish the primary processes and to determine whether the previously derived mechanism could be extended to this system. We wish to present here the results of this investigation.

Experimental

The apparatus, the general vacuum technique, the analytical technique, and the actinometric determinations were similar to those employed in the previous studies (4, 5). Hydrogen atoms were generated by the mercury-photosensitized decomposition of H_2; the mean value of the light intensity absorbed was 0.012 μeinstein min^{-1}.

Purification procedures for H_2 (Airco) and C_2H_4 (Matheson) were the same as before (4, 5). Diethylsulfide (Eastman) was purified by gc using a 10 ft 10% tricresylphosphate on Chromosorb W column operated between 60 and 65°C using helium as the carrier gas. The purity was always checked by gc prior to each experiment.

The major reaction products were identified by comparison of gc retention times and mass spectrometric analysis of the gc effluents with those of authentic samples.

In these experiments the fraction volatile at −160°C, consisting of C_2H_4 and C_2H_6, was analyzed on an 8 ft poropak N column at 59°C, while the fraction volatile at −130°C, consisting of C_4H_{10} and C_2H_5SH, on a 10 ft tricresylphosphate column at 25°C. The remaining condensable fraction at −130°C was analyzed by gc on the tricresylphosphate column by temperature programming (5° min^{-1}) to 120°C. In order to ascertain whether methane was formed in the reaction, the hydrogen fraction volatile at −210°C was passed through a 3 Å molecular sieve column kept at −196°C. After pumping off the hydrogen through the column, the column was heated to 100°C and the evolved gas was analyzed on a 10 ft 3 Å molecular sieve column.

Results

When hydrogen atoms are generated by the $Hg(^3P_1)$-sensitized decomposition of H_2 in the presence of $C_2H_5SC_2H_5$, the observed products are C_2H_5SH, C_2H_4, C_2H_6, C_4H_{10}, 4-methyl-3-thiahexane (MTH), 4,5-dimethyl-3,6-dithiaoctane (DMDTO), and some polymer at longer illumination times. The extent of quenching of the excited mercury atoms by $C_2H_5SC_2H_5$ was estimated to be

0008-4042/81/233226-06$01.00/0
©1981 National Research Council of Canada/Conseil national de recherches du Canada

Can. J. Chem. Downloaded from www.nrcresearchpress.com by 210.87.254.105 on 09/06/12
For personal use only.

TABLE 1. Effect of $P(C_2H_5SC_2H_5)$ on the product quantum yields[a]

$P(C_2H_5SC_2H_5)$ (Torr)	$\phi(C_2H_6)$	$\phi(C_2H_4)$	$\phi(C_4H_{10})$	$\phi(C_2H_5SH)$
1.00	0.421±0.005	0.0625±0.0030	0.276±0.006	0.987±0.03(2)[b]
10.00	0.630±0.004	0.0982±0.0025	0.407±0.004	1.53±0.01(2)
20.00	[c]	[c]	[c]	1.53±0.01(2)
30.00	0.630±0.005	0.0980±0.0021	0.408±0.005	1.53±0.02(2)

[a] Temperature = 25–26°C; $P(H_2)$ = 580 ± 10 Torr; photolysis time = 45 min; I_a (μeinstein min^{-1}) × 10^2 = 1.06.
[b] Number of experiments.
[c] Not determined.

TABLE 2. Effect of temperature and substrate pressure on the quantum yields of products[a]

Temperature (°C)	$P(C_2H_5SC_2H_5)$ (Torr)	φ					
		C_2H_6	C_2H_4	C_4H_{10}	MTH	C_2H_5SH	Σ[b]
170	31.6	1.51	0.114	0.197	~0	2.01	2.02
170	20.0	1.49	0.107	0.197	~0	2.00	1.99
167	10.0	1.45	0.0982	0.236	~0	2.01	2.02
150	20.0	1.19	0.110	0.291	0.136	2.01	2.02
130	20.0	0.984	0.107	0.321	0.272	2.01	2.01
110	20.0	0.652	0.104	0.363	0.527	2.01	2.01
25	20.0	0.630	0.0982	0.407	~0	1.53	1.54

[a] $P(H_2)$ = 580±10 Torr; I_a (μeinstein min^{-1}) × 10^2 = 1.06; photolysis time = 45 min; V = 200 cm^3.
[b] $\Sigma = \phi(C_2H_6) + \phi(C_2H_4) + 2\phi(C_4H_{10}) + \phi(MTH)$.

Can. J. Chem. Downloaded from www.nrcresearchpress.com by 210.87.254.105 on 09/06/12
For personal use only.

less than 5% in all cases. Control experiments in the range 25–188°C showed that $C_2H_5SC_2H_5$ was thermally stable.

In Table 1, the quantum yields of C_2H_5SH, C_2H_4, C_2H_6 and C_4H_{10} are presented as a function of $C_2H_5SC_2H_5$ pressure from 1 to 30 Torr. As seen, they all increase at low pressures with increasing substrate pressure but level off and become constant above 10 Torr $C_2H_5SC_2H_5$.

$\phi(C_2H_5SH)$ was determined at various time intervals at 25°C and at 20 Torr $C_2H_5SC_2H_5$, and was found to be independent of the time of illumination; therefore C_2H_5SH must be a primary product.

Next the effect of temperature on the product yields was investigated in the range 25 to 170°C and the results are given in Table 2. The yield of ethane increases with increasing temperature, while that of butane decreases; the ethylene yield, on the other hand, shows only moderate temperature dependence. $\phi(C_2H_5SH)$ first increases with increasing temperature but at 110°C reaches the value of 2.0 and from there on remains constant. The yield of MTH goes through a maximum at 110°C, but is negligibly small at 25 and 167°C.

Finally, in order to determine the rate parameters, temperature studies of the H + $C_2H_5SC_2H_5$ reaction have also been carried out with added ethylene, utilizing the addition reaction H + C_2H_4 → C_2H_5 as reference, for which reliable kinetic data are available. In the presence of ethylene no additional products were detected, but polymer formation was greatly reduced. The quantum yields of C_2H_5SH obtained in the presence of varying amounts of ethylene at different temperatures are listed in Table 3. As seen $\phi(C_2H_5SH)$ decreases with increasing ethylene pressure owing to the competitive scavenging of hydrogen atoms by the ethylene.

Discussion

The yield of C_2H_5SH is directly proportional to the exposure time, indicating that C_2H_5SH is a primary product. Therefore the initial step, by analogy to the H + CH_3SCH_3 reaction (3), is postulated to be

[1] $H + C_2H_5SC_2H_5 \rightarrow C_2H_5SH + C_2H_5$

followed by combination and disproportionation of the C_2H_5 radicals:

[2] $2C_2H_5 \rightarrow C_2H_6 + C_2H_4$

[3] $\rightarrow C_4H_{10}$

For C_2H_5 the accepted value for the k_d/k_c ratio is 0.14 (8). Assuming that C_2H_4 is formed exclusively in reaction [2] the data in Table 2 give k_2/k_3 = 0.24 at 25°C and 0.58 at 170°C. The room temperature value is rather high and the value at 170°C is at variance with the reported (9) very small temperature dependence of k_d/k_c for ethyl radicals.

$\phi(C_2H_6)$ is about an order of magnitude greater than $\phi(C_2H_4)$, indicating the existence of an efficient source of C_2H_6 in addition to reaction [2]. One of these additional C_2H_6-producing reactions

Can. J. Chem. Downloaded from www.nrcresearchpress.com by 210.87.254.105 on 09/06/12
For personal use only.

TABLE 3. Effect of C_2H_4 pressure and temperature on $\phi(C_2H_5SH)$[a]

$P(C_2H_4)$ (Torr)	$[C_2H_4]/[C_2H_5SC_2H_5]$	$\phi(C_2H_5SH)$	$1/\phi(C_2H_5SH)$
	25°C		
0.00	0.000	1.53	0.654
0.50	0.050	1.15	0.870
1.00	0.100	0.917	1.09
1.50	0.150	0.769	1.30
2.00	0.200	0.658	1.52
	96°C		
0.00	0.000	2.00	0.500
0.50	0.050	1.49	0.671
1.00	0.100	1.32	0.758
1.50	0.150	1.11	0.901
2.00	0.200	1.00	1.00
	132°C		
0.00	0.000	2.03	0.493
0.50	0.050	1.63	0.614
1.00	0.100	1.39	0.719
1.50	0.150	1.26	0.794
2.00	0.200	1.07	0.935
2.00	0.200	1.12	0.893
	170°C		
0.00	0.000	2.00	0.500
0.50	0.050	1.72	0.581
1.00	0.100	1.51	0.662
1.20	0.120	1.44	0.694
1.50	0.150	1.36	0.735
2.00	0.200	1.22	0.820
	188°C		
0.00	0.000	2.01	0.498
1.00	0.100	1.62	0.618
2.00	0.200	1.24	0.806
3.00	0.300	1.04	0.962

[a] $P(H_2) = 580$ Torr; $P(C_2H_5SC_2H_5) = 10.0$ Torr; I_a (μeinstein min^{-1}) × $10^2 = 1.06$; photolysis time = 45 min.

must be hydrogen abstraction from the substrate:

[4] $C_2H_5 + C_2H_5SC_2H_5 \rightarrow C_2H_6 + CH_3\dot{C}HSC_2H_5$

The site of the abstraction is most probably at the methylene moiety since the C—H bond here is weaker (~ 92 kcal mol^{-1}) than in the methyl group (98 kcal mol^{-1}), and moreover, MTH and DMDTO were identified among the products but the corresponding products from the expected reactions of the $CH_3CH_2SCH_2CH_2$ radical were not. The reaction sequence is completed by the combination and disproportionation reactions [5] to [9]:

[5] $C_2H_5 + CH_3\dot{C}HSC_2H_5 \rightarrow C_2H_6 + CH_2{=}CHSC_2H_5$

[6] $\rightarrow C_2H_4 + C_2H_5SC_2H_5$

[7] $\rightarrow C_2H_5\underset{\displaystyle CH_3}{\underset{|}{C}}HSC_2H_5$(MTH)

[8] $2CH_3\dot{C}HSC_2H_5 \rightarrow C_2H_5SCH(CH_3)CH(CH_3)SC_2H_5$(DMDTO)

[9] $\rightarrow CH_2{=}CHSC_2H_5 + C_2H_5SC_2H_5$

The formation of C_2H_4 in reaction [6] explains the high values obtained for k_2/k_3 from the uncorrected data in Table 2.

Ethylvinylthioether was not identified as a product, probably because reactions [5] and [9] are relatively slow. However, even if it were formed in small quantities, gc analysis for ethylvinylthioether in a mixture containing a large excess of $C_2H_5SC_2H_5$ would be difficult since the two compounds would probably have similar elution times.

From the above mechanism the following relationship for the product quantum yields can be derived:

[10] $\phi(C_2H_5SH) = \phi(C_2H_6) + \phi(C_2H_4) + 2\phi(C_4H_{10}) + \phi(MTH)$

The sums of the quantum yields on the right hand side at various temperatures are listed in Table 2, and are in very good agreement with $\phi(C_2H_5SH)$, providing further support for the postulated primary step, reaction [1].

Although H atoms are completely scavenged in the system at 10 Torr $C_2H_5SC_2H_5$ (Table 1), the data in Table 2 show that $\phi(C_2H_5SH)$ reaches its maximum value of 2.0 only at 110°C. Hence at room temperature the intervention of H-scavenging reactions in the mechanism must be considered.

A number of reactions may come to mind, of which the only relevant one in the present context is hydrogen abstraction from the substrate,

[11] $H + C_2H_5SC_2H_5 \rightarrow H_2 + CH_3\dot{C}HSC_2H_5$

To be important at 25°C but unoperative at 110°C, this should then have an activation energy considerably smaller than that of reaction [1], which is 3.6 kcal/mol (*vide infra*). In fact the activation energy of the abstraction reaction should have a negative value of ~ −9 kcal/mol which cannot be the case. This is in contrast to the $H + C_2H_5OC_2H_5$ reaction where hydrogen abstraction is the only major reaction.

Therefore it appears that at 25°C H atoms are lost in reactions such as

$$H + CH_3\dot{C}HSC_2H_5 \rightarrow C_2H_5SC_2H_5$$
$$H + C_2H_4 \rightarrow C_2H_5$$
$$H + CH_2{=}CHSC_2H_5 \rightarrow CH_3\dot{C}HSC_2H_5$$
$$H + C_2H_5SH \rightarrow C_2H_5S + H_2$$
$$H + C_2H_5SH \rightarrow C_2H_5 + H_2S, \text{ etc.}$$

which all have activation energies ≤3.6 kcal/mol. The combination reaction with ethyl radicals

$$H + C_2H_5 \rightarrow C_2H_6$$

however, is too slow to have any significance.

The Arrhenius parameters for the hydrogen

Can. J. Chem. Downloaded from www.nrcresearchpress.com by 210.87.254.105 on 09/06/12
For personal use only.

abstraction of ethyl radicals [4] can be determined from the data on the basis of the above mechanism.

The total rate of ethane formation can be expressed as

[12] $R_{C_2H_6} = R_2 + R_4 + R_5$

Similarly, the total rate of ethylene formation is

[13] $R_{C_2H_4} = R_2 + R_6$

and assuming that $R_5 = R_6$

[14] $R_{C_2H_6} = R_{C_2H_4} + R_4$

Thus the values of R_4 can be calculated directly from the quantum yields of C_2H_6 and C_2H_4 listed in Table 2. The observed and derived values of R_3 and R_4 over the temperature range 25 to 170°C are listed in Table 4 together with the ratio $R_4/R_3^{1/2}$.

The Arrhenius plot of $R_4/R_3^{1/2}$, shown in Fig. 1, is linear. It is to be noted that the value at 25°C is a good fit to the straight line, lending support to the mechanism. From the slope and intercept, and taking $A_3 = 1.0 \times 10^{13}$ cm^3 mol^{-1} s^{-1} and $E_3 = 0$ kcal mol^{-1} (10), the value of k_4 is calculated to be $(7.4 \pm 0.5) \times 10^{13} \exp[-(6860 \pm 98)/RT]$ cm^3 mol^{-1} s^{-1}.

The value of E_4 seems reasonable when compared to those reported for other similar reactions, collected in Table 5. The somewhat lower activation energy for the diethylsulfide than for the ether reaction may be a consequence of the higher efficiency of sulfur to stabilize the incipient radical through electron-releasing conjugative effects (14):

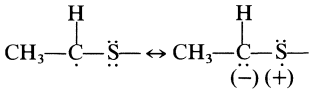

Our measured value of E_4 for the $C_2H_5 + C_2H_5SC_2H_5$ reaction is twice as high as that derived by Knight and Smith (15) from the photolysis of ethylsulfide vapor at 253.7 nm:

[15] $C_2H_5SC_2H_5 \xrightarrow{h\nu} C_2H_5S + C_2H_5$

However, reaction [15] is exothermic by 41 kcal mol^{-1} at 253.7 nm and the ethyl radicals are formed with about 19 kcal excess energy. The low activation energy determined in this system is probably due to the involvement of "hot" ethyl radicals.

E_a for the abstraction reaction $C_2H_5S + C_2H_5SSC_2H_5$ is 3.6 kcal mol^{-1} and seems rather low in comparison to the other activation energies listed in Table 5. It was calculated (5) on the assumption that $k_d/k_c = 0.13$ for the C_2H_5S radical but this value is probably low and using a higher value would increase the activation energy correspondingly.

In the presence of ethylene, reaction [1] competes with reaction [16]:

[16] $H + C_2H_4 \rightarrow C_2H_5$

In regard to the fate of the ethyl radicals produced in [16] the addition of C_2H_5 radicals to ethylene

[17] $C_2H_5 + C_2H_4 \rightarrow C_4H_9$

is a relatively slow process ($\log k_{17} = 8.17 - 7560/2.303RT$) (17) compared to the other reactions involving C_2H_5; furthermore, butene, the disproportionation product of C_4H_9 radicals

[18] $2C_4H_9 \rightarrow C_4H_8 + C_4H_{10}$

was demonstrably absent. Also the polymerization reaction

[19] $C_4H_9 + nC_2H_4 \xrightarrow{CH_3\dot{C}HSC_2H_5}$ polymer

could not be important since polymer formation was greatly reduced in the presence of ethylene.

Simple steady-state treatment yields the following expression:

[20] $$\phi(C_2H_5SH)^{-1} = \tfrac{1}{2}\left(1 + \alpha + \frac{k_{16}[C_2H_4]}{k_1[C_2H_5SC_2H_5]}\right)$$

where $\alpha = R_{loss}/R_1$. Using the data from Table 3, eq. [20] is plotted at different temperatures in Fig.

TABLE 4. Effect of temperature on $R_{C_2H_6}/R_{C_4H_{10}}^{1/2}$ [a]

Temperature (°C)	Rates, μmol min^{-1}		
	$C_2H_6(R_4)$	$C_4H_{10}(R_3) \times 10^3$	$R_4/R_3^{1/2}$
25	0.000463	4.32	0.00706
110	0.00598	3.85	0.0964
130	0.00930	3.40	0.159
150	0.0115	3.08	0.207
167	0.0143	2.50	0.286
170	0.0146	2.09	0.319
170	0.0148	2.09	0.324

[a] $P(H_2) = 580 \pm 10$ Torr; I_a (μeinstein min^{-1}) $\times 10^2 = 1.06$; photolysis time = 45 min; $[C_2H_5SC_2H_5] = 9.48 \times 10^{-4}$ mol L^{-1}

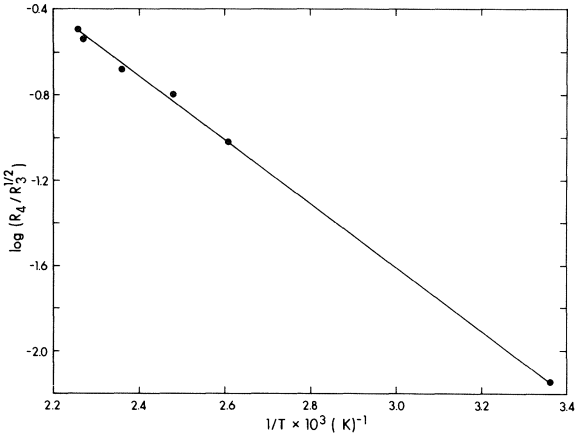

FIG. 1. Arrhenius plot of $R_4/R_3^{1/2}$ versus $1/T$.

TABLE 5. Activation energies for methylene hydrogen abstraction by C_2H_5 radicals

Reaction	E_a (kcal mol^{-1})	Temperature range (°C)	Method	Ref.
$C_2H_5 + C_2H_5OC_2H_5 \rightarrow C_2H_6 + CH_3\dot{C}HOC_2H_5$	9.0	87–218	γ-Radiolysis	11
$C_2H_5 + C_2H_5COC_2H_5 \rightarrow C_2H_6 + CH_3\dot{C}HCOC_2H_5$	7.3	25–225	Photolysis	12
$C_2H_5 + C_2H_5NNC_2H_5 \rightarrow C_2H_6 + CH_3\dot{C}HNNC_2H_5$	7.5	30–171	Photolysis	13
$C_2H_5 + C_2H_5SC_2H_5 \rightarrow C_2H_6 + CH_3\dot{C}HSC_2H_5$	3.4	30–90	Photolysis	15
$C_2H_5 + C_2H_5SC_2H_5 \rightarrow C_2H_6 + CH_3\dot{C}HSC_2H_5$	6.9	25–170	Hg* sensitization	This work
$C_2H_5 + CH_3CH_2CH_2CH_2CH_2CH_3 \rightarrow C_2H_6 + CH_3\dot{C}H(CH_2)_3CH_3$	10.1	87–252	Photolysis	16
$C_2H_5S + C_2H_5SSC_2H_5 \rightarrow C_2H_5SH + CH_3\dot{C}HSSC_2H_5$	3.6	25–145	Hg* sensitization	5

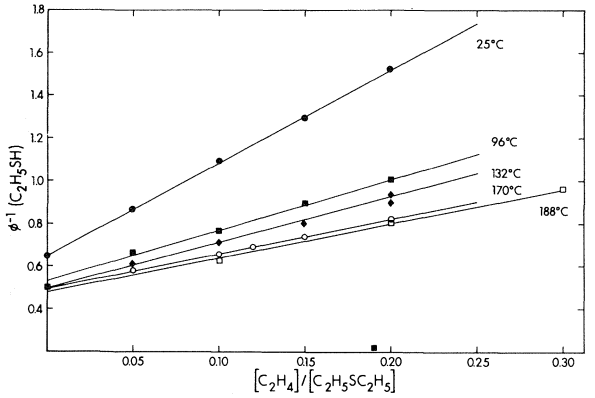

FIG. 2. $\phi(C_2H_5SH)^{-1}$ versus $[C_2H_4]/[C_2H_5SC_2H_5]$ at different temperatures.

2. The plots are all linear within the temperature range examined; the intercepts and slopes of the lines are listed in Table 6. The plots in Fig. 2 have an intercept of about 0.5 in the range 96 to 188°C indicating that for $T \geq 96$°C α is close to zero. At 25°C, on the other hand, the intercept is 0.654 which gives $\alpha = 0.3$, in agreement with the experimental value obtained at room temperature:

$$(2 - \phi(1))/\phi(1) = 0.47/1.53 = 0.31$$

The slopes of the straight lines in Fig. 2 are equal to $k_{16}/2k_1$ at the corresponding temperatures. When the k_{16}/k_1 ratios, listed in Table 6, are plotted in the Arrhenius form (Fig. 3) a good straight line is obtained from which

$$\log (k_{16}/k_1) = -(0.332 \pm 0.040) + (1731 \pm 69)/2.303RT$$

Using the value of Lee *et al.* (18) for the limiting high pressure rate constant of reaction [16],

$$k_{16} = (2.2 \pm 0.4) \times 10^{13} \exp[-(2066 \pm 83)/RT] \text{ cm}^3 \text{ mol}^{-1} \text{ s}^{-1}$$

TABLE 6. Slopes and intercepts of the plots in Fig. 2[a]

T (°C)	Slope	Intercept	k_{16}/k_1
25	4.32±0.02	0.654±0.002	8.64±0.02
96	2.46±0.14	0.520±0.018	4.92±0.14
132	2.05±0.10	0.502±0.014	4.10±0.10
170	1.59±0.02	0.501±0.002	3.18±0.01
188	1.58±0.09	0.484±0.017	3.16±0.09

[a] The errors are standard deviations.

the absolute rate constant for reaction [1] is

$$k_1 = (4.7 \pm 0.9) \times 10^{13} \exp[-(3797 \pm 152)/RT] \text{ cm}^3 \text{ mol}^{-1} \text{ s}^{-1}$$

The experimental entropy of activation calculated from the A factor is −22.1 eu for the standard state of 1 atm. This value is very close to $\Delta S^{\neq} = -24.1$ eu obtained for the $H + CH_3SCH_3$ reaction (3), suggesting that the transition states in the two reactions have a similar structure. Using Benson's method (19) the experimental activation entropy can indeed be reproduced by assuming a transition state similar to that proposed for the $H + CH_3SCH_3$ reaction (3):

$$H + C_2H_5SC_2H_5 \rightarrow [C_2H_5—\underset{\vdots}{\underset{H}{S}}\cdots C_2H_5]^{\neq} \rightarrow C_2H_5 + C_2H_5SH$$

which involves an initial interaction between the H atom and the non-bonding $3p$ orbital of the sulfur atom.

According to Benson's method (19)

$$\begin{aligned}\Delta S^{\neq} &= S_0{}^{\neq} - S_0(C_2H_5SC_2H_5) - S_0(H)\\ &= S_0(C_2H_5SC_2H_5) + R \ln 2 + x - S_0(C_2H_5SC_2H_5) - S_0(H)\\ &= R \ln 2 + x - S_0(H) = 1.4 + x - 27.4\\ &= -26 + x\end{aligned}$$

$$x = 26 - 22.1 = 3.9 \text{ eu}$$

The 3.9 eu could reasonably be attributed to

Can. J. Chem. Downloaded from www.nrcresearchpress.com by 210.87.254.105 on 09/06/12
For personal use only.

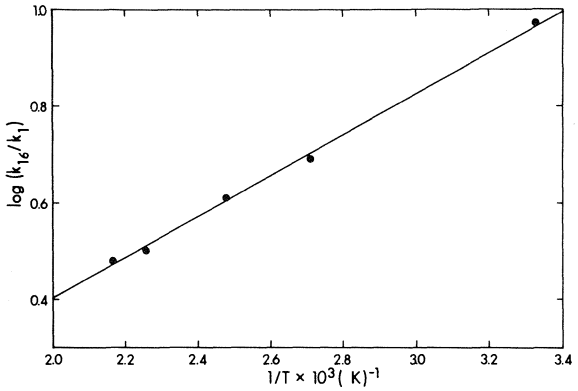

FIG. 3. Arrhenius plot of k_{16}/k_1 versus $1/T$.

contributions from the two new vibrational modes formed by the S···H bond in the activated complex.

The higher activation energy for reaction [1] is opposite to the trend in the C—S bond energy: $D(CH_3—SCH_3) = 77 \pm 1.5$ kcal mol^{-1} and $D(C_2H_5—SC_2H_5) = 74 \pm 2$ kcal mol^{-1} (20). This may be a consequence of the intramolecular H-bond formed between the non-bonding $3p$ orbital of the S atom and the H atoms of the alkyl groups in the molecule. A stronger H-bond in diethylsulfide as compared to dimethylsulfide could have a larger influence on the activation energy than the small difference in the C—S bond dissociation energies since the H-bonding would be weakened or broken in the activated complex.

It is interesting to note that although the methylene moieties in $C_2H_5SC_2H_5$ are expected to be rather amenable to hydrogen abstraction, no such reaction occurs. Instead, the attack takes place exclusively on the sulfur atom. This is in contrast to the reaction of hydrogen atoms with diethylether where the primary step is hydrogen abstraction (21):

[21] $H + C_2H_5OC_2H_5 \rightarrow H_2 + CH_3\dot{C}HOC_2H_5$

The rate coefficient reported (21) for reaction [21] is

$$k_{21} = (7.4 \pm 3.6) \times 10^{12} \exp[-(3240 \pm 100)/RT] \text{ cm}^3 \text{ mol}^{-1} \text{ s}^{-1}$$

A similar value for the rate constant of the hydrogen abstraction reaction from $C_2H_5SC_2H_5$, reaction [11], would result in a strong competition with the primary substitution reaction at room temperature. The non-occurrence of [11] is due to the shadowing effect of the protruding non-bonding p orbital of the sulfur atom on the α hydrogens reducing the rate constant k_{11} to a value considerably lower than k_{21}.

Acknowledgments

We thank the Natural Sciences and Engineering Research Council of Canada and the Canada–Alberta Energy Resources Research Fund for financial support.

1. S. TSUNASHIMA, T. YOKOTA, I. SAFARIK, H. E. GUNNING, and O. P. STRAUSZ. J. Phys. Chem. **79**, 775 (1975).
2. T. YOKOTA, M. G. AHMED, I. SAFARIK, O. P. STRAUSZ, and H. E. GUNNING. J. Phys. Chem. **79**, 1759 (1975).
3. T. YOKOTA and O. P. STRAUSZ. J. Phys. Chem. **83**, 3196 (1979).
4. M. M. EKWENCHI, A. JODHAN, and O. P. STRAUSZ. Int. J. Chem. Kinet. **12**, 431 (1980).
5. M. M. EKWENCHI, I. SAFARIK, and O. P. STRAUSZ. Int. J. Chem. Kinet. **13**, 799 (1981).
6. W. A. PRYOR and E. G. OLSEN. J. Am. Chem. Soc. **100**, 2852 (1978).
7. O. HORI, J. NISHINO, and A. AMANO. Int. J. Chem. Kinet. **10**, 1043 (1978).
8. K. J. IVIN and E. W. R. STEACIE. Proc. R. Soc. **208**A, 25 (1951).
9. J. A. KERR. *In* Free radicals. Vol. 1. *Edited by* J. K. Kochi. J. Wiley and Sons, New York, NY. 1973. pp. 14–22.
10. H. ADACHI, N. BASCO, and D. G. L. JAMES. Int. J. Chem. Kinet. **11**, 995 (1979).
11. K. M. BANSAL and G. R. FREEMAN. J. Am. Chem. Soc. **88**, 4326 (1966).
12. K. O. KUTSCHKE, M. H. J. WIJEN, and E. W. R. STEACIE. J. Am. Chem. Soc. **74**, 714 (1952).
13. P. AUSLOOS and E. W. R. STEACIE. Bull. Soc. Chim. Belg. **63**, 87 (1954).
14. W. TAGAKI. *In* Organic chemistry of sulfur. *Edited by* S. Oae. Plenum Press, New York. NY. 1977. p. 284.
15. C. S. SMITH and A. R. KNIGHT. Can. J. Chem. **51**, 780 (1973).
16. P. J. BODDY and E. W. R. STEACIE. Can. J. Chem. **39**, 13 (1961).
17. K. W. WATKINS and L. A. O'DEEN. J. Phys. Chem. **73**, 4094 (1969).
18. J. H. LEE, J. V. MICHAEL, W. A. PAYNE, and L. J. STIEF. J. Chem. Phys. **88**, 1817 (1978).
19. S. W. BENSON. Thermochemical kinetics. 2nd ed. Wiley, New York, NY. 1976.
20. S. W. BENSON. Chem. Rev. **78**, 23 (1978).
21. C. FAUBEL, K. HOYERMAN, E. STRÖFER, and H. GG. WAGNER. Ber. Bunsenges. Phys. Chem. **83**, 532 (1979).

Can. J. Chem. Downloaded from www.nrcresearchpress.com by 210.87.254.105 on 09/06/12
For personal use only.

Conformational aspects of L-histidine

R. RAMANI AND RUSSELL J. BOYD[1]

Department of Chemistry, Dalhousie University, Halifax, N.S., Canada B3H 4J3

Received June 15, 1981

R. RAMANI and RUSSELL J. BOYD. Can. J. Chem. **59**, 3232 (1981).

Ab initio molecular orbital (MO) calculations at the STO-3G level are reported for selected conformations of L-histidine. The minimum energy conformations are chosen on the basis of force-field calculations on the χ^1–$\chi^{2,1}$ plane of the side chain of histidine. The MO relative energies are observed to be substantially larger than the force-field values. With one exception both theoretical methods are consistent with the results of X-ray diffraction studies on L-histidine. The exception occurs in the case of the force-field calculations which suggest that the (60,80) conformation may be accessible contrary to the MO results and experiment. And finally the *ab initio* charge distribution is used to account for the fact that the $N^{\varepsilon 2}$ atom is always protonated in the crystal structures of L-histidine.

R. RAMANI et RUSSELL J. BOYD. Can. J. Chem. **59**, 3232 (1981).

On rapporte les calculs ab initio d'orbitales moléculaires du niveau STO-3G pour des conformations choisies de la L-histidine. On a choisi les conformations à énergie minimum en se basant sur les calculs du champ de force dans le plan χ^1–$\chi^{2,1}$ de la chaîne latérale de l'histidine. On a observé que les énergies relatives de l'O.M. sont substantiellement plus élevées que les valeurs du champ de force. À une exception, près les deux méthodes théoriques sont en accord avec les résultats des études de diffraction de rayons X sur la L-histidine. L'exception apparaît dans le cas des calculs du champ de force, ce qui suggère que la conformation (60,80) peut être accessible contrairement à l'expérience et aux résultats des OM. Finalement, on a utilisé la distribution de charge ab initio pour tenir compte du fait que l'atome $N^{\varepsilon 2}$ est toujours protoné dans les structures cristallines de la L-histidine.

[Traduit par le journal]

Introduction

Histidine, a functional amino acid, is well known as a proton donor, proton acceptor, and a nucleophilic reagent. The significance of histidine in protein chemistry is associated with the frequency with which it occurs at the active site of enzymes. It is known that histidine is directly involved in the proteolytic mechanisms of enzymes such as papain, subtilisin, chymotrypsin, and trypsin and in the coordination of zinc in zinc insulin (1). This is due to the facile transfer of protons to and from the nitrogen atoms in the imidazole ring of the side chain (Fig. 1).

In order to relate the conformation of histidine to its reactivity, several X-ray crystallographic studies have been reported (2). Some representative results are summarized in Table 1. In this paper we present an extensive conformational study of L-histidine. Force-field calculations are first used to determine the preferred conformations and then *ab initio* molecular orbital (MO) calculations are carried out for the minimum energy conformations. The MO relative energies are compared with the force-field values, and the theoretical conformations are compared with the results of X-ray diffraction studies on L-histidine. And finally the *ab initio* charge distribution is used to compute the electrostatic potential in the plane of the imidazole ring for the two tautomeric forms of histidine.

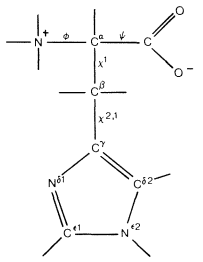

FIG. 1. Structural formula of histidine in the zwitterionic form.

Method

The requirements for computer time were reduced by use of force field calculations for the initial conformational analysis of L-histidine. The nonbonded interactions due to van der Waals forces were treated by use of the Lennard–Jones (6–12) potential function for which standard parameters were adopted (3). For the electrostatic interactions, partial charges were taken from the MO calculations. Torsional barriers to rotation about single bonds were modeled by assuming a threefold barrier for the χ^1 variation (see Fig. 1) while the barrier to variation of $\chi^{2,1}$ was assumed to be zero (3).

Standard single determinant *ab initio* MO theory, according to which closed shells are treated by the spin restricted Hartree–Fock (RHF) procedure (4), was used in this work. All calculations were carried out on a Control Data Cyber 170-720 system by use

[1]To whom all correspondence should be addressed.

0008-4042/81/233232-05$01.00/0

©1981 National Research Council of Canada/Conseil national de recherches du Canada

Can. J. Chem. Downloaded from www.nrcresearchpress.com by 210.87.254.6 on 09/06/12
For personal use only.

TABLE 1. Observed conformational parameters of histidine[a]

Compound	ψ	χ^1	$\chi^{2,1}$	Site of protonation	Reference
L-His ($P2_1$)	−27	303	58	$N^{\varepsilon 2}$	12
L-His ($P2_12_12_1$)	−26	301	57	$N^{\varepsilon 2}$	13
DL-His	−10	273	292	$N^{\varepsilon 2}$	14
L-N-Acetyl His·H_2O					8
Mol (1)	−19	80	284	$N^{\delta 1}$,$N^{\varepsilon 2}$	
Mol (2)	015	297	273	$N^{\delta 1}$,$N^{\varepsilon 2}$	
L-His·HCl·H_2O	−2	71	240	$N^{\delta 1}$,$N^{\varepsilon 2}$	15
	−1	72	239	$N^{\delta 1}$,$N^{\varepsilon 2}$	16
DL-His·HCl·$2H_2O$	−17	298	289	$N^{\delta 1}$,$N^{\varepsilon 2}$	17
L-His·2HCl	−27	307	285	$N^{\delta 1}$,$N^{\varepsilon 2}$	18
L-Pyro Glu L-His (methyl ester)	−41	180	57	$N^{\varepsilon 2}$	19
L-His·L-Asp·H_2O					9
His A	−26	167	76	$N^{\delta 1}$,$N^{\varepsilon 2}$	
His B	−8	65	240	$N^{\delta 1}$,$N^{\varepsilon 2}$	
His AS	−32	168	78	$N^{\delta 1}$,$N^{\varepsilon 2}$	
His BS	−12	61	240	$N^{\delta 1}$,$N^{\varepsilon 2}$	
D-histidino-L-histidino Co(II)·$2H_2O$	−15	64	341	$N^{\varepsilon 2}$	20
Bis-L-histidino Co(II)·H_2O	−8	65	338	$N^{\varepsilon 2}$	21
D-Histidino-L-histidino Co(III)·$2H_2O$	−16	71	324	$N^{\varepsilon 2}$	20
Bis-(L-histidino) Co(II)·H_2O	−10	75	333	$N^{\varepsilon 2}$	21
Tosyl-α-chymotrypsin		93	256		22
Trypsin		62	257		23
Tosyl-elastase		312	45		24
Subtilisin		194	248		25
Ribonuclease-S		143	69		26

[a] Dihedral angles are defined in Fig. 1.

of the Gaussian 76 program (5). The minimal STO-3G (6) basis set was used.

Results and Discussion

The structural formula of histidine in its zwitterionic form is shown in Fig. 1 and the assumed bond lengths and bond angles are listed in Table 2. The atoms and dihedral angles have been labelled in accord with the IUPAC-IUB Commission of Biochemical Nomenclature (7).

Before considering our calculations we would like to point out that analysis of the conformational properties of 18 examples of histidine from 12 crystal structures (Table 1) indicates that the dihedral angle ψ always assumes a small negative value and ranges from −1° to −41°, possibly due to steric hindrance between the oxygen atom of the carboxyl group and the C^β atom of the side chain. The values of χ^1 indicate three staggered conformations of the side chain about the C^α—C^β bond, while the $\chi^{2,1}$ values indicate that two distinct ranges (± 90°) are preferred by the imidazole ring about the C^β—C^γ bond. These comformations of the imidazole ring with respect to the backbone are such that the intramolecular constant distances between the C^α and $N^{\delta 1}$ atoms and the C^α and $C^{\delta 2}$ atoms are near or below the sum of the corresponding van der Waals radii (see Fig. 2), but above the respective normal limiting distances (3). In such a situation the nonbonded forces would stabilise a conformation for the imidazole ring with $\chi^{2,1} \approx \pm 90°$.

TABLE 2. Bond lengths (Å) and bond angles (degrees) adopted for calculations on histidine

Bond	Length	Bond	Angle
N—C^α	1.470	NC^αC′	110.8
C^α—C′	1.535	N$C^\alpha C^\beta$	109.8
C′—O	1.249	C^αC′O	117.5
C^α—C^β	1.537	OC′O	125.0
C^β—C^γ	1.499	$C^\alpha C^\beta C^\gamma$	112.7
C^γ—$N^{\delta 1}$	1.373	$C^\beta C^\gamma N^{\delta 1}$	124.2
$N^{\delta 1}$—$C^{\varepsilon 1}$	1.325	$C^\gamma N^{\delta 1} C^{\varepsilon 1}$	109.2
$C^{\varepsilon 1}$—$N^{\varepsilon 2}$	1.315	$N^{\delta 1} C^{\varepsilon 1} N^{\varepsilon 2}$	108.7
$N^{\varepsilon 2}$—$C^{\delta 2}$	1.370	$C^{\varepsilon 1} N^{\varepsilon 2} C^{\delta 2}$	108.7
$C^{\delta 2}$—C^γ	1.356	$N^{\varepsilon 2} C^{\delta 2} C^\gamma$	107.4
		$N^{\delta 1} C^\gamma C^{\delta 2}$	106.0

Throughout this work the bond lengths and bond angles were kept constant (8, 9) since a complete search for the optimum geometry is prohibitively expensive. The amino acid was assumed to be in the zwitterionic form, with the NH_3^+ group having a staggered conformation about the N—C^α bond. Several additional assumptions were made for the force-field calculations. The angle ϕ was not varied; while ψ was kept at −20°, which is the average of the observed range (see Table 1). The other two

Can. J. Chem. Downloaded from www.nrcresearchpress.com by 210.87.254.6 on 09/06/12
For personal use only.

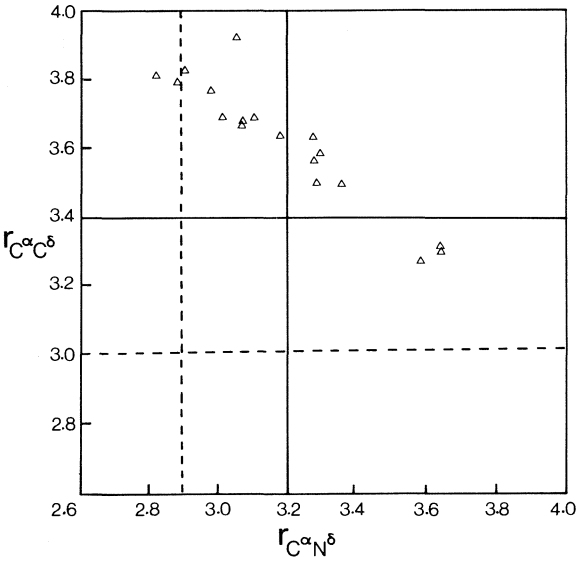

FIG. 2. Plot of observed contact distances between the C^α and $N^{\delta 1}$ atoms versus observed contact distances between the C^α and $C^{\delta 2}$ atoms. The sum of the van der Waals radii are indicated by the solid lines. The normal limiting distances are indicated by the dashed lines.

dihedral angles χ^1 and $\chi^{2,1}$ were varied stepwise and independently from 0° to 360°. No barrier to rotation about the C^β—C^γ bond was assumed, but a three-fold barrier of 3 kcal/mol was considered for rotation about the C^α—C^β bond. Here we should stress that we have taken the full imidazole ring into consideration, unlike an earlier calculation (10).

Table 3 lists the positions of minima and relative conformational energies for the two tautomeric forms of the imidazole ring as obtained from the force-field calculations and the MO calculations. A force-field conformation energy map on the χ^1–$\chi^{2,1}$ plane of the side chain is shown in Fig. 3 for the case where the $N^{\varepsilon 2}$ atom is protonated. The experimental observations from the crystal structures, summarized in Table 1, have been marked on the map. The general agreement between these observations and the theoretical calculations is evident. It is interesting to note, however, that no experimental observations lie in the region of the minimum at about $\chi^1 = 60°$ and $\chi^{2,1} = 80°$, whereas observations have been made in the regions of the other minima. This lack of experimental observations is corroborated by the MO calculations which place the (60,80) minimum above the other minima. Unfortunately a complete calculation of the MO conformational energy map is prohibitively expensive. Of the selected MO calculations we have carried out at the conformations corresponding to the force-field minima, the (60°,270°) conformation yields the lowest energy in agreement with the force-field prediction for the location of the global minimum. Similar agreement is observed for the protonation of $N^{\delta 1}$ (see Table 3). In both cases the MO calculations lead to larger energy differences for the selected conformations although we should stress that the minima have not been searched for by means of MO calculations and may therefore be over-estimated.

TABLE 3. Relative conformational energies of the two tautomeric forms of L-histidine[a]

	χ^1	$\chi^{2,1}$	Force-field	STO-3G
$N^{\varepsilon 2}$ atom protonated				
	60	270	0	0[b]
	300	110	1	3.5
	300	310	1	4.3
	60	80	2	12.2
	180	80	2	6.8
	180	250	3	10.5
$N^{\delta 1}$ atom protonated				
	60	80	0	0[c]
	60	260	1	10.1
	180	60	2	9.1
	180	250	2	7.3
	300	110	2	5.5
	300	310	2	4.6

[a] Relative energies are in kcal/mol.
[b] STO-3G total energy is −538.38304 au.
[c] STO-3G total energy is −538.38314 au.

Atomic charges in the two tautomeric forms of L-histidine are recorded in Table 4. While most of the atoms have nearly the same atomic charges, the

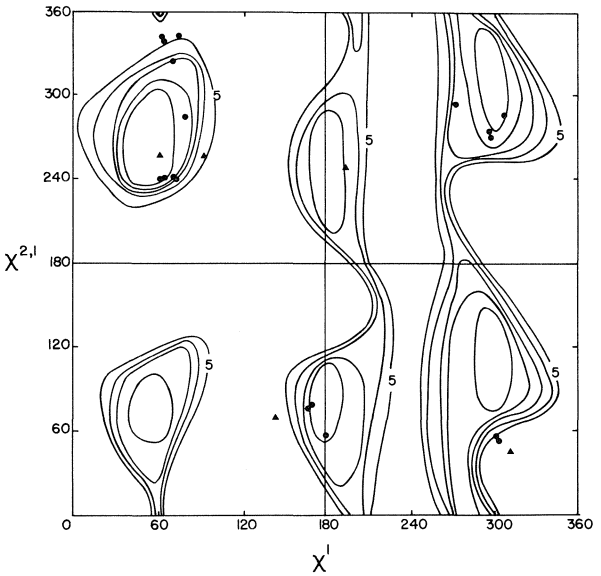

FIG. 3. Conformational energy map on the χ^1–$\chi^{2,1}$ plane of the side chain of histidine for the case where the $N^{\varepsilon 2}$ atom is protonated. Contours are shown at 1 kcal/mol intervals. Observed conformations are indicated by (●) in small crystal structures and by (▲) in active sites of enzymes.

Can. J. Chem. Downloaded from www.nrcresearchpress.com by 210.87.254.6 on 09/06/12
For personal use only.

Can. J. Chem. Downloaded from www.nrcresearchpress.com by 210.87.254.6 on 09/06/12
For personal use only.

TABLE 4. Atomic charges of the two tautomeric forms of L-histidine

Atom	$N^{\delta 1}$ atom protonated	$N^{\varepsilon 2}$ atom protonated
N	−0.370	−0.369
C^{α}	0.020	0.018
C^{1}	0.237	0.236
O1	−0.475	−0.481
O2	−0.440	−0.439
C^{β}	−0.120	−0.116
C^{γ}	0.086	0.052
$N^{\delta 1}$	−0.317	−0.273
$C^{\varepsilon 1}$	0.086	0.128
$N^{\varepsilon 2}$	−0.261	−0.319
$C^{\delta 2}$	0.082	−0.060
H(N)	0.328	0.326
H(N)	0.298	0.293
H(N)	0.322	0.318
H^{α}	0.069	0.083
$H_1{}^{\beta}$	0.078	0.069
$H_2{}^{\beta}$	0.126	0.130
$H(C^{\varepsilon 1})$	0.100	0.093
$H(C^{\delta 2})$	0.088	0.082
$H(N^{\delta 1})$	0.230	—
$H(N^{\varepsilon 2})$	—	0.228

charges of the $N^{\delta 1}$ and $N^{\varepsilon 2}$ atoms are observed to interchange. The difference is, however, only of the order of 0.06e. The classical electrostatic potential in the plane of the imidazole ring is shown in Figs. 4 and 5. In both of the tautomeric forms, a strong negative potential of the order of −200 to −250 kcal/mol is observed near the $N^{\varepsilon 2}$ atom, while the electrostatic potential near the $N^{\delta 1}$ atom remains at −85 kcal/mol. This calculation explains why in all the examples shown in Table 1 the $N^{\varepsilon 2}$ atom is always protonated. As an analogy, we point out the preference for the $N^{\varepsilon 2}$—H tautomer in aqueous solutions of histamine monocation (11). For a discussion of the reliability of electrostatic potentials for the determination of protonation sites we refer to the work of Andrews and Defina (27) and references therein.

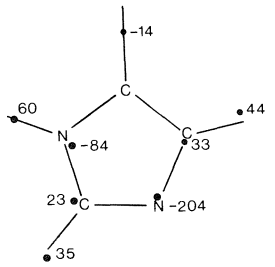

FIG. 4. Electrostatic potential (kcal/mol) in the plane of the imidazole ring for the case where the $N^{\delta 1}$ atom is protonated.

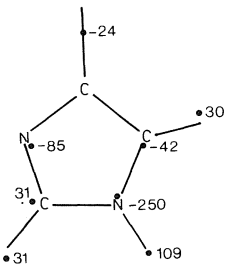

FIG. 5. Electrostatic potential (kcal/mol) in the plane of the imidazole ring for the case where the $N^{\varepsilon 2}$ atom is protonated.

In conclusion, this paper presents the first *ab initio* MO study on L-histidine. In an earlier MO study (28) of the protonation of simple amino acids, histidine was modelled by a methyl group attached to the imidiazole ring. Calculations for such a model lead to a difference of about 1.4 kcal/mol in the proton affinities for the two protonation sites. Our calculations on the complete molecule, however, yield a difference of only 0.1 kcal/mol (see Table 3). No doubt the use of model geometries in this and previous work (28) affects the computed proton affinities.

Acknowledgements

The financial support of the Natural Sciences and Engineering Research Council of Canada and the Research Development Fund of Dalhousie University is gratefully acknowledged. We also wish to thank the Dalhousie University Computer Centre for providing excellent computing facilities.

1. C. TANFORD and J. EPSTEIN. J. Am. Chem. Soc. **76**, 2170 (1954).
2. H. C. FREEMAN. Adv. Protein Chem. **22**, 257 (1976).
3. G. N. RAMACHANDRAN and V. SASISEKHARAN. Adv. Protein Chem. **23**, 283 (1968).
4. C. C. J. ROOTHAAN. Rev. Mod. Phys. **23**, 69 (1951).
5. J. S. BINKLEY, R. A. WHITEHEAD, P. C. HARIHARAN, R. SEEGER, and J. A. POPLE. QCPE **11**, 368 (1978).
6. W. J. HEHRE, R. F. STEWART, and J. A. POPLE. J. Chem. Phys. **51**, 2657 (1969).
7. IUPAC-IUB COMMISSION ON BIOCHEMICAL NOMENCLATURE. Biochemistry, **9**, 3471 (1970).
8. T. J. KISTENMACHER, D. J. HUNT, and R. E. MARSH. Acta Crystallogr. B**28**, 3352 (1972).
9. T. N. BHAT and M. VIJAYAN. Acta Crystallogr. B**34**, 2556 (1978).
10. P. K. PONOWSWAMY and V. SASISEKHARAN. Int. J. Protein Res. III, 9 (1971).
11. W. G. RICHARDS and J. WALLIS. Eur. J. Med. Chem. **14**, 9 (1979).
12. J. J. MADDEN, E. L. MCGANDY, and N. C. SEEMAN. Acta Crystallogr. B**28**, 2377 (1972).
13. M. S. LEHMAN, T. F. KOETZLE, and W. C. HAMILTON. Int. J. Pep. Protein Res. **4**, 229 (1972).
14. P. EDINGTON and M. M. HARDING. Acta Crystallogr. B**30**, 204 (1974).
15. K. ODA and H. KOYAMA. Acta Crystallogr. B**28**, 639 (1972).
16. H. FUESS, D. HOHLWEIN, and S. A. MASON. Acta Crystallogr. B**33**, 654 (1977).

17. I. BENNET, A. G. H. DAVIDSON, M. M. HARDING, and I. MORELLE. Acta Crystallogr. B**26**, 1722 (1970).
18. T. J. KISTENMACHER and T. SORELL. Cryst. Struct. Commun. **2**, 673 (1973).
19. M. COTRAIT and M. ALLARD. C.R. Acad. Sci. Ser. C, **276**, 1671 (1973).
20. R. CANDLIN and M. M. HARDING. J. Chem. Soc. (A), 384 (1970).
21. M. M. HARDING and H. A. LONG. J. Chem. Soc. 2554 (1968).
22. J. J. BERKTOFT, B. W. MATHEWS, and D. M. BLOW. Biochem. Biophys. Res. Commun. **36**, 131 (1969).
23. R. HUBER, D. KUKLA, W. BODE, P. SCHWAGER, K. BARTELS, J. DEISENHOFER, and W. STEIGEMANN. J. Mol. Biol. **89**, 73 (1974).
24. L. SAWYER, D. M. SHOTTON, and H. C. WATSON. Biochem. Biophys. Res. Commun. **53**, 944 (1973).
25. J. KRAUT, J. D. ROBERTUS, J. J. BIRKTOFT, R. A. ALDEN, P. E. WILCOX, and J. C. POWERS. Cold Spring Harbour Symp. Quant. Biol. **36**, 117 (1971).
26. H. W. WYCKOFF, D. TSERNOGLOU, A. W. HANSON, J. R. KNOX, B. LEE, and F. M. RICHARDS. J. Biol. Chem. **245**, 305 (1970).
27. P. R. ANDREWS and J. A. DEFINA. Int. J. Quantum Chem. Quant. Biol. Symp. **7**, 297 (1980).
28. P. G. MEZEY, J. J. LADIK, and S. SUHAI. Theoret. Chim. Acta, **51**, 323 (1979).

Can. J. Chem. Downloaded from www.nrcresearchpress.com by 210.87.254.6 on 09/06/12
For personal use only.

Chemical and electrochemical reduction of pyrazino[2,3-*b*]quinoxalines

JOSEPH ARMAND, LINE BOULARES, AND KHALED CHEKIR

Laboratoire de Physicochimie des Solutions, LA CNRS 161, Université Pierre et Marie Curie, Bâtiment F, 8 Rue Cuvier, 75230 Paris, Cedex 05, France

AND

CHRISTIAN BELLEC

Laboratoire de Chimie des Hétérocycles, Université Pierre et Marie Curie, 4, Place Jussieu, 75230 Paris, Cedex 05, France

Received April 3, 1981

JOSEPH ARMAND, LINE BOULARES, KHALED CHEKIR, and CHRISTIAN BELLEC. Can. J. Chem. **59**, 3237 (1981).

The hydrogenation of 2,3-dimethylpyrazino[2,3-*b*]quinoxaline **1** and 2-phenylpyrazino[2,3-*b*]quinoxaline **2** leads to the corresponding 5,10-dihydroderivatives **3***b* and **4***b*. $LiAlH_4$ reduction of **2**, of 2,3-dimethyl-6,7-diphenylpyrazino[2,3-*b*]pyrazine **8** and 2,6,7-triphenylpyrazino[2,3-*b*]pyrazine **9** furnishes the corresponding 1,2,3,4-tetrahydroderivatives **7**, **10**, and **11**. $NaBH_4$ reduction of **2** leads to a mixture of **4***b* and **7**. In hydroorganic medium **1** and **2** are electrochemically reduced to **3***b* and **4***b* with which they form a redox system.

JOSEPH ARMAND, LINE BOULARES, KHALED CHEKIR et CHRISTIAN BELLEC. Can. J. Chem. **59**, 3237 (1981).

L'hydrogénation de la diméthyl-2,3 pyrazino[2,3-*b*] quinoxaline **1** et de la phényl-2 pyrazino[2,3-*b*] quinoxaline **2** conduit aux dérivés dihydro-5,10 correspondants **3***b* et **4***b*. La réduction par $LiAlH_4$ de **2**, de la diméthyl-2,3 diphényl-6,7 pyrazino[2,3-*b*] pyrazine **8** et de la triphényl-2,6,7 pyrazino[2,3-*b*] pyrazine **9** fournit les dérivés tetrahydro-1,2,3,4 correspondants **7**, **10** et **11**. La réduction de **2** par $NaBH_4$ donne un mélange de **4***b* et **7**. En milieu hydroorganique, **1** et **2** sont réduits électrochimiquement en **3***b* et **4***b* avec lesquels ils forment un système rédox.

Can. J. Chem. Downloaded from www.nrcresearchpress.com by 210.87.254.5 on 09/06/12
For personal use only.

Although the synthesis of pyrazino[2,3-*b*]quinoxalines has been investigated (1) neither their chemical nor their electrochemical reduction has been studied.

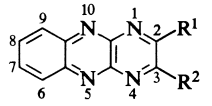

1 $R^1 = R^2 = CH_3$ **2** $R^1 = C_6H_5$, $R^2 = H$

We report the hydrogenation, the reduction with $LiAlH_4$ and $NaBH_4$, and the electrochemical reduction of compounds **1** and **2**. Concerning the electrochemical reduction, the presence of two condensed pyrazine rings made possible two reaction paths, either a reduction into a 1,4- (or 5,10-) dihydro derivative as in the case of pyrazines, or a behaviour similar to that of flavines leading to a 1,5- (or 4,10-) dihydro compound.

Hydrogenation

In the presence of Pd/C, hydrogenation of **1** and **2** leads to the dihydro derivatives **3***b* and **4***b*, the structures of which were determined by nmr (Table 1). The reduction products of **1** and **2** have two amino protons which are readily exchanged by addition of D_2O so that the isomeric structures shown below have to be considered:

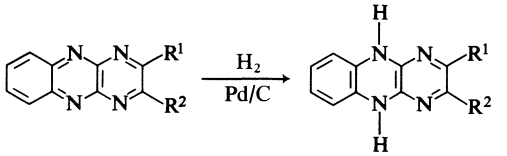

1 $R^1 = R^2 = CH_3$ **3***b* $R^1 = R^2 = CH_3$
2 $R^1 = C_6H_5$, $R^2 = H$ **4***b* $R^1 = C_6H_5$, $R^2 = H$

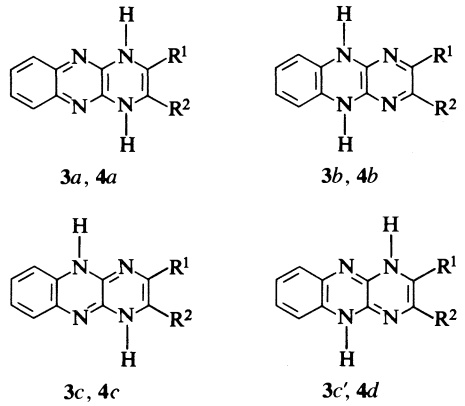

3*a*, **4***a* **3***b*, **4***b*

3*c*, **4***c* **3***c*′, **4***d*

A rapid equilibrium on the nmr time scale of the two tautomers **3***c* and **3***c*′ cannot be excluded on the grounds of the nmr spectrum. However, acetylation gives a diacetylated compound to which the nmr spectrum permits assigning the 1,4-diacetyl-1,4-dihydro structure or the 5,10-diacetyl-5,10-dihydro structure (see Experimental). Thus, the reduction product of **1** must have a plane of symmetry, which rules out structure **3***c*. Structures **3***a* and **3***b* can be discriminated by examination of the chemical shifts. The aromatic protons of 1,2,3,4-tetrahydrophenazine **5** give evidence of a multiplet

0008-4042/81/233237-04$01.00/0

©1981 National Research Council of Canada/Conseil national de recherches du Canada

TABLE 1. Nuclear magnetic resonance data[a,b] for **3***b* and **4***b*

Compound		δ		
3*b*	2-CH_3 3-CH_3	1.93	s	6H
	6-H,7-H 8-H,9-H	6.28	AA'BB' pattern	4H
	5-H,10-H	8.54	s[c,d]	2H
4*b*	6-H,7-H 8-H,9-H	6.38	m	4H
	C_6H_5	7.32 7.70	m m	3H 2H
	3-H	7.40	s	1H
	5-H,10-H	8.88	s[c,d]	2H

[a] Solvent DMSO-d_6.
[b] δ values in ppm relative to internal TMS.
[c] Broad, exchanged with D_2O.
[d] Irradiation of these protons shows that there is no coupling with the methyl protons of **3***b* nor with the 3-H of **4***b*.

between 7.50 and 8.10 ppm (2) while those of 5,10-bis(*n*-propyl)-5,10-dihydrophenazine **6** appear as a multiplet between 6.06 and 6.70 ppm (3). In our case a multiplet is observed between 6.1 and 6.5 ppm. Structure **3***b* is the only one which can account for these results.

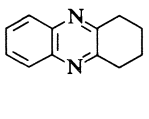

5

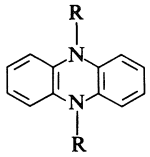

6 R = *n*-propyl

In the same way, the nmr spectrum of the reduction product of **2**, together with the results of an acetylation yielding a diacetylated compound with two nearly equivalent CO—CH_3 groups, permits assigning structure **4***b* to this compound.

This behaviour is different from that of pyrazines and quinoxalines. The hydrogenation of pyrazines (4, 5) gives 1,2-dihydro or 1,2,3,4-tetrahydro derivatives or piperazines; the hydrogenation of quinoxalines (6, 7) furnishes 1,2,3,4-tetrahydro derivatives.

Reduction by $LiAlH_4$ and $NaBH_4$

The reaction of $LiAlH_4$ with **1** gives only gummy products while **2** gives in good yields the 1,2,3,4-tetrahydro compound **7**.

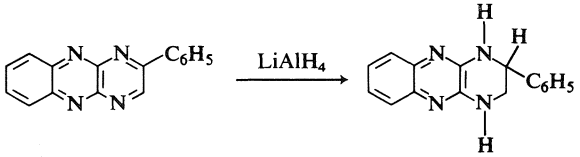

2 **7**

In view of this result, we reacted $LiAlH_4$ with pyrazino[2,3-*b*]pyrazines. The 2,3-dimethyl-6,7-diphenylpyrazino[2,3-*b*]pyrazine **8** as well as the 2,6,7-triphenylpyrazino[2,3-*b*]pyrazine **9** lead to the corresponding 1,2,3,4-tetrahydro derivative. Examination of the nmr spectrum of **10** shows that the two methyl groups have the *cis* configuration. Indeed, 2-H and 3-H give a multiplet at 3.48 ppm and Archer and Mosher (8) have shown that 2-H and 3-H are observed at 3.48 ppm in the case of *cis*-2,3-dimethyl-1,2,3,4-tetrahydroquinoxaline and at 2.98 ppm in the case of the *trans* derivative. The reduction of **8** is stereospecific as in the case of 2,3-dimethylquinoxaline (6).

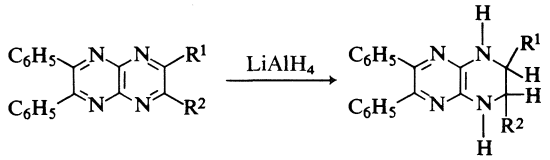

8 $R^1 = R^2 = CH_3$
9 $R^1 = C_6H_5$, $R^2 = H$

10 $R^1 = R^2 = CH_3$
11 $R^1 = C_6H_5$, $R^2 = H$

The reduction of **1** by $NaBH_4$ gives only a resinous product but **2** furnishes a 68:32 mixture of **4***b* and **7**.

Electrochemical Reduction

In hydroorganic medium (50% aqueous dimethylformamide) **1** and **2** are unstable at pH lower than 3. Between pH 3 and 12 they present a 2 F wave which corresponds to the reduction into 5,10-dihydro derivatives **3***b* and **4***b* as shown by preparative electrolysis. These last two compounds present a 2 F anodic wave, the half wave potential of which is very near that of the first cathodic waves of **1** and **2**. The half wave potentials are linearly dependent upon the pH: $E_{1/2}(V) = 0.19 - 0.060\,pH$ for **1** and $E_{1/2}(V) = 0.24 - 0.060\,pH$ for **2**. The reduction scheme is:

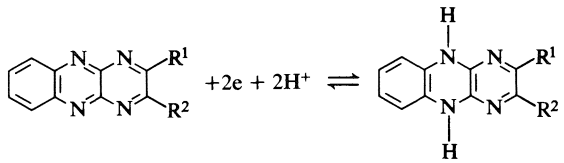

1 $R^1 = R^2 = CH_3$
2 $R^1 = C_6H_5$, $R^2 = H$

3*b*
4*b*

The first cathodic wave of **1** and **2** is followed by a second, ill-defined wave very near the background discharge (at pH 5, $E_{1/2} \sim -1.1$ V). The height of this wave decreases upon increasing the pH; it is close to 4 F in acidic medium and disappears at pH 10. This same wave is also observed on the polarograms of **3***b* and **4***b*; it must correspond to the reduction of these 5,10-dihydro compounds. However, preparative electrolysis of **3***b* and **4***b* gave only gummy products, thus preventing the possible establishment of a sound reaction scheme.

Can. J. Chem. Downloaded from www.nrcresearchpress.com by 210.87.254.5 on 09/06/12
For personal use only.

Can. J. Chem. Downloaded from www.nrcresearchpress.com by 210.87.254.5 on 09/06/12
For personal use only.

The observation of the redox couples **1**–**3***b* and **2**–**4***b* indicates that the electrochemical behaviour of pyrazino[2,3-*b*]quinoxalines is different from that of flavines, but similar to that of phenazine which forms a redox couple with the 5,10-dihydrophenazine (9). Besides, our results are in good agreement with the reduction scheme which we had proposed for the pyrazino[2,3-*b*]pyrazines (10). In this last case the dihydro derivatives were too oxidizable to be isolated; by analogy with what is observed in the case of quinoxalines we had assigned a 1,4- (or 5,8-) dihydro structure to these compounds and had excluded a 1,5- (or 4,8-) structure.

In aprotic medium (acetonitrile) the cyclic voltammogram of **2** shows two reversible monoelectronic peaks I_c and II_c at $E_{p_{c1}} = -0.72$ V and $E_{p_{c2}} = -1.37$ V.

As in the case of pyridopyrazines (11) this voltammogram corresponds to the following reduction scheme

$$2 \overset{e^-}{\rightleftarrows} 2^{\cdot -} \overset{e^-}{\rightleftarrows} 2^{2-}$$

Upon addition of phenol, the second couple progressively disappears while the first cathodic and anodic peaks increase in height up to a bielectronic behaviour while shifting to more positive potentials, e.g., for a 5×10^{-2} *M* concentration of phenol $E_{p_c} = -0.53$ V and $E_{p_a} = -0.43$ V. The cathodic peak corresponds to the reduction to **4***b*. Indeed a preparative electrolysis of **1** ($c = 2 \times 10^{-3}$ *M*); *c*(phenol) = 0.1 *M*, $E = -0.9$ V consumes 2 F per mol and gives **4***b* (75%).

A similar behaviour is evidenced in the case of **1** ($E_{p_c} = -0.92$ and -1.42 V in acetonitrile and $E_{p_c} = -0.78$ V in the presence of 5×10^{-2} *M* of phenol).

Experimental

Melting points are uncorrected. The ^{1}H nmr spectra were obtained on a Bruker WH 80 spectrometer using tetramethylsilane (TMS) as internal standard. The apparatus and techniques used for the electrochemical studies and pH measurements have been described previously (11); all the potentials are referred to the saturated calomel electrode; the temperature of the solutions was 20°C. The microanalyses were performed by M. E. Dorme (Service de Microanalyse, Université Pierre et Marie Curie). All the compounds described gave correct elemental analyses. The following abbreviations are used in reporting nmr results: s = singlet, d = doublet, t = triplet, q = quadruplet, m = multiplet.

Preparation of Pyrazino[2,3-b]quinoxalines and Pyrazino-[2,3-b]pyrazines

2,3-Dimethylpyrazino[2,3-b]quinoxaline **1** was prepared by condensation of 2,3-diaminoquinoxaline (12) with diacetyl according to ref. 1; mp > 190°C dec.; lit. (1) mp 193°C dec; nmr (DMSO-d_6): 2-CH_3 and 3-CH_3, s, 2.84 ppm (6H); 6-H, 7-H, 8-H, 9-H, AA'BB' pattern at 8.02 ppm, m (2H) and 8.30 ppm, m (2H).

2-Phenylpyrazino[2,3-b]quinoxaline **2**

Phenylglyoxal hydrate (1.5 g) was added to a suspension of 2,3-diaminoquinoxaline (1.6 g) in ethanol (40 mL). The mixture was stirred at room temperature for 5 h. The solid material was filtered, washed with ethanol, and dried to give 2.32 g (90%) of **2**; mp 215°C dec.; nmr (DMSO-d_6): 2-Ph, m, 7.68 ppm (3H) and 8.08 ppm (2H); 6-H, 7-H, 8-H, 9-H, m, 8.3–8.6 ppm (4H); 3-H, s, 10.06 ppm (1H).

2,3-Diamino-5,6-diphenylpyrazine

The experimental procedure of ref. 13 has been improved. A mixture of 2.5 g of 2,3-dibromo-5,6-diphenylpyrazine (14), 35 mL of methanol, and 35 mL of ammonium hydroxide solution in water ($d = 0.92$) and 100 mg of Cu powder was heated in a 125 mL steel bomb at 140°C for 24 h. The precipitate was filtered, washed with water, and dried to give 1.3 g (77%) of the diamine; mp > 270°C dec.; lit. (13) mp 275–282°C dec.

2,3-Dimethyl-6,7-diphenylpyrazino[2,3-b]pyrazine **8**

A mixture of 2,3-diamino-5,6-diphenylpyrazine (0.75 g) and diacetyl (5 g) in 15 mL ethanol was refluxed under nitrogen for half an hour. The solution was poured in 250 mL of water. The precipitate was filtered, washed with water, dried, and crystallized in ethanol to give 300 mg of **8** (34%); mp 230°C; lit. (15) mp 228–230°C; nmr ($CDCl_3$): 2-CH_3 and 3-CH_3, s, 2.81 ppm (6H); 6-Ph and 7-Ph, m, 7.2–7.7 ppm (10H).

2,6,7-Triphenylpyrazino[2,3-b]pyrazine **9**

A mixture of 2,3-diamino-5,6-diphenylpyrazine (0.87 g) and 1 g of phenylglyoxal hydrate in 60 mL ethanol was stirred at 0°C for 20 min. Stirring was continued for 3 h at room temperature. The solid material was filtered and crystallized in ethanol to give 0.74 g (62%) of **9**; mp 246°C; nmr ($CDCl_3$): 2-Ph + 6-Ph and 7-Ph, m, 7–8.5 ppm (15H); 3-H, s, 9.60 ppm (1H).

Hydrogenation of ***1*** *and* ***2****: Preparation of* ***3****b and* ***4****b*

A catalytic hydrogenation was carried out at room temperature with 350 mg of **1** in 100 mL dimethylformamide in the presence of 100 mg of 10% Pd/C. After 3 h of stirring and consumption of one mol of H_2 per mol of **1** the solution was filtered and poured in 300 mL of water. The precipitate was filtered, washed with water, and dried to give 295 mg of **3***b* (84%); mp 235°C dec.; nmr: see Table 1. With the same procedure 350 mg of **2** gave 310 mg (88%) of **4***b*: mp 225°C dec.; nmr: Table 1.

Acetylation of ***3****b and* ***4****b*

A solution of 200 mg of **3***b* in 4 mL of acetic anhydride was refluxed for 1 h, poured in water, and filtered to give the diacetyl derivative (180 mg; mp 160°C dec.); nmr (DMSO-d_6): 2-CH_3 + 3-CH_3 + 5-$COCH_3$ + 10-$COCH_3$, 2s, 2.42 and 2.50 ppm (6H + 6H); 6-H + 7-H + 8-H + 9-H, AA'BB' pattern between 7.18 and 7.83 ppm. With the same procedure **4***b* yielded a diacetyl derivative (165 mg; mp 170°C dec.); nmr (DMSO-d_6): 5-$COCH_3$ + 10-$COCH_3$, 2s, 2.48 and 2.53 ppm (6H); 3-H + 2-Ph + 6-H + 7-H + 8-H + 9-H, m, 7.1–8.3 ppm (10H).

Reduction with $LiAlH_4$ *of* ***2****,* ***8****, and* ***9****. Preparation of* ***7****,* ***10****, and* ***11***

$LiAlH_4$ (300 mg) was added slowly to a solution of **2** (516 mg) in freshly distilled tetrahydrofuran (75 mL). After 4 h of stirring at room temperature, the mixture was quenched with 5 mL of water and filtered. Tetrahydrofuran was evaporated and the solid which precipitated was filtered, washed with water, and dried. Compound **7**: 450 mg (86%); mp 215°C dec.; nmr (DMSO-d_6 + D_2O): 3-H, dd, 3.40 ppm ($J_{3-3'} = 12$ Hz; $J_{2-3} = 6$ Hz) (1H); 3'-H, dd, 3.72 ppm ($J_{2-3'} = 4$ Hz) (1H); 2-H, t, 4.82 ppm (1H); 2-Ph + 6-H, 7-H, 8-H, 9-H, m, 7.1–7.7 ppm (9H). In DMSO-d_6, the nmr spectrum presents a broad signal at 7.87 ppm (N*H*) and two multiplets centered at 4.82 and 3.40 ppm which simplify

after exchange of NH protons with D_2O; this result evidences a coupling between NH protons and 2-H, 3-H, and 3′-H.

With the same procedure 160 mg of **8** in 40 mL of tetrahydrofuran and 100 mg of $LiAlH_4$ gave 120 mg (74%) of **10**: mp 236°C dec.; nmr ($CDCl_3$ + D_2O): 2-CH_3 + 3-CH_3, d, 1.05 ppm (6H); 2-H + 3-H, m, 3.48 ppm (2H); 6-Ph + 7-Ph, m, 7.1–7.6 ppm (10H). In the same way, 160 mg of **9** in 40 mL of tetrahydrofuran and 100 mg of $LiAlH_4$ gave 104 mg (65%) of **11**; mp 192°C dec.; nmr (DMSO-d_6 + D_2O): 3-H + 3′-H, m, 3.40 ppm (2H); 2-H, m, 4.82 ppm (1H); 2-Ph + 6-Ph + 7-Ph, m, 6.6–7.6 ppm (15H).

Reduction with $NaBH_4$ of 2

$NaBH_4$ (300 mg) was added to a suspension of **2** (300 mg) in ethanol (30 mL). After 16 h of stirring at room temperature, the mixture was poured in 100 mL of water. Ethanol was evaporated and the solid which precipitated was filtered, washed with water, and dried to yield 240 mg of a solid which was shown by nmr to be a mixture of **4***b* (68%) and **7** (32%).

Electrolysis of 1 and 2 in Hydroorganic Medium

Electrolysis was carried out according to the technique described previously (11) at pH = 6.5 and $E = -0.5$ V (sce). The cathodic compartment contained 210 mg of **1** in 100 mL of solution (dimethylformamide 50%). At the end of electrolysis (2.1 F per mol) the catholyte was poured in 200 mL of water and the precipitate was filtered, washed with water, and dried to give 165 mg (78%) of **3***b*.

With the same work-up, 258 mg of **2** led to 216 mg (83%) of **4***b*.

1. E. B. Nyquist and M. M. Moullie. J. Chem. Soc. 947 (1968), and references cited therein.
2. J. Stating, S. Reiffers, and H. Wynberg. Synthesis, 211 (1971).
3. G. F. Bettinetti, S. Maffei, and S. Pietra. Synthesis, 748 (1976).
4. J. R. Williams, J. J. Cossey, and M. Adler. J. Org. Chem. **37**, 2963 (1972).
5. J. Armand, K. Chekir, and J. Pinson. Can. J. Chem. **52**, 3971 (1974), and references cited therein.
6. R. C. De Selms and H. S. Mosher. J. Am. Chem. Soc. **82**, 3762 (1960), and references cited therein.
7. J. Figueras. J. Org. Chem. **31**, 803 (1966).
8. R. A. Archer and H. S. Mosher. J. Org. Chem. **32**, 1378 (1967).
9. D. N. Bailey, D. M. Hercules, and D. K. Roe. J. Electrochem. Soc. **116**, 190 (1969).
10. J. Armand, K. Chekir, and J. Pinson. C. R. Acad. Sci. Ser. C, **284**, 391 (1977).
11. J. Armand, K. Chekir, and J. Pinson. Can. J. Chem. **56**, 1804 (1978).
12. A. H. Gowenlock, G. T. Newbold, and F. S. Spring. J. Chem. Soc. 622 (1945).
13. R. H. Martin and Z. Tarasiejska. Bull. Soc. Chim. Belg. **66**, 136 (1957).
14. G. Karmas and P. E. Spoerri. J. Am. Chem. Soc. **78**, 4071 (1956).
15. C. K. Cain. Fr. Patent No. 6,196 (1968); Chem. Abstr. **72**, 12767e (1970).

Can. J. Chem. Downloaded from www.nrcresearchpress.com by 210.87.254.5 on 09/06/12
For personal use only.

Replacement of the butenolide moiety of digitoxigenin by cyclic Michael acceptor systems[1,2]

ANGEL GUZMAN
Syntex, S.A., Division de Investigacion, Apartado Postal 10-820, Mexico 10, D.F.
JOSEPH M. MUCHOWSKI[3]
Syntex Research, Institute of Organic Chemistry, Palo Alto, CA 94304
ARTHUR M. STROSBERG
Department of Pharmacology, Institute of Clinical Medicine, Syntex Research, Palo Alto, CA 94304
AND
JOHN M. SIMS
Syntex Research, Institute of Biological Sciences, Palo Alto, CA 94304
Received February 3, 1981[4]

ANGEL GUZMAN, JOSEPH M. MUCHOWSKI, ARTHUR M. STROSBERG, and JOHN M. SIMS. Can. J. Chem. **59**, 3241 (1981).
A series of digitoxigenin analogues was prepared in which the butenolide moiety was replaced by other 5- or 6-membered cyclic Michael acceptor systems. Three compounds, **1***b*, **1***c*, and **1***d* showed weak to moderate cardiotonic activity.

ANGEL GUZMAN, JOSEPH M. MUCHOWSKI, ARTHUR M. STROSBERG et JOHN M. SIMS. Can. J. Chem. **59**, 3241 (1981).
On a préparé une série d'analogues de la digitoxigénine dans lesquelles on remplace le fragment buténolide par d'autres systèmes cycliques à 5 ou 6 chainons pouvant agir comme accepteurs dans des réactions de Michael. Les composés **1***b*, **1***c* et **1***d* présentent une activité cardiotonique varient de faible à modérée.

[Traduit par le journal]

In connection with our interest in steroid cardiac stimulants containing a modified butenolide ring (1) we wished to study the effect on the cardiotonic activity of the substitution of the butenolide moiety of digitoxigenin by other cyclic Michael acceptor systems. A similar strategy has been employed by Boutagy *et al.* (2) and others (3), whereby the replacement of the unsaturated latone ring with analogous open chain structures has led to compounds with substantial cardiotonic activity. This paper describes our efforts to synthesize the digitoxigenin analogues **1***b–g*, **1***j*, and **1***l–o* bearing 5- or 6-membered conjugated unsaturated systems at C-17. After this study was commenced (1975), several publications (5–7) describing the synthesis of certain lactam analogues of cardioactive steroids have appeared. Where overlap has occurred, the results described herein agree well with those already reported.

The point of departure for the synthetic studies described herein was the α-ketomethanesulfonate **2***b* which was prepared from the α-ketol **2***a*, a readily available (8) degradation product of digitoxigen acetate **1***a*.

The preparation of the aza analogue **1***b* of digitoxigenin acetate was accomplished using the method of Stork and Matthews (9). For this purpose, the azide **2***c*, derived from the methanesulfonate **2***b*, was catalytically reduced to the amine **2***d*, which was acylated with diethyl phosphonoacetic acid in the presence of dicyclohexylcarbodiimide. The phosphonate **2***e*, obtained in this way, underwent an internal Wadsworth–Emmons reaction to give the unsaturated lactam **1***b* in 50% yield. This compound was also recently synthesized by Guntert *et al.* (5) by a slightly different route. The *N*-methyl derivative **1***c* was prepared by alkylation of **1***b* with methyl iodide in dimethylformamide solution containing sodium hydride.

A reaction sequence, similar to that described above, was employed to prepare the thiolactone **1***d*. The α-mercaptoketone **2***f*, obtained from **2***b* and sodium hydrosulfide, was acylated with diethylphosphonoacetic acid, and the phosphonate **2***g* thus produced was converted in low (15%) yield into the unsaturated thiolactone **1***d*, with sodium hydroxide in aqueous tetrahydrofuran.

The 2,5-dihydrothiophene derivative **1***e*, a potential precursor of the sulfoxide **1***f* and the sulfone **1***g*, was generated according to the method of

[1]Contribution No. 572 from the Syntex Institute of Organic Chemistry.
[2]Presented in part at the XV Congreso Mexicano de Quimica Pura y Aplicada, Acapulco, Gro., Mexico, October 19–23, 1980.
[3]To whom all correspondence should be addressed.
[4]Revision received August 13, 1981.

0008-4042/81/233241-07$01.00/0
©1981 National Research Council of Canada/Conseil national de recherches du Canada

Can. J. Chem. Downloaded from www.nrcresearchpress.com by 210.87.254.42 on 09/06/12
For personal use only.

Can. J. Chem. Downloaded from www.nrcresearchpress.com by 210.87.254.42 on 09/06/12
For personal use only.

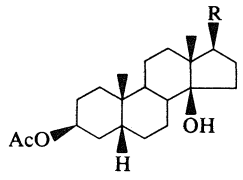

1

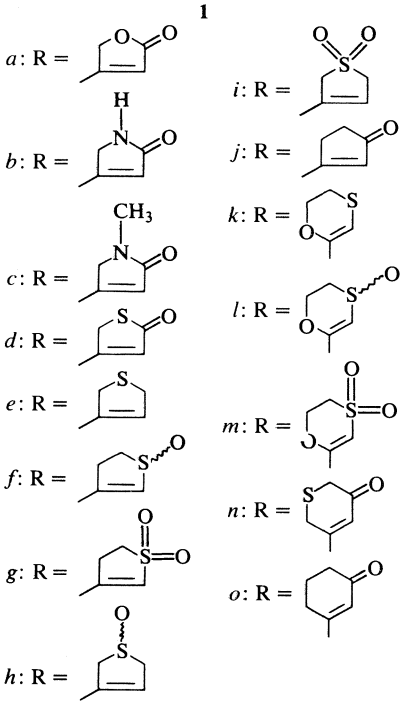

McIntosh *et al.* (10), by an intramolecular Wittig reaction of the ylid derived from the putative phosphonium salt **2***h*. This salt, which was not characterized, was prepared by the reaction of **2***b* with the sodium salt of 2-mercaptoethyltriphenylphosphonium bromide, a substance which in turn was generated *in situ* from sodium hydrosulfide and vinyltriphenylphosphonium bromide. Selective oxidation of the dihydrothiophene derivative **1***e* with sodium metaperiodate gave a stereoisomeric mixture of sulfoxides **1***h* which was converted into the sulfone **1***i* with *m*-chloroperbenzoic acid. Various attempts to transform **1***h* and **1***i* into the conjugated isomers **1***f* and **1***g* under basic conditions failed. Mild conditions (sodium hydride/dimethoxyethane/0°C) resulted in recovery of the starting material or hydrolysis of the acetate moiety (sodium hydroxide/aqueous methanol/25°C), while more vigorous treatment (sodium hydride/dimethoxyethane/25°C) caused the formation of multiple products.

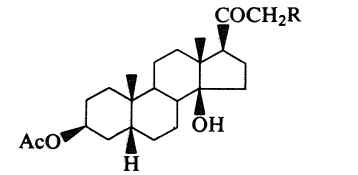

2

a: R = OH
b: R = OSO_2CH_3
c: R = N_3
d: R = $NH_2 \cdot HCl$
e: R = $NHCOCH_2PO(OEt)_2$
f: R = SH
g: R = $SCOCH_2PO(OEt)_2$
h: R = $SCH_2CH_2\overset{+}{P}(C_6H_5)_3Br^-$
i: R = $CH_2COCH_2PO(OMe)_2$
j: R = $CH(CO_2Et)COCH_3$
k: R = CH_2COCH_3
l: R = SC_6H_5
m: R = SCH_2CH_2OH
n: R = SCH_2COCH_3
o: R = $SO_2C_6H_5$
p: R = $CH_2CH_2COCH_3$

Several attempts to prepare the cyclopentenone analogue **1***j* of digitoxigenin acetate failed. For example, the reaction of the sulfonate **2***b*, or the corresponding iodide, with the dianion of dimethyl-2-oxopropylphosphonate (11) did not produce the cyclopentenone **1***j* or the diketophosphonate precursor **2***i* thereof. Furthermore, although ethyl acetoacetate was readily alkylated by **2***b*, or the related α-iodoketone, cyclization of the keto ester **2***j* so produced could not be affected under a variety of basic conditions (sodium hydride, DBN, sodium methoxide, etc.), nor could **2***j* be converted into the 1,4-diketone **2***k*. Finally, although it was expected that the desulfurization of the 1,4-diketosulfide **3***a* would provide **2***j*, this process could not be examined because the alkylation of the phenylthioketone **2***l*, with bromoacetone, gave complex mixtures of products in the presence of diverse bases.

The reaction of sodium-2-hydroxyethanethiolate with **2***b* gave the hydroxyethyl sulfide **2***m* which was transformed into the dihydro-1,4-oxathiin **1***k* when a dichloromethane solution of the sulfide, containing *p*-toluenesulfonic acid, was heated at reflux temperature. The cyclic vinylogous sulfinate **1***l* and sulfonate **1***m* were derived from the oxathiin by oxidative processes identical to those utilized for the synthesis of **1***h* and **1***i*.

In contrast to the difficulties encountered during the attempted synthesis of the cyclopentenone **1***j*, the sodium methoxide induced aldolization of the diketosulfide **2***n* to the 2,6-dihydrothiopyran-5-one derivative **1***n* occurred without incident, albeit in very modest yield.

The synthesis of the cyclohexenone derivative **1***o*, related to the thiopyrone **1***n*, was also effected by an intramolecular aldol condensation. Thus, brief (≤1 h) contact of the 1,5-diketone **2***p* with sodium methoxide in boiling methanol gave the expected cyclohexenone **1***o*. Longer reaction periods resulted in substantial isomerization of this compound to the 17α-epimer **3***b*. The two isomers were readily identified by their characteristic ^{13}C spectra which showed the anticipated upfield shifts for carbon 14 (85.50 ppm) and carbon 18 (15.71 ppm)

TABLE 1. Comparison of effects on myocardial contractility and inhibition of Na^+, K^+ – ATPase

Compound	Positive inotropic effect relative to digitoxigenin	Inhibition of Na^+, K^+ – ATPase potency relative to digitoxigenin
Digitoxigenin	1.0	1.0
1*b*	0.015	0.02
1*c*	0.015	0.15
1*d*	0.05	Not tested
1*e*	Negative inotropic effect (18%)[a]	0.075
1*h*	Negative inotropic effect (39%)[b]	0.014
1*i*	0.002	0.029
1*l*	Negative inotropic effect (25%)[b]	0.0006
1*m*	Negative inotropic effect (20%)[b]	0.003
1*n*	Inactive	0.007
1*o*	Inactive	0.002
3*b*	Not tested	0.002

[a] At 3.5×10^{-5} *M*.
[b] At 1.0×10^{-4} *M*.

in the 17β-epimer **1***o* with respect to the absorptions for the corresponding carbon atoms (86.31, 18.66 ppm) in the 17α-compound **3***b*. Furthermore, as expected (12), C-20 in **1***o* was deshielded to the extent of 3 ppm, by the 14β-hydroxyl group, as compared to that observed for this carbon (166.61 ppm) in **3***b*. Analogous data have been reported (13) for digitoxigenin acetate and the 17α-isomer thereof.

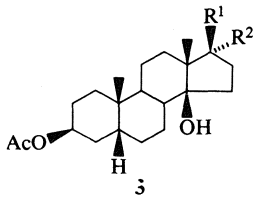

3

a: R^1 = $COCH(SC_6H_5)CH_2COCH_3$; R^2 = H

b: R^1 = H; R^2 =

c: R^1 = $COCH(SO_2C_6H_5)CH_2CH_2COCH_3$; R^2 = H

The 1,5-diketonic precursor **2***p* of the cyclohexenone **1***o* was obtained by reductive desulfonylation (14) of **3***c* with zinc and acetic acid. This latter material was prepared by Michael addition of the α-ketosulfone **2***o* to methyl vinyl ketone.

The digitoxigenin analogues were examined for inotropic activity in driven left atria of guinea pigs (2*c*) and for their ability to inhibit bovine kidney Na^+, K^+ – ATPase.[5] The data in Table 1 indicate that of the ten compounds tested for inotropic effects, four showed a moderate to weak stimulatory action, four depressed the force of contraction, and two were inactive. The most active stimulants were the lactams **1***b* and **1***c* and the thiolactone **1***d*, whereas **1***n* and **1***o* showed no activity. Thus this datum is another illustration (3*c*) of a lack of parallelism between the myocardial contractility and the reactivity of the Michael acceptor (16). This statement also holds for the inhibition of the Na^+, K^+ – ATPase.

[5] Bovine kidney Na^+, K^+ – ATPase was used because it is readily available in substantial amounts, possesses high activity, and the heart and kidney enzyme activities are of the same order (15*a*). The assay method used was that of Barnett (15*b*).

Experimental

The melting points were determined in a Mel-Temp melting point apparatus and are not corrected. The infrared spectra were measured with a Perkin-Elmer Model 237 grating infrared spectrophotometer. The ultraviolet spectra were recorded on a Perkin-Elmer Model 402 ultraviolet visible spectrophotometer. The ^1H nmr spectra were measured with a Varian T-60 or a Varian HA-100 spectrometer and are expressed as parts per million (δ) from internal tetramethylsilane. The ^{13}C nmr spectra were recorded in chloroform solution with a Bruker WH-90 Pulse Fourier Transform spectrometer. The mass spectra were measured with an Atlas CH-4 spectrometer. All optical rotations were measured at ambient temperature.

Unless specified otherwise, the extracts of the reaction mixtures were dried over anhydrous sodium sulfate.

Synthesis of 3β-Acetoxy-14β-hydroxy-21-methanesulfonyloxy-5β-pregnan-20-one **2**b

Methanesulfonyl chloride (0.173 g) was added, in a dropwise manner at 0°C, to a stirred solution of 3β-acetoxy-14β,21-dihydroxy-5β-pregnan-20-one **2***a* (0.495 g) in anhydrous dichloromethane (10 mL) containing triethylamine (0.167 g). After 0.5 h at 0°C, the reaction was diluted with dichloromethane (40 mL); the solution was washed successively with saturated sodium bicarbonate solution and water, dried over sodium sulfate, and evaporated *in vacuo*. The residue was crystallized from benzene to give the product (0.479 g, 80%) mp 149–150°C; $[\alpha]_D$ + 37.9° (c 0.303, $CHCl_3$) *Anal.* calcd. for $C_{24}H_{38}O_7S$: C 61.27, H 8.08, S 6.08; found: C 61.34, H 7.83, S 6.84.

Preparation of 3β-Acetoxy-14β-hydroxy-21-azido-5β-pregnan-20-one, **2**c

A solution of the methanesulfonate **2***b* (0.227 g) in anhydrous acetone (20 mL) containing sodium azide (0.650 g) was stirred at room temperature for 30 h. The mixture was poured into cold water, and extracted with ethyl acetate. The extract was washed with water, dried, and evaporated *in vacuo*. The residue was

Can. J. Chem. Downloaded from www.nrcresearchpress.com by 210.87.254.42 on 09/06/12
For personal use only.

Can. J. Chem. Downloaded from www.nrcresearchpress.com by 210.87.254.42 on 09/06/12
For personal use only.

subjected to thin layer chromatography (tlc) on silica gel using dichloromethane–hexane (3:2) as the developing solvent. After crystallization from dichloromethane–hexane, the azide (0.146 g, 70%) had mp 163–164°C dec.; $[\alpha]_D$ + 63° (c 0.500, $CHCl_3$) *Anal.* calcd for $C_{23}H_{35}N_3O_4$: C 66.18, H 8.39, N 10.07; found: C 66.01, H 8.38, N 10.07.

*Synthesis of 4-(3β-Acetoxy-14β-hydroxy-5β-androstan-17β-yl)-3-pyrrolin-2-one, 1*b

Palladium on charcoal (10%, 0.20 g), suspended in methanol (50 mL), was prehydrogenated at atmospheric pressure and the azido compound **2***c* (2.00 g) was added and hydrogenation was continued for 2 h. The catalyst was removed by filtration, the filtrate was mixed with a solution of hydrogen chloride (0.14 g) in methanol (5 mL) and the whole mixture was evaporated *in vacuo* to give the amine hydrochloride **2***d* which was immediately used in the next step.

The hydrochloride **2***d*, described above, was suspended in dry dichloromethane (50 mL) and dicyclohexylcarbodiimide (1.03 g) and a solution of diethyl phosphonoacetic acid (0.982 g) in dichloromethane (20 mL) were added in succession with stirring. Agitation was continued for 14 h, the mixture was poured into water, the organic phase was washed successively with a saturated sodium bicarbonate solution and water, dried, and evaporated. The residue was subjected to tlc on silica gel (ethyl acetate – hexane, 9:1) to give the phosphonate **2***e* (0.970 g, 70%) as a foam; $[\alpha]_D$ + 25° (c 0.206, $CHCl_3$); ir ($CHCl_3$) 3420, 1730, 1675 cm^{-1}; nmr ($CDCl_3$) δ 0.90 (s, 18 – CH_3), 0.94 (s, 19 – CH_3), 1.32 (t, J = 7.1 Hz, CH_3CH_2O of phosphonate), 2.01 (s, CH_3CO), 2.88 (d, J = 20 Hz, $COCH_2P$), 4.15 (m, 21 – CH_2 and CH_3CH_2O of phosphonate), 5.04 (m, H—3), 7.34 (m, W_H = 9 Hz, exchanged with D_2O); mass spectrum *m/e* 569 (M^+). This compound was homogeneous (by tlc) and was used without further purification or characterization in the next step.

To a suspension of sodium hydride (prepared from 50% sodium hydride (0.096 g) in mineral oil and washed free of the carrier with hexane) in dry dimethylformamide (3 mL) was added the phosphonate **2***e* (0.569 g) and the mixture was stirred for 1 h at room temperature. The mixture was poured into ice–water, and after acidification with 0.5 *N* hydrochloric acid the product was extracted into dichloromethane. The extract was washed with water, dried, and evaporated *in vacuo*. The residue was subjected to tlc on silica gel (ethyl acetate – acetone – dichloromethane, 8:2:1) to give the lactam **1***b* as a solid (0.300 g, 50%) which had mp 256–258°C (lit. (5) 253–257°C) $[\alpha]_D$ + 29° (c 0.135, $CHCl_3$); uv (MeOH) 216 nm (ε 9800); ir ($CHCl_3$) 3460, 1730, 1680 cm^{-1}; nmr ($CDCl_3$) δ 0.83 (s, 18—CH_3), 0.94 (s, 19—CH_3), 2.02 (s, CH_3CO), 2.66 (m, H—17), 4.03 (m, 21—CH_2), 5.02 (m, H—3), 5.86 (m, H—22), 6.36 (m, NH); mass spectrum *m/e* 416 (M^+) *Anal.* calcd. for $C_{25}H_{37}NO_4$: C 72.25, H 8.98, N 3.37; found: C 72.30, H 9.01, N 3.25.

*Synthesis of 1-Methyl-4-(3β-acetoxy-14β-hydroxy-5β-androstan-17β-yl)-3-pyrrolin-2-one, 1*c

A solution of the lactam **1***b* (0.208 g) in anhydrous dimethylformamide (30 mL) was added to a suspension of sodium hydride (derived from 50% sodium hydride (0.026 g) which had been washed with hexane) in dry dimethylformamide (20 mL). After 1 h, methyl iodide (1 mL) was added and the mixture was stirred for 24 h. The solution was poured into water, the product was extracted into dichloromethane, the extract was washed with water, dried, and evaporated *in vacuo*. The residue was subjected to tlc on silica gel to give the *N*-methylated lactam **1***c* (0.086 g, 40%) as a solid which had mp 193–194°C after crystallization from hexane–benzene; $[\alpha]_D$ + 31° (c 0.225, $CHCl_3$); uv (MeOH) 217 nm (ε 13 000); ir ($CHCl_3$) 3620, 3420, 1730, 1670 cm^{-1}; nmr ($CDCl_3$) δ 0.82 (s, 18—CH_3), 0.97 (s, 19—CH_3), 2.03 (s, CH_3CO), 2.69 (m, H—17), 2.95 (s, NCH_3), 3.95 (s, 21—CH_2), 5.00 (m, H—3), 5.78 (m, H—22); mass spectrum *m/e* 429 (MH^+) *Anal.* calcd. for $C_{26}H_{39}NO_4$: C 72.69, H 9.15, N 3.26; found: C 72.86, H 9.17, N 3.09.

*Synthesis of 2,5-Dihydro-4-[3β-acetoxy-14β-hydroxy-5β-androstan-17β-yl)-thiophen-2-one, 1*d

A solution of the methanesulfonate **2***b* (1.88 g) in dimethoxyethane (5 mL) was added at 0°C to a solution of sodium hydrosulfide (0.112 g) in methanol (50 mL). After 15 min the solution was diluted with dichloromethane, the solution was washed with water, dried over sodium sulfate, and evaporated *in vacuo* to give the crude mercapto compound **2***f* (0.980 g); ir ($CHCl_3$) 3400, 1721 cm^{-1}; nmr ($CDCl_3$) δ 1.00 (s, 18—CH_3, 19—CH_3), 2.09 (s, CH_3CO), 3.33 (s, 21—CH_2), 5.08 (m, H—3). This material was used without further purification in the next step.

A solution of the mercapto compound **2***f* in dichloromethane (25 mL) was added to a stirred solution of dicyclohexylcarbodiimide (1.648 g) in anhydrous dichloromethane (50 mL) containing diethyl phosphonoacetic acid (1.568 g). After stirring for 24 h the reaction mixture was poured into saturated sodium bicarbonate solution (50 mL) and the solid which separated was collected by filtration. The filtrate was separated into aqueous and organic phases and the aqueous phase was extracted with dichloromethane. The organic phases were combined, washed with water, dried over sodium sulfate, and evaporated *in vacuo*. The residue, on subjection to tlc on silica gel, (ethyl acetate – hexane – acetone, 8:2:1) gave the crude phosphonate **2***g* (2.08 g); $[\alpha]_D$ + 45° (c 0.245, $CHCl_3$); ir ($CHCl_3$) 3440, 1730 cm^{-1}; nmr ($CDCl_3$) δ 0.94 (s, 18—CH_3, 19—CH_3), 1.32 (t, J = 7.1 Hz, CH_3CH_2O of phosphonate), 2.01 (s, CH_3CO), 3.64–4.29 (m, 21—CH_2 and CH_3CH_2O of phosphonate), 5.40 (m, H—3); mass spectrum *m/e* 390 [M^+ – $PO(OCH_2CH_3)_2$]. This compound was homogeneous by tlc and was used without further purification in the next step.

A sodium hydroxide solution (2.95 mL, 1 *N*) was added to a stirred and cooled (0°C) solution of the phosphonate **2***g* (1.70 g) in tetrahydrofuran (40 mL). The reaction was allowed to reach room temperature and after 30 min it was neutralized by the addition of acetic acid. The solution was diluted with dichloromethane, washed with water, dried, and evaporated *in vacuo*. The crude reaction mixture showed the presence of at least five spots, in addition to that corresponding to the desired compound, on examination by tlc. The desired product was isolated from this mixture by tlc (hexane – ethyl acetate, 7:3) and after crystallization from acetone–hexane a solid (0.192 g, 15%) mp 212–214°C was obtained; $[\alpha]_D$ + 10° (c 0.530, $CHCl_3$); uv (MeOH) 237 nm (ε 12 300); ir ($CHCl_3$) 3600, 3440, 1730, 1670 cm^{-1}; nmr ($CDCl_3$) δ 0.82 (s, 18—CH_3), 0.94 (s, 19—CH_3), 2.00 (s, CH_3CO), 2.77 (m, H—17), 4.08 (m, 21—CH_2), 5.00 (m, H—3), 6.09 (m, H—22); mass spectrum *m/e* 432 (M^+). *Anal.* calcd. for $C_{25}H_{36}O_4S$: C 69.44, H 8.33, S 7.40; found: C 69.54, H 8.47, S 7.30.

*Synthesis of 2,5-Dihydro-4-(3β-acetoxy-14β-hydroxy-5β-androstan-17β-yl)thiophene, 1*e

Vinyl triphenylphosphonium bromide (5.54 g) was added to a stirred solution of sodium hydrosulfide (0.70 g) in methanol (50 mL). After 10 min a solution of the methanesulfonate **2***b* (1.175 g) in tetrahydrofuran (30 mL) was added and when a further 1 h had elapsed the solvent was removed *in vacuo*. The residue was suspended in anhydrous tetrahydrofuran (40 mL) and sodium hydride (0.696 g, 50% in mineral oil) was added. The mixture was stirred for 3 h, and then poured into water. The product was extracted into ethyl acetate, the extract was dried and the solvent was evaporated. The residue was subjected to tlc on silica gel (hexane – ethyl acetate; 7:3) to give a solid (0.375 g, 40%) which was the 3-hydroxy compound corresponding to the desired product; mp 93–95°C, $[\alpha]_D$ + 11° (c 0.136,

Can. J. Chem. Downloaded from www.nrcresearchpress.com by 210.87.254.42 on 09/06/12
For personal use only.

$CHCl_3$); ir ($CHCl_3$) 3450 cm^{-1}; nmr ($CDCl_3$) δ 0.88 (s, 18—CH_3), 0.93 (s, 19—CH_3), 3.69 (m, CH_2SCH_2), 5.54 (m, C=CH); mass spectrum *m/e* 358 ($M^+ - H_2O$). This material was not easily manipulated and it was therefore immediately acetylated with acetic anhydride in pyridine at room temperature. The desired acetate **1***e* was thus obtained in 36% overall yield. After crystallization from methanol, it had mp 183–185°C, $[\alpha]_D$ + 11.7° (c 0.367, $CHCl_3$); ir ($CHCl_3$) 3625, 3540, 1734 cm^{-1}; nmr ($CDCl_3$) δ 0.89 (s, 18—CH_3), 0.96 (s, 19—CH_3), 2.01 (s, CH_3CO), 2.57 (m, H—17), 3.69 (s, CH_2SCH_2), 5.01 (m, H—3), 5.52 (s, H—22); mass spectrum *m/e* 400 ($M^+ - H_2O$). *Anal.* calcd. for $C_{25}H_{38}O_3S$: C 71.77, H 9.09, S 7.65; found: C 71.99, H 9.17, S 7.71.

*Synthesis of 2,5-Dihydro-4-(3β-acetoxy-14β-hydroxy-5β-androstan-17β-yl)thiopene sulfoxide, 1*h

A solution of sodium metaperiodate (0.028 g) in water (0.25 mL) was added, with stirring, to the sulfide **1***e* (0.027 g) dissolved in methanol (2 mL). After 1 h the reaction mixture was poured into water and the product was extracted into dichloromethane. The extract was washed with water, dried, and evaporated *in vacuo*. The residue (0.0225 g, 80%), which was a mixture of stereoisomeric sulfoxides, on crystallization from hexane–benzene had mp 203°C; $[\alpha]_D$ + 30° (c 0.180, $CHCl_3$); ir ($CHCl_3$) 3400, 1730 cm^{-1}; nmr ($CDCl_3$) δ 0.80, 0.90 (singlets, 18—CH_3), 0.93 (s, 19—CH_3), 2.00 (s, CH_3CO), 3.60–3.80 (m, CH_2SOCH_2), 5.05 (m, H—3), 5.60 (m, C=CH); mass spectrum *m/e* 416 ($M^+ - H_2O$). *Anal.* calcd. for $C_{25}H_{38}O_4S$: C 69.09, H 8.81, S 7.36; found: C 69.37, H 8.70, S 7.23.

*Synthesis of 2,5-Dihydro-4-(3β-acetoxy-14β-hydroxy-5β-androstan-17β-yl)thiophene sulfone 1*i

m-Chloroperbenzoic acid (0.259 g) was added at 0°C to a stirred solution of the sulfoxide **1***h* (0.434 g) in anhydrous dichloromethane (30 mL). After 1 h at this temperature, dichloromethane (50 mL) was added and the solution was washed successively with a saturated sodium bicarbonate solution and water. The extract was then dried and evaporated *in vacuo* to give a solid (0.330 g, 73%) which, after crystallization from methanol, had mp 213–215°C; $[\alpha]_D$ + 18.6° (c 0.207, $CHCl_3$); ir ($CHCl_3$) 3540, 1730 cm^{-1}; nmr ($CDCl_3$) δ 0.84 (s, 18—CH_3), 0.92 (s, 19—CH_3), 2.00 (s, CH_3CO), 2.51 (m, H—17), 3.34–4.28 (m, $CH_2SO_2CH_2$), 5.05 (m, H—3), 5.67 (m, H—22); mass spectrum *m/e* 433 ($MH^+ - H_2O$). *Anal.* calcd. for $C_{25}H_{38}O_5 \cdot 0.25H_2O$: C 66.00, H 8.47, S 7.04; found: C 65.88, H 8.47, S 7.14.

*3β-Acetoxy-14β-hydroxy-21-hydroxethythio-5β-pregnan-20-one, 2*m

2-Mercaptoethanol (0.195 g) was added to a stirred solution of sodium methoxide (prepared from sodium (0.0575 g)) in methanol (5 mL) at 0°C. After 15 min the methanesulfonate **2***b* (0.235 g) in methanol (5 mL) was added and stirring at 0°C was continued for a further 30 min. The reaction mixture was diluted with dichloromethane, the solution thus obtained was washed with water, dried, and evaporated *in vacuo*. The residue was crystallized from hexane–dichloromethane to give the sulfide **2***m* (0.158 g, 70%), mp 97–98°C; $[\alpha]_D$ + 55° (c 0.233, $CHCl_3$); ir ($CHCl_3$) 3420, 1730, 1715 cm^{-1}; nmr ($CDCl_3$) δ 0.95 (s, 18—CH_3, 19—CH_3), 2.00 (s, CH_3CO), 2.63 (t, *J* = 5.9 Hz, SCH_2), 3.07 (m, H—17), 3.28 (s, CH_2CO), 3.70 (t, *J* = 5.9 Hz, CH_2O), 5.05 (m, H—3); mass spectrum *m/e* 434 ($M^+ - H_2O$). *Anal.* calcd. for $C_{25}H_{40}O_5S \cdot 1.5H_2O$: C 62.63, H 8.971, S 6.68; found: C 62.57, H 8.61, S 6.63.

*2,3-Dihydro-6-(3β-acetoxy-14β-hydroxy-5β-androstan-17β-yl)-1,4-oxathion 1*k

A solution of the sulfide **2***m* (1.00 g) in anhydrous dichloromethane (250 mL) containing *p*-toluenesulfonic acid monohydrate (0.010 g) was heated at reflux temperature for 2 h. The cooled solution was washed with water, dried, and evaporated. The residue was subjected to tlc on silica gel (hexane – ethyl acetate, 7:3) to give a solid (0.700 g, 72%) which, on crystallization from hexane–benzene, had mp 207–208°C; $[\alpha]_D$ + 75° (c 0.204, $CHCl_3$); uv (CH_3OH) 231 nm (ε 9200); ir ($CHCl_3$) 3500, 1730 cm^{-1}; nmr ($CDCl_3$) δ 0.91 (s, 18—CH_3), 0.95 (s, 19—CH_3), 2.00 (s, CH_3CO), 2.26 (m, H—17), 2.90 (t, *J* = 4.5 Hz, CH_2S), 4.32 (t, *J* = 4.5 Hz, CH_2O), 4.94 (s, (C=CH), 5.04 (m, H—3); mass spectrum *m/e* 434 (M^+). *Anal.* calcd. for $C_{25}H_{38}O_4S$: C 69.12, H 8.75, S 7.37; found: C 68.92, H 8.69, S 7.42.

*2,3-Dihydro-6-(3β-acetoxy-14β-hydroxy-5β-androstan-17β-yl)-1,4-oxathiin sulfoxide 1*l

A solution of sodium metaperiodate (0.690 g) in water (5 mL) was added to a stirred solution of the sulfide **1***k* (0.700 g) in a mixture (1:1) of methanol and tetrahydrofuran (20 mL). After 2 h the solution was diluted with water, the product was extracted into dichloromethane, the extract was washed with water, dried, and evaporated *in vacuo*. The residue was subjected to tlc on silica gel (acetone–methanol, 95:5) to give the sulfoxide **1***l* (0.400 g, 55%) as a mixture of epimers. After crystallization from ethyl acetate the product had mp 193°C; $[\alpha]_D$ + 61° (c, 0.258, $CHCl_3$); uv (MeOH) 231 nm (ε 9800); ir ($CHCl_3$) 3540, 1730 cm^{-1}; nmr ($CDCl_3$) δ 0.87, 0.96 (singlets, 18—CH_3), 0.96 (s, 19—CH_3), 2.01 (s, CH_3CO), 2.34 (m, H—17), 2.59–2.98 (m, CH_2SO), 4.49, 4.58 (multiplets, CH_2O), 5.06 (m, H—3), 5.75, 5.77 (singlets, C=CH); mass spectrum *m/e* 450 (M^+). *Anal.* calcd. for $C_{25}H_{38}O_5S$: C 66.66, H 8.44, S 7.11; found: C 66.46, H 8.56, S 6.82.

*2,3-Dihydro-6-(3β-acetoxy-14β-hydroxy-5β-androstan-17β-yl)-1,4-oxathiin sulfate, 1*m

m-Chloroperbenzoic acid (0.216 g) was added to a stirred solution of the sulfoxide **1***l* (0.255 g) in dichloromethane (25 mL). After 1 h the reaction was worked up as described for **1***i* and the crude product was subjected to tlc (hexane – ethyl acetate, 1:1) to give the sulfone **1***m* (0.140 g, 60%) as a solid which, after crystallization from methanol, had mp 209–210°C; $[\alpha]_D$ + 34° (c 0.177, $CHCl_3$); uv (MeOH) 222 nm (ε 9550); ir ($CHCl_3$) 3560, 1730, 1615 cm^{-1}; nmr ($CDCl_3$) δ 0.95 (s, 18—CH_3, 19—CH_3), 2.02 (s, CH_3CO), 3.25 (m, CH_2SO_2), 4.75 (m, CH_2O), 5.06 (m, H—3), 5.72 (s, C=CH); mass spectrum *m/e* 466 (M^+). *Anal.* calcd. for $C_{25}H_{38}O_6S$: C 64.37, H 8.15, S 6.86; found: C 64.32, H 8.28, S 6.77.

*3β-Acetoxy-14β-hydroxy-21-acetonylthio-5β-prenan-20-one, 2*n

Mercaptoacetone ((17), 0.270 g) was added, with stirring at 0°C, to a solution of sodium methoxide (prepared from sodium (0.058 g)) in methanol (15 mL). After 5 min a solution of the methanesulfonate **2***b* (0.235 g) in a mixture of methanol and tetrahydrofuran (1:1, 10 mL) was added. In 10 min the reaction was complete and the solution was poured into water, the product was extracted with dichloromethane, the extract was washed with water, dried, and evaporated. Crystallization of the residue from methanol gave the desired compound (0.163 g, 71%), mp 130–131°C; $[\alpha]_D$ + 47° (c 0.233, $CHCl_3$); ir ($CHCl_3$) 3440, 1725 cm^{-1}; nmr ($CDCl_3$) δ 0.96 (s, 18—CH_3, 19—CH_3), 2.05 (s, CH_3CO), 2.27 (s, CH_3CO), 3.27 (s, SCH_2), 3.37 (s, SCH_2), 5.08 (m, H—3); mass spectrum *m/e* 446 ($M^+ - H_2O$). *Anal.* calcd. for $C_{26}H_{40}O_5S$: C 67.24, H 8.62, S 6.89; found: C 67.26, H 8.60, S 7.01.

*5-(3β-Acetoxy-14β-hydroxy-5β-androstan-17β-yl)-thiopyran-4-en-3-one, 1*n

The sulfide **2***n* (0.093 g) was added to a solution of sodium methoxide (prepared from sodium (0.015 g)) in anhydrous methanol (6 mL) and the solution was heated at reflux tempera-

Can. J. Chem. Downloaded from www.nrcresearchpress.com by 210.87.254.42 on 09/06/12
For personal use only.

ture for 1 h. The solution was poured into 0.01 *N* hydrochloric acid (20 mL) and the product was extracted into dichloromethane. The extract was washed with water, dried, and evaporated *in vacuo*. The product (0.013 g, 15%) was obtained from the residue by tlc (hexane – ethyl acetate, 7:3). After crystallization from acetone it had mp 231–232°C; $[\alpha]_D$ + 15° (c 0.258, $CHCl_3$); uv (MeOH) 251 nm (ε 10 700); ir ($CHCl_3$) 3500, 1730, 1660 cm^{-1}; nmr ($CDCl_3$) δ 0.88 (s, 18—CH_3), 0.94 (s, 19—CH_3), 2.02 (s, CH_3CO), 2.49 (m, H—17), 3.24 (q, J = 16.8 Hz, SCH_2CO), 3.52 (q, J = 17.3 Hz, SCH_2), 5.06 (m, H—3), 5.93 (m, C=CH); mass spectrum *m/e* 428 ($M^+ - H_2O$) *Anal.* calcd. for $C_{26}H_{38}O_4S$: C 69.95, H 8.52, S 7.17; found: C 69.88, H 8.52, S 7.03.

3β-Acetoxy-14β-hydroxy-21-phenylthio-5β-pregnan-20-one, 2l

Thiophenol (1.155 g) was added to a solution of sodium methoxide (prepared from sodium (0.241 g)) in anhydrous methanol (10 mL). The solution was cooled to 0°C and the methanesulfonate **2***b* (1.00 g) dissolved in 1:1 methanol–tetrahydrofuran (10 mL) was added. The mixture was stirred for 0.5 h, poured into water, and the product was extracted into dichloromethane. The extract was washed with water, dried, and evaporated *in vacuo*. The residue was crystallized from methanol to give the product (0.880 g, 86%) mp 123–124°C; $[\alpha]_D$ + 26° (c 0.260, $CHCl_3$); ir ($CHCl_3$) 3440, 1730, 1690 cm^{-1}; nmr ($CDCl_3$) δ 0.90 (s, 18—CH_3), 0.96 (s, 19—CH_3), 2.03 (s, CH_3CO), 3.15 (m, H—17), 3.68 (s, CH_2S), 5.06 (m, H—3), 7.18–7.48 (m, C_6H_5); mass spectrum *m/e* 484 (M^+). *Anal.* calcd. for $C_{29}H_{40}O_4S$: C 71.90, H 8.26, S 6.61; found: C 71.78, H 8.26, S 6.66.

3β-Acetoxy-14β-hydroxy-21-phenylsulfonyl-5β-pregnan-20-one, 2o

m-Chloroperbenzoic acid (80%, 0.236 g) was added, with stirring at 0°C, to a solution of the thioether **2***h* (0.242 g) in dichloromethane (10 mL). The solution was left to come to room temperature and after 1 h it was diluted with dichloromethane, washed successively with saturated sodium bicarbonate solution and water, dried, and evaporated. The residue was subjected to tlc (dichloromethane – ethyl acetate, 95:5) to give the product (0.220 g, 86%) as a foam; $[\alpha]_D$ + 46° (c, 0.249, $CHCl_3$); ir ($CHCl_3$) 3460, 1730 cm^{-1}; nmr ($CDCl_3$) δ 0.89 (s, 18—CH_3), 0.93 (s, 19—CH_3), 2.01 (s, CH_3CO), 3.16 (m, H—17), 4.23 (q, J = 1.6 Hz, CH_2SO_2), 5.06 (m, H—3), 7.45–7.93 (m, C_6H_5). *Anal.* calcd. for $C_{29}H_{40}O_6S$: C 67.44, H 7.75; found: C 67.43, H 7.96.

3β-Acetoxy-14β-hydroxy-21-(3-oxobutyl)-5β-pregnan-20-one, 2p

A solution of the sulfone (0.258 g), in tetrahydrofuran (2.5 mL) containing methyl vinyl ketone (0.350 g) and tetramethylguanidine (0.115 g), was stirred for 4 h. It was then neutralized with acetic acid, diluted with dichloromethane, washed with water, dried, and evaporated. The residue was subjected to tlc (ether–hexane, 7:3) to give the Michael adduct **3***c* (0.146 g, 50%) as a foam; ir ($CHCl_3$) 3450, 1720, 1345 cm^{-1}; nmr ($CDCl_3$) δ 0.96 (s, 18—CH_3, 19—CH_3), 2.04, 2.06 (singlets, CH_3CO and 3—CH_3CO_2), 4.45 (t, J = 6.0 Hz, 21—CH), 5.08 (m, H—3), 7.50–7.90 (m, C_6H_5). The crude product was used immediately as described below.

To a solution of **3***c* (0.0586 g) in ethyl acetate (0.6 mL) containing ethanol (0.2 mL) and acetic acid (0.2 mL) was added zinc dust (0.059 g) and the mixture was heated at reflux temperature with stirring for 2 h. The mixture was diluted with ethyl acetate, washed successively with a sodium bicarbonate solution and water, dried, and evaporated. The residue was submitted to tlc (hexane – ethyl acetate, 7:3) to give the product (0.0178 g, 40%) which, after crystallization from ethyl acetate – hexane, had mp 117–119°C; $[\alpha]_D$ + 42.4° (c 0.205, $CHCl_3$); ir ($CHCl_3$) 3400, 1710 cm^{-1}; nmr ($CDCl_3$) δ 0.92 (s, 18—CH_3), 0.96 (s, 19—CH_3), 2.05 (s, CH_3CO), 2.13 (s, CH_3CO), 2.48 (t, J = 6.7 Hz, CH_2CO), 2.54 (t, J = 7.2 Hz, CH_2CO), 2.87 (m, H—17), 5.08 (m, H—3); mass spectrum *m/e* 446 (M^+). *Anal.* calcd. for $C_{27}H_{42}O_5$: C 72.64, H 9.41; found: C 72.61, H 9.66.

1-(3β-Acetoxy-14β-hydroxy-5β-androstan-17β-yl)-cyclohexen-3-one, 1o

The 1,5-diketone **2***p* (0.223 g) was added to a solution of sodium methoxide (prepared from sodium (0.223 g)) in anhydrous methanol (8 mL) and the solution was heated at reflux temperature for 1 h. Acetic acid (0.2 mL) was added followed by dichloromethane. The mixture was washed with water, dried over sodium sulfate, and the dichloromethane was removed *in vacuo*. The residue was acetylated with acetic anhydride in pyridine at room temperature (2 h) and after the usual workup and crystallization from ethyl acetate the desired product (0.064 g, 30%) was obtained, mp 235–237°C; $[\alpha]_D$ – 3° (c 0.227, $CHCl_3$); uv (MeOH) 245 nm (ε 16 600); ir ($CHCl_3$) 3625, 3480, 1733, 1660, 1612 cm^{-1}; nmr ($CDCl_3$) δ 0.87 (s, 18—CH_3), 0.97 (s, 19—CH_3), 2.03 (s, CH_3CO), 5.08 (s, H—3), 5.97 (s, C=CH); mass spectrum *m/e* 428 (M^+). *Anal.* calcd. for $C_{27}H_{40}O_4$: C 75.66, H 9.41; found: C 75.58, H 9.21.

If the reaction was extended to more than 1 h, isomerization of **1***o* to the 17α-isomer, 1-(3β-acetoxy-14β-hydroxy-5β-androstan-17α-yl)cyclohexen-3-one, **3***b*, became significant. At the end of 3 h the 17α-isomer became the principal product. After the usual workup and acetylation, this compound could be isolated by tlc (hexane–acetone, 7:3) in *ca.* 15% yield. After crystallization from ethyl acetate – hexane it had mp 210°C; $[\alpha]_D$ + 36.8° (c 0.242, $CHCl_3$); uv (MeOH) 247 nm (ε 17 400); ir ($CHCl_3$) 3580, 3450, 1725, 1660, 1612 cm^{-1}; nmr ($CDCl_3$) δ 0.98 (s, 18—CH_3), 1.04 (s, 19—CH_3), 2.04 (s, CH_3CO), 5.10 (H—3), 5.96 (s, C=CH); mass spectrum *m/e* 428 (M^+). *Anal.* calcd. for $C_{27}H_{40}O_4$: C 75.66, H 9.41; found: C 75.34, H 9.30.

1. A. Cruz, A. Guzman, J. Iriarte, R. Medina, J. M. Muchowski, and M. L. Maddox. J. Org. Chem. **44**, 3511 (1979).
2. (*a*) J. S. Boutagy and R. E. Thomas. Aust. J. Chem. **24**, 2723 (1971); Aust. J. Pharm. Sci. NS1, 67 (1972); NS2, 9 (1973); J. Boutagy, A. Gelbart, and R. Thomas. Aust. J. Pharm. Sci. NS2, 42 (1973); (*b*) R. Thomas, J. Boutagy, and A. Gelbart. J. Pharmacol. Exp. Ther. **191**, 219 (1974); (*c*) A. Gelbart, J. Boutagy, and R. Thomas. J. Med. Chem. **22**, 287 (1979).
3. (*a*) W. Eberlein, J. Heider, and J. Machleidt. Chem. Ber. **107**, 1275 (1974); (*b*) G. Bodem and K. Wirth. Arzneim. Forsch. (Drug Res.) **26**, 1253 (1976); (*c*) D. S. Fullerton, M. C. Pankaskie, K. Ahmad, and A. H. L. From. J. Med. Chem. **19**, 1330 (1976).
4. R. Megges, H. Timm, H. J. Portius, P. Franke, R. Hintsche, and K. Repke. East German Patents 126,092; 126,093 (1977).
5. T. W. Guntert, H. H. A. Linde, M. S. Ragab, and S. Spengel. Helv. Chim. Acta, **61**, 977 (1978).
6. R. Megges, H. Timm, H. J. Portius, E. Glusa, and K. Repke. East German Patent 129,795 (1978).
7. R. Megges, H. J. Portius, and K. R. G. Pepke. Pharmazie, **34**, 328 (1979).
8. K. Meyer and T. Reichstein. Helv. Chim. Acta, **30**, 1508 (1947).
9. G. Stork and R. Matthews. Chem. Commun. 445 (1970).
10. J. H. McIntosh and R. S. Steevensz. Can. J. Chem. **55**, 2442 (1977), and references therein.

11. P. GRIECO and C. S. POGANOWSKI. Synthesis, 425 (1973).
12. S. H. GROVER, J. P. GUTHRIE, J. B. STOTHERS, and C. T. TAN. J. Magn. Reson. **10**, 227 (1973); W. A. AYER, L. M. BROWNE, S. FUNG, and J. B. STOTHERS. Can. J. Chem. **54**, 3272 (1976) and references therein.
13. K. TORI, H. ISHII, Z. W. WOLKOWSKI, C. CHACHATY, M. SNAGARE, F. PIRIOUS, and G. LUKACS. Tetrahedron Lett. 1077 (1973).
14. L. PAVLICKOVA, B. KOUTCK, J. VELEK, and M. SOUCEK. Coll. Czech. Chem. Commun. **39**, 1216 (1974).
15. (*a*) Y. R. CHOI and T. AKERA. Biochem. Biophys. Acta. **508**, 313 (1978); L. K. LAVE, J. H. COPENHAUER, G. E. LINDENMEYER, and A. SCHWARTZ. J. Biol. Chem. **248**, 7197 (1973); (*b*) R. E. BARNETT. Biochemistry, **9**, 4644 (1970).
16. H. SHENHAV, A. RAPPOPORT, and S. PATAI. J. Chem. Soc. B, 469 (1970).
17. F. ASINGER, W. SCHAFER, G. BAUMGARTE, and P. F. MUTING. Liebigs Ann. **661**, 104 (1963).

Can. J. Chem. Downloaded from www.nrcresearchpress.com by 210.87.254.42 on 09/06/12
For personal use only.

Viscosity of ternary mixtures. IV. Urea – *tert*-butyl alcohol – water at 25°C

MARC PALMA AND JEAN-PIERRE MOREL

Laboratoire d'Etudes des Interactions Solutés–Solvants, Groupe de Chimie Physique, Université de Clermont II, Bât. 6 Chimie, B.P. 45, 63170 Aubière, France

Received April 16, 1981

MARC PALMA and JEAN-PIERRE MOREL. Can. J. Chem. **59**, 3248 (1981).

We have measured, at 25°C, the viscosities of urea and *tert*-butyl alcohol ternary aqueous solutions for total concentrations reaching about 4 *M* and various ratios of the solutes. We have also determined *B* coefficients of the Jones–Dole law for urea in water–*tert*-butyl alcohol mixtures and for *tert*-butyl alcohol in water–urea mixtures. The results can be fitted in the form:

$$\eta_r = 1 + B_1 m_1 + B_2 m_2 + D_{11} m_1^2 + D_{22} m_2^2 + D_{12} m_1 m_2 + \ldots.$$

where η_r is the viscosity relative to water and subscripts 1 and 2 characterise the two solutes. B_1 and B_2 are determined in water and the additional *D* parameters appear as pair-interaction contributions of the solutes to the viscosity of the system. Some relations are established and verified between the previous parameters and the *B* coefficients of *1* and *2* determined, respectively, in the aqueous mixtures of *2* and *1*.

MARC PALMA et JEAN-PIERRE MOREL. Can. J. Chem. **59**, 3248 (1981).

Nous avons mesuré, à 25°C, la viscosité des solutions aqueuses d'urée et d'alcool *tert*-butylique pour des concentrations totales allant jusqu'à environ 4 *M* et des proportions différentes de l'un et l'autre des deux solutés. D'autre part, nous avons déterminé les coefficients *B* de la loi de Jones–Dole de l'urée dans les mélanges eau – alcool *tert*-butylique et de l'alcool *tert*-butylique dans les mélanges eau–urée. Les résultats obtenus peuvent s'exprimer à l'aide d'une relation de la forme:

$$\eta_r = 1 + B_1 m_1 + B_2 m_2 + D_{11} m_1^2 + D_{22} m_2^2 + D_{12} m_1 m_2 + \ldots.$$

où η_r est la viscosité relative par rapport à l'eau et les indices 1 et 2 caractérisent les deux solutés. Les différents paramètres *D* qui figurent en plus des coefficients B_1 et B_2 déterminés dans l'eau apparaissent comme caractéristiques des contributions par paires des solutés à la viscosité du système. Des relations sont établies et vérifiées entre les paramètres précédents et les coefficients *B* de *1* et *2* déterminés, respectivement, dans les mélanges aqueux de *2* et *1*.

Introduction

It has been shown (1) that the viscosity of ternary mixtures water – electrolyte (E) – *tert*-butyl alcohol (N) in the water-rich region can be represented by

$$[1] \quad \eta_r = 1 + A_E m_E^{1/2} + B_E m_E + B_N m_N + D_{EE} m_E^2 + D_{NN} m_N^2 + D_{EN} m_E m_N + \ldots.$$

where η_r is the viscosity of the solution relative to water, m_E and m_N the molalities of the electrolyte and the nonelectrolyte, A_E, B_E, and B_N the coefficients of the classical Jones–Dole law (2), respectively, obtained from the viscosity studies of binary solutions of electrolyte and of nonelectrolyte. The *D* parameters are supplementary terms of significant weight at high concentrations. D_{EE} and D_{NN} are obtained from binary solutions of E and N in water, but D_{EN} is a supplementary term characteristic of ternary solutions. D_{EN} is additive for different ionic pairs and it can be correlated to the entropic coefficient of pair interaction (1); thus it seems to reflect some pair-interaction contribution to the excess viscosity of ternary mixtures.

There is no theory related to transport properties, like McMillan–Mayer theory for thermodynamics, which justifies relation [1]. Therefore, it appears interesting to verify the generality of this formalism and to see if it deserves theoretical speculations.

In our previous study (1), D_{EN} parameters were determined from the viscosities of ternary solutions of equal molality of electrolyte and nonelectrolyte, the best precision on D_{EN} being obtained when $m_E = m_N$. It is, of course, necessary to check the validity of relation [1] for various ratios m_E/m_N to state its generality.

The classical viscosity studies of electrolytes in binary water–co-solvent mixtures have described the variations of the *B* coefficient of the electrolyte with the concentration of co-solvent in water (3, 4). When this concentration becomes of the same magnitude as m_E, both N and E play symmetrical solute roles in water. The formalism of relation [1] which permits one to express the relative viscosity with respect to water is then more adequate. We shall show how the coefficients obtained through these two approaches are related.

We have chosen for this study the ternary system water – urea – *tert*-butyl alcohol. By using two nonelectrolytes we get rid of the A_E coefficient of Falkenhagen (5) that takes into account ionic interactions. The two selected nonelectrolytes urea and *tert*-butyl alcohol are of different natures: the first is hydrophilic and a water-structure breaker, the second is hydrophobic and considered a water-

0008-4042/81/233248-04$01.00/0

©1981 National Research Council of Canada/Conseil national de recherches du Canada

Can. J. Chem. Downloaded from www.nrcresearchpress.com by 210.87.254.40 on 09/06/12
For personal use only.

TABLE 1. Densities and relative viscosities of ternary solutions urea (*1*) – *tert*-butyl alcohol (*2*) – water (*3*) at 25°C*

r = 0.299					r = 1.00					r = 3.32				
		η_r					η_r					η_r		
m	ρ	(*1*)	(*2*)	(*3*)	m	ρ	(*1*)	(*2*)	(*3*)	m	ρ	(*1*)	(*2*)	(*3*)
1.978	0.98611	1.916	1.957	1.918	1.915	1.00336	1.877	1.887	1.877	0.7485	1.02215	1.380	1.358	1.382
1.818	0.98678	1.836	1.867	1.837	1.872	1.00322	1.855	1.866	1.856	0.6820	1.02021	1.345	1.328	1.347
1.789	0.98692	1.822	1.851	1.822	1.748	1.00280	1.797	1.804	1.796	0.6207	1.01835	1.314	1.300	1.314
1.666	0.98741	1.759	1.783	1.760	1.701	1.00261	1.774	1.780	1.774	0.5118	1.01486	1.257	1.250	1.258
1.502	0.98814	1.679	1.695	1.678	1.618	1.00231	1.735	1.740	1.734	0.4693	1.01351	1.236	1.230	1.236
1.426	0.98844	1.641	1.656	1.641	1.409	1.00156	1.635	1.638	1.634	0.4276	1.01217	1.215	1.211	1.215
1.011	0.99036	1.441	1.446	1.441	1.177	1.00076	1.526	1.527	1.525	0.3629	1.01006	1.182	1.180	1.182
0.9577	0.99059	1.416	1.420	1.416	0.9730	1.00012	1.431	1.432	1.431	0.3431	1.00945	1.173	1.170	1.173
0.9100	0.99084	1.394	1.398	1.394	0.7070	0.9993	1.310	1.310	1.309	0.3269	1.00892	1.165	1.163	1.165

*$m = m_2$; $r = m_1/m_2$. For η_r, experimental values in columns *1*, calculated values from [4] without E terms in columns *2*, calculated values from [4] with E terms in columns *3*.

structure promoter. On the other hand, the thermodynamic properties of the ternary solutions of these nonelectrolytes have been previously studied (6).

Experimental

Apparatus and Products

The general technique and instrumentation for the viscosity and density measurements have been described previously (3, 7).

Urea (Merck, analysis) was dried under vacuum at 50°C for 48 h. The purification of *tert*-butyl alcohol (Prolabo) has been described elsewhere (8). All solutions were prepared by weight with triply-distilled water and then filtered (glass porosity 4). All measurements were made at 25.000 ± 0.001°C.

Results

Binary Mixtures

In earlier work (1) the relative viscosities of *tert*-butyl alcohol solutions in water enabled us to write (up to m = 2.5 mol kg^{-1}).

$$[2] \quad \eta_r = 1 + 0.386m + 0.054m^2 - 0.0044m^3$$

By similar study of urea–water solutions, we have found here

$$[3] \quad \eta_r = 1 + 0.038m + 0.0015m^2$$

In the concentration range $0 < m < 3$, this expression fits all measurements within experimental error (see Tables 2 and 3).

Ternary Mixtures

Let us call m_1 and m_2 the molalities of urea and *tert*-butyl alcohol in water, respectively. We first carry out measurements of relative viscosities with respect to water of various solutions such that $m_1/m_2 = r$ = constant. In Table 1 are listed the molalities $m = m_2$ and the corresponding relative viscosities and densities for three different ratios r. On the other hand, we have reported in Table 2, for different molalities of water–urea system, the density, the relative viscosity, and the classical Jones–Dole B coefficients of *tert*-butyl alcohol in these systems. In Table 3 are listed the parallel values for water – *tert*-butyl alcohol mixtures and the B coefficients of urea in these mixtures (ρ in g cm^{-3} and m in mol kg^{-1}).

TABLE 2. Densities, relative viscosities of urea (*1*) – water mixtures and B coefficients of *tert*-butyl alcohol (*2*) in these mixtures*

		η_r		$^{(w+1)}B_2$	
m_1	ρ	(*1*)	(*2*)	(*3*)	(*4*)
0	0.99705	1.000	1.000	0.386	0.386
0.50	1.0049	1.019	1.019	0.377	0.374
1.00	1.0122	1.038	1.039	0.373	0.366
2.00	1.0258	1.082	1.082	0.358	0.356
3.00	1.0381	1.127	1.127	0.352	0.360
4.00	1.0497	1.176	1.176	0.341	0.378
5.00	1.0601	1.227	1.227	0.333	0.409

*Experimental values in columns (*1*) and (*3*), calculated values from eq. [3] in column (*2*), from eq. [12] in column (*4*).

TABLE 3. Densities, relative viscosities of *tert*-butyl alcohol (*2*) – water mixtures and B coefficients of urea (*1*) in these mixtures*

		η_r		$^{(w+2)}B_1$	
m_2	ρ	(*1*)	(*2*)	(*3*)	(*4*)
0	0.99705	1.000	1.000	0.038	0.038
0.71	0.98888	1.290	1.300	0.009	0.009
1.50	0.98196	1.677	1.685	−0.019	−0.016
2.38	0.97520	2.133	2.165	−0.042	−0.038
3.37	0.96682	2.644	2.745	−0.048	−0.059
5.78	0.94532	3.537	4.185	−0.040	−0.120
8.99	0.92214	4.333	5.637	−0.027	−0.230

*Experimental values in columns (*1*) and (*3*), calculated from eq. [2] in column (*2*), from eq. [12] in column (*4*).

Discussion

Extended Jones–Dole Law Approach

By analogy with expression [1], we shall write the relative viscosity of the ternary systems studied here as follows

Can. J. Chem. Downloaded from www.nrcresearchpress.com by 210.87.254.40 on 09/06/12
For personal use only.

Can. J. Chem. Downloaded from www.nrcresearchpress.com by 210.87.254.40 on 09/06/12
For personal use only.

[4] $$\eta_r(m_1,m_2) = \eta(m_1,m_2)/\eta_0 = 1 + B_1m_1 + B_2m_2 + D_{11}m_1^2 + D_{22}m_2^2 + D_{12}m_1m_2 + E_{111}m_1^3 + E_{112}m_1^2m_2 + \ldots$$

where η_0 is the absolute viscosity of water, B_1, D_{11} and B_2, D_{22} are determined by expressing the extended Jones–Dole law equations for both water–urea and water – *tert*-butyl alcohol binary systems.

[5] $$\eta_r(m_1) = \eta(m_1)/\eta_0 = 1 + B_1m_1 + D_{11}m_1^2 + E_{111}m_1^3 + \ldots$$

[6] $$\eta_r(m_2) = \eta(m_2)/\eta_0 = 1 + B_2m_2 + D_{22}m_2^2 + E_{222}m_2^3 + \ldots$$

By setting $m_1/m_2 = r$ and $m_2 = m$, measurements of $\eta_r(m)$ in a well-defined concentration range allow us to determine the D_{12} value. This coefficient can be obtained from the intercept of

[7] $$G(m) = \{\eta_r - 1 - (rB_1 + B_2)m\}/m^2 = (D_{11}r^2 + D_{12}r + D_{22}) + (E_{111}r^3 + E_{112}r^2 + E_{122}r + E_{222})m$$

Since B_1, D_{11}, B_2, D_{22} may be deduced from the results of binary mixtures (relations [2], [3]), a least-squares treatment gives $D_{12} = -0.034$, -0.034, -0.035 respectively for $r = 0.299$, 3.32, and 1.00. We must point out that the same value is found for D_{12} whatever the ratio value r; we shall adopt in the present calculations $D_{12} = -0.035$, which is obtained in the best conditions. The range of concentration studied to determine the D coefficients is of primary importance and has been discussed elsewhere (1). In fact, the problem is that of the independent determination of the various coefficients; it has been resolved in the case of B coefficient (9), and we intend to apply an extended form of this method in further work.

The relative viscosities, η_r, calculated from eq. [4], reduced to the B and D coefficients are listed in Table 1 (columns *2*). Agreement with experimental values (columns *1*) is generally better than 2%. It would seem reasonable to expect a better agreement with the use of the E coefficients. The different values of r permit a rough estimation of these terms and we found: $E_{112} = 0.007$ and $E_{221} = -0.004$. Hence, the complete eq. [4] allows us to calculate again η_r (columns *3*). The agreement with experimental results is now about 0.1%. In other words, the expression of the relative viscosity $\eta_r(m_1, m_2)$ given by eq. [4] is valid whatever the relative concentrations of the mixture constituents. This result reinforces our assumption that D_{12} are pair-interaction terms and E triplet ones. Nevertheless, we ought to point out that a better knowledge of these coefficients needs a more appropriate method for their more correct determination.

Relation with Classical Approach

It is usual to measure the variations of the B coefficient of a solute in the mixture of water with a co-solvent. Such results are given in Tables 2 and 3 for our system. Let us show that a relation exists between these B coefficients and the parameters defined by our previous formalism.

Starting from the expressions [4], [5], [6] of the relative viscosities of binary and ternary solutions with respect to water, the B, D, and E coefficients are defined at infinite dilution in water. If we call ${}^{(w+1)}B_2$ the B coefficient of the solute *2* in a solution of the co-solvent *1* at molality m_1 in water, we can write, within the range of validity of the Jones–Dole law (dilute solution of *2*)

[8] $$\eta(m_1,m_2)/\eta(m_2) = 1 + {}^{(w+1)}B_2\,{}^{(w+1)}m_2$$

where ${}^{(w+1)}m_2$ is the molality of *2* in the aqueous mixture of *1*. This molality is related to the molality in water

[9] $${}^{(w+1)}m_2 = m_2/(1 + 10^{-3}M_1m_1)$$

where M_1 is the molecular weight of *1*. We can write

[10] $$\frac{\eta(m_1,m_2) - \eta(m_1)}{\eta_0} = \frac{\eta(m_1)}{\eta_0}\left[\frac{\eta(m_1,m_2)}{\eta(m_1)} - 1\right]$$

and relations [4], [5], [8] lead to

[11] $$B_2m_2 + D_{12}m_1m_2 + E_{112}m_1^2m_2 + \ldots = \eta_r(m_1)^{(w+1)}B_2\,{}^{(w+1)}m_2$$

because, for dilute solutions of *2*, expression [4] is limited to the terms which only contain one subscript 2. Hence, we can write, with [9],

[12] $${}^{(w+1)}B_2 = (B_2 + D_{12}m_1 + E_{112}m_1^2 + \ldots) \times (1 + 10^{-3}M_1m_1)/\eta_r(m_1)$$

and see that ${}^{(w+1)}B_2$ is obtained from B_2 (value in pure water), $\eta_r(m_1)$ the relative viscosity of the hydroorganic solvent and the various D_{12}, E_{112}, ... coefficients. We can also express the limiting slope, when $m_1 = 0$, of the tangent at the ${}^{(w+1)}B_2$ versus m_1 curve, as

[13] $$\frac{d^{(w+1)}B_2}{dm_1} = D_{12} + B_2(10^{-3}M_1 - B_1)$$

Now, we must note that symmetrical relations can be obtained by replacing subscript 1 by 2 and

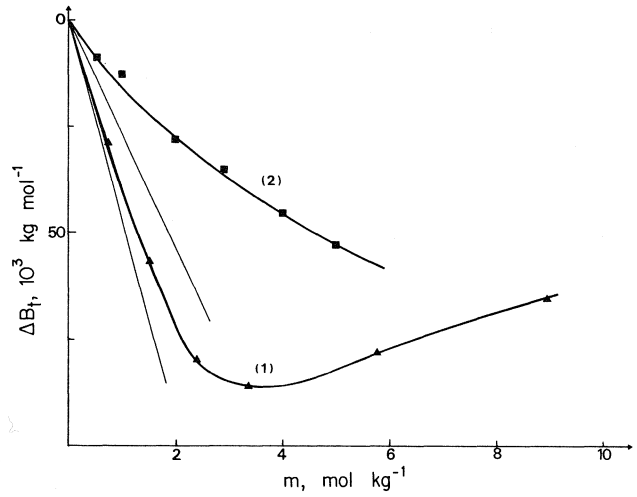

FIG. 1. Variation of B coefficients of urea (*1*) in water – *tert*-butyl alcohol (*2*) mixtures and of *tert*-butyl alcohol (*2*) in water–urea (*1*) mixtures. $\Delta B_{t_1} = {}^{(w+2)}B_1 - B_1$ versus m_2 (curve *1*); $\Delta B_{t_2} = {}^{(w+1)}B_2 - B_2$ versus m_1 (curve 2).

vice versa in eqs. [8] to [13]. In Fig. 1, we have drawn the variations of the B coefficient of urea in water – *tert*-butyl alcohol ($\Delta B_{t_1} = {}^{(w+2)}B_1 - B_1$ versus m_2) and of the B coefficient of *tert*-butyl alcohol in water–urea ($\Delta B_{t_2} = {}^{(w+1)}B_2 - B_2$ versus m_1). The slopes of the two straight lines are respectively −0.047 and −0.026, these values being calculated by relation [13]; it appears that the two straight lines may be taken as the tangents at the origin of the experimental curves. On the other hand, ${}^{(w+2)}B_1$ and ${}^{(w+1)}B_2$ values calculated with relation [12] are given in Tables 2 and 3 for comparison with experimental determinations. The agreement is very satisfying considering the low precision on our evaluation of E_{112} and E_{221}; the weight of these and higher terms is very important for solutions containing more than 3 m co-solvent leading, consequently, to a bad agreement.

Conclusion

The relation [4] which we have proposed for the relative viscosity of the solution of two nonelectrolytes in water is valid whatever the proportions of these two solutes. This strengthens our assumption considering D parameters as pair-interaction contributions to the excess viscosity of the solution. On the other hand, the different terms of relation [4] can be correlated to the classical B coefficient of one solute in a water mixture of the other solute. Here again, the good agreement with the experimental values shows the coherence of the proposed formalism.

1. M. PALMA and J. P. MOREL. J. Solution Chem. **8**, 767 (1979).
2. G. JONES and M. DOLE. J. Am. Chem. Soc. **51**, 2950 (1929).
3. M. PALMA and J. P. MOREL. Can. J. Chem. **55**, 1521 (1977).
4. M. PALMA and J. P. MOREL. Can. J. Chem. **57**, 3247 (1979).
5. M. FALKENHAGEN and E. L. VERNON. Z. Phys. **33**, 140 (1932).
6. J. E. DESNOYERS, G. PERRON, L. AVEDIKIAN, and J. P. MOREL. J. Solution Chem. **5**, 631 (1976).
7. M. PALMA and J. P. MOREL. J. Chim. Phys. **73**, 645 (1976).
8. J. P. MOREL and J. MORIN. J. Chim. Phys. **67**, 2018 (1970).
9. N. MARTINUS, C. D. SINCLAIR, and C. A. VINCENT. Electrochim. Acta, **22**, 1183 (1977).

Can. J. Chem. Downloaded from www.nrcresearchpress.com by 210.87.254.40 on 09/06/12
For personal use only.

Acid catalysed rearrangements of 8,8-dimethyl-2,3-homotropone

RONALD F. CHILDS[1] AND ARAVAMUTHAN VARADARAJAN

Department of Chemistry, McMaster University, Hamilton, Ont., Canada L8S 4M1

Received July 2, 1981

RONALD F. CHILDS and ARAVAMUTHAN VARADARAJAN. Can. J. Chem. **59**, 3252 (1981).

The Brønsted and Lewis acid catalysed rearrangements of 8,8-dimethyl-2,3-homotropone, **2**, have been examined. Four major products have been identified: 2-isopropyltropone, **6**; isobutyrophenone, **7**; 2-isobutenylphenol, **8**; and 8,8-dimethylbicyclo[3.2.1]-octa-3,6-dien-2-one, **5**. The relative amounts of these products differ very markedly as the acid medium changes. Mechanisms are proposed to account for these reactions.

RONALD F. CHILDS et ARAVAMUTHAN VARADARAJAN. Can. J. Chem. **59**, 3252 (1981).

On a examiné les transpositions catalysées par les acides de Brønsted et Lewis de la diméthyl-8,8 homo-2,3 tropone (**2**). On a identifié quatre produits majoritaires: l'isopropyl-2 tropone (**6**), l'isobutyrophénone (**7**), l'isobutényl-2 phénol (**8**) et la diméthyl-8,8 bicyclo[3.2.1] octadiène-3,6 one-2 (**5**). Les quantités relatives de ces produits varient largement avec les changements d'acidité du milieu. On propose des mécanismes pour expliquer ces réactions.

[Traduit par le journal]

Hydroxyhomotropylium cations undergo a variety of photochemical and thermal isomerizations (1–3). Thermally induced rearrangements include *exo–endo* interconversion of substituents on the bridging C(8) carbon by a ring flipping process (1, 4), isomerizations to protonated aromatic ketones (2–4), and circumambulatory rearrangements of the bridging carbon (2, 5). This latter process becomes facile when the bridging carbon bears charge stabilizing groups. An example of these circumambulatory rearrangements is shown in Scheme 1 for the 8,8-dimethyl substituted systems (2).

One feature of the reactions shown in Scheme 1 is that the ultimate product is the protonated bicyclo[3.2.1]octadienone, **5H**. Thus **1H**, **2H**, and **4H** all isomerize to **5H**.[2] At first glance the thermodynamic stability of **5H** is surprising inasmuch as this cation can formally be regarded as "antibishomoaromatic" (6), while **1H**, **2H**, **3H**, and **4H** are homoaromatic ions (2, 7). However, there is a considerable difference in strain energy expected between the two types of cation and this could override any difference in stability due to delocalization.

As part of a program designed to quantitatively probe the importance of strain and delocalization energies in these systems it was desirable to establish the relative stability of the ketones **2** and **5**. This could be achieved by establishing an equilibrium between the two ketones and measuring the equilibrium constant. To this end we examined the acid catalysed reactions of **2** and have uncovered a further series of isomerizations.

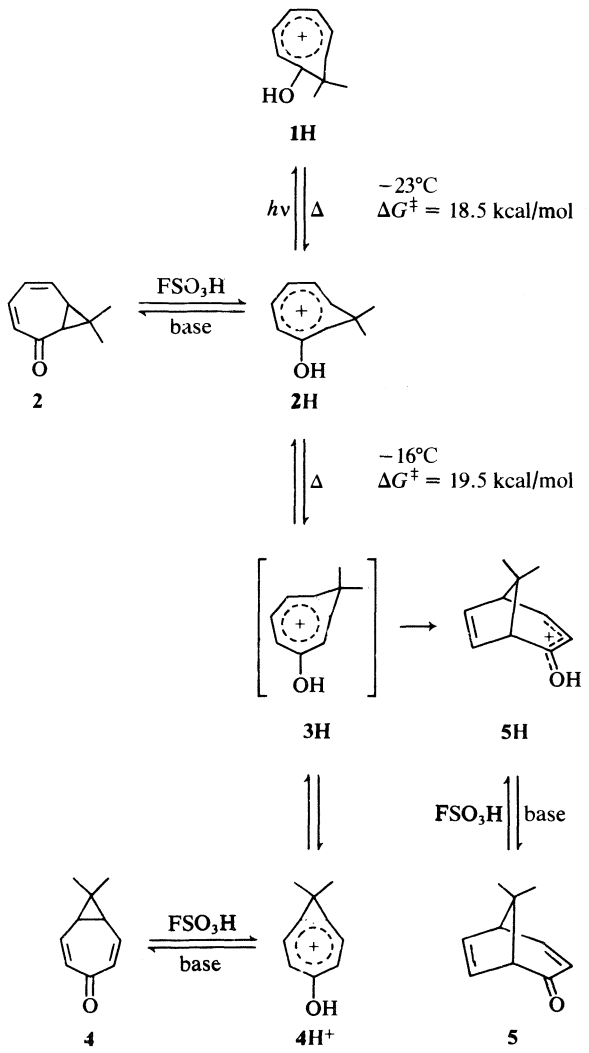

SCHEME 1

[1]Author to whom correspondence may be addressed.

[2]At elevated temperatures in FSO_3H, **5H** undergoes further, as yet uncharacterized, rearrangements.

0008-4042/81/233252-04$01.00/0

©1981 National Research Council of Canada/Conseil national de recherches du Canada

Can. J. Chem. Downloaded from www.nrcresearchpress.com by 210.87.254.40 on 09/06/12
For personal use only.

TABLE 1. Products obtained on isomerization of **2**

Acid medium	Acid concentration (*M*)	Ketone concentration (*M*)	Temperature °C	Time,[a] h	Products (%)[b] 5	6	7	8
FSO_3H	—	0.20	0	2	100	—	—	—
CF_3COOH/CCl_4	0.18	0.14	70	16	—	100	—	—
CF_3COOH/CCl_4	6.0	0.07	70	16	—	53	47	—
CF_3COOH	—	0.05	25	4	—	<2	82[c]	—
CCl_3COOH/CCl_4	0.6	0.20	70	10	—	100	—	—
$HCl/CDCl_3$	—	0.07	25	1	—	100	—	—
$TSOH.H_2O/CCl_4$[d]	0.01	0.14	75	3	—	—	—	100
$BCl_3/CDCl_3$	0.012	0.09	25	<1	—	—	—	100[e]
$BCl_3/CDCl_3$	0.26	0.05	25	<1	—	—	—	100[e]
$BF_3.O(Et)_2/CCl_4$	0.07	0.14	70	3	50	—	50	—
$BF_3/CDCl_3$	<0.1	0.05	25	1	100	—	—	—
$BBr_3/CDCl_3$	0.02	0.08	25	4	—	—	—	100[d]
$TiCl_4/CDCl_3$	0.006	0.07	25	0.5	—	—	—	100[d]
$SbCl_5/CDCl_3$	0.11	0.06	25	0.5	100	—	—	—

[a] Times given are approximately those required for complete reaction.
[b] Yields are based on ^1H nmr and glc analyses. Recovered yields are about 10% lower.
[c] Other minor products present.
[d] *p*-Toluenesulfonic acid. The acid was not completely soluble in CCl_4.
[e] 4,5-Benzo-2,2-dimethyldihydrofuran is also produced on further reaction of **8**. This is included with **8** in terms of product distribution.

Results

8,8-Dimethyl-2,3-homotropone, **2**, (8) was reacted with a variety of Brønsted acids. The reactions were carried out on a small scale and monitored directly by ^1H nmr spectroscopy on the solutions. The acids and acid concentrations were chosen such that **2** was not completely protonated and converted to **2H**. It became apparent from these preliminary observations that **5** was not being formed but rather a series of other compounds, Table 1.

With 0.15 *M* CF_3COOH in CCl_4, **2** was found to isomerize cleanly to 2-isopropyltropone, **6**. The structure of **6** was established by comparison with an authentic sample prepared by the reaction of tropone with isopropylmagnesium iodide and subsequent oxidation of the resulting products (9). Solutions of HCl in $CDCl_3$ and CCl_3COOH in CCl_4 caused the clean isomerization of **2** to **6**.

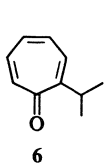

6

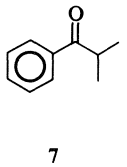

7

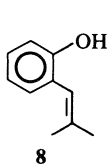

8

As the concentration of CF_3COOH in CCl_4 was increased beyond 0.15 *M*, an additional product was observed. This was identified as **7** on the basis of comparison of its spectroscopic properties and glc retention times with an authentic sample. When CF_3COOH itself was used as solvent, **7** was the major product present and only traces of **6** could be detected. Ketones **6** and **7** were not interconverted under the reaction conditions.

Yet another product was found when *p*-toluenesulfonic acid hydrate was used as the acid catalyst. Heating **2** in the presence of this acid led to the production of the phenol **8** with no detectable amounts of **6** or **7** being produced. Again the structure of **8** was established by comparison of its properties with an independently synthesized material (10).

Lewis acid catalysts were also examined. The same products were obtained with Lewis acids as with the Brønsted acids described above. One complicating feature was that the phenol **8** underwent a cyclization to give the benzodihydrofuran **9** with the stronger Lewis acids (11). (For the sake of simplicity the amounts of this further product have been combined with those of **8** in Table 1.)

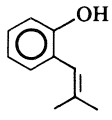

8

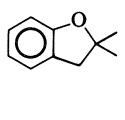

9

With either catalytic amounts or a molar excess of BCl_3, the only products observed were phenol **8** or furan **9**. Similarly, catalytic amounts of BBr_3 or $TiCl_4$ again led to **8**/**9**. Catalytic amounts of BF_3 etherate, on the other hand, led to the formation of **5** and **7** in equal proportions, while an excess of BF_3 or $SbCl_5$ in $CDCl_3$ caused **2** to isomerize cleanly to **5**. With molar excesses of the Lewis acids, it would appear from ^1H nmr evidence that the ketone **2** is completely complexed. Control experiments showed that apart from the conversion of **8** → **9**, the

Can. J. Chem. Downloaded from www.nrcresearchpress.com by 210.87.254.40 on 09/06/12
For personal use only.

products did not interconvert in the presence of the Lewis acids.

Discussion

It is clear from the results presented above that it is not possible to measure an equilibrium constant between **2** and **5** using either weak protic acid or Lewis acid catalysts to equilibrate the two ketones. Instead we have uncovered a variety of isomerization pathways and a remarkable acid dependence on the relative energies of these paths. In FSO_3H, where the various ketones are fully protonated, **2H** isomerized essentially exclusively to **3H** and then to either **4H** or **5H** (2). None of the products found under the acid catalysed conditions used here was detected on rearrangement of **2H** in FSO_3H. This suggests that with the weaker protic acids and certain Lewis acids, the rearrangements of **2** to **6**, **7**, and **8** do not simply involve cationic intermediates but that various unobserved covalent intermediates are also formed. Thus although the aromatic ketone **7** could be formed by isomerization of **2H** to **1H** by a cyclopropyl walk followed by the known isomerization of the **1H** to protonated ketone **7H**, eq. [1] (2–4), the absence of such a reaction in FSO_3H makes it difficult to see why such a pathway should operate with the weaker acids.

[1] $2 \overset{H^+}{\rightleftharpoons} 2H \rightleftharpoons 1H \rightleftharpoons 7H \rightleftharpoons 7$

Instead we suggest that with a weaker acid it is likely that **1H** can lose a proton to give cyclooctatrienone **1**. It is known that **1** exists preferentially as its valence tautomer **10** (12) and that this on protonation irreversibly yields **7H**, eq. [2] (2).

[2] 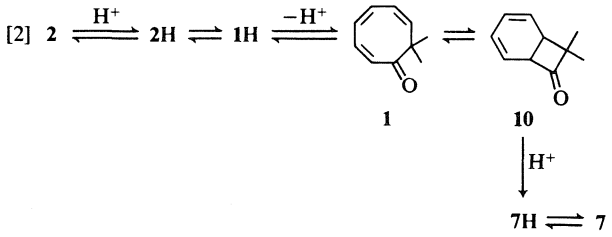

Likewise, formation of **6** could have been considered to arise by a hydride shift from C(1) to C(8) of **2H** or an ion closely related to **2H** involved in the circumambulatory rearrangements of these cations. It is known that there is considerable localization of positive charge on C(8) during this migration and Hehre has suggested that partial hydrogen bridging might occur in the "allowed" transition state for cyclopropyl circumambulation (13). However, as **6** (or **6H**) is only formed in the weaker acids it is suggested that a more appropriate mechanism might be as shown in eq. [3], in which nucleophilic capture at C(8) occurs to give **11**. This would be followed by ketonization of the intermediary enol. This is known to occur by protonation preferentially at C(2) as shown (14). This is followed by loss of X^-, a hydride shift and proton loss.

[3] 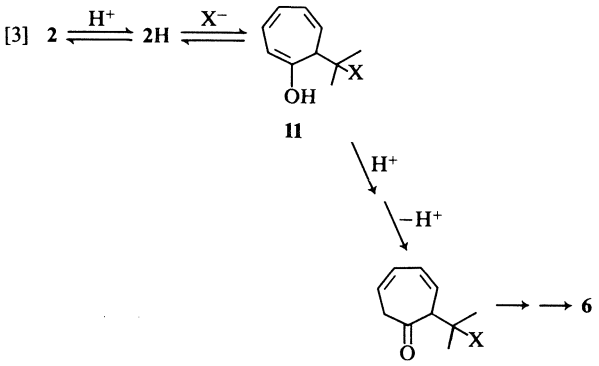

From the data in Table 1 it can be seen that with trifluoroacetic acid both **6** and **7** are produced from **2**. The tropone **6** predominates when small amounts of the acid are used in a nonpolar medium (CCl_4) where ion pairing would be maximized and nucleophilic attack likely. As the amount of trifluoroacetic acid is increased the solvent polarity would be enhanced. Consequently less nucleophilic capture, to give **11** and an increase in the relative amount of **7**, might be expected.

An alternative course of reaction for **11** would be its reionization prior to ketonization. Sargent has shown that cycloheptatriene carbinyl systems ionize from their norcaradiene valence tautomers to yield styrene derivatives (15). As is shown in eq. [4], this would yield a potential route to the phenol **8**.

[4] 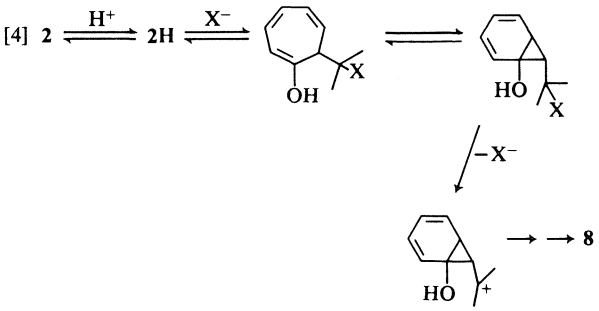

Some measure of support for these suggestions comes from the Lewis acid catalysed reaction. With an excess of a strong Lewis acid such as BF_3 or $SbCl_5$, a situation similar to that occurring with FSO_3H pertains. With catalytic amounts of BF_3, however, decomplexation of **1**.BF_3 could occur. This would be expected to lead to **7** as is observed. BCl_3, BBr_3, and $TiCl_4$ all lead to the quantitative formation of **8**. This, we would suggest, occurs by the attack of halide at C(8) of the complexes of **2**. Certainly in the cases of BCl_3 and BBr_3 this is not unexpected and probably also occurs from the

Can. J. Chem. Downloaded from www.nrcresearchpress.com by 210.87.254.40 on 09/06/12
For personal use only.

Can. J. Chem. Downloaded from www.nrcresearchpress.com by 210.87.254.40 on 09/06/12
For personal use only.

bisketone complex of $TiCl_4$. With a Lewis acid such as BF_3, the -OBF_3^- or BF_4^- groups would not be expected to dissociate a fluoride which could then nucleophilically add to the complex. In the absence of a protic acid, ketonization of **11** could well be slower than reionization and formation of **8**.

In conclusion it is of interest to reconsider the reactions observed in FSO_3H, Scheme 1. In this acid **1H** thermally rearranged to **2H**, indicating that the latter cation is thermodynamically more stable than **1H**. At higher temperatures **2H** further rearranged to **4H** and **5H** via **3H**. The results obtained in this work suggest that the barrier for the isomerization of **2H** to **1H**, a reaction not observed in FSO_3H because of the equilibrium position between the two cations, is lower than that for the conversion of **2H** to **3H**. This suggests that the ground state energy difference between **1H** and **2H** can only be of the order of 1 kcal/mol.

Experimental

The ^1H nmr spectra were recorded on Varian EM-390 and Bruker WP-80 spectrometers. Infrared spectra were obtained with a Perkin–Elmer model 283 instrument. Varian A-90-P3 and 3700 gas chromatographs, respectively, were used for preparative and analytical glpc.

General Isomerization Procedure

8,8-Dimethyl-2,3-homotropone, **2** (5–20 mg), was dissolved in $CDCl_3$ or CCl_4 (0.7 mL) in an nmr tube, the solution cooled to −78°C, and the appropriate amount of acid added under an argon blanket. The mixture was warmed to the appropriate temperature and the reaction monitored by ^1H nmr spectroscopy. After reaction the mixture was poured into a saturated solution of $NaHCO_3$ and the organic materials extracted into CH_2Cl_2 (3 × 5 mL) and the combined extracts dried over $MgSO_4$. The solvent was removed *in vacuo* and the residue subjected to glpc and ^1H nmr analysis. The results are summarized in Table 1.

Product Characterizations

(a) Rearrangement Catalysed by Trifluoroacetic Acid

Ketone **2** (20 mg) in CCl_4 (1 mL) and trifluoroacetic acid (20 mg) were mixed and heated at 70°C for 16 h. The reaction mixture was neutralized with $NaHCO_3$, the product extracted into CH_2Cl_2 and dried as above. Removal of the solvent and bulb to bulb distillation (80°C/0.1 Torr) gave **6** (19 mg); ir (film): 2960, 1630, 1580, 1520, 780, 690 cm^{-1}; ^1H nmr (CCl_4, TMS) δ: 6.81 (vinyl H, 5H, m), 3.34 (methine H, m, J = 6 Hz), 1.14 (CH_3, d, J = 6 Hz). The ir and ^1H nmr spectra of **6** were identical to an authentic sample prepared by the method of Noyori *et al.* (9).

(b) Rearrangement Catalysed by p*-Toluenesulfonic Acid*

Ketone **2** (20 mg) in CCl_4 (1 mL) was treated with *p*-toluenesulfonic acid hydrate (2 mg). The reaction was heated at 75°C for 3 h and subsequently worked up as described above. Removal of the solvent gave the crude phenol **8** (10 mg). The phenol was purified by extraction into aqueous NaOH, acidification and reextraction into ether, drying ($MgSO_4$), and solvent removal. Infrared (CS_2): 3540, 2960, 750, 695 cm^{-1}; ^1H nmr ($CDCl_3$, TMS) δ: 7.0 (aromatic H, 4H, m), 6.2 (vinyl H, 1H, s), 5.17 (OH, 1H, s), 2.0 and 1.72 (CH_3, each 3H, s). The ^1H nmr and ir spectra and glpc retention times of **8** were identical to an independently prepared sample (10).

(c) Rearrangement Catalysed by BCl_3

BCl_3 (30 mg) was condensed into a frozen solution of **2** (13 mg) in $CDCl_3$ (1 mL) at −78°C. The mixture was warmed to 25°C. After 1 h at this temperature the reaction mixture was quenched and worked up as described above. Removal of the solvent and bulb to bulb distillation (150°C/15 Torr) gave 2,3-dihydro-2,2-dimethylbenzofuran. Infrared (film): 2920, 1595, 1455, 1260, 1205, 890, 745 cm^{-1}; ^1H nmr ($CDCl_3$) δ: 7.17 and 6.83 (aromatic H, 4H, m), 3.03 (CH_2, 2H, s), 1.46 (CH_3, 6H, s). The ^1H nmr and ir spectra and glpc retention times were identical to those of an authentic sample prepared by the method of Martini *et al.* (11).

(d) Rearrangement Catalysed by BF_3/OEt_2

Ketone **2** (20 mg) in CCl_4 (mL) was treated with $BF_3.OEt_2$ (1 mg) and heated at 70°C for 3 h. Working up the reaction as described above gave a mixture of **5** and **7** (10 mg). These were separated by preparative glpc (15% SE30 on Chromosorb W; retention times: **5**, 5.8 m, and **7**, 6.6 m, at 130°C). The properties of **5** were identical to those previously described (2). Isobutyrophenone, **7**, ir (film): 2980, 1690, 1600, 1582, 1480, 1430, 1315, 1225, 1160, 970, 788, 696 cm^{-1}; ^1H nmr ($CDCl_3$) δ: 7.86 and 7.43 (aromatic H, 5H, m), 3.45 (CH, 1H, h, J = 7 Hz), 1.15 (CH_3, 6H, d, J = 7 Hz). The properties of **7** were identical to a commercial sample.

Acknowledgement

This work was supported by the Natural Sciences and Engineering Research Council of Canada.

1. R. F. Childs and C. V. Rogerson. J. Am. Chem. Soc. **98**, 6391 (1976).
2. R. F. Childs and C. V. Rogerson. J. Am. Chem. Soc. **102**, 4159 (1980); **100**, 649 (1978).
3. M. S. Brookhart, M. Ogliaruso, and S. Winstein. J. Am. Chem. Soc. **89**, 1965 (1967).
4. M. S. Brookhart and M. A. M. Atwater. Tetrahedron Lett. 4399 (1972).
5. L. T. Scott and W. R. Brunsvold. J. Am. Chem. Soc. **100**, 6535 (1978).
6. H. Hart and M. Kuzuya. J. Am. Chem. Soc. **98**, 1545 (1976); A. F. Diaz, M. Sakai, and S. Winstein. J. Am. Chem. Soc. **92**, 7477 (1970).
7. S. Winstein. Q. Rev. Chem. Soc. **23**, 141 (1969); P. M. Warner. *In* Topics in nonbenzenoid aromatic chemistry. Vol. 2. *Edited by* T. Nozoe, R. Breslow, K. Hafner, S. Ito, and I. Morata. Hirokawa, Tokyo. 1976; L. A. Paquette. Angew Chem. Int. Ed. Engl. **17**, 106 (1978).
8. M. Franck-Neumann and D. Martina. Tetrahedron Lett. 1759 (1975).
9. R. Noyori, S. Makino, T. Okita, and N. Hayakawa. J. Org. Chem. **40**, 806 (1975).
10. H. Pauly and R. Frh. V. Butlar. Ann. Chem. **383**, 230 (1911).
11. A. T. Shulgin and A. W. Baker. J. Org. Chem. **28**, 2469 (1963); J. C. Martini, N. W. Franke, and G. M. Singerman. J. Org. Chem. **35**, 2904 (1970).
12. G. N. Schrauzer. J. Am. Chem. Soc. **83**, 2966 (1961); A. Davison, W. McFarlane, W. Pratt, and G. Wilkinson. J. Chem. Soc. 4821 (1962).
13. W. J. Hehre. J. Am. Chem. Soc. **96**, 5207 (1974).
14. K. E. Hine and R. F. Childs. J. Am. Chem. Soc. **95**, 3289 (1973); W. E. Parham, R. W. Soeder, and R. M. Dodson. J. Am. Chem. Soc. **84**, 1755 (1962); E. Garbisch. J. Org. Chem. **30**, 2109 (1965).
15. G. D. Sargent, N. Lowry, and S. D. Reich. J. Am. Chem. Soc. **89**, 5885 (1967); W. A. Bonner, E. K. Raunio, and D. M. Bowen. J. Org. Chem. **31**, 912 (1966).

The electroreduction of aromatic aldehydes in aprotic solvents

W. RONALD FAWCETT

Guelph-Waterloo Centre for Graduate Work in Chemistry (Guelph Campus), Department of Chemistry, University of Guelph, Guelph, Ont., Canada N1G 2W1

AND

ANDRZEJ LASIA

Department of Chemistry, University of Warsaw, ul. Pasteura 1, 02-093 Warsaw, Poland

Received April 30, 1981

W. RONALD FAWCETT and ANDRZEJ LASIA. Can. J. Chem. **59**, 3256 (1981).

The mechanism of electroreduction of aromatic aldehydes was investigated by cyclic voltammetry in dimethylformamide and acetonitrile in the presence of tetraethylammonium, potassium, and sodium perchlorates. It was found that the reaction products disappear in a dimerization reaction. Rate constants for the subsequent dimerization and association constants for ion pair intermediates were determined. The reactivity of the anion radicals initially formed decreases in the sequence: 9-anthraldehyde > benzaldehyde > 2-naphthaldehyde > 1-naphthaldehyde. The Hückel molecular orbital method was used to explain the reactivity sequence and the properties of the radical intermediates.

W. RONALD FAWCETT et ANDRZEJ LASIA. Can. J. Chem. **59**, 3256 (1981).

Faisant appel à la voltamétrie cyclique, on a étudié le mécanisme d'électoréduction des aldéhydes aromatiques dans le diméthylformamide et dans l'acétonitrile en présence des perchlorates de tétraéthylammonium, de potassium et de sodium. On a trouvé que le produit de la réaction disparaît dans une réaction de dimérisation. On a déterminé la constante de vitesse de la dimérisation et les constantes d'association de la paire d'ions intermédiaire. La réactivité des radicaux anions qui se forment initialement décroît dans l'ordre suivant: antraldéhyde-9 > benzaldéhyde > naphtaldéhyde-2 > naphtaldéhyde-1. On a utilisé la méthode d'orbitale moléculaire de Hückel pour expliquer l'ordre de réactivité et les propriétés des radicaux intermédiaires.

[Traduit par le journal]

Introduction

The reaction mechanism for the electroreduction of aromatic aldehydes, in particular, benzaldehyde, has been widely studied in protic solutions (see ref. 1 and references therein). It was found that electron transfer to benzaldehyde is a fast process with an apparent rate constant of the order 0.1 cm s^{-1} (2). The reduction mechanism involves protonation of the resulting anion radical and dimerization (3, 4). Nekrasov *et al.* (5) suggested that the products of dimerization are pinacols and other substances with a quinoid structure.

The reduction of aromatic aldehydes in aprotic solvents has been studied in less detail (6–17). Anthoine *et al.* (6) presented half-wave potentials of aldehydes in dimethylformamide (DMF) and found a linear relationship between the energy of the lowest empty molecular orbital and the half-wave potential, $E_{1/2}$. They also found that the first reduction step is reversible in cyclic voltammetric experiments carried out at high sweep rates (20 Hz). Most papers were concerned with the reduction of benzaldehyde (7–17). Large scale electrolysis in DMF at the potentials corresponding to the first polarographic wave gave pinacol as a main product (8, 9). Vykhodtseva and Nekrasov (15) suggested that in DMSO not only pinacols but also other dimers with a quinoid structure are formed.

The kinetics of dimerization of benzaldehyde was investigated by Armstrong *et al.* (13, 14) in sulfolane. In the presence of 0.1 tetrabutylammonium perchlorate the second order rate constant was equal to $2.4 \times 10^3 M^{-1}$ s^{-1}. The possibility of dimerization of two radical anions or of the radical anion with the parent molecule was discussed by Yeh (18) for *p*-cyanobenzaldehyde in DMSO.

Kalinowski (17) studied the reduction of benzaldehyde in DMF in the presence of alkali metal and alkaline earth metal perchlorates and found a linear relationship between the half-wave potential and the ionic potential (defined as the ratio of the charge on the cation to its radius). This result was attributed to ion pair formation between anion radicals and cations of the supporting electrolyte with subsequent dimerization of the ion pairs.

The purpose of the present study was to investigate the mechanism of electroreduction of simple aromatic aldehydes: benzaldehyde (BA), 1-naphthaldehyde (1NA), 2-naphthaldehyde (2NA), and 9-anthraldehyde (AA), and to assess the influence of ion association on that process.

Experimental

Chemicals

Spectroquality DMF (Matheson, Coleman, and Bell) was purified as described earlier (19). Spectroquality acetonitrile

0008-4042/81/233256-05$01.00/0

©1981 National Research Council of Canada/Conseil national de recherches du Canada

Can. J. Chem. Downloaded from www.nrcresearchpress.com by 210.87.254.6 on 09/06/12
For personal use only.

Can. J. Chem. Downloaded from www.nrcresearchpress.com by 210.87.254.6 on 09/06/12
For personal use only.

(ACN) (Matheson, Coleman, and Bell) was dried with 3A molecular sieves and P_2O_5 and then distilled under a nitrogen atmosphere. All perchlorates were dried according to previous procedures (19). The aldehydes were distilled or sublimated under reduced pressure before use. The concentration of the supporting electrolyte was 0.1 *M* in all experiments. Peak potentials were measured against an aqueous saturated calomel electrode (SCE). All measurements were performed at 21 ± 1°C.

Apparatus

The apparatus for voltammetry consisted of a PAR Model 173 potentiostat, a PAR Model 175 waveform generator, and a PDP-11 minicomputer. Positive feedback iR compensation was used in the experiments with fast scan rate. In the kinetic measurements sweep rates varied from 1 to 100 V s^{-1}. The peak potentials were measured from the voltammetric curves recorded at a sweep rate of 0.04 V s^{-1} using an X–Y recorder.

Estimates of the anodic to cathodic current ratio were obtained by comparing the voltammetric curves observed for a given system with the curves for *p*-dicyanobenzene (20) obtained at the same scan rate and depolarizer concentration but with 0.1 *M* tetraethylammonium perchlorate (Et_4NClO_4) as a supporting electrolyte.

The working electrode was a platinum disk (diameter 0.1 cm) electrolytically covered by a thin layer of silver and amalgamated by dipping in mercury.

The cell for kinetic measurements contained a Luggin capillary with a W wire as a pseudo-reference electrode (21) and a Hg pool as an auxiliary electrode. The cell for potential measurements was described previously (22). Peak potentials were determined for at least six curves, standard deviations being less than or equal to 1 mV.

Data Analysis

Analysis of the kinetic data was performed using the theoretical results calculated by Olmstead *et al.* (23) for cyclic voltammetry in which the product of the electron transfer process undergoes subsequent dimerization:

[1] $O + ne \rightarrow R$

[2] $R + R \rightarrow Z$

The second order rate constant k_{eff} defined by the equation

[3] $-dc_R/dt = 2k_{eff}c_R^2$

was determined by studying the variation in the ratio of anodic peak current to cathodic peak current with τ, the time interval between the standard potential on the cathodic sweep and the potential at which the sweep is reversed (23, 24). The value of $k_{eff}c_O^0\tau$, and thus k_{eff} itself, can be determined from the current ratio (23, 24), c_O^0 being the bulk concentration of O.

TABLE 1. The dependence of the dimensionless peak potential ξ_p on the kinetic parameter λ for a subsequent dimerization reaction in linear potential sweep voltammetry

λ	$-\xi_p$
0.25	1.00
0.50	0.91
1.0	0.765
1.5	0.65
2.0	0.575
4.0	0.365

In order to separate the ion pairing effects from the effects of dimerization of the reaction products, one must be able to estimate the shift in the peak potential from the standard potential due to each effect. Olmstead *et al.* (23) presented a plot $\xi_p/f = n(E_p^k - E^0)$ against $\lambda = k_{eff}c_O^0/nfv$ where E_p^k is the peak potential in the presence of dimerization (no ion pairing), E^0, the standard potential, v, the voltage sweep rate and $f = F/RT$. Since data of sufficient precision cannot be obtained from the graph, values of ξ_p and λ were calculated by the finite difference method described in the literature (25) with the integrated kinetic term (26); the new values are recorded in Table 1. For $\lambda > 2$, ξ_p may also be estimated by the approximate relationship (23)

[4] $\xi_p = (\ln 2\lambda - 3.12)/3$

to a precision better than ±0.02.[1]

Having estimated the shift in peak potential due to dimerization, $\Delta E_p^k = E_p^k - E_p^0$ where E_p^0 is the peak potential in the absence of a subsequent reaction and ion pair formation, one may find the contribution due to ion pairing ΔE_p^{ip} from the total observed shift in peak potential, ΔE_p:

[5] $\Delta E_p = \Delta E_p^{ip} + \Delta E_p^k$

The ion pair association constants are calculated from the slope of plots of exp ($f\Delta E_p^{ip}$) against metal ion concentration, [M^+] (22). Error estimates in the derived association constants were obtained from least-squares regression analysis.

Results

The cyclic voltammetric measurements performed in DMF in the presence of 0.1 *M* Et_4NClO_4 at a sweep rate of 0.1 V s^{-1} show that BA and AA form unstable ion radicals which disappear in subsequent dimerization reactions. In acetonitrile in the presence of the same supporting electrolyte all aldehydes form unstable radicals. The dimerization rate constants determined by the cyclic voltammetric method are presented in Table 2.

In the presence of alkali metal perchlorates, a shift of the peak potential in the positive direction is observed and the subsequent dimerization reaction proceeds more rapidly. The results of kinetic measurements in DMF are shown in Table 3. In the last column the shift of the peak potential (defined as the difference between the peak potential in the presence of alkali metal perchlorates and in 0.1 *M* Et_4NClO_4) is presented.

The data in Table 3 indicate that the rate constants for dimerization increase with increase in alkali metal cation concentration because of the formation of reactive ion associates. To analyse the mechanism of dimerization it is assumed (22,

[1]It should be noted that in the paper of Olmstead *et al.* (23) eq. [3] was written without the factor 2 normally used in defining the rate constant for reaction [2], so that k_{eff} in that work is twice that defined here. Since the definitions of λ given here is the same, the values of ξ_p recorded in Table 1 do not correspond to those which may be read from the graph in ref. 23.

Can. J. Chem. Downloaded from www.nrcresearchpress.com by 210.87.254.6 on 09/06/12
For personal use only.

TABLE 2. The rate constants for the dimerization reaction of 1×10^{-3} *M* aldehydes in 0.1 *M* Et_4NClO_4

Aldehyde	$k_{eff}/M^{-1}\,s^{-1}$ DMF	$k_{eff}/M^{-1}\,s^{-1}$ ACN
BA	8.5×10^3	9.5×10^4
1NA	[a]	7.0×10^3
2NA	[a]	1.7×10^4
AA	1.0×10^5	$>4 \times 10^5$

[a] Reversible at a sweep rate of 0.1 V s^{-1}.

TABLE 3. The rate constants and the shifts of peak potential of aldehydes in DMF in the presence of alkali metal perchlorates (ionic strength maintained constant at 0.1 with addition of Et_4NClO_4)

Aldehyde	Cation	$[Me^+]/M$	$k_{eff}/M^{-1}\,s^{-1}$	$\Delta E_p/V$
BA	K^+	0.005	9.7×10^4	0.030
		0.01	1.8×10^5	0.038
1NA	K^+	0.03	8.15×10^3	0.024
		0.05	1.65×10^4	0.029
		0.07	2.4×10^4	0.032
		0.09	2.75×10^4	0.033
		0.11[a]	3.6×10^4	0.036
	Na^+	0.01	1.0×10^4	0.026
		0.02	2.8×10^4	0.036
		0.03	5.5×10^4	0.045
		0.03	4.9×10^4	
		0.043	7.5×10^4	0.052
		0.05	1.05×10^5	0.056
		0.06	1.5×10^5	0.059
2NA	K^+	0.01	2.0×10^4	0.026
		0.02	4.5×10^4	0.037
		0.03	1.0×10^5	0.044
		0.04	1.15×10^5	0.050
		0.05	1.35×10^5	0.055
		0.061	1.95×10^5	0.060

[a] Ionic strength = 0.11.

27–32) that the reaction proceeds in three parallel pathways:

$$\left.\begin{array}{ll} [6] & 2R^{\cdot -} \xrightarrow{k_1} \\ [7] & R^{\cdot -} \ldots M^+ + R^{\cdot -} \xrightarrow{k_2} \\ [8] & 2R^{\cdot -} \ldots M^+ \xrightarrow{k_3} \end{array}\right\} \text{products}$$

The observed rate constant k_{eff} can be described by the equation (27–32):

$$[9] \quad k_{eff} = \frac{k_1 + k_2 K_{ass}[M^+] + k_3 K_{ass}^2 [M^+]^2}{(1 + K_{ass}[M^+]^2}$$

In order to analyze the data in Table 3 on the basis of eq. [9], the value of the ion pairing association constant K_{ass} was determined from the peak potential measurements as described above. This calculation first involved estimating k_{eff}, and then the corresponding value ΔE_p^k by interpolation in the table of values of λ and ξ_p (Table 1). The association constants were estimated from values of ΔE_p^{ip} obtained by subtracting ΔE_p^k from the observed value of ΔE_p.

TABLE 4. Association constants and rate constants for the dimerization reaction (reactions [7] and [8]) of aromatic aldehydes in DMF

Aldehyde	Cation	K_{ass}/M^{-1}	$k_2/M^{-1}\,s^{-1}$	$k_3/M^{-1}\,s^{-1}$
1NA	K^+	0.95±0.2	4.0×10^5	—
	Na^+	9.5 ±0.6	1.7×10^4	1.0×10^6
2NA	K^+	10.9 ±0.5	8.9×10^4	1.0×10^6
BA	K^+	63 ±8		

The rate constants k_1, k_2, and k_3 were determined by fitting the function $k_{eff}(1 + K_{ass}[M^+])^2$ to a quadratic equation in $[M^+]$ using least squares. Because the slopes of plots of E_p against log $[M^+]$ were smaller than 59 mV, the existence of associates more complex than 1-to-1 can be excluded for the concentration range studied (22). In all cases k_1 was negligible, indicating that dimerization involving the unassociated anion radicals can be neglected. The values of k_2 and where measurable, k_3, are recorded in Table 4. The estimated error in the rate constants is at least 30%.

Discussion

The comparison of the kinetic results indicate that $k_1 < k_2 < k_3$. It follows that the reaction of two ion pairs is the fastest and two ion radicals the slowest one and that Coulomb interactions have a large influence on the kinetics of the dimerization reaction.

From the data presented in Tables 2–4, it follows that the reactivity of ion radicals and ion pairs increases in the order: 1NA < 2NA < BA < AA. In order to explain this result, HMO calculations were performed assuming $\beta_{C=O} = 1.55\beta$ and $\alpha_O = \alpha + 1.7\beta$ (11). The spin densities obtained using the McLachlan modification (33) of the HMO method (with $\lambda = 1.2$) are presented in Table 5. In the dimerization reaction, the spin density at the reaction site is the main factor which influences the rate of reaction. The spin densities on the carbonyl carbon atom increase in the order: AA < 1NA < 2NA < BA. Thus, only the AA radical is out of order in comparing spin densities with reaction rates. However, one should take into account the possibility that dimers other than pinacols are formed. The highest spin density in the AA anion radical is at position 10, and it is possible that dimerization proceeds between the carbonyl carbon atom 1a and carbon 10 or between two radicals in position 10. A similar reaction for 2NA in position 1 should be more difficult because of steric hindrances. In fact, it was found that 2-acetylnaph-

Can. J. Chem. Downloaded from www.nrcresearchpress.com by 210.87.254.6 on 09/06/12
For personal use only.

TABLE 5. Spin densities calculated by the McLachlan modification of the HMO technique

Radical	Atom No.	Spin density
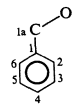	1a	0.3527
	1	0.0648
	2	0.1665
	3	−0.0526
	4	0.2374
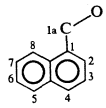	1a	0.1930
	1	0.0755
	2	0.2031
	3	−0.0396
	4	0.2963
	5	0.1256
	6	−0.0140
	7	0.0684
	8	0.0457
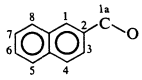	1a	0.2167
	1	0.3564
	2	0.0542
	3	−0.0219
	4	0.0534
	5	0.0322
	6	0.1117
	7	−0.0376
	8	0.1680
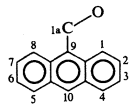	1a	0.1025
	1	0.0195
	2	0.0789
	3	−0.0179
	4	0.1212
	10	0.3833

thalene during macroelectrolysis in aqueous solutions forms only pinacols (34) whereas 1-acetylnaphthalene forms more complicated dimers (35). Reactions of BA and 1NA radicals at position 4 cannot be excluded. The possibility of the formation of such dimers for benzaldehyde was proposed by Nekrasov and co-workers (5, 15). Calculating the maximum sums of the spin densities one obtains: 2NA (C(1a) + C(1a) 0.4334, C(1) + C(1) 0.7128), 1NA (C(4) + C(4) 0.5926), BA (C(1a) + C(1a) 0.7054), AA (C(10) + C(10) 0.7666). This order (excluding the possibility of the reaction of 2NA in position 1) is in agreement with the observations in acetonitrile. However, one should remember that the HMO calculations are rather approximate and do not take into account the change in the spin density distribution due to the formation of ion pairs and the influence of the solvent. In order to substantiate the proposed mechanisms, further investigations are planned.

The results shown in Table 4 indicate that the association constants of ketyl radicals with the potassium cation in DMF increase in the sequence 1NA < 2NA < BA. This phenomenon may be attributed to the difference in electron distribution in the radical anions. The HMO calculations (36, 37) indicate that in the ion pairs of the carbonyl radicals, the metal atom is located over the CO bond close to oxygen atom. However, more accurate *ab initio* (38) and SCF LHP (39) calculations show two minima: one over the carbonyl oxygen and a deeper one on the line of the C—O bond (in the plane). Using the HMO method and assuming sp^2 hybridization in the molecules and an O—Me^+ distance equal to 3 Å, association energies were calculated for the two above locations of the metal ion. For 1NA and 2NA two possible orientations of the carbonyl group were taken into account:

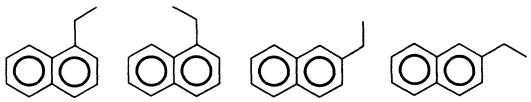

I II III IV

The calculated association energies are shown in Table 6. When the cation is located over the oxygen atom, the sequence of the change of association energies is in agreement with that observed experimentally. But, for the other location of the metal cation, the sequence of 1NA and 2NA is reversed. The simple HMO method does not take into account the influence of the solvent, and the calculated structure of the ion pair *in vacuo* may be different from the structure in the dipolar solvent. Miertus *et al.* (38) tried to account for the influence of the solvent but the simple physical model which they used seems to be insufficient because it does not consider specific donor–acceptor interactions. Thus, the model in which the metal ion is located over the oxygen atom is able to explain the experimental results more satisfactorily.

From the kinetic measurements it follows that in ACN all anion radicals are unstable and the subsequent reactions are faster in ACN than in DMF. This result may be rationalized on the basis of

TABLE 6. Association energies of free radicals with a monovalent cation, $r_{O—M^+} = 3$ Å

Radical	E_{ass}/β	
	Cation over oxygen	Cation on C—O line
BA	1.748	1.667
1NA(I)	1.689	1.605
1NA(II)	1.693	1.657
2NA(III)	1.716	1.632
2NA(IV)	1.712	1.614
AA	1.650	1.628

solute–solvent interactions. Considering the donor (DN) and acceptor (AN) numbers of DMF (DN = 26.6, AN = 16.0) and ACN (DN = 14.1, AN = 18.9) (40), it follows that ACN interacts somewhat more strongly with anions and DMF much more strongly with cations. These facts are also verified by the difference in free energies of solvation of Cl^- and K^+ in DMF and ACN ($\Delta\Delta G_{sv}(Cl^-) = 1.22$ kcal, $\Delta\Delta G_{sv}(K^+) = -3.6$ kcal) (41, 42). Thus, the reactivity of cations is greater in ACN than in DMF, and ion pairs are much more associated in ACN (40–42) and therefore, more reactive.

The results presented above indicate that the ion association process plays an important role in the electroreduction of aromatic aldehydes and that the simple HMO method may be helpful in explaining the properties and reactivity of the radical intermediates.

Acknowledgement

The financial support of the Natural Sciences and Engineering Research Council of Canada is gratefully acknowledged.

1. D. H. Evans. *In* Encyclopedia of electrochemistry of the elements. Vol. 12. *Edited by* A. J. Bard and H. Lund. Marcel Dekker, New York. 1978. p. 1.
2. J. M. Saveant and D. Tessier. J. Phys. Chem. **82**, 1723 (1978).
3. L. Nadjo and J. M. Saveant. J. Electroanal. Chem. **33**, 419 (1971).
4. F. Ammar, L. Nadjo, and J. M. Saveant. J. Electroanal. Chem. **47**, 146 (1973).
5. L. N. Nekrasov, L. I. Vykhodtseva, A. P. Korotkov, and L. P. Yupeva. Elektrokhimiya, **13**, 735 (1977).
6. G. Anthoine, J. Nasielski, and B. Wilmet-Devos. Bull. Soc. Chim. Belg. **78**, 465 (1969).
7. H. Letaw, Jr. and A. H. Gropp. J. Phys. Chem. **57**, 964 (1953).
8. S. Wawzonek and A. Gundersen. J. Electrochem. Soc. **107**, 537 (1960).
9. P. H. Given and M. E. Peover. J. Chem. Soc. 385 (1960).
10. P. H. Rieger and G. K. Fraenkel. J. Chem. Phys. **37**, 2811 (1962).
11. N. Steinberger and G. K. Fraenkel. J. Chem. Phys. **40**, 723 (1964).
12. S. G. Mairanovskii, I. E. Valashek, and G. I. Samokhalov. Elektrokhimiya, **3**, 611 (1967).
13. N. R. Armstrong, R. K. Quinn, and N. E. Vanderborgh. Anal. Chem. **46**, 1759 (1974).
14. N. R. Armstrong, N. E. Vanderborgh, and R. K. Quinn. J. Electrochem. Soc. **122**, 615 (1975).
15. L. N. Vykhodtseva and L. N. Nekrasov. Elektrokhimiya, **14**, 1439 (1978).
16. V. P. Gultyai, S. G. Mairanovskii, and T. Ya. Rubinskaya. Elektrokhimiya, **14**, 1880 (1978).
17. M. K. Kalinowski. Chem. Phys. Lett. **8**, 378 (1971).
18. L.-S. R. Yeh. J. Electroanal. Chem. **84**, 159 (1977).
19. B. G. Chauhan, W. R. Fawcett, and A. Lasia. J. Phys. Chem. **81**, 1476 (1977).
20. A. Baranski and W. R. Fawcett. J. Electroanal. Chem. **100**, 185 (1979).
21. W. R. Fawcett and A. Lasia. J. Phys. Chem. **82**, 1114 (1978).
22. A. Lasia. J. Electroanal. Chem. **102**, 117 (1979).
23. M. L. Olmstead, R. G. Hamilton, and R. S. Nicholson. Anal. Chem. **41**, 260 (1969).
24. Z. Galus. Electroanalytical methods of determining physiocochemical parameters. Panstwowe Wydawnictwo Naukowe, Warsaw. 1970. Chapt. 7.
25. S. W. Feldberg. *In* Electroanalytical chemistry. Vol. III. *Edited by* A. J. Bard. Marcel Dekker, New York. 1969. p. 199.
26. C. Amatore and J. M. Saveant. J. Electroanal. Chem. **102**, 21 (1979).
27. A. Lasia. J. Electroanal. Chem. **43**, 253 (1973).
28. M. D. Ryan and D. H. Evans. J. Electrochem. Soc. **121**, 881 (1974).
29. M. J. Hazelrigg, Jr. and A. J. Bard. J. Electrochem. Soc. **122**, 211 (1975).
30. J. Chodkowski, A. Chrzanowski, and M. K. Kalinowski. J. Electroanal. Chem. **74**, 235 (1976).
31. A. Kapturkiewicz and M. K. Kalinowski. Rocz. Chem. **51**, 1483 (1977).
32. A. Kapturkiewicz and M. K. Kalinowski. J. Phys. Chem. **82**, 1141 (1978).
33. A. D. McLachlan. Mol. Phys. **3**, 233 (1960).
34. J. Grimshaw and E. J. F. Rea. J. Chem. Soc. 683 (1971).
35. J. Grimshaw and E. J. F. Rea. J. Chem. Soc. 2628 (1967).
36. L. Pasimeni, M. Brustolon, and C. C. Corvaja. J. Chem. Soc. Faraday Trans. II, 223 (1972).
37. A. Lasia. Ph.D. Thesis, University of Warsaw, Warsaw, Poland. 1975.
38. S. Miertus, O. Kysel, and P. Mach. Collect. Czech. Chem. Commun. **45**, 351 (1980).
39. F. Bernardi and G. F. Pedulli. J. Chem. Soc. Perkin II, 194 (1975).
40. W. R. Fawcett and T. M. Krygowski. Can. J. Chem. **54**, 3283 (1976).
41. U. Mayer. Coord. Chem. Rev. **21**, 159 (1976).
42. U. Mayer. Pure Appl. Chem. **51**, 1697 (1979).

Can. J. Chem. Downloaded from www.nrcresearchpress.com by 210.87.254.6 on 09/06/12
For personal use only.

Muonium addition to vinyl monomers

J. M. STADLBAUER, B. W. NG, AND D. C. WALKER

Department of Chemistry and TRIUMF, University of British Columbia, Vancouver, B.C., Canada V6T 1Y6

Y. C. JEAN

Department of Physics, University of Missouri-Kansas City, Kansas City, MO 64110 U.S.A.

AND

Y. ITO

Research Center for Nuclear Science and Technology, University of Tokyo, 2-11-16 Yayoi, Tokyo, Japan

Received June 1, 1981

J. M. STADLBAUER, B. W. NG, D. C. WALKER, Y. C. JEAN, and Y. ITO. Can. J. Chem. **59**, 3261 (1981).

The chemical rate constants for the addition of the muonium atom (Mu) across the vinyl double bonds of acrylamide, acrylic acid, acrylonitrile, methylmethacrylate, and styrene were determined in aqueous solution; they are, respectively, $k_M = 1.9 \times 10^{10} M^{-1} s^{-1}$, $1.6 \times 10^{10} M^{-1} s^{-1}$, $1.1 \times 10^{10} M^{-1} s^{-1}$, $9.5 \times 10^{9} M^{-1} s^{-1}$, and $1.1 \times 10^{9} M^{-1} s^{-1}$. Since muonium can be considered a very light isotope of hydrogen, the kinetic isotope effects, k_M/k_H, for acrylamide (1.1) and acrylonitrile (2.8) were calculated. The muonium rate constants of these monomers are also compared to those of hydroxyl and methyl radical additions where available. The muonium substituted free radical formed by reaction with styrene is represented by two peaks in the Fourier Transform of the μSR spectrum at 500, 1500, and 2500 G with a hyperfine coupling constant of 213.5 MHz. This spectrum shows that Mu addition to styrene occurs at the vinyl bond only and not at the benzene ring.

J. M. STADLBAUER, B. W. NG, D. C. WALKER, Y. C. JEAN et Y. ITO. Can. J. Chem. **59**, 3261 (1981).

On a déterminé en solution aqueuse, les constantes de vitesse chimique de l'atome de muonium (Mu) à travers la double liaison vinylique de l'acrylamide, de l'acide acrylique, de l'acrytonitrile, du méthacrylate de méthyle et du styrène. Ces constantes sont respectivement de $K_M = 1{,}9 \times 10^{10} M^{-1} s^{-1}$, $1{,}6 \times 10^{10} M^{-1} s^{-1}$, $1{,}1 \times 10^{10} M^{-1} s^{-1}$, $9{,}5 \times 10^{9} M^{-1} s^{-1}$ et $1{,}1 \times 10^{9} M^{-1} s^{-1}$. Puisque le muonium peut être considéré comme un isotope très léger de l'hydrogène, on a calculé les effets isotopiques cinétiques k_M/k_H pour l'acrylamide (1,1) et l'acrylonitrile (2,8). On a également comparé les constantes de vitesse du muonium avec ces monomères à celles qui sont disponibles pour les additions radicalaires de l'hydroxyle et du méthyle. Le radical libre substitué du muonium formé par la réaction avec le styrène est représenté par deux pics dans la transformation de Fourier du spectre μSR à 500, 1500 et 2500 G avec une constante de couplage hyperfin de 213,5 MHz. Le spectre révèle que l'addition du Mu sur le styrène se produit seulement au niveau de la double liaison vinylique et non sur le noyau benzénique.

[Traduit par le journal]

Introduction

The muonium atom (Mu), one ninth the mass of ^1H but with the same Bohr radius and ionization potential, can be considered a very light radioactive isotope of hydrogen. It can, therefore, be used as a hydrogen-like probe to study addition, redox, abstraction, and spin conversion reactions. Muonium is formed when an energetic positive muon (μ^+) abstracts an electron from the stopping media and combines with it to form a bound state. The muon, a product of a pion decay, has a 2.2 μs lifetime which allows enough time to study the chemical reactions of muonium in many chemical systems (1–3).

Muonium Spin Rotation (MSR), the method used to observe the presence of the atom, monitors the muonium spin precession frequency under external magnetic fields. The Larmor frequency for the Mu precession under a transverse magnetic field is 1.39 MHz/G, while the precession frequency for the free muon is 13.6 kHz/G. The factor of 102 between the two frequencies distinguishes Mu from muons in other chemical states. Further descriptions of the MSR technique have been detailed elsewhere (2).

Mu atoms have been observed to form in pure liquids such as water (3), alcohols (4), and hydrocarbons (5). The relatively long lived (up to 4 μs in water) precession signals of Mu in these pure liquids indicate that spin depolarization reactions between Mu and the liquids are relatively unimportant. However, if these liquids are used as solvents for various solutes of interest, the chemical reactivity of Mu towards those solutes can be easily measured. As the free triplet Mu reacts with the solute its precession signal is damped and a muonium decay constant, λ, can be obtained. From these decay constants second order chemical rate constants can be calculated and then compared with the related hydrogen atom rate constant (when available) to determine kinetic isotope effects.

Experimental

(A) MSR: Muonium Spin Rotation Measurements

At the M20 channel at TRIUMF a beam of 4.1 MeV surface muons was made to strike the sample target, which consisted of approximately 80 mL of solution contained in a shallow Teflon

0008-4042/81/233261-06$01.00/0

©1981 National Research Council of Canada/Conseil national de recherches du Canada

Can. J. Chem. Downloaded from www.nrcresearchpress.com by 210.87.254.5 on 09/06/12
For personal use only.

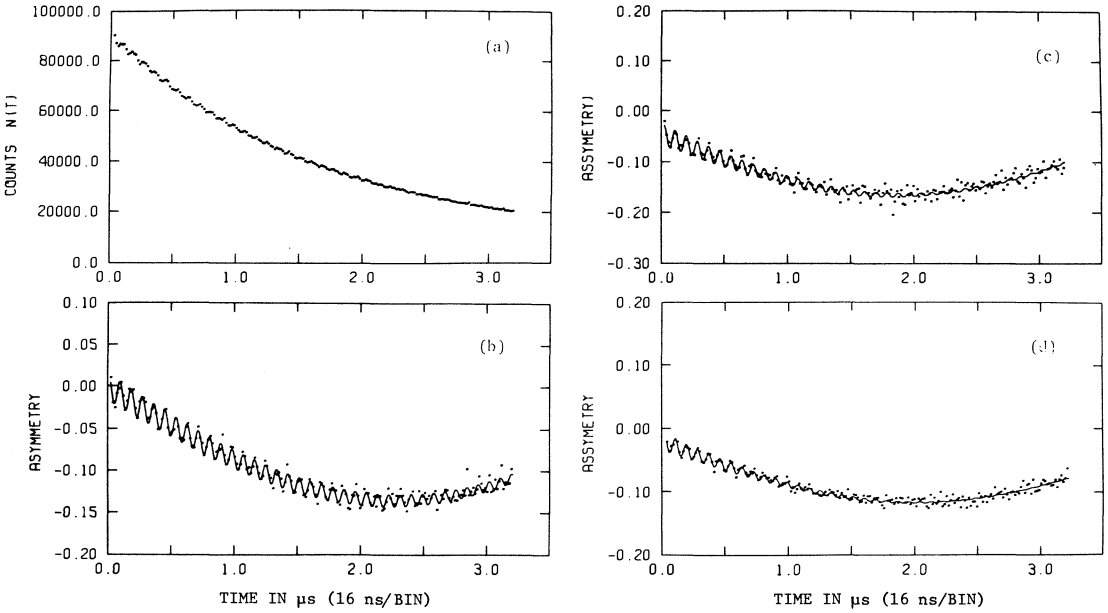

FIG. 1. (*a*) Raw data histogram for water at 8G before MINUIT fit; (*b*) the same data computer fitted to eq. [1]; (*c*) computer fitted histogram for 0.02 m*M* acrylamide; and (*d*) 0.05 m*M* acrylamide aqueous solution.

cell with 0.007 cm mylar as muon window. With a range of 150 mg cm^{-2} almost all of the incident muons came to rest in the target solution. Helmholtz coils provided transverse magnetic fields of 80 G for diamagnetic muon data and 8 G for paramagnetic muonium data.

The MSR experimental histograms were computer processed with a χ^2-minimization program (MINUIT) to fit an eight-parameter function. Equation [1] shows that function with the background and muon decay subtracted out.

$$[1]\quad A(t) = A_\mu \cos(\omega_\mu t + \phi_\mu) + A_M \exp(-\lambda t)\cos(\omega_M t - \phi_M)$$

where A_μ and A_M are the muon and muonium amplitudes, ω_μ and ω_M their frequencies, ϕ_μ and ϕ_M their initial phases, and λ the muonium spin polarization decay constant. Figure 1 shows typical histograms of both raw and fitted data. The bimolecular rate constant, k_M, for the reaction between muonium and the solute, of concentration [S], can be calculated from λ by eq. [2].

$$[2]\quad \lambda = \lambda_0 + k_M[S]$$

The decay constant for the pure water solvent, λ_0, has a value of about $(2.4 \pm 0.6) \times 10^5$ s^{-1} (4–6). The λ values for the separate left and right (or top and bottom, depending on field orientation) detectors are plotted against the solute concentration and the slope, k_M, of the best line determined.

(B) MRSR: Muonium Radical Spin Rotation

For an initial look at muonium radicals in pure styrene, high energy muons (24 MeV) were made to strike the samples sealed in glass cells held in transverse magnetic fields up to 2500 G. Dissolved oxygen was removed from the bulk monomer by the freeze–pump–thaw method before sealing. Resultant data were examined by a Fast Fourier Transform (FFT) computer program to obtain radical frequencies and the hyperfine coupling constant, as described elsewhere (7, 8). Similar radical studies in styrene were also performed using the surface muons in conjunction with the thin Teflon cells at fields up to 500 G.

(C) Chemicals

Acrylamide and acrylic acid were supplied by Eastman and were transferred directly from the reagent bottle. Acrylonitrile, methylmethacrylate, and styrene were purchased from Aldrich and purified before use. The acrylic acid contained 200 ppm *p*-methoxyphenol as an inhibitor. At the solute concentrations used, 5×10^{-5} *M* and 7.4×10^{-5} *M*, the inhibitor would be present only at $\sim 10^{-8}$ *M* so it could not contribute significantly to the decay of muonium because the reaction with acrylic acid turns out to be near the diffusion-controlled limit of 2×10^{10} M^{-1} s^{-1}.

All aqueous solutions were bubbled immediately before and during the experiment with high purity helium to remove dissolved oxygen. Because of the volatile nature of the acrylic and styrene monomers the gas was passed through a prebubbler containing a solution of the same concentration as the target sample.

Results

Table 1 shows the muonium rate constants, k_M, obtained in this study for the five monomers investigated. These values were obtained from the measurement of λ at two solute concentrations, prepared individually, and at each concentration there were two independent (left and right or top and bottom) histograms. Each value of k_M, therefore, arose from the averaging of four values of λ. Though the statistical error on each value of λ arising from the computer fits range, in these experiments, from 5% to 17%, the overall actual probable errors are taken to be about ±25%. As often transpires in MSR measurements there are unknown random irreproducibilities arising from

Can. J. Chem. Downloaded from www.nrcresearchpress.com by 210.87.254.5 on 09/06/12
For personal use only.

TABLE 1. Reaction rate data for Mu addition to vinyl monomers in aqueous solution

Monomer	[S]/M	$\lambda/10^6\ s^{-1}$	$k_M^*/10^{10}\ M^{-1}\ s^{-1}$
Acrylamide	2.0×10^{-5}	0.83	1.90±0.13
	5.0×10^{-5}	1.23	
Acrylic acid	5.0×10^{-5}	0.89	1.55±0.25
	7.4×10^{-5}	1.63	
Acrylonitrile	2.0×10^{-5}	0.45	1.14±0.20
	5.0×10^{-5}	0.88	
Methylmethacrylate	2.6×10^{-5}	0.58	0.95±0.19
	5.0×10^{-5}	0.80	
Styrene	5.0×10^{-5}	0.38	0.11±0.01
	8.0×10^{-5}	0.41	

*Errors quoted are the computed statistical errors; but, as pointed out in the text, the actual reproducibilities may be ~±25 %.

the cell positioning, muon beam asymmetry, detector thresholds, background counts, sample contamination, and error in the evaluation of sample concentrations, which together seem to contribute some ±25% to the overall reliability of a k_M value (6). Within the broad context of rate constant data obtained by direct physical techniques or competitive rate methods, this level of reproducibility is quite good.

Figure 2 shows the FFT spectra of the styrene sample at 500, 1500, and 2500 G. At 1500 G the radical frequencies at 83.5 MHz and 130.1 MHz add to give the hyperfine coupling constant, A_μ = 213.6 MHz. The same coupling constant is obtained from the radical frequencies of 70.3 MHz and 143.2 MHz at 2500 G, and 92.3 MHz and 121.6 MHz at 500 G. Acrylonitrile and methylmethacrylate as pure liquids were examined briefly (~2 million events) and also showed muonium radicals. The FFT spectra indicated that the hyperfine coupling constants were 281 and 279 MHz respectively for acrylonitrile and methylmethacrylate.

Discussion

It can be seen that k_M ranges from $1\times10^{10}\ M^{-1}\ s^{-1}$ to $2\times10^{10}\ M^{-1}\ s^{-1}$ for the acrylic vinyl bonds and is $1\times10^{9}\ M^{-1}\ s^{-1}$ for styrene. The reaction type is undoubtedly that of addition to the vinyl bond. The net result of addition is likely to be the radical shown in [3],

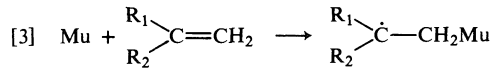

where R_1 = H, R_2 = $CONH_2$ for acrylamide; R_1 = H, R_2 = CO_2H for acrylic acid; R_1 = H, R_2 = CN for acrylonitrile; R_1 = CH_3, R_2 = CO_2CH_3 for methylmethacrylate; and R_1 = H, R_2 = C_6H_5 for styrene. Roduner *et al.* (7) have shown that muonium radicals such as in reaction [3] produce a Fourier Transform spectrum containing three peaks. The most intense is the diamagnetic muon, the other two are due to the radical. The addition of the frequencies of these two radical peaks gives a value for the hyperfine coupling constant, a_μ, that is

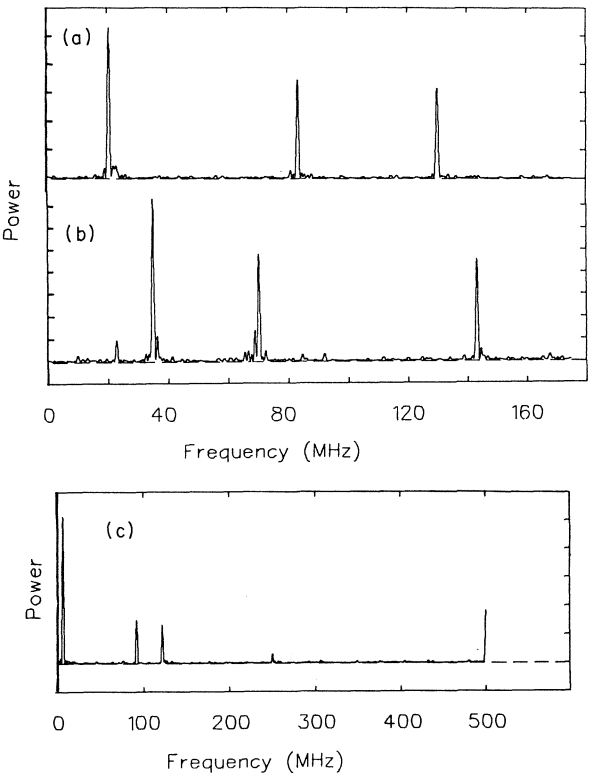

FIG. 2. Fast Fourier Transform spectra of styrene radical from muonium addition to vinyl bond; (*a*) at 1500G, (*b*) at 2500G, and (*c*) at 500G. The latter utilized surface (4.1 MeV) muons. (In the Fourier transform spectrum of (*c*) the peaks at 500 and 250 Hz should be ignored. They are spurious effects arising from the 1GHz clock as beat frequencies.)

Can. J. Chem. Downloaded from www.nrcresearchpress.com by 210.87.254.5 on 09/06/12
For personal use only.

TABLE 2. Monomer reactions with other simple free-radicals where available*

Monomer	Rate constant/M^{-1} s^{-1} k_H	k_M/k_H	k_{OH}	$(k_2/k_1)_{Me}$†
Acrylamide	1.8×10^{10} (11)	1.1	$(2.0\pm0.5)\times10^9$ (15)	
Acrylic acid			1.4×10^9 (13)	
Acrylonitrile	$(4.0\pm0.5)\times10^{10}$ (12)	2.8	3.4×10^9 (20) $(2.9\pm0.3)\times10^9$ (12)	1730 ± 50 (18) 1370 (19)
Methylmethacrylate				1440 ± 65 (18) 1250 (19)
Styrene			$(6.0\pm0.6)\times10^9$ (13)	792 (19)

*Reference citations in parentheses.
†k_2 = methyl addition, k_1 = hydrogen abstraction by methyl radical. N.B. For muonium, this ratio is also $\sim10^3$, based on a comparison of maleic acid versus formate (6).

independent of the magnetic field. The styrene spectra presented in Fig. 2 clearly show that such a radical is produced in bulk styrene with a field independent coupling constant of $a_\mu = 213.5$ MHz. This observation strongly confirms (see later) that addition across the vinyl bond occurred. Furthermore, the evidence of Fig. 2(*c*) shows that only one radical is observed and that there is negligible production of cyclohexadienyl radicals which are expected to have hyperfine coupling constants of ~500 MHz (7). The radicals are observed in the μSR time-window of 10^{-7} to 10^{-5} s, so it is conceivable that they are not the primary radicals but result from rearrangements.

That "addition" rather than "abstraction" occurred is certainly indicated by these observed muonium radicals. This is also in accord with the kinetic data with regard to both the absolute rate constants and the kinetic isotope effect relative to H. Thus addition reactions typically have $k_M \sim 10^{10}\ M^{-1}$ s^{-1} whereas H-abstraction reactions have $k_M \sim 10^7$–$10^8\ M^{-1}$ s^{-1}; and additions have isotope effects close to unity whereas for abstraction of H-atoms k_M/k_H has been found to be of the order of 10^{-2} (2, 4, 6).

The k_M values obtained for the acrylic monomers ($1–2 \times 10^{10}\ M^{-1}$ s^{-1}) are similar to those determined by Percival *et al.* (4) for muonium addition to the vinyl bond in maleic and fumaric acids. The reaction with maleic acid has also been shown to have an activation energy of ~17 kJ mol^{-1}, corresponding to the activation for diffusion in water (6). We conclude, therefore, that the reaction with the acrylic compounds is within a factor of two or so of the diffusion-controlled limit. The question then arises, why do the various acrylic monomer rates differ slightly and what factors, such as electrophilicity and steric hindrance, reduce the rate constant slightly below the diffusion limited value? In the case of styrene the k_M value is more than one order of magnitude less than the diffusion limited value; but here π-delocalization may play a dominant role. A comparison of these initiation rates with those obtained previously for H, OH, and CH_3 radicals could also be of importance. These matters are discussed below.

From Table 1 the order of reactivity of the four acrylic monomers can be seen to be methylmethacrylate (MMA) ≤ acrylonitrile (AN) < acrylic acid (AA) < acrylamide (AM). MMA, the least reactive of the four, has the least accessible double bond due to the "blocking" effect of the methyl group on the α carbon. The other three are three-carbon straight-chain conjugated compounds with the vinyl bond equally open to attack. Of these, acrylamide and acrylic acid, having the carbonyl oxygen to withdraw electron shielding from the target carbons, would be expected to react slightly faster than acrylonitrile with muonium—a nucleophile. Between acrylamide and acrylic acid a difference lies in that unbuffered acrylic acid solution (pK_a =4.25) (9), is 64% dissociated at a solute concentration of $5.0 \times 10^{-5}\ M$. One would expect to see a somewhat slower reaction rate for the acid anion, compared to the undissociated acid, because the delocalized anionic charge could increase the carbon target shielding.

Styrene, with $k_M = 1.1 \times 10^9\ M^{-1}$ s^{-1}, is the least reactive of the five monomers studied. It also has the highest degree of conjugation and the largest π-delocalization of any of these monomers. Therefore, we must conclude that this delocalization stabilizes the molecule thereby reducing the efficiency of muonium addition.

From absorption band labelling, Swallow (10) inferred that for H atom addition reactions with styrene, the hydrogen possibly added to the ring 85% of the time and to the vinyl bond 15% of the time. This indicates that the conjugated π-electron cloud is delocalizing the H atom attack over the

Can. J. Chem. Downloaded from www.nrcresearchpress.com by 210.87.254.5 on 09/06/12
For personal use only.

Can. J. Chem. Downloaded from www.nrcresearchpress.com by 210.87.254.5 on 09/06/12
For personal use only.

entire molecule. This, however, we believe to be incorrect. If H adds to the ring as well as to the vinyl bond of styrene then Mu should also. One would therefore expect two radicals to be formed with distinctive hyperfine coupling constants, one around 200 MHz for the vinyl radical and one around 500 MHz for the ring radical. Roduner *et al.* have shown that the cyclohexadienyl radicals from the Mu addition to benzene and the tetramethylethane radical from the Mu addition to tetramethylethylene have coupling constants of 514.6 MHz and 161.3 MHz, respectively (7, 8). We have calculated the coupling constants of the styrene, acrylonitrile, and methylmethacrylate radicals to be 213.6 MHz, 281 MHz, and 279 MHz, respectively. From the tetramethylethane and acrylic radical constants, almost half the magnitude of the cyclohexadienyl radical coupling constant, we conclude that Mu is adding to the vinyl double bond of styrene rather than to the molecule's benzene ring.

Table 2 lists some rate constants for hydrogen and hydroxyl additions, and methyl radical rate constant ratios, for these same monomers. The only H atom rate constants found were for acrylamide and acrylonitrile, $k_H = 1.8 \times 10^{10}\ M^{-1}\ s^{-1}$ (11) and $(4.0 \pm 0.5) \times 10^9\ M^{-1}\ s^{-1}$ (12), respectively. Using these we calculate kinetic isotope effects, k_M/k_H, of 1.1 ± 0.4 for acrylamide and 2.8 ± 1.0 for acrylonitrile. The first agrees nicely with the k_M/k_H of 1.4 calculated for maleic acid (4, 6) which indicate no mass effect on these addition reactions. At the diffusion-controlled limit, it is a matter of current interest as to whether the Stokes–Einstein relationship should apply to particles as small as H and Mu, or whether there should be an isotope effect of 3, as with acrylonitrile, because the mean velocity of Mu (with a mass 1/9 that of H) is three times that of H (6). However, there is no obvious reason for the k_M/k_H values for these two addition reactions to be different. Therefore, and because of the limited amount of H atom addition rate constant data, we reserve judgement on the matter of kinetic isotope effects at this time.

The hydroxyl radical data shows a trend that points toward OH being less nucleophilic than Mu. For OH the order of reactivity towards the monomers is reversed, with styrene having a rate constant $k_{OH} = 6 \times 10^9\ M^{-1}\ s^{-1}$ (13, 14) while acrylamide and acrylic acid have the smaller specific rates at $2 \times 10^9\ M^{-1}\ s^{-1}$ (15) and $1.4 \times 10^9\ M^{-1}\ s^{-1}$ (13, 16), respectively. This is also expected as the hydroxyl oxygen will decrease that radical's nucleophilicity compared to hydrogen or muonium atoms. The increased reactivity of styrene toward the more electrophilic hydroxyl radical compared to the acrylic monomers is further supported by the earlier cationic, anionic, and radical initiated polymerization studies (17). These data show that (*i*) styrene and the acrylics polymerize equally when radical initiated (50:50 mixtures of styrene and MMA produce a copolymer containing equal proportions of the two monomers), (*ii*) styrene prefers cationic polymerization (the same 50:50 mixture produces only polystyrene), and (*iii*) MMA prefers anionic polymerization (the polymer produced contains only MMA). The cationic propagation of styrene shows that it undergoes electrophilic attack, while the anionic data show that MMA, and presumably the other acrylic monomers, undergo nucleophilic attack. A comparison of our muonium data with the published hydroxyl (electrophilic) rate data therefore supports the conclusion that muonium acts as a nucleophilic reagent in its addition reactions.

In the case of the methyl radical additions, the rate constant for the addition, k_2, is given relative to the rate constant for the H-abstraction by the radical, k_1 (18, 19). The three monomer–methyl reaction constant ratios listed (see Table 2) for acrylonitrile, methylmethacrylate, and styrene show the same trend in reactivity as do the muonium specific rates. In fact the ratio of the muonium rate constants for acrylonitrile and methylmethacrylate (k_MAN/k_MMMA) and the ratio of their methyl addition constants (k_2AN/k_2MMA) are both 1.2. This ratio of the reactivities of these two monomers might be a useful indicator of the steric hindrance of the H vs. CH_3 substitution on the α carbon. Such a comparison between styrene and MMA, however, does not hold true. This is expected because the hydrogen addition band labelling studies (10) indicate that all accessible carbons in styrene are attacked and there is a higher probability for H atom abstraction from styrene by methyl radicals than from MMA. The latter factor would decrease the apparent reactivity gap between styrene and MMA for methyl additions (k_1 styrene > k_1MMA) but not for muonium additions.

Conclusion

Though the five muonium rate constants reported are rather similar, we believe the preceding arguments based on electrophilic and steric factors can explain their differences and their falling just short of the diffusion-controlled limit. Although we reserve judgement on the kinetic isotope effects in the Mu compared to H addition reactions, the only ones for which H atom data are available are close to the diffusion controlled limit. It would be interesting to know k_M/k_H for the styrene reaction

which, at least for Mu, occurs at more than an order of magnitude slower than the collision frequency due to the π-delocalization.

Since there is a scarcity of data on the initiation of polymerization of monomers by the simplest atom, the hydrogen atom, perhaps these muonium atom data will fill a real need. Once the kinetic isotope effect is fully understood, the MSR method could supercede the more tedius H-atom techniques in this and other areas.

Acknowledgements

We wish to thank T. Suzuki and P. W. Percival for their kind assistance. The financial support by the Natural Sciences and Engineering Research Council of Canada is gratefully acknowledged.

1. (*a*) V. W. Hughes. Ann. Rev. Nucl. Sci. **16**, 445 (1966); (*b*) J. H. Brewer and K. M. Crowe. Ann. Rev. Nucl. Part. Sci. **28**, 239 (1978).
2. D. G. Fleming, D. M. Garner, L. C. Vaz, D. C. Walker, J. H. Brewer, and K. M. Crowe. Adv. Chem. Ser. **175**, 279 (1979).
3. P. W. Percival, H. Fischer, M. Camani, F. N. Gygax, W. Ruegg, A. Schenck, H. Schilling, and H. Graf. Chem. Phys. Lett. **39**, 333 (1976).
4. (*a*) P. W. Percival, E. Roduner, and H. Fischer. Adv. Chem. Ser. **175**, 335 (1979); (*b*) P. W. Percival, E. Roduner, H. Fischer, M. Camani, F. N. Gygax, and A. Schenck. Chem. Phys. Lett. **47**, 11 (1977).
5. Y. Ito, B. W. Ng, Y. C. Jean, and D. C. Walker. Can. J. Chem. **58**, 2395 (1980).
6. B. W. Ng, Y. C. Jean, Y. Ito, T. Suzuki, J. H. Brewer, D. G. Fleming, and D. C. Walker. J. Phys. Chem. **85**, 454 (1981).
7. (*a*) E. Roduner, P. W. Percival, D. G. Fleming, J. Hochmann, and H. Fischer. Chem. Phys. Lett. **57**, 37 (1978); (*b*) E. Roduner. Ph.D. Thesis, Universität Zürich. 1979.
8. E. Roduner and H. Fischer. Chem. Phys. **54**, 261 (1981).
9. V. Madhaven, N. N. Lichtin, and E. Hayon. J. Org. Chem. **41**, 2320 (1976).
10. A. J. Swallow. Adv. Chem. Ser. **82**, 499 (1968).
11. K. W. Chambers, E. Collinson, and F. S. Dainton. Trans. Faraday Soc. **66**, 142 (1970).
12. G. V. Buxton, P. G. Ellis, and T. F. W. Mckillip. J. Chem. Soc. Faraday Trans. 1, **75**, 1050 (1979).
13. F. Ross and A. B. Ross. Report 1977 NSRDS-NBS-59.
14. O. Brede, W. Helmstreit, and R. Mehnert. J. Prakt. Chem. **316**, 402 (1974).
15. K. W. Chambers, E. Collinson, F. S. Dainton, W. A. Seddon, and F. Wilkinson. Trans. Faraday Soc. **63**, 1699 (1967).
16. C. Walling and B. M. El-Taliawi. J. Am. Chem. Soc. **95**, 855 (1973).
17. (*a*) D. S. Trifan and P. D. Bartlett. J. Am. Chem. Soc. **81**, 5573 (1959); (*b*) C. Walling, E. R. Briggs, W. Cummings, and F. R. Mayo. J. Am. Chem. Soc. **72**, 48 (1950); (*c*) F. R. Mayo and C. Walling. Chem. Rev. **46**, 278 (1950); (*d*) F. R. Mayo and F. M. Lewis. J. Am. Chem. Soc. **66**, 1594 (1944).
18. L. Herk, A. Stefani, and M. Szwarc. J. Am. Chem. Soc. **83**, 3008 (1961).
19. F. Leavitt, V. Stannett, and M. Szwarc. J. Polym. Sci. **31**, 193 (1958).
20. O. K. Borggaard. Acta Chem. Scand. **26**, 3398 (1972).

Can. J. Chem. Downloaded from www.nrcresearchpress.com by 210.87.254.5 on 09/06/12
For personal use only.

Triphenylphosphine complexes of cadmium(II) perchlorate, nitrate, and trifluoroacetate preparation, characterization, and spectral studies

RAM G. GOEL AND NARENDRA K. JHA[1]

Guelph Waterloo Centre for Graduate Work in Chemistry, University of Guelph, Guelph, Ont., Canada N1G 2W1

Received May 11, 1981

RAM G. GOEL and NARENDRA K. JHA. Can. J. Chem. **59**, 3267 (1981).

1:2 complexes, $CdX_2(PPh_3)_2$, where X = ClO_4, NO_3, CF_3CO_2 and 1:1 complex, $Cd(CF_3CO_2)_2PPh_3$, have been isolated and characterized by elemental analysis and by vibrational and $^{31}P—\{^1H\}$ nmr spectral measurements. Conductance measurements show that the complexes behave as non-ionic species in dichloromethane. The vibrational spectra of the perchlorato complex are consistent with a six-coordinate structure in the solid state as well as in solution but it is difficult to deduce the structures of the nitrato and trifluoroacetato complexes from the spectral data. Assignments for the metal–ligand stretching frequencies for all the four complexes have been proposed. The $^{31}P—\{^1H\}$ nmr spectra of the four complexes have been discussed. Formation of the 1:3 and 1:4 complexes, $Cd(ClO_4)_2(PPh_3)_3$ and $Cd(ClO_4)_2(PPh_3)_4$, in solution, has also been established by $^{31}P—\{^1H\}$ nmr spectral measurements.

RAM G. GOEL et NARENDRA K. JHA. Can. J. Chem. **59**, 3267 (1981).

On a isolé les complexes 1:2 du type $CdX_2(PPh_3)_2$ où X = ClO_4, NO_3, CF_3CO_2 et le complexe 1:1 du type $Cd(CF_3CO_2)_2$ PPh_3 et on les a caractérisé par l'analyse élémentaire et par les mesures des spectres de vibration et de rmn du $^{31}P—\{^1H\}$. Des mesures de conductance montrent que les complexes se comportent dans le dichlorométhane comme des espèces non ioniques. Les spectres de vibration du complexe perchloré sont en accord avec une structure hexacoordonnée aussi bien à l'état solide qu'en solution, mais il est difficile de déduire la structure des complexes nitrés ou trifluoroacétyés à partir des données spectrales. On a identifié les fréquences d'élongation métal–ligand des quatres complexes. On discute des spectres de rmn du $^{31}P—\{^1H\}$ des quatres complexes. On a également mis en évidence la formation des complexes 1:3 et 1:4 du type $Cd(ClO_4)_2(PPh_3)_3$ et $Cd(ClO_4)_2(PPh_3)_4$ en solution en utilisant les données spectrales de la rmn du $^{31}P—\{^1H\}$.

[Traduit par le journal]

Introduction

Tertiary phosphine complexes of cadmium(II) and mercury(II) halides were first reported (1) more than 40 years ago. In the intervening years phosphine complexes of several other mercury(II) derivatives such as pseudohalides (2–11), carboxylates (12–16), nitrate (2, 17–19), and perchlorate (2, 20, 21) have been prepared and investigated by spectroscopic as well as X-ray diffraction studies. Surprisingly, phosphine complexes of cadmium(II) derivatives other than the halides have remained virtually unexplored.

Cadmium(II) halides are known to form only 1:2 complexes with triphenyl phosphine (1, 22) as well as with *para*- and *meta*-substituted triarylphosphines (23). These complexes are indicated (22–24) to be molecular species with a pseudotetrahedral coordination around cadmium. Recent work in this laboratory showed that cadmium(II) thiocyanate, unlike cadmium(II) halides, forms only 1:1 complexes with triarylphosphines (25) as well as with trialkylphosphines such as tricyclohexylphosphine (25) and tri-*tert*-butylphosphine (26). The work reported herein was undertaken to seek information on triphenylphosphine complexes of cadmium(II) salts of oxy-anions such as perchlorate, nitrate, carboxylates, and to compare the properties of such complexes with the analogous mercury(II) complexes.

Results and Discussion

Cadmium(II) perchlorate as well as the nitrate, like the halides, gave only the 1:2 complexes upon treatment with triphenylphosphine. Attempts to isolate 1:1 complex of either salt gave the 1:2 complex and the unreacted cadmium(II) salt. The failure to isolate 1:1 complexes of cadmium(II) perchlorate and nitrate is thus in marked contrast with the behaviour of mercury(II) perchlorate and nitrate both of which form readily isolable 1:2 as well as 1:1 complexes (2) with triphenylphosphine. Cadmium(II) trifluoroacetate, like mercury(II) trifluoroacetate (14), readily gave 1:1 as well as 1:2 complexes. However, cadmium(II) acetate, in marked contrast with mercury(II) acetate (14), did not react with triphenylphosphine as shown by the infrared and $^{31}P—\{^1H\}$ nmr spectral measurements of the products obtained upon treating cadmium(II) acetate with varying amounts of the phosphine.

The analytical data, melting points, molar conductances, and the characteristic infrared frequencies due to the anionic groups for the four complexes isolated in the present study are given in Table 1. All four complexes are white crystalline solids. The

[1]Permanent address: Department of Chemistry, Indian Institute of Technology, Delhi, New Delhi–110016, India.

0008-4042/81/233267-06$01.00/0

©1981 National Research Council of Canada/Conseil national de recherches du Canada

Can. J. Chem. Downloaded from www.nrcresearchpress.com by 210.87.254.40 on 09/06/12
For personal use only.

TABLE 1. Analytical data, melting points, conductance, and characteristic infrared frequencies (cm^{-1}) due to the anionic ligands

Compound	Melting point	C		H		Λ_M*	Infrared frequencies†
		Calcd.	Found	Calcd.	Found		
$Cd(ClO_4)_2(PPh_3)_2$	190‡	51.72	52.02	3.62	3.67	5.05	1165s, 1120s, 998s, 888s, 630m, 618m, 605m, 484sh
$Cd(NO_3)_2(PPh_3)_2$	245§	56.81	57.29	3.97	4.01	2.99	1465s, 1266s, 1017ms 810m, 736ms, 685s
$Cd(CF_3CO_2)_2(PPh_3)_2$	218	55.66	55.02	3.50	3.52	0.38	1690m, 1648s
$Cd(CF_3CO_2)_2PPh_3$	246	43.98	44.25	2.51	2.51	0.28	1690s, 1650m

*In ohm^{-1} cm^2 mol^{-1} at 25°C for $\sim 10^{-3}$ *M* solution in dichloromethane.
†In cm^{-1} for the solid state.
‡Compound exploded.
§Compound decomposed.

trifluoroacetato complexes are air-stable but the nitrato and perchlorato complexes are sensitive to atmospheric moisture. All the complexes are soluble in polar organic solvents like acetone and dichloromethane and insoluble in pentane or light petroleum ether. The complexes of cadmium(II) trifluoroacetate are also soluble in benzene. Molar conductance of 10^{-3} *M* solutions of the trifluoroacetato complexes, in dichloromethane, were less than 0.4 ohm^{-1} cm^2 mol^{-1} indicating no ionization of these complexes in solution. The Λ_M values for the nitrato and perchlorate complexes were 3 and 5 ohm^{-1} cm^2 mol^{-1}, respectively, showing slight ionization; the molar conductance for the 1:1 electrolyte NEt_4ClO_4, in dichloromethane, was found to be 40 $ohms^{-1}$ cm^2 mol^{-1}.

The infrared spectra of the complexes were examined in the 4000 to 50 cm^{-1} region, in the solid state. The infrared frequencies due to the anionic ligands for each complex were assigned with reasonable certainty by comparing the spectra with that of free phosphine. As shown by the data in Table 1, the infrared spectrum of the perchlorate complex showed strong bands at 1165, 1120 and 998, and 888 cm^{-1} and medium bands at 630, 618, 605, and 484 cm^{-1} due to the vibrations of the perchlorate groups. It is, therefore, evident that the perchlorate groups in this complex act as bidentate ligands (27*a*). The infrared spectrum of a dichloromethane solution of the complex in the 1200 to 800 cm^{-1} region showed bands similar to those observed in the solid state; the perchlorate bands were at 1160, 1125, 998, and 890 cm^{-1}. Thus, the observed reduction in the perchlorate symmetry cannot be attributed to the solid state effects and the complex is indicated to contain octahedrally coordinated cadmium in the solid state as well as in solution. The infrared spectrum of the nitrato complex showed strong or medium bands at 1465, 1266, 1017, 810, 736, and 685 cm^{-1} due to the internal vibrations of the nitrate groups (27*b*). Thus, the symmetry of the nitrate groups in the nitrato complex is also not higher than C_{2v}. Although it is difficult to distinguish between unidentate and bidentate nitrato groups on the basis of infrared data alone, the observed infrared frequencies due to the nitrate groups in $Cd(NO_3)_2(PPh_3)_2$ are similar to those reported for $Cu(NO_3)(PPh_3)_2$ (28) which contains bidentate nitrato group as shown by an X-ray crystallographic study (29). The infrared bands at 1465 and 1266 cm^{-1} observed for $Cd(NO_3)_2(PPh_3)_2$ in the solid state were also observed in the spectrum of its solution in dichloromethane. Thus, like the perchlorato complex, the nitrato complex is also indicated to maintain its solid state structure in solution.

The vibrational frequencies due to the internal vibrations of the trifluoroacetate group have been established and attempts have been made to correlate these frequencies with the mode of its bonding (30). Since the number of infrared or Raman bands observed for a trifluoroacetate group is independent of its environment, the antisymmetric and symmetric CO_2 stretching frequencies and their separation have been used to infer the mode of its bonding. As shown by the data in Table 1, the infrared spectra for both the 1:1 and 1:2 complexes of cadmium(II) trifluoroacetate showed bands at ca. 1650 and 1690 cm^{-1} which are attributable to the antisymmetric CO_2 stretching vibration of the coordinated trifluoroacetate groups. The relative intensities of these bands in the two complexes were, however, reversed. Unfortunately, the symmetric CO_2 stretching frequency could not be ascertained for either compound due to the presence of several phenyl bands in this region. It is, therefore, difficult to ascertain the mode of bonding of the trifluoroacetate groups in either complex. The antisymmetric CO_2 stretching frequencies for both the complexes were not significantly altered in

Can. J. Chem. Downloaded from www.nrcresearchpress.com by 210.87.254.40 on 09/06/12
For personal use only.

TABLE 2. Infrared and Raman spectral data‡ in the 400–50 cm^{-1} region

$Cd(ClO_4)_2(PPh_3)_2$		$Cd(NO_3)_2(PPh_3)_2$		$Cd(CF_3CO_2)_2(PPh_3)_2$		$Cd(CF_3CO_2)_2(PPh_3)$		
Ir	Raman	Ir	Raman	Ir	Raman	Ir	Raman	Assignment
394mw*	394vw*			396w*		395mw*		
				390m*		391mw*		
	284m*					280vs,b†		
	272m*	274m*	276w*	275vs,b†	272w*		273w*	
	259m*			257w*	259mw*		259mw*	
	252m*	252m*	254m*					
				248m	249mw	248m*	250mw*	
243mw*	246m*	245w*	246w*					
	227sb*							
	222m*	222sh*	222w*					
216mw*	214m*				216w*	215mw*	216mw*	
		205vs,b						ν(Cd—O)
				205mw*	208w*			
	198mw*			194w*	192w*		194mw*	
190vs,b				168s		188vs,b		ν(Cd—O)
	189w*	189sh*	188w*					
154ms								
	141s		124s		128ms		152ms	ν(Cd—P)
		145ms		147s		144s		
				120sh		120ms		
90–70s,vb				98s		96s		
				72m		72sh		
		65s		62sh		63sh		

*Bands due to the internal vibrations of PPh_3
†Bands due to internal modes of CF_3CO_2
‡In cm^{-1} for the solid state. Abbreviations: Ir, infrared; R, Raman; b, broad; m, medium; s, strong; sh, shoulder; v, very; w, weak; ν, stretching mode

solution in dichloromethane. Thus, the structures of these complexes, like the perchlorate and the nitrato complexes, do not seem to be altered in going from solid state to solution. The ^{19}F nmr spectra of both the 1:1 and 1:2 complexes at 213 K were almost identical and showed a single resonance at ca. 74.15 ppm upfield of $CFCl_3$. Although some workers have claimed (31) that the ^{19}F chemical shift can be used to ascertain the mode of coordination of the trifluoroacetate group, the ^{19}F chemical shifts for trifluoroacetates of some twenty different metals are reported (30) to fall in the narrow range of −74 to −79 ppm. We, therefore, believe that the ^{19}F nmr data also do not seem to provide much useful structural information.

The observed infrared as well as Raman frequencies for the four complexes in the 400 to 50 cm^{-1} region, in the solid state, are listed in Table 2. Since neither the perchlorate nor the nitrate group is expected to give rise to any infrared or Raman frequency in this region, the observed frequencies for the perchlorato and the nitrato complexes are attributable either to the internal vibrations of the phosphine (32) or to the skeletal vibrations of the complex or to the lattice modes. The infrared and Raman frequencies due to the internal vibrations of triphenylphosphine are identified, with reasonable certainty, by comparison of the spectra of the complexes with those for free phosphine. Although little is known about skeletal vibrational frequencies for cadmium(II) complexes, the strong and broad infrared band at 190 cm^{-1} for the perchlorato complex and a similar band at 205 cm^{-1} for the nitrato complex are tentatively assigned to the vibrations involving stretching of the Cd—O bonds. The assignments are consistent with those for the Cd—N stretching frequencies for cadmium(II) thiocyanate (33) which has been shown to contain octahedrally coordinated cadmium(II) (34). A lower Cd—O stretching frequency for the perchlorato complex is consistent with a weaker coordinating ability of the perchlorate ligand. The Raman bands at 141 and 124 cm^{-1} are assigned to the symmetric Cd—P stretching frequency by comparison with the assignments for the cadmium(II) halide complexes, $CdX_2(PR_3)_2$ (23). The higher Cd—P stretching frequency for the perchlorato complex is consistent with its lower Cd—O stretching frequency. Assignments for the infrared bands at 154 and 90–70 cm^{-1} for the perchlorato complex and at 145 and 65 cm^{-1} for the nitrato complex are not so clear-cut.

The strong infrared band in the 270–280 cm^{-1} region in the spectra of the trifluoroacetato complexes is attributable to an internal mode of the CF_3CO_2 group (30). The strong infrared bands at

Can. J. Chem. Downloaded from www.nrcresearchpress.com by 210.87.254.40 on 09/06/12
For personal use only.

Can. J. Chem. Downloaded from www.nrcresearchpress.com by 210.87.254.40 on 09/06/12
For personal use only.

TABLE 3. ^{31}P—$\{^1H\}$ nmr spectral data*

Complex	δ,ppm	Δδ†	$^1J(^{113}Cd—^{31}P)$, Hz	$^1J(^{111}Cd—^{31}P)$, Hz
$Cd(ClO_4)_2(PPh_3)_4$	9.64	17.48	1129	1078
$Cd(ClO_4)_2(PPh_3)_3$	9.54	17.38	1574	1504
$Cd(ClO_4)_2(PPh_3)_2$	9.75	17.59	2292	2192
$Cd(NO_3)_2(PPh_3)_2$‡	7.84	16.88	1958	1872
$Cd(CF_3CO_2)_2(PPh_3)_2$	5.32	13.16	1875	1799
$Cd(CF_3CO_2)_2PPh_3$	4.92	12.76	2629	2517

*At 213 K for solutions in dichloromethane containing 10% $CDCl_3$ unless stated otherwise.
†$\Delta\delta = \delta_{complex} - \delta_{PPh_3}$.
‡At 183 K for solutions in dichloromethane containing 10% $CDCl_3$.

188 and 144 cm^{-1} for the 1:1 complex and similar bands at 168 and 147 cm^{-1} for the 1:2 complex are tentatively assigned to the stretching modes involving Cd—O bonds; assignments for the remaining infrared bands are uncertain. The Raman bands at 152 and 128 cm^{-1} are assigned to the Cd—P stretching frequency.

The ^{31}P—$\{^1H\}$ nmr spectra of the four complexes, like those for the cadmium(II) halide complexes, at ambient temperatures, consisted of a single resonance without any satellite showing that the complexes undergo fast ligand exchange on the nmr time scale. Well-resolved satellites due to the ^{113}Cd—^{31}P and ^{111}Cd—^{31}P spin–spin couplings were observed at 213 K for the perchlorato and the trifluoroacetato complexes but the nitrato complex had to be cooled to 183 K to observe the satellites. The observed ^{31}P nmr chemical shifts and the $^1J(^{113}Cd—^{31}P)$ and $^1J(^{111}Cd—^{31}P)$ values for the complexes are listed in Table 3. As can be seen from the data in Table 3, the ratio $^1J(^{113}Cd—^{31}P)/^1J(^{111}Cd—^{31}P)$ is in excellent agreement with the theoretical value of 1.046. The data also show that the magnitude of $^1J(Cd—P)$ decreases in the order: $ClO_4 > NO_3 > CF_3CO_2$. The effective nuclear charge at cadmium is also expected to decrease in this order. Thus, the magnitude of $^1J(Cd—P)$ for these complexes, like the cadmium(II) halide complexes (23), increases with an increase in the effective nuclear charge at the cadmium. Consistent with this trend, the magnitude of $^1J(^{111}Cd—^{31}P)$ for the 1:1 complex, $Cd(CF_3CO_2)_2PPh_3$, is markedly higher than that for the 1:2 complex.

Contrary to the views of other workers (15, 35), recent work in this laboratory (14, 23) has shown that there is no meaningful correlation between the coordination chemical shift, $\Delta\delta$ ($\delta_{complex} - \delta_{PPh_3}$), and the magnitude of metal phosphorus nuclear spin–spin coupling, $^1J(M—P)$. This is further supported by the data in Table 3 which show that although the magnitude of $^1J(Cd—P)$ for $Cd(CF_3CO_2)_2PPh_3$ is markedly higher than that for $Cd(CF_3CO_2)_2(PPh_3)_2$, the $\Delta\delta$ values for the two complexes are not significantly different.

Low temperature ^{31}P—$\{^1H\}$ nmr spectral measurements on solutions containing $Cd(ClO_4)_2(PPh_3)_2$ and varying amounts of PPh_3 provided evidence for the formation of 1:3 as well as 1:4 complexes. The spectral parameters for these complexes are included in Table 3. The ^{31}P—$\{^1H\}$ nmr spectrum of a solution containing $Cd(ClO_4)_2(PPh_3)_2$ and PPh_3, in 1:1 mole ratio, at 213 K, consisted of a main resonance (δ = 9.54 ppm) flanked by satellite doublets on each side due to ^{113}Cd—^{31}P and ^{111}Cd—^{31}P spin–spin coupling; the $^1J(^{113}Cd—^{31}P)$ and $^1J(^{111}Cd—^{31}P)$ values were 1574 and 1504 Hz respectively. From the marked decrease in the $^1J(Cd—P)$ values (as compared to those observed for the 1:2 complex) and the absence of any other ^{31}P resonance, it is evident that the 1:2 complex is completely converted into the 1:3 complex upon addition of one mole-equivalent of PPh_3. Addition of another mole-equivalent of PPh_3 to the solution gave a spectrum showing a main resonance (δ = 9.54 ppm) with two satellite doublets on each side, corresponding to $^1J(^{113}Cd—^{31}P)$ values of 1574 and 1129 Hz and $^1J(^{111}Cd—^{31}P)$ values of 1504 and 1078 Hz, respectively. Another resonance peak (δ = −7.84 ppm) with no satellite was also present in the spectrum. The latter resonance signal was about half as intense as the former and is undoubtedly due to free PPh_3. The observed $^1J(Cd—P)$ values are thus indicative of the presence of both $Cd(ClO_4)_2(PPh_3)_3$ and $Cd(ClO_4)_2(PPh_3)_4$. Relative intensities of the satellite signals due to the 1:3 and 1:4 complexes indicted that the 1:4 complex undergoes considerable dissociation as represented by the equation given below and that the equilibrium lies towards the left.

$$Cd(ClO_4)_2(PPh_3)_3 + PPh_3 \rightleftharpoons Cd(ClO_4)_2(PPh_3)_4$$

The ^{31}P—$\{^1H\}$ nmr spectrum of a solution containing $Cd(ClO_4)_2(PPh_3)_2$ and PPh_3 in 1:4 mole ratio showed resonances at 9.64 and −7.8 ppm with almost equal intensity. Two satellite doublets showing the presence of both the 1:3 and 1:4 complexes were still present on each side of the 9.64 ppm peak but the intensity of the satellite due to the 1:4

Can. J. Chem. Downloaded from www.nrcresearchpress.com by 210.87.254.40 on 09/06/12
For personal use only.

complex was about twice that the satellites due to 1:3 complex. The $^1J(^{113}Cd—^{31}P)$ or $^1J(^{111}Cd—^{31}P)$ values for the $Cd(ClO_4)_2(PPh_3)_2$, $Cd(ClO_4)_2(PPh_3)_3$, and $Cd(ClO_4)_2(PPh_3)_4$ complexes are approximately in the 1:0.66:0.50 ratio. If one assumes that the Cd—P bonds in the 1:2 complex use *sp* hybrid cadmium orbitals, the Cd—P bonds in the 1:3 and 1:4 complexes are indicated to use sp^2 and sp^3 hybrid cadmium orbitals, respectively. Similar $\Delta\delta$ values for the three perchlorate complexes provide further support to our proposal that no meaningful correlation exists between $\Delta\delta$ and the magnitude of $^1J(M—P)$.

The $^{31}P—\{^1H\}$ nmr spectrum of a solution containing $Cd(NO_3)_2(PPh_3)_2$ and one mole-equivalent of PPh_3 showed a broad resonance which was accompanied by a broad and unresolved satellite peak on each side. Unfortunately, the spectrum could not be recorded at a lower temperature which caused precipitation of the complex. $^{31}P—\{^1H\}$ nmr spectrum of solutions containing $Cd(CF_3CO_2)_2(PPh_3)_2$ and PPh_3, in 1:1, 1:2, and 1:3 mole ratios, gave a broad resonance signal without any satellites due to $^{113}Cd—^{31}P$ or $^{111}Cd—^{31}P$ spin–spin coupling at 213 K or 183 K. At 178 K, the spectrum showed broad resonances due to the 1:2 complex and free phosphine indicating no reaction between the two components. Addition of a large excess of phosphine (1:8 mole ratio) gave a spectrum showing a broad single resonance.

Experimental

Materials and Solvents

Triphenylphosphine was recrystallized twice from ethanol and its purity was established by ^{31}P nmr measurement. Reagent grade cadmium(II) perchlorate hexahydrate, cadmium(II) nitrate tetrahydrate, silver trifluoroacetate, and triethylorthoformate were used as received. The solvents were purified by standard methods.

Preparations of the Complexes

Complexes of Cadmium(II) Perchlorate

$Cd(ClO_4)_2 \cdot 6H_2O$ (1 mmol) was dissolved in triethylorthoformate and the solution was allowed to stand for 2 h in an atmosphere of dry nitrogen. Triphenylphosphine (2 mmol) was added slowly, with stirring, to this solution to give a clear solution which after standing for an hour yielded white crystalline powder of $Cd(ClO_4)_2(PPh_3)_2$. The product was filtered, washed with pentane, and dried *in vacuo*. Attempts to prepare 1:1 or 1:3 complexes by a similar procedure also gave the 1:2 complex as shown by the infrared and $^{31}P—\{^1H\}$ nmr data.

Complexes of Cadmium(II) Nitrate

$Cd(NO_3)_2 \cdot 4H_2O$ (1 mmol) was dissolved in triethylorthoformate and the solution was left to stand for 2 h under dry nitrogen. A solution of triphenylphosphine (2 mmol) in ethanol was added slowly, with stirring to the above solution and the resulting mixture was cooled in an ice bath to give $Cd(NO_3)_2(PPh_3)_2$ as white crystalline powder which was filtered, washed with pentane, and dried *in vacuo*. Attempts to prepare the 1:1 complex following a similar procedure gave a white solid which gave correct C, H, and N analyses for $Cd(NO_3)_2PPh_3$ but the infrared and $^{31}P—\{^1H\}$ nmr spectra as well as the X-ray powder photograph of the product showed it to be a mixture of $Cd(NO_3)_2(PPh_3)_2$ and $Cd(NO_3)_2$.

Complexes of Cadmium(II) Trifluoroacetate

A solution of cadmium(II) trifluoroacetate (1 mmol) was prepared from the reaction of silver trifluoroacetate with cadmium(II) iodide in ethanol. Precipitated silver iodide was filtered off and a solution of triphenylphosphine (2 mmol) in ethanol was added dropwise to the filtrate with stirring. White precipitate of $Cd(CF_3CO_2)_2(PPh_3)_2$ was obtained upon concentrating the reaction mixture *in vacuo*. The product was washed with pentane and recrystallized from a mixture of dichloromethane and pentane.

To a solution of $Cd(CF_3CO_2)_2$ (1 mmol) in ethanol (prepared in the same way as above), a solution of triphenylphosphine (1 mmol) in ethanol was added dropwise, and the mixture was stirred for an hour to give a clear solution. Removal of the solvent gave a white solid which was recrystallized from a mixture of ethanol and petroleum ether to give pure $Cd(CF_3CO_2)_2PPh_3$.

Physical Measurements

Microanalyses were performed by Guelph Chemical Laboratories, Guelph. Melting points were determined with a Gallenkamp melting point apparatus. Conductance measurements were made at 25°C using a Yellow Springs conductivity bridge and a glass conductivity cell with platinized platinum electrodes. Infrared spectra were recorded in the 4000–50 cm^{-1} region using a Perkin-Elmer 180 spectrophotometer. Spectra, in the solid state, were measured on mulls in Nujol and halocarbon oil using KRS-5 windows or polyethylene discs. Solution spectra were recorded using 0.1 mm path length demountable liquid cells with AgBr windows. Raman spectra were measured in the solid state with a Jarrell Ash spectrophotometer using 5145A exciting line of an argon ion laser. The infrared and Raman frequencies are accurate within ± 2 cm^{-1}. $^{31}P—\{^1H\}$ and ^{19}F nmr spectra were measured in the Fourier-transform mode using Bruker WP-60 and Bruker HFX-90 spectrometers, respectively. All the measurements were carried out on solutions in dichloromethane containing 10% $CDCl_3$. External H_3PO_4 and $CFCl_3$ were used as references for the ^{31}P and ^{19}F nmr spectral measurements, respectively. The positive chemical shifts are downfield from the reference.

Acknowledgements

Thanks are due to the Natural Sciences and Engineering Research Council of Canada for operating and travel grants (to R.G.G.). The work was written up during the tenure of a Visiting Professorship awarded (to R.G.G.) by the Indian Institute of Technology, Delhi, India.

1. R. C. Evans, F. G. Mann, H. S. Peiser, and D. Purdie. J. Chem. Soc. 1209 (1940).
2. A. R. Davis, C. J. Murphy, and R. A. Plane. Inorg. Chem. **9**. 423 (1970).
3. R. C. Makhija, A. L. Beauchamp, and R. Rivest. J. Chem. Soc. Dalton Trans. 2447 (1973).
4. H. Schmidbaur, and K. H. Rathlein. Chem. Ber. **106**, 2491 (1973).
5. F. G. Moers and J. P. Langhout. Rec. Trav. Chim. Pays. Bas, **92**, 996 (1973).
6. E. C. Alyea, S. A. Dias, R. G. Goel, and W. O. Ogini. Can. J. Chem. **55**, 4227 (1977).

7. E. C. ALYEA, G. FERGUSON, and R. J. RESTIVO. J. Chem. Soc. Dalton Trans. 1845 (1977).
8. E. C. ALYEA, S. A. DIAS, R. G. GOEL, W. O. OGINI, P. PILON, and D. W. MEEK. Inorg. Chem. **17**, 1697 (1978).
9. R. G. GOEL, W. P. HENRY, and W. O. OGINI. Can. J. Chem. **57**, 762 (1979).
10. C. GAGNON and A. L. BEAUCHAMP. Acta Crystallogr. B**35**, 166 (1979).
11. R. C. MAKHIJA, R. RIVEST, and A. L. BEAUCHAMP. Can. J. Chem. **57**, 2555 (1979).
12. W. O. OGINI. M.Sc. Thesis. University of Guelph, Guelph, Ont. Canada, 1976.
13. P. J. ROBERTS, G. FERGUSON, R. G. GOEL, W. O. OGINI, and R. J. RESTIVO. J. Chem. Soc. Dalton Trans. 253 (1978).
14. T. ALLMAN, R. G. GOEL, and P. PILON. Can. J. Chem. **57**, 91 (1979).
15. E. C. ALYEA and S. A. DIAS. Can. J. Chem. **57**, 83 (1979).
16. E. C. ALYEA, S. A. DIAS, G. FERGUSON, M. A. KHAN, and P. J. ROBERTS. Inorg. Chem. **18**, 2433 (1979).
17. S. H. WHITLOW. Can. J. Chem. **52**, 198 (1974).
18. E. C. ALYEA, S. A. DIAS, G. FERGUSON, and R. J. RESTIVO. Inorg. Chem. **16**, 2329 (1977).
19. E. C. ALYEA, S. A. DIAS, G. FERGUSON, and M. PARVEZ. Inorg. Chim. Acta **37**, 45 (1979).
20. T. ALLMAN and R. G. GOEL. Inorg. Nucl. Chem. Lett. **15**, 199 (1979).
21. E. C. ALYEA, S. A. DIAS, G. FERGUSON, and M. A. KHAN. J. Chem. Res. Symp. 360 (1979).
22. G. B. DEACON, J. H. S. GREEN, and D. J. HARRISON. Spectrochim. Acta, Part A, **24**a 1921 (1968).
23. R. G. GOEL, W. P. HENRY, and R. C. SRIVASTAVA. Inorg. Chem. **20**, 1727 (1981).
24. A. F. CAMERON, K. P. FORREST, and G. FERGUSON. J. Chem. Soc. A, 1286 (1971).
25. R. G. GOEL, W. P. HENRY, M. J. OLIVIER, and A. L. BEAUCHAMP. Inorg. Chem. In press.
26. R. G. GOEL and W. O. OGINI. Inorg. Chem. **16**, 1968 (1977).
27. K. NAKAMOTO. Infrared spectra of inorganic and coordination compounds, 3rd ed. Wiley Interscience, New York. 1978. (*a*) p. 242 and references therein; (*b*) p. 242 and references therein.
28. W. A. ANDERSON, A. J. CARTY, G. J. PALENIK, and G. SCHERIBER. Can. J. Chem. **49**, 761 (1971).
29. G. G. MESSMER and G. J. PALENIK. Inorg. Chem. **8**, 2750 (1969).
30. C. D. GARNER and B. HUGHES. Adv. Inorg. Chem. Radiochem. **17**, 1 (1975) and references therein.
31. G. S. GIROLANI, V. V. MAINZ, and R. A. ANDERSEN. Inorg. Chem. **19**, 805 (1980).
32. K. SHOBATAKE, C. POSTMUS, J. R. FERRARO, and K. NAKAMOTO. Appl. Spectrosc. **23**, 12 (1969).
33. R. G. GOEL. Spectrochim. Acta, Part A. **37**A, 557 (1981).
34. (*a*) M. S. CANNAS, G. CARTA, A. CRISTINI, and G. MARONGIU. J. Chem. Soc. Dalton Trans. 300 (1976); (*b*) G. SRDANOV, R. HERAK, B. PRELESNIK, and M. JEREMIC. Bull. Soc. Chim. Beograd. **44**, 561 (1979).
35. S. O. GRIM, P. J. LUI, and R. L. KEITER. Inorg. Chem. **13**, 342 (1974).

Can. J. Chem. Downloaded from www.nrcresearchpress.com by 210.87.254.40 on 09/06/12
For personal use only.

Nucleophilic substitution of 5,5-dimethyl-2-cyclopentenyl derivatives. Lack of S_N2' reaction[1]

KARL R. KOPECKY AND CYRIL LEVINE

Department of Chemistry, University of Alberta, Edmonton, Alta., Canada T6G 2E1

Received April 3, 1981

KARL R. KOPECKY and CYRIL LEVINE. Can. J. Chem. **59**, 3273 (1981).

Treatment of tetramethyl-1,3-cyclobutanedione with two equivalents of allyl oxide anion at 140°C yields 2,2-dimethyl-4-pentenoic acid which is cyclized via the acid chloride with aluminum chloride to 5,5-dimethyl-2-cyclopentenone, **4**. Reduction of **4** with aluminum hydride provides 5,5-dimethyl-2-cyclopentenol **1**-OH which is pyrolyzed to 5,5-dimethyl-1,3-cyclopentadiene in dimethylsulfoxide. Reduction of **4** with tri-*t*-butoxyaluminum hydride at −70°C gives 2,2-dimethylcyclopentanone.

The 2,6-dichlorobenzoate ester of **1**-OH failed to yield S_N2' products under a variety of conditions. The rate constants for solvolysis of the *p*-nitrobenzoate esters of **1**-OH, 2-cyclopentenol and *Z*-2-methyl-4-hexene-3-ol in 80% ethanol at 80°C are 20.2, 523, and 0.63×10^{-6} s^{-1}, respectively, and the main products of solvolysis are 5-ethoxy-3,3-dimethylcyclopentene, 3-ethoxycyclopentene, and *E*-2-ethoxy-5-methyl-3-hexene, respectively. There is steric hindrance to solvation during ionization of the *p*-nitrobenzoate of **1**-OH.

KARL R. KOPECKY et CYRIL LEVINE. Can. J. Chem. **59**, 3273 (1981).

La tétraméthylcyclobutanedione-1,3 réagit avec deux équivalents d'anion allyloxyde à 140° en donnant l'acide diméthyl-2,2 pentène-4 oique. Ce dernier réagit avec le chlorure d'aluminium en donnant le chlorure d'acide qui par cyclisation conduit à la diméthyl-5,5 cyclopentène-2 one (**4**). La réduction du composé **4** par l'hydrure d'aluminium permet d'obtenir le diméthyl-5,5 cyclopentene-2 ol (OH-**1**) que l'on pyrolyse en diméthyl-5,5 cyclopentadiène-1,3 dans le diméthylsulfoxyde. La réduction du composé **4** par l'hydrure de tri-*tert*-butoxyaluminium à 70°C donne la diméthyl-2,2 cyclopentanone.

Soumis à diverses conditions, l'ester dichloro-2,6 benzoate de OH-**1** n'a pas donné de produits de type S_N2'. Les constantes de vitesse des solvolyses des esters *p*-nitrobenzoates du OH-**1**, du cyclopentène-2 ol et du (*Z*)-méthyl-2 hexène-4 ol-3 à 80°C dans l'éthanol à 80% sont respectivement 20.2, 523 et 0.63×10^{-6} s^{-1} et les produits principaux de ce solvolyses sont respectivement l'éthoxy-5 diméthyl-3,3 cyclopentène, l'éthoxy-3 cyclopentène et le (*E*)-éthoxy-2 méthyl-5 hexène-3. Il y a un encombrement stérique à la solvatation lors de l'ionisation du *p*-nitrobenzoate de OH-**1**.

[Traduit par le journal]

The recent flurry of activity in the study of the S_N2' reaction (1) prompts the present report of the unsuccessful attempt to observe this reaction in the 5,5-dimethyl-2-cyclopenten-1-yl system **1**, reaction [1],

[1] 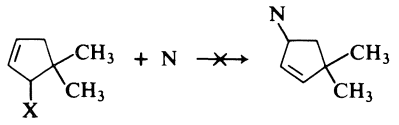

1 **2**

using conditions under which the corresponding 6-alkyl-2-cyclohexen-1-yl derivatives produce S_N2' products (2). In the latter reactions there was a *syn* relationship between the entering and leaving groups. However, a possible *anti* reaction might have been hindered because of a possible unfavorable conformation of the cyclohexenyl system chosen (3). The present research was prompted by a desire to investigate the stereochemistry of the S_N2' reaction in a system much more rigid than the cyclohexenyl system and in which there would be no impediment to an *anti* reaction. Use of racemic **1** would have given no information about the stereochemistry of the reaction, but had an S_N2' reaction been observed for racemic **1** further studies with optically active **1** would have been carried out.

While the original objective of this study was not met an efficient synthesis for 2,2-dimethyl-4-pentenoic acid **3** was developed during the course of this work. This allows 2,2-dimethylcyclopentanone **5** and 5,5-dimethyl-1,3-cyclopentadiene **6** to be easily prepared on a large scale. The solvolysis of the *p*-nitrobenzoate ester **1**-OPNB and two analogues was also studied briefly.

Results

The preparation of 5,5-dimethyl-2-cyclopenten-1-ol **1**-OH, Scheme 1, proceeds via cyclization of the acid chloride of **3** with aluminum chloride. Large amounts of **3** can be prepared readily in a one-pot reaction with inexpensive materials by treatment of tetramethylcyclobutan-1,3-dione with two equivalents of allyl oxide anion at 140°C. This reaction probably represents the most convenient large scale synthesis of **3** (4) using inexpensive, readily available materials, and is based on the observation (5) that allyl 2,2,4-trimethyl-3-oxopentanoate is cleaved by methoxide ion to a

[1](*a*) This research was supported by the National Research Council of Canada. (*b*) Abstracted from the Ph.D. dissertation of C. Levine, University of Alberta. 1969.

0008-4042/81/233273-07$01.00/0

©1981 National Research Council of Canada/Conseil national de recherches du Canada

Can. J. Chem. Downloaded from www.nrcresearchpress.com by 210.87.254.5 on 09/06/12
For personal use only.

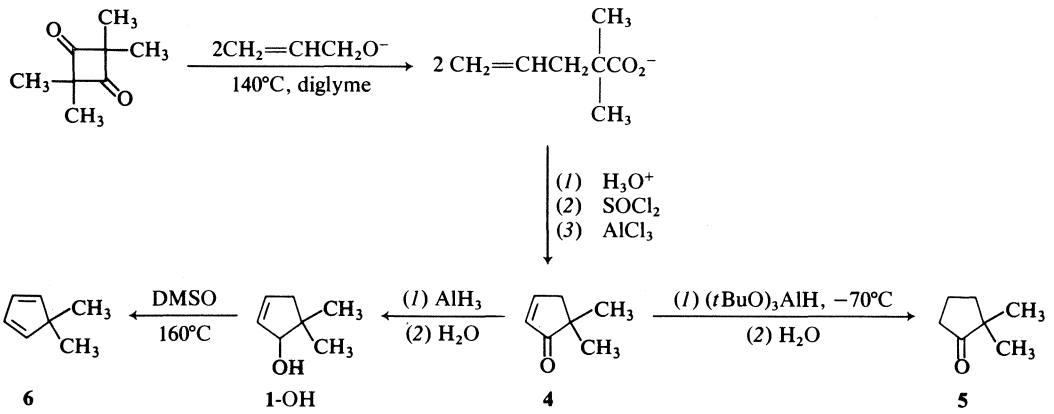

SCHEME 1

mixture of the anion of **3** and methyl 2-methylpropanoate.

In addition to 5,5-dimethyl-2-cyclopentenone **4** (52%), the cyclization of the acid chloride of **3** produced 3-chloro-2,2-dimethylcyclopentanone **7** (~25%) and 2,3-dimethyl-2-cyclopentenone **8** (~15%). Formation of products such as **7** in acylation reactions of this kind is well known (6). In the present work the cyclization reaction was carried out in a nitromethane – methylene chloride solvent mixture.

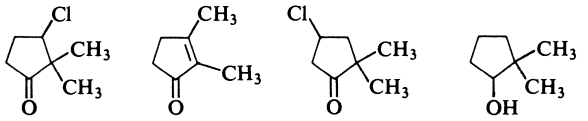

7 **8** **9** **10**

The isomeric chloroketone **9**, but neither **7** nor **8**, is reported to be formed when the reaction is carried out in carbon disulfide (7).

Considerable difficulty was experienced in finding a suitable method for the reduction of **4** to the allylic alcohol **1**-OH. The method of choice proved to be aluminum hydride in ether (8). The saturated ketone **5** or the saturated alcohol **10** were the exclusive products when **4** was treated with lithium tri-*t*-butoxyaluminum hydride at −70°C or with sodium borohydride, respectively. Pyrolysis of the alcohol **1**-OH in dimethylsulfoxide (9) forms **6**. Overall, the syntheses presented here appear to be the most efficient for the preparation of **4** (7, 10), **5** (10, 11), and **6** (12).

The 2,6-dichlorobenzoate of the cyclohexenyl system first studied (6) required rather drastic conditions for reaction so preparation of **1** containing a more reactive leaving group was attempted. Preliminary experiments with the more readily available acyclic model compound 4,4-dimethyl-1-penten-3-ol **11**-OH were first carried out. The phenylmethanesulfonate ester **11**-OPMS was prepared and treated with tetrabutylammonium acetate TBA in carbon tetrachloride, reaction [2].

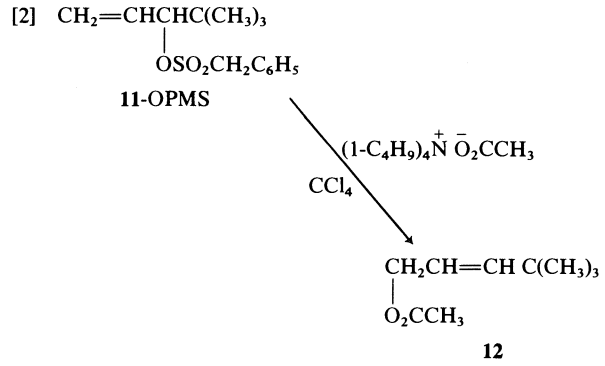

After 5 h at 40–45°C, ~50% of **11**-OPMS had been converted to **12**, as judged from the nmr spectrum of the reaction mixture. A doublet at τ5.30, J = 8 Hz, due to the methine proton of **11**-OPMS, was decreased in intensity, while a new doublet J = 5.5 Hz, assigned to the methylene group of **12**, appeared at τ5.60. It appeared that the product was exclusively the rearranged acetate **12**.

Further identification was not made and after these preliminary results attempts were made to isolate the phenylmethanesulfonyl ester **1**-OPMS of the dimethylcyclopentenyl system. However, these were not successful. The ester apparently formed but rapidly decomposed, even at −30°C, in the reaction mixture to yield the diene **6** among other, unidentified, products.

The 2,6-dicholorobenzoate ester **1**-ODCB was then prepared and a series of qualitative experiments was carried out to determine conditions under which the S_N2' reaction would occur. No evidence for the S_N2' reaction was obtained. The ester was recovered unchanged after treatment

Can. J. Chem. Downloaded from www.nrcresearchpress.com by 210.87.254.5 on 09/06/12
For personal use only.

Can. J. Chem. Downloaded from www.nrcresearchpress.com by 210.87.254.5 on 09/06/12
For personal use only.

with TBA in carbon tetrachloride for 9 h at 90°C (TBA was destroyed), with thiourea in dimethylformamide for 40 h at 100°C, and with diethyl malonate anion in dimethylformamide for 36 h at 100°C. In piperidine solution at 130°C the ester was slowly destroyed and had disappeared after 90 h. The nmr spectrum of the reaction mixture showed no signals attributable to the desired product of rearrangement **2**, N=piperidyl. Mainly the diene **6** appeared to be formed when the ester was treated with cyanide or with thiocyanate ion in dimethylformamide at 150°C.

After this unsuccessful search for an S_N2' reaction, a brief study of the solvolysis of the *p*-nitrobenzoate ester **1**=OPNB was made to determine whether this system was unusually unreactive. For comparison the rates of solvolysis of *Z*-2-methyl-4-hexen-3-yl *p*-nitrobenzoate **13**-OPNB and 2-cyclopentenyl *p*-nitrobenzoate **14**-OPNB were also measured. The esters were allowed to solvolyze in 80% aqueous ethanol, Table 1. The reactions

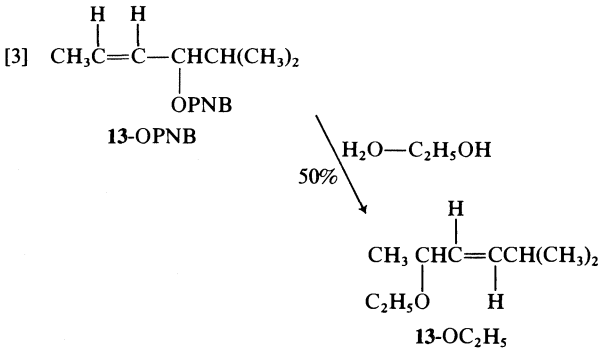

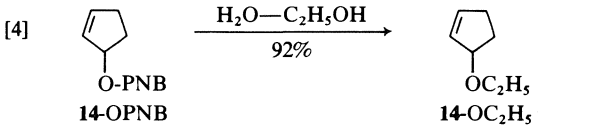

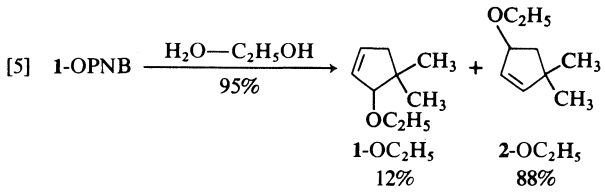

were followed to at least 80% completion and obeyed first order kinetics throughout. There is internal return upon ionization of **1**-OPNB. After one half-life of reaction of **1**-OPNB ~25% of the *p*-nitrobenzoate ester that was recovered consisted of the rearranged compound **2**-OPNB. Since first-order kinetics were obeyed during solvolysis of **1**-OPNB for over three half-lives the rearranged ester must undergo solvolysis at a rate quite similar to that of **1**-OPNB. No rearranged ester could be detected after one half-life of solvolysis of **13**-OPNB.

The major products of solvolysis of the esters are the ethyl ethers, reactions [3]–[5], which from **1**- and **13**-OPNB are mainly the rearranged compounds. Several other products were detected by gc from solvolysis of **13**-OPNB, but these were not identified.

Discussion

The order of solvolytic reactivity, **14**-OPNB > **13**-OPNB, is consistent with previous work (13) in which it was found that 3-bromocyclopentene undergoes solvolysis 210 times as rapidly as 4-bromo-2-pentene in 80% ethanol at 0°C. The moderately slower rate of solvolysis of **1**-OPNB as compared with that of **14**-OPNB is likely due to steric inhibition of solvation (14) during ionization of **1**-OPNB. There is thus no remarkable lack of reactivity of **1**-OPNB under solvolytic conditions.

The failure to observe S_N2' substitution reactions with **1**-ODCB was not expected. Good yields of S_N2' reaction products were obtained under reaction conditions similar to those used here from the original cyclohexenyl systems studied (2). It may be that the *gem*-dimethyl groups in the rigid **1**-ODCB present enough of a steric barrier so as to make the S_N2' reaction considerably more sluggish than in the more flexible cyclohexenyl systems. Little work appears to have been done to evaluate steric effects in substitution reactions in cyclopentyl systems. Steric effects in pyrazoline decompositions are quite pronounced (15). Steric effects in 5-membered rings may be greater than in analogous acyclic or cyclohexyl compounds. A clearer assessment of the steric effects in S_N2' reactions of cyclopentenyl systems might be made from a study of the *cis*- and *trans*-4-methyl-2-cyclopenten-1-yl analogues.

Experimental

Melting points and boiling points are uncorrected. Refractive indices were measured on a Bausch and Lomb Abbe-3L refractometer. Infrared spectra were recorded on Perkin-Elmer Model 421 and 337 spectrophotometers, and only characteristic absorption bands are given. Nuclear magnetic resonance spectra were recorded on Varian analytical spectrometers, Models A-60, A-60A, and HR-100. Gas chromatography was carried out on a Perkin-Elmer Vapor Fractometer using a 5 ft × 1/4 in. column of 20% SE-30 on 60/80 chromosorb W.

Anhydrous ethanol was prepared by the method of Fieser (16). Eighty volumes of this at 25°C were mixed with 20 volumes of water, which had been distilled from potassium permanganate in all all-glass apparatus at 25.0°C to make the 80% ethanol.

Can. J. Chem. Downloaded from www.nrcresearchpress.com by 210.87.254.5 on 09/06/12
For personal use only.

Elemental analyses were performed in the microanalytical laboratories of the Chemistry Department under the supervision of Darlene Mahlow.

Solutions were dried with magnesium sulfate.

*2,2-Dimethyl-4-pentenoic acid, **3***

To a stirred suspension of 5.67 g (0.26 mol) of sodium hydride in 200 mL purified (17) diglyme was added 207 g (3.6 mol) of dry (molecular sieve) allyl alcohol over a 20 min period while keeping the temperature below 30°C. After hydrogen evolution ceased the clear, red solution was cooled to 10°C and 250 g (1.79 mol) of tetramethyl-1,3-cyclobutanedione was added in small portions at such a rate as to keep the temperature below 30°C. The resultant solution was stirred 1 h, transferred to a dropping funnel, and added to a stirred suspension of 90.7 g (3.69 mol) sodium hydride in 450 mL purified diglyme at 110°C. The rate of addition was such as to maintain the solution at 120–140°C without external heating. The mixture was stirred at 140°C for 1 h after the addition was complete, cooled and treated cautiously with water until the excess sodium hydride was destroyed. More water was added and the resulting solution was extracted with 3 × 200 mL ether. The aqueous layer was poured slowly into a mixture of ice and 450 mL concentrated hydrochloric acid. The resultant mixture was shaken with 500 mL pentane and the resulting aqeuous layer was shaken twice with 200 mL pentane. The combined pentane extracts were dried, concentrated through a Vigreux column, and the residual oil distilled through a 30 cm Vigreux column to give 60 g of forerun, bp 30–104°C/17 Torr and 299 g (65%) of **3** bp 104–109°C/17 Torr, n_D^{28} 1.4301 (lit bp 104–108°C/20 Torr (4*a*), n_D^{25} 1.4318 (18)).

*5,5-Dimethyl-2-cyclopentenone, **4***

Anhydrous aluminum chloride, 160 g (1.20 mol), was slowly added with stirring to 250 mL nitromethane and the resulting suspension was diluted with 900 mL methylene chloride. A solution of 181 g (1.23 mol) of the acid chloride of **3** in 1100 mL methylene chloride was added dropwise to the refluxing suspension over 10 h, and the resulting mixture was heated under reflux for 2 h more. The mixture was cooled and poured slowly into a stirred mixture of ice and concentrated hydrochloric acid. The aqueous layer was shaken with 2 × 400 mL methylene chloride and the combined organic layers were shaken with brine, aqueous sodium bicarbonate, brine, and dried. Solvent was removed through a Vigreux column and the residue was distilled through an annular Teflon spinning-band column to give, in addition to a forerun of nitromethane, 71 g (52%) of **4**, bp 150–152°C/700 Torr, n_D^{25} 1.4550 (lit bp 104–108°C/20 Torr (4*a*) n_D^{20} 1.4337 (4*b*)) and 55 g of a fraction, bp 186–188°C/700 Torr, that was shown by gc to consist of two major components in a ratio of about 1.7:1 and two minor components. The major components were identified as indicated below.

*3-Chloro-2,2-dimethylcyclopentanone **7***

The high boiling fraction from the preparation of **4** was stored at −10°C for several months and the supernatant liquid was decanted from the crystals that formed. The crystals were melted and refrozen. The decantation, melting, and freezing process was repeated twice more after which the product was distilled to give 5 g of a colorless oil, bp 95–97°C/30 Torr; mp 16.8–17.0°C; n_D^{29} 1.4661; ir (CCl_4): 1745, 1365, and 1385 cm^{-1}; ^{1}Hnmr (CCl_4): τ5.83 (m, 1H, —C*H*Cl—), 7.4–8.0 (broad m, 4H, —CH_2CH_2—); 8.92 (two s, 6H). *Anal.* calcd for $C_7H_{11}ClO$: C 57.35, H 7.59; found: C 57.41, H 7.80.

This compound possesses a pleasant camphor-like odor, and was unaffected after treatment with silver nitrate in ethanol at 77°C for 24 h, with silver nitrate in acetic acid at 110°C for 40 h, or with *N*,*N*-dimethylaniline at 190°C for 20 h. Heating this material with silver nitrate in boiling benzoic acid (235°C) for 8.5 h destroyed 50% of it to give a 25% yield of **4** and an unidentified compound. This lack of reactivity is more likely to be expected of **7** than of **9**.

The other major component of the high boiling fraction was isolated from the effluent of the gc using a 20 ft × 1/4 in. column of 20% ethylene glycol succinate on 60/80 chromosorb W at 150°C, and was identified as **8**, n_D^{29} 1.4774; ν_{max} (CCl_4): 1701 and 1655 cm^{-1}; uv (C_6H_{12}) λ_{max} 225 nm (6750); ^{1}Hnmr (CCl_4): τ7.4–8.1 (broad m, 4H), 8.04 (m, 3H), 8.40 (m, 3H). These spectroscopic properties are in good agreement with those reported (19).

*5,5-Dimethyl-2-cyclopentenol **1**-OH*

A solution of 27.7 g (0.25 mol) **4** in 500 mL ether was added over 1 h to a stirred mixture of aluminum hydride prepared (8) from 5.28 g (0.14 mol) lithium aluminum hydride and 6.0 g (0.05 mol) aluminum chloride in 500 mL ether. The resulting mixture was stirred overnight and then hydrolyzed by cautious addition of saturated ammonium chloride solution. The liquid was decanted and the salts were washed with ether. The combined ether solutions were dried, concentrated, and the residual oil was distilled to give 23 g (82%) of **1**-OH, bp 65.6–66.5°C/20 Torr; n_D^{25} 1.4598; ν_{max} (CCl_4) 3590, 3340, 1610 cm^{-1}; ^{1}Hnmr (CCl_4): τ4.30 (m, 2H), 5.95 (s, 1H, —C*H*—OH), 6.90 (s, 1H, O*H*), 7.88 (m, 2H), 8.95 (two close s, 6H). A satisfactory analysis was not obtained.

The *p*-nitrobenzoate was prepared, mp 66.3–67.0°C. *Anal.* calcd. for $C_{14}H_{15}NO_4$: C 64.36, H 5.79, N 5.36; found: C 64.13, H 5.74, N 5.36.

The 3,5-dinitrobenzoate was prepared, mp 71–72°C. *Anal.* calcd for $C_{14}H_{14}N_2O_6$: C 54.90, H 4.61, N 9.15; found: C 54.87, H 4.57, N 9.25.

*5,5-Dimethyl-2-cyclopentenyl 2,6-dichlorobenzoate, **1**-ODCB*

Treatment of **1**-OH with 2,6-dichlorobenzoyl chloride in pyridine solution (2) failed to produce any of the desired ester.

A solution of 4.36 g (0.039 mol) of **1**-OH in 10 mL tetrahydrofuran was added to a hot suspension of 4.8 g (0.2 mol) sodium hydride in 100 mL tetrahydrofuran at such a rate as to maintain gentle reflux. The resulting mixture was cooled to −11°C and a solution of 8.15 g (0.039 mol) 2,6-dichlorobenzoyl chloride (2) in 30 mL tetrahydrofuran was added over 25 min while keeping the temperature below −8°C. The cooling bath was removed, the reaction mixture stirred overnight and then filtered. The precipitate was triturated with tetrahydrofuran, the filtrates were combined, dried, and concentrated under 10 Torr. Hexane was added to the oily residue and 1.36 g of what appeared to be 2,6-dichlorobenzoic anhydride crystallized out. After three crystallizations from hexane this had mp 154–155°C, ν_{max} (CCl_4): 1820 and 1760 cm^{-1}; ^{1}Hnmr (CCl_4): τ2.60(s). The filtrate was concentrated to 25 mL and left at −10°C. The product was recrystallized from hexane to give 7.9 g (71%) of colorless crystals, mp 56–57°C; ν_{max} (CCl_4) 1735 cm^{-1}; ^{1}Hnmr (CCl_4): τ2.63 (s, 3H), 3.55–3.96 (m, 1H), 3.96–4.25 (m, 1H): 4.32 (m, 1H), 7.75 (m, 2H), 8.81 (two close s, 6H). *Anal.* calcd for $C_{14}H_{14}Cl_2O_2$: C 58.97, H 4.95, Cl 24.86; found: C 59.86, H 5.18, Cl 24.57.

*2,2-Dimethylcyclopentanone, **5***

A solution of 3.0 g (0.027 mol) of **4** in 35 mL tetrahydrofuran was added over a 1 h period to a stirred mixture of 13.8 g (0.055 mol) lithium tri-*t*-butoxyaluminum hydride and 45 mL tetrahydrofuran at −78°C. The resulting mixture was stirred 2 h at −78°C, and a further 16 h after removal of the cooling bath. A solution of Rochelle salt was added slowly with cooling. The upper of the two layers which formed was extracted into pentane. The pentane extract was dried, concentrated, and the

Can. J. Chem. Downloaded from www.nrcresearchpress.com by 210.87.254.5 on 09/06/12
For personal use only.

residue was distilled to give 2.0 g (66%) of **5**, bp 65°C/70 Torr, n_D^{25} 1.4306 ((lit. 12*a*) bp 140–143/745 Torr; $n_D^{22.5}$ 1.4312).

*2,2-Dimethylcyclopentanol, **10***

A solution of 3.2 g (0.029 mol) of **4** in 30 mL 2-propanol was added to a boiling solution of 2.32 g (0.061 mol) sodium borohydride in 40 mL 2-propanol over a 40 min period and the resulting solution was heated under reflux for 4 h. Then 125 mL water was added and this solution was heated under reflux overnight, cooled, and shaken with 2 × 600 mL pentane. The pentane layers were combined, dried, concentrated, and the residue distilled to give 2.65 g (80%) of **10**, bp 70°C/27 Torr, n_D^{25} 1.4518 ((lit. 12*a*) bp 151–152°C/760 Torr, n_D^{20} 1.4532).

*4,4-Dimethyl-1-penten-3-yl phenylmethanesulfonate, **11**-OPMS*

Treatment of dimethylpropanal with vinylmagnesium chloride (20) followed by workup of the reaction mixture produced 4,4-dimethyl-1-penten-3-ol in 16% yield, bp 128–129°C/700 Torr, n_D^{25} 1.4286 (lit (21) bp 131°C/760 Torr, n_D^{25} 1.4282). Some reduction product, 2,2-dimethyl-1-propanol, was also formed (4.5%).

A solution of 0.414 g (4 mmol) triethylamine in 5 mL carbon tetrachloride was added over 10 min to a stirred mixture of 0.224 g (2 mmol) of the above allylic alcohol and 0.374 g (2 mmol) of phenylmethanesulfonyl chloride (22) in 10 mL carbon tetrachloride at 22°C. Stirring was continued for 1 h and the mixture filtered. The precipitate was triturated with carbon tetrachloride, the filtrates were combined and concentrated at 0°C to a red oil which solidified at −10°C and then remained solid at 22°C. This solid was treated with pentane which left a dark red oil. The pentane was decanted, cooled to −11°C, and the resultant white crystals were filtered at −5°C under dry nitrogen. Four recrystallizations from pentane gave 0.223 g (42%) of slightly yellow needles, mp 38.5–39.5°C; ^{1}Hnmr (CCl_4): τ2.59 (s, 5H), 3.95–4.85 (m, 3H), 5.30 (m, 1H), 5.77 (s, 2H), 9.10 (s, 9H). *Anal.* calcd. for $C_{14}H_{20}O_3S$: C 62.66, H 7.51; found: C 62.13, H 7.41.

This compound was very unstable, decomposing within 10 min at 22°C, but could be stored for months at −10°C. All apparatus involving its preparation and other operations was rinsed with isopropylamine before use.

2-Cyclopentenyl p-*Nitrobenzoate, **14**-OPNB*

This was prepared by treatment of 2-cyclopentenol (23) with *p*-nitrobenzoyl chloride in the presence of trimethylamine, mp 79.5–80.2°C; ^{1}Hnmr (CCl_4): τ1.75 (s, 4H), 3.65–4.20 (m, 3H), 7.35–8.15 (m, 4H). *Anal.* calcd. for $C_{12}H_{11}NO_4$: C 61.80, H 4.75, N 6.01; found: C 61.93, H 4.76, N 6.12.

Z-2-Methyl-4-hexen-3-yl p-*nitrobenzoate, **13**-OPNB*

Hydrogenation of 2-methyl-4-hexyn-3-ol (24) in pyridine solution over palladium on barium sulfate produced *Z*-2-methyl-4-hexen-3-ol which was converted directly without workup to **13**-OPNB, mp 64.1–65.0°C; ^{1}Hnmr ($CDCl_3$): τ1.75 (s, 4H), 4.05–4.65 (m, 3H), 8.25 (d, J = 5 Hz, 3H), 7.90–8.40 (m, 1H), 9.05 (d, J = 7 Hz, 64). *Anal.* calcd. for $C_{14}H_{17}NO_4$: C 63.86, H 6.51, N 5.32; found: C 63.77, H 6.50, N 5.45.

3-Ethoxy-4,4-dimethylcyclopentene

A solution of 18 g (0.11 mol) iodoethane in 30 mL dimethylformamide was added to a stirred suspension containing the anion of **1**-OH prepared from 5.73 g (0.05 mol) **1**-OH and 6.5 g (0.27 mol) sodium hydride in 100 mL dimethylformamide. The mixture was stirred overnight, water was cautiously added, and the resulting solution was extracted with 3 × 100 mL pentane. The pentane extracts were combined, shaken with 2 × 150 mL water, dried, concentrated, and the residual oil distilled to give 2.1 g (29%) of a colorless oil, bp 58.0–58.5°C/43 Torr; n_{25}^D 1.4295; ^{1}Hnmr (CCl_4): τ4.25 (m, 2H), 6.20 (m, 1H), 6.58 (m, 2H, —O—CH_2—), 7.9 (m, 2H), 8.75 (s, 3H), 8.95 (t, J = 7 Hz, 3H, overlapping with s, 3H): ms *m/e*: 140.1200 ($M^{+\cdot}$, calcd for $C_9H_{16}O$: 140.1201).

Z-4-Ethoxy-5-methyl-2-hexene

This was prepared using a procedure similar to that described for the above ether, except that the reaction was carried out in tetrahydrofuran. From 4.0 g *Z*-2-methyl-4-hexen-3-ol, obtained by saponification of **13**-OPNB, 2.67 g (54%) of the ether was obtained, bp 52–53°/35 Torr; n_D^{26} 1.4148; ^{1}Hnmr (CCl_4): τ4.10–5.00 (m, 2H), 6.20–7.00 (m, 3H), 8.35 (dd, J = 1.5 and 7Hz, 3H), 8.9–9.50 (m, 10H); ms *m/e*: 142.1358 ($M^{+\cdot}$, calcd. for $C_9H_{18}O$: 142.1358).

E-*5-Methyl-3-hexen-2-yl* p-*Nitrobenzoate*

The fraction boiling at 78–81°C/51 Torr, n_D^{24} 1.4293, 32 g (0.28 mol) of the product of reduction of 99 g *E*-5-methyl-3-hexen-2-one (24) with aluminum hydride (8) was treated with 57.5 g (0.28 mol) *p*-nitrobenzoyl chloride in 300 mL dry pyridine at 0°C and the mixture stirred overnight. The usual workup and several recrystallizations from hexane at −20°C gave 18.7 g (25%) product, mp 47.7–48°C; ^{1}Hnmr (CCl_4): τ1.80 (s, 4H) 3.90–4.60 (m, 3H), 7.50–7.90 (m, 1H): 8.52 (d, J = 7 Hz, 3H), 8.90 (d, J = 7 Hz, 6H). *Anal.* calcd. for $C_{14}H_{13}NO_4$: C 63.87, H 6.51, N 5.32; found: C 63.86, H 6.89, N 5.58.

E-*2-Ethoxy-5-methyl-3-hexene*

Saponification of *E*-5-methyl-3-hexen-2-yl *p*-nitrobenzoate gave *E*-5-methyl-3-hexen-2-ol, bp 86–88°C/74 Torr, n_D^{24} 1.4310, which was converted to the ethyl ether using the procedure described for the preparation of 3-ethoxy-4,4-dimethylcyclopentene. A pure sample was isolated by gc, bp 63°C/73 Torr; n_D^{25} 1.4168; ^{1}Hnmr (CCl_4): τ4.50–5.00 (m, $J_{3,4}$ = 15 Hz, 2H), 6.40–7.00 (m, 3H, —O—CH_2— and >C*H*O), 7.85 (m, 1H), 9.10 (m, 12H); ms *m/e*: 142.1358 ($M^{+\cdot}$, calcd. for $C_9H_{18}O$: 142.1358).

Rate Studies

Solutions (0.03 *M*) of the *p*-nitrobenzoate ester in 80% ethanol were charged into ampoules which were sealed and inserted into thermostatted heating baths. From time to time ampoules were removed, equilibrated to 25.0°C, and broken open. Aliquots, 5 mL, were removed with calibrated automatic pipettes, drained into 50 mL methanol, α-naphtholbenzein was added, and titration carried out with 0.03 *M* sodium hydroxide solution. The runs were all followed to more than 80% completion and at least seven points were taken. The values of the first order rate constants were calculated from the expression

$$k = \frac{2.303}{t} \log \frac{V_\infty - V_0}{V_\infty - V_t}$$

where V_0, V_t, and V_∞ are the volumes of titrant at time $t = 0$, t, and infinity, respectively. The first ampoule was removed from the heating bath after 4–5 min, this time taken as zero time and the volume of titrant taken as V_0. The instantaneous values of k within each run were averaged, the average deviation of each point from this average k_t was computed, and any point further than an arbitrarily chosen three times the average deviation from the mean was rejected from the computation. Refinement of the data was continued this way until a suitably precise result emerged. In no case were more than two points rejected. The activation parameters were then calculated (25). The results are presented in Table 1.

Products of solvolysis

(A) From 1-OPNB

A solution of 0.605 g **1**-OPNB in 75 mL 80% ethanol was heated at 100°C for one half-life of solvolysis and then the

TABLE 1. Rates of solvolysis of 0.03 *M* **1**-, **13**-, **14**-OPNB in 80% ethanol

Ester	Temperature (°C)	$10^6 k$, s^{-1}	Relative rate	E_a, (kcal/mol)	$\Delta S^{\neq}$ eu (80°C)
1-OPNB	80.1	20.2±0.9	32	26.7±1	7±3
	100.0	157±8			
13-OPNB	80.1	0.632±0.04	1	27.8±1.1	11±3
	100.0	5.24±0.16			
14-OPNB	50.1	23.5±0.7		23.3±0.6	10±2
	70.0	197±7			
	80	523[a]	828		

[a] Extrapolated rate constant.

solvent was thoroughly evaporated under reduced pressure. The residue 0.475 g (95.6%, based on 50% ester remaining and 50% *p*-nitrobenzoic acid produced) was analyzed by ^{1}Hnmr ($CDCl_3$). From the relative areas of the aromatic protons of **1**-OPNB and **2**-OPNB at τ1.75 and 1.83, respectively, and also of olefinic and methine protons it was estimated the recovered ester consisted of ~75% **1**-OPNB and ~25% **2**-OPNB.

A solution of 0.202 g **1**-OPNB in 25 mL 80% ethanol was heated at 100°C for 18 half-lives of solvolysis in a sealed ampoule. A weighed quantity of cumene was added to a 10 mL portion of the solution which was then analyzed by gc. Calibration was carried out with known mixtures of cumene and **1**-OC_2H_5. The remainder of the solvolysis mixture was poured into an equal volume of water and the resulting solution concentrated with 3 × 80 mL dichloromethane. The combined extract was shaken with potassium hydroxide and brine, and dried and carefully concentrated through a Vigreux column with a partial reflux head. Gas chromatographic analysis disclosed three peaks in a ~90:5:5 ratio. The major component was collected from the effluent of the gc and shown by nmr to be a mixture of **1**- and **2**-OC_2H_5, the composition of which was determined from the ratios of the areas of the peaks due to the methine protons. ^{1}Hnmr for **2**-OC_2H_5 (CCl_4): τ4.46 (s, 2H), 5.70 (dd, J = 7.0 and 5.0 Hz, 1H), 6.72 (q, J = 7.5 Hz, 2H), 8.30 (dd, J = 13.0 and 7.0 Hz, 1H), 8.52 (dd, J = 13.0 and 5.0 Hz, 1H); 8.99 (t, J = 7.5 Hz, 3H), 8.99 (s, 3H), 9.10 (s, 3H).

(B) From 13-OPNB

The procedure was operationally similar to that described above. Examination of the nmr spectrum of the ester isolated from the interrupted solvolysis disclosed that no rearranged *p*-nitrobenzoate had been formed. The major product of solvolysis was isolated from the effluent of the gc and shown by nmr to be *E*-2-ethoxy-5-methyl-3-hexene.

(C) From 14-OPNB

Using the methods described above the product of solvolysis was shown to be **14**-OC_2H_5 by comparison of the nmr spectrum with that of an authentic (26) sample.

Tetrabutylammonium Acetate TBA

A solution of 164 g TBA-hydrate (27), mp 14.7–14.9°C (lit. (27) mp 15.1°C) in 200 mL ethanol was allowed to stand 7 days over 200 g 3A molecular sieve, decanted, and then concentrated. The residue was heated overnight with rotation under 7 Torr at 45°C. The residue then crystallized on cooling with evolution of much heat, mp 45–48°C, and was shown by nmr to contain 3% water, corresponding to TBA·½ H_2O. Treatment with molecular sieve was repeated except that the final pumping out was done at 80°C. The resulting solid, mp 70–72°C, was extraordinarily hygroscopic and all operations were carried out under dry nitrogen. A water content corresponding to 10TBA·H_2O was deduced from integration of the nmr spectrum which showed the water peak at τ2.1 (CCl_4). This material was used in the S_N2' experiments.

Reaction between 11-OPMS and TBA

A carbon tetrachloride solution 0.4 *M* in **11**-OPMS and 0.45 *M* in TBA was placed in nmr tube and the nmr spectrum taken at various times. The results have been described in the text.

Attempted S_N2' Reactions of 1-ODCB

Solutions 0.4 *M* in 1-ODCB and 0.5 *M* in various nucleophiles or in piperidine in nmr tubes were heated as described in the text and analyzed from time to time by nmr. The results have been given in the text.

1. (*a*) G. STORK and A. F. KREFT, III. J. Am. Chem. Soc. **99**, 3850 (1977); (*b*) G. STORK and A. F. KREFT, III. J. Am. Chem. Soc. **99**, 3851 (1977); (*c*) A. A. DOBBIE and K. H. OVERTON. J. Chem. Soc., Chem. Commun. 722 (1977); (*d*) R. M. MAGID and O. S. FRUCHEY. J. Am. Chem. Soc. **99**, 8368 (1977); (*e*) N. IKOTA and B. GANEM. J. Am. Chem. Soc. **100**, 351 (1978); (*f*) W. KIRMSE, F. SCHEIDT, and H.-J. VATER. J. Am. Chem. Soc. **100**, 3945 (1978); (*g*) R. M. MAGID and O. S. FRUCHEY. J. Am. Chem. Soc. **101**, 2107 (1979); (*h*) S. E. DENMARK and A. ESCHENMOSER. Abstracts. 181st National Meeting of the American Chemical Society, Atlanta, Ga., March 29–April 3. 1981. ORGN 104.
2. G. STORK and W. N. WHITE. J. Am. Chem. Soc. **78**, 4609 (1956).
3. (*a*) J. D. PARK, J. R. LACHER, and J. R. DICK. J. Org. Chem. **31**, 1116 (1966); (*b*) E. TOROMANOFF. Tetrahedron, **34**, 1665 (1978); (*c*) R. M. MAGID. Tetrahedron, **36**, 1901 (1980); (*d*) E. TOROMANOFF. Tetrahedron, **36**, 2809 (1980).
4. (*a*) R. F. BROWN and N. M. VAN GULICK. J. Am. Chem. Soc. **77**, 1092 (1955); (*b*) K. C. BRANNOCK, H. S. PRIDGEON, and B. THOMPSON. J. Org. Chem. **25**, 1815 (1960); (*c*) P. L. CREGER. J. Am. Chem. Soc. **89**, 2500 (1967).
5. R. H. HASEK, R. D. CLARK, E. V. ELAM, and R. J. NATIONS. J. Org. Chem. **27**, 3106 (1962).
6. M. F. ANSELL and S. S. BROWN. J. Chem. Soc. 2955 (1958).
7. W. C. AGOSTA and A. B. SMITH, III. J. Am. Chem. Soc. **93**, 5513 (1971).
8. M. J. JORGENSON. Tetrahedron Lett. 559 (1962).
9. V. J. TRAYNELIS, W. L. HERGENROTHER, J. L. LIVINGSTON, and J. A. VALICENTI. J. Org. Chem. **27**, 2377 (1962).
10. T. MATSUMOTO, H. SHIRAHAMA, A. ICHIHARA, H. SHIN, K. KAGAWA, F. SAKAN, S. NISHIDA, S. MATSUMOTO, K. SAITO, and H. HASHIMOTO. Bull. Chem. Soc. Jpn. **45**, 1140 (1972).
11. (*a*) F. G. GAULT, J. E. GERMAIN, and J. M. CONIA. Bull. Soc. Chim. Fr. 1064 (1957); (*b*) R. T. CONLEY. Rec. Trav. Chim. Pays-Bas **81**, 198 (1962); (*c*) H. O. HOUSE and B. M. TROST. J. Org. Chem. **30**, 2502 (1965); (*d*) V. A. MIRONOV, A. A. IVANOV, and A. A. AKHREM. Izv. Akad. Nauk SSSR. Ser. Khim. 363 (1973); (*e*) M. LACHEVEQUE, A. DEBAL, and T. CUVIGNY. J. Organomet. Chem. **87**, 25 (1975).
12. (*a*) C. F. WILCOX, JR. and M. MESIROV. J. Org. Chem. **25**,

Can. J. Chem. Downloaded from www.nrcresearchpress.com by 210.87.254.5 on 09/06/12
For personal use only.

1841 (1960); (*b*) R. S. ROUSE and W. E. TYLER. J. Org. Chem. **26**, 3525 (1961); (*c*) P. EILBRACHT and P. DAHLER. Justus Liebigs Ann. Chem., 1890 (1979); (*d*) C. W. JEFFORD, T. W. WALLACE, M. T. H. CAN, and C. G. RIMBAULT. J. Org. Chem. **44**, 689 (1979).
13. E. F. KIEFER, and J. D. ROBERTS. J. Am. Chem. Soc. **84**, 784 (1962).
14. (*a*) J. L. FRY, C. J. LANCELOT, L. K. M. LAM, J. M. HARRIS, R. C. BINGHAM, D. J. RABER, R. E. HALL, and P. v. R. SCHLEYER. J. Am. Chem. Soc. **92**, 2538 (1970); (*b*) J. L. FRY, J. M. HARRIS, R. C. BINGHAM, and P. v. R. SCHLEYER. J. Am. Chem. Soc. **92**, 2540 (1970); (*c*) P. v. R. SCHLEYER, J. L. FRY, L. K. M. LAM, and C. J. LANCELOT. J. Am. Chem. Soc. **92**, 2542 (1970); (*d*) A. PROSS and R. KOREN. Tetrahedron Lett. 1949 (1974).
15. (*a*) R. J. CRAWFORD and A. MISHRA. J. Am. Chem. Soc. **88**, 3963 (1966) (*b*) R. J. CRAWFORD and H. TOKUNAGA. Can. J. Chem. **52**, 4033 (1974); (*c*) P. S. ENGEL and L. SHEN. Can. J. Chem. **52**, 4040 (1974).
16. L. F. FIESER. Experiments in organic chemistry. 3rd ed. D. C. Heath and Co., Boston. 1957. p. 285.
17. H. C. BROWN, E. J. MEAD, and B. C. SUBBA RAO. J. Am. Chem. Soc. **72**, 6212 (1955).
18. N. O. BRACE. J. Org. Chem. **29**, 1247 (1964).
19. A. J. BELLAMY. J. Chem. Soc. B, 449 (1969).
20. H. E. RAMSDEN, J. R. LEEBRICK, S. D. ROSENBERG, E. H. MILLER, J. J. WALBURN, A. E. BALINT, and R. CSERR. J. Org. Chem. **22**, 1602 (1957).
21. P. B. D. DE LA MARE, E. D. HUGHES, P. C. MERRIMAN, L. PICHET, and C. A. VERNON. J. Chem. Soc. 2563 (1958).
22. E. MARKER, O. KAMM, J. LUCIUS, and T. S. OAKWOOD. J. Am. Chem. Soc. **59**, 1837 (1937).
23. K. ALDER and F. H. FLOCK. Chem. Ber. **89**, 1737 (1956).
24. R. HEILMANN, G. DE GAUDEMARIS, P. ARNAUD, and G. SCHEUERBRANDT. Bull. Soc. Chim. Fr. 112 (1957).
25. J. F. BUNNETT. *In* Rates and mechanisms of reactions. Vol. VIII. Part 1 of Technique of organic chemistry. 2nd ed. *Edited by* A. Weissberger. Interscience, New York. 1961. pp. 199–201.
26. R. YA. LEVINA, T. I. GODOVIKOVA, and V. M. VINOGRADOVA. Vestn. Mosk. Univ. Khim. **14**, 171 (1959); Chem. Abstr. **54**, 10888*b* (1960).

Can. J. Chem. Downloaded from www.nrcresearchpress.com by 210.87.254.5 on 09/06/12
For personal use only.

A theoretical study of the CSH_4 and CPH_5 hypersurfaces. Geometries, tautomerization, and dissociation of sulfonium and phosphonium ylides

DAVID JOHN MITCHELL AND SAUL WOLFE
Department of Chemistry, Queen's University, Kingston, Ont., Canada K7L 3N6
AND
H. BERNHARD SCHLEGEL[1]
Department of Chemistry, Wayne State University, Detroit, MI 48202, U.S.A.
Received June 10, 1981

Can. J. Chem. Downloaded from www.nrcresearchpress.com by 210.87.254.6 on 09/06/12
For personal use only.

DAVID JOHN MITCHELL, SAUL WOLFE, and H. BERNHARD SCHLEGEL. Can. J. Chem. **59**, 3280 (1981).

Calculations have been performed at four basis set levels (STO-3G, STO-3G*, 4-31G, 4-31G*) on the model ylides methylenesulfurane (CH_2SH_2) and methylenephosphorane (CH_2PH_3), their stable tautomers (CH_3SH and CH_3PH_2), their dissociation products (SH_2, PH_3 and CH_2), and the protonated species $CH_3SH_2^+$ and $CH_3PH_3^+$. At each basis set level all geometries have been optimized fully, using the FORCE method. The conformational behaviour of the ylides as a function of C—X bond-stretching, C—X torsion, and CH_2 (or SH_2) bending has been examined in some detail. The experimental properties (i.e., geometries, relative stabilities, proton affinities, rotation–inversion behaviour) of sulfonium and phosphonium ylides are reproduced well by the model calculations with the 4-31G* basis set, which contains *d*-type functions on both carbon and sulfur (or phosphorus). All other basis sets are deficient in different ways and for different reasons, which are discussed in detail. The principal result of this work is the conclusion that *d*-type functions are essential for a proper description of the hypervalent species CH_2SH_2 and CH_2PH_3, but not for the normal-valent species SH_2, PH_3, CH_3SH, and CH_3PH_2. The conclusion concerning hypervalent species reverses our earlier views. The role of the *d*-type functions is to concentrate charge into the C—X region of the ylides, and thus to stabilize the system. Evidence for this effect has been obtained from quantitative perturbational molecular orbital (PMO) analyses of interactions associated with the carbon lone pair, as well as comparisons of electron density plots with and without the *d* AO's. A second conclusion is that the imposition of various geometrical constraints such as assumed C—X, C—H, or X—H bond lengths, and HCH or XH_n bond angles, as was necessary for computational reasons in all previous work on such systems, has major and previously unrecognized consequences. For example, the assumption that the CH_2 moiety is planar in CH_2SH_2 leads to very similar geometries with and without *d* AO's, although only in the latter case does such a geometry at carbon correspond to the true energy minimum; in the absence of *d* AO's the C—S bond length is maintained by a symmetry-enforced barrier to dissociation. These and other consequences of geometrical constraints at carbon, sulfur, or phosphorus are analyzed in detail.

DAVID JOHN MITCHELL, SAUL WOLFE et H. BERNHARD SCHLEGEL. Can. J. Chem. **59**, 3280 (1981).

Utilisant quatre ensembles de base (STO-3G, STO-3G*, 4-31G, 4-31G*), on a effectué des calculs sur des modèles d'ylures de méthylenesulfurane (CH_2SH_2) et de méthylenephophorane (CH_2PH_3), sur leurs tautomères stables (CH_3SH et CH_3PH_2), sur leurs produits de dissociation (SH_2, PH_3 et CH_2) et sur leurs espèces protonées CH_3SH_2, $CH_3PH_3^+$. Faisant appel à la méthode de FORCE, on a optimisé pleinement toutes les géométries pour tous les ensembles de base. On a examiné soigneusement le comportement conformationnel des ylures en fonction de l'élongation de la liaison C—X, de la torsion de cette liaison et de la déformation du CH_2 (ou du SH_2). On a reproduit convenablement les propriétés expérimentales (i.e. les géométries, les stabilités relatives, les affinités pour le proton, le comportement à la rotation–inversion) des ylures de sulfonium et de phosphonium en utilisant des calculs modèles de la base 4-31* qui contient les fonctions de type-*d* sur le carbone et le soufre (ou sur le phosphore). Tous les autres ensembles de base sont déficients de différentes façons et pour des raisons différentes que l'on discute en détail. Le résultat principal de ce travail permet de conclure que les fonctions-*d* sont essentielles pour une description adéquate des espèces hypervalentes CH_2SH_2 et CH_2PH_3 mais ne le sont pas dans le cas des espèces à valence normale SH_2, PH_3, CH_3SH et CH_3PH_2. La conclusion relative aux espèces hypervalentes renverse notre première idée. Les fonctions de type-*d* concentrent la charge dans la région de C—X des ylures et stabilisent alors le système. On a obtenu la preuve de cette action à partir des analyses quantitatives des pertubations d'orbitale moléculaires (POM) des interactions associées au doublet libre du carbone ainsi qu'à partir des comparaisons des courbes de densité électronique avec ou sans les OA *d*. On conclut également que l'imposition de contraintes géométriques variées telles qu'assumées par les longueurs de liaison C—X, C—H, ou X—H et par les angles HCH ou XH_n qui étaient nécessaires pour des raisons de calculs dans tous les travaux antérieurs portant sur de tels systèmes, ont des conséquences importantes et inconnues. Par exemple, l'hypothèse relative à la planéité de la portion CH_2 du CH_2SH_2 conduit à deux géométries très semblables avec ou sans les OA *d* bien que ce soit seulement dans le deuxième cas qu'une telle géométrie du carbone corresponde à l'énergie minimum réelle. En l'absence des OA *d*, la longueur de liaison C—S est maintenue par une barrière à la rotation induite par la symmétrie. On analyse en détail ces faits et d'autres conséquences relatives aux contraintes géométriques au niveau du carbone, du soufre ou du phosphore.

[Traduit par le journal]

---

[1]Fellow of the Alfred P. Sloan Foundation, 1981–1983.

0008-4042/81/233280-13$01.00/0
©1981 National Research Council of Canada/Conseil national de recherches du Canada

Can. J. Chem. Downloaded from www.nrcresearchpress.com by 210.87.254.6 on 09/06/12
For personal use only.

Introduction

The participation of low-lying virtual atomic *d*-orbitals ("outer" *d*-orbitals (1)) in molecular bonding has been studied extensively (2). Attention has focused, especially, upon hypervalent molecules (3), i.e., molecules having Lewis structures with more than eight valence electrons about a central atom (e.g., silicon, phosphorus, sulfur, chlorine) (4–12).

Included in the class of hypervalent molecules are the sulfonium and phosphonium ylides (13*a*), also known as methylenesulfuranes and methylenephosphoranes, which are isoelectronic with the corresponding sulfoxides (13*b*) and phosphine oxides. The importance of such ylides in organic synthesis (13*c*) has led to numerous theoretical investigations at both the semi-empirical (14) and *ab initio* levels (15, 16). All of the *ab initio* studies have employed either idealized geometries or have included a limited geometry optimization subject to some constraints.

One of the objectives of the present work is to reexamine the two model ylides methylenesulfurane (CH_2SH_2) and methylenephosphorane (CH_2PH_3) at the *ab initio* level, with complete geometry optimization. A second objective is to perform computations with and without *d*-atomic orbitals (*d* AO's) in the basis set, to evaluate the degree and manner of the participation of *d* AO's in the bonding in both ylides. Certain other points on the CSH_4 and CPH_5 hypersurfaces have also been examined, to assess the consequences of various geometrical constraints. The calculated relative energetics have been placed within the context of known experimental quantities by computation of the protonation energies and sulfur inversion barriers of selected species.

To facilitate the discussion, certain points will be highlighted using qualitative arguments based on the perturbational molecular orbital (PMO) method (17). As will be seen, the PMO treatment of these ylides is dominated by the presence of the lone pair on carbon.

Computational Details

The *ab initio* calculations were performed using either the GAUSSIAN 80 program system (18) or a modified version of GAUSSIAN 76 (19). All geometry optimizations were performed using the FORCE method (20), a gradient relaxation procedure now incorporated into GAUSSIAN 80. Setting the convergence on the RMS gradient at 0.0025 mdyne gave bond lengths accurate to 0.001 Å and bond angles accurate to 0.1°.

The basis sets used were the standard STO-3G (21), STO-3G* (10), 4-31G (22*a*), and 4-31G* (22*b*) basis sets of Pople. The 4-31G* basis set contains six second-order Gaussian functions (xx, yy, zz, xz, yz, xy) on all heavy atoms. The *d*-orbital exponents for sulfur and phosphorus were optimized variationally for the lowest energy conformations of CH_2SH_2 ($\alpha_d = 0.59$) and CH_2PH_3 ($\alpha_d = 0.51$), and were then used unchanged in subsequent calculations. The *d*-orbital set on carbon was not modified.

The program used to plot electron density difference maps was adapted from Jorgensen's PSI/77 (23). Energy surfaces were generated using the program 3DPLOT (20).

In those sections of the discussion which deal with a quantitative PMO analysis, the fragment orbital energies and the properties of these orbitals necessary for the computation of orbital interaction energies were obtained by the procedure described earlier (24). The two-orbital, four-electron interaction energies were calculated using eq. [1] where e_i^0 and e_j^0 are the energies of the fragment orbitals ϕ_i^0 and ϕ_j^0, and S_{ij} and Δ_{ij} are the overlap integral and the interaction matrix element between them, respectively. The two-orbital, two-electron interaction energies were calculated by direct solution of the appropriate secular determinant (eq. [2]).[2]

$$[1] \quad \Delta e_{ij} = 2S_{ij}[-2\Delta_{ij} + (e_i^0 + e_j^0)S_{ij}]/(1 - S_{ij}^2)$$

$$[2] \quad \begin{vmatrix} e_i^0 - e & \Delta_{ij} - S_{ij}e \\ \Delta_{ij} - S_{ij}e & e_j^0 - e \end{vmatrix} = 0$$

Results and Discussion

1. Ab initio *Calculations*

Thermodynamic Aspects of the CSH_4 and CPH_5 Hypersurfaces

Calculations with full geometry optimization were performed at the four different basis set levels for selected conformations of the two ylides CH_2SH_2 and CH_2PH_3, the staggered conformations of the stable tautomers CH_3SH and CH_3PH_2, and the dissociation products H_2S, PH_3, and CH_2. Calculations are also reported for the staggered conformations of the protonation products $CH_3SH_2^+$ and $CH_3PH_3^+$. The various geometries and total energies of the two heavy-atom sulfur and phosphorus

[2] The usual equation [3], which approximates the solution to [2],

$$[3] \quad \Delta e_{ij} = 2(\Delta_{ij} - e_i^0 S_{ij})^2/(e_i^0 - e_j^0)$$

could not be used because of the unusually large stabilizing interactions in these molecules.

TABLE 1. Geometries[a] and total energies[b] of selected CSH_4 Systems and $CH_3SH_2^+$

Molecule	Parameter	Basis set			
		STO-3G	STO-3G*	4-31G	4-31G*
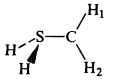 1	r(CS)	1.690	1.596	1.732	1.627
	r(CH$_1$)	1.057	1.069	1.062	1.067
	r(CH$_2$)	1.059	1.069	1.062	1.068
	r(SH)	1.361	1.354	1.376	1.355
	∠(SCH$_1$)	114.7	115.3	113.6	114.7
	∠(SCH$_2$)	119.1	124.2	119.1	122.9
	∠(CSH)	109.2	111.5	112.5	113.2
	∠(HSH)	90.7	88.9	93.4	90.4
	E_T	−432.68254	−432.79874	−437.00816	−437.11947
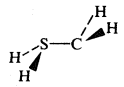 2	r(CS)	2.060	1.812	2.451	2.049
	r(CH)	1.111	1.105	1.100	1.097
	r(SH)	1.333	1.332	1.349	1.327
	∠(SCH)	94.1	97.6	91.3	95.6
	∠(HCH)	101.0	103.1	104.8	102.9
	∠(CSH)	97.9	100.2	93.0	97.3
	∠(HSH)	93.6	91.9	96.0	94.0
	E_T	−432.71598	−432.77518	−437.02679	−437.10304
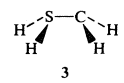 3	r(CS)	2.118	1.807	2.610	2.385
	r(CH)	1.113	1.098	1.101	1.097
	r(SH)	1.335	1.334	1.353	1.329
	∠(SCH)	93.5	101.4	87.8	91.1
	∠(HCH)	100.5	104.9	104.9	102.5
	∠(CSH)	105.4	108.5	107.9	106.1
	∠(HSH)	93.0	90.2	95.6	93.5
	E_T	−432.70806	−432.76839	−437.02090	−437.09783
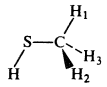 4	r(CS)	1.798	1.782	1.886	1.815
	r(CH$_1$)	1.085	1.088	1.077	1.081
	r(CH$_{2,3}$)	1.087	1.089	1.076	1.081
	r(SH)	1.331	1.320	1.356	1.330
	∠(SCH$_1$)	108.6	108.2	105.7	106.8
	∠(SCH$_{2,3}$)	112.2	112.5	110.1	111.3
	∠(CSH)	95.4	95.1	97.8	97.3
	ω(H$_1$CSH$_{2,3}$)	119.0	118.7	118.7	118.5
	E_T	−432.89607	−432.92985	−437.18375	−437.25261
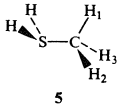 5	r(CS)	1.841	1.805	1.944	1.833
	r(CH$_1$)	1.089	1.091	1.074	1.077
	r(CH$_{2,3}$)	1.089	1.092	1.075	1.079
	r(SH)	1.349	1.339	1.353	1.332
	∠(SCH$_1$)	109.7	110.7	108.2	110.2
	∠(SCH$_{2,3}$)	107.0	107.4	104.4	106.3
	∠(CSH)	100.1	98.4	102.4	100.7
	ω(H$_1$SCH$_{2,3}$)	120.8	121.0	121.1	121.3
	ω(H$_1$CSH)	49.0	47.5	51.0	49.1
	E_T	−433.27243	−433.33228	−437.46857	−437.55983

[a] Bond lengths in Å, bond angles in degrees.
[b] In hartrees.

systems are collected in Tables 1 and 2, respectively. Results for the simple hydrides are reported in Table 3. The relative energies are summarized in Tables 4 and 5.

A number of points can be made concerning the CSH_4 and CPH_5 surfaces. The experimental energy difference for the equilibrium process of eq. [4] is reasonably well reproduced at both the 4-31G

[4] $CH_3XH_n \rightleftarrows {}^1A_1CH_2 + XH_{n+1}$

and 4-31G* levels. Thus, addition of *d* AO's to a split-valence basis set has only a modest effect upon this net proton transfer – dissociation process. An analogous result is obtained at the STO-3G and STO-3G* levels, but the energy is greatly overestimated by these minimal basis sets. The problem is caused by a lack of flexibility within such basis sets, and also by basis set superposition (29).

Since the *tautomerization* energy of CH_2SH_2 is *greater* than that of CH_2PH_3, and, at the same time, the *dissociation* energy of CH_2SH_2 is *less* than that

Can. J. Chem. Downloaded from www.nrcresearchpress.com by 210.87.254.6 on 09/06/12
For personal use only.

TABLE 2. Geometries[a] and total energies[b] of selected CPH_5 systems and $CH_3PH_3^+$

Molecule	Parameter	Basis set			
		STO-3G	STO-3G*	4-31G	4-31G*
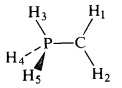 6	r(CP)	1.674	1.601	1.701	1.641
	$r(CH_1)$	1.058	1.068	1.065	1.070
	$r(CH_2)$	1.058	1.069	1.065	1.071
	$r(PH_3)$	1.372	1.371	1.405	1.389
	$r(PH_{4,5})$	1.393	1.391	1.438	1.414
	$\angle(PCH_1)$	117.6	118.8	117.6	118.3
	$\angle(PCH_2)$	119.5	122.6	120.6	122.0
	$\angle(CPH_3)$	112.3	111.4	110.8	110.9
	$\angle(CPH_{4,5})$	120.8	122.0	121.7	122.1
	$\omega(H_1CPH_{4,5})$	119.6	119.1	118.8	119.0
	E_T	−377.03267	−377.16908	−380.87381	−380.99523
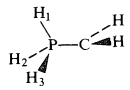 7	r(CP)	1.897	1.607	1.721	1.652
	r(CH)	1.101	1.071	1.069	1.074
	$r(PH_1)$	1.387	1.399	1.461	1.428
	$r(PH_{2,3})$	1.373	1.376	1.410	1.394
	$\angle$(PCH)	100.0	119.7	117.2	118.3
	$\angle(CPH_1)$	132.1	127.4	129.1	128.8
	$\angle(CPH_{2,3})$	110.9	113.7	112.2	112.8
	$\omega(H_1PCH)$	52.8	80.2	75.9	75.9
	$\omega(H_1CPH_{2,3})$	124.5	120.5	121.4	120.7
	E_T	−377.05050	−377.17013	−380.87503	−380.99680
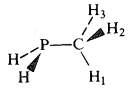 8	r(CP)	1.841	1.830	1.915	1.861
	$r(CH_1)$	1.084	1.085	1.079	1.082
	$r(CH_{2,3})$	1.083	1.086	1.080	1.084
	r(PH)	1.381	1.379	1.435	1.410
	$\angle(PCH_1)$	113.1	113.4	112.2	113.2
	$\angle(PCH_{2,3})$	110.2	110.0	108.6	109.2
	$\angle$(CPH)	96.1	95.7	97.5	97.5
	$\omega(H_1CPH_{2,3})$	120.8	121.0	121.1	121.3
	$\omega(H_1CPH)$	47.2	46.7	47.9	47.4
	E_T	−377.22385	−377.27661	−381.01277	−381.09103
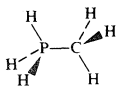 9	r(CP)	1.834	1.795	1.886	1.810
	r(CH)	1.086	1.090	1.078	1.082
	r(PH)	1.380	1.378	1.401	1.385
	$\angle$(PCH)	109.0	109.3	108.4	109.2
	$\angle$(CPH)	111.5	111.5	111.6	111.8
	E_T	−377.63158	−377.69947	−381.33341	−381.43344

[a] Bond lengths in Å, bond angles in degrees.
[b] In hartrees.

of CH_2PH_3, it follows that the sulfonium ylide is intrinsically the less stable species. This is in accord with experiment (30).

The most important finding is that inclusion of *d* AO's on the second row atoms has a large effect upon the stabilities of the ylides. With the split-valence basis set the stabilization is nearly 27 kcal/mol in both cases. Consequently, deletion of the *d* AO's forces the ylides to lie too close to their dissociation limits. Indeed, as seen in Table 4, the sulfonium ylide **1** is actually calculated to be less stable than the dissociation products, even without correction for basis set superposition.

On the other hand, the energy differences associated with the normal valent species of eq. [4] do not depend greatly upon the presence of *d* AO's, as already noted. This indicates that the concept of hypervalence may be of some value in defining those species that require *d* AO's for a proper description.

Table 6 compares the proton affinities calculated for the two ylides and their stable tautomers. The experimental proton affinities of methanethiol and methylphosphine are also included for comparison. It is clear that the 4-31G* basis set predicts this experimental quantity quite well (31). The very similar proton affinities of CH_2SH_2 and CH_2PH_3 with the *d*-orbital basis sets are noteworthy. Apparently, PH_3^+ and SH_2^+ substituents have almost the same effect upon the protonation of an adjacent carbanionic centre.

Structures of the Ylides

CH_2SH_2

The data of Table 1 reinforce the observations already made concerning the role of *d* AO's spec-

Can. J. Chem. Downloaded from www.nrcresearchpress.com by 210.87.254.6 on 09/06/12
For personal use only.

Can. J. Chem. Downloaded from www.nrcresearchpress.com by 210.87.254.6 on 09/06/12
For personal use only.

TABLE 3. Geometries[a] and total energies[b] of CH_2, H_2S, and PH_3 at the 4-31G* basis set level[c]

Molecule	Parameter	
$^1A_1$ CH_2	r(CH)	1.097
	∠(HCH)	102.9
	E_T	−38.83140
$^1\Delta$ CH_2[d]	r(CH)	1.054
	∠(HCH)	180.
	E_T	−38.79835
H_2S	r(SH)	1.329
	∠(HSH)	93.7
	E_T	−398.25771
PH_3	r(PH)	1.409
	∠(HPH)	94.1
	E_T	−342.09026

[a] Bond lengths in Å, bond angles in degrees.
[b] In hartrees.
[c] Results for these systems at the STO-3G, STO-3G*, and 4-31G levels may be found in ref. 10*a* (H_2S, PH_3) and in ref. 10*b* (CH_2).
[d] Complex orbitals were used.

ifically in the description of the hypervalent species methylenesulfurane (cf. 13*b*). Thus, the geometries of methanethiol **4** and methylsulfonium cation **5** show only minor dependence on the basis set; the principal trends are longer C—S bond lengths at the split-valence level, and the shortening of this bond upon addition of *d* AO's (10). In contrast, the geometries of the ylides depend greatly upon the choice of basis set.

Computations were performed initially on conformation **1**, in which the carbon centre is constrained to planarity and the HCH plane bisects the H_2S plane. These constraints result in somewhat similar structures with the different basis sets, and the C—S bond length varies in the manner already described for **4** and **5**.

Release of all constraints, to allow both pyramidalization at carbon and C—S torsion, illustrates the effect of the *d*AO's. When these functions are present, the carbon centre remains planar and no rotation occurs, so that **1** is the true minimum. In the absence of these functions, the carbon centre becomes strongly pyramidal, the C—S bond lengthens to values greater than 2 Å and the molecule rotates to the anti structure **2**. It is noteworthy that optimization of the *anti* conformation using the *d* AO-containing basis sets also reveals pyramidalization at carbon and C—S bond lengthening; however, **2** then becomes a rotational maximum. The *syn* conformation **3** was also examined. It is a rotational maximum with all basis sets.

Therefore, at the STO-3G* and 4-31G* levels, **1** is the only minimum on the conformational hypersurface. It lies in a deep well with respect to C—S torsion (see below). On the other hand, at the STO-3G and 4-31G levels, **2** is the most stable conformation, and is 5.0 and 3.7 kcal/mol, respectively, more stable than the *syn* conformation **3**, which remains the maximum on the rotational potential. No distinguishable minimum corresponding to a *gauche* conformation (e.g. **10**) exists at 4-31G, although a careful search did reveal an extremely shallow minimum 1.3 kcal/mol above **2** at STO-3G.

TABLE 4. Relative energies[a] of selected points on the singlet CSH_4 surface

System	Basis set				Expt.[b]
	STO-3G	STO-3G*	4-31G	4-31G*	
4	0.	0.	0.	0.	0.
1	134.0	82.3	110.2	83.5	
2	113.0	97.1	98.5	94.5	
$^1A_1$ $CH_2 + H_2S$	133.1	133.7	106.3	103.2	101.1
$^1\Delta CH_2 + H_2S$	163.6	164.2	119.3	123.3	

[a] In kcal/mol (theoretical values are uncorrected for zero-point vibration).
[b] The heats of formation of CH_3SH and H_2S were taken from ref. 27, and $^3B_1$ CH_2 from ref. 25. The CH_2 $^3B_1 - {}^1A_1$ separation was taken from ref. 26.

TABLE 5. Relative energies[a] of selected points on the singlet CPH_5 surface

System	Basis set				Expt.[b]
	STO-3G	STO-3G*	4-31G	4-31G*	
8	0.	0.	0.	0.	0.
7	108.8	66.8	86.4	59.1	
6	120.0	67.5	87.2	60.1	
$^1A_1$ $CH_2 + PH_3$	135.0	137.0	111.0	106.3	(108.8)
$^1\Delta CH_2 + PH_3$	165.5	167.5	123.9	127.0	

[a] In kcal/mol (theoretical values are uncorrected for zero-point vibration).
[b] The heat of formation of PH_3 was taken from ref. 27, and that of CH_3PH_2 was taken from ref. 28. See also footnote *b* of Table 4.

TABLE 6. Proton affinities[a,b] of CSH_4 and CPH_5 species

System	Basis set				Expt.[c]
	STO-3G	STO-3G*	4-31G	4-31G*	
CH_3SH	236.2	252.5	178.7	192.8	188.6
CH_2SH_2	349.2	334.8	277.2	276.3	
CH_3PH_2	255.9	265.3	201.2	214.9	204.8
CH_2PH_3	364.6	332.2	287.6	274.0	

[a] In kcal/mol.
[b] Theoretical values are derived from the most stable conformation with each basis set.
[c] Values taken from ref. 32.

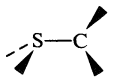

10

These results are of some importance in assessing the validity of a model proposed recently for the prediction of the relative acidities of diastereotopic protons in sulfonium salts (33). This model is derived from an examination of the C—S rotational potential of $CH_2S(CH_3)_2$ at the 4-31G level with the following major assumptions: (*i*) a pyramidal carbon; (*ii*) a 1.85 Å C—S bond length; (*iii*) 105° angles at sulfur; (*iv*) rigid rotation. With these various assumptions, the computations of Graham and Heathcock lead to a *gauche* minimum. It should be clear that this result is an artifact for two reasons, viz., the neglect of *d* AO's and the choice of geometry.

Figure 1 illustrates further the consequences of the imposition of geometrical constraints and the usefulness of a computational procedure which allows ready optimization of all parameters. The figure shows C—S torsion of **2** at the STO-3G level with rigid rotation of the fully optimized structure (r_{CS} = 2.06 Å) and of the structures having r_{CS} = 1.86 Å and 1.66 Å. It can be seen that a *gauche* minimum could be made to exist by the artificial choice of an appropriately short C—S bond length and, presumably, other arbitrary constraints.[3] There is a parallel between the artificial behaviour achieved in Fig. 1 and the experimental properties of nonhypervalent A_2X_4 systems. In hydrazines (r_{NN} ~ 1.45 Å) (34), the *gauche* conformation is adopted, while diphosphines (r_{PP} ~ 2.20 Å) and diarsines (r_{AsAs} > 2.4 Å) (35) prefer the *anti* conformation.

In view of the large effect of *d* AO's upon the energy of CH_2SH_2 it seems, at first glance, surprising that the geometries computed for **1** under C_s symmetry at STO-3G or 4-31G are close to the fully optimized values obtained at STO-3G* or 4-31G*.

[3] In fact, holding r_{CS} = 1.66 Å and optimizing all other parameters of **2** and **10** at the STO-3G level produces *gauche* minima lying 9.8 and 18.6 kcal/mol, respectively, *below* the *anti* structure.

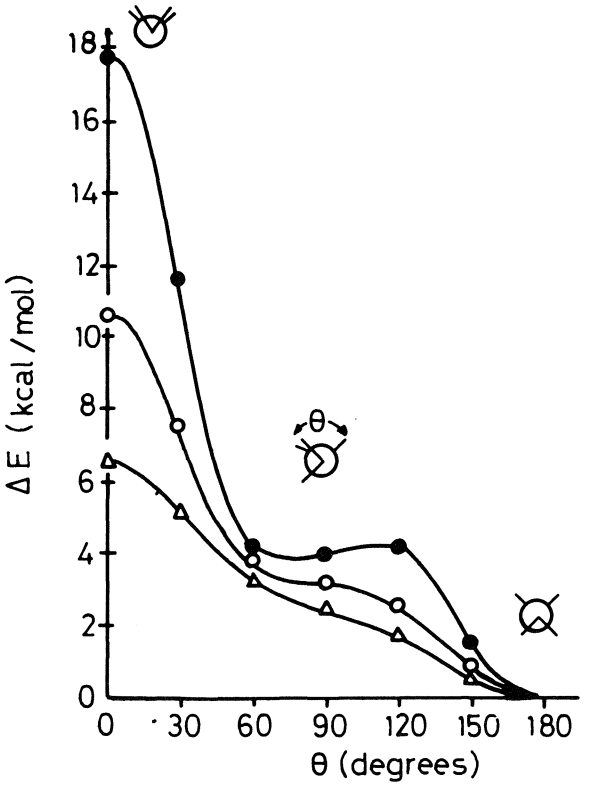

FIG. 1. Effect of geometrical constraint upon the C—S torsional potential of **2** at the STO-3G level. △, r_{C-S} = 2.06 Å (fully optimized); ○, r_{C-S} = 1.86 Å; ●, r_{C-S} = 1.66 Å.

The reason for this is that, when carbon is planar, dissociation of the ylide along only a C—S stretching coordinate would require the formation of CH_2 in the excited $^1\Delta$ state. This causes the CSH_4 energy surface along this stretching coordinate to rise steeply from **1**; therefore, at the STO-3G and 4-31G levels the ylide exists within the symmetry of **1** because of a large symmetry-enforced barrier to separation of the fragments. Such barriers have been recognized previously by Trinquier and Malrieu in their pseudopotential study of CH_2PH_3 (15*f*).

Pyramidalization at carbon provides a mechanism for dissociation which avoids the high-energy

Can. J. Chem. Downloaded from www.nrcresearchpress.com by 210.87.254.6 on 09/06/12
For personal use only.

Can. J. Chem. Downloaded from www.nrcresearchpress.com by 210.87.254.6 on 09/06/12
For personal use only.

ridge of the surface. Nevertheless, complete dissociation does not occur because the C—S bond stretching – carbon pyramidalization surface contains a minimum corresponding to **10**, which transforms to **2** when rotation is permitted to occur. The calculated topology of this surface in the absence of *d* AO's is shown in Fig. 2. In agreement with this assessment, the structures obtained for **2** have long C—S bonds and HSH and HCH planes nearly perpendicular to this bond axis. Therefore, **2** is best regarded as $^1A_1$ carbene solvated by hydrogen sulfide. Such behaviour is reminiscent of that exhibited by so-called oxonium ylides (15*g*, 36).

When *d* AO's are added to the basis set, **1** is no longer a saddle point on the conformational hypersurface but, as already seen, the minimum. Dissociation is now entirely endothermic, as can be seen in Fig. 3. The enantiomeric dissociation paths p and p′ are directly comparable to Fig. 2 of ref. 15*f*.

This analysis also accounts for the very modest effect of *d* AO's upon the P—O bond length of H_3PO observed by Wallmeier and Kutzelnigg in their study of hypervalent oxides (37). As pointed out by these workers, direct dissociation of H_3PO leads to an excited state of atomic oxygen. This corresponds to the effect seen here for the isoelectronic CH_2. However, in the case of H_3PO, no symmetry-breaking path exists and no dramatic bond lengthening occurs upon deletion of the *d* AO's.

Finally, Table 7 lists the STO-3G* and 4-31G* energies computed for pyramidal inversion at sulfur for $CH_3SH_2^+$ and CH_2SH_2. Comparison of the 4-31G* data with experimental results shows satisfactory agreement.

CH_2PH_3

The phosphorus analog of **1** is **6** (Table 2), in

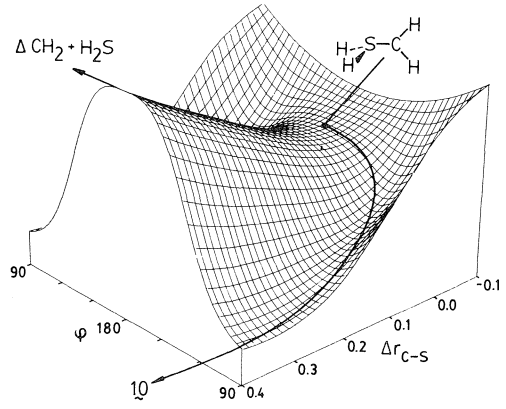

FIG. 2. Dissociation of CH_2SH_2 by a combination of C—S bond stretching and pyramidalization at carbon when *d* AO's are omitted.

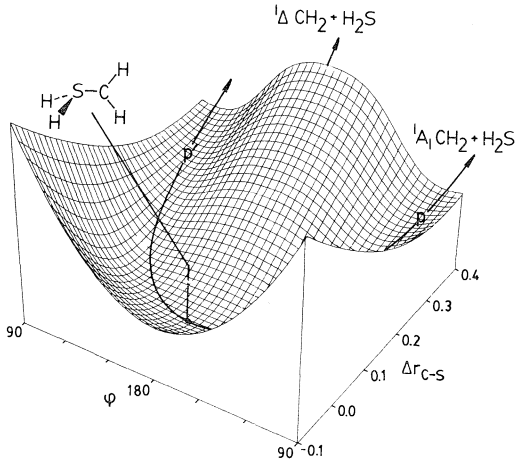

FIG. 3. Effect of *d* AO's upon the C—S bond stretching – carbon pyramidalization surface of CH_2SH_2.

which a P—H bond formally replaces a sulfur hybrid lone pair. As with the sulfonium ylide, addition of the *d* AO's causes a small decrease in the C—P bond length of **6** and the carbon centre is planar.

With all basis sets, **7** is the rotational minimum. The very nonplanar carbon geometry and C—P bond lengthening obtained at STO-3G is mainly a result of the effects already described for the sulfonium ylide. With all other basis sets, and in general agreement with Lischka (15*d*), Strich (15*e*), and Dixon and co-workers (15*g*), the carbon centre of **7** is nearly planar.

The 4-31G* C—P bond length in **7**, 1.652 Å, is in excellent agreement with previous theoretical (15) and experimental (38) determinations. An interesting feature of the geometries of **6** and **1** is the substantial deviation of the PH_3 moiety from local C_{3v} symmetry. The rotational barrier for CH_2PH_3 (**7** → **6**) is relatively small (0.7 kcal/mol at the STO-3G* level and 1.0 kcal/mol at the 4-31G* level), but larger than calculated previously (15) because the geometry at the PH_3 moiety has been taken into account. The reasons for this unusual geometry are discussed below in some detail.

The bond stretching – carbon inversion energy

TABLE 7. Pyramidal inversion barriers[a] at sulfur in methylsulfonium cation and methylenesulfurane

System	Basis set		Expt.[b]
	STO-3G*	4-31G*	
$CH_3SH_2^+$	47.4	29.6	25–29
CH_2SH_2	32.6	15.9	19–23

[a] In kcal/mol.
[b] Experimental values taken from refs. 39 and 40.

Can. J. Chem. Downloaded from www.nrcresearchpress.com by 210.87.254.6 on 09/06/12
For personal use only.

surface of Fig. 2 is also appropriate for methylenephosphorane at the STO-3G level although, even without *d* AO's, the saddle point **6** lies below $^1A_1$ CH_2 + PH_3. With all other basis sets, a surface analogous to that shown in Fig. 3 better describes the dissociation of **6**.

The ability of the 4-31G basis set to provide a reasonable description of the geometry of CH_2PH_3 (but not CH_2SH_2) illustrates the importance of obtaining accurate relative energies for the ylides and the dissociation products. The very poor energy for **1** relative to $^1A_1$ CH_2 + H_2S at the STO-3G and 4-31G levels renders these surfaces very unstable towards dissociation. This process is prevented because of the existence of a dative-bonded complex **2**. Since CH_2PH_3 is intrinsically more stable than CH_2SH_2, the dissociation limit lies well above the ylide even without *d* AO's, and much less bond lengthening occurs. Nevertheless, the *d* AO's are necessary for the description of the relative energetics of the phosphorus system; their absence simply has less of a geometrical consequence than in the sulfur system.

II. PMO Analyses

All of the *ab initio* results are consistent with the view that stabilization of the carbon lone pair of an ylide is a major factor affecting the energy differences between CH_2SH_2 and CH_2PH_3 and their more stable tautomers. This can be seen more clearly from a PMO analysis of the geometrical and basis set factors which influence the interaction of a CH_2 group with an adjacent H_nX system.

Bonding

The PMO analysis of the model ylide CH_2XH_n consists of the fragmentation $H_2C\cdots XH_n$ and evaluation of the energies associated with the allowed interactions between the two sets of group orbitals. Although many valence orbital interactions are present (e.g., twelve in the case of $H_2C\cdots SH_2$), attention will be focused upon only those interactions associated with n_C, the carbon lone pair. This choice follows from the dominant contribution of this orbital to the HOMO's of these ylides, and the dominant contribution of the two-electron and four-electron interactions associated with this lone pair to the total interaction energies (17*c*). Although the other interaction energies are not zero, they are overwhelmed by the effects of the carbon lone pair.

Figure 4 shows the interaction diagram for conformation **6** of CH_2PH_3. Interaction *a* is a four-electron destabilizing interaction between the carbon lone pair (n_C) and the bonding π-type orbital of the PH_3 group (π_y). Interaction *b* is a two-electron stabilizing interaction between n_C and the antibonding PH_3 orbital, π_y^*. This latter interaction is large because n_C is high-lying and π_y^* is low-lying. Figure 5 shows the interaction diagram which results from a 90° rigid rotation of the CH_2 group (i.e., **7**). For a PH_3 group having C_{3v} symmetry, interactions *a* and *b* of Fig. 5 are identical to interactions *a* and *b* of Fig. 4, because the π-type orbitals are doubly degenerate. Therefore, this qualitative argument suggests no conformational preference in CH_2PH_3. This idealized picture is in accord with the low barrier computed for this ylide, which may be attributed to small variations in the σ-system.

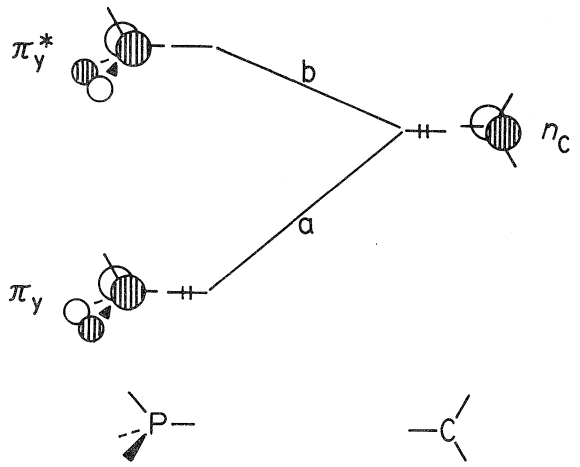

FIG. 4. Frontier orbital interactions in conformation **6** of CH_2PH_3.

The corresponding interaction diagrams for CH_2SH_2 are shown in Figs. 6 and 7. Figure 6, which refers to **1**, is entirely analogous to Fig. 4 for **6**; however, Fig. 7, which represents a 90° rigid

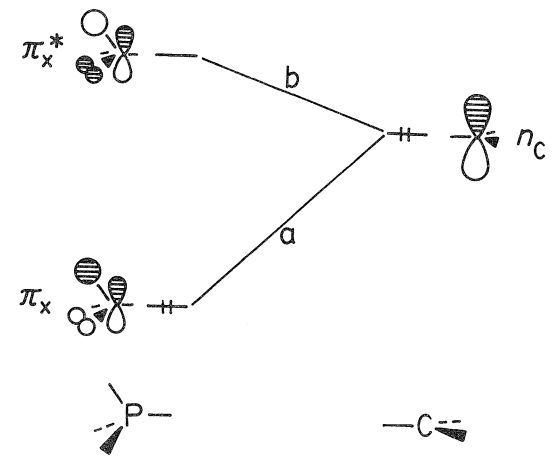

FIG. 5. Frontier orbital interactions in conformation **7** of CH_2PH_3.

Can. J. Chem. Downloaded from www.nrcresearchpress.com by 210.87.254.6 on 09/06/12
For personal use only.

rotation of **1** is very different from Fig. 5. Interaction *a* takes place between n_C and the sulfur lone pair, n_S, while interaction *b* takes place between n_C and the antibonding orbital σ_{SH_2}*. The n_C–n_S interaction is more destabilizing than n_C–π_y because n_S lies higher in energy than π_y; the n_C–σ_{SH_2}* interaction is much less stabilizing than n_C–π_y* because the overlap is smaller and σ_{SH_2}* lies higher than π_y*. The result is a strong preference for conformation **1**.

Rotation of **1** by 90° leads to an increase in the C—S bond length and pyramidalization at carbon since the strong n_C–π_y* interaction is lost and the destabilizing n_C–n_S interaction is reduced by such changes. Conformation **2** is the result.

The qualitative PMO analysis just presented has focused on the net effects of an XH_n fragment upon one common orbital, n_C, of an adjacent CH_2 moiety. If this treatment is reasonable, the relative magnitudes of the stabilization (or destabilization) by SH_2 and PH_3 should be related to the intrinsic stabilities of the two ylides, i.e., the tautomerization and dissociation energies. Table 8 reports the results of a quantitative PMO analysis on **1** and **6** with the different basis sets. This indicates that **6** is more stabilized than **1** in all cases. The same trend was seen in the tautomerization energies.

The function of the *d* AO's is to polarize or rehybridize the π-type antibonding acceptor orbitals of XH_n into the C—X region. As can be seen by comparison of the magnitudes of interaction *b* for **1** and **6** from Table 8, the *d* orbital polarization of the π* orbitals increases the overlap with n_C and greatly strengthens the stabilization.

That such a polarization exists can be demonstrated by examination of electron density plots.

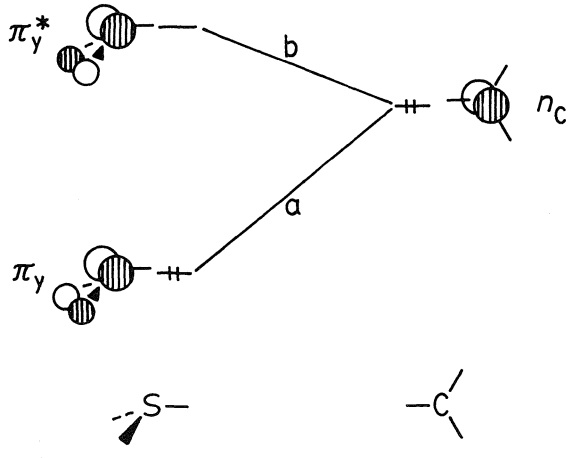

FIG. 6. Frontier orbital interactions in conformation **1** of CH_2SH_2.

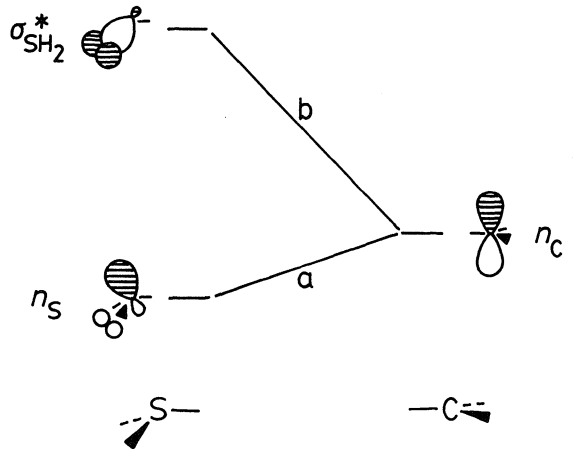

FIG. 7. Frontier orbital interactions in CH_2SH_2 following a 90° rotation of conformation **1**.

Figures 8 and 9 show the electron density in the HOMO (taken in the *yz* plane) of the sulfonium ylide **1** at the 4-31G and 4-31G* levels, respectively. Clearly the *d* AO's have not altered the nodal characteristics of this predominantly *p*-type lone pair on carbon. Their effect only becomes evident in the density difference plot. Figure 10 shows the electron density difference in the HOMO for **1** at the 4-31G* – 4-31G level; an identical result is observed for **6**. This figure now demonstrates that the effect of the *d* AO's is to concentrate charge into the C—S or C—P π-bonding region.

The form of this figure is dominated by the *d* AO's on sulfur; thus, in the 4-31G* HOMO of **1** the coefficients of the two contributing carbon *d* AO's are 0.002 and 0.023, while those of the corresponding sulfur *d* AO's are 0.060 and −0.136. In addition, deletion of the *d* AO's from carbon has no significant effect upon the sulfur *d* and carbon *p* coefficients computed at 4-31G*. The effect of the analysis presented here is to cast the role of *d* AO participation in a somewhat different language than is customary in the concept of p_π–d_π bonding, with its implication of conjugation with "free standing" *d* orbitals.

Geometric Consequences

The orbital interactions considered in Figs. 4–7 also provide insight into the origins of the geometric distortions in the XH_n fragments of these ylides. Each of these interactions will lead to distortion of XH_n to permit minimization of the four-electron destabilization or maximization of the two-electron stabilization. Such effects have been discussed recently for methyl groups by Radom and coworkers (41).

Figure 11 shows interactions *a* and *b* of **1**.

TABLE 8. Quantitative PMO analyses of CH_2SH_2 and CH_2PH_3

Basis set	Molecule	Interaction energy[a]			Difference[c]
		Interaction *a*	Interaction *b*	Total	
STO-3G[b]	**1**	31.7	−57.0	−25.3	−8.8
	6	26.7	−60.8	−34.1	
STO-3G*	**1**	28.2	−107.5	−79.3	−18.6
	6	18.7	−116.6	−97.9	
4-31G[b]	**1**	47.6	−31.9	15.7	−9.5
	6	39.3	−33.1	6.2	
4-31G*	**1**	44.0	−45.1	−1.1	−12.2
	6	31.6	−44.9	−13.3	

[a] In kcal/mol.
[b] Calculated at the geometry optimized using *d* AO's.
[c] ΔE_{PMO} (**6** − **1**).

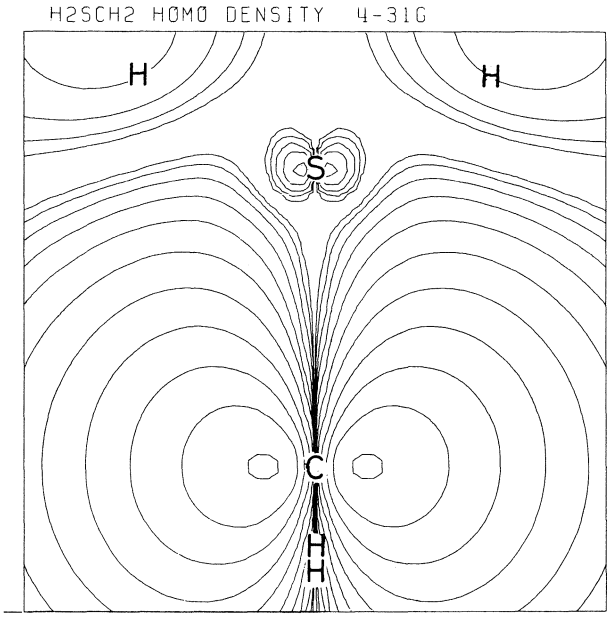

FIG. 8. Total electron density plot of the 4-31G HOMO of CH_2SH_2 in the plane perpendicular to the HCH plane with the C—S bond along the *z*-axis. Contour levels are at 0.0001, 0.00022, 0.00047, 0.001, 0.0022, 0.0047, 0.01, 0.022, 0.047, 0.1, 0.22e.

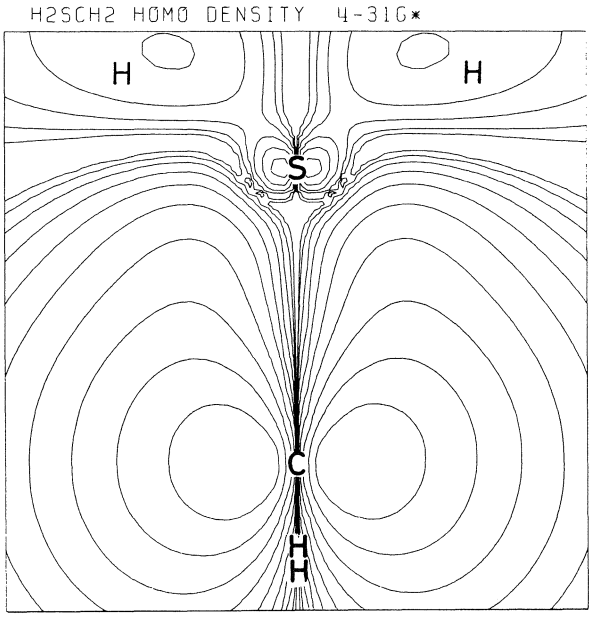

FIG. 9. As for Fig. 8 but at the 4-31G* level.

Secondary overlap is depicted by double-headed arrows. In *a* this secondary overlap will cause the HSH plane to tilt away from carbon, so as to decrease the unfavourable overlap associated with the destabilizing interaction. The tilt is in the same direction in *b*, so as to *increase* the overlap associated with the *stabilizing* interaction. The angular distortion resulting from these reinforcing effects leads to CSH angles in **1** which range from 109.2°–113.2° for the four basis sets. The corresponding angle in **4** is 95.1°–97.8° and in **5** it is 98.4°–102.4°.

An additional consequence of interaction *b* is lengthening of the S—H bonds of **1**, because charge is delocalized into an S—H antibonding region. Inspection of Table 1 reveals that this effect amounts to ca. 0.03 Å, the S—H bond of **1** being longer than those of **2**–**5**.

Figure 11 also describes interactions *a* and *b* of **6**. In this case, the distortion of PH_3 is greater than that of SH_2. Thus $\angle CPH_{4,5}$ of **6** ranges from 120.8°–122.1°, compared to a ∠CPH range in **8** of 95.7°–97.5°. This suggests that a PH_3 group is more readily deformed than an SH_2 group,[4] but interaction *b* is also stronger in **6** than in **1**. The disparity between the two different ∠CPH angles of **6**

[4] The calculated diagonal force constant for this rocking mode is k_{rock} = 1.05 mdyne Å/rad² for **6** and k_{rock} = 1.24 mdyne Å/rad² for **1**.

Can. J. Chem. Downloaded from www.nrcresearchpress.com by 210.87.254.6 on 09/06/12
For personal use only.

Can. J. Chem. Downloaded from www.nrcresearchpress.com by 210.87.254.6 on 09/06/12
For personal use only.

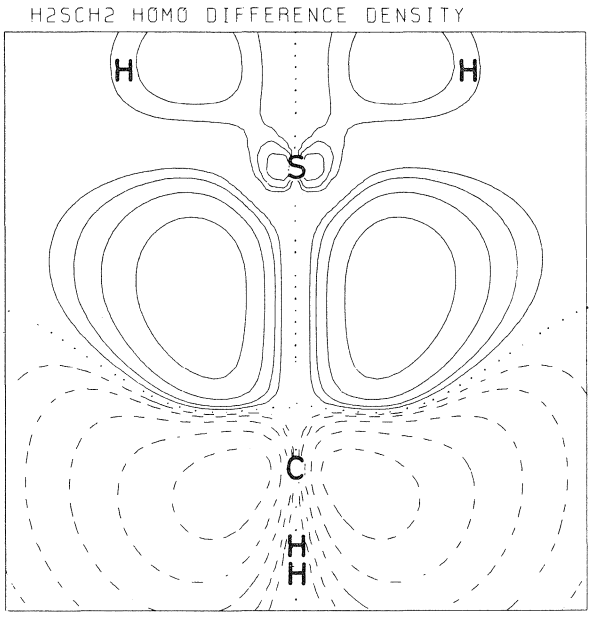

FIG. 10. Electron density difference plot (4-31G* − 4-31G) for the HOMO of CH_2SH_2 in the plane perpendicular to the HCH plane with the C—S bond along the z-axis. Solid contours refer to regions which gain electron density upon addition of d-orbitals; dashed contours represent regions which lose electron density. Dotted lines represent nodes. Contour levels are at ±0.001, ±0.0022, ±0.0047, ±0.01, ±0.022e.

corresponds to a tilt angle (the angle between the nominal C_3 axis of the PH_3 group and the C—P bond[5]) of +7.6° at the 4-31G* level. Interaction **6** also leads to selective weakening of the P—$H_{4,5}$ bonds compared to P—H_3, as can be seen in the 0.02 Å–0.03 Å difference recorded in Table 2 (cf. 24*b*).

As depicted in Fig. 12, a tilt of the PH_3 group is also expected in **7**, but in the opposite sense to that of **6**. In this case, an approximately *16° difference* between ∠CPH_3 and ∠CP$H_{4,5}$ is found, corresponding to a tilt angle of *−10.4°*. These results indicate that the assumption of local C_{3v} symmetry for the PH_3 group about the P—C axis is a much greater approximation than was previously supposed and would have significant effects upon calculated rotational barriers (15*a*, *d*, *f*, *g*) and the experimental structure refinement of $CH_2P(Me)_3$ (30). An additional feature of interaction *b* in **7** is the prediction that P—H_3 should be longer than P—$H_{4,5}$ (cf. 24*b*); this effect is seen in the data of Table 2.

Summary and Conclusions

The first *ab initio* molecular orbital calculations on sulfur-containing carbanions were reported in

[5]Calculated using 3 cos (α_1 + 2α) = 4 cos α_2 − cos α_1 where α = tilt angle, α_1 = ∠CPH_3, and α_2 = ∠CP$H_{4,5}$. See ref. 41.

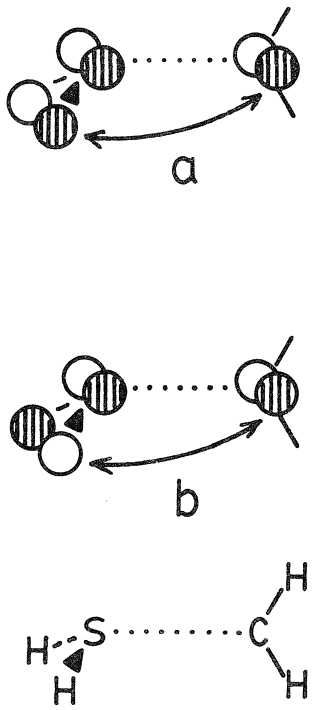

FIG. 11. Secondary frontier orbital interactions in conformation **1** of CH_2SH_2 or conformation **6** of CH_2PH_3 showing the origin of the tilt of the XH_n group.

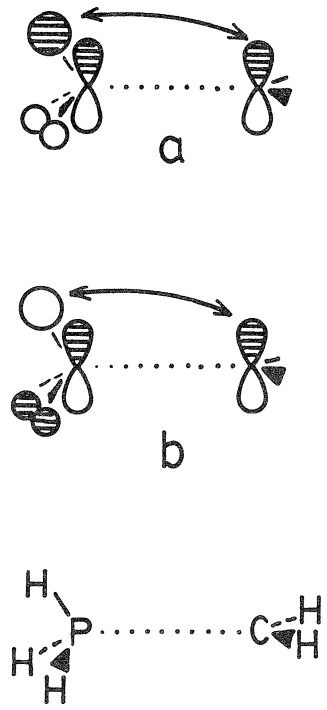

FIG. 12. Secondary frontier orbital interactions in conformation **7** of CH_2PH_3 showing a tilt of PH_3 in the opposite direction from that in **6**.

Can. J. Chem. Downloaded from www.nrcresearchpress.com by 210.87.254.6 on 09/06/12
For personal use only.

1969 (42, 43). At that time it was necessary to employ minimal level basis sets and experimental or idealized bond lengths and bond angles. As a result of that work on alpha-sulfinyl and alpha-sulfonyl systems and subsequent, more detailed computations on alpha-thio and alpha-oxycarbanions (44), it was concluded that *"the asymmetry of alpha-sulfinyl and alpha-sulfonylcarbanions need not be related to a possible existence of 3*d*-orbital conjugation"* (43), but that *"small basis set calculations were ... necessary forerunners to the more extensive and elaborate calculations that now have to be done"* (42).

The present work provides some indication of the type of study that will be needed and is now feasible. The experimental properties (geometries, relative stabilities, proton affinities, rotation–inversion behaviour) of sulfonium and phosphonium ylides are reproduced well by the model calculations with the 4-31G* basis set, which contains *d*-type functions on carbon, sulfur, and phosphorus. All other basis sets are deficient, in different ways, and for different reasons. The necessity of *d* AO's to *stabilize* these hypervalent molecules, and the mechanism of this stabilization, have become clear. At the same time, it has been found that a proper manifestation of the *d*-orbital effects upon the *stereochemical properties* of these systems depends upon the initial choice of geometry. If the C—X bond length is incorrect, incorrect carbon valence angles or torsional angles about the C—X bond are predicted, whether *d* AO's are present or not. On the other hand, the assumption of planarity at carbon leads to very similar bond lengths and torsional angles with and without *d* AO's, although only in the latter case does such a geometry at carbon correspond to the true energy minimum. In the absence of *d* AO's, this assumption leads to an acceptable C—X bond length because of a symmetry-enforced barrier to dissociation. The existence of such a barrier then obscures the effects of the *d* AO's.

Consequently, a reinvestigation of the geometrical properties of alpha-sulfinyl and alpha-sulfonylcarbanions, and the effects of *d* AO's upon these properties, will require full geometry optimization of all structures at several basis set levels. Depending on the adequacy of the earlier geometrical assumptions (42, 43), the 1969 rotation–inversion behaviour may yet prove to be reliable. However, the conclusions concerning the role of the *d* AO's will probably have to be revised.

Acknowledgements

This research has been supported by grants from the Natural Sciences and Engineering Research Council of Canada and the Petroleum Research Fund, administered by the American Chemical Society. The authors gratefully thank the Advisory Research Committee of Queen's University, Wayne State University, and Merck, Sharp and Dohme Research Laboratories for generous allocation of computing funds.

1. C. A. COULSON. Nature (London), **221**, 1106 (1969).
2. (*a*) E. E. BALL, M. A. RATNER, and J. R. SABIN. Chem. Scr. **12**, 128 (1977); (*b*) M. A. RATNER and J. R. SABIN. J. Am. Chem. Soc. **99**, 3954 (1977), and references cited therein.
3. (*a*) J. I. MUSHER. Angew. Chem. **81**, 68 (1969); (*b*) J. I. MUSHER. J. Am. Chem. Soc. **94**, 1370 (1972).
4. V. B. KOUTECKY and J. I. MUSHER. Theor. Chim. Acta, **33**, 227 (1974).
5. R. E. RUNDLE. Surv. Prog. Chem. **1**, 81 (1963).
6. R. HOFFMANN, J. M. HOWELL, and E. L. MUETTERTIES. J. Am. Chem. Soc. **94**, 3047 (1972).
7. G. M. SCHWENZER and H. F. SCHAEFER III. J. Am. Chem. Soc. **97**, 1393 (1975).
8. A. RAUK, L. C. ALLEN, and K. MISLOW. J. Am. Chem. Soc. **94**, 3035 (1972).
9. M. M. L. CHEN and R. HOFFMANN. J. Am. Chem. Soc. **98**, 1647 (1976).
10. (*a*) J. B. COLLINS, P. v. R. SCHLEYER, J. S. BINKLEY, and J. A. POPLE. J. Chem. Phys. **64**, 5142 (1976); (*b*) W. A. LATHAN, W. J. HEHRE, L. A. CURTISS, and J. A. POPLE. J. Am. Chem. Soc. **93**, 6377 (1971).
11. A. STRICH and A. VEILLARD. J. Am. Chem. Soc. **95**, 5574 (1973).
12. (*a*) I. H. HILLIER and V. R. SAUNDERS. Mol. Phys. **22**, 193 (1971); (*b*) M. F. GUEST, M. B. HALL, and I. H. HILLIER. J. Chem. Soc. Faraday Trans. II, **69**, 1829 (1973).
13. (*a*) J. I. MUSHER. Tetrahedron, **30**, 1747 (1974); (*b*) P. G. MEZEY and A. KAPUR. Can. J. Chem. **58**, 559 (1980); (*c*) B. M. TROST and L. S. MELVIN. *In* Sulfur ylids: emerging synthetic intermediates. Academic Press, New York. 1975. S. TRIPPETT. Special Periodical Report: Organo-phosphorus Chem. **9** (1978).
14. (*a*) R. HOFFMANN, D. B. BOYD, and S. Z. GOLDBERG. J. Am. Chem. Soc. **92**, 3929 (1970); (*b*) R. HOFFMANN and D. B. BOYD. J. Am. Chem. Soc. **93**, 1064 (1971); (*c*) K. A. OSTOJA STARZEWSKI, H. TOM DIECK, and H. BOCK. J. Organomet. Chem. **65**, 311 (1974); (*d*) K. A. OSTOJA STARZEWSKI and H. BOCK. J. Am. Chem. Soc. **98**, 8486 (1976); (*e*) K. A. OSTOJA STARZEWSKI, W. RICHTER, and H. SCHMIDBAUR. Chem. Ber. **109**, 473 (1976).
15. (*a*) I. ABSAR and J. R. VAN WAZER. J. Am. Chem. Soc. **94**, 2382 (1972); (*b*) M.-H. WHANGBO and S. WOLFE. Can. J. Chem. **54**, 949 (1976); (*c*) F. BERNARDI, H. B. SCHLEGEL, M.-H. WHANGBO and S. WOLFE. J. Am. Chem. Soc. **99**, 5633 (1977); (*d*) H. LISCHKA. J. Am. Chem. Soc. **99**, 353 (1977); (*e*) A. STRICH. Nouv. J. Chim. **3**, 105 (1979); (*f*) G. TRINQUIER and J. P. MALRIEU. J. Am. Chem. Soc. **101**, 7169 (1979); (*g*) R. A. EADES, P. G. GASSMAN, and D. A. DIXON. J. Am. Chem. Soc. **103**, 1066 (1981).
16. (*a*) K. TATSUMI, Y. YOSHIOKA, K. YAMAGUCHI, and T. FUENO. Tetrahedron, **32**, 1705 (1976); (*b*) R. M. MINYAEV, V. I. MINKIN, I. D. SADEKOV, and V. I. NADDAKA. Zh. Obshch. Khim. **47**, 1294 (1977); (*c*) G. BARBARELLA, P. DEMBECH, A. GARBESI, F. BERNARDI, A. BOTTONI, and A. FAVA. J. Am. Chem. Soc. **100**, 200 (1978).
17. (*a*) L. SALEM. J. Am. Chem. Soc. **90**, 543 (1968); R. HOFFMANN. Acc. Chem. Res. **4**, 1 (1971); B. M. GIMARC.

Acc. Chem. Res. **7**, 384 (1974); S. DAVID, O. EISENSTEIN, W. J. HEHRE, L. SALEM, and R. HOFFMANN. J. Am. Chem. Soc. **95**, 3806 (1973); (*b*) I. FLEMING. *In* Frontier orbitals and organic chemical reactions. Wiley–Interscience, New York. 1976; G. KLOPMAN (*Editor*). Chemical reactivity and reaction paths. Wiley–Interscience, New York. 1974; R. F. HUDSON. Angew. Chem. Int. Ed. Engl. **12**, 36 (1973); M. J. S. DEWAR and R. C. DOUGHERTY. *In* The PMO theory of organic chemistry. Plenum Press, New York. 1975; (*c*) M.-H. WHANGBO and S. WOLFE. Israel J. Chem. **20**, 36 (1980).

18. J. S. BINKLEY, R. A. WHITESIDE, R. KRISHNAN, R. SEEGER, D. J. DEFREES, H. B. SCHLEGEL, S. TOPIOL, L. R. KHAN, and J. A. POPLE. Submitted to Quantum Chemistry Program Exchange (1980).
19.. J. S. BINKLEY, R. A. WHITEHEAD, P. C. HARIHARAN, R. SEEGER, and J. A. POPLE. QCPE. **11**, 368 (1978).
20. H. B. SCHLEGEL. Ph.D. thesis, Queen's University. 1975.
21. W. J. HEHRE, R. F. STEWART, and J. A. POPLE. J. Chem. Phys. **51**, 2657 (1969).
22. (*a*) R. DITCHFIELD, W. J. HEHRE, and J. A. POPLE. J. Chem. Phys. **54**, 724 (1971); (*b*) P. C. HARIHARAN and J. A. POPLE. Theor. Chim. Acta, **28**, 213 (1973).
23. W. L. JORGENSEN. QCPE. **10**, 340 (1977).
24. (*a*) M.-H. WHANGBO, H. B. SCHLEGEL, and S. WOLFE. J. Am. Chem. Soc. **99**, 1296 (1977); (*b*) D. KOST, H. B. SCHLEGEL, D. J. MITCHELL, and S. WOLFE. Can. J. Chem. **57**, 729 (1979).
25. JANAF thermochemical tables. 1975 Suppl. J. Phys. Chem. Ref. Data, **4**, 1 (1975).
26. R. K. LENGEL and R. N. ZARE. J. Am. Chem. Soc. **100**, 7495 (1978).
27. S. W. BENSON. *In* Thermochemical kinetics. 2nd ed. Wiley, New York. NY. 1976.
28. Y. WADA and R. W. KISER. J. Phys. Chem. **68**, 2290 (1964).
29. S. F. BOYS and F. BERNARDI. Mol. Phys. **19**, 553 (1970).
30. A. W. JOHNSON. *In* Ylid chemistry. Academic Press, New York. 1966.
31. (*a*) P. KOLLMAN and S. ROTHENBERG. J. Am. Chem. Soc. **99**, 1333 (1977); (*b*) J. CHANDRASEKHAR, J. G. ANDRADE, and P. v. R. SCHLEYER. J. Am. Chem. Soc. **103**, 5609 (1981).
32. D. H. AUE and M. T. BOWERS. *In* Gas phase ion chemistry. Vol. 2. *Edited by* M. T. Bowers. Academic Press, New York, NY. 1979.
33. S. L. GRAHAM and C. H. HEATHCOCK. J. Am. Chem. Soc. **102**, 3713 (1980).
34. J. R. DURIG, B. M. GIMARC, and J. D. ODOM. *In* Vibrational spectra and structure. Vol. 2. *Edited by* J. R. Durig. Marcel Dekker, New York, NY. 1973.
35. A. H. COWLEY, M. J. S. DEWAR, D. W. GOODMAN, and M. C. PADOLINA. J. Am. Chem. Soc. **96**, 2648 (1974).
36. L. B. HARDING, H. B. SCHLEGEL, R. KRISHNAN, and J. A. POPLE. J. Phys. Chem. **84**, 3394 (1980).
37. H. WALLMEIER and W. KUTZELNIGG. J. Am. Chem. Soc. **101**, 2804 (1979).
38. (*a*) J. C. J. BART. J. Chem. Soc. B, 350 (1969); (*b*) E. A. V. EBSWORTH, T. E. FRASER, and D. W. H. RANKIN. Chem. Ber. **110**, 3494 (1977).
39. D. DARWISH and R. L. TOMILSON. J. Am. Chem. Soc. **90**, 5938 (1968).
40. S. WOLFE, P. CHAMBERLAIN, and T. F. GARRARD. Can. J. Chem. **54**, 2847 (1976).
41. A. PROSS, L. RADOM, and N. V. RIGGS. J. Am. Chem. Soc. **102**, 2253 (1980).
42. A. RAUK, S. WOLFE, and I. G. CSIZMADIA. Can. J. Chem. **47**, 113 (1969).
43. S. WOLFE, A. RAUK, and I. G. CSIZMADIA. J. Am. Chem. Soc. **91**, 1567 (1969).
44. F. BERNARDI, I. G. CSIZMADIA, A. MANGINI, H. B. SCHLEGEL, M.-H. WHANGBO, and S. WOLFE. J. Am. Chem. Soc. **97**, 2209 (1975).

Can. J. Chem. Downloaded from www.nrcresearchpress.com by 210.87.254.6 on 09/06/12
For personal use only.

Palladium compounds of pyrimidine and pyridine derivatives – proposed structure assignment changes

PI-CHANG KONG AND F. D. ROCHON

Département de chimie, Université du Québec à Montréal, C.P. 8888, Montréal (Qué.), Canada H3C 3P8

Received May 8, 1981

PI-CHANG KONG and F. D. ROCHON. Can. J. Chem. **59**, 3293 (1981).

The complexes $[PdL_2X_2]$ where L = cytosine, 1-methylcytosine, cytidine, 2-amino-4-methylpyrimidine, 2-hydroxy-4-methylpyrimidine, 4-methylpyrimidine, 2-hydroxypyrimidine, 2,4-diethoxy-5-methylpyrimidine, 2-hydroxypyridine, and methyl-4-picolinate, and X = Cl and Br, were prepared from the reaction of K_2PdCl_4 and L in aqueous solution. When L = cytosine, the *cis*-isomer was obtained. *trans*-Compounds were obtained with all other ligands. The *trans*-isomer of cytosine was prepared from the *cis*-isomer. The configuration of the reported compounds of cytidine and methyl-4-picolinate has been reassigned.

PI-CHANG KONG et F. D. ROCHON. Can. J. Chem. **59**, 3293 (1981).

Les complexes $[PdL_2X_2]$ où L = cytosine, méthyl-1 cytosine, cytidine, amino-2 methyl-4 pyrimidine, hydroxy-2 méthyl-4 pyrimidine, méthyl-4 pyrimidine, hydroxy-2 pyrimidine, diéthoxy-2,4 méthyl-5 pyrimidine, hydroxy-2 pyridine et picolinate-4 de méthyle et X = Cl et Br, ont été préparés par la réaction de K_2PtCl_4 et L en solution aqueuse. Lorsque L = cytosine, l'isomère *cis* a été obtenu. Les complexes *trans* ont été obtenus avec tous les autres ligands. Le composé *trans* de la cytosine a été préparé à partir de l'isomère *cis*. La configuration des deux composés rapportés dans la littérature, avec cytidine et picolinate-4 de méthyle, a été réattribuée.

Introduction

Since the discovery of the antitumour properties of some platinum amine complexes $[Pt(am)_2Cl_2]$, a great number of platinum compounds have been tested for antitumour activity. The screening results have shown that the active compounds have the *cis*-configuration while the *trans*-isomers have no activity. Several authors have been looking for many years for other active metal complexes. Recently, Kirschner *et al.* reported some palladium complexes which seemed to be active (1). Previous studies on the chemistry of palladium complexes have shown that *cis*-$[Pd(am)_2Cl_2]$ isomerizes easily to the *trans*-isomer (2–4). It is therefore important that these isomerization reactions be well understood before drawing any conclusion from the antitumour activity results, especially when some of these tests are performed in non-aqueous solvents like DMF. Recently we have been interested in the isomerization reactions of platinum pyrimidine complexes (5). We now want to report a study of palladium complexes with pyrimidine and pyridine derivatives and reassign the configuration of two complexes which have already been reported.

Experimental

$PdCl_2$ was bought from Strem Chemical Inc. 2-Aminopyrimidine was obtained from Eastman and purified as previously described (5). Other pyrimidine derivatives were purchased from Aldrich or Biochemical and used without purification. The infrared spectra were measured in Nujol with cesium iodide plates on a Perkin-Elmer 621.

Solution of K_2PdX_4, X = Cl or Br

$PdCl_2$ and potassium halide were mixed together in 1:4 molar ratio. After 24 h, all $PdCl_2$ was digested. The solution was filtered and the filtrate was ready for use. The concentration of K_2PdX_4 was made approximately 0.1 *M*.

$[PdL_2X_2]$

Ligand (2 mmol) was added to 10 mL of the K_2PdX_4 solution (1 mm Pd). After stirring 3–5 h, the precipitate was filtered off, washed with water, air-dried, then washed with ether and dried.

The ligands used in this method are cytosine (cyto), cytidine (cyti), 1-methylcytosine (1Mcyto), 2-amino-4-methylpyrimidine (2A4Mpm), 2-hydroxy-4-methylpyrimidine (2H4Mpm), 4-methylpyrimidine (4Mpm), 2,4-diethoxy-5-methylpyrimidine (2,4E5Mpm), 2-hydroxypyrimidine (2Hpm), 2-hydroxypyridine (2Hpy), and methyl-4-picolinate (4Mpy).

trans-*$[Pd(cyto)_2Cl_2]$*

cis-$[Pd(cyto)_2Cl_2]$ was refluxed in water with cytosine in 1:2 molar ratio until the suspension became a yellow solution. After cooling to room temperature, the solution was filtered. Concentrated hydrochloric acid was added dropwise to the filtrate until the concentration of HCl was about 0.5 *M*. The mixture was stirred for 30 min. The yellow precipitate was filtered off, washed with 0.5 *M* HCl solution, and air-dried.

trans-*$[Pd(cyto)_2Br_2]$*

K_2PdBr_4 solution (10 mL, 1 mmol) was slowly added dropwise to a 75 mL solution of cytosine (4 mmol) at 75°C. A yellow solution was first formed, and then a precipitate appeared. The mixture was stirred for 30 min and then cooled to room temperature. The product was collected by filtration and washed with water. Yield 52%. The filtrate was acidified with a dilute HCl solution and a yellow precipitate was obtained. The product was isolated by filtration and washed with water. Yield 30%. Infrared spectroscopy showed that the two products were the same.

Ethanolic Solution of Li_2PdCl_4

An aqueous solutions of Li_2PdCl_4 was first prepared by the

0008-4042/81/233293-04$01.00/0

©1981 National Research Council of Canada/Conseil national de recherches du Canada

Can. J. Chem. Downloaded from www.nrcresearchpress.com by 210.87.254.105 on 09/06/12
For personal use only.

Can. J. Chem. Downloaded from www.nrcresearchpress.com by 210.87.254.105 on 09/06/12
For personal use only.

method described to prepare K_2PdCl_4. The solution was then evaporated to dryness and dissolved in ethanol.

Attempt to Prepare cis-*[Pd(4Mpm)$_2$Cl$_2$]*

The ethanolic solution of Li_2PdCl_4 and 4-methylpyrimidine dissolved in ethanol were separately cooled in a dry ice – acetone bath. The pyrimidine solution was then added dropwise to the solution of Li_2PdCl_4 and a yellow precipitate appeared immediately. The product was isolated by filtration and washed with cooled ethanol and ether. The infrared spectrum of this compound was the same as that of *trans*-[Pd(4Mpm)$_2$Cl$_2$] isolated from water.

Results and Discussion

Infrared spectroscopy is a very effective method for distinguishing the *cis* from the *trans*-isomers of palladium complexes because there are marked differences in their spectra especially in the region of the skeleton vibrations of the complexes (3, 6). Recently, the structure of a pyrimidine complex, dichloro-bis(1-methylcytosine)palladium(II), was determined by X-ray diffraction (7). It was found to be the *trans*-isomer. We have prepared this compound and measured its infrared spectrum. The Pd—Cl stretching vibrations showed a single sharp band. This is consistent with a *trans*-configuration. N(3) is the binding site. The infrared spectrum of this *trans*-compound was used as reference to assign the configuration of other palladium compounds, which were prepared by a method similar to that of 1-methylcytosine, i.e. by the reaction of K_2PdCl_4 and the ligands in water.

All the ligands used in this study, except cytosine, gave compounds whose infrared spectrum showed a single Pd—Cl stretching band. They were therefore assigned to the *trans*-configuration (see Fig. 1 and Table 1). Kukushkin *et al.* (8) investigated several palladium complexes with various nitrogen bases (L). They reached the conclusion that the *cis*-isomer, PtL_2Cl_2, formed for the reaction of K_2PdCl_4 and L in water, isomerized rapidly, because of the higher stability of the *trans*-isomer. *cis*-[Pd(NH$_3$)$_2$Cl$_2$] (9) and *cis*-[Pd(py)$_2$Cl$_2$] (3) were isolated at low temperature but isomerized to the *trans*-compounds even in the solid state (2, 3). This would explain why the *cis*-isomers of palladium are quite rare. We attempted to prepare a *cis*-compound with 4-methylpyrimidine, by the reaction to Li_2PdCl_4 and the ligand in an ethanolic solution at low temperature. We had no success, since the *trans*-isomer was obtained.

The infrared spectrum of the cytosine compound showed two Pd—Cl stretching bands at 348 and 330 cm^{-1}. This is characteristic of *cis*-compounds. *trans*-Platinum pyridine complexes can usually be prepared by the following reactions (10):

[1] *cis*-[Pt(py)$_2$Cl$_2$] $\xrightarrow{py}$ [Pt(py)$_4$]Cl$_2$ $\xrightarrow{HCl}$ *trans*-[Pt(py)$_2$Cl$_2$]

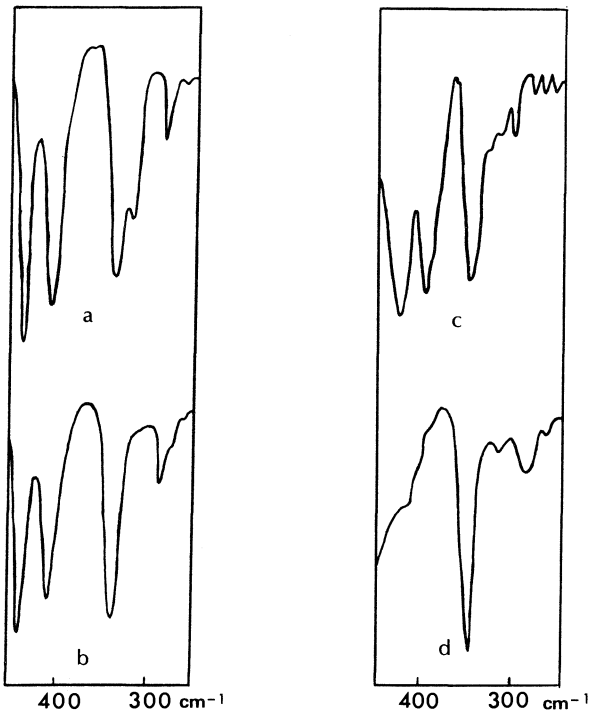

FIG. 1. Infrared spectra of (*a*) *cis*-[Pd(cyto)$_2$Cl$_2$], (*b*) *trans*-[Pd(cyto)$_2$Cl$_2$], (*c*) *trans*-[Pd(1Mcyto)$_2$Cl$_2$], and (*d*) *trans*-[Pd(cyti)$_2$Cl$_2$].

In order to obtain additional evidence on the *cis*-configuration of the cytosine compound, we attempted to prepare the *trans*-isomer by the above reactions. *trans*-[Pd(cyto)$_2$Cl$_2$] was obtained and its infrared spectrum showed just one single sharp Pd—Cl stretching band at 349 cm^{-1} (Fig. 1). A few *cis*-compounds, *cis*-[PdL$_2$X$_2$] where L = imidazole and X = Cl, Br (4) and L = benzimidazole, X = Br (8) have been reported. All these compounds showed two Pd—X stretching bands in their infrared spectra. The infrared spectra of both isomers of [Pd(cyto)$_2$X$_2$] are also different in the fingerprint region. Both isomers of the chloro compounds are yellow while the bromo isomers can be easily distinguished visually. The *cis*-compound is orange while the *trans*-isomer is yellow. *cis*-[Pd(cyto)$_2$Br$_2$] also differs from the *trans*-compound in its reaction with potassium iodide and perchloric acid. In dimethylformamide (DMF) solution, *cis*-[Pd(cyto)$_2$Br$_2$] reacts with KI to give a black colour within 1 h, while the *trans*-isomer has no apparent change after 2½ h (0.01 g of compound dissolved in 5 mL DMF + 0.15 g KI dissolved in 5 mL DMF). *cis*-[Pd(cyto)$_2$Br$_2$] in $HClO_4$ solution decomposes within 5 min while the *trans*-isomer starts to decompose 45 min later (0.02 g of compound in 5 mL of 0.6 *M* $HClO_4$).

TABLE 1. Element analyses and ν_{Pd-Cl} of the palladium complexes*

Compound	Element analyses C	H	N	X	ν_{Pd-Cl} (cm^{-1})
cis-$[Pd(cyto)_2Cl_2]$	24.00	2.50	21.00	17.75	347 vs
	23.75	2.81	20.70	18.07	328 s
trans-$[Pd(cyto)_2Cl_2]$	24.00	2.50	21.00	17.75	348 s
	23.61	2.75	21.23	17.88	
trans-$[Pd(1Mcyto)_2Cl_2]$	28.04	3.27	19.63	16.59	354 s
	27.59	3.13	20.40	16.81	
trans-$[Pd(4Mpm)_2Cl_2]$	32.86	3.31	15.33	19.40	356 s
	32.69	3.27	16.04	19.81	
trans-$[Pd(2A4Mpm)_2Cl_2]$	30.30	3.13	21.21	17.93	330 vs
	29.25	3.57	21.83	18.95	
trans-$[Pd(2H4Mpm)_2Cl_2]$	30.15	3.02	14.07	17.84	350 s
	29.76	3.13	15.00	18.50	
trans-$[Pd(2Hpm)_2Cl_2]$	26.01	2.18	15.16	19.19	330 m
	25.82	2.37	14.52	19.14	
trans-$[Pd(2Hpy)_2Cl_2]$	32.68	2.74	7.62	19.29	330 vs
	32.53	2.86	6.85	19.19	
trans-$[Pd(2,4E5Mpm)_2Cl_2]$	39.91	5.20	10.34	13.09	334 vs
	39.94	5.10	9.50	13.38	
cis-$[Pd(cyto)_2Br_2]$	19.67	2.06	17.21	32.72	
	19.47	2.19	18.05	31.78	
trans-$[Pd(cyto)_2Br_2]$	19.67	2.06	17.21	32.72	
	19.89	2.28	16.87	32.13	
trans-$[Pd(4Mpy)_2Br_2]$	31.05	2.59	5.18	29.57	
	31.30	2.71	6.02	29.84	

*Calculated value of element analysis in first row.

A few years ago, $[Pd(4Mpy)_2Cl_2]$ (4Mpy = 4-$CH_3OC(O)C_5H_4N$), was reported (11*a*). Its infrared spectrum showed two stretching Pd—Cl bonds at 365 and 337 cm^{-1}. Therefore the compound was assigned as the *cis*-isomer by the authors. However, its bromo analogue has an infrared band at 340 cm^{-1}, which may be assigned as a bending mode of CH_3—O—C (12). We might conclude then, that the band at 337 cm^{-1} observed for the chloro compound is not caused by a Pd—Cl stretching but by the bending of CH_3—O—C. Therefore, there would be only one Pd—Cl stretching band, characteristic of the *trans*-configuration. The compound with 4-picolinic acid which has no ester group, *trans*-$[Pd(4\text{-}OHC(O)C_5H_4N)_2Cl_2]$, has only one Pd—Cl band at 369 cm^{-1} (11*a*). Furthermore the chloro compound was refluxed in the presence of the free pyridine ligand, and it was found to be unchanged. Because of reaction [1], this behaviour is not consistent with other *cis*-compounds. Complexes of the type $[ML_2X_2]$ (where M = Pd or Pt, L = nitrogen base, and X = halide) undergo *cis*-to-*trans* isomerization when heated (13), catalysed by an impurity (14) or by the free ligand (15, 16). There is no known case of isomerization in the opposite direction, *trans*-to-*cis*. It may therefore be assumed that the reactions are as follows:

$$[MX_4]^{2-} \xrightarrow{L} \textit{cis}\text{-}[ML_2X_2] \rightarrow \textit{trans}\text{-}[ML_2X_2]$$

When M = Pd, the *cis*-intermediate is often unstable and can be rarely isolated. We can therefore conclude that the compound $[Pd(4\text{-}CH_3OC(O)C_5H_4N)_2Cl_2]$ is the *trans*-isomer.

The synthesis of $[Pd(cyti)_2Cl_2]$ was reported (17). It was assigned as the *cis*-isomer without any comment. No infrared spectrum was reported. We have prepared this compound and its infrared spectrum was similar to other *trans*-complexes. One single band was observed in the Pd—Cl stretching region (Fig. 1*d*). Therefore it should be assigned as the *trans*-isomer.

Palladium and platinum coordinate to 1-methylcytosine and cytidine through N(3) (7, 18, 19). Cytosine coordinates to copper through N(3) (7). When N(1) is not deprotonated, usually N(3), which is a pyridine-type nitrogen, is the preferred coordination site. Therefore cytosine should also coordinates to palladium through N(3). N(1) of 4-methylpyrimidine, 2-amino-4-methylpyrimidine,

Can. J. Chem. Downloaded from www.nrcresearchpress.com by 210.87.254.105 on 09/06/12
For personal use only.

2-hydroxy-4-methylpyrimidine, and 2,4-diethoxy-5-methylpyrimidine has less steric hindrance and should be the binding site (5).

The infrared spectrum of the palladium complex of 2-hydroxypyridine showed a strong ν_{O-H} stretching band at a frequency of 3420 cm^{-1} with a shoulder at 3480 cm^{-1}. Two strong bands at 1602 and 1580 cm^{-1} may be assigned as the stretching vibrations of the aromatic ring (11*b*). No other band appears higher than 1602 cm^{-1}, indicating that the ligand is not in the ketone form. A strong band at 262 cm^{-1} might tentatively be assigned as Pd—N stretching. All pyrimidine complexes have an absorption band in the 250–300 cm^{-1} region. This band is weak except for the 2-amino-4-methylpyrimidine and 2-hydroxy-4-methylpyrimidine complexes where the absorption band is medium. We cannot at the moment assign it unambiguously as a Pd—N stretching.

Both *cis*- and *trans*-$[Pd(cyto)_2Cl_2]$ react with thiourea (tu) to give $[Pd(tu)_4]Cl_2$, i.e. they do not respond to Kurnakov's test:

$$cis\text{-}[ML_2Cl_2] \xrightarrow{tu} [M(tu)_4]Cl_2 + 2L$$

$$trans\text{-}[ML_2Cl_2] \xrightarrow{tu} trans\text{-}[ML_2(tu)_2]Cl_2$$

Kurnakov's test should be used with extreme care because many isomers like *cis*- and *trans*-$[Pd(cyto)_2Cl_2]$ do not respond to the test, or at least the appropriate conditions for the reactions have not been found (16). The well known *trans*-compound of pyridine *trans*-$[Pd(py)_2Cl_2]$ liberates pyridine immediately in water, at room temperature, when mixed with thiourea. Correct information on the configuration of a compound therefore cannot be obtained by just testing one isomer which would give $[M(tu)_4]Cl_2$ (20). Infrared spectroscopy is probably a more reliable method.

1. S. Kirschner, A. Maurer, and C. Dragulescu. J. Clin. Hematol. Oncol. **7**, 190 (1977).
2. R. Layton, D. W. Sink, and J. R. Durig. J. Inorg. Nucl. Chem. **28**, 1965 (1966).
3. J. R. Durig, B. R. Mitchell, D. W. Sink, and J. N. Willis. Spectrochim. Acta, **23**A, 1121 (1967).
4. (*a*) J. Reedijk and J. K. de Ridder. Inorg. Nucl. Chem. Lett. **12**, 585 (1976); (*b*) C. G. Van Kralingen, J. K. De Ridder, and J. Reedijk. Inorg. Chim. Acta, **36**, 69 (1979).
5. P. C. Kong and F. D. Rochon. Can. J. Chem. **57**, 526 (1979).
6. J. S. Coe and A. A. Malik. Inorg. Nucl. Chem. Lett. **3**, 99 (1967) and references therein.
7. E. Sinn, C. M. Flynn, and R. B. Martin. Inorg. Chem. **16**, 2403 (1977).
8. Y. N. Kukushkin, G. N. Sedova, L. Y. Pyzhova, R. A. Vlasova and A. D. Garnovskii. Russ. J. Inorg. Chem. **24**, 1257 (1979) and references therein.
9. C. H. Perry, D. P. Athans, E. F. Young, J. R. Durig, and B. R. Mitchell. Spectrochim. Acta, **23**A, 1137 (1967).
10. G. B. Kauffman. Inorg. Synth. **7**, 249 (1963).
11. M. Pfeffer, P. Braunstein, and J. Dehand. Spectrochim. Acta, (*a*) **30**A, 341 (1974); (*b*) **30**A, 331 (1974).
12. T. M. Mijazawa. Bull. Chem. Soc. Jpn. **34**, 691 (1961).
13. Y. N. Kukushkin, G. N. Sedova, and A. N. Belyaev. Russ. J. Inorg. Chem. **23**, 1165 (1978) and references therein.
14. J. R. Durig and B. R. Mitchell. Appl. Spectrosc. **21**, 221 (1967).
15. L. Cattalini and M. Martelli. J. Am. Chem. Soc. **91**, 312 (1969).
16. P. C. Kong and F. D. Rochon. Can. J. Chem. **56**, 441 (1978).
17. G. Pneumatikakis, N. Hadjiliadis, and T. Theophanides. Inorg. Chem. **17**, 915 (1978).
18. C. J. L. Lock, R. A. Speranzini, and J. Powell. Can. J. Chem. **54**, 53 (1976).
19. R. Melanson and F. D. Rochon. Inorg. Chem. **17**, 679 (1978).
20. N. Hadjiliadis and T. Theophanides. Inorg. Chim. Acta, (*a*) **16**, 67 (1976); (*b*) **16**, 77 (1976); (*c*) G. Pneumatikakis. Inorg. Chim. Acta, **46**(B1), 243 (1980).

Can. J. Chem. Downloaded from www.nrcresearchpress.com by 210.87.254.105 on 09/06/12
For personal use only.

High resolution nuclear magnetic resonance studies of platinum(II) – guanosine-5′-monophosphate interactions in aqueous solutions

MOSCHOS POLISSIOU,[1] MINH TAN PHAN VIET, MAURICE ST-JACQUES,[2] AND THEOPHILE THEOPHANIDES[2]

Université de Montréal, Département de Chimie, Montréal, (Qué.), Canada H3C 3V1

Received June 23, 1981

MOSCHOS POLISSIOU, MINH TAN PHAN VIET, MAURICE ST-JACQUES, and THEOPHILE THEOPHANIDES. Can. J. Chem. **59**, 3297 (1981).

A detailed 400 MHz ^{1}H nmr study was carried out on platinum complexation products of GMP by K_2PtCl_4. Coupling constant values show that platination on N7 induces a conformational change on the ribose moiety: the ^3E form of the ring and the gt conformer about the C(4′)—C(5′) bond are favoured upon complexation. The results are compared to the conformational changes induced by N7 protonation and methylation.

MOSCHOS POLISSIOU, MINH TAN PHAN VIET, MAURICE ST-JACQUES et THEOPHILE THEOPHANIDES. Can. J. Chem. **59**, 3297 (1981).

Faisant appel à la spectroscopie de rmn à 400 MHz, on a étudié les produits provenant de la complexation du MPG par le K_2PtCl_4. Les valeurs des constantes de couplage montrent que l'introduction du platine sur l'azote en position 7 provoque des changements de conformation sur le fragment ribose; la complexation favorise la forme ^3E du cycle et le conformère gt autour de la liaison C(4′)—C(5′). On a comparé ces résultats aux changements de conformation provoqués par la protonation et la méthylation de l'azote en position 7.

[Traduit par le journal]

Introduction

Platinum complexes and their interactions with purine and pyrimidine nuclosides and nucleotides as well as with nucleic acids have been the subject of extensive investigations in recent years (1). Interest in such interactions stems from the discovery that platinum compounds (e.g. *cis*-$Pt(NH_3)_2Cl_2$, *cis*-dichlorodiammineplatinum) show antitumor activity (2) and are being used in cancer treatment (3).

Most of the quantitative structural data on platinum–nucleotide interactions have been derived from X-ray diffraction and spectroscopic studies in the solid state (4, 5). These solid state studies reveal several interesting structural and conformational features of the nucleotides, such as sugar-ring pucker, rotation of the exocyclic methylene group and the phosphate group, as well as the orientation of these groups with respect to the platinum square plane. Reported X-ray results, mainly on 1:2 complexes of platinum with guanine nucleotides, such as *cis*-$[Pt(ammine)_2(nucleotide)_2]^{2+}$ have shown that the platinum atom is coordinated to N7 of guanine (6, 7).

Guanosine-5′-monophosphate (G^5′p), was chosen in this nmr study because of the recognized affinity of the guanosine base for platinum salts (8). Potassium tetrachloroplatinate(II) (K_2PtCl_4) was selected as complexing agent with G^5′p because it is one of the simplest ionic platinum salts available from which fundamental information about the effects of complexation could be derived by ^{1}H nmr measurements.

In the present work we report high resolution 400 MHz ^{1}H nmr spectra of D_2O solutions of K_2PtCl_4 and G^5′p for various metal/nucleotide concentrations. The chemical shifts of the H(8) proton of guanine provide information on the site of platinum binding to guanine while the chemical shifts of the sugar protons together with spin-coupling constants suggest that complexation perturbs the conformational equilibrium of the ribose ring significantly and causes the phosphate group to rotate with respect to the sugar ring.

Experimental

Guanosine-5′-monophosphate disodium salt was purchased from Sigma Chemical Company. K_2PtCl_4 was obtained from Johnson Matthey and Mallory Ltd. and the D_2O(99.996%) was supplied by Kor Isotopes.

The ^{1}H nmr spectra were obtained with a Bruker High Resolution WH-400 Spectrometer located at the Laboratoire régional de RMN à haut champ at Université de Montréal. Typically, a total of 200–500 transients were acquired in 32K of memory using a pulse width of 5 μs (corresponding to a flip angle of 60–70°). For coupling constant measurements, the 3000 Hz spectral width used results in an acquisition time of 5.472 s and in a digital resolution no better than 0.18 Hz. Probe temperature was about 20°C. The chemical shifts are referenced relative to the internal standard, sodium 2,2-dimethyl-2-silapentane-5-sulfonate (DSS). The pD of the solutions was measured both before and after recording the nmr spectra with a Fisher Accumet 630 pH meter. The samples of G^5′p in D_2O were lyophilized

[1]On leave from the Agricultural College of Athens, Laboratory of General Chemistry, Votanikos, Athens, Greece.

[2]Authors to whom correspondance should be addressed.

0008-4042/81/233297-06$01.00/0

©1981 National Research Council of Canada/Conseil national de recherches du Canada

Can. J. Chem. Downloaded from www.nrcresearchpress.com by 210.87.254.5 on 09/06/12
For personal use only.

twice to reduce the HDO concentration. A partial exchange of H(8) was observed after lyophilization.

Samples of $[(PtCl_3)G^5'p]^-$ and $(PtCl_2)(G^5'p)_2$ (abbreviated: $Pt^7G^5'p$ and $Pt^7(G^5'p)_2$, respectively) were prepared using different ratios, $r = [Pt]/[G^5'p]$. The reaction of K_2PtCl_4 and $G^5'p$ in D_2O was slowed down by the addition of NaCl in order to follow the spectral changes of the new species formed. A typical nmr solution was prepared by mixing a solution of (5 or 10 m*M*) K_2PtCl_4 in D_2O in the presence of NaCl (20 m*M*) with a solution of $G^5'p$ (20 m*M*) in D_2O and the reaction was followed by ^1H nmr spectroscopy with time.

Excess of $G^5'p$ was used to avoid the formation of small quantities of paramagnetic polymeric blue complexes which broaden the nmr resonances (9). The blue complexes are predominant at high platinum-to-$G^5'p$ ratios, high reaction temperatures, and at pH above 9. The addition of 20 m*M* of NaCl in the solutions was necessary to slow down the substitution reaction by the base in the first coordination sphere of the platinum atom. The substitution of the second chloride in the *cis*-position was slower. Furthermore, aquation studies (9) of $[PtCl_4]^{2-}$ show that for concentrations of the order of 10^{-2} to 10^{-3} *M* the most predominant aquated species in solution is $[PtCl_3(H_2O)]^-$, the diaquated species, $PtCl_2(H_2O)_2$, exists in smaller quantities and is further suppressed by the presence of the chloride ions in solution. Aquation of the monosubstituted complex $[PtCl_3(G^5'p)]^-$ to form $[PtCl_2(H_2O)(G^5'p)]$ is also assumed to be very slow and comparable to diaquation of $[PtCl_4]^{2-}$. In fact, with a ratio of 4:1, $G^5'p$ to K_2PtCl_4 the monosubstituted complex is present in significant amount after 24 h at room temperature, whereas the disubstituted forms slowly and is dominant after about one week. Finally, the reaction of K_2PtCl_4 with $G^5'p$ can still be slowed down by lowering the pH (pD = 1) of the solutions and therefore have the platinum competing with the proton for the N7 site.

Results and Discussion

High resolution 400 MHz ^1H nmr spectra of samples of $G^5'p$ and of $G^5'p$–K_2PtCl_4 mixtures in D_2O were studied. The spectrum reported in Fig. 1 was taken 24 h after mixing and it reveals signals compatible with a mixture of two species, the major one being free $G^5'p$ and the minor one being the reaction complex $[PtCl_3(G^5'p)]^-$. The signal assignments shown are the same as that reported by Davies and Danyluk (10). Phosphorus decoupling simplifies the signals of H(4′) and H(5′,5″) as also shown in Fig. 1. The various chemical shift values are summarized in Table 1 while the coupling constants are collected in Table 2, where the data reported for the disubstituted species were obtained 160 h after mixing.

The high field spectra were analyzed by the first order method, which for $G^5'p$ gave parameters, are identical to those obtained from computer fits of spectra recorded at lower field (10, 11). In the case of $[PtCl_3(G^5'p)]^-$ and $[PtCl_2(G^5'p)_2]$, however, the signal of H(3′) appears as a triplet instead of a quartet. In such a situation, the two coupling constants involved ($^3J_{2',3'}$ and $^3J_{3',4'}$) are not necessarily equal and their individual values cannot be determined accurately by first order analysis. In

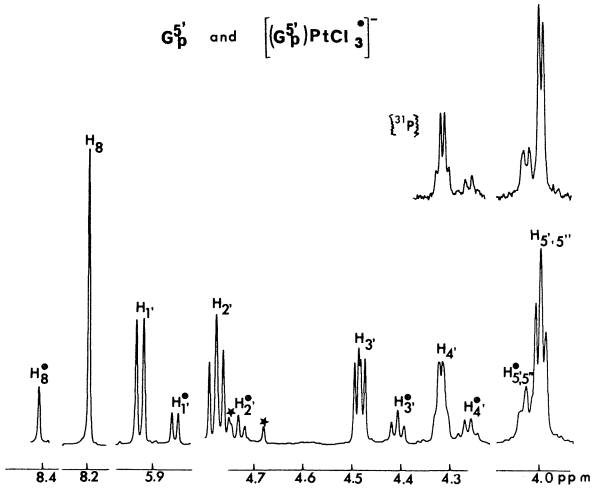

FIG. 1. 400 MHz ^1H nmr spectrum of a mixture of $G^5'p$ and $[PtCl_3(G^5'p)]^-$ (signals marked with a dot) in D_2O at 20°C. The inset shows the effect of ^{31}P irradiation. The * identifies spinning side bands of the residual HOD signal.

fact such "approximate" triplets yield only the sum of the two coupling constants involved. Homonuclear and ^{31}P decoupling experiments were used to simplify the analysis and the coupling constants obtained are given in Table 2. Among these a few are mean values.

The experimental results (Fig. 1 and Table 1) clearly show that H(8) and H(5′,5″) are displaced downfield whereas the sugar-ring protons H(1′), H(2′), H(3′), and H(4′) are all shifted upfield upon reaction and complexation with K_2PtCl_4. Chemical shifts for the disubstituted platinum complex $[PtCl_2(G^5'p)_2]$ recorded 160 h after mixing follow the same trend as observed for $[PtCl_3(G^5'p)]^-$. In fact, the upfield shift of the sugar-ring protons is even more pronounced.

The downfield shift of H(8) for $[PtCl_3(G^5'p)]^-$ appears to be a direct consequence of platinum binding at N7 which produces a polarizing effect of the C—H(8) bond towards the imidazole ring causing it to become electron deficient (11, 12), hence the use of the abbreviation $Pt^7G^5'p$. The downfield shift of 0.202 ppm observed for $Pt^7G^5'p$ is somewhat less than the value of 0.858 ppm determined for protonation of $G^5'p$ at N7 (Table 1) but is nevertheless compatible with a certain degree of positive character on the imidazole ring.

Support for the above conclusion is provided by the crystal structures of several metal–purine reaction complexes which reveal that binding of Pt occurs preferentially at N7 of the imidazole ring. For example, Kong and Theophanides have shown by ^1H nmr that the complexes $[Pt(Guo)_2(en)_2]^{2+}$

Can. J. Chem. Downloaded from www.nrcresearchpress.com by 210.87.254.5 on 09/06/12
For personal use only.

TABLE 1. ^{1}H nmr chemical shifts[a] for guanosine-5′-monophosphate and its derivatives

Compounds	pD	T (°C)	Chemical shift 8	1′	2′	3′	4′	5′	5″
$G^{5'}p$	8.3	20	8.201	5.920	4.783	4.483	4.314	3.983	3.983
$Pt^7G^{5'}p$	7.8	20	8.403	5.852	4.730	4.405	4.262	4.022	4.022
		Δδ	+0.202	−0.068	−0.053	−0.078	−0.052	+0.039	+0.039
$Pt^7(G^{5'}p)_2$	7.7	20	8.690	5.817	4.669	4.384	4.266	4.018	4.018
		Δδ	+0.489	−0.103	−0.114	−0.099	−0.048	+0.035	+0.035
$H^7G^{5'}p$	1.0	20	9.032	6.097	4.734	4.482	4.415	4.337	4.222
		Δδ	+0.831	+0.177	−0.049[b]	−0.001	+0.101	+0.354	+0.239
$m^7G^{5'}p$	7.0[c]	Δδ	—	+0.131	−0.156	−0.002	+0.048	+0.139	0.031

[a] The chemical shifts were determined relative to DSS.
[b] The values reported here for $H^7G^{5'}p$ are very similar to those reported in ref. 16 except for H(2′). However, the spectra shown in the paper suggest that our value is correct and that a typographical error exist in Table 1 or ref. 16.
[c] The values for $m^7G^{5'}p$ are all taken from ref. 11.

and $[Pt(Guo)_2(NH_3)_2]^{2+}$ are characterized by Pt binding to N7 of the guanine base in solution (8). These structures have been confirmed later by X-ray diffraction analysis (6, 7).

The crystal structure of the monosubstitution complex $Pt^7G^{5'}p$ is not known, although it has been observed that guanosine (G) reacts with K_2PtCl_4 to form 1:1 and 2:1 complexes (9). Mononucleoside platinum complexes have been shown to form in solution (8), and in some cases they have been isolated in the solid state (13). In the former study (9) K_2PtCl_4 has been found to give polynuclear paramagnetic blue or green substances at high temperatures, high pH values, and high $Pt/G^{5'}p$ ratios. For this reason the reaction conditions employed here were mild in order to avoid the formation of any polymeric species in solution which might perturb the proton resonances.

Initially the reaction of tetrachloroplatinate$^{(2-)}$ ion with $G^{5'}p$ yields predominantly $[PtCl_3(G^{5'}p)]^-$ in aqueous solution. With time the monosubstituted complex is transformed into the disubstituted derivative most likely according to the following reactions:

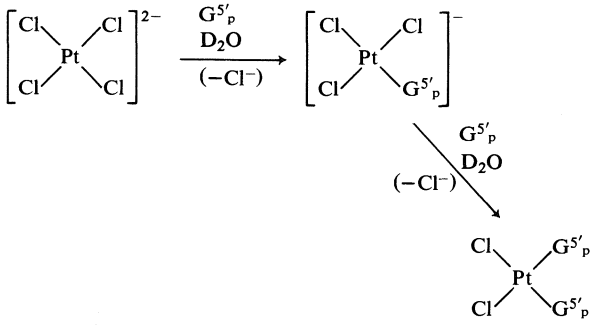

The above reaction is well known to proceed in two steps, firstly aquation and then substitution of the water molecule by $G^{5'}p$. The substitution process could in principle continue until all four chlorine atoms have been substituted by $G^{5'}p$ molecules (9). However, with excess chloride ions (NaCl) in solution the reaction rate is controlled and the above two steps are slowed down sufficiently to follow the evolution of each species by ^{1}H nmr spectroscopy. It is deduced that the second molecule of $G^{5'}p$ is complexed in the *cis*-geometry because the *trans* effect of chlorine atoms is higher than the —N= of the pyrole ring.

The disposition of the two $G^{5'}p$ units in the disubstituted complex can be determined from the chemical shift data. Only in the *cis*-form can the purine base be close enough to each other so that they may experience mutual shielding created by the ring currents in the purine moiety (14). Consequently such an effect is expected to lead to the additional upfield shift of H(8), H(1′), H(2′) of the disubstituted complex for which the two $G^{5'}p$ are *cis*.

Table 2 reveals that the coupling constants change significantly upon coordination of the platinum atom to N7 of $G^{5'}p$. Only the value of $J_{1',2'}$ decreases; all others ($J_{2',3'}$, $J_{3',4'}$, $J_{4',5'}$, and $J_{5',P}$) increase. It is now well known that the behavior of these parameters provides insight on the conformation of the sugar ring (15). Furthermore, results for protonation (16) and methylation (11) on N7 of $G^{5'}p$ ($H^7G^{5'}p$ and $m^7G^{5'}p$ respectively) provide useful references to which the effect of platination can be compared. Table 2 shows that $J_{1',2'}$ decreases from 6.1 for $G^{5'}p$ to 4.9 Hz for $Pt^7G^{5'}p$ whereas it has been reported that for $H^7G^{5'}p$ and $m^7G^{5'}p$ the values are 3.4 and 3.6 Hz respectively. The reduction of 1.2 Hz for $Pt^7G^{5'}p$ instead of ~2.5 Hz determined for the two model compounds is compatible with a reduced electronegativity of the guanine base owing to the fact that complexation with $PtCl_3^-$ is less electron demanding from N7 and the imidazole ring than is protonation or methylation.

Can. J. Chem. Downloaded from www.nrcresearchpress.com by 210.87.254.5 on 09/06/12
For personal use only.

TABLE 2. Coupling constants (Hz)[a] of guanosine-5′-monophosphate and its derivatives

Compound	pD	T (°C)	Coupling constant 1′2′	2′3′	3′4′	4′5′	4′5″	5′p	5″p
G^{5}′p	8.3	20	6.1	5.2	3.4	3.7[b]	3.7[b]	4.6[b]	4.6[b]
$Pt^{7}G^{5}$′p	7.8	20	4.9	5.5	4.8	5.1[b]	5.1[b]	5.0[b]	5.0[b]
$Pt^{7}(G^{5}p)_2$	7.7	20	5.5	5.3	4.4	5.3[b]	5.3[b]	—[c]	—[c]
$H^{7}G^{5}$′p	1.0	20	3.4	4.9	5.4	2.4	2.9	4.7	5.7
$m^{7}G^{5}$′p	7.0[d]	20	3.6	4.9	5.1	2.3	2.0	4.5	4.5

[a] The couplings given are accurate to ±0.2 Hz.
[b] These values represent averaged coupling constants.
[c] Signal overlap prevented the analysis of the H(5′,5″) multiplet for $Pt^{7}(G^{5}p)_2$.
[d] The values for $m^{7}G^{5}$′p are all taken from ref. 11.

TABLE 3. Conformational populations for guanosine-5-monophosphate and derivatives

Compound	pD	T (°C)	Conformational isomers: Ribose ^{3}E	C(4′)—C(5′) gg	C(4′)—C(5′) gt[a]	C(5′)—O(5′) g′g′	C(5′)—O(5′) g′t′[b]
G^{5}′p	8.3	20	36	65	35	76	24
$Pt^{7}G^{5}$′p	7.8	20	51	36	64	72	28
$Pt^{7}(G^{5}p)_2$	7.7	20	45	38	62	—	—
$H^{7}(G^{5}p)$	1.0	20	57	87	13	70	30
$m^{7}(G^{5}p)$	7.0[c]	20	54	97	3	77	23

[a] Combined population of gt (ψ = 180°) and tg (ψ = 300°).
[b] Combined population of g′t′ (ϕ = 60°) and tg′ (ϕ = 300°).
[c] All values for $m^{7}G^{5}$′p were taken from ref. 11.

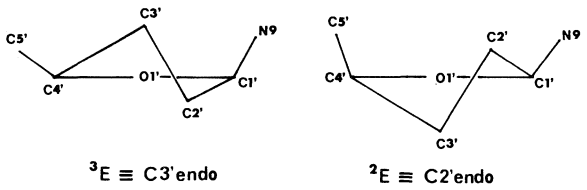

$^{3}E \equiv$ C3′endo $\quad$ $^{2}E \equiv$ C2′endo

Conformational populations for different segments of G^{5}′p were determined by methods explained below and are summarized in Table 3. Lee *et al.* (17) and Ezra *et al.* (11) have proposed a method to estimate the population of each of the C(2′)–endo (^{2}E) and C(3′)–endo (^{3}E) conformers of the ribose ring from the sum of $J_{1',2'}$ and $J_{3',4'}$. The value of 10.1 Hz determined for $Pt^{7}G^{5}$′p differs from the standard value of 9.5 Hz and can be ascribed to charge perturbations in the imidazole ring brought about by complexation. Because $J_{3',4'}$ is not expected to be affected significantly by electronegativity changes of the base, the $^{3}E/^{2}E$ ratios were determined using values of $J_{3',4'}$ and the standard sum of 9.5 Hz for $J_{1',2'} + J_{3',4'}$ (11).

The results given in Table 3 show that platination on N7 causes a change in the $^{2}E \rightleftharpoons {}^{3}E$ equilibrium whereby the proportion of the ^{3}E conformer increases from ~36% to ~51% for $Pt^{7}G^{5}$′p. This 15% increase is comparable to the 18% change observed for $m^{7}G^{5}$′p. Similar conformation changes were estimated for $H^{7}G^{5}$′p (16). Thus it appears that, notwithstanding differences in charge distribution in these three compounds, the ribose ring is shown to undergo a similar conformational change in favor of the ^{3}E form.

On the other hand Table 2 reveals that some differences do exist between the coupling constants of $Pt^{7}G^{5}$′p and $m^{7}G^{5}$′p. The mean value, $(J_{4',5'} + J_{4',5''})/2$, increases upon platination from 3.7 to 5.1 Hz while for $m^{7}G^{5}$′p a decrease from 3.6 to 2.1 Hz was reported (11). This difference is indeed very striking. In addition, the respective coupling constants of H(5′,5″) with ^{31}P could also be different; $^{3}J_{4',5'}$ and $^{3}J_{4',5''}$ are known with greater precision from the ^{31}P-decoupled ^{1}H nmr spectrum and their interpretation should be most significant.

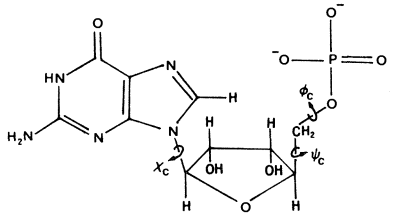

3

Structure 3 illustrates the symbols employed to describe the various conformational features of G^{5}′p; χ_c describes the rotation of the glycosidic

Can. J. Chem. Downloaded from www.nrcresearchpress.com by 210.87.254.5 on 09/06/12
For personal use only.

bond, ψ_c the rotation of the C(4′)—C(5′) bond, and ϕ_c the rotation of the C(5′)—O(5′) bond.

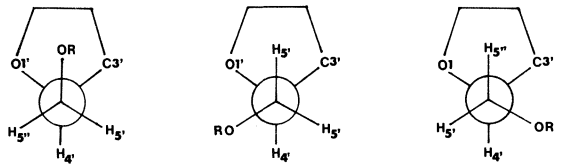

gg gt tg

The population of the gg, gt, and tg conformers about the C(4′)—C(5′) bond can be computed from $\sum = (J_{4',5'} + J_{4',5''})$ using the expression suggested by Lee and Sarma (18). Similarly the three rotameric populations about the C(5′)—O(5′) bond can be estimated from $\sum' = (J_{5'P} + J_{5''P})$.

The data in Table 3 show that the population change about the C(5′)—O(5′) bond is relatively small and because of the larger error in determining $\sum'$ for $Pt^7G^5'p$, the difference is not significant and will not be discussed further.

The conformational change about the C(4′)—C(5′) bond is, on the other hand, very significant. It is seen that the proportion of the gg form decreases from 65% for $G^5'p$ to 36% for $Pt^7G^5'p$. This change is to be contrasted with the increase to 97% of gg for $m^7G^5'p$ and 87% for $H^7G^5'p$. Thus N7 platination and methylation (or protonation) of $G^5'p$ produce opposite conformational changes. The conformational change determined for $m^7G^5'p$ was explained in terms of an electrostatic attraction involving the positively charge imidazole ring and the phosphate group (11). The opposite conformational change determined for $Pt^7G^5'p$ (from gg → gt (or tg)) can adequately be rationalized in terms of an electrostatic repulsion between the phosphate group and the platinum halide moiety. A similar interaction would exist with the $PtCl_2(G^5'p)$ moiety in $Pt^7(G^5'p)_2$ because here too the population of gg has decreased.

It is therefore quite interesting to note that while the $^2E \rightarrow {}^3E$ ribose conformation change is found to be very similar for platination and methylation on N7, the conformational change about the C(4′)—C(5′) bond is opposite and found to favour gg for $m^7G^5'p$ vs. gt (or tg) for $Pt^7G^5'p$. It would therefore appear that conformational interdependence between the ribose ring and the C(4′)—C(5′) bond, if it exists as suggested by Hruska (19), breaks down for nucleotides with a charged imidazole ring.

Alternatively, this result could provide support for the suggestion that a correlation exists only between the ribose ring conformation and the glycosidic bond orientation (χ_c). Of the various conformational features of nucleotides, rotation of the glycosidic bond (base orientation) has been most difficult to characterize quantitatively in solution although useful information was obtained in the crystalline state (4, 15).

Table 1 illustrates the effect of protonation, platination, and methylation of $G^5'p$ on ^1H chemical shifts. While protonation and methylation produce similar chemical shift changes relative to $G^5'p$ for the ribose ring proton, platination leads to striking differences. If compared to $H^7G^5'p$ and $m^7G^5'p$, H(3′) of $Pt^7G^5'p$ is more shifted upfield (about 0.076 ppm) and H(1′) and H(4′) show a sign reversal on platination compared to protonation and methylation.

There is no doubt that chemical shift differences can arise in part from a perturbation of the ribose ring conformation, rotation of the C(4′)—C(5′) conformation, and base reorientation. In spite of this complexity many attempts have focused on using the chemical shifts of H(1′) and H(2′) as probes for χ_c variations. The method used is based on semi-empirical calculations of shielding constants (20) in terms of several contributions such as ring current effects, diamagnetic and paramagnetic parts of atomic anisotropy of the bases as well as of the sugar phosphate backbone, polarization of bonds by molecular charge distribution, etc ... This approach has been applied with some success to non-complexed nucleic acid derivatives (20). For $m^7G^5'p$, it led to the conclusion that a small *syn* → *anti* shift of the conformational equilibrium takes place on methylation.

Unfortunately results for $Pt^7G^5'p$ show that H(1′) moves in opposite direction on platination (upfield) compared to methylation and protonation (downfield). Nevertheless, the upfield shift of the H(2′) signal for all three species as shown in Table 1 could suggest that changes in base orientation are similar for all three complexes as was found to be the case for the conformational change ($^2E \rightarrow {}^3E$) of the ribose ring provided the anisotropy effect of the $PtCl_3^-$ moiety is not dominant. It is therefore tempting to suggest that the differences observed for the chemical shifts of H(1′), H(3′), and H(4′) do not reflect significant differences in base reorientation.

Furthermore, it appears reasonable to expect that the gg → gt (or tg) change about the C(4′)—C(5′) bond will most affect the chemical shifts of H(3′) and H(4′) which are nearest to the rotated bond. This conformational change is therefore believed to be responsible in large part for the upfield shift of H(3′) and H(4′) relative to $m^7G^5'p$ and $H^7G^5'p$.

The upfield shift of H(1′) is more difficult to rationalize since complexation at N7 is expected to

Can. J. Chem. Downloaded from www.nrcresearchpress.com by 210.87.254.5 on 09/06/12
For personal use only.

increase the electronegativity of the imidazole ring and thereby produce a downfield shift, although this effect is expected to be smaller than for protonation and methylation as is indicated from the behavior of H(8). This observation could argue against the validity of the hypothesis of a small anisotropy effect for the $PtCl_3^-$ moiety. On the other hand, a smaller H(1′) downfield shift on platination coupled to an upfield shift caused by the gg → gt change of the C(4′)—C(5′) bond could account for the observed chemical shift change of H(1′).

It must, however, be stressed that qualitative interpretation of small chemical shift differences in terms of specific conformational changes in metal-complexed nucleotides is not straightforward and may lead to erroneous conclusions whereas conformational changes deduced from variations in coupling constants are usually more reliable.

It therefore appears reasonable to conclude that platination of G5′p produces a small $^2E \rightarrow {}^3E$ ribose ring conformational change and a small perturbation of the purine base orientation similar to those produced by protonation and methylation on N7 but that different conformational changes are noted at the C(4′)—C(5′) bond. Platination therefore produces a gg → gt (or tg) rotation whereas protonation and methylation produce an opposite rotation gt (or tg) → gg.

Acknowledgments

We are grateful to the Natural Sciences and Engineering Research Council of Canada for financial support. M. T. Phan Viet is thankful to NSERC for a NATO scholarship. Finally, we thank Dr. H. Beierbeck, manager of the High Field NMR Regional Laboratory in Montreal for technical assistance in recording some of the nmr spectra.

1. T. G. Spiro (*Editor*). Nucleic acid – metal ion interactions. Vol. 1. Wiley-Interscience, New York, NY. 1980.
2. B. Rosenberg. Biochimie, **60**, 859 (1978).
3. (*a*) T. Theophanides. Chem. Can. **32**, 30 (1980); (*b*) A. W. Prestayko, S. T. Crooke, and S. K. Carter (*Editors*). Cisplatin—current status and new developments. Academic Press, New York. NY. 1980.
4. R. W. Gellert and R. Bau. *In* Metal ions in biological systems. Vol. 8. 1979. Chapt. 1. p. 1.
5. L. G. Marzilli. Prog. Inorg. Chem. **23**, 255 (1977).
6. R. W. Gellert and R. Bau. J. Am. Chem. Soc. **97**, 7379 (1975).
7. R. E. Cramer and P. O. Dahlstrom. J. Clin. Hematol. Oncol. **7**, 330 (1977).
8. P. C. Kong and T. Theophanides. Inorg. Chem. **13**, 1167 (1974); Bioinorg. Chem. **5**, 51 (1975).
9. N. Hadjiliadis and T. Theophanides. Inorg. Chim. Acta, **16**, 67 (1976); **16**, 77 (1976).
10. D. B. Davies and S. S. Danyluk. Biochemistry, **21**, 4417 (1974).
11. C. H. Kim and R. H. Sarma. J. Am. Chem. Soc. **100**, 1571 (1978).
12. A. T. M. Marcelis, C. G. van Kralingen, and J. Reedijk. J. Inorg. Biochem. **13**, m 213 (1980).
13. P. C. Kong and F. D. Rochon. J. Chem. Soc. Chem. Commun. 599 (1975).
14. C. Giessner-Prettre and B. Pullman. J. Theoret. Biol. **65**, 171 (1977); **65**, 189 (1977).
15. D. B. Davis. Prog. NMR Spectrosc. **12**, 135 (1979).
16. S. Tran-Dinh and W. Guschlbauer. Nucl. Acid Res. **2**, 873 (1975).
17. C. H. Lee, F. S. Ezra, N. S. Konda, R. H. Sarma, and S. S. Danyluk. Biochemistry, **16**, 3627 (1976).
18. C. H. Lee and R. H. Sarma. J. Am. Chem. Soc. **98**, 3541 (1976).
19. F. E. Hruska. *In* Conformations of biological molecules and polymers. *Edited by* E. D. Bergmann and B. Pullman. Academic Press. 1973. p. 345.
20. C. K. Mitra, M. H. Sarma, and R. H. Sarma. Biochemistry, **20**, 2036 (1981).

Can. J. Chem. Downloaded from www.nrcresearchpress.com by 210.87.254.5 on 09/06/12
For personal use only.

Can. J. Chem. Downloaded from www.nrcresearchpress.com by 210.87.254.6 on 09/06/12
For personal use only.

Thermally induced crossed aldol condensations

JOHN A. FINDLAY, DIXIT N. DESAI, AND JOHN B. MACAULAY
Department of Chemistry, University of New Brunswick, Fredericton, N.B., Canada E3B 6E2

Received August 4, 1981

JOHN A. FINDLAY, DIXIT N. DESAI, and JOHN B. MACAULAY. Can. J. Chem. **59**, 3303 (1981).

A relatively efficient, noncatalytic method for effecting crossed aldol condensations between cyclic ketones and aldehydes and between cyclic 1,3-diones and methyl vinyl ketone is reported.

JOHN A. FINDLAY, DIXIT N. DESAI et JOHN B. MACAULAY. Can. J. Chem. **59**, 3303 (1981).

On rapporte une méthode, non catalytique, relativement efficace qui permet d'effectuer des condensations aldoliques croisées entre des cétones cycliques et des aldéhydes et également entre des diones cyclique-1,3 et la méthylvinylcétone.

[Traduit par le journal]

In the course of studies successfully directed at the total synthesis of the phytoalexin phytuberin we noted (1) the thermally induced C2 epimerization of 2-hydroxy methyl-2-methyl-5-isopropenylcyclohexanone **1***a* to **3***a* by heating at 185°C for 15 min in a sealed Pyrex tube (2), providing a 5:4 mixture of the diastereomers. We have now established that prolongation of the reaction time to 3 h provides dihydrocarvone **2** (3) plus the diastereomeric mixture **1***b*, **3***b* at the expense of the **1***a*/**3***a* yield. Pyrolysis of dihydrocarvone and paraformaldehyde under the same conditions gives a similar mixture (see Table 1). Performing these reactions in Pyrex vessels pretreated with trimethylsilylchloride does not alter the rate of reaction and thus it appears that the operative mechanism is the dealdolization–aldolization depicted in Scheme 1 in which the enol form of the cyclohexanone ring is the key intermediate.

Similar crossed condensations have now been

TABLE 1. Thermally induced crossed aldol condensations

Reactants	Temperature (°C)	Time (h)	Products[a]	Yield (%)
+ $(HCHO)_n$	185	3	**1***a* **3***a* **1***b* + **3***b*	23 45 10
+ $(HCHO)_n$	150	3	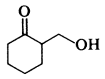 **4**	68
+ $(CH_3(CH_2)_6CHO$	150	3	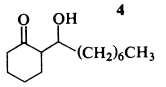 **5**	41
+ $CH_3(CH_2)_8CHO$	150	3	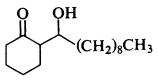 **6**	45
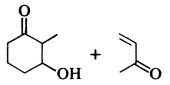	185	6	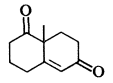 **7**	80
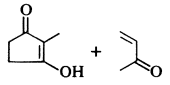	150	3	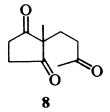 **8**	65

[a] All products were fully characterized after purification and gave spectral data consistent with the assigned structures.

0008-4042/81/233303-02$01.00/0
©1981 National Research Council of Canada/Conseil national de recherches du Canada

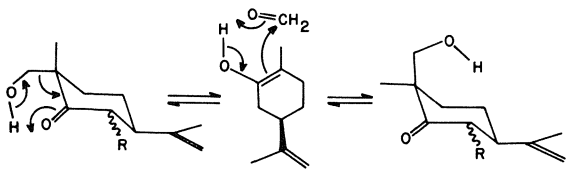

SCHEME 1. Dealdolization–aldolization mechanism.

effected by us between cyclohexanone and a number of aldehydes and between 2-methyl-1,3-cyclohexanedione and methyl vinyl ketone to provide an improved synthesis of the known (4) 3,4,8,8a-tetrahydro-8a-methyl-1,6(1*H*,7*H*)-naphthalenedione **7**.

We have not observed any competing crossed or self-condensation products in the examples studied and starting compounds constituted the bulk of the balance of recovered materials in all cases. Attempted isolation of compounds **5** and **6** using silica gel chromatography led exclusively to their corresponding dehydration products while compound **7** was recovered directly from the reaction mixture.

Attempts to condense acetone or acetophenone with aldehydes under the conditions described were unsuccessful and this is consistent with the belief that the thermally induced aldolization proceeds via a six-membered ring transition state employing the enol form of the ketone (see Scheme 1) since the enol form of cyclic ketones is known (5) to be more prevalent than that of acyclic carbonyl systems. It is also possible that the failure in some cases may be due to unfavourable equilibria between aldol product and starting materials.

Acknowledgements

The authors are grateful to the Natural Sciences and Engineering Research Council of Canada for financial support and to D. Jean Burnell for suggesting the preparation of **7**.

1. JOHN A. FINDLAY, DIXIT N. DESAI, GREG C. LONERGAN, and PETER S. WHITE. Can. J. Chem. **58**, 2827 (1980).
2. DIXIT N. DESAI. Ph.D. Thesis, University of New Brunswick, Fredericton, N.B., 1981.
3. G. C. LONERGAN. Ph.D. Thesis, University of New Brunswick, Fredericton, N.B., 1978.
4. JAMES A. MARSHALL, DAVID E. SEITZ, WILLIAM R. SCHNEIDER, and BARRY GOLDBERG. Synth. Commun. **4**, 79 (1974).
5. (*a*) J. PETER GUTHRIE and PATRICIA A. CULLIMORE. Can. J. Chem. **57**, 240 (1979); (*b*) WOLF-ECKART NOACK. Theor. Chim. Acta Berlin, **53**, 101 (1979).

Can. J. Chem. Downloaded from www.nrcresearchpress.com by 210.87.254.6 on 09/06/12
For personal use only.

Mixtures of methyl isobutyl ketone with three butanols at various temperatures

ROQUE RIGGIO, JUAN F. RAMOS, MARIANA HERNANDEZ UBEDA, AND JOSÉ A. ESPINDOLA

Departamento de Ciencias Exactas, Universidad Nacional de Salta, Salta, Argentina

Received August 15, 1980[1]

ROQUE RIGGIO, JUAN F. RAMOS, MARIANA HERNANDEZ UBEDA, and JOSÉ A. ESPINDOLA. Can. J. Chem. **59**, 3305 (1981).

The viscosities, densities, and refractive indices at 20, 25, 30, and 35°C were determined for the systems: methyl isobutyl ketone – *n*-butanol (MIK–B_1), methyl isobutyl ketone – *sec*-butanol (MIK–B_2), and methyl isobutyl ketone – isobutanol (MIK–B_3). From the experimental results the excess volume, excess viscosity, and excess molar free energy of activation of flow were calculated. The deviations from ideality for the excess thermodynamic function are more important for the system (MIK – B_2) than for the systems (MIK–B_3) and (MIK–B_1). This fact is explained by the existence of hydrogen bonds in the alcohols, stronger in the primary alcohols than in *sec*-butanol.

ROQUE RIGGIO, JUAN F. RAMOS, MARIANA HERNANDEZ UBEDA et JOSÉ A. ESPINDOLA. Can. J. Chem. **59**, 3305 (1981).

Les valeurs de la viscosité, densité et indice de réfraction ont été determinées à 20, 25, 30 et 35°C pour les sytèmes: methyle isobutyle cétone – *n*-butanol (MIK – B_1), méthyle isobutyle cétone – butanol secondaire (MIK – B_2) et méthyle isobutyle cétone – isobutanol (MIK – B_3). Les fonctions de l'écoulement ont été calculées à partir des données expérimentales. Les déviations de l'idéalité pour les fonctions thermodynamiques d'excès sont plus importantes pour le systeme (MIK – B_2) que pour les systèmes (MIK –B_3) et (MIK – B_1). Ce fait est expliqué par l'existence de ponts hydrogene moins forte dans les alcools primaires que ceux dans le butanol secondaire.

Introduction

Viscosities of binary liquid–nonelectrolyte mixtures have been studied to obtain information about the type and degree of interaction between molecules of the components of some binary systems. Positive deviations from ideal behavior mean strong interaction between unlike molecules, but if negative deviations are present, dispersion forces are dominant (1).

The following systems: methyl isobutyl ketone + *n*-butanol (MIK–B_1), methyl isobutyl ketone + *sec*-butanol (MIK–B_2), and methyl isobutyl ketone + isobutanol (MIK–B_3) were chosen because the alcohols show hydrogen bonding and the methyl isobutyl ketone has polar characteristics.

Densities, viscosities, and refractive indices for the three systems at different molar fractions were measured at 20, 25, 30, and 35°C. Some data for these three physical constants of the pure compounds are tabulated in the literature.

From the experimental results the following thermodynamic functions have been calculated: ΔV^E (excess molar volume), $\Delta\eta^E$ (excess of viscosity), and ΔG^{*E} (excess molar free energy of activation of flow).

Experimental

Density

Densities were determined with a Robertson specific gravity bottle (2). The total pycnometer volume was about 20 mL and was calibrated with doubly distilled water at various temperatures. All weighing operations were made on a Mettler balance H-311 with an accuracy of ± 0.0001 g, and corrected to vacuum.

Viscosity

Viscosities of pure liquids and mixtures have been determined with a Cannon Feske viscosimeter calibrated with doubly distilled water, benzene, and sucrose solutions (3).

Refractive Index

The refractive indices for the sodium D line of the pure components and mixtures were measured with a Jena refractometer with an accuracy of ± 0.00002. In the three cases a thermostatically controlled bath, constant to ± 0.01°C, was used.

Materials and Solutions

Methyl isobutyl ketone, *n*-butanol, *sec*-butanol, and isobutanol, all Merck Darmstadt p.a., were twice distilled over dried K_2CO_3 under a nitrogen atmosphere with a Vigreux column, and only the middle half of each distillation was recovered and used in the experiments.

The physical properties of the components are compared with those reported in the literature (Table 1).

Results

The experimental molar fraction, densities, viscosities, and refractive indices[2] for all the systems at 20, 25, 30, and 35°C were used to calculate the excess thermodynamic functions with the following equations (4):

$$\Delta\eta^E = \eta - (x_1\eta_1 + x_2\eta_2)$$

$$\Delta V^E = V - (x_1V_1 + x_2V_2)$$

$$\Delta G^{*E} = RT\ln\eta V - (x_1\ln\eta_1 V_1 + x_2\ln\eta_2 V_2)$$

where η, η_1, and η_2 are the viscosity of the mixture and of the pure components; V, V_1, and V_2 are the molar volume of the mixture and of the pure

[1]Revision received September 2, 1981.

[2]A complete set of data is available, at a nominal charge, from the Depository of Unpublished Data, CISTI, National Research Council of Canada, Ottawa, Ont., Canada K1A 0S2.

0008-4042/81/243305-04$01.00/0

©1981 National Research Council of Canada/Conseil national de recherches du Canada

Can. J. Chem. Downloaded from www.nrcresearchpress.com by 210.87.254.42 on 09/06/12
For personal use only.

Can. J. Chem. Downloaded from www.nrcresearchpress.com by 210.87.254.42 on 09/06/12
For personal use only.

TABLE 1. Physical properties of components in present work and in the literature

Component	Temperature °C	$\rho_{exp.}$	$\rho_{lit.}$	$n_{D exp}$	$n_{D lit.}$	$\eta_{exp.}$	$\eta_{lit.}$
Methyl isobutyl ketone	20	0.8010	0.8008(8)	1.39576	1.3962(10)	0.575	—
	25	0.7963	0.7961(8)	1.39362	1.3933(8)	0.543	0.542(8)
	30	0.7920	—	1.39145	—	0.518	—
	35	0.7868	—	1.38929	—	0.494	—
n-Butanol	20	0.8098	0.8098(11)	1.39929	1.3993(8)	2.922	2.948(8)
	25	0.8060	0.8060(8)	1.39741	1.3973(8)	2.581	—
	30	0.8023	—	1.39563	—	2.243	2.30(11)
	35	0.7979	—	1.39347	—	1.996	2.00(9)
sec-Butanol	20	0.8066	0.8069(8)	1.39706	1.3972(8)	3.598	—
	25	0.8025	0.8026(8)	1.39530	1.3950(8)	3.028	3.018(8)
	30	0.7987	—	1.39342	—	2.518	—
	35	0.7938	—	1.39155	—	2.083	—
Isobutanol	20	0.8017	0.8017(8)	1.39591	1.3959(8)	4.023	4.028(10)
	25	0.7980	0.7978(8)	1.39389	1.3939(8)	3.404	—
	30	0.7942	0.7943(9)	1.39201	—	2.888	—
	35	0.7901	—	1.39042	—	2.473	—

TABLE 2. Coefficients for least-squares fit of results by eq. [1] (units $cm^3\ mol^{-1}$)

System	Temperature (°C)	C_1	C_2	C_3	C_4	C_5	10^4
Excess volume							
MIK–B_1	20	−0.3688	−0.0274	0.1944	0.0480	−0.1157	17.57
	25	−0.4034	−0.0384	0.1239	0.0486	−0.0442	9.00
	30	−0.4398	−0.0451	0.0644	0.0711	0.0420	9.85
	35	−0.4771	−0.0291	0.0264	0.0104	0.1685	1.47
MIK–B_2	20	1.1978	0.0121	−0.0004	0.2654	0.4087	19.02
	25	1.3133	−0.0478	0.0182	0.4094	0.4421	45.38
	30	1.4250	0.0568	0.1013	0.2459	0.6001	33.06
	35	1.5626	0.0071	0.3999	0.4384	0.7153	61.76
MIK–B_3	20	−0.0345	0.0017	0.0284	−0.0204	−0.0626	2.12
	25	−0.0741	−0.0185	0.0233	0.0141	−0.0086	4.83
	30	−0.0914	−0.0048	−0.0044	0.0060	0.0061	4.71
	35	−0.1392	0.0211	0.0504	−0.0382	−0.0192	3.71
Excess viscosity							
MIK–B_1	20	−3.302	−2.174	−1.538	0.158	1.106	74.55
	25	−2.809	−1.747	−1.088	−0.273	0.335	68.86
	30	−2.401	−1.355	−0.494	−0.559	−0.682	21.02
	35	−2.081	−1.159	−0.503	−0.629	−0.724	20.74
MIK–B_2	20	−4.879	−3.425	−2.307	−3.303	−2.884	116.00
	25	−3.975	−2.659	−2.114	−2.651	−1.915	22.72
	30	−3.151	−2.255	−1.753	−1.646	−1.050	87.94
	35	−2.486	−1.519	−1.028	−1.548	−1.188	28.08
MIK–B_3	20	−5.431	−4.104	−3.277	−2.089	−0.473	57.75
	25	−4.459	−3.154	−2.169	−2.309	−1.660	39.56
	30	−3.594	−2.446	−1.485	−1.751	−1.590	48.71
	35	−2.993	−2.002	−1.276	1.379	−1.243	56.81

components; R is the gas constant; T is the absolute temperature.

The molar volume of the mixture is defined by

$$V = \frac{x_1 M_1 + x_2 M_2}{\rho}$$

where M_1 and M_2 are the molecular weights of the components.

Each set of results was fitted with a Redlich Kister equation of the type:

$$[1] \quad X^E = x_1 (1 - x_1) \sum_{j=1}^{n} a_j (1 - 2 x_1)^{j-1}$$

where X^E represents ΔV^E or $\Delta\eta^E$ and x_1 is the molar fraction of methyl isobutyl ketone. In each case,

Can. J. Chem. Downloaded from www.nrcresearchpress.com by 210.87.254.42 on 09/06/12
For personal use only.

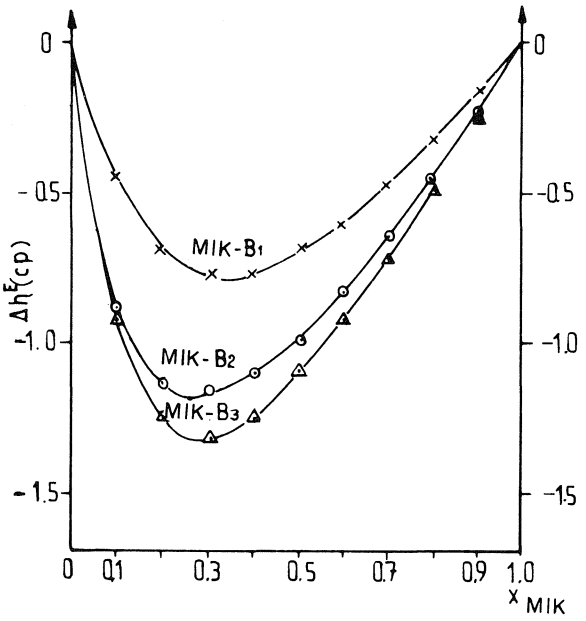

FIG. 1. $\Delta\eta^E$ vs. X_{MIK} at 25°C.

the standard error of the estimate defined by

$$\sigma x = \left[\sum (x_{obs} - x)^2/(n_{obs} - n)\right]^{1/2}$$

was determined (where n_{obs} is the number of measurements.) The optimum number of coefficients was ascertained from an examination of the variation of the standard error of the estimate with n.

The values adopted for the coefficients a_j and the standard error of the estimate are summarized in Table 2. These values are in good agreement with previous results for the (MIK–B_1) system (5, 6).

Only $\Delta\eta^E$, ΔV^E, and ΔG^{*E} at 25°C are shown in Fig. 1, 2, and 3; for the other temperatures the curves are similar.

In order to determine the minimum values of $\Delta\eta^E$ the Newton–Raphson method (7) was applied to eq. [1]. The values obtained were 0.268 for the (MIK–B_2) system, 0.284 for (MIK–B_3), and 0.340 for (MIK–B_1).

Discussion

The experimental values of viscosities show a relatively high decrease after the initial addition of

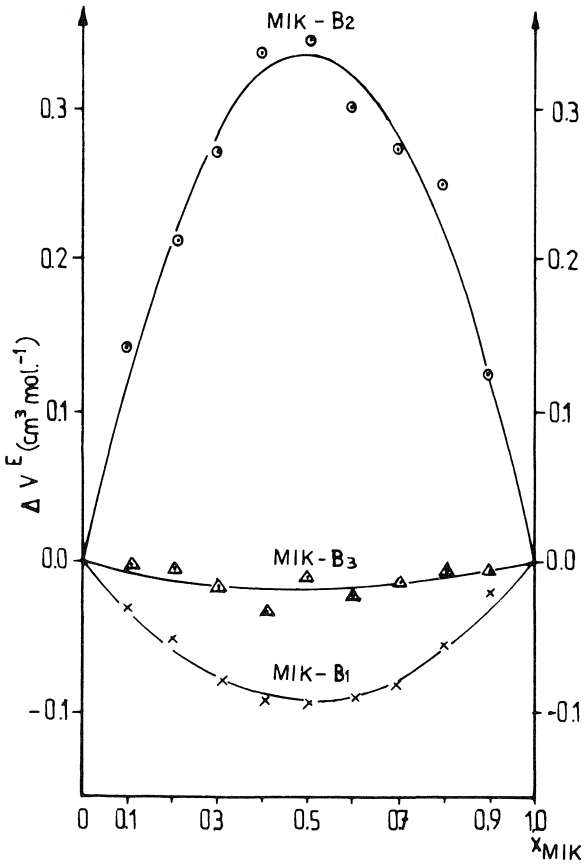

FIG. 2. ΔV^E vs. X_{MIK} at 25°C.

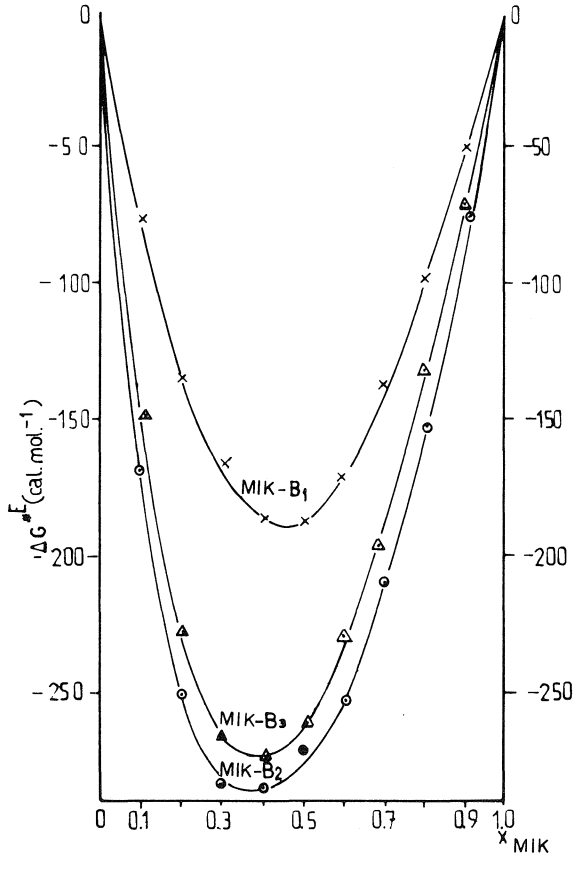

FIG. 3. ΔG^{*E} vs. x_{MIK} at 25°C.

the alcohols. This behavior is characteristic of systems in which at least one of the components exhibits hydrogen bonding.

On account of the very important values of the MIK concentration in the initial mixtures, this component has a predominant effect and causes the hydrogen bonding of the alcohols to break.

This behavior suggests that the hydrogen bonding between the *sec*-butanol molecules is the most labile of all, in good agreement with the literature on secondary alcohols (12). Isobutanol shows more negative values of $\Delta\eta^E$ than *n*-butanol owing to the fact that isobutanol has a methyl group at the α-carbon. These conclusions are strengthened by the values obtained for $\Delta\eta^E$ in these systems.

One expects (Fig. 2) breaking of hydrogen bonding in the alcohols to result in curves of ΔV^E with positive deviations for the systems (MIK–B_1) and (MIK–B_3). The negative values obtained for such systems show that there is an apreciable association between the different molecules.

For the (MIK–B_2) system we do observe a positive deviation. This behavior can be attributed to a neat rupture of association complexes between the alcohol molecules and the small possibility of forming other types of complexes between the MIK and B_2 owing to the position of OH^- group in the alcohol molecule.

On the basis of Fig. 3, we observe increasingly negative deviations in the order (MIK–B_2) > (MIK–B_3) > (MIK–B_1). This behavior is in good agreement with the discussion of the preceding paragraph.

The almost linear variation of the refractive indices for the three systems in terms of the composition is in agreement with the conclusion of Loiselier (13) for a large number of ideal and nonideal systems.

Neither the polar characteristic of the MIK nor the existence of hydrogen bonding in alcohols seem to have any important effect on the linear dependence of this property with concentration.

Acknowledgements

The authors wish to express their thanks to Hector Eduardo Martinez for experimental assistance. This work was supported by the Consejo de Investigación de la Universidad Nacional de Salta.

1. R. J. FORT and W. R. MOORE. Trans. Faraday Soc. **62**, 1112 (1966).
2. G. R. ROBERTSON. Ind. Eng. Chem. **11**, 464 (1939).
3. International critical tables. Vol. V. McGraw-Hill Book Co., Inc. 1929.
4. P. K. KATTI and M. CHAUDRI. J. Chem. Eng. Data, **9**, 442 (1964).
5. P. DAKSHINAMURTY, C. CHIRANJIVI, and V. SEETHARAMASWAMY. J. Chem. Eng. Data, **17**, 98 (1972).
6. P. DAKSHINAMURTY, K. RAO, P. RAO, and C. CHIRANJIVI. J. Chem. Eng. Data, **18**, 39 (1973).
7. B. CARNAHAN. Applied numerical methods. Wiley, New York. 1969. p. 319.
8. J. A. RIDDIC and W. B. BUNGER. Organic solvents. Vol. II. 3rd ed. Wiley–Interscience, New York. 1970.
9. G. J. JANZ and R. P. T. TOMKINS. Nonaquous electrolytes handbook. Vol. I. Academic Press, New York. 1972.
10. K. RAZNJEVIC. Handbook of thermodynamic tables and charts. McGraw-Hill Book Co., Inc. 1976.
11. J. WEAST. Handbook of chemistry and physics. 58th ed. C.R.C. Press., Inc., Cleveland, OH. 1977.
12. N. L. ALLINGER *et al.* Organic chemistry. Worth Publishers, Inc., New York. 1971.
13. H. LOISELEUR. These de Doctorat-es-Sciences. Lyon. 80. 1965.

Can. J. Chem. Downloaded from www.nrcresearchpress.com by 210.87.254.42 on 09/06/12
For personal use only.

Isotopic exchanges in the treatment of cyclopentane or cyclohexane with some deuterated or tritiated acids

CHOI CHUCK LEE AND ERIC C. F. KO

Department of Chemistry and Chemical Engineering, University of Saskatchewan, Saskatoon, Sask., Canada S7N 0W0

Received May 26, 1981

CHOI CHUCK LEE and ERIC C. F. KO. Can. J. Chem. **59**, 3309 (1981).

The exchange between the H atoms of cyclopentane (**3**) or cyclohexane (**4**) and the labeled acid protons of CF_3SO_3D (**2**-*d*), $[^3H]CF_3SO_3H$ (**2**-*t*), $[^3H]H_2SO_4$ (**1**-*t*), or $ZnCl_2$–$[^3H]HCl$ (**5**-*t*) has been investigated. Results from the treatment of **3** or **4** with **2**-*d* at 0° or 20°C, respectively, gave rise to polydeuterated cycloalkanes, indicating that all H atoms of **3** or **4** could be involved in the exchange. The rates of incorporation of the T-label into the hydrocarbon layer from the tritiated acids were found to be directly related to acid strength. After treatment of **3** or **4** with **2**-*t*, quenching of the acid layer and analysis by isotope dilution showed the presence of cyclopentanol or cyclohexanol. A carbocationic chain mechanism for the exchange, as well as the mechanism for the formation of the cycloalkyl cation from the cycloalkane, are discussed.

CHOI CHUCK LEE et ERIC C. F. KO. Can. J. Chem. **59**, 3309 (1981).

On a étudié la réaction d'échange entre les atomes d'hydrogène du cyclopentane (**3**) ou du cyclohexane (**4**) et les protons acides marqués des composés suivants: CF_3SO_3D (*d*-**2**), $[^3H]CF_3SO_3H$ (*t*-**2**), $[^3H]H_2SO_4$ (*t*-**1**) ou $ZnCl_2$–$[^3H]HCl$ (*t*-**5**). Les produits issus de la réaction des composés **3** ou **4** avec le composé *d*-**2** à 0° ou 20°C respectivement sont des cycloalcanes polydeutérés, indiquant par là que tous les atomes d'hydrogène des composés **3** ou **4** peuvent être impliqués dans l'échange. On a trouvé que les vitesses d'incorporation des marqueurs au tritium dans la phase hydrocarbonée à partir des acides tritiés sont reliés directement à la force de l'acide. Le piégeage de la phase d'acide, après la réaction des composés **3** ou **4** avec le composé *t*-**2**, suivi d'une analyse par dilution isotopique révèle la présence de cyclopentanol et de cyclohexanol. On discute d'un mécanisme en chaine de type carbocationique pour l'échange, ainsi que d'un mécanisme de formation du cation cycloalkyle à partir du cycloalcane.

[Traduit par le journal]

The treatment of cyclopropane with D_2SO_4 (**1**-*d*) (1) or $[^3H]H_2SO_4$ (**1**-*t*) (2) led to the formation of 1-propyl products with the isotopic label distributed over all three carbon positions, and these results were attributed to the involvement of equilibrating protonated cyclopropane intermediates (3, 4). The treatment of cyclobutane with **1**-*t*, CF_3SO_3D (**2**-*d*), or $[^3H]CF_3SO_3H$ (**2**-*t*) failed to give any significant amount of open chain butyl product, but a facile incorporation of the T-label from **2**-*t* into the hydrocarbon layer was observed (5). This exchange was recently shown to involve a carbocationic chain mechanism and quenching with H_2O led to the detection of cyclobutanol, cyclopropylcarbinol, and allylcarbinol, indicating the formation of the bicyclobutonium ion (6). The results from cyclobutane thus resemble closely the earlier finding of Otvos *et al.* (7), reported in 1951, that the treatment of isobutane with **1**-*d* gave rise to the *tert*-butyl cation, and that exchange occurred with all 9 α-hydrogens. It is of interest to ascertain what would take place when cycloalkanes other than the small ring hydrocarbons are treated with acids under similar conditions. Hence in the present work, studies were made on the exchange reactions between cyclopentane (**3**) or cyclohexane (**4**) with some deuterated or tritiated acids.

The treatment of **3** or **4** with **2**-*d* followed by mass spectral analysis showed the presence of polydeuterated species in the region of the molecular ions, and the results are summarized in Tables 1 and 2. In measuring the relative composition of the various deuterated species given in these tables, while the errors in some cases could be as high as ± 5–10% of the recorded values, all of the observed peaks were definitely present. Although the relative composition of the d_{10} species from **3** was only $0.2 \pm 0.02\%$ and that of the d_{12} species from **4** was $0.1 \pm 0.01\%$, their presence was real. The results in Tables 1 and 2 thus indicate that all of the H atoms of **3** or **4** could be involved in the H–D exchange, a behavior that was also observed in similar studies with cyclobutane and **2**-*d* (6).

Upon treatment of **3** or **4** with **2**-*t*, incorporation of the T-label into the hydrocarbon through H–T exchange also took place, again as was observed in the treatment of cyclobutane with **2**-*t* (6). Since all of the H atoms of the cycloalkane could be involved in the exchange as was demonstrated in studies with **2**-*d*, at infinite time, a complete mixing of all H isotopes could be assumed and the specific activity of the recovered **3** or **4** after complete exchange, x_∞, could then be calculated (6). At different reaction times, the specific activities of the recovered cycloalkane were determined and the ratio, x/x_∞, would give a measure of the extent of exchange. Such results from the reaction of **2**-*t* with **3** and with **4**, at 20° and 40°C, respectively, are summarized in

0008-4042/81/243309-04$01.00/0

©1981 National Research Council of Canada/Conseil national de recherches du Canada

Can. J. Chem. Downloaded from www.nrcresearchpress.com by 210.87.254.6 on 09/06/12
For personal use only.

Can. J. Chem. Downloaded from www.nrcresearchpress.com by 210.87.254.6 on 09/06/12
For personal use only.

TABLE 1. Relative compositions of deuterated cyclopentanes from the treatment of cyclopentane (**3**) with CF_3SO_3D (**2**-*d*) at 0°C[a]

Reaction time (h)[b]	Composition (%)[c]										
	d_0	d_1	d_2	d_3	d_4	d_5	d_6	d_7	d_8	d_9	d_{10}
1.0	91.0	4.6	1.2	0.6	0.5	0.4	0.4	0.4	0.4	0.4	—
2.0	86.2	2.0	1.1	0.8	0.8	1.2	1.8	2.3	2.2	1.4	0.2
3.0	78.4	2.6	1.4	1.1	1.6	2.4	3.3	3.8	3.3	2.0	0.2
4.5	77.8	2.1	1.7	1.6	2.0	2.8	3.6	3.6	2.9	1.6	0.2
7.5	58.6	4.9	3.1	3.9	7.0	7.2	6.0	4.6	2.9	1.6	0.2

[a] From mass spectral analysis of 0.20 mL aliquots of the hydrocarbon layer withdrawn periodically from an initial mixture of 3.00 mL of **3** and 6.00 mL of **2**-*d* mechanically shaken at 0°C, the d_0 species being at *m/e* 70 for C_5H_{10}.
[b] There was an induction period and no D incorporation into the hydrocarbon was observed at reaction times of up to 45 min.
[c] Corrected for $p + 1$ and $p + 2$ due to ^{13}C.

TABLE 2. Relative compositions of deuterated cyclohexanes from the treatment of cyclohexane (**4**) with CF_3SO_3D (**2**-*d*) at 20°C[a]

Reaction time (h)[b]	Composition (%)[c]												
	d_0	d_1	d_2	d_3	d_4	d_5	d_6	d_7	d_8	d_9	d_{10}	d_{11}	d_{12}
2.0	97.5	1.4	—	0.1	0.1	—	—	0.1	0.2	0.2	0.2	0.1	—
3.0	97.4	0.7	0.1	0.1	0.1	0.1	0.1	0.2	0.3	0.3	0.3	0.2	—
4.0	95.6	1.9	0.2	0.2	0.2	0.2	0.2	0.2	0.3	0.4	0.4	0.3	—
5.5	93.9	2.6	0.2	0.2	0.3	0.3	0.3	0.3	0.4	0.5	0.5	0.4	—
7.5	90.0	4.0	0.5	0.4	0.4	0.4	0.5	0.6	0.7	0.8	0.9	0.7	0.1
24.0	64.8	3.7	2.4	2.6	3.2	4.1	4.7	4.7	4.1	3.1	1.6	0.8	0.1
30.0	51.8	4.3	4.5	5.2	6.5	7.1	6.6	5.5	3.9	2.6	1.3	0.6	0.1

[a] From mass spectral analysis of 0.20 mL aliquots of the hydrocarbon layer withdrawn periodically from an initial mixture of 3.00 mL of **4** and 6.00 mL of **2**-*d* mechanically shaken at 20°C, the d_0 species being at *m/e* 84 for C_6H_{12}.
[b] There was an induction period and no D incorporation into the hydrocarbon was observed at reaction times of up to 1.5 h.
[c] Corrected for $p + 1$ and $p + 2$ due to ^{13}C.

Tables 3 and 4. From plots of ln $[1 - (x/x_\infty)]$ vs. reaction time, straight lines were obtained, the negative slopes of which gave the first order rate constants, k, for the appearance of T in the recovered **3** or **4** (6, 7). The k values obtained were 2.6×10^{-5} s^{-1} and 1.5×10^{-5} s^{-1}, respectively, for the incorporation of T into **3** at 20°C and into **4** at 40°C (Tables 3 and 4). When **3** or **4** was treated with **2**-*t* for 24 h at 20° or 40°C, respectively, the nmr spectrum of the hydrocarbon layer showed the presence of only **3** or **4**. After quenching the acid layer with H_2O, analysis by isotopic dilution showed the presence of only cyclopentanol or cyclohexanol, indicating the formation of the cyclopentyl or cyclohexyl cation from **3** or **4**, respectively, and no methylcyclopentyl cation from **4** was detected.

On treating **3** or **4** with **1**-*t* at 85°C in sealed tubes, H–T exchange was also found to have taken place, but the incorporation of T into the cycloalkane was much slower than in the reactions with **2**-*t*. The results are given in Tables 5 and 6, the k values for the appearance of T in **3** or **4** on treatment with **1**-*t* at 85°C being 4.9×10^{-7} s^{-1} and 1.5×10^{-7} s^{-1}, respectively. Attempts were also made to ascertain whether exchange would occur between **3** or **4** and tritiated Lucas reagent (ZnCl–[^{3}H]HCl, **5**-*t*). When mixtures of **3** or **4** and **5**-*t* in sealed tubes were heated at 85°C as in the experiments with **1**-*t*, there was a high tendency for the tubes to break. Consequently, only two experiments were carried out with **3** at reflux temperature. When a stirred mixture of 3.0 mL of **3** and 9.0 mL of tritiated Lucas reagent was heated under reflux in a water bath at

TABLE 3. Incorporation of T into the hydrocarbon layer in the treatment of cyclopentane (**3**) with [^{3}H]CF_3SO_3H (**2**-*t*) at 20°C[a]

Reaction time (min)	Specific activity x (10^{-7} dpm/mmol)		x/x_∞	
	Run 1	Run 2	Run 1	Run 2
0[b]	0.150	0.187	0.0405	0.0505
20	—	0.433	—	0.117
30	0.567	—	0.153	—
40	—	0.699	—	0.189
60	0.844	0.876	0.228	0.237
80	—	1.07	—	0.289
90	1.08	—	0.292	—
100	—	1.22	—	0.330
120	1.43	—	0.387	—
150	2.22	—	0.600	—
		10^5k(s^{-1})	2.6	2.6

[a] Initially, 5.00 mL of **3** and 10.00 mL of **2**-*t* with specific activity of 2.10×10^7 dpm/mmol were shaken at 20°C. The calculated specific activity of the cyclopentane layer at complete exchange, x_∞, was 3.70×10^7 dpm/mmol.
[b] The zero time was arbitrarily chosen after the initial induction period of about 45 min has passed.

Can. J. Chem. Downloaded from www.nrcresearchpress.com by 210.87.254.6 on 09/06/12
For personal use only.

TABLE 4. Incorporation of T into the hydrocarbon layer in the treatment of cyclohexane (**4**) with [^{3}H]CF_3SO_3H (**2**-*t*) at 40°C[a]

Reaction time (min)	Specific activity x (10^{-7} dpm/mmol)		x/x_∞	
	Run 1	Run 2	Run 1	Run 2
0[b]	0.0576	0.104	0.0134	0.0242
20	0.0839	—	0.0195	—
30	—	0.168	—	0.0391
60	0.161	0.198	0.0374	0.0460
90	—	0.646	—	0.150
120	0.418	1.01	0.0972	0.235
150	—	1.08	—	0.251
180	1.08	1.37	0.251	0.319
240	1.42	—	0.330	—
		$10^5k(s^{-1})$	1.5	1.5

[a] Initially 5.00 mL of **4** and 10.00 mL of **2**-*t* with specific activity of 2.10×10^7 dpm/mmol were shaken at 40°C. The calculated specific activity of the cyclohexane layer at complete exchange, x_∞, was 4.30×10^7 dpm/mmol.
[b] The zero time was arbitrarily chosen after the initial induction period of about 60 min has passed.

TABLE 5. Incorporation of T into the hydrocarbon layer in the treatment of cyclopentane (**3**) with [^{3}H]H_2SO_4(**1**-*t*) at 85°C[a]

Reaction time (h)	Specific activity x (10^{-5} dpm/mmol)	x/x_∞
0[b]	0.375	0.0062
4.0	1.65	0.0275
17.5	5.32	0.0885
24.0	6.01	0.100
41.5	9.70	0.161
48.0	9.64	0.160
65.5	1.23	0.205
	$k(s^{-1})$	4.9×10^{-7}

[a] Samples each containing 1.00 mL of **3** and 2.00 mL of **1**-*t* with specific activity of 2.82×10^6 dpm/mmol were shaken in sealed tubes at 85°C. The calculated x_∞ was 6.01×10^6 dpm/mmol C_5H_{10}.
[b] To allow for the induction period, each sample was shaken for 1.5 h before being regarded as having reached its zero time.

50°C for 2 or 4 days, the recovered **3** showed x/x_∞ values of 1.2×10^{-4} and 2.2×10^{-4}, respectively, indicating that only a very small amount of exchange has taken place.

From the results described above, it is clear that cyclopentane (**3**) or cyclohexane (**4**), when treated with the various deuterated or tritiated acids, showed behaviors quite similar to those observed for cyclobutane (6), and these results may be interpreted by a carbocationic chain mechanism as originally suggested by Otvos *et al.* (7). The chain initiation is the formation of a carbocation, the cyclopentyl or cyclohexyl cation from **3** or **4**. A slow formation of such a cation in the initiation step may thus account for the observation, in the present and previous studies (6, 7), of a variable induction period. The carbocationic chains are

TABLE 6. Incorporation of T into the hydrocarbon layer in the treatment of cyclohexane (**4**) with [^{3}H]H_2SO_4 (**1**-*t*) at 85°C[a]

Reaction time (h)	Specific activity x (10^{-5} dpm/mmol)	x/x_∞
0[b]	0.061	0.0009
17	1.88	0.0267
24	2.90	0.0413
41	3.90	0.0555
48	3.87	0.0551
65	6.00	0.0853
	$k(s^{-1})$	1.5×10^{-7}

[a] Samples each containing 0.50 mL of **4** and 1.00 mL of **1**-*t* with specific activity of 2.82×10^6 dpm/mmol were shaken in sealed tubes at 85°C. The calculated x_∞ was 7.03×10^6 dpm/mmol C_6H_{12}.
[b] To allow for the induction period, each sample was shaken for 1.5 h before being regarded as having reached its zero time.

then propagated through intermolecular transfers of hydride ions between the cation and the cycloalkane ($R^+ + RH \rightleftarrows RH + R^+$). During the lifetime of the carbocation, H–D or H–T exchange may occur, presumably at the carbons α to the positive charge, since in the studies with isobutane and **1**-*d* (7) the 9 α-H atoms, but not the tertiary H atom, were found to undergo H–D exchange. The involvement of all H atoms of **3** or **4** in the exchange observed in the present work may be explained by the occurrence of 1,2-hydride shifts around the ring in the cyclopentyl or cyclohexyl cation, thus allowing the H atoms at all carbon positions to become α to the positive charge and to undergo exchange.

It is of interest to note that Olah and Lukas (8) have found that protonation of **3** in FSO_3H–SbF_5 or HF–SbF_5 solution at above −10°C yielded, via cleavage and rearrangement, the *tert*-amyl cation. At temperatures below −10°C and in solution diluted with SO_2ClF, the cyclopentyl cation was obtained from **3** and the ^{1}H nmr spectrum of this cation showed only one singlet, indicating rapid 1,2-hydride shifts around the ring, thus rendering all H atoms equivalent. The treatment of **4** with FSO_3H–SbF_5 (8) at room temperature was found to give rise to a 9:1 mixture of the methylcyclopentyl and 2,3-dimethyl-2-butyl cations resulting from rearrangement and cleavage of the incipient cyclohexyl cation. The present work has shown that by the use of ordinary acids such as CF_3SO_3H or H_2SO_4, instead of the super-acids employed by Olah and Lukas, and at ordinary temperatures, the cyclopentyl or cyclohexyl cation could be generated from **3** or **4**. Under these conditions, proton exchanges could occur but there was little cleavage to give acyclic products. The present results also would suggest that if a nonspecifically labeled cycloalkane were to be prepared, a treatment with

Can. J. Chem. Downloaded from www.nrcresearchpress.com by 210.87.254.6 on 09/06/12
For personal use only.

a deuterate or tritiated acid such as **2**-*d* or **2**-*t* under quite mild conditions would be an easy route to produce such a labeled cycloalkane.

The formation of a carbocation from the corresponding hydrocarbon would, of course, involve an overall oxidation or hydride abstraction (6–8). In the present work, it was found that the treatment of **3** with tritiated Lucas reagent did give rise to a very small, but detectable, amount of exchange. Since Lucas reagent could not act as an oxidizing agent, this finding would suggest the possibility that a direct chemical oxidation may not be the mechanism responsible for the carbocation formation. The rates of incorporation of T through exchange between the acid proton and the cycloalkyl cation have clearly been shown to be $CF_3SO_3H > H_2SO_4 > ZnCl_2$–HCl, and these findings could be considered as being consistent with Olah's proposal (9) of an electrophilic protolysis of a C—H bond to give a pentacoordinated carbonium ion as a key step in the eventual formation of the tricoordinated carbocation.

Experimental

Materials

[^{3}H]H_2SO_4 (**1**-*t*), [^{3}H]CF_3SO_3H (**2**-*t*), and CF_3SO_3D (**2**-*d*) were prepared as described previously (6). The tritiated Lucas reagent, **5**-*t*, was made up by combining equimolar amounts of $ZnCl_2$ and concentrated HCl containing [^{3}H]HCl. Cyclopentane (**3**) and cyclohexane (**4**) were of spectroquality and were washed with cold concentrated H_2SO_4 and redistilled or purified by preparative vpc.

Treatment of ***3*** *or* ***4*** *with* ***2***-d

A mixture of 3.00 mL of **3** and 6.00 mL of **2**-*d* was shaken mechanically in a stoppered glass tube kept at 0°C in an ice–water bath. Periodically, 0.20 mL aliquots of the hydrocarbon layer were withdrawn and analyzed by mass spectrometry to give the results recorded in Table 1. Similarly, from a mixture of 3.00 mL of **4** and 6.00 mL of **2**-*d* shaken at 20°C, analysis of 0.20 mL aliquots of the organic layer withdrawn periodically gave the results summarized in Table 2.

Treatment of ***3*** *or* ***4*** *with* ***2***-t

A mixture of 5.00 mL (3.75 g, 53.5 mmol) of **3** and 10.00 mL (17.15 g, 114.3 mmol) of **2**-*t*, with a specific activity of 2.10×10^7 dpm/mmol, was shaken mechanically in a stoppered glass tube kept in a water bath maintained at 20°C. After the induction period had passed, 0.20 mL and 0.40 mL aliquots, respectively, of the hydrocarbon and acid layers were withdrawn at different times. Each hydrocarbon aliquot was redistilled and its activity determined. In this way, the relative amounts of hydrocarbon to acid, and hence the theoretical specific activity in the hydrocarbon layer at complete exchange, x_∞, would remain constant throughout the experiment.

In this experiment, the total amount of activity involved was $114.3 \times 2.70 \times 10^7 = 2.40 \times 10^9$ dpm, and the total amount of H involved was $(53.5 \times 10) + 114.3 = 649.3$ mg atoms.

At complete exchange, the specific activity, x_∞, would be $(2.40 \times 10^9)/649.3 = 3.70 \times 10^6$ dpm/mg atom H or 3.70×10^7 dpm/mmol C_5H_{10}.

Using the specific activity x determined for the hydrocarbon aliquots at different times, x/x_∞ values were calculated. The results are given in Table 3.

In a similar manner, treatment of 5.00 mL (3.90 g, 46.3 mmol) of **4** with 10.00 mL (17.15 g, 114.3 mmol) of **2**-*t* at 40°C gave the results summarized in Table 4.

After a mixture of **3** or **4** and **2**-*t* under the conditions described above was shaken at 20° or 40°C, respectively, for 24 h, the nmr and mass spectra of the recovered hydrocarbon showed it to be unchanged **3** or **4**, with singlet nmr absorption at 1.43 or 1.40 ppm and molecular ion at *m/e* 70 or 84 for **3** or **4**, respectively. Quenching of 1.00 mL aliquots of the acid layer with 10.0 mL of H_2O containing 1.0 mL of cyclopentanol or cyclohexanol as carrier, followed by vpc purification of the recovered alcohol and its conversion to the α-naphthylurethane in a manner as described previously (6), showed that the urethane derivative was radioactive, the mean specific activity of the α-naphthylurethane of the cyclopentanol or cyclohexanol obtained under these conditions being 1.60×10^3 or 8.90×10^3 dpm/mmol, respectively.

Treatment of ***3*** *or* ***4*** *with* ***1***-t

The treatment was carried out at 85°C in individual sealed tubes each containing 1.00 mL (751 mg, 10.7 mmol) of **3** and 2.00 mL (3.88 g, 39.6 mmol) of **1**-*t* or 0.50 mL (390 mg, 4.63 mmol) of **4** and 1.00 mL (1.44 g, 19.8 mmol) of **1**-*t*. The reaction mixtures were shaken at 85°C for 1.5 h before being considered as having reached zero time. At different times after this arbitrarily chosen induction period, the incorporations of T into the hydrocarbon layer were measured to give the results summarized in Tables 5 and 6.

Treatment of ***3*** *with* ***5***-t

A mixture of 3.00 mL (2.25 g, 32.1 mmol) of **3** and 9.00 mL (30.3 mmol HCl) of tritiated Lucas reagent (**5**-*t*) with a specific activity of 3.25×10^6 dpm/mmol was heated with stirring and under reflux in a water bath at 50°C for 2 or 4 days. The recovered hydrocarbon was washed with a 5% NaOH solution, dried with $MgSO_4$, and redistilled. Its activity was found to be 334 and 607 dpm/mmol, respectively, for the samples recovered after 2 and 4 days. Under these conditions, the calculated x_∞ was 2.80×10^6 dpm/mmol, hence x/x_∞ values for the recovered **3** after reaction times of 2 and 4 days were 1.2×10^{-4} and 2.2×10^{-4}, respectively.

Acknowledgements

The financial support given by the Natural Sciences and Engineering Research Council of Canada and the technical assistance of Craig A. Obafemi are sincerely acknowledged.

1. R. L. Baird and A. A. Aboderin. J. Am. Chem. Soc. **86**, 252 (1964).
2. C. C. Lee and L. Gruber. J. Am. Chem. Soc. **90**, 3775 (1968).
3. C. J. Collins. Chem. Rev. **69**, 543 (1969).
4. C. C. Lee. Prog. Phys. Org. Chem. **7**, 129 (1970).
5. C. C. Lee and E. C. F. Ko. Can. J. Chem. **54**, 1722 (1976).
6. C. C. Lee and E. C. F. Ko. Can. J. Chem. **58**, 1 (1980).
7. J. W. Otvos, D. P. Stevenson, C. D. Wagner, and O. Beeck. J. Am. Chem. Soc. **73**, 5741 (1951).
8. G. A. Olah and J. Lukas. J. Am. Chem. Soc. **90**, 933 (1968).
9. G. A. Olah, Y. Halpern, J. Shen, and Y. K. Mo. J. Am. Chem. Soc. **95**, 4960 (1973).

A ^1H and ^{13}C nmr study of the radiation-induced degradation products of 2′-deoxythymidine derivatives: N-(2′-deoxy-β-D-erythropentofuranosyl) formamide

J. CADET, R. NARDIN,[1] AND L. VOITURIEZ

Laboratoires de Chimie, Département de Recherche Fondamentale, Centre d'Etudes Nucléaires de Grenoble, 85 X, F.38041 Grenoble Cedex, France

M. REMIN

Department of Biophysics, Institute of Experimental Physics, The University of Warsaw, Warszawa 02-089, Poland

AND

F. E. HRUSKA

Chemistry Department, The University of Manitoba, Winnipeg, Man., Canada R3T 2N2

Received May 18, 1981

J. CADET, R. NARDIN, L. VOITURIEZ, M. REMIN, and F. E. HRUSKA. Can. J. Chem. **59**, 3313 (1981).

N-(2′-Deoxy-β-D-*erythro*pentofuranosyl) formamide is an ionizing radiation-induced degradation product of 2′-deoxythymidine. This work describes a facile chemical synthesis of this molecule, and discusses the results of an ^1H and ^{13}C nmr study. The rotational barrier to *cis–trans* isomerization about the amide linkage is calculated, and details of the molecular conformation of the *cis* and *trans* isomers in aqueous solution are presented.

J. CADET, R. NARDIN, L. VOITURIEZ, M. REMIN et F. E. HRUSKA. Can. J. Chem. **59**, 3313 (1981).

La dégradation de la déoxy-2′ thymédine induite par une radiation ionisante conduit au *N*-(déoxy-2′β-D-*erythro* pentofuranosyl) formamide. Ce travail décrit une synthèse chimique facile de cette molécule; on discute aussi des résultats obtenus lors de son étude par la rmn du ^1H et du ^{13}C. On a calculé la barrière à la rotation de l'isomérisation *cis–trans* autour du lien amide et on fournit des détails relatifs à la conformation des isomères *cis* et *trans* en solution aqueuse.

[Traduit par le journal]

Introduction

Exposure of nucleic acids to ionizing radiation leads to a modification of their constituents and to local functional and conformational alterations in polynucleotides (1). *N*-(2′-deoxy-β-D-*erythro*-pentofuranosyl) formamide (dF, Fig. 1) and its derivatives appear to be the main, stable products of ionizing irradiation of dT (2), 5′dTMP (3), d(TpT) (4), and the thymine moieties of DNA (5) in aerated, aqueous solution.[2] The formation of dF probably involves α-hydroxy peroxide cleavage (6), followed by hydrolytic cleavage, of the hydroxy-hydroperoxy intermediates which were initially formed through attack on dT by the hydroxyl radicals generated from radiolytic decomposition of water (7).

From the viewpoint of nucleoside stereochemistry, the formamide product poses an interesting problem since the restricted rotation of the amide bond leads to separate nmr spectra for the *cis* and *trans* isomers. Here we discuss a facile chemical synthesis of dF, and the data of a ^1H and ^{13}C nmr study, including nuclear Overhauser effect (NOE) and ^1H relaxation time (T_1) measurements. Spectral assignments are made, and the *cis–trans* isomer ratio and the energy barrier to amide bond rotation are determined. Comparison of the data with those of 2′-deoxyuridine provides information

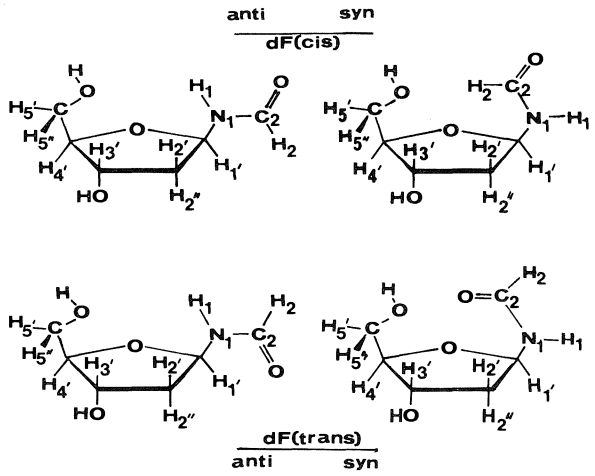

FIG. 1. Structure of *N*-(2′-deoxy-β-D-*erythro*pentofuranosyl formamide (dF). Top: *cis* isomer about the N_1—C_2 amide bond in the *anti* (left) and *syn* (right) conformations about the $C_{1'}$—N_1 bond. Bottom: *trans* isomer about the N_1—C_2 amide bond in the *anti* (left) and *syn* (right) conformation about the $C_{1'}$—N_1 bond.

[1]Détaché du Centre de Recherches sur les Macromolécules Végétales (CNRS) au Centre Grenoblois de Resonance Magnétique (C.G.R.M.), Département de Recherche Fondamentale, Centre d'Etudes Nucléaires de Grenoble.

[2]Abbreviations used: dF(*cis*) and dF(*trans*) for the *cis* and *trans* isomers of the title compound; dT, 5′dTMP, and d(TpT): 2′-deoxythymidine, its 5′-monophosphate and 3′,5′-dideoxynucleosidemonophosphate; dU: 2′-deoxyuridine.

0008-4042/81/243313-06$01.00/0

©1981 National Research Council of Canada/Conseil national de recherches du Canada

Can. J. Chem. Downloaded from www.nrcresearchpress.com by 210.87.254.42 on 09/06/12
For personal use only.

about the relation between sugar conformation and nature of the aglycone. This study should also provide insight into the stereochemical properties of similar amide *ribo*nucleotide derivatives which are intermediates in purine biosynthesis (8).

Experimental

Materials

dT was purchased from Merck (Darmstadt, F.R.G.). dF was synthesized by a modification of the earlier procedure of Cadet and Teoule (9). Bromine (600 μL) was added dropwise to a well-stirred solution of dT (2 g) in water (30 mL, 0°C). Then pyridine (30 mL) was added and the mixture warmed for 1 h 30 min at 60°C. After evaporation to dryness under reduced pressure the resulting oily residue was dissolved in a solution of sodium metaperiodate (10 g) in water (50 mL). The mixture was shaken overnight at room temperature and then evaporated to dryness. A fraction of the salts was precipitated by addition of methanol (2 × 10 mL) and removed by filtration. The filtrate was evaporated under reduced pressure and the resulting oil dissolved in 20 mL of water. The solution was rendered neutral by the addition of sodium acetate leading to a further precipitation of salts. The filtrate was concentrated to 20 mL and then analyzed (2 × 10 mL) by preparative high-performance liquid chromatography on a ^{18}C-reverse phase column using a LC 500 Prep. chromatograph (Waters Ass., Milford, MA,) equipped with a refractive index detector. The main peak ($k' = 1.0$) was collected and combined (2 × 200 mL). Evaporation to dryness afforded 596 mg (yield 45%) of homogeneous dF as a syrup.

Nuclear Magnetic Resonance Experiments

Continuous wave ^{1}H nmr spectra were obtained on a 250 MHz CAMECA TSN Spectrometer at a probe temperature of 30°C. D_2O or DMSO-d_6 (containing respectively 3-(trimethylsilyl) propionate-2,2,3,3-d_4 (TSP) or tetramethylsilane (TMS) as the internal standard) were used as the solvent and provided the internal deuterium lock.

Nuclear magnetic resonance measurements in the Fourier transform mode were made with a Varian XL-100-15 NMR spectrometer equipped with a deuterium lock for field stabilization. Carbon and proton resonances were observed at 25.1 and 100.1 MHz respectively.

The ^{1}H spin–lattice relaxation time measurements were made on the Varian XL-100-15 spectrometer with a 32 K Informatek 620 L-100 computer as complementary equipment. The proton T_1 values were determined using the inversion recovery pulse sequence (180°–t–90°–T_∞). The delay between pulses (T_∞) was in all cases at least $5T_1$. The relative uncertainty in the ^{1}H T_1 values was about ±5%.

The NOE enhancements were measured with the electronic integrator of the spectrometer since changes in the peak height could not be used due to the occurrence of a small scalar coupling between the formyl and anomeric protons. The optimal H_2 intensity level was determined by ensuring complete decoupling of the $H_{2'}$ and $H_{2''}$ patterns when $H_{1'}$ was irradiated. The NOE is expressed as the percentage change in the peak intensity when the formyl proton was saturated and when the double resonance field was applied off resonance, c.a. 10 ppm down field of the formyl proton resonance. About 20 measurements were made in each case. The temperature was regulated by the Varian temperature accessory and was checked before and after each experiment with a copper–constantan thermocouple. The potential difference was measured with a Philips PM 2435 millivoltmeter. For the NOE and T_1 measurements the nucleoside was lyophilized three times from 99.8% D_2O (Commissariat Energie Atomique, France), then dissolved in 99.95% D_2O to a concentration of 0.2 M and the resulting solution carefully degassed.

Table 1 lists, for the major and minor isomers, the ^{1}H and ^{13}C chemical shifts (δ) and the ^{1}H–^{1}H coupling constants. The ^{1}H data were obtained by spectral analysis using iterative LAOCOON (10).

Results and Discussion

Assignment of the ^{1}H and ^{13}C nmr Spectra

Figure 2 shows the 250 MHz spectrum of the isomer mixture in D_2O (30°C) accompanied by a computer-simulated spectrum. The isomer ratio (major:minor = 3:2) was determined by integration of the well-separated formyl proton (H_2) resonances at lowest field (major: 8.12 ppm; minor: 8.22 ppm from TSP, Table 1). The assignments of the 2′-deoxyribose protons, to the major and minor components, were based on line intensity considerations and extensive spin-decoupling experiments, and are in line with published data for a large number of 2′-deoxyribosides (11). For example, irradiation of the major H_2 band confirmed the location of the major $H_{1'}$ band (5.89 ppm) and the presence of a $^4J_{21'}$ coupling (0.9 Hz). Irradiation of this $H_{1'}$ band then led to location of the $H_{2'}$ and $H_{2''}$ bands, and so on. The distinction between the $H_{2'}$ and $H_{2''}$ bands for the same isomer was based on coupling constant arguments (12, 13), while the $H_{5'}$ and $H_{5''}$ assignments followed from arguments by Remin and Shugar (14) and the selective deuteration studies of Ritchie and Perlin (15).

The 25.1 MHz ^{13}C nmr spectrum of dF exhibited distinct pairs of signals for the C_2, $C_{1'}$, and $C_{2'}$ carbons, whereas single signals were observed for $C_{3'}$, $C_{4'}$, and $C_{5'}$ carbons distant from the formamide group. The assignments were made by "off-resonance" and selective heteronuclear (^{1}H) decoupling experiments.

Isomer Assignment

Several criteria (16) were used to assign the major and minor components to the *trans* and *cis* rotamers of dF, respectively (Fig. 1), the most reliable being the nuclear Overhauser effect (NOE) method (17–19). In NOE measurements at 12°C (Table 2), in which the minor $H_{1'}$ proton was irradiated, a 17% increase in the integrated intensity of the minor H_2 band was observed; no increase in intensity in the major H_2 band was detected. However, irradiation of the major $H_{1'}$ band had no effect on the integrated intensities of either H_2 band. Given the r^{-6} dependence of the enhancements, the results are in line with a close approach of $H_{1'}$ and H_2 (minor), possible only in the dF(*cis*) isomer in its *anti* conformation about the *N*-glycosyl link (see below). The minor form must therefore be dF(*cis*).

Can. J. Chem. Downloaded from www.nrcresearchpress.com by 210.87.254.42 on 09/06/12
For personal use only.

TABLE 1. ^1H and ^{13}C chemical shifts (δH, δC) and ^1H–^1H coupling constants (J(H,H)) of the minor (dF(*cis*)) and major (dF(*trans*)) forms of *N*-(2′-deoxy-β-D-*erythro*pentofuranosyl) formamide[a,b]

δ(H)	Major	Minor	dU[c]	J(H,H)	Major	Minor	dU	δ(C)	Major	Minor
H-2	8.119	8.217	—	2,1′	0.9	0.2	—	2	165.0	168.1
H-1′	5.892	5.626	6.285	1′,2′	7.2	7.7	6.5	1′	79.2	84.7
H-2′	2.141	2.160	2.379	1′,2″	6.0	6.1	6.7	2′	39.1	39.4
H-2″	2.271	2.308	2.437	1′,3′	−0.6	−0.6	—	3′	71.9	71.9
H-3′	4.394	4.379	4.474	1′,4′	≃0.1	≃0.1	—	4′	86.5	86.5
H-4′	3.957	3.950	4.060	2′,2″	−14.0	−14.0	−13.9	5′	62.3	62.3
H-5′	3.667	3.682	3.846	2′,3′	6.2	6.2	6.8			
H-5″	3.619	3.617	3.771	2″,3′	3.2	3.2	3.5			
				3′,4′	3.0	3.0	4.0			
				4′,5′	4.2	4.2	3.4			
				4′,5″	5.3	5.3	5.1			
				5′,5″	−12.2	−12.2	−12.6			

[a] Proton data at 250 MHz in ppm from TSP; J in Hz; 0.1 *M* nucleoside in D_2O at 30 ± 1°C. See Fig. 1 for numbering.
[b] Carbon data (30°C) at 25.1 MHz. δ measured relative to external C_6H_6 and converted to TMS scale. $\delta_{TMS} = \delta_{C_6H_6} - 128.1$. Nucleoside in D_2O at 25% w/v.
[c] dU at 23°C (220 MHz) from ref. 27.

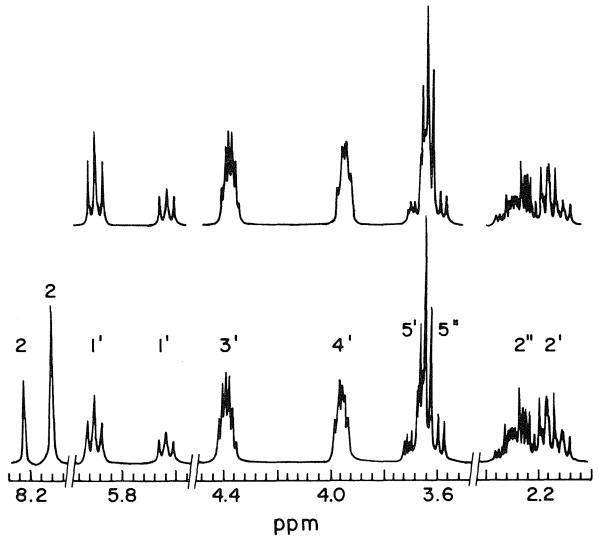

FIG. 2. Bottom: 250 MHz ^1H nmr spectrum of the *cis* and *trans* isomers of the title compound (dF) in D_2O (30°C). Numbering scheme in Fig. 1. Separate major (*trans*) and minor (*cis*) bands observed for H_2 and $H_{1'}$. Overlap in remaining bands. Top: Computer-simulated spectrum.

TABLE 2. NOE enhancement measurements for dF(*cis*) and dF(*trans*) in aqueous solution[a]

T (°C)	Irradiated proton ($H_{1'}$)	Observed proton (H_2) dF(*cis*)	dF(*trans*)
12	dF(*cis*)	17	—
	dF(*trans*)	—	—
31	dF(*cis*)	7	9
	dF(*trans*)	6	7

[a] See Experimental section for details.

TABLE 3. Longitudinal relaxation times (T_1, s) of $H_{1'}$ and H_2, and life times (τ,s) of the dF(*cis*) and dF(*trans*) rotamers[a]

T (°C)	T_1 ($H_{1'}$) dF(*cis*)	T_1 ($H_{1'}$) dF(*trans*)	T_1 (H_2) dF(*cis*)	T_1 (H_2) dF(*trans*)	τ
12	1.3	3.4	2.2	7.2	66
31	2.5	5.2	4.7	10.9	7.6

[a] In D_2O. See Experimental section for details.

Support for this assignment is provided as follows.

(*a*) The shorter longitudinal relaxation times (T_1) of the $H_{1'}$ and H_2 protons of the minor form, relative to the corresponding proton of the major form (Table 3), are consistent with the close approach of these protons in the dF(*cis*) form in its *anti* conformation.

(*b*) With slow exchange in DMSO-d_6 solution, the amide proton (H_1) resonances can be observed at 7.99 ppm (major) and 8.11 ppm (minor) from TMS, with a 3:2 relative, total intensity. Double resonance experiments confirmed that the splittings of 11.2 Hz in the minor H_1 and H_2 bands, and of 1.2 Hz in the major H_1 and H_2 bands, were due to vicinal $^3J_{12}$ interactions. The couplings are in line with the *trans* H_1, H_2 orientation in dF(*cis*) (minor) and their *cis* orientation in dF(*trans*) (major) (16, 20, 22). No crossover of the major and minor H_2 bands occurs in D_2O, so the isomer assignment must be the same as in DMSO-d_6.

(*c*) Support also comes from the four-bond coupling interactions between the anomeric $H_{1'}$ and formyl H_2 protons ($^4J_{1'2}$:0.9 Hz, major; 0.2 Hz, minor, Table 1). Their relative magnitudes conform with the stereochemical trends defined by ^4J interactions seen in *N*-methyl and *N*,*N*-dimethyl formamides (16).

In general, the *trans* form is favored in *N*-alkyl formamides when the alkyl substituent is small (e.g. methyl); the amount of the *cis* form increases with increasing substituent size due to steric inter-

Can. J. Chem. Downloaded from www.nrcresearchpress.com by 210.87.254.42 on 09/06/12
For personal use only.

Can. J. Chem. Downloaded from www.nrcresearchpress.com by 210.87.254.42 on 09/06/12
For personal use only.

actions with the carbonyl oxygen atom (16). In spite of its size, the 2′-deoxyribose sugar does not lead to a preference for the *cis* form. This we suggest points to a preference for the *anti* conformation about the *N*-glycosyl link which minimizes interactions between the sugar and formamide (see below). It would be interesting to study the ribose analog of dF and determine the influence of the 2′-hydroxyl on the isomer ratio.

In NOE experiments at 31°C irradiation of *either* the minor or the major $H_{1'}$ band led to an enhancement (6%–9%) of the intensities of *both* the minor and major H_2 bands (Table 2). This absence of selectivity in the NOE at this higher temperature can be rationalized in terms of saturation transfer since the T_1 values of the $H_{1'}$ and H_2 protons in each rotamer (2.5–9 s) are similar to the rotamer lifetimes (8 s; Table 3). Thus, on the chemical shift difference time scale, the rotamer lifetimes (τ) must be long (since separate rotamer spectra are observed), but must be of intermediate magnitude on the ^1H relaxation time scale ($\tau \approx T_1$, see below). A similar situation, leading to magnetization transfer, has been observed for a variety of amides (22).

Barrier to Amide Bond Rotation

Estimates of the energy barrier to *cis–trans* interconversion should provide insight into the stereochemistry of purine biosynthesis which involves amides analogous to dF (8). To evaluate the free energy of activation ($\Delta G^{\ddagger}$) for rotation about the amide bond, coalescence temperatures were measured for the formyl proton (H_2) in D_2O (T_c = 369 K) and for the formyl carbon (C_2) in DMSO (T_c = 378 K). The barrier was calculated from the Eyring equation (23)

$$[1] \quad \Delta G^{\ddagger}\,(\text{kcal mol}^{-1}) = 4.57\, T_c \left(9.67 + \log \frac{T_c}{\Delta\nu}\right)$$

where T_c is in degrees K and $\Delta\nu$ is the chemical shift difference (Hz) for a given nucleus in the two isomers when the exchange is slow. Thus, from the H_2 data (T_c = 369 K; $\Delta\nu$ = 24.0 Hz) $\Delta G^{\ddagger}$ = 18.3 kcal mol^{-1} in D_2O; from the C_2 data (T_c = 378 K; $\Delta\nu$ = 94.2 Hz), $\Delta G^{\ddagger}$ = 17.7 kcal mol^{-1}. Thus a small solvent effect on $\Delta G^{\ddagger}$ is apparent. Also, the barrier is considerably smaller than that measured for dimethylformamide (21 kcal mol^{-1}; average for several solvents (16)). The reason for this difference is not immediately apparent to us.

Conformation about $C_{1'}$—N_1

As in normal nucleosides, two broad *anti* and *syn* ranges of conformational angles about $C_{1'}$—N_1, defining the relative orientation of the formamide and sugar moieties, should be accessible to dF(*cis*) and dF(*trans*) (Fig. 1). Our data point to a preference for the *anti* form in both the *cis* and *trans* isomers. The preference for *anti* in dF(*trans*) is suggested by the upfield shift (0.24 ppm) of $H_{2'}$ relative to $H_{2'}$ of dU. If the conformation were predominantly *syn*, $H_{2'}$ should experience a large downfield shift (≃ 0.5 ppm) due to the juxtaposed carbonyl oxygen (24–26). The effects of *cis–trans* isomerization on the sugar proton and carbon chemical shifts also point to a dominant *anti* conformer for both dF(*cis*) and dF(*trans*). Thus, the $H_{1'}$ chemical shifts are sensitive to the isomerization (*cis–trans* difference: 0.266 ppm; Table 1). The shifts of the remaining sugar protons (in particular, $H_{2'}$) are relatively insensitive to isomerization (largest *cis–trans* difference: 0.037 ppm). Likewise, the $C_{2'}$, $C_{3'}$, $C_{4'}$, and $C_{5'}$ shifts are relatively insensitive (largest *cis–trans* difference: 0.3 ppm). Now note (*a*) the large increase in separation between $H_{1'}$ and the keto oxygen upon isomerization of *anti* dF(*trans*) to *anti* dF(*cis*) and (*b*) the presence of H_1 over the sugar ring (in proximity with $H_{2'}$, etc.) in the two *anti* forms (Fig. 1).

The *anti* conformation in dF(*cis*) is also suggested by the NOE and T_1 measurements which reveal that $H_{1'}$ and H_2 are near. No NOE enhancement of the $H_{3'}$, $H_{4'}$, $H_{5'}$, and $H_{5''}$ signals was noted upon irradiation of H_2 in dF(*cis*), in line with the *anti* conformation. The vicinal $H_{1'}$—$C_{1'}$—N_1—H_1 couplings which can be measured in DMSO solution (9.0 Hz in dF (*trans*); 9.6 Hz in dF(*cis*)) point to a similarity in the *N*-glycosyl angle distribution for the two isomers, but are not easily treated in terms of conformer distributions.

Sugar Pucker

Comparison of the sugar ^1H–^1H coupling constants of our molecules (with fragmented bases) and those of dU (taken from ref. 27) provides insight into the influence of the aglycone on the sugar pucker. For dF(*cis*) and dF(*trans*), the corresponding *cis* couplings ($J_{1'2''}$, $J_{2'3'}$) and *trans* couplings ($J_{2''3'}$, $J_{3'4'}$) are identical to within 0.2 Hz while the *trans* $J_{1'2'}$ couplings differ by 0.5 Hz (Table 1). Thus, the sugar conformations are not very sensitive to the amide bond orientation. Relative to dU, the $J_{1'2'}$ couplings of the dF isomers are larger by 0.7–1.2 Hz whereas $J_{2''3'}$ and $J_{3'4'}$ are smaller by 0.3–0.7 Hz. These trends indicate a small shift towards the *S*-pucker (28). (Following Remin *et al.* (29) we estimate from $J_{3'4'}$ 70% *S* for dU and 80% *S* for the dF isomers.) Also relative to dU, the *cis* couplings, $J_{1'2''}$ and $J_{2'3'}$, of the dF isomers are smaller by 0.6–0.7 Hz. This means that on a time-averaged basis the torsion angles about the $C_{1'}$—$C_{2'}$ (τ_1) and $C_{2'}$—$C_{3'}$ (τ_2) bonds are larger

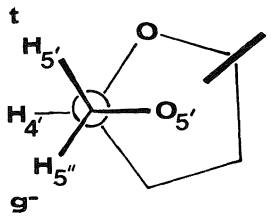

FIG. 3. Newman projection viewed along the C5′—C4′ bond. The g^+ conformer is shown. t and g^- give location of $O_{5'}$ in the t and g^- conformers, respectively.

in dF (28). These increases could be a result of changes in the pseudorotational parameters (P_N, P_S) and/or in the degrees of pucker ($\tau_m(N)$, $\tau_m(S)$), but disentanglement of the contributions is difficult (28).

Recently Gerlt and Youngblood (30) studied a series of furanosides which are not substituted at $C_{1'}$ with a heterocyclic base, namely methyl-β-D-ribofuranoside, its 5′-phosphate, and the corresponding 2′-deoxyribose derivatives.[3] In these molecules unusually small coupling constants between the $C_{1'}$ and $C_{2'}$ protons were noted, due, perhaps largely, to the electronegativity of the O-atom of the methoxy substituent at $C_{1'}$. Comparison of these couplings with our corresponding data is hazardous. However, the $J_{3'4'}$ data can safely be compared in conformational terms since electronegativity effects should be small here. Thus, $J_{3'4'}$ is 5.5 Hz and 6.1 Hz in uridine and methyl-β-D-ribofuranoside, respectively (30), suggesting a slight shift towards an *N*-type pucker in the latter. $J_{3'4'}$ is 4.0 Hz in dU and in methyl-β-D-2′-deoxyribofuranoside, indicating that the sugar conformations are identical, at least insofar as the $C_{3'}$—$C_{4'}$ bond is concerned. Thus, it seems that a uracil base, in a preferred *anti* conformation, does not have any profound influence on the pucker of a ribose or 2′-deoxyribose ring when compared with the smaller formamide and methoxyl groups.

Conformation about the $C_{4'}$—$C_{5'}$ Bond

We have used the Haasnoot *et al.* parameterization (31) to determine the conformer distribution (Fig. 3) for dU, dF(*cis* and *trans*) and methyl-β-D-2′-deoxyribofuranoside (Table 4). The data reveal that the g^+ conformer dominates in dU (50%) while g^- is least occupied. In dF(*cis* and *trans*) a reduction (to ~ 40%) occurs. This stabilizing influence of the uracil base, relative to the formamide group, is probably a consequence of an attraction between the electron deficient 6-carbon (32) and the 5′-hydroxyl. For methyl-β-D-2′-deoxyribofuranoside,

[3]To facilitate comparison of the formamides and the (deoxy)-nucleosides, we have used "primed" numbers for the atoms of the Gerlt-Youngblood molecules.

TABLE 4. Calculated rotamer populations (%) for $C_{4'}$—$C_{5'}$ bond[a]

	Population		
Compound	g^+	t	g^-
dU	50	38	22
dF(*cis*)	40	39	21
dF(*trans*)	41	38	21
dM[b]	22	56	22

[a]Calculated from the *J* data in Table 1 following Haasnoot *et al.* (31).
[b]Methyl-β-D-2-deoxyribofuranoside. Data taken from Gerlt and Youngblood (30).

the large decrease in the g^+ population (to 22%), and the concomitant increase in t population (to 56%) could be due to repulsion between the oxygen atoms of the 5′-hydroxyl and methoxy groups.

Conclusion

In the present work we have studied the formamide derivative obtained by radiation-induced degradation of dT. Hindered rotation about the amide bond (energy barrier $\Delta G^* \simeq 18$ kcal mol^{-1}) is revealed by separate ^{1}H and ^{13}C spectra for the *cis* (minor) and *trans* (major) isomers at room temperature. Fragmentation of the pyrimidine base leads to an enhancement of the *S* (2′ *endo*) pucker and a destabilization of the g^+ ($C_{4'}$—$C_{5'}$) conformation.

Acknowledgements

This work was supported in part by an operating grant from the Natural Sciences and Engineering Research Council of Canada and from the Polish Academy of Science (09·7·1). We acknowledge Mr. Henri Reutenauer (Centre Grenoblois de Résonance Magnétique Nucléaire) for the 250 MHz ^{1}H nmr spectra.

1. G. SCHOLES. *In* Photochemistry and photobiology of nucleic acids. *Edited by* S. Y. Wang. Academic Press, New York. 1976. p. 521.
2. J. CADET and R. TEOULE. Bull. Soc. Chim. Fr. 891 (1975).
3. J. CADET, R. DUCOLOMB, and R. TEOULE. C. R. Acad. Sci. Paris, **279**C, 549 (1974).
4. J. CADET and L. VOITURIEZ. *In* Symposium on radiation chemistry of DNA and DNA model compounds. Book Abstracts, Mulheim. 1979. p. 65.
5. R. TEOULE, C. BERT, and A. BONICEL. Radiat. Res. **72**, 190 (1977).
6. H. S. ISBELL, H. L. FRUSH, and Z. ORHANOVIC. Carbohydr. Res. **43**, 93 (1975).
7. R. TEOULE and J. CADET. *In* Molecular biology, biochemistry and biophysics. Vol. 27. *Edited by* J. Hutterman, W. Kohnlein, R. Teoule, and A. J. Bertinchamps. Springer, Berlin. 1978. p. 171.
8. A. L. LEHNINGER. Biochemistry. 2nd ed. Worth Publishers, Inc., New York. 1970. p. 730.
9. J. CADET and R. TEOULE. Tetrahedron Lett. 3229 (1972).
10. Program No. 101, Q.C.P.E., Indiana University, Bloomington, IN.

Can. J. Chem. Downloaded from www.nrcresearchpress.com by 210.87.254.42 on 09/06/12
For personal use only.

11. D. B. DAVIES. Prog. Nucl. Magn. Reson. Spectrosc. **12**, 135 (1978).
12. D. J. WOOD, F. E. HRUSKA, and K. K. OGILVIE. Can. J. Chem. **52**, 3353 (1974).
13. D. J. WOOD, K. K. OGILVIE, and F. E. HRUSKA. Can. J. Chem. **53**, 2781 (1975).
14. M. REMIN and D. SHUGAR. Biochem. Biophys. Res. Commun. **48**, 636 (1972).
15. R. G. S. RITCHIE and A. S. PERLIN. Carbohyd. Res. **55**, 121 (1977).
16. W. E. STEWART and T. H. SIDDAL. Chem. Rev. **70**, 517 (1970).
17. F. A. L. ANET and A. J. R. BOURN. J. Am. Chem. Soc. **87**, 5250 (1965).
18. J. K. SAUNDERS and R. A. BELL. Can. J. Chem. **48**, 512 (1970).
19. A. H. LEWIN and M. FRUCHT. Org. Magn. Reson. **7**, 206 (1975).
20. L. H. PIETTE, J. D. RAY, and R. A. OGG. J. Mol. Spectrosc. **2**, 66 (1958).
21. L. A. LA-PLANCHE and M. T. ROGERS. J. Am. Chem. Soc. **86**, 337 (1964).
22. S. COMBRISSON and B. P. ROQUES. Tetrahedron Lett. **32**, 1507 (1976).
23. M. L. MARTIN, G. J. MARTIN, and J.-J. DELPUECH. Practical NMR spectroscopy. Heyden, London. 1980. p. 340.
24. J. CADET, R. DUCOLOMB, and C. TAIEB. Tetrahedron Lett. 3455 (1975).
25. A. L. GEORGE, F. E. HRUSKA, K. K. OGILVIE, and A. HOLY. Can. J. Chem. **56**, 1170 (1978).
26. W. NIEMCZURA, F. E. HRUSKA, K. L. SADANA, and P. C. LOEWEN. Biopolymers, **20**, 1671 (1981).
27. T. SCHLEICH, B. J. BLACKBURN, R. D. LAPPER, and I. C. P. SMITH. Biochemistry, **11**, 137 (1972).
28. C. ALTONA and M. SUNDARALINGAM. J. Am. Chem. Soc. **95**, 2333 (1973).
29. M. RÉMIN, I. EKIEL, and D. SHUGAR. Eur. J. Biochem. **53**, 197 (1975).
30. J. A. GERLT and A. V. YOUNGBLOOD. J. Am. Chem. Soc. **102**, 7433 (1980).
31. C. A. G. HAASNOOT, F. A. A. M. DE LEEUW, H. P. M. DE LEEUW, and C. ALTONA. Recl. Trav. Chim. Pays-Bas. **98**, 576 (1979).
32. B. PULLMAN and A. PULLMAN. Quantum biochemistry. Interscience, New York. 1963. pp. 714, 832.

Can. J. Chem. Downloaded from www.nrcresearchpress.com by 210.87.254.42 on 09/06/12
For personal use only.

Erratum: Studies in general acid and general base catalysis. Rate–acidity profiles for prototropic processes

ROSS STEWART AND R. SRINIVASAN
Department of Chemistry, University of British Columbia, Vancouver, B.C., Canada V6T 1Y6

(Ref.: Can. J. Chem. **59**, 957 (1981))
Received September 21, 1981

On page 962 the sentence beginning "It can be readily shown that hydroxide ion catalysis becomes manifest ...", and the following sentence, should read "It can be readily shown that hydroxide ion catalysis becomes manifest when $pH = pK_{H_2O} - \log dpf$; at this pH the dominant path changes from one in which water is the base to one in which hydroxide ion is the base. Furthermore, when $pH = pK_{ZH^+} + \log paf$ the dominant path changes from one in which ZH^+ is the substrate to one in which Z is the substrate".

In the second sentence from the end of the same paragraph $pH_{(a)}$ should be $pH_{(b)}$, and vice versa.

Formation and characterization of transitory platinum–ammonia complex ions using pulse radiolysis

HASAN M. KHAN, WILLIAM L. WALTZ,[1] AND ROBERT J. WOODS

Department of Chemistry and Chemical Engineering and the Saskatchewan Accelerator Laboratory, University of Saskatchewan, Saskatoon, Sask., Canada S7N 0W0

AND

JOCHEN LILIE

Hahn-Meitner-Institut für Kernforschung Berlin GmbH, Bereich Strahlenchemie, D-1000 Berlin 39, Federal Republic of Germany

Received July 13, 1981

HASAN M. KHAN, WILLIAM L. WALTZ, ROBERT J. WOODS, and JOCHEN LILIE. Can. J. Chem. **59**, 3319 (1981).

The reactions of tetraammineplatinum(II) complex ion with the hydrated electron and hydrogen atom have been investigated in aqueous media using the technique of pulse radiolysis coupled with absorption and conductivity detection. Analysis has also been carried on pulse-irradiated solutions for the formation of free ammonia and for changes in concentration of Pt(II). The hydrated electron and hydrogen atom react with the complex at near diffusion-controlled rates, with the respective rate constant being $1.9 \pm 0.1 \times 10^{10}\ M^{-1}\ s^{-1}$ and $2.8 \pm 0.3 \times 10^{10}\ M^{-1}\ s^{-1}$. The nascent products of these reactions are shown to be different transitory species. For the electron reaction, the initial product is $Pt(NH_3)_4^+$ in which the metal center is formally Pt(I). In acidic media, there is a subsequent and rapid release of two ammonia ligands, with only the second step being measurable ($k = 4.2 \pm 1.7 \times 10^4\ s^{-1}$). In the reaction of H atom, the results support the occurrence of an addition process, giving rise to a hydrido type product. This species undergoes a first-order reaction ($k = 2.2 \pm 0.6 \times 10^4\ s^{-1}$); however the process is not associated with a change in conductivity, and thus it is not one involving loss of ammonia. Subsequent to this process, the loss of one ammonia ligand is observed, with $k = 2.0 \pm 0.6 \times 10^3\ s^{-1}$. The natures of these transients and the long term behavior of these systems are discussed.

HASAN M. KHAN, WILLIAM L. WALTZ, ROBERT J. WOODS et JOCHEN LILIE. Can. J. Chem. **59**, 3319 (1981).

Faisant appel à la technique de radiolyse par impulsion couplée avec la détection par absorption et par conductivité, on a étudié les réactions de l'ion complexe platine(II) tétrammine avec l'électron hydraté et l'atome d'hydrogène. On a également analysé des solutions irradiées par impulsion afin d'évaluer la formation d'ammoniac libre et les changements de concentration en Pt(II). L'électron hydraté et l'atome d'hydrogène réagissent avec le complexe au voisinage des vitesses contrôlées par la diffusion avec des constantes de vitesse respectives de $1{,}9 \pm 0{,}1 \times 10^{10}\ M^{-1}\ s^{-1}$ et de $2{,}8 \pm 0{,}3 \times 10^{-10}\ M^{-1}\ s^{-1}$. On montre que les produits naissants de ces réactions sont des espèces transitoires différentes. Dans le cas de la réaction de l'électron, le produit initial est l'ion $Pt(NH_3)_4^+$ dans lequel le Pt est formellement le métal central. En milieu acide, il se produit une rapide libération additionnelle de deux ligands d'ammoniac, dont seulement la vitesse de la deuxième étape peut être mesurée ($k = 4{,}2 \pm 1{,}7 \times 10^4\ s^{-1}$). Lors de la réaction des atomes d'hydrogène, les résultats confirment l'existence d'une réaction d'addition donnant lieu à un produit de type hybride. Cette espèce réagit selon une cinétique d'ordre un ($k = 2{,}2 \pm 0{,}6 \times 10^4\ s^{-1}$); cependant on n'associe pas la réaction à un changement de conductivité et dans ces conditions elle ne libère pas d'ammoniac. A la suite de cette réaction, on observe la perte d'un ligand d'ammoniac, avec $k = 2{,}0 \pm 0{,}6 \times 10^3\ s^{-1}$. On discute de la nature de ces intermédiaires et de leur comportement à long terme.

[Traduit par le journal]

Introduction

Both the hydrated electron, e_{aq}^-, and hydrogen atom represent two of the most elementary reagents available for investigating the oxidation–reduction mechanisms of transition-metal coordination compounds. These radical species are formed as primary products along with hydroxyl radical when aqueous solutions are exposed to ionizing radiation such as high energy electrons (2–20 MeV in this work)

[1] $H_2O \xrightarrow{e^-} e_{aq}^-,\ H,\ OH,\ H^+$

The hydrated electron and hydrogen atom are also interrelated in the manner of a conjugate acid – base pair,

[2] $H \rightleftharpoons H^+ + e_{aq}^-$

with pK_a of 9.7 (1). Through the use of the fast reaction technique of pulse radiolysis, a number of studies have been carried out on the electron reactions with metal complexes, generally processes leading to the reduction of the metal center (2–4). In some instances, this has afforded the unique opportunity to investigate transitory products in which the metal is formally in an unusual oxidation state, for example platinum(I), a feature of this study.

By way of contrast, relatively few reports exist concerning the reactions of H atom with metal complexes; however, the results do indicate that the processes can involve not only single electron reduction as for e_{aq}^- but also ones of addition and atom transfer (3, 5). The potential differences as well as similarities in reaction mechanisms between e_{aq}^- and H atom are exemplified in their

[1]To whom all correspondence should be addressed.

0008-4042/81/243319-07$01.00/0

©1981 National Research Council of Canada/Conseil national de recherches du Canada

Can. J. Chem. Downloaded from www.nrcresearchpress.com by 210.87.254.40 on 09/06/12
For personal use only.

Can. J. Chem. Downloaded from www.nrcresearchpress.com by 210.87.254.40 on 09/06/12
For personal use only.

reactions with square-planar platinum(II) complex ions. Pulse radiolysis studies using uv–visible absorption detection have shown that a common product arises from their reactions with $Pt(Cl)_4^{2-}$ (6, 7). With complexes containing bi- and tridentate amines or glycine as ligands and that of $Pt(CN)_4^{2-}$, the nascent products are different, implying a difference in mechanism (7–10).[2] These studies and one on the reaction of e_{aq}^- with *cis*-$Pt(NH_3)_2(Cl)_2$ (11) indicate that the initial products are capable of undergoing further and rapid reactions involving, for example, ligand substitution. The final products from these reactions have generally not been characterized, due in part to the very low concentrations formed in pulse radiolysis experiments; however, based upon some of the kinetic results and the detection of metallic platinum, dismutation processes have been proposed. Additional interest in the occurrence and properties of Pt(I) species has been engendered by the role of platinum compounds in radiation sensitization of cellular materials where the sensitizing action may be in part derived from the reactions of Pt(I) with organic substrates and/or the release of toxic ligands such as ammonia (11, 12).

The present study was undertaken to compare the reactions of e_{aq}^- and H atom with $Pt(NH_3)_4^{2+}$ and to characterize the reaction products and their subsequent chemical behavior. In so doing, we have endeavored to enlarge the scope of such investigations in part through the use of conductivity as well as absorption detection techniques. The former has been particularly useful in elucidating the nature and reaction properties of the intermediates, for which the platinum center is formally in an unusual oxidation state. The kinetic studies have been supplemented by product analysis on pulse-irradiated solutions for the formation of free ammonia and for changes in total Pt(II) concentrations.

Experimental Section

Materials and Solutions

Tetraammineplatinum(II) perchlorate was prepared from the chloride salt, obtained commercially (Platinum Chemicals, Alfa Division of Ventron Corp., K and K Labs of ICN Pharmaceuticals, Inc.) (13), and the compound was characterized by comparison of its uv absorption spectrum with that reported (14) and by elemental analysis (15). All solutions used for pulse radiolysis experiments, carried out at about 23°C, were prepared just prior to use with triply distilled water or water purified by a Millipore Super-Q system. The solutions were deaerated by procedures which are described elsewhere (16) and which employed argon, helium, or nitrous oxide gases. The pH of the solutions was adjusted by addition of reagent grade perchloric acid or sodium hydroxide, and was measured by pH-meter, calibrated with certified buffer solutions. All other materials were of reagent grade.

Product Analysis

Pulse-irradiated solutions were analyzed for uncoordinated ammonia and for changes in total Pt(II) content by the following spectrophotometric methods. The determination of free ammonia was based upon its reaction with hypochlorite and phenol to give indophenol, the absorption of which was measured at 625 nm in basic media at 25°C (15, 17). Analysis for changes in total Pt(II) concentration upon irradiation made use of the oxidation of Pt(II) to Pt(IV) in 0.2 *M* HCl and 0.2 *M* NaCl solutions at 25°C by $K_2[Ir(Cl)_6]$ (15, 18). The decrease in the intense absorption peak of the oxidant, $Ir(Cl)_6^{2-}$, at 487 nm, a wavelength where other species present do not absorb significantly, was used to measure the concentration of Pt(II). While some colloidal platinum metal was formed upon irradiation, its presence under our conditions did not appear to interfere with the analysis: removal by filtration of the suspension prior to analysis did not alter the results. Our findings for solutions containing $Pt(NH_3)_4^{2+}$ (50–250 μM) or *cis*-$Pt(NH_3)_2(H_2O)_2^{2+}$ (123 μM) and that of others on related Pt(II) complex ions (18, 19) would indicate that this analytical test provides a valid measure of the total concentration of Pt(II).[3]

Pulse Radiolysis Apparatus and Dosimetry

The apparatus employing conductivity and optical detection methods and the associated dosimetry have been described previously (16). Of note is that the transient signals represent differences between those of the unirradiated and the pulsed solutions. Such differences were calibrated against one of the following dosimetry solutions: ferrocyanide, thiocyanate, or tetranitromethane. The absorption spectra were recorded on a point-to-point basis, generally at 10 nm intervals, using an optical cell of 3.93 cm light path. Contributions to the absorption changes owing to the absorption of $Pt(NH_3)_4^{2+}$ were minor as this complex ion absorbs only weakly over the wavelength range investigated, and thus the spectra have not been corrected for this (or for minor contributions by alcohol radicals below 300 nm (20)). The *G*-values (number of a given species formed or lost per 100 eV of energy absorbed) used were $G_{e^-} = G_{H^+} = 2.66$ and $G_H = 0.55$ (21). In the study of the reaction of H atom and $Pt(NH_3)_4^{2+}$, conditions were maintained so that e_{aq}^- reacted predominantly with the proton, and thus the effective *G*-value for H atom was now the sum of G_{e^-} and G_H. The equivalent ionic conductivity values for H^+, OH^-, and NH_4^+ were taken as 350, 198, and 74 Ω^{-1} cm^2 equiv^{-1} respectively, and those for the platinum complex ions were anticipated to be about 50 Ω^{-1} cm^2 equiv^{-1} (22, 23).

Results

Reactions Associated with e_{aq}^- and $Pt(NH_3)_4^{2+}$

The reaction of the hydrated electron with $Pt(NH_3)_4^{2+}$ was followed by monitoring the decrease in the electron absorption at 578 nm in solutions at a natural pH of about 5.6 and containing 0.1 *M* isopropanol. This alcohol is a facile

[2]Results of a recent low temperature, esr study on $Pt(CN)_4^{2-}$ indicate that *in methanol* the electron product, $Pt(CN)_4^{3-}$, undergoes proton addition to yield the same complex, H—$Pt(CN)_4^{2-}$, as formed by H atom reaction in aqueous sulfuric acid matrices (10).

[3]Owing to the low concentrations of other Pt(II) complex ions which might be formed under pulsed-irradiation conditions, it was not feasible to identify their specific compositions although such possible products are likely to be aquated species such as *trans*- and *cis*-$Pt(NH_3)_2(H_2O)_2^{2+}$ (11).

Can. J. Chem. Downloaded from www.nrcresearchpress.com by 210.87.254.40 on 09/06/12
For personal use only.

scavenger of both hydrogen atom and hydroxyl radical (5, 24). Under the condition where the concentration of complex ion (15–174 μ*M*) was considerably in excess of that for e_{aq}^-, the optical decay obeyed a pseudo first-order rate law. A plot of the observed rate constant versus complex concentration was linear, and from the slope of the plot, the second-order rate constant was calculated to be $1.9 \pm 0.1 \times 10^{10} M^{-1} s^{-1}$. The products derived from this reaction exhibited optical absorption at shorter wavelengths as shown in Fig. 1. The studies of these products were carried out over a pH range of 4.1 to 11.4 on solutions containing 0.1–0.2 *M* isopropanol or 0.2 *M* *tert*-butyl alcohol. The concentration of $Pt(NH_3)_4^{2+}$ used was now in general higher (100–524 μ*M*) than that employed to study the disappearance of e_{aq}^- so as to minimize any possible interference by the electron reaction to subsequent events.

For these conditions, a prompt increase in absorption occurred following the irradiation pulse (Fig. 1 at 1 μs). Following this, there transpired a decrease in absorption at wavelengths below 350 nm and a concomitant increase at longer wavelengths. Addition of N_2O, used as a scavenger of e_{aq}^- (4), eliminated these changes except for small levels of residual absorption at shorter wavelengths, having the properties characteristic of the alcohol radicals that are formed by the reactions of OH and H with the alcohols (5, 20, 24). This observation confirms that the species observed in Fig. 1 are ones derived from the electron reaction. Furthermore, it implies that the alcohol radicals are unreactive towards $Pt(NH_3)_4^{2+}$, a feature that has also been noted for other Pt(II) complex ions (6–9). Below pH 7, the absorption changes obeyed a first-order rate law with a rate constant of $4.9 \pm 1.7 \times 10^4 s^{-1}$. This value was found to be independent of dose (10-fold), concentration of complex (5-fold), the nature and concentration of the alcohol although the values were somewhat higher (ca. 50%) in the region of 300–340 nm. On the same time scale as the optical change, there was a decrease in conductivity to $-190\,\Omega^{-1}\,cm^2\,equiv^{-1}$ as shown in Fig. 2*a*. This change exhibited first-order kinetics with a rate constant of $3.6 \pm 0.1 \times 10^4 s^{-1}$, which is within experimental error the same as that for the absorption change. At longer times (0.1 s scale), relatively minor alterations in absorption and conductivity took place. This situation may, however, be more apparent than real because both here and in the case of the H atom reaction with $Pt(NH_3)_4^{2+}$, suspensions of metallic platinum were observed after irradiation.

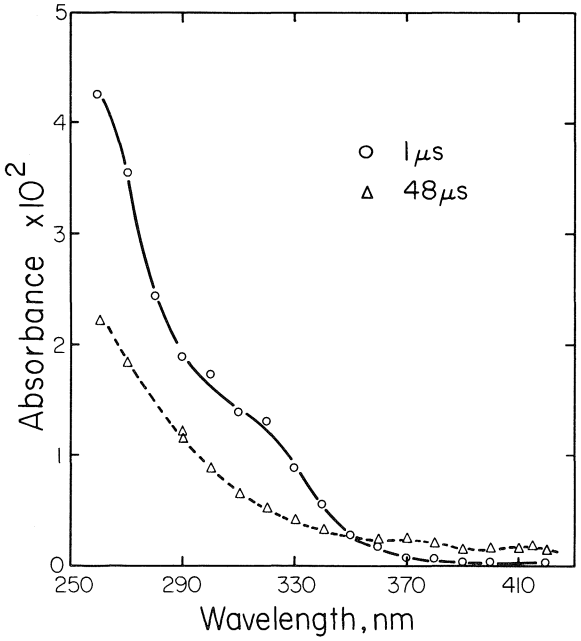

FIG. 1. Absorption spectra arising from reaction of e_{aq}^- and $Pt(NH_3)_4^{2+}$. (○) at 1 μs; (△) at 48 μs for 408 μ*M* $Pt(NH_3)_4^{2+}$, ca. 2.8 μ*M* e_{aq}^-, 2.0 *M* isopropanol at natural pH of ca. 5.6.

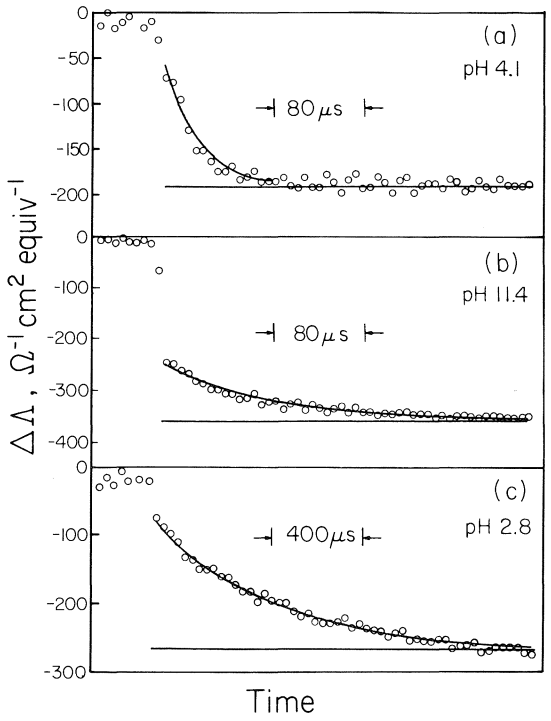

FIG. 2. Equivalent conductivity changes with time: (*a*) and (*b*), reaction of e_{aq}^- and $Pt(NH_3)_4^{2+}$: 495 μ*M* $Pt(NH_3)_4^{2+}$, 2.0 *M* isopropanol, pH 4.1 and 11.4 respectively; (*c*) reaction of H atom and $Pt(NH_3)_4^{2+}$: 96 μ*M* $Pt(NH_3)_4^{2+}$, 0.10 *M* *tert*-butyl alcohol, pH 2.8.

Can. J. Chem. Downloaded from www.nrcresearchpress.com by 210.87.254.40 on 09/06/12
For personal use only.

The foregoing absorption results show that the nascent product of the electron reaction, which is expected to be $Pt(NH_3)_4^+$ (2, 3), undergoes subsequent reactions. The observed decrease in conductivity at short time scales demonstrates that more than one ammonia ligand is released from $Pt(NH_3)_4^+$, even though only one kinetic step could be discerned. If only one NH_3 had been lost from this Pt(I) species, then the rapid reaction of the NH_3 with the proton formed via the irradiation process, reaction [1], would have resulted in essentially no net change in conductivity in contrast to the observed decrease. Support for the presence of free ammonia is also provided by its detection in substantial amounts as a final product. For product analysis, solutions containing 60–260 μM $Pt(NH_3)_4^{2+}$ and 0.1–2.0 M isopropanol at a pH of ca. 5.6 were pulse-irradiated (1–11 successive pulses) to an extent of about 15 to 75% reaction, based upon the amount of the electron reacted. For three separate measurements, the concentration ratio of free ammonia formed to that of the cumulative amount of e_{aq}^- was (3.7 ± 0.6)/1, and the corresponding ratio for loss in Pt(II) relative to that of the electron was (1.1 ± 0.1)/1.

In alkaline media (pH 11.4 and 2.0 M isopropanol), the absorption features were essentially the same as those at lower pH (Fig. 1). There was however an immediate decrease in conductivity to about $-240\,\Omega^{-1}\,cm^2\,equiv^{-1}$ at the end of the irradiation pulse, followed by a further decrease of $-110\,\Omega^{-1}\,cm^2\,equiv^{-1}$ (Fig. 2*b*). (No subsequent changes occurred at times up to 1 s.) For the latter process, both the absorption and conductivity signals obeyed first-order rate laws with a rate constant of 1.2 ± 0.3 × $10^4\,s^{-1}$, a value smaller by three-fold than that obtained at pH 4.1. At pH 11.4, free NH_3 will not undergo protonation as the pK_a of NH_4^+ is 9.24 (25), nor will there be extensive ionization of isopropanol radical with a pK_a of 12.2 (20). While it was not feasible to carry out investigations at higher pH, this secondary decrease in conductivity suggests that the platinum transient(s) has acidic properties. The prompt decrease of $-240\,\Omega^{-1}\,cm^2\,equiv^{-1}$ is accounted for by the rapid neutralization of the proton formed during the irradiation pulse, and by the reaction of e_{aq}^- with $Pt(NH_3)_4^{2+}$.

Reactions Associated with H Atom and $Pt(NH_3)_4^{2+}$

These investigations were carried out at pH's between 1.1 and 2.9 and at low enough levels of $Pt(NH_3)_4^{2+}$ to insure that the predominant electron reaction was with proton to give hydrogen atom (4).

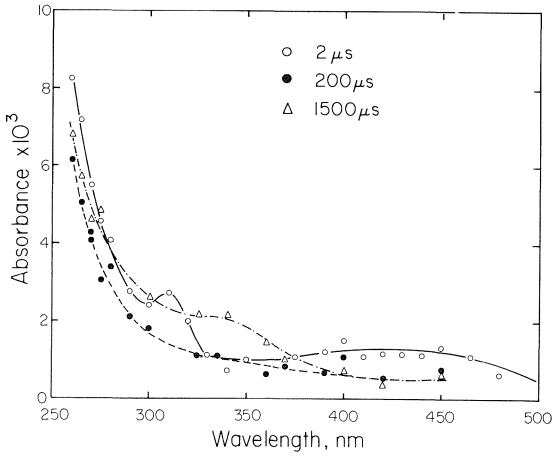

FIG. 3. Absorption spectra arising from the reaction of H atom and $Pt(NH_3)_4^{2+}$. (○) at 2 μs; (●) at 200 μs; (△) at 1500 μs for 112 μM $Pt(NH_3)_4^{2+}$, ca. 3.1 μM H atom, 0.21 M *tert*-butyl alcohol at pH 2.3.

Sufficient *tert*-butyl alcohol (0.1–0.2 M) was present to scavenge OH but not to react unduly with H atom (5, 24). The concentrations of the platinum complex ranged between 15 and 245 μM. The results described below were found to be independent of the concentration of alcohol, pH, and dose (5-fold). As shown in Fig. 3, irradiation led to the formation of absorption spectra in the region of 260 to 500 nm. Addition of 2.1 M isopropanol, a scavenger of H atom, eliminated the absorption in this region aside from minor amounts at short wavelengths, which are attributable in the main to the alcohol radicals (20). The rates of the initial growth in absorption were measured at 260–300, 420, and 425 nm. Under the condition where the complex concentration (15–100 μM) was considerably in excess of that for H atom, the growth in absorption followed a pseudo first-order rate law. The values of the associated rate constant increased linearly with the concentration of complex, and from this behavior, the second-order rate constant was determined to be 2.8 ± 0.3 × $10^{10}\,M^{-1}\,s^{-1}$ for the reaction of H and $Pt(NH_3)_4^{2+}$.

The initial absorption spectrum (Fig. 3 at 2 μs) is considerably different in its features (peaks at about 310 and 430 nm) and in its level of absorption (ca. 4-fold less on a normalized basis at 260 nm) from that of the electron case (Fig. 1). The differences between the two cases also extended to the kinetic aspects. For the hydrogen atom situation, two intervening absorption changes were observed (Fig. 3), with both obeying first-order rate laws: a general decrease in absorption at intermediate

Can. J. Chem. Downloaded from www.nrcresearchpress.com by 210.87.254.40 on 09/06/12
For personal use only.

times ($k = 2.2 \pm 0.6 \times 10^4\ s^{-1}$),[4] followed by a slower growth in absorption at wavelengths below 400 nm ($k = 1.9 \pm 0.6 \times 10^3\ s^{-1}$). In contrast to the two absorption changes, only one conductivity step was found as shown in Fig. 2*c* ($\Delta\Lambda_{final} = -260\ \Omega^{-1}\ cm^2\ equiv^{-1}$), and this process conformed to a first-order rate law with $k = 2.1 \pm 0.2 \times 10^3\ s^{-1}$. Of note is that the conductivity step correlates with the *second* absorption change (growth).

At longer times, there was a general decrease in the absorption spectrum, the kinetics of which were not describable by simple rate law expressions. The conductivity was now constant up to 0.1 s. As with the electron reaction, this situation may be complicated by the development of the observed platinum suspensions. Pulse-irradiation (6–11 successive pulses) of 200 μM $Pt(NH_3)_4^{2+}$ solutions to an extent of about 25 to 80% reaction of the complex also gave rise to free ammonia as a final product. The ratio of ammonia concentration to that of H atom formed was (1.6 ± 0.4)/1 (3 trials). Relatively small losses in Pt(II) concentration occurred, and the results of two trials suggest that the ratio of Pt(II) loss to that of H atom formed probably does not exceed 0.3/1.

Discussion

The foregoing kinetic results and product analyses indicate that the reactions of e_{aq}^- and H atom with $Pt(NH_3)_4^{2+}$ give rise to situations that are different from each other, both from the perspective of the short- and long-term processes involved. For the electron reaction, the nascent product is expected to be the platinum(I) species, $Pt(NH_3)_4^+$ (2–4). The events associated with its occurrence show that at fast time scales, this species undergoes ligand substitution. In particular, the conductivity results indicate the release of two ammonia ligands occurs sequentially

[3] $Pt(NH_3)_4^+ + H_2O \rightarrow Pt(NH_3)_3(H_2O)^+ + NH_3$

[4] $Pt(NH_3)_3(H_2O)^+ + H_2O \rightarrow Pt(NH_3)_2(H_2O)_2^+ + NH_3$

The first step, represented by reaction [3], is presumed to be fast based upon the following observations. At high concentrations of $Pt(NH_3)_4^{2+}$ where the rate of electron reaction with the complex is very rapid (half-life < 0.1 μs), only one kinetic step was discernible subsequent to the prompt development of absorption in the near-uv region (Fig. 1). In addition at pH 4.1, no net conductivity change was observed immediately after the irradiation pulse. This latter feature is consistent with the rapid release of one ammonia whose reaction with an amount of proton equivalent to that formed by irradiation (reaction [1]) forestalls a noticeable change in conductivity. (In the absence of such a neutralization process, a substantial increase in conductivity, due primarily to the radiolytically generated proton, would have been recorded.) Within this context, the initial absorption spectrum of Fig. 1 should be representative in the main of that for $Pt(NH_3)_3(H_2O)^+$. The substitution of an ammonia ligand in this species is associated with the observed changes in conductivity and absorption, having an average first-order rate constant of $4.2 \pm 1.7 \times 10^4\ s^{-1}$. Protonation of the released ammonia is anticipated to lead to an overall decrease in conductivity of about $-250\ \Omega^{-1}\ cm^2\ equiv^{-1}$, in reasonable agreement with that found, Fig. 2*a*.

This two-step sequence parallels that observed in the case of the reaction of e_{aq}^- and *cis*-$Pt(NH_3)_2(Cl)_2$ although in this instance the steps pertain to chloride substitution (11). The loss of the first chloride ligand was prompt, and was followed by release of a second chloride ion ($k = 4.9 \times 10^3\ s^{-1}$). In both studies, the resulting diamino Pt(I) species appear to be relatively stable within the time domain of pulse radiolysis. With reference to their compositions, we have portrayed them above as being four coordinate, on the basis that other d^9 metal complexes such as those of Ag(II) exhibit this (or a higher) coordination number (26, 27), and that our results found in basic media suggest the presence of coordinated water.

In this latter circumstance (pH 11.4), protonation of free NH_3 will be minimal (25). The level of the prompt decrease in conductivity ($-240\ \Omega^{-1}\ cm^2\ equiv^{-1}$) shown in Fig. 2*b* is near that expected ($-250\ \Omega^{-1}\ cm^2\ equiv^{-1}$) owing to the electron reaction and the neutralization of radiolytically produced proton, under the assumption that extensive ionization of $Pt(NH_3)_3(H_2O)^+$ did not occur. The subsequent absorption and conductivity changes, which proceeded at a somewhat slower rate (ca. 3-fold) than that in acidic media, suggest two additional facets, namely that reaction [3] may now reflect a rapid approach towards equilibrium and that $Pt(NH_3)_2(H_2O)_2^+$ undergoes ionization to yield a base form such as $Pt(NH_3)_2(H_2O)(OH)$. Rapid formation of this base form would give rise to the observed decrease in conductivity. The magnitude of this change ($-110\ \Omega^{-1}\ cm^2\ equiv^{-1}$) would imply a pK_a of the order of 11, which might reasonably be

[4]Between 290–310 nm, the rate constants were higher by a factor of three than that cited here for higher and lower wavelengths, and this may indicate the presence of an additional transient.

Can. J. Chem. Downloaded from www.nrcresearchpress.com by 210.87.254.40 on 09/06/12
For personal use only.

anticipated from the pK_a values (4–8) encountered for the analogous platinum(II) complexes of $Pt(NH_3)_2(H_2O)_2^{2+}$ (28).

Both the hydrated electron and hydrogen atom can function as strong, single-electron reducing agents although for the latter other modes are also possible (2–5). For their reactions with $Pt(Cl)_4^{2-}$, a common initial product was observed optically (6, 7) whereas with platinum(II) complexes containing organic amines, glycine or cyano ligand systems, the products arising from the electron and H atom reactions exhibited different optical and kinetic properties (7–10). Our conductivity and absorption results concerning the corresponding reactions of $Pt(NH_3)_4^{2+}$ place this system in the second category. If the reaction of H atom with this complex was to involve a charge transfer mechanism (in analogy to the electron reaction), then the proton so generated would cause in acidic media a prompt and large increase in conductivity, in contrast to our observation of essentially no net, initial change. While the absence of such a change might be masked in a kinetic sense by a rapid release and protonation of NH_3, in a process analogous to reaction [3], the observed product should be $Pt(NH_3)_3(H_2O)^+$. If so, then common spectral and kinetic features (as well as final products) should now prevail between the two situations. This expectation is not in accord with our findings.

A mechanism that encompasses the findings, in particular the occurrence of no initial conductivity change and the discernment of two subsequent absorption steps with the slower one coinciding with a process involving a conductivity decrease, is

[5] $H + Pt(NH_3)_4^{2+} \rightarrow H—Pt(NH_3)_4^{2+}$

[6] $H—Pt(NH_3)_4^{2+} \rightarrow [H—Pt(NH_3)_4]^{2+}$ (rearrangement)

[7] $[H—Pt(NH_3)_4]^{2+} + H_2O \rightarrow H—Pt(NH_3)_3(H_2O)^{2+} + NH_3$

The near diffusion-controlled rate constant associated with reaction [5] is compatible with this step being one of hydrogen atom addition to the metal center. (Such addition reactions are frequently faster than those pertaining to abstraction and charge transfer processes (5).) The resulting five coordinate product, $H—Pt(NH_3)_4^{2+}$, may undergo structural rearrangement such as a transformation from a square-pyramidal form to one of a trigonal-bipyramidal type. Such a process would be in keeping with the observed, first absorption change not being accompanied by an alteration in conductivity. The products of reactions [5] and [6] formally contain a hydrido ligand, a species well known for its *trans* activating capacity in ligand substitution reactions. Its presence in a complex of trigonal-bipyramidal form would be expected to promote labilization of the ammonia ligand in the *trans* position to it, and so give rise to reaction [7], followed by rapid protonation of the released ammonia (pH 2). The latter reaction would yield a conductivity decrease of about $-270\,\Omega^{-1}\,cm^2\,equiv^{-1}$, in good agreement with the experimental value of $-260\,\Omega^{-1}cm^2\,equiv^{-1}$.

For both the electron and hydrogen atom cases, the subsequent processes leading to the disappearance of the intermediates are less readily characterized, in large measure because only minor changes in absorption and conductivity occurred during the longer time periods (upwards of 1 s). Clearly changes did eventually occur as evidenced by the development of colloidal platinum metal (an indication of further reduction) and by the detection of amounts of free ammonia in excess of those that can be accounted for by the intervening processes of reactions [3], [4], and [7]. Pulse radiolysis results concerning the behavior of related platinum complexes have intimated that Pt(I) species decay by disproportionation to yield equal amounts of Pt(0) and Pt(II) (6–9, 11). Within this context, the expected ratio for loss in Pt(II) relative to each e_{aq}^- reacting to produce Pt(I) would be 0.5/1. Our observed ratio of 1.1 ± 0.1 for the electron reaction is substantially higher, and as such implicates for the case of $Pt(NH_3)_4^{2+}$ the occurrence of either processes in addition to disproportionation or a different mechanistic sequence. One possible sequence could involve the oxidation of water (or ammonia) and concomitant reduction of Pt(I) to metallic platinum (Pt(I) is isoelectronic with Ag(II), a strong oxidant (26)). This scheme would be representative of a noncomplementary redox situation. A likely consequence would be the occurrence of several reaction steps, the rates of which may be slow and thus not necessarily observable on our time scales. By way of contrast to the electron case, the overall loss in Pt(II) and formation of free ammonia associated with the hydrogen atom reaction were substantially less. These differences not only underscore the dissimilarity between the two situations but also suggest that decay of the hydrido species leads in part to regeneration of Pt(II), perhaps in association with the formation of molecular hydrogen.

Acknowledgements

One of us (H.M.K.) wishes to thank the University of Saskatchewan for a Graduate Scholarship. Assistance from the Natural Sciences and Engineering Research Council of Canada is also acknowledged.

1. A. HENGLEIN, W. SCHNABEL, and J. WENDENBERG. Einführung in die Strahlenchemie. Verlag Chemie GmbH, Weinheim/Bergstr, Germany. 1969. p. 140.
2. E. J. HART and M. ANBAR. The hydrated electron. Wiley-Interscience, New York. 1970. Chapt. 5.
3. G. V. BUXTON and R. M. SELLERS. Coord. Chem. Rev. **22**, 195 (1977).
4. (*a*) M. ANBAR, M. BAMBENEK, and A. B. ROSS. Natl. Stand. Ref. Data Ser. U.S. Natl. Bur. Stand. NSRDS-NBS43. 1973; (*b*) A. B. ROSS. Natl. Stand. Ref. Data Ser. U.S. Natl. Bur. Stand. NSRDS-NBS43, Supplement. 1975.
5. M. ANBAR, FARHATAZIZ, and A. B. ROSS. Natl. Stand. Ref. Data Ser. U.S. Natl. Bur. Stand. NSRDS-NBS51. 1975.
6. G. E. ADAMS, R. K. BROSZKIEWICZ, and B. D. MICHAEL. Trans. Faraday Soc. **64**, 1256 (1968).
7. A. S. GHOSH-MOZUMDAR and E. J. HART. Int. J. Radiat. Phys. Chem. **1**, 165 (1969).
8. D. K. STORER, W. L. WALTZ, J. C. BRODOVITCH, and R. L. EAGER. Int. J. Radiat. Phys. Chem. **7**, 693 (1975).
9. W. L. WALTZ, J. C. BRODOVITCH, and K. P. KUNDU. Radiat. Phys. Chem. **10**, 77 (1977).
10. M. C. R. SYMONS, M. M. ALY, and J. L. WYATT. J. Chem. Soc. Chem. Commun. 176 (1981).
11. R. C. RICHMOND and M. G. SIMIC. Br. J. Cancer, Suppl. III, **37**, 20 (1978).
12. E. B. DOUPLE and R. C. RICHMOND. *In* Cisplatin: current status and new developments. *Edited by* A. Prestakeys, S. T. Crooke, and S. K. Carter. Academic Press, New York. 1980. Chapt. 8.
13. W. R. MASON and R. C. JOHNSON. Inorg. Chem. **4**, 1258 (1965).
14. W. R. MASON and H. B. GRAY. J. Am. Chem. Soc. **90**, 5721 (1968).
15. H. M. KHAN, W. L. WALTZ, J. LILIE, and R. J. WOODS. Inorg. Chem. To be published.
16. W. L. WALTZ, J. LILIE, R. T. WALTERS, and R. J. WOODS. Inorg. Chem. **19**, 3284 (1980).
17. W. T. BOLLETER, C. J. BUSHMAN, and P. W. TIDWELL. Anal. Chem. **33**, 592 (1961).
18. J. HALPERN and M. PRIBANIĆ. J. Am. Chem. Soc. **90**, 5941 (1968).
19. A. V. LOGINOV, V. A. YAKOULEV, and G. A. SHAGISULTANOVA. Koord. Khim. **5**, 733 (1979).
20. M. SIMIC, P. NETA, and E. HAYON. J. Phys. Chem. **73**, 3794 (1969).
21. K. SEHESTED, H. CORFITZEN, and H. FRICKE. J. Phys. Chem. **74**, 211 (1970).
22. W. J. MOORE. Physical chemistry. 3rd ed. Prentice-Hall, Englewood Cliffs, NJ. 1962. p. 337.
23. R. C. JOHNSON, F. BASOLO, and R. G. PEARSON. J. Inorg. Nucl. Chem. **24**, 59 (1962).
24. L. M. DORFMAN and G. E. ADAMS. Natl. Stand. Ref. Data Ser. U.S. Natl. Bur. Stand. NSRDS-NBS46. 1973.
25. L. G. SILLÉN and A. E. MARTELL. Stability constants of metal–ion complexes, Special Publication 17. The Chemical Society, London. 1964.
26. F. A. COTTON and G. WILKINSON. Advanced inorganic chemistry. 4th ed. John Wiley and Sons, New York. 1980.
27. A. KUMAR and P. NETA. J. Phys. Chem. **83**, 3091 (1979).
28. F. BASOLO and R. G. PEARSON. Mechanisms of inorganic reactions. 2nd ed. J. Wiley and Sons, Inc., New York. 1967. pp. 32–33.

Can. J. Chem. Downloaded from www.nrcresearchpress.com by 210.87.254.40 on 09/06/12
For personal use only.

Single drop square wave polarography

LOUIS RAMALEY[1] AND WEE TEE TAN

Trace Analysis Research Centre, Department of Chemistry, Dalhousie University, Halifax, N.S., Canada B3H 4J3

Received March 12, 1981

LOUIS RAMALEY and WEE TEE TAN. Can. J. Chem. **59**, 3326 (1981).

The theory of square wave voltammetry for reversible electrode reactions is expanded to include average currents and currents flowing to a growing drop (single drop square wave polarography) using an expanding plane model. Excellent agreement between theory and experiment was found for the reduction of Fe(III), good agreement for the reduction of Cd(II). The expanding plane model proved superior, but not greatly superior to the simpler theory. For the case of average current the effect on the polarogram of the times at which integration is started and stopped is discussed. Integration decreases sensitivity but increases signal-to-noise ratio. The conditions for maximum analytical usefulness are presented.

LOUIS RAMALEY et WEE TEE TAN. Can. J. Chem. **59**, 3326 (1981).

En utilisant un modèle plan élargi, on a développé la théorie de la voltamétrie en signaux carrés pour des réactions reversibles d'électrode dans le but d'inclure les courants moyens et les courants circulants dans une goutte en formation (polarographie en signaux carrés d'une goutte unique). L'accord est excellent entre la théorie et l'expérience dans le cas de la réduction de Fe(III) et il est bon dans le cas de la réduction de Cd(II). Le modèle plan élargi se révèle supérieur, mais il ne surpasse pas la théorie la plus simple. On discute de l'effet, du temps de départ et d'arrêt de l'intégration, sur le polarogramme dans le cas du courant moyen. L'intégration diminue la sensibilité mais augmente le rapport signal/bruit. On propose des conditions qui confèrent à ce modèle une grande utilité du point de vue analytique.

[Traduit par le journal]

Introduction

Traditionally, pulse and square wave polarography have been techniques in which the current is sampled at only one potential on each mercury drop. Construction of the entire polarogram thus requires several hundred drops. Even with very short drop times, such analyses are quite lengthy. Superimposition of a square wave on a potential sweep and application of the result to a stationary electrode has been used to reduce analysis time considerably (1, 2). More recently (3–6), entire polarograms have been recorded on a single drop at the dropping mercury electrode (dme). The use of the dme reduces the effect of electrode surface contamination but requires faster sweep rates. Commercial instruments have been modified (7, 8) and circuits designed (9) to provide such fast sweep rates. A flow detector based on single drop square wave polarography (SDSWP) has been described (10) and an alternate drop technique which provides a flatter baseline in SDSWP has been proposed (11). Drake *et al.* (12) have indicated that cyclic square wave voltammetric methods might be very useful in the study of electrode processes as well as in chemical analysis.

At this time, it would be appropriate to examine more closely the theory of square wave polarography at an expanding mercury drop and compare the theory to experiment. Commercial instruments and many laboratory-constructed polarographs (4, 13) use gated integration to improve the experimental signal-to-noise ratio, yet no theoretical treatment has been presented for average currents. In addition, no treatment exists for currents at an expanding electrode. These problems are treated in this paper.

Theory

Ramaley and Krause (1) solved the diffusion equations using the Laplace transform and the superposition principle to provide equations for both the instantaneous and differential current in square wave voltammetry at a stationary, plane electrode. Christie *et al.* (5) expanded the treatment to include non-symmetrical pulse trains (differential pulse voltammetry). They applied their model to a dropping electrode by multiplying the current calculated for a plane, stationary electrode by a factor proportional to the change in area of the growing drop. Rifkin and Evans (14) showed that these treatments could be completely generalized for any type of pulse sequence and could be obtained by employing the Heaviside unit function rather than the superposition principle.

In the following, reference is made only to square wave polarography. The potential applied to the test electrode is the sum of a true square wave of amplitude ΔE and half period τ and a staircase ramp with a

[1]To whom all correspondence should be addressed.

0008-4042/81/243326-08$01.00/0

©1981 National Research Council of Canada/Conseil national de recherches du Canada

Can. J. Chem. Downloaded from www.nrcresearchpress.com by 210.87.254.105 on 09/06/12
For personal use only.

step amplitude of E_s and period 2τ. The resulting nomenclature is simpler and, in practice, there is little or no advantage to using unsymmetrical waveforms, especially in chemical analysis. The electrode reaction

[1] $O + n\,e \leftrightarrows R$

will be assumed to be reversible and diffusion will be considered semi-infinite. The initial concentration of R will be set to zero, the usual case in square wave polarography. The more generalized treatments (5, 14) can be used to include non-symmetrical waveforms or different initial conditions.

The average current flowing between times t_a and t_b is obtained from the law of the mean.

$$[2] \quad i_{av} = \frac{1}{t_b - t_a}\int_{t_b}^{t_a} i\,dt$$

Applying this law to eq. [3] of ref. 1 gives the average current flowing during the jth half-period of the applied square wave at a stationary, plane electrode.

$$[3] \quad (i_{av})_j = \frac{2nFAD_0{}^{1/2}C^*}{\pi^{1/2}(\beta_b - \beta_a)\tau^{1/2}}\sum_{k=1}^{j}[(j - k + \beta_b)^{1/2} - (j - k + \beta_a)^{1/2}](Q_{k-1} - Q_k)$$

with

$$[4] \quad Q_j = \frac{\exp[(E_j - E_{1/2})nF/RT]}{1 + \exp[(E_j - E_{1/2})nF/RT]}$$

and

$$[5] \quad E_{1/2} = E^0 + \frac{RT}{2nF}\ln(D_r/D_0)$$

In the above, A is the electrode area, D_0 and D_r the respective diffusion coefficients, C^* the bulk concentration of the oxidized species, E_j the applied potential during the jth half-period of the square wave, β_a the fraction of τ at which integration begins, and β_b the fraction of τ at which integration ends,

$$[6] \quad 0 \leq \beta_a < \beta_b \leq 1$$

The remaining terms have their usual meaning and Q_0 equals unity. By comparison (1), the instantaneous current is given by

$$[7] \quad i_j = \frac{nFAD_0{}^{1/2}C^*}{\pi^{1/2}\tau^{1/2}}\sum_{k=1}^{j}\frac{(Q_{k-1} - Q_k)}{(j - k + \beta)^{1/2}}$$

where β is the fraction of τ at which the current is measured,

$$[8] \quad 0 \leq \beta \leq 1$$

Equations [3] and [7] can be applied to dropping electrodes when the diffusion layer thickness is small compared to the radius of curvature so that planarity is a reasonable approximation, and when the electrode does not expand appreciably during the period of integration. The growth of the electrode can be taken into account by substituting for A the area of the mercury drop.

$$[9] \quad A = 4.836\,(mt/\rho)^{2/3}$$

where m is the mass flow rate and ρ the density of mercury. Assuming that the drop area remains constant during a single half-period of the square wave

$$[10] \quad A = 4.836\,(m/\rho)^{2/3}(t_d + j\tau)^{2/3}$$

where t_d is the time between the beginning of drop life and the start of the experiment. Thus [3] and [7] become respectively

$$[11] \quad (i_{av})_j = \frac{5.457nF(m/\rho)^{2/3}(t_d + j\tau)^{2/3}D_0{}^{1/2}C^*}{(\beta_b - \beta_a)\tau^{1/2}}\sum_{k=1}^{j}[(j - k + \beta_b)^{1/2} - (j - k + \beta_a)^{1/2}](Q_{k-1} - Q_k)$$

Can. J. Chem. Downloaded from www.nrcresearchpress.com by 210.87.254.105 on 09/06/12
For personal use only.

and

$$[12]\quad i_j = \frac{2.728nF(m/\rho)^{2/3}(t_d + j\tau)^{2/3}D_0{}^{1/2}C^*}{\tau^{1/2}} \sum_{k=1}^{j} \frac{(Q_{k-1} - Q_k)}{(j + k - \beta)^{1/2}}$$

A more accurate treatment of the cell current that flows at a dme can be provided by using the expanding plane model (15, 16) originally used in the derivation of the Ilkovic equation. In this model, the electrode is allowed to expand; however, the curvature of the electrode surface is ignored. In dc polarography this assumption results in inaccuracies very early in drop life when the radius of curvature of the dme is very small and for very long drop times when the thickness of the diffusion layer approaches the radius of curvature of the dme. In SDSWP the sweep is delayed well into drop life avoiding the first difficulty and the sweep is usually carried out in a very short time so that the diffusion layer never becomes very thick, avoiding the second difficulty even for very long drop times. The results of the use of this model, derived in the appendix, are

$$[13]\quad (i_{av})_j = \frac{3.572nF(m/\rho)^{2/3}D_0{}^{1/2}C^*}{(\beta_b - \beta_a)\tau} \sum_{k=1}^{j} \{([t_d + (j - 1 + \beta_b)\tau]^{7/3} - [t_d + (k - 1)\tau]^{7/3})^{1/2} - ([t_d + (j - 1 + \beta_a)\tau]^{7/3} - [t_d + (k - 1)\tau]^{7/3})^{1/2}\}(Q_{k-1} - Q_k)$$

and

$$[14]\quad i_j = 4.168nF(m/\rho)^{2/3}[t_d + (j - 1 + \beta)\tau]^{4/3}D_0{}^{1/2}C^* \times \sum_{k=1}^{j} \frac{(Q_{k-1} - Q_k)}{([t_d + (j - 1 + \beta)\tau]^{7/3} - [t_d + (k - 1)\tau]^{7/3})^{1/2}}$$

The above equations give the actual cell current whereas the differential cell current is usually what is desired, especially in chemical analysis. One method for calculating the differential current is as follows:

$$[15]\quad i_{dif} = i_{j-1} - i_j \qquad j = 2, 4, 6 \text{ etc.}$$

and by convention i_{dif} will be positive if the even half-periods are the more anodic.

Experimental

Apparatus

A block diagram of the instrument is shown in Fig. 1. It is a conventional operational amplifier potentiostat provided with digital control and interfaced to a dedicated minicomputer. The computer interface, staircase generator, control logic, and differential autoranging amplifier, A, are similar to modules described elsewhere (17–20). The output of A, which is proportional to cell current, is integrated by I to provide the average current for acquisition by the computer. The control logic divides each square wave half-period into eight equal segments (19). Integration can start at any of these segments and continue for as many segments as desired until the half-period ends. The staircase generator provides a wide variety of sweep rates and step sizes. In this study, sweep rates varied from 1.563 to 0.04883 V/s and step sizes of 2.00 and 4.00 mV were used. The computer system consisted of a Hewlett-Packard 2114B minicomputer with paper tape and magnetic tape peripherals and a point plotter. All control programs were written in assembly language.

Unthermostated borosilicate glass cells of 10 mL capacity were employed. A conventional saturated calomel electrode (sce) was connected to the cell through a side arm filled with supporting electrolyte. The dme consisted of a 10 second capillary sealed above a 6 mm soft glass tube which was drawn to a fine tip. Electrical contact was made below the capillary. This arrangement avoids the shielding and capillary resistance of the normal dme. No drop dislodging device was employed; the breaking of a light beam by the free-falling drop signalled the beginning of a new drop and was used to synchronize the start of a sweep. A variable delay between drop fall and sweep origin was provided, the usual delay time being 5.00 s. Measurements were carried out between 23 and 25°C.

Specific details of the instrument, the computer system, and the programming can be obtained from the authors by request.

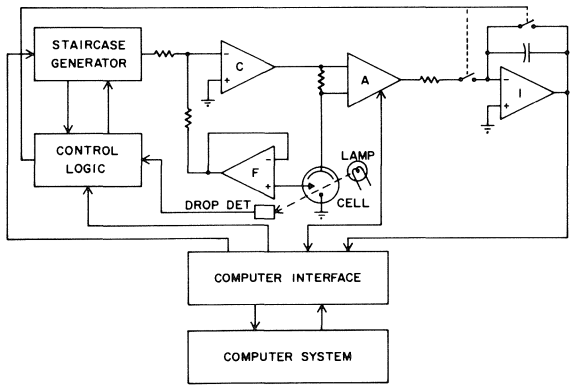

FIG. 1. Block diagram of the computer controlled potentiostat.

Can. J. Chem. Downloaded from www.nrcresearchpress.com by 210.87.254.105 on 09/06/12
For personal use only.

Can. J. Chem. Downloaded from www.nrcresearchpress.com by 210.87.254.105 on 09/06/12
For personal use only.

Reagents

All chemicals were reagent grade and were used without further purification except KCl, which was crystallized once from distilled water. Cadmium(II) in 1.00 *M* KCl medium was employed as an example of an amalgam forming species and Fe(III) in 0.500 *M* $K_2C_2O_4$ at pH 5.00 served as an example in which both halves of the redox couple are soluble in solution. Stock Fe(III) solutions were prepared by oxidation of the Fe(II) in $Fe(NH_4)_2(SO_4)_2 \cdot 6H_2O$ taken as a primary standard; stock Cd(II) solutions were prepared from $Cd(NO_3)_2 \cdot 4H_2O$ and were standardized by EDTA titration. Laboratory distilled water was run through activated charcoal and distilled once more from an all-glass still before use.

Results and Discussion

The general shape of square wave polarograms and the effects of C^*, ΔE and E_s, and n on those polarograms have already been well-covered (1, 2, 5, 6, 14, 21) for the case of instantaneous current measurements. No changes occur in these effects when integration is used to provide average current. Figure 2 shows the agreement between theory and experiment for the average differential current in the reduction of Fe(III). A diffusion coefficient of 6.31×10^{-6} cm^2 s^{-1} (22) for Fe(III) was used in the theoretical calculation. Simple theory, [11], and the expanding plane theory, [14], give results which are almost indistinguishable and which agree very well with experiment. Figure 3 demonstrates the agreement when the actual cell current is displayed. The upper curve is the current flowing on the more cathodic half-cycles; the lower is that flowing on the more anodic half-cycles. Agreement is still good, but differences are evident, especially on the cathodic tail of the wave. The expanding plane theory gives

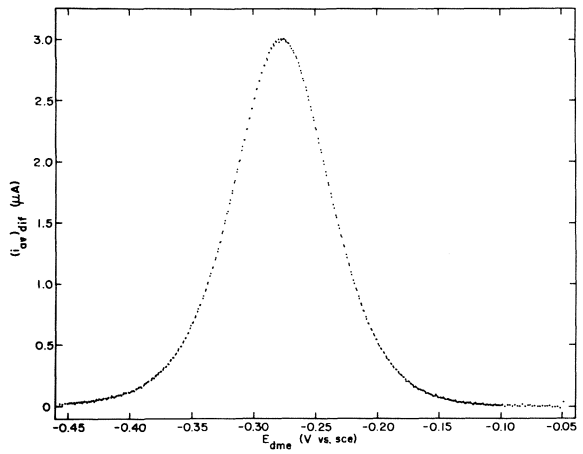

FIG. 2. Theoretical and experimental differential square wave polarograms of the reduction of 2.00×10^{-4} *M* Fe(III) in 0.50 *M* $K_2C_2O_4$ at a pH of 5.01; $\Delta E = 10$ mV, $E_s = 2$ mV, sweep rate = 0.0488 V s^{-1}, $\tau = 20.48$ ms, $\beta_a = 0.125$, $\beta_b = 0.250$, $m = 1.35$ mg s^{-1}, $t_d = 4$ s.

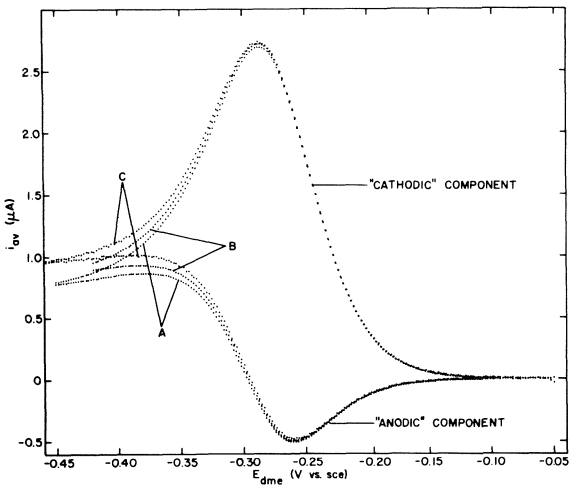

FIG. 3. Theoretical and experimental square wave polarograms. Conditions as in Fig. 2. *A* = corrected stationary electrode model, *B* = expanding plane model, *C* = experiment.

closer agreement as expected; however, the differences between the simple and more complex theories are not as great as might be expected. These differences decrease as τ decreases, again as expected since the drop better approximates a stationary electrode as sweep times become shorter. All calculations were carried out on the laboratory computer and required the use of extended precision arithmetic (48 bit) and a period about ten times as long for the calculation of the expanding plane data as compared to the data for the simple theory which could be satisfactorily computed with 32 bit arithmetic. Considering the increased complexity of calculations using the expanding plane theory, use of the simple theory is advisable except where very subtle differences are being investigated.

The data for Cd(II) reduction are similar to those for Fe(III) except that a diffusion coefficient of 9.8×10^{-6} cm^2 s^{-1} was required to provide an adequate fit between theory and experiment. The accepted experimental value is 7.91×10^{-6} cm^2 s^{-1} (5). A wider difference between theory and experiment is observed near the cathodic tail of the peak than in the case of Fe(III). The cause of this discrepancy was not uncovered by the data taken in this study. Further experimentation may provide an explanation of this effect.

Simple theory predicts that, since τ does not appear in the summations of [11] and [12], the peak differential current, i_p, should be proportional to $\tau^{-1/2}$ provided that β or β_a and β_b are constant and provided that t_d is adjusted so that $(t_d + j\tau)$ at the peak is constant. Although it is not obvious from

Can. J. Chem. Downloaded from www.nrcresearchpress.com by 210.87.254.105 on 09/06/12
For personal use only.

the forms of [13] and [14], the expanding plane theory produces the same result. In practice, instantaneous current measurements should be made or integration started as soon as the double layer charging current has decayed to a suitable level. Thus β or β_a will increase as τ decreases. In this case, theory predicts that a plot of i_p vs. $\tau^{-1/2}$ should deviate negatively from linearity. This was borne out by experiments using both Cd(II) and Fe(III). At the highest sweep rates used, 0.781 and 1.56 V s^{-1}, the experimental currents were slightly higher than those calculated from theory. No obvious explanation is proposed for this behaviour; instrument response may be the cause of the discrepancy between theory and experiment.

The effect of β on the square wave polarogram is more complicated when integration is considered. It was first pointed out by Ramaley and Krause (1) and later confirmed by Christie *et al.* (5) that for instantaneous current measurement greater sensitivity is achieved by making β as small as possible and lengthening τ rather than making τ as small as possible while setting β to unity. When integration is introduced, the effect of integration time must be considered. Defining sensitivity as the ratio of peak current to concentration, sensitivity decreases as integration time increases (β_b increases) holding β_a and τ constant. Furthermore, integration always produces a lower sensitivity than measurement of instantaneous current, provided β_a equals β. If integration time is held constant, increasing τ while beginning integration as soon as possible leads to increased sensitivity as in the case of instantaneous current measurement. However, the above statements do not take into account the effect of integration on noise reduction. In chemical analysis, signal-to-noise ratio (S/N) is the parameter of importance since it determines detection limits and the ability to make accurate estimates of quantity.

Although integration decreases sensitivity, it also decreases noise and thus may increase S/N. With our apparatus, this is exactly what is observed as demonstrated in Fig. 4 for solutions of 1.00×10^{-5} M Cd(II) where τ equals 2.56 ms, β_a equals 0.125 and integration times of 0.32, 0.96, 1.60, and 2.24 ms were used. The sensitivities decrease with increasing integration time from 0.216 to 0.114 AL mol^{-1}, but S/N increases from 104 to 288 for the data of Fig. 4. The noise was determined by calculating the standard deviations of two sets of fifty data points along the baseline on either side of the peak and averaging these two values. If integration is begun as soon as possible after decay of the charging current and continued until the end of the half-period, sensitivity falls as τ increases. As above, however, S/N increases. Allowing 0.64 ms between the beginning of a new

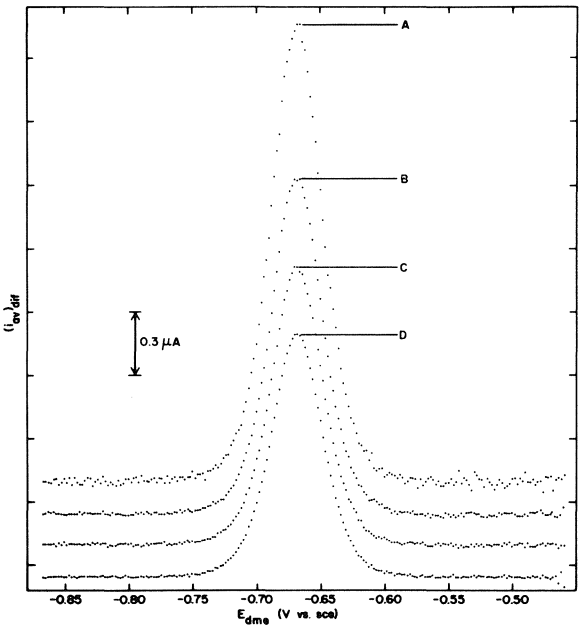

FIG. 4. Experimental differential square wave polarograms of the reduction of 1.00×10^{-5} M Cd(II) in 1.0 M KCl; ΔE = 10 mV, E_s = 2 mV, sweep rate = 0.391 V s^{-1}, τ = 2.56 ms, β_a = 0.125, m = 1.35 mg s^{-1}, t_d = 8 s. Integration period: A = 0.32 ms, B = 0.96 ms, C = 1.60 ms, D = 2.24 ms.

half-period and the start of integration, the sensitivity decreases from 0.0923 to 0.0594 AL mol^{-1} as τ increases from 1.28 to 5.12 ms, but S/N increases from 275 to 697. Although the actual value of S/N will depend on the instrument used, the above indicates that maximum S/N, and thus best detection limits, will be obtained by making β_a as small as possible, β_b equal unity, and τ as large as possible. An increase in τ alone results in a proportional decrease in sweep rate and can only be carried out until sweep time becomes an appreciable percentage of drop time. τ can be increased with no change in sweep rate by increasing E_s, which causes a decrease in resolution. Thus, a compromise must be established between maximum S/N, resolution, and drop time.

It has been proposed that square wave polarography be employed in investigations of electrode mechanisms (12). The similarity of the current–voltage profiles of ac and square wave polarography suggest a comparison. Square wave polarography is more sensitive and might find use in a few cases where concentrations could not be made high enough to use ac polarography. However, exact mathematical treatment is more difficult for the square wave case and much less has been done in this regard than for ac polarography. In addition to the differential current, the individual components

Can. J. Chem. Downloaded from www.nrcresearchpress.com by 210.87.254.105 on 09/06/12
For personal use only.

of the current, the "cathodic" and "anodic" components as shown in Fig. 3, are available in square wave polarography and could also be used in electrochemical investigations. Unfortunately, the distinctive features of these components, peak position and height, vary considerably as a function of β and integration time for a simple reversible reaction as shown in Figs. 5 and 6. In general, as β_a goes to zero and β_b approaches β_a, the peak potentials both approach $E_{1/2}$ and the peak heights become equal but opposite in sign. The "anodic" features are the most sensitive to various parameter changes. These features are also functions of ΔE and E_s and the peak heights depend directly on $\tau^{-1/2}$, but the positions are independent of τ. This complexity may make the application of square wave polarography less useful as a diagnostic tool in electrochemical investigations; the final answer must await the development of theory for cases other than a simple reversible reaction. An excellent beginning in this regard has recently been made by O'Dea *et al.* (23).

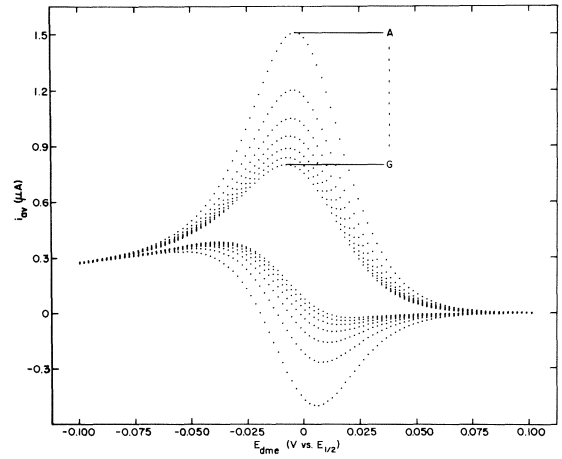

FIG. 5. Theoretical square wave polarograms; $n = 2$, $C^* = 1 \times 10^{-5}$ M, $D_0 = 1 \times 10^{-5}$ cm^2 s^{-1}, $m = 1.5$ mg s^{-1}, $t_d = 5$ s, $\Delta E = 10$ mV, $E_s = 2$ mV, sweep rate $= 0.5$ V s^{-1}, $\tau = 2$ ms, integration time $= 0.25$ ms. β_a increases from 0.125 to 0.875 in steps of 0.125 from A to G.

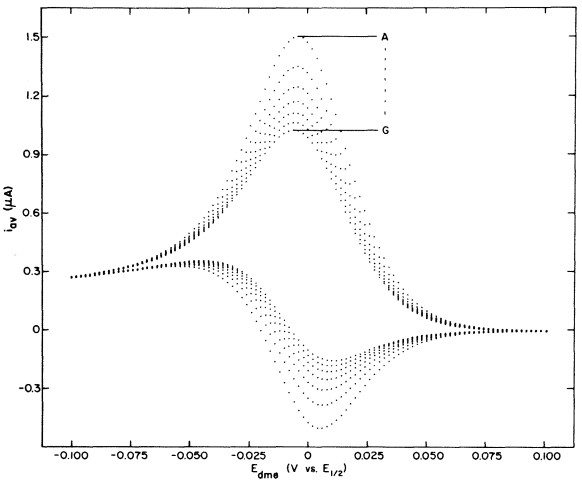

FIG. 6. Theoretical square wave polarograms; conditions as in Fig. 5 except $\beta_a = 0.125$. Integration time increases from 0.25 to 1.75 ms in 0.25 ms steps from A to G.

Acknowledgements

The authors thank the Faculty of Graduate Studies at Dalhousie University for financial support of this project. One of us (W.T.T.) wishes to thank the Universiti Pertanian Malaysia for granting study leave to pursue this research.

1. L. RAMALEY and M. S. KRAUSE, JR. Anal. Chem. **41**, 1362 (1969).
2. M. S. KRAUSE, JR. and L. RAMALEY. Anal. Chem. **41**, 1365 (1969).
3. L. RAMALEY and D. P. SURETTE. Paper #27, 58th Conference of the Chemical Institute of Canada, Toronto, May 1975.
4. L. RAMALEY and D. P. SURETTE. Paper #118, Centennial American Chemical Society Meeting, San Francisco, August 1976.
5. J. H. CHRISTIE, J. A. TURNER, and R. A. OSTERYOUNG. Anal. Chem. **49**, 1899 (1977).
6. J. A. TURNER, J. H. CHRISTIE, M. VUKOVIC, and R. A. OSTERYOUNG. Anal. Chem. **49**, 1904 (1977).
7. R. H. ABEL, J. H. CHRISTIE, L. L. JACKSON, and J. G. OSTERYOUNG. Chem. Instrum. **7**, 123 (1976).
8. L. L. JACKSON, CH. YARNITZKY, R. A. OSTERYOUNG, and J. OSTERYOUNG. Chem. Biomed. Environ. Instrum. **10**, 175 (1980).
9. B. D. YEAKEL, K. C. BURROWS, and M. C. HUGHES. Chem. Biomed. Environ. Instrum. **9**, 239 (1979).
10. J. WANG, E. OUZIEL, CH. YARNITZKY, and M. ARIEL. Anal. Chim. Acta, **102**, 99 (1978).
11. J. A. TURNER and R. A. OSTERYOUNG. Anal. Chem. **50**, 1496 (1978).
12. K. F. DRAKE, R. P. VAN DUYNE, and A. M. BOND. J. Electroanal. Chem. **89**, 231 (1978).
13. J. H. CHRISTIE, L. L. JACKSON, and R. A. OSTERYOUNG. Anal. Chem. **48**, 242 (1976).
14. S. C. RIFKIN and D. H. EVANS. Anal. Chem. **48**, 1616 (1976).
15. V. G. LEVICH. Physiochemical hydrodynamics. Prentice Hall, Inc., Englewood Cliffs, NJ. 1962. Chapt. X.
16. D. D. MACDONALD. Transient techniques in electrochemistry. Plenum Press, New York. 1977. Chapt. 3.
17. L. RAMALEY and G. S. WILSON. Anal. Chem. **42**, 606 (1970).
18. L. RAMALEY. Chem. Instrum. **2**, 415 (1970).
19. L. RAMALEY. Chem. Instrum. **6**, 119 (1975).
20. L. RAMALEY and D. P. SURETTE. Chem. Instrum. **8**, 181 (1978).
21. S. C. RIFKIN and D. H. EVANS. Anal. Chem. **48**, 2174 (1976).
22. M. L. OLMSTEAD and R. S. NICHOLSON. Anal. Chem. **38**, 150 (1966).
23. J. J. O'DEA, J. OSTERYOUNG, and R. A. OSTERYOUNG. Anal. Chem. **53**, 695 (1981).
24. R. V. CHURCHILL. Operational mathematics. 2nd ed. McGraw-Hill Book Co., Inc., New York. 1958. Chapt. 2.

Appendix

For electrode reaction [1] Fick's second law of diffusion for an expanding plane can be written (15, 16)

[16] $\partial C_0/\partial t = D_0(\partial^2 C_0/\partial x^2) + (2x/3t)(\partial C_0/\partial x)$

where x is the distance from the electrode surface into the solution. The initial and boundary conditions that prevail are as follows:

[17] $C_0 = C^*$, $C_r = 0$ for $0 \leq t \leq t_d$ and $0 \leq x \leq \infty$

[18] $C_0 \rightarrow C^*$, $C_r \rightarrow 0$ as $x \rightarrow \infty$ for $t > t_d$

[19] at $x = 0$, $C_0 = C_1$ for $t_d < t < t_1$

$C_0 = C_2$ for $t_1 < t < t_2$

. .

. .

. .

$C_0 = C_{j-1}$ for $t_{j-2} < t < t_{j-1}$

$C_0 = C_j$ for $t_{j-1} < t$

Conditions [17] and [19] can be written

at $x = 0$, $C_0 = I_0 C^*$ where $I_0 = 1$ for $0 \leq t < t_d$, zero otherwise

.

.

.

$C_0 = I_j C_j$ where $I_j = 1$ for $t > t_{j-1}$, zero otherwise

or

[20] at $x = 0$, $C_0 = \sum_{k=0}^{j} I_k C_k$ where $C_0 = C^*$

Using the substitutions

[21] $z = xt^{2/3}$

[22] $g = (3D_0/7)t^{7/3}$

Equations [16], [18], and [20] become respectively

[23] $\partial C_0/\partial g = \partial^2 C_0/\partial z^2$

[24] $C_0 \rightarrow C^*$ as $z \rightarrow \infty$ for $g > g_d$

[25] at $z = 0$, $C_0 = \sum_{k=0}^{j} I_k C_k$ where $I_0 = 1$ for $0 \leq g \leq g_d$ etc.

Solution is achieved by transforming [23] to [25] into Laplace space where [23] becomes a simple differential equation. The following transforms using the unit finite impulse function (24) or Heaviside unit function are useful in transforming [25] and back transforming the result.

[26] $F(t) = 1$ for $0 < t < k$ $\quad f(s) = \dfrac{1 - \exp(-ks)}{s}$

$= 0$ for $t > k$

[27] $F(t) = 1$ for $k_1 < t < k_2$ $\quad f(s) = \dfrac{\exp(-k_1 s) - \exp(-k_2 s)}{s}$

$= 0$ otherwise

Can. J. Chem. Downloaded from www.nrcresearchpress.com by 210.87.254.105 on 09/06/12
For personal use only.

[28] $F(t) = 1 \text{ for } t > k \qquad f(s) = \dfrac{\exp(-ks)}{s}$

$= 0 \text{ for } 0 \leq t < k$

where s is the Laplace variable and $f(s)$ is the Laplace transform of $F(t)$. The final solution in Laplace space is

[29] $$\bar{C}_0 = \frac{C^*}{s} + \exp(-s^{1/2}z)\left(\frac{C^* \exp(-g_0 s)}{s} + \frac{1}{s}\sum_{k=1}^{j-1} C_k[\exp(-g_{k-1}s) - \exp(-g_k s)] + \frac{C_j \exp(-g_{j-1}s)}{s}\right)$$

Upon reverse transformation and back substitution of [21] and [22] the result is

[30] $$C_0 = C_j + \sum_{k=1}^{j} (C_{k-1} - C_k) \operatorname{erf} \frac{(7/3)^{1/2} x t^{2/3}}{2D_0{}^{1/2}(t^{7/3} - t_{k-1}{}^{7/3})^{1/2}}$$

[31] $$i = nFAD_0(\partial C_0/\partial x)_{x=0}$$

Applying [31] to [30], substituting [9] for A and using [4] as follows

[32] $$C_k = C^* Q_k$$

which is valid for a reversible reaction, yields

[33] $$i_j = 4.168nF(m/\rho)^{2/3} t^{4/3} D_0{}^{1/2} C^* \sum_{k=1}^{j} \frac{(Q_{k-1} - Q_k)}{(t^{7/3} - t_{k-1}{}^{7/3})^{1/2}}$$

Average current is obtained by integrating [33] according to [2] which produces

[34] $$(i_{av})_j = \frac{3.572nF(m/\rho)^{2/3} D_0{}^{1/2} C^*}{t_b - t_a} \sum_{k=1}^{j} ([t_b{}^{7/3} - t_{k-1}{}^{7/3}]^{1/2} - [t_a{}^{7/3} - t_{k-1}{}^{7/3}]^{1/2})(Q_{k-1} - Q_k)$$

Equations [33] and [34] are completely general in that any potential or time sequence may be applied — symmetry with regard to potential changes or time periods is not required — and they may be used for linear or cyclic sweeps with symmetric or asymmetric pulse trains. When a symmetric pulse train is used (square wave polarography), the following equations apply:

[35] $t = t_d + (j - 1 + \beta)\tau$ for instantaneous current

[36] $t_a = t_d + (j - 1 + \beta_a)\tau$ for average current

[37] $t_b = t_d + (j - 1 + \beta_b)\tau$ for average current

[38] $t_{k-1} = t_d + (k - 1)\tau$ for all cases

When these equations are appropriately substituted into [33] and [34] eqs. [14] and [13] result.

The potential program applied to the electrode can be written in several ways. The program used in this work is given by

[39] $$E_j = E_i + \{(j - 1)/2\}E_s + (-1)^j \Delta E/2$$

where E_i is the potential applied when $0 < t < t_d$ and the term $\{(j - 1)/2\}$ represents the greatest integer not exceeding $(j - 1)/2$.

Can. J. Chem. Downloaded from www.nrcresearchpress.com by 210.87.254.105 on 09/06/12
For personal use only.

Adsorption enhancement in square wave polarography

LOUIS RAMALEY,[1] JOHN A. DALZIEL,[2] AND WEE TEE TAN
Trace Analysis Research Centre, Department of Chemistry, Dalhousie University, Halifax, N.S., Canada B3H 4J3

Received June 25, 1981

LOUIS RAMALEY, JOHN A. DALZIEL, and WEE TEE TAN. Can. J. Chem. **59**, 3334 (1981).

Reduction peaks in single drop square wave polarography (SDSWP) for metal ions such as Cd(II) and Pb(II) in the presence of picolinic acid gave peak currents that can be an order of magnitude or more greater than diffusion-limited peaks. Various studies using techniques such as controlled-potential electrolysis, tast polarography, staircase voltammetry, and SDSWP demonstrated that this enhancement effect was due to the adsorption of metal–picolinate complexes on the electrode surface. Since it provides a detection limit of about 0.2 ppb with ions such as Cd(II), adsorption enhancement appears to be of use in trace analysis under certain circumstances. Linearity is observed only up to 1×10^{-5} *M* and any substance capable of adsorption is a potential interferent.

LOUIS RAMALEY, JOHN A. DALZIEL et WEE TEE TAN. Can. J. Chem. **59**, 3334 (1981).

Les pics de réduction dans la polarographie à onde carrée sur goutte pendante (POCGP) d'ions métalliques tels le Cd(II) et le Pb(II) en présence de l'acide picolinique donnent des courants de pointe qui peuvent plus grands que les pics limites par la diffusion par un ordre de grandeur ou plus. Plusieurs études utilisant des techniques comme l'électrolyse à potentiel controlé, la polarographie échantillonnée, la voltamérie à impulsions surimposés d'amplitudes croissantes et la POCGP ont démontré que cet effet d'augmentation est due à l'adsorption des complexes picolinate-métal à la surface de l'électrode. Puisqu'elle fournit une limite de détection de 0,2 ppb avec des ions comme le Cd(II), l'augmentation de l'adsorption apparaît utile dans l'analyse des traces dans certaines circonstances. On observe une linéarité seulement jusqu'à 1×10^{-5} *M* et toute substance capable d'adsorber pourrait éventuellement interférer.

[Traduit par le journal]

Introduction

Complexing reagents are often used to selectively shift the reduction potentials of metal ions. In a study of this effect using single drop square wave polarography (SDSWP) it was observed that addition of common complexing reagents such as citric acid or ethylene diamine to solutions containing Cd(II) with chloride or sulfate salts as supporting electrolyte caused cathodic shifts in the peak reduction potential and no change or a decrease in the peak current. This is the expected behaviour. However, the addition of picolinic acid (pyridine-2-carboxylic acid) caused not only the predicted cathodic potential shift but also an increase in current by a factor of six to ten. One explanation for this behaviour could be the involvement of Cd(II) in a catalytic or kinetic reduction of picolinic acid. It has been reported that picolinic acid is reduced to the aldehyde under conditions similar to those used in this study (1, 2). However, no experimental evidence was found to support a kinetic or catalytic mechanism as the cause of the current enhancement.

Adsorption of electroactive species on the electrode also leads to increased faradaic currents in some electrochemical techniques. In dc polarography adsorption can cause shifts in wave position (3) but little or no enhancement in measured current. However, techniques that use rapid potential sweep rates such as cyclic voltammetry (4) or oscillopolarography (5), or techniques which employ pulse waveforms such as normal (6, 7) or differential pulse polarography (DPP) (8), produce both wave shifts and enhanced currents. In general, the faster the sweep rate or the shorter the measurement time after application of the pulse, the greater the enhancement. Qualitatively the enhancement is caused by the presence of excess electroactive species right at the electrode surface which can oxidize or reduce without a time consuming diffusion step.

Adsorption current enhancement has been observed in several chemical systems. The inorganic complexes formed by Cd(II) in iodide solution (8) or Pb(II) in bromide solution (6) produce this effect. In systems involving an organic ligand either the metal, as in the case of the nickel–dimethylglyoxime complex (9), or the ligand, for the Al(III) or Be(II) complexes of diazo compounds (10, 11), may be the electroactive species. Mixed systems involving metal ions with both inorganic and organic ligands have also been investigated (5). Uncomplexed species, usually uncharged organics, behave in the same manner (3, 4).

The experimental conditions employed in SDSWP should make it well suited for observation and analytical use of adsorption effects. Turner *et al.* (12) have observed enhancements using SDSWP

[1]To whom all correspondence should be addressed.
[2]Present address: Bedford Institute of Oceanography, Dartmouth, N.S., Canada B2Y 4A2.

0008-4042/81/243334-07$01.00/0
©1981 National Research Council of Canada/Conseil national de recherches du Canada

Can. J. Chem. Downloaded from www.nrcresearchpress.com by 210.87.254.40 on 09/06/12
For personal use only.

Can. J. Chem. Downloaded from www.nrcresearchpress.com by 210.87.254.40 on 09/06/12
For personal use only.

while working with Cd(II) in iodide medium. Similar techniques such as classical square wave polarography (6) and DPP (8, 9, 13) also provide large, potentially analytically useful current enhancements.

Exact theoretical treatment of adsorption requires the inclusion of an adsorption isotherm (which may not correspond to reality) and some form of potential dependence of adsorption coefficient in the mathematics. Wopschall and Shain have presented a treatment for certain types of adsorption in linear and cyclic voltammetry (4). Laviron has derived equations for the cyclic voltammetry of both reversible and irreversible electrochemical reactions involving adsorption of reactant and product at a dropping mercury electrode (dme) (3). Barker and Bolzan present results for normal pulse polarography and an approximate expression for classical square wave polarography which predicts an increase of four in sensitivity caused by adsorption (6). Anson and co-workers have both solved the boundary value problem mathematically and applied digital simulation in investigating adsorption in normal pulse polarography (7), DPP (8, 13), and the behaviour of reagents confined to the electrode surface (14), a situation similar to strong adsorption of product and reactant. Usually in these treatments one or, at most, several different adsorption isotherms were assumed and the adsorption coefficient was considered independent of potential.

Even though to the authors' knowledge no specific theoretical treatment has been published for adsorption behaviour in SDSWP, certain predictions can be made from the treatments of other, similar techniques. Adsorption requires inclusion of an extra capacitance term (pseudocapacitance) in the faradaic impedance. It might thus seem unusual that a technique such as SDSWP, which is relatively insensitive to capacitive effects, should produce large adsorption enhancements. This phenomenon was first explained by Barker and Bolzan (6) in their treatment of adsorption in normal pulse polarography. For a reversible electrode process in which only the oxidized (or reduced) species is adsorbed, the oxidant can be reduced as rapidly as charge can be supplied to the electrode since oxidant need not diffuse to the surface. However, reductant must diffuse away from the surface. Since the ratio of concentrations at the surface is fixed by the Nernst equation, the rate at which oxidant can be reduced is limited by the rate at which reductant diffuses from the surface, allowing the observation of an enhanced current in SDSWP. In the case where oxidized and reduced species are both about equally strongly adsorbed, the behaviour should be capacitive (14) and the type of enhancement described above should not be observed.

In SDSWP the dme is held at a constant potential, E_i, for a period of time, t_d, before applying a potential scan consisting of a staircase waveform superimposed on a square wave. If reactant is adsorbed at E_i, the surface concentration of reactant, Γ_0 (assuming the reactant to be the oxidized species), is given by the Koryta equation (15).

$$[1] \quad \Gamma_0 = 0.739 D_0^{1/2} C^* t^{1/2}$$

where C^* is the bulk concentration of oxidant, D_0 its diffusion coefficient, and t the time from the beginning of drop life. Equation [1] applies under conditions where all reactant molecules or ions arriving at the surface are adsorbed (strong adsorption); thus the bulk concentration must be below that at which the surface saturates at the time in question. Under these conditions reactant continuously diffuses to the electrode from the beginning of drop life. The solution concentration of reactant near the electrode is very low, while the surface concentration continues to increase, the drop acting as a preconcentration site. When the sweep is applied and reduction occurs, virtually all current is supplied by adsorbed oxidant with little contribution from diffusion. Increasing the bulk concentration increases the contribution of adsorption while that of diffusion remains small until surface saturation is approached. At this point concentration of reactant near the surface is no longer negligible and diffusion begins to contribute to the reduction current. For any further increase in bulk concentration the contribution of adsorption remains fixed while that of diffusion now increases until the reaction appears to be totally controlled by diffusion.

The fractional surface coverage is given by

$$[2] \quad \theta = A_m N \Gamma_0$$

in which A_m is the area occupied by a molecule of adsorbate and N is Avogadro's number. On substitution of [1] this becomes

$$[3] \quad \theta = 0.739 A_m N D_0^{1/2} C^* t^{1/2}$$

which applies under the same conditions as [1]. Substituting typical values for A_m (100 Å^2), D_0 (1×10^{-5} cm^2 s^{-1}) and t (5 s) and setting θ equal to unity produces a value for C^* of 3.2×10^{-5} M, the bulk concentration at which surface saturation occurs. Since the boundary at which diffusion begins to

Can. J. Chem. Downloaded from www.nrcresearchpress.com by 210.87.254.40 on 09/06/12
For personal use only.

play a part will be diffuse rather than sharp, especially if the adsorption is not particularly strong, one would expect diffusion effects to begin to be observed at concentrations somewhat less than 3×10^{-5} *M*.

For a reversible, diffusion controlled SDSWP experiment (16) with all parameters except electrode area held constant

$$[4] \quad i_p = K_1 A_p = K_2 t_p^{2/3}$$

and with all parameters except square wave half-period, τ, held constant

$$[5] \quad i_p = K_3 \tau^{-1/2} = K_4 \nu^{1/2}$$

In these expressions i_p is the peak differential current, ν is the sweep rate, and A_p and t_p are the electrode area and time during drop life at which i_p is measured. The "*K*'s" are proportionality constants.

For a system in which the reactant is adsorbed and provides the major contribution to reduction current, assuming that peak current is proportional both to electrode area and to surface concentration,

$$[6] \quad i_p = K_5 A_p \Gamma_0 = K_6 (t_p^{2/3})(t_p^{1/2}) = K_6 t_p^{7/6}$$

As in the case of other electrochemical techniques involving adsorption (4), one would expect that peak current would approach a first power dependence on sweep rate as opposed to the half power dependence observed for diffusion control.

Experimental

Apparatus

The computer-controlled potentiostat and cell system used have been previously described (16). All potentials were measured versus the saturated calomel reference electrode and experiments were carried out between 23 and 25°C. Delay times, t_d, were normally 5 s, mercury flow rate was 1.5 mg s^{-1}, staircase step height was 2 mV, and square wave amplitude was 10 mV.

Reagents

All chemicals were reagent grade and were used without further purification except KCl, which was crystallized once from distilled water. Stock Cd(II) and Pb(II) solutions were prepared from $Cd(NO_3)_2 \cdot 4H_2O$ and $Pb(NO_3)_2$. Picolinic acid (J. T. Baker or Aldrich Chem. Co.) was purified by crystallization and by sublimation. There was little difference in behaviour between purified and unpurified picolinic acid and the majority of experiments were performed with the unpurified acid. Laboratory distilled water was passed through activated charcoal and distilled once more from an all-glass still before use.

Results and Discussion

Initial studies were carried out using controlled potential electrolysis with a conventional laboratory-built potentiostat in conjunction with spectral methods of analysis to determine what species were being reduced under the conditions that produced a current enhancement in SDSWP. Electrolyses were performed on 0.0010 *M* Cd(II) solutions in 1.0 *M* KCl electrolyte in the absence and in the presence of 0.010 *M* picolinic acid. The mercury pool potential was set at −0.90 V, a value well negative to the reduction peak in both cases. The charge passed in both cases was identical and was equivalent to two faradays per mole of Cd(II). Ultraviolet spectra were obtained on the solutions which contained picolinic acid before and after electrolysis at wavelengths where the acid and picolinaldehyde could be readily identified. Electrolysis produced no change in the spectra and no evidence was obtained for the presence of any picolinaldehyde after electrolysis. Finally the electrolyzed solutions were subjected to atomic absorption analysis for Cd(II). The results indicated that over 97% of the Cd(II) had been removed by electrolysis. It was therefore concluded that Cd(II) was the only species undergoing reduction.

A qualitative experiment involving Triton X100, a strong surfactant, was performed to determine what effect adsorption was having on the observed current enhancement. No enhancement was observed for tast polarograms of 1.0×10^{-5} *M* Cd(II) with 0.010 *M* picolinic acid. Addition of up to 0.0025% Triton X100 produced no changes in the tast polarography of Cd(II) with or without added picolinic acid or in the SDSWP of Cd(II) solutions without picolinic acid. However, for the SDSWP of 1.0×10^{-5} *M* Cd(II) with 0.010 *M* picolinic acid, addition of 0.0005% surfactant caused the sixfold current enhancement to decrease by 20%, and addition of 0.001% surfactant caused a 50% decrease. Since adsorption does not cause current enhancement in dc polarography, these observations are consistent with a mechanism in which adsorption is responsible for the enhancement in SDSWP.

The effect of pH on enhancement was studied in 1.0 *M* KCl electrolyte. No enhancement occurred at pH values less than about 3.0. Enhancement increased rapidly to a pH of 5.0 and continued a more gradual increase up to pH 9.0. All experiments described below were carried out between pH 5 and 6 using picolinic acid itself to buffer the solutions, since its pK_a is 5.23 (17). Table 1 presents the effect of supporting electrolyte on the enhancement. Of the electrolytes studied, KCl gave the smallest enhancement and the smallest peak current (in the presence of picolinic acid) while NaF provided the largest of both. Ammonium sulfate produced an almost equal enhancement and the second largest peak current. For this

TABLE 1. Effect of supporting electrolyte on enhancement of peak current for 1.0×10^{-5} *M* Cd(II) in 1.0×10^{-2} *M* picolinic acid (PA) at pH of 6.0

	i_p (μA)		E_p (V)		
Electrolyte	No PA	PA	No PA	PA	Enhancement
1.0 *M* KCl	1.77	8.86	−0.641	−0.747	5.0
1.0 *M* KNO_3	1.62	10.44	−0.588	−0.739	6.4
0.50 *M* $(NH_4)_2SO_4$	1.40	12.60	−0.606	−0.740	9.0
1.0 *M* $(NH_4)ClO_4$	1.17	11.00	−0.590	−0.731	9.4
0.50 *M* NaF	1.64	15.60	−0.602	−0.754	9.5

reason, and because it is a more benign material than NaF, it was used in a majority of the enhancement studies. Potassium chloride was also used in some studies because Cd(II) showed the most ideal behaviour in this medium in the absence of picolinic acid.

Figure 1 depicts the effect of varying the concentration of Cd(II) on peak current at constant picolinic acid concentration. Linearity is observed below 1.0×10^{-5} *M*, while the expected change from adsorption to diffusion control is noted above this concentration. Figure 2 demonstrates the behaviour when picolinic acid concentration varies and that of Cd(II) is held constant. Maximum enhancement occurs at a picolinic acid concentration of 5×10^{-3} *M*.

The variation in drop time during a set of tast polarograms run at various concentrations of picolinic acid is shown in Fig. 3. As the acid concentration is raised, drop time, and thus surface tension, is decreased at more positive potentials. However, at potentials on the diffusion plateau, all drop times are the same, indicating that the surfactant causing the lowering of surface tension has been removed.

If all experimental parameters are held constant except delay time, a plot of ln (i_p) vs. ln (t_p) should have a slope of 0.67 for diffusion control and 1.17

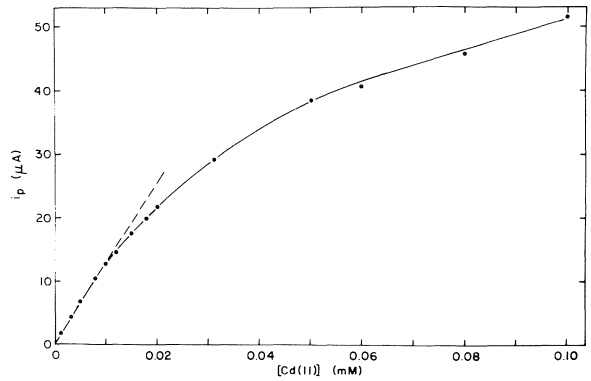

FIG. 1. Variation of peak current in SDSWP with Cd(II) concentration; 1.0×10^{-2} *M* PA, 0.50 *M* $(NH_4)_2SO_4$, pH 6.0, sweep rate 0.781 V s^{-1}.

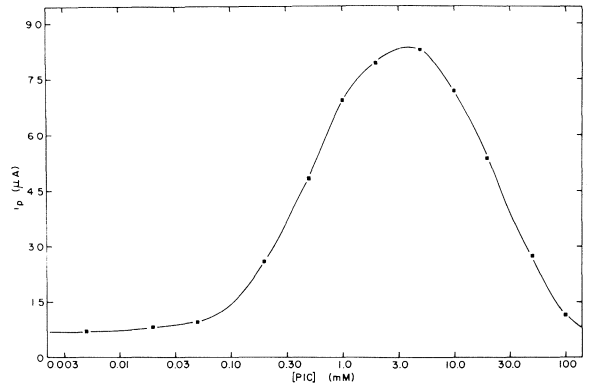

FIG. 2. Variation of peak current in SDSWP with picolinic acid concentration; 1.0×10^{-5} *M* Cd(II), 0.50 *M* $(NH_4)_2SO_4$, pH 6.0, sweep rate 0.781 V s^{-1}.

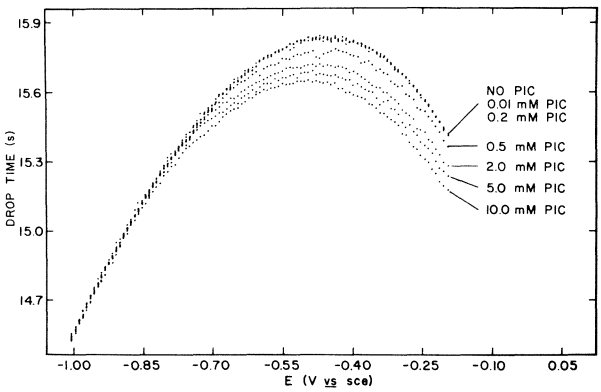

FIG. 3. Variation of drop time with potential in tast polarography at various picolinic acid concentrations; 1.0×10^{-5} *M* Cd(II), 0.50 *M* $(NH_4)_2SO_4$.

for adsorption control (from [4] and [6] above). Diffusion conditions produced a good straight line of slope 0.74, while adsorption conditions resulted in a line with slight negative curvature and a least-squares slope of 1.01. The slope for diffusion control is greater than expected, possibly because at larger delay times the drop is less spherical and the shielded area is a smaller fraction of the total area, both effects causing the electrode area to increase more rapidly than expected. The slope for

Can. J. Chem. Downloaded from www.nrcresearchpress.com by 210.87.254.40 on 09/06/12
For personal use only.

Can. J. Chem. Downloaded from www.nrcresearchpress.com by 210.87.254.40 on 09/06/12
For personal use only.

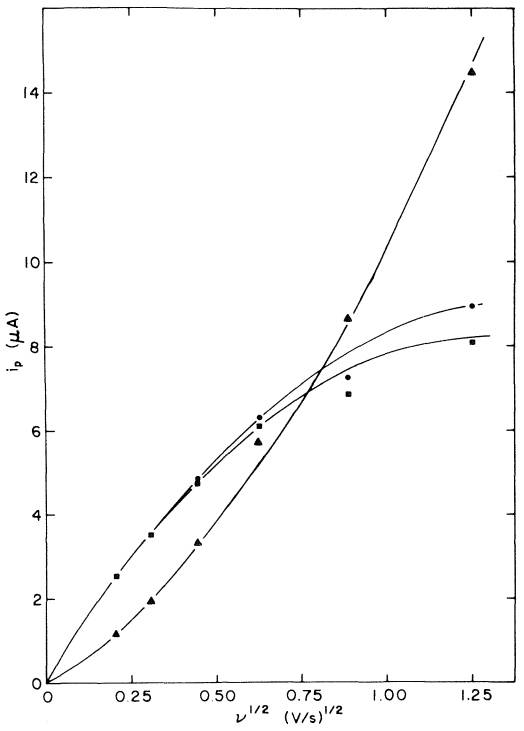

FIG. 4. Dependence of peak current in SDSWP with sweep rate; 0.50 M $(NH_4)_2SO_4$; ●, theory for 1.0×10^{-4} M Cd(II); ■, experimental data for 1.0×10^{-4} M Cd(II); ▲, 1.0×10^{-5} M Cd(II) with 0.010 M PA.

adsorption control is considerably larger than that for diffusion, as expected, but is less than that predicted from [6]. This may be due to the adsorption not being strong enough for the Koryta equation to be rigorously applied.

The effect of variation in sweep rate is demonstrated in Fig. 4. Diffusion control should produce a linear plot, provided that all experimental parameters are held constant, including peak time, t_p, and the portions of the square wave half-period over which the current is integrated. Unfortunately, our instrument cannot hold these two parameters constant over a wide range in sweep rate, the result being a non-linear graph. Theoretical calculations agree well with the experimental data for diffusion control except that they are consistently high at higher sweep rates. For adsorption control, peak current is related to sweep rate by a power greater than one-half, as expected, but somewhat less than the predicted value of one.

All of the above data point to specific adsorption of a complex of Cd(II) with picolinic acid (PA) as the cause of enhanced currents in SDSWP. The most likely complex would be the neutral $Cd(PA)_2$ complex in which the ligands assume a square planar configuration around the metal ion. Loss of a ligand (perhaps water) from one of the two remaining coordination sites would allow both aromatic rings to lie flat against the electrode surface when adsorbed. Some evidence for this can be inferred from Fig. 2. Calculations using the appropriate stability constants (17, 18) predict that $[Cd(PA)_2]$ will be maximum in 0.50 M $(NH_4)_2SO_4$ at a ligand concentration of 0.004 M; Fig. 2 indicates a maximum at 0.005 M. That the adsorption is not particularly strong is indicated by the less than first power dependence of i_p on ν and the less than 7/6 power dependence of i_p on t_p. The data in Table 1 indicate that the effect depends on double layer structure and the ability of the supporting electrolyte to compete with picolinic acid as a ligand. As the electrolyte anion competes less and/or specifically adsorbs less, the magnitude of the enhancement effect increases. This also indicates that the adsorption of complex is not particularly strong.

Further evidence for adsorption is provided by cyclic staircase voltammetry as shown in Fig. 5. In the absence of picolinic acid, the voltammogram is normal. When ligand is added, the cathodic peak is greatly enhanced, is more symmetrical and closer in potential to the anodic peak which still has the shape of a diffusion peak. For comparison the individual current components in SDSWP are shown in Fig. 6. Without picolinic acid the curve is normal and agrees with theory. In the presence of the acid the anodic or reverse component remains truly anodic for almost the entire peak, indicating a large amount of metal which can be reoxidized into solution on the anodic or reverse half-cycle. Without added ligand the currents stay cathodic well

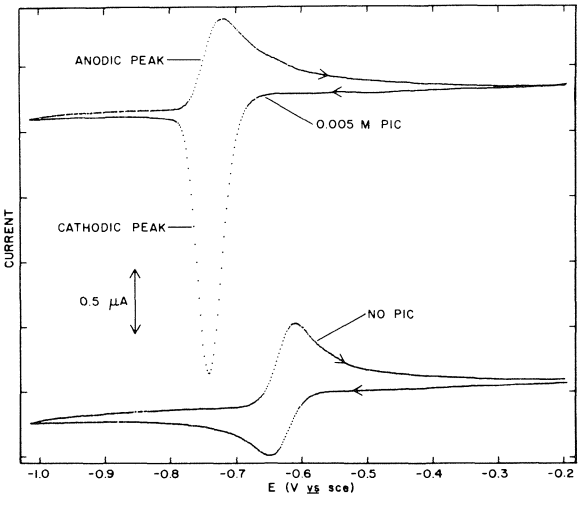

FIG. 5. Staircase cyclic voltammograms of 1.0×10^{-5} M Cd(II) in 0.50 M $(NH_4)_2SO_4$; sweep rate, 0.781 V s^{-1}.

Can. J. Chem. Downloaded from www.nrcresearchpress.com by 210.87.254.40 on 09/06/12
For personal use only.

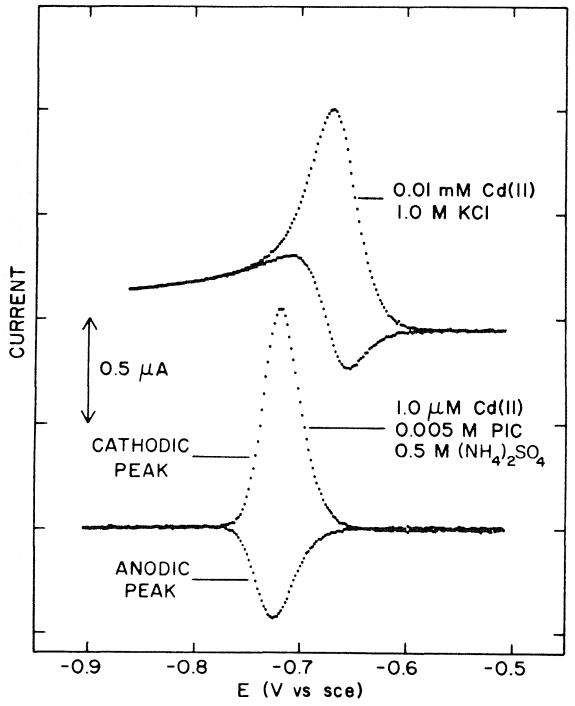

FIG. 6. Individual current components in SDSWP of Cd(II).

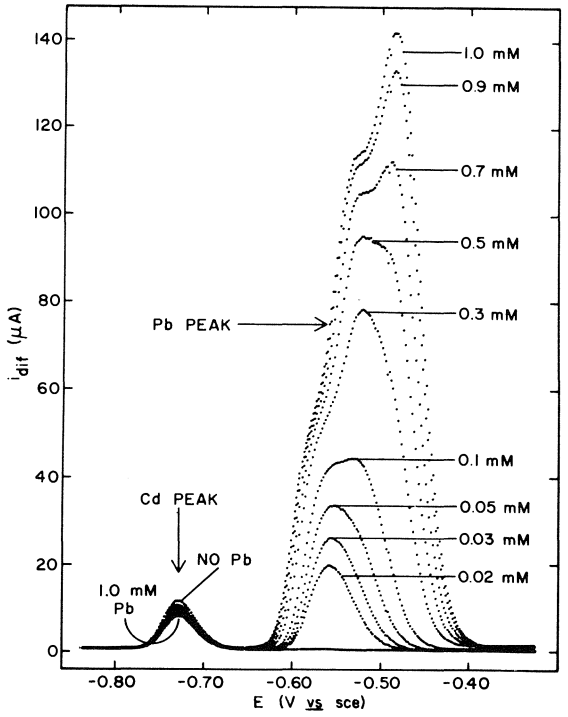

FIG. 7. SDSWP of 1.0×10^{-5} *M* Cd(II) with added Pb(II) in 1.0 *M* KNO_3 and 0.010 *M* PA; sweep rate 0.781 V s^{-1}.

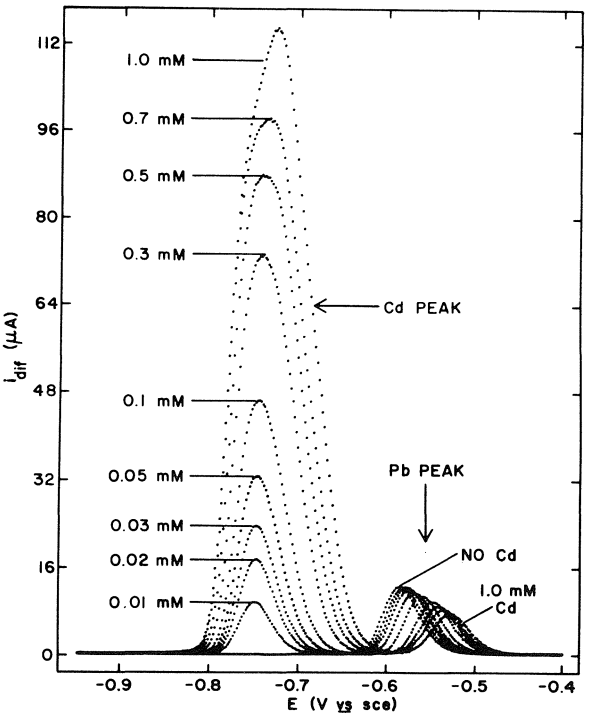

FIG. 8. SDSWP of 1.0×10^{-5} *M* Pb(II) with added Cd(II) in 1.0 *M* KNO_3 and 0.010 *M* PA; sweep rate 0.781 V s^{-1}.

after the peak due to continued diffusion of metal ion to the electrode; with ligand the currents return almost to zero after the peak since the diffusion layer is much thicker, having existed since the beginning of drop life rather than since the beginning of the peak. This effect may also be partially responsible for the reverse component of current staying anodic for the entire peak. Interestingly, the peak for the anodic component is more cathodic than that for the cathodic component.

During the course of this study it became obvious that metal ions other than Cd(II) exhibit an enhancement with picolinic acid, Pb(II) being a good example. A high concentration of one adsorbable ion should interfere with the enhancement of a second such ion. This interference is demonstrated in Figs. 7 and 8, in which [Cd(II)] is held constant while [Pb(II)] is varied and vice versa. In the absence of picolinic acid no interference between ions is observed. With picolinic acid addition of one ion suppresses the peak for the other, and in the case of the addition of Cd(II) to a solution containing fixed Pb(II), the potential of the Pb(II) peak also shifts to more anodic values. This occurs because Cd(II) competes with Pb(II) for the ligand and for the electrode surface sites, both effects tending to cause a shift in peak potential. The reason that a similar shift is not observed in the case where Pb(II) is added to a Cd(II) solution is explained by noting

Can. J. Chem. Downloaded from www.nrcresearchpress.com by 210.87.254.40 on 09/06/12
For personal use only.

that since Cd(II) is reduced after Pb(II), when Cd(II) undergoes reduction there is no Pb(II) remaining on or near the electrode surface to compete for ligand or surface sites. Depression of peak current is still observed because the surface concentration of Cd(II) is lowered by Pb(II) which is present during drop growth up to a fraction of a second before Cd(II) reduction. This effect cannot be explained by differences in the formation constants of lead and cadmium picolinates since they are almost identical (17).

The magnitude of the enhancement raises the question of its usefulness as an aid to trace metal analysis. SDSWP is a very sensitive method in its own right and can be made a factor of ten more sensitive using the adsorpion enhancement effect of picolinic acid. Figure 9 demonstrates the sensitivity attainable. All supporting electrolytes used contained enough Pb(II) and Cd(II) impurities to be easily detectable. Standard additions of sufficient Cd(II) stock solution to cause changes in solution concentration of 2.0×10^{-9} *M* produced the curves shown in Fig. 9. From these data the detection limit for Cd(II) was determined to be 2×10^{-9} *M* or 0.2 ppb (signal twice the standard deviation of the background noise) and the concentration of Cd(II) in the supporting electrolyte was found to be 9×10^{-9} *M*. With such high sensitivity, the technique has obvious merit. However, caution should be exercised since linearity is observed only up to 1×10^{-5} *M* and the presence of any other substance capable of adsorption will interfere. Such substances include other adsorbable metal ions or neutral organics at concentrations above 1×10^{-5} *M*. Thus the ability to increase sensitivity through addition of picolinic acid or other such reagents will be highly matrix dependent. On the other hand adsorption of electroactive species may be more common in some practical samples than suspected and can lead to errors in quantitation when using trace techniques such as DPP or SDSWP if not recognized. In addition to any analytical applications, the use of reagents like picolinic acid coupled with pulse techniques such as SDSWP may provide a simple and sensitive method to obtain electrochemical information on adsorption as indicated by the data of Table 1 and Figs. 7 and 8.

Studies are continuing to determine which other metal ions exhibit adsorption enhancement with picolinic acid and similar ligands.

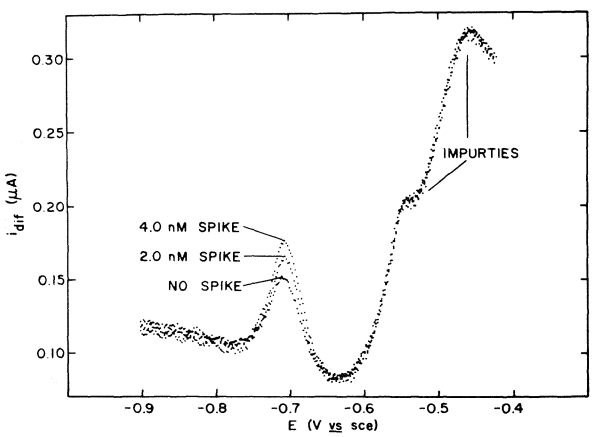

FIG. 9. SDSWP of Cd(II) in 0.50 *M* $(NH_4)_2SO_4$ and 0.0050 *M* PA; t_d 8 s; square wave amplitude 50 mV; sweep rate 0.195 V s^{-1}, 20 runs averaged.

Acknowledgements

The authors thank the Natural Science and Engineering Research Council of Canada and the Faculty of Graduate Studies at Dalhousie University for financial support of this project. One of us (W.T.T.) wishes to thank the Universiti Pertanian Malaysia for granting study leave to pursue this research.

1. E. KNOBLOCK. Collect. Czech. Chem. Commun. **22**, 1777 (1957).
2. O. R. BROWN, J. A. HARRISON, and K. S. SASTRY. J. Electroanal. Chem. **58**, 387 (1975).
3. E. LAVIRON. J. Electroanal. Chem. **52**, 355 (1974).
4. R. H. WOPSCHALL and I. SHAIN. Anal. Chem. **39**, 1514 (1967).
5. R. KALVODA, W. ANSTINE, and M. HEYROVSKY. Anal. Chim. Acta, **50**, 93 (1970).
6. G. C. BARKER and J. A. BOLZAN. Z. Anal. Chem. **216**, 215 (1966).
7. J. B. FLANAGAN, K. TAKAHASHI, and F. C. ANSON. J. Electroanal. Chem. **85**, 257 (1977).
8. F. C. ANSON, J. B. FLANAGAN, K. TAKAHASHI, and A. WAMADA. J. Electroanal. Chem. **67**, 253 (1976).
9. C. J. FLORA and E. NIEBOER. Anal. Chem. **52**, 1013 (1980).
10. T. M. FLORENCE. J. Electroanal. Chem. **52**, 115 (1974).
11. A. G. FOGG, J. L. KUMAR, and D. T. BURNS. Analyst, **94**, 262 (1969).
12. J. A. TURNER, J. H. CHRISTIE, M. VUKOVIC, and R. A. OSTERYOUNG. Anal. Chem. **49**, 1904 (1977).
13. J. B. FLANAGAN, K. TAKAHASHI, and F. C. ANSON. J. Electroanal. Chem. **81**, 261 (1977).
14. A. P. BROWN and F. C. ANSON. Anal. Chem. **49**, 1589 (1977).
15. J. KORYTA. Collect. Czech. Chem. Commun. **18**, 206 (1953).
16. L. RAMALEY and W. T. TAN. Can. J. Chem. **59**, 3326 (1981).
17. A. E. MARTEL and R. M. SMITH. Critical stability constants. Vol. 1. Plenum Press, New York. 1974.
18. A. E. MARTEL and R. M. SMITH. Critical stability constants. Vol. 4. Plenum Press, New York. 1976.

Détermination d'un champ de force de valence pour le chloro-3 triazole-1,2,4[4H] et ses dérivés deutériés (a)

MALIKA SAIDI-IDRISSI[1] ET CHANTAL GARRIGOU-LAGRANGE[2]
Centre de Recherche Paul Pascal, Domaine Universitaire, 33405 Talence Cedex, France
ET
CLAUDE POUCHAN
I.U.R.S. Chimie Structurale, Avenue Philippon, 64000 Pau, France
Reçu le 15 juin, 1981

MALIKA SAIDI-IDRISSI, CHANTAL GARRIGOU-LAGRANGE et CLAUDE POUCHAN. Can. J. Chem. **59**, 3341 (1981).
Un champ de force de valence du chloro-3 triazole-1,2,4[4H] a été calculé à partir des spectres de vibration de la molécule et de ses dérivés deutériés. Les attributions précédentes sont discutées.

MALIKA SAIDI-IDRISSI, CHANTAL GARRIGOU-LAGRANGE and CLAUDE POUCHAN. Can. J. Chem. **59**, 3341 (1981).
The vibrational frequencies of chloro-3 triazole-1,2,4[4H] and its deuterated derivatives have been used to calculate a valence force field. Previous assignments are discussed.

Can. J. Chem. Downloaded from www.nrcresearchpress.com by 210.87.254.105 on 09/06/12
For personal use only.

Introduction

A la suite de nos travaux sur les spectres de vibration du triazole-1,2,4 et de quelques uns de ses dérivés (1–5), nous nous sommes proposés de définir un champ de force susceptible de rendre compte des données expérimentales relatives à la molécule de chlorotriazole[3] et de ses trois dérivés deutériés.

Mel'nikov *et al.* avaient déjà effectué un tel calcul en utilisant une géométrie ClTA[1H] (6) analogue à celle du triazole-1,2,4 (7).

Les récentes études cristallographiques entreprises sur cette molécule ont montré que la structure du ClTA correspond à une configuration [4H] (2), aussi le champ de force proposé par Mel'nikov est-il contestable. L'objet de notre travail consistera donc, à partir des nouvelles attributions des spectres infrarouges et de la structure du cristal précédemment publiées, de proposer une fonction potentielle pour le ClTA et ses trois homologues deutériés.

Conditions de calcul

Pour le calcul des modes normaux de vibration de la molécule de ClTA et de ses homologues deutériés sélectivement sur l'azote ClTA[D]-4, sur le carbone ClTA[D]-5 dideutérié sur l'azote et le carbone ClTA[D]$_2$-4,5, nous avons utilisé la méthode de Wilson *et al.* (8) dans l'hypothèse d'un champ de force de valence. Le programme employé est celui écrit par Schachtschneider (9) modifié par Forel.[4]

La géométrie introduite est celle déterminée par rayons X et la molécule est supposée isolée dans le réseau cristallin. Cette approximation fait implicitement entrer dans le champ de force des paramètres liés à la force des interactions intermoléculaires et en particulier aux liaisons hydrogènes.

Nous avons décrit la matrice **F** de l'énergie potentielle dans la même approximation que la matrice **G** de l'énergie cinétique, c'est à dire en posant nulles les constantes de force d'interaction entre vibrateurs sans atome commun.

Choix des coordonnées

La notation des coordonnées internes est indiquée sur la figure 1.

L'analyse vibrationnelle ayant été faite dans l'approximation des vibrations de groupe, nous avons choisi pour les vibrations de déformation autour des atomes C_3, N_4 et C_5 les coordonnées suivantes:

$$\theta_i = \frac{1}{\sqrt{6}}(2\alpha_i - \phi_i - \phi_i') = \text{déformation des angles } i \text{ du cycle}$$

$$\beta_i = \frac{1}{\sqrt{2}}(\phi_i - \phi_i') = \text{déformation } \delta\text{NH, } \delta\text{CH ou } \delta\text{CCl}$$

$$\rho_i = \frac{1}{\sqrt{3}}(\alpha_i + \phi_i + \phi_i') = 0 \text{ coordonnée redondante}$$

[1]Adresse permanente: Laboratoire de spectroscopie infrarouge, Dept de chimie, Faculté des Sciences, Rabat, Maroc.
[2]Auteur à qui doit être envoyée la correspondance.
[3]Dans ce travail, le chlorotriazole-1,2,4 sera noté ClTA.
[4]M. T. Forel, travaux non publiés.

0008-4042/81/243341-05$01.00/0
©1981 National Research Council of Canada/Conseil national de recherches du Canada

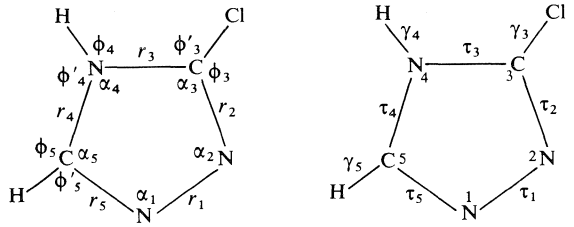

FIG. 1. Coordonnées internes du ClTA.

Les torsions τ ont été définies en considérant pour chaque lien valenciel tous les angles dièdres mis en jeu.

Champ de force

La fonction potentielle initiale a été définie à partir des constantes de force proposées pour le triazole-1,2,4 (10). Pour le vibrateur C—Cl, nous avons transféré les paramètres publiés pour le chloro-2 thiazole (11). L'amélioration du champ de force ainsi initialisé s'est révélée difficile; en effet, comme l'avait suggérée l'analyse des spectres, les modes normaux mettent presque tous en jeu plusieurs vibrations de groupe.

La comparaison des spectres calculés avec les spectres expérimentaux ainsi que l'examen des termes de la matrice **G**, nous ont amenés à introduire des constantes de force d'interaction supplémentaires, puis à modifier les valeurs de ces constantes de force à partir d'un processus itératif stoppé lorsque nous avons jugé satisfaisant l'accord obtenu pour les quatre composés.

TABLEAU 1. Champ de force de valence du ClTA* comparé à celui du triazole-1,2,4 (TA)

Constantes de forces†	TA (10)	ClTA (PT)
Mouvements dans le plan (A′)		
$F(\nu NH)$	3,88	4,20
$F(\nu CH)$	5,25	5,30
$F(\nu CCl)$	—	4,10
$F(r_2)$	7,2	7,0
$F(r_1) = F(r_3)$	6,5	6,75
$F(r_4)$	7,2	6,75
$F(r_5)$	6,5	7,0
$F(\theta_1) = F(\theta_2) = F(\theta_4) = F(\theta_5)$	1,90	1,90
$F(\theta_2) = F(\theta_4) = F(\theta_5)$	1,90	1,90
$F(\theta_3)$	1,90	2,00
$F(\delta NH)$	0,42	0,52
$F(\delta CH)$	0,38 et 0,285	0,48
$F(\delta CCl)$	—	0.96
$f(r_1, r_2) = f(r_2, r_3) = f(r_3, r_4) = f(r_4, r_5)$	0,30	0,20
$f(r_5, r_1)$	0,30	0,15
$f(\theta_1, \theta_2) = f(\theta_5, \theta_1)$	0,50	0,10
$f(\theta_2, \theta_3) = f(\theta_3, \theta_4) = f(\theta_4, \theta_5)$	0,50	0,30
$f\lvert(r_1,\theta_3),(r_1,\theta_5)\rvert = f\lvert(r_2,\theta_4),(r_2,\theta_1)\rvert = f\lvert(r_5,\theta_2),(r_5,\theta_4)\rvert$	—	−0,80
$f\lvert(r_3, \theta_2), (r_3, \theta_5)\rvert = f\lvert(r_4, \theta_1), (r_4, \theta_3)\rvert$	—	−0,70
$f\lvert(r_2, \delta NH), (r_5, \delta NH)\rvert$	−0,14	0,06
$f\lvert(r_3, \delta NH), (r_4, \delta NH)\rvert$	0,14	0,15
$f\lvert(r_1, \delta CH), (r_3, \delta CH)\rvert$	−0,14	−0,10
$f\lvert(r_4, \delta CH), (r_5, \delta CH)\rvert$	0,14	0,14
$f(\theta_3, \nu CCl)$	—	−0,52
$f(\delta NH, \delta CCl)$	—	0,10
$f\lvert(r_2, \delta CCl), (r_3, \delta CCl)\rvert$	—	0,10
Mouvements hors du plan (A″)		
$F(\gamma NH)$	0,435	0,35
$F(\gamma CH)$	0,275 et 0,33	0.29
$F(\gamma CCl)$	—	0,45
$F(\tau_1)$	0,34	0,34
$F(\tau_2) = F(\tau_4)$	0,68	0,40
$F(\tau_3)$	0,51	0,40
$F(\tau_5)$	0,34	0,44
$f\lvert(\tau_3, \gamma NH), (\tau_4, \gamma NH)\rvert$	−0,10	−0,10
$f\lvert(\tau_4, \gamma CH), (\tau_5, \gamma CH)\rvert$	−0,14	−0,08
$f\lvert(\tau_1, \gamma CH), (\tau_3, \gamma CH)\rvert$	—	0,04
$f\lvert(\gamma NH, \gamma CH)\rvert$	—	0,02
$f\lvert(\tau_2, \gamma CCl), (\tau_3, \gamma CCl)\rvert$	—	−0,07

*Unités: Elongations des liaisons et interactions liaison–liaison: m dyne Å $^{-1}$; déformations des angles, torsions et interactions angle-angle: m dyne Å rad^{-2}; interactions angle–liaison: m dyne rad^{-1}.
†Les notations utilisées sont celles du ClTA.

Can. J. Chem. Downloaded from www.nrcresearchpress.com by 210.87.254.105 on 09/06/12
For personal use only.

TABLEAU 2. Nombres d'onde observés et calculés pour la molécule de ClTA et attributions

ν_{exp} (cm^{-1})	ν_{calc} (cm^{-1})	DEP 100 $L_{ik}^2 F_{ii}/\lambda_k$*	Attribution
3 130	3 129	99ν(CH)	νCH
2 800	2 770	98ν(NH)	νNH
1 535	1 540	27ν(r_2), 20ν(r_4), 18δ(NH)	R_1
1 480	1 529	21ν(r_3), 18ν(r_5), 10(θ_3), 20δ(CH), 28δ(NH)	R_2
1 390	1 392	30ν(r_2), 26ν(r_3), 29ν(r_4), 17ν(r_5), 19δ(NH)	R_3
1 290	1 309	52ν(r_1), 23ν(r_5)	R_4
1 260	1 268	20ν(CCl), 18ν(r_2), 20ν(r_3), 18ν(r_5), 25(θ_3), 15δ(NH)	R_5 ou δCH
1 185	1 173	36ν(r_4), 16ν(r_5), 16(θ_5), 12δ(NH)	δNH
1 085	1 115	26ν(r_1), 51δ(CH)	δCH ou R_5
1 000	1 028	23(θ_3), 43(θ_4), 36(θ_5)	R_6
975	973	38(θ_1), 37(θ_2), 13(θ_3)	R_7
895	904	76γ(NH), 33(τ_3), 11(τ_4)	γNH
870	846	20γ(NH), 77γ(CH), 51(τ_4), 18(τ_5)	γCH ou R_8
710	707	36γ(CCl), 21(τ_4), 27(τ_5)	R_8 ou γCH
635	601	25γ(CCl), 11(τ_4), 21(τ_5)	R_9
505	488	64ν(CCl), 14(θ_3)	νCCl
345	354	90δ(CCl)	δCCl
290	248	42(τ_2), 36γ(CCl), 28(τ_3)	γCCl

*Seules sont indiquées les DEP supérieures à 10.

Présentation et discussion des résultats

Le champ de force final que nous avons obtenu pour le ClTA comparé à celui du triazole-1,2,4 (10) est donné dans le tableau 1. Seize constantes de force principales et dix huit constantes d'interaction ont été nécessaires pour rendre compte des 69 fréquences expérimentales.

Nous avons reporté dans les tableaux 2 à 5 les fréquences calculées et observées, les distributions d'énergie potentielle (DEP) par rapport aux constantes de force principales ainsi que les attributions que nous avons proposées pour les quatre molécules de ClTA.

Analyse du champ de force

Le champ de force final est constitué de 23 constantes de force qui ont permis de rendre compte de 52 fréquences A′ et de 11 relatives aux 17 modes A″ observés.

Ces constantes de force restent relativement proches de celles du triazole-1,2,4 (tableau 1). Rappelons cependant que le calcul se rapporte pour le triazole à la forme [1H] (10) et pour le ClTA à la forme [4H]. En outre, la substitution de l'atome d'hydrogène en position 3 par un atome de chlore est de nature à modifier la structure électronique du cycle. Nous avons donc été amenés à introduire, en plus des constantes de force de valence et de déformation de la liaison C—Cl, de nouvelles constantes d'interaction et à différencier certaines constantes de forces principales relatives au squelette triazolique.

C'est ainsi que nous avons donné une valeur plus élevée pour $F(\theta_3)$ que pour les autres $F(\theta_i)$. Cette modification se justifie, en particulier, par la présence du chlore en position 3 du cycle. En plus, nous avons fait intervenir des constantes de force d'interaction entre liaison du cycle triazolique et angle de déformation du cycle avec un atome commun; les constantes de force ont une valeur assez élevée et sont négatives.

Nous avons dû également tenir compte d'une interaction entre les modes γCH et γNH que l'on peut rapprocher de celle qui existe entre γNH et rCH_2 dans le δ valérolactame (12) ainsi que d'une interaction entre les modes γCH et τ avec un atome commun.

Les valeurs des constantes de force F(νCCl), F(δCCl) et F(γCCl) sont comparables à celles reportées dans le cas du chloro-2 thiazole (11). Les constantes d'interaction $f|(r_2, \delta CCl), (r_3, \delta CCl)|$ et $f|(\tau_2, \gamma CCl), (\tau_3, \gamma CCl)|$ ont été introduites par analogie avec celles mettant en jeu les vibrations de déformation dans et hors du plan des groupements NH et CH.

En outre, il a été nécessaire de faire intervenir des interactions entre νCCl et θ_3 et entre δNH et δCCl. L'introduction de cette dernière constante de force se justifie par le voisinage sur le cycle des deux vibrateurs NH et CCl et par la masse relativement importante du chlore qui peut entraîner le NH dans son déplacement.

Attribution et répartition d'énergie potentielle

Les distributions d'énergie potentielle reportées sur les tableaux 2 à 5 confirment en la nuançant l'interprétation que nous avons proposée précédemment.

Comme nous l'avons signalé, les fréquences situées entre 1550 et 1050 cm^{-1} correspondent à des

Can. J. Chem. Downloaded from www.nrcresearchpress.com by 210.87.254.105 on 09/06/12
For personal use only.

TABLEAU 3. Nombres d'onde observés et calculés pour la molécule de ClTA(D)-4 et attributions

ν_{exp} (cm^{-1})	ν_{calc} (cm^{-1})	DEP 100 $L_{ik}^2 F_{ii}/\lambda_k$	Attribution
3 130	3 129	99ν(CH)	νCH
2 200	2 067	91ν(ND)	νND
1 520	1 516	10ν(r_2), 20ν(r_3), 14ν(r_4), 27δ(CH)	R_1
1 480	1 477	10ν(CCl), 41ν(r_2), 19ν(r_5), 14(θ_3), 10δ(ND)	R_2
1 390	1 367	12ν(r_2), 48ν(r_3), 44ν(r_4), 10δ(ND)	R_3
1 285	1 301	57ν(r_1), 17ν(r_2), 34ν(r_5)	R_4
1 220	1 219	20ν(CCl), 15ν(r_4), 16ν(r_5), 10(θ_3), 15δ(CH)	R_5 ou δCH
1 075	1 123	31ν(r_1), 16ν(r_5), 41δ(CH)	δCH ou R_5
1 030	945	10ν(r_4), 57δ(ND)	δND
995	1 002	16(θ_1), 10(θ_3), 34(θ_4), 45(θ_5)	R_6
960	976	24(θ_1), 27(θ_2), 24(θ_3), 11δ(ND)	R_7
886	857	79γ(CH), 21(τ_4), 21(τ_5)	γCH ou R_8
710	731	34γ(CCl), 48γ(ND), 17(τ_4), 12(τ_1)	R_8 ou γCH
632	673	54γ(ND), 16(τ_3), 21(τ_5), 18(τ_1)	γND
—	575	26γ(CCl), 11(τ_3), 28(τ_4), 13(τ_5)	R_9
502	486	63ν(CCl), 14(θ_3)	νCCl
337	342	89δ(CCl)	δCCl
280	246	36γ(CCl), 42(τ_2), 30(τ_3)	γCCl

TABLEAU 4. Nombres d'onde observés et calculés pour la molécule de ClTA(D)-5 et attributions

ν_{exp} (cm^{-1})	ν_{calc} (cm^{-1})	DEP 100 $L_{ik}^2 F_{ii}/\lambda_k$	Attribution
2 800	2 770	98ν(NH)	νNH
2 350	2 337	94ν(CD)	νCD
1 510	1 527	31ν(r_2), 12ν(r_4), 37δ(NH)	R_1
1 460	1 492	38ν(r_3), 18ν(r_5), 10δ(CD), 12δ(NH)	R_2
1 360	1 390	27ν(r_2), 19ν(r_3), 32ν(r_4), 22ν(r_5), 18δ(NH)	R_3
1 290	1 292	72ν(r_1), 15ν(r_2), 19ν(r_5)	R_4
1 235	1 262	18ν(CCl), 12ν(r_2), 21ν(r_3), 13ν(r_5), 21(θ_3), 23δ(NH)	δNH
1 140	1 139	12ν(r_1), 31ν(r_4), 26ν(r_5), 10(θ_5)	R_5
1 005	1 024	28(θ_3), 43(θ_4), 35(θ_5)	R_6
975	976	36(θ_1), 34(θ_2), 15(θ_5)	R_7
860	848	79δ(CD)	δCD
880	898	92γ(NH), 36(τ_3), 27(τ_4)	γNH
705	741	19γ(CCl), 35γ(CD), 12(τ_4), 27(τ_1)	γCD ou R_8
—	656	32γ(CCl), 56γ(CD), 11(τ_5)	R_9
570	564	30(τ_4), 51(τ_5), 11γ(CCl)	R_8 ou γCD
510	488	63ν(CCl), 14(θ_3)	νCCl
340	348	89δ(CCl)	δCCl
280	240	36γ(CCl), 41(τ_2), 27(τ_3)	γCCl

mouvements mettant en jeu le cycle triazolique et de façon plus ou moins importante les vibrateurs CH (ou CD) et NH (ou ND). On observe bien pour le ClTA[D]-4, le couplage entre une vibration de noyau R_5 et δCH. Pour le ClTA, l'interaction est plus complexe et met également en jeu le mode situé à 1185 cm^{-1}. Les vibrations δCD par contre semblent relativement pures. Il en est de même des vibrations νCCl et δCCl.

Comme nous l'avions suggéré précédemment (2), les fréquences calculées à 707, 731, 564 et 541 cm^{-1} pour les ClTA, ClTA[D]-4, ClTA[D]-5 et ClTA$[D]_2$-4,5 respectivement, correspondent à des modes normaux relativement semblables. Cependant, il ne nous a pas été possible de traduire par le calcul le caractère γCH (ou γCD) que la comparaison des spectres nous avait conduit à envisager.

Enfin, nous n'avons pas réussi à situer correctement la vibration de plus basse fréquence.

Ces divergences entre calcul et expérience, qui se manifestent surtout dans le cas des vibrations A″, doivent être liées vraisemblablement à l'autoassociation importante du ClTA, à la forte anharmonicité qui en résulte pour les vibrations γNH et γND et aux couplages intermoléculaires qui doivent se manifester pour ces modes, mais que nous n'avons pas pu observer à cause de leur intensité nulle sur nos spectres Raman.

Can. J. Chem. Downloaded from www.nrcresearchpress.com by 210.87.254.105 on 09/06/12
For personal use only.

TABLEAU 5. Nombres d'onde observés et calculés pour la molécule de ClTA$(D)_2$-4,5 et attributions

ν_{exp} (cm^{-1})	ν_{calc} (cm^{-1})	DEP 100 $L_{ik}^2 F_{ii}/\lambda_k$	Attribution
2 300	2 337	94ν(CD)	νCD
2 200	2 066	92ν(ND)	νND
1 513	1 484	37ν(r_2), 19ν(r_3), 13ν(r_4)	R_1
1 460	1 459	13ν(CCl), 19ν(r_2), 13ν(r_3), 29ν(r_5), 18(θ_3)	R_2
1 385	1 362	41ν(r_3), 51ν(r_4), 12ν(r_5), 10δ(ND)	R_3
1 285	1 289	72ν(r_1), 20ν(r_2), 24ν(r_5)	R_4
1 150	1 178	17ν(CCl), 12ν(r_4), 26ν(r_5)	R_5
1 040	1 006	12ν(r_1), 12(θ_2), 28(θ_3), 10δ(CD), 21δ(ND)	δND
970	992	17(θ_1), 32(θ_4), 50(θ_5)	R_6
955	953	21(θ_1), 23(θ_2), 27δ(ND)	R_7
856	827	69δ(CD), 14δ(ND)	δCD
705	758	28γ(CCl), 17γ(ND), 18γCD), 21(τ_1)	γCD ou R_8
635	695	76γ(ND), 43γ(CD), 12(τ_3), 28(τ_4)	γND
—	634	17γ(CCl), 10γ(ND), 32γ(CD), 15(τ_3), 24(τ_5)	R_9
570	549	17γ(CCl), 43(τ_4)	R_8 ou γCD
505	485	63ν(CCl), 14(θ_3)	νCCl
340	338	88δ(CCl)	δCCl
280	238	35γ(CCl), 41(τ_2), 30(τ_3)	γCCl

En outre, vu le petit nombre de fréquences expérimentales dont nous disposions pour ces vibrations A″, nous n'avons pas estimé raisonnable d'introduire des constantes d'interaction supplémentaires pour améliorer notre champ de force.

Remerciements

Nous remercions Messieurs H. Sauvaitre et M. Chaillet, Professeurs à la Faculté des Sciences de Pau, pour les discussions dont ils nous ont fait bénéficier.

1. M. SAIDI-IDRISSI. D.E.S. Rabat (1977).
2. M. SAIDI-IDRISSI, M. SENECHAL, H. SAUVAITRE, M. COTRAIT et C. GARRIGOU-LAGRANGE. J. Chim. Phys. **77**, 195 (1980).
3. M. SAIDI-IDRISSI, P. LALANNE et C. GARRIGOU-LANGRANGE. J. Chim. Phys. **78**, 511 (1981).
4. M. SAIDI-IDRISSI, H. SAUVAITRE et C. GARRIGOU-LAGRANGE. J. Chimistes Arabes. Sous presse.
5. M. SAIDI-IDRISSI. Thèse, Rabat (1981).
6. V. V. MEL'NIKOV, V. V. STOLPAKOVA et B. V. GIDASPOV. Khim. Geterotsikl. Soedin. 1567 (1972).
7. P. GOLDSTEIN, J. LADEL et G. ABOWITZ. Acta. Crystallogr. Sect. B, **25**, 135 (1969).
8. E. B. WILSON, J. C. DECIUS et P. C. CROSS. Molecular vibrations. McGraw-Hill Book Co., New York. 1955.
9. J. H. SCHACHTSCHNEIDER. Projets no. 31450; Technical Reports no. 231–264 (1964) et 57–65 (1964). Shell Development Cie., Emeryville, CA.
10. D. BOUGEARD, N. LE CALVE, B. SAINT ROCH et A. NOVAK. J. Chem. Phys. **64**, 5152 (1976).
11. T. AVIGNON, E. J. VINCENT, J. RAYMOND et M. CHAILLET. J. Mol. Struct. **21**, 319 (1974).
12. M. REY-LAFON, M. T. FOREL et C. GARRIGOU-LAGRANGE. Spectrochim. Acta, Part A, **29**, 471 (1973).

Can. J. Chem. Downloaded from www.nrcresearchpress.com by 210.87.254.105 on 09/06/12
For personal use only.

Coulometric determination of several water-insoluble aromatic nitro compounds with electrogenerated chromium(II)

I. M. AL-DAHER[1] AND B. KRATOCHVIL

Department of Chemistry, University of Alberta, Edmonton, Alberta, Canada T6G 2G2

Received January 31, 1981[2]

I. M. AL-DAHER and B. KRATOCHVIL. Can. J. Chem. **59**, 3346 (1981).

The electrochemical reduction of a series of water-insoluble aromatic nitro compounds with coulometrically generated chromium(II) has been investigated. Samples ranging from 0.2 to 0.5 μmol could be determined for several substances with a precision and accuracy of about 1%. The number of electrons involved in the reductions corresponded in most cases to the formation of hydroxylamines or amines, but in some instances to dihydrazo products.

I. M. AL-DAHER et B. KRATOCHVIL. Can. J. Chem. **59**, 3346 (1981).

On a étudié la réduction électrochimique d'une série de composés aromatiques nitrés insolubles dans l'eau par le chrome(II) produit par coulométrie. Dans des échantillons dont la concentration varie de 0,2 à 0,5 μmol, on peut déterminer plusieurs substances avec une précision d'environ 1%. Le nombre d'électrons impliqués dans les réductions correspond, dans la plupart des cas, à la formation des hydroxylamines ou des amines; dans certains cas, il correspond à des produits dihydrazo.

[Traduit par le journal]

Can. J. Chem. Downloaded from www.nrcresearchpress.com by 210.87.254.5 on 09/06/12
For personal use only.

Electrochemically generated chromium(II) at a mercury cathode has been applied to the determination of a number of aromatic nitro compounds in our laboratory (1). We became interested in determining whether this method could be applied to other water-insoluble nitro compounds, both to extend the analytical applicability of the system and to study the effect of various functional groups on the ease of reduction of the nitro group. The same procedure has also been used successfully for the determination of some herbicides and insecticides containing the nitro function (2).

An important feature of the method is the use of constant current potentiometry for end-point detection, since conventional potentiometry does not respond adequately to the organic species being titrated, and the titration solution is too intensely colored by the chromium(III) bromide from which the chromium(II) is generated for indicators to be employed.

Experimental

Chemicals

Chromium(III) bromide (K & K Laboratories) was washed twice with ethyl ether, the excess ether removed by suction, and the solid dried under vacuum at room temperature. This material yields the rapidly reducible $CrBr(H_2O)_5^{2+}$ species at a mercury cathode (3). A solution 0.1 *M* in $CrBr(H_2O)_5^{2+}$ and 1.5 *M* in HCl was used as the catholyte in the coulometric cell (1). *p*-Nitroethylbenzene (K & K Laboratories), nitrobenzene (Fisher), and *o*-nitrophenetole (Aldrich Chemical Co.) were distilled under vacuum and the middle portions of the distillates used. *o*- and *m*-Nitrobenzaldehyde (Aldrich Chemical Co.) were used as received. The following compounds were recrystallized from ethanol until melting points within ±1°C of reported values were obtained: *o*- and *m*-nitrocinnamic acid, *p*-nitrosotoluene, 2-nitronaphthalene, *p*-nitroanisole, and 2-methyl-1-nitronaphthalene (Aldrich Chemical Co.); *p*-nitrophenetole, 2,4-dinitrophenetole, and 2,6-dinitrothymol (Eastman). 1,8-Dinitronaphthalene (K & K Laboratories) was recrystallized from chloroform. Cacotheline (Fluka AG) was used as received as was chloromycin obtained from L. Chatten, Faculty of Pharmacy, University of Alberta. Acetonitrile (Matheson, Coleman and Bell) was purified by distillation from calcium hydride; only the middle fraction was retained.

Apparatus

The coulometer, titration cell, and catholyte composition were as previously described (1). A 20-mA coulometric current, found to be satisfactory in earlier work, was employed (1), as was the constant current potentiometric system for end point detection, a pair of electrodes with a 10 μA current passing between them.

Titration Procedure

Into the anode compartment of the coulometry cell place 50 mL of 0.01 *M* HCl – 1.0 *M* KCl solution. Into the cathode compartment place 70 mL of a solution 0.1 *M* in $CrBr(H_2O)_5^{2+}$ and 1.5 *M* in HCl. Deaerate both solutions for 15 min with oxygen-free nitrogen. Then direct the nitrogen over the surface of the catholyte and introduce the mercury pool cathode. Run a blank by generating chromium(II) at the mercury cathode at a current level of about 20 mA, continuously at first and then in increments of 5 to 10 s near the end point, until the potential between the polarized pair of platinum microelectrodes begins to decrease. Record the potential and time readings for several points just before and beyond the potential decrease. Then inject about 1 g of approximately millimolar sample solution by hypodermic syringe and generate chromium(II), recording the time and potential readings as for the blank. Weigh the syringe before and after sample injection to determine the amount of sample delivered. Plot the readings against time of current generation and locate the end point by linear extrapolation (1). The amount of chromium(II) to be generated beyond the end point depends on the compound being determined. With sharp

[1]Present address: Department of Chemistry, University of Al-Mustansiriyah, Baghdad, Iraq.

[2]Revision received August 21, 1981.

0008-4042/81/243346-04$01.00/0

©1981 National Research Council of Canada/Conseil national de recherches du Canada

Can. J. Chem. Downloaded from www.nrcresearchpress.com by 210.87.254.5 on 09/06/12
For personal use only.

end points only about a 2% excess is needed; for more sluggish reactions about a 25% excess may be necessary.

When products of the first titration do not interfere, inject a second weighed portion of sample solution and repeat the titration, calculating the time of current generation from the previous end-point value.

Results and Discussion

Results of the titrations studied are summarized in Table 1. With some compounds four or five samples can be titrated in the same catholyte before it must be replaced, but with other compounds it is possible to analyse one sample only. The first sample run in the fresh catholyte solution sometimes must serve as a blank to establish an initial end point, and in these instances should not be used in the calculations. The total time required for titration of individual samples after injection into the cell ranged from 6 to 25 min. Sample solutions were always titrated within a few hours of preparation. Acetonitrile was used as solvent for all the compounds in Table 1 except cacotheline, for which water was used.

Rates of reaction varied widely with the compound; *p*-nitrophenetole, *p*-nitroethylbenzene, and 1,8-dinitronaphthalene were the most rapid. Where the reactions are rapid, the end points are usually sharp, and the error small. An exception was *o*-nitrosotoluene, which gave results about 5% high for a 2-electron reduction even though the end point was excellent. The error may be due to the presence of nitrotoluene formed by aerial oxidation during the recrystallization from hot ethanol, since the melting point after recrystallization, 70°C, is somewhat lower than the reported value of 72–75°C. Oxidation after recrystallization is also a possible contributing factor.

Cacotheline, nitrobenzene, and chloromycin react too slowly to be determinable; all give sloping end points with drifting potentials. The stoichiometry of 2,6-dinitrothymol and 2,4-dinitrophenetole suggests that one of the nitro groups undergoes a 6-electron reduction to the amine and the other a 5-electron reduction to a coupled hydrazo species. A 5-electron reduction was observed previously for 5-nitro-1-naphthylamine (1). 1,8-Dinitronaphthalene is involved in an overall 10-electron reduction. If the nitro group in the 1 position undergoes a 6-electron reduction as in 1-nitronaphthalene (1), then the nitro group in the 8 position may be reduced to the hydroxylamine for a total of ten electrons per molecule.

On the basis of previous (1, 2) and present results on the reduction of aromatic nitro compounds, all under the same conditions, we can summarize the relation between the molecular structure of a given aromatic nitro compound and reduction by chromium(II) as follows. Those compounds which contain methoxy or ethoxy groups on the benzene ring are easily reduced to the corresponding hydroxylamines or amines. The end points are sharp, and the potential difference between the indicator electrodes after the end point is stable. For *o*-nitroanisole reduction takes place with 4 electrons to the hydroxylamine, which may be stabilized by formation of a hydrogen bond to the oxygen of the anisole. The related compounds *p*-nitroanisole and *p*-nitrophenetole undergo 6-electron reduction to the corresponding amines. Although *o*-nitrophenetole reacts cleanly and sharply, the results of 12 determinations (rel. std. dev. 0.2%) were 8.7% higher than expected for a 4-electron reduction, and did not change when an additional distillation from a spinning band column at reduced pressure was performed on the material before titration. Further, a mass spectrum of the purified material showed only a parent peak and fragments corresponding to dissociation of the parent.

Methyl groups on the aromatic ring have an effect on the reduction of nitro groups similar to that of the methoxy group. *o*-Nitrotoluene, *m*-nitrotoluene, and 2-methyl-1-nitronaphthalene all undergo reduction only to the hydroxylamine with sharp end points. Potentials between the polarized platinum electrodes are stable at the end point for these compounds, especially if the methyl group is located *ortho* to the nitro group. The ease of reduction decreases if the nitro group is in the para position, as in *p*-nitrotoluene. However, the reduction of *p*-nitroethylbenzene, though rapid, requires only 5 electrons.

1-Nitronaphthalene undergoes rapid and stoichiometric reduction to the amine, but reduction of 2-nitronaphthalene is slow and nonstoichiometric, despite a well-defined end point. On the other hand, 1,8-dinitronaphthalene undergoes a rapid 10-electron reduction with a clean, sharp end point.

Dinitro compounds possessing a hydroxyl and methyl or butyl group on the aromatic ring undergo 12-electron reduction to the corresponding diamines; 4,6-dinitro-*o*-cresol and the herbicide dinoseb (2-(1-methylpropyl)-4,6-dinitrophenol) fall into this class (2). On the other hand, a ketone group in the *ortho*, *meta*, or *para* position decreases the ease of reduction of nitro groups. Thus *o*-, *m*-, and *p*-nitrobenzoic acid, *o*- and *m*-benzaldehyde, and 4-nitrophthalic acid all undergo 4-electron reduction, but with slow, poor end points that are unsatisfactory for analytical use. The introduction

Can. J. Chem. Downloaded from www.nrcresearchpress.com by 210.87.254.5 on 09/06/12
For personal use only.

TABLE 1. Summary of results of titrations of aromatic nitro compounds with coulometrically generated chromium(II)

Compound	No. of electrons	No. of determinations	Ave. error, %	Rel. std. dev., %	No. of titrations per catholyte	Product postulated	Comments
o-Nitrosotoluene	2	10	+4.3	1.0	1	RNHOH	End point sharp
2-Methyl-1-nitronaphthalene	4	6	+0.2	0.8	2	RNHOH	Reaction sluggish near end point
o-Nitrobenzaldehyde	4	2	−0.3	—	1	RNHOH	Reaction sluggish near end point
m-Nitrobenzaldehyde	4	3	+0.1	0.5	1	RNHOH	Reaction sluggish near end point
o-Nitrophenetole	4	12	+8.7	0.2	1	RNHOH	Reaction rapid near end point
o-Nitrocinnamic acid	4	2	+17.6	—	1	RNHOH	Reaction rapid, end point sharp
m-Nitrocinnamic acid	4	4	~15	6	1	RNHOH	Slow reaction, poor end point
p-Nitroethylbenzene	5	3	−0.5	0.6	1	RNHNHR	Reaction rapid, end point sharp
2-Nitronaphthalene	6	3	−23	3.5	1	RNH_2	Slow reaction, poor end point
p-Nitrophenetole	6	9	−0.3	0	5	RNH_2	End point sharp, reaction rapid
p-Nitroanisole	6	3	−0.2	0.4	1	RNH_2	Some drift on end point
Nitrazepam	6	3	−0.2	1.2	1	RNH_2	Reaction rapid, end point sharp
1,8-Dinitronaphthalene	10	3	−0.5	0.2	1	$H_2NRNHOH$	Reaction rapid, end point sharp
2,6-Dinitrothymol	11	14	+0.1	0.7	4	$H_2NRNHNHRNH_2$	End point sharp
2,4-Dinitrophenetole	11	10	+0.8	0.9	4	$H_2NRNHNHRNH_2$	End point sharp, use first sample in catholyte as blank

of a side chain containing a carboxylic group and a carbon–carbon double bond results in a reduction of between 4 and 5 electrons. This was observed with both *o*- and *m*-nitrocinnamic acid. *o*-Nitrophenol behaves in a similar way. A hydroxyl group in the *meta* or *para* position, however, yields reduction to the corresponding amines, as with *m*- and *p*-nitrophenol.

Acknowledgements

Financial support by the National Sciences and Engineering Research Council of Canada and by the University of Alberta is gratefully acknowledged.

1. I. M. AL-DAHER and B. G. KRATOCHVIL. Anal. Chem. **51**, 1408 (1979).
2. B. G. KRATOCHVIL and I. M. AL-DAHER. Analyst. **106**, 196 (1981).
3. D. A. AIKENS and S. M. CARLITA. Anal. Chem. **37**, 459 (1965).

Can. J. Chem. Downloaded from www.nrcresearchpress.com by 210.87.254.5 on 09/06/12
For personal use only.

Studies related to biological detoxification of Kraft pulp mill effluent. II. The biotransformation of isopimaric acid with *Mortierella isabellina*

JAMES P. KUTNEY, MAHATAM SINGH, EUGENE DIMITRIADIS, GARY M. HEWITT, PHILIP J. SALISBURY, AND BRIAN R. WORTH

Department of Chemistry, University of British Columbia, 2036 Main Mall, University Campus, Vancouver, B.C., Canada V6T 1Y6

AND

JAMES A. SERVIZI, DENNIS W. MARTENS, AND ROBERT W. GORDON

Sweltzer Creek Salmon Research Laboratory, International Pacific Salmon Fisheries Commission, Cultus Lake, B.C., Canada V3L 4X9

Received June 30, 1981

JAMES P. KUTNEY, MAHATAM SINGH, EUGENE DIMITRIADIS, GARY M. HEWITT, PHILIP J. SALISBURY, BRIAN R. WORTH, JAMES A. SERVIZI, DENNIS W. MARTENS, and ROBERT W. GORDON. Can. J. Chem. **59**, 3350 (1981).

A study related to the biological detoxification of Kraft pulp mill effluent is presented. Several fungal and bacterial preparations were evaluated for their action on isopimaric acid (IPA), one of the effluent constituents toxic to fish. *Mortierella isabellina* was the organism selected for the biodegradation of IPA and subsequent chemical studies established the structures of three diterpenoid substances with very much lower acute toxicity.

JAMES P. KUTNEY, MAHATAM SINGH, EUGENE DIMITRIADIS, GARY M. HEWITT, PHILIP J. SALISBURY, BRIAN R. WORTH, JAMES A. SERVIZI, DENNIS W. MARTENS et ROBERT W. GORDON. Can. J. Chem. **59**, 3350 (1981).

On présente une étude sur la désintoxication biologique des résidus provenant des moulins à papier. On a évalué l'action de plusieurs préparation bactériennes et fongiques sur l'acide isopimarique (AIP), un des constituants du résidu toxique pour les poissons. On a choisi l'organisme *Mortierella isabellina* pour dégrader l'AIP et des études chimiques qui ont suivi ont permis d'établir les structures de trois substances diterpéniques ayant une toxicité beaucoup plus faible.

[Traduit par le journal]

Introduction

Of the major toxicants in Kraft pulp mill effluent (KME), dehydroabietic acid (DHA; **1**) has been shown to be efficiently transformed into non-toxic compounds by the fungus *Mortierella isabellina* (1). In this earlier work, specific biotransformation products from **1** were identified and quantified and a major pathway of DHA transformation was elucidated. *M. isabellina* proved to be a stable and readily produced organism potentially useful as a supplement to existing biobasins for the detoxification of DHA. Preliminary tests indicated that the metabolites produced had no significant toxicity to sockeye salmon fry or to juvenile *Daphnia pulex*.

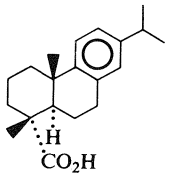

1

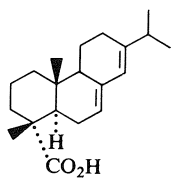

3

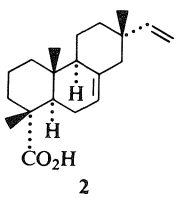

2

A second major toxicant of KME is isopimaric acid (IPA; **2**) (2, 3). IPA is a highly toxic resin acid with a 96-h LC_{50} for rainbow trout of 0.4 mg/L[3]. It also appears to be more resistant to biodegradation than other resin acids. For example, in studies of the biodegradation of the sodium salts of resin acids (4), the IPA salt was most recalcitrant to breakdown by the natural, mixed micro-flora of an activated sewage sludge and of the waters of two rivers.

In the present study, several bacteria and fungi were screened for their abilities to degrade IPA. As in the case of DHA, *M. isabellina* was most effective.

Methods, results, and discussion

Culture growth

In preliminary screening experiments, *M. isabellina* was the only organism among five fungi and six bacteria (Table 1) to degrade IPA. Shake flask, batch cultures of *M. isabellina* were used to further examine IPA degradation. When grown in dextrose–yeast extract broth (Fig. 1), there was a 12 h lag followed by rapid growth resulting in a maximum dry weight of 3.7 mg/mL after 24 h incuba-

0008-4042/81/243350-06$01.00/0

©1981 National Research Council of Canada/Conseil national de recherches du Canada

Can. J. Chem. Downloaded from www.nrcresearchpress.com by 210.87.254.5 on 09/06/12
For personal use only.

TABLE 1. Microorganisms screened for the ability to degrade isopimaric acid (IPA)*

Fungi	Bacteria
Cephalosporium sp.†‡	*Pseudomonas indoloxidans* (*acidovorans*) ATCC 9355
Fusarium culmorum CBS 171.28	*Pseudomonas aeruginosa* ATCC 1066
Geotrichum sp.†‡	4 isolates‡
Mortierella isabellina UBC #129	
pink yeast isolate	

*CBS, Centraalbureau voor Shimmelcultures; UBC, University of British Columbia culture collection in Botany; ATCC, American Type Culture Collection.
†Provisional identification.
‡Isolated from Kraft pulp mill effluent (KME).

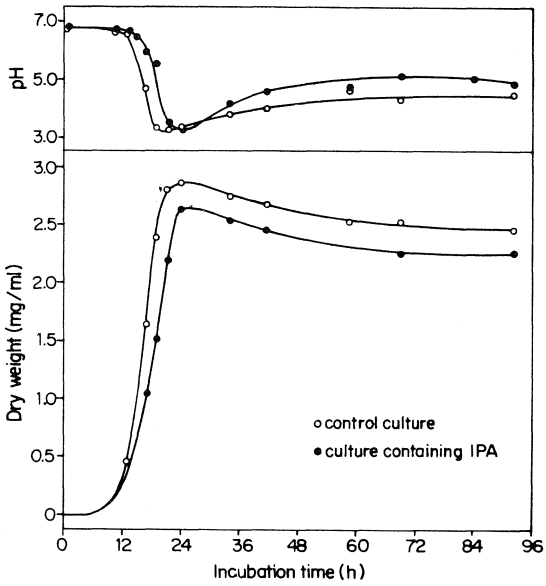

FIG. 1. Growth of *M. isabellina* in DYE and DYE plus IPA (80 mg/L) at 35°C.

tion. Inclusion of IPA at 80 mg/L caused a slight extension of the lag phase and a small reduction in the final biomass yield. A further extension of the lag phase occurred if the inoculum was not preconditioned to IPA. The cultures experienced a growth-associated decrease in pH.

Quantitative analysis

It was thought that a specific analytical technique that simultaneously evaluates the concentrations of several toxic resin acids would be useful in applications to the natural environment (e.g. KME). Therefore, a method was developed for the simultaneous measurement of DHA, IPA, abietic acid (ABA; **3**), and the metabolites derived from these compounds. Since IPA, unlike DHA and abietic acid, lacks an ultraviolet chromophore to facilitate simple detection (1), the acid was converted to its relatively stable imidazolide **4** by reaction with 1,1′-carbonyldiimidazole. The imidazolides of all three resin acids were sufficiently stable to be analysed in aqueous methanol without detectable decomposition. The actual analyses were performed by quantitative hplc on reverse phase C-8 columns, with methanol/water mixtures. Standard curves for the analysis of the three resin acids **1**, **2**, and **3** as their imidazolides are given in Fig. 2.

Optimization of the separation of the imidazolides of **1**, **2**, and **3** (see Experimental) gave k' values of 15.8, 21.5, and 23.5, respectively. The imidazolides of **2** and **3** were resolved to $R \simeq 1$, using methanol/water (77:23) on a Waters Associates C-8 radial pak at 2 mL/min, with detection at 280 nm. For the purposes of the present study, the IPA imidazolide standard curve shown in Fig. 2 was used for monitoring the disappearance of IPA and the appearance of its metabolites in cultures.

The imidazolides of the metabolites of IPA were assumed to have the same response factors as those of **2** since no new chromophores were introduced during biotransformation (see Experimental). Collectively, the standard curves in Fig. 2 will allow similar monitoring of **1**, **2**, and **3** during the detoxification of KME.

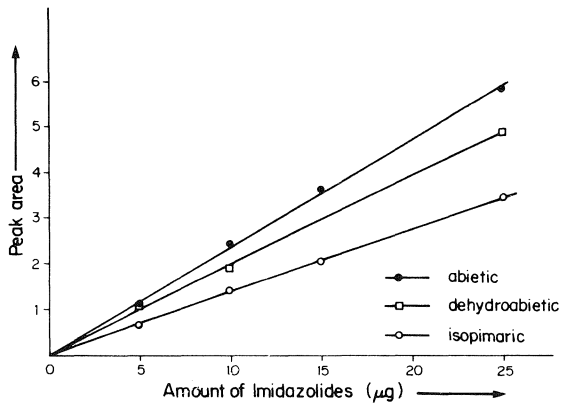

FIG. 2. Hplc quantitation of abietic, dehydroabietic, and isopimaric acids as their imidazolides: column: C8-reverse phase (radial pak A); solvent: CH_3OH/H_2O (77:23); flow rate: 2 mL/min; detector: Waters model 440 uv, (280 nm).

Can. J. Chem. Downloaded from www.nrcresearchpress.com by 210.87.254.5 on 09/06/12
For personal use only.

Can. J. Chem. Downloaded from www.nrcresearchpress.com by 210.87.254.5 on 09/06/12
For personal use only.

Biotransformation of IPA by M. isabellina

IPA (80 mg/L) was fed to cultures of *M. isabellina* in dextrose–yeast extract broth and the biotransformation of IPA over 96 h was followed using hplc analysis (Fig. 3). Most of the IPA was converted during the first 24 h of incubation. Three major metabolites were present in approximately equal concentrations at about 17 h, however, only one metabolite reached a plateau and remained in the culture until the end of the sampling period (Fig. 4).

Identification and isolation of the IPA metabolites

A large-scale incubation of *M. isabellina* containing approximately 480 mg of IPA was allowed to proceed for 17 h, at which time the cultures were harvested. The presence of the three major metabolites was confirmed by hplc analysis and each was separated from the crude mixture by preparative layer chromatography. On the assumption that the carboxylic acid function was not altered by *M. isabellina*, the metabolites (**5**, **9**, and **12**) were converted to their methyl esters (**6**, **10**, and **13**, respectively) for purification and identification.

The methyl ester **6** had molecular formula $C_{21}H_{32}O_3$ indicating the introduction of one additional oxygen to the IPA skeleton. The ir spectrum indicated hydroxyl stretching at 3700–3400 cm^{-1}. The ^{1}Hmr spectrum revealed a nine line, one proton absorbance at δ 3.9 for a ring proton geminal to a hydroxyl group. The splitting pattern (tt., J_{aa} = 12 Hz, J_{ae} = 4.0 Hz) was consistent with an axial proton split by two adjacent methylenes. These data indicated that a hydroxyl group was introduced at the $C_{2\alpha}$ position. To obtain further proof of this structure, the lactone, **7**, was formed by treatment of **5** with *p*-toluene sulphonic acid in refluxing benzene. Infrared absorption at 1770 cm^{-1} confirmed the γ-lactone function. Furthermore, oxidation of **6** with pyridinium chlorochromate gave **8** which exhibited an ir stretching band at 1708 cm^{-1} in addition to a saturated ester stretching at 1722 cm^{-1}. From these results, the possibility of an α,β-unsaturated ketone arising from oxidation of a C_6-hydroxyl group, which could also have formed a γ-lactone, was eliminated. Therefore, the first-formed major metabolite had structure **5**.

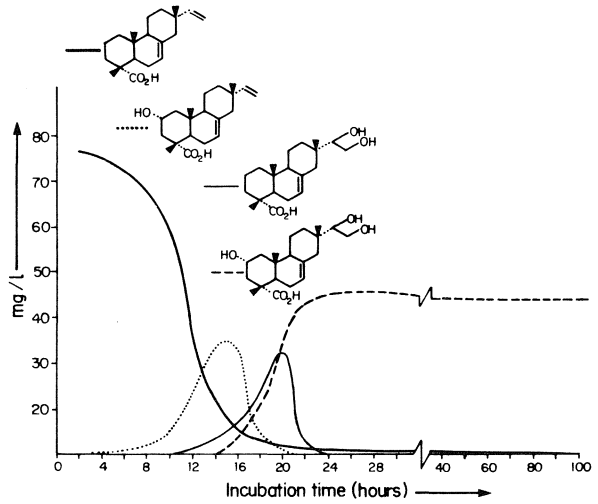

FIG. 3. Isopimaric acid biodegradation sequence by *M. isabellina*: column: C8-reverse phase (radial pak A); solvent: CH_3OH/H_2O (77:23); flow rate: 2 mL/min; detector: Waters model 440 uv, (280 nm).

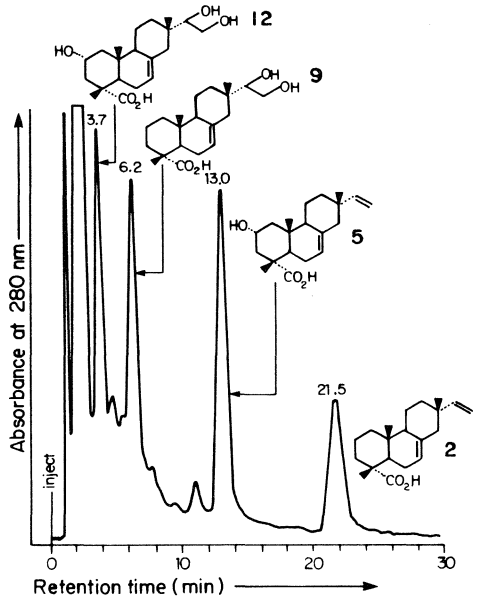

FIG. 4. Plot of absorbance at 280 nm of **2**, **5**, **9**, **12** versus retention time: column: C8-reverse phase (radial pak A); solvent: CH_3OH/H_2O (77:23); flow rate: 2 mL/min; detector: Waters model 440 uv, (280 nm).

The methyl ester **10** of the second product of the biotransformation of IPA was a dihydroxy compound with molecular formula $C_{21}H_{34}O_4$, indicating the addition of two hydroxyl groups to the parent IPA skeleton. This may have occurred by dihydroxylation at one of the double bonds or by the addition of a molecule of water across a double bond plus monohydroxylation elsewhere. The latter possibility was excluded by analysis of the ^{1}Hmr spectrum which included only one vinyl proton multiplet at δ 5.35 and a three proton multiplet at δ 3.35–3.77, suggesting the side chain double bond had undergone dihydroxylation. This was supported by the fact that **10** gave an acetonide (**11**) on refluxing with acetone in the presence of anhydrous copper sulphate. Furthermore, the ^{1}Hmr spectrum of **11** is identical with that of a synthetic

Can. J. Chem. Downloaded from www.nrcresearchpress.com by 210.87.254.5 on 09/06/12
For personal use only.

sample made by selective hydroxylation of the side chain double bond of IPA by osmium tetroxide. The second metabolite, therefore, had structure **9**.

The methyl ester **13** of the third metabolite had molecular formula $C_{21}H_{34}O_5$, indicating addition of three hydroxyls to the parent IPA skeleton. The ir spectrum showed hydroxyl stretching at 3700–3400 cm^{-1}, while the ^{1}Hmr spectrum again indicated a $C_{2\alpha}$-hydroxylation. In addition, the hydroxy acid **12** gave the lactone **16** when heated in benzene containing *p*-toluene sulphonic acid and acetone. A three proton multiplet at δ 3.55–3.77 and a single proton multiplet at δ 5.35 suggested C_{15}–C_{16} double bond dihydroxylation. Further confirmation of this feature was obtained from additional chemical transformations. When the methyl ester **13** was heated under reflux in the presence of anhydrous copper sulphate the acetonide **14** was formed which upon pyridinium chlorochromate oxidation furnished the ketoacetonide **15**. These latter compounds were characterized by their various spectral data. Considering the foregoing information, **12** was determined to be the structure of the third biotransformation product.

The experiments outlined above clearly indicate the tendency for *M. isabellina* to oxygenate IPA at $C_{2\alpha}$, C_{15}, and C_{16} positions. Introduction of the $C_{2\alpha}$ hydroxyl group is initiated first, followed by attack at the C_{15} and C_{16} positions. The two processes appear to proceed independently in that **5** is not a precursor of **9**, or vice versa. The trihydroxylated IPA (**12**) arises from each of the first-formed metabolites. the reaction sequence may be described as follows:

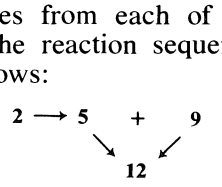

The last formed compound (12) resists further biotransformation by *M. isabellina* up to 96 h under the culture conditions described above.

Preliminary toxicity measurements (using juvenile *Daphnia pulex*) of the crude degradation mixture indicate very efficient detoxification of IPA by *M. isabellina*. Quantitative evaluation is presently underway, as are studies into the detoxification of abietic acid.

Experimental

Ultraviolet spectra were recorded on a Cary 15 spectrophotometer. Low resolution mass spectra were recorded on either an Atlas CH-4B or an AEI MS-902 spectrometer. High resolution mass data were measured on an AEI MS-902 instrument. The ^{1}Hmr spectra were recorded on Varian XL-100 and Nicolet Oxford H-270 instruments. Chemical shifts are reported as ppm from tetramethylsilane, used as internal standard. Microanalyses were performed by P. Borda, Microanalytical Laboratory, University of British Columbia. Melting points are uncorrected.

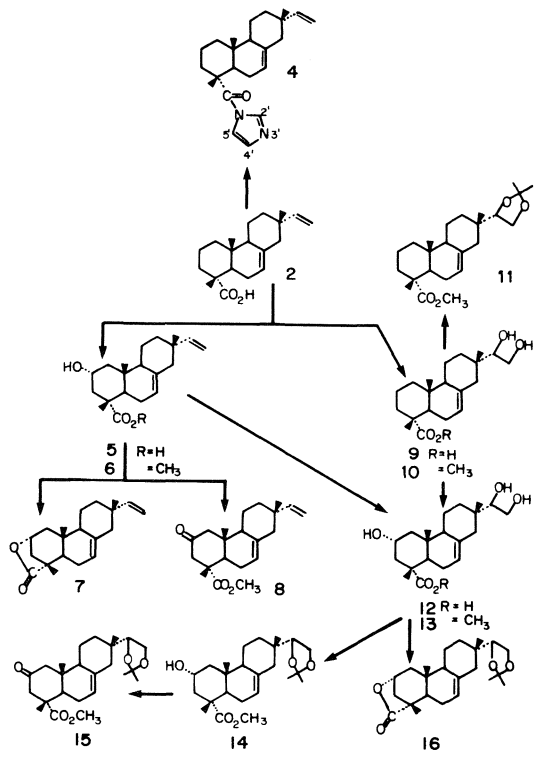

Screening of microorganisms for the ability to degrade IPA

Liquid media containing IPA at 50 mg/L (50 mL of medium per 250 mL Erlenmeyer flask) were inoculated with 1 mL of cell suspensions prepared by washing the surface of six-day old slant cultures with 5 mL of sterile Aerosol OT solution (Fisher Scientific: 450 μL per L distilled water). Cultures were incubated at room temperature (21 to 25°C) and 200 rpm on a rotary shaker. Bacterial cultures were harvested after 48 h and fungal cultures after 96 h. The presence of IPA was determined after derivatization, using hplc. Fungi were maintained as slant cultures on potato–dextrose agar (Difco) and were tested against IPA in dextrose–yeast extract broth (DYE) (5.0 g D-glucose, 0.5 g yeast extract (Difco), 1.0 g KH_2PO_4, 1.0 g $(NH_4)_2HPO_4$, 1.0 g NaCl, and 0.5 g $MgSO_4.7H_2O$ per L distilled water). Bacteria were kept as slant cultures on nutrient agar (Difco) and were tested against IPA in nutrient broth (Difco).

Biotransformation of IPA by M. isabellina

Cultures to be used as inocula were grown on 100 mL of potato–dextrose agar supplemented with 10 mg/L IPA in Roux bottles at 25°C. Inocula were prepared by washing the surface of a confluent mature culture (older than 10 days but younger than two months) with 50 mL of sterile Aerosol OT solution. The resulting suspension containing approximately 10^6 spores per mL (as determined using a Howard mold counting chamber) was inoculated into DYE at a volumetric ratio of 1:50. Controls contained no IPA, while cultures used to follow IPA degradation contained IPA at 80 mg/L which was added as a filter sterilized solution made slightly alkaline with NaOH. All cultures were 100 mL in 250 mL Erlenmeyer flasks. The cultures were incubated at 35°C and 200 rpm on a rotary shaker. To obtain a sample, a whole culture was harvested. Culture dry weights

Can. J. Chem. Downloaded from www.nrcresearchpress.com by 210.87.254.5 on 09/06/12
For personal use only.

were measured using membrane filtered (0.45 μm cellulose acetate filters, Millipore Corp.), freeze-dried cells.

Quantitative analysis for DHA, IPA, and ABA

Stock solutions (1.0 mg/mL) of DHA, IPA, and ABA were prepared in anhydrous acetonitrile (distilled from P_2O_5). Aliquots were taken to make up the following standards.

Acid (mg/3 mL)	Sample #1	2	3	4	5
DHA	2.5	1.0	0.5	0.0	0.0
IPA	0.5	1.0	0.0	2.5	1.5
ABA	0.0	1.0	2.5	0.5	1.5

A solution (0.5 mL) of 1,1′-carbonyldiimidazole (32 mg/mL) in anhydrous acetonitrile was added to each and the vials sealed and kept at room temperature for 1 h. The resin acid imidazolides were then analysed by analytical hplc (Waters Associates Data Module, System Controller and WISP Automatic injector coupled to a Radial Compression Module carrying a C_8 reverse phase column, and with a Model 440 UV detector operating at 280 nm and at 254 nm). Optimum resolution was obtained using the solvent system methanol/water (77:23) at 2 mL/min. The k' values, retention times, and response ratios were as follows:

		Relative response ratio	
Acid imidazolide	k'	280 nm	254 nm
DHA imidazolide	15.8 (16 min)	1.00	1.00
IPA imidazolide	21.5 (21.8 min)	0.82	0.90
ABA imidazolide	23.5 (23.8 min)	0.58	4.30

Peak areas, calculated electronically, were used to derive the standard curves shown in Fig. 2.

Analysis of cultures

Harvested cultures (50 mL each) were acidified to pH 2 and extracted with ethyl acetate (3 × 25 mL). The combined extracts were washed with water (10 mL), dried ($MgSO_4$), and concentrated *in vacuo*. The dried residues were dissolved in a solution (3.5 mL) of 1,1′-carbonyldiimidazole (16 mg) in dry acetonitrile, kept at room temperature for 1 h, and analysed by hplc. The polar products from IPA were eluted before the acid (**2**) (Fig. 3), and had k' values of 13.16 (**5**), 6.23 (**9**), and 3.75 (**12**).

*Isopimaric acid imidazolide (**4**)*

IPA (**2**) (30 mg) was reacted with 1,1′-carbonyldiimidazole (50 mg) in dry dichloromethane (2 mL). The excess reagent and imidazole was removed by washing with 1% $NaHCO_3$ solution. The organic layer was dried (Na_2SO_4) and concentrated *in vacuo*. The unstable imidazolide (**4**) was isolated (90%) as a viscous oil; uv (MeOH) λ_{max} 248 (1400); ir (film) ν_{max} 1720, 1650, 1480, 930, 745 cm^{-1}; ^{1}Hmr ($CDCl_3$) δ 0.98 (3H, s, C20—methyl), 1.00 (3H, s, C19—methyl), 1.50 (3H, s, C17—methyl), 4.9–5.1 (2H, m, C16—vinyl), 5.30 (1H, m, C7—H), 5.85 (1H, m, C15—H), 7.10 (1H, d, J = 1 Hz, C4′—H), 7.66 (1H, d, J = 1 Hz, C5′—H), 8.40 (1H, s, C2′—H); ms *m/e* 352 (M^+), 337, 316, 257, 119, 121, 88, 84.

*Methyl 2α-hydroxyisopimarate (**6**)*

The title compound was obtained as a white solid; mp 103–107°C (ether – petroleum ether); ir ($CHCl_3$) ν_{max} 3700–3300, 1722 cm^{-1}; ^{1}Hmr ($CDCl_3$) δ 0.8 (3H, s, C20—methyl), 0.96 (3H, s, C19—methyl), 1.32 (3H, s, C17—methyl), 3.68 (3H, s, CO_2CH_3), 3.92 (1H, tt, J = 12, 4 Hz, C2β—H), 4.82–5.12 (2H, m, C16—vinyl), 5.3–5.4 (1H, m, C7—H), 5.68–6.04 (1H, m, C15—H); ms *m/e* 332 (M^+), 314, 299, 255, 239, 201. *Anal.* calcd. for $C_{21}H_{32}O_3$: C 75.90; H 9.63; found: C 75.43, H 9.36. High resolution molecular weight determination, calcd. 332.2343, found 332.2353.

*Methyl 15,16-dihydro-15,16-dihydroxyisopimarate (**10**)*

The ester **10** was obtained as a white solid; mp 68–72°C (ether – petroleum ether); ir ($CHCl_3$) ν_{max} 3700–3300, 1725 cm^{-1}; ^{1}Hmr ($CDCl_3$) δ 0.77 (3H, s, C20—methyl), 0.9 (3H, s, C19—methyl), 1.27 (3H, s, C17—methyl), 3.35–3.77 (3H, m, C15—H and C16—H_2), 3.65 (3H, s, CO_2CH_3), 5.25–5.35 (1H, m, C7—H); ms *m/e* 350 (M^+), 299, 290, 289, 288, 257, 229. *Anal.* calcd. for $C_{21}H_{34}O_4$: C 72.0, H 9.71; found: C 71.83, H 9.49. High resolution molecular weight determination, calcd. 350.2448; found 350.2460.

*Methyl 15,16-dihydro-2α, 15,16-trihydroxyisopimarate (**13**)*

The ester **13** was obtained as a white solid; mp 135–140°C (ether); ir ($CHCl_3$) ν_{max} 3700–3300, 1725 cm^{-1}, ^{1}Hmr ($CDCl_3$) δ 0.77 (3H, s, C20—methyl) 0.92 (3H, s, C19—methyl), 1.3 (3H, s, C17—methyl), 3.33–3.75 (4H, m, C2β—H, C15—H and C16—H_2), 3.67 (3H, s, CO_2CH_3), 5.25–5.45 (1H, m, C7—H); ms *m/e* 366 (M^+), 305, 287, 255, 227, 185, 159, 157, 145, 131, 128. *Anal.* calcd. for $C_{21}H_{34}O_5$: C 68.85, H 9.28; found C 68.27, H 9.06. High resolution molecular weight determination, calcd. 366.2397, found 366.2416.

*2α-Isopimaric acid lactone (**7**)*

p-Toluene sulphonic acid (5 mg) was added to a refluxing solution of the hydroxy acid (**5**) (14 mg) in dry benzene (25 mL). The solution was refluxed for 30 min, cooled, washed with water, dried ($MgSO_4$), and concentrated *in vacuo*. Chromatography on silica gel gave lactone (**7**) (8 mg, 59%); ir ($CHCl_3$) ν_{max} 1770 cm^{-1}; ^{1}Hmr ($CDCl_3$) δ 0.80 (3H, s, C20—methyl), 1.15 (3H, s, C19—methyl), 1.32 (3H, s, C17—methyl), 4.5–4.7 (1H, m, $W/2$ = 13 Hz, C2β—H), 4.0–4.5 (3H, m, C15—H, C16—H_2), 5.3–5.45 (1H, m, C7—H); ms *m/e* 300 (M^+), 285, 271, 256, 241. High resolution molecular weight determination, calcd. 300.2082, found 300.2081.

*Methyl 2-oxoisopimarate (**8**)*

A solution of **6** (15 mg) in dichloromethane (1.5 mL) was added to a suspension of pyridinium chlorochromate (25 mg) in dichloromethane (2 mL) at room temperature and the mixture stirred for 1.5 h, diluted with ether (25 mL), filtered, and concentrated *in vacuo*. Chromatography on silica gel gave the ketone (**8**) (10.4 mg, 69%): ir ($CHCl_3$) ν_{max} 1725, 1710 cm^{-1}; ^{1}Hmr ($CDCl_3$) δ 0.76 (3H, s, C20—methyl), 0.92 (3H, s, C19—methyl), 1.26 (3H, s, C17—methyl), 3.70 (3H, s, CO_2CH_3), 4.80–5.10 (2H, m, C16—H_2), 5.25–5.45 (1H, m, C7—H), 5.60–6.00 (1H, m, C15—H); ms *m/e* 330 (M^+), 315, 271, 255, 213, 187. High resolution molecular weight determination: calcd. 330.2187, found 330.2196.

*Acetonide (**11**)*

Anhydrous $CuSO_4$ (500 mg) and the dihydroxy ester (**10**) (22 mg) were stirred in dry acetone (5 mL) at room temperature for 16 h. The mixture was filtered and the filtrate concentrated *in vacuo*. Chromatography on silica gel gave **11** (18.5 mg, 75%); ir ($CHCl_3$) ν_{max} 1722 cm^{-1}; ^{1}Hmr ($CDCl_3$) δ 0.75 (3H, s, C20—methyl), 0.87 (3H, s, C19—methyl), 1.25 (3H, s, —CH_3), 1.32 (3H, s, C17—methyl), 1.37 (3H, s, —CH_3), 3.62 (3H, s, CO_2CH_3), 3.65–3.85 (3H, m, C15—H, C16—H_2), 5.20–5.40 (1H, m, C7—H); ms *m/e* 390 (M^+), 375, 332, 317, 314, 255. *Anal.* calcd. for $C_{24}H_{38}O_4$: C 73.84, H 9.74; found C 73.49, H 9.67. High resolution molecular weight determination, calcd. 390.276, found 390.2771.

*The acetonide lactone (**16**)*

The trihydroxy acid (**12**) (35 mg), *p*-toluene sulphonic acid (10 mg) and anhydrous $CaCl_2$ (20 mg) were heated in refluxing, dry acetone (20 mL) for 20 min. The mixture was cooled, and evaporated. Benzene (15 mL) was added to the residue and the mixture refluxed for 20 min, cooled, filtered, washed with water, dried ($MgSO_4$), and concentrated *in vacuo*. Chromatography on

silica gel gave **16** (26 mg, 70%) mp 164–167°C (ether – petroleum ether); ir ($CHCl_3$) ν_{max} 1770 cm^{-1}; ^{1}Hmr ($CDCl_3$) δ 0.76 (3H, s, C20—methyl), 1.14 (3H, s, C19—methyl), 1.18 (3H, s, —CH_3), 1.34 (3H, s, C17—methyl), 1.40 (3H, s, —CH_3), 3.60–3.90 (3H, m, C15—H, C16—H_2), 4.60–4.80 (1H, m, $W/2$ = 13 Hz, C2β—H), 5.25–5.50 (1H, m, C7—H); ms *m/e* 374 (M^+), 316, 298, 272. *Anal*. calcd. for $C_{23}H_{34}O_4$: C 73.79, H 9.09; found: C 73.81, H 8.98. High resolution molecular weight determination, calcd. 374.2448; found 374.2442.

*The acetonide (**14**)*

Acetonide (**14**) was obtained in 86% yield by stirring a mixture of the ester **13** (37 mg), and anhydrous $CuSO_4$ (500 mg) in acetone (20 mL) for 12 h at room temperature as above; ir ($CHCl_3$) ν_{max} 3700–3300, 1722 cm^{-1}; ^{1}Hmr ($CDCl_3$) δ 0.75 (3H, s, C20—methyl), 0.92 (3H, s, C19—methyl), 1.30 (3H, s, —CH_3), 1.40 (3H, s, C17—methyl), 1.45 (3H, s, —CH_3), 3.67 (3H, s, CO_2CH_3), 3.56–4.00 (4H, m, C2β—H, C15—H, C16—H_2), 5.25–5.50 (1H, m, C7—H); ms *m/e* 406 (M^+), 391, 348, 330, 315, 286, 272, 253. *Anal*. calcd. for $C_{24}H_{38}O_5$: C 70.93, H 9.35; found C 70.74, H 9.16. High resolution molecular weight determination, calcd. 406.2709, found 406.2716.

*The acetonide (**15**)*

The hydroxyacetonide **14** was oxidised using pyridinium chlorochromate, as described above, to give **15** in 84% yield; ir ($CHCl_3$) ν_{max} 1722, 1708 cm^{-1}; ^{1}Hmr ($CDCl_3$) δ 0.76 (3H, s, C20—methyl), 0.92 (3H, s, C19—methyl), 1.26 (3H, s, —CH_3), 1.36 (3H, s, C17—methyl), 1.40 (3H, s, —CH_3), 3.70–3.95 (3H, m, C15—H, C16—H_2), 3.72 (3H, s, CO_2CH_3), 5.30–5.50 (1H, m, C7—H); ms *m/e* 404 (M^+), 389, 346, 331, 328, 302, 287, 269, 243. *Anal*. calcd. for $C_{24}H_{36}O_5$: C 71.28, H 8.91; found: C 71.19, H 8.63. High resolution molecular weight determination: calcd. 404.2553; found 404.2561.

Acknowledgements

Financial aid from the Natural Sciences and Engineering Research Council of Canada is gratefully acknowledged. We also wish to thank Drs. J. W. Rowe and D. F. Zinkel, U.S. Department of Agriculture, Forest Products Laboratory, Madison, WI, for generous gifts of isopimaric acid.

1. J. P. KUTNEY, M. SINGH, G. HEWITT, P. J. SALISBURY, B. R. WORTH, J. A. SERVIZI, D. W. MARTENS, and R. W. GORDON. Can. J. Chem. **59**, 2334 (1981).
2. I. H. ROGERS. Pulp Paper Mag. Can. **74**(9), T303 (1973).
3. J. M. LEACH and A. N. THAKORE, *Tappi*, **59**(2), 129 (1971).
4. R. W. HEMMINGWAY and H. GREAVES, *Tappi*, **56**(12), 189 (1973).

Can. J. Chem. Downloaded from www.nrcresearchpress.com by 210.87.254.5 on 09/06/12
For personal use only.

Nucleic acid related compounds. 35. Synthesis of 5-bromo- and 5-deuterio-3-deazauridine[1]

MORRIS J. ROBINS, CHISATO KANEKO,[2] AND MASAKATSU KANEKO[3]
Department of Chemistry, The University of Alberta, Edmonton, Alta., Canada T6G 2G2

Received May 20, 1981

MORRIS J. ROBINS, CHISATO KANEKO, and MASAKATSU KANEKO. Can. J. Chem. **59**, 3356 (1981).

Bromination of 3-deazauracil (4-hydroxy-2-pyridinone) (**1**) gave the 3,5-dibromo compound (**2**). Selective debromination of **2** gave 5-bromo-4-hydroxy-2-pyridinone (**3**). Trimethylsilylation of **3** and condensation of the product (**4**) *in situ* with tetra-*O*-acetyl-β-D-ribofuranose (**5**) using tin(IV) chloride as catalyst gave 1-(2,3,5-tri-*O*-acetyl-β-D-ribofuranosyl)-5-bromo-4-hydroxy-2-pyridinone (**7**). Deprotection of **7** gave 5-bromo-3-deazauridine (**6**). Catalytic hydrogenolysis of **7** gave 3-deazauridine triacetate (**8***a*) and deuteriolysis gave the 5-deuterio product (**8***b*). Deprotection of **8***b* gave the isotope-labeled anticancer agent, 5-deuterio-3-deazauridine (**9**). Biochemical and clinical implications are discussed.

MORRIS J. ROBINS, CHISATO KANEKO et MASAKATSU KANEKO. Can. J. Chem. **59**, 3356 (1981).

La bromation du déaza-3 uracile (hydroxy-4 pyridinone-2) (**1**) conduit au composé dibromé en positions 3 et 5 (**2**). Une débromation sélective du composé **2** donne la bromo-5 hydroxy-4 pyridinone-2 (**3**). La triméthylsylilation du composé **3** suivie de la condensation *in situ* du composé **4** obtenu sur le tétra-*O*-acétyl β-D-ribofurannose (**5**) en utilisant le chlorure d'étain(IV) comme catalyseur permet d'obtenir la (tri-*O*-acétyl-2,3,5 β-D-ribofurannosyl)-1 bromo-5 hydroxy-4 pyridinone-2 (**7**). La déprotection du composé **7** conduit à la bromo-5 déaza-3 uridine (**6**). Par hydrogénolyse catalysée, le composé **7** conduit au triacétate de la deaza-3 uridine (**8***a*) et par deutérolyse, on obtient le produit deutéré en position 5 (**8***b*). La déprotection de ce dernier donne l'agent anticancérigène marqué isotopiquement: la deutéro-5 déaza-3 uridine (**9**). On discute des implications biochimiques et cliniques.
[Traduit par le journal]

The synthesis of 3-deazauridine (4-hydroxy-1-β-D-ribofuranosyl-2-pyridinone) was described by us several years ago (2). This nucleoside analogue was found to possess significant antileukemia activity in cell culture and also in infected experimental animals (3). A remarkable collateral sensitivity to 3-deazauridine was observed in a leukemia cell line that had developed resistance to the widely used clinical drug araC (1-β-D-arabinofuranosylcytosine) (4). It was found that 3-deazauridine is phosphorylated rapidly by cellular enzymes. Its 5′-triphosphate product functions as a potent inhibitor of cytidine triphosphate (CTP) synthetase, the enzyme that effects the sole *de novo* pathway into cytosine nucleotide metabolism (5). It has been observed very recently that significantly elevated levels of CTP synthetase occur in certain tumors (6). Cytidine and deoxycytidylate dearminases were found to be inhibited by 3-deazauridine and its 5′-monophosphate, respectively (7). These combined effects of blockage of *de novo* CTP production and depression of deamination of cytosine-type nucleosides and nucleotides provide a strong rationale for combination chemotherapy employing 3-deazauridine plus araC (8, 9) or 5-azacytidines (10, 11).

Successful pharmacological evaluation in animals led to introduction of 3-deazauridine into human clinical trials (9, 12). A very recent report notes a term clinical remission in a leukemia patient whose disease had become resistant to standard araC therapy (9).

Incorporation of 5-bromouracil into nucleic acids results in enhanced mutation frequencies (13). No incorporation of 3-deazauridine into cellular RNA or DNA was detected previously (14). However, 5-bromo-3-deazauridine had not been synthesized and the level of radioactivity achieved previously in labeled 3-deazauridine was insufficient for certain biochemical and metabolic studies. Therefore, we sought routes to make these compounds available.

Bromination of protected 3-deazauridine occurs readily at C-3 (15). However, attempted 3,5-dibromination resulted in decomposition of the protected nucleoside. Rapid hydrogen exchange with protic solvents occurs at C-3 (2), which precludes this position for labeling. We have employed the Vorbrüggen silyl ether coupling procedure (16) with 5-bromo-3-deazauracil and acetylated ribofurnanose to provide the needed product nucleosides.

Bromination of 3-deazauracil (4-hydroxy-2-pyridinone) (**1**) gave 3,5-dibromo-4-hydroxy-2-pyridinone (**2**) in 71% yield as described by den Hertog (17). Compound **2** was selectively debrominated at C-3 with aniline in aqueous hydrobromic acid to give 5-bromo-4-hydroxy-2-pyridinone (**3**) in 82% yield as described (18). The ^{1}H nmr and elemental

[1]For the previous paper in this series see ref. 1.
[2]Postdoctoral Fellow 1980–1981.
[3]On leave from Sankyo Co., Ltd., Tokyo, Japan 1979–1981.

0008-4042/81/243356-04$01.00/0
©1981 National Research Council of Canada/Conseil national de recherches du Canada

Can. J. Chem. Downloaded from www.nrcresearchpress.com by 210.87.254.42 on 09/06/12
For personal use only.

Can. J. Chem. Downloaded from www.nrcresearchpress.com by 210.87.254.42 on 09/06/12
For personal use only.

Reaction Scheme

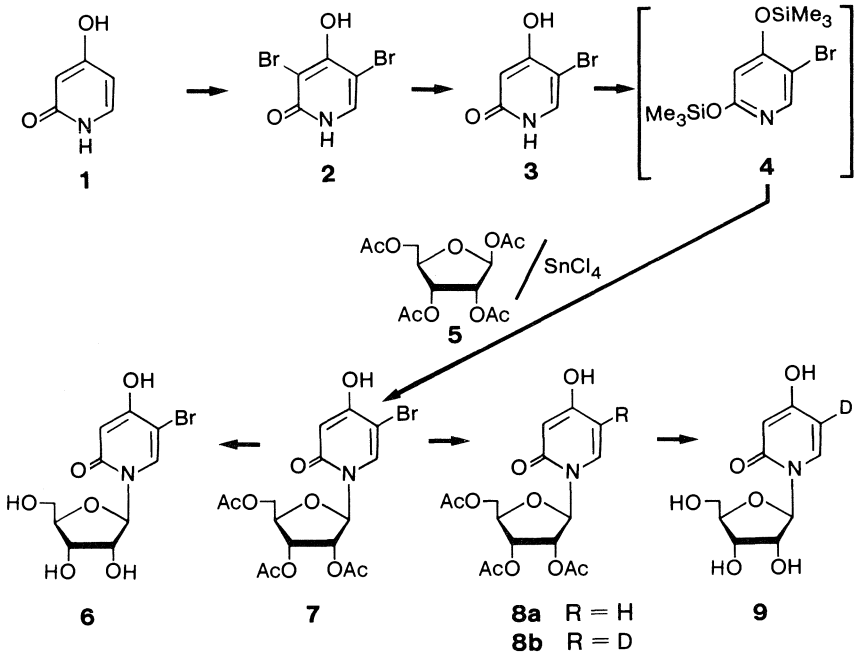

analysis data confirmed the structures of **2** and **3**, whose melting point behavior was divergent from reported values.

Treatment of **3** with a catalytic amount of chlorotrimethylsilane in hexamethyldisilazane gave an oily product (presumed **4**) that was condensed with 1,2,3,5-tetra-*O*-acetyl-β-D-ribofuranose (**5**) in the presence of tin(IV) chloride (16). A 97% yield (78% recrystallized) of 1-(2,3,5-tri-*O*-acetyl-β-D-ribofuranosyl)-5-bromo-4-hydroxy-2-pyridinone (**7**) was obtained. Deprotection of **7** with methanolic ammonia gave 5-bromo-3-deazauridine (**6**) as a crystalline monoacetamide complex in 51% yield. Removal of the acetamide was effected by chromatography on Dowex 1-X2 (OH^-). However, the free **6** resisted crystallization under a variety of conditions. A solid sample of **6** was obtained by lyophilization of a solution in benzene. Addition of one equivalent of acetamide to a solution of the free nucleoside again resulted in crystallization of a **6**·monoacetamide complex.

Catalytic hydrogenolysis of **7** gave 3-deazauridine triacetate (**8*a***) in 80% yield. This product was identical to a sample prepared from 3-deazauridine, which confirmed the N-1 attachment site and β configuration of **6–8**. Identical treatment of **7** in monodeuterioacetic acid (DOAc) with deuterium gas gave **8*b*** cleanly in 88% yield. Deuteriolysis of **7** in glacial acetic acid resulted in partial incorporation of protium at C-5. Deprotection of **8*b*** with methanolic ammonia gave 5-deuterio-3-deazauridine (**9**) in 83% yield. The H-6 and H-3 protons gave rise to clean singlets in the nmr spectrum of **9**.

The present work has provided the previously unknown 5-bromo-3-deazauridine[4] (**6**) and makes readily available a convenient precursor for labeling 3-deazauridine with hydrogen isotopes at a chemically stable site (C-5). Such a tritium-labeled product with high specific activity[5] was urgently needed for biomedical studies.

Experimental

General

Melting points were obtained on a Reichert microstage block and are uncorrected. Ultraviolet (uv) spectra were recorded on a Cary 15 spectrophotometer. The ^1H nmr spectra were determined on a Varian 100-MHz spectrometer with Me_4Si as internal reference. Mass spectra (ms) were measured at 70 eV with an AEI MS-50 instrument with coupled computer analysis using direct probe sample introduction at 150–250°C by the mass

[4]Evaluation of compound **6** in a murine leukemia L1210 cell culture indicated no inhibitory activity at a concentration of 100 μ*M*.

[5]Now available from Moravek Biochemicals, Brea, CA 92621, U.S.A.

Can. J. Chem. Downloaded from www.nrcresearchpress.com by 210.87.254.42 on 09/06/12
For personal use only.

spectral laboratory of this department. Elemental analyses were determined by the microanalytical laboratory of this department. Evaporations were effected with a Buchler rotary evaporator equipped with a Dewar "Dry-Ice" condenser at mechanical oil pump (*in vacuo*) or water aspirator vacuum.

The 4-hydroxy-2-pyridinone (2,4-dihydorxypyridine, 3-deazauracil) was purchased from Aldrich Chemical Co. and the 1,2,3,5-tetra-*O*-acetyl-β-D-ribofuranose from Raylo Chemicals Ltd., Edmonton, Alberta.

*3,5-Dibromo-4-hydroxy-2-pyridinone (**2**)*

A 1.1 g (9.9 mmol) sample of 4-hydroxy-2-pyridinone (**1**) was brominated with 1.1 mL (20 mmol) of Br_2 essentially as described (17) to give 1.88 g (71%) of **2**. Recrystallization from 98% EtOH gave colorless needles of **2**, mp 259–262°C (after becoming dark colored from 235–245°C) (lit. (17) mp ~ 245°C (dec.), mp (19) 225–240°C (dec.)); nmr (Me_2SO-d_6) δ: 7.67 (s, 1, H-6). *Anal.* calcd. for $C_5H_3Br_2NO_2$: C 22.34, H 1.12, N 5.21; found: C 22.28, H 1.14, N 5.27.

*5-Bromo-4-hydroxy-2-pyridinone (**3**)*

A 0.54 g (2 mmol) sample of **2** was heated with 0.19 g (2 mmol) of aniline in 5 mL of 47% HBr/H_2O at 100°C for 4 h in a sealed tube. Processing as described previously (18) and recrystallization from 95% EtOH gave 0.31 g (82%) of white needles of **3**, mp 250–251°C (lit. (20) mp 226.5–227.5°C); nmr (Me_2SO-d_6) δ: 5.72 (s, 1, H-3), 7.56 (s, 1, H-6). *Anal.* calcd. for $C_5H_4BrNO_2$: C 31.61, H 2.12, N 7.37; found: C 31.71, H 2.21, N 7.44.

*1-(2,3,5-Tri-O-acetyl-β-D-ribofuranosyl)-5-bromo-4-hydroxy-2-pyridinone (**7**)*

A 1.71 g (9 mmol) sample of **3** was suspended in 7 mL of hexamethyldisilazane and 3 drops of chlorotrimethylsilane was added. The mixture was heated at reflux with exclusion of moisture for 3 h. A clear solution was obtained and solid NH_4Cl was deposited in the reflux condenser. The volatile materials were evaporated *in vacuo* at 40°C to give the presumed bis-trimethylsilyloxypyridine derivative (**4**) as a colorless viscous oil.

A solution of the oily **4** in 5 mL of 1,2-dichloroethane was added to a solution of 2.75 g (8.6 mmol) of 1,2,3,5-tetra-*O*-acetyl-β-D-ribofuranose (**5**) in 50 mL of dichloroethane. The vigorously stirred mixture was cooled in an ice-bath and then 0.75 mL (6.5 mmol) of redistilled $SnCl_4$ was added. The pale yellow solution was allowed to stand at room temperature for 18 h while protected from moisture. The solution was diluted with 20 mL of 1,2-dichloroethane and then was shaken with 40 mL of saturated $NaHCO_3/H_2O$. The resulting emulsion was filtered using a layer of Celite. The Celite cake was washed with 10 mL of $CHCl_3$. Dilute HBr/H_2O was added to the combined filtrate to pH ~ 4 (indicator paper). NaCl was added to saturate the aqueous layer and the mixture was extracted with 3 × 40 mL of $CHCl_3$. The combined organic phase was washed with saturated $NaCl/H_2O$, dried over Na_2SO_4, filtered, and evaporated. The resulting amorphous residue was purified by chromatography on silica using 3% $MeOH/CHCl_3$ for elution to give 3.75 g (97%) of **7** as an amorphous colorless solid. Crystallization from absolute EtOH gave 3.02 g (78%) of white needles of **7**, mp 195–196°C; uv (0.1 *N* HCl): max 295 nm (ε 3900), min 262 nm (ε 1100); (H_2O): max 268, 286 (sh) nm (ε 4900, 4000), min 248 nm (ε 3700); nmr (Me_2SO-d_6) δ: 2.05 (s, 3, OAc), 2.07 (s, 6, two OAc's), 4.28 (m, 3, H-4′, 5′, 5″), 5.28–5.50 (m, 2, H-2′, 3′), 5.74 (s, 1, H-3), 6.02 (d, $J_{1'-2'}$ = 4.0 Hz, 1, H-1′), 7.95 (s, 1, H-6); ms *m/z*: 449.0127 (5.1%, M^+ [^{81}Br] = 449.0144), 447.0160 (4.6%, M^+ [^{79}Br] = 447.0165). *Anal.* calcd. for $C_{16}H_{18}BrNO_9$: C 42.88, H 4.05, N 3.13; found: C 42.74, H 4.03, N 3.00.

*5-Bromo-4-hydroxy-1-β-D-ribofuranosyl-2-pyridinone (5-Bromo-3-deazauridine) (**6**)*

To 30 mL of MeOH saturated with NH_3 at 0°C was added 868 mg (1.94 mmol) of **7**. The mixture was allowed to stand for 18 h in a refrigerator at 4°C and then was evaporated to give a white solid foam. This residue was crystallized from isopropanol to give 379 mg (51%) of white needles of a **6**·monoacetamide complex, mp 180–181°C; uv (0.1 *N* HCl): max 293 nm (ε 4000), min 261 nm (ε 1300); (H_2O): max 284, 270 nm (ε 4000, 4200), min 278, 249 nm (ε 3900, 3500); (0.1 *N* NaOH): max 264, 270 (sh), 286 (sh) nm (ε 7400, 7200, 4200), min 244 nm (ε 5000); nmr (Me_2SO-d_6) δ: 1.78 (s, 3, acetamide methyl), 3.66 (m, 2, H-5′, 5″), 3.96 (m, 3, H-2′, 3′, 4′), 4.98, 5.20, 5.34 (br singlets, three OH's), 5.75 (s, 1, H-3), 5.94 (d, $J_{1'-2'}$ = 3.8 Hz, 1, H-1′), 6.63 and 7.25 (br, 1 & 1, acetamide NH's), 8.30 (s, 1, H-6); ms *m/z*: 322.9835 (3.3%, M^+ [^{81}Br] = 322.9829), 320.9847 (3.1%, M^+ [^{79}Br] = 320.9848). *Anal.* calcd. for $C_{10}H_{12}BrNO_6 \cdot C_2H_5NO$: C 37.82, H 4.50, N 7.35; found: C 37.83, H 4.52, N 7.27.

An aqueous solution of 500 mg (1.31 mmol) of **6**·monoacetamide complex was applied to a column of 20 mL of Dowex 1-X2 (OH^-) resin. The column was washed with water to remove the acetamide and then was eluted with 1% $HOAc/H_2O$. Fractions containing **6** were pooled and evaporated *in vacuo*. The residue failed to crystallize under a variety of conditions. It was dissolved in a minimum amount of methanol, diluted with dry benzene, and lyophilized to give 395 mg (89%) of **6** as an amorphous white solid containing ~ 0.2 equivalents of benzene solvate; uv (0.1 *N* HCl): max 294 nm (ε 4100), min 262 nm (ε 1300); (H_2O): max 287, 273 nm (ε 4000, 3900), min 278, 252 nm (ε 3800, 3300); (0.1 *N* NaOH): max 265, 285 (sh) nm (ε 7300, 4200), min 245 nm (ε 4800); the nmr (Me_2SO-d_6) spectrum was identical to that of the above **6**·monoacetamide complex except for the absence of peaks for acetamide and the presence of ~ 1.2 H from residual benzene; ms *m/z*: 322.9840 (6.3%, M^+ [^{81}Br] = 322.9829), 320.9853 (6.0%, M^+ [^{79}Br] = 320.9848). *Anal.* calcd. for $C_{10}H_{12}BrNO_6 \cdot 0.2\ C_6H_6$: C 39.83, H 3.94, N 4.15; found: C 39.85, H 4.12, N 3.91.

*1-(2,3,5-Tri-O-acetyl-β-D-ribofuranosyl)-5-deuterio-4-hydroxy-2-pyridinone (**8**b)*

A suspension of 500 mg of 5% Pd·C catalyst in 8 mL of acetic acid-d_1 (DOAc) was stirred vigorously for 20 min in a deuterium atmosphere with intermittent bubbling of D_2 through the mixture. A 500 mg (1.12 mmol) sample of **7** was added and the mixture was stirred vigorously for 5 h at room temperature under 1 atm pressure of D_2. The mixture was filtered, 410 mg (5 mmol) of NaOAc was added to the filtrate, and this solution was evaporated *in vacuo*. The residue was treated with 10 mL of $CHCl_3$ and 5 mL of H_2O and the organic layer was separated. The aqueous phase was extracted with 2 × 10 mL of $CHCl_3$. The combined organic phase was washed with 10 mL of H_2O, dried over Na_2SO_4, filtered, and evaporated. The resulting pale violet residue (365 mg, 88%) was dissolved in dry benzene and lyophilized to give a powder. The powder was crystallized from dry benzene to give violet tinted needles of **8***b*, mp 155–155.5°C; uv (0.1 *N* HCl): max 282, 228 (sh) nm (ε 4500, 3200), min 252 nm (ε 1500); (H_2O): max 282 nm (ε 4800), min 250 nm (ε 1800); nmr ($CDCl_3$) δ: 2.09 (s, 6, two OAc's), 2.14 (s, 3, OAc), 4.38 (br, 3, H-4′, 5′, 5″), 5.33 (br, 2, H-2′, 3′), 5.96 (s, 1, H-3), 6.28 (d, $J_{1'-2'}$ = 3.8 Hz, 1, H-1′), 7.45 (s, 1, H-6); ms *m/z*: 370.1117 (8.0%, M^+ = 370.1123). *Anal.* calcd. for $C_{16}H_{18}DNO_9$ (by H_2O/HDO gas volume analysis): C 51.90, H 5.17, N 3.78; found: C 51.95, H 5.13, N 3.65.

*1-(2,3,5-Tri-O-acetyl-β-D-ribofuranosyl)-4-hydroxy-2-pyridinone (**8**a)*

A 100 mg (0.223 mmol) sample of **7** was subjected to the identical procedure for the above conversion of **7** → **8***b* (but employing ^{1}H isotope in place of deuterium) to give 66 mg (80%) of amorphous **8***a*. This product was crystallized from absolute EtOH to give colorless prisms of **8***a*, mp 153–155°C; uv (same as for **8***b*); nmr ($CDCl_3$) (sugar protons same as for **8***b*) δ: 5.96 (d,

J_{3-5} = 2.0 Hz, 1, H-3), 6.10 (d of d, J_{5-3} = 2.0 Hz, J_{5-6} = 7.0 Hz, 1, H-5), 7.47 (d, J_{6-5} = 7.0 Hz, 1, H-6); ms *m/z*: 369.1052 (6.4%, M^+ = 369.1060). *Anal.* calcd. for $C_{16}H_{19}NO_9$: C 52.04, H 5.19, N 3.79; found: C 52.03, H 5.13, N 3.70.

This compond was identical to a sample prepared from 3-deazauridine (M. Kaneko, to be published) by mp, ir, ^{1}H nmr, and mass spectral comparisons.

5-Deuterio-4-hydroxy-1-β-D-ribofuranosyl-2-pyridinone (5-Deuterio-3-deazauridine) (9)

To 30 mL of MeOH saturated with NH_3 at 0°C was added 365 mg (0.986 mmol) of **8***b*. The mixture was allowed to stand for 18 h in a refrigerator at 4°C and then was evaporated. The residual pale yellow foam was dissolved in H_2O and applied to a column of 10 mL of Dowex 1-X2 (OH^-) resin. The column was washed with 500 mL of H_2O, 1000 mL of 30% MeOH/H_2O, and then was eluted with 500 mL of 0.5% HOAc/H_2O. Appropriate fractions were pooled and evaporated *in vacuo*. The residue was dissolved in a minimum volume of MeOH, diluted with dry benzene, and lyophilized to give 200 mg (83%) of **9** as a pale yellow powder. This material was crystallized from MeOH to give off-white prisms of **9**, mp 248–249°C; uv (0.1 *N* HCl): max 280, 272 (sh), 230 nm (ε 5000, 4800, 4900), min 250, 223 nm (ε 2300, 4500); (H_2O): max 281 nm (ε 6300), min 250 nm (ε 2200); (0.1 *N* NaOH): max 255, 270 (sh) nm (ε 10 000, 7300), min 232 nm (ε 4800); nmr (Me_2SO-d_6) δ: 3.63 (br, 2, H-5′, 5″), 3.96 (m, 3, H-2′, 3′, 4′), 5.00 (br, 2, two OH's), 5.27 (br, 1, OH), 5.57 (s, 1, H-3), 5.98 (d, $J_{1'-2'}$ = 3.8 Hz, 1, H-1′), 7.80 (s, 1, H-6), 13.0 (br, 1, pyridine-4-OH); ms *m/z*: 244.0812 (1.3%, M^+ = 244.0805). *Anal.* calcd. for $C_{10}H_{12}DNO_6$ (by H_2O/HDO gas volume analysis): C 49.19, H 5.37, N 5.74; found: C 49.07, H 5.33, N 5.64.

Acknowledgments

We thank the National Cancer Institute of Canada, the Natural Sciences and Engineering Research Council of Canada (A5890), and The University of Alberta for generous financial support.

1. M. J. Robins and B. Uznański. Can. J. Chem. **59**, 2608 (1981).
2. M. J. Robins and B. L. Currie. Chem. Commun. 1547 (1968).
3. (*a*) M. J. Robins, B. L. Currie, R. K. Robins, and A. Bloch. Proc. Am. Assoc. Cancer Res. **10**, 73 (1969); (*b*) A. Bloch, G. Dutschman, B. L. Currie, R. K. Robins, and M. J. Robins, J. Med. Chem. **16**, 294 (1973).
4. R. W. Brockman, S. C. Shaddix, M. Williams, J. A. Nelson, L. M. Rose, and F. M. Schabel, Jr. Ann. N.Y. Acad. Sci. **255**, 501 (1975).
5. R. P. McPartland, M. C. Wang, A. Bloch, and H. Weinfeld. Cancer Res. **34**, 3107 (1974).
6. H. Kizaki, J. C. Williams, H. P. Morris, and G. Weber. Cancer Res. **40**, 3921 (1980).
7. J. C. Drake, K. R. Hande, R. W. Fuller, and B. A. Chabner. Biochem. Pharmacol. **29**, 807 (1980).
8. C. Mills-Yamamoto, G. J. Lauzon, and A. R. P. Paterson. Biochem. Pharmacol. **27**, 181 (1978).
9. B. Barlogie, W. Plunkett, M. Raber, J. Latreille, M. Keating, and K. McCredie. Cancer Res. **41**, 1227 (1981).
10. R. L. Momparler, J. Veselý, L. F. Momparler, and G. E. Rivard. Cancer Res. **39**, 3822 (1979).
11. S. Grant and E. Cadman. Cancer Res. **40**, 4000 (1980).
12. (*a*) K. B. McCredie, G. P. Bodey, M. J. Keating, M. Valdivieso, S. Yap, and E. J. Freireich. Proc. Am. Assoc. Cancer Res. **20**, 405 (1979); (*b*) J. A. Benvenuto, S. W. Hall, D. Farquhar, D. J. Stewart, R. S. Benjamin, and T. L. Loo. Cancer Res. **39**, 349 (1979); (*c*) D. J. Stewart, J. A. Benvenuto, M. Leavens, S. W. Hall, R. S. Benjamin, W. Plunkett, K. B. McCredie, M. A. Burgess, and T. L. Loo. Cancer Res. **39**, 4119 (1979).
13. E. Freese. J. Mol. Biol. **1**, 87 (1959).
14. M. C. Wang and A. Bloch. Biochem. Pharmacol. **21**, 1063 (1972).
15. B. L. Currie, M. J. Robins, and R. K. Robins. J. Heterocycl. Chem. **8**, 221 (1971).
16. U. Niedballa and H. Vorbrüggen. J. Org. Chem. **39**, 3654 (1974).
17. H. J. den Hertog. Recl. Trav. Chim. Pays-Bas, **64**, 85 (1945).
18. H. J. den Hertog, W. P. Combé, and C. R. Kolder. Recl. Trav. Chim. Pays-Bas, **73**, 704 (1954).
19. G. Errera. Chem. Ber. **31**, 1682 (1898).
20. H. J. den Hertog, J. C. M. Schogt, J. de Bruyn, and A. de Klerk. Recl. Trav. Chim. Pays-Bas, **69**, 673 (1950).

Can. J. Chem. Downloaded from www.nrcresearchpress.com by 210.87.254.42 on 09/06/12
For personal use only.

Nucleic acid related compounds. 36. Synthesis of the 2′-*O*-methyl and 3′-*O*-methyl ethers of guanosine and 2-aminoadenosine and correlation of *O*′-methylnucleoside ^{13}C nmr spectral shifts[1]

MORRIS J. ROBINS, FRITZ HANSSKE,[2] AND SALWA E. BERNIER[3]

Department of Chemistry, The University of Alberta, Edmonton, Alta., Canada T6G 2G2

Received May 20, 1981

Can. J. Chem. Downloaded from www.nrcresearchpress.com by 210.87.254.6 on 09/06/12
For personal use only.

MORRIS J. ROBINS, FRITZ HANSSKE, and SALWA E. BERNIER. Can. J. Chem. **59**, 3360 (1981).

A modified trimethylsilylation of guanosine (**1**) followed by *in situ* replacement of the 6-trimethylsilyloxy group with ammonia at 150°C gave 2,6-diamino-9-β-D-ribofuranosylpurine (**2**) in 92% yield. Treatment of **2** with diazomethane in the presence of tin(II) chloride dihydrate gave the 2′-*O*-methyl (**3**) and 3′-*O*-methyl (**4**) ethers of **2** in 98% combined yield. The ratios of **3**/**4** could be varied from 51:47 to 34:64 by changing the amount of catalyst used. Treatment of **3** and **4** with adenosine deaminase resulted in clean conversion of these 2-aminoadenosine ethers to 2′-*O*-methylguanosine (**5**) and 3′-*O*-methylguanosine (**6**), respectively, in optimized yields of 40% and 54% overall from **1**. The ^{13}C nmr data for six ribonucleosides and their isomeric methyl ether derivatives have been correlated to provide a convenient method of identification.

MORRIS J. ROBINS, FRITZ HANSSKE et SALWA E. BERNIER. Can. J. Chem. **59**, 3360 (1981).

Une triméthylsilylation de guanosine (**1**) suivie d'une réaction *in situ* avec l'ammoniac à 150°C conduit, par déplacement du groupe triméthylsilyloxy-6, à la diamino-2,6 β-D-ribofurannosyl-9 purine (**2**) avec un rendement de 92%. Le composé **2** réagit avec le diazométhane en présence du dihydrate du chlorure d'étain(II) pour en donner les éthers *O*-méthyl-2′ (**3**) et -3′ (**4**) avec un rendement combiné de 98%. On peut faire varier le rapport **3**/**4** de 51:47 à 34:64 en changeant la quantité de catalyseur utilisé. En faisant réagir les composés **3** et **4** avec la désaminase de l'adénosine, on transforme ces éthers de l'amino-2 adénosine en *O*-méthyl-2′ guanosine (**5**) et *O*-méthyl-3′ guanosine (**6**) avec des rendements globaux respectifs optimisées de 40 et de 54%. On a établi une corrélation entre les données de la rmn du ^{13}C de six ribonucléosides et de leurs éthers méthyliques isomères de façon à obtenir une méthode convenable d'identification.

[Traduit par le journal]

The 2′-*O*-methyl ethers of the four major ribonucleosides occur as ubiquitous "minor components" in all types of ribonucleic acids (RNA's) (2). Recently, an extreme thermophile, *Thermus thermophilus* HB27, was found to have markedly enhanced levels of 2′-*O*-methylguanosine in its tRNA when grown at 80°C. It was inferred that the enzyme activity of a specific methyl transferase in the bacterium was higher at the elevated temperature (3). The 5′-triphosphate of synthetic 3′-*O*-methylguanosine was shown to effect termination of biosynthesis of RNA catalyzed by a RNA polymerase. This termination technique has been applied to sequencing studies of RNA and DNA (4).

Convenient and high yield methods have been devised for synthesis of the 2′-*O*- and 3′-*O*-methyl ethers of adenosine, cytidine, and uridine (see the discussion and references quoted in ref. 5). However, guanosine has presented significant difficulties. Khwaja and Robins (6) treated 2-amino-6-chloro-9-β-D-ribofuranosylpurine with diazomethane followed by sodium hydrogen sulfide to give 2′-*O*-methyl-6-thioguanosine. This product was converted to 2′-*O*-methylguanosine in ~14% yield overall from guanosine. Goodman and co-workers first prepared 3′-*O*-methylguanosine by a multistep carbohydrate synthesis and base–sugar coupling (7). We had obtained the 2′-*O*- and 3′-*O*-methylguanosines in ~15% yield, each, by careful treatment of guanosine with diazomethane and stannous chloride as catalyst. However, tedious chromatographic separation and isolation were involved (5). Kusmierek and Shugar (8) converted guanosine to its 6-ethoxy analogue. Treatment of this product with diazomethane/tin(II) chloride followed by separation of isomers and hydrolysis gave low overall yields of 2′-*O*- (7%) and 3′-*O*-methylguanosine (5%). Ekborg and Garegg very recently have reported overall yields of the 2′-*O*- (13%) and 3′-*O*-methyl (28%) isomers by treatment of 5′-*O*-*tert*-butyldiphenylsilylguanosine with diazomethane/stannous chloride followed by chromatography and fractional crystallization (9). We now report a convenient procedure that allows complete separation of isomers on the Dekker column (10) (Dowex 1-X2 (OH^-) resin) and gives good overall yields of 2′-*O*- (40%) and 3′-*O*-methylguanosine (54%) from guanosine.

The acidic cyclic amide function of guanosine

[1]For the previous paper in this series see ref. 1.

[2]Deutsche Forschungsgemeinschaft Postdoctoral Fellow 1977–1979; University of Alberta Research Associate 1980–present.

[3]NSERC Summer Undergraduate Research Participant 1980.

0008-4042/81/243360-05$01.00/0

©1981 National Research Council of Canada/Conseil national de recherches du Canada

Can. J. Chem. Downloaded from www.nrcresearchpress.com by 210.87.254.6 on 09/06/12
For personal use only.

Reaction Scheme

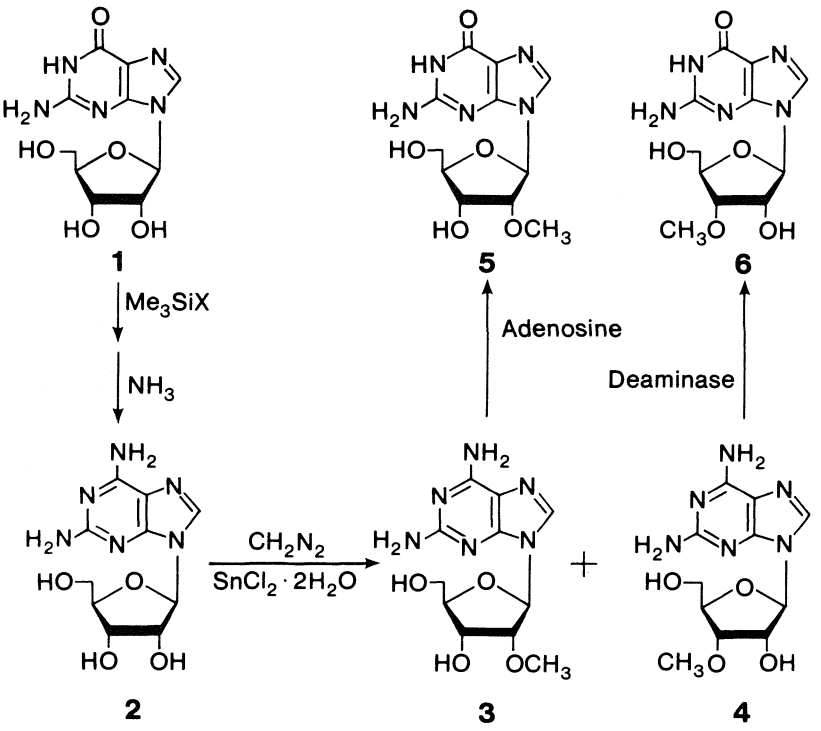

($pK_a = 9.16$) was converted to a weakly basic cyclic amidine by modification of the procedure of Vorbrüggen and Krolikiewicz (11). Guanosine (**1**) was exhaustively trimethylsilylated and treated *in situ* with anhydrous ammonia in toluene at 150°C to give 2,6-diamino-9-β-D-ribofuranosylpurine (2-aminoadenosine) (**2**) in 92% yield. Methylation of **2** with diazomethane/stannous chloride dihydrate (5) in warm *N*,*N*-dimethylformamide (DMF) proceeded to completion. The 2′-*O*- (**3**) and 3′-*O*-methyl-2-aminoadenosine (**4**) products were resolved cleanly on the Dekker column in a combined yield of 98% after crystallization. The ratio of **3**/**4** could be varied from 51:47 to 34:64 by altering the quantity of catalyst. Attempts to alter the product ratio using other inorganic catalysts (12) were not productive.

Conversion of **3** and **4** to the corresponding guanine nucleosides **5** and **6** was effected smoothly using adenosine deaminase, as demonstrated previously with the parent nucleosides **2** → **1** (13). In parallel with rates of the enzymatic deamination of 2′-*O*- and 3′-*O*-methyladenosine,[4] the conversion of **3** → **5** proceeded more rapidly than **4** → **6**. The overall conversion of **1** → **5** was effected in 40% yield and **1** → **6** in 54% with catalyst optimization for each isomer.

The ^1H nmr and mass spectral properties of these *O*′-methyl isomers are in harmony with previously noted trends (5). The 2′-identifying mass spectral ion at B + 44 (2′-OH) or B + 58 (2′-OCH_3) is distinctive. Minor proton shifts (~0.15 ppm) are characteristic as noted by Reese and co-workers (14). However, the small magnitudes of these shifts would make assignment extremely tenuous unless both methylated isomers were available.

The ^{13}C nmr shifts in the *O*′-methyl nucleosides provide a clear means of identification even if only one isomer and the parent nucleoside are available. Table 1 contains ^{13}C nmr data for the four major naturally occurring ribonucleosides plus 2-aminoadenosine (**2**) and 6-thioinosine. Table 2 lists ^{13}C data for the six 2′-*O*-methyl compounds and Table 3 that for their 3′-*O*-methyl isomers. Resonance assignments for the parent nucleosides are in harmony with those of Grant and co-workers (15) with the positions for C-2′ and C-3′ reversed (16) as corrected by Mantsch and Smith (17).

No major effects on the ^{13}C resonances of the base carbons occur upon methylation of the sugar hydroxyl groups. Methylation of O-2′ results in a

[4]F. Hansske, unpublished observation.

TABLE 1. ^{13}C nmr chemical shifts for ribonucleosides

Compound[a]	C-6	C-2	C-4	C-8	C-5	C-1′	C-4′	C-2′	C-3′	C-5′
1	156.81	153.67	151.34	135.63	116.70	86.41	85.23	73.72	70.41	61.45
2	160.14	156.41	151.50	136.64	113.70	87.34	85.70	73.34	70.84	61.84
Ado	156.09	152.31	149.00	139.87	119.30	87.90	85.83	73.41	70.59	61.61
6-TI	175.93	145.13	143.76	141.10	135.30	87.48	85.53	74.15	70.06	61.01
Cyd	141.55	155.50	165.59	—	93.97	89.23	84.14	74.01	69.47	60.69
Urd	140.75	150.77	163.12	—	101.76	87.73	84.86	73.56	69.91	60.88

[a] Abbreviations used are: Ado = adenosine, 6-TI = 6-thioinosine, Cyd = cytidine, Urd = uridine.

TABLE 2. ^{13}C nmr chemical shifts for 2′-*O*-methylribonucleosides

Compound	C-6	C-2	C-4	C-8	C-5	C-1′	C-4′	C-2′	C-3′	C-5′	2′-OCH_3
5	156.75	153.72	151.18	135.36	116.60	85.86	84.35	82.74	68.67	61.29	57.50
3	160.18	156.32	151.43	136.22	113.52	86.25	85.22	82.41	69.02	61.71	57.46
2′-*O*MeAdo	156.10	152.41	148.94	139.57	119.21	86.32	85.76	82.39	68.75	61.41	57.39
2′-*O*Me-6-TI	176.08	145.12	143.55	140.78	135.29	86.03	85.50	83.00	68.53	60.84	57.44
2′-*O*MeCyd	141.24	155.07	165.68	—	93.88	87.51	84.31	83.30	68.41	60.51	57.58
2′-*O*MeUrd	140.31	150.42	162.94	—	101.76	85.91	85.02	82.56	68.19	60.44	57.41

TABLE 3. ^{13}C nmr chemical shifts for 3′-*O*-methylribonucleosides

Compound	C-6	C-2	C-4	C-8	C-5	C-1′	C-4′	C-3′	C-2′	C-5′	3′-OCH_3
6	156.73	153.66	151.27	135.46	116.69	86.43	82.72	79.64	72.92	61.31	57.57
4	160.03	156.30	151.39	136.39	113.59	87.29	83.02	80.60	72.63	61.74	57.59
3′-*O*MeAdo	156.20	152.36	149.33	139.73	119.56	88.23	83.45	80.09	73.02	61.77	57.66
3′-*O*Me-6-TI	176.02	144.97	143.67	140.79	135.32	87.65	83.12	79.22	73.18	60.93	57.43
3′-*O*MeCyd	141.48	155.37	165.68	—	93.80	89.99	82.18	79.00	72.86	60.98	57.46
3′-*O*MeUrd	140.42	150.63	163.00	—	101.61	87.86	82.39	78.92	72.53	60.73	57.48

marked downfield shift of the signal for C-2′ relative to that of the parent nucleoside (average $\Delta\delta$ −9.04 ppm with a range of −8.85 to −9.29 ppm for the six compounds). Upfield shifts for C-1′ (average $\Delta\delta$ 1.37, range 0.55 to 1.82 ppm) and C-3′ (average $\Delta\delta$ 1.62, range 1.06 to 1.84 ppm) occur consistently. Methylation of O-3′ results in the pronounced downfield shift of the signal for C-3′ (average $\Delta\delta$ −9.37, range −9.01 to −9.76 ppm) and upfield shifts for C-2′ (average $\Delta\delta$ 0.84, range 0.39 to 1.15 ppm) and C-4′ (average $\Delta\delta$ 2.40, range 1.96 to 2.68 ppm).

A small upfield shift for C-5′ was observed with all the 2′-*O*-methyl isomers and all but two of the 3′-*O*-methyl compounds. Shifts for C-4′ in the 2′-*O*-methyl and C-1′ in the 3′-*O*-methyl series were small generally, and were not consistent in direction.

This study has provided a convenient route to 2′-*O*-methylguanosine (**5**) and its 3′-*O*-methyl isomer (**6**). The overall yields from guanosine (**1**) are three times greater for **5** and double for **6** those obtained by prior methods. Clean resolution of isomers **3** and **4** was effected on the Dekker column. The ^{13}C nmr shifts provide rapid identification of the methylated isomers. A pronounced downfield shift of ~−9 ppm for C-2′ and upfield shifts of ~1.4 ppm for C-1′ and ~1.6 ppm for C-3′ are diagnostic for the 2′-*O*-methyl compounds. A marked downfield shift of ~−9.4 ppm for C-3′ and upfield shifts of ~0.8 ppm for C-2′ and ~2.4 ppm for C-4′ are observed with the 3′-*O*-methyl isomers, which causes a "cross-over" for the C-2′ and C-3′ resonances in this series relative to the parent and 2′-*O*-methylnucleosides.

Experimental

General

Most general procedures and instrumentation used are given in ref. 1. All nmr spectra were determined in Me_2SO-d_6 with Me_4Si as internal standard. The ^{13}C nmr spectra were obtained at ~22.6, ~50.3, or ~100.6 MHz with broad band ^1H decoupling on Bruker HFX-90, WH-200, or WH-400 spectrometers by the high field nmr laboratory of this department. All uv spectra were measured at pH 7.0 in an aqueous phosphate buffer. Samples for analysis were dried over P_2O_5 at 100°C for three days *in vacuo*. Thin-layer electrophoresis (tle) was performed on 0.1 mm cellulose 300 UV_{254} plates from Macherey & Nagel with a 0.1 *M* aqueous sodium borate buffer (pH 10.0) using a Desaga tle

Can. J. Chem. Downloaded from www.nrcresearchpress.com by 210.87.254.6 on 09/06/12
For personal use only.

Can. J. Chem. Downloaded from www.nrcresearchpress.com by 210.87.254.6 on 09/06/12
For personal use only.

double chamber apparatus at 800–1000 V for 1–1.5 h. The tle mobilities are given relative to the migration of guanosine (R_{Guo} = 1.0), which migrated toward the positive (+) electrode.

2,6-Diamino-9-β-D-ribofuranosylpurine (2-Aminoadenosine) (2)

A mixture of 45 g (0.16 mol) of dried guanosine (**1**), 600 mL of hexamethyldisilazane, and 20 mL of chlorotrimethylsilane was stirred at reflux for 16 h while protected from moisture under dry nitrogen. Volatile materials were distilled at atmospheric pressure and the silylation procedure was repeated on the residual syrup. The second solution was evaporated *in vacuo* and the yellow syrup was dissolved in 250 mL of anhydrous toluene. This solution was transferred quickly into a dried Parr pressure bomb under dry nitrogen, sealed, and cooled to −40°C in a "Dry-Ice"/acetone bath. The bomb was opened under dry nitrogen and 40 mL of hexamethyldisilazane, 3.75 g of trimethylsilyl trifluoromethanesulfonate ($CF_3SO_3SiMe_3$), and 22 mL of anhydrous liquid ammonia were added. The bomb was sealed quickly, heated at 150°C for 3 days, and cooled. The ammonia was vented and 500 mL of MeOH/H_2O (1:1) was added. The mixture was stirred at reflux for 4 h and the MeOH removed by evaporation. Water (300 mL) was added and the hot mixture decolorized with charcoal. The filtrate was chilled to give 37.4 g (83%) of colorless crystals of **2**. This filtrate was concentrated and applied to a column (2.5 × 30 cm) of Dowex 1-X2 (OH^-) resin. The column was washed with H_2O. Elution with MeOH/H_2O (6:4) gave an additional 3.7 g of crystallized product for a total yield of 41.1 g (92%) of **2**, mp 250–252°C (lit. (11) mp 242–244°C); tle R_{Guo} = 0.34 (+); uv max: 280, 256, 216 nm (ε 10 900, 10 000, 25 600); ^{1}H nmr δ: 3.57 (m, 2, H-5′,5″), 3.90 (m, $J_{4'-3'}$ = 3 Hz, $J_{4'-5',5''}$ ~7 Hz, 1, H-4′), 4.09 (m, $J_{3'-3'OH}$ = 4.5 Hz, $J_{3'-2'}$ = 5 Hz, 1, H-3′), 4.50 (m, $J_{2'-2'OH}$ = 6 Hz, $J_{2'-1'}$ = 6 Hz, 1, H-2′), 5.06 (d, 1, 3′-OH), 5.32 (d, 1, 2′-OH), 5.43 (t, $J_{5'OH-5',5''}$ = 6 Hz, 1, 5′-OH), 5.67 (br s, 2, 2-NH_2), 5.69 (d, 1, H-1′), 6.72 (br s, 2, 6-NH_2), 7.87 (s, 1, H-8); ms *m/z*: 282.1075 (8.8%, M^+ = 282.1077), 193.0837 (9.7%, B + 43 = 193.0838), 150.0655 (100%, B = 150.0654). *Anal.* calcd. for $C_{10}H_{14}N_6O_4$: C 42.55, H 5.00, N 29.78; found: C 42.32, H 4.99, N 29.83.

2,6-Diamino-9-(2-O-methyl-β-D-ribofuranosyl)purine (3) and 2,6-Diamino-9-(3-O-methyl-β-D-ribofuranosyl)purine (4)

To a stirred solution of 2.26 g (8 mmol) of **2** in 150 mL of hot DMF was added 324 mg (1.44 mmol) of $SnCl_2 \cdot 2H_2O$. The mixture was stirred at 50–55°C (to maintain solubility of **2**) and 120 mL of ~0.2 *M* CH_2N_2 in 1,2-dimethoxyethane was added dropwise over 3–4 h. The resulting yellow solution became cloudy, and stirring at 50°C was continued overnight. Complete disappearance of **2** with formation of two products was observed by tle. The mixture was evaporated, the residue dissolved in water, and the solution applied to a column (3 × 34 cm) of Dowex 1-X2 (OH^-). The column was washed with water and then **3** (1.21 g, 51%) was eluted with MeOH/H_2O (1:9). Elution with MeOH/H_2O (3:7) gave 1.11 g (47%) of **4**. These pure samples (recrystallized once each from MeOH) were recovered in a combined yield of 98% and had for **3**, mp 122–123°C; tle R_{Guo} = 0.68 (−); uv max: 280, 256, 216 nm (ε 11 000, 10 500, 26 500); ^{1}H nmr δ: 3.28 (s, 3, 2′-OCH_3), 3.58 (m, 2, H-5′,5″), 3.93 (m, 1, H-4′), 4.26 (m, 2, H-2′,3′), 5.14 (d, $J_{3'OH-3'}$ = 4.5 Hz, 1, 3′-OH), 5.43 (t, $J_{5'OH-5',5''}$ = 6 Hz, 1, 5′-OH), 5.71 (br s, 2, 2-NH_2), 5.83 (d, $J_{1'-2'}$ = 6 Hz, 1, H-1′), 6.74 (br s, 2, 6-NH_2), 7.92 (s, 1, H-8); ms *m/z*: 296.1239 (13%, M^+ = 296.1233), 207.0998 (29%, B + 58 = 207.0994), 150.0651 (100%, B + H = 150.0654). *Anal.* calcd. for $C_{11}H_{16}N_6O_4$: C 44.59, H 5.44, N 28.36; found: C 44.71, H 5.51, N 28.54.

Isomer **4** had mp 234–235°C; tle R_{Guo} = 0.50 (−); uv max: 280, 255, 216 nm (ε 10 500, 10 000, 25 600); ^{1}H nmr δ: 3.40 (s, 3, 3′-OCH_3), 3.57 (m, 2, H-5′,5″), 3.80 (m, $J_{4'-3'}$ = 3 Hz, $J_{4'-5',5''}$ ~ 4.5 Hz, 1, H-4′), 3.99 (m, $J_{3'-2'}$ = 6 Hz, 1, H-3′), 4.64 (m, $J_{2'-2'OH}$ = 6 Hz, $J_{2'-1'}$ = 6 Hz, 1, H-2′), 5.36 (d, 1, 2′-OH), 5.44 (dd, $J_{5'OH-5'}$ = 5,5 Hz, $J_{5'OH-5''}$ = 6.5 Hz, 1, 5′-OH), 5.69 (br s, 2, 2-NH_2), 5.69 (d, 1, H-1′), 6.74 (br s, 2, 6-NH_2), 7.89 (s, 1, H-8); ms *m/z*: 296.1244 (20%, M^+ = 296.1233), 193.0846 (13%, B + 44 = 193.0839), 150.0656 (100%, B + H = 150.0654). *Anal.* calcd. for $C_{11}H_{16}N_6O_4$: C 44.59, H 5.44, N 28.36; found: C 44.25, H 5.43, N 28.43.

Repetition of the above methylation of **2** using 216 mg (0.96 mmol) of $SnCl_2 \cdot 2H_2O$ gave 1.0 g (42%) of **3** and 1.33 g (56%) of **4**. A run using 108 mg (0.48 mmol) of $SnCl_2 \cdot 2H_2O$ gave 0.81 g (34%) of **3** and 1.52 g (64%) of **4**.

2′-O-Methylguanosine (5)

A mixture of 888 mg (3 mmol) of **3** dissolved in 30 mL of Me_2SO, 75 mL of 0.1 *M* aqueous sodium phosphate buffer (pH 7.4), and 20 mg of adenosine deaminase (Sigma Chemical Co., crude, type II) was stirred at ambient temperature for 3 days. Progress of the deamination reaction was monitored by tle. The solution was applied to a column (2.5 × 20 cm) of Dowex 1-X2 (OH^-) and the column was washed well with H_2O. Elution of **5** was effected using 0.03 *M* aqueous triethylammonium bicarbonate buffer (pH 7.5). Fractions containing **5** were pooled, evaporated, and the buffer salt volatilized by repeated addition and coevaporation of H_2O. The resulting solid was recrystallized from H_2O and then from MeOH to give 767 mg (86%) of **5**, mp 235–237°C (lit. mp (for **5**·MeOH) (5) 234–236°C, (9) 229–232°C); tle R_{Guo} = 0.25 (−); uv max: 253, 270 (sh) nm (ε 13 900, 9800); ^{1}H nmr data were in accord with literature values (5); ms *m/z*: 297.1078 (8.5%, M^+ = 297.1073), 208.0871 (20%, B + 58 = 208.0835), 151.0493 (100%, B + H = 151.0494). *Anal.* calcd. for $C_{11}H_{15}N_5O_5$: C 44.44, H 5.09, N 23.56; found: C 44.20, H 5.04, N 23.85.

3′-O-Methylguanosine (6)

A 888 mg (3 mmol) sample of **4** was treated identically to the above conversion of **3** → **5** to give 820 mg (92%) of recrystallized **6**, mp > 265°C (dec.) (lit. (5) mp > 258°C (dec.), (7) 263–300°C (dec.)); tle R_{Guo} = 0.18 (−); uv max 253, 270 (sh) nm (ε 14 000, 9900); ^{1}H nmr data were in accord with literature values (5); ms *m/z*: 297.1087 (5.5%, M^+ = 297.1073), 194.0677 (5.4%, B + 44 = 194.0678), 151.0496 (100%, B + H = 151.0494). *Anal.* calcd. for $C_{11}H_{15}N_5O_5$: C 44.44, H 5.09, N 23.56; found: C 44.21, H 5.04, N 23.85.

Acknowledgments

We thank the Natural Sciences and Engineering Research Council of Canada (A5890), the National Cancer Institute of Canada, and The University of Alberta for generous financial support.

1. M. J. ROBINS, C. KANEKO, and M. KANEKO. Can. J. Chem. **59**, 3356 (1981).
2. (*a*) R. H. HALL. The modified nucleosides in nucleic acids. Columbia University Press, New York. 1971; (*b*) M. J. ROBINS, M. MACCOSS, and A. S. K. LEE. Biochem. Biophys. Res. Commun. **70**, 356 (1976), and references quoted therein.
3. I. KUMAGAI, K. WATANABE, and T. OSHIMA. Proc. Natl. Acad. Sci. U.S.A. **77**, 1922 (1980).
4. V. D. AXELROD, R. M. VARTIKYAN, V. A. AIVAZASHVILI, and R. SH. BEABEALASHVILI. Nucleic Acids Res. **5**, 3549 (1978).

5. M. J. ROBINS, S. R. NAIK, and A. S. K. LEE. J. Org. Chem. **39**, 1891 (1974).
6. T. A. KHWAJA and R. K. ROBINS. J. Am. Chem. Soc. **88**, 3640 (1966).
7. G. L. TONG, W. W. LEE, and L. GOODMAN. J. Org. Chem. **32**, 1984 (1967).
8. J. T. KUŚMIEREK and D. SHUGAR. Nucleic Acids Res. Special Publication No. 4, s73 (1978).
9. G. EKBORG and P. J. GAREGG. J. Carbohydr. Nucleos. Nucleot. **7**, 57 (1980).
10. C. A. DEKKER. J. Am. Chem. Soc. **87**, 4027 (1965).
11. H. VORBRÜGGEN and K. KROLIKIEWICZ. Justus Liebigs Ann. Chem. 745 (1976).
12. M. J. ROBINS, A. S. K. LEE, and F. A. NORRIS. Carbohydr. Res. **41**, 304 (1975).
13. (*a*) O. P. CHILSON and J. R. FISHER. Arch. Biochem. Biophys. **102**, 77 (1963); (*b*) H.-P. BAER, G. I. DRUMMOND, and E. L. DUNCAN. Mol. Pharmacol. **2**, 67 (1966).
14. D. M. G. MARTIN, C. B. REESE, and G. F. STEPHENSON. Biochemistry, **7**, 1406 (1968).
15. A. J. JONES, D. M. GRANT, M. W. WINKLEY, and R. K. ROBINS. J. Am. Chem. Soc. **92**, 4079 (1970).
16. M.-T. CHENON, R. J. PUGMIRE, D. M. GRANT, R. P. PANZICA, and L. B. TOWNSEND. J. Am. Chem. Soc. **97**, 4627 (1975).
17.. H. H. MANTSCH and I. C. P. SMITH. Biochem. Biophys. Res. Commun. **46**, 808 (1972).

Can. J. Chem. Downloaded from www.nrcresearchpress.com by 210.87.254.6 on 09/06/12
For personal use only.

The synthesis of 2,3,5,6-*endo,endo,endo,endo*-tetrakis-substituted bicyclo[2.2.1]heptanes

DOUGLAS N. BUTLER AND TIMOTHY J. MUNSHAW
Chemistry Department, York University, Downsview, Ont., Canada M3J 1P3

Received June 22, 1981

DOUGLAS N. BUTLER and TIMOTHY J. MUNSHAW. Can. J. Chem. **59**, 3365 (1981).

Oxidation of the readily available diketone **2** affords high yields of the symmetrical dilactone **5**, from which the *all-endo*-tetrakis(hydroxymethyl)norbornane **10** can be made. A related tetrol **22** is also described. These tetrols are dehydrated to polycyclic di-ethers **12**, **13**, and **23** which constrain their oxygen atoms in rigid proximity within their structures.

DOUGLAS N. BUTLER et TIMOTHY J. MUNSHAW. Can. J. Chem. **59**, 3365 (1981).

L'oxydation de dicétone **2**, que l'on peut obtenir facilement conduit avec d'excellents rendements à la dilactone symétrique **5** à partir de laquelle on peut préparer le tétrakis (hydroxyméthyl) norbonanes (**10**) complètement *endo*. On décrit également le tétrol apparenté (**22**). La déshydratation de tétrols conduit aux diéthers polycycliques **12**, **13** et **23** dans lesquels les atomes d'oxygène sont maintenus dans un voisinage rigide à l'intérieur de leurs structures.

[Traduit par le journal]

Can. J. Chem. Downloaded from www.nrcresearchpress.com by 210.87.254.42 on 09/06/12
For personal use only.

The anticipated congestion of the *endo* face requires that any scheme directed toward the preparation of a 2,3,5,6-*all-endo*-tetrasubstituted norbornane must mark the prevention of epimerization of one (or more) of the substituents of any of the intermediates of the synthesis into the more stable *exo* stereochemistry. The caveat is successfully countered by using the readily available photo-cage **1** (1) from the cyclopentadiene/benzoquinone Diels–Alder adduct as the starting point of the synthesis only if the necessary carbon–carbon disconnections within **1** can be effected by processes which exclude any possibility of such an isomerization, preferably intramolecular events which maintain the *all-endo* stereochemistries until nonepimerizable functionalities are in place.

A 2,3,5,6-tetrakis(hydroxymethyl) derivative of norbornane has been described (2), the origins of which suggest 2,3-*endo,endo*-5,6-*exo,exo* as the likely stereochemistry. The objective of this work was to prepare the *all-endo* isomer in order to study the chemical and physical consequences of the congestion imposed on the functionalities by this geometry. The dissolving-metal reduction (3) of the cage dione **1** required refluxing conditions (4) in our hands in order to produce **2**. Curiously, very little chemistry has been described for this diketone, although it is easily prepared and ideal for the purpose at hand. Initially, we envisioned functionalizing the two methylene carbons α to the carbonyls as a logical strategy; however, selenium dioxide oxidation to the anticipated tetraketone **3** failed. A stereospecific bromination proceeded very efficiently to give a dibromide to which we ascribe the structure **4** from steric and spectroscopic rationalizations. The acetate and hydroxide anionic nucleophiles did not change **4** under the conditions tried and a stronger base (methoxide) slowly produce a rearranged monobromoketo-ester of unknown structure (presumably via a Favorskii mechanism).

Although unreactive to *m*-chloroperbenzoic acid, **2** reacted cleanly with trifluoroperacetic acid at room temperature to produce a mixture of dilactones. Fortunately, this mixture was predominantly one isomer (> 95%) whose structure was unambiguously assigned as **5** from spectroscopic evidence. The other symmetrical dilactone **6** was isolated from the mother liquors in low yield. The major dilactone **5**, whilst only slightly soluble in cold water, can be easily recrystallized from hot water. Remarkably, it is freely soluble in cold dilute aqueous alkali to give solutions which show different ^{1}H and ^{13}C nmr signals from those of hot aqueous solutions of **5**. Since acidification reprecipitates the dilactone immediately, we propose **7** as the alkaline hydrolysis product and we are currently studying the kinetics of this most facile hydrolysis.

The success of the Baeyer–Villiger reaction on **2** led us to attempt similar oxidations of **1** and **4**. The cage diketone **1** gave a mixture of dilactones, again with one symmetrical isomer predominating and for which we favour structure **8** over **9** (5).

Once again an extremely rapid hydrolysis is observed for this compound. We could not find any literature precedent for the peracid oxidation of an α-bromoketone; however, in the event, we did not observe any reaction of **4** with trifluoroperacetic acid either at room temperature or at reflux in methylene chloride.

The excellent overall yields of dilactones **5** and **8** from such readily available precursors render these compounds highly accessible synthons for *all-*

0008-4042/81/243365-07$01.00/0
©1981 National Research Council of Canada/Conseil national de recherches du Canada

Can. J. Chem. Downloaded from www.nrcresearchpress.com by 210.87.254.42 on 09/06/12
For personal use only.

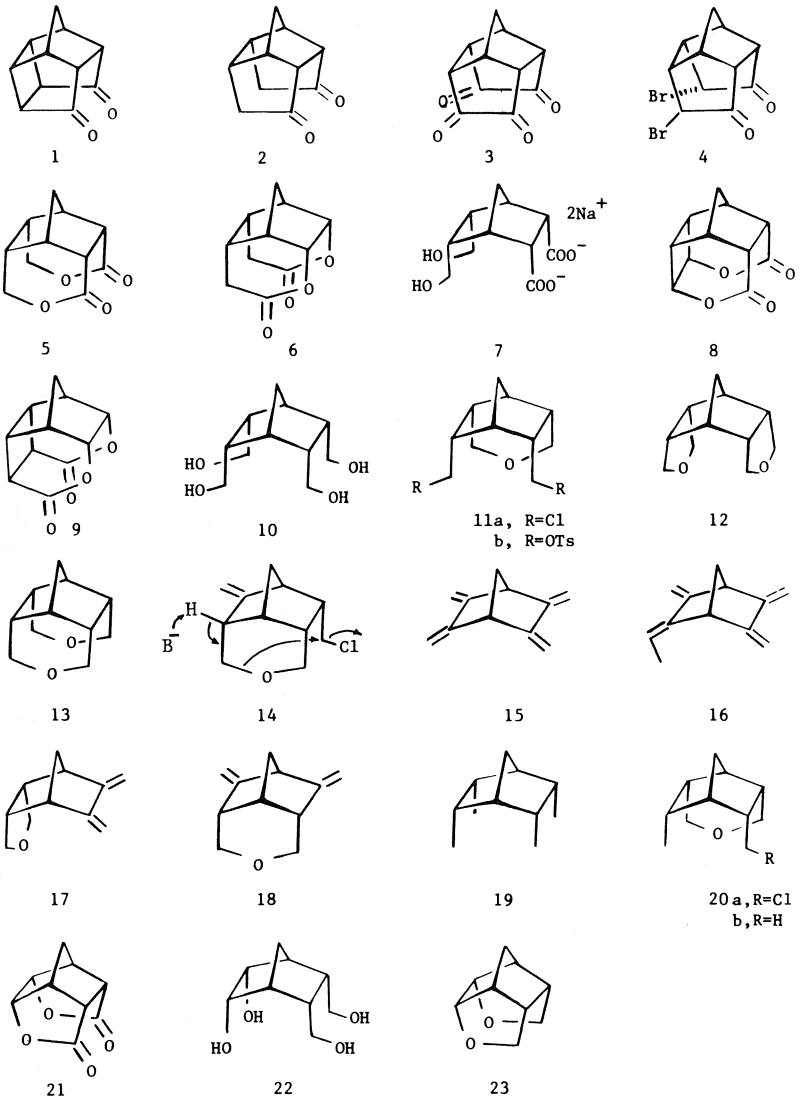

endo-2,3,5,6-tetrasubstituted bicyclo[2.2.1]heptanes (see also ref. 5). It might also be noted that more than 20 photo-cage isomers of various diene/quinone adducts are reported in the literature (1, 6) although apparently only two of these have been reduced to their dihydro derivatives (3, 4). Thus, a considerable scope of synthetic utility is predictable for this sequence.

The reduction by lithium aluminum hydride of the dilactone **5** and the isolation of the *all-endo* tetrol **10** presented several difficulties. Partial reduction readily occurred but complete reduction was slow, requiring 48 h at reflux in 1,2-dimethoxyethane. The course of the reduction was followed by hydrolysing aliquots of the reaction mixture, acetylating, and subjecting these to gas chromatographic/mass spectrometric (gc–ms) analysis. The isolation of the tetrol from the hydrolysed reaction mixture was complicated by the presence of aluminium salts in the aqueous extracts; however, with care, a 63% yield of the tetrol **10** was realized. The protons on the oxygen-bearing carbons showed temperature variable line shapes arising from restricted rotation and/or hydrogen bonding; however, the four line ^{13}C nmr spectrum confirmed the molecular symmetry and ruled out any possible epimerization during reaction.

Whilst from **10** the tetra(trimethylsilyl) ether and the tetra-acetate formed readily, thionyl chloride produced an ether dichloride, **11***a*, as the major product along with minor amounts of both the diethers **12** and **13** and an elimination product **14**

Can. J. Chem. Downloaded from www.nrcresearchpress.com by 210.87.254.42 on 09/06/12
For personal use only.

(*vide infra*). The identity of **11***a* as a six-ring ether was established by its seven line ^{13}C nmr spectrum. Both diethers **12** and **13** can also be formed from **10**, either by heating in dimethyl sulfoxide (7) or by treatment with carbon tetrachloride/triphenyl phosphine (8). The identity of **12** and **13** as the bis-five- and bis-six-ring ethers respectively was inferred from consideration of the shapes of the A_2B_2 patterns of the methylene hydrogens attached to the oxygen-bearing carbon atoms. Thus in all the compounds having a six-ring ether partial structure (e.g. **11***a*, **11***b*, **13**, **18**, and **20***b*) this A_2B_2 was a clean first-order pattern with $J_{AB} \approx 12$ Hz, whereas in the five-ring ether examples (e.g. **12** and **17**) the corresponding pattern was more complex (see Fig. 1). Inspection of molecular models supports this assignment in terms of the dihedral angles of the vicinal protons involved. These isomers have only been isolated by preparative gas chromatography. An attempt at tetratosylate formation resulted likewise in the formation of an ether ditosylate **11***b*.

Several base-promoted eliminations were carried out on **11***a* and **11***b*. Thus heating **11***a* with potassium *tert*-butoxide in dimethyl sulfoxide produced a complex mixture of products which was separated by preparative gas chromatography into the known tetraene **15** (2), a methylated tetraene **16** (presumably by methylene transfer[1] from dimsyl anion), and the two ether dienes **17** and **18**. These two dienes were also formed from the ether ditosylate **11***b* using the same elimination reagent (9). Again these diene structural assignments followed from the seven line ^{13}C nmr spectrum of the major elimination product (from both precursors) namely **18**.

The identity of the minor elimination product **14** mentioned above, arising from the treatment of the tetrol **10** with thionyl chloride, was secured when it was found that it was converted by KO^{t}Bu/DMSO into the two dienes **17** and **18** in about the same ratio (8:2) as in the double elimination of **11***a* under the same conditions. Thus **14** is the logical precursor to both dienes with the new allylic hydrogen being abstracted by the base to initiate the elimination-rearrangement to provide **17** as shown on structure **14**.

In an attempt to prepare the *all-endo*-tetramethyl hydrocarbon **19**, the dichloride **11***a* was slowly reduced by lithium aluminium hydride in hot monoglyme to the dimethyl ether **20***b* via the monochloride **20***a*. A variety of reagents including trimethylsilyl iodide (10) were tried in an effort to cleave the ether of **20***b* but they all were ineffective under normal conditions or destroyed the compound under forcing conditions. Other routes to **19** are currently being studied.

A second series of *all-endo*-tetrasubstituted bi-

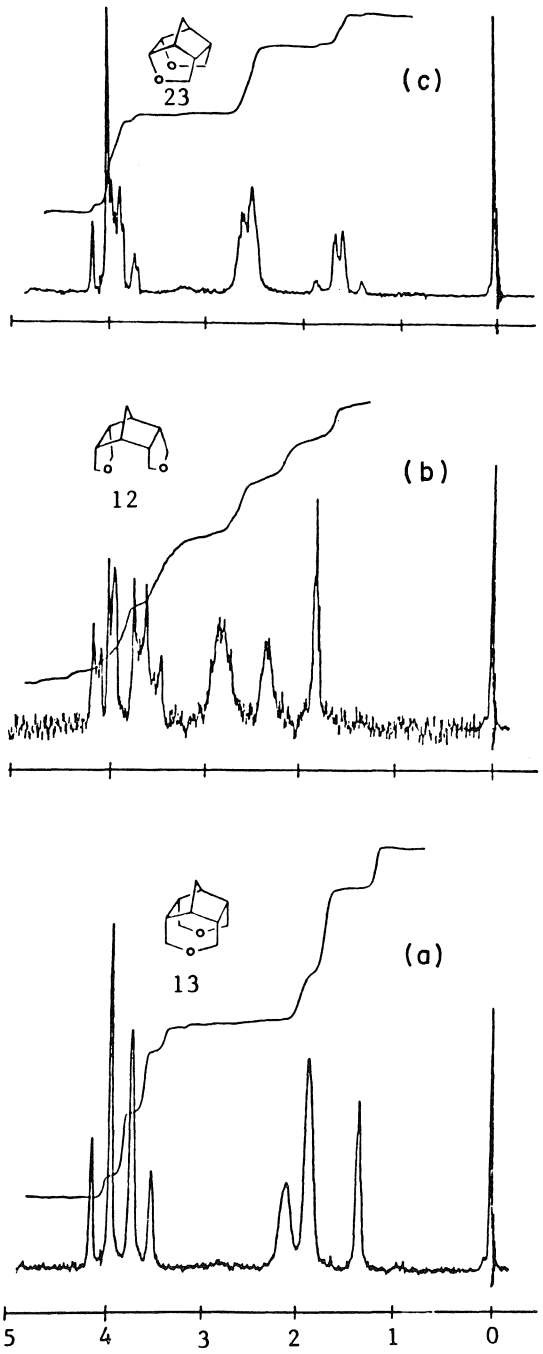

FIG. 1. The 60 MHz ^1H nmr spectra of (a) **13**, (b) **12**, and (c) **23** in $CDCl_3$.

[1]From the ^1H nmr data we assign the structure of **16** as shown. We have observed similar methylations in bis-tosylate eliminations using KO^{t}Bu in DMSO.

Can. J. Chem. Downloaded from www.nrcresearchpress.com by 210.87.254.42 on 09/06/12
For personal use only.

cyclo[2.2.1]heptanes was prepared from the known dilactone **21**. Several synthetic methods for this dilactone are reported (11); however, in our hands none of these gave reliable yields of large quantities and we have modified one of these procedures (**11***b*) (see Experimental).

Reduction of **21** with lithium aluminium hydride afforded good yields of the tetrol **22** which formed a tetra-acetate and a tetra(trimethylsilyl) derivative and which was dehydrated by heating in dimethyl sulfoxide (7) or by thionyl chloride into the di-ether **23** (see Fig. 1).

The special spatial characteristics of the two oxygen atoms in each of the three di-ethers **12**, **13**, and **23** provoke questions relating to their ability to complex electrophilic species e.g. H^+, CH_3^+, or metal ions. Of the three, **23** is the most rigid with the two oxygen atoms about 2.3 Å apart (from Drieding models). From the models, **12** appears to be the most sterically congested and because it is formed in minor amount and has only been purified by preparative gas chromatography it has not yet been further studied. Both **13** and **23** appear to be protonated in 6 *M* sulfuric acid as judged by the appearance of their respective ^1H nmr spectra as the acidity was increased by dropwise addition of sulfuric acid to D_2O solutions or, in reverse, as D_2O was added to concentrated sulfuric acid solutions of these two di-ethers. Thus **13** and **23** appear to be more basic than even tetrahydrofuran (12) and it is tempting to propose a shared proton between both ether oxygens somewhat reminiscent of "proton sponge" (13). Further studies are underway relating to the ability of these di-ethers to complex electrophiles and to nonbonding electron interactions as revealed by photo-electron spectroscopy. Interestingly, all three di-ethers are soluble in water and organic solvents and bind strongly to silica as compared to comparable mono-ethers.

Finally there remains the intriguing possibility of positional scrambling within the oxonium salt **24** derived from the ether dichloride **11***a* as shown in Scheme 1. Early results are inconclusive and we are continuing a study of this possibility.

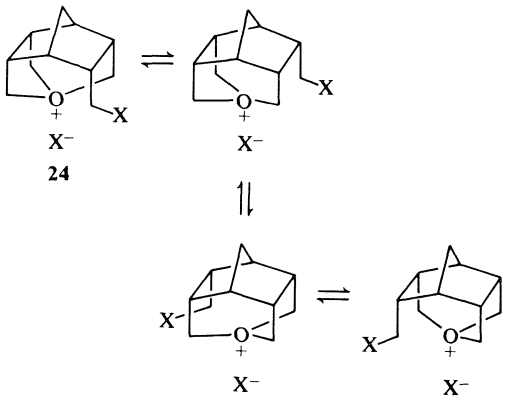

SCHEME 1

Experimental

All melting points are uncorrected. The ir spectra were taken on a Unicam SP1000 instrument as liquid films or Nujol mulls. The ^1H nmr and ^{13}C nmr spectra were recorded on Varian EM360 and CFT20 instruments respectively. The uv spectra were recorded on a Unicam SP800A spectrophotometer. Mass spectra were taken at 70 eV using a Hitachi–Perkin–Elmer RMU-6E mass spectrometer. Both the analytical and the preparative gas chromatography were carried out on a Varian Aerograph Series 1700 instrument on a 6 ft. × 1/4 in. od glass column packed with 2.5% SE30 + 3.5% QF1 on Chromosorb W (acid washed), 60–80 mesh (HMDS treated).

Tetracyclo[6.3.0.0^{4,11}.0^{5,9}]undeca-2,7-dione **2**

The photo-dione **1** (1) (20 g) was dissolved in glacial acetic acid (1 L) in a 2-*L* three-necked flask equipped with an overhead stirrer, reflux condenser, and stopper. Freshly activated zinc dust (50 g) (prepared by suspending the zinc in aqueous 2% hydrochloric acid for 1 min, filtering, washing under nitrogen with degassed, distilled water until neutral, washing with ethanol and ether, and drying under vacuum) was then added with stirring and the mixture brought to and then held at reflux for 5 h. The zinc was then removed by filtration on the water pump, washed with methylene chloride (2 × 50 mL), and the bulk of the solvents removed on a rotary evaporator at water-pump pressure. The residue was mixed with an equal volume of water and extracted with methylene chloride (4 × 100 mL). The combined organic phase was washed with dilute (10%) aqueous sodium hydroxide solution until the water phase remained alkaline and then the organic phase was separated, dried (Na_2SO_4), and filtered through a 2.5 cm filter containing a 5 cm column of silica. Evaporation of the solvent left light-brown crystals which were sublimed under vacuum to afford **2** (16 g; 80%), mp 255–257°C; ir: 1725, 1755 cm^{-1}; ^1H nmr ($CDCl_3$) δ: 1.92 (s, 2H), 2.26 (s, 4H), 2.7–2.8 (s + sh, 6H); ^{13}C nmr ($CDCl_3$) δ: 34.2 (t, J = 133.6 Hz), 38.2 (d, J = 141.6 Hz), 39.7 (t, J = 133.6 Hz), 47.4 (d, J = 149.3 Hz), 58.0 (d, J = 154.0 Hz), and 217.3 (s); mass spectrum: m/e = 176 (M^+).

Dibromide **4**

The diketone **2** (9.0 g) was dissolved in methylene chloride (100 mL) in a flask equipped for magnetic stirring and reflux. A 15% solution of bromine in carbon tetrachloride (100 mL) was added slowly with stirring through the open end of the reflux condenser together with 5 drops of concentrated aqueous hydrobromic acid (48%). The mixture evolved HBr gas with vigorous refluxing over a 1/2 h period, then it was transferred to a rotary evaporator and the solvent and excess bromine removed to leave the crude product. This was recrystallized from chloroform to yield the pure dibromide **4** (14 g; 85%) as a fine white solid, mp 217–218°C; ir: 1730, 1760 cm^{-1}; ^1H nmr ($CDCl_3$) δ: 2.05 (s, 2H), 3.03 (s, 4H), 3.45 (s, 2H), and 4.36 (s, 2H); ^{13}C nmr ($CDCl_3$) δ: 34.0 (t, J = 134.3 Hz), 46.2 (d, J = 150.1 Hz), 47.1 (d, J = 158.0 Hz), 50.4 (d, J = 150.1 Hz), 57.9 (d, J = 142.2 Hz), and 200.8 (s); mass spectrum: m/e = 332, 334, 336 (M^+).

*5,6-*endo,endo-*Bis(hydroxymethyl)bicyclo[2.2.1]heptane-2,3-*endo,endo-*dicarboxylic Acid Dilactone* **5**

To the diketone **2** (7 g) dissolved in methylene chloride (200 mL) was added with stirring a solution of trifluoroperacetic

Can. J. Chem. Downloaded from www.nrcresearchpress.com by 210.87.254.42 on 09/06/12
For personal use only.

acid (prepared by adding trifluoroacetic anhydride (13 mL) to a well-stirred, ice-cold mixture of 90% H_2O_2 and methylene chloride (50 mL) – *careful: vigorous reaction with foaming*) and the mixture allowed to stand overnight. The pale yellow oil remaining after the solvent had been removed (under vacuum) was rubbed with pentane (200 mL) with cooling in an ice-bath until the crop of light-brown granular crystals had formed. The pentane was decanted, carbon tetrachloride (150 mL) was then added followed by absolute ethanol (5 mL) to give the product as a white precipitate. After thorough chilling this was filtered off, washed with cold carbon tetrachloride, dried, and recrystallized from methanol/acetone (1:1) to afford fine crystals of the pure dilactone **5** (6 g; 75%) mp > 350°C; ir: 1730 cm^{-1}; ^1H nmr (hot $CDCl_3$) δ: 1.8 (AB pattern, 2H), 2.5 (bd s, 2H), 2.8 (bd s, 2H), 3.2 (bd s, 2H), and 4.6 (bd s, 4H); ^{13}C nmr (hot D_2O (70°C) referenced to sodium 2,2-dimethyl-2-silapentane-5-sulfonate = −1.1 ppm) δ: 34.8, 39.4, 40.5, 46.4, 71.7, C=O not observed; mass spectrum: *m/e* = 208 (M^+). *Anal.* calcd. for $C_{11}H_{12}O_4$: C 63.45, H 5.81%; found: C 63.61, H 5.78%.

The filtrates from three of the above preparations were combined and evaporated to give a thick amber oil (5 g) which was fractionally crystallized using methanol/methylene chloride. After the separation of several small crops of impure **5**, the filtrates were evaporated to a white solid (0.2 g, mp 287–295°C) which (by its ^1H nmr spectrum) was mainly the isomeric dilactone **6** still contaminated with **5**. A pure sample of **6** was not obtained; ir: 1730 cm^{-1}; ^1H nmr ($CDCl_3$) δ: 1.8 (AB pattern, 2H), 2.3 (s, 2H), 2.75 (bd s, 2H), 2.9 (s, 4H), and 4.53 (s, 2H).

2,3,5,6-endo,endo,endo,endo-*Tetrakis(hydroxymethyl)-bicyclo[2.2.1]heptane* ***10***

The finely ground dilactone **5** (10 g) was suspended in dry monoglyme (100 mL) and added slowly to lithium aluminium hydride (8 g) in ice-cold monoglyme (150 mL) with stirring. This mixture was subjected to reflux for 48 h under anhydrous conditions. After cooling in ice, the reaction mixture was quenched by the careful addition of aqueous 2 *N* sodium hydroxide solution (100 mL) and the resultant slurry washed by decantation with hot methanol (4 × 100 mL) with vigorous stirring during each of the wash steps. The combined aqueous and methanol extracts were evaporated to dryness under vacuum, the resulting solid dissolved in a minimum of hot methanol, and dry ether added until the solution became cloudy with a fine precipitate of alumina. Solid Dry Ice (20 g) was added, allowed to evaporate, and the resulting slurry filtered (or centrifuged) to remove the inorganic material. Evaporation of the filtrate to dryness left a gummy solid upon which the above treatment was repeated several times until the evaporated extracts became a clear amber-coloured syrup. This was dissolved again in a minimum volume of hot methanol and dry ether added until a faint cloudiness appeared. This mixture was then set aside in a refrigerator until the product crystallized. Three repetitions of this recrystallization afforded **10** (6.5 g; 63%) as small colorless plates, mp 127.5–128.5°C; ir (Nujol mull): 2600–3500, 1090, 1005 cm^{-1}; ^1H nmr (D_2O referenced to HOD = 4.72 ppm) δ: 1.45 (s, 2H), 2.30–2.38 (s, sh, 6H), and 3.30–3.95 (m, 8H); ^{13}C nmr (D_2O internally referenced to dioxane = 67.4 ppm) δ: 42.2 (t, J = 118.7 Hz), 44.3 (d, J = 116.6 Hz), 44.7 (d, J = 111.3 Hz), and 67.40 (t, J = 111.3 Hz). *Anal.* calcd. for $C_{11}H_{20}O_4$: C 61.09, H 9.32%; found: C 60.85, H 9.18%.

Tetra-acetate: colorless plates from dry ether, mp 96–97°C. Tetrakis(trimethylsilyl)ether: white solid, mp 123–125°C; mass spectrum: *m/e* = 504 (M^+).

6,10-endo,endo-*Bis(chloromethyl)-3-oxatricyclo[5.2.1.0^{5,9}]-decane* ***11***a

The tetrol **10** (2 g) was added portionwise to thionyl chloride (40 mL) and this mixture subjected to reflux under anhydrous conditions for 6 h. The excess thionyl chloride was then removed under vacuum to afford an orange syrup, gc–ms analysis of which revealed it to be a mixture of **14** (13.5%), **12** (9%), **13** (12%), and **11***a* (65.5%) which separated by vacuum distillation into a forerun boiling up to 84°C/0.02 Torr and the main fraction bp 84–95°C/0.02 Torr. Sufficient of the forerun was separated by preparative gas chromatography to allow spectroscopic characterization of the three minor components **14**, **13**, and **12** (in order of elution); **14**, an amber liquid, ir(film): 3040, 2900, 1660, 1460, 1270, 1150, 1095, 1040, 880, and 730 cm^{-1}; ^1H nmr ($CDCl_3$) δ: 1.52 (s, 2H), 1.90 (s, 1H), 2.3 (m, 3H), 2.95 (s, 1H), 3.2–4.1 (overlapping multiplets, 6H), 4.91 (s, 1H), and 5.08 (narrow m, 1H); mass spectrum: *m/e* = 198, 200 (M^+). For **13** and **12**, see details below. The main fraction solidified on cooling and scratching and was recrystallized from pentane to give **11***a* (1.2 g; 55%) as clear plates, mp 44–45°C; ir (Nujol mull): 1300, 1270, 1140 med shp, 1090, 1080, 1015 str br; ^1H nmr ($CDCl_3$) δ: 1.42 (s, 2H), 1.88 (bd s, 1H), 2.32 (bd s, 2H), 2.54 (bd s, 2H), and 3.2–4.25 (overlapping multiplets, 8H); ^{13}C nmr ($CDCl_3$) δ: 34.1 (d, J = 139.7 Hz), 39.6 (t, J = 127.0 Hz), 41.0 (d, J = 133.5 Hz), 44.4 (t, J = 152.4 Hz), 45.6 (d, J = 140.0 Hz), 46.3 (d, J = 133.5 Hz), and 65.7 (t, J = 133.0 Hz); mass spectrum: *m/e* = 234, 236, 238 (M^+).

endo, endo-*3,8-Dioxatetracyclo[8.3.0.0^{5,13}.0^{6,11}]tridecane* ***13*** *and* endo, endo-*4,10-Dioxatetracyclo[5.5.1.0^{2,6}.0^{8,12}]-tridecane* ***12***

DMSO Method

The tetrol **10** (0.50 g) was heated in dimethyl sulfoxide (4 mL) at 170°C for 15 h under a reflux condenser fitted with a drying tube. The bulk of the solvent was removed from the black reaction mixture under vacuum (0.02 Torr) to leave a black residue which was shown by gas chromatography to be a mixture of the two di-ethers **13** and **12** in a 82:18 ratio. Passage of this dark mixture in ether through a short silica column allowed the black impurities to pass through whilst retaining the two di-ethers. These in turn were eluted with methanol and were obtained by evaporation under vacuum as a gummy residue (0.36 g; 86%). Sufficient of this mixture was subjected to preparative gas chromatography to allow spectroscopic characterization. Compound **13**, mp 120–135°C; ir(Nujol mull): 1165, 1080, and 1003 cm^{-1}; ^1H nmr ($CDCl_3$) δ: 1.41 (s, 2H), 1.90 (bd s, 4H), 2.19 (bd s, 2H), 3.65 (d, J = 12 Hz), and 4.00 (d, J = 12 Hz) (see Fig. 1); ^{13}C nmr ($CDCl_3$) δ: 36.4 (d, J = 131.7 Hz), 37.6 (t, J = 131.7 Hz), 41.9 (d, J = 137.5 Hz), and 63.5 (t, J = 143.8 Hz); mass spectrum: *m/e* = 180 (M^+), 79 (base peak). Compound **12**, mp 135–138°C; ir (Nujol mull): 1083, 1010, and 955 cm^{-1}; ^1H nmr ($CDCl_3$) δ: 1.80 (s, 2H), 2.32 (bd s, 2H), 3.62 (m, 4H), and 4.07 (m, 4H) (see Fig. 1); ^{13}C nmr ($CDCl_3$) δ: 43.6, 48.0, 51.1, and 67.6; mass spectrum: *m/e* = 180 (M^+), 79 (base peak).

Triphenylphosphine/Carbon Tetrachloride Method

The tetrol **10** (0.2 g) and triphenylphosphine (0.5 g) were dissolved in carbon tetrachloride (30 mL) and dry tetrahydrofuran (5 mL) and this mixture subjected to reflux under anhydrous conditions for 24 h. The solvents were evaporated off under vacuum and the residue extracted with pentane (200 mL). The precipitated triphenylphosphine oxide was filtered off and the filtrate evaporated to a clear oil which was shown by gas chromatographic analysis to be a 3:2 mixture of **13** and **12**.

6,10-endo, endo-*Bis(hydroxymethyl)-3-oxatricyclo[5.2.1.0^{5,9}]-decane Di*-p-*toluene Sulfonate* ***11***b

The tetrol **10** (0.25 g) and *p*-toluene sulfonyl chloride (0.9 g) were taken up in pyridine (10 mL) and kept for 5 days in the refrigerator. Water (70 mL) was then added and the mixture stirred magnetically for 3 h after which time it was extracted with methylene chloride (3 × 25 mL). The combined organic

Can. J. Chem. Downloaded from www.nrcresearchpress.com by 210.87.254.42 on 09/06/12
For personal use only.

phases were back-extracted with 1 *N* aqueous hydrochloric acid until the aqueous phase remained acid, dried, and evaporated under vacuum to a gummy residue which was taken up in a minimum volume of warm methanol and water added until just cloudy. This was set aside in the refrigerator until the product precipitated. The collected solid was recrystallized from methanol to give **11***b* (0.34 g; 54%), mp 121–123°C; ir (Nujol mull): 1180, 1100, 950, and 840 cm^{-1}; ^1H nmr ($CDCl_3$) δ: 1.45 (s, 2H), 1.8–2.0 (m, 4H), 2.45 (s, 6H), 3.35 (A_2 of A_2B_2 pattern, 2H), 3.80 (B_2 of A_2B_2 pattern, 2H), 4.31 (m, 4H), 7.4 (d, 4H), and 7.8 (d, 4H).

Elimination Reactions

*From Ether Dichloride 11*a

The dichloride **11***a* (0.53 g) was dissolved in DMSO (10 mL) and freshly prepared potassium *tert*-butoxide (1.1 g) was added. This mixture was heated to reflux for 5 min, cooled, water (5 mL) added, and extracted with pentane (3 × 5 mL). Analysis of this extract revealed the presence of four products and these were individually collected by preparative gas chromatography with the column temperature set at 150°C. In order of elution these were **15** (2) (6%); ^1H nmr ($CDCl_3$) δ: 1.65 (s, 2H), 3.40 (s, 2H), 4.95 (s, 4H) and 5.21 (s, 4H); mass spectrum: *m/e* = 144 (M^+); **16** (9%); uv (hexane): λ_{max} 246, sh 261 nm; ^1H nmr ($CDCl_3$) δ: 1.70 (s, 2H), 1.87 (d, *J* = 8 Hz, 3H), 3.49 (bd s, 1H), 4.72 (bd s, 1H), 5.0 (m, 4H), 5.2 (d, *J* = 1.6 Hz, 2H), and 5.81 (q, *J* = 8 Hz, 1H); mass spectrum: *m/e* = 158; **18**, clear liquid (63%); uv (hexane): λ_{max} = 244 nm; ir (film): 3090, 2860, 1720, 1660, 1160, and 1090 cm^{-1}; ^1H nmr ($CDCl_3$) δ: 1.55 (s, 2H), 2.14 (s, 3H), 3.25 (s, 1H), 3.60 (A_2 of A_2B_2 pattern, 2H), 4.00 (B_2 of A_2B_2 pattern, 2H), 4.87 (s, 2H), and 5.08 (d, *J* = 2 Hz, 2H); ^{13}C nmr ($CDCl_3$) δ: 39.1, 39.9, 40.5, 56.0, 68.3, 103.4, and 156.4; and **17**, clear liquid (22%); uv (hexane): λ_{max} = 251 nm; ir (film): 3020, 2900, 1625, 1075, 1020, 980, and 860 cm^{-1}; ^1H nmr ($CDCl_3$) δ: 1.60 (s, 2H), 2.78 (bd s, 4H), 3.45 (A_2 of A_2B_2 pattern, 2H), 3.70 (B_2 of A_2B_2 pattern, 2H), 4.79 (s, 2H), and 5.30 (s, 2H).

*From Ether Ditosylate 11*b

The ether ditosylate **11***b* (0.124 g) was dissolved in DMSO (5 mL) and potassium *tert*-butoxide (0.5 g) added; the mixture was stirred at room temperature for 24 h, then added to water (40 mL) and extracted with pentane (3 × 10 mL). The pentane extract was dried and evaporated to a low volume (≈ 0.25 mL) and this was separated by preparative gas chromatography at 150°C into **13** (14.6 mg; 36.6%) and **12** (9.7 mg; 24.3%).

6,10-endo, endo-*Dimethyl-3-oxatricyclo[5.2.1.0^{5,9}]decane* ***20***b

A solution of the dichloride **11***a* (0.20 g) in dry monoglyme (3 mL) was added to lithium aluminium hydride (0.1 g) in the same solvent (10 mL) and this mixture stirred under reflux for 72 h. The reduction was monitored by hydrolysing small aliquots approximately every 12 h, extracting with a small volume of pentane, and analysing this using gc–ms. The sequence **11***a* → **20***a* → **20***b* was readily followed and when complete the reaction was worked up by the addition of aqueous 2 *N* sodium hydroxide (0.5 mL) and the white suspension extracted with pentane (3 × 10 mL). The combined extracts were passed through a short Florisil column and eluted with ether. Evaporation under vacuum afforded **20***b* as a white solid, mp 38–40°C (0.088 g; 62%); ir (film): 2900, 1450, 1370, 1260, 1230, 1165, 1090, 1035, 1000, 970, 900, 840, and 720 cm^{-1}; ^1H nmr ($CDCl_3$) δ: 1.18 (s, 2H), 1.20 (s, 6H), 1.62 (s, 1H), 1.8–2.2 (m, 5H), 3.48 (A_2 of A_2B_2 pattern, 2H), and 3.90 (B_2 of A_2B_2 pattern, 2H); ^{13}C nmr ($CDCl_3$) δ: 13.6, 35.4, 37.8, 40.3, 41.0, 49.0, and 66.4.

endo,endo-*5,6-Dihydroxybicyclo[2.2.1]heptane*-endo,endo-*2,3-dicarboxylic Acid Dilactone* ***21*** *(12)*

exo,exo-5,6-Dibromobicyclo[2.2.1]heptane-*endo,endo*-2,3-dicarboxylic anhydride (40 g) (14) was added to a solution of sodium carbonate decahydrate (36 g) in water (350 mL) and this mixture was subjected to reflux for 3 h during which time the pH was maintained at approximately 10 by the addition of more sodium carbonate (if required). This clear solution was acidified with aqueous 2 *N* hydrochloric acid to pH 2 and then evaporated under vacuum to dryness to leave a white solid which was gently heated at 0.02 Torr with a free flame until dehydration was complete. The white residue was freed from inorganic salts by washing with cold water (50 mL) on the filter pump, resuspended in cold ethanol (50 mL), filtered, and washed with cold dry ether to leave the pure dilactone **21** (20.5 g; 92%), mp 266–268°C; ^1H nmr ($CDCl_3$–$C_6H_5NO_2$ 4:1) δ: 2.05 (s, 2H), 3.15 (s, 2H), 3.50 (s, 2H), and 4.86 (s, 2H); mass spectrum: *m/e* = 180 (M^+).

endo,endo-*2,3-Bis(hydroxymethyl)*-endo,endo-*5,6-dihydroxybicyclo[2.2.1]heptane* ***22***

The dilactone **21** (19.4 g) suspended in dry monoglyme (80 mL) was slowly added to excess lithium aluminium hydride (16 g) with stirring and this mixture refluxed for 72 h under anhydrous conditions. After cooling in an ice-bath, aqueous 2 *N* sodium hydroxide (50 mL) was carefully added with vigorous stirring and the whole reaction mixture diluted to a total volume of 1.5 L with methanol and then centrifuged in 4 × 375 mL portions. The combined supernatant liquid was evaporated to a white slurry under vacuum, dissolved in a minimum volume of hot methanol, and ether added until cloudy. Then solid Dry Ice (5 g) was added and the mixture recentrifuged. This process was repeated until the supernatant liquid evaporated to a clear viscous liquid (≈ 8 times), which was subjected to vacuum (0.02 Torr) at 80°C for 2 h to remove any water as this interfered with crystallization. The clear residue was taken up in a minimum of hot methanol, dry ether added until just cloudy, and stored in the refrigerator for 16 h. The product crystallized as small prisms and was collected by filtration. Further dilution of the mother liquors with dry ether produced two further crops, total yield 17.4 g. This was recrystallized using methanol/dry ether to give the pure tetrol **22** (14.4 g; 71%), mp 209–212°C; ir (Nujol mull): 3310, 3140, 1150, 1115, 1090, 1020, and 990 cm^{-1}; ^1H nmr (D_2O referenced to HOD = 4.72 ppm) δ: 1.35 (s, 2H), 2.45–2.55 (s + sh, 4H), and 4.15 (m, 6H); ^{13}C nmr (D_2O referenced to internal dioxane = 67.4 ppm) δ: 32.9 (t, *J* = 136.7 Hz), 43.4 (d, *J* = 126.0 Hz), 46.2 (d, *J* = 149.9 Hz), 62.0 (t, *J* = 143.9 Hz), and 70.8 (d, *J* = 145.2); mass spectrum: *m/e* = 188 (M^+).

Tetra-acetate, mp 85–86°C (dry ether).

2,6-Dioxatetracyclo[6.3.0.0^{1,10}.0^{7,8}]undecane ***23***

DMSO Method

The tetrol **22** (0.90 g) was heated in DMSO (10 mL) at 150°C for 15 h under anhydrous conditions. The bulk of the solvent was then removed from the black reaction mixture by vacuum (0.02 Torr) transfer and the residue directly subjected to preparative gas chromatography at 170°C. The product so collected was sublimed at 115°C and 20 Torr to give the diether **23** (0.23 g; 32%), mp 120–125°C; ir (film): 1350, 1290, 1240, 1070, 1010, 900 cm^{-1}; ^1H nmr ($CDCl_3$) δ: 1.55 (AB q, *J* = 13 Hz, 2H), 2.45–2.60 (2 bd s, 4H), 3.80 (A_2 of A_2B_2 pattern, 2H), 3.98 (s, 2H), and 4.01 (B_2 of A_2B_2 pattern, 2H); ^{13}C nmr ($CDCl_3$) δ: 24.6 (t, *J* = 132.5 Hz), 41.2 (d, *J* = 145.1 Hz), 44.9 (d, *J* = 145.2 Hz), 69.1 (t, *J* = 145.0 Hz), and 77.9 (d, *J* = 151.4 Hz); mass spectrum: *m/e* = 152 (M^+).

Thionyl Chloride Method

The tetrol **22** (0.25 g) was heated to reflux for 2 h with thionyl chloride (5 mL) and the mixture evaporated under vacuum to an orange gum. This was dissolved in dry ether and applied to a silica column (0.5 × 8 cm) packed in ether. After eluting with ether to remove any by-products, the column was washed with methanol and this eluate evaporated to leave behind the crude

product which was purified by sublimation as before to give clear, granular crystals of the di-ether **23** (0.082 g; 41%), mp 120–123°C.

Dilactone 8 (or 9) from Photo-dione 1

The photo-dione **1** (1) (5 g) was dissolved in methylene chloride (50 mL) and trifluoroperacetic acid, prepared by carefully adding trifluoroacetic anhydride (8.5 mL) to 90% hydrogen peroxide (1.4 mL) in methylene chloride (25 mL), was added and the mixture kept at room temperature for 15 h. This was reduced to a volume of 5 mL under vacuum and the clear amber oil so obtained taken up in carbon tetrachloride (100 mL) and then absolute ethanol (20 mL) was added with shaking and ice-cooling. The fine, white precipitate was collected and washed with dry ether to leave the crude product (4.7 g; 79%) which was recrystallized from methylene chloride to give **8** (or **9**) as needles, mp 250–255°C; ir (Nujol mull): 1755, 1725, 1250, 1180, 1080, 945, and 850 cm^{-1}; ^1H nmr ($CDCl_3$) δ: 1.8 (s, 2H), 2.95 (bd s, 4H), 3.30 (s, 2H), and 5.20 (m, 2H); ^{13}C nmr ($CDCl_3$) δ: 36.2 (d, J = 157.1 Hz), 39.4 (t, J = 135.1 Hz), 39.7 (d, J = 144.5 Hz), 45.1 (d, J = 150.8 Hz), 73.9 (d, J = 163.4 Hz), and 169.7 (s); mass spectrum: m/e = 206 (M^+).

1. R. C. Cookson, E. Crundwell, R. R. Hill, and J. Hudec. J. Chem. Soc. 3062 (1964).
2. A. Florey and P. Vogel. Helv. Chim. Acta, **58**, 1488 (1975).
3. E. Wenkert and J. E. Yoder. J. Org. Chem. **35**, 2986 (1970).
4. L. A. Paquette, R. A. Snow, J. L. Muthard, and T. Cynkowski, J. Am. Chem. Soc. **101**, 6991 (1979).
5. G. Mehta, V. Singh, P. N. Pandey, B. Chandhury, and H. Duddeck. Chem. Lett. (Japan), 59 (1980).
6. (*a*) A. R. Marchand and T-C. Chau. Tetrahedron, **31**, 2655 (1975); (*b*) G. Mehta, A. V. Reddy, and A. Srikrishna. Tetrahedron Lett. 4863 (1979); (*c*) J. C. Barborak, L. Watts, and R. Pettit. J. Am. Chem. Soc. **88**, 1328 (1966); (*d*) A. S. Kushner. Tetrahedron Lett. 3275 (1971); (*e*) W. K. Appel, T. J. Greenhough, J. R. Scheffer, J. Trotter, and L. Walsh. J. Am. Chem. Soc. **101**, 1158 (1980); **101**, 1160 (1980); (*f*) G. A. Craze and I. Watt. J. Chem. Soc. Chem. Commun. 147 (1980).
7. B. T. Gillis and P. E. Beck. J. Org. Chem. **28**, 1388 (1963).
8. R. Appel. Angew. Chem. Int. Ed. Engl. **14**, 801 (1975).
9. D. N. Butler and R. A. Snow. Can. J. Chem. **50**, 795 (1972).
10. M. E. Jung and M. A. Lyster. J. Org. Chem. **42**, 3761 (1977).
11. (*a*) E. J. Corey and A. W. Gross. Tetrahedron Lett. 1819 (1980); (*b*) A. Winston and P. Wilder. J. Am. Chem. Soc. **76**, 3045 (1954); (*c*) K. Alder and G. Stein. Ann. **514**, 1 (1934).
12. E. M. Arnett. Prog. Phys. Org. Chem. **1**, 223 (1963).
13. R. W. Alder, P. S. Bowman, W. R. P. Steele, and D. R. Winterman. J. Chem. Soc. Chem. Commun. 723 (1968).
14. P. D. Bartlett and A. Schnieder. J. Am. Chem. Soc. **68**, 3045 (1945).

Can. J. Chem. Downloaded from www.nrcresearchpress.com by 210.87.254.42 on 09/06/12
For personal use only.

Structure of a trichlorocyclohexenone from bleached kraft chlorination-stage effluent

A. Bruce McKague
B.C. Research, 3650 Wesbrook Mall, Vancouver, B.C., Canada V6S 2L2
Steven J. Rettig and James Trotter
Department of Chemistry, University of British Columbia, Vancouver, B.C., Canada V6T 1Y6
and
George R. Douglas
Mutagenesis Section, Environmental and Occupational Toxicology Division, Health and Welfare Canada, Ottawa, Ont., Canada K1A 0L2

Received August 20, 1981

A. Bruce McKague, Steven J. Rettig, James Trotter, and George R. Douglas. Can. J. Chem. **59**, 3372 (1981).

Several compounds suspected to be mutagenic have been isolated by large scale fractionation of chlorination-stage effluent from a bleached kraft pulp mill. When reacted with diazomethane, one of these compounds yields a crystalline material, **1**. Crystals of **1** are triclinic, $a = 7.8814(7)$, $b = 8.3988(8)$, $c = 10.309(1)$ Å, $\alpha = 71.529(8)$, $\beta = 80.002(7)$, $\gamma = 62.587(9)°$, $Z = 2$, space group $P\bar{1}$. The structure was solved by Patterson and Fourier techniques and was refined by full-matrix least-squares procedures to $R = 0.030$ and $R_w = 0.036$ for 1795 reflections with $I \geq 3\sigma(I)$. The structure analysis has unambiguously identified compound **1** as 1,6-dioxa-4,4,10-trichlorodispiro[2.1.4.3]dodec-10-en-12-one, implying that the material originally present was 1-oxa-6,10,10-trichlorospiro[4.5]dec-6-en-8,9-dione.

A. Bruce McKague, Steven J. Rettig, James Trotter et George R. Douglas. Can. J. Chem. **59**, 3372 (1981).

Certains composés mutagéniques ont été isolés par fractionnement à grande echelle des effluents de l'étage de chloruration d'une usine de blanchiment de pâte à papier (bleached Kraft). Par réaction avec le diazomethane, l'un de ces composés donne un produit cristallin **1**. Les cristaux de **1** sont tricliniques, $a = 7.8814(7)$, $b = 8.3988(8)$, $c = 10.309(1)$ Å, $\alpha = 71.529(8)$, $\beta = 80.002(7)$, $\gamma = 62.587(9)°$, $Z = 2$, group d'espace $P\bar{1}$. On a déterminé la structure par les méthodes de Patterson et de Fourier et on l'a précisée par la méthode des moindres carrés (matrice entière) jusqu'à des valeurs de $R = 0.030$ et $R_w = 0.036$ pour 1795 réflexions avec $I \geq 3\sigma(I)$. Cette analyse nous a permis d'identifier sans l'ambiguité le composé 1 comme étant dioxa-1,6 trichlor-4,4,10 dispiro [2.1.4.3]dodec-10-en-12-one, ce qui suppose que le produit primitif était l'oxa-1 trichloro-6,10,10 spiro[4.5]dec-6-en-8,9-dione.
[Traduit par le journal]

Introduction

Since chlorination-stage effluents from bleached kraft pulp mills were first reported to be mutagenic (1), interest in their chemical composition has increased. During the past two years several publications have appeared describing the identification and testing of mutagenic compounds found in this effluent (2–7). As a result of a large scale fractionation of chlorination-stage effluent from an interior B.C. mill we have obtained a number of compounds possibly associated with the mutagenicity. One of these compounds gave a crystalline product when reacted with diazomethane. The structure of the product has been determined by X-ray crystallography as the trichlorocyclohexenone **1**, suggesting the corresponding cyclohexenedione **2** was originally present.

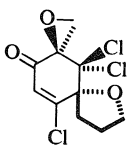

1

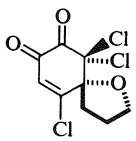

2

Experimental

Concentration of the Chlorination-stage Effluent

Three-litre columns of XAD-2 resin were prepared by washing with methanol (2 L), ether (6 L), methanol (4 L), and water (30 L). A sample of chlorination-stage effluent (105 L) was passed through three columns, 35 L/column at a rate of 3 L/h. Each column was eluted with ether (10 L) to recover the adsorbed material. The solvent was removed under reduced pressure on a rotary evaporator with use of a bath temperature below 50°C. the evaporated ether eluate was dissolved in ether (500 mL), dried ($MgSO_4$), and re-evaporated.

Fractionation of the Ether Eluate on Silica Gel

A portion of the ether eluate from the chlorination-stage sample equivalent to 25 L effluent (4.5 g) was separated into 5 fractions by chromatography on silica gel (300 g, 60/200 mesh). The column was eluted successively with hexane (1.5 L), hexane:ether 9:1 (1.5 L), hexane:ether 1:1 (1.5 L), ether (2 L), and methanol (1.5 L). Solvents were evaporated under reduced pressure as previously described. Material eluted by hexane:ether 1:1 was further fractionated in three successive chromatographic steps on silica gel, in each instance using a 1:90 weight ratio of material:silica gel and a fraction volume equal to the weight of silica gel. In the first step the column was eluted with hexane:ether 9:1 (5 fractions), hexane:ether 4:1 (5 fractions) and hexane:ether 2:1 (5 fractions). Fractions 7–11 were combined for the second step where the column was eluted with hexane:ether 9:1 (22 fractions) and hexane:ether 4:1 (8 fractions). Fractions 22–27 were combined and in the final step the column was eluted with hexane:ether 7:1 to provide an orange

0008-4042/81/243372-04$01.00/0
©1981 National Research Council of Canada/Conseil national de recherches du Canada

Can. J. Chem. Downloaded from www.nrcresearchpress.com by 210.87.254.5 on 09/06/12
For personal use only.

Can. J. Chem. Downloaded from www.nrcresearchpress.com by 210.87.254.5 on 09/06/12
For personal use only.

oil which was one spot by tlc (silica gel, benzene:ethyl acetate 9:1, uv or 2,4-DNP visualization). The compound had ms (chemical ionization, corrected for ionizing gas) *m/e* (% relative intensity); 272(13) $M^+ + 4$, 270(28) $M^+ + 2$, 268(29) M^+, 204(100); ir (cm^{-1}); 3400, 1710; uv (nm): 238.

Trichlorocyclohexenone, 1

Diazomethane, generated from *N*-nitrosomethylurea, was bubbled through a solution of the material obtained above (40 mg) in ether (2 mL) for 1 h. After standing another hour the ether was evaporated with a stream of N_2 and the residue fractionated by preparative thin layer chromatography on silica gel (benzene:ethyl acetate 95:5). The major uv absorbing band ($R_f \sim 0.8$) was recovered, triturated with hexane, and crystallized from ether–hexane giving colourless needles, mp 87–89°C; ms (electron impact) *m/e* (% relative intensity): 284(6) $M^+ + 2$, 282(6) M^+, 136(100); ir (cm^{-1}): 1700; uv(nm): 242.

X-ray Crystallographic Analysis of the Trichlorocyclohexenone, 1

A crystal ca. 0.40 × 0.30 × 0.12 mm in size was mounted in a general orientation. Unit-cell parameters were refined by least-squares on 2 sin θ/λ values for 25 reflections measured on a diffractometer with Mo Kα radiation (λ = 0.71073 Å). Crystal data at 22°C are:

$C_{10}H_9Cl_3O_3$ f.w. = 283.54

Triclinic, $a = 7.8814(7)$, $b = 8.3988(8)$, $c = 10.309(1)$ Å, $\alpha = 71.529(8)$, $\beta = 80.002(7)$, $\gamma = 62.587(9)°$, $V = 574.2(1)$ Å^3, $Z = 2$, $\rho_c = 1.640$ g cm^{-3}, $F(000) = 288$, μ(Mo Kα) = 18.4 cm^{-1}. Absent reflections: none, space group $P\bar{1}$ (C_i^1,No. 2, lattice constants refer to reduced cell) from structure analysis.

Intensities were measured with graphite-monochromated Mo Kα radiation on an Enraf-Nonius CAD4-F diffractometer. An ω–2θ scan at 1.26–10.06° min^{-1} over a range of (0.60 + 0.35 tan θ) degrees in ω (extended by 25% on both sides for background measurement) was employed. Data were measured to 2θ = 55°. The intensities of three check reflections, measured every 3600 s throughout the data collection, remained constant to within 4%. After data reduction, an absorption correction was applied using the Gaussian integration method (8, 9). Transmission factors ranged from 0.598 to 0.811 for 188 sampling points. Of the 2617 independent reflections measured, 1795 (68.6%) had intensities greater than $3\sigma(I)$ above background where $\sigma^2(I) = S + 2B + (0.03(S - B))^2$ with S = scan count and B = background count.

The centrosymmetric space group $P\bar{1}$ was indicated by both the *E*-statistics and by the Patterson function. The positions of the three chlorine atoms were determined from the Patterson function and those of the remaining non-hydrogen atoms from a subsequent difference map. After full-matrix least-squares refinement of the non-hydrogen atoms with anisotropic thermal parameters to $R = 0.046$, a difference map gave the positions of all nine hydrogen atoms which were included in subsequent cycles of refinement with isotropic thermal parameters. The scattering factors of ref. 10 were used for non-hydrogen atoms and those of ref. 11 for hydrogen atoms. Anomalous scattering factors from ref. 12 were used for the Cl atoms. The weighting scheme, $w = 1/\sigma^2(F)$ where $\sigma^2(F)$ is derived from the previously defined $\sigma^2(I)$, gave uniform average values of $w(|F_o| - |F_c|)^2$ over ranges of $|F_o|$ and was employed in the final stages of refinement. Convergence was reached at $R = 0.030$ and $R_w = 0.036$ for 1795 reflections with $I \geq 3\sigma(I)$. For all 2617 reflections $R = 0.059$ and $R_w = 0.038$. The function minimized was $\sum w(|F_o| - |F_c|)^2$, $R = \sum||F_o| - |F_c||/\sum|F_o|$ and $R_w = (\sum w(|F_o| - |F_c|)^2/\sum w|F_o|^2)^{1/2}$.

On the final cycle of refinement the mean and maximum parameter shifts corresponded to 0.03 and 0.34σ, respectively. The mean error in an observation of unit weight was 1.797. A final difference map showed no unusual features. The final positional and thermal parameters appear in Tables 1 and 2[1] respectively. Measured and calculated structure factors have been placed in the Depository of Unpublished Data.[1]

TABLE 1. Final positional (fractional × 10^5, H × 10^3) and isotropic thermal parameters ($U \times 10^3$ Å^2) with estimated standard deviations in parentheses

Atom	*x*	*y*	*z*	U_{eq}/U_{iso}
Cl(1)	51813(6)	−19947(7)	27679(6)	48
Cl(2)	28220(8)	−16387(8)	7424(6)	53
Cl(3)	−20631(8)	36119(7)	16650(7)	59
O(1)	16834(19)	10864(17)	35739(13)	37
O(2)	31411(20)	−44478(18)	37856(16)	45
O(3)	−7325(21)	−30927(22)	34007(18)	56
C(1)	26611(37)	22540(35)	33660(27)	51
C(2)	23705(47)	33769(37)	18953(28)	61
C(3)	23010(38)	20830(32)	11769(24)	49
C(4)	15621(26)	8169(25)	23081(18)	33
C(5)	27914(24)	−12882(25)	23878(19)	33
C(6)	19464(23)	−25083(24)	34026(19)	32
C(7)	25355(31)	−34522(29)	48232(24)	44
C(8)	−981(27)	−19535(28)	31279(21)	38
C(9)	−12661(27)	426(30)	25903(21)	41
C(10)	−5329(26)	12722(25)	22158(19)	37
H(1a)	398(4)	143(3)	356(3)	54(7)
H(1b)	213(3)	297(3)	400(3)	50(6)
H(2a)	110(4)	453(4)	183(3)	59(7)
H(2b)	339(4)	364(4)	156(3)	80(9)
H(3a)	357(4)	133(4)	84(3)	61(7)
H(3b)	140(4)	273(4)	43(3)	65(8)
H(7a)	356(3)	−328(3)	509(2)	47(6)
H(7b)	165(3)	−381(3)	547(2)	49(6)
H(9)	−260(4)	40(3)	250(2)	58(7)

The ellipsoids of thermal motion for the non-hydrogen atoms are shown in Fig. 1. The thermal motion has been analysed in terms of the rigid-body modes of translation, libration, and screw motion (13). The rms standard error in the temperature factors σU_{ij} (derived from the least-squares analysis) is 0.009 Å^2. Analysis of all non-hydrogen atoms gave rms $\Delta U_{ij} = 0.0028$ Å^2 and physically reasonable rigid-body parameters. The appropriate bond distances have been corrected for libration (14), using shape parameters q^2 of 0.08 for all atoms involved. Corrected bond lengths appear in Table 3 along with the uncorrected values; corrected bond angles do not differ by more than 1σ from the uncorrected values given in Table 4. Intra-annular torsion angles defining the conformations of the five- and six-membered rings are listed in Table 5. Tables 6–8, containing bond lengths and angles involving hydrogen atoms and a complete list of torsion angles, have been deposited.[1]

Results and Discussion

The crystal structure of **1** consists of discrete molecules separated by normal van der Waals distances. Each molecule (Fig. 1) contains a system

[1]The structure factor table, Table 2 (anisotropic thermal parameters), and other material mentioned in the text are available, at a nominal charge, from the Depository of Unpublished Data, CISTI, National Research Council of Canada, Ottawa, Ont., Canada K1A 0S2.

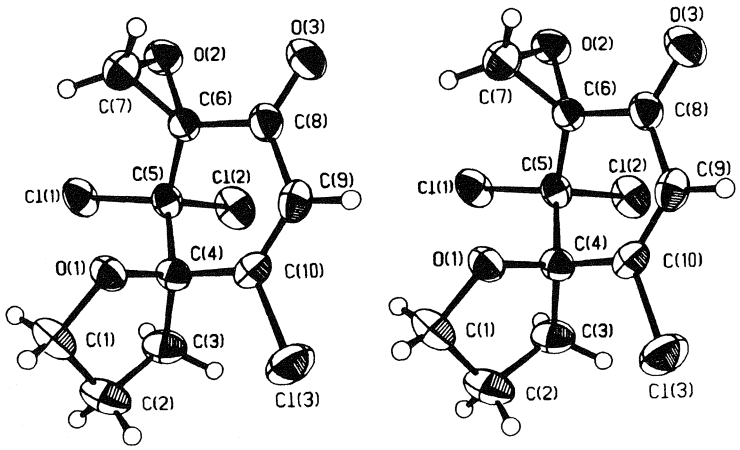

FIG. 1. Stereo view of **1**, 50% probability thermal ellipsoids are shown for the non-hydrogen atoms. Hydrogen atoms have been assigned artificially small thermal parameters for the sake of clarity.

TABLE 3. Bond lengths (Å) with estimated standard deviations in parentheses

	Length			Length	
Bond	Uncorr.	Corr.	Bond	Uncorr.	Corr.
Cl(1)—C(5)	1.770(2)	1.775	C(2)—C(3)	1.520(3)	1.524
Cl(2)—C(5)	1.806(2)	1.812	C(3)—C(4)	1.542(3)	1.547
Cl(3)—C(10)	1.728(2)	1.733	C(4)—C(5)	1.559(2)	1.564
O(1)—C(1)	1.451(2)	1.455	C(4)—C(10)	1.527(3)	1.532
O(1)—C(4)	1.419(2)	1.425	C(5)—C(6)	1.515(3)	1.521
O(2)—C(6)	1.416(2)	1.420	C(6)—C(7)	1.466(3)	1.469
O(2)—C(7)	1.447(3)	1.450	C(6)—C(8)	1.509(2)	1.514
O(3)—C(8)	1.211(2)	1.215	C(8)—C(9)	1.460(3)	1.464
C(1)—C(2)	1.502(4)	1.508	C(9)—C(10)	1.330(3)	1.334

TABLE 4. Bond angles (deg) with estimated standard deviations in parentheses

Bonds	Angle (deg)	Bonds	Angle (deg)
C(1)—O(1)—C(4)	109.88(15)	C(4)—C(5)—C(6)	112.17(14)
C(6)—O(2)—C(7)	61.61(12)	O(2)—C(6)—C(5)	116.81(14)
O(1)—C(1)—C(2)	105.3(2)	O(2)—C(6)—C(7)	60.23(12)
C(1)—C(2)—C(3)	103.8(2)	O(2)—C(6)—C(8)	115.80(15)
C(2)—C(3)—C(4)	103.7(2)	C(5)—C(6)—C(7)	123.8(2)
O(1)—C(4)—C(3)	107.26(15)	C(5)—C(6)—C(8)	113.27(15)
O(1)—C(4)—C(5)	107.94(14)	C(7)—C(6)—C(8)	116.6(2)
O(1)—C(4)—C(10)	105.39(14)	O(2)—C(7)—C(6)	58.16(12)
C(3)—C(4)—C(5)	112.5(2)	O(3)—C(8)—C(6)	121.6(2)
C(3)—C(4)—C(10)	115.1(2)	O(3)—C(8)—C(9)	122.9(2)
C(5)—C(4)—C(10)	108.25(14)	C(6)—C(8)—C(9)	115.5(2)
Cl(1)—C(5)—Cl(2)	107.80(9)	C(8)—C(9)—C(10)	122.4(2)
Cl(1)—C(5)—C(4)	110.50(12)	Cl(3)—C(10)—C(4)	115.72(14)
Cl(1)—C(5)—C(6)	111.21(13)	Cl(3)—C(10)—C(9)	118.56(15)
Cl(2)—C(5)—C(4)	108.89(12)	C(4)—C(10)—C(9)	125.6(2)
Cl(2)—C(5)—C(6)	106.05(12)		

of three spiro-fused rings. The central cyclohexenone ring adopts a sofa conformation with C(5) (crystallographic numbering), which is bonded to two chlorine atoms, displaced from the approximate plane defined by the five remaining ring atoms. The conformation of the five-membered oxolane ring is best described as an "envelope", with C(2) displaced from the rough plane of the four other atoms. As expected, the oxirane and oxolane rings are oriented approximately at right angles to the central ring.

The geometry of the oxirane ring, which has an

Can. J. Chem. Downloaded from www.nrcresearchpress.com by 210.87.254.5 on 09/06/12
For personal use only.

TABLE 5. Intra-annular torsion angles (deg) standard deviations in parentheses

Atoms	Value (deg)
C(10)—C(4)—C(5)—C(6)	−46.0(2)
C(5)—C(4)—C(10)—C(9)	20.5(3)
C(4)—C(5)—C(6)—C(8)	55.3(2)
C(5)—C(6)—C(8)—C(9)	−34.7(2)
C(6)—C(8)—C(9)—C(10)	7.6(3)
C(8)—C(9)—C(10)—C(4)	−1.1(3)
C(4)—O(1)—C(1)—C(2)	24.7(2)
C(1)—O(1)—C(4)—C(3)	−7.0(2)
O(1)—C(1)—C(2)—C(3)	−32.0(3)
C(1)—C(2)—C(3)—C(4)	27.3(3)
C(2)—C(3)—C(4)—O(1)	−13.1(2)

area of 0.905 Å^2, agrees well with that reported for a number of other epoxy groups (15, 16). The geometry of the remainder of the molecule is generally as expected, distortions from "normal" geometry being explicable in terms of intramolecular steric effects. The three sp^2 hybridized carbon atoms (C(8), C(9), and C(10)) are all slightly, but significantly, displaced from the planes of their substituents (by 0.024(2), 0.012(2) and 0.029(2) Å, respectively). The double bonds of the α,β-unsaturated ketone fragment (O(3)=C(8)—C(9)=C(10)) are essentially localized, the central C(8)—C(9) bond at 1.464(3) Å being somewhat shorter than the expected C(sp^2)—C(sp^2) single bond distance of 1.485 Å. Some of this shortening, however, may result from hybridization effects. The bonds C(4)—C(5) and C(4)—C(10) are both lengthened by intramolecular steric interactions involving chlorine atoms.

A number of mechanisms may be postulated to explain the formation of a spirochlorocyclohexenedione such as **2** during bleaching of kraft pulp with chlorine. The compound could be formed either by direct degradation of lignin, a polymer of coniferyl alcohol (17) or by oxidation and chlorination of one of the monomeric phenols containing a three carbon side chain associated with pulping processes.

Acknowledgments

This work was funded by a contract with the Environmental and Occupational Toxicology Division, Environmental Health Directorate, Health Protection Branch, Health and Welfare Canada. X-ray crystallographic analysis was made possible by financial support from the Natural Sciences and Engineering Research Council of Canada and the Xerox Corporation, and assistance from the University of British Columbia Computing Centre.

1. P. ANDER, K-E. ERIKSSON, M-C. KOLAR, K. KRINGSTAD, U. RANNUG, and C. RAMEL. Svensk Papperstidn. **80**, 454 (1977).
2. A. BJØRSETH, G. E. CARLBERG, and M. MØLLER. Sci. Total Environ. **11**, 197 (1979).
3. E. R. NESTMANN, E. G-H. LEE, T. I. MATULA, G. R. DOUGLAS, and J. C. MUELLER. Mutation Res. **79**, 203 (1980).
4. L. STOCKMAN, L. STRÖMBERG, and F. DE SOUSA. Cell. Chem. Technol. **14**, 517 (1980).
5. B. R. HOLMBOM, R. H. VOSS, R. D. MORTIMER, and A. WONG. Tappi, **64**, 172 (1981).
6. K. P. KRINGSTRAD, P. O. LJUNGQUIST, F. DE SOUSA, and L. M. STRÖMBERG. Environ. Sci. Technol. **15**, 562 (1981).
7. A. B. MCKAGUE, E. G-H. LEE, and G. R. DOUGLAS. Mutation Res. Lett. **91**, 301 (1981).
8. P. COPPENS, L. LEISEROWITZ, and D. RABINOVICH. Acta Crystallogr. **18**, 1035 (1965).
9. W. R. BUSING and H. A. LEVY. Acta Crystallogr. **22**, 457 (1967).
10. D. T. CROMER and J. B. MANN. Acta Crystallogr. Sect. A, **24**, 321 (1968).
11. R. F. STEWART, E. R. DAVIDSON, and W. T. SIMPSON. J. Chem. Phys. **42**, 3175 (1965).
12. D. T. CROMER and D. LIBERMAN. J. Chem. Phys. **53**, 1891 (1970).
13. V. SCHOMAKER and K. N. TRUEBLOOD. Acta Crystallogr. Sect. B, **24**, 63 (1968).
14. D. W. J. CRUICKSHANK. Acta Crystallogr. **9**, 747 (1956); **9**, 754 (1956); **14**, 896 (1961).
15. C. FOCES-FOCES, F. H. CANO, and S. GARCIA-BLANCO. Acta Crystallogr. Sect. B, **33**, 3521 (1977).
16. M. L. MARTINEZ, F. H. CANO, and S. GARCIA-BLANCO. Acta Crystallogr. Sect. B, **33**, 3913 (1977).
17. K. V. SARKANEN and C. H. LUDWIG. Lignins, occurrence, formation, structure and reactions. Wiley-Interscience, New York. 1971.

Can. J. Chem. Downloaded from www.nrcresearchpress.com by 210.87.254.5 on 09/06/12
For personal use only.

Can. J. Chem. Downloaded from www.nrcresearchpress.com by 210.87.254.40 on 09/06/12
For personal use only.

Separation of fluorescent impurities from Amphotericin B

NILS O. PETERSEN AND PAUL F. HENSHAW
Department of Chemistry, University of Western Ontario, London, Ont., Canada N6A 5B7

Received August 13, 1981

NILS O. PETERSEN and PAUL F. HENSHAW. Can. J. Chem. **59**, 3376 (1981).

Reverse phase high pressure liquid chromatography of Amphotericin B samples provides one means of cleanly separating Amphotericin B from a strongly fluorescent contaminant. Purified Amphotericin B does not exhibit any fluorescence.

NILS O. PETERSEN et PAUL F. HENSHAW. Can. J. Chem. **59**, 3376 (1981).

On décrit la séparation efficace par chromatographie liquide à haute pression en phase renversée de l'amphotéricine B et de son contaminant fluorescent. L'amphotéricine B ne présente aucune fluorescence.

[Traduit par le journal]

Amphotericin B is one of a series of polyene antibiotics isolated from several species of *Streptomycetes* (1). Amphotericin B is purported to interact with sterols, notably ergosterol and cholesterol, in cell membranes to form cylindrical complexes with hydrophilic channels along their axes (2). Hereby, Amphotericin B and similar polyene antibiotics generate conductive paths for Na^+ and K^+ ions across the membrane. The resultant loss of osmotic control can lead to cell lysis and death.

Amphotericin B and several of the other polyene antibiotics are currently being investigated for their potential use as anti-tumor agents (3) and for their role as immunoadjuvants in mice (4). All actions of polyene antibiotics are thought to depend critically on their binding affinities to sterols in membranes. *In vitro* studies of polyene antibiotic – sterol binding have exploited changes in both optical and fluorescence properties (5, 6). We report here on our findings that, contrary to published data (6), Amphotericin B does not exhibit intrinsic detectable fluorescence in any of several solvent systems. Rather, the fluorescence arises from an impurity easily separable by high pressure liquid chromatography.

Figure 1*A* shows the optical spectrum (---) (Varian Assoc. Cary 219), the fluorescence emission spectrum (·····), and the fluorescence excitation spectrum (—) (Perkin Elmer MPF-4) of a sample of Amphotericin B (Lot #800254, Calbiochem, La Jolla, CA) in dimethyl sulfoxide. It is apparent that the optical spectrum and the fluorescence excitation spectrum do not match, suggesting that the fluorescing and absorbing species are different. Simple polyenes generally show good correlations between optical and fluorescence excitation spectra, and the lowest energy allowed transition ($A_g \rightarrow B_u$) corresponds to the strongest fluorescent band (7).

In order to ascertain whether Amphotericin B was the fluorescing species, the material was purified by analytical high pressure liquid chromatography (Varian Instruments Model 5000) on a reverse phase column (Waters Assoc. Column model 8C1810μ) eluting at 2 mL per min with a buffer mixture containing 35% (v/v) acetonitrile and 65% (v/v) 0.05 *M* aqueous sodium citrate buffered at pH = 5.3. The elution profile (monitored continuously at 254 nm) is shown in Fig. 2*A* trace *b* compared to the elution of the dimethylsulfoxide solvent in trace *a*. The elution profile is similar to that reported (8) for Amphotericin B in a different reverse phase system and shows three minor peaks (I–III) and a major band (IV) which is slightly asymmetric. Two millilitre fractions (labelled 1–20) were collected as marked in Fig. 2. Each fraction was diluted 1:1 (v/v) with the elution buffer. Optical and fluorescence emission and excitation spectra were recorded. The optical (---), fluorescence emission (·····) and excitation (—) spectra of a 10 μL sample of stock solution in dimethyl sulfoxide diluted into 5 mL elution buffer is shown in Fig. 1*B*. The corresponding spectra for fractions 2 and 14 are shown in Figs. 1*C* and 1*D*, respectively. Based on the absorption spectra of fractions 13–15 (Fig. 1*D*) we assign peak IV to Amphotericin B. Further characterization by chemical means and by biological activity assays should confirm this assignment. Clearly, the fluorescence in fraction 2 does not co-chromatograph with the absorption in fraction 14. This is illustrated more clearly in Fig. 2*B*, which shows the peak

0008-4042/81/243376-03$01.00/0
©1981 National Research Council of Canada/Conseil national de recherches du Canada

Can. J. Chem. Downloaded from www.nrcresearchpress.com by 210.87.254.40 on 09/06/12
For personal use only.

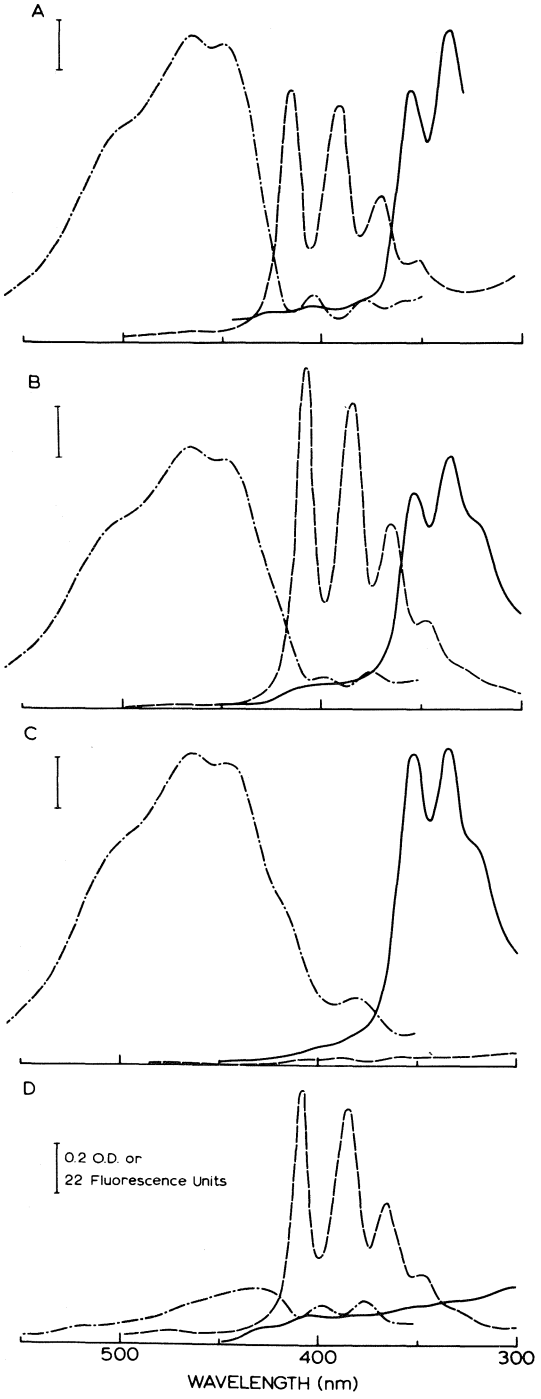

FIG. 1. Optical spectra (---), fluorescence emission spectra (-·-·-), and fluorescence excitation spectra (—) of Amphotericin B in dimethylsulfoxide at 7.0 μg/mL (*A*) and in elution buffer at 11.6 μg/mL (*B*) and of fractions 2 (*C*) and 14 (*D*) from the high pressure liquid chromatography elution. The fluorescence emission was measured with λ_{EX} = 335 nm while the fluorescence extinction was measured with λ_{em} = 465 nm. In each graph the bar represents 0.2 OD units or 22 fluorescence units as indicated in *D*.

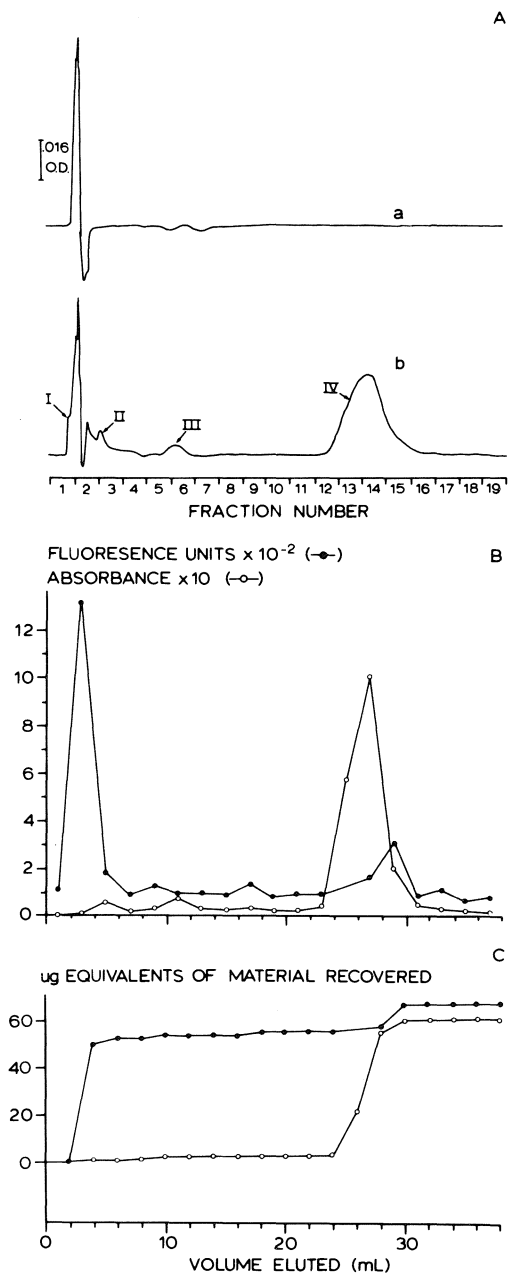

FIG. 2. (*A*) Elution profiles monitored at 254 nm of 10 μL dimethylsulfoxide (trace *a*) and of about 58 μg Amphotericin B in 10 μL dimethylsulfoxide. Peaks I to IV are absent in the pure solvent and are attributed to Amphotericin B (peak IV) and impurities (peaks I to III). Peak I co-chromatographs with the solvent and is the predominant fluorescent impurity. (*B*) Absorbance amplitude at 408 nm (—○—) and fluorescence emission amplitude at 465 nm (λ_{EX} = 335 nm) (—●—) as a function of elution volume from the reverse phase column. The peak fluorescence appears in fraction 2 while the peak absorbance occurs in fraction 14. (*C*) The total amount of material recovered as a function of elution volume in microgram equivalents based on the fluorescence (—●—) and the absorbance (—○—) of Fig. 2*B*.

amplitude of the fluorescence emission at 465 nm ((—•—), λ_{EX} = 335) and the absorbance at 408 nm (—○—). Fractions 2 and 3 contained most of the fluorescence whereas fractions 13–15 contained all of the absorbance. A small amount of fluorescence is detectable in fractions 14 and 15 (Fig. 2*B*) but this appears to elute slightly later than the major absorbance. Although the resolution is insufficient to provide strong evidence, we believe this fluorescence does not arise from Amphotericin B but rather from yet another impurity.

The extinction at 408 nm in the elution buffer is approximately 0.118 OD units per (μg/mL) of the impure material. Similarly, the fluorescence emission at 465 nm (λ_{EX} = 335 nm) is approximately 10 fluorescence units per (μg/mL) of the impure material. Using these numbers and the measured absorbance and emission of each fraction, it was possible to calculate the microgram "equivalents" of the original material recovered in each fraction as measured by the optical and fluorescence properties respectively. These data are shown in Fig. 2*C* and demonstrate that most of the fluorescence (—•—) added to the column is recovered in fraction 2 whereas all of the absorbance (—○—) is recovered in fractions 13–15. The recovery is quantitative since 58 ± 5 μg material was added, while 66 μg equivalents of fluorescent material was recovered and 60 μg equivalents of absorbant material was recovered. This quantitative recovery of both fluorescence and absorbance, together with the lack of observable changes in either the fluorescence or absorption spectra, provide strong evidence that the materials eluted from the column were present prior to injection on the column. We, therefore, feel it is unlikely that any of the elution peaks arise from chemical degradation or reaction on the column.

These experiments demonstrate unambiguously that virtually all the fluorescence observed from Amphotericin B solutions prepared prior to high pressure liquid chromatography purification arises from a highly polar impurity which co-chromatographs with the solvent (dimethylsulfoxide) in this system. Even solutions which are allowed to sit in the dark contain larger proportions of this fluorescent species, as judged both from the fluorescence emission amplitude relative to the optical spectrum, and from the peak areas of the high pressure liquid chromatography elution profiles. It is possible that this impurity represents a degradation product of Amphotericin B. The fluorescence spectra properties are similar to those of tetraenes (5, 6).

We conclude that Amphotericin B does not exhibit significant intrinsic fluorescence in any of the solvents tested (dimethylsulfoxide, *N,N*-dimethylformamide, ethanol, methanol, water, and aqueous buffers). We still need to investigate whether complexes of Amphotericin B and sterols can exhibit fluorescence particularly when formed in membranes.

Incomplete studies of other polyene antibiotics suggest that many, and perhaps all, of these are intrinsically fluorescent. It is then possible that Amphotericin B is unique in its non-fluorescent properties among the class of polyene antibiotics.

Acknowledgements

N.O.P. is an NSERC University Research Fellow, P.F.H. was an NSERC Undergraduate Research Fellow for 1981. This work was supported by NSERC grant U0109 to N.O.P. and by National Institute of Health (NCI) grant CA15665. We acknowledge valuable discussion with Larry Gaudioso of University of Illinois (Urbana) and thank Dr. G. Medoff of Washington University (St. Louis) for an Amphotericin B sample.

1. A. W. NORMAN, A. M. SPIELVOGEL, and R. G. WONG, Adv. Lipid Res. **14**, 127 (1976).
2. P. VAN HOOGEVEST and B. DEKRUIJFF. Biochim. Biophys. Acta, **511**, 397 (1978).
3. F. VALERIOTE, R. LYNCH, G. MEDOFF, and B. V. KUMAR. J. Natl. Cancer Inst. **56**, 557 (1976).
4. J. R. LITTLE, E. J. PLUT, J. KOTLER-BRAJTBURG, G. MEDOFF, and G. S. KOBAYASHI. Immunochemistry, **15**, 219 (1978).
5. J. PATTERSON, J. HOLLAND, and L. L. BIEBER. J. Antibiotics, **32**, 646 (1979).
6. R. BITTMAN and S. A. FISCHKOFF. Proc. Natl. Acad. Sci. U.S.A., **69**, 3795 (1972).
7. B. HUDSON and B. KOHLER. Annual Rev. Phys. Chem. **25**, 437 (1974).
8. W. MECHLINSKI and C. P. SCHAFFNER. J. Chromatogr. **99**, 619 (1974).

Can. J. Chem. Downloaded from www.nrcresearchpress.com by 210.87.254.40 on 09/06/12
For personal use only.

Homoenolization and H/D exchange in tricyclic ketones. Rearrangement via a γ-enolate[1]

A. K. CHENG,[2] A. K. GHOSH, I. (TSE) SHEEPY, AND J. B. STOTHERS
Department of Chemistry, The University of Western Ontario, London, Ont., Canada N6A 5B7

Received August 24, 1981

A. K. CHENG, A. K. GHOSH, I. (TSE) SHEEPY, and J. B. STOTHERS. Can. J. Chem. **59**, 3379 (1981).

Under homoenolization conditions (*t*-BuO$^-$, *t*-BuOH, 185°C), 7,7-dimethyltricyclo[3.2.1.0^{2,4}]octan-6-one (**5**) readily rearranges to 4,4-dimethyltricyclo[3.3.0.0^{2,8}]octan-3-one (**6**) which subsequently suffers reduction of the three-membered ring, presumably by electron transfer from the *tert*-butoxide anion for which some evidence has been obtained. The conversion of **5** to **6** constitutes one of very few examples of rearrangement via a γ-enolate. From reactions in *tert*-butyl alcohol-*O*-d_1, deuterium incorporation at the several sites in **5** and **6** undergoing H/D exchange was directly monitored by ^{2}Hmr spectroscopy; these results shed light on the stereochemistry of homoenolate formation and cleavage.

A. K. CHENG, A. K. GHOSH, I. (TSE) SHEEPY et J. B. STOTHERS. Can. J. Chem. **59**, 3379 (1981).

Dans des conditions d'homoénolisation (*t*-BuO$^-$, *t*-BuOH, 185°C), la diméthyl-7,7 tricyclo[3.2.1.0^{2,4}]octanone-6 (**5**) se transpose facilement en diméthyl-4,4 tricyclo[3.3.0.0^{2,8}]octanone-3 (**6**) dont le cycle à 3 chaînons est réduit ensuite probablement par transfert d'électron de l'anion *tert*-butylate; nous avons obtenu quelques données supportant cette hypothèse. La transformation du composé **5** en composé **6** constitue un des rares exemples de transposition par l'intermédiaire d'un γ-énolate. A partir des réactions dans le *tert*-butanol-*O*-d_1 on a pu enregistrer directement, par rmn du ^{2}H, l'échange H/D conduisant à l'incorporation du deutérium dans plusieurs positions des composés **5** et **6**; ces résultats permettent de mieux comprendre la stéréochimie et le clivage des homoénolates.

[Traduit par le journal]

Since the initial discovery (1) that a ketonic carbonyl group can activate proton abstraction from remote carbon atoms in strong base (homoenolization), several examples in acyclic and cyclic systems have been described as recently reviewed (2). In the majority of cases, proton abstraction occurs at β-carbons, i.e. β-enolization, but there are a few examples involving γ-carbons. The latter include the rearrangement of half-cage ketone **1** to its isomer **2** upon treatment with *t*-BuO$^-$/*t*-BuOH at elevated temperatures, the typical homoenolization conditions, and for which it was established that homoketonization of the bird-cage alcohol **3** gave the same mixture of **1** and **2** (3). Also, H/D exchange at the *syn*-methyl (C-8) of camphor (4) and at C-6 and -7 in 3,3-dimethylbicyclo[3.3.0]octan-2-one (5) is consistent with the formation of γ-enolates. In fact for the former system strong support has been provided by the synthesis of the corresponding alcohol **4** by reductive cyclization of 8-bromocamphor, homoketonization of which in a deuterated medium provided 8-deuteriocamphor exclusively (6). A γ-enolate may also be implicated in the conversion of *sym*-tetramethyldiphenylacetone to 2-isopropylbenzoic acid (7). Our interest in homoenolization has led us to examine systems potentially able to rearrange via γ-enolates and in this communication we wish to describe preliminary results from the study of 7,7-dimethyltricyclo[3.2.1.0^{2,4}]octan-6-one (**5**). We have found that **5** is readily transformed to 4,4-dimethyltricyclo[3.3.0.0^{2,8}]octan-3-one (**6**) upon treatment with *t*-

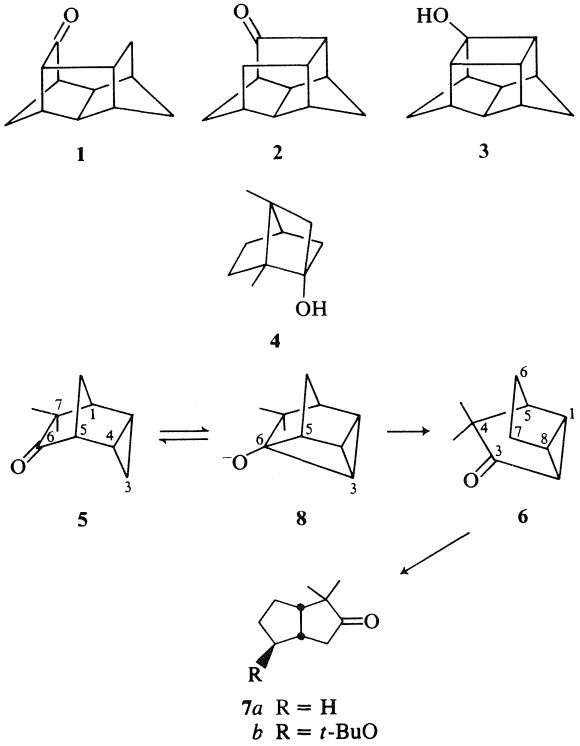

[1]Part XXXIV of Nuclear magnetic resonance studies; for Part XXXIII see ref. 12.

[2]Present address: Department 367, Beckman Instruments, Fullerton, CA.

0008-4042/81/243379-03$01.00/0

©1981 National Research Council of Canada/Conseil national de recherches du Canada

Can. J. Chem. Downloaded from www.nrcresearchpress.com by 210.87.254.6 on 09/06/12
For personal use only.

Can. J. Chem. Downloaded from www.nrcresearchpress.com by 210.87.254.6 on 09/06/12
For personal use only.

BuO^-/t-BuOH at 185°C, constituting a third example of rearrangement via γ-enolization. Furthermore **6** is unstable under these conditions and is slowly converted to a mixture of the bicyclic octanone **7***a* and its *exo*-6-*tert*-butoxy derivative **7***b*. Experiments in *tert*-butyl alcohol-*O*-d_1 permitted identification of the sites of H/D exchange in **5** and **6**.

Ketone **5** (8) was dissolved in anhydrous t-BuO^-/t-BuOH (1.27 *M*) to furnish a solution 0.26 *M* in ketone; aliquots were transferred to glass tubes under nitrogen, sealed under vacuum, and heated at 185°C for various times. Gas–liquid chromatography (glc) of the neutral product (pentane extraction, >80% yields) revealed the presence of three new ketones in addition to starting material, isolable by preparative glc. (Three minor components constituting <5% of the product in the longest runs were not identified.) The major new component **6** in the earlier samples reached a maximum concentration which then decreased progressively. With increasing reaction times the proportion of the other two new ketones **7** increased (see Table 1).

Ketone **6** (1713 cm^{-1}, $CHCl_3$) gave the following ^{1}Hmr data (δ, $CDCl_3$): 0.85 (s, 3H), 1.10 (s, 3H), 2.66 (bq, 1H), 2.43 (bt, 1H), 1.35 (m, 1H), and complex absorption 1.6–2.1 (5H). Its ^{13}Cmr spectrum contained 10 signals: methyl (2), methylene (2), methine (4), quaternary (1), and one carbonyl peak. *Exact Mass* calcd. for $C_{10}H_{14}O$: 150.1044; found (high resolution ms); 150.1044. These data are consistent with **6** and the structure was confirmed by methylation ($NaNH_2$–CH_3I) of the parent ketone, prepared as described by Monti *et al.* (9).

The major ketone (1730 cm^{-1}) in the later samples exhibited a ^{1}Hmr spectrum (δ, $CDCl_3$) containing two methyl singlets (1.03, 1.08), with multiplets centred at 2.70 (2H), 2.25 (1H), 2.04 (1H), and complex absorption 0.9–1.9 (6H). Its ^{13}Cmr spectrum contained 10 signals: methyl (2), methylene (4), methine (2), quaternary (1), and one carbonyl peak. *Exact Mass* calcd. for $C_{10}H_{16}O$: 152.1206; found (high resolution ms): 152.1200. These data indicated this ketone to be **7***a* and identical material could be generated by reduction of **6** with potassium in alcohol followed by CrO_3 oxidation of the resulting alcohols. The remaining ketonic product (1740, 1130 cm^{-1}) appeared to contain an ethereal linkage. Its ^{1}Hmr spectrum included (δ, $CDCl_3$): 1.00 (s, 3H), 1.05 (s, 3H), 1.20 (s, 9H), 3.80 (m, 1H), and 1.30–3.00 (complex absorptions, 8H). The ^{13}Cmr spectrum contained 3 methyl signals, one of which was ~3 times as intense as the others, 3 methylene, 3 methine, 2 quaternary, and a carbonyl signal. *Exact Mass* calcd. for $C_{14}H_{24}O_2$: 224.1775; found (high resolution ms): 224.1764. These data accord well with structure **7***b*. Upon treatment with t-BuO^-/t-BuOH at 185°C, **6** is smoothly converted to a mixture of **7***a* and **7***b*.

TABLE 1. Distribution [a] of components in the neutral product obtained upon treatment of **5** with t-BuO^-/t-BuOH at 185°C

Time (h)	**5**	**6**	**7***a*	**7***b*
6	55	27	15	Trace
13	45	36	18	Trace
30	19	50	22	8
47	8	58	24	9
63	3	57	29	10
76	—	48	33	16
95	—	40	38	17

[a]Determined as % of the total by glc using a 6% FFAP column at 155°C.

The transformation of **5** → **6** must involve proton abstraction from C-3 leading to γ-enolate **8**, which can suffer cleavage of the original C-5, C-6 bond to furnish **6** or return to starting material. Evidence that the formation of **8** is reversible was furnished by experiments in t-BuOD. Treatment of **5** with t-BuO^-/t-BuOD at 185°C for 6 h gave samples of **5**-d_x and **6**-d_x which were examined by ^{2}Hmr. The ^{2}H spectrum of **5**-d_x contained four signals establishing that H/D exchange occurred, in order of decreasing reactivity, at C-5, -4, -3, and the *exo*-methyl carbon.[3] Exchange at C-3 is stereospecific with deuterium found only in the *exo*-orientation, indicative of the reversible formation of **8**, and opening with *inversion* to return to **5**. This is the first such example; all other γ-homoketonizations for which the stereochemistry has been examined proceed with *retention* (2). Bridgehead (C-5) and stereoselective methyl exchange is analogous to our earlier findings for the closely-related 7,7-dimethylbicyclo[3.2.1]octan-6-one (10). The inductive effect of the carbonyl group presumably activates C-4 exchange. From these experiments **6** had seven ^{2}H signals, three of which will arise from exchange in **5** before conversion to **6**. The ^{2}H spectra of **6**-d_x contained signals for ^{2}H at C-1, -2, -7, -8, and both methyls. Since incorporation of ^{2}H in **6** results from prior exchange in **5** and from exchange after its formation, the latter processes were examined separately by treatment of **6** with t-BuO^-/t-BuOD at 185°C. The ^{2}H spectra of these **6**-d_x samples differed significantly in that only four

[3]The ^{2}H assignments were confirmed by comparison of ^{1}H and ^{2}H spectra of solutions containing Eu(fod)$_3$ in the presence of which the ^{1}H shieldings could be determined using spin-decoupling to establish individual assignments. The *exo* and *endo* methyl groups were distinguishable by selective decoupling of the ^{13}C spectrum.

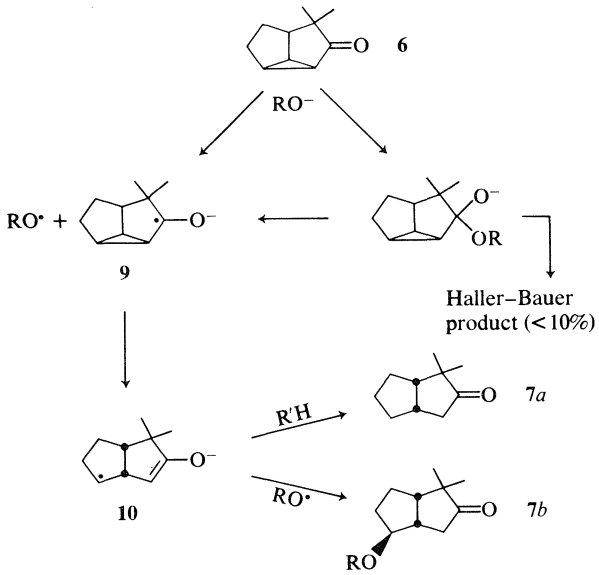

SCHEME 1

signals were apparent after a 30 h treatment. No deuterium was detectable at the *endo*-methyl or at C-7! The absence of ^2H at C-7 establishes that the opening of **8** → **6** is irreversible. Only the hydrogens bonded to the *exo*-methyl and the cyclopropyl carbons undergo exchange;[3] thus, there is no evidence of γ-enolization in **6**.

The conversion **6** → **7** requires a reducing agent but we have been unable to detect an oxidized product. With lithium aluminium hydride, **6** is reduced to a mixture of the corresponding epimeric alcohols which may be oxidized to **6**; as noted above, **6** is readily reduced with K metal in *t*-BuOH to a 2:1 mixture of two bicyclic alcohols which can be oxidized to furnish **7***a*. Treatment of **6** with *t*-BuO⁻/*t*-BuOH at reflux gave no reaction even after 135 h. Thus the formation of **7***b* via Michael addition of *t*-BuO⁻ to **6** seems unlikely. Our current view is summarized in Scheme 1. We suggest that **6** → **7** occurs by electron transfer from *t*-BuO⁻, either directly or by homolysis of the addition product formed by attack of *t*-BuO⁻ at the carbonyl of **6**; Haller–Bauer cleavage of this addition product to form an ester is not a major pathway since it gives < 10% of the total product after the longest reaction times. In the resulting ketyl **9**, the three-membered ring can open to form **10**, which subsequently gains a hydrogen atom from solvent giving **7***a* or reacts with *tert*-butoxide radical formed in the generation of **9** to yield **7***b*. Other evidence for electron transfer from *t*-BuO⁻ has been presented (11).

From these results we conclude that γ-enolization occurs reversibly from **5** but the cleavage of the resulting γ-enolate **8** to **6** is unidirectional. Experiments to determine the relative rates of ^2H incorporation in **5** and **6** require lower reaction temperatures and these are in progress, as well as further work to substantiate our suggestion for the **6** → **7** transformation.

Acknowledgements

We wish to thank the Natural Sciences and Engineering Research Council of Canada for financial support of this work. We are indebted to Mary Ellen Sturgeon for technical assistance and we are grateful to D. H. Hunter, D. D. Tanner, and E. W. Warnhoff for valuable discussions.

1. A. NICKON and J. L. LAMBERT. J. Am. Chem. Soc. **84**, 4604 (1962); **88**, 1905 (1966).
2. D. H. HUNTER, J. B. STOTHERS, and E. W. WARNHOFF. *In* Rearrangements in ground and excited states. Vol. 1. *Edited by* P. de Mayo. Academic Press, New York. 1980. pp. 410–437.
3. R. HOWE and S. WINSTEIN. J. Am. Chem. Soc. **87**, 915 (1965); T. FUKUNAGA. J. Am. Chem. Soc. **87**, 917 (1965); T. FUKUNAGA and R. A. CLEMENT. J. Org. Chem. **42**, 270 (1977).
4. A. NICKON, J. L. LAMBERT, J. E. OLIVER, D. F. COVEY, and J. MORGAN. J. Am. Chem. Soc. **98**, 2593 (1977).
5. A. L. JOHNSON, N. O. PETERSEN, M. B. BRAMPERSAD, and J. B. STOTHERS. Can. J. Chem. **52**, 4143 (1974).
6. W. A. DADSON and T. MONEY. Can. J. Chem. **58**, 2524 (1980).
7. R. A. DYLLICK-BRENZINGER and J. B. STOTHERS. J. Chem. Soc. Chem. Commun. 108 (1979).
8. A. K. CHENG and J. B. STOTHERS. Org. Magn. Reson. **9**, 355 (1977).
9. S. A. MONTI, D. J. BUCHECK, and J. C. SHEPARD. J. Org. Chem. **34**, 3080 (1969).
10. A. K. CHENG, J. B. STOTHERS, and C. T. TAN. Can. J. Chem. **55**, 447 (1977).
11. K. A. BILEVITCH, N. N. PUBNOV, and O. Y. OKHLOBYSTIN. Tetrahedron Lett. 3465 (1968).
12. Y. HOYANO, A. STOESSL, and J. B. STOTHERS. Can. J. Chem. **58**, 1894 (1980).

Can. J. Chem. Downloaded from www.nrcresearchpress.com by 210.87.254.6 on 09/06/12
For personal use only.